Organic sulfur mechanisms. 27. A reexamination of the reaction of thiirane 1,1-dioxide with aqueous hydroxide[1]

JAMES FREDERICK KING, JOHN HENRY HILLHOUSE, AND KISHAN CHAND KHEMANI
Department of Chemistry, University of Western Ontario, London, Ont., Canada N6A 5B7

Received April 30, 1984

JAMES FREDERICK KING, JOHN HENRY HILLHOUSE, and KISHAN CHAND KHEMANI. Can. J. Chem. **63**, 1 (1985).

Reaction of thiirane 1,1-dioxide (**1**) with aqueous barium hydroxide gives chiefly barium ethanesulfonate (**3**) together with some ethylene and barium sulfite, and only a small amount (<5%) of barium 2-hydroxyethanesulfinate (**2**), the material previously described by Hesse *et al.* as the major product of this reaction. Reaction of **1** with potassium hydroxide proceeds analogously except for the formation of barium 2-sulfinatoethanesulfonate (**6**) from reaction of potassium sulfite with unreacted **1**. This revision, when taken with what is already known of the final step of the Ramberg–Bäcklund reaction, provides a consistent picture of the reaction of thiirane 1,1-dioxides with hydroxide. For this reaction we suggest a common intermediate with a pentacoordinated sulfur for formation of both the sulfonate anion and the olefin, though an attempt to confirm the existence of such a species using $H_2{}^{18}O$ was unsuccessful.

JAMES FREDERICK KING, JOHN HENRY HILLHOUSE et KISHAN CHAND KHEMANI. Can. J. Chem. **63**, 1 (1985).

La réaction du dioxyde-1,1 de thiiranne (**1**) avec l'hydroxyde de baryum aqueux donne principalement l'éthanesulfonate de baryum (**3**) avec un peu d'éthylène et de sulfite de baryum et une faible quantité (<5%) d'hydroxy-2 éthanesulfinate de baryum (**2**), le produit décrit antérieurement par Hesse *et al.*, comme produit principal de cette réaction. La réaction du composé **1** avec l'hydroxyde de potassium se produit d'une façon analogue, à l'exception du fait qu'il se forme du sulfinato-2 éthanesulfonate de baryum (**6**) qui provient de la réaction du sulfite de potassium avec le composé **1** qui n'aurait pas réagi. Cette nouvelle étude, entreprise à la lumière de ce qui est connu de la dernière étape de la réaction de Ramberg–Bäcklund, permet de développer une image cohérente de la réaction des dioxydes-1,1 de thiirannes avec l'hydroxyde. Nous suggérons donc que cette réaction implique un soufre pentacoordonné comme intermédiaire commun tant pour la formation de l'anion sulfonate que pour celle de l'oléfine et ce en dépit du fait qu'on n'a pas réussi à confirmer l'existence d'un tel intermédiaire en utilisant $H_2{}^{13}O$.

[Traduit par le journal]

In 1957 Hesse *et al.* (2) reported that thiirane 1,1-dioxide (ethylene sulfone) (**1**), on reaction with aqueous barium hydroxide, gave barium 2-hydroxyethanesulfinate (**2**) plus a small amount of ethylene and barium sulfite; the sulfinate (**2**) was described as being thermally unstable, decomposing rapidly to ethylene and barium sulfite above 50°C. Recently, while exploring possible routes to 2-hydroxyethanesulfonyl chloride (3), we had occasion to repeat some of these experiments and found them to be seriously in error; in particular, we found that **2** constitutes only a small part of product from **1** and, in addition, is thermally quite stable. We now describe our investigation and discuss its relevance to the mechanism of the final step of the Ramberg–Bäcklund reaction.

Results and discussion

Reaction products

Repetition of the reaction of **1** with aqueous barium hydroxide in our hands gave, as shown in Scheme 1 and Table 1, barium ethanesulfonate (**3**) as the major product, along with some ethylene and barium sulfite, plus a small quantity of the 2-hydroxyethanesulfinate (**2**). Similar reaction with potassium hydroxide gave potassium ethanesulfonate (**5**), ethylene, a small amount of the 2-hydroxyethanesulfinate (**4**), and a further product shown to be potassium 2-sulfinatoethanesulfonate (**6**).

Ethylene and barium sulfite were identified by comparison of ir spectra of the isolated products with those of authentic materials. The formation of barium ethanesulfonate (**3**) was proved by (a) the presence of the characteristic ^{1}Hmr and ^{13}Cmr signals of authentic **3** in the spectra of the reaction product, and (b) conversion of the crude reaction product via ethanesulfonyl chloride into crystalline ethanesulfon-*p*-toluidide, identical to a specimen prepared by a standard method. The presence of a small amount of the 2-hydroxyethanesulfinate salts (**2** and **4**) was indicated by a pair of triplets, at 2.60 and 3.92 ppm in the ^{1}Hmr spectrum, and by peaks at 65.9 and 59.1 ppm in the ^{13}Cmr spectrum of the crude product, the same signals having been observed already with authentic 2-hydroxyethanesulfinate (see experimental section and ref. 3).

An early indication that the crude potassium hydroxide product contained **6** was obtained by aqueous chlorination, which converted it into potassium 1,2-ethanedisulfonate, as shown by the replacement of the peaks ascribed to **6** by characteristic singlets in the ^{13}Cmr and ^{1}Hmr spectra, at 49.3 and 3.26 ppm, respectively. The 2-sulfinatoethanesulfonate anion was then characterized in the form of its potassium (**6**) and sodium salts. The latter was made simply by treating **1** with aqueous sodium sulfite; the recrystallized material showed appropriate ^{1}H and ^{13}Cmr and ir spectra and good elemental analyses. Conversion of this salt to the acid by ion exchange followed by neutralization with KOH gave **6**, which also gave correct elemental

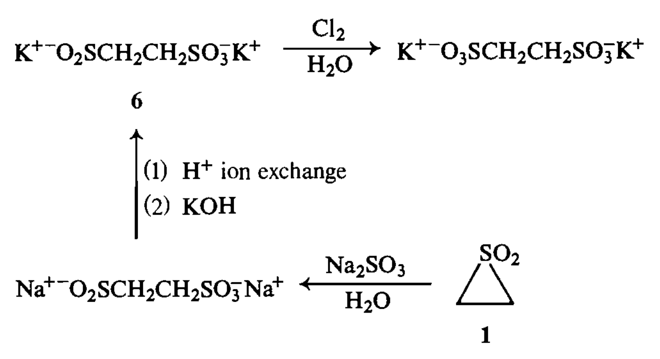

analyses and the same ir and ^{13}Cmr and ^{1}Hmr spectra as the sodium salt. This preparation also, of course, provides the

[1]For part 26 see ref. 1.

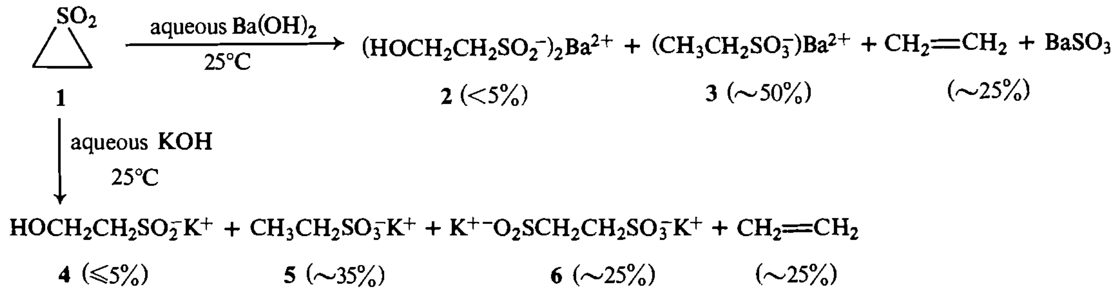

See Table 1 for conversions and yields in individual runs

SCHEME 1

TABLE 1. The reaction of thiirane 1,1-dioxide (**1**) with aqueous barium and potassium hydroxides

Reactants and conditions[a]				Percentage yields of products (% conversions[b])			
M	[OH^-]	[**1**]	Time (h)	$CH_3CH_2SO_3^-M^+$ (**3** or **5**)	$CH_2{=}CH_2$[c]	$HOCH_2CH_2SO_2^-M^+$ (**2** or **4**)	Recovered **1**
Ba/2	0.33	0.16	24	49 (53)	14 (15)	3 (3)	7
	0.36	0.18	48	53 (53)	31 (31)	3 (3)	0
K	0.31[d]	0.28[d]	34	34 (48)	26 (37)	5 (6)	3
	0.45	0.45	42	28 (42)	24 (36)	3 (5)	10
	0.34[e]	0.17[e]	24	42 (54)	22 (28)	3 (4)	0

[a]At room temperature in 5 mL of H_2O, except as noted.
[b]That is, yield after correcting for recovered **1**, and, for the KOH reactions, the formation of potassium 2-sulfinatoethanesulfonate (**6**). Recovery of **1** is probably not quantitative and the conversions given are therefore likely somewhat underestimated.
[c]Ethylene production was not determined directly; the numbers given are the yields of the co-product, i.e. $BaSO_3$ from the $Ba(OH)_2$ reactions, and **6** from KOH.
[d]Ten millilitres of H_2O.
[e]At the end of the reaction the mixture was extracted with CH_2Cl_2 and the aqueous layer brought to pH 7.00 with 1 *M* HCl and worked up; the weight of the product (148 mg after drying) was corrected for the KCl present (estimated from the volume of HCl added) to give an estimated product weight (105 mg) which was used (with the ^{1}Hmr spectrum) in calculating these yields.

explanation for the difference in products found with the reaction of **1** with potassium and barium hydroxides. The reaction with hydroxide anion gives ethylene and sulfite anion in both cases, but whereas SO_3^{2-} simply precipitates as barium sulfite in the one case, it remains in solution and reacts with **1** in the other. Analogous ring opening of **1** by such nucleophiles as bromide or thiophenoxide ions has been reported by Vilsmaier and co-workers (4,5). The small amount of **2** and **4**, noted in the reactions of **1** with hydroxide presumably also arises similarly though, in accord with the pattern expected from hard–soft acid–base theory, this is only a very minor pathway with this nucleophile.

The numbers in Table 1 given as "percentage conversion" give the percentages of products after correction for unreacted **1** and, in the reaction with KOH, diversion of **1** to form **6**. Note that each molecule of $BaSO_3$ or **6** must be accompanied by a molecule of ethylene, and, as indicated in Table 1, it is on this basis that the (minimum) yields of ethylene are assigned. If in fact these reactions simply involve hydroxide anion without the countercations, we would expect the numbers under the above heading to be the same for both the barium and potassium hydroxides. The values in Table 1 indicate that the products from the two reagents are the same within the uncertainty of the rather complex and imprecise procedures used, and there is clearly no basis for suspecting any counterion effect.

Our experiments on the cleavage of **1** with hydroxide were carried out a number of times and found to be reproducible within the limits of the analytical method. Since we regard the identity of the products as established beyond reasonable doubt, it is pertinent to consider why Hesse *et al.* report such different results. Their elemental analyses, of course, fit **3** as well as **2**, but their assertion that their product above 50°C is rapidly decomposed into ethylene and barium sulfite is more difficult to explain. We have found that authentic **2** is not readily decomposed below 350°C (3) and is stable at 98°C for at least 5 h; **3** is also completely unaffected by temperatures much higher than 50°C. We note, however, that in our hands work-up of the reaction of **1** with $Ba(OH)_2$ after 1 h (the reaction time used by these authors) showed only partial reaction; specifically **3** was formed in <20% yield and a good deal of unreacted **1** was recovered. Noting also that their experiments were carried out before ^{1}Hmr or even ir spectra were generally used to examine crude reaction products, we are inclined to suspect that unreacted thiirane 1,1-dioxide (**1**), perhaps with residual base, is the source of the ethylene produced on heating above 50°C as reported by Hesse *et al.* (2).

The mechanism of the final step of the Ramberg–Bäcklund reaction

Cleavage of a thiirane 1,1-dioxide (episulfone) is, of course, the final step in the well-known Bordwell mechanism (6,7) of the Ramberg–Bäcklund reaction (6–9). This process commonly gives an olefin (and presumably sulfite anion), though (saturated) sulfonate anions have been observed when (a) the original substrate has two or three α-halogen atoms (10,11), and (b) as a minor product in the reaction of chloromethyl ethyl sulfone (12). Whereas the report of Hesse *et al.* (2) describes behavior of the parent thiirane 1,1-dioxide entirely different from that of its alkylated derivatives, our findings fit well with the picture of episulfone cleavage adduced from study of the Ramberg–Bäcklund reaction. It would appear that up to one alkyl group (or else one or more halogen atoms) on the thiirane 1,1-dioxide permits a measure of cleavage to the sulfonate salt, whereas more alkyl groups lead more or less entirely to olefin formation.

Bordwell *et al.* have suggested that a species analogous to **7** is an intermediate in the methoxide-promoted desulfonylation[2] of *cis*-2,3-diphenylthiirane 1,1-dioxide (13), and Paquette (8) has proposed that formation of β-chloroalkanesulfonate anions arises by "attack of hydroxide at the sulfur atom with C–S bond cleavage to give more stable carbanion". We find it particularly attractive to combine these two pictures and to view the two sets of products as proceeding from a common species, e.g. **7** and (or) possibly **8**; a species such as **7**, by having two reaction pathways (other than reversal to starting material)

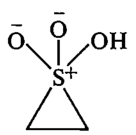

7

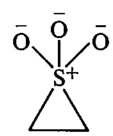

8

must therefore have a finite lifetime, and thus be a genuine intermediate. Although such hypervalent sulfur species have been subjects of discussion for many years and well-characterized oxygenated 10-S-5 anions have in fact been prepared (19,20), the existence of such species as actual intermediates in the reactions of ordinary sulfones or sulfonic or sulfuric esters has not been established. A good case for such intermediates has been presented by Kice (21), but, on the other hand, the conclusion in one recent examination of the reaction of aryl arenesulfonates is that the reaction probably does not proceed by way of an intermediate of finite lifetime (22).

The formation of such a hypervalent species (**7** or **8**) is expected (13) to be easy, relative to one from an unstrained precursor, owing to the release of considerable ring strain, provided that the form of **7** with one carbon apical and the other equatorial is formed.[3] It should be noted that this version of **7** is less symmetrical than **1** and that cleavage to the ethanesulfonate (**3** or **5**) might be expected to arise by cleavage of the relatively weak sulfur – apical carbon bond, probably in a general acid-promoted process akin to that suggested by Thibblin and Jencks (25) for the opening of cyclopropanols and related species. For the synthetically important extrusion to form the olefin, Bordwell *et al.* have suggested that the hypervalent intermediate cleaves by way of a short-lived biradical species. This proposal was made after the enunciation of orbital symmetry rules for cheletropic reactions but before the possibility of nonlinear cheletropic cleavage of three-membered rings had been put forward; in the light of Dewar's very recent pronouncement that "multibond reactions cannot normally be synchronous" (26), however, we would not presume to examine the mechanism of the cheletropic extrusion further at this stage.

In the hope of obtaining experimental verification of the existence of **7** as a species of finite lifetime, we tried carrying out the cleavage of **1** in ^{18}O-water. As with the others before us who have carried out related experiments (27,28), however, we found no incorporation of ^{18}O in the recovered starting sulfonyl compound. As has already been clearly noted by Kaiser (29), failure to observe ^{18}O-exchange does not rule out the intermediacy of the pentacoordinated species, but merely that if such a species (e.g. **7**) is formed, either equilibration of the oxygens or return to **1** must be slow relative to its further reaction.

[2]Although the thermal decomposition of episulfones has been extensively studied (see ref. 14 for a summary), it is evident that the relatively neglected base-promoted process is the important pathway under the usual conditions of the Ramberg–Bäcklund reaction. For example, although the conversion of *cis*-2,3-diphenylthiirane 1,1-dioxide to *cis*-stilbene is known to take place readily under mild conditions (e.g. in 1 h in CS_2 at 46°C) (13,15–17), for the reaction in methanol at 25°C Bordwell *et al.* note that "a [methoxide] concentration of 10^{-5} *M* is sufficient to make the half-lives of the first-order and second-order decompositions equal" (13). In agreement with Mock's activation data (18), which show the desulfonylation of neat **1** to be very slow at room temperature ($k = 2.1 \times 10^{-8}$ s^{-1} at 25°C), we find that the ^{1}Hmr signal of **1** in D_2O is undiminished after 1 week at room temperature; our base-promoted reactions were 90% complete within 5 min to 48 h depending on the hydroxide concentration.

[3]The C—S—C angle in **1** is reported to be 54.6° (23) in contrast to the "unstrained" angle in dimethyl sulfone of about 103° (24); conversion to this form of **7** would therefore effect a considerable reduction in ring strain since the C—S—C angle in the corresponding unstrained system would be expected to be around 90° or perhaps slightly less (cf. ref. 20).

Experimental

Reagent grade chemicals and solvents were used without additional purification unless otherwise noted. Melting points were determined on a Kofler Hot Stage and are uncorrected. Infrared spectra were obtained with a Beckman 4250 spectrophotometer and, unless otherwise stated, refer to KBr discs. The ^{1}Hmr spectra were obtained using Varian T60 and XL100 spectrometers, with all reported chemical shifts from the latter instrument; ^{13}Cmr spectra were determined on a Varian XL200 instrument using a sweep width of 5 K with 32 K transforms. Mass spectra were run on a Varian MAT-311A spectrometer. Solvent evaporation on work-up was carried out using a Büchi rotary evaporator connected to a water aspirator. Thiirane 1,1-dioxide (**1**) was prepared by the method of Hesse *et al.* (2) and purified by distillation (78°C/1.5 Torr; 1 Torr = 1.33 Pa). The colorless liquid so obtained gave, on cooling, white crystals, mp 18–19°C, and the following spectra: ir ($CHCl_3$) ν_{max}: 3100 (m), 3020 (m), 1390 (m), 1375 (m), 1325 (vs), 1210 (w), 1175 (vs), 1005 (m), 750 (m, br) cm^{-1}; ^{1}Hmr ($CDCl_3$) δ: 3.15 (s); ^{13}Cmr ($CDCl_3$) δ: 31.6. The ^{1}Hmr spectra of a solution of **1** in D_2O (with TSP as the chemical shift and integration standard), before and after standing 1 week at room temperature, were identical. Sodium 2-hydroxyethanesulfinate, prepared as described previously (3), showed ^{13}Cmr signals at δ(D_2O) 65.8 and 59.0.

Reaction of thiirane 1,1-dioxide (1) with base

(a) *Potassium hydroxide*

A 10-mL round bottom flask containing thiirane 1,1-dioxide (**1**) (205 mg, 2.2 mmol) and KOH (125 mg, 2.2 mmol) dissolved in water (5 mL) was evacuated (2 Torr) and connected to an evacuated ir gas cell (NaCl plates, 10-cm path length) via an adaptor fitted with a stopcock which was opened from time to time over a 2-h period to collect the evolved gas in the cell. The ir spectrum showed peaks at ν_{max} 3120 (w), 3020 (vw), 1920 (w), 1440 (s), 945 (s) cm^{-1}, as observed also in the spectrum of authentic ethylene (Linde). The reaction mixture was allowed to react a further 40 h, after which it was extracted with CH_2Cl_2 (4 × 50 mL). The organic extracts were combined, dried with anhydrous $MgSO_4$, and the solvent evaporated to give unreacted **1** (20 mg, 0.22 mmol, 10%). The aqueous layer was evaporated and the last traces of water removed by azeotropic distillation with benzene and then by keeping under vacuum (5 Torr) for 24 h. The white powder (263 mg) thus obtained gave the following ^{1}Hmr spectrum (D_2O) δ: 1.27 (t), 2.92 (q), 2.59−3.22 (symmetrical A_2B_2 multiplet), 2.60 (t), 3.92 (t). The peaks were assigned from comparison with authentic spectra to potassium ethanesulfonate (**5**) (1.27 and 2.92 ppm), potassium 2-sulfinatoethanesulfonate (**6**) (2.59−3.22 ppm), and potassium 2-hydroxyethanesulfinate (**4**) (2.60 and 3.92 ppm), with the ratio of the peak areas coresponding to relative amounts of 50, 44, and 6% of **5**, **6**, and **4**, respectively. The ^{13}Cmr spectrum of this mixture confirmed the presence of these compounds with peaks at 57.7 and 46.8 assigned to **6**, at 48.2 and 11.2 due to **5**, and 65.9 and 59.1 ppm due to **4**. This material showed the presence of water (presumably of crystallization) in the ir spectrum; ν_{max}: 3400 (s, br), 2920 (w), 1620 (w), 1170 (vs, br), 1030 (s), 970 (w, br), 740 (m), 690 (w), 580 (w), 510 (w, br), 420 (w) cm^{-1}. Upon drying at 145°C/5 Torr for 36 h, the peak at 3400 cm^{-1} was largely removed, and the product mixture weighed 237 mg, which, when taken with the relative proportions deduced from the ^{1}Hmr spectrum, corresponds to yields of 24% of **6**, 28% of **5**, and 3% of **4**.

The presence of **6** in the reaction mixture was further demonstrated as follows. Chlorine gas was bubbled for 2 min into a solution of 50 mg of the reaction product in water (1 mL) at room temperature. The yellow solution so obtained was washed with CH_2Cl_2, the aqueous layer then evaporated, and the residual solid dried as before; the white powder (55 mg) thus obtained showed peaks at 3.3 in the ^{1}Hmr and 49.3 ppm in the ^{13}Cmr spectra characteristic of potassium 1,2-ethanedisulfonate (42%), in addition to those at 2.9 and 1.26 ppm (^{1}Hmr) and at 48.3 and 11.3 (^{13}Cmr) due to unchanged potassium ethanesulfonate (**5**) (58%). In a separate experiment, authentic **6** (27 mg, 0.12 mmol) was oxidized as above by bubbling chlorine (2 min) into a D_2O solution (0.5 mL) at room temperature. The ^{1}Hmr spectrum of the resulting solution showed peaks at 3.3(s) and 3.4−4.5 ppm (apparent A_2B_2). On standing (1 h), the complex set of peaks at 3.4−4.5 ppm almost completely disappeared, with corresponding growth of the singlet at 3.3 ppm (assigned, from comparison with authentic material, to potassium 1,2-ethanedisulfonate); the complex set of peaks at 3.4−4.5 is tentatively assigned to potassium 2-(chlorosulfonyl) ethanesulfonate, $K^+\bar{O}_3SCH_2CH_2SO_2Cl$, which hydrolyses on standing.

(b) *Barium hydroxide*

Thiirane 1,1-dioxide (**1**, 75 mg, 0.815 mmol), $Ba(OH)_2.8H_2O$ (257 mg, 0.815 mmol), and water (5 mL) were combined and the gas evolved collected over a 2-h interval and identified (as ethylene) as described above. The reaction mixture was allowed to react a further 22 h, after which the precipitated white solid was collected by filtration and dried (25 mg, 0.115 mmol, 14%); the ir spectum, with peaks at ν_{max} 1880 (w), 1630 (w), 1100 (w), 940 (vs, br), 640 (m), 500 (m) cm^{-1}, was identical to that of an authentic specimen of $BaSO_3$ (prepared by mixing solutions of Na_2SO_3 and $BaCl_2$ and collecting and drying the precipitate). The filtrate was extracted with CH_2Cl_2 (4 × 50 mL); the organic extracts were combined, dried with anhydrous $MgSO_4$, and the solvent evaporated to yield unreacted **1** (5 mg, 0.054 mmol, 7%). CO_2 was bubbled into the water layer and the precipitated $BaCO_3$ filtered off (and, after drying, identified by ir). The aqueous filtrate was then evaporated and the last traces of water removed as before. The white powder (95 mg) so obtained showed (a) ^{1}Hmr peaks at δ (D_2O) 1.29 (t, 3H), 2.95 (q, 2H), 2.60 (t, 2H), and 3.90 (t, 2H), indicating (by comparison with authentic spectra) the presence of **3** and **2** in relative proportions of 94% and 6% respectively, (b) the following ir spectrum, ν_{max}: 3400 (m, br), 2980 (w), 2940 (w), 1650 (w), 1450 (w), 1425 (w), 1200 (vs, br), 1050 (s), 780 (w), 750 (m), 520 (s) cm^{-1}, and (c) ^{13}Cmr peaks at δ (D_2O) 65.9 and 59.1 ppm assigned to **2**, and 48.2 and 11.2 ppm due to **3**. Upon drying at 145°C/5 Torr for 36 h, the peak at 3400 cm^{-1} was largely removed and the product mixture weighed 92 mg, which, when taken with the relative proportions deduced from the ^{1}Hmr spectrum and corrected for $BaCO_3$ present (see below), corresponds to 49% and 3% yields of **3** and **2** respectively. The $BaCO_3$ above apparently arose because of the solubility of $Ba(HCO_3)_2$; the quantity was estimated at 16 mg (of the 92 mg above) on the basis of a control experiment in which a known comparable amount of $Ba(OH)_2$ was treated with CO_2 as above and the weight of the precipitate (78%) and the material remaining in solution (22%) determined; the ir spectra of both (after drying) were identical to that of authentic $BaCO_3$.

In another experiment, **1** (1.2 g, 13 mmol) and $Ba(OH)_2.8H_2O$ (2.4 g, 7.6 mmol) in water (37 mL) were allowed to react for 1 h. Excess CO_2 was then bubbled into the mixture and the precipitate of $BaCO_3$ and $BaSO_3$ (as shown by ir) collected by filtration, and the filtrate evaporated (below 35°C) to yield a cream-coloured solid (0.92 g), the ^{1}Hmr spectrum (D_2O, T60) of which showed two singlets, a quartet, and a triplet (ratios roughly 12:6:2:3) corresponding to water, **1**, and **3** in the molar ratio 6:3:1, or about 400 mg (17% yield) of **3**. Attempts to remove the water completely considerably increased the ratio of **3** to **1**, presumably by volatilizing the latter; the ^{1}Hmr spectrum (XL100, D_2O), in addition to the peaks at 4.65 (s, HOD), 3.38 (s, **1**), 2.92 (q, **3**), and 1.27 (t, **3**), also showed peaks at 2.58 and 3.90 ppm corresponding to **2** (about 8 mol% of the amount of **3** or ~1% yield). An aqueous solution of this material was passed through a column of Rexyn 101 (H) and evaporated to yield a brown syrup. Thionyl chloride (50 mL) and a few drops of *N*,*N*-dimethylformamide were added and the mixture refluxed for 3 h, whereupon the excess $SOCl_2$ was removed by evaporation to give a brown liquid (0.4 g). To this liquid a solution of *p*-toluidine (0.5 g, 4.7 mmol) and triethylamine (1.0 mL, 7.2 mmol) in benzene (15 mL) was added. After standing overnight the solution was extracted with 1.0 *M* HCl (2 × 10 mL) and water (10 mL). The benzene layer was dried, filtered, and the solvent evaporated to yield a brown oil (0.16 g) which was recrystallized from benzene − petroleum ether (60−80°C) to yield off-white crystals (10 mg), mp 79−80°C; mixture mp with authentic etl.:nesulfon-*p*-toluidide gave no depression; ^{1}Hmr and ir were identical to those of an authentic specimen, mp 79−80°C (30).

(c) *$K^{18}OH$ in $H_2{}^{18}O$*

A solution of $K^{18}OH$ was made by dissolving small pieces of potassium (39 mg, 1 mmol) in 0.32 mL of $H_2{}^{18}O$ (97.5 at.% ^{18}O), supplied by MSD Isotopes division of Merck Frosst Canada Inc., Montreal, Canada, under a slow stream of nitrogen at 0°C. Thiirane 1,1-dioxide (**1**) (92 mg, 1 mmol) was then added to the above solution with stirring at room temperature. Gas evolution started immediately. After 30 s, the reaction mixture was extracted with CH_2Cl_2 (4 × 20 mL). The organic extracts were combined, dried with anhydrous $MgSO_4$, and the solvent evaporated to yield unreacted **1** (30 mg), which upon analysis by mass spectrometry showed SO_2 peaks at *m/e* 64 and 66 in the ratio 100 to 5.6; natural abundance thiirane 1,1-dioxide showed the same peaks in the ratio 100 to 5.2.

Preparation of sodium and potassium 2-sulfinatoethanesulfonates

Thiirane 1,1-dioxide (**1**) (191 mg, 2.08 mmol) and sodium sulfite (anhydrous, 225 mg, 1.79 mmol) dissolved in D_2O (0.5 mL) were allowed to react for 1.5 h, the reaction being monitored by ^{1}Hmr. The unchanged **1** was removed by extraction with chloroform, and the D_2O solution then evaporated and the white solid so obtained dried as before, to yield sodium 2-sulfinatoethanesulfonate (385 mg, 99% based on Na_2SO_3). The analytical specimen was recrystallized from ethanol−water and dried at 125°C/1 Torr for 24 h; mp >360°C (dec.); ir ν_{max}: 2910 (m), 2820 (w), 1190 (s), 1040 (s), 980 (w), 962 (w), 932 (w), 755 (m), 690 (w), 590 (w), 540 (w) cm^{-1}; ^{1}Hmr (D_2O) δ: 2.61−3.22 (m, A_2B_2); ^{13}Cmr (D_2O) δ: 57.6, 46.8. *Anal.* calcd. for $C_2H_4O_5S_2Na_2$: C 11.01, H 1.83, S 29.36; found: C 11.02, H 1.82, S 29.31.

A portion of the above salt was converted to the potassium salt (**6**) by passing the aqueous solution through Rexyn 101(H) (Fisher) cation exchange resin and neutralizing to pH 7.0 with 1 *M* KOH solution. Evaporation of the water gave a white solid which was recrystallized from ethanol−water and dried as before; mp 319−320°C (dec.); ir identical to that of the sodium salt. *Anal.* calcd. for $C_2H_4O_5S_2K_2$: C 9.59, H 1.60, S 25.56; found: C 9.63, H 1.57, S 25.43.

Preparation of potassium 1,2-ethanedisulfonate

This was made by the reaction of aqueous K_2SO_3 with 1,2-dibromoethane (31). The compound so obtained gave the following spectra: ir, ν_{max}: 3400 (m, br), 3020 (m), 2960 (w), 2940 (w), 1210 (vs, br), 1040 (s), 770 (s), 560 (s) cm^{-1}; ^{1}Hmr (D_2O) δ: 3.3 (s); ^{13}Cmr (D_2O) δ: 49.1.

Preparation of barium ethanesulfonate (3)

Ethanesulfonyl chloride (1.0 g, 7.8 mmol) was stirred with $Ba(OH)_2.8H_2O$ (2.3 g, 7.3 mmol) in water (100 mL) for 3 h at room temperature. The water was removed by evaporation and the off-white residue (2.0 g) so obtained recrystallized from 95% alcohol to give **3** as colorless needles, mp >395°C; ir (Nujol) ν_{max}: 1255 (m), 1220 (w), 1187 (s), 1162 (s), 1052 (s), 784 (m), 575 (m) cm^{-1}; ^{1}Hmr (D_2O) δ: 1.29 (t, 3H), 2.94 (q, 2H); ^{13}Cmr (D_2O) δ: 48.2, 11.2 ppm.

Stability of barium 2-hydroxyethanesulfinate (2)

Barium 2-hydroxyethanesulfinate (**2**) (49 mg, 0.28 mmol) prepared as described elsewhere (3) was kept at 98°C for 5 h, at the end of which time the ^{1}Hmr spectrum of the material (48 mg, 98%) was that of unchanged **2**; **2** shows no mp but decomposes above 350°C (3).

Acknowledgement

We thank the Natural Sciences and Engineering Research Council of Canada for financial support of this work.

1. J. F. KING, J. H. HILLHOUSE, and S. SKONIECZNY. Can. J. Chem. **62**, 1977 (1984).
2. G. HESSE, E. REICHOLD, and S. MAJMUDAR. Chem. Ber. **90**, 2106 (1957).
3. J. F. KING, and J. H. HILLHOUSE. Can. J. Chem. **61**, 1583 (1983).
4. E. VILSMAIER, R. TROPITZSCH, and O. VOSTROWSKY. Tetrahedron Lett. 3275 (1974).
5. E. VILSMAIER and G. BECKER. Synthesis, 55 (1975).
6. F. G. BORDWELL and G. D. COOPER. J. Am. Chem. Soc. **73**, 5187 (1951).
7. F. G. BORDWELL and N. P. NEUREITER. J. Am. Chem. Soc. **85**, 1209 (1963).
8. L. A. PAQUETTE. Org. React. **25**, 1 (1977).
9. D. H. HUNTER, J. B. STOTHERS, and E. W. WARNHOFF. *In* Rearrangements in ground and excited states, Vol. 1. *Edited by* P. de Mayo. Academic Press, New York. 1980. p. 391.
10. L. A. PAQUETTE, L. S. WITTENBROOK, and V. V. KANE. J. Am. Chem. Soc. **89**, 4487 (1967).
11. L. A. PAQUETTE and L. S. WITTENBROOK. J. Am. Chem. Soc. **90**, 6790 (1968).
12. B. BÄCKLUND. Doctoral dissertation, University of Uppsala, 1945, as quoted in ref. 13.
13. F. G. BORDWELL, J. M. WILLIAMS, JR., E. B. HOYT, JR., and B. B. JARVIS. J. Am. Chem. Soc. **90**, 429 (1968).
14. W. L. MOCK. *In* Pericyclic reactions Vol. II. *Edited by* A. P. Marchand and R. E. Lehr. Academic Press, New York. 1977. p. 141.
15. J. F. KING and T. DURST. Can. J. Chem. **44**, 819 (1966).
16. L. A. CARPINO and L. V. MCADAMS III. J. Am. Chem. Soc. **87**, 5804 (1965).
17. N. TOKURA, T. NAGAI, and S. MATSUMURA. J. Org. Chem. **31**, 349 (1966).
18. W. L. MOCK. J. Am. Chem. Soc. **97**, 3673 (1975).
19. P. H. W. LAU and J. C. MARTIN. J. Am. Chem. Soc. **100**, 7077 (1978).
20. C. W. PERKINS and J. C. MARTIN. J. Am. Chem. Soc. **105**, 1377, (1983).
21. J. L. KICE. Adv. Phys. Org. Chem. **17**, 65 (1980).
22. S. THEA and A. WILLIAMS. J. Chem. Soc. Perkin Trans. 2, 72 (1981).
23. Y. NAKANO, S. SAITO, and Y. MORINO. Bull. Chem. Soc. Jpn. **43**, 368 (1970).
24. I. HARGITTAI. Sulphone molecular structures, lecture notes in chemistry. Vol. 6. Springer Verlag, Berlin and Heidelberg. 1978.
25. A. THIBBLIN and W. P. JENCKS. J. Am. Chem. Soc. **101**, 4963 (1979).
26. M. J. S. DEWAR. J. Am. Chem. Soc. **106**, 209 (1984).
27. D. R. CHRISTMAN and S. OAE. Chem. Ind. (London), 1251 (1959).
28. E. T. KAISER and O. R. ZABORSKY. J. Am. Chem. Soc. **90**, 4626 (1968).
29. E. T. KAISER. *In* Organic chemistry of sulfur. *Edited by* S. Oae. Plenum Press, New York and London. 1977. Chapt. 12. p. 649, esp. pp. 654 and 672.
30. N. N. MEL'NIKOV, E. M. SOKOLOVA, and P. P. TRUNOV. Z. Obshch. Khim. **29**, 529 (1959).
31. P. W. CLUTTERBUCK and J. B. COHEN. J. Chem. Soc. **121**, 120 (1922).

Radiation-induced binding of 2,2,6,6-tetramethyl-1,4-piperidone-*N*-oxyl to thymidine in oxygen-free aqueous solutions. Isolation and characterization of the adducts

MAURICE BERGER AND JEAN CADET[1]

Laboratoires de Chimie, Département de Recherche Fondamentale, Centre d'Études Nucléaires de Grenoble, 85 X, F.38041 Grenoble Cedex, France

AND

JACQUES ULRICH

Service d'Études Analytiques, Centre d'Études Nucléaires de Grenoble, 85 X, F.38041 Grenoble Cedex, France

Received March 9, 1984

MAURICE BERGER, JEAN CADET, and JACQUES ULRICH. Can. J. Chem. **62**, 6 (1984).

Steady-state γ-radiolysis of deaerated aqueous solutions of thymidine has been carried out in the presence of 2,2,6,6-tetramethyl-1,4-piperidone-*N*-oxyl (TAN), a well-known radiosensitizing agent. The eight main radiation-induced TAN addition products to thymidine have been isolated and characterized by ^{1}H and ^{13}C nmr, cd, and fast-atom bombardment mass spectrometry measurements.

MAURICE BERGER, JEAN CADET et JACQUES ULRICH. Can. J. Chem. **62**, 6 (1984).

La radiolyse γ en régime stationnaire de solutions aqueuses désaérées de thymidine a été effectuée en présence de tétraméthyl-2,2,6,6-pipéridone-4-*N*-oxyl (TAN) qui est un agent de radiosensibilisation. Les huit produits d'addition radio-induite de la molécule de TAN avec la thymidine ont été isolés et identifiés par diverses méthodes spectroscopiques: rmn ^{1}H et ^{13}C, dc et spectrométrie de masse par bombardement avec des atomes rapides.

Introduction

Various nitroxyl free radicals including nor-pseudopelletierine-*N*-oxyl (NPPN) and 2,2,6,6-tetramethyl-1,4-piperidone-*N*-oxyl (TAN) have been shown to sensitize hypoxic living cells to the lethal action of ionizing radiations (1, 2). The radiosensitizing ability of TAN appears to be higher in bacterial cells than in mammalian cells (3, 4). Two mechanisms which involve DNA as the major cellular target have been proposed for the biological action of several classes of radiosensitizers (5). The first postulates the oxidation of DNA anionic radicals (generated as anion–cation radical pairs by the direct action of ionizing radiation in purine and pyrimidine bases) through electron transfer reactions with TAN or NPPN. This would prevent the recombination of anion and cation radicals, resulting in permanent damage to the biopolymer. A second reaction is the covalent binding with radiation-induced DNA radicals (6). The formation of covalent TAN–DNA adducts has been reported upon irradiation either in aqueous solutions of DNA (7) or within living cells (8). Such lesions, the structures of which remain unknown, have been detected in Chinese hamster cells as *M. luteus* sensitive sites (9). Pulse radiolysis experiments have shown that the second-order reaction rate of TAN with the radicals resulting from the addition of OH radicals across the 5,6 bond of pyrimidine DNA components is an efficient process (10). The two main addition products of TAN to radiation-induced 5-hydroxy-5,6-dihydrothymin-6-yl and 6-hydroxy-5,6-dihydrothymin-5-yl radicals have been isolated and characterized (11). In the present study, thymidine has been used as a DNA model compound for a further investigation of the binding of TAN with the various nucleoside radicals induced by the water radiolysis species. We show that the bulk of the adducts result from the binding reaction of TAN with the radicals derived from addition of OH radicals at either carbon C(5) or carbon C(6).

Results

Steady-state γ-radiolysis of oxygen-free aqueous solutions of 1 m*M* thymidine containing 2 m*M* 2,2,6,6-tetramethyl-1,4-piperidone-*N*-oxyl (TAN) led to the formation of a complex mixture of nucleosides and thymine derivatives. These compounds were separated by two-dimensional thin-layer chromatography on silica gel plates (12). Eight nucleosides which exhibit high chromatographic mobility gave a coloration characteristic of carbonyl-containing compounds by spraying the chromatoplates with the 2,4-dinitrophenylhydrazine reagent (13). This is consistent with the presence of the piperidone moiety in the above nucleosides. These TAN–thymidine adducts were further purified and separated from the radiation-induced diastereoisomers of 5,6-dihydrothymidine and 5,6-dihydroxy-5,6-dihydrothymidine by preparative thin-layer chromatography on silica gel, followed by reversed–phase high performance liquid chromatography. These TAN–thymidine adducts, which represent about 50% of the overall radiation-induced degradation products (Table 1), were further characterized on the basis of various spectroscopic measurements. Further confirmation was provided by comparison with the adducts generated in alternate chemical routes.

The eight thymidine derivatives **2**–**9** showed no absorption around 260 nm, in line with the saturation of the 5,6-pyrimidine bond of these nucleosides (14). The six more stable thymidine–TAN adducts **2**–**7** were analyzed by fast-atom bombardment (FAB) mass spectrometry. This soft ionization technique is particularly suitable for the mass spectrometry measurement of polar and fragile molecules, such as the TAN adducts (Fig. 1). A prominent pseudo-molecular ion $(M + Na)^+$ at $m/z = 452$ was observed in the positive mass spectrum of each of the six nucleosides **2**–**7**. The pseudo-molecular ion $(M - H)^-$ exhibited in the negative ionization mode at $m/z = 428$ is of relatively low intensity. These spectroscopic data strongly suggest that these compounds result from the addition of a hydroxyl radical and of a TAN molecule to the starting thymidine. The same conclusions can be deduced from the observation of a pseudo-molecular ion in the field desorption (FD) and the desorption by chemical ionization (DCI) spectra of compounds **2** and **3** respectively. In addition, the fragmentation patterns of these adducts, particularly those obtained in

[1]Author to whom all correspondence should be addressed.

TABLE 1. Yield of the radiation-induced TAN addition products **2–9** to thymidine in oxygen free aqueous solution[a]

Nucleosides	G value[b]
trans-(5*S*,6*S*)-5-hydroxy-6-(2,2,6,6,-tetramethyl-4-oxo-1-piperidinoxy)-5,6-dihydrothymidine (**2**)	0.11
trans-(5*R*,6*R*)-5-hydroxy-6-(2,2,6,6,-tetramethyl-4-oxo-1-piperidinoxy)-5,6-dihydrothymidine (**3**)	0.10
cis-(5*S*,6*R*)-5-hydroxy-6-(2,2,6,6,-tetramethyl-4-oxo-1-piperidinoxy)-5,6-dihydrothymidine (**4**)	0.05
cis-(5*R*,6*S*)-5-hydroxy-6-(2,2,6,6,-tetramethyl-4-oxo-1-piperidinoxy)-5,6-dihydrothymidine (**5**)	0.06
trans-(5*S*,6*S*)-6-hydroxy-5-(2,2,6,6,-tetramethyl-4-oxo-1-piperidinyl-*N*-oxide)-5,6-dihydrothymidine (**6**)	0.05
trans-(5*R*,6*R*)-6-hydroxy-5-(2,2,6,6,-tetramethyl-4-oxo-1-piperidinyl-*N*-oxide)-5,6-dihydrothymidine (**7**)	0.03
(5*R**) and (5*S**)-5-(2,2,6,6,-tetramethyl-4-oxo-1-piperidinyl-*N*-oxide)-5,6-dihydrothymidine (**8**, **9**)	0.07
Thymidine (**1**)	−0.89

[a]Absorbed dose: 1.5 kGy; 1 mM thymidine and 2 mM TAN aqueous solutions.

[b]Number of molecules formed or destroyed per an absorbed dose of 1 Gy. The G values are the average of four independent measurements (accuracy to ±5%).

FD-ms, provide significant structural information. Thus the base peak at $m/z = 259$ corresponds to the loss of the TAN radical, whereas major fragments can be assigned to the TAN residue ($m/z = 170$) and the deoxyribose residue ($m/z = 117$) respectively. Mass spectrometric analyses of the two other nucleosides **8** and **9** were not so conclusive due to extensive thermal decomposition of the samples.

The 250-MHz ^{1}H nmr spectra of the thymidine–TAN adducts **2–7** in D_2O confirm the presence of the piperidine moiety. In particular, they exhibit four singlets in the range 1.04–1.44 ppm which correspond to the resonance signals of the methyl substituents of the piperidone ring. We also note the presence at a slightly higher field (1.55–1.70 ppm) of an additional singlet which was assigned as the pyrimidine methyl group. The chemical shift of this signal and those of the H(6) pyrimidine proton (5.23–5.40 ppm) are characteristic of 5,6-dihydrothymine derivatives. Similar ^{1}H nmr features are observed for the nucleosides **6** and **7**, suggesting an isomeric relationship for the adducts **2–7**. On the other hand, the two last products **8** and **9** have a different structure with a methylene group ($J_{gem} = -14$ Hz) at the C(6) carbon and the TAN residue attached to the C(5) carbon.

Site of attachment of the TAN moiety

Considerations of the ^{1}H nmr chemical shift values of the H(6) proton and of the thymine methyl group are not of interest for determining the site of attachment of the piperidone ring, either at the C(5) or the C(6) positions (Fig. 2). The comparison of the chemical shift values of H(6) for the adducts **2–7** does not show any significant differences which could be related to the α or β position of the TAN substituent. The lack of any selective downfield shift effect associated with other electronegative α substituents such as a hydroperoxide group has been previously noted for 5,6-dihydrothymidine derivatives (15). It must also be mentioned that the chemical shift of the pyrimidine H(6) proton is sensitive to the orientation of the aglycone about the *N*-glycosidic bond (16). On the other hand, ^{13}C nmr has been shown to be a suitable spectroscopic method for investigating the effects of substituents at carbons C(5) and C(6) in various 5,6-dihydrothymine derivatives (17). The relevant ^{13}C chemical shift values of the six thymidine–TAN adducts **2–7** and of various 5,6-dihydrothymidine derivatives are listed in Table 2. The comparison of the C(5) and C(6) chemical shifts of the compounds **2–7** with the corresponding carbons of the *cis* and *trans* diastereoisomers of 5,6-dihydroxy-5,6-dihydrothymidine shows that the C(6) resonance signal of compounds **2–5** is shifted downfield by about 9 or about 13 ppm. A similar deshielding effect is observed for the C(5) of the thymidine–TAN adducts **6** and **7**. This strongly suggests that the TAN substituent is at position 5 in nucleosides **6** and **7** and at position 6 in adducts **2–5**. The magnitude of the α effect of the TAN substituents (as determined by using 5-hydroxy-5,6-dihydrothymidine and 6-hydroxy-5,6-dihydrothymidine as the reference compounds) is 41–45 ppm for the C(6) carbon and about 38 ppm for the C(5) carbon. The lower value for the latter carbon may be due to the more severe crowding of this carbon which is suggested by the molecular model. The variation in the magnitude of the α effect at the C(6) carbon could be the result of changes in the *syn–anti* conformation of the nucleobase with respect to the sugar moiety, as discussed in more detail in the second paper (18). Polarization effects resulting from the close vicinity of the O(1′) atom with the C(6) carbon in compounds **2** and **5** would be at the origin of this shielding effect.

Further confirmation of the assignment of the position of the TAN substituent was provided by the radiation-induced synthesis of the various thymidine–TAN adducts **2–9** from 5,6-saturated thymidine derivatives. In the first series of reactions, the γ-radiolysis of oxygen-free aqueous solutions of (−)-*trans*-(5*S*,6*S*)-5-bromo-6-hydroxy-5,6-dihydrothymidine (**12**) (18) in the presence of 4.7 mM TAN and 0.1 M *tert*-butanol gives rise to the adduct **6**, whereas irradiation of the (+)-*trans*-5-bromo-6-hydroxy-5,6-dihydrothymidine (**13**) generates the adduct **7** (Fig. 3). A reasonable mechanism for their formation would involve, in the initial step of the reaction, the departure of the Br atom through an electron capture dissociation process (20). A recombination reaction between the resulting 6-hydroxy-5,6-dihydrothymid-5-yl radical and the TAN molecule would generate, with retention of configuration at the C(6) carbon (21), the adducts **6** and **7** respectively.

In the second series of reactions, evidence is provided for the adducts **2–5**. The two pairs of *cis* and *trans* diasteroisomers of C(6) addition products, **5**,**3** and **4**,**2** respectively, can be prepared in a selective way by using a radiation-induced procedure. γ-Irradiation of deaerated aqueous solutions of the 5*R* diasteroisomer of 5-hydroxy-5,6-dihydrothymidine (**11**) containing 2 mM TAN generates adducts **3**,**5**, whereas the two other adducts **2**,**4** are obtained from (5*S*)-5-hydroxy-5,6-dihydrothymidine (**10**). In addition, a mixture of both the 5*R** and 5*S** adducts, **8** and **9**, the absolute configuration of which has not been determined, is produced in both irradiated solutions. Under the experimental conditions used, the hydroxyl radical is the main radiolysis-reactive species which may abstract a hydrogen at carbon C(6) or lead to the loss of a hydroxyl group at carbon C(5). Similar abstraction of a hydroxyl group has been observed in X-irradiated 5-hydroxy-5-methylbarbituric acid (22). A recombination reaction of the resulting oxyl radical with TAN (23) gives rise to a pair of *cis* and *trans* diastereoisomers of C(6) adducts **5**,**3** or **4**,**2** with retention of the C(5) configuration (Fig. 4). It should be noted that the addition of the TAN molecule to the carbon C(6) is less stereoselective than to carbon C(5). This loss of stereospecificity is

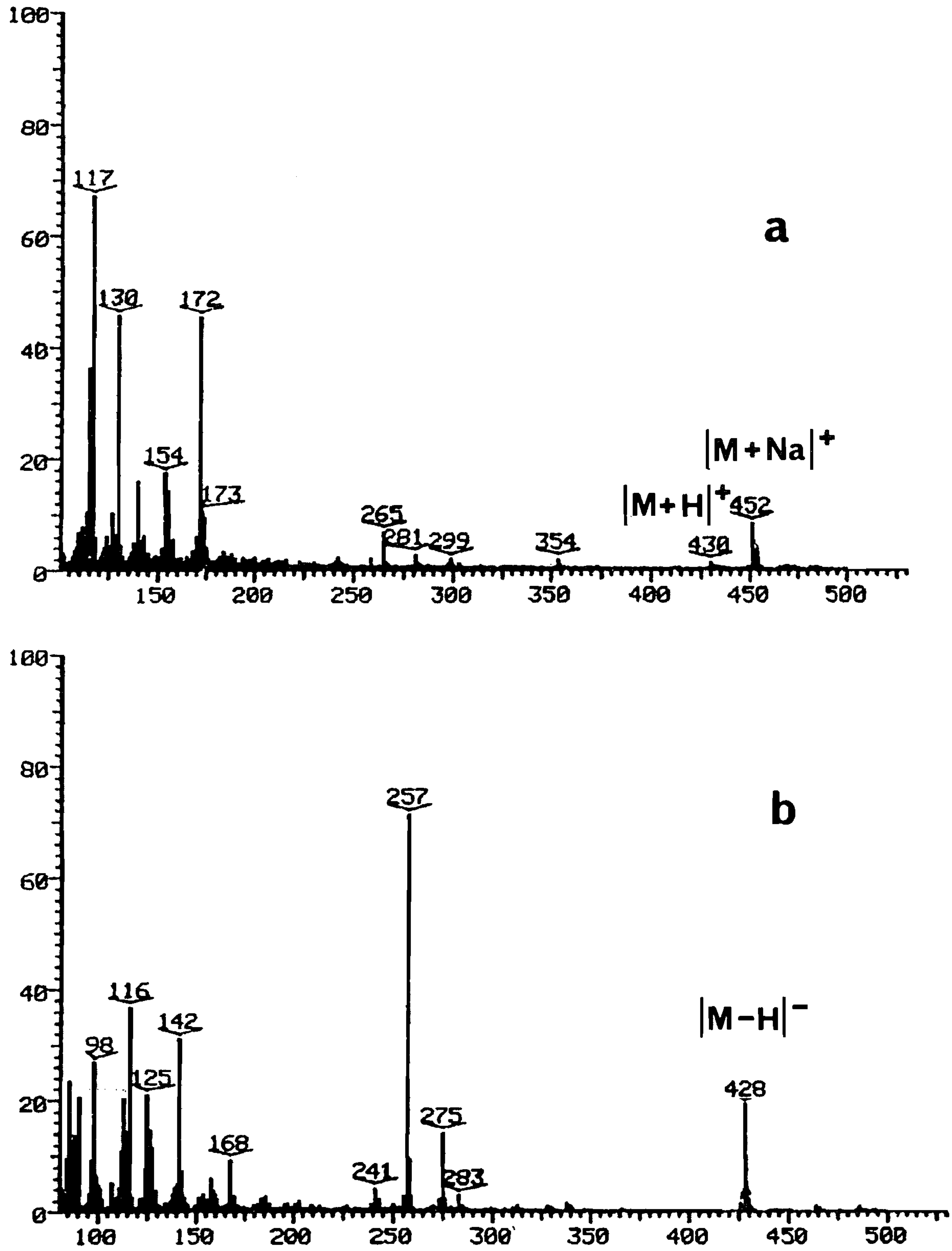

FIG. 1. FAB-ms spectra of the TAN−thymidine adduct **5**: (a) positive mode; (b) negative mode.

probably due to the presence of the two bulky substituents on the carbon C(5) preventing the preferential *trans* radical addition which is usually observed with respect to the 5- or 6-monosubstituted carbon within the pyrimidine ring (24).

Nature of the linkage to the TAN substituent

The covalent addition of nitroxyl radicals to carbon-centered radicals may generate either hydroxylamine derivatives (25) or *N*-oxide type compounds (26). Chemical transformations of the adducts **2**−**9** provided the most convincing evidence that the TAN moiety is linked via the nitroxyl oxygen to carbon C(6) in nucleosides **2**−**5** (hydroxylamine) and via the nitroxyl nitrogen to carbon C(5) in nucleosides **6**−**9** (*N*-oxide). Catalytic hydrogenation is expected to convert the substituted hydroxyl-

TABLE 2. ^{13}C Chemical shifts (δ, ppm) of relevant pyrimidine carbons of TAN–thymidine adducts and various diastereoisomers of 5,6-dihydrothymidine derivatives in D_2O[a]

Nucleosides	CH_3	C(5)	C(6)
trans-(5*S*,6*S*)-5-hydroxy-6-(2,2,6,6-tetramethyl-4-oxo-1-piperidinoxy)-5,6-dihydrothymidine (**2**)	20.1	70.7	89.1
trans-(5*R*,6*R*)-5-hydroxy-6-(2,2,6,6-tetramethyl-4-oxo-1-piperidinoxy)-5,6-dihydrothymidine (**3**)	19.8	70.7	93.7
cis-(5*S*,6*R*)-5-hydroxy-6-(2,2,6,6-tetramethyl-4-oxo-1-piperidinoxy)-5,6-dihydrothymidine (**4**)	23.8	73.2	93.4
cis-(5*R*,6*S*)-5-hydroxy-6-(2,2,6,6-tetramethyl-4-oxo-1-piperidinoxy)-5,6-dihydrothymidine (**5**)	24.0	73.6	89.1
trans-(5*S*,6*S*)-6-hydroxy-5-(2,2,6,6-tetramethyl-4-oxo-1-piperidinyl-*N*-oxide)-5,6-dihydrothymidine (**6**)	14.6	80.9	79.5
trans-(5*R*,6*R*)-6-hydroxy-5-(2,2,6,6-tetramethyl-4-oxo-1-piperidinyl-*N*-oxide)-5,6-dihydrothymidine (**7**)	15.0	80.1	80.8
(−)-(5*S*)-5-hydroxy-5,6-dihydrothymidine (**10**)	22.3	69.5	48.3
(+)-(5*R*)-5-hydroxy-5,6-dihydrothymidine (**11**)	22.7	69.6	48.2
(+)-(5*R*)-5,6-dihydrothymidine	13.3	35.8	43.2
(−)-(5*S*)-5,6-dihydrothymidine	12.8	35.8	43.1
(+)-*cis*-(5*S*,6*R*)-6-hydroxy-5,6-dihydrothymidine	10.5	42.2	77.6
(−)-*cis*-(5*R*,6*S*)-6-hydroxy-5,6-dihydrothymidine	10.4	42.5	76.7
(+)-*cis*-(5*S*,6*R*)-5,6-dihydroxy-5,6-dihydrothymidine	22.8	73.6	80.7
(−)-*cis*-(5*R*,6*S*)-5,6-dihydroxy-5,6-dihydrothymidine	22.9	73.5	79.9
(+)-*trans*-(5*R*,6*R*)-5,6-dihydroxy-5,6-dihydrothymidine	19.2	72.2	80.8
(−)-*trans*-(5*S*,6*S*)-5,6-dihydroxy-5,6-dihydrothymidine	19.3	72.1	80.2

[a]All chemical shifts were referenced to external TMS.

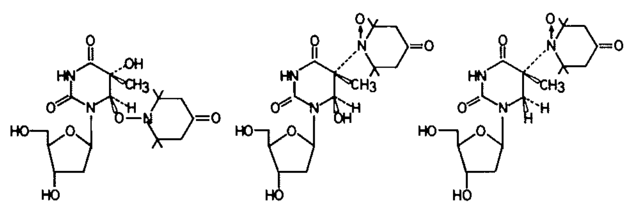

(5R,6R) 3 (5R,6R) 7 (5R) 9

FIG. 2. Structure of three possible TAN–thymidine adducts with a 5*R* stereoconfiguration.

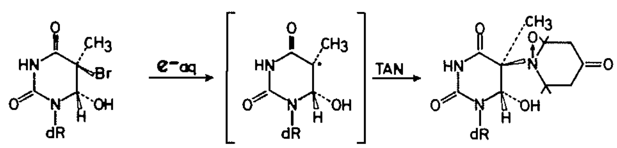

(5S,6S) 12 (5S,6S) 6

FIG. 3. Specific synthesis of the thymidine–TAN adduct **6** by γ-radiolysis of deaerated aqueous solution of (−)-*trans*-5-bromo-6-hydroxy-5,6-dihydrothymidine **12**.

amine derivative to an alcohol and an amine through heterolysis of the N—O bond according to an S_N2 mechanism (27). Hydrogenolysis of the four adducts **2**–**5**, in the presence of Pd/C, generated in a quantitative way the thymidine glycols and the 2,2,4,4-tetramethylpiperidone. However, the two C(5) thymidine–TAN addition products **6** and **7** remain unchanged under these hydrogenolysis conditions.

The latter compounds **6** and **7** are unstable in solutions and undergo various transformations which can be rationalized on the basis of the postulated *N*-oxide structure. In particular, they show extensive decomposition after standing for 48 h in neutral

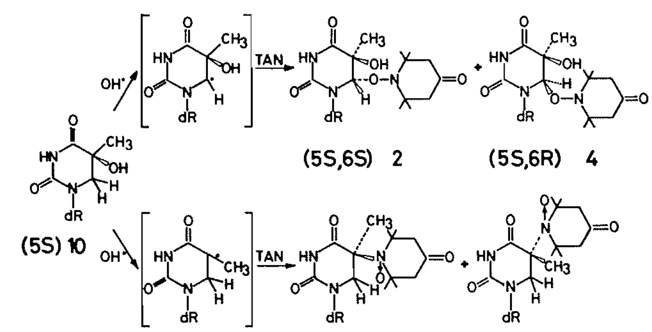

(5S,6S) 2 (5S,6R) 4

(5S) 10

(5S) 8 (5R) 9

FIG. 4. Preparation of the thymidine–TAN adducts **2**, **4**, **8**, and **9** by γ-irradiation of oxygen-free aqueous solutions of (5*S*)-5-hydroxy-5,6-dihydrothymidine (**10**).

aqueous solution at 20°C. The major degradation product was characterized as 5-hydroxymethyl-2′-deoxyuridine (**14**) by comparison of some of its spectroscopic features (uv, EI-ms, ^1H and ^{13}C nmr) with those of the authentic sample synthesized according to Baker *et al.* (28). A likely mechanism for its formation would involve a Cope rearrangement, which is characteristic of *N*-oxide type compounds (29). Hydrogen abstraction from the methyl by the N—O function through a planar pentagonal transient state and subsequent departure of the piperidone substituent would generate a nucleoside with a methylene group (Fig. 5). Elimination of the hydroxyl at carbon C(6) would give rise to a reactive carbonium ion, which by reaction with water is converted to 5-hydroxymethyl-2′-deoxyuridine (**14**). In H_2O_2 the corresponding hydroperoxide **15** is obtained as the result of the nucleophilic attack by the perhydroxyl ion on the carbonium ion intermediate (30). It is interesting to note that similar reaction mechanisms have been proposed in the biosynthetic pathway of 5-hydroxy-

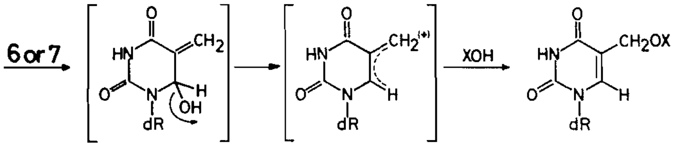

X = H, 14
X = OH, 15

FIG. 5. Cope rearrangement of the thymidine–TAN adduct **6** or **7** to hydroxymethyl-2′-deoxyuridine (**14**) or hydroperoxymethyl-2′-deoxyuridine (**15**).

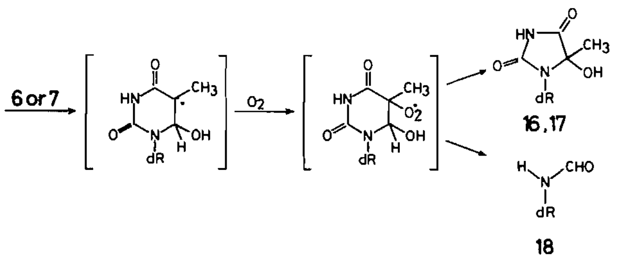

FIG. 6. Rearrangement of the thymidine–TAN adduct **6** or **7** to $5R^*$ and $5S^*$-1(2-deoxy-β-D-*erythro*-pentofuranosyl)-5-hydroxy-5-methyl hydantoin (**16**, **17**) and *N*-(2-deoxy-β-D-*erythro*-pentofuranosyl) formamide (**18**).

methyl-2′-deoxyuridine-5′-monophosphate which is catalyzed by dUMP hydroxymethylase (31). We may note that *N*-1-(2-deoxy-β-D-*erythro*-pentofuranosyl) barbituric acid (32), which would result from initial hydrogen abstraction reaction at carbon C(6), is produced, but in very low yield. This lower yield could be explained by the lack of planarity for the pentagonal transient state, due to the half-chair conformation of the 5,6-saturated pyrimidine ring. The formation of thymidine (**1**) from the other C(5) thymidine–TAN adducts **8** and **9** in aqueous solution would also strongly suggest a *N*-oxide type structure for these compounds. A Cope rearrangement appears as a likely mechanism for the generation of **1**.

Radical reactions, as the result of homolytic scission of the C—N bond of adduct **6** or **7** (*vide infra*) are predominant in aerated aqueous pyridine solutions. The major decomposition products were characterized as thymidine (**1**) (10%), the four *cis* and *trans* diastereoisomers of 5,6-dihydroxy-5,6-dihydrothymidine (20%), the *N*-(2-deoxy-β-D-*erythro*-pentofuranosyl) formamide (**18**) (33), and the $5R^*$ and $5S^*$ diastereoisomers of *N*-(2-deoxy-β-D-*erythro*-pentofuranosyl)-5-hydroxy-5-methylhydantoin (**16**, **17**) (34). The formation of the two latter classes of products may involve a Meisheimer mechanism (35) which would generate the 6-hydroxy-5,6-dihydrothymid-5-yl radical from homolytic scission of the C(5)—N bond. Subsequent fast reaction of this pyrimidine radical with molecular oxygen would give rise to the corresponding hydroxyhydroperoxyl thymidine radical (36). Disproportionation reactions between these peroxyl radicals are expected to produce oxyl radicals (37), which through subsequent β scission reactions would lead to the opening of the pyrimidine ring (Fig. 6). N^1-(2-deoxy-β-D-*erythro*-pentofuranosyl)-N^1-formyl-N^2-pyruvylurea is the expected product of this reaction. Hydrolysis of this unstable intermediate gives rise to the formamide compound **18** in 40% yield, whereas recyclization generates the hydantoin nucleosides **16**, **17** in about 20% yield.

The loss of oxygen from the molecular ion in electron impact mass spectrometric analysis may be diagnostic for the *N*-oxide structure (38). This particular ion ($M - 16$) has not been observed in the FAB mass spectrometry measurements of adducts **2**–**7**, which show little fragmentation.

Determination of the absolute configuration of adducts 2–7

As mentioned above, the radiation-induced degradation of the $5R$ diastereoisomer of 5-hydroxy-5,6-dihydrothymidine (**11**) in the presence of TAN gives rise to the *trans* and *cis* C(6) adducts **3** and **5** with retention of the initial $5R$ configuration. In the same way, the two $5S$ diastereoisomers **2** and **4** have been prepared from the ($5S$)-diastereoisomer of 5-hydroxy-5,6-dihydrothymidine (**10**) (39). The *cis* and *trans* configuration of the two nucleosides of each pair of $5R$ and $5S$ diastereoisomers could be deduced by considering the γ-effect of the C(6) TAN substituent on the ^{13}C nmr chemical shift value of the pyrimidine methyl group. An upfield shift effect of about 3 ppm is observed for the *trans* thymine glycol (11) and the corresponding 2′-deoxyribonucleoside derivatives (Table 2) when the C(6) hydroxyl group is in a *gauche* relationship with the C(5) methyl substituent. A similar upfield shift effect is noted for the adducts **2** and **3** by comparison with the second $5S$ and $5R$ diastereoisomers **4** and **5** respectively. The magnitude of this γ-effect is higher than for the 5,6-dihydroxy-5,6-thymidine, as expected for a bulky C(6) substituent. As a result, a $6R$ configuration and $6S$ configuration can be deduced for **3**,**4** and **2**,**5** respectively.

The assignment of the C(6) configuration of the TAN–thymidine adducts **6** and **7** is also based on their selective preparation in 90% yield from the corresponding ($5S$,$6S$) and ($5R$,$6R$) 5-bromo-6-hydroxy-5,6-dihydrothymidine (**12** and **13**). As discussed above, a *trans* addition of the TAN molecule to the 6-hydroxy-5,6-dihydrothymid-5-yl radical is expected to take place preferentially, giving rise to the ($5S$,$6S$) and ($5R$,$6R$) TAN–thymidine adducts **6** and **7**, respectively.

Mechanisms of the radiation-induced formation of the adducts 2–9

Interaction of the γ-rays with dilute aqueous solutions of thymidine and TAN leads to the formation of three reactive species (40): OH radicals ($G = 2.72$), solvated electrons ($G = 2.63$), and hydrogen atoms ($G = 0.55$). Under the experimental conditions used, about 40% of the OH radicals will react with thymidine (41): $k_{OH+dThd} = 3.9 \times 10^9\ M^{-1}\ s^{-1}$. The remaining 60% are scavenged by the TAN molecules (42): ($k_{OH+TAN} = 6.3 \times 10^9\ M^{-1}\ s^{-1}$). The pyrimidine ring of the nucleoside is the preferential site of reaction of the OH$^{\cdot}$ radicals through addition at the carbons C(5) and C(6) as shown by esr flow experiments (43). Recombination reactions of these radicals with the TAN molecule give rise to the C(5) adducts and the four *cis* and *trans* diastereoisomers of the C(6) addition products. The reaction of the solvated electrons with thymidine takes place mostly on the pyrimidine moiety (41). The resulting anionic radical is exposed to be quantitatively oxidized to the starting thymidine, since pulse radiolysis experiments have shown that electron transfer reaction from electron pyrimidine adduct to TAN is an efficient process (6, 8). The formation of the two adducts **8** and **9** may also be accounted for by the recombination reaction of 2,2,6,6-piperidone-*N*-oxyl with the radiation-induced 5,6-dihydrothymid-5-yl radical (42). This radical arises from the preferential addition of the hydrogen atom to the carbon C(6) within the thymine moiety (44). It should be noted that, in the present work, adducts with TAN covalently bound to the sugar moiety of thymidine were not detected. On the other hand, this latter class of adducts has been shown to be relatively important when purine 2′-deoxyribonucleosides are exposed to γ-rays in deaerated aqueous solution containing *N*-oxyl radicals (45).

Conclusion

The main radiation-induced TAN adducts to thymidine have been isolated and characterized as recombination products between TAN and transient 5-hydroxy-5,6-dihydrothymid-6-yl or 6-hydroxy-5,6-dihydrothymid-5-yl radicals. This constitutes a first step to further studies dealing with the radiation-induced binding of TAN to the thymine moiety within isolated DNA. In particular, the knowledge of the structure and chemical properties of these various thymidine−TAN adducts will facilitate their detection in enzymatic hydrolysates of DNA which has been irradiated in the presence of TAN.

Experimental

Materials

Thymidine was purchased from Sigma (St. Louis, Missouri) and used without further purification. 2,2,6,6-Tetramethylpiperidone was obtained from Aldrich (Beerse, Belgium). 2,2,6,6-Tetramethylpiperidone *N*-oxyl was synthesized according to Briere *et al.* (46). The two *trans* diastereoisomers of 5-bromo-6-hydroxy-5,6-dihydrothymidine (**12**, **13**) were prepared by addition of Br_2 to an aqueous solution of thymidine (19) and separated by preparative reversed-phase high performance liquid chromatography.

The four *cis* and *trans* diastereoisomers of 5,6-dihydroxy-5,6-dihydrothymidine (47), the two *cis* (5*S*,6*R*) and (5*R*,6*S*) diastereoisomers of 6-hydroxy-5,6-dihydrothymidine (48), and the 5*R* and 5*S* diastereoisomers of 5-hydroxy-5,6-dihydrothymidine (**11**, **10**) (49) were prepared according to literature procedures. The (−)-(5*S*)-dihydrothymidine has been obtained according to Kondo and Witkop (14), whereas the (+)-(5*R*)-diastereoisomer has been prepared by hydrogenation of an aqueous solution of thymidine in the presence of Pd/C as the catalyst (50). 5-Hydroxymethyl-2′-deoxyuridine has been synthesized according to Baker *et al.* (28). [^{14}CH$_3$]thymidine has been obtained from the Service des Molécules Marquées du Commissariat à l'Energie Atomique (Saclay, France). The radioactive nucleoside was purified prior to use on a Nucleosil octadecylsilyl silica gel column to remove self-radiolysis decomposition products.

Spectroscopic measurements

The uv absorption spectra were registered on a Beckman spectrophotometer Model 5230. The ir spectra using the KBr micropellet method were obtained on a Perkin−Elmer spectrophotometer Model 177. Field desorption mass spectra were obtained on a Varian-Mat 311 spectrometer. (The intensity of the current of desorption was 10 mA.) Fast-atom bombardment (FAB) mass spectrometry was carried out in a Model MS 50 spectrometer equipped with a commercially available FAB gun. Desorption of the molecules was obtained by exposure to a beam of 8-keV xenon atoms in a glycerol mull. Chemical ionization mass spectra using NH_3 as the reactant gas were performed on a Nermag R 10-10 C apparatus. The ^{1}H nmr and ^{13}C nmr spectra operating at 250 MHz and 62.83 MHz respectively were obtained on a CAMECA TSN 250 apparatus in the Fourier transform mode. Deuterium oxide was used as the solvent with 3-(trimethylsilyl)-propionate-2,2,3,3-*d*$_4$ as the internal reference. Circular dichroïsm spectra (cd) were registered on a Roussel Jouan III dichrograph using methanol as the solvent.

Irradiation procedure

The γ-radiolysis experiments were carried out with three ^{60}Co sources located in a pool. The dose rate, which was determined according to Fricke's method, was 110 Gy/min. The flasks which were used for the irradiation experiments were previously filled with bidistilled water (pH 6.5) and exposed to high doses of γ-rays (10^5Gy) in order to destroy the organic impurities within the glass. The aqueous solutions of thymidine were deaerated by bubbling nitrogen for 15 min prior to irradiation.

Chromatographic analyses

Analytical two-dimensional separations of radiation-induced decomposition products of thymidine were carried out on precoated silica gel 60 F_{254} plates (Merck, Darmstadt, G.F.R.) with the two following solvent systems (12): I. lower phase of chloroform−methanol−water (4:2:1) to which was added 5% of methanol; II. ethyl acetate − 2-propanol − water (75:16:9). Preparative thin-layer chromatography was performed on thick precoated silica gel plates (Merck). Detection of far-uv absorbing compounds was made by fluorescence quenching with a 254-nm emitting Desaga mineral lamp. The 2′-deoxyribonucleosides were visualized as pink spots after spraying the plates with the cysteine − sulfuric acid reagent and subsequent heating for 3 min at 100°C. The carbonyl-containing compounds were detected on the chromatogram by using the 2,4-dinitrophenylhydrazine spray reagent (13).

Quantitative analysis

The [^{14}C] radio-labelled compounds were detected on the thin-layer silica gel plates by autoradiography using Kodak NS-2T X-ray sensitive films. Detection of radioactivity as low as 0.01 μCi/cm^2 was made after overnight exposure. The detected radioactive compounds were further scraped off the silica gel and suspended in 1 mL water for 2 h. Under these conditions, the radioactive recovery was nearly quantitative. The β scintillation counting was accomplished on a Packard model 2425 Tricarb spectrometer.

Isolation and characterization of the radiation-induced TAN−thymidine adducts

A solution of 1 m*M* thymidine (484 mg) and 2 m*M* TAN (680 mg) in 2 L of deaerated water was irradiated for 45 min with ^{60}Co γ-rays (absorbed dose: 4950 Gy). The solution was evaporated to dryness under reduced pressure. The resulting residue was dissolved in 2 mL of aqueous methanol (1:1) and applied to 5 preparative thick-layer chromatoplates. The developing solvent was a mixture of chloroform and methanol (9:1). The faster-moving broad uv-absorbing zone (R_f 0.35), which gives rise to a yellow coloration with the 2,4-dinitrophenylhydrazine spray reagent, was extracted with 50% aqueous methanol (3 × 10 mL). Evaporation of the solution to dryness gave a syrup (129 mg) which was deposited on 5 thin-layer precoated silica gel plates. Two uv absorbing zones were resolved (R_f 0.53 and 0.43 respectively) by using chloroform−methanol (9:1) as the developer. The fastest eluting uv absorbing zone (R_f 0.53) was shown to contain a mixture of three thymidine−TAN adducts **4**, **8**, and **9** (46 mg) after being extracted with 50% aqueous methanol (3 × 6 mL). The slower eluting uv absorbing zone (R_f 0.43) was scraped off and the silica gel was further extracted with 50% aqueous methanol (3 × 6 mL). Evaporation to dryness of the resulting solution yielded 67 mg of a colorless syrup which contains the four thymidine−TAN adducts **2**, **3**, **5**, and **7**.

cis-*(5*S*,6*R*)-5-hydroxy-6-(2,2,6,6-tetramethyl-4-oxo-1-piperidinoxy)-5,6-dihydrothymidine (**4**)*

The oily residue (46 mg) which is a mixture of adducts **4**, **8**, and **9** was extracted from the faster uv-absorbing zone and applied to 3 precoated silica gel plates. The tlc plates were developed with ethyl acetate as the solvent. Two main zones which give a positive coloration with the cysteine−H_2SO_4 or the 2,4-dinitrophenylhydrazine spray reagents were detected by fluorescence quenching at 254 nm. The fastest eluting zone (R_f 0.62) was scraped off and the resulting silica gel was extracted with 3 × 5 mL of water−methanol (1:1). Evaporation to dryness of the filtrates yields 14 mg (1.7%) of an oily compound which was shown to be homogeneous by reversed-phase high performance liquid chromatography analysis on a C-18 Nucleosil column using a mixture of water−methanol (7:3) as the solvent (k' = 1.50); uv (λ_{max} H_2O): 206 nm; ^{1}H nmr (D_2O, TSP) δ: 1.14 (s, 3, CH_3), 1.21 (s, 3, CH_3), 1.32 (s, 3, CH_3), 1.44 (s, 3, CH_3), 1.59 (s, 3, CH_3 thymine), 2.42 (ddd, 1, H-2″), 2.94 (m, 1, H-2′), 3.74 (dd, 1, H-5″), 3.82 (dd, 1, H-5′), 4.0 (m, 1, H-4′), 4.47 (m, 1, H-3′), 5.41 (s, 1, H-6), 5.78 (dd, 1, H-1′); ^{13}C nmr (D_2O, TMS) δ: 19.8 (q, CH_3 thymine), 23.7, 24.3, 32.3, 33.8 (q, 4 × CH_3 piperidone), 38.7 (t, C-2′), 53.6 (t, CH_2 piperidone), 53.7 (t, CH_2 piperidone), 63.0 (t, C-5′), 66.1 (s, C-2, C-6 piperidone), 70.7 (s, C-5 thymine), 72.3 (d, C-3′), 87.0 (d, C-4′), 92.8 (d, C-1′), 93.7 (d, C-6 thymine); cd (*c* 1.4, methanol): $[\theta]_{280}$ ±0, $[\theta]_{270}$ −140, $[\theta]_{260}$ −1720, $[\theta]_{249}$ −4650, $[\theta]_{240}$ −1720, $[\theta]_{288}$ ±0, $[\theta]_{230}$ +3500; FAB-ms, *m/e* (relative intensity), positive mode: 452 (30, M^+ + Na), 430 (8, M^+ + H), 265 (20), 172 (15, TAN + 2H), 117 (58, 2-deoxyribose); negative mode: 428 (12, M^- − H), 283 (17), 257 (41, M^- − TAN), 241 (6, thymidine-H), 142 (15,5-hydroxy-5,6-dihydrothymine), 125 (18, thymine-H), 116 (14, 2-deoxyribose-H).

(5R) and (5S*)-5-(2,2,6,6-tetramethyl-4-oxo-1-piperidinyl-*N*-oxide)-5,6-dihydrothymidine (8, 9)*

Extraction of the slowest uv-absorbing zone (R_f 0.31) yielded 23 mg of a mixture of thymidine−TAN adducts **8** and **9** which were further separated on the C-18 Nucleosil octadecylsilyl silica gel column under the above conditions. Two main fractions corresponding to nucleosides **8** (k' = 4.36) and **9** (k' = 4.85) were collected. Evaporation to dryness of the aqueous methanol solutions gave respectively 9 mg of **8** (1.1%) and 8 mg of **9** (1%) as oily compounds.

Compound 8: ^{1}H nmr (D_2O, TSP) δ: 1.18 (s, 3, CH_3), 1.21 (s, 3, CH_3), 1.22 (s, 3, CH_3), 1.27 (s, 3, CH_3), 1.57 (s, 3, CH_3 thymine), 2.18 (ddd, 1, H-2″), 2.35 (ddd, 1, H-2′), 3.57 (d, 1, H-6a), 3.70 (dd, 1, H-5″), 3.76 (dd, 1, H-5′), 3.92 (m, 1, H-4′), 4.17 (d, 1, H-6b), 4.41 (m, 1, H-3′), 6.31 (dd, 1, H-1′).

Compound 9: ^{1}H nmr (D_2O, TSP) δ: 1.16 (s, 3, CH_3), 1.22 (s, 3, CH_3), 1.23 (s, 6, 2 × CH_3), 1.56 (s, 3, CH_3 thymine), 2.16 (ddd, 1, H-2″), 2.28 (ddd, 1, H-2′), 3.48 (d, 1, H-6a), 3.73 (dd, 1, H-5′), 3.76 (dd, 1, H-5″), 3.92 (m, 1, H-4′), 4.12 (d, 1, H-6b), 4.41 (m, 1, H-4′), 6.29 (dd, 1, H-1′).

cis-*(5R,6S)-5-hydroxy-6-(2,2,6,6-tetramethyl-4-oxo-1-piperidinoxy)-5,6-dihydrothymidine (5)*

The mixture (67 mg) of the four thymidine−TAN adducts **2**, **3**, **5**, and **7** was extracted from the second 2′-deoxyribonucleoside-containing band (R_f 0.42), applied to 5 silica gel precoated plates, and eluted with ethyl acetate as the solvent. Extraction of the fastest eluting band (R_f 0.61) provided a mixture (25 mg) of the TAN-addition products **5** and **7**, which were further separated by reversed-phase hplc on the C-18 Nucleosil column as reported above. Evaporation to dryness of the methanolic aqueous solution containing the fastest eluting compound (k' = 1.14) yielded 12 mg of **5** (1.4%) as an oily compound; uv (λ_{max} H_2O): 216 nm; ^{1}H nmr (D_2O, TSP) δ: 1.09 (s, 3, CH_3), 1.24 (s, 3, CH_3), 1.29 (s, 3, CH_3), 1.42 (s, 3, CH_3), 1.54 (s, 3, CH_3 thymine), 2.35 (ddd, 1, H-2″), 3.15 (ddd, 1, H-2′), 3.76 (m, 2, H-5′ and H-5″), 3.93 (m, 1, H-3′), 4.48 (m, 1, H-4′), 5.36 (dd, 1, H-1′); ^{13}C nmr (D_2O, TMS) δ: 24.0 (q, CH_3 thymine), 24.2 (q, 2, × CH_3 piperidone), 32.4 (q, 2 × CH_3 piperidone), 38.6 (t, C-2′), 53.5 (t, 2 × CH_2 piperidone), 63.0 (t, C-5′), 66.0 (s, C-2 and C-6 piperidone), 72.5 (d, C-3′), 73.6 (s, C-5 thymine), 85.5 (d, C-1′), 86.3 (d, C-4′), 89.1 (d, C-6 thymine); cd (*c* 1.2, methanol): $[\theta]_{310}$ ±0, $[\theta]_{280}$ +310, $[\theta]_{260}$ +2480, $[\theta]_{250}$ +6470, $[\theta]_{246}$ +7100, $[\theta]_{240}$ +4920, $[\theta]_{234}$ ±0; FAB-ms *m/e* (relative intensity), positive mode: 452 (10, M^+ + Na), 430 (3, M^+ + H), 265 (7), 172 (46 TAN + 2H), 117 (67, 2-deoxyribose); negative mode: 428 (20, M^- − H), 275 (16), 257 (73, M^- − TAN), 241 (4, thymidine-H), 142 (31, 5-hydroxy-5,6-dihydrothymine), 125 (22, thymine-H), 116 (37, 2-deoxyribose-H).

trans-*(5R,6R)-6-hydroxy-5-(2,2,6,6-tetramethyl-4-oxo-1-piperidinyl-*N*-oxide)-5,6-dihydrothymidine (7)*

The slowest eluting fractions (k' = 3.50) were collected and evaporated to dryness, yielding 11 mg of **7** (1.3%) as an oily compound; uv (λ_{max} H_2O): 215 nm; ^{1}H nmr (D_2O, TSP) δ: 1.08 (s, 6, 2 × CH_3), 1.17 (s, 3, CH_3), 1.29 (s, 3, CH_3), 1.64 (s, 3, CH_3 thymine), 2.27 (ddd, 1, H-2″), 2.36 (ddd, 1, H-2′), 3.74 (dd, 1, H-5″), 3.79 (dd, 1, H-5′), 3.95 (m, 1, H-4′), 4.44 (m, 1, H-3′), 5.32 (d, 1, H-6), 6.25 (dd, 1, H-1′); ^{13}C nmr (D_2O, TMS) δ: 15.0 (q, CH_3 thymine), 23.6 (q, CH_3), 23.7 (q, CH_3), 33.9 (q, CH_3), 34.0 (q, CH_3), 39.1 (t, C-2′), 53.9 (t, CH_2 piperidone), 54.3 (t, CH_2 piperidone), 62.6 (t, C-5′), 67.3 (s, C-2 or C-6 piperidone), 68.0 (s, C-6 or C-2 piperidone), 72.0 (d, C-3′), 80.1 (d, C-6), 80.8 (s, C-5), 86.2 (d, C-1′), 86.7 (d, C-4′); cd (*c* 1.6, methanol): $[\theta]_{320}$ ±0, $[\theta]_{300}$ −200, $[\theta]_{294}$ −220, $[\theta]_{289}$ ±0, $[\theta]_{270}$ +2900, $[\theta]_{253}$ +6230, $[\theta]_{240}$ 4450; FAB-ms *m/e* (relative intensity), positive mode: 452 (15, M^+ + Na), 430 (6, M^+ + H), 172 (48, TAN + 2H), 154 (18), 130 (48), 117 (2-deoxyribose); negative mode: 428 (22, M^- − H), 275 (18), 257 (76, M^- − TAN), 142 (32), 125 (22, thymine − H), 116 (36, 2-deoxyribose − H).

trans-*(5S,6S)-5-hydroxy-6-(2,2,6,6-tetramethyl-4-oxo-1-piperidinoxy)-5,6-dihydrothymidine (2)*

The silica gel containing the slowest eluting thymidine−TAN adducts **2** and **3** (R_f 0.30) was extracted with 50% aqueous methanol (3 × 6 mL). The evaporation of the resulting solution to dryness gave 26 mg of the two nucleosides **2** and **3** which were applied to the C-18 Nucleosil column and eluted with methanol−water (7:3) as the solvent. The fractions containing the fastest eluting nucleoside (k' = 3.43), as monitored by its uv absorption at 230 nm, were collected. Evaporation to dryness of the aqueous methanol solution yielded 15 mg of **2** (1.8%) as an oily compound; uv (λ_{max} H_2O): 206 nm; ^{1}H nmr (D_2O, TSP) δ: 1.04 (s, 3, CH_3), 1.07 (s, 3, CH_3), 1.23 (s, 3, CH_3), 1.43 (s, 3, CH_3), 1.69 (s, 3, CH_3 thymine), 2.34 (ddd, 1, H-2″), 3.14 (ddd, 1, H-2′), 3.72 (dd, 1, H-5″), 3.80 (dd, 1, H-5′), 3.88 (m, 1, H-4′), 4.47 (m, 1, H-3′), 5.24 (d, 1, H-6), 6.29 (dd, 1, H-1′); ^{13}C nmr (D_2O, TMS) δ: 20.1 (q, CH_3 thymine), 23.6 (q, 2 × CH_3), 32.8 (q, CH_3), 33.0 (q, CH_3), 53.8 (t, CH_2 piperidone), 53.9 (t, CH_2 piperidone), 62.5 (t, C-5′), 64.4 (s, C-2 or C-4 piperidone), 65.8 (s, C-4 or C-2 piperidone), 70.7 (s, C-5 thymine), 71.7 (d, C-3′), 85.5 (d, C-1′), 86.0 (d, C-4), 89.1 (d, C-6 thymine); cd (*c* 1.2, methanol): $[\theta]_{310}$ ±0, $[\theta]_{280}$ +190, $[\theta]_{260}$ +2840, $[\theta]_{253}$ +3800, $[\theta]_{246}$ +2830, $[\theta]_{240}$ ±0, $[\theta]_{230}$ −8400; FAB-ms, *m/e* (relative intensity), positive mode: 452 (35, M^+ + Na), 430 (12, M^+ + H), 354 (6), 265 (20), 172 (22, TAN + 2H), 117 (40, 2-deoxyribose); negative mode: 428 (22, M^- − H), 283 (15), 257 (42, M^- − TAN), 241 (8, thymidine − H), 142 (16, 5-hydroxy-5,6-dihydrothymine − H), 125 (16, thymine − H), 115 (15, 2-deoxyribose − H); FD-ms, *m/e* (relative intensity): 430 (40, M^+ + H), 259 (100, M^+ − TAN), 170 (75, TAN), 117 (15, 2-deoxyribose).

trans-*(5R,6R)-5-hydroxy-6-(2,2,6,6-tetramethyl-4-oxo-1-piperidinoxy)-5,6-dihydrothymidine (3)*

The fractions containing the slowest eluting thymidine−TAN adduct **3** (k' = 4.57) were collected and evaporated to dryness, yielding 14 mg (1.7%) of an oily compound; uv (λ_{max} H_2O): 214 nm; ^{1}H nmr (D_2O, TSP) δ: 1.07 (s, 3, CH_3), 1.17 (s, 3, CH_3), 1.26 (s, 3, CH_3), 1.44 (s, 3, CH_3), 1.66 (s, 3, CH_3 thymine), 2.42 (ddd, 1, H-2″), 2.96 (ddd, 1, H-2′), 3.73 (dd, 1, H-5″), 3.79 (dd, 1, H-5′), 3.99 (m, 1, H-4′), 4.45 (m, 1, H-3′), 5.34 (s, 1, H-6), 5.75 (dd, 1, H-1′); ^{13}C nmr (D_2O, TMS) δ: 19.8 (q, CH_3 thymine), 23.7 (q, CH_3), 24.3 (q, CH_3), 32.3 (q, CH_3), 33.8 (q, CH_3), 53.6 (t, CH_2 piperidone), 53.7 (t, CH_2 piperidone), 63.0 (t, C-5′), 66.1 (s, C-2 and C-6 piperidone), 70.7 (s, C-5 thymine), 72.3 (d, C-3′), 87.0 (d, C-4′), 92.8 (d, C-1′), 93.7 (d, C-6 thymine); cd (*c* 1.8, methanol): $[\theta]_{290}$ ±0, $[\theta]_{270}$ −300, $[\theta]_{260}$ −1480, $[\theta]_{255}$ −1780, $[\theta]_{249}$ −1290, $[\theta]_{244}$ ±0, $[\theta]_{230}$ +8200; FAB-ms, *m/e* (relative intensity), positive mode: 452 (28, M^+ + Na), 430 (11, M^+ + H), 265 (18), 172 (51, TAN + 2H), 117 (82, 2-deoxyribose); negative mode: 428 (29, M^- − H), 257 (58, M^- − TAN), 241 (8, thymidine − H), 142 (26, 5-hydroxy-5,6-dihydrothymine − H), 125 (37, thymine − H), 115 (25, 2-deoxyribose − H); DCI-ms (NH_3) *m/e* (relative intensity), positive mode: 430 (40, M^+ + H), 276 (10, M^+ − TAN + NH_3), 243 (11, thymidine + H), 172 (42, TAN + 2H).

trans-*(5S,6S)-6-hydroxy-5-(2,2,6,6-tetramethyl-4-oxo-1-piperidinyl-*N*-oxide)-5,6-dihydrothymidine (6)*

The main uv absorption band (R_f 0.22), which contained the starting thymidine (**1**) and the thymidine−TAN addition product **6**, was scraped off and the two nucleosides were extracted with 50% aqueous methanol (3 × 6 mL). The resulting solution was evaporated to dryness and applied to the C-18 Nucleosil reversed-phase column. The eluent was a mixture of water and methanol (7:3) and the detection of the nucleosides was monitored at 230 nm. The latest eluting nucleoside consisted of thymidine (k' = 1.05). The fractions containing the thymidine–TAN adduct (k' = 4.58) were collected and evaporated to dryness, giving 12 mg of a colorless oily compound (1.4%); uv (λ_{max} H_2O): 214; ^{1}H nmr (D_2O, TSP) δ: 1.10 (s, 6, 2 × CH_3), 1.21 (s, 3, CH_3), 1.31 (s, 3, CH_3), 1.65 (s, 3, CH_3 thymine), 2.20 (ddd, 1, H-2″), 2.44 (ddd, 1, H-2′), 3.74 (dd, 1, H-5″), 3.79 (dd, 1, H-5′), 3.96 (m, 1, H-4′), 4.46 (m, 1, H-3′), 5.39 (s, 1, H-6), 6.26 (dd, 1, H-1′); ^{13}C nmr (D_2O, TMS) δ: 14.6 (q, CH_3 thymine), 23.6 (q, 2 × CH_3), 33.8 (q, 2 × CH_3), 37.8 (t, C-2′), 53.8 (t, CH_2 piperidone), 54.3 (CH_2 piperidone), 63.1 (t, C-5′), 63.8 (s, C-2 or C-4 piperidone), 64.2 (C-4 or C-2 piperidone), 72.5 (d, C-3′), 79.5 (d, C-6 thymine), 80.9 (s, C-5 thymine), 85.1 (d, C-4′), 86.6 (d, C-1′); cd (c 1.3, methanol): $[\theta]_{319}$ ±0, $[\theta]_{309}$ +80, $[\theta]_{283}$ +600, $[\theta]_{276}$ ±0, $[\theta]_{269}$ −1500, $[\theta]_{240}$ −3870, $[\theta]_{229}$ −3760; FAB-ms m/e (relative intensity), positive mode: 452 (18, M^+ + Na), 430 (10, M^+ + H), 172 (40, TAN + 2H); negative mode: 428 (20, M^- − H), 257 (70, M^- − TAN), 116 (40, 2-deoxyribose − H).

*Decomposition studies of the adducts **2**–**7** in aqueous solutions*

The TAN–thymidine adduct **6** (45 mg) was dissolved in 100 mL of water (pH 6.5) and the resulting aerated solution was stirred for 48 h at 30°C. Two-dimensional thin-layer chromatographic analysis of an aliquot of the solution shows, besides the starting compound, the presence of a far-uv absorbing nucleoside. Preparative separation of this nucleoside was made on two thick silica gel tlc plates by using solvent system II. Extraction of the silica gel (R_f 0.35) with methanol (3 × 6 mL) provided 11.5 mg of a nucleoside which was characterized as 5-hydroxymethyl-2′-deoxyuridine (**14**) by comparison of its uv, ^{1}H nmr, and FAB mass spectrometric features with those of the authentic sample (28).

Under the same experimental conditions, the partial decomposition of **7** (~60%) generated 5-hydroxymethyl-2-deoxyuridine (**14**) in 45% yield as the major product.

It has to be pointed out that the other TAN–thymidine adducts **2**–**5** did not undergo any detectable degradation in the above conditions, even at a higher temperature (60°C).

*Conversion of the adducts **6** and **7** to 5-hydroperoxymethyl-2′-deoxyuridine (**15**)*

The solution of the adduct **6** (35 mg) in 80 mL of 30% aqueous hydrogen peroxide was stirred for 15 h at 30°C. The solution was evaporated to dryness under reduced pressure (10^{-3} Torr; 1 Torr = 133.3 Pa) to remove H_2O_2. The resulting residue was deposited on three thin-layer precoated silica gel plates which were further eluted with the solvent system II. The silica gel containing the main uv absorbing band (R_f 0.50), which gave a positive test for a peroxidic compound by spraying the chromatogram with a methanolic solution of KI, was scraped off and extracted with 3 × 6 mL of methanol. Evaporation of the methanolic solution yielded 8.8 mg of 5-hydroperoxymethyl-2′-deoxyuridine (39%), which showed uv and ^{1}H nmr spectroscopic properties identical to those of the authentic sample (30). Work-up in a similar way of the minor uv absorbing band gave 1.2 mg of 5-hydroxymethyl-2′-deoxyuridine (**14**) (5%).

Treatment of the adduct **7** under the above conditions yielded 5-hydroperoxy-2′-deoxyuridine (**15**) and 5-hydroxymethyl-2′-deoxyuridine (**14**) in 35% and 6% yields, respectively.

*Stability studies of the thymidine adducts **2**–**7** in pyridine–water solutions*

The TAN addition product to thymidine, **6** (85 mg), was dissolved in 100 mL of 50% aqueous pyridine. The resulting solution was stirred, open to the air, for 3 h at 60°C. The solution was evaporated to dryness and the resulting residue was applied on two precoated silica gel plates. Solvent system II was used as the developer. Six main bands, which gave a pink coloration after spraying the chromatoplates with the cysteine – sulfuric acid reagent, were extracted with 3 × 5 mL of methanol. Evaporation to dryness of the resulting solutions yielded six homogeneous nucleosides which were characterized by comparison of their uv, ^{1}H nmr, cd, and mass spectrometric features with those of the corresponding authentic samples: *N*-(2-deoxy-β-D-*erythro*-pentofuranosyl) formamide (**18**) (R_f 0.22; 22.2 mg, 40%); (+)-*cis*-(5*S*,6*R*)-5,6-dihydroxy-5,6-dihydrothymidine (R_f 0.30; 9.8 mg, 10%); (−)-*cis*-(5*R*,6*S*)-5,6-dihydroxy-5,6-dihydrothymidine (R_f 0.33; 9.4 mg, 10%); thymidine (**1**) (R_f 0.52; 7.9 mg, 9%); (+)-(5*R**)-1-(2-deoxy-β-D-*erythro*-pentofuranosyl)-5-hydroxy-5-methylhydantoin (**16**) (R_f 0.57; 7.9 mg, 9%); (−)-(5*S**)-1-(2-deoxy-β-D-*erythro*-pentofuranosyl)-5-hydroxy-5-methylhydantoin (**17**) (R_f 0.61; 8.5 mg, 10%).

Under similar experimental conditions, the degradation of the adduct **7** gave rise to the following compounds, which were separated by thin-layer chromatography on precoated silica gel plates as reported above: *N*-(2-deoxy-β-D-*erythro*-pentofuranosyl) formamide (**18**) (R_f 0.22; 29.3 mg, 41%); (+)-*cis*-(5*S*,6*R*)-5,6-dihydroxy-5,6-dihydrothymidine (R_f 0.30; 8.4 mg, 9%); (−)-*cis*-(5*R*,6*S*)-5,6-dihydroxy-5,6-dihydrothymidine (R_f 0.33; 8.6 mg, 9%); (+)-(5*R**)-1-(2-deoxy-β-D-*erythro*-pentofuranosyl)-5-hydroxy-5-methylhydantoin (**16**) (R_f 0.57; 7.7 mg, 9%); (−)-(5*S**)-1-(2-deoxy-β-D-*erythro*-pentofuranosyl)-5-hydroxy-5-methylhydantoin (**17**) (R_f 0.61; 8.4 mg, 10%).

The other adducts **2**–**5** are stable in pyridine–water at 60°C. In particular, no detectable decomposition of these adducts was observed after storage under the above conditions over a period of 24 h.

*γ-Radiolysis of deaerated aqueous solutions of 5-bromo-6-hydroxy-5,6-dihydrothymidine (**12**) or (**13**) in the presence of TAN*

A 0.1 *M* *tert*-butanol solution of 200 mg of (+)-*trans*-5-bromo-6-hydroxy-5,6-dihydrothymidine (**13**) and 200 mg of TAN in 250 mL of bi-distilled water (pH 6.5) was deaerated by bubbling with a stream of nitrogen for 15 min and subsequently exposed to γ-rays from the ^{60}Co source of 2.5 h (absorbed does 16.5 kGy). The solution was evaporated to dryness and the resulting residue was applied on a preparative high performance silica gel column SI 500 (Waters, Milford). Elution was carried out with solvent system II at a flow-rate of 50 mL per minute. The separation of the major adduct **7** from the starting bromohydrin and TAN was achieved after one recycle. Evaporation of the corresponding fraction (k' = 2.24) as detected by refractive index yielded 154 mg of **7** (61%) which was shown to be homogeneous by analytical reversed-phase high performance liquid chromatography and two-dimensional silica gel thin-layer chromatography (eluents I and II). Its ^{1}H nmr and FAB mass spectrometric data were identical to those obtained for the adduct **7** (*vide supra*).

γ-Irradiation of the aqueous solution of the (−)-*trans* diastereoisomers of 5-bromo-6-hydroxy-5,6-dihydrothymidine (**12**) in the presence of 4.7 m*M* TAN and 0.1 *M* *tert*-butanol gave rise to the TAN–thymidine adduct **6** in a 64% yield.

γ-Irradiation of an aqueous solution of 5-hydroxy-5,6-dihydrothymidine containing TAN

Two hundred milliliters of a degassed aqueous solution of 52 mg of (5*S*)-5-hydroxy-5,6-dihydrothymidine (**10**) and of 70 mg of TAN was irradiated with the γ-rays of ^{60}Co for 1 h (absorbed dose 6600 kGy). The solution was evaporated to dryness and the resulting syrup was deposited on a preparative silica gel thin-layer plate. The developing solvent was a mixture of chloroform and methanol (9:1). The broad band (R_f 0.42) which gave a positive coloration with both the 2,4-dinitrophenylhydrazine and cysteine – sulfuric acid sprays, which are characteristic of carbonyl containing compounds and 2′-deoxyribosides respectively, was extracted with 3 × 4 mL of methanol. Evaporation to dryness of the resulting solution yielded 11 mg of a yellow syrup. This residue was dissolved in 1 mL of 70% aqueous methanol and 0.2 mL of this solution was applied per analysis on the ODS-3 reversed-phase hplc column. Elution was carried out with a mixture of water and methanol (7:3) as the solvent. Four main fractions were detected by their uv absorption at 220 nm and collected. Evaporation to dryness yielded the four homogeneous TAN–thymidine adducts, which were characterized by comparison of their ^{1}H nmr and FAB mass spectroscopic features with those obtained for the authentic samples (*vide supra*): fraction 1 (k' = 1.50), 3.2 mg of

4; fraction 2 (k' = 3.42), 3.5 mg of **2**; fraction 3 (k' = 4.34), 1.2 mg of **8**; and fraction 4 (k' = 4.84), 1.4 mg of **9**.

Under similar experimental conditions, the γ-irradiation of 52 mg of the 5*R* diastereoisomer of 5-hydroxy-5,6-dihydrothymidine (**11**) in the presence of TAN generated four thymidine–TAN adducts. Initial thin-layer analysis, followed by reversed-phase high performance liquid chromatography, provided four main fractions: fraction 1 (k' = 1.15), 3.4 mg of **5**; fraction 2 (k' = 4.57), 3.7 mg of **3**; fraction 3 (k' = 4.35), 1.5 mg of **8**; and fraction 4 (k' = 4.85), 1.4 mg of **9**.

Hydrogenolysis of thymidine–TAN adducts

The nucleoside (10 mg) to be hydrogenolysed was dissolved in 10 mL of methanol; 300 mg of previously hydrogenated Pd/C (Merck, Darmstad, GFR) were added to this solution. Hydrogenolyses were carried out under 50 bars (1 bar = 100 kPa) for 5 h, while stirring the solution. The methanolic solution was then filtered through a Celite pad and evaporated to dryness. The oily residue was analyzed by tlc on silica gel and (or) hplc on the C-18 reversed phase column.

Acknowledgments

The authors thank H. Reutenauer (Centre Grenoblois de Résonance Magnétique Nucléaire) for carrying out the ^{1}H nmr experiments, and Dr. F. E. Hruska for fruitful discussions. They also acknowledge the "Association pour le Développement de la Recherche sur le Cancer" for partial support (Grant ADRC GR. 762.964).

1. P. T. EMMERSON and P. HOWARD-FLANDERS. Radiat. Res. **26**, 54 (1965).
2. N. M. BLACKETT, W. R. WOLLISCROFT, E. M. FIELDEN, and S. C. LILLICRAP. Radiat. Res. **30**, 841 (1974).
3. R. P. HILL, E. M. FIELDEN, S. C. LILLICRAP, and J. A. STANLEY. Int. J. Radiat. Biol. **27**, 499 (1975).
4. K. A. SKOV, B. PALCIC, and L. D. SKARSGARD. Int. J. Radiat. Biol. **37**, 529 (1976).
5. G. E. ADAMS and M. S. COOKE. Int. J. Radiat. Biol. **15**, 457 (1969).
6. P. B. ROBERTS and E. M. FIELDEN. Int. J. Radiat. Biol. **20**, 363 (1971).
7. K. F. NAKKEN, T. BRUSTAD, and E. TAMAS. Advances in chemical radiosensitization. International Atomic Energy, Vienna. 1974. p. 37.
8. E. WOLD and T. BRUSTAD. Int. J. Radiat. Biol. **25**, 225 (1974).
9. K. A. SKOV, B. PALCIC, and L. D. SKARSGARD. Radiat. Res. **92**, 113 (1982).
10. E. WOLD and T. BRUSTAD. Int. J. Radiat. Biol. **24**, 153 (1973).
11. J. CADET, M. BERGER, M. GUTTIN-LOMBARD, and M. J. BOBENRIETH. Tetrahedron, **35**, 2743 (1972).
12. J. CADET and R. TEOULE. J. Chromatogr. **76**, 407 (1973).
13. A. MEHLITZ, K. GIERSCHNER, and TH. MINAS. Chem. Ztg. **87**, 573 (1963).
14. Y. KONDO and B. WITKOP. J. Am. Chem. Soc. **90**, 764 (1968).
15. J. CADET and R. TEOULE. Biochem. Biophys. Res. Commun. **59**, 1047 (1974).
16. J. ZEMLICKA and J. P. HORWITZ. J. Am. Chem. Soc. **97**, 4089 (1975).
17. A. M. GIROUD, J. CADET, and R. DUCOLOMB. Nouv. J. Chim. **4**, 657 (1980).
18. F. E. HRUSKA, M. BERGER, J. CADET, and M. REMIN. Can. J. Chem. **63**, 15 (1985).
19. J. CADET and R. TEOULE. Carbohydr. Res. **29**, 345 (1973).
20. A. HISSUNG, M. ISILDAR, C. VON SONNTAG, and H. WITZEL. Int. J. Radiat. Biol. **39**, 185 (1981).
21. M. BERGER. PhD Thesis, Grenoble, 1982.
22. P. GUTIERREZ and B. BENSON. Radiat. Res. **58**, 141 (1974).
23. P. T. EMMERSON. *In* Advances in radiation chemistry. Vol. 3. *Edited by* M. Burton and J. L. Magee. Wiley–Interscience, New York. 1972. p. 209.
24. R. TEOULE and J. CADET. *In* Molecular biology, biochemistry and biophysics. Vol. 27. *Edited by* J. Hütterman, W. Kohnlein, R. Teoule, and A. J. Bertinchamps. Springer, Berlin. 1978. p. 171.
25. K. MURAYAMA, S. MORIMURA and T. YOSHIOKA. Bull. Chem. Soc. Jpn. **42**, 1640 (1969).
26. G. D. MENDENHALL and K. U. INGOLD. J. Am. Chem. Soc. **95**, 6395 (1973).
27. E. TESTA, B. J. R. NICOLAUS, L. MARIANI, and F. PAGANI. Helv. Chim. Acta, **46**, 766 (1963).
28. B. R. BAKER, T. T. SCHWAN, and D. V. SANTI. J. Med. Chem. **9**, 66 (1966).
29. A. C. COPE, T. T. FOSTER, and P. H. TOWLE. J. Am. Chem. Soc. **71**, 3929 (1949).
30. J. CADET and R. TEOULE. Bull. Soc. Chim. Fr. 879 (1975).
31. D. V. SANTI and C. F. BREWER. Biochemistry, **12**, 2416 (1973).
32. J. CADET, R. DUCOLOMB, and C. TAIEB. Tetrahedron Lett. **40**, 3455 (1975).
33. J. CADET, R. NARDIN, L. VOITURIEZ, M. REMIN, and F. E. HRUSKA. Can. J. Chem. **59**, 3313 (1981).
34. J. CADET and R. TEOULE. J. Chem. Res. (S) 296 (1977).
35. A. R. LEPLEY, P. M. COOK, and G. F. WILLARD. J. Am. Chem. Soc. **92**, 1101 (1970).
36. M. ISILDAR, M. N. SCHUCHMANN, D. SCHULTE-FROHLINDE, and C. VON SONNTAG. Int. J. Radiat. Biol. **41**, 525 (1982).
37. D. LINDSAY, J. A. HOWARD, E. C. HORSWILL, L. ITON, K. U. INGOLD, T. COBBLEY, and A. LL. Can. J. Chem. **51**, 870 (1973).
38. R. GRIGG and B. G. ODELL. J. Chem. Soc. B, **3**, 218 (1966).
39. A. GRAND and J. CADET. Acta Crystallogr. Sect. B, **34**, 1524 (1978).
40. E. J. HART. Radiat. Res. Rev. **3**, 285 (1972).
41. G. SCHOLES, P. SHAW, R. L. WILLSON, and M. EBERT. *In* Pulse radiolysis. *Edited by* M. Ebert, J. P. Keene, A. J. Swallow, and J. H. Baxendale. Academic Press, New York. 1965. p. 151.
42. R. L. WILLSON. Int. J. Radiat. Biol. **21**, 401 (1972).
43. H. DERTINGER and C. NICOLAU. Biochim. Biophys. Acta, **199**, 316 (1970).
44. L. S. MYERS, JR. and L. H. THEARD. J. Am. Chem. Soc. **92**, 2868 (1970).
45. M. BERGER AND J. CADET. Proceedings 7th International Congress of Radiation Research, Amsterdam, July 3–8, 1983. Abstract A3-03.
46. R. BRIERE, H. LEMAIRE, and A. RASSAT. Bull. Soc. Chim. Fr. 3273 (1965).
47. J. CADET, J. ULRICH, and R. TEOULE. Tetrahedron, **31**, 2057 (1975).
48. J. CADET, R. DUCOLOMB, and R. TEOULE. Tetrahedron, **33**, 1603 (1977).
49. J. CADET and M. BERGER. Proceedings 7th International Congress of Radiation Research, Amsterdam, July 3–8, 1983. Abstract A3-09.
50. J. CADET, A. BALLAND, and M. BERGER. Int. J. Radiat. Biol. **39**, 119 (1981).

A conformational study of the adducts of 2′-deoxythymidine and 2,2,6,6-tetramethyl-1,4-piperidone-*N*-oxyl by [1]H and [13]C nuclear magnetic resonance

FRANK E. HRUSKA,[1] MAURICE BERGER, AND JEAN CADET

Laboratoires de Chimie, Département de Recherche Fondamentale, Centre d'Études Nucléaires de Grenoble, 85 X, F. 38041 Grenoble Cedex, France

AND

MIECZYSLAW REMIN

Department of Biophysics, Institute of Experimental Physics, The University of Warsaw, 02-089 Warszawa, Poland

Received March 9, 1984

FRANK E. HRUSKA, MAURICE BERGER, JEAN CADET, and MIECZYSLAW REMIN. Can. J. Chem. **63**, 15 (1985).

γ-Irradiation of oxygen-free, aqueous solutions of 2′-deoxythymidine in the presence of the organic nitroxide free radical, 2,2,6,6-tetramethyl-1,4-piperidone-*N*-oxyl (TAN), leads to a complex mixture of products in which the TAN moiety is linked to the C5 or C6 position of a 5,6-saturated thymine ring. Extensive [1]H and [13]C nmr data are provided for the eight TAN−dT adducts which are produced in the largest amounts. The results show that the conformational properties of the sugar moiety are dependent on the point of attachment of the TAN group and the configuration of the saturated thymine ring.

FRANK E. HRUSKA, MAURICE BERGER, JEAN CADET et MIECZYSLAW REMIN. Can. J. Chem. **63**, 15 (1985).

La radiolyse γ de solutions aqueuses de désoxy-2′-thymidine et d'un radical libre nitroxyde, la tétraméthyl-2,2,6,6 pipéridone-4 oxyle-1 (TAN), engendre un mélange complexe de produits qui résultent de l'addition de la molécule de TAN sur les carbones 5 ou 6 pyrimidiniques. Une étude détaillée de rmn [1]H et [13]C a été effectué par les huit dérivés d'addition radio-induite du TAN avec la thymidine. Les propriétés conformationnelles du fragment osidique de ces produits dépendent du site d'attachement de la molécule de TAN et de la configuration du carbone (6) du cycle pyrimidinique.

Introduction

The free radical reactions in γ-irradiated aqueous solutions of 2′-deoxythymidine (dT) in the presence of the organic nitroxide free radical, 2,2,6,6-tetramethyl-4-piperidone-*N*-oxyl (triacetoneamine-*N*-oxide, or TAN), lead to a complex array of products with the TAN moiety linked to a 5,6-saturated thymine base. In the previous, companion paper extensive chemical, mass spectrometric, and [1]H and [13]C nmr data were used for

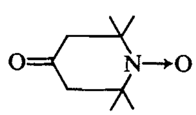

structural and configurational assignments of several series of adducts with a TAN group at the C5 or C6 position of the pyrimidine ring (1). In vitro evidence (2,3) indicates that TAN, and other organic nitroxides, can react with hydroxyl radical-induced transients in DNA, but the nature of the products has not been determined. The adducts of the type described (1) are likely candidates, though addition of TAN to other bases, or to the sugar, cannot be discounted (4). The addition of the TAN group to the thymine base, with the concomitant 5,6-saturation of the ring, would have profound effects on its hydrogen bonding and stacking properties, and on the stereochemistry of the sugar phosphate backbone of a polynucleotide, but no information on its effects is available. Similarly, no structural data for any TAN adduct has been provided by X-ray crystallography. In this study we discuss [1]H and [13]C nmr data which provide information about the conformation of the TAN−dT adducts in aqueous solution and should contribute to our growing knowledge of modified nucleosides. Furthermore, our data should be useful for identifying any TAN adduct isolated from DNA.

[1]Permanent address: Chemistry Department, The University of Manitoba, Winnipeg, Manitoba, Canada.

In Fig. 1 are shown the four diastereoisomeric forms of 5-TAN-6-hydroxy-5,6-dihydro-2′-deoxythymidine (5T series) and the four diastereoisomeric forms of 5-hydroxy-6-TAN-5,6-dihydro-2′-deoxythymidine(6T series). Structures are shown for the adduct in each series, 5T1 and 6T1, which has the *R* configuration at C5 and C6. For the six remaining molecules only the C5—C6 fragment is given to show their configurations at C5 and C6: 5*S*,6*R* in 5T2 and 6T2; 5*R*,6*S* in 5T3 and 6T3; 5*S*, 6*S* in 5T4 and 6T4. It is important to note that evidence (1) points to linkage at C5 via the nitroxyl N-atom in the 5T series and at C6 via the nitroxyl O-atom in the 6T series. Note also that in each series (5T, 6T) the T1 and T4 bases constitute, in isolation, an enantiomeric pair with a *trans* relationship between the TAN and hydroxyl groups, whereas the T2 and T3 bases constitute a *cis* enantiomeric pair. As pointed out (1), the four 6T isomers, but only two of the 5T isomers, could be isolated in quantities sufficient for study; arguments were presented that the two are the *trans* isomers, 5T1 and 5T4. Space-filling models reveal more severe crowding of substituents on the pyrimidine ring in the 5T series. Thus, the absence of significant amounts of the *cis* isomers, 5T2 and 5T3, may be a reflection of the more critical stereochemical requirements for the formation of the 5T molecules. The *cis* isomers may, however, be present in the additional fraction of as yet unidentified products of γ-irradiation.

Figure 2 shows the structure of two additional adducts isolated in sufficient quantity, the diastereoisomers of 5-TAN-5,6-dihydro-2′-deoxythymidine with a TAN group linked to C5 via the nitroxyl N-atom and with a C6-*methylene* function. The molecules are denoted 5T*R* and 5T*S* according to their *R* or *S* configuration at C5, but we could make no absolute configurational assignment with the available spectroscopic data (1).

Essential for our discussion of the data for the 5T and 6T series are the four diastereoisomers of 5,6-dihydroxy-5,6-dihydro-2′-deoxythymidine which are major products of γ-irradiation of *aerated*, aqueous solutions of dT (5). They are

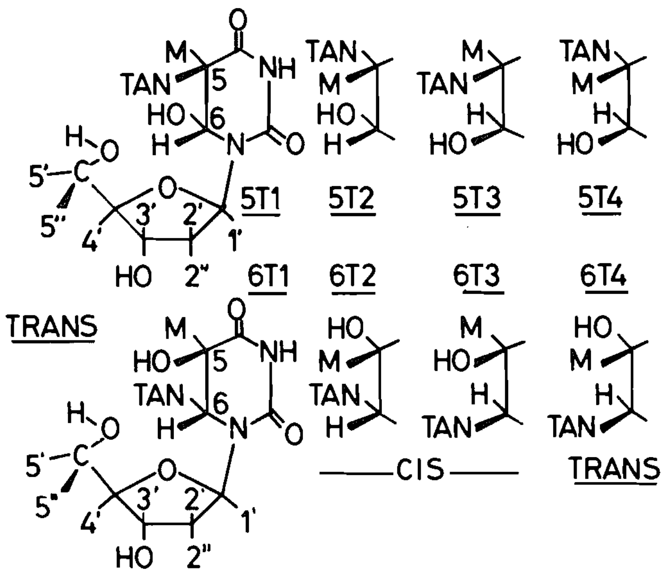

FIG. 1. Structures of the 5T and 6T series of 2′-deoxythymidine – TAN adducts. The linkage is to the nitroxyl N- and O-atoms in 5T and 6T, respectively. In each series the T1 and T4 bases are, in isolation, enantiomers with *trans*-oriented TAN and hydroxyl groups; the T2 and T3 bases are enantiomers with *cis*-oriented TAN and hydroxyl groups. The bases are represented in the *anti* conformer range about the *N*-glycosyl link; rotation by 180° makes them *syn*. M is CH_3. Absolute configurations of C5 and C6: T1 (*R*,*R*); T2 (*S*,*R*); T3 (*R*,*S*); T4 (*S*,*S*).

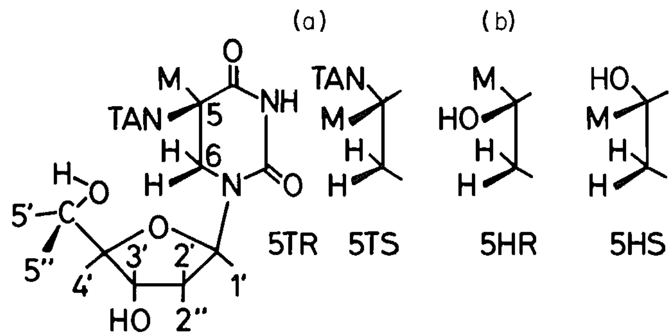

FIG. 2. Structures of (a) the 5T(*RS*) series of TAN adducts, 5T*R* and 5T*S* (linked via the nitroxyl N-atom), and (b) the 5H series of derivatives, 5H*R* and 5H*S*. M is CH_3. *R* and *S* refer to the C5 configuration. The bases are drawn in the *anti* conformer range about the *N*-glycosyl link. The absolute configurations have been determined for the 5H series but not for the 5T(*R*,*S*) series.

denoted D1, D2, D3, and D4, which have respectively the 5*R*,6*R*, 5*S*,6*R*, 5*R*,6*S*, and 5*S*,6*S* configurations at C5 and C6. Replace TAN by a hydroxyl group in the 5T (or 6T) series to obtain the correspondingly numbered D isomer (Fig. 1). Thus, 5T1, 6T1, and D1 all have the 5*R*,6*R* configuration, and so on. Note that the D1 – D4 and D2 – D3 base pairs in isolation are enantiomers with *trans* and *cis* oriented hydroxyl groups, respectively. ^{1}H nuclear magnetic resonance data have been reported for the D molecules (6). Similarly useful for comparison with the data of 5T*R* and 5T*S* are the two diastereoisomers of 5-hydroxy-5,6-dihydro-2′-deoxythymidine, generated also in γ-irradiated, aerated aqueous solutions and labelled 5H*R* and 5H*S* according to their configuration at C5 (Fig. 2). A detailed ^{1}H and ^{13}C nmr study of this 5H series has not been presented. In conjunction with the crystallographic structure available for the 5H*S* isomer (7), our solution spectroscopic data could be used to assign the configurations of the two 5H diastereoisomers (1).

Experimental

Materials

The 5T, 6T, and 5T (*RS*) series of TAN adducts (Figs. 1, 2) were prepared by γ-radiolysis of oxygen-free solutions of dT (1 m*M*) containing 2 m*M* TAN, and purified as described (1,8). The 5H*R* and 5H*S* isomers (Fig. 2) were prepared by γ-radiolysis of deaerated, aqueous solutions of dT (10 m*M*) containing 20 m*M* cysteine as described (9).

Nuclear magnetic resonance experiments

The nucleoside samples were lyophilized three times from 99.9% D_2O (Commissariat Energie Atomique, Saclay) and dissolved in 99.9% D_2O to a concentration of 0.1 *M*. (3-Trimethylsilyl)propionate-2,2,3,3-d_4 (TSP) was used as internal reference. Metal ions were removed using Chelex 100 resin columns (Bio-Rad, Richmond, CA). For the ^{1}H T_1 and nOe measurements the nmr tubes (5-mm od) were sealed under nitrogen. The ^{1}H nmr spectra were obtained at 250 MHz (Cameca TSN 250, FT mode, 20°C). Homonuclear decoupling experiments facilitated the spectral assignment. H2′ and H2″ were assigned following coupling constant arguments (10); H5′ and H5″ were assigned from chemical shift trends (11) and selective deuteration experiments (12). Spectral analysis (LAOCOON III) and computer-simulated spectra were the final test of the chemical shift (δ) and coupling constant (*J*) data, and are listed in Tables 1 and 2. The uncertainties in δ and *J* are estimated to be about 0.1 Hz at 250 MHz.

The proton T_1 data (30°C) were obtained by the inversion recovery pulse sequence ($180°-t-90°-T_d$) with a pulse delay of at least $5T_1$ between sequences (13). Ten spectra with delay times *t* in the range 0.1 s to 15 s were collected; peak heights as a function of *t* served as input for a least-squares computer program (probable uncertainty ~5%). The homonuclear ^{1}H nOe experiments were carried out as described elsewhere (14). The nOe enhancements were expressed as the percentage change in peak height of the H6 (or H1′) resonances upon saturation of the H1′ (or H6) resonances. The enhancements are averages of twenty measurements, reproducible to ±3%. The T_1 and nOe data are given in relevant sections below. Unfortunately, due to the rapid decomposition of the 5-TAN derivatives and the difficulties encountered in their synthesis and isolation, only their conventional ^{1}H (and ^{13}C) nmr spectra, but no T_1 or nOe data, were obtainable.

^{1}H-Decoupled ^{13}C nmr spectra were obtained at 25.1 MHz (Varian XL-100-15; 21°C) on aqueous solutions (~0.1 *M* in nucleoside containing about 1% dioxane as internal reference). The assignment of the spectra was made by comparison with published data (15, 16), off-resonance ^{1}H-decoupling, and, for C1′, C4′, and C6, selective ^{1}H-decoupling experiments. The $\delta(^{13}C)$ data in Table 3 are reported in ppm downfield from external TMS with internal dioxane measured at 67.86 ppm. With the available material, the weak carbonyl resonances could not be detected in reasonable times.

Results and discussion

Geometry of the pyrimidine and TAN rings

Evidence points to a distorted half-chair conformation for 5,6-saturated pyrimidines in which C5 and C6 lie on opposite sides of the mean plane defined by N1—C2—N3—C4 (7, 17 – 19). Of the molecules considered here, crystallographic data are available only for 5H*S*, which shows a half-chair with the 5-hydroxyl and 5-methyl groups in pseudo-axial and pseudo-equatorial positions, respectively (7). Conventional methods for determining solution conformations (vicinal *J*(HH)) are not applicable to the ring systems of the molecules under study (Figs. 1, 2). Space-filling models of the 6T molecules suggest a ring pucker with the bulky TAN group in an axial position. The models also suggest that, to accomodate the

TABLE 1. Proton chemical shifts for radiation-induced TAN−thymidine addition products[a]

Nucleoside[b]	CH_3 (base)	CH_3 (piperidine)	H6	H1′	H2′	H2″	H3′	H4′	H5′	H5″
6T1	1.66	1.07 1.17 1.26 1.44	5.34	5.75	2.96	2.42	4.45	3.99	3.79	3.73
6T2	1.59	1.14 1.21 1.32 1.44	5.41	5.78	2.94	2.42	4.47	4.00	3.82	3.74
6T3	1.54	1.09 1.24 1.29 1.42	5.36	6.35	3.15	2.35	4.48	3.93	3.76	3.76
6T4	1.69	1.04 1.07 1.23 1.43	5.24	6.29	3.14	2.34	4.47	3.88	3.80	3.72
5T1	1.64	1.08 (x2) 1.17 1.29	5.32	6.25	2.36	2.27	4.44	3.95	3.79	3.74
5T4	1.65	1.10 (x2) 1.21 1.31	5.39	6.26	2.44	2.20	4.46	3.96	3.79	3.74
5T*R*	1.57	1.18 1.21 1.22 1.27	3.57 4.17	6.31	2.35	2.18	4.41	3.92	3.76	3.70
5T*S*	1.56	1.16 1.22 1.23 (x2)	3.48 4.12	6.29	2.28	2.16	4.41	3.92	3.76	3.73
5H*R*	1.47	—	3.48[c]	6.27	2.29	2.15	4.37	3.91	3.77	3.71
5H*S*	1.47	—	3.43 3.51	6.27	2.30	2.16	4.38	3.91	3.77	3.69

[a]Chemical shifts in ppm from TSP as internal reference to an accuracy of ±0.1 Hz.
[b]0.10 *M* in D_2O at 20 ± 1°C.
[c]The C6 protons are isochronous.

TABLE 2. Proton coupling constants (Hz) for the sugar moiety of 2′-deoxyribonucleosides in aqueous solution (20°C)

Nucleoside	1′,2′	1′,2″	2′,2″	2′,3′	2″,3′	3′,4′	4′,5′	4′,5″	5′,5″
6T1	7.1	6.5	−13.6	6.5	3.4	3.3	4.0	5.9	−12.1
6T2	7.2	6.5	−13.6	6.6	3.2	3.5	4.1	5.6	−12.1
6T3	8.4	6.4	−14.5	6.8	3.1	2.7	3.5	3.5[a]	−12.5[b]
6T4	8.1	6.5	−14.8	7.0	3.0	3.0	3.0	4.2	−12.5
5T1	7.9	6.0	−13.6	6.2	3.3	3.0	3.4	4.0	−12.3
5T4	9.2	5.6	−14.0	5.9	2.2	2.4	4.4	4.6	−12.3
5T*R*	7.9	6.5	−14.0	6.2	3.6	3.1	4.1	4.6	−12.4
5T*S*	7.7	6.4	−14.1	6.3	3.8	2.9	3.9	4.9	−12.3
5H*R*	7.8	6.5	−14.0	6.8	3.4	3.4	4.1	5.2	−12.3
5H*S*	7.7	6.6	−14.2	6.8	3.5	3.6	4.0	5.5	−12.3

[a]Only the sum of connected coupling constants $J(4'5')$ and $J(4'5'')$ ( ) is significant when $\delta(5') \approx \delta(5'')$.
[b]Estimated; not measurable when $\delta(5') \approx \delta(5'')$.

6-TAN group in this orientation, the torsion angle about the C6—O bond in the C5—C6—O—N fragment (which defines the relative orientation of the pyrimidine and TAN groups) must be in the antiperiplanar range (180° ± 30°). Rotation out of this range leads to severe crowding of the TAN methyl groups and the substituents on the base and sugar moieties. Crowding of groups is even more severe in the 5-TAN adducts since the TAN group is accompanied on C5 by the bulky 5-methyl group. (The absence of the *cis* adducts, 5T2 and 5T3, in the products of γ-radiolysis is probably a reflection of this more serious crowding.) Molecular models suggest that considerable distortion of the pyrimidine ring would be required to accommodate the 5-TAN group in the *trans* isomers, 5T1 and 5T4, as well as in 5T*R* and 5T*S*.

In the absence of vicinal H—H coupling interactions, only limited structural information about the TAN moiety can be

TABLE 3. ^{13}C chemical shifts (δ,ppm) of radiation-induced TAN−thymidine adducts in aqueous solution[a]

								Thy	TAN		
Nucleosides[b]	1′	2′	3′	4′	5′	5	6	CH_3	CH_3	—CH_2	—C—
6T1	92.8	38.7	72.3	87.0	63.0	70.7	93.7	19.8	23.7 24.3 32.3 33.8	53.7 53.6	66.1(2)
6T2	92.6	38.8	72.2	87.0	63.0	73.2	93.4	23.8	23.7 24.4 32.1 33.3	53.3 53.5	63.0 64.9
6T3	85.5	38.6	72.5	86.3	63.0	73.6	89.1	24.0	24.2(2) 32.4(2)	53.5(2)	66.0(2)
6T4	85.5	38.6	71.7	86.0	62.5	70.7	89.1	20.1	33.0 32.8 23.6	53.8 53.9	64.4 65.8
5T1	86.2	39.1	72.0	86.7	62.6	80.8	80.1	15.0	23.6 23.7 33.9 34.0	53.9 54.3	67.3 68.0
5T4	86.6	37.8	72.5	85.1	63.1	80.9	79.5	14.6	23.6(2) 33.8(2)	53.8 54.3	63.8 64.2

[a]These spectra were obtained using the Varian XL-100-15 (25.15 MHz) and the Cameca TSN 250 (62.87 MHz) spectrometers. All chemical shifts were referenced to external TMS.
[b]20% w/v in D_2O. Ambient probe temperature 21°C.

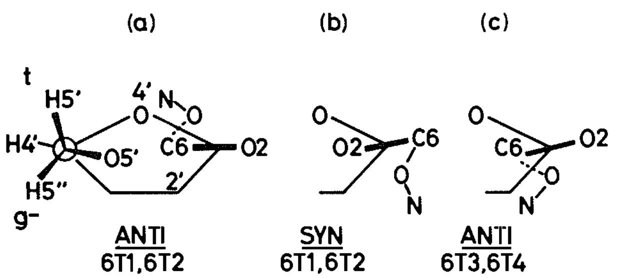

FIG. 3. View of the 6T molecules which shows the position of the 6-TAN group and 2-keto oxygen of the base relative to the sugar moiety in the *anti* and *syn* conformations. TAN is represented by O—N. The view of *syn* 6T3 and 6T4 (not shown) resembles *anti* 6T1 and 6T2 in the position of the TAN group. To obtain views of the correspondingly numbered 5T or D molecule, replace TAN by OH. The diagram on the left shows a projection along C4′—C5′ with the g^+ conformation. t and g^- give the location of O5′ in the t and g^- conformations.

gleaned from our ^1H nmr data. It is interesting that, in the —CH_2—CO—CH_2— portion of the spectrum (an ABXY pattern with geminal coupling constants of 13.5 Hz), a four-bond coupling of 2.2 Hz is noted between one pair of protons, with a smaller coupling of about 0.7 Hz between the other pair. This suggests that one of the four-bond H—C—C—C—H fragments approaches an all-*trans* conformation favorable for coupling (20), whereas the second fragment assumes a less favorable conformation. It is noteworthy that just this situation obtains in the twist-boat conformation found for the TAN molecule in organic solvents (21, 22).

Conformation about the N-*glycosyl bond* (χ)

Steric interactions involving the sugar ring with H6, the 2-keto oxygen, and the TAN methyl groups should have the largest direct role in determining the preferred conformations about the χ bond in the 6T series. Space-filling models suggest that, with an antiperiplanar C5—C6—O—N fragment, rotation about the *N*-glycosyl link is highly hindered and that relatively narrow ranges of χ angles are accessible to the 6T molecules. Thus for the 6*R* pair, 6T1 and 6T2, relatively few contacts are made in a conformation represented in Fig. 3(a) ($\chi \approx -130°$; *anti* domain) which places the TAN group off the sugar ring to its O4′ side. (See Davies and Dixon (23) for definitions of torsion angles.) A second conformation (Fig. 3(b); $\chi \approx 50°$; *syn* domain) places the TAN group off the sugar and near to the C2′ protons. For the 6*S* pair, 6T3 and 6T4, an acceptable conformation is found in the *anti* domain (Fig. 3(c); $\chi \approx -130°$) which places the TAN group near to the C2′ protons in a region similar to that in Fig. 3(b). A *syn* conformation for the 6*S* pair ($\chi \approx 50°$) also seems possible; a perspective is not given but it places the TAN group in a region near O4′, similar to that in Fig. 3(a). Other conformations, which place the 6-TAN group over the sugar ring, seem unlikely.

A variety of data lead us to conclude, in a qualitative way, that the 6*R* adducts, 6T1 and 6T2, prefer the *syn* domain of χ angles whereas the 6*S* pair, 6T3 and 6T4, prefer the *anti* domain. Thus, in nOe experiments in aqueous solution (30°C), saturation of H1′ of 6T1 or 6T2 led to an 11% enhancement of the integrated intensity of the corresponding H6 singlet; similar enhancements in H1′ intensity were noted when the H6 proton was saturated. This suggests proximity of the H6 and H1′ protons, which is achieved in the *syn* conformation (Fig. 3(b)) (24, 25). On the other hand, in the same experiments on the 6*S* pair, 6T3 and 6T4, no significant intensity changes (≈1%) were noted for either H1′ or H6, consistent with the separation of these atoms in the *anti* conformation (Fig. 3(c)).

Following the structural studies by ^1H spin-lattice relaxation time measurements of Preston and Hall (26) and Chachaty and Langlet (27), we find further evidence in Table 4 for the proximity of H1′ and H6. In dT, the parent, unsaturated nucleoside, a relatively long T_1 (H1′) is observed (≈3 s); saturation of the pyrimidine ring to form the D2 glycol leads to a small decrease

TABLE 4. [1]H longitudinal relaxation times (T_1,s) of nucleosides[a]

	6T1	6T2	6T3	6T4	D2	dT
H-1′	0.67	0.49	1.02	1.15	2.54	3.07
H-2′	0.47	0.34	0.28	0.33	0.61	0.80[b]
H-2″	0.49	0.45	0.50	0.55	0.66	0.80
H-3′	2.00	1.90	2.10	1.55	1.88	2.27
H-4′	1.60	0.92	1.10	1.38	2.23	2.48
H-5′,H-5″	0.53	0.41	0.44	0.53	0.66	0.76
CH_3(Thy)	0.49	0.43	0.54	0.40	0.80	1.41
H-6	0.47	0.36	0.48	0.52	1.33	1.88
CH_3 (a)	0.24	0.23	0.24	0.22	—	—
CH_3 (b)	0.41	0.32	0.37	0.45	—	—
CH_3 (c)	0.29	0.25	0.28	0.26	—	—
CH_3 (d)	0.41	0.31	0.36	0.43	—	—
CH_2 (a)	0.41	0.36	0.60	0.45	—	—
CH_2 (b)	0.43	0.35	0.61	0.38	—	—

[a]In D_2O at 30°C.
[b]Isochronous protons.

(17%) in T_1 (H1′). But formation of the 6T adducts leads to a sharp drop in T_1 (H1′) to 0.49 s − 1.15 s. This trend to shorter T_1 values for H1′ (and for the other protons on the nucleoside fragment, in general) is presumably a reflection, in part, of the longer correlation times for the heavier TAN adducts. However, much shorter T_1 (H1′) values are noted for 6T1 (0.67 s) and 6T2 (0.49 s) than for 6T3 (1.02 s) and 6T4 (1.15 s). This additional relaxation process in the *syn* 6*R* pair can be assigned to interactions with H6 which are not possible in the *anti* 6*S* pair. The striking difference between the 6*R* and 6*S* pairs is not, however, seen in the T_1 (H6) data. We think that, for two reasons, T_1 (H6) might be less sensitive to a *syn*, *anti* conversion. First, H6 should be most strongly relaxed by dipolar interactions with the TAN methyl and 5-methyl protons, which are independent of the χ angle. (Note that T_1 (H6) is always shorter than T_1 (H1′) (Table 4).) Second, the contribution to the H6 relaxation from H1′ in the *syn* conformation is replaced by a comparable contribution from H2′ in the *anti* conformation. (Table 4 also contains T_1 data for the remaining protons which serve to further characterize the molecules and may be of interest to readers).

With normal, unsaturated pyrimidine bases qualitative information about the χ angle has been obtained from chemical shift comparisons, particularly for the H2′ sugar proton, which experiences a large deshielding in the *syn* conformation due to the juxtaposition of the 2-keto oxygen (28−32). To show more clearly the effects of the TAN modification, correlation diagrams (Fig. 4) were constructed with the δ data for the methyl (M), H6, H1′, H2′, and H2″ protons of the 6T, 5T, and D molecules (Table 1 and ref. 6). Data for H3′, H4′, H5′, and H5″ are not given since they show smaller variations. Data are also shown for H1′, H2′, and H2″ of dT and m^{6}dU (6-methyl-2′-deoxyuridine), which prefer the *anti* and *syn* conformations, respectively, in the crystal and aqueous solution states (10, 29, 32, 33).

A striking feature of the diagram is the similarity, for 6T1 and 6T2 on the one hand and for 6T3 and 6T4 on the other hand, in the data for H1′, H2′, and H2″, the sugar protons of which are expected to sense most strongly the shielding effects of the TAN and base moieties. Within each pair the differences in δ are on average only 0.02 ppm, whereas differences in δ between the pairs is large (ca. 0.5, 0.2, and 0.08 ppm for H1′, H2′, and H2″, respectively). Particularly noteworthy are the large deshielding effects of H2′ relative to the data for the dT, D, and 5T molecules (ca. 0.5 ppm for the 6*R* pair and 0.7 ppm for the 6*S* pair) and the large shielding effects of H1′ for the 6*R* pair (ca. 0.5 ppm). In line with the T_1 and nOe measurements, these trends suggest a similarity in χ for 6T1 and 6T2, and for 6T3 and 6T4; that is, in the 6T series the conformation about the *N*-glycosyl bond depends strongly on the configuration at C6 but not at C5. Furthermore, in line with the proposal that 6T1 and 6T2 are *syn*, their H2′ protons resonate downfield by 0.55 ppm from dT and, in fact, only 0.01 ppm from H2′ of m^{6}dU. It is also interesting that the upfield shift of H1′ in the 6*R* pair relative to the 6*S* pair parallels the change in H1′ in m^{6}dU (*syn*) relative to dT (*anti*), though the effect is much larger in the TAN series (0.55 ppm versus 0.1 ppm). The relatively smaller variations in δ(H2″) are less useful as conformational probes.

The similarity in δ(H1′) for dT, 6T3, and 6T4 is in line with the proposed *anti* conformation for the 6*S* pair (Fig. 4). Of considerable concern, however, is the large deshielding (ca. 0.75 ppm) of their H2′ protons relative to dT. The effect is larger than that for the 6*R* pair and in isolation would have led us to assign a *syn* type conformation to the 6*S* pair as well. We attempt to reconcile this effect with the *anti* conformation in the following way. Space-filling models reveal that, with an antiperiplanar C5—C6—O—N fragment, H6 and the TAN methyl protons form a shallow cavity in which is located the nitroxyl nitrogen. In the *anti* conformation of the 6*S* pair, with the TAN group at the C2′ side of the sugar, H2′ can comfortably enter the cavity and approach the N-atom, which we propose is the origin of its strong deshielding. We are not aware of discussions of the shielding properties of N-atoms singly-bonded to three substituents, one of which is oxygen. However, evidence that N-atoms can strongly deshield a nearby proton is provided by the 2.1 ppm deshielding of the chloroform proton in its association with *N*-methylpyrrolidine (34). Of course, we do not suggest hydrogen bonding interactions for H2′, no more here than to the 2-keto oxygen in the *syn* conformation of the 6*R* pair.

Unfortunately, only conventional nmr spectra (but no nOe or T_1 data) could be obtained for the 5-TAN adducts since they are relatively unstable in solution. However, little variation (0.14 ppm or less) is seen in the shielding of any sugar proton for the entire collection of 5T, 5T(*R*,*S*), 5H, and D molecules (Table 1 and Fig. 4). Furthermore, the values for H1′ and H2′ are identical to the corresponding value in dT to within about 0.1 ppm, whereas the δ(H2″) values are typically only 0.1−0.2 ppm upfield from that of dT. Thus a predominantly *anti* conformation is assigned to this group of 5,6-saturated nucleosides. This conclusion is supported by the observation that 5H*S* is *anti* in the crystal state (7). It seems, then, that whereas the 6*S* to 6*R* configurational change in the 6T series effects a rotation from the *anti* to the *syn* conformation, no such effect is apparent for the 5T and D molecules. Thus, it seems that the 6-TAN can only be accommodated on the C2′ side of the sugar (Figs. 3(b), (c)), whereas the steric requirements of the smaller 6-hydroxyl group of the 5T and D molecules are much less critical.

Pucker of the sugar ring

The data in Table 2 show that the values of the *cis* coupling constant $J(1'2'')$ are remarkably similar for the majority of the 5,6-saturated systems (6.4−6.6 Hz) with slightly smaller values for 5T1 (6.0 Hz) and 5T4 (5.6 Hz). In the D series (6)

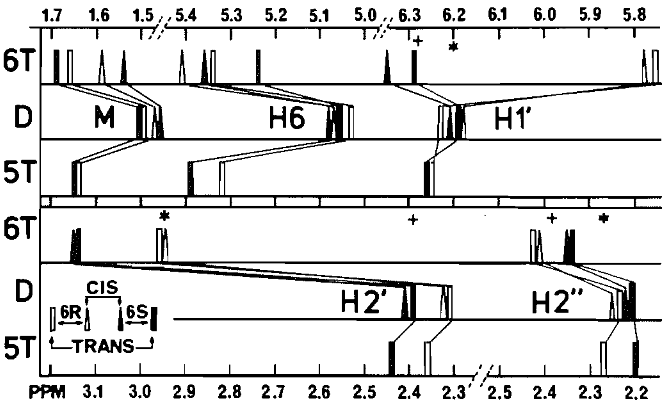

FIG. 4. Chemical shifts of the methyl (M), H6, H1′, H2′, and H2″ protons of the 6T, D, and 5T series. δ in ppm from TSP (Table 1). For each series: isomer 1 (open rectangle); isomer 2 (open triangle); isomer 3 (solid triangle); isomer 4 (solid rectangle). See also legend in lower left corner. δ for H1′, H2′, and H2″ for dT(+) and m^{6}dU(*) shown at the 6T levels.

TABLE 5. Calculated populations of the 2′-*endo* (*S*) pucker[a] and of the g$^+$, t, g$^-$ rotamers about the C4′—C5′ bond[b]

Nucleoside	*S*	g$^+$	t	g$^-$
6T1	70	37	45	18
6T2	67	39	41	19
6T3	73	67	—	—
6T4	74	64	30	6
5T1	74	62	26	11
5T4	82	47	29	23
5T*R*	73	50	30	20
5T*S*	75	48	34	17
5H*R*	68	43	37	19
5H*S*	66	41	41	18
dU	60	51	37	12
m^{6}dU	44	35	51	14

[a]%*S* = (8.4 − *J*(3′4′))/7.3 as in ref. 41, which follows ref. 42, and 10*J*(3′4′) for m^{6}dU.
[b]Following ref. 43.

J(1′2′) lies in the range 6.1−6.7 Hz with D1 and D2 at the upper end of the range, and D3 and D4 at the lower end. The values of the *cis* coupling *J*(2′3′) are in the ranges 6.5−7.0 Hz for the 6T and 5H molecules and 5.9−6.3 Hz for the 5T and 5T(*R*,*S*) molecules. In the D series (6) *J*(2′3′) is in the range 6.4−7.0 Hz. Overall, only small changes in the *cis* couplings are seen relative to those of dU (2′-deoxyuridine) (*J*(1′2″) = 6.7 Hz; *J*(2′3′) = 6.8 Hz (35)), suggesting that the formation of the 5,6-saturated derivatives does not lead to large changes in the pseudorotational parameters (P, τ_m) (36, 37). That the *cis* couplings of dU are similar to those of 6T1 and 6T2 for which a *syn* conformation is proposed is interesting, since in the *syn* nucleoside m^{6}dU increases are observed in *J*(1′2″) (8.6 Hz) and *J*(2′3′) (8.2 Hz) (29). Such increases can be rationalized by shifts in the values of *P*(*N*) and *P*(*S*) towards to O4′-*endo* conformation (38). It may be that these changes in pucker, which do not accompany the *syn* 6T1 and 6T2 bases, are characteristic of 5,6-unsaturated pyrimidine nucleosides. A study of the 5,6-saturated derivatives of m^{6}dU could provide useful information about this possibility.

The *trans* coupling constants for the molecules in Table 2 (as well as for the D series (6)) show the overall trend *J*(1′2′) > *J*(2″3′) ≈ *J*(3′4′), which indicates a preference for the *S*(2′-*endo*) pucker over *N*(3′-*endo*) (Table 5) which is noted for normal 2′-deoxyribosides (39, 40). In less pronounced trends, the *J*(1′2′) couplings are similar in the 6T1, 6T2 pair (7.1 Hz, 7.2 Hz) and are similar in the 6T3, 6T4 pair (8.4 Hz, 8.1 Hz). A parallel trend is noticed for *J*(1′2′) in the D1, D2 pair (7.5 Hz, 7.2 Hz) and in the D3, D4 pair (8.5 Hz). For the remaining molecules *J*(1′2′) falls in the narrow range 7.8 ± 0.1 Hz, except for 5T4 (9.2 Hz). *J*(2″3′) and *J*(3′4′) fall into the narrow range 2.2−3.8 Hz and show the inverse correlation with *J*(1′2′) observed for normal 2′-deoxyribosides.

The calculated %*S* values in Table 5 show that, relative to dU, all of the 5,6-saturated systems show a greater bias for 2′-*endo*, the largest being 82% for 5T4. A similar trend toward higher %*S* in the 5,6-saturated system is also noted for the *ribosides*, uridine (U) and 5,6-dihydrouridine (h^{2}U) (19). In the *syn* nucleoside, m^{6}dU, a destabilization of 2′-*endo* occurs, and a bias now exists for 3′-*endo*. This shift towards 3′-*endo* is not seen for 6T1 and 6T2, suggesting again that in the *syn* conformation, 5,6-unsaturated and 5,6-saturated pyrimidine bases may, in general, have different effects on sugar pucker.

C4′—C5′ conformation

Interesting trends in the C4′—C5′ conformation (Fig. 3(a)) are apparent in the sum *J*(4′5′) + *J*(4′5″) (Σ) (Table 2). In one group of molecules Σ varies from 8.7 Hz to 9.9 Hz and is larger than the value for dU (8.5 Hz) (35) and dT (8.6 Hz) (10). At the upper extreme are the Σ values for 6T1 and 6T2, which are similar to that of m^{6}dU (10.1 Hz) (29, 30). In the second group, which comprises 5T1 and the 6S pair, 6T3 and 6T4, Σ is in the narrow range 7.2 ± 0.2 Hz and resembles the value for the riboside U (7.4 Hz) (44). Relative to dU, the molecules in the first group show a diminished contribution from the g$^+$ conformer (Table 5). The largest decrease is seen for 6T1 and 6T2 whose conformer distribution approaches that of m^{6}dU, where a bias for t over g$^+$ is noted. The destabilization of g$^+$ in *syn*, 5,6-unsaturated pyrimidine nucleosides has been attributed to repulsion of the 5′-hydroxyl and 2-keto groups (28−30). However, it is clear from, in particular, the data for 5H*S* that 5,6-saturation of an *anti* base can lead to comparable decreases in %g$^+$. The nmr studies also point to a destabilization of g$^+$ upon 5,6-saturation of pyrimidine *ribo*sides (19).

In contrast, the second group of 5,6-saturated derivatives (5T1, 6T3, 6T4) show an enhanced %g$^+$ relative to dU. A bias towards g$^+$ is apparent with an overall conformer distribution resembling that of U (g$^+$: 62%; t: 32%; g$^-$: 5%; calculated from data in ref. 44). No interactions which should enhance %g$^+$ are apparent to us in molecular models and thus we can only state the obvious: the overall conformation of these molecules is the result of complex steric and electronic factors. However, it is interesting to note that in the *anti* conformation of the 6*S* pair, 6T3 and 6T4, van der Waals contact is made between the 5′-hydroxyl group of the sugar and the protons of a TAN methyl group; in the *syn* conformation of the 6*R* pair, 6T1 and 6T2, this contact is prevented by the intervening 2-keto oxygen of the base. Also, with 5T4 aside, there is the prevailing trend in the TAN molecules for %g$^+$ to increase with increasing %S, the converse of a previously noted correlation (45).

The calculated values of %g$^-$ (Table 5) are interesting in the light of data for ribosides and other 2′-deoxyribosides (41, 46, 47). In both the ribose and deoxyribose series, the g$^-$ con-

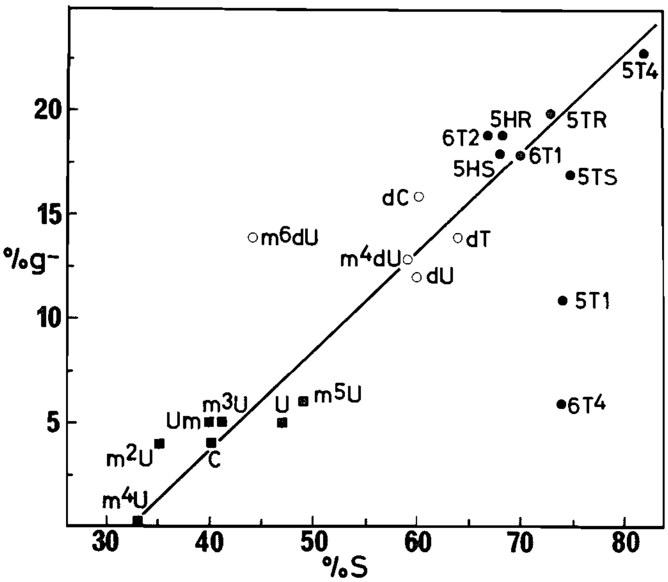

FIG. 5. Plot of %g⁻ versus %S for a series of pyrimidine nucleosides. Solid circles: 5,6-saturated TAN adducts. Open circles: 5,6-unsaturated 2′-deoxyribosides (data from refs. 41, 47). Solid squares: 5,6-unsaturated ribosides, cytidine (C), uridine (U), uridine methylated on the base (m^2U, m^3U, m^4U, m^5U), and at the 2′-position of the sugar (Um).

formation is the least likely, but g^- is more completely suppressed in the ribosides. Figure 5 shows that, with the exception of the data for m^6dU, 5T1, and 6T4, a reasonable correlation is obtained between %g^- and %*S*. The plot suggests that g^- is highly unlikely in a 3′-*endo* sugar. Extrapolation indicates that a maximum of about 40% can be obtained for g^- in a sugar which is 100% S. These solution studies agree with observations on crystalline nucleosides and tRNA which demonstrate that g^- is likely only for 2′-*endo* sugars (48, 49). The exclusion of g^- in 3′-*endo* sugars probably stems from crowding of the 3′- and 5′-hydroxyl groups, which is analogous to the unfavorable parallel 1,3-interactions between oxygens in acyclic sugar derivatives (50), the alleviation of which is an important conformational factor in these systems. (Presumably for similar reasons, the g^- conformation of the hydroxymethyl group of glucopyranosides is also unimportant (51–53).) The crowding of the hydroxyl groups in 3′-*endo*, g^- is removed by a change in the pucker, or by rotation into g^+ or t. A thorough analyses of the C4′—C5′ rotamer populations has been presented (41).

^{13}C chemical shifts

The effects of TAN modification and of configurational changes at C5 and C6 on the ^{13}C chemical shifts (Table 3) are more clearly seen in Fig. 6, which shows the data for the methyl (M), C5, C6, and C1′ carbons. Data for the remaining carbon atoms are not reproduced since they show smaller variations. Using the glycols (D series) as the reference points, one can note a number of interesting trends.

1. In the 6T series, TAN substitution has a small effect on δ(M) and δ(C5) (<1.5 ppm) relative to the corresponding D isomer. M is more shielded in the *trans* isomers (T1, T4) than in the *cis* isomers (T2, T3), by about 4 ppm in the 6T series and in the D series as well. Viewed differently, this means that, in the 6T and D series, the 5*R* to 5*S* configurational change causes a 4-ppm *deshielding* of M when C6 is *R* but a 4-ppm *shielding*

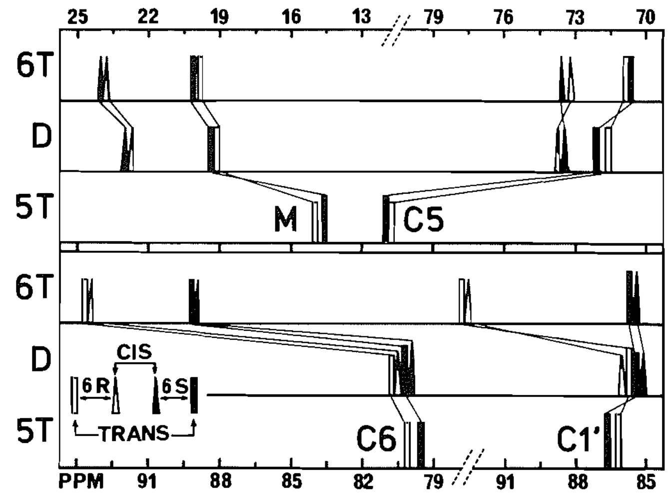

FIG. 6. Chemical shifts of the methyl (M), C5, C6, and C1′ carbons of the 6T, D, and 5T series in ppm from external TMS (Table 3). For each series: isomer 1 (open rectangle); isomer 2 (open triangle); isomer 3 (solid triangle); isomer 4 (solid rectangle). See also legend in lower left corner.

when C6 is *S*. Thus, δ(M) reflects significantly the configuration at C5 and C6, but less so the nature of the C6 substituent (OH or TAN). Similar but attenuated trends also develop in δ(C5).

2. In the D series, δ(C6) is essentially independent of the configuration at C5 and C6, with an overall spread of only 1 ppm for the four isomers. 6-TAN substitution effects a large deshielding of C6, the extent of which depends on the configuration of C6, i.e. 13 ppm for the 6*R* pair and 9 ppm for the 6*S* pair. Furthermore, the 6*R* to 6*S* change causes an upfield shift of about 4.5 ppm in C6, whereas a configurational change at C5 has little effect (compare 6T1 with 6T2, and 6T3 with 6T4). Thus, in contrast with δ(M) and δ(C5), δ(C6) in the 6T series reflects most strongly the nature of the 6-substituent (OH or TAN) and to a lesser extent the configuration at C6, with the configuration at C5 being unimportant.

3. In the D series, δ(C1′) is essentially independent of configuration at C5 or C6 with an overall spread of about 1 ppm for the four isomers. 6-TAN substitution in the 6*R* configuration deshields C1′ by about 7 ppm, but 6-TAN substitution in the 6*S* configuration has no effect on δ(C1′) (<1 ppm). Thus the change in configuration 6*R* to 6*S* causes an upfield shift of about 7 ppm in C1′, but configurational changes at C5 have minimal effect (<0.3 ppm). Though these ^{13}C shifts are not easily related to conformation, it is interesting to note that the *anti* conformation was assigned to the D isomers and the 6*S* pair of 6T isomers, but the *syn* conformation was assigned to the 6*R* pair.

4. A remarkable feature of Fig. 6 is that in the 6T series the M and C5 chemical shifts are "paired" according to the *cis* or *trans* geometry of the pyrimidine ring. That is, we see a similarity in δ(C5) for the *cis* isomers (6T2: 73.2 ppm; 6T3: 73.6 ppm) and for the *trans* isomers (6T1: 70.7 ppm; 6T4: 70.7 ppm), and a parallel behavior for δ(M). In striking contrast, δ(C6) and δ(C1′) are paired according to the configuration C6 rather than to the *cis* or *trans* nature of the ring. That is, we see a similarity in δ(C6) for the 6*R* pair (6T1: 93.7 ppm; 6T2: 93.4 ppm) and for the 6*S* pair (6T3: 89.1 ppm; 6T4: 89.1 ppm), with parallel behavior for δ(C1′). In a qualitative way, one can rationalize the presence of these two pairing

schemes by noting that in isolation the T1 and T4 bases are *trans* enantiomers, whereas the T2 and T3 bases are *cis* enantiomers (Fig. 1). In the absence of differential shielding effects from the sugar, corresponding base carbons in an "enantiomeric pair" will be identically shielded. The pairing of δ(M) and δ(C5) according to *cis* and *trans* geometries suggests the absence of significant shielding of C5 and M by the sugar, in line with the separation of the groups. The pairing of δ(C6) according to the *R* and *S* configurations at C6 indicates that, unlike C5 and M carbons, C6 experiences important shielding effects of the sugar. Furthermore, we are inclined to suggest that the pairing of δ(C6) is a reflection of the differences in conformation about the *N*-glycosyl link for the 6*R* pair (*syn*) and 6*S* pair (*anti*). This view is supported by the observation that the atoms of the *sugar moiety,* which are expected to sense configurational changes at C6 and conformational changes in the *N*-glycosyl link (C1′ (Fig. 6) as well as H1′, H2′, and H2″ (Fig. 4)), have chemical shifts paired in the same way as C6.

5. Comparing that data for 5T1 and 5T4 with the D isomers, we see that 5-TAN substitution causes a 9-ppm deshielding of the C5 carbon which is comparable to the effect of the 6-TAN group on C6 for 6T1 and 6T2 (~9 ppm) but less than the effect on C6 for 6T3 and 6T4 (~13 ppm). Comparison of these effects is complicated, however, because of the differences in conformation for 6*R* (*syn*) and 6*S* (*anti*) pairs of 6T isomers. 5-TAN substitution has a large shielding effect on the 5-methyl group (4−5 ppm), in contrast with the minor deshielding effect of a 6-TAN group (<1 ppm). C6 and C1′ (and the other carbons) experience only small changes upon 5-TAN substitution (>1 ppm). The similarity in the chemical shifts for corresponding carbons of 5T1 and 5T4 demonstrates that the sugar has no important configuration-dependent shielding effects on the base carbons.

Acknowledgements

This work was supported in part by grants from l'Association pour le Développement de la Recherche sur le Cancer (M.B., J.C.) and the Polish Academy of Sciences. F.E.H. acknowledges the support of the Canada−France Scientific Exchange Program and the Natural Sciences and Engineering Research Council of Canada for a travel grant. We thank Mr. Henri Reutenauer (Centre Grenoblois de Résonance Magnétique) for acquiring the nmr spectra.

1. M. BERGER, J. CADET, and J. URLICH. Can. J. Chem. **63**, 6 (1985).
2. F. F. NAKKEN, T. SIKKELAND, and T. BRUSTAD. FEBS Lett. **8**, 33 (1970).
3. E. WOLD and T. BRUSTAD. Acta Chem. Scand. Ser. B, **29**, 781 (1975).
4. M. BERGER and J. CADET. Proceedings of the 7th International Congress of Radiation Research, Amsterdam, July 3−8, 1983. Abstract A3-03.
5. J. CADET and R. TEOULE. Bull. Soc. Chim. Fr. 891 (1975).
6. J. CADET, R. DUCOLOMB, and F. E. HRUSKA. Biochim. Biophys. Acta, **563**, 206 (1979).
7. A. GRAND and J. CADET. Acta Crystallogr. Sect. B, **34**, 1524 (1978).
8. J. CADET, M. BERGER, M. GUTTIN-LOMBARD, and M. J. BOBENRIETH. Tetrahedron, 35, 2743 (1979).
9. M. BERGER. PhD Thesis, Grenoble, 1982.
10. D. J. WOOD, F. E. HRUSKA, and K. K. OGILVIE. Can. J. Chem. **52**, 3353 (1974).
11. M. REMIN and D. SHUGAR. Biochem. Biophys. Res. Commun. **48**, 636 (1972).
12. R. G. S. RITCHIE and A. S. PERLIN. Carbohydr. Res. **55**, 121 (1977).
13. R. FREEMAN and H. D. W. HILL. J. Chem. Phys. **54**, 3367 (1971).
14. J. CADET, R. NARDIN, L. VOITURIEZ, M. REMIN, and F. E. HRUSKA. Can. J. Chem. **59**, 3313 (1981).
15. A. J. JONES, M. W. WINKLEY, D. M. GRANT, and R. K. ROBINS. Proc. Natl. Acad. Sci. U.S.A. **65**, 27 (1970).
16. J. CADET, C. TAIEB, M. REMIN, W. P. NIEMCZURA, and F. E. HRUSKA. Biochim. Biophys. Acta, **608**, 435 (1980).
17. J. EMERSON and M. SUNDARALINGAM. Acta Crystallogr. Sect. B, **36**, 537 (1980).
18. A. R. KATRITZKY, M. R. NESBIT, B. J. KURTEV, M. LYAPOVA, and I. G. POJARLIEFF. Tetrahedron, **25**, 3807 (1969).
19. R. DESLAURIERS, R. D. LAPPER, and I. C. P. SMITH. Can. J. Chem. **49**, 1279 (1971).
20. M. BARFIELD and B. CHAKRABARTI. Chem. Rev. **69**, 757 (1969).
21. R. BRIERE, H. LEMAIRE, and A. RASSAT. Bull. Soc. Chim. Fr. 3273 (1965).
22. R. BRIERE, H. LEMAIRE, A. RASSAT, P. REY, and A. ROUSSEAU. Bull. Soc. Chim. Fr. 4479 (1967).
23. D. B. DAVIES and H. B. F. DIXON. Eur. J. Biochem. **131**, 9 (1983).
24. P. A. HART and J. P. DAVIS. J. Am. Chem. Soc. **93**, 753 (1971).
25. R. K. NANDA, R. TEWARI, G. GOVIL, and I. C. P. SMITH. Can. J. Chem. **52**, 371 (1974).
26. C. M. PRESTON and L. D. HALL. Carbohydr. Res. **37**, 267 (1974).
27. C. CHACHATY and G. LANGLET. FEBS Lett. **68**, 181 (1976).
28. M. P. SCHWEIZER, E. B. BANTA, J. T. WITKOWSKI, and R. K. ROBINS. J. Am. Chem. Soc. **95**, 3770 (1973).
29. J. CADET, R. DUCOLOMB, and C. TAIEB. Tetrahedron Lett. 3955 (1975).
30. A. L. GEORGE, F. E. HRUSKA, K. K. OGILVIE, and A. HOLY. Can. J. Chem. **56**, 1170 (1978).
31. C. GIESSNER-PRETTRE and B. PULLMAN. J. Theor. Biol. **65**, 171 (1977).
32. G. I. BIRNBAUM, F. E. HRUSKA, and W. P. NIEMCZURA. J. Am. Chem. Soc. **102**, 5586 (1980).
33. D. W. YOUNG, P. TOLLIN, and H. R. WILSON. Acta Crystallogr. Sect. B, **25**, 1423 (1969).
34. R. K. HARRIS. Nuclear magnetic resonance spectroscopy. Pitman Books Ltd., London. 1983. p. 200.
35. T. SCHLEICH, B. J. BLACKBURN, R. D. LAPPER, and I. C. P. SMITH. Biochemistry, **11**, 137 (1972).
36. C. ALTONA and M. SUNDARALINGAM. J. Am. Chem. Soc. **94**, 8205 (1972).
37. C. ALTONA and M. SUNDARALINGAM. J. Am. Chem. Soc. **95**, 2333 (1973).
38. W. P. NIEMCZURA, F. E. HRUSKA, K. L. SADANA, and P. C. LOEWEN. Biopolymers, **20**, 1671 (1981).
39. D. B. DAVIES. Prog. Nucl. Magn. Spectrosc. **12**, 135 (1978).
40. M. SUNDARALINGAM. Jerusalem Symp. Quantum Chem. Biochem. **5**, 417 (1973).
41. M. REMIN. J. Biomol. Struct. Dyn. 1984. In press.
42. C. A. G. HAASNOOT, F. A. A. M. DE LEEUW, and C. ALTONA. Tetrahedron, **36**, 2783 (1980).
43. C. A. G. HAASNOOT, F. A. A. M. DE LEEUW, H. P. M. DE LEEUW, and C. ALTONA. Recl. Trav. Chim. Pays-Bas, **98**, 576 (1979).
44. B. J. BLACKBURN, A. A. GREY, I. C. P. SMITH, and F. E. HRUSKA. Can. J. Chem. **48**, 2866 (1970).
45. F. E. HRUSKA. Jerusalem Symp. Quantum Chem. Biochem. **5**, 345 (1973).
46. F. E. HRUSKA and W. J. BLONSKI. Can. J. Chem. **60**, 3026 (1982).

47. B. D. ALLORE, A. QUEEN, W. J. BLONSKI, and F. E. HRUSKA. Can. J. Chem. **61**, 2397 (1983).
48. M. SUNDARALINGHAM. *In* Conformation in biology. *Edited by* R. Srinivasan and R. H. Sarma. Adenine Press, New York. 1982. p. 191.
49. A. JACK, J. E. LADNER, D. RHODES, R. S. BROWN, and J. KLUG. J. Mol. Biol. **111**, 315 (1977).
50. J. DEFAYE, D. GAGNAIRE, and D. HORTON. Carbohydr. Res. **21**, 407 (1972).
51. D. GAGNAIRE, D. HORTON, and F. R. TARAVEL. Carbohydr. Res. **27**, 363 (1973).
52. R. U. LEMIEUX and J. C. MARTIN. Carbohydr. Res. **13**, 139 (1970).
53. M. SUNDARALINGAM. Biopolymers, **6**, 189 (1968).

The conformational dependence of ${}^6J_p^{F,C}$ in some 4-fluorophenyl derivatives of methane, ethene, and cyclohexane

TED SCHAEFER, JAMES PEELING,[1] GLENN H. PENNER, ALBERTA LEMIRE, AND RUDY SEBASTIAN

Department of Chemistry, University of Manitoba, Winnipeg, Man., Canada R3T 2N2

Received May 3, 1984

TED SCHAEFER, JAMES PEELING, GLENN H. PENNER, ALBERTA LEMIRE, and RUDY SEBASTIAN. Can. J. Chem. **63**, 24 (1985).

The spin–spin coupling over six bonds between ${}^{19}F$ and ${}^{13}C$ nuclei on the sidechain in thirteen 4-fluorophenyl derivatives appears to be mediated by a $\sigma-\pi$ mechanism. Its magnitude depends somewhat on the hybridization state of the carbon atom carrying the coupled nucleus, as well as on the electronegativity of substituents attached to this carbon atom. A consistent behaviour of this coupling is observed if its value is assumed to be proportional to $\sin^2\theta$, where θ is the angle by which the bond carrying the coupled carbon nucleus twists out of the ring plane. However, in 4-fluorostyrene ${}^6J_p^{F,C}$ is a π electron coupling in the planar form, so that its magnitude decreases as the vinyl group twists out of the benzene plane. The $\sigma-\pi$ contribution to this coupling is smaller than the π component. ${}^6J_p^{F,C}$ is used to assess the conformational preferences of a number of compounds, including 4-fluoro-α-methylstyrene, 4,4′-difluorodiphenylmethane, 1,1-dichloro-2,2-bis(4-fluorophenyl)ethane, and 1-(4-fluorophenyl)-*N*-methylcyclohexylamine.

TED SCHAEFER, JAMES PEELING, GLENN H. PENNER, ALBERTA LEMIRE et RUDY SEBASTIAN. Can. J. Chem. **63**, 24 (1985).

Le couplage de spin à travers six liaisons entre les noyaux du ${}^{19}F$ et du ${}^{13}C$ des chaînes latérales de 13 dérivés fluoro-4 phényles semble être contrôlé par un mécanisme de type $\sigma-\pi$. Son amplitude dépend en partie de l'état d'hybridation de l'atome de carbone portant le noyau couplé et aussi de l'électronégativité des substituants fixés sur ce carbone. On observe un comportement consistant de ce couplage si on admet que sa valeur est proportionnelle à $\sin^2\theta$, où θ est l'angle de torsion hors plan de la liaison portant le noyau de carbone couplé. Cependant, dans le cas du fluoro-4 styrène, le couplage ${}^6J_p^{F,C}$ est un couplage d'électrons π dans une forme planaire; il en résulte que son amplitude diminue lorsque le groupe vinyle subit une torsion hors du plan du benzène. La contribution $\sigma-\pi$ à ce couplage est plus faible que celle de la composante π. On a utilisé la valeur de ${}^6J_p^{F,C}$ pour déterminer les préférences conformationnelles de plusieurs composés comprenant les fluoro-4 α-méthylstyrène, difluoro-4,4′ diphénylméthane, dichloro-1,1 bis(fluoro-4 phényl)-2,2 éthane et (fluoro-4 phényl)-1 *N*-méthylcyclohexylamine.

[Traduit par le journal]

Introduction

In the study of long-range spin–spin coupling constants, their mechanisms, and their application to conformational problems (1–16), it has been shown (5) that ${}^6J_p^{H,CH}$ varies as $\sin^2\theta$ in toluene derivatives. Here θ is the angle by which the α C—H bond twists out of the benzene plane. The coupling proceeds via a $\sigma-\pi$ mechanism and involves the sidechain proton and the *para* ring proton. Similarly, ${}^5J_p^{C,CH}$, the coupling between the sidechain proton and the *para* carbon-13 nucleus also varies as $\sin^2\theta$ (17, 18), implying that this parameter allows an extension (8) of the *J* method (1) as a conformational tool. In this method, a hindered rotor model provides a relationship between the expectation value of $\sin^2\theta$ and the barrier to rotation about the Csp^2—Csp^3 bond. The expectation value and the observed coupling are simply related by eq. [1], in which ${}^nJ$ can be ${}^6J_p^{H,CH}$ or ${}^5J_p^{C,CH}$ and ${}^nJ_{90}$ is the value of ${}^nJ$

$$[1] \quad {}^nJ = {}^nJ_{90}\langle\sin^2\theta\rangle$$

when θ is 90° in **1**. The *J* method can also discriminate among

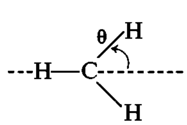

1

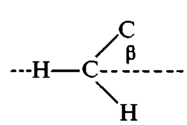

2

preferred ground-state conformations. For example, **3** and **4** can be established as the low-energy forms of ethylbenzene (19) and cumene (20), respectively.

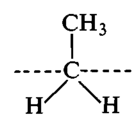

3

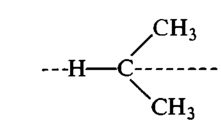

4

${}^6J_p^{F,CH}$ has also been investigated as a conformational indicator for *p*-fluorotoluene derivatives (21). The conformational barriers obtained for identical sidechains differed somewhat from those found by the use of ${}^6J_p^{H,CH}$, although identical preferred conformations were identified. Part of the discrepancy possibly may be attributed to a non $\sigma-\pi$ component of ${}^6J_p^{F,CH}$, but this could not be proved. Perhaps a *para* fluorine substituent alters the barriers by altering hyperconjugative interactions of the sidechain C—H and C—C bonds with the benzene system. Another possibility is that the $\sigma-\pi$ component of ${}^6J_p^{F,CH}$ varies somewhat between compounds, ${}^6J_p^{F,CH_3}$ being more sensitive to ring substituent perturbations than is ${}^6J_p^{H,CH_3}$ (22).

It seems sensible, therefore, to extend the investigations to ${}^6J_p^{F,C} \equiv {}^6J$(C-β,F) in compounds of type **2**. The mechanism of this coupling might emerge and a comparison with ${}^6J_p^{H,CH}$, ${}^6J_p^{F,CH}$, and, indeed, ${}^5J_p^{C,CH}$ may establish its viability in conformational work. Because the coupling is measurable in the ${}^{13}C$ nmr spectrum under conditions where ${}^1H$ is decoupled, the experimental work is relatively simple and can be relatively easily done with low-field FT nmr spectrometers.

Experimental

Most of the compounds were obtained from Aldrich Chem. Co. The 4-fluoro-n-propylbenzene, and 4-fluoro-*tert*-butylbenzene were prepared from the *p*-amino derivatives via the diazonium salts. The 4-fluoroethylbenzene was synthesized from the 2-(4-fluorophenyl)-

[1] On sabbatical leave from the University of Petroleum and Minerals, Dhahran, Saudi Arabia, in 1982–1983.

TABLE 1. ^{13}C, ^{19}F spin–spin coupling constants in Hz in some 4-fluorophenyl compounds

Sidechain	^1J	^2J	^3J	^4J	^5J	$^6J^d$
$CH_3{}^a$	241.4	21.16	7.74	3.22	0.73	—
$CH_2CH_3{}^a$	241.3_5	21.13	7.78	3.17	0.67	1.023(19)
$CH(CH_3)_2{}^a$	241.7	21.04	7.76	3.12	0.64	0.804(11)
$C(CH_3)_3{}^a$	242.1	20.79	7.70	3.17	0.58	0.602(3)
$CH_2CH_2CH_3{}^b$	—	21.11	7.72	—	—	1.108(10)
$CH_2CH_2OH^b$	242.0	21.09	7.81	3.13	0.59	1.262(9)
CH_2COOH^b	242.9	21.40	8.07	3.30	0.71	1.179(8)
$CH_2COCH_3{}^b$	242.9	21.40	8.00	3.22	0.61	1.201(8)
1-$NHCH_3$-c-$C_6H_{10}{}^b$	242.7	20.76	7.67	3.15	0.47	0.47
CH_2—$C_6H_4F^b$	242.6	21.30	7.91	3.21	0.66	0.942(2)
$C(CH_3){=}CH_2{}^a$	—	21.41	8.00	3.29	0.39	0.27^e
$C(c\text{-}C_3H_5){=}CH_2{}^c$	244.8	21.40	7.99	3.27	—	$0.369(1)^f$
$CH{=}CH_2{}^a$	—	21.71	8.08	3.31	0.59	2.245(30)
$CH(4\text{-}F$—$C_6H_4)(CHCl_2)^{b,h}$	244.8	21.52	8.10	3.31	^{g}	$0.801(2)^i$

^{a}50 v/v % in acetone-d_6.
^{b}30 v/v % in acetone-d_6.
^{c}40 v/v % in acetone-d_6.
^{d}Numbers in parentheses are averages of deviations from the mean.
^{e} ^6J to the methylene carbon is 1.57(2) Hz.
^{f} ^6J to the methylene carbon is 1.42 Hz.
^{g}The aliphatic ^{13}C nmr peaks are broad.
^{h}This is 1,1-dichloro-2,2-bis(p-fluorophenyl)ethane (DFDD).
^{i}Coupling to phenyl carbon of the second ring.

ethanol via the bromide and its Grignard reagent. The ^{13}C nmr spectra were acquired at 305 K on a Bruker WH 90 FFT nmr spectrometer. A typical run involved 64 acquisitions into 16K and a spectral window of 400 Hz. The sample concentrations and solvents employed are noted in Table 1. The ^1H transitions were strongly irradiated in all these experiments, so that spectral analytical complexities did not arise.

However, the ^1H nmr spectrum of 4-fluoroethylbenzene had not been previously analyzed and yielded to a LAME analysis (23, 24).

The ^{13}C nmr spectrum of 4-fluorobenzyl cyanide was too broad to extract $^6J_p^{F,C}$, no doubt as a consequence of partially relaxed coupling to ^{14}N, whose spin-lattice relaxation time must fall into a range in which the T_2 of C-β becomes inconveniently short.

INDO MO FPT computations (25, 26) were done on an Amdahl V/8 system.

Results and discussion

(a) *Coupling parameters*

In Table 1 the observed $^nJ^{F,C}$ (n = 1–6) values are given for fourteen 4-fluorophenyl derivatives. In fluorobenzene the $^nJ^{F,C}$ values are −245.1, 21.02, 7.79, and 3.20 Hz for n = 1–4, respectively (28), and are no doubt of the same sign for the compounds in Table 1; the magnitudes vary only slightly from compound to compound. Coupling constants of this kind have been discussed previously in some detail (29). $^5J^{F,C}$ in 4-fluorotoluene is of unknown sign and, in view of previous discussions for $^5J_p^{F,H}$ in fluorobenzene (22, 30), may well contain σ and π components of opposite sign.[2] $^6J^{F,C}$ values are discussed in detail below.

Table 2 gives the ^1H nmr spectral parameters for 4-fluoroethylbenzene, not previously reported.

TABLE 2. The ^1H nmr spectral parameters for a solution of 4-fluoroethylbenzene in acetone-d_6 at 90.020 MHz and 305 K

Parameter	Value	Parameter	Value
$\nu_{CH_3}{}^{a,b}$	−76.668(14)	$^4J_o^{H,CH_2}$	−0.618(3)
ν_{CH_2}	50.569(4)	$^5J_{25}$	0.393(3)
ν_2	464.187(8)	$^5J_m^{H,CH_2}$	0.302(3)
ν_3	446.575(6)	$^6J_p^{F,CH_2}$	0.812(3)
$^3J(CH_2,CH_3)$	$7.597(2)^c$	Peaks	162
$^3J_{23}$	8.474(8)	Transitions assigned	255
$^3J_{3F}$	9.010(4)		
$^4J_{26}$	2.398(7)	Largest difference	0.052
$^4J_{35}$	2.866(4)	RMS deviation	0.020
$^4J_{2F}$	5.462(4)		

^{a}In Hz at 90.020 MHz to low field of the ^1H nmr peak of acetone-d_6.
^{b}In order to estimate shifts relative to tetramethylsilane, add 183.64 Hz to these ν values.
^{c}Numbers in parentheses are standard deviations in the last significant figure.

(b) *The coupling mechanism of* $^6J^{F,C}$

Because $^6J_p^{H,CH}$ and $^5J_p^{C,CH}$ in toluene and its derivatives (5–8), $^6J_p^{H,CC\text{-}\beta}$ in an ethylbenzene derivative (8), and $^6J_p^{F,CH}$ in 4-fluorotoluene and its derivatives (21) are most likely dominated by a σ–π mechanism, it appears likely that $^6J_p^{F,C}$ will behave similarly.

Certainly, INDO MO FPT calculations of the above σ–π couplings confirm their $\sin^2\theta$ dependence (5, 8). Such calculations on 4-fluoroethylbenzene yield eq. [2] for standard geometries (27)

$$[2] \quad {}^6J_p^{F,C}\ \text{Hz} = 0.055 + 0.862\sin^2\theta$$

As argued for other couplings previously (5, 8), the number 0.055 is an artifact of the computation, so that eq. [2] should become eq. [3], where 0.055 Hz is subtracted from 0.862 Hz.

[2]The sign of $^5J^{F,C}$ in 4-fluorotoluene, as well as for analogous couplings in other 4-fluorophenyl derivatives, is under study here.

TABLE 3. Values of ${}^6J_{90}^{F,C}$ estimated from ${}^6J_p^{H,CH_2}$ and ${}^6J_p^{F,CH_2}$ in toluene derivatives

Sidechain	${}^6J_p^{H,CH}$	$\langle\sin^2\theta\rangle_H^H$	$\langle\sin^2\theta\rangle_F^C$	${}^6J_p^{F,C}$	${}^6J_{90}^{F,C}$	${}^6J_p^{F,CH}$	$\langle\sin^2\theta\rangle_F^H$	$\langle\sin^2\theta\rangle_F^C$	${}^6J_p^{F,C}$	${}^6J_{90}^{F,C}$
CH_3	−0.62[a]	0.500	—	—	—	1.12[f] (1.15)	0.5	—	—	—
CH_2CH_3	−0.477(3)[b]	0.385[d]	0.730[e]	1.023(19)	1.401	0.812(3)[g]	0.363[h]	0.775[j]	1.023	1.320
	−0.45[c]	0.363[d]	0.774[e]	1.023(19)	1.321					(1.289)
$CH(CH_3)_2$	−0.253[i]	0.204	0.648[e]	0.804(11)	1.241	0.560(10)[g]	0.250[h]	0.625[j]	0.804	1.286 (1.280)
$C(CH_3)_3$						—	—	0.500	0.602(3)	1.204

[a] In toluene (6) in Hz.
[b] In 3,5-dibromoethylbenzene (19).
[c] In ethylbenzene (33).
[d] Assuming ${}^6J_{90}^{H,CH_2} = -1.24$ Hz.
[e] $\langle\sin^2\theta\rangle_F^C = 1.5 - 2\langle\sin^2\theta\rangle_H^H$.
[f] In 4-fluorotoluene (21), 1.12 in CS_2, 1.15 Hz in acetone-d_6.
[g] In the 4-fluorotoluene derivatives.
[h] Assuming ${}^6J_{90}^{F,CH_2} = 2.28$ Hz.
[i] In 3,5-dibromoisopropylbenzene (20).
[j] $\langle\sin^2\theta\rangle_F^C = 0.75 - 0.5\langle\sin^2\theta\rangle_F^H$.

$$[3]\quad {}^6J_p^{F,C}\text{ Hz} = {}^6J_{90}^{F,C}\sin^2\theta = 0.807\sin^2\theta$$

In other words, INDO MO FPT computations imply a $\sigma-\pi$ mechanism for ${}^6J_p^{F,C}$, where θ is the angle by which the C—C bond of the sidechain twists out of the benzene plane. As expected on the basis of the known positive signs of ${}^6J_p^{F,CH}$ and ${}^5J_p^{CCH}$ (17, 22), ${}^6J_p^{F,C}$ is computed as positive.

However, ${}^6J_{90}^{F,C}$ is no doubt computed as too small in magnitude, just as is ${}^6J_{90}^{F,CH}$ in 4-fluorotoluene (5). This discrepancy has to do with the INDO parameterization, which should not perturb the functional form of eq. [3]. An artificial way of reproducing a correct ${}^6J_{90}^{F,C}$ would be to alter the C—F bond length, because such a coupling will depend on the overlap of the π orbitals at C-4 with the fluorine orbitals. In fact, ${}^6J_p^{F,C}$ depends exponentially on the C—F bond length, a situation previously noted for other $\sigma-\pi$ couplings, for example, ${}^6J_p^{H,BH}$ in a pyridine–borane complex (31). The discussion below suggests that eq. [4] agrees with experiment.

$$[4]\quad {}^6J_p^{F,C}\text{ Hz} = (1.29 \pm 0.06)\langle\sin^2\theta\rangle_F^C$$

A second question concerns the dependence of ${}^6J_{90}^{F,C}$ on a substituent attached to the coupled carbon. INDO MO FPT computations yield eq. [5] for 2-(4-fluorophenyl)ethanol, in which the electronegative hydroxyl group is attached to the coupled carbon atom.

$$[5]\quad {}^6J_p^{F,C}\text{ Hz} = 0.046 + 1.066\sin^2\theta$$

Relative to 4-fluoroethylbenzene the ${}^6J_{90}^{F,C}$ value has increased by 26%. As before, write eq. [6] in which the angle independent term is deleted on the basis of previous experience. The

$$[6]\quad {}^6J_p^{F,C}\text{ Hz} = 1.02\sin^2\theta$$

calculated increase in the presence of an electronegative substituent has its experimental counterpart in the increase of ${}^1J^{H,C}$ in methane derivatives, interpreted as originating in an enhanced s-electron density at the carbon-13 nucleus caused by the polar substituent (32).

The experimental deduction of ${}^6J_{90}^{F,C}$ now proceeds as follows. Table 3 contains ${}^6J_p^{H,CH}$ and ${}^6J_p^{F,CH}$ values and the $\langle\sin^2\theta\rangle$ values for a series of toluene derivatives in which the sidechain is CH_3, CH_2CH_3, $CH(CH_3)_2$, or $C(CH_3)_3$. The $\langle\sin^2\theta\rangle$ values are given on the assumption that ${}^6J_p^{H,CH}$ and ${}^6J_p^{F,CH}$ are $\sigma-\pi$ couplings and are obtained from ${}^6J$(observed) $= {}^6J_{90}\langle\sin^2\theta\rangle$, where $\langle\sin^2\theta\rangle$ is the expectation value of $\sin^2\theta$. The $\langle\sin^2\theta\rangle_F^C$ numbers follow from $\langle\sin^2\theta\rangle_F^C = 1.5 - 2\langle\sin^2\theta\rangle$ for ethyl substituents and from $\langle\sin^2\theta\rangle_F^C = 0.75 - 0.5\langle\sin^2\theta\rangle$ for isopropyl substituents if **3** and **4** are considered to be the preferred conformations of the two sidechains. The observed ${}^6J_p^{F,C}$ parameters then yield ${}^6J_{90}^{F,C}$ in the last column of Table 3.

The ${}^6J_p^{F,C}$ magnitudes range from 1.20 to 1.40 Hz, the eight values yielding an average of 1.29 ± 0.06 Hz, where 0.06 Hz is the standard deviation. In view of measurement errors in all the couplings involved and of the fact that 4-fluorophenyl are treated on the same footing as 3,5-dibromophenyl groups, a smaller uncertainty in ${}^6J_{90}^{F,C}$ is not expected. It might be argued, for example, that ${}^6J_{90}^{F,C}$ appears to decrease monotonically with an increase in the number of methyl substituents and that this implies an intrinsic dependence of ${}^6J_{90}^{F,C}$ on the substituent β to the coupled carbon, in constrast to the calculated increase above in ${}^6J_p^{C,F}$ caused by an α substituent on the coupled carbon. This dependence may exist but, in our opinion, is unproven and is difficult to establish from the present data set.

An example of the errors in the twofold barriers caused by the uncertainty in ${}^6J_{90}^{F,C}$ comes from ethylbenzene. A ${}^6J_{90}^{F,C}$ of 1.29 Hz implies a V_2 of 1.8 kcal/mol (1 cal ≡ 4.184 J), whereas 1.40 Hz leads to 1.2_5 kcal/mol. This last number, of course, is that deduced from ${}^6J_p^{H,CH}$ in 3,5-dibromoethylbenzene (19). If ${}^6J_p^{H,CH}$ is 0.45 Hz, as reported for ethylbenzene (33), then V_2 follows as 1.6 kcal/mol.

A conservative conclusion is that ${}^6J_{90}^{F,C}$ is predominantly a $\sigma-\pi$ coupling, and that it yields the preferred conformation of the sidechain and also a rough estimate of the barrier to internal rotation about the exocyclic carbon–carbon bond for these alkyl substituents.

(c) *Conformational applications of* ${}^6J_p^{F,C}$

(i) *4,4′-Difluorodiphenylmethane*

Here ${}^6J_p^{F,C}$ involves an sp^2 carbon atom in the second benzene ring, in contrast to the sp^3 carbon atoms discussed in the previous section. However, ${}^6J_p^{H,CH}$ and ${}^6J_p^{F,CH}$ have been used to study the preferred conformations of diphenylmethane derivatives (34), so that the following comparisons may be made. The latter couplings implied that the gable conformation, **5**, having

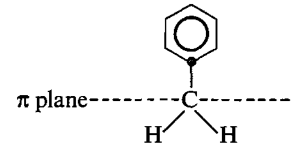

5

C_{2v} symmetry, obtained from a heavy-atom coplanar conformation by rotation of each benzene ring by 90° about the sp^2–sp^3 carbon–carbon bond, was preferred. In other words, C-1 of the second benzene ring lies preferably in a plane perpendicular to the plane of the first benzene ring. As far as $^6J_p^{F,C}$ is concerned, the preferred conformation is therefore analogous to **3** for ethylbenzene.

$^6J_{90}^{F,C}$ for 4,4′-difluorodiphenylmethane is 0.942(2) Hz. Therefore $\langle \sin^2 \theta \rangle_F^C$ is 0.942/1.29 or 0.730 ± 0.035, assuming $^6J_{90}^{F,C}$ as unaltered from its value for an sp^3 carbon and its error as 0.06 Hz. The V_2 is implied as $1.2_5 \pm 0.2_5$ kcal/mol for rotation about the sp^2–sp^3 bond. The temperature dependence of $^6J_p^{F,CH}$ yielded V_2 as $1.5_5 \pm 0.25$ kcal/mol, whereas $^6J_p^{H,CH}$ in 3,5-dibromodiphenylmethane gave V_2 as 1.1 ± 0.3 kcal/mol (34). These results imply that $^6J_{90}^{F,C}$ is not very sensitive to the hybridization state of the carbon atom carrying the coupled nucleus.

$^6J_p^{F,C}$ confirms that the preferred conformation of diphenylmethane has the C_1—C—C_1' plane perpendicular to the benzene planes. If the preferred conformation were one in which this plane lay *in* a benzene plane, then $^5J_p^{F,C}$ would most likely have a magnitude of less than 0.5 (1.29) or 0.65 Hz instead of the observed 0.94 Hz. See refs. 34 and 35 for a fuller discussion of other suggested conformations. The use of $^6J_p^{F,C}$ as an indicator of preferred conformations in *ortho*-substituted diphenylmethanes appears sensible, as it does for diphenylethanes.

(ii) *1,1-Dichloro-2,2-bis(4-fluorophenyl)ethane (DFDD)*

$^6J_p^{F,C}$ in DFDD is 0.801(2) Hz and again involves a carbon atom of the second benzene ring, suggesting a conformation closely related to that of diphenylmethane. In the crystal, the benzene rings do indeed lie in face-to-face positions (36) and corresponding atoms in these rings are related by reflection across a mirror plane containing the HCCH atoms of the aliphatic fragment. The latter has very nearly tetrahedral bond angles. If **5** corresponded to the preferred conformation in solution, that is, if θ_{min} were 90°, and if the rotation about the sp^2–sp^3 carbon–carbon bond were naively treated as twofold, then the internal barrier would be deduced as about 0.6 kcal/mol ($\langle \sin^2 \theta \rangle_F^C = 0.801/1.29$), about 1 kcal/mol lower than in the difluorodiphenylmethane above. That this interpretation would be erroneous can be seen as follows.

First, in solution the C—H bonds of the aliphatic fragment can also take on *gauche* conformations with respect to each other. Thus, in a 5 mol% solution in CCl_4 at 305 K, $^3J^{H,H}$ is only 7.76(8) Hz. The usual approach to the estimation of the magnitudes of the *trans* and *gauche* couplings (37–39), together with a $^3J_t^{H,H}$ of 10.5 Hz in sym-tetrachloroethane (40) and 11.3 Hz in sym-tetraphenylethane (41*a*), and a $^3J_g^{H,H}$ of 2.2 Hz in the former, implies a $^3J_t^{H,H}$ of about 10.9 Hz and a $^3J_g^{H,H}$ of 2.3 Hz in DFDD. A 2-site treatment then yields the *trans* population as 63%. In an acetone-d_6 solution the *trans* population increases to 82%, $^3J^{H,H}$ having increased to 9.35(3) Hz.

Furthermore, $^4J_o^{H,CH}$, $^5J_m^{H,CH}$, and $^6J_p^{F,CH}$ are −0.451(5), 0.233(3), and 0.25(2) Hz, respectively, in the acetone solution. These numbers imply (1, 7, 21) that not **5**, but a conformation with θ nearer 60°, is that of lowest energy. For a twofold barrier one may write (7) $^5J_m^{H,CH} = 0.336 \langle \sin^2 \theta \rangle_H^H + 0.188$, so that $\langle \sin^2 \theta \rangle_H^H$ becomes 0.134. Also (21), $^6J_p^{F,CH} = 2.27 \langle \sin^2 \theta \rangle_F^H$, yielding $\langle \sin^2 \theta \rangle_F^H$ as 0.110. The mean value is 0.122, implying a barrier of 2.9 kcal/mol. An empirical plot (41*b*) of $^4J_o^{H,CH}$ versus V_2 values suggests a twofold barrier of 3.0 kcal/mol. An estimate of $\langle \sin^2 \theta \rangle_F^C$ then follows as 0.75 − 0.5 (0.122), or 0.69, and $^6J_p^{F,C}$ becomes 0.69(1.29), or 0.89 Hz. The observed value is 0.80 Hz.

Of course, better agreement is not expected because the barrier can hardly be purely twofold, the *gauche* and *trans* conformations are treated as having the same conformation about sp^2–sp^3 bonds, and because the barriers in the two forms need not be the same. However, the argument does demonstrate DFDD as more rigid than 4,4′-difluorodiphenylmethane and that θ_{min} is much nearer 60° than 90°. A detailed investigation in which additional long-range couplings, such as $^nJ^{C,H}$ (8), are measured in solutions of varying polarity, may well lead to a sensible description of the internal dynamics of DFDD.

(iii) *2-(4-Fluorophenyl)ethanol and 1-(4-fluorophenyl)-propane*

In these compounds an electronegative substituent, hydroxy or methyl, is attached to the coupled carbon. The INDO MO FPT computations above imply a 26% increase in $^6J_{90}^{F,C}$ in the presence of the hydroxyl substituent. Assuming a linear dependence of $^6J_{90}^{F,C}$ on E_X, the electronegativity of the substituent, where $E_H = 2.1$, $E_{CH} = 2.5$, $E_{OH} = 3.5$, and assuming that $^6J_{90}^{F,C}$ is 1.29 Hz when X = H and 1.63 Hz when X = OH, leads to a $^6J_{90}^{F,C}$ of 1.39 Hz for X = CH_3.

In the propane derivative, $^6J_p^{F,C}$ is 1.11(1) Hz, implying $\langle \sin^2 \theta \rangle_F^C$ as 0.799 and V_2 as $1.8_5 \pm 0.3$ kcal/mol, based on a 0.06-Hz uncertainty in $^6J_{90}^{F,C}$. In the 3,5-dibromo derivative (42) of 1-phenylpropane, $^6J_p^{H,CH}$ is −0.428(2) Hz, leading to a barrier of 1.9 ± 0.2 kcal/mol. Of course, the existence of *gauche* and *trans* conformers about the sp^3–sp^3 carbon–carbon bond has been ignored in this comparison, which is meant only to suggest $^6J_{90}^{F,C}$ as a feasible conformational marker. The detailed discussion (42) of the barriers about the sp^2–sp^3 carbon–carbon bonds in the *trans* and *gauche* forms, given for $^6J_p^{H,CH}$ measurements, applies to $^6J_p^{F,C}$ also and need not be repeated here, except to note that the *gauche* is much larger than the *trans* barrier.

Turning to the ethanol derivative, one has $\langle \sin^2 \theta \rangle_F^C$ as 1.26/1.63 or 0.773 and therefore a V_2 of 1.6 ± 0.3 kcal/mol. In CS_2 solution, $^6J_p^{H,CH}$ in 2-(3,5-dibromophenyl)ethanol is −0.380(4) Hz (42) and leads to an average V_2 for the *trans* and *gauche* conformers of 3.1 ± 0.3 kcal/mol. Of course, in the CS_2 solution the proportion of *trans* and *gauche* forms varies with concentration (42), intermolecular self-association of 2-phenylethanol favoring the *trans* form.

For the fluorophenylethanol derivative, $^6J_p^{F,C}$ is here quoted for a 30 v/v % solution in acetone-d_6 (Table 1), in which the *trans* conformer will be favored strongly by intermolecular hydrogen bonding to solvent and other solute molecules. The *trans* form, of course, has a smaller barrier than does the *gauche* form, the latter having considerable steric hindrance to rotation due to the proximity of the phenyl and hydroxyl substituents. Consequently the average V_2 of 1.6 kcal/mol found from $^6J_{90}^{F,C}$ in acetone-d_6 solution is reasonable, implying, in fact (42), that 2-(4-fluorophenyl)ethanol exists predominantly in the *trans* conformation in acetone solution.[3] The *trans* form has a barrier of near 1.2 kcal/mol, while that in the *gauche* form must be greater than 4 kcal/mol (42) in CS_2 solution.

(iv) *4-Fluoro-α-methylstyrene and α-cyclopropyl-4-fluorostyrene*

These compounds do not have a proton necessary for the measurement of ${}^6J_p^{H,CH}$ or ${}^6J_p^{F,CH}$, so that ${}^6J_p^{F,C}$ remains as a conformational indicator. Now, although styrene is probably planar in the ground state (43, 44), the present compounds most likely are not, the α substituents entailing destabilization of a coplanar arrangement of the benzene and olefinic moieties. Furthermore, the internal rotational potential may not be twofold. Nevertheless, some conformational information is available from ${}^6J_p^{F,C}$.

In the α-methyl styrene, ${}^6J_p^{F,C}$ is 0.27 Hz. A *naive* approach, in which ${}^6J_p^{F,C}$ is taken to indicate *a* conformation, goes as follows. Assume ${}^6J_p^{F,C}$ is a σ–π coupling as suggested by INDO MO FPT calculations, also indicating that ${}^6J_p^{F,C}$ for this bonding situation is somewhat smaller than ${}^6J_p^{F,C}$ for an ethyl substituent, and that ${}^6J_{90}^{F,C}$ is therefore 1.13 Hz. It follows that $\sin^2\theta$ is 0.235 and that θ is 29°, the angle by which the CH_3 group twists out of plane. This number happens to agree with the 30° (45*a*) deduced from ultraviolet spectral extinction coefficients and from transition frequencies of the conjugation bands. Photoelectron spectral data imply a θ of 29 ± 6° in α-methylstyrene (45*b*). The same approach for the α-cyclopropylstyrene yields θ as 35°, employing a ${}^6J_p^{F,C}$ of 0.369(1) Hz (α-*tert*-butylstyrene (45*a*) apparently has θ = 64°).

If θ = 0° were to represent the preferred conformation and the internal barrier to rotation about the sp^2–sp^2 carbon–carbon bond were twofold, then the ${}^6J_p^{F,C}$ values would yield barriers of 1.4 and 0.8 kcal/mol for the methyl and cyclopropyl derivatives, respectively. That θ = 90° is not the preferred conformation is evident from the ${}^6J_p^{F,C}$ numbers, which are *less* than 0.5 $J_{90}^{F,C}$ for both compounds, the latter being the value in the limit of a vanishing barrier for a potential minimum at θ = 90°; this conclusion is independent of the barrier symmetry.

If a twofold steric barrier exists in the α-methylstyrene analogous to that in ethylbenzene of stable perpendicular form **3**, it opposes the twofold conjugational barrier favoring planarity. It may therefore be that the net barrier is lower than in styrene itself, estimated as twofold and ranging from 1.0 to 2.2 kcal/mol (43, 46), with an outlier at 0.5 kcal/mol.

No reliable value of V_2 is available for 4-fluorostyrene. ${}^6J_p^{F,C}$ is 2.24_5 (30) Hz. INDO MO FPT computations have it that ${}^6J_p^{F,C}$ is of maximum magnitude when θ is 0° and decreases as θ increases, no doubt because the coupling is dominated by a pure π mechanism involving the electrons of the olefinic double bond. The decrease goes as $\sin^2\theta$ and is calculated as

$$[7] \quad {}^6J_p^{F,C}\ \text{Hz} = 1.54 - 0.85 \sin^2\theta$$

Of course, it may well be that a σ–π mechanism comes into play as θ increases from zero, so that this ${}^6J_p^{F,C}$ would not go to zero at θ = 90°. It is interesting, therefore, that ${}^6J_p^{FCH}(CH_3)$ in 4-fluoro-α-methylstyrene is computed as 0.71 Hz at θ = 90° (σ–π mechanism) whereas ${}^6J_p^{F,C}$ (=CH_2) is 0.69 Hz for eq. [7]. In other words, the INDO MO FPT computations imply that the coupling to the olefinic carbon nucleus consists of two positive contributions, both dependent on $\sin^2\theta$. The contributions differ by 90° in their maxima, the π component being the larger.

The important conclusion is that ${}^6J_p^{F,C}$ for the β-olefinic carbon nucleus decreases as θ increases, as observed for the α-methyl and α-cyclopropyl derivatives, being 1.57 and 1.42 Hz, respectively; this is smaller than the 2.24 Hz in 4-fluorostyrene, whose ground state conformation is presumably planar. These observations are in qualitative agreement with the indication above that the π is larger than the σ–π component of ${}^6J_p^{F,C}$.

The assumption of a twofold internal barrier, together with the harmonic approximation for the torsion about the exocyclic bond, leads to a V_2 of 0.5 or 1.0 kcal/mol from the microwave spectrum (44) of 4-fluorostyrene, and 1.0 kcal/mol from vibrational assignments in the 288-nm absorption spectrum (43). Heat capacity data (47) give V_2 as 2.87 kcal/mol. An MO calculation suggests 3.9 kcal/mol (48). The latter barrier would imply that the observed ${}^6J_p^{F,C}$ is within a few percent of its maximum value, that is, at θ = 0. Further work is needed, possibly involving long-range couplings from sidechain ^1H, ^{13}C nuclei and ^{19}F, ^1H, ^{13}C nuclei in the benzene ring.[4]

(v) *1-(4-Fluorophenyl)*-N-*methylcyclohexylamine*

In phenylcyclohexane the low-energy conformer contains the α C—H bond in the plane of the benzene ring, analogous to **4** for 2-phenylpropane, and ${}^6J_p^{H,CH}$ entails a twofold barrier to rotation about the exocyclic carbon–carbon bond of 2.1 ± 0.3 kcal/mol (49). In the presence of an *N*-methyl substituent on the α carbon atom, the phenyl group attached to this atom will most likely prefer a conformation obtained by a rotation of 90° from the bisected conformer in phenylcyclohexane, namely **6**. The angle θ will be 30° for a conformation in which the phenyl group is axial *or* equatorial.

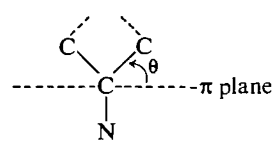

6

${}^6J_p^{F,C}$ is 0.46_9 Hz and therefore $\langle\sin^2\theta\rangle_F^C$ is 0.364 ± 0.017 if ${}^6J_{90}^{F,C}$ is taken as 1.29 ± 0.06 Hz, as used above for tetrahedral carbon linkages. This value of $\langle\sin^2\theta\rangle_F^C$, being less than 0.5, confirms **5** as the preferred conformer and V_2 follows as 1.6 ± 0.3 kcal/mol. Whether the internal barrier is indeed twofold is not certain, so that this number must be treated with circumspection. The identification of **6** as the ground state seems certain, however.

(vi) *4-Fluorophenylacetic acid and 4-fluorophenylacetone*

In these compounds, ${}^6J_p^{F,C}$ involves a trigonal carbon atom

[3] Given sufficient sensitivity of the spectrometer, ${}^6J_p^{F,C}$ may therefore be the most convenient indicator of *trans*/*gauche* ratios in molecules of this kind, its measurement being straightforward compared to the analyses of spectra from complex spin systems.

[4] It is amusing that 1.57/2.24, the ratio of the couplings to the β olefinic carbon in the α-methyl derivative and the 4-fluorostyrene itself, yields 33° as the angle of twist in the former, as also deduced from the coupling to the methyl carbon (30°). For the α-cyclopropyl compound, θ is then 37°, compared to the 35° deduced from the ${}^6J_p^{F,C}$ for the coupling to the carbon nucleus in the 3-membered ring. These results may well indicate that the coupling to the β olefinic carbon nucleus is near zero at θ = 90°. However, a proper dynamical model is needed, together with a reliable potential energy profile for the internal rotation.

attached to electronegative substituents. Whatever the value of $^{6}J_{p}^{F,C}$ at $\theta = 90°$, from the values of 1.20 and 1.18 Hz for the ketone and acid, respectively, it is clear that the perpendicular form, of type **3**, is very stable. $^{6}J_{90}^{F,C}$ is expected to be larger than the 1.13 Hz assessed above for an olefinic carbon, by analogy with the 26% increase in $^{6}J_{90}^{F,C}$ for an aliphatic carbon caused by an attached electronegative substituent. If a similar increase applied to the carbonyl bond, $^{6}J_{90}$ would be 1.42 Hz. In that event, the barrier to rotation about the sp^2–sp^3 carbon–carbon bond, assumed twofold, would be about 2.3 kcal/mol for both the ketone and the acid. Obviously, this is a very rough estimate of V_2.

Therefore, $^{6}J_{p}^{F,CH}$ was measured for these two compounds in acetone-d_6, yielding 0.67(2) and 0.70(2) Hz for the ketone and acid, respectively. The electronegativity of the COOH group is 2.8 (50), and $^{6}J_{90}^{F,CH}$ is therefore estimated as 2.12 Hz by the procedure described for $^{6}J_{90}^{H,CH}$ (1). Then $\langle \sin^2 \theta \rangle_F^H$ is 0.323 ± 0.018 Hz and V_2 becomes 2.5 ± 0.5 kcal/mol, where $^{6}J_{p}^{F,CH}$ for the two compounds is averaged to $0.68_5 \pm 0.03$ Hz. It appears that $^{6}J^{F,C}$ and $^{6}J^{F,CH}$ yield similar conclusions about the conformational dynamics of these two compounds, agreeing that the low-energy conformer is analogous to **3**.

Acknowledgements

We are grateful to the Natural Sciences and Engineering Research Council of Canada and to UPM for financial support.

1. W. J. E. PARR and T. SCHAEFER. Acc. Chem. Res. **13**, 400 (1980).
2. R. HOFFMAN. Mol. Phys. **1**, 326 (1958).
3. M. BARFIELD and R. CHAKRABARTI. J. Am. Chem. Soc. **91**, 4346 (1969).
4. C. J. MACDONALD and W. F. REYNOLDS. Can. J. Chem. **48**, 1002 (1970).
5. R. WASYLISHEN and T. SCHAEFER. Can. J. Chem. **50**, 1852 (1972).
6. M. P. WILLIAMSON, R. KOSTELNIK, and S. M. CASTELLANO. J. Chem. Phys. **49**, 2218 (1968).
7. T. SCHAEFER and R. LAATIKAINEN. Can. J. Chem. **61**, 2785 (1983).
8. T. SCHAEFER, J. PEELING, and G. H. PENNER. Can. J. Chem. **61**, 2773 (1983).
9. M. BARFIELD, C. J. FALLICK, K. HATA, S. STERNHELL, and P. W. WESTERMAN. J. Am. Chem. Soc. **105**, 2178 (1983).
10. R. E. WASYLISHEN and M. BARFIELD. J. Am. Chem. Soc. **97**, 4545 (1975).
11. T. SCHAEFER, T. A. WILDMAN, and R. SEBASTIAN. Can. J. Chem. **60**, 1924 1982).
12. T. SCHAEFER, K. MARAT, J. PEELING, and R. P. VEREGIN. Can. J. Chem. **61**, 2779 (1983).
13. R. LAATIKAINEN. J. Magn. Reson. **52**, 293 (1983).
14. A. R. ENGELMANN, R. H. CONTRERAS, and J. C. FACELLI. Theor. Chim. Acta (Berlin), **59**, 17 (1981).
15. H. FUKUI, K. MIURA, K. OHTA, and T. TSUJI. J. Chem. Phys. **76**, 5169 (1982).
16. M. BARFIELD. J. Am. Chem. Soc. **102**, 1 (1980).
17. M. HANSEN and H. J. JAKOBSEN. J. Magn. Reson. **20**, 520 (1975).
18. L. ERNST, V. WRAY, V. A. CHERTKOV, and N. M. SERGEYEV. J. Magn. Reson. **25**, 123 (1977).
19. T. SCHAEFER, L. KRUCZYNSKI, and W. NIEMCZURA. Chem. Phys. Lett. **38**, 498 (1976).
20. T. SCHAEFER, W. J. E. PARR, and W. DANCHURA. J. Magn. Reson. **25**, 167 (1977).
21. T. SCHAEFER, W. DANCHURA, W. NIEMCZURA, and J. PEELING. Can. J. Chem. **56**, 2442 (1978).
22. R. WASYLISHEN and T. SCHAEFER. Can. J. Chem. **49**, 94 (1971).
23. S. CASTELLANO and A. A. BOTHNER-BY. J. Chem. Phys. **41**, 3863 (1964).
24. C. W. HAIGH. Annu. Rep. Nucl. Magn. Reson. Spectrosc. **4**, 311 (1971).
25. J. A. POPLE, J. W. MCIVER, and N. S. OSTLUND. Chem. Phys. Lett. **1**, 465 (1967).
26. P. A. DOBOSH. Quantum Chemistry Program Exchange, **11**, 142 (1979).
27. J. A. POPLE and M. S. GORDON. J. Am. Chem. Soc. **89**, 4253 (1967).
28. F. J. WEIGERT and J. D. ROBERTS. J. Am. Chem. Soc. **93**, 2361 (1971).
29. D. DODDRELL, M. BARFIELD, W. ADCOCK, M. AURANGZEB, and D. JORDAN. J. Chem. Soc. Perkin Trans. 2, 402 (1976).
30. W. S. BREY, L. W. JAQUES, and H. J. JAKOBSEN. Org. Magn. Reson. **12**, 243 (1979).
31. T. SCHAEFER, W. NIEMCZURA, W. DANCHURA, and T. A. WILDMAN. Can. J. Chem. **57**, 1881 (1979).
32. D. M. GRANT and W. M. LITCHMAN. J. Am. Chem. Soc. **87**, 3994 (1965).
33. W. E. HULL. To be published.
34. T. SCHAEFER, W. NIEMCZURA, W. DANCHURA, and T. A. WILDMAN. Can. J. Chem. **57**, 1881 (1979).
35. G. MONTAUDO, S. CACCAMESE, and P. FINOCCHIARO. J. Am. Chem. Soc. **93**, 4202 (1971).
36. G. SMITH, C. H. L. KENNARD, and J. WHITNALL. Cryst. Struct. Commun. **6**, 131 (1977).
37. R. J. ABRAHAM and G. GATTI. J. Chem. Soc. B, 961 (1969).
38. L. PHILLIPS and V. WRAY. J. Chem. Soc. Perkin Trans. 2, 536 (1972).
39. W. F. REYNOLDS and D. J. WOOD. Can. J. Chem. **51**, 2659 (1973).
40. R. J. ABRAHAM and M. A. COOPER. J. Chem. Soc. B, 202 (1967).
41. (*a*) D. A. DOUGHERTY, K. MISLOW, J. F. BLOUNT, J. B. WOOTEN, and J. JACOBUS. J. Am. Chem. Soc. **99**, 6149 (1977); (*b*) T. SCHAEFER, L. J. KRUCZYNSKI, and W. J. E. PARR. Can. J. Chem. **54**, 3210 (1976).
42. T. SCHAEFER, L. J. KRUCZYNSKI, B. KRAWCHUK, R. SEBASTIAN, J. L. CHARLTON, and D. M. MCKINNON. Can. J. Chem. **58**, 2452 (1980).
43. J. M. HOLLAS, E. KHALILIPOUR, and S. N. THAKUR. J. Mol. Spectrosc. **73**, 240 (1978).
44. W. M. RALOWSKI, P. J. MYÖBERG, and S. O. LJUNGGREN. J. Mol. Struct. **30**, 1 (1976).
45. (*a*) G. K. HAMER, I. R. PEAT, and W. F. REYNOLDS. Can. J. Chem. **51**, 915 (1973); (*b*) T. KOBAYASHI, T. ARAI, H. SAKURAGI, K. TOKUMARU, and C. UTSUNOMIYA. Bull. Chem. Soc. Jpn. **54**, 1658 (1981).
46. T. SCHAEFER and W. J. E. PARR. J. Mol. Spectrosc. **61**, 479 (1976), and references therein.
47. B. SINGH, J. B. DHAWAN, and R. M. P. JAISWAL. Indian J. Phys. **47**, 69 (1973).
48. W. M. RALOWSKI, P. J. MJÖBERG, and J. E. ALMLOF. J. Chem. Soc. Faraday Trans. 2, **71**, 1109 (1975).
49. T. SCHAEFER, W. NIEMCZURA, and W. DANCHURA. Can. J. Chem. **57**, 355 (1979).
50. P. R. WELLS. Prog. Phys. Org. Chem. **6**, 111 (1968).

The radiation chemistry of 2-mercaptoethanol

MANOHAR LAL
Chemistry Division, Bhabha Atomic Research Centre, Bombay – 400085, India

AND

DAVID A. ARMSTRONG
Chemistry Department, University of Calgary, Calgary, Alta., Canada T2N 1N4

Received April 5, 1984

MANOHAR LAL and DAVID A. ARMSTRONG. Can. J. Chem. **63**, 30 (1985).

Hydrogen, hydrogen sulphide, mercaptoethanol disulphide, and ethanol yields from the radiolysis of 2-mercaptoethanol are consistent with the same mechanism postulated for other sulphydryl-containing molecules. In all cases studied g_H in neutral solution appears to be enhanced ($g_H = 0.7-0.9$ molecule per 100 eV). However, there is no basis for attributing this to reaction [10] which was postulated in earlier work:

[10] $e_{aq}^- + RSH \xrightarrow{H^+} RS\cdot + H_2$

but is not supported by independent data from H atom studies.

MANOHAR LAL et DAVID A. ARMSTRONG. Can. J. Chem. **63**, 30 (1985).

Les rendements en hydrogène, en sulfure d'hydrogène, en disulfure de mercaptoéthanol et en éthanol, obtenus lors de la radiolyse du mercapto-2 éthanol, sont en accord avec le mécanisme postulé pour d'autres molécules contenant des groupes sulfhydryles. Dans tous les cas étudiés, il semble que la valeur de g_H en solution neutre soit augmentée ($g_H = 0{,}7-0{,}9$ molécule par 100 eV). Toutefois, il n'y a aucune donnée expérimentale qui puisse permettre d'attribuer ce résultat à la réaction [10] qui avait été postulée dans un travail antérieur

[10] $e_{aq}^- + RSH \xrightarrow{H^+} RS\cdot + H_2$

mais ces résultats n'ont pas été confirmés par des données indépendantes obtenues à partir d'études sur des atomes d'hydrogènes.

[Traduit par le journal]

Introduction

Sulphydryl groups play an important role in many cellular processes (1). At the same time they are known to be highly susceptible to ionising radiation, and low molecular weight sulphydryl-containing molecules have been shown to act as sacrificial protectors (2). Their reactions with the free radicals formed in irradiated aqueous solutions are therefore of considerable interest. The following reaction mechanism, with RSH as the sulphydryl molecule, has been shown to adequately describe the products observed for cysteine (3, 4), penicillamine (5), and glutathione (6) in 1 to 10 mM aqueous solutions subjected to ^{60}Co or fast electron radiolysis. These are also the main primary reactions in

[1] $H_2O \rightsquigarrow 2.7\ \cdot OH + 2.6\ e_{aq}^- + 0.6\ \cdot H + 0.7\ H_2O_2 + 0.5\ H_2$

[2] $e_{aq}^- + H^+ \rightarrow \cdot H$

[3] $RSH + \cdot OH \rightarrow RS\cdot + H_2O$

[4] $RSH + \cdot H \rightarrow RS\cdot + H_2$

[5] $RSH + \cdot H \rightarrow R\cdot + H_2S$

[6] $RSH + e_{aq}^- \rightarrow R\cdot + SH^-$

[7] $RSH + R\cdot \rightarrow RS\cdot + RH$

[8] $RS\cdot + RS\cdot \rightarrow RSSR$

[9] $2RSH + H_2O_2 \rightarrow RSSR + 2H_2O_2$

dithiothreitol, but in that case there are some additional secondary reactions (7, 8). Reaction [9] is slow except at high pH and can usually be neglected in acid solutions (3, 9).

At pH 4–7 reaction [2] can be neglected and, since the contribution of reaction [5] is small in this pH range, the mechanism then predicts $G(H_2S) = G(RH) \simeq g_{e_{aq}^-}$ (3–6). While this was observed with the sulphydryl molecules noted above, the values of $G(H_2S)$ and $G(RH)$ from 2-mercaptoethanol, although equal, were reported to be only half of $g_{e_{aq}^-}$ (10). Jayson, Stirling, and Swallow attributed that observation to the occurrence of reaction [10]:

[10] $e_{aq}^- + RSH \xrightarrow{H^+} H_2 + RS\cdot$

Intuitively this seems to require the existence of a relatively long-lived RSH^- ion:

[11] $e_{aq}^- + RSH \rightarrow RSH^-$

[12] $RSH^- + H^+ \rightarrow RS\cdot + H_2$

and no evidence for that has been reported for aqueous systems.

The apparent difference between 2-mercaptoethanol and the other sulphydryl-containing molecules was obviously of fundamental interest. Also, since the former compound is often used as a model sulphydryl species, it is important that its mechanism of radiolysis be well understood. We have therefore reinvestigated the radiation chemistry of aqueous mercaptoethanol. A detailed study of the pH dependence of the hydrogen yields was made, since reaction [10] (or [11]–[12]) would significantly augment $G(H_2)$ in the pH range 4–7. Hydrogen sulphide, RSSR, and RH (i.e. ethanol) yields were also determined. Experiments were performed at both the Bhabha Atomic Research Centre (BARC) and at the University of Calgary.

Experimental

Materials

Mercaptoethanol (Sigma Chemical Co. pure grade) was subjected

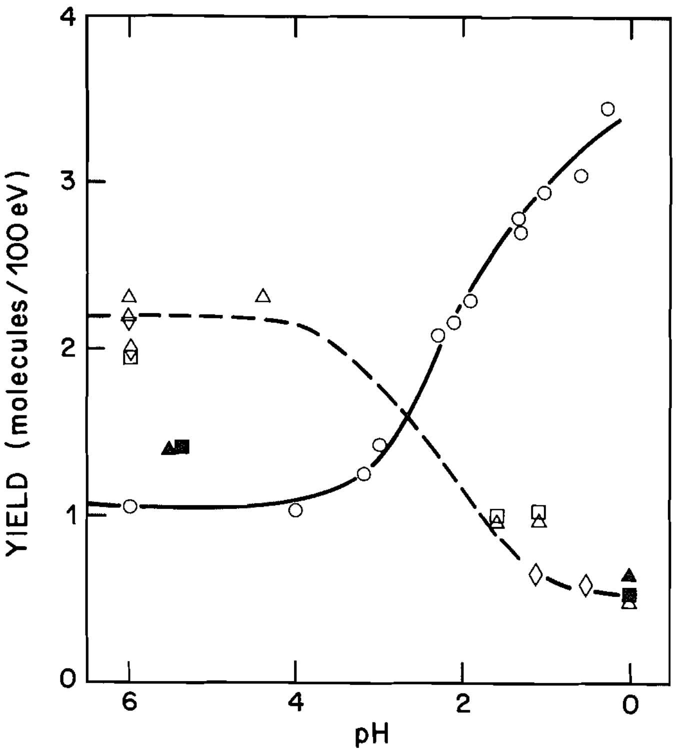

FIG. 1. Product yields as a function of pH for H_2 ○, EtOH □, H_2S △ in 10^{-2} *M* RSH and EtOH ◇ and H_2S ▽ in 2×10^{-3} *M* RSH, this study; filled symbols — as above from ref. 10.

to distillation under vacuum before use in the earlier experiments, but later it was found to be satisfactory to use it directly. Nitrogen used for preliminary deaeration of solutions at BARC, Bombay, was IOLAR-2 from the Indian Oxygen Co. Ltd. Water was triply distilled by standard methods. Fresh solutions were made for each experiment and final degassing was carried out by freeze, pump, thaw cycles (3).

Irradiations

These were performed in ^{60}Co sources, which gave dose rates of 40 or 9×10^{19} eV min^{-1} dm^{-3} (BARC, Bombay) and 7×10^{18} eV min^{-1} dm^{-3} (Calgary). Analyses were carried out immediately after irradiations.

Analyses

Hydrogen: Aliquots of degassed solution in cells fitted with break seals were connected to a vacuum system, which was used to extract the gases volatile at liquid nitrogen temperature (3) and collect them in a standard volume. Hydrogen was then analysed by gas chromatography with a 2 m × 0.66 cm diameter stainless steel column filled with 30–60 mesh SA molecular sieve at room temperature and with N_2 as carrier gas (BARC) or by following the drop in pressure when the hydrogen was allowed to diffuse through a heated palladium thimble (Calgary (3)).

Ethanol: This analysis was carried out by gas chromatography with N_2 carrier gas on a Carbowax number 6 column (10% chromosorb WAW) in a 1.6 m 0.66 cm diameter copper tube at 85°C.

Hydrogen sulphide: This was determined by both the ammonium molybdate and methylene blue methods (3).

Disulphide: Concentrations of RSSR in the irradiated solutions were obtained from the absorbances at 248 nm using an extinction coefficient of 324 M^{-1} cm^{-1}. In this case the ^{60}Co γ dose rate was 4×10^{20} eV min^{-1} dm^{-3}.

Results

As in the case of cysteine, product concentration versus dose plots were linear in the region below 10^{22} eV dm^{-3}. Yields of

TABLE 1. Yields of H_2 and ethanol as a function of pH

Concentration of 2-mercaptoethanol (*M*)	pH	$G(H_2)$	G(ethanol)
0.06 −0.13	6.0 ± 0.2	1.0_0 ± 0.05	2.2_5 ± 0.0_5
0.06 −0.10	1.1 ± 0.1	2.3 ± 0.1	1.0_3 ± 0.0_5
0.06 −0.10	0.4 ± 0.1	2.5 ± 0.1	1.0 ± 0.1

products in molecules per 100 eV of radiation energy absorbed were obtained from their slopes. Hydrogen, H_2S, and ethanol yields for 2×10^{-3} and 10^{-2} *M* 2-mercaptoethanol solutions are presented as a function of pH in Fig. 1. Yields for more concentrated solutions are contained in Table 1.

Discussion

The effects of pH exhibited by the yields for high and low concentrations in Table 1 and Fig. 1 are similar, and the trends seen are in agreement with those observed with cysteine (3, 4). The yields of hydrogen sulphide and ethanol reported by Jayson, Stirling, and Swallow for 2-mercaptoethanol at pH 5.5 and 0.0 have been included in Fig. 1. Their results at the lower pH's are in good agreement with the present data. On the other hand, at pH 5.5 their values of $G(H_2S)$ and G(ethanol) are much less than the ones reported here for pH 4 to 6 in Fig. 1 and Table 1. The reason for this is not clear. However, if the lower yields of $G(H_2S)$ and G(ethanol) at pH ~5 *were* correct and reaction [10] had occurred to the extent postulated in ref. 10, the hydrogen yields would have been higher than $g_H + G^M_{H_2}$ (see below) by one molecule per 100 eV and close to 2 molecules per 100 eV. Clearly this is not the case. If g_H is taken as 3.6_5 at pH ≤ 1.3 (11) and $G^{H_2}_M$ as 0.3_0 in 10^{-2} *M* 2-mercaptoethanol solutions, then the mechanism given in the Introduction predicts $G(H_2S)$ or G(ethanol) + $G(H_2) = 3.6_5 + 0.3_0 = 3.9_5$ (11). The sum of the yields from the smoothed curves in Fig. 1 at pH 0.5 is 3.8_5, in reasonable agreement. Likewise k_4/k_5 is given by $(G(H_2) - 0.30_0)\,(G(H_2S))^{-1}$ (3). The value of 5 thus estimated from the 10^{-2} *M* solution yields at pH 0.5 is typical of primary sulphydryl compounds such as cysteine and methyl mercaptan (3, 12). The mechanism also predicts $G(\mathrm{RSSR}) = (1/2)\,[g_{e^-_{aq}} + g_H + g_{OH}]$, which is 3.1 molecules per 100 eV for 10^{-2} *M* RSH, taking into account the solute reactivity (5). The result obtained here at pH 6 was 3.4 molecules per 100 eV, which is in agreement, and is the same as the experimental yield reported in ref. 10. It was also similar to the disulphide yields from other sulphydryl molecules (3, 6).

The similarity to these other thiol compounds may be further demonstrated. At pH 6 the mechanism predicts that $\{G(H_2S)$ or G(ethanol) + $G(H_2)\}$ should be equal to $(g_e + g_H + G^M_{H_2})$ which is 3.2 + 0.30 = 3.6 (5). The sum of the experimental yields is $2.2_5 + 1.0_5 = 3.3$, which is also in satisfactory agreement. The yield of hydrogen should be equal to $G^M_{H_2} + g_H \times k_4/(k_4 + k_5)$. If $G^M_{H_2}$ is taken as 0.3 and $k_4/(k_4 + k_5)$ is assumed to be pH independent, then g_H must be ≃ 0.9 molecule per 100 eV. This is significantly larger than the normally accepted value of 0.6 (11). However, a similar discrepancy has been observed for cysteine and methyl mercaptan, for which the hydrogen yields in 10^{-2} *M* solutions are also ~1.0 molecule per 100 eV (3).

The origin of this extra hydrogen is not clear. Wilkening *et* *al.* (3) have argued against the occurrence of reaction [13] on the basis of Littman, Carr, and Brady's report (13) that reaction [14] is relatively efficient,

[13] $e^-_{aq} + RSH \rightarrow RS^- + H\cdot$

[14] $\cdot H + RS^- \rightarrow R\cdot + SH^-$

an observation which demonstrates that the exit channel to $R\cdot + SH^-$ is more favourable than that to $H\cdot + RS^-$. Alternative explanations of the excess hydrogen are the absorption of energy from subexcitation electrons (14) and the scavenging of dry electrons in reaction [15],

[15] $e^- + RSH \rightarrow RS^- + H\cdot$

for which the energetics would be different from [10]. Further experiments will be required to resolve this problem.

Acknowledgements

The authors are grateful to M. Wieser and V. Wilkening for assistance in the earlier phases of this work.

1. Y. M. TORCHINSKII. Sulphydryl and disulphide groups of proteins. *Translated by* H.B.F. Dixon. Consultants Bureau, New York. 1974.
2. J. E. PACKER. The chemistry of the thiol group. Part 2. *Edited by* S. Patai. Wiley, London. 1974. p. 481.
3. D. A. ARMSTRONG and V. G. WILKENING. Can. J. Chem. **42**, 2631 (1964); V. G. WILKENING, M. LAL, M. ARENDS, and D. A. ARMSTRONG. Can. J. Chem. **45**, 1209 (1967); V. G. WILKENING, M. LAL, M. ARENDS, and D. A. ARMSTRONG. J. Phys. Chem. **72**, 185 (1968).
4. A. AL-THANNON, R. M. PETERSON, and C. N. TRUMBORE. J. Am. Chem. Soc. **72**, 2395 (1968).
5. G. C. GOYAL and D. A. ARMSTRONG. Can. J. Chem. **54**, 1938 (1976); J. Phys. Chem. **80**, 1848 (1976).
6. M. LAL, D. A. ARMSTRONG, and M. WIESER. Radiat. Res. **37**, 246 (1969).
7. M. LAL. Radiat. Phys. Chem. **15**, 649 (1980).
8. A. J. ELLIOT and F. C. SOPCHYSHYN. Radiat. Phys. Chem. **19**, 417 (1982).
9. M. LAL. Radiat. Eff. **2**, 225 (1970).
10. G. G. JAYSON, D. A. STIRLING, and A. J. SWALLOW. Int. J. Radiat. Biol. **19**, 143 (1971).
11. I. G. DRAGANIĆ and Z. D. DRAGANIĆ. The radiation chemistry of water. Academic Press, New York. 1971.
12. T.-L. TUNG and R. KUNTZ. Radiat. Res. **55**, 10 (1973); W. L. SEVERS, P. A. HAMILTON, T.-L. TUNG, and J. A. STONE. Int. J. Radiat. Phys. Chem. **8**, 461 (1973).
13. F. E. LITTMAN, E. M. CARR, and A. P. BRADY. Radiat. Res. **7**, 107 (1957).
14. M. A. J. RODGERS and W. M. GARRISON. J. Am. Chem. Soc. **72**, 758 (1968).

A nuclear magnetic resonance study of the formation and conformational equilibria of symmetrical and mixed disulfides of captopril

DALLAS L. RABENSTEIN[1] AND YVON THERIAULT
Department of Chemistry, University of Alberta, Edmonton, Alta., Canada T6G 2G2

Received March 8, 1984

DALLAS L. RABENSTEIN and YVON THERIAULT. Can. J. Chem. **63**, 33 (1985).

The oxidation of captopril (CpSH, 1-(D-3-mercapto-2-methylpropanoyl)-1-proline) by glutathione disulfide (GSSG) via thiol/disulfide exchange to form, in the first step, CpSSG and GSH and, in the second step, CpSSCp and GSH, has been studied in aqueous solution by ^{1}H nmr. Due to slow rotation around the amide bond(s) of CpSH and CpSSCp and of the captopril part of CpSSG, separate resonances are observed for the *cis* and *trans* conformations across these bonds. Conformational equilibrium constants were estimated as a function of pH for CpSH, CpSSCp, and CpSSG from the intensities of resonances for the *cis* and *trans* isomers. These equilibrium constants were used in the determination of equilibrium constants for the two steps in the oxidation of CpSH by GSSG. The results suggest that CpSH has a greater tendency to reduce disulfide bonds by thiol/disulfide exchange at physiological pH, and thus form mixed disulfides, than do the thiol groups in amino acids. Also, the conformational equilibrium constants indicate that, at physiological pH, approximately two thirds of the captopril, either free or in a disulfide form, has the *trans* conformation.

DALLAS L. RABENSTEIN et YVON THERIAULT. Can. J. Chem. **63**, 33 (1985).

Faisant appel à la rmn du ^{1}H et opérant en solutions aqueuses, on a étudié l'oxydation du captoprile (CpSH, (D-mercapto-3 méthyl-2 propanoyl)-1 proline-1) par le disulfure de glutathion (GSSG) via un échange thio/disulfure qui permet de former le CpSSG et le GSH dans une première étape et le CpSSCp et le GSH dans une deuximème étape. A cause de la rotation lente autour des liaisons amide(s) du CpSH, du CpSSCp et de la partie captoprile du CpSSG, on a pu observer des résonances distinctes pour les conformations *cis* et *trans* par rapport à ces liaisons. Utilisant les intensités des résonances des isomères *cis* et *trans*, on a évalué les constantes d'équilibres conformationnels du CpSH, du CpSSCp et du CpSSG en fonction du pH. On a utilisé ces constantes d'équilibre pour déterminer les constantes d'équilibre des deux étapes de l'oxydation du CpSH par le GSSG. Les résultats suggèrent que, par comparaison avec les thiols des acides aminés, le CpSH a une plus grande tendance à réduire les liaisons disulfures, par un échange thiol/disulfure à pH physiologique, et ainsi à former des disulfures mixtes. Les constantes d'équilibres conformationnels indiquent également, à pH physiologique, qu'approximativement les deux tiers du captoprile, tant sous la forme libre que sous la forme de disulfure, existe sous une conformation *trans*.

[Traduit par le journal]

Introduction

Captopril, 1-(D-3-mercapto-2-methylpropanoyl)-1-proline, is used clinically for the treatment of hypertension (1–3). Antihypertensive activity is thought to result from inhibition of angiotensin I-converting enzyme, with the thiol group of captopril binding to the active site of the enzyme (1–3). The thiol group is also the key functional group in the metabolism of captopril, with major metabolites being captopril disulfide and mixed disulfides with thiol-containing amino acids, peptides, and proteins (4–7).

Captopril exists in solution as an equilibrium mixture of *trans* (**1**) and *cis* (**2**) isomers with respect to the conformation

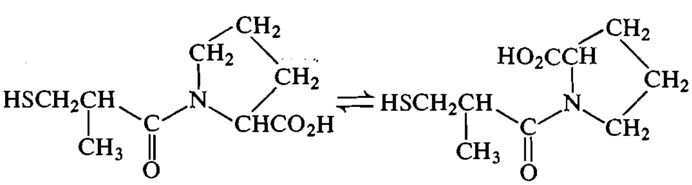

1 2

across the peptide bond (8). Although the conformational equilibrium of captopril has been characterized in detail (8), the chemistry of formation of disulfides from captopril and their conformational equilibria have not. This is of interest since it has been suggested that disulfide metabolites may play a role in determining the nature and time course of adverse reactions to captopril (9). In this paper, we report the results of an ^{1}H nmr study of the formation of symmetrical and mixed disulfides by

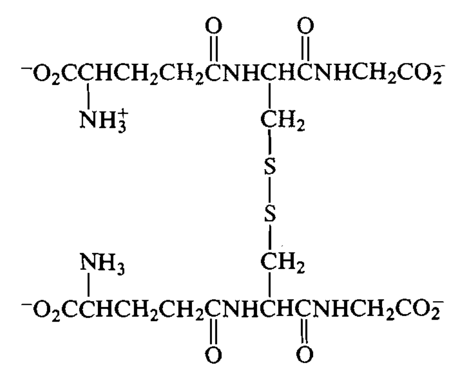

3

oxidation by glutathione disulfide (**3**) via thiol/disulfide exchange as described by eqs. [1] and [2].

[1] CpSH + GSSG ⇄ CpSSG + GSH

[2] CpSH + CpSSG ⇄ CpSSCp + GSH

where CpSH, CpSSCp, GSH, GSSG, and CpSSG are captopril, captopril disulfide, glutathione, glutathione disulfide, and captopril–glutathione mixed disulfide, respectively. As part of this study, the *cis–trans* conformational equilibrium across the amide bond(s) of CpSH and CpSSCp and the captopril part of CpSSG have also been characterized by ^{1}H nmr.

Glutathione disulfide was chosen for this study because it occurs naturally (10), captopril–glutathione mixed disulfide (CpSSG) has been detected as a metabolite of captopril (4, 5), and, with the cystine between two amino acid residues, GSSG

[1] Author to whom correspondence should be addressed.

serves to a first approximation as a model for disulfide bonds in proteins.

Experimental

The captopril and captopril disulfide used in this study were gifts from The Squibb Institute for Medical Research, Princeton, N.J. Glutathione disulfide was obtained from Sigma Chemical Co. The 99.7% D_2O, 40% NaOD in D_2O, and 35% DCl in D_2O were obtained from Merck Sharp and Dohme, Ltd.

The ^1H nmr spectra were measured at 360 MHz on a Bruker WM-360 spectrometer operating in the pulse/Fourier transform mode. The probe temperature was 25 ± 1°C. Chemical shifts were measured relative to internal *tert*-butyl alcohol and are reported relative to the methyl resonance of sodium 2,2-dimethyl-2-silapentane-5-sulfonate (DSS). The resolution was increased in some spectra with the Gaussian resolution enhancement routine in the Aspect 2000 software.

The pH measurements were made at 25°C with a Fisher Accumet pH meter equipped with a standard glass electrode and a fiber-tipped, saturated calomel reference electrode, or a microcombination electrode. Fisher certified standard solutions having nominal pH values of 4.00, 7.00, and 10.00 were used for calibrating the pH meter. The exact pH of each standard solution was determined by comparison with freshly prepared N.B.S. pH standard solutions (11). pH values reported are the meter readings; to indicate that pH readings for D_2O solutions were not corrected for the deuterium isotope effect (12), they are reported as pH*.

Solutions were prepared in 99.7% D_2O containing 1 *M* KCl and approximately 0.0001 *M* *tert*-butyl alcohol. Na_2H_2EDTA (0.003 *M*) was also added to solutions containing thiols, e.g. the equilibrium mixture resulting from the reaction of CpSH with GSSG, to complex traces of heavy metals which would catalyze the oxidation of the thiols (13). The solvent mixture was deoxygenated by bubbling with argon or nitrogen before addition of thiol to minimize oxidation by dissolved oxygen. Inert gas was also blown over the solution during adjustment of pH, and nmr tubes were flushed out with the gas before transfer of an aliquot of solution to the tube. To ensure that no air oxidation of thiol occurred in the measurement of equilibrium constants for thiol/disulfide exchange reactions of CpSH with GSSG, the sample solutions were degassed further by taking them, in an nmr tube, through at least three freeze–pump–thaw cycles on a vacuum line.

Results

In aqueous solution, captopril and its disulfides exist in a conformational equilibrium due to *cis/trans* isomerization across the captopril amide bond. To quantitatively characterize the oxidation of CpSH by GSSG, it was necessary to first characterize these conformational equilibria for CpSH, CpSSCp, and CpSSG.

Conformational equilibria

The 360-MHz ^1H nmr spectra of captopril and captopril disulfide are shown in Fig. 1. Each spectrum consists of two highly coupled spin systems: the —CH_2CHCH_3 spin system from the 3-mercapto-2-methylpropanoyl part and the —$CH_2CH_2CH_2CH$— spin system from the proline residue. The spectra are further complicated by the presence of *cis* and *trans* isomers with respect to the conformation across the amide bond. This results in a doubling of the resonances in the spectrum of captopril, as is clearly evident in the multiplet patterns at 3.4–3.9 and 4.26–4.39 ppm for the hydrogens on C_δ and C_α respectively of the proline residue and the methyl resonances at 1.12–1.17 ppm (Fig. 2). In the 3.4–3.9 ppm region, the resonances at 3.4–3.66 and 3.66–3.9 ppm are from the *cis* and *trans* isomers respectively (8). In the 4.26–4.39 and 1.12–1.17 ppm regions, the more intense multiplets are from the *trans* isomer. The assignment of the other resonances for captopril are: 1.8–2.4 ppm, the hydrogens on C_β and C_γ of the proline residue; 2.48–3.06 ppm, the two hydrogens on C3 and the one hydrogen on C2 of the 3-mercapto-2-methylpropanoyl part. The spectrum of captopril disulfide is composed of the spectrum for the captopril unit in four different environments due to the *cis–trans* isomerism: $CpSSCp_{(tt)}$ in which both amide bonds are *trans*, $CpSSCp_{(tc)}$ in which one amide bond is *cis* and the other is *trans*, and $CpSSCp_{(cc)}$ in which both amide bonds are *cis*. This results in an apparent lower resolution over the 1.9–2.4 and 3.2–3.8 ppm regions due to the overlap of resonances for the two *trans* environments ($CpSSCp_{(tt)}$ and $CpSSCp_{(tc)}$) and overlap of resonances for the two *cis* environments ($CpSSCp_{(tc)}$ and $CpSSCp_{(cc)}$). Four doublets from the four different environments are observed in the methyl region (Fig. 2). The assignments are given in Table 1; the basis of these assignments is discussed below.

Fractional concentrations of the two isomers of captopril were determined as a function of pH* from the relative intensities of the two methyl doublets and from the relative intensities of the resonances for the hydrogens on C_δ of the proline residue in the *cis* and *trans* isomers. The fractional concentrations of the *trans* isomer are 0.87 ± 0.01, 0.63 ± 0.01, and 0.71 ± 0.01 for the fully-protonated, monoprotonated, and deprotonated forms of captopril, which correspond to the equilibrium constants, $K_{1c/t} = [cis]/[trans]$, listed in Table 2.

The fractional concentrations of the three isomers of captopril disulfide were determined from the relative intensities of the methyl resonances (Fig. 2). Equations [3]–[6] describe the equilibria between the three forms of captopril disulfide.

TABLE 1. Identification of captopril-containing species

Species	Conformation of the captopril amide bond(s)	Species number
$CpSH_{(t)}$	*trans*	1
$CpSH_{(c)}$	*cis*	2
$CpSSCp_{(tt)}$	*trans, trans*	3
$CpSSCp_{(tc)}$	*trans, cis*	4
$CpSSCp_{(cc)}$	*cis, cis*	5
$CpSSG_{(t)}$	*trans*	6
$CpSSG_{(c)}$	*cis*	7

TABLE 2. *cis–trans* Conformational equilibrium constants for proline-containing molecules[a]

Compound	Low pH[b]	Neutral pH[c]	High pH[d]
Glycyl-L-proline[e]	0.19	0.54	0.72
Glycyl-L-hydroxyproline[e]	0.14	0.52	0.59
L-Alanyl-L-proline[e]	0.12	0.54	0.89
Captopril	0.15	0.59	0.41
Captopril disulfide	0.20[f]	0.39[f]	0.39[f]
Captopril–glutathione mixed disulfide	0.16	0.49	0.35

[a]Defined as $K_{c/t} = [cis]/[trans]$ where *cis* and *trans* refer to the conformation across the proline amide bond.
[b]Carboxyl, thiol, and amino groups, if present, are protonated.
[c]Carboxyl groups deprotonated; thiol and amino groups, if present, protonated.
[d]Carboxyl, thiol, and amino groups, if present, deprotonated.
[e]Reference 13.
[f]$K_{c/t} = [cis]_{total}/[trans]_{total}$.

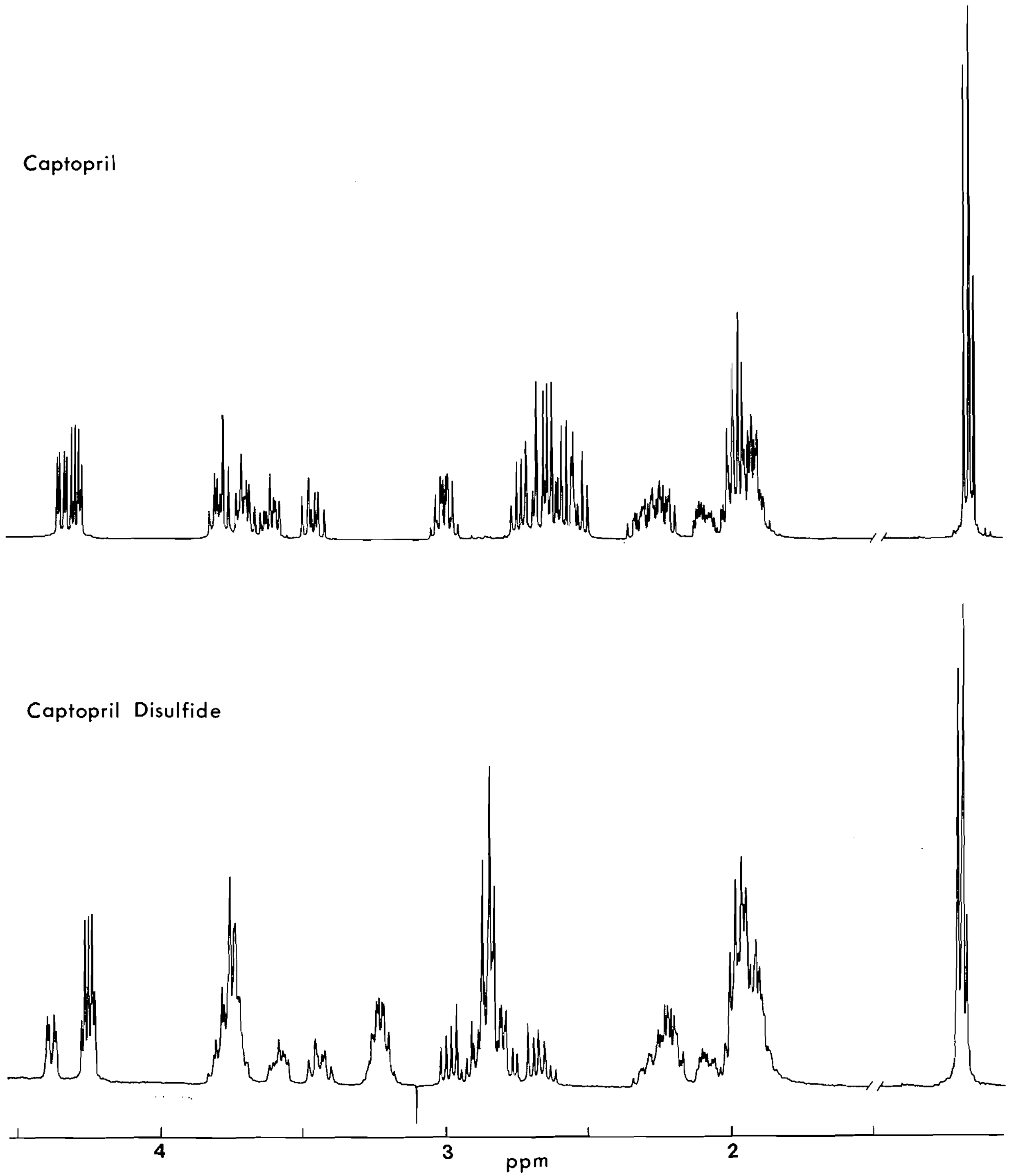

FIG. 1. The 360-MHz ^{1}H nmr spectra of 0.062 *M* captopril (pH* 6.0) and 0.042 *M* captopril disulfide (pH* 6.0). The gain was reduced by 2 in the 1–1.5-ppm region.

$$[3] \qquad \begin{array}{ccc} & \mathrm{CpSSCp}_{(tt)} & \\ \rightleftarrows & & \rightleftarrows \\ \mathrm{CpSSCp}_{(tc)} & \rightleftharpoons & \mathrm{CpSSCp}_{(cc)} \end{array}$$

$$[4] \qquad K_{cc/tt} = \frac{[\mathrm{CpSSCp}_{(cc)}]}{[\mathrm{CpSSCp}_{(tt)}]}$$

$$[5] \qquad K_{tc/tt} = \frac{[\mathrm{CpSSCp}_{(tc)}]}{[\mathrm{CpSSCp}_{(tt)}]}$$

$$[6] \qquad K_{cc/tc} = \frac{[\mathrm{CpSSCp}_{(cc)}]}{[\mathrm{CpSSCp}_{(tc)}]}$$

Equilibrium constants were determined at pH* 5.90, 5.99, and 6.10 and the results are: $K_{cc/tt} = 0.144 \pm 0.005$, $K_{tc/tt} = 0.84 \pm 0.01$, and $K_{cc/tc} = 0.171 \pm 0.006$. Total fractional concentrations of the *cis* and *trans* environments[2] were also deter-

[2] Fractional concentration of *trans* = $(2[\mathrm{CpSSCp}_{(tt)}] + [\mathrm{CpssCp}_{(tc)}])/2[\mathrm{CpSSCp}]_{\mathrm{total}}$.

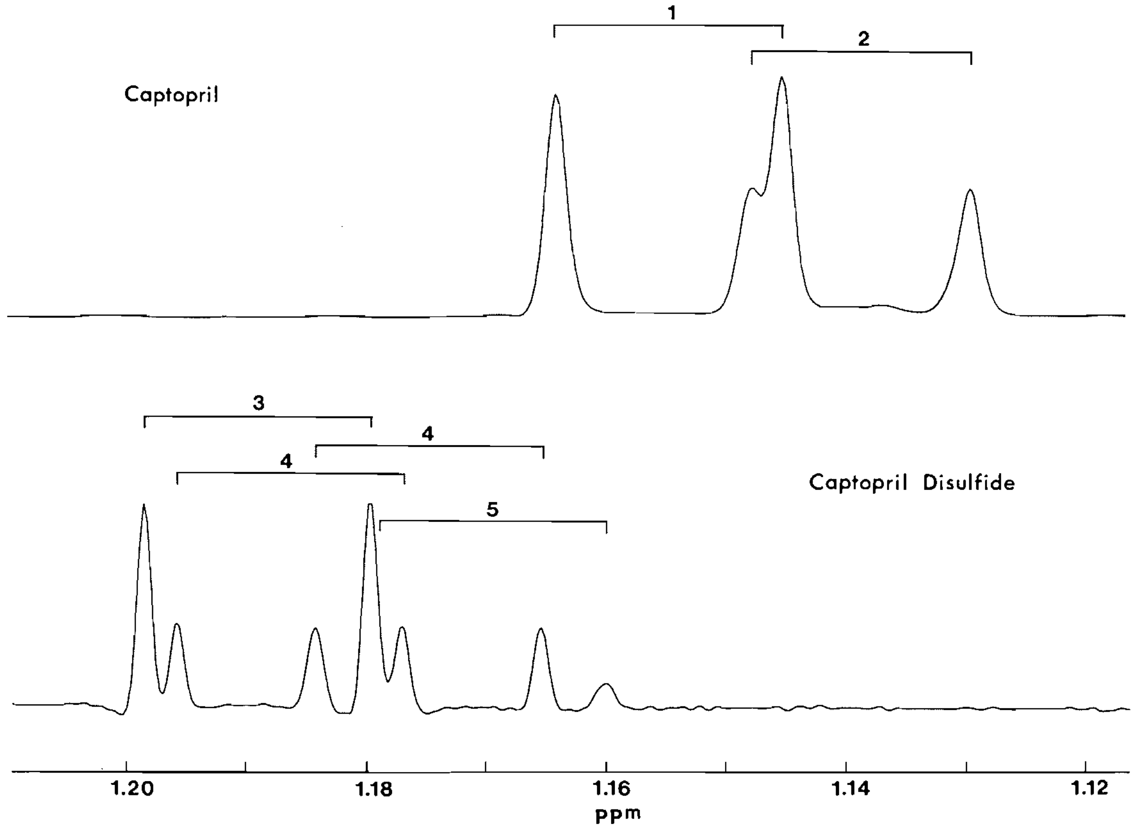

FIG. 2. The methyl resonances for the solutions described in the legend to Fig. 1. Resolution was enhanced by doing a Gaussian multiplication with the Bruker Aspect 2000 software. Resonance assignments are given in Table 1.

mined as a function of pH* directly from relative intensities of the *cis* and *trans* C_δ—H resonances. The fractional concentration of the *trans* conformation is 0.72 ± 0.03, independent of pH over the pH* range 3.75–11.02, corresponding to an equilibrium constant, $K_{c/t} = [cis]_{total}/[trans]_{total}$, of 0.39 ± 0.05. This is in excellent agreement with the value predicted by the above values for $K_{cc/tt}$, $K_{tc/tt}$, and $K_{cc/tc}$.[3] As the pH is decreased and the carboxylate groups are protonated, the fractional concentration of the *trans* isomer increases to 0.83 at pH* 0.75, corresponding to $K_{c/t} = 0.20$.

To obtain a solution containing CpSSG for the study of its conformational equilibrium (eq. [7]) 0.009 *M* CpSH was reacted with 0.18 *M* GSSG at pH* 7.1 in 1 *M* KCl solution. CpSSG, GSH, and CpSSCp were formed by thiol/disulfide exchange, as described by eqs. [1] and [2]. After reaction for 15 min, the solution was stirred in air for 18 days to oxidize CpSH to CpSSCp and GSH to GSSG to simplify the nmr spectrum. The methyl region of the ^1H nmr spectrum is shown in Fig. 3 and the assignments are given in Table 1. As indicated in Fig. 3, the dominant resonances are from CpSSG. Using the

[7]

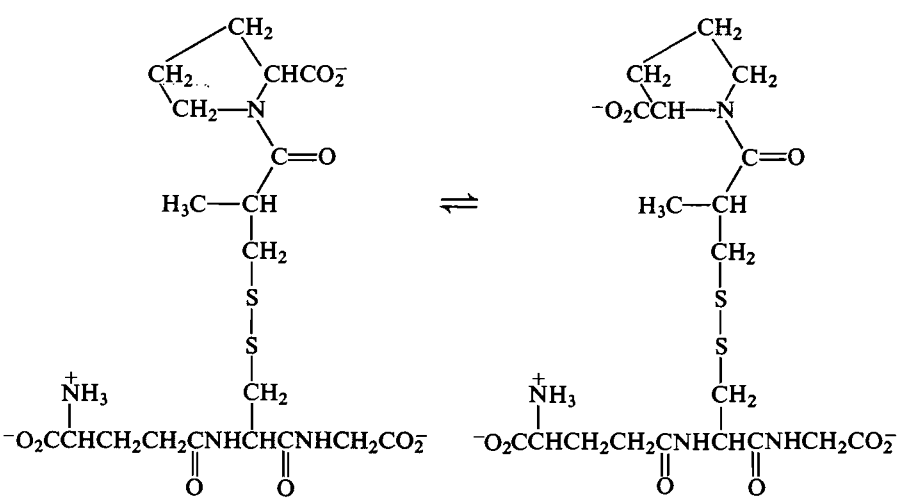

[3] $K_{c/t} = (2K_{cc/tt} + K_{tc/tt})/(2 + K_{tc/tt})$.

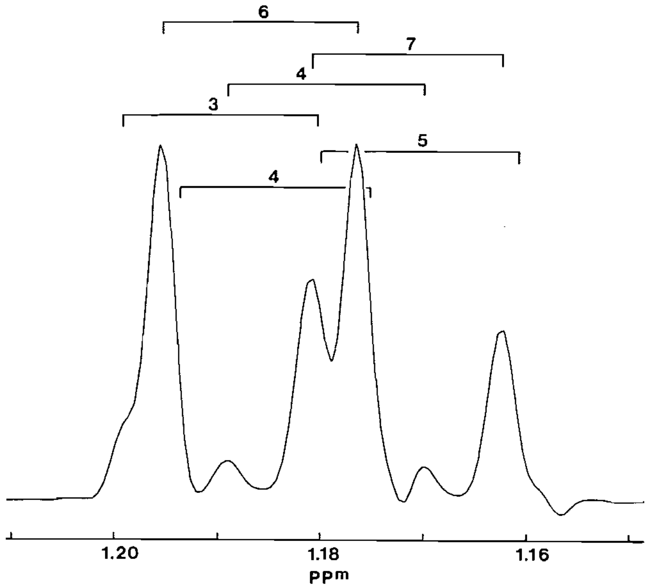

FIG. 3. The methyl region of the ^{1}H nmr spectrum of a pH* 7.0 solution contaning captopril–glutathione mixed disulfide and captopril disulfide. Details of the preparation of the mixed disulfide are given in the text. Resolution was enhanced by doing a Gaussian multiplication with the Bruker Aspect 2000 software.

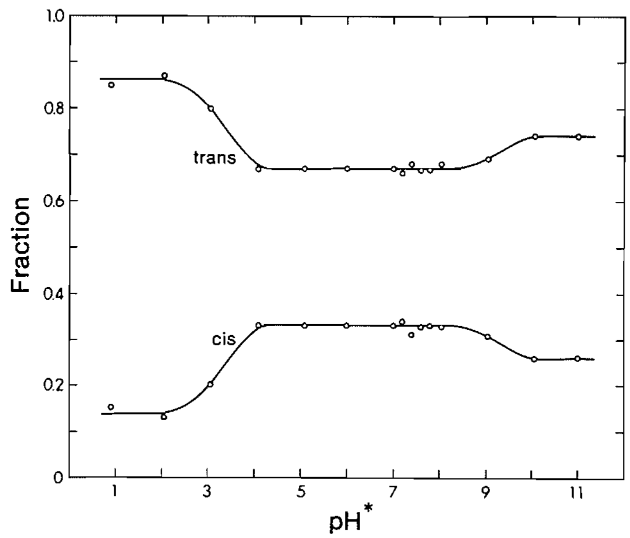

FIG. 4. The fractional concentrations of captopril–glutathione mixed disulfide in which the amide bond of the captopril part has the *trans* and *cis* conformations.

relative intensities of the methyl doublets for CpSSG, the fractional concentrations of the *trans* and *cis* forms of CpSSG were determined as a function of pH* over the pH* range 0.92–10.98 (Fig. 4). The equilibrium constants listed in Table 2 were obtained from these fractional concentrations.

Oxidation of CpSH by GSSG

To characterize the oxidation of CpSH by GSSG, equilibrium constants were determined for the reactions described by eqs. [1] and [2]. CpSH was reacted with GSSG in sealed nmr tubes, which had been degassed by the freeze–pump–thaw technique to minimize air oxidation, and then concentrations at equilibrium were determined by ^{1}H nmr. Figure 5 shows the methyl region of the nmr spectrum for a pH*

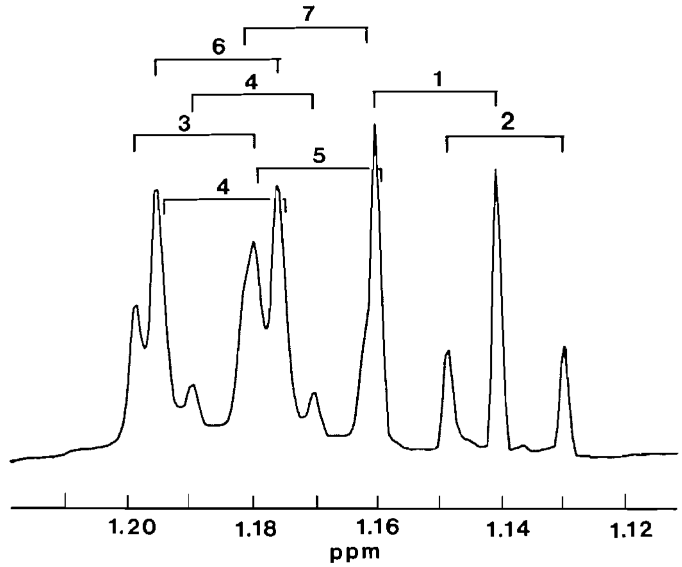

FIG. 5. The methyl region of the ^{1}H nmr spectrum of a solution prepared by reacting 0.045 *M* CpSH with 0.041 *M* GSSG at pH* 6.0 for 341 h in a degassed, sealed nmr tube. Resolution was enhanced by doing a Gaussian multiplication. Resonance assignments are given in Table 1.

6.0 solution at equilibrium; the spectrum was obtained 341 h after mixing the reactants to ensure that equilibrium had been achieved. As indicated in Fig. 5, the spectrum contains resonances for the *cis* and *trans* forms of CpSH, CpSSCp, and CpSSG. The concentrations of the various species were determined from the relative intensities of the resonances in Fig. 5 and the initial reactant concentrations. Using the determined concentrations, the conditional equilibrium constants, K_{1c} and K_{2c}, as defined by eqs. [8] and [9] and the equilibrium reactions in Fig. 6, were calculated.

$$[8] \quad K_{1c} = \frac{[\mathrm{CpSSG}]_{\mathrm{total}}[\mathrm{GSH}]}{[\mathrm{CpSH}]_{\mathrm{total}}[\mathrm{GSSG}]}$$

$$[9] \quad K_{2c} = \frac{[\mathrm{CpSSCp}]_{\mathrm{total}}[\mathrm{GSH}]}{[\mathrm{CpSH}]_{\mathrm{total}}[\mathrm{CpSSG}]_{\mathrm{total}}}$$

where $[\mathrm{CpSH}]_{\mathrm{total}}$, $[\mathrm{CpSSCp}]_{\mathrm{total}}$, and $[\mathrm{CpSSG}]_{\mathrm{total}}$ are the total concentration (*cis* + *trans*) of CpSH, CpSSCp, and CpSSG. The procedure involved determining the fractions of the total area of the methyl resonances due to CpSH, CpSSCp, and CpSSG. The total area of the resonances for CpSH was obtained by doubling the sum of the areas of its resonances at 1.13 and 1.14 ppm. That due to CpSSCp was calculated from the area of its resonances at 1.17 and 1.19 ppm and the values determined above for $K_{tc/tt}$, $K_{cc/tt}$, and $K_{cc/tc}$, and that for CpSSG was calculated as the difference between the total methyl resonance area and the areas for the CpSH and CpSSCp resonances. Using these fractions of the total methyl resonance area and the initial concentration of CpSH, the concentrations of CpSH, CpSSCp, and CpSSG were obtained. From these concentrations and the initial GSSG concentration, the concentrations of GSH and GSSG were calculated. The values calculated for K_{1c} and K_{2c} from three separate experiments in the pH* range 5.9–6.1 are 2.1 ± 0.1 and 1.5 ± 0.6 respectively. The rather large uncertainties reflect the accumulation of errors that results from obtaining concentrations by difference.

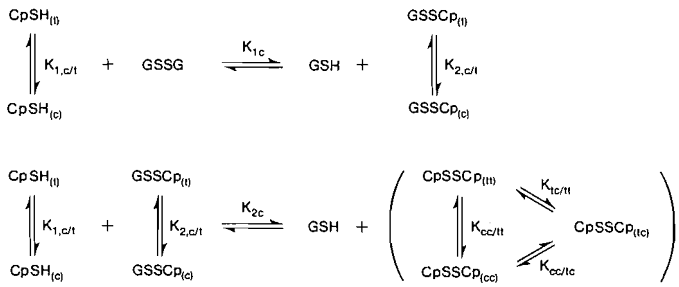

FIG. 6. The thiol/disulfide exchange equilibria and CpSH, CpSSCp, and CpSSG conformational equilibria occurring in a solution prepared by reacting CpSH and GSSG. The subscripts *t* and *c* indicate *trans* and *cis* conformations across the amide bond(s) of captopril in CpSH and CpSSCp or the captopril part of CpSSG.

Discussion

Conformational equilibria

Assignment of the *trans* conformation to the more abundant isomer(s) of CpSSCp and CpSSG is based on previous findings that the *trans* conformation is the more abundant for proline-containing dipeptides and related molecules, e.g. *tert*-butyloxycarbonyl-glycyl-L-proline-benzylester (14), glycyl-L-proline, glycyl-L-hydroxyproline, L-alanyl-L-proline, *N*-acetylsarcosine, glycylsarcosine (15), and captopril (8), and that the fractional concentration of the *trans* conformation increases when the carboxylate group is protonated (15). For example, the fractional concentration of the *trans* conformation of glycyl-L-proline increases from 0.65 to 0.84 when the carboxylate group is protonated (15), which is very similar to the increases found in this study for the more abundant isomers of CpSSCp and CpSSG.

The *cis/trans* equilibrium constants for the carboxyl-protonated (low pH) forms of CpSH, CpSSCp, and CpSSG are quite similar to each other and to those for dipeptides in which proline is the C-terminal residue, as indicated by the results in Table 2. The enhanced stability of the *trans* isomer at low pH probably results from intramolecular hydrogen bonding between the carboxylic acid hydrogen and the captopril amide carbonyl oxygen, which is not possible in the *cis* isomer. Evidence has been presented previously which indicates this to be the origin of the enhanced stability of the *trans* isomer of peptides in which protonated proline or sarcosine is the C-terminal residue (15–17). It is interesting to note that $K_{c/t}$ is approximately the same for the high pH forms of CpSH, CpSSCp, and CpSSC but is somewhat less than for the high pH forms of the proline-containing dipeptides. The origin of the enhanced stability of the *trans* conformation in the captopril unit at high pH is not obvious.

The magnitude of the *cis/trans* equilibrium constants for the neutral pH forms of CpSH, CpSSCp, and CpSSG suggests that, at physiological pH, approximately two thirds of the captopril has the *trans* conformation, regardless of whether it is free or in a disulfide form.

Oxidation of CpSH by GSSG

The reactive species in the oxidation of CpSH by GSSG via thiol/disulfide exchange (eqs. [1] and [2]) is presumably CpS^-, since it is well established that thiol/disulfide exchange proceeds via the thiolate anion (18–27). At pH 6, only a small fraction of CpSH is in the form of CpS^-, and thus the constants obtained in this work for eqs. [1] and [2] are conditional equilibrium constants. Conditional equilibrium constants for thiol/disulfide exchange in related systems are essentially pH independent up to pH values at which deprotonation of the thiol groups begins to occur (18), suggesting that the conditional equilibrium constants obtained in this work describe the reaction of CpSH with GSSG up to at least pH ~8.

The conditional equilibrium constant for the overall reaction (eq. [10])

[10] $2CpSH + GSSG \rightleftarrows CPSSCp + 2GSH$

K_{3c}, is calculated to be 3.2 ± 1.2 using the relation $K_{3c} = K_{1c}K_{2c}$. If the equilibrium position were governed by random distribution, K_{1c} and K_{2c} would be 2 and 0.5 respectively and K_{3c} would be 1. For comparison with the values for the reaction of CpSH with GSSG, $K_1 = 1.27$, $K_2 = 0.27$, and $K_3 = 0.34$ for the reaction of cysteine (CSH) with GSSG at pH 6.6 and 25°C (27) and $K_{1c} = 1.36$, $K_{2c} = 0.039$, and $K_{3c} = 0.053$ for the reaction of penicillamine (PSH) with GSSG at pH 7.4 and 25°C (18). The values for K_3 for the reactions involving CpSH and CSH are within a factor of 3 of the random distribution value, whereas that for PSH is somewhat smaller. PSH differs from CpSH and CSH in that it has two bulky methyl groups next to its thiol group, which hinders its reaction with penicillamine–glutathione mixed disulfide in the second step (18).

The overall equilibrium constant K_{3c} is related to the difference between the formal electrode potentials, $E^{0'}$, of the GSSG/GSH and CpSSCp/CpSH couples according to eq. [11].

[11] $$\Delta E^{0'} = E^{0'}_{GSSG/GSH} - E^{0'}_{CpSSCp/CpSH} = \frac{RT}{nF} \ln K_{3c}$$

With the value of 3.2 for K_{3c}, $\Delta E^{0'}$ is calculated to be 0.015 V. For comparison, $E^{0'}_{GSSG/GSH} - E^{0'}_{CSSC/CSH}$, where CSSC is cystine, is reported to be in the range −0.013 to −0.018 V at pH 6.6–7.0 (21, 23, 27) and $E^{0'}_{GSSG/GSH} - E^{0'}_{PSSP/PSH}$, where PSSP is penicillamine disulfide, is −0.0378 V at pH 7.4 (18). Values reported for $E^{0'}_{GSSG/GSH}$ are −0.205 V vs. the standard hydrogen electrode at 30°C and pH 7 (19) and −0.24 V at 40°C and pH 7 (28). These results indicate that CpSH has a greater tendency to reduce disulfide bonds by thiol/disulfide exchange than do the thiol groups in amino acids and that, if the disulfide bond in GSSG is similar to those in proteins, CpSH is capable of reducing protein disulfide bonds. These conclusions are supported by the finding that CpSH can activate papain by reduction of a disulfide bond at the active site and that CpSH is a more efficient activator of papain than is cysteine (29).

Acknowledgements

This research was supported by the Natural Sciences and Engineering Research Council of Canada, the Alberta Heritage Foundation for Medical Research, and the University of Alberta. Financial support of Y.T. by an AHFMR Studentship is gratefully acknowledged.

1. M. A. ONDETTI, B. RUBIN, and D. W. CUSHMAN. Science, **196**, 441 (1977).
2. D. W. CUSHMAN, H. S. CHEUNG, E. F. SABO, and M. A. ONDETTI. Biochemistry, **16**, 5484 (1977).
3. D. W. CUSHMAN, H. S. CHEUNG, E. F. SABO, and M. A. ONDETTI. Prog. Cardiovasc. Dis. **21**, 176 (1978).
4. S.-J. LAN, S. H. WEINSTEIN, and B. H. MIGDALOF. Drug Metab. Dispos. **10**, 306 (1982).

5. B. K. PARK, P. S. GRABOWSKI, J. H. K. YEUNG, and A. M. BRECKENRIDGE. Biochem. Pharmacol. **31**, 1755 (1982).
6. O. H. DRUMMER, P. J. WORLAND, and B. JARROTT. Biochem. Pharmacol. **32**, 1563 (1983).
7. J. H. K. YEUNG, A. M. BRECKENRIDGE, and B. K. PARK. Biochem. Pharmacol. **32**, 2467 (1983).
8. D. L. RABENSTEIN and A. A. ISAB. Anal. Chem. **54**, 526 (1982).
9. S. J. HOORNTJE, C. S. KALLENBERG, J. J. WEENING, A. J. M. DONKEN, T. H. THE, and P. J. HOEDEMAEKER. Lancet, 1212 (1980).
10. P. C. JOCELYN. Biochemistry of the SH group. Academic Press, London. 1972.
11. R. G. BATES. Determination of pH: theory and practice. Wiley, New York. 1973.
12. P. K. GLASOE and F. A. LONG. J. Phys. Chem. **64**, 188 (1960).
13. J. F. ROESLER, J. LESLIE, and G. GORIN. J. Org. Chem. **29**, 1488 (1964).
14. C. M. DEBER, F. A. BOVEY, J. P. CARVER, and E. R. BLOUT. J. Am. Chem. Soc. **92**, 6191 (1970).
15. C. A. EVANS and D. L. RABENSTEIN. J. Am. Chem. Soc. **96**, 7312 (1974).
16. J. T. GERIG. Biopolymers, **10**, 2435 (1971).
17. S. MIZUSHIMA. Adv. Protein Chem. **9**, 299 (1954).
18. D. L. RABENSTEIN and Y. THERIAULT. Can. J. Chem. **62**, 1672 (1984).
19. J. M. WILSON, R. J. BAYER, and D. J. HUPE. J. Am. Chem. Soc. **99**, 7922 (1977).
20. R. P. SZAJEWSKI and G. M. WHITESIDES. J. Am. Chem. Soc. **102**, 2011 (1980).
21. I. M. KOLTHOFF, W. STRICKS, and R. C. KAPOOR. J. Am. Chem. Soc. **77**, 4733 (1955).
22. L. ELDJARN and A. PIHL. J. Am. Chem. Soc. **79**, 4589 (1957).
23. P. JOCELYN. Eur. J. Biochem. **2**, 327 (1967).
24. A. PIHL, L. ELDJARN, and K. NAKKEN. Acta Chem. Scand. **12**, 1357 (1958).
25. L. ELDJARN and A. PIHL. J. Biol. Chem. **225**, 499 (1957).
26. G. GORIN, G. DOUGHTY, and R. GIDEON. J. Chem. Soc. B, 729 (1967).
27. G. GORIN and G. DOUGHTY. Arch. Biochem. Biophys. **126**, 547 (1968).
28. J. ROST and S. RAPOPORT. Nature, **201**, 185 (1964).
29. R. P. IGIC, J. T. GAFFORD, and E. G. ERDÖS. Biochem. Pharmacol. **30**, 683 (1981).

Hydrogen bonding of *n*-alcohols of different chain lengths

LUCIE WILSON
Département de Chimie, Université de Montréal, Montréal (Qué.), Canada H3C 3V1

R. BICCA DE ALENCASTRO
Instituto de Quimica, Universidade Federal Do Rio de Janeiro, Ilha Do Fundao, Rio de Janeiro, Brasil 21 910

AND

C. SANDORFY
Département de Chimie, Université de Montréal, Montréal (Qué.), Canada H3C 3V1

Received April 18, 1984

LUCIE WILSON, R. BICCA DE ALENCASTRO, and C. SANDORFY. Can. J. Chem. **63**, 40 (1985).

The anesthetic potency of *n*-alcohols exhibits a somewhat irregular dependence on the length of the hydrocarbon chain. An attempt has therefore been made to ascertain if this is related to the relative tendency for hydrogen bond formation by these alcohols. No such relationship was found. The result was rather that the degree of association by hydrogen bond formation of dissolved alcohols appears to be independent of the chain length, that is of the extent of other interactions that exist in these solutions.

LUCIE WILSON, R. BICCA DE ALENCASTRO et C. SANDORFY. Can. J. Chem. **63**, 40 (1985).

Le pouvoir anesthésique des alcools normaux dépend d'une manière quelque peu irrégulière de la longueur de la chaîne paraffinique. Nous avons par conséquent examiné la possibilité que cela soit lié à la tendance relative des alcools de former des liaisons hydrogène. Les résultats montrent que tel n'est pas le cas. Par contre il a pu être démontré que le degré d'association par liaisons hydrogène est indépendant de la longueur de leur chaîne paraffinique, c'est-à-dire des autres interactions intermoléculaires qui s'exercent dans ces solutions.

Introduction

The anesthetic potency of *n*-alcohols has been recognized by Posternak and Arnold in 1954 (1). This potency varies with the length of the paraffin chains of the *n*-alcohols, increasing steadily from methanol (C_1) to dodecanol (C_{12}). Then a surprising observation is made: tetradecanol (C_{14}) has no anesthetic potency at all. Tridecanol (C_{13}) has been reported to be intermediate between C_{12} and C_{14} or having no potency at all (2–5).

General anesthesia is known to be a matter of molecular associations. The current "hydrophobic theory" coupled with the "unitary hypothesis" stems from the Meyer–Overton rule which is based on the smooth relationship between anesthetic potency and solubility in lipids. According to this theory anesthetics exert their action in the hydrophobic part of the lipids in the neuron membranes. (For reviews see refs. 6–8.) We have challenged this view and proposed instead a pluralistic theory (9–12). According to it hydrophobic interactions can induce only weak anesthetic action while strong anesthetic action implies changes in polar interactions (hydrogen bonds) at ion-channels. Strong experimental indication for this on model gramicidin ion-channels has been provided by Urry and co-workers (13) (ion–channels are formed in proteins crossing the lipid membrane).

Whatever the case might be, it is of interest to examine the effects of alcohols on the neuron membrane. According to Richards and co-workers (2–4), *n*-alcohols with less than ten carbon atoms (C_1–C_9) decrease the gel to liquid crystal transition temperature (T_t) of the membrane and increase its fluidity. Alcohols with more than ten carbon atoms act in the opposite way: they increase the transition temperature and decrease the fluidity of the membrane. Decanol has no appreciable effect on either. These observations do not parallel anesthetic potency and cast doubt on the validity of the lipid solubility theories of anesthesia.

Miller and co-workers (5) took a different view. According to these authors, as well as Lawrence and Gill (14), the disordering effect of *n*-alcohols on the membrane decreases steadily with increasing chain length. They explain the cutoff by a rapid decrease, to below anesthetic levels, of the attainable concentration in the bilayer.

Now, alcohols can associate hydrophobically wih their hydrocarbon chains and by H-bonding using their OH groups. Since the possible role of H-bonding in the anesthetic properties of alcohols has not been considered by previous authors, we have undertaken a comparative study of H-bonding in *n*-alcohols from C_1 to C_{18}. While this work has not provided an explanation for the "cutoff" an intriguing result has been obtained which may have a bearing on our understanding of the anesthetic potency as well as of certain physicochemical properties of *n*-alcohols.

Outline of the work

The method used was infrared and near-infrared spectroscopy. The part of the spectrum due to the OH stretching vibrations was recorded for the *n*-alcohols from C_1 to C_{18} in carbon tetrachloride solutions. This was done at 23°C and then at 37°C, to approach physiological conditions and at 5°C where a larger proportion of the alcohol molecules is self-associated.

Subsequently we recorded the spectra of the alcohols using saturated hydrocarbons of different chain lengths as the solvent. This was done in order to explore the effect of solute–solvent interactions on the extent of self-association by H-bonding.

At the next stage binary mixtures of alcohols were studied. The alcohols were chosen in such a way that one of them had less than 10 and the other more than 10 carbons. As mentioned above (2–4), these should be antagonistic as to membrane disordering (fluidization) and the raising or lowering of the temperature of the membrane phase transition.

Finally spectra of mixtures of alcohols and carboxylic esters of different chain lengths were recorded. Esters contain a carbonyl group which, as a proton acceptor, is similar to those that alcohols might encounter if they enter the cell membrane.

Analogous measurements have been carried out in the near-infrared on ν(OH) overtones.

Experimental

Alcohols were purchased from the Aldrich Chemical Company or the Sigma Chemical Company and were 99% pure or better. They were further purified by distillation. The alkanes, from the Sigma Chemical Co. were passed through a silica gel column dried over magnesium sulfate and distilled under dry nitrogen atmosphere. The esters and *N,N*-diethylpalmitamide were Eastman products and were used without further purification.

Spectrograde carbon tetrachloride was supplied by A & C American Chemicals. Tetrachloroethylene (Eastman) was distilled under vacuum in order to eliminate traces of phosgene, and was protected from light.

The purity of the compounds was checked by recording their uv spectra or by gas phase chromatography. All samples were kept in a dry box under nitrogen atmosphere. Solutions were prepared gravimetrically and the spectra were recorded immediately afterwards.

The infrared spectra were recorded with a Perkin-Elmer model 621 instrument, using cells of 0.320 and 0.577 mm with silver chloride windows. The overtones were recorded on a Cary-17 instrument using silica cells of 1.07 and 3.00 cm. Resolution was about 2 cm^{-1} for both instruments.

Temperature was made constant by using a MGW Lauda-Thermostat. For maintaining 5°C a mechanical pump immersed in melting ice was used. Temperatures were measured by a copper–constantan thermocouple.

The spectrum of the solvent was recorded in the same cell and at the same temperature as the spectrum of the solution and was subtracted from the latter. The apparent molar absorption coefficients were computed by using the total alcohol concentration since the concentrations of the various monomer, dimer, . . . species cannot be determined with precision.

The calibration of the cells was regularly checked against benzene bands: 1960 cm^{-1} for cells whose optical path was less than 0.1 mm; for thicker cells the 845 cm^{-1} band was used.

Results and discussion

The ν(OH) bands in the solution spectra of alcohols have been the object of numerous investigations (refs. 15, 16, see ref. 17 for an early review). The "free" (non-hydrogen bonded) OH group has its band at about 3640 cm^{-1}, in methanol about 5–10 cm^{-1} higher. At higher concentration a band at about 3485 cm^{-1} belongs to the (linear) dimer. When the concentration is further increased the broad and intense "polymer" band appears, centered at about 3350 cm^{-1}, due to the internal OH groups which are both proton donors and proton acceptors. The end OH groups of dimers and polymers contribute to the apparent intensity of the free band. The dimer is well defined in a narrow concentration range only, since at higher concentration it is overlapped and covered by the broad and intense polymer band.

The relative intensities of the related overtones are very different. While in the fundamental region the polymer band is much more intense than the free band, in the overtone region the opposite usually holds (18–20). The reasons for this were the object of previous studies (21). (In H-bonded species mechanic and electric anharmonicities can make contributions of opposite sign to the intensity of the overtones.) In addition to the weakness of the overtones of H-bonded OH groups, we encounter another difficulty: this is the presence of strong ν(OH) + ν(CH) combination tones (22). Both CH and OH deuteration and low temperature measurements were needed in

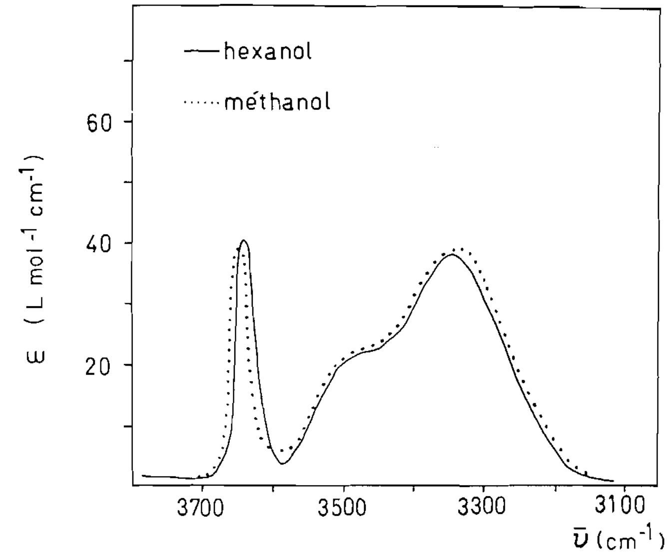

FIG. 1. The OH stretching region of the infrared spectra of methanol (dashed line) and *n*-hexanol (solid line) in 0.2 *M* carbon tetrachloride solutions.

order to assign the overtones for the H-bonded OH groups (20). For all these reasons only the free band was used in the work reported here. This free band is located near 7100 cm^{-1}. As the fundamental, it might receive contributions from the end OH groups of dimers and polymers.

Self-association of n-*alcohols* (C_1–C_{18})

Figure 1 shows the OH stretching region of the ir spectrum of a 0.20 *M* solution of *n*-hexanol in carbon tetrachloride. The monomer, dimer, and polymer bands are easily recognized at 3640, 3480, and 3345 cm^{-1}, respectively. The spectrum of methanol also given in Fig. 1 is slightly different. All the other *n*-alcohols from C_3 to C_{18} taken at 0.20 *M* concentration give spectra which are practically superimposable to that of *n*-hexanol. Thus, since both the free and polymer bands have evidently the same half-width from C_3 to C_{18}, the molar absorption coefficients may be considered proportional to the intensities. Table 1 lists the ϵ values for both bands for all the alcohols which were studied. Obviously, they are all equal within the limits of experimental error.

This result quite certainly does not constitute a basis for an explanation for the anesthetic "cutoff" observed. Nor does it make the changes in gel to liquid crystal transition temperature or the degree of fluidization that alcohols induce in the neuron membrane understandable.

This seems to indicate that the extent of H-bonding is not the fact underlying the variations of the anesthetic potency with chain length or of the membrane deforming effect of *n*-alcohols. The astonishing observation is that the extent of association by H-bond formation is independent of the number of carbon atoms in *n*-alcohols.

The spectra were also recorded at 37°C and at 5°C. The results are shown in Tables 2 and 3. While the values of the apparent molar absorption coefficients are, of course, different, from the point of view of the present discussion the result is the same: ϵ_A is independent of the number of carbons.

Only methanol and to a lesser extent, ethanol exhibits some slight differences; ϵ_A values of the free band are lower and those of the polymer band are higher than that of the alcohols C_3 to C_{18} indicating a somewhat higher degree of association (Table 1).

TABLE 1. Absorbances and apparent molar absorption coefficient (ϵ_A) of free (3640 cm^{-1}) and associated (3345 cm^{-1}) OH stretching vibrations of *n*-alcohols (0.2 *M* in CCl_4 at 23°C)

n-Alcohols	Absorbance of the free band (±0.01)	Absorbance of the polymer band (±0.01)	ϵ_A of the free band (±2.7)	ϵ_A of the polymer band (±2.7)
C_1	0.289	0.290	39.0	39.2
C_2	0.278	0.288	37.6	38.9
C_3	0.300	0.278	40.5	37.4
C_4	0.298	0.280	40.3	37.8
C_5	0.302	0.279	40.8	37.7
C_6	0.298	0.281	40.1	38.0
C_7	0.298	0.281	40.2	38.0
C_8	0.302	0.278	40.9	37.6
C_9	0.302	0.279	40.6	37.9
C_{10}	0.302	0.281	40.5	38.0
C_{11}	0.300	0.280	41.0	37.8
C_{12}	0.300	0.278	40.5	37.5
C_{13}	0.301	0.279	40.4	37.7
C_{14}	0.298	0.281	40.3	38.0
C_{16}	0.299	0.281	40.4	38.1
C_{18}	0.301	0.281	40.7	38.0
Mean value of ϵ_A for *n*-alcohols C_3 to C_{18}			40.5	37.8

TABLE 2. Apparent molar absorption coefficients (ϵ_A) of the free (3640 cm^{-1}) and associated (3485 and 3370 cm^{-1}) OH stretching vibrations of *n*-alcohols (0.2 *M* in CCl_4 at 37°C)

n-Alcohols	ϵ_A of the free band (±2.7)	ϵ_A of the dimer band (±2.6)	ϵ_A of the polymer band (±2.7)
C_4	44.9	16.8	18.6
C_6	44.6	16.7	18.8
C_7	44.5	16.6	19.0
C_8	44.6	17.0	18.7
C_{10}	44.4	16.9	18.6
C_{11}	44.7	16.5	19.1
C_{12}	44.5	17.1	18.5
C_{14}	45.0	17.0	18.8
C_{16}	44.5	16.6	18.9
Mean value of ϵ_A	44.6	16.8	18.8

TABLE 3. Apparent molar absorption coefficients (ϵ_A) of the free (3635 cm^{-1}) and associated (3325 cm^{-1}) OH stretching vibrations of *n*-alcohols (0.2 *M* in CCl_4 at 5°C)

n-Alcohols	ϵ_A of the free band (±2.0)	ϵ_A of the polymer band (±2.0)
C_1	31.6	70.3
C_2	28.9	70.2
C_3	33.8	70.2
C_4	33.9	70.2
C_5	34.0	70.0
C_6	34.0	70.3
C_7	33.7	70.1
C_8	33.6	70.4
C_9	33.9	70.2
C_{10}	34.1	70.0
C_{11}	33.8	70.4
C_{12}	33.9	70.3
C_{13}	33.9	70.5
C_{14}	33.7	70.2
C_{16}	33.9	70.2
C_{18}	34.0	70.1
Mean value of ϵ_A for *n*-alcohols C_3 to C_{18}	33.9	70.2

n-*Alcohols in* n-*alkanes of different chain length*

The question to which we sought an answer is as follows: is the extent of H-bond association of alcohols influenced by van der Waals interactions between the alkane solvent and the alcohols? For providing an answer the OH stretching region has been recorded for 0.2 *M* solutions of the alcohols C_4, C_6, C_8, C_{10}, C_{12}, and C_{13} in *n*-hexanol, *n*-dodecane, and *n*-tetradecane. Table 4 shows the results.

It is of interest to note that the mean molar absorption coefficient of the free band is 17.8 in *n*-heptane while it is 40.5 in CCl_4. As to the polymer band the corresponding values are $\epsilon_A = 68.7$ for *n*-heptane and 37.8 for CCl_4. This demonstrates the known fact (23–26) that in Cl-containing solvents the degree of H-bond self-association of alcohols is less than in hydrocarbon solvents.

A glance at Table 4 shows that the degree of H-bond self-association is independent of both the length of the chain of the *n*-alkane used as a solvent and the length of the chain in the alcohol.

Thus while halogenated solvents do interfere with H-bond formation, the latter appears to be independent of the length of the hydrocarbon chain.

Mixtures of "antagonistic" alcohols

If short chain alcohols (C_1 to C_9) on the one hand and alcohols having longer chains (C_{11} to C_{14}) on the other exert opposite influence on the physicochemical properties of lipid bilayers, it is logical to expect that binary mixtures of alcohols, one chosen from C_1–C_9 and the other from C_{11}–C_{14} will behave as antagonists as to their anesthetic action. Richards *et al.* found, however, that the effect in any of the pairs studied is

TABLE 4. Apparent molar absorption coefficients (ϵ_A) of the free (3640 cm^{-1}) and associated (3330 cm^{-1}) OH stretching vibrations of *n*-alcohols dissolved in different *n*-alkanes (0.2 *M* at 23°C)

n-Alcohols/ *n*-alcanes	ϵ_A of the free band (±3.2)	ϵ_A of the polymer band (±3.1)
C_4/C_7	17.8	68.6
C_{12}	17.7	68.9
C_{14}	17.6	68.5
C_6/C_7	17.7	68.7
C_{12}	17.8	68.6
C_{14}	17.8	68.6
C_8/C_7	18.0	68.9
C_{12}	17.7	68.5
C_{14}	17.7	68.7
C_{10}/C_7	17.9	68.7
C_{12}	17.8	68.7
C_{14}	18.0	68.8
C_{12}/C_7	17.6	68.6
C_{12}	17.9	68.6
C_{14}	17.9	68.7
C_{13}/C_7	17.7	68.6
C_{12}	17.9	68.7
C_{14}	17.8	68.7
Mean value of ϵ_A	17.8	68.7

TABLE 5. Apparent absorption coefficients (ϵ_A) of the free (3640 cm^{-1}) and associated (3345 cm^{-1}) OH stretching vibrations of binary mixtures of "antagonistic" *n*-alcohols (0.1 *M* for each component in CCl_4 at 23°C)

Binary mixtures of *n*-alcohols	ϵ_A of the free band (±2.6)	ϵ_A of the polymer band (±2.5)
$C_6 + C_{11}$	40.5	38.0
$C_7 + C_{11}$	40.6	37.6
$C_6 + C_{12}$	40.3	38.1
$C_8 + C_{12}$	40.6	37.9
$C_6 + C_{13}$	40.9	37.9
$C_8 + C_{14}$	40.7	37.8
Mean value of ϵ_A	40.6	37.9

additive, not antagonistic (2–4). In an attempt to ascertain whether or not there exists a parallel trend in the free/associated intensity ratio in the ir spectra we recorded (at 23°C) the OH stretching region for a number of such pairs in CCl_4 solutions, each of the components having a concentration of 0.1 *M*. The result obtained is that the intensities are perfectly additive. No indication has been found for antagonism. The results shown in Table 5 are practically the same as found for solutions containing a single alcohol at 0.2 *M* concentration (Table 1).

Mixtures of alcohols and esters or amides

Alcohols entering the lipid bilayer might form H-bonds of the O—H···:C=O type with the carbonyl groups of the lipids. In order to study this possibility (ref. 27 and references therein), we have examined the spectra of the ethyl esters of myristic, lauric, capric, and caprylic acids. The solutions contained 1.0 *M* of one of these esters and 0.2 *M* of an *n*-alcohol in CCl_4. Under these conditions the self-association of the alcohols diminishes considerably. Figure 2 gives as an example the spectrum of a solution containing *n*-heptanol and ethyl myristate. The polymer band at 3345 cm^{-1} has almost entirely disappeared. The free OH band has lost nearly half of its intensity. Instead, a new band appears at 3545 cm^{-1} which has been previously assigned to the OH stretching motion in the O—H···:O=C hydrogen bond (27). Its relatively high frequency indicates a weak H-bond. (The band at 3455 cm^{-1} is the first overtone of the carbonyl band whose fundamental is at 1735 cm^{-1}.)

All alcohols from C_3 to C_{18} behave in the same way, the spectra which we obtained are superimposable. This shows that at the same concentration the length of the chain has no appreciable influence on the degree of alcohol–ester H-bond formation. This is the same result as what has been obtained for alcohol–alcohol association.

Similar results have been obtained for amide–alcohol association. Only one example is given: that of *N*,*N*-diethylpalmitamide. Certain lipids, like sphingomyelin contain an amide group instead of an ester group. The H-bond is of the same type: O—H···:O=C. The length of the chain in the alcohols had no apparent influence on the OH stretching bands. Only methanol and ethanol exhibited slight differences with respect to the others (cf. Lesikar (28)).

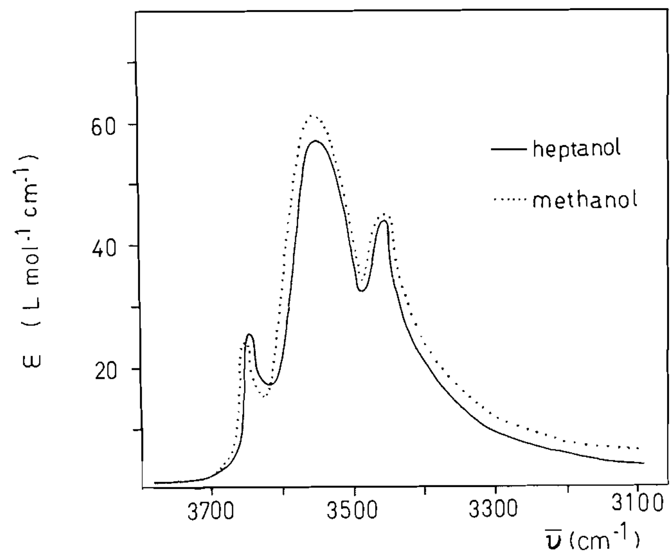

FIG. 2. The OH stretching region of the infrared spectra of a mixture of methanol (0.2 *M*) or *n*-heptanol (0.2 *M*) and ethyl myristate (1.0 *M*) in CCl_4 solution at 23°C.

In order to increase the chances of association the series of alcohol–ester spectra were also recorded at 5°C. Since at this temperature the free OH band disappears completely for 1.0 *M* solutions, the concentration of the esters was decreased to 0.5 *M* while that of the alcohols was kept at 0.2 *M*. Under the circumstances the O—H···:O=C band is found at 3520 instead of 3545 cm^{-1}. (The carbonyl overtone is at 3445 cm^{-1}.) The free OH band shifts from 3640 to 3635 cm^{-1}, the polymer band from 3345 to 3325 cm^{-1}. Typical examples are shown in Tables 6, 7, and 8 for esters at 23°C and at 5°C and for amides at 23°C, respectively. They exhibit no dependence on the length of the chain in the alcohols. The same applies to the chain length in the esters. Again methanol and ethanol exhibit slight differences with respect to the other alcohols.

Overtone studies

The first overtone of the free OH stretching vibration ($\nu = 0 \rightarrow \nu = 2$) of *n*-alcohols gives a well-defined band near 7100

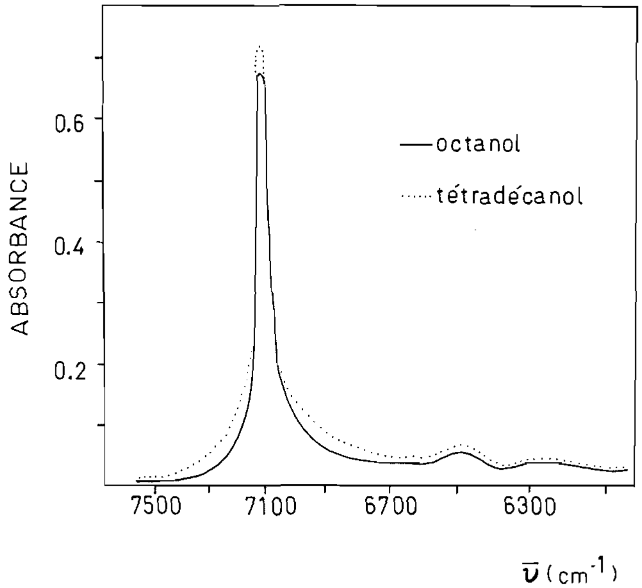

FIG. 3. The first overtone of the free OH stretching vibration of n-octanol and n-tetradecanol (0.2 M in tetrachloroethylene at 23°C).

TABLE 6. Apparent molar absorption coefficients (ϵ_A) of the free OH stretching vibration (3640 cm^{-1}) and the OH...O=C association band for mixtures of n-alcohols (0.2 M) and ethyl laurate (1.0 M) in CCl_4 at 23°C

n-Alcohols	ϵ_A of the free band (±2.0)	ϵ_A of the O—H...O=C band (±2.1)
C_1	23.7	61.0
C_2	23.0	60.8
C_3	24.4	56.7
C_4	24.0	56.8
C_5	24.6	56.7
C_6	24.3	56.9
C_7	24.2	56.8
C_8	24.4	56.7
C_9	24.5	56.5
C_{10}	24.1	56.9
C_{11}	24.4	56.8
C_{12}	24.7	56.6
C_{13}	24.4	57.0
C_{14}	24.4	56.9
C_{16}	24.3	56.8
C_{18}	24.5	56.9
Mean value of ϵ_A for n-alcohols C_3 to C_{18}	24.4	56.8

cm^{-1}. An example is given in Fig. 3. The first overtone of the associated OH stretching vibration is very weak, broad, and ill-defined. In the present work only the first overtone of the free OH band has been used.

First, the OH overtones of 0.2 M solutions in tetrachloroethylene were recorded for the whole series. Unfortunately, the coincidence of the free OH overtone band with a CH_2 combination band introduces an additional source of error. (This band contains two quanta of a CH_2 stretching vibration and one quantum of the CH_2 scissoring vibration.) In the related n-alkanes the intensity of this CH_2 combination increases linearly with the number of CH_2 groups. Actually, when we subtracted

TABLE 7. Apparent molar absorption coefficients (ϵ_A) of the free (3635 cm^{-1}) and associated (3325 cm^{-1}) OH stretching vibration and of the OH...O=C association band for mixtures of n-alcohols (0.2 M) and ethyl laurate (0.5 M) in CCl_4 at 5°C

n-Alcohols	ϵ_A of the free band (±2.0)	ϵ_A of the O—H...O=C band (±2.0)	ϵ_A of the polymer band (±2.0)
C_1	21.4	57.2	41.2
C_2	19.8	52.1	44.1
C_3	23.5	52.1	44.2
C_5	23.6	52.4	44.5
C_7	23.3	52.0	44.1
C_9	23.5	52.1	44.0
C_{11}	23.5	52.5	44.3
C_{12}	23.7	52.6	44.1
C_{13}	23.5	52.0	44.4
C_{14}	23.5	52.0	44.0
C_{16}	23.4	52.1	44.1
C_{18}	23.6	52.1	44.0
Mean value of ϵ_A for n-alcohols C_3 to C_{18}	23.5	52.2	44.2

TABLE 8. Apparent molar absorption coefficients (ϵ_A) of the free (3640 cm^{-1}) OH stretching vibration and of the OH...O=C association band for mixtures of n-alcohols (0.2 M) and N,N-diethylpalmitamide (1.0 M) in CCl_4 at 23°C

n-Alcohols	ϵ_A of the free band (±2.0)	ϵ_A of the O—H...O=C band (±2.1)
C_1	23.7	61.0
C_2	23.1	60.8
C_3	24.4	56.8
C_4	24.6	56.7
C_5	24.2	56.9
C_6	24.2	56.7
C_7	24.5	56.7
C_8	24.4	56.9
C_9	24.4	56.8
C_{10}	24.2	56.5
C_{11}	24.8	56.8
C_{12}	24.6	56.7
C_{13}	24.3	56.9
C_{14}	24.5	56.8
C_{16}	24.5	56.9
C_{18}	24.4	56.9
Mean value of ϵ_A for n-alcohols C_3 to C_{18}	24.4	56.8

from the alcohol spectrum that of the respective alkane we found again that the intensity of the OH band is independent of the number of CH_2 groups in the alcohols. While this corroborates the results yielded by the fundamentals at the same concentration, this procedure is, for the above mentioned reason, less accurate. Therefore we renounce giving the numerical data.

The intrinsic intensity of the free band

The following objection could be made to the above interpretation of our results: it is conceivable that the intrinsic intensity of the free band decreases gradually with increasing chain length while that of the polymer band increases propor-

TABLE 9. Integrated band areas for the free OH band of 0.04 *M* solutions of *n*-alcohols in carbon tetrachloride

Alcohol	Band areas (cm^{-2} L mol^{-1})	Relative band areas with respect to	
		C_1	C_4
C_1	712±35	1.00±0.10	0.90±0.09
C_2	720±55	1.01±0.12	0.91±0.12
C_4	795±45	1.12±0.12	1.00±0.11
C_8	813±55	1.14±0.12	1.00±0.13
C_{10}	885±55	1.24±0.12	1.11±0.13
C_{12}	859±40	1.20±0.11	1.07±0.11
C_{13}	835±35	1.17±0.11	1.05±0.12
C_{14}	763±20	1.07±0.08	0.96±0.08
C_{15}	755±35	1.06±0.11	0.95±0.12

tionately and that these trends are compensated for by a parallel decrease in the H-bonded/free ratio as the chain length increases. (The opposite situation would also be conceivable.) In order to test this possibility, the integrated intensities of very dilute (0.04 *M*) solutions of ten of our alcohols were determined.

The solvent, carbon tetrachloride, was dried on anhydrous magnesium sulfate until complete disappearance of the infrared water bands. Two solutions were prepared for each alcohol and the spectrum was recorded several times between 3700 and 3200 cm^{-1}. The band areas, between 3660 and 3612 cm^{-1}, were determined with a polar compensation planimeter (model KP-27, Koizumi, Japan) calibrated with a rectangle of known surface area, close to that of the bands. The integration was carried out six times for each curve and the average of the results was taken. In view of the great similarity of all the bands, slit or wing corrections were not applied; the integration was extended from 3660 and 3612 cm^{-1} in all cases.

The results are given in Table 9. Clearly, the differences that are observed are within the limits of experimental error. If experimental error is disregarded, a trend appears whereby the intensity of the free band increases gradually until C_{10}, then it decreases until C_{17}. We cannot attach to this any significance at this stage although many years ago Mullins (29) found a similar trend in the activity coefficients. The cutoff at C_{14} certainly cannot be explained by these results.

Conclusions

We now have to answer the question: can the degree of H-bonding of alcohols be related to their anesthetic potency? The answer is clearly no in as much as self-association is concerned in either carbon tetrachloride or in paraffins of different lengths; the same applies to H-bonds between alcohols and esters or amides. An important observation can be made, however, the degree of association by H-bond formation in dissolved alcohols appears to be independent of the extent of other van der Waals or hydrophobic interactions that might exist in these solutions. The OH group does not seem to be the active factor in the anesthetic action of alcohols and one can speculate that their strong tendency for H-bond formation probably makes it difficult for them to reach the ion channels.

Neither hydrophilic, nor hydrophobic interactions seem to explain the curious dependence of the anesthetic potency of alcohols on their chain length. They are not so favorable a test case for the theories of anesthesia as they might appear to be at first sight.

Acknowledgements

Financial help from the Natural Sciences and Engineering Research Council of Canada and the Ministère de l'Éducation du Québec and from the Conselho Nacional de Desenvolvimento Cientifico e Tecnologico (CNPq), Brasil, is gratefully acknowledged. Our thanks are due to Professor D. D. Patterson of McGill University and to Dr. P. Menassa and Dr. M. Costas for helpful discussions.

1. J. POSTERNAK and E. ARNOLD. J. Physiol. **46**, 502 (1954).
2. T. R. HESKETH, C. A. KEIGHTLEY, J. L. METCALFE, and C. D. RICHARDS. J. Physiol. **278**, 5P (1978).
3. J. C. METCALFE and C. D. RICHARDS. J. Physiol. **278**, 35P (1978).
4. C. D. RICHARDS, C. A. KEIGHTLEY, T. R. HESKETH, and J. C. METCALFE. *In* Molecular mechanisms of anesthesia. Vol. 2. *Edited by* B. Raymond Fink. Raven Press, New York. 1980. p. 337.
5. M. J. PRINGLE, K. B. BROWN, and K. W. MILLER. Mol. Pharmacol. **19**, 49 (1981).
6. J. J. HALSEY. *In* Anesthetic uptake and action. *Edited by* E. I. Eger. Williams and Wilkins, Baltimore. 1974. p. 45.
7. J. C. MILLER and K. W. MILLER. *In* MTP international review of science: biochemistry. Series One. Vol. 12. *Edited by* H. K. F. Blaschko. Butterworth, London. 1975. p. 33.
8. R. D. KAUFMAN. Anesthesiology, **46**, 49 (1977).
9. G. TRUDEAU, J. M. DUMAS, P. DUPUIS, M. GUÉRIN, and C. SANDORFY. Top. Curr. Chem. **93**, 91 (1980).
10. C. SANDORFY. Anesthesiology, **48**, 357 (1978).
11. G. TRUDEAU, K. C. COLE, R. MASSUDA, and C. SANDORFY. Can. J. Chem. **56**, 1681 (1978).
12. C. SANDORFY. *In* Molecular mechanism of anesthesia. Vol. 2. *Edited by* B. Raymond Fink. Raven Press, New York. 1980. p. 337.
13. D. W. URRY, K. U. PRASAD, and T. L. TRAPANE. Proc. Natl. Acad. Sci. U.S.A. **79**, 390 (1982).
14. D. K. LAWRENCE and E. W. GILL. Mol. Pharmacol. **11**, 595 (1975).
15. F. A. SMITH and E. C. CREITZ. J. Res. Natl. Bur. Stand. **46**, 154 (1951).
16. R. N. JONES. Can. J. Chem. **40**, 321 (1962).
17. R. N. JONES and C. SANDORFY. *In* Chemical applications of spectroscopy. Technique of organic chemistry. Vol. 9. *Edited by* A. Weissberger and W. West. Interscience, New York. 1956.
18. W. A. P. LUCK and W. DITTER. J. Mol. Struct. **1**, 261 (1967–1968); **1**, 339 (1967–1968).
19. A. BURNEAU and J. CORSET. J. Chim. Phys. **69**, 171 (1972).
20. C. BOURDÉRON and C. SANDORFY. J. Chem. Phys. **59**, 2527 (1973).
21. T. DI PAOLO, C. BOURDÉRON, and C. SANDORFY. Can. J. Chem. **50**, 3161 (1972).
22. W. A. P. LUCK and W. DITTER. Ber. Bunsenges. Phys. Chem. **72**, 365 (1978).
23. W. KLEMPERER, M. W. CRONYN, A. H. MAKI, and G. C. PIMENTEL. J. Am. Chem. Soc. **76**, 5846 (1954).
24. K. B. WHETSEL. Spectrochim. Acta, **17**, 614 (1961).
25. M. GOMEL. Ann. Chim. **3**, 415 (1968).
26. M. C. BERNARD-HOUPLAIN and C. SANDORFY. J. Chem. Phys. **56**, 3412 (1972).
27. P. MERCIER, C. SANDORFY, and D. VOCELLE. J. Phys. Chem. **87**, 3670 (1983).
28. A. V. LESIKAR. J. Chem. Phys. **63**, 2297 (1975); **66**, 4263 (1977).
29. L. J. MULLINS. Chem. Rev. **54**, 289 (1954).

Complexation du cuivre(II) par les phénylsérines *thréo* et *érythro*: étude thermodynamique

PATRICK SHARROCK

Département de chimie, Faculté des sciences, Université de Sherbrooke, Sherbrooke (Qué.), Canada J1K 2R1

Reçu le 24 avril 1984

PATRICK SHARROCK. Can. J. Chem. **63**, 46 (1985).

Les complexes cuivriques de la phénylsérine *thréo* et *érythro* ont été étudiés en solution par conductimétrie et potentiométrie. Les constantes de formation de complexes ont été obtenues en fonction de la température. La déprotonation en milieu basique du groupement OH des acides aminés β-hydroxylés est favorisée par la présence de l'ion métallique. La phénylsérine *thréo* a donné à 298 K les constantes de formation suivantes: Cu(L), K_1 = 7,99; Cu(L)$_2$, K_2 = 6,71; Cu(L$_2$H$_{-1}$), K_3 = −9,51; Cu(L$_2$H$_{-2}$), K_4 = −10,83. Les constantes correspondantes pour l'isomère *érythro* sont: K_1 = 7,70; K_2 = 6,70; K_3 = −9,82 et K_4 = −11,20. Les paramètres thermodynamiques pour la formation des complexes successifs Cu(L) et Cu(L)$_2$ sont: $-\Delta H$ = 21,3 et 44,7 kJ mol^{-1}; ΔS = 82 et 132 J K^{-1} mol^{-1}, respectivement, pour la forme *thréo* ainsi que $-\Delta H$ = 20,7 et 44,1; ΔS = 79 et 129 pour la forme *érythro*. Une enthalpie additionnelle de −21 kJ mol^{-1} correspond à la déprotonation des complexes. Ces résultats et les structures des complexes sont commentés.

PATRICK SHARROCK. Can. J. Chem. **63**, 46 (1985).

Conductimetric and potentiometric measurements in aqueous solution as a function of temperature show that cupric ions promote the deprotonation of the hydroxy side chain of *threo* and *erythro* β-phenylserines. The *threo* ligand yields at 298 K the formation constants: Cu(L), K_1 = 7.99; Cu(L)$_2$, K_2 = 6.71; Cu(L$_2$H$_{-1}$), K_3 = −9.51; Cu(L$_2$H$_{-2}$), K_4 = −10.83. The *erythro* isomer yields the corresponding constants: K_1 = 7.70, K_2 = 6.70, K_3 = −9.82, and K_4 = −11.20. Thermodynamic parameters for the first two complexation steps are $-\Delta H$ = 21.3 and 44.7 kJ mol^{-1}; ΔS = 82 and 132 J K^{-1} mol^{-1}, respectively, for the *threo* form and $-\Delta H$ = 20.7 and 44.1, ΔS = 79 and 129 for the *erythro* form. Deprotonation of the complexes corresponds to an additional enthalpy of −21 kJ mol^{-1}. These results and the structures of the complexes are discussed.

Introduction

La première synthèse de la phénylsérine fut décrite par Erlenmeyer en 1892 (1). La phénylsérine reste un acide aminé rare et a été peu étudiée en présence d'ions métalliques mis à part quelques travaux sur ses bases de Schiff utilisées comme modèles enzymatiques (2). Une étude rapporte la formation de complexes cuivriques avec la phénylsérine (3) mais comme il existe deux isomères de la phénylsérine, à savoir les formes *thréo* et *érythro*, il nous a paru utile de clarifier l'étude des complexes des phénylsérines pures, ce qui n'a encore jamais été fait. Shaw et Fox réussirent à séparer les deux isomères dès 1953 (4) et la *thréo* phénylsérine (L) fut reliée via une décarboxylation enzymatique à la (−) artérénol (5). Le chloramphénicol est un bactéricide dont la structure est reliée à celle de la phénylsérine, ce qui laisse présager des propriétés biologiques intéressantes pour cet acide aminé. Nous avons déjà décrit une synthèse de la *thréo* phénylsérine via une condensation catalysée par les ions cuivriques (6), synthèse qui passe par l'intermédiaire d'une isoxazolidine complexée aux ions cuivriques. Nous rapportons maintenant l'étude physicochimique en solution aqueuse de l'interaction des phénylsérines *thréo* et *érythro* avec les ions cuivriques.

Partie expérimentale

Synthèse

L'acide 2-amino, 3-hydroxy, 3-phénylpropanoïque, soit la phénylsérine, a été synthétisée par la méthode de Shaw et Fox (4) avec un rendement de 70%. La forme *érythro* a été obtenue avec une modification du protocole comme suit. Dans 150 mL d'eau on dissout 30 g de glycine et 24 g de NaOH. On ajoute 82 mL de benzaldéhyde et on refroidit la solution à 8°C. Un précipité se forme après 4 min et après 10 min, on laisse la température monter jusqu'à 20°C juste assez longtemps pour que tout le mélange se liquéfie. On refroidit de nouveau entre 8 et 10°C tout en agitant pendant 4 h. On acidifie lentement avec HCl glacé en mélangeant régulièrement. Les grosses boules de produit coagulé sont lavées avec 250 mL EtOH 95% froid, suivi d'éthanol absolu bouillant. À ce stade on a de la phénylsérine brute dont le rapport *thréo*/*érythro* (déterminé par rmn et chromatographie) est d'environ 1. L'isomère *thréo* recristallise dans 400 mL d'eau bouillante alors qu'après concentration et addition de 400 mL de dioxane–eau 50% on obtient l'isomère *érythro* avec un rendement de 47%.

Nous avons également obtenu les hydrochlorures des esters éthyliques des isomères *thréo* et *érythro* avec des rendements respectifs de 98 et 83% en partant des acides aminés hydratés, par la méthode de Fisher. Ces hydrochlorures d'ester sont intéressants car ils ne sont pas hydroscopiques et redonnent les acides aminés de départ par simple hydrolyse. L'hydrochlorure d'ester *thréo* est très soluble dans l'éthanol, tandis que celui de la forme *érythro* ne l'est pratiquement pas, ce qui permet de confirmer la séparation des deux isomères. Nous n'avons pas réussi à séparer les deux isomères de cette façon car la forme *érythro* devient soluble en présence de la forme *thréo*.

Mesures physiques

Les mesures de conductivité ont été effectuées avec une électrode CMO5g de Tacussel et un conductimètre de type CD6N de Solea (Lyon). Les surfaces de 5 mm^2 et distantes de 5 mm étaient fraîchement réactivées et calibrées avec du KCl 0,10 *M*.

Pour les mesures potentiométriques, nous avons préparé une solution NaOH ≈ 0,1 *M* dans de l'eau fraîchement distillée que nous avons conservé sous azote et standardisé avec KHP. L'acide nitrique utilisé pour abaisser le pH entre 2,2 et 2,5 avant les titrages a été titrée par la solution de NaOH. Les solutions d'acides aminés et de nitrate de cuivre ont été préparées immédiatement avant les titrages qui ont été effectués avec KNO_3 0,10 *M* comme électrolyte de support. Des rapports de ligand à métal de 1:1 à 2,5:1 ont été utilisés avec une concentration d'ions cuivriques de l'ordre de 0,01 *M*. La cellule de titrage thermostatée était munie d'un capuchon Metrohm par lequel passait des électrodes au calomel et de verre (Sargent Welch 150 MΩ) et une arrivée d'azote. Les lectures de pH effectuées avec un "Ionalyser Orion Research Model 801 Digital pH meter" étaient précises à ±0,002.

Nous avons délivré le titrant par l'intermédiaire d'un tube spécial en Teflon rigide provenant d'une seringue d'autoburette ABU 12 de Radiometer (Copenhagen). L'autoburette se lit au centième de millilitre et les résultats, enregistrés sur papier graphique avec un Fisher Recordall series 100, ont été accumulés entre 17 et 45°C par intervalle de 5°C en calibrant le pH-mètre à chaque température à pH 4 et pH 10. Les données en vue de l'affinement des constantes de formation ont été obtenus à partir des courbes de titrage avec un "Bendix datagrid digitizer" relié à un miniordinateur. Sur le coordinatographe, l'axe de pH était pris pour l'axe y et l'axe x était ajusté pour correspondre avec l'axe de volume. Les données x en fonction de y ont été prélevées par le coordinatographe avec des incréments mesurés le long des deux axes (mode $\Delta x + \Delta y$). Près des points équivalents, le mode Δx a été utilisé, ce qui diminue le nombre de points prélevés lors de grandes variations de pH. L'effet d'eventuelles erreurs analytiques est ainsi minimisé. Le programme SCØGS a été modifié afin que les matrices puissent accommoder jusqu'à 200 lectures par expérience. Nous avons utilisé un coefficient d'activité pour l'ion hydrogène de 0,78 et avons tenu compte de la variation avec la température de la valeur du produit ionique de l'eau.

Dans un premier temps les constantes K_1 et K_2 ont été affinées pour les ligands. Un graphique a été construit des logarithmes des constantes de dissociation en fonction de la température et les valeurs retenues comprenaient trois décimales et une erreur estimée à ±0,005. Dans un deuxième temps, ces constantes ont été utilisées en conjonction avec les estimés provenant de la méthode graphique de la fonction de formation ($\bar{n}$ α log A^-), pour affiner les valeurs des constantes de formation de complexes. Les deux premières constantes de formation ont été obtenues en éliminant les données à pH ≥ 10. Les données à pH basique ont été réintroduites en même temps que deux estimés pour les constantes de déprotonation des complexes. Ces deux dernières constantes ont été affinées indépendemment des quatre autres impliquées.

Les valeurs de ΔH et ΔS, ajustées par moindres carrés, ont été obtenues d'après la pente et l'intercept des graphiques de log K vs. $1/T$. Les courbes de distribution des espèces ont été dessinées d'après les résultats du programme SCØGS.

Résultats

Les courbes de titrages conductimétriques permettent généralement de mettre en évidence la formation successive de complexes 1:1 et 2:1. Cependant des titrages d'ions cuivriques par des solutions d'acide aminé de divers pH n'ont pas donné de bons résultats. Nous avons donc procédé au titrage conductimétrique de solutions contenant des rapports stoichiométriques ligand/métal de 2:1 par de la soude de titre connu. Ainsi, après correction pour les conductivités équivalentes des ions sodium ajoutés et correction pour les conductivités des ions H^+ et OH^- effectuées après mesure du pH, nous avons observé une augmentation de la résistance avec augmentation du pH, suivi d'une diminution en milieu basique. Les courbes de titrage présentées dans la fig. 1 montrent des brisures dans la pente des droites pour des rapports stoichiométriques des ions Na^+/Cu^{2+} de 1, 2 et 4.

Les courbes de titrages potentiométriques sont typiques des courbes observées lors de titrages de complexes cuivriques. Nous remarquons cependant que dans le cas d'un rapport ligand/métal de 1, on observe la formation d'un précipité d'hydroxyde cuivrique qui provoque un plateau vers pH neutre correspondant à la disproportionation en complexe 2:1 et en $Cu(OH)_2$ insoluble. Il est intéressant de noter la dissolution du précipité, ce qui conduit progressivement à une solution limpide en milieu fortement basique. Même s'il est impossible de calculer une constante de formation de complexe dans ces conditions, les données indiquent la formation d'une espèce distincte en milieu basique. Nous avons retenu la formation des complexes CuA^+, CuA_2, $CuH_{-1}A_2^-$ et $CuH_{-2}A_2^{2-}$ où H_2A représente le ligand protoné aux fonctions carboxyliques et aminées. Quelques titrages en fonction de la dilution n'ont pas permis de détecter la formation de dimères du genre M_2A_4.

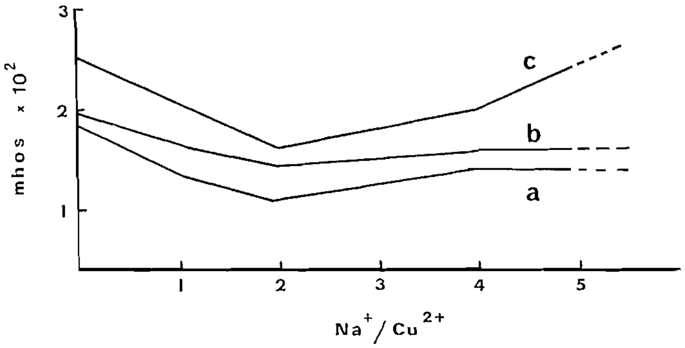

FIG. 1. Courbes de titrages conductimètriques pour les complexes cuivriques de la phénylsérine *thréo* (a) et *érythro* (b). La courbe (c) correspond au complexe de la sérine. Les concentrations de complexes sont ~0,01 *M*.

Les constantes de formation sont regroupées dans le tableau 1. On constate que les valeurs diminuent progressivement lorsque la température augmente et qu'elles sont légèrement plus petites pour la phénylsérine *érythro* que pour la forme *thréo*. Il est à noter que les constantes cumulatives log β_3 et log β_4 diminuent par rapport à log β_2. Ceci provient de la nature de log K_3 et log K_4 qui sont négatives car elles correspondent à des constantes de déprotonation des complexes.

Les courbes de distribution des espèces sont représentées à la fig. 2. La différence principale entre la complexation par l'isomère *thréo* et celle par l'isomère *érythro* réside dans le pH de formation des espèces déprotonées, celles-ci se formant plus facilement avec la *thréo* phénylsérine.

Les valeurs des paramètres thermodynamiques ΔG^0, ΔH^0 et ΔS^0 obtenues d'après la variation en fonction de la température des constantes d'équilibre paraissent dans le tableau 2. Dans ce tableau nous présentons aussi les enthalpies de formation des complexes CuA^+ et CuA_2 décomposées en termes électrostatiques et covalents d'après les équations [1] à [3]:

$$[1] \quad \Delta H_c = \Delta H - \Delta H_c$$

$$[2] \quad \Delta H_c = (T - \nu)(\Delta S + \Delta n\, R \ln 55.5)$$

$$[3] \quad \Delta G_c = -\nu(\Delta S + \Delta n\, R \ln 55.5)$$

ν est une constante obtenue à partir de la variation de la constante diélectrique du solvant en fonction de la température (ν = 219 K pour H_2O), Δn représente le changement dans le nombre de particules de soluté au cours de la réaction. De même ΔG_c, la contribution électrostatique à l'énergie libre qui

$$[4] \quad \Delta G = \Delta n\, RT \ln 55.5 + \Delta G_c + \Delta G_c$$

dépend de la température et ΔG_c, la contribution covalente invariable en fonction de la température sont données d'après [4]. Dans notre cas, la formule [5] permet de trouver la température T^0 ≥ 100°C et puisque nos réactions de formation de complexes sont exothermiques, log K diminue avec augmentation de la température et on s'attend à une importante

$$[5] \quad T^0 = \nu(1 + \Delta G_c/\Delta G^0_c)$$

contribution des forces covalentes. Nous remarquons dans le tableau 2 que les ΔH_c ne varient pas entre la formation du monochélate et du dichélate et sont caractéristiques des acides aminés utilisés. La variation observée dans ΔH pour les complexes successifs est donc attribuable à la variation dans ΔH_c. Pour préciser les résultats, nous avons corrigé la différence ΔG_r

TABLEAU 1. Constantes de formation des complexes cuivriques de la phénylsérine

Isomère *thréo*	Température (°C) 45	40	35	30,7	25	21,7	17,4
pK_1	8,550	8,630	8,710	8,782	8,870	8,926	8,995
pK_2	10,200	10,295	10,390	10,470	10,575	10,637	10,705
$\log K_1$	7,77	7,80	7,84	7,91	7,99	8,05	8,12
$\log K_2$	6,46	6,53	6,63	6,67	6,71	6,75	6,80
$\log \beta_2$	14,23	14,33	14,47	14,58	14,70	14,80	14,92
$-\log K_3$	9,28	9,34	9,42	9,44	9,51	9,57	9,62
$\log \beta_3$	4,95	4,99	5,05	5,14	5,19	5,23	5,30
$-\log K_4$	10,35	10,44	10,55	10,68	10,79	10,87	10,98
$-\log \beta_4$	5,40	5,45	5,50	5,54	5,60	5,64	5,68
Isomère *érythro*							
pK_1	8,365	8,450	8,530	8,605	8,700	8,760	8,827
pK_2	9,948	10,044	10,140	10,225	10,355	10,403	10,485
$\log K_1$	7,53	7,60	7,62	7,70	7,74	7,77	7,86
$\log K_2$	6,42	6,48	6,51	6,63	6,70	6,71	6,75
$\log \beta_2$	13,95	14,10	14,21	14,25	14,40	14,46	14,62
$-\log K_3$	9,48	9,59	9,68	9,67	9,78	9,78	9,86
$\log \beta_3$	4,47	4,51	4,53	4,58	4,62	4,68	4,76
$-\log K_4$	6,38	6,42	6,47	6,51	6,57	6,60	6,64
$-\log \beta_4$	10,85	10,93	11,00	11,09	11,19	11,28	1,140

TABLEAU 2. Paramètres thermodynamiques pour la formation des complexes cuivriques d'acides aminés β-hydroxylés

Réaction[a]	$-\Delta G^{0\,b}$	$-\Delta H^0$	ΔS^0	ΔH^0_e	$-\Delta H^0_c$
Cu^{2+} + TPS → $(CuTPS)^+$	45,8	21,2	82	9,1	30,4
$(CuTPS)^+$ + TPS → $CuTPS_2$	38,5	23,5	50	6,6	30,1
Cu^{2+} + 2TPS → $CuTPS_2$	84,2	44,7	132	15,7	60,5
Cu^{2+} + EPS → $(CuEPS)^+$	44,4	20,7	79	8,9	29,6
$(CuEPS)^+$ + EPS → $CuEPS_2$	38,3	23,4	50	6,6	30,0
Cu^{2+} + 2EPS → $CuEPS_2$	82,7	44,1	29	15,5	59,6
Cu^{2+} + SER → $(CuSER)^+$	44,8	23,0	73	8,4	31,4
$(CuSER)^+$ + SER → $CuSER_2$	37,9	25,6	41	5,9	31,5
Cu^{2+} + 2SER → $CuSER_2$	82,6	48,6	114	14,3	62,9
Cu^{2+} + PS → $(CuPS)^+$	44,2	20,9	78	8,8	29,7
$(CuPS)^+$ + PS → $CuPS_2$	36,1	22,9	45	6,1	29,1
Cu^{2+} + 2PS → $CuPS_2$	80,4	43,9	122	14,9	58,8

[a] TPS = thréophénylsérine, EPS = érythrophénylsérine. SER et PS sont sérine et phénylsérine de la réf. 15.
[b] Les unités sont: ΔG et ΔH en kJ mol^{-1} et ΔS en J K^{-1} mol^{-1}. Les erreurs sont estimées à ±0,2 kJ mol^{-1} et ±1 J K^{-1} mol^{-1}.

$= \Delta G_1 - \Delta G_2$ pour tenir compte de l'effet statistique pour la réaction [6]

$$[6] \quad Cu^{2+} + CuL_2 \overset{K_r}{\rightleftharpoons} 2\,Cu\,L^+$$

K_{stat} serait la valeur de K_r si la réaction procédait suivant une loi purement statistique. Les équations utilisées sont [7] à [10] et les résultats sont consignés au tableau 3, avec $K_{stat} = 4$.

$$[7] \quad \Delta G_r = -RT \ln K_{stat} + \Delta G_{r,c} + \Delta G_{r,c}$$

$$[8] \quad \Delta H_{r,c} = (T - \nu)(\Delta S_r - R \ln K_{stat})$$

$$[9] \quad \Delta H_{r,c} = \Delta G_{r,c} = \Delta H_r - \Delta H_{r,c}$$

$$[10] \quad \Delta S_{r,t} = \Delta S_r - \Delta S_{stat}$$

Discussion

Les complexes cuivriques des phénylsérines ont des conductivités équivalentes faibles, ce qui indique qu'ils sont faiblement dissociés, en accord avec les constantes de formation trouvées assez grandes. Les phénylsérines agissent comme la sérine (7) et différemment de la glycine qui ne montre aucune discontinuité dans la valeur de la conductivité en fonction de la quantité de base ajoutée après le rapport molaire Na^+/Cu^{2+} 2:1. Ceci indique que dans le cas des acides aminés β-hydroxylés, il s'opère un changement particulier quand deux moles de base ont été ajoutées par mole d'acide aminé. Ceci peut s'expliquer par un changement dans la dimension ou la mobilité des complexes, ou par la formation de complexes déprotonés ou hydroxylés. Dans la mesure où la formation de complexes hydroxylés n'est pas détectée dans le cas de la glycine et qu'elle devrait dépendre du pH et non de la quantité stoechiométrique de base ajoutée, on peut affirmer qu'il y a déprotonation des fonctions β-hydroxylées et formation de complexes cuivriques anioniques.

TABLEAU 3. Comparaison des complexes successifs

Ligand	log K_r	ΔG_r^c	ΔH_r	ΔS_r	$\Delta G_{r,t}$	$\Delta S_{r,t}$	$\Delta G_{r,e}$	$\Delta H_{r,e}$	$\Delta G_{r,e}$	$\Delta H_{r,e}$
Sérine[a]	1,20	−6,8	2,4	31	−3,4	20	−4,4	1,6	1,0	0,8
Sérine[b]	1,23	−7,2	2,5	32	−3,8	21	−4,6	1,6	0,8	0,8
PS[a]	1,42	−8,1	2,0	34	−4,6	22	−4,9	1,7	0,3	0,2
TPS	1,27	−7,3	2,3	32	−3,8	20	−4,5	1,6	0,7	0,7
EPS	1,04	−6,1	2,7	29	−2,6	18	−3,9	1,4	1,3	1,3
Glycine[b]	1,42	−8,1	2,5	33	−4,6	24	−5,3	1,9	0,7	0,6

[a] Valeurs calculées d'après les données de la réf. 15.
[b] Valeurs provenant de la réf. 19.
[c] Ces unités sont: ΔG et ΔH en kJ mol^{-1} et ΔS en J K^{-1} mol^{-1}.

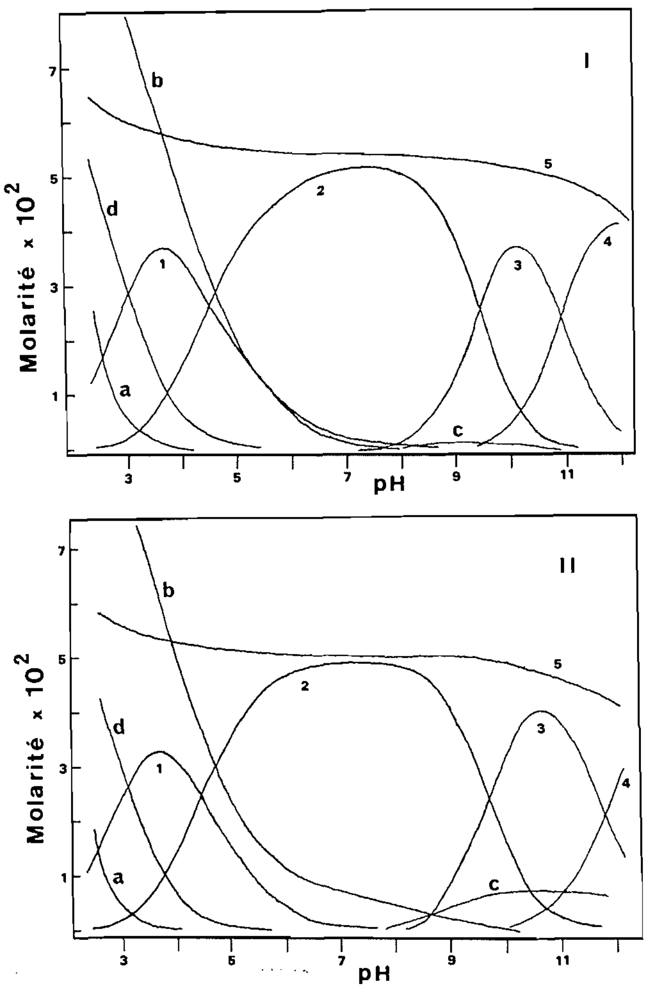

FIG. 2. Courbes de répartition des espèces en fonction du pH pour les complexes cuivriques de la phénylsérine *thréo* (I) et *érythro* (II). Les complexes sont 1: $[CuL]^+$; 2: CuL_2; 3: $[CuL_2H_{-1}]^-$ et 4: $[CuL_2H_{-2}]^{2-}$; 5: représente la concentration totale de cuivre et d, la concentration d'ions Cu^{2+} libres. a, b et c sont respectivement l'acide aminé protoné, le zwitterion et l'acide aminé déprotoné non complexés.

L'étude potentiométrique confirme la formation de plusieurs espèces. Les différences entre les titres calculés et observés sont minimisées avec le programme SØCGS en tenant compte des complexes CuA^+, CuA_2 et $CuH_{-1}\ A_2^-$ et $CuH_{-2}\ A_2^{2-}$. La détection de complexes déprotonés ou hydroxylés n'est pas nouvelle (7–10), ce phénomène ayant déjà été décrit pour la sérine et la thréonine. On ne s'attend pas à ce que des complexes hydroxylés soient solubles, ce qui favorise la conclusion qu'il s'agisse d'une déprotonation du ligand coordiné. Les ions cuivriques peuvent aussi déprotoner le carbone α dans des complexes analogues (11).

Pour les acides aminés, nous observons que les pK_1 et pK_2 sont plus petits pour la forme *érythro* (8,70 et 10,35) que pour la forme *thréo* (8,87 et 10,57) de la phénylsérine. Ceci est en accord avec les tendances générales observées et en particulier le cas de la thréonine et la allo-thréonine. L'ordre décroissant de pK_1 et pK_2 est sérine > thréonine > allo-thréonine > *thréo*-phénylsérine > *érythro*-phénylsérine. L'ordre de stabilité des complexes est Cu(thréonine)$^+$ > Cu(*thréo*-phénylserine)$^+$ > Cu(sérine)$^+$ > Cu(allo-thréonine)$^+$ > Cu(*érythro*-phénylsérine)$^+$; et aussi Cu(thréonine)$_2$ > Cu(*thréo*-phénylserine)$_2$ > Cu(sérine)$_2$ > Cu(*érythro*-phénylsérine)$_2$ > Cu(allo-thréonine)$_2$. Cet ordre n'est pas le même que l'ordre de basicité des ligands et on peut en déduire que les effets structuraux sont importants. En effet, par rapport aux complexes de la sérine (qui ne peut exister que sous une seule forme), les complexes avec les acides aminés substitués en position α sont plus stables lorsque la substitution donne une forme *thréo* et ils sont moins stables dans le cas d'une forme *érythro*. Ceci implique que la stabilité des complexes dépend non seulement de l'influence des groupes fonctionnels des ligands mais aussi de la géométrie globale des complexes résultants.

Des résultats thermodynamiques montrent que les paramètres ΔH et ΔS obtenus pour les complexes d'acides aminés hydroxylés sont semblables à ceux obtenus pour les acides aminés ordinaires. Raju et Mathur ont étudié les complexes de la sérine et de la thréonine avec une série de métaux de transition (12). Ils trouvèrent que les valeurs de ΔG et de ΔS étaient beaucoup plus grandes pour le cuivre qui formait des complexes plus stables. Par ailleurs, ils trouvèrent que c'était dans le cas du cuivre qu'il y avait la plus petite différence entre les valeurs observées pour la sérine et la α-alanine d'une part, et la thréonine et l'acide α-aminobutyrique d'autre part. Ils conclurent de ces observations que les complexes du cuivre étaient stabilisés par le champ cristallin et que le groupement OH n'entrait pas dans la première sphère de coordination. La comparaison de leurs résultats avec ceux de Stack et Skinner (13) révéla une différence anormalement large dans les valeurs de ΔH et ΔS pour la formation de Cu(sérine)$_2$. Ils trouvaient 40,1 kJ mol^{-1} et 142 J K^{-1} mol^{-1} alors que Stack et Skinner donnaient 58,9 kJ mol^{-1} et 79 J K^{-1} mol^{-1}, respectivement. Ils expliquèrent alors la différence comme étant attribuable aux conditions expérimentales. En effet, Stack et Skinner avaient utilisé un assez considérable excès d'acide aminé et avaient supposé la formation d'un complexe du cuivre avec plus de deux acides aminés. Ils avaient par conséquent appliqué une correction pour obtenir une valeur de ΔH correspondant exclusivement à la formation de CuA_2.

Thornton et Skinner étudièrent de nouveau les mêmes complexes (14) dans une série de mesures plus détaillées et se rendirent compte alors qu'il y avait un changement brusque dans ΔH dès que le pH dépassait 10. $-\Delta H$ était de l'ordre de 54 kJ mol^{-1} pour la formation de Cu(sérine)$_2$ et de Cu(thréonine)$_2$ à pH $\leq$ 10, ce qui se compare bien avec les valeurs pour Cu(glycine)$_2$ ($\simeq$ 56 kJ mol^{-1}) et pour Cu(alanine)$_2$ ($\simeq$ 48 kJ mol^{-1}). Ces valeurs montaient à 96 et 102 kJ mol^{-1} à pH = 12 pour la sérine et la thréonine respectivement. Donc, en milieu basique, les réactions étaient presque deux fois plus exothermiques. Ceci n'arrivait pas dans le cas des complexes de Ni ou du Zn, où des précipités apparaissaient en milieu basique. Les auteurs conclurent que leurs données démontraient la formation d'autres espèces en plus de Cu(sérine)$_2$ en milieu alcalin et proposèrent des complexes polyhydroxylés et polynucléaires. Cependant ils remarquèrent que le complexe Cu(glycine)$_2$ donnait un précipité en milieu basique et aucun changement de ΔH en fonction du pH et ne purent expliquer ces faits.

Letter et Bauman étudièrent les complexes du Cu et du Ni avec une série d'acides aminés reliés à la sérine (15) et à la tyrosine (16). Les enthalpies de formation des complexes successifs étaient toutes comprises entre 20 et 26 kJ mol^{-1}, la formation du deuxième complexe étant toujours un peu plus exothermique que la formation du premier (d'environ 2 kJ mol^{-1}). Les entropies variaient de 58 à 75 J K^{-1} mol^{-1} pour la formation du premier complexe et de 42 à 50 J K^{-1} mol^{-1} pour le deuxième. Ils expliquèrent leurs résultats comme suit:

1. L'enthalpie négative est attribuée principalement à la formation des liens cuivre–azote (la moitié des enthalpies de complexation du cuivre avec l'éthylènediamine étant de 27 kJ mol^{-1} pour CuL et de 26 kJ mol^{-1} pour CuL_2).

2. L'entropie positive est relié au départ des molécules d'eau coordonnées lors de la neutralisation des charges du cuivre par les groupements carboxyliques (la moitié de l'entropie de complexation de Cu^{2+} avec l'ion oxalate étant de 59 J K^{-1} mol^{-1}). Ils concluèrent que leurs données ne leur permettaient pas de retenir l'hypothèse de la formation de liens cuivre hydroxyles car les interactions cuivre–azote et cuivre – acide carboxylique semblaient adéquates et suffisantes.

Gergely *et al.* étudièrent de nouveau une série de complexes en partant du principe qu'il fallait considérer la possibilité des liaisons métal – groupement hydroxyle (17). Ils observèrent que tous les métaux étudiés (Co, Ni, Cu et Zn) et en particulier le cuivre, avaient une enthalpie de formation de complexe plus exothermique dans le cas de la sérine et de la thréonine que dans le cas de l'alanine et de l'acide α-aminobutyrique. Ils objectèrent à la comparaison de Letter et Bauman entre l'isosérine et les autres acides aminés hydroxylés, préférant baser leurs conclusions sur des comparaisons entre les acides aminés où —CH_2OH était remplacé par —CH_3.

L'inspection des différences pH – log K montra que les complexes des acides aminés hydroxylés étaient relativement plus stables que ceux des acides aminés non hydroxylés. De plus, les complexes de la thréonine paraissaient encore plus stables que ceux de la sérine. Cette stabilité accrue se réflétait par des réactions plus exothermiques pour les acides aminés hydroxylés. Pourtant, l'effet inductif du groupement OH était naturellement d'affaiblir les liens Cu $\leftarrow$ N. Gergely *et al.* concluèrent donc: "The greater enthalpy change resulting in spite of this can be explained only by the formation of a further bond". Ils proposèrent par conséquent que les groupements OH non ionisés des acides aminés en question participaient à la formation de liens faibles à l'intérieur de la première sphère de coordination du métal.

D'autres auteurs ont étudié les complexes cuivriques de la sérine sans détecter les complexes déprotonés à pH basique (18 19). Nos résultats sur la phénylsérine *thréo* et *érythro* (voir tableau 2) sont semblables à ceux de Letter et Bauman sur la sérine et la phénylsérine. Nous remarquons que les ΔH_c sont caractéristiques des acides aminés et ne varient pas entre la formation du monochélate et du dichélate. Ces observations concordent avec les résultats de I et Nancollas (19). La variation observée dans ΔH pour les complexes successifs est donc attribuable à la variation dans ΔH_c.

Nous observons que $\Delta G_{r,c}$ est négatif, ce qui s'explique comme suit: les répulsions électrostatistiques entre ligands réduisent la stabilité des complexes dichélatés et favorisent la formation des monochélates. Par contre, les valeurs de $\Delta G_{r,c}$ (ou $\Delta H_{r,c}$) sont positives et reflètent les interactions covalentes et l'influence mutuelle des ligands. I et Nancollas (19) ont expliqué cet effet comme probablement relié à la plus grande facilité d'enlever l'eau de coordination du monocomplexe que de l'ion Cu^{2+}. Letter et Bauman ont montré que pour tous les complexes d'acides aminés, ΔH_2 est plus exothermique que ΔH_1. Ceci montre que la coordination du premier acide aminé facilite le départ des molécules d'eau restantes. Les changements d'entropie corroborent ces conclusions car ΔS_1 est beaucoup plus grand que ΔS_2. La formation du monocomplexe, comparé à la deuxième étape, correspond donc à la libération d'une plus grande quantité d'eau, avec un accroissement correspondant du désordre résultant. Les changements d'entropie positifs sont essentiellement reliés aux différences dans la solvatation des espèces participant aux réactions d'association.

Nancollas a considéré que la sérine était un acide aminé ordinaire (bidentate) mais il a remarqué que toutes les valeurs de $\Delta S_{r,t}$ étaient semblables à l'exception de celles pour les complexes de la sérine. Nos résultats montrent que la phénylsérine *thréo* et *érythro* ressemble à la sérine, c'est-à-dire qu'ils diffèrent eux aussi des valeurs observées pour les acides aminés ordinaires. Voici l'explication de Nancollas: "The lower value of $\Delta S_{r,t}$ for serine can be attributed to the electron-withdrawing property of the hydroxyl group in the β-position which renders the net positive charge on $Cu(ser)^+$ higher than for the other mono (amino acid) complexes. Interaction with the solvent will therefore be stronger in the case of $Cu(ser)^+$ resulting in a lower $\Delta S_{r,t}$". Cet argument est tendancieux, car si l'effet inductif est important dans le cas du monocomplexe, il doit être important aussi dans le cas de Cu(serine)$_2$. Autrement dit, on ne peut observer dans la différence qu'est $\Delta S_{r,t}$, aucune particularité attribuable à l'effet inductif, à moins que cet effet disparaisse dans le dichélate, ce qui semble douteux. A notre avis, les résultats thermodynamiques peuvent être expliqués raisonnablement si on postule que les acides aminés β-hydroxylés sont tridentates, avec le groupe OH en position axiale. Les structures proposées par les complexes sont présentées dans la fig. 3. On ne s'attend pas à une grande différence entre l'enthalpie d'un lien Cu—H_2O et d'un lien Cu—ROH où R représente le reste de l'acide aminé. Par conséquent, on peut même s'attendre à un équilibre, en solution aqueuse, entre des complexes avec soit H_2O, soit ROH coordonnés.

La question des changements d'entropie est plus délicate. En effet, la formation d'un chélate entraîne normalement un ΔS plus grand résultant en une plus grande stabilité d'un complexe

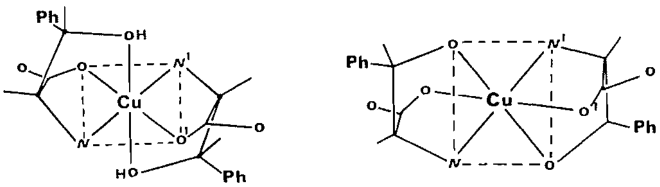

A B

FIG. 3. Structures proposées pour les complexes cuivriques de la phénylsérine. A à un pH neutre, B à un pH basique.

chélaté par rapport à un complexe analogue non cyclique. L'effet chélate est justement un effet d'entropie. Pourtant on observe encore une fois des valeurs de ΔS typiques de ligands bidentates seulement. Cependant, les acides aminés β-hydroxylés existent déjà sous forme cyclique en solution, (20–22), cycle formé par une liaison hydrogène entre les groupements OH et NH_3. Il est donc difficile d'interpréter les changements d'entropie lors de la formation du chélate métallique.

Conclusion

En conclusion, l'hypothèse que la sérine et la phénylsérine sont des acides aminés tridentates offre une meilleure explication des résultats thermodynamiques. Cette hypothèse explique pourquoi les acides aminés β-hydroxylés ont des ΔG (et des constantes de formation de complexes) proches des ΔG observés pour les acides aminés ordinaires. De plus elle suggère une bonne possibilité pour la formation des complexes déprotonés: la déprotonation du groupement OH coordonné et la formation d'un lien Cu–alcoxyde en milieu basique expliquerait l'augmentation de l'exothermicité de la réaction cuivre + acide aminé au dessus de pH 10. D'après la variation de log β_3 et log β_4 en fonction de la température, nous obtenons une valeur voisine de 21 kJ mol^{-1} pour chaque déprotonation (-23 et -19 ± 2 kJ mol^{-1} pour la phénylsérine *thréo* et *érythro*, respectivement). On retrouve donc l'augmentation totale de -42 kJ mol^{-1} découverte par Thornton et Skinner pour le cas des complexes de la sérine (14). Des études complémentaires par spectroscopie visible montrent un acroissement de la force du champ cristallin à pH basique. De plus des résultats rpe montrent l'apparition d'une structure hyperfine à 5 raies pour le complexe déprotonné, en accord avec la transformation de l'acide aminé en un ligand tridentate moins labile à pH basique. Les temps de relaxation en rmn concordent aussi avec les conclusions thermodynamiques et feront le sujet d'une autre publication.

Nos expériences sur la phénylsérine représentent la troisième occurrence de la détection de complexes déprotonés et tend à confirmer la généralité de ce phénomène pour les acides aminés β-hydroxylés.

Remerciements

Nous remercions le CRSNG pour l'aide financière accordée à ce travail.

1. E. ERLENMEYER. Ber. 3445 (1892).
2. K. TATSUMOTO et A. E. MARTELL. J. Am. Chem. Soc. **100**, 5549 (1978); M. S. MOHAN et E. H. ABBOTT. Inorg. Chem. **17**, 3083 (1978).
3. P. SHARROCK. Synthèse de la phénylsérine et étude de ses complexes cuivriques. Thèse de Ph.D., Faculté des sciences, Université de Sherbrooke (1976).
4. K. SHAW et S. W. FOX. J. Am. Chem. Soc. **75**, 3417 (1953); **75**, 3421 (1953).
5. J. GREENSTEIN et M. WINITZ. Chemistry of the amino-acids. J. Wiley, New York. 1961. pp. 2595–2602.
6. P. SHARROCK et S. ARABI. Arab Gulf J. Sci. Res. **1**, 105 (1983).
7. P. SHARROCK et R. HARAN. J. Coord. Chem. **11**, 117 (1981).
8. P. GRENOUILLET, R. P. MARTIN, A. ROSSI et M. PTAK. Biochim. Biophys. Acta, **322**, 185 (1973).
9. H. C. FREEMAN et R. P. MARTIN. J. Biol. Chem. **18**, 4823 (1969).
10. T. P. KRUCK et B. SARKAR. Can. J. Chem. **51**, 3555 (1973).
11. P. SHARROCK. Polyhedron, **2**, 11 (1983).
12. E. V. RAJU et H. B. MATHUR. J. Inorg. Nucl. Chem. **30**, 2181 (1968).
13. W. F. STACK et H. A. SKINNER. Trans. Faraday Soc. **63**, 1136 (1967).
14. A. C. R. THORNTON et H. A. SKINNER. Trans. Faraday Soc. **65**, 2044 (1969).
15. J. E. LETTER et J. E. BAUMAN. J. Am. Chem. Soc. **92**, 437 (1970).
16. J. E. LETTER et J. E. BAUMAN. J. Am. Chem. Soc. **92**, 443 (1970).
17. A. GERGELY, J. MOJZES et ZS. KASSAI BAZSA. J. Inorg. Nucl. Chem. **34**, 1277 (1972).
18. D. R. WILLIAMS. J. Chem. Soc. Dalton Trans. 1064 (1973).
19. T. P. I. et G. NANCOLLAS. Inorg. Chem. 2414 (1972).
20. J. MARCHAND, M. PAIS et F. X. JARREAU. Bull. Soc. Chim. Fr. 3742 (1971).
21. S. FUTAGAWA, T. INUI et T. SHIBA. Bull. Chem. Soc. Jpn. 3308 (1973).
22. H. OGURA, Y. ARATA, et S. FUJIWARA. J. Mol. Spectrosc. **23**, 76 (1967).

Copper(II) acetates: from dimer to monomer

PATRICK SHARROCK
Département de chimie, Faculté des sciences, Université de Sherbrooke, Sherbrooke (Qué.), Canada J1K 2R1

AND

MILAN MELNÍK[1]
Department of Inorganic Chemistry, Slovak Technical University, CS 81237 Bratislava, Czechoslovakia

Received April 4, 1984

PATRICK SHARROCK and MILAN MELNÍK. Can. J. Chem. **63**, 52 (1985).

The epr spectra at various frequencies of copper(II) acetate anhydrous, monohydrate, monoacetic acid, and water – acetic acid adduct are presented and analysed. The presence of copper hyperfine splittings in the solid state epr spectra of this series of compounds is discussed. The frozen solution spectrum of copper(II) acetate in acetic acid solution containing ~2% water shows an exceptional resolution of $A_\perp$ hyperfine of 24 G. This is attributed to a key intermediate which explains the monomer–dimer dissociation mechanism. The influence of distortions on the structures of these compounds is presented.

PATRICK SHARROCK et MILAN MELNÍK. Can. J. Chem. **63**, 52 (1985).

Les spectres rpe à diverses fréquences de l'acétate cuivrique anhydre, monohydraté et des composés d'addition avec l'acide acétique et l'eau et l'acide acétique sont présentés et analysés. La présence de couplages hyperfins avec les noyaux ^{63}Cu et ^{65}Cu sont discutés. Le spectre rpe d'une solution gelée d'acétate cuivrique dans l'acide acétique contenant ~2% d'eau ont une résolution inhabituelle de $A_\perp$ de 24 G. Ceci est attribué à un intermédiaire clef qui explique bien le mécanisme de dissociation dimère–monomère. Nous présentons l'importance des distortions sur les structures de ces composés.

Introduction

Binuclear metal centers are known to be present in copper(II) carboxylates (1). The bridged binuclear structure, first documented by Van Niekerk and Schoening (2) for copper(II) acetate monohydrate, is now an ubiquitous feature in coordination chemistry. The magnetic properties of exchanged-coupled paramagnetic centers is of considerable interest (3). Bleaney and Bowers first recognized the triplet state epr spectrum of copper(II) acetate monohydrate (4) and solved the $S = 1$ spin Hamiltonian parameters. There is strong antiferromagnetic coupling in such dimers and a $-2J$ value of 298 ± 4 cm^{-1} was determined recently by direct spectroscopic measurements by neutron scattering (5).

A thermodynamic study (6) of solvation (in water/acetic acid) of copper(II) acetate shows that the dimer prefers coordination of water to that of acetic acid in the axial position. Also, water is reported to stabilize the dimer in solution despite the fact that water shifts the monomer–dimer equilibrium towards the monomer. Conflicting reports exist in the literature dealing with the presence or absence of epr signals for solutions of copper(II) acetate (7, 8), and even on the composition of the adducts present in water – acetic acid mixtures (6, 9).

We now wish to report the synthesis and characterization of copper(II) acetate adducts with acetic acid and water. We present the first epr spectrum for $Cu(OAc)_2 \cdot H_2O \cdot HOAc$ as well as a frozen solution spectrum with resolved hyperfine along $g_\perp$. We compare the spectroscopic parameters for the series of adducts.

Experimental

Preparation of compounds

Copper(II) acetate monohydrate was purchased from J.T. Baker Co. and used without further purification. The anhydrous compound was prepared by monitoring the weight loss on the monohydrate by gentle heating until constant weight. The sample was then sealed in the quartz epr tube.

Copper(II) acetate·acetic acid was prepared by adding acetic anhydride to a glacial acetic acid solution of copper(II) acetate. The solution was heated to dissolve the solids and put aside for crystallisation.

Copper(II) acetate·hydrate·acetic acid was prepared by equilibrating a suspension of copper(II) acetate monohydrate in acetic acid containing 1% water as measured by nmr. Following a one week period the solid product was filtered off and stored without drying in tightly sealed containers.

Physical measurements

Copper contents were checked by atomic absorption analyses. Thermal analyses were performed with a Setaram electrobalance and fully programmable oven. The samples weighed 100 mg and were under a nitrogen flow of 50 mL/min; the average heating rate was 2°/min.

Electron parameter resonance spectra were recorded on Varian E-9 spectrometers operating at X-band and Q-band and Jeol spectrometer at K-band. Standard cryostats and Varian temperature control units were used for the low temperatures.

Results

We found that careful dehydration of the monohydrate yields an anhydrous copper(II) acetate with only a small amount of mononuclear species. The acetic acid adduct also contains small amounts of mononuclear species and must be prepared in the rigorous absence of water and protected from atmospheric humidity. The water – acetic acid adduct cannot be dried in air without decomposition leading to formation of the monohydrate. This mixed-ligand adduct can only be obtained by a slow heterogeneous reaction as described in the Experimental section.

Atomic absorption and thermogravimetric analyses confirm the compositions of the compounds. *Anal.* calcd. for $Cu(CH_3COO)_2 \cdot CH_3COOH$: Cu 26.29; found: Cu 26.17. *Anal.* calcd. for $Cu(CH_3COO)_2 \cdot H_2O \cdot CH_3COOH$: Cu 24.46; found: Cu 24.32. All compounds begin to decompose at 250°C and yield copper metal mixed with small amounts of copper oxide. The acetic acid adduct loses its axial ligand readily beginning at temperatures as low as 40°C. Between 40 and 60°C the observed weight loss is 25.0%, which corresponds closely to the theoretical value of 24.85%. The monohydrate loses water near 100°C (observed weight loss of 9.1%, theoretical value

[1] Present address: Département de chimie, Université de Sherbrooke, Sherbrooke (Qué.), Canada J1K 2R1.

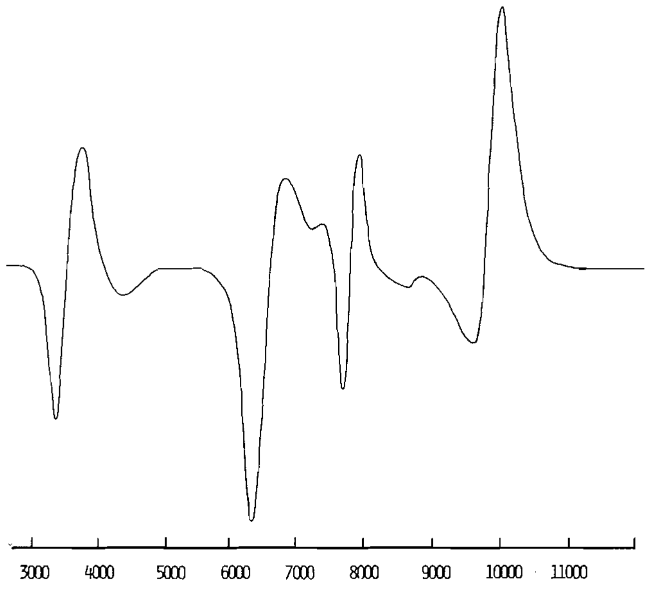

FIG. 1. K-band spectrum (24.725 GHz) of $[Cu(CH_3COO)_2 \cdot CH_3COOH]_2$ at room temperature.

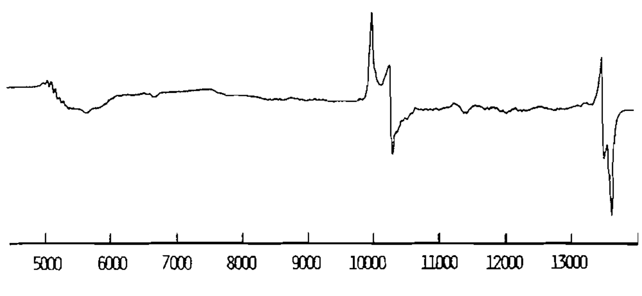

FIG. 2. Q-band spectrum (37.25 GHz) of $[Cu(CH_3COO)_2 \cdot H_2O \cdot CH_3COOH]_2$ at 110 K.

9.02%). Two steps were observed in the water – acetic acid adduct derivative of the decomposition curve between 40 and 100°C. The overall weight loss observed (29.4%) corresponds well with the calculated values for water and acetic acid (30.06%). Acetic acid is eliminated in the first step, followed by water in the second step. Reproducible results were obtained only by drying the compound to constant weight under a stream of dry nitrogen directly in the electrobalance sample holder immediately prior to the experiment.

At X-band frequencies and room temperature, powdered $Cu(OAc)_2 \cdot HOAc$ shows three broad absorption bands similar to those found in $Cu(OAc)_2 \cdot H_2O$. However, the anhydrous copper(II) acetate only shows one broad epr absorption near $g = 2$, and of peak-to-peak width of about 1 000 G. $Cu(OAc)_2 \cdot H_2O \cdot HOAc$ shows the three typical well-resolved absorption bands due to the triplet state transitions observable when $h\nu \simeq 0.3\ cm^{-1}$. These spectra are governed by the usual $S = 1$ spin Hamiltonian

$$\mathcal{H} = \beta H \cdot g \cdot S + D(S_z^2 - (1/3)S(S+1)) + E(S_x^2 - S_y^2)$$

where D and E are the zero-field splitting parameters which determine the energy levels along the three principal axes. The experimental D values are related to the interaction between the two coupled electrons by both the direct magnetic dipole–dipole interaction inversely dependant on the separation distance and by the pseudo dipolar interaction occuring via the bridging ligand's molecular orbitals. The E values reflect the rhombic component of the crystalline field. Of the six principal resonance field positions expected for $\Delta M_s = \pm 1$, the three corresponding to H_{z1}, $H_{\perp 2}$, and H_{z2} are detected at X-band. Increasing the quantum of energy allows a more complete observation of the spectrum as illustrated in Fig. 1.

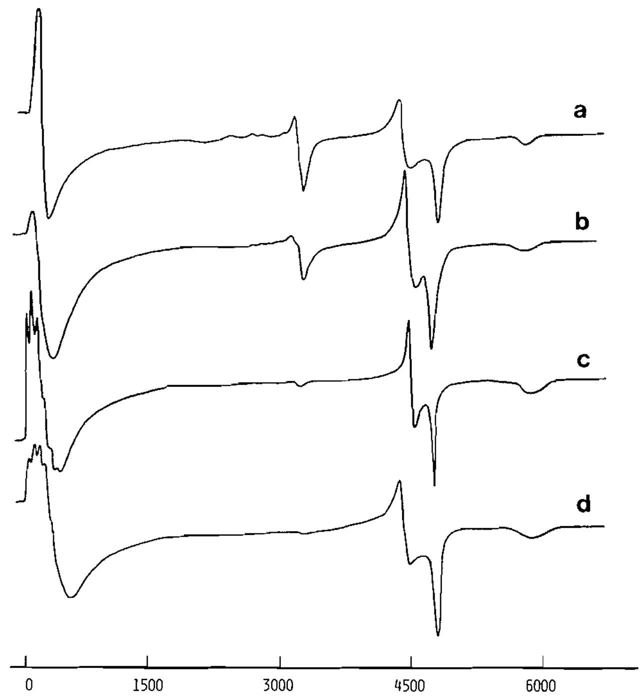

FIG. 3. X-band spectra (9.130 GHz) of $[Cu(CH_3COO)_2]_2$ (*A*), $[Cu(CH_3COO)_2 \cdot CH_3COOH]_2$ (*B*), $[Cu(CH_3COO)_2 \cdot H_2O \cdot CH_3COOH]_2$ (*C*), and $[Cu(CH_3COO)_2 \cdot H_2O]_2$ (*D*) at 110 K.

At K-band and room temperature (Fig. 1), $Cu(OAc)_2 \cdot HOAc$ shows a $\Delta M_s = \pm 2$ transition at 3 600 G in addition to the $H_{\perp 1}$ and $H_{\perp 2}$ transitions at 6 450 and 10 100 G, respectively. The absorption at 7 870 G is a $S = \frac{1}{2}$ monomer signal near $g = 2$. Lowering the temperature results in resolution of the rhombic field components. Figure 2 shows the low temperature Q-band epr spectrum of $Cu(OAc)_2 \cdot H_2O \cdot HOAc$. It also shows a $\Delta M_s = \pm 2$ transition with a seven-line dicopper nuclear hyperfine splitting in addition to the H_{x1}, H_{y1}, H_{x2}, and H_{y2} transitions. In this case, the weaker H_z absorptions were not detected because of the small sample size imposed at high frequency.

The epr spectra at 110 K obtained at X-band for the four copper(II) acetates studied are compared in Fig. 3. The four transitions observed are assigned to H_{z1}, H_{x2}, H_{y2}, and H_{z2} absorptions occurring from low to high field. The anhydrous compound which showed a featureless broad signal at room temperature shows a sharp peak for H_{z1}. $Cu(OAc)_2 \cdot HOAc$ has a H_{z1} absorption broadened by unresolved nuclear hyperfine structure, which was partly resolved, however, around 150 K. Both $Cu(OAc)_2 \cdot H_2O \cdot HOAc$ and $Cu(OAc)_2 \cdot H_2O$ show resolved seven-line splitting patterns on H_{z1}. The various spin Hamiltonian parameters derived from these spectra are listed in Table 1.

TABLE 1. Triplet epr parameters for dimer copper(II) acetates

Compound	$g_\perp$	$g_\parallel$	g_{ave}	$\lvert D \rvert$ (cm^{-1})	E (cm^{-1})	Reference
$Cu(CH_3COO)_2$	2.084	2.385	2.189	0.338		12
	2.080	2.382	2.186	0.340	0.006	This work
$Cu(CH_3COO)_2 \cdot H_2O$	2.073	2.344	2.167	0.345	0.007	13
	2.076[a]	2.397	2.188			14
	2.073	2.344	2.167	0.345	0.01	15
	2.077	2.365	2.177	0.343	0.007	This work
$Cu(CH_3COO)_2 \cdot CH_3COOH$	2.063	2.364	2.168	0.322	0.005	This work
$Cu(CH_3COO)_2 \cdot H_2O \cdot CH_3COOH$	2.070	2.370	2.170	0.344	0.006	This work
g_x	2.060[b]	—	—	0.331	0.007	This work
g_y	2.085					

[a] By μ-irradiation of the parent compound.
[b] ν = 37.25 GHz.

TABLE 2. Doublet epr data for monomer copper(II) acetates

$Cu(CH_3COO)_2 \cdot H_2O$ (in)	$g_\perp$	$g_\parallel$	g_{ave}[a]	$A_\parallel$ (G)	$A_\perp$ (G)	Reference
H_2O	2.069	2.361	2.166	150		This work
Ethyleneglycol	2.077	2.375	2.176	135		This work
1.88% H_2O + HAc	2.069	2.350	2.163	150	24	This work
15% H_2O + 85% HAc[b]	2.087	2.372	2.182	135	0	16
20% H_2O + HAc			2.178			16
20% H_2O + HAc			2.167			17
25% H_2O + HAc			2.185			17

[a] $g_{ave} = (2g_\perp + g_\parallel)/3$.
[b] At −186°C.

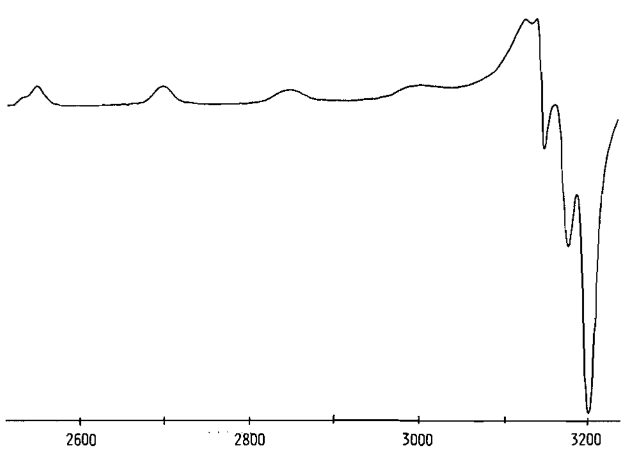

FIG. 4. Glassy state epr spectrum of $Cu(CH_3COO)_2$ in CH_3COOH with 1.88% H_2O at 110 K.

Solution spectra of copper(II) acetate at room temperature show no absorption in pure glacial acetic acid or very weak absorptions in DMSO, or ethyleneglycol. However, an ill-resolved four-line pattern appears when small amounts of water (or pyridine) are present in these solvents. Saturated copper(II) acetate in pure water shows an isotropic spectrum of 140 G peak-to-peak width, and a 0.01 M aqueous solution shows partly resolved hyperfine and $g_0 = 2.182$.

Frozen solution spectra of copper(II) acetate in water or ethyleneglycol only show $S = \frac{1}{2}$ transitions typical of mononuclear copper(II) complexes with metal hyperfine structure resolved along $g_\parallel$ and one strong absorption corresponding to $g_\perp$. In glacial acetic acid solutions, analogous features are found, but when small quantities of water (near 2% by volume) are present an exceptionally well-resolved spectrum yields $A_\parallel$, $A_\perp$, and partially separated ^{63}Cu and ^{65}Cu absorptions at low field (Fig. 4). The epr parameters calculated for the mononuclear copper(II) acetates are listed in Table 2. In glacial acetic acid solutions from 273 K to 77 K a triplet state spectrum similar to that obtained for the solid complex is observed with spin Hamiltonian parameters which show no variation with temperature and yield: $g_\parallel = 2.350$, $g_\perp = 2.066$, $g_{ave} = 2.165$, [D] = 0.326 cm^{-1}, E = 0.005 cm^{-1}.

Discussion

Copper(II) monohydrate (2) and acetic acid adduct (10) are both well-characterized. However, the water – acetic acid adduct has been previously formulated as $Cu_2(OAc)_4 \cdot H_2O \cdot HOAc$ (11) or as $Cu(OAc)_2 \cdot H_2O \cdot HOAc$ (6, 9). It is clear from both our thermogravimetric and atomic absorption analyses that the correct formula is the latter one. This compound has not been previously studied in the solid state because of difficulties in drying the compound without loss of acetic acid.

The epr spectra for the four compounds shown in Fig. 3 and the parameters listed in Table 1 are in good agreement with previous results (18). The broad single absorption observed for anhydrous copper(II) acetate is a common feature found in other anhydrous copper(II) carboxylates (19, 20). This broadening is attributed to interdimer magnetic interaction. It is known from the structure of copper(II) butyrate (21) that the axial sites are occupied by oxygen atoms of neighboring dimer molecules, providing a polymeric network and pathway for exchange. The [D] value of about 0.3 cm^{-1} is large compared to magnetic quantities (~3 000 G) but is small compared to vibrational frequencies. At room temperature nearly 50% of the dimers are in the thermally populated triplet state. Therefore interdimer dipolar couplings may also be expected to be significant at room temperature.

Figure 3 shows that all the compounds presented have axial symmetry with rhombic distortion. The anhydrous and acetic acid adduct do not show the seven-line hyperfine splitting on H_{z1}. This is also observed in a variety of other carboxylates with axial or rhombic symmetry, with or without axial ligands (22). From the observed narrow linewidth of 13 G (peak-to-peak of derivative) we conclude the absence of copper hyperfine is not due to inhomogeneous broadening but can be assigned to exchange interactions which, at low temperature are stronger than the hyperfine interaction but weaker than the g-anisotropy. The water and water – acetic acid adducts show resolved hyperfine splitting of about 60 G. As expected for exchange-coupled dimer systems this coupling is about half the value observed in monomer species. The resolution is attributed to isolation of the dimers by axial water ligands. In addition, a seven-line pattern is resolved in the low temperature Q-band spectrum (Fig. 2) on the $\Delta M_s = \pm 2$ transition which is observed only at higher frequencies.

The liquid solutions yield no epr absorption in solvents where copper(II) acetate retains the dinuclear structure. The $S = \frac{1}{2}$ spectra obtained in the presence of water are due to dissociation of the dimers. This is in agreement with excessive broadening of the triplet signal because of the large value of the anisotropic zero field splitting.

Frozen solution spectra reveal no significant variations in either the g values or appearance of the $A_{\parallel}$ hyperfine. The spectrum in Fig. 4 is unusual in showing resolved $A_{\perp}$ copper hyperfine. Well-resolved $A_{\perp}$ is often seen for other O-donor systems (23), but hyperfine structure along $g_{\perp}$ is absent in previous reports on copper carboxylates. This can be attributed to inhomogeneous broadening due to unresolved hyperfine and some sort of chemical exchange process leading to multiplicity of the complexes present. $Cu(H_2O)_4OAc_2$ has been proposed previously (9). Scheme 1 presents the various compounds present in solution. Compound **4**, with two coordinated water molecules exists in pure water or in other solvents containing water in the absence of other Lewis bases stronger than water. Compound **1** exists in glacial acetic acid solution and acetic acid axially coordinates to the dimer structure, leading to appreciable distortions as found in the solid state (10, 21). When the solvent is acetic acid containing ~2% water, compound **3** is found in equilibrium with compound **2**. Compound **2** is not expected to yield a visible triplet state spectrum and insufficient water is available to obtain **4**. This explains why **3** yields a well-resolved spectrum pertaining to one well-defined species. Furthermore, a compound of same composition as **2** can be isolated in the solid state and this is a key intermediate in explaining monomer–dimer equilibria. From Nyberg's data (17), the greatest line-width variation of the hyperfine lines is found precisely in acetic acid solutions containing 2% water, indicating a longer correlation time in a solvent of this composition. This was attributed to acetic acid replacing water as axial ligand in monomers, leading to large hydrodynamic radii (16), but should in fact be related to aggregation of **3** to form **2**. We propose for **2** similar distortions as known in compound **1**. The bridging acetate has one short Cu*—O* bond (darkline)

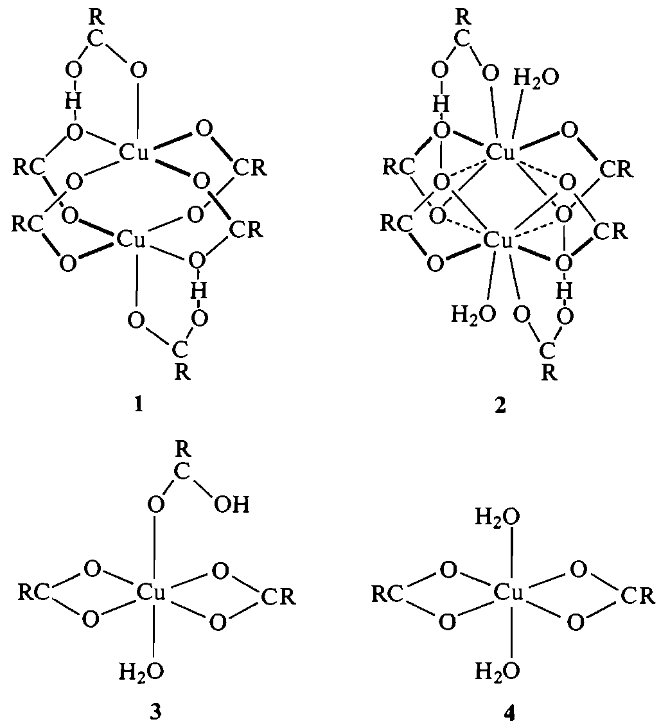

SCHEME 1

and one long Cu—O (dotted line). This long Cu—O bond can easily be broken with formation of a Cu*—O bond yielding chelating acetate ligands as shown by the thin lines (Scheme 1, compounds **2** and **3**).

Conclusion

Despite intensive study of copper(II) carboxylates, no comprehensive mechanism of formation or of dissociation of the dimer species had been presented yet. We believe our results point to distortions as the main factor governing the transformation. Our isolation of a complete series of copper(II) acetates clarifies the characterization of the species present both in solution and in the solid state and highlights the structural features which influence the epr spectra.

Acknowledgments

This work was supported by grant No. A1127 (NSERCC) and subvention EQ-2441 (FCAC QUEBEC). We acknowledge this essential financial help.

1. M. MELNÍK. Coord. Chem. Rev. **36**, 1 (1981); **42**, 259 (1982); and references therein.
2. J. N. VAN NIEKERK and F. R. L. SCHOENING. Acta Crystallogr. **6**, 227 (1953).
3. S. NAKATSUKA, K. OSAKI, and N. URYU. Inorg. Chem. **21**, 4332 (1982).
4. B. BLEANEY and K. D. BOWERS. Proc. R. Soc. Ser. A, **214**, 451 (1952).
5. H. U. GUDEL, A. STEBLER, and A. FURRER. J. Am. Chem. Soc. **18**, 1021 (1979).
6. A. T. A. CHENG and R. A. HOWALD. Inorg. Chem. **14**, 546 (1975).
7. B. M. RODE and W. S. KITTL. Inorg. Chim. Acta, **38**, 203 (1980).
8. H. D. HARDT and G. STREIT. Z. Anorg. Allg. Chem. **350**, 84 (1967).
9. K. SANVED. J. Chem. Soc. 2967 (1927).

10. V. M. RAO, D. N. SATHYANARAYANA, and H. MANOHAR. J. Chem. Soc. Dalton Trans. 2167 (1983).
11. H. GRASDALEN and I. SVARE. Acta Chem. Scand. **5**, 1089 (1971).
12. YU. V. YABLOKOV, A. V. ABLOV, L. N. MILKOVA, and L. N. ROMANENKO. Dokl. Acad. Nauk SSSR, **180**, 659 (1968).
13. A. K. GREGSON, R. L. MARTIN, and S. MITRA. Proc. R. Soc. Ser. A, **230**, 473 (1971).
14. W. SAKAGUCHI, Y. ARATA, and S. FUJIWARA. J. Chem. Phys. **53**, 464 (1970).
15. D. COLLISON and F. E. MABBS. J. Chem. Soc. Dalton Trans. 1565 (1982).
16. H. GRASDALEN. J. Magn. Res. **9**, 166 (1973).
17. G. NYBERG. J. Phys. Chem. **75**, 2228 (1971).
18. G. F. KOKOSZKA and R. W. DUERST. Coord. Chem. Rev. **5**, 209 (1970).
19. R. UGGLA and M. MELNÍK. Acta Chem. Scand. **25**, 1790 (1971).
20. M. MELNÍK and R. UGGLA. Suom. Kemistil. B, **44**, 5 (1971).
21. M. Y. BIRD and T. R. LOMER. Acta Crystallogr. Sect. B, **28**, 242 (1972).
22. P. SHARROCK, M. DARTIGUENAVE, and Y. DARTIGUENAVE. Bioinorg. Chem. **9**, 3 (1978).
23. M. MAKOTO and H. YOKOI. J. Chem. Soc. Dalton Trans. 2344 (1977).

Niobium(IV) methoxide complexes with phosphorus donor ligands

MILAN MELNÍK[1]
Department of Inorganic Chemistry, Slovak Technical University, CS 81237 Bratislava, Czechoslovakia

AND

PATRICK SHARROCK
Département de chimie, Faculté des sciences, Université de Sherbrooke, Sherbrooke (Qué.), Canada J1K 2R1

Received June 20, 1984

MILAN MELNÍK and PATRICK SHARROCK. Can. J. Chem. **63**, 57 (1985).

Niobium(IV) methoxide was synthesized by prolonged electroreduction of niobium pentachloride in methanol. Electron paramagnetic resonance spectra at room temperature and 77 K show the expected 10-line patterns of ^{93}Nb at $\bar{g} = 1.95$ and $\Delta M_s = 2$ absorptions indicating the presence of dimer species. The spectroscopic parameters obtained in the presence of a series of phosphorus donor ligands are presented and discussed in terms of mononuclear and dinuclear structures.

MILAN MELNÍK et PATRICK SHARROCK. Can. J. Chem. **63**, 57 (1985).

Nous avons préparé le tétraméthoxide de niobium(IV) par électroréduction lente du pentachlorure de niobium en solution méthanolique. Les spectres rpe à 298 K et 77 K montrent la structure hyperfine à 10 raies typique du ^{93}Nb à $\bar{g} = 1.95$ et aussi l'absorption $\Delta M_s = 2$ à $g = 4$ correspondant à des espèces dimères. Les paramètres rpe observés en présence d'une série de ligands phosphorylés sont présentés et discutés en termes de structures monomères et dimères pour les complexes du niobium(IV).

Introduction

Niobium(V) alkoxides are known to form dimeric, or polymeric compounds (1). Early transition metal alkoxides autoassociate in preference to complex formation with other ligands to reach coordination number six (2). Diamagnetic niobium(V) alkoxides were investigated by nmr (3) and factors controlling the coordination chemistry were discussed (4). Niobium(IV) alkoxides have been rarely investigated (5) and we now wish to report the first characterization of niobium alkoxide dimerisation observed by epr (6). We also present data demonstrating weak coordination of a variety of phosphine and phosphite ligands to the tetraalkoxoniobium species.

Experimental

Niobium pentachloride was purchased from Ventron, and kept under an atmosphere of dry nitrogen. All the phosphines used were of commercial origin (Organometallics, Inc. New Hampshire) and stored in Schlenk tubes.

Niobium tetramethoxide was prepared by dissolving niobium pentachloride in dry methanol and reducing the solution under a nitrogen atmosphere by electrolysis with graphite electrodes. Initially the deep wine–red to purple niobium(IV) chloro-methoxo species are formed, but after prolonged electroreduction in a cell equipped with a large porous-glass membrane separating the two electrode compartments, chloride ions migrate and are oxidized to chlorine gas as evidence by the appearance of the pale yellow–green solution in the other compartment. Following a three-day period with a large overpotential (5 to 8 V), the brown solution was filtered and concentrated under vacuum. A dark brown to black solid could be isolated with the characteristic infrared absorptions (ν(M—O) 870 cm^{-1}; ν(OCH_2) 985 and 1025 cm^{-1}) (7). Chloride ion determinations by silver nitrate titrations showed only 0.6% chloride by weight was present in the methoxide. Niobium content was determined as Nb_2O_5 after ignition in oxygen and confirmed isolation of $Nb(OCH_3)_4$. *Anal.* calcd.: Nb 42.8; found: Nb 42.2). *Anal.* calcd. for $Nb(OCH_3)_4$: C 22.14, H 5.57; found: C 21.86, H 5.61.

Samples for epr analysis were prepared and sealed under nitrogen in 3 mm quartz tubes. A varian E-9 spectrometer operating at X-band was used to obtain the epr spectra. Low temperatures were obtained using a cryostat technique previously reported (8). The frequency was measured with a digital frequency meter and the magnetic field calibrated with a Systron-Doner NMR gaussmeter.

Results

We observed that magnesium metal rapidly reduces niobium(V) in methanol, but the resulting products contain complex alkoxides. The formula $MgNb(OMe)_6$, analogous to the reported double alkoxide of niobium(V) (9), can be proposed for these compounds which were not further investigated. Electroreduction yields the desired tetramethoxoniobium(IV) which can be isolated as a dark brown solid insoluble in common organic solvents. It is relatively stable towards oxygen but hydrolyses readily in solution. It is insoluble in pure liquid phosphines but dissolves in liquid phosphites or toluene solutions of phosphites. A small amount of methanol is needed to dissolved niobium(IV) methoxide in toluene. The products of the reaction of niobium(IV) methoxide with phosphites are yellow to brown oils. With phosphines, brown to green viscous products are obtained which slowly separate out of the toluene solvent.

The room temperature epr spectrum of niobium(IV) methoxide is presented in Fig. 1. High gains and power and a strong modulation amplitude are needed to obtain spectrum (*a*) which shows a clearly resolved absorption near 1700 G in addition to the ten-line pattern centered near 3450 G. The spectrum (*b*) in Fig. 1 results when a small amount of dry HCl is bubbled into the same methanol solution used to obtain spectrum (*a*) (Fig. 1). This concentrated niobium(IV) solution does not show a half-field resonance but shows an intense absorption centered near $g = 2$. This somewhat distorted spectrum changes to the classical 10-line spectrum (*c*) as shown in Fig. 1, when diluted with toluene.

Oxygen-containing solvents tend to decompose niobium(IV) methoxide slowly but an epr spectrum could be obtained in THF, which consisted of a single broad resonance centered at $g = 2.0$. The spectroscopic parameters for the room-temperature spectra are listed in Table 1 together with data derived from the phosphine and phosphite ligands. Most of the phosphine adducts gave weak room-temperature signals and

[1] Present address: Département de chimie, Université de Sherbrooke, Sherbrooke (Qué.), Canada J1K 2R1.

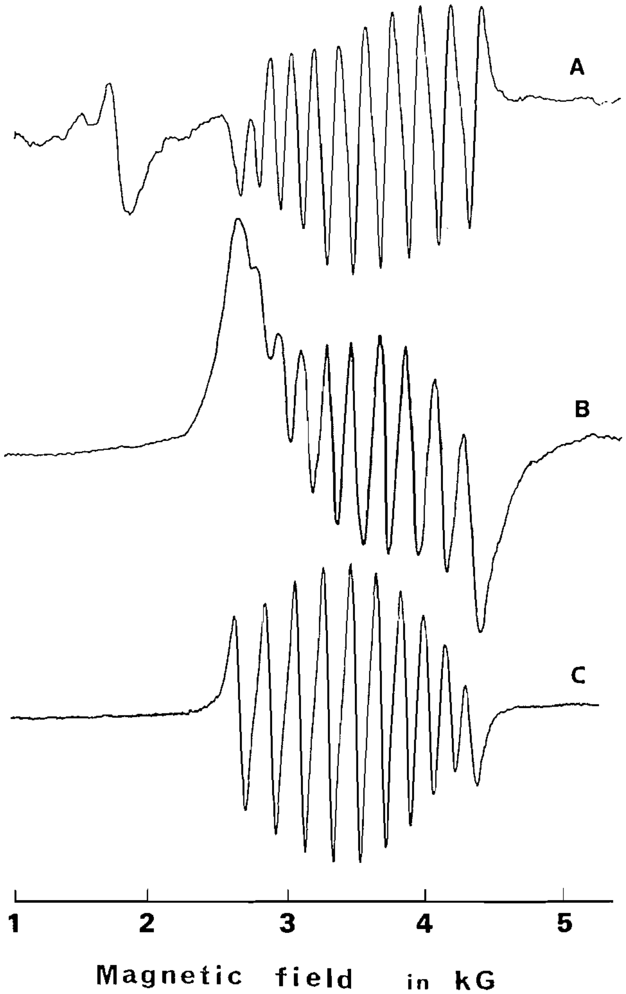

FIG. 1. Electron proton resonance spectra of niobium(IV) methoxide at room temperature (*a*) in methanol solution; (*b*) same as (*a*) with a small amount of dry HCl; (*c*) same as (*b*) diluted in toluene.

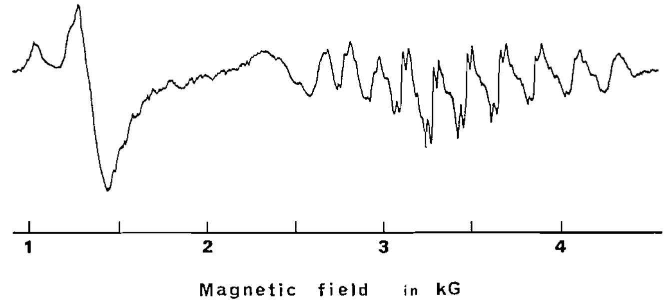

FIG. 2. Room temperature epr spectrum of niobium(IV) methoxide with dimethylphenylphosphine.

TABLE 1. Electron spin resonance data for niobium(IV) methoxide complexes at 298 K

Compound[a]	g_i	$A_{\parallel}$ (gauss)	$\Delta M_s = 2$
$Nb(OCH_3)_4$	1.950	182	4.0
+ HCl	1.930	177	—
+ THF	2.0	—	—
$Nb(OCH_3)_4$ + PMe_3	1.989	139[b]	4.0
+ MeOH(DMF)	—	—	—
$Nb(OCH_3)_4$ + PEt_3	1.90	—	—
+ THF	—	—	—
$Nb(OCH_3)_4$ + PBu_3	1.90	—	—
+ PMe_2Ph	1.99	144[c]	4.0
+ $PMePh_2$	—	144	4.0
+ HCl	1.95	174	[d]
$Nb(OCH_3)_4$ + $PHPh_2$	—	—	4.0
+ HCl	1.95	174	—
$Nb(OCH_3)_4$ + PPh_3	—	—	—
$Nb(OCH_3)_4$ + $Ph_2P(CH_2)PPh_2$	1.95	187	4.0
+ HCl	1.952	185	—
$Nb(OCH_3)_4$ + Ph_2PPPh_2	1.96	175	4.0
+ HCl	1.951	175	[d]
$Nb(OCH_3)_4$ + $OPPh_3$	1.950	182	4.0
+ $P(OMe)_3$	1.936	182	—
+ $(EtO)_2P(O)P(OEt)_2$	1.951	190	4.0
+ HCl	1.95	182	4.0
$Nb(OCH_3)_4$ + $P(OCH_2)_3CCH_3$	—	—	4.0
+ HCl	1.956	177	—

[a] THF = tetrahydrofuran; PMe_3 = trimethylphosphine; DMF = dimethylformamide; PEt_3 = triethylphosphine; PMe_2Ph = dimethylphenylphosphine; $PMePh_2$ = diphenylmethylphosphine; $PHPh_2$ = diphenylphospine; PPh_3 = triphenylphosphine; $Ph_2P(CH_2)PPh_2$ = bis(diphenylphosphine) methane; Ph_2PPPh_2 = tetraphenyldiphosphine; $OPPh_3$ = triphenylphosphine oxide; $P(OMe)_3$ = trimethylphosphite; PBu_3 = tributylphosphine; $(EtO)_2P(O)P(OEt)_2$ = tetraethylpyrophosphite; $P(OCH_2)_3CCH_3$ = trimethylolpropane phosphite.
[b] Phosphorous hyperfine of 25 G.
[c] Phosphorous hyperfine of 23 G.
[d] Weak signal.

showed half-field signals. In some cases no signal at all could be detected. For example triphenylphosphine, tri-*n*-butylphosphine, triethylphosphine in THF, or trimethylphosphine in DMF.

Trimethylphosphine, pure or diluted in toluene, yielded triplet ligand hyperfine splitting on each one of the ten niobium hyperfine lines. The dimethylphenylphosphine yielded phosphorus hyperfine partly resolved on the strongest niobium lines in the center of the spectrum, as shown in Fig. 2. Triethylphosphine gave a very broad and distorted 500 G peak-to-peak width absorption near g = 1.90.

Triphenylphosphine oxide gave a room-temperature spectrum identical to the ligand-free case. The phosphites used did not reveal ligand hyperfine structure in the epr of their niobium(IV) adducts. Dry HCl gas usually increased the intensity of the g = 2 spectra to the expense of the g = 4 absorptions, but with little improvement in the resolution.

The low temperature spectra of niobium(IV) methoxide showed features typical of anisotropic hyperfine with axial symmetry. Figure 3 showed the frozen-solution spectrum of niobium(IV) methoxide in methanol. The g = 4 feature at low field present in spectrum *a* disappears in spectrum *b* (Fig. 3), after HCl is introduced into the solution. Also the decrease in intensity in the central sharp peak is significant and is related to an absorption occuring together with the half-field line, as will be shown later. The frozen THF spectrum comprised a sharp peak at g = 2.0, the usual g =4 absorption and a strong and broad absorption centered at g = 2.7.

Difficulties were encountered in obtaining low-temperature epr signal for the phosphine adducts. For example, triethylphosphine produced a broad line with ill-resolved $A_{\perp}$. $A_{\parallel}$ was resolved and allowed the calculation of $g_{\parallel}$, but $g_{\perp}$ could not be obtained. When THF, acetone, methanol, or DMF was added to the phosphine adduct, the spectrum changed entirely to give a g = 4 absorption paired with a sharp axial-type absorption at g = 2.0. Figure 4 illustrates this pair of signals obtained in the case of tri-*n*-butyl phosphine. This spectrum could in turn be

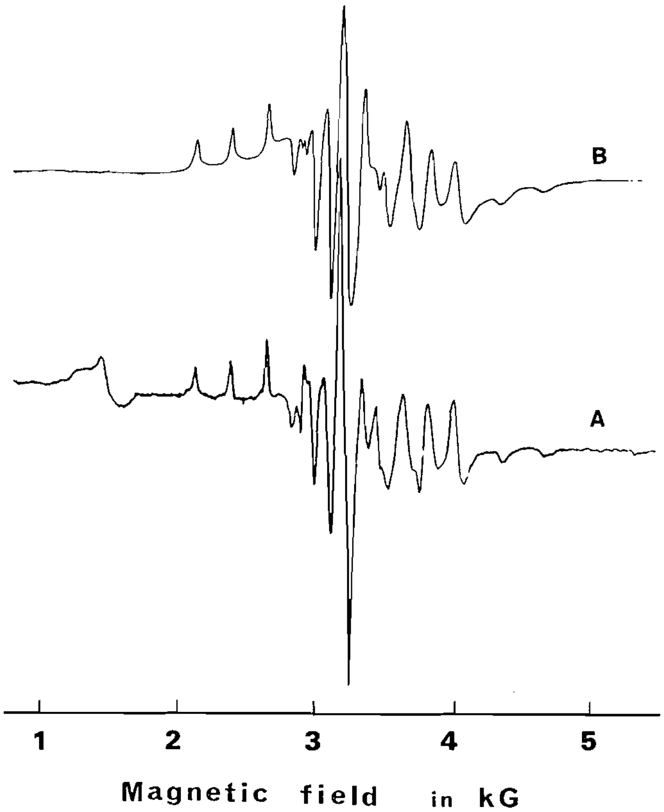

FIG. 3. The frozen-solution epr spectra of niobium(IV) methoxide; (*a*) in methanol solution, (*b*) same as (*a*) with a small amount of dry HCl.

eliminated by the addition of a small amount of HCl gas, but the spectra then reverted to those of the phosphine-free case.

Triphenylphosphine oxide showed a 77 K spectrum almost identical to the pure niobium methoxide, but a clearly resolved doublet on the lowest field $A_{\|}$ absorption demonstrated that two compounds are present with nearly identical epr parameters. The phosphite gave interesting results with tetraethyl pyrophosphite yielding two superimposed spectra. Figure 5 shows the epr spectrum obtained in the case of trimethylphosphite. The observed linewidths are significantly smaller than for the parent compound, illustrated in Fig. 3.

Discussion

Vanadium(IV) or vanadyl halide species form phosphine complexes which have been studied by epr (10). Few epr studies were conducted on niobium(IV) or tantalum complexes (11, 12), one problem being the loss of resolution observed for the heavier metals, attributed in part to the greater quadrupolar moment of their nuclei (13).

Electrolytically reduced niobium solutions have been reported in the literature (14–16), and niobium(IV) has also been produced by reduction with zinc (17) or aluminium foil (13). Discrepancies exist in the literature regarding the various species present in aqueous HCl or alcoholic HCl solutions. $NbCl_6^{2-}$ anion does not give an epr spectrum, indicating a pure octahedral configuration and a degenerate ground state (17). In tetrahedral organometallic niobium(IV) complexes the free electron lies in the $4d_{x^2-y^2}$ orbital and the epr spectrum is well-resolved (18). According to the Jahn–Teller Theorem and when the epr spectrum is observable at room and moderately low temperature, the free electron must lie in the d_{xy} non-

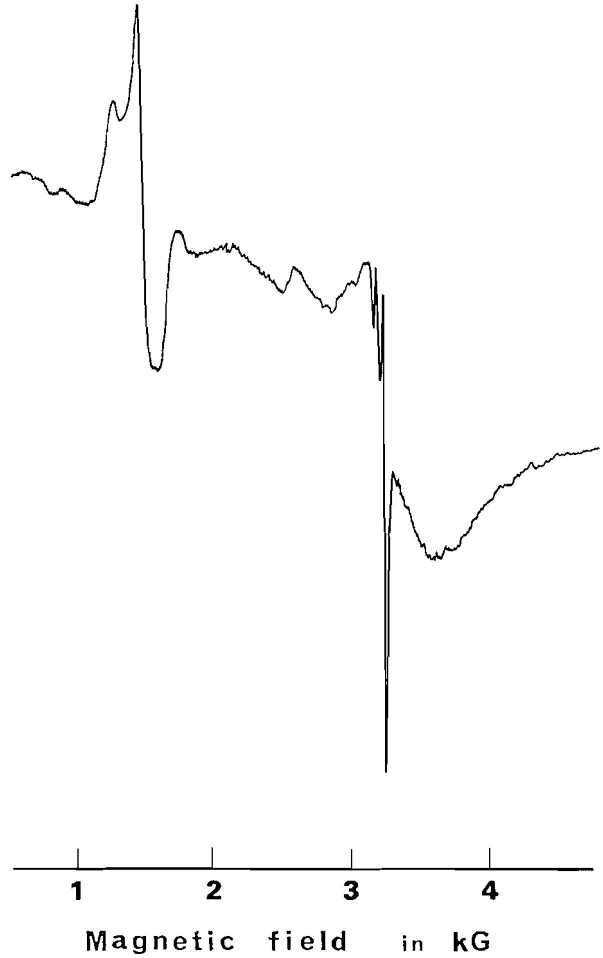

FIG. 4. The frozen-solution epr spectrum of niobium(IV) methoxide with tri-*n*-butylphosphine.

degenerate orbital in octahedral niobium(IV) complexes of D_{4h} molecular symmetry (19).

The ten-line room-temperature patterns observed for the complexes is consistent with the expected 100% ^{93}Nb metal hyperfine arising from nuclear spin $I = 9/2$. The coupling constant of about 180 G is in agreement with previous observations (13, 17). The low solubility of the parent complex and addition compounds points to the polymeric nature of the methoxide. The $g = 4$ signal can be attributed to a forbidden $\Delta M_s = 2$ absorption resulting from the presence of dimers held together by methoxo bridges. Many diamagnetic niobium(IV) complexes are known in the solid state (20) indicating polymeric compounds with strong magnetic interactions. This could also account for the absence of epr spectra or the weak signals observed in some of our solutions, despite the visible absorptions which demonstrate niobium(IV) complexation. The small value of the superhyperfine coupling constants shows weak niobium–phosphorus interactions. In analogy to the structure proposed for niobium(V) alkoxides, we propose the structures of Scheme 1. The triplet superhyperfine patterns are in agreement with two equivalent phosphine ligands coordinated in a *trans* axial geometry, but a *cis* geometry cannot be ruled out because of the absence of phosphorus splittings in the anisotropic spectra. In any case, the equilibrium is strongly in favor of the dimer, and only the smaller phosphines showed evidence for two coordinated ligands. Symmetry considerations rule out direct interaction of "σ" phosphorus orbitals

TABLE 2. Electron paramagnetic resonance data for niobium(IV) methoxide compounds at 77 K

Compound	$g_{\perp}$	$g_{\parallel}$	g_{ave}	$A_{\perp}$	$A_{\parallel}$	A_{ave}	$\Delta M_s = 2$
$Nb(OCH_3)_4$	1.950	1.955	1.951	135	270	180	—
+ THF	—	—	2.0	—	—	—	4.0
$Nb(OCH_3)_4$ + PMe_3	—	—	2.0	—	—	—	4.0
$Nb(OCH_3)_4$ + PEt_3	[a]	1.90	—	[a]	280	—	—
+ THF	—	—	2.0	—	—	—	4.0
$Nb(OCH_3)_4$ + PBu_3	—	—	2.0	—	—	—	4.0
+ THF	—	—	—	—	—	—	4.0
$Nb(OCH_3)_4$ + PMe_2Ph	—	—	2.0	—	—	—	4.0
+ THF	—	—	2.0	—	—	—	4.0
$Nb(OCH_3)_4$ + $Ph_2P(CH_2)PPh_2$	—	—	[b]	—	—	—	4.0
+ HCl	1.950	1.955	1.951	135	272	181	—
$Nb(OCH_3)_4$ + Ph_2PPPh_2 + HCl	1.950	1.955	1.951	135	272	181	—
$Nb(OCH_3)_4$ + $OPPh_3$	1.950	1.955	1.951	135	272	181	—
$Nb(OCH_3)_4$ + $PHPh_2$	—	—	2.0	—	277		4.0
+ HCl	—	—	[b]	—	277		[b]
$Nb(OCH_3)_4$ + $P(OMe)_3$	1.960	1.929	1.946	138	283	186	—
$Nb(OCH_3)_4$ + $(EtO)_2P(O)P(OEt)_2$	[c] 1.962	1.907	1.943	148	307	201	[b]
	[d] 1.962	1.898	1.940	153	320	209	—
$Nb(OCH_3)_4$ + $P(OCH_2)_3CCH_3$	—	—	2.0	—	—	—	4.0

[a] Unresolved signal.
[b] Weak signal.
[c] Major component.
[d] Minor component.

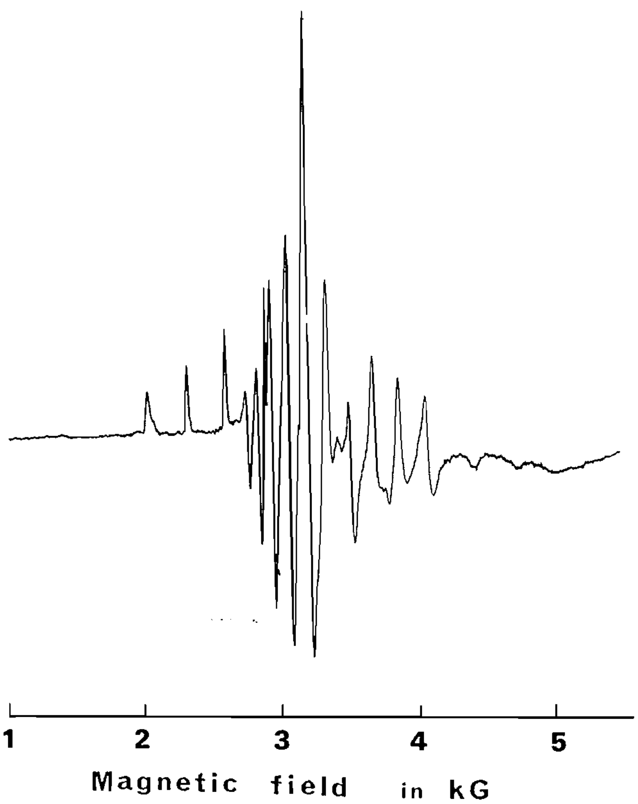

FIG. 5. Electron spin resonance spectrum of niobium(IV) methoxide with trimethylphosphite.

with the niobium d_{xy} orbital and spin-polarization may account for much of the coupling mechanism. Polar solvents shift the equilibrium towards dimer formation whereas HCl gas tends to destroy the dimers by formation of monomeric mixed chloromethoxo complexes. HCl also has the effect of eliminating excess phosphine used as solvent by producing phosphinium chlorides, and changing the dielectric constant. In agreement

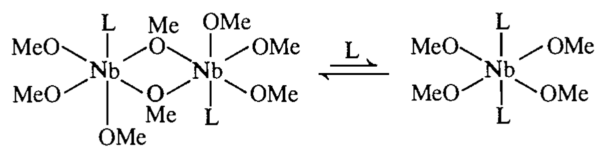

SCHEME 1

with previous work on niobium(V) alkoxides (3), this has a pronounced effect on complex formation. However, niobium(IV) has a stronger tendency to form addition compounds than does niobium(V). The di-octahedral edge-shared dimer structure found for niobium(V) methoxide is coordinatively saturated whereas the same structure has room for one ligand (L in Scheme 1) in the case of niobium(IV). The bulkier phosphines fail to yield bis-adducts of monomer structure, and so do the bidentate phosphines used despite the expected chelate effect stabilization. We feel niobium(IV) methoxide is a polymer in the solid state, with each octahedral unit sharing two edges with neighboring molecules. Methanol may break up this insoluble structure and produce dimer or oligomer structures responsible for the $\Delta M_s = 2$ signals observed in solution. The axial peaks at $g = 2.0$ are so sharp they must be attributed to exchange-narrowed signals.

The low-temperature spectra can be explained assuming the same structures as presented in Scheme 1. The dimer or polymer signals at $g = 4$ and $g = 2$ are very strong, but superimposed on a broad absorption centered near 3300 G, as shown for example in Fig. 4. The sharp lines found for the trimethylphosphite adduct presented in Fig. 5 are attributed to slower methoxo group exchange in this species compared to the parent compound which shows broader features. Niobium(V) methoxide shows significant variations in its low-temperature nmr chemical shifts corresponding to various non-equivalent methoxide groups in exchange (21). The low temperature spectrum obtained for niobium(IV) methoxide in the presence of triphenylphosphine oxide shows spectroscopic parameters identical to the ligand free system, as listed in Table 2. However, the small but clearly visible splitting of the lowest field

$A_{\parallel}$ component indicates two similar compounds are present. Triphenylphosphine oxide is reported to react with niobium(V) alkoxide (1) to make an addition compound, but with niobium pentachloride, a niobium oxytrichloride adduct is formed by oxygen abstraction (5). Because triphenylphospine oxide is the only phosphorus-containing donor which we found to cause such a splitting, we may tentatively conclude it produces also a niobium oxymethoxocomplex. Tetraethylpyrophosphite yields two species which are attributed to the presence of excess phosphite which can thus form a *bis* complex and a *mono* adduct containing bidentate ligand.

In general, the phosphites produce larger $A_{\parallel}$ splitting constants than the phosphines. Inspection of the data listed in Table 2 also shows that the large hyperfines coincide with the smaller g values. This trend should follow variations in the strength of metal–ligand bonding but most of the spectra observed show great similarities in the spectroscopic parameters related to monomers. No differences are detected in spectra attributed to dimer species.

Conclusion

Niobium(IV) methoxide shows features analogous to niobium(V) alkoxides. The results point to a polymeric network for the structure of this compound, and a dimer structure in equilibrium with some monomer in solution. Weak interactions with phosphorus containing donors also result in the predominance of dimer adducts. Electron paramagnetic resonance spectra are useful in confirming that early transition metal alkoxides prefer to self-associate rather than form complexes with donor ligands. Further work showing stronger bonding in mixed niobium(IV) chloro-methoxo complexes will be reported elsewhere.

Acknowledgments

Financial help is gratefully acknowledged from NSERC (A1127) and FCAC Québec (EQ−2441).

1. L. G. Hubert-Pfalzgraf, J. Guion, and J. G. Riess. Bull. Soc. Chim. Fr. 3855 (1971).
2. D. C. Bradley. Progress in inorganic chemistry. Vol. II. *Edited by* F. A. Cotton. Interscience, New York. 1960. p. 203.
3. L. G. Hubert-Pfalzgraf and J. G. Riess. J. Chem. Soc. Dalton, 585 (1974); D. C. Bradley and C. E. Holloway. J. Chem. Soc. A, 219 (1968).
4. L. G. Hubert-Pfalzgraf. Inorg. Chim. Acta, **12**, 229 (1975).
5. R. C. Mehrotra, A. K. Rai, P. N. Kapoor, and R. Bohra. Inorg. Chim. Acta, **16**, 237 (1976).
6. P. Sharrock and M. Melník. Ann. de l'ACFAS, **51**, 47 (1984).
7. V. Katovic and C. Djordjevic'. Inorg. Chem. **9**, 1720 (1970).
8. N. D. Chasteen. J. Magn. Reson. **27**, 349 (1977).
9. R. C. Mehrotra, M. M. Agrawal, and P. N. Kapoor. J. Chem. Soc. A, 2673 (1968).
10. G. H. Olivé and S. Olivé. J. Am. Chem. Soc. **93**, 4154 (1971).
11. N. H. Kilmer and C. H. Brubaker, Jr. Inorg. Chem. **10**, 3283 (1971).
12. R. J. Burt, C. J. Leigh, and D. L. Hughes. J. Chem. Soc. Dalton, 793 (1981).
13. G. Labauze, E. Samuel, and J. Livage. Inorg. Chem. **19**, 1384 (1980).
14. M. Lardon and H. H. Gunthard. J. Chem. Phys. **44**, 2010 (1966).
15. I. F. Gainullin, N. S. Garifyanov, and B. M. Kozyrev. Dokl. Acad. Nauk SSSR, **180**, 878 (1968).
16. R. A. D. Wentworth and C. H. Brubaker, Jr. Inorg. Chem. **2**, 551 (1963).
17. D. P. Johnson and R. D. Bereman. J. Inorg. Nucl. Chem. **33**, 679 (1971).
18. C. P. Stewart and A. L. Porte. J. Chem. Soc. Dalton, 722 (1973).
19. K. A. Rubinson. J. Am. Chem. Soc. **98**, 5188 (1976).
20. J. C. Bailar, J. J. Emeleus, R. Nyholm, and A. F. Trotman-Dickenson. Comprehensive inorganic chemistry. Vol. 3. Pergamon Press. 1973. p. 553.
21. J. G. Riess and L. G. H. Pfalzgraf. J. Chim. Phys. **70**, 646 (1973).

The photolysis of 2,3- and 3,3-dimethyl-1-butene at 147.0 and 184.9 nm

HÉLÈNE DESLAURIERS AND GUY J. COLLIN[1]

Département des Sciences Fondamentales, Université du Québec à Chicoutimi, Chicoutimi (Qué.), Canada G7H 2B1

Received March 26, 1984

HÉLÈNE DESLAURIERS and GUY J. COLLINS. Can. J. Chem. **63**, 62 (1985).

The photofragmentation of 2,3-dimethylbutene and 3,3-dimethylbutene has been studied at 147 and 184.9 nm in the gas phase. The main primary decomposition process at both wavelengths involves the rupture of a β(C—C) bond. The quantum yield for this process is higher than 0.7 at 147 nm and is probably even higher at 184.9 nm. All dimethallyl radicals formed at 147 nm in this process decompose at low pressure, but some of them isomerize from the α,β- to the α,α- structure (and vice versa) — via a 1,4-H transfer — before decomposition. At 184.9 nm, the same primary process is used to get a rough value for the lifetime of the photoexcited molecule, compared with the one made with RRKM calculations by assuming that all the photon energy resides in the vibrational framework of the fundamental electronic state. These lifetimes are about one nanosecond or less.

HÉLÈNE DESLAURIERS et GUY J. COLLINS. Can. J. Chem. **63**, 62 (1985).

On a étudié la photolyse des diméthyl-2,3- et -3,3-butène-1 à 147 et à 184,9 nm. Le principal mode de fragmentation de la molécule photoexcitée implique la rupture d'un lien C—C situé en position β. Le rendement quantique de ce processus primaire est supérieur à 0,7 à 147 nm et peut-être plus élevé encore à 184,9 nm. À 147 nm, tous les radicaux diméthallyles se décomposent à basse pression, mais certains le font après isomérisation par transfert interne 1,4 d'un atome d'hydrogène. À 184,9 nm le même processus primaire est utilisé pour déterminer le temps de vie de la molécule photoexcitée. Ce temps de vie, de l'ordre ou moins de la nanoseconde, est comparé avec celui que l'on peut obtenir à l'aide de calculs RRKM en supposant que toute l'énergie du photon est distribuée dans le tissu vibrationnel de la molécule.

Introduction

We have recently studied the gaseous photolysis of tetramethylethylene and 1-hexene at 184.9 nm. At low pressures (1 Torr = 1330 N m^{-2}), both photoexcited molecules decompose. The photoexcited 1-hexene molecule gives rise to the rupture of the β(C—C) bond (1) and that of the tetramethylethylene — a molecule without the β(C—C) bond — gives rise to the rupture of either a β(C—H) or a α(C—C) bond (2) with similar probability. Moreover, at high pressure (above 100 Torr), isomers are formed with rather high quantum yields in the tetramethylethylene case: Φ(isomers) = 0.34 in the presence of high propane pressure (3). Conversely, the isomerization processes are very low or not even observed in the 1-hexene case: Φ(isomers) ≤ 0.01 (1).

This work has two main purposes. First, we shall examine in other C_6 terminal olefins the validity of the rupture of the β(C—C) bond at low pressure, and, if possible, we shall estimate the lifetime of the photoexcited molecule. Second, we shall try to reconcile the apparent conflict observed above at high pressure: does the photoexcited molecule isomerize? We have chosen 2,3-dimethylbutene (23DMB) and 3,3-dimethylbutene (33DMB) for this study. It is hoped that any structural effect inside the C_6 family of terminal olefins will be exemplified.

Experimental section

Experimental details were essentially the same as those reported in previous papers from this laboratory (1–3). This include the Hg-lamp and actinometry (1). 23DMB and 33DMB are API products: 99.93 ± 0.03% and 99.98 ± 0.02%, respectively. All the irradiations were performed at room temperature (T ≃ 20°C). The analyses of the starting materials reveal only traces of lighter compounds (≤50 ppm). However, some C_6 hydrocarbons are present. They are 3- and 4-methyl-1-pentene (0.01%), 1-hexene (0.035%), and 2-methyl-2-pentene (0.055%) in 23DMB; 2,2-dimethylbutane (17.5 ppm) and 2,3-dimethyl-1,3-butadiene (?) (19.5 ppm) in 33DMB. The relatively large amount of impurity in 23DMB may be the result of an artifact: we observed an increase in impurity content (ca. 1%) when the gas chromatograph was used at T = 50°C. All these analyses were routinely made on two gas-chromatographs (dual flame ionization detector) one equipped with a squalane column (4) and the other one with a UCON column maintained at room temperature (23DMB case) or at 50°C (33DMB case) (5).

The RRKM calculations were made as reported in a previous paper from this laboratory (6). The vibrational models for 33DMB were taken from the literature (complex **2**) (7).

Results

The photolyses of 23DMB and 33DMB yield a number of hydrocarbon products which are reported in the tables along with their quantum yields. Within experimental conditions the percentage of conversion is kept well below 1%. Oxygen or nitric oxide at a sufficient concentration level (≃10%) remove free radicals from the reaction zone and does not significantly absorb the incident photon beam. Deuterium iodide was also used to scavenge free radicals. This technique was only possible with 33DMB. In the presence of 23DMB, the addition of DI results in an orange liquid formation.

At 147 nm

In both systems and in the presence of 10% oxygen, the main product is isoprene (Fig. 1) with pressure-dependant quantum yields between 0.35 and 0.8. A few other products, having lower quantum yield, are sensitive to an increase in the pressure. They are 1,2-butadiene (Fig. 2) and 2-methyl-2-butene formed in the 23DMB case: its quantum yield decreases from 0.03 at 5 Torr to 0.015 at 150 Torr. Several products formed with low yields are rather insensitive to an increase in pressure (Table 1). In the pure systems, the products are more numerous (Table 2). Ethane and 2,2,3-trimethylbutane are among the major ones. The addition of DI has substantially increased the methane yield (Table 3). Finally, isomers were not observed in either system in the presence of 10% oxygen.

At 184.9 nm

Except for isoprene (Fig. 3), all the quantum yields measured in the presence of oxygen are lower than 0.01. Table 4

[1]To whom all correspondence should be addressed.

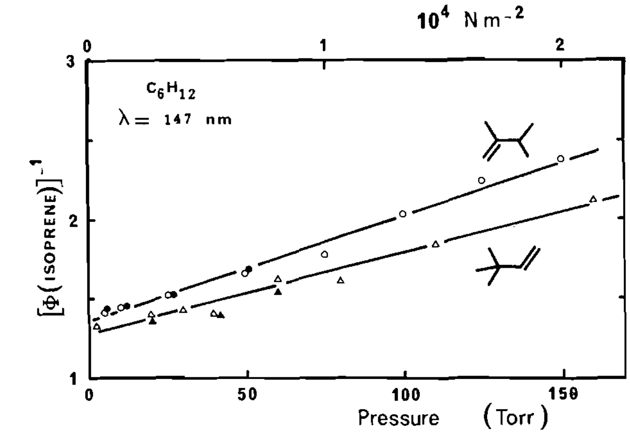

FIG. 1. Photolyses of 23DMB (○,●) and 33DMB (△,▲) at 147 nm either pure (○,△) or in the presence of 10% oxygen (●,▲). The straight lines are calculated from linear regressions: ○: $y = 1.358 + 0.0067x$, $r^2 = 0.983$; △: $y = 1.262 + 0.0051x$, $r^2 = 0.978$.

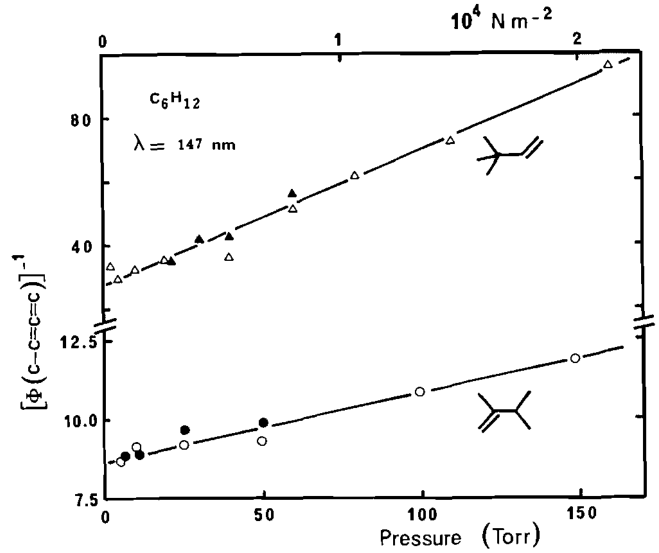

FIG. 2. Photolyses of 23DMB (○,●) and 33DMB (△,▲) at 147 nm either pure (○,△) or in the presence of 10% oxygen (●,▲). The straight lines are calculated from linear regressions: ○: $y = 8.6 + 0.021x$, $r^2 = 0.942$; △: $y = 27.6 + 0.41x$, $r^2 = 0.981$.

gives the main products formed in the pure systems. Again, isomers were not observed in the presence of 10% added oxygen even in the cases where 2–6 atm of propane were added to 50 Torr of monomer. Absorption coefficients of the 184.9 nm line were measured (base 10): ε(23DMB) = 7 200 (±5%) and ε(33DMB) = 5 900 (±5%) $dm^3\ mol^{-1}\ cm^{-1}$, in agreement with values taken from the literature (8).

Discussion

(a) Fragmentation of the photoexcited molecules and excited intermediates

At 147.0 nm

The energy of the incident photon at this wavelength is about 810 kJ $Einstein^{-1}$. Thus, the photoexcited molecules have much more internal energy than what it is needed for a C—C bond rupture. For example,

[1] 23DMB or 33DMB + $h\nu \rightarrow$ 23DMB** or 33DMB**

TABLE 1. Quantum yields of the photolyses of 23DMB and 33DMB in the presence of 10% oxygen at 147 nm[a]

Products	Quantum yield 23DMB	33DMB
Methane	0.03 ± 0.01	0.04 ± 0.01
Acetylene	$0.01_3 \pm 0.00_2$	$0.13 \pm 0.01_5$
Ethylene	0.04 ± 0.01	$0.04 \pm 0.01_5$
Propene	0.10 ± 0.01	0.06 ± 0.01
Propyne	0.10 ± 0.02	0.00
Allene	$0.05_5 \pm 0.01$	0.00
Isobutane	0.00	$0.02_4 \pm 0.00_5$
1,3-Butadiene	$0.01_5 \pm 0.00_5$	0.05 ± 0.01

[a] Pressure of the monomer is between 10 and 100 Torr; all quantum yields are the same in the pure systems except those of methane, propene, and isobutane (see Table 2).

[2] $23DMB^{**} \rightarrow CH_3^* + \underbrace{\overline{CH_2C(CH_3)CHCH_3}^*}_{A^*}$

[3] $33DMB^{**} \rightarrow CH_3^* + \underbrace{CH_3\overline{C(CH_3)CHCH_2}^*}_{B^*}$

$$\Delta H([2]) \simeq \Delta H([3]) \simeq 290 \text{ kJ mol}^{-1} \quad (9)$$

The excess energy is about 520 kJ mol^{-1} and must be shared between the fragments. Part of the C_5H_9* radicals (**A*** or **B***) carry away sufficient energy to overcome the energy barrier of the following process:

[4] **A*** or **B*** $\rightarrow H + CH_2{=}C(CH_3)CH{=}CH_2$ $\quad E_A \simeq 200$ kJ mol^{-1}

[5] **A*** or **B*** + M → M + **A** or **B**

This simple mechanism is known as a Stern–Volmer one (processes [1]–[5]) and the reverse of the isoprene quantum yield is a linear function of the pressure (10) (Fig. 1). At zero pressure, the Φ(isoprene) values, measured in the presence of 10% oxygen, are 0.74 and 0.79 in the 23DMB and 33DMB systems, respectively. Since the ϕ(process [2] or [3]) value is less than unity, the majority of **A*** or **B*** decomposes at zero pressure. Another compound observed in the presence of oxygen and having a Stern–Volmer behavior is 1,2-butadiene (Fig. 2). Its quantum yield is smaller than that of isoprene and smaller in the 33DMB than in the 23DMB system. Since allene is formed in the decomposition process of the excited β-methallyl radicals (11, 12), it may be proposed that the α,β-dimethallyl radicals also decompose only partially in 1,2-butadiene.

[6] $\overline{CH_2C(CH_3)CHCH_3}^* \rightarrow CH_2{=}C{=}CHCH_3 + CH_3$

[7] $\overline{CH_2C(CH_3)CHCH_3}^* + M \rightarrow M + \overline{CH_2C(CH_3)CHCH_3}$

Conversely, excited α-methallyl radicals are not known to decompose in allene. Thus, α,α-dimethallyl radicals are not expected to produce 1,2-butadiene. Moreover, a structural isomerization process must take place somewhere in order for this to happen. An easy way to explain such 1,2-butadiene formation is to assume an isomerization process involving **A*** and **B***.

Since these allylic radicals are far from cold, they have an internal energy probably sufficient to allow the occurrence of a 1,4-hydrogen atom transfer:

[8] **A*** ⇌ **B***

TABLE 2. Quantum yields of the photolyses of pure 23DMB and 33DMB at 147 nm[a]

	23DMB			33DMB		
Pressure (Torr)	10	50	100	10	50	100
Methane	0.14	0.14	0.14	0.09	0.04	0.04
Ethane	0.29	0.32	0.33	0.31	0.36_5	0.31
Propene	0.12	0.12	0.11_5	0.06	0.06_5	0.05_5
Propane	0.02	0.03	0.03	0.00	0.00	0.00
Isobutane	0.04	0.05	0.05_5	0.03_5	0.03_5	0.03
Neopentane	0.00	0.00	0.00	0.02	0.02	0.02
C_4H_8[b]	0.00	0.01	0.00_5	0.03	0.03_5	0.06
2,3-Dimethylbutane	0.18	0.17	0.14_5	0.00	0.00	0.00
3,3-Dimethylbutane	0.00	0.00	0.00	0.07	0.06	0.03
2-Methyl-2-pentene	0.00_8	0.01	0.02_3	0.04	0.10	0.13
33DMB	0.01	0.03	0.00_5	—	—	—
23DMB	—	—	—	0.01_5	0.01_3	0.01
3-Methyl-2-pentene	0.02	0.12_4	0.11_5	0.02	0.02_7	0.03_8
2,2,3-Trimethylbutane	0.19	0.15	0.13_5	0.35_7	0.21	0.22
2-Ethyl-3-methyl-1-butene	0.01_7	0.03	0.03	0.00	0.00	0.00

[a]All quantum yields vanish in the presence of 10% oxygen except in the cases of methane, propene, and isobutane; see Table 1.
[b]Isobutene + 1-butene.

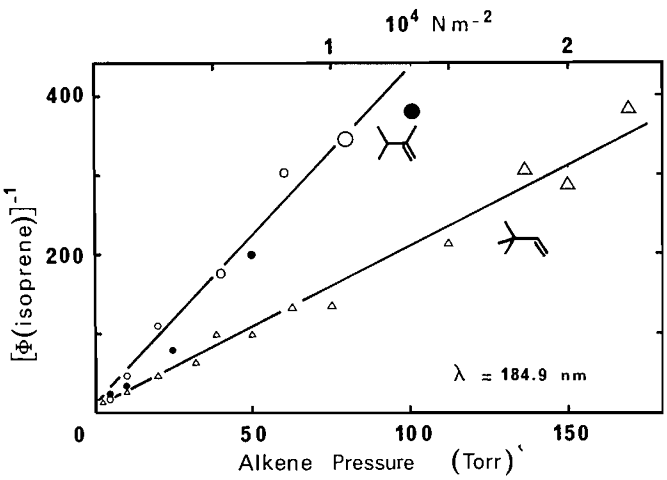

FIG. 3. Photolyses of 23DMB (○,●) and 33DMB (△,▲) at 184.9 nm either pure (○,△) or in the presence of 10% oxygen (●,▲). The straight lines are calculated from linear regressions: ○: $y = 16.19 + 4.03x$, $r^2 = 0.956$; △: $y = 7.0 + 2.0x$, $r^2 = 0.997$.

Other minor primary fragmentation processes must be proposed to take account of the results. For example, the occurrence of the rupture of a α(C—C) bond results in various compounds.

[9] $\quad 23DMB^{**} \rightarrow CH_3\dot{C}HCH_3^* + CH_2{=}\dot{C}CH_3^*$

[10] $\quad 33DMB^{**} \rightarrow t\text{-}C_4H_9^* + \dot{C}H{=}CH_2^*$

Again the major excess energy of the incident photon must be distributed among the fragments and the majority of them may decompose at low pressure. Thus, propylene (13), propyne, and allene (14), and acetylene (15) are expected even in the presence of oxygen (Table 1). At higher pressure and in the pure systems, propane and isobutene must be formed in the 23DMB system, as well as neopentane and propene in the 33DMB (Table 2). 1,3-Butadiene must be formed jointly with two methyl radicals since no ethane is formed in the presence of DI (Table 3). Finally, an unusual primary process seems to occur in the 33DMB system. In the presence of 10% oxygen,

TABLE 3. Quantum yields of the photolysis of 33DMB in the presence of DI

	147 nm		184.9 nm		
33DMB (Torr)	10	20	10	25	50
DI (Torr)	2	4	1	2.5	5
Methane	0.86	0.96	0.89	0.54	0.48
Ethylene	0.07	0.07	0.03	0.06	0.10
Isobutane	0.10	0.10	0.02	0.06	0.09
3-Methyl-1-butene	0.01	0.02	0.04	0.06	0.07
2-Methyl-1-butene	0.02_5	0.04_5	0.01_2	0.01_7	0.01_6
2-Methyl-2-butene	n.m.[a]	n.m.	0.16	0.28	n.m.
2,2-Dimethylbutane	0.23	0.16	n.m.	0.26	n.m.

[a]Not measured.

tiny amounts of isobutane are formed.

[11] $\quad 33DMB^{**} \rightarrow iso\text{-}C_4H_{10} + C_2H_2$

At 184.9 nm

At this wavelength products are formed in lesser quantities than reported at 147 nm (Table 4). Figure 3 shows the variation of the reverse of the isoprene quantum yield versus the pressure. The Stern–Volmer behavior of these plots is similar to the observation made at 147 nm. However, the quantum yields measured at zero pressure are lower: $\Phi(\text{isoprene}) = 0.06_2$ and 0.27_6 in the 23DMB and 33DMB, respectively. In addition, the dependence of the pressure of these quantum yields is much stronger. Much more significant is the decrease of the methyl quantum yield with an increment of pressure. Compare for example Φ(ethane) in Tables 2 and 4 and Φ_{DI}(methane) in Table 3. By adding up the quantum yields of the products formed from methyl—methyl and methyl—**A** or —**B** radicals reactions, the $\Phi(CH_3)$ values may be estimated at each pressure. These values are reported in a Stern–Volmer way in Fig. 4. Again the $\Phi_0(CH_3)$ values measured at zero pressure are close to unity. In a first approximation, all the formation of methyl radicals may be ascribed to the primary processes. Thus Fig. 4 may be used to estimate the rate constant of the mono-

TABLE 4. Quantum yields of the photolysis of pure 23DMB and 33DMB at 184.9 nm

	23DMB			33DMB		
Pressure (Torr)	10	50	100	10	50	100
Methane	0.02	0.03	0.04	0.02_7	0.01_5	0.00_8
Ethane	0.24	0.13_5	0.10	0.30	0.22	0.16
Isobutane	0.00_4	0.00_2	0.00_1	0.00_1	0.00_1	0.00_1
2-Methyl-2-pentene	0.01_5	n.m.	n.m.	0.17	0.21	0.17
3-Methyl-2-pentene (*cis* + *trans*)	0.24	0.14	0.10_5	0.01_6	0.00_7	0.00_5
2,2,3-Trimethylbutane	0.01	0.01	0.01_4	0.00_8	0.00_4	0.00_3
2-Ethyl-3-methyl-1-butene	0.00_7	0.00_8	0.00_3	0.00	0.00	0.00

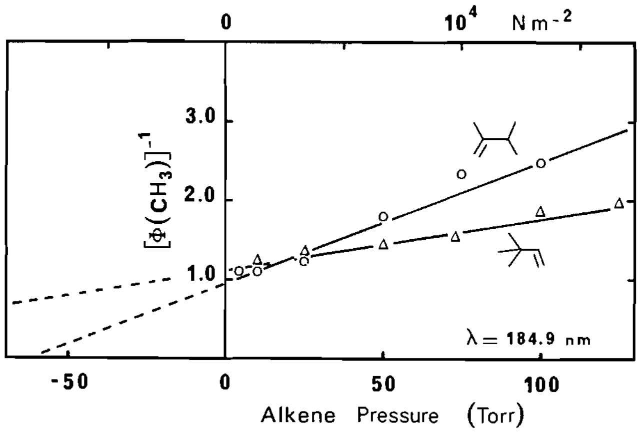

FIG. 4. Photolyses of pure 23DMB (○) and 33DMB (△) at 184.9 nm. The straight lines are calculated from linear regressions: ○: $y = 0.96 + 0.014x$, $r^2 = 0.95$; △: $y = 1.11 + 0.0065x$, $r^2 = 0.92$.

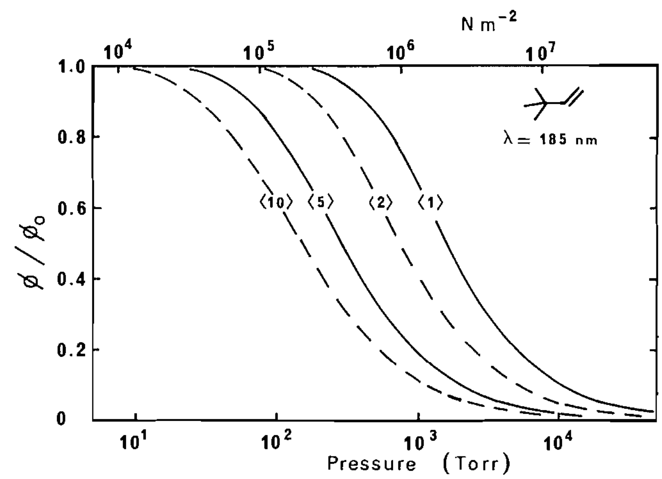

FIG. 5. Effect of the pressure on the fragmentation of 33DMB photoilluminated at 184.9 nm as determined through RRKM calculations. Stepladder models: ⟨10⟩ . . . are energies in kcal mol^{-1} transferred on each collision: see ref. 6.

molecular fragmentation process of the photoexcited molecule. In fact, the intercept of the Stern–Volmer plot with the pressure axis is a measure of the k_2/k_{12} and k_3/k_{12} ratios[2] (negative value: see Fig. 4).[3]

[12] $C_6H_{12}^{**} + M \rightarrow M + C_6H_{12}$

The intercepts are −60 and −170 Torr in the 23DMB and 33DMB systems, respectively. A similar value determined for the stabilization of photoexcited 1-hexene molecules was found about −30 Torr (1). The experimental k_{12} values are k_{12}(1-hexene) = 0.5 10^9, k_{12}(23DMB) = 1 10^9, and k_{12}(33DMB) = 2.75 10^9 s^{-1}. Thus in the C_6 1-alkene group, it appears that the lifetime of the photoexcited molecule decreases with an increase in the degree of ramification of the monomer. Figure 5 shows the results of RRKM calculations applied to process [9] of 33DMB (7). When a stepladder model is used for the stabilization of the photoexcited molecule where all the energy of the photon may be found in the vibrational framework of the ground state, it turns out that half of the excited molecules are stabilized at a pressure of 155 Torr, provided an energy step of 10 kcal mol^{-1} is chosen. The lessening of the lifetime of the vibrationally excited molecule is probably a direct consequence of the number of available reaction channels (1 in 1-hexene, 2 in 23DMB, and 3 in 33DMB) and also the slight decrease of activation energy with an increase of the ramification of the parent molecule (see footnote 3 and ref. 17).[3] The agreement with the experimental value is good, although it may be fortuitous. This constitutes an indication that the lifetime of the electronic excited states formed upon photoexcitation is much shorter.

(b) Radical reactions

At 147 nm

The effect of the addition of molecular oxygen has a drastic effect on the formation of various products (footnote *a*, Table 2). Thus it may be proposed that several products are formed in radical–radical reactions. The ethane quantum yield of 0.3 suggests a rather high yield for the methyl radical formation. Other radicals are also present. As seen in Table 2 as well as the DI experiments in Table 3, hydrogen atoms and allylic C_5H_9 radicals are formed. In fact, the H atom adds itself very efficiently to the double bond of the monomers and gives rise to the formation of a methyl-substituted C_6H_{13} radical (18). The combination of the latter with the methyl is responsible for the 2,2,3-trimethylbutane formation in both systems, 2,3- and 3,3-dimethylbutane are partly formed in disproportionation processes involving a C_6H_{13} and another radical.

---

[2] The rate constant subscripts refer to the reaction numbers.

[3] A referee made a valuable comment at that point. In the 23DMB case, the Stern–Volmer equation is

$$[\Phi(CH_3)]^{-1} = \phi_2^{-1} + \phi_2^{-1}(k_{12}/k_2)[M]$$

where ϕ_2 is the quantum yield of the primary process [2]. Since this ϕ_2 value is close or equal to 1, the slope, k_{12}/k_2, is the inverse of the negative intercept. Of course, the same comment applies in the 33DMB system.

[13] $H + 23DMB \rightarrow (CH_3)_2CCH(CH_3)_2$ **C**

[14] $H + 33DMB \rightarrow (CH_3)_3C\dot{C}HCH_3$ **D**

[15] **C** or **D** + $CH_3 \rightarrow (CH_3)_3CCH(CH_3)_2$

In experiments where DI is added, methyl radicals as well as **D**, abstract D atoms from DI: methane and 2,2-dimethylbutane are formed, respectively (19, 20). Obviously, allylic C_5H_9 radicals are also present: 3-methyl-2-pentene (*cis* + *trans*) and 2-methyl-2-pentene are the results of the combination of methyl and either α,β- or α,α-dimethallyl radicals in 23DMB and 33DMB, respectively.

[16*a*] $\overline{CH_2C(CH_3)CHCH_3} + CH_3 \rightarrow CH_3CH{=}C(CH_3)C_2H_5$

[16*b*] **A** $\rightarrow$ 23DMB

[17*a*] $CH_3\overline{C(CH_3)CHCH_2} + CH_3 \rightarrow (CH_3)_2C{=}CHC_2H_5$

[17*b*] **B** $\rightarrow$ 33DMB

[18] **A** or **B** + $CH_3 \rightarrow CH_4 + CH_2{=}C(CH_3)CH{=}CH_2$

The k_{16a}/k_{16b}, k_{17a}/k_{17b}, and $\Delta(CH_3,\mathbf{B})$ values were reported (16). They are 1.81 ± 0.04, 6.1 ± 0.6, and 0.1, respectively. Other radicals are formed in smaller amounts. For example, DI reveals the presence of methylsubstituted C_4H_9 radicals (19, 20) in the 33DMB system (Table 3) and their structure may be inferred from the neopentane formation (Table 2). In the 23DMB system, the presence of isopropyl radicals may be shown from the isobutane formation. Finally, β-isopropylallyl radicals probably appear in the 23DMB system. By combination reaction with methyl radicals they are responsible for the 2-ethyl-3-methyl-1-butene formation. They are probably formed through the abstraction reaction of an allylic hydrogen atom by a radical, although definitive proof is lacking. This reaction would explain part of the methane formation observed in the presence of oxygen (Table 1).

At this point it must be said that the above mechanism explains neither the formation of 2-methyl-2-pentene and 33DMB in the 23DMB system nor the formation of 3-methyl-2-pentene and 23DMB in the 33DMB system. An easy way to reconcile the observations with the above mechanism consists of calling upon the isomerization process involving the C_5H_9 radicals, and reported above (process [8]). One may add that this isomerization process is probably not at equilibrium, since a pressure effect is evident (Table 2). The amount of the isomerization decreases with an increase in the pressure.

At 184.9 nm

The main difference observed between experiments done at 147 and 184.9 nm is the relatively less yields of products at the longer wavelength: see for example, in Tables 2 and 4, the methane, ethane, . . . , 2,2,3-trimethylbutane quantum yields. However methyl as well as allylic C_5H_9 radicals are still present. One should add the absence of dimethylbutanes, 23DMB, and 33DMB. Thus it can be said either that hydrogen atoms are not formed or that their quantum yields are too low to measure. If the previously indicated mechanism for the fragmentation of the photoexcited molecules is still acceptable, hydrogen atoms are mainly formed in secondary processes. The excess energy of the photon is now reduced to ca. 350 kJ mol^{-1}. Then, excited $C_5H_9{}^*$ radicals bear away less internal energy at 184.9 nm compared to the situation described in the vacuum uv region. Their lifetime must be longer, so that stabilizing processes are more efficient. In the pure systems, at 147 nm, the isomeric 33DMB and 23DMB were assumed to be formed in radical processes following isomerization of the α,β-dimethallyl radicals towards the α,α- structure and vice versa. Again, the lower energy content of the $C_5H_9{}^*$ precludes this isomerization process, and these isomers are not observed at 184.9 nm.

TABLE 5. Quantum yields of the primary processes of the photolyses of 23DMB and 33DMB at 147 nm

$C_6H_{12}{}^{**} \rightarrow$	23DMB	33DMB
$CH_3 + C_5H_9{}^*$		
$\hookrightarrow H$ + isoprene	0.74	0.79
$\hookrightarrow \dot{C}H_3 + CH_2{=}C{=}CHCH_3$	0.11_6	0.03_6
$i\text{-}C_3H_7 + CH_2{=}\dot{C}CH_3{}^*$		
$\hookrightarrow H + CH_3C{\equiv}CH$	0.10	—
$\hookrightarrow H + CH_2{=}C{=}CH_2$	0.05_5	—
$t\text{-}C_4H_9 + \dot{C}H{=}CH_2{}^*$		
$\hookrightarrow H + CH{\equiv}CH$	—	0.10_6
$CH_2{=}CHCH{=}CH_2 + 2\dot{C}H_3$	0.01_5	0.05
$iso\text{-}C_4H_{10} + CH{\equiv}CH$	—	0.02_4
$\Sigma =$	1.02_6	1.00_6

[a] All the quantum yields are indicated at zero pressure.

Conclusion

From the discussion given above, and the results shown in the tables, a fragmentation pattern may be proposed (Table 5). The total is close to unity, but uncertainties on values make the Σ value no more accurate than ±10%. A theoretical methyl radical quantum yield may be calculated: $\Phi(CH_3) = 1.1$ and 0.96 in 23DMB and 33DMB systems, respectively. As seen in Table 2, more precisely from the products formed in the methyl radical reactions, $\Phi(CH_3)$ values may be calculated and are close to unity at low pressure. Unfortunately, not all the pertinent disproportionation/combination ratios are available. However, a rough estimate leads to $\Phi_{meas}(CH_3)$ values such as 1.1 ± 0.2 and 1.0 ± 0.2 in each system. The agreement is particularly good. For the other radicals, similar calculations are much more difficult, and indeed impossible, since not all the pertinent products have been measured. For example, the measurements of the hydrogen atom quantum yield requires the measurements of all products coming from the C_6H_{13} radical reactions, and among them are the $C_{12}H_{26}$ molecules.

Acknowledgment

We thank the "Fonds de Formation de Chercheurs et d'Actions Concertées" (F.C.A.C.) for its financial assistance throughout this work.

1. H. DESLAURIERS, G. J. COLLIN, and B. SIMARD. J. Photochem. **21**, 19 (1983).
2. G. J. COLLIN, H. DESLAURIERS, and A. WIĘCKOWSKI. J. Phys. Chem. **85**, 944 (1981).
3. G. J. COLLIN and H. DESLAURIERS. Can. J. Chem. **61**, 1510 (1983).

4. R. A. HIVELY and R. E. HIPTON. J. Gas Chromatogr. **6**, 203 (1968).
5. J. GAWŁOWSKI, J. NIEDZIELSKI, and A. BIERZYNSKI. Chem. Anal. **15**, 721 (1970).
6. J. GAWŁOWSKI and G. J. COLLIN. J. Photochem. **23**, 241 (1983).
7. D. C. MONTAGUE. J. Chem. Soc. Faraday Trans. **I**, **71**, 398 (1975).
8. L. C. JONES, JR. and L. W. TAYLOR. Anal. Chem. **27**, 228 (1955).
9. A. B. TRENWITH. Trans. Faraday Soc. **66**, 2805 (1970).
10. J. A. BARLTROP and J. D. COYLE. *In* Principles of photochemistry. J. Wiley and Sons, New York. 1978. Particularly p. 150–155.
11. A. B. TRENWITH and S. P. WRIGLEY. J. Chem. Soc. Faraday Trans. I, **73**, 817 (1977).
12. G. J. COLLIN and H. DESLAURIERS. Int. J. Chem. Kinet. **12**, 17 (1980).
13. B. S. RABINOVITCH and D. W. SETSER. Adv. Photochem. **3**, 1 (1964).
14. J. NIEDZIELSKI, J. GAWŁOWSKI, and T. GIERCZAK. J. Photochem. **21**, 195 (1983).
15. D. G. KIEL, K. P. LYNCH, J. A. COWFER, and J. V. MICHAEL. Int. J. Chem. Kinet. **8**, 825 (1976).
16. D. C. MONTAGUE. Int. J. Chem. Kinet. **5**, 513 (1973).
17. W. TSANG. Int. J. Chem. Kinet. **1**, 245 (1969); A. B. TRENWITH. Int. J. Chem. Kinet. **5**, 67 (1973).
18. J. A. KERR and M. J. PARSONAGE. *In* Evaluated kinetic data on gas phase addition reaction. CRC Press, Cleveland OH. 1972. Particularly pp. 19–39 and references cited therein.
19. P. AUSLOOS and S. G. LIAS. J. Chem. Phys. **44**, 521 (1966).
20. P. AUSLOOS, R. B. REBBERT, and S. G. LIAS. J. Photochem. **2**, 267 (1973/74).

A calorimetric study of trimethylene oxide and its structure I and structure II clathrate hydrates in the temperature range 85 to 270 K[1]

Y. P. HANDA

Division of Chemistry, National Research Council of Canada, Ottawa, Ont., Canada K1A 0R9

Received May 30, 1984

Y. P. HANDA. Can. J. Chem. **63**, 68 (1985).

Heat capacities and dissociation properties of trimethylene oxide and its structure I and structure II clathrate hydrates in the temperature range 85 to 270 K were determined using a Tian–Calvet heat flow calorimeter. The hydrates dissociate incongruently. The heat capacities of the hydrates are similar in magnitude to those observed for other structure I and structure II hydrates. For the structure I hydrate two thermal anomalies were observed. The one centered at 107 K can be identified as due to ordering of the trimethylene oxide dipoles along the $\bar{4}$ axes of the cages as suggested by the previous dielectric and nmr relaxation studies. The second centered at 168 K is interpreted as due to trimethylene oxide rich eutectic rather than due to some restructuring of the host lattice as has recently been suggested.

Y. P. HANDA. Can. J. Chem. **63**, 68 (1985).

Utilisant un calorimètre à écoulement de chaleur du type Tian–Calvet et opérant à des températures allant de 85 à 270 K, on a déterminé les capacités calorifiques et les propriétés de dissociation de l'oxyde de triméthylène et de ses hydrates de clathrates de structures I et II. Les modes de dissociation des hydrates ne sont pas congruents. Les capacités calorifiques des hydrates sont du même ordre de grandeur que celles observés pour d'autres hydrates de structures I ou II. On observe deux anomalies thermiques dans le cas de l'hydrate ayant la structure I. L'une d'elle est centrée à 107 K et on peut l'attribuer au fait que les dipoles de l'oxyde de triméthylène se réorientent le long des axes $\bar{4}$ de la cage, comme il a été suggéré par des études diélectriques et de relaxation en rmn qui ont été effectuées antérieurement. Contrairement à ce qui a été suggéré récemment, on croit que la deuxième anomalie, qui est centrée à 168 K, serait due à un eutectique riche en oxyde de triméthylène plutôt qu'à une certaine restructuration du réseau hôte.

[Traduit par le journal]

Introduction

Trimethylene oxide (TMO) is one of the few guest species known to form both structure I and II clathrate hydrates. This has been confirmed by X-ray diffraction studies (1–3). The compositions of the structures I and II are reported to be $TMO \cdot 7.67H_2O$ and $TMO \cdot 17H_2O$ respectively (2). The phase diagrams (4, 5), dielectric (2, 6, 7), continuous-wave nmr (2), and far infrared absorption (3, 8) studies for both structures and heat capacities (9) for structure I have also been reported.

The structure I TMO hydrate is the only clathrate hydrate for which two unique transitions, one relating to the guest and the other to the host lattice, have been reported. From their dielectric and nmr study, Gough *et al.* (2) suggested that at about 105 K, the TMO guest molecules undergo an ordering transition whereby below 105 K the nearest neighbour TMO dipoles acquire a predominantly parallel alignment along the $\bar{4}$ axes of the 14-hedral cages. This transition was not detected in any of the other studies. From their heat capacity measurements, Comper *et al.* (9) found a thermal anomaly at 169 K and attributed it to some restructuring of the host lattice. No such transition was detected in any of the studies on TMO hydrates. However, a metastable eutectic at 165 K corresponding to conversion of structure II hydrate and solid TMO into TMO-rich (81% by mass) liquid and a stable eutectic at 172 K corresponding to conversion of structure I hydrate and solid TMO into TMO-rich (93% by mass) liquid (4) has been reported. The absence of an independent evidence for any restructuring of the structure I host lattice leaves open the possibility that the transition observed by Comper *et al.* (9) may simply be due to eutectic melting. In the light of these reports, it was decided to re-examine the TMO hydrates.

In this paper the results of heat capacity and dissociation runs on pure TMO and on solid samples of composition $TMO \cdot 7.30H_2O$, $TMO \cdot 7.65H_2O$, $TMO \cdot 8.06H_2O$, and $TMO \cdot 17H_2O$ are presented and discussed in terms of the two transitions noted above. In view of the compositions of structures I and II hydrates (2) and the phase diagram of TMO–water mixture (4), sample $TMO \cdot 7.30H_2O$ should consist of solid TMO and structure I hydrate and sample $TMO \cdot 8.06H_2O$ should consist of a mixture of structures I and II hydrates.

Experimental

TMO was obtained from Fluka Chemical Corp. A gas chromatographic analysis showed it to contain methanol, ethanol, and 1-hexene as impurities. It was purified using a preparative gas chromatograph (F & M Model 775). The gas chromatographic analysis of the final sample did not show any detectable impurities. Water used was distilled and deionized. Solutions of composition $TMO \cdot 7.30H_2O$, $TMO \cdot 7.65H_2O$, $TMO \cdot 8.06H_2O$, and $TMO \cdot 17H_2O$ were prepared from degassed components directly in the calorimeter cells. The sample size in each case was about 5 g. Hydrates were prepared by keeping a sample about 1 K below its dissociation temperature (4, 5) for 2 days and then at a temperature about 10 K below it for another 2 days. This procedure was continued for 10 days after which the sample was kept at 235 K for another 50 days.

The calorimeter and its operating technique has been described elsewhere (10). It is a Tian–Calvet heat flow calorimeter (SETARAM, Model BT), the operation of which has been automated by connecting it to a computer and a data acquisition system. Before loading a sample, the calorimeter was cooled to 10 K below the dissociation temperature of the sample. It was subsequently cooled to 78 K over a period of 8 h and maintained at this temperature for 12 to 48 h before initiating a run. All measurements were made in the temperature scanning mode using scan rates of 9 K h^{-1} for the heat capacity and 3 K h^{-1} for the dissociation runs. The thermopile output was collected every 60 s for the heat capacity and every 15 s for the dissociation runs.

Results and discussion

TMO

For melting temperature, we obtained a value of (173.2 ±

[1]NRCC No. 23665.

TABLE 1. Experimental values of dissociation temperatures for various samples of TMO hydrates

Compound	T_{dso}/K 1st peak	2nd peak
$TMO\cdot7.30H_2O$	250.2	257.0
$TMO\cdot7.65H_2O$	250.9	256.3
$TMO\cdot8.06H_2O$	251.5	259.6
$TMO\cdot17H_2O$	251.1	262.4

0.1) K which is identical with the value reported in the literature (11). For enthalpy of melting, we obtained a value of (6.273 ± 0.050) kJ mol^{-1}. In the temperature range 85 to 160 K, the heat capacity, C_p, results were fitted by the method of least-squares to give the equation

$$[1]\quad C_p/(\mathrm{J\ K^{-1}\ mol^{-1}}) = 40.30 + 1.081 \times 10^{-2}\,(T/\mathrm{K}) + 1.581 \times 10^{-3}\,(T/\mathrm{K})^2$$

with a standard deviation of 0.50 J K^{-1} mol^{-1}. The heat capacity of the liquid in the range 185 to 195 K was virtually constant with a value of 98.6 J K^{-1} mol^{-1}. We are not aware of any literature data on enthalpy of melting and C_p of TMO to compare our results with.

TMO hydrates

The dissociation temperature, T_{dso}, observed for various samples are summarised in Table 1. For each hydrate sample two dissociation peaks were obtained. For the samples $TMO\cdot7.30H_2O$, $TMO\cdot7.65H_2O$, and $TMO\cdot8.06H_2O$ the temperature for the first peak corresponds to the peritectic point at which the structure I hydrate is converted into structure II hydrate and TMO-rich liquid. The temperature for the second peak corresponds to conversion of structure II hydrate into ice and TMO-rich liquid. For the sample $TMO\cdot17H_2O$, the first peak is due to the presence of a small amount of structure I hydrate as reflected by its T_{dso} value. The temperature for the second peak corresponds to the peritectic point at which the structure II hydrate is converted into ice and TMO-rich liquid. The present results are in good agreement with the literature values of 252.3 K (4) and 253 K (9) and of 264 K (4) for the incongruent dissociation of structures I and II hydrates, respectively.

The experimental results of heat capacity measurements are shown in Fig. 1 along with the heat capacities for $TMO\cdot7.67H_2O$ reported by Comper *et al.* (9). Since the C_p values were determined 0.15 K apart, the present results appear as continuous curves. The C_p values of the hydrates studied in this work are very close to each other and for the sake of clarity the curves for $TMO\cdot7.65H_2O$, $TMO\cdot8.06H_2O$, and $TMO\cdot17H_2O$ have been shifted downwards by 6, 8, and 8 J K^{-1} (mol $H_2O)^{-1}$, respectively. For the structure II hydrate, the C_p values are very similar to those for the structure II tetrahydrofuran hydrate (10). For the structure I hydrate, the C_p values are slightly higher than the structure I ethylene oxide hydrate (12). Such a result is to be expected in the light of the recent finding (13) that the C_p of the clathrate hydrates increases slightly with an increase in the unit cell size. The cubic cell parameter for structure I TMO hydrate is 12.02 Å at 143 K (2) and for ethylene oxide hydrate is 11.89 Å at 173 K (14). However, the C_p values of Comper *et al.* for $TMO\cdot7.67H_2O$ are, on the average, 35% higher than the present results for $TMO\cdot7.65H_2O$ at temperatures outside the transition regions.

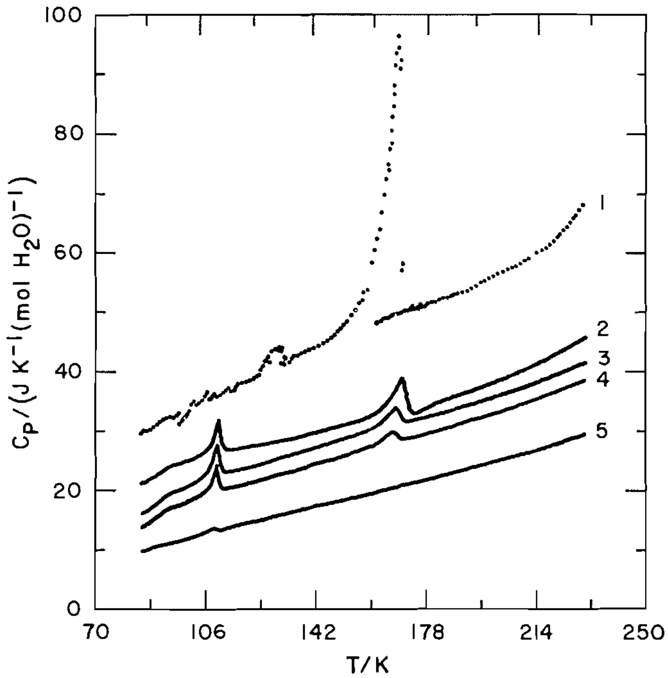

FIG. 1. Experimental heat capacities vs. temperature for trimethylene oxide hydrates. Curve *1*: $TMO\cdot7.67H_2O$ from ref. 9; curve *2*: $TMO\cdot7.30H_2O$; curve *3*: $TMO\cdot7.65H_2O$; curve *4*: $TMO\cdot8.06H_2O$; curve *5*: $TMO\cdot17H_2O$. Curves *3*, *4*, and *5* have been shifted downwards by 6, 8, and 8 J K^{-1} (mol $H_2O)^{-1}$, respectively.

As seen in Fig. 1, all the structure I samples show a transition at 162.6 K with the peak maximum temperature of 168.1 K. The corresponding values from the work of Comper *et al.* are 162 K and 169 K. The transition is very close to the solid TMO-structure I hydrate-TMO rich liquid eutectic observed at 172 K (4). The magnitude of the enthalpy of transition is maximum for $TMO\cdot7.30H_2O$ and corresponds to fusion of 0.042 mol of TMO whereas excess TMO present in the sample was 0.043 mol. The magnitude of the transition is smallest for $TMO\cdot8.06H_2O$ which contains a mixture of hydrates of structures I and II. No transition is observed for $TMO\cdot17H_2O$. The transition observed for $TMO\cdot7.65H_2O$ corresponds to the presence of about 2% unclathrated TMO. This suggests the presence of unreacted ice in the sample. However, the presence of ice can not be detected as according to the phase diagram (4), the melting of ice occurs in the same temperature range as the second dissociation peak observed in our work and thus any information related to melting of a small amount of ice will be buried in the main dissociation peak.

TMO occupies only the larger cages in both structure I and II hydrates. The mean free diameters of the 14-hedral cages which occur in structure I and the 16-hedral cages which occur in structure II are 5.8 Å and 6.6 Å, respectively (15) and the largest van der Waals diameter for TMO is about 6.2 Å (8). Thus whereas enclathration of TMO in the 16-hedral cages should be easy, the relatively large size of TMO makes it difficult to be incorporated in the 14-hedral cages of structure I. The difficulty of enclathration of TMO in the 14-hedral cages is further reflected by the slightly larger unit cell size of $TMO\cdot7.67H_2O$ as compared with other structure I hydrates (2). Thus even when one starts with a solution of proper composition, TMO + $7.67H_2O$, complete enclathration of TMO is not always guaranteed. This, in fact, is a general problem with clathrate hydrates and can occur even in cases where hydrate formation is supposed to take place rather easily, e.g., ethylene oxide and tetrahydrofuran hydrates (12). Since structure II hydrate is stable at a higher temperature than structure I hydrate, the formation of structure I hydrate may proceeed through formation of structure II hydrate first. Gough *et al.* (2) found that samples of structure I hydrate prepared from solution of composition TMO + $7.67H_2O$ always contained a small amount of structure II hydrate. This will lead to the presence of a small excess of unclathrated TMO. From these considerations and from the results presented above, we conclude that the transition observed at 168 K is due to TMO eutectic rather than due to any restructuring of the host lattice as suggested by Comper *et al.* (9).

For structure I hydrate, an order–disorder transition at about 105 K has been reported by Gough *et al.* (2) according to whom at temperatures below 105 K, the TMO dipoles in the 14-hedral cages align themselves parallel to the $\bar{4}$ axes of the cages. No such transition was observed in the structure II hydrate. As seen in Fig. 1, a transition is observed in the present C_p results at 107 K. A small transition peak seen in the structure II hydrate is due to the presence of a small amount of structure I hydrate in the sample as noted above. Similarly a slightly smaller magnitude of the transition observed in TMO·$8.06H_2O$ is due to the required presence of a small amount of structure II in the sample. The dielectric measurements (2) showed that the order–disorder transition process is quite slow and complete equilibrium was not attained even after a period of 12 days. In this work, the samples were conditioned at 78 K for 12 to 48 h and thus only qualitative results can be obtained from the transition peak. The enthalpy change associated with the transition at 107 K is calculated to be 140 J $(\text{mol TMO})^{-1}$ for TMO·$7.65H_2O$. The entropy change for the transition is 1.3 J K^{-1} $(\text{mol TMO})^{-1}$ which suggests that there are about 20% more orientations available to the TMO molecule in the cage above 107 K than below it.

Acknowledgement

The author thanks Mr. C. J. Halpin for purifying and analysing trimethylene oxide.

1. D. F. Sargent and L. D. Calvert. J. Phys. Chem. **70**, 2689 (1966).
2. S. R. Gough, S. K. Garg, and D. W. Davidson. Chem. Phys. **3**, 239 (1974).
3. J. E. Bertie and S. M. Jacobs. J. Chem. Phys. **69**, 4105 (1978).
4. J.-C. Rosso and L. Carbonnel. Compt. Rend. Acad. Sci. Paris, **274C**, 1108 (1972).
5. L. Carbonnel and J.-C. Rosso. J. Solid State Chem. **8**, 304 (1973).
6. R. E. Hawkins and D. W. Davidson. J. Phys. Chem. **70**, 1889 (1966).
7. S. R. Gough, R. E. Hawkins, B. Morris, and D. W. Davidson. J. Phys. Chem. **77**, 2969 (1973).
8. J. E. Bertie and S. M. Jacobs. Can. J. Chem. **55**, 1777 (1977).
9. J. Comper, A. Quesnel, C. A. Fyfe, and R. K. Boyd. Can. J. Chem. **61**, 92 (1983).
10. Y. P. Handa, R. E. Hawkins, and J. J. Murray. J. Chem. Thermodyn. **16**, 623 (1984).
11. H. H. Sisler and P. E. Perkins. J. Am. Chem. Soc. **78**, 1135 (1956).
12. D. G. Leaist, J. J. Murray, M. L. Post, and D. W. Davidson. J. Phys. Chem. **86**, 4175 (1982).
13. Y. P. Handa. J. Chem. Thermodyn. In press.
14. J. E. Bertie, F. E. Bates, and D. K. Hendricksen. Can. J. Chem. **53**, 71 (1975).
15. D. W. Davidson. *In* Water: a comprehensive treatise. Vol. 2. *Edited by* F. Franks. Plenum Press, New York. 1973. Chapt. 3.

Molecular orbital calculations for dialuminum and disilicon hydrides and related systems

N. COLIN BAIRD
Department of Chemistry, University of Western Ontario, London, Ont., Canada N6A 5B7

Received March 12, 1984

N. COLIN BAIRD. Can. J. Chem. **63**, 71 (1985).

Ab initio MO calculations for Si_2H_2 are reviewed and discussed in qualitative terms. New calculations are reported, by MNDO for Si_2H_2 and Si_2H_4, and using both MNDO and *ab initio* methods (including electron correlation at the MP2 level) for various possible structures for Al_2H_2 (**3**). As with the analogous silicon dihydride, a dibridged structure **3***a* is found to be superior to classical structures **3***b*, **3***c*, and **3***d*. MNDO calculations for derivatives of Al_2H_2 are reported. Finally, some implications of the calculations for the surface structures of partially-hydrogenated elemental aluminum and silicon are discussed.

N. COLIN BAIRD. Can. J. Chem. **63**, 71 (1985).

On a réévalué les calculs *ab initio* d'OM effectués sur le Si_2H_2 et on en discute sur une base qualitative. On rapporte de nouveaux calculs MNDO effectués sur le Si_2H_2 et sur le Si_2H_4 ainsi que d'autres, basés tant sur les méthodes MNDO qu'*ab initio* (incluant une corrélation électronique au niveau MP2), effectués sur diverses structures possibles du Al_2H_2 (**3**). Comme avec le dihydrure de silicium analogue, on a trouvé que la structure doublement pontée **3***a* est supérieure aux structures classiques **3***b*, **3***c* et **3***d*. On rapporte les résultats des calculs MNDO effectués sur des dérivés du Al_2H_2. On discute finalement des quelques implications des calculs pour les structures de surface de l'aluminium et du silicium élémentaire partiellement hydrogénés.

[Traduit par le journal]

Introduction

Second-row analogs to the "saturated" first row hydrides A_2H_m are well-known. Thus for example H_3SiSiH_3, H_2PPH_2, and HSSH have long been known, and are analogs to ethane, hydrazine, and hydrogen peroxide. The situation with respect to "unsaturated" hydrides is much less well-developed. A few compounds are known which have silicon–silicon or phosphorus–phosphorus double bonds, but all are derivatives in which all hydrogen atoms are substituted by large organic groups (1).

Although the $R_2Si{=}SiR_2$ and RP=PR molecules synthesized to date have structures which resemble the corresponding $R_2C{=}CR_2$ and RN=NR systems, there are indications from recent theoretical calculations that the silicon analog of acetylene and perhaps other second row hydrides have unusual structures (2). These results have provoked our interest in the field, and we wish to report here some MO calculations (both *ab initio* and semiempirical) for the "double bonded" hydride of aluminum, Al_2H_2, as well as semiempirical explorations (to complement existing *ab initio* results) for Si_2H_2 and Si_2H_4. Finally, the results are used as a basis for some speculations concerning possible structures near the surface of partially-hydrogenated elemental aluminum and silicon.

All *ab initio* calculations were performed using the methods and GAUSSIAN 82 computer program of Pople and coworkers. Geometry searches were performed using the 3-21G* basis for the aluminum atoms (3*a*) and the 31-G basis for hydrogen (3*b*); thus a set of Gaussian *d* orbitals is present on each Al atom, its other valence orbitals (3*s* and 3*p*) are each expanded by three GTOs (split into two sets) and the valence orbital of hydrogen is represented by four GTOs. Final energies were recomputed using the more sophisticated 6-31G* basis (3*c*). The major differential effects of electron correlation were incorporated by performing second-order perturbation calculations using the Moller–Plesset theory ("MP2") for the 6-31G* wavefunction (3*d*) obtained using the Hartree–Fock theory (unrestricted in the case of triplet states).

The MNDO calculations (4) were performed using Thiel's MNDOC computer program. (MNDO rather than the older but sometimes more reliable MINDO/3 method was employed since parameters for aluminum apparently are unavailable for the latter technique.) Our hope was that MNDO results would sufficiently parallel the *ab initio* results and experiment so that systems with three or more second-row atoms could be studied by the much less computationally-expensive semiempirical technique.

We have attempted to understand all the results by recourse to simple theoretical concepts such as bond strength, atomic promotion energy, and delocalization energies in the hope that non-theoreticians can usefully employ and generalize these computations.

Discussion and results

Recently a number of very sophisticated *ab initio* MO calculations, which include treatment of correlation energy, have been reported for Si_2H_2 (2). The global minimum is found to be the dibridged structure **1***a*, which contains a silicon–silicon single bond:

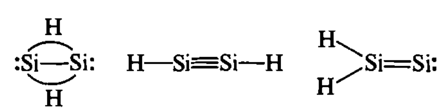

1*a* **1***b* **1***c*

This isomer is preferred energetically to the acetylene analog **1***b*, as well as to **1***c*. This preference can usefully be analyzed in simple terms. Structure **1***a* possesses two divalent, formally s^2p^2 silicon atoms, a single SiSi σ bond and two Si—H single bonds, each of which have been strengthened by delocalization of the bonding electron pair into an empty orbital of the other silicon. Structure **1***b* contains two tetravalent Si atoms (i.e. ones in which an *s* electron has formally been promoted to a *p* orbital to give the s^1p^3 configuration), one σ and two π SiSi bonds, and two localized SiH single bonds. Thus the strength of two π bonds here must be less than two times the sum of the

TABLE 1. MNDO calculations for Si and Al hydrides[a]

Structure		ΔH_f	Geometry
Si_2H_2			
1*a*,	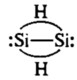	+57.6	SiH = 1.631 SiSi = 2.086 ∠SiHSi = 79.5° ∠HSiH = 76.0° ∠SiH—SiH = 49.5°
1*b*,	H—Si≡Si—H	Collapses to **1***a*	—
1*c*,	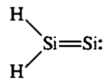	+90.7	SiH = 1.432 SiSi = 1.990 ∠HSiSi = 128.0° Planar molecule
Si_2H_4			
2*a*,	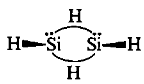	+2.3	SiH = 1.613 SiH_b = 1.426 ∠SiSiH = 102.4° ∠SiH_bSi = 102.0° ∠SiH_b—SiH_b = −10.5° ∠H_bSi—SiH = 81.8°
2*b*,	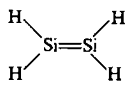	+35.4	SiH = 1.426 SiSi = 2.330 ∠HSiSi = 118.5° ∠H_2Si plane to SiSi vector = 44.3° ∠HSi—SiH = 64.1°, 180.0°
2*c*,	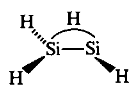	+20.4	SiH_b = 1.649 H_bSi' = 1.588 Si′H = 1.421 HSi = 1.431 ∠SiH_bSi' = 91.0° ∠$H_bSi'H$ = 94.0° ∠$HSiH_b$ = 100.1°, 99.3° ∠SiH_b—Si′H = −96.8° ∠$Si'H_b$—SiH = +130.9°, −129.4°
2*d*,	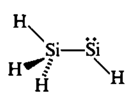	+31.6	HSi = 1.437* Si′H = 1.413 SiSi′ = 2.262 ∠HSi′Si = 96.6° ∠Si′SiH = 116.8°* ∠HSi′—SiH = 180.0°, +59.7°, −59.1°
Al_2H_2			
3*a*,	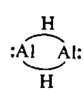	+69.2	AlH = 1.638 ∠AlHAl = 103.4° ∠AlH—AlH = 0.0
3*b* (triplet)	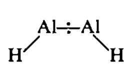	+110.6	AlH = 1.410 AlAl = 2.283 ∠HAlAl = 130.5° ∠HAl—AlH = 28.1°
3*c*,	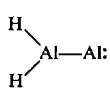	+82.7	AlH = 1.421 AlAl = 2.366 ∠HAlAl = 125.9° Planar molecule
3*d*, see Table 3			

TABLE 1. (*Concluded*)

	Structure	ΔH_f	Geometry
Al_2H_4			
4*a*,	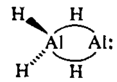	+47.3	AlH_b = 1.562 H_bAl = 1.712 AlH = 1.410 $\angle AlH_bAl$ = 99.9° $\angle HAlAl$ = 119.0° $\angle AlH_b—AlH_b$ = 0° $\angle H_bAl—AlH$ = ±90°
4*b*,	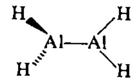	+60.9	AlH = 1.408 AlAl = 2.299 $\angle HAlAl$ = 121.9° $\angle HAl—AlH$ = 90.0°
Al_2H_6			
5,	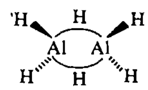	+34.8	AlH_b* = 1.622 AlH = 1.403 $\angle AlH_bAl$ = 99.6° $\angle AlAlH$ = 117.4° $\angle AlH_b—AlH_b$ = 0° $\angle H_bAl—AlH$ = ±90°

[a]Distances are in Å. Average results indicated by *. Bridged hydrogen indicated as H_b.

silicon promotion energy and the delocalization energy (of the SiH bond). Of course the opposite must be true for carbon, since only structures of type **1***b* are found in neutral hydrocarbons. The difference in behavior between the two elements is due primarily to the (expected) weakness of π bonds involving silicon and other atoms in its row of the Periodic Table. Structure **1***c* involves promotion for only one silicon, but compared to **1***a* only one π bond is gained and delocalization for both SiH bonds is lost. Nevertheless, the energy for **1***c* is only about 11 kcal mol^{-1} above that for **1***a*, whereas **1***b* lies about 40 kcal mol^{-1} above **1***a* (2*b*).

MNDO calculations (4) for Si_2H_2 which we have performed agree with the *ab initio* results in that **1***a* is predicted to be the minimum on the surface; type **1***b* structures collapse to **1***a* spontaneously. Structure **1***c* is calculated to be 33.1 kcal mol^{-1} less stable than **1***a* (see Table 1).

The optimum structure calculated by *ab initio* methods (which include correlation corrections) for Si_2H_4 is the ethylene analog **2***b*, although the SiH_2 groups are slightly flapped (5). The MNDO structure for **2***b* has a much greater angle of flap for the SiH_2 groups than does that from the *ab initio* calculations; the SiH_2 planes make a 44° angle with the SiSi vector according to MNDO. In the experimental structure for tetramesityldisilene, the corresponding angle is 18° (6).

Structures for Si_2H_4 which do not involve *s* to *p* electron promotion at both silicons include **2***a* (neither Si promoted) and **2***c* and **2***d* (one Si promoted).

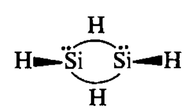

2*a*

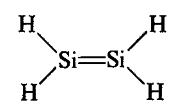

2*b*

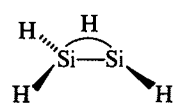

2*c*

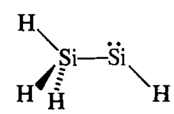

2*d*

The contrast of **2***b* to **2***a* is formally identical to that of **1***b* to **1***a*, except that it is one σ and one π SiSi bond, rather than two π bonds, which are absent in the dibridged structure. Apparently the energetic superiority of σ over π SiSi bonds is sufficient to tip the balance here in favour of the classical structure. The *ab initio* calculations indicate that the classical structure **2***d* is in fact almost isoenergetic with **2***b* (3*a*); thus the π bond energy in **2***b* is not much greater than is the $s \rightarrow p$ promotion energy.

MNDO calculations we have performed predict that **2***a* is the global minimum on the Si_2H_4 surface. In contrast to **1***a*, the four-membered ring in **2***a* is predicted to be almost planar; the non-bridged hydrogens are located *cis* to each other. The preferred *cis* conformation in **2***a* is 1.0 kcal mol^{-1} more stable than the *trans*. The geometry at divalent, three-coordinate Si, and at univalent, two-coordinate Al, can be reconstructed qualitatively by requiring that one *p* orbital of the metal point toward each of the coordinated atoms. The predicted heat of formation for **2***a* is 33.1 kcal mol^{-1} superior to that for **2***b* and 18.1 kcal mol^{-1} superior to **2***c* — see Table 1. The **2***a* structure is predicted to be 50.2 kcal mol^{-1} more stable than two SiH_2 units, and 29.3 more stable than the classical structure **2***d*. (Apparently structures of type **2***a* were not considered in the previous MNDO calculations reported for Si_2H_4, since only **2***b* was discussed (7).)

Structure **2***c* is obtained from **2***d* by conversion of one of the three localized SiH bonds formed by the tetravalent silicon into a three-center Si--H--Si unit by delocalizing it into the empty 3*p* orbital of the divalent silicon. Although **2***c* is a minimum on the MNDO energy surface, it presumably represents the transition state between **2***b* and **2***d* on *ab initio* surfaces. Relative to *ab initio* results, MNDO appears to overestimate the energetic advantage of SiH bond delocalization and $s \rightarrow p$ promotion energies, and to underestimate the energy of SiSi bonds — compare results for **2***a* versus **2***b*, and **2***c* versus **2***b* and **2***d*.

Based upon the calculations and comparisons given above, we expect that the choice between structures having promoted

TABLE 2. *Ab initio* results for Al hydrides

Molecule		Energy (au) by smaller basis[a]	6-31G* (MP2)	Geometry[b] (smaller basis[a])
AlH		−241.1691	−242.4380 (−242.4799)	AlH = 1.65
Al_2H_2				
3*a*,	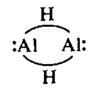	−482.3726	−484.9074 (−485.0047)	AlH = 1.817 ∠AlHAl = 108.2° ∠AlH—AlH = 0°
3*b* (triplet),	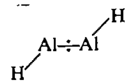	−482.3632	−484.8946 (484.9762)	AlH = 1.569 AlAl = 2.38 ∠HAlAl = 148.0 ∠HAl—AlH = 180°
3*c*,	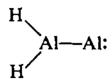	—	−484.8759 (−484.9675)	AlH = 1.57[c] AlAl = 2.44[c] ∠HAlAl = 108°[c] Planar molecule[c]
3*d*,	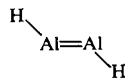	−482.3515	−484.8858 (−484.9824)	AlH = 1.61 AlAl = 2.67 ∠HAlAl = 121° Planar, *trans* molecule[c]

[a]See ref. 6 for details.
[b]Distances are in Å.
[c]Assumed.

atoms which can form π bonds, and unpromoted, low-valent atoms which then form multicenter bonds using vacant *p* orbitals, will be determined by subtle electronic factors since apparently there is little difference energetically between them.

Given the above considerations, some rather intriguing chemistry is expected for compounds of silicon and aluminum, and perhaps even of magnesium, which have relatively low hydrogen-to-metal ratios. Thus, we have performed *ab initio* MO calculations (initially without any inclusion of configuration interaction or other correction for electron correlation) for Al_2H_2 in three possible structures **3***a*, **3***b*, and **3***c* and semi-empirical MNDO calculations for Al_2H_2 and also for other derivatives Al_2X_2.

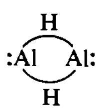  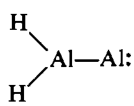 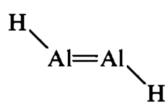

3*a* 3*b* 3*c* 3*d*

Both the *ab initio* calculations (Table 2) and the MNDO (8) calculations (Table 1) predict that a planar dibridged structure **3***a* is the most stable structure for **3**. It is predicted to be 21.6 kcal mol^{-1} more stable than 2AlH monomers using the smaller basis set, 19.7 kcal mol^{-1} superior by the 6-31G* basis (using the same geometry), 28.2 superior by MP2 calculations with this basis, and 22.8 superior by MNDO. The optimum energy calculated for **3***c* is 13.5 kcal mol^{-1} less stable than for **3***a* according to MNDO. Using an assumed geometry (see Table 2), the estimated energy preference for **3***a* compared to **3***c* according to *ab initio* 6-31G* and MP2/6-31G* calculations is 19.8 and 23.4 kcal mol^{-1}, respectively. The calculated AlH distances in **3***a* are 1.817 Å and 1.638 Å respectively, and the AlHAl angles are 108.2° and 103.4°, respectively, according to *ab initio* and MNDO methods. (MNDO underestimates by 0.22 Å the bond distance in diatomic AlH, whereas using the present basis set *ab initio* predictions give 1.649 Å, which is in excellent agreement with the experimental value of 1.648 Å (8). Thus we expect the *ab initio* value for Al_2H_2 to be realistic, but the MNDO value to be rather too short.)

Although the linear double bond structure **3***b* appears favourable since the two singly-occupied π MOs produce a triplet state, it is predicted to be 10.6 (*ab initio*) or 49.5 (MNDO) kcal mol^{-1} less stable than is the dibridged singlet. MNDO calculations indicate that the optimum structure for the triplet in fact is not linear, but almost *cis* bent with HAlAl angles of 130.5° and a dihedral angle between the HAl vectors of 28°. One of the unpaired electrons occupies an MO which is best described as a combination of bonding π and antibonding σ; it contains substantial contributions from the 3*s* orbitals from the Al atoms. By the distortion from linearity, the 3*s* orbitals gain extra electron density (to yield a total of 1.45e) even at the expense of destruction of some of AlAl bonding, both σ and π. The energy improvement due to distortion from linearity is 8.1 kcal mol^{-1}. The *ab initio* results for the Al_2H_2 triplet are stable to these geometric distortions, but are unstable with respect to distortion to a planar *trans* structure with an HAlAl angle of 148°. As in the MNDO calculations, the incentive for nonlinearity is the increase in aluminum 3*s* orbital population which results. Clearly, though, both types of theory predict that AlAl π bonds are rather weak. The final energy for the nonlinear triplet at the optimum geometry is inferior to that for the dibridged singlet by 5.9 kcal mol^{-1} with the smaller basis, by 8.0 with 6-31G* and by 17.9 at the MP2/6-31G* level. The optimum AlAl distance in the linear triplet is 2.288 Å and in the *trans* is 2.38 Å; by comparison the single bond value obtained using the 3-21G* basis for Al_2 is 2.10 Å.

We have performed MNDO calculations for the dibridged and the classical X—Al=Al—X structures (closed shell singlet only) for Al_2F_2 and Al_2Cl_2 as well as Al_2H_2; the results are summarized in Table 3. In all three cases, the optimum classi-

TABLE 3. MNDO calculations for singlet Al_2X_2 systems

Molecule	ΔH_f	Planar, dibridged geometry		ΔH_f	Planar, *trans* geometry	
Al_2H_2 (3*d*)	69.2	AlH	1.638	87.7	AlH	1.421
		∠AlHAl	103.4°		AlAl	2.542
					∠HAlAl	131.5°
Al_2F_2	−198.3	AlF	1.751	−167.9	AlF	1.560
		∠AlFAl	104.2°		AlAl	3.007
					∠FAlAl*	132.7°
Al_2Cl_2	−69.5	AlCl	2.314	−56.2	AlCl	2.069
		∠AlClAl	93.4°		AlAl	2.957
					∠ClAlAl*	138.9°
					∠ClAl—AlCl	2.7°

[a]Distances are in Å. Average result indicated by *.

cal structure is the *trans* planar molecule, but this is less stable (by 30.4, 13.3 and 18.5 kcal mol^{-1}, respectively) than the dibridged structure. The dibridged dimers are more stable than two monomers by 31.0, 13.5, and 22.8 kcal mol^{-1}, respectively. Thus the classical structures are only slightly bound relative to the monomers; this is consistent with the long AlAl distances predicted for them by MNDO (Table 3). An *ab initio* structure for (singlet) **3***d* in the *trans* planar geometry gave a long AlAl bond, 2.67 Å, and an AlH distance and HAlAl angle of 1.61 Å and 121.0°, respectively. This classical double bond structure is 13.2 kcal mol^{-1} less stable than **3***a*, and by 13.5 and 14.0 at the 6-31G* and MP2/6-31G* levels, respectively.

The calculations for the disilicon and dialuminum hydrides have interesting implications regarding the surface structure for samples of elemental silicon and aluminum which have chemisorbed small amounts of hydrogen (though the possible dangers of extrapolation from results for two atoms to a multiatom surface are clear). For example, any univalent surface Al atoms can add H_2 to yield a dibridged structure **4***a* or a classical structure **4***b*:

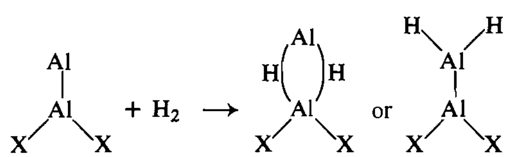

4*a* **4***b*

MNDO results for Al_2H_4 (i.e. **4** with X = H) predict the dibridged to be superior by 13.6 kcal mol^{-1}; however, this result could be spurious if MNDO's overestimate of the strength of delocalized Si—H bonds relative to Si—Si bonds (see S_2H_4 results above) extends also to aluminum. If two trivalent Al atoms at the surface are singly-bonded, an added H_2 could bridge the atoms (**5***a*) or add one hydrogen to each to give the classical structure **5***b*. MNDO calculations for Al_2H_6 and its monomers indicate that the dimer is preferred by 13.5 kcal mol^{-1} to two monomers. Thus from MNDO calculations we predict that hydrogen atoms will be always shared between aluminum atoms in a dibridged sense, whether or not this occurs between two Al atoms of the surface layer or between one of the first and one of the second layer.

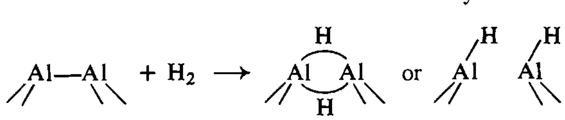

5*a* **5***b*

With respect to the surface of silicon, it is clear that it could well consist of divalent silicon atoms, since the tendency of Si toward tetravalence is not nearly as acute as is that for carbon. If two Si atoms at the surface are singly-bonded to each other, and singly-bonded to (tetravalent) atoms in the next layer, one can conceive of hydrogen addition yielding classical structures in two ways; either one H to each of the Si atoms, to yield an ethylenic structure **6***b* with a formal double bond and the HSiSiH plane perpendicular to the surface plane, or both H atoms adding to the same Si atoms, to yield an analog **6***c* of the **2***d* structure. *Ab initio* calculations for Si_2H_4 indicate that these

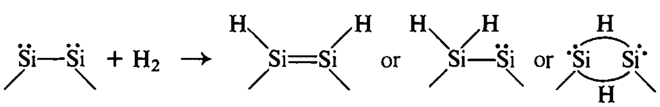

6*b* **6***c* **6***a*

two structures will be preferred to bridged systems, and that the two will be almost equal in stability. On the other hand, MNDO calculations would presumably predict that the H atoms form a dibridged structure **6***a* with two surface silicon atoms, i.e., structure **2***a* with the classical, terminal *cis* SiH bonds replaced by SiSi bonds to two Si atoms in the second layer. High-quality *ab initio* calculations, including allowance for electron correlations effects, clearly are desirable for the *cis*, symmetrical dibridged structure **2***a* of Si_2H_4 in order to ascertain the real energy difference between it and the classical ethylene analog, since only such results can provide a realistic idea of the likelihood of finding dibridged hydrogen structures on the surface.

Conclusions

Both the semiempirical and *ab initio* calculations indicate that Al_2H_2, like Si_2H_2, has a dibridged singlet ground state rather than a classical multiply-bonded structure, and is bound relative to two AlH monomers. The driving forces which favour the nonclassical structures for these molecules include the weakness of π bonding between second row elements, and the energetic cost of $s \rightarrow p$ electron promotion. Unfortunately, MNDO calculations appear to overemphasize the strength of delocalized SiH bonds and to underemphasize the strength of SiSi bonds, and thus yield a nonclassical structure even for Si_2H_4. Further investigations concerning the structure of unsaturated aluminum or silicon hydrides should therefore use high quality *ab initio* calculations.

Acknowledgements

The author is grateful to Cheryl Kay and Gail Parkhill for assistance with the calculations, to the Natural Sciences and Engineering Research Council of Canada for financial support, and to Drs. Goddard, Lischka, and Krogh-Jespersen for supplying preprints and advice.

1. A. H. COWLEY. To be published.
2. (*a*) H. LISCHKA and H-J. KOHLER. J. Am. Chem. Soc. **105**, 6646 (1983); (*b*) J. S. BINKLEY. J. Am. Chem. Soc. **106**, 603 (1984); (*c*) J. KALCHER, A. SAX, and G. OLBRICH. Int. J. Quantum. Chem. **25**, 543 (1984).
3. (*a*) W. J. PIETRO, M. M. FRANCL, W. J. HEHRE, D. J. DEFREES, J. A. POPLE, and J. S. BINKLEY. J. Am. Chem. Soc. **104**, 5039 (1982); (*b*) R. DITCHFIELD, W. J. HEHRE, and J. A. POPLE. J. Chem. Phys. **54**, 724 (1971); (*c*) M. M. FRAND, W. J. PIETRO, W. J. HEHRE, J. S. BINKLEY, M. S. GORDON, D. J. DEFREES, and J. A. POPLE. J. Chem. Phys. **77**, 3654 (1982); (*d*) J. A. POPLE, J. S. BINKLEY, and R. SEEGER. Int. J. Quantum. Chem. Sym. **10**, 1 (1976).
4. M. J. S. DEWAR, M. L. MCKEE, and H. S. RZEPA. J. Am. Chem. Soc. **100**, 3607 (1978).
5. (*a*) R. A. POIRIER and J. D. GODDARD. Chem. Phys. Lett. **80**, 37 (1981); (*b*) H. LISCHKA and H-J. KOHLER. Chem. Phys. Lett. **85**, 467 (1982); (*c*) H-J. KOHLER and H. LISCHKA. J. Am. Chem. Soc. **104**, 5884 (1982); (*d*) K. KROGH-JESPERSEN. J. Phys. Chem. **86**, 1492 (1982); Chem. Phys. Lett. **93**, 327 (1982).
6. M. J. FINK, M. J. MICHALCZYK, K. J. HALLER, R. WEST, and J. MICHL. J. Chem. Soc. Chem. Commun. 1010 (1983).
7. W. S. VERWOERD. J. Comput. Chem. **3**, 445 (1982).
8. L. P. DAVIS, R. M. GUIDRY, J. R. WILLIAMS, M. J. S. DEWAR, and H. S. RZEPA. J. Comput. Chem. **2**, 433 (1981).

Intramolecular fluorescence energy transfer in nitrobenzoxadiazole derivatives of polyene antibiotics

NILS O. PETERSEN

Department of Chemistry, University of Western Ontario, London, Ont., Canada N6A 5B7

Received April 11, 1984

NILS O. PETERSEN. Can. J. Chem. **63**, 77 (1985).

Spectroscopic properties of the polyene antibiotic Nystatin and its nitrobenzoxadiazole derivative have been characterized by lifetime and quantum yield measurements. The data suggest that Nystatin and other polyene antibiotics exhibit spectral features common to other linear polyenes such as diphenylhexatriene and parinaric acid, and support the conclusion that the strong absorption (ϵ_{max} ~70 000 M^{-1} cm^{-1}; λ = 306 nm) is due to a symmetry-allowed transition to a higher excited state while the red-shifted emission occurs from a lower lying excited state through a weak, symmetry-forbidden transition.

Nitrobenzoxadiazole derivatives also exhibit efficient intramolecular fluorescence energy transfer from the polyene chromophore to the nitrobenzoxadiazole chromophore (λ_{em} = 535 nm). The lifetime and quantum yield measurements suggest that the predominant mechanism of energy transfer is via a Dexter type transfer in a fraction of molecules with appropriate conformations.

NILS O. PETERSEN. Can. J. Chem. **63**, 77 (1985).

Faisant appel à des mesures de rendements quantiques et de temps de demi-vie, on a caractérisé les propriétés spectroscopiques de l'antibiotique de nature polyénique, la Nystatine, ainsi que celles de son dérivé nitrobenzoxadiazole. Les donnés suggèrent que la Nystatine ainsi que les autres antibiotiques de nature polyéniques présentent des caractéristiques spectrales communes à celles des autres polyènes linéaires, comme le diphénylhexatriène et l'acide parinarique, et elles sont en accord avec la conclusion selon laquelle la forte absorption (ϵ_{max} d'environ 70 000 M^{-1} cm^{-1}; λ = 306 nm) est due à une transition, permise par la symétrie, vers un état plus excité tandis que l'émission dipolaire vers le rouge se produit à partir d'un état faiblement excité et par le biais d'une transition faible qui est prohibée en raison de symétrie.

Les dérivés nitrobenzoxadiazoles permettent également de transférer d'une façon efficace et intramoléculaire de l'énergie du chromophore du polyène vers le chromophore nitrobenzoxadiazole (λ_{em} = 535 nm). Les mesures de temps de demi-vie et de rendements quantiques suggèrent que le mécanisme prédominant du transfert d'énergie implique un transfert de type Dexter dans une fraction des molécules ayant des conformations appropriées.

[Traduit par le journal]

Introduction

Polyene antibiotics (Fig. 1) are naturally-occurring compounds which can associate with sterols in membranes causing enhanced ion permeabilities (1). Some polyene antibiotics cause several physiological effects distinguishable by their dose response (2). *In vitro*, low doses stimulate DNA and RNA synthesis and are mitogenic, intermediate doses cause ion leakage, and high doses are cytotoxic (2–4). *In vivo*, many polyene antibiotics potentiate the effects of antitumor agents (5) and exhibit immunoadjuvant properties (6) in mice. It is possible that the multitude of effects originate from a single mechanism such as formation of specific pores (7, 8) through association with sterols, but it is likely that there are several sites in cell membranes where the polyene antibiotics can act. We are studying the membrane distribution and dynamics of a few polyene antibiotics, specifically Amphotericin B, Nystatin, and Pimaricin, in order to shed further light on their mechanism of action in culture cells. We are particularly interested in fluorescence photobleaching measurements of the dose dependence of the diffusion of these polyene antibiotics in cell membranes and have recently reported on the synthesis of a nitrobenzoxadiazole derivative of Amphotericin B (AmB) and its diffusion in L-cells at low doses (9). We also presented evidence suggesting that intramolecular fluorescence energy transfer could occur in this derivative. We have since prepared similar derivatives of Nystatin and Pimaricin and report here on quantum yield and lifetime measurements which provide evidence that intramolecular energy transfer in these three compounds occur principally by an electron exchange mechanism (Dexter transfer).

Experimental

Syntheses

N-Methyl-*N*-(7-nitrobenz-2-oxa-1,3-diazol-4-yl)-6-aminohexanoyl (NBD-6-MAHA) derivatives of Amphotericin B (NBD-AmB), Nystatin (NBD-Nys), and Pimaricin (NBD-Pim) were prepared, purified, and characterized as previously reported (9) with only minor modifications. The condensations with Nystatin and Pimaricin were carried out in dimethyl formamide (DMF) rather than dimethyl sulfoxide (DMSO) and their purification by high performance liquid chromatography were effected with slightly different proportions of the elution buffer.

Instrumentation

Fluorescence spectra were recorded as corrected spectra on either an MPF-4 or a model 650 fluorescence spectrophotometer (Perkin Elmer). Quantum yield measurements were made relative to 1.28 × 10^{-6} M quinine sulphate (recrystallized from water) in 0.1 N H_2SO_4 using the quantum yield of 0.52 (10). The quantum yields were corrected for refractive index differences between this solution and the particular solvent employed (10, 11). The quantum yields were calculated from areas of fluorescence emission curves by an integration program available in the Perkin Elmer 650 data station accessory. Absorbance spectra were measured on a Cary 219 UV-Visible spectrophotometer using more concentrated solutions (subsequently diluted accurately). No changes in extinction coefficient are observed upon dilution except for the case of AmB in water where changes in aggregation affect the spectrum above 10^{-6} M. Fluorescence lifetime measurements were made using single photon counting equipment in Professor W. R. Ware's laboratory. A picosecond laser system with frequency doublers were used for excitation in the 300 nm region while a Photochemical Research Associates Model 3000 nanosecond system was used for excitation in the 470 nm region. These systems have been described elsewhere (12). The laser system provides a cw

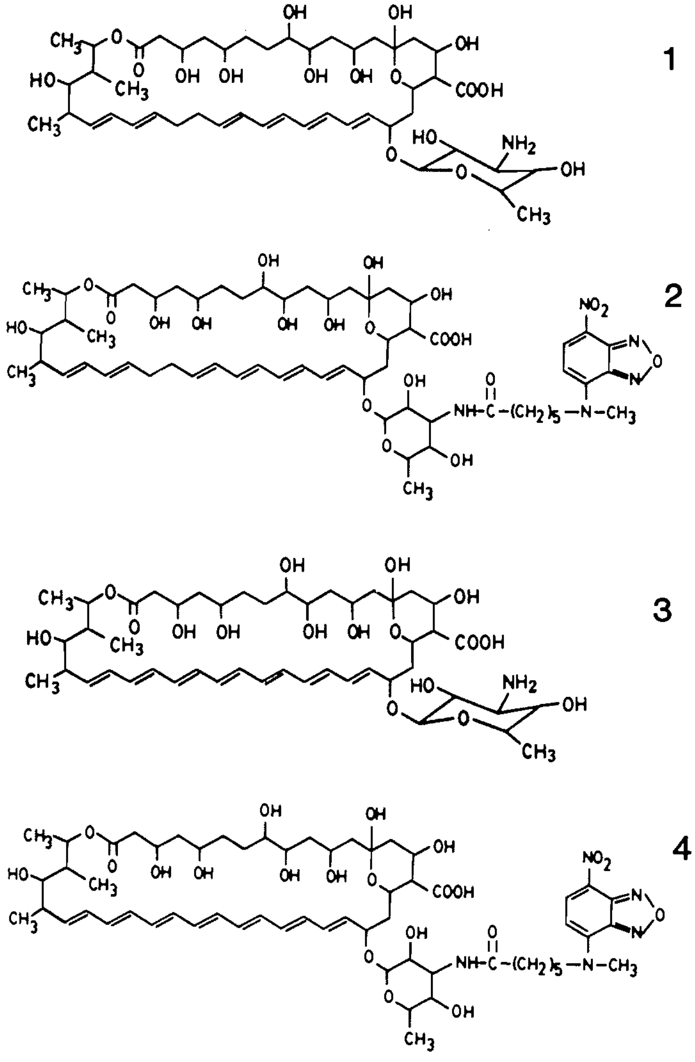

FIG. 1. Chemical structure of Nystatin (1), Amphotericin B (3) and their nitrobenzoxadiazole derivatives: NBD-Nys (2) and NBD-AmB (4). Note the polyene chromophore in the macrolide ring and the amphiphilic character of these molecules. Amphotericin B is a heptaene while Nystatin is spectroscopically a tetraene. The six carbon spacer and the mycosamine ring provide sufficient flexibility to permit close contact between the polyene chromophore and the nitrobenzoxadiazole ring in certain conformations.

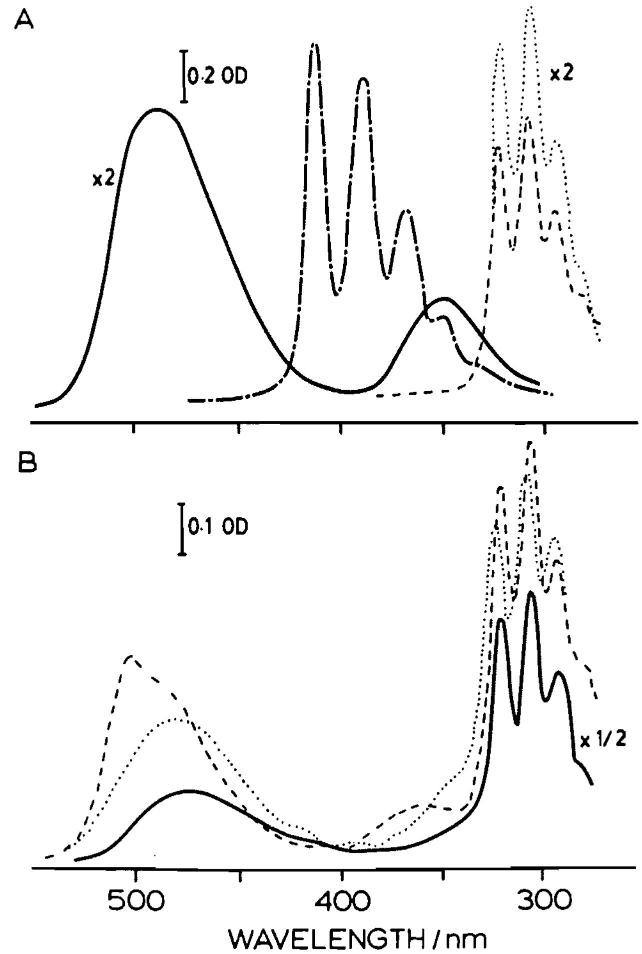

FIG. 2. (*A*) Absorbance spectra of 16 μ*M* Nystatin (---); 15 μ*M* Pimaricin (·····); 9 μ*M* Amphotericin B(-·-·-) and 25 μ*M* NBD-6-MAHA (—) all in DMF. (*B*) Absorbance spectra of 16 μ*M* NBD-Nys in THF (—); 14 μ*M* NBD-Nys in H_2O (---) and 14 μ*M* NBD-Nys in benzene (···). Note the characteristic red-shifted absorbance at 505 nm in H_2O.

power on the sample of less than about 10^3 W m^{-2} with pulse separations of 11 ns. Thus two-photon processes are unlikely in this system. The lifetimes were estimated from fitting by standard procedures of the fluorescence decay data to single or double exponential decays and the fits with reduced χ^2 values closest to unity were retained. De-oxygenating the samples by bubbling argon gas through the sample for 10–20 min had no measurable effects on either quantum yields or lifetimes.

Results

The optical spectra of the three polyene antibiotics prior to chemical modification are shown in Fig. 2, which also illustrates the solvent effect on the optical spectrum of NBD-Nys. Similar solvent shifts are found for all of the polyene antibiotics. The corresponding extinction coefficients are summarized in Table 1 which also shows the extinction coefficient of the NBD-6-MAHA intermediate used for preparing the fluorescent derivatives.

Representative fluorescence emission and excitation spectra of NBD-6-MAHA, Nystatin, NBD-Nys, and NBD-AmB are shown in Fig. 3. The emission corresponding to the NBD-chromophore is similar for all the derivatives. This emission is solvent sensitive and is red-shifted in more polar solvents (compare Fig. 3*c* and *d*). The excitation spectra (for emission at ~535 nm) are superpositions of the absorption spectra of the NBD-chromophore and the polyene chromophore but at different intensity ratios than observed in the absorption spectra of the derivatives. This suggests that absorption by the polyene chromophore results in emission from the NBD-chromophore, but this process occurs with less than unity efficiency.

The emission and excitation spectra are obtained from solutions of the derivative at very low concentrations (10^{-6} *M* and less) where intermolecular associations are unlikely. Moreover, the shape of the spectra, and therefore the relative intensities of the peaks in the excitation spectra, are insensitive to the concentration over a range from 4×10^{-6} *M* to 8×10^{-8} *M* except for small changes due to self-absorption at the higher concentrations. These latter effects are minimal for concentrations less than 10^{-6} *M*. These data suggest very strongly that the energy transfer process is *intramolecular*. In support of this conclusion, we can add that we have so far failed to

TABLE 1. Extinction coefficients of the polyene antibiotics and the nitrobenzoxadiazole precursor: NBD-6-MAHA, as a function of solvent

	$\epsilon/10^4\ M^{-1}\ cm^{-1}$ (λ_{max}/nm)					
Compound/solvent	H_2O	EtOH	DMF	DMSO	THF	Benzene
Nystatin	5.3(321)	6.7(320)	6.1(323)	—	6.3(321)	2.73(325)
molar mass: 924 g mol^{-1}	6.0(307)	7.6(305)	6.8(308)	—	6.8(307)	3.6(308)
	4.1(294)	5.1(292)	4.5(295)	—	4.7(295)	—
Pimaricin	5.3(320)	6.0(318)	4.8(321)	5.0(324)	4.5(321)	—
molar mass: 666 g mol^{-1}	5.9(305)	6.5(302)	5.3(307)	5.4(309)	4.9(306)	—
	3.9(292)	4.3(290)	3.5(294)	3.4(296)	2.9(295)	—
Amphotericin B	2.4(408)	14.2(408)	15.1(412)	12.1(416)	13.2(411)	—
molar mass: 922 g mol^{-1}	2.9(385)	12.9(383)	13.5(388)	11.0(392)	11.7(386)	—
	2.8(364)	7.7(364)	8.0(368)	6.6(371)	6.9(367)	—
	6.1(332)[a]	3.6(345)	3.4(350)	3.0(353)	3.2(348)	—
NBD-6-MAHA	3.4(504)	2.5(479)	2.4(490)	2.5(491)	2.1(474)	2.1(470)
molar mass: 308 g mol^{-1}	0.73(364)	0.87(342)	0.85(351)	0.79(353)	0.83(339)	0.81(340)

[a]This spectrum reflects changes in extinction due to aggregation of Amphotericin B in H_2O.

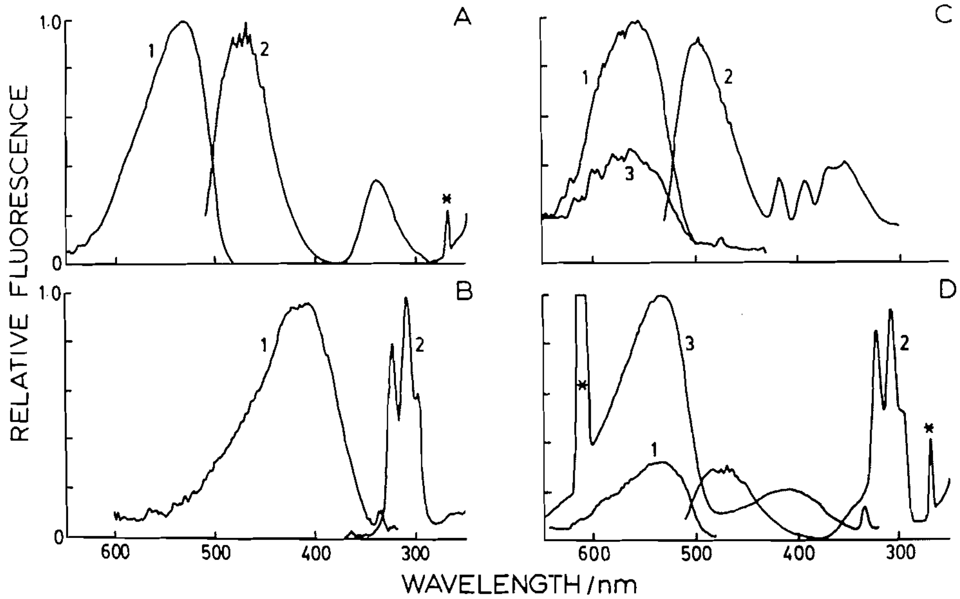

FIG. 3. Corrected fluorescence emission and excitation spectra of (*A*) 1.6 μ*M* NBD-6-MAHA in THF; (*B*) 1.1 μ*M* Nystatin in THF; (*C*) 1.3 μ*M* NBD-AmB in DMSO, and (*D*) 0.82 μ*M* NBD-Nys in THF. A-1, emission spectrum for excitation at 470 nm; A-2, excitation spectrum for emission at 530 nm; B-1, emission spectrum for excitation at 306 nm; B-2, excitation spectrum for emission at 405 nm; C-1, emission spectrum for excitation at 490 nm; C-2, excitation spectrum for emission at 550 nm; C-3, emission spectrum for excitation at 416 nm; D-1, emission spectrum for excitation at 470 nm; D-2, excitation spectrum for emission at 530 nm; D-3, emission spectrum for excitation at 306 nm. The peaks marked by (*) are due to scattering. The fine structure at 470 nm in the excitation spectra (A-2, C-2, and D-2) arises from imperfect corrections for the spectrophotometer.

observe intermolecular energy transfer from the parent polyene antibiotic to either NBD-6-MAHA or NBD-MANC, the latter being a cholesterol derivative which should complex with the polyenes even at $10^{-5}-10^{-6}$ *M* concentrations ($K \sim 10^5\ M^{-1}$ (13)).

Figure 3 illustrates that in pure Nystatin there is an emission which peaks at λ = 405 nm. A similar fluorescence can be observed for Pimaricin but, as we have shown previously (14), pure Amphotericin B exhibits no detectable emission. One can, however, show (15) (data not presented) that the fluorescence and absorbance are both due to the Nystatin molecule since both are observed in the same peaks upon reverse-phase high performance liquid chromatography in several solvent systems. This is in contrast to Amphotericin B where a fluorescent species is clearly separated from the absorbance attributed to AmB (14). The quantum yield data presented below also indicate that the fluorescence emission at 405 nm for Nystatin arises from its polyene chromophore.

More careful analysis of emission spectra from purified Amphotericin B and the instrumental sensitivity show that the quantum yield is less than 0.002. In contrast, the quantum yield for Nystatin in THF is about 0.046. For these reasons, we have chosen to concentrate on characterizing the energy transfer process for NBD-Nys rather than NBD-AmB. It should be noted that even though the quantum yield for fluorescence of Amphotericin B is low, the energy transfer is still possible with reasonable efficiency as the spectra demonstrate (Fig. 3*c*).

Table 2 shows the fluorescence quantum yield and lifetimes

TABLE 2. Measured quantum yield and lifetime values and calculated rate constants for emission in THF at ambient temperature for Nystatin, NBD-6-MAHA, and NBD-Nys

Compound	λ_{ex}/nm	λ_{em}/nm	ϕ	τ/ns	$k_F/10^8\ s^{-1}$	$k_{NR}/10^8\ s^{-1}$
Nystatin	306	320–600	0.046	—		
	295	405	—	2.60	0.175	3.62
NBD-6-MAHA	470	480–650	0.054	—		
	470	535	—	0.61	0.886	15.5
NBD-Nys	306	320–600	0.011[a]	—		
	295	405	—	2.35[b]	—	—
	470	480–650	0.056	—		
	470	535	—	0.52	1.08	18.1
	306	480–650	0.040	—		
	295	530	—	0.73	—	—

[a]Corrected for contribution from Nystatin emission in the region from 480–600 nm which overlaps the NBD emission.
[b]The best fit includes a very fast (0.1 ns) decay accounting for 10% of the intensity.

for Nystatin, NBD-6-MAHA, and NBD-Nys in THF at various combinations of excitation and emission wavelengths. The quantum yield measurements are relative to quinine sulphate in 0.1 N H_2SO_4 (ϕ = 0.52 (10)) and are corrected for the refractive index difference between 0.1 N H_2SO_4 and THF (10, 11). The emission spectra of Nystatin and of NBD-6-MAHA overlap in the region from about 480 nm to about 600 nm. The quantum yield of NBD-Nys emission for excitation at 306 nm was calculated allowing for this overlap correction. The lifetime measurements with excitation at 295 nm were done using a picosecond fluorescence lifetime apparatus by frequency doubling the emission at 590 nm from a Rhodamine dye laser pumped with a mode-locked argon ion laser tuned to 515 nm. The excitation at 295 nm minimizes overlap with the uv absorption of the NBD-chromophore which peaks at 340 nm. All tests show that the quantum yield for Nystatin is independent of the excitation wavelength between 290 nm and 323 nm. The 306 nm excitation used in the quantum yield measurements was the optimum choice based on three considerations: (*1*) it is the strongest absorption band thus giving the best signal-to-noise ratio, (*2*) it does not overlap severely with the 340 nm NBD absorption, and (*3*) the scattered light in these dilute solutions is sufficiently intense that it is detected at twice the wavelength (Fig. 3). For 306 nm excitation the light scattering peak is at 612 nm which is at the tail of the emission and therefore does not interfere seriously with the quantum yield measurements. For 295 nm excitation the light scattering peak is closer to the emission peak, increasing the uncertainty in the area measurement. (The light scattering peak was subtracted in all area measurements but this nevertheless introduces a small uncertainty.)

Several points can be made about the quantum yield data in Table 2. First, the quantum yields of emission for Nystatin and NBD-6-MAHA are similar. Second, the quantum yield of fluorescence from the NBD-chromophore arising from direct excitation at 470 nm is not affected by the chemical linkage to Nystatin (or to AmB). Third, in the NBD-Nystatin derivative the quantum yield for emission at 405 nm is decreased relative to that in pure Nystatin, while the quantum yield of new emission at 530 nm for excitation at 306 nm is approaching that of the NBD-chromophore when excited at 470 nm.

From these emission data we can calculate the quantum efficiency of energy transfer in two independent ways (16) as illustrated below for NBD-Nys in THF. First the transfer efficiency ϕ_{ET} may be calculated from the donor quantum yields in the absence (ϕ) and presence (ϕ') of the acceptor as

$$\phi_{ET} = 1 - \frac{\phi'}{\phi} = 1 - \frac{0.011}{0.046} = 0.76$$

Alternatively it may be calculated from the acceptor quantum yields in the absence (ϕ_A) and presence (ϕ'_A) of the donor as

$$\phi_{ET} = \frac{\phi'_A}{\phi_A} = \frac{0.040}{0.056} = 0.71$$

These are independent measures of the same quantity and the mutual agreement increases our confidence that the ϕ_{ET} measurement is accurate and therefore representative. These quantum yield measurements are determined from the areas of the fluorescence emission spectra. It is also possible to get an approximate estimate of the efficiency of energy transfer by measuring the *ratio* of the peak amplitudes in the corrected fluorescence excitation spectra and normalizing them to the appropriate extinction coefficients, i.e.,

$$\phi_{ET} = \frac{F_{306}/E_{306}}{F_{470}/E_{470}} = 0.70$$

This measurement is a third independent measurement of ϕ_{ET} and agrees well with the more correct area measurements. Utilizing the excitation spectra is particularly convenient for dilute solutions or highly scattering solutions if one can assume the absorption spectra are invariant. Obviously the measurement is extremely sensitive to self-absorption effects and requires good corrections for the spectrophotometer.

Table 2 also provides the lifetime measurements. These are from fits to single exponential decays in all cases but one, namely the emission from NBD-Nys at 405 nm when excited at 295 nm. In this case a small (~10%) but very rapid (~0.1 ns) component appeared. The major component decayed at 2.4 ns which is comparable to the lifetime of pure Nystatin at 2.6 ns. The lifetimes for emission at 530–535 nm are between 0.51 and 0.73 ns with the longest lifetime observed for the process involving the energy transfer process. Although the decay times have statistical uncertainties of less than 0.1 ns, it is likely that these processes have fundamentally the same decay rate.

The energy transfer efficiencies were measured in several solvents and are listed in Table 3. For the pure solvents there is a very large variation from 0.73 in THF to 0.04 in benzene.

TABLE 3. Fluorescence energy transfer efficiency for NBD-Nys in various solvents at ambient temperature

Solvent	ϕ_{ET}
THF	0.73
EtOH	0.57
DMF	0.33
H_2O	0.18
Benzene	0.04
100:0 EtOH:H_2O	0.60
60:40 EtOH:H_2O	0.60
40:60 EtOH:H_2O	0.62
20:80 EtOH:H_2O	0.45
2:98 EtOH:H_2O	0.31
0:100 EtOH:H_2O	0.18

The solvent-dependent changes in the optical spectra are smaller and cannot account for the variation in energy transfer efficiency through changes in the overlap integral. Interestingly enough, the energy transfer efficiency is lowest in benzene (0.04) where the quantum yield for emission by NBD-6-MAHA is the greatest. Table 3 also includes the variation in energy transfer efficiency with the composition of the solvent in mixtures of ethanol and water. It is evident that the efficiency is very sensitive to ethanol at low concentrations (2–20%) and fairly insensitive at higher concentrations of ethanol. We believe the solvent sensitivity arises from differences in conformation and state of aggregation of the NBD-Nys in each of the solvents. It should be noted that there appears to be no correlation between the efficiency of energy transfer and any of the standard solvatochromism scales (e.g. Z or E_T (17)).

The energy transfer efficiencies for NBD-AmB were measured by the ratio of emission areas at 535 nm by excitation at either 410 nm or 470 nm or by the ratio of the fluorescence intensities at 410 and 470 nm in the corrected excitation spectra (methods 2 and 3 above) in both cases correcting for the extinction ratio. In DMSO $\phi_{ET} = 0.05$ while in ethanol $\phi_{ET} = 0.07$. These are much smaller than the corresponding energy transfer efficiencies for NBD-Nystatin (in DMF and ethanol) which probably reflects a difference in the overlap integral in the two sets of chromophores. The energy transfer efficiency for NBD-Pim in ethanol is 0.49 which is slightly smaller than that for NBD-Nys (0.57). Since the spectral parameters are very similar, this difference likely represents a different conformational arrangement in the two molecules rather than a different overlap integral.

We have initiated studies of the energy transfer process in model membrane systems. Although these are incomplete, we have found that the energy transfer efficiency is greatest in dimyristoylphosphatidyl choline bilayers below the gel-to-liquid crystal transition ($\phi_{ET} = 0.90$) and lowest in dipalmitoyl phosphatidyl choline bilayers above the phase transition ($\phi_{ET} = 0.06$). It is difficult to get accurate measurements of the absorbance spectra in these samples because of the large amount of scattering from them due to the membrane suspension. Nevertheless, it is clear that the efficiency of energy transfer is greatest below the phase transition and greater in the less rigidly packed DMPC bilayer. Moreover, there is a shift in the excitation spectrum of the NBD-chromophore at higher temperatures which suggest a greater exposure to an aqueous environment. Thus the decrease in energy transfer efficiency is a combination of a change in bilayer structure and an increase in water content in the bilayer, both known to occur at the phase transition. At this point we cannot be certain which is the dominant effect.

Discussion

Nystatin spectroscopy

The photophysics of polyene antibiotics has not been studied in detail although their fluorescence properties have been utilized in several studies (18–20). Other polyenes, notably diphenylpolyenes such as diphenylhexatriene and diphenyloctatetraene and polyenic fatty acids such as *cis*- and *trans*-parinaric acid, have been studied intensively in part because of their utility in fluorescence depolarization measurements (21–24). Our results with Nystatin and other polyene antibiotics indicate that they share many of the characteristic spectroscopic features of other polyenes.

Diphenylpolyenes exhibit large Stoke's shifts and poor symmetry relations between the absorption and emission spectra (21, 22). The lifetimes measured by fluorescence decay are short (<5 ns) while the corresponding quantum yields are low (<0.1). The intrinsic or natural lifetimes are typically significantly longer than those estimated from the oscillator strength of the absorbance, i.e. from the integrated absorbance (21, 22). These observations have been interpreted in the past by considering two singlet excited states of different symmetry (^1B_u and ^1A_g in the $2/m$ (C_{2h}) group) where the ^1A_g state is at lower energy than the ^1B_u state. The ground state has ^1A_g symmetry, so the strong absorbance spectra (ϵ ~80–100000 M^{-1} cm^{-1}; $f \sim 1$) are associated with the $^1B_u \leftarrow {}^1A_g$ transition to the upper excited state. A rapid internal conversion causes relaxation to the excited ^1A_g state which is relatively long-lived because the $^1A_g \leftarrow {}^1A_g$ transition is symmetry forbidden. This ordering of the first two excited states accounts for the apparent discrepancy between the large oscillator strength and the long lifetime; for the large Stoke's shift (because the energy gap between the two excited states contributes to the red-shift of the emission) and for the loss of mirror symmetry between the absorption and emission spectra. The model has been confirmed in the case of diphenyloctatetraene in a glass at low temperatures by direct excitation of the $^1A_g \leftarrow {}^1A_g$ transition (22).

Parinaric acid (octadecatetranoic acid), specifically the isomers α(9,11,13,15-*cis*, *trans*, *trans*, *cis*) and β(9,11,13,15-*all-trans*) exhibit many of the spectroscopic features outlined above for the diphenylpolyenes (24). Although indirect, the evidence strongly supports an excited state ordering in the parinaric acids similar to that in the diphenylpolyenes. The data presented in this report for Nystatin are very similar to those of the parinaric acids. Specifically, their absorbance wavelength is solvent-sensitive while the emission wavelength is not; the emission is about 90 nm red-shifted (compared to 100 nm for parinaric acid); the intrinsic lifetime is about 57 ns (compared to 100 ns for parinaric acid) which is longer than the 8 ns estimated from the strong absorbance spectrum. The measured lifetime of 2.6 ns in THF is comparable to that of parinaric acid of 3.2 ns in dioxane; the quantum yield is 0.046 compared to 0.051 for parinaric acid. Considering these comparisons and accepting the conclusions about the excited state ordering for diphenylpolyenes and polyenic fatty acids, we conclude that the tetraene antibiotic Nystatin has similar excited state ordering and symmetry relationships between the states. Nystatin is a more complex molecule than either the diphenylpolyenes or the parinaric acids, so we are reluctant to attach the symmetry descriptions of ^1A_g and ^1B_u to the states. For the

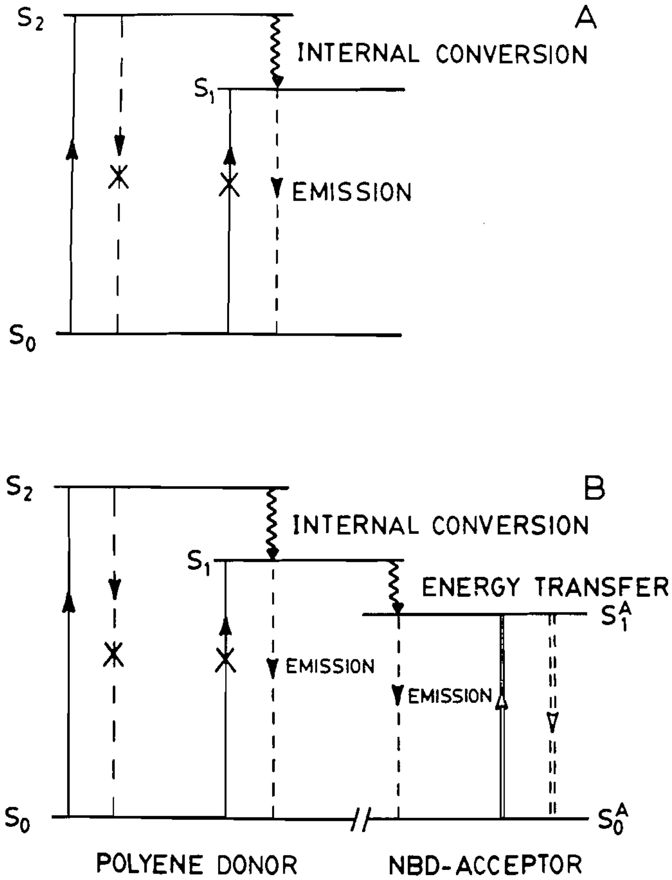

FIG. 4. *A*, Schematic representation of the transitions in the polyene chromophore of Nystatin. The emission from S_2 is not detected because of the rapid internal conversion to S_1. The direct absorption into S_1 is too weak to be detected. *B*, Schematic representation of the transitions in NBD-Nys. The polyene chromophore of Nystatin acts as a donor in the energy transfer from S_1 to the $S_1{}^A$ state of the NBD chromophore. The double arrows indicate the direct absorption and emission processes for the NBD chromophore. The energy transfer occurs rapidly in 70% of the molecules while the other 30% emit as in the parent Nystatin molecule.

purpose of the remainder of this discussion we will refer to the excited states as S_1 and S_2 with the understanding that S_2 is at higher energy than S_1 and that the $S_2 \leftarrow S_0$ transition is a symmetry-allowed transition observed in the absorption spectrum while the $S_0 \leftarrow S_1$ transition corresponds to a symmetry-forbidden transition observed in the emission spectrum. We will further presume that the internal conversion $S_1 \leftarrow S_2$ is rapid ($k_{IC} > 10^{12}\ s^{-1}$ (24)), so that energy transfer is most likely to occur from S_1. Figure 4*A* illustrates graphically the possible transitions in the Nystatin chromophore.

All the polyene antibiotics we have so far looked at (representing tetraenes (Nystatin, Etruscomycin, Pimaricin) and pentaenes (Chainin, Fungichromin (≡ lagosin ≡ cogomycin) (25)) and heptaenes (Amphotericin B)) exhibit the characteristically large Stoke's shifts and have very solvent-sensitive absorption spectra. Based on this limited evidence it is tempting to suggest that all the polyene antibiotics will follow the pattern of other polyenes including Nystatin. Of course, with the heptaenes the emission is so weak that any conclusions about the excited state ordering is dangerous.

NBD-Nystatin spectroscopy

The fluorescence emission spectrum of NBD-Nys in the region from 350 nm to 480 nm for excitation at 306 nm is the same as that of Nystatin except for a four-fold reduced quantum yield. Correspondingly, the excitation spectrum for emission at 405 nm is the same as that of Nystatin but with a four-fold lower intensity. These observations suggest that the state ordering of the Nystatin polyene chromophore is not affected by the conjugation of the NBD-chromophore. The reduction in quantum yield is due to energy transfer as discussed below. Moreover, the excitation spectrum in the region from 250 nm to 325 nm for emission at 535 nm is the same as that of Nystatin but with different intensities. This confirms that the emission from the NBD-chromophore is coupled to an energy transfer from the same excited states involved in the polyene spectroscopy. We suspect that the energy transfer occurs from S_1 in NBD-Nystatin.

The energy transfer process

The quantum yield and lifetime of acceptor (NBD) emission in NBD-Nys are similar to those in NBD-6-MAHA (Table 2) suggesting that there is no back-transfer from the NBD-chromophore to the polyene and that the radiative and non-radiative rate constants of the acceptor are essentially unaffected by the intramolecular interactions in NBD-Nys.

The emission at 535 nm arising from excitation at 306 nm is dependent on the kinetics of three consecutive processes, namely, internal conversion from S_2 to S_1 in the donor, energy transfer, and acceptor emission (Fig. 4*B*). Internal conversion is rapid and not rate-limiting. Standard kinetic arguments (26) predict an emission decay comparable to the slower and therefore rate-limiting of the two other processes. The measured lifetime for the total energy transfer and emission is only slightly larger than the lifetime of acceptor emission due to direct excitation (Table 2), suggesting that the emission step rather than the energy transfer step is rate-limiting. A consecutive reaction scheme also predicts an initial increase in the concentration of the intermediate which would be observed as an initial growth in the emission decay curve, unless the first step (energy transfer) is very rapid relative to the timescale of the measurement. The measured decay curve (Fig. 5) shows no evidence of an initial growth supporting the conclusion that energy transfer is rapid. From the data we estimate that the rate constant for energy transfer would have to exceed about $10^{10}\ s^{-1}$.

The donor emission quantum yield is about four times smaller in NBD-Nys than in Nystatin whereas the lifetime is about 10% smaller (Table 2). These data are mutually inconsistent or in conflict with the rapid energy transfer predicted by the acceptor emission data in any model which assumes that all molecules behave equivalently. Specifically, the measured quantum yield, ϕ, and lifetime, τ, of donor emission must change in proportion (16) since $\phi = k_F \cdot \tau = k_F/(k_F + k_{NR})$ in the absence of energy transfer and $\phi' = k'_F \cdot \tau' = k'_F/(k'_F + k'_{NR} + k'_{ET})$ with energy transfer. Here k_F, k_{NR}, and k_{ET} are the radiative, non-radiative, and energy transfer rate constants, respectively, and the primes indicate the values in the presence of energy transfer. If the donor radiative rate constant is not affected by the donor–acceptor interactions in NBD-Nys ($k'_F = k_F$), a four-fold decrease in quantum yield requires a four-fold decrease in lifetime. This is not observed. Conversely, the radiative rate constant would have to decrease about four-fold to accommodate the small change in lifetime actually observed. The resulting energy transfer rate constant of $3 \times 10^8\ s^{-1}$ is smaller than the rate of decay of the acceptor

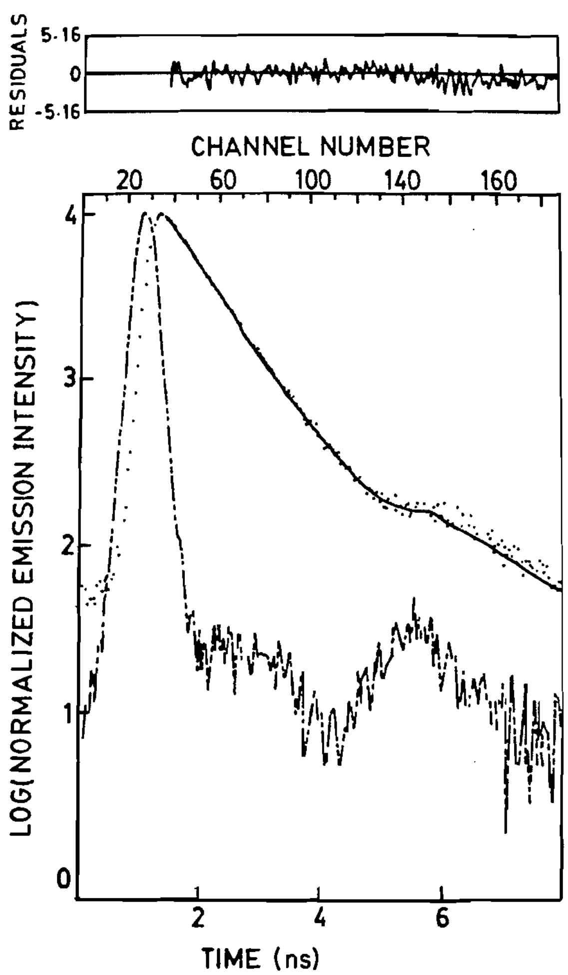

FIG. 5. Decay of emission from NBD-Nystatin measured at 530 nm while exciting at 295 nm. The dashed curve represents the laser pulse profile. Note the absence of a slow build-up as predicted for the Förster transfer process. The deconvolution yields a good fit to a single exponential decay with a time constant of 0.71. The residuals are shown above the curve.

emission ($k = 1.4 \times 10^9\ s^{-1}$) and much smaller than the energy transfer rate constant estimated from the acceptor emission data. Hence a decrease in radiative rate constant of donor emission would make the energy transfer process, rather than the acceptor emission, the rate-limiting step. This is contrary to the data for the acceptor emission (Fig. 5, Table 2). Furthermore, a large change in the radiative rate constant of the donor should be observable in its absorption spectrum since the integrated absorbance is related to the radiative lifetime (16).[1] Since there are no differences in extinction coefficients or wavelengths of maximum absorption of the polyene chromophore between Nystatin and NBD-Nys (Fig. 2) it is unlikely that the radiative rate constant is decreased significantly. Clearly, there are inconsistencies in the data whether or not we assume an invariant radiative rate constant. Models for the energy transfer process which assume that all molecules are affected equivalently must, therefore, be rejected for the NBD-Nys system.

The simplest alternative is the case where one population of molecules exhibits energy transfer exclusively and another population exhibits no energy transfer. The former do not contribute to the donor emission and are "dark-complexes" which still absorb and contribute to the observed acceptor emission. The latter are the only source of donor emission and since they are not affected by the energy transfer process, the measured lifetime of donor emission is unchanged. However, the measured quantum yield of donor emission must decrease to reflect the mole fraction, X, of unaffected molecules remaining. Specifically, the measured quantum yield will be

$$\phi' = X \cdot k_F/(k_F + k_{NR}) + (1 - X)k'_F/(k'_F + k'_{NR} + k'_{ET})$$

In the limit where $k'_{ET} \gg k'_F + k'_{NR}$, i.e., when energy transfer is rapid this reduces to $\phi' = X \cdot k_F/(k_F + k_{NR}) = X \cdot \phi$. The energy transfer efficiency becomes

$$\phi_{ET} = 1 - \frac{\phi'}{\phi} = 1 - X$$

and is now a direct measure of the mole fraction of the population of molecules which exhibit rapid energy transfer. The four-fold decrease in quantum yield then indicates approximately a 1:3 distribution of the two populations. The acceptor emission due to energy transfer arises from the population where energy transfer must be rapid so the acceptor emission step is rate-limiting and no growth in the decay curve is expected, in accord with the acceptor emission data (Table 2, Fig. 5). All the data are, therefore, wholly consistent with a system of two populations which are spectroscopically distinct and which interconvert slowly on the nanosecond time scale.

The conformational model

Examination of the structure of NBD-Nys (Fig. 1) suggests that two conformations could exist: a fully extended conformer in which the polyene and NBD-chromophore are separated by between 23 and 28 Å and a folded conformer in which the NBD-chromophore is positioned along the hydrophobic polyene-section of the macrolide ring. We propose that in THF these are the predominant conformers of NBD-Nys and that in the extended conformer energy transfer is inefficient because of the separation and relative orientation of the chromophores while in the folded conformer energy transfer occurs rapidly because of the proximity of the chromophores. The energy transfer efficiency then measures the mole fraction of the folded conformer and the large variation in energy transfer in different solvents (Table 3) reflects a different equilibrium between the conformers in each solvent.

Although this model will account for the quantum yield and lifetime data, three observations indicate that there likely is a small contribution to energy transfer from the extended conformer also. First, we have found no solvents in which the energy transfer could be completely suppressed. This could indicate that there is always at least some of the folded conformer present in solvents as different as H_2O or benzene, but it is also possible that the extended conformer is contributing to this emission. Second, the lifetime of donor emission decreases in THF by about 10%. This would be expected if energy transfer is a slow competing process in the extended conformer. Third, the separation of the chromophore in the extended conformer is small enough that some energy transfer by a Förster-type mechanism is expected.

It is possible to estimate the characteristic separation, R_0, at which 50% energy transfer would occur by a Förster mechanism since (27)

[1]This argument is complicated by the fact that the absorbing and emitting electronic states are different (Fig. 4) but some effects should be observed.

$$R_0 = C(\kappa^2 \cdot \phi \cdot \eta^{-4} \cdot J)^{1/6}$$

where C is a constant ($C = 9.786 \times 10^{-5}$), κ^2 is a factor dependent on the time-averaged relative orientation of the chromophores, ϕ is the quantum yield of donor emission, η is the refractive index of the medium, and J is the overlap integral given by (27, 28)

$$J = \frac{\int \epsilon(\lambda)F(\lambda)\lambda^4 d\lambda}{\int F(\lambda)d\lambda}$$

In this expression $\epsilon(\lambda)$ is the molar extinction coefficient of the acceptor, $F(\lambda)$ is the donor emission intensity, and λ is the wavelength. For the NBD–tetraene chromophore pair in THF we calculate

$$J = 3.10 \times 10^{-14} \text{ cm}^6 \text{ mmol}^{-1}$$

using a summation over 1 nm intervals. Assuming an orientation factor for an isotropic relative orientation ($\kappa^2 = 2/3$ (27, 28)) the characteristic separation is

$$R_0 = 25.8 \text{ Å}$$

It is likely that the intramolecular linkage would restrict the chromophore reorientations and the R_0 value could be an upper limit. Nevertheless, the extended conformer could in principle exhibit up to 50% energy transfer.

Given the likelihood that the extended conformer exhibits some energy transfer, we can use the observed decrease in lifetime to estimate the energy transfer rate constant, k_{ET}, and efficiency, ϕ_{ET}, in this conformer. Assuming no changes in radiative and non-radiative rate constants $\tau = 1/(k_F + k_{NR} + k_{ET})$ so $k_{ET} = 1/\tau - k_F - k_{NR} = (4.25 - 0.175 - 3.62) \times 10^8$ s^{-1} = 4.6×10^7 s^{-1} and $\phi_{ET} = k_{ET} \cdot \tau = 4.6 \times 10^7 \text{ s}^{-1}\, 2.35 \times 10^{-9} \text{ s} = 0.11$. Thus in THF the extended conformer may exhibit a slow energy transfer with an efficiency up to about 11%.

The folded conformer we postulate as one in which the NBD-chromophore has folded back over the mycosamine so that its π-ring system is parallel to the polyene chromophore. This will provide the close contact necessary for energy transfer by an electron-exchange mechanism. Because of the proximity we assume that energy transfer is occurring at unit efficiency by the Dexter-type mechanism. The total observed energy transfer is then given by the sum of the contribution from each conformer weighted by the respective mole fractions, i.e.,

$$\begin{aligned}\phi_{ET}\,(\text{total}) &= X \cdot \phi_{ET}\,(\text{extended}) + (1 - X)\phi_{ET}\,(\text{folded}) \\ &= X \cdot \phi_{ET}\,(\text{extended}) + (1 - X)\end{aligned}$$

For NBD-Nys in THF this yields (using ϕ_{ET} (extended) = 0.11), $X = 0.32$ and $(1 - X) = 0.68$. In other words, 32% of the NBD-Nys are in an extended conformation while 68% are folded.

The proposed conformational model for energy transfer in NBD-Nys is summarized in the following kinetic scheme where D represents the donor (Nystatin) and A the acceptor (NBD):

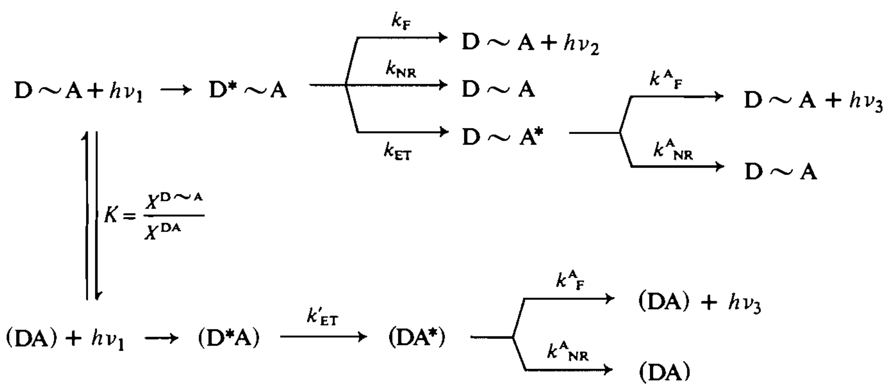

Here the internal conversion step ($S_2 \rightarrow S_1$) in the donor has been omitted for clarity. The extended conformer is represented by D ~ A. Upon excitation at $h\nu_1$, the donor can decay by emission of light (at $h\nu_2$), by non-radiative processes or by energy transfer to give D ~ A* which in turn can decay by acceptor emission (at $h\nu_3$). The folded conformer is represented by (DA). Upon excitation at $h\nu_1$, the donor transfers energy with unit efficiency to the acceptor which then decays by emission at $h\nu_3$. The conformers exist in equilibrium in the ground state, but the rate of interconversion is slower than the photophysical decay paths and therefore the conformers are observed as spectroscopically distinct species. We propose that the equilibrium constant is solvent dependent, which accounts for the variation in energy transfer efficiency (Table 3). We then interpret the variation in energy transfer efficiency in the mixed ethanol:water system and in the lipid membrane system as a reflection of changes in the equilibrium constant for the two predominant conformers. We hope to exploit this in studies of binding of steroids to NBD-Nys, since binding is likely to shift the equilibrium and thus alter the observed energy transfer efficiency.

Conclusions

Polyene antibiotics have intrinsic chromophores whose spectroscopic properties when properly understood may be exploited in studies of their mechanism of action in cell membranes. The photophysical behaviour of the tetraene Nystatin can be shown to resemble closely that of other polyenes, particularly the parinaric acids. On the basis of this comparison we suggest that the pattern of excited state ordering observed in other polyenes extends to the polyene antibiotics.

Nitrobenzoxadiazole derivatives of the polyene antibiotics exhibit efficient intramolecular energy transfer from the polyene chromophore to the nitrobenzoxadiazole chromophore. Lifetime and quantum efficiency measurements are consistent with a model in which there is an equilibrium between a fully extended conformer (D ~ A) and a folded conformer (DA). The former exhibit energy transfer by a Förster type energy transfer mechanism through Coulombic interactions of the transition dipoles. The latter exhibit energy transfer by a Dexter type energy transfer mechanism at a very fast rate. The total transfer efficiency depends on the relative proportion of the conformers which is sensitive to the solvent. For NBD-Nys in tetrahydrofuran the folded conformer represents about two-thirds of the molecules and accounts for more than 90% of the observed transfer. In other solvents the fraction of folded conformer is less.

The dependence of the energy transfer efficiency on the proportion of each conformer may provide a sensitive spectroscopic tool for studies of polyene−sterol interactions, since these are expected to affect the equilibrium distribution of extended and folded conformers (7, 8). Moreover, the spectroscopic properties of the chromophores suggest that it might be possible to observe intermolecular energy transfer between NBD-chromophores and polyene antibiotics if the complexes formed bring the chromophores within about 15−20 Å.

Acknowledgements

Some of the preparative work were done by Andy van Ginniken and Robert Semmler as NSERC Undergraduate Research Scholars. The author appreciates the assistance of Professor W. R. Ware and members of his research group in performing the lifetime measurements. Professor Ware's critical reading of the manuscript was very helpful. The work was supported by NSERC grant U0109 and National Institute of Health (NCI) grant CA15665.

1. A. W. NORMAN, A. M. SPIELVOGEL, and R. G. WONG. Adv. Lipid Res. **14**, 127 (1976).
2. G. MEDOFF, J. BOLARD, J. BRAJTBURG, and G. S. KOBAYASHI. Ann. Rev. Pharmacology and Toxicology. Vol. 23. *Edited by* R. George, R. Okun, and A. K. Cho. Palo Alto, CA. 1983. p. 303.
3. J. BRAJTBURG, G. MEDOFF, G. S. KOBAYASHI, S. ELBERG, and C. FINEGOLD. Antimicrob. Agents Chemother. **18**, 586 (1980).
4. J. R. LITTLE, A. ABEGG, and E. PLUT. Cellular Immunology, **78**, 224 (1983).
5. G. MEDOFF, F. VALERIOTE, and J. DIECKMAN. J. Natl. Canc. Inst. **67**, 131 (1981).
6. J. R. LITTLE, G. MEDOFF, S. F. SHIRLEY, and T. E. SHINE. The immune system. Vol. 1. *Edited by* I. Levkovitz, N. K. Jerne, and C. M. Steinberg. Karger, Basel. 1981. p. 256.
7. B. DEKRUIJFF, W. J. GERRITSEN, A. OERLEMANS, R. A. DEMEL, and L. L. M. VAN DEENEN. Biochim. Biophys. Acta, **339**, 30 (1974).
8. P. VAN HOOGEVEST and B. DEKRUIJFF. Biochim. Biophys. Acta, **511**, 397 (1978).
9. N. O. PETERSEN. Spectrosc. Internatl. J. **2**. 408 (1983).
10. S. R. MEECH and D. PHILLIPS. J. Photochem. **23**, 193 (1983).
11. C. A. PARKER. Photoluminescence of solutions. Elsevier Publ. Co., Amsterdam. 1968. p. 263.
12. W. R. WARE, M. PRATINIDHI, and R. K. BAUER. Rev. Sci. Instrum. **54**, 1148 (1983).
13. I. GRUDA, P. NADEAU, J. BRAJTBURG, and G. MEDOFF. Biochim. Biophys. Acta, **602**, 260 (1980).
14. N. O. PETERSEN and P. F. HENSHAW. Can. J. Chem. **59**, 3376 (1981).
15. T. DRAPER. B.Sc. Thesis. The University of Western Ontario, London, Ont. 1981.
16. N. J. TURRO. Modern molecular photochemistry. Benjamin/Cummings Publ. Co., Menlo Park, CA. 1978.
17. J. A. HIRSCH. Concepts in theoretical organic chemistry. Allyn and Bacon, Inc., Boston. 1974. Chapt. 9.
18. J. M. PATTERSON, J. HOLLAND, and L. L. BIEBER. J. Antibiot. **32**, 646 (1979).
19. R. BITTMAN and S. A. FISCHKOFF. Proc. Natl. Acad. Sci. (US) **69**, 3795 (1972).
20. J. M. PATTERSON, M. R. OLINGER, J. F. HOLLAND, and L. L. BIEBER. J. Antibiot. **32**, 1193 (1979).
21. B. HUDSON and B. KOHLER. Ann. Rev. Phys. Chem. **25**, 437 (1974).
22. B. S. HUDSON and B. E. KOHLER. J. Chem. Phys. **59**, 4984 (1973).
23. M. SHINITZKY and Y. BARENHOLTZ. J. Biol. Chem. **249**, 2652 (1974).
24. L. A. SKLAR, B. S. HUDSON, M. PETERSEN, and J. DIAMOND. Biochemistry, **16**, 813 (1977).
25. R. C. PANDY, E. C. GUENTHER, A. A. ASZALOS, and J. BRAJTBURG. J. Antibiot. **35**, 988 (1982).
26. K. J. LAIDLER. Chemical kinetics. 2nd ed. McGraw-Hill Book Co., New York, NY. 1965.
27. R. E. DALE, J. NOVROS, S. ROTH, M. EDIDIN, and L. BRAND. *In* Fluorescent probes. *Edited by* G. S. Beddard and M. A. West. Academic Press. 1981. p. 159.
28. L. C. CANTLEY, JR., and G. G. HAMMES. Biochemistry, **14**, 2976 (1975).

Réactivité du nucléophile azoture vis à vis de cations hétérocycliques aromatiques. VI. Cas des triaryl-2,4,6 oxaziniums-1,3

JEAN-CLAUDE CHERTON, PAUL-LOUIS DESBENE, MARC BAZINET, MARC LANSON, ODILE CONVERT ET JEAN-JACQUES BASSELIER

Laboratoire de Chimie Organique Structurale, Université Pierre et Marie Curie, 4, Place Jussieu, 75230 Paris Cedex 05, France

Reçu le 25 janvier 1984

JEAN-CLAUDE CHERTON, PAUL-LOUIS DESBENE, MARC BAZINET, MARC LANSON, ODILE CONVERT et JEAN-JACQUES BASSELIER. Can. J. Chem. **63**, 86 (1985).

La réaction du nucléophile azoture avec les triaryl-2,4,6 oxazinium-1,3 conduit en haut rendement aux β tétrazolo-*trans*-benzalacétophénones. La formation de ces tétrazoles implique l'intervention des azido-2 2*H*-oxazines-1,3 correspondantes. Un mécanisme de réarrangement de ces azides mettant en jeu deux tautoméries cycle–chaîne autour des intermédiaires iminoazides est proposé. Sous réserve que les azido-2 2*H*-oxazines-1,3 sont bien les produits cinétiques de l'attaque de N_3^-, les résultats présentés constituent un rare exemple de régiosélectivité de l'attaque d'un nucléophile sur le pôle C2 d'oxazinium-1,3.

Le problème de la réactivité du système oxazinium-1,3/azoture est discuté en référence au couple triphényl-2,4,6 pyrylium/N_3^-.

JEAN-CLAUDE CHERTON, PAUL-LOUIS DESBENE, MARC BAZINET, MARC LANSON, ODILE CONVERT, and JEAN-JACQUES BASSELIER. Can. J. Chem. **63**, 86 (1985).

Nucleophilic attack of sodium azide on 2,4,6-triaryl-1,3-oxazinium species gives high yields of β-tetrazolo-*trans*-benzalacetophenones from the corresponding 2-azido-1,3-oxazines. The rearrangement of the azido oxazines likely proceeds via tautomerism of the intermediate iminoazides. If the formation of the 2-azido-1,3-oxazines is under kinetic control, these results are a rare example of high regioselectivity in nucleophilic attack at the C2 carbon of 1,3-oxazinium species.

The reaction behaviour of the 1,3-oxazinium/N_3^- system is discussed, together with results obtained from the 2,4,6-triphenylpyrilium/N_3^-.

Nous nous intéressons depuis quelques années à la réaction du nucléophile azoture avec divers cations hétérocycliques aromatiques de type pyrylium. Les recherches ont ainsi été menées tant en raison de l'intérêt théorique de la réaction (1, 2) que des possibilités qu'elle offre sur le plan de la synthèse de composés hétérocycliques à sept chaînons (1, 3 à 9). (cf. schéma 1).

Les cations oxazinium-1,3 **1** ou azapyrylium-1,3 sont comme les cations pyrylium déficients en électrons, et comme tels réagissent avec de nombreux nucléophiles (10 à 13). A l'issue de ces réactions des oxaziniums-1,3, trois types d'oxazines: les 6*H*-oxazines **2**, les 4*H*-oxazines **3**, les 2*H*-oxazines **4** sont envisageables a priori en raison de la différenciation des pôles 2 et 6 en α de l'oxygène (cf. schéma 2).

Cependant, il ressort des travaux de R. R. Schmidt et coll. d'une part (10 et réf. citées) et de I. Shibuya et coll. d'autre part (11 à 13) que l'attaque d'une grande variété de nucléophiles sur le cation triphényl-2,4,6 oxazinium-1,3 **1***a* conduit exclusivement ou en prépondérance à des composés de type 6*H*-oxazine-1,3, c'est à dire de type **2** ou à des produits résultant de leur réarrangement (cf. schéma 2).

Le comportement du couple cation **1**/azoture n'avait pas encore été abordé. Compte tenu des résultats obtenus précédemment par nous mêmes en série pyrylium (1, 3 et 8) et par Schmidt et coll. (10) avec d'autres nucléophiles en série oxazinium-1,3, on pouvait attendre: soit une "non attaque" au sens covalent du terme avec formation d'un complexe de type donneur–accepteur comme observé dans le cas du couple triphényl-2,4,6 pyrylium/N_3^- (1, 3, 8); soit une attaque de N_3^- sur le pôle C6 du cation **1**. Au quel cas, l'evolution de l'azide covalent **2***a* (Nu = N_3) permettrait éventuellement l'accession à des homologues "aza" d'oxazépines-1,3, (cf. schéma 1) en l'occurence des *oxadiazépines* (14).

Nous présentons ici les premiers résultats concernant le comportement de triaryl-2,4,6 oxaziniums-1,3 **1** vis à vis du nucléophile azoture.

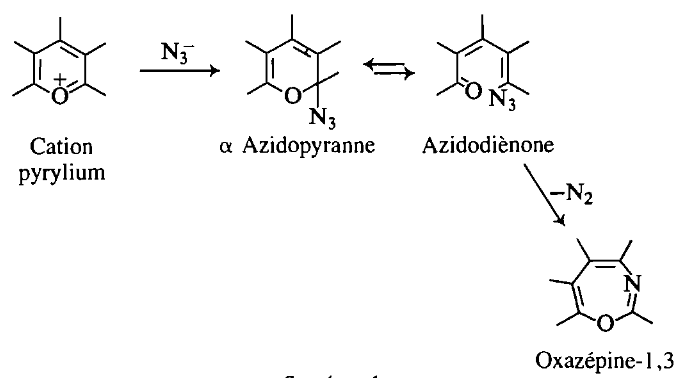

SCHÉMA 1

Résultats et discussion

L'action de l'azoture de sodium sur une solution de perchlorate de triphényl-2,4,6 oxazinium-1,3 **1***a* (10) dans l'acétonitrile anhydre se manifeste tout d'abord par une exaltation de coloration malheureusement trop brève pour être analysée par exemple par spectroscopie uv–visible, suivie d'une décoloration progressive du mélange réactionnel. Il s'agit donc d'une réaction d'attaque de N_3^-, mais la possibilité de formation transitoire ou simultanée d'un complexe donneur–accepteur, comme le laisse supposer l'exaltation de coloration n'est pas exclue. Au bout de quelques heures on isole un composé unique: le [diphényl-1,3 oxo-3 propène-1-yl (*E*)]-1 phényl-5 tétrazole que l'on dénommera désormais tétrazole **5***a* (Rdt 92%) (cf. schéma 2).

I. *Structure du tétrazole* 5a

Ce composé $C_{22}H_{16}N_4O$ résulte de l'incorporation de trois atomes d'azote au squellette du cation **1***a*. Toutefois les structures des produits primaires envisageables: **2***a*, **3***a* ou **4***a* (Nu = N_3, cf. schéma 2) sont à écarter en raison de l'absence de la bande d'absorption azido vers 2100 cm^{-1} dans le spectre infra-

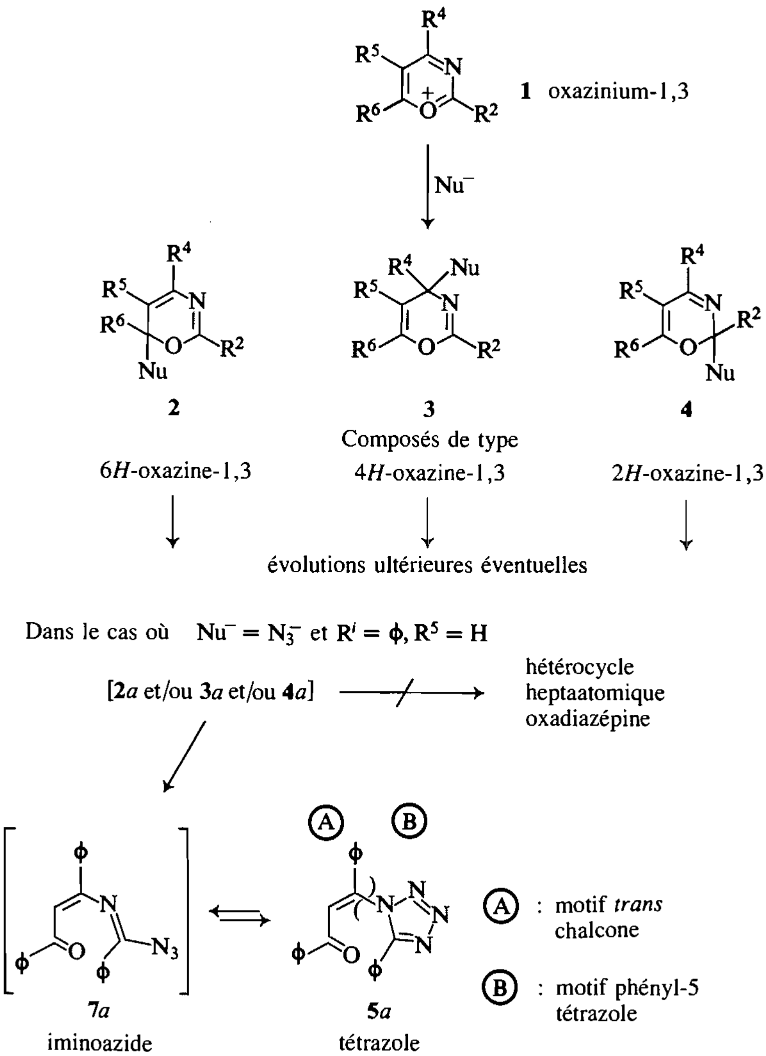

SCHÉMA 2

rouge (15). Après examen de ses propriétés chimiques[1] et spectroscopiques, nous avons attribué à ce composé la structure **5***a* associant les deux motifs: phényl-5 tétrazole et *trans* chalcone (cf. schéma 2).

Les arguments d'ordre spectroscopique sont les suivants: *la présence du motif* trans *chalcone* est établie par les analogies observées entre les spectres d'absorption uv–visible, infrarouge, de rmn ^{1}H et de rmn ^{13}C du composé **5***a* et ceux de la *trans* benzalacétophénone **6** (cf. partie expérimentale); le *motif tétrazole* est décelé en spectroscopie infra-rouge par l'observation d'un ensemble de bandes caractéristiques dans la région des empreintes (17, 18). En spectroscopie de masse, l'observation des ions moléculaires n'est pas possible par la technique de l'impact électronique I.E. à 70 eV ni même à plus basse énergie. L'ion de masse la plus élevée est alors celui résultant de la perte de N_2. Dans le cas du tétrazole **5***a*, une fragmentation $M^{+\cdot} - N_3^{\cdot}$ est également notée, elle conduit au cation oxazinium (M^+ 310, *Masse Exacte*). Pour les autres tétrazoles, les même hypothèses de fragmentations semblent raisonnables, d'autant que des observations similaires ont été faites dans le cas d'aryl et d'alkyl tétrazoles (19, 20). Le recours à l'ionisation chimique (IC) permet d'observer les ions quasi moléculaires (cf. partie expérimentale).

II. *Mécanisme d'obtention du tétrazole* 5a

La formation de ce tétrazole pose deux questions: celle du mécanisme d'isomérisation de l'azido-2 2*H*-oxazine-1,3 **4***a* dont il dérive manifestement – et celle de savoir si cette oxazine **4***a* est bien le produit cinétique de l'attaque de N_3^- sur l'oxazinium-1,3 **1***a*.

1. *Filiation oxazine 4*a *→ tétrazole 5*a

Nous proposons, pour rationaliser l'obtention du tétrazole **5***a*, deux tautoméries cycle–chaîne impliquant l'imino-azide **7***a* (1, 3, 8, 21, 22) (cf. schéma 2) jusqu'ici rencontrées séparément pour des systèmes voisins. (*i*) La tautomérie **4***a* $\leftrightarrows$ **7***a* s'apparente aux classiques équilibres diènone $\leftrightarrows$ α pyranne (cf. schéma 1) qui ont pu être notés lors de l'étude de l'action de nucléophiles (23) et en particulier de l'ion azoture (1, 3, 8) sur les cations pyrylium. (cf. schéma 1). (*ii*) La tautomérie **7***a* $\rightleftharpoons$ **5***a* est un équilibre du type iminoazide–tétrazole dont on connaît de nombreux exemples (21, 22).

L'obtention des tétrazoles **5***a* constitue une dérivation au schéma réactionnel initialement envisagé:

[1] L'étude détaillée du comportement thermique et photochimique des tétrazoles fait l'objet d'un article à part soumis pour publication au Can. J. Chem. (16).

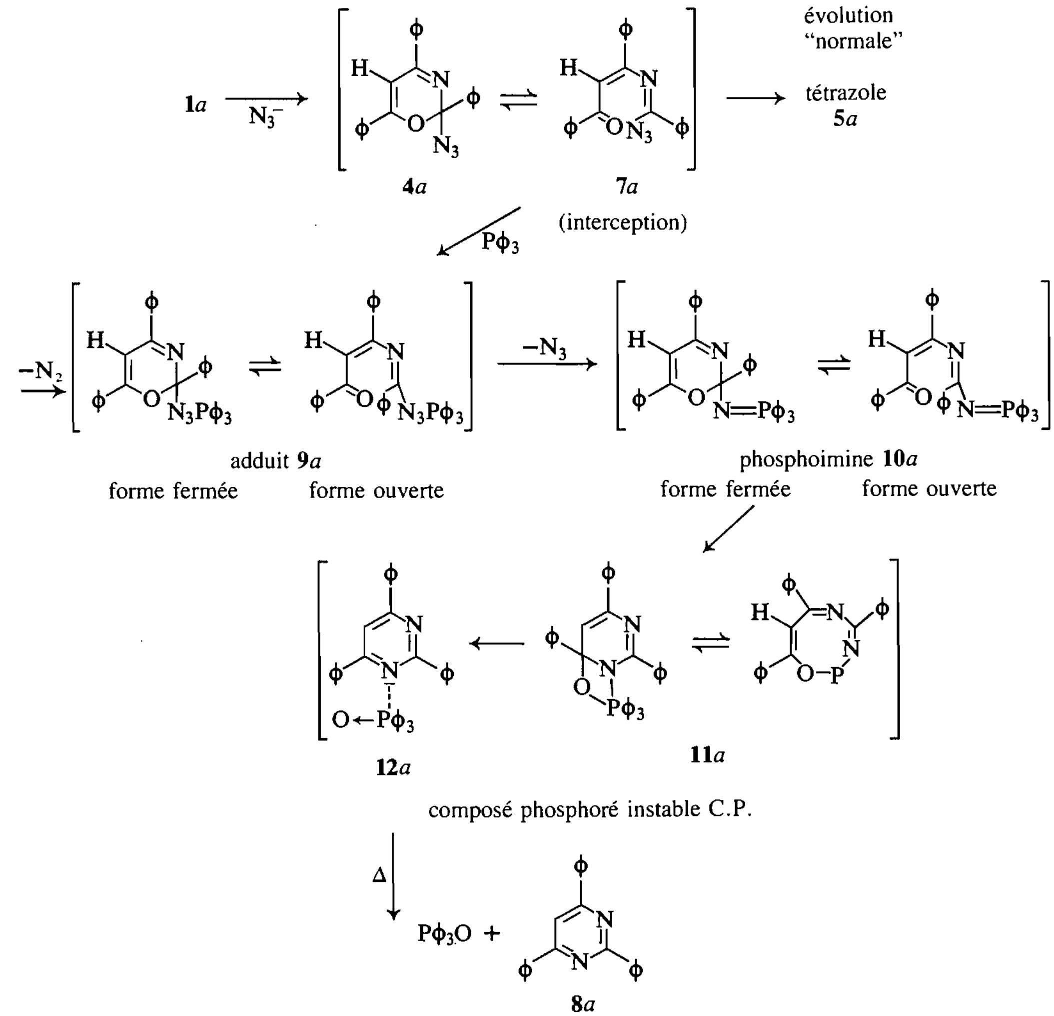

SCHÉMA 3

TABLEAU 1. Résonance magnétique nucléaire du ^{13}C des pôles d'attaque des oxaziniums-1,3 **1**. Réactivité vis à vis de N_3^-

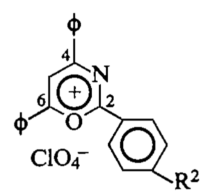

1

Composé **1**	δ ^{13}C, TMS, (CF_3COOH) C2	C4	C6	Attaque de N_3^- Réactivité	%5
b $R^2 = OCH_3$	177,5	170,1	175,2	1*b*	90
a $R^2 = H$	178,1	170,5	176,2	↘ croît	92
c $R^2 = NO_2$	178,4	168,2	178,0	1*c*	75

$$\text{Cation aromatique hétérocyclique} \xrightarrow{N_3^-} \text{azide hétérocyclique} \xrightarrow[-N_2]{\Delta} \text{hétérocycle azoté heptaatomique}$$

puisqu'elle inhibe la formation des hétérocycles heptaatomiques. Toutefois le mécanisme que nous proposons (cf. schéma 2) pour leur obtention laisse entrevoir des possiblilités de retour vers l'iminoazide ou l'azido-2 2*H*-oxazine-1,3 qui

TABLEAU 2. Spectres de masse des oxazines-1,3 **3** et **14** (I.E.; 70 eV)

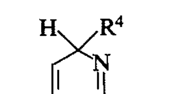

Composé	Spectre de masse
3*a* $R^2 = H$, $R^4 = C_6H_5$	311(8); *208*(100); 207(85); 179(10); 131(28); 130(11); 105(60); 103(70); 77(77)
3*b* $R^2 = OCH_3$, $R^4 = C_6H_5$	341(8); *208*(100); 207(96); 179(18); 165(5); 133(50); 131(39); 130(13); 105(48); 103(61); 77(96)
3*c* $R^2 = NO_2$, $R^4 = C_6H_5$	356(2); 208(53); 207(60); 179(10); 165(5); 148(3); 131(22); 130(10); 118(14); 105(35); 103(38); *77*(100)
14 (33) $R^2 = H$, $R^4 = H$	253(1); 149(7); 145(5); 132(3); 121(20); 120(18); *105*(100); 103(15); 77(80)

sont les formes intéressantes du schéma réactionnel général. A ce titre, a été entreprise une étude des différents facteurs intervenant sur les deux tautoméries impliquées dans la formation des tétrazoles (16).

2. *Mode d'action de N_3^- sur les oxaziniums-1,3 **1***

Afin de savoir si l'azido-2 2*H*-oxazine-1,3 **4***a* est ou non le

TABLEAU 3. Spectres de résonance magnétique nucléaire du ^{13}C des 2,4,6 polyaryloxazines-1,3 **3**[a]

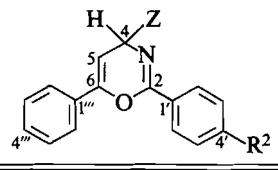

		3 Z = 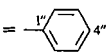 *a* R^2 = H	*b* $R^2 = OCH_3$[f]	*c* $R^2 = NO_2$	**14**[d] Z = H R^2 = H	**15**[e] Z = CH_3 R^2 = H
Carbones quaternaires	C2	152,2	152,0	150,6	151,4	150,6•
	C6	146,2	146,3	146,5	145,7	148,8•
	C1′	132,8*	124,9 (123,9)[c]	138,1 (138,8)[c]	130,4	132,9•
	C1″	144,4	144,6	143,7	—	145,1•
	C1‴	132,4*	132,9	132,3	131,0	132,5•
Carbones[b] tertiaires	C4′	131,0	162,0 (161,2)[c]	149,5 (150,6)[c]	128,9	
	C4	56,6	56,5	56,9	41,4[g]	
	C5	100,8	100,0	100,6	95,0	
	C4″	127,2	127,2	127,6	—	
	C4‴	128,3	128,9	129,8	126,7	

* Peuvent être inversés.
• Nos attributions.

[a] Déplacements chimiques en ppm/TMS interne, solutions dans $CDCl_3$.
[b] En raison de la complexité des spectres, les carbones tertiaires des groupes aryles n'ont pas été attribués, excepté les carbones *para* (identifiables par leur intensité et pour 4′ par la substitution).
[c] Déplacements calculés par incrémentation (30) à partir des δ ^{13}C de **3***a*.
[d] Diphényl-2,6 oxazine-1,3 **14** (29) facilitant l'attribution du carbone C1″ des oxazines **3**.
[e] Diphényl-2,6 méthyl-4 oxazine-1,3 **15**: spectre de ^{13}C publié sans attribution (31).
[f] δ ^{13}C OCH_3 = 55,3 ppm.
[g] Carbone secondaire.

produit cinétique de l'attaque de N_3^- sur l'oxazinium **1***a*, nous avons tenté de répondre en procédant à diverses démarches.

(a) *Action de NaN_3 sur* **1***a à basse température*

On ne décèle dans ces conditions aucune modification de la réaction: ni diminution notable du rendement en **5***a*, ni formation de nouveaux composés. Ce résultat signifie que l'oxazine **4***a* est probablement le produit cinétique de l'attaque.

(b) *Action de NaN_3 à basse température et en présence de triphényl phosphine*

Nous avons tenté d'intercepter à froid le précurseur du tétrazole **5***a* en procédant à l'attaque de l'oxazinium **1***a* par N_3^- en présence de $P(\phi)_3$. La triphénylphosphine est en effet connue pour capter les azides organiques en conduisant à des adduits 1 : 1 ou bien encore aux phosphoimines correspondantes par perte d'azote moléculaire (24).

Dans ces conditions, le cours "normal" de la réaction est modifié, une interception se produit effectivement puisqu'on observe: une diminution du rendement en tétrazole **5***a* de 92 à 47% (l'interception n'est que partielle), et la formation d'un composé phosphoré noté C.P. correspondant d'après l'analyse centésimale à la perte d'une molécule d'azote et à la fixation de $P(\phi)_3$ en partant d'une azidooxazine **2**, **3**, ou **4** ou de tout autre azide isomère (cf. schéma 3).

L'analyse centésimale n'a pu être réalisée que sur le composé C.P. brut car les essais de purification (recristallisation, chromatographie sur couche mince) conduisent immanquablement à une décomposition plus ou moins prononcée en mélange de $(\phi)_3PO$ et de triphényl 2,4,6-pyrimidine **8** (25) (cf. schéma 3). La fragilité de ce composé C.P. n'a pas facilité la détermination de sa structure. Cependant, aussi bien sa décomposition que diverses données spectroscopiques (comme: absence de carbonyle en infra-rouge, certaines fragmentations en spectrométrie de masse, présence dans le spectre de rmn ^{31}P d'un signal compatible avec un phosphore engagé dans un cycle (26)) nous conduisent à admettre pour ce composé C.P. une structure d'hétérocycle phosphoré. Dans le schéma 3 est représentée l'hypothèse la plus vraisemblable selon laquelle le précurseur intercepté à froid serait effectivement l'azido-2 2*H*-oxazine-1,3 **4***a*. Le produit de l'interception serait alors l'adduit $RN_3P(\phi)_3$ **9***a* sous forme ouverte ou cyclique dont le réarrangement direct ou par l'intermédiaire de la phosphoimine **10***a* (forme ouverte ou cyclique) conduirait au composé C.P. de structure **11***a* ou **12***a*.

Ces résultats confirment l'intervention d'un azide intermédiaire dans la formation du tétrazole **5***a* (cf. schéma 2) et s'accordent avec l'hypothèse de l'azido-2 2*H*-oxazine-1,3 **4** comme produit cinétique de l'attaque de N_3^-. Ils permettent d'écarter l'hypothèse d'un mécanisme concerté de l'attaque de N_3^- sur le pôle C2 de l'hétérocycle avec simultanéité de l'ouverture de cet hétérocycle et de la formation du cycle tétrazolique.

(c) *Effets de la substitution du pôle C2 sur la réactivité de N_3^- vis à vis des oxaziniums-1,3* **1**

Nous avons synthétisé de nouveaux oxaziniums-1,3

TABLEAU 4. Spectres de résonance magnétique nucléaire ^{13}C des triaryl-2,4,6 oxaziniums-1,3 **1**[a]

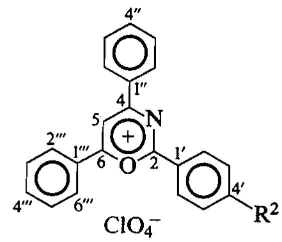

		1			[d] 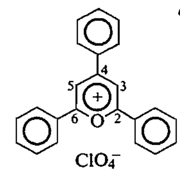
Carbones		*a* $R^2 = H$	*b* $R^2 = OCH_3$	*c* $R^2 = NO_2$	
	C2	178,1	177,5	178,4*	173,4
	C4	170,5	170,1	168,2	169,3
Carbones	C6	176,1	175,2	178,0*	173,4
quaternaires	C1′	128,8	120,9 (119,9)[c]	135,1 (134,8)[c]	129,8
	C1″	133,9	134,0	133,8	134,1
	C1‴	128,8	128,9	128,8	129,8
	C4′	139,8*	170,4 (170,0)[c]	154,6 (159,4)[c]	137,6
Carbones	C4″	140,8*	140,3		137,6
tertiaires[b]	C4‴	139,8	139,2	140,7	137,6
	C5	109,4	108,0	109,8	et C3 115,8

* Peuvent être inversés.

[a] Déplacements chimiques en ppm/TMS interne, solutions dans CF_3COOH.
[b] En raison de la compléxité des spectres, les carbones tertiaires des groupes aryles n'ont pas été attribués, exceptés les carbones *para* (identifiables par leur intensité et pour 4′ par la substitution).
[c] Déplacements calculés par incrémentation (30) à partir des δ ^{13}C du composé **1***a*.
[d] Triphényl-2,4,6 pyrylium utilisé comme modèle (1, 8).

présentant en C2 un groupement aryle C_6H_4p-R^2 – soit électrodonneur et désactivant (**1***b*, $R^2 = OCH_3$) – soit électroattracteur (**1***c*, $R^2 = NO_2$), (cf. tableau 1).

De façon tout à fait qualitative, on constate que l'oxazinium anisylé **1***b* est moins réactif vis à vis de N_3^- que les sels **1***a* et **1***c*.

Le recours à le spectroscopie uv–visible comme moyen de comparaison des vitesses d'attaque des trois sels **1***a* à **1***c* n'a pas permis un classement plus précis de leurs réactivités. En effet, à de telles concentrations, intervient de façon non négligeable la réaction concurrente d'hydrolyse des sels, en particulier dans le cas de l'oxazinium nitré **1***c*, qui conduit aux "pseudo-bases" correspondantes: les β benzamido-*trans*-benzalacétophénones **13** (cf. partie expérimentale).

En revanche, le recours à des réactions compétitives d'attaque de N_3^- sur des mélanges de sels d'oxazinium **1** fournit le classement indicatif suivant (basé sur une analyse des mélanges réactionnels par rmn ^1H, cf. partie expérimentale): **1***c* ($R^2 = NO_2$), **1***a* ($R^2 = H$) > **1***b* ($R^2 = OCH_3$).

Cette séquence suggère l'hypothèse selon laquelle la réactivité de l'ion azoture vis à vis des oxaziniums serait tributaire dans une mesure restant à déterminer, de la charge du pôle C_2. En effet, l'examen a priori de la substitution R^2 sur les carbones hétérocycliques montre que l'effet mésomère du groupe nitro n'affecte pratiquement pas les pôles d'attaque, cependant que celui du groupe méthoxyle est désactivant. Il est évident que cette constatation ne constitue qu'une indication grossière de l'influence de la substitution et que bien sûr l'ensemble des effets électroniques doit être pris en compte.

Dans un premier temps, nous avons fait appel au déplacement chimique ^{13}C pour situer, de façon approchée, la densité électronique des différents pôles des cations oxazinium, sous réserve de la validité d'une telle relation pour ces cations (27). Néanmoins, nous avons montré que pour des cations hétérocycliques voisins: pyryliums et thiopyryliums, existait une relation linéaire δ ^{13}C et charge π.H.M.O (1, 8).

En ce qui concerne les oxaziniums-1,3 **1**, les données de la rmn ^{13}C (cf. tableau 1) semblent confirmer l'hypothèse d'une influence importante du facteur densité de charge des pôles éventuels d'attaque sur la réactivité de l'ion N_3^-. On observe en effet que le pôle C2 est le plus déblindé (voire le plus chargé) et qu'un certain parallélisme existe entre le δ ^{13}C du pôle C2 et la réactivité du cation correspondant vis à vis de N_3^- (cette dernière croissant du sel **1***b* au sel **1***c*).

Cette hypothèse amène à considérer comme moins favorable une attaque sur le pôle C4 qui s'avère être le moins déblindé voire le moins chargé des pôles d'attaque. En revanche, dans le cas de l'oxazinium nitré **1***c*, elle conduit à envisager la simultanéité d'une attaque de N_3^- sur les pôles C2 et C6 qui porteraient selon la rmn ^{13}C des charges voisines. Un composé supplémentaire a d'ailleurs été isolé en procédant à l'attaque du sel **1***c* à basse température. Son trop faible rendement n'a toutefois pas permis d'en préciser la structure ni, bien sûr, l'origine (attaque en C2 ou C6).

Un traitement théorique de la réactivité du système oxazinium-1,3/N_3^- analogue à celui déjà effectué dans le cas

TABLEAU 5. Spectres de résonance magnétique nucleaire du ^{13}C des pseudobases triarylées **13**[a]

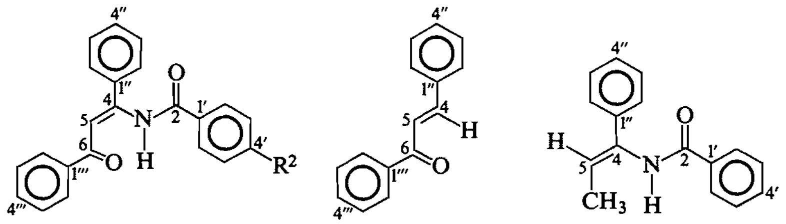

13 **6** **16**

Carbones		13 *a* $R^2 = H$	13 *b* $R^2 = OCH_3$	13 *c* $R^2 = NO_2$	**6**[d]	**16**[e]
	C2	165,2	164,7	165,2		164,8
	C4	157,1	157,5	156,4	144,6	138,3
Carbones	C6	192,0	191,9	192,4	190,2	
quaternaires	C1′	133,5	125,6 (124,6)[c]	138,9 (139,5)[c]		134,1 *
	C1″	136,4	136,5	135,7	134,8	134,8 *
	C1‴	138,6	138,6	138,3	138,1	
	C4′	132,8*	163,2 (163,0)[c]	150,3 (152,4)[c]		132,2
Carbones	C4″	129,8	129,7	130,1	130,4	128,1
tertiaires[b]	C4‴	132,8	132,6	133,1	132,7	
	C5	105,4	104,9	106,2	122,0	120,5

* Peuvent être inversés.

[a] Déplacements chimiques en ppm/TMS interne, solutions dans $CDCl_3$.
[b] En raison de la complexité des spectres, les carbones tertiaires des groupes aryles n'ont pas été attribués, exceptés les carbones *para* (identifiables par leur intensité et pour 4′ par la substitution).
[c] Déplacements calculés par incrémentation (30) à partir des déplacements du composé **13***a*.
[d] *trans*-Benzalacétophénone **6** utilisée comme modèle du système ènonique.
[e] **16** (31) modèle de benzamide secondaire.

de système pyrylium/N_3^- (1, 2) est actuellement entrepris. Tout d'abord il devrait permettre de vérifier la validité des hypothèses émises, comme celle d'une relation linéaire δ ^{13}C/densité de charges des pôles éventuels d'attaque des oxaziniums et celle d'une réactivité des cations **1** fortement tributaire des charges, selon laquelle les azido-2 oxazines-1,3 seraient les produits cinétique de l'attaque. Enfin, il devrait renseigner sur l'éventualité d'un complexe donneur–accepteur du type de ceux observés (1, 8) dans le cas de pyryliums peu encombrés, que nous avions envisagée pour interpréter l'exaltation de coloration observée au début de la réaction entre N_3^- et l'oxazinium **1***a*.

Partie expérimentale

Les spectres d'absorption ultraviolet–visible et infrarouge ont été respectivement enregistrés sur des appareils Hewlett Packard 8450 ou Philips SP8-250 et Philips SP3-200. Les spectres de rmn ^1H et rmn ^{13}C ont été enregistrés sur appareils Varian EM360 ou Bruker WP80 et sur appareils Bruker SY80 et WM250. Quant aux spectres de masse, ils ont été effectués par Mesdemoiselles J. Mercier et C. Lange que nous remercions, respectivement – au Centre de Mesures Physiques de Paris sur un spectromètre AEI MS50 – au laboratoire sur un spectrographe quadrupolaire NERMAG R10-10C. Les analyses élémentaires ont été effectuées par le Centre de Microanalyse du C.N.R.S. ou au Laboratoire de Microanalyse de l'Université Pierre et Marie Curie. Les points de fusion non corrigés ont été déterminés de façon instantanée au banc de Köfler.

1. *Synthèse et structure des triaryl-2,4,6 oxaziniums-1,3 1*

La structure des oxaziniums-1,3 **1** repose tant sur leurs propriétés spectroscopiques que sur celles de leurs précurseurs, les 4*H*-oxazines-1,3 **3** (Nu = H), et celles de leurs produits d'hydrolyse, les β-benzamido-*trans*-benzalacétophénones **13**. Une étude spectroscopique de ces trois classes de composés a donc été menée en recourant notamment à la rmn ^{13}C.

(a) *Propriétés des 4*H*-oxazines-1,3 3 (Nu = H)*

Les oxazines **3***a* et **3***b* étaient déjà connues (10, 28) ainsi que l'oxazine **14** (29) qui a servi de modèle pour les attributions de déplacements en rmn ^{13}C. *L'oxazine nitrée* **3***c* nouvelle a été préparée selon Schmidt (10): (60%); Fi 134°C (éther); ir cm^{-1} (KBr): 1690, 1640, 1605, 1580, 1520, 1500, 1455 et 1350; UV λ_{max} nm (ϵ_{max}), (éther): 214 (4,32), 272 (4,32); rmn ^1H ($CDCl_3$) δ ppm/TMS: 5,75 (syst. AB, 2H, J = 3 Hz). *Anal.* calc. pour $C_{22}H_{16}N_2O_3$: C 74,14, H 4,53, N 7,86; tr.: C 74,04, H 4,70, N 8,01. Spectre de masse: cf. tableau 2; rmn ^{13}C des oxazines: cf. tableau 3.

(b) *Obtention et propriétés des triaryl-2,4,6 oxaziniums-1,3 1*

Seul l'oxazinium **1***a* était connu (10). Les oxaziniums **1***b* et **1***c* ont été obtenus selon la même méthode (10) par oxydation des 4*H*-oxazines-1,3 **3** correspondantes.

*Perchlorate de diphényl-4,6 paraméthoxyphényl-2 oxazinium-1,3 1*b: (60%); Fi 265–267°C (CH_3CN, éther); ir cm^{-1} (KBr): 2850, 1615, 1590, 1530, 1095; uv–visible (CH_3CN) λ_{max} nm (log ϵ_{max}): 375

TABLEAU 6. Propriétés spectroscopiques des tétrazoles **5**

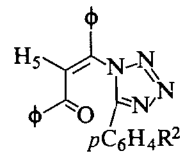

5

Spectre		**5***a* R^2 = H			**5***b* R^2 = OCH_3			**5***c* R^2 = NO_2		
Infra-rouge[a] (KBr) cm^{-1}		1665, 1620 1600, 1590			2840, 1665 1610, 1580			1665, 1610, 1580		
Ultraviolet–visible (éther) λ_{max} nm (log ϵ_{max})		228 (4, 11) 290 (4, 06)			247 (3, 56) 331 (3, 49)					
Résonance magnétique nucléaire du ^{1}H δ ppm/TMS interne Solution $CDCl_3$		7,85–7,65 (m, 4H) 7,6 (s, H_5)[b] 7,55–7,25 (m, 11H)			7,9–6,8 (m, 15H) 3,75 (s, 3H)			8,5–8,1 (m, 4H) 8,1–7,3 (m, 11H)		
Masse (*M*)		(352)			(382)			(397)		
D.I.C. (NH_3; 0,1 Torr) ions quasi moléculaires		$(M + 1)^+$ 353			$(M + 1)^+$ 383			$(M + 1)^+$ 415 $(M + 1)^+$ 398		
I.E. 70 eV		324(10), 310(6)[c] 247(3), *105*(100), 77(70)			354(3), 340(2) 277(1), 135(25) 105(94), *77*(100)			369(10), 355(30) 292(5), 150(10) 105(55), *77*(100)		
		C	H	N	C	H	N	C	H	N
Analyse	% calc.	74,98	4,58	15,90	72,23	4,74	14,65	66,49	3,80	17,63
	% tr.	74,62	4,49	15,68	72,42	4,81	14,76	66,38	3,88	17,88

[a]On note entre 1340 et 690 cm^{-1} la présence d'un ensemble de bandes caractéristiques du noyau tétrazolique (17, 18).
[b]Position confirmée par la rmn à haut champ (250 MHz), par l'emploi de $Eu(fod)_3$ et par effet de solvant ASIS (34), (C_6D_6): 7,9–7,4 (m, 4H), 7,15 (s, $^3H_5$), 7,1–6,8 (m, 11H).
[c]*Masse Exacte* calc. pour $C_{22}H_{16}NO$: 310, 1231; tr.: 310, 1236.

1*a* + **1***b*
5×10^{-5} mol 5×10^{-5} mol

1*c* + **1***b*
5×10^{-5} mol 5×10^{-5} mol

↓ Action à l'abri de la lumière de 20 mg NaN_3 ~ 3×10^{-4} mol ↓
$5\ cm^3$ de CH_3CN pendant 5 min à −5°C

Mélange réactionnel
5*a* + **5***b* + **1***a* + **1***b*

Mélange réactionnel
5*c* + **5***b* + **1***c* + **1***b*

↓ Hydrolyse ↓

Pseudobases **13***a* + **13***b*
Tétrazoles **5***a* + **5***b*

Pseudobases **13***c* + **13***b*
Tétrazoles **5***c* + **5***b*

↓ Silice séparation ccm tétrazoles/pseudobases ↓

\+ Tétrazole **5***a*
Tétrazole **5***b*

\+ Tétrazole **5***b*
Tétrazole **5***c*

↓ Dosage rmn ^{1}H $CDCl_3$

Dosage rmn ^{1}H DMSO-d_6 ↓

Résultat: **5***b*/**5***a* = 0,80

Résultat: **5***b*/**5***c* = 0,78

SCHÉMA 4

TABLEAU 7. Spectres de résonance magnétique nucléaire du ^{13}C des tétrazoles 5[a]

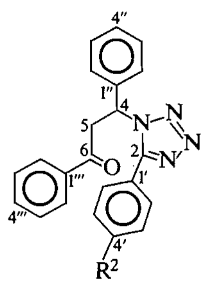

5

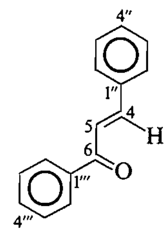

6

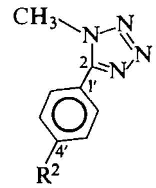

17

		5 *a* R^2 = H	5 *b* $R^2 = OCH_3$	5 *c* $R^2 = NO_2$	6[d]	17[e] *a* R^2 = H	17[e] *c* $R^2 = NO_2$
Carbones quaternaires	C2	155,9	155,4	154,3		154,2	152,7
	C4	142,7	142,6	142,0	144,5		
	C6	189,1	188,9	189,9	190,0		
	C1′	124,8	116,6 (115,9)[c]	120,9 (130,8)[c]		123,2	129,9 (129,2)[c]
	C1″	134,5	134,4	134,1	134,6		
	C1‴	138,2	138,0	137,7	137,9		
Carbones tertiaires[b]	C4′	131,8* }	162,9 (162,0)[c]	149,9 (151,4)[c]		131,3	148,8 (150,9)[c]
	C4″	132,2 }	132,4	132,6	130,3		
	C4‴	134,3	134,4	134,7	132,7		
	C5	123,9	124,3	124,6	122,0		

*Peuvent être inversés.

[a]Déplacements chimiques en ppm/TMS interne, solutions dans CD_3COCD_3.
[b]En raison de la compléxité des spectres, les carbones tertiaires des groupes aryles n'ont pas été attribués exceptés les carbones *para* (identifiables par leur intensité et pour 4′ par la substitution).
[c]Déplacements calculés par incrémentation (30) à partir des déplacements du composé **5***a*.
[d]*trans*-Benzalacétophénone **6** utilisée comme modèle du système énonique.
[e]**17** (35): modèle de tétrazoles.

(5,38), 436 (5,03); rmn ^{13}C: cf. tableau 4. *Anal.* calc. pour $C_{23}H_{18}N_1O_6$ Cl: C 62,80, H 4,13, N 3,18, Cl 8,06; tr.: C 62,49, H 4,23, N 3,30, Cl 7,83.

Perchlorate de diphényl-4,6 paranitrophényl-2 oxazinium-1,3 **1***c*: (85%); Fi 275–280°C (CH_3CN, éther); ir cm^{-1} (KBr): 1625, 1590, 1520, 1350, 1100; uv–visible (CH_3CN) λ_{max} nm (log ϵ_{max}): 274 (4,36), 352 (4,41), 404 (4,44); rmn ^{13}C: cf. tableau 4. *Analyse*: composé ne pouvant être isolé pur, cf. analyse centésimale de son produit d'hydrolyse la pseudobase **13***c*.

Pour les attributions des signaux δ ^{13}C des oxaziniums-1,3 **1** nous nous sommes basés sur la comparaison de l'oxazinium triphénylé **1***a* avec le pyrylium correspondant pour lequel δC4 < δC2 et δC6 (1, 8). Nous avons supposé que pour les oxaziniums-1,3 le même ordre était conservé et que le carbone C2 était le plus déblindé en raison de sa situation entre deux hétéroatomes. Ceci a été confirmé en procédant à l'enregistrement du spectre de **1***a* sans découplage des protons. On observe alors que le carbone le plus déblindé est le moins couplé (il s'agit de C2 qui apparaît sous forme de triplet), cependant que le signal suivant apparaît sous forme d'un quadruplet (C6 subit un couplage avec H2‴ et H6‴ et un couplage supplémentaire voisin avec H5). Pour les oxaziniums-2,4,6 triarylés la séquence des pôles éventuels d'attaque apparaît donc comme δC2 > δC6 > δC4. On constate que ces positions sont plus déblindées que celles des pyryliums (8, 32).

(c) β-*Benzamido* trans-*benzalacétophénones* **13**: *pseudo bases des oxaziniums* **1**

L'hydrolyse en milieu acétonitrile aqueux des oxaziniums **1***a* à **1***c* conduit aux pseudo bases **13***a* à **13***c* (33). Ces composés sont de configuration Z et présentent une liaison hydrogène intramoléculaire entre le carbonyle et le groupe amidique. Ceci se manifeste – en infra-rouge: bande de NH associé vers 3200 cm^{-1} et bande de C=O conjugué et associé vers 1620–1625 cm^{-1} – et en rmn ^{1}H: présence d'un signal très déblindé vers 13 ppm.

β-p-*Méthoxybenzamido*-trans-*benzalacétophénone* **13**b (70%); Fi 90–92°C (CH_3CN, éther); ir cm^{-1} (KBr): 3200, 2840, 1690, 1620, 1590, 1575; uv–visible (éther) λ_{max} nm (log ϵ_{max}): 213 (4,43), 283 (4,46) 344 (4,48); rmn ^{1}H ($CDCl_3$) δ ppm/TMS: 13,4 (s, 1H, éch. D_2O), 6,5 (s, 1H), 3,9 (s, 1H); rmn ^{13}C: cf. tableau 5). *Anal.* calc. pour $C_{23}H_{19}N_1O_3$: C 77,29, H 5,36, N 3,92; tr.: C 77,04, H 5,51, N 4,02; masse *m/e*: M^+ 357 (3), 252 (75), 207 (5), 135 (40), 92 (20), 77 (100).

β-p-*Nitrobenzamido*-trans-*benzalacétophénone* **13**c: (80%); Fi 192–194°C (CH_3CN, éther); ir cm^{-1} (KBr): 3200, 1690, 1625, 1590, 1350; rmn ^{1}H ($CDCl_3$) δ ppm/TMS: 13,4 (s, 1H, éch. D_2O), 6,5 (s, 1H); rmn ^{13}C: cf. tableau 5. *Anal.* calc. pour $C_{22}H_{16}N_2O_4$: C 77,29, H 5,36, N 3,92; tr.: C 77,04, H 5,51, N 4,02; masse *m/e*: M^+ 372 (1), 261 (21), 267 (100), 237 (20), 105 (40), 77 (60).

II. *Réaction de NaN_3 avec les triaryl-2,4,6 oxaziniums-1,3* **1**

A. *Obtention des tétrazoles* **5**

1. *Action de NaN_3 à température ambiante*

A une mmol de perchlorate de triaryl-2,4,6 oxazinium-1,3 **1***a* à **1***c* en solution dans 10 cm^3 d'acétonitrile sec est ajouté un excès de NaN_3 (2 à 3 fois la quantité stoechiométrique). Le mélange réactionnel est agité à la température ambiante sous atmosphère inerte et à l'obscurité pendant 2 h. Il est repris à l'eau, extrait à l'éther. La phase éthérée est séchée sur $MgSO_4$ puis évaporée à température ambiante sous vide.

Les tétrazoles *5a* à *5c* sont obtenus avec les rendements respectifs de 92%, 90% et 75%. Dans le cas de l'oxazinium **1***c*, on isole également 5% de pseudobase **13***c* ainsi qu'un composé supplémentaire non identifié lorsqu'on opère à froid (environ 5 mg).

2. *Action de NaN_3 à basse température*

A une solution de 100 mg (0,22 mmol) de sel **1***a* dans 5 cm^3 de CH_3CN sec sont ajoutés à froid (environ −40°C) 35 mg de NaN_3. Au bout de 48 h l'analyse par chromatographie sur couche mince de silice (ccm) n'indique qu'un seul produit. Le traitement habituel conduit à 84 mg (97%) de tétrazole **5***a*.

3. *Action de NaN_3 à basse température et en présence de $P(Ph)_3$*

A une solution de 100 mg (0,24 mmol) de sel **1***a* dans 5 cm^3 de CH_3CN sec sont ajoutés à froid ($\theta = -40$°C) 100 mg de $P(Ph)_3$ et 45 mg de NaN_3. Au bout de 48 h, le solvant est chassé et le résidu analysé par chromatographie préparative sur couche mince de silice, on isole dans l'ordre d'élution (cyclohexane/acétate d'éthyle 8:2): $P(\phi)_3$ en excès, le composé C.P. (100 mg) légèrement contaminé par $P(\phi)_3$, la triphényl-2,4,6 pyrimidine **8** (2,5 mg, 3,5%) identifiée à un échantillon authentique (10), le tétrazole **5***a* (40 mg, 48%), la pseudobase **13***a* (22 mg, 28%) et $P(\phi)_3O$ (3 mg, 3%) isolé par lavage à l'éther des 60 mg constituant le dépôt de ccm.

*Composé phosphoré C.P.: 11*a *ou 12*a: Fi ~ 190°C; ir (KBr) pas de carbonyle; rmn ^1H pas de signal caractéristique en dehors des H arom. *Anal.* calc. pour $C_{40}H_{31}OPN_2$ ($P(\phi)_3O$ + **8**): C 81,73, H 5,45, N 4,60; tr.: C 81,89, H 5,32, N 4,77. *Spectroscopie de masse*: impact électronique: on n'observe pas l'ion moléculaire $M^{+\cdot}$ 586 mais on retrouve l'intégralité des spectres de $P(Ph)_3O$ et de la pyrimidine **8**; *rmn ^{31}P* (101,25 MHz) δ ppm/H_3PO_4: 28,3 ($P\phi_3O$); −6,4 (C.P.).

4. *Classement de la réactivité des oxaziniums-1,3 1*a *à* c

Nous avons réalisé deux mélanges dans l'acétonitrile de sels ayant l'oxazinium anisylé **1***b* en commun (cf. schéma 4).

Sur chacun de ces mélanges il est procédé à l'action de NaN_3 pendant un court laps de temps (temps inférieur au temps nécessaire à la réaction totale du plus réactif). On procède alors à l'hydrolyse des sels n'ayant pas réagi. Les pseudobases **13** sont séparées (ccm) des tétrazoles **5** qui sont alors dosés par rmn ^1H en prenant comme référence les intégrations du signal méthoxyle du tétrazole **5***b* formé.

Il apparaît donc que le tétrazole **5***b* est obtenu en plus faible rendement que les tétrazoles **5***a* et **5***c*, ce qui signifie que le sel **1***b* réagit plus lentement avec N_3^- que les sels **1***a* et **1***c* qui ne peuvent toutefois pas être différenciés.

(B) *Propriétés spectroscopiques des tétrazoles*

Les données spectroscopiques: uv–visible, infra-rouge et masse sont consignées dans le tableau 6; *rmn ^{13}C* cf. tableau 7. L'interprétation des spectres des tétrazoles est facilitée par leur comparaison à ceux de deux composés modèles: la *trans*-benzalacétophénone **6** et les méthyl-1 aryl-5 tétrazoles **17** (35).

L'attribution des signaux voisins de 190 et 155 ppm se fait sans ambiguïté aux carbones notés C6 et C2. L'ordre des δ ^{13}C des carbones quaternaires notés C1′, C1″ et C1‴ pour le composé **5***a* découle de la comparaison avec les molécules modèles **6** et **17***a*. Les carbones C4′ et C4″ du composé **5***a* présentent des déplacements voisins de ceux des carbones correspondants des modèles **6** et **17***a*.

L'attribution du carbone C4 (δ = 142,7 ppm pour **5***a*) a été confirmée par l'enregistrement d'un spectre sans découplage des protons. C4 apparaît alors comme le plus couplé des carbones quaternaires: couplages avec H2″, H6″ et H5 et élargissement dû au voisinage de l'azote.

En conclusion, on est amené à considérer le motif tétrazole comme un groupement azoté très particulier: contrairement au motif benzamido, son introduction en position β sur la *trans*-benzalacétophénone n'a pratiquement pas d'influence sur le système ènonique.

1. P-L. DESBENE. Thèse d'Etat, Paris. 1979.
2. P-L. DESBENE, D. RICHARD, J-C. CHERTON et P. CHAQUIN. Tétrahedron. Sous presse.
3. J-P. LE ROUX, J-C. CHERTON et P-L. DESBENE. C. R. Acad. Sci. **280**, 37 (1975).
4. J-P. LE ROUX, J-C. CHERTON et P-L. DESBENE. C. R. Acad. Sci. **278**, 1389 (1974).
5. J-P. LE ROUX, P-L. DESBENE et M. SEGUIN. Tetrahedron Lett. **36**, 3141 (1976).
6. J-P. LE ROUX, P-L. DESBENE et J-C. CHERTON. J. Heterocycl. Chem. **18**, 847 (1981).
7. P. L. DESBENE et J-C. CHERTON. Tetrahedron. Sous presse.
8. P. L. DESBENE, J-P. LE ROUX, J-C. CHERTON et J-J. BASSELIER. Tetrahedron. Sous presse.
9. P. L. DESBENE et J-C. CHERTON. Tetrahedron. Sous presse.
10. R. R. SCHMIDT. Synthesis, 333 (1972) et réf. citées.
11. I. SHIBUYA et M. KURABAYASHI. Bull. Chem. Soc. Jpn. **46**, 3903 (1973).
12. I. SHIBUYA et M. KURABAYASHI. Bull. Chem. Soc. Jpn. **48**, 73 (1975).
13. I. SHIBUYA. Bull. Chem. Soc. Jpn. **54**, 2387 (1981).
14. D. TKACZYNSKA. Wiad. Chem. **26**, 757 (1972).
15. L. J. BELLAMY. The infrared spectra of complex molecules. 1ère éd. John Wiley and Sons Inc., New York. 1954. p. 223.
16. J. C. CHERTON, M. BAZINET, M. M. BOLZE, M. LANSON et P. L. DESBENE. Can. J. Chem. Soumis.
17. A. WENTRUP. Helv. Chim. Acta, **59**, 262 (1970).
18. E. LIEBER, D. LEVERING et L. PATTERSON. Anal. Chem. **23**, 1954 (1951).
19. R. R. FRASER et K. E. HAQUE. Can. J. Chem. **46**, 2855 (1968).
20. D. M. FORKEY et W. R. CARPENTER. Org. Mass. Spectrosc. 433 (1969).
21. W. LWOWSKI. *Dans* The chemistry of the azidogroup. *Edité par* S. Patai. Interscience, New York. 1971. p. 503.
22. R. N. BUTLER. Adv. Hétérocycl. Chem. **21**, 402 (1977).
23. J-P. LE ROUX, G. LETERTRE, P-L. DESBENE et J-J. BASSELIER. Bull. Soc. Chim. Fr. 4059 (1971).
24. (*a*) J. E. LEFFLER, U. HONSBERG, Y. TSUNO et I. FORSBLAD. J. Org. Chem. **26**, 4810 (1961); (*b*) L. F. KASUKHIN, M. P. PONOMARCHUK, T. I. KLEPA, V. PLYSENKO et YU GOLOBOY. Zh. Obshch. Khim. **47**, 2188 (1977).
25. R. R. SCHMIDT. Chem. Ber. **98**, 334 (1965).
26. (*a*) F. RAMIREZ et N. B. DESAI. J. Am. Chem. Soc. **85**, 3254 (1963); (*b*) E. L. CLENNAN et POH CHOO HEAH. J. Org. Chem. 4107 (1981).
27. G. A. OLAH, P. W. WESTERMAN et D. A. FORSYTH. J. Am. Chem. Soc. **97**, 3419 (1975).
28. R. R. SCHMIDT. Justus Liebigs Ann. Chem. **12**, 2010 (1973).
29. S. GABRIEL. Justus Liebigs Ann. Chem. **409**, 305 (1915).
30. J. B. STOTHERS. Carbon-13 nmr. Academic Press, New York. 1972.
31. S. AURICCHIO, O. VAJNADEPAVA et E. VERA. Synthesis, 116 (1979).
32. A. T. BALABAN et V. WRAY. Org. Magn. Reson. **9**, 16 (1977).
33. R. R. SCHMIDT, D. SCHWILLE et U. SOMMER. Justus Liebigs Ann. Chem. **723**, 111 (1969).
34. P. BAAS et H. CERFONTAIN. Tetrahedron, **33**, 1509 (1977).
35. R. N. BUTLER et T. M. MACEVOY. J. Chem. Soc. Perkin Trans. 2, 1087 (1978).

A laser diffraction and nuclear magnetic resonance investigation of the cholesteric potassium *N*-dodecanoylalaninate mesophase system

KEITH RADLEY AND ALAN S. TRACEY
Department of Chemistry, Simon Fraser University, Burnaby, B.C., Canada V5A 1S6

Received February 28, 1984

KEITH RADLEY and ALAN S. TRACEY. Can. J. Chem. **63**, 95 (1985).

Nematic and twisted nematic mesophases have been prepared from various mixtures of potassium *N*-dodecanoyl-*l*-alaninate and its racemate. The induced pitch was determined as a function of optical purity as were nmr spectra from a variety of additives including several inorganic salts and *d,l*-alanine. Dipolar couplings from the $CHCH_3$ moiety of the alaninate headgroup were studied, as were quadrupole splittings from the N—D of the amido group and the D_2O of the water. It was proposed that with development of cholesteric behaviour on proceeding in a stepwise fashion from the *d,l* to *l* amphiphile, the individual disk-like micelles twisted into a chiral shape, then aggregated to form domain-like structures. The major axis of these aggregates is the axis along which the helix propagates and this local axis serves as the director axis for the aggregates. The individual aggregates reorient as a unit when placed in the magnetic field of an nmr spectrometer. As a consequence of this, the diamagnetic anisotropy of the mesophase prepared from the *l* amphiphile is positive in sign while that of the *d,l* analogue is negative. Despite this observed change in diamagnetic anisotropy, the alignment of the individual micelles is not different for the chiral and racemic materials.

KEITH RADLEY et ALAN S. TRACEY. Can. J. Chem. **63**, 95 (1985).

On a préparé des mésophases nématiques et nématiques croisées à partir de divers mélanges de *N*-dodécanoyl *l*-alaninate de potassium et de son racémate. On a déterminé le pas induit en fonction de la pureté optique ainsi que les spectres rmn obtenus par l'addition de divers produits incluant plusieurs sels inorganiques et la *d,l*-alanine. On a étudié les couplages dipolaires de la portion $CHCH_3$ de l'alaninate de tête ainsi que les couplages quadrupolaires N—D du groupe amido et du D_2O de l'eau. Il a été proposé que, si on développe le caractère cholestérique lorsqu'on procède par étape de l'amphiphile *d,l* vers le *l*, les micelles individuelles en forme de disques se croisent pour prendre une forme chirale et elles s'agglutinent ensuite pour former des structures en forme de domaines. L'axe principal de ces aggrégats est l'axe le long duquel l'hélice se propage et cet axe local sert d'axe directeur pour ces aggrégats. Les aggrégats individuels se réorientent sous forme d'unité lorsqu'ils sont placés dans le champ magnétique d'un spectromètre rmn. A cause de cette réorientation, l'anisotropie diamagnétique de la mésophase préparée à partir du *l*-amphiphile est de signe positif alors que celle de l'analogue *d,l* est négative. En dépit de ce changement observé dans l'anisotropie diamagnétique, il n'y a pas de différence dans l'alignement des micelles individuelles des substances chirales et racémiques.

[Traduit par le journal]

Introduction

The twisted nematic or cholesteric liquid crystalline materials were the first class of liquid crystals to be recognized (1). The term "cholesteric" designates the fact that early examples of this case of mesomorphic materials were prepared from derivatives of cholesterol. The most striking characteristic of these compounds is their selective reflection of incident light, thereby providing an intense irridescence. This behaviour derives from a helical arrangement of the constituent molecules induced by the specific interactions between chiral centres of adjacent molecules.

In the lyotropic mesophases employed in this study, cholesteric behaviour arises by a much more complex behaviour. The nematic state is characterized by micellar aggregates dispersed through an aqueous medium. In twisted nematics, the individual micelles are organized into a helical arrangement via interactions with other micelles. This implies that there must be a high degree of molecular order within each micelle, similar to that for the thermotropic twisted nematic mesophases, and that information concerning this molecular order is transferred from one micelle to another. The mechanism of transfer of this information is of interest. The interactions between micelles generate a helical axis giving rise to reflectance bands in the infrared rather than in the visible light region. The wavelength of reflected light, λ_0, is directly proportional to the pitch, P, of the helical axis and is dependent on the average of the refractive indices, $\eta_\parallel$ and $\eta_\perp$ so that eq. [1] is obtained. In this expression $\parallel$ and $\perp$ refer to an axis parallel or perpendicular to the helix

$$[1] \quad \lambda_0 = \frac{\eta_\parallel + \eta_\perp}{2} P$$

axis respectively.

The pitch of the helix can also be readily measured by microscopy (2); however, it is sometimes more convenient to use diffraction of laser light where the twist ($1/P$) is given by Bragg's Law for diffraction

$$[2] \quad 1/P = \sin \sigma/\lambda_0$$

where λ_0 is the frequency of the incident light and σ is the angle of light diffraction. Laser diffraction allows samples prepared for nuclear magnetic resonance (nmr) spectroscopy to be investigated without disturbing them. This is particularly convenient when samples have been homogeneously aligned by the magnetic field of the nmr spectrometer through their diamagnetic anisotropy, since the aligned samples give sharp diffraction bands.

Both twisted nematic and nematic lyotropic mesophases have been studied by microscopy using polarized light (2–6) and by nmr spectroscopy (6–9). The texture observed under the microscope is dependent on aggregate shape and thus microscopy can differentiate between nematic mesophases formed from the disk-like lamellar aggregates or the rod-shaped cylindrical aggregates (3). This information is necessary for the interpretation of the results from the nmr experiments.

The sign of the diamagnetic anisotropy of the individual micelles is important when studying twisted nematics. If this quantity is negative, the micellar aggregates align with their major axis perpendicular to the magnetic induction, B_0, which defines the z axis. Because B_0 is cylindrically symmetric, the helical arrangement is free to propagate along this axis. The symmetry in B_0, of course, may effectively be destroyed in the conventional iron-core magnet spectrometers by spinning the sample, thus providing a unique axis perpendicular to B_0. Such sample spinning will, in general, destroy the helical arrangement provided, of course, that aligning forces are stronger than twisting forces; if not, two-dimensional order of the micelles will then be obtained. If the diamagnetic anistropy of the micelles is of positive sign, they align with their major axis, the director, parallel to B_0. In this case, the cholesteric behaviour may be destroyed when the helical axis propagates perpendicular to the director.

Nuclear magnetic resonance spectroscopy is a powerful tool for investigating the details of interactions in liquid crystalline systems. Such information may be inferred from dipolar couplings and quadrupole splittings which provide information concerning molecular alignment (10, 11). This alignment, being determined by specific interactions, can be used to investigate those interactions. Of interest in this regard is the specificity of interactions between centres of optical activity, in particular the interactions between *d,l* isomers of simple molecules and an optically pure centre (*d* or *l*) of a micellar constituent. Work with *d* and *l* alanine in a mesophase prepared from optically resolved sodium decyl-2-sulphate has demonstrated the feasibility of this approach (7).

Recently, twisted nematic mesophases prepared from potassium *N*-dodecanoylalaninate have been described (4) and these materials provide suitable systems to work with. They are easily prepared in optically pure form and are readily obtained chemically pure by recrystallization.

Experimental

The *N*-dodecanoylalanine used in this study was prepared from commercially provided *l* and *d,l*-alanine by reaction with dodecanoyl chloride, as has been described (12), and that procedure differs little from the procedure utilized here. The purity of the amide was monitored by ^{13}C magnetic resonance, which indicated that several recrystallizations from petroleum ether (60–80) were required in order to remove dodecanoic acid. The product was made alkaline with KOH to provide the potassium *N*-dodecanoylalaninate, which was recrystallized three times from ethyl acetate/ethanol. It was necessary to take care that solutions were not made excessively basic since hydrolysis occurred to give potassium dodecanoate, which was not readily separated from the desired product by recrystallization. The purity of the product was checked by ^{13}C nmr and, if potassium dodecanoate was detected, the free amide was regenerated by acidification and purification carried out before recycling to the salt.

The liquid crystalline samples were prepared by weighing the various components into test tubes with a constriction in the centre. The tubes were then sealed and a homogeneous material formed by repetitively warming and centrifuging through the constriction. The liquid crystalline materials so prepared were transferred to nmr tubes, which were then sealed.

Table 1 provides the compositions of the various samples used in this study. For preparation B of this table, samples were prepared so that they proceeded from the racemic amphiphile to optically pure amphiphile in a stepwise manner. Two mesophases of composition C were prepared, C_1 from the racemic amphiphile and C_2 from the optically pure amphiphile.

The nmr measurements were made at 303 K. This slight warming of the samples allowed alignment in the nmr spectrometer to proceed at a relatively much more rapid pace, thus considerably shortening the spectrometer time required for this study. Variable temperature studies were performed on several samples and no unexpected behaviour was observed. For this study, ^1H, ^2H, alkali metal ion, and halide ion nmr spectra were obtained using a 400-MHz nmr spectrometer.

TABLE 1. Compositions used to form the various mesophases utilized in this study. Compositions are given in percentages by weight

Sample	KDDA[a]	Decanol	D_2O	Salt
A	22.70	6.38	70.92[b]	
B	27.81	5.94	66.25[b]	
C	26.85	6.04	60.40[c]	6.04 CsCl, 2.67 NaOAc

[a]KDDA refers to potassium *N*-dodecanoylalaninate which was changed in a stepwise manner from the racemate to the *l*-detergent.
[b]D_2O contains NaCl, 1%; LiCl, 0.67%; CsCl, 1.6%; RbCl, 1%; *d,l*-alanine, 0.5%; and *l*-alanine, 0.5% by weight.
[c]D_2O contains *d,l*-alanine, 0.67% and *l*-alanine, 0.17% by weight.

Various samples used in this study were investigated by microscopy using polarized light. All observations were made at ambient temperature ≈294 K and samples were contained in unsealed CAMLAB microslides or between a microscope slide and a cover slip. Concentration gradients were obtained when water evaporated at the exposed edge of the samples. This allowed mesophases that are adjacent, in the phase diagram, to the nematic (or twisted nematic) to be identified.

The pitches of the helical axis in the cholesteric materials were measured by laser diffraction. The wavelength of the light from the laser used was 6.328×10^{-5} cm. The samples used in the diffraction measurement were generally the same as those used for obtaining nmr spectra. Such highly aligned samples gave very sharp diffraction bands. The temperature of the samples was controlled by placing them in a brass block suitably drilled for water flow, sample placement, and an optical path. The temperature was then controlled with circulating water from a thermostated water bath. The temperature of the brass block was determined to within 0.1° using a calibrated thermocouple thermometer.

Results and discussion

Micelle structure

Two samples were prepared according to composition C of Table 1. One sample was prepared from potassium *N*-dodecanoyl-*d,l*-alaninate, the second from the corresponding *l* detergent. The samples were placed individually on microslides, covered with a coverslip, and investigated with a microscope. The first sample initially showed a schlieren texture which, following spontaneous alignment of the nematogen, became pseudo isotropic, characteristic of the nematic disk-like lamellar mesophase. The second sample provided the fingerprint texture associated with a twisted nematic mesophase. Both samples dried from the edges of the coverslip to give pseudo isotropic textures and oily, streak mosaic textures which are characteristic of lamellar layers. This indicates the nematic and twisted nematic mesophases are closely related to the lamellar phase, in accord with disk-like micelles (3). The pseudo isotropic textures of the nematic phases were investigated using a Bertrand lens and a full-wave retardation plate. The interference figures observed were consistent with positive birefringence, which is characteristic of disk-like rather than the cylindrical micelles (13). Similarly, investigation of the twisted nematic mesophase provided interference figures consistant with negative birefringence. This change in sign of birefringence with introduction of twist is characteristic of thermotropic materials (14).

The sign of the diamagnetic anisotropy of mesophases prepared from the resolved detergent was established by obtaining

TABLE 2. Quadrupole splittings and dipolar couplings observed from various components of the mesophase

Detergent[a,b]			Water[a,c]					
$\Delta\nu_{ND}$	D_{HCH_3}	D_{HH} (CH_3)	$\Delta\nu_{Li}$	$\Delta\nu_{Na}$	$\Delta\nu_{Cs}$	$\Delta\nu_{Cl}$	$\Delta\nu_{D_2O}$	D_{HH} (CH_3)
17.8	0.245	−0.535	0.49	5.30	0.25	2.17	0.27	0.056

[a]All splittings are in kHz. The maximum deviation from the average was ±5% for any component. Splittings are independent of the proportion of optical resolution of the chiral detergent.
[b]Detergent splittings were obtained for the headgroup only; signs of splittings are relative.
[c]The CH_3 dipolar coupling is from the alanine methyl group.

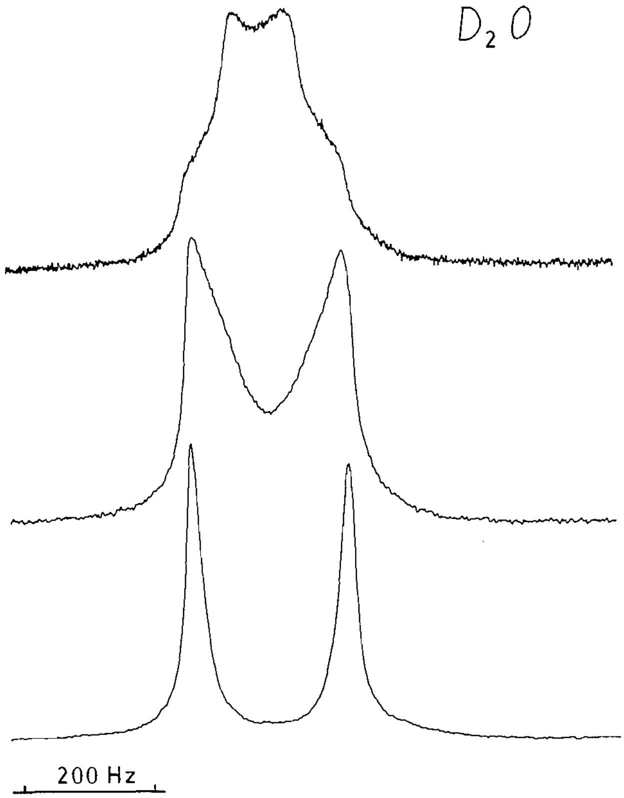

FIG. 1. Deuterium nmr spectra showing the change in deuterium signal as the twisted nematic mesophase progressively aligns in the magnetic field of the nmr spectrometer.

^{2}H nmr spectra from the D_2O immediately after placing a sample in the nmr spectrometer and at later time intervals. The first spectrum in a series typically showed a slight distortion from a true powder spectrum because a spectrum could not be obtained rapidly enough to eliminate all contributions from partially aligned material. Except for this, the first spectrum is characteristic of a random orientation of microcrystallites, while the others showed the development of signal intensity corresponding to alignment parallel to the magnetic field axis. The diamagnetic anistropy is therefore positive. Figure 1 shows the progressive effects of increasing alignment on the nmr powder spectrum. Signal intensity develops at the extremes of the spectrum, a result caused by the spontaneous alignment of the director along the magnetic field axis.

The above experiment could not be repeated for the racemate since it was found to align too quickly in the nmr spectrometer to provide a powder spectrum. However, when the sample was placed in an iron-core spectrometer and allowed to orient while spinning, a sharp D_2O doublet was obtained, as was a well-resolved alanine spectrum. This can only occur if the diamagnetic anistropy is negative, a result in accordance with that previously reported for this mesophase (4). The twisted nematic and nematic mesophase clearly are of opposite diamagnetic anisotropies. The mesophase prepared from the racemate consists of disk-like lamellar micelles of negative diamagnetic anisotropy, is nematic in character, and is designated as N_D^-.

An interesting aspect of these materials is the behaviour as a range of samples were prepared for which the amphiphile varied from pure potassium *N*-dodecanoyl-*l*-alaninate to the racemic compound. It was found that the samples prepared from the racemic detergent were highly fluid and aligned rapidly in the nmr spectrometer, while those prepared from the *l* material were significantly more viscous and aligned slowly in the spectrometer. Samples of intermediate compositions showed a gradual change in viscosity on proceeding stepwise from the racemic to the *l* detergent. It seems clear that this behaviour is related directly to the induced twist since measurements of the headgroup alignment, both at the amido position (given by the deuterium quadrupole splitting) and at the methyl group (given by the HH dipolar splitting), were constant throughout the range of *d,l* to *l* amphiphiles. Such constancy in alignment was also observed for the alkali metal and halide ions incorporated into the mesophase and for the D_2O solvent. The *d* and *l*-alanine also contained in the mesophase showed a constant average alignment although, in this case, *d* and *l*-alanine gave independent spectra that coalesced into one for the racemic detergent mesophase. The averages obtained for the various measured parameters are given in Table 2. Deviations from the average are less than 5%, dependent on the sample.

Figure 2 shows the change in twist ($1/P$) as a function of the proportion of *l* detergent and also the % change in alignment of the methyl group of the *d* and *l*-alanine from the averaged alignment for the two isomers, $\Delta s\%$. The behaviour of the twist with proportion of *l* detergent is similar to that previously reported (4). The change in pitch induced by change in temperature (Fig. 3) is quite surprising since the pitch increases with increase in temperature. This is in direct contrast with thermotropic cholesteric liquid crystals where, except in certain mixtures, the pitch always decreases with increase in temperature (14). It is also seen from Fig. 3 that the difference in the alignment of the *d* and *l*-alanines increases with increase in temperature.

For cholesteric thermotropic mesophases, two mechanisms have been proposed for the variation of twist with temperature (14). Both are based on the increase in thermal motion which leads to an increase in molar volume. This increase in molar volume affects the structure of the helix by either increasing (*i*) the intermolecular distance along the helix axis, thus increasing

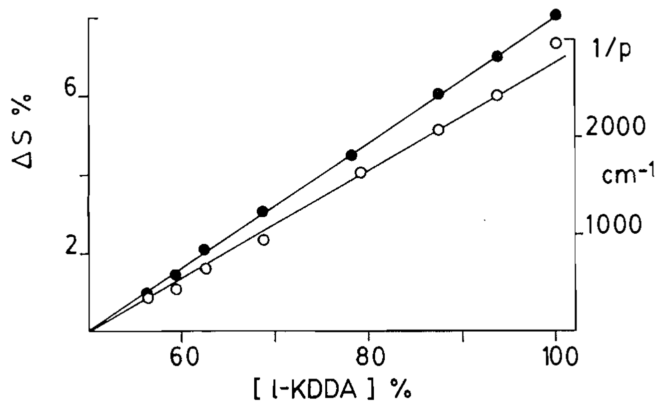

FIG. 2. The magnitude of the twist ($1/P$) induced in the mesophase as the amphiphile is changed in a stepwise manner from the racemate to the *l* derivative (○). The corresponding percentage change from the average alignment of the *d* and *l* isomers of alanine incorporated into the mesophase is also shown (●).

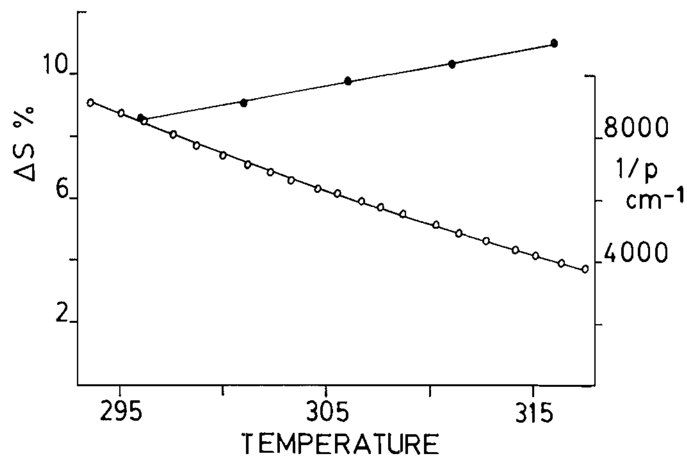

FIG. 3. The effect of temperature on twist (○) and on the difference in alignment of *d* and *l*-alanine is depicted (●).

the pitch, or (*ii*) by increasing the average displacement angle of the director of one nematogen with respect to the next, therefore decreasing the pitch. Although in principle the first mechanism could account for the observations obtained here, the explanation does not seem likely, at least on a molecular basis, because of the structure of a nematic lyotropic mesophase itself.

This mesophase consists of disk-like fragmented lamellae dispersed into an aqueous medium and interacting strongly with that medium via the polar headgroups of the individual detergent molecules. The individual micelles are separated by the interstitial water and will tend to stay separated since the micelles carry an electrostatic charge. If the effect of the asymmetry within one micelle is transmitted through the intervening aqueous solution to a second micelle by way of pairwise interactions (2) then a mechanism similar to the first, proposed for thermotropic mesophases, might be operative.

There is evidence to suggest that the micellar surface on the molecular level does not appear asymmetric from a distance. For instance, the individual components of racemic serine, tartaric acid, and other chiral molecules that are very hydrophilic in nature do not provide well-separated nmr spectra corresponding to the individual isomers.[1] On the other hand, slightly more hydrophobic species such as alanine do provide individual spectra. This indicates that the mechanism giving rise to the individual spectra is one of direct contact; a *d* to *l* interaction is different from an *l* to *l* interaction and this is reflected in the nmr spectrum where the dipolar coupling provides a direct measure of this difference.

On the basis of the argument advanced here, an increase in temperature of the mesophase should lead to a greater difference between the two spectra from *d* and *l*-alanine. As the temperature is increased, alanine will have an increased tendency to partition into the micelle and thus spend more time in contact with the optical centre of the individual amphiphiles. The increasing difference between the two spectra is clearly observed as shown by Fig. 3.

These results from solute molecules demonstrate that information concerning chirality within the micellar surface is not efficiently transmitted into the interstitial water of the mesophase. This conclusion provides little support for the pairwise interaction model, which suggests that specific interactions between molecules within different micelles generates the twist (2). The possibility of distorting a micelle into a chiral shape was also suggested by those authors but rejected tentatively on the basis of cholesteric behaviour versus distribution of chiral molecules within the micelle. However, a distortion model has been advanced by other workers (4) and distortion is supported by the work here.

The distortion model proposed here has the following salient features. The individual micelles are distorted into a chiral shape. Chiral micelles aggregate to form domains. The helical axis propagates along the major axis of the micellar aggregates. The twist characteristic of each domain is the same as that obtained by the twist measurements on the macroscopic sample.

The above characteristics are supported by several lines of evidence. The mesophase becomes progressively more viscous and requires longer periods of time in the nmr spectrometer before sharp nmr transitions are obtained as one proceeds in a stepwise fashion from the *d,l* to *l* amphiphile. This implies that increase in viscosity is caused by a progressive stabilization of a domain structure, although it could be a consequence of the different symmetry in the two materials. There is no evidence to suggest a significant change in micelle size. Indeed the constancy of the measured parameters in Table 2 seems to preclude such changes. The diamagnetic anisotropy determined for the mesophase prepared from the *l*-alaninate is opposite in sign to that determined for the racemate. Since the helical axis generated by the chiral amphiphile is parallel to the magnetic induction, it follows that the principle axis of the diamagnetic anisotropy tensor is parallel to the helical axis. This axis is the local alignment axis and as such is the director axis for the mesophase, rather than an axis attached to the individual micelles, as in the racemic material. This situation arises because the intermicellar forces generating the twist are strong enough that the micelles do not act as individuals when a magnetic field is applied; instead, the aggregates of micelles rearrange as the structural unit. The behaviour of the nematic and cholesteric materials is best pictured by considering two powder spectra, the first, derived from the racemic materials (nematic) having some specified width, the second, corresponding to the chiral material (cholesteric) having a width one-half that for the racemate. As alignment is allowed to

[1] A. S. Tracey and K. Radley, unpublished results.

proceed, the first powder spectrum grows at the maxima of the powder spectrum, 90° orientation, while the second spectrum grows at the extrema of the powder spectrum, corresponding to 0° orientation. When alignment is complete the two spectra are indistinguishable. This description is in accordance with all observations.

The decreasing pitch with decrease in temperature reflects the operation of a process similar to that of mechanism (*i*) described for the thermotropic mesophases. The individual twisted miceles within each domain pack closer together as temperature decreases. This shortens the pitch because the distance along the helix axis corresponding to one complete rotation of micelle directors is decreased as the micelles become closer together.

The decrease in mesophase viscosity with rise in temperature and the corresponding faster rates of alignment could reflect a smaller domain size as temperature is raised, but more probably it just reflects the fact that there is more thermal motion. This is supported by the fact that there is a memory associated with these materials. If a sample is aligned at 30°C in the nmr spectrometer, then removed, and laser diffraction used to measure its pitch (also measured at 30°C), a sharp diffraction pattern is obtained. With change in temperature, by say ±10°C, the diffraction bands are significantly broadened. When the sample is returned to 30°C, sharp diffraction bands are again obtained.

It is suggested that these liquid crystals be designated Ch_D^+ to specify that they are cholesteric mesophases of positive diamagnetic anisotropy originating from disk-like fragmented lamellae.

Conclusions

Lyotropic mesophases prepared from aqueous solutions of potassium *N*-dodecanoyl-*l*-alaninate and its racemate have been studied. A model for cholesteric behaviour in these systems has been proposed.

Microscope studies shows that the nematic mesophase prepared from the racemic amphiphile is composed of disk-like lamellae. With increasing optical purity of amphiphile, individual disk-like fragments develop a chiral shape which, through interactions with adjacent micelles, induces the formation of aggregates of micelles. In conjunction with this aggregation, the diamagnetic anisotropy changes from negative to positive. This change reflected the fact that the director for the mesophase has become the axis of the domain along which the helix propagates rather than the directors of the micelles themselves.

The alignment of the individual micelles is insensitive to the development of domains, a conclusion in accordance with the observation that quadrupole splittings and dipolar couplings from components incorporated into the aqueous region and from the amphiphiles of the micelles remain constant, independent of whether the amphiphile is racemic or optically resolved.

Acknowledgements

Thanks are gratefully extended to the Natural Sciences and Engineering Research Council of Canada for its financial support of this work.

1. F. Reinitzer. Monatsh. Chem. **9**, 421 (1888).
2. K. Radley and A. Saupe. Mol. Phys. **35**, 1405 (1978).
3. M. C. Holmes, N. Boden, and K. Radley. Mol. Cryst. Liq. Cryst. **100**, 93 (1983).
4. P. S. Covello, B. J. Forrest, M. E. Marcondes Helene, L. W. Reeves, and M. Vist. J. Phys. Chem. **87**, 176 (1983).
5. M. R. Alcantara, M. V. Marques Correia de Melo, V. R. Paoli, and J. A. Vanin. Mol. Cryst. Liq. Cryst. **90**, 335 (1983).
6. K. Radley and A. Saupe. Mol. Cryst. Liq. Cryst. **44**, 227 (1978).
7. A. S. Tracey and P. Diehl. FEBS Lett. **59**, 139 (1975).
8. K. Radley, L. W. Reeves, and A. S. Tracey. J. Phys. Chem. **80**, 174 (1976).
9. M. Acimis and L. W. Reeves. Can. J. Chem. **58**, 1533 (1980).
10. C. L. Khetrapal, A. C. Kunwar, P. Diehl, and A. S. Tracey. NMR Basic Princ. Prog. **9** (1975).
11. C. L. Khetrapal and P. Diehl. NMR Basic Princ. Prog. **1** (1969).
12. E. Jungermann, J. F. Gerecht, and I. J. Krems. J. Am. Chem. Soc. **78**, 172 (1956).
13. N. H. Hartshorne. The microscopy of liquid crystals. Microscope Publications Ltd., London, Chicago. 1974.
14. H. W. Gibson. *In* Liquid crystals – the fourth state of matter. *Edited by* F. D. Saeva. Marcel Dekker, Inc., New York. 1979. p. 113.

COMMUNICATION

Secondary α-deuterium kinetic isotope effects for the E2 reaction of the 2-phenylethyl halides with *tert*-butoxide ion in *tert*-butyl alcohol

PETER JAMES SMITH[1] AND KANCHUGARAKOPPAL S. RANGAPPA
Department of Chemistry, University of Saskatchewan, Saskatoon, Sask., Canada S7N 0W0

AND

KENNETH CHARLES WESTAWAY
Department of Chemistry, Laurentian University, Sudbury, Ont., Canada P3E 2B6

Received August 2, 1984

PETER JAMES SMITH, KANCHUGARAKOPPAL S. RANGAPPA, and KENNETH CHARLES WESTAWAY. Can. J. Chem. **63**, 100 (1985).

Secondary α-deuterium kinetic isotope effects have been determined for the elimination reactions of 2-phenylethyl halides with *tert*-butoxide in *tert*-butyl alcohol at 40°C in the presence and absence of the crown ether 18C6. The second-order rate constant k_2 and the normal $(k^H/k^D)_\alpha$ effect remained constant when the *tert*-butoxide concentration was varied for reaction of the iodo and bromo compounds. However, both the magnitude of k_2 and the secondary α-deuterium isotope effect were significantly dependent on [t-BuO$^-$] when chlorine and fluorine are the leaving groups. It is noteworthy that $(k^H/k^D)_\alpha$ is *inverse* for the reaction of both the chloro and fluoro compounds at "low" base concentrations and normal at "high" base concentrations. These results are discussed in terms of both *syn*- and *anti*-elimination pathways promoted by various associated and dissociated base species. It is suggested that the $(k^H/k^D)_\alpha$ effect may be useful as a criterion for determining the stereochemistry of E2 elimination reactions.

PETER JAMES SMITH, KANCHUGARAKOPPAL S. RANGAPPA et KENNETH CHARLES WESTAWAY. Can. J. Chem. **63**, 100 (1985).

Opérant à 40°C et en présence ou en l'absence de l'éther couronne 18C6, on a déterminé les effets isotopiques cinétiques secondaires des deutérium en α sur les réactions d'élimination des halogénures de phényl-2 éthyles par la *tert*-butylate dans l'alcool *tert*-butylique. Dans les cas des composés iodés ou bromés, la constante de vitesse du deuxième ordre (k_2) ainsi que l'effet normal $(k^H/k^D)_\alpha$ demeurent constants lorsqu'on fait varier la concentration du *tert*-butylate. Toutefois, lorsque les groupes nucléofuges sont soit le fluor ou le chlore, l'amplitude de k_2 ainsi que l'effet isotopique secondaire des deutérium en α varient d'une façon importante avec la concentration de l'ion *tert*-butylate. Il est notable que, pour les réactions des composés fluorés ou chlorés à de "basses" concentrations de base, la valeur $(k^H/k^D)_\alpha$ est *inverse*; toutefois, à des concentrations "élevées" de base, cette valeur est normale. On discute de ces résultats en fonction de voies d'éliminations *syn* et *anti* qui sont favorisées par diverses espèces basiques associées et dissociées. On suggère que l'effet $(k^H/k^D)_\alpha$ pourrait être un critère utile pour déterminer la stéréochimie des réactions d'éliminations E2.

[Traduit par le journal]

The elimination reaction of the 2-arylethyl derivatives with different leaving groups Y, $ArCH_2CH_2Y$, has been extensively studied (1–6) under a variety of solvent/base conditions. It has been established that the majority of the reactions proceed by way of the E2 mechanism following the *anti* pathway (5,7). Experimental studies (8–14) have demonstrated that the structures of the respective E2 transition states vary significantly in accord with theoretical predictions (15–20).

The reaction of the 2-arylethyl quaternary ammonium ions with base has been shown to have considerable carbanionic character at the E2 transition state (1,11,21), while the corresponding reaction of the 2-phenylethyl halides has been considered (11,16) to involve a more central E2 transition state where the extent of the carbon–hydrogen and carbon – leaving group bond rupture processes has progressed in a more synchronous fashion.

In order to gain a direct measure of the relative amount of hybridization change at the α carbon at the E2 transition state (double-bond character), we have determined the secondary α-deuterium kinetic isotope effects for the reaction of the 2-phenylethyl halides with *tert*-butoxide in *tert*-butyl alcohol at 40°C, eq. [1].

$$[1]\quad PHCH_2CH_2X + t\text{-BuO}^- \xrightarrow{t\text{-BuOH}} PHCH{=}CH_2$$
$$X = F, Cl, Br, I$$

[1]Author to whom correspondence should be addressed.

The reactions, which were shown to give the styrene product in 100 ± 1% yield, were studied under pseudo-first-order conditions where the *tert*-butoxide concentration was at least in twenty-fold excess. The progress of the reactions was determined by monitoring the product spectrophotometrically (λ_{max} = 248 nm). The analysis was done after the reaction solutions had been quenched at appropriate times with a dilute solution of sulfuric acid in 95% ethanol. This was done to eliminate the appreciable absorption of *tert*-butoxide ion at this wavelength. For reactions involving the crown ether 18C6, the reference cell in the spectrophotometer contained a solution of potassium *tert*-butoxide and the crown ether 18C6 in *tert*-butyl alcohol, both at the same concentrations as used in the kinetic experiments in order to compensate for the absorption of the complexed t-BuOK at 248 nm.

The second-order rate constants for the reaction of the 2-phenylethyl halides with different *tert*-butoxide concentrations in *tert*-butyl alcohol, both in the absence and presence of the crown ether 18C6, are given in Table 1 along with the observed values of the secondary α-deuterium kinetic isotope effects, $(k^H/k^D)_\alpha$. The theoretical maximum values (22–25) of the isotope effect corresponding to complete hybridization change from sp^3 to sp^2 at the transition state for the different leaving groups are also included.

It is generally considered that the reaction of the 2-phenylethyl halides with ethoxide in ethanol proceeds by way of the E2 mechanism (13,26–29). Since a plot of log k_2 (rate con-

TABLE 1. Secondary α-deuterium isotope effects for reaction of the 2-phenylethyl halides with t-BuO$^-$ in t-BuOH in the absence and presence of 18C6 at 40°C

Leaving group	[t-BuO$^-$], M	[18C6], M	k_2^H, M^{-1} s^{-1}	$(k^H/k^D)_\alpha^*$	$(k^H/k^D)_\alpha^*$ (theoretical maximum)
I	0.01648		7.02×10^{-2}	1.040±0.014†	1.188
	0.03296		7.25×10^{-2}	1.047±0.016	
Br	0.01688		1.92×10^{-2}	1.170±0.015	1.266
	0.03376		1.99×10^{-2}	1.165±0.011	
Cl	0.01320		5.43×10^{-4}	0.820±0.020	1.323
	0.08960		5.54×10^{-4}	0.808±0.004	
	0.2300		6.46×10^{-4}	0.966±0.008	
	0.2664		6.58×10^{-4}	1.047±0.014	
	0.3060		7.16×10^{-4}	1.149±0.010	
	0.3536		8.31×10^{-4}	1.165±0.010	
	0.01296	0.01377	0.413	1.170±0.010	
F	0.1767		8.11×10^{-5}	0.862±0.012	1.488
	0.4066		9.80×10^{-5}	1.036±0.019	
	0.01523	0.01523	3.07×10^{-2}	1.073±0.014	

*For two deuteriums.
†The error in the isotope effect is calculated using the formula:

$$\text{Error} = \pm(k^H/k^D)\,[(\Delta k^H/k^H)^2 + (\Delta k^D/k^D)^2]^{1/2}$$

where Δk^H and Δk^D are the standard deviations for the rate constants for the undeuterated and deuterated reactants, respectively.

stants found at "high" base concentration) for reaction with *tert*-butoxide in the present study against log k_2 (EtO$^-$) (30) is linear,[2] it is reasonable to conclude that reaction with *tert*-butoxide ion also proceeds via the concerted mechanism.

It is seen (Table 1) that the second-order rate constants for both the iodo and bromo[3] substrates do not change significantly when the [t-BuO$^-$] is doubled. However, there is a significant increase in k_2 in the reactions of the chloro and fluoro compounds when the *tert*-butoxide concentration is increased within certain limits; i.e., for the bromo compound, k_2 = 1.92×10^{-2} and 1.99×10^{-2} M^{-1} s^{-1} when [t-BuO$^-$] = 0.01688 and 0.03376 M, respectively, while for the fluoro compound $k_2 = 8.11 \times 10^{-5}$ and 9.80×10^{-5} M^{-1} s^{-1} when [t-BuO$^-$] = 0.1767 and 0.4066 M, respectively.

Addition of the crown ether 18C6 to the reaction of the chloro compound leads to the expected large increase in the magnitude of the second-order rate constant; i.e. $k_2 = 5.43 \times 10^{-4}$ M^{-1} s^{-1} when [t-BuO$^-$] = 0.01320 M while k_2 = 0.413 M^{-1} s^{-1} when [t-BuO$^-$] = 0.01296 M in the presence of 0.01377 M 18C6. It is known (31) that 18C6 complexes the potassium of t-BuOK converting the ion pair or larger aggregates to non-associated ions which are more effective (stronger) bases.

It is seen that the secondary α-deuterium isotope effects, like the k_2 values, do not vary with base concentration for the reactions of both the iodo and bromo compounds. On the other hand, both the α-deuterium isotope effects and the k_2 values, for the reactions of both the chloro and fluoro compounds with t-BuO$^-$ in the absence of 18C6, vary over a particular range of *tert*-butoxide concentrations. Of particular significance, however, is the observation that the secondary α-deuterium isotope effects are *inverse* at low base concentrations. To our knowledge, this is the first example of an inverse secondary α-deuterium isotope effect in an elimination reaction proceeding via the one-step concerted E2 pathway.

The reactions of both the chloro and fluoro substrates with *tert*-butoxide ion at the "higher" base concentrations, Table 1, have normal secondary α-deuterium isotope effects. As well, when the crown ether is added to the reaction solutions containing "low" concentrations of *tert*-butoxide, where inverse α-d_2 effects are found, the observed isotope effects are normal and are similar in magnitude to those found at "high" base concentrations.

An approximate measure of the degree of double bond formation (extent of C—X bond rupture) at the transition state for reaction of the four substrates can be determined by comparing the observed α-deuterium isotope effects, found for reaction carried out at "high" base concentrations, with the calculated theoretical maximum values for each leaving group, Table 1. The percent of the theoretical maxima for the leaving groups are 7, 51, 62, and 25 for F, Cl, Br, and I, respectively. This variation in the extent of double-bond formation with a change in leaving group can be rationalized in terms of the More O'Ferrall (17) – Jencks (19) energy surface diagrams if it is considered that the reaction of the fluoro compound proceeds via an E1cb-like E2 transition state while the iodo substrate reacts via a more central E2 activated complex.[4]

A reasonable explanation for the observed experimental results is that the reaction involving the best two leaving groups (I and Br) proceeds via the usual *anti* pathway at all base concentrations even though the extent of base association varies. The reactions involving the more electronegative (poorer) Cl and F leaving groups proceed via two distinct stereochemical pathways, the *anti* and *syn*, with the relative proportions of each pathway depending on the *tert*-butoxide concentration (32–34).

[2]The irreversible E1cb mechanism is also consistent with a linear plot. However, since it has been established (14, 39) that both the F and Br substrates react with t-BuO$^-$ in t-BuOH via the concerted E2 pathway, it is reasonable to conclude that all four substrates react via the same mechanism under these experimental conditions.

[3]Other workers (9, 39) also concluded that there was no significant drift in the second-order rate constants for reaction of the bromo compound in the t-BuO$^-$ in t-BuOH.

[4]A more detailed discussion can be found in a full paper to follow in this journal.

When the *tert*-butoxide concentration is "low" and *t*-BuOK exists to a significant degree as an associated base (ion pair), reaction of both the Cl and F substrates proceeds via a *syn*-elimination pathway where the loss of the leaving group and the β-hydrogen are assisted by the *t*-BuOK ion pair. For such a transition state **1**, which is expected to have considerable carbanionic character (35), sufficient negative charge could develop on the β-carbon so that inversion occurs at both C_β and C_α. Such a pathway is consistent with the observed inverse isotope effects which arise from an *increase* in the C_α—H out-of-plane bending frequencies at the transition state (22–25, 36, 37, and footnote 4).

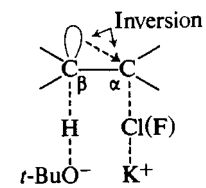

1

The effect of *tert*-butoxide concentration on the magnitude of both k_2 and $(k^H/k^D)_\alpha$ is shown by the data in Table 1 for the reaction of the chloro substrate. It is seen that both the rate constant k_2 and the magnitude of $(k^H/k^D)_\alpha$ initially increase from their values at "low" base concentration, when *tert*-butoxide concentration is increased, and level off at "high" base concentration. A possible rationalization of these results is that an increase in *tert*-butoxide concentration leads to a decrease in the amount of associated base species (which favours *syn*-elimination) and an increase in the concentration of multiple ions such as negatively charged ion triplets, $(RO^-)_2M^+$, which may be considered as a free base (38). The bulky triple ion would presumably favour *anti*-elimination, for steric reasons, and a normal isotope effect and an increased rate of reaction would be observed because the triple ion is a stronger base than the associated species.

The effect of the addition of 18C6 to the reaction medium is consistent with the above explanation. The crown ether will complex the potassium ion and liberate a free *tert*-butoxide ion, an effective base, which removes the β-hydrogen via the *anti*-pathway. It is interesting to note that the magnitude of the secondary α-deuterium isotope effect is essentially the same for reaction of the chloro compound at "high" base concentration (triple ion as abstracting base) and under conditions of "low" base concentration in the presence of the crown ether where free *t*-BuO^- acts as the base. This suggests that the transition state structure is similar for reaction under the above conditions, in agreement with studies on the reaction of 2-phenylethyl bromide with dissociated and associated *tert*-butoxide ions (39). Finally, it appears that an inverse secondary α-deuterium kinetic isotope effect may be useful as a criterion for determining the stereochemistry of E2 elimination reactions; i.e., an inverse isotope effect is consistent with a *syn*-elimination and a normal kinetic isotope effect is diagnostic of a normal *anti*-coplanar E2 mechanism.

Acknowledgements

The authors gratefully acknowledge the financial support provided by the Natural Sciences and Engineering Research Council of Canada.

1. C. H. DePuy and C. A. Bishop. J. Am. Chem. Soc. **82**, 2535 (1960).
2. W. H. Saunders, Jr., D. G. Bushman, and A. F. Cockerill. J. Am. Chem. Soc. **90**, 1775 (1968).
3. D. V. Banthorpe. Elimination reactions. Elsevier, New York. 1963.
4. J. E. Bunnett. Surv. Prog. Chem. **5**, 53 (1969).
5. W. H. Saunders, Jr. and A. F. Cockerill. Mechanisms of elimination reactions. Wiley–Interscience, New York. 1973.
6. A. F. Cockerill and R. G. Harrison. *In* The chemistry of double-bonded functional groups. Part I. *Edited by* S. Patai. Wiley–Interscience, New York. 1977. pp. 155–189.
7. A. N. Bourns and A. C. Frosst. Can. J. Chem. **48**, 133 (1970).
8. R. Baker and M. S. Spillett. J. Chem. Soc. (B), 481 (1969).
9. A. F. Cockerill, S. Rottschaefer, and W. H. Saunders Jr. J. Am. Chem. Soc. **89**, 901 (1967).
10. P. Schmid and A. N. Bourns. Can. J. Chem. **53**, 3513 (1975).
11. P. J. Smith and A. N. Bourns. Can. J. Chem. **52**, 749 (1974).
12. J. R. Gandler and W. P. Jencks. J. Am. Chem. Soc. **104**, 1937 (1982).
13. J. R. Gandler and T. Yokoyama. J. Am. Chem. Soc. **106**, 130 (1984).
14. H. F. Koch, W. Tumas, and R. Knoll. J. Am. Chem. Soc. **103**, 5423 (1981).
15. E. R. Thornton. J. Am. Chem. Soc. **89**, 2915 (1967).
16. D. A. Winey and E. R. Thornton. J. Am. Chem. Soc. **97**, 3102 (1975).
17. R. A. More O'Ferrall. J. Chem. Soc. (B), 274 (1970).
18. J. E. Chritchlow. J. Chem. Soc. Faraday Trans. 1, **68**, 1774 (1972).
19. W. P. Jencks. Chem. Rev. **72**, 705 (1972).
20. D. A. Jencks and W. P. Jencks. J. Am. Chem. Soc. **99**, 7948 (1977).
21. S. Alunni and W. P. Jencks. J. Am. Chem. Soc. **102**, 2052 (1980).
22. M. Wolfsberg and M. J. Stern. Pure Appl. Chem. (*a*) **8**, 225 (1964); (*b*) **8**, 325 (1964).
23. V. J. Shiner, Jr., M. W. Rapp, E. A. Halevi, and M. Wolfsberg. J. Am. Chem. Soc. **90**, 7171 (1968).
24. V. J. Shiner, Jr. *In* Isotope effects in chemical reactions. *Edited by* C. J. Collins and N. S. Bowman. ACS Monograph 167, Van Nostrand Reinhold Co., New York, NY. 1970. Chapt. 2.
25. L. Melander and W. H. Saunders, Jr. Reaction rates of isotopic molecules. Wiley–Interscience, New York. 1980.
26. J. R. Keefe and W. P. Jencks. J. Am. Chem. Soc. **105**, 265 (1983).
27. H. F. Koch, D. J. McLennan, J. G. Koch, W. Tumas, B. Dobson, and N. H. Koch. J. Am. Chem. Soc. **105**, 1930 (1983).
28. F. G. Bordwell. Acc. Chem. Res. **5**, 377 (1972).
29. W. H. Saunders, Jr. Acc. Chem. Res. **9**, 21 (1976).
30. C. H. De Puy and A. L. Schultz. J. Org. Chem. **39**, 878 (1974).
31. R. A. Bartsch, G. M. Pruss, O. M. Cook, E. L. Buswell, B. A. Bushaw, and K. E. Wiegers. J. Am. Chem. Soc. **95**, 6745 (1973).
32. J. Sicher, J. Zavada, and M. Pankova. Collect. Czech. Chem. Commun. **33**, 1278 (1968).
33. D. S. Bailey and W. H. Saunders, Jr. J. Am. Chem. Soc. **92**, 6904 (1970).
34. D. S. Bailey, F. C. Montgomery, G. W. Chodak, and W. H. Saunders, Jr. J. Am. Chem. Soc. **92**, 6911 (1970).
35. C. H. DePuy, D. L. Storm, J. T. Frey, and C. G. Naylor. J. Org. Chem. **35**, 2746 (1970).
36. A. Fry. Chem. Soc. Rev. **1**, 163 (1970).
37. A. Fry. Pure Appl. Chem. **8**, 409 (1964).
38. R. A. Bartsch and J. Zavada. Chem. Rev. **80**, 453 (1980).
39. S. Alunni, E. Baciocchi, and P. Perucci. J. Org. Chem. **41**, 2636 (1976).

Conformational features of bisphenol-A polycarbonate

P. R. SUNDARARAJAN
Xerox Research Centre of Canada, 2660 Speakman Drive, Mississauga, Ont., Canada L5K 2L1

Received December 23, 1983

This paper is dedicated to the 10th anniversary of the Xerox Research Centre of Canada

P. R. SUNDARARAJAN. Can. J. Chem. **63**, 103 (1985).

Conformational energies have been estimated for the segments of the bisphenol polycarbonate chain, using the Lennard-Jones and Hill's empirical force field type of functions. It is found that the conformation of the carbonate group, defined by the torsion angle ζ, is restricted to the range of 45° to 65°. The rotations χ and χ' of the methyl groups also show similar limited flexibility. However, accessible conformations of the diphenyl propane (DPP) segment, defined by torsion angles ϕ and ψ, span a wide area of the (ϕ,ψ) surface, with the restriction that the rotations ϕ and ψ be synchronized such that $\phi + \psi \approx 90°$ or 270°. These features explain the slow thermal crystallization behaviour of the polycarbonate chains. The variability of the conformations of the repeat unit is illustrated with a series of figures.

P. R. SUNDARARAJAN. Can. J. Chem. **63**, 103 (1985).

Faisant appel aux fonctions empiriques de Lennard-Jones et Hill, de type champ de force, on a évalué les énergies conformationnelles de segments de la chaîne de polycarbonate de bisphénol. On a trouvé que la conformation du groupe carbonate, définie par l'angle de torsion ζ, est restreinte à l'intervalle de 45 à 65°. Les rotations χ et χ' des groupes méthyles présentent une flexibilité limitée analogue. Cependant, les conformations accesibles du segment diphénylpropane (DPP), telles que définies par les angles de torsion ϕ et ψ couvrent une plus grande proportion de la surface (ϕ,ψ); on doit toutefois imposer la restriction à l'effet que les rotations ϕ et ψ doivent être synchronisées de telle sorte que $\phi + \psi \approx 90°$ ou 270°. Ces caractéristiques expliquent le comportement des chaînes de polycarbonate lors de leur cristallisation thermique lente. On illustre la variabilité des conformations de l'unité de base à l'aide d'une série de figures.

[Traduit par le journal]

Introduction

The bisphenol-A polycarbonate (BPAPC), represented schematically in Fig. 1, possesses a high T_g (~150°C) and T_m (~280°C). Its transparency in the film form and its dimensional stability contribute to its utility as a commercial material. Crystallization of BPAPC by thermal methods is difficult. Often, annealing for over 200 h at 190°C is required in order to crystallize it (1, 2). This inability to readily crystallize, combined with the dimensional stability, makes it a suitable material for various commercial applications.

The slow crystallizing tendency of BPAPC has been interpreted (3) as due to the fact that the thermal crystallization has to be preceded by certain morphological changes in the polymer matrix: preliminary ordering of the chains or a change in the polymer conformation. This characteristic of BPAPC makes it an ideal candidate for studies on the polymer glassy state. Several investigations on thermal transitions, molecular motion, etc., have been reported in the literature (4-6). Although thermal crystallization of BPAPC is a slow process, it crystallizes readily upon exposure to vapours of organic solvents such as acetone, carbon tetrachloride, methanol, etc. (7-9), or in the presence of plasticizers (10, 11).

Bonart (12) reported the crystal structure of BPAPC, with a unit cell of dimensions a = 12.3 Å, b = 10.1 Å, c (chain axis) = 20.8 Å, and γ = 84°. Two monomer units comprise the fiber identity period and four chains are contained in the unit cell, in the space group C_s^2.

Conformational energy calculations on segments of the BPAPC chain are reported here. These were undertaken in order to determine the extent of freedom of rotation enjoyed by the segments of the molecule and to verify if the concept of unhindered rotation for the phenyl and methyl groups is valid. Similar calculations have been reported by Tonelli (13). An appreciation of the accessible conformations and flexibility via the conformational energy calculations would lead to the understanding of not only the crystallization behavior, mechanical properties, etc., but also the type of interactions, at the short range level, which precipitate when the chain is associated with small molecule plasticizers. For example, Dulmage *et al.* (14) have studied the structure of the complex of aryl-substituted thiapyrylium salt with 4,4'-isopropylidenediphenyl-bis-phenyl carbonate, a model compound for BPAPC.

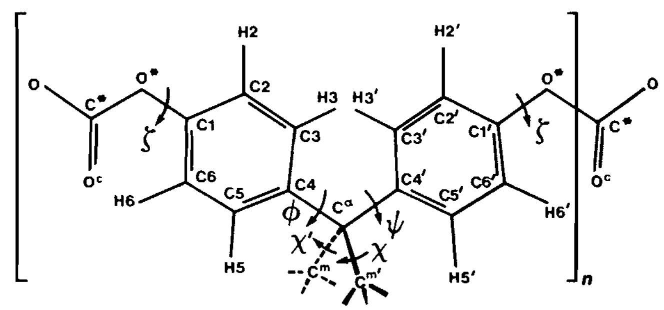

FIG. 1. Schematic representation of a segment of the BPAPC polycarbonate chain. The planar conformation is shown here. The relevant torsion angles are marked.

While this work was in progress, a paper on the optical anisotropy of polycarbonate analogs was published by Flory and co-workers (15). The calculations of optical anisotropy were based on the conformations of the carbonate and the diphenyl segments.

Energy calculations

1. *Geometrical parameters*

A portion of the polycarbonate chain is shown in Fig. 1, with the *trans-trans* conformation of the carbonate group. Calculations of Williams and Flory (16) indicate that the *cis-trans* or *trans-cis* forms are of low incidence. Hence, calculations described here were carried out with the *trans-trans* form exclusively. The bond lengths and bond angles used in this study are given in Table 1. These (Set I) were taken from

TABLE 1. Bond lengths and bond angles used in this study*†

	Length (Å)			Angle (deg)	
Bond	Set I	Set II	Atoms in bond	Set I	Set II
O—C*	1.34	1.32	O—C*—O*	114	108
C*—O*	1.34	1.32	O—C*—O^{c}	123	126
C*—O^{c}	1.22	1.21	C*—O*—C1	113	121
O*—C1	1.36	1.42	C^{ar}—C^{ar}—C^{ar}	120	120
C^{ar}—C$^{\alpha}$	1.52	1.51	C^{ar}—C$^{\alpha}$—C^{ar}	(a) 112 (b) 109.5	109.5
C—H	1.10	1.10			
C$^{\alpha}$—C	1.52	1.53	C^{ar}—C$^{\alpha}$—C C—C$^{\alpha}$—C	(a) 108.9 (b) 109.5	109.5
C^{ar}—C^{ar}	1.39				
C1—C2 C1—C6 C3—C4 C5—C4		1.37			
C2—C3 C5—C6		1.40			

* See Fig. 1 for designation of atoms.
† Set I from refs. 16 and 17. Set II from ref. 15 and footnote 1.

Bowen and Sutton (17), and Williams and Flory (16). Also included (Set II) are the values used by Erman *et al.* (15) based on a crystal structure analysis of diphenyl carbonate.[1] Both sets of parameters have been used in the present calculations. The bond lengths and bond angles differ between Set I and Set II. The partial double bond character of the O—C* and C*—O* bonds leads to a bond length of 1.34 Å on the average (Set I). This distance was found to be 1.32 Å in the crystal structure of diphenyl carbonate.[1] The average of the O*—C1 bond length, taken from various structures, is 1.36 Å, whereas it is 1.42 Å in the above crystal structure. Quite significant are the differences in the bond angles of the carbonate group. Such large differences affect the results of the calculations, as discussed below. The geometrical parameters derived by Dulmage *et al.* (14) are not used here. Comparing them with the parameters reported by Erman *et al.* (15), it is found that there are appreciable differences in the bond angles of the carbonate group as well as the 2,2-diphenyl propane segment. The bond angles in the phenyl group, for example, vary from 120° to as small as 111.8°, and a pronounced nonplanarity of the phenyl is indicated.

The conformation of the carbonate group with respect to the phenyl was determined by varying the torsion angle ζ around the O*—C1 bonds (cf. Fig. 1). The planar *trans* conformation of the C*—O* and the C1—C2 bonds defines $\zeta = 0°$. The *trans* planarity about the C*—O* bond was maintained. The relative conformations of the contiguous phenyl groups were determined as a function of the rotations ϕ and ψ about the C4—C$^{\alpha}$ and C$^{\alpha}$—C4′ bonds. The eclipsed conformation of the C4—C3 and the C$^{\alpha}$—C4′ bonds corresponds to $\phi = 0°$. Likewise, for $\psi = 0°$, the C4—C$^{\alpha}$ bond eclipses the C4′—C3′. In these calculations, the minimum energy conformations of ζ and (ϕ,ψ) were determined independently.

Considering the appendage of the C$^{\alpha}$—C^{m} bonds, when the angle θ = C4—C$^{\alpha}$—C4′ is enlarged to 112°, if C^{m}—C$^{\alpha}$—C4 and C^{m}—C$^{\alpha}$—C4′ are kept at tetrahedral values, the angle C^{m}—C$^{\alpha}$—C$^{m'}$ would decrease to 106.7°. In order to distribute the strain equally between all the bond angles involving C^{m}, we impose the condition that C^{m} and C$^{m'}$ be attached to C$^{\alpha}$ such that the bond angles C^{m}—C$^{\alpha}$—C$^{m'}$, C^{m}—C$^{\alpha}$—C4, C^{m}—C$^{\alpha}$—C4′, C$^{m'}$—C$^{\alpha}$—C4, C$^{m'}$—C$^{\alpha}$—C4′ are equal, and denoted by θ'. Incorporating this condition in eq. 2 of Suter and Flory (18) leads to:

$$[1] \quad \cos\theta' = \frac{1 \pm \sqrt{1 + 4x}}{2x}$$

where:

$$[2] \quad x = \frac{4}{(1 + \cos\theta)}$$

With this formula, if $\theta = 112°$, θ' will be 108.96°. The methyl hydrogens were kept at mutually tetrahedral angles. One of the methyl hydrogens eclipsing the C$^{\alpha}$—C4 bond defines $\chi = 0°$. For each value of (ϕ,ψ), the torsion angles χ and χ' defining the positions of the methyl hydrogens were varied at intervals of 10° each and the positions corresponding to minimum energy were included in subsequent calculations.

TABLE 2. Parameters used for the potential energy functions

	L–J function			Hill's function	
Atom	α (Å^3)	N	R (Å)	ϵ (kcal mol^{-1})	$d^*/2$ (Å)
C	0.93	5	1.70	0.116	1.50
C^{ar}	1.23	5	1.85	0.060	1.95
C^{carb}	1.23	5	1.70	0.033	1.85
H	0.42	0.9	1.20	0.060	1.50
O	0.70	7	1.50	0.070	1.54
O^{carb}	0.84	7	1.50	0.070	1.54

2. *Energy functions*

The nonbonded interactions were estimated using the Lennard–Jones (L–J) 6–12 potential function and the Hill's empirical force-field function. The L–J function of the form:

$$[3] \quad E_{nb}(i, j) = -\frac{A_{ij}}{r_{ij}^{6}} + \frac{B_{ij}}{r_{ij}^{12}}$$

has been extensively used in the conformational analysis of various types of polymers (19–21). The parameters A_{ij} and B_{ij} were evaluated in the usual manner (19–21), using the polarizability (α), effective number of electrons (N), and the van der Waals radius (R_0). The values of α, N, and R_0 used in the present calculations are given in Table 2.

The Hill's function is similar to the Buckingham 6-exp function and is given by (22):

$$[4] \quad E_{nb} = \epsilon_{ij}\left[8.3 \times 10^{5} \exp\left(-13.6\frac{r_{ij}}{d_{ij}^*}\right) - 2.25\frac{r_{ij}}{d_{ij}^*}^{-6}\right]$$

Here ϵ_{ij} is an "energy" parameter which is taken to be the geometric mean of parameters ϵ_i and ϵ_j for the interacting atoms, and d_{ij}^* is the characteristic distance derived as an arithmetic mean of the diameters d_i^* and d_j^* assigned to the atoms.

The Hill's function was modified into a one-parameter function by Kitaigorodsky (23). The Hill's function has been widely used in the molecular mechanics calculations on organic small molecules (24) and has been incorporated in standard minimization computer programs. The parameters ϵ_i and d_i^* used in the present calculations are given in Table 2 and were taken

[1] D. Y. Yoon and P. J. Flory, cited in ref. 15.

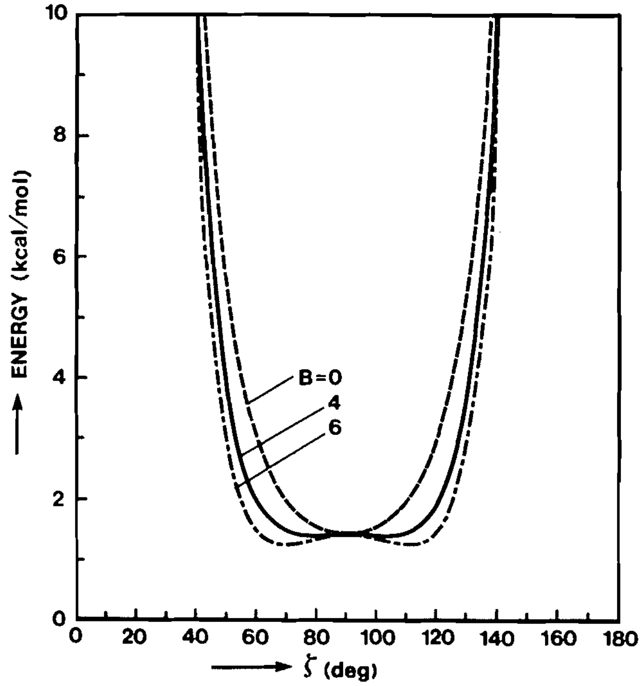

FIG. 2. The variation of energy with ζ is shown, for select values of *B*. The Lennard–Jones function was used here. The angle C*—O*—Cl is 113° (Set I parameters, see text).

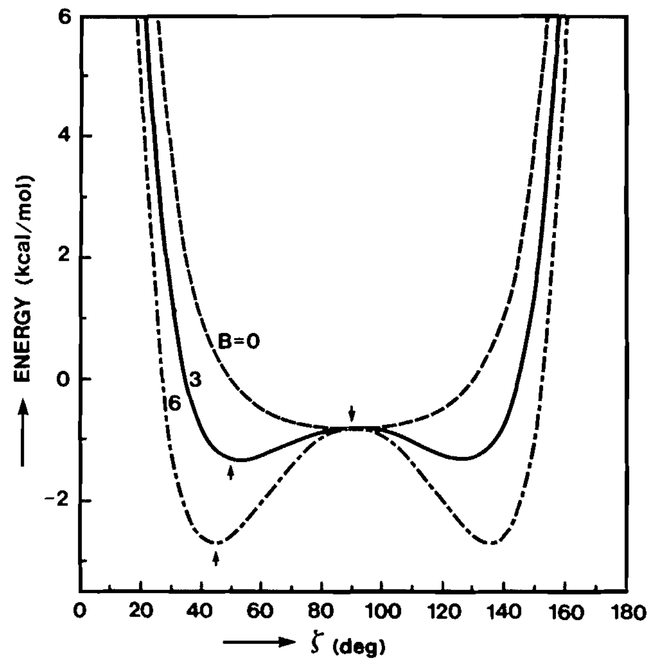

FIG. 3. The variation of energy with ζ is shown for select values of *B*. The Lennard–Jones function was used. The angle C*—O*—Cl is 121° (Set II parameters, see text).

from Allinger *et al.* (24), Hummel and Flory (25), and Andose and Mislow (26).

Another contribution to be considered for the estimation of the energies is that due to electron delocalization. The nonbonded interaction between O^c and the *ortho* hydrogen (H6 in Fig. 1) would oppose coplanarity of the carbonate group with the phenyl and would lead to a preferred value of $\zeta = 90°$. On the other hand, the electron delocalization would favour the planar conformation. Hence, the combined contribution due to both of these effects has to be included. The electron delocalization energy was estimated according to (25):

$$[5] \quad E_{\mathrm{deloc}} = -B\cos^2\zeta$$

where *B* is a parameter, in kcal mol^{-1}. An inherent threefold torsional potential with a barrier of 3 kcal mol^{-1} was assigned to the C—CH_3 bonds. The torsional potential was not included for rotations ϕ and ψ due to the negligible barrier for such a rotation in toluene.

Results and discussion

The calculations showed that the energies corresponding to ϕ and ψ in the accessible region are unaffected by the preferred ranges of ζ. Although the rotation of the phenyl via, for example, the ϕ would affect the carbonate group to the extent that its preferred relative disposition with respect to the phenyl has to be maintained, the interactions which arise between the two phenyl groups are determined by only the rotations ϕ and ψ. Hence the rotations (ϕ,ψ) and ζ can be treated independently, for the present discussion.

1. *The carbonate group*

The carbonate group is planar and predominantly *trans*. While the electronic delocalization would favour the coplanarity of the carbonate group with the plane of the phenyl, the steric repulsion between the carbonyl oxygen and the *ortho* CH group would oppose the coplanarity. In the crystal structure (27) of *p*-phenylenediacrylic acid diphenyl ester, $\zeta = 65°$, and in the structure of diphenyl carbonate,[1] $\zeta = 45°$.

The variation of energy with ζ, calculated with Set I geometry and L–J function, is shown in Fig. 2. The angle C*—O*—Cl is 113° here. While, as expected, the minimum in energy occurs at $\zeta = 90°$ with $B = 0$, it shifts to 80° and 70° with $B = 4$ and 6 kcal mol^{-1} respectively. Due to the predominant interaction between O^c and H6, a value of $B = 18$ is required in order to obtain the minimum at $\zeta \approx 50°$. The calculations of Hummel and Flory (25) on model compounds of *p*-phenylene polyesters and polyamides show that values of *B* in the range of 3 to 7 kcal mol^{-1} are required to reproduce the crystallographically observed torsion angles. A similar range of *B* can be expected to be valid for the carbonate group. The high value of 18 kcal mol^{-1} required to obtain a minimum at $\zeta = 50°$ is a consequence of the small value of 113° assigned to the angle C*—O*—Cl.

The variations of energy with ζ, calculated with Set II geometry (Flory parameters) using the L–J and Hill's functions, are shown in Figs. 3 and 4 respectively. The variations of some of the nonbonded distances with ζ are shown in Fig. 5. Note that with Set II geometry, the angle C*—O*—Cl is 121°. Comparison of Figs. 3 and 4 shows that with $B = 6$ kcal mol^{-1}, minima occur at $\zeta = 50°$ and 45° using the Hill's function and the L–J function, respectively. Figure 5 shows that the distances O^c - - - H6, C* - - - H6, and O* - - - C6 increase reasonably close to the sum of the van der Waals radii or the *characteristic* distance d^* in the range of $\zeta = 45$ to 55°. Comparison of the results obtained with Set I and Set II geometries shows that an enlargement of the angle C*—O*—Cl to nearly 121° is necessary to obtain the minimum in energy at $\zeta \approx 50°$, with values of *B* in the range of 4–6 kcal mol^{-1}. In the crystal structure[1] of diphenyl carbonate, the angle C*—O*—Cl is 121°, whereas it is 117.6° in the structure of *p*-phenylenediacrylic acid diphenyl ester (27). In any event, a value greater than 113° (which

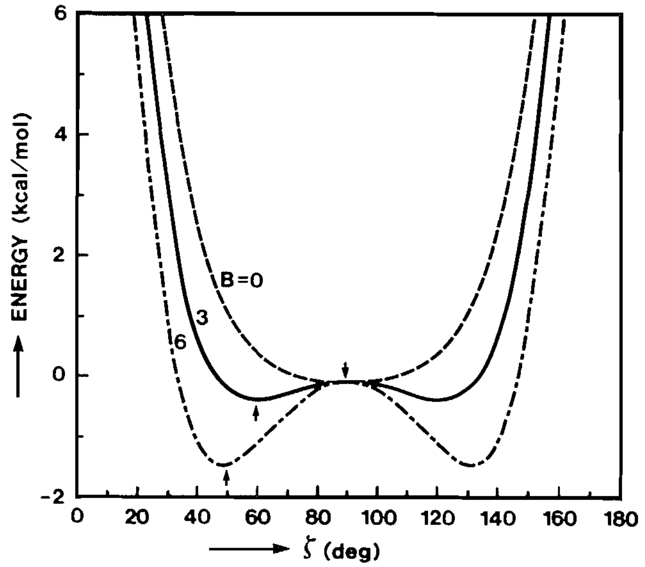

FIG. 4. Same as Fig. 3, but with Hill's functions for evaluating nonbonded interactions.

was used by Williams and Flory (16)) is indicated. The present calculations as well as the crystal structure studies cited above show that the preferred value of ζ is limited to 45–65°.

With B = 6 kcal mol^{-1}, and the Hill's function, the energy values at ζ = 0, 50, and 90° are 14, −1.5, and −0.1 kcal mol^{-1}, respectively, leading to a barrier of 15.5 kcal mol^{-1} at ζ = 0° and 1.4 kcal mol^{-1} at ζ = 90°. Similarly, with the L–J function and B = 6 kcal mol^{-1}, the energies at ζ = 0,45, and 90° are 20.2, −2.7, and −0.8 kcal mol^{-1}, respectively, resulting in a barrier of 22.9 kcal mol^{-1} at ζ = 0° and 1.9 kcal mol^{-1} at ζ = 90°. Adjustments of geometrical parameters could lower these energies somewhat. Pochan *et al.* (28), on the basis of dielectric relaxation measurements, deduced an activation energy of 17.7 kcal mol^{-1} for combined (sub T_g) β and γ relaxations of BPAPC and 8.1 kcal mol^{-1} for γ relaxation of bisphenol-A – diphenyl carbonate. The latter was associated with the carbonate group. Massa and Rusanowsky (29) reported a value of 9.8 kcal mol^{-1} for the γ relaxation. Although Yee and Smith (30) obtained 13 kcal mol^{-1} for the γ relaxation, they have shown that this relaxation is not attributable to the carbonate group exclusively, but rather to the monomer unit as a whole. Hence, it would seem that unambiguous comparison of the theoretical and experimental values of the barrier corresponding to the carbonate group is not possible at this time. However, the above experimental values for the activation energy can perhaps be accounted for by combining the energy barrier of ~2 kcal mol^{-1} mentioned above for the carbonate group at ζ = 90° and the barrier for the phenyl rotation discussed in the next section.

The results reported by Flory and co-workers (15) show that with the same geometrical parameters (Set II), and the Hill's function, the minimum occurs at ζ = 45° with B = 2 kcal mol^{-1}. However, according to our calculations shown in Fig. 4, when using a value of B = 2 kcal mol^{-1}, the minimum occurs at ζ = 65° and a value of B > 6 is needed to derive a minimum at ζ = 45°. It seems that these differences are due to the allowance made for bond angle variations for each ζ, in the work of Flory *et al.* (P. J. Flory, private communication).

2. *Conformation of the 2,2-diphenylpropane (DPP) segment*

The conformation of the DPP segment is defined by the

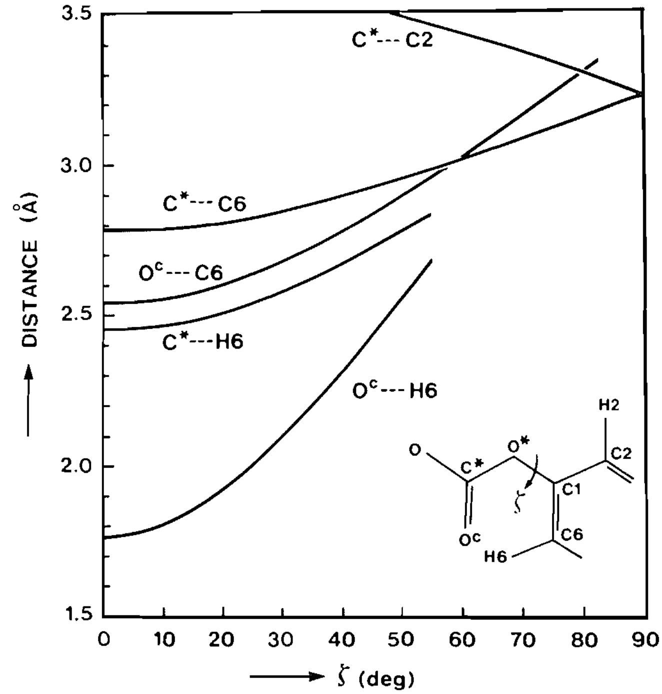

FIG. 5. The variations of significant nonbonded distances with ζ are shown here.

torsion angles ϕ and ψ (Fig. 1). The coplanar conformation of the phenyls incurs severe overlap of the *ortho* hydrogens. When $\phi = \psi$ = 0°, the distances H3---H3′, C3---H3′ (or C3′---H3) and C3---C3′ are 0.22, 1.3, and 2.2 Å respectively.

Energies calculated for the DPP segment in terms of ϕ and ψ are shown in Figs. 6 and 7, for the L–J and the Hill's functions respectively. The exact Flory geometry (Set II) was used. The torsion angles χ and χ' were varied for each (ϕ,ψ) and the methyl hydrogens were kept in their minimum energy conformation. It is seen from Figs. 6 and 7 that the minimum in energy occurs at (ϕ,ψ) = (45°,75°) and (75°,45°) with the L–J function and at (ϕ,ψ) = (25°,75°) and (75°,25°) with the Hill's function. Further, it is seen from Fig. 7 that all the conformations for which $\phi + \psi \approx$ 90° or 270° are within 1 kcal mol^{-1} from the minimum. The calculations with the L–J function (Fig. 6) also show a similar feature, with $\phi + \psi \approx$ 120° or 240°. The small variations in energy over a large domain are responsible for slight shifts in minima and the allowed range when different potential functions are compared. At the intervals of 5° in ϕ and ψ chosen for these maps, 35% of the conformational space is within 1 kcal mol^{-1} in Fig. 6 and 25% in Fig. 7. In the crystal structure (31) of diglycidyl ether of bisphenol-A, the values of (ϕ,ψ) are (64.3°,49°). This conformation occurs within the contour of 0.5 kcal mol^{-1} in Fig. 6. The energy corresponding to (ϕ,ψ) = (90°,90°) is 7.5 kcal mol^{-1} in Fig. 6 using the L–J function and 30.9 kcal mol^{-1} in Fig. 7, with Hill's function, relative to the respective minima. The value obtained with Hill's function is perhaps too high due to the higher emphasis that the parameters for this function place for the H---H interaction (see below). Combining the 7.5 kcal mol^{-1} for the barrier at (ϕ,ψ) = (90°,90°) and the ~2 kcal mol^{-1} derived for the barrier at ζ = 90°, the total energy is close to the value of ~9.0 kcal mol^{-1} deduced experimentally for γ relaxation. This theoretical energy is the maximum value of the barrier, as obtained by the present calcu-

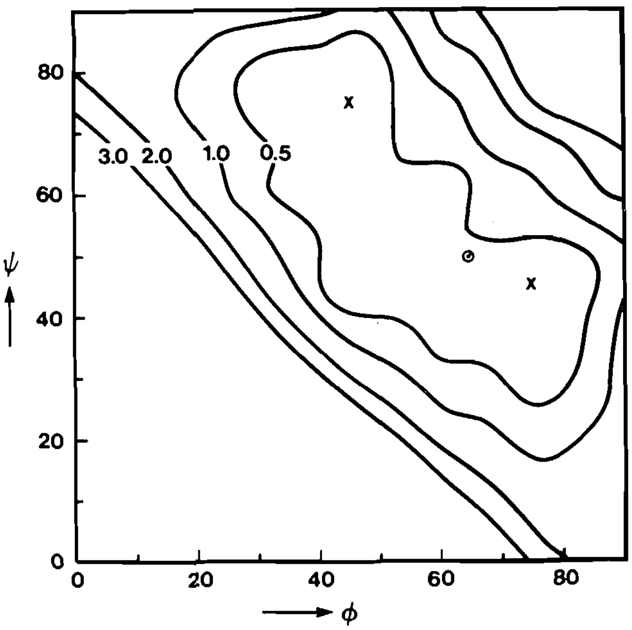

FIG. 6. The iso-energy contours are shown for the DPP segment, in terms of rotations φ and ψ, with respect to the minimum marked by ×. The L–J function was used. The symmetrically related part of the map can be seen as in Fig. 8. The conformation corresponding to the crystal structure of diglycidyl ether of bisphenol-A is marked by ⊙.

lations. A least-energy path for the conformational transition is possible, as discussed later.

Although intuitively one would expect the minimum to occur at (φ,ψ) = (60°,60°), the shifts of the minima from such a position in Figs. 6 and 7 need clarification. In Fig. 6, the difference in energy between (φ,ψ) = (45°,75°) and (60°,60°) is only 0.2 kcal mol^{-1}, and cannot be attributed to any unique predominant interaction. However, in Fig. 7, the energy difference between (φ,ψ) = (25°,75°) and (60°,60°) is 4.7 kcal mol^{-1}. The higher energy of the latter is not due to unfavorable interactions between the skeletal atoms but is due to those involving the methyl hydrogens. For purposes of discussion, let us denote the hydrogens attached to C^m by H_a, H_b, and H_c, and those appended to C^{m} by H_a', H_b', and H_c'. For (φ,ψ) = (25°,75°), with the hydrogens kept at positions corresponding to the minimum energy, the distances H_b---H_5', H_b'---H_5, and H_c---H3 are 2.13, 2.11, and 3.05 Å, respectively. These distances reduce to 2.01, 2.01, and 2.21 Å, respectively, at (φ,ψ) = (60°,60°), contributing to the energy difference of ~4 kcal mol^{-1}. Such a large contribution to the energy was traced to the nature of the Hill's function. The parameters chosen (24–26) (Table 2) for this function accentuate the interactions involving the hydrogen atoms, compared to the L–J function. For H---H interaction, R = 1.2 Å and $d^*/2$ = 1.5 Å are used. For a H---H distance of 2.4 Å, energies of −0.12 and 0.42 kcal mol^{-1} are obtained with L–J and Hill's functions respectively. However, at a distance of 2 Å, the energy is 0.36 kcal mol^{-1} with the L–J function and 4.2 kcal mol^{-1} with Hill's function. Thus, for the contact pairs listed above for (φ,ψ) = (25°,75°) and (60°,60°), the emphatic contribution to the energy of the latter is due to the nature of the Hill's function and the parameters chosen for the hydrogen atom. Adjustment of the parameters to establish correspondence between the two functions is not attempted here.

The (φ,ψ) map corresponding to a value of 112° for the

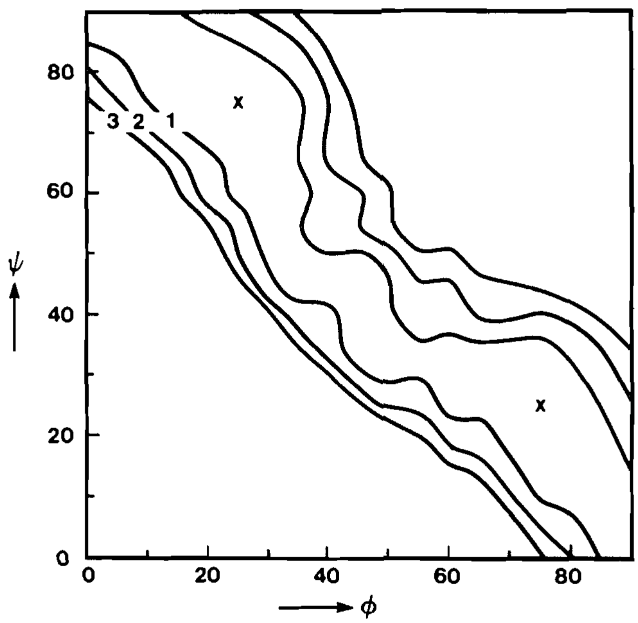

FIG. 7. Same as Fig. 6, but with Hill's function.

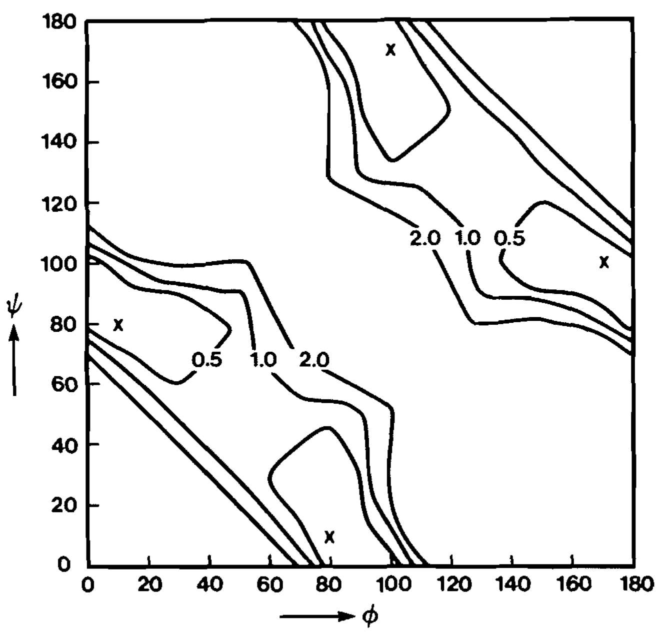

FIG. 8. Same as Fig. 6, but with a value of 112° for the C4—C^{α}—C4′ bond angle.

skeletal bond angle C4—C^{α}—C4′, constructed using the L–J function, is shown in Fig. 8. It is seen here that the minimum has shifted to (φ,ψ) = (10°,80°) and (80°,10°). The energy at (φ,ψ) = (90°,90°) is 7 kcal mol^{-1}. The large accessible area remains similar to those in Figs. 6 and 7. In fact, 49% of the conformations on the (φ,ψ) space are within 1 kcal mol^{-1} from the minimum. The small variation in energy (within 1 kcal mol^{-1}) over a large domain of the (φ,ψ) surface is responsible for the shift of the position of the minimum when either the potential functions or the geometrical parameters are changed.

The large accessible area on the (φ,ψ) surface qualifies the DPP segment to be classified as a fairly flexible portion of the polycarbonate chain. However, the rotations are *not* unhindered. The accessible conformations are such that the rota-

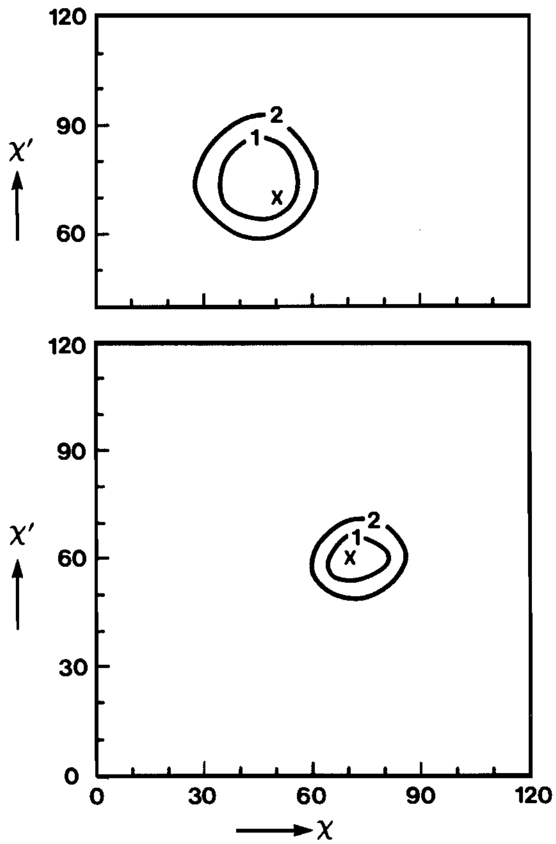

FIG. 9. The iso-energy contours are shown, for the methyl group rotation, in terms of χ and χ'. The (ϕ,ψ) values are (60°,40°) for the bottom figure and (0°,90°) for the top. The L–J function was used here.

tions ϕ and ψ have to be synchronized to meet the condition that $\phi + \psi \approx 90$–120° or 240–270°. In considering the molecular motion of the phenyls and their reorientation in BPAPC, the π flip or reorientation through small diffusive steps have been suggested as possibilities (32, 33). Figures 6–8 show that the reorientation of the phenyls can occur with coordinated rotations, along the path defined by $\phi + \psi \approx 90°$, without having to overcome a high energy barrier.

The energies associated with the rotations χ and χ' of the methyl groups are shown in Fig. 9, for two select values of (ϕ,ψ), using the L–J function. It is seen that with (ϕ,ψ) = (60°,40°), the minimum occurs at (χ,χ') = (70°,60°), which corresponds to the staggered disposition of the C—H bonds with respect to the contiguous skeletal bonds. With (ϕ,ψ) = (0°,90°), the minimum occurs at (χ,χ') = (50°,70°). The energy contours in Fig. 9 also show that within an energy of 2 kcal mol^{-1}, only a range of about 20° is accessible for χ and χ', for each (ϕ,ψ) conformation. The various values of (χ,χ') obtained with L–J and Hill's functions for conformations with $\phi + \psi = 90°$ are given in Table 3. This table shows that with the L–J function, χ and χ' vary from (50°,70°) to (70°,50°) as the values of (ϕ,ψ) change from (0°,90°) to (90°,0°). A larger range of (40°,80°) to (80°,40°) is obtained with the Hill's functon. In the above ranges, the energy of interaction of the methyl groups with the rest of the molecule varies very little with the L–J function, whereas a change in energy of 4.1 kcal mol^{-1} is noted with the Hill's function. These results show that while a certain range of conformations is accessible to the methyl hydrogens, the variations in χ and χ' depend on the values of ϕ and ψ.

TABLE 3. Values of χ and χ' derived for minimum energy positions of methyl hydrogens, for a few select values of ϕ and ψ

	L–J function		Hill's function	
ϕ,ψ (°)	χ,χ'	E*	χ,χ'	E*
0,90	50,70	0.2	40,80	0
10,80	50,70	0	50,80	1.1
20,70	50,70	0.2	50,80	2.0
30,60	60,70	0	60,80	2.8
40,50	70,70	0.3	70,80	4.1
50,40	70,70	0.3	80,70	4.1
60,30	70,60	0	80,60	2.8
70,20	70,50	0.2	80,50	2.0
80,10	70,50	0	80,50	1.1
90,0	70,50	0.2	80,40	0

* The energies, in kcal mol^{-1}, are given relative to the lowest energy (χ,χ') conformation in each case.

Garfield (34) suggested, based on the results of wide-line nmr studies, that the motions of the methyl groups and phenyls are cooperative. Jones and Bisceglia (5) arrived at the same conclusion.

The energy map for the DPP segment, reported by Flory *et al.* (Fig. 6 of ref. 15), shows that the minimum occurs at (ϕ,ψ) = (46°,46°) $(\psi_A,\psi_B$ in the notation of ref. 15). The contours therein also imply that the rotations ϕ,ψ are highly restricted. This is in contrast to Figs. 6–8 presented here, which show that a wide range of ϕ,ψ is accessible. This difference has been traced to the fact that Flory *et al.* used a constant value of $\chi = \chi' = 6°$ for constructing the energy map (P. J. Flory, private communication), whereas, in the present calculations, χ and χ' were minimized for each ϕ,ψ conformation. Since Flory *et al.* were concerned with the averages $\langle\cos^2 \phi\rangle$ and $\langle\cos^2 \psi\rangle$, this difference is not of significant consequence in their results on the optical anisotropy.

The inability of polycarbonate to crystallize readily is rationalized by the large accessible conformational domain derived from the present calculations. Further, the suggestion (3) that the chain has to adopt several intermediate conformations prior to crystallization is also supported by our work.

3. *Molecular shapes*

Robertson and co-workers (35) have discussed the nomenclature for the description of the conformations usually adopted by bridged diphenyls in crystal structures. These are generally described in terms of planar, butterfly, twist, and skew conformations as shown schematically in Fig. 10. None of the compounds studied so far by X-ray crystallography adopts the planar conformation, whatever the nature of the bridge atom: C, O, or S. This is mainly due to the repulsion between the *ortho* hydrogens as described earlier. Most diphenyls with ether linkage and sulfides adopt the skew and twist conformations; the ketones show only the twist conformation; the sulfoxides only the butterfly, sulfones the twist and butterfly, and methanes, the skew and twist. The reader is referred to the paper by Robertson and co-workers (35) for the identity of these compounds. These results show that the bridged diphenyls are found in a variety of conformations, depending upon both intra and intermolecular packing effects. The accessible conformations of the DPP segment of the BPAPC chain, discussed above, show that twist and skew conformations are

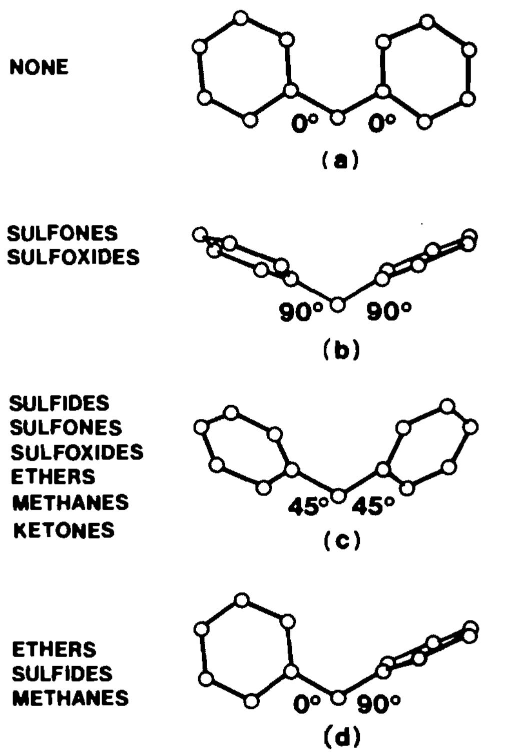

FIG. 10. Schematic representation of the nomenclature used for the description of the conformations of bridged diphenyls: (a) planar, (b) butterly, (c) twist, and (d) skew. The ideal (ϕ,ψ) values are marked (adapted from ref. 35).

possible. It is noteworthy that most of the compounds surveyed in ref. 35, with the C—C—C type linkage, occur along the zone defined by $\phi + \psi \approx 90°$.

The shapes of the segment of the BPAPC chain were drawn, in orthogonal projection, using a computer program developed for the Diablo Multiwriter. The shapes of one repeat unit of the BPAPC, for conformations with $\phi + \psi = 90°$, are shown in Fig. 11 (A–I). The (ϕ,ψ) corresponding to each shape is marked. These are only a few select conformations among those accessible to the repeat unit. Comparing with Fig. 10, the twist and skew shapes are obvious. Figure 11 clearly shows the variety of conformations which is accessible to the repeat unit in solution or in the amorphous state. With such a diversity of conformations, the long annealing time required for crystallization is understandable. The technique of molecular graphics is being used increasingly in conformational analysis of biopolymers, enzyme–substrate interactions, drug design, and organic synthetic chemistry. The variability in the shapes of the polycarbonate and similar chains can be best understood by such means.

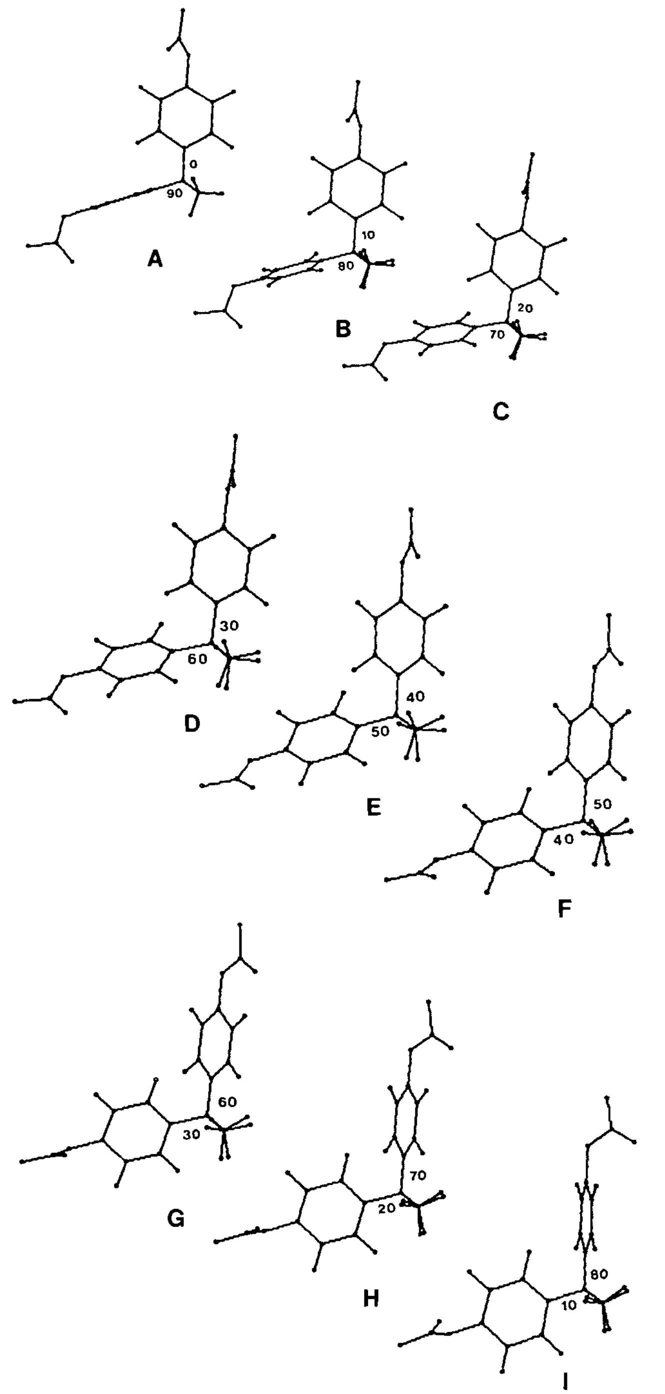

FIG. 11. (A–I): The variability of the conformation of the DPP segment is illustrated in terms of a series of shapes. The values of (ϕ,ψ) are marked. The molecule is shown in projection. The (χ,χ') conformations correspond to those derived using Hill's function (see Table 3).

Conclusions

The conformational calculations show that although the accessible area of the (ϕ,ψ) surface for the DPP segment is large, the rotations ϕ and ψ should be synchronized. Uninhibited free rotation is not possible. The carbonate group has a restricted freedom of rotation, to within 20°. The methyl group also has only a limited freedom of rotation. Free rotation is not indicated for these portions of the molecule. The slow crystallization upon annealing can be attributed to the conformational flexibility of the DPP segment, and the cooperativity needed for conformational rearrangement. The synchronized rotations of the phenyls can lead to diffusive reorientation. The general conformational features are discussed here and not the specific one pertaining to the crystal structure. The shapes of the repeat unit shown in Fig. 11 give pictorial representation to the stereochemical jargon.

Acknowledgement

The author is grateful to Dr. P. J. Flory for clarifying the origin of the differences noted between his work and the present results.

1. E. TURSKA, W. PRZYGOCKI, and K. MASLOWSKI. J. Polym. Sci., Part C, **16**, 3373 (1968).
2. H. SCHNELL. Chemistry and physics of polycarbonates. Wiley Interscience, New York. 1964.
3. E. TURSKA, J. HUREK, and L. ZMUDZINSKI. Polymer, **20**, 321 (1979).
4. J. SCHAEFER, E. O. STEJSKAL, and R. BUCHDAHL. Macromolecules, **10**, 384 (1977); J. SCHAEFER, E. O. STEJSKAL, T. R. STEGER, M. D. SEFEIK, and R. A. MCKAY. Macromolecules, **13**, 1121 (1980); **13**, 1127 (1980).
5. A. A. JONES and M. BISCEGLIA. Polym. Prepr. **20**, 227 (1979).
6. K. VARADARAJAN and R. F. BOYER. J. Polym. Sci. Polym. Phys. Ed. **20**, 141 (1982), and references therein.
7. R. P. KAMBOUR, F. E. KARASZ, and J. H. DAANE. J. Polym. Sci. Part A2, **4**, 327 (1966).
8. E. TURSKA and H. JANECZEK. Polymer, **20**, 855 (1979).
9. R. A. WARE, S. TRITOWIDJOJO, and C. COHEN. J. Appl. Polym. Sci. **26**, 2975 (1981).
10. F. GALLEZ, R. LEGRAS, and J. P. MERCIER. J. Polym. Sci. Polym. Phys. Ed. **14**, 1367 (1976).
11. R. LEGRAS and J. P. MERCIER. J. Polym. Sci. Polym. Phys. Ed. **15**, 1283 (1977).
12. R. BONART. Makromol. Chem. **92**, 149 (1966).
13. A. E. TONELLI. Macromolecules, **5**, 558 (1972).
14. W. J. DULMAGE, W. A. LIGHT, S. J. MARINO, C. D. SALZBERG, D. L. SMITH, and W. J. STAUDENMAYER. J. Appl. Phys. **49**, 5543 (1978).
15. B. ERMAN, D. C. MARVIN, P. A. IRVINE, and P. J. FLORY. Macromolecules, **15**, 664 (1982).
16. A. D. WILLIAMS and P. J. FLORY. J. Polym. Sci. Part A2, **6**, 1945 (1968).
17. H. J. M. BOWEN and L. E. SUTTON. Tables of interatomic distances and configurations in molecules and ions. The Chemical Society, London. 1958.
18. U. W. SUTER and P. J. FLORY. Macromolecules, **8**, 765 (1975).
19. P. R. SUNDARARAJAN. Macromolecules, **13**, 512 (1980).
20. R. H. MARCHESSAULT and P. R. SUNDARARAJAN. Pure Appl. Chem. **42**, 399 (1975).
21. (*a*) P. J. FLORY. Statistical mechanics of chain molecules. Interscience, New York. 1969; (*b*) A. J. HOPFINGER. Conformational properties of macromolecules. Academic Press, New York. 1973.
22. T. L. HILL. J. Chem. Phys. **16**, 399 (1948).
23. A. I. KITAIGORODSKY. Tetrahedron, **14**, 230 (1961).
24. N. L. ALLINGER, J. A. HIRSCH, M. A. MILLER, and I. J. TYMINSKI. J. Am. Chem. Soc. **91**, 337 (1969); N. L. ALLINGER, M. T. TRIBBLE, and M. A. MILLER. Tetrahedron, **28**, 1173 (1972); N. L. ALLINGER and D. Y. CHUNG. J. Am. Chem. Soc. **98**, 6798 (1976).
25. J. P. HUMMEL and P. J. FLORY. Macromolecules, **13**, 479 (1980).
26. J. D. ANDOSE and K. MISLOW. J. Am. Chem. Soc. **96**, 2168 (1974).
27. H. NAKANISHI, K. UENO, and Y. SASADA. Acta Crystallogr. Sect. B, **34**, 2036 (1978).
28. J. M. POCHAN, H. W. GIBSON, M. F. FROIX, and D. F. HINMAN. Macromolecules, **11**, 165 (1978).
29. D. J. MASSA and P. P. RUSANOWSKY. Polym. Prepr. **17**, 184 (1976).
30. A. F. YEE and S. A. SMITH. Macromolecules, **14**, 54 (1981).
31. J. L. FLIPPEN-ANDERSON and R. GILARDI. Acta Crystallogr. Sect. B, **37**, 1433 (1981).
32. A. N. GARROWAY, W. M. RITCHEY, and W. B. MONIZ. Macromolecules, **15**, 1051 (1982).
33. P. T. INGLEFIELD, R. M. AMICI, J. F. O'GARA, C.-C. HUNG, and A. A. JONES. Macromolecules, **16**, 1552 (1983).
34. L. J. GARFIELD. J. Polym. Sci. Part C, **30**, 551 (1970).
35. S. P. N. VAN DER HEIJDEN, E. A. H. GRIFFITH, W. D. CHANDLER, and B. E. ROBERTSON. Can. J. Chem. **53**, 2084 (1975).

Mechanisms and models for homogeneous copper mediated ligand exchange reactions of the type: CuNu + ArX → ArNu + CuX[1]

CHRISTIANE COUTURE AND ANTHONY JAMES PAINE[2]
Xerox Research Centre of Canada, 2660 Speakman Drive, Mississauga, Ont., Canada L5K 2L1

Received January 24, 1984

This paper is dedicated to the 10th anniversary of the Xerox Research Centre of Canada

CHRISTIANE COUTURE and ANTHONY JAMES PAINE. Can. J. Chem. **63**, 111 (1985).

The title reactions are an important class of copper mediated nucleophilic aromatic substitution processes, which constitute a useful tool in the molecular design and synthesis of small molecules. We report the results of extensive investigation of these processes, primarily focussing on cyanodeiodination (ArI + CuCN → CuI + ArCN). Among the interesting features of these processes are: (a) an unusual rate equation involving autocatalysis by CuI product; (b) retardation by both excess nucleophile (as KCN) and excess leaving group (as KI), which compete with ArX to complex with CuNu; (c) only cuprous nucleophiles are active (ligand exchanged products from cupric salts arise from prior redox equilibria which form CuNu); (d) the halogen effect is large ($k_I \sim 40-100\ k_{Br} \sim 300-5000\ k_{Cl}$) but the Hammett ρ value is zero; (e) *ortho*-alkyl groups do not hinder the reaction (and actually cause mild acceleration by relief of steric strain). Finally, the introduction of an *ortho*-COO^- group accelerates the reaction by a factor of 10^4-10^5, but the general features of the accelerated reactions are also the same, again indicating a common mechanism, with entropic acceleration by *ortho*-carboxylate. Both kinetic and thermodynamic factors were considered in detail, the latter apparently for the first time. Applications to practical syntheses are considered, and novel mechanistic models for these interesting processes are discussed.

CHRISTIANE COUTURE et ANTHONY JAMES PAINE. Can. J. Chem. **63**, 111 (1985).

Les réactions mentionnées dans le titre constituent une classe importante de réactions de substitutions nucléophiles aromatiques catalysées par le cuivre qui sont un outil utile pour la conception moléculaire et la synthèse des petites molécules. Nous rapportons les résultats d'une étude poussée de ces réactions au cours de laquelle on a mis l'accent, en premier lieu, sur la cyanodéiodation: (ArI + CuCN → CuI + ArCN). Parmi les caractéristiques intéressantes de ces réactions on peut noter, entre autre, le fait que: (a) ces réactions présentent une équation de vitesse inhabituelle qui implique une autocatalyse par le CuI qui est produit; (b) la vitesse de la réaction est retardée à la fois par un excès de nucléophile (comme le KCN) ou de nucléofuge (comme le KI) qui entre en compétition avec le composé ArX pour complexer le CuNu; (c) le fait que seuls les nucléophiles cuivreux soient actifs (les produits provenant d'un échange de ligands se forment au cours d'un équilibre rédox antérieur qui forme du CuNu; (d) l'effet des halogènes soit grand (k_I = 40 à 100 k_{Br} = 300 à 5000 k_{Cl}) alors que la valeur ρ de Hammett est égale à zéro; (e) les groupes alkyles en position *ortho* n'encombrent pas la réaction (et qu'ils provoquent en fait une légère accélération grâce à une diminution de la contrainte stérique). Finalement l'introduction d'un groupe COO^- en position *ortho* accélère la réaction par un facteur de 10^4 à 10^5; toutefois les caractéristiques générales des réactions accélérées sont les mêmes que les autres et ce fait indique l'existence d'un mécanisme commun qui subit une accélération entropique due à la présence du groupe carboxylate en *ortho*. On a considéré en détail les facteurs cinétiques et thermodynamiques; il semble que ces derniers ont été examinés pour la première fois. On considère les applications de ces réactions dans des synthèses pratiques et on discute de nouveaux modèles mécanistiques pour ces réactions intéressantes.

[Traduit par le journal]

Introduction

Aromatic substitution reactions are important tools in the molecular design and synthesis of small molecules. Substitution methodologies may be of electrophilic, nucleophilic, or radical character, the last of which is relatively rarely applied to synthetic problems. Electrophilic aromatic substitution (EAS) is the most common, and is supported by a wide literature. Nucleophilic aromatic substitution (NAS) usually requires a suitable leaving group, X, plus activation by electron-withdrawing substituents, which stabilize the intermediate negative charge in the classic addition–elimination mechanism (1). Nucleophilic aromatic substitution on unactivated rings is relatively rare, but may be effected in the presence of copper. There are two major classes of copper mediated reactions which are formal nucleophilic aromatic substitutions: copper catalysed reactions (known as Ullmann condensations), where copper is present as the metal, a salt, or an oxide; and copper ligand exchange reactions (1, 2). These reactions are fairly general, and some of the possibilities are shown in eqs. [1] and [2]. There is evidence that cuprous nucleophile species are intermediates in the catalytic reactions, and therefore, these processes likely share the same mechanism (3–5).

$$[1]\quad \mathrm{CuNu + ArX \rightarrow CuX + ArNu} \qquad \text{(ligand exchange)}$$

$$[2]\quad \mathrm{NuH + ArX \xrightarrow{Cu^+} ArNu + HX} \qquad \text{(catalysis)}$$

Nu = X, CN, SCN, OAc, OH, ArO, ArS, ArSe, ArNH, Ar_2N, Ar. . . .
X = I, Br, Cl.

Although these reactions have been known for many decades, there has been little systematic investigation of the reaction mechanism (2, 6, 7). The literature is characterized by questionable conclusions drawn with only a minimum of data, using relative yield measurements, or final product analyses (e.g. ref. 8) – techniques which cannot distinguish between rate and equilibrium effects (which, as will be shown, are quite important). In order to broaden mechanistic understanding of copper mediated NAS in general, and to improve its scope as a synthetic tool, we have begun by investigating the kinetically simpler ligand exchange reaction. In this case CuNu is a measurable reactant, rather than a hypothetical transient intermediate. In particular we focussed on copper mediated cy-

[1] Presented, in part at the 66th Canadian Chemical Conference, Calgary, Alberta as paper OR14-9 (June, 1983).
[2] Author to whom correspondence should be addressed.

anodeiodination (replacement of iodide with cyanide using cuprous cyanide) in detail, although we also examined a variety of other nucleophiles and leaving groups to ensure the generality of the work.

Experimental

Most substrates and products were commercially available and were purified by distillation or recrystallization to >99% purity by analytical hplc. 2,4,6-Tri-*tert*-butylbromobenzene was prepared by the method of Pearson *et al.* (9). Sodium salts of aromatic carboxylic acids were prepared by standard methods, and recrystallized from water.

Synthesis of 2,4,6-trimethyliodobenzene

Following the general procedure of Martin *et al.* (10), 2,4,6-trimethylbenzene (12.1 g; 0.10 mol), iodine (6.4 g; 0.025 mol), and ammonium persulfate (6.9 g; 0.031 mol) were added to a solvent consisting of acetic acid (135 mL), water (25 mL), and sulfuric acid (6 mL) in a 250-mL round bottom blask. The reaction mixture was stirred and heated at 80°C for 4 h, poured on ice (300 g), and worked up into methylene chloride. The coloured impurities were removed by elution through a short column of silica gel in hexane. The product was isolated from excess starting material by fractional distillation (bp 128°C/13 Torr) (1 Torr = 133.3 Pa) to give a low-melting white crystalline solid (7.1 g; 0.029 mol; 58% yield; mp 29.5–31°C (lit. (11) mp 29–30°C)). 2,4,6-Tri-*tert*-butyliodobenzene could not be prepared by this method.

*Synthesis of 2,4,6-tri-*tert*-butylbenzonitrile*

CuCN (0.48 g; 50 mmol) and 2,4,6-tri-*tert*-butylbromobenzene (0.20 g; 0.61 mmol) were heated in 50 mL DMA at 137°C for $4\frac{1}{2}$ days, then cooled and worked up into methylene chloride. The solvent was dried and evaporated to give a green oil which was chromatographed on silica gel, with hexane as eluent, to give impure white crystals (crude yield 0.10 g; 0.37 mmol; 60% yield). Pure product obtained by crystallization from MeOH (mp 150–151.5°C (lit. (12) mp 151–152°C)) had ir, ^{1}Hmr, Cmr, and ms consistent with the structure and the literature.

General kinetic method

Dimethylacetamide (DMA; Burdick and Jackson Company, Distilled in Glass grade) was the solvent selected. DMA from alternative suppliers gave the same results. Analytical hplc correction factors (KFs) were determined with reference to internal standard biphenyl (or *N,N*-diphenylformamide for the carboxylic substrate series), which gave the concentrations of substrate and product directly.

$$[\text{Compound}] = \frac{\text{Area counts compound} \times \text{KF compound} \times [\text{Internal STD}]}{\text{Area counts internal STD}}$$

Unfortunately, there was a relatively narrow operating window of reagent concentrations determined by the balance between the limited solubility of the cuprous nucleophiles and the requirement for moderately high iodobenzene concentrations to achieve a reasonable conversion rate. These windows were $[\text{CuCN}]_0 = 50–160$ mM and $[\text{PhI}]_0 = 15–45$ mM. Product cuprous iodide was less soluble and often precipitated from solution. For kinetic analysis, the following relationship was assumed: $[\text{CuNu}]_t = [\text{CuNu}]_0 - [\text{ArNu}]_t$.

Five or six reactions were usually conducted simultaneously in a temperature controlled oil bath fitted with independent magnetic stirrers. In a typical reaction CuCN (350 mg; 3.55 mmol) and biphenyl (internal standard; 3 mg; 0.02 mmol) were brought to temperature (usually 137°C) in 20 mL DMA. Iodobenzene (100 mg; 0.50 mmol in 1.00 mL DMA) was added and 10–20 aliquots (~50 μL) were taken from the reaction flask over 5–100% conversion. The aliquots were quenched in 68% CH_3CN/H_2O, filtered, and analysed by analytical hplc using a Varian 5020 liquid chromatograph, CDS 401 Vista data station, and 8055 auto-sampler (Column: Applied Science 3μ Excalibar adsorbosphere C_{18} or Spherisorb ODS reverse phase; 150 × 4.6 mm. Mobile phase: typically 68% CH_3CN/H_2O (+2% HOAc for carboxylate substrates); 1.5 mL/min. Detection: 254 nm and variable wavelength).

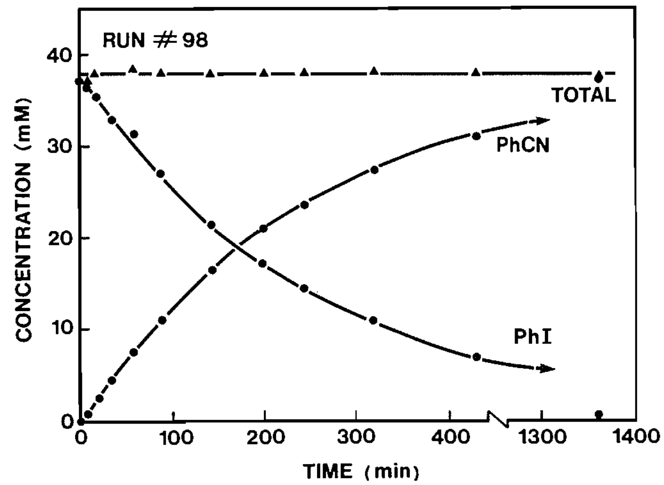

FIG. 1. Typical reaction profile for cyanodeiodination.

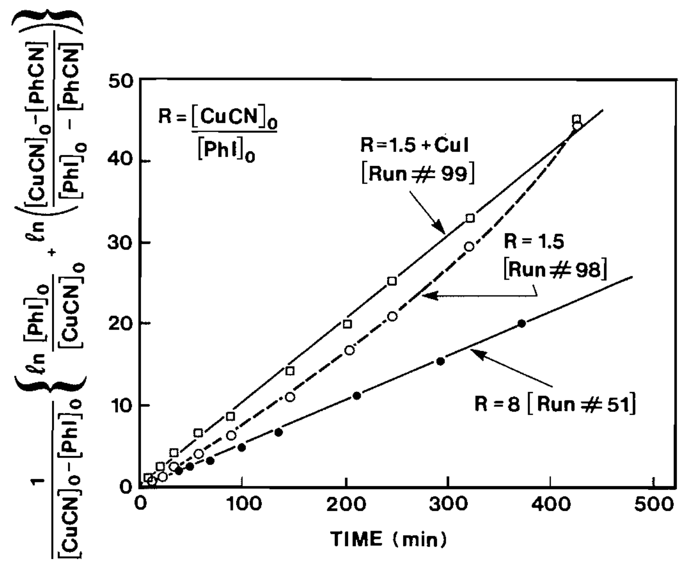

FIG. 2. Second-order kinetic plots for cyanodeiodination.

Analysis of kinetic results

The hplc data were corrected for thermal volume expansion of DMA (measured to be 1.2×10^{-3} K^{-1}) and used to prepare reaction profiles for over 170 runs (example in Fig. 1). These profiles were not well fit by the expected second-order kinetic expressions (see Fig. 2), so initial rates were determined over the first 10–30% of reaction from the slope, $k_{0,1}$, of plots of $-\ln [\text{ArX}]$ vs. time as follows.

$$[3] \quad \text{Initial rate} = (\text{d}[\text{ArCN}]/\text{d}t)_0 = k_{0,n+1}[\text{ArX}]_0[\text{CuCN}]_0^n$$

$$[4] \quad \text{Initial pseudo first-order rate constant} \equiv k_{0,1} = -\text{d}(\ln [\text{ArX}])/\text{d}t = \frac{(\text{d}[\text{ArCN}]/\text{d}t)_0}{[\text{ArX}]_0} = k_{0,n+1}[\text{CuCN}]_0^n$$

The order in CuCN, n, was determined from a log–log plot (Fig. 3) to be 0.64 ± 0.04. We have elected to represent the initial rate equation as 3/2 order ($n = 1/2$), so the initial 3/2-order rate constant is given by:

$$[5] \quad k_{0,3/2} = \frac{k_{0,1}}{[\text{CuCN}]_0^{1/2}} = \frac{-\text{d}(\ln[\text{ArX}])/\text{d}t}{[\text{CuCN}]_0^{1/2}}$$

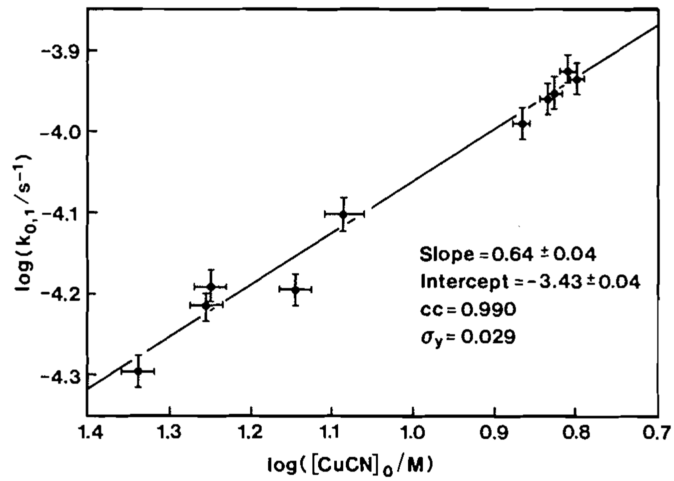

FIG. 3. Determination of the kinetic order in CuCN.

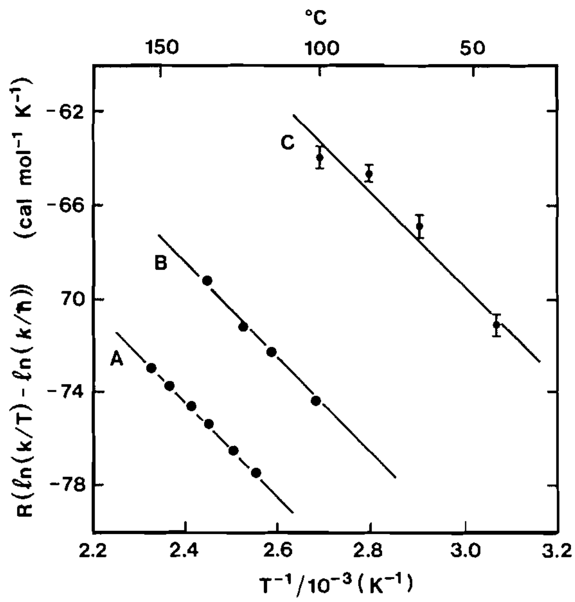

FIG. 4. Activation parameter plots for copper mediated cyanodehalogenations. (Labels A, B, and C correspond to the columns in Table 1.)

Unless otherwise noted, all rate constants presented in this work are the initial 3/2-order rate constants, $k_{0,3/2}$, in units of $L^{1/2}$ $mol^{-1/2}$ s^{-1}, and are designated simply as k, without subscripts.

Determination of activation parameters

Transition state theory gives the relation $k = \kappa(\mathrm{k}T/\hbar)$ [exp $(-\Delta G^{\ddagger}/RT)$], where k is the rate constant, κ the transmission coefficient, k the Boltzmann constant, and the other symbols have their usual meaning (13). Substitution of $\Delta G^{\ddagger}$ by $\Delta H^{\ddagger} - T\Delta S^{\ddagger}$, and reorganization of this equation leads to the linear relation in eq. [6], where the slope and intercept give the enthalpy and entropy of activation, respectively.

[6] $R[\ln (k/T) - \ln (\mathrm{k}/\hbar)] = (-\Delta H^{\ddagger}/T) + \Delta S^{\ddagger}$

$$y = mx + b; \quad x = 1/T$$

Activation parameter plots are shown in Fig. 4 and the results summarized in Table 1.

Competitive reactions

Some competitive reactions were performed in which the relative reactivity of A vs. B was obtained by extrapolating the measured product ratio $[P_A]/[P_B]$ back to time = 0, and correcting for the initial concentration of A and B as follows: $k_A/k_B = ([P_A]/[P_B])_0 \times ([B]_0/[A]_0)^m$, where $m = 1$ if A and B were aromatic halides, and $m = 1/2$ if A and B were cuprous nucleophiles.

TABLE 1. Summary of activation parameters for cyanodehalogenation

	A	B	C
ArX	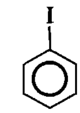	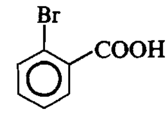	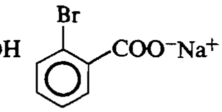
$\Delta H^{\ddagger}$ (kcal mol^{-1})	20 ± 1	21 ± 3	19 ± 1
$\Delta S^{\ddagger}$ (cal mol^{-1} K^{-1})	−26 ± 2	−19 ± 5	−12 ± 4

Results

The rate equation

Second-order kinetic plots for cyanodeiodination exhibited upward curvature (see Fig. 2). This curvature is greater in reactions performed with nearly stoichiometric amounts of reagents ($R \equiv [CuCN]_0/[PhI]_0 \sim 1$) than in cases where a large excess of CuCN was employed (e.g. $R = 8$), which become almost pseudo-first order. Interestingly, the $R = 1.5$ (Run 98) and $R = 8$ (Run 51) lines in Fig. 2 appear to have the same *initial* slope, but the $R = 1.5$ line diverges upwards with time, indicating significant acceleration.

More than a dozen kinetic models were examined in an attempt to quantitatively describe the kinetics. Of these models, only two could rationalize upward curvature of this type:

[7] Model 1: $v = k_{3/2}[CuCN]^{1/2}[PhI]$; 3/2 order
RMS error ~ 1.5%

and (or)

[8] Model 2: $v = k_2[CuCN][PhI] + k_3[CuCN][PhI][CuI]$
RMS error ~ 0.3%

The 3/2-order model appears to best describe the initial rate, but the 3rd-order autocatalytic term in [CuI] in the second model (eq. [8]) is the only explanation for the slight accelerating effect of added CuI (*vide infra* and Table 2), as shown in Run 99 of Fig. 2. Run 99, saturated with added CuI, had an excellent 2nd-order plot ($v = k_{obs}[CuCN][PhI]$, where $k_{obs} = k_2 + k_3[CuI]_{sat}$). Integrating the Model 2 rate equation led to the result that ~35% of the $R = 1.5$ reaction proceeded via the 3rd-order term while less than ~12% of the $R = 8$ reaction went that way. The phenomenon of autocatalysis appears to be general: added CuBr also accelerates cyanodebromination of 2-bromobenzoic acid (for example, when [CuBr] ~ 16 × [2 BrPhCOOH], cyanodebromination is about twice as fast as in the absence of CuBr).

Other results

Reaction rates were compared in the presence and absence of various added substances, as shown in Table 2. Within experimental error, common electron or radical traps 1,1-diphenylethylene, 1,4-dinitrobenzene, and 1,6-di-*tert*-butyl-4-methylphenol had no effect on the rate of reaction between iodobenzene and CuCN, even when added in very large excess. Similar results were obtained for reaction of *o*-bromobenzoic acid with CuCN at 137°C in DMA (7.1 equiv. DNB gave a

TABLE 2. Effect of added substances on cyanodeiodination at 137°C in DMA

Added Substance	$[PhX]_0$ (mM)	Ratio $[CuCN]_0/[PhX]_0$	Ratio $[add]_0/[PhX]_0$	k_{rel} (k_{add}/k_{ref})
None[a]	18–46	2–8	—	1.0 ± 0.1[b]
$Ph_2C{=}CH_2$	18.6	7.9	13	1.1
BHT[c]	18.6	8.1	10	1.0
DNB[d]	18.6	8.0	5.9	0.88
H_2O	40.9	2.0	5% in DMA	1.6
CuI	17.9	8.2	<8.1[e]	1.5
	40.8	1.5	<10[e]	1.5
PhCOOH	20.5	7.2	17	1.0
		7.6	17	1.2
$PhCOOCH_3$	20.5	7.2	17	1.1
		7.4	17	0.95
PhCN	17.5	8.7	12	1.0
	19.2	7.8	13	0.43
KI	19.2	7.9	13	0.41
	42.4	1.7	10	0.29
KCN	42.4	1.4	<10[e]	0.12
	42.5	1.4	<2.6[e]	0.13

[a] Average of 11 runs.
[b] $k_{ref} = 2.75 \times 10^{-4}$ $L^{1/2}$ $mol^{-1/2}$ s^{-1}. Error limits refer to standard deviation of the sample.
[c] 1,6-Di-*tert*-butyl-4-methylphenol (butylated hydroxytoluene).
[d] 1,4-Dinitrobenzene.
[e] Not all the added substance dissolved, so these were saturated solutions.

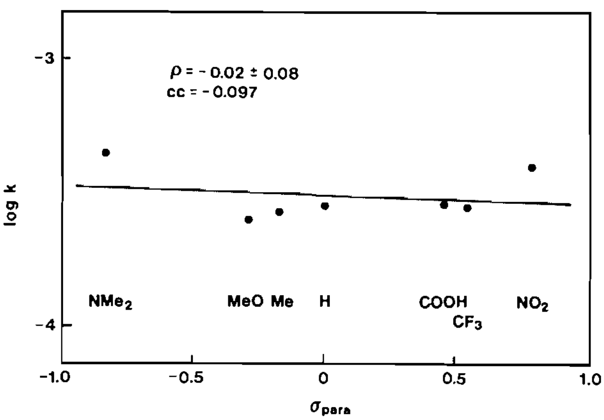

FIG. 5. Hammett plot for cyanodeiodination at 137°C in DMA.

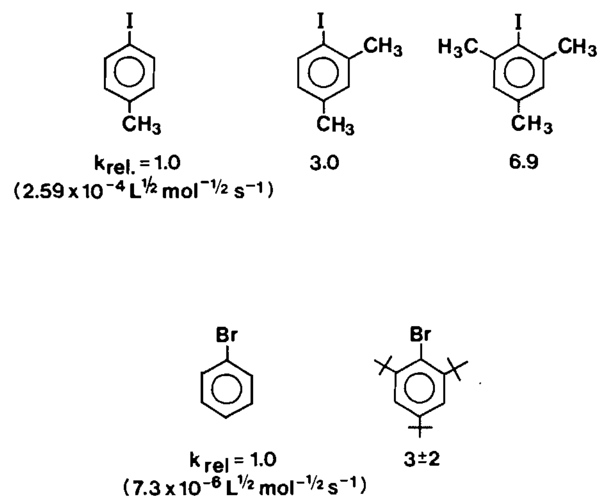

SCHEME 1. *ortho*-Substituent effects on cyanodehalogenation at 137°C in DMA.

relative rate of 1.2 ± 0.25 (4 experiments)).

An equilibrium was observed for the reaction between iodobenzene and cuprous bromide (CuBr + PhI $\leftrightharpoons$ CuI + PhBr) at 137°C in DMA. Equilibrium was initially observed for a reaction, involving stoichiometric amounts of reagents, which stopped at only 85% conversion, and then confirmed by approach to equilibrium from the other direction. Unfortunately, the limited range of accessible compositions made it difficult to determine whether the equilibrium was bimolecular (K_2 = ([CuI][PhBr])/([CuBr][PhI])) or 3/2-order ($K_{3/2}$ = $([CuI]^{1/2} \times [PhBr])/([CuBr]^{1/2}[PhI])$). Equilibrium constants calculated for 5 runs performed at different compositions averaged 14 ± 3 for K_2, and 6.5 ± 1.4 for $K_{3/2}$. A single run of the same I/Br exchange in sodium *ortho*-halobenzoates was performed at 53°C, giving $K_2 \sim 6.3$ and $K_{3/2} \sim 3.1$. Cyanodeiodination, in contrast, goes to >99.99% conversion.

The effect of *para*-substituent on reactions of the type ArI + CuCN → ArCN + CuI was negligible (the Hammett plot in Fig. 5 has a ρ value of −0.02 ± 0.08), and *ortho*-methyl or even -*tert*-butyl groups have very little effect, causing a mild acceleration, as reflected in the data in Scheme 1. The relatively large error in the reaction rate for 2,4,6-tri-*tert*-butylbromobenzene is due to side reactions, apparently dealkylation, which destroy the mass balance.

Ortho- and *para*-diiodobenzene react sequentially, first forming the monosubstituted iodobenzonitrile, which builds up to 40–60% yield before conversion into the disubstituted product. Rate data for fits of these reaction profiles (not shown) are as follows: for *p*-diiodobenzene, k_1 (first substitution) = 1.24×10^{-3} and k_2 (second substitution) = 5.26×10^{-4}; for *o*-diiodobenzene, $k_1 = 5.48 \times 10^{-3}$ and $k_2 = 5.99 \times 10^{-4}$ $L^{1/2}$ $mol^{-1/2}$ s^{-1} at 137°C in DMA. These rate constants were determined by Runge–Kutta fits of the reaction profiles (RMS error ~2–3%), and are not initial rate constants.

In contrast to the relatively minor impact of all *para*-substituents and *ortho*-methyl, -*tert*-butyl, -iodo, and -cyano groups, there is an enormous *ortho*-carboxylate effect, and a

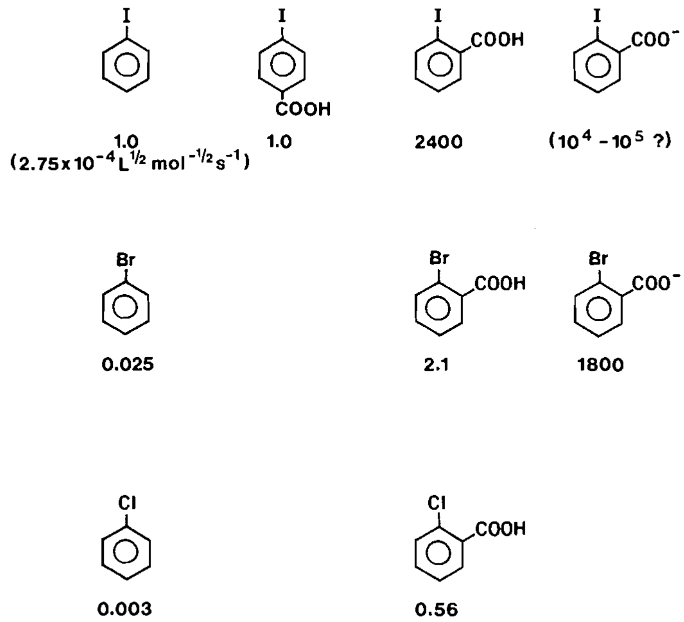

SCHEME 2. Relative rates of cyanodehalogenation at 137°C in DMA.

large halogen leaving group effect, as summarized in Scheme 2. The data in the scheme has been rendered to a common temperature, and the bracketted value for sodium 2-iodobenzoate has been estimated from the trend in the bromo series.

The reactivity of several cuprous salts was compared to CuCN to explore the effect of the nucleophile on the rate, and the results for nucleodeiodination are summarized in Table 3. Both CuBr and $CuBr_2$ react with PhI to form PhBr (Table 4). The addition of excess Br_2 to either reaction effectively inhibits the exchange, indicating an equilibrium of the type $CuBr_2 \rightleftarrows CuBr + 1/2\ Br_2$, where only CuBr is active in the ligand exchange reaction.

Discussion

Full reaction profiles, similar to the example in Fig. 1, were determined by analytical hplc, using an internal standard to test for the maintenance of a mass balance. Except where noted, the reactions were clean, and went to >99.99% conversion, with no side reactions detectable (hydrodehalogenation to form benzene: <0.5%; Ullmann coupling to form biphenyl: <0.02%). Mass balance failure occurred with some *ortho*-carboxylate systems and with 1,3,5-tri-*tert*-butylbromobenzene. These problems were attenuated somewhat by the use of initial rates.

Among the major identifiable classes of proposed mechanisms for copper mediated NAS reactions are the concerted mechanism, the benzyne mechanism, the $S_{RN}1$ radical chain mechanism (14), other non-chain electron transfer or radical mechanisms, and other forms of catalysed addition–elimination mechanisms. The concerted mechanism has frequently been proposed in the face of lack of evidence for any intermediates (particularly benzyne or radical ions (6, 7)). For example, the benzyne mechanism has been clearly ruled out by the well-known retention of position of substitution on the ring. Our unoriginal observation that copper mediated NAS is not inhibited by normal radical or electron traps rules out the $S_{RN}1$ mechanism (14) and any non-chain electron transfer or radical mechanism involving "free" radicals or radical ion intermediates. Furthermore, although we did observe weak esr signals at the beginning of a cyanodeiodination reaction, they were due to ~2% Cu^{2+} initially present in the CuCN (a common impurity in cuprous salts). The fact that cyanodeiodination of *o*- and *p*-diiodobenzene clearly occurs with the detectable buildup and decay of substantial amounts of the monocyano intermediate species also rules out the $S_{RN}1$ chain mechanism (14*a*, *c*).

TABLE 3. Relative reactivity of some cuprous nucleophiles in deiodinations

CuNu[a]	$[PhI]_0$ (*mM*)	Ratio $[CuNu]_0/[PhI]_0$	$k_{rel} \pm 10\%$
CuSPh[a]	13.3	7.5	7.5
CuBr[b]	18–53	0.4–7	6.2
CuCN[c]	18–46	2–8	1.0
CuCl	12.0	8.1	0.78
CuOAc[a]	15.3	8.5	<0.013[d]

[a] All CuNu species, except CuSPh and CuOAc, seemed completely soluble in DMA. The relative reactivity shown in the table assumes complete solubility.
[b] Average of 5 runs.
[c] Average of 11 runs. $k_{rel} = 2.75 \times 10^{-4}\ L^{1/2}\ mol^{-1/2}\ s^{-1}$.
[d] Yield of ~15% after 6 days.

TABLE 4. Comparison of bromodeiodination yields with CuBr and $CuBr_2$[a]

Reagent	$[Br_2]_0$ (*M*)	Ratio $[Cu]_0/[PhI]_0$	24-Hour yield of PhBr (%)
CuBr	—	0.53	91
$CuBr_2$	—	0.49	31
CuBr	0.16	0.54	9.5
$CuBr_2$	0.13	0.48	7

[a] All runs with $[PhI]_0 = 0.045\ M$; at $T = 135°C$.

The rate equation

Second-order kinetics normally prevail for exchange reactions run under homogeneous conditions,[3] but Fig. 2 shows that second-order plots had upward curvature, consistent with the observed mild catalysis by cuprous iodide. Because *n*, the order in CuCN, at 0.64, was closer to 1/2 than to 1, and because the mechanistically significant *relative* rates were insensitive to variations in *n*, all results have been reported in terms of a simpler 3/2-order rate equation ($n = 1/2$) for the *initial* rate.

More than a dozen kinetic models were tested on individual runs, with the best fits obtained by two-term equations of the form $v = k_1[PhI][CuCN]^n + k_2[PhI][CuI][CuCN]^n$ for $n = 1/2$ or 1 (RMS error ~0.3%). One possible interpretation of $n = 1/2$ could be reversible dissociation of inactive, largely dimeric Cu_2CN_2:

$$[9]\quad \underset{\text{inactive}}{Cu_2CN_2} \overset{K}{\rightleftarrows} \underset{\text{active}}{2\ CuCN} \xrightarrow{PhI} PhCN + CuX$$

$$[10]\quad K = [CuCN]^2/[Cu_2CN_2]$$

$$[11]\quad v = k[PhI][CuCN] \sim k[PhI]\ (K[CuCN]_{stoich})^{1/2}$$

[3] Bacon and Hill found second-order kinetics to prevail in most copper mediated ligand exchange processes (using $R \sim 2-10$), except for cyanodeiodination, where their second-order rate constant also increased with time (6). They did not attempt to explain the observation.

TABLE 5. Results of competitive reactions performed in DMA at 137°C. The ratio of absolute rate constants (determined from ordinary experiments) is shown in the last column for comparative purposes

Reaction competitors A	B	Co-reagent	Ratio $[A]_0/[B]_0$	$[ArI]_{tot}$ (mM)	Ratio $R = [CuNu]_0/[ArI]_0$	k_{rel} k_A/k_B Competition	k_{rel} k_A/k_B Absolute
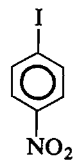	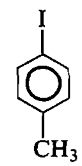	CuCN	0.79	42.4	1.5	2.0	1.6
			0.83	15.7	7.9	2.1	1.7
CuBr	CuCN	PhI	0.86	40.0	1.1	1.0	6.1
			0.85	42.3	1.1	1.2	6.1
			0.90	16.5	8.0	1.6	6.5
			1.02	17.4	7.4	1.8	6.5

if the extent of dissociation is small. CuCN may dimerize at low temperatures, or in the solid state (15); however, at 137°C in DMA solution, dissociation should be extensive for entropy reasons. Detailed curve fitting of reaction profiles to general kinetic models allowing this dissociation, with K as a second adjustable parameter, gave worse results than the two-term models above. Furthermore, if CuCN actually dimerizes in solution, some consideration of potential Cu_2ICN species would be required, further complicating the quantitative analysis. For all these reasons, the rate equation was not pursued further, and the following discussion relies on the initial rate measurements using the empirical 3/2-order rate equation. Fortunately, *the broad conclusions drawn from these results are independent of the precise form of the initial rate equation.* Furthermore, the impact of the third-order term describing CuI autocatalysis could be attenuated significantly by comparing initial rates for reactions run with excess cuprous cyanide ($[CuCN]_0/[PhI]_0 \sim 8$, which approaches pseudo-first-order kinetics).

One of the interesting features of the $S_{RN}1$ mechanism in particular, and chain reactions in general, is the observation that relative rates measured in competitive reactions are very much different than relative rates determined by the ratio of absolute rate constants (14*b*). We applied this test of mechanism to these reactions (Table 5). In competition of *p*-nitro and *p*-methyliodobenzenes for cuprous cyanide, the competitive rate ratio was about the same as the ratio of absolute rate constants (2.05 vs. 1.65; both $\pm$ 15%). However, when CuBr and CuCN competed for iodobenzene, the competitive rate ratio was smaller than the absolute rate ratio (1–2 vs. 6–7). Since CuI catalyses CuCN reactions, the combination of two cuprous nucleophile species in the same solution may give rise to complex interaction effects, making it doubtful that this rate ratio discrepancy indicates a chain component to the reaction mechanism. The role of cuprous iodide autocatalysis may be assistance for removal of halide ion in the rate-limiting step, forming CuI_2^- as a superior leaving group.

Effect of other added substances

Basic mechanistic information may often be garnered from the effect various substances have on reaction rates. There is a rather strong solvent effect on copper mediated ligand exchange reactions which has been attributed to the ability to dissolve and solvate the cuprous species (6). For example, the rate in DMA was one-half that in DMF. The cuprous nucleophiles are insoluble in solvents like hydrocarbons, chlorocarbons, ethers, etc., so there is no reaction in those solvents. Table 2 lists the impact of various substances added at 10 to 20 times the initial iodobenzene concentration. 5% Water in DMA accelerates the reaction about 60%, probably a solvent effect. Benzoic acid, methyl benzoate, and benzonitrile have essentially no effect on cyanodeiodination. The absence of any effect with PhCOOH appears to contradict results of Cohen on reaction of *o*-iodo-*N*,*N*-dimethylbenzamide with CuCl and CuCN, where benzoic acid diverts the reaction to hydrodehalogenation (8). Unfortunately, Cohen gives no details on which to base a discussion of this difference. Interestingly, the addition of either excess nucleophile, in the form of KCN, or excess leaving group, as KI, retards the rate significantly. This observation effectively rules out any dissociative mechanisms, which should show common ion effects.

Other features

Scheme 2 summarizes the impact of halogen on cyanodehalogenation reactions. For both ordinary and *o*-COOH substituted systems, aryl iodides are about 40–100 times more reactive than aryl bromides, which, in turn, are more reactive than aryl chlorides. This series parallels leaving group ability of the halide ions ($I^- > Br^- > Cl^-$), and has been interpreted as indicative of rate limiting CX rupture (5, 6). It is noteworthy that the opposite order of reactivity is observed for unmediated nucleophilic aromatic substitution, proceeding via the well known addition–elimination mechanism with rate limiting attack by the nucleophile on the activated aromatic ring (16). In contrast to the relatively large aromatic halide leaving group effect, the cuprous nucleophile effect is quite small for soluble cuprous salts (Table 3), again consistent with rate limiting breakdown of an intermediate.

There is mounting evidence that only cuprous ion is active in copper mediated reactions, although cupric reagents may sometimes give product (5, 17).[4] In the case of ligand exchange observed with cupric bromide, the formation of bromobenzene from iodobenzene was traced to a redox equilibrium (eq. [12]), followed by subsequent reaction of cuprous bromide (eq. [13]). Crude thermodynamic estimates indicate that eq. [12] is probably thermoneutral at 140°C ($\Delta H^0 \sim 9$ kcal mol^{-1} (18) but $\Delta S^0 \sim 20$ cal mol^{-1} K^{-1} gives $\Delta G^0 \sim 0$).

[12] $CuBr_2 \leftrightharpoons CuBr + 1/2\ Br_2$

[13] $CuBr + PhI \rightarrow PhBr + CuI$

[4] Also A. J. Paine, unpublished data.

The Hammett ρ value for cyanodeiodination was found to be zero, within experimental error, for 7 *para*-substituents (Fig. 5). Copper mediated reactions typically have ρ values in the range 0–1 (6, 7, 19). This is also in marked contrast to unmediated nucleophilic aromatic substitution, where electron withdrawing groups like nitro are required to stabilize the incipient negative charge as it develops on the ring during attack by the nucleophile, leading to ρ values of 3–5 (7, 20). Clearly the copper mediation results in a mechanism which completely avoids the build-up of negative charge.

The effect of *ortho*-alkyl groups on the reaction was probed with the idea that steric retardation might indicate a concerted mechanism, because the transition state would be very crowded. Interestingly, both *o*-methyl and *o-tert*-butyl groups demonstrate a mild steric *acceleration*, perhaps indicative of relief of steric strain in the transition state. Thus, the overall absence of steric retardation appears to speak against a fully concerted mechanism.

ortho-*Carboxylate effect*

In spite of the fact that electronic substituent effects and *ortho*-alkyl steric effects are small, there is a widely recognized *ortho*-carboxylate effect (1, 2, 6): sodium *ortho*-iodobenzoate reacts ~10^4–10^5 times faster than iodobenzene (Scheme 2). *p*-Carboxylate has no effect, and the *ortho* salt is about 40–100 times more reactive than the free acid. The trend is the same in the bromo and chloro series as well. Of particular interest here is whether the *ortho*-carboxylate acceleration occurs via the same basic mechanism or by a completely new mechanism. This problem was considered in detail, and the general features of the *ortho*-acid series were found to parallel those in the simple haloaromatic series in all aspects: the rate equation, the halogen effect, the effect of added substances, cuprous iodide autocatalysis, etc. Thus we conclude that the accelerated reactions must have essentially the same mechanism. What then accounts for the huge rate difference?

It appears that the difference is primarily in the activation *entropy*. The plot of activation parameters in Fig. 4 shows that iodobenzene, *ortho*-bromobenzoic acid, and sodium *ortho*-bromobenzoate reactions with cuprous cyanide give three essentially parallel lines (same $\Delta H^{\ddagger}$) with different intercepts, $\Delta S^{\ddagger}$ (see Table 1). The $\Delta S^{\ddagger}$ obtained for the reaction of iodobenzene with CuCN is ~−26 entropy units, typical of second-order reactions, and is associated with the need for the reagents to diffuse together. On the other hand, a much more entropically neutral $\Delta S^{\ddagger} \sim -12$ eu for reaction of bromocarboxylate with CuCN suggests that the two reagents are already substantially associated in the ground state (perhaps by complexation of cuprous ion in the vicinity of the halide leaving group). On the other hand, the *enthalpy* of activation, corresponding to the bond breaking and forming steps, is the same as for the normal copper mediated reaction (19–21 kcal).

Thermodynamics and reversibility

Thus far, the discussion has considered the results of kinetic measurements and presented some pseudo-thermodynamic parameters. It is also useful to examine the thermodynamic parameters, particularly with regard to potential reversibility of these processes. Table 6 shows the reaction enthalpies, ΔH^0, calculated for generalized bimolecular copper ligand exchange equilibria of the type shown, using the relatively rare literature data on these compounds (18). Although they are quite crude, these appear to be the first such thermodynamic estimates, presently limited to the cases X, Y = F, Cl, Br, I, CN, N_3, and

TABLE 6. Estimated reaction enthalpies for assumed bimolecular ligand exchange reactions. (The standard states are the solid and liquid phases for the cuprous and aromatic species, respectively. The units are kcal mol^{-1}.)

$$CuX + PhY \xrightarrow{\Delta H^0} PhX + CuY$$

NUCLEOPHILES

LEAVING GROUPS: Y \ X	F	Cl	Br	I	CN	N_3
F	○ 0	25	30	34	△ 6	10
Cl	○ -25	○ 0	△ 4	9	○ -19	○ -15
Br	○ -30	○ -4	○ 0	△ 4	○ -23	○ -19
I	○ -34	○ -9	○ -4	○ 0	○ -28	○ -24
CN	○ -6	19	23	28	○ 0	○ -4
N_3	○ -10	15	19	24	△ 4	○ 0

○ Feasible ($\Delta H^0 \leq 0$)

△ Possible ($0 \leq \Delta H^0 \leq 7$)

to solid or liquid standard states. The resulting table of 21 possible ligand exchange reactions is useful for correlation and prediction. For example, equilibrium constants, K_{eq}, may be estimated using the relation $\Delta H^0 \sim -RT \ln K_{eq}$ (assuming $\Delta S^0 \sim 0$). If ΔH is too large (>5 kcal mol^{-1}) then the reaction is predicted to be too endothermic to be feasible. If ΔH is negative, then the reaction becomes thermodynamically possible (but may still be kinetically slow). Synthetically useful reactions must be thermodynamically downhill, and, indeed, cyanodehalogenation is found to be so. In cases where $\Delta H \sim 0$, reversible equilibria may result, lowering the synthetic yield. For example, Table 6 predicts possible equilibria for Cl/Br or Br/I exchange, which was tested in the latter case, measuring $\Delta H^0 = -2.15$ kcal mol^{-1} (vs. prediction of -4 ± 2 in Table 6). This appears to be the first fully established case of reversibility in these reactions and it reinforces the notion that the proposed mechanism must have a *symmetrical*, high energy intermediate or transition state, which does not distinguish between the nucleophile and the leaving group.

The thermodynamic data in Table 6 show the following leaving group order: I > Br > Cl (> N_3 > CN > F); where the last 3 are usually endothermic. This series agrees with the kinetic leaving group ability. The thermodynamic nucleophilic reactivity is in the reverse order (obviously), but the kinetic nucleophile effects (SPh ≥ Br > CN ~ Cl, Table 3) are much smaller than the kinetic leaving group effects. This series differs from the kinetic nucleodebromination results of Bacon (6): Cl > Br > I > CN ~ SPh > SCN. Thus, it is evident that both thermodynamic considerations ($\Delta H < 0$) and kinetic considerations ($k_{ArI} > k_{ArBr}$) are required to design practical syntheses using copper mediated NAS.

Reaction mechanism

Any proposed mechanism must account for the following:

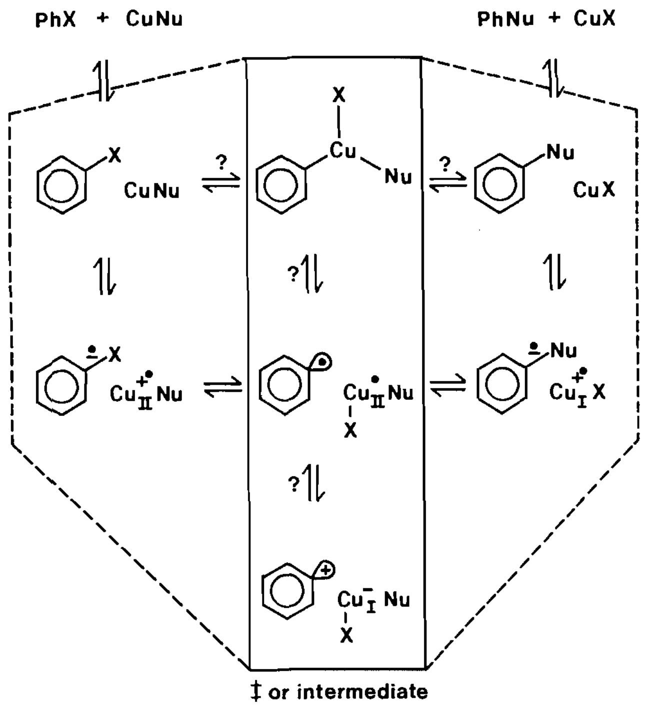

SCHEME 3. Intimate electron transfer mechanism for copper mediated NAS.

the halogen effect; the lack of *para*-substituent effect; the negligible *ortho* steric effect; entropic acceleration by *ortho*-carboxylate (but not by *para*-carboxylate); absence of radical chains or free radicals; cuprous iodide autocatalysis; and the retarding effect of potassium cyanide and postassium iodide. Finally, any proposed mechanism must obey the Principle of Microscopic Reversibility, and because of the symmetry of the ligand exchange, must involve a symmetrical transition state or intermediate which does not distinguish between the incoming nucleophile and the leaving group. It is in fact quite difficult to propose a chemically reasonable mechanism consistent with all these requirements, and this may explain why the literature abounds with concerted mechanisms. However, at this stage, we propose two fairly reasonable working hypotheses which are offered to stimulate further research.

Intimate electron transfer mechanism

The first alternative to a fully concerted mechanism is a special kind of electron transfer mechanism. More and more nucleophilic reactions are found to involve electron transfer instead of nucleophilic attack. In this system, however, the absence of any effect of electron traps means that electron transfers which do occur must be very rapidly reversible, or rapidly product generating, so that no "free" radical ions escape the solvent cage. Thus, a mechanism also capable of accounting for many of the results is shown in Scheme 3: cuprous nucleophile and aromatic halide drift around in solution until they come together in an encounter complex in a solvent cage. Such complexes have lifetimes of 500–1000 vibrations, during which time the action inside the large dotted area in the scheme must occur.

Suppose there were an electron transfer from the cuprous nucleophile to the aromatic halide. Such a transfer should be to the σ^* orbital, as opposed to a π^* orbital, because diiodo substrates first give monosubstituted products (a classical test to rule out the $S_{RN}1$ electron transfer mechanism (14*a*, *c*)). This radical ion then gives up a halide ion to form a cupric odd-electron species and a phenyl radical, still trapped in the same solvent cage. Presumably the interaction between these proximate unpaired electrons stabilizes the complex, and perhaps leads to bonding, giving rise to the possibility of the tri-substituted organocopper intermediate shown in the top centre of the scheme.[5] Whatever the form of the symmetrical intermediate shown in the central box, it merely reverses the formation process to give the ligand exchanged material.

This associative mechanism for ligand exchange has the advantage that leakage of phenyl radical can explain the benzene which is sometimes observed as a hydrodehalogenation side product (2). Also, cupric copper might further oxidize the phenyl radical to a cation, perhaps accounting for dealkyation in *tert*-butylated substrates. An electron transfer mechanism of this type might have less rigid stereochemical requirements than a concerted mechanism. Both KI and KCN retard the reaction by competing with ArX as ligands for the cuprous ion. Finally, the *entropic* role of the *ortho*-carboxylate substituent in this mechanism would be to complex the cuprous and cupric ions in the vicinity of the halide, thereby extending the lifetime of the encounter complex in the solvent cage, and increasing the probability of reaction. (The *enthalpic* role of *ortho*-carboxylate, if any, would be to stabilize the transition state by complexation with the copper.) On the other hand, the problems with this mechanism are: (a) the need for intimacy of electron transfer; and (b) the need for electron transfer to the σ^* vs. π^* orbital.

π-Complexed organocuprate intermediates

Another mechanism capable of rationalizing many of the experimental results is a refined version of Weingarten's proposal (5) involving π-complexed organocuprate intermediates (eq. [14]). The key intermediate in this process is the h^6, 18-electron complex between the cuprous nucleophile and the 6 π-electrons of the aryl halide (cuprous ion is d_{10}). From this complex, intramolecular attack of the nucleophile gives the tetrahedral intermediate, where the negative charge that would otherwise be borne in the ring, is neutralized by the 16-electron π-complexed copper atom, which sucks all of the excess electron density out of the ring (hence no substituent effect). The rate determining step would be loss of halide, followed by rapid collapse to final products.

[14] 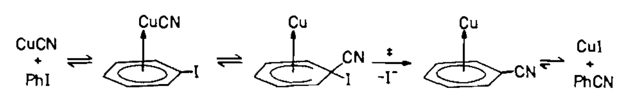

This mechanism offers a ready explanation for the retarding effect of KCN and KI, which are known to form higher coordinate anions ($Cu(CN)_2^-$ or $CuCNI^-$ (21)) which would be inactive in this model because they already have 14 electrons, and therefore cannot form the necessary h^6 18-electron complex.

This mechanism appears to be supported by parallels to nucleophilic aromatic substitution reactions in stable iron, chromium, molybdenum, and manganese arene carbonyl complexes known in the literature (5, 22). In fact, the tetrahedral

[5] A referee has noted that thermodynamic E^0 values for electron transfer from cuprous species to iodobenzenes are ~2 eV (i.e. at least twice as great as the enthalpy of activation of the ligand exchange process). However, the E^0 values refer to separated ions in solution, and stabilization within the cage (particularly if bonding is involved) could lower the activation energy from the E^0 value.

intermediate in eq. [15] has been isolated and characterized by X-ray crystallography (22c). Cuprous h^6 complexes are rare (23), but not unknown (24). Unfortunately, the arene carbonyl complexes undergo NAS with the following leaving group order: F > Cl > Br, opposite to that observed here (22). To account for this apparently conflicting order of reactivity, complexation of CuNu and ArX would have to be favoured in the order I ≫ Br ≫ Cl, in order to overcome the reactivity preference of the complex. If that were so, one would expect a larger substituent effect in general, because h^6 complexation should see the halide as just another substituent. Thus, this inconsistency diminishes the value of the parallel to other transition metal arene complexes.

[15] 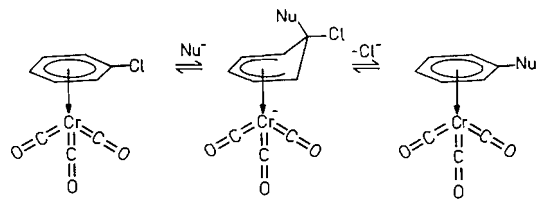

There are some minor problems with microscopic reversibility in the simple picture in eq. [14], but they can be overcome if the stereochemical integrity at the ipso carbon is allowed to scramble by reversible halide loss.

There are two possible explanations for the *ortho*-carboxylate effect in this reaction, both based on anchimeric assistance (25). The *ortho*-carboxylate may displace halide first, facilitating attack by cyanide (eq. [16]), or the carboxylate might assist removal of iodide, without ipso scrambling, through formation of a transient carboxyl hypoiodite (eq. [17]).

[16] 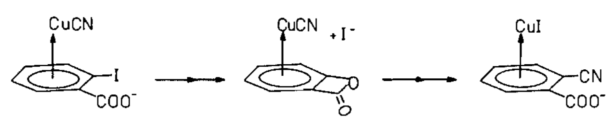

[17] 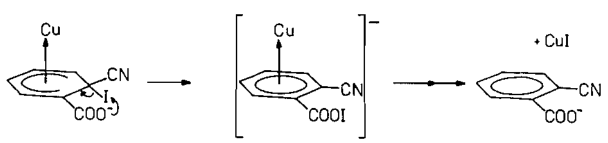

Neither of these possibilities is well supported at present: the first because of the strained 4-membered ring β-lactone intermediate (~25 kcal uphill (26)); and the second because of the extra electron density pushed into the ring upon formation of the hypoiodite. Furthermore, any anchimeric assistance mechanism is inconsistent with the *increased* (less negative) entropy of activation observed for *ortho*-carboxylate systems. $\Delta S^{\ddagger}$ should *decrease* for anchimeric assistance because of the loss of entropy on forming the 4- or 5-membered ring transition state or intermediate ($\Delta S^0_{\mathrm{cyclization}} \sim -(10-15)$ eu (26)), so the primary neighbouring group effect in this kind of reaction should be on $\Delta H^{\ddagger}$. Attractive though these anchimeric assistance explanations are for the *ortho*-carboxylate effect, they seem to be inconsistent with the observed activation parameter data.[6]

Thus, the problems with the π-complexed organocuprate intermediate mechanism are: (a) questionable parallels to NAS in other transition metal arene complexes; and (b) the inability to rationalize the *ortho*-carboxylate effect.

Final comments

Both of these mechanisms implicitly assume that CuNu is monomeric in solution. This is a crucial requirement for the *active* species in the π-complexed organocuprate proposal, but may be relaxed for the intimate electron transfer mechanism. Although the assumption is both reasonable and common, the problems with defining the rate equation serve as a reminder that this was an assumption, and may not be true.

A key mechanistic question is the nature of the initial interaction of ArX with CuNu: is it halogen complexation or π-type complexation? An obvious way to attempt to measure the relative affinity of cuprous ion for X or Ar in ArX would be through a systematic study of the solubility of cuprous salts in various ArX (e.g. PhH, PhI, PhBr, PhCl, 2,4,6-tri-*tert*-butylbromobenzene, etc.). If solubility were assumed a direct consequence of complexation, then trends in the solubilities would indicate the site of complexation. Attractive as this idea might seem, cuprous iodide was found to be insoluble in iodobenzene, for example, with a probable solubility of $<10^{-6}$ *M*, indicating an enthalpy barrier to dissolution and complexation of $> -RT \ln([\mathrm{CuI}]/[\mathrm{PhI}]) = 9.6$ kcal mol^{-1} at 25°C. (Compare to $\Delta H^0 \sim 2.9$ kcal for CuI in acetonitrile (35 g/kg solution (21))). These enthalpy numbers are *composite* figures, accounting for overcoming lattice energy *and* forming the complex, but the lattice energy term is the same for dissolution in either solvent, so complexation of CuI with PhI is >6.7 kcal more endothermic than complexation with CH_3CN. Thus it is not surprising that there is no reported spectroscopic evidence for complexed intermediates in these exchange reactions.

Although the 170 runs reported here probably constitute the most thorough investigation of copper mediated ligand exchange reactions to date, they are not adequate to completely specify the operable mechanism. Two working hypothesis mechanisms have emerged which should be further tested and refined. Further progress on this complex issue requires: a clarified rate equation from a clearer definition of the copper species in solution (monomer/dimer/oligomer and solvation state); more accurate thermodynamic estimates (particularly experimental data on other CuNu species); a better unravelling of entropy and enthalpy rate effects (via more accurate activation parameters); and measurement of association equilibria of CuNu with $ArCOO^-$. Furthermore, theoretical calculations may have some relevant input. The π-complexation mechanism may be tested by intramolecular reactions (systems which are sufficiently inflexible that CuNu cannot lie over the aromatic ring of ArX).[7]

Neither of the proposed mechanisms is completely satisfactory. Perhaps there is a combination process where initial halogen–copper complexation evolves into h^6 complexation. Given the plethora of mechanisms for unmediated NAS (28), it is possible that more than one mechanism operates in mediated reactions as well. These very interesting and useful processes pose an extremely complex and difficult problem, but new light has been shed on the issue and promising research directions identified.

[6] It may be that this inconsistency arises from the comparison of iodo and bromo aromatics in Fig. 4. A more accurate comparison would employ the same halogen.

[7] In fact, some intramolecular reactions are known (23, 27), but to interpret the results requires good models for intermolecular rates. Some of the known examples involve substrates which appear to be sufficiently flexible to position CuNu over the aromatic ring anyway.

1. (*a*) F. TERRIER. Chem. Rev. **82**, 77 (1982); (*b*) J. F. BUNNETT and R. E. ZAHLER. Chem. Rev. **49**, 392 (1951).
2. R. G. R. BACON and H. A. O. HILL. Q. Rev. 95 (1965).
3. T. YAMAMOTO and Y. KURATA. Can. J. Chem. **61**, 86 (1983).
4. T. KAWAKI and H. HASHIMOTO. Bull. Chem. Soc. Jpn. **45**, 1499 (1972).
5. H. WEINGARTEN. J. Org. Chem. **29**, 3624 (1964).
6. R. G. R. BACON and H. A. O. HILL. J. Chem. Soc. 1097 (1964).
7. V. V. LITVAK and S. M. SHEIN. J. Org. Chem. USSR **10**, 555 (1974); **10**, 2373 (1974).
8. T. COHEN, J. WOOD, and A. G. DIETZ, JR. Tetrahedron Lett. 3555 (1974).
9. D. E. PEARSON, M. G. FRAZER, V. S. FRAZER, and L. C. WASHBURN. Synthesis, 621 (1976).
10. T. I. MARTIN, P. SZABO, and S. R. TURNER. US Patent No. 4,240,987 (1980).
11. A. MCKILLOP, J. S. FOWLER, M. J. ZELESKO, J. D. HUNT, E. C. TAYLOR, and G. MCGILLIVRAY. Tetrahedron Lett. 2427 (1969).
12. W. RUNDEL. Chem. Ber. **108**, 1779 (1975).
13. H. EYRING. Chem. Rev. **17**, 65 (1935).
14. (*a*) R. A. ROSSI. Acc. Chem. Res. **15**, 164 (1982); (*b*) R. G. SCAMEHORN and J. F. BUNNETT. J. Org. Chem. **44**, 2604 (1979); (*c*) J. F. BUNNETT. Acc. Chem. Res. **11**, 413 (1978); (*d*) R. G. SCAMEHORN and J. F. BUNNETT. J. Org. Chem. **42**, 1449 (1977).
15. (*a*) A. WERNER, P. FERCHLAND, W. SCHMUJLOW, A. MAIBORN, and M. STEPHANI. Z. Anorg. Chem. **15**, 1 (1897); (*b*) E. BECKMANN and W. GABEL. Z. Anorg. Chem. **51**, 236 (1906).
16. J. F. BUNNETT, E. W. GARBISCH, JR., and K. M. PRUITT. J. Am. Chem. Soc. **79**, 385 (1957).
17. T. D. HUONG and M. HIDA. Bull. Chem. Soc. Jpn. **44**, 765 (1971).
18. (*a*) J. A. DEAN (*Editor*). Lange's handbook of chemistry. 12th ed. McGraw Hill Co., New York, NY. 1979. pp. 9–20; (*b*) J. D. COX and G. PILCHER. Thermochemistry of organic and organometallic compounds. Academic Press, London, UK. 1970.
19. V. I. STANKO and N. G. IROSHNIKOVA. Zh. Obshch. Khim. **49**, 2076 (1979).
20. D. M. BREWIS, N. B. CHAPMAN, J. S. PAINE, and J. SHORTER. J. Chem. Soc. Perkin Trans. 2, 1802 (1974).
21. F. A. COTTON and G. WILKINSON. Advanced inorganic chemistry. 3rd ed. Wiley–Interscience, New York, NY. 1972. pp. 903–922.
22. (*a*) A. C. KNIPE, S. J. MCGUINNESS, and W. E. WATTS. J. Chem. Soc. Chem. Commun. 842 (1979); (*b*) P. J. C. WALKER and R. J. MAWBY. Inorg. Chim. Acta, **7**, 621 (1973); (*c*) M. F. SEMMELHACK, H. T. HALL, JR., R. FARINA, M. YOSHIFUJI, G. CLARK, T. BARGAR, K. HIROTSU, and J. CLARDY. J. Am. Chem. Soc. **101**, 3535 (1979); (*d*) V. V. LITVAK, L. S. FILATOVA, G. A. SELIVANOVA, and V. D. SHTEINGARTS. J. Org. Chem. USSR **16**, 303 (1978); (*e*) A. ALEMAGNA, P. D. BUTTERO, C. GORINI, D. LANDINI, E. LICANDRO, and S. MAIORANA. J. Org. Chem. **48**, 605 (1983).
23. (*a*) W. CARRUTHERS. *In* Comprehensive organometallic chemistry, Vol. 7. *Edited by* G. Wilkinson. Pergammon Press, Oxford, UK. 1982. Chapt. 49. pp. 661–729; (*b*) G. VAN KOTEN and J. G. NOLTES. *In* Comprehensive organometallic chemistry, Vol. 2. *Edited by* G. Wilkinson. Pergammon Press, Oxford, UK. 1982. Chapt. 14. pp. 709–763; (*c*) A. CAMUS, N. MARSICH, G. NARDIN, and L. RANDACCIO. Inorg. Chem. Acta, **23**, 131 (1977).
24. F. A. COTTON and T. J. MARKS. J. Am. Chem. Soc. **91**, 7281 (1969).
25. B. CAPON and S. P. MCMANUS. Neighboring group participation. Plenum Press, New York, NY. 1976.
26. M. I. PAGE. Chem. Soc. Rev. **2**, 295 (1973).
27. R. JOYEAU, Y. DUGENET, and M. WAKSELMAN. J. Chem. Soc. Chem. Commun. 431 (1983).
28. C. F. BERNASCONI. Chimia, **34**, 1 (1980).

Kinetics and equilibrium in the ammonolysis of substituted phthalimides

ROBERT A. MCCLELLAND AND N. ESTHER SEAMAN
Department of Chemistry, University of Toronto, Toronto, Ont., Canada M5S 1A1

AND

JAMES M. DUFF AND R. E. BRANSTON
Xerox Research Centre of Canada, 2660 Speakman Drive, Mississauga, Ont., Canada L5K 2L1

Received April 16, 1984

This paper is dedicated to the 10th anniversary of the Xerox Research Centre of Canada

ROBERT A. MCCLELLAND, N. ESTHER SEAMAN, JAMES M. DUFF, and R. E. BRANSTON. Can. J. Chem. **63**, 121 (1985).

Kinetic studies are reported for the base hydrolysis to phthalamic acid anions (H) and ammonolysis to phthalamides (A) for seven phthalimides (P): **1**, unsubstituted; **2**, 4-NO_2; **3**, 4-Cl; **4**, 4-*t*Bu; **5**, 3-NO_2; **6**, 3-Me; **7**, 3-Me_3Si. The hydrolysis kinetics require two mechanisms, one which is first order in neutral imide and first order in hydroxide ion, and a second, which is important only in quite concentrated NaOH, which is first order in neutral phthalimide and second order in hydroxide ion. Ammonolysis kinetics for **1–5** revealed the rate law: Rate = k_N [Unionized phthalimide] $[NH_3][OH^-]$. A mechanism is proposed with rate-determining breakdown of the anionic form of the tetrahedral intermediate derived by addition of NH_3 to the phthalimide. The ammonolysis is reversible. The phthalamide hydrolyzes to the phthalamic acid via cyclization to an intermediate phthalimide, which is detected in concentrated base where its formation from phthalamide is more rapid than its subsequent hydrolysis. Rate constants for the cyclization follow the rate law: Rate = k_{cyc} [Phthalamide]$[OH^-]$. This reaction is the microscopic reverse of the ammonolysis, and the ratio k_N/k_{cyc} provides the equilibrium constant K_{eq} for the reaction P + NH_3 = A. Values for **1–5** lie in the range $2 \times 10^2 - 4 \times 10^3$. With 3-methylphthalimide, kinetics in aqueous ammonia do not obey a first-order relationship, but they could be analyzed by a scheme whereby the phthalimide is converted reversibly to the phthalamide and simultaneously undergoes an irreversible hydrolysis. The value of K_{eq} in the system is 1.8. With 3-trimethylsilylphthalimide the value of K_{eq} is further reduced to 0.01. The ammonolysis reaction does occur more quickly than hydrolysis but the equilibrium is so unfavorable that even in concentrated ammonia only a small amount of the phthalamide is ever formed.

ROBERT A. MCCLELLAND, N. ESTHER SEAMAN, JAMES M. DUFF et R. E. BRANSTON. Can. J. Chem. **63**, 121 (1985).

On rapporte des études cinétiques relatives à l'hydrolyse basique conduisant aux anions de l'acide phtalamique (H) ainsi qu'à l'ammonolyse conduisant aux phtalamides (A) de sept phtalimides (P) soit non substituée **1** ou substituées par des groupements NO_2-4 **2**, Cl-4 **3**, *t*-Bu-4 **4**, NO_2-3 **5**, Me-3 **6**, Me_3Si-3 **7**. Les cinétiques d'hydrolyse nécessitent deux mécanismes dont l'un est d'ordre un en imide neutre et d'ordre un en ions hydroxydes alors que le deuxième mécanisme, qui n'est important qu'en milieu très concentré en NaOH, est d'ordre un en phtalimide neutre et d'ordre deux en ion hydroxyde. La loi de vitesse des cinétiques d'ammonolyse des composés **1–5** peut être représentée par l'équation suivante: Vitesse = k_N [Phtalimide non ionisée]$[NH_3][OH^-]$. On propose un mécanisme dont l'étape déterminante est la rupture de la forme anionique de l'intermédiaire tétraédrique provenant de l'addition du NH_3 sur la phtalimide. L'ammonolyse est réversible. La phtalamide s'hydrolyse en acide phtalamique par le biais d'une cyclisation conduisant à une phtalimide intermédiaire que l'on peut déceler lorsque la réaction est réalisée en présence de base concentrée; dans ces conditions la formation de cet intermédiaire est plus rapide que son hydrolyse subséquente. Les constantes de vitesse pour la cyclisation peuvent être représentées par l'équation suivante: Vitesse = k_{cyc} [Phtalamide]$[OH^-]$. Sur une base microscopique, cette réaction constitue l'inverse de l'ammonolyse et le rapport k_N/k_{cyc} fournit la constante d'équilibre K_{eq} de la réaction P + NH_3 = A. Les valeurs de K_{eq} pour les composés **1** à **5** s'étalent de 2×10^2 à 4×10^3. Dans le cas de la méthyl-3 phtalimide en milieu ammoniacal aqueux, la cinétique n'obéit pas à la relation d'ordre un; on peut toutefois rationaliser ses données cinétiques en faisant appel à un mécanisme impliquant une transformation réversible de la phtalimide en phtalamide accompagnée d'une hydrolyse irréversible simultanée. La valeur de K_{eq} dans ce système est égale à 1,8. Dans le cas de la triméthylsilyl-3 phtalimide, la valeur de K_{eq} est réduite à 0,01. La réaction d'ammonolyse est plus rapide que celle d'hydrolyse mais l'équilibre est tellement défavorisé que, même en milieu ammoniacal concentré, il ne se forme que de très faibles quantités de phtalamide.

[Traduit par le journal]

Introduction

As well as being one of the most commonly used types of blue-green organic colourants, the phthalocyanine class of compounds are used in a number of electronic applications as a result of their well-known semiconductive properties (1). As part of a systematic investigation of the effect of substituents on the optical and electronic properties of phthalocyanines we have synthesized and characterized a variety of substituted phthalocyanines (J. M. Duff and R. E. Branston, unpublished results). The general route chosen involved as many as 6 steps (*o*-xylene → phthalic acid → phthalic anhydride → phthalimide → phthalamide → phthalonitrile → phthalocyanine), depending on the availability of starting materials. While most of these reactions proceeded as expected and we were able to devise optimized syntheses for most intermediates, a pronounced substituent effect, particularly at the 3-position, was found in the aqueous ammonolysis of phthalimide to phthalamide. Thus the unsubstituted phthalimide, all 4-substituted compounds studied, and the 3-nitro compound gave excellent yields of the corresponding diamide. The 3-methylphthalamide was finally synthesized in reasonable yield in a pressure reactor using liquid ammonia at 90°C. On the other hand, numerous attempts to convert the 3-trimethylsilylphthalimide to the amide in ammonia at a variety of pressures and temperatures afforded, at best, a few percent of amide (spectroscopically identified), which spontaneously formed the imide at room temperature.[1]

We report here a kinetic study of the aqueous ammonolysis (eq. [1]) undertaken in order to evaluate the effect of substituents on the course of the reaction, particularly substituents at the 3-position.

[1] 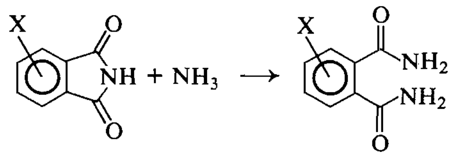

Seven phthalimides have been subjected to investigations: X = H (**1**); 4-NO_2 (**2**); 4-Cl (**3**); 4-*t*-Bu (**4**); 3-NO_2 (**5**); 3-Me (**6**); 3-Me_3Si (**7**).

Results and discussion

Kinetic studies were conducted using uv spectroscopy, monitoring the disappearance (or appearance) of the phthalimide at its λ_{max} near 300 nm. As illustrated in Fig. 1, neither the phthalamide product of ammonolysis nor the phthalamic acid anion product of hydrolysis have significant absorbance at this wavelength (with the exception of the two nitro compounds). Imide concentrations were 10^{-3} molar or less, ensuring pseudo-first-order conditions of constant pH and ammonia concentration. Conditions in general were aqueous solutions at 25.0°C and 1 *M* ionic strength. The exception is the 3-Me_3Si derivative, which for solubility reasons was studied in 25% acetonitrile. The parent phthalimide was also studied in this solution for comparison purposes.

Hydrolysis kinetics

Hydrolysis of the phthalimides to phthalamic acids competes with ammonolysis under aqueous conditions, and its importance obviously needs to be evaluated. A number of studies of imide hydrolysis have appeared (4–7), although a detailed investigation involving a series of substituted phthalimides has not been carried out. The hydrolysis was investigated in sodium hydroxide solutions (pH > 11), carbonate buffers (pH 8.5–11), and phosphate buffers (pH 7.8–8.5). Excellent pseudo-first-order kinetic plots were obtained in all cases. Weak catalysis by the carbonate and phosphate buffers was observed. In these cases observed rate constants were extrapolated to zero buffer concentration or obtained in dilute buffers (0.005–0.01 *M*) where catalysis is unimportant. (Even in 0.5 *M* buffer solutions the contributions to the overall rate from the buffer catalysis is only of the order of 10–20%.) Typical plots showing the variation of the first-order rate constant with pH are shown in Fig. 2. Three separate regions can be observed in these profiles, a region A at low pH with a first-order dependence in hydroxide ion, which gives way in more concentrated base to a pH-independent region B, followed then in very concentrated base by a region C, again with a first-order dependence on hydroxide ion. The last region is most pronounced with electron-withdrawing substituents, and is not observed with the 3-Me_3Si substituent.

The general behaviour exhibited in weakly basic solutions,

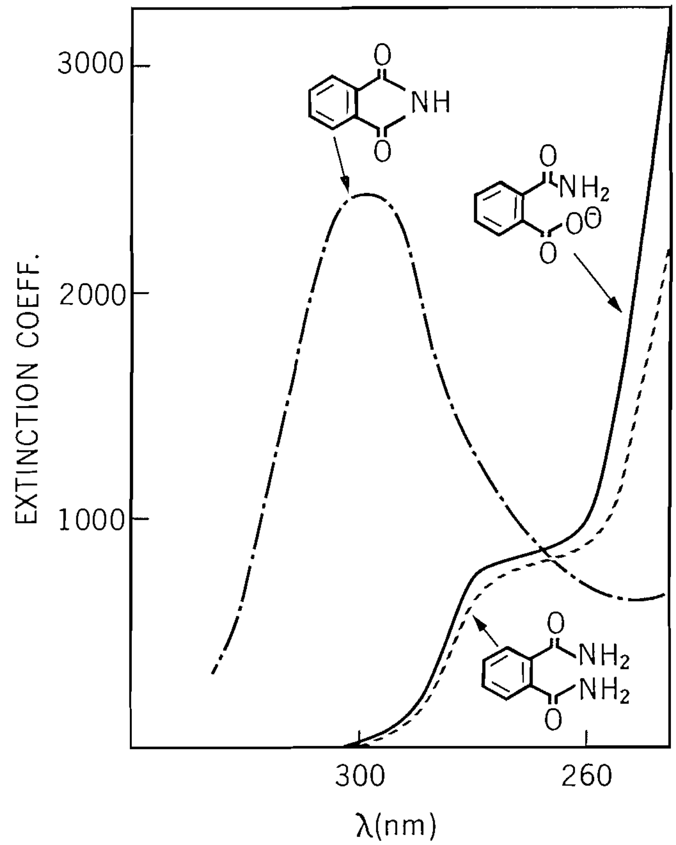

FIG. 1. Ultraviolet spectra of phthalimide and its products of ammonolysis and hydrolysis.

regions A and B, has been observed previously (4), and is explained by the reaction of hydroxide ion and the neutral phthalimide, with deprotonation of the imide occurring around pH 9–10, so that the rate constant levels, once the unreactive phthalimide ion is formed.

[2] 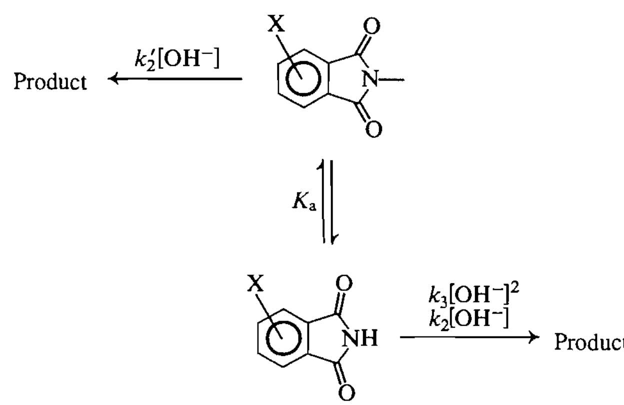

The additional dependency on hydroxide ion observed in more concentrated base solution has been reported for the parent phthalimide on two occasions (5, 7). Butler (5) suggested that this was associated with the reaction of hydroxide ion with the phthalimide anion (k_2' process of eq. [2]), while Khan and Khan (6) favoured a kinetically equivalent reaction which is first order in unionized phthalimide and second order in hydroxide ion (k_3 process of eq. [2]). The latter interpretation seems more likely in light of the large number of studies of amide and anilide hydrolysis which have shown second-order terms in hydroxide ion (8). We have removed the ambiguity in

[1] These results are in conflict with those of Hopff and Gallegra (3), who describe the synthesis of both 3- and 4-trimethylsilylphthalamide in high yield using aqueous ammonia. Our results suggest that the 3-substituted amide was not formed as claimed and that the nitrile and phthalocyanine subsequently prepared from this material are of questionable existence.

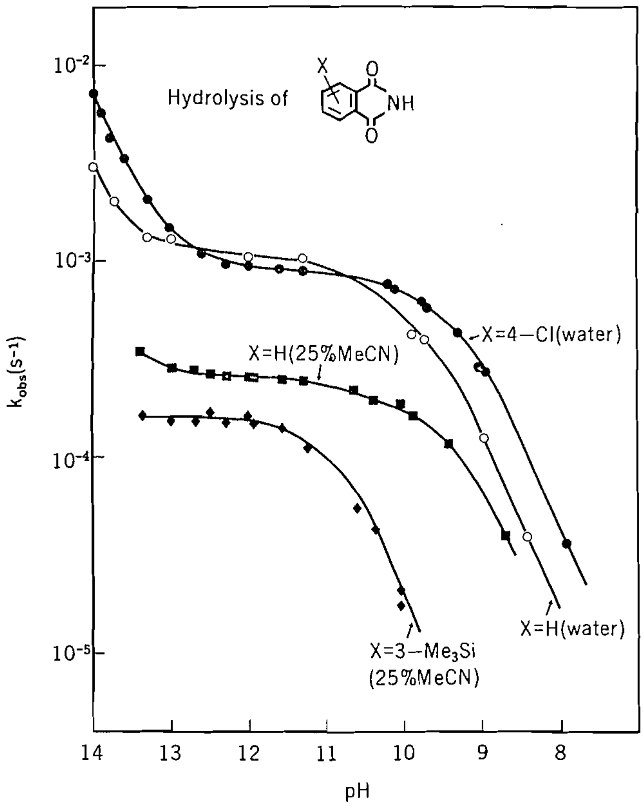

FIG. 2. Rate–pH profiles for phthalimide hydrolysis. Points are experimental. Curves are drawn according to eq. [4] using constants defined in Table 1.

the present case by studying *N*-methylphthalimide, an imide which cannot ionize. First- and second-order terms in hydroxide ion are required in the rate law for this imide, eq. [3],

[3] $\text{Rate} = (k^2_{\text{OH}}[\text{OH}^-] + k^3_{\text{OH}}[\text{OH}^-]^2)\,(N\text{-methylphthalimide})$

with $k^2_{\text{OH}} = 22.8\ M^{-1}\ s^{-1}$ and $k^3_{\text{OH}} = 8.0\ M^{-1}\ s^{-1}$. Mechanistically the overall third-order process is explained (7, 8) by a rate-determining decomposition of the dianionic form of the tetrahedral intermediate.

[4]
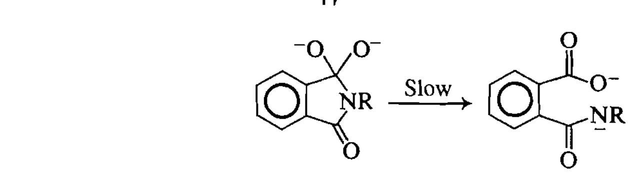

The following rate expression accounts for the overall rate profiles in terms of constants defined in eq. [2].

[5] $$k_{\text{obs}} = \frac{k_2[\text{OH}^-] + k_3[\text{OH}^-]^2}{1 + (K_a/K_w)[\text{OH}^-]}$$

Using an iterative computer program, values of k_2, k_3, and K_a

TABLE 1. Rate constants for the hydrolysis of substituted phthalimides and kinetically determined dissociation constants (T = 25°C, ionic strength = 1.0)

Substituent	k_2, $M^{-1}\ s^{-1}$	k_3, $M^{-2}\ s^{-1}$	pK_a
4-NO_2	65.1	3.3×10^3	8.68
4-Cl	14.4	100	9.48
H	4.8	8.5	10.06
4-*t*Bu	2.9	4.4	10.21
3-NO_2	85.6	2.9×10^3	8.80
3-Me	1.69	1.50	10.49
3-Me_3Si (25% MeCN)	0.23	—	11.2
H (25% MeCN)	4.3	7.2	10.1

have been determined that provide the best fit to the experimental data. These are listed in Table 1. Hammett ρ values based on the data for the 4-substituted phthalimides[2] are 1.5 (±0.2) for k_2 and 3.4 (±0.2) for k_3. These reflect the different charge nature of the transition states for these two processes, a monoanionic transition state being involved with the k_2 process and the dianionic transition state of eq. [4] for k_3.

Ammonolysis kinetics – normal behaviour

In these experiments the disappearance of the phthalimide was monitored as a function of time in NH_4^+/NH_3 buffers. With the exception of the 3-Me and 3-Me_3Si phthalimides, excellent pseudo-first-order kinetic plots are observed, and in concentrated (1 *M*) buffers, the rate is significantly faster (by factors of about 10) than the hydrolysis rate at the same pH. This increase in rate can be attributed to the ammonolysis reaction of eq. [1]. The possibility does exist that some fraction of this rate increase is due to an ammonia-catalyzed hydrolysis, that is, ammonia acting as a general base, not a nucleophile. We feel, however, that this contribution cannot be very important. Excellent yields of phthalamides are obtained in aqueous ammonolysis. Moreover, general base catalysis by carbonate buffers is very small.

Serial buffer dilutions at constant pH were carried out for ammonia buffers with NH_4^+/NH_3 concentration ratios varying from 4:1 to 1:4. At constant pH the pseudo-first-order rate constant for phthalimide disappearance increases in a linear fashion with increasing NH_3 concentration (see Fig. 3).

$$K_{\text{obs}} = k^{\text{app}}_{\text{NH}_3}[\text{NH}_3] + k_0$$

The intercept rate constants k_0 obviously refer to hydrolysis, and these values do fit well into the hydrolysis rate profiles. The term in NH_3 represents the ammonolysis, and the feature of this is that the apparent second-order rate constants $k^{\text{app}}_{\text{NH}_3}$ are not constant, but increase with increasing pH (see insert to Fig. 3). This occurs in spite of a decreasing concentration of the neutral phthalimide, since the pH values of the ammonia buffers lie in the range 9–10 where the phthalimides are becoming ionized. The kinetics are, however, satisfied by a third-order ammonolysis, first order in neutral phthalimide, first order in ammonia, and first order in hydroxide ion. Taking into account the phthalimide ionization, the overall rate expression for ammonolysis becomes

[2] The σ values employed in determining this parameter are 0.76 (4-NO_2), 0.30 (4-Cl), 0 (H), and −0.14 (4-*t*Bu). These are the average of the *meta* and *para* values of the particular substituents. In the unsymmetrical phthalimides it was not determined to which carbonyl group the hydroxide anion or ammonia becomes attached.

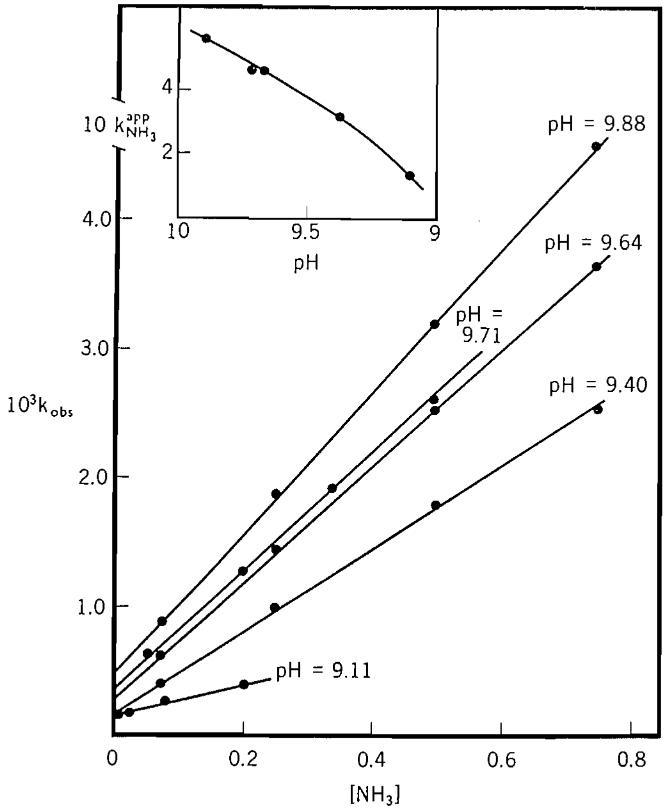

FIG. 3. Pseudo-first-order rate constants (s^{-1}, 25°C, ionic strength = 1.0) for disappearance of phthalimide in ammonia buffers. The insert plots the slopes $k^{app}_{NH_3}$ versus pH.

$$[6]\quad \text{Rate} = \frac{k_N[\text{Imide}][NH_3][OH^-]}{1 + (K_a/K_w)[OH^-]}$$

and the apparent second-order rate constant is

$$[7]\quad k^{app}_{NH_3} = \frac{k_N[OH^-]}{1 + (K_a/K_w)[OH^-]}$$

The third-order requirement for ammonolysis is reminiscent of the third-order hydrolysis and it signifies that the formation of a tetrahedral intermediate by addition of ammonia to the imide carbonyl cannot be rate limiting. We propose a scheme with rate-determining breakdown of the tetrahedral intermediate, involving ring opening of the anionic intermediate T^-.

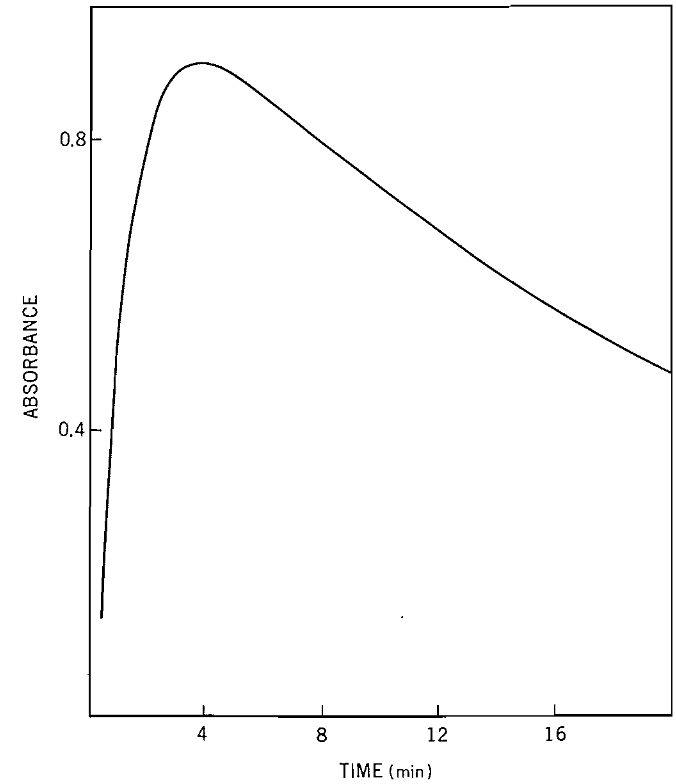

FIG. 4. Absorbance at 300 nm showing the formation and decay of phthalimide to acid on addition of phthalamide to 0.06 M NaOH.

The term in hydroxide ion appears in the kinetic expression because of the requirement for deprotonation of the initially formed zwitterionic intermediate $T^{\pm}$ prior to the rate-determining step. An alternative interpretation involves a rate-determining formation of the anionic intermediate T^-, either in a concerted mechanism where hydroxide ion assists the addition of amonia by removing a proton as the carbon–nitrogen bond is formed, or in a "trapping" mechanism (9) where conversion of $T^{\pm}$ to T^- is rate-determining. These mechanisms have a proton transfer in the rate-determing step, so that hydroxide ion is acting as a general base. The argument against them is that general base catalysis by a second ammonia molecule is not observed. This requires a second-order term in ammonia,[3] and would appear as an upward curvature on plots

[8]

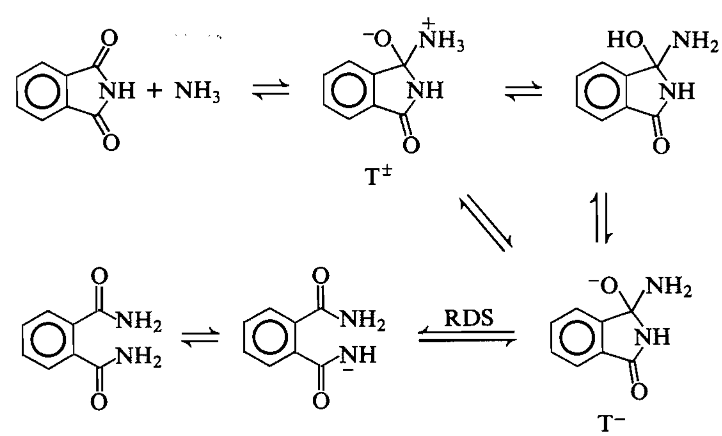

[3]The formation of an amide from an amine and ester occurs at high pH with the rate-determining formation of a tetrahedral intermediate, and does show general base catalysis by a second molecule of amine (ref. 2).

TABLE 2. Rate constants and equilibrium constants for the ammonolysis of substituted phthalimides (T = 25°C, ionic strength = 1.0)

Substituent	k_N, M^{-2} s^{-1}	k_{cyc}, M^{-1} s^{-1}	K_{eq}, M^{-1}
4-NO_2	3.7×10^3	2.78	1.3×10^3
4-Cl	2.3×10^2	0.59	3.9×10^2
H	70.6	0.29	2.4×10^2
4-*t*Bu	35.1	0.12	2.8×10^2
3-NO_2	2.9×10^3	3.6	8.1×10^2
3-Me	7.3	4.2	1.8
3-Me_3Si (25% MeCN)	0.3	24	0.01
H (25% MeCN)	14	0.4	35

of k_{obs} versus NH_3 concentration. A mechanism involving the addition of NH_2^- to the phthalimide is also excluded bcause of the extremely low concentration of this anion. It can also be noted that the conversion of trihaloacetones into acetamide and the halohydrin also exhibts third-order kinetics, with a term in hydroxide ion appearing in the rate law (10).

Values of k_N have been determined from eq. [7], using K_a values determined in the fit to the hydrolysis kinetics,[4] and are listed in Table 2. A substantial substituent effect (ρ = 2.3) is observed, consistent with the proposed anionic transition state. A comment can also be made about the competing hydrolysis. The ratio of the rate of ammonolysis of a phthalimide to the rate of its hydrolysis is simply $k_N[NH_3]/k_2$. This ratio is independent of pH, since both species require hydroxide ion, and proceed on unionized phthalimide. The relationship obviously breaks down at very high pH where hydrolysis is second-order in hydroxide ion. Using values determined here for k_N and k_2, one calculates for the parent phthalimide that reaction in a 1 M NH_3 solution will give 94% phthalamide and 6% hydrolysis product. In 10 M NH_3 the phthalamide yield goes to 99%.

Reversibility of phthalamide formation

As reported with the parent system by Crooy and Bruylants (11), phthalamides when placed in NaOH solutions show the rapid formation and subsequent decay of the phthalimide uv peak at 300 nm (Fig. 4). The decay rates are identical to those measured under the same conditions for the hydrolysis of the phthalimide. The formation process must therefore represent cyclization. The net result is the hydrolysis of one of the amide groups.

The cyclization of the phthalamide corresponds to the reverse of the phthalimide ammonolysis. Cyclization rate constants have been measured in concentrated NaOH solutions where the cyclization is much faster than the subsequent phthalimide hydrolysis. As noted by Crooy and Bruylants (11), the following rate law is observed.

$$[9] \quad \text{Rate} = k_{cyc}[\text{Phthalamide}][\text{OH}^-]$$

This is consistent with a mechanism which is the microscopic reverse of that proposed for phthalimide ammonolysis (eq. [8]) – pre-equilibrium deprotonation of one of the amide groups, followed by rate-limiting nucleophilic addition of the anion so-formed to the neighbouring amide. We were unable to detect any deviation from the rate law of eq. [9] even in 0.5 M NaOH solutions, and conclude therefore that the concentration of the deprotonated phthalamide remains small throughout.[5]

Values of k_{cyc} are listed in Table 2. The availability of the rate constants in both directions now means that the equilibrium constant for the system

[10] 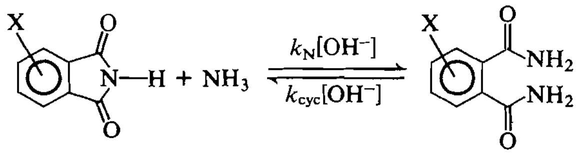

can be determined as the ratio of forward and reverse rate constants

$$K_{eq} = \frac{[\text{Phthalamide}]}{[\text{Phthalimide}][\text{NH}_3]} = \frac{k_N}{k_{cyc}}$$

Values of K_{eq} are also listed in Table 2. The equilibrium constants are large for the 4-substituted and 3-nitrophthalimides **1–5**, consistent with the ease of ammonolysis of these compounds.

A significant substituent effect is observed, electron-withdrawing substituents increasing the equilibrium concentration of phthalamide (ρ = +0.9 on K_{eq}). Electron-withdrawing groups should interact unfavourably with the carbonyl groups in both the phthalimide and phthalamide, and the indication therefore is that this interaction is less important in the amide form. A possible explanation is that the carbonyl groups in the amide are twisted with respect to the plane of the benzene ring, whereas the imide is constrained to be planar. This would mean that the phthalamide would have a diminished resonance interaction of the carbonyls and the 4-substituents. Another feature is the similarity of the 3-NO_2 and 4-NO_2 systems, this being particularly interesting in light of the results to be discussed with the two other 3-substituted imides. The implication is that the steric effect of the 3-NO_2 group is minimal. This may arise from a twisting of this group out of coplanarity with the benzene ring, so that the two oxygen atoms are directed away from the carbonyl groups. There also appears to be a significant solvent effect, the value of K_{eq} for the parent system being eight times smaller in 25% acetonitrile. There is no obvious explanation for this, but it seems to indicate that the phthalamide is a more polar molecule. It should also be noted that K_{eq} as defined in eq. [11] refers to neutral imide, and in base the equilibrium will shift significantly to the imide side because of its deprotonation. This is illustrated for the parent system in Table 3.

TABLE 3. Equilibrium concentrations of phthalamide and total phthalimide in 1 M NH_3 solutions

pH	Phthalamide / ([Phthalimide] + [Phthalimide anion])
7.06	240
8.06	238
9.06	218
10.06	120
11.06	22
12.06	2.4
13.06	0.2

[4] Values of k_N were also determined by fitting the experimental $k^{app}_{NH_3}$ data to eq. [7] with k_N and K_a as unknowns, and show good agreement. We preferred, however, to use the K_a determined in the hydrolysis kinetics, since a much greater pH range was covered in this study, so that the value of K_a should be more accurate.

[5] pK_a values for amide dissociation typically lie in this region. See ref. 19.

Ammonolysis kinetics – 3-methylphthalimide

When the ammonolysis of 3-methylphthalimide was investigated, decidely nonlinear first-order kinetic plots invariably resulted (see insert to Fig. 5). Imide disappearance occurs in two stages, an initial decrease followed by a somewhat slower decrease. This is explained by the following kinetic scheme,

$$\text{[12]}\quad \text{3-Methylphthalimides (I)} \begin{cases} \overset{k_1}{\underset{k_{-1}}{\rightleftharpoons}} \text{3-methylphthalamide (A)} \\ \xrightarrow{k_2} \text{3-methylphthalamic acid anion (H)} \end{cases}$$

with the imide being converted reversibly to the amide and irreversibly to the hydrolysis product. In simple terms, the initial rapid decrease represents the ammonolysis equilibration, where imide does not totally disappear since the equilibrium does not lie completely to the phthalamide side. The subsequent slower decrease corresponds to the hydrolysis of the imide in the imide–amide mixture, until only hydrolysis product remains. It can be noted that in any aqueous ammonolysis the latter product is the product of thermodynamic control.

In rigorous terms the analysis is more complex since the kinetic stages are not at all separated, signifying that the rate constants of eq. [12] are of the same order of magnitude so that all processes are occurring simultaneously. The differential equations for the kinetic system of eq. [12] can be solved (12). We have fitted the experimental curves of absorbance versus time to the appropriate equation[6] to obtain values of the constants k_1, k_{-1}, and k_2 which best satisfy the data. The constant k_2 refers to imide hydrolysis, and indeed the values obtained on the curve fitting were in excellent agreement with those directly measured for hydrolysis. The constants k_I and k_{-1} also take the appropriate form,[7] and provide values of k_N, k_{cyc}, and K_{eq} for the system (Table 2).

The value of K_{eq} is significantly decreased, being over 100-fold smaller than the value in the unsubstituted system. The decrease arises because of a 5-fold slower ammonolysis rate and a 40-fold faster cyclization rate. The effect arises because of greater steric congestion in the amide than in the imide, caused by the introduction of the 3-methyl group. This stabilization of a cyclic form relative to an acyclic one through the introduction of bulky substituents is fairly common (see, for example, ref. 13). In the present case, the phthalamide has three nonbonded groups on adjacent carbon atoms of the benzene ring. Cyclization to the imide releases some of the steric ocngestion caused by this arrangement.

Concentration–time profiles for the three species involved in the system are depicted in Fig. 6 for two aqueous ammonia solutions. The data shown in Fig. 6A represent the situation in the kinetics experiment. This shows that a maximum of only 35% 3-methylphthalamide is formed after 0.5 h, falling to only 12% after 3 h. As shown in Fig. 6B, however, quite high yields can be obtained in concentrated ammonia solutions.

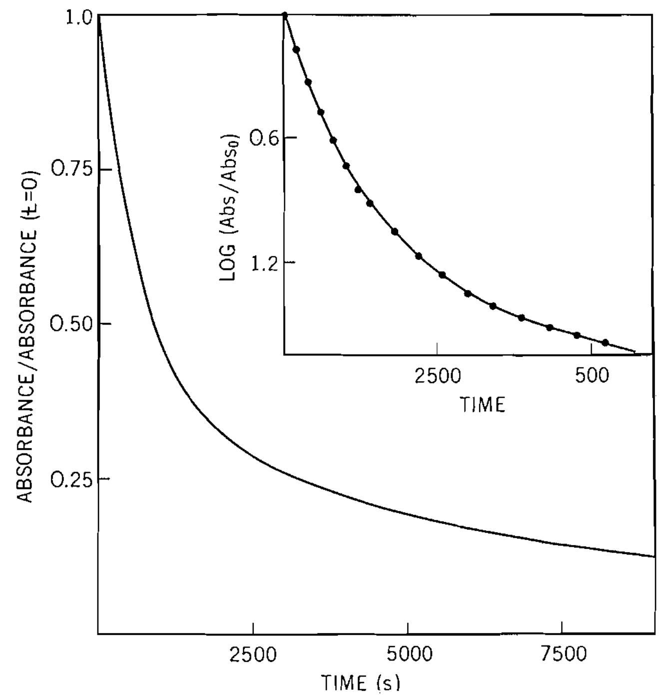

FIG. 5. 3-Methylphthalimide disappearance (λ = 305 nm) in a solution with $[NH_3]$ = 0.75, $[NH_4^+]$ – 0.25, pH = 9.88. Final absorbance is 0.00.

Reversibility is not as great a problem with the more reactive 4-substituted and 3-nitrophthalimides, **1–5**. The very favourable ammonolysis equilibrium drives the equilibrium to the phthalamide side and, particularly in concentrated aqueous ammonia, maintains it there so that the formation of hydrolysis product from the phthalimide is relatively unimportant.

Ammonolysis kinetics – 3-trimethylsilylphthalimide

With 3-trimethylsilylphthalimide, kinetic studies in the ammonia solutions used with the other compounds showed no acceleration in the rate beyond that of the hydrolysis reaction. This implies that ammonolysis is not occurring in these solutions and no phthalamide is forming. In more concentrated ammonia solutions, however, reproducible traces were obtained in which a more rapid initial decrease in absorbance is observed, accounting for about 5–10% of the total phthalimide, followed then by a slower absorbance decrease occurring at essentially the hydrolysis rate (Fig. 7). These curves are similar to those associated with the 3-methylphthalimide (Fig. 5), and they can be analyzed in the same way to provide rate and equilibrium constants for the ammonolysis (Table 2). The equilibrium constant is found to be very small here, being 100-fold smaller than the value for 3-methyl, and 3500 times smaller than the constant for the parent phthalimide in the same solvent. This effect is obviously associated with the increased steric bulk of the trimethylsilyl group, and is not unexpected on the basis of the results obtained with the smaller 3-methyl group. In kinetic terms, the 3500 factor is made up of a 50-fold slower ammonolysis rate coupled with a 65-fold faster cyclization. In terms of the ammonia solution in Fig. 6, the maximum yield of 3-trimethylphthalamide is only 6.5%, obtained after about 1000 s. Over 90% imide remains at this point, hydrolysis product accounting for only 2.4% of the mixture. Thus ammonolysis is more efficient than hydrolysis, but the equilibrium position is unfavourable.

---

[6] With the boundary conditions that at zero time $[I] = [I]_0$, $[A] = 0 = [H]$; then $[I]/[I]_0 = (\lambda_1 - k_{-1})\exp(-\lambda_1 t)/(\lambda_1 - \lambda_2) + (k_{-1} + \lambda_2)\exp(-\lambda_2 t)/(\lambda_1 - \lambda_2)$; $[A]/[I]_0 = k_I \exp(-\lambda_2 t)/(\lambda_1 - \lambda_2) - k_I \exp(\lambda_1 t)/(\lambda_1 - \lambda_2)$; $[H]/[I]_0 = 1 - (\lambda_1 - k_1 - k_{-1})\exp(-\lambda_1 t)/(\lambda_1 - \lambda_2) + (k_1 + k_{-1} - \lambda_2)\exp(-\lambda_2 t)/(\lambda_1 - \lambda_2)$.

[7] $k_I = k_I[NH_3][OH^-]/(1 + (k_w[OH^-]/k_a))$; $k_{-1} = k_{cyc}[OH^-]$.

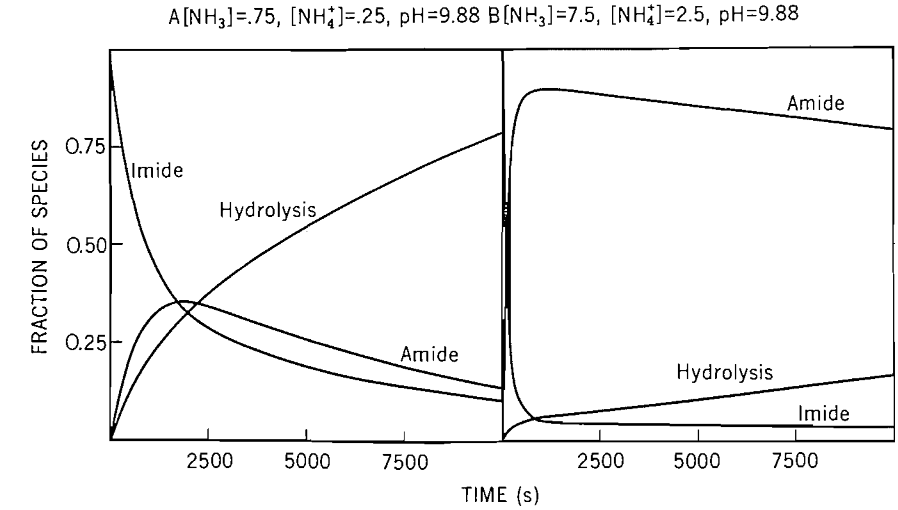

FIG. 6. Concentration of species as a function of time for 3-methylphthalimide in aqueous ammonia (A = dilute, B = concentrated).

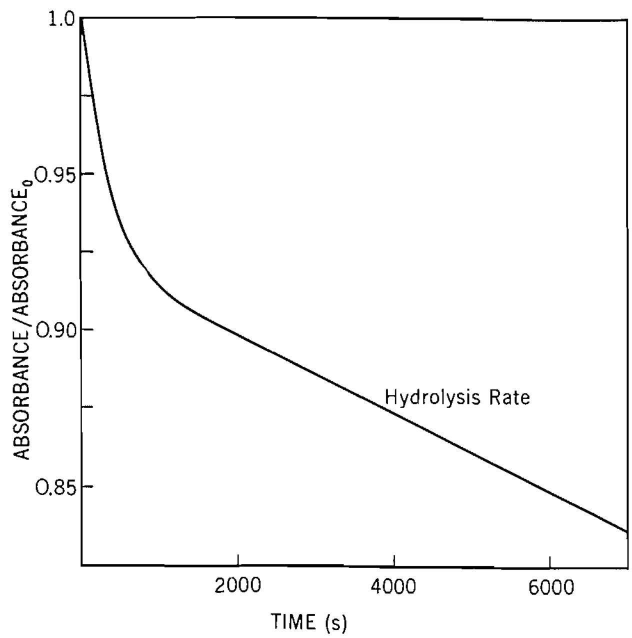

FIG. 7. Disappearance of 3-trimethylsilylphthalimide in concentrated aqueous ammonia $[NH_3] = 7.5$, $[NH_4^+] = 0.25$, pH = 10.6, 25% MeCN, 25°C).

Experimental

Synthesis of starting materials

Reagent grade phthalimide, 4-nitrophthalimide, 3-nitrophthalimide, and phthalamide were purchased from Fisher Scientific and were used without further purification. All products were characterized by ir (in Nujol) and ^{1}H or ^{13}C nmr spectroscopy using a Bruker 250 MHz instrument. Elemental analyses were performed by Galbraith Laboratoires, Knoxville, Tennessee.

4-Chlorophthalimide 3

A. 4-Chlorophthalic acid monosodium salt (100.01 g, 0.449 mol) was added to thionyl chloride (250 mL). The resultant solution was heated at reflux for 2 h, then the excess thionyl chloride was removed under reduced pressure. The remaining orange-yellow solid was heated with 2 L of boiling hexane and the hot suspension was filtered. The cooled filtrate afforded 57.4 g (70%) of 4-chlorophthalic acid anhydride, mp 67–68°C; ir cm^{-1}: 1860, 1790, 1760 (O=C—O—C=O).

B. The 4-chlorophthalic anhydride (55.9 g, 0.339 mol) was mixed with urea (17.8 g, 0.296 mol) and the mixture was gently heated with a Meker burner for 40 min. The liquid cooled to form a yellow solid, which was crushed and dissolved in 400 mL of DMF. Dropwise addition of water (800 mL in total) to the stirring DMF solution, followed by filtration and drying, gave 54.8 g (98%) of pale yellow crystals; mp 209–210°C (lit (14), mp 210°C); ir cm^{-1}: 3195 (N—H) 1787, 1705 (C=O).

3-Methylphthalimide 6

Urea (7.8 g, 0.130 mol) was mixed with 3-methylphthalic acid anhydride (24 g, 0.146 mol) and the mixture was gently heated with a Meker burner for 40 min. The melt was cooled, crushed, and suspended in water (200 mL) for 1 h. The brown solid was filtered off and dissolved in 100 mL of DMF to which decolorizing carbon (0.5 g) was added. The suspension was stirred for 1 h, then filtered. Dropwise addition of water (400 mL) to the DMF solution yielded 16.5 g (70%) of a beige solid; mp 186–188°C (lit (15) mp 188–189°C); ir cm^{-1}: 3220 (N—H), 1780, 1730 (C=O).

*4-*tert*-butylphthalimide, 4*

4-*tert*-Butylphthalic acid anhydride (61.4 g, 0.30 mol), prepared in three steps from *o*-xylene, was mixed with urea (18.0 g, 0.30 mol) and gently heated with a Meker burner for 30 min. The melt was cooled, and dissolved in 125 mL of DMF. Dropwise addition of water (375 mL) produced 57.8 g (94.5%) of a beige solid; mp 136–138°C (lit. (16) mp 131–132°C); ir cm^{-1}: 3220 (N—H), 1782, 1720 (C=O).

3-Trimethylsilylphthalimide, 7

3-Trimethylsilylphthalic acid anhydride (87.4 g, 0.397 mol), prepared in six steps from *o*-xylene (3) was mixed with urea (23.8 g, 0.397 mol). The reagents were kept in a nitrogen atmosphere, while being heated to produce a melt, for 30 min. The liquid melt was cooled, crushed, and stirred in water (600 mL) for 19 h. The crude product was filtered off, washed with water (500 mL), and dried in a vacuum oven for 4 h. The solid was dissolved in acetone (400 mL) and decolorizing carbon (2 g) was added to the solution. The suspension was filtered after 30 min. Dropwise addition of water (1.2 L) to the acetone solution, followed by filtration and water washing (3 × 500 mL), yielded 74 g (85%) of a white crystalline solid; mp 148.5–150.5°C; ir cm^{-1}: 3190 (N—H), 1769, 1722 (C=O). *Anal.* calcd. for $C_{11}H_{13}NO_2Si$: C 60.24, H 5.97, N 6.39, Si 12.81; found: C 60.44, H 5.93, N 6.48, Si 12.59.

4-Nitrophthalamide

4-Nitrophthalimide (100.5 g, 0.520 mol) was added to concentrated ammonium hydroxide (530 mL) and the suspension was stirred for 6 h, then cooled to 0°C for 19 h. The suspension was filtered and the product was washed with ether, then dried, yielding 107 g (99%) of a white powder; mp 196–198°C; ir cm^{-1}: 3440, 3440 (NH_2), 1668, 1587 (C=O).

4-Chlorophthalamide

4-Chlorophthalimide (53.2 g, 0.293 mol) was added to concentrated ammonium hydroxide and the suspension was stirred for 5 h, filtered, and dried, producing 41.6 g (72%) of a pale yellow powder; mp 196–198°C (lit. (17) mp 194–196°C); ir cm^{-1}: 3420, 3320, 3160 (NH_2), 1660, 1592 (C=O).

4-tert-Butylphthalamide

4-*tert*-Butylphthalimide (56.1 g, 0.274 mol) was suspended in concentrated ammonium hydroxide (825 mL). The stirred beige suspension quickly formed a dirty yellow solution which immediately became a milky suspension. At this point, more concentrated ammonium hydroxide (200 mL) was added since the mixture was too thick to stir, and stirring was continued for 3 h. The product was filtered off, washed with water (3 × 300 mL), and dried, giving 60.7 g (79.7%) of a white solid; mp 177–178°C (lit. (16) mp 180–181°C); ir cm^{-1}: 3300, 3190 (NH_2), 1670, 1595 (C=O).

3-Nitrophthalamide

3-Nitrophthalimide (256 g, 1.33 mol) was added to concentrated ammonium hydroxide (3225 mL). The yellow suspension gradually became white in color as the mixture was stirred, for 21 h. The reaction mixture was cooled to 0°C for 19 h, then filtered, washed with water (2 × 500 mL), and dried, giving 82.7 g (93%) of a white powder; mp 200–201°C (lit (18) mp 204–205°C); ir cm^{-1}: 3430, 3340, 3210 (NH_2), 1671 (C=O). *Anal.* calcd. for $C_8H_7N_3O_3$: C 45.94, H 3.38, N 20.08; found: C 45.69, H 3.48, N 19.94.

3-Methylphthalamide

3-Methylphthalimide (15 g, 0.084 mol) was added to liquid ammonia (100 mL) which had been condensed into a 300-mL Parr pressure reactor. The reactor was sealed and the temperature was raised to 90°C (840 psi; 1 psi = 6.89 kPa) in 1 h. The reaction mixture was stirred for 20 h, then cooled to less than −50°C. When the pressure in the reactor was close to 1 atm (101.3 kPa) the vessel was opened and the ammonia was allowed to evaporate off, producing a beige solid (15 g). An ir spectrum indicated the product was a mixture of 3-methylphthalimide and 3-methylphthalamide. A Soxhlet extraction of the crude product was carried out, with methylene chloride, for 23 h. The ir spectrum of the solid remaining in the thimble indicated there was only 9.17 g (56%) 3-methylphthalamide remaining. A sample (1.2 g) of the product was recrystallized from methanol; mp 182–184°C. *Anal.* calcd. for $C_9H_{10}N_2O_2$: C 60.66, H 5.66, N 15.72; found: C 60.79, H 5.78, N 15.54.

Attempt to synthesize 3-trimethylsilylphthalamide

3-Trimethylsilylphthalimide (15 g, 0.068 mol) was added to ammonia (150 mL) which had been condensed into a 300-mL Parr pressure reactor. The reactor was sealed, and heated to 90°C (860 psi) for 20 h. The vessel was then cooled to less than −50°C and the ammonia was allowed to evaporate away. A ^{13}C nmr spectra of the remaining beige solid (14.26 g) indicated that the product was ~90% starting material.

Kinetic methods

Kinetic measurements were made on a Unicam SP 1800 spectrophotometer, equipped with a jacketed multiple cell block maintained at 25.0 ± 0.01°C by an external water bath. A 3-μL solution of the phthalimide or phthalamide substrate was injected into 30 mL of the appropriate solution pre-thermostatted at 25°C, and the change in absorbance at 305 nm (330 nm for nitro compounds) monitored as a function of time. For phthalimide hydrolysis and ammonolyses, first-order rate constants were evaluated as slopes of plots of ln $(A - A_0)$ versus time. First-order rate constants for phthalimide appearance from phthalamide were determined using the Guggenheim method.

1. F. H. MOSER and A. L. THOMAS. Phthalocyanine Compounds. Reinhold, New York. 1963.
2. G. M. BLACKBURN and W. P. JENCKS. J. Am. Chem. Soc. **90**, 2638 (1968).
3. H. HOPFF and P. GALLEGRA. Helv. Chim. Acta, **51**, 253 (1968).
4. J. TIRAUFLET and E. LETROUIT. C. R. Acad. Sci. **241**, 1053 (1955); J. T. EDWARDS and K. A. KERRY. J. Chem. Soc. 3527 (1956); P. PAPOFF, U. MAZZUCATO, A. FOFFANI, and G. PIAZZA. Ann. Chim. (Rome), **50**, 530 (1960); S. CHAMPY-HATEM. C. R. Acad. Sci. **261**, 271 (1965).
5. A. R. BUTLER. J. Chem. Soc. Perkin Trans. 2, 1239 (1974).
6. M. N. KHAN and A. A. KHAN. J. Org. Chem. **40**, 1793 (1975); J. Chem. Soc. Perkin Trans. 2, 1009 (1976); 1093 (1979).
7. M. N. KHAN and A. A. KHAN. J. Chem. Soc. Perkin Trans. 2, 796 (1979).
8. S. S. BIECHLER and R. W. TAFT. J. Am. Chem. Soc. **79**, 4927 (1957); S. O. ERIKSSON. Acta Pharm. Suec. **6**, 139 (1969); D. DRAKE, R. L. SCHOWEN, and H. JAYARAMAN. J. Am. Chem. Soc. **95**, 454 (1973); R. M. POLLACK and T. C. DUMSHA. J. Am. Chem. Soc. **95**, 4463 (1973); **97**, 377 (1975); R. M. POLLACK. J. Org. Chem. **39**, 2108 (1974); J. KAVALEK and V. STERBA. Collect. Czech. Chem. Commun. **40**, 1176 (1975); O. S. TEE, M. TRANI, R. A. MCCLELLAND, and N. E. SEAMAN. J. Am. Chem. Soc. **104**, 7219 (1982).
9. W. P. JENKS. Acc. Chem. Res. **13**, 161 (1980).
10. W. STANCZYK. J. CHMIELECKA, and T. CHOJNOWSKI. J. Org. Chem. **47**, 3757 (1982).
11. P. CROOY and A. BRUYLANTS. Bull. Soc. Chim. Belg. **73**, 44 (1964).
12. C. D. RITCHIE. Physical organic chemistry – The Fundamental Concepts. Marcel Dekker, New York, NY 1975. p. 27.
13. M. CASWELL and G. L. SCHMIR. J. Am. Chem. Soc. **102**, 4815 (1980; P. S. HILLERY and L. A. COHEN. J. Chem. Soc. Chem. Commun. 403 (1973); S. MILSTEIN and L. A. COHEN. J. Am. Chem. Soc. **94**, 9158 (1972); B. CAPON. Q. Rev. **18**, 45 (1964).
14. L. M. YAGUPOL'SKII and R. V. BELIMSKAYA. Zh. Obshch. Khim. **33**, 2358 (1963).
15. P. A. S. SMITH and R. O. KAN. J. Org. Chem. **29**, 2261 (1964).
16. S. A. MIKHALENKO, S. V. BARKANOVA, O. L. LEBEDEV, and E. A. LUK'YANETS. J. Gen. Chem. USSR (Engl. Trans.) **41**, 2735 (1971).
17. F. S. SPRING and J. C. WOODS. J. Chem. Soc. 625 (1945).
18. M. HAYASHI, S. TSURUOKA, I. MORIKAWA, and H. NAMIKAWA. Bull. Chem. Soc. Jpn. **11**, 184 (1936).
19. D. O. PERRIN. Dissociation constants of organic bases in aqueous solution. Butterworths, London. 1965.

Phosphorescence of naphthalene-labelled colloidal polymer particles. The α-methyl relaxation of one microphase in a multicomponent material[1]

MITCHELL A. WINNIK[2] AND ONDER PEKCAN[3]
Lash Miller Chemical Laboratories, Department of Chemistry, University of Toronto, Toronto, Ont., Canada M5S 1A1

AND

M. D. CROUCHER
Xerox Research Centre of Canada, 2660 Speakman Drive, Mississauga, Ont., Canada L5K 2L1

Received February 23, 1984

This paper is dedicated to the 10th anniversary of the Xerox Research Centre of Canada

MITCHELL A. WINNIK, ONDER PEKCAN, and M. D. CROUCHER. Can. J. Chem. **63**, 129 (1985).

Nonaqueous dispersions of poly(methyl methacrylate) (PMMA) particles, sterically stabilized with polyisobutylene (PIB), were prepared with naphthalene (N) groups covalently incorporated into the PMMA chains. These materials have a complex morphology of phase-separated PMMA and PIB microdomains, with the N groups in the PMMA microphases. The phosphorescence intensity and decay times of the N groups were measured as a function of temperature over the range 77–295 K for dispersions in methylcyclohexane and for freeze-dried powder samples. An Arrhenius treatment of the radiationless decay rate showed a change in slope at −35°C. The activation energy for the radiationless decay process is 3.8 kcal/mol in the −35 – +22°C temperature region, identical to that found for pure PMMA by nmr for chain motion associated with the α-methyl relaxation process. We believe that the phosphorescence experiment is sensitive to the diffusion of oxygen and other impurities in the sample. These rates increase as the temperature is raised, enhancing the rate of phosphorescence quenching. These experiments indicate that phosphorescence measurements on labelled samples are suitable for studying relaxation processes within individual microphases of a polyphasic composite material.

MITCHELL A. WINNIK, ONDER PEKCAN et M. D. CROUCHER. Can. J. Chem. **63**, 129 (1985).

On a préparé des dispersions non aqueuses de particules de poly(méthacrylate de méthyle) (PMAM) stabilisées stériquement par du polyisobutylène (PIB) et dans lesquelles des groupes naphtalènes (N) ont été incorporés d'une façon covalente dans les chaînes de PMAM. Ces composés ont une morphologie complexe comportant des microdomaines séparés de phases de PMAM et de PIB avec les groupes N situés dans les microphases de PMAM. Opérant à des températures allant de 77–295 K et pour des dispersions dans le méthylcyclohexane et des échantillons de poudres lyophilisées, on a mesuré l'intensité de la phosphorescence et le temps de décroissance de l'émission des groupes N en fonction de la température. Si on traite les vitesses de décroissance non radiative par le méthode d'Arrhénius, on observe un changement de pente à −35°C. L'énergie d'activation pour le processus de décroissance non radiative est de 3,8 kcal/mol dans l'intervalle allant de −35°C – +22°C; cette valeur est identique à celle trouvée par rmn, dans le cas du PMAM à l'état pur, pour le mouvement de chaîne associé au processus de relaxation du méthyle en α. Nous croyons que l'expérience de phosphorescence est sensible à la diffusion de l'oxygène et d'autres impuretés présentes dans l'échantillon. Ces vitesses augmentent avec la température, augmentant ainsi la vitesse avec laquelle la phosphorescence est piégée. Ces expériences indiquent que les mesures de phosphorescence sur des échantillons marqués conviennent bien à l'étude des processus de relaxation à l'intérieur de microphases individuelles d'un matériel composite à phases multiples.

[Traduit par le journal]

Phosphorescence measurements on polymer samples doped or labelled with appropriate dye molecules provide powerful means for studying properties of polymers in the solid state. Over the past 20 years various research groups have used these techniques to study the dynamics of gas permeability (1–3), and to detect various relaxation processes (4–7) in polymer films. A careful reading of these papers suggests that both the phosphorescence intensity of a dye and its phosphorescence decay time are sensitive to many of the processes which occur in the glassy state of polymers. One can observe the glass transition (at temperature T_g), the β transition (T_β), and in some instances the α′ transition due to local mode relaxation of the main polymer chain. Examples of sensitivity to sample history including hysteresis effects are known. Activation energies for polymer relaxation pathways can be determined, and these are comparable to those obtained by solid state nmr techniques.

One of the curious features of these experiments is that nearly all of them have been reported by research groups specializing in luminescence spectroscopy or photochemistry. Either the usefulness of these methods is not appreciated by the polymer community in general or they consider the techniques to be difficult, complex, or arcane. Perhaps it is felt that one needs optically transparent samples and sophisticated equipment. Our results reported here may serve as an incentive to others contemplating such experiments. We report phosphorescence intensity and decay measurements, obtained with rather primitive equipment, and with samples which are powders, suspensions, and dispersions, placed in cylindrical quartz tubes.

The system we are investigating is a particle ca. 2 μm in diameter, composed of two incompatible polymers, poly(methyl methacrylate) (PMMA) and polyisobutylene (PIB) (8–11). Nonaqueous dispersions of these particles have important industrial applications, particularly in electrostatic imaging technology (12). Although this material is commonly considered to have a "core-shell" structure, we have shown that its real morphology is more complex and more interesting. We have proposed a "microphase model" for its structure (10), with threads of PIB forming a connected interpenetrating network

[1] Luminescence of Polymer Colloids 6.
[2] Author to whom correspondence should be directed.
[3] Current address, Department of Physics, Hacettepe University, Ankara, Turkey.

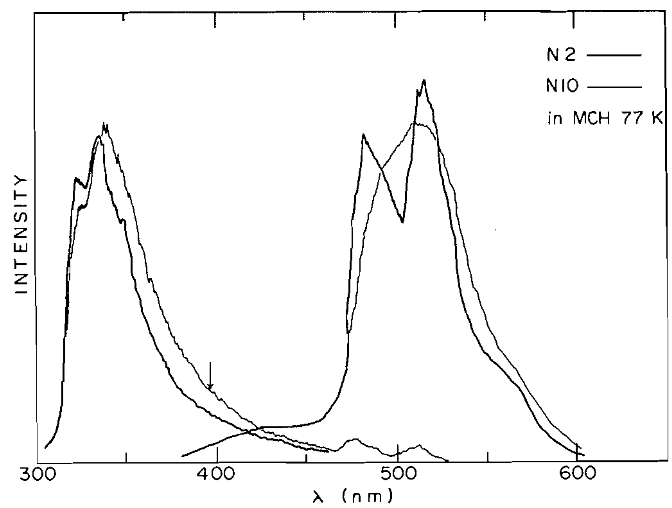

FIG. 1. The fluorescence and phosphorescence spectra of N2 and N10 dispersions in methylcyclohexane at 77 K.

throughout the interior of the particle.

This model was proposed to explain apparently contradictory results of fluorescence quenching experiments carried out on particles labelled in the PMMA chains with naphthalene (N) groups or anthracene (A) groups. The particles were dispersed in hydrocarbon solvents and small molecule quenchers were added to the liquid. When the quencher was very soluble in PIB and could communicate with the excited N* groups over substantial distances (e.g. 20–40 Å by a Förster energy transfer mechanism), we observed that quenching occurred within minutes of sample preparation, even for N groups deep within the core of the particle (8, 10). Quite different behavior was seen for quenchers that were soluble in PMMA and poorly soluble in PIB, particularly when quenching involved short range interactions (e.g. 4–5 Å, by exciplex formation) (11). Here it took days or weeks for the sorption process to come to equilibrium.

Because the N groups were introduced into the particle as an N-substituted methacrylate during a step in particle synthesis involving PMMA polymerization, the N groups must be covalently linked to the PMMA chains. Phosphorescence at room temperature from the particles indicates that the N groups are located in glassy PMMA phases. The N groups thus serve as molecular spies for events transpiring within the PMMA microdomains. Luminescence spectra of these labelled materials are shown in Fig. 1.

In this report we describe the phosphorescence intensity and phosphorescence decay times of these N-labelled PMMA particles as they are affected by changes in temperature and by the presence of hydrocarbon solvents. These experiments permit the α-methyl transition within the PMMA microphases to be identified.

Experimental

The synthesis and characterization of the particles have been reported previously (8–11). The particles, 2 μm in diameter, have compositions containing monomer units in mole ratios of isobutylene/methyl methacrylate/naphthylmethyl methacrylate of 13:100:2 and 13:100:10. We have referred to these materials as N2 and N10, respectively.

Phosphorescence measurements were carried out on a Hitachi–Perkin–Elmer MPF2 spectrofluorimeter. Intensity measurements were made in conjunction with a rotating mechanical chopper to remove prompt fluorescence. Phosphorescence decay measurements were made in a rather primitive fashion by blocking the excitation source of the spectrometer and recording the time profile of the intensity decay at 500 nm on a strip chart recorder (9, 13). These traces were digitized with a digitizing x,y-plotter and fitted to an exponential function by a nonlinear least-squares method. While reproducibility was excellent for decays on the order of 1–3 s, the method gives only the first decade of the intensity decay. Small departures from exponentiality would not have been detected (13).

Samples were prepared in quartz tubes fitted with a graded seal. Those samples in which oxygen was rigorously removed, by evacuating 3 – 5 h at 35°C on a vacuum line at 1×10^{-5} Torr (1 Torr = 133.3 Pa), were sealed under vacuum. Dispersions of N2 were prepared by weighing 6-mg samples of N2 into the sample tubes and adding 1 mL of methylcyclohexane. These were sonicated for ca. 1 min using a low-power ultrasonic cleaning bath.

Results and discussion

Spectroscopic considerations

Triplet states of organic molecules are extremely sensitive to quenching by oxygen and other impurities. As a consequence, phosphorescence is normally observed only in very viscous media – in crystalline hosts and glassy polymer films at ordinary temperatures, and in glassy matrices formed from organic solvents at low temperatures. Early sudies (14) focussed on two viscosity regimes in simple organic media: a low viscosity domain where the triplet lifetime ${}^3\tau$ was determined largely by diffusion processes involving quenchers, and a high viscosity region where ${}^3\tau$ depended upon the unimolecular rate constants for radiative (k_p) and non-radiative (k_{nr}) decay.

This view is somewhat oversimplified (15). If the impurity concentration is significant, static quenching can contribute to the radiationless decay rate. Similarly at high enough chromophore concentration, self-quenching becomes important (9), even in the absence of mass diffusion. When these bimolecular processes become dominant, one observes decreases in the phosphorescence quantum efficiency (ϕ_p) without concomitant changes in ${}^3\tau$: Some excited states, adjacent to a quencher, are quenched essentially instantaneously, and thus do not contribute to the signal used to determine ${}^3\tau$.

Extensive studies have shown that the unimolecular decay rates of aromatic triplet states are sensitive to temperature (1). Lifetimes decrease by about a factor of two between room temperature and 150 K. Below 150 K, both ${}^3\tau$ and ϕ_p remain constant. For many molecules, ϕ_p^0 (the superscript ^{0} implying the low temperature value) is quite small. For naphthalene, $\phi_p^0 = \phi_{ST}^0\, k_p/(k_p + k_{nr}^0) = 0.05$, where ϕ_{ST}^0, the triplet formation efficiency, is significantly larger than 0.05. Since k_p is independent of temperature (1, 15), this indicates that k_{nr} has both temperature-dependent and temperature-independent components.

The theory of radiationless triplet decay has been examined by a number of authors including Lin and Bersohn (16), Jortner and Berry (17), and Dexter and Powder (18). These groups give an expression for k_{nr} of the form

$$[1] \quad k_{nr} = k_{nr}^0\,(1 + A\mathrm{e}^{-E_a/kT})$$

which, in conjunction with the expression ${}^3\tau^{-1} = k_p + k_{nr}$, leads to the expression

$$[2] \quad \tau^0/\tau - 1 = a\mathrm{e}^{-(E_a/kT)}$$

The parameters A, a, and E_a are constants related to the vibrational levels of the matrix into which the excitation energy is dissipated.

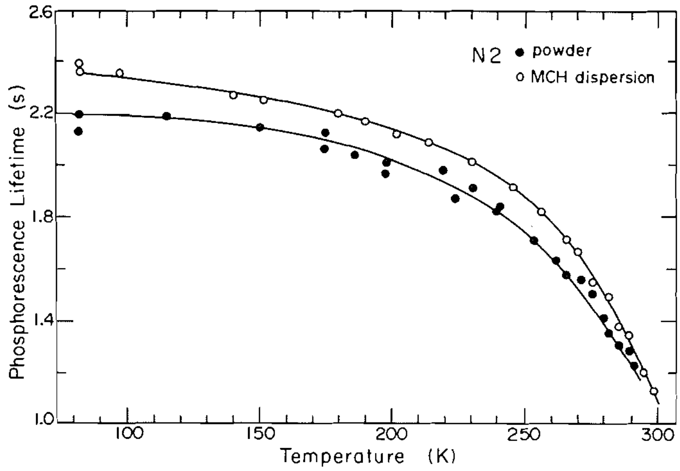

FIG. 2. Phosphorescence lifetimes of N2 as a function of temperature for (○) dispersions in methylcyclohexane and for (●) solid powder samples.

The case of naphthalene in PMMA has been investigated extensively by Jones and Siegel (1). They examined thin films (10 μm) which were carefully degassed and extensively annealed under vacuum. Exponential decays and simple Arrhenius behavior over the temperature range 77–300 K was observed only if these precautions were taken.

Oxygen was not the only quencher initially present in the sample. Residual monomer was also implicated. These authors treated their data according to eq. [2], taking the 77 K lifetime as the ${}^3\tau^0$ value. They found an E_a value of 500 cm^{-1} (1.4 kcal/mol). The temperature-dependent component of the radiationless decay was attributed to coupling of the decay to low-frequency bending vibrations in the PMMA matrix.

Through their care in removing quenching impurities, Jones and Siegel (1) simplified their experiments and data interpretation. Their ${}^3\tau$ values were insensitive to mechanical relaxation processes within the polymer film. If one takes less care in sample preparation, other factors, including diffusive quenching, contribute to the value of ${}^3\tau$. The magnitudes of these factors are sensitive to mechanical relaxation processes within the polymer. As we discuss below, impurities act to reveal, via phosphorescence quenching, various relaxation phenomena characteristic of the polymer matrix.

Triplet lifetime measurements in N2

Triplet lifetimes of freeze-dried N2 particles, in the powder form, were measured at temperatures between 77 K and room temperature. The samples were chilled rapidly in liquid nitrogen and measurements were taken from time to time as the sample warmed. Dispersions of N2 in methylcyclohexane were treated similarly. As Fig. 2 indicates, at temperatures below 150 K, the phosphorescence lifetimes are essentially independent of temperature.

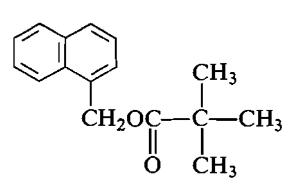

1

One of the interesting features of the data is that the phosphorescence lifetimes depend upon the local concentration of N groups in the PMMA phase. This aspect has been examined in detail previously (9). Thus ${}^3\tau$ (N10) is shorter than ${}^3\tau$ (N2), which in turn is somewhat shorter than ${}^3\tau$ for a model compound, 1-naphthylmethyl pivalate (**1**), at 10^{-4} *M* in methylcyclohexane, or in a PMMA film at 77 K. The process of self-

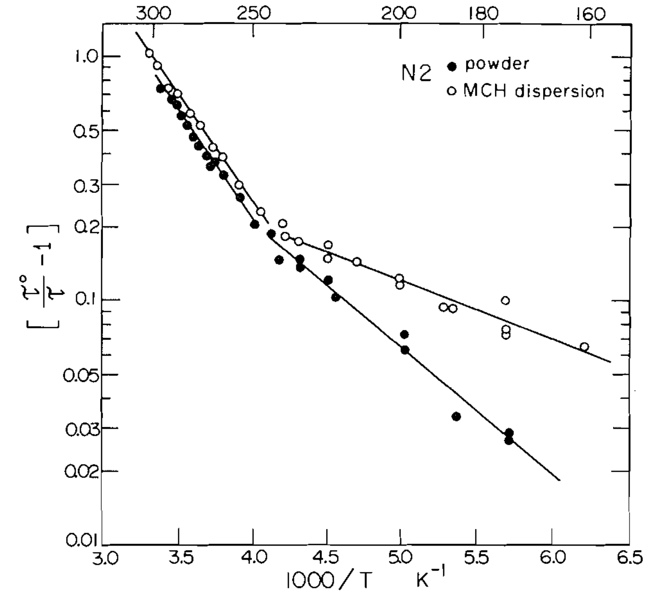

FIG. 3. Plot of log (τ^0/τ − 1) vs. $1/T$ for the data from Fig. 2.

[3] $N + N^* \rightarrow 2N$

quenching, eq. [3], provides an additional radiationless pathway, presumably via triplet excimer formation, to shorten the triplet lifetime.

The fact that ${}^3\tau$ in N2 is longer at 77 K in the methylcyclohexane dispersion than in the dry powder implies that the solvent acts to increase the mean separation between N groups in the particle. Curiously, the lifetime differences are exacerbated at low temperatures and disappear as the respective samples are allowed to warm. This result is in accord with separate observations on the fluoroescence of N groups in N2 and N10. One finds that the fluorescence lifetimes at room temperature are also sensitive to the local N concentration, but are nearly unchanged when N2 or N10 powders are dispersed in methylcyclohexane.[4]

Our interpretation of the triplet lifetime results is that the alkane solvent does not swell the PMMA microphases at room temperature. Rather it penetrates into various sites of free volume[5] and acts to retard the contraction of the PMMA phases as they are cooled.

The α-methyl relaxation process

The triplet lifetime data from N2 as a function of temperature are replotted in an Arrhenius fashion according to eq. [2] in Fig. 3. While the plots are curved, both are fit quite reasonably to two intersecting straight lines. The intersection temperature for both curves is approximately −35°C. This temperature corresponds to a relaxation process in PMMA as determined by wide-line ^{1}H nmr (20). This relaxation process corresponds to commencement of backbone methyl (α-methyl) group rotation in the polymer.

[4] O. Pekcan, unpublished observations.
[5] For an important discussion of non-solvent penetration into glassy polymers and its consequence on chain motion see ref. 19.

The activation energies E_a^{HT} of the high temperature portion of Fig. 3 are 1320 cm^{-1} (3.8 kcal/mol) for the N2 powder and 1460 cm^{-1} (4.2 kcal/mol) for the dispersion of N2 in methylcyclohexane. The former is very close to the value of 1260 cm^{-1} determined by Kawai (20*a*) from the temperature dependence of ^{1}H nmr correlation time for the α-methyl group relaxation process in solid PMMA.

In our opinion, the agreement of the phosphorescence experiments with the nmr data is not entirely coincidence. Rather, we believe that the $^3\tau$ values between −35°C and 25°C are sensitive to the conformational mobility of the backbone methyl groups in PMMA. The origin of this sensitivity is most likely related to the onset of diffusive quenching of N^{*3} by oxygen and other impurities in the matrix (22). Diffusion is enhanced by free volume fluctuations coupled to the increasing rotational mobility of the α-methyl groups at temperatures above −35°C.

These results pose a singular dilemma. Although the apparent onset temperature of −35°C from the phosphorescence lifetime measurements corresponds to $T_{\alpha\text{-Me}}$ determined by ^{1}H nmr for the α-methyl group rotation, the two experiments refer to very different time scales. The nmr experiment is sensitive to methyl group rotations in the megahertz frequency range (20, 21). The phosphorescence lifetimes are sensitive to impurity diffusion on the time scale of seconds. The 10^6 difference in experimental frequency should lead to a large (ca. 40°) difference in the value of $T_{\alpha\text{-Me}}$. The apparent E_a values for both measurements, however, should be the same.

This dilemma can be resolved by recognizing that the break in the Arrhenius plot in Fig. 3 does not necessarily represent a critical temperature of the system. Rather, it represents the temperature at which the rate of process with E_a = 1320 cm^{-1} overtakes the rate of a lower temperature process with E_a = 830 cm^{-1}. While impurity diffusion in a polymer matrix below T_g can lead to enhanced phosphorescence quenching, impurity diffusion itself is slow. Free volume increases which enhance the rate of α-methyl group rotation also enhance diffusion rates. Our experiments indicate that long range diffusion of impurities becomes efficient at reaching excited chromophores on a time scale of seconds when the free volume of the system is sufficient to permit α-methyl group rotation rates in the MHz range. The coincidence is that the break in the Arrhenius plot in Fig. 3 occurs at the same temperature as the $T_{\alpha\text{-Me}}$ found by ^{1}H nmr T_1 measurements.

Below −35°C, important differences appear in the phosphorescence decay times of N2 in the presence or absence of methylcyclohexane. The $^3\tau$ values decrease less with temperature in the alkane dispersion than in the dry powder. Activation energies are presented in Table 1. We have previously suggested that methylcyclohexane retards the volume contraction of the PMMA phase as the temperature is lowered. This implies some solvent penetration into the PMMA, although the details of the process are unclear.

If the preceding explanation is correct, bimolecular self-quenching ($N^{*3} + N \rightarrow 2N$) makes an important contribution to $^3\tau$ under these conditions, since contraction of the PMMA phases decreases the mean separation between N groups. This is a testable hypothesis, since self-quenching will no longer be important in particles containing less than 0.1% N groups. Particles of that composition are currently being prepared.

TABLE 1. Activation energies for radiationless decay rates for naphthalene groups in N2

	E_a (cm^{-1})	
Temperature range (°C)	Solid powder	Methylcyclohexane dispersion
−35 – 25	1320 ± 70	1470 ± 70
−180 – −35	830 ± 30	370 ± 20

Phosphorescence intensity measurements

While it is difficult to make quantitative luminescence intensity measurements on powder samples or turbid solutions, reasonable measurements of intensity versus temperature can be made on individual samples. We have carried out five sets of measurements on N phosphorescence as a function of temperature. These measurements involved N10 powder samples and N10 dispersions in methylcyclohexane, some samples degassed and sealed under vacuum, and other identical samples stoppered in the presence of air at room temperature. In addition we examined a dilute solution (10^{-4} *M*) of 1-naphthylmethyl pivalate (**1**) in methylcyclohexane. These samples were chilled rapidly to liquid nitrogen temperature. The phosphorescence intensity at 500 nm was monitored as the samples were allowed to warm.

These results are presented in Fig. 4. The top part (a) shows the intensity vs. temperature plots for the degassed N10 samples; (b), the same samples in the presence of air; and (c), the model compound **1** in aerated methylcyclohexane. There are numerous interesting and peculiar features present, not all of which can be interpreted at the present time.

The most straightforward to understand is that of **1** in methylcyclohexane. When chilled to 77 K, the solvent forms a transparent glass (T_g = 87 K) (23), where impurity diffusion is slow. As the sample warms, it begins to crystallize (24). The microcrystals formed serve to protect the chromophores from quenching, either by trapping them or by increasing the effective microscopic viscosity of the medium. At higher temperatures, (i.e. above −145°C) solvent mobility is such that larger crystals form, excluding both impurities and **1**. Quenching becomes more effective. Above the melting point of the solvent (−126°C), there is very little phosphorescence.

In the N10 powder samples, the intensity vs. temperature plots are rather featureless. The small dip at ca. −150°C seems to be reproducible. Whether or not it originates in some molecular relaxation process (25) in the PMMA is a matter of speculation. Phosphorescence persists to higher temperature in the degassed rather than the aerated samples.

The N10 dispersions show a number of peaks and valleys. These features are consistently reproducible. Their interpretation is difficult, and it is important to keep in mind that one cannot compare absolute intensities among different samples. The powder and dispersion samples, in Figs. 4(a) and (b), for example, have been normalized to equal intensity at 77 K. In our opinion, these features reflect aspects of quencher diffusion in the PMMA microdomains and interphase regions. Since these features do not appear in the phosphorescence lifetime experiments, quencher diffusion must be localized. It must occur on time scales much faster (less than 0.1 s) than our decay measurements permit us to detect.

Perhaps the most important aspect of these results is that the presence of a non-solvent for PMMA has such an influence on diffusive processes within the PMMA phases. The nature of this influence is still unclear and perhaps will become more apparent as our work progresses.

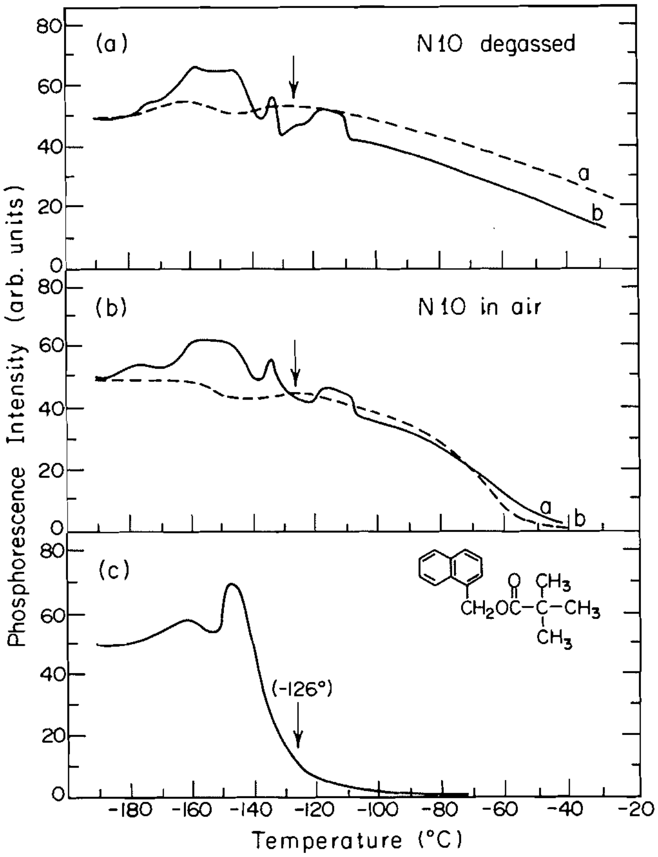

FIG. 4. Plot of phosphorescence intensity at 500 nm vs. temperature. (a) degassed samples of N10 (- - - - powder, —— dispersion in methylcyclohexane); (b) aerated samples of N10 (- - - - powder, —— dispersion); (c) aerated solution of 1-naphthylmethyl pivalate (**1**) in methylcyclohexane.

Conclusions

Phosphorescence decay times in PMMA phases labelled covalently with naphthalene groups are sensitive to mechanical relaxation processes in the glassy polymer. This sensitivity arises from impurity diffusion, which is coupled to the molecular motion of the polymer chains. The activation energy for diffusive quenching which we obtain corresponds to that previously determined by nmr methods for chain motion in PMMA (20). What is remarkable about our experiments is that the N groups were incorporated into the PMMA chains of a heterogeneous material composed of PMMA, polyisobutylene (PIB), and a graft of PMMA branches onto PIB. These results indicate that the PMMA chains demix into microphases. While the apparent T_g of this material has decreased to ca. 75°C compared to 105°C for pure PMMA, the activation energy for the α-methyl group relaxation within the PMMA microphase is unchanged from its value in the pure homopolymer.

These results offer encouragement that fluorescence and phosphorescence methods will provide means for studying relaxation processes within the individual microphases of blends and other composite polymer systems.

1. P. F. JONES and S. SIEGEL. J. Chem. Phys. **50**, 1134 (1969).
2. P. F. JONES. Polym. Lett. **6**, 487 (1968).
3. (*a*) S. CZARNECKI and M. KRYSZEWSKI. J. Polym. Sci. A, **1**, 3067 (1963); (*b*) E. I. HORMATS and F. C. UNTERLEITNER. J. Phys. Chem. **69**, 3677 (1965); (*c*) G. SHAW. Trans. Faraday Soc. **63**, 2181 (1967).
4. K. HORIE and I. MITA. Chem. Phys. Lett. **93**, 61 (1982).
5. A. C. SOMMERSALL, E. DAN, and J. E. GUILLET. Macromolecules, **7**, 233 (1974).
6. (*a*) H. RUTHERFORD and I. SOUTAR. J. Polym. Sci. Polym. Phys. Ed. **18**, 1021 (1980); (*b*) F. E. EL-SAYED, J. R. MACCALLUM, P. J. POMERY, and T. M. SHEPHERD. J. Chem. Soc. Faraday Trans. 2, **75**, 79 (1979).
7. (*a*) W. H. MELHUISH. Trans. Faraday Soc. **62**, 3384 (1966); (*b*) W. E. GRAVES, R. H. HOFELDT, and S. P. MCGLYNN. J. Chem. Phys. **56**, 1309 (1972).
8. (*a*) O. PEKCAN, M. A. WINNIK, L. EGAN, and M. D. CROUCHER. Macromolecules, **16**, 699 (1983); (*b*) M. A. WINNIK. Polym. Eng. Sci. **24**, 87 (1984).
9. O. PEKCAN, M. A. WINNIK, and M. D. CROUCHER. J. Coll. Interface Sci. **95**, 420 (1983).
10. O. PEKCAN, M. A. WINNIK, and M. D. CROUCHER. J. Polym. Sci. Polym. Lett. **21**, 1011 (1983).
11. M. A. WINNIK, M. H. HUA, B. HOUGHAM, B. WILLIAMSON, and M. D. CROUCHER. Macromolecules, **17**, 262 (1984).
12. M. D. CROUCHER, K. P. LOK, R. W. WONG, S. DRAPPEL, J. DUFF, A. L. PUNDSACK, and M. L. HAIR. J. App. Poly. Sci. In press.
13. U. MAHARAJ and M. A. WINNIK. J. Am. Chem. Soc. **103**, 2328 (1981).
14. J. W. HILPERN, G. PORTER, and L. J. STIEF. Proc. Roy. Soc. A, **277**, 437 (1964).
15. J. B. BIRKS. Photophysics of aromatic molecules. J. Wiley and Sons, New York. 1971.
16. S. H. LIN and R. BERSOHN. J. Chem. Phys. **48**, 2732 (1968).
17. J. JORTNER and R. S. BERRY. J. Chem. Phys. **48**, 2758 (1968).
18. D. L. DEXTER and W. B. POWDER. J. Chem. Phys. **47**, 1379 (1967).
19. Z. VEKSLI, W. G. MILLER, and E. L. THOMAS. J. Polym. Sci. Symposium No. 54, 299 (1976).
20. (*a*) T. KAWAI. J. Phys. Soc. Jpn. **6**, 1220 (1961); (*b*) J. G. POWLES and P. MANSFIELD. Polymer, **3**, 336 (1962).
21. N. G. MCCRUM, B. E. READ, and G. WILLIAMS. Inelastic and dielectric effects in polymer solids. J. Wiley and Sons, New York. 1900. Chapt. 8.
22. D. R. PAUL. Ber. Bunsenges. Phys. Chem. **83**, 294 (1979).
23. M. R. CARPENTER, D. B. DAVIES, and A. J. MATHESON. J. Chem. Phys. **46**, 2451 (1967).
24. M. A. WINNIK and O. PEKCAN. Macromolecules, **16**, 1021 (1983).
25. P. G. BORDANI, M. NUOVO, and L. VERDINI. Nuovo Cimento, **20**, 667 (1961).

Photoconductivity studies of perylene tetracarboxyl-diimides

ZORAN D. POPOVIC, RAFIK O. LOUTFY, AND AH-MEE HOR
Xerox Research Centre of Canada, 2660 Speakman Drive, Missassauga, Ont., Canada L5K 2L1

Received April 16, 1984

This paper is dedicated to the 10th anniversary of the Xerox Research Centre of Canada

ZORAN D. POPOVIC, RAFIK O. LOUTFY, and AH-MEE HOR. Can. J. Chem. **63**, 134 (1985).

Photoconductivity of a series of perylene tetracarboxyl-dimides has been studied by delayed-collection-field and electric field induced fluorescence quenching techniques. It has been shown that these materials exhibit both extrinsic (impurity controlled) and intrinsic carrier generation originating from the first excited singlet state. Perylene tetracarboxyl-diimides are photoactive in the visible spectral range and their carrier generation efficiencies compare well with generation efficiencies in the best known organic photoconductors. This makes them suitable for xerographic applications using visible light.

ZORAN D. POPOVIC, RAFIK O. LOUTFY et AH-MEE HOR. Can. J. Chem. **63**, 134 (1985).

Faisant appel à des techniques de piégeage de la fluorescence induite par un champ électrique et par un champ à collection retardée, on a étudié la photoconductivité d'une série de pérylènes tétracarboxyl-diimides. On montre que ces matériaux peuvent générer des transporteurs, à la fois d'une façon extrinsèque (controlée par les impuretés) et d'une façon intrinsèque; ces propriétés auraient leur origine dans le premier état singulet excité. Les pérylènes tétracarboxyl-diimides sont photoactifs dans la région du visible et leurs efficacités pour générer des transporteurs se compare bien avec les efficacités de génération des photoconducteurs organiques les mieux connus. On peut donc les considérer pour des applications xérographiques utilisant de la lumière visible.

[Traduit par le journal]

Introduction

In recent years the interest in photoconductivity in organic materials has ceased to be purely academic. This was mainly due to successful applications of organic photoconductors in xerography. After the pioneering work on the PVK–TNF system (1), many classes of photoconductive organic compounds have been found which can be used in xerographic photoreceptors. These include phthalocyanines (2), squaraines (3), thiopyrilium dyes (4), etc. Recently it has been shown that N,N'-bis-substituted perylene 3,4,9,10-tetracarboxyl-diimides exhibit high photoconductivity in both photovoltaic and xerographic applications (5). In the present study we have chosen to investigate in some depth the photoconductive behaviour of this class of compounds.

In a recent series of papers on X and β polymorphs of metal-free phthalocyanine, delayed-collection-field and electric field induced fluorescence quenching experiments were used to elucidate the mechanism of carrier generation (6–9). In the present work we will apply these techniques to study the carrier generation mechanism and also the influence of molecular structure and impurities on carrier generation in perylene derivatives.

Experimental

Materials

The chemical structures of the four compounds we investigated are given in Fig. 1. These materials were synthesized via the reaction of perylene 3,4,9,10-tetracarboxylic dianhydride with the desired amine. Products were purified by temperature gradient sublimation (10). The last compound (IV) is obtained as a mixture of two isomers shown in Fig. 1. The sublimed crystals therefore probably contained both isomers. The polymer binder used for fabrication of sandwich cells was polycarbonate (GE/Merlon) and the solvent used to prepare casting solutions was spectral grade methylene chloride.

Cell fabrication

Samples consisted of about 5 wt.% dispersion of the pigment in the polymer matrix draw-bar coated onto NESA glass slides. The coating solution was prepared by ball-milling the polymer, pigment, and solvent for 24 h. On top of the organic film Al was evaporated as the second electrode. Film thickness, which was between 1.5 μm and 2 μm, was determined from capacitance measurements assuming the composite relative dielectric constant of 2.9 (11). Optical micrographs of the cells showed that most of pigment particles were about 1 μm in size, with a few larger particles also present. The schematic representation of the sandwich cell is shown in Fig. 2.

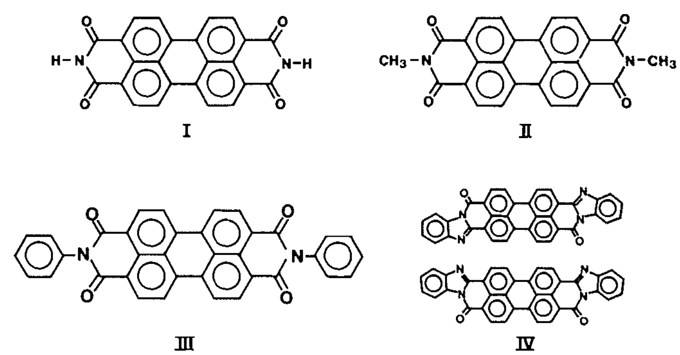

FIG. 1. Structural formulas of perylene diimides investigated in this work. In the text they are referred to as perylene I, II, III, and IV.

Measurements

Relative photoresponse, R, was determined by the delayed-collection-field technique (12). It was obtained as:

$$[1] \quad R = \frac{\Delta V}{I_{\text{light}}}$$

where ΔV is light induced voltage drop on the sample and I_{light} is the incident light intensity.

In the delayed-collection-field experiment the sample is illuminated with a short laser pulse (5 ns) under specified external voltage bias, which determines the electric field, E_{appl}, applied to the sample at the moment of illumination. After a short delay (typically 0.1 μs for our experimental set-up) a strong collection field, E_{coll}, is applied, which separates the photogenerated carriers. In order for the delayed-collection-field measurement to be meaningful, the relative photoresponse should saturate as the collection field is increased.

Electric field induced fluorescence quenching, $\Phi(E)$, is determined by the equation:

$$[2] \quad \Phi(E) = \frac{I_f(0) - I_f(E)}{I_f(0)}$$

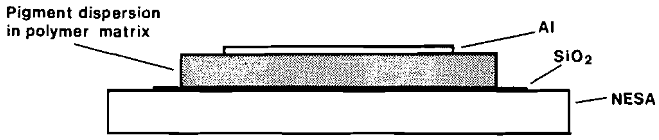

FIG. 2. Schematic diagram of the sandwich cell used in the measurements.

where $I_f(E)$ is the fluorescence signal normalized to the incident laser pulse intensity at the electric field E applied to the sample. Both R and Φ were measured simultaneously using a computerized signal averaging system described previously (8).

Fluorescence spectra were measured by exciting the sample by 5-ns light pulses from a Molectron nitrogen laser – dye laser system. The detection system consisted of a JY-20 monochromator, RCA C31034 GaAs photomultiplier tube, and PAR Model 162 boxcar integrator. For action spectra measurements (wavelength dependence of the photoresponse) Photochemical Research Associates Model 610C pulsed Xenon lamp and JY-20 monochromators were used providing 2.5-μs light pulses. All different instruments were controlled by a Cromemco System III microcomputer and every experimental point is typically an average of 100 measurements.

Results and discussion

In Figs. 3 and 4 action spectra and fluorescence spectra of compounds I–IV (Fig. 1) are presented. Action spectra were measured under the following electric field conditions: $E_{appl} = E_{coll} = E$. The apparent quantum efficiency, η', was obtained using the equation (13).

$$[3] \quad \eta' = \frac{C\Delta V}{eN_\Phi}\frac{1}{f_p}$$

where C is the total capacitance of the measuring circuit, ΔV is the voltage drop induced in the sample by pulsed illumination, e is the electron charge, N_Φ the number of light quanta falling on the sample, and f_p the relative volume of the sample occupied by photoconductive particles. As discussed in detail in ref. 13, the apparent quantum efficiency given by eq. [3] is approximately equal to the true carrier generation efficiency for illumination wavelengths which are strongly absorbed in photoconductive particles. It is interesting to note that there is a small but systematic discrepancy between sample photoresponse obtained for positive and negative bias of the semitransparent NESA electrode, with the negative bias giving consistently smaller photoresponse. This may be caused by either the existence of surface sensitized photoconductivity for holes or by slight differences in charge trapping and surface recombination parameters for electrons and holes. In general, action spectra (Figs. 3 and 4) resemble the absorption spectra (not shown) and the fluorescence appears as a mirror image of the absorption spectra.

In Fig. 5, the dependence of the relative photoresponse as a function of the collection field is given for samples I–III. These measurements were performed with no field applied to the sample at the moment of illumination $E_{appl} = 0$). As seen from Fig. 5, as the collection field is increased, the photoresponse saturates. In all subsequent experiments collection fields were chosen corresponding to the onset of saturation.

In Fig. 6 the dependence of the relative photoresponse on the collection field is given for sample no. IV for different fields, E_{appl}, applied at the time of illumination. In contrast to samples I–III, no clear saturation of the photoresponse is observed when $E_{appl} = 0$ (Fig. 6, curve (a)). However, there is a "distinct" shoulder around $E_{coll} = 10$ V/μm, after which photo-

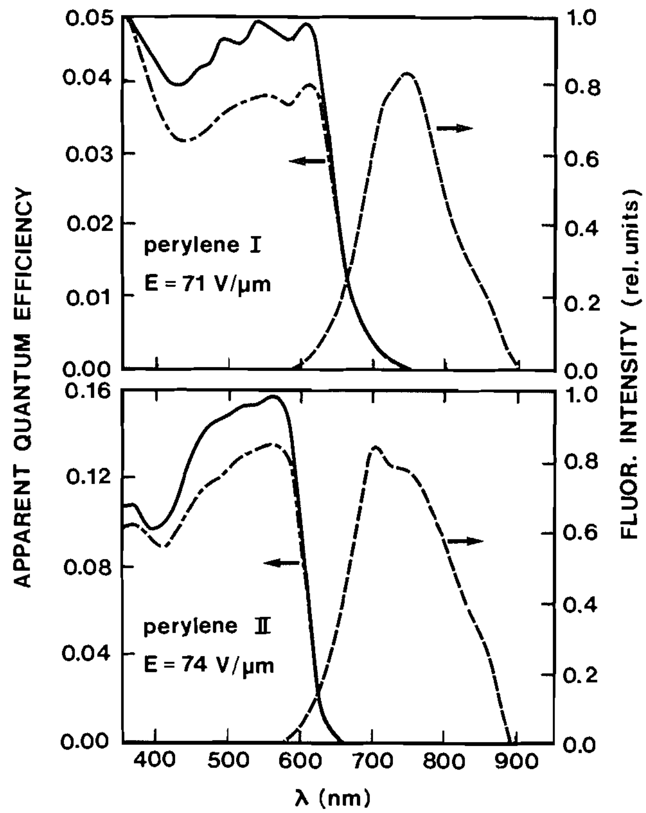

FIG. 3. Action spectra (—— NESA positive, ····· NESA negative) and fluorescence (– –) of perylenes I and II.

response increases relatively slowly. At higher E_{appl}, however, a clear saturation is observed for $E_{coll} > 10$ V/μm (Fig. 6, curves (b) and (c)). In subsequent measurements on this sample we have chosen $E_{coll} = 20$ V/μm, which is in the saturation range for higher fields.

At present we do not understand why sample no. IV behaves differently than samples I–III. It is interesting that only this compound has two structural isomers, which may be leading to increased trap density and to the observed anomalous behaviour in the photoresponse dependence on the collection field.

Before proceeding with discussion of further experimental data we will briefly discuss the correlation expected between fluorescence quenching and carrier generation in materials where the photoconductivity process occurs from the first excited singlet state. The fluorescence quenching efficiency (eq. [2]) is connected to the efficiency of the charge transfer state (geminate electron-hole pair) formation, η_{CT}, through the relation (7, 9)

$$[4] \quad \Phi(E) = \frac{\eta_{CT}(E) - \eta_{CT}(0)}{1 - \eta_{CT}(0)}$$

The carrier generation efficiency is given by

$$[5] \quad \eta(E) = \eta_{CT}(E) \cdot \Omega(E)$$

where $\Omega(E)$ is the probability that the CT dissociates into free carriers. At high fields $\Omega(E) = 1$ and linear correlation is expected between fluorescence quenching and carrier generation. As carrier generation is proportional to the relative photoresponse

$$[6] \quad \eta(E) = C \cdot R(E)$$

at high field we can write

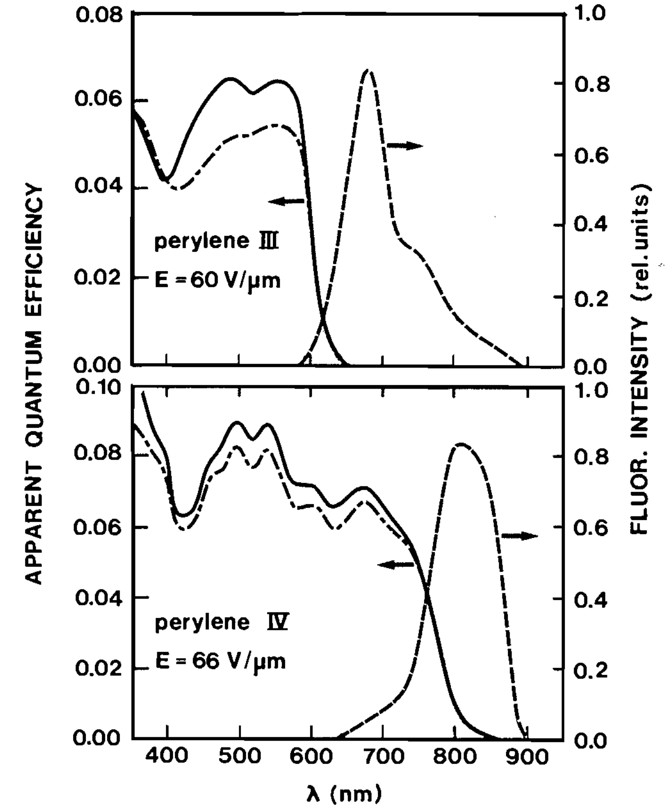

FIG. 4. Action spectra (—— NESA positive, ----- NESA negative) and fluorescence (– –) of perylenes III and IV.

$$[7] \quad \Phi(E) = \frac{C}{1 - \eta_{CT}(0)} R(E) - \frac{\eta_{CT}(0)}{1 - \eta_{CT}(0)}$$

If we now plot Φ as a function of R, from the intercept, i,

$$[8] \quad i = -\frac{\eta_{CT}(0)}{1 - \eta_{CT}(0)}$$

and slope, one can obtain both the proportionality constant C and $\eta_{CT}(0)$ and using [6] determine the true quantum efficiency $\eta(E)$. It is important to note that, alternatively, carrier generation efficiency can be calculated using eq. [3].

In Figs. 7a–10a the dependence of carrier generation efficiency and electric field induced fluorescence quenching on the applied field is given. For samples I and II, two material batches (before and after purification) have been studied. In Figs. 7b–10b correlation curves between fluorescence quenching efficiency and carrier generation are presented. Good correlation is observed in all cases, with some small discrepancies occuring at low fields. In Figs. 7–10 the scaling factor between R and η has been obtained as described in the preceding discussion.

It is interesting to compare carrier generation efficiencies obtained using combined fluorescence quenching and relative photoresponse measurements with the values obtained directly (as an absolute measurement) using eq. [3]. The comparison for purified materials is given in Table 1. The agreement between values obtained by the two methods is very good for samples II–IV, with only significant difference (a factor of two) observed in the case of sample I. For this sample optical microscopy reveals a relatively large proportion of large particles ($\gg$1 μm) which will not contribute significantly to the photoresponse, as they are larger than film thickness. There-

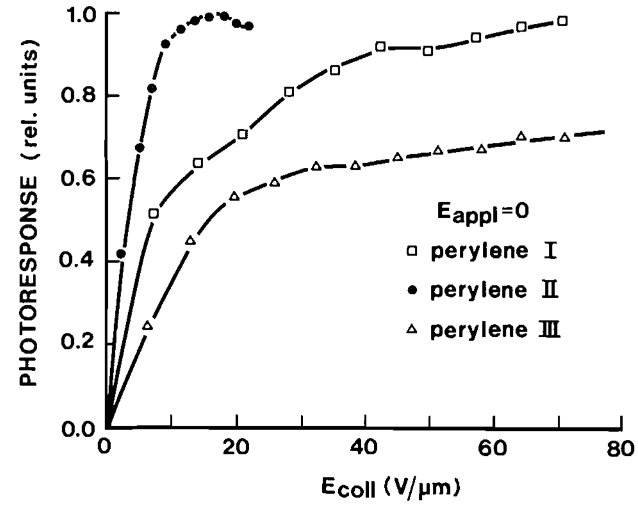

FIG. 5. Relative photoresponse obtained for zero field applied to the sample at the moment of illumination as a function of the collection field for perylenes I, II, and III.

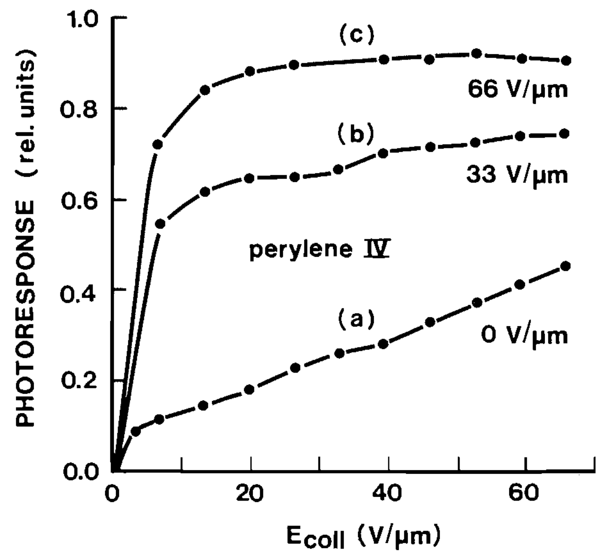

FIG. 6. The dependence of the relative photoresponse (at selected applied fields) on the collection field for perylene IV.

fore f_p in eq. [3] is overestimated, leading to the observed discrepancy.

A general feature of all fluorescence quenching curves is that they exhibit quadratic dependence at low applied fields. This can be easily understood in the framework of singlet decay (and concomitant fluorescence decrease) by production of CT states. Quadratic dependence is a direct consequence of possible formation of CT states in two opposite directions.

Some CT states are formed even at zero applied field. As they basically represent geminate electron-hole pairs, they can be separated by the application of a strong collection field in the delayed-collection-field experiment. Indeed, all our samples show non-zero carrier generation efficiency at no external field applied to the sample at the moment of illumination. As a rule in purified samples, the zero field carrier generation is relatively small. On the other hand, in non-purified samples it is much larger (Figs. 7 and 8). This enhancement of the zero field carrier generation must therefore be an impurity effect. It therefore appears that, in perylenes, both intrinsic and extrinsic

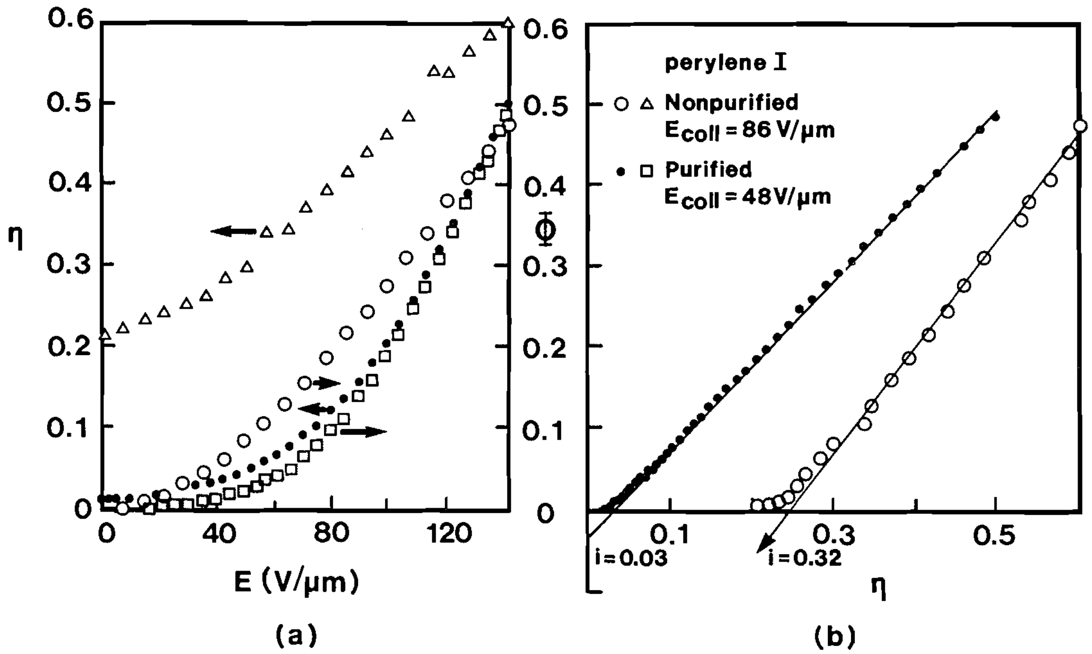

FIG. 7. Measurements on perylene I, before and after purification. (a) Field dependence of carrier generation efficiency and fluorescence quenching. (b) Correlation curves between fluorescence quenching and carrier generation.

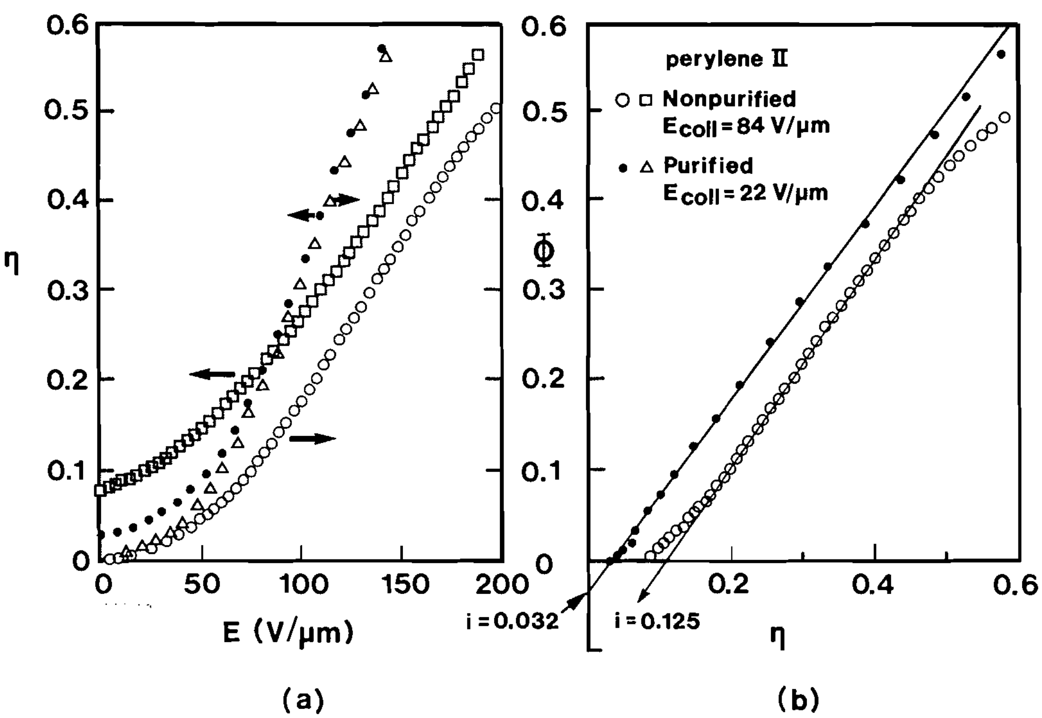

FIG. 8. Measurements on perylene II, before and after purification. (a) Field dependence of carrier generation and fluorescence quenching. (b) Correlation curves between fluorescence quenching and carrier generation.

(impurity controlled) carrier generation occurs. This is really not surprising, as the existence of sensitized photogeneration has been well documented in the literature (14).

From the point of view of practical applications like xerography, the existence of impurity controlled photogeneration can be quite detrimental, depending on the system. It is important to note that high fields are needed to separate carriers photogenerated at zero applied field. This, combined with the possibility that the carrier of one sign can be immobile, may lead to the increase in dark decay in subsequent xerographic cycles and accumulation of the trapped charge which increases background potential, and therefore decreases the contrast potential.

In xerography the shape of PIDC (photoinduced discharge curve) is predominantly governed by field dependence of carrier generation of the photoconductive component. This is strictly true when charge carriers have ranges of the order of photoreceptor thickness and, in dual layer structures, injection efficiency from the generator layer to the transport layer is

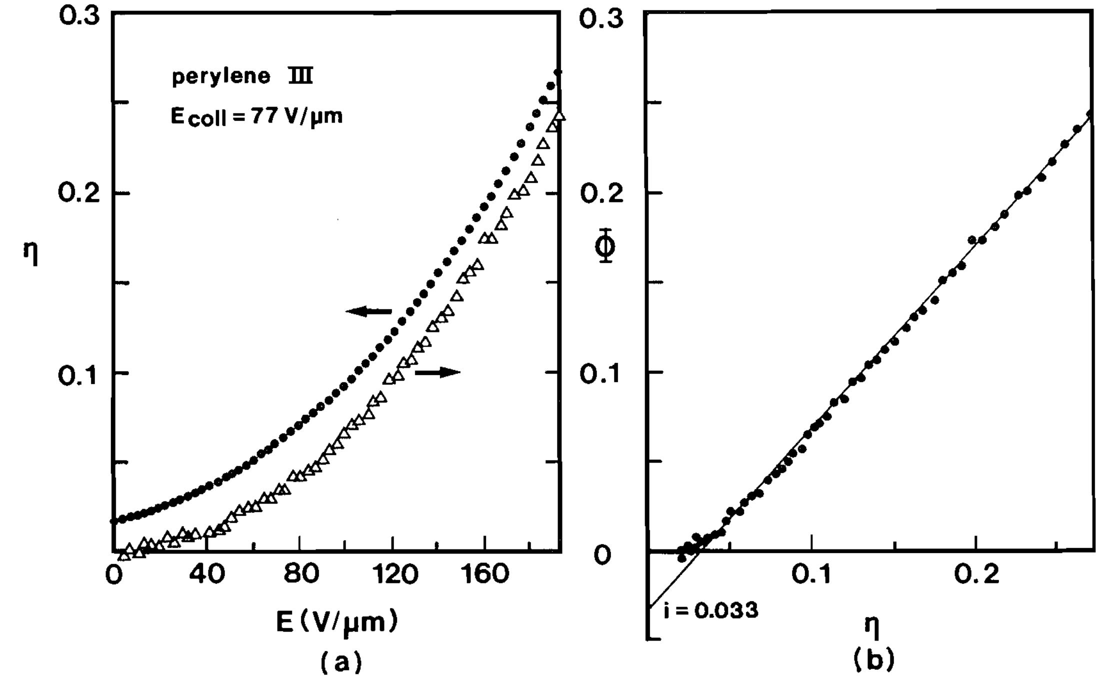

FIG. 9. Measurements on perylene III. (a) Field dependence of carrier generation and fluorescence quenching. (b) Correlation curve between fluorescence quenching and carrier generation.

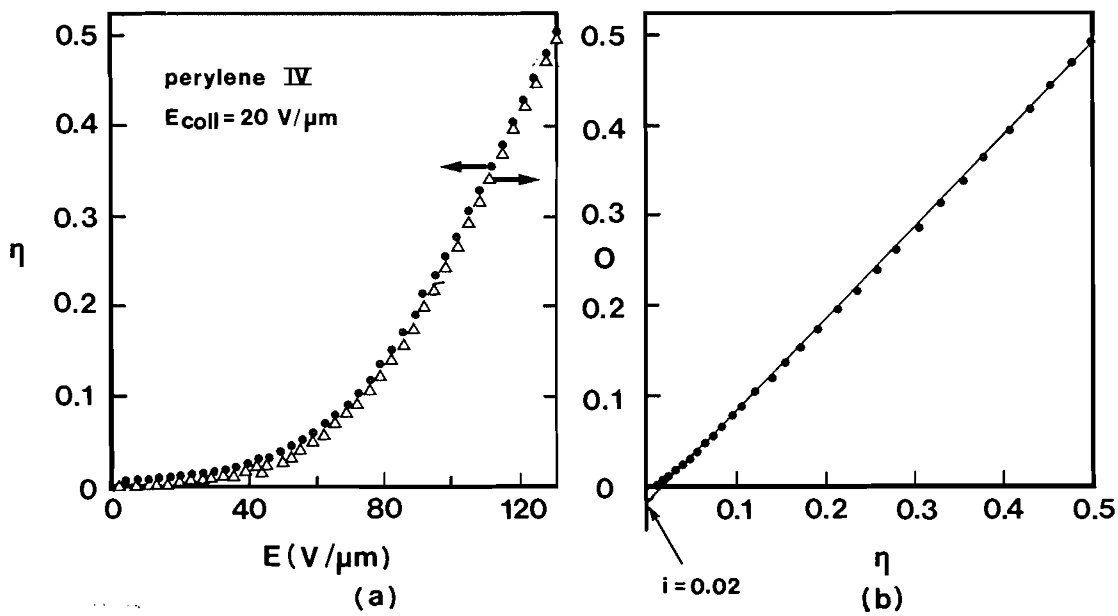

FIG. 10. Measurements on perylene IV. (a) Field dependence of carrier generation and fluorescence quenching. (b) Correlation curve between fluorescence quenching and carrier generation.

TABLE 1. Comparison of carrier generation efficiencies obtained as an absolute measurement from action spectra (η') and deduced from combined relative photoresponse and fluorescence quenching measurements (η)

		Carrier generation	
Compound	E_{appl} (V/µm)	η' (−, + NESA bias)	η
I	71	0.04–0.05	0.086
II	74	0.14–0.16	0.16
III	60	0.055–0.065	0.056
IV	66	0.08–0.09	0.08

unity. Therefore the obtained carrier generation data shown in Figs. 7–10 can be used to predict the performance of these materials when incorporated in photoreceptor structures.

The comparison of generation efficiencies of the perylene derivatives with selected organic photoconductors is given in Table 2. Thiopyrylium aggregate photoreceptor, hydroxy squarylium, and x-metal-free phthalocyanine all exhibit carrier generation efficiencies approaching unity at electric fields larger than 100 V/µm. The perylenes studied in the present work also exhibit high carrier generation, although it is typically about 50% lower than the carrier generation in previously discussed compounds. Perylenes are, however, much more photoconductive than β-H_2Pc, PVK, and PVK–TNF systems.

TABLE 2. Comparison of carrier generation efficiencies in perylene diimides with selected organic photoconductors, at three different applied fields

Material	η(%) E_{appl} = 100 V/μm	E_{appl} = 50 V/μm	E_{appl} = 20 V/μm	Reference
Perylene I	21	5	1.5	This work
II	32	10	4.5	This work
III	9	4	2.5	This work
IV	36	4	1	This work
Thiopyrylium aggregate p/r	50	34	14	4
Hydroxy squarylium	70	22	7	16
x-H_2Pc	40	18	8	7
β-H_2Pc	8	3.5	2.5	9
PVK	4.5	1.5	0.25	15
PVK–TNF	8	2	0.4	1

Conclusions

We have applied pulsed photoconductivity and electric field induced fluorescence quenching techniques to study photogeneration in perylene diimides. Results showed that both extrinsic (impurity controlled) and intrinsic carrier generation exist in these materials. The intrinsic component of photoconductivity is consistent with the model of carrier generation in which the first excited singlet state is the direct precursor of the photogenerated carriers. This is manifested in excellent linear correlation between carrier generation and fluorescence quenching measured at different electric fields.

We have also demonstrated that simultaneous measurements of relative photoresponse and fluorescence quenching lead to determination of true carrier generation efficiency which is in good agreement with the values determined by absolute measurements on particle dispersions.

In summary, the data presented in this work show that perylene diimides are highly photoconductive in the visible spectral range and therefore represent useful materials for xerographic applications using visible light.

Acknowledgements

We want to thank C. K. Hsiao for synthesizing the materials investigated in this work.

1. P. J. MELZ. J. Chem. Phys. **57**, 1694 (1972).
2. C. F. HACKET. J. Chem. Phys. **55**, 3178 (1971); S. GRAMMATICA and J. MORT. Appl. Phys. Lett. **38**, 445 (1981).
3. R. B. CHAMP and M. D. SHATTUCK. U.S. Patent No. 3,824,099 (1974); H. W. ANDERSON and M. T. MOR. U.S. Patent No. 4,140,987 (1979); H. KAMFER. U.S. Patent No. 3,617,270 (1971).
4. W. J. DULMAGE, W. A. LIGHT, S. J. MARINO, C. D. SALZBERG, D. L. SMITH, and W. J. STAUDENMAYER. J. Appl. Phys. **49**, 5543 (1978); P. M. BORSENBERGER, A. CHOWDRY, D. C. HOESTEREY, and W. MEY. J. Appl. Phys. **49** 5555 (1978).
5. E. G. SCHLOSSER. J. Appl. Phot. Eng. **4**, 118 (1978); C. W. TANG. Eur. Patent No. 0000829 A: (1980); W. WIEDEMANN. Eur. Patent No. 0040402 (1981); S. R. FORREST, M. L. KAPLAN, P. H. SCHMIDT, W. L. FELDMANN, and E. XANOWSKI. Appl. Phys. Lett. **41**, 90 (1982).
6. Z. D. POPOVIC. J. Chem. Phys. **76**, 2714 (1982).
7. Z. D. POPOVIC. J. Chem. Phys. **78**, 1552 (1983).
8. Z. D. POPOVIC. Chem. Phys. Lett. **100**, 227 (1983).
9. Z. D. POPOVIC. Chem. Phys. **86**, 311 (1984).
10. H. J. WAGNER, R. O. LOUTFY, and C. K. HSIAO. J. Mater. Sci. **17**, 2781 (1982).
11. W. J. ROFT, J. R. SCOTT, and J. PACITTI. Handbook of common polymers. CRC, Cleveland, OH. 1971.
12. F. K. DOLEZALEK and W. E. SPEAR. J. Phys. Chem. Solids, **36**, 819 (1975); R. ENCK and G. PFISTER. Photoconductivity and related phenomena. *Edited by* J. Mort and D. M. Pai. Elsevier, Amsterdam. 1976. pp. 224, 225.
13. Z. D. POPOVIC. J. Appl. Phys. **52**, 6197 (1981).
14. R. LOUTFY and E. R. MENZEL. J. Am. Chem. Soc. **102**, 4967 (1980).
15. P. M. BORSENBERGER and A. I. ATEYA. J. Appl. Phys. **49**, 4035 (1978).
16. R. O. LOUTFY, C. K. HSIAO, and P. M. KAZMAIER. Photogr. Sci. Eng. **27**, 5 (1983).

Dominance of irregular structures in the formation of intramolecular antiparallel β sheets by homopolyamino acids

WAYNE L. MATTICE
Department of Chemistry, Louisiana State University, Baton Rouge, LA 70803, U.S.A.

AND

EOK LEE AND HAROLD A. SCHERAGA
Baker Laboratory of Chemistry, Cornell University, Ithaca, NY 14853, U.S.A.

Received January 6, 1984

This paper is dedicated to the 10th anniversary of the Xerox Research Centre of Canada

WAYNE L. MATTICE, EOK LEE, and HAROLD A. SCHERAGA. Can. J. Chem. **63**, 140 (1985).

A matrix formulation of the conformational partition function is used to assess the influence of irregular structures on the formation of intramolecular antiparallel β sheets. An antiparallel sheet is considered to be irregular if any pair of contiguous strands has an unequal number of residues. The regular structures in the model consist of antiparallel sheets in which every strand contains the same number of residues. Aside from a growth parameter t, the model contains two parameters that account for the influence of edge effects. Each tight turn contributes a factor δ, and each residue in the sheet that does not have a partner in a preceding strand contributes a factor τ. When $\tau < \delta = 1$, preferred sheets consist of an extremely large number of very short strands. Such sheets resemble those found in cross-β fibers. Irregular structures increase the cooperativity of the formation of cross-β fibers. They cause the fibers that are formed to be longer (have more strands) and thicker (have more residues per strand) than if all antiparallel sheets were regular. A much different result is obtained if end effects are modified so that the antiparallel sheets formed resemble those found in globular proteins. Formation of antiparallel sheets remains cooperative, but irregular sheets now markedly reduce the cooperativity of the transition. At high antiparallel-sheet content, irregular structures cause typical antiparallel sheets to be smaller. The behavior of the conformational partition function shows that irregular structures make the dominant contribution to both transitions. Therefore, formulations that restrict consideration to regular structures may provide a misleading picture of antiparallel-sheet formation.

WAYNE L. MATTICE, EOK LEE et HAROLD A. SCHERAGA. Can. J. Chem. **63**, 140 (1985).

On a utilisé une formulation matricielle de la fonction de partition de conformation pour déterminer l'influence des structures irrégulières sur la formation de couches β intramoléculaires et antiparallèles. On considère qu'une structure feuilletée antiparallèle est irrégulière si l'une quelconque des paires de filaments contigues a un nombre inégal de résidus. Les structures régulières du modèle sont les couches antiparallèles dans lesquelles chaque filament contient le même nombre de résidus. En plus d'un paramètre de croissance, t, le modèle comporte deux paramètres qui tiennent compte de l'influence des effets d'arête. La contribution de chaque spire hermétique est un facteur δ et celle de chaque résidu dans la couche qui n'a pas de partenaire dans le filament précédent est un faceur τ. Lorsque $\tau < \delta = 1$, les couches privilégiées correspondent à un très grand nombre de filaments très courts. De telles couches ressemblent à celles trouvées dans des fibres réticulées de type β. Les structures irrégulières provoquent une augmentation de la coopérativité de formation de chaînes réticulées β. Les fibres qui se forment dans de telles conditions sont plus longues (il y a plus de filaments) et plus épaisses (il y a plus de résidus par filaments) que celles qui se forment lorsque toutes les couches antiparallèles sont régulières. On obtient un résultat très différent si les effets d'extrémités sont modifiés de telle sorte que les couches antiparallèles formées ressemblent à celles trouvées dans les protéines globulaires. La formation de couches antiparallèles reste soumise à l'effet de forces agissant dans le même sens, toutefois la présence de couches irrégulières réduit d'une façon importante la coopération de transition. Lorsque la teneur en couches antiparallèles est élevée, les structures irrégulières conduisent à la formation de couches antiparallèles typiques qui sont plus petites. Le comportement de la fonction de partition conformationnelle montre que les structures irrégulières contribuent de façon majoritaire aux deux transitions. En conséquence, les formulations qui se restreignent uniquement à une considération des structures régulières peuvent fournir une fausse image de la formation des couches antiparallèles.

[Traduit par le journal]

1. Introduction

The intramolecular antiparallel β sheet (1) is a structure commonly found in fibrous and globular proteins. We recently described a tractable matrix treatment for formation of intramolecular antiparallel β sheets with tight bends in homopolymers having a finite degree of polymerization (2). Three statistical weights are utilized. One, denoted by t, is assigned to every residue in the antiparallel sheet. The remaining two statistical weights, δ and τ, reflect the consequences of end effects. Each bend contributes a factor δ, and each residue that does not have a partner in a preceding strand contributes a factor τ. Previous illustrative calculations for homopolymers defined conditions that give rise to several different types of antiparallel sheets (2). Three types of particular interest here are (a) "sheets" consisting of isolated extended strands, (b) cross-β fibers, which are antiparallel sheets having a high axial ratio due to the presence of a large number of very short strands, and (c) antiparallel sheets composed of several strands in which the average strand contains approximately five residues. The third type of antiparallel sheet has a size and shape typical of those seen in globular proteins (3, 4). This type of sheet is not identical with those found in all globular proteins because it does not contain parallel strands, and contiguous strands cannot be connected by loops larger than tight bends. Cross-β fibers occur in several fibrous structures (5–7).

The general formulation (2) (which is easily extendible to specific-sequence heteropolymers) imposes no artificial constraints on the relationship between the numbers of residues in adjacent strands of the antiparallel sheet. However, the general treatment is easily modified so that every strand in a particular antiparallel sheet must have the same number of residues. In such antiparallel sheets, the number of residues in all strands is specified by the number of residues in the initial strand. These antiparallel sheets are described here as regular. In contrast, an antiparallel sheet in which any pair of adjacent strands has different numbers of residues will be designated as irregular. Several earlier descriptions of intramolecular antiparallel-sheet formation considered all antiparallel sheets to be regular (8–10). Two treatments (8, 9) employed antiparallel sheets in which all internal strands contained i residues, while the first and last strands had $i/2$ residues. These antiparallel sheets are defined here as being regular because the number of residues in all strands is specified by the number of residues in the first strand. It is of interest to establish the manner in which irregular antiparallel sheets contribute to statistical mechanical averages of conformational properties. The results presented here demonstrate that the presence of irregular antiparallel sheets has a profound influence on the formation of cross-β fibers and also on antiparallel sheets of the type found in globular proteins.

2. Calculations

The matrix formulation of the conformational partition function has been described in detail (2). The conformational partition function, Z, for a homopolymer comprised of n residues is written as

$$[1] \quad Z = \text{row}\,(1, \mathbf{0})\,\mathbf{U}^{n}\,\mathbf{U}\,\text{col}\,(1, \mathbf{0})$$

Here $\mathbf{U}$ is the statistical weight matrix, and $\mathbf{0}$ denotes a rectangular null submatrix whose dimensions are determined by the requirement that all matrices be conformable for multiplication. The terminating column, $\mathbf{U}$ col (1, $\mathbf{0}$), is identical with the first column in $\mathbf{U}$. All computations described here were performed for a homopolymer of 300 residues. A chain of 300 residues was selected because it is typical of that found in several large proteins. This number of residues is not sufficient to produce the behavior expected for an infinitely long chain when δ and τ are both small (11).

The statistical weight matrix is square and of dimensions $I(I + 3)/2$, where I is the maximum number of residues permitted in a strand. Ultimate interest is in the behavior of statistical mechanical averages in the limit where I goes to n. For most cases of interest here, that limit is attained in excellent approximation when I is 20. Special attention will be given in Section 6 to one circumstance in which a larger value for I would be required in order to produce a good approximation to the desired limit. For $I = 20$, the dimensions of $\mathbf{U}$ are 230 × 230, and the dimensions increase to 350 × 350 when I is 25. These large matrices are not constructed and manipulated in the computer. Instead a completely equivalent, but much more efficient, computation is performed by taking advantage of the sparseness of $\mathbf{U}$ and of summarizing rules which specify the locations of all nonzero elements (2). Conformational averages are extracted from Z by means of the usual statistical mechanical operations (12, 13).

The minimum number of residues per strand is two. Figure 1(A) depicts a regular antiparallel sheet containing six strands with two residues per strand. There are five bends. If one residue were to be removed from each strand, the resulting structure would be viewed as a single isolated strand of six residues and no bends. It is not considered to be an antiparallel sheet composed of six strands (each containing one residue) and five bends.

A disordered "c" residue is selected as the reference state and assigned a statistical weight of 1. The weighting scheme for

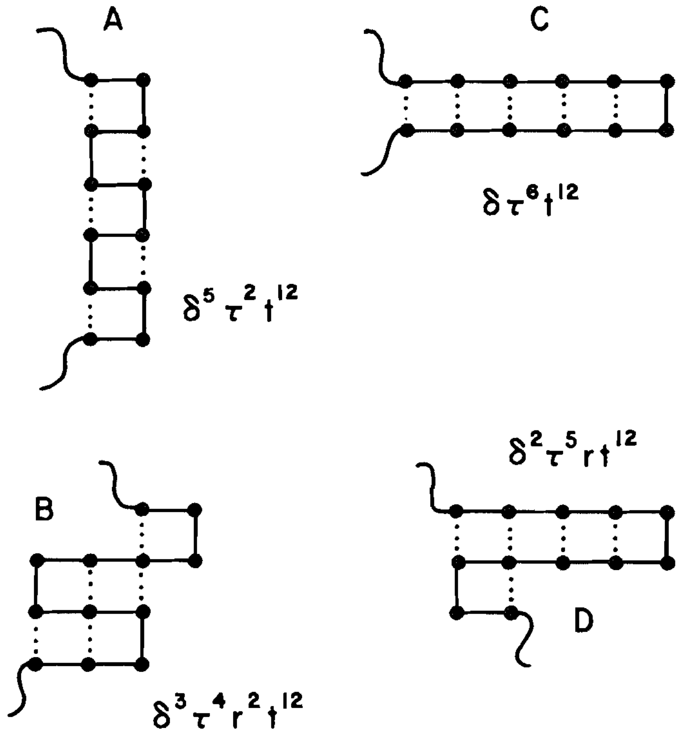

FIG. 1. Four illustrative antiparallel sheets of twelve residues, along with their statistical weights.

antiparallel sheets is illustrated in Fig. 1. This figure depicts four antiparallel sheets, two of which (A and C) are regular, while two (B and D) are irregular. The statistical weight is indicated for each antiparallel sheet. This weight can be written as

$$\delta^{n_{\mathrm{Bend}}/2}\,\tau^{n_{\mathrm{b}}}\,r^{n_{\mathrm{r}}}\,t^{n_{\mathrm{b+B}}}$$

Here $n_{\mathrm{b+B}}$ is the number of residues in the antiparallel sheet, n_{b} is the number of residues in the sheet that do not have a partner in the preceding strand, n_{r} is the number of pairs of contiguous strands which contain unequal numbers of residues, and n_{Bend} is the number of residues located at bends. Residues which contribute a factor τ are denoted by "b". The remaining residues in the antiparallel sheets are denoted by "B". Those residues situated at bends are considered to be part of the antiparallel sheet.

The value of n_{r} is of no consequence when $r = 1$. This assignment allows for the presence of both regular and irregular antiparallel sheets. All irregular antiparallel sheets are rejected when the assignment is changed from $r = 1$ to $r = 0$. Thus, if $r = 0$, the structures in Figs. 1B and 1D are rejected. There is no effect on the relative weighting of surviving antiparallel sheets because all regular antiparallel sheets have $n_{\mathrm{r}} = 0$ (we assume $x^0 = 1$ even when x is zero).

3. Transition from disordered chain to antiparallel sheet

Sheet formation in chains of 300 residues, arising from changes in t, is depicted in Fig. 2 for four combinations of δ and τ. A maximum of twenty residues is permitted in a strand. The transitions depicted by solid lines were initially described by Mattice and Scheraga (2).

Cooperativity provides a convenient means of classifying the transitions. The maximum of $\mathrm{d}f_{\mathrm{b+B}}/\mathrm{d}t$ (where $f_{\mathrm{b+B}}$ is the fraction of b + B states) will be taken as a measure of the cooperativity of a transition. A noncooperative transition is obtained

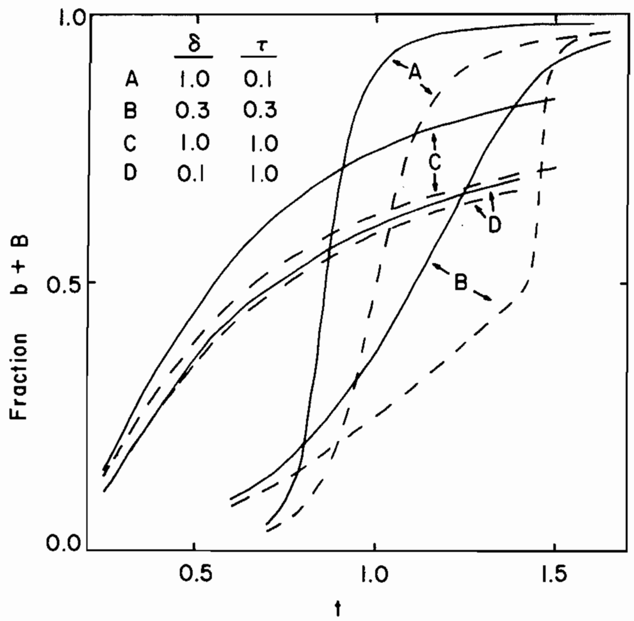

FIG. 2. Fraction of the residues in "b" or "B" states for the indicated values of δ and τ. Solid curves are obtained when there is no distinction between regular and irregular antiparallel sheets (r = 1), while dashed curves denote results obtained when all antiparallel sheets are regular (r = 0). All transitions were computed using n = 300 and l = 20.

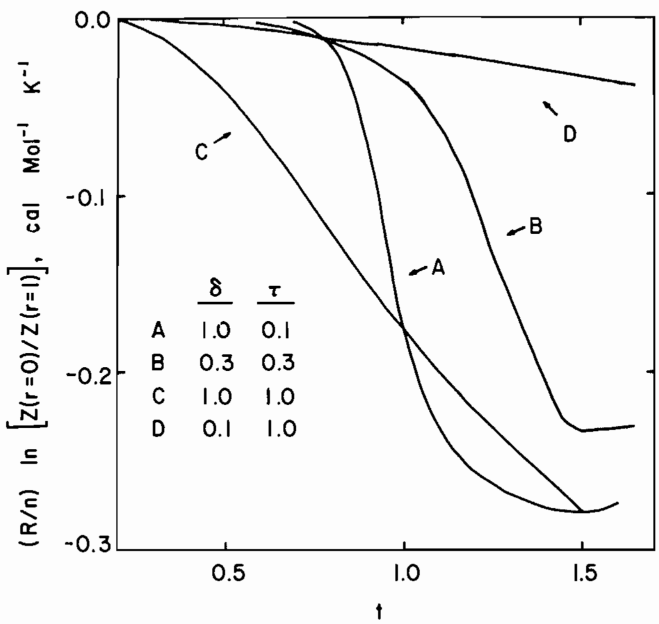

FIG. 3. $(R/n)\ln[Z(r = 0)/Z(r = 1)]$ for the indicated transitions when n = 300 and l = 20.

when δ = τ = 1. Comparison of curves C and D in Fig. 2 shows a similar lack of cooperativity when δ = 0.1, τ = 1. At a specified t, antiparallel sheet content in the noncooperative transitions is reduced if irregular antiparallel sheets are rejected. The reduction becomes less dramatic when δ is decreased from 1 to 0.1. In the limit where δ goes to zero, bends are completely suppressed and each "sheet" consists of an isolated extended strand (2). The statistical weight denoted by r is excluded from Z when δ is zero because no sheet contains multiple strands. Multistranded antiparallel sheets retain a small contribution to Z when δ is 0.1, and some of the antiparallel sheets are irregular. Consequently the change from r = 1 to r = 0 has a small effect when δ = 0.1. A larger effect is seen at δ = 1 because multistranded antiparallel sheets make a larger contribution to Z when bends are not penalized; hence, the effect of eliminating a significant number of irregular sheets is larger.

Sheet formation shows a higher degree of cooperativity when δ = 1, τ = 0.1, and when δ = τ = 0.3. The antiparallel sheets formed can be described as cross-β fibers in the former case (2). The initial strand is short because each residue in it is penalized when τ = 0.1. Many short strands can follow the initial strand without further penality because bends are not penalized when δ = 1. Antiparallel sheets resembling those found in globular proteins can be formed when δ = τ = 0.3. These antiparallel sheets contain several strands with about five residues per strand (3, 4). Onset of antiparallel sheet formation in the cooperative transitions demands a larger t if irregular antiparallel sheets are rejected. The cooperativity of the formation of cross-β fibers is slightly reduced if the fiber must be regular. In contrast, antiparallel sheet formation at δ = τ = 0.3 becomes significantly more cooperative when all antiparallel sheets are regular.

The greatest cooperativity is seen in the latter stages of the transition with δ = τ = 0.3, r = 0. A slightly greater cooperativity would be exhibited in the latter portion of this transition if the strands were allowed to contain more than twenty residues. Justification for this statement will be presented in Section 6. Additional calculations, the results of which are not presented here, show that the transition with δ = τ = 0.3, r = 0, at large t is the only one in Fig. 2 for which l = 20 does not provide an excellent approximation to the limit as l goes to 300.

Attention now turns to a consideration of the details of noncooperative antiparallel sheet formation (δ = τ = 1), cooperative cross-β fiber formation (δ = 1, τ = 0.1), and cooperative formation of the types of antiparallel sheets seen in globular proteins (δ = τ = 0.3).

4. Noncooperative sheet formation

Special interest attends the circumstance δ = τ = t = 1. All allowed conformations then have a statistical weight of one, and Z is simply the number of conformations. Numerical values of Z with n = 300 and l = 20 are 1×10^{90} when r = 1 and 4×10^{78} when r = 0. There are nearly 10^{12} conformations containing irregular antiparallel sheets for every conformation in which all antiparallel sheets are regular. If a large number of residues in a long chain is arranged in antiparallel sheets of the types seen in Fig. 1, the overwhelming majority of chain conformations will contain at least one sheet in which contiguous strands have different numbers of residues.

The relationship between Z at r = 1 and Z at r = 0 was evaluated for other values of t for the noncooperative transitions. Figure 3 depicts the results as $(R/n)\ln[Z(r = 0)/Z(r = 1)]$, which can be viewed as an entropic contribution expressed per mole of residues. It is on the order of -0.1 cal mol^{-1} K^{-1} at the midpoint of the transition to an antiparallel sheet (t near 0.6, Fig. 2) when δ = τ = 1. In contrast, it is on the order of -0.01 cal mol^{-1} K^{-1} at the midpoint of noncooperative antiparallel sheet formation when δ = 0.1 and τ = 1. The entropic effect is smaller in the latter case because the small value of δ/τ discourages formation of bends.

The average number of residues per antiparallel sheet is depicted in Fig. 4. The average antiparallel sheet is small when

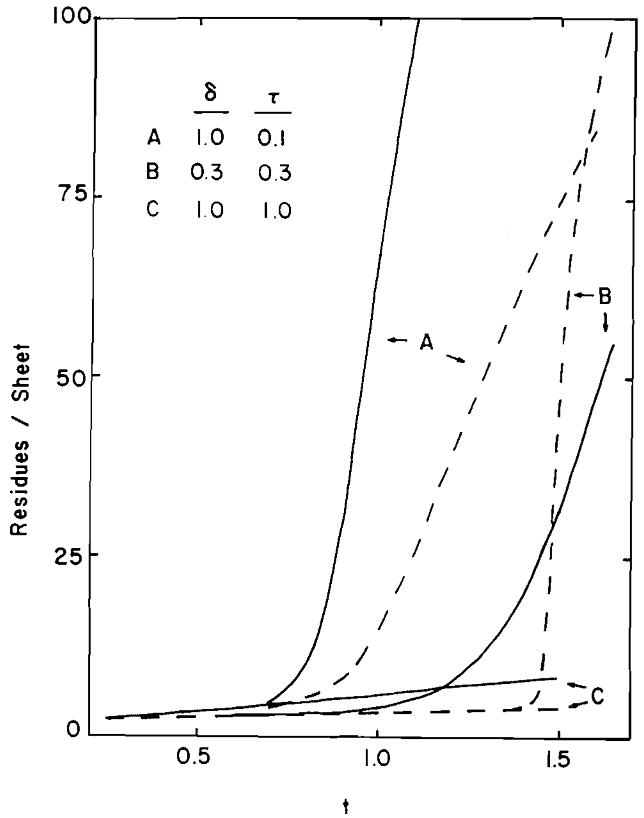

FIG. 4. Average number of residues per antiparallel sheet for the indicated values of δ and τ. Solid and dashed curves pertain to $r = 1$ and $r = 0$, respectively. All transitions were computed using $n = 300$ and $l = 20$.

$\delta = \tau = 1$. It becomes significantly smaller at large t if irregular antiparallel sheets are rejected. There is only a trivial effect on the number of residues per strand. At $t = 1.5$, the average number of residues per strand falls from 3.17 to 3.08 when irregular antiparallel sheets are eliminated. The change in the size of the average antiparallel sheet arises primarily from a reduction in the number of strands per antiparallel sheet, as shown in Fig. 5. At $t = 1.5$, there is an average of 2.72 strands per antiparallel sheet when irregular antiparallel sheets are allowed, but the average drops to 1.39 if irregular antiparallel sheets are excluded. The decrease in the number of strands per antiparallel sheet occurs because it is unlikely that adjacent strands will contain the same number of residues when antiparallel sheets form noncooperatively.

Differences in the average number of strands per antiparallel sheet have a large effect on the fraction of the residues situated at bends (Fig. 6). Rejection of irregular antiparallel sheets is accompanied by a large reduction in the number of bends because most of the surviving "sheets" consist of a single extended strand.

5. Cooperative cross-β fiber formation

An example of a set of end effects giving rise to cooperative formation of cross-β fibers is provided by the transition obtained with $\delta = 1$, $\tau = 0.1$. Comparison of Figs. 2 and 3 shows that $Z(r = 0)/Z(r = 1)$ undergoes a dramatic change as t passes through the region where fiber formation occurs. Differences in characteristics of the fibers are brought out in Figs. 4–7. If irregular antiparallel sheets are retained, the fibers are larger (contain more residues, Fig. 4), longer (have

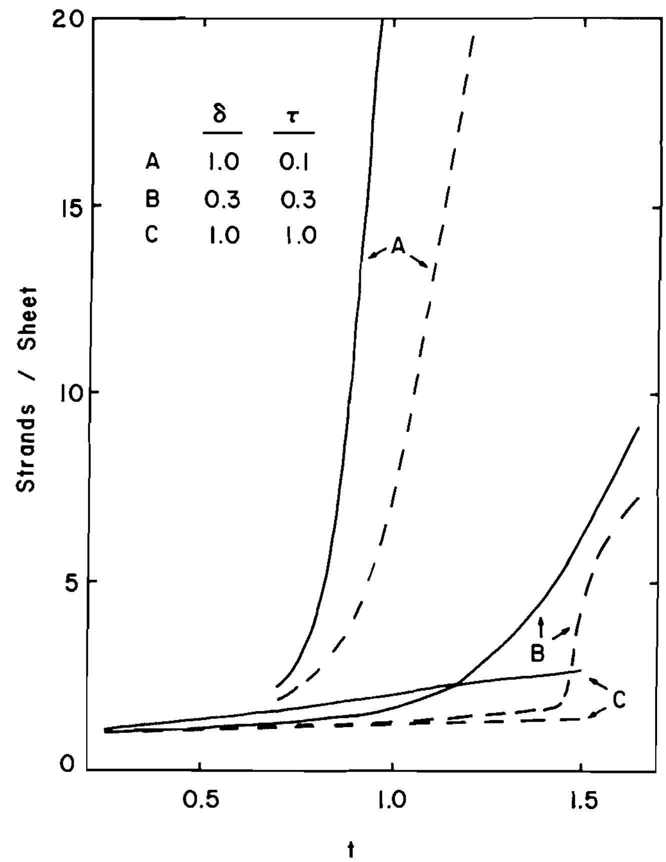

FIG. 5. Average number of strands per antiparallel sheet for the indicated values of δ and τ. Solid and dashed curves pertain to $r = 1$ and $r = 0$, respectively. All transitions were computed using $n = 300$ and $l = 20$.

more strands per antiparallel sheet, Fig. 5), and thicker (possess more residues per strand, Fig. 7). Differences in the average number of residues per strand are particularly important. There is an average of two residues per strand if irregular antiparallel sheets are rejected. Most antiparallel sheets then consist of a large number of in-register strands comprised of two residues each. Fig. 1(A) depicts a prototype of this fiber. All internal residues in this antiparallel sheet participate in bend formation. Consequently the fraction of residues situated at bends approaches 1 at large t (Fig. 6).

The average number of residues per strand approaches three when irregular antiparallel sheets are allowed (Fig. 7). Since the middle residue in a three-residue strand cannot participate in bend formation, the value of f_{Bend} at large t is considerably smaller than that when irregular antiparallel sheets are permitted (Fig. 6). While the average number of residues per strand is three, it would be incorrect to infer that the typical fiber consists of a large number of in-register strands containing exactly three residues each. If such fibers were truly to dominate the ensemble having $r = 1$, they would also dominate the ensemble with $r = 0$. Since they do not readily survive this change in r, the typical cross-β fiber occurs in a chain conformation which contains at least one pair of contiguous strands having unequal numbers of residues.

6. Cooperative sheet formation when $\delta = \tau = 0.3$

Antiparallel sheets resembling those commonly seen in globular proteins are formed when δ and τ are both less than one and

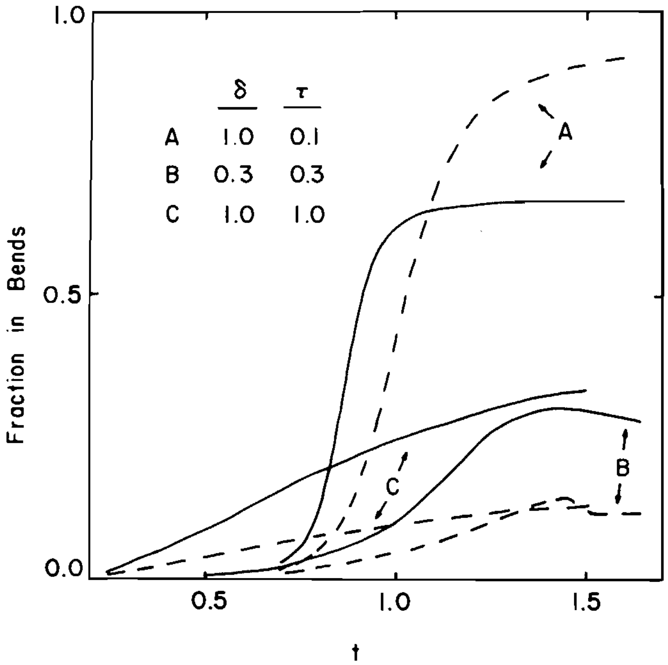

FIG. 6. Average number of residues located at bends for the indicated values of δ and τ. Solid and dashed curves pertain to $r = 1$ and $r = 0$, respectively. All transitons were computed using $n = 300$ and $I = 20$.

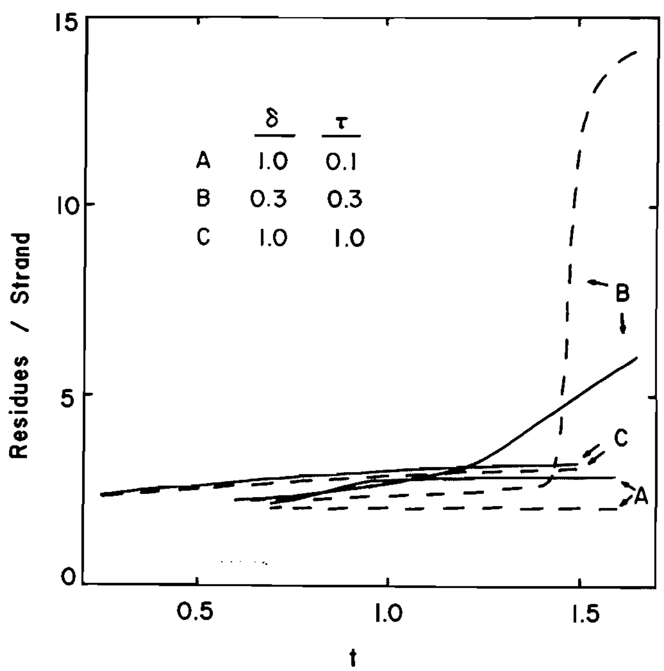

FIG. 7. Average number of residues per strand for the indicated values of δ and τ. Solid and dashed curves pertain to $r = 1$ and $r = 0$, respectively. All transitions were computed using $n = 300$ and $I = 20$.

not too different from one another (2). Comparison of curves depicted in Figs. 2 and 3 shows that (R/n) ln $[Z(r = 0)/Z(r = 1)]$ decreases as sheets are formed when $\delta = \tau = 0.3$. A striking feature of the transition obtained with $r = 0$ is the extremely sharp rise in f_{b+B} as t rises above 1.4. No comparable jump is seen when irregular antiparallel sheets contribute to the transition.

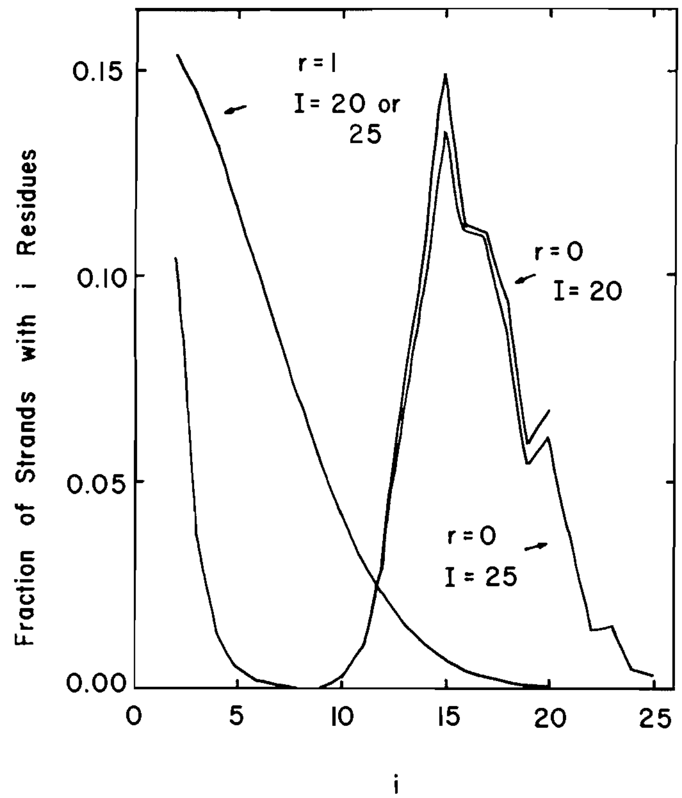

FIG. 8. Fraction of the strands containing the indicated number of residues when $\delta = \tau = 0.3$, $t = 1.6$, $n = 300$. The values of r and I are indicated for each curve.

The contrasting behaviors seen in Fig. 2 have their counterparts in the dimensions of the antiparallel sheets formed. Figure 4 shows that rejection of irregular antiparallel sheets is accompanied by a substantial reduction in the average number of residues per antiparallel sheet when t is in the range 1.0–1.4. However, the reverse becomes true as t approaches 1.5, due to an extremely rapid increase in the average size of the regular antiparallel sheets. This dramatic increase in the size of regular antiparallel sheets coincides with the rapid rise in f_{b+B} in Fig. 2. Inspection of Figs. 5 and 7 shows that the rapid rise in the size of regular antiparallel sheets has contributions from increases in the average number of strands per antiparallel sheet and average number of residues per strand.

In Section 2, it was stated that $I = 20$ provides a satisfactory approximation to the true behavior for all but one of the models considered here. The single exception is provided by regular antiparallel sheets formed at high t when $\delta = \tau = 0.3$. The basis for this statement is provided by examination of distribution functions for the number of residues per strand. Four distribution functions are depicted in Fig. 8. All are for $\delta = \tau = 0.3$ and a chain of 300 residues. The value of t is 1.6, which is slightly higher than the t that provides the maximum value of df_{b+B}/dt in Fig. 2.

Two distribution functions are for ensembles which retain irregular antiparallel sheets. The maximum number of residues permitted in a strand is 20 in one computation and 25 in the other. These two distribution functions resemble one another so closely that they are not distinguishable on the scale used in preparation of Fig. 8. Both distribution functions exhibit a monotonic decline as the length of the strands increases. They decay to very small values for chains containing as many as twenty residues per strand. The average number of residues per strand changes slightly (from 5.77 to 5.79) when l increases from 20 to 25.

Figure 8 also depicts a distribution function computed using $r = 0$ and $l = 20$. Two important differences are apparent upon comparison of the two distribution functions calculated using a maximum of 20 residues per strand. When irregular antiparallel sheets are present, the distribution function exhibits a monotonic decay at small values of i, but elimination of irregular antiparallel sheets causes the distribution function to become biphasic. The biphasic distribution function exhibits maxima for strands containing two and fifteen residues. At the beginning of Section 4, it was noted that the ensemble contains many more chain conformations when irregular sheets are allowed. Ensembles specified by $r = 0$ and $r = 1$ differ not only in the number of chain conformations, but also in the sizes of the strands that are present in these conformations. The presence of irregular structures causes a greater portion of the conformations to have sheets containing 6–9 residues per strand than would have been the case if all sheets were regular. The ensemble with $r = 1$ contains a greater fraction of conformations that are potential stable intermediates if δ and τ are assigned so that sheets contain more than 9 residues per strand as t becomes infinite. The presence of more stable intermediates causes the transition to have less of an "all or none" character when irregular sheets are present. The second difference is seen upon examination of the value of the distribution function for the longest (20 residues) allowed strand. The distribution function has decayed to a negligible value when irregular antiparallel sheets are retained, but it remains quite large when irregular antiparallel sheets are rejected. There is an implication that the ensemble with $r = 0$ would take advantage of the opportunity to form even longer strands if that opportunity were presented.

That implication is verified by the fourth distribution function, computed using $r = 0$ and $l = 25$. The increase in l from 20 to 25 causes the average number of residues per strand to rise from 13.87 to 14.27. When $r = 0$, the limiting behavior as l approaches n requires a value of l greater than 20. The consequences of the use of $l = 20$, rather than some larger value, can be summarized as follows: for $\delta = \tau = 0.3$, $r = 0$, and large t, the height and cooperativity of the sharp rise in f_{b+B} (Fig. 2), and the sizes of the resulting regular antiparallel sheets (Figs. 4, 5, and 7) are all underestimated.

Distribution functions were also examined using $t = 1.3$, which lies slightly before the marked rise in f_{b+B} in Fig. 2. At this value of t, all four distribution functions show a maximum for a strand of two residues, undergo a monotonic decay as one proceeds to longer strands, and fall to a negligible value when strands contain as many as twenty residues. These distribution functions are unaffected by changing l from 20 to 25.

An examination of the numerical values for Z facilitates an understanding of the origin of the effects seen in Fig. 8. The first two entries in Table 1 are for ensembles in which all antiparallel sheets are regular. The increase in l from 20 to 25 does not eliminate any conformations from the ensemble. Instead it adds chain conformations having 21–25 residues per strand. The added conformations cause Z to increase by a factor of 1.1.

No chains are eliminated from the ensemble if r is changed from 0 to 1 at constant l. Instead, conformations containing irregular antiparallel sheets are introduced into the ensemble. At $l = 20$ or 25, addition of the irregular antiparallel sheets

TABLE 1. Conformational partition functions when $n = 300$, $\delta = \tau = 0.3$, $t = 1.6$

r	l	Z
0	20	5.3×10^{44}
0	25	6.0×10^{44}
1	20	7.0×10^{59}
1	25	7.0×10^{59}

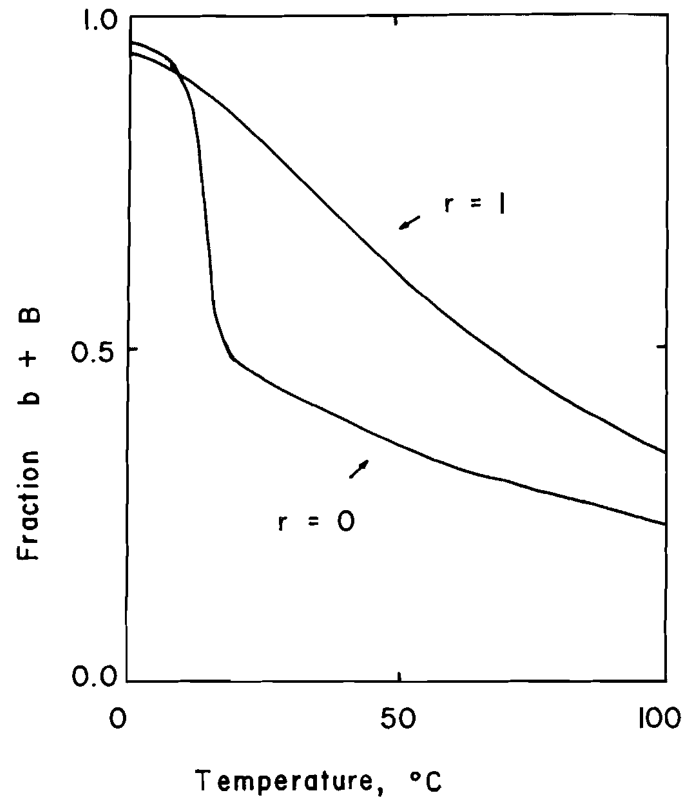

FIG. 9. Illustrative thermal transitions for the case where $n = 300$, $l = 20$, $\delta = \tau = 0.3$. The only temperature-dependent parameter is t. It is 1.6 at 0°C, with a temperature dependence corresponding to $\Delta H^0 = -1$ kcal mol^{-1}.

increases the value of Z by a factor of 10^{15}. The huge increase in the size of Z implies that completely regular antiparallel sheets have negligible influence on the properties of the new ensemble. Using "Σ_{irreg}" to denote the sum of the statistical weights for all chain conformations containing irregular sheets, we have

$$[2] \quad Z(r = 1) = Z(r = 0) + \Sigma_{\text{irreg}}$$

The last term exceeds $Z(r = 0)$ by a factor of 10^{15}. This factor would have been 10^{12} if all conformations were weighted equally (see Section 4). Conformations containing irregular antiparallel sheets completely dominate the ensemble due primarily to their overwhelming numbers, but in part due to the influence of the weighting of chain conformations. The presence of a multitude of chains containing irregular antiparallel sheets markedly reduces the cooperativity of the transition and the sizes of the antiparallel sheets formed.

Data depicted in Fig. 2 are replotted in Fig. 9 in a manner which emphasizes the potentially important consequences of irregular antiparallel sheets in thermally induced transitions. For purposes of illustration, all parameters except t are assumed to be independent of temperature. The value of t is assumed to be 1.6 at 0°C, with $d \ln t/d(1/T) = -\Delta H^0/R$ and ΔH^0 having the temperature-independent value of -1 kcal mol^{-1}. Irregular antiparallel sheets cause melting to extend continuously over a broader temperature range. If all antiparallel sheets must be regular, there is a rather sharp transition at low temperature, corresponding to the highly cooperative melting of the large regular antiparallel sheets, followed by a much less cooperative melting of small regular antiparallel sheets. The two melting curves are qualitatively different.

7. Conclusions

The number of irregular sheets accessible to a long chain far exceeds the number of regular sheets. Irregular structures make important contributions to average properties of two important classes of antiparallel sheets formed by homopolypeptides. They increase slightly the cooperativity of the formation of cross-β fibers. They also cause the fibers formed to be wider and longer. Irregular structures have a different effect on the transition which produces antiparallel sheets containing several strands with an average of about five residues per strand. Here, irregular structures bring about a dramatic reduction in the cooperativity of the transition and the size of the antiparallel sheets formed. Theoretical formulations in which all structures are regular may provide a misleading picture of antiparallel sheet formation in globular proteins.

Acknowledgment

This research was performed while W.L.M. was on sabbatical leave at Cornell University during 1983–1984. W.L.M. gratefully acknowledges sabbatical support from the National Institutes of Health (Senior National Research Service Award 1 F33-AM-07296-01). This research was also supported by research grants to H.A.S. from the National Institutes of Health (AM-08465) and from the National Science Foundation (PCM 79-20279) and to W.L.M. from the National Science Foundation (PCM 81-18197).

1. L. PAULING and R. B. COREY. Proc. Natl. Acad. Sci. U.S.A. **39**, 253 (1953).
2. W. L. MATTICE and H. A. SCHERAGA. Biopolymers. **23**, 1701 (1984).
3. M. J. E. STERNBERG and J. M. THORNTON. J. Mol. Biol. **110**, 285 (1977).
4. J. S. RICHARDSON. Nature, **268**, 495 (1977).
5. W. T. ASTBURY, S. DICKINSON, and K. BAILEY. Biochem. J. **29**, 2351 (1935).
6. A. J. GEDDES, K. D. PARKER, E. D. T. ATKINS, and E. BEIGHTON. J. Mol. Biol. **32**, 343 (1968).
7. N. M. GREEN, N. G. WRIGLEY, W. C. RUSSELL, S. R. MARTIN, and A. D. MCLACHLAN. EMBO J. **2**, 1357 (1983).
8. F. KANÔ. J. Phys. Soc. Jpn. **41**, 219 (1976).
9. H. WAKANA, T. SHIGAKI, and N. SAITÔ. Biophys. Chem. **16**, 275 (1982).
10. W. L. MATTICE. Macromolecules, **17**, 407 (1984).
11. W. L. MATTICE and H. A. SCHERAGA. Macromolecules. In press.
12. D. POLAND and H. A. SCHERAGA. Theory of helix-coil transitions in biopolymers. Academic, New York. 1970.
13. P. J. FLORY. Macromolecules, **7**, 381 (1974).

Synthesis, molecular and electron transport properties of 2-alkyltrinitrofluoren-9-ones

BENG S. ONG,[1] BARKEV KEOSHKERIAN, TREVOR I. MARTIN, AND GORDON K. HAMER
Xerox Research Centre of Canada, 2660 Speakman Drive, Mississauga, Ont., Canada L5K 2L1

Received February 10, 1984

This paper is dedicated to the 10th anniversary of the Xerox Research Centre of Canada

BENG S. ONG, BARKEV KEOSHKERIAN, TREVOR I. MARTIN, and GORDON K. HAMER. Can. J. Chem. **63**, 147 (1985).

2-Alkyltrinitrofluoren-9-ones **2** were conveniently synthesized by controlled nitration of 2-alkylfluoren-9-ones **5** with a mixture of red fuming HNO_3 and concentrated H_2SO_4 at 0–25°C. The precursors **5** were derived from the corresponding 2-acylfluorenes by appropriate reduction of the acyl function, followed by base-catalysed O_2-oxidation at the C-9 position. The regiochemistry of nitration was interesting: with a sterically bulky substituent in **5**, nitration occurred at C-4, -5, and -7 positions, affording 2-alkyl-4,5,7-trinitrofluoren-9-one in over 35% yield; on the other hand, **5** with a primary alkyl function underwent nitration predominantly at C-3, -5, and -7 positions. By virtue of its alkyl function, 2-alkyltrinitrofluoren-9-one **2** displayed better solubility and polymer compatibility characteristics than its non-alkylated analog, TNF. However, the charge transfer interactions of **2** with electron donors were weaker than those of TNF, despite the fact that they both have the same electron affinity. Both **2** and TNF exhibited good electron transport properties in poly(*N*-vinylcarbazole) matrices.

BENG S. ONG, BARKEV KEOSHKERIAN, TREVOR I. MARTIN et GORDON K. HAMER. Can. J. Chem. **63**, 147 (1985).

On a synthétisé les alkyl-2 trinitrofluorènones-9 (**2**) en procédant à une nitration contrôlée des alkyl-2 fluorènones-9 **5** à 25°C et à l'aide de HNO_3 fumant et de H_2SO_4 concentré. Les dérivés **5** sont obtenus par une réduction appropriée de la fonction acyle des acyl-2 fluorènes correspondants qui est suivie d'une oxydation par O_2, catalysée par les bases, de la position C-9. La régiochimie de la nitration est intéressante: si le composé **5** porte un substituant stériquement volumineux, la nitration se produit aux positions C-4, C-5 et C-7 et l'on obtient les alkyl-2 trinitro-4,5,7 fluorènones-9 avec un rendement dépassant 35%; par ailleurs, si le composé **5** porte un groupe alkyle primaire, la nitration se produit principalement dans les positions C-3, C-5 et C-7. Grâce à la présence de leurs fonctions alkyles, les alkyl-2 trinitrofluorènones-9 (**2**) sont plus solubles et plus compatibles avec les polymères que leurs analogues qui ne sont pas alkylés. Toutefois, les interactions de transfert de charge des composés **2** avec les produits donneurs d'électrons sont plus faibles que celles de la TNF et ce même si ces composés ont tous la même affinité électronique. Les composés **2** ainsi que la TNF présentent tous de bonnes propriétés comme transporteurs d'électrons dans des matrices de poly(*N*-vinylcarbazole).

[Traduit par le journal]

Nitrofluoren-9-ones and their derivatives have received growing interest as a unique class of electron acceptors. These molecules readily form charge-transfer complexes with electron donors (1–3) and have been extensively employed as photosensitizers and active constituents of photosensitive composites (4–7). Of this class of acceptors, 2,4,7-trinitrofluoren-9-one **1** (TNF) appears to be the most investigated molecule, presumably because of its relatively strong π-acid strength as well as its efficient photosensitization effect and electron transport capability (6, 7). Unfortunately, TNF has low solubility in organic solvents and exhibits poor compatibility with common matrix polymers; many applications requiring high concentrations of TNF cannot therefore be fulfilled. Moreover, TNF is mutagenic, and its use in the public domain is therefore discouraged.

In this paper we describe the synthesis, and molecular and electron transport properties of 2-alkyltrinitrofluoren-9-ones **2** – a structure which is expected to possess higher solubility characteristics than TNF by virtue of its alkyl substituent. The presence of a weakly electron-donating alkyl function in **2** and the difference in the regiochemistry of the nitro groups of **2** and that of TNF are not, however, expected to lead to a distinctive

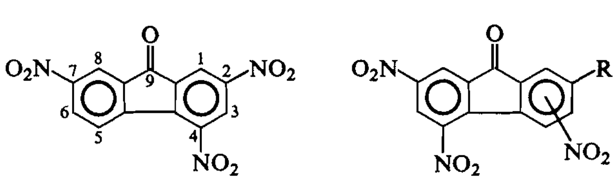

1 **2**

[1] Author to whom correspondence should be addressed.

difference in their electronic properties, in particular, the energy of their LUMO's (i.e., electron affinities (8)). On the other hand, it is possible that the presence of an alkyl substituent in **2** may render the structure non-mutagenic.

Results and discussion

Synthesis

While polynitration conditions are generally drastic, and oxidative degradations are common in these reactions, direct nitration of 2-alkylfluoren-9-one **5** appears to be the obvious route to **2**. What is required is a selective nitration reaction which is strong enough to trinitrate **5**, but mild enough not to cause significant degradation of its alkyl function. We felt that such a selective trinitration could be achieved by using a shorter reaction time and lower temperature conditions.

2-Alkylfluoren-9-one **5** was synthesized from 2-acylfluorene **3** by appropriate reduction of its acyl function to 2-alkylfluorene **4**, followed by oxidation at C-9 (Scheme 1). Thus, a Wolff–Kishner reduction of **3** with NH_2NH_2/KOH in ethylene glycol at 130–200°C afforded the corresponding 2-alkylfluorene **4***c* in good yield. On the other hand, the dimethylated species **4***a* or **4***b* was obtained by reductive methylation using the mild reductive methylating agent, $Al(CH_3)_3$ (9). Owing to the relatively high acidity of the C-9 protons ($pK_a \sim 23$, (10)), subsequent oxidation of **4** at C-9 was effectively accomplished by base-catalysed O_2-oxidation using Triton B in pyridine (11).

Nitration of 2-alkylfluoren-9-one **5** under standard polynitration conditions (e.g., 90% HNO_3/concentrated H_2SO_4, heat (12, 13)) did not yield the desired trinitro species. Under these conditions, **5** with a primary alkyl side chain (i.e., **5***c*) gave an intractable mixture of compounds, while **5***a* and **5***b*

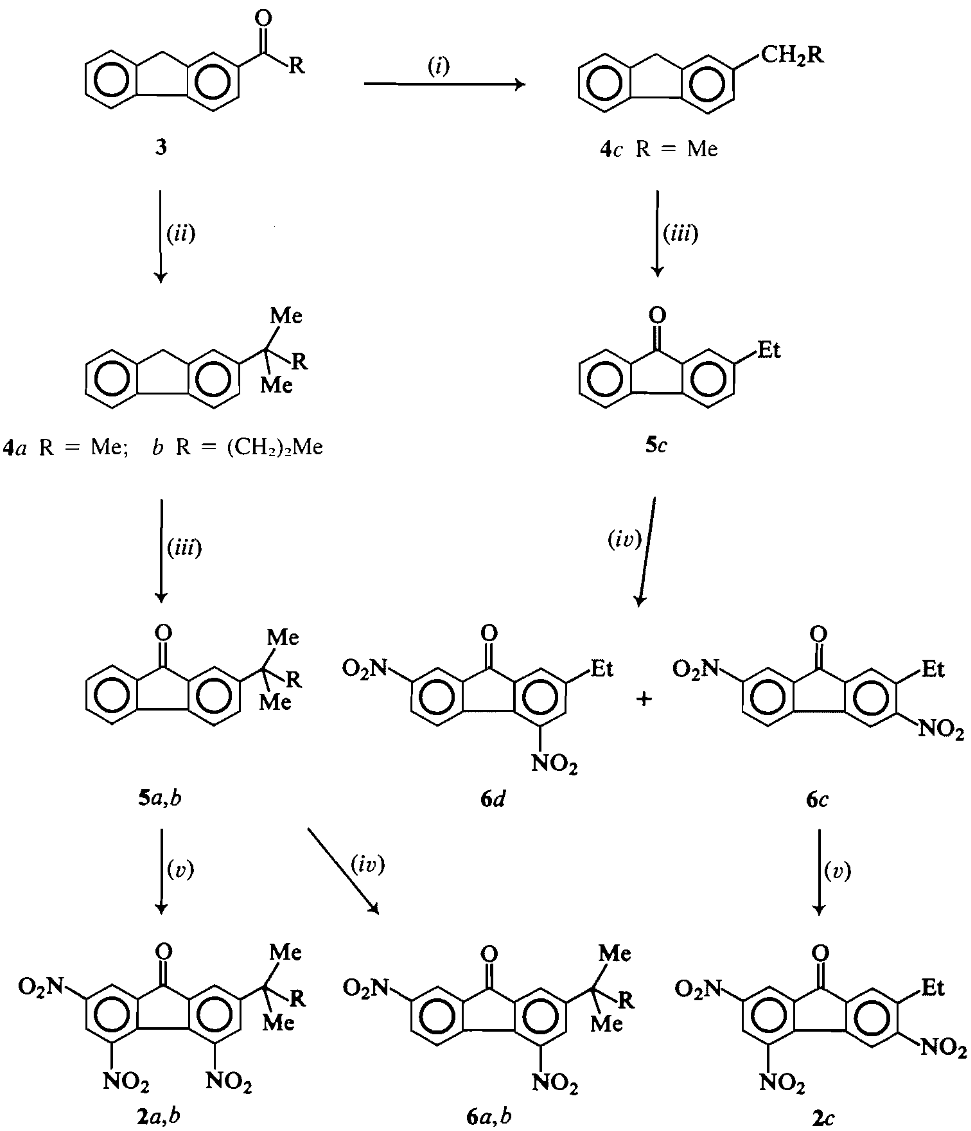

Reaction conditions: (*i*) NH_2NH_2/KOH, 130–200°C; (*ii*) $Al(Me)_3$/cat. AcOH, 0–140°C; (*iii*) O_2/Triton B, pyridine; (*iv*) red fuming HNO_3, 0–25°C; (*v*) red fuming HNO_3/conc. H_2SO_4, 0–25°C.

SCHEME 1

with α-tertiary alkyl substituents afforded mainly 2,4,5,7-tetranitrofluoren-9-one. The latter apparently resulted from dealkylation of **5** and its nitrated intermediates during the course of the reaction. Even at room temperature and below, the desired product could not be detected in the reaction mixture. However, we found that the desired trinitration could be achieved by employing a stronger nitrating agent such as a mixture of red fuming HNO_3 and concentrated H_2SO_4. Thus, when **5***a* or **5***b* was treated with this nitrating agent, first at 0°C and then at room temperature, the trinitrated product, 2-alkyl-4,5,7-trinitrofluoren-9-one (**2***a* or **2***b*) was obtained in over 35% yield. The dinitro species, 2-alkyl-4,7-dinitrofluoren-9-one (**6***a*, *b*) could be isolated by terminating the reaction earlier or simply by treating **5** with red fuming HNO_3 at room temperature. The regiochemistry of the nitro functions in these products was unambiguously determined by nmr spectroscopy and is consistent with the reactivity of the fluoren-9-one structure in electrophilic substitution reactions (13). With **5***c*, the above conditions did not prove to be satisfactory; a complex mixture containing even the tetranitrated 2-alkylfluoren-9-one (as detected by mass spectrometry) was obtained. Nevertheless, if **5***c* was first treated with red fuming nitric acid at ice-bath temperature to generate the dinitro species, followed by addition of concentrated H_2SO_4 at room temperature, the desired trinitrated product, **2***c*, could be obtained in about 20% yield. Two other dinitrated compounds, namely 2-ethyl-3,7-dinitrofluoren-9-one **6***c* and 2-ethyl-4,7-dinitrofluoren-9-one **6***d* were also isolated in over 10% yields. The regiochemistry of nitration in this case is interesting; with a less bulky primary alkyl side chain, nitration also occurred at the weakly activated C-3 position. However, under the above conditions, it was difficult to nitrate the sterically congested C-4 and C-5 positions both at the same time. Accordingly, only **6***c* (and not **6***d*) was further nitrated at C-5 to give the corresponding trinitro derivative. The moderate

TABLE 1. ^{1}H nuclear magnetic resonance spectral data of 2-alkylnitrofluoren-9-ones

2-Alkylnitrofluoren-9-one	δ, ppm ($CDCl_3$)
(*2a*) R = $C(CH_3)_3$ 4,5,7-Trinitro-	1.50 (s, 9H), 8.15 (AB, $J_{1,3}$ = 1.9 Hz, 2H), 8.75 (A of AB, $J_{6,8}$ = 2.2 Hz, 1H), 8.85 (B of AB, 1H)
(*2b*) R = $C(CH_3)_2CH_2CH_2CH_3$ 4,5,7-Trinitro-	0.85 (t, 3H), 1.20 (m, 2H), 1.40 (s, 6H), 1.70 (m, 2H), 8.10 (AB, $J_{1,3}$ = 1.9 Hz, 2H), 8.75 (A′ of A′B′, $J_{6,8}$ = 2.2 Hz, 1H), 8.90 (B′ of A′B′, 1H)
(*2c*) R = CH_2CH_3 3,5,7-Trinitro-	1.35 (t, 3H), 2.95 (q, 2H), 7.95 (A of AB, $J_{1,4}$ = 0.4 Hz, 1H), 8.55 (B of AB, 1H), 8.75 (A′ of A′B′, $J_{6,8}$ = 2.1 Hz, 1H), 9.05 (B′ of A′B′, 1H)*
(*6a*) R = $C(CH_3)_3$ 4,7-Dinitro-	1.45 (s, 9H), 8.0 (A of AB, $J_{1,3}$ = 1.9 Hz, 1H), 8.05 (B of AB, 1H), 8.12 (A of AMX, $J_{5,6}$ = 8.5 Hz, $J_{5,8}$ = 0.6 Hz, 1H), 8.35 (M of AMX, $J_{6,8}$ = 2.3 Hz, 1H), 8.45 (X of AMX, 1H)
(*6b*) R = $C(CH_3)_2CH_2CH_2CH_3$ 4,7-Dinitro-	0.85 (t, 3H), 1.15 (m, 2H), 1.40 (s, 6H), 1.70 (m, 2H), 8.0 (A of AB, $J_{1,3}$ = 1.9 Hz, 1H), 8.05 (B of AB, 1H), 8.10 (A of AMX, $J_{5,6}$ = 8.5 Hz, $J_{5,8}$ = 0.6 Hz, 1H), 8.35 (M of AMX, $J_{6,8}$ = 2.3 Hz, 1H), 8.45 (X of AMX, 1H)
(*6c*) R = CH_2CH_3 3,7-Dinitro-	1.35 (t, 3H), 2.95 (q, 2H), 7.75 (A of AMX, $J_{5,6}$ = 8.2 Hz, $J_{5,8}$ = 0.6 Hz, 1H), 7.80 (A of AX, $J_{1,4}$ = 0.3 Hz, 1H), 8.10 (X of AX, 1H), 8.50 (M of AMX, $J_{6,8}$ = 2.2 Hz, 1H), 8.55 (X of AMX, 1H)*
(*6d*) R = CH_2CH_3 4,7-Dinitro-	1.30 (t, 3H), 2.85 (q, 2H), 7.9 (A of AB, $J_{1,3}$ = 1.7 Hz, 1H), 8.0 (B of AB, 1H), 8.20 (A of AMX, $J_{5,6}$ = 8.6 Hz, $J_{5,8}$ = 0.5 Hz, 1H), 8.40 (M of AMX, $J_{6,8}$ = 2.3 Hz, 1H), 8.50 (X of AMX, 1H)*

*Parameters for **2***c*, **6***c*, and **6***d* from the methylene proton-decoupled 250-MHz spectra.

yields of these 2-alkylnitrofluoren-9-ones are respectable in view of the extensive degradation commonly observed in polynitration reactions.

Spectroscopic properties

All the nitrofluoren-9-ones display ir absorptions at ~1345 and 1550 cm^{-1} typical of aromatic nitro compounds. The carbonyl absorption appears at approximately 1740 cm^{-1}, which is 30 cm^{-1} higher than that of fluoren-9-one; this is consistent with the electron-deficient carbonyl function of these compounds. Mass spectra of these molecules all exhibit molecular ions, together with fragmentations expected of the structures.

The ^{1}H nmr spectra of these compounds are regiochemically informative. The spectra of the trinitro derivatives display, besides their alkyl signals, two distinct AB quartets for their aromatic protons. Both **2***a* and **2***b* exhibit *meta*-coupling constants of ~1.9–2.2 Hz. Coupling constants for **2***c*, on the other hand, are 2.1 and 0.4 Hz for the *meta* and *para*-couplings respectively. The chemical shifts of the aromatic protons of **2** are extremely sensitive to solvent effects, particularly with benzene and dimethylformamide, which are capable of forming charge transfer complexes with **2**. The 80-MHz ^{1}H nmr spectra of the dinotro derivatives **6** are complex. While the disubstituted ring displays an AB (**6***d*) or AX (**6***c*) quartet (long-range coupling to the side-chain methylene protons is also observed), the proton signals of the monosubstituted ring are complex second-order ABC. However, at 250 MHz, the spectra are reduced to approximately first-order AMX, and the chemical shifts and coupling constants can be measured directly (Table 1).

Solubility and polymer compatibility characteristics

With an alkyl substituent in its structure, **2** was observed to display better molar solubility in organic solvents than its corresponding non-alkylated counterpart, TNF. The solubility characteristics of three trinitrofluoren-9-ones are summarized in Table 2.

TABLE 2. Solubilities of trinitrofluoren-9-ones in organic solvents at 22°C (mmol/mL)

	CH_3CN	CH_2Cl_2	$CHCl_3$	Acetone	EtOAc	THF
TNF	0.09	0.15	0.14	0.13	0.07	0.50
2*a*	0.13	0.34	0.33	0.21	0.13	0.65
2*b*	0.23	0.34	0.44	0.24	0.23	0.69

Although the trinitrofluoren-9-ones are compatible with strongly electron-donating polymers such as poly(*N*-vinylcarbazole), **2** generally displays better polymer compatibility characteristics than TNF with other common matrix polymers. For instance, while the solvent-cast films of TNF in Lexan (polycarbonate) and Flexiclad (polyester) at relatively high loadings of ~3 mmol/g of polymer exhibit signs of TNF crystallization on standing for a few days at room temperature, the same polymer matrices containing **2***a* and **2***b* under similar conditions are stable for months. Undoubtedly, the presence of an alkyl group, particularly one that is sterically bulky, imparts not only good solubility but also good polymer compatibility characteristics to the trinitrofluoren-9-one structure.

Electrochemical and charge-transfer properties

The electrochemical properties of nitrofluoren-9-ones were examined by cyclic voltammetric techniques. The cyclic voltammetric measurements were carried out in methylene chloride at room temperature using a hanging-mercury-drop working electrode and a Ag/AgCl reference electrode. Figure 1 depicts typical cyclic voltammograms for **2***b* and TNF under similar conditions. Both **2** and TNF exhibited two reversible one-electron reductions separated by ~0.3 V. The first half-wave reduction potentials of **2** and TNF are essentially identical. Their cyclic voltammograms showed a reversible re-

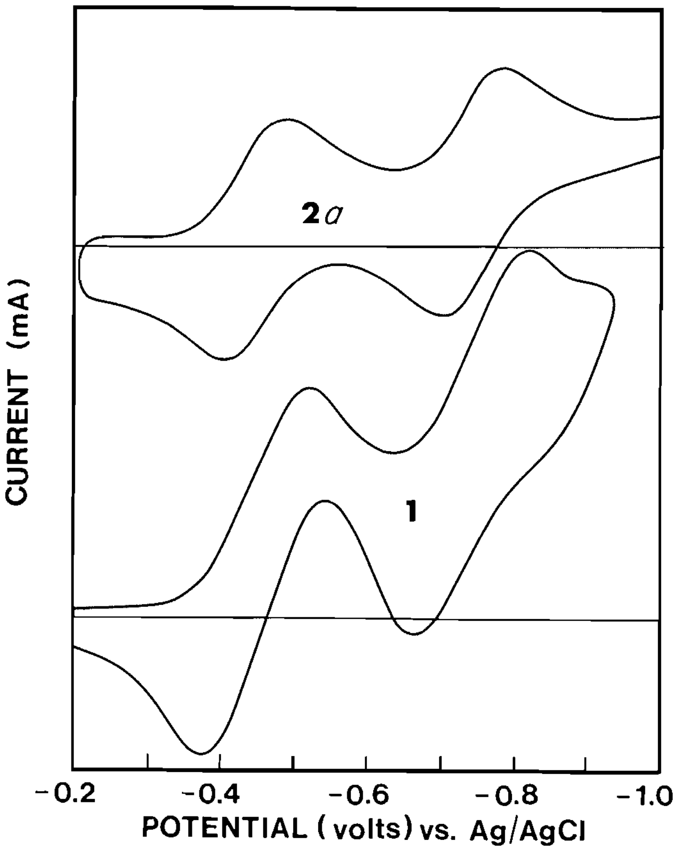

FIG. 1. Typical cyclic voltammograms of TNF (**1**) and 2-(1,1-dimethylbutyl)-4,5,7-trinitrofluoren-9-one (**2***b*) in methylene chloride at 25°C.

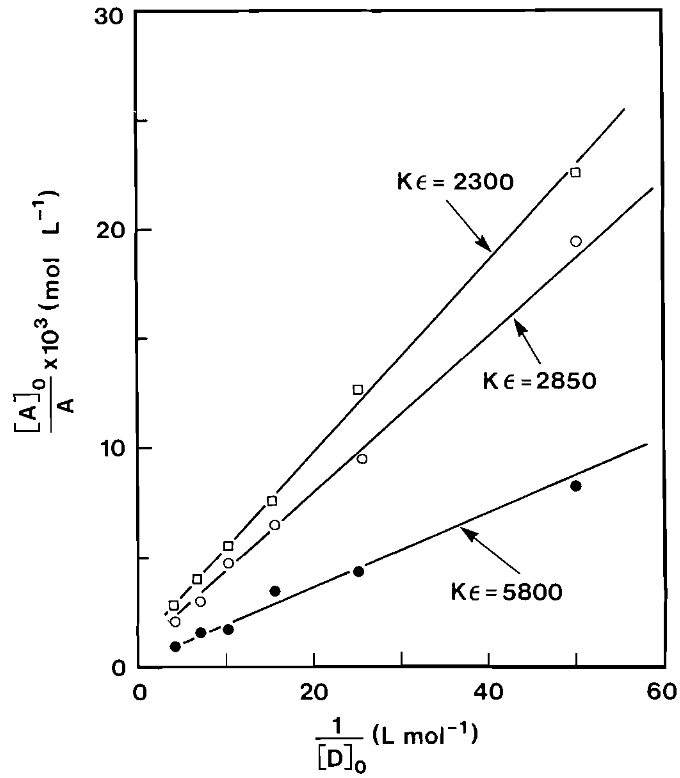

FIG. 2. Benesi–Hildebrand plots of charge-transfer interactions of TNF (**1**, ●), 2-*tert*-butyl-4,5,7-trinitrofluoren-9-one (**2***a*, ○), and 2-(1,1-dimethylbutyl)-4,5,7-trinitrofluoren-9-one (**2***b*, □) with *N*-ethylcarbazole in THF (λ_{max} ~ 435 nm, 1-cm cell, 25°C); $[A]_0$ = total acceptor concentration; [D] = total donor concentration; *A* = absorbance.

sponse, with a separation of 70 mV between cathodic and anodic peak potentials independent of scan rate (10–200 mV/s). These results indicate a simple, kinetically diffusion-controlled reduction of the molecules to the corresponding radical anions, which were stable within the time scale of measurement. Accordingly, it can be concluded that the presence of a weakly electron-donating alkyl substituent in **2** does not significantly perturb the energy of its LUMO from that of the basic trinitrofluoren-9-one structure. This is particularly important in that the electron transport capability of the structure depends profoundly on its electron affinity (14). From this perspective, **2** is therefore expected to be as good an electron transport system as TNF. Interestingly, the dinitro derivatives (e.g., **6***b*) also displayed two reversible one-electron reductions; the first reduction, however, occurred at −0.76 V.

Although **2** has the same electron affinity as TNF, it displays weaker charge-transfer interactions with electron donors than the latter. This is especially true in the case of **2***a* or **2***b* where a sterically demanding tertiary alkyl substituent is present. Figure 2 depicts the Benesi–Hildebrand plots of the charge-transfer interactions of **2** and TNF with *N*-ethylcarbazole. The selection of the latter as a donor was to ensure a strong CT interaction because of its reasonably high electron donor strength, structural planarity, as well as extended π-network. As can be noted, the product *K*ε's for **2** are significantly lower than that for TNF. For effective charge transfer interaction, a close spatial relationship of electron donor and acceptor is mandatory. The presence of a bulky group in **2***a* and **2***b* obviously hampers close association with donor molecules, and thus a weaker charge-transfer interaction results.

Electron Transport Properties

The electron transport properties of **2** and TNF were investigated by the xerographic discharge technique under space charge limited conditions (14–16). Figure 3 shows a schematic representation of the photoconductive layered device used in these studies. The device is comprised of a thin layer (0.5 μm) of amorphous selenium (a-Se) photogenerator, a relatively thick transport layer (10–15 μm) of a trinitrofluoren-9-one in poly(*N*-vinylcarbazole) (PVK), and a conductive substrate.

Figure 4 depicts the typical time-resolved photoinduced discharge curves (PIDC's) of **2***b* and, for comparison of TNF. The PIDC characteristics of **2***a*, **2***b*, and TNF are very similar, although a sharper initial discharge is noted in the case of **2**. This was probably the result of a better dispersion of **2** in the transport layer. The slight differences in the residual potentials for **2** and TNF are primarily due to variations in the thickness of the experimental devices. The estimated electron drift mobilities are tabulated in Table 3. It appears that under equivalent molar loading conditions, **2** has a higher electron drift mobility. Whether this is an intrinsic property of **2** or is merely due to the better dispersibility of **2** in the transport layer cannot be unambiguously answered.

Conclusions

We have shown that the direct nitration of 2-alkylfluoren-9-ones is a feasible route to the novel 2-alkyltrinitrofluoren-9-ones. The incorporation of an alkyl function into the basic trinitrofluoren-9-one structure not only results in an enhancement of its solubility but also its polymer compatibility

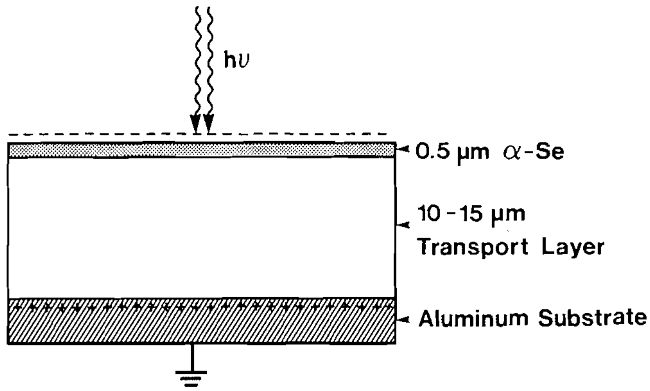

FIG. 3. Schematic diagram of the layered device for electrical characterization of trinitrofluoren-9-ones.

TABLE 3. Electron drift mobilities of trinitrofluoren-9-ones in poly(*N*-vinylcarbazole) matrices at applied electric field of 2×10^5 V/cm

Trinitrofluoren-9-one	Matrix loading (mol/g PVK)	Electron mobility (cm^2/V s)
TNF	3.2×10^{-3}	4×10^{-8}
2*a*	2.7×10^{-3}	1.4×10^{-8}
2*b*	3.2×10^{-3}	1×10^{-7}

characteristics. Of significance in this structural modification is that the electron affinity of the basic TNF structure is preserved in the alkylated analogs even though the regiochemistry of their nitro functions differs from that of TNF. In line with this, it is observed that both TNF and the alkylated analogs exhibit similar electron transport properties.

Experimental

All the solvents used in the reactions were Reagent Grade; unless otherwise stated, they were dried by refluxing with appropriate drying agents, followed by distillation before use (chlorinated solvents, xylene (P_2O_5); THF ($LiAlH_4$); pyridine (CaH_2)). Infrared spectra were recorded on a Beckmann IR-4250 spectrophotometer with polystyrene as the calibration standard; solid samples were taken as KBr pellets, liquid samples as thin films (neat). Electronic absorption spectra were obtained on Hewlett Packard 8450A uv/visible spectrophotometer. The ^{1}H nmr spectra were recorded in $CDCl_3$ on Bruker WP-80 and WM-250 spectrometers with tetramethylsilane as an internal standard. Mass spectra were obtained on a Finnigan 4000 quadrupole instrument. All melting points were measured on a Thomas–Hoover melting point apparatus and are uncorrected. Elemental analyses were performed by Galbraith Laboratories, Inc., Knoxville, Tennesse, U.S.A.

2-Acylfluorene (3)

2-Acylfluorene was prepared by Friedel–Crafts acylation of fluorene according to literature procedures (12). The reaction was conducted on a 0.6-mol scale with carboxylic anhydride/$AlCl_3$ as the acylating agent and dichloroethane as the reaction medium.

2-tert-Butylfluorene (4a)

A suspension of 2-acetylfluorene (4.16 g, 0.02 mol) in xylene (60 mL) and 5 drops of acetic acid was stirred at ice-bath temperature under a nitrogen atmosphere. 2 *M* trimethylaluminum solution in toluene (40 mL, 0.08 mol) was added slowly over a period of 15–20 min. After addition, the mixture was heated under reflux for 4 h. The reaction mixture was cooled, diluted with 50 mL ether, and hydrolyzed by pouring into a mixture of ether and dilute aqueous HCl solution. The aqueous layer was separated and extracted with ether. The combined organic solution was dried and evaporated to give the solid crude product. Column chromatography of the crude product on silica gel (hexane) gave the pure 2-*tert*-butylfluorene as a white crystalline solid (3.32 g, 75%), mp 115–116°C; ^{1}H nmr δ: 1.40 (s, 9H), 3.25 (s, 2H), 7.2–7.9 (m, 7H); ms (*m*/*e*): 222 (M^+). *Anal.* calcd. for $C_{17}H_{18}$: C 91.84, H 8.16; found: C 91.58, H 8.22.

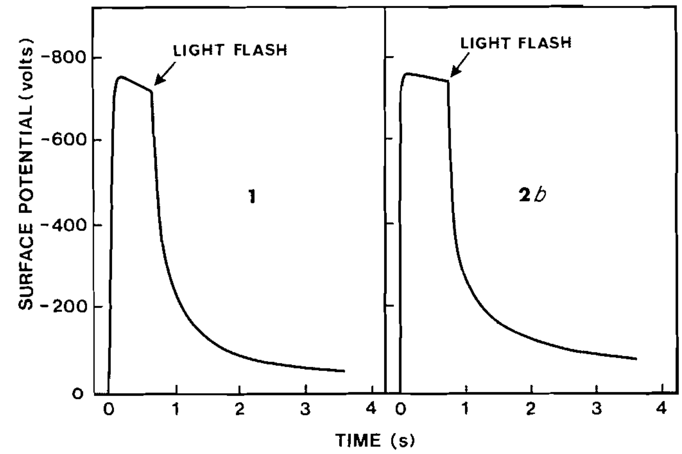

FIG. 4. Typical time-resolved photoinduced discharge curves for TNF (**1**) and 2-(1,1-dimethylbutyl)-4,5,7-trinitrofluoren-9-one (**2***b*)-based photoreceptors.

2-(1,1-Dimethylbutyl)fluorene (4b)

The title compound was prepared in a similar manner as **4***a*, in 82% yield. It was purified by recrystallization from methanol, mp 62–63°C; ^{1}H nmr δ: 0.80 (t, 3H), 1.10 (m, 2H), 1.35 (s, 6H), 3.85 (s, 2H), 7.20–7.80 (m, 7H). *Anal.* calcd. for $C_{19}H_{22}$: C 91.14, H 8.85; found: C 91.04, H 8.84.

2-Ethylfluorene (4c)

A mixture of 2-acetylfluorene (10.4 g, 0.05 mol), 85% NH_2NH_2 (5 g, 0.15 mol), and 8.4 g KOH in ethylene glycol (120 mL) was heated at 130–140°C for 2 h. Water generated from the reaction and excess NH_2NH_2 were removed by distillation at this temperature. The reaction mixture was then gradually brought to reflux over a period of 1 h and held at this temperature for another 4 h. After cooling and diluting with 65 mL of water, the mixture was poured into 100 mL dilute aqueous HCl solution. The solid product was collected, washed with water, and dried. Recrystallization from acetone–hexane afforded pure 2-ethylfluorene in 75% yield, mp 99–99.5°C; ^{1}H nmr δ: 1.30 (t, 3H), 2.70 (q, 2H), 3.85 (s, 2H), 7.1–7.8 (m, 7H); ms (*m*/*e*): 194 (M^+). *Anal.* calcd. for $C_{15}H_{14}$: C 92.74, H 7.26; found: C 92.68, H 7.18.

2-tert-Butylfluoren-9-one (5a)

A solution of 2-*tert*-butylfluorene **4***a* (2.83 g, 12.7 mmol) in dried pyridine (15 mL) was stirred in a 50-mL round-bottom flask under an oxygen atmosphere at room temperature. The reaction flask was connected separately to an oxygen source and a gas regulatory apparatus by means of rubber tubing such that the oxygen pressure in the system could be maintained at near atmospheric pressure during the reaction. A solution of 40% Triton B in pyridine (0.32 mL) was added to the reaction vessel by means of a syringe. An exothermic reaction was observed upon addition; the reaction mixture turned black instantaneously, and a fast consumption of oxygen was noted. The extent of reaction was conveniently monitored by tlc. After the reaction (~40 min), the mixture was pipetted into water with vigorous stirring. The yellow precipitate was collected, washed with water, and dried. Recrystallization from petroleum ether afforded pure **5***a* as a bright yellow solid (2.81 g, 94%), mp 99.5–100.5°C; ir (KBr): 1710 cm^{-1}; ^{1}H nmr δ: 1.35 (s, 9H), 7.2–7.7 (m, 7H); ms (*m*/*e*): 236 (M^+). *Anal.* calcd. for $C_{17}H_{16}O$: C 86.41, H 6.82; found: C 86.23, H 6.91.

2-(1,1-Dimethylbutyl)fluoren-9-one (5b)

The title compound was prepared from 2-(1,1-dimethylbutyl)-

fluorene *4b* in the same manner as *5a*. It was purified by column chromatography on silica gel using ethyl acetate – heptane (1:20) as the eluting solvent. Compound **5***b* was obtained as an oil in 86% yield; ir (neat): 1710 cm^{-1}; ^1H nmr δ: 0.80 (t, 3H), 1.10 (m, 2H), 1.30 (s, 6H), 1.60 (m, 2H), 7.2–7.7 (m, 7H). *Anal.* calcd. for $C_{19}H_{20}O$: C 86.32, H 5.81; found: C 86.25, H 5.69.

2-Ethylfluoren-9-one (5c)

The title compound was obtained from 2-ethylfluorene **4***c*, as in the case of **5***b*, in 92% yield; ir (neat): 1715 cm^{-1}; ^1H nmr δ: 1.20 (t, 3H), 2.60 (q, 2H), 7.0–7.7 (m, 7H); ms (*m/e*): 208 (M^+). *Anal.* calcd. for $C_{15}H_{12}O$: C 86.51, H 5.81; found: C 86.25, H 5.69.

2-tert-Butyl-4,5,7-trinitrofluoren-9-one (2a)

A mixture of red fuming HNO_3 (S.G. = 1.6, 40 mL) and concentrated H_2SO_4 (20 mL) was added slowly to 3.7 g (10 mmol) of powdered **5***a* in a 100-mL round-bottom flask at ice-bath temperature. The flask was constantly swirled during addition to ensure proper mixing of the reagents. The initial addition was carried out very slowly because of the highly exothermic reaction. After 20 mL of the nitrating agent was added, the mixture was removed from the ice bath, and the remaining nitrating agent then added. The resulting reaction mixture was further stirred at room temperature for 25 min before being pipetted into 500 mL of well-stirred ice-cold water. The solid yellow product was collected, washed with water, and air dried. Purification by preparative hplc on silica gel (methylene chloride – hexane 1:1) afforded 1.37 g (37%) of pure **2***a* as a bright yellow crystalline solid, mp 212–212.5°C; ir (KBr): 1345, 1550 (C—NO_2), 1742 (C═O) cm^{-1}; ms (*m/e*): 371 (M^+). *Anal.* calcd. for $C_{17}H_{13}N_3O_7$: C 54.99, H 3.53, N 11.32; found: C 55.12, H 3.47, N 11.21.

2-(1,1-Dimethylbutyl)-4,5,7-trinitrofluoren-9-one (2b)

The title compound was prepared from 2-(1,1-dimethylbutyl)-fluoren-9-one *4b* according to the same procedure as for *2a* on a 40-mmol scale in 43% yield, mp 188–190°C; ir (KBr): 1345, 1550 (C—NO_2), 1740 (C═O) cm^{-1}; *Anal.* calcd. for $C_{19}H_{17}N_3O_7$: C 57.14, H 4.29, N 10.51; found: C 56.88, H 4.34, N 10.31.

Nitration of 2-ethylfluoren-9-one (5c)

Red fuming nitric acid (16 mL) was added to 2-ethylfluoren-9-one **5***c* (0.416 g, 2 mmol) in a 50-mL round-bottom flask at ice-bath temperature with constant swirling over a period of 10 min. After addition, the mixture was stirred at room temperature for 1 h before 8 mL of concentrated H_2SO_4 was added. The mixture was allowed to react for another hour before being worked up as before. Preparative thin layer chromatography on silica gel (methylene chloride – hexane 2:1) yielded 0.15 g (22%) of 2-ethyl-3,5,7-trinitrofluoren-9-one **2***c* as a viscous oil (R_f 0.15); ir (neat): 1345, 1540 (C—NO_2), 1740 (C═O) cm^{-1}; ms (*m/e*): 343 (M^+); hplc analysis showed that the purity of **2***c* was about 95%, with some contamination from the dinitro derivatives.

Also isolated from the mixture were 0.065 g (11%) of 2-ethyl-3,7-dinitrofluoren-9-one **6***c* (R_f 0.24) and 0.083 g (14%) of 2-ethyl-4,7-dinitrofluoren-9-one **6***d* (R_f 0.39). Both of the products exhibit ir absorpitions at 1345, 1540, and 1740 cm^{-1}.

2-tert-Butyl-4,7-dinitrofluoren-9-one (6a)

Red fuming HNO_3 (20 mL) was added slowly to 1.0 g (4.2 mmol) of powdered **5***a* in a 50-mL round-bottom flask at ice-bath temperature over a period of 15 min with constant stirring. After addition, the reaction mixture was further stirred at room temperature for 20 min before being pipetted into 50 mL of ice-cold water. The yellow precipitate was collected, washed with water, and air dried. Column chromatography on silica gel (methylene chloride – hexane 2:1) gave 0.66 g (48%) of pure **6***a* as bright yellow crystals, mp 172–173°C; ir (KBr): 1345, 1540 (C—NO_2), 1740 (C═O) cm^{-1}. *Anal.* calcd. for $C_{17}H_{14}N_2O_5$: C 62.58, H 4.32, N 8.59; found: C 62.65, H 4.11, N 8.54.

2-(1,1-Dimethylbutyl)-4,7-dinitrofluoren-9-one (6b)

The title compound was prepared from 2-(1,1-dimethylbutyl)-fluoren-9-one **5***b*, in the same manner as **6***a*, in 53% yield as a bright yellow solid, mp 130.5–131.5°C; ir (KBr): 1345, 1540 (C—NO_2), 1740 (C═O) cm^{-1}. *Anal.* calcd. for $C_{19}H_{18}N_2O_5$: C 64.40, H 5.12, N 7.91; found: C 64.65, H 5.03, N 8.01.

Charge-transfer interaction

The charge-transfer measurements were performed on freshly prepared solutions in THF using a Hewlett Packard 8450A uv/visible spectrophotometer. The concentrations of the donor, *N*-ethylcarbazole, were varied from 2.0×10^{-2} *M* to 2.5×10^{-1} *M*, while those of trinitrofluoren-9-ones were kept constant at $\sim 2.2 \times 10^{-4}$ *M*. The λ_{max} of the CT band appeared at ~435 nm.

Electrochemical measurements

Electrochemical measurements were carried out on a PAR 174A polarographic analyzer connected to a PAR 175 universal programmer. A PAR model 303 static mercury drop electrode assembly was used. The system was equipped with a hanging-mercury-drop working electrode, a Ag/AgCl reference electrode, and a platimum wire auxiliary electrode. Sample concentrations were 10^{-3} *M*. Tetrabutylammonium perchlorate in methylene chloride was employed as the supporting electrolyte.

Electrical characterization

The electrical characterization of trinitrofluoren-9-ones as electron transport molecules was performed using the xerographic discharge technique under space charge limited conditions (14–16). The photoconductive layered device used for measurement was prepared as follows: a transport layer (10–15 μm) comprising a trinitrofluoren-9-one in PVK was solvent cast onto an aluminium substrate using a Bird film applicator. A 0.5-μm thick layer of amorphous selenium was vacuum evaporated on top of the transport layer to serve as the photogenerator. The device was corona charged to a negative surface potential and was discharged by exposing it to a light flash of wavelength of 4330 Å. The resulting photoinduced discharge of the device was monitored by a capacitively coupled probe. Under these conditions, one of the parameters controlling the rate of discharge is the electron mobility in the transport layer.

Acknowledgements

The authors are indebted to Dr. R. O. Loutfy for electrochemical studies and for helpful discussion. Sincere gratitude is extended to Dr. D. M. Pai and Mr. T. B. McAneney for electrical characterization.

1. (*a*) M. ORCHIN and E. O. WOOLFOLK. J. Am. Chem. Soc. **68**, 1727 (1946); (*b*) M. ORCHIN, L. REGGEL, and E. O. WOOLFOLK. J. Am. Chem. Soc. **69**, 1225 (1947).
2. A. R. LEPLEY. J. Am. Chem. Soc. **84**, 3577 (1962).
3. R. FOSTER. Organic charge-transfer complexes. Academic Press, New York. 1969.
4. H. HOEGL. J. Phys. Chem. **69**, 755 (1965); British Patent No. 990,368 (1965).
5. K. NISHIDE and T. EIDA. U.S. Patent No. 3,864,126 (1965).
6. (*a*) J. MORT and R. L. EMERALD. J. Appl. Phys. **45**, 175 (1974); (*b*) R. L. EMERALD and J. MORT. J. Appl. Phys. **45**, 3943 (1974).
7. D. W. GILL. J. Appl. Phys. **43**, 5031 (1972).
8. G. BRIEGLEB. Angew. Chem. Int. Ed. Engl. **3**, 617 (1964).
9. A. MEISTER and T. MOLE. Aust. J. Chem. **27**, 1655 (1974).
10. J. C. STOWELL. Carbanions in organic synthesis. John Wiley, New York. 1979.
11. Y. SPRINZAK. J. Am. Chem. Soc. **80**, 5449 (1958).
12. M. S. NEWMAN and H. BODEN. Org. Synth. Coll. Vol. **5**, 1029 (1973).
13. T. SULZBERG and R. J. COTTER. J. Org. Chem. **35**, 2762 (1970).
14. J. E. KUDER, J. M. POCHAN, S. R. TURNER, and D. F. HINMAN. J. Electrochem. Soc. **125**, 1750 (1978).
15. R. M. SCHAFFERT. Electrophotography. 2nd ed., Wiley, New York. 1975.
16. M. STOLKA, D. M. PAI, D. S. RENFER, and J. F. YANUS. J. Polym. Sci. Polym. Chem. Ed. **21**, 969 (1983).

Phase transfer catalysis in the *tert*-butyloxycarbonylation of alcohols, phenols, enols, and thiols with di-*tert*-butyl dicarbonate

F. HOULIHAN, F. BOUCHARD, AND J. M. J. FRÉCHET[1]
Ottawa-Carleton Institute, Graduate Studies and Research, Department of Chemistry, University of Ottawa, Ottawa, Ont., Canada K1N 9B4

AND

C. G. WILLSON
IBM Research Laboratory, Department K42-282, 5600 Cottle Road, San Jose, CA 95193, U.S.A.

Received February 6, 1984

This paper is dedicated to the 10th anniversary of the Xerox Research Centre of Canada

F. HOULIHAN, F. BOUCHARD, J. M. J. FRÉCHET, and C. G. WILLSON. Can. J. Chem. **63**, 153 (1985).

It is shown that the *tert*-butyloxycarbonylation of phenols, alcohols, enols, and thiols can be accomplished by reaction of these functionalities with di-*tert*-butyl dicarbonate under phase transfer conditions. The reactions proceed in high yield and can also be used for the introduction of *t*-BOC groups onto functionalized polymer backbones such as novolac or poly(*p*-hydroxystyrene). In addition, a study is made of the selectivity towards *tert*-butyloxycarbonylation of various polyfunctional compounds.

F. HOULIHAN, F. BOUCHARD, J. M. J. FRÉCHET et C. G. WILLSON. Can. J. Chem. **63**, 153 (1985).

On démontre que l'on peut effectuer une réaction de *tert*-butyloxycarbonylation des phénols, des alcools, des énols et des thiols en faisant réagir ces diverses fonctions avec du bicarbonate de di-*tert*-butyle dans des conditions de transfert de phase. Les réactions se produisent avec des rendements élevés et elles peuvent être utilisées pour introduire des groupements *t*-BOC sur les squelettes de polymères comme le novolac ou le poly(*p*-hydroxystyrène). De plus, on a étudié la sélectivité de divers composés polyfonctionnels par rapport à la réaction de *tert*-butyloxycarbonylation.

[Traduit par le journal]

Introduction

While the *tert*-butyloxycarbonyl group (*t*-BOC) is used widely as an amino protecting group, particularly in peptide synthesis following the work of Carpino and others (1–5), it has not, until recently, found any application as a protecting group for hydroxyl or thiol functionalities.

Our recent work on the preparation of poly(*p*-hydroxystyrene) (6) and poly(*p*-hydroxy-a-methylstyrene) (7) through the polymerization of the corresponding *t*-BOC protected vinyl phenols has shown the versatility of the *t*-BOC group for the protection of phenolic compounds. For example, the *t*-BOC group is resistant to both the conditions of the Wittig reaction and of cationic polymerization in liquid sulfur dioxide where other more classical protecting groups such as the acetoxy group fail. In addition, the unique ability of the *t*-BOC group to be removed by thermolysis or by the action of a catalytic amount of strong acid has proved critical in the preparation of pure poly(*p*-hydroxystyrene) (6) and is the basis for the use of poly(*p*-*t*-BOC-hydroxystyrene) in a new photoimaging system exhibiting the phenomenon of chemical amplification (8).

Results and discussion

Several different pathways have been tested for the *tert*-butyloxycarbonylation of hydroxyls and thiols (9–13); three of the most commonly used are shown in Scheme 1. All three are characterized by generally low yields and the use of extremely toxic or unstable reagents. In contrast to the paucity of methods for the preparation of *t*-BOC derivatives of alcohols, the preparation of *t*-BOC derivatives of amines has been studied extensively as the *t*-BOC group has proven extremely useful in peptide synthesis. In recent years numerous preparations have used di-*tert*-butyl dicarbonate as an *N*-*tert*-butyloxycarbonylation reagent due to the ease with which it reacts with amines to form the corresponding *t*-BOC derivatives in essentially quantitative yields. The reaction is accompanied by evolution of gas, as both carbon dioxide and isobutylene are released as the amine attacks the dicarbonate. Di-*tert*-butyl dicarbonate is a readily available crystalline reagent (14) which is safe and is easily handled. Our initial experiments were designed to explore the utility use of *t*-BOC groups for the protection of hydroxyls and involved the reaction of simple phenolates with di-*tert*-butyl dicarbonate.

tert-*Butyloxycarbonylation of phenols*

The reaction of phenols with di-*tert*-butyl dicarbonate (Scheme 2) proceeds readily under a variety of conditions and requires the presence of an equivalent amount of base. The reaction is fastest under phase transfer catalysis using liquid–liquid or liquid–solid reaction conditions. For example, phenol reacts very rapidly and quantitatively with di-*tert*-butyl dicarbonate in THF, ethyl acetate, or dichloromethane, in the presence of a catalytic amount of 18-crown-6 and an equivalent amount of powdered anhydrous potassium carbonate. Under liquid–liquid phase transfer conditions in dichloromethane solution, with aqueous sodium hydroxide or potassium carbonate as base and tetrabutyl ammonium hydrogen sulfate as catalyst, the reaction is also complete in an hour or less. Alternately, the phase transfer catalyst can be omitted completely for easier processing; the reaction with powdered anhydrous potassium carbonate and di-*tert*-butyl dicarbonate gives excellent yields of the desired product, albeit at much slower rates than the catalyzed reaction (Table 1). Phenolic substrates with functionalities such as aldehydes or ketones can be modified successfully without side reactions, as shown in the preparation of the *O*-*tert*-butyloxycarbonyl derivatives of *p*-hydroxybenzaldehyde and *p*-acetylphenol, **2***a* and **3***a* (Table 1), which are two useful precursors in the synthesis of reactive polymers (6,

[1] Author to whom correspondence should be addressed.

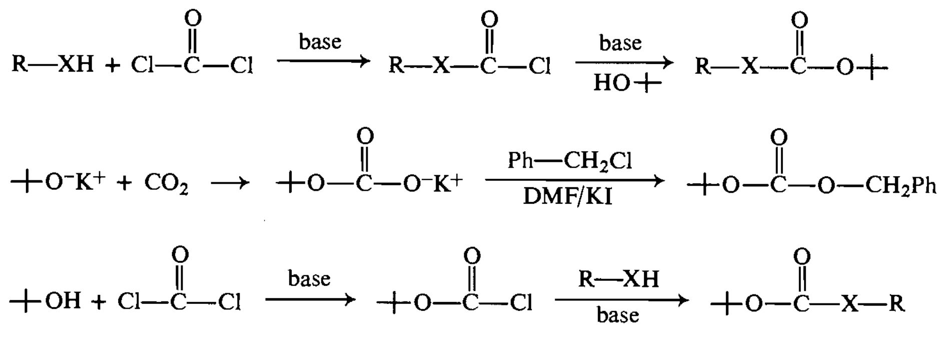

R = alkyl or aryl X = O or S

SCHEME 1

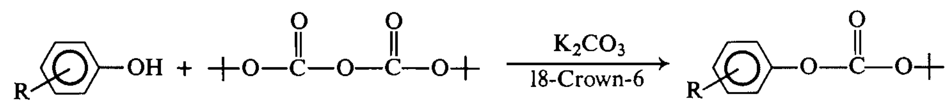

R = H, CHO, $COCH_3$

SCHEME 2

7). The presence of substituents in the *ortho* position of the phenols causes a noticeable decrease in the reaction rate as the size of the substituent increases from methyl to *tert*-butyl. With 2,6-di-*tert*-butyl phenol, the reaction occurs, but at a very slow rate, and only a very low conversion (ca. 10%) is achieved, even in the presence of 18-crown-6 and after two days of stirring. While much of the 2,6-di-*tert*-butyl phenol remains unchanged in this reaction (ca. 70%), a significant amount of the diphenoquinone dimerization product is also isolated; such diphenoquinones are also obtained as by-products in the oxidative polymerization of phenols with bulky *ortho* substituents (15).

All of the low molecular weight aryl *tert*-butyl carbonates which were prepared by this method exhibit strong carbonyl bands near 1760 cm^{-1} in their infrared spectra. Their mass spectra all include a characteristic pattern for the loss of *t*-BOC (m/e 100) and a peak at m/e 57. Full spectral data are given in Table 4.

The *tert*-butyloxycarbonylation of phenolic polymers such as poly(*p*-hydroxystyrene) and novolac is also successful using the reaction conditions described above, faster reaction rates being observed in the presence of phase transfer catalysts. However, as the uncatalyzed reactions in the presence of powdered anhydrous potassium carbonate also give the *t*-BOC-substituted polymer in quantitative yield, it is the preferred method, as the purification of the final polymer is greatly simplified since no removal of the phase transfer catalyst from the precipitated polymer is necessary. With *m*-cresol novolacs containing *ortho–ortho* linkages, the reaction is slower than with the unhindered poly(*p*-hydroxystyrene) but proceeds nevertheless to completion even when no excess of dicarbonate reagent is present. Partial functionalization of a phenolic polymer is readily acomplished using less than a stoichiometric amount of dicarbonate; the dicarbonate is used quantitatively and without side reaction and this method is useful for the preparation of phenolic polymers containing varying proportions of free and *t*-BOC-protected hydroxyls.

In addition to analysis by nmr and ir spectroscopies, the *tert*-butyloxycarbonylated phenolic resins can be analyzed by thermogravimetry. This analytical technique is particularly useful in determining the exact degree of functionalization of partly *tert*-butyloxycarbonylated polymers, as the thermal reversion to the phenolic polymer occurs at 200°C with a sharp and easily measurable weight loss. For example, a novolac resin which had been allowed to react with 20% of the stoichiometric amount of di-*tert*-butyl dicarbonate lost 15% (100% of theory) of its weight upon heating to 200°C, confirming that 20% of the polymer's hydroxyl groups had been substituted in the reaction with the dicarbonate.

tert-Butyloxycarbonylation of alcohols

The reaction of alcohols with di-*tert*-butyl dicarbonate is much slower than that of phenols and requires the use of a phase transfer catalyst. Excellent results are obtained with liquid–liquid phase transfer catalysis using tetrabutyl ammonium hydrogen sulfate and aqueous sodium hydroxide; solid–liquid phase transfer catalysis is also suitable and affords essentially the same results. Allylic, benzylic, or primary alcohols react with the dicarbonate in a matter of hours, while secondary alcohols may require a day or more to react fully and tertiary alcohols are unreactive (Table 1). Reactions with the less reactive alcohols are best carried out using a 20% excess of the dicarbonate, as some of the reagent is slowly consumed in a side reaction with the aqueous sodium hydroxide. The infrared spectra of the carbonates show strong carbonyl bands near 1740 cm^{-1}, reflecting the lower energy of the carbonate bond of these alcohols compared to those of the phenolic compounds described above. Other spectral data are shown in Table 4.

tert-Butyloxycarbonylation of thiols

Both thiophenol and butanethiol react rapidly with di-*tert*-butyl dicarbonate under phase transfer conditions using the anhydrous potassium carbonate 18-crown-6 system, and afford good yields of the *t*-BOC derivatives. In contrast, the reaction with aqueous sodium hydroxide and tetrabutyl ammonium hydrogen sulfate does not lead to product, as the thiocarbonates which are formed are immediately hydrolyzed back to the starting thiols. Like phenol, thiophenol reacts with di-*tert*-butyl dicarbonate even in the absence of a phase transfer catalyst, provided anhydrous potassium carbonate is present. The reac-

TABLE 1. *tert*-Butyloxycarbonylation of phenols, alcohols, and thiols with di-*tert*-butyl dicarbonate

Starting material	Molar ratio[a]	Solvent	Catalyst	Base	Time[b] (h)	Product	Yield (%)
PhOH **1**	1.2	CH_2Cl_2	$(Bu)_4NHSO_4$	30% NaOH	1	PhO—*t*-BOC **1***a*	89
PhOH **1**	1.0	THF	18-Crown-6	K_2CO_3	<1[c]	**1***a*	99
PhOH **1**	1.0	THF	None	K_2CO_3	24	**1***a*	97
p-(CHO)PhOH **2**	1.1	CH_2Cl_2	$(Bu)_4NHSO_4$	30% NaOH	2	*p*-(CHO)PhO—*t*-BOC **2***a*	84
p-(CH_3CO)PhOH **3**	1.0	CH_2Cl_2	$(Bu)_4NHSO_4$	30% NaOH	<1	*p*-(CH_3CO)PhO—*t*-BOC **3***a*	94
2,6-Di-(*t*-Bu)PhOH **4**	1.2	CH_2Cl_2	$(Bu)_4NHSO_4$	30% NaOH	48	**4***a*	Trace
2,6-Di-(*t*-Bu)PhOH **4**	1.2	CH_2Cl_2	18-Crown-6	K_2CO_3	48	**4***a*	7[e]
o-(*t*-Bu)PhOH **5**	1.0	THF	18-Crown-6	K_2CO_3	20	*o*-(*t*-Bu)PhO—*t*-BOC **5***a*	98
o-(CH_3)PhOH **6**	1.0	THF	18-Crown-6	K_2CO_3	2	*o*-(CH_3)PhO—*t*-BOC	92
PhCH=CHCH_2OH (*trans*) **7**	1.2	CH_2Cl_2	$(Bu)_4NHSO_4$	30% NaOH	<1	PhCH=CHCH_2O—*t*-BOC (*trans*) **7***a*	93
PhCH_2CH_2OH **8**	1.2	CH_2Cl_2	$(Bu)_4NHSO_4$	30% NaOH	6	PhCH_2CH_2O—*t*-BOC **8***a*	91
CH_2=CHCH_2OH **9**	1.2	CH_2Cl_2	$(Bu)_4NHSO_4$	30% NaOH	2	CH_2=CHCH_2O—*t*-BOC **9***a*	81
PhCH_2OH **10**	1.2	CH_2Cl_2	$(Bu)_4NHSO_4$	30% NaOH	1.5	PhCH_2O—*t*-BOC **10***a*	80
Cyclohexanol **11**	1.2	CH_2Cl_2	$(Bu)_4NHSO_4$	30% NaOH	24	C_6H_{11}O—*t*-BOC **11***a*	30
$CH_3(CH_2)_{10}CH_2OH$ **12**	1.6	CH_2Cl_2	$(Bu)_4NHSO_4$	30% NaOH	6	$CH_3(CH_2)_{10}CH_2O$—*t*-BOC **12***a*	52
HOC$(CH_3)_2CH_2CH_2$—C$(CH_3)_2$OH **13**	2.0	CH_2Cl_2	$(Bu)_4NHSO_4$	30% NaOH	No reaction		
HOC$(CH_3)_2CH_2CH_2$—C$(CH_3)_2$OH **13**	2.0	THF	18-Crown-6	K_2CO_3	No reaction		
PhSH **14**	1.2	CH_2Cl_2	$(Bu)_4NHSO_4$	30% NaOH	2	PhS—*t*-BOC **14***a*	66
PhSH **14**	1.0	THF	18-Crown-6	K_2CO_3	<1[c]	**14***a*	96
PhSH **14**	1.0	THF	None	K_2CO_3	<1[c]	**14***a*	90
$CH_3CH_2CH_2CH_2SH$ **15**	1.2	CH_2Cl_2	$(Bu)_4NHSO_4$	30% NaOH	24	$CH_3CH_2CH_2CH_2S$—*t*-BOC **15***a*	Trace[d]
$CH_3CH_2CH_2CH_2SH$ **15**	1.0	CH_2Cl_2	18-Crown-6	K_2CO_3	2	**15***a*	90

[a] Molar ratio di-*tert*-butyl dicarbonate/ROH or RSH.
[b] Reaction mixture cooled to 0°C while mixing reactants, then allowed to come to room temperature.
[c] Evolution of gas observed during reaction.
[d] Product lost through hydrolysis.
[e] Product not isolated, yield estimated from nmr spectrum.

TABLE 2. *tert*-Butyloxycarbonylation of enols with di-*tert*-butyl dicarbonate

Starting material	Molar ratio[a]	Solvent	Catalyst	Base	Time[b] (h)	Product	Mol%	Yield (%)
$CH_3COCH_2COCH_3$ **16**	1.2	CH_2Cl_2	18-Crown-6	K_2CO_3	2	$CH_3COCH{=}C(CH_3)O$—*t*-BOC **16*a*** (*Z*)	23	90
						$CH_3COCH{=}C(CH_3)O$—*t*-BOC **16*b*** (*E*)	77	
16	1.2	THF	18-Crown-6	K_2CO_3	24	$CH_3COCH{=}C(CH_3)O$—*t*-BOC **16*a*** (*Z*)	37	48
						$CH_3COCH{=}C(CH_3)O$—*t*-BOC **16*b*** (*E*)	63	
16	1.2	CH_2Cl_2	$(Bu)_4NHSO_4$	30% NaOH	48	No reaction		
$CH_3COCH_2CO_2CH_2CH_3$ **17**	1.2	CH_2Cl_2	18-Crown-6	K_2CO_3	2	CH_3CH_2—$COCH{=}C(CH_3)O$—*t*-BOC **14*a*** (*E*)	100	90
$PhCOCH_3$ **18**	1.2	THF	None	NaH	1	$CH_2{=}C(Ph)O$—*t*-BOC **18*a***		66
18	1.2	THF	18-Crown-6	K_2CO_3	48	$CH_2{=}C(Ph)O$—*t*-BOC **18*a***		12
18	1.2	CH_2Cl_2	18-Crown-6	K_2CO_3	160	$CH_2{=}C(Ph)O$—*t*-BOC **18*a***		47

[a]Molar ratio di-*tert*-butyl dicarbonate/enol.
[b]Reaction mixture cooled to 0°C while mixing reactants, then allowed to come to room temperature.

tion with thiophenol can also be followed visually as it is accompanied by visible gas evolution. This evolution of carbon dioxide and 2-methyl propene is also observed in the reaction of di-*tert*-butyl dicarbonate with amines and in the reaction of phenol catalyzed by 18-crown-6, but is was not observed during reactions with alcohols or substituted phenols.

tert-*Butyloxycarbonylation of enols*

The *tert*-butyloxycarbonylation reaction was carried out with some readily enolizable compounds including acetyl acetone, ethyl acetoacetate, and acetophenone. Best results in these reactions (Table 2) were obtained using the crown ether – anhydrous potassium carbonate route. With ethyl acetoacetate, attack occurs exclusively at the acyl oxygen with formation of the (*E*) *t*-BOC derivative. Similar reactions of ethyl acetoacetate with acyl chlorides under phase transfer conditions are also known to give high percentages of the (*E*) *O*-acylated product (16). In contrast, acetyl acetone affords a 3 : 1 mixture of the (*E*) and (*Z*) *t*-BOC derivatives. Structural assignments for the two isomers of the *t*-BOC derivative of acetylacetone were made by a combination of spectral methods. Thus, it is known that the olefinic proton of similar compounds (11, 16) is observed at lower fields for the (*E*) isomer than for the (*Z*) isomer. In addition, a detailed FT-ir study shows that one of the isomers gives two carbonyl bands at 1704 and 1673 cm^{-1}, while the other isomer shows a single carbonyl band at 1702 cm^{-1}. An examination of molecular models confirms that while two possible orientations can occur for the (*Z*) isomer (structures A and B, Scheme 3), only one is likely for the (*E*) isomer (structure C, Scheme 3) as the other (D) is sterically hindered; therefore only one carbonyl band is expected for the (*E*) isomer. A similar result is obtained by consideration of the olefinic bands of the various isomers. This interpretation is further confirmed by the mass spectral data. Although the chemical ionization mass spectra of the isomers are nearly identical, that of the least abundant isomer shows an additional strong signal at m/e 127. This can be explained by a process in which the protonated cation resulting from loss of 2-methyl propene loses water and undergoes cyclization to form an aromatic cation (Scheme 4). This process is only possible with the (*Z*) isomer. Detailed spectral data can be found in Table 4.

The reaction with acetophenone gives best results when sodium hydride is used to form the enolate in a stoichiometric reaction, since the reaction under phase transfer catalysis, though successful, is too slow to be of practical value (Table 2).

Reactions with polyfunctional molecules

Having succeeded in the *tert*-butyloxycarbonylation of hydroxyls and thiols and enols, we looked briefly at the selectivity of the reaction by using polyfunctional molecules. A series of reactions was carried out with tyrosine ethyl ester, tyramine, *p*-aminophenol, and *p*-hydroxybenzyl alcohol. With *p*-aminophenol, excellent selectivity is observed as *N-tert*-butyloxycarbonylation is obtained in the absence of base, while in the presence of NaOH the reaction occurs mainly at oxygen (Table 3). This result is not unexpected since the nucleophilicity of the phenolate ion is much higher than that of the amino group of this substituted aniline.

As expected, different results are obtained with a molecule such as tyrosine, which has a more nucleophilic amino group as well as the reactive phenolic functionality. To simplify the reaction, tyrosine ethyl ester was chosen as the substrate. The reaction cannot be carried out with aqueous NaOH under phase

TABLE 3. *tert*-Butyloxycarbonylation of difunctional organic moieties

Starting material	Molar ratio[a]	Solvent	Catalyst	Base	Time[b] (h)	Product	(Mol.%)	Yield[c] (%)
19	1.2	CH_2Cl_2	$(Bu)_4NHSO_4$	30% NaOH	2	**19***a*	94	74 (85)
						19*b*	6	
20	1.0	CH_2Cl_2	$(Bu)_4NHSO_4$	30% NaOH	2	**20***a*	100	99 (50)
20	1.0	THF	None	None	1	**20***a*	20	100 (17)
						20*b*	80	
21	1.2	CH_2Cl_2	$(Bu)_4NHSO_4$	30% NaOH	2	**21***a*	43	84 (64)
						21*b*	57	
21	1.0	CH_2Cl_2	18-Crown-6	K_2CO_3	12	**21***a*	87	100 (89)
						21*b*	13	
21	1.0	Ethyl acetate	None	K_2CO_3	96	**21***a*	27	87 (51)
						21*b*	73	
22	2.0	Ethyl acetate	$(Bu)_4NHSO_4$	60% K_2CO_3	1	**22***a*	100	80 (80)
23	2.0	Ethyl acetate	$(Bu)_4NHSO_4$	60% K_2CO_3	2	**23***a*	100	83 (83)
23	1.0	Ethyl acetate	18-Crown-6	K_2CO_3	17	**23***b*	100	85 (0)

[a] Molar ratio di-*tert*-butyl dicarbonate/ROH or RSH.
[b] Reaction mixture cooled to 0°C while mixing reactants, then allowed to come to room temperature.
[c] First number indicates %conversion of di-*tert*-butyl dicarbonate and number in parenthesis indicates %conversion for phenolic or thiol functionalities.

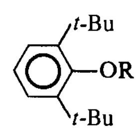

4 R = H
4*a* R = *t*-BOC

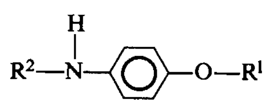

19 R^1, R^2 = H
19*a* R^1, *t*-BOC
R^2 = H
19*b* R^1, R^2 = *t*-BOC

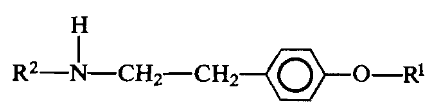

20 R^1, R^2 = H
20*a* R^1, R^2 = *t*-BOC
20*b* R^1 = H, R^2 = *t*-BOC

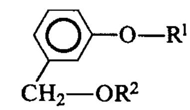

21 R^1, R^2 = H
21*a* R^1 = *t*-BOC
R^2 = H
21*b* R^1, R^2 = *t*-BOC

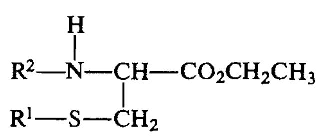

22 R^1, R^2 = H
22*a* R^1, R^2 = *t*-BOC

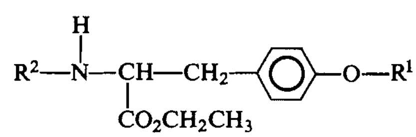

23 R^1, R^2 = H
23*a* R^1, R^2 = *t*-BOC
23*b* R^1 = H
R^2 = *t*-BOC

transfer conditions because the ester group is rapidly hydrolyzed. Reaction with the 18-crown-6 potassium carbonate system resulted in *N*-*tert*-butyloxycarbonylation. Selective *O*-*tert*-butyloxycarbonylation was not achieved. A similar reaction with tyramine using aqueous NaOH with tetrabutyl ammonium hydrogen sulfate resulted in protection at both the phenolic and the amino groups. Direct reaction of the phenolate of tyramine with di-*tert*-butyl dicarbonate afforded the same result, which confirms that selective *tert*-butylcarbonylation of the phenolic group cannot be achieved in the presence of strongly nucleophilic amino groups. In fact, the reaction affords a mixture of both the mono *N*-*tert*-butyloxycarbonyl and the di-*tert*-butyloxycarbonyl derivatives of tyramine even in the absence of added base, as the amino group of the tyramine acts as a base to assist in the *O*-*tert*-butyloxycarbonylation reaction. This result is not observed with *p*-aminophenol, which has a less basic amino group. Detailed spectral characteristics of the various *t*-BOC derivatives are given in Table 4.

To determine whether selectivity can be achieved in systems containing both phenol and aliphatic hydroxyl functionalities, the reaction of *m*-hydroxy-benzyl alcohol with di-*tert*-butyl dicarbonate was attempted under a variety of reaction conditions (Table 3). Aqueous NaOH in the presence of tetrabutyl ammonium hydrogen sulfate led to the formation of much disubstituted product. A higher percentage of reaction at the phenolic site was observed when the reaction was carried out with 18-crown-6 in the presence of powdered potassium carbonate; this limited selectivity was lost when the crown ether was omitted in the reaction with powdered potassium carbonate (Table 3). Finally, although the bis-*tert*-butyloxycarbonylation of L-cysteine has been accomplished previously (13) using *tert*-butyl chlorocarbonate, the reaction is much more convenient using di-*tert*-butyl dicarbonate.

Experimental

Infrared spectra were recorded using a Nicolet MX-1 Fourier-

TABLE 4. Physical and spectral

Product	Melting point (°C)	Infrared (cm^{-1})[b]	^{1}H nmr (ppm from TMS)[a,c]
1*a*	Liquid	1759	7.21(m,5H), 1.56(s,9H)
2*a*	69–71	1764, 1705	9.33(s,1H), 7.25(d,2H), 7.82(d,2H), 1.55(s,9H)
3*a*	60–61.5	1756, 1682, 1599	7.92(d,2H), 7.18(d,2H), 2.55(s,3H), 1.56(s,9H)
5*a*	Liquid	1759	6.83–7.40(m,4H), 1.55(s,9H), 1.39(s,9H)
6*a*	Liquid	1758	7.40(s,4H), 2.20(s,3H), 1.53(s,9H)
7*a*	Liquid	1743	7.23(s,5H), 5.93–6.77(m,2H), 4.63(d,2H), 1.47(s,9H)
8*a*	Liquid	1741	7.22(s,5H), 4.18(t,2H), 2.88(t,2H), 1.47(s,9H)
9*a*	Liquid	1744	5.80(m,1H), 5.27(m,2H), 4.52(d,2H), 1.43(s,9H)
10*a*	Liquid	1741	7.30(s,5H), 5.05(s,2H), 1.50(s,9H)
11*a*	Liquid	1737	4.15(s(broad),1H), 1.53(s,9H), 1.2–1.8(m,10H)
12*a*	Liquid	1743	4.00(t,2H), 1.51(s,9H), 1.30(s,20), 0.86(t,3H)
14*a*	Liquid	1724, 1584	7.31(m,5H), 1.52(s,9H)
15*a*	Liquid	1718, 1702	2.66(t,2H), 1.40(s,9H), 1.05–1.78(m,4H), 0.82(t,3H)
16*a*	Liquid	1758, 1704, 1673, 1637	5.73(s,1H), 2.18(s,3H), 2.02(s,3H), 1.55(s,9H)
16*b*	Liquid	1758, 1702, 1630 1616	6.13(s,1H), 2.31(s,3H), 2.20(s,3H), 1.56(s,9H)
17*a*	Liquid	1760, 1724, 1670	5.70(s,1H), 3.12(q,2H), 2.23(s,3H), 1.52(s,9H), 1.25(t,3H)
18*a*	Liquid	1759, 1645	7.13, 7.60(m,5H), 5.35(d,1H), 5.02(d,1H), 1.50(s,9H)
19*a*	113.5–114.5	3475, 3384, 1744	6.85(d,2H), 6.50(d,2H), 3.53(s,2H), 1.53(s,9H)
19*b*	135–137	1754, 1746, 1704, 1523	7.26(d,2H), 6.97(d,2H), 6.45(s,1H), 1.53(s,9H), 1.48(s,9H),
20*a*	76–77.5	1752, 1694	7.11(s,4H), 4.52(s,1H), 3.33(q,2H), 2.74(t,2H), 1.54(s,9H), 1.44(s,9H)
20*b*	74–75	3377, 1687, 1667	6.83(q,4H), 6.63(s(broad),1H), 4.53(m(br),1H), 3.27(q,2H), 2.63(t,2H), 1.43(s,9H)
21*a*	Liquid	3400, 1758	6.72–7.82(m,4H), 4.57(s,2H), 2.07(s,1H), 1.52(s,9H)
21*b*	Liquid	1759, 1744	7.18(m,4H), 5.03(s,2H), 1.56(s,9H), 1.53(s,9H)
22*a*	76.5–77.5	3394, 1747, 1718, 1706, 1693, 1516	5.43(d,1H), 4.20–4.63(m,1H), 4.15(q,2H), 3.22(d,2H), 1.50(s,9H), 1.43(s,9H), 1.27(t,3H)
23*a*	84–86	3380, 1758, 1741, 1716	7.03(s,4H), 4.93(d,1H), 4.33–4.67(m,1H), 4.08(q,2H), 3.03(d,2H), 1.56(s,9H), 1.40(s,9H), 1.20(t,3H)
23*b*	82–83	3384, 3342, 1727, 1692	7.03(s,1H), 7.00(d,2H), 6.63(d,2H), 5.03(d,1H), 4.16–4.63(m,1H), 4.10(q,2H), 3.93(d,2H), 1.20(t,3H)

[a] Chemical shift in ppm from TMS, the numbers in parenthesis refer to the multiplicity of the lines and the
[b] Liquids done neat on NaCl disks and solids done as a KBr pressed disk.
[c] m = multiplet, s = singlet, d = doublet, t = triplet, q = quartet.
[d] vs = very strong, s = strong, m = medium, w = weak, vw = very weak.
[e] Value obtained from chemical ionization with methanol.
[f] Value obtained from chemical ionization with isobutane.
[g] Elemental analysis for C,H,N,S indicated for new compounds only; "calcd." refers to the calculated values, and

transform infrared spectrometer. The nmr spectra were recorded on Varian EM-360, CFT-80, and XL-200 instruments using $CDCl_3$ as solvent and TMS as reference. Mass spectra were measured on a VG-7070E double-focusing mass spectrometer using chemical ionization where appropriate. Thermogravimetric analyses (tga) were performed on a DuPont 1090 instrument under nitrogen atmopshere. Di-*tert*-butyl dicarbonate was purchased from Sigma Chemicals and used without further purification. Solvents used in solid–liquid phase transfer reactions with anhydrous potassium carbonate were dried prior to use. Poly(*p*-hydroxystyrene) was obtained from Maruzen Oil properties of products

Mass spectrum[d]	Elemental analysis[g]
(M^+) absent, 179(w), 94(s), 77(m), 57(vs)	Reference 13
(M^+) absent, 207(w), 122(m), 166(w), 57(vs)	Reference 6
($M^+ + 1$) 237(vw), 137(w), 136(vw), 121(w), 57(vs)	Reference 7
(M^+) 250(w), 235(w), 191(m), 150(s), 135(s), 107(m), 91(s), 57(vs)	C,H: 72.40, 8.97 Calcd.: 72.69, 9.15
(M^+) 193(w), 149(m), 108(s), 107(m), 91(s), 57(vs)	C,H: 68.98, 8.02 Calcd.: 69.20, 7.74
(M^+) 234(w), 178(s), 134(m), 133(m), 117(s), 57(vs)	C,H: 71.62, 7.81 Calcd.: 71.77, 7.74
($M^+ + 1$)[e] 223, 122(m), 104(s), 91(s), 57(vs)	C,H: 70.09, 8.27 Calcd.: 70.25, 8.16
(M^+) absent, 102(s), 99(s), 58(s), 57(vs), 41(vs)	Reference 17
(M^+) 208, 152(m), 108(m), 107(m), 91(vs), 57(vs)	Reference 12
($M^+ + 1$)[e] 201, 145(w), 99(m), 82(m), 57(s)	Reference 18
($M^+ + 1$)[e] 287, 168(w), 57(s)	C,H: 71.31, 12.16 Calcd.: 71.28, 11.96
(M^+) 210(w), 110(vs), 109(vs), 195(w), 137(m)	Reference 13
($M^+ + 1$)[f] 191, 147,[f] 135[f]	Reference 13
(M^+) absent, 127(vs), 100(s), 101(m), 83(m), 85(s), 57(vs)	C,H: 60.14, 8.06 Calcd.: 59.98, 8.05
(M^+) absent, 100(m), 101(m), 85(m), 83(m), 57(vs)	C,H: 59.81, 7.89 Calcd.: 59.98, 8.05
($M^+ + 1$)[f] 231, 130(w), 113(w), 102(vw), 85(m), 56(vs)	C,H: 57.11, 7.62 Calcd.: 57.38, 7.88
($M^+ + 1$) 221(vw), (M^+) 220(w), 120(s), 103(s), 105(m), 165(vw), 164(vw)	C,H: 66.90, 6.89 Calcd.: 66.65, 6.88
(M^+) 209(w), 153(w), 194(w), 109(vs), 57(s)	C,H,N: 63.09, 7.16, 6.41 Calcd.: 63.14, 7.23, 6.69
($M^+ + 1$)[f] 310, (M^+)[f] 309, 209(m), 194(w), 153(s), 109(s), 57(vs)	C,H,N: 61.88, 7.36, 4.55 Calcd.: 62.12, 7.49, 4.52
($M^+ + 1$) 338,[e] 237(w), 266(w), 222(w), 181(s), 120(vs), 57(vs)	C,H,N: 64.10, 8.25, 3.99 Calcd.: 64.07, 8.07, 4.15
(M^+) 237(w), 181(m), 120(s), 57(vs)	C,H,N: 65.64, 8.29, 5.84 Calcd.: 65.80, 8.07, 5.90
($M^+ + 1$)[f] 225, 165(w), 124(s), 209(vw), 107(w), 57(vs)	C,H: 63.97, 7.10 Calcd.: 64.24, 7.19
($M^+ + 1$)[f], 325, 224(w), 207(m), 168(m), 124(m), 107(m), 57(vs)	C,H: 63.13, 7.54 Calcd.: 62.94, 7.46
($M^+ + 1$)[f] 350, 237(w), 220(m), 193(m), 176(m), 132(s), 57(vs)	C,H,N,S: 51.56, 7.79, 4.01, 9.17 Calcd.: 51.36, 7.87, 3.98, 9.31
($M^+ + 1$)[f] 410, 294(w), 280(w), 253(w), 252(w), 236(w), 192(s), 136(s), 107(s), 57(vs)	C,H,N: 61.43, 7.42, 3.30 Calcd.: 61.16, 7.63, 3.42
($M^+ + 1$) 310,[e] 253(vw), 209(vw), 192(m) 107(vs), 57(s)	Reference 19

integration.

is given to compounds already reported.

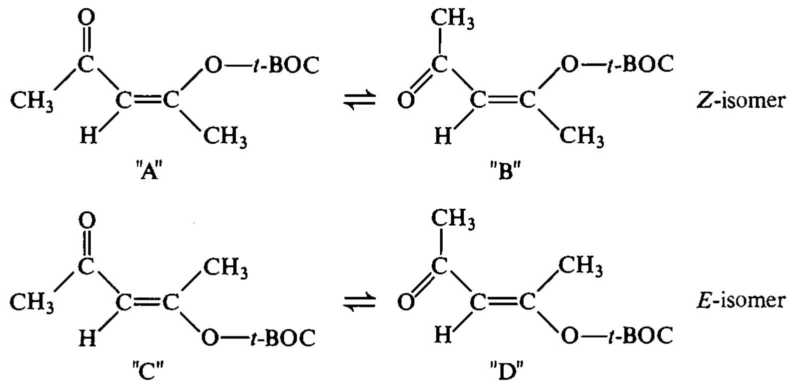

SCHEME 3

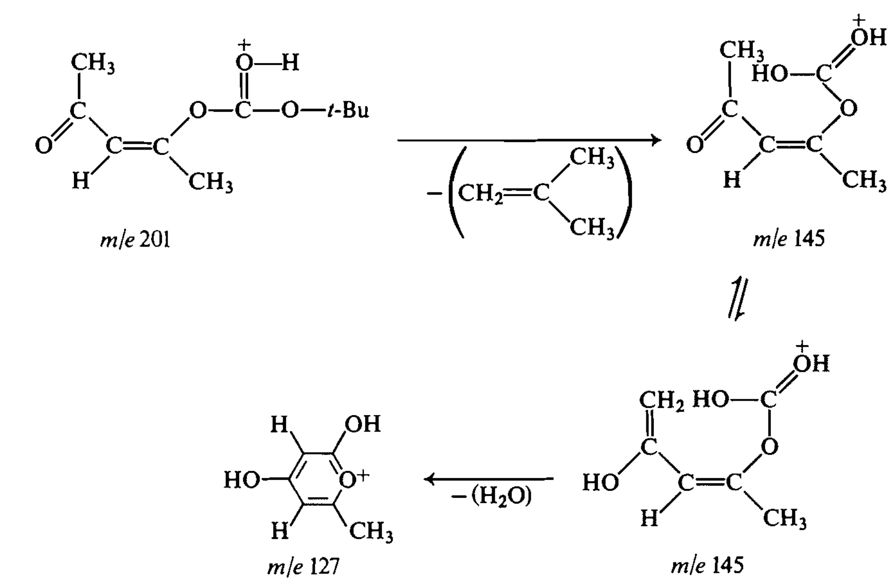

SCHEME 4

Co. (resin M); the dark colored material had a broad molecular weight distribution with M_n approximately 6,000. Several grades of novolac obtained from Eastman Kodak were used successfully, most had molecular weights (M_n) less than 1000. All of the yields which are reported are for isolated compounds; in the case of polyfunctional molecules, Table 3 reports the %conversion for the dicarbonate as well as for the phenolic or thiol functionalities.

tert-*Butyloxycarbonylation of alcohols*

In a typical reaction, cinnamyl alcohol (1 g, 7.45 mmol) was dissolved in 2 mL dichloromethane containing di-*tert*-butyl dicarbonate (1.94 g, 8.89 mmol) and a catalytic amount of tetrabutyl ammonium hydrogen sulfate (0.073 g, 0.22 mmol). After cooling to 0°C, ice-cold 30% aqueous NaOH (3.7 mL) was added with vigorous stirring. After 90 min stirring, tlc indicated that the reaction was complete. The organic phase was diluted with dichloromethane, washed with a saturated brine solution, then dried over magnesium sulfate. After evaporation of the solvent, the product was purified by passing over a short silica gel column using 5% ethyl acetate in petroleum ether as eluting solvent; 1.65 g (93%) of the pure product was obtained as an oil; ir: carbonyl at 1741 cm^{-1}; ^{1}H nmr: 7.23 (s, phenyl), 6.66–6.23 (ABX_2 pattern, vinyl), 4.63 (d, CH_2), 1.47 (s, *tert*-butyl); mass spectrum: *M* + 234 (weak), 178 (strong, M − CH_2=$C(CH_3)_2$), 134 (medium, additional loss of CO_2), 133, 117, 57.

Similar reactions with other alcohols were carried out using a 10–15% excess of the dicarbonate reagent. The products which were obtained had spectral properties which are shown in Table 4.

tert-*Butyloxycarbonylation of phenols*

A suspension of 20.0 g anhydrous potassium carbonate in 20.0 mL dry THF containing 10.0 g phenol (0.1 mol) was cooled to 0°C, then treated with 23.2 g di-*tert*-butyl dicarbonate (0.1 mol) containing a catalytic amount of 18-crown-6. Chromatographic monitoring of the reaction showed that the dicarbonate was consumed in less than 1 h and the mixture was worked up as described above to afford 21 g (99% yield) of pure phenyl *tert*-butyl carbonate. The spectral characteristics of the product are given in Table 4. A parallel reaction done in the absence of 18-crown-6 proceeded somewhat more slowly, but afforded an excellent yield of the desired product.

tert-*Butyloxycarbonylation of novolac*

A solution of 5 g novolac in 20 mL ethyl acetate was treated with 3.5 g powdered anhydrous potassium carbonate and 4.55 g of di-*tert*-butyl dicarbonate. The mixture was stirred for 24 h at room temperature, then filtered. After evaporation of the solvent under reduced pressure, the residue was dissolved in a minimum of THF and the polymer was precipitated in water. After redissolution in dichloromethane, washing with water, and drying over anhydrous magnesium sulfate, the solvent was evaporated to yield the partly *tert*-butyloxycarbonylated novolac (6.7 g) as a hard foam. The *t*-BOC content of the polymer was 50% measured by nmr as well as by tga, as expected from the stoichiometry of the reaction. In other experiments the *t*-BOC content of the polymer was varied at will from a low of 3% to 100% by simple adjustments in the amount of di-*tert*-butyl dicarbonate available for the reaction. The functionalization reaction was also carried out using THF as a solvent; this resulted in an easier work-up as the polymer could be precipitated directly from the after-reaction mixture. The infrared spectra of the products show a carbonyl band at 1760 cm^{-1}, accompanied by a hydroxyl band at 3300 cm^{-1} in the case of the partly functionalized polymers only.

tert-Butyloxycarbonylation of poly(p-hydroxystyrene)

The reaction with resin M was carried out as described above for Novolac using 3.25 g of poly(*p*-hydroxystyrene) in 12 mL ethyl acetate with 4 g powdered anhydrous K_2CO_3 and 6 g di-*tert*-butyl dicarbonate to yield 5.5 g (93% yield) of fully substituted poly(*p-tert*-butyloxycarbonyl styrene). The polymer has spectral characteristics similar to those of an authentic sample (10). Partial *tert*-butyloxycarbonylation of poly(*p*-hydroxystyrene) can be accomplished readily as above, using less than a stoichiometric amount of the dicarbonate reagent.

tert-Butyloxycarbonylation of thiophenols

The reaction was carried out exactly as described above for the *tert*-butyloxycarbonylation of phenol. Effervescence occurred immediately upon addition of the dicarbonate and the reaction was complete within minutes. The desired product, obtained in 96% yield, has the spectral characteristics given in Table 4.

tert-Butyloxycarbonylation of enols

The reaction was carried out as above for the preparation of **1***a* but requires a longer reaction time. In typical cases most of the reaction is completed in 5–6 h and a small amount of colored tarry material is formed. This is removed by precipitation in petroleum ether followed by the usual work-up.

The spectral characteristics of the various products are given in Table 4.

tert-Butyloxycarbonylation of p-aminophenol

To a suspension of 1.00 g (9.16 mmol) of *p*-aminophenol in 5 mL dichloromethane was added 0.16 g (0.60 mmol) tetrabutyl ammonium hydrogen sulfate and 5.0 mL 30% aqueous NaOH. After stirring the mixture until a clear two-phase system is obtained and cooling to 0°C, 2.43 g (11.12 mmol) of di-*tert*-butyl dicarbonate was added. The stirred mixture turned dark and, after a few hours, chromatographic monitoring revealed that the reaction was over. After work-up, a mixture of two products was obtained. This mixture afforded 1.54 g of *O-tert*-butyloxycarbonyl-*p*-aminophenol **19***a* (80% yield) as well as 0.14 g of the *O,N*-bis-*tert*-butyloxycarbonylated derivative **19***b*. This result shows that 85% of the original phenolic groups have reacted, while conversion of the di-*tert*-butyl dicarbonate into the two isolated products reached 74%. A similar reaction carried out on the phenolate of *p*-aminophenol in homogeneous medium gave a slightly lower yield of **19***a* with only a trace (less than 1%) of **19***b*.

tert-Butyloxycarbonylation of tyramine

The reaction was carried out as above using 0.5 g (3.65 mmol) tyramine in 2 mL dichloromethane containing 0.05 g tetrabutyl ammonium hydrogen sulfate. After addition of an equal volume of 30% aqueous NaOH, the mixture was stirred until a clear two-phase system was obtained, 0.795 g di-*tert*-butyl dicarbonate was added, and the mixture was stirred rapidly at 0°C. The reaction was over in a few hours and the mixture was processed as above to yield 0.61 g of bis-*O,N-tert*-butyloxycarbonylated tyramine **20***a* (quantitative yield with respect to dicarbonate). A similar reaction using the preformed phenolate of tyramine and di-*tert*-butyl dicarbonate afforded the same di-protected product. In the absence of added base the reaction proceeded as follows: to 0.5 g tyramine (3.65 mmol) suspended in 2 mL THF at 0°C is added an equimolar amount (0.795 g) of di-*tert*-butyl dicarbonate. Effervescence occurred with complete dissolution of the solid materials. Work-up after 2 h of standing afforded 0.21 g of the bis-*t*-BOC derivative **20***a* (0.62 mmol) and 0.57 g of the *N-t*-BOC compound **20***b* (2.4 mmol). The overall conversion for this reaction was 100% for the dicarbonate and only 17% for the phenolic groups.

tert-Butyloxycarbonylation of m-hydroxybenzyl alcohol

The reaction was carried out as above with 1 g (8.05 mmol) *m*-hydroxybenzyl alcohol, 5 mL dichloromethane, 0.136 g tetrabutyl ammonium hydrogen sulfate, 5 mL 30% NaOH, and 2.108 g (9.66 mmol) di-*tert*-butyl dicarbonate at 0°C. The dicarbonate was consumed within 2 h and the mixture was subjected to the usual work-up to yield 0.96 g of the bis-*t*-BOC derivative **21***b* and 0.49 g of **21***a* for an overall conversion of 64% of the phenolic groups and 84% of the dicarbonate. A similar reaction carried out on equimolar amounts of *m*-hydroxy benzyl alcohol (1 g, 8.05 mmol) and di-*tert*-butyl dicarbonate (1.76 g) in 4 mL dichloromethane with 3 g anhydrous potassium carbonate and 0.4 mmol 18-crown-6 afforded a larger proportion of the mono-*t*-BOC derivative **21***a* (1.39 g) and a smaller amount (13 mol% of total or 0.31 g) of th bis-*t*-BOC derivative **21***b* with a quantitative conversion of the dicarbonate and 89% conversion of the phenolic groups.

tert-Butyloxycarbonylation of tyrosine ethyl ester

A suspension of 1.0 g (4.07 mmol) of tyrosine ethyl ester hydrochloride in 15 mL ethyl acetate was stirred with 0.050 g 18-crown-6 and 2.50 g anhydrous potassium carbonate until the tyrosine derivative was fully dissolved. Upon addition of 0.888 g (4.07 mmol) di-*tert*-butyl dicarbonate, effervescence was observed and the reaction mixture was processed immediately as above to yield *N-tert*-butyloxycarbonyl tyrosine ethyl ester (1.07 g, 85% yield) with mp 82–84°C. A similar reaction with two equivalents of the dicarbonate afforded the results listed in Table 3.

tert-Butyloxycarbonylation of a cysteine derivative

A solution of 1 g L-cysteine ethyl ester hydrochloride (5.4 mmol) in 2 mL water was treated with 4 g potassium carbonate. After addition of 2.36 g di-*tert*-butyl dicarbonate (10.8 mmol) and 0.13 g tetrabutyl ammonium hydroxide, the mixture was stirred. Heat was evolved and the reaction proceeded to completion very rapidly. After the usual work-up, the bis-protected cysteine ethyl ester was obtained as white crystals melting at 76.5–77.5°C.

Acknowledgements

Partial financial support of this research from the Natural Sciences and Engineering Research Council of Canada is gratefully acknowledged.

1. L. A. Carpino. J. Am. Chem. Soc. **79**, 98 (1957).
2. F. C. McKay and N. F. Albertson. J. Am. Chem. Soc. **79**, 4686 (1957).
3. G. W. Anderson and A. C. McGregor. J. Am. Chem. Soc. **79**, 6180 (1957).
4. L. A. Carpino. Acc. Chem. Res. **6**, 191 (1973).
5. M. Bodanski, Y. Klaussner, and M. A. Ondetti. Peptide synthesis. 2nd ed. Wiley–Interscience, New York. 1976. p. 25.
6. J. M. J. Fréchet, E. Eichler, H. Ito, and C. G. Willson. Polymer, **24**, 995 (1983).
7. H. Ito, C. G. Willson, J. M. J. Fréchet, M. J. Farrall, and E. Eichler. Macromolecules, **16**, 510 (1983).
8. C. G. Willson, H. Ito, J. M. J. Fréchet, and F. Houlihan. Proceedings 28th IUPAC Macromolecular Symposium, Amherst, Mass. 1982. p. 448.
9. L. A. Carpino, D. Collins, S. Gowecke, J. Mayo, S. D. Thatte, and F. Tibbets. Org. Synth. Coll. Vol. **5**, 166 (1973).
10. T. Nagasawa, K. Kuroiwa, K. Norita, and Y. Isowa. Bull. Chem. Soc. Jpn. **46**, 1269 (1973); J. W. Scott. Org. Prep. Proceed. Int. **12**, 242 (1980).
11. R. Gelin, S. Gelin, and A. Gallaud. Bull. Soc. Chim. Fr. **12**, 3416 (1973); S. Sahakibara, I. Honda, K. Takada, M. Miyoshi, T. Ohnishi, and K. Okamura. Bull. Chem. Soc. Jpn. **42**, 809 (1969).
12. V. F. Pozdnev and I. A. Nishnova. Zh. Org. Khim. **12**, 1407 (1976).
13. L. A. Carpino, B. A. Carpino, C. A. Giza, R. W. Murray, A. A. Santilli, and P. H. Terry. Org. Synth. **44**, 22 (1964); L. Schutte and A. Van der Heijden. J. Agric. Food Chem. **21**,

226 (1973).
14. B. M. POPE, Y. YAMAMOTO, and D. S. TARBELL. Org. Synth. **57**, 45 (1977).
15. H. L. FINBEINER, A. S. HAY, and D. M. WHITE. *In* Polymerization processes. *Edited by* C. E. Schildknetch. Wiley–Interscience, New York. 1977. Chapt. 15.
16. R. ALAN JONES, S. NOKKEO, and S. SIMEH. Synth. Commun. **7**, 195 (1977).
17. K. SHIKATA and T. SHIGEMUNE. Ger. Offen. 2,838,701. 1979; Chem. Abstr. **90**, 186402u (1979).
18. M. YANAGI, K. SANO, and I. NAKAMURA. Japan Kokai, 7332, 997, 1973; Chem. Abstr. **79**, 126922b (1973).
19. W. KULLMAN. J. Biol. Chem. **256**, 1301 (1981).

Chemistry of spectinomycin: its total synthesis, stereocontrolled rearrangement, and analogs[1]

STEPHEN HANESSIAN AND RENÉ ROY[2]
Department of Chemistry, Université de Montréal, Montreal, P.Q., Canada H3C 3V1

Received March 9, 1984

This paper is dedicated to the 10th anniversary of the Xerox Research Centre of Canada

STEPHEN HANESSIAN and RENÉ ROY. Can. J. Chem. **63**, 163 (1985).

The total stereocontrolled synthesis of the antibiotic spectinomycin is described, based on the regiospecific functionalization and manipulation of appropriate starting materials. The tertiary ketol rearrangement of the antibiotic and its derivatives was studied and the stereochemical identity of spectinoic acid was established by chemical correlation. Dihydrospectinomycin derivatives undergo unusual solvolysis reactions.

STEPHEN HANESSIAN et RENÉ ROY. Can. J. Chem. **63**, 163 (1985).

La synthèse totale et stéréocontrôlée de l'antibiotique spectinomycine est décrite en se basant sur une stratégie de fonctionnalisation et manipulation spécifique de produits de départs appropriés. Le réarrangement des α-cétols tertiaires de la spectinomycine et ses dérivés a été étudié et l'identité stéréochimique de l'acide spectinoïque a été établie par des corrélations chimiques. Les dérivés de la dihydrospectinomycine donnent lieu à des réactions de solvolyses intéressantes.

Spectinomycin is a structurally unique antibiotic which is formally classified among the aminocyclitol group (1). Isolated from several fermentation broths in the early sixties, it was originally given the name actinospectacin (2; for a recent review on the chemistry of spectinomycin, see ref. 3) and is presently used in the veterinary area. It is also widely used in human medicine because of its potent activity against some strains of *Neisseria gonorrhoeae*. It may be the drug of choice against penicillin resistant strains of *Neisseria gonorrhoeae* (4) or for patients allergic to β-lactam antibiotics. Another interesting feature concerning the biological profile of spectinomycin is the fact that it exhibits a greater degree of therapeutic effect in infected animals than might be expected on the basis of its in vitro activities. Extensive studies concerned with structure modification in order to induce greater antibiotic activity were carried out in several laboratories (5, 6). Unfortunately, except for the recently announced 4-amino-4-(*R*)-dihydro derivative (7*a*), and some alkyl spectinomycin analogs (7*b*), efforts to improve the biological profile of spectinomycin have been somewhat disappointing.

The constitutional structure (8, 9), stereochemistry, and absolute configuration (10), as well as the biosynthesis (11) of spectinomycin have been the subject of elegant studies over the years. Its unique structural, conformational, and functional features are depicted in Scheme 1. The tricyclic structure harbors nine chiral carbon atoms, each of which bears at least one hetero atom. Stereoelectronic factors are dominant in view of the presence of three contiguous acetal type linkages (12) and the fused ring systems provide classical cases of the manifestation of natural anomeric stereoselection (13). This feature may be appreciated by considering the conformational depiction of spectinomycin in Scheme 1 where it can be seen that, in the solid state structure (10), one of the oxygen atoms at C4a and C10a has an axial disposition with respect to the other on the same carbon atom (*gauche* orientation), as dictated by the stereoelectronic requirements of the anomeric effect (for a discussion of the anomeric effect, see ref. 14). Deslongchamps, Descotes and their respective groups (15) have found that bicyclic acetals having an axial orientation of alkoxy anomeric substituents are stabilized by at least 1.5 kcal/mol compared to the alternate anomer.

Spectinomycin adopts a "bent" shape in the solid state as well as in solution, and the resulting topological features in terms of functional groups, sidedness, and electronic properties may have an important bearing on its mode of action in inhibiting protein biosynthesis at the ribosomal level.

Surprisingly, little if any effort was reported on the total synthesis of spectinomycin prior to 1977. Thus, Suami *et al.* (16) reported on the synthesis of a tetrahydrospectinomycin derivative by glycosylation of a suitably protected actinamine. Several syntheses of actinamine, the cyclitol portion, were already available at the time (17; actinamine is also easily accessible from spectinomycin, see ref. 8) although by far the quickest access to this compound is by acidic hydrolysis of the antibiotic (9). In 1979, two independent and conceptually different total syntheses of spectinomycin were announced. The Upjohn synthesis (18) utilized L-glucose as starting material and involved a series of unique transformations. Our own synthesis, announced in preliminary form (13*b*, 19), was based on the systematic chemical manipulation of D-glucose and took advantage of some reactions anticipated to occur with a high degree of regiocontrol. It also relied in its final stages on a biomimetically-related process. Our strategy called for the synthesis of one of the four possible tetrahydrospectinomycins (20), namely, the 4*R*,4a*R* isomer (Scheme 1), which, by virtue of a predisposed arrangement of hydroxyl groups was expected to provide the necessary regio- and stereochemical control in subsequent operations leading to a pivotal 4a-keto derivative, and eventually to spectinomycin. With such a precursor in hand, we further expected the critical intramolecular ketalization to be diastereoselective because of the stereoelectronic requirements (12) of the anomeric effect (14).

In this paper, we give a full account of this synthesis, and we report on subsequent work (21) dealing with a unique stereocontrolled rearrangement of spectinomycin. The retrosynthetic analysis shown in Scheme 1 calls for the availability of a derivative of a 4,6-dideoxyhexose, which represents the chiral tetrahydropyran portion of the molecule. The fortuitous D-nature of the corresponding sugar directed our attention to D-glucose as a precursor. An initial objective, therefore, was to

[1] Taken in part from the Ph.D. thesis of René Roy, Université de Montréal, 1981.

[2] NSERCC Predoctoral fellow 1978–1981.

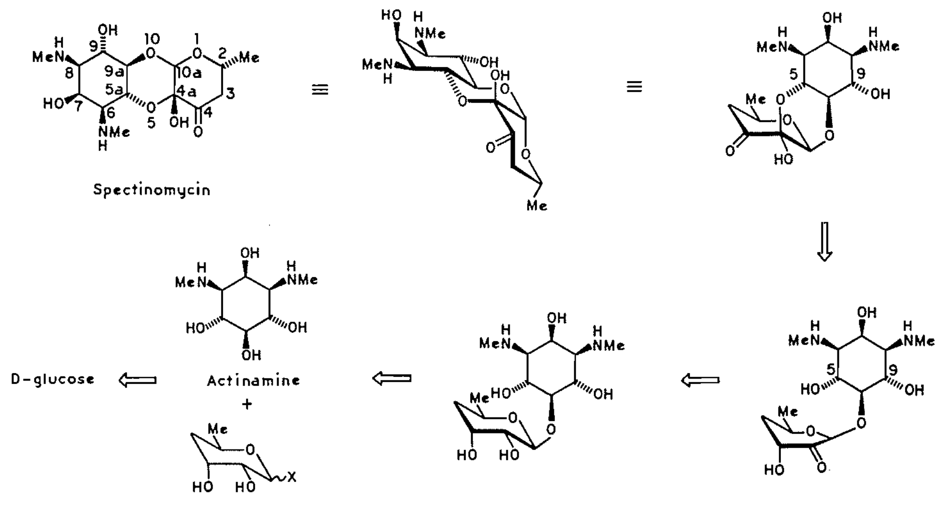

SCHEME 1

find expedient and practical methods to convert this readily available sugar into a dideoxy derivative with a predisposed orientation of hydroxyl groups at C-2 and C-3, as expressed in the structure of the glycoside **3** (Scheme 2). Note that the α-orientation of the *cis*-diol unit commits the synthetic scheme to proceed via a specific tetrahydrospectinomycin as dictated by our original strategy (Scheme 1). The availability of a two-step deoxygenation process (22) at C-4 and C-6 of methyl α-D-glucopyranoside via the intermediacy of the corresponding 4,6-dichloro derivative allowed us to have substantial quantities of the desired intermediate **1**. Attainment of the *cis*-diol orientation necessitated an inversion of configuration at C-3 and the most practical way was a two-step process involving oxidation at C-3 and reduction of the corresponding ketone. Thus, we were faced with the task of selective protection of the C-2 hydroxyl group, a process which was easily accomplished by taking advantage of the nucleophilic enhancement of oxygen atoms in trialkyltin ethers and their selective reaction with electrophiles (23, 24). Upon treatment of **1** with bis(tributyltin) oxide, the intermediate 2-*O*-tributlytin ether was formed selectively due to coordination with the anomeric methoxyl group (24). Reaction with benzoyl chloride gave the known 2-benzoate derivative (25) in 94% yield. Oxidation then gave the crystalline derivative **2** (25), which was reduced to **3**. The outcome of the reduction was predictable because of the α-orientation to the aglycone. Debenzoylation, acetolysis, and transformation into the glycosyl chloride were done in high-yielding steps to provide the reactive intermediate **5**. We were now faced with a stereocontrolled glycosidation with a suitably protected actinamine derivative, and the first of a series of protecting groups that would be compatible with the remainder of the synthetic sequence had to be chosen. Moreover, inspection of the structure of the intended glycoside intermediate placed some stringent requirements with regard to regio and stereocontrol. Thus, only the central hydroxyl group in the symmetrical actinamine molecule must be considered, in a condensation that should lead to a 1,2-*trans* orientation of substituents in the resulting glycoside. Such stereoselectivity can be expected by anticipating the intermediacy of 1,2-acyloxonium ions in the glycoside-forming step (for some reviews on glycoside synthesis, see ref. 26). The regioselectivity, on the other hand, could be achieved by appropriate protection–deprotection procedures so as to free the required hydroxyl group. Clearly this would unduly lengthen the synthesis. It was reasoned that by placing reasonably bulky substituents on the amino groups, the order of reactivity would greatly favor the hydroxyl group in question since it would be the least congested. Such was the case when *N,N'*-[(benzyloxy)carbonyl]-actinamine (16) was allowed to react with **5** in the presence of silver trifluoromethanesulfonate in dichloromethane at 40°C. Selective glycoside formation took place to give the expected product **6** in 60–65% yield. The choice of catalyst was evidently important (27), since a related glycosidation was accomplished in less than 10% yield when silver carbonate was used under typical Koenigs–Knorr conditions (16). Deacetylation of **6** gave the known *N,N'*-[(benzyloxy)carbonyl]-4(*R*),4a(*R*)-tetrahydrospectinomycin **7** (20).

Having thus secured the stereochemical identity of glycosidic linkage in our synthetic sample **6**, we considered various options for manipulating the hydroxyl groups en route to our next target, namely dihydrospectinomycin. To achieve this, it was necessary to set the stage for preferential oxidation at C-2 of the sugar and for intramolecular ketalization. The *cis*-diol unit in 7, comprising an axial–equatorial orientation of hydroxyl groups, proved to be a judicious choice for the synthetic operations to be performed. These called for the formation of a cyclic orthoester **9***b* which was expected to undergo a site-selective solvolysis to give the axial ester – equatorial alcohol **1***a* (28). At the same time the interplay between protecting groups and reaction conditions became, once again, an important issue. In order to achieve selective protection of the actinamine hydroxyl groups, **7** was first transformed into the corresponding isopropylidene derivative and a search for O-protecting groups was initiated, bearing in mind that the resulting derivative should withstand the rigors of aqueous acid,[3] while being susceptible to mild conditions of deprotection. The seldom used trichloroethoxycarbonate group (see, for example, ref. 29) was found to be ideal for these transformations. With these considerations in mind, we set out to test their outcome in the laboratory. The desired derivative **9** was easily prepared from the diol **7** by an uneventful sequence involving the isopropylidene derivative **8**, which upon acid hydrolysis gave the selectively protected diol. The latter was then transformed into

[3] In our original publication, we had used acetates as protecting groups. However, unless carefully controlled, their hydrolysis was accompanied by some intramolecular cyclic carbamate formation, ref. 19.

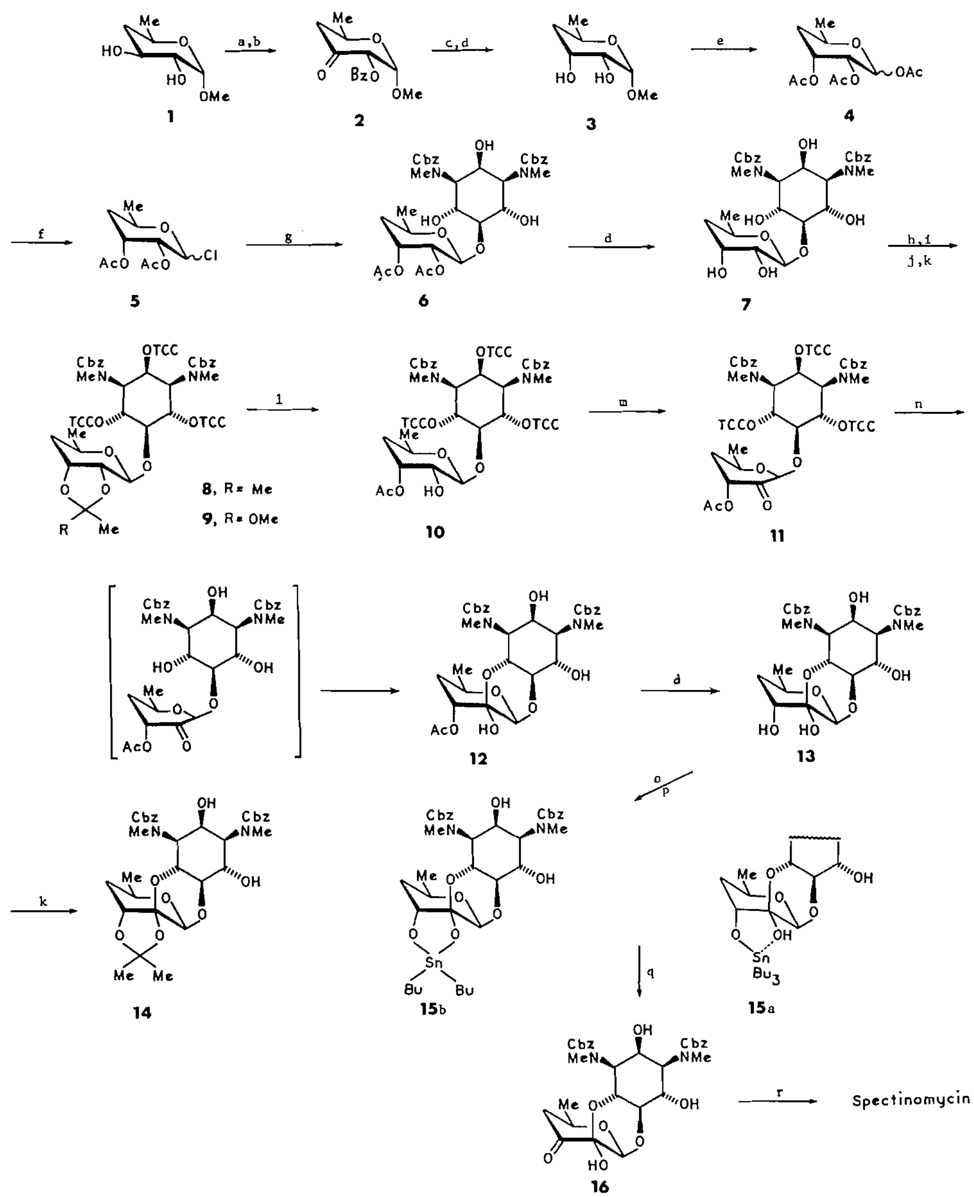

SCHEME 2. a: $(Bu_3Sn)_2O$, then BzCl; b: PCC; c: $NaBH_4$; d: NaOMe; e: Ac_2O, BF_3; f: HCl, ether; g: Cbz-actinamine, silver triflate, THF, −40°C; h: $Me_2C(OMe)_2$, TsOH; i: $ClCH_2CH_2OCOCl$, pyr., DMAP; j: aq. TsOH, H_2O–MeOH; k: $MeC(OMe)_3$, TsOH; l: aq. AcOH; m: PCC, benzene, reflux; n: Zn dust, AcOH; o: Bu_2SnO, MeOH reflux; p: $(Bu_3Sn)_2O$, benzene; q: NBS or Br_2; r: Pd/C H_2.

the orthoester **9**. Treatment of **9** with dilute acetic acid gave the amorphous monoacetate **10**, in which the acetate group was axial. Thus, the anticipated regiochemistry in the solvolysis of the orthoester ring had been indeed attained. Oxidation of **10** by a recent modification (30) of the Corey–Suggs procedure (31) gave the unstable keto derivative **11** as a syrup. Treatment of **11** with zinc dust in tetrahydrofuran cleanly removed the trichloroethoxycarbonyl groups and regenerated the triol system in the actinamine portion, with concomitant intramolecular ketalization, to give the monoacetyl derivative **12** in high yield. Mild base treatment then gave *N,N'*-[(benzyloxy)carbonyl]-4(*R*)-dihydrospectinomycin **13**, identical in all respects with authentic material. The corresponding acetonide **14** (13*a*, 32) was also easily prepared. Thus, the intermediate keto polyol underwent stereoselective ketalization with only one of the two possible, symmetrically disposed hydroxyl groups in the actinamine portion. This preference can be logically rationalized on stereoelectronic grounds (12, 14), much in the same way as for the free antibiotic itself (13, 18), and it is an anticipated event in this sequence.

Having reached this penultimate stage in our synthesis, we were in a position to address the next critical step in the sequence, namely, the oxidation of **13** to *N,N'*-[(benzyloxy)-carbonyl]spectinomycin **16**. The challenge that we faced was once more one of selectivity. How could one effect preferential oxidation of the 4(*R*)-hydroxyl group in the presence of a pair of axially (C-7) and equatorially (C-9) disposed hydroxyl groups, while maintaining the structural integrity of the molecule? Having explored a number of possible solutions to this problem, we turned once again to organotin chemistry where a unique opportunity for achieving a selective oxidation became evident, particularly in view of the *cis*-disposition of the vicinal diol unit. The oxidation of tributyltin ethers to carbonyl compounds (33) and of dibutyltin acetals to α-hydroxyketones (34) in the presence of bromine were known in the literature (23). This reaction appeared to be admirably suited to our needs,

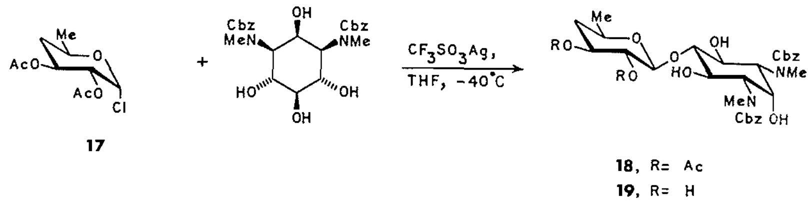

SCHEME 3

although its adaptation to acetals originating from tertiary and secondary hydroxyl groups was yet to be tested. Treatment of **13** with bis(tri-n-butyltin) oxide, followed by NBS, smoothly led to the desired *N,N'*-[(benzyloxy)carbonyl]spectinomycin **16** in high yield, presumably via the intermediacy of an intramolecularly coordinated tributyltin ether such as **15***a*. Alternatively, **13** could be transformed into the stannylidene acetal **15***b*, then treated with bromine to give the desired products. The former method was found to give cleaner products and could be better controlled, particularly in view of the tendency for the product to over-oxidize to give a by-product, which will be discussed later.

Vital to this successful oxidation was the original choice of a 4(*R*)-axial alcohol since, by its very nature the intermediate tin ether or acetal could only be oxidized at C-4, which has a favorably situated equatorial hydrogen atom.[4] Finally, hydrogenation of **16** under carefully monitored conditions led to the intended target, isolated as the crystalline dihydrochloride pentahydrate in high yield. This product was found to be identical to the natural product in all respects.

During the course of our studies, we also prepared the 4-epi tetrahydro *N,N'*-[(benzyloxy)carbonyl]tetrahydro-4(*S*),4a(*R*)-spectinomycin **19** (Scheme 3). Thus, acetolysis of **1** and glycosyl halide formation led to 2,3-di-*O*-acetyl-4,6-dideoxy-α-D-*xylo*-hexopyranosyl chloride **17** which, when condensed with *N,N'*-[(benzyloxy)carbonyl]actinamine as previously described, gave, after purification, the crystalline derivative **18** in 67% yield. Deacetylation at pH 8.5 gave the crystalline tetrol **19** (16), mp 260–265°C; $[\alpha]_D$ −3.2° ($CHCl_3$).

Stereocontrolled rearrangements

During the course of our oxidation studies of **13** in the presence of bis(dibutyltin) oxide and bromine, we had observed the formation of a secondary product which migrated close to the desired *N,N'*-[(benzyloxy)carbonyl]spectinomycin **16** (21). The same product was also formed when samples of **16** were treated with silica gel, or on prolonged standing in ethyl acetate. The spectroscopic properties of this new product were sufficiently different from those of **16** to warrant further inquiry, and it soon became apparent that a new entity was produced. The constitutional identity of this product was secured from chemical evidence and eventual correlation with a known degradation product of spectinomycin itself. Thus, treatment with sodium ethoxide in tetrahydrofuran led to a methyl ester, while treatment with aqueous sodium hydroxide followed by hydrogenolysis gave the known crystalline spectinoic acid dihydrochloride **20** (Scheme 4) (8). It was therefore evident that the new product was the seven-membered lactone **22**, which presumably arose by a process related to an α-ketol

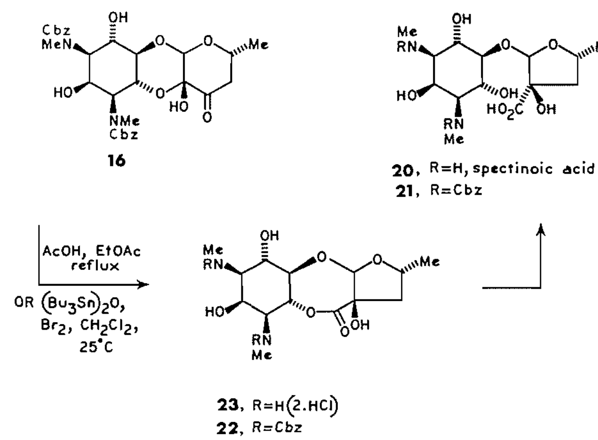

SCHEME 4

rearrangement (for a review, see ref. 35). Such rearrangements are well known to occur under acidic, basic, and solvolytic conditions and may be reversible processes (see, for example, ref. 36). However, many attempts to induce reversibility in our case were unsuccessful, possibly because of an unfavorable alignment of bonds in the lactone. The forward rearrangement process, however, can be nicely visualized to occur by activation of the C-4 carbonyl oxygen atom by an electrophile, and migration of the antiperiplanar C-4a—C-10 bond. The rearrangement did not occur with bis(dibutyltin) oxide or bromine alone, or when the substrate was converted to the 4,4-dimethylacetal derivative. It is therefore possible that the reaction is caused by initial formation of Bu_3SnOBr (33), which can supply a base as well as an electrophile. That a tertiary ketol rearrangement was indeed operative was also demonstrated when the same lactone was formed from **16** in the presence of 10% acetic acid in refluxing ethyl acetate.

Hydrogenolysis of the lactone **22** led to the corresponding amino derivative **23**, which was tested and found to be devoid of activity as an antibacterial agent. It is of interest to note in this regard that **23** is isomeric with spectinomycin and it can be considered as a variant in which the central ring has been expanded and the original α-ketol functionality transposed.

When spectinomycin was treated with strong base, there was formed an acidic degradation product which was called actinospectinoic acid (spectinoic acid) (9) and its formation was explained based on a tertiary ketol rearrangement. Although this substance was crystalline and a new asymmetric center was created at the carbon atom bearing the carboxyl group, no effort was made over the years to secure its configurational identity. The discovery of the acid-catalyzed rearrangement of **16** into the lactone **22** and its correlation with spectinoic acid **20** prompted us to establish the configurational identity of the latter. It had already been known (9) that methanolysis of spectinoic acid gave a mixture of methyl glycosides **24** and the lactone **25** (of unknown absolute configuration at C-2) (Scheme

[4] Vicinal *trans*-disposed stannylidene acetals are also subject to oxidation with bromine (ref. 34). It is also possible that we might be dealing with oligomeric ethers or acetals, rather than discrete derivatives such as **15***a,b*.

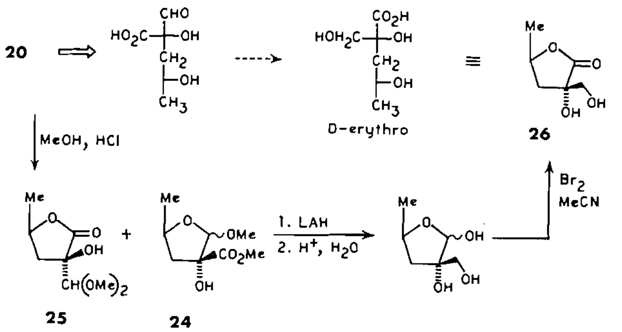

SCHEME 5

5). Thus if either product were successfully correlated with a known substance, then the task of assigning an absolute stereochemistry would be greatly simplified. We recognized the structural resemblance of α-D-isosaccharino-1,4-lactone to either methanolysis product **24** or **25**. In the hope of achieving structural and stereochemical convergence, we proceeded with a chemical modification program on two fronts. Thus, **24** was converted in three steps into the lactone **26** by standard methodology. The conversion of lactone **27**[5] derived from lactose (37) into our target required a deoxygenation at the terminal primary hydroxymethyl group, which was achieved in straightforward manner by a series of reactions shown in Scheme 6. Comparison of the physical properties of this crystalline *p*-nitrobenzoate ester **29**, derived from both the synthetic and degradation-derived lactone, established their complete convergence. The tertiary ketol rearrangement of spectinomycin therefore produces a single acid, whose absolute configuration at the newly formed asymmetric center is *R*. This, in fact, is the anticipated stereochemical result, based on a stereocontrolled migration of the C-4a—C-10 bond. With the establishment of the stereochemical identity of spectinoic acid some 23 years after its isolation, the last remaining structural problem concerning the parent antibiotic can be considered fully addressed.

In the course of our synthetic studies, we had become intrigued by the prospects of effecting a number of stereocontrolled fragmentation and substitution reactions, particularly with the unique anti-periplanar arrangement of bonds in 4-substituted dihydrospectinomycins (Scheme 7) (for examples of Grob-type fragmentations, see ref. 38). It was therefore of interest to attempt the experiments with the mesylate **31** derived from the 4-(*S*)-dihydro isomer **30** (Scheme 8). At first, heating the mesylate to its melting point did not result in the formation of new products. Consequently solvolytic studies were undertaken. Treatment of **31** with silver carbonate (39) in aqueous acetone gave the 4-(*R*)-dihydro isomer **13** in 47% yield, accompanied by *N,N'*-[(benzyloxy)carbonyl]actinamine. Clearly, solvolysis with net inversion has taken place under these conditions. When the same mesylate was treated with sodium acetate in anhydrous trifluoromethanol (40) at reflux temperature, there was formed the inverted acetate derivative **12** in 38% yield, accompanied by two unidentified side-products. Once again, apparent inversion of configuration had occurred in this reaction. However, when **31** was treated with sodium azide in 1.5% aqueous trifluoromethanol, the corresponding 4-(*S*)-azido derivative **32** was isolated in 30% yield, along with starting material and two unknown by-products. Thus, in this case a net retention of configuration was observed. Catalytic hydrogenation of **32** led to 4-amino-4-(*S*)-dihydrospectinomycin **33**, which was found to be devoid of antibacterial activity,[6] unlike its 4-(*R*) epimer **34** (7). Thus, what appeared to have been an alternative entry into the biologically active series was thwarted by the unexpected. Inspection of molecular models clearly indicates a severly restricted backside approach at C-4 in the conformationally rigid tricyclic system. Two possibilities can be considered for the displacement reactions. The mesylate could, in fact, react in the α-ketomesylate rather than the ketol form in which a much higher order of reactivity is expected (41) to give inverted products. In the case of the α-azido (Scheme 9) derivative, a subsequent base-catalyzed epimerization and subsequent intramolecular ketalization could take place to give the observed product. Alternatively, an intermediate epoxide can be envisaged to be transiently formed and attacked by the nucleophile, regiospecifically, with net retention of configuration. The results in the case of acetate ion and silver carbonate can be rationalized, based on attack of the α-keto mesylate followed by ketalization (without epimerization, or by another mechanism via initial attack on the carbonyl group, followed by an intramolecular reaction leading to the ejection of the mesylate and the formation of an intermediate acetoxonium ion).

These reactions were unsuccessful when the corresponding 4a-methoxy derivative was used, which strongly implies the involvement of the carbonyl group in the open form, or the tertiary hydroxyl group in a cyclic form.

Experimental

Melting points are uncorrected. Optical rotations were measured on a Perkin–Elmer automatic spectropolarimeter, model 141. The ^{1}H nmr spectra were recorded on Varian EM-360 and Bruker WH-90 and 400-MHz instruments using deuterochloroform as solvent unless otherwise stated. The ^{13}C nmr spectra were recorded at 22.6 MHz. Mass spectra were recorded on an AE1-902 mass spectrometer at low resolution unless otherwise indicated. Column chromatography was done using silica gel G254 with application of moderate suction or by the flash technique. Work-up with usual processing signifies extraction with an appropriate organic solvent, washing, drying the organic phase with magnesium sulfate, and evaporation.

*Methyl 2-O-benzoyl-4,6-dideoxy-α-D-*erythro*-hexopyranosid-3-ulose, 2*

A solution of **1** (22) (3.88 g, 24 mmol) in 100 mL of anhydrous toluene containing 9 mL (18 mmol, 0.75 equiv.) of bis(tributyltin) oxide was heated under reflux with a Dean–Stark trap. After 3 h, the solution was cooled to room temperature and benzoyl chloride (3.4 mL, 28 mmol) was added. After stirring 1 h, methanol was added and the solvent evaporated to give a residue which crystallized upon trituration with petroleum ether to give 6 g (94%) of the known 2-benzoate (25), mp 103–105°C; $[\alpha]_D$ +158.6 (*c* 1.21, $CHCl_3$).

A solution of this product (1.06 g, 4 mmol) was added to a suspension of pyridinium chlorochromate (16 mmol) and sodium acetate (656 mg, 8 mmol) in 50 mL of dichloromethane. After stirring for 15 h, ether was added to the dark suspension, the salts were filtered, and the filtrate was evaporated to a syrup (1.18 g; ~quantitative); $[\alpha]_D$ +65.2° (*c* 0.15, $CHCl_3$) (lit. (25) $[\alpha]_D$ +66°).

*Methyl 4,6-dideoxy-α-D-*ribo*-hexopyranoside, 3*

The preceding product (2.9 g, 11 mmol) in 100 mL of methanol was treated with sodium borohydride (492 mg, 13 mmol) and the solution was stirred for 10 min. Excess hydride was destroyed by addition of

[5] We thank Prof. R. B. Yeats, Bishop's University, Lennoxville, Quebec for a generous sample of **27**.

[6] Courtesy of Abbott Laboratories, North Chicago, Illinois.

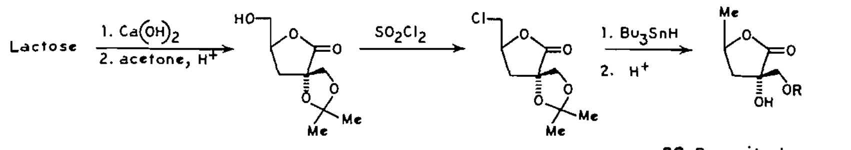

27 28 29, R=p-nitrobenzoate

SCHEME 6

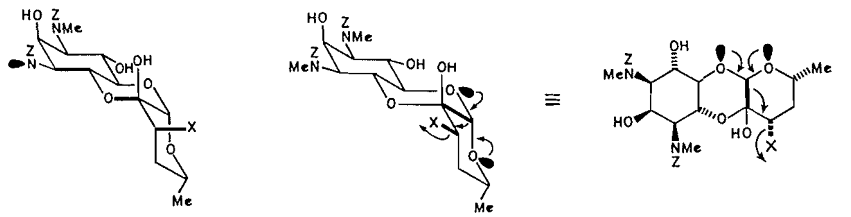

4(R) 4(S)

SCHEME 7

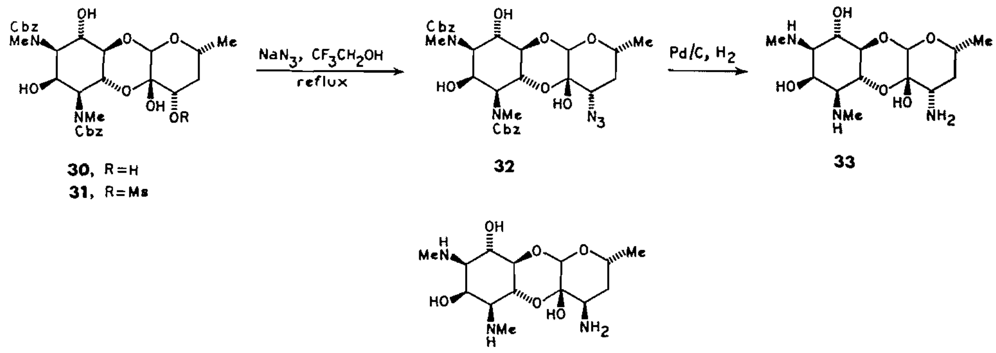

30, R=H
31, R=Ms
32 33 34

SCHEME 8

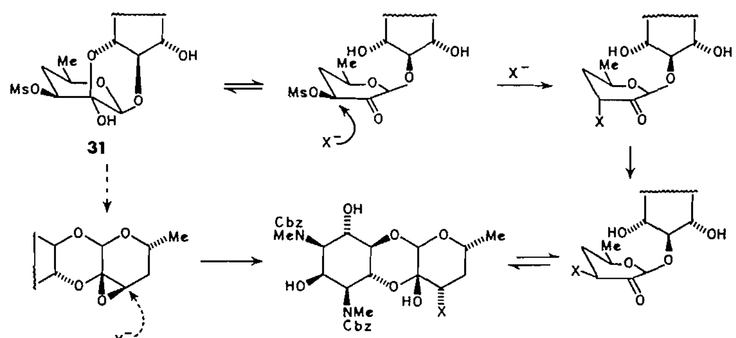

31 4(S)

SCHEME 9

aqueous acetic acid to pH 6, the solution was evaporated to dryness, and the residue was extracted with ether. Usual processing gave a syrup which was dissolved in methanol and treated with sodium methoxide. After 24 h, the solution was treated with Dowex-50 (H^+), filtered, and the filtrate was evaporated to dryness. Flash column chromatography gave the pure product **3** as a colorless syrup in almost quantitative yield; $[\alpha]_D$ +112° (*c* 0.56, $CHCl_3$); ^1H nmr (60 MHz, ppm): 1.19 (d, Me, $J_{5,6}$ = 6 Hz), 1.37–2.21 (m, H-4'4', J = 13 Hz), 3.36 (OH), 3.42 (s, OMe), 3.50–4.30 (m, H2, H3, H5), 4.70 (d, H-1, $J_{1,2}$ = 1.3 Hz); ^{13}C nmr (22.6 MHz, ppm): 101.5, 68.8, 68.1, 58.8, 55.9, 39.06, 20.6.

1,2,3-Tri-O-acetyl-4,6-dideoxy-α-D-ribo-hexopyranose, 4

The preceding diol (840 mg, 5.2 mmol), acetic anhydride (5 mL), and $BF_3 \cdot Et_2O$ (0.3 mL) were stirred at 0°C for 24 h. The solution was poured into aqueous saturated sodium bicarbonate, and the solution extracted with chloroform and processed as usual to give a syrup which crystallized upon trituration with ethanol to give 563 mg (39%) of the crystalline β-anomeric acetate, mp 131.5–133°C (EtOH); $[\alpha]_D$ −53.3° (*c* 3.32, $CHCl_3$); ^1H nmr (60 MHz, ppm): 1.21 (d, C-Me, $J_{5,6}$ = 6 Hz), 1.77 (m, H-4,4', J = 13 Hz); 2.00, 2.07 (OAc); 4.14 (m, H5), 4.80 (dd, H-2, $J_{1,2}$ = 8 Hz; $J_{2,3}$ = 8 Hz), 5.44 (m, H-3), 6.01 (d, H-1); ms *m/e*: 215 (M^+ − OAc). The mother liquors were chromatographed on silica (hexanes – 10% ethyl acetate) to give 1.07 g (75%) of an anomeric mixture of acetates. *Anal.* calcd. for $C_{12}H_{18}O_7$: C 52.55, H 6.61; found: C 52.80, H 6.63.

2,3-Di-O-acetyl-4,6-dideoxy-α,β-D-ribo-hexopyranosyl chloride, 5

The mixture of anomeric triacetates **4** (500 mg, 1.82 mmol) was dried overnight under vacuum (desiccator). It was dissolved in 50 mL of ether (freshly distilled, LAH), cooled to 0°C, and a stream of HCl gas was bubbled through the solution during 2 h. The solvent was evaporated and the residue was repeatedly coevaporated with dry toluene. This product was kept under argon in THF solution. An aliquot was analyzed by ^{1}H nmr (60 MHz, ppm): 1.20 and 1.35 (d, C-Me, two anomers); 2.09, 2.13, 2.15, 2.17 (OAc, 2 anomers); 5.53 (d, H-1, $J_{1,2}$ = 8 Hz, β-anomer), 6.09 (d, H-1, $J_{1,2}$ = 4 Hz, α-anomer).

4,4a-Di-O-acetyl-N,N'-[(benzyloxy)carbonyl]-4(R),4a(R)-tetrahydrospectinomycin, ***6***

The chloride **5** prepared from 1 g (3.65 mmol) of triacetate **4** was transferred via a double-tip needle into a dry separatory funnel in a total volume of 40 mL of THF. A solution containing *N,N'*-[(benzyloxy)carbonyl]actinamine (2.6 g, 5.46 mmol, 1.5 equiv., previously dried from THF via Dean–Stark) and silver trifluoromethanesulfonate (1.4 g, 5.46 mmol, 1.5 equiv. (Fluka)), in 50 mL of dry THF was stirred at 0°C under argon. The temperature was lowered to −40°C, and the chloride added dropwise over a period of 1 h. The reaction mixture was stirred at −40°C for 3 h, then 1 g of sodium bicarbonate followed by 5 mL of aqueous saturated sodium chloride were added. The mixture was diluted with 150 mL of chloroform, filtered over Celite, and the organic layer was processed as usual to give a foam which was chromatographed over silica (hexanes–EtOAc, 3:7). Those fractions which showed a positive uv absorption test and a negative benzidine–periodate test were combined and processed to give 1.56 g (62%) of the title compound as an amorphous solid; $[\alpha]_D$ −8.2° (*c* 0.11, $CHCl_3$); ir ν_{max} ($CHCl_3$): 3480 (OH), 1750 (OAc), 1685 (Cbz) cm^{-1}; ^{1}H nmr (90 MHz, ppm): 1.26 (d, C-Me, J = 6 Hz), 1.78 (m, H-3,3'); 1.99, 2.05 (OAc); 3.09 (s, NMe_2), 4.81 (dd, H-4a, $J_{4a,10a}$ = 8 Hz, $J_{4a,4}$ = 3 Hz), 4.91 (d, H-10a, $J_{10a,4a}$ = 8 Hz), 5.15 (s, CH_2Ph), 5.52 (m, H-4), 7.35 (s, OH, Ph), etc. *Anal.* calcd. for $C_{34}H_{44}O_{13}$: C 59.29, H 6.44, N 4.07; found: C 58.98, H 6.39, N 3.98.

N,N'-[(benzyloxy)carbonyl]-4(R),4a(R)-tetrahydrospectinomycin, ***7***

A solution of **6** (700 mg, 1.02 mmol) in 10 mL of methanol was cooled to 0°C and treated with a small chip of sodium metal to give a pH ~ 8.5. After 15 min at 25°C, Dowex-50 (H$^+$) was added, the mixture filtered, and the filtrate was evaporated to dryness. Purification by chromatography (EtOAc) gave a solid which was recrystallized from acetone to give the title compound, (~quantitative), identical in all respects to authentic material (20) (mp, mixture mp, X-ray powder diffraction diagram, $[\alpha]_D$, ir, nmr); mp 189–192°C; $[\alpha]_D$ −31.3° (*c* 0.53, MeOH). *Anal.* calcd. for $C_{30}H_{40}N_2O_{11}$: C 59.59, H 6.67, N 4.63; found: C 59.55, H 6.78, N 4.46.

7,9-Tri-O-(2,2,2-trichloroethoxycarbonyl)-4,4a-O-isopropylidene-N,N'-[(benzyloxy)carbonyl]-4(R),4a(R)-tetrahydrospectinomycin, ***8***

The preceding compound (600 mg, 1 mmol) was suspended in 10 mL of benzene, 1 mL of 2,2-dimethoxypropane and 10 mg of *p*-TsOH were added, and the homogenous solution was stirred at 25°C for 1 h. The acid was neutralized with Dowex-1 (OH$^-$), the suspension filtered, and the filtrate was evaporated to dryness. Purification by silica gel chromatography (hexanes–EtOAc, 4:1, then 1:1) gave the expected acetonide derivative as colorless crystals (526 mg, 78%); mp 189–193°C; $[\alpha]_D$ −46.1° (*c* 0.94, $CHCl_3$); ir ν_{max} (KBr): 3450 (OH), 1680 (Cbz) cm^{-1}; ^{1}H nmr (90 MHz, ppm): 1.26 (d, C-Me); 1.37, 1.51 (s, CMe_2); 1.79 (dd, H-3,3'), 2.14 (d, H-3 eq.), 3.09 (s, NMe_2), 4.51 (d, H-10a, $J_{10a,4a}$ = 7 Hz), 5.14 (s, CH_2Ph), 7.35 (OH, Ph); ms *m/e*: 644 (M$^+$), 626 (M$^+$ − H_2O), etc. *Anal.* calcd. for $C_{33}H_{44}N_2O_{11}$: C 61.48, H 6.88, N 4.34; found: C 60.92, H 6.82, N 4.19.

A solution of the preceding compound (315 mg, 0.47 mmol) in 20 mL of dry pyridine containing 30 mg of *N,N*-dimethylaminopyridine was treated at 0°C with trichloromethyl chloroformate (1 mL, 7 mmol). The solution was left at 25°C overnight, excess reagent was destroyed by adding ice-water (30 min), and the mixture was evaporated in the presence of toluene to eliminate the pyridine. The residue was extracted with ether, the latter was washed successively with aqueous ammonium chloride, then water, and the organic phase was processed as usual. Chromatography over silica (hexanes–EtOAc, 7:3) gave the title compound as a glassy semi-crystalline solid (434 mg, 67%); mp 100–105°C; $[\alpha]_D$ −16.9° (*c* 1.16, $CHCl_3$); ir ν_{max} (KBr): 1765 (OCO_2), 1700 (Cbz) cm^{-1}; ^{1}H nmr (90 MHz, ppm): 1.22 (d, C-Me); 1.34, 1.49 (s, CMe_2); 2.80 (s, NMe_2), 4.48 (d, H-10a, $J_{10a,4a}$ = 7 Hz), 4.75 (s, CH_2CCl_3), 5.13 (s, CH_2Ph), etc. *Anal.* calcd. for $C_{42}H_{43}Cl_9N_2O_{17}$: C 43.23, H 3.71, Cl 27.34, N 2.40; found: C 43.78, H 4.27, Cl 27.19, N 2.38.

4-O-acetyl-7,9-O-(2,2,2-trichloroethoxycarbonyl)-N,N'-[(benzyloxy)carbonyl]-4(R),4a(R)-tetrahydrospectinomycin, ***10***

Compound **8** (300 mg, 0.22 mmol) was dissolved in a mixture of THF (5 mL) and 9:3 methanol–water (10 mL) containing 40 mg of *p*-TsOH. After stirring for 48 h the acid was neutralized with Dowex-1 (OH$^-$), the mixture was filtered, and the filtrate was evaporated to dryness to given an amorphous solid (280 mg); $[\alpha]_D$ −7.9° (*c* 0.26, $CHCl_3$); ir ν_{max} (KBr): 3450 (OH), 1765 (OCO_2), 1705 (Cbz) cm^{-1}; ^{1}H nmr (90 MHz, ppm): 1.19 (d, C-Me), 2.82 (s, NMe_2), 5.15 (s, CH_2Ph), 7.34 (s, Ph), etc.

The preceding compound (280 mg, 0.248 mmol), in 10 mL of benzene, was treated with 0.5 mL of trimethylorthoacetate and 10 mg of *p*-TsOH. The solution was stirred at 25°C for 1 h, the acid was neutralized with dry Dowex-1 (OH$^-$), and the suspension was filtered. Evaporation of the filtrate gave a syrup consisting of **9**, which was dissolved in 10 mL of 80% aqueous acetic acid, and the solution was stirred for 30 min. The solvent was evaporated and the residue treated with toluene several times (with evaporation), to give a syrup that was chromatographed (hexane–EtOAc, 7:3). The desired acetate was obtained as an amorphous solid (hexanes) (270 mg, ~quantitative); $[\alpha]_D$ −21.0° (*c* 0.63, $CHCl_3$); ir ν_{max} (KBr): 3500 (OH), 1770 (OCO_2), 1740 (OAc), 1710 (Cbz) cm^{-1}; ^{1}H nmr (90 MHz, ppm): 1.20 (d, C-Me), 2.11 (s, OAc), 2.82 (s, NMe_2), 3.41 (dd, H-4a, $J_{4a,10a}$ = 8 Hz, $J_{4a,4}$ = 4 Hz), 4.75 (s, CH_2CCl_3), 5.14 (s, CH_2Ph), 7.34 (s, OH, Ph). *Anal.* calcd. for $C_{41}H_{45}Cl_9N_2O_{13}$: C 41.99, H 3.87, N 2.39; found: C 41.53, H 3.85, N 2.31.

4-O-acetyl-N,N'-[(benzyloxy)carbonyl]-4(R)-dihydrospectinomycin, ***12***

(a) *From* ***10***

The preceding (160 mg, 0.14 mmol) was oxidized in the presence of PCC (90 mg, 6 equiv.) in refluxing benzene (10 mL) for 1 h. Excess ether was added, the suspension was filtered over "Florisil", and the filtrates and washing were processed as usual to give a syrup that was chromatographed (hexanes–EtOAc, 7:5). The unstable intermediate 4a-keto derivative **11** was collected in appropriate fractions, and immediately used in the next step. Thus, the resulting syrup was dissolved in 10 mL of glacial acetic acid, 130 mg of zinc dust (freshly activated by washing with 1 *N* HCl), and the mixture was stirred for 30 h. The reaction mixture was poured into aqueous saturated sodium bicarbonate – EtOAc, and the organic extracts were washed and processed as usual to give the title compound. This was purified by preparative thick layer chromatography on silica gel (EtOAc) (syrup, 60 mg, 64%), and was identical in all respects with material prepared from the natural product.

(b) *From N,N'-[(benzyloxy)carbonyl]-4(R)-dihydrospectinomycin*

The title compound (600 mg, 1 mmol), readily available from spectinomycin (13a, 32), was suspended in 15 mL of benzene, 1 mL of trimethylorthoacetate and 10 mg of *p*-TsOH were added, and the mixture was stirred for 1 h. The homogeneous solution was then treated with Dowex-1 (OH$^-$) and filtered. Processing the filtrate gave a syrup which was dissolved in 20 mL of 80% aqueous acetic acid (30 min). Evaporation and chromatography as previously described gave the 4-*O*-acetyl derivative **12** as a syrup (494 mg, 77%); $[\alpha]_D$ +27.2° (*c* 1.30, $CHCl_3$); ir ν_{max} ($CHCl_3$): 3600, 3640 (OH); 1730 (OAc), 1690 (Cbz) cm^{-1}; ^{1}H nmr (90 MHz, ppm): 1.26 (d, C-Me), 1.69 (m, H-3,3'), 2.14 (s, OAc); 3.04, 3.07 (s, NMe_2); 4.82 (s, H-10a), 4.95 (t, H-4), 5.15 (s, CH_2Ph), 7.34 (s, Ph).

N,N'-[(benzyloxy)carbonyl]-4(R)-dihydrospectinomycin, ***13***

The acetate **12** (100 mg, 0.155 mmol) was dissolved in 5 mL of methanol containing 0.05 mL of a 1 *N* sodium methoxide solution (pH ~8) and the solution was stirred at 25°C for 15 min. The base was neutralized with Dowex-50 (H^+), the mixture was filtered, and the filtrate was processed as usual to give an amorphous solid (93 mg, ~quantitative), mp 157–160°C; $[\alpha]_D$ +27.5° (*c* 0.50, $CHCl_3$); ir ν_{max} (KBr): 3420 (OH), 1680 (Cbz) cm^{-1}; ^1H nmr (90 MHz, ppm): 1.22 (d, C-Me), 1.69 (m, H-3,3′); 3.02, 3.07 (s, NMe_2); 4.84 (s, H-10a), 5.13 (s, CH_2Ph), 7.33 (OH, Ph).

This product was found to be identical with a sample prepared from spectinomycin (13*a*, 32) (tlc, $[\alpha]_D$, ir, nmr, ms).

Treatment of **13** (30 mg) with 2,2-dimethoxypropane in benzene containing *p*-TsOH gave the corresponding 4,4a-acetonide derivative **14** in 96% yield, identical with material prepared from spectinomycin; glassy amorphous solid, $[\alpha]_D$ +29.6° (*c* 0.27, $CHCl_3$) (lit. (13*a*, 32) $[\alpha]$ +31.17 ($CHCl_3$).

N,N′-*[(benzyloxy)carbonyl]spectinomycin (**16**)*

A solution containing 298 mg (1 equiv.) of bis(tri-n-butyltin) oxide and **13** (300 mg, 0.5 mmol) in 20 mL of benzene was stirred at 25°C for 1 h, then treated with NBS (134 mg, 1.5 equiv.). After stirring for 10 h, hexanes were added to precipitate the title compound in almost pure form as an amorphous solid (240 mg, 80%). Chromatography on silica gel (hexanes–EtOAc, 2:3) gave pure product, identical with a sample prepared from the antibiotic; $[\alpha]_D$ −4.6° (*c* 0.28, $CHCl_3$); ir ν_{max} (KBr): 3460 (OH), 1685 (Cbz) cm^{-1}; ^1H nmr (90 MHz, ppm): 1.41 (d, C-Me), 1.51 (m, H-3e), 1.65 (m, H-3a); 2.98, 3.08 (NMe_2); 4.70 (s, H-10a), 5.14 (s, CH_2Ph), 7.34 (OH, Ph), etc; ms *m/e*: 600 (M^+), 492 (M^+ − $PhCH_2OH$), 4.65 (M^+ − $PhCH_2OCO$), etc.

The oxidation of **13** (200 mg, 0.33 mmol) was also done in the presence of di-n-butyltin oxide (90 mg, 1.1 equiv.). The mixture was refluxed in methanol (10 mL) for 1 h, evaporated, benzene added, and the solution evaporated again to give a syrup. The stannylidene derivative was dissolved in 5 mL of dichloromethane containing 0.12 mL (1.1 equiv.) of tri-n-butyltin methoxide (24) and the solution was cooled to 0°C. This was treated with a solution of bromine (1.1 equiv., 2% in CH_2Cl_2) dropwise, over a period of 1 h. Residual bromine was destroyed with cyclohexene and the crude product was isolated by precipitation with hexanes to give an amorphous solid (184 mg, 92%). Chromatography as described above gave 139 mg (70%) of pure product.

(+)-Spectinomycin dihydrochloride

A solution of the previous compound (140 mg, 0.23 mmol) in a mixture of 2-propanol and water (~1:1, 5 mL) was hydrogenated in the presence of 100 mg of 5% palladium-on-charcoal, while monitoring the effluent gas for cessation of CO_2 evolution (aqueous $Ca(OH)_2$). The catalyst was filtered, the filtrate was evaporated, and the residue was dissolved in water (3 mL) and acidified with HCl to pH 3. Repeated evaporation with toluene gave a solid which was recrystallized from aqueous acetone (~5 mL). After standing at 0°C overnight, beautiful colorless needles of (+)-spectinomycin dihydrochloride·$5H_2O$ were obtained (104 mg, 90%), mp 205–207°C (dec.); $[\alpha]_D$ +14.8° (*c* 0.42, H_2O), identical to the authentic natural product (9); ir ν_{max} (KBr): 3300 (OH), 1740 (C=O, weak) cm^{-1}, etc.; ^1H nmr (90 MHz, ppm, D_2O): 1.25 (d, C-Me); 2.79, 2.82 (s, NMe_2); 4.86 (s, H-10a); ^{13}C nmr (22.6 MHz, ppm, D_2O): 94.4 (C4a, C10a), 92.6 (C4), 70.6 (C9a), 69.2 (C2), 66.9 (C9), 66.5 (C5a), 62.3 (C8), 60.3 (C7), 59.4 (C6), 42.6 (C3), 31.5 (N8-Me), 31.1 (N6-Me), 20.5 (C2-Me); see also ref. 11; X-ray Cu-powder diffraction diagram (mm distance, m, medium, s, strong): 16.1 m, 24.5 ms, 28 m, 29.2 m, 31.8 s, 42 m, 44.7 m, 51.0 m, 52.9 mm, 54.8 mm, 59.7.

N,N′-*[(benzyloxy)carbonyl]spectinoic acid, **21***

A solution of **16** (1 g, 1.67 mmol) in 25 mL of THF and 2.5 mL of *N* NaOH was stirred for 1 h, then the solution was neutralized with Dowex-50 (H^+). The resin was filtered, and the filtrate was evaporated to a syrup which was dissolved in ethyl acetate. Addition of hexanes gave the title compound as an amorphous solid (950 mg, 92%); $[\alpha]_D$ −47.3° (*c* 2.06, $CHCl_3$); ir ν_{max} ($CHCl_3$): 3440 (OH, CO_2H), 1730 (CO_2H), 1685 (Cbz) cm^{-1}; ^1H nmr (90 MHz, ppm): 1.36 (d, C-Me), 2.19 (m, H-4, 4′); 2.9, 2.04 (s, NMe_2); 5.30 (s, H-2), 5.10 (s, CH_2Ph), 7.30 (Ph), etc.; ms *m/e*: 600 (M^+ − H_2O).

Esterification of **21** with diazomethane in a mixture of ether and THF gave the corresponding methyl ester, isolated as an amorphous solid; $[\alpha]_D$ −48.2 (*c* 0.71, $CHCl_3$); ms *m/e*: 632 (M^+).

Alternatively, treatment of **16** (1 g, 1.67 mmol) with a solution of sodium methoxide (20 mL, pH 8.5, 30 min), followed by neutralization with Dowex-50 (H^+) and processing, gave the ester (787 mg, 75%) as an amorphous solid.

N,N′-*[(benzyloxy)carbonyl]spectinoic acid lactone, **22***

(a) *From **16** under acid catalysis*

A solution containing **16** (600 mg, 1 mmol) in 25 mL of EtOAc and 2 mL of glacial acetic acid was refluxed overnight. A new product was formed with a slightly higher tlc mobility ($CHCl_3$–MeOH, 9:1). The solution was evaporated to dryness in the presence of toluene and the residue was chromatographed over silica gel (hexanes–EtOAc, 2:3) to give 457 mg (76%) of the title lactone as an amorphous solid; $[\alpha]_D$ +67° (*c* 1.45, $CHCl_3$); ir ν_{max} ($CHCl_3$): 3360, 3320 (OH); 1750 (lactone), 1685 (Cbz) cm^{-1}; ^1H nmr (90 MHz, ppm, DMSO-d_6): 1.25 (d, C-Me), 2.20 (m, H-4,4′); 2.95, 299 (s, NMe_2); 5.35 (s, H-2); 5.13, 5.16 (s, CH_2Ph); 7.37 (s, Ph), etc.; ms *m/e*: 600 (M^+), 601 (M^+ + 1), etc.

(b) *From **16** in presence of $(Bu_3Sn)_2O$ and Br_2*

A mixture containing bis(tri-n-butyltin) oxide (596 mg, 1 mmol, 1 equiv.) and **16** (400 mg, 0.67 mmol) in 10 mL of dichloromethane was stirred for 2–3 min, then treated dropwise with 0.05 mL of bromine in 1 mL of dichloromethane under argon. The desired product was formed after 4 h at 25°C. The solution was evaporated to a small volume and the product was precipitated with hexanes, leaving the tin by-products in solution. The solid thus obtained was chromatographed to give 330 mg (83%) of lactone **22**.

(c) *From **13** in presence of bis(tri-n-butyltin) oxide and bromine*

A solution of **13** (200 mg, 0.33 mmol) and 258 mg (0.43 mmol, 1.3 equiv.) of the tin derivative in 10 mL of dichloromethane was treated with bromine (0.02 mL, 1.3 equiv. in 1 mL of dichloromethane) dropwise under argon. After similar treatment as described above, the desired lactone was obtained (170 mg, 85%).

*Chemical transformations of the lactone **22***

(a) *Methanolysis*

Treatment of **22** (105 mg, 0.18 mmol) in 15 mL of methanol containing 50 mg of potassium carbonate (or sodium methoxide), followed by neutralization with Dowex-50 (H^+), after 10 min gave the methyl ester of **21** (see above) (118 mg, ~quantitative); $[\alpha]_D$ −48.2° (*c* 0.48, $CHCl_3$).

(b) *Base hydrolysis*

A solution of the lactone **22** (500 mg, 0.67 mmol) in 10 mL of THF was cooled to 0°C and treated with *N* NaOH (1 mL, 1.5 equiv.); neutralization with Dowex-50 (H^+), followed by processing, gave **21** (413 mg, ~quantitative) as an amorphous solid.

*Spectinoic acid lactone dihydrochloride **23***

A solution of **22** (400 mg, 0.67 mmol) in 10 mL of 2-propanol containing 1 mL of water and 1.6 mL *N* HCl was hydrogenated in the presence of 10% palladium-on-charcoal (100 mg). After 1 h the catalyst was filtered, and the filtrate was processed as usual by coevaporation of the solvent with toluene to give an amorphous solid (225 mg, 83%); $[\alpha]_D$ −64.3° (*c* 1.12, H_2O); ir ν_{max} (KBr): 1720 (C=O) cm^{-1}; ^{13}C nmr (22.6 MHz, ppm, D_2O): 21.8, 31.7, 41.0, 60.1, 61.9, 68.1, 69.4, 77.8, 81.1, 86.9, 108.8, 174.9.

*Methanolysis of spectinoic acid. Isolation of **24** and **25***

This experiment was done essentially according to a literature procedure (8). A solution containing 10 g of spectinomycin free base (liberated from the salt with Dowex-1) and 20 g of barium hydroxide in 500 mL of water was stirred at room temperature for 24 h. The suspension was filtered, excess barium ions were precipitated with *N* H_2SO_4 until pH ~ 5.5, and the mixture was filtered over Celite. The filtrate was evaporated in the presence of methanol and the resulting spectinoic acid **20** was used in the next step. The residue was then dissolved in methanol (600 mL) containing 95 mL of acetyl chloride (**caution!**). After 48 h of stirring, ether was added to precipitate actinamine dihydrochloride (7 g). The filtrate was neutralized with sodium methoxide until pH 6–7, the salts were filtered off, and the filtrate was evaporated to dryness. The residue was extracted with ethyl acetate, washed with water, and the organic phase was processed as usual to give 3.06 g (58%) of a colorless syrup. Flash chromatography (hexanes–EtOAc, 3:2) gave an anomeric mixture of glycosides **24** (2.31 g, 75%) and the lactone **25** (0.77 g, 25%). The mixture of glycosides **24** (showed α_D −67.4° $CHCl_3$) (lit. (8) $[\alpha]_D$ −65.5° for a product distilled at 51–54°C (0.05 Torr; 1 Torr = 133.3 Pa)). The lactone **25** showed $[\alpha]_D$ +3.3° (*c* 0.55, $CHCl_3$); ir ν_{max} (film): 3400 (OH), 1770 (γ-lactone) cm^{-1}; ^1H nmr (90 MHz, ppm): 1.43 (d, C-Me); 1.85, 2.79 (dd, H-3, J_{gem} = 13 Hz, J_{vic} = 7.9 Hz); 3.53, 3.63 (s, OMe); 3.55 (s, OH), 4.40 (s, $CH(OMe)_2$), 4.63 (m, H4). The crystalline *p*-nitrobenzoate derivative (DMAP, *p*-nitrobenzoyl chloride) showed mp 123.5–125°C (ether–hexanes); $[\alpha]_D$ −20.0° (*c* 0.19, $CHCl_3$).

Transformation of ***24*** *into the lactone* ***26***

A solution containing the mixture of glycosides **24** (210 mg, 1.06 mmol) in 10 mL of ether was reduced with lithium aluminium hydride (130 mg, 2.67 mmol). After 30 min, water was carefully added to the cooled reaction mixture, then excess ether. The organic phase was separated and processed as usual to give a syrup (170 mg, 93%). This product was hydrolyzed in a mixture of THF and *N* HCl (10 mL, 1:1) by refluxing for 1.5 h. After neutralization with Dowex-1 (OH^-), filtration, and evaporation, a syrup was obtained which was purified by flash column chromatography ($CHCl_3$–MeOH, 95%) to give 130 mg (85%) of a chromatographically homogeneous product. Oxidation of a portion (90 mg, 0.60 mmol) in 7 mL acetonitrile, containing 166 mg (0.84 mmol) of barium carbonate, with 0.04 mL (0.72 mmol) of bromine diluted in 1 mL of acetonitrile gave, after 4 h, the desired lactone. Addition of cyclohexene, filtration, and evaporation gave a syrup corresponding to the lactone **26**. The crystalline *p*-nitrobenzoyl derivative **29** was prepared in the usual manner, mp 127–129°C (ether–hexanes); $[\alpha]_D$ +20.9° (*c* 0.87, $CHCl_3$); ir ν_{max} (KBr): 3500 (OH), 1745 (γ-lactone), 1729 (ester); 1520, 1340 (NO_2) cm^{-1}; ^1H nmr (90 MHz, ppm): 1.49 (d, C-Me); 2.02, 2.57 (dd, H-3,3′, J_{gem} = 14 Hz, J_{vic} = 6, 8 Hz); 3.03 (s, OH), 4.59 (d, CH_2OH), 4.88 (m, H-4), 8.26 (m, arom); ms *m/e*: 295 (M^+). *Anal.* calcd. for $C_{13}H_{13}NO_7$: C 52.86, H 4.44, N 4.74; found: C 52.66, H 4.54, N 4.59.

α-D-Isosaccharino-1,4-lactone acetonide, ***27***

α-D-Isosaccharino-1,4-lactone (37) (324 mg, 2 mmol) was dissolved in a 1:5 mixture of 2,2-dimethoxypropane and acetone, and 15 mg of *p*-TsOH was added. After stirring 1 h, the acid was neutralized with Dowex-15 (OH^-), the mixture filtered, and the filtrate was processed as usual to give the title compound as colorless crystals (398 mg, 99%), mp 53–55°C (ether–hexanes); $[\alpha]_D$ +41.5° (*c* 0.46, $CHCl_3$) (lit. (42) mp 56–57°C).

5-Chloro-5-deoxy-α-D-isosaccharino-1,4-lactone acetonide, ***28***

The preceding compound (311 mg, 1.54 mmol) was dissolved in 2 mL of $CHCl_3$ and 2 mL of pyridine, then heated with 0.2 mL of sulfuryl chloride at 0°C. After stirring overnight, the solution was diluted with water, then chloroform, and the organic phase was separated and processed. Evaporation gave a pale yellow syrup which was purified by column chromatography (hexanes–EtOAc, 7:3) to give 292 mg (86%) of the title product as a colorless syrup, $[\alpha]_D$ +28.8° (*c* 0.72, $CHCl_3$).

Transformation of ***28*** *into lactone* ***26***

An amount of the chloro derivative **28** (687 mg, 3.1 mmol) was dissolved in 30 mL of toluene and 3.27 mL (12.4 mmol) of tri-n-butyltin hydride was added, followed by 20 mg of azobisisobutyronitrile (AIBN). The mixture was refluxed for 4 h, cooled, the solvents evaporated, and the resulting oily residue was triturated with hexanes to remove a large portion of tin by-products. The residue was dissolved in acetonitrile, hexane added to deposit an oil, and the upper phase decanted. Evaporation of excess solvent gave the 5-deoxy derivative as a syrup (547 mg, 95%); $[\alpha]_D$ +31.7° (*c* 1.03, $CHCl_3$). Hydrolysis of the acetonide (547 mg, 2.94 mmol) was done with 80% aqueous acetic acid at 80°C for 30 min. Evaporation of the solvent and column chromatography gave the desired lactone **26** (430 mg); $[\alpha]_D$ +34.4° (*c* 0.22, $CHCl_3$). Transformation into the *p*-nitrobenzoate derivative **29** was done in the usual manner (DMAP) to give material identical in all respects with a sample obtained from the methanolysis and oxidation of spectinoic acid (mp, mixture mp, $[\alpha]_D$, ir, nmr).

4-O-methanesulfonyl-N,N′-[(benzyloxy)carbonyl]-4-(S)-dihydrospectinomycin, ***31***

To a solution of *N,N′*-[(benzyloxy)carbonyl]-4-(*S*)-dihydrospectinomycin **30**, readily available by catalytic hydrogenation of spectinomycin (43), followed by *N*-benzyloxycarbonylation (600 mg, 1 mmol) in 10 mL of pyridine, was added methanesulfonyl chloride (0.12 mL, 1.3 equiv.) at 0°C. The mixture was stirred at 0°C for 18 h, then ice-water was added, followed by extraction with ethyl acetate. Processing of the organic phase gave a residue which was chromatographed on silica gel ($CHCl_3$–MeOH, 97%) to give 530 mg (79%) of the title compound as an amorphous solid, $[\alpha]_D$ +2.60 (*c* 0.73, $CHCl_3$); ir ν_{max} ($CHCl_3$): 3560, 3390 (OH); 1685 (Cbz); 1340, 1170 (SO_2Me) cm^{-1}; ^1H nmr (90 MHz, ppm, DMSO-d_6): 1.21 (d, C-Me); 2.95, 2.97 (s, NMe_2); 3.20 (s, Ms), 4.62 (s, H-10a), 5.11 (s, CH_2Ph), 7.36 (O, H, Ph), etc.; ms *m/e*: 584 (M^+ − $MeSO_3H$). Calcd.: 584.236; found: 584.236.

Solvolysis studies with ***31***

(a) *With silver carbonate*

A solution of **31** (50 mg, 0.073 mmol) in 10 mL of 1:1 acetone–water mixture was refluxed in the presence of 100 mg of freshly prepared silver carbonate. The suspension was filtered over Celite, the filtrate was evaporated in the presence of 2-propanol, and the residue was chromatographed over thick layer plates (EtOAc). The major product, 21 mg (47%), was found to be *N,N′*-[(benzyloxy)carbonyl]-4-(*R*)-dihydrospectinomycin **13**, identical in all respects with authentic material. Another product (3 mg, 9%) was identified as *N,N′*-[(benzyloxy)carbonyl]actinamine.

(b) *With sodium acetate*

Compound **31** (50 mg, 0.073 mmol) was dissolved in 3 mL of anhydrous trifluoromethanol containing 96 mg (10 equiv.) of anhydrous sodium acetate. After refluxing for 18 h, the solvent was evaporated and the residue was chromatographed on thick layer plates (EtOAc). The major product (18 mg, 38%) was identified as the 4-*O*-acetyl derivative **12** (ir, $[\alpha]_D$, nmr). Deacetylation of this product gave **13**.

(c) *With sodium azide*

A solution of **31** (340 mg, 0.5 mmol) in 20 mL of trifluoromethanol containing 1.5% water was treated with finely powdered sodium azide (4.89 mg, 1.5 equiv.) and the mixture refluxed for 4 h. Filtration and evaporation gave a syrup which was chromatographed on silica (hexanes–EtOAc, 3:7) to give the 4-azido derivative **32** (syrup, 93 mg, 30%) and unreacted starting material (128 mg). The azide showed $[\alpha]_D$ +20.1° (*c* 0.38, $CHCl_3$); ir ν_{max} ($CHCl_3$): 3600, 3200 (OH); 2100 (N_3), 1685 (Cbz) cm^{-1}.

4-Amino-4-deoxy-(S)-dihydrospectinomycin dihydrochloride, ***33***

A solution containing 70 mg (0.11 mmol) of the azide **32** in 7 mL of ethanol and 0.1 mL of aqueous HCl was hydrogenated in the presence of 25 mg of 10% palladium-on-charcoal. After 3 h, the catalyst was filtered, and the filtrate was processed as usual to give a syrup. The latter was taken up in a small volume of ethanol and ether was added to precipitate the product. The hygroscopic solid was separated from the supernatant by decantation, then it was dried in a desiccator to give 45 mg (92%) of the title compound as an amorphous solid, mp 198–200°C (dec.); $[\alpha]_D$ +11.4° (*c* 0.49, H_2O); ^1H nmr (400 MHz, ppm, D_2O): 1.36 (d, C-Me), 1.77 (dd, H-3ax, $J_{3ax,3eq}$ = 12.7 Hz, $J_{3ax,4}$ = 3.9 Hz, $J_{3eq,2}$ = 1.7 Hz), 2.88 (s, NMe_2), 3.32 (dd, H-6, $J_{6,5a}$ = 10.1 Hz, $J_{6,7}$ = 2.9 Hz), 3.61 (dd, H-8, $J_{8,9}$ = 11.0 Hz, $J_{8,7}$ = 2.84 Hz), 3.71 (dd, H-4), 3.95 (m, H-2), 4.01 (dd, H5a, $J_{5a,9a}$ =

10.1 Hz), 4.11 (dd, H-9a, $J_{9a,9}$ = 10.0 Hz), 4.37 (dd, H-9), 4.79 (dd, H-7), 4.96 (s, H-10a); ms m/e: 334 (M^+ + 1, 315 ($M^+ - H_2O$), etc.

Acknowledgements

We wish to thank the Natural Sciences and Engineering Research Council of Canada and Le Ministère de l'Éducation du Québec for financial assistance and post-graduate fellowships to R. Roy. We also acknowledge the technical assistance by Michel Therien and Daniel Delorme. Many thanks are due to Dr. W. Rosenbrook, Jr. (Abbott Laboratories) for a gift of spectinomycin and its derivatives as well as for interesting discussions.

1. J. REDEN and W. DURKHEIMER. Topics Curr. Chem. **83**, 105 (1979); D. A. COX, K. RICHARDSON, and B. C. ROSS. Topics Antibiot. Chem. **1**, 2 (1977); S. UMEZAWA. Adv. Carbohydr. Chem. Biochem. **30**, 111 (1974); S. HANESSIAN and T. H. HASKELL. *In* The carbohydrates. 2nd ed. *Edited by* W. Pigman and D. Horton. Academic Press, New York. 1970. p. 139.
2. D. J. MASON, A. DIETZ, and R. M. SMITH. Antibiot. Chemother. **11**, 118 (1961).
3. W. ROSENBROOK, JR. J. Antibiot. **32**, Suppl. S-211 (1979), and references cited therein.
4. Science, **194**, 1395 (1976).
5. C. J. MARING and D. R. WHITE. Tetrahedron Lett. **21**, 4065 (1980).
6. L. FOLEY, J. T. S. LIN, and M. WEIGELE. J. Antibiot. **31**, 985 (1978).
7. (*a*) R. MAIER, F. WOLTUN, W. REUTER, B. WELTZEL, H. GOETH, and U. LECHNER. Europ. Patent No. 78, 101,542 (1979); (*b*) D. R. WHITE, C. J. MARING, and G. A. CAIN. J. Antibiot. **36**, 339 (1983), and references cited therein.
8. P. F. WILEY, A. D. ARGOUDELIS, and H. HOEKSMA. J. Am. Chem. Soc. **85**, 2652 (1963).
9. A. L. JOHNSON, R. H. GOURLAY, D. S. TARBELL, and R. L. AUTREY. J. Org. Chem. **28**, 300 (1983).
10. T. G. COCHRAN, D. J. ABRAHAM, and L. L. MARTIN. J. Chem. Soc. Chem. Commun. 494 (1972).
11. L. A. MITSCHER, L. L. MARTIN, D. R. FELLER, J. R. MARTIN, and A. W. GOLDSTEIN. Chem. Commun. 1541 (1971); R. M. STROSHAN, M. TANIGUCHI, K. L. RINEHART, JR., J. P. ROLLS, W. J. HAAR, and B. A. RUFF. J. Am. Chem. Soc. **98**, 3025 (1976).
12. P. DESLONGCHAMPS. Stereoelectronic effects in organic chemistry. *Edited by* J. E. Baldwin. Pergamon, Oxford. 1982. p. 4.
13. (*a*) L. FOLEY and M. WEIGELE. J. Org. Chem. **43**, 4355 (1978); (*b*) S. HANESSIAN and R. ROY. J. Antibiot. **32**, Suppl. S-73 (1979), and references cited therein.
14. R. U. LEMIEUX and S. KOTO. Tetrahedron, **30**, 1933 (1974), and references cited therein.
15. N. BEAULIEU, R. A. DICKINSON, and P. DESLONGCHAMPS. Can. J. Chem. **58**, 2531 (1980); G. DESCOTES, M. LISSAC, J. DELMAU, and J. DUPLAN. C. R. Acad. Sci. Ser. C, **267**, 1240 (1968).
16. T. SUAMI, S. NISHIYAMA, H. ISHIKAWA, H. ODADA, and T. KINOSHITA. Bull. Chem. Soc. Jpn. **50**, 2754 (1977).
17. M. NAKAJIMA, N. KURIHARA, A. HASEGAWA, and T. KUROKAWA. Justus Liebigs Ann. Chem. **689**, 2443 (1965); F. LICHTENTHALER, H. LEINERT, and T. SUAMI. Chem. Ber. **100**, 383 (1967); S. OGAWA, T. ABE, H. SANO, K. KOTTERA, and T. SUAMI. Bull. Chem. Soc. Jpn. **40**, 2405 (1967).
18. D. R. WHITE, R. D. BIRKENMEYER, R. C. THOMAS, S. A. MIZSAK, and V. H. WILEY. Tetrahedron Lett. 2737 (1979).
19. S. HANESSIAN and R. ROY. J. Am. Chem. Soc. **101**, 5839 (1979).
20. J. C. KNIGHT and H. HOEKSEMA. J. Antibiot. **28**, 136 (1975).
21. S. HANESSIAN and R. ROY. Tetrahedron Lett. **22**, 1005 (1971).
22. B. T. LAWTON, W. A. SZAREK, and J. K. N. JONES. Carbohydr. Res. **14**, 255 (1970); H. PAULSEN, B. SUMFLETH, and H. REDLICH. Chem. Ber. **109**, 1362 (1976).
23. S. DAVID and S. HANESSIAN. Tetrahedron. In press, and references cited therein.
24. D. WAGNER, J. P. H. VERHEYDEN, and J. G. MOFFATT. J. Org. Chem. **39**, 24 (1974); R. M. MUNAVU and H. H. SZMANT. J. Org. Chem. **41**, 1832 (1976); T. OGAWA and M. MATSUI. Carbohydr. Res. **56**, C1 (1977).
25. J. S. BRIMACOMBE, J. MINSHALL, and C. W. SMITH. J. Chem. Soc. Perkin Trans. 1, 682 (1975).
26. K. IGARASHI. Adv. Carbohydr. Chem. Biochem. **34**, 243 (1977); A. F. BOCHKOV and G. E. ZAIKOV. Chemistry of the *O*-glycosidic bond. Pergamon Press, Oxford. 1979.
27. S. HANESSIAN and J. BANOUB. Carbohydr. Res. **53**, C13 (1977); Adv. Chem. Series No. 39, 36 (1976); F. J. KRONZER and C. SCHUERCH. Carbohydr. Res. **27**, 379 (1973).
28. R. U. LEMIEUX and H. DRIGUEZ. J. Am. Chem. Soc. **97**, 4069 (1975).
29. S. RAKHIT, J. B. BAGLI, and R. DEGHENGHI. Can. J. Chem. **47**, 2906 (1969); T. GREENE. Protective groups in organic chemistry. J. Wiley, New York. 1981.
30. D. H. HOLLENBERG, R. S. KLEIN, and J. J. FOX. Carbohydr. Res. **67**, 491 (1978).
31. E. J. COREY and J. W. SUGGS. Tetrahedron Lett. 2647 (1975).
32. W. ROSENBROOK, JR., R. E. CARNEY, R. S. EGAN, R. S. STANASZEK, M. CIROVIC, T. NISHINAGA, K. MOCHIDA, and Y. MORI. J. Antibiot. **28**, 960 (1975).
33. K. SAIGO, A. MORIKAWA, and T. MUKAIYAMA. Bull Chem. Soc. Jpn. **49**, 1656 (1976); Chem. Lett. 154 (1975).
34. S. DAVID. C. R. Acad. Sci. Ser. C, **278**, 1051 (1974); S. DAVID and A. THIEFFREY. J. Chem. Soc. Perkin Trans. 1, 1568 (1979); A. Y. UENO and M. OKAWARA. Tetrahedron Lett. 4597 (1976).
35. S. SELMAN and J. F. EASTHAM. Rev. **14**, 221 (1960).
36. N. L. WENDLER. *In* Molecular rearrangements. Vol. II. *Edited by* P. De Mayo. John Wiley & Son, New York, NY. 1964. p. 1019; D. H. G. CROUT, C. H. HASSALL, and T. L. JONES. J. Chem. Soc. 2187 (1964), and references cited therein; Y. MAZUR and M. NUSSIM. Tetrahedron Lett. 817 (1961); N. L. WENDLER, D. TAUB, and R. W. WALKER. Tetrahedron, **11**, 163 (1960); R. B. TURNER. J. Am. Chem. Soc. **75**, 484 (1953); V. DAVE and E. W. WARNHOFF. J. Org. Chem. **43**, 4622 (1978).
37. R. L. WHISTLER and J. N. BEMILLER. Methods Carbohydr. Chem. **2**, 477 (1963).
38. C. A. GROB. Angew. Chem. Int. Ed. Engl. **8**, 535 (1969); **6**, 1 (1967).
39. T. NAKATA, G. SCHMID, B. VRANESIC, M. OKIGAWA, T. SMITH-PALMER, and Y. KISHI. J. Am. Chem. Soc. **100**, 2933 (1978).
40. J. KASPI and Z. RAPPOPORT. J. Am. Chem. Soc. **102**, 3830 (1980).
41. X. CREARY and A. J. ROLLIN. J. Org. Chem. **44**, 1798 (1979); D. S. SIMOND, JR., M. PONS, and D. F. JOHNSON. J. Org. Chem. **45**, 3084 (1980).
42. R. L. WHISTLER and J. N. BEMILLER. J. Org. Chem. **26**, 2886 (1961); J. C. SOWDEN, M. G. BLAIR, and D. J. KAENNE. J. Am. Chem. Soc. **79**, 6450 (1957).
43. W. ROSENBROOK, JR. and R. E. CARNEY. J. Antibiot. **28**, 953 (1975).

Packing analysis of carbohydrates and polysaccharides. 16. The crystal structures of celluloses IV_I and IV_{II}

ERIC S. GARDINER AND ANATOLE SARKO[1]

Department of Chemistry and the Cellulose Research Institute, State University of New York, College of Environmental Science and Forestry, Syracuse, NY 13210, U.S.A.

Received February 20, 1984

This paper is dedicated to the 10th anniversary of the Xerox Research Centre of Canada

ERIC S. GARDINER and ANATOLE SARKO. Can. J. Chem. **63**, 173 (1985).

The crystal structures of cellulose polymorphs IV_I and IV_{II} have been determined by X-ray fiber diffraction analysis combined with stereochemical model refinement. Both structures crystallize in a two-chain unit cell of essentially identical parameters. The most probable space group in both cases is $P1$. The chain conformations, although close to two-fold helical, are marked by unequal rotational positions of the O(6) hydroxyl groups in adjacent residues. Despite identical unit cell parameters, the structures differ in chain polarity: in cellulose IV_I both chains of the unit cell are parallel, whereas in cellulose IV_{II} they are antiparallel. The difference in polarity is further substantiated by the results of chemical conversions which show that cellulose IV_I is converted to cellulose I, and cellulose IV_{II} is converted to cellulose II, via parallel and antiparallel cellulose triacetates, respectively. The reliability of the structure analyses is indicated by the residual $R'' = 0.115$ for cellulose IV_I and 0.094 for cellulose IV_{II}, for data sets of 41 and 43 reflections, respectively.

ERIC S. GARDINER et ANATOLE SARKO. Can. J. Chem. **63**, 173 (1985).

Faisant appel à une analyse de la diffraction des rayons-X par les fibres combinée avec une affinement du modèle stéréochimique, on a déterminé les structures cristallines des polymorphes IV_I et IV_{II} de la cellulose. Les deux structures cristallisent dans une cellule unitaire à deux chaînes et les paramètres de chacune de ces cellules sont essentiellement identiques. Dans chacun des cas, le groupe d'espace le plus probable est $P1$. Les conformations des chaînes sont pratiquement toutes les deux sous formes d'hélices binaires; toutefois, les groupes hydroxyles en (O)6 des résidus adjacents sont dans des positions rotationnelles différentes. Même si les paramètres de la cellule unitaire sont identiques, la polarité des chaînes diffère suivant les structures: dans la cellulose IV_I, les deux chaînes de l'unité cellulaires sont parallèles alors que dans la cellulose IV_{II} elles sont antiparallèles. La différence de polarité est confirmée par les résultats de conversions chimiques qui montrent que la cellulose IV_I peut être transformée en cellulose I et la cellulose IV_{II} est transformée en cellulose II par le biais de triacétates de cellulose qui sont respectivement parallèles et antiparallèles. La fiabilité des analyses structurales est indiquée par les valeurs de R'' qui sont 0,115 et 0,094 repectivement pour les celluloses IV_I et IV_{II} et qui sont basées sur des ensembles de données de 41 et 43 réflexions.

[Traduit par le journal]

Introduction

The existence of cellulose in the form of four polymorphic crystalline structures, designated celluloses I, II, III, and IV, has been known for some time (1). Of these polymorphs, only cellulose I is the native form, and all others are conversion products of it. However, only cellulose IV is obtained under high temperature conditions. This suggests a measure of stability for its structure, not unlike that of cellulose I and cellulose II (the most stable polymorph). Indeed, though celluloses I and II appear to be the most stable structures, cellulose IV can only be converted back to cellulose I or II by resorting to drastic treatments such as mercerization or boiling in acid (2). In contrast, the cellulose III polymorphs revert to celluloses I and II by simply warming in water.

Previous crystallographic analyses of various cellulose polymorphs have shown that their structures fall into two classes: one based on parallel chains (celluloses I and III_I), and the other on antiparallel chains (celluloses II and III_{II})[2] (3). Within each category there is reversibility between the polymorphs; however, the parallel to antiparallel conversion is irreversible.

Cellulose IV can be most easily prepared by heating cellulose III, and therefore, two polymorphs of it also exist — celluloses IV_I and IV_{II} — obtained, respectively, from celluloses III_I and III_{II} (4). The diffraction diagrams of both cellulose IV polymorphs are very similar (cf. Fig. 1). Nonetheless, reversible transformations to cellulose triacetate have shown that the two structures are not identical. Cellulose IV_I, upon heterogeneous acetylation, yields cellulose triacetate I (CTA I), whereas cellulose IV_{II} yields CTA II (5). Crystallographic structure analyses have shown that CTA I possesses a parallel-chain structure (6) while CTA II is antiparallel (7). It has further been shown that CTA I prepared from cellulose IV_I deacetylates to cellulose I while CTA II obtained from cellulose IV_{II} deacetylates to cellulose II (5). These observations strongly indicate that the two cellulose IV polymorphs differ in chain polarity.

A full crystallographic structure analysis of both polymorphs was undertaken in order to delineate their structural differences and to gain some understanding of their stability. From an industrial point of view, cellulose IV is an important minor component in various cellulose products, where it tends to modify their properties.

Experimental

Fibrous cellulose IV_I was prepared from ramie cellulose I by first converting the latter to cellulose III_I, followed by heating. The conversion to cellulose III_I was accomplished by swelling the fibers in 75% aqueous ethylene diamine for 5 h at 35°C, followed by washing with anhydrous methanol (8). The process was repeated three times. The conversion to cellulose IV_I was done by heating in glycerol, at 260°C for 20 min (9). Although cellulose IV_{II} can be prepared from cellulose III_{II} using the same method, the sample used here was a commercial one, produced by regenerating cellulose xanthate at 100°C. (This sample was provided by Dr. R. H. Marchessault of Xerox Research Centre of Canada.)

X-ray diffraction diagrams of both samples were recorded in an

[1]Author to whom correspondence should be addressed.
[2]The subscript indicates the polymorph of origin.

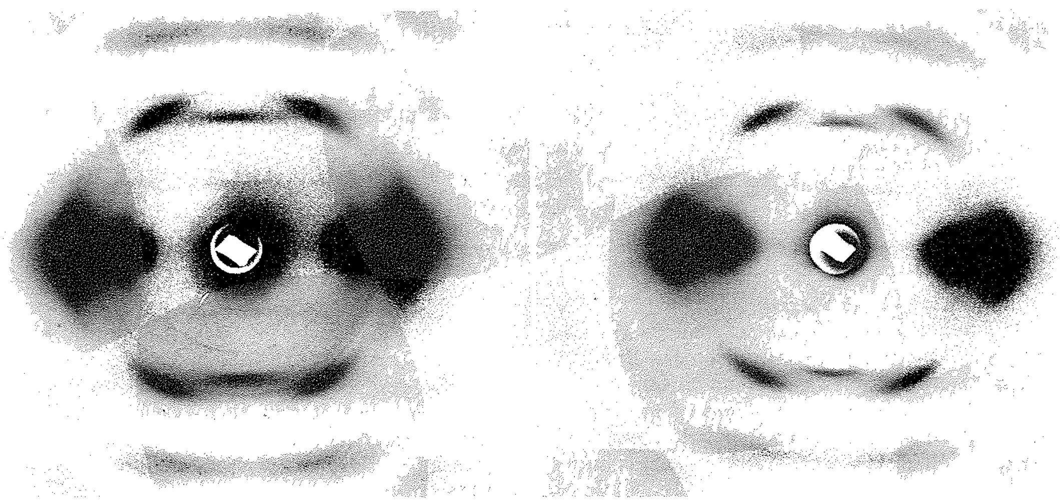

FIG. 1. X-ray diffraction diagrams of (left) cellulose IV_I, (right) cellulose IV_{II}. Fiber axis is vertical.

evacuated Searle toroidal focusing camera, using Ni-filtered CuKα radiation and Ilford Type G Industrial X-ray Film. Multiple-film exposures were used for intensity determinations and powdered NaF was used for the calibration of the films intended for d-spacing measurements. The unit cell parameters were refined against measured d-spacings using least-squares procedures. The intensities were measured with a Joyce-Loebl recording microdensitometer, using straight-line scans along the layer lines. Overlapping intensity envelopes were resolved with a least-squares curve resolution program. The individual intensities were corrected for Lorentz and polarization factors, reflection arcing, distance of diffracted ray to film, tracing direction other than radial, and the Franklin artificial temperature factor (10), and were converted to relative structure factor amplitudes. A total of 16 observed structure factors were obtained for cellulose IV_I, which included the contributions of 30 planes. An additional 7 observed structure factors, representing 11 planes, were obtained in the same manner from intensities assigned one-half of the minimum observable intensity. For cellulose IV_{II}, the corresponding numbers were: 15 observed, 32 planes; 7 unobserved, 11 planes. Meridional reflections were not included in the measurements, because of the well-known difficulties in applying the necessary intensity corrections. During the structure refinement, most of the observed structure factors were equally weighted at 1.0, while the unobserved and some observed structure factors from weak and diffuse reflections were weighted at 0.5.

Results and discussion

Diffraction measurements

The diffraction diagrams of both polymorphs are shown in Fig. 1. Based on the d-spacing measurements of 15 reflections for cellulose IV_I and 16 reflections for cellulose IV_{II}, the unit cell parameters obtained by least-squares refinement are given in Table 1. The less than 1% difference in the parameters indicates the two unit cells to be identical within experimental error. Agreement between the measured and calculated d-spacings, also shown in Table 1, is good.

As previously observed with other cellulose structures, the space groups of the two cellulose IV polymorphs could not be determined unequivocally and were, therefore, assumed to be $P1$. The frequently used space group $P2_1$ with the screw axis in the chain direction was not considered because faint odd-order meridional reflections 001 and 003 were observable. However, as discussed later, the space group $P2_1$ with the screw axis at right angles to the chain axes was considered. As it turned out, after the completion of structure refinement, the space group $P1$ appeared to be the correct choice for both polymorphs.

TABLE 1. Unit cell parameters and observed and predicted d-spacings (in Å) for cellulose IV_I and IV_{II}

Cellulose IV_I			Cellulose IV_{II}		
a = 8.03 ± 0.05 Å b = 8.13 ± 0.05 Å c = 10.34 ± 0.10 Å			a = 7.99 ± 0.05 Å b = 8.10 ± 0.05 Å c = 10.34 ± 0.10 Å		
hkl	*d* (obs)	*d* (calcd.)	*hkl*	*d* (obs)	*d* (calcd.)
110	5.67	5.71	110	5.67	5.69
020, 200	4.03	4.07, 4.01	020, 200	4.05	4.05, 4.00
130, 310	2.58	2.57, 2.54	130, 310	2.6	2.56, 2.53
230, 320	2.22	2.25, 2.24	230, 320	2.25	2.24, 2.23
121, 211	3.40	3.42, 3.40	121, 211	3.35	3.41, 3.39
031, 301	2.63	2.62, 2.59	031, 301	2.62	2.61, 2.58
131, 311	2.49	2.49, 2.47	131, 311	2.48	2.48, 2.46
012, 102	4.36	4.36, 4.35	012, 102	4.36	4.36, 4.34
112	3.82	3.83	112	3.75	3.83
022, 202	3.21	3.20, 3.17	022, 202	3.24	3.19, 3.16
122, 212	2.98	2.97, 2.95	122, 212	2.99	2.96, 2.95
013, 103	3.19	3.17, 3.17	013, 103	3.18	3.17, 3.17
113	2.96	2.95	113	3.00	2.95
023, 203	2.61	2.63, 2.62	023, 203	2.61	2.63, 2.61
123, 213	2.49	2.50, 2.49	123, 213	2.49	2.49, 2.48
			223	2.19	2.19

Structure solution and refinement

As was done in all other cellulose crystal structure analyses, the method was one of model refinement. The generation of starting models was considerably simplified owing to the availability of detailed structural data for other cellulose polymorphs. The similarity of the unit cells of all cellulose structures indicates common conformational and packing features, viz., chains conforming exactly or nearly to a two-fold screw axis along the chain, and a crystalline packing marked by a sheet-like arrangement of chains in the $b-c$ plane of the unit cell. As is true of all other cellulose polymorphs, the calculated and observed densities (approx. 1.6 g/cm^3) dictate that two chains pass through each unit cell, with the most probable arrangement of one chain at the corner of the cell and the other in the center. With these constraints in place, the choice of

TABLE 2. Characteristics of possible models

Parameter	Model: IV_I Antiparallel		IV_I Parallel	IV_{II} Antiparallel		IV_{II} Parallel
Space group	$P1$	$P2_1$	$P1$	$P1$	$P2_1$	$P1$
R''	0.119	0.125	0.115	0.094	0.120	0.130
B (temp. factor)	6.8	7.3	5.8	18.1	19.0	21.7
Chain 1 rotation[a] (deg)	−143.7	−53.5	40.9	−139.8	−50.3	48.1
Chain 2 rotation[a] (deg)	−38.9	—	48.0	−43.3	—	39.9
Chain 2 translation[a] (Å)	−5.319	2.665	−2.864	−4.562	2.317	−2.672
O(6) rotations[b] (deg)	136.2, 143.3 127.2, 134.1	130.9 147.4	158.9, 139.7 164.3, 124.1	137.3, 162.5 122.8, 170.8	137.2 167.8	166.4, 151.1 165.4, 148.8
ϕ (deg)[c]	22.0, 22.0	21.9, 21.8	22.0, 22.1	26.2, 22.7	23.3, 21.8	21.9, 22.0
ψ (deg)[c]	−24.5, −24.3	−24.5, −24.0	−24.4, −24.6	−28.1, −24.6	−24.5, −24.5	−24.4, −24.4
τ (bridge angle) (deg)	115.8, 115.8	115.7, 115.8	115.8, 115.8	115.9, 115.9	115.9, 115.9	115.8, 115.8
V.B.[d] (Å)	5.450, 5.450	5.450, 5.442	5.447, 5.449	5.450, 5.450	5.448, 5.452	5.450, 5.450
Hydrogen bonds[e]	10 + 4	5 + 4	6 + 6	7 + 6	6 + 6	6 + 8
Short contacts	0	0	0	0	0	0

[a]Chain 1 is the corner chain, chain 2 is the center chain. The 0° position of the chain rotation for space group $P1$ is when $O(4)_1$ is on the $-y$ axis for the corner chain (and in analogous position for the center chain). For $P2_1$, the corresponding positions are on the $-x$ axis. Chain 2 translation is measured relative to chain 1.

[b]O(6) rotations refer to the torsion angle O(5)—C(5)—C(6)—O(6). The 0° position is when atoms O(5) and O(6) are eclipsed. The first two angle values are for residues 1 and 2 (chain 1), the second two are for residues 3 and 4 (chain 2).

[c]ϕ = 0° when the bond sequence $H(1)_1$—$C(1)_1$—$O(4)_2$—$C(4)_2$ is *cis*; ψ = 0° when the bond sequence $C(1)_1$—$O(4)_2$—$C(4)_2$—$H(4)_2$ is *cis*. A positive angle is for the far bond clockwise relative to the near bond.

[d]The *virtual bond* (V.B.) is the vector connecting successive glycosidic oxygens (bridge oxygens, O(4)).

[e]The first number counts the intermolecular bonds, the second intramolecular bonds, per unit cell.

initial models was essentially limited to two: (1) both chains parallel, and (2) corner and center chains antiparallel. In the latter case, a further distinction into two models could be made: one in which both chains were independent, and another in which the chains were related by a two-fold screw axis along either the a or the b axis of the unit cell. In all models, the two glucopyranose residues comprising the fiber repeat were considered to be independent, i.e., the structures were assumed to be based on a cellobiose residue.

The model refinement procedure was identical with that used previously with other cellulose structures (11–13). Initially, all models were refined to acceptable stereochemical parameters, with all bond lengths, bond angles, torsion angles, and hydrogen bond lengths within the observed ranges as seen in carbohydrate crystal structures (14). The refinement was carried out with the molecular mechanics computer program PS79 (15), by minimizing the function

$$[1] \quad E = \sum[(a_i - a_{oi})/S.D._i]^2 + W \sum w_{ij}(d_{ij} - d_{oij})^2$$

where a_i are the bond lengths, bond angles, and torsion angles; a_{oi} and $S.D._i$ are the corresponding standard values and standard deviations, respectively; d_{ij} are the nonbonded distances; d_{oij} are the corresponding equilibrium distances; w_{ij} are appropriate weights; and W is the weight of the nonbonded repulsion term in the function. The standard values a_{oi} and d_{oij} have been previously published (15).

The stereochemically sound models were subsequently refined against the set of observed structure factor amplitudes, F_o, by minimizing the weighted crystallographic residual

$$[2] \quad R'' = \left[\sum w(|F_c| - |F_o|)^2/\sum w|F_o|^2\right]^{1/2}$$

(In this equation, F_c are the calculated structure factor amplitudes, and w are weights assigned to individual reflections.)

Because the number of reflections was relatively small, the refinable parameters during these refinement cycles included only the chain positioning parameters (i.e., rotation about the chain axes and translation along the c axis), all chain and ring torsion angles, and selected bond angles (bridge angles at the two glycosidic oxygens of the cellobiose residue and bond angles in the hydroxymethyl groups). All other bond angles and bond lengths remained invariant at values obtained by stereochemical refinement. During the final cycles of refinement, the function

$$[3] \quad \Phi = 100fR'' + (1 - f)E$$

was minimized, in order to forestall the development of short nonbonded contacts which may arise when refinement with a small number of reflections is attempted. (The fraction f ranged from 0.92 to 0.95, designed to weight both terms in eq. [3] equally.) In addition, during the final cycles of refinement, an overall, isotropic temperature factor of the form exp $(-B \sin^2 \theta/\lambda^2)$ was applied to the calculated structure factor amplitudes, with the term B included among the refinable parameters.

The results of the refinement of all three models for both cellulose IV_I and cellulose IV_{II} are shown in Table 2. As expected on the basis of virtually identical unit cells and diffraction diagrams, almost equally good parallel and antiparallel chain models were obtained in both cases. In the absence of any additional information, it would have been difficult to decide which of the models represented the correct structure solution. But, as described above, chemical conversion evidence, obtained through acetylation and deacetylation of the cellulose IV polymorphs, had definitely indicated that cellulose IV_I was a parallel and cellulose IV_{II} was an antiparallel structure. Therefore, of the three solutions shown in Table 2 for cellulose IV_I, only the parallel model should be correct, while it remained to be decided which of the two antiparallel models was the correct

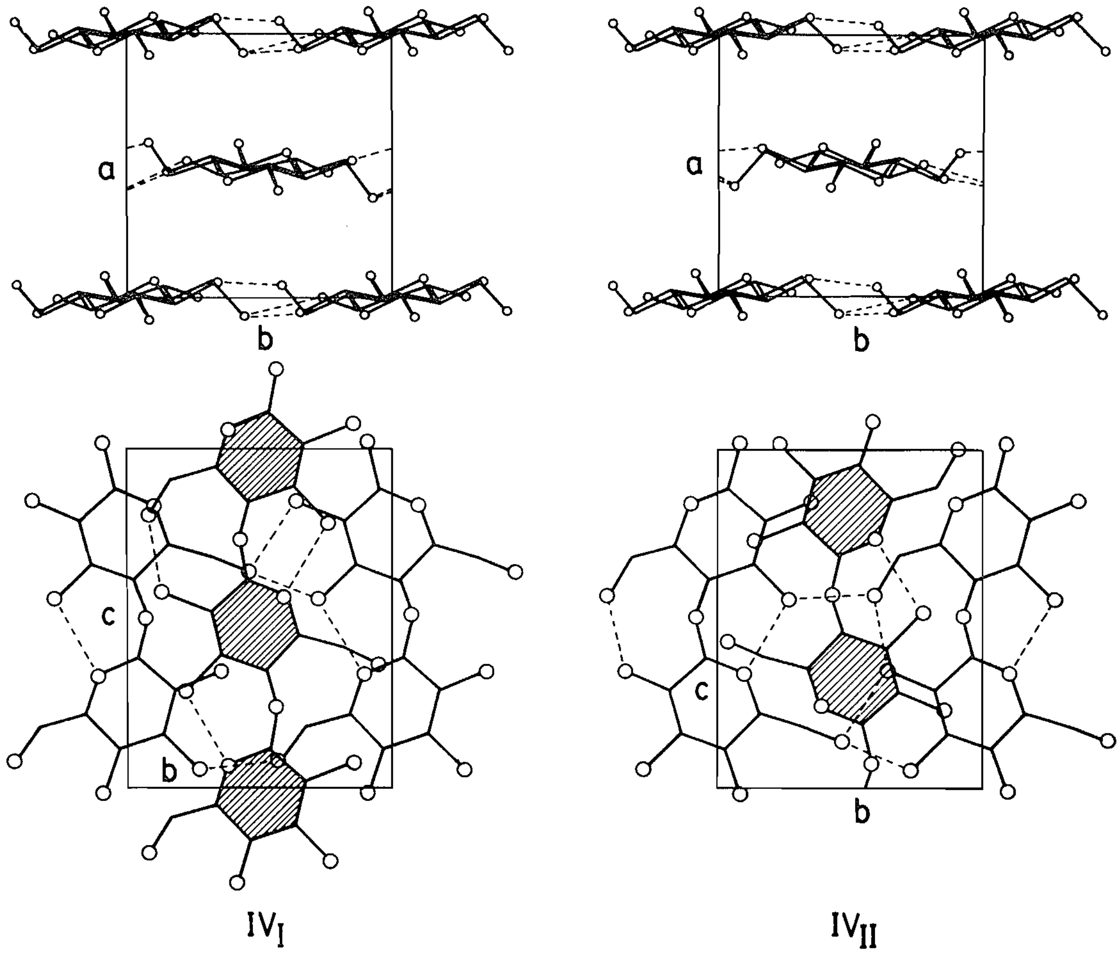

FIG. 2. Projections of the crystal structures of cellulose IV_I and IV_{II}. Hydrogen atoms are omitted and hydrogen bonds are shown by dashed lines.

solution for cellulose IV_{II}. Fortunately, in the case of cellulose IV_{II}, the decision could be made on the basis of the X-ray refinement which clearly favored the model in space group $P1$. The R'' index for the $P1$ structure was 0.094, while the index for the $P2_1$ structure was 0.120, or 28% higher. (This difference in the R''-factor is significant at a 75% confidence level, using the Hamilton statistical test as a criterion (16).)

A similar analysis failed for cellulose IV_I, for which both parallel and antiparallel models yielded an almost identical R'' index. As pointed out above, however, the parallel $P1$ structure should be the correct solution based on chemical conversion results.

The final structures of both polymorphs are shown in Fig. 2. Comparisons of calculated and observed structure factor amplitudes are given in Table 3, the atom coordinates are listed in Table 4, and the hydrogen bonds are shown in Table 5.

Structural characteristics

It is interesting that both cellulose IV polymorphs appear to crystallize in space group $P1$, i.e., they possess no symmetry. The lack of symmetry in the case of cellulose IV_I is clearly evident: the two chain rotations ("setting angles") differ by ~7°, and the O(6) rotation angles in adjacent residues differ by approximately 20° and 40° in the two chains, respectively. For cellulose IV_{II} the lack of symmetry is not as accentuated, but is observable in some other features of the structure. The chain setting angles are within approximately 3° of the position found for the model with $P2_1$ symmetry, i.e., with a two-fold screw axis parallel to the a axis of the unit cell. (To compare chain setting angles of $P2_1$ and $P1$ models, add 90° to the values of the latter.) Similarly, the translational positions of the two chains along the c axis differ by only 0.072 Å between the $P1$ and $P2_1$ models (4.562 to 2 × 2.317 Å; cf. Table 2). But the chain conformation angles (ϕ, ψ) and the O(6) rotation angles differ considerably more in this case.

In other respects, the cellulose IV_I and IV_{II} structures resemble other cellulose polymorphs. As an example, the chain conformations are very close to obeying two-fold screw symmetry — in all aspects but the O(6) rotation angles. This is shown by the generally similar ϕ, ψ, and τ (bridge) angles, and the lengths of the *virtual bonds* (V.B.) for the individual residues (cf. Table 2). The two-fold screw symmetry is definitely eliminated by the differences in the O(6) rotation, which probably arise because of a higher degree of hydrogen-bonding that this affords. For example, in the cellulose I structure where all O(6) rotations are nearly identical, eight intramolecular and four intermolecular hydrogen bonds, for a total of 12 per unit cell, are possible (11). In the cellulose IV_I and IV_{II} structures, where the unequal O(6) rotational positions allow essentially the same number of hydrogen bonds (12 and 13, respectively), there are more intermolecular bonds. In cellulose IV_{II}, there is even one intersheet hydrogen bond (cf. Table 5). This increased level of two- and three-dimensional hydrogen bonding must contribute to the stability of both polymorphs. A similar

TABLE 3. Comparison of calculated and observed structure factor amplitudes

hkl	*F*	*F* (calcd)[a]	*F* (obs)
Cellulose IV_I:			
010, 100	(0.9, 0.6)	1.1	2.[b]
110		152.7	155.7
020, 200	(8.8, 263.9)	264.1	269.3
120, 210	(5.4, 35.0)	35.4	40.6[c]
220		25.8	16.2[b]
030, 300	(0.7, 3.6)	3.6	9.7[b]
130, 310	(17.7, 67.1)	69.4	65.7
011, 101	(17.7, 22.4)	28.5	12.2[b]
111		26.6	12.2[b]
021, 201	(10.7, 27.7)	29.7	12.2[b]
121, 211	(8.8, 58.4)	59.0	31.6[c]
221		30.7	20.3[b]
031, 301	(59.8, 32.9)	68.2	61.6
131, 311	(48.8, 45.8)	66.9	73.0
012, 102	(40.5, 56.8)	69.8	59.2
112		5.7	11.4
022, 202	(5.5, 7.8)	9.6	17.8
122, 212	(34.1, 35.1)	48.9	44.6
013, 103	(31.5, 21.8)	38.3	46.2
113		60.5	48.7
023, 203	(70.8, 8.8)	71.4	87.6
123, 213	(58.8, 49.5)	76.9	68.9
223, 033, 303	(44.7, 20.2, 19.0)	52.6	64.1[c]
001		5.3	Very weak
002		8.7	Medium
003		13.0	Weak
004		59.3	Medium
Cellulose IV_{II}:			
010, 100	(4.8, 1.4)	5.0	2.9[b]
110		140.7	147.1
020, 200	(7.9, 219.3)	219.4	220.4
120, 210	(7.2, 39.6)	40.3	37.7[c]
220		11.8	9.6[b]
030, 300	(1.0, 2.8)	3.0	10.5[b]
130, 310	(12.7, 38.9)	40.9	37.7
011, 101	(14.6, 20.1)	24.9	16.8[b]
111		22.4	18.9[b]
021, 210	(8.9, 7.6)	11.7	21.0[b]
121, 211	(11.5, 27.8)	30.1	25.2[c]
221		7.0	8.4[b]
031, 301, 131, 311	(23.0, 27.7, 51.9, 23.8)	67.5	83.8
012, 102	(34.7, 44.2)	56.2	50.3
112		11.2	16.8
022, 202	(24.5, 8.2)	25.8	18.4
122, 212	(8.1, 31.1)	32.2	33.1
013, 103	(14.3, 14.5)	20.4	31.4
113		48.6	39.4
023, 203	(44.0, 5.9)	44.4	40.2
123, 213	(35.7, 13.8)	38.3	37.3
223, 033, 303, 133, 313	(22.7, 3.7, 9.6, 26.9, 21.1)	42.3	36.9[c]
001		7.4	Very weak
002		30.0	Medium
003		4.3	Weak
004		3.7	Medium (?)

[a] F (calcd.) = $(\Sigma F^2)^{1/2}$.
[b] Unobserved reflection, weight = 0.5.
[c] Weight = 0.5.

situation exists in the cellulose II structure (12). The unequal O(6) rotations also account for the weak odd-order meridional reflections (001 and 003) that are visible in the diffraction diagrams of both polymorphs.

The general similarity of the ϕ, ψ angles in the two cellulose IV polymorphs, as well as their similarity to other cellulose structures, does not support the proposal by Hayashi *et al.* that the cellulose I and II families differ principally in measurable

TABLE 4. Cartesian atomic coordinates (in Å)

Cellulose IV_I				Cellulose IV_{II}		
x	y	z	Atom	x	y	z
Chain 1:						
−0.043	0.340	3.916	$C(1)_1$	0.060	−0.352	4.458
0.186	1.478	2.933	$C(2)_1$	−0.148	−1.490	3.470
−0.389	1.109	1.583	$C(3)_1$	0.433	−1.102	2.129
0.129	−0.239	1.122	$C(4)_1$	−0.126	0.228	1.662
−0.073	−1.294	2.200	$C(5)_1$	0.059	1.288	2.747
0.538	−2.626	1.831	$C(6)_1$	−0.573	2.614	2.388
−0.413	2.668	3.426	$O(2)_1$	0.475	−2.670	3.962
−0.058	2.102	0.610	$O(3)_1$	0.155	−2.102	1.147
−0.565	−0.651	−0.047	$O(4)_1$	0.557	0.658	0.493
0.545	−0.861	3.416	$O(5)_1$	−0.544	0.846	3.968
−0.319	−3.357	0.943	$O(6)_1$	0.417	3.547	1.934
−1.072	0.198	4.066	$H(1)_1$	1.089	−0.193	4.594
1.219	1.635	2.830	$H(2)_1$	−1.178	−1.666	3.360
−1.435	1.056	1.666	$H(3)_1$	1.474	−1.011	2.229
1.153	−0.159	0.905	$H(4)_1$	−1.148	0.122	1.449
−1.102	−1.423	2.365	$H(5)_1$	1.086	1.434	2.909
0.703	−3.189	2.701	$H(6a)_1$	−1.065	3.006	3.228
1.458	−2.458	1.354	$H(6b)_1$	−1.275	2.461	1.622
0.052	−0.353	9.088	$C(1)_2$	−0.051	0.345	9.628
−0.181	−1.492	8.100	$C(2)_2$	0.157	1.482	8.640
0.400	−1.125	6.753	$C(3)_2$	−0.424	1.094	7.296
−0.122	0.223	6.289	$C(4)_2$	0.135	−0.236	6.832
0.081	1.281	7.371	$C(5)_2$	−0.049	−1.297	7.917
−0.531	2.615	7.005	$C(6)_2$	0.582	−2.621	7.558
0.413	−2.686	8.593	$O(2)_2$	−0.464	2.662	9.132
0.074	−2.118	5.778	$O(3)_2$	−0.145	2.094	6.317
0.574	0.636	5.122	$O(4)_2$	−0.511	−0.696	5.663
−0.539	0.848	8.588	$O(5)_2$	0.554	−0.854	9.138
0.467	3.514	6.506	$O(6)_2$	−0.219	−3.327	6.601
1.082	−0.212	9.236	$H(1)_2$	−1.079	0.819	9.779
−1.215	−1.644	7.994	$H(2)_2$	1.187	1.656	8.531
1.445	−1.069	6.841	$H(3)_2$	−1.466	1.004	7.395
−1.146	0.142	6.071	$H(4)_2$	1.160	−0.125	6.634
1.110	1.410	7.537	$H(5)_2$	−1.077	−1.433	8.079
−0.989	3.035	7.851	$H(6a)_2$	0.688	−3.205	8.424
−1.258	2.465	6.262	$H(6b)_2$	1.531	−2.446	7.146
Chain 2:						
4.013	4.408	1.052	$C(1)_3$	4.036	4.407	−8.034
4.379	5.509	−0.069	$C(2)_3$	3.766	5.533	−7.046
3.763	5.214	−1.281	$C(3)_3$	4.368	5.176	−5.705
4.112	3.812	−1.742	$C(4)_3$	3.882	3.818	−5.238
3.782	2.790	−0.664	$C(5)_3$	4.124	2.770	−6.323
4.226	1.394	−1.033	$C(6)_3$	3.564	1.412	−5.964
3.931	6.764	0.562	$O(2)_3$	4.324	6.744	−7.538
4.213	6.159	−2.254	$O(3)_3$	4.036	6.160	−4.723
3.373	3.488	−2.911	$O(4)_3$	4.587	3.426	−4.069
4.449	3.144	0.552	$O(5)_3$	3.497	3.178	−7.544
3.354	0.821	−2.016	$O(6)_3$	4.615	0.443	−5.835
2.973	4.394	1.202	$H(1)_3$	5.072	4.304	−8.170
5.424	5.538	−0.034	$H(2)_3$	2.729	5.652	−6.937
2.197	5.289	−1.197	$H(3)_3$	5.412	5.142	−5.805
5.139	3.766	−1.959	$H(4)_3$	2.855	3.869	−5.025
2.745	2.789	−0.499	$H(5)_3$	5.517	2.680	−6.485
4.231	0.789	−0.174	$H(6a)_3$	2.891	1.102	−6.708
5.199	1.438	−1.425	$H(6b)_3$	3.053	1.484	−5.050
4.022	3.709	6.224	$C(1)_4$	3.962	3.705	−13.204
3.651	2.607	5.236	$C(2)_4$	4.232	2.581	−12.216
4.273	2.900	3.889	$C(3)_4$	3.631	2.937	−10.872
3.920	4.302	3.425	$C(4)_4$	4.117	4.296	−10.408

TABLE 4. (concluded)

4.251	5.327	4.507	$C(5)_4$	3.875	5.345	−11.493
3.806	6.726	4.141	$C(6)_4$	4.434	6.701	−11.134
4.094	1.349	5.729	$O(2)_4$	3.676	1.369	−12.708
3.828	1.954	2.914	$O(3)_4$	3.963	1.954	−9.893
4.661	4.627	2.258	$O(4)_4$	3.447	4.720	−9.239
3.582	4.973	5.724	$O(5)_4$	4.501	4.935	−12.714
4.935	7.595	3.991	$O(6)_4$	3.708	7.281	−10.043
5.061	3.723	6.373	$H(1)_4$	2.928	3.806	−13.355
2.607	2.583	5.131	$H(2)_4$	5.270	2.463	−12.107
5.316	2.827	3.977	$H(3)_4$	2.586	2.971	−10.971
2.894	4.347	3.208	$H(4)_4$	5.147	4.240	−10.210
5.287	5.329	4.673	$H(5)_4$	2.842	5.435	−11.655
3.173	7.100	4.891	$H(6a)_4$	4.378	7.336	−11.969
3.279	6.691	3.234	$H(6b)_4$	5.440	6.593	−10.855

TABLE 5. Hydrogen bonds of the final structures

Model	Hydrogen bond and length in Å[a]		
Cellulose IV_I	$O(3)_1$—$O(6)_1$	2.71	(Intermolecular)
	$O(2)_2$—$O(6)_2$	2.84	(Intermolecular)
	$O(3)_2$—$O(6)_2$	2.63	(Intermolecular)
	$O(3)_3$—$O(6)_3$	2.93	(Intermolecular)
	$O(2)_4$—$O(6)_4$	2.70	(Intermolecular)
	$O(3)_4$—$O(6)_4$	2.93	(Intermolecular)
	$O(3)_{1,3}$—$O(5)_{2,4}$	2.72	(Intramolecular)
	$O(3)_{2,4}$—$O(5)_{1,3}$	2.72	(Intramolecular)
	$O(2)_2$—$O(6)_1$	2.87	(Intramolecular)
	$O(2)_4$—$O(6)_3$	2.75	(Intramolecular)
Cellulose IV_{II}	$O(2)_1$—$O(6)_1$	2.77	(Intermolecular)
	$O(3)_1$—$O(6)_1$	2.59	(Intermolecular)
	$O(3)_2$—$O(6)_2$	2.70	(Intermolecular)
	$O(2)_3$—$O(6)_3$	2.50	(Intermolecular)
	$O(3)_3$—$O(6)_3$	2.70	(Intermolecular)
	$O(3)_4$—$O(6)_4$	2.79	(Intermolecular)
	$O(5)_1$—$O(6)_3$	2.91	(Intermolecular)
	$O(3)_{1,3}$—$O(5)_{2,4}$	2.69	(Intramolecular)
	$O(3)_{2,4}$—$O(5)_{1,3}$	2.69	(Intramolecular)
	$O(2)_1$—$O(6)_2$	2.81	(Intramolecular)
	$O(2)_3$—$O(6)_4$	2.63	(Intramolecular)

[a]Subscripts 1 and 2 designate residues of corner chain, 3 and 4 of center chain.

differences in chain conformations (4).

As noted above, the two chains of the unit cell were placed at the corner and the center, respectively, in both structures. After completing refinement with this chain placement, the x and y parameters of the center chain axis were included as refinable parameters. This resulted in no significant movement of the chain in the $a-b$ plane and no further lowering of the R''-factor. It is concluded, therefore, that the second chain of the unit cell is centered in both cellulose IV polymorphs, as it appears to be in all other cellulose structures.

Stability of celluloses IV_I and IV_{II}

The stereochemical molecular mechanics techniques employed here had previously been used in an attempt to predict the unit cells of all cellulose polymorphs (17). The calculations were done on the assumption that the polymorphs resided in crystalline packing energy minima. The results generally supported this assumption, showing the existence of energy minima corresponding to celluloses I, II, III_I, III_{II}, and IV_{II}. Furthermore, cellulose II resided in a global minimum, in agreement with crystallographic and other experimental observations. Cellulose IV_{II} was predicted to reside in a reasonably deep energy minimum, which also agrees with experimental facts. Among the latter is the observation that single crystals of cellulose grow in the cellulose IV_{II} lattice at high temperatures rather than in the cellulose II lattice which occurs at low temperatures (18). In addition, it has been shown that cellulose IV_{II} can be converted to cellulose II, but only through a drastic treatment of boiling in hydrochloric acid (2).

A similar energy minimum for a parallel cellulose IV_I was not predicted; instead, the minimum coincided with the unit cell of cellulose I. The position of the cellulose IV_I unit cell was up-slope relative to cellulose I, which agrees with the experimental observation that cellulose IV_I can be converted to cellulose I (although, again, only be boiling HCl (2)). The claim that cellulose IV is not a unique crystalline polymorph but is a poorly crystalline mixture of two or more crystal lattices (19), is clearly not in accord with the results of crystallographic analysis and other observations. It is thus curious that even a shallow energy well corresponding to cellulose IV_I was not found. The energy surface in the region surrounding the unit cell of cellulose IV_I was recalculated on a finer grid, but the results were not significantly different. At best, a small "shelf" in the energy surface exists in that region. It is concluded that the stereochemical calculations used in our method either are not sufficiently sensitive or that there are contributions to stability that are not taken into account in the calculations. The latter alternative appears to be the more probable of the two.

Conclusions

With the completion of this study, all cellulose polymorphs except III_{II} have now been crystallographically analyzed. The results, which include the analyses of CTA I and CTA II, clearly support the conclusion that the cellulose crystal structures fall into two families that differ in chain polarity. The parallel-chain family, comprised of celluloses I, III_I, and IV_I, owes its existence solely to the mode of biosynthesis of cellulose I, as has been demonstrated by Brown and co-workers (20). In the biosynthetic mechanism, multiple cellulose chains are synthesized simultaneously and extended in parallel, apparently crystallizing immediately without rearrangement.

Regardless of the chain polarity, the crystal structures of all cellulose polymorphs are similar. The chain conformation is in all cases either exactly two-fold helical or is very close to it. The deviation from two-fold screw symmetry is principally caused by differences in the rotational positions of the O(6) hydroxyls. Even then, in all polymorphs including the present two, almost all of the O(6) rotational positions are not far from *tg*,[3] which for a long time was thought to be an unfavorable position because of its absence in carbohydrate crystal structures.

Other features of the cellulose crystal structures are, likewise, similar. The chains are arranged in sheets, with two-dimensional hydrogen-bonding within the sheets accounting for their stability. In all polymorphs, most of the hydrogen bonds are the intramolecular O(3)—O(5)′ and O(6)—O(2)′, and intermolecular O(3)—O(6). In all polymorphs except cellulose II (and to some extent, cellulose IV_{II}), intersheet hydrogen bonds are either lacking or are very weak. Consequently, the relative stagger of adjacent sheets along the *c* direction of the unit cell shows the most variability of all features among the different structures.

The unit cells of all polymorphs appear to be true two-chain cells and not sub-cells in a larger lattice. This is certainly true for the polymorphs that can be grown in single crystal form, such as cellulose II and IV_{II} (18). The possible exception may be *Valonia* cellulose which appears to crystallize in an eight-chain unit cell, although an alternative, two-chain, triclinic cell has been proposed (21). It is still of interest to determine the true unit cell of *Valonia* cellulose and the differences in its crystalline packing relative to other polymorphs.

The space groups of the crystalline celluloses are more difficult to determine with accuracy. For the most part, they appear to be $P1$, or in some cases, perhaps $P2_1$. Certainly, no more symmetry is evident in any of the structures than is afforded by the latter space group. Even in cases where $P2_1$ appears to be applicable, very weak odd-order meridional reflections can be detected.

The crystal structure analysis of celluloses, as well as of polymers in general, has made great strides during the past 10−15 years. To a large extent this is due to exhaustive model analysis made possible by computer methods. The next challenges in cellulose structure analysis lie in two broad areas. The first is in trying to gain a better understanding of the structure of the amorphous phase and the morphology of the cellulose fiber, and the second is in determining the mechanisms of cellulose interconversions, such as mercerization. Some work concerning the latter is in progress (22). Likewise, there is a challenge in trying to devise more accurate methods for predicting polysaccharide conformations and crystal lattices. As the case of cellulose IV_I illustrates, our methods in this regard may be inadequate. However, as a recent report by Pertsin *et al.* (24) points out, the use of more rigorous potential energy functions may be helpful, at least for the prediction of probable conformational models. Whether the same holds true for the prediction of complete crystal structures remains to be seen. In our hands, the results with respect to the latter have been inconclusive, regardless of the types of functions employed.

[3]For a description of this terminology, see ref. 23.

Acknowledgment

This work has been supported by National Science Foundation grants No. CHE7727749 and CHE8107534.

1. R. H. Marchessault and A. Sarko. Adv. Carbohydr. Chem. **22**, 421 (1967).
2. P. K. Chidambareswaran, S. Sreenivasan, N. B. Patil, and H. T. Lokhande. J. Appl. Polm. Sci. **27**, 709 (1982).
3. A. Sarko. Tappi, **61**, 59 (1978).
4. J. Hayashi, T. Yamada, and K. Kimura. Appl. Polym. Symp. **28**, 713 (1976).
5. E. S. Gardiner and A. Sarko. Appl. Polym. Symp. **37**, 303 (1983).
6. A. J. Stipanovic and A. Sarko. Polymer, **19**, 3 (1978).
7. E. Roche, H. Chanzy, M. Boudeulle, R. H. Marchessault, and P. R. Sundararajan. Macromolecules, **11**, 86 (1978).
8. H. T. Lokhande, S. R. Shukla, P. K. Chidambareswaran, and N. B. Patil. J. Polym. Sci. Polym. Lett. **15**, 97 (1977).
9. J. Hayashi and A. Sufoka. J. Polym. Sci. Polym. Lett. **13**, 23 (1975).
10. R. E. Franklin and R. G. Gosling. Acta Crystallogr. **6**, 678 (1953).
11. C. Woodcock and A. Sarko. Macromolecules, **13**, 1183 (1980).
12. A. J. Stipanovic and A. Sarko. Macromolecules, **9**, 851 (1976).
13. A. Sarko, J. Southwick, and J. Hayashi. Macromolecules, **9**, 857 (1976).
14. S. Arnott and W. E. Scott. J. Chem. Soc. Perkin Trans. 2, 324 (1972).
15. P. Zugenmaier and A. Sarko. ACS Symposium Series, No. 141. American Chemical Society, Washington, DC. 1980. p. 225.
16. W. C. Hamilton. Acta Crystallogr. **18**, 502 (1965).
17. A. Sarko. Appl. Polym. Symp. **28**, 729 (1976).
18. A. Buleon and H. Chanzy. J. Polym. Sci. A-2, **18**, 1209 (1980).
19. R. H. Atalla. Appl. Polym. Symp. **28**, 659 (1976).
20. C. H. Haigler, R. M. Brown, and M. Benziman. Science, **210** 903 (1980).
21. A. Sarko and R. Muggli. Macromolecules, **7**, 486 (1974).
22. A. Sarko and T. Okano. SPCI Report No. 38, IV, 91 (SPCI, Stockholm, 1981).
23. A. Sarko and R. H. Marchessault. J. Polym. Sci. Part C, **28**, 317 (1969).
24. A. J. Pertsin, O. K. Nugmanov, G. N. Marchenko, and A. I. Kitaigorodsky. Polymer, **25**, 107 (1984).

Liquid crystal polymers. 17. Thermotropic properties of random copolyesters of monotropic and enantiotropic polymers

Q.-F. ZHOU,[1] J.-I. JIN,[2] AND R. W. LENZ
Chemical Engineering Department, University of Massachusetts, Amherst, MA 01003, U.S.A.

Received January 31, 1984

This paper is dedicated to the 10th anniversary of the Xerox Research Centre of Canada

Q.-F. ZHOU, J.-I. JIN, and R. W. LENZ. Can. J. Chem. **63**, 181 (1985).

A series of random copolyesters containing two different aromatic ester triads and a decamethylene flexible spacer was prepared and characterized for the effect of comonomer composition on glass, crystalline and liquid crystalline state properties. The homopolymer of one of the triads was enantiotropic, but the other was not. However, a copolymer containing 90 mol% of the latter units and 10 mol% of the former showed thermotropic behaviour, which suggested that the latter homopolymer was probably monotropic. The effects of comonomer content on glass, melting and isotropization temperatures of the copolymers were very different for the three transitions.

Q.-F. ZHOU, J.-I. JIN et R. W. LENZ. Can. J. Chem. **63**, 181 (1985).

Dans le but de déterminer l'effet de la composition du comonomère sur les propriétés des états vitreux, cristallin et cristal liquide des copolyesters, on a préparé et caractérisé une série de copolyesters désordonnés contenant deux triades différentes d'esters aromatiques et un décaméthylène qui introduit un espacement flexible. L'homopolymère de l'une des triades est énantiotope, mais l'autre ne l'est pas. Cependant un copolymère contenant 90 mol% de ces dernières unités et 10 mol% des premières montre un comportement thermotrope qui suggère que le dernier homopolymère est probablement monotrope. L'effet de la teneur en comonomère sur l'état vitreux, les températures de fusion et d'isotropisation des copolymères est très différent dans les trois transitions.

[Traduit par le journal]

Introduction

In a recent investigation in this laboratory, a series of thermotropic polyesters was prepared and characterized for the effect of lateral substituents on their liquid crystalline properties. The polymers contained an aromatic ester triad with a central hydroquinone unit, on which was placed a single substituent, and a decamethylene flexible spacer, as shown in the structure below (1, 2):

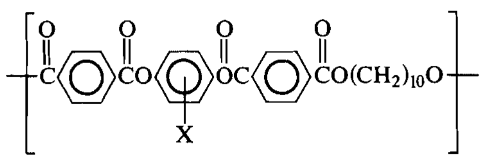

In this series, X was either a *n*-alkyl group (1) (C_nH_{2n+1}, n = 1–6, 8, 10) or a polar group (2), the latter including the CN, NO_2, Br, and OCH_3 groups.

Most of the polymers in this series showed nematic behaviour as indicated by their textures on the polarizing microscope. The exceptions were those polymers with the longer alkyl groups (n = 8 or 10) and, surprisingly, that with the methoxy group. It was possible, however, that these non-enantiotropic polymers were monotropic in their behaviour, but attempts to observe this property by controlled cooling experiments did not show clear evidence of thermotropic behaviour.

It was decided, therefore, to prepare a series of copolymers containing decreasing amounts of the non-enantiotropic methoxy units with one of the enantiotropic units (the cyano monomer unit) in order to estimate the possible isotropization temperature of the methoxy containing homopolymer if it was indeed monotropic. This approach had been taken with success by Iannelli, Roviello, and Sirigu (5) on two series of substituted benzalazine polymers containing flexible spacers, which were closely related to each other and had the following structures:

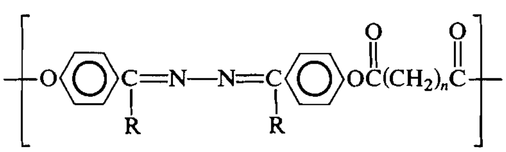

The homopolymers in which R was methyl and n = 8, 10, 12, or 14 were liquid crystalline, as indicated from their analysis by DSC and by polarizing microscopy, but none of the polymers in the series in which R was ethyl were thermotropic. For the latter, it was concluded that the polymers, most likely, were monotropic; that is, that their liquid crystalline behaviour and anisotropization transitions were masked or prevented by crystallization. By examining instead the copolymers containing units with R = CH_3 and with R = C_2H_5 groups having a single flexible spacer, an isotropization temperature could be estimated. This temperature was also confirmed by analyzing copolymers of R = C_2H_5 with two different flexible spacers. For both series of copolymers, isotropization temperatures could be observed in polymers of high ethyl group content because of depression of the melting point of the ethyl substituted homopolymer.

The former approach was taken in this study in that copolymers containing both cyano and methoxy substituted units, varying in composition from 0.5 to 0.9 mole fraction of the non-enantiotropic methoxy units, m, were prepared and characterized for their liquid crystalline properties.

Results and discussion

Thermal transition data as determined by DSC analysis, and confirmed by observations of the samples on the hot stage of a polarizing microscope, are collected in Table 1 for a series of copolymers of the following structure:

[1]Present address: Chemistry Department, Beijing University, Beijing, China.
[2]Present address: Chemistry Department, Korea University, 1-Anam Dong Seoul 132, South Korea.

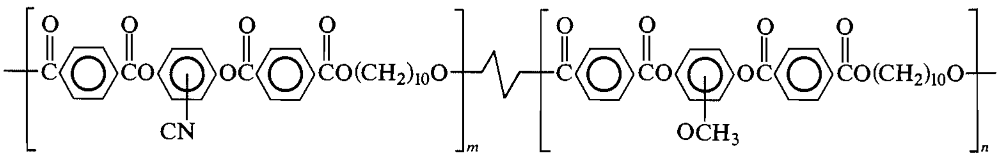

Transition temperatures

As shown by the data in Table 1, the glass transition temperatures, T_g, of the copolymers were all lower than those of either of the two homopolymers, and an apparently non-linear variation of T_g with composition was observed. The cause of this unusual relationship between copolymer composition and T_g is unknown, but the glass phases of these polymers and copolymers may well retain at least a partial nematic order, and it has been observed that a polymer with a mesophase glass has a different T_g value than with an amorphous glass (4).

The melting points, T_m, of the copolymers were found to vary in a uniform manner with composition, and the copolymers were crystalline over the entire range of compositions studied. The value of T_m of the methoxy unit polymer component decreased with increasing cyano unit content and probably passed through a minimum for the copolymer at or near the equimolar composition of the two different substituted hydroquinone units. The same type of behaviour was observed for the substituted benzalazine copolymers discussed above (3).

In contrast to the melting points, the isotropization temperatures (or clearing points), T_i, of the copolymers increased continuously, with increasing content of the mesogenic cyano unit throughout the composition range studied, and the thermal stability of the mesophase, ΔT, showed the same behaviour. In contrast, for the benzalazine copolymers discussed above, the equimolar copolymer showed that the widest temperature range of mesophase stability (3).

As clearly indicated by the data in Table 1, the effect of copolymerizing these two closely related, potentially mesogenic monomers on the transition temperatures of their copolymers is much greater on T_i than on T_m, and the two different transitions apparently follow different thermodynamic rules. Indeed, at this stage of our investigation very little is known, and no theory has yet been developed, about the thermodynamic behaviour of the liquid crystalline phase of main chain copolymers (5). Similar observations to these on differential effects on T_m and T_i have been made by Blumstein and co-workers on a series of main chain copolyesters containing azoxybenzene mesogenic units and flexible spacers (6).

TABLE 1. Physical properties of homopolyesters and copolyesters containing cyano and methoxy hydroquinone units

Polymer composition, mole fraction			Thermal transitions, °C			
n (OCH_3)	m (CN)	$\eta_{inh.}$ (dL/g)[a]	T_g[b]	T_m[c]	T_i[c]	ΔT[d]
1.0	0.0	0.61	50	158	—[e]	—
0.9	0.1	0.31[f]	39	150	154	3
0.8	0.2	0.26	37	140	157	17
0.6	0.4	0.27	45	134	165	31
0.5	0.5	0.39	42	133	177	44
0.0	1.0	0.56	47	157	219	62

[a]Inherent viscosity measured in tetrachloromethane at 40°C and 0.5 g/dL.
[b]Glass transition observed in first heating cycle.
[c]Melting, T_m, and isotropization, T_i, temperatures taken as the peak of the endotherm in the first heating cycle.
[d]Thermal stability of the mesophase: $\Delta T = T_i - T_m$.
[e]Anisotropization temperature peak observed at 148°C with recrystallization at 116°C.
[f]GPC analysis of this polymer in solution in THF indicated a molecular weight of approximately 9 000 relative to polystyrene standards.

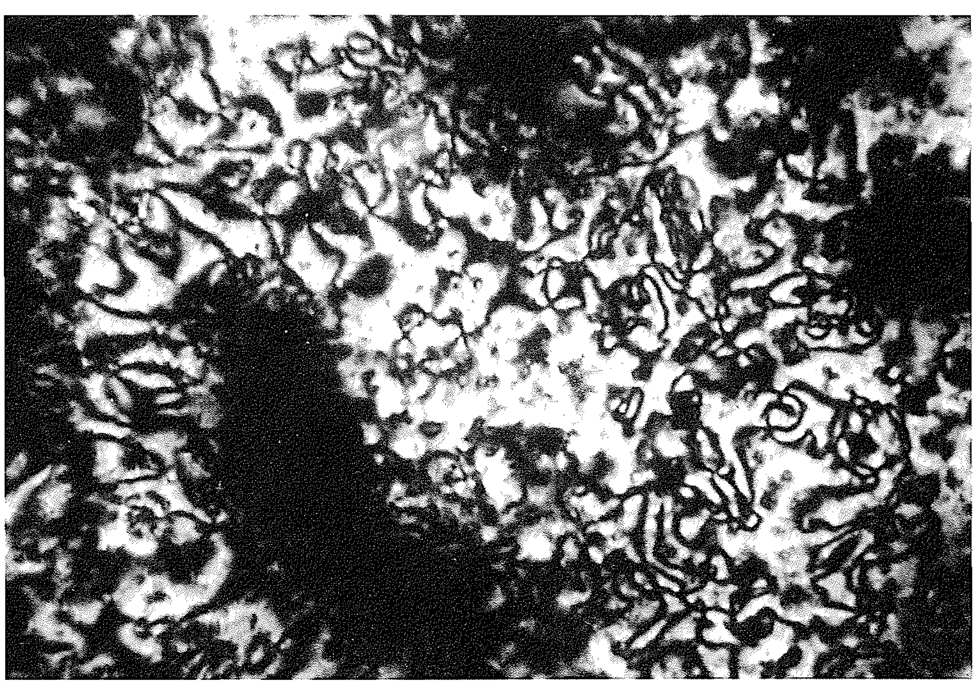

FIG. 1. Photomicrograph of copolymer with 0.90 mole fraction of methoxy triad units at 160°C; 320× magnification.

By extrapolating the relationship between T_i and methoxy unit content of the copolymers, a possible value of T_i for the homopolymer of that unit can be estimated, and it was found to be approximately 151°C. When only 10 mol% of the comonomer cyano units were inserted into the polymer, the melting point was depressed from 158 to 150°C, and the formation of a liquid crystalline phase on melting was observed. A photomicrograph of this phase, as observed on the polarizing microscope at 160°C, is shown in Fig. 1. The mesophase appears to be poorly organized, but the crude threaded Schlieren texture observed suggests the presence of a nematic phase. The occurrence of this type of monotropic behaviour was previously reported by this laboratory for polyesters containing dyad mesogenic units (7) and is well known for low molar mass liquid crystalline compounds (8).

In the DSC curve, the isotropization transition of the copolymer containing 10 mol% cyano units appeared only as a shoulder on the melting peak, but on cooling the sample from the isotropic melt state, a clearly separated exothermic deisotropization temperature, T_d, peak was observed at 148°C because of the normal supercooling of the crystallization process. That is the exothermic recrystallization peak for this copolymer was observed at 116°C, which is well below T_d.

It is also of interest to note that the copolymers containing 20 to 50 mol% of the cyano units showed little or no crystallization in the cooling cycle of the DSC curve. Instead crystallization occurred during the second heating cycle in most cases.

Experimental

The monomers were prepared by procedures previously described (2). A typical polymerization reaction was carried out in the following manner:

A solution of 1.143 g (2.25 *m*) of 1,10-*bis*(p-chloroformylbenzyloxy)decane in 15 mL of tetrachloromethane, TCE, was added dropwise with vigorous stirring to a solution of 2.25 *m* of the hydroquinone monomer in 5 mL of TCE and 5 mL of pyridine. The reaction was carried out at room temperature for 20–24 h under a nitrogen atmosphere, after which the mixture was poured into a large volume of acetone to precipitate the polymers. The solid product was washed successively with acetone, water, and acetone and dried under vacuum at room temperature.

Polymer characterization

The solution viscosities of the copolymers were measured with a Ubbelohde Viscometer at 40°C at a solution concentration of 0.5 g/dL in TCE. GPC analysis of one of the copolymer samples in a THF solution was made on a Waters instrument. The molecular weight and polydispersity index were determined by comparison with polystyrene standards. Thermal properties of the copolymers were studied using a Perkin-Elmer DSC II instrument under a nitrogen atmosphere with heating and cooling rates of 10°C/min. Thermotropic behaviour and optical textures of the polymers were examined on the hot stage (Mettler FP-2) of a polarizing microscope (Leitz, Orthoux).

Acknowledgements

We gratefully acknowledge the support of this work by the Air Force Office of Scientific Research under Grant Number 80-0101, by the NSF sponsored Materials Research Laboratory of the University of Massachusetts and by the Korea Science and Engineering Foundation. Q.-F. Zhou also wishes to express his appreciation to the government of the People's Republic of China for the financial support of his study in the U.S.A.

1. Q.-F. ZHOU and R. W. LENZ. J. Polym. Sci. Polym. Chem. Ed. **21**, 3313 (1983).
2. Q.-F. ZHOU, R. W. LENZ, and J.-I. JIN. *In* Polymer liquid crystals. *Edited by* A. Blumstein. Plenum Press. In press.
3. P. IANNELLI, A. ROVIELLO, and A. SIRIGU. Eur. Polym. J. **18**, 753 (1982).
4. J. MENCZEL and B. WUNDERLICH. Polymer, **22**, 778 (1981).
5. P. IANNELLI, A. ROVIELLO, and A. SIRIGU. Eur. Polym. J. **18**, 745 (1982).
6. A. BLUMSTEIN, S. VILASAGAR, S. PONRATHUAN, S. B. CLOUGH, and R. B. BLUMSTEIN. J. Polym. Sci. Polym. Phys. Ed. **20**, 877 (1982).
7. C. OBER, R. W. LENZ, G. GALLI, and E. CHIELLINI. Macromolecules, **16**, 1034 (1983).
8. J. S. DEWAR and M. J. S. DEWAR. J. Chem. Soc. 4305 (1955); M. VOGEL, E. M. BARRAL, and C. P. MIGNOSA. Mol. Cryst. Liq. Cryst. **15**, 49 (1971).

Heat conduction in thermal transfer printing

D. J. SANDERS
Xerox Research Centre of Canada, 2660 Speakman Drive, Mississauga, Ont., Canada L5K 2L1

Received January 31, 1984

This paper is dedicated to the 10th anniversary of the Xerox Research Centre of Canada

D. J. SANDERS. Can. J. Chem. **63**, 184 (1985).

The physical properties of thermal transfer materials are reviewed. Thermal conductivities and thermal contact resistances were measured for commercial Ink Donor Films (IDF's) with base films of condenser paper or polyethylene terephthalate, and for experimental base materials such as regenerated cellulose, polypropylene, and polyimide. Theoretical models of heat transport in IDF's are presented to demonstrate how the intrinsic thermal properties affect the IDF's performance in thermal transfer printing. To a first order approximation, the sensitivity of an IDF can be characterized by the time taken for heat to diffuse across it. Thermal transfer test patterns for commercial and experimental IDF's were evaluated for sensitivity, and the experimental results were compared to the theoretical predictions.

D. J. SANDERS. Can. J. Chem. **63**, 184 (1985).

On réexamine les propriétés physiques des matériaux de transfert thermique. On a mesuré les conductibilités thermiques et les résistances de contact thermique de Films Donneurs d'Encre commerciaux (IDF) portés par des films de base de papier de condensateur ou de téréphthalate de polyéthylène ainsi que celles des matériaux de base experimentale comme la cellulose regénérée, le polypropylène et la polyimide. On présente des modèles théoriques de transport de chaleur dans les IDF pour démontrer comment les propriétés thermiques intrinsèques affectent la performance des IDF dans l'impression par transfert thermique. En première approximation, on peut caractériser la sensibilité d'un IDF par le temps nécessaire pour que la chaleur puisse diffuser à travers du film. On a évalué les tendances observées lors des essais de transfert thermique effectués sur des IDF commerciaux et expérimentaux afin de déterminer la sensibilité et on a comparé les résultats expérimentaux avec les prédictions théoriques.

[Traduit par le journal]

I. Introduction

Thermal transfer printing (1–3) is a thermal printing process that uses plain paper rather than a specially coated thermal marking paper. Transfer printing employs an Ink Donor Film (IDF) consisting of a thin base film coated with a solid waxy ink. The ink side of the IDF is placed in contact with a plain paper receiver sheet and heat from a thermal printhead is applied to the base film. This locally melts the ink layer which then wets the receiver sheet and resolidifies. Since the receiver is usually much rougher than the smooth base film, the resolidified ink adheres preferentially to the receiver sheet. Subsequent separation of the sheets leaves transferred ink on the imaged areas of the plain paper.

The printing performance of a particular Ink Donor Film is determined by the physical properties of its constituent materials. The transferable ink is typically composed of Carnauba and other waxes with approximately 20% by weight carbon black pigment (1, 2). For high printing speeds and long printhead life, the temperature to which the printhead elements are cycled should be minimized. Therefore, the ink should have a low melting point, yet still be environmentally stable. Typically T_m is between 60 and 80°C (1–3). At the melting point, the ink viscosity should drop sharply to below 100 cP to promote wetting of the receiver sheet (1–3). Below T_m the ink should have a fairly high tensile strength so that it will not transfer under pressure to the receiver sheet without heating (2). The base material must be available as a film less than 50 μm thick. It should be smooth to promote release of the transferred ink, and it must be strong enough to be handled in a thermal printer without tearing. It must also be able to withstand high printhead temperatures for short periods (up to 300°C for several ms) without melting or charring. This requirement eliminates many polymeric materials.

Commercial IDF's use base films of polyethylene terephthalate (PET) (1–3), or "condenser" paper (3) of the type used in electrical capacitors. Typically the base film is 10–20 μm thick and the ink layer is 5–10 μm. Since the IDF is a one-use consumable item, the materials cost is also a factor in choosing a base film. Oki Electric Co. has developed a thermal transfer printer that uses a recoatable Ink Donor Film (4). The base film forms a continuous belt which is repeatedly passed through a heated inking system that reforms the ink layer. In this case, a heat-resistant 25 μm polyimide film was used (4).

This report concentrates on the thermal transport properties of the IDF. Since heat must be conducted from the thermal printhead to the surface of the ink layer, the total thermal resistance of the IDF should be minimized. This means it must be as thin as possible, it should have a high intrinsic thermal conductivity, and it should be smooth so as to minimize its thermal contact resistance with the printhead. The relationship between the thermal transport properties of the IDF and its printing performance has been examined for several commercial IDF's with condenser paper and PET base films, and various experimental IDF's with base films of regenerated cellulose, polypropylene, polyimide, and aluminum foil. In Section II, measurements of the thermal conductivites and other thermal parameters of the IDF materials are presented. Simple theoretical models of heat transport in thermal transfer printing are developed in Section III. The theoretical predictions are demonstrated experimentally in Section IV by measurements of the thermal printing sensitivities of the various IDF's.

II. Thermal properties of thermal transfer materials

The principal difficulty in measuring the thermal conductivity of a thin film is the problem of distinguishing between its bulk thermal conductivity and the thermal contact resistance between the film surface and the heating or cooling elements. This problem has been solved by using a pressure cell apparatus which is described in detail elsewhere (5). Basically, the cell

TABLE 1. Thermal properties of thermal transfer materials

Material	l (μm)	ρ (g/cm³)	K (mW/cm °C)	g (μm)	T_m (°C)	ρC (J/cm³ °C)	D (10^{-3} cm²/s)
Receiver paper	96	0.80	1.67	4.7	240[a]	1.5	1.1
Ink	5	1.0	3.9	0.8	70[b]	2.5–28.5[b]	0.25[b]
Condenser paper	14	1.34	1.67	1.1	240[a]	1.67[a]	1.0
PET	10	1.32	1.48	0.6	255[a,c]	1.49[a,c]	1.0
Cellulose film	19	1.40	2.67	0.8	240[a]	1.9[a]	1.4
Polypropylene	13	0.90	1.25	1.0	155[a]	1.85[a,c]	0.68
Polyimide	26	1.46	2.0	0.9	>500	1.65[c]	1.21
Aluminum foil	9	2.45	2.0×10^3[d]	—	660[d]	2.4[d]	880
Glass	10	2.5[d]	10[e]	—	—	2.0[e]	5.0[e]

[a]Reference 7.
[b]Includes the heat of fusion $\rho\Delta H$ = 130 J/cm³ as a specific heat peak between 60 and 70°C. D is calculated from the average ρC = 15.5 J/cm³ °C.
[c]Reference 8.
[d]Reference 6.
[e]Reference 1.

consists of two thermally insulated brass columns placed one on top of the other, each fitted with two temperature sensors. Heat is supplied at a known rate at the top of one column, and removed by water cooling at the bottom of the other, thus establishing a steady-state temperature gradient. The thin film sample is placed between the optically polished faces of the two columns, creating a discontinuity in the temperature gradient which represents the total temperature drop across the sample. Since the heat flux down the column is known, the apparent thermal resistivity of the sample can be calculated.

The top column is connected to a hydraulic piston so that the apparent resistivity R_T can be monitored as a function of the pressure P_0 applied to the sample up to a maximum pressure of 1700 psi. It has been shown (5) that this effectively eliminates the thermal contact resistance between the sample and brass surfaces. Therefore, the resistivity measured at high pressure represents the true bulk thermal resistivity R (inverse conductivity) of the sample. On the other hand, the total apparent resistivity at zero pressure is just

[1] $R_T = R + 2r/l$

where r is the coefficient of thermal contact resistance and l is the sample thickness. Since the contact resistance is due mainly to the roughness of the sample surface, it is useful to express it as the thickness of an equivalent air gap given by $g = K_a r$, where $K_a = 2.6 \times 10^{-4}$ W/cm °C is the thermal conductivity of air (6).

Typical results are illustrated by Fig. 1. The closed circles indicate the thermal resistivity of a commercial IDF with a 14 μm condenser paper base and a 5 μm ink layer. The open circles represent measurements for an uncoated sample of the base paper prepared by removing the ink layer with acetone. Since the complete IDF has a lower resistivity than the paper alone, this indicates that the ink has a higher thermal conductivity than condenser paper. The thermal conductivities and contact resistances of both the ink and the base paper can be calculated from these results (5). Similar measurements were performed for a PET based commercial IDF, for a typical office-grade bond paper receiver sheet, and for experimental base film materials such as cellulose, polypropylene, and polyimide.

These results are summarized in Table 1 along with other thermal parameters taken from various sources in the literature (6–8). The second column l represents the sample thickness,

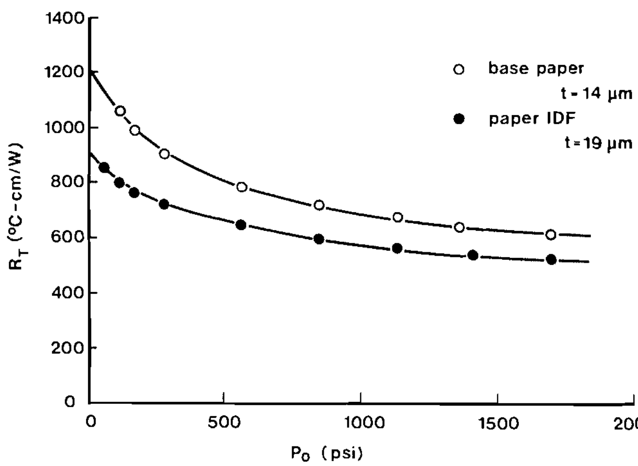

FIG. 1. Apparent thermal resistivity of a condenser paper based IDF. The closed circles represent the coated film, and the open circles represent the uncoated base paper.

ρ is the measured density, K is the bulk thermal conductivity, g is the effective air gap, T_m is the melting point or temperature of thermal decomposition, ρC is the heat capacity per unit volume, and $D = K/\rho C$ is the thermal diffusivity. All quantities listed without a reference were experimentally measured. The IDF ink has a heat of fusion $\rho\Delta H$ = 130 J/cm³ typical of paraffin waxes (9). This can be included as a temperature-dependent specific heat which rises from its base value of 2.5 J/cm³ °C (6) at 60°C to 28.5 J/cm³ °C at 70°C. The thermal diffusivity was calculated from the average specific heat ρC = 15.5 J/cm³ °C. The pressure cell is not suitable for measuring a thin film with a thermal conductivity greater than that of brass, so no attempt was made to measure the aluminum foil. The glass referred to in the last row of Table 1 is the protective overglaze coating which covers the resistive heating elements in a thermal printhead (10). Thus, reading from bottom to top, Table 1 represents the various layers through which heat must pass during thermal transfer printing. One can also compare the effective air gaps of the IDF materials. All the base films have roughnesses of 1 μm or less, while the receiver sheet is much rougher.

It is interesting to compare the thermal conductivities of the three cellulosic materials — receiver paper, condenser paper,

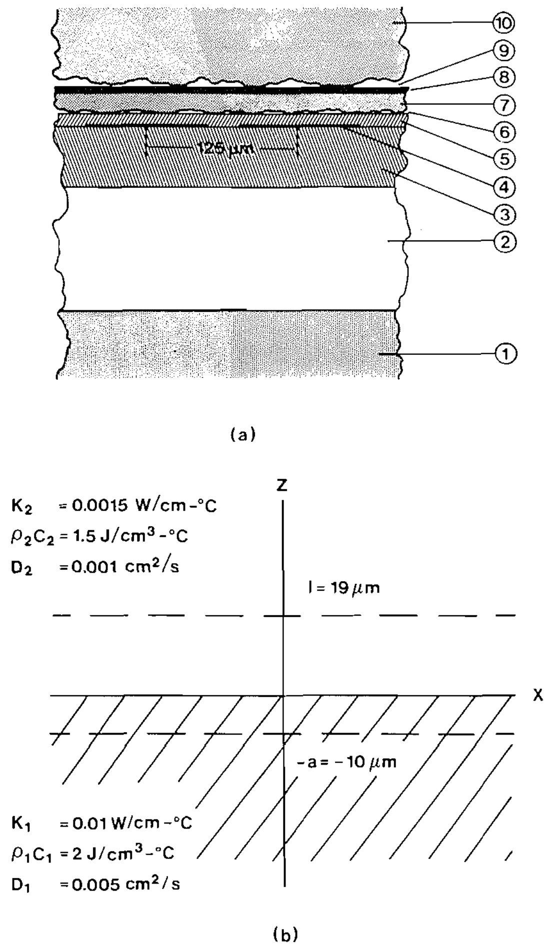

FIG. 2. Geometry of thermal transfer printing. (*a*) 200 spi thin-film thermal printhead. The layers are (*1*) 1 mm aluminum substrate, (*2*) 800 μm Al_2O_3 heat sink, (*3*) 50 μm glass underglaze, (*4*) 2 μm heating element, (*5*) 10 μm overglaze, (*6*) 1 μm air gap, (*7*) 14 μm base film, (*8*) 5 μm ink layer, (*9*) 5 μm air gap, (*10*) 100 μm receiver sheet. (*b*) Simplified two layer model for thermal transfer printing.

and cellulose film. Condenser paper is highly compressed so that it is almost as dense as the cellulose film, but its thermal conductivity is only 60% that of the regenerated film and in fact, is the same as the conductivity of the much less dense receiver sheet. This is because even a highly compressed paper has a structure of matted paper fibers. The principal direction of heat flow will be along the fibers, most of which are oriented in the plane of the sheet: In a regenerated film, however, the cellulose has been dissolved to a molecular level, so heat can flow directly across the thickness of the film.

III. Heat transport in IDF's

The heat flow in thermal transfer printing is more complicated than the steady-state heat flow used to measure thermal conductivity. Figure 2*a* illustrates the thermal printing geometry for a 200 spots/inch thin-film thermal printhead (10). The heating elements are deposited on top of a 50 μm glass underglaze layer which separates them from the ceramic and aluminum heat sinks, and are covered with a 10 μm protective overglaze layer. We wish to determine the transient response of this system to a pulse of heat applied to one of the heating elements.

The multilayered problem can only be solved numerically; however, the main features of the heat flow can be illustrated by a much simpler model that can be solved analytically. Shortly after the application of the heating pulse, all the heat will be concentrated in the layers close to the heating element. The thermal parameters of the overglaze and the glass underglaze are equal so they can be approximated by a single layer. Similarly, the thermal parameters of the IDF and the receiver paper are also nearly equal. Therefore, to a first order approximation, the system can be described by a two layer model. Since the heating element is wider (125 μm) than the thickness of the IDF (19 μm) or the underglaze (50 μm), the heat source is approximately planar. The simplified model is shown in Fig. 2*b*. Semi-infinite medium 1 (glass) extends below the *xy* plane, and medium 2 (paper) above it. At time $t = 0$ a heat source of q J/cm^2 is produced at the plane $z = -a$. According to Carslaw and Jaeger (11) the temperature rise T at any subsequent time t and any point z in either medium is given by

$$[2] \quad T_1(z, t) = \frac{q}{2\rho_1 C_1 \sqrt{\pi D_1 t}} \left\{ \exp\left[-(z + a)^2/4D_1 t\right] + \frac{d - k}{d + k} \exp\left[-(z - a)^2/4D_1 t\right] \right\}$$

and

$$[3] \quad T_2(z, t) = \frac{d^2}{d + k} \frac{q}{\rho_1 C_1 \sqrt{\pi D_2 t}} \exp\left[-(z + da)^2/4D_2 t\right]$$

where d and k are the ratios

$$d = \sqrt{D_2/D_1} \text{ and } k = K_2/K_1$$

In a thermal printhead, heat is not created instantaneously, but is generated during a pulse of width t_p. For a finite pulse, eqs. [2] and [3] must be modified to

$$[4] \quad T_1(z, t) = \frac{p}{2\rho_1 C_1 \sqrt{\pi D_1}} \left\{ \int_0^{t_0} \frac{\exp\left[-(z + a)^2/4D_1(t - t')\right]}{(t - t')^{1/2}} dt' + \frac{d - k}{d + k} \int_0^{t_0} \frac{\exp\left[-(z - a)^2/4D_1(t - t')\right]}{(t - t')^{1/2}} dt' \right\}$$

and

$$[5] \quad T_2(z, t) = \frac{d^2}{d + k} \frac{p}{\rho_1 C_1 \sqrt{\pi D_2}} \int_0^{t_0} \frac{\exp\left[-(z + da)^2/4D_2(t - t')\right]}{(t - t')^{1/2}} dt'$$

where

$$t_0 = t,\ t < t_p$$
$$= t_p,\ t > t_p$$

and $p = q/t_p$ is the power density supplied to the printhead.

Calculated temperature profiles in the printhead and IDF are shown in Fig. 3 for a pulse width of 1 ms. The thermal parameters for the printhead and IDF are those listed in Fig. 2*b*. The power density in the printhead was taken to be p = 1.9 mW/cm^2, as specified for a 200 spi printhead with a 1 ms pulse. With this choice of parameters, the calculation predicts a maximum printhead temperature of 300°C, which decays in about 10 ms.

The simple model can illustrate the effects of varying the IDF thermal parameters. Figure 4 shows how the temperature of the ink − receiver paper interface changes with time. The solid line corresponds to the parameters of Fig. 2*b*, i.e., an IDF with thickness l = 19 μm and the conductivity of paper K_2 =

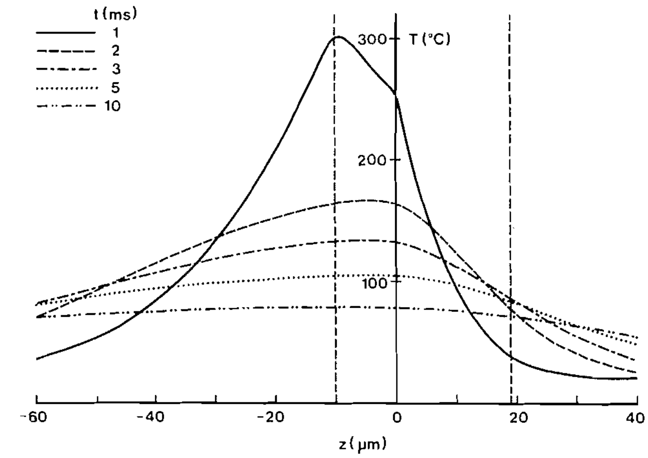

FIG. 3. Temperature profiles in a thermal printhead ($z < 0$) and ink donor film ($0 < z < 19$ μm) at various times after a 1 ms heating pulse at $z = -10$ μm.

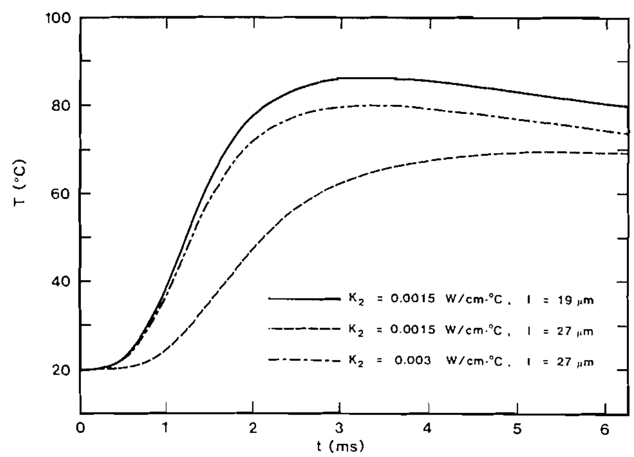

FIG. 4. Time evolution of the temperature at the IDF ink surface for various IDF thicknesses l and thermal conductivities K_2.

1.5 mW/cm °C. The ink temperature reaches a maximum of 86°C after a diffusion time $t_D = 3$ ms. If the IDF thickness were increased by a factor of $\sqrt{2}$ to 27 μm, the diffusion time increases to 5 ms as shown by the dashed line in Fig. 4. Moreover, since heat has more time to dissipate in the printhead, the ink temperature reaches a maximum of only 69°C. If the ink melting point is 70°C, this means that the thicker IDF would not transfer ink. However, if the IDF conductivity is doubled to $K_2 = 3$ mW/cm °C for a thickness of 27 μm, the situation is shown by the dash–dot line in Fig. 4. The diffusion time again is 3 ms and the maximum temperature is 80°C which is almost as high as the original case. Therefore, T_{max} is determined not by the thickness of the IDF, but rather by its effective thermal thickness as measured by its diffusion time t_D.

This can be demonstrated by the following approximations. Since T_{max} occurs after the heating pulse, the finite width of t_p can be neglected. From eq. [3], the temperature at the ink surface $z = l$ reaches a maximum after a diffusion time given by

$$[6] \quad t_D = (l + da)^2/2D_2$$

and the maximum temperature is

$$[7] \quad T_{max} = (2/e\pi)^{1/2} \frac{d^2}{d + k} \frac{q}{\rho_1 C_1 (l + da)}$$

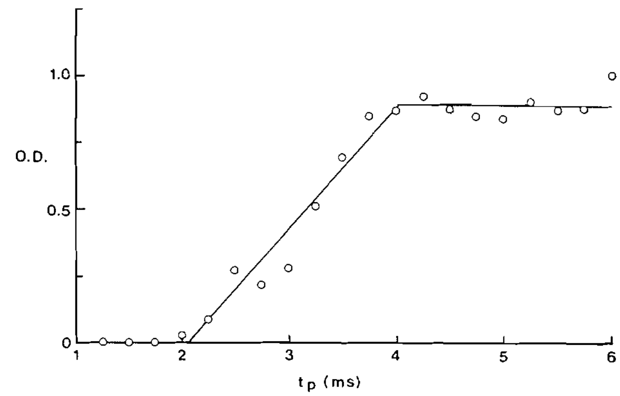

FIG. 5. Variation in optical density with heating pulse width for a thermal transfer test pattern. The IDF consists of a 14 μm condenser paper base with a 5 μm ink layer.

If $K_1\rho_1C_1 \gg K_2\rho_2C_2$, and $da \ll l$, this reduces to

$$[8] \quad T_{max} \simeq (2/e\pi)^{1/2}(D_2/K_1\rho_1C_1)^{1/2}q/l$$

But the diffusion time is just $t_D \simeq l^2/2D_2$. Therefore, for a given thermal printhead, the maximum ink surface temperature depends only on the heat density q, and the diffusion time t_D, i.e.

$$[9] \quad T_{max} \propto q/\sqrt{t_D}$$

IV. IDF sensitivity

The thermal transfer characteristics of a variety of IDF's were measured using a simple thermal imaging test fixture. This employs a printhead consisting of 10 elements arranged in a column with 60 spi spacing, producing a heated area of 0.4 × 4.0 mm. Under microcomputer control it creates a bar test pattern by energizing the printhead with voltage pulses of constant amplitude but progressively increasing pulse width. Figure 5 shows the results of measuring the optical densities of a typical test pattern with a scanning microdensitometer consisting of a Zeiss universal microscope with a photometer head. The O.D. was measured in reflection over a 0.1 × 1.0 mm slit. The test pattern of Fig. 5 was created with the standard IDF shown in Fig. 1, i.e., a 14 μm condenser paper base and a 5 μm ink layer. The power level was 2.6 W per element, and the pulse width t_p was increased from 1.25 to 6 ms in 0.25 ms steps. After a threshold is passed, the O.D. increases approximately linearly with pulse width until complete transfer occurs and the O.D. saturates.

Similar test patterns were created for a variety of commercial IDF's. To the naked eye, each pattern consists of a series of bars ranging from very faint to uniform black, as the amount of ink transfer increases. The sensitivity of each IDF was ranked relative to the standard IDF of Fig. 5 by shifting its test pattern relative to the standard pattern until bars of equal perceived optical density were aligned. The resulting shift in pulse width was translated into the difference in energy density Δq required to produce an image with each IDF relative to the standard. Results of these measurements are listed in Table 2. The base film thickness is l_f and the ink thickness is l_i. L is an effective thermal thickness for the IDF, defined as follows. From eq. [9], in order to produce a T_{max} equal to the ink melting temperature T_m, the heat density must be $q \propto T_m l/\sqrt{D}$. For a bilayer IDF this can be generalized to

$$[10] \quad q \propto T_m(l_f/\sqrt{D_f} + l_i/\sqrt{D_i}) = T_m L/\sqrt{D_f}$$

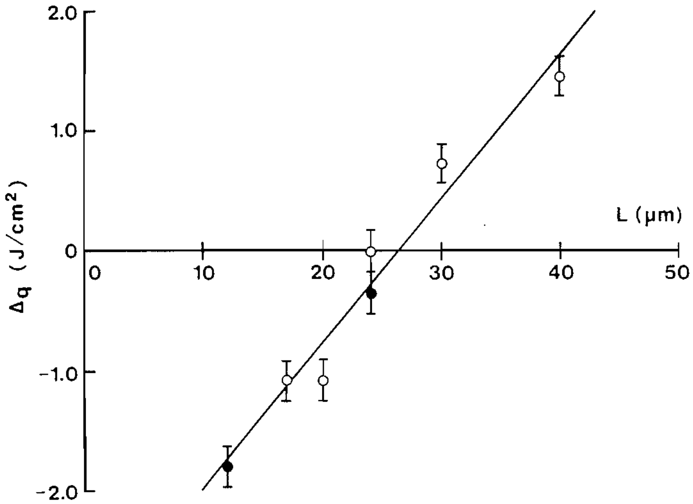

FIG. 6. Relative thermal transfer sensitivity Δq vs. effective thermal thickness L for 7 commercial IDF's. The open circles are condenser paper based IDF's, and the closed circles PET based.

TABLE 2. Relative sensitivities of commercial IDF's

Base material	l_f (μm)	l_i (μm)	L (μm)	Δq (J/cm^2)
1. Condenser paper	14	5	24	0
2. PET	10	5	20	−1.08
3. Condenser paper	16	7	30	+0.72
4. Condenser paper	11	3	17	−1.08
5. PET	6	3	12	−1.80
6. Condenser paper	18	3	24	−0.36
7. Condenser paper	32	4	40	+1.44

TABLE 3. Relative sensitivities of experimental IDF's

Base material	l_f (μm)	l_i (μm)	L (μm)	Δq (J/cm^2)	$L/\sqrt{D_f}$ (s$^{1/2}$)
1. Condenser paper	13	13	30	0	0.123
2. Cellulose	19	12	47.4	+0.36	0.127
3. Polypropylene	13	9	27.8	+0.36	0.107
4. Polyimide	26	8	43.6	+2.88	0.125
5. Aluminum foil	9	10	602	+1.80	0.064

where $L = l_f + (D_f/D_i)^{1/2} l_i$ is the effective thermal thickness of the IDF. Using the data of Table 1, $L = l_f + 2l_i$ for both condenser paper and PET based IDF's. Because of its heat of fusion, the ink layer has a greater thermal thickness than an equal layer of base film, in spite of the higher thermal conductivity of the ink. The results listed in Table 2 are illustrated in Fig. 6. As predicted by eq. [10], there is a linear relationship between the IDF sensitivity as measured by Δq and the effective thermal thickness L.

Thermal transfer sensitivity was also measured for a series of experimental IDF's consisting of various base films coated in-house with a pigmented waxy ink. The results are listed in Table 3. Δq is a measure of the sensitivity of each IDF relative to the condenser paper based IDF. Since these materials have quite different thermal diffusivities, Δq does not correlate with the effective thickness L. However, eq. [10] predicts that Δq should correlate with the diffusion time given by $L/\sqrt{D_f}$. Comparing the last two columns of Table 3, it can be seen that this is true for the first three IDF's. They all have approximately equal sensitivities and equal diffusion times. In the case of the cellulose based IDF, the higher thermal conductivity of cellulose compensates for the greater film thickness. For the polypropylene IDF, the thinner ink layer compensates for the lower conductivity of the base film.

This correlation does not hold for the polyimide and aluminum foil based IDF's. In the case of the 26 μm polyimide film, it may be that the base film is too thick for a simple 1-dimensional heat flow analysis to be valid, and a numerical 3-dimensional analysis is required. This is certainly the case for aluminum foil. The transferred bars of the test pattern have a rounded appearance, indicating that heat has diffused laterally in the aluminum base film because it has a higher thermal conductivity than the printhead overglaze. This results in a loss of resolution and sensitivity.

In summary it can be stated that, for maximum sensitivity, an ink donor film should be as thin as possible, particularly the ink layer, and the base film should have a high thermal diffusivity, provided it is not higher than that of the printhead.

Acknowledgement

Maya Stevanovic is gratefully acknowledged for providing the experimental ink donor films.

1. Y. TOKUNAGA and K. SUGIYAMA. IEEE Trans. Electron. Devices ED-27, 218 (1980).
2. Y. TOKUNAGA and R. TAKANO. J. Appl. Photogr. Eng. **7**, 10 (1981).
3. T. OHNO, M. MIZUGUCHI, Y. YAMAGUCHI, T. INOUE, T. OHZEKI, and M. NAGASHIMA. J. Appl. Photogr. Eng. **7**, 171 (1981).
4. S. NAKAYA, K. TANOSHIMA, I. NOSE, and T. TAKEDA. SID Digest, **83**, 56 (1983).
5. D. J. SANDERS and R. C. FORSYTH. Rev. Sci. Instrum. **54**, 238 (1983).
6. J. A. DEAN (*Editor*). Lange's handbook of chemistry. 12th ed. McGraw-Hill, New York. 1979.
7. J. BRANDUP (*Editor*). Polymer handbook. 2nd ed. John Wiley, New York. 1975.
8. M. J. HOWARD (*Editor*). Plastics 1980, Cordura Publications, La Jolla CA. 1980.
9. R. C. WEAST (*Editor*). CRC handbook of chemistry and physics. CRC Press, Boca Raton, FL. 1981.
10. Y. TOKUNAGA, M. YOSHIDA, and M. KIZAWA. IEEE Trans. Components, hybrids, and manufacturing technology CHMT-4, 148 (1981).
11. H. S. CARSLAW and J. C. JAEGER. Conduction of heat in solids. 2nd ed. Oxford University Press, Oxford. 1959.

Influence of molecular structure on the dynamic thermoelasticity of polyphasic polymer systems

ROBERT H. MARCHESSAULT, TERRY L. BLUHM, HRIRE M. GHARAPETIAN, AND PUDUPADI R. SUNDARARAJAN

Xerox Research Centre of Canada, 2660 Speakman Drive, Mississauga, Ont., Canada L5K 2L1

Received February 1, 1984

This paper is dedicated to the 10th anniversary of the Xerox Research Centre of Canada

ROBERT H. MARCHESSAULT, TERRY L. BLUHM, HRIRE M. GHARAPETIAN, and PUDUPADI R. SUNDARARAJAN. Can. J. Chem. **63**, 189 (1985).

The relationship between the dynamic thermoelastic behavior and molecular morphology of polyphasic polymer systems was studied. A sensitive tensometer equipped with a 50W/12V heating lamp provided uniform and controlled heat pulses to one side of the film. For various extension ratios, the stress change ($\Delta\sigma$) as a function of the sample temperature, was recorded, both for increasing and decreasing extension ratios.

The amount of increase in stress $\Delta\sigma$ with temperature was different for Kraton GX-6500 samples cast from either toluene, cyclohexane, or heptane. The variation of $\Delta\sigma$ with temperature was dependent on the extension ratio and was always greater for increasing extension. The slope of $\Delta\sigma$ with temperature decreased at 100–150% elongation in all Kraton GX-6500 samples during increasing extension. However, this slope increased at higher elongations. Small angle X-ray scattering studies on Kraton GX-6500 showed the presence of lamellar, rod shape, and spherical structures in samples cast from toluene, cyclohexane, and heptane solvents, respectively. The extreme dependence of elastomeric behavior on polyphasic morphology caused Kraton samples to show a strong decline in thermoelastic response with cycling.

X-ray studies on the films of Spandex, cast from dimethyl formamide, at different extension ratios showed the onset of crystallization at about 150% elongation. The thermoelastic studies performed on Spandex films also showed an increase in slope of $\Delta\sigma$ vs. T at 150–170% elongations, which was attributed to the influence of increased crystalline orientation on thermoelastic response. X-ray studies on unstretched and stretched Hytrel films showed the presence of crystallinity. The magnitude of $\Delta\sigma$ and variation with temperature for Hytrel films was greater than that of either Spandex, Kraton GX-6500, or cross-linked natural rubber.

By comparison with the latter, only Hytrel was superior in the magnitude of $\Delta\sigma$ variations with temperature. This was attributed to intrinsic crystallinity and the orientation which developed on stretching. At extension ratios $\lambda = 2$, $\Delta\sigma$ for Hytrel was an order of magnitude greater than for cross-linked natural rubber.

ROBERT H. MARCHESSAULT, TERRY L. BLUHM, HRIRE M. GHARAPETIAN, et PUDUPADI R. SUNDARARAJAN. Can. J. Chem. **63**, 189 (1985).

On a étudié la relation qui existe entre le comportement thermoélastique dynamique et la morphologie moléculaire de systèmes de polymères à plusieurs phases. Un tensomètre sensible, équipé d'une lampe chauffante 50W/12V, a permis d'appliquer des pulsations contrôlées et uniformes à une face du film. Pour divers rapports d'élongation, tant pour des rapports croissants que pour des rapports décroissants, on a enregistré le changement de stress ($\Delta\sigma$) en fonction de la température de l'échantillon.

Dans le cas d'échantillons de Kraton GX-6500, le taux d'augmentation du stress $\Delta\sigma$ avec la température varie suivant que le solvant utilisé pour préparer les échantillons est le toluène, le cyclohexane ou l'heptane. La variation du $\Delta\sigma$ avec la température dépend du rapport d'élongation et cette valeur est toujours plus élevée lorsque l'élongation est croissante. Avec tous les échantillons de Kraton GX-6500 examinés alors que l'élongation était croissante, la pente du $\Delta\sigma$ en fonction de la température diminue lorsque l'élongation est de 100 à 150%. Toutefois, cette pente augmente à nouveau lorsque les élongations sont plus élevées. Faisant appel à la diffraction des rayons-X à de petits angles, on a examiné divers échantillons de Kraton GX-6500; suivant que le solvant utilisé pour préparer les échantillons est le toluène, le cyclohexane ou l'heptane, on observe la présence de structures en lamelles, en forme de bâtonnets ou sous formes sphériques. La dépendance extrême du comportement élastomère sur la morphologie polyphasique fait que la réponse thermoélastique d'échantillons de Kraton subit une forte diminution.

Des films de Spandex, préparés à partir de solutions dans le diméthyl formamide, ont été étudiés par diffraction des rayons-X à différents rapports d'élongation; ces études ont permis de montrer que la cristallisation commence à environ 150% d'élongation. Les études thermoélastiques effectuées sur les films de Spandex ont aussi montré la présence d'une augmentation dans la courbe du $\Delta\sigma$ vs. T à des élongations de 150 à 170%; on attribue cette propriété à l'influence d'une orientation cristalline accrue sur la réponse thermoélastique. Des études par diffraction des rayons-X sur des films de Hytrel tendus et non-tendus ont permis de montrer la présence d'une cristallinité. Par comparaison avec les valeurs obtenues avec le Spandex, le Kraton GX-6500 ou le caoutchouc naturel réticulé, la valeur de l'amplitude du $\Delta\sigma$ — et sa variation avec la température — observée avec des films de Hytrel est beaucoup plus élevée.

Par comparaison avec les autres, le Hytrel est le seul à présenter une supériorité dans l'amplitude des variations du $\Delta\sigma$ avec la température. On attribue cette propriété à une cristallinité intrinsèque et à l'orientation qui se développe par élongation. A des rapports d'élongation $\lambda = 2$, la valeur du $\Delta\sigma$ est au moins dix fois plus élevée que celle du caoutchouc naturel réticulé.

[Traduit par le journal]

Introduction

Thermoelasticity is an increase in force with temperature for strained elastomeric systems. This is opposite to the behavior of most solids, especially metals, and has long been recognized as a fundamental characteristic of elastomers. The possibility of using the thermoelastic phenomenon to convert heat into mechanical work has been explored (1, 2). The extent of the thermal contraction of elastomers under tension, is directly related to their molecular structure, chain configurations, and the morphology (3, 4). In the thermodynamic treatment of thermoelasticity, the tensile force (*f*) required to maintain a constant extension is presented as the sum of the internal energy and entropy (5). The thermoelastic properties are usually studied by following the temperature dependence of the tensile force at constant length, for various extensions, and under equilibrium conditions. The energetic and entropic components and their variation with extension in relation to the structure of the polymer can be derived from these data (5). In the present studies, the dynamic thermoelastic behavior of three thermoplastic elastomers and natural rubber were studied by applying uniform, controlled heat pulses of 10 s duration while recording the variation of tensile force with temperature at different extensions.

Usually, thermoplastic elastomers are block copolymers containing segregated chain segments of relatively low glass transition temperature. These segments, which are responsible for the elastomeric behavior of the copolymers, are referred to as "*soft*" segments. The other part of the copolymer chains consist of portions, which are capable of undergoing intermolecular association, thereby constraining the polymer chains without the need of covalent crosslinks. These parts are referred to as "*hard*" segments. At least two such hard segments per molecule are necessary for development of a three-dimensional pseudo-network structure.

Three thermoplastic elastomers, Kraton-GX6500, DTEX-Spandex, Hytrel-4056, and vulcanized natural rubber, as reference material, were used in the present studies. The elastomeric copolymers differ from one another not only in their molecular structure, but also in their morphologies. Kraton is not crystalline and does not crystallize under strain. Spandex is also not crystalline but exhibits strain-induced crystallization. Hytrel is crystalline in both unstretched and stretched states.

Kraton-GX6500 (Shell) is a hydrogenated, styrene–butadiene–styrene block copolymer containing 29 mol% of styrene. From small-angle X-ray scattering studies on solvent-cast Kraton films, it is known (6) that, depending on the casting solvent, the films possess spherical, cylindrical, or lamellar microdomains, which are obtained in the order of increasing solvent affinity for polystyrene. Thermo-mechanical studies (6) on Kraton, show that, under strain, films with spherical domains behave like natural rubber, while films with cylindrical and lamellar domains exhibit stress softening and yielding, respectively.

DTEX-Spandex fibres consist of polyurethane and inorganic fillers. Polyurethane elastomers may be considered block copolymers composed of relatively short areas of urethane "*hard*" segments and longer, flexible polyester or polyether "*soft*" blocks. The polarity of the "*hard*" segments may cause formation of hydrogen bonds, resulting in microphase separation (7). The "*soft*" blocks of some polymers have crystalline structure (8, 9), but other soft segments are amorphous and can undergo crystallization upon stretching, especially when the molecular weight is high. Linear polyether- or polyester-urethane elastomers based on aromatic diisocyanates and chain extended with low molecular weight diols under different extensions exhibit X-ray diffraction patterns corresponding to the onset of crystallization at about 150% elongation (10).

Hytrel (DuPont) is a thermoplastic elastomer. It is produced in a range of compositions of poly (tetramethyleneoxy) "*soft*" and tetramethylene terephthalate "*hard*" segments. Hytrel Type 4056 was used in the present studies. Mole fraction of the

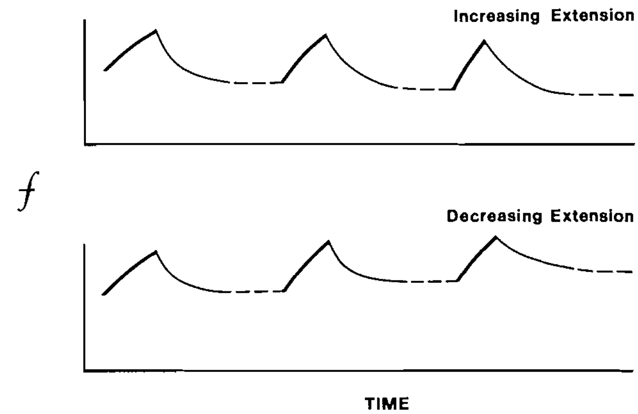

FIG. 1. Schematic of the variation of tensile force with time, for increasing and decreasing extensions. The heavy line represents the period when the heat lamp is on.

hard segments of this copolymer (11), determined by ^{13}C nmr has been reported to be 0.8. Electron microscopy studies have shown that Hytrel exhibits a two-phase morphology (12). The structure of the polymer consists of interpenetrating and continuous amorphous and crystalline phases rather than discrete domain structures as observed in styrene–butadiene copolymers (6). Small-angle light scattering and optical microscopy studies have shown that the crystalline phase is basically spherulitic (13). Application of stress to Hytrel produces orientation of the crystallites with their long axes perpendicular to the drawing direction (12). This orientation is most likely the effect of destructuring of the crystalline lamellae during drawing and is not recoverable upon the release of the applied force. It has also been observed that irreversible disruption of crystalline regions results in pronounced stress softening (12).

A sample of cross-linked natural rubber was also used in these studies for comparison. It is known that natural rubber is capable of undergoing strain-induced crystallization (3). However, the network structure of cross-linked natural rubber is affected by strain at much higher extensions than for thermoelastic elastomers.

Experimental

Thermoelasticity measurements

The thermoelasticity measurements were performed using a computerized tensometer setup. Each sample was initially subjected to stepwise increasing, followed by decreasing, extensions. At each extension, 4–6 heat pulses of 10 s duration, with 20 min relaxation time between each two consecutive pulses, were applied to the samples. The increase in the temperature for each heat pulse of 10 seconds duration was 31–33°C, which was measured by a thermocouple placed underneath the sample. The change in the tensile force during each thermal stimulation and after relaxation of 20 min was recorded.

It was observed that, for the initial 2–3 heat pulses applied at each extension, the tensile force after relaxation (f') was smaller than the tensile force before applying the previous heat pulse (f), if the pulse was applied after an increasing extension, and vice versa if the pulse was applied after a decreasing extension. However, the difference between f and f' decreased continuously at a given extension, and after 4–5 heat pulse–relaxation periods f' became almost equal to f. This is schematically shown in Fig. 1.

Preparation of the films

The films were cast by evenly coating the smooth surface of a Teflon block with a solution of the polymer. The coated block was placed horizontally in a chamber saturated with solvent vapour. The

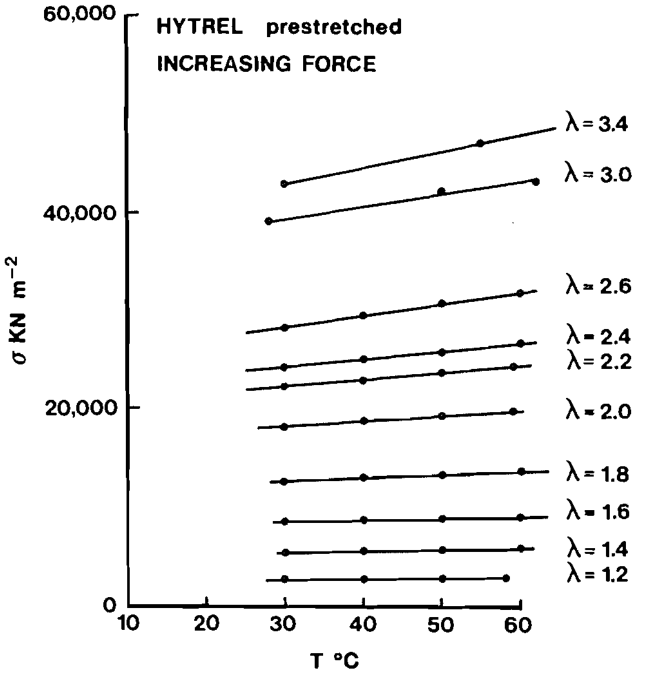

FIG. 2. Variation of stress (σ) with temperature, for different elongation ratios (λ) are shown for Hytrel.

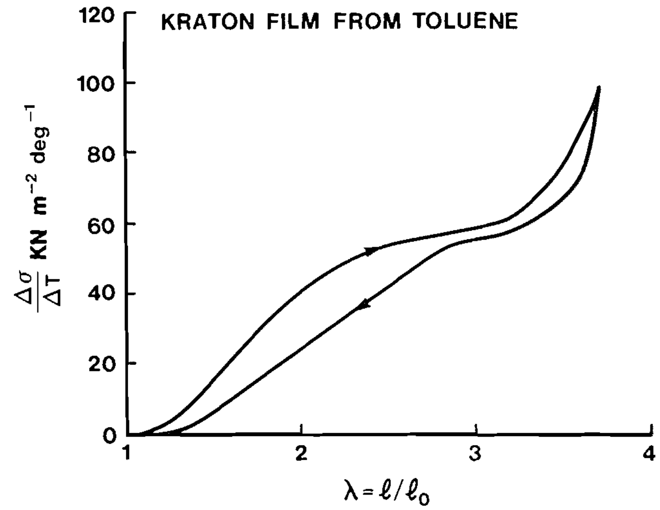

FIG. 3. Plots of variation of $\Delta\sigma$ with extension ratios (λ), for increasing and decreasing λ are shown for Kraton films cast from toluene.

vapour concentration was gradually lowered allowing the coating to dry slowly and form a uniform film. The films were then placed in an oven at about 100°C for 4 h. Rectangular samples, 130 mm × 70 mm in size, were cut from the films which were 0.1 to 0.2 mm thick. The thickness and width of the films were measured, at each extension, with a micrometer before applying the heat pulse.

The Hytrel films were prepared from the solution of the polymer in 1,2-dichloroethane, at room temperature. Toluene, cyclohexane, and heptane were used for Kraton. The Spandex solution was prepared by heating the Spandex fibres in dimethyl formamide at 100°C followed by removal of the inorganic fillers by sedimentation.

Hytrel films were also prepared by heat pressing the polymer granules between 2 mm thick Teflon sheets under a gradually applied pressure up to 6 psi at 160°C followed by rapid cooling to room temperature. Since these samples "necked" on stretching, all samples of Hytrel were cold-stretched until necking was completed (about 300-500%). X-ray examination showed a small degree of uniaxial orientation of the crystalline phase after this operation.

Small-angle X-ray scattering data were collected using a Kratky camera, equipped with a proportional counter, pulse height analyzer, and a step scanner. Wide-angle diffraction patterns were recorded using a Warhus flat plate camera. In both cases, CuK_α (λ = 1.5418 Å) radiation was used.

Results and discussion

In the thermoelasticity measurements, the variation of the stress (σ) with the rise in temperature (T) for the polymer films subjected to 10-s heat pulses at different extensions was recorded. At each extension (λ), 4–6 heat pulses were applied to the samples. However, only the data obtained from the last thermal stimulation at each extension were used in the present studies. Some typical results on variation of σ vs. T at different extensions are presented in Fig. 2. The data on the variation of σ with T for various values of λ was used to construct the curves of $\Delta\sigma/\Delta T$ vs. λ. Here, $\Delta\sigma/\Delta T$ is the change in the stress due to the change in the temperature from 30 to 50°C during the last heat pulse at an extension λ. The magnitude of $\Delta\sigma/\Delta T$ and the variation of the slopes of the plots of $\Delta\sigma/\Delta T$ vs. λ were correlated with sample microstructures derived by X-ray diffraction and scattering techniques as well as microscopic examination.

Small-angle X-ray scattering (SAXS) studies performed on solution-cast Kraton samples from toluene, cyclohexane, and heptane showed that these polymer films contained lamellar, cylindrical, and spherical structures, respectively, in agreement with previous conclusions (6).

Plots of $\Delta\sigma/\Delta T$ vs. λ for the Kraton samples are presented in Figs. 3–5. It is seen that the slopes in these cases decrease between 120–180% elongations.

SAXS curves recorded for the films cast from toluene, cyclohexane, and heptane are shown in Figs. 6, 7, and 8 respectively. In all cases, the data were collected before and after an extension of 125%. Fig. 6*a* shows a maximum at $s = (2 \sin \theta)/\lambda = 3.1 \times 10^{-3}$ Å^{-1}, which corresponds to a periodicity of about 320 Å in this film, which is known to possess lamellar structure. However, upon stretching 125%, this maximum vanishes. This phenomenon is reversible, i.e., when the film is relaxed, the maximum reappears. Accordingly, the phenomenon has been interpreted as due to the orientation of the lamellae in the plane of the film upon stretching. Since the plane of the X-ray beam is normal to the plane of the film, any periodicity normal to the plane of the film is not observed. Partial alignment of lamellar domains has been observed by other investigators (14). Figure 7*a*, corresponding to the cylindrical morphology, shows a maximum at $s = 3.4 \times 10^{-3}$ Å^{-1} and this results in an inter-cylinder distance of 290 Å. Upon stretching, this maximum is lost. However, another broad maximum is recorded at $s = 6.25 \times 10^{-3}$ Å^{-1} inter-cylinder distance of 150 Å. It is possible that, compared to the case of the unstretched sample, the alignment of the cylinders upon stretching reduces the inter-cylinder distance, following an affine deformation mechanism. The orientation is not nearly as complete as in the lamellar case , as evidenced by the continued presence of a scattering maximum, although it is greatly reduced in intensity. Figure 8 for the case of the spherical morphology shows that the dimensions increase in the direction of stretch, in direct correspondence with film extension.

Since orientation of the microstructure of the different Kraton samples at different extensions is observed by X-ray

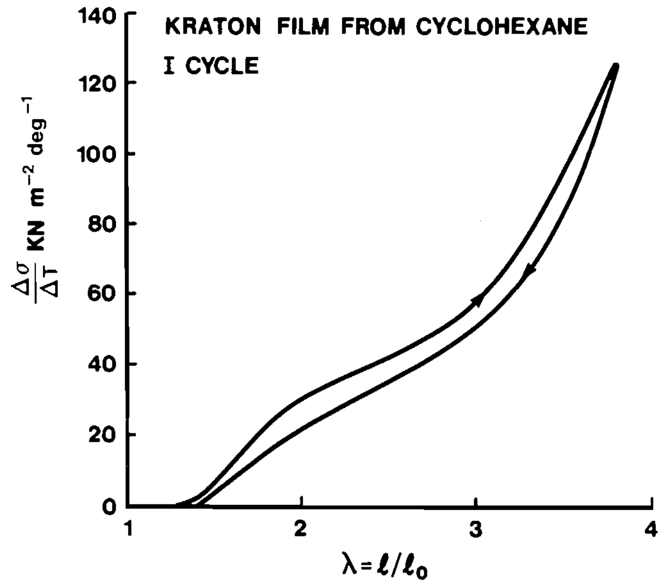

FIG. 4. Same as Fig. 3, but during the first cycle of measurement on Kraton film cast from cyclohexane (see also Fig. 9).

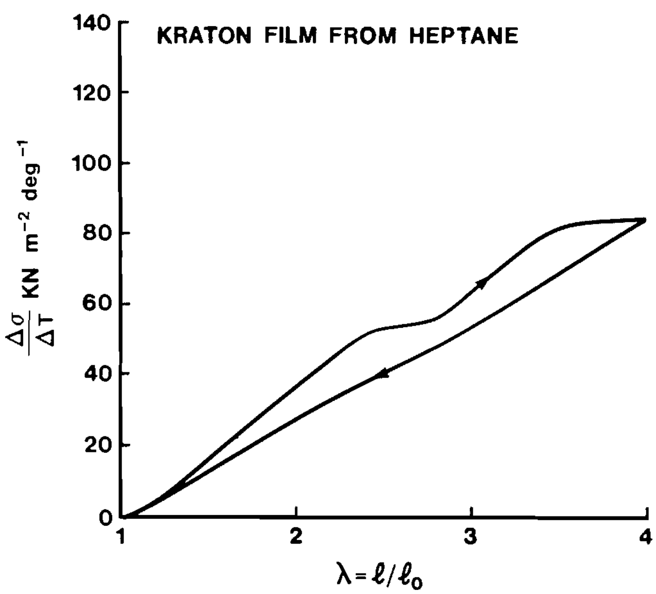

FIG. 5. Same as Fig. 3, but for Kraton film cast from heptane.

scattering studies, it is suggested that the decrease in the rate of increase of the $\Delta\sigma/\Delta T$ with λ (range of 120–180% elongation) is related to microdestructuring which negatively affects the thermoelasticity of these materials. At higher extensions, alignment of the stable domains is high and this sharply increases the slopes of the curves of $\Delta\sigma/\Delta T$ vs. λ. The extent of the "*low slope*" region was greatest for the sample cast from toluene and shortest for the one cast from heptane. The latter observation may be attributed to the linear extent of the lamellar and cylindrical microstructure and consequent orientation effects compared with the absence of microstructure anisotropy for the spherical domains during extension.

The rapid decrease in the slope of the curves of $\Delta\sigma/\Delta T$ vs. λ observed in the measurements performed during decreasing extensions were attributed to the orientation of the microstructure and stress softening during increasing extension of the samples. The plot of $\Delta\sigma/\Delta T$ vs. λ for the second cycle of

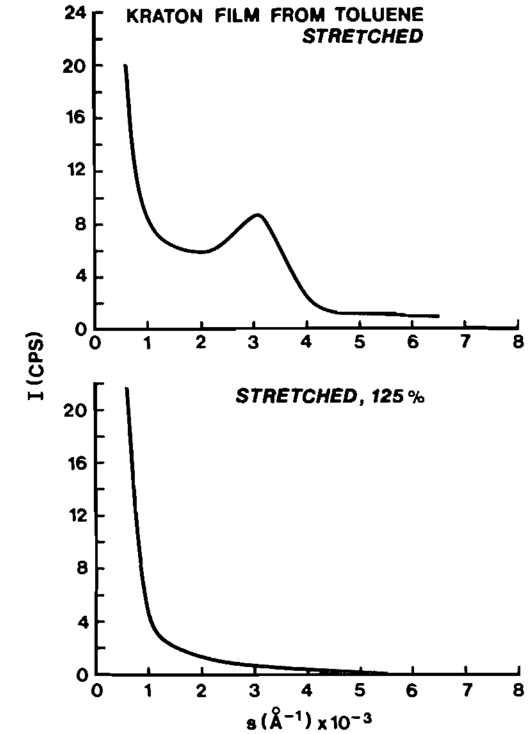

FIG. 6. Small-angle X-ray scattering curves for Kraton film cast from toluene, before and after stretching.

measurements, performed on the Kraton film cast from cyclohexane, is presented in Fig. 9. It was observed that the first cycle of studies considerably influences the thermoelastic properties of the material. The slope in the plot of $\Delta\sigma/\Delta T$ vs. λ, compressed to the first cycle, indicates partial destructuring of the polymeric microstructure after completion of the first cycle.

It is known that polyurethane undergoes strain-induced crystallization (11). X-ray scattering studies performed on the films prepared from Spandex fibres also showed strain-induced crystallization of the "*soft*" segments at an elongation of 150%. From thermoelastic measurements on the film cast from a solution of Spandex in dimethyl formamide, it is observed (Fig. 10) that the slope of the curve of $\Delta\sigma/\Delta T$ vs. λ increases rather abruptly at elongations of 140–160%. The generation of a crystalline phase in the strained Spandex sample is responsible for increasing the thermoelastic response of the sample above elongations of 140–160%. The increase in thermoelastic response can be attributed to thermally induced melting in the "*soft*" segments. The rapid drop in slope of $\Delta\sigma/\Delta T$ with λ during decreasing extensions is attributed to the reversal of strain-induced crystallization. In theory, the slope of the reverse curve is a function of rate of decrease of strain but this was not investigated in detail.

For both solution-cast and heat-pressed Hytrel films necking occurred during stretching, resulting in unidirectional orientation. For this reason the thermoelasticity measurements were performed on prestretched films. The extent of thermal contraction manifested by the magnitude of $\Delta\sigma/\Delta T$ at different extensions was greatest for Hytrel, compared with the other samples (cf. Fig. 11). The slopes of the curves of $\Delta\sigma/\Delta T$ vs. λ, for both Hytrel films, show a sharp increase above elongations of 120–140%. Wide angle X-ray diffraction patterns from prestretched (necked) and unstretched samples in the relaxed state show the presence of a crystalline phase in both

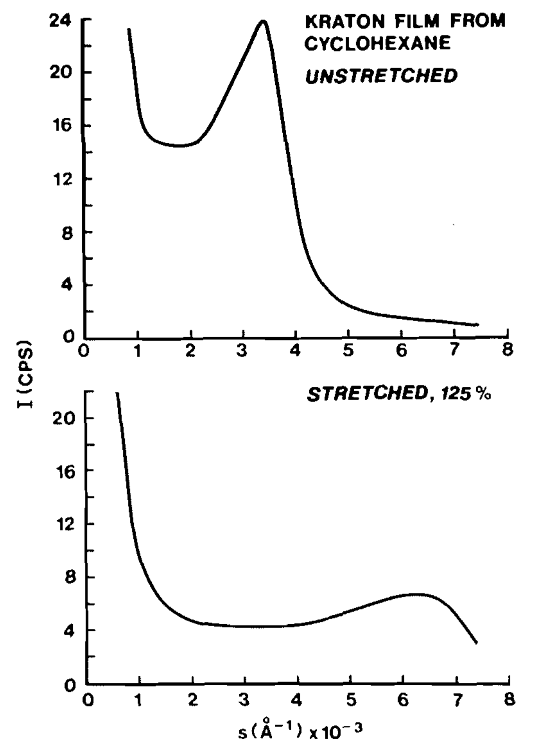

FIG. 7. Same as Fig. 6, but for Kraton film cast from cyclohexane.

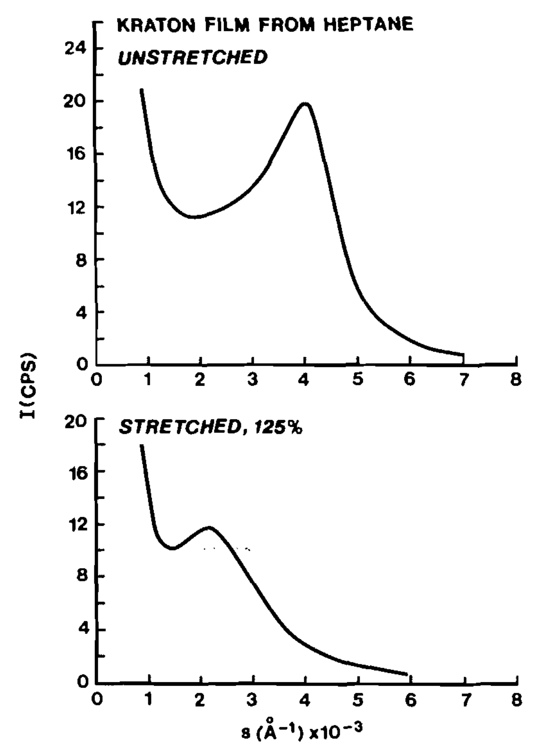

FIG. 8. Same as Fig. 6, but for Kraton film cast from heptane.

cases, and fibre-type orientation in prestretched samples. The superior thermoelastic response of Hytrel is attributed to the presence of homogeneously distributed, thermally stable, and partially oriented crystallites. The increase in the slope of the curves of $\Delta\sigma/\Delta T$ vs. λ at elongations of 120–140% could be due to the strain-induced crystallization.

The plot of $\Delta\sigma/\Delta T$ vs. λ for natural rubber is presented in

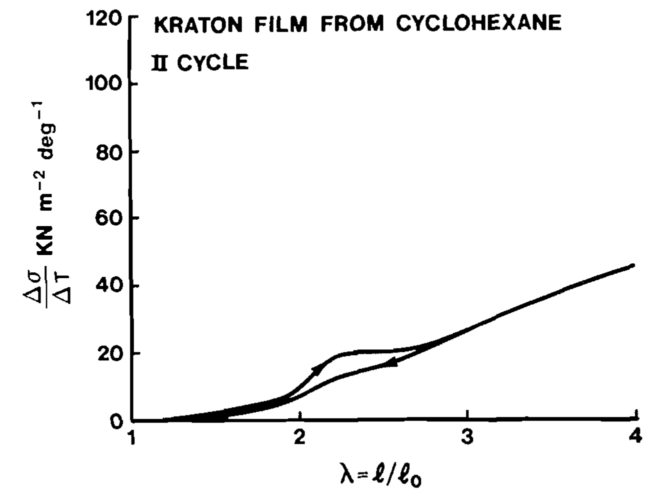

FIG. 9. Plots of variation of $\Delta\sigma$ with extension ratio (λ), for increasing and decreasing λ, are shown for the second cycle of measurement on Kraton film cast from cyclohexane (see also Fig. 4).

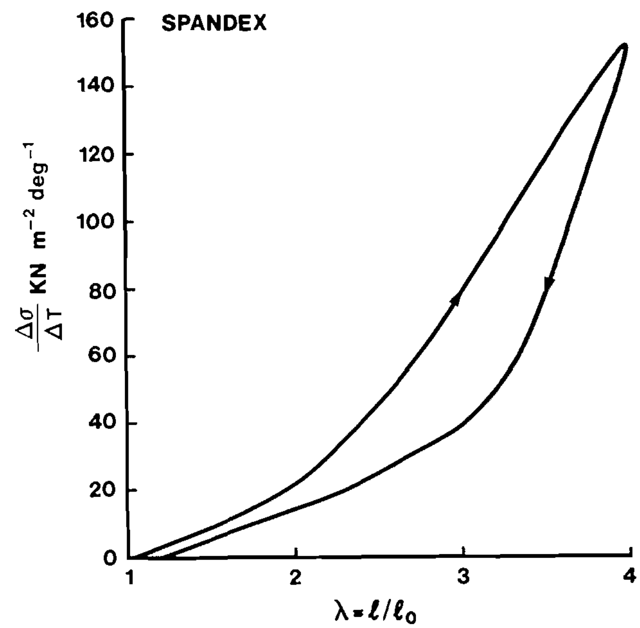

FIG. 10. Plots of variation of $\Delta\sigma$ with extension ratio (λ), for increasing and decreasing λ, for Spandex film cast from dimethyl formamide.

Fig. 12. It is observed that there is a relatively small change in the slope of the curve for increasing or decreasing extensions at elongations of about 120%. Compared with similar changes for films or Kraton, Hytrel, and Spandex, the changes for natural rubber are less significant, and this could be attributed to the affine behavior of an amorphous, covalently crosslinked structure, which undergoes very little textural change during extension. Also, it is well known that strain-induced crystallization does not occur in natural rubber at the low extension ratios employed here.

Conclusions

A comparison of the thermoelastic behavior of the four elastomers under investigation shows that increasing strain (with consequent orientation of microstructure and/or strain-induced crystallization of "soft" segments) has a positive influence on

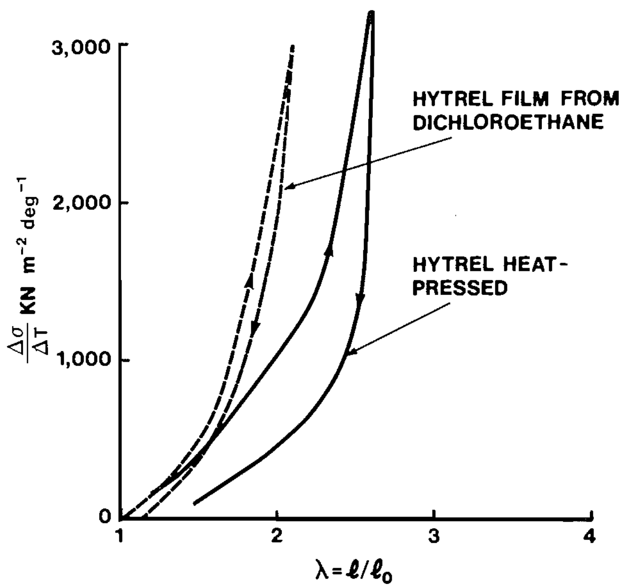

FIG. 11. Same as Fig. 10, but for heat-pressed and dichloroethane-cast films of Hytrel.

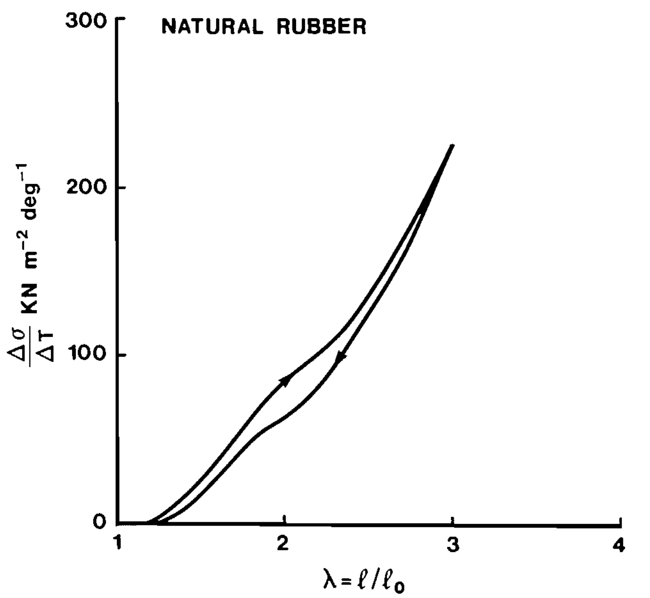

FIG. 12. Same as Fig. 11, but for natural rubber.

the extent of thermal contraction. Permanent orientation (e.g. prestretched Hytrel) also has a positive influence on thermoelastic properties probably because of removal of a spherulitic texture. Strain-induced crystallization of "soft" segments greatly increases the thermal response due to thermal melting of the crystallites and the concomitant increase in entropy during the application of a heat pulse.

Of the four materials, Hytrel best demonstrated the benefit to be derived from permanent crystallites ("hard" segments), preorientation and strain-induced crystallization of "soft" segments. Spandex also crystallizes upon stretching, but reversibly with stress. The "hard" segments in Spandex do not form a separate crystalline phase and hence permanent cross-links do not exist. Clearly, the permanent cross-links, oriented in the stretch direction, as in Hytrel, are the desirable contributors for a strong thermoelastic response.

In the case of natural rubber, the effect of moderate strains on thermoelastic behavior is well documented. The results of Fig. 12 are surprising only by comparison with the data for Hytrel, which at $\lambda = 2$ show a $\Delta\sigma/\Delta T$ which is an order of magnitude greater. The most obvious explanation is in terms of the above referenced cross-links. The near-reversibility of the curves in Fig. 11 suggests that strain encourages the development of intermolecular forces between Hytrel macromolecules to provide a pseudo-network with a distribution of crosslink strengths. This develops a network with a memory, at least up to strains of $\lambda = 2-3$ and probably well beyond.

In comparison to Hytrel, Kraton samples show less pronounced thermoelastic behavior. This can be attributed to a microtexture which is based on weak segment interaction, compared to crystallization forces. Entropy contributions to the thermoelasticity are low. Extension disrupts the microtexture and recovery is exceedingly time-dependent. Accordingly, the thermoelasticity of Kraton is difficult to exploit.

Again, in comparison to Hytrel, Spandex exhibits a softer thermoelastic behavior. It is probably optimized for comfort factors in garment application. Cross-linked natural rubber is similar in behavior and would probably show the rapid rise in thermoelastic response of Hytrel with extension but only at much higher λ where crystallization is known to develop. At that point both permanent and pseudo-crosslinks would be intermeshed.

In the case of the ideal rubber, stress-strain behavior is predictable if there is affine deformation and no intermolecular interaction. The present study suggests that maximum thermoelastic response is dependent on affine deformation with development of reversible intersegment forces as extension takes place. The very large difference in thermoelastic response of Hytrel compared to crosslinked natural rubber demonstrates the remarkable difference between crystallite networks vs. covalent networks in elastomers. Given the imagination of polymer chemists, the limits of elastomer technology are probably still far away.

For non-ideal elastomers there are both entropy and enthalpy contributions to the stress. The measurement of $\Delta\sigma/\Delta T$ provides one with a means of separating the entropy and enthalpy contributions to the stress at constant λ given by

$$\sigma_s = T(\delta\sigma/\delta T)_{p,l}$$

$$\sigma_e = (\delta H/\delta L)_{p,T} = \sigma - \sigma_s$$

where T is the absolute temperature, and p, s, H, and L represent the pressure, entropy, enthalpy, and length, respectively. Thus, thermoelastic data gathered using a tensometer as described here can be used to compare elastomers on the basis of these entropy contributions to the developed stress. Although these equations are only strictly accurate when constant pressure is replaced by constant volume, they are very nearly correct at small extensions, where affine deformations occur.

1. R. J. FARRIS. Polym. Eng. Sci. **17**, 737 (1977).
2. E. D. RAY. U.S. Patent 4,075,847 (1978).
3. L. R. G. TRELOAR. The physics of rubber elasticity. 3rd ed. Calderon Press, Oxford. 1975; H. HAPPY (*Editor*). Applied fibre science. Vol. 2. Academic Press, New York. 1979.
4. P. J. FLORY. Principles of polymer chemistry. Cornell University Press, Ithaca, NY. 1953.
5. J. E. MARK. Macromol. Rev. **11**, 135 (1976).
6. R. SEGUELA and J. PRUD'HOMME. Macromolecules, **11**, 1007 (1978).
7. (*a*) R. BONART, L. MORBITZER, and G. HENTZE. J. Macromol.

Sci. B**2**, 337 (1969); (*b*) R. BONART. J. Macromol. Sci. B**2**, 115 (1968).
8. J. M. SAUNDERS and K. C. FRISCH. Polyurethanes, chemistry and technology. Part I, Wiley Interscience, New York. 1962.
9. D. PUETT. J. Polymer. Sci. Part A2, **5**, 839, (1967).
10. S. B. COUGH, N. S. SCHNEIDER, and A. O. KING. J. Macromol. Sci. B**2**, 553 (1968).
11. L. W. JELINSKI, F. C. SCHILLING, and F. A. BOVEY. Macromolecules, **14**, 581 (1981).
12. R. J. CELLA and W. H. BUCK. Polym. Prep. **15**, 159 (1974).
13. A. LILAONITKUL, J. C. WEST, and S. L. COOPER. J. Macromol. Sci. B**12**, 563 (1976).
14. J. A. ODELL and A. KELLER. Polym. Eng. Sci. **17**, 544 (1977).

Particles in polymers: surface chemistry of their nucleation, growth, configuration, and interactions with the matrix

G. J. KOVACS AND P. S. VINCETT

Xerox Research Centre of Canada, 2660 Speakman Drive, Mississauga, Ont., Canada L5K 2L1

Received February 3, 1984

This paper is dedicated to the 10th anniversary of the Xerox Research Centre of Canada

G. J. KOVACS and P. S. VINCETT. Can. J. Chem. **63**, 196 (1985).

The surface chemistry and thermodynamics of the nucleation, growth, configuration, and host–guest interactions of small particles within softenable substrates is investigated. It is found that novel subsurface particle monolayers form rather generally when inorganic materials are appropriately deposited onto softened (or subsequently softened) organic polymer substrates; partially embedded structures are generally formed by organic particulate materials, although these can also be embedded by exposure to a solvent vapour. For both rigid preformed particles spread onto the polymer surface, and for flexible growing clusters (as occur in vacuum deposition), the tendency for complete immersion is thermodynamically determined by the same simple inequality among the surface and interfacial tensions. Modelling of the polymer molecule configurations in the vicinity of subsurface particles predicts a novel entropic force of sufficient magnitude to explain why the particles form a monolayer a few tens of nm below the surface, rather than dispersing throughout the polymer, and why this structure is remarkably stable on extended heating. With the convenient fabrication technique of vacuum deposition, subsurface formation is further limited kinetically, by growth mode and sinking rate considerations, to generally low melting point inorganics and to certain ranges of deposition conditions; once subsurface particles are formed, their subsequent growth during the deposition process generally occurs at constant (nearly close-packed) surface coverage by a combination of material-capture and coalescence. After these nearly monodisperse particles grow beyond ~0.4 μm, they begin to bridge into a continuous subsurface structure. These vacuum-deposition phenomena are quantitatively explained by kinetic models of the formation and growth mechanisms.

G. J. KOVACS et P. S. VINCETT. Can. J. Chem. **63**, 196 (1985).

On a étudié la chimie de surface et la thermodynamique de la nucléation, de la croissance, de la configuration et des interactions "hôte–récepteur" de petites particules à l'intérieur de substrats qui peuvent être ramollis. On a trouvé que, si des produits inorganiques sont déposés d'une façon appropriée sur des polymères organiques ramollis (ou qui ont subséquement été ramollis), il se forme d'une façon assez générale de nouvelles monocouches de particules sous la surface; généralement, les particules organiques forment des structures qui sont partiellement incrustées même si ces composés peuvent être incrustés par une simple exposition à des vapeurs de solvant. Tant pour les particules rigides préformées étendues sur la surface du polymère que pour les agglomérats flexibles croissants (qui se produisent par un dépot sous vide), la tendance à obtenir une immersion totale est déterminée par la même inégalité simple entre les tensions de surface et interfaciales. A l'aide de modèles des configurations de la molécule de polymère près des particules sous la surface, on peut prédire l'existence d'une nouvelle force entropique dont l'amplitude est telle qu'elle peut expliquer pourquoi les particules forment une monocouche à quelques nm sous la surface plutôt que de se disperser à travers tout le polymère et pourquoi cette structure est si stable lorsqu'on la chauffe d'une façon prolongée. Compte-tenu de l'existence, d'une part, de la technique commode de fabrication par dépot sous vide et, d'autre part, de considérations cinétiques relatives à la méthode de croissance et aux vitesses d'enfoncement, la formation sous la surface est généralement limitée à des composés inorganiques de bas point de fusion et à certaines conditions de dépot; lorsqu'il y a eu formation de particules sous la surface, une combinaison de capture de matériel et de coalescence fait que leur croissance subséquente, au cours du processus de dépot, se produit généralement avec une couverture de la surface qui est constante (pratiquement tassée). Lorsque ces particules pratiquement monodispersées atteignent des dimensions d'environ 0,4 μm, elles commencent à se joindre pour former une structure continue sous la surface. On peut expliquer quantitativement ces phénomènes de dépot sous vide en faisant appel à des modèles cinétiques pour les mécanismes de formation et de croissance.

[Traduit par le journal]

1. Introduction

The surface chemistry of thin film formation during vacuum deposition onto rigid substrates has been studied extensively for the past half century (1). However, structures formed on/in softenable substrates have received very little consideration, save for one technologically important process involving the vacuum deposition of the photoconductive material Se (2). In this process, the substrate is a thermoplastic material which is heat-softened during Se deposition. Within a rather broad "window" of substrate temperature and deposition rate, the Se can form into a nearly close-packed monolayer of submicron, nearly monodisperse amorphous spheres embedded a few tens of nm under the polymer surface. This unique structure, illustrated in Fig. 1, is remarkably stable under extended heating. It can also readily be formed from a wide range of materials if they are incident as a smoke (3) onto a heated thermoplastic, or if appropriate particles are merely spread over the surface which is subsequently heat- or vapour-softened. However, with the very convenient technique of vacuum deposition onto heated thermoplastics, kinetic factors somewhat limit the formation of subsurface particles, usually to low-melting materials; even then, kinetic factors further limit it to certain ranges of substrate temperature and deposition rate. These unique vacuum-deposited structures possess other very unusual properties. The structure is very nearly independent of substrate temperature and deposition rate over very large ranges, within the "window" mentioned above. The diameter of the spheres can be varied from very low values up to at least ~0.4 μm *at constant surface (projected-area) coverage,* merely by varying the total quantity Q of material deposited per unit substrate area; this of course implies that a continual aggregation/coalescence process is occurring. Very strikingly, the diameter of the spheres is simply proportional to Q.

Structures of this kind may have major technological appli-

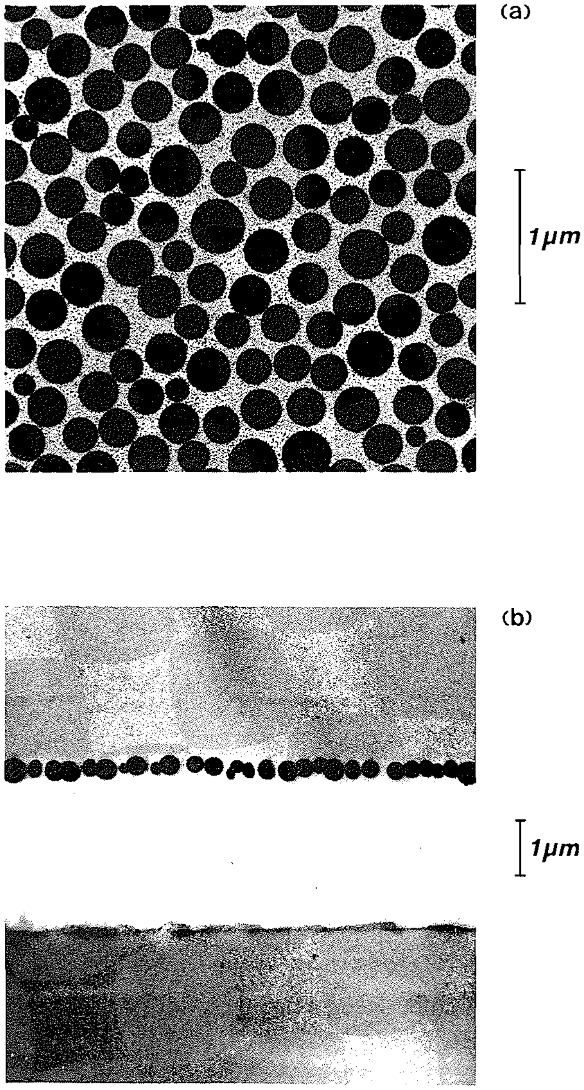

FIG. 1. TEM of Se, vacuum deposited onto heated thermoplastic, looking (*a*) normal to substrate surface, (*b*) parallel to substrate surface.

cations. For example, the Se material, shown in Fig. 1, has important uses as an electrophotographic film which is usually developed by a migration imaging process to form a visible image (2, 4–6). The many remarkable properties and demonstrated applications of this unique material have recently been reviewed (7).

In this paper we analyze the surface chemistry of the novel subsurface and related structures, including a detailed analysis of the interactions between particles and polymers; we also model the kinetics of the formation and growth mechanisms during vacuum deposition. The experimental observations are summarized in section 2. The roles of the surface and interfacial tensions of the particle and substrate materials in determining the thermodynamically most favourable structures are investigated in section 3. The configurations (8) of the polymer molecules and their interfacial interactions (9) with the particle surfaces are modelled in section 4, and are shown to result in a novel entropic force of sufficient magnitude to explain why particles form a monolayer rather than dispersing throughout the polymer, and why this structure is remarkably stable on extended heating. Kinetic models of the formation mechanism during vacuum deposition onto softenable substrates and also

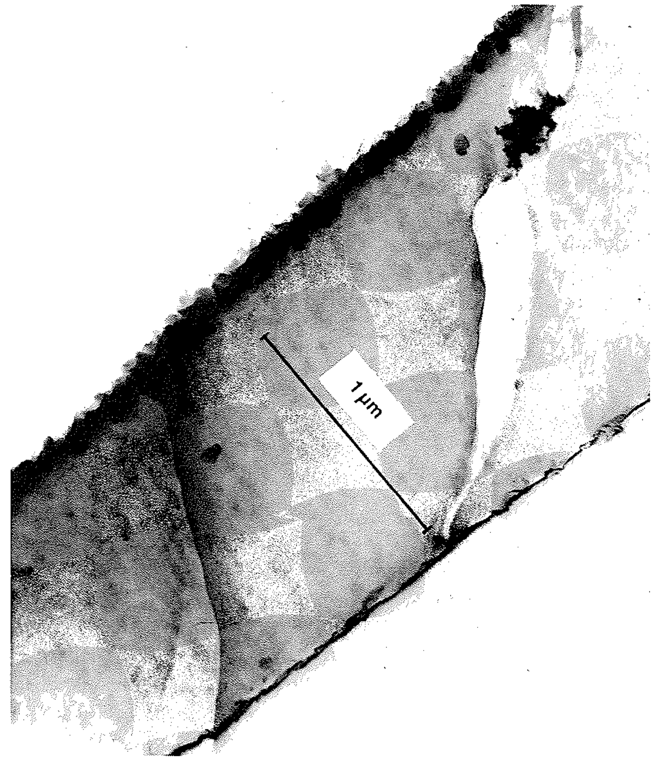

FIG. 2. TEM of vanadyl phthalocyanine, vacuum deposited onto heated thermoplastic, looking parallel to the substrate surface.

of the subsequent growth of subsurface particles are given in section 5.

2. Summary of experimental data

Apart from vacuum deposition, which we discuss below, there are several methods of forming subsurface structures from almost any particulate material. For example, we have formed such structures from both inorganic and organic materials (principally phthalocyanines), by a novel spreading technique. The phthalocyanine or other particulate is finely dispersed in a liquid (e.g. methanol) which is a non-solvent for the polymer substrate. The dispersion is then coated as a thin liquid film by a gravure coating technique. After the liquid evaporates, a thin powder film is left which can easily be wiped off and is therefore clearly above the substrate surface. If the substrate is now softened by heating, inorganic particles now form the subsurface monolayer. Organic particles, however, become partially embedded, much as in Fig. 2; in this state, a substantial amount of pigment can still be wiped off the film surface with a light paper tissue. However, if the polymer substrate is instead softened by exposure to a vapour which is a solvent for the polymer, complete embedding of the organic particles is achieved, generally within a few seconds. Typical solvents suitable for the styrene–hexylmethacrylate copolymer generally used in the technological applications (7) of the Se material are toluene, methylene chloride, and 1,1,1-trichloroethane. After vapour exposure, the polymer surface has a shiny glazed finish and since the particles are completely submerged the film can no longer be wiped off. Such embedded organic particulate structures, like their Se counterparts, have application as an electrophotographic film, in this case infrared-sensitive. In addition to vacuum deposition and the spreading technique, embedded particulate structures can also be made from a wide range of inorganic materials by a smoke (3) method. Material is evaporated in a high (atmospheric) background pressure of flowing nitrogen. Under these conditions, the material forms into a smoke which is carried by the gas flow onto a heated polymer substrate. The particle deposition can also be carried out by cascade and electrophoretic techniques. In the cascade technique, colloidal-size particles are produced by standard methods and are then picked up triboelectrically onto xerographic carrier beads. The beads are cascaded over the polymer substrate surface to deposit the particles. Particle sinking is then accomplished by either heat or vapour softening of the substrate, as discussed above. In the electrophoretic technique, the colloidal-size particles are suspended in an insulating liquid medium. They are then deposited onto the polymer substrate, which is in contact with the liquid, by applying an electric field through the liquid and thereby driving the naturally-charged particles to the polymer substrate. With appropriate suspending liquids, the particles may already become embedded at this stage. If not, after evaporation of the liquid, the polymer substrate may be either heat- or vapour-softened as above to effect embedding.

Turning now to the vacuum deposition technique, we have made a rather comprehensive experimental study of the formation of vacuum-deposited structures on heated thermoplastic substrates. The evaporants included a wide range of inorganic and organic materials and the experimental details have been given elsewhere (10). In general, two types of embedded structures have been observed, which appear to represent cases of thermodynamic equilibrium.

The first equilibrium structure, and by far the most important, is a monolayer of completely embedded spheres; an example is shown in the TEM of Fig. 1(*b*), for which the evaporant was Se and the substrate a heated styrene–hexylmethacrylate copolymer. The second equilibrium structure consists of partially embedded particles. This has been observed in the evaporation of vanadyl phthalocyanine onto the heated copolymer, the embedded lower portion of the particles being clearly seen in Fig. 2. The structure of Fig. 1(*b*) is readily obtained with low melting inorganic evaporants (10–12) but, at best, only partially submerged structures can be obtained with organic evaporants.

The subsurface monolayer structure was found to possess remarkable thermal stability. Continued heating of the polymer substrate at 115°C in vacuum for 3 days after formation of a subsurface Sn structure (similar to the Se structure in Fig. 1) failed to produce even the slightest migration of the nearly single-crystalline Sn particles into the polymer, as determined by electron microscopy of microtomed sections. A simple calculation (10) shows that this period of time should be more than ample for random Brownian motion to scatter the particles throughout the 1.5 μm-thick polymer matrix, in the absence of a restraining force.

The kinetics of subsurface particle formation (13–17) and growth (17) have also been determined for vacuum deposition. The formation data is summarized in Fig. 3, where the solid line gives the transition between surface and subsurface particle formation for Se on the well characterized (15) styrene–hexylmethacrylate copolymer substrate. The dashed lines represent the same transition for Sn on this copolymer substrate. At low deposition rates, the surface/subsurface transition lines for the two evaporants are nearly identical, with an activation energy of ~50 kcal/mol, which is also equal to the polymer's activation energy for viscous flow. At high deposition rates, the

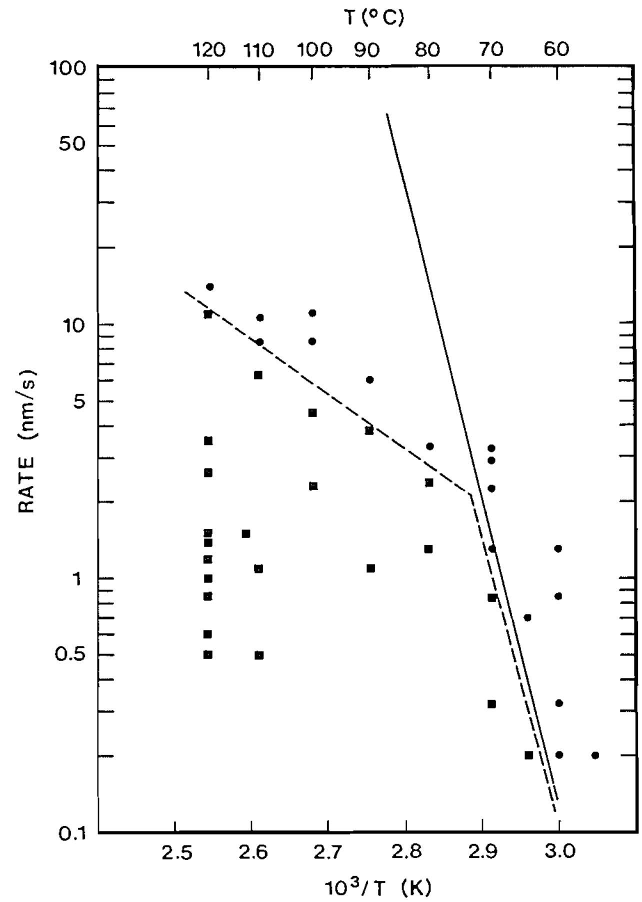

FIG. 3. Subsurface particle formation conditions for Se and Sn on our styrene-rich copolymer. Solid line separates region of surface film formation (right) and subsurface particle formation (left) for Se on the polymer. Dots represent surface Sn deposits and squares represent subsurface Sn deposits with the dashed curve dividing these two regions for Sn.

activation energy for the Se transition remains at 50 kcal/mol, but that for Sn drops to ~10 kcal/mol. Many other high-melting inorganic evaporants were studied, and formed only surface deposits under all accessible deposition conditions, as illustrated by the V deposit shown in Fig. 4. An interesting feature of this V film, common to virtually all above-surface deposits of inorganic materials on soft substrates, is that it consists of a thin continuous underlayer followed by superposed island structures. (The structure observed between the large dark islands is definitely due to a thin continuous film, since the underlying polymer has been dissolved away (10).) This normally-rare Stranski–Krastanov (S–K) growth mode (1) is thought to be one important factor limiting subsurface particle formation with inorganic evaporants (13).

The growth data for subsurface Se spheres is given in Fig. 7 of ref. 17. The projected area coverage $N\pi\langle a\rangle^2$ of the spheres remains remarkably constant over a rather large range. The average sphere radius, $\langle a\rangle$, and the number of particles per unit area, N, correlate with deposition time, t (at constant deposition rate), according to $\langle a\rangle \propto t$ and $N \propto t^{-2}$, at least up to a fairly large value of $\langle a\rangle$ ~0.2 μm. However, for larger values of $\langle a\rangle$, bridging of subsurface spheres begins, with eventual formation of a continuous *subsurface* film as shown in Fig. 5. The particulate structures obtained are almost independent of deposition rate and temperature over very large ranges, so long as one

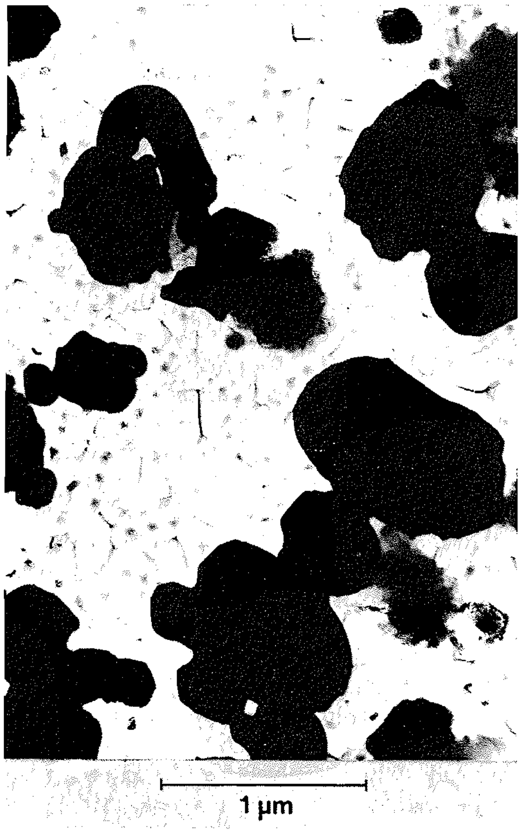

FIG. 4. TEM of V surface film deposited onto our heated styrene-rich copolymer, looking normal to the polymer surface.

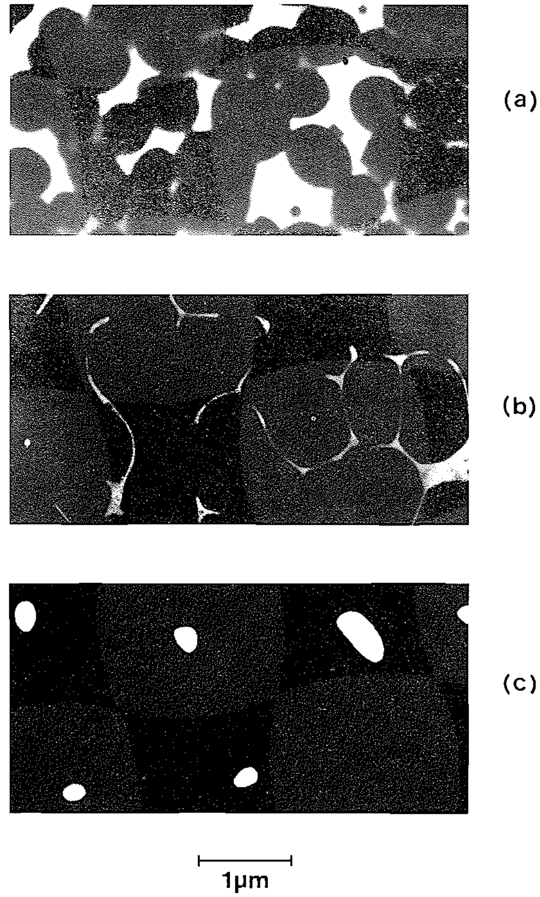

FIG. 5. TEM's of successive stages of the growth of subsurface Se spheres into a continuous surbsurface film.

remains within the "window" within which subsurface structures are formed at all.

3. Thermodynamic analysis of embedding

Thermodynamically, the most favourable state for any isochoric, isothermal system is the state with the lowest Helmholtz free energy, F (18). This free energy has both a volume and a surface contribution. We assume that the former is constant in our systems, corresponding to constant internal morphology within each material, so that only the surface contribution varies according to the particle-substrate configuration. To keep our analysis simple, we consider only homogeneous materials with isotropic surface tensions. For very small particles, gravitational forces are negligible compared with surface tension forces.

The surface free energy per unit area of a material is equivalent to its surface tension, γ, which is also equivalent to the isothermal work required to create a unit area of surface (19). The work of adhesion between two materials, W_{12}, is defined as the work necessary to separate the two materials at their interface. W_{12} is related to the surface tensions of the materials, γ_1, γ_2, by the relationship (19)

$$[1] \quad W_{12} = \gamma_1 + \gamma_2 - \gamma_{12}$$

where γ_{12} is the interfacial tension. It follows that the work of cohesion of a material, W_{11}, is simply $2\gamma_1$. It should also be noted that γ_{12} between two incompatible materials is positive. A negative γ_{12} implies a tendency for one material to dissolve in the other.

We start by considering subsurface structure formation by vacuum deposition. The case of a flexible cluster on a rigid substrate is generally taken as the starting point in treatments of thin film nucleation phenomena (1). The equilibrium cluster configuration is a spherical cap, with the contact angle determined by balancing the surface and interfacial tension components parallel to the rigid substrate, resulting in the well known Young equation (1). We restrict our discussion to the novel case of a soft substrate.

If the substrate is softened in the presence of a flexible cluster, the equilibrium cluster shape becomes a surface lens (20) as shown in Fig. 6. In this case, the surface tension components both parallel and normal to the substrate surface must be balanced at equilibrium. These two conditions give two equations which can be solved for the contact angles θ_1 and θ_2:

$$[2] \quad \cos\theta_2 = (\gamma_2^2 + \gamma_1^2 - \gamma_{12}^2)/2\gamma_2\gamma_1$$

and

$$[3] \quad \cos\theta_1 = (\gamma_2^2 + \gamma_{12}^2 - \gamma_1^2)/2\gamma_2\gamma_{12}$$

From Fig. 6, it is clear that the lens material will remain partially exposed above the substrate provided $\cos\theta_2 < 1$ (or equivalently $\cos\theta_1 > -1$). However, if the rhs of eq. [2] is >1 (or the rhs of eq. [3] is < -1), the lens material will become completely submerged into the substrate material and (for isotropic surface forces) will assume a spherical shape. From eqs. [2] and [3], these conditions for complete immersion reduce to the inequality

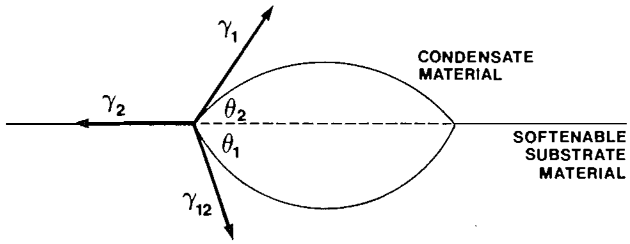

FIG. 6. Equilibrium lens configuration of a soft cluster in a soft substrate. The surface tension components both parallel and perpendicular to the substrate are in balance.

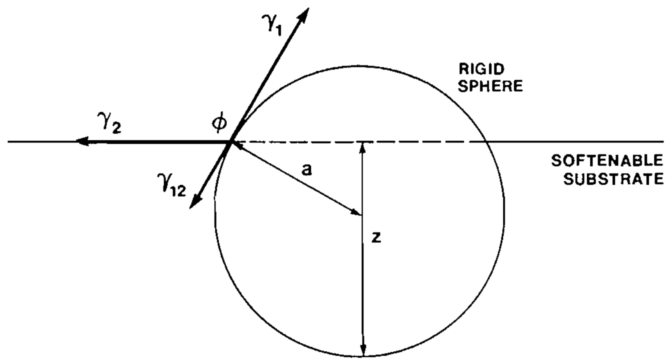

FIG. 7. Equilibrium position of a rigid sphere embedded in a soft substrate as determined by surface and interfacial tensions, related (as an example) according to $\gamma_1 = \gamma_2 = 2\gamma_{12}$.

$$[4] \quad \gamma_1 > \gamma_2 + \gamma_{12}$$

We now consider the case of a rigid preformed particle (for simplicity a sphere) in contact with a soft substrate (applicable to the case of structures formed by spreading, smoke, or electrophoretic techniques). For this case, the system will be in equilibrium when the surface tension components parallel to the *rigid* surface, i.e. parallel to the particle surface, are in balance. (The components perpendicular to the rigid surface remain unbalanced, analogous to the situation, described by the Young equation, of a liquid drop on a rigid substrate.) The situation is depicted in Fig. 7. The balance condition is given by

$$[5] \quad \gamma_1 + \gamma_2 \cos \varphi = \gamma_{12}$$

where φ is the angle between γ_2 and γ_1 on the line of contact between substrate and sphere surfaces. Since, for a sphere, the embedded depth z and the angle φ are geometrically related according to

$$[6] \quad z = a(1 - \cos \varphi)$$

where a is the radius of the sphere, the equilibrium embedded depth, z_{eq}, is seen to be given by

$$[7] \quad z_{eq} = a(\gamma_1 + \gamma_2 - \gamma_{12})/\gamma_2 \; (= 2aW_{12}/W_{22})$$

From eq. [7] it is readily seen that the equilibrium configuration is again a completely embedded sphere if and only if inequality [4] holds. It is a straightforward extension of the above analysis to show that inequality [4] is the general condition for complete immersion of an arbitrarily shaped rigid particle (21).

It can therefore be concluded that at equilibrium a particle, either rigid or soft, in contact with a soft substrate, will be completely embedded provided inequality [4] holds; otherwise, partial embedding represents the equilibrium configuration. It is interesting to note that inequality [4] can be expressed in terms of the relevant works of cohesion and adhesion as defined in eq. [1]. Inequality [4] is equivalent to the relationship, $W_{12} > W_{22}$. Therefore, a material will tend to completely embed itself in a soft substrate provided that the work of adhesion between the two materials is greater than the work of cohesion of the substrate, an intuitively reasonable result.

While the surface tensions of many materials are known, the interfacial tensions for most material combinations have not been determined. The dispersion force interaction theory developed by Fowkes (9) was used to calculate the interfacial tensions for systems of interest. In general, inequality [4] is found to hold for virtually any inorganic material on an organic polymer substrate (12, 21), but the reverse inequality holds in general for organic materials on organic polymer substrates (21).

These thermodynamic predictions are in fact confirmed by the experimental data. Completely embedded equilibrium structures as in Fig. 1 were formed by low melting inorganic evaporants where no kinetic limitations intervened, and by virtually any inorganic particulate when the spreading technique was used. Partially embedded structures as in Fig. 2 were formed by organic evaporants when no kinetic factors intervened, and by virtually any organic particulate when the spreading technique was used with only heat-softening. However if, instead, polymer solvent vapour exposure was used, then organic particulates as well as inorganic particulates would form a completely embedded structure.

The effect of polymer solvent vapour on particle embedding can be understood by noting that on vapour absorption the surface tension of the polymer–solvent system becomes that of the polymer solution. With sufficient uptake of a low surface tension solvent vapour, the surface tension of the polymer–solvent system approaches that of the pure solvent (21). In our experiments, the surface tension of the polymer (similar to polystyrene) is significantly higher than that of the solvent (e.g. toluene), so that absorption of a relatively small amount of solvent by the polymer can lower the surface tension of the substrate, γ_2, very close to that of the pure solvent (γ_{12} is not expected (21) to change appreciably). Therefore $\gamma_2 + \gamma_{12}$ can be lowered significantly by introduction of the solvent vapour, inequality [4] can now be satisfied, and complete immersion results.

4. Analysis of monolayer stability

In addition to the large free energy change associated with embedding an inorganic particle into the polymer as discussed in the previous section, there are at least two smaller contributions to the free energy; these vary with the depth of the sphere below the surface, and for convenience we reference them relative to a deeply embedded sphere. The first of these, ΔU_{VdW}, represents the Van der Waals attraction between the sphere and polymer half-space, which acts to pull the sphere deeper into the polymer. In addition we have attempted to treat the difficult problem of the detailed interactions between the sphere and polymer; this treatment suggests that there is a second (entropic) energy, $-T\Delta S$, tending to reject the particle. The sum of these two energy contributions with opposing gradients possesses a minimum for the sphere situated a specific distance below the polymer surface.

The Van der Waals (dispersion) interaction between the sphere and the polymer is a very long-range force. It the top of a sphere of radius a is located a distance l below the polymer surface, then by symmetry the net attractive force on the sphere by the polymer within the surface slab of thickness $2a + 2l$ is zero. However, all the polymer below this slab will exert an uncompensated attraction on the sphere. This interaction energy, ΔU_{vdW}, between a sphere and a half-space can be written down immediately (22):

$$[8] \quad \Delta U_{\mathrm{vdW}} = A_{12}/6\{(2 + 2x)/(2x + x^2) + \ln[x/(2 + x)]\}$$

where $x = l/a$ and A_{12} is the appropriate Hamaker constant describing the interaction between the sphere and polymer material. ΔU_{vdW} monotonically decreases to zero as the sphere moves away from the polymer surface.

As discussed in the previous section, when complete particle submersion is thermodynamically favourable, the work of adhesion of the polymer material to the particle is greater than the work of cohesion of the polymer ($W_{12} > W_{22}$). According to Fowkes' view of the interface, this implies that the polymer chain elements immediately adjacent to the particle surface should be in a state of compression with density slightly higher than the rest of the bulk polymer (12). Modern theories of polymer conformations (23) involving free volume effects also predict a higher polymer density at the particle surface. We shall make the simplifying assumption that the relaxation of this local high polymer density about the sphere surface can be described by random walk statistics (8), and we calculate the variation in entropy of the polymer as the sphere approaches the polymer–air (or polymer–vacuum) surface. Generally speaking, a compression of the polymer should reduce its entropy, and a long-chain material will not relax this compression for some considerable distance from the particle. Thus, we might expect the proximity of the air surface to diminish the extent of this compression, effectively allowing the compression to relax at the surface. In this case, the polymer's entropic contribution to the free energy of the system would tend to push the sphere toward the surface to maximize the entropy.

To calculate the internal entropy of the polymer, we use the diffusion equation approach (8, 24) with boundary conditions appropriate to the above view of the sphere–polymer interface. The details of this calculation may be found elsewhere (12). We give here only the final result for ΔS, the change in polymer entropy for a sphere at distance l from the polymer surface relative to the entropy when the sphere is deeply embedded:

$$[9] \quad \Delta S = kV_m(b^2/6)4\pi a\epsilon\left\{1 - \sinh\beta_0 \sum_{n=0}^{\infty} \exp\left[-\left(n + \frac{1}{2}\right)\beta_0\right] \Big/ \cosh\left[\left(n + \frac{1}{2}\right)\beta_0\right]\right\}$$

In eq. [9], k is Boltzmann's constant, V_m is the monomer volume, b is the average length of a link in the polymer chain (commonly called the Kuhn statistical length), ϵ is a positive dimensionless parameter related to the increased density at the sphere interface, and β_0 is given by $\sinh^{-1}\{[x(x + 2)]^{1/2}\}$. Numerical evaluation shows that ΔS steadily increases as the sphere moves toward the surface.

From eqs. [8], [9], the free energy variation with depth below the surface, ΔF_p, can be calculated according to the relation:

$$[10] \quad \Delta F_p = \Delta U_{\mathrm{vdW}} - T\Delta S$$

Parameters suitable for Se and Sn spheres in polystyrene have been determined (12) and the results for ΔF_p are given in Fig. 8 for spheres of radius $a = 0.15$ μm. The energy minima occur at the depths $l_{\min}(\mathrm{Se}) = 120$ nm and $l_{\min}(\mathrm{Sn}) = 98$ nm. The order of magnitude and relative size of these distances are in qualitative agreement with what is observed experimentally. The depths of the wells are 2.5×10^{-13} and 4.5×10^{-13} erg. These energies are about ten to twenty times $(kT/2)$ $(2.7 \times 10^{-14}$ erg) and should therefore be sufficient to stabilize a given sphere against random thermal fluctuations; this explains why the monolayer structure forms, and also its remarkable thermal stability on extended heating. Long range Van der Waals interactions of a given sphere with its neighbours should cause an additional self-stabilizing effect on the monolayer (12).

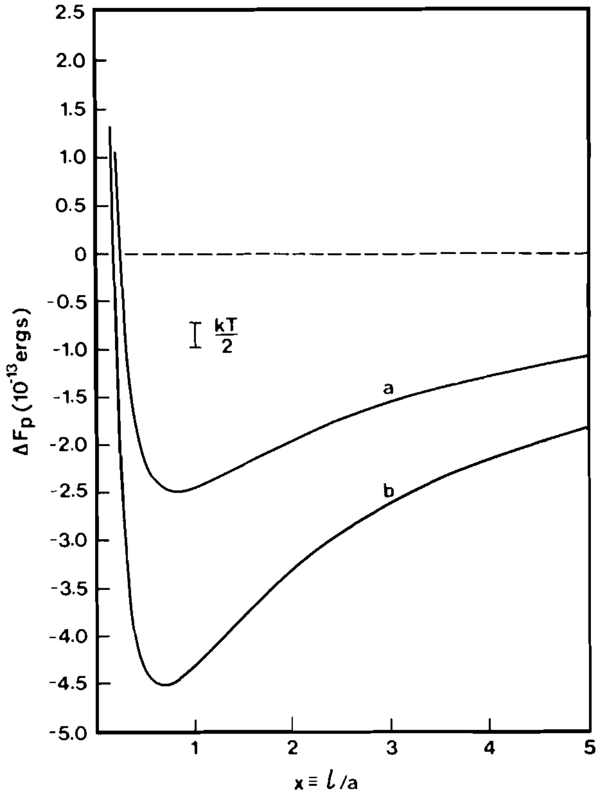

FIG. 8. Plots of ΔF_p given by eq. [10], as a function of the reduced depth of the sphere, $x = l/a$. Curves (a) and (b) were computed using the parameters given in ref. 12 appropriate for Se–polystyrene and Sn–polystyrene systems, respectively. The temperature in eq. [10] was taken as 120°C.

5. Kinetic analysis of formation and growth mechanisms during vacuum deposition

5.1 Formation mechanism

The Se transition curve in Fig. 3 is thought to be determined by particle sinking rate as controlled by polymer substrate viscosity and surface tension forces. If we assume the usual Volmer–Weber (V–W) growth mode (i.e. initial nucleation of the evaporant into an island structure) (1) with complete evaporant condensation into N spherical islands per unit area in a time negligible compared with that for island sinking, and also assume the viscous drag on a sinking sphere of radius a to be given by Stokes' formula (25), then the rate Ω at which material sinks below the surface is given by (13):

$$[11] \quad \Omega = (4\pi\gamma_2 Na^2/9\eta)\ln[(\gamma_1 + \gamma_2 - \gamma_{12})/(\gamma_1 - \gamma_2 - \gamma_{12})]$$

where η is the viscosity of the polymer. If the deposition rate

R is greater than Ω, an above surface film should form (i.e. the islands get buried by incoming evaporant before they can sink). Ω increases with surface coverage $N\pi a^2$ and should be a maximum at the largest practical surface coverage which does not impose significant additional restraints on sinking time. Using known values for η (15) and the γ's (12), and assuming $N\pi a^2 \sim 0.6$ (the result for randomly packed spheres (26)), an exact fit to the Se transition curve is obtained, using no disposable parameters.

A similar analysis gives a good description of the Sn transition curve in Fig. 3 for lower deposition rates; however, at high rates the transition from V–W to S–K growth (initial formation of the evaporant into a two-dimensional monolayer) gives initial continuous layers, which prevent subsurface Sn formation. (A similar transition is predicted for Se, but only at very high R values.) Theoretical considerations predict this transition when the saturation cluster density, N_s (the highest density of evaporant clusters reached on the polymer surface before neighbouring clusters begin to merge (27)), approaches the number of available adsorption sites/unit area N_0. That is, the transition is predicted when, at saturation, each cluster consists of only a few atoms (i.e. $\alpha = 0.1–0.5$ where α is defined as N_s/N_0) (28). This transition curve has an activation energy equal (28) to the surface diffusion energy E_d of the evaporant:

$$[12] \quad \ln (R/V_a) = \ln (\alpha^3 \delta q_0 \nu N_0/C) - E_d/kT$$

where V_a is the atomic volume, ν is a typical atomic vibration frequency $\sim 10^{12}$ s^{-1}, C is the number of nearest neighbour sites around a given adsorption site, and δ and q_0 are dimensionless parameters related to the rates at which stable nuclei grow into contact and stable clusters capture diffusing atoms, respectively (27).

To use eq. [12], we must estimate E_d. Now, if one considers the evaporant atoms to be adsorbed into the "tacky" polymer surface then one is able to account for an *adsorption* energy for Se equal to the unusually high value found experimentally (15). This tacky adsorption model also suggests a greatly increased surface diffusion energy E_d, and gives $E_d \sim 10$ kcal/mol for Sn. With this value of E_d, eq. [12] correctly predicts the slope of the high-R portion of the experimental Sn transition curve (Fig. 3). Moreover, using $\delta q_0 \sim 10^{-2}$ (appropriate for the diffusion-limited cluster growth process (27) thought to be applicable to low melting materials like Sn), we obtain agreement with the absolute values in Fig. 3 for $\alpha = 0.2$; this is well within the predicted range of 0.1–0.5. We thus have exact numerical agreement between theory and all parts of Fig. 3, essentially without the use of disposable parameters. Using $\delta q_0 \sim 10^{-7}$ (calculated (27) for the incorporation-limited cluster growth process, thought to be applicable to *high melting point* materials like Cr, Fe, V, etc.) we predict transition lines far below that of Sn, i.e., only the S–K growth mode is predicted to occur within accessible deposition conditions for these materials; this is exactly as observed experimentally (10). For such materials, calculations based on eq. [12] suggest that $T \geq 400$°C is necessary to give subsurface structures at $R \geq 0.1$ nm s^{-1}. Low surface tension polymers usually undergo severe degradation at such temperatures; in one case, however, we were indeed able to produce subsurface structures from a high melting material (Ag), by using relatively high values of T and special polymers (10).

5.2 *Growth mechanisms*

Let us now consider the *growth* of vacuum-deposited subsurface spheres, once a reasonably close-packed subsurface particulate monolayer is formed. In this situation, additional material impinging on the polymer surface will be captured by existing spheres, leading to their growth. When two adjacent spheres touch, a coalescence process will occur to form a new sphere in a time τ determined by their surface and bulk self-diffusivity (17). For Se, for example, at the temperatures used for the vacuum deposition process ($\sim$110°C), τ can be calculated to be generally very small ($\sim$ms), i.e. we have essentially instantaneous formation of the new sphere. In this case, the growth process can be considered as (a) growth of the stationary spheres (due to evaporant capture), leading to increase in the projected-area coverage $N\pi\langle a\rangle^2$ of the monolayer, and (b) continual random impaction and instant coalescence of neighbouring spheres, leading to a reduction in the coverage. Since the rate of sphere-sphere impingement will increase as the coverage increases, with no other dependence on the deposition rate, and since τ is negligible, it is clear that the situation will come to a dynamic equilibrium at a constant projected-area coverage, exactly as observed (section 2). That is to say:

$$[13] \quad N\pi\langle a\rangle^2 = \text{numerical constant}$$

The total volume of evaporant material (per unit area of substrate), Q, is of course given by:

$$[14] \quad N(4/3)\pi\langle a\rangle^3 = Q$$

Dividing eq. [14] by eq. [13] yields the extraordinarily simple proportionality between $\langle a\rangle$ and Q mentioned in section 1. Moreover, it is clear that in this regime the final structure will depend only on Q, not on the deposition rate or on temperature (so long as the subsurface structure is formed at all), also as observed. In addition, for constant deposition rate in this regime we have the relation $\langle a\rangle \propto t$, and (combining this with eq. [13]) $N \propto t^{-2}$. This is again exactly as observed (17).

Finally, it can be shown by consideration of the surface free energies (surface tensions) that, at high projected-area coverage, a continuous subsurface film is thermodynamically favourable compared with subsurface spheres (21). However, it is known from the previous discussion that the spheres grow at constant projected-area coverage with nearly instantaneous coalescence, over a rather large range. It therefore follows that a continuous film should be formed only after the coalescence time τ ceases to be negligible. In turn, since τ is expected to be proportional (17) to a^m ($m = 3$ or 4), this should only happen once the spheres exceed some minimum size. This is indeed observed in practice. With Se, for example, no deviation from sphericity is observed for sphere diameters up to about 0.4 μm; if more Se is deposited however, Fig. 5 shows that the structure becomes more and more two-dimensional, a continuous subsurface film eventually being formed.

Acknowledgements

We would like to thank A. L. Pundsack for the electron micrographs and K. M. Hong for helpful discussions.

1. B. LEWIS and J. C. ANDERSON. Nucleation and growth of thin films. Academic, New York. 1978.
2. W. L. GOFFE. Photogr. Sci. Eng. **15**, 304 (1971).
3. W. L. GOFFE, P. J. CERLON, A. L. PUNDSACK, M. LEVY, D. A.

BUCKLEY, and F. G. BELLI. U.S. Patent 3,598,644 (1971).
4. S. TUTIHASI. Photogr. Sci. Eng. **18**, 394 (1974).
5. A. L. PUNDSACK. Photogr. Sci. Eng. **18**, 642 (1974).
6. P. S. VINCETT, A. L. PUNDSACK, G. C. HARTMANN, R. K. HUNTER, JR., and W. D. MCCRARY. J. Appl. Photogr. Eng. **6**, 97 (1980).
7. P. S. VINCETT. J. Appl. Photogr. Eng. **9**, 38 (1983); A. L. PUNDSACK, P. S. VINCETT, P. H. SODEN, M. C. TAM, G. J. KOVACS, and D. S. NG. J. Imaging Technology, In press.
8. K. M. HONG and J. NOOLANDI. Macromolecules, **13**, 964 (1980).
9. F. M. FOWKES. Ind. Eng. Chem. **56**, 40 (1964).
10. G. J. KOVACS, P. S. VINCETT, C. TREMBLAY, and A. L. PUNDSACK. Thin Solid Films, **101**, 21 (1983).
11. G. J. KOVACS and P. S. VINCETT. J. Vac. Sci. Technol. **20**, 419 (1982).
12. G. J. KOVACS and P. S. VINCETT. J. Colloid Interface Sci. **90**, 335 (1982).
13. G. J. KOVACS and P. S. VINCETT. J. Vac. Sci. Technol. A, **1**, 369 (1983).
14. D. A. BUCKLEY, F. G. BELLI, and G. A. BROWN. Surf. Technol. **10**, 157 (1980).
15. D. A. BUCKLEY, F. G. BELLI, and J. H. LENNON. Surf. Technol. **9**, 241 (1979).
16. D. A. BUCKLEY, G. A. BROWN, and F. G. BELLI. Surf. Technol. **12**, 257 (1981).
17. D. ROBERTSON and A. L. PUNDSACK. J. Appl. Phys. **52**, 455 (1981).
18. M. W. ZEMANSKY. Heat and thermodynamics, McGraw-Hill, New York. 1968. p. 279.
19. I. N. SNEDDON (*Editor*). Encyclopaedic dictionary of mathematics for engineers and applied scientists. Pergamon, Oxford. 1976. p. 654.
20. L. D. LANDAU and E. M. LIFSHITZ. Statistical physics. 2nd ed. Pergamon, Oxford. 1970. p. 471.
21. G. J. KOVACS and P. S. VINCETT. Thin Solid Films. **111**, 65 (1984).
22. J. MAHANTY and B. W. NINHAM. Dispersion forces. Academic, New York/London. 1976. p. 16.
23. K. M. HONG and J. NOOLANDI. Macromolecules, **14**, 1229 (1981).
24. E. HELFAND. J. Chem. Phys. **62**, 999 (1975).
25. L. D. LANDAU and E. M. LIFSHITZ. Fluid mechanics. Pergamon, London. 1959. p. 66.
26. G. D. SCOTT and D. M. KILGOUR. J. Phys. D, **2**, 863 (1969).
27. V. N. E. ROBINSON and J. L. ROBINS. Thin Solid Films, **20**, 155 (1974).
28. D. KASHCHIEV. Thin Solid Films, **55**, 399 (1978).

Photogeneration of hydrogen peroxide in aqueous TiO_2 dispersions

JOHN R. HARBOUR, JOHN TROMP, AND MICHAEL L. HAIR

Xerox Research Centre of Canada, 2660 Speakman Drive, Mississauga, Ont., Canada L5K 2L1

Received February 9, 1984

This paper is dedicated to the 10th anniversary of the Xerox Research Centre of Canada

JOHN R. HARBOUR, JOHN TROMP, and MICHAEL L. HAIR. Can. J. Chem. **63**, 204 (1985).

Evidence is presented which demonstrates that titanium dioxide does in fact photogenerate H_2O_2 in the presence of the donor sodium formate. However, this H_2O_2 has only a transient existence in aqueous dispersions. This was confirmed by experiments in which H_2O_2 was injected into the dispersion. The reasons for the lability of H_2O_2 are discussed and possible mechanisms presented. Electron paramagnetic resonance experiments using spin traps reveal that photolysis of TiO_2 dispersion generates $\cdot OH$ radicals in the donor-free case while $\cdot CO_2^-$ radicals are observed in the presence of formate. These results are also consistent with H_2O_2 generation.

JOHN R. HARBOUR, JOHN TROMP et MICHAEL L. HAIR. Can. J. Chem. **63**, 204 (1985).

On présente des données qui indiquent que le dioxyde de titane, en présence d'un donneur comme le formate de sodium, provoque une photogénération du H_2O_2. Cependant, dans des dispersions dans l'eau, ce H_2O_2 n'existe que d'une façon transitoire. On a confirmé ce fait grâce à des expériences au cours desquelles on a injecté du H_2O_2 dans la dispersion. On discute de la cause de la labilité de ce H_2O_2 et on présente un mécanisme possible. Des expériences de résonance paramagnétique électronique, utilisant des capteurs de spin, révèlent que la photolyse d'une dispersion de TiO_2 génère des radicaux $\cdot OH$ dans le cas où il n'y a pas de donneur alors qu'on obtient des radicaux $\cdot CO_2$ en présence de formate. Les résultats sont également en accord avec la production de H_2O_2.

[Traduit par le journal]

Introduction

In the past decade there has been a resurgence of interest in the photochemistry and photoelectrochemistry of semiconducting materials (1−15). Much of this work has been associated with solar energy applications and photochemical energy conversion devices. In particular, there has been much work done on titanium dioxide. Although this pigment would not be useful for solar energy conversion due to its large band gap (~3 eV), it is known to be quite stable when it is illuminated in contact with water. This is to be contrasted with other common semiconducting pigments such as ZnO, CdS, and GaAs which undergo photo-corrosion (4). It is well known that when aqueous dispersions of such pigments are irradiated with band gap radiation that hydrogen peroxide is formed in the external solution in measurable quantities. This does not appear to be the case, however, for unreduced titanium dioxide and, despite numerous experiments (2, 16−19), its photochemical formation has yet to be proven. Rao *et al.* (20), however, have demonstrated H_2O_2 generation using reduced TiO_2 while Pappas and Fischer (6) have reported H_2O_2 formation (using a surface treated TiO_2) detected with *o*-ansidine and horse radish peroxidase.

When semiconducting oxides are irradiated with light of energy greater than the semiconductor band gap then an electron from the valance band can be excited to the conduction band thus creating an electron−hole pair (21). These electrons and holes can then, if they do not recombine, reduce or oxidise species in the external electrolyte solution. The semiconductor thus acts as an electron pump driving electrons from a low to a higher energy level. The flat band potentials of zinc oxide and titanium dioxide are shown in Fig. 1 together with the redox energy levels of reactions potentially occurring in hydrogen peroxide synthesis. It is noted that the potentials of titanium dioxide and zinc oxide are very similar. As it is well established in the case of zinc oxide that hydrogen peroxide is formed as a result of the reduction of dissolved molecular oxygen by the conduction band electrons it is difficult to explain why hydrogen peroxide is not formed by a similar mechanism at the titanium dioxide − water interface.

In order to clarify some of the reaction mechanisms which are occurring, a series of experiments have been carried out utilizing the techniques of spin trapping, oxygen uptake from solution, and the transient detection of hydrogen peroxide during catalase injection. The results obtained with titanium dioxide are compared with similar data obtained for analogous zinc oxide systems.

Experimental

No convenient, non-destructive in situ method of H_2O_2 determination is known, thus it is not possible to monitor a system directly for H_2O_2 formation. However, addition of the enzyme catalase to a system containing H_2O_2 causes the dismutation of H_2O_2 to H_2O and oxygen. If the system is closed, the changes in oxygen concentration can be monitored and then doubled to get the H_2O_2 concentration. For this purpose a YSI model 5331 oxygen probe and YSI model 53 electronic unit were used and the oxygen concentration vs. time curves recorded on a strip chart recorder as described previously (8, 22). The oxygen probe used was a Clark type polarographic electrode with a semi-permeable membrane which allows the O_2 to diffuse to the electrode. The membrane is temperature-sensitive (~4% O_2/°C) and the whole system is enclosed within a constant temperature bath. The use of the oxygen electrode has the added advantage that changes in the dissolved oxygen concentration under illumination can also be measured. For example, it has previously been shown (8) that illumination of ZnO dispersions can result in a 1:1 relationship between oxygen consumption and H_2O_2 formation (3) if an electron donor such as formate ion is present in the solution.

Illumination for all systems was provided by a filtered G.E. Quartzline projection lamp. For the photon efficiency measurements, a 380 nm narrow band pass filter was used. For all other experiments a Corning CS 0-52 filter was used. During illumination the temperature of the oxygen monitor sample cells rose by up to 5°C, as seen by an apparent initial increase in the O_2 concentration after the start of illumination due to the temperature sensitivity of the probe (Fig. 2). This temperature increase in only temporary and the temperature falls when illumination is stopped.

All chemicals were used as received and were reagent quality. The anatase polymorph of TiO_2 was used as it is reported to be more photoactive than rutile and was obtained from Fisher. Its BET surface

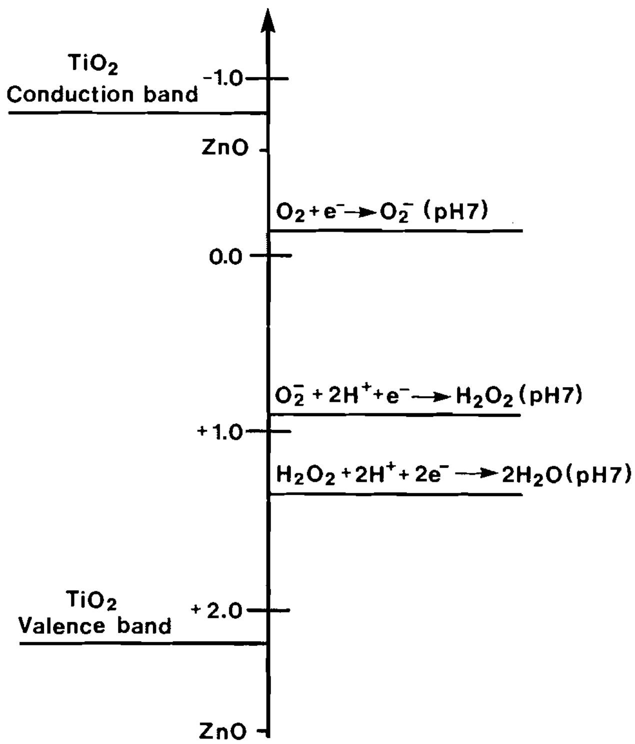

FIG. 1. Energy level diagram for TiO_2 (5). Also included for reference is the conduction and valence band levels for ZnO (5) and reduction processes in solution.

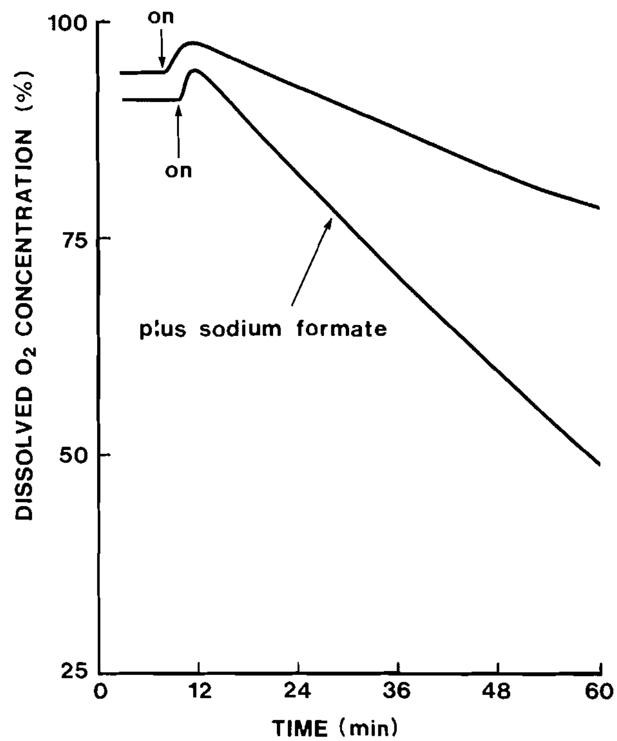

FIG. 2. Photo-induced oxygen uptake curves for TiO_2 in H_2O and TiO_2 in 0.1 *M* sodium formate solution.

area was determined to be 10.8 m^2/g. SEM showed the particle size to be between 0.2 and 0.5 μm.

Particle dispersions were prepared by adding TiO_2 and an appropriate amount of other reagents (usually to ~0.1 *M* concentration) to purified water and irradiating ultrasonically with a Heat System model 350 sonicator. Final TiO_2 concentration was 1 mg per 1 mL (pH = 6.5).

Spin trapping (23) experiments were carried out as described previously (8) using 5,5-dimethyl-1-pyrrolinyl-1-oxy (DMPO) (24) as the spin trap.

Results and discussion

(i) O_2 uptake

When an aqueous dispersion of TiO_2 (1 mg/1 mL) is illuminated such that a band-gap transition occurs (λ = 380 nm), the oxygen dissolved in the aqueous external solution is consumed. The rate of oxygen uptake (Fig. 2) in this closed system is 1.7%/min. (This is reported as the percentage decrease in the O_2 concentration of 5 mL of dispersion per min and corresponds to a photon efficiency of ~0.02.) If catalase is injected after illumination is stopped, no O_2 is liberated and therefore no H_2O_2 is free in solution. This is contrary to results with CdS or ZnO in which H_2O_2 is detected through catalase addition after illumination (7,8).

Addition of sodium formate at 0.1 *M* causes the rate of photoinduced O_2 uptake to increase to 4%/min or to a photon efficiency of ~0.05 (Fig. 2). Again, catalase addition *after* illumination ceased did not result in O_2 evolution. This lack of detection of H_2O_2 with TiO_2 is consistent with previous experiments (2, 16–19).

If H_2O_2 is being continuously generated in this system but is present only as a transient, then it is argued that injection of catalase at a point during illumination should reveal its presence. The catalase will cause dismutation of the H_2O_2 releasing oxygen and thus causing an apparent reduction in the rate of oxygen uptake. When this experiment was carried out in the donor-free system, no peak associated with O_2 evolution was observed. If anything, the rate of O_2 uptake increased slightly (depending on the amount of catalase injected). In any event, a reduction in the rate of O_2 uptake was not observed.

However, when the electron donor sodium formate was present in the system, addition of catalase at a point during illumination did provide evidence for H_2O_2 presence. At the point of injection, a small but reproducible peak associated with O_2 evolution was observed (Fig. 3). As expected, further additions of catalase or water as a control did not give this peak. After this peak of O_2 evolution, the rate of O_2 uptake was approximately halved (Fig. 3). This is the result one would expect if catalase causes the dismutation of transient H_2O_2 in this system. These results suggest that H_2O_2 is being generated when formate is present but, in the donor-free case, free H_2O_2 is not observed. (Similar results are obtained with the donor EDTA.)

If H_2O_2 (~10^{-4} *M*) is added to a TiO_2/H_2O dispersion during irradiation, evolution of oxygen is first observed and this gradually returns to oxygen consumption at the same initial rate. Addition of catalase at this point shows no change in the O_2 concentration demonstrating that all of the H_2O_2 had been removed from solution. Similar results were obtained in the presence of sodium formate (Fig. 4). These results show that H_2O_2 is not stable to the environment of illuminated TiO_2 either in the presence or absence of donor. Hence, it is not surprising that H_2O_2 is not readily detected in these systems since it is rapidly destroyed under these conditions.

In the formate case, illumination for 72 min of an O_2-saturated dispersion resulted in 65% of the total O_2 being consumed. For our 5 mL dispersion this amounts to a consumption of 1.9×10^{18} molecules of O_2. The surface area of the TiO_2 is

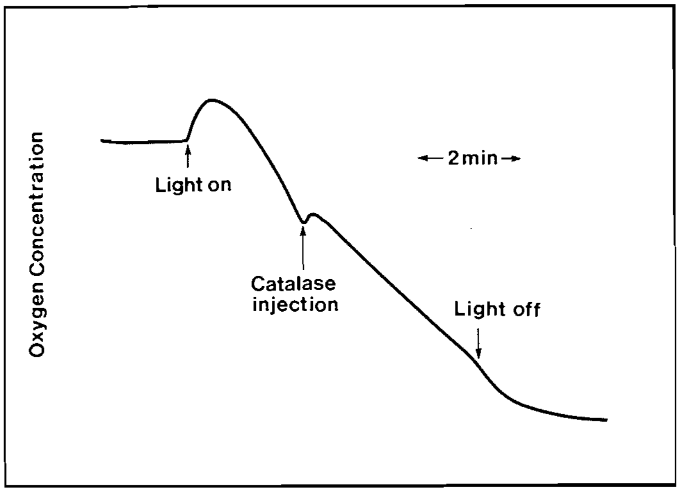

FIG. 3. The effect of injecting catalase during illumination of a TiO_2 dispersion of 0.1 *M* sodium formate.

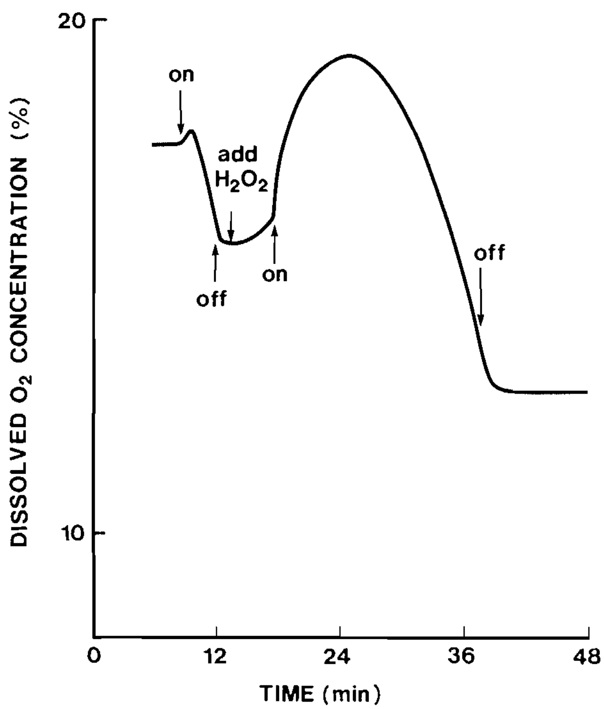

FIG. 4. Effect of adding H_2O_2 (~1 μmol) to a TiO_2 dispersion (5 mL) containing 0.1 *M* sodium formate. Note that the rate of O_2 uptake eventually returns to the value of the initial rate.

10.8 m^2/g and thus our 5 mg sample contributes 5.4×10^{18} Å^2 of surface. The oxygen uptake is thus equivalent to 35 molecules of H_2O_2 per 100 Å^2! In addition, the rate of uptake showed no sign of saturation which indicates that 35 molecules/100 Å^2 is certainly only a minimum value.

A similar experiment with the donor-free system showed that after 172 min, 40% of the total O_2 was consumed and the rate of O_2 uptake at this point was about half the initial value. This corresponds to 22 molecules H_2O_2 per 100 Å^2.

(ii) Electron spin resonance results

When the spin trap DMPO was added to the donor-free system and irradiation begun, an esr spectrum of the DMPO·OH radical adduct (25) was observed (Fig. 5) providing clear evidence that ·OH radicals are produced in this photo-

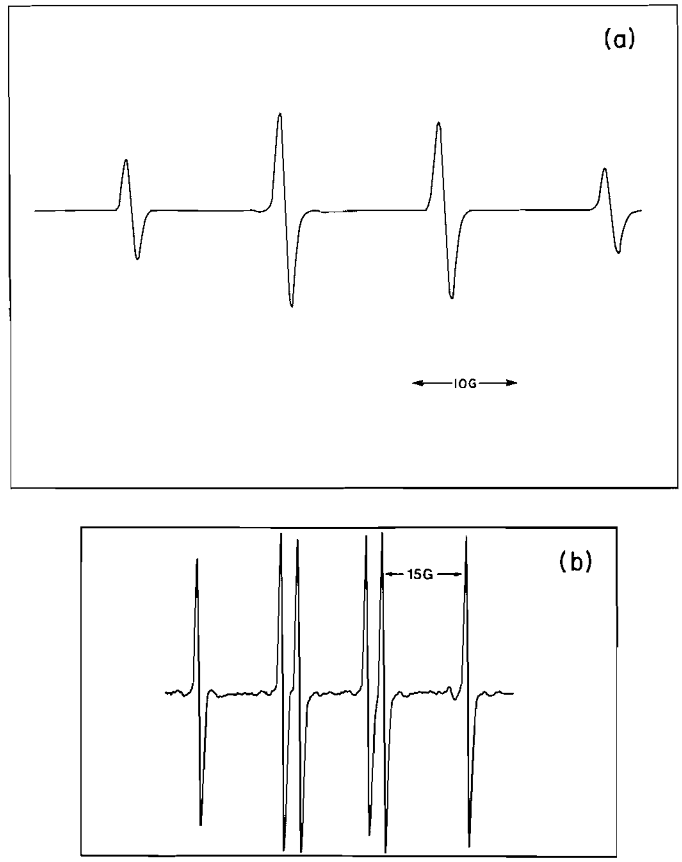

FIG. 5. The esr spectra of the (*a*) ·OH radical adduct of DMPO and (*b*) the $\cdot CO_2^-$ radical adduct of DMPO.

reaction. This production of ·OH radicals was a function of dissolved O_2 concentration. These results are analogous to those reported previously for ZnO suspensions. We found no evidence for the presence of O_2^- radicals in contradistinction to the results of Jaeger and Bard (26) who report the presence of trapped $HO_2\cdot$ and ·OH radicals when carrying out a similar experiment but using a different spin trap and *reduced* TiO_2.

In the case where formate was present, the spin trapping experiment revealed that excitation to TiO_2 produced the $\cdot CO_2^-$ radical adduct (27) (Fig. 5) while the hydroxyl radical adduct was no longer present. This has been observed (28) in other pigment systems (both CdS and ZnO) reflecting the oxidation of formate to $\cdot CO_2^-$ and/or the reaction of ·OH radicals with formate with a concomitant increase in H_2O_2 generation. Thus, the spin trapping experiments are also consistent with other systems in which H_2O_2 is being photogenerated. It is noted that the intensity of the signal is dependent on oxygen concentration and purging with nitrogen reduces both CO_2^- and ·OH signal to very small levels.

Boonstra and Mutsaers (29, 30) suggest that the photoactivity of titanium dioxide (in the gas phase) is described by the formation of a hydrogen radical rather than by formation of the hydroxyl radical which has been postulated in many previous studies. We would point out that in our spin trapping experiments at no time did we detect H· radical adduct.

It is clear from these results that in the presence of the donor, sodium formate, TiO_2 photocatalytically generates H_2O_2. The mechanism is summarized in reactions [1] — [10] (Table 1). However, in the case of TiO_2 without added donors, no evidence for H_2O_2 was found, yet oxygen is being consumed

TABLE 1. Reactions that generate or remove H_2O_2

Reduction	
[1]	$O_2 + e \rightarrow (O_2^-)_s$
[2]	$(O_2^-)_s + H^+ \leftrightharpoons (HO_2\cdot)_s$
[3]	$(HO_2\cdot)_s + e \rightarrow (HO_2^-)_s$
[4]	$(HO_2^-)_s + H^+ \leftrightharpoons (H_2O_2)_s$
or	
[5]	$2(HO_2\cdot)_s \rightarrow (H_2O_2)_s + O_2$
[6]	$(H_2O_2)_s \leftrightharpoons H_2O_2$
Oxidation	
[7]	$OH^- + h^+ \rightarrow \cdot OH$
	$\cdot OH$ + surface/impurities $\rightarrow$ oxidised product
or	
[8]	$Ti_sOH + h^+ \rightarrow Ti_s^r + \cdot OH$
For formate	
[9]	$HCO_2^- + \cdot OH \rightarrow H_2O + \cdot CO_2^-$
or	
[10]	$HCO_2^- + h^+ \rightarrow H^+ + \cdot CO_2^-$
H_2O_2 removal	
[11]	$H_2O_2 + 2e + 2H^+ \rightarrow 2H_2O$
[12]	$H_2O_2 + 2h^+ \rightarrow O_2 + 2H^+$
[13]	$Ti_s—O—Ti_s + H_2O_2 \rightarrow Ti_s—OH + Ti_sOOH$
[14]	$e + H_2O_2 \rightarrow \cdot OH + OH^-$
[15]	$\cdot CO_2^- + H_2O_2 \rightarrow \cdot OH + OH^- + CO_2$

during photolysis. Finally TiO_2, both with and without donor, destroys added H_2O_2 during photolysis.

There appears to be two plausible mechanisms for the photodestruction of H_2O_2. The first involves photoinduced redox reactions in which H_2O_2 can be reduced and/or oxidized by the electrons and holes. The second possibility involves an interaction of the TiO_2 surface with H_2O_2 which effectively consumes the H_2O_2 through a modification of the TiO_2 surface. Both of these mechanisms will be briefly discussed.

In the case of redox reactions, H_2O_2 can be reduced and/or oxidized at the TiO_2 surface (reactions [11], [12]). For reduction, the product would be H_2O (reaction [11]) and the O_2 uptake explained by the reduction of O_2 to H_2O_2 (reactions [1]–[6]) which is subsequently reduced to H_2O. On the other hand, oxidation of H_2O_2 would yield $2H^+$ and O_2. The fact that oxygen is evolved initially when TiO_2 is illuminated in the presence of added H_2O_2 suggests that oxidation of H_2O_2 is occurring. However, in order for oxygen uptake to be observed, the rate of reduction of H_2O_2 would have to exceed the rate of oxidation of H_2O_2. This is certainly plausible in the presence of a strong donor such as formate. It is also interesting to note that the measured photon efficiency is only 0.04 for TiO_2 compared to 0.70 previously reported for ZnO under similar conditions (8). This suggests that with TiO_2, much of the photocatalytic activity simply converts the generated product H_2O_2 back to water and oxygen.

Another redox reaction capable of removing H_2O_2 is given by reaction [15]. In this case $\cdot CO_2^-$ is the reducing agent. However, previous work (8) with aqueous ZnO dispersions has shown that $\cdot CO_2^-$ formation in no way diminishes the H_2O_2 which is photogenerated in that system. In fact, a conversion ratio of 1 is obtained (8). It therefore appears unlikely that reaction [15] plays any significant role in the destruction of H_2O_2.

The second possibility is the incorporation of H_2O_2 into the TiO_2 itself with the formation of a gel-like surface. This possibility appears to be most applicable to the donor-free case of TiO_2. It is well recognized that ZnO and TiO_2 have differing surface chemistry and, although it is difficult to speculate on the species which are formed and the exact surface structure that exists at the complex solid/solution interface, some insights may be obtained from the literature data generated on the gas/solid interface in the absence of donor (29–32). In particular the work of Boonstra and Mutsaers (30–32) is cited. These workers have examined the adsorption and thermal desorption of hydrogen peroxide in the presence of oxygen and water using both spectroscopic and volumetric techniques. It was found that hydrogen peroxide could be chemisorbed on a titania surface to a concentration of approximately 2×10^{14} molecules/cm^2 (2 H_2O_2 molecules/100 Å^2). H_2O_2 did not adsorb on zinc oxide. Boonstra and Mutsaers suggest that this difference in adsorption behaviour may explain why hydrogen peroxide is not detected when TiO_2 suspensions are irradiated and we agree that this behaviour could contribute to the observations in our experiments. Thus, it is suggested that the hydrogen peroxide formed from dissolved oxygen (reactions [1]–[4]) is either not able to desorb from the surface after it is formed (cf. reaction [6]) or, undergoes a reaction to become chemisorbed on adjacent sites. Unfortunately this facile utilisation of Boonstra and Mutsaers results cannot be correct in detail—the quantitative uptake numbers do not coincide. Thus Boonstra and Mutsaers observe an adsorption of 2 molecules of H_2O_2/nm^2. According to their proposed model the chemisorbed species is $Ti_s—O—O—H$ and thus 4 sites/nm^2 are involved (see reaction [13]).

In our simplest experiment with irradiation of the TiO_2/H_2O_2/O_2 suspension at least 1.2×10^{18} molecules of O_2 disappear from the system. This corresponds to 22 molecules of H_2O_2/nm^2, clearly an unlikely situation. It is therefore suggested that the TiO_2 surface becomes internally hydroxylated.

Further experimentation must be undertaken in order to determine which of these mechanisms is most important. In particular, changes in the chemical nature of the TiO_2 would be observed if incorporation of H_2O_2 into the surface/bulk is an important mechanism.

1. T. R. RUBIN, J. G. CALVERT, G. T. RANKIN, and W. MACNEVIN. J. Am. Chem. Soc. **75**, 2850 (1953).
2. M. C. MARKHAM and K. J. LAIDLER. J. Phys. Chem. **57**, 363 (1953).
3. J. G. CALVERT, K. THEURER, G. T. RANKIN, and W. MACNEVIN. J. Am. Chem. Soc. **76**, 2576 (1954).
4. T. FREUND and W. P. GOMES. Catal. Rev. **3**, 1 (1969).
5. H. GERISCHER. *In* Solar power and fuels. *Edited by* J. R. Bolton. Academic Press, New York. 1977.
6. S. P. PAPPAS and R. M. FISCHER. J. Paint Tech. **46**, 65 (1974).
7. J. R. HARBOUR and M. L. HAIR. J. Phys. Chem. **81**, 1791 (1977).
8. J. R. HARBOUR and M. L. HAIR. J. Phys. Chem. **83**, 652 (1979).
9. M. L. HAIR and J. R. HARBOUR. *In* Advances in chemistry series. No. 184, M. S. Wrighton. *Edited by* American Chemical Society, Washington. 1980.
10. D. R. DIXON and T. W. HEALY. Aust. J. Chem. **24**, 1193 (1971).
11. A. J. BARD. Photochemistry, **10**, 59 (1979).
12. A. B. ELLIS, S. W. KAISER, and M. S. WRIGHTON. J. Am. Chem. Soc. **98**, 6855 (1976).
13. P. CLECHET, C. MARTELET, J. R. MARTIN, and R. OLIER. Electrochimica Acta, **24**, 457 (1979).
14. M. GRATZEL. Acc. Chem. Res. **14**, 376 (1981).
15. A. HELLER. Acc. Chem. Res. **14**, 154 (1981).
16. G. A. KORSUNOVSKI. J. Phys. Chem. Mosk. **39**, 1139 (1965).
17. G. IRICK. J. Appl. Polymer Sci. **16**, 2387 (1972).
18. I. S. MCLINTOCK and M. RITCHIE. Trans. Faraday. Soc. **61**, 1007 (1961).

19. R. B. CUNDALL, R. RUDHAM, and M. S. SALIM. J. Chem. Soc. Faraday Trans. **1**, 1642 (1976).
20. M. V. RAO, K. RAJESHWAR, V. R. PAIKERNEKER, and J. DUBOW. J. Phys. Chem. **84**, 1987 (1980).
21. H. GERISCHER. J. Electroanal. Chem. Interfacial Electrochem. **58**, 263 (1975).
22. J. R. HARBOUR, J. R. TROMP, and M. L. HAIR. J. Am. Chem. Soc. **102**, 1874 (1980).
23. E. G. JANZEN. Acc. Chem. Res. **4**, 31 (1971).
24. E. G. JANZEN and J. I-P. LIU. J. Mag. Reson. **9**, 510 (1973).
25. J. R. HARBOUR, V. CHEN, and J. R. BOLTON. Can. J. Chem. **52**, 3549 (1974).
26. C. D. JAEGER and A. J. BARD. J. Phys. Chem. **83**, 3146 (1979).
27. J. R. HARBOUR and M. L. HAIR. Can. J. Chem. **57**, 1150 (1979).
28. J. R. HARBOUR and M. L. HAIR. *In* Magnetic resonance in colloid and interface science. *Edited by* J. P. Fraissard and H. A. Resing. D. Reidel, Dordrecht. 1980.
29. K. TANAKA and J. M. WHITE. J. Phys. Chem. **86**, 4708 (1982).
30. A. H. BOONSTRA and C. A. H. A. MUTSAERS. J. Phys. Chem. **79**, 2025 (1975).
31. A. H. BOONSTRA and C. A. H. A. MUTSAERS. J. Phys. Chem. **79**, 1940 (1975).
32. A. H. BOONSTRA and C. A. H. A. MUTSAERS. J. Phys. Chem. **79**, 1694 (1975).

Particle size control in dispersion polymerization of polystyrene

KAR P. LOK AND CHRISTOPHER K. OBER
Xerox Research Centre of Canada, 2660 Speakman Drive, Mississauga, Ont., Canada L5K 2L1

Received February 20, 1984

This paper is dedicated to the 10th anniversary of the Xerox Research Centre of Canada

KAR P. LOK and CHRISTOPHER K. OBER. Can. J. Chem. **63**, 209 (1985).

In a dispersion polymerization process, the reaction mixture starts out as a homogeneous solution and the resulting polymer precipitates as spherical particles, stabilized by a steric barrier of dissolved polymer. The final polymer particle size is determined by the inherent polymer aggregation behaviour under a given set of conditions. In the present study styrene polymerization was studied in various solvents using cellulosic derivatives as the steric stabilizer. Some of these solvents in certain combinations allowed the direct preparation of particles in the micron size and their size distribution appeared to be highly dependent on the monomer–solvent–initiator system. Investigations of these factors have suggested that monodisperse particles up to 12 μm can be prepared in a single step; studies of several systems are delineated.

KAR P. LOK et CHRISTOPHER K. OBER. Can. J. Chem. **63**, 209 (1985).

Dans un processus de polymérisation par dispersion, le mélange réactionnel de départ se présente sous forme d'une solution homogène et le polymère qui en résulte précipite sous forme de particules sphériques stabilisées par une barrière stérique du polymère dissous. Avec un ensemble donné de conditions de réactions, la grosseur des particules du polymère final est déterminée par un comportement inhérent au polymère vis-à-vis de l'aggrégation. Dans cette publication, nous étudions la polymérisation du styrène dans divers solvants en utilisant des dérivés de la cellulose comme stabilisateurs. Certaines combinaisons de ces solvants permettent de préparer directement des particules dont la taille est de l'ordre du micron; il semble que la répartition de leur taille dépende fortement du système monomère–solvant–initiateur. L'étude de ces facteurs suggère que l'on peut préparer, en une seule étape, des particules monodispersées dont la grosseur va jusqu'à 12 μm. On rapporte les résultats obtenus avec plusieurs systèmes.

[Traduit par le journal]

Introduction

There has been substantial interest in monodisperse polymer particles ever since J. W. Vanderhoff and E. B. Bradford announced their preparation of polystyrene particles with highly uniform particle size in 1955 (1). Monodisperse particles are finding a wide variety of applications including instrument calibration standards, standards for the determination of pore size and the efficiency of filters, column packing material for chromatographic separation, support materials for biochemicals, and so on. The level of success in each of these applications is ultimately dependent upon the particle size and its distribution, the morphology of the particles and the surface characteristics among numerous other factors.

Control of particle size and its uniformity has been a major area of interest; it proves to be particularly challenging to prepare monodisperse polymer particles in the micron size range (2–20 μm). Traditionally the attempt to prepare micron size particles has been to break up monomer droplets into the micron size range by homogenization in the presence of a stabilizer, and subsequently, polymerize the monomer by a suspension polymerization (2). This proves to be an inefficient method of achieving monodispersity because of the inherent size distribution in the mechanical homogenization step.

Monodisperse micron size polymer particles could not be prepared in reasonable quantities until Ugelstad *et al.* developed a method of growing sub-micron particles using a two-step swelling technique (3). In this method, submicron polymer seed particles are made by surfactant-free emulsion polymerization. The seed particles are subsequently suspended in a new medium and swelled by the addition of an emulsion of low molecular weight compound which diffuses from the emulsion droplets into the polymer particles. This small molecule is insoluble in water and does not normally diffuse through water, so a low boiling point water soluble aprotic solvent is used to facilitate the transport. The addition of the aprotic solvent permits the otherwise insoluble compound to diffuse and upon removal of the aprotic solvent, the small molecule is locked into the particle. Owing to the entropic dilution effect, this small molecule allows further swelling of the particle by monomer which, upon subsequent polymerization, gives rise to micron size particles as large as 50 μm. This technique provides a very elegant route to micron size particles but it is very tedious and difficult to carry out. There is sufficient interest in such particles that Vanderhoff and co-workers have been contemplating the growth of polymer particles to the micron size range aboard the space shuttle in microgravity (4, 5).

A second approach to preparing micron size particles is by dispersion polymerization. This method has been very thoroughly reviewed by Barrett (6) and it has been shown to produce particles with a very narrow size distribution. The process involves the polymerization of a monomer dissolved in a medium in the presence of a graft copolymer dispersant (or its precursor) to produce insoluble polymer dispersed in the medium. The graft copolymer functions as a steric stabilizer which can prevent flocculation and aggregation of the particles being formed. Since this method depends on incipient aggregation of the polymerizing species at the early stages of the polymerization, the number of particles are determined by these growing nuclei. The final size and distribution are largely determined by the amount of monomer introduced and the ability of the stabilizer to maintain the colloidal stability of the growing particles. Using a variation of this approach, M. Levy *et al.* have successfully prepared monodisperse polymer particles in the range of 1–6 μm (7). Their method involves the use of a polymeric steric stabilizer in combination with a quaternary ammonium salt which the authors claimed acts as an electrostatic co-stabilizer.

This paper discusses recent developments in the dispersion polymerization of styrene using nonionic cellulosic derivatives as steric stabilizers in a variety of solvent systems. Micron size

TABLE 1. Comparison of the different types of particulate polymerization

	Emulsion	Dispersion	Suspension
Monomer	Droplets Micelles/particles Little in medium	Particles Mostly in medium	Droplets Little in medium
Initiator	Mostly in medium	Particles and medium	Particle/droplet
Stabilizer	May be present	Necessary	Necessary
Surfactant	Present	None	None
Initial Homogeneity	Multiple phase	Single phase	Dual phase

particles can be prepared without the use of an electrostatic costabilizer, resulting in an uncharged dispersion. Such polymer particles can be made to be very uniform in size or to have a wider but defined particle size range, depending upon the solvency of the dispersion medium. In addition, the particle nucleation and growth mechanism will be delineated.

Experimental

The styrene monomer, dimethoxyethane, cellosolve, and benzoyl peroxide (BPO) were supplied by Aldrich. The methyl cellosolve came from several suppliers including J. T. Baker, Aldrich, and BDH. BDH *Omnisolve* ethanol was used, but other alcohols were obtained from Fisher Scientific. Tetrahydrofuran was stock from Caledon. The hydroxypropylcellulose (HPC, mw = 100 000), cellulose propionate and ethyl cellulose came from Scientific Polymer Products. All materials were used without further purification.

2.1. *Alcohol–ether/ethanol*

In a typical reaction, hydroxypropyl cellulose (HPC, 7.5 g) was dissolved in ethanol (EtOH, 175 mL) and methyl cellosolve (2-methoxyethanol, MeCell, 250 mL) under nitrogen in a three-necked round bottom flask with mechanical stirring over 30 min at 65°C. At that time, benzoyl peroxide (BPO, 3.0 g) dissolved in styrene monomer (75 mL) was added. The homogeneous mixture became cloudy after 5 min. After 2 h, the temperature of the reaction was raised to 75°C. The reaction was allowed to proceed for 24 h and then cooled. The particles were isolated by centrifuging the reaction mixture, decanting the supernatant, redispersing the particles in water, and finally freeze-drying them on a Labconco FreezeDry-12 giving a final product of monodisperse 10 μm spheres.

2.2. *Alcohol/water*

As an example, HPC (5.0 g) was dissolved in ethanol (500 mL) and water (300 mL) at 80°C using the flask and stirring conditions used above. Then solid BPO (1.0 g) was added. After 1 h, 50 mL of styrene monomer was added all at once, and heating was continued at 78°C for 7 h. A stable milky latex dispersion was obtained.

2.3. *Ether/ethanol*

In this reaction, HPC (7.5 g) was dissolved in THF (75 mL) and ethanol (350 mL) at 65°C. A solution of BPO (3.0 g) dissolved in styrene (75 mL) was added. After reacting for 48 h, a volume equal to 1.5 times the volume of THF present was distilled off using a rotary evaporator. A product with a particle size of approximately 8 μm resulted.

2.4. *Characterization*

Particle size measurements were performed on an optical microscope using calibrated photomicrographs for a given sample. In most cases these values were compared with those obtained using the ISI Mini-Scanning Electron Microscope. In addition, Coulter Counter measurements were performed on the samples with particle diameters 3 μm and above, and Nanosizer measurements were made on particles less than 3 μm.

Molecular weights were calculated using a Waters GPC (Model #M6000A, M440 and R401) operating at room temperature with columns in methyl ethyl ketone or THF solvent. Columns were packed with μ-Styragel with pore sizes of 100, 500, 10^5, 10^4, and 10^3 Å in diameter. A flow rate of 1.0 mL per min and both the uv and refractive index detectors were used.

Conversion kinetics were followed on a Varian GC Model 2830 using an FID detector. Helium was used as carrier gas in an isothermal experiment where the reaction mixture was injected directly into the instrument. The quantity of styrene monomer could be measured with respect to the solvent medium.

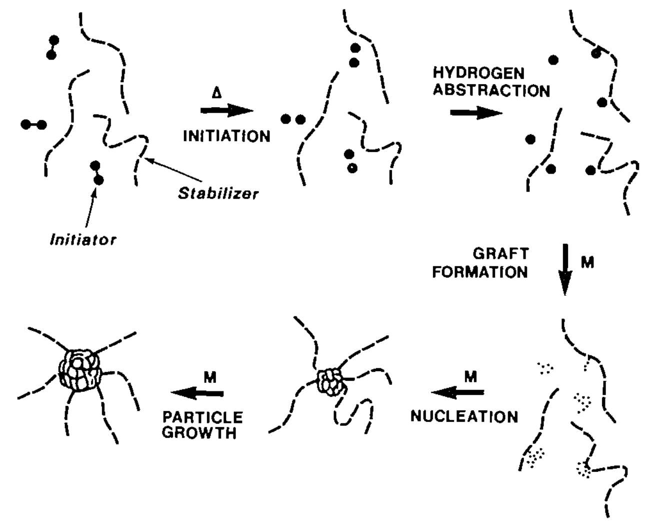

FIG. 1. Schematic representation of nucleation and growth in a dispersion polymerization.

3. Discussion

All of the different methods of particulate polymerization discussed in the introduction have properties that make them unique from each other. These differences are especially dependent on the way in which the reagents are located in the reaction medium as outlined in Table 1. The striking feature of dispersion polymerization is that there is initially only one phase and therefore the monomer is distributed throughout the reaction medium. In contrast, the other methods of polymerization start out as multiphase systems and as a result have different routes to nucleation and growth. Figure 1 shows a schematic for the nucleation and growth of sterically stabilized particles by dispersion polymerization.

Polystyrene particles can be prepared in a wide variety of solvent combinations by dispersion polymerization. The reaction requires that the monomer, initiator, and stabilizer are all soluble in the starting medium, and that the product polymer precipitates during the reaction. This puts certain constraints on the types of solvents that can be used in combination with the styrene monomer and stabilizer. However, once the polymer particles are formed, the initiator and monomer can be expected to partition between the solvent and polymer phases and the

TABLE 2. Solubility parameters of selected solvents

Solvent	Dielectric constant	Dipole Moment (D)	δ*†	δ_d*‡	δ_p*‡	δ_H*‡
Dimethoxyethane	—	—	8.6	—	—	—
Tetrahydrofuran	7.32	1.63	9.1	8.2	2.8	3.9
Styrene	—	—	9.3	9.1	0.5	2.0
Cellosolve	—	2.08	10.5	7.8	4.5	7.0
t-Butanol	10.9	1.66	10.6	—	—	—
Methyl Cellosolve	16	2.2	11.4	7.9	4.5	8.0
Isopropanol	18.3	1.66	11.5	—	—	—
Ethanol	24.3	1.69	12.7	7.7	4.3	9.5
Methanol	32.6	1.70	14.5	7.4	6.0	10.9
Water	78.5	1.84	23.4	6.0	15.3	16.7
Polystyrene	2.5	—	8.9	—	—	—

*In $(\text{cal/cm}^3)^{1/2}$.
† $\delta^2 = \delta_d^2 + \delta_p^2 + \delta_H^2$.
‡ δ_d = dispersion forces, δ_p = polar forces, δ_H = H-bonding forces. Values from ref. 14.

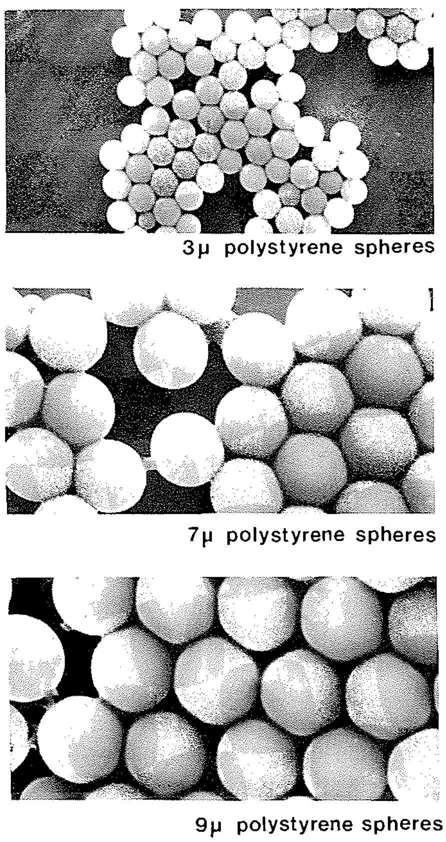

FIG. 2. Scanning electron micrograph of particles prepared with HPC stabilizer.

relative amount in each phase is determined by the choice of reaction conditions.

Particle size control is therefore a function of several thermodynamic and kinetic factors, and these include: (*1*) monomer–polymer solubility, (*2*) reactant composition, (*3*) temperature, and (*4*) solvent medium among others. Temperature, of course, influences both the thermodynamic factors such as solubility as well as the kinetics of initiator decomposition, which in turn determines the rate of polymerization and particle nucleation.

Several of these parameters controlling particle size were explored while preparing particles composed of a polystyrene core and cellulosic stabilizers. The solvent systems studied were water miscible, and could be classified as alcohols, ethers, and ether–alcohols. These materials possess a wide range of solubilities and systematic variations in the chemical structure, and this permits a better qualitative understanding of the effects of medium on the polymerizing mixture.

The properties of these liquids are listed in Table 2 and include their dielectric constant, dipole moment, and solubility parameter. Also included in the table is a three component parameter based upon covalent, dipolar, and hydrogen bonding forces, the presence of which is intended to show that even though the solubility parameter can be the same for two solvents, the contributing factors can be quite different. The solvents are ranked in increasing polarity according to their solubility parameter. As the table indicates, the least polar solvent used, and a solvent for polystyrene, was dimethoxyethane while the most polar liquid was water.

3.1. Ether–alcohol/alcohol mixtures

Methyl cellosolve (2-methoxyethanol or MeCell) is a member of the cellosolve or ether–alcohol family of commercial solvents, and is a solvent for hydroxypropyl cellulose (HPC) while being a non-solvent for polystyrene, the polymer prepared in the polymerization reaction. The solubility parameter, δ, of MeCell is 11.4 (14). In the systems studied, when MeCell was used alone, solvent-swollen 5 to 50 μm particles were obtained that could not be isolated without substantial coalescence, whereas ethanol (δ = 12.7) alone produced 0.5 to 3 μm particles.

The addition of ethanol, a stronger non-solvent for polystyrene, to MeCell enabled the preparation of particles in the 5–10 μm range. Both the ratio of the monomer to suspending medium was varied as well as the proportion of MeCell to ethanol. It was found that within a narrow window of relative concentrations it was possible to obtain particles with a monodisperse size distribution. By varying the relative amount of MeCell to ethanol the ultimate particle size could be controlled. Some of these monodisperse particles are illustrated in Fig. 2, and their molecular weights and diameters are listed in Table 3. The particles shown in Fig. 2 were taken from the unpurified reaction mixture which included ungrafted HPC as well as MeCell and ethanol. The bridging observed in the figure is due to excess HPC which can be easily removed during the washing

TABLE 3. Diameters and molecular weights of particles prepared with HPC stabilizer

Stabilizer	Diameter (μm) OM	SEM	Coulter counter	(GSD)	$M_n \times 10^3$	$M_w \times 10^3$	M_w/M_n
HPC	3*	3	2.7	1.11	9.33	20.7	2.18
HPC	7	7	6.2	1.13	5.44	15.3	2.81
HPC	10	10	9.1	1.07	5.98	14.6	2.44

*Coulter Nanosizer diameter was 2.7, PDI = 1.

TABLE 4. Particle sizes versus methyl cellosolve concentration

Concentration (vol.%) Styrene	Ethanol	Methyl cellosolve	Particle size† (μm)	Solubility parameter δ_i (cal/cm^3)$^{1/2}$
10	51	39	1–3	11.9
15	71	14	1–4	12.1
15	60	25	3‡	11.9
15	42.5	42.5	7‡	11.7
15	30	55	9‡	11.5
15	14	71	1–50	11.3
20	40	40	5–20	11.6
26	44	30	5–20	11.5
26	74	—	1–5	11.9
33	67	—	7–9	11.7

*All reactions at 65°C, HPC:styrene = 1:10, 3.0 g benzoyl peroxide.
†Particle sizes by optical and electron microscopy.
‡Monodisperse samples.

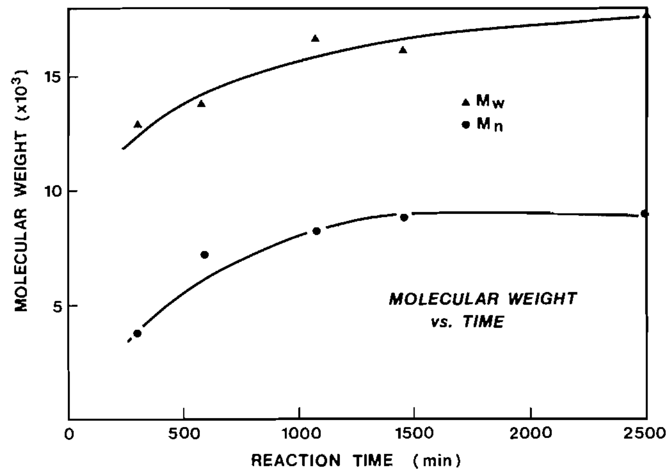

FIG. 3. Molecular weight changes as a function of time for polymerization in methylcellosolve/ethanol.

prior to the freeze-drying process. Once the HPC is removed, bridging has been found to be absent.

Shown in Table 4 are the reaction conditions used to produce monodisperse particles as well as those conditions producing polydisperse particles in MeCell–ethanol. As the amount of methyl cellosolve was increased, corresponding to a decrease in the polarity of the reaction medium, the size of the particles increased. Changes in styrene monomer concentration also led to polydispersity with more or less monomer producing larger particles. Interestingly, the amount of stabilizer had only a small effect on the final particle size. When the amount of HPC was halved, the resulting particles showed monodispersity of the large particles, but also the presence of some smaller particles. This suggests that stabilization may have been somewhat less effective with reduced HPC levels. Doubling the quantity of stabilizer produced effectively no change in particle size, indicating that the reaction is tolerant of excess stabilizer. In contrast, when less initiator was used, the resulting particles possessed a very large polydispersity and the rate of polymerization was much slower.

The molecular weight of both the HPC-stabilized polymer particles and the oligomer remaining in solution was determined by GPC in THF solvent. A plot of molecular weight versus time is shown in Fig. 3, and there it can be seen that as the reaction proceeds, the molecular weight of the particles increases initially and then levels off. This increase is probably an artifact of the particle isolation procedure at low conversions, and in fact particle molecular weight is level throughout the reaction. The molecular weights of the monodisperse particles produced in MeCell–EtOH are lower than those of polydisperse particles produced in the EtOH–water system discussed later and suggests that there are differences in the polymerization mechanism between the two systems at higher conversion.

The chromatograms of isolated particles, and the suspending medium at the end of the polymerization are given in Fig. 4. It is evident that the material left in solution (dashed line) was of lower molecular weight, except for the second peak appearing at lower elution volumes observable only on the RI detector. This material may be grafted HPC with enough styrene to give the material detectability by refractive index changes. The HPC remaining in solution and making up most of the dissolved polymer was otherwise not detected in either curve. The presence of the oligomer (peak maximum ~ 2500 MW) in solution shows that a critical molecular weight must be reached before nucleation can occur or else the polymer will remain in solution. This molecular weight is probably higher than 2 500 due to the larger amount of monomer at the beginning of the reaction causing increased solubility. A separate experiment has shown that polystyrene of 9 000 molecular weight is totally soluble in the starting reaction mixture while polystyrene of 35 000 molecular weight or more is insoluble. This observation indicates that the precipitating component has a molecular weight greater than 9 000. Interestingly, runs giving monodisperse and polydisperse particles both gave products with similar molecular weight properties.

Two other cellulosic stabilizers, ethyl cellulose and cellulose propionate, were studied in the MeCell–EtOH reaction medium. These polymeric stabilizers were soluble in the reaction medium and could be used to produce monodisperse particles. However, when the same conditions employed with HPC were used for these stabilizers the resulting particle sizes were quite different. The conditions used to generate 3 μm particles with

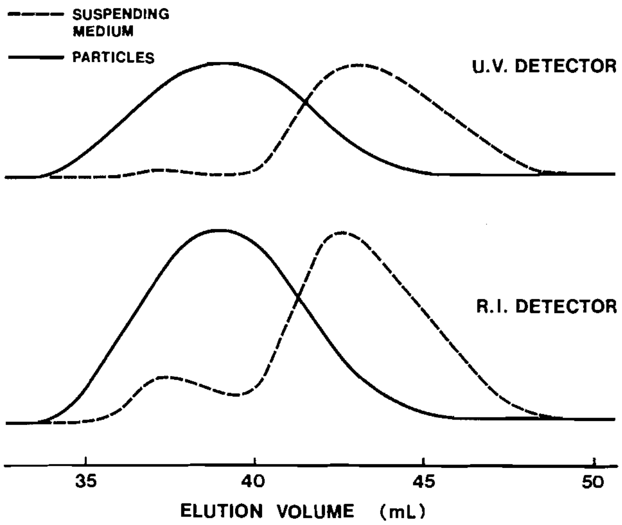

FIG. 4. GPC curves of isolated particles and reaction medium.

TABLE 5. Sizes of particles prepared in ether solvents

Solvent concentration (vol. %)*		δ_i $(cal/cm^3)^{1/2}$	Particle size (μm)
Ethanol	Cellosolve		
42.5	42.5	11.3	1–10
53	32	11.6	1–5
63	22	11.7	1–4
Ethanol	THF		
76.5	8.5	12.0	1–5
70	15	11.8	3–12
Ethanol	DME		
63	22	11.4	8–10
70	15	11.7	1–4

* 15% styrene at 65°C, 7.5 g HPC, 3.0 g BPO.

HPC stabilizer produced much larger particles (6 μm) with ethyl cellulose and cellulose propionate. Similarly when the conditions for the synthesis of 10 μm monodisperse HPC-stabilized particles were used, particles with a wide distribution and sizes ranging from 5 to 50 μm were produced with the other two stabilizers. Such differences between stabilizers may be due to changes in the degree of grafting expected to occur during the polymerization or in the solubility of the cellulosic function in the reaction medium. The ability of the stabilizer to inhibit coalescence would be affected in both cases.

Another ether–alcohol was investigated for its particle forming properties. Cellosolve (2-ethoxyethanol, $\delta = 10.5$) is chemically similar to methyl cellosolve, but cellosolve replaces the methoxy group of methyl cellosolve with an ethoxy group, making it somewhat less polar than methyl cellosolve. The size distribution of the cellosolve particles was perhaps the widest of those produced using the various solvent pairs, and was certainly never as narrow as that produced using methyl cellosolve. As shown in Table 5, increased amounts of ethanol produced smaller particles, in agreement with the MeCell–ethanol results.

3.2. Ether/alcohol mixtures

Two ether class solvents, dimethoxyethane (DME, $\delta = 8.6$) and tetrahydrofuran (THF, $\delta = 9.1$), were used in conjunction with ethanol as polymerization media. Of the solvents studied,

TABLE 6. Properties of particles prepared in alcohol media

Pure alcohol medium	δ_i $(cal/cm^3)^{1/2}$	Diameter (μm)*
Methanol	14.0	1.11 (2)
Ethanol	12.3	1.40 (2)
Isopropanol	11.3	1.02 (3)
tert-Butanol	10.5	2.27 (5)

* Number in parentheses is Coulter Nanosizer polydispersity index, 12% monomer by volume.

TABLE 7. The effect of solvent changes on particle sizes

Aqueous ethanol	δ_i $(cal/cm^3)^{1/2}$	Diameter (μm)*
100%	12.3	1.40 (2)
85%	14.2	1.08 (2)
75%	15.4	1.05 (2)
65%	16.5	0.91 (2)

* 12% monomer, number in parentheses is Coulter Nanosizer polydispersity index.

these were the most non-polar and were both swelling solvents for polystyrene, the particle core. Using THF and ethanol, particles of about 10 μm could be prepared as shown in Table 5. Regardless of the final particle size, the particles were swollen by solvent which could be removed by distillation without leading to coalescence. While swollen particles had a smooth surface, the deswelled particles possessed a wrinkled surface. Small changes in the relative amount of THF to ethanol caused a much larger change in size and distribution than in the case of MeCell or cellosolve, but in no case was monodispersity observed even though a relatively narrow distribution was produced.

The even less polar solvent, DME, was used as a co-solvent with ethanol to produce polystyrene particles. Like the other solvent pairs, more ethanol led to smaller particles, and like the THF medium the particle size distribution was narrow but not monodisperse. It is probable that if different monomer levels were used, other effects on particle size and size distribution could be observed; however, the examples illustrate what can be expected when polymerization occurs in the presence of solvents for the polymer core.

3.3. Alcohol/water mixtures

Particles with a polystyrene core and HPC stabilizer could be made in methanol, ethanol, isopropanol, *tert*-butanol, or mixtures of these alcohols and water by dispersion polymerization. In pure alcohol, particle size increased from methanol ($\delta = 14.5$) to ethanol ($\delta = 12.7$) to *tert*-butanol ($\delta = 10.6$). In addition, the *tert*-butanol particle size distribution was also much wider. The smallest particle size was obtained in isopropanol ($\delta = 11.5$), as noted in Table 6. Based upon solubility alone, the isopropanol would have been expected to produce particles in the range between the ethanol and *tert*-butanol systems.

As one decreased the concentration of alcohol in ethanol–water systems, the particle size became smaller without much change in the polydispersity as shown in Table 7. This property was related to the polarity of the solvent system as observed in Table 2. By changing the systems shown in Table 8 from the most polar methanol–water system to ethanol–water to isopropanol–water and finally the least polar *tert*-butanol–water system, a similar trend of particle size in-

TABLE 8. The effect of changes of monomer concentration on particle size

Cosolvents (3:1 ratio)	Monomer concentration (vol. %)	δ_i $(cal/cm^3)^{1/2}$	Diameter* (μm)
MeOH–H_2O	12%	16.4	0.82 (1)
EtOH–H_2O	6%	15.7	0.61 (1)
	12%	15.4	1.05 (1)
	24%	14.7	2.14 (4)
	35%	14.0	2.85 (6)
iso-PrOH–H_2O	12%	14.8	1.11 (2)
tert-BuOH–H_2O	12%	14.3	1.64 (1)

*Number in parentheses is Coulter Nanosizer polydispersity index.

crease was observed. The size increase from ethanol–water to isopropanol–water was relatively small compared with the increase from isopropanol–water to *tert*-butanol–water.

Monomer, since it is part of the initial solvent system, plays an important role in the resulting particle size. An increase in the initial monomer concentration leads to bigger particles and a wider size distribution. These effects, demonstrated with the ethanol–water system and shown in Table 8 and Fig. 5, can be summarized as follows: (*i*) increased monomer levels can sustain growth to give larger particles, (*ii*) solvency is changed since the monomer is in this case a solvent for its polymer, and (*iii*) the amount of monomer affects the equilibrium distribution of monomer between the polymer phase and the medium leading to a modification of the growth mode.

Another interesting observation is that both the molecular weight and the molecular weight distribution increase in the ethanol–water system as the polymerization proceeds as illustrated in Fig. 6. These are results that might be expected for a suspension polymerization and are quite different from those of an emulsion polymerization. The increase in molecular weight is also consistent with the Tromsdorf effect. This effect is quite strong in this solvent system, but not evident with MeCell–EtOH. In the latter case the Tromsdorf effect may be undetected due to polymerization in the medium, which masks an increase in the rate of polymerization expected to occur within the particles. In ethanol/water systems most of the monomer is located in the growing particle whereas in the ethanol/MeCell case, substantial quantities of monomer remain in the medium and these differences are reflected in the relative rates of polymerization.

In order to test the predictive properties of the solubility parameter, a solvent system having the same value as the MeCell–ethanol mixture was investigated. The solubility parameter value for isopropanol happens to be almost identical to that of MeCell, so two runs prepared by substituting isopropanol for MeCell with 15% monomer by volume were studied. The runs used a 50:50 isopropanol–ethanol (IPA–EtOH) mixture in the first case and a 70:30 IPA–EtOH mixture in the second case. The resulting particles (2.6 μm) were indeed found to be monodisperse in the first set of conditions, but quite a bit smaller than those particles prepared in MeCell–EtOH. In the second case the particles were somewhat larger (6 μm), but polydisperse. These observations show the importance of solubility to the ultimate particle size. However, the precise role of solvent polarity on final particle size is clouded somewhat by the observation that smaller particles are formed in the presence of isopropanol as compared to MeCell. Such inconsistencies demonstrate the existence of a different

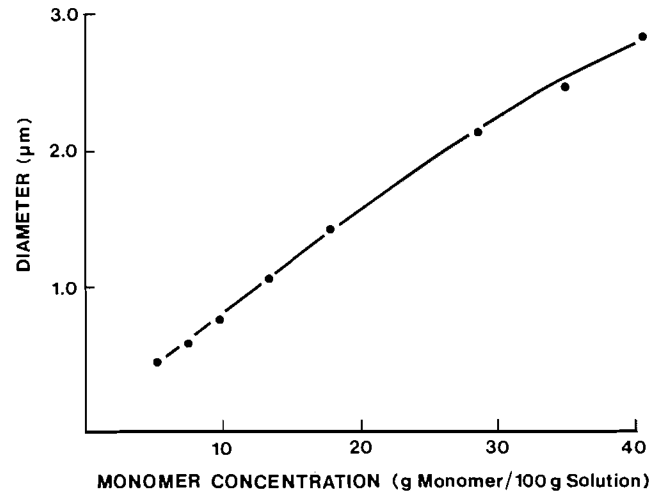

FIG. 5. Monomer concentration versus particle size in ethanol/water media.

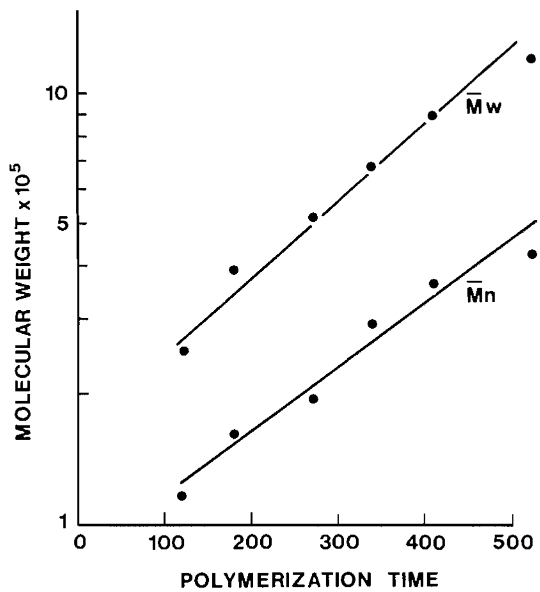

FIG. 6. Particle molecular weight versus conversion in ethanol/water media.

solvent property besides that reflected by the solubility parameter. The effect of solvent therefore is certainly not limited to solubility alone.

3.4. *Particle growth*

The unique feature of this polymerization technique is that it permits the direct polymerization of monodisperse micron-size particles when the appropriate conditions are used. The rate and mode of growth of these large monodisperse micron size particles are therefore of some interest and were studied quantitatively.

The current literature refers to several researchers who have dealt with monodisperse particles, but these particles were generally prepared in emulsion systems (8–13). In contrast to dispersion polymerization which entails nucleation from a homogeneous environment (11), emulsion polymerization begins as a multiphase system (8). Other differences are outlined in Table 1 and show the way that initiator and monomer is distributed differently in the two systems. In addition, it should be

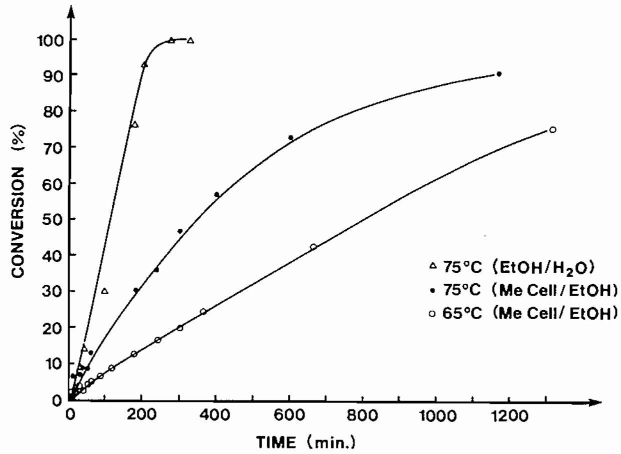

FIG. 7. Conversion versus time in particulate polymerization.

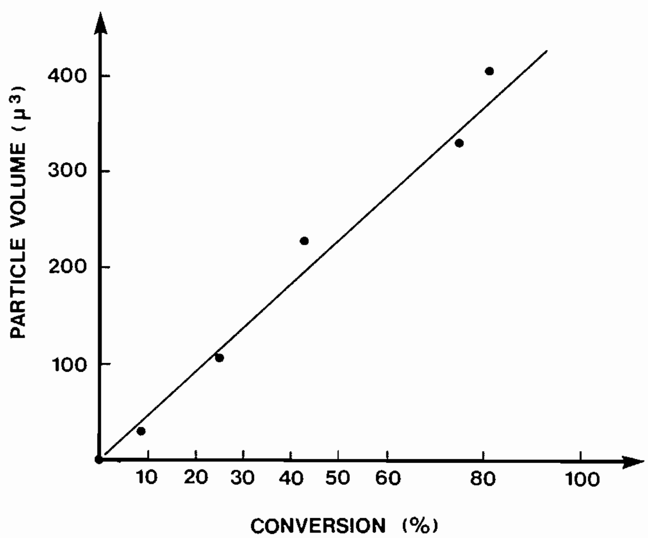

FIG. 8. Particle volume versus conversion during growth of monodisperse particles.

noted that oligomer formed in the homogeneous phase can be considered to either nucleate or be captured by growing emulsion particles, but may remain in solution in a dispersion polymerization depending on which reaction medium is used.

Figure 7 shows a plot of conversion (p) versus time (t) for two reactions in methyl cellosolve–ethanol at 65 and 75°C and for comparison a reaction in ethanol–water at 75°C is also shown. The conversion was measured by monitoring the disappearance of the monomer peak by gc as a function of time relative to the MeCell or ethanol peak. The ethanol–water system showed the highest rate of conversion indicating that there was a strong auto-acceleration or Tromsdorf effect typical of the kinetics of suspension polymerization and was consistent with the molecular weight results reported above. This could be related to the polarity of the solvent medium since in the ethanol–water system, both the non-polar styrene monomer and initiator quickly diffused into the particle nucleus and sustained faster particle growth. In the less polar MeCell–EtOH system, much slower rates resembling solution polymerization were observed, possibly because the monomer was present to a larger extent in both phases and the slower growth was determined by diffusion.

The final particle size depended on the amount of initiator and the temperature of reaction. If the amount of initiator was reduced, particle size and size dispersity increased. Temperature was also critical to the size distribution of the final product. Even though the reaction profiles of both runs in methyl cellosolve – ethanol at 75 and 65°C are similar, only the lower temperature run gave monodispersity. Starting temperatures of 75 and 55°C instead produced polydisperse samples. However, if the temperature was increased from 65 to 75°C after only 10% conversion the rate of polymerization could be increased without changing the dispersity of the product. This indicates that the temperature was critical to the particle formation stage, but not so crucial to the growth stage.

The increase in particle size during the course of the polymerization would be expected to be proportional to conversion provided that (a) all or a constant fraction of polymer was incorporated into the particles and (b) little or no coalescence occurred between particles of the same size. The relationship between particle volume (V_p) and conversion (p) is given in Fig. 8, which shows a plot of particle volume versus conversion for a monodisperse run where volume was calculated from the diameter of the particles as measured by optical microscopy. There is indeed an apparently linear relationship between particle volume and conversion. The linearity of the curve indicates that the number of particles is essentially constant from even the earliest stages of the reaction, and therefore nucleation must take place only in those early stages.

3.5. *Particle size control*

The initial medium solvency is important in determining the final particle size, since particle formation is restricted to the early stages of the polymerization. The ultimate particle size and distribution are also a function of the amount of coalescence that occurs during and after the particle formation stage. In the case of the monodisperse particles, coalescence between large particles is negligible and therefore a narrow size distribution is retained.

The importance of the initial solvency of the reaction medium can be seen in Table 4 where the solubility parameter (δ_i) of the starting reaction medium is listed. The solubility parameter is a value derived from the heat of vaporization of a solvent and its molar volume. All δ values reported here are in units of $(\mathrm{cal/cm^3})^{1/2}$. The solubility parameter was calculated as the root-mean-square volume weighted average of the solubility parameters of the cosolvents and monomer (15). The contributions of stabilizer and initiator were neglected because they were present in very low levels with respect to the other components.

The trend of particle size decrease with solvent polarity increase can be observed in this table, and was consistent for all observed reactions. The reaction conditions for MeCell–ethanol systems were plotted in Fig. 9, a three-coordinate plot where the axes are the volume percentages of ethanol, methyl cellosolve, and styrene. Also shown are two iso-solubility curves with δ equal to 11.5 and 11.9. Particles prepared at $\delta \geq 11.9$ were in the range of 3 μm diameter or less while those prepared at $\delta \leq 11.5$ were 10 μm or more. This observation was consistent over the range of monomer levels used, that is between 10 and 33% styrene. When monomer was reacted at concentrations as high as 50%, the polymerization system tended to gel and therefore no reactions are reported in this range. The three reaction mixtures represented by open circles are those that produced monodisperse particles. No satisfactory explanation can be presently offered as to why these

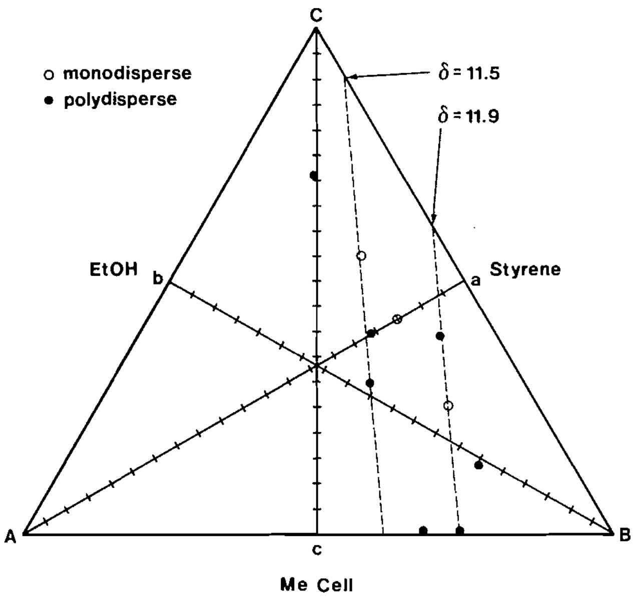

FIG. 9. Effect of composition of methyl cellosolve-ethanol-styrene reaction mixture on particle size and distribution.

particular reactions gave products with such narrow size distributions.

The initial solubility parameter of the other reported solvent systems was also calculated and is listed in Tables 5 to 8. The trend of particle size with polarity was consistent with the results reported above within a given solvent system. Note that a solubility parameter of 11.8 gave ~ 10 μm particles with THF–ethanol while the other systems in Tables 4 and 5 gave particles ranging from 1–4 μm to 7–9 μm with δ_i equal to 11.7. It is difficult therefore to correlate these results among substantially different solvent systems.

The reaction conditions listed in Tables 6, 7, and 8 also showed good consistency within a given system when comparing particle size with solubility. Comparing different systems again revealed that while particles of comparable size were produced at a given solubility parameter, direct comparison was not possible. These differences may be ascribed to the interaction that the solvent system has with the propagating free radical, and with the steric stabilizer. Differences in the chain transfer properties of the solvent, and the effect of solvent on the solubility of the stabilizer would both be expected to alter the ultimate particle size. This reconfirms the earlier observation that the effect of solvent on final particle size was not limited to solubility alone.

1. R. M. FITCH (*Editor*). Polymer colloids, Plenum Press, New York. 1971.
2. Y. ALMOG and M. LEVY. J. Polym. Sci. Polym. Chem. Ed. **20**, 417 (1982).
3. J. UGELSTAD, P. C. MORK, K. H. KAGGERUD, T. ELLINGSEN, and A. BERGE. Adv. Colloid. Interf. Sci. **13**, 101 (1980).
4. A. M. LOVELACE, J. W. VANDERHOFF, F. J. MICALE, M. S. EL-ASSER, and D. M. KORNFELD. U.S. Patent #4247434 (1981).
5. J. Coating Techn. **54**, 691, 12 (1982).
6. K. E. J. BARRETT (*Editor*). Dispersion polymerization in organic media. Wiley, London. 1975.
7. Y. ALMOG, S. REICH, and M. LEVY. Brit. Polym. J. **14**, 131 (1982).
8. R. M. FITCH. *In* Emulsion polymer and emulsion polymerization. *Edited by* D. Bassett and A. Hamielec. Am. Chem. Soc. Washington. 1981.
9. J. W. VANDERHOFF. Preprints, ACS Div. Org. Coatings Plastic Chem. **24**(2), 223 (1964).
10. D. H. NAPPER. J. Colloid Interface Sci. **58**, 390 (1977).
11. J. F. STAGEMAN. Ph.D. Thesis, University of Bristol, UK. 1978.
12. F. K. HANSEN and J. UGELSTAD. J. Polym. Sci. Polym. Chem. Ed. **17**, 3033 (1979).
13. F. K. HANSEN and J. UGELSTAD. J. Polym. Sci. Polym. Chem. Ed. **16**, 1953 (1978).
14. J. BRANDRUP and E. H. IMMERGUT. Polymer handbook. Wiley-Interscience, Toronto. 1975.
15. (*a*) C. M. HANSEN and A. BEERBOWER. *In* Encyclopedia of chemical technology: Suppl. Vol. *Edited by* A. Stander. Interscience, New York. 1971; (*b*) D. R. LLOYD, T. PRADO, K. KINZER, J. P. WIGHTMAN, and J. E. MCGRATH. Proc. Pol. Mat. Sci. Eng. **50**, 152 (1984).

Nature and distribution of radicals in rf and dc silane discharges; effects on deposition rate and physical properties of a-Si:H

F. JANSEN, J. MORT, AND M. MORGAN
Xerox Webster Research Center, Webster, NY 14580, U.S.A.

Received February 27, 1984

This paper is dedicated to the 10th anniversary of the Xerox Research Centre of Canada

F. JANSEN, J. MORT, and M. MORGAN. Can. J. Chem. **63**, 217 (1985).

Anodic and cathodic processes for rf and dc excited plasmas of silane gas differ in the relative role of charged and neutral radical species. By studying the thickness distribution of films deposited on substrates immersed in the plasma, the relative importance of these species as contributors to the film thickness is assessed. In addition, the impact of the different deposition processes on the spin density in the deposited hydrogenated amorphous silicon films and a key photoelectronic property, the hole range, is discussed.

F. JANSEN, J. MORT et M. MORGAN. Can. J. Chem. **63**, 217 (1985).

Les processus anodiques et cathodiques des plasmas de silanes gazeux excités par des f.r. et par du c.d. diffèrent par les rôles relatifs des espèces radicalaires neutres et chargées. L'étude de la répartition des épaisseurs des filmes déposés sur les substances immergés dans le plasma a permis d'établir l'importance relative de ces espèces en tant que responsables de l'épaisseur du film. De plus, on discute de l'impact des différents processus de dépôt sur la densité de spin des films amorphes de silicium hydrogéné déposés et sur une propriété photoélectronique fondamentale, la grandeur de la cavité.

[Traduit par le journal]

Introduction

Any physical vapor deposition process for thin films requires the generation of radicals which are transported to a substrate on which the film condenses. Condensable radicals are commonly generated by the vaporization of precursor solids and liquids in vacuum. Examples of such deposition techniques are thermal evaporation and sputtering. If the precursor material is already in gaseous form, condensable radicals can be created by thermal decomposition (CVD) or by plasma decomposition (plasma enhanced CVD) of an appropriate gas. The latter deposition method is also known as plasma or glow discharge deposition. This method has become increasingly important over the last decade because the use of gaseous starting materials offers significant and unique advantages over other physical vapor deposition methods. The glow discharge process is ideally suited for the uniform deposition of a wide variety of materials in single and multi-layers over large areas. In addition, materials that can be deposited by the glow discharge process often have unique properties which may be difficult if not impossible to duplicate by other fabrication processes. This is especially true for the alloys based on the group IV elements, such as amorphous hydrogenated silicon (a-Si:H), plasma silicon nitride (SiN_x), silicon oxide (SiO_x) and others. There is wide spread interest in devices based on these materials including solar cells, photoreceptors, and thin film transistors and correlations between process/material properties are therefore of considerable importance.

Despite this intense and growing interest in these materials and the considerable understanding of the physics of the devices which can be fabricated by the glow discharge process, relatively little is known about the mechanisms active during the deposition process itself. Diagnostic measurements such as mass spectroscopy and optical emission spectroscopy are commonly used to determine the presence of neutral and ionic species in glow discharge plasmas. These measurements have, in the case of silane, revealed the existence of a wide variety of such species in the plasma (1, 2) but have not been very useful in determining their importance and relative contribution to the growing film. It is generally assumed that the contribution of ions to the growth of a film in a plasma deposition process is much smaller than that of neutral radicals. The reasoning which leads to this consideration is based on the comparison of molecular dissociation and ionization energies where the first is generally much smaller than the latter. With a near Maxwellian distribution of electron energies, the generation rate for neutral radicals can be estimated to exceed the ionization rate by more than an order of magnitude for typical operating conditions. However, this argument may be misleading because the mass transport processes for ions and neutrals are fundamentally different. The relative concentrations of condensable neutrals and ions in the plasma are not necessarily simply related to the relative amounts of neutrals and ions which contribute to film growth.

Of special interest are the regions and plasma conditions close to the electrodes where, it is assumed, the film material of interest is deposited. These conditions are generally different at the cathode and the anode. As a consequence, the deposition rate and material properties of anodic and cathodic films are often different. Charged and neutral radical species arrive at the substrate surface with different energies and can impact various physical properties of the film due to differences in bonding, mechanical damage, or ablation. Differences in anodic and cathodic deposition rates can in principle be understood when charged condensable species contribute significantly to the deposition process. However, even if only neutral radicals contribute to the growing film, an imbalance in the cathodic and anodic deposition rate can result if the neutral species are not created uniformly in the gap.

Significantly different conditions can be externally and controllably imposed on any deposition system by the excitation mode of the plasma. Direct current (dc) and radio frequent (rf) plasma excitation are commonly used in capacitively coupled reactors. Very little is known about the relative deposition rates and the properties of the films deposited under these different conditions on the anode and the cathode.

The object of this paper is to compare and contrast the anodic and cathodic processes for rf and dc excited plasmas using information derived from the condensed species distribution in and across the discharge gap of a deposition reactor. In addition, measurements have been made of a key photoelectronic

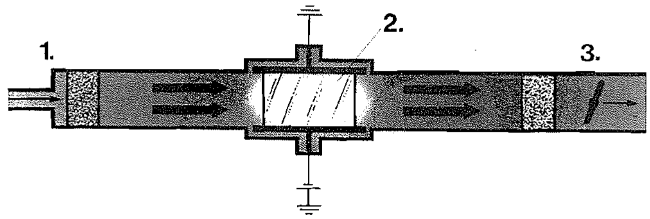

FIG. 1. Schematic of the experimental arrangement: (*1*) gas inlet and dispersion filter, (*2*) discharge region with glass slide, and (*3*) throttle valve and exhaust.

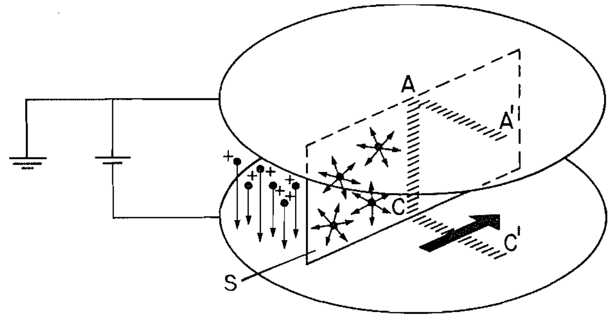

FIG. 2. Detail of the electrode arrangement. A thin glass substrate is placed between the electrodes, parallel to the gas flow (arrow). The line A'ACC' indicates the line over which the thickness distribution of the deposit was measured. Ionic and neutral mass transport process are schematically indicated.

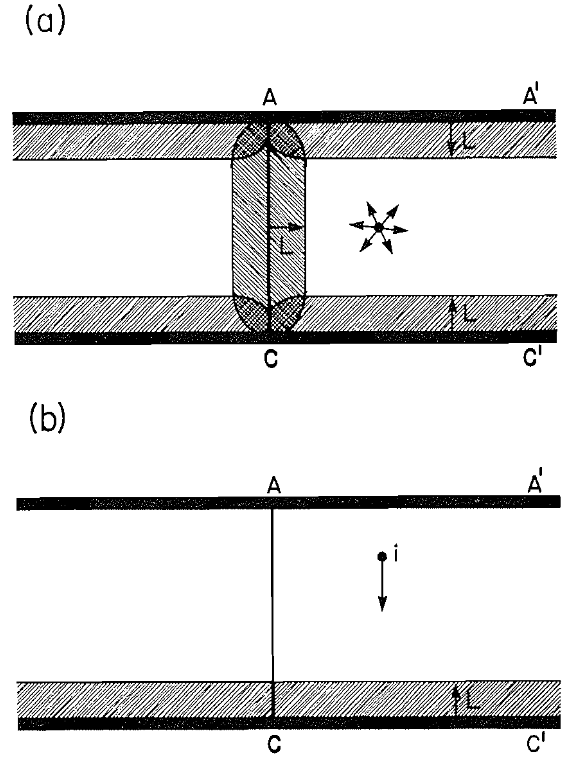

FIG. 3. Film thickness distribution on the three substrate surfaces for (*a*) mass transport of neutral radicals by diffusion and (*b*) transport of ions in the electric field.

parameter, viz the carrier range (3) for holes $\mu\tau_h$ (μ is the electronic drift mobility and τ_h is the deep trapping lifetime) for material produced under different conditions.

Experimental method

In a plasma, a variety of neutral and charged condensable radicals is created in the discharge gap by electron impact fragmentation of the precursor gas. To discriminate between the collective of neutral and the collective of ionic radical species, one can advantageously use the difference in the mass transfer mode of these species. The transport of charged species conforms primarily to the electric field lines whereas neutrals diffuse isotropically from their point of origin. A specific experimental arrangement which has been used in this work to study silane plasmas is shown in Fig. 1 and a more detailed drawing of the electrode area is presented in Fig. 2. A dielectric slab, S, called the "gap substrate" is placed in the discharge gap perpendicular to the parallel anode, A, and cathode, C, and parallel to the direction of gas flow. The dielectric plane is thin in order to minimize the flow disturbance. Its placement parallel with the electric field lines does not disturb the electric field distribution outside the slab. As convective transport is parallel to any of the surfaces under consideration, one can, to first order, neglect its effect on the thickness distribution of the condensed films. The line A'ACC' indicates the line over which the thickness of the deposited film was measured.

Characteristic hypothetical thickness distributions are shown in Fig. 3 for the extreme cases of deposition by exclusively neutral radicals (Fig. 3*a*) and exclusively ions (Fig. 3*b*). In the first case, neutral radicals are asumed to be uniformly created in the discharge gap by electron impact dissociation of gas molecules. These neutral radicals are transported to the walls of the confinement by diffusion. Even for the case of uniform radical generation in the discharge gap, the film thickness decreases close to the intersection lines of the electrodes and the gap substrate (points A and C in Fig. 3). The first reason for this decrease follows from geometrical considerations. Far away from the right angles between electrodes and the gap substrate, each point at the film surface receives vapor isotropically from the half space above it. Moving within distances d toward the right angles A and C, the half space contribution gradually diminishes to quarter space contribution in the corner. This geometrical effect causes therefore the film thickness to be half of the value which it would have without gap substrate. A second reason why the measured film thickness on the electrodes and the gap substrate decreases close to A and C is the sink effect of the walls on the condensable radicals. A concentration gradient between the neutral radical concentration in the plasma and the walls of the confinement is caused by the continuous disappearance of the condensable radicals close to the walls. This sink effect causes, just as the geometrical effect, gradients which extend over the order of the neutral radical diffusion length from A and C. These effects confound the interpretation of the measured thickness distributions and have to be taken into account. Mathematical modelling of the diffusion process is required to deconvolute the observed gap gap distribution in order to derive the gap distribution of neutrals. The mathematical formalisms have been developed by Chen (4) for various reactor geometries.

A significant simplification of the considerations results when only a small volume of space close to the intersection lines through A and C is considered. A volume can always be found in which the neutral radical distribution can be considered to be constant. In the case where only isotropic diffusion processes are active, the film thicknesses at A and C will be the same for the electrode and the gap substrate (Fig. 3*a*). This situation changes drastically when the predominant contribution to the deposition is by ionic species, a case which is schematically illustrated in Fig. 3*b*. Here, charged radicals of only one polarity are assumed to be created somewhere in the discharge gap by electron impact ionization. These ions are primarily transported along the electric field lines, thus contributing only to the buildup of material on one of the electrodes. The resulting thickness distribution pattern is quite different from the previous case and this difference can, at least in principle, be used to determine the relative contribution of neutral and charged radicals to the growing film.

It is emphasized that the previous considerations apply only to the idealized condition where the effects of self bias of the different surfaces in contact with the plasma are negligible with respect to the

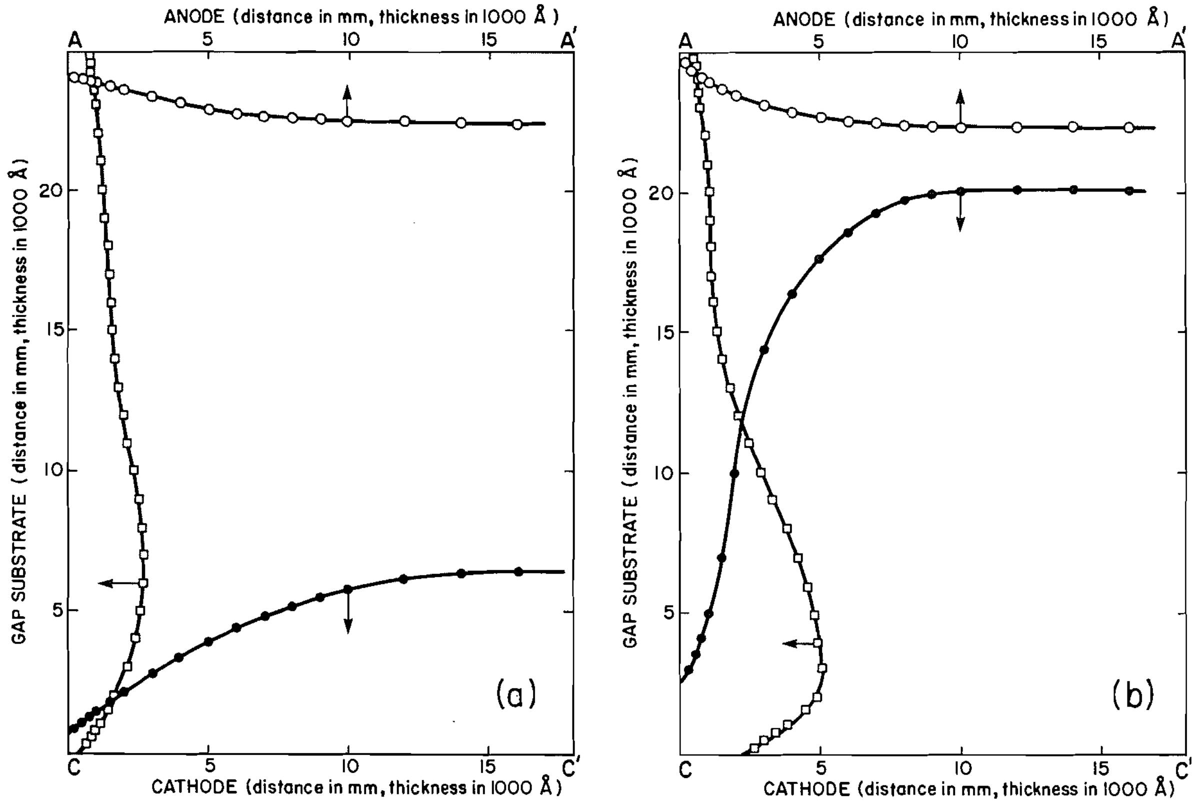

FIG. 4. (a) The film thickness distributions on the cathode (●), the anode (○), and the gap substrate (□) for a rf 10 min discharge of 100 sccm of silane at 250 mTorr and at a power input of 10 W; (b) The film thickness distributions on the cathode (●), anode (○), and gap substrate (□) for a 10 min dc discharge of 100 sccm of silane at 250 mTorr and at a current density of 0.1 mA/cm^2.

effects of the externally applied potentials. In reality, insulating surfaces, such as the gap substrate, assume a local potential which equalizes the electron and ion flux to the surface. Ions will then diffuse to this surface with an ambipolar diffusion coefficient which magnitude is of the order of the diffusion coefficient for neutral species. The contribution of ambipolar ion diffusion to the film thickness on the cross gap substrate has been neglected with respect to the combined effects of ion diffusion and ion drift in the externally applied electric field. Figure 3b is only an approximation of the practical situation and the deposition of a thin film on the gap substrate has to be expected.

In this paper the specific case of amorphous silicon deposition from silane gas has been studied. Knowledge about the condensable radical distribution in the discharge gap is essential for the realistic modeling of the mass transfer process active during deposition of this technologically important material. In addition, the effect of the externally applied bias on some of the properties of the deposited film have been determined. The spin density, as determined by electron spin resonance (esr) techniques, is generally taken as a measure for the dangling bond density. Furthermore, the range of photogenerated holes in the deposited films was measured by standard time of flight techniques (5) using samples ~10 μm thick. The hole range depends both on the mobility and the lifetime of these charge carriers, both of which parameters are related to the density of states in the forbidden gap of the material.

Experimental details and results

The entire electrode area (40 cm^2) of the anode and cathode of a small plasma deposition reactor was covered with glass with an electrically conductive film of indium-tin-oxide (ITO). The ITO film is hard enough to allow reliable thickness measurements to be made over grooved areas where the film has been removed by scratching of the material with a stainless steel pin. The electrical power was supplied to the electrodes and the ITO film. The interelectrode distance was kept constant at 2.5 cm. The electrode temperature was maintained at room temperature during deposition on substrates used for thickness measurements. Samples which were to be evaluated electrically were deposited on aluminum substrates at 230°C. The gap substrate was formed by a 100 μm thick glass plate mechanically clamped perpendicular to the electrodes at the anode. Silane gas was introduced into the reactor through a dispenser at a constant flow rate of 100 sccm. The gas was exhausted through a throttle valve arrangement such that its pressure was maintained at 250 mTorr. The deposition arrangement is schematically shown in Fig. 1.

The rf power and negative dc voltage, supplied between the cathode and grounded anode, were adjusted to a level where comparable amounts of polysilanes were formed by the discharge. The polysilane formation was measured by the rate of weight increase of a downstream filter and was of the order of 0.5 g/h under the present rf and dc operating conditions. The rf power was supplied at 5 W and 13.56 MHz whereas the dc current density was maintained at a level of 0.1 mA/cm^2 which corresponds to an intergap voltage of about 750 V.

Film thickness distributions were measured with a mechanical stylus instrument on the anode and cathode ITO substrates and the gap substrate over the line A′ACC′ as indicated in Fig. 2. The results are shown in Fig. 4. These results do not depend on which of the electrodes was used as anode or cathode, indicating uniformity of the gas flow in the gap area. The detailed shape of the thickness distributions and particularly the relative cathodic and anodic deposition rates depend somewhat on the reactor geometry, the interelectrode gap distance, and the pressure. The results obtained for different reactor geometries and operating conditions are qualitatively the same. The dc cathodic deposition rates are about a factor of 3–4 higher than the cathodic rf rates at comparable levels of polysilane formation. The anodic rates for dc and rf deposition are comparable under those circumstances and always smaller than the cathodic rates.

Table 1 lists the results of electron spin resonance measurements

TABLE 1. Hole range values for a-Si:H samples prepared in different plasmas

Plasma type	Electron spin resonance (cm^{-3})	Mobility*, $\mu(cm^2/V\ s)$	$\mu\tau_h$* (cm^2/V)
dc cathodic	5×10^{16}	5×10^{-4}	9×10^{-8}
dc anodic	5×10^{16}	3×10^{-4}	3×10^{-7}
rf cathodic	4×10^{16}	—	—
rf anodic	8×10^{15}	1.9×10^{-3}	1.3×10^{-6}

*These samples were made from SiH_4 admixed with 10 ppm B_2H_6.

and measurements of the hole range, $\mu\tau_h$, for samples made in rf and dc (anodic and cathodic) glow discharges.

Discussion

The differences between the measured and the hypothetical distribution of Fig. 3*b*, where ionic species were assumed to contribute primarily, include a significant film growth on the gap substrate and anode. This film growth is in the case of rf as well as dc discharges skewed towards the cathode where the electric field is expected to be relatively high. This indicates that, independent of the excitation mode, neutral radicals, rather than ions, are the dominant contributing species to the deposition process. Moreover, at A and C the film thickness on the gap substrate is the same as on the electrodes in all cases, again indicative of the diffusion of neutral species, the concentration of which is uniform close to A and C. Yet, the measured thickness distributions are quite different from the hypothetical distribution in Fig. 3*a*. The gap distributions are not symmetric with respect to the midgap position. This indicates that the neutral radicals are not uniformly created throughout the discharge gap as assumed for Fig. 3*a*. The fact that the cathodic deposition rates are always higher than the anodic rates is consistent with the fact that the generation of the neutral radicals takes placed relatively close to the cathode for both rf and dc discharges. However, there are significant and consistent differences in the film thickness distribution on the gap substrate between rf and dc excited plasma discharges. The gap substrate thickness is more uniformly distributed and the maximum is further away from the cathode for the case of an rf excited discharge. In the case of a dc discharge, the gap thickness distribution decreases only close to the cathode to about one half of the maximum value, which has to be expected from geometrical considerations alone. This is indicative of a high neutral radical distribution close to the dc cathode, consistent with the high cathodic deposition rates for that excitation mode.

The observed differences between the rf and dc discharge thickness distributions are compatible with the mechanisms through which these discharges are sustained. In the case of a rf discharge, the high frequency oscillation of electrons in the bulk of the plasma causes the molecular dissociation and ionization processes. This is in contrast to the case of a dc plasma which is sustained through secondary electron emission from ion impact on the cathode. The impacting ions do not contribute significantly to the thickness of the growing film. However, the electronic properties of the condensed film could critically depend on the effects of ion impact during growth. Even at ion concentrations which are three orders of magnitude smaller than the neutral radical concentration, the gap state density of the material would be of the order of 10^{18} cm^{-3} if each impacting ion could create a localized electronic state.

The anodic rf material consistently gives higher values of $\mu\tau_h$ compared with anodic or cathodic dc material. The relatively poor quality of the dc material may be associated with the bombardment of the film surface during the deposition process. Although damage of the material might be expected from the ion bombardment processes at the cathode, it is surprising that the anodic material, subject to predominantly electron bombardment, is of similar poor quality. At this point it can not be excluded that radiation damage associated with the dc process is responsible for the relatively high density of dangling bonds. Independent measurements of the drift mobility μ show that the mobility values for rf samples are consistently higher than dc samples whereas little difference is found between the dc cathodic and anodic samples. The primary change in the range, $\mu\tau_h$, for anodic and cathodic dc samples therefore appears associated with variation of the deep trapping lifetime τ_h, and hence the density of deep traps.

Conclusion

From the study of the film thickness distribution on substrates immersed in rf and dc silane plamas, it is concluded that in both types of discharge the predominant condensing species are neutral. These neutral radicals are in the case of dc discharges created closer to the cathode than for rf discharges. The dc cathodic deposition rate is therefore relatively high compared to an rf discharge at a comparable power level. This difference in the spatial distribution of condensable species in the discharge gap is compatible with the fact that rf discharges are predominantly sustained by electrons created in the bulk of the plasma whereas dc discharges are sustained by secondary electron emission from ion impact on the cathode. Although the impacting electrons do not contribute significantly to the thickness of the growing film, they do affect the electronic properties of the film by causing a relatively large concentration of deep gap states in dc cathodic films.

1. G. TURBAN, Y. CATHERINE, and B. GROLLEAU. Thin Solid Films, **67**, 309 (1980).
2. R. W. GRIFFITH, F. J. KAMPAS, P. E. VANIER, and H. D. HIRSCH. J. Non-cryst. Solids, **35/36**, 391 (1980).
3. J. MORT, S. GRAMMATICA, J. C. KNIGHTS, and R. LUJAN. Photogr. Sci. Eng. **24**, 241 (1980).
4. I. CHEN. Thin Solid Films, **101**, 41 (1983).
5. M. D. TABAK and P. J. WARTER. Phys. Rev. **173**, 899 (1968).

Molecular weight – viscosity relationships for a broad molecular weight distribution polymer

H. KH. MAHABADI AND L. ALEXANDRU
Xerox Research Centre of Canada, 2660 Speakman Drive, Mississauga, Ont., Canada L5K 2L1

Received February 28, 1984

This paper is dedicated to the 10th anniversary of the Xerox Research Centre of Canada

H. KH. MAHABADI and L. ALEXANDRU. Can. J. Chem. **63**, 221 (1985).

A novel and simple method is described for evaluation of molecular weight – viscosity relationships for a polymer where only broad molecular weight distribution samples are available. The method demands measurement of the intrinsic viscosity and GPC chromatograms of several samples. Results of applying the procedure to bisphenol A – Diethyleneglycol (50:50) copolycarbonate are presented.

H. KH. MAHABADI et L. ALEXANDRU. Can. J. Chem. **63**, 221 (1985).

On décrit une nouvelle méthode simple permettant d'évaluer les relations poids moléculaire vs viscosité de polymères pour lesquels on ne dispose que des échantillons pour lesquels la distribution des poids moléculaires est large. La méthode implique des mesures de viscosité intrinsèque et des chromatogrammes en phase gazeuse de plusieurs échantillons. On rapporte les résultats obtenus lorsqu'on a appliqué la méthode à un échantillon de polymère de bisphénol – A/diéthylèneglycol (50/50).

[Traduit par le journal]

Introduction

In order to interpret a gel permeation chromatograph (GPC) of any polymer sample in terms of its molecular weight distribution, it is necessary to establish a quantitative relationship between molecular weight M and elution volume v. It is well-known that well-characterized narrow distribution polymer samples are the most appropriate for GPC calibration purposes. Such samples are, however, difficult to prepare with the exception of polystyrene, for which good standards are readily available. The $M-v$ relationship for any other polymer can be obtained using the familiar universal calibration procedure (1, 2) and a reliable pair of k and α constants for the Mark–Houwink–Sakurada equation.

The evaluation of the Mark–Houwink constants k and α for a particular polymer–solvent system normally requires the preparation of a series of samples having a wide range of molecular weights and their subsequent characterization by light scattering and dilute-solution viscosity. However, gel permeation chromatography (GPC), i.e., size exclusion chromatography can provide a convenient alternative route to k and α (3–10). In this case k and α can be estimated using unfractionated polymer samples of known $\bar{M}_n$ or $\bar{M}_w$ and intrinsic viscosity.

In this work a new and simple method which permits the facile determination of the Mark–Houwink constants using hydrodynamic average molecular weight, $\bar{M}_x$ (11), is presented. The method described uses a combination of gel permeation chromatography and intrinsic viscosity measurements for several broad molecular weight distribution samples.

As an example of the use of this method, molecular weight – viscosity relationships for bisphenol A – diethyleneglycol copolycarbonate were found.

Theory

In a recent publication by Rudin *et al.* (11), the use of a new molecular weight average, $\bar{M}_x$, to characterize polymer samples of heterogeneous composition have been proposed. $\bar{M}_x$, the hydrodynamic volume average, is defined according to

$$[1]\quad \bar{M}_x = \frac{\Sigma\omega_i[\eta]_iM_i}{\Sigma\omega_i[\eta]_i} = \frac{\Sigma\omega_iJ_i}{[\eta]}$$

where ω_i and $[\eta]_i$ are the weight fraction and intrinsic viscosity, respectively, of all species which exit the GPC columns with elution volume v_i. The denominator in eq. [1] is equal to the intrinsic viscosity $[\eta]$, of the whole sample GPC solvent. The values in numerator are available from GPC chromatogram and universal calibration curve. $J_i = [\eta]_iM_i$ can be read directly from the universal calibration curve and ω_i is equated to the ratio of the area of the GPC detector response at elution volume v_i to the total area under the GPC chromatogram.

For a polydisperse polymer, the Mark–Houwink equation relates $[\eta]$ to the viscosity average molecular weight $\bar{M}_v$

$$[2]\quad [\eta] = K\bar{M}_v^{\alpha}$$

If the whole polymer is considered to be composed of a mixture of monodisperse species each with molecular weight M_i, weight fraction ω_i, and intrinsic viscosity $[\eta]_i$ in GPC solvent, then

$$[3]\quad \bar{M}_v = (\Sigma\omega_iM_i^{\alpha})^{1/\alpha}$$

and

$$[4]\quad J_i = [\eta]_iM_i = KM_i^{\alpha+1}$$

Equation [2] can be written in terms of $\bar{M}_x$

$$[5]\quad [\eta] = K_x\bar{M}_x^{\alpha} = \delta K\bar{M}_x^{\alpha}$$

where δ is given by (12)

$$[6]\quad \delta = (\Sigma\omega_iJ_i^{\alpha/\alpha+1})^{\alpha+1}/(\Sigma\omega_iJ_i)^{\alpha}$$

If the parameter δ remains constant through the change of $[\eta]$ and $\bar{M}_x$, then a log–log plot of $[\eta]$ vs. $\bar{M}_x$ gives the expected straight line relationship. The constants α and K_x can be obtained from the slope and intercept of such lines, respectively. Then constant $k = K_x/\delta$ can be estimated utilizing eq. [7].

As reported earlier (12) δ, for polymer samples having the same polydispersity or having very broad MWD ($\bar{M}_w/\bar{M}_n \geq 4$), is constant.

Experimental

Copolycarbonate synthesis

Bisphenol A (BPA) – diethyleneglycol (DEG) copolycarbonates

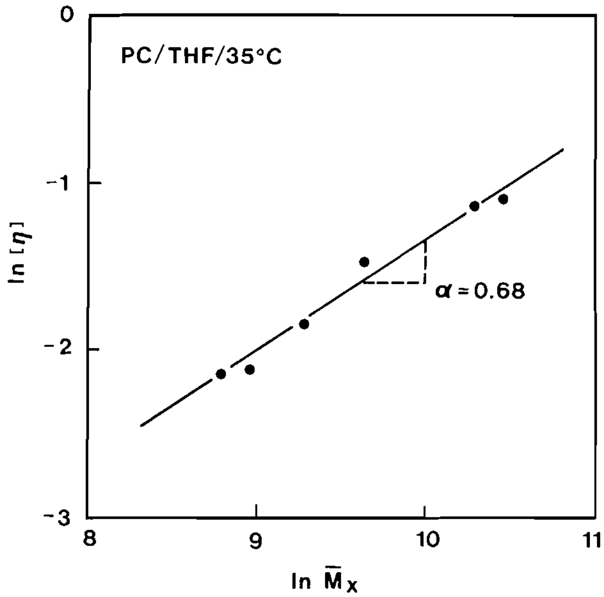

FIG. 1. ln [η] vs. ln $\bar{M}_x$ for cpc in THF at 35°C ($\bar{M}_w/\bar{M}_n \geq 4.5$).

were synthesized by solution polycondensation of BPA and DEG bischloroformate using CH_2Cl_2 as solvent and pyridine as the acid acceptor. The polymerization was carried out at low temperature and atmospheric pressure. The polymer molecular weight was changed by varying the concentration of DEG bischloroformate. All polymers synthesized are linear and have very broad molecular weight distribution ($\bar{M}_w/\bar{M}_n \geq 4.5$).

Gel permeation chromatography

A Water Associates GPC equipped with a high pressure solvent delivery (model 150C) was used. THF solutions of concentration less than 2 mg/mL were used. The flow rate, through a set of six μ styragel packed columns was 1 mL/min. The nominal size (in A) of μ styragel packings were 100, 500, 10^3, 10^4, 10^5, 10^6. A calibration curve based on elution volumes of 11 polystyrene standards from Pressure Chemical Company was constructed. The relation between molecular weight of PS and elution volume was obtained using a third degree polynomial. The coefficient of this polynomial was adusted for axial dispersion effects using an optimization method reported in the literature (13). Then, the corrected relationship between molecular weight of PS and elution volume was transferred to a universal calibration curve using the intrinsic viscosity of PS standards.

Intrinsic viscosity measurements

The intrinsic viscosities were determined using a Canon-Ubbelohde viscometer. All viscosities were obtained in THF and at 35°C (GPC conditions).

Results and discussion

The hydrodynamic volume average molecular weights of the polymer, $\bar{M}_x$, were estimated using eq. [1]. The right-hand side of eq. [1] was evaluated by treating the normalized GPC chromatogram data in a computer program. The calculated values of $\bar{M}_x$ along with [η] data were applied to eq. [5] and using least square analysis K_x and α were estimated. A log–log plot of [η] vs. $\bar{M}_x$ for BPA–DEG polycarbonate is shown in Fig. 1. Using GPC chromatogram and estimated value of α along with eq. [6], δ and therefore K for each sample was estimated. The results are summarized in Table 1. It is clear that variation for the calculated values of δ is less than 3%. The fact that δ is independent of MW and MWD of these samples indicate an accurate K and α estimation. The calculated values of K and α can be used to establish a relationship between [η] and molecular weight of copolycarbonate. This relationship can be written as:

TABLE 1. Calculated values of δ and k

Copolycarbonate samples	δ^a	$10^5 k^b$ (dL/g)
1	0.694	31.7
2	0.687	32.0
3	0.705	31.2
4	0.684	32.2
5	0.689	31.9
6	0.690	31.9
	$\delta = 0.692 \pm 0.007$	$\bar{K} = (31.8 \pm 0.3) \times 10^{-5}$

^{a}δ calculated from eq. [6] using α = 0.68.
^{b}K calculated from $K = k_x/\delta$ using K_x = 0.00022 dL/g.

TABLE 2. Viscosity results of copolycarbonate samples

Copolycarbonate samples	[η] measured (dL/g)	[η] calculated (dL/g)	% Difference
CPC 121	0.740	0.764	+3.2
CPC 108	0.139	0.130	−6.5

$$[7] \quad [\eta]\ \mathrm{dL/g} = 0.00032\ \bar{M}_x^{0.68}\ \mathrm{THF/35°C}$$

Using this relationship and universal calibration curve any average molecular weight of this copolymer can be calculated.

The precision of the proposed methods which use $\bar{M}_x$–[η] data to calculate K and α is tested here by comparing measured and calculated [η]. Two additional copolycarbonate samples were used for this purpose. Using the estimated values of K and α and GPC chromatogram, $\bar{M}_v$ and then [η] of these two samples were calculated. Good agreement is observed between measured and calculated [η] values as shown in Table 2. The difference between corresponding [η] values are small considering possible experimental uncertainties.

In summary, the proposed method for determination of molecular weight viscosity relationship outlined in this report has the advantage of being fast, convenient, and eliminates all fractionation problems related to monodisperse sample preparation and should be very useful for the characterization of highly specialized polymer products.

1. Z. GRUBISIC, P. REMPP, and H. BENOIT. J. Polym. Sci. B, **5**, 753 (1967).
2. A. RUDIN and H. L. W. HOLGY. J. Polym. Sci. A-1, **10**, 217 (1972).
3. A. R. WEISS and E. C. GINSBERG. J. Polym. Sci. B, **7**, 349 (1969).
4. A. L. SPATORICO and B. COUTLER. J. Polym. Sci. Phys. Ed. **11**, 1139 (1973).
5. H. K. MAHABADI and K. F. O'DRISCOLL. J. Appl. Polym. **21**, 1283 (1977).
6. C. J. B. DOBBIN, A. RUDIN, and M.F. TCHIR. J. Appl. Polym. Sci. **25**, 2985 (1980).
7. X. ZHONGDE, S. MINGSHI, N. HADJICHRISTIDIES, and L. J. FETTERS. Macromolecules **14**, 1591 (1981).
8. M. SZESZTY and F. TUDO'S. Polym. Bulletin, **5**, 429 (1981).
9. P. SZEWCZYK. J. Appl. Polym. Sci. **26**, 2727 (1981).
10. H. KH. MAHABADI. J. Polym. Sci. Phys. Ed. **22**, 449 (1984).
11. J. M. GOLDWASSER, A. RUDIN, and W. L. ELSDON. J. Liquid Chromatogr. **1–5**, 2253 (1982).
12. H. KH. MAHABADI. J. Appl. Polym. Sci. In press.
13. J. N. CARDENAS and K. F. O'DRISCOLL. J. Polym. Sci. Polym. Lett. Ed. **13**, 657 (1975).

Thermodynamic miscibility of polystyrene–poly(2,6-dimethyl-1,4-phenylene oxide) blends

GIUSEPPA DIPAOLA-BARANYI AND JOCELYN RICHER[1]
Xerox Research Centre of Canada, 2660 Speakman Drive, Mississauga, Ont., Canada L5K 2L1

AND

WILLIAM M. PREST, JR.
Xerox Corporation, 800 Phillips Road, Webster, NY 14580, U.S.A.

Received March 8, 1984

This paper is dedicated to the 10th anniversary of the Xerox Research Centre of Canada

GIUSEPPA DIPAOLA-BARANYI, JOCELYN RICHER, and WILLIAM M. PREST, JR. Can. J. Chem. **63**, 223 (1985).

Inverse gas chromatography was used to investigate the miscibility behaviour of molten polystyrene–poly(2,6-dimethyl-1,4-phenylene oxide) blends as a function of composition (0, 25, 50, 75, 85, and 100 wt.% PS). Specific retention volumes were measured for various solutes in pure and mixed stationary phases of these polymers at 240°C. Infinite dilution weight fraction activity coefficients and Flory–Huggins polymer–solute (χ) and polymer–polymer (χ_{23}') interaction parameters were derived from these data.

Negative polymer–polymer interaction parameters were obtained for blends containing more than 60 wt.% PS, suggesting strong intermolecular interactions in the molten state. This is in accord with the well-known compatibility of PS–PPO blends. However, positive χ_{23}' values were observed for blends containing less than 60 wt.% PS. This suggests weak intermolecular interactions, and perhaps some microheterogeneity in PS–PPO blends with a low PS content. In view of the single, composition dependent T_g measured for each of these blends the microheterogeneity or microphase separation must be on a finer scale than that measured by the glass transition.

GIUSEPPA DIPAOLA-BARANYI, JOCELYN RICHER et WILLIAM M. PREST, JR. Can. J. Chem. **63**, 223 (1985).

On a utilisé la chromatographie en phase gazeuse inversée pour étudier le comportement, du point de vue de la miscibilité, de mélanges fondus de polystyrène–poly(diméthyl-2,6 oxyde de phénylène-1,4) en fonction de la composition (0, 25, 50, 75, 85 et 100% en poids de PS). Opérant à 240°C, on a mesuré, pour chacun des polymères, les volumes spécifiques de rétention de divers solutés dans des phases stationnaires pures et dans des phases stationnaires mixtes. A partir de ces données, on a déduit les coefficients d'activités de fraction en poids à dilution infinie ainsi que les paramètres d'interaction polymère–soluté (χ) et polymère–polymère (χ_{23}') de Flory–Huggins.

On a obtenu des paramètres d'interactions polymère–polymère négatifs pour les mélanges contenant plus de 60% en poids de PS; ceci suggère qu'il existe de fortes interactions moléculaires dans l'état fondu. Ceci est en accord avec la compatibilité bien connue des mélanges PS–PPO. Cependant, on a observé des valeurs positives de χ_{23}' pour des mélanges contenant moins de 60% en poids de PS. Cette observation suggère l'existence d'interactions moléculaires faibles et peut-être aussi quelques microhétérogénéités dans les mélanges de PS–PPO à faible teneur en PS. En se basant sur le fait que, pour chacun de ces mélanges, on ne mesure qu'une seule valeur de T_g, qui est indépendante de la composition, on peut croire que la micro-hétérogénéité ou la séparation de la microphase doit être dans une échelle plus précise que celle qui est mesurée par la transition du verre.

[Traduit par le journal]

Introduction

The technique of inverse gas chromatography (IGC) has recently been proven to be a very useful tool for obtaining polymer – small molecule and polymer–polymer interaction data (1–6). This method provides a fast and convenient route to reliable thermodynamic information on concentrated polymer systems in the molten state.

Polystyrene–poly(2,6-dimethyl-1,4-phenylene oxide) blends are classic examples of compatible polymer blends. However, recent calorimetric work by Prest suggests that there may be some microheterogeneity in PS–PPO blends with low PS content (7).

Therefore, a systematic study of PS–PPO blends was carried out over the whole composition range using IGC. The focal point of this work was the determination of polymer–polymer interaction parameters (χ_{23}') for various blend compositions. These data will be useful in evaluating the thermodynamic miscibility of these blends.

[1]Co-op student, Université de Sherbrooke, Quebec.

Experimental

Materials

All solutes were reagent or chromatoquality grade and were obtained from standard lab supply sources. Chromosorb G, AW-DMCS treated (70–80 mesh), was obtained from Johns-Manville. Polystyrene ($\bar{M}_w$: 110 000; $\bar{M}_w/\bar{M}_n < 1.06$) came from Polysciences Inc. The PPO sample was obtained from General Electric Co. ($\bar{M}_w$ = 69 000; $\bar{M}_w/\bar{M}_n$ = 2.1).

Column preparation

Coatings were prepared by coating the polymers onto Chromosorb G. Benzene (150 mL) was slowly evaporated from a solution containing polymer(s) (~2.7 g) and support (~23 g). The coated support was then dried in a vacuum oven (80°C) for 4 days and resieved before use (60/80 mesh). The percent loading of polymer on support (weight of polymer/weight of polymer plus support) was determined by calcination of 1–1.5 g of coating. A correction was made for the loss of volatiles from the uncoated support. The relative concentration of polymers in the blends was assumed to be identical with that in the original solution prior to deposition on the support. Columns were prepared from 1/4 in. o.d. copper tubing plugged at each end by silanized glass wool. To provide even packing, the column was constantly vibrated during filling. Columns were conditioned under N_2 at

TABLE 1. Stationary phase and column parameters

Polymer	Loading (wt.%)	Wt. polymer (g)	Column length (cm)
PS	7.45	1.1778	152
PPO	11.39	1.7624	140
PS/PPO blends			
25 wt.% PS	11.19	1.8076	147
50 wt.% PS	10.19	1.6551	152
75 wt.% PS	10.81	1.7726	147
85 wt.% PS	9.20	1.5229	152

250°C for 3 h before use. A complete description of the columns is given in Table 1.

Instrumentation

The IGC measurements were carried out with a Hewlett-Packard 5830A gas chromatograph equipped with a dual flame ionization detector. The oven temperature was measured with a precision of ±0.01°C with a Hewlett–Packard platinum resistance thermometer. Carrier gas (prepurified nitrogen) flow rates were measured from the end of the column with a water-jacketted soap bubble flowmeter. The net retention time of the probe (±0.01 min) was determined from the peak maxima retention times for the probe and methane (a marker to correct for dead volume in the column). Column inlet and outlet pressures were read from a mercury manometer (±0.05 mm Hg).

The solutes and marker were injected manually with a 10-μL Hamilton syringe (<0.01 μL). The solutes were characterized by symmetrical elution peaks and generally exhibited little sample size dependence at low injection volumes, low carrier gas flow rates (5–20 cm^3/min) and moderate column loading (7–10%). Galin and Rupprecht (22) have shown that under these conditions the opposite influences of surface adsorption and gas flow rate are nearly equivalent, so that the experimental V_g^0 value is quite close to the bulk V_g^0 value.

Data reduction

Specific retention volumes, V_g^0 (cm^3/g), were computed from the familiar expression of Littlewood *et al.* (8)

$$[1] \quad V_g^0 = t_N F J / w_L$$

where t_N is the net retention time for the probe, F is the carrier gas flow rate at 0°C and 1 atm (STP), J is a correction factor for gas compressibility, and w_L is the weight of polymer in the column.

At temperatures above T_g, the magnitude of V_g^0 is a measure of the solubility of the probe in the stationary phase. By applying thermodynamic theory to gas chromatography, one can relate the measured V_g^0 to the weight fraction activity coefficient at infinite dilution of the probe, $(a_1/w_1)^\infty$, a fundamental parameter of solution thermodynamics which indicates deviation from ideal solution behavior (9).

$$[2] \quad \ln (a_1/w_1)^\infty = \ln \frac{(273.16R)}{V_g^0 p_1^0 M_1} - \frac{p_1^0}{RT}(B_{11} - V_1)$$

where V_1, M_1, p_1^0 refer to the solute molar volume, molecular weight, and saturated vapor pressure respectively, R is the gas constant, T is the column temperature (K), and B_{11} is the second virial coefficient, which is used to correct for vapor phase nonideality of the probe. Values of B_{11} were estimated from corresponding equations of state (10, 11). Solute vapor pressures were obtained from Dreisbach's compilation (12). Solute densities were obtained from various sources, including the compilations by Orwoll and Flory (13) and Timmermans (14) as well as the International critical tables (15).

From the Flory–Huggins treatment of solution thermodynamics (16), one can obtain the χ parameter, which is a measure of the residual free energy of interaction between solute and polymer (9). χ is determined from the relationship

$$[3] \quad \chi_{12} = \ln (273.16 R v_2 / V_g^0 p_1^0 V_1) - (1 - V_1/V_2)\varphi_2 - p_1^0(B_{11} - V_1)/RT$$

TABLE 2. Specific retention volume, V_g^0 (cm^3/g), for various solutes in PS/PPO blends at 240°C

Solute	wt.% PS 0	25	50	75	85	100*
n-Octane	1.60	1.93	2.11	1.89	2.03	2.22
n-Decane	3.25	3.79	4.29	3.75	3.96	4.12
3,4,5-Trimethylheptane	2.36	3.55	5.88	3.58	3.81	3.95
n-Butylcyclohexane	5.22	6.48	7.20	6.33	6.73	6.95
cis-Decalin	10.12	12.71	14.12	12.54	13.50	13.69
Toluene	3.42	3.96	4.33	3.84	4.06	4.13
n-Butylbenzene	8.42	9.72	10.67	9.43	10.04	10.09
Chlorobenzene	5.45	6.40	6.93	6.07	6.38	6.61
Acetophenone	12.84	15.27	17.02	15.34	16.52	16.49
Cyclohexanol	5.43	6.54	6.99	6.25	6.63	6.53

*Extrapolated from 170–190°C range.

where v_2, V_2, and φ_2 refer to the specific volume, molar volume, and volume fraction of the polymer. All other symbols have their usual meanings. For high molecular weight polymer and infinite dilution of probe the second term of eq. [3] (i.e., $(1 - V_1/V_2)\varphi_2$) approaches 1.

It has been shown (17) using Scott's ternary solution treatment (18) of Flory–Huggins theory that the overall interaction parameter between the volatile probe (1) and the binary stationary phase (2, 3) is given by

$$[4] \quad \chi_{1(23)} = \ln \frac{(273.16R(w_2 v_2 + w_3 v_3))}{V_g^0 p_1^0 V_1} - \left(1 - \frac{V_1}{V_2}\right)\varphi_2 - \left(1 - \frac{V_1}{V_3}\right)\varphi_3 - \frac{p_1^0}{RT}(B_{11} - V_1)$$

where w_2 and w_3 refer to the weight fractions of PS and PPO in the blend.

The volumetric data for the blends were determined by assuming that the specific volume of the blend is the weight average of the specific volumes of the parent homopolymers (19, 20).

Results and discussion

Specific retention volumes V_g^0 (cm^3/g) were measured for a variety of polar and apolar probes in molten PS, PPO, as well as four blends of varying ratios of these two homopolymers (i.e., 25, 50, 75, and 85 wt.% PS). In order to ensure the attainment of thermodynamic equilibrium for each polymer melt, measurements were carried out at 240°C, well above the glass transition of each homopolymer. The reliability of the V_g^0 values is better than 3%, except for 3,4,5-trimethylheptane for which the uncertainty is ±5%. Table 2 summarizes the measured V_g^0 values. The derived infinite dilution weight fraction activity coefficients $(a_1/w_1)^\infty$ are tabulated in Table 3.

Flory–Huggins χ parameters were determined from the measured retention data in order to examine the extent of polymer – small molecule (eg. probe) and polymer–polymer interaction in various PS–PPO mixtures. These values are summarized in Tables 4 and 5 at 240°C.

Polymer–probe miscibility

The data in Table 2 indicate that V_g^0 values for the probes investigated are consistently higher for PS than for PPO. These results indicate that the interaction between the aliphatic or aromatic probes and PS are stronger than with PPO. Figure 1 illustrates the dependence of V_g^0 on blend composition for six selected probes. With the exception of the 75% PS blend, higher values of V_g^0 are observed for these blends than would be predicted by addition of the homopolymer values.

TABLE 3. Infinite dilution weight fraction activity coefficient $(a_1/w_1)^\infty$, for various solutes in PS/PPO blends at 240°C

	wt.% PS					
Solute	0	25	50	75	85	100*
n-Octane	14.97	12.47	11.36	12.60	11.85	10.13
n-Decane	13.88	11.97	10.53	11.97	11.45	10.26
3,4,5-Trimethylheptane	16.43	11.01	10.03	10.83	10.25	9.24
n-Butylcyclohexane	9.98	8.15	7.25	8.26	7.84	7.17
cis-Decalin	6.99	5.59	5.03	5.63	5.28	4.92
Toluene	6.43	5.57	5.10	5.71	5.45	5.10
n-Butylbenzene	6.65	5.79	5.27	5.91	5.62	5.27
Chlorobenzene	4.69	4.02	3.70	4.20	4.03	3.71
Acetophenone	6.74	5.69	5.08	5.59	5.25	4.98
Cyclohexanol	4.67	3.89	3.64	4.03	3.85	3.81

*Extrapolated from 170–190°C range.

TABLE 4. Flory–Huggins $\chi_{1(23)}$ interaction parameter for various solutes in PS/PPO blends at 240°C

	wt.% PS					
Solute	0	25	50	75	85	100
n-Octane	0.936	0.776	0.703	0.827	0.776	0.673
n-Decane	0.972	0.846	0.739	0.888	0.853	0.778
3,4,5-Trimethylheptane	1.203	0.825	0.752	0.850	0.804	0.748
n-Butylcyclohexane	0.829	0.641	0.550	0.696	0.653	0.582
cis-Decalin	0.601	0.400	0.315	0.449	0.392	0.392
Toluene	0.330	0.208	0.142	0.275	0.237	0.214
n-Butylbenzene	0.483	0.340	0.294	0.429	0.386	0.341
Chlorobenzene	0.355	0.223	0.160	0.308	0.276	0.215
Acetophenone	0.654	0.525	0.433	0.550	0.496	0.464
Cyclohexanol	0.266	0.105	0.060	0.182	0.145	0.149

TABLE 5. Polymer–polymer interaction parameter χ_{23}' for PS/PPO blends at 240°C

	wt.% PS			
Solute	25	50	75	85
n-Octane	0.46	0.38	−0.52	−0.55
n-Decane	0.38	0.53	−0.36	−0.40
3,4,5-Trimethylheptane	1.32	0.86	−0.03	0.07
n-Butylcyclohexane	0.62	0.60	−0.32	−0.31
cis-Decalin	0.74	0.71	−0.19	−0.06
Toluene	0.47	0.51	−0.19	−0.06
n-Butylbenzene	0.54	0.46	−0.34	−0.34
Chlorobenzene	0.48	0.49	−0.31	−0.21
Acetophenone	0.40	0.49	−0.23	−0.05
Cyclohexanol	0.66	0.58	−0.03	0.17

Positive deviations of V_g^0 from linearity have previously been observed for some polystyrene–poly(*n*-butylmethacrylate) blends which are characterized by weak intermolecular interactions (4).

Values of $(a_1/w_1)^\infty$ are the highest for pure PPO irrespective of the solute used. This shows that the probes are less soluble in PPO than in PS. Measured values range from 4 to 16. The probe that shows highest $(a_1/w_1)^\infty$ in PPO is 3,4,5-trimethylheptane, 16.43 (i. e., a poor solvent). The lowest value in PPO, 4.67, is observed for cyclohexanol (i.e., a good solvent). In PS, the highest activity coefficient is observed for *n*-decane, 10.26, (i.e., a poor solvent), and the lowest value is 3.71, for

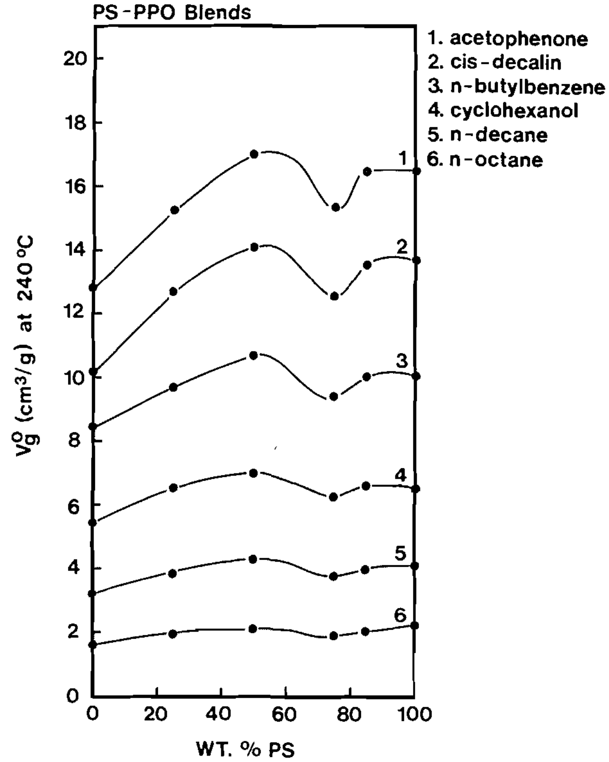

FIG. 1. Composition dependence of V_g^0 for various solutes in PS–PPO blends at 240°C.

chlorobenzene (i.e., a good solvent).

Flory–Huggins χ interaction parameters, which were derived from measured specific retention volumes, are summarized in Table 4. For any given solute, χ is larger (i.e., more positive) for pure PPO than for PS or its blends. This is consistent with the trend observed in the V_g^0 and $(a_1/w_1)^\infty$ data and indicates that the probe-polymer interaction is stronger for PS than for PPO. All χ parameters measured for these systems are greater than 0. Most of the χ values in PPO are greater than 0.5 (critical value) except for toluene, *n*-butylbenzene, chlorobenzene, and cyclohexanol. The reverse is true for PS. Most of the χ parameters here are less than 0.5 except for *n*-octane, *n*-decane, 3,4,5-trimethylheptane, and *n*-butylcyclohexane. Although the aromatic probes are good solvents for both PPO and PS, the interactions are more favorable with PS.

Polymer–polymer miscibility

Polymer–polymer interaction parameters (χ_{23}') were calculated from the measured polymer–probe interaction (Table 4) in corresponding pure and mixed stationary phases (4, 6).

$$[5] \quad \chi_{1(23)} = \chi_{12}\varphi_2 + \chi_{13}\varphi_3 + \chi_{23}'\varphi_2\varphi_3$$

where $\chi_{23}' = \chi_{23}V_1/V_2$.

The interaction parameter χ_{23}' is thus normalized to the size of the probe molecule. A negative interaction parameter is required in order to ensure miscibility of two high molecular weight polymers. Table 5 summarizes χ_{23}' values (240°C) obtained for the 10 probes for each of the four blend compositions.

As noted in previous chromatographic investigations of polymer–polymer miscibility (4, 6), probe-to-probe variations are observed. This is probably due to the assumptions inherent in eq. [5], i.e., random mixing of the two polymers in the stationary phase and/or random sensing of the polymer–

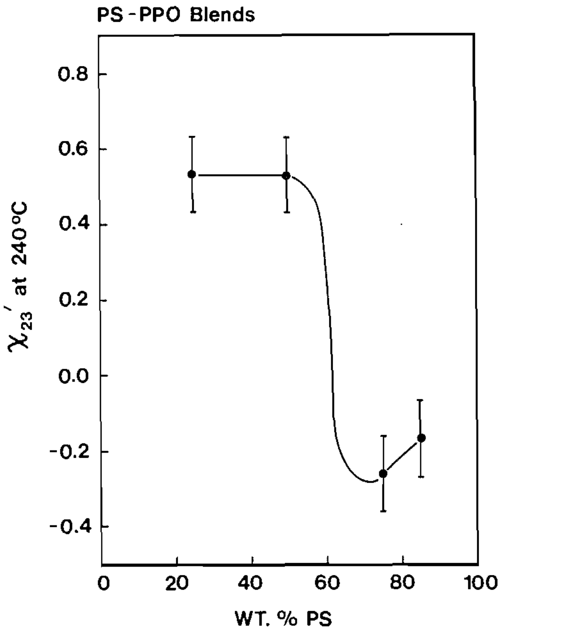

FIG. 2. Composition dependence of χ_{23}' in PS–PPO blends at 240°C.

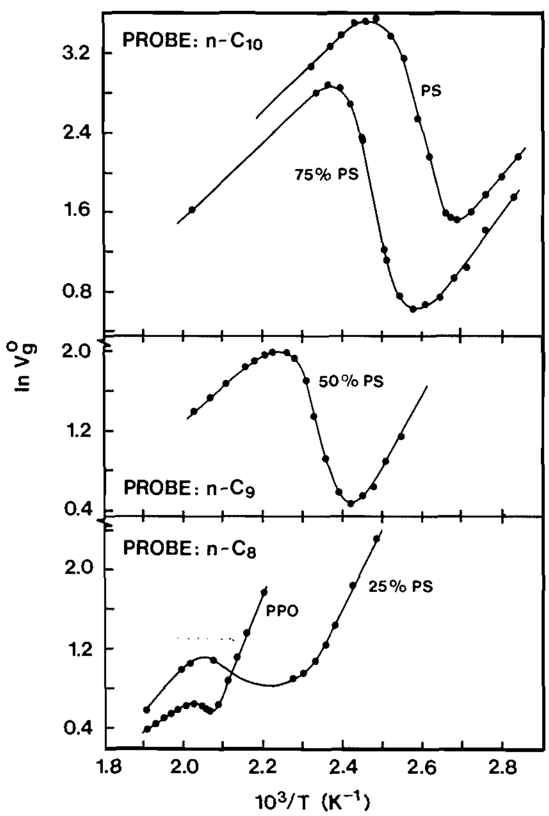

FIG. 3. Retention diagrams for PS–PPO blends of varying compositions.

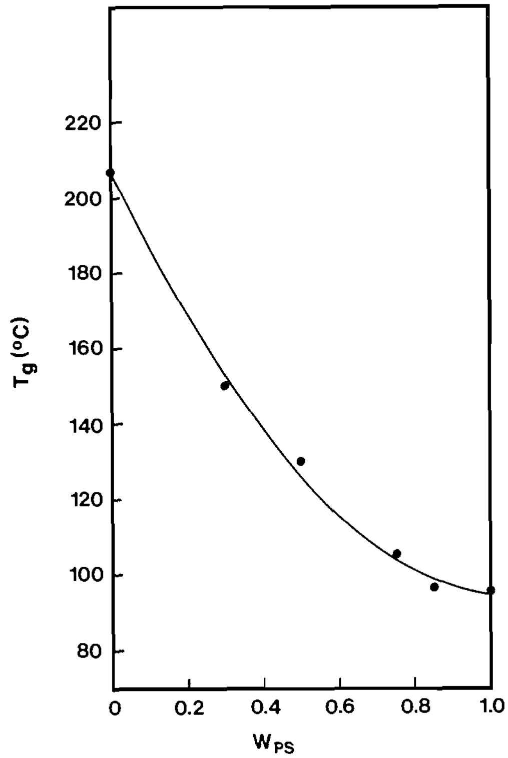

FIG. 4. Composition dependence of T_g.

polymer interaction by the probe.

For each blend composition, the measured χ_{23}' values were averaged for nine probes (3,4,5-trimethylheptane exhibits large deviations and was not considered in the averaging procedure) and are plotted in Fig. 2. In general, blends containing 25 and 50 wt.% PS exhibit positive χ_{23}' values (ca. 0.5); blends containing 75 and 85 wt.% PS exhibit negative χ_{23}' values (ca. −0.2). Thus PS–PPO blends with a high polystyrene content (>60 wt.% PS) are characterized by a strong specific interaction ($\chi_{23}' < 0$) in the molten state. This is in accord with the well-known compatibility of PS–PPO blends. Blends with a low polystyrene content (<60 wt.% PS) appear to exhibit weak intermolecular interactions at 240°C ($\chi_{23}' > 0$).

IGC studies show only one T_g for each blend over the whole composition range (Fig. 3 and 4), suggesting that PS and PPO are miscible at the segmental level.

However, Prest's DSC data indicate a broadening of the T_g transition with decreasing PS content which can be interpreted as increasing microheterogeneity in these blends (7). A similar conclusion was reached by MacKnight *et al.* (21) from dielectric relaxation studies.

The present thermodynamic data are in agreement with the postulate of increasing microheterogeneity in PS–PPO blends with decreasing PS content. The measured χ_{23}' values probably reflect interactions on a much finer scale than that reflected by the T_g transition. Electron microscopic studies should shed some further light on the level of miscibility in PS–PPO blends.

1. O. OLABISI, L. M. ROBESON, and M. T. SHAW. Polymer–polymer miscibility. Academic Press, New York. 1979.
2. D. G. GRAY. Prog. Polym. Sci. **5**, 1 (1977).
3. G. DIPAOLA-BARANYI. Macromolecules, **14**, 683 (1981).
4. G. DIPAOLA-BARANYI and P. DEGRÉ. Macromolecules, **14**, 1456 (1981).
5. G. DIPAOLA-BARANYI. Macromolecules, **15**, 622 (1982).
6. G. DIPAOLA-BARANYI, S. J. FLETCHER, and P. DEGRÉ. Macromolecules, **15**, 885 (1982).
7. W. M. PREST, JR., D. J. LUCA, and F. J. ROBERTS, JR. Thermal analysis in polymer characterization. *Edited by* E. A. Turi. Heyden and Son Inc., Philadelphia, PA. p. 24.
8. A. B. LITTLEWOOD, C. S. G. PHILLIPS, and D. T. PRICE.

J. Chem. Soc. 1480 (1955).
9. D. PATTERSON, Y. B. TEWARI, H. P. SCHREIBER, and J. E. GUILLET. Macromolecules, **4**, 356 (1971).
10. M. L. MCGLASHAN and D. J. B. POTTER. Proc. R. Soc. London, Ser. A, **267**, 478 (1962).
11. E. A. GUGGENHEIM and C. J. WORMALD. J. Chem. Phys. **42**, 3775 (1965).
12. D. R. DREISBACH. Adv. Chem. Ser. No. 15 (1955); No. 22 (1959); No. 29 (1961).
13. R. A. ORWOLL and P. J. FLORY. J. Am. Chem. Soc. **89**, 6814 (1967).
14. J. TIMMERMANS. Physico-chemical constants of pure organic compounds. Elsevier, New York. Vol. I 1958; Vol. 2. 1965.
15. International critical tables. Vol. 3. McGraw-Hill, New York. 1928.
16. P. J. FLORY. Principles of polymer chemistry. Cornell University Press. New York. 1953.
17. D. D. DESHPANDE, D. PATTERSON, H. P. SCHREIBER, and C. S. SU. Macromolecules, **7**, 530 (1974).
18. R. L. SCOTT. J. Chem. Phys. **17**, 279 (1949).
19. H. HOCKER, G. J. BLAKE, and P. J. FLORY. Trans. Faraday Soc. **67**, 2251 (1971).
20. O. G. LEWIS. Physical constants of linear homopolymers. Springer-Verlag, New York. 1968.
21. W. J. MACKNIGHT, J. STOELTING, and F. E. KARASZ. Advances in chemistry series. No. 99. *Edited by* R. F. Gauld. 1971.
22. M. GALIN and M. C. RUPPRECHT. Polymer, **19**, 506 (1978).

Picosecond measurements of geminate charge pair recombination in photoionized liquids

T. W. SCOTT[1]

Exxon Research and Engineering Company, Corporate Research Science Laboratories, Annandale, NJ 08801, U.S.A.

AND

C. L. BRAUN

Department of Chemistry, Dartmouth College, Hanover, NH 03755, U.S.A.

Received March 20, 1984

This paper is dedicated to the 10th anniversary of the Xerox Research Centre of Canada

T. W. SCOTT and C. L. BRAUN. Can. J. Chem. **63**, 228 (1985).

The recombination dynamics of geminate cation−electron pairs in liquid hexane is studied by combining picosecond photoionization and infrared-stimulated charge dissociation measurements. The observed yield of free charge is determined by the product of the charge pair survival probability and the probability for infrared-stimulated charge dissociation. Experimental results are compared with transient solutions of the Smoluchowski equation governing diffusive recombination in a Coulomb well. Reasonable agreement with experiment can be reached by allowing for a radial distribution of initial pair separations. However, the stimulated dissociation yield exhibits a functional dependence on pair separation which complicates the analysis. A simple model of geminate charge pair dissociation by infrared stimulation is presented and its implications for these experiments are discussed.

T. W. SCOTT et C. L. BRAUN. Can. J. Chem. **63**, 228 (1985).

Faisant appel à une combinaison de mesures de photoionisations au niveau de la picoseconde et de dissociations de charges stimulées par l'infrarouge, on a étudié la dynamique de la recombinaison de paires de cation/électron géminées dans l'hexane liquide. On a déterminé le rendement observé de la charge libre en faisant le produit de la probabilité de survie de la paire chargée et de la probabilité de dissociation de charge stimulée par l'infrarouge. On compare les résultats expérimentaux avec des solutions transitoires de l'équation de Smoluchowski décrivant la recombinaison diffusante dans un puit de Coulomb. On peut obtenir un bon accord avec les résultats expérimentaux si l'on fait l'hypothèse qu'il se produit une distribution radiale des séparations initiales des paires. Toutefois, il existe une dépendance fonctionnelle du rendement de dissociation stimulée avec la séparation de la paire et ce fait complique l'analyse. On présente un modèle simple de la dissociation par stimulation infrarouge des paires chargées géminées et on discute des implications des ces expériences.

[Traduit par le journal]

Introduction

Photocarrier generation in organic materials frequently involves a transient charge pair as the immediate precursor of free charge carriers (1−6). Each pair consists of a parent positive ion and a localized photoelectron which are strongly correlated by their mutual coulombic attraction. The Onsager theory of geminate recombination gives the probability that a charge pair will dissociate into free carriers (7). In non-polar organic materials, at least for small values of the applied field, the separation probability is small and most pairs suffer rapid geminate annihilation. The influence of temperature and applied electric fields on the free carrier yield has been extensively studied in a large number of materials. In most cases the escape probability is well described by the Onsager model.

More recently, efforts to probe the time dependence of geminate recombination have been reported. The recombination dynamics of cation−anion pairs, where the anion is formed by electron attachment, has been studied using pulsed electron beam excitation (8−10). It has also been shown that the first half-life of electron−cation pairs is less than 100 ps in liquid hexane (11). A number of theoretical treatments of the time-dependent recombination process are also available. Following a series of approximate solutions (12), an exact treatment of geminate pair dynamics within the Onsager model is now available (13). This model assumes that the recombination process involves mutual diffusion of the geminate electron and cation through a uniform dielectric medium under the influence of their coulombic field. The work described here is an attempt to directly observe charge pair recombination dynamics in simple non-polar liquids and thereby test the validity of applying diffusion theory to this problem.

In a previous communication we reported picosecond recombination of photogenerated cation−electron pairs in liquid hexane (14). A new experimental approach was employed whereby geminate charge pairs are photodissociated by an intense infrared light pulse (15). With the improved time resolution attainable using mode locked lasers, we found that the first half-life in liquid hexane was no more than 9 ps. We report here a more detailed analysis of the geminate pair photodissociation process as well as a semiempirical fit of the observed charge pair annihilation dynamics in terms of transient solutions of the Brownian motion of the charge pair. In order that this diffusion theory (13) adequately fit the observed decay kinetics, it is necessary to assume that thermalization of the photogenerated electron results in a distribution of initial charge pair separations.

Experimental

Geminate charge pairs were formed in liquid n-hexane by resonant two-photon ionization of anthracene at 351 nm. The 351 nm light pulse with a 6−8 ps duration delivered 0.05 mJ of uv light over 2 mm^2 cross section of the sample. The uv pulses were obtained from the third harmonic of a mode locked Nd^{3+}-phosphate laser. After the arrival of the uv pulse, a 0.5 mJ probe pulse at 1053 nm interrogated the ionized sample for a period of 8− 10 ps. We recorded ionic photocurrent transients lasting several milliseconds after irradiation of the

[1]This work was completed during a post doctoral appointment at AT&T, Bell Laboratories, Murray Hill, NJ 07974, U.S.A.

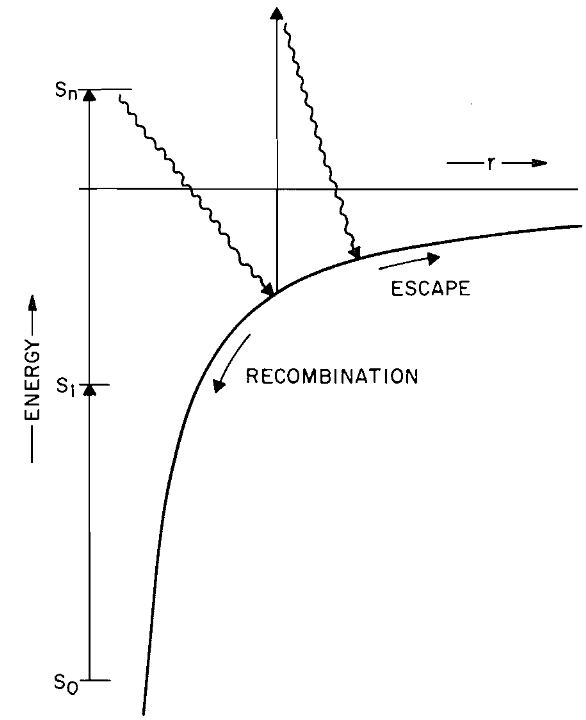

FIG. 1. A model for infrared-assisted dissociation of geminate electron–cation pairs. Two 351 nm photons generate a 7.1 eV singlet state of anthracene, S_n, which ionizes to form a geminate charge pair. Photoexcitation of the geminate electron initiates a second thermalization process which on average enhances the charge pair separation probability.

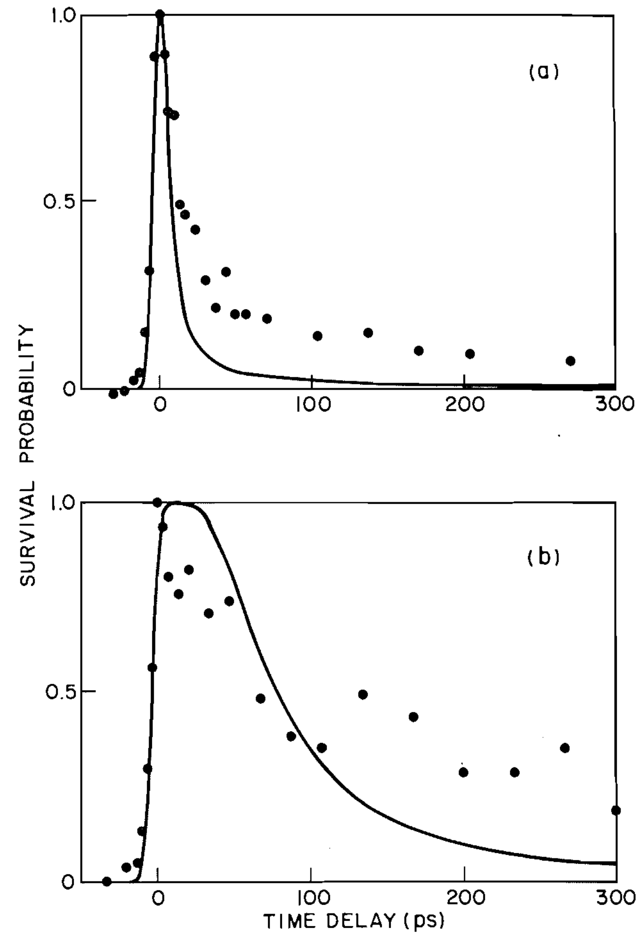

FIG. 2. Time dependence of ir-stimulated charge dissociation at 296 K (*a*) and 214 K (*b*). Each curve has been scaled to unity at its maximum. The solid curves are Hong and Noolandi's transient solutions of the Onsager problem for an initial charge pair radius of 45 Å. The dielectric constant used for hexane was 1.885 at 296 K and 2.01 at 214 K. The electron diffusion constant was 1.91×10^{-3} cm^2/s at 296 K and 9.4×10^{-5} cm^2/s at 214 K.

solution with a sequence of uv and ir pulses. The photocurrent amplitude was determined by the total number of free charge carriers generated by cooperative action of the two light pulses. The ir pulse enhances photoconduction by laser-assisted dissociation of the charge pairs formed by uv excitation. The time-dependent geminate pair survival probability was identified with the change in photocurrent amplitude as a function of the optical delay between the uv ionization pulse and the ir photodissociation pulse.

Zone-refined anthracene was dissolved in liquid hexane at a concentration of 7.5×10^{-6} mol L^{-1}. The solvent was dried over silica gel and passed through a 0.2 μm Teflon filter. A tandem photoconductivity cell allowed measurements of the charge carrier yield with and without ir excitation during each laser firing. The uv light pulse passed between two sets of parallel plate electrodes, each with an inter-electrode spacing of 3 mm and biased at 1500 V. The ir pulse overlapped the uv pulse in the first ionization cell, but was prevented from entering the second cell by an ir blocking color filter. The relative photoionization response of the two cells was determined by temporarily blocking the ir beam.

Discussion

Geminate charge pair annihilation dynamics were monitored by the process of infrared-enhanced photogeneration (14, 15). A schematic illustration of this technique is presented in Fig. 1. A uv photoionization pulse at 351 nm creates thermalized electron–cation pairs by resonant two-photon ionization of anthracene in liquid hexane. When only the uv pulse enters the sample, a photocurrent is observed from the fraction of charge pairs which surmount the Coulomb barrier and separate. When the uv pulse is folowed by an intense infrared pulse at 1053 nm, an increased yield of free charge is observed which depends strongly on the relative timing of the two optical pulses. It has been suggested (14, 15) that the infrared pulse acts by exciting the geminate electron which has an absorption cross-section of 3×10^{-17} cm^2 at 1053 nm (16). Since the ir photon has an energy of 1.2 eV while the Coulomb binding energy only amounts to 0.1–0.2 eV, ir excitation promotes the charge pair well above its dissociation limit. With the available infrared intensity of 10^{28} photons/cm^2 s the probability of exciting each geminate electron in the sample is near unity.

Apparently the subsequent dissociation of the infrared-excited geminate pair is an inefficient process. Typical thermal dissociation efficiencies of charge pairs in organic liquids are on the order of 0.1% (6). Anthracene in liquid hexane exhibits efficiencies of this size (15). Infrared excitation of the geminate electron is found to increase the dissociation yield by only a factor of 5 to 6. Enhancements on the order of 1000 would be expected if each optically excited geminate electron separated with unit probability. The smaller observed efficiencies can be rationalized by assuming that the optically excited electron re-thermalizes at an electron–cation separation where Coulomb driven charge annihilation remains the dominant decay mechanism (see Fig. 1).

Figure 2 shows how the cooperative ionization of anthracene in liquid hexane depends on the time delay between the uv and

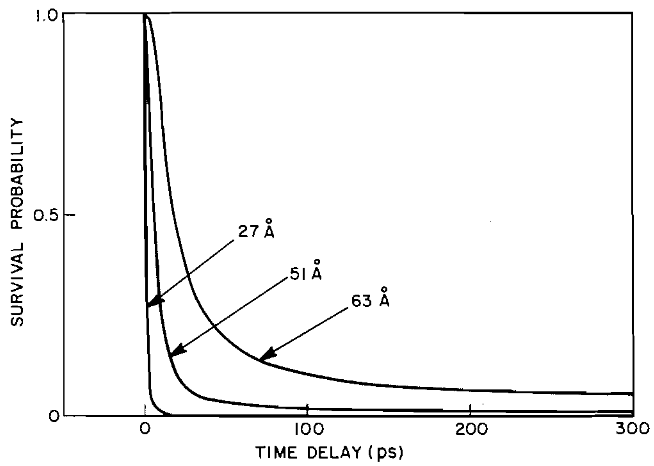

FIG. 3. Hong–Noolandi solutions of the time dependent charge pair survival probabilities for different initial separations at 296 K.

ir pulses at two temperatures. The vertical axis represents the difference in free charge yield when the uv pulse is accompanied by delayed ir excitation and when the uv pulse enters the sample alone. The steep rise and decay near time zero represents the recombination kinetics convoluted with the laser pulse width (8 ps at 1053 nm and 6 ps at 351 nm FWHM). The solid lines represent Hong and Noolandi's solutions (13) of the time-dependent Onsager problem for a single charge pair initially separated by 45 Å. Theoretical decay curves for other initial separations are shown in Fig. 3. The simulated decay curves in Fig. 2 take into account the finite laser pulse widths assuming Gaussian time profiles. It can be seen in Fig. 2 that cooling the solution from 296 to 214 K dramatically extends the first half-life. Each curve in Fig. 2 is normalized to unity at time zero. The actual magnitude of the infrared enhancement was seen to increase by a factor of five at low temperatures. The temperature dependence of the enhancement shows that the ir pulse generates at least some charge pairs with a larger separation than those formed by the uv pulse alone. This is consistent with the model presented in Fig. 1. The increased half-life seen upon cooling is captured by the Hong–Noolandi decay curves. We previously pointed out that the slower decay at 214 K results from the temperature dependence of the electron mobility in liquid hexane (14).

Although the theoretical decay curves shown in Fig. 2 agree qualitatively with experiment, it is apparent that the observed decay is faster at early times and slower at longer times than predicted for a 45 Å radius pair. This discrepancy can be rationalized by assuming that photoionization results in a distribution of charge pair separations. The radial distribution function

$$[1] \quad g(r) = r^2 \exp(-r/L)$$

when convoluted with Hong and Noolandi's theoretical decays gives good agreement with experiment at both temperatures for L = 14 Å (see Fig. 4). The mean charge pair radius occurs at $3L$ = 42 Å according to eq. [1]. This should be compared with the value of 45 Å obtained when temperature dependence studies are analyzed in terms of a single charge pair radius (15). Prior to convolution with the laser pulse width, the theoretical recombination curves give a half-life of approximately 3.5 ps at 298 K and 68 ps at 214 K.

The comparison of the time-dependent photodissociation

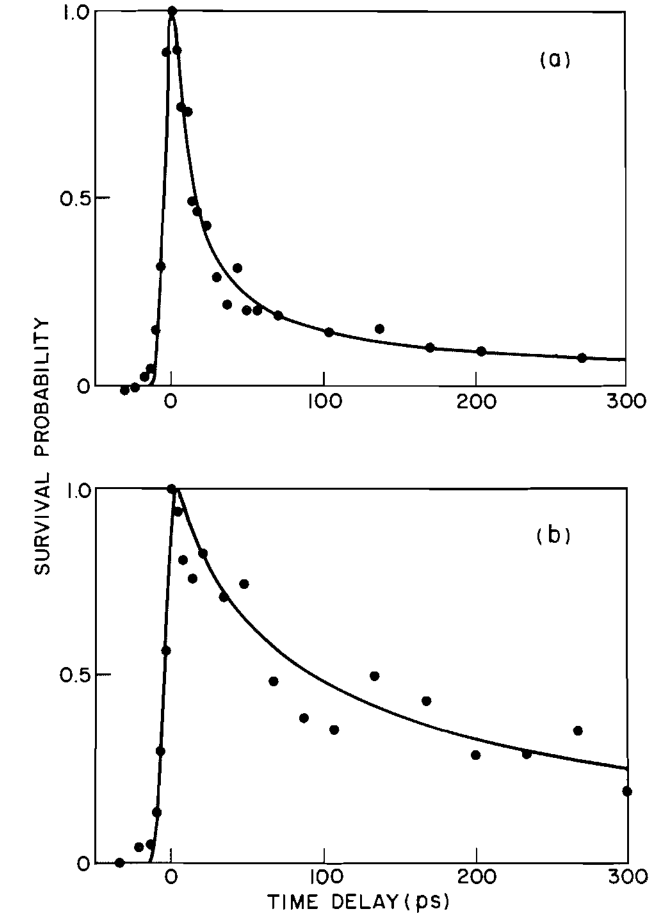

FIG. 4. Comparison of theoretical (—) survival probabilities and experimental (●) dissociation yields at 296 K (a) and at 214 K (b). Each curve has been scaled to unity at its maximum. The theoretical decay functions allow for a distribution of initial charge pair separations according to eq. [1] of the text. The simulations are shown for L = 14 Å (mean radius = 42 Å) at each temperature.

curves with transient solutions of the Onsager problem (Figs. 2, 4) assumes that the infrared-enhanced photogeneration process provides a direct measure of the charge pair survival probability. To test this assumption a simple analysis of the change in photocurrent due to infrared excitation of the geminate electron can be developed based on the model presented in Fig. 1. In the absence of the infrared photodissociation pulse, the escape probability (P_0) of a single charge pair at zero applied field is given by the well known relation (13).

$$[2] \quad P_0(r_0, T) = \exp(-r_c/r_0)$$

where r_0 is the initial charge pair separation and $r_c = e^2/4\pi\epsilon\epsilon_0 kT$ is the Onsager radius. Assuming that rethermalization after infrared excitation is not significantly perturbed by the Coulomb field of the cation, the probability of finding the rethermalized electron at some distance r from its initial position will be spherically symmetric about the original electron position. The new escape probability is then given by

$$[3] \quad P_{h\nu}(r_0, T) = \int g'(r)[\exp(-r_c/d)]r^2 \sin\theta \; dr d\theta d\phi$$

where (r, θ, ϕ) describes the position of the rethermalized electron in terms of a coordinate system centered at the initial

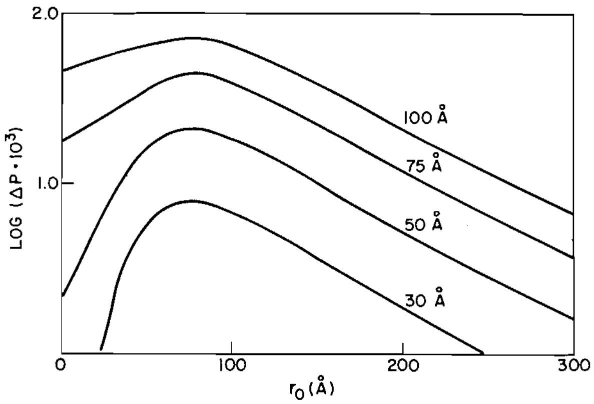

FIG. 5. Logarithm of the change in geminate pair escape probability, ΔP, after ir stimulation, as a function of initial pair separation, r_0. A series of curves are shown for different values of the secondary thermalization length at 296 K.

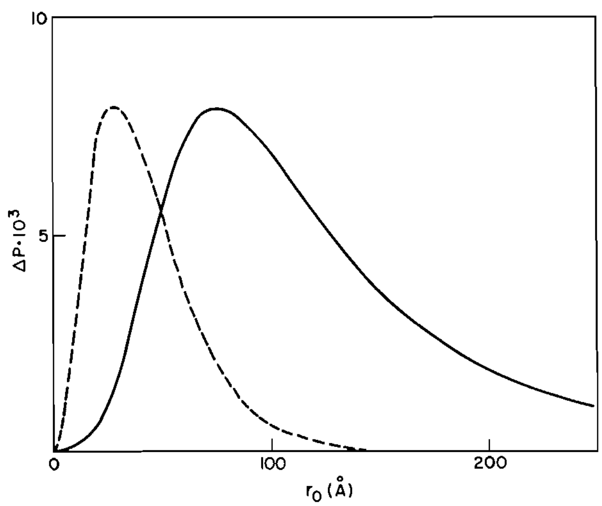

FIG. 6. Plot of the radial dependence of the initial pair distribution $g(r)$ for L = 14 Å (dashed line) and the change in escape probability for a secondary thermalization length of 30 Å (solid line). The vertical scale gives the numerical value of ΔP, while $g(r)$ has been scaled for ease of viewing.

position of the electron and where $g'(r)$ denotes the radial distribution of secondary thermalization lengths. The function $d(r,\theta,\phi)$ in eq. [3] is the distance between the cation and the rethermalized electron. (We note that the treatment of infrared photogeneration presented here differs from that in ref. 15 in that the previous work assumed that rethermalization would be symmetric about the parent cation.) In the absence of any detailed information on the secondary distribution of thermalization lengths, $g'(r)$, we will evaluate $P_{h\nu}$ for rethermalization on a spherical shell of radius r. Making the change of variables

$$x = [r^2 + r_0^2 - 2rr_0 \cos \theta]^{-1/2}$$

in eq. [3] we obtain

$$[4] \quad P_{h\nu}(r, r_0, T) = \frac{1}{2rr_0}\int_{|r_0+r|^{-1}}^{|r_0-r|^{-1}} \frac{1}{x^3} [\exp(-r_c x)]\mathrm{d}x$$

Numerical integration of eq. [4] shows how the infrared-enhanced escape probability $\Delta P = P_{h\nu} - P_0$ depends on the initial charge pair separation and the secondary thermalization length. Figure 5 shows a series of ΔP versus r_0 curves for different values of r. The enhancement shows a maximum in the range r_0 = 70–80 Å. ΔP goes to zero as r_0 becomes very large because both $P_{h\nu}$ and P_0 approach unity. For very small values of r_0, ΔP is again small unless the rethermalization lengths are large enough to substantially increase the charge pair separation.

A secondary thermalization length of ~30 Å accounts for the magnitude of the infrared enhancements seen in this work at both 296 K and 214 K. Figure 6 compares the radial dependence of ΔP with the distribution of initial separations described by eq. [1]. It is apparent that the measurement technique employed in this work does not sample all members of the initial distribution with equal probability and that the fit in Fig. 4 will be somewhat in error, particularly at early times. A more critical assessment of the importance of radial selectivity in geminate pair photodissociation will require an examination of the time evolution of the radial distribution of charge pairs (13).

Aknowledgements

The authors thank J. Noolandi, Xerox Research Center of Canada, and William J. McNeil for generating the theoretical decay curves shown in Figs. 2, 3, and 4. Grant DE-AC02-83ER13102 from the Department of Energy provided partial support for this work.

1. R. H. BATT, C. L. BRAUN and J. F. HORNIG. J. Chem. Phys. **49**, 1967 (1968); R. H. BATT, C. L. BRAUN, and J. F. HORNIG. Appl. Opt. Suppl. **3**, 20 (1969); R. R. CHANCE and C. L. BRAUN. J. Chem. Phys. **59**, 2269 (1973); **64**, 3573 (1976).
2. A. C. ALBRECHT. Acc. Chem. Res. **3**, 238 (1970).
3. R. A. HOLROYD and R. L. RUSSELL. J. Phys. Chem. **78**, 2128 (1974).
4. R. C. JARNAGIN. Acc. Chem. Res. **4**, 420 (1971).
5. D. M. PAI and R. C. ENCK. Phys. Rev. B **11**, 5163 (1975).
6. D. S. SETHI, H. T. CHOI, and C. L. BRAUN. Chem. Phys. Lett. **74**, 223 (1980); H. T. CHOI, D. S. SETHI, and C. L. BRAUN. J. Chem. Phys. **77**, 6027 (1982).
7. L. ONSAGER. Phys. Rev. **54**, 554 (1938).
8. M. C. SAUER, JR. and C. D. JONAH. J. Phys. Chem. **84**, 2539 (1980); C. D. JONAH, M. C. SAUER, R. COOPER, and A. D. TRIFUNAC. Chem. Phys. Lett. **63**, 535 (1979); J. P. SMITH and A. D. TRIFUNAC. J. Phys. Chem. **85**, 1645 (1981).
9. C. A. M. VAN DEN ENDE, L. H. LUTHJENS, J. M. WARMAN, and A. HUMMEL. Radiat. Phys. Chem. **19**, 455 (1982); C. A. M. VAN DEN ENDE, L. NYIKOS, J. M. WARMAN, and A. HUMMEL. Radiat. Phys. Chem. **15**, 273 (1980).
10. S. TAGAWA, Y. TABATA, H. KOBAYASHI, and M. WASHIO. Radiat. Phys. Chem. **19**, 193 (1982); Y. KATSUMURA, Y. TABATA, and S. TAGAWA. Radiat. Phys. Chem. **19**, 267 (1982); S. TAGAWA, M. WASHIO, Y. TABATA, and H. KOBAYASHI. Radiat. Phys. Chem. **19**, 277 (1982); S. TAGAWA, Y. KATSUMURA, and Y. TABATA. Radiat. Phys. Chem. **19**, 125 (1982).
11. C. D. JONAH. Radiat. Phys. Chem. **21**, 53 (1983).
12. A. MOZUMDER. J. Chem. Phys. **61**, 780 (1974).
13. G. C. ABELL, A. MOZUMDER, and J. L. MAGEE. J. Chem. Phys. **56**, 5422 (1972); K. M. HONG and J. NOOLANDI. J. Chem. Phys. **68**, 5163 (1978), **69**, 5026 (1978).
14. C. L. BRAUN and T. W. SCOTT. J. Phys. Chem. **87**, 4776 (1983).
15. L. V. LUKIN, A. V. TOLMACHEV, and B. S. YAKOVLEV. Chem. Phys. Lett. **81**, 595 (1981).
16. J. H. BAXENDALE and E. J. RASBURN. J. Chem. Soc. Faraday Trans. 1, **70**, 705 (1974).

High-resolution ^{13}C CP/MAS solid-state nmr investigation of the thermal degradation of poly(methylvinylketone)

C. A. FYFE[1] AND M. S. MCKINNON

The Guelph-Waterloo Centre for Graduate Work in Chemistry, Department of Chemistry, University of Guelph, Guelph, Ont., Canada N1G 2W1

Received April 19, 1984

This paper is dedicated to the 10th anniversary of the Xerox Research Centre of Canada

C. A. FYFE and M. S. MCKINNON. Can. J. Chem. **63**, 232 (1985).

The structural changes occurring in poly(methylvinylketone) when exposed to high temperatures have been investigated by high-resolution ^{13}C solid-state nmr. The degradation proceeds via the aldol condensation of pendant ketone groups to form a cyclic β-hydroxy ketone which is dehydrated to the cyclic α,β-unsaturated ketone. As the degradation continues there is the formation of polycyclic structures and aromatization of the sample.

C. A. FYFE et M. S. MCKINNON. Can. J. Chem. **63**, 232 (1985).

Faisant appel à la rmn du ^{13}C à l'état solide, on a étudié la nature des changements structuraux qui se produisent lorsqu'on soumet de la poly(méthylvinyl cétone) à des températures élevées. La dégradation se produit par le biais d'une condensation aldolique de la fonction cétonique disponible qui conduit initialement à une β-hydroxycétone cyclique qui se déshydrate par la suite en une cétone cyclique α,β-insaturée. Au fur et à mesure de la dégradation, il y a formation de structures polycycliques et aromatisation de l'échantillon.

[Traduit par le journal]

Introduction

The coloration which occurs during the thermally initiated degradation of poly(methylvinylketone) (PMVK) (**I**) was first reported by Marvel and co-worker (1). The chemical process was thought to be a cyclization resulting from an aldol condensation between pendant ketone groups. Previous workers (2–5) have employed uv and ir spectroscopy to study structural changes during the degradation, giving data in general agreement with this postulated reaction.

We wish to report the application of high resolution solid-state ^{13}C CP/MAS spectroscopy to study the structural changes which occur during the thermal degradation of PMVK. Schaefer and Stejskal (6) first demonstrated that by employing a combination of cross-polarization (7) and magic angle spinning (8) with high-power decoupling, spectra of moderate to good resolution could be obtained from solid materials (9). The spectra yield the isotropic average value of the chemical shift (for the solid state) and can be used for structural elucidations utilizing chemical shift correlations from solution nmr studies. This technique is particularly useful for samples which are insoluble or for amorphous materials where X-ray diffraction techniques are not applicable. It is also possible to separate the contributions to the spectra from protonated and non-protonated carbons in the sample by using a pulse sequence developed by Opella and Frey (10), giving additional structural information.

The purpose of this work is to follow the structural changes occurring during the thermal degradation of PMVK by ^{13}C CP/MAS nmr to determine the nature of the solid products formed and elucidate a degradation mechanism.

Experimental

^{13}C CP/MAS spectra were recorded at 22.6 MHz using a Bruker CXP 100 spectrometer equipped with a home-built probe. Samples were run as powders in spinners (capacity ~460 μL) constructed of KEL-F (polychlorotrifluoroethylene) in an Andrew-Beams type spinning apparatus. Samples were spun at ~3 kHz using air as a driving gas.

[1] To whom all correspondence should be addressed.

Poly(methylvinylketone) was a commercially available sample (Aldrich). Heat treatments were conducted in air for the times and temperatures specified in the text. After treatment, ^{13}C solid-state spectra were recorded using CP/MAS techniques to obtain both the total spectra and those of the nonprotonated carbons using the non-protonated carbon selection procedure (10). All ^{13}C CP/MAS spectra were recorded using a 1 ms contact time and a 1 s delay between pulse sequences with a decoupling field of 12 G. The spectra are semi-quantitative under these conditions. Nonprotonated spectra were recorded under similar conditions but with the decoupler gated off for 50 μs between the cross-polarization sequence and the acquisition of the free induction decay. During the time when the decoupler is off the magnetizations of those carbons with directly bonded protons decay rapidly due to the large dipolar interactions and are not detected during the acquisition period.

Results and discussion

^{13}C solid-state chemical shift assignments were based on the ^{13}C solution chemical shifts of model compounds (cyclohexanone, cyclohexenone, 3-methylcyclohexenone). In cases where suitable model compounds could not be found, assignments were based on the expected shift for the particular functional group.

Figure 1 shows the spectra of poly(methylvinylketone) during the various stages of thermal degradation. In each case, the spectrum on the left is that of the simple CP/MAS experiment and the corresponding spectrum on the right was recorded employing the nonprotonated carbon selection experiment and therefore shows signals from only the nonproton bearing carbons in the system.

Figure 1, parts *A*, *B* show spectra of the solid, untreated polymer, with the chemical shifts indexed with respect to TMS. As indicated in Fig. 1 and in Table 1, the resonance at $\delta = 211$ ppm may be assigned to the ketone functionality and the absorption at $\delta = 49$ ppm to the methine carbons. The resonance at $\delta = 29$ ppm consists of two components, one due to the methylene carbons and one from the methyl carbons. The use of the nonprotonated carbon selection experiment discriminates between these two components, yielding the assignment given in the figure (methyl resonances still appear after this selection although with reduced intensity, due to their particular relax-

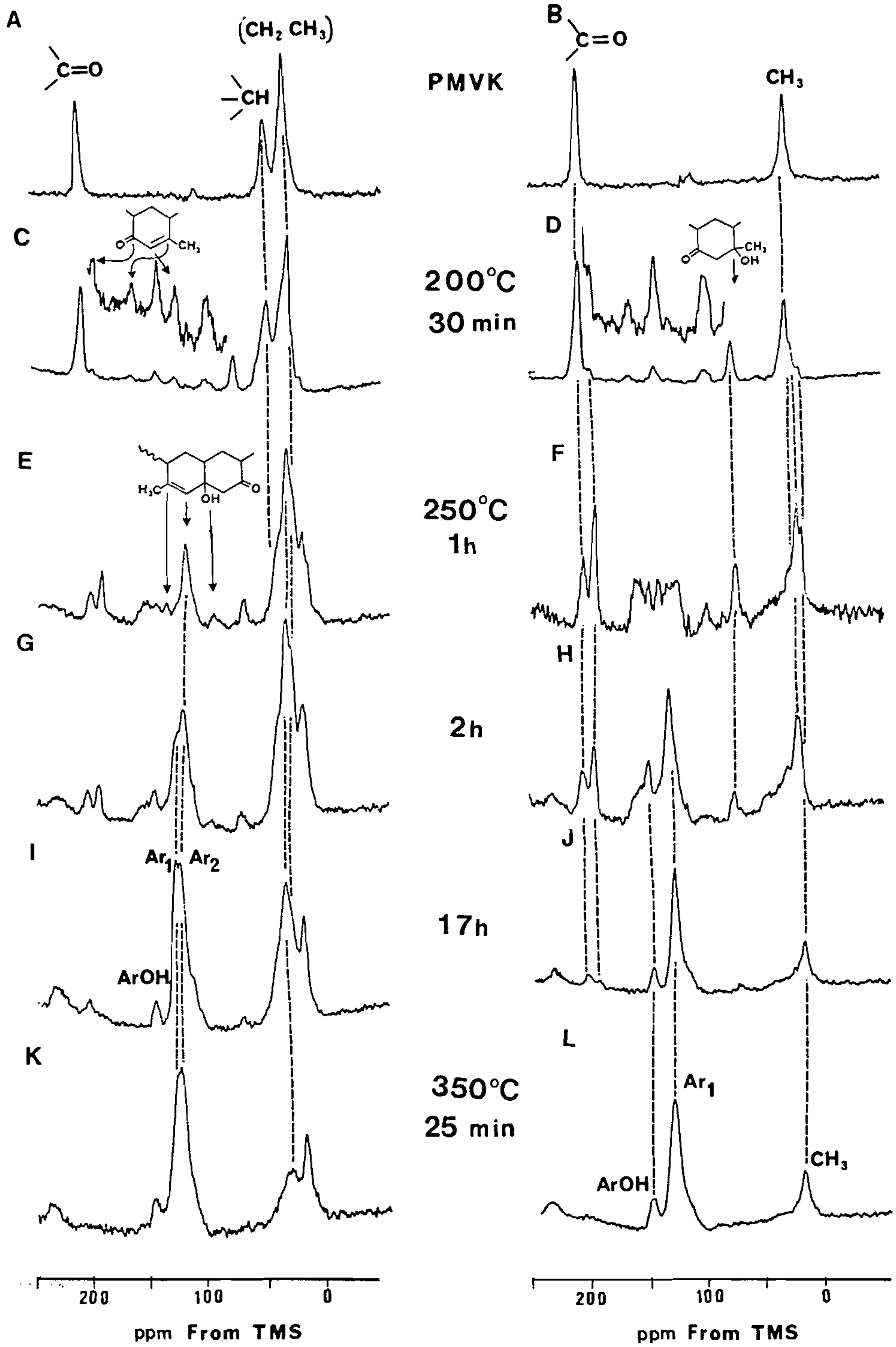

FIG. 1. ^{13}C CP/MAS spectra of PMVK during various stages of degradation. All spectra obtained with 1 ms contact and 1 s recycle delay: (*A*) undegraded polymer, 3 600 scans; (*B*) same sample as (*A*) only nonprotonated carbon selection, 16 000 scans; (*C*) spectrum of PMVK heated at 200°C in air for 30 min, 10 000 scans; (*D*) same sample as (*C*) only nonprotonated carbon selection, 33 000 scans; (*E*) spectrum of PMVK heated at 250°C in air for 1 h, 3 600 scans; (*F*) same sample as (*E*) only nonprotonated carbon selection, 6 000 scans; (*G*) spectrum of PMVK heated at 250°C in air for 2 h, 3 600 scans; (*H*) same sample as (*G*) only nonprotonated carbon selection, 13 000 scans; (*I*) spectrum of PMVK heated at 250°C in air for 17 h, 3 600 scans; (*J*) same sample as (*I*) only nonprotonated carbon selection, 6 800 scans; (*K*) spectrum of PMVK heated at 350°C in air for 25 min, 5 500 scans; (*L*) same as (*K*) only nonprotonated carbon selection, 6 000 scans.

ation properties (10)).

The effect of heating in air at 200°C for 30 min is illustrated in Fig. 1 parts *C* and *D*. The spectra indicate clearly that the degradation proceeds via the aldol condensation of adjacent $COCH_3$ groups. The small peak at δ = 201 ppm is due to a cyclic α,β-unsaturated ketone (**II**). This corresponds to the

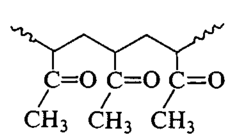

I

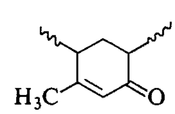

II

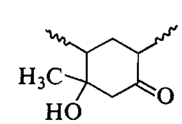

III

ketone group in 2-cyclohexen-1-one which absorbs at δ = 197.1 (11). The absorption at δ = 76 ppm is due to the hydroxyl bearing carbon of the cyclic β-hydroxy ketone (**III**). The resonance due to the carbonyl in this β-hydroxy ketone occurs at 211 ppm and is obscured by the large absorption due to the uncyclized ketone groups. Resonances at δ = 164 and 129 ppm are also assigned to the presence of the cyclic α,β-unsaturated ketone (**II**) as indicated in Fig. 1. The corresponding carbons in 3-methyl-2-cyclohexen-1-one give rise to absorptions at δ = 162 and δ = 126.5 (12). There is also a small absorption at 99 ppm thought to be due to the polycyclic alcohol (**IV**). The olefin in this structure is thought to give rise

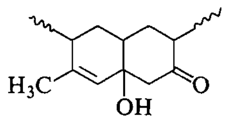

IV

to the resonances at δ = 144 ppm and contributes to the absorption at δ = 129 ppm. From the nonprotonated spectra three types of methyls can be observed. The resonance at δ = 30 ppm is due to undegraded polymer, the absorption at δ = 22 ppm is due to methyl groups adjacent to a hydroxy-bearing carbon and the peak at δ = 19 ppm results from methyl groups adjacent to an olefinic group. Table 2 summarizes the chemical shift assignments for the degraded polymer.

Heating at 250°C (Fig. 1*E*, *F*) results in further degradation of the sample. There is a substantial loss in the carbonyl absorption at δ = 211 ppm and an increase in the absorption at δ = 201 ppm due to the cyclized ketone (**II**). The major component of the resonance at δ = 211 ppm is now due to the β-hydroxyketone (**III**). There is also the appearance of additional peaks at δ = 126 and 132 ppm indicating the formation of aromatic rings which must involve loss of hydrogen along the backbone of the polymer. A peak at δ = 154 ppm indicates the formation of phenol rings from the cyclic ketone. There is a large absorption due to methylene carbons from cyclized sections of the polymer as well as between cyclized sections at δ = 34 ppm. The intensity of the phenol resonance compared with the aliphatic absorption suggests that the terminal ketone rings are the first to be aromatized. As degradation continues there is an increase in the intensity of the absorptions in the aromatic region along with a corresponding loss in the aliphatic resonances (Fig. 1, *G*, *H*, *I*, and *J*), yielding a highly aromatic structure after 17 h.

At 350°C degradation is much more rapid. Figure 1 parts *K* and *L* show spectra of a sample heated at 350°C for 25 min. The sample is now mainly aromatic in nature and contains a number of phenol rings. There are also a number of methylene groups which form the links between the aromatic sections and methyl functionalities from the terminal rings at the opposite end of the cyclized sections from the phenol ring. At this stage the spectra of the degraded poly(methylvinylketone) resemble the spectra obtained from thermally degraded phenol–formaldehyde resins (13). This indicates a similarity in the types of functionalities formed during the degradation process. Thus, from the analysis of the ^{13}C solid-state nmr spectra considerable information is obtained on the nature of the degradation process and the mechanism of degradation summarized in Scheme 1. The initial step in the degradation appears to be an aldol condensation between pendant $COCH_3$ groups to form cyclic β-hydroxyketones. This is followed by dehydration to form the

TABLE 1. ^{13}C solid-state chemical shifts (ppm from TMS) for poly(methylvinylketone) (**I**)

Functional group	Chemical shift
>C=O	211
—C(—)—H	48
$—CH_2—$	34
$—CH_3$	30

TABLE 2. ^{13}C solid-state chemical shifts (ppm from TMS) for the different functionalities observed in thermally degraded poly(methylvinylketone) samples

Functional group		Chemical shift
β-Hydroxyketone		211
α,β-Unsaturated ketone		201
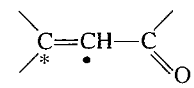	*	164
	•	129
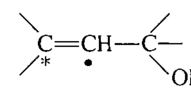	*	144
	•	129
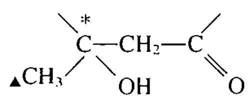	*	76
	▲	22
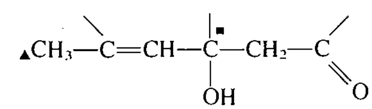	■	99
	▲	19
Ar—OH		154
Ar—H		126
Ar—C		132

cyclic α,β-unsaturated ketone. The aldol condensation then continues to ultimately form polycyclic structures. This agrees in general with the ladder-type structures proposed by other workers.

As degradation continues there appears to be formation of phenol rings, followed by a gradual aromatization of the sample. After heating at 350°C the sample consists of segments of aromatic rings (**V**). The ring at the ketone end of the segment will have a phenolic structure. At the opposite end of the segment the terminal ring will have a pendant methyl group. The sample also contains a number of methylene groups which link the aromatic sections.

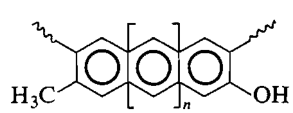

V

Conclusions

By employing the techniques of high resolution solid-state ^{13}C nmr spectroscopy it is possible to follow the reactions

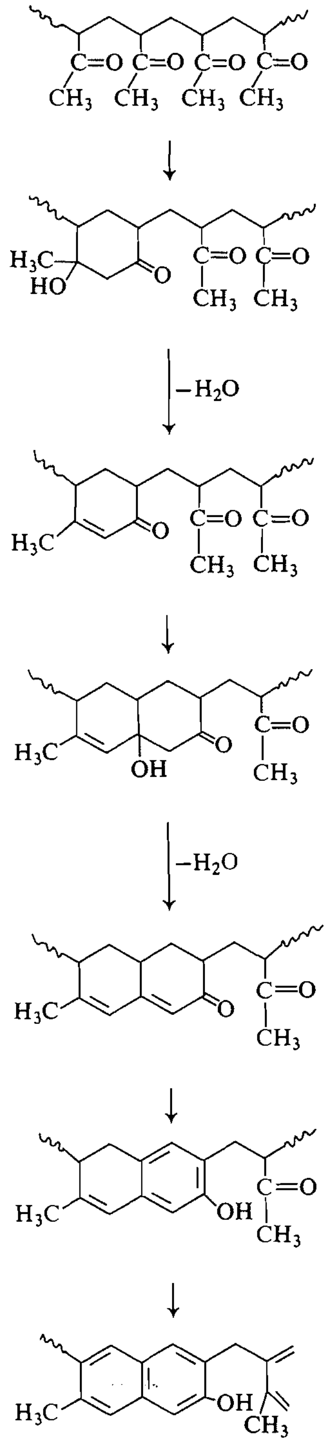

SCHEME 1

occurring during the thermal degradation of poly(methylvinylketone). The solid state spectra give considerable structural information on the nature of the solid products formed during the degradation process and on the mechanism of the degradation reaction itself.

The initial step appears to involve an aldol condensation between pendant ketone groups to form a cyclic β-hydroxy ketone, which is subsequently converted to the α,β-unsaturated ketone. The degradation continues to form polycyclic structures. At higher temperatures there is formation of phenol rings and a gradual aromatization of the sample. At 350°C the sample consists mainly of aromatic rings with a few linking methylene groups along with methyl groups.

Acknowledgement

We acknowledge the financial support of the Natural Sciences and Engineering Research Council of Canada in the form of an operating grant (C.A.F.) and a Graduate Fellowship (M.McK).

1. C. S. MARVEL and C. L. LEVESQUE. J. Am. Chem. Soc. **60**, 280 (1938).
2. J. N. HAY. Makromol. Chem. **67**, 31 (1963).
3. K. MATSUZAKI and T. C. LAY. Makromol. Chem. **110**, 185 (1967).
4. K. MATSUZAKI and S. OHSHIMA. Makromol. Chem. **164**, 269 (1973).
5. H. TANAKA and T. OTSU. J. Macromol. Sci.-Chem. **A11**, 1685 (1977).
6. J. SCHAEFER and E. O. STEJSKAL. J. Am. Chem. Soc. **98**, 1031 (1976).
7. M. G. GIBBY, A. PINES, and J. S. WAUGH. Chem. Phys. Lett. **16**, 296 (1972); A. PINES, M. G. GIBBY, and J. S. WAUGH. Chem. Phys. Lett. **16**, 273 (1972); A. PINES, M. G. GIBBY, and J. S. WAUGH. J. Chem. Phys. **59**, 569 (1973).
8. E. R. ANDREW. Prog. Nucl. Magn. Reson. Spectrosc. **8**, 1 (1971).
9. J. SCHAEFER and E. O. STEJSKAL. Topics in carbon-13 NMR spectroscopy. Vol. 3. John Wiley and Sons. 1979; Nuclear magnetic resonance in solids. The Royal Society of London. 1981; J. R. LYERLA. Contemporary topics in polymer science. Vol. 3. Plenum Publishing Corporation. 1979; W. W. FLEMING, C. A. FYFE, R. D. KENDRICK, J. R. LYERLA, H. VANNI, and C. S. YANNONI. Am. Chem. Soc. Symp. Ser. **142**, 193 (1980); R. E. WASYLISHEN and C. A. FYFE. Ann. Rev. NMR, **12**, 1 (1982).
10. S. J. OPELLA and M. J. FREY. J. Am. Chem. Soc. **101**, 5854 (1979).
11. D. H. MARR and J. B. STOTHERS. Can. J. Chem. **43**, 596 (1965).
12. J. B. STOTHERS and P. C. LAUTERBUR. Can. J. Chem. **42**, 1563 (1964).
13. C. A. FYFE, M. S. MCKINNON, A. RUDIN, and W. J. TCHIR. J. Polym. Sci.-Polym. Lett. **21**, 249 (1983); Macromolecules, **16**, 1216 (1983).

The localization of injected charges in polymers and molecular solids

CHARLES B. DUKE

Xerox Webster Research Center, 800 Phillips Road, Bldg. 114, Webster, NY 14580, U.S.A.

Received May 24, 1984

This paper is dedicated to the 10th anniversary of the Xerox Research Centre of Canada

CHARLES B. DUKE. Can. J. Chem. **63**, 236 (1985).

Polymers and molecular solids are characterized by two fundamental features: the retention of molecular identity in the solid state and the occurrence of relatively weak interactions between the individual molecular entities. The weak interactions lead to a high degree of disorder caused both by defects and by thermally induced motions of the molecules. A model of charges injected into polymers and molecular solids is developed. Photoemission and transport measurements are utilized to evaluate the parameters in this model. Results for metal free phthalocyanine are presented as an illustrative example. For molecular glasses and aromatic pendant-group polymers this analysis predicts that disorder causes injected charges to form a Fermi glass of self-trapped polarons, i.e., they occupy localized states characterized by a high degree of local atomic and electronic polarization. Successful interpretations of photoemission spectra, contact charge exchange, and injected carrier drift mobilities verify this prediction. The boundary of the Fermi-glass region of localized-state molecular-ion behavior is identified by consideration of molecular crystals in which injected charges may occupy extended energy-band states at low temperatures.

CHARLES B. DUKE. Can. J. Chem. **63**, 236 (1985).

Les polymères et les solides moléculaires présentent deux caractéristiques fondamentales: la rétention de leur identité moléculaire à l'état solide et l'existence d'interactions faibles entre les entités moléculaires individuelles. Les interactions faibles conduisent à beaucoup de désordre qui est causé tant par les défauts que par les mouvements induits thermiquement des molécules. On a développé un modèle des charges injectées dans les polymères et les solides moléculaires. On a utilisé des mesures de photoémission et de transport pour évaluer les paramètres de ce modèle. A titre d'exemple, on rapporte les résultats obtenus avec des phtalocyanines ne contenant pas de métal. Dans le cas des verres moléculaires et des polymères portant un groupe aromatique, cette analyse permet de prédire que, sous l'influence du désordre, les charges injectées forment un verre de Fermi composé de polarons auto-piégés, à savoir qu'ils occupent des états localisés caractérisés par un degré élevé de polarisation électronique et atomique locale. Des interprétations satisfaisantes de spectres de photoémission, d'échange de charge de contact et de mobilités de déplacement de substances ajoutées permettent de vérifier cette prédiction. On peut identifier la limite de la région du verre de Fermi du comportement ion-moléculaire de l'état localisé en considérant des cristaux moléculaires dans lesquels des charges injectées peuvent occuper, à basse température, des états étendus de bande d'énergie.

[Traduit par le journal]

Introduction

This paper is devoted to the construction and validation of a model for the dynamics of charge carriers injected into polymers and molecular, especially organic, films. Our theme is that most organic materials which exhibit semiconducting behavior are *not* organic semiconductors in the traditional sense of energy-band theory. Misunderstandings of this topic have persisted for decades (1), thereby greatly delaying progress in the design of commercially useful organic semiconductors (2). Our results are of particular interest because they establish an explicit link between current ideas about the role of disorder in solid state physics and traditional chemical concepts concerning the molecular origin of the electronic properties of polymers and molecular solids (3, 4). Specifically, they establish the domain of model parameters called the Fermi-glass limit, for which injected charges form molecular ions (rather than occupy extended energy-band states) the spectroscopy and dynamics of which are governed by molecular-ion chemistry.

We proceed by first examining the distinguishing features of the molecular solid state and constructing models suitable for the description of injected charges therein. Then the validity of these models in the limit of strong disorder is verified by demonstrating that they provide quantitative descriptions of valence electron photoemission, contact charge exchange, and carrier drift mobilities in pendant-group polymers and molecular glasses. Finally, we discuss the boundary of the strong-disorder (Fermi-glass) limit by considering electron drift mobilities in single-crystal naphthalene.

The molecular solid state

Molecular solids are characterized by two fundamental features: the retention of molecular identity in the solid state and the occurrence of relatively weak interactions between the individual molecular entities. The weak interactions lead to a high degree of disorder caused both by defects and by thermally-induced motions of the molecules. In addition, the hopping integrals for an excess charge carrier to move from one molecule to its neighbors are small, typically about 0.01 eV, whereas the relaxation energy of these charges due to their polarization of both the molecules on which they reside and the surrounding dielectric medium is quite large, typically over 1 eV. The combination of large relaxation energies, small hopping integrals, and copious disorder suggests that charge carriers in organic solids form a Fermi glass of self-trapped polarons, i.e., they occupy localized states characterized by a high degree of local atomic and electronic polarization (4, 5).

Models of injected charges

One-electron models

The local or extended nature of molecular-ion states in molecular solids is determined by a competition between fluctuations in the local site energies of these states (which tend to localize them) and the hopping integrals for inter-site excitation transfer (which tend to delocalize them). In order to define this fluctuation-induced localization concept more precisely, consider the one-electron Hamiltonian

$$[1] \quad H = \sum_{i,\beta} \epsilon_i(\beta) a_{i\beta}{}^{+} a_{i\beta} + \sum_{i \neq i',\beta} (t_{ii'} a_{i'\beta}{}^{+} a_{i\beta} + \text{h.c.})$$

in which i is a site index; β indicates the molecular orbital; $t_{ii'}$ designate the intermolecular hopping integrals; and $a_{i\beta}$ is the annihilation operator for an electron occupying orbital β at site i. The important new feature of polymers and molecular glasses, not present in periodic crystal lattices, is that the site energies $\{\epsilon_i\}$ and the hopping integrals $\{t_{ij}\}$ form distributions. For example, the probability of finding an eigenvalue ϵ_i with value ϵ is typically taken to be (3, 4)

$$[2] \quad P(\epsilon) = (\pi\sigma^2)^{-1/2} \exp(-[\epsilon - \epsilon(\beta)]^2/\sigma^2)$$

in which σ^2 is the sum of a number of contributions associated with various types of disorder, and $\epsilon(\beta)$ is an average eigenvalue associated with the molecular-ion state labelled by the orbital index β. Because both the $\{\epsilon_i\}$ and $\{t_{ij}\}$ form distributions, the Hamiltonian [1] is specified statistically and hence can exhibit localized as well as extended eigenstates (2–5).

The eigenfunctions and eigenvalues of Hamiltonian [1] for prescribed (e.g., experimentally measured) distributions of the $\{\epsilon_i\}$ and $\{t_{ij}\}$ cannot be determined analytically at the present time. Some qualitative results have, however, been established numerically. The features of interest here can be specified in terms of a mean site energy, ϵ, the rms deviation from this mean, $\Delta = [\langle(\epsilon_i - \epsilon)^2\rangle_{AV}]^{1/2}$, and a mean hopping integral, t (5). Injected charges are localized, i.e., they form molecular cations or anions with the solid, if

$$[3] \quad \Delta > czt \equiv cW$$

in which W is the one-electron band width and c is a dimensionless number of the order of unity which depends both on the connectivity (i.e., dimensionality) of the system and on the distribution of the $\{t_{ij}\}$. Typically $c \sim 2.5$ for (isotropic) three-dimensional systems, 1.5 for two-dimensional systems, and zero for one-dimensional systems, although some confusion currently exists in the case of two dimensions (6). Inequality [3] is believed to be satisfied in molecular glasses and in certain aromatic polymers (3–5). In these cases electrons and holes injected into the material form local, molecular radical anions and cations, respectively, rather than extended states like those characteristic of crystalline covalent semiconductors. Consequently, under these circumstances the electrons and holes are more accurately visualized as molecular ions in solution which move by carrier hopping rather than by ionic diffusion.

The traditional energy-band model describes the opposite limit when $\Delta \equiv 0$. A schematic diagram of the nature of the eigenvalue spectrum associated with eq. [1] in the various limiting cases of relative magnitudes of Δ and W is given in Fig. 1. Different classes of polymers and molecular solids exhibit systematically distinct ranges of values of Δ and W. For typical pendant-group and molecularly doped polymers, 0.1 eV $\leq \Delta \leq$ 1 eV, and $W \ll 0.1$ eV. Therefore, $\Delta \gg cW$ is clearly satisfied for these materials and, as noted above, injected charges form intrinsic local molecular ion states in pendant-group polymers or analogous extrinsic states in molecularly doped polymers. This "Fermi-glass" limit is described in panel (c) of Fig. 1. For polymers with larger hopping integrals within the individual macromolecular chains, e.g., polyacetylene, polyethylene, and polyphenylene, Δ is less than W for motion along the chain. If interchain hopping were neglected, injected charges still would be localized in these materials because c = 0 for one-dimensional systems. If strong interchain hopping

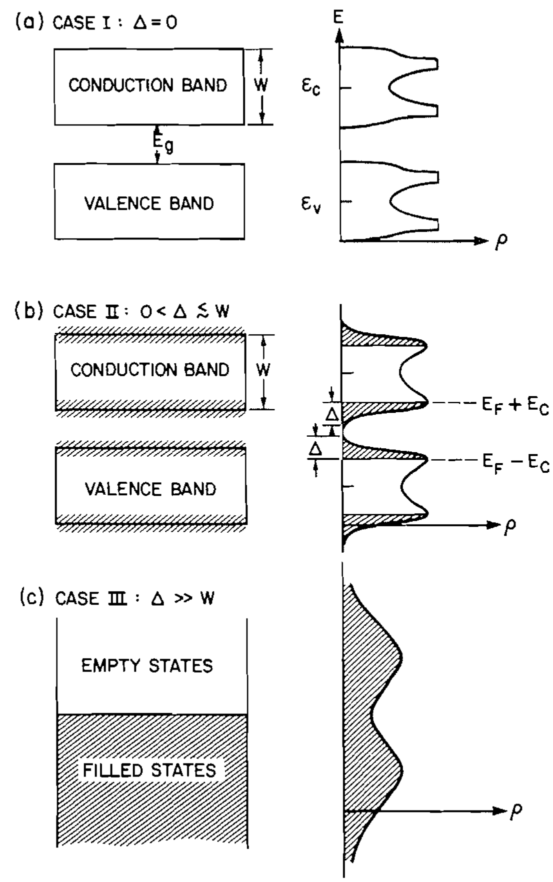

FIG. 1. Schematic indication of the consequences of static diagonal disorder (i.e., $\Delta \neq 0$, see text above inequality [3]) on the localization of one-electron states in a nominally three-dimensional solid. The symbol ρ designates the one-electron density of states. Panel (a): Case I, $\Delta = 0$, describes the traditional energy-band model. Panel (b): Case II, $\Delta < W$, where W is the one-electron bandwidth, describes the localization of electronic states at the edges of the band but not the center. E_c designates the mobility edge and E_F the bulk electrochemical potential. States closer to the band centers are extended whereas those further removed are localized. The localized states are indicated by shaded areas in the figure. Panel (c): Case III, $\Delta \gg W$, describes the situation in which all electronic states are localized and the concept of energy bands has lost its meaning (the Fermi glass model).

occurs, the polymer can become two- or three-dimensional, depending upon the packing of the macromolecular chains. This situation is described in panel (b) of Fig. 1. Such interchain interactions are thought to occur in polymers that exhibit metallic conductivity, e.g., polythiazyl, $[SN]_n$, and heavily doped polyacetylene (2).

Molecular orbital models

Since the molecular ions of interest in practical xerographic materials are "large" (i.e., azepines, benzidines, pendant-group polymers like polystyrene and poly(2-vinyl pyridine)) a description of their electronic properties requires the use of semiempirical molecular orbital methods. A spectroscopic CNDO-level model is used both for large molecules (7) and for macromolecules, i.e., polymers (8). This model affords a quantitative description of the photoemission and uv absorption spectra of over 100 polymers and large molecules (7, 8) and hence is useful for screening large classes of materials. It provides the starting point for constructing quantitative models of the electronic structure of molecular solids (4), triboelectric charge transfer (3), and transport in pendant-group and molecularly-doped polymers (9). Thus, the model affords a practical and reliable vehicle for describing the properties which are essential in electrophotographic applications. It also provides a useful way to calculate electron–molecular-vibration coupling constants (10): a critical ingredient in models of photoemission and transport in molecular solids (4, 9). A typical example of the application of the model to calculate the molecular cation density of states for comparison with photoemission (PES) data is shown in Fig. 2 for metal-free phthalocyanine, a molecule used as a photogenerator material in organic photoconductors (2).

Electron–vibration coupling: dynamic disorder and polarons

Given the existence of localized molecular ions in molecular solids, their small-polaron dynamics is established primarily by the interaction of the excess charge with those induced in the polymer matrix (4, 9). For such a purpose the Hamiltonian of eq. [1] must be extended to become

$$[4]\quad H = \sum \epsilon_i a_i^+ a_i^+ + \sum_{i \neq j} (t_{ij} a_i^+ a_j + h.c.) + \sum_{i,n} g_{in} \hbar\omega_n a_i^+ a_i (b_n + b_n^+) + \sum \hbar\omega_n (b_n^+ b_n + 1/2)$$

In eq. [4], a_i^+ designates the creation operator of an electron in an orbital of energy ϵ_i at site i, and b_n^+ that of a normal mode of vibration of energy $\hbar\omega_n$ coupled to the electronic state labelled by i via the dimensionless coupling constant g_{in}. The most obvious $\hbar\omega_n$ are the intramolecular vibrations of the molecular ions themselves (10). More important, however, are the dielectrically active normal modes of the molecular medium in which we envision the sites to be embedded. The $\hbar\omega_n$ associated with these "longitudinal polarization fluctuation" modes are obtained from the measured dielectric response of the polymer and g_{in} are specified in terms of a classical electrostatics analysis of the interaction of a charge in a prescribed molecular orbital with the dielectrically active normal modes (4). This model has been applied successfully to interpret valence-electron photoemission and uv absorption spectra of polystyrene and poly(2-vinyl pyridine), as well as photoemission from a wide variety of molecular glasses (4). Transport data are less widely available, but the model is consistent with the limited data base currently in the literature (4, 9). We conclude, therefore, that in molecular glasses (e.g., condensed ethyl benzene), pendant-group polymers (e.g., polystyrene), and molecularly-doped polymers (e.g., polycarbonate doped with trinitrofluorenone) the model defined by eq. [4] with the $\{g_{in}\}$ and $\{\hbar\omega_n\}$ obtained from measured polymer dielectric response is both necessary and sufficient for the description of the small-polaron dynamics of charges injected into these materials.

Valence electron photoemission

The main evidence for the validity of the relaxation-localization model defined by eq. [4] arises from the analysis of valence electron photoemission: a measure of eigenvalue spectrum of photogenerated molecular cations. In the Fermi-glass limit (Case III, panel (*c*), Fig. 1) the model makes three observable predictions (4). First, for molecules whose radical cation geometries are expected to be the same in the gaseous and solid phases, the valence electron photoemission spectrum in the solid state is predicted to be shifted rigidly to lower binding energies by an intermolecular relaxation energy 1 eV $\lesssim E_r$ (inter) $\lesssim$ 2 eV and broadened considerably. Second, in contrast to traditional models of solvation energies, E_r is predicted to be identical for polar and non-polar isoelectronic molecules. Third, the broadening of the spectra, although dominated by static disorder, should exhibit a characteristic temperature dependence associated with the excitation of low-frequency molecular motions upon the photogeneration of the radical cation from the neutral molecule. All three predictions have been verified, as indicated below.

Valence electron photoemission spectra from both gas-phase (11) and thin-film (12, 13) metal-free phthalocyanine are shown in Fig. 3. The fact that to within experimental reproducibility the thin film spectra are rigidly shifted and broadened versions of the gas-phase spectra is evident from the figure. In addition, all of these spectra are well described by the CNDO/S3 model (7) whose predictions already were shown in Fig. 2. Thus, we see for this particular case of a xerographic photogenerator the validity of the first prediction of the Fermi-glass limit of eq. [4]. This result also has been established for other molecular solids comprised of relatively rigid molecules (14, 15). In the case of less rigid molecules, e.g., triphenylamine and phenylenediamines, the geometry of the molecular cations can change between the gaseous and solid states, so that more complex differences occur between the valence electron photoelectron spectra characteristic of these two phases (16). Even in these cases, however, the spectra of condensed molecular films are essentially those of localized molecular cations. Therefore the task of any model of molecular cation states in condensed media (both glassy and crystalline) is the prediction of the relaxation energy shifts and large increases in widths of the photoionization lines in the condensed relative to the gaseous phase.

It might be anticipated that the intermolecular relaxation energies would be simply the static polarization energies of a molecular cation in the condensed medium given, for example, by the Born model of solvation (17). That such cannot be the case is immediately evident upon noting that nonpolar polystyrene and condensed ethyl-benzene exhibit the same relaxation-energy shifts, E_r(inter) = 1.5 eV, as polar poly(2-vinyl pyridine) and condensed 2-ethyl pyridine (4). The static dielectric constants of the polar materials are over twice those of the non-polar ones, demonstrating that static models of the relaxation energy are clearly incompatible with the observations. The relaxation-localization model specified by eq. [4] correctly predicts this result by revealing that only the high-frequency electronic branches of the longitudinal polarization spectrum, contribute to E_r(inter).

The analysis of the widths, σ, of the condensed phase photoionization lines is more complex because both static and dynamic disorder contribute to σ. Schematically, we can write

$$[5]\quad \sigma^2 = \sigma^2(\text{ins}) + \sigma^2(\text{intra}) + \sigma^2(\text{inhom}) + \sigma^2(\text{hom})$$

The instrumental width, σ(ins), is typically less than about 0.02 eV for a well designed ultraviolet photoemission spectrometer (4). The intramolecular contributions to the widths, σ(intra), vary from one molecular-ion state to another, lying in the range 0.2 eV $\lesssim \sigma$(intra) $\lesssim$ 0.4 eV (4). Usually the predominant contribution to the width in the condensed state is the inhomogeneous width σ(inhom), caused by spatial fluctuations of the electronic contributions to the relaxation energy. Typically 0.4 eV $\lesssim \sigma$(inhom) $\lesssim$ 0.6 eV depending upon sample

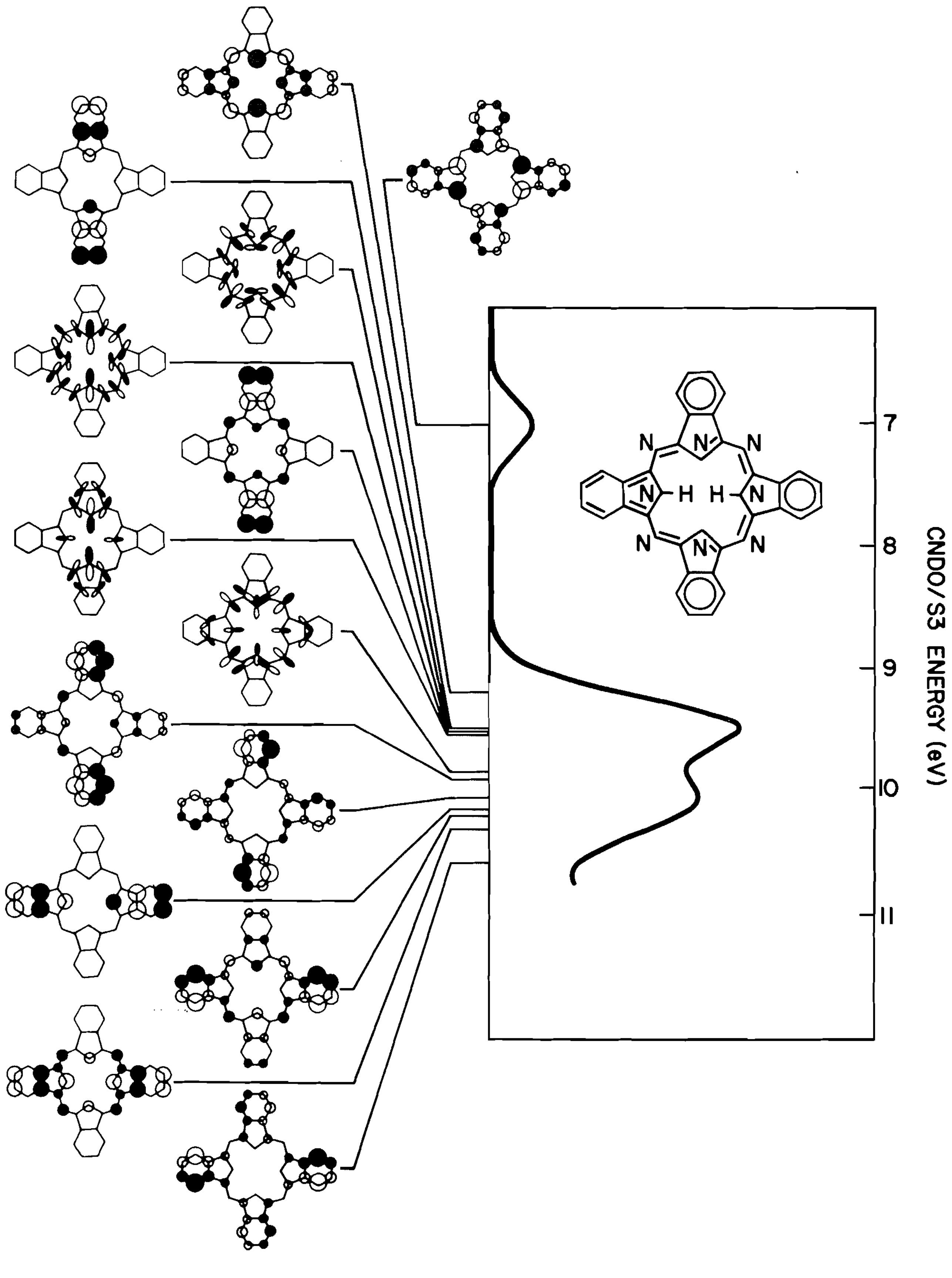

FIG. 2. Molecular-ion-state orbitals, eigenvalues, and density of states for metal free phthalocyanine predicted by the CNDO/S3 molecular orbital model (7).

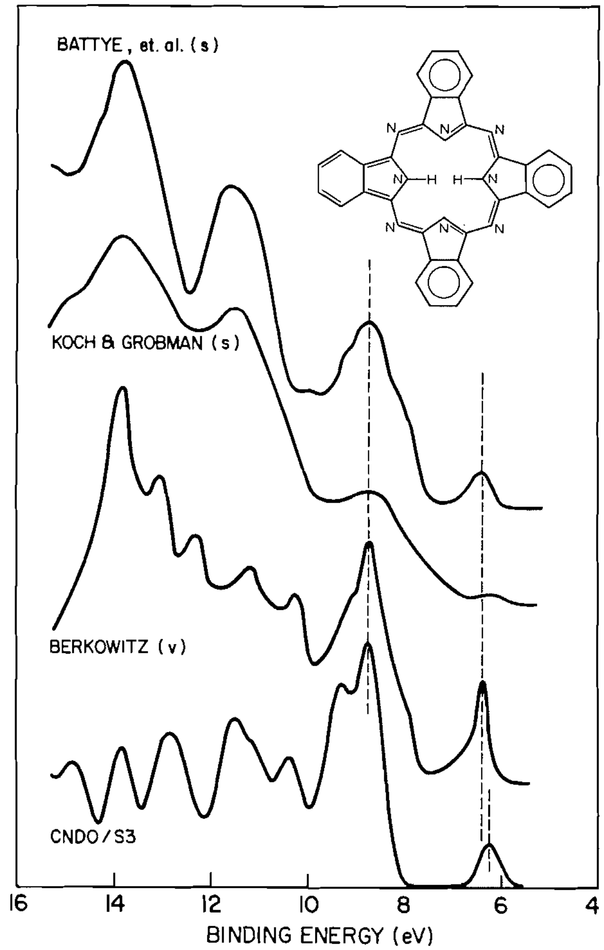

FIG. 3. Comparison of measured photoemission spectra from condensed thin-film (top two panels (12, 13)) and vapor-phase (third panel (11)) metal free phthalocyanine with the density of states calculated using the CNDO/S3 model (7). All spectra have been shifted to align the peak 8.75 eV with the vapor-phase spectrum. This procedure yields a relaxation energy shift of 5.0 eV for the thin film spectrum of Battye *et al.* (12) and of 1.3 eV for that of Koch and Grobman (13).

preparation conditions. Finally, the homogeneous contributions may be written as

$$[6] \quad \sigma^2(\text{hom}) = \sigma^2(\text{ir}) + c^2\,\kappa T$$

in which κ is Boltzmann's constant and T is the temperature. The first term arises from infrared active vibrations on all molecules including the one on which the molecular ion is formed. The second is caused by thermally excited longitudinal polarization fluctuations. It was predicted by the relaxation-localization model *a priori* (18), and subsequently observed for condensed isopropyl benzene (19) and violanthrene A (20). The model predicts 0.1 eV $\lesssim \sigma(\text{ir}) \lesssim$ 0.3 eV, but the contributions to σ from $\sigma(\text{ir})$ and $\sigma(\text{inhom})$ have not yet been separated experimentally.

Charge transport

Drift mobilities in pendant-group polymers and molecular glasses: the Fermi-glass limit

The relaxation-localization model has been applied to derive explicit expressions for electron (hole) transfer probabilities between two molecular sites in pendant-group and molecularly-doped polymers (9). These probabilities are the input data used in multiple-hopping models of measured transport properties, e.g., drift mobilities and photoconductivity. Consequently, they constitute the link between observed transport properties and the microscopic electronic structure of polymers. In particular, the model has proven useful in quantifying the trade-offs between the electrical and mechanical properties of polymers used in electrophotographic copying machines and in suggesting improved materials for such applications (9).

The model's important prediction is that of the influence of each of the different branches of the longitudinal polarization fluctuation spectrum on the electron-transfer probability. The high-frequency electronic branches, which are responsible for the photoemission relaxation energies, exert only a minor influence on electron-transfer by virtue of a temperature-independent prefactor. The low-frequency branches contribute to the activation energy for the electron transfer process as well as to the temperature-dependent widths of photoemission lines via eq. [6]. The ir branches cause the apparent activation energies to increase with increasing temperature. Thus, the model has clarified the physical basis of electron-transfer processes in condensed media as well as provided a new, more accurate mathematical expression for the transfer probabilities themselves. Its predictions are consistent with available experimental data (9).

Contact charge exchange between polymers

Although over a century of research has been devoted to contact charge exchange between insulators, prior to 1978 no model had been proposed which successfully predicted the quantitative magnitude of this charge exchange. That year a phenomenological version of the relaxation-localization model was proposed which predicted quantitatively the polymer–polymer charge exchange among various copolymers of polystyrene and poly(methyl methacrylate) in terms of effective spatially-averaged densities of molecular ion-states per unit energy, $\rho(E)$, for each polymer determined from metal-polymer contact charge exchange experiments (3). This model also predicted correctly the difference in contact charge exchange between pigmented and unpigmented polymers, and later was extended to encompass copolymers of polystyrene and poly(methyl methacrylate) with poly(2-vinyl pyridine), and copolymers of $(C_2F_3Cl)_m$ and $(C_2H_3F)_n$ (i.e., "Kel F-800") (21, 22). In addition, new data for polystyrene, poly(methyl methacrylate), and polyethylene subsequently were reported which purportedly contradicted the relaxation-localization average-density-of-states model interpretation (23). The differences between the data sets were attributed to the presence of extrinsic states and to the absence of a sufficient number of contacts to achieve adequate spatial averaging (24), however, so the original model thus far has withstood the test of time.

The relationship between the chemical properties of the polymers in question and the steady-state contact charge exchange is embedded in the parameters characteristic of the average density of states $\rho(E)$. Typically $\rho(E)$ is the form (3, 9):

$$[7] \quad \rho(E) = \rho_A(E) + \rho_D(E)$$

in which the $\rho_i(E)$ are given by eq. [2], D designates electron donors and A electron acceptors. Good donors exhibit small radical cation energies, ϵ_D, and good acceptors large radical anion energies, ϵ_A. Polar media lead to σ_i which are large and which have a temperature dependence as described in eq. [6] with large values of c. The structure of the polymer host enters

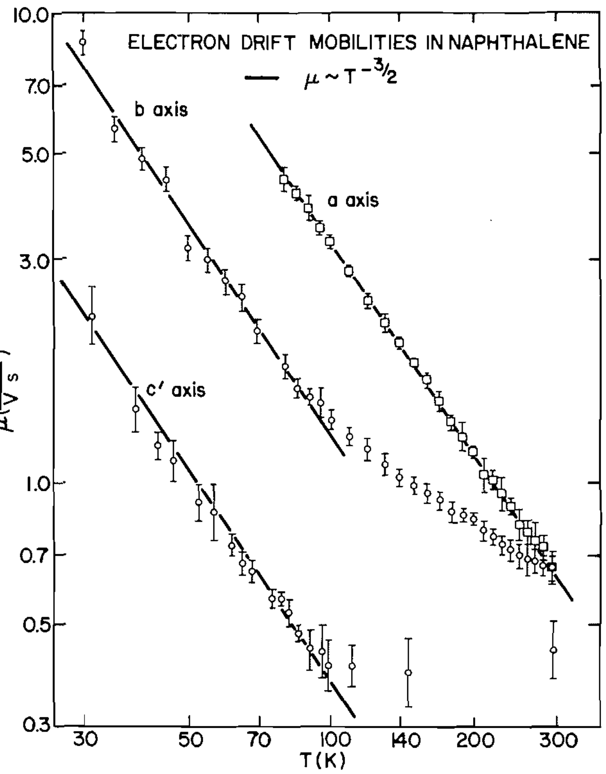

FIG. 4. Measured electron drift mobilities along the a, b, and c' directions in naphthalene as functions of temperature. The error bars are obtained as the averages of repeated runs under nominally identical conditions. The solid lines indicating $\mu \sim T^{-3/2}$ are the predictions of a Boltzmann equation analysis in which injected electrons occupy Bloch energy band states and their motion is limited via scattering by acoustical lattice vibrations (i.e., phonons) (after Andersen, Duke, and Kenkre (33), courtesy of the American Physical Society).

by virtue of more rigid (e.g., crystalline) materials tending to reduce ϵ_A, to increase ϵ_D, and to reduce σ_i^2 for a given acceptor or donor species, *ceteris paribus*. The correlation of the resulting contact charge exchange properties with measures of chemical reactivity and molecular structure have been discussed elsewhere (25). These correlations are consistent with triboelectric charge transfer occurring between relaxed molecular-ion states, typically intrinsic states localized on the pendant group moieties for polymers like polystyrene, poly(methyl methacrylate), and poly(2-vinyl pyridine).

Drift mobilities in naphthalene: the localized-extended-state boundary

The theory of the drift mobilities of charge carriers injected into semiconducting organic crystals has been a subject of debate for many years because of the occurrence in several materials of temperature and field independent mobilities (26–28) which initially proved inexplicable by either band or hopping models (26, 29). Interest in this subject was greatly stimulated when it was discovered that for exceptionally pure and perfect crystals of naphthalene the electron mobilities in the c' direction began to rise rapidly with decreasing temperature below $T \simeq 100$ K: a phenomenon interpreted as evidence for the long-anticipated band-to-hopping transition because in these materials $\Delta^2 \sim \kappa T$ so that a transition from the situation described by panel (b) in Fig. 1 to that described by panel (c) is expected with increasing temperature (30). Subsequently, additional drift-mobility data were accumulated for naphthalene, rendering it by far the most comprehensively characterized organic crystal in this regard, but the original interpretation (30) of the c' direction mobility data was questioned by virtue of the construction of a model in which the behavior exhibited by these mobilities was attributed to hopping between quasi-one-dimensional chains of naphthalene molecules (31). Thus, it seemed possible that naphthalene exhibited quasi-one-dimensional injected electron motion along the a axis at all temperatures rather than exhibiting a band-to-hopping transition at $T \simeq 100$ K for motion in the b and c' directions (29, 31, 32).

Although this saga is not yet over, its latest episode consists of a reinterpretation of the original drift mobility data in light of the recently expanded data base to reveal that a model embodying three-dimensional band motion is uniquely compatible with all the data for $T < 100$ K (33). These data and their description by acoustical-phonon-scattering limited band motion, i.e., $\mu \sim T^{3/2}$, for $T < 100$ K in all directions are shown in Fig. 4. A transition in the character of the electron motion at $T \simeq 100$ K is evident from these data which are compatible with the quasi-one-dimensional motion model for $T \gtrsim 300$ K (32). This transition is thought to constitute the boundary between localized and extended states specified by inequality [3]. The data for $T > 100$ K remain incomplete, however, so no quantitative analysis thereof is possible at this time (33).

Synopsis

Disorder-induced localization constitutes the bridge between solid-state physics and molecular-ion chemistry in condensed molecular media. Practical organic "semiconductors" typically are characterized by the Fermi-glass limit (Fig. 1, Case III, panel (c)) in which injected charges form localized molecular ions rather than occupy extended Bloch energy band states characteristic of traditional semiconductors. This fact renders local molecular-ion chemistry rather than energy-band models the appropriate predictors of the behavior of charges injected into xerographic materials. The boundary of the Fermi-glass region remains imprecisely defined, however, as revealed by the example of electron mobilities in naphthalene.

1. H. MEIER. Organic semiconductors. Verlag Chemie, Weinheim. 1974.
2. C. B. DUKE and H. W. GIBSON. *In* Kirk-Othmer: encyclopedia of chemical technology. 3rd ed. Vol. 18. John Wiley, New York. 1982. pp. 755–793.
3. C. B. DUKE and T. J. FABISH. J. Appl. Phys. **49**, 315 (1978).
4. C. B. DUKE. *In* Extended linear chain compounds. Vol. 2. *Edited by* J. S. Miller, Plenum Press, New York. 1982. pp. 59–125.
5. C. B. DUKE. Surf. Sci. **70**, 674 (1978).
6. D. WEAIRE. *In* Fundamental physics of amorphous semiconductors. *Edited by* F. Yonezawa. Springer-Verlag, Berlin. 1981. pp. 155–163.
7. C. B. DUKE. Int. J. Quant. Chem. Quant. Chem. Symp. **13**, 267 (1979).
8. C. B. DUKE and W. K. FORD. Int. J. Quant. Chem. Quant. Chem. Symp. **17**, 597 (1983).
9. C. B. DUKE and R. J. MEYER. Phys. Rev. B, **23**, 2111 (1981).
10. C. B. DUKE. Ann. N. Y. Acad. Sci. **313**, 166 (1978).
11. J. BERKOWITZ. J. Chem. Phys. **70**, 2819 (1979).
12. F. L. BATTYE, A. GOLDMAN, and L. KASPER. Phys. Stat. Sol. (b) **80**, 425 (1977).
13. E. E. KOCH and W. D. GROBMAN. J. Chem. Phys. **67**, 837 (1977).
14. C. B. DUKE, W. R. SALANECK, A. PATON, K. S. LIANG, N. O.

LIPARI, and R. ZALLEN. *In* Structure and excitations of amorphous solids. *Edited by* G. Lucovsky and F. L. Galeener. American Institute of Physics, New York. 1976. pp. 23–27.
15. W. D. GROBMAN and E. E. KOCH. *In* Photoemission in solids. Vol. 2. *Edited by* L. Ley and M. Cardona. Springer-Verlag, Berlin. 1979. pp. 261–298.
16. C. B. DUKE, J. W-P. LIN, A. PATON, W. R. SALANECK, and K. L. YIP. Chem. Phys. Lett. **61**, 402 (1979).
17. R. R. DOGONADZE and A. A. KORNSHEV. J. Chem. Soc. Faraday Trans. II, **70**, 1121 (1974).
18. C. B. DUKE. Mol. Cryst. Liq. Cryst. **50**, 63 (1979).
19. W. R. SALANECK, C. B. DUKE, W. EBERHARDT, E. W. PLUMMER, and H. FREUND. Phys. Rev. Lett. **45**, 280 (1980).
20. N. SATO, K. SEKI, H. INOKUCHI, Y. HARADA, and T. TAKAHASHI. Solid State Commun. **41**, 759 (1982).
21. T. J. FABISH. Crit. Rev. Solid State Mater. Sci. **8**, 383 (1979).
22. T. J. FABISH and H. R. THOMAS. Macromolecules, **13**, 1487 (1980).
23. G. A. COTTRELL, J. LOWELL, and A. C. ROSE INNES. J. Appl. Phys. **50**, 374 (1979).
24. T. J. FABISH, C. B. DUKE, M. L. HAIR, and H. M. SALTSBURG. J. Appl. Phys. **51**, 1247 (1980).
25. H. W. GIBSON. *In* Modification of polymers. *Edited by* C. E. Carraher, Jr. and I. A. Moore. Plenum, New York. 1983. pp. 353–372.
26. L. B. SCHEIN. Phys. Rev. B, **15**, 1024 (1977).
27. L. B. SCHEIN. Chem. Phys. Lett. **48**, 571 (1977).
28. L. B. SCHEIN and A. R. MCGHIE. Chem. Phys. Lett. **62**, 356 (1979).
29. C. B. DUKE. Festkörperprobleme, **22**, 21 (1982).
30. L. B. SCHEIN, C. B. DUKE, and A. R. MCGHIE. Phys. Rev. Lett. **40**, 197 (1978).
31. H. SUMI. J. Chem. Phys. **75**, 2987 (1981).
32. C. B. DUKE. *In* Organic molecular aggregates. *Edited by* P. Reineker, H. Haken, and H. C. Wolf. Springer-Verlag, Berlin. 1983. pp. 11–19.
33. J. D. ANDERSEN, C. B. DUKE, and V. M. KENKRE. Phys. Rev. Lett. **51**, 2202 (1983).

X-ray methods for quantitative determination of inorganic fillers in paper

TERRY L. BLUHM, ARTHUR Y. JONES, AND YVES DESLANDES
Xerox Research Centre of Canada, 2660 Speakman Drive, Mississauga, Ont., Canada L5K 2L1

Received December 30, 1983

TERRY L. BLUHM, ARTHUR Y. JONES, and YVES DESLANDES. Can. J. Chem. **63**, 243 (1985).

X-ray diffraction methods have been investigated as means of quantifying filler contents of paper. Both an "internal standard method" and an "absorption−diffraction method" were applied. Because of preferential orientation of the filler particles in commercial paper samples, the "internal standard method" was modified to include an empirical evaluation of the proportionality constant, K. Values of K specific for each filler material investigated (clay, calcite, talc, and titanium dioxide) were obtained by X-ray diffraction intensity measurements on standard papers containing different amounts of each filler. These values of K were then used to calculate the filler content of various commercial papers. The filler contents of these same commercial papers were also determined using the X-ray "absorption−diffraction method" and ash determination. Comparisons made among results from all these methods indicated that both X-ray methods give acceptable agreement with ash determination, but that the "absorption−diffraction method" is preferred due to its ease of application. In addition, the X-ray methods are more rapid and versatile than ash determination.

TERRY L. BLUHM, ARTHUR Y. JONES et YVES DESLANDES. Can. J. Chem. **63**, 243 (1985).

Deux méthodes de diffraction des rayons-X, "méthode du standard interne" et "absorption−diffraction," ont été utilisées pour la quantification des pigments inorganiques dans le papier. A cause de la présence d'une orientation préférentielle des particules de pigments dans des feuilles de papier commerciaux, la "méthode du standard interne" a été modifiée en utilisant une évaluation empirique de la constante de proportionalité K. Pour chaque pigment étudié (argile, calcite, talc et dioxide de titane) une valeur de K a été obtenue par la mesure des intensités rayons-X obtenus de papiers expérimentaux qui contenaient différentes quantités de pigments. Ces valeurs de K ont ensuite été utilisées pour évaluer la quantité en pigments dans des papiers commerciaux. Les contenus en pigments de ces derniers ont également été déterminés par la méthode "absorption−diffraction" et par détermination des cendres. Après comparaison des résultats obtenus par ces trois méthodes, il apparaît que la méthode "absorption−diffraction" soit préférée à cause de sa facilité d'application. De plus, les méthodes utilisant la diffraction des rayons-X sont plus rapides et plus versatiles que la méthode classique de détermination des cendres.

Introduction

Paper is composed of a mat of wood fibers bonded together by surface hydrogen bonds. It also contains some filler materials, usually incorporated to improve the optical properties (whiteness, opacity, etc.) of the sheet (1, 2). Typical plain xerographic paper made in North America consists of about 80% wood fiber, of which one quarter is softwood and three quarters are hardwood. The sheet also contains about 10% clay fillers and titanium dioxide, 5% starch, 5% water, and small amounts of various chemical additives such as rosin size and retention aids. However, the materials used as fillers around the world vary according to their availability and economic factors. Important considerations for the selection of a filler include optical properties, low cost, and compatibility with the paper-making process.

Most xerographic papers made in North America contain approximately 10% kaolin ($Al_2O_3 \cdot 2SiO_2 \cdot 2H_2O$), which is commonly known as clay, a naturally occuring, fine grain, well crystallized mineral composed of platelet-like particles. This hydrated aluminum silicate is extracted from the ground in various grades. Small amounts of titanium dioxide particles (~1 μm in diameter) are incorporated in paper to increase the whiteness of the sheet. The "anatase" crystal form is usually used in paper since it is cheaper than the "rutile" form. TiO_2 is, however, more expensive than clay and is therefore usually found only in small quantities in paper.

In Europe, calcite ($CaCO_3$) is extensively used as filler. European xerographic papers contain large quantities of calcite which is relatively inexpensive and compatible with the alkaline sizing treatment widely used in Europe. Particle size may vary from 1 to 10 μm. Calcium carbonates can be found occurring naturally or precipitated from limestone.

Most Japanese papers contain significant quantities of talc as filler. In Japan, talc costs about 50% less than clay. The designation of talc covers a wide range of natural products. The theoretical formula corresponds to a weight ratio of MgO to SiO_2 of about 1:2, but in actual samples this ratio may reach 1:1. Since the composition of talc is variable, it is understandable that there are many grades offered as commercial pigments.

In view of the large variety of fillers that are found in various xerographic as well as non-xerographic papers, we have undertaken a study examining the usefulness of X-ray analytical techniques for the quantitative determination of inorganic fillers in paper. It is clear that other analytical methods have been known for many years, but they suffer from various drawbacks. For example, ash determination (3), currently used in the paper industry, provides only the value of total ash, independent of the chemical composition. For analysis of each individual component, a complex "wet" chemistry method must be used (3), making the whole process very time consuming unless the laboratory is well equipped for continuous analysis. More sophisticated techniques such as energy dispersive X-ray analysis (EDAX) can be extremely accurate, but they do not provide an overall measure of filler content since EDAX is a surface technique (penetration of 3 μm only). X-ray fluorescence is a valuable method for elemental determination of fillers in paper, however, quantitative determination of the actual individual mineral phases cannot be made. For instance, the rutile and anatase forms of TiO_2 cannot be distinguished using this method, and since both clay and talc contain silicon atoms, these phases cannot be uniquely determined. The combination of X-ray diffraction and EDAX methods has been used successfully for the identification of both crystalline and amorphous fillers (4). Finally, fillers have also been analyzed by microscopic methods. However, these methods only provide qualitative information (5).

X-ray diffraction methods (6) have been used for a long time as a qualitative means of identification of inorganic fillers in paper and are extensively used for quantitative determination of mixed crystalline powder phases. Therefore, we have sought to extend these quantitative methods to the analysis of paper sheets. We report here results using two methods of X-ray quantitative analysis; (*i*) an internal standard method and (*ii*) absorption–diffraction method, for determination of inorganic fillers in cut paper sheets.

Methods

It has been widely observed that the intensity of diffraction peaks arising from various crystalline components in a mixture are greatly affected by the X-ray absorptivity of the components in the mixture. Peaks of the weakly absorbing component appear relatively weak and those of the strongly absorbing species are relatively stronger. Alexander and Klug (7) first arrived at a mathematical relationship relating the intensity of diffraction lines to the absorptivity of the sample as follows:

$$[1] \quad I_{iJ} = \frac{K_{iJ}x_J}{\rho_J\mu^*}$$

where I_{iJ} = intensity of peak i of component J of a mixture, x_J = weight fraction of component J in a mixture, ρ_J = density of solid component J, μ^* = mass absorption coefficient of the sample, and K_{iJ} = a constant depending on the nature of component J and the geometry of the diffractometer. The mass absorption coefficient of the sample, μ^*, can be related to the mass absorption coefficient of the Jth component, μ^*_J and that of the matrix surrounding the Jth component, μ^*_M, as follows:

$$[2] \quad \mu^* = x_J\mu^*_J + (1 - x_J)\mu^*_M$$

For paper where the Jth component is a filler $\mu^*_J \neq \mu^*_M$. μ^*_J can be calculated from a table of mass absorption coefficients for the various elements assuming that the elemental composition of the Jth component is known:

$$[3] \quad \mu^*_J = \sum x_i\mu^*_i$$

where the x_i are the weight fraction of the elements and the μ^*_i are the mass absorption coefficients for the elements in the compound J. However, μ^*_M can not be calculated as the composition of the matrix is not known. These circumstances necessitate the use of indirect methods of analysis by use of an internal standard.

Internal standard method

In using the internal standard method a known amount of a standard component, S_1 is added to the sample. Without going into the mathematics, a detailed discussion of which can be found in ref. 7, the following equations are obtained:

$$[4] \quad \frac{I_{iJ}}{I_{kS}} = K\frac{x_J}{x_S}$$

where I_{iJ} = intensity of the ith peak of component J in the matrix, I_{kS} = intensity of the kth peak of the internal standard in the mixture, x_J = weight fraction of component J, x_S = weight fraction of the internal standard added, and K = constant dependent on the mass absorption coefficients of the matrix and Jth component.

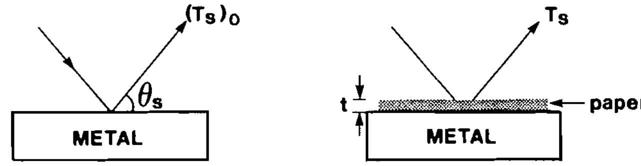

FIG. 1. Schematic of the arrangement used for the absorption–diffraction method.

$$[5] \quad K = \frac{(I_{iJ})_0\mu_J}{(I_{kS})_0\mu_S}$$

where μ_J = mass absorption coefficient of component J, μ_S = mass absorption coefficient of internal standard, $(I_{iJ})_0$ = intensity of ith peak of pure component J, and $(I_{kS})_0$ = intensity of kth peak of pure internal standard.

Equation [5] presented above is valid only when the particles in the sample are small (<3–5 μm) and no preferred orientation of particles is present in the sample. In paper, filler particles are often larger than 3–5 μm in size and they can not be ground to smaller size without completely destroying the paper sheet. Also, in the case of some fillers (i.e., kaolin and talc) the particle shape is anisotropic and some preferred orientation of the particles along the oriented wood fiber network is often present (8). Therefore, we chose to use a semi-empirical approach to the problem. Instead of calculating the value of K by using eq. [5], several sheets of paper were made containing various fillers, as described in the Experimental section, and K was determined from the slope of plots of x_J/x_S vs. I_{iJ}/I_{kS}. The value of K determined in this manner will henceforth be referred to as K'.

Absorption–diffraction technique

From eq. [1] it can be shown that

$$[6] \quad x_J = \frac{\mu^* I_{iJ}}{\mu_J^*(I_{iJ})_0}$$

In this equation the only unknown quantity is μ^*, the mass absorption coefficient of the mixture. If μ^* can be measured for the mixture using an X-ray powder diffractometer in the same geometry as that with which I_{iJ} and $(I_{iJ})_0$ are measured, the weight fraction, x_J, of a component can be determined. A method has been developed (9) using a thin layer of powder mounted on the surface of a fine grained metal where diffracted X-rays from the metal are attenuated by the powder (Fig. 1). The ratio of the intensities of a metal diffraction peak with, and without, the powder layer in place is given by the following equation;

$$[7] \quad \frac{T_s}{(T_s)_0} = e^{-2t\mu^*\rho/\sin\theta_s}$$

where T_s = intensity of metal diffraction with powder layer, $(T_s)_0$ = intensity of metal diffraction without powder layer, t = thickness of the powder layer, ρ = bulk density, θ_s = Bragg angle of the diffraction peak, and μ^* = mass absorption coefficient of the powder.

Combining eqs. [6] and [7] and introducing the parameters, A, the cross-sectional area of the beam at the sample; B, the area of the sample illuminated; and W, the weight of the paper sample illuminated, one obtains

$$[8] \quad x_J = \frac{-I_{iJ}}{(I_{iJ})_0} \times \frac{B\sin\theta_s}{AW} \times \frac{\log\,[T_s/(T_s)_0]}{1 - [T_s/(T_s)_0]^r}$$

in which $r = \sin\theta_s/\sin\theta_{iJ}$.

If we define

$$[9] \quad P_{iJ} = (I_{iJ})_0 \frac{A}{B}$$

then

$$[10] \quad x_J = \frac{-I_{iJ}\sin\theta_s}{WP_{iJ}} \times \frac{\log\,[T_s/(T_s)_0]}{1-[T_s/(T_s)_0]^r}$$

and P_{iJ} is constant for a given diffraction peak i of component J when A and B are invariant.

Paper is an ideal sample for the absorption–diffraction technique since the thickness is uniform and easily measured. Use of this method also eliminates the need to add an internal standard to the paper sheets which is often troublesome and introduces inaccuracy to the measurement.

Experimental

Three sets of standard papers were prepared using the Centrifugal Dynamic Vertical Sheet Former (Allimand 38140, Rives, France) which allows the preparation of papers having filler distributions similar to commercial papers (10). The basic furnish consisted of a 70:30 mixture of hardwood kraft pulp and softwood kraft pulp. Each set of papers consisted of five sheets with each sheet containing different amounts of fillers. The first set of papers contained varying amounts of calcite and clay (kaolin), the second set contained calcite and talc, while the third set contained calcite and titanium dioxide (anatase). These standard sets were used for the determination of K' values described in the Method section above. In our model papers, calcite was always present because we wanted to use the X-ray methods for determination of at least two fillers in the presence of each other. The quantity of filler added to a paper furnish is not totally retained in the final paper sheet. Therefore, the filler content actually present in the finished paper sheet was determined by ashing. Since calcite liberates CO_2 at around 600°C, it is possible to determine the percentage of both fillers by ashing at 575°C and at 925°C. Also, the four materials examined, clay, calcite, talc, and titanium dioxide, are the most commonly found fillers in xerographic papers.

X-ray diffraction data were collected using a Philips Automated X-ray Powder Diffractometer Model PW 1050/80 fitted with a proportional counter, pulse-height analyzer, and a graphite crystal monochromator placed in the diffracted beam. The design of the powder diffractometer is shown schematically in Fig. 2. The radiation used was Ni filtered CuK_α ($\lambda = 0.1542$ nm).

For the internal standard method, the internal standard chosen was finely ground NaCl producing a strong diffraction line at $2\theta = 31.7°$, not overlapping with lines from any of the filler analytes. The internal standard was added to the paper by pressing the finely divided powder into the surface of the sheet. The amount of sodium chloride added to each sheet was determined by weighing. Sample stacks consisting of four sheets each cut into squares 3 cm on a side were used for X-ray measurements. These paper squares were placed in a standard X-ray powder diffractometer sample holder as provided by Philips Electronics.

In the X-ray absorption–diffraction method of analysis no internal standard was required. The standard silicon wafer provided with the X-ray powder diffractometer was used for standard intensity measurement of the $2\theta = 26.1°$ diffraction line. Single thickness paper sheets cut approximately 2 cm × 2 cm were placed on top of the silicon wafer for measurement of diffraction line intensities as described in the Methods section. All intensities were determined by scanning across the diffraction peak at a 2θ scan rate of 1 deg per min and collecting the total number of counts recorded by the proportional counter. Background corrections were made by adding the number of counts collected during one-half of the scan time at each side of the diffraction peak and, subsequently, subtracting this total from the number of counts obtained while scanning across the peak.

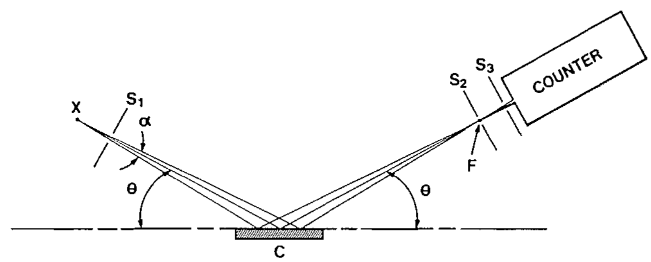

FIG. 2. Optical arrangement of a typical vertical goniometer of the powder diffractometer. S_1, collimating slit; S_2 and S_3, receiving slits; C, sample; X, X-ray source.

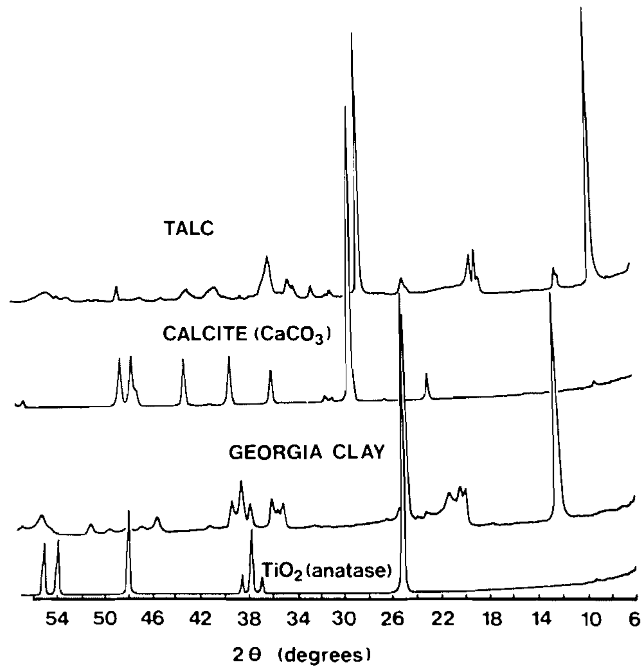

FIG. 3. X-ray diffraction traces of common paper fillers.

Results

Figure 3 shows the X-ray powder diffractometer traces of the four most widely encountered fillers in paper. Each material is characterized by a unique trace with peaks observed at specific values of 2θ. It is possible to use these traces to identify the components present in the sheet, and then, by measuring the intensity of the selected peaks, to estimate the quantity of each inorganic material.

(a) Internal standard method

Figures 4 to 6 represent X-ray powder diffractometer traces of representative samples for each of the three standard paper sets described in the Experimental section. On these traces, it is possible to identify the peaks due to cellulose, the major component of wood, and the peaks due to the filler materials. Only the peaks used for the quantification are identified on the figures.

Table 1 summarizes the data obtained from these control sheets. Diffraction peaks for measurement of I_{iJ} were chosen so as not to overlap severely with the peak of NaCl at $2\theta = 31.7°$. In these measurements, since a proportional counter was used, the errors in the I_{iJ} values are equal to $(I_{iJ})^{1/2}$.

A plot of the ratio of the intensity of the peak of the filler to the peak of the standard versus the ratio of the weight fraction

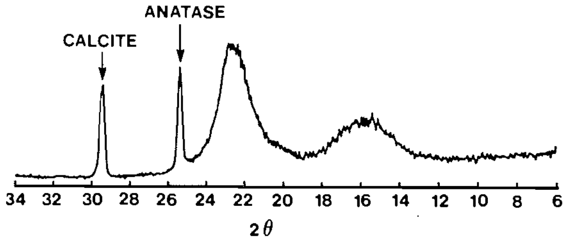

FIG. 4. X-ray diffractometer trace of paper sample containing titanium dioxide (anatase) and calcium carbonate.

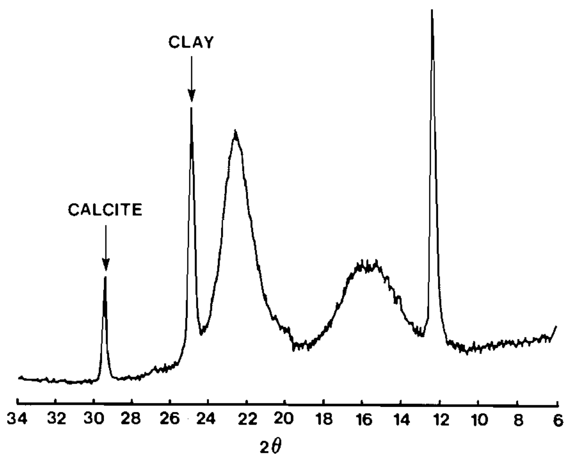

FIG. 5. X-ray diffractometer trace of paper sample containing clay and calcium carbonate.

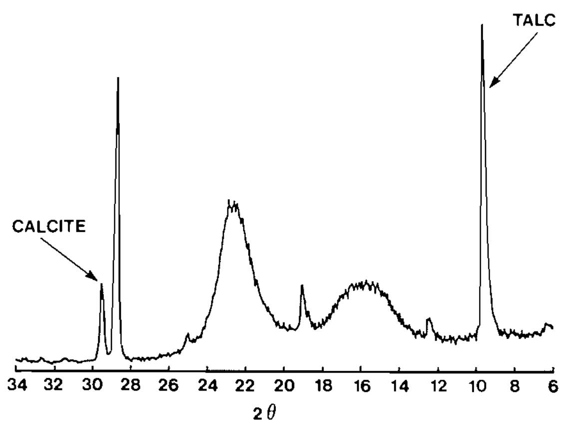

FIG. 6. X-ray diffractometer trace of paper sample containing talc and calcium carbonate.

TABLE 1. Experimental data collected from the standard paper samples, all intensities reported in counts.

(*a*) Anatase ($2\theta_{iJ}$ = 25.3°; $2\theta_{ks}$ = 31.7°)

Sample No.	I_{iJ}	I_{ks}	x_s	x_J (ash)
1	4067	238	0.011	0.158
2	1963	172	0.008	0.117
3	1411	301	0.015	0.075
4	636	459	0.019	0.031
5	1380	307	0.018	0.077

(*b*) Calcite ($2\theta_{iJ}$ = 29.3°; $2\theta_{ks}$ = 31.7°)

Sample No.	I_{iJ}	I_{ks}	x_s	x_J (ash)
1	570	330	0.015	0.043
2	770	400	0.017	0.084
3	1575	285	0.013	0.125
4	2173	300	0.020	0.163
5	1032	286	0.015	0.084
6	325	238	0.011	0.033
7	775	172	0.008	0.075
8	958	307	0.018	0.074
9	1875	459	0.019	0.156
10	1289	301	0.015	0.118
11	700	1938	0.035	0.030
12	2304	1382	0.247	0.190
13	2040	1258	0.173	0.160
14	1697	1975	0.103	0.080
15	684	694	0.039	0.040

(*c*) Clay ($2\theta_{iJ}$ = 24.8°; $2\theta_{ks}$ = 31.7°)

Sample No.	I_{iJ}	I_{ks}	x_s	x_J (ash)
1	1026	1938	0.048	0.040
2	474	1382	0.073	0.050
3	990	1258	0.054	0.080
4	2656	1975	0.060	0.140
5	2129	706	0.027	0.110

(*d*) Talc ($2\theta_{iJ}$ = 9.2°; $2\theta_{ks}$ = 31.7°)

Sample No.	I_{iJ}	I_{ks}	x_s	x_J (ash)
1	6630	330	0.015	0.154
2	3580	400	0.017	0.113
3	2316	285	0.013	0.073
4	867	300	0.020	0.030
5	2830	286	0.015	0.073

of the filler (as determined by ashing) to the weight fraction of the internal standard (as determined by gravimetric analysis) are shown in Figs. 7 to 10. Values of K', which are determined by calculating the slope of these curves, are tabulated in Table 2. These values of K' can now be used in the determination of unknown filler content in other paper sheets.

The measured values of K' were then used to determine the amount of fillers in five selected samples of xerographic papers again using NaCl as internal standard. Diffractometer traces of these samples, labelled sample A, B, C, D, and E, are shown in Fig. 11. The total filler content of these papers was also obtained by ash determination. The results of this analysis along with results of ash determination are shown in Table 3. In the cases where more than one filler component was found in the paper, only the total filler content can be determined by ash determination.

(b) Absorption–diffraction method

The absorption–diffraction method was evaluated by determining the filler content of the same xerographic papers listed above. Values of P_{iJ} were calculated from the known geometrical parameters of the diffractometer and using values of $(I_{iJ})_0$ measured under the same conditions as for measurement of I_{iJ} values. The standard anatase, calcite, clay, and talc samples used were the same as those commonly used in the paper-making process. Equation [10] was used for calculation of the weight fraction of fillers. Values of A, B, $(I_{iJ})_0$, and P_{iJ} are reported in Table 4. The filler content in the five xerographic

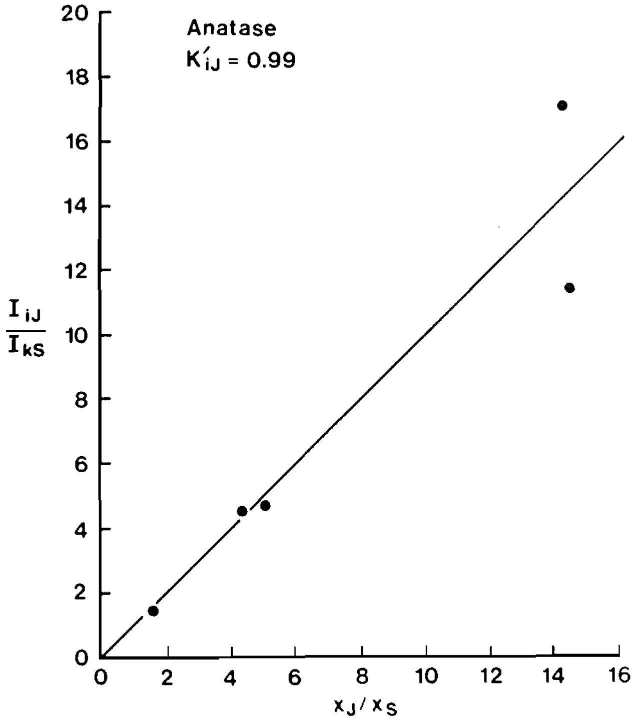

FIG. 7. Plot of I_{iJ}/I_{kS} versus x_J/x_S for anatase.

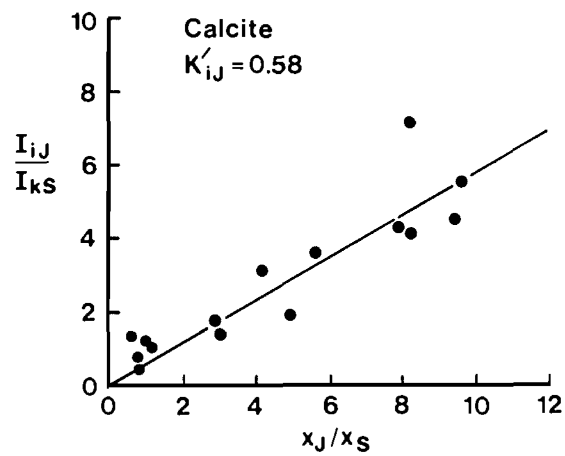

FIG. 8. Plot of I_{iJ}/I_{kS} versus x_J/x_S for calcium carbonate in paper.

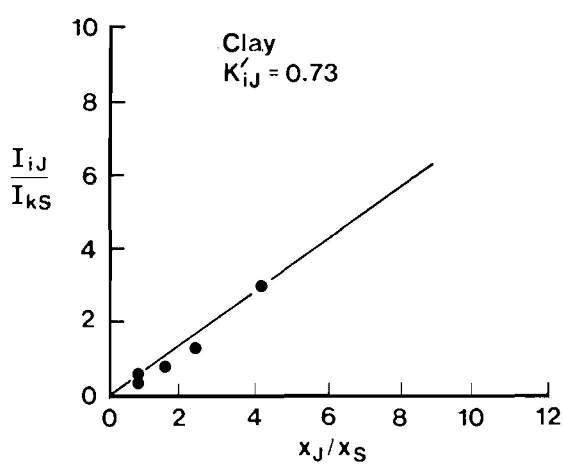

FIG. 9. Plot of I_{iJ}/I_{kS} versus x_J/x_S for clay.

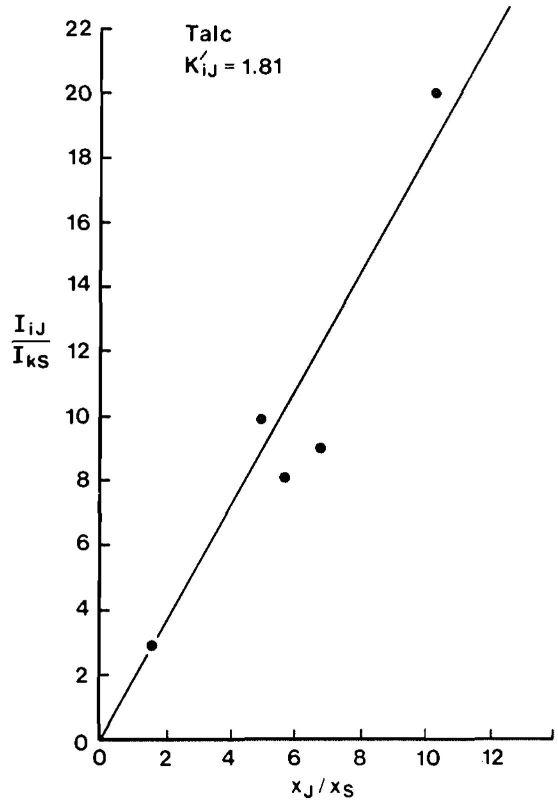

FIG. 10. Plot of I_{iJ}/I_{kS} versus x_J/x_S for talc.

TABLE 2. Measured values of K' for the different fillers investigated

Filler	K'
Anatase	0.99
Calcite	0.58
Clay	0.73
Talc	1.81

papers determined using this method are reported in Table 5 along with those from ash determination.

Conclusions

Quantitative results of the method using an internal standard are very comparable with results obtained from the absorption–diffraction technique. Also, in almost all papers investigated, the agreement between ash and X-ray results is fairly good with the exception of sample B where high values of calcite content are found by both the absorption–diffraction and internal standard X-ray methods. Since this paper is made in Europe, it is possible that differences in crystallinity exist between calcite used in Europe and in North America. Since the evaluation of K' for the internal standard method and of $(I_{iJ})_0$ for the absorption–diffraction method were made using papers containing North American calcite, it is possible that these values cannot be used to analyze papers made with a calcite from different sources. This observation points to the fact that one should determine the parameters mentioned above with the same fillers as are actually used in the analyzed papers.

The average deviation between results from X-ray diffraction analysis and results from ash determination for both meth-

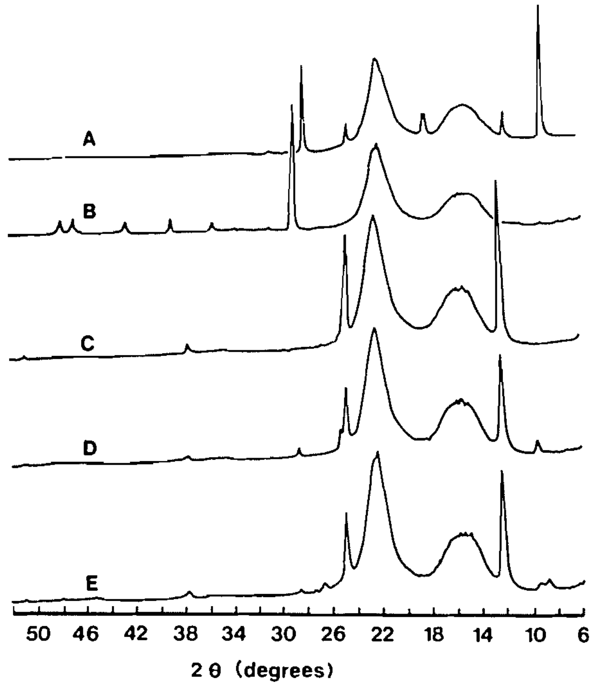

FIG. 11. X-ray diffractometer traces of five commercial xerographic papers.

TABLE 3. Filler concentration in five commercial xerographic papers as determined by X-ray diffraction (internal standard method) and ash determination

Xerographic paper	Filler	x_j (X-ray)		x_j (ash)
Sample A	Clay	0.028	0.097	0.093
	Talc	0.069		
Sample B	Calcite	0.269		0.190
Sample C	Clay	0.116		0.094
Sample D	Anatase	0.012	0.107	0.101
	Clay	0.091		
	Talc	0.004		
Sample E	Clay	0.098	0.100	0.096
	Talc	0.002		

ods of X-ray analysis is 15%, which seems acceptable in view of the heterogeneity of paper and its fluctuating water content. However, in our view the use of an internal standard is more difficult in practice since great care must be used in adding the internal standard and it is necessary to prepare a set of standard papers. Use of eq. [5] for calculation of K' was not successful, presumably because of preferred orientation and microabsorption effects in the paper samples.

TABLE 4. Values of the parameters used in the absorption–diffraction method

Filler	A (cm^2)	B (cm^2)	$(I_{ij})_0$ (counts)	P_{ij} (× 10^3)
Anatase	0.45	2.10	18629	3.99
Calcite	0.45	1.78	20104	5.08
Clay	0.45	2.10	26638	5.71
Talc	0.45	3.00	10310	1.55

TABLE 5. Filler concentration in five commercial xerographic papers as determined by X-ray diffraction (absorption–diffraction method) and ash determination

Xerographic paper	Filler	x_j (X-ray)		x_j (ash)
Sample A	Clay	0.013	0.115	0.093
	Talc	0.102		
Sample B	Calcite	0.246		0.190
Sample C	Clay	0.102		0.094
Sample D	Anatase	0.011	0.094	0.101
	Clay	0.066		
	Talc	0.017		
Sample E	Clay	0.079	0.084	0.096
	Talc	0.005		

Therefore, we conclude that the absorption–diffraction method of quantitative analysis using X-rays provides a rapid and moderately accurate method of determination of inorganic fillers in paper. This method is preferred over the use of an internal standard.

1. K. W. BRITT. Handbook of pulp and paper technology. Van Nostrand Reinhold Company, New York. 1970.
2. T. C. PATTON. Pigment handbook. Wiley-Interscience, John Wiley and Sons, New York. 1973.
3. B. L. BROWNING. Analysis of paper. 2nd ed. Marcel Dekker Inc., New York, NY. 1977.
4. R. A. PARHAM and J. D. HULTMAN. TAPPI, **59**(1), 152 (1976).
5. H. C. KOCH, C. E. BRANDON, and K. P. GEOHEGAN. TAPPI, **34**(6), 265 (1951).
6. C. L. GAREY and J. W. SWANSON. TAPPI, **43**(10), 813 (1960).
7. L. ALEXANDER and H. P. KLUG. Anal. Chem. **20**, 886 (1948).
8. P. R. SUNDARARAJAN. TAPPI, **64**, 111 (1981).
9. P. P. WILLIAMS. Anal. Chem. **31**, 1842 (1959).
10. E. ANCZUROWSKI, A. Y. JONES, and D. F. RUTLAND. Pulp and paper Canada, **84(12)**, 112 (1983).

Styrene/butadiene block copolymer micelles in heptane

T. L. BLUHM AND M. D. WHITMORE[1]

Xerox Research Centre of Canada, 2660 Speakman Drive, Mississauga, Ont., Canada L5K 2L1

Received May 24, 1984

This paper is dedicated to the 10th anniversary of the Xerox Research Centre of Canada

T. L. BLUHM and M. D. WHITMORE. Can. J. Chem. **63**, 249 (1985).

The radius of gyration of poly(styrene-*b*-butadiene) block copolymer micelles in *n*-heptane is measured by small angle X-ray scattering (SAXS). The results are compared with theoretical predictions, and good agreement is found, particularly for the appropriate scaling relations. It is argued that the radius of gyration of the micelles depends on both the molecular weight and the composition of the copolymers. The dominant factors which determine the micelle core and corona dimensions are identified.

T. L. BLUHM et M. D. WHITMORE. Can. J. Chem. **63**, 249 (1985).

Faisant appel à la dispersion des rayons-X à petits angles (DXPA), on a mesuré les rayons de giration des micelles de copolymères en bloc de poly(styrène-*b*-butadiène) dans le *n*-heptane. On a comparé les résultats avec les prévisions théoriques et l'accord est satisfaisant, particulièrement pour les relations d'échelles appropriées. On pense que le rayon de giration des micelles dépend à la fois du poids moléculaire et de la composition des polymères. On a identifié les facteurs principaux qui déterminent le centre de la micelle et les dimensions de la couronne.

[Traduit par le journal]

Introduction

In the recent past, much experimental work has been done on diblock copolymer micelle formation in both selective solvents (1–5), and in a homopolymer corresponding to one of the copolymer blocks (6). More recently, a theoretical model has been developed for predicting the structural properties of these systems from equilibrium statistical mechanics (7, 8). For given molecular weights and chemical compositions of the copolymers and of the solvent or the homopolymer, the properties of interest include the sizes of the insoluble core and soluble corona, their swelling by the solvent or homopolymer, the stretching of each block of the copolymer, and the number of copolymer molecules per micelle. In addition to the overall magnitudes of the quantities, the ways in which they scale with the molecular weights of each block of the copolymer and of the homopolymer (if present), and with temperature, are of particular interest.

In this paper, we consider a system consisting of poly(styrene-*b*-butadiene) block copolymers in *n*-heptane, a selective solvent for the butadiene. In earlier work, Plestil and Baldrian (2) used small-angle X-ray scattering (SAXS) to determine the micelle parameters in this system over the temperature range 18 to 50°C, for copolymers of number average molecular weight $\bar{M}_N$ = 64 700 with 24% polystyrene by weight. Noolandi and Hong (7) developed a simple model involving one fitted Flory interaction parameter; their calculations were in good agreement with these results, including the temperature dependence.

A similar system has been studied by small angle neutron scattering (SANS), namely poly(styrene-*b*-butadiene) copolymers in polybutadiene homopolymer (6). In that work, four copolymers of different molecular weights and compositions, and three different molecular weight homopolymers were used. The measured quantity was the radius of the core, l_B, which was found to increase with increasing mw of the styrene block of the copolymer (or the homopolymer), but decreases with increasing mw of the butadiene block. In an extension and refinement of the model of ref. 7, Whitmore and Noolandi (8) obtained theoretical values for l_B which were in good overall agreement with these experiments and in particular, the scaling of l_B with the molecular weights of *each* block of the copolymer and with the homopolymer agreed very well. There were no fitted parameters in that case.

For the present work, we had available block copolymers of narrow dispersity and three different molecular weights and compositions. We have made room temperature SAXS measurements of the radius of gyration of the micelles formed in *n*-heptane, R_M, and extracted the dependence of R_M on the molecular weights of each block. This provides a test of the theoretical model which is complementary to the earlier work; we have a measure of the overall micelle size through R_M (not just the core radius l_B), and how it varies with the individual block molecular weights (not temperature). In addition, using the model we develop additional insight into the experimental results.

Experimental

The three poly(styrene-*b*-butadiene) copolymers used in this study were obtained from Professor Dale Meier, Michigan Molecular Institute, Midland, MI. They are materials originally supplied by Shell Development Company (9). The three polymers were designated by the code number SB(22-55), SB(12-71), and SB(12.5-93) referring to diblock copolymers with block molecular weights in thousands corresponding to the initials in the code. For example, SB(22-55) is the code for a styrene-butadiene block copolymer with a 22 000 molecular weight styrene block and a 55 000 molecular weight butadiene block. The Shell product numbers corresponding to these polymers are TR-41-2673, 967-250, and 982-250, respectively. The polydispersities in all cases are narrow (9) (Pd < 1.1).

Solutions of these copolymers were prepared in *n*-heptane (reagent grade) at room temperature and allowed to stand overnight before SAXS curves were measured. The solutions were turbid and remained stable for several weeks. Several solutions of each polymer were prepared with concentrations varying from 2 to 10 g L^{-1}. Radii of gyration obtained from the SAXS data were extrapolated to zero concentration to remove any concentration effect. All samples were run twice in order to ascertain the experimental errors. Small angle X-ray scattering curves were obtained using a Kratky camera with a 40 μm entrance slit, a 75 μm receiving slit and CuKα radiation (λ = 1.5418 Å). Scattered intensity was measured by means of a propor-

[1] Permanent address: Department of Physics, Memorial University of Newfoundland, St. John's, Nfld., Canada A1B 3X7.

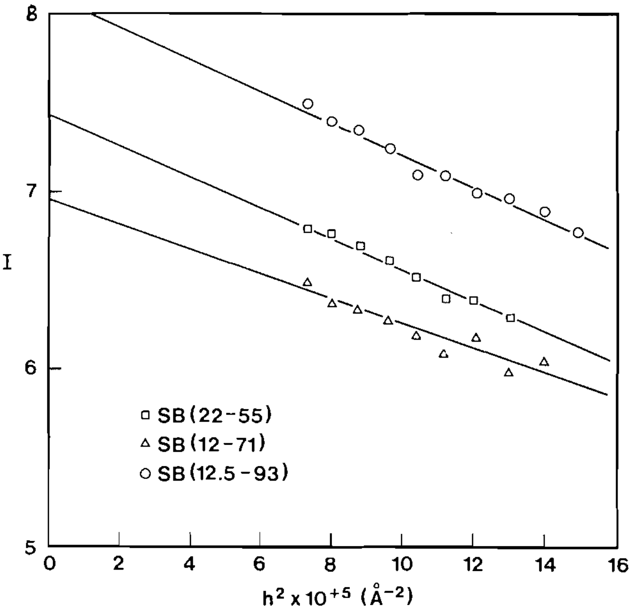

FIG. 1. Guinier plots of diblock copolymers (SB(12.5-93), SB(22-5), and SB(12-71) all at a concentration of 10 g L^{-1} in *n*-heptane. The radii of gyration are 182 Å, 177 Å, and 162 Å at 10 g L^{-1}, respectively.

TABLE 1. Experimental and theoretical properties of the micelles

Sample code	SB(22-55)	SB(12-71)	SB(12.5-93)
Molecular weight	77 000	83 000	105 500
Z_{CB}	210	115	120
Z_{CA}	1 020	1 315	1 720
R_M (Å) experimental	171 ± 4	173 ± 4	195 ± 4
Theoretical properties			
R_M (Å)	206	204	233
l_B (Å)	117	77	79
l_A (Å)	199	211	246
α_B	1.95	1.76	1.76
α_A	1.58	1.49	1.51
$\varphi_{CB}^{(1)}$	0.92	0.93	0.93
$\varphi_{CA}^{(2)}$	0.14	0.12	0.11
d (Å)	5.4	5.3	5.3

tional counter equipped with a pulse height analyzer. The solutions were placed in beryllium glass capillaries (2.0 mm diameter) and the data were collected at room temperature. The intensity scattered by a solvent blank was subtracted in each case. Sufficient counts were measured at each point during step-scanning so that the counting error was less than 1%. Radii of gyration were then determined from Guinier plots constructed using the slit smeared intensity data directly.

Guinier's approximation (10) of the scattering curve at very small angles can be written as:

$$[1] \quad I(h) = I(O)\exp(-h^2 R_M^2/3)$$

where

$$[2] \quad h = \frac{4\pi\theta}{\lambda}$$

θ equals one-half the scattering angle and λ is the wavelength of the incident radiation. The radius of gyration, R_M, is obtained from the slope of a plot of ln $I(h)$ versus h^2. It should be noted that this treatment according to Guinier's Law is valid only for $h^2R_M^2 \ll 1$ and that the radius of gyration obtained is a *z*-average radius. The radii of gyration measured for the three copolymer micelle systems are reported in Table 1. The Guinier plots in all cases are linear indicating that the micelles are most probably spherical and monodisperse (see Fig. 1) as one might expect from nearly monodisperse copolymers. The presence of the monodisperse micelles allows us to make direct comparisons with theory developed for monodisperse systems.

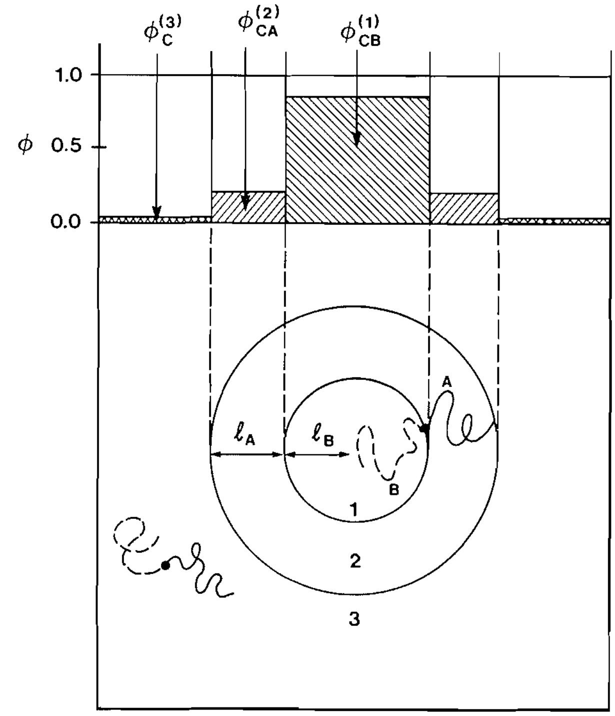

FIG. 2. Cross section of the model micelle, consisting of diblock copolymers in solvent. The core region, of radius l_B, is assumed to consist of B blocks of the copolymer (volume fraction $\varphi_{CB}^{(1)}$) plus solvent; the corona, of thickness l_A, consists of A blocks of the copolymer (volume fraction $\varphi_{CA}^{(2)}$) plus solvent; the outer region is calculated to consist almost enirely of solvent (although the model does allow for a finite copolymer volume fraction $\varphi_C^{(3)}$ in this region). Each of the three regions is assumed to be uniform.

Analysis

The results reported in Table 1 are now used to test the model referred to earlier, which in turn is then used to further analyze these results and deduce additional structural properties of the micelles. This model is essentially that developed originally by Noolandi and Hong (7); it incorporates the refinements introduced by Whitmore and Noolandi (8), but they turn out to be unimportant for this case. The model is fully described in refs. 7 and 8; here we describe it only briefly, generally writing out equations only when they differ from those in refs. 7 and 8. The model micelle is shown schematically in Fig. 2.

Each micelle is assumed to consist of a uniform core, referred to as region 1, and a uniform corona, region 2. The core consists of polystyrene blocks of the copolymer (B blocks) and solvent, with volume fractions $\varphi_{CB}^{(1)}$ and $\varphi_S^{(1)}$, respectively. Similarly, the uniform corona consists of polybutadiene blocks of the copolymer (A block) and solvent, with volume fractions $\varphi_{CA}^{(2)}$ and $\varphi_S^{(2)}$. Region 3, lying between the micelles, contains randomly distributed copolymers $\varphi_C^{(3)}$ and solvent $\varphi_S^{(3)}$. It is also assumed that the system is incompressible, so that in each region the volume fractions sum to unity.

In the procedure, the first step consists of obtaining an expression for the free energy of this system with micelles relative to the random state,

$$[3] \quad \Delta g = \frac{G_{\text{micelle}} - G_{\text{random}}}{\rho_{OS} k_B T V}$$

Here V is the volume of the system, T the temperature, k_B is Boltzmann's constant, and ρ_{OS} a reference density taken to be that of the pure solvent. The free energy difference depends on the degrees of polymerization of each of the two blocks of the copolymers, Z_{CB} (core) and Z_{CA} (corona), the densities of each of the corresponding pure systems (ρ_{OS}, ρ_{OB}, ρ_{OA}), three Flory interaction parameters and the overall copolymer volume fraction $\varphi_C{}^0$. In addition, Δg depends on four independent parameters which specify the structural properties of the micelles. They are the radius of the core, which we call l_B, the corona thickness l_A, the unit cell radius R, and the fraction of copolymers which condenses to form the micelles, $F_M{}^C$. (The remaining fraction $F_3{}^C = 1 - F_M{}^C$ remains in solution between the micelles.) The equilibrium values of these four parameters are the set that minimize Δg; the procedure thus consists of minimizing Δg with respect to them.

We express Δg as a sum of six terms. The first is the change in interaction energy.

$$[4] \quad \Delta g_{\text{int}} = -\chi_{AB} f_A f_B (\varphi_C{}^O)^2 [1 - (F_3{}^C)^2/G_3{}^V]$$
$$-\chi_{AS} f_A \varphi_C{}^O \varphi_S{}^O [1 - F_2{}^S F_M{}^C/G_2{}^V - F_3{}^S F_3{}^C/G_3{}^V]$$
$$-\chi_{BS} f_B \varphi_C{}^O \varphi_S{}^O [1 - F_1{}^S F_M{}^C/G_1{}^V - F_3{}^S F_3{}^C/G_3{}^V]$$

In eq. [4], $f_K = (Z_{CK}\rho_{OC})/(Z_C \rho_{OK})$ for each component with $Z_C = Z_{CA} + Z_{CB}$, and ρ_{OC} is given by $(Z_C/\rho_{OC}) = (Z_{CA}/\rho_{OA}) + (Z_{CB}/\rho_{OB})$. $F_i{}^S$ is the fraction of solvent in region i, and $G_i{}^V$ is the fraction of the total volume occupied by region i. The room temperature molar densities were taken to be $\rho_{OA} = 0.0165$ cm^{-3} (11), $\rho_{OB} = 0.0103$ cm^{-3} (12), and $\rho_{OS} = 0.00684$ cm^{-3} (2). Choosing ρ_{OS} for the reference density, the Flory χ parameters are $\chi_{AB} = 0.24$ (8, 13), $\chi_{AS} = 0.53$ (7), and $\chi_{BS} = 1.9$ (7).

The core-corona interface of each micelle contributes an interfacial energy, which has the form

$$[5] \quad g_I = \frac{\gamma}{\rho_{OS} k_B T} \frac{3 l_B{}^2}{R^3}$$

with the interfacial tension given as a simple function of $\varphi_{CB}{}^{(1)}$ and $\varphi_{CA}{}^{(2)}$ as well as the Flory χ parameters. The width of the interface, d, is given approximately by

$$[6] \quad \frac{d}{b} = \left(\frac{\varphi_{CB}{}^{(1)} + \varphi_{CA}{}^{(2)}}{6}\right) \left(\frac{\gamma}{\rho_{OS} k_B T}\right)^{-1}$$

when b is an average Kuhn statistical length. For the present case, the lengths (11) are $b_A = 6.8$ Å and $b_B = 7.1$ Å.

The third and fourth contributions are due to the reduction in entropy when fractions of each component are restricted to the different regions, including the localization of the copolymer joints to the interface. The stretching of the copolymer blocks is incorporated via the Flory expression for the elastic energy and depends on the relative extension of each block α_A and α_B, defined by $\alpha_K = (3/Z_{CK})^{1/2}\, l_K/b_K$ in each case. Finally, the small term which is due to the translational entropy of the micelles constitutes the sixth contribution to Δg.

The model as described provides theoretical values for the micelle parameters. For direct comparison with the experimental results, the radius of gyration of the micelles was calculated (2).

$$[7] \quad R_M{}^2 = \frac{3}{5} \frac{a_A(l_M{}^5 - l_B{}^5)/(l_M{}^3 - l_B{}^3) + a_B(f_B/f_A)\, l_B{}^2}{a_A + (f_B/f_A) a_B}$$

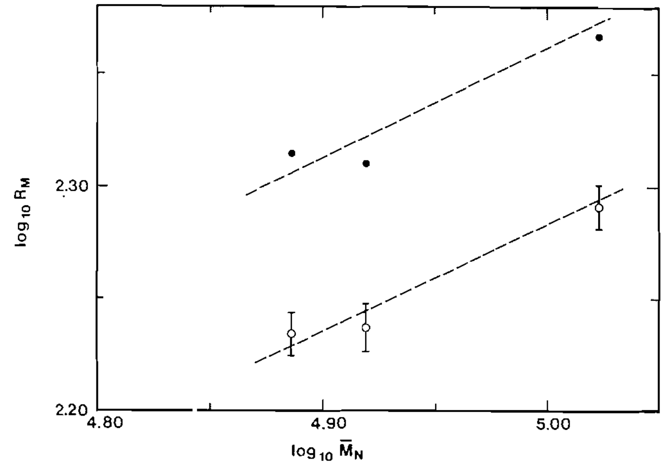

FIG. 3. Micelle radii of gyration as a function of $\bar{M}_N$ for the copolymers studied. The upper points are the theoretical values, and the lower ones are the experimental. As argued in the text, due to the different compositions of the blocks the two sets of points are not expected to lie on straight lines. However calculating the slopes of the straight lines as shown gives an overall power law of $R_M \propto \bar{M}_N{}^{0.44}$ both theoretically and experimentally.

where $l_M = l_A + l_B$, and a_A and a_B represent the density of "excess" electrons of polybutadiene and polystyrene, respectively.

These theoretical values of R_M are included in Table 1. The first point to note is the reasonable overall agreement with the measurements being consistently about 20% larger. (Recall that there are no fitted parameters.) Second, the overall general increase in R_M with molecular weight is in agreement. Finally, note that for the second sample, R_M is predicted to be slightly *less* than for the first, even though the molecular weight is somewhat *greater*. This, in fact, is not inconsistent with the measurements; a decrease of this small magnitude is well within the estimated error.

This last observation further illustrates a point emphasized in ref. 8, namely, that even the total micelle radius (or R_M) is determined by the degree of polymerization of each block of the copolymer, Z_{CA} and Z_{CB}, not just the total d.p. Z_C; it is clear from Table 1 that Z_C and the total molecular weight are larger for sample 2 than for sample 1.

Although the experimental uncertainty precludes verification of the prediction of a slightly smaller R_M for sample SB(12-71) as compared with SB(22-55), we can quantify the comparison of the theory and experiment by least-squares fitting a straight line to the two sets of points. Based on the above argument, we *expect* that the points should not lie on a straight line, but this procedure does act as a test of the model. The result is illustrated in Fig. 3; remarkably (and no doubt fortuitously), both theory and experiment give an average overall dependence of $R_M \propto \bar{M}_N{}^{0.44}$. This agreement implies the model predicts well the scaling of the entire micelle size. Furthermore, Whitmore and Noolandi found good agreement for the scaling of the core of the micelles (in homopolymer). We are thus lead to have considerable confidence in the scaling laws predicted by this model.

Based on this evidence, we can extract from the model some additional features. Table 1 lists the theoretical values for the radii (or thicknesses), stretching parameters and copolymer volume fractions in each region of the micelles, and the widths of the interfacial regions, d. Due to the somewhat large values of R_M obtained theoretically one or both of l_B and l_A is presumably overestimated, with corresponding effects on α_B and α_A. The small values of $\varphi_{CA}^{(2)}$ are largely due to geometry; even if the A blocks were unstretched, for the values of l_B found we would have $\varphi_{CA}^{(2)} \simeq 0.3$. We point out that the copolymer volume fraction remaining in solution is always very small, $\varphi_C^{(3)} < 10^{-10}$.

Next, we examine the scaling of l_B and l_A. Over the range of Z_{CB} and Z_{CA} used in these measurements, we find (theoretically),

[8*a*] $l_B \propto Z_{CB}^{0.67} Z_{CA}^{-0.01}$

[8*b*] $l_A \propto Z_{CA}^{0.54} Z_{CB}^{0.12}$

The picture that emerges is thus very similar to that found when a homopolymer was present in place of the solvent. The dominant behaviour is that the core radius scales with Z_{CB}, with a power very close to 2/3, and the corona thickness with Z_{CA} with a power somewhat larger than 1/2. These two scaling laws are perfectly consistent with a decrease in R_M with increasing $\bar{M}_N$ or Z_C, if the composition also changes. As well, they are certainly consistent with the average scaling $R_M \propto \bar{M}_N^{0.44}$, since the composition changes over the range.

It is also interesting to compare the A block stretching found here with the case of the AB copolymer in the A type homopolymer. In that case, there is no increase in interaction energy when the homopolymer penetrates the corona, leading to more stretching and hence a larger α_A than found in the present case.

One of these copolymers, SB(22-55), has been investigated using a new technique involving degradation of the polybutadiene matrix surrounding the polystyrene core (14). The degradation is achieved using ozone produced by an ozone generator. Thin copolymer films were first cast from octane solution, producing spherical structures, placed on stainless electron microscope grids, and then exposed to ozone. The result was polystyrene cores, separated completely from any matrix materials, which could then be shadowed with Pt—C and observed in the transmission electron microscope. The resulting micrographs obtained from SB(22-55) so treated revealed polystyrene cores with radii of approximately 115 Å in excellent agreement with the predicted values of l_B in Table 1. However, it should be pointed out that values of l_B from electron micrographs of stained copolymer films were found in the same study to range from 130 to 200 Å.

Conclusion

We have measured the radius of gyration of polystyrene/polybutadiene block copolymer micelles in *n*-heptane, and found an *average* power law dependence $R_M \propto \bar{M}_N^{0.44}$. We have modelled the system theoretically, and found the same power law dependence. However, it is argued that the composition of the blocks is also important, and that we should *not* expect all data points to obey this relationship because of their varying composition, a conclusion which is consistent with the measurements. Theoretically, we find the scaling of the core radius and corona thickness to be approximately $Z_{CB}^{2/3}$ and $Z_{CA}^{1/2}$, respectively, and that these relations are consistent with the average dependence of R_M on $\bar{M}_N$ found experimentally.

Acknowledgements

We wish to thank Dr. J. Noolandi for suggesting these measurements, and Dr. D. Meier of the Michigan Molecular Institute for supplying the copolymers.

1. C. Price and D. Wood. Eur. Polym. J. **9**, 827 (1973).
2. J. Plestil and J. Baldrian. Makromol. Chem. **176**, 1009 (1975).
3. Z. Tuzar and P. Kratochirl. Adv. Colloid Interface Sci. **6**, 201 (1976).
4. T. Kotaka, T. Tanaka, M. Hattori, and H. Inagoki. Macromolecules, **11**, 138 (1978).
5. C. J. Stacy and G. Krans. Polym. Eng. Sci. **17**, 627 (1977).
6. J. Selb, P. Marie, A. Rameau, R. Duplessix, and Y. Gallot. Polym. Bull. **10**, 444 (1983).
7. J. Noolandi and M. Hong. Macromolecules, **16**, 1443 (1983).
8. M. D. Whitmore and J. Noolandi. Macromolecules. In press.
9. D. Meier. Private communication.
10. A. Guinier. Ann. Phys. Paris, **12**, 161 (1939).
11. J. Brandrup and E. G. Immergut (*Editors*). Polymer handbook. Vols. 1, 3. 2nd ed. Interscience: New York. 1975.
12. M. J. Richardson and N. G. Savill. Polymer, **18**, 3 (1977).
13. R.-J. Roe and W.-C. Zin. Macromolecules, **13**, 1221 (1980).
14. D. R. Smith. M.Sc. Thesis. Case Western Reserve University. August, 1983.

Detailed copolymer characterization using ultraviolet spectroscopy

L. H. GARCIA-RUBIO[1] AND N. RO
Xerox Research Centre of Canada, 2660 Speakman Drive, Mississauga, Ont., Canada L5K 2L1

Received January 12, 1984[2]

This paper is dedicated to the 10th anniversary of the Xerox Research Centre of Canada

L. H. GARCIA-RUBIO and N. RO. Can. J. Chem. **63**, 253 (1985).

A method is demonstrated for the interpretation of the ultraviolet spectra of styrene-containing copolymers. This method is based on the use of model molecules to approximate the absorption behaviour of the known chromophores and on the statistical estimation of the average spectra of the unknown chromophores. The analysis yields directly the copolymer composition and an estimate of the background spectra which arise from the different arrangements of the styril units along the polymer chains. It is shown that reliable composition estimates are obtained for styrene – methyl methacrylate and styrene–acrylonitrile copolymers. The results from the interpretation of the spectra are discussed and compared with results obtained from the statistical copolymerization models.

L. H. GARCIA-RUBIO et N. RO. Can. J. Chem. **63**, 253 (1985).

On présente une méthode permettant d'interpréter les spectres ultraviolets de copolymères contenant du styrène. Cette méthode est basée sur l'utilisation de molécules modèles qui permettent de déterminer approximativement le comportement, vis-à-vis de l'absorption, de chromophores connus ainsi que sur l'évaluation statistique du spectre moyen de chromophores inconnus. L'analyse permet d'obtenir directement la composition du copolymère et d'évaluer les spectres de fond qui découlent des différents arrangements des unités styriles le long des chaînes de polymères. On démontre que, pour les copolymères styrène/méthacrylate de méthyle et styrène/acrylonitrile, on obtient des évaluations fiables de la compositions. On discute des résultats obtenus par l'interprétation des spectres et on les compare avec les résultats obtenus à partir de modèles statistiques de la copolymérisation.

[Traduit par le journal]

Introduction

The application of ultraviolet spectroscopy to the analysis of styrene-containing copolymers has been extensively reported in the literature (1–13). Band shifts, solvent effects, and hypochromic effects have been observed as functions of the copolymer composition and the microstructure of the polymer chains (2–8). The band shifts, solvent effects, and other anomalies observed in the absorption behaviour of polymers have precluded the development of analytical techniques which can yield composition estimates directly from the uv spectra (4). Existing techniques have to resort to assumptions regarding the copolymerization kinetics or to independent measurements of the copolymer microstructure (8–11). In this paper, a method is demonstrated which yields directly both the copolymer composition and an estimate of the background spectra which arise from the different arrangements of the styril units along the polymer chains. The method proposed is based on the use of model molecules to approximate the absorption patterns of the known chromophores and on the statistical estimation of the average spectra of the unknown chromophores. The technique reported is shown to give reliable estimates of the copolymer composition for styrene – methyl methacrylate and styrene–acrylonitrile copolymers. The preliminary assignment of absorption patterns is discussed and compared with previous literature reports and with the results of statistical copolymerization models.

Literature review

Studies on the absorption behaviour of styrene-containing copolymers have shown significant deviations from Beer's Law and from the assumption of additivity of the absorption of the individual components. These deviations have been attributed to the microstructure of the polymer chains (3, 4, 8, 10, 11) and in some cases to the conformation of the molecules in solution (2, 6, 9). Vala and Rice (2) observed that the extinction coefficient of isotactic polystyrene at certain wavelengths is smaller than the corresponding extinction coefficients for atactic polystyrene. This reduction in extinction coefficient (hypochromism) was attributed to the anisotropic effect of the phenyl rings. A similar hypochromic effect on the steric isomerism has been observed in the case of polymethyl methacrylate (14) and poly(2-methylbutyl methacrylate) (15). Hypochromic effects on styrene copolymers were first reported by O'Driscoll *et al.* (3) from observations made in the analysis of styrene – methyl methacrylate copolymers (SMMA). These authors suggested that the differences in the extinction coefficients were due to differences in the length of the styrene sequences present in the polymer chains. Brussau and Stein (4) investigated the effect of the sequence length of the uv absorption of styrene–butadiene (SB), styrene – maleic anhydride (SMA), and styrene–acrylonitrile (SAN) copolymers at several wavelengths in chloroform and THF. They also concluded that the response of the uv detector appears to be a function of the length of the styrene sequences. Stutzel *et al.* (8) investigated SMMA copolymers in THF and dioxane solutions. From their analysis using styrene dimers they concluded that the hypochromic effects are probably not due to differences in conformation. Rather, they suggested that hypochromic effects arise from the sequential arrangement of the monomer units in the chain, in agreement with O'Driscoll's and Brussau's conclusions.

More recently, the assumption that the extinction coefficient is correlated with the sequence length has been used by Gruber and Knell (10) in the analysis of styrene – butyl acrylate and styrene – *n*-butyl methacrylate copolymers and by Garcia-Rubio *et al.* (11) for the development of the GPC (gel permeation chromatography) technique for the analysis of SAN

[1]Current address: College of Engineering, University of South Florida, Tampa, Florida 33620.
[2]Revision received August 3, 1984.

copolymers.

Russo and co-workers (6, 7)[3] concluded, from studies on the hypochromism of SMMA copolymers in ester solutions, that the hypochromism in SMMA copolymers seems to be produced by inter- and intramolecular interactions between carbonyl groups and the phenyl rings and, therefore, it is governed by the number (sequence length) and intensity (solvent dielectric constant) of such interactions. These authors experimentally demonstrated that the hypochromism in SMMA copolymers can be effectively eliminated at 269.2 nm by using ester-type solvents. Recent studies (12, 13) on the estimation of copolymer extinction coefficients have also shown that, within the limits of experimental error, Beer's Law and the assumption of additivity of chromophores appear to be valid for a variety of styrene homopolymers and copolymers. This suggests that the hypochromic effects and the deviations from Beer's Law are due to unidentified chromophores present in the polymer molecules. The general concensus, however, favours the hypothesis that recognizes the length of the styrene sequences as the most important factor in explaining the observed deviations from Beer's Law. This implies that uv spectrophotometers cannot be used as concentration detectors for copolymer analysis without prior calibrations, which include the necessary corrections for the copolymer microstructure (4, 8, 11) or, alternatively, that a suitable solvent system should be found for each copolymer system, which will minimize the microstructure effects on the absorption behavior of the polymer. Either approach is unsatisfactory for chromatography experiments, where it would be desirable to interpret the detector responses directly, without having to make assumptions regarding the microstructure of the copolymer or without having to collect fractions for further analysis. Therefore, there is incentive for the development of the necessary methodology for the interpretation of the uv spectra.

Method of analysis

The estimation of copolymer compositions from uv spectroscopy data can be divided into several aspects: 1. the identification and quantification of chromophores embedded along the polymer chains that may have different absorption patterns, depending on their local environment and position in the chain; 2. the selection of model molecules which can adequately represent at least some of the chromophores present; 3. the statistical estimation of the polymer compositions and an average representation of the unidentified chromophores.

Based on the recent reports which suggest that: (a) Beer's Law is valid for chromophores present in the polymer molecules (12) and (b) that model compounds can be used to represent equivalent chromophores attached to the polymer molecules (13), the first problem can be postulated as a statistical identification process, where the objective is to obtain an accurate representation of the spectra of all the species present in the polymer molecules. The simplest criterion for the identification is to select those model molecules that best predict the spectra of the unknown mixture of chromophores, i.e. to eliminate statistically those components that, within the limits of the experimental error, cannot reduce the residual sum of squares between the measured and the calculated spectra. The calculated spectra are obtained from Beer's Law applied to all the concentrations over all the measured wavelengths, i.e.:

[3]M. Nencioni and S. Russo. Private communication.

$$[1] \quad A_j = \sum_{n=1}^{N} \epsilon_{nj} p_n C l$$

The objective function for the minimization process is given by:

$$[2] \quad \text{Min: } \sum_i \sum_j \frac{\phi^2_{ij}}{\sigma^2_{ij}}$$

where

$$\phi_{ij} = A_{ij} - \sum_n^N \epsilon_{nj} p_n C_i l$$

$$\sigma^2_{ij} = \text{var}\,(A_{ij}) + \sum_n^N [l C_i p_n]^2 \text{ var}\,(\epsilon_{n,j}) + \left[l \sum_n^N p_n \epsilon_{nj}\right]^2 \text{var } C_i$$

Alternatively, the differences between the measured (ϵ_j^{o}) and calculated extinction coefficients can also be used in the objective function. For this case, eq. [2] becomes:

$$[3] \quad \text{Min: } \sum_j^{\lambda} \left[\left(\epsilon_j^{\text{o}} - \sum_n^N \epsilon_{nj} p_n\right)^2 \Big/ \text{var}\,(\epsilon_j^{\text{o}}) + \sum_n^N p_n^2 \text{ var}\,(\epsilon_{nj})\right]$$

where the variances of the extinction coefficients are estimated from the absorption measurements. The solution of the nonlinear equations [2] or [3] for the identified number of components yields the composition estimates, as shown for the initiator fragments present in polystyrene molecules (13).

In the case of copolymers and other complex polymers, the spectra (ϵ_{nj}) which correspond to some of the species present can be obtained directly from the homopolymers of the monomers used to synthesize the polymer. If there are no effects on the absorption behaviour due to inter- and intramolecular interactions between the functionalities present in the solvent and in the polymer molecule, the direct application of [2] or [3] together with the spectra of the homopolymers and the initiator fragments should yield the copolymer composition estimates. However, if interactions are present, as in the case of styrene copolymerized with polar comonomers (4), the spectra of the chromophores present may be altered in an, as yet unknown, fashion. In order to aid the identification of the effects due to interactions, it is desirable to estimate the spectrum of the distorted or the unknown species. For this purpose the following assumptions are made.

(a) The distorted spectra of chromophores which result from interactions with the comonomer or with the solvent are considered to be separate species obeying Beer's Law.

(b) The spectra of the identified species are assumed to be independent of both the microstructure and the copolymer composition.

Given these two assumptions, it follows that if $N - 1$ species have been identified, or are known to be present in the polymer, it is possible, by applying simultaneously eqs. [2] or [3] to K different polymer samples, to obtain estimates of the composition for the K samples and the extinction coefficients for the Nth species (i.e. ϵ_{nj}: $j = 1, \ldots, \lambda$).

In other words, it is possible to obtain the composition estimates and an estimate of the extinction coefficient for the Nth component conditional upon the identification of $N - 1$ components, and the availability of K different polymer samples.

TABLE 1. Data on styrene – methyl methacrylate and styrene–acrylonitrile copolymers

Samples	f_{10} (mol%)	X_w	Copolymer composition: % Styrene	Copolymer composition: Method of analysis	References
SMMA01	60	4.5	55.1	^{1}H nmr*	17, 20
SMMA02	35	4.6	40.4	^{1}H nmr	
SMMA03	35	24.1	42.1	^{1}H nmr	
SMMA04	60	26.1	56.2	^{1}H nmr	
SMMA05	60	55.6	58.3	^{1}H nmr	
SMMA06	35	35.1	40.6	^{1}H nmr	
SMMA07	60	4.7	57.4	^{1}H nmr	
SMMA08	60	27.3	59.0	^{1}H nmr	
SMMA09	60	49.6	59.5	^{1}H nmr	
SMMA10	60	70.0	59.6	^{1}H nmr	
SAN01			75.0	Reported by manufacturer	Scientific Polymer Products 494
SAN02			70.0	Reported by manufacturer	Scientific Polymer Products 495
SAN03			76.8	Reported by manufacturer	Monsanto Standard 18
SAN90	90	94.3	94.37	Gas chromatography/^{1}H nmr†	18
SAN80	80	69.9	85.23	Gas chromatography/^{1}H nmr	18
SAN50	50	10.0	72.09	Gas chromatography/^{1}H nmr	18

*The standard error for the nmr measurements is 1.75% (refs. 17, 18 and 26).
†The standard error for the gc measurements is 1.0% (ref. 18).

The total number of parameters to be estimated in this case is given by:

$$[4] \quad N_p = \lambda + KN$$

The total number of observations available from K samples measured at I concentrations and λ wavelengths is given by:

$$[5] \quad N_{ob} = \lambda KI$$

If eq. [3] is applied, then the number of observations becomes:

$$[6] \quad N_{ob} = \lambda K$$

A necessary condition for the estimation of N_p parameters is:

$$[7] \quad N_p \leq N_{ob}$$

It follows from eq. [7] that:

$$[8] \quad K > \frac{\lambda}{\lambda - N}$$

Therefore, if $\lambda \gg N$, a minimum of two samples should suffice to estimate the N_p parameters. The solution to the nonlinear eq. [2] or [3] for N_p parameters can be accomplished using any of the nonlinear least-squares estimation techniques (16). From the estimated background, the appropriate model molecule may be selected, or alternatively the estimated absorption pattern may be used directly for the estimation of composition in other samples.

Experimental

Materials

The model molecules butylbenzene, *tert*-butylbenzene, and ethyl benzoate were purchased from Eastman Kodak and Aldrich Chemicals respectively. The solvent, spectral grade tetrahydrofuran, was obtained from Burdick and Jackson Laboratories. The polymer samples were synthesized via free radical polymerization using benzoyl peroxide and 2,2′-azobisisobutyronitrile as initiators in the temperature range of 40 to 60°C (17, 18). Table 1 lists the properties of the materials investigated.

Measurements

The uv spectra for the polymers and model compounds in THF were determined in a H.P. Diode array 8450 uv/vis spectrophotometer at room temperature with a 1-cm path length cell. Up to seven concentrations plus replicates were used to obtain good estimates of the extinction coefficients as well as the measurement errors. Special care was taken to ensure that the measurements were always within the linear range of the instrument. The raw absorption data were transferred to a Data General S-230 Eclipse computer for further processing. The linear behaviour of the absorption with respect to concentration was statistically verified for all the substances used. Estimation of the extinction coefficients was done on a weight basis to minimize propagation of the experimental error (13).

Analysis of all the polymer samples was restricted to the spectral region between 250–300 nm. This was done to reduce the dimensionality of the statistical estimation problem when using eq. [2] or [3].

Results and discussion

Ultraviolet spectra of polystyrene and model compounds

Comparison of the absorption spectra of polystyrene with two similar chromophores, butylbenzene and its stereoisomer, *tert*-butylbenzene (Figs. 1 and 2), indicates the importance of steric effects in modifying the absorption pattern of a single chromophore. It seems that the ability of the phenyl rings, or the molecules containing them, to align themselves in the presence of the uv light has a definite effect on both the absorption pattern and the magnitude of the extinction coefficient. The fact that the absorption behavior of butylbenzene and polystyrene is very similar in form and intensity suggests that the phenyl groups in the polystyrene molecules are arranged in an oderly structure that maximizes the interaction between the phenyl rings. As the steric hindrance for such an arrangement increases (*tert*-butylbenzene), the absorption pattern changes and the absorption intensity decreases (Fig. 2). A similar observation has been made by Stutzel and Miyamoto from their studies on *meso*- and *d,l*-2,4-diphenylpentanes and isotactic and syndiotactic rich polystyrenes (8). These authors also show that the

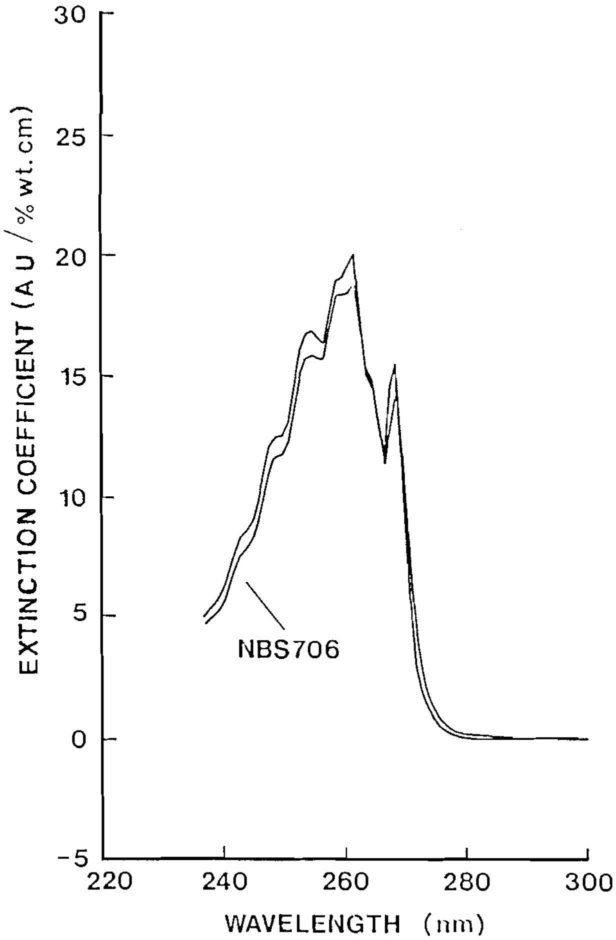

FIG. 1. Absorption spectra of butylbenzene and the National Bureau of Standards polystyrene NBS706.

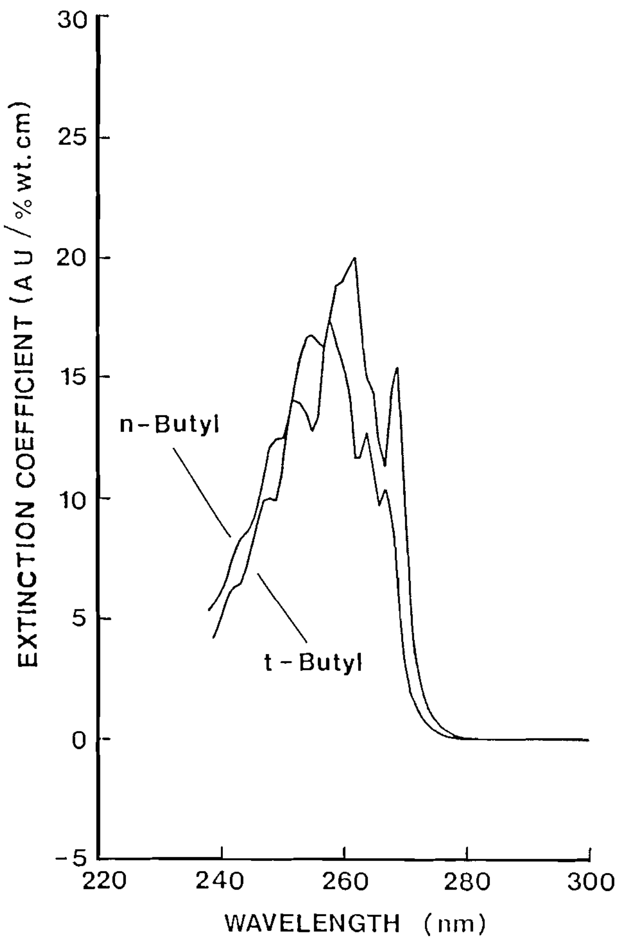

FIG. 2. Comparison of the absorption spectra of butylbenzene and *tert*-butylbenzene.

spectra of the polystyrenes and of the isomers decrease in intensity with increasing temperatures and converge to a shape similar to the *tert*-butyl benzene absorption pattern. The conclusion from the above observations is that the mutual position in space of adjacent phenyl rings seems to control the extinction coefficient as well as the shape and the form of the absorption spectrum. Therefore, depending on the chemical and steric nature of the comonomer, an absorption pattern intermediate between polystyrene and *tert*-butyl benzene could be expected as a result of the statistical estimation process.

Analysis of styrene – methyl methacrylate copolymers

The analysis of the SMMA copolymers shown in Table 1 was conducted in two stages. In the first stage the least-squares solution of eq. [3], using the data from samples SMMA01 to SMMA06 (Fig. 3) and the model molecules of polystyrene, *tert*-butylbenzene, and ethyl benzoate, gave the corresponding copolymer compositions (Table 2) and an average spectrum of the unidentified background (Fig. 4). Using the estimated background and the same model molecules, the analysis of the remaining samples (i.e. SMMA07-10) was done applying eq. [3] directly to each sample.

The estimation of the background was done conditional upon the following assumptions.

(a) The spectrum of polystyrene adequately represents some of the styril units present in polystyrene sequences, particularly those present in long styrene sequences.

(b) The spectrum of *tert*-butylbenzene can be used as a good approximation of the styril units that are either isolated or sterically hindered. This assumption was made based on the similarity between the spectrum of *tert*-butylbenzene and the spectra of high methyl methacrylate SMMA copolymers (compare Figs. 2 and 3).

(c) The spectrum of ethyl benzoate was used to approximate the benzoate groups resulting from the decomposition of benzoyl peroxide (13).

The initial guesses for the simultaneous solution of eq. [3] in the first stage (samples 01–06) were obtained directly from the same equation applied to each individual polymer using only three components: polystyrene, *tert*-butylbenzene, and ethyl benzoate. (Methyl methacrylate has negligible absorption in the wavelength region of interest, 230–300 nm.) Subsequently, several combinations of initial guesses were used to ensure that a global minimum, and therefore the solution to eq. [3], had been found. The estimated absorption pattern for the unknown chromophores is shown in Fig. 4. The compositions for samples 07–10 were obtained using the previously estimated absorption pattern (S_3) and the spectra of polystyrene NBS706 (S_1), *tert*-butyl benzene (S_2), and ethyl benzoate. The copolymer compositions obtained are reported in Table 2. Very good agreement between the measured and the calculated spectra was obtained in every case, as shown in Figs. 5 and 6. Comparison of the columns labelled total styrene and nmr in Table 2 indicates that the estimates of the styrene content by uv spectroscopy are within the limits of the experimental error for nmr measurements. The standard error for the

TABLE 2. Composition analysis of styrene – methyl methacrylate copolymers*

			Copolymer composition (wt.%)							
				Styrene						
Sample	f_{10} (mol%)	X_w	BPO fragment	S_1	S_2	S_3	Total	nmr	MMA	σ_{AB}
SMMA01	60	4.5	0.166	13.06	24.66	21.11	58.83	55.1	41.0	0.461
SMMA07	60	4.7	0.113	13.07	24.34	21.17	58.57	57.4	41.3	0.465
SMMA04	60	26.1	0.075	13.23	23.81	20.84	57.88	56.2	42.04	0.467
SMMA08	60	27.3	0.227	12.65	24.71	21.66	59.02	59.0	40.76	0.467
SMMA09	60	49.6	0.141	12.51	24.28	21.53	58.33	59.5	41.53	0.470
SMMA05	60	55.6	0.161	12.88	21.88	20.91	58.66	58.3	41.18	0.468
SMMA10	60	70	0.043	13.25	23.61	21.17	58.03	59.6	41.92	0.473
SMMA02	35	4.6	0.201		22.81	18.89	41.70	40.4	58.10	0.453
SMMA03	35	24.1	0.165		22.14	18.67	40.81	42.1	59.02	0.458
SMMA06	35	69.6	0.067		20.96	18.02	38.88	40.6	61.04	0.463

*Standard error for the uv measurements is 0.4% on a weight basis. Standard error for the nmr measurements is 1.75% on a weight basis.

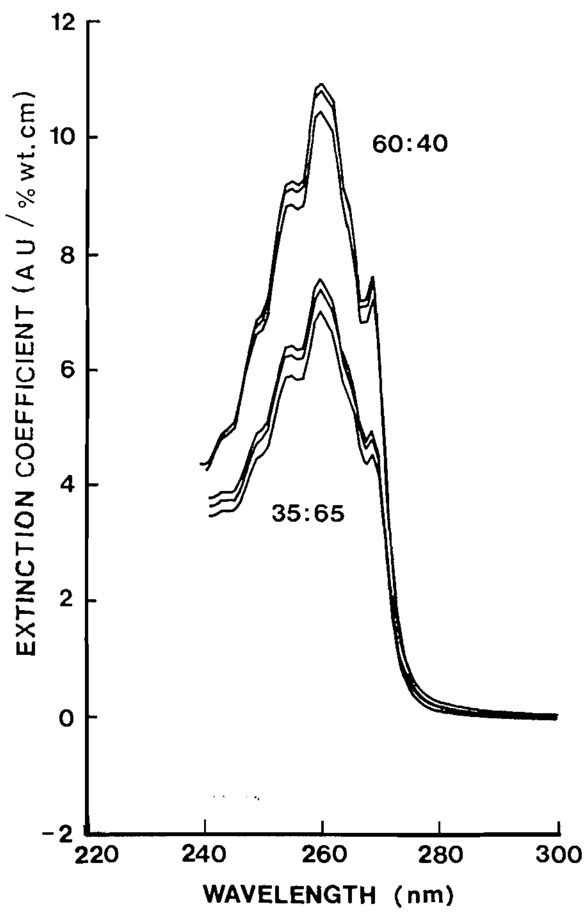

FIG. 3. Absorption spectra of styrene – methyl methacrylate copolymers. Feed compositions as indicated (styrene/methyl methacrylate).

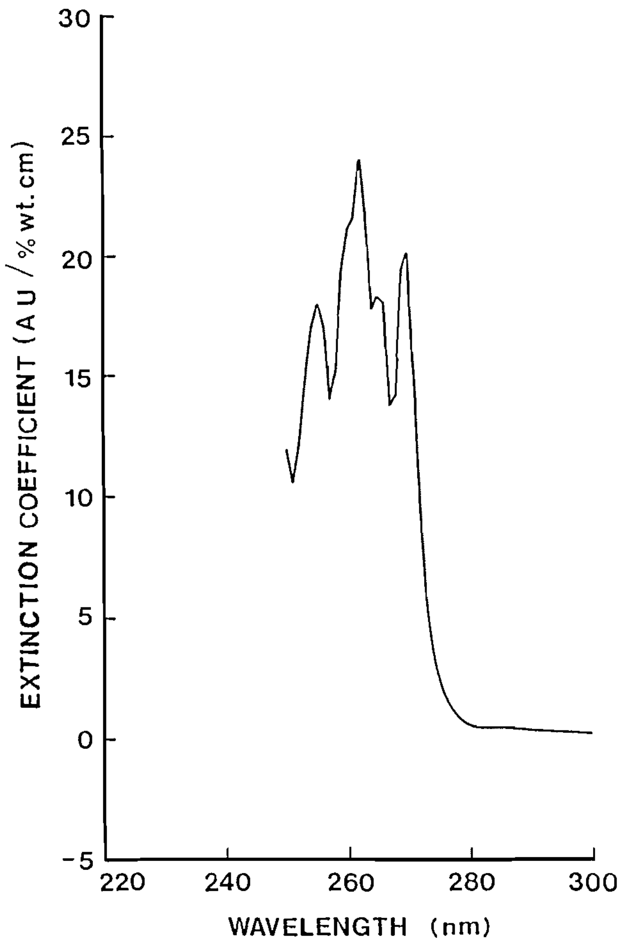

FIG. 4. Estimated background spectra for styrene – methyl methacrylate copolymers (S_3).

styrene content obtained from the pooled variance of replicate uv measurements is ±0.4 on a wt.% basis, whereas for the nmr the standard error was estimated at ±1.75 on the same basis. (Note that the standard error for the nmr measurements is in good agreement with previously reported values (19, 26)). Clearly, the approach suggested here can yield reliable quantitative information on the styrene content for SMMA copolymers.

Interpretation of the results for styrene – methyl methacrylate copolymers

As a first step in the interpretation of the results, the reactivity ratios from the composition data shown in Table 1 were estimated using the "Error in variables" models applied to the integrated form of the Mayo and Lewis equation (18, 20). The values obtained, r_1 = 0.4971, r_2 = 0.4639, were used to compute the concentration of monads, diads, triads, etc., from

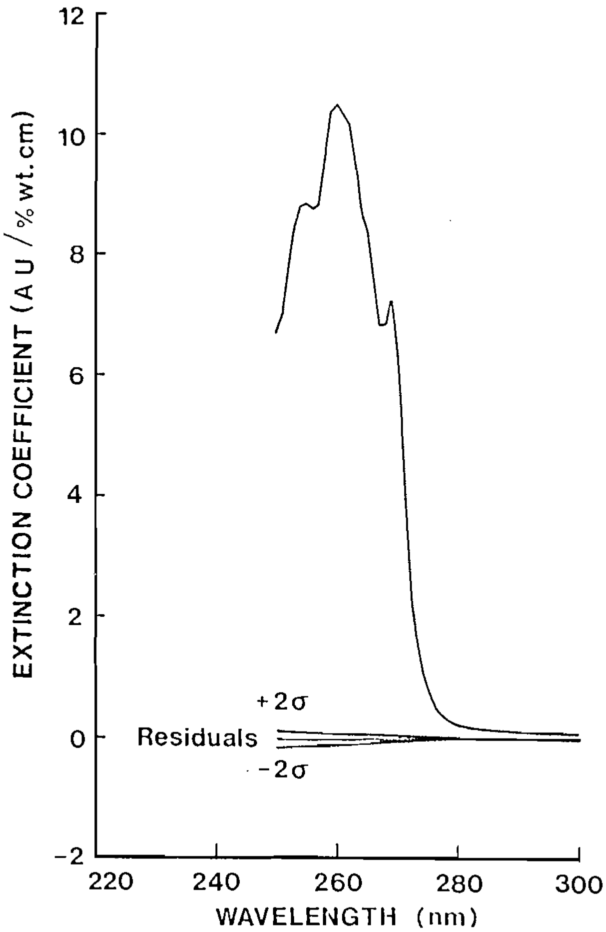

FIG. 5. Comparison between measured and calculated spectra for sample SMMA04. The residuals from the estimation and the 95% confidence interval on the measurements are indicated.

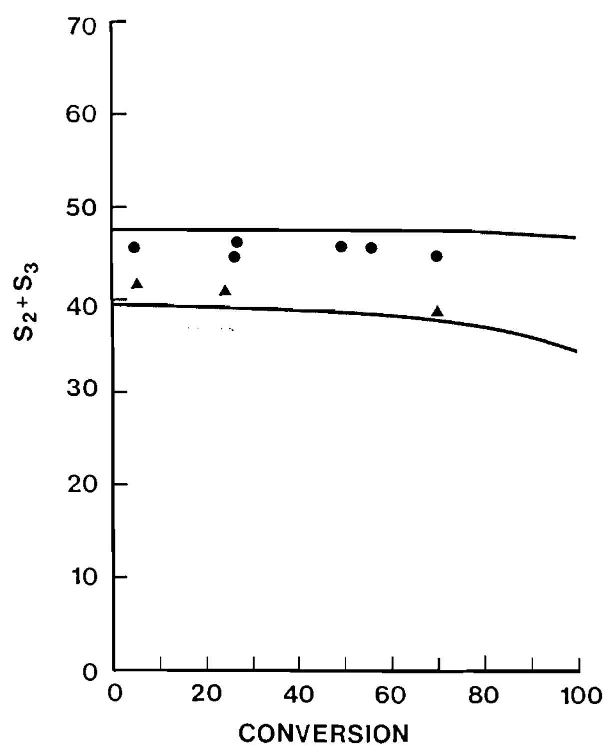

FIG. 6. Comparison between the measured and the calculated spectra for sample SMMA02.

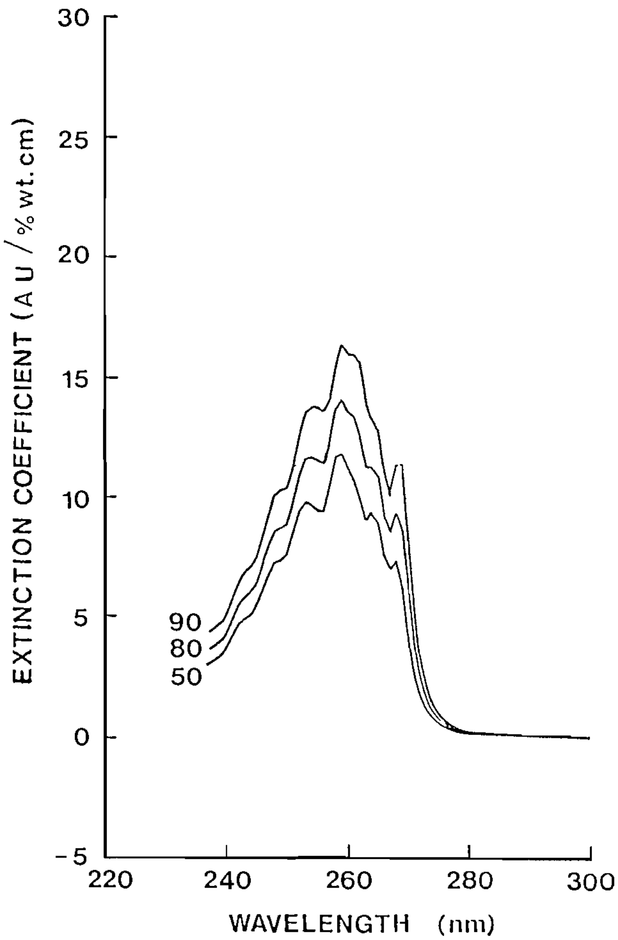

FIG. 7. Weight fraction of styrene contained in styrene − methyl methacrylate links as function of the weight conversion. Feed composition: (○) 60:40, (△) 35:65 styrene/methyl methacrylate. Solid lines, calculated values with $r_1 = 0.4971$ and $r_2 = 0.4639$.

the standard probability equations integrated as functions of conversion (18). The calculated concentrations were then compared with those obtained from the uv analysis: the results reported by Stutzel and Miyamoto (8) suggested good agreement between the calculated styrene centered triads (MSM, MSS, and SSS) and the uv measured concentrations. This, however, was not the case. Concentration differences beyond the limits of the experimental error were observed in all cases. Closer inspection of the estimated background spectrum (Fig. 4) indicates a red shift in the peaks at approximatley 267 and 272 nm relative to polystyrene's 264 and 269 nm. Since these red shifts are normally associated with solvent or substituent effects (21), we assume that the estimated background arises from styril units close to the carbonyl moiety of the methyl methacrylate units. That is, the estimated spectrum (Fig. 4) arises from coisotactic styrene − methyl methacrylate linkages. If it is further assumed that the species represented by *tert*-butylbenzene correspond to cosyndiotactic placements, then the sum of these two species (columns S_2 and S_3 in Table 2) represents the total concentration of styrene in styrene − methyl methacrylate diads, and the ratio $\sigma_{AB} = S_3/(S_2 + S_3)$ represents the fraction of the Sty−MMA diads which are coisotactic.

The mass fraction of styrene contained in Sty−MMA and MMA−Sty diads can be readily calculated from the standard

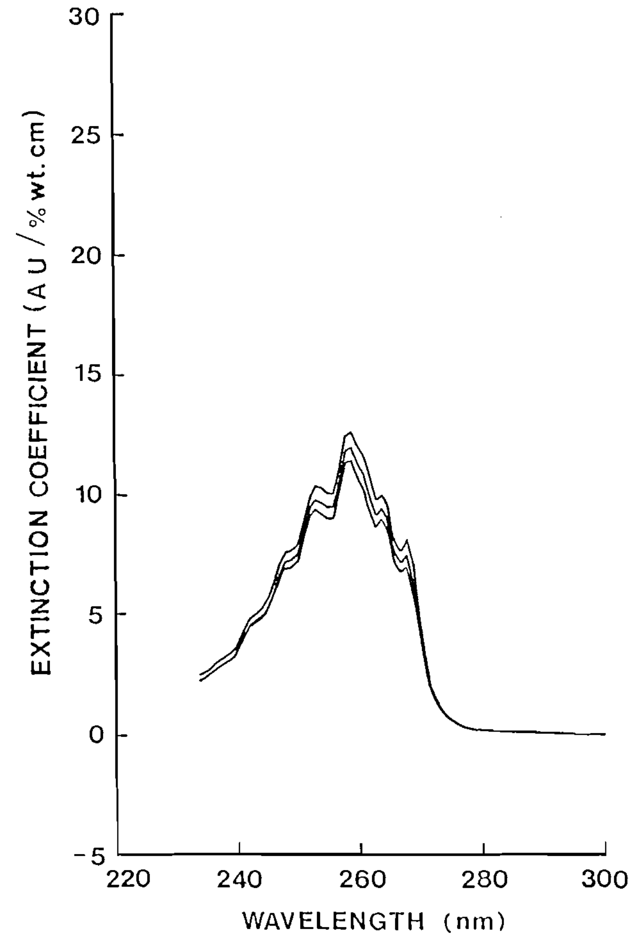

FIG. 8. Absorption spectra of bulk polymerization styrene–acrylonitrile copolymers. Feed composition as indicated in mol% styrene.

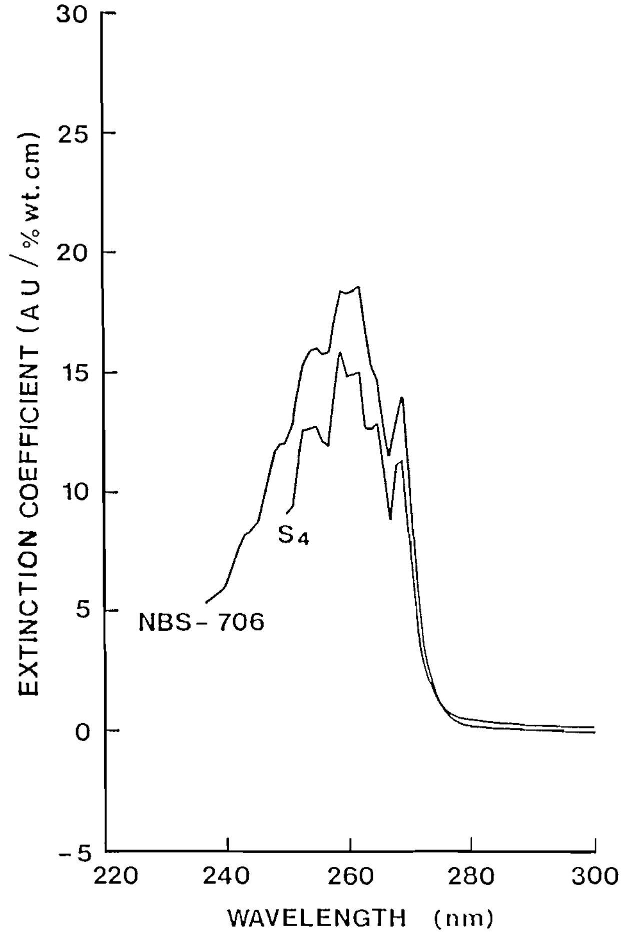

FIG. 9. Absorption spectra of commercial samples of styrene–acrylonitrile copolymers.

probability approach (22):

$$[9] \quad A_{AB} = \frac{1 - Paa^2}{1 + \dfrac{Pab}{Pba}}$$

where:

$$Pab = \frac{f_A}{r_b f_B + f_A}; \quad Paa = 1 - Pba$$

$$Pba = \frac{f_A}{r_B f_B + f_A}; \quad Pbb = 1 - Pba$$

Equation [9] can be numerically integrated along the conversion trajectory to give the cumulative concentration of styrene contained in Sty–MMA links:

$$[10] \quad A_{AB}(X) = \frac{1}{X}\int_0^X A_{AB}(X')\,dX'$$

Figure 7 shows the comparison between the measured fractions ($S_2 + S_3$) and the values calculated from eq. [10]. The agreement is satisfactory considering that only the total styrene content was used for the estimation of the reactivity ratios (20).

There is also very good agreement between the values for the coisotacticity parameter calculated from the uv measurements (Table 2) and the literature value of $\sigma_{AB} = 0.47 \pm 0.02$ (23–25) obtained from the ^{1}H nmr analysis of the methoxy resonance bands. This agreement supports the assignment of the S_2 to the cosyndiotactic Sty–MMA placements and S_3 to the coisotactic diads. Note that since the Sequence Length Distribution is proportional to the number of Sty–MMA diads, these assignments also explain previously reported correlations between the moments of the Sequence Length Distribution and the hypochromic effects (3, 8, 10, 11).

Analysis of styrene–acrylonitrile copolymers

The analysis of styrene–acrylonitrile (SAN) copolymers was, as in the case of SMMA copolymers, divided into two stages.

(a) The background spectrum and the compositions were estimated simultaneously for samples SAN90, SAN80, and SAN50 (Fig. 8) for which the conversion and composition were known (18).

(b) Using the estimated spectrum (Fig. 10), the compositions for the commercially available copolymers SAN 01–03 (Fig. 9) were obtained directly from the application of eq. [3] to each individual sample.

The assumptions made in the analysis were the same ones previously made for SMMA copolymers. That is, species S_1 and S_2, approximated by the spectrum of NBS-706 polystyrene and *tert*-butylbenzene respectively, are also present in SAN copolymers. The compositions obtained from the optimization procedure are reported in Table 3. Figure 10 shows the estimated absorption pattern for the unidentified chromophores, and Figs. 11 and 12 show typical comparisons between mea-

TABLE 3. Composition analysis of styrene–acrylonitrile copolymer

Sample	Styrene content (wt.%) S_1	S_2	S_4	Total	Reported	$S_2 + S_4$	A_{AB_w} calculated Terminal	Penultimate	η% Isotactic styrene
SAN01	2.55	36.91	33.96	73.42	75.0	70.87			46.25
SAN02	0.00	38.40	31.99	70.39	70.0	70.39			45.45
SAN03	6.25	34.13	36.82	77.20	76.8	70.95			47.69
SAN90	53.17	13.94	27.17	94.28	94.37	41.11	20.99	20.00	28.82
SAN80	20.41	26.68	37.99	85.08	85.23	64.67	53.26	51.25	44.65
SAN50	3.25	36.31	33.23	72.79	72.09	69.54	66.38	61.71	45.65

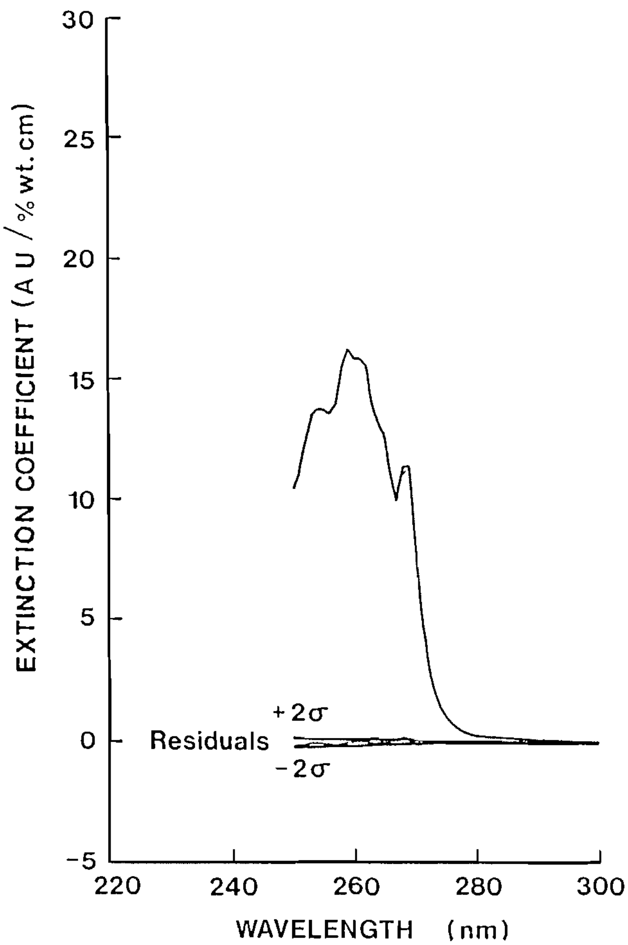

FIG. 10. Comparison between the estimated background spectrum of SAN copolymers (S_4) and the National Bureau of Standards polystyrene NBS706.

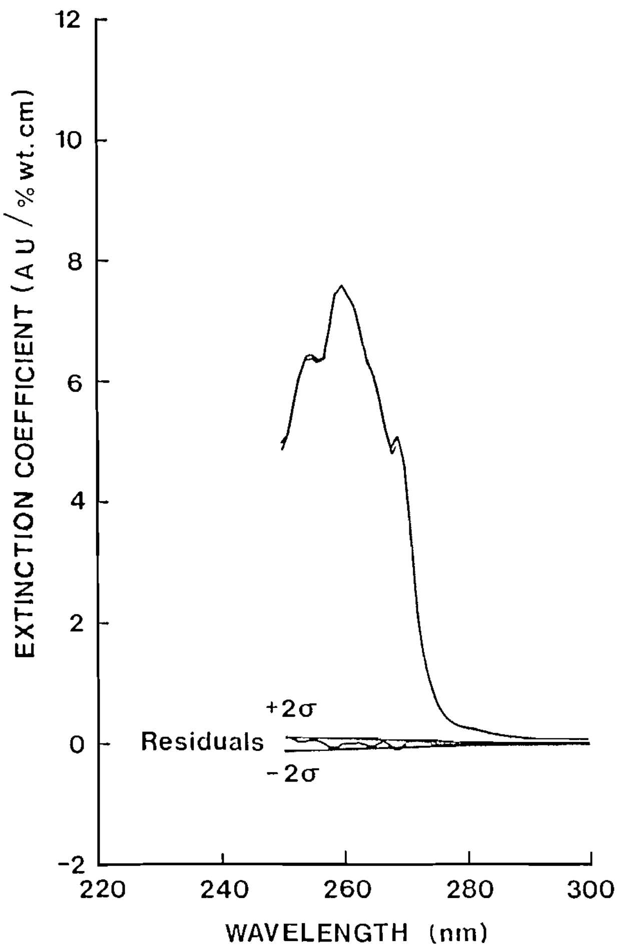

FIG. 11. Comparison between the measured and the calculated spectra of styrene–acrylonitrile copolymer SAN90. The residuals from the estimation and the 95% confidence interval on measurements are indicated.

sured and calculated spectra for samples SAN90 and SAN02 (the highest and the lowest in styrene content). Clearly, the total styrene content measured by uv spectroscopy is in good agreement with the values reported from other measurement techniques (see Tables 1 and 3). In addition, there is very good agreement, within the limits of the experimental error, between the measured and the calculated uv spectra. This indicates that the estimated spectrum constitutes a good average representation of the unidentified chromophores.

Interpretation of the results for SAN copolymers

Close inspection of the estimated background spectrum (Fig. 10) shows that it has common features with the spectrum of isotactic polystyrene (8). This suggests that the presence of the acrylonitrile units may induce tacticity in the styrene sequences, or, as in the case of Sty–MMA copolymers, the observed absorption pattern may arise from coisotactic styrene/acrylonitrile diads. In order to assign the envelopes S_1, S_2, and S_4, the analysis done for SMMA copolymers with eqs. [9] and [10] was repeated. The reactivity ratios used were those for bulk styrene – acrylonitrile polymerizations (18) (i.e., $r_A = 0.37$ and $r_B = 0.0664$). As in the case of SMMA, no correspondence between a specific sequence length fraction and the uv-measured compositions could be obtained. A significant difference between the measured and calculated concentration of styrene in styrene–acrylonitrile diads was also observed (see Table 3 under Terminal). Therefore the esti-

TABLE 4. Microstructure parameters for SAN copolymers

Sample	Terminal model				Penultimate model			
	P_{IW} calc.	A_{ABw}	σ_{AB}	σ_{AA}	P_{IW} calc.	A_{ABw}	σ_{AB}	σ_{AA}
SAN90	94.29	20.99	0.336	0.275	94.3	20.0	0.303	0.284
SAN80	85.08	53.26	0.515	0.444	85.03	51.25	0.479	0.397
SAN50	71.60	66.38	0.435	0.493	72.04	61.71	0.412	0.707

mated background cannot be attributed to coisotactic styrene–acrylonitrile diads if the copolymerization kinetics follow the terminal copolymerization model. Recent ^{13}C nmr studies on the mechanism of styrene–acrylonitrile copolymerization suggest that the molecular microstructure is better described by the Penultimate copolymerization model (22). Using this model, the total concentration of styrene in styrene–acrylonitrile diads is given by:

$$[11] \quad A_{AB} = \frac{1 + Pbaa}{\dfrac{Pbaa}{Paab} + 2 + \dfrac{Pabb}{Pbba}}$$

where:

$$Paab = \frac{f_B}{r_A f_A + f_B}; \quad Pbba = \frac{f_B}{r_B f_B + f_A}$$

$$Pbaa = \frac{r'_A f_A}{r'_A f_A + f_B}; \quad Pabb = \frac{r'_B f_B}{r'_B f_B + f_A}$$

Replacing eq. [9] with eq. [11], the concentration of styrene groups which are next to a nitrile group can be evaluated as a function of conversion. The values obtained for samples SAN 90, 80, and 50 are reported in Table 3 under "Penultimate". The reactivity ratios were those recently reported by Hill *et al.* (26), $r_A = 0.229$, $r'_A = 0.634$, $r_B = 0.039$, and $r'_B = 0.091$. The predicted concentrations based on the penultimate model are also smaller than the uv measured values. This indicates that the observed concentrations cannot be completely explained by either the Terminal or the Penultimate copolymerization model. Therefore another explanation for the observed background must be found. Based on the similar spectral features of isotactic polystyrene and the estimated background, it can be assumed that the estimated spectrum is an average representation of the coisotactic styrene/acrylonitrile and styrene/styrene diads. Under this assumption it is possible to calculate both the coisotacticity parameter σ_{AB} and the styrene isotacticity parameter σ_{AA}:

$$[12] \quad \sigma_{AB} = 1 - \frac{S_2}{A_{ABw}}$$

$$[13] \quad \sigma_{AB} = 1 - \frac{S_2}{P_{IW} - A_{ABw}}$$

where P_{IW} is the total weight fraction of styrene in the copolymer, and A_{ABw} is the weight fraction of styrene in Sty–AN diads (eqs. [10] and [11]). The values for σ_{AB} and σ_{AA} calculated from the copolymerization equations and the uv measurements are reported in Table 4 for the Terminal and the Penultimate copolymerization models. Both the Terminal and the Penultimate copolymerization models predict that the concentration of the S_1 species should drop with the styrene content in the copolymer (or the corresponding feed compositions) to a value close to zero as the Number Average Sequence length

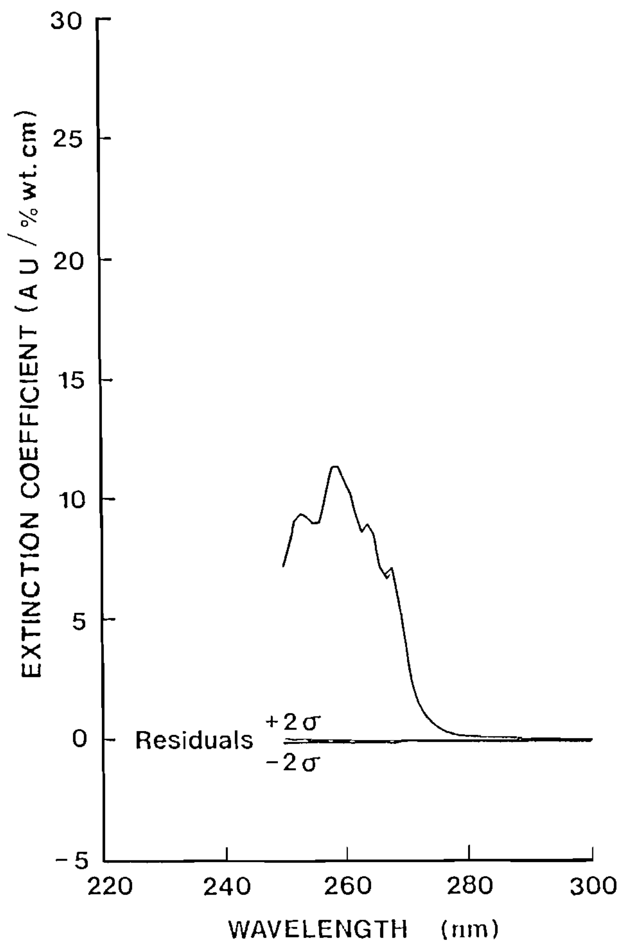

FIG. 12. Comparison between the measured and the calculated spectra of the commercial styrene–acrylonitrile sample SAN02.

approaches 1. Figure 13 shows that the variation of the species S_1, S_2, and S_4 is consistent with this assumption. Based on the above, the envelope S_4 can be tentatively assigned to the sum of the coisotactic Sty–AN and the isotactic Sty–Sty diads. The validity of the proposed assignments can be tested by demonstrating consistency between the uv concentrations and the corresponding assignments on the nmr spectrum of SAN copolymers. Work in this area is ongoing and it will be reported separately.

Summary and conclusions

A method has been proposed for the analysis of styrene-containing copolymers which yields the composition estimates directly from ultraviolet spectroscopy data. The compositions obtained from the uv measurements for styrene – methyl methacrylate and styrene–acrylonitrile copolymers have been com-

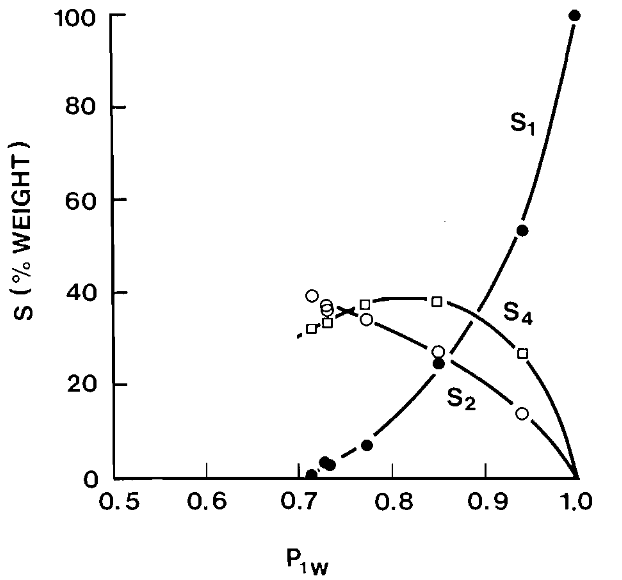

FIG. 13. Variation of the weight fraction of the styrene configurations S_1, S_2, and S_4 as function of styrene content in styrene–acrylonitrile copolymers.

pared with composition values determined with other measurement techniques. The agreement found was satisfactory within the limits of experimental error for the techniques involved. As a result of applying the proposed technique, an estimate of the spectrum of the unidentified chromophores is also obtained. This spectrum can be applied directly to the estimation of compositions in unknown samples and to the identification of the unknown structures giving rise to the measured spectrum. A tentative assignment of the estimated spectra has been made based on the well-known copolymerization models and published values of the coisotacticity parameter. In the case of SMMA, good agreement was found between the coisotacticity parameter estimates for uv spectroscopy and published ^{1}H nmr results. In the case of SAN copolymers there are no quantitative experimental data reported that allow the confirmation of the assignments. However, the concentrations of the species identified follow expected behaviour as a function of the copolymer composition.

The approach proposed here gives results which depend upon the model compounds selected to approximate the absorption of the known chromophores. The choice of the model molecules can, nevertheless, be verified by the consistency between the uv results and other measurement techniques such as ^{1}H and ^{13}C nmr. Once the model molecules and the residual spectra have been identified they can be used, routinely, for the analysis of unknown samples, as demonstrated in the analysis of the commercial SAN copolymers. The extension of this technique to GPC or SEC (size exclusion chromatography) experiments is therefore straightforward. It is clear that the uv spectra of polymers contain significant amounts of structural information which is yet to be explored. The use of the method demonstrated here in conjunction with other spectroscopy techniques appears to be a very promising tool for the elucidation of polymer microstructure and for the study of the conformation of molecules in solution.

Acknowledgments

The authors are indebted to Mr. L. Kale and Dr. K. F. O'Driscoll of the University of Waterloo for providing the styrene – methyl methacrylate copolymers, to Drs. J. F. MacGregor and A. E. Hamielec of McMaster University for providing the bulk polymerization styrene–acrylonitrile copolymers, and in particular to Dr. J. Fernandez of the Chemistry Department at the University of South Florida for his many useful suggestions.

1. E. J. MEEHAN. J. Polym. Sci. **1**, 175 (1945).
2. M. T. VALA and S. A. RICE. J. Chem. Phys. **39**, 2348 (1963).
3. K. F. O'DRISCOLL, W. WERTZ, and A. J. HUSAR. J. Polym. Sci. **5**, 2159 (1967).
4. R. J. BRUSSAU and D. J. STEIN. Angew. Makromol. Chem. **12**, 59 (1970).
5. J. L. ACOSTA and R. SASTRE. Rev. Plast. Mod. **24**, 67 (1973).
6. B. M. GALLO and S. RUSSO. J. Makromol. Sci. Chem. **33**, 521 (1974).
7. B. M. GALLO and S. RUSSO. Adv. Chem. Ser. **142**, 85 (1974).
8. B. STUTZEL, T. MIYAMOTO, and H. CANTOW. Polym. J. **8**(3), 1976 (1976).
9. C. NOEL and L. MONNERIE. Polym. J. **8**(4), 319 (1976).
10. E. GRUBER and W. L. KNELL. Makromol. Chem. **179**, 733 (1978).
11. L. H. GARCIA-RUBIO, A. E. HAMIELEC, and J. F. MACGREGOR. ACS Symposium Series. Vol. 197. *Edited by* T. Provder. 1982. p. 151.
12. L. H. GARCIA-RUBIO. J. App. Polym. Sci. **27**, 2043 (1982).
13. L. H. GARCIA-RUBIO, N. RO, and R. PATEL. Macromolecules, **17**, 1998 (1984).
14. L. KANG-JEN, J. S. LINOWSKI, and R. ULLMAN. Makromol. Chem. **105**, 18 (1967).
15. K. OHARA. Polymer Journal, **2**, 109 (1971).
16. Y. BARD. Non linear parameter estimation. Academic Press, New York. 1970.
17. L. KALE. Ph.D. Thesis in Progress, Chemical Engineering Department, University of Waterloo, Waterloo, Ont.
18. L. H. GARCIA-RUBIO. Ph.D. Thesis, McMaster University, Hamilton, Ont. 1981.
19. P. W. TIDWELL and G. A. MORTIMER. J. Macromol. Sci. Rev. Macromol. Chem. **4**, 281 (1970).
20. K. F. O'DRISCOLL, L. T. KALE, and L. H. GARCIA-RUBIO. J. Polym. Sci. Submitted.
21. R. M. SILVERSTEIN and G. C. BASSLER. Spectrometric identification of organic compounds. Wiley–Interscience, New York. 1967.
22. K. ITO and Y. YAMASHITA. J. Polym. Sci. Part A, **3**, 2165 (1965).
23. K. ITO and Y. YAMASHITA. J. Polym. Sci. Polym. Lett. Ed. **3**, 625 (1965).
24. J. PODESVA and DOSKOCILOVA. Makromol. Chem. **178**, 2383 (1977).
25. J. SAN ROMAN, E. L. MADRUGA, and M. A. DEL PUERTO. Angew. Makromol. Chem. **78**, 129 (1979).
26. D. J. HILL, J. H. O'DONNELL, and P. W. O'SULLIVAN. Macromolecules, **15**, 960 (1982).

Appendix

List of symbols

A	Absorption (au)
A_{AB}	Mole fraction of monomer A present in A.B links
C	Concentration (wt.% unless otherwise indicated)
f_A	Mole fraction of monomer A in the monomer mixture
K	Number of samples
l	Cell path length (cm)
N	Number of species present in the solution
N_{ob}	Number of observations or measurements
N_p	Number of parameters
p_i	Weight fraction of the ith species in the solution

P_{IW} Weight fraction of styrene in the copolymer
r_{AB} Reactivity ratio for monomer A or B
r'_{AB} Reactivity ratios for monomer A or B
X Molar conversion

Greek symbols
η Fraction of styrene contained in isotactic and coisotactic diads
λ Number of wavelengths
ϵ Extinction coefficient (au/wt.% cm)
σ_{AA} Isotacticity parameter
σ_{AB} Coisotacticity parameter

Subscripts
i ith concentration
j jth wavelength
M Molar
n nth component
o Initial value
w On weight basis

Cationic polymerization of 1,3-dioxolane and 1,3-dioxepane. Application to graft and block copolymer synthesis

LÉONARD C. REIBEL, CLAUDE P. DURAND, AND EMILE FRANTA

Centre de Recherches sur les Macromolécules (CNRS), 6, rue Boussingault, 67083 Strasbourg Cedex, France

Received February 27, 1984[1]

This paper is dedicated to the 10th anniversary of the Xerox Research Centre of Canada

LÉONARD C. REIBEL, CLAUDE P. DURAND, and EMILE FRANTA. Can. J. Chem. **63**, 264 (1985).

The cationic polymerization of 1,3-dioxolane and 1,3-dioxepane has been investigated to prepare "living" polymers and then to use them for copolymerization. Carbenium hexafluoroantimonate salts that are good initiators for tetrahydrofuran polymerization have been tested but produce unsatisfactory results with these acetals. In contrast, triflic anhydride, another good initiator for tetrahydrofuran polymerization, allows molecular weight control. Attempts to prepare block copolymers of two acetals by adding the second one to the first one under living conditions were unsuccessful because of randomization through transacetalization. Block copolymers containing a central block of polydioxepane and outer blocks of 1,2-dimethoxyethylene could be prepared by addition of the latter to living polydioxepane. Active polydioxolane reacts readily with polystyrene and leads to the formation of graft copolymers in the absence of gel.

LÉONARD C. REIBEL, CLAUDE P. DURAND et EMILE FRANTA. Can. J. Chem. **63**, 264 (1985).

Nous avons étudié la polymérisation cationique d'acétals cycliques tels que le dioxolanne-1,3 et le dioxepanne-1,3 en vue de préparer des systèmes vivants et, partant de là, d'obtenir des copolymères. Les sels (hexafluoroantimoniates) de carbénium qui s'étaient avérés être de bons amorceurs pour la polymérisation du tétrahydrofuranne donnent des résultats décevants avec les acétals cycliques. Par contre l'emploi de l'anhydride de l'acide triflique, un autre bon amorceur de la polymérisation du tétrahydrofuranne, permet de contrôler la masse moléculaire des polyacétals formés. Nous avons tenté d'obtenir des copolymères séquencés de deux acétals cycliques en préparant d'abord un poly-acétal vivant avec l'un des monomères et en ajoutant ensuite le deuxième acétal cyclique. Cependant le copolymère obtenu présente une distribution statistique des deux monomères due aux réactions de transacétalisation. Par contre un copolymère triséquencé ayant une séquence centrale de polydioxepanne a pu être préparé en faisant réagir sur du polydioxepanne-α,ω vivant du diméthoxy-1,2 éthylène. Des copolymères greffés ont également été obtenus en faisant réagir du polydioxolanne, porteur d'un site actif par chaîne polymère, sur du polystyrène.

Introduction

Tetrahydrofuran (THF) has been known to polymerize through an oxonium active site which remains stable, provided that the counter anion is stable (e.g., SbF_6^-, PF_6^-, $CF_3SO_3^-$). We have shown that organic halides of various types, when reacted with a silver salt such as silver hexafluoroantimonate, induce by addition a fast, quantitative initiation of the THF polymerization. This is true for mono- and plurifunctional aliphatic and aromatic acyl halides as well as for allyl iodide, 2-iodopropane, chlorodiphenylmethane, etc. (1). We have also studied in detail the mechanism of initiation and shown that, for some other halides,initiation is slow either because of the slow formation of the initiating carbenium ions or because though the formation of the latter is fast, even quantitative (e.g. tertiobutyl iodide), they undergo immediate proton elimination; the protons formed are slow initiators and, besides, not suitable for our purpose because if the particular halide studied is carried by a polymer they lead to homopolymers instead of the desired copolymers.

These findings obtained from model molecules have been applied in the preparation of block and graft copolymers: it has been shown that acyl halides carried by a backbone are very good initiators (2), just like the model acyl halide studied. But when the model molecules exhibit proton elimination it has been shown that the corresponding polymers exhibit proton elimination to an even greater extent, probably because of increased steric hindrance (3).

We have tried to use the same approach for the polymerization of cyclic acetals, which have some common character with a cyclic ether such as THF but still differ from it in many ways which we tried to utilize. First, in order to initiate the polymerization of these acetals, we used some carbocations that were successful in the case of THF; then we tried triflic anhydride. In a second series of experiments we made use of the results obtained to prepare block and graft copolymers.

Cyclic acetal homopolymerization

It has been shown that THF polymerization proceeds through a cyclic tertiary oxonium ion, but for dioxolane[2] the structure of the growing center has been proposed to exist under two different forms in equilibrium, namely, oxonium and alkoxy carbenium (4):

[1]

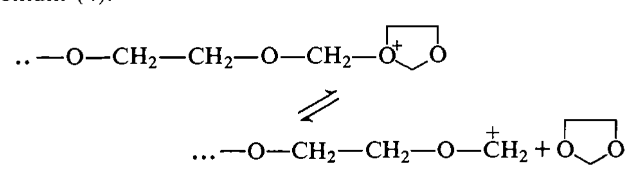

the equilibrium being shifted very strongly to the left so that propagation occurs mostly through oxonium-type ions. The dual nature of the active sites introduces a new feature as compared to THF, since one can expect active poly-DXL to be able to induce other reactions because of the higher electro-

[1]Revision received September 20, 1984.

2

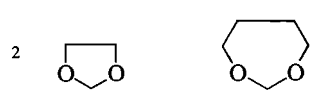

1,3-Dioxolane (DXL) 1,3-Dioxepane (DXP)

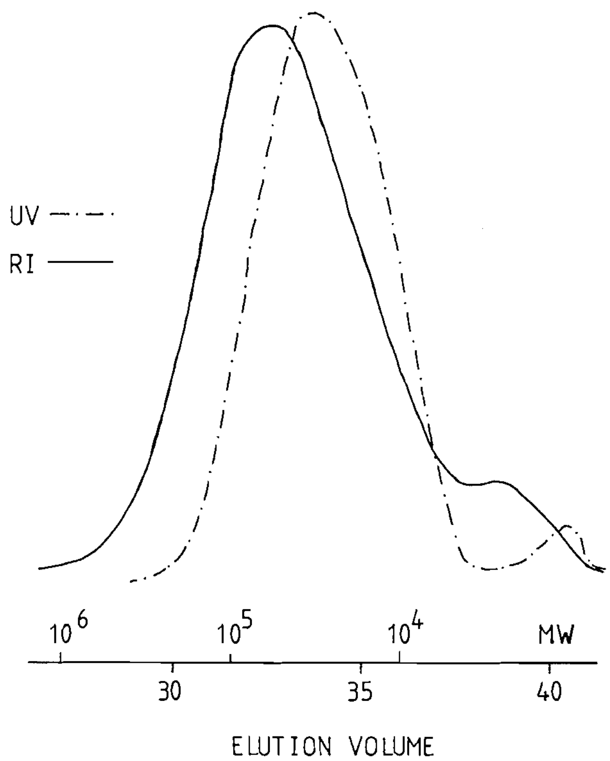

FIG. 1. The GPC curves of poly-DXL initiated by the diphenylmethylium cation; refractometric (RI) and ultraviolet (UV) detection at 260 nm (2 Shodex A-80 M columns; THF solvent; 1 mL/min flow rate).

philicity of the alkoxycarbenium ion. But, before such synthetic application can be envisioned, it is important to find the proper conditions to produce living poly-DXL systems where initiation is fast and quantitative and propagation is without transfer to monomer and without termination. Molecular weights can then be controlled and new synthetic routes are open.

1,3-Dioxolane (DXL) or 1,3-dioxepane[2] are known to produce side reactions (4); transfer to polymer is important and causes extensive formation of small rings by intramolecular and intermolecular transfer.

We are going to present our results concerning several initiators in relation to our search for living poly-DXL and apply the results to the preparation of block and graft copolymers using different comonomers and various methods.

Carbocations as initiators for DXL

Chlorodiphenylmethane has been reacted with silver hexafluoroantimonate stoichiometrically in the presence of DXL (5.2 *M*) at −55°C in CH_2Cl_2 solvent for 1 h. The polymer is recovered by precipitation in methanol at −30°C; the precipitated polymer is characterized by gel permeation (GPC) chromatography using the universal calibration; the soluble part is recovered after evaporation and characterized by vapor phase chromatography coupled to a mass spectrometer. The yield is ≃87%.

The precipitated fraction exhibits a number average molecular weight of 15 000 whereas the theoretical $\bar{M}_n$ is 55 000 and UV determinations show that only 70% of the initial chromophore has been incorporated.

The GPC determinations using both differential refractive index, RI, and UV detections (Fig. 1) show that the chromophore is present in all of the sample except for the lower molecular weight fraction: this could be an indication that it is composed of cycles. The UV peak at very low molecular weight corresponds probably to diphenylmethane but this has not been checked. After normalization of the curves a plot is made of the ratio of the UV absorption to the RI absorption multiplied by the $\bar{M}_n$ determined by GPC; the plot of ln $|\bar{M}_n \times (UV/RI)|$ obtained versus time of elution (Fig. 2) is an efficient way to estimate the relative incorporation of the chromophore into the polymer; if a particular polymer carries a chromophore at the chain end, the polydispersity of the sample will make the plot − using this representation − a straight horizontal line. This ideal situation is very close to that observed; it means that the chromophore is equally present on smaller and longer poly-DXL samples. Nevertheless, considering that only 70% of the chromophore is incorporated and that the experimental $\bar{M}_n$ is way below the theoretical one, we have to admit that some chain transfer occurred, probably involving the monomer through some unknown reaction, and that this side reaction was equally active on smaller and longer poly-DXL chains.

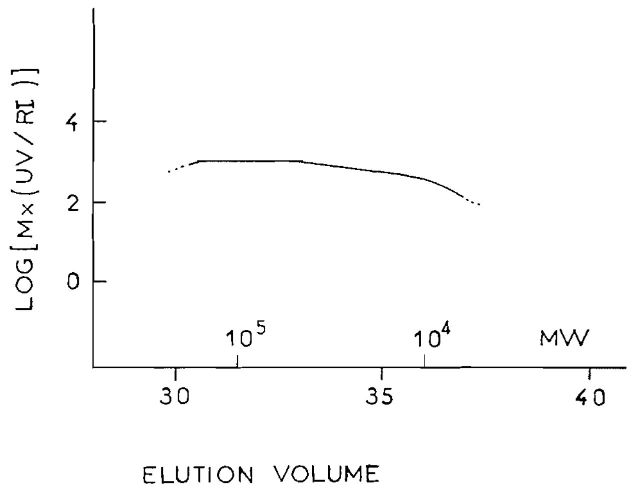

FIG. 2. Relative incorportion of the initiator moiety per polymer chain as a function of the chain length (RI, UV: normalized refractometric and ultraviolet signals; MW: molecular weight as given by the GPC universal calibration).

The soluble fraction analyzed by vp (vapor phase) chromatography and mass spectroscopy shows the presence of diphenylmethane: about 30% of the initially present chlorodiphenylmethane is present in this latter (eq. [2]). This suggests that initiation through hydride abstraction is quite significant:

[2] 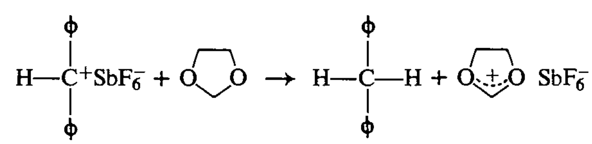

[3] 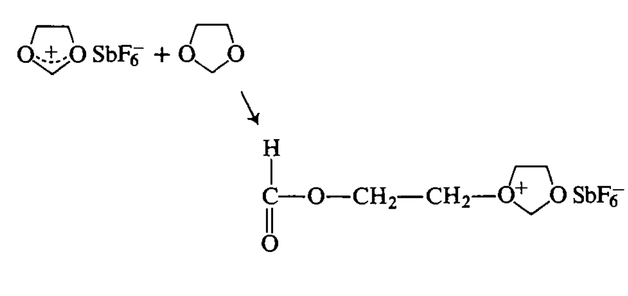

TABLE 1. Polymerization of DXL by reacting organic halides with silver hexafluoroantimonate in CH_2Cl_2

Organic halide	Concentration of the halide (mol L^{-1})	Temperature and time of polymerization	Polymer yield (%)	$\bar{M}_{n.exp.}$ (GPC)	$\bar{M}_{n.th.}$
Chlorodiphenylmethane	5×10^{-3}	−55°C 1 h	87	15 000	55 000
2-Iodopropane	10^{-3}	−55°C 1 h	76	5 000	140 000
Benzyl bromide	13×10^{-3}	−15°C 1 h	79	10 000	32 000

From these observations, one can conclude that diphenylmethylium hexafluoroantimonate initiates the polymerization of DXL through two distinct mechanisms: addition and hydride abstraction (eq. [4]). Besides, extensive side reactions create smaller chains, just after initiation, and transfer takes place during propagation: an explanation of these findings is to be found in the lower nucleophilicity of dioxolane as compared to THF; the equilibrium is shifted to the left (as compared to the THF case)

[4] 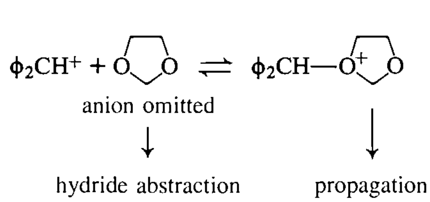

and the competition between the two processes − addition or hydride abstraction − makes the latter important. This is to be compared to the situation with THF where ϕ_2CH^+ is an excellent initiator by addition and ϕ_3C^+ initiates mostly through hydride abstraction. This result can be compared to that obtained when trityl salts react on THF: long ago it was established that hydride abstraction occurs in quantitative yield (5) and proposed that the tetrahydrofuran-2 ylium formed loses a proton (6) that is the true initiator of the THF polymerization.

The reaction of *2-iodopropane* with silver hexafluoroantimonate produced another good initiator of THF; we tried it also for DXL. 2-Iodopropane was reacted with the same silver salt, stoichiometrically in the presence of DXL (2.5 *M*), in methylene chloride at −55°C for 1 h to induce polymerization; deactivation was carried out with an excess of sodium benzylate (Table 1).

The solvent and unreacted monomer were evaporated: yield was 76%. The sample obtained was precipitated in methanol at −30°C, which separates the polymer from some low molecular weight material in solution. The recovered sample represented 77% of the starting sample and was characterized by GPC:

$$\bar{M}_{n.exp.GPC} = 5\,000$$
$$\bar{M}_{w.exp.GPC} = 88\,000$$
$$\bar{M}_{n.theor.} = 140\,000$$
$$\bar{M}_{n.exp.UV} = 40\,000 \text{ after excess benzylate elimination}$$

$\bar{M}_n$ determined by GPC is much lower than the theoretical value of 140 000, equal to the molar ratio of monomer consumed to initial 2-iodopropane; the polydispersity is quite high. The $\bar{M}_{n.exp.UV}$ which was determined by UV spectrometry is much higher than the $\bar{M}_{n.exp.GPC}$, which is an indication that very few active chains reacted with the deactivation agent. Double detection GPC (RI and UV) shows, as for diphenylmethylium, that the chromophore is present in all of the sample and also fairly regularly distributed.

Here again one observes that transfer to monomer prevails and that no living contribution can be found.

Benzylium hexafluoroantimonate was prepared by reaction of *benzylbromide* with $AgSbF_6$ stoichiometrically in the presence of DXL (7 *M*) in CH_2Cl_2 at −15°C, and the reaction proceeded for 1 h; termination was carried out with an excess of sodium methanolate. The yield was 79% (Table 1); the product was precipitated in methanol at −30°C where 74% was recovered as a high poymer, the rest (26%) was soluble.

Molecular weights were determined by GPC and by UV spectroscopy making use of the initiating chromophore; we found:

$$\bar{M}_{n.exp.GPC} = 10\,000$$
$$\bar{M}_{n.exp.UV} = 56\,000$$
$$\bar{M}_{n.theor.} = 32\,000$$

Here again the experimental $\bar{M}_n$ determined by GPC is much lower than the theoretical one, assuming complete initiation and absence of side reactions; i.e., transfer occurred. The high value of $\bar{M}_n$ determined by UV spectroscopy shows that only a small percentage (16%) of the initial chromophore has been incorporated into the polymer chains; the rest remains in the methanol-soluble fraction under various forms that we did not try to identify.

In conclusion, our attempts to use initiators containing the hexafluoroantimonate counter-ion − that had proved successful for THF polymerization − for the polymerization of dioxolane, ended without finding the proper conditions to obtain living samples; initiation was incomplete, and transfer significant.

Triflic anhydride as initiator

Penczek and co-workers (7) used triflic anhydride as an initiator for the polymerization of DXL and DXP; they showed that the concentration of active sites determined by a trapping agent (e.g. Ph_3P) corresponds to the initial concentration of initiator used within a few percent error. They also determined that the experimental $\bar{M}_n$'s agree with the theoretical ones so that they concluded that these systems are living; i.e. the total concentration of all active species is equal to the initial concentration of initiator. Since we needed well-defined polyacetals for copolymer synthesis we investigated this system and present below our findings.

Our main goal was to define experimental conditions where the theoretical and experimental $\bar{M}_n$'s would agree and where oligomer concentration would be minimal. We changed the initial monomer concentration, the temperature, and the reaction time. The GPC was used to determine the proportion of oligomers present and to calculate the $\bar{M}_n$'s of the higher molecular weight fraction, without taking into account the oligomers.

TABLE 2. Determination of the number average molecular weight in the polymerization of 1,3-dioxepane using triflic anhydride as an initiator versus time and temperature of reaction

Temperature (°C)	$[DXP]_0$ mol L^{-1}	$[Initiator]_0 \times 10^3$ mol L^{-1}	Time of reaction*	$\bar{M}_{n,theor.} \times 10^{-3}$	$\bar{M}_{n,exp.}$† $\times 10^{-3}$	$\bar{M}_w/\bar{M}_n$†	Remarks
−78	0.86	4.5	14	13.9	100	2.0	Large quantity of oligomers
−78	0.89	1.01	16.30	62	600	3.3	
−72	0.95	1.71	2.45	36	450	2.0	
			25	36	450	2.0	
−40	0.93	1.70	2.40	40	50	3.0	Small quantity of oligomers
			25	40	350	2.9	Large quantity of oligomers
−40	3.0	6.0	2	42	55	1.9	Very viscous reaction mixture
−40	1.0	2.0	2	40	48	1.7	Using 2,6-ditertiobutyl-4 methyl pyridine (10^{-2} mol L^{-1})

*Hours · minutes.
†Determined on the higher molecular weight fraction by GPC using the universal calibration.

The molecular weight determination by GPC is based on the universal calibration. The experiments described have been carried out with DXP. Table 2 shows our results.

Reactions carried out around −70°C are far from satisfactory since the molecular weights determined by GPC are markedly higher than the theoretical ones and large quantities of oligomers, probably rings, are present.

Reactions at −40°C give better results: molecular weights are close to the expected ones. The proportion of oligomers is very small (<5%). When monomer concentration is higher (e.g. 3 mol L^{-1}) viscosity increases considerably so that, in order to be able to stir, a compromise has to be found, and for our later experiments we chose initial monomer concentrations between 1 and 1.5 mol L^{-1}.

We used also an efficient proton scavenger, 2,6-ditertiobutyl-4-methylpyridine, in order to determine whether protons were involved in the initiation or propagation. Table 2 shows that no significant difference was found, and we can conclude that protons do not interfere with the polymerization.

When the reaction mixture is left standing for longer periods of time (e.g. 25 h) the molecular weight distribution changes very much; one observes an important increase of the proportion of oligomers and the $\bar{M}_n$ of the polymer increases drastically (e.g. from 50 000 to 350 000, Table 2). The polydispersity of the poly-DXP formed is quite important in every experiment and varies from 1.7 to 3.3.

In conclusion, we found that triflic anhydride can be used to prepare poly-DXP under conditions in which the molecular weights are controlled and only a small percentage of oligomers is present. This implies a careful choice of the temperature, of the time of reaction, and of the initial monomer concentration.

Copolymer synthesis

Penczek and co-workers have shown that the use of triflic anhydride leads to the formation of living poly-DXP (7); this was demonstrated by nmr, applying the ion trapping technique. We have seen above that one can control the molecular weight of the polymer formed; we can then try various possibilities to prepare block and graft copolymers.

Copolymers of two cyclic acetals

When DXL has been polymerized to prepare a dicationically living polymer, a small percentage of cycles are present because of the particular thermodynamic conditions. After addition of a second acetal, 1,3-dioxepane, polymerization ensues:

TABLE 3. Living polyacetals + vinylic monomers

Monomer		$10^{-3} \times \bar{M}_n$, I Stage		$10^{-3} \times \bar{M}_n$, II Stage		Yield* (%)
I	II	calcd.	found	calcd.	found	
DXP	DME	30.2	37.7	73.1	77.5	50
DXP	n.BVE	46.4	34.8	111.4	30.9	~100
DXP	St.	50.0	47.5		45.5	0
DXP	α-MeSt	91.2			87.0	0
DXP	Indene	73.5	87.7		81.0	0

*II stage. DME: 1,2-dimethoxyethylene; n.BVE: n.butylvinylether; St.: styrene; α-MeSt: α-methylstyrene.

removal of the lower molecular weight fraction of the macrocyclics leaves a copolymer which has a $\bar{M}_n$ close to the theoretical one — assuming a living copolymerization — within 10−15%.

The analysis of the microstructure (by ^1H and ^{13}C nmr) shows that, after the second monomer has been added, some block formation takes place but that these convert rapidly into random copolymer (7, 8). Clearly one cannot expect to prepare block copolymers using two acetals under living conditions because of the fast transacetalization occurring.

Copolymers using a vinylic comonomer

In order to avoid randomization through this side reaction we have used a second monomer whose active species are sufficiently stabilized to be unable to attack the polyacetal already formed during the second stage of the polymerization.

The first stage of the polymerization is always relative to poly-1,3-dioxepane initiated with triflic anhydride under the living conditions described above. After about 20 h the second monomer was added and left for 123 h. The polymers were then recovered and analyzed. Results are shown in Table 3.

Living cyclic DXP cannot initiate the polymerization of styrene, α-methylstyrene, and indene but can initiate the polymerization of n-butylvinyl ether, where a 100% conversion is observed. The molecular weights determined, nevertheless, do not correspond to the theoretical ones assuming a side reaction free system; the lower $\bar{M}_n$ observed in stage II stems from transfer to monomer so that, besides the copolymer formed, extensive transfer leads to homo-n-butylvinyl ether.

1,2-Dimethoxyethylene is an interesting case: the yield under our experimental conditions is usually of the order of 50%

TABLE 4. Reaction of active polydioxolane with various polymers

Experiment	Polymer	$\bar{M}_w/\bar{M}_n$	Polymer $\bar{M}_n$	$\psi = \lvert O^+ \rvert / \lvert PS \rvert$	Nature of the soluble part	Weight fraction of the insoluble part* (%)	Nature of the insoluble part
I	Polystyrene	1.1	160000	63	Some graft	60	Polystyrene + traces of poly-DXL
II	Polystyrene	1.1	10000	5.5	Graft copolymer + homopoly-DXL	No	—
III	Polystyrene	1.1	10000	15.6	Graft copolymer + homopoly-DXL	No	—
IV	Poly-α-methyl-styrene	1.2	81000	70.6	Some graft copolymer	≤5	Poly-α-methylstyrene + traces of poly-DXL
V	Polyvinyl-mesitylene	1.4	133000	83	Poly-DXL	99	Polyvinylmesitylene + traces of poly-DXL

*As compared to the initial phenyl-containing polymer introduced.

and it is not clear whether or not this comes from spontaneous deactivation. The samples obtained have been characterized by GPC, which shows a mononodal distribution, and membrane osmometry; the $\bar{M}_n$'s determined agree closely with the calculated ones (e.g. 77 500 and 73 100 respectively); fractionation with methylene chloride as solvent and iso-octane as nonsolvent has been carried out; each fraction obtained has been characterized by ^{1}H nmr to determine its content in both blocks, and selective solvent extraction has been carried out. It appears that no extractible homopolymer is present and that each fraction contains both DXP and DME. This demonstrates that direct initiation of a vinylic monomer by a living polyacetal is possible and that it can lead to a true block copolymer formation in the absence of homopolymer (9). Nevertheless the application of the method remains limited in its scope.

"Grafting onto" experiments

We have tried to make use of the dual nature of the active sites by reacting living polyacetal samples onto polystyrene, expecting to obtain a new way to prepare graft copolymers because of the possible Friedel–Crafts type reaction of the alkoxycarbenium onto the phenyl rings. Some preliminary experiments were carried out using diphenylmethylium hexafluoroantimonate as the initiator for dioxolane polymerization: we observed that a large fraction of the polystyrene was transformed into an insoluble network and that some poly-DXL was grafted on some soluble polystyrene. This finding definitely showed that growing poly-DXL has a reactivity much higher than that of oxonium ions since these latter are not capable of attacking a phenyl ring. This corroborated the possibility of existence of the proposed alkoxycarbenium.

The initiator used in the preliminary experiments has been shown since then to be poor for DXL polymerization so we turned to benzoylium hexafluoroantimonate, which, according to Kubisa and Penczek, is a satisfactory initiator (10).

The reactions were carried out in two steps: first, preparation of a growing poly-DXL which was characterized on an aliquot sample, then division of the batch into five parts which were reacted separately with a polymer containing phenyl rings; each experiment was then treated the same way and the products analyzed.

Preparation of an active poly-dioxolane

Benzoyl chloride (1.9×10^{-2} *mol* L^{-1}) was reacted stoichiometrically with silver hexafluoroantimonate in methylene chloride at −15°C in the presence of DXL (3.8 *M*); the reaction proceeded for 2 h. A sample aliquot was taken out and the reaction terminated with sodium methanolate: silver chloride was eliminated by centrifugation, the solvent and monomer left evaporated, and the product characterized by GPC. One peak plus some (<10%) oligomers were observed. The molecular weight was calculated without taking into account the oligomers; we found:

yield in polymer: 56%
$\bar{M}_n$: 13 500
$\bar{M}_w$: 22 500
$\bar{M}_{theor.}$: 8 500

Reaction of active poly-dioxolane onto various backbones

The solution of active poly-DXL was divided into five different aliquot samples, each containing the desired quantity of active sites for each particular experiment. The poly-DXL was then poured into five flasks containing the various polymers to be studied as backbones; after addition the concentration in DXL was 2.9 mol L^{-1}.

The reactions were carried out for 24 h at −15°C. Then sodium methanolate was added to terminate the reactions; silver chloride was centrifuged out. When some insoluble material was present it was isolated by filtration and treated with THF in a Soxhlet-type apparatus to remove the soluble fraction. The solvent was evaporated, the polymers dried and characterized by ^{1}H nmr and GPC.

Polystyrene, poly α-methylstyrene, and polyvinylmesitylene samples are used as polymers containing phenyl rings. The results are collected in Table 4. Refluxing 2-methoxyethanol, a solvent for poly-DXL and a nonsolvent for polystyrene, was used to separate homopolystyrene; refluxing ethanol was used to separate homopoly-DXL. Experiment I where the number of active poly-DXL sites per polystyrene chain is high ($\psi = \lvert O^+ \rvert / \lvert PS \rvert = 63$) yields mostly an insoluble network, but experiments II and III where ψ is much smaller show that the grafting efficiency for the polystyrene is 100%; only 20% of the poly-DXL present has been grafted.

In experiment IV the soluble fraction shows that it contains poly-DXL and some higher molecular weight material corresponding to ill-defined grafted poly α-methylstyrene.

Experiment V is relative to polyvinylmesitylene; 99% is recovered as an insoluble network and exemplifies the influence of a hindered phenyl ring.

In order to rationalize these results we propose that, when active poly-DXL is reacted on the polymers tested, two reactions are in competition, namely, a Friedel and Crafts attack of the alkoxycarbenium ion on the benzene ring, which leads to grafting, as in experiments I, II, III, and IV; hydride abstraction from the benzylic position can also occur and give a benzylic ion which can then attack a phenyl ring on another macromolecule, leading eventually to a network formation. This latter mechanism operates in experiments I and V.

In the case of poly α-methylstyrene, when there is no benzylic hydrogen, this process cannot take place and only the first one is operative: the existence of some small fraction of insoluble polymer could be explained by the Friedel–Crafts type attack of the benzenium onto a phenyl. An alternate explanation would involve some transfer to polymer involving the polyacetal itself, as has been observed in the case of poly THF.

In experiment I, both mechanisms are operative: grafting is observed because of the first one and network formation because of the second one, the number of active poly-DXL sites per polystyrene chain being high (63): the reason why experiments II and III do not exhibit this undesirable side reaction resting on the smaller number of active sites per chain.

In conclusion, the reaction of active poly-DXL on phenyl-carrying polymers can lead to graft copolymer formation in high yield, provided that experimental conditions are properly chosen, especially concerning the concentration of active sites per chain, which should remain small.

1. E. FRANTA and L. REIBEL. ACS Meeting, St. Louis, Missouri, U.S.A. 1984. Preprints 233.
2. E. FRANTA, L. REIBEL, J. LEHMANN, and S. PENCZEK. J. Polym. Sci. (Symp.) **56**, 139 (1976).
3. J. C. SCHWEICKERT. Thesis, Strasbourg (1980).
4. S. PENCZEK, P. KUBISA, and K. MATYJASZEWSKI. Adv. Polym. Sci. **37**, 45 (1980).
5. C. E. H. BAWN, R. M. BELL, and A. LEDWITH. Polym. **6**, 95 (1965).
6. M. P. DREYFUSS, J. C. WESTFAHL, and P. DREYFUSS. Macromolecules, **1**, 437 (1968).
7. W. CHWIALKOWSKA, P. KUBISA, and S. PENCZEK. Makromol. Chem. **183**, 753 (1982).
8. P. KUBISA, K. BRZEZINSKA, S. PENCZEK, L. REIBEL, and E. FRANTA. IUPAC 6th Int. Symp. on Cationic Polymerization, Ghent, Belgium. 1983. Preprints 185.
9. S. PENCZEK, P. KUBISA, L. REIBEL, and E. FRANTA. To be published.
10. P. KUBISA and S. PENCZEK. Makromol. Chem. **179**, 445 (1978).

COMMUNICATION

^{13}C CP/MAS nuclear magnetic resonance of crystalline methylxylopyranosides

MICHAEL G. TAYLOR AND ROBERT H. MARCHESSAULT
Xerox Research Centre of Canada, 2660 Speakman Drive, Mississauga, Ont., Canada L5K 2L1

SERGE PEREZ
Centre de Recherches sur les Macromolecules Vegetales, 53 X-38041, Grenoble, Cedex, France

AND

PETER J. STEPHENSON AND COLIN A. FYFE
The Guelph–Waterloo Center for Graduate Work in Chemistry, University of Guelph, Guelph, Ont., Canada N1G 2W1

Received January 31, 1984

This paper is dedicated to the 10th anniversary of the Xerox Research Centre of Canada

MICHAEL G. TAYLOR, ROBERT H. MARCHESSAULT, SERGE PEREZ, PETER J. STEPHENSON, and COLIN A. FYFE. Can. J. Chem. **63**, 270 (1985).

The ^{13}C nmr spectra of solids, acquired using the Cross Polarization/Magic Angle Spinning (CP/MAS) technique, are very sensitive to the detailed nature of crystalline packing. These effects are illustrated in the CP/MAS spectra of the α and β anomers of methyl-D-xylopyranoside. In the spectrum of the α anomer, which crystallizes with two molecules per unit cell, individual spectra can be resolved for the two molecules in the asymmetric unit of this crystal.

MICHAEL G. TAYLOR, ROBERT H. MARCHESSAULT, SERGE PEREZ, PETER J. STEPHENSON et COLIN A. FYFE. Can. J. Chem. **63**, 270 (1985).

Les spectre rmn du ^{13}C de solides, obtenus à l'aide de la technique Cross Polarization/Magic Angle Spinning (CP/MAS), sont très sensibles à la nature détaillée de l'entassement des cristaux. On a illustré ces effets en déterminant les spectres CP/MAS des anomères α et β du D-xylopyrannoside de méthyle. Dans le spectre de l'anomère α, qui cristallise avec deux molécules par maille unitaire, les spectres individuels peuvent être résolus pour chacune des deux molécules présentes dans l'unité asymétrique de ce cristal.

[Traduit par le journal]

Introduction

Nuclear magnetic resonance has been widely applied to the study of carbohydrates. The solution ^{1}H and ^{13}C nmr spectra provide details of the chemical structures and conformational features. It is also possible to obtain high resolution ^{13}C spectra of solid carbohydrates using the Cross Polarization/Magic Angle Spinning (CP/MAS) technique (1). The CP/MAS spectra are similar to the corresponding solution spectra, although the resolution achieved in the solid state is generally lower. The ability to observe spectra of solids promises to be useful in the study of insoluble carbohydrate polymers, especially in relation to their native, solid states. For many biopolymers, insolubility in water must be the result of simultaneous or near-simultaneous biosynthesis and crystallization, a phenomenon which may well result in a non-minimum energy state in the native material.

The chemical shifts observed in solution are characteristic of the time-averaged, isotropic environments of the nuclei. Isotropic shifts are also observed in the solid state, under magic angle spinning. However, in the solid state, the chemical shifts can be influenced by features due to the manner in which the materials crystallize. For example, crystallization may "*lock in*" conformational features which alter the chemical shifts. In addition, interactions with near neighbors depend on the crystalline conformation. Solid state effects on chemical shifts have been noted in a number of systems, including carbohydrates (2, 3). The manifestation can be in terms of simple displacement of a given signal as a function of polymorphic form or it can be in terms of multiplicities which are seen for some, but not necessarily all, of the signals. In general multiplicities will be seen if: (*i*) the site symmetry in the crystal is less than the molecular symmetry for the isolated molecule; (*ii*) the unit cell contains more than one chemically equivalent molecule. In short, one should see a signal for each atom whose position must be specified in order to define the unit cell.

In the case of simple carbohydrates where a crystal can contain more than one isomer, the technique has proven to be a valuable supplement for the crystallographer (2, 3). In the case of homopolysaccharides where a disaccharide is often the crystallographic repeat, the method can provide direct evidence of small conformational and (or) crystal field effect differences between the two chemically equivalent units.

To add to our understanding of the factors which affect chemical shift, we have examined the ^{13}C CP/MAS spectra of the methyl α- and β-D-xylopyranosides. The crystal structures of these sugars are known (4–6) and are quite different. In particular, the β-xyloside crystallizes with one molecule in the asymmetric unit, while the α-xyloside has two independent molecules in the asymmetric unit.

Experimental

Crystals of both compounds were crystallized from alcohol/water mixtures. Solution state ^{13}C nmr (7) was used to verify the anomeric identity of each sugar. The crystals were then ground into homogeneous powders. X-ray powder diffractometry indicated the unit cell dimensions previously found (4–6). Solid state ^{13}C nmr spectra were obtained at 50.3 MHz using a Bruker CXP-200 spectrometer. The spectra were acquired with dipolar decoupling and cross polarization with radio frequency field strengths of approximately 65 kHz for Hartmann–Hahn matching and proton decoupling. Recycle times of 20 s were used in the cross-polarization pulse sequence. A rotor of the Andrew–Beams design was used for Magic Angle Spinning at approximately 4 kHz. The setting of the Magic Angle was monitored by

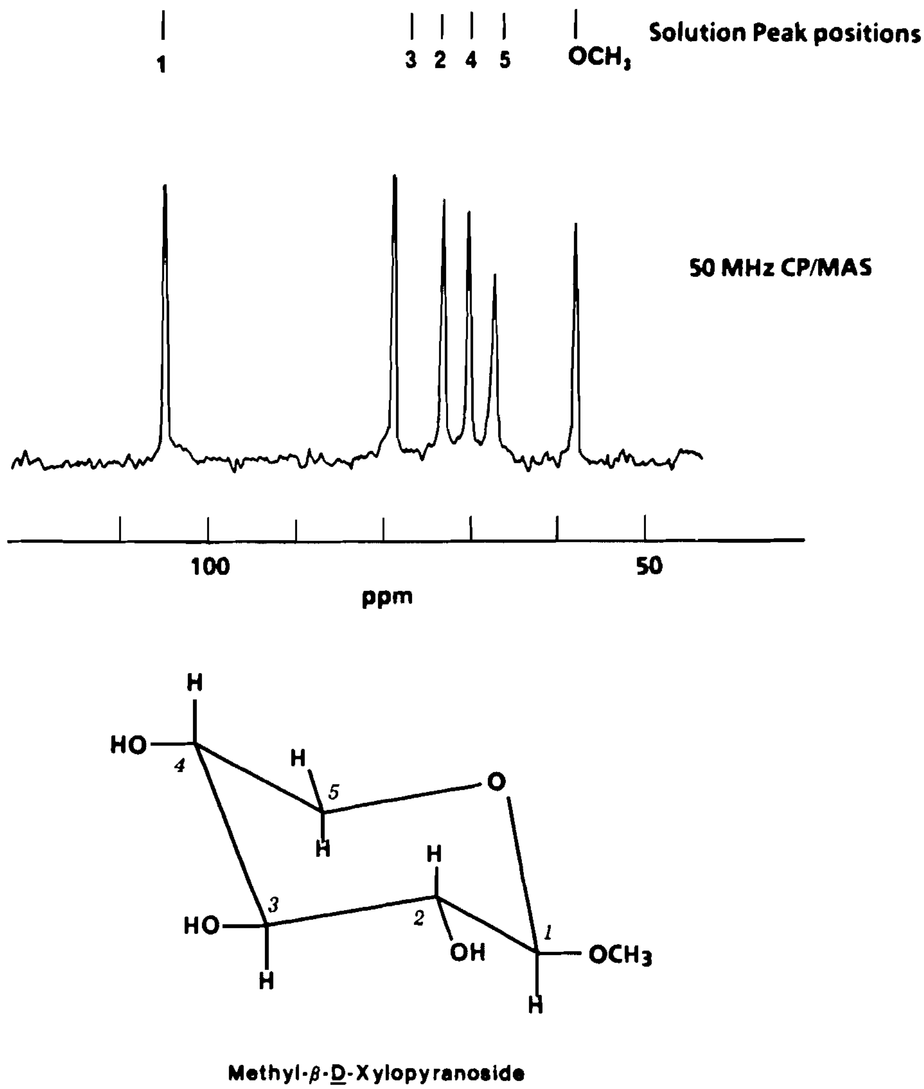

FIG. 1. Structure and ^{13}C CP/MAS nmr spectrum of methyl β-D-xylopyranoside. The solution chemical shifts (7) are included at the top of the figure.

the ^{79}Br nmr spectrum of KBr (8) incorporated in the rotor. A small amount of linear polyethylene ($\delta^{13}C$ = 33.6 ppm) was also included in the sample to provide a chemical shift reference (9).

Results and discussion

The ^{13}C CP/MAS spectra of solid samples of the methyl β- and α-D-xylopyranosides are shown in Figs. 1 and 2, respectively. In both figures, the solution state chemical shifts (7) are included for reference. The observed chemical shifts are given in Table 1. In the spectrum of the β anomer, a well-resolved six-line spectrum is observed. In the spectrum of the α anomer, eleven lines are resolved. The resonance multiplicity in the spectrum of the α anomer reflects the inequivalence of the two molecules in the asymmetric unit of this crystal. The magnetic environments of chemically equivalent carbon sites in the two molecules are different, so that individual resonances are resolved for each molecule.

A recent paper on the crystal structure of lactulose (2) convincingly showed how configurational multiplicity derived from solid state nmr was invaluable in arriving at the full three-dimensional crystal structure. In the present case, we

TABLE 1. ^{13}C chemical shifts of methyl α- and β-D-xylopyranosides*

α-Methylxylopyranoside		β-Methylxylopyranoside	
Solid state	Solution assignment	Solid state	Solution assignment
101.7 100.3	C-1	105.1	C-1
74.5 73.5 72.6 71.6 69.8	C-3, C-2, C-4	79.1 73.4 70.4	C-3 C-2 C-4
62.7 61.7	C-5	67.6	C-5
57.9 55.4	CH_3	58.3	CH_3

*Solid state shifts are measured relative to linear polyethylene at δ = 33.6 ppm. Solution assignments (7) may not correspond exactly to the solid state shifts due to differences in isotropic shifts in the two states.

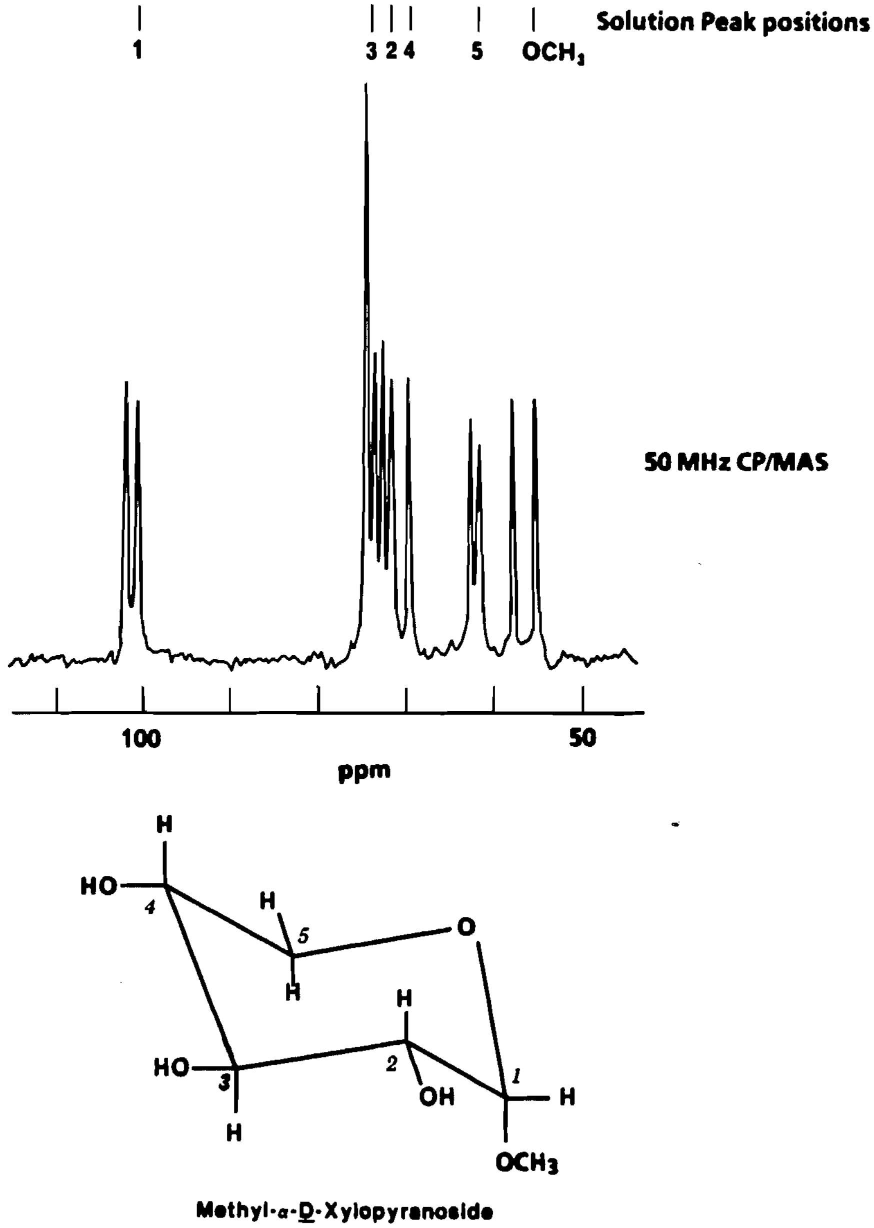

FIG. 2. Structure and ^{13}C CP/MAS nmr spectrum of methyl α-D-xylopyranoside. The solution chemical shifts (7) are included at the top of the figure.

have examined materials which have been well characterized by X-ray and neutron diffraction and the CP/MAS spectra serve to confirm the X-ray diffraction data. However, the remarkable sensitivity of this spectroscopic tool to the small differences in the shapes of the two molecules in the methyl α-xyloside is to be noted. The X-ray diffraction data (4) indicate that the only large conformational difference between the two crystalline forms of the α-xyloside is in the ϕ dihedral angle (O-5—C-1—O—CH_3). The small conformational differences, along with variations in intermolecular interactions, are sufficient to result in significantly different chemical shifts for chemically equivalent carbon sites in the two molecules. The methyl group shifts are particularly sensitive to the crystallographic inequivalence of the two molecules. The examination of other well-characterized systems may provide at least qualitative trends for the effects of the variation of crystal structure on the ^{13}C CP/MAS nmr spectra. It has been shown that a correlation exists between the C-6 chemical shift and the exocyclic C-5—C-6 torsion angle (10) in a number of sugars. It may be possible to derive other empirical relationships between the CP/MAS spectra and solid state conformational properties. Such information would be useful in aiding in the interpretation of the solid state spectra of material such as cellulose, where the spectra show characteristic features dependent on polymorphic form or the natural source of the material (11).

1. J. SCHAEFER and E. O. STEJSKAL. *In* Topics in carbon-13 nmr spectroscopy. *Edited by* G. C. Levy. Wiley–Interscience. New York. 1979. pp. 284–324.
2. G. A. JEFFREY, R. A. WOOD, P. E. PFEFFER, and K. B. HICKS. J. Am. Chem. Soc. **105**, 2128 (1983).
3. L. M. WINGERT, J. R. RUBLE, and G. A. JEFFREY. Carbohydrate Res. Submitted.

4. S. TAKAGI and G. A. JEFFREY. Acta Crystallogr. Sect. B, **34**, 3104 (1978).
5. S. TAKAGI and G. A. JEFFREY. Acta Crystallogr. Sect. B, **33**, 3033 (1977).
6. C. J. BROWN, G. COX, and F. J. LLEWELLYN. J. Chem. Soc. (A), 922 (1966).
7. P. A. GORIN and M. MAZUREK. Can. J. Chem. **53**, 1212 (1975).
8. J. S. FRYE and G. E. MACIEL. J. Magn. Reson. **48**, 125 (1982).
9. D. L. VANDERHART. J. Magn. Reson. **44**, 117 (1981).
10. F. HORII, A. HIRAI, and R. KITAMARU. Polym. Bull. **10**, 357 (1983).
11. C. A. FYFE, R. L. DUDLEY, P. J. STEPHENSON, Y. DESLANDES, G. K. HAMER, and R. H. MARCHESSAULT. J. Macromol. Sci. Rev. Macromol. Chem. Phys. C, **23**, 187 (1983).

Oxidation of elemental mercury by hydroperoxides in aqueous solution

DONALD C. WIGFIELD AND SHERRY L. PERKINS
The Ottawa-Carleton Institute for Research and Graduate Studies in Chemistry, Department of Chemistry, Carleton University, Ottawa, Ont., Canada K1S 5B6

Received February 8, 1984

DONALD C. WIGFIELD and SHERRY L. PERKINS. Can. J. Chem. **63**, 275 (1985).

The recent development of techniques in this and other laboratories has allowed the exploration of elemental mercury oxidations by compounds bearing the —O—O—H moiety. The peracid group appears to be a far more effective oxidant of mercury than the peroxide group, and both peracetic acid and *m*-chloroperbenzoic acid oxidize mercury at the trace level to both mercurous and mercuric forms.

DONALD C. WIGFIELD et SHERRY L. PERKINS. Can. J. Chem. **63**, 275 (1985).

La mise au point de nouvelles techniques, tant dans notre laboratoire qu'ailleurs, a permis d'étudier l'oxydation du mercure élémentaire par des composés portant l'unité —O—O—H. Par rapport au groupe peroxyde, le groupe peracide semble être un oxydant beaucoup plus efficace du mercure: les acides paracétique et *m*-chloroperbenzoïque oxydent tous les deux le mercure à l'état de trace pour le transformer en composés mercureux et mercuriques.

[Traduit per lar jounral]

In recent communications we have shown that mercury signals in the cold vapor atomic absorption analysis (c.v.a.a.) under non-reducing conditions arise from elemental mercury and the mercurous ion, but not from mercuric ion, and furthermore that the signals from elemental mercury cannot exceed those corresponding to the solubility limit of mercury in water (63 ppb) (1−3). A signal in the c.v.a.a. under non-reducing conditions that exceeds 63 ppb may therefore be assigned as being due, at least in part, to the mercurous ion (3), and we have recently shown that, although most mercury oxidations do not display such a signal, oxidation by peracetic acid does (3). This observation, coupled with the development of the signal assignment mentioned above, allows the exploration of previously inaccessible mercury-peroxide chemistry at the trace level. This article reports our findings in this area.

Results and discussion

The combination of cold vapor atomic absorption analysis (c.v.a.a.) of mercury, together with the so-called "uptake" experiments involving the diffusion of mercury from the side-arm of a Thunberg flask, has been a particularly powerful methodology for studying metabolic oxidation of elemental mercury. This technique, devised by Magos, Clarkson, and their collaborators (4) involves having mercury in the side-arm of a Thunberg flask, separated from potential oxidants in aqueous solution which are located in the main body of the flask. Reaction and oxidation of the mercury is achieved by the mercury diffusing to the main body of the flask, thus eliminating the problem of trying to dissolve elemental mercury in aqueous solution. The contents of the flask are subsequently analysed by c.v.a.a. This analysis can be done either with the addition of stannous chloride, to reduce all forms of mercury to elemental mercury and thus give the total mercury content of solution, or in the absence of reducing agent, in which case the analysis is specifically for volatile mercury. These aspects have previously been fully described elsewhere (1, 4−6).

Although we have reported studies of mercury oxidation under fully homogeneous conditions (5), these studies are clearly limited to having a mercury concentration of less than 63 ppb (solubility limit of mercury in water). In this regard the non-homogeneous side-arm diffusion method offers a distinct advantage, and allows not only the possibility of a far greater concentration of mercury diffusing from the side-arm and being oxidized in solution, but also the opportunity of observing the signal, under non-reducing conditions, exceeding 63 ppb, indicative of the presence of mercurous ion. Using this mercury diffusion − c.v.a.a. technique with various peroxides as the oxidant in the main body of the flask, we have been able to explore mercury-peroxide reactions. The commercially available compounds which incorporate the —O—O—H functionality are hydrogen peroxide, ethyl hydroperoxide, *tert*-butyl hydroperoxide, peracetic acid, and *m*-chloroperbenzoic acid. Oxidations of mercury by all of these reagents at various concentrations have been studied, and the results are summarized in Table 1.

Perusal of these data reveals a number of interesting points. Firstly, the reactions with H_2O_2, C_2H_5OOH, and t-C_4H_9OOH show little oxidation and the results of these experiments are basically the diffusion-controlled formation of a Hg^0 aqueous solution coupled with a small amount of oxidation. In some cases (e.g. *t*-BuOOH, 20.7×10^{-5} M) the total mercury in solution is greater than 63 ppb, but this is mostly in the mercuric ion form, and there is no suggestion of the non-reducing c.v.a.a. signal exceeding, or approaching this value. These observations are consistent with our previous chemical and enzymic oxidations of mercury (3). Secondly, the oxidations by the two peracids, in contrast, give substantial uptake and oxidation of mercury, in some cases approaching 2000 ppb. Thirdly, although most of this mercury signal appears only on the c.v.a.a. analysis under reducing conditions, and is therefore mercury in the Hg^{2+} oxidation state (1, 2), oxidations, both peracetic acid and by *m*-chloroperbenzoic acid at several concentrations show c.v.a.a. signals under non-reducing conditions substantially in excess of 63 ppb. This observation shows the presence of the mercurous ion in these oxidations. Finally, within the concentration range studied, there appears to be an interesting contrast between oxidations by peracetic acid and by *m*-chloroperbenzoic acid. Oxidations by peracetic acid show the formation of mercurous ion at $[CH_3CO_3H] = 10.5 \times 10^{-5}$ M and at higher concentrations this mercurous signal continues to increase. In contrast, the oxidations with *m*-chloroperbenzoic acid also show the mercurous ion becoming evident at approximately $[RCO_3H] = 10 \times 10^{-5}$ M, but then rising to a maximum value at approximately $[RCO_3H] = 20 \times 10^{-5}$ M and dropping at higher $[RCO_3H]$. At very high $[RCO_3H]$ the signal is once again submerged below the solu-

TABLE 1. Cold vapor atomic absorption analysis of mercury oxidized by various peroxide reagents

Oxidant	Concentration × 10^5 (M)	Signal* non-reducing conditions (Hg^0, Hg_2^{2+}) (ppb)	Reducing conditions Hg(total) (ppb)
None	—	36.2±1.7	26.6±0.3
Acetic acid	23.3	42.6±1.0	30.6±0.6
Benzoic acid	27.3	39.7±1.9	32.8±1.1
Peracetic acid	1.40	40.3±1.0	66.5±2.6
	10.5	64.6±0.1	218±7
	17.5	105±2	397±8
	26.3	153±3	528±15
	35.1	237±3	671±6
m-Chlorobenzoic acid	2.90	36.8±1.5	33.4±2.5
	11.6	109±7	1080±10
	19.3	189±14	2100±10
	38.6	120±5	1700±10
	193	28.7±2.7	1930±60
Hydrogen peroxide	2.94	36.0±0.6	33.6±2.2
	11.8	30.8±1.6	35.9±4.9
	23.5	35.5±1.7	31.7±0.8
tert-Butyl hydroperoxide	2.59	36.1±2.5	27.3±0.4
	20.7	36.5±1.3	93.5±2.1
Ethyl hydroperoxide	2.68	35.1±1.6	25.3±3.0
	10.7	33.9±2.3	35.8±2.0
	21.5	36.3±1.4	27.1±2.1

*The signal under non-reducing conditions can sometimes appear to exceed that under reducing conditions due to unavoidable time lag between determinations and resulting loss of Hg^0. This is of consequence only where Hg(total) is very small.

bility limit of Hg^0.

A number of conclusions appear to follow from these observations. Firstly, the peracids are evidently far more effective oxidants than the peroxides and, since these "acids" are not particularly acidic (pK_a 7.1−8.2 (7)), it appears likely that the carbonyl group may well be playing a role in the peracid oxidations. Although a cyclic mechanism involving mercury and the carbonyl group, such as shown in Fig. 1 is an attractive notion, and one which would be restricted to the peracids, there are certainly other mechanistic possibilities which would account for the greater oxidative capability of the peracid group. Oxidation to the mercurous ion is also an intriguing mechanistic question. Clearly the technique used in this study, while allowing chemistry to be delineated, does not permit any mechanistic insight to be gained.

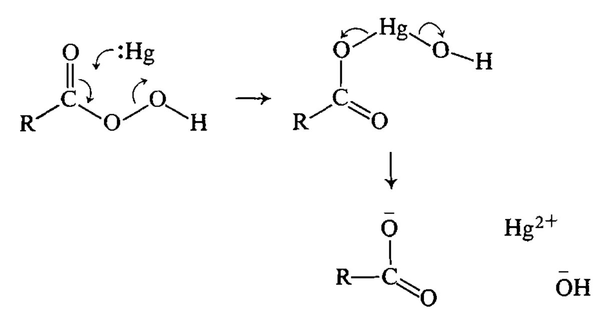

FIG. 1. Cyclic mechanism for mercury oxidation.

Experimental

Solutions and reagents

t-*Butyl hydrogen proxide*: *t*-butyl hydrogen peroxide solutions were prepared by serial dilution of *t*-butyl hydroperoxide-70 (Wallace and Tiernan Inc., Buffalo, NY).

Ethyl hydrogen peroxide: solutions were prepared by serial dilutions of 10% aqueous ethyl hydrogen peroxide (Polysciences Inc., Warrington, PA).

Peracetic acid: 40% peracetic acid (FMC Corporation, Buffalo, NY) was sequentially diluted to produce reagent solutions.

Hydrogen peroxide: 30% A.C.S. reagent grade hydrogen peroxide (Anachemia, Montreal, Canada) was serially diluted to produce reagent solutions.

m-*Chloroperoxybenzoic acid*: 0.5 g *m*-chloroperoxybenzoic acid (Aldrich Chemical Company, Milwaukee, WI) was dissolved in 10.0 mL absolute ethanol (Consolidated Alcohols Ltd., Toronto, Canada). Reagent solutions were prepared by serial dilutions of this stock solution with distilled water.

Incubation and analysis

Distilled water (3.0 mL) was placed in the main body of each Thunberg flask. The test reagent (20 μL) was added and the flasks were stoppered with a side-arm containing metallic mercury (0.1 mL). The flasks were incubated overnight in a metabolic shaker. At the end of the incubation period the side-arms were removed, flasks were sealed with parafilm, and solutions were analyzed by double Magos determination (1).

Control experiments

Oxidations with carboxylic acids were tested (see Table 1) in order to ensure that oxidations with peracids were not proceeding by initial reduction to the carboxylic acid which in turn acted as the main oxidant.

Errors

Error limits quoted are standard deviations on triplicate determinations.

Acknowledgements

We gratefully acknowledge the financial support of the Natural Sciences and Engineering Research Council of Canada in the form of continuing operating grants (to D.C.W.) and an NSERC Scholarship (to S.L.P.).

1. D. C. WIGFIELD and S. L. PERKINS. J. Anal. Toxicol. **6**, 279 (1982).
2. D. C. WIGFIELD and S. L. PERKINS. Anal. Chim. Acta. In press.
3. D. C. WIGFIELD and S. L. PERKINS. J. Appl. Toxicol. In press.
4. L. MAGOS, S. HALBACH, and T. W. CLARKSON. Biochem. Pharm. **27**, 1373 (1978).
5. D. C. WIGFIELD and S. L. PERKINS. J. Appl. Toxicol. **3**, 185 (1983).
6. D. C. WIGFIELD, S. M. CROTEAU, and S. L. PERKINS. J. Anal. Toxicol. **5**, 52 (1981).
7. C. R. NOLLER. Chemistry of organic compounds. 3rd ed. W. B. Saunders Company, Philadelphia. 1966. p. 201.

Etude de l'anharmonicité électrique dans $^{12}C^{16}O_2$

PHILIPPE MILLIÉ
Département de Physico-Chimie, CEN/SACLAY, 91191 Gif-sur-Yvette Cedex, France

Reçu le 24 avril 1984

PHILIPPE MILLIÉ. Can. J. Chem. **63**, 278 (1985).

Le développement du moment dipolaire dans la molécule $^{12}C^{16}O_2$ en fonction des coordonnées normales est déterminé jusqu'au quatrième ordre par ajustement sur les valeurs expérimentales des intensités de transition. La convergence du développement est rapide, mais les termes d'ordre trois jouent un rôle très important si on veut obtenir une précision de l'ordre de 20%.

PHILIPPE MILLIÉ. Can. J. Chem. **63**, 278 (1985).

The dipole moment derivatives up to the fourth order are determined for the $^{12}C^{16}O_2$ molecule by fitting the experimental values of several transition intensities. The convergence is fast, but the third order is significant in order to obtain an acceptable accuracy (~20%).

Introduction

Le moment dipolaire d'une molécule polyatomique peut être décrit dans n'importe quel système de coordonnées représentant le déplacement des atomes par rapport à la configuration d'équilibre. Cependant, en général, on utilise un développement en puissance en fonction des coordonnées normales sans dimension (q_s)

$$[1]\quad M^\alpha = M_e^\alpha + \sum_s P_s^\alpha q_s + \frac{1}{2}\sum_{s,s'} P_{ss'}^\alpha q_s q_{s'} + \ldots$$

avec

$$P_s^\alpha = \left(\frac{\partial M^\alpha}{\partial q_s}\right)_e, \quad P_{ss'}^\alpha = \left(\frac{\partial^2 M^\alpha}{\partial q_s \partial q_{s'}}\right)_e \ldots \quad \alpha = x,y,z$$

La question essentielle est la rapidité de convergence d'un tel développement, c'est-à-dire le rôle de l'anharmonicité électrique dans les intensités de transition.

La molécule de bioxyde de carbone se prête particulièrement bien à une telle étude, car d'une part, sa fonction potentiel est bien connue (1), d'autre part, l'intensité d'un grand nombre de ses transitions a été déterminée (2).

Cette étude se distingue des études précédentes (3, 4) sur le même sujet sur trois plans: (*i*) l'utilisation d'une fonction potentiel plus raffinée, (*ii*) le nombre de transitions utilisées pour déterminer les coefficients P_s, P_{ss}, etc.., beaucoup plus grand (7 à 10 fois), et (*iii*) la fonctionnelle utilisée: on a cherché à reproduire au mieux les intensités de transition et non les moments dipolaires.

L'emploi de ces derniers pose en effet le problème du signe des valeurs expérimentales, et oblige, soit à tester tous les jeux de signe possibles, soit à ne garder que les transitions les plus intenses pour lesquelles le signe est certain (3), ce qui restreint l'échantillonnage dans les deux cas.

Considérations théoriques

1. *Principe général*

L'intensité d'une transition donnée entre deux états vibrationnels ψ_i et ψ_j est proportionnelle à

$$\langle\psi_i|M|\psi_j\rangle^2$$

Compte tenu de l'éq. [1], on obtient:

$$\langle\psi_i|M^\alpha|\psi_j\rangle^2 = \left[\sum_s P_s^\alpha \langle\psi_i|q_s|\psi_j\rangle + \frac{1}{2}\sum_{s,s'} P_{ss'}^\alpha \times \langle\psi_i|q_s q_{s'}|\psi_j\rangle + \ldots\right]^2$$

Si on connaît par ailleurs les fonctions d'ondes ψ_i et ψ_j, on peut aisément calculer $\langle\psi_i|q_s|\psi_j\rangle$, $\langle\psi_i|q_s q_{s'}|\psi_j\rangle$, etc. $\langle\psi_i|M^\alpha|\psi_j\rangle^2$ devient une fonction des seuls paramètres P_s^α, P_{ss}^α, etc.. et ces derniers sont alors obtenus à partir d'un échantillonnage de valeurs expérimentales de $\langle\psi_i|M^\alpha|\psi_j\rangle^2$.

2. *Obtention des fonctions d'ondes*

Elle consiste à écrire les fonctions d'ondes comme des produits des fonctions harmoniques et à diagonaliser l'hamiltonien $T + V$ dans cette base. Le potentiel utilisé est celui déterminé par A. Chedin (1). La validité de ce potentiel, la convergence des fonctions d'ondes et des éléments de matrice de l'opérateur moment dipolaire ont été discutées dans un article précédent (5). La dimension de la base utilisée est de 246 pour chacune des symétries Σ_g^+, Σ_u^+, Π_g, Π_u, Δ_g, Δ_u alors que les intensités des transitions utilisées ne font intervenir au maximum que les vingt premiers niveaux dans chaque symétrie.

3. *Développement du moment dipolaire*

Le développement, au quatrième ordre, en fonction des coordonnées normales sans dimension compte tenu des restrictions dues à la symétrie, s'écrit sous la forme (*i*) pour les transitions parallèles ($\Sigma_g^+ \leftrightarrow \Sigma_u^+$, $\Pi_g \leftrightarrow \Pi_u$, $\Delta_g \leftrightarrow \Delta_u$)

$$M_\parallel = P_3 q_3 + P_{13} q_1 q_3 + P_{113} q_1^2 q_3 + P_{223} q_2^2 q_3 + P_{333} q_3^3 + P_{1113} q_1^3 q_3 + P_{1223} q_1 q_2^2 q_3 + P_{1333} q_1 q_3^3$$

(*ii*) pour les transitions perpendiculaires ($\Pi_{g,u} \leftrightarrow \Sigma_{u,g}^+$, $\Delta_{g,u} \leftrightarrow \Pi_{u,g}$), si on utilise les coordonnées polaires ρ et φ, on obtient:

$$M_\perp = e^{i\varphi}(P_2\rho + P_{12} q_1\rho + P_{112} q_1^2\rho + P_{233}\rho q_3^2 + P_{222}\rho^3 + P_{1112} q_1^3\rho + P_{1233} q_1\rho q_3^2 + P_{1222} q_1\rho^3)$$

Conduite du calcul et résultats

1. *Choix de l'échantillonnage*

Bien qu'on ne puisse pas définir un critère absolu de choix, cet échantillonnage doit répondre aux qualités suivantes:

(a) Le nombre d'echantillons doit être nettement supérieur au nombre de paramètres, ici huit.

(b) Les transitions choisies doivent permettre une détermination significative des paramètres. Elles doivent donc faire intervenir ces derniers avec des poids comparables sur l'ensemble à déterminer. Il est notamment nécessaire pour cela de choisir aussi bien des transitions intenses que des transitions très faibles.

TABLEAU 1. Coefficients du développement du moment dipolaire en fonction des coordonnées normales (en 10^{-2} e Å). Cas des transitions parallèles. F: Valeur de la fonctionnelle utilisée

Paramètre	Ce travail					Réf. 3	Réf. 4
P_3	−12,0690	−9,8613	−9,9270	−9,9312	−9,8910[a]	−9,937	−9,7910
P_{13}	—	0,3078	0,4287	0,4265	0,4107	0,534	0,3125
P_{113}	—	—	0,0110	0,0176	0,0169	—	—
P_{223}	—	—	0,0530	0,0657	0,0644	0,058	—
P_{333}	—	—	0,0072	0,0064	0,0068	—	0,0333
P_{1113}	—	—	—	0,0011	0,0012	—	
P_{1223}	—	—	—	0,0062	0,0074	—	0,0271
P_{1333}	—	—	—	−0,0020	−0,0019	—	0,0085
F	0,217	0,079	0,033	0,016	0,023		

[a] Valeurs obtenues pour une variation aléatoire d'au maximum 15% des valeurs expérimentales.

TABLEAU 2. Cas des transitions perpendiculaires

Paramètre	Ce travail					Réf. 3
P_2	−3,3539	−4,1746	−3,9548	−3,9164	−3,8880[a]	−3,823
P_{12}		0,1762	0,1785	0,1753	0,1741	0,148
P_{112}			0,0077	0,0070	0,0069	—
P_{233}			0,0021	0,0021	0,0020	—
P_{222}			0,0197	0,0191	0,0187	0,014
P_{1112}			—	−0,0002	−0,0002	
P_{1233}			—	−0,0001	−0,0002	
P_{1222}			—	0,0001	0,0001	
F	3,05	1,88	0,080	0,059	0,059	

(c) On doit éliminer les transitions faisant intervenir des états vibrationnels très fortement perturbés par interaction de Coriolis (puisqu'on a négligé cette dernière dans l'hamiltonien) ainsi que celles pour lesquelles les erreurs expérimentales sont trop importantes.

On arrive ainsi à un total de 100 (après en avoir éliminé huit par le critère (c) pour les transitions parallèles et de 66 pour les perpendiculaires (après en avoir éliminé six) (à comparer à 9 pour la réf. 3 et à 15 pour la réf. 4).

2. *Choix de la fonctionnelle et conduite du calcul*

Soit expe(k) et theor(k) les valeurs expérimentales et théoriques du carré du moment dipolaire de la $K^{\text{ième}}$ transition considérée.

On recherche, par la méthode de Newton, les valeurs des paramètres P_1, P_2... qui minimisent la fonctionnelle

$$F = \frac{1}{n} \sum_{k=1}^{n} (\text{theor}(k) - \text{expe}(k))^2/\text{theor}(k) \cdot \text{expe}(k)$$

c'est-à-dire la somme des carrés des erreurs relatives. Les valeurs expérimentales sont tirées de la référence 2.

Pour s'assurer que l'on atteint le minimum minimorum, le processus itératif de Newton est répété pour un certain nombre de valeurs de départ différentes des paramètres.

On obtient, par cette méthode, la valeur absolue et le signe de chaque paramètre à condition d'attribuer un signe au paramètre le plus grand (P_1 ou P_2). La détermination antérieure de ce signe (3) permet de lever totalement l'ambiguité.

Discussion des résultats

Les résultats sont rassemblés dans les tableaux 1 (transitions parallèles) et 2 (transitions perpendiculaires).

On peut remarquer: (*i*) le bon accord entre cette détermination et les déterminations antérieures pour le premier terme aussi bien pour les transitions parallèles que pour les perpendiculaires; (*ii*) la rapide décroissance (environ un facteur 10 à chaque ordre) des termes successifs, notamment dans le cas des transitions perpendiculaires, où l'ordre quatre est pratiquement négligeable, ce qui justifie le choix d'un développement en fonction des coordonnées normales; (*iii*) l'amé-

TABLEAU 3. Valeurs expérimentales et théoriques de la force oscillatrice des dix transitions les plus intenses et des dix transitions les plus faibles (en 10^{-4} (e Å)^2)

ψ_i	ψ_j	$\langle\psi_i\|M\|\psi_j\rangle^2_{\text{exp.}}$	$\langle\psi_i\|M\|\psi_j\rangle^2_{\text{th.}}$
$(0,0^0,0)$	$(4,0^0,1)$V	6,593 10^{-7}	5,090 10^{-7}
$(0,0^0,0)$	$(4,0^0,1)$IV	2,279 10^{-8}	2,833 10^{-8}
$(0,0^0,0)$	$(4,0^0,1)$III	1,439 10^{-6}	1,386 10^{-6}
$(0,0^0,0)$	$(4,0^0,1)$II	3,885 10^{-7}	4,003 10^{-7}
$(0,0^0,0)$	$(4,0^0,1)$I	2,096 10^{-8}	2,067 10^{-8}
$(0,0^1,0)$	$(1,1^1,3)$II	7,157 10^{-6}	5,624 10^{-6}
$(0,1^1,0)$	$(3,2^2,0)$III	6,686 10^{-7}	6,825 10^{-7}
$(0,0^0,0)$	$(3,1^1,0)$IV	5,139 10^{-8}	6,499 10^{-8}
$(0,1^1,0)$	$(4,0^0,0)$IV	3,157 10^{-7}	3,416 10^{-7}
$(0,0^0,0)$	$(0,1^1,2)$	8,634 10^{-6}	8,230 10^{-6}
$(0,0^0,0)$	$(0,0^0,1)$	47,145	47,762
$(1,0^0,0)$II	$(1,0^0,1)$II	49,141	46,780
$(1,0^0,0)$I	$(1,0^0,1)$I	49,545	46,343
$(0,2^2,0)$	$(0,2^2,1)$	49,886	47,500
$(1,1^1,0)$I	$(2,0^0,0)$I	18,315	16,210
$(0,0^0,0)$	$(0,1^1,0)$	14,314	15,052
$(1,0^0,0)$I	$(1,1^1,0)$I	21,091	20,981
$(2,0^0,0)$I	$(2,1^1,0)$I	31,833	29,217
$(2,0^0,0)$II	$(2,1^1,0)$II	23,077	23,324
$(1,1^1,0)$II	$(1,2^2,0)$II	34,757	36,920

lioration très nette de la valeur minimale de la fonctionnelle F en fonction du nombre de paramètres et notamment l'importance du troisième ordre pour obtenir une erreur relative moyenne inférieure à 30%; (*iv*) la bonne fiabilité des résultats obtenus en fonction des erreurs expérimentales: un changement aléatoire de toutes les valeurs expérimentales (limitée à 15% au maximum) ne modifie que peu les valeurs obtenues, même les plus faibles (comparer les colonnes 4 et 5 des tableaux 1 et 2). On peut ainsi estimer notre erreur à 1% sur le 1er terme et à 5% sur les autres. (*v*) le bon accord que l'on obtient avec les valeurs expérimentales aussi bien pour des transitions très intenses que pour des transitions de très faible intensité (huit ordres de grandeur) (voir tableau 3).

Conclusion

Comme il a été déjà discuté (5), le potentiel utilisé dans ce travail semble apte à reproduire théoriquement les intensités de transition observées. Le large échantillonnage utilisé permet d'améliorer la fiabilité du développement du moment dipolaire, notamment pour les plus petits termes qui jouent un rôle important pour les transitions presque interdites.

Une évaluation a priori, d'intensités de transitions non encore observées dans CO_2, semble maintenant possible avec une précision de l'ordre de 20%.

1. A. CHEDIN. J. Mol. Spectrosc. **76**, 430 (1979).
2. A. CHEDIN, N. HUSSON, N. A. SCOTT, I. COHEN-HALLALEH et A. BERROIR. Tables Geisa Laboratoire de Météorologie Dynamique du C.N.R.S. Notes internes n$^{\circ}$s 108, 113 et 116 (1982).
3. I. SUZUKI. J. Mol. Spectrosc. **80**, 12 (1980).
4. J. BORDE. J. Phys. **39**, 369 (1978).
5. PH. MILLIÉ. Can. J. Chem. **62**, 736 (1984).

Thermodynamic control in the reactions of gas phase anions. An *ab initio* and ion cyclotron resonance study of the reactions of anions with diborane

O. EISENSTEIN[1]
Department of Chemistry, University of Michigan, Ann Arbor, MI 48109, U.S.A.

M. KAYSER[2]
Département de Chimie, Université de Moncton, Moncton, N.B., Canada E1A 3E9

M. ROY AND T. B. MCMAHON[3,4]
Department of Chemistry, University of New Brunswick, Fredericton, N.B., Canada E3B 6E2

Received April 3, 1984

O. EISENSTEIN, M. KAYSER, M. ROY, and T. B. MCMAHON. Can. J. Chem. **63**, 281 (1985).

The gas phase ion molecule reactions of a number of anions, X^-, with diborane, B_2H_6, have been investigated using ion cyclotron resonance spectroscopy. Two distinct reaction channels are observed in addition to simple proton transfer. The first of these is production of BH_4^- and BH_2X while the second is formation of BH_3X^- and BH_3. In order to determine the importance of thermodynamic factors in the course of reaction *ab initio* calculations have been carried out on the species involved to obtain the relative stabilities of the two possible pairs of products. The 4-31+G basis set incorporating additional flat *s* and *p* functions has been used since this basis set has been demonstrated to give the most accurate description of anions to date. The results obtained indicate that the thermochemical factors are instrumental in determining the reaction pathway.

O. EISENSTEIN, M. KAYSER, M. ROY et T. B. MCMAHON. Can. J. Chem. **63**, 281 (1985).

Faisant appel à la spectroscopie de résonance de l'ion dans un cyclotron, on a étudié les réactions ion molécule en phase gazeuse d'un certain nombre d'anions, X^-, avec le diborane B_2H_6. On a observé deux voies distinctes de réaction en plus du simple transfert de proton. La première voie conduit à la formation de BH_4^- et de BH_2X alors que la seconde fournit du BH_3X^- et du BH_3. Dans le but de déterminer l'importance des facteurs thermodynamiques pendant la réaction, on a effectué des calculs *ab initio* sur les espèces impliquées afin d'obtenir les stabilités relatives des deux paires possibles de produits. On a utilisé l'ensemble de base 4-31+G incluant des fonctions additionnelles *s* et *p* planes puisque cet ensemble de base a donné jusqu'à présent la description la plus correcte des anions. Les résultats obtenus indiquent que les facteurs thermodynamiques contribuent à déterminer le processus réactionnel.

[Traduit par le journal]

Introduction

Despite the widespread synthetic utility of borohydride reductions the details of the mechanism by which BH_4^- reacts with carbonyl groups is not well understood (1–3). Recent *ab initio* calculations (4) have shown that the reaction of isolated BH_4^- with formaldehyde to produce methoxide ion and BH_3, reaction [1],

[1] $BH_4^- + CH_2O \rightarrow CH_3O^- + BH_3$

should be *endothermic* by 36 kcal mol^{-1}. In addition, exploration of the potential energy surface for this reaction also revealed a substantial activation barrier. This is in considerable contrast to the experimental observations which show that in solution borohydride reductions of carbonyl groups proceed rapidly with little or no activation energy and with evolution of substantial quantities of heat.

In order to explore the mechanism of reaction between naked BH_4^- and CH_2O we undertook an investigation of the gas phase reactions of BH_4^- with CH_2O using ion cyclotron resonance spectroscopy (ICR) (5). As predicted by *ab initio* calculations (4) no hydride transfer occurred. Furthermore, even in the case of reaction of BH_4^- with CF_2O, in which the carbonyl group is substantially activated, no hydride transfer was observed, reaction [2].

[2] $BH_4^- + F_2CO \rightarrow F_2CHO^- + BH_3$

In the course of our study reactions of BH_4^- with a wide variety of aliphatic aldehydes and ketones were also attempted and, while no hydride transfer was observed an extremely interesting new reaction was discovered.

Borohydride ion, BH_4^-, was generated in our system by reaction of F^- with diborane, B_2H_6, reaction [3].

[3a] $F^- + B_2H_6 \rightarrow BH_4^- + BH_2F$

[3b] $F^- + B_2H_6 \rightarrow BH_3F^- + BH_3$

Under usual experimental conditions proton abstraction by F^- from the aldehyde or ketone under investigation was also observed in those species possessing an α hydrogen. For example, with acetone the acetone enolate ion was readily formed, reaction [4]

[4] 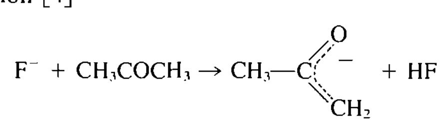

This ion was observed to subsequently react with diborane to produce a new species of boron enolate, reaction [5].

[5] 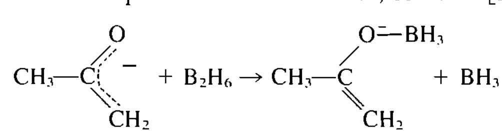

[1] Present address: Laboratoire de Chimie Theorique, Batiment 490, C.N.R.S., Centre d'Orsay, 91405, Orsay, France.

[2] Present address: Département de Chimie, Université de Quebec à Montreal, C.P. Succursale A, Montreal (Que.), Canada H3C 3P0.

[3] Present address: The Guelph Waterloo Centre for Graduate Work in Chemistry, Waterloo Campus, Department of Chemistry, University of Waterloo, Waterloo, Ont., Canada N2L 3G1.

[4] To whom all correspondence should be addressed.

Trialkyl boron enolates are well known synthetic reagents for important reactions such as stereoselective aldol condensations (6, 7).

Having observed reaction [5], and to a smaller extent the analogous reaction of F^-, reaction [3*b*], it was felt that the reaction of CH_3O^- with diborane might then yield $CH_3OBH_3^-$, the postulated intermediate in the borohydride reduction of formaldehyde. However, when CH_3O^- was reacted with B_2H_6 the only product observed was BH_4^-, reaction [6].

$$[6] \quad CH_3O^- + B_2H_6 \rightarrow BH_4^- + CH_3OBH_2$$

The realization that there are two very different ways in which anions can react with diborane, reactions [7] and [8] led us to investigate a large number of anion–diborane reactions to

$$[7] \quad X^- + B_2H_6 \rightarrow BH_4^- + BH_2X$$
$$[8] \quad X^- + B_2H_6 \rightarrow XBH_3^- + BH_3$$

determine the factors affecting the species produced in these two general pathways. In order to determine the importance of the relative thermodynamic stabilities of the two sets of products on the product distribution, *ab initio* calculations for several key reactions representing different extents of pathways [7] and [8] were carried out. The results reported in the present study show an excellent agreement between theoretical calculations and experimental findings and provide strong evidence for thermochemical control in gas phase anion–diborane reactions.

Experimental

All experiments were carried out using an ion cyclotron resonance spectrometer of basic Varian V-5900 design extensively modified to permit routine operation in both conventional drift and trapped ion modes (8). Ion cyclotron resonance spectroscopic techniques have been described in detail elsewhere (9, 10).

Pure gaseous diborane was generated according to a modified method described by Dunbar (11) in which finely powdered KBH_4 (0.32 g) was added to 85% phosphoric acid (6 mL) which was frozen in liquid nitrogen. The reaction flask was then attached to a vacuum line, evacuated, and allowed to warm to room temperature. The B_2H_6 product was collected continuously by pumping through a dry-ice acetone trap into a liquid nitrogen trap. Mass spectrometric analysis revealed no higher boron hydrides and no other impurities.

All other chemicals were commercial materials of highest purity obtainable and were used without further purification other than degassing by successive freeze–pump–thaw cycles.

Although Dunbar (11) has reported that BH_4^- is obtained by dissociative electron impact on diborane, reaction [9], at the pressures

$$[9] \quad B_2H_6 + e^- \rightarrow BH_4^- + BH_2$$

at which our experiments were carried out the cross section for formation of BH_4^- by this mode relative to those for formations of the other anions of interest was so low that no direct production of BH_4^- was observed. Fluoride ion, F^-, was produced by dissociative electron attachment to NF_3; alkoxide ions, RO^-, were generated by dissociative attachment to alkyl nitrites, RONO; and CN^- by electron impact on cyanogen iodide, ICN. All other anions studied were generated by proton abstraction from the appropriate conjugate acid, by either F^- or CH_3O^-, reaction [10].

$$[10] \quad X^- + AH \rightarrow A^- + HX$$

Computational method

Ab initio molecular orbital calculations were carried out using the GAUSSIAN 80 program package (12). All calculations on molecules and ions were at the SCF level. All structures were fully optimized using the 4-31+G basis set described by Schleyer and co-workers (13) using an analytical gradient technique (14). The only geometric constraint imposed was freezing of rotation about the B—O bond in $CH_3OBH_3^-$ such that the ion was constrained to the most stable, staggered configuration.

The 4-31+G basis set with additional flat *s* and *p* Gaussian functions on all heavy atoms has been shown by Schleyer and co-workers (13, 14) to give a much more accurate description of energetics of anions than other split valence basis sets previously used.

TABLE 1. Products observed for reactions of anions with diborane

BH_4^- only	BH_4^- and XBH_3^-	XBH_3^- only
CH_3O^-	F^-	CF_3^-
$C_2H_5O^-$	CH_3S^-	CF_3O^-
i-$C_3H_7O^-$	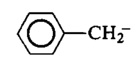	$CH_2NO_2^-$
t-$C_4H_9O^-$	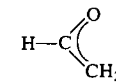	CH_2CN^-
$CF_3CH_2O^-$	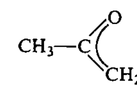	$CH_3CO_2^-$
	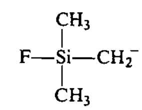	CN^-
		NO_2^-
		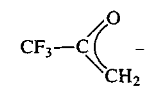
		
		$CH_3—C\equiv C^-$

Results and discussion

The reactions of anions, X^-, with diborane can be divided into three broad categories: (*i*) those producing only BH_4^-; (*ii*) those producing both BH_4^- and XBH_3^- in varying proportions; (*iii*) those producing only XBH_3^-. The results obtained for the anions investigated in the present work are summarized in Table 1 according to these categories. Representative data are shown in Fig. 1 for reaction of CH_3O^- with B_2H_6, in Fig. 2 for reactions of F^- with B_2H_6, and in Fig. 3 for reaction of CN^- with B_2H_6.

These results suggest that the reactions of anions with B_2H_6 may be interpreted as occurring through a common, intermediate $XB_2H_6^-$ complex from which dissociation to products may occur as shown in Scheme 1. The structure of the inter-

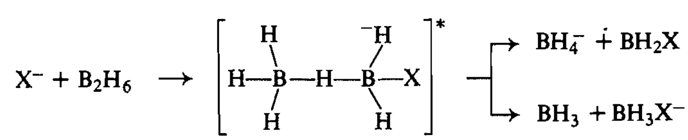

SCHEME 1

mediate complex with a linear B—H—B bond is chosen by analogy to the $B_2H_7^-$ anion which has been shown by X-ray crystallographic (15) and *ab initio* studies (16–18) to have a symmetrical structure with a single, linear B—H—B bridge bond. The decomposition path will then depend upon the position of the central hydrogen atom in the B—H—B linkage, which, in turn, is dictated by the electronic properties of the X substituent. When X is a strongly electron donating substituent the central H will be displaced towards the boron to which X

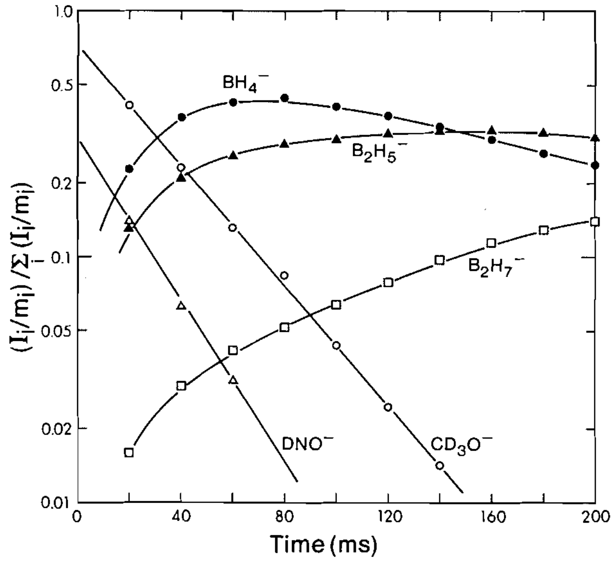

FIG. 1. Variation of relative ionic abundances with reaction time for a 2:1 mixture of CH_3ONO and B_2H_6 at total pressure of 1.5×10^{-6} Torr following a 5 ms, 70 eV electron beam pulse. Products of reactions of anions with CD_3ONO are omitted for clarity.

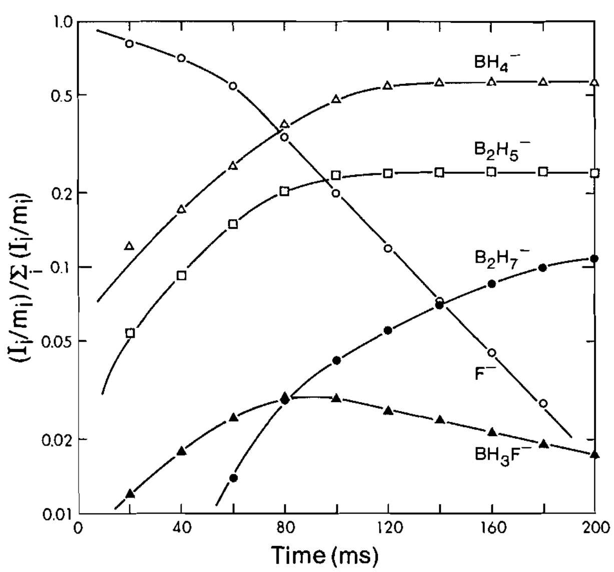

FIG. 2. Variation of relative ionic abundances with reaction time for a 3.3:1 mixture of NF_3 and B_2H_6 at a total pressure of 1.7×10^{-6} Torr following a 5 ms, 70 eV electron beam pulse.

is not bound, as in **I**, thus facilitating a decomposition to produce BH_4^- and BH_2X. Conversely, when X is an electron-withdrawing group the central hydrogen atom will be displaced toward the boron to which X is bonded, as in **II**, thus favoring

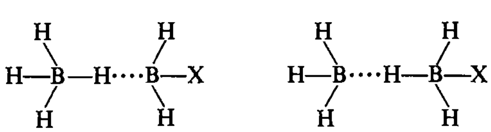

I **II**

a dissociation to BH_3 and BH_3X^-. Finally, substituents which are neither intrinsically good electron-withdrawing nor donating groups will yield intermediates in which the central hydrogen atom remains close to the center of the bond, giving rise to

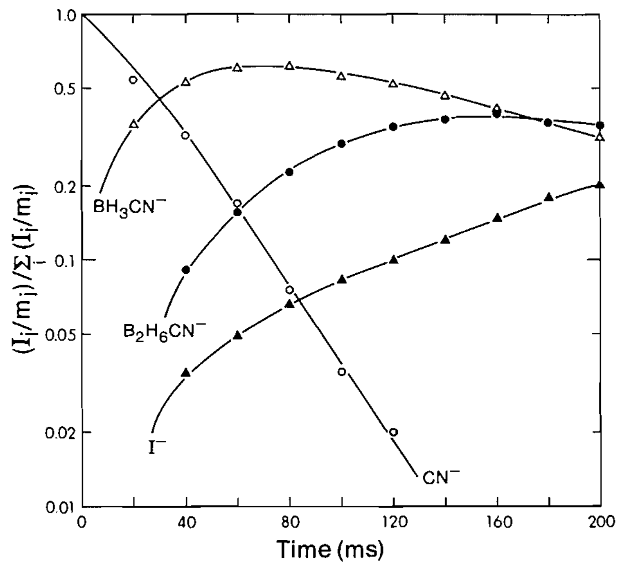

FIG. 3. Variation of relative ionic abundances with reaction time for a 1.4:1 mixture of ICN and B_2H_6 at a total pressure of 1.9×10^{-6} Torr following a 5 ms, 70 eV electron beam pulse.

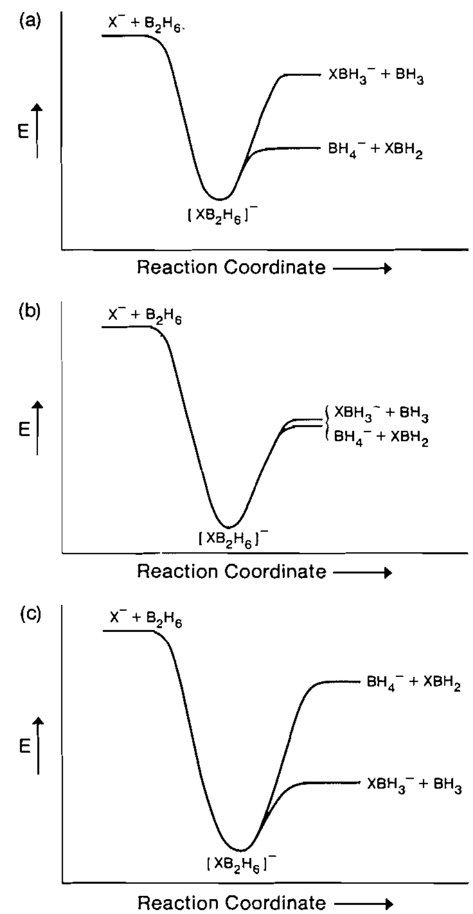

FIG. 4. Hypothetical reaction coordinate diagrams for the three possible situations arising from the reactions of anions, X^-, with diborane, B_2H_6.

a mixture of products. It is interesting to note that according to this classification F must be regarded as a more electron donating than withdrawing substituent on boron since 95% of the products of reaction of F^- are BH_4^- + BH_2F. This result is

TABLE 2. Optimized geometries and total energies using 4-31+G basis set

BH_3	B—H = 1.184 Å	E = −26.350023 au
BH_4^-	B—H = 1.240 Å	E = −26.9360665 au
BH_2F	B—F = 1.362 Å B—H = 1.177 Å ∠HBF = 117.332°	E = −125.168469 au
BH_3F^-	B—F = 1.517 Å B—H = 1.231 Å ∠HBF = 108.486°	E = −125.7591873 au
BH_2CN	B—C = 1.533 Å C—N = 1.147 Å B—H = 1.177 Å ∠HBC = 118.995°	E = −117.972091 au
BH_3CN^-	B—C = 1.613 Å C—N = 1.155 Å B—H = 1.229 Å ∠HBC = 108.765°	E = −118.60325 au
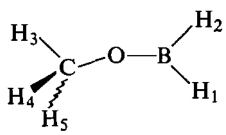	B—O = 1.355 Å B—H_1 = 1.192 Å B—H_2 = 1.181 Å C—O = 1.434 Å C—H_3 = 1.075 Å C—H_4,H_5 = 1.080 Å ∠H_1BO = 120.156° ∠H_2BO = 117.743° ∠COB = 127.600° H_3CO = 105.917° $H_{4,5}$CO = 110.260° ωH_4COB = 60.657°	E = −140.14529 au
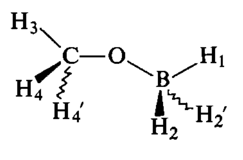	B—O = 1.522 Å B—H_1 = 1.227 Å B—H_2 = 1.248 Å C—O = 1.401 Å C—H_3 = 1.087 Å C—H_4 = 1.092 Å ∠H_1BO = 108.544° ∠H_2BO = 110.013° ∠COB = 117.703° ∠H_3CO = 109.095° ∠H_4CO = 111.789° ωH_2BOH = 120.575° ωH_4COB = 60.238°	E = −140.7039776 au

consistent with previous ICR investigations of isoelectronic gaseous carbonium ions (19, 20) which show F is a strongly stabilizing substituent by virtue of donation of F $2p$ electron density into the vacant $2p$ lobe of a carbonium ion center. The borane groups in this work are isoelectronic analogues of substituted methyl cations and it is then logical that stabilization of intermediates and products by F via $p-\pi$ donation can occur. This situation may be regarded formally as resulting from contributions from the valence bond structures **III** and **IV**.

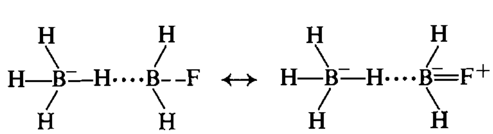

III **IV**

It is also of interest to note the change in product distribution as the degree of charge delocalization is varied in a series of similar substituents. For example, the CH_3O^- ion yields only BH_4^- as a product ion whereas the CF_3O^-, in which negative charge is dispersed by inductive withdrawal through the σ framework of the molecule, yields only $CF_3OBH_3^-$. Similarly, a comparison of acetaldehyde, acetone, and trifluoroacetone enolates and acetate ion reveals that the least delocalized species, $HCOCH_2^-$, produces over 90% BH_4^- while the more delocalized, $CH_3COCH_2^-$, yields 70% BH_4^- and 30% $CH_3COCH_2BH_3^-$. As the degree of negative charge delocalization increases still further in $CF_3COCH_2^-$ and $CH_3CO_2^-$, no BH_4^- is observed and only XBH_3^- product is formed.

The factors affecting the stability of the intermediate complexes also apply to the product species and thus the competition between the two reactions might be regarded as the result of thermodynamic control. The three different situations may be represented by the three reaction coordinate diagrams shown in Fig. 4. In every case formation of both sets of products is exothermic; however, when there is a large difference in

TABLE 3. Total energies of possible products formed in reaction of selected anions with diborane

X	Neutral (BH_2X) energy (au)	Anion (BH_3X^-) energy (au)
H	−26.350023	−26.9360665
CH_3O	−140.14529	−140.7039776
F	−125.168469	−125.7591873
CN	−117.970091	−118.60325

TABLE 4. Energy changes for isodesmic hydride transfer reactions $BH_3X^- + BH_3 \rightarrow BH_4^- + BH_2X$

X	ΔE (kcal mol^{-1})
CH_3O	−17.2
F	+2.9
CN	+28.3

exothermicity of formation of the two sets of products the more stable products are formed virtually exclusively (Fig. 4*a* and 4*b*). Conversely, when the exothermicities of both reactions are comparable (Fig. 4*c*) both pairs of products are produced, with the slightly more energetically favored pathway giving rise to somewhat more product.

In order to investigate this possibility of thermochemical control of the product distribution high quality *ab initio* calculations were carried out for products of reaction of CH_3O^-, F^-, and CN^-. These anions are representative of each of the three possible situations above. The optimized geometries of each of the possible ionic and neutral products are summarized in Table 2. The total energies obtained using the 4-31+G basis set and optimized geometries are listed in Table 3. The degree to which thermodynamic control operates in these reactions is seen most easily from an examination of the isodesmic hydride transfer reaction, eq. [11]. Energy changes for each of the situations

$$[11] \quad XBH_3^- + BH_3 \rightarrow BH_4^- + XBH_2$$

examined are shown in Table 4. As expected, when the enthalpy change for reaction [11] is large and negative as for CH_3O^-, reaction [7] producing exclusively BH_4^- is the only reaction observed. When the enthalpy change for reaction [11] is large and positive, as for CN^-, reaction [8], producing exclusively BH_3CN^-, is the only reaction observed. However, when the enthalpy change for reaction [11] is relatively small and either positive or negative both possible products might be expected. This situation is illustrated by the reaction of F^- with B_2H_6 where both BH_4^- (95%) and BH_3F^- (5%) are produced. According to the calculations at the 4-31+G level production of BH_3F^- is found to be 2.9 kcal mol^{-1} more energetically favorable than BH_4^- production. Thus from the *ab initio* results a *reverse* order of product abundances would have been predicted. This is most likely a consequence of slight deficiencies of the 4-31+G basis set which lead to a poorer representation of fluorine-containing neutrals relative to anions. As can be seen from the data in the Appendix the 6-31G* basis set predicts a B—F bond length of 1.29 Å in BH_2F while our 4-31+G calculations yield a B—F bond length of 1.36 Å. In order to test this possibility the energy change for the isodesmic reaction [11] where X = F was also determined at the 6-31G* level and BH_4^- was found to be slightly favored as the ionic product. In

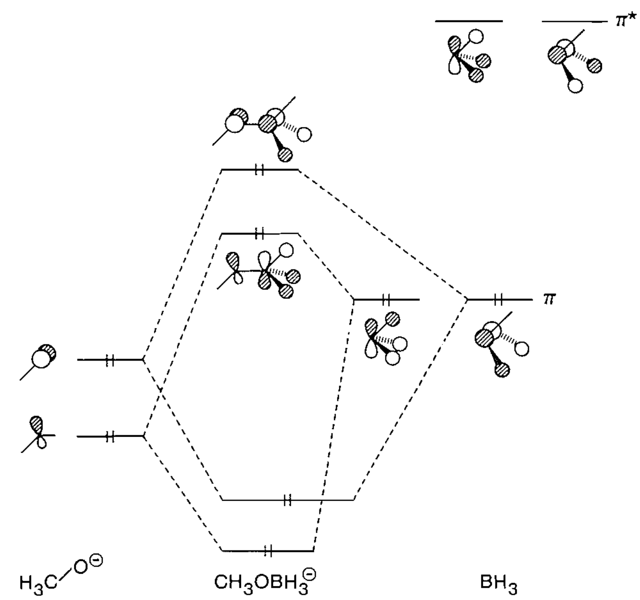

FIG. 5. Orbital interactions between CH_3O^- and the BH_3 fragment in $CH_3OBH_3^-$. Only those orbitals contributing to the destabilization of species are illustrated.

the absence of experimental data for the geometry of BH_2F it is not possible to say which basis set more adequately describes BH_2F; however, our experimental data clearly show that BH_4^- is the more energetically favorable product. In cases such as this where the energetic difference between possible products is very small it thus seems likely that *ab initio* calculations will have difficulty in determining the more stable products. It is important to note that in all cases *ab initio* calculation predicts that production of *both* sets of products is exothermic. These results are thus clear evidence of the importance of thermodynamic control in determination of product distribution in the reaction of anions with diborane.

An alternative method of analysing the above ion molecule reactions is to examine the orbital interactions stabilizing or destabilizing all possible products. The inspection of the anionic products listed in Table 1 shows that we can discriminate between the two types of BH_3X^- anions: those in which BH_3 fragment is linked to a non-stabilized anion with high energy orbitals (example, —OCH_3) and those in which BH_3 is attached to an anion possessing the low-lying empty orbitals.

An examination of the interactions between BH_3 and X^- fragments in the BH_3X^- anions shows that the BH_3 group contains a degenerate set of π_{BH_3} and $\pi^*_{BH_3}$ orbitals (Fig. 5). The latter set (π^*) is of high energy due to the low electronegative character of the boron atom, and consequently may be neglected. Thus, the only interactions of importance are those between the π_{BH_3} and the occupied and empty orbitals of X^- fragment.

When X^- has a *high energy HOMO and no accessible LUMO* orbitals as is the case of CH_3O^-, the interaction of X^- with BH_3 leads to a four electron repulsion between the two fragments. Such a limiting case is illustrated by the $CH_3OBH_3^-$ anion as shown in Fig. 5. Here, the methoxy anion has three lone pairs, one of which is implicated in the σ bonding with BH_3. The remaining two interact in an antibonding fashion with symmetry compatible π_{BH_3} orbitals (Fig. 5). On the other hand, if X^- is characterized by low-lying occupied orbitals, as well as *low-lying empty* orbitals, for example CN^- or NO_2^-, the

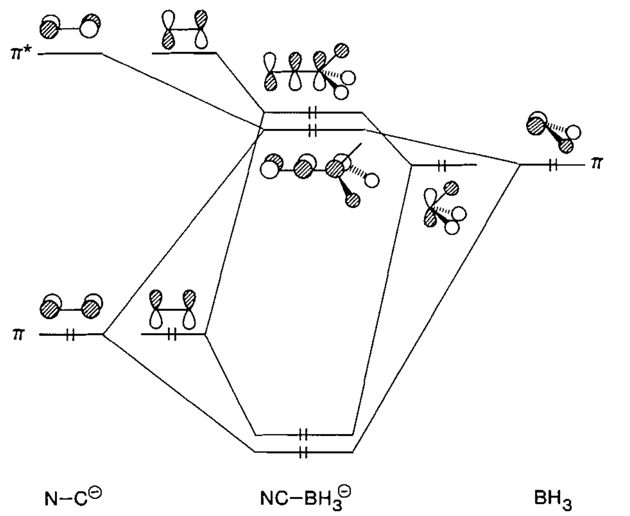

FIG. 6. Orbital interactions between CN^- and the BH_3 fragment in $NCBH_3^-$. Only those orbitals contributing to the stabilization and destabilization of the species are illustrated.

TABLE 5. Energies of the highest occupied molecular orbitals (HOMO) of the calculated XBH_3^- anions

Anion XBH_3^-	HOMO ϵ(au)
HBH_3^-	−0.19001
$NCBH_3^-$	−0.22265
FBH_3^-	−0.20029
$CH_3OBH_3^-$	−0.16315

effect of the four electron repulsion is minimal, while the system is stabilized by the two electron interaction between π_{BH_3} and the LUMO of the anionic fragment (Fig. 6).

The above analysis is confirmed by the relative energy levels of the highest occupied molecular orbitals (HOMO) of the calculated anions listed in Table 5. The highest HOMO (Fig. 5, Table 5) is found in the most destabilized species — $CH_3OBH_3^-$, while the $NCBH_3^-$, the most stabilized anion, possesses a low-lying HOMO (Fig. 6, Table 5). The HOMO of our reference anion BH_4^- is situated in-between those two extreme cases. This illustrates the absence of the stabilizing or destabilizing effects in the BH_4^- anion.

The stability of the neutral species (XBH_2) is the result of the electronic back donation from the occupied orbital of X fragment into the empty orbital of BH_2 fragment. The magnitude of this effect is related to the energy level of the occupied orbital of the X group and consequently is larger for CH_3OBH_2 than for $NCBH_2$.

The above orbital considerations also correspond closely to the gas-phase, ion–molecule reaction results shown in Table 1. Alkoxides, thiolates, and fluoride ion, characterized by high energy lone pair and inaccessible empty orbitals yield predominantly XBH_2 and BH_4^- products. On the other hand, the strongly stabilized anions such as CF_3O^-, cyclopentadienyl, and trifluoro acetone enolate which possess low-lying orbitals give XBH_3^- and BH_3 as products. In between those two extremes lie enolates, benzyl, and the slightly less stabilized anions such as $(CH_3)_2FSiCH_2^-$.

Conclusion

The experimental results presented above show that two possible competitive reaction channels exist for reactions of anions with diborane. The uniformity of these reaction pathways suggests that both reactions occur via a common $XB_2H_6^-$ complex reaction intermediate. The *ab initio* calculations performed reveal that the relative stabilities of the two possible products controls the reaction channel. This conclusion is further supported by considerations of the electronic donating and withdrawing properties of various substituent groups X and considerations of orbital interactions betwen X^- and BH_3. This, and similar studies, reveal the tremendous value to be gained from the parallel investigation of gas phase ion molecule reactions by both experimental and *ab initio* methods.

Acknowledgements

Generous financial support of this work was provided by grants from N.A.T.O. (O.E. and M.M.K.) and N.S.E.R.C. (Canada) (T.B.M.). O.E. would also like to thank the donors of the Petroleum Research Fund administered by the American Chemical Society for support of this research.

1. H. C. BROWN. Boranes in organic chemistry. Cornell University Press, Ithaca, New York. 1972.
2. D. C. WIGFIELD. Tetrahedron, **35**, 449 (1979).
3. M. M. KAYSER, S. ELIEV, and O. EISENSTEIN. Tetrahedron Lett. **24**, 1015 (1983).
4. O. EISENSTEIN, H. B. SCHLEGEL, and M. M. KAYSER. J. Org. Chem. **47**, 2886 (1982).
5. M. M. KAYSER and T. B. MCMAHON. Tetrahedron Lett. To be published.
6. C. H. HEATHCOCK and C. T. WHITE. J. Am. Chem. Soc. **101**, 7076 (1979).
7. S. MASAMUNE, W. CHOY, F. A. J. KERDESKY, and B. IMPERCALI. J. Am. Chem. Soc. **103**, 1566 (1981).
8. T. B. MCMAHON and J. L. BEAUCHAMP. Rev. Sci. Instrum. **43**, 509 (1973).
9. J. L. BEAUCHAMP. Ann. Rev. Phys. Chem. **22**, 517 (1971).
10. T. A. LEHMAN and M. M. BURSEY. Ion cyclotron resonance spectroscopy. Wiley Interscience, New York, NY. (1976).
11. R. C. DUNBAR. J. Am. Chem. Soc. **90**, 567 (1968).
12. J. S. BINKLEY, R. A. WHITESIDES, R. KRISHNAN, R. SEEGER, D. J. DEFREES, H. B. SCHLEGEL, S. TOPIOL, L. R. KAHN, and J. A. POPLE. Q.C.P.E. **13**, 406 (1981).
13. G. W. SPITZNAGEL, T. CLARK, J. CHANDRASEKHAR, and P. v. R. SCHLEYER. J. Comput. Chem. **3**, 363 (1982).
14. H. B. SCHLEGEL. J. Comput. Chem. **3**, 214 (1982).
15. S. G. SHORE, S. H. LAWRENCE, M. I. WATKINS, and R. BAU. J. Am. Chem. Soc. **104**, 7669 (1982).
16. J. H. HALL, D. S. MARYNICK, and W. N. LIPSCOMB. Inorg. Chem. **11**, 3126 (1972).
17. C. HOHEISEL and W. KUTZELNIGJ. J. Am. Chem. Soc. **97**, 6970 (1975).
18. B. BIGOT, R. M. LEGUAN, and A. DEVAQUET. Nouv. J. Chim. **2**, 449 (1978).
19. T. B. MCMAHON, R. J. BLINT, D. P. RIDGE, and J. L. BEAUCHAMP. J. Am. Chem. Soc. **94**, 834 (1972).
20. R. J. BLINT, T. B. MCMAHON, and J. L. BEAUCHAMP. J. Am. Chem. Soc. **96**, 1269 (1974).
21. F. BERNARDI, A. BOTTONI, and N. D. EPIOTIS. J. Am. Chem. Soc. **100**, 7205 (1978).
22. C. MINOT and T. A. NGUYEN. Tetrahedron Lett. 3905 (1975).
23. J. D. DILL, P. v. R. SCHLEYER, and J. A. POPLE. J. Am. Chem. Soc. **97**, 3402 (1975).
24. P. PULAY, G. FOYANASI, F. PAUG, and J. E. BOGGS. J. Am. Chem. Soc. **101**, 2550 (1979).

25. A. PROSS and L. RADOM. Tetrahedron, **36**, 673 (1980).
26. O. EISENSTEIN and J. D. DUNITZ. Israel J. Chem. **19**, 292 (1980).
27. D. S. MARYNICK, L. THROCKMORTON, and R. BACQUET. J. Am. Chem. Soc. **104**, 1 (1982).

Appendix

Geometries

Since these are the first calculations of which we are aware employing the 4-31+G basis set on the species described here, it is of some interest to compare the geometries obtained with results using other basis sets.

1. BH_3. The B—H bond length is found to vary 1.16 Å (STO-3G) to 1.22 Å in a double zeta quality calculation (21–23). At the 6-31G** level the B—H bond length was found to be 1.1822 Å (24), in excellent agreement with the present value of 1.1836 Å.

2. BH_4^-. The borohydride ion, BH_4^-, has received a great deal of theoretical attention. Experimental results show a B—H bond length of 1.25 Å. Calculations at the 4-31G* level give 1.239 Å (25) and at the 6-31G level a value of 1.247 Å (26). Our value of 1.200 Å is thus in good agreement.

3. BH_2F. At the 6-31G* level the B—F bond length in BH_2F is found to be 1.293 Å (21, 23) while the present 4-31+G calculations yield 1.362 Å. Differences are also noted in the H—B—F bond angle 121.0° at the 6-31G* level and 117.3° at the 4-31+G level.

4. BH_3F^-. In BH_3F^-, as expected, the B—F bond length is considerably lengthened relative to BH_2F. At the 4-31G level the B—F bond length is 1.482 Å (25) while at the 4-31+G level 1.517 Å is found. B—H bond lengths for BH_2F and BH_3F^- are similar for all basis sets. This suggests that the B—F bond is very sensitive to the basis set used. In the absence of any experimental data for BH_3F^- it is not possible to determine which basis set provides the best description of B—F bonding.

5. BH_2CN and BH_3CN^-. Recently Marynick and co-workers (27) have carried out calculations using the 4-31G basis set for BH_3CN^- and its isomer BH_3NC^-. They found BH_3CN^- to be the more stable species and obtained a partially optimized geometry in good agreement with our present fully optimized geometry. To our knowledge no calculations on BH_2CN have been carried out. As expected the B—C bond length in the neutral molecule is shorter than that in the anion.

6. CH_3OBH_2 and $CH_3OBH_3^-$. No previous studies of either of these species could be found, however, a comparison to the corresponding hydroxy derivatives is of interest. Both BH_2OH (21, 23) and the BH_2OC— fragment are found to be planar. A staggered configuration in the CH_3 group was assumed. The B—O bond length in BH_2OH was found to be 1.334 Å (23) in good agreement with that found here for CH_3OBH_2 of 1.355 Å. The B—H bonds in CH_3OBH_2 were found to be slightly longer than those in BH_2OH. Calculations at the 4-31G level give a B—O bond length in BH_3OH^- of 1.522 Å, in exact accord with that found here for $CH_3OBH_3^-$.

The influence of a base on the methylation of aminoalcohols

CHOJI KASHIMA,[1] KAZUO HARADA, AND YOSHIMORI OMOTE
Department of Chemistry, University of Tsukuba, Sakura-mura, Niihari-gun, Ibaraki 305, Japan

Received May 14, 1984

This paper is dedicated to Professor Peter Yates on the occasion of his 60th birthday

CHOJI KASHIMA, KAZUO HARADA, and YOSHIMORI OMOTE. Can. J. Chem. **63**, 288 (1985).

A selective methylation towards N and O atoms on aminoalcohols was observed using metal hydride reagents as the base, and the predominant factors for the selectivity were investigated in detail.

CHOJI KASHIMA, KAZUO HARADA et YOSHIMORI OMOTE. Can. J. Chem. **63**, 288 (1985).

Lorsqu'on utilise des hydrures métalliques comme bases, on observe une sélectivité de la réaction de méthylation pour les sites N et O d'amino-alcools. On a étudié en détail les facteurs prépondérants qui déterminent cette sélectivité.

[Traduit par le journal]

We reported previously on the selective alkylation towards N and O atoms of hydroxylamine in the presence of various bases (1). Here, in relation to the above, the methylation of aminoalcohols, which are the methylene analogues of hydroxylamine, was carried out using metal hydride reagents such as NaH, LiH, and CaH_2, and a selectivity in the methylation towards N and O atoms was observed.

The methylation of aminoalcohols was carried out as shown in Scheme 1. To a THF solution of the aminoalcohols, a molar equivalent amount of NaH, LiH, or CaH_2 was added and stirred at room temperature for an hour. To this mixture, a molar equivalent amount of dimethyl sulfate was added and stirred for another hour. After usual work-up, the yields were determined by means of gas chromatography. In the case of methyl iodide as the electrophile, the yields were generally lower.

The methylation of 2-aminoethanol (**1***a*) using NaH led mainly to O-methylated products (**4***a*, **5***a*, and **6***a*), while the use of LiH and CaH_2 led exclusively to N-methylated products (**2***a* and **3***a*) (Scheme 1, Table 1). The stirring with supersonic vibration, the higher reaction temperature, the use of various amounts of the base, the concentration of the substrates, and the polarity of the solvent were all ineffective in the selectivity of the methylation.

In order to clarify the predominant factor controlling the selectivity, the ability of the lithium cation to form a complex with aminoalcohols was measured by ^{7}Li nmr (2). 2-Aminoethanol (**1***a*), which possesses an ethyl alcohol moiety and an ethylamine moiety intramolecularly, was added to an ethanol solution of lithium ethoxide, and the signal of lithium ethoxide was shifted downfield. On the other hand, no remarkable shift could be observed in a mixture of lithium ethoxide and diethylamine, where an alcohol moiety and an amine moiety exist intermolecularly. These data suggested the formation of complexes due to the chelation between the aminoalcohol and the lithium cation. Similarly, 3-aminopropanol (**2***a*), 5-aminopentanol (**7**), and the N- and O-methylated derivatives of 2-aminoethanol (**2***a*–**6***a*) caused the downfield shifts summarized in Table 2. From Table 2, the magnitude of the shift was largest in 2-aminoethanol and decreased by the introduction of methyl groups on **1***a*, especially on the O atom. However, 1-phenyl-1,3-butanedione (**8**), where the stability constant (log *K*) of its lithium complex is reported to be 5.95 (3), showed a very large downfield shift. Therefore, even in the case of 2-aminoethanol, the complexation should be a very weak one.

TABLE 1. Methylation of 2-aminoethanol (**1***a*)

$$NH_2CH_2CH_2OH + Me_2SO_4 \xrightarrow{\text{Base}}$$

	Conv. (%)	N-Me:O-Me*
NaH	69	4:96
LiH	53	100:0
CaH_2	64	100:0
MeLi	66	100:0
MeMgI	65	100:0
No base	60	100:0

*The ratios of (**2***a* + **3***a*):**4***a* are shown.

The ratio of N-methylated products (**2***b* and **3***b*) to the O-methylated product (**4***b*) in ther methylation reaction of 3-aminopropanol (**1***b*) by the use of NaH, LiH, and CaH_2 were 23:77, 100:0, and 100:0, respectively (Scheme 1, Table 3). Next, the methylation of an equimolar mixture of 2-phenylethylamine (**9**) and 2-phenylethanol (**10**) (Scheme 2), where the influence of chelation is excluded, was carried out by the use of equimolar amounts of dimethyl sulfate. The ratios of N-methylated products (**11** and **12**) to O-methylated products (**13**) using NaH, LiH, and CaH_2 were 37:63, 100:0, and 100:0, respectively (Table 3). These results are very similar to those of the 2-aminoethanol (**1***c*) (Table 1), indicating that the complexation does not take part in the selective methylation.

Furthermore, the amount of hydrogen released in the methylation of 2-aminoethanol (**1***a*) in the presence of a metal hydride was measured, and the results are shown in Fig. 1. When NaH was used as the base, on addition of 2-aminoethanol (**1***a*) to the hydride, a vigorous evolution of hydrogen was observed simultaneously, and no hydrogen was released on addition of dimethyl sulfate. On the contrary, in the case of LiH and CaH_2, hydrogen was released only after the addition of dimethyl sulfate.[2] That is, although NaH reacted vigorously with 2-aminoethanol (**1***a*) to form aminoalkoxide anion, the reaction of LiH and CaH_2 with 2-aminoethanol (**1***a*) did not seem to occur at all. Since alkyllithiums are homogeneous and much

[1]Author to whom correspondence may be addressed.

[2]The evolution of methane by the reaction of LiH or CaH_2 with dimethyl sulfate can be ruled out from the fact that no gas evolved in control experiments.

$$\underset{\mathbf{1}a,b}{NH_2(CH_2)_nOH} \xrightarrow[\text{THF, r.t., 1 h}]{\text{Base (1 equiv.)}} \xrightarrow[\text{r.t., 1 h}]{Me_2SO_4\text{ (1 equiv.)}} \xrightarrow[\text{(2) 10\% aq. NaOH sol.}]{\text{(1) EtOH}}$$

$$\underset{\mathbf{2}a,b}{MeNH(CH_2)_nOH} + \underset{\mathbf{3}a,b}{Me_2N(CH_2)_nOH} + \underset{\mathbf{4}a,b}{NH_2(CH_2)_nOMe} + \underset{\mathbf{5}a,b}{MeNH(CH_2)_nOMe} + \underset{\mathbf{6}a,b}{Me_2N(CH_2)_nOMe}$$

a; $n = 2$, *b*; $n = 3$
Base; NaH, LiH, CaH_2

SCHEME 1. The methylation of aminoalcohols (**1***a*,*b*)

$$\underset{\mathbf{9}}{PhCH_2CH_2NH_2} + \underset{\mathbf{10}}{PhCH_2CH_2OH} + Me_2SO_4 \xrightarrow{\text{Base}} \left\{ \begin{array}{l} \underset{\mathbf{11}}{PhCH_2CH_2NHMe} \\ + \underset{\mathbf{12}}{PhCH_2CH_2NMe_2} \\ + \underset{\mathbf{13}}{PhCH_2CH_2OMe} \end{array} \right.$$

Base: NaH, LiH, CaH_2

SCHEME 2. The methylation of an equimolar mixture of **9** and **10**

TABLE 2. ^{7}Li nuclear magnetic resonance measurements

Substrate	Δδ (Hz)
$NH_2(CH_2)_2OH$	0.98
Et_2NH	0.00
$EtNH(CH_2)_2OH$	0.71
Et_3N	0.10
$Et_2N(CH_2)_2OH$	0.49
$NH_2(CH_2)_3OH$	0.59
$NH_2(CH_2)_5OH$	0.49
$MeNH(CH_2)_2OH$	0.78
$Me_2N(CH_2)_2OH$	0.88
$NH_2(CH_2)_2OMe$	0.29
$MeNH(CH_2)_2OMe$	0.29
$Me_2N(CH_2)_2OMe$	0.19
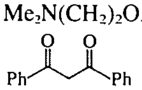	55.85

TABLE 3. The methylation of various aminoalcohols

	N-Me:O-Me (Conv. (%))		
Aminoalcohol	NaH	LiH	CaH_2
$MeNHCH_2CH_2OH$	30:70 (92)	100:0 (81)	100:0* (90)
$NH_2CH_2CH_2CH_2OH$	23:77 (85)	100:0 (61)	100:0† (54)
$PhCH_2CH_2OH$ + $PhCH_2CH_2NH_2$	37:63 (57,18)	100:0 (0,37)	100:0‡ (0,59)

*The ratios of **3***a*:**5***a* are shown.
†The ratios of (**2***b* + **3***b*):**4***b* are shown.
‡The ratios of (**11** + **12**):**13** are shown.

more active as lithiating reagents, the formation of aminoalkoxide was attempted using methyllithium as the base. Actually, a drastic reaction occurred by the treatment of 2-aminoethanol (**1***a*) with methyllithium accompanied by temperature elevation and gas evolution. However, the ratio for the N- and O-methylated products in this reaction was very similar to that of LiH (Table 1).

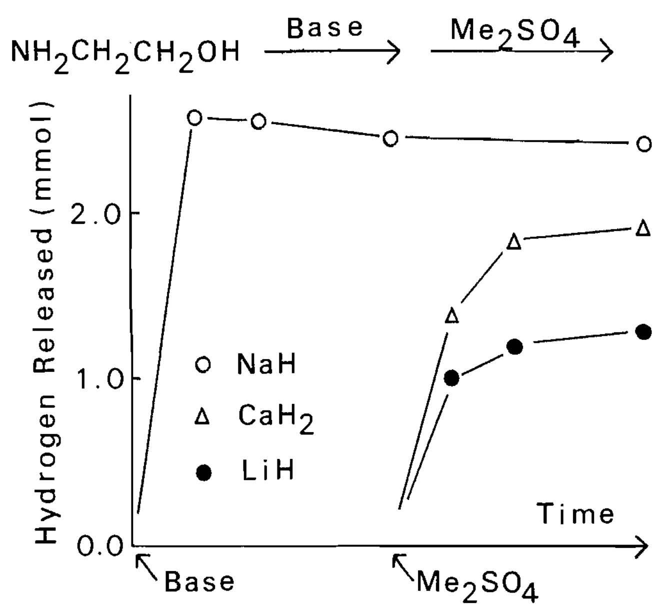

FIG. 1. Hydrogen released in the methylation of 2-aminoethanol (**1***a*).

The results of the methylation reactions, using hydride reagents alone, may be interpreted simply as the difference in basicity of the hydride reagents (4). However, in the methylation reactions using MeLi and MeMgI, gas evolution similar to the case of NaH was observed, while the product ratio resembled that of LiH. Therefore at the present stage no consistent explanation which stands for all the above results can be proposed. However, it is very interesting that NaH and LiH showed such a remarkable difference in selectivity in the methylation reaction.

Experimental

Methylation of aminoalcohols with metal hydrides

To a solution of the aminoalcohol (4 mmol) in 5 mL of THF, a molar equivalent amount of NaH, LiH, or CaH_2 was added and stirred at room temperature for 1 h. To this mixture a molar equivalent amount of dimethyl sulfate or methyl iodide was added and stirred for another hour. The reaction was quenched with ethanol, and an aqueous 10% sodium hydroxide solution was added in the case of 2-aminoethanol. The yields were determined by gas chromatography on a Shimadzu GC-4CM gas chromatograph using *N,N*-dimethylaniline as an internal standard. 10% PEG 20M and 5% KOH on Celite 545 was used as the stationary phase, and the column temperature was raised from 60 to 150°C at 10°/min.

Methylation of ethanolamine with methyl lithium and methyl magnesium iodide

A THF solution of ethanolamine (10 mmol) was added dropwise to a molar equivalent amount of MeLi or MeMgI in ether, which was accompanied by vigorous gas evolution. After stirring at room temperature for 2.5 h, a molar equivalent amount of dimethyl sulfate in THF was added and stirred for another 1.5 h. The reaction was quenched first with ethanol, and next with a 10% aqueous sodium hydroxide solution. The yields were determined by gas chromatography as described above.

*Measurement of the hydrogen released in the methylation of 2-aminoethanol (**1**a)*

The metal hydride (4 mmol) was placed in a flask fitted with a gas burette. A solution of 2-aminoethanol (**1***a*) (4 mmol) in 7 mL of THF was added and stirred at room temperature for 30 min. Next, a solution of dimethyl sulfate (2 mmol) in 3 mL of THF was added and stirred for another 30 min. As a control experiment, the above procedure was carried out in the absence of 2-aminoethanol (**1***a*). The amount of hydrogen released was measured by a gas burette with time, and the values were plotted as shown in Fig. 1.

Measurements of ^{7}Li nuclear magnetic resonance

The ^{7}Li nmr measurements were carried out on a JEOL-100 spectrometer at 30°C employing a D-lock to avoid any slight magnetic field drifts. The chemical shift measurements were made in spinning 10-mm tubes, and a solution of lithium chloride in D_2O was used as an external standard. The samples were prepared by addition of a molar equivalent of the substrate to an ethanol solution of lithium ethoxide (0.25 mmol of lithium hydride/mL of dry ethanol). The $\Delta\delta$ values shown in Table 2 are the differences in the chemical shifts of the samples and those of lithium ethoxide. Since all substrates exhibited a downfield shift based on the chemical shift of lithium ethoxide, the downfield direction was specified as plus.

1. C. Kashima, N. Yoshihara, and Y. Omote. Tetrahedron Lett. **23**, 2955 (1982).
2. J. W. Akitt and M. Parekh. J. Chem. Soc. (A), 2195 (1968).
3. W. C. Fernelius and L. G. Van Uitert. Acta Chem. Scand. **8**, 1726 (1954).
4. C. A. Brown. J. Org. Chem. **39**, 3913 (1974).

Brown algal polyphenols: synthesis of "fucophlorethol A" octamethyl ether (2,2′,4,6,6′-pentamethoxy-4′-(2,4,6-trimethoxyphenoxy)biphenyl)

Mark A. Ragan

Atlantic Research Laboratory, National Research Council of Canada, 1411 Oxford Street, Halifax, N.S., Canada B3H 3Z1

Received February 27, 1984

Mark A. Ragan. Can. J. Chem. **63**, 291 (1985).

Vanadium tetrachloride-catalyzed dimerization of 3,5-dimethoxyphenol yields the key intermediate 2,2′,6,6′-tetramethoxy-4,4′-dihydroxybiphenyl, from which the octamethyl ether of the brown algal metabolite "fucophlorethol A" (2,2′,4,6,6′-pentamethoxy-4′-(2,4,6-trimethoxyphenoxy)biphenyl, **6**) is synthesized by Ullmann condensation and Hakomori methylation.

Mark A. Ragan. Can. J. Chem. **63**, 291 (1985).

La dimérisation du diméthoxy-3,5 phénol, catalysée par la tétrachlorure de vanadium, conduit au tétraméthoxy-2,2′,6,6′ dihydroxy-4,4′ biphényle, un intermédiaire clé à partir duquel on a synthétisé, par une condensation de Ullmann et une méthylation de Hakomori, l'éther octaméthylique du "fucophloréthol A" (pentaméthoxy-2,2′,4,6,6′ (triméthoxy-2,4,6 phénoxy)-4′ biphényle, **6**), un métabolite extrait d'algues brunes.

[Traduit par le journal]

Introduction

Marine brown algae (class Phaeophyceae) accumulate large quantities of polyphenolic materials which may help protect the alga against predators or epiphytes (1). Most of these materials exist as intermediate-molecular weight "oligomers" (mol. wt. $\approx 10^3-10^4$) and high-molecular weight "polymers" (mol. wt. $\geq 10^4$) based on phloroglucinol (2–6); low-molecular weight congeners such as phloroglucinol itself, "dimers" (e.g. 2,2′,4,4′,6,6′-hexahydroxybiphenyl and 2,3′,4,5′,6-pentahydroxybiphenyl ether), "trimers", etc. (7, 8) are usually present in much smaller amounts. In Nova Scotian *Fucus vesiculosus* L., the "trimeric" polyphloroglucinol fraction consists almost exclusively of 2,2′,4,6,6′-pentahydroxy-4′-(2,4,6-trihydroxyphenoxyl)biphenyl (9), which has been given the trivial name "fucophlorethol A" (10).

Until now no synthesis has been reported for fucophlorethol A, nor for its isomer fucophlorethol B (8, 10) or for higher congeners (8, 10) in the fucophlorethol series. The commercial availability of bromo-2,4,6-trimethoxybenzene (**4**) made it appealing to approach the problem as an Ullmann ether synthesis (condensing **4** with 2,2′,6,6′-tetramethoxy-4,4′-dihydroxybiphenyl (**2**); see diagram), thereby taking advantage of the relatively low yields of the Ullmann ether reaction (11) to limit 4,4′-diphenoxy ether formation. Synthesis of **2** was more problematic; the Ullmann biaryl synthesis (by far the best standard procedure for forming 2,2′,6,6′-tetrasubstituted biphenyls) is incompatible with free or lightly protected 4,4′-hydroxyl groups, while biaryl syntheses based on Kharasch reactions (12, 13), the Wurtz reaction (14), organothallium intermediates (15), organoboranes (16), or various transition metal complexes (reviewed briefly in ref. 17) may have the same limitation and (or) fail to produce 2,2′,6,6′-tetrasubstituted products in significant yield.

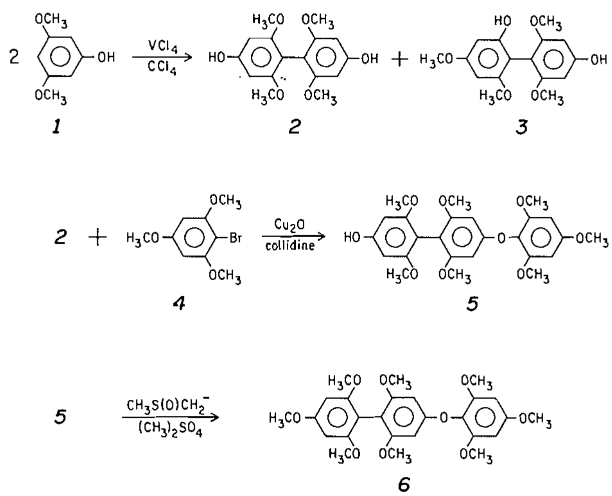

On the other hand, reports of VCl_4- or $VOCl_3$-catalyzed dehydrodimerization predominantly in the *para* position of unprotected phenols (18, 19), including the production in one instance of 2,2′-dihydroxybinaphthyl (19), suggested that **2** might be directly synthesized by treating the commercially available 3,5-dimethoxyphenol (**1**) with VCl_4 or $VOCl_3$. The three-step synthesis of **6** reported herein should serve as a pattern for eventual synthetic approaches to the "tetrameric" fucodiphlorethol A and the higher homologues.

Experimental

Electron impact mass spectra were recorded, and accurate mass determination made by peak-matching with ions of perfluorokerosene, on a Dupont-CEC 21-110B instrument. The ^{1}H nmr and ^{13}C nmr spectra were recorded on Varian HA-100 and FT-80 spectrometers respectively. Elemental analyses were performed by Mikroanalytisches Laboratorium (Bonn, FRG) and Microanalysis Laboratories Ltd. (Markham, Ont.).

2,2′,6,6′-Tetramethoxy-4,4′-dihydroxybiphenyl (2) and 2,2′,4,6′-tetramethoxy-4′,6-dihydroxybiphenyl (3)

3,5-Dimethoxyphenol (**1**) (6.16 g, 40 mmol; Aldrich) was dissolved in CCl_4 (50 mL) under N_2 in a 500-mL 3-necked flask. VCl_4 (6.5 mL, 62 mmol; Alfa/Ventron) was added with stirring during 5 min, and the reaction mixture was stirred under N_2 at ≈25°C for 1 h.[2] Then 2 *N* aqueous H_2SO_4 (100 mL) was added, and the mixture was stirred vigorously under N_2 for 10 min (19). Partitioning between the acidic aqueous phase and $CHCl_3$ (75 mL) gave a yellow-brown organic layer,

[1]NRCC No. 23425.

[2]**CAUTION!** VCl_4 is toxic and corrosive. Use an efficient fume hood, and wear strong plastic-covered gloves and apron (VCl_4 attacks neoprene). VCl_4 is moisture sensitive. Spills may be neutralized with water. Physical data: see ref. 20.

a turquoise aqueous layer, and a water-insoluble, acetone-soluble precipitate. Thin-layer chromatography (tlc) on silica gel (75:20:5 by vol. hexane$-CH_2Cl_2-$isopropanol) revealed two major products, the more abundant (R_f 0.31) occurring in high concentration in the acetone-soluble precipitate, the less abundant (R_f 0.43) present in similar concentrations in both the precipitate and the $CHCl_3$ extract. Silica gel column chromatography (gradient 82:15:3 to 75:20:5 by vol. hexane$-CH_2Cl_2-$isopropanol) yielded the R_f 0.31 isomer (**2**; 512 mg) and the R_f 0.43 isomer (**3**; 133 mg).

2,2′,6,6′-Tetramethoxy-4,4′-dihydroxybiphenyl (2)

Crystallization from acetone gave colourless prisms, mp (cap., uncorr.) 285.0–291.0°C (dec.); ^{1}H nmr (acetone-d_6) δ: 6.14 (4H, ring H), 3.56 (12H, 2,2′,6,6′-OMe) ppm; ^{13}C nmr (acetone-d_6) δ_C: 160.3 (m; C-2,2′,6,6′), 158.8 ($^2J_{CH}$ ≈4 Hz, t; C-4,4′), 105.3 (poorly relaxed; C-1,1′), 93.2 ($^1J_{CH}$ = 157.8 Hz, d; $^3J_{CH}$ = 4.5 Hz, d; C-3,3′,5,5′), 55.8 ($^1J_{CH}$ = 143.1 Hz, q; 2,2′,6,6′-OMe) ppm; ms (250°C): 307.1139 ± 0.0009 (18%; required for $^{12}C_{15}{}^{13}CH_{18}O_6$, 307.1136), 306.1096 ± 0.0009 (M^+; 100%; required for $C_{16}H_{18}O_6$, 306.1103), 260 (18%), 167 (38%), 154 (13%), 153 (11%), 107 (11%), 69 (27%). *Anal.* calcd.: C 62.74, H 5.92, O 31.34; found: C 62.63, H 6.34, O 31.2.

2,2′,4,6′-Tetramethoxy-4′,6-dihydroxybiphenyl (3)

Crystallization from acetone or methanol gave tiny colourless prisms, mp (cap., uncorr.) 211.0–212.5°C; ^{1}H nmr (acetone-d_6) δ: 6.16 (2H; 3′,5′-H), 6.09 (2H; 3,5-H), 3.75 (3H, 4-OMe), 3.60 (9H; 2,2′,6′-OMe) ppm; ^{13}C nmr (acetone-d_6) δ_C: 161.4 (m; C-2), 160.7 (m; C-2′,6′), 160.4 ($^2J_{CH}$ ≈4? Hz, t; C-4), 159.6 ($^2J_{CH}$ ≈4.2 Hz, t; C-4′), 157.2 (m; C-6), 104.3 (poorly relaxed; C-1′), 102.8 (poorly relaxed; C-1), 94.3 ($^1J_{CH}$ ≈160 Hz, d; $^3J_{CH}$ poorly resolved d; C-3), 93.3 ($^1J_{CH}$ = 158.3 Hz, d; $^3J_{CH}$ = 4.7 Hz, d; C-3′,5′), 91.5 ($^1J_{CH}$ = 158.4 Hz, d; $^3J_{CH}$ = 5.2 Hz, d; C-5), 55.8 ($^1J_{CH}$ = 143.5 Hz, q; 2′,6′-OMe and 2-OMe), 55.3 ($^1J_{CH}$ = 143.5 Hz, q; 4-OMe) ppm; ms (195°C): 307.1139 ± 0.0009 (21%; required for $^{12}C_{15}{}^{13}CH_{18}O_6$, 307.1136), 306.1102 ± 0.0009 (M^+; 100%; required for $C_{16}H_{18}O_6$, 306.1103), 275 (12%), 260 (11%), 245 (12%), 167 (14%), 69 (22%). *Anal.* calcd.: C 62.74, H 5.92, O 31.34; found: C 61.45, H 5.99, O 31.35.

2,2′-6,6′-Tetramethoxy-4-hydroxy-4′-(2,4,6-trimethoxyphenoxy)biphenyl (5)

Bromo-2,4,6-trimethoxybenzene (**4**) (432 mg, 1.75 mmol), **2** (269 mg, 0.88 mmol), and dry Cu_2O (800 mg) were added to collidine (5 mL) in a 10-mL flask. Dry N_2 was bubbled through the suspension, then the mixture was heated to reflux for 44.5 h under N_2 (cf. ref. 12). The mixture was cooled, acidified (concentrated HCl – ice), and organic products were extracted into diethyl ether (3×) and ethyl acetate (3×), concentrated under N_2, and dried over Na_2SO_4. Vacuum sublimation at increasing temperatures yielded 1,3,5-trimethoxybenzene (≈10% of recovered organic matter), **4** (≈55%), **2** (≈15%), a major product (≈15%) having R_f 0.52 on silica gel (75:20:5 by vol. hexane$-CH_2Cl_2-$isopropanol), and numerous minor products (Σ ≈5%) including brominated (M^+ 384, 386) and dibrominated (M^+ 462, 464, 466) derivatives of **2**, a brominated derivative of **5** (M^+ 550, 552), a compound with M^+ 638 (presumably 2,2′,6,6′-tetramethoxy-4,4′-di(2,4,6-trimethoxyphenoxy)biphenyl), and its brominated derivative(s) (M^+ 716, 718). The R_f 0.52 material (**5**) was further purified by preparative silica gel tlc (Whatman PLK5F), and was crystallized from acetone + methanol. Yield isolated after three crystallizations, 15 mg (3.6% based on **2**); mp (biref. stage) 256.0–258.8°C; ^{1}H nmr (acetone-d_6) δ: 6.37 (2H; 3″, 5″-H), 6.15 (2H; 3,5-H), 6.09 (2H; 3′,5′-H), 3.83 (3H; 4″-OMe), 3.78 (6H; 2″,6″-OMe), 3.57 (6H; 2,6-OMe), 3.51 (6H; 2′,6′-OMe) ppm; ^{13}C nmr (acetone-d_6) δ_C: 160.8 (C-4′), 160.2 (C-2,6), 160.1 (C-2′,6′), 159.0 and 158.8 (C-4 and C-4″), 155.0 (C-2″,6″), 126.8 (poorly relaxed; C-1″), 105.0 (poorly relaxed; C-1 and C-1′), 93.2 (C-3,5), 92.8 (C-3′,5′?), 92.7 (C-3″,5″?), 56.4 (2″,6″-OMe?), 56.0 (2,6-OMe?), 55.8 (2′,6′-OMe? and 4″-OMe) ppm; ms (190°C): 473.1752 ± 0.0015 (23%; required for $^{12}C_{24}{}^{13}CH_{28}O_9$, 473.1766), 472.1735 ± 0.0015 (M^+; 100%; required for $C_{25}H_{28}O_9$, 472.1733), 303 (54%), 183 (13%), 155 (10%).

2,2′,4,6,6′-Pentamethoxy-4′-(2,4,6-trimethoxyphenoxy)biphenyl (fucophlorethol A octamethyl ether; 6)

Thrice-crystallized **5** (14 mg, ≈0.03 mmol) was dissolved in dry, redistilled DMSO (0.3 mL) under Ar. Sodium methylsulfinylcarbanion (22) was prepared from NaH (1.0 g of 80% dispersion in oil; BDH) and dry, redistilled DMSO (14 mL) under Ar by the method of Sjöberg (23), and 0.04 mL (0.06 mequiv.) was added under Ar to the solution of **5**. After 10 min of stirring, $(CH_3)_2SO_4$ (ca. 0.01 mL) was added; thereafter a white insoluble material formed in the reaction vessel. Additions of base (0.04 mL) and of $(CH_3)_2SO_4$ (≈0.01 mL) were repeated at 50 and 60 min, respectively. After a total of 270 min, the product was partitioned between CH_2Cl_2 and H_2O and, after further washings with H_2O, the organic phase was dried. Crystallization from absolute ethanol gave thin, elongated platelets, mp (biref. stage) 205.0–207.5°C. Yield isolated after three crystallizations, 96%; ^{1}H nmr ($CDCl_3$) δ: 6.22 (2H) and 6.21 (2H) (3,5-H and 3′,5′-H), 6.17 (2H; 3″,5″-H), 3.83 (3H) and 3.82 (3H) (4- and 4″-OMe), 3.80 (6H; 2″,6″-OMe), 3.68 (6H; 2,6-OMe), 3.60 (6H; 2′,6′-OMe) ppm; ^{13}C nmr ($CDCl_3$) δ_C: 160.5 ($^2J_{CH}$ ≈4 Hz, t; C-4′), 159.8 ($^2J_{CH}$ ≈5 Hz?, t; C-4), 159.2 (m; C-2,6), 159.0 (m; C-2′,6′), 157.6 ($^2J_{CH}$ ≈4.5 Hz, t; C-4″), 154.0 (m; C-2″,6″), 126.3 ($^2J_{CH}$ ≈8 Hz, t; C-1″), 105.5 and 105.4 (poorly relaxed; C-1 and C-1′), 92.2 ($^1J_{CH}$ = 159.8 Hz, d; $^3J_{CH}$ ≈5 Hz, d; C-3′,5′), 91.9 ($^1J_{CH}$ ≈159 Hz, d; $^3J_{CH}$ ≈5 Hz, d; C-3″,5″), 91.6 ($^1J_{CH}$ = 158.7 Hz, d; $^3J_{CH}$ ≈5 Hz, d; C-3,5), 56.3 ($^1J_{CH}$ = 144.4 Hz, q; 2″,6″-OMe), 56.2 ($^1J_{CH}$ = 143.3 Hz, q; 2,6-OMe), 56.0 ($^1J_{CH}$ = 143.6 Hz, q; 2′,6′-OMe), 55.5 q; 4-OMe) ppm (7); ms (145°C): 487.1917 ± 0.0015 (26%; required for $^{12}C_{25}{}^{13}CH_{30}O_9$, 487.1923), 486.1884 ± 0.0015 (M^+; 100%; required for $C_{26}H_{30}O_9$, 486.1890), 317 (16%). *Anal.* calcd.: C 64.19, H 6.21; found: C 64.15, H 6.07.

Assignments of ^{13}C nmr signals were made in the following manner: comparison of ^{13}C chemical shifts in **1** and 1,3,5-trimethoxybenzene allowed the effect of replacing one —OMe by —OH in this system to be calculated (*ipso*, +4.1 ppm; *ortho*, −1.6 ppm; *meta*, +0.1 ppm; *para*, −0.4 ppm; *meta*-OMe, −0.1 ppm). For **2**: these values, together with ^{13}C shifts for 2,2′,4,4′,6,6′-hexamethoxybiphenyl (cf. ref. 9), were used to calculate expected shifts for ^{13}C nuclei. The C-4,4′ signal was distinguished from that for C-2,2′,6,6′ by integration (recorded under a variety of conditions) and by its sharp symmetrical triplet in the nondecoupled spectrum. For **3**: signals for C-1′ through C-6′ were assigned by comparison with **2**, C-1 through C-6 by calculation from 2,2′,4,4′,6,6′-hexamethoxybiphenyl as above, and 4-OMe by integration and by comparison with 4,4′-OMe in 2,2′,4,4′,6,6′-hexamethoxybiphenyl. C-3′,5′ was distinguished from C-3 and C-5, and C-2′,6′ from C-4, by integration under a variety of conditions; C-4 and C-4′ gave sharp symmetrical triplets in the nondecoupled spectrum. Comparison of ^{13}C chemical shifts in **1** and 1,3,5-trimethoxy-2-(3,5-dimethoxyphenoxy)benzene (**7**; ref. 4, p. 83) allowed the effect of replacing —OH by 1,3,5-trimethoxyphenoxy to be calculated (*ipso*, +3.3 ppm; *ortho*, −1.0 ppm; *meta*, −0.2 ppm; *para*, +0.2 ppm; *meta*-OMe, −0.2 ppm). For **5**: these values, together with ^{13}C shifts for **2**, were used to calculate expected shifts for C-1′ through C-6′. Signals corresponding to C-1 through C-6 were assigned by comparison with **2**, and signals of the trimethoxyphenoxy group carbons (C-1″ through C-6″) by comparison with **7**. C-4, C-4′, and C-4″ were further distinguished from C-2,6, C-2′,6′, and C-2″,6″ by integration. Assignments for signals at 160.2 (C-2,6: expected, 160.3) and 160.1 (C-2′,6′: expected, 160.1 ppm) may be interchanged. For **6**: signals for C-1 through C-6 and C-1′ through C-6′ were assigned by comparison with 2,2′,4,4′,6,6′-hexamethoxybiphenyl, and C-1″ through C-6″ by comparison with **5** and **7**. C-4, C-4′, and C-4″ were further distinguished by integration and by the comparatively sharp triplets seen in the nondecoupled spectrum; assignments for signals at 56.3, 56.2, and 56.0 ppm may be interchanged.

Results and discussion

Vanadium tetrachloride-catalyzed dehydrodimerization of **1** under the conditions described above produces both the *para,para-* (**2**) and *ortho,para-* (**3**) coupled products, in approximately 4:1 ratio, with a combined isolated yield of 10.5% of theoretical. Although this is a modest yield, the major product **2** requires no further modification or deprotection prior to use in the Ullmann diaryl ether synthesis. The isolated yield (3.6%) of monocondensed product **5** from the diaryl ether synthesis compares reasonably well with the yield (9.9%) reported for the condensation of **4** with 3,4,5-trimethoxyphenol (11); moreover, the inefficiency of diaryl ether formation minimizes formation of 2,2′,6,6′-tetramethoxy-4,4′-di(2,4,6-trimethoxyphenoxy)biphenyl. Although the work of Sattler and Glombitza (11) suggests that diaryl ether formation could have been made more efficient by reacting 2,4,6-trimethoxyphenol with 2,2′,6,6′-tetramethoxy-4,4′-dibromobiphenyl, the latter is not directly available from Ullmann-type condensation, and would have to be synthesized indirectly through a tetramethoxybenzidine. The essentially quantitative methylation of **5** to **6** once again (see ref. 24) illustrates that the Hakomori procedure, normally used with carbohydrates (25), is ideal for methylation of polyphloroglucinols as well. Under the conditions described above, ring-methylation (24) was minimal.

Condensation of **2** with bromo-2,6-dimethoxy-4-(2,4,6-trimethoxyphenoxy)benzene would give "fucodiphlorethol A", the next higher homologue (8, 10) in this series of natural products.

Acknowledgements

I thank A. G. McInnes for helpful advice, D. J. Embree for mass measurements, and J. Van Ingen for 100-MHz ^{1}H nmr spectra.

1. M. A. RAGAN and A. JENSEN. J. Exp. Mar. Biol. Ecol. **34**, 245 (1978), and references therein.
2. K. FRETHEIM. Thesis, Norges Tekniske Høgskole, Trondheim (1974).
3. E. SATTLER. Thesis, Rheinische Friedrich-Wilhelms-Universität, Bonn (1974).
4. M. A. RAGAN. Thesis, Dalhousie University, Halifax, N.S. (1976).
5. M. A. RAGAN and J. S. CRAIGIE. Can. J. Biochem. **54**, 66 (1976).
6. E. SATTLER, K.-W. GLOMBITZA, F. W. WEHRLI, and G. ECKHARDT. Tetrahedron, **33**, 1239 (1977).
7. K.-W. GLOMBITZA. *In* Marine natural products chemistry. *Edited by* D. J. Faulkner and W. H. Fenical. Plenum, New York. 1977. pp. 194–204.
8. K.-W. GLOMBITZA. *In* Marine algae in pharmaceutical sciences. *Edited by* H. A. Hoppe, T. Levring, and Y. Tanaka. Walter de Gruyter, Berlin. 1979. pp. 303–342.
9. J. S. CRAIGIE, A. G. MCINNES, M. A. RAGAN, and J. A. WALTER. Can. J. Chem. **55**, 1575 (1977).
10. K.-W. GLOMBITZA, H.-W. RAUWALD, and G. ECKHARDT. Planta Med. **32**, 33 (1977).
11. E. SATTLER and K.-W. GLOMBITZA. Arch. Pharm. **308**, 813 (1975).
12. M. S. KHARASCH and E. K. FIELDS. J. Am. Chem. Soc. **63**, 2316 (1941).
13. J.-P. MORIZUR. Bull. Soc. Chim. Fr. **1964**, 1331 (1964).
14. W. E. BACHMANN and H. T. CLARKE. J. Am. Chem. Soc. **49**, 2089 (1927).
15. A. MCKILLOP, L. F. ELSOM, and E. C. TAYLOR. Tetrahedron, **26**, 4041 (1970).
16. S. W. BREUER and F. A. BROSTER. Tetrahedron Lett. 2193 (1972).
17. A. MCKILLOP, A. G. TURRELL, D. W. YOUNG, and E. C. TAYLOR. J. Am. Chem. Soc. **102**, 6504 (1980).
18. W. L. CARRICK and G. L. KARAPINKA. U.S. Pat. No. 3,322,838 (1967); Chem. Abstr. **67**, 99853y (1967).
19. W. L. CARRICK, G. L. KARAPINKA, and G. T. KWIATKOWSKI. J. Org. Chem. **34**, 2388 (1969).
20. J. H. SIMONS and M. G. POWELL. J. Am. Chem. Soc. **67**, 75 (1945).
21. K.-W. GLOMBITZA, H.-U. RÖSENER, and D. MÜLLER. Phytochemistry, **13**, 1115 (1975).
22. E. J. COREY and M. CHAYKOVSKY. J. Am. Chem. Soc. **84**, 866 (1962).
23. K. SJÖBERG. Tetrahedron Lett. 6383 (1966).
24. M. A. RAGAN. Can. J. Chem. **63**, 294 (1985).
25. S.-I. HAKOMORI. J. Biochem. (Tokyo) **55**, 205 (1964).

The high molecular weight polyphloroglucinols of the marine brown alga *Fucus vesiculosus* L.: degradative analysis[1,2]

MARK A. RAGAN

Atlantic Research Laboratory, National Research Council of Canada, 1411 Oxford Street, Halifax, N.S., Canada B3H 3Z1

Received February 27, 1984

MARK A. RAGAN. Can. J. Chem. **63**, 294 (1985).

The high-molecular-weight polyphloroglucinol tannin of *Fucus vesiculosus* has been islated in pure form as judged by ^{1}H and ^{13}C nmr. Acetate and methyl derivatives were prepared and examined by uv and ir spectroscopy. Calcium – liquid ammonia degradation of the methyl ether derivative liberated numerous aryl compounds including fragments arising from ether-linked phloroglucinol end groups, internal *ortho*-, *meta*-, and *para*-oriented diethers, *vic*- and (tentatively identified) *sym*-triethers, internal phloroglucinol-derived biphenyls (three isomers), probable terminal biphenyls, terphenyl(s), and from quaterphenyl(s). No evidence was found for *vic*-trihydroxylated end groups. In all, 63 fragments were identified by gc–ms, and abundances of the major fragments were estimated by quantitative gc. The data indicate that the *F. vesiculosus* tannins – or at least the portion represented by these fragments – are highly branched structures consisting entirely of phloroglucinol units.

MARK A. RAGAN. Can. J. Chem. **63**, 294 (1985).

Si l'on se base sur les spectres rmn du ^{1}H et du ^{13}C, c'est à l'état pur que l'on a isolé du *Fucus vesiculosus* le tannin polyphloroglucinol de haut poids moléculaire. On en a préparé les dérivés acétate et méthylique et on les a étudiés par les spectroscopies uv et ir. La dégradation du dérivé méthylique par du calcium dans de l'ammoniac liquid libère plusieurs composés aromatiques dont des phloroglucinols terminaux qui étaient liés par des fonctions éthers, des diéthers internes orientés en positions *ortho*, *méta* et *para*, des triéthers *vic* et *syn* (attribution préliminaire), des biphényles internes dérivant du phloroglucinol (trois isomères), des biphényles qui sont probablement terminaux, des terphényles et des quaterphényles. On n'a pas pu mettre en évidence l'existence de groupes terminaux *vic*-trihydroxylés. Au total, on a identifié 63 fragments par cpg/sm et on a évalué les abondances relatives des fragments principaux en faisant appel à la cpg. Les données indiquent que les tannins du *F. vesiculosus* – ou du moins la portion représentée par ces fragments – ont des structures fortement ramifiées qui sont entièrement constituées d'unités phloroglucinol.

[Traduit par le journal]

Introduction

Microscopic examination of the cells of brown algae (Phaeophyceae) reveals numerous small vesicles which stain intensely red with vanillin in strong mineral acid. Early investigators correctly concluded that these vesicles or "physodes" contain phloroglucinol or related compounds (1, 2). The roles (if any) of the physodes and their polyphenolic constituents in brown algal physiology remain unclear (3); however, at least some of these polyphenols possess antibacterial (4), antilarval (5), and antialgal (6, 7) activities, inhibit feeding by herbivores (8), and have properties of tannins (2, 9) and chelate ions of heavy metals (10, 11). The polyphenols are released into the surrounding seawater by living brown algae during stress (12) or solar irradiation (13), and by chelating toxic metal ions may influence the growth of phytoplankton (14) and other marine life.

Chemical investigation of the brown algal polyphenols has revealed a variety of low-, intermediate-, and high-molecular-weight compounds composed of phloroglucinol units. The low-molecular-weight fraction (operationally defined as those polyphenols which can be individually separated by chromatographic techniques) includes phloroglucinol itself (14, 15); "dimers" of phloroglucinol joined by direct carbon–carbon (e.g. 2,2′,4,4′,6,6′-hexahydroxybiphenyl) or ether bonds (e.g. 2,3′,4,5′,6-pentahydroxybiphenyl ether); and related "trimers", "tetramers", etc. similarly containing directly bonded and (or) ether- linked units (17, 18). Elaborations of this basic pattern include vicinal trihydroxylation (18), chloro substitution (19), esterification by sulfate (20, 21), and the presence of alkenyl side chains (22, 23).

Although the low-molecular-weight polyphenols have received much attention, they often constitute only a minor (<5%) portion of the total polyphenolic material of brown algae. The high-molecular-weight fraction (operationally defined as those soluble polyphenols remaining inside a dialysis tube during extended dialysis against distilled water) is by contrast the major fraction which has been isolated, comprising approximately 15–25% of the total extractable polyphenols (the intermediate-molecular-weight fraction, presumably the remaining 75% of the total polyphenols, is lost during dialysis and has never been directly examined). The high-molecular-weight fraction, although not particularly toxic to bacteria or yeasts (*vide infra*), is an excellent chelator of several heavy metal ions, particularly Cu^{2+} and Pb^{2+} (ref. 11; also, Guevremont and Ragan, unpublished), and is probably present in exudates from marine brown algae (24). The isolation, purification, preparation of derivatives, and degradative analyses of this high-molecular-weight polyphloroglucinol ("polymer") fraction are described in this report. The accompanying paper (25) describes direct investigations by nuclear magnetic resonance spectroscopy on the structure of the intact polymer.

Experimental

Fucus vesiculosus L. (25 kg f.w.), collected near Morris Point, Halifax Country on 15 July 1980, was transported on ice to the laboratory, where it was cleaned of macroscopic epiphytes and immediately frozen in liquid N_2. Portions were broken off, covered with EtOH (95%) in a large Waring Blendor (4.5 L), and macerated thoroughly. The green suspension was collected in large glass carboys, sparged exhaustively with N_2, and stored with occasional stirring under N_2 at 3°C in the dark for ≈48 h. Particles were removed on glass-wool filters to give 105 L of extract, which was concentrated *in vacuo* to 15 L using a 50-L continuous-flow "cyclone" evaporator.

[1] Issued as NRCC no. 23430.

[2] Part 4 in the series "Physodes and the phenolic compounds of brown algae". For part 3, see ref. 17.

The brownish, mostly aqueous concentrate was filtered (Whatman no. 1 paper), then was dialyzed to waste by cycling continuously through 2 m of $\frac{1}{4}$-in. diameter dialysis tubing (130 h, 3°C, N_2 atmosphere in reservoir; the returning, less-dense solution was carefully layered atop the liquid in the reservoir, and dense solution from the bottom of the reservoir was pumped to the dialysis tubing, to increase efficiency of operation). The dialyzed solution (≈23 L) was lyophilized, redissolved in distilled water (1.5 L), further dialyzed (48 h) against N_2-sparged distilled water, and again lyophilized to yield 84.6 g of crude polymer. Approximately 28-g portions were each dissolved in 50% aqueous MeOH (≈80 mL), sorbed onto "Avicel" microcrystalline cellulose, and loaded atop a dry-packed column (10 × 43 cm) of Avicel (16). Elution with MeOH–acetone (2:1 v/v) yielded a total of 68.2 g of purified polymer. Unless otherwise specified, all experiments reported herein were conducted on this preparation. Subsequent elution of the column with pyridine yielded only a further 2.7 g of highly discolored material which was not extensively analyzed.

Smaller batches of the polymer were prepared similarly (26, 27) from another collection of *F. vesiculosus* (Morris Point, Halifax County, 3 July 1974), from Nova Scotian *Ascophyllum nodosum* (L.) Le Jol. (Morris Point, 22 July 1975), and from Norwegian *A. nodosum* (Østmarkneset, Trondheim, 2 November 1976).

Purity of high-molecular-weight polyphloroglucinols prepared in this manner was indicated by the absence of all ^1H nmr signals except those in the range δ_H = 6.0–6.5 ppm, and the absence of all ^{13}C nmr signals except those in the ranges δ_C = 92–103, 123–131, and 148–162 ppm (11, 25). If carbohydrate signals were observed (^1H nmr: δ_H = 3.4–4.1 ppm; ^{13}C nmr: $\delta_C \approx$ 60–75 ppm), chromatography on Avicel columns was repeated to remove the contaminants.

Acetylation of the "polymer" (600 mg) was performed in excess Ac_2O (105°C, ≈1 h) with freshly fused NaOAc as catalyst. Remaining Ac_2O was destroyed with water (room temperature, 2 h), the $CHCl_3$-soluble product was washed by shaking against a saturated aqueous solution of NaCl, and residual HOAc was removed *in vacuo* (40°C); yield, 892 mg. Complete acetylation of —OH groups was confirmed by infrared spectrometry (Fig. 1).

Methylation was accomplished by a modification of the Hakomori (28) procedure. An aliquot of the polymer (600 mg) was dissolved in dry DMSO (redistilled from CaH_2; 10 mL) under N_2, and was cooled to 18 ± 1°C. Sodium dimethylsulfinylcarbanion (29) was prepared under a N_2 or Ar atmosphere by the method of Sjöberg (30). Additions (under N_2) of base and of $(CH_3)_2SO_4$ were made at intervals with stirring: methylsulfinylcarbanion base (1.40 mequiv. mL^{-1}; 14.0 mL, t = 0), $(CH_3)_2SO_4$ (1.8 mL, t = 30 min), base (8.0 mL, t = 4 h), and $(CH_3)_2SO_4$ (1.1 mL, t = 4.5 h). The temperature was allowed to increase slowly to 22°C (t = 30 min) and 25°C (t = 4.5 h), then was raised to 44°C for 1 h beginning at t = 24 h, and finally was reduced to ≈22°C. Careful attention to temperature was crucial for successful methylation. The product was placed into a wet dialysis tube, dialyzed against distilled water for 6–8 h, collected on a glass filter disc (GF/C, Whatman), and dried *in vacuo* (37°C) to constant weight (712 mg). Complete methylation of —OH groups was confirmed by infrared spectrometry (Fig. 1).

Esterification with diethyl phosphate groups was achieved by adding $CHCl_3$ (4.0 mL) to an efficiently cooled (≈25°C) solution of the polymer (210 mg) in diethyl phosphite (Aldrich; 3.0 mL) and Et_3N (1.1 mL), then stirring overnight at room temperature. The product was dialyzed repeatedly against distilled water (precipitates) and absolute EtOH (redissolves), and finally was dried *in vacuo* (37°C). The yellowish-brown, $CHCl_3$-soluble powder contained almost no free —OH groups (Fig. 1). Attempts to reduce the diethyl phosphate ester to the corresponding hydrocarbon (cf. ref. 31), and to cleave its ether bonds by treatment with alkali metals in NH_3, were unsuccessful.

Cleavage of aryl–aryl ether bonds was accomplished by dropwise addition of a solution of the methylated polymer (25 mg) in dry, redistilled THF (10 mL) to a stirred solution of Ca metal (BDH; 25–100 mg) in liquid NH_3 (≈15 mL). Additional Ca was added after 5–10 min to a total of 50–200 mg. After the blue color had persisted for 10–20 min, the solution was poured onto crushed ice in a separatory funnel, and carefully acidified (concentrated HCl – ice) to pH ≈2. Organic material was extracted into EtOAc, CH_2Cl_2, and (or) Et_2O, concentrated under N_2 at reduced temperature, and analyzed by tlc, gc, and gc–ms. Use of Na instead of Ca gave similar results. An alternative work-up procedure likewise gave similar results: the blue solution was transferred to a large Erlenmeyer flask, redistilled absolute EtOH (ref. 32; 30 mL) and solid CO_2 were added, the solution was clarified by centrifugation, and the products were concentrated under N_2 at reduced temperature prior to analysis by gc.

Products obtained from Ca–NH_3 cleavage were in some cases butylated by the Williamson procedure: an aliquot (e.g. 90%) of the organic phase from the cleavage reaction was dried under N_2, redissolved in NaOEt (0.32 g Na in 15 mL absolute EtOH), stirred under an atmosphere of N_2 for ≈10 min, then refluxed with n-butyl bromide (Anachemia; 2.8 mL) for ≈5 h; additional NaOEt (5 mL) and n-BuBr (1.0 mL) were added at t = 160 min. The product was cooled, filtered (GF/C), evaporated *in vacuo* (no external heating), then partitioned between CH_2Cl_2 and aqueous 6 N HCl. Butylation efficiency, estimated from capillary column gc, was ca. 98.5%. An aliquot of the product was subsequently treated once again with Ca in NH_3.

In other experiments, the fragments from Ca—NH_3 cleavage were trimethylsilylated (27) using "Tri-Sil" (Pierce).

Synthesis of reference compounds

The syntheses of 2,2′,6,6′-tetramethoxy-4,4′-dihydroxybiphenyl (33), 2,4′,6,6′-tetramethoxy-2′,4-dihydroxybiphenyl (33), 3,3′,-4,5,5′-pentamethoxybiphenyl ether (26), 2,2′,4,4′,6,6′-hexamethoxybiphenyl (16), and 2,2′,4,6,6′-pentamethoxy-4′-(2,4,6-trimethoxyphenoxy)biphenyl (33) have been described elsewhere. 2,4,6-Trimethoxyphenol and 1,2,3,5-tetramethoxybenzene were prepared by (partial) methylation of 2,6-dimethoxy-1,4-dihydroxybenzene (dissolved in acetone or DMSO) with CH_2N_2 (vigorous agitation, room temperature, 4 h), and were distinguished from 3,4,5-trimethoxyphenol by comparison with authentic 3,4,5-trimethoxyphenol on capillary column gc–ms (see below).

Iodo-2,2′,4,4′,6,6′-hexamethoxybiphenyl (**1**) was synthesized from 2,2′,4,4′,6,6′-hexamethoxybiphenyl (**2**) by Suzuki iodination (cf. ref. 34). Resublimed I_2 (2.06 g, 8.1 mmol), **2** (6.68 g, 20.0 mmol), and $HIO_4 \cdot 2H_2O$ (0.91 g, 4.0 mmol) were combined well. In a second flask, HOAc (67 mL), H_2O (11 mL), and concentrated H_2SO_4 (0.8 mL) were heated together (45°C), then were added to the solids in the first flask. The vigorously stirred solution was heated to 67°C during 150 min, then the reaction was quenched by pouring into ice water (ca. 250 mL), and the products were extracted into $CHCl_3$. The product **1** (≈60% of recovered organic matter) was separated from unreacted **2** (≈25%), diiodo-2,2′,4,4′,6,6′-hexamethoxybiphenyl(s) (M^+ 586; ≈10%), and more complex products by chromatography on silica gel (hexane–THF–CH_2Cl_2, gradient 80:10:10 v/v/v to 70:15:15 v/v/v). Crystallization from acetone gave tiny white crystals, mp (cap., uncorr.) 166–168°C; isolated yield, 22%; ^1H nmr ($CDCl_3$) δ_H: 6.37 (1H, H-5), 6.22 (2H, H-3′,5′), 3.90 (3H, 4-OCH_3), 3.84 (3H, 4′-OCH_3), 3.72 and 3.70 (9H, 2′,6,6′-OCH_3), 3.62 (3H, 2-OCH_3) ppm; ^{13}C nmr ($CDCl_3$) δ_C: 161.1 (m; C-4′), 160.0 (m; C-4), 159.7 (m; C-2), 159.0 (m; C-2′,6′), 158.8 (m; C-6), 111.0 (poorly relaxed; $^3J_{CH}$ = 5.4 Hz, d; C-1), 104.7 (poorly relaxed; $^3J_{CH}$ = 5.3 Hz, t; C-1′), 92.5 ($^1J_{CH}$ = 158.3 Hz, d; C-5), 90.9 ($^1J_{CH}$ = 159.0 Hz, d; $^3J_{CH}$ = 4.7 Hz, d; C-3′,5′), 73.4 ($^3J_{CH}$ = 7.4 Hz, d; C-3), 60.2 ($^1J_{CH}$ = 144.6, q; 2-OMe), 56.4 ($^1J_{CH}$ = 144.5 Hz, q; 4-OMe), 56.3 ($^1J_{CH}$ = 143.9 Hz, q; 6-OMe), 55.9 ($^1J_{CH}$ = 143.8 Hz, q; 2′,6′-OMe), 55.2 ($^1J_{CH}$ = 143.8 Hz, q; 4′-OMe) (assignments for C-2, C-4, C-4′, and C-6 are tentative) ppm; ms (190°C): 460 (M^+, 100%), 303 (11%), 302 (10%), 181 (9%), 69 (15%). *Anal.* calcd.: C 46.97, H 4.60, O 20.86, I 27.57; found: C 46.90, H 4.63, O 20.7, I 27.60.

2,2′,2″,4,4′,4″,6,6′,6″-Nonamethoxyterphenyl (**3**) and 2,2′,2″,2‴,-4,4′,4″,4‴,6,6′,6″,6‴-dodecamethoxy-(1,1′:3′,1″:3″:1‴)quaterphenyl (**4**) were synthesized by "crossed-Ullmann" reaction of **1** and iodo-2,4,6-trimethoxybenzene (16). Iodo-2,4,6-trimethoxybenzene (1.6 g, 5.5 mmol), **1** (2.0 g, 4.4 mmol), and 3.75 g EDTA-activated Cu

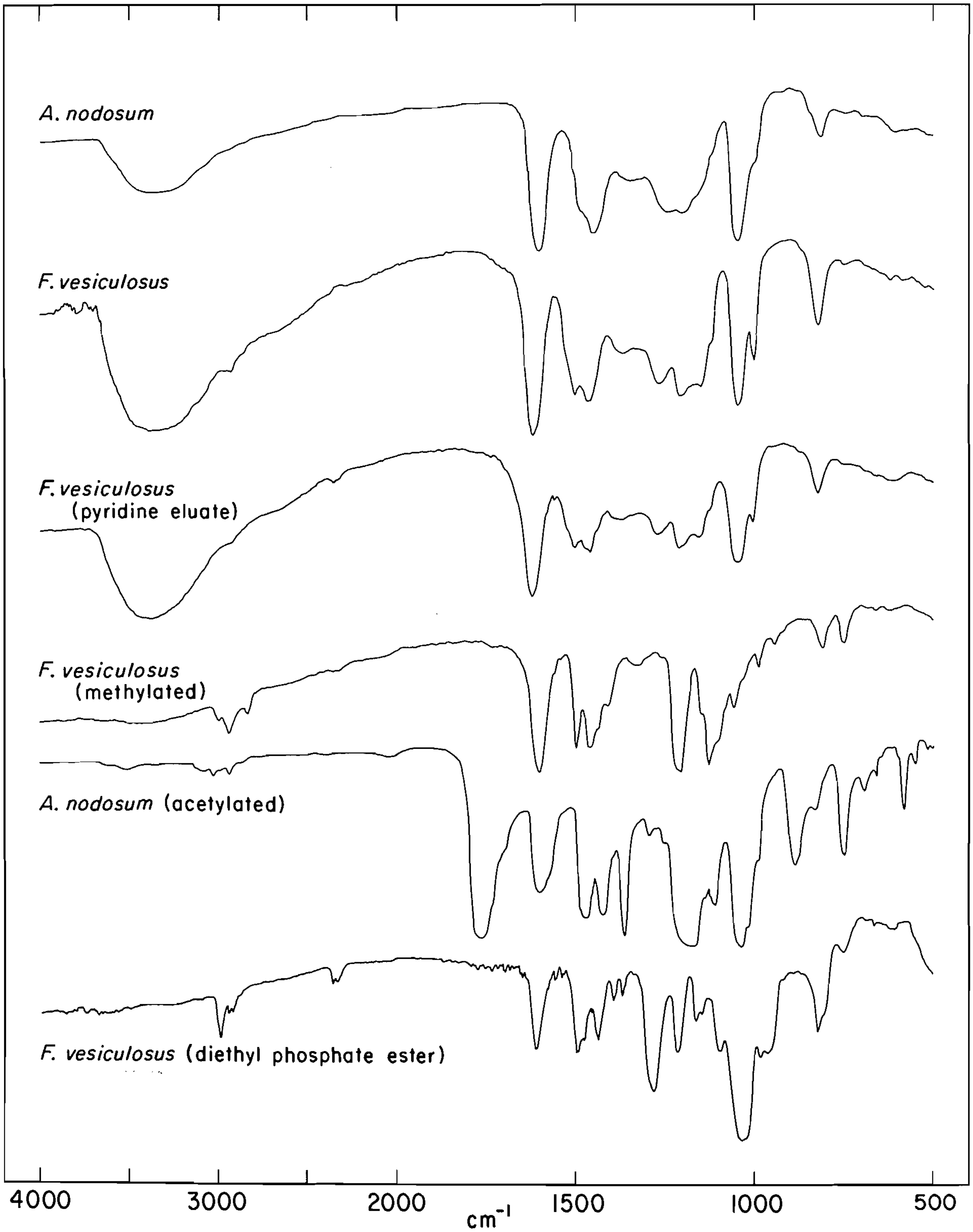

FIG. 1. Infrared spectra of high-molecular-weight polyphloroglucinols and derivatives.

powder (35) were combined thoroughly. The temperature was increased from 110°C to 295°C during 4.5 h while the reaction mixture was stirred vigorously with a heavy copper wire. Thereafter the mixture was cooled, crushed, and extracted with boiling EtOH (2 portions of 1 L). Column chromatography on silica gel (hexane–THF–CH_2Cl_2, gradient 80:10:10 v/v/v to 62.5:12.5:25 v/v/v) yielded **3** (≈30% of recovered organic products) and **4** (≈20%), together with **2** (≈30%), unreacted **1** (≈15%), and minor products (≈5%). Compounds **3** and **4** were further purified by preparative tlc (E. Merck silica gel 60F-254, 45:25:30 v/v/v hexane–THF–CH_2Cl_2). Isolated yields: 0.55 g of **3**, 0.34 g of **4**.

2,2′2″,4,4′,4″,6,6′,6″-Nonamethoxyterphenyl (3)

Crystallization from acetone gave white prisms, mp (birefringence stage) 209.5–210.0°C. ^1H nmr ($CDCl_3$) δ_H: 6.43 (1H, H-5′), 6.22 (4H, H-3,3″,5,5″), 3.82 (6H, 4,4″-OMe), 3.76 (6H, 4′,6′-OMe), 3.72

TABLE 1. Elemental analysis and apparent molecular weights of high-molecular-weight polyphloroglucinols

Alga, source, drying temperature (*in vacuo*)	C%	H%	N%	S%	Apparent molecular weight
A. nodosum, Nova Scotia 1975, 105°C	52.38	4.32	0.30	N/D[a]	N/D
A. nodosum, Norway 1976, 105°C	52.05	4.51	0.91	0.64	N/D
F. vesiculosus, Nova Scotia 1974, 61°C	45.12	5.36	0.16	N/D	$3.71-6.50 \times 10^5$[b]
F. vesiculosus, Nova Scotia 1980, 61°C	50.51	5.37	0.40	N/D	2.70×10^5
F. vesiculosus, Nova Scotia 1980, 105°C	54.37	4.56	N/D	N/D	N/D
F. vesiculosus, Nova Scotia 1980, (pyridine eluate), 105°C	53.96	4.35	0.98	N/D	N/D
	C%	H%	O%	OCH_3%	
F. vesiculosus, Nova Scotia 1980 (methylated), 61°C	59.79	5.88	28.5	32.35	

[a]Not determined.
[b]See ref. 16.

(12H, 2,2″,6,6″-OMe), 3.14 (3H, 2′-OMe) ppm; ^{13}C nmr ($CDCl_3$) δ_C: 160.6 (m; C-4,4″), 159.2 (m; C-2,2″,6,6″ and C-2′), 158.2 (m; C-4′,6′), 109.1 (poorly relaxed: $^3J_{CH}$ = 5.8 Hz, d; C-1′-3′), 105.9 (poorly relaxed; $^3J_{CH} \approx 5.6$ Hz, t; C-1,1″), 91.8 ($^1J_{CH}$ = 156.7 Hz, d; C-5′), 91.3 ($^1J_{CH}$ = 158.6 Hz, d; $^3J_{CH}$ = 4.8 Hz, d; C-3,3″,5,5″), 60.1 ($^1J_{CH}$ = 143.6 Hz, q; 2′-OMe), 56.0 ($^1J_{CH}$ = 143.6 Hz, q; 2,2″,6,6″-OMe), 55.8 ($^1J_{CH}$ = 143.4 Hz, q; 4′,6′-OMe), 55.2 ($^1J_{CH}$ = 143.6 Hz, q; 4,4″-OMe) ppm; ms (165°C): 500.2052 ± 0.0015 (M^+; 100%; required for $C_{27}H_{32}O_9$, 500.2046), 454 (5%), 250 (4%). *Anal.* calcd.: C 64.79, H 6.44, O 28.77; found: C 64.58, H 6.44, O 28.45.

2,2′,2″,2‴,4,4′,4″,4‴,6,6′,6″,6‴-Dodecamethoxy-(1,1′:3′,1″:3″,1‴)quaterphenyl (4)

Crystallization from acetone or methyl ethyl ketone gave white prisms, mp (birefringence stage) 201.0–202.0°C. ^{1}H nmr ($CDCl_3$) δ_H: 6.43 (2H, H-5′,5″), 6.22 and 6.20 (4H; H-3,3‴,5,5‴), 3.82 (6H; 4,4‴-OMe), 3.78 (6H; 4′,6″- or 4″,6′-OMe), 3.74 (12H; 2,2‴,6,6‴-OMe), 3.62 (6H; 4′,6″- or 4″,6′-OMe), 3.24 (6H; 2′,2″-OMe) ppm; ^{13}C nmr ($CDCl_3$) δ_C: 160.6 (J_{CH} = 3.2 Hz, "q"; C-4,4‴), 159.2 (m; C-2′,2″), 159.12 and 159.09 (m; C-2,2‴,6,6‴), 158.25 and 158.15 (m; C-4′,6″ and C-4″,6′), 110.1 (poorly relaxed; $^3J_{CH}$ = 5.3 Hz, d; C-1″,3′), 109.3 (poorly relaxed; $^3J_{CH}$ = 5.1 Hz, d; C-1′,3″), 106.0 (poorly relaxed; $^3J_{CH}$ = 5.0 Hz, t; C-1,1‴), 91.7 ($^1J_{CH}$ = 156.3 Hz, d; C-5′,5″), 91.15 ($^1J_{CH}$ = 158.4 Hz, d; $^3J_{CH}$ = 4.4 Hz, d; C-3,3‴,5,5‴), 60.0 ($^1J_{CH}$ = 143.8 Hz, q; 2′,2″-OMe), 55.9 ($^1J_{CH}$ = 143.4 Hz, q; 2,2‴,6,6‴-OMe), 55.8 ($^1J_{CH}$ = 143.3 Hz, q; 6′,6″-OMe), 55.6 ($^1J_{CH}$ = 143.4 Hz, q; 4′,4″-OMe), 55.1 ($^1J_{CH}$ = 143.6 Hz, q; 4,4‴-OMe) ppm; ms (210°C): 666.2658 ± 0.0020 (M^+; 100%; required for $C_{36}H_{42}O_{12}$, 666.2673), 333 (16%). *Anal.* calcd.: C 64.85, H 6.35, O 28.80; found: C 63.52, H 6.43, O 29.25.

Compound **4** was also synthesized directly from **1**; **1** (3.0 g, 6.5 mmol) and EDTA-activated (35) Cu powder (2.6 g) were combined thoroughly, and the Ullmann condensation was conducted (heating from 125°C to 285°C during 5.5 h) and worked up as above. The product was further purified by chromatography on silica gel (as above) and was crystallized from acetone. Yield, 10%. The product co-chromatographed under a variety of conditions with **4** prepared by the crossed-Ullmann reaction.

A variety of acetylated and *n*-butylated reference compounds were prepared from the corresponding free phenols by the methods outlined above.

Gas chromatography was carried out on packed columns of 3% SE-30 (3.05 m × 3.2 mm id) with temperature programming from 100°C (held 2 min) to 280°C at 4 or 6°C min^{-1} using Hewlett–Packard 5731A and 5750 instruments with flame ionization detection. Mass spectra were recorded on a Dupont-CEC 21-110B instrument (70 eV) with electron-multiplier detection; high resolution mass measurements were made by peak matching, using perfluorokerosene as internal standard. Combined gc–ms was carried out (70 eV) on a Finnigan model 4000 instrument with an INCOS data system; gc–ms analysis of fragments from Ca– (or Na–)NH_3 degradation of the methylated polymer, and of reference compounds, utilized a high-capacity quartz capillary column (3% OV-1, ≈25 m, 0.3 mm id; Hewlett–Packard) with He carrier gas and a ≈10:1 injection splitter. The temperature was programmed from 75°C (held 1 min) to 275°C at 8° min^{-1}. Some gc–ms experiments utilized a packed column (3% SE-30, 3.05 m) with direct injection. Ultraviolet spectra were recorded on a Unicam SP8000 spectrophotometer using matched quartz 10-mm cuvettes. Infrared spectra were recorded on Perkin–Elmer model 283B and model 180 instruments; samples were prepared as films on AgCl discs. The ^{1}H and ^{13}C nmr spectra of reference compounds were recorded on a Varian FT-80 instrument using 5-mm or 10-mm sample tubes, internal ^{2}H pulse lock, and tetramethylsilane as internal reference; proton-noise-decoupled spectra were recorded using 8K data points, and high-resolution ("nondecoupled") spectra with 16K data points. Elemental analyses were done by Microanalytisches Laboratorium (Bonn, FRG) and by Microanalysis Laboratories Ltd. (Markham, Ontario). Metal analysis by plasma emission spectroscopy was done by Berringer Magenta Ltd. (Rexdale, Ontario). Determination of molecular weight by equilibrium ultracentrifugation was carried out on a Beckman model E instrument (0.1 *M* phosphate buffer, pH 7.00, 15°C, concentration ca. 0.2% w/v, 5.2×10^3 rpm ($\omega^2 = 2.965 \times 10^5$ rad^2 s^{-2})) equipped with Schlieren optics. Antibiotic screening was conducted by BioResearch Laboratories (Senneville, P.Q.), and antitumor testing by the U.S. National Cancer Institute (Bethesda, MD).

Results

Physical and spectroscopic properties

The purified high-molecular-weight polymer was a light-brown amorphous solid, extremely soluble (1 g mL^{-1}) in water, also soluble in DMSO, MeOH, and diethyl phosphite, and insoluble in other organic solvents or in SO_2 or NH_3. Aqueous solutions of the polymer gave reactions typical of tannins, e.g. precipitated proteins and alkaloids, tasted astringent, and formed insoluble complexes with excess Fe^{3+} ion. Colorimetric behaviour has been described elsewhere (36). Elemental analyses and apparent molecular weights are given in Table 1. Heterogeneity of molecular weights was indicated by the deviation from linearity of the plot of ln $(1/r)$ (dc/dr) vs. r^2, particularly at values of $r^2 > 50.3$ cm^2. Metal analysis showed Cu (10.7 ppm), Mg (231 ppm), and Si (10 ppm), while levels of Ag, Al, Ba, Be, Ca, Cd, Co, Cr, Fe, K, Mn, Mo, Na, Ni, P, Pb, Sr, Th, Ti, V, Zn, and Zr were below the limits of detection.

The ultraviolet spectrum (in H_2O) is dominated by "end-absorption", although a small absorption due to aromatic nuclei is present at λ = 268 nm; the $E^{1\%(w/v)}_{268\ nm}$ is 109 ± 10 units in distilled water (24). Infrared spectra of the purified polymers from *A. nodosum* and *F. vesiculosus* are virtually identical (Fig. 1), showing a strong bonded O—H stretching band (≈3400 cm^{-1}) which is removed by derivatization, as well as

TABLE 2. Fragments recovered after Ca–NH_3 degradation of methylated "polymer": identification and capillary column gc–ms behaviour. Asterisk denotes identification using authentic standard (see Supplementary Material)

Fragments recovered	Relative retention time (rrt)	Mass spectra (ms)	*n*-Butylation product rrt	*n*-Butylation product ms
Mononuclear fragments				
1,3,5-Trimethoxybenzene*	≡1.000	168,139,125	≡1.000	168,139,125
2,4,6-Trimethoxytoluene*	1.131	182,167,151	1.135	182,167,151
2,4,6-Trimethoxy-*m*-xylene	1.195	196,181	1.198	196,181
3,5-Dimethoxyphenol*	1.090	154,125,111	1.425	210,154,125
Methyl-3,5-dimethoxyphenol	1.176	168,153,137	1.524	224,168,137
Methyl-3,5-dimethoxyphenol	1.228	168,153,137		
Dimethyl-3,5-dimethoxyphenol	1.247	182,167,151	1.571	238,182,167
Dimethyl-3,5-dimethoxyphenol	1.257	182,167	1.600	238,182,167
p-Methoxyphenol*	0.663	124,109	1.057	180,124,109
m-Methoxyphenol*	0.682	124		
Methyl-methoxyphenol	0.786	138,123,107	1.179	194,138,123
Methyl-*m*-methoxyphenol[a]	0.803	138,123	1.191[a]	194,138,123
Methyl-*m*-methoxyphenol[a]	0.827	138,123,107		
2,6-Dimethoxy-1,4-dihydroxybenzene*	1.361	170,155,127	1.937	(282)
Dimethoxy-dihydroxybenzene[b]	1.145	170,155,127	?	—
Methyl-dimethoxy-dihydroxybenzene	1.211	184,169,141	Not seen[c]	—
1,3-Dimethoxybenzene*	0.582	138,109	0.586	138,109
Methyl-dimethoxybenzene[d]	0.739	152,137,121	0.742	152,137,121
Methyl-dimethoxybenzene	0.950	152,137,121	0.956	152,137,121
2,4,6-Trimethoxyphenol*	1.278	184,169,141	1.544(?)[c]	240,184,169
Methyl-trimethoxyphenol(?)	Not seen	—	1.551	(—, 198)
Dimethylphenol[e]	0.577	122,105	0.849	178,122
Methoxytoluene	0.591	122,107,105	0.595	122,107,105
Dimethoxyphenol[f]	0.867	154,139,111	1.327	210,154,139
Binuclear fragments				
Pentamethoxybiphenyl[g]	2.057	304,151,129.5	2.062	304,151,129.5
Methyl-pentamethoxybiphenyl	2.074	318,151,136.5	2.078	318,151,136.5
Methyl-pentamethoxybiphenyl	2.081	318,165,136.5	2.086	318,165,136.5
Dimethyl-pentamethoxybiphenyl	2.102	332	2.108	332
Dimethyl-pentamethoxybiphenyl	2.109	332	2.115	332
2,2′,4,4′,6,6′-hexamethoxybiphenyl(**2**)*	2.297	334,181,167	2.300	334,181,167
3-Methyl-2,2′,4,4′,6,6′-hexamethoxybiphenyl	2.309	348,174,151.5	2.315	348,174,151.5
Dimethyl-2,2′,4,4′,6,6′-hexamethoxybiphenyl	2.330	362,306,275	2.336	362,306,275
Dimethyl-2,2′,4,4′,6,6′-hexamethoxybiphenyl(?)	2.287	362,319	?	—
Hexamethoxybiphenyl(?)	2.373	334,273,181	2.378	334,320,273
Methyl-hexamethoxybiphenyl(?)	2.366	348	2.371	348
Pentamethoxy-hydroxybiphenyl[h]	2.380	320,167,160	2.542	376,320,167
Methyl-pentamethoxy-hydroxybiphenyl	2.394	334,288,167	2.552	390,334,167
Dimethyl-pentamethoxy-hydroxybiphenyl	2.399	348	2.571	404
Methyl-pentamethoxy-hydroxybiphenyl	Not seen	—	2.720	390
Dimethyl-pentamethoxy-hydroxybiphenyl	Not seen	—	2.732	404
Dimethyl-pentamethoxy-hydroxybiphenyl	2.366	348,174	2.561	404,348
Tetramethoxy-hydroxybiphenyl	2.140	290,145	2.322	346,290
Methyl-tetramethoxy-hydroxybiphenyl	2.173	304,165,125	2.338	360,304
Methyl-tetramethoxy-hydroxybiphenyl	Not seen	—	2.344	360
Dimethyl-tetramethoxy-hydroxybiphenyl	Not seen	—	2.349	374
Tetramethoxybiphenyl	1.786	274	1.790	274
Methyl-tetramethoxybiphenyl	1.819	288	1.824	288
2,4′,6,6′-Tetramethoxy-2′,4-dihydroxybiphenyl*	2.430	306,260,167	2.758	418,362,306,260
Methyl-2,4′,6,6′-tetramethoxy-2′,4-dihydroxybiphenyl	Not seen	—	2.770	432
Methyl-2,4′,6,6′-tetramethoxy-2′,4-dihydroxybiphenyl	Not seen	—	2.779	432
Methyl-2,4′,6,6′-tetramethoxy-2′,4-dihydroxybiphenyl	Not seen	—	2.784	432
Dimethyl-2,4′,6,6′-tetramethoxy-2′,4-dihydroxybiphenyl	2.487	334,292	2.781	446,281,223
Dimethyl-2,4′,6,6′-tetramethoxy-2′,4-dihydroxybiphenyl	Not seen	—	2.791	446,281
Tetramethoxy-dihydroxybiphenyl(?)	2.461	306,191,153	2.614(?)	(362,306,207)
Methyl-tetramethoxy-dihydroxybiphenyl(?)	Not seen	—	2.656	432
Methyl-tetramethoxy-dihydroxybiphenyl(?)	Not seen	—	2.689	432,389
2,2′,6,6′-Tetramethoxy-4,4′-dihydroxybiphenyl*	2.442	306,275,191	2.654	418,362,306,275
Methyl-2,2′,6,6′-tetramethoxy-4,4′-dihydroxybiphenyl	2.475	320,160,154	2.665	432,376

TABLE 2. (*Concluded*)

Fragments recovered	Relative retention time (rrt)	Mass spectra (ms)	*n*-Butylation product	
			rrt	ms
Tri- and tetranuclear fragments				
2,2′,2″,4,4′,4″,6,6′,6″-Nonamethoxyterphenyl(**3**)*	3.268	500,250	3.285	500,250
Methyl-2,2′,2″,4,4′,4″,6,6′,6″-nonamethoxyterphenyl	3.325	514	3.341	514
Octamethoxyterphenyl	2.941	470	2.950	470
Octamethoxyterphenyl	3.152	470	3.166	470
2,2′,2″,2‴,4,4′,4″,4‴,6,6′,6″,6‴-Dodecamethoxy-(1,1′:3′,1″3″,1‴)quaterphenyl(**4**)*		—		—

[a]Ring-methylated methoxyphenols at rrt ≈0.803 and 0.827 were seen in commercial preparations of *m*-methoxyphenol; after butylation, ring-methylated methoxyphenyl butyl ethers were seen at rrt 1.185 and 1.192. Then, after subsequent re-treatment with Ca—NH_3, a trace of a possible fourth (debutylated) methyl-methoxyphenol was observed at rrt = 0.812.
[b]Probably 1,2-dihydroxy-3,5-dimethoxybenzene (see text).
[c]A possible monobutyl ether of methyl-dimethoxy-dihydroxybenzene was seen at rrt = 1.547.
[d]Probably methyl-1,3-dimethoxybenzene.
[e]Possibly 2,4-dimethylphenol (see text).
[f]Probably 2,4-dimethoxyphenol (see text).
[g]Probably 2,2′,4,6,6′-pentamethoxybiphenyl (see text).
[h]Probably 4-hydroxy-2,2,4′,6,6′-pentamethoxybiphenyl (see text).
[i]Not seen on capillary column but demonstrable (rrt ≈5.8) during packed-column gc.

bands arising from aromatic C—H stretching (≈2920, 2850 cm^{-1}, weak), aromatic ring skeletal vibrations (1605 cm^{-1}), aryl ether stretching (≈1470, 1200, 1050 cm^{-1}), and C—H out-of-plane bending in 1,3,5-substituted nuclei (815, 705 cm^{-1}) (37).

Derivatives

Acetylation of the high-molecular-weight polymer yielded a light-colored product soluble in $CHCl_3$, acetone, dioxane, THF, and Ac_2O/HOAc. No uv absorbance maximum (other than "end-absorption") was evident. Infrared spectroscopy (Fig. 1) demonstrated the absence of hydroxyl groups (loss of 3400 cm^{-1} band) and the presence of acetoxy groups (2935 cm^{-1}, acetate methyl C—H stretching; 1760 cm^{-1}, acetate carbonyl C=O stretching; 1185–1165 cm^{-1}, stretching), and in addition showed bands arising from aromatic C—H stretching (3090, 3025 cm^{-1}), aromatic ring skeletal vibrations (1605 cm^{-1}), aryl ether stretching (and aromatic nuclear in-plane bending?) (1475, 1140, 1110, 1035, 1020 cm^{-1}), and C—H out-of-plane bending in highly substituted (890 cm^{-1}) and 1,3,5-substituted (830, 695 cm^{-1}) nuclei.

Methylation of the purified polymer gave a light tan-colored product which was readily soluble in $CHCl_3$, CH_2Cl_2, and DMSO; soluble in THF and acetone; mostly soluble in dioxane; and insoluble in water, Et_3N, or NH_3. Infrared spectroscopy (Fig. 1) demonstrated the absence of hydroxyl groups, indicated the presence of methyl groups (C—H stretching, 2940 and (or) 2840 cm^{-1}; C—H bending, 1500 cm^{-1}), and showed bands arising from aromatic ring skeletal vibrations (1605 cm^{-1}), ether stretching (1465, 1440, 1220, 1205, 1125, 1055 cm^{-1}), and ring C—H out-of-plane bending (810 cm^{-1}).

Degradative analysis

Treatment of the methylated polymer with Ca in NH_3 (cf. ref. 38) produced a very complex mixture. Silica gel tlc (using a variety of solvent systems) allowed only partial resolution of ca. 15 components, but demonstrated the presence of relatively immobile (polar and (or) higher-molecular-weight) compounds which also absorbed at λ = 254 nm. Judging from the behaviour of reference compounds in these tlc systems and on gc, most of these relatively immobile fragments would not have been sufficiently volatile, even after butylation or trimethylsilylation, to have been seen during gc or gc–ms analysis.

A total of 63 fragments arising from the methylated polymer were identified by gc and gc–ms analysis of the Ca–NH_3 degradation product and the subsequent butylation mixture. Capillary gc–ms of the initial degradation product resolved at least 150 compounds, mostly of very minor abundance. Of the 123 most abundant in the reconstructed ion current (RIC) under these scanning and ionization conditions, 51 were identified as methoxylated and (or) methylated phenolic or aryl fragments (Table 2), 63 (mostly minor peaks, totalling 19.1 ± 7.2% of the total area of the RIC) were identified as column or septum bleed compounds, phthalate esters, etc., and 9 relatively small peaks could not be identified. The gc–ms of the *n*-butylated reaction mixture under the same conditions resolved at least 170 compounds; of the 150 most abundant, 59 were identified as methoxylated and (or) methylated aryl or phenyl butyl ether fragments (Table 2), 84 (almost entirely minor peaks) arose from column bleed, phthalate esters, etc., and 7 could not be identified. After further treatment of the butylated mixture with Ca–NH_3, gc–ms revealed an essentially identical pattern, with the exception that some debutylation had occurred. In all, 62 fragments arising from the methylated polymer were identified by gc–ms; the 63rd, **4** (Table 2), was insufficiently volatile for analysis on the capillary column, but was identified by its retention time on the packed SE-30 column. The permethoxy ether of a second phloroglucinol-related quaterphenyl reported (39) to occur in brown algae, 2,4,6-trimethoxy-1,3,5-*tris*-(2,4,6-trimethoxyphenyl)benzene, was not available for reference.

Identification of the former 62 fragments was made in the following manner. *Methoxyarenes* were initially located by scanning for expected molecular ions using the INCOS program "CHROMATOGRAM"; the individual methoxyarenes were then identified by comparison with reference compounds (when available; Supplementary Material[3]), examination of the

[3]This supplementary material is available, at a nominal charge, from the Depository of Unpublished Data, CISTI, National Research Council of Canada, Ottawa, Ont., Canada K1A 0S2.

mass spectra (with computer enhancement for the least abundant compounds), inferences drawn from ring-methylation (see below), and appearance of the compound at the same relative retention time (rrt) in chromatograms of the butylated reaction mixtures, both before and after the second $Ca-NH_3$ cleavage reaction. *Phenolic fragments* were identified similarly, except that the peak in the chromatogram of the initial reaction mixture was required to be absent from the butylation products, and instead to correspond to a new peak appearing at longer rrt and having an appropriate mass spectrum (including the molecular ion, major fragments of the parent phenol, and the required number of 56-amu fragmentations reflecting loss of butyl groups). The gc peak intensities from the butylated reaction mixture corresponded very well with intensities for the identical or parent compounds in the nonbutylated mixture. Problematic identifications are treated below.

The abundance of ring-methylated fragments, together with the total absence of infrared (see above) or nmr (25) evidence for any methyl groups in the native "polymer", indicates that extensive ring-methylation of the "polymer" had occurred, as expected from earlier studies (16). Although the presence of ring-methylated fragments greatly complicates the chromatograms, in some instances (abundances permitting) the pattern of ring-methylation provides useful corroboration of proposed structures as in the following instances.

(a) The appearance of only two mono- and only two dimethyl derivatives of the major fragment at rrt 1.090 (3,5-dimethoxyphenol) helps to rule out four of the six possible dimethoxyphenols: the 2,3-, 2,4-, 2,5-, and 3,4- dimethoxy isomers each should show three mono- and three di(ring-)methylated derivatives if all three ring positions were available for methylation in the native "polymer". The 2,6- (rrt 0.895) and 3,5- (rrt 1.091) isomers have only two possible mono- and two dimethyl derivatives.

(b) The presence of only two monomethyl derivatives of the abundant pentamethoxybiphenyl at rrt 2.057, together with the presence of **2** (rrt 2.297) and 2,2′,6,6′-tetramethoxy-4,4′-dihydroxybiphenyl (rrt 2.442), argues strongly that the former fragment has 2,2′,4,6,6′-methoxylation and was originally linked to the rest of the "polymer" by (at least) an ether bond at C-4′. If so, the hydroxypentamethoxybiphenyl at rrt 2.380 is probably 4-hydroxy-2,2′,4′,6,6′-pentamethoxybiphenyl.

(c) The obviously congeneric group of three methyl- and two dimethyl-tetramethoxydibutoxybiphenyls (rrts 2.770–2.791) may be provisionally correlated with 2,4′,6,6′-tetramethoxy-2′,4-dihydroxybiphenyl (three possible mono- and four di(ring-)methyl derivatives) at rrt 2.430 in the nonbutylated mixture, rather than with its 2,2′,6,6′-tetramethoxy-4,4′-dihydroxy isomer (one possible mono- and two dimethyl derivatives) at rrt 2.442.

Of the 24 parent (without ring-methylation) fragments found (Table 2), 21 were positively identified by the criteria described above. Both *m*- and *p*-methoxyphenols were found in the $Ca-NH_3$ reaction mixture and were positively identified by comparison of rrts and mass spectra with those of authentic compounds (Supplementary Material[3]), by computer matching with spectra in the 25409-compound National Bureau of Standards library,[4] and by their absence from the same positions in the chromatogram after butylation. The appearance of only one peak for butyl methoxyphenyl ether(s) after butylation (rrt 1.057) presumably results from the lack of resolution of *m* and *p* isomeric butyl methoxyphenyl ethers (Supplementary Material[3]). The three tentative identifications among parent fragments are a dimethoxydihydroxybenzene at rrt 1.145 (of modest abundance; no corresponding dimethoxydibutoxybenzene found), a hexamethoxybiphenyl at rrt 2.373 (of extremely minor abundance, incompletely resolved from the pentamethoxyhydroxybiphenyl at rrt 2.380), and a tetramethoxydihydroxybiphenyl at rrt 2.461 (of modest abundance and occurring in a very congested region of the chromatogram near two (other?) isomeric tetramethoxydihydroxybiphenyls and related ring-methylated compounds). One further problem involved the resolution of only one methyl-dimethoxybutoxybenzene peak despite the prior well-demonstrated presence of two ring-methylated 3,5-dimethoxyphenols. These and other problematic or tentative identifications (indcated by a "?" in Table 2) concern fragments of minor abundance, and the uncertainty of identification does not affect the subsequent discussion.

Semiquantitative estimation of the recovered fragments was made in the following manner: first, the 15 peaks resolved by packed column gc and detected by flame ionization were quantified using standard curves from reference compounds chromatographed under identical conditions. Second, the efficiency of recovering each fragment from the $Ca-NH_3$ reaction mixture was estimated, where possible, from the identical work-up of sham reactions spiked with known amounts of authentic references. Finally, the proportion of the total recovered fragments represented by these 15 peaks was approximated, by analysis of the reconstructed ion current distribution among the fragments resolved by capillary column gc–ms (Incos program "QUANTITATION"); the major fragments, together with their isomers and ring-methylated derivatives which were not separated by gc on packed columns, were responsible for 70.3 ± 1.7% of the total RIC under the scanning and ionization conditions employed. The results, summarized in Table 3, suggest that ca. 20% of the methylated "polymer" was released as mono-, di-, tri-, and tetranuclear fragments detectable by gc. Of these, ≈71% (by weight) are mononuclear (arising from ether-linked phloroglucinol units), ≈27% binuclear (arising from biphenyls linked to the remainder of the polymer by one or more ether bonds), and ≈2% tri- or tetranuclear.

Exact quantitation of the fragments was not possible. The efficiencies of recovery of fragments from the reaction mixture were variable (Table 3), with greatest variation seen among the most volatile fragments. Quantitative studies involving packed-column gc were complicated by incomplete resolution of fragments and by poor peak shape of phenolic components, while dependable quantitative results from capillary gc(–ms) were precluded by the use of an injection splitter.

Biological activity

The native, nonderivatized high-molecular-weight polymer was not significantly inhibitory at concentrations of 0.05–25 mg mL^{-1} to the growth of *Escherichia coli* (ATCC 10536), *Pseudomonas aeruginosa* (ATCC 15442), *Staphylococcus aureus* (ATCC 6538), *Streptococcus faecalis* (ATCC 10541), or *Saccharomyces cerevisiae* (ATCC 2601) in suspension cultures, and showed no activity against mouse P388 lymphocytic leukemia (5 daily injections of 12.5–200 mg kg^{-1} $injection^{-1}$).

Discussion

All spectroscopic and degradative data presented in this pa-

[4] Library as supplied by Finnigan-MAT Corp. (Sunnyvale, Calif.) and stated to be identical with the "EPA/NIH Mass Spectral Data Base" (see ref. 40).

TABLE 3. Recoveries and quantitation (using packed-column gc) of major fragments from Ca–NH_3 degradation of methylated "polymer"

Compound(s)[a]	rrt[b]	Rel. amt. ±s.d.[c]	n[d]	% Recovery[e]	n[d]	Estimate of amount released from 25 mg "polymer": mg	(wt%)
Dimethoxybenzenes	≈0.40	0.09[f]	1	34.5 ± 1.1[g]	4	0.1	(0.4%)
Methoxyphenols	≈0.62	0.10 ± 0.10[f]	3	31.0 ± 19.5[h]	2	0.1	(0.5%)
1,3,5-Trimethoxybenzene	≡1.00	1.99 ± 0.65	6	52.5 ± 12.6	8	1.4	(5.7%)
3,5-Dimethoxyphenol	1.21	2.63 ± 0.45	5	69.9 ± 15.8	3	1.4	(5.6%)
2,4,6-Trimethoxytoluene	1.31	0.21 ± 0.08	6	49.2 ± 0.5	2	0.15	(0.6%)
Tetramethoxybiphenyl	2.33	0.08 ± 0.03	5	N/D	–	0.05[j]	(0.1%)
2,2′,4,6,6′-Pentamethoxybiphenyl	2.67	1.08 ± 0.45	6	N/D	–	0.5[j]	(2.0%)
Tetramethoxyhydroxybiphenyl	2.83	Trace	–	N/D	–	Trace	(<0.1%)
2,2′,4,4′,6,6′-Hexamethoxybiphenyl	3.02	≡1.00	6	81.0 ± 23.2	8	0.45	(1.8%)
Pentamethoxyhydroxybiphenyl	3.19	Trace[i]	–	N/D	–	Trace	(<0.1%)
Tetramethoxydihydroxybiphenyls	≈3.33	Trace	–	N/D	–	Trace	(<0.1%)
Octamethoxyterphenyl$_1$	3.79	0.04	1	N/D	–	0.02[j]	(0.1%)
Octamethoxyterphenyl$_2$	4.00	0.04	1	N/D	–	0.02[j]	(0.1%)
3	4.21	0.10	1	76.0 ± 16.8	7	0.05	(0.2%)
4	≈5.8	Trace	–	N/D	–	Trace	(<0.1%)
						≈4.3 mg	(17.4%)[k]

[a] Including unresolved isomers and ring-methylated derivatives.
[b] On 3% SE-30 on 60–80 mesh GasChrom Q; 3.05 m × 3.2 mm id columns; He flow 30 mL min^{-1}; flame ionization detection; temperature program 100°C (2 min) to 280°C (hold) at 6°/min.
[c] From standard curves of authentic reference compounds.
[d] Number of independent experiments from which quantitative data could be obtained.
[e] Recovery of internal reference (bromo-2,4,6-trimethoxybenzene) was 79.5 ± 3.7%.
[f] Occasionally seen in much larger quantities; *meta* isomers used for standardization.
[g] *meta*, 35.1 ± 0.2%; *ortho*, 33.9 ± 1.0%.
[h] *meta* Isomer.
[i] Much more abundant in capillary-column separations (RIC).
[j] Efficiency of recovery assumed to be 81%.
[k] From capillary-column separations, the minor fragments (not seen on packed-column gc) may be estimated to constitute a further ≈2.6% of the initial "polymer."

per suggest that the high-molecular-weight tannin of *F. vesiculosus* is based entirely on phloroglucinol. Previous hydrolytic experiments (16, 26) had revealed no carbohydrates and only traces of amino acids and ammonia; now, gc–ms analyses of the alkali metal – liquid ammonia degradations have revealed a variety of $(C_6)_n$-based fragments, but no C_6C_3 units which might be expected from a brown algal "lignin" (41–45), nor $C_6C_1C_6$ units characteristic of phloroglucinols in ferns and some higher plants (46), nor phenol or *o*-methoxyphenol as reported by Reznikov *et al.* (45). No evidence has been found for carboxy, alkenyl (cf. refs. 22, 23), or halo (cf. ref. 19) substitution in the polymer (although the Ca–NH_3 degradation would have caused dehalogenation). The efficient derivatizations by acetic anhydride and by sodium methylsulfinylcarbanion imply that all free hydroxyl groups (i.e. not involved in diaryl ether bonds) are readily "available" to the surrounding medium.

Both directly bonded and ether-linked units were demonstrated. Due to the low overall recovery of material from the Ca–NH_3 cleavage reaction, it is not possible to estimate the ratio of direct C—C to diaryl ether bonds in the parent molecule (see ref. 25); however, approximately 29% of the recovered phloroglucinol groups bore one or more direct C—C bonds (Table 3), whereas a minimum of 85% (71/1 + 27/2 + 2/3%) must have been linked to the rest of the molecule by one or more diaryl ether bonds. Oligoaryl regions donated a much smaller proportion (≈2%) of the recovered fragments. Thus to the extent that the results (Tables 2, 3) are characteristic of the entire polymer, it appears that the latter is composed of phloroglucinol units linked predominantly by ether bonds, with a smaller (but significant) proportion of direct C—C linkages.

It is also possible to identify certain fragments as having arisen from end groups (linked to the rest of the "polymer" by only one diaryl ether bond) and from "in-chain" groups (linked by two or more diaryl ether bonds). The only fragment unequivocally coming from end groups is 2,4,6-trimethoxy-*m*-xylene; however, as it is extremely unlikely (given the observed degree of ring-methylation) that every terminal phloroglucinol group would be methylated at both free ring positions, it is probable that much of the non- and mono-(ring-)-methylated 1,3,5-trimethoxybenzene observed also arose from end groups. Consistent with this conclusion is the absence of dihydroxytrimethoxybenzene fragments. If so, it becomes likely that most or all of the 2,4,6-trimethoxyphenol fragments have also arisen from terminal phloroglucinol groups. Other fragments perhaps arising from end groups include the pentamethoxy-, pentamethoxyhydroxy-, and hexamethoxybiphenyls (and their ring-methylated derivatives), although the only evidence bearing on their origin is the absence of dihydroxy derivatives in the reaction mixture.

"In-chain" groups include all those fragments bearing two hydroxy groups, and may be further categorized on the basis of the relative orientations of ether linkages: *para* (2,6-dimethoxy-1,4-dihydroxybenzene); *meta* (*m*-methoxyphenol, assuming its origin from a 1,3,5-trisubstituted group); *ortho* (the dimethoxydihydroxybenzene at rrt 1.145, which if possessing

1,3,5-substitution is probably 1,2-dihydroxy-3,5-dimethoxybenzene, as in the diether-linked ring of the 4-(2″-(2‴,-4‴,6‴-trihydroxyphenoxy)-4″,6″-dihydroxyphenoxy)-2,2′,4′,-6,6′-pentahydroxybiphenyl reported earlier (17), and the dimethoxyphenol (presumably 2,4-dimethoxyphenol) at rrt 0.867, which would arise from the same type of nucleus in the polymer); and possible *vic*- (*p*-methoxyphenol, assuming its origin from a 1,3,5-substituted unit) and *sym*-triethers (*p*-methoxyphenol; also, the presumed 2,4-dimethylphenol at rrt 0.577). The major fragment probably representing internal positions, 3,5-dimethoxyphenol, must arise from both *ortho*- and *para*-ether linked environments, because both possible mono- and both possible di-(ring-)methylated derivatives are present. In addition, and in contrast to the report by Glombitza and Lentz (47), evidence for internal biphenyl groups was found as well: three dihydroxytetramethoxybiphenyls, one tetramethoxyhydroxybiphenyl, and one tetramethoxybiphenyl (the latter two assumed to have arisen from 2,2′,4,4′,6,6′-hexasubstituted biphenyl nuclei), together with their ring-methylated derivatives.

Glombitza and Lentz (47) have studied a mixture of EtOAc-soluble "phlorotannins" (of unspecified medium to high molecular weights) from *F. vesiculosus* by $Na-NH_3$ cleavage and chromatography, finding six of the fragments reported here (1,3,5-trimethoxybenzene; 3,5-dimethoxyphenol; 2,4,6-trimethoxyphenol; **2**; 4-hydroxy-2,2′,4′,6,6′-pentamethoxybiphenyl; and 2,2′,4,6,6′-pentamethoxybiphenyl) as well as five biphenyl ethers and polar fragments relatively immobile during tlc. No biphenyl ethers could be demonstrated in the study reported herein. In agreement with the results of Glombitza and Lentz (47), no evidence was found here for the occurrence of *vic*-trihydroxy phenoxy end groups.

Information on the $Ca-NH_3$ cleavage reaction itself can also be deduced from the fragmentation observed: (a) cleavage of a diaryl ether bond *ortho* to two methoxy groups, and *para* to a third, liberates much more arene than phenol from that group, as also found by Glombitza and Lentz (47). Examples include the large quantity of 1,3,5-trimethoxybenzene (and its ring-methylated derivatives) produced, contrasted to the much smaller amount of 2,4,6-trimethoxyphenol recovered; and correspondingly, the large amount of **2** (and its ring-methylated derivatives) vis-à-vis the apparent absence of 2,2′,4,4′,6,6′-hexamethoxyhydroxybiphenyl from the fragments recovered.

(b) During cleavage of a 2,6-dimethoxy-1,4-diphenoxy group, the *meta* (4-) oxygen is retained intact whereas the *ortho* (1-) oxygen may or may not be lost. The presence of such units in the polymer is indicated by the appearance of 2,6-dimethoxy-1,4-dihydroxybenzene among the $Ca-NH_3$ reaction products. Some, but not all, of the 3,5-dimethoxyphenol fragments could have arisen from such units also (4-methylated and 2,4-dimethylated 3,5-dimethoxyphenols were observed); however, 2,6-dimethoxyphenol fragments were not seen. The 1,3-dimethoxybenzene observed could have arisen from loss of the 1,4-phenoxy oxygens, but given the absence of 2,6-dimethoxyphenol is more likely to be derived from 1,2-diphenoxy-3,5-dimethoxy groups.

(c) In contrast to the above, the *meta* (1-) oxygen of 1,2-diphenoxy-3,5-dimethoxy units may be lost during $Ca-NH_3$ cleavage, producing the presumed 2,4-dimethoxyphenol (rrt 0.867, see above). Loss of the 2-phenoxy oxygen could produce 3,5-dimethoxyphenol, and loss of both phenoxy oxygens, 1,3-dimethoxybenzene; however, each of the latter two fragments may have arisen from several different environments in the "polymer".

(d) Cleavage of the ether bond in a 4-phenoxy-2,2′,4′,6,6′-pentamethoxybiphenyl unit yields both 4-hydroxy-2,2′,4′,-6,6′-pentamethoxybiphenyl and 2,2′,4,6,6′-pentamethoxybiphenyl in approximately equal quantities (estimated from capillary column gc–ms experiments; on packed-column gc, the former fragment was found only in trace amounts).

High-molecular-weight polyphloroglucinols have been reported to occur in a variety of brown algae (26). The application of the methods described in this paper and similar methods independently developed by Glombitza and Lentz (47), together with ^{13}C nmr (25), may be expected to provide interesting structural and comparative data on these molecules.

Acknowledgements

I thank G. Kulbotten, P. Shacklock, L/Cdr K. G. Nesbit, Lt. B. MacLean, and the crew of the submarine HMCS Okanagan for assistance with collections; D. J. Embree, C. Flinn, W. D. Jamieson, and E. Lewis for assistance with gc–ms; J. A. Verpoorte for performing the ultracentrifugation experiments; A. Taylor for operating the "cyclone" evaporator; K.-W. Glombitza for communicating results from ref. 47 prior to publication; and J. S. Craigie, A. Jensen, and A. G. McInnes for advice and encouragement.

1. E. CRATO. Ber. Dtsch. Bot. Ges. **10**, 295 (1892).
2. H. KYLIN. Ber. Dtsch. Bot. Ges. **36**, 10 (1918).
3. M. A. RAGAN. Bot. Mar. **19**, 145 (1976).
4. J. McN. SIEBURTH. Adv. Microbiol. Sea, **1**, 63 (1968).
5. J. T. CONOVER and J. McN. SIEBURTH. Proc. Int. Seaweed Symp. **5**, 99 (1966).
6. J. McLACHLAN and J. S. CRAIGIE. Can. J. Bot. **42**, 287 (1964).
7. R. L. FLETCHER. Nature (London) **253**, 534 (1975).
8. J. A. GEISELMAN and O. J. McCONNELL. J. Chem. Ecol. **7**, 1115 (1981).
9. C. OGINO and Y. TAKI. J. Tokyo Univ. Fish. **43**, 1 (1957).
10. K. M. KHAILOV. Dokl. Akad. Nauk SSSR, Biol. Sci. **155**, 237 (1964) (English translation).
11. M. A. RAGAN, O. SMIDSRØD, and B. LARSEN. Mar. Chem. **7**, 265 (1979).
12. J. McN. SIEBURTH and A. JENSEN. J. Exp. Mar. Biol. Ecol. **3**, 275 (1969).
13. M. A. RAGAN and A. JENSEN. J. Exp. Mar. Biol. Ecol. **36**, 91 (1979).
14. M. A. RAGAN, C. M. RAGAN, and A. JENSEN. J. Exp. Mar. Biol. Ecol. **44**, 261 (1980).
15. K.-W. GLOMBITZA, H. U. RÖSENER, H. VILTER, and W. RAUWALD. Planta Med. **24**, 301 (1973).
16. M. A. RAGAN and J. S. CRAIGIE. Can. J. Biochem. **54**, 66 (1976).
17. J. S. CRAIGIE, A. G. McINNES, M. A. RAGAN, and J. A. WALTER. Can. J. Chem. **55**, 1575 (1977).
18. K.-W. GLOMBITZA. *In* Marine algae in pharmaceutical science. *Edited by* H. A. Hoppe, T. Levring, and Y. Tanaka. Walter de Gruyter, Berlin and New York. 1979. pp. 303–342.
19. K.-W. GLOMBITZA, M. KOCH, and G. ECKHARDT. Phytochemistry, **16**, 796 (1977).
20. A. JENSEN and M. A. RAGAN. Tetrahedron Lett. 847 (1978).
21. M. A. RAGAN and A. JENSEN. Phytochemistry, **18**, 261 (1979).
22. R. P. GREGSON, R. KAZLAUSKAS, P. T. MURPHY, and R. J. WELLS. Aust. J. Chem. **30**, 2527 (1977).
23. R. KAZLAUSKAS, L. KING, P. T. MURPHY, R. G. WARREN, and R. J. WELLS. Aust. J. Chem. **34**, 439 (1981).
24. M. A. RAGAN and J. S. CRAIGIE. J. Exp. Mar. Biol. Ecol. **46**, 231 (1980).
25. A. G. McINNES, M. A. RAGAN, D. G. SMITH, and J. A. WALTER.

Can. J. Chem. **63**, 304 (1985).
26. M. A. RAGAN. Ph.D. thesis, Dalhousie University, Halifax, N.S. 1976.
27. M. A. RAGAN and J. S. CRAIGIE. *In* Handbook of physological methods: physiological and biochemical methods. *Edited by* J. A. Hellebust and J. S. Craigie. Cambridge Univ. Press, London. 1978. pp. 157–179.
28. S.-I. HAKOMORI. J. Biochem. (Tokyo) **55**, 205 (1964).
29. E. J. COREY and M. CHAYKOVSKY. J. Am. Chem. Soc. **84**, 866 (1962).
30. K. SJÖBERG. Tetrahedron Lett. 6383 (1966).
31. R. A. ROSSI and J. F. BUNNETT. J. Org. Chem. **38**, 2314 (1973).
32. A. I. VOGEL. Practical organic chemistry. 3rd ed. Longman, London. 1970.
33. M. A. RAGAN. Can. J. Chem. **63**, 291 (1985).
34. H. SUZUKI. Bull. Chem. Soc. Jpn. **44**, 2871 (1971).
35. A. H. LEWIN, M. J. ZOVKO, W. H. ROSEWATER, and T. COHEN. Chem. Commun. 80 (1967).
36. M. A. RAGAN and A. JENSEN. J. Exp. Mar. Biol Ecol. **30**, 209 (1977).
37. R. N. JONES. Infrared spectra of organic compounds: summary charts of principal group frequencies. NRC Bulletin 6, National Research Council, Ottawa. 1959.
38. J. H. CHAPMAN, J. ELKS, G. H. PHILLIPPS, and L. J. WYMAN. J. Chem. Soc. 4344 (1956).
39. K.-W. GLOMBITZA, H.-W. RAUWALD, and G. ECKHARDT. Phytochemistry, **14**, 1403 (1975).
40. S. R. HELLER and G. W. A. MILNE. NSRDS–NBS 63, Volumes 1–4, U.S. Government Printing Office, Washington, D.C. 1978.
41. S. SCHMIDT-NIELSEN and A. ASTAD. K. Nor. Vidensk. Slsk. Forh. **9**, 89 (1936).
42. K. K. LEBEDEV, O. I. CHERNYAEVA, M. A. RAKITINA, and Z. N. ZHELEZNYAKOVA. Sb. Tr. Tsentr. Nauchno-Issled. Proektn. Inst. Lesokhim. Promsti. No. 16. 259 (1965).
43. R. RIPA and L. M. BORQUEZ. Scientia, **34**, 36 (1967).
44. L. P. GOL'MAN, M. F. MIKHASEVA, and V. M. REZNIKOV. Dokl. Akad. Nauk BSSR **17**, 1031 (1973).
45. V. M. REZNIKOV, M. F. MIKHASEVA, and M. A. ZIL'BERGLEIT. Khim. Prirod. Soed. **5**, 645 (1978).
46. C.-J. WIDEN, H. PYYSALA, and P. SALOVAARA. J. Chromatogr. **188**, 213 (1980).
47. K.-W. GLOMBITZA and G. LENTZ. Tetrahedron, **37**, 3861 (1981).

The high molecular weight polyphloroglucinols of the marine brown alga *Fucus vesiculosus* L. ^{1}H and ^{13}C nuclear magnetic resonance spectroscopy[1,2]

A. GAVIN MCINNES, MARK A. RAGAN,[3] DONALD G. SMITH, AND JOHN A. WALTER

Atlantic Research Laboratory, National Research Council of Canada, 1411 Oxford Street, Halifax, N.S., Canada B3H 3Z1

Received February 27, 1984

A. GAVIN MCINNES, MARK A. RAGAN, DONALD G. SMITH, and JOHN A. WALTER. Can. J. Chem. **63**, 304 (1985).

^{1}H and ^{13}C nuclear magnetic resonance spectroscopy of the high-molecular-weight ($>10^4$) polyphenol fraction from *Fucus vesiculosus*, before and after acetylation or methylation, demonstrates that it is composed of phloroglucinol units (48.9 ± 3.5%) and 2,2′,4,4′,6,6′-hexahydroxybiphenyl, 2,2′,2″,4,4′,4″,6,6′,6″-nonahydroxy-1,1′:3′1″-terphenyl, and related quater- and polyphenyl groups (together, 51.1 ± 3.5%) linked by ether bonds, each bond involving the carbinol and methine carbons of different units and the formal loss of a molecule of hydrogen. The polymer is highly branched, with ca. 20–22% of the constituent units being chain termini; there is no evidence for large rings of units. Approximately 5–10% of the phloroglucinol and 54–82% of the directly bonded units occur on the exterior of the molecule, whereas the interior backbone consists predominantly of ether-linked phloroglucinol units.

A. GAVIN MCINNES, MARK A. RAGAN, DONALD G. SMITH et JOHN A. WALTER. Can. J. Chem. **63**, 304 (1985).

Sur la base des résultats obtenus à l'aide de la rmn du ^{1}H et du ^{13}C appliquée à la fraction polyphénolique (tant à l'état naturel qu'après une acétylation ou une méthylation) de poids moléculaire élevé ($>10^4$) isolée du *Fucus vesiculosus*, on peut conclure que ce produit est formé d'unités phloroglucinols (48,9 ± 3,5%), d'hexahydroxy-2,2′,4,4′,6,6′ biphényle, de nonahydroxy-2,2′,2″,4,4′,4″,6,6′,6″ terphényles et de groupements quater- et polyphényles qui leurs sont reliés (formant ensemble 51,1 ± 3,5%); toutes ces unités sont reliées par des liaisons éthers alors que chaque liaison implique le carbinol et les carbones méthines des différentes unités avec la perte formelle d'une molécule d'hydrogène. Le polymère est fortement ramifié et il comporte environ 20–22% d'unités constituantes qui terminent des chaînes; sur la base de nos données, il ne semble pas y avoir de grands arrangements cycliques des unités. Environ 5–10% du phloroglucinol et de 54–82% des unités qui sont directement attachées se retrouvent sur la partie extérieure de la molécule, alors que le squelette intérieur est formé principalement d'unités de phloroglucinol qui sont reliées par des liaisons éthers.

[Traduit par le journal]

Introduction

Polyphenols constitute as much as 15% of the dry matter of marine brown algae (Phaeophyceae) (1–3). Phloroglucinol, 2,2′,4,4′,6,6′-hexahydroxybiphenyl, and other MW (molecular weight) $<10^3$ phloroglucinol-based polyphenols have been identified as cellular constituents of *Fucus vesiculosus* (4–7) and other brown algae (4). However, as much as 95% of the total polyphenols of many brown algae have MW $>10^3$, and in *F. vesiculosus* approximately 25% have MW $>10^4$ (3, 5, 8). The gc–ms analysis of Ca–NH_3 degradation fragments of this highest MW fraction (9) has indicated that the molecules in this fraction contain phloroglucinol, 2,2′,4,4′,6,6′-hexahydroxybiphenyl, and smaller amounts of the corresponding hydroxyterphenyl and -quaterphenyl groups, linked together through oxygen. These observations suggest that the MW $>10^4$ polyphenols may be regarded as formally derived from phloroglucinol, although there is at present no supporting biosynthetic evidence. In this communication we present evidence from ^{13}C and ^{1}H nmr to characterize further the structure of the MW $>10^4$ polyphenols ("polymer") of *F. vesiculosus*.

Throughout this discussion, the term "unit" refers to hydroxylated benzene rings within the polymer, whereas the term "group" refers to two or more such units linked by direct carbon–carbon bonds to form hydroxy bi- or polyphenyls.

Experimental

Preparation of the polymer fraction, its derivatives, and reference compounds has been described in the previous paper (9). The additional reference compound hexaacetoxybenzene was synthesized from tetrahydroxy-*p*-quinone (Aldrich) by the procedure of Fatiadi and Sager (10) and was dissolved in trifluoroacetic acid-^{2}H for nmr. Unless otherwise specified, other nmr spectra were recorded in D_2O containing a small amount of DMSO as internal reference (for the native polymer and the corresponding reference compounds), or in $CDCl_3$ containing tetramethylsilane (TMS) (for acetoxyl and methoxyl derivatives). Chemical shifts are reported as ppm downfield from TSP (sodium 3-trimethylsilylpropionate 2,2,3,3-$^2H_4$) or TMS, respectively.

The ^{1}H nmr spectra were recorded at 80 and 100 MHz on Varian FT-80 and HA-100 instruments, respectively. The ^{13}C nmr spectra with broadband ^{1}H-decoupling were recorded at 20.11 MHz (Varian FT-80), 25.16 MHz (Varian XL-100), and 90.80 MHz (Nicolet Magnetics 360) at ambient temperatures, using an internal lock to ^{2}H. Conditions varied: flip angles 30°–55°, acquisition times 0.8–1.0 s, and delays between acquisitions 0–2.2 s. To ensure that spectral integrals were representative of the numbers of ^{13}C nuclei, in some experiments the relaxation reagents tris(ethylenediamine)chromium(III)chloride (CREN, 5 mg mL^{-1} D_2O solution) or chromium(III) acetylacetonate (10 mg mL^{-1} $CDCl_3$ solution) were used together with nOe suppression by "inverse-gated decoupling" (11) (decoupler off during the delay between acquisiitons). Within error, integrals were unchanged by these additional precautions, and hence may be taken as representative.

"EDIT" experiments (12) were carried out on Varian XL-100 (modified by addition of a Nicolet 1280 computer and 293B pulse programmer) and Nicolet Magnetics 360 instruments. The delay between 90° and 180° pulses at the ^{13}C frequency in the EDIT sequence was 2.99 ms, corresponding to an average $^1J_{CH}$ of 167 Hz.

Model structures used in the analysis of ^{13}C and ^{1}H spectra included the free hydroxy (suffix "*a*"), acetoxy (suffix "*b*"), and methoxy (suffix "*c*") forms of all possible phloroglucinol-based tri- (**1–3**), tetra- (**4–9**), penta- (**11–16**), and hexa-*O*-substituted (**18–21**) benzenes, tri- (**22–27**), tetra- (**28–35**), and penta-*O*-substituted (**36–41**) phenyl units, representative simple hydroxy ter- and quaterphenyls (**42–45**), and two other hydroxylated structures (**10, 17**) reported by

[1]NRCC No. 23431.

[2]Part 5 in the series "Physodes and the phenolic compounds of brown algae". For Part 4, see ref. 9.

[3]Author to whom correspondence should be addressed.

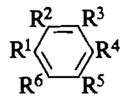

Phloroglucinol units

1 R^1 = —O—, R^2 = R^4 = R^6 = H, R^3 = R^5 = OH
2 R^1 = R^3 = —O—, R^2 = R^4 = R^6 = H, R^5 = OH
3 R^1 = R^3 = R^5 = —O—, R^2 = R^4 = R^6 = H

4 R^1 = R^3 = R^5 = OH, R^2 = —O—, R^4 = R^6 = H
5 R^1 = R^2 = —O—, R^3 = R^5 = OH, R^4 = R^6 = H
6 R^1 = R^3 = OH, R^2 = R^5 = —O—, R^4 = R^6 = H
7 R^1 = R^2 = R^3 = —O—, R^4 = R^6 = H, R^5 = OH
8 R^1 = R^2 = R^5 = —O—, R^3 = OH, R^4 = R^6 = H
9 R^1 = R^2 = R^3 = R^5 = —O—, R^4 = R^6 = H
10 R^1 = R^2 = R^3 = OH, R^4 = R^6 = H, R^5 = —O—

11 R^1 = R^3 = R^5 = OH, R^2 = R^6 = —O—, R^4 = H
12 R^1 = R^2 = R^6 = —O—, R^3 = R^5 = OH, R^4 = H
13 R^1 = R^5 = OH, R^2 = R^3 = R^6 = —O—, R^4 = H
14 R^1 = R^2 = R^3 = R^6 = —O—, R^5 = OH, R^4 = H
15 R^1 = OH, R^2 = R^3 = R^5 = R^6 = —O—, R^4 = H
16 R^1 = R^2 = R^3 = R^5 = R^6 = —O—, R^4 = H
17 R^1 = R^2 = R^3 = OH, R^5 = R^6 = —O—, R^4 = H

18 R^1 = R^3 = R^5 = OH, R^2 = R^4 = R^6 = —O—
19 R^1 = R^2 = R^4 = R^6 = —O—, R^3 = R^5 = OH
20 R^1 = R^2 = R^4 = R^5 = R^6 = —O—, R^3 = OH
21 R^1 = R^2 = R^3 = R^4 = R^5 = R^6 = —O—

Hexahydroxybiphenyl units

22 R^1 = —,* R^2 = R^4 = R^6 = OH, R^3 = R^5 = H
23 R^1 = —, R^2 = —O—, R^3 = R^5 = H, R^4 = R^6 = OH
24 R^1 = —, R^2 = R^6 = OH, R^3 = R^5 = H, R^4 = —O—
25 R^1 = —, R^2 = R^6 = —O—, R^3 = R^5 = H, R^4 = OH
26 R^1 = —, R^2 = R^4 = —O—, R^3 = R^5 = H, R^6 = OH
27 R^1 = —, R^2 = R^4 = R^6 = —O—, R^3 = R^5 = H

28 R^1 = —, R^2 = R^4 = R^6 = OH, R^3 = —O—, R^5 = H
29 R^1 = —, R^2 = R^3 = —O—, R^4 = R^6 = OH, R^5 = H
30 R^1 = —, R^2 = R^6 = OH, R^3 = R^4 = —O—, R^5 = H
31 R^1 = —, R^2 = R^4 = OH, R^3 = R^6 = —O—, R^5 = H
32 R^1 = —, R^2 = R^3 = R^4 = —O—, R^5 = H, R^6 = OH
33 R^1 = —, R^2 = R^3 = R^6 = —O—, R^4 = OH, R^5 = H
34 R^1 = —, R^2 = OH, R^3 = R^4 = R^6 = —O—, R^5 = H
35 R^1 = —, R^2 = R^3 = R^4 = R^6 = —O—, R^5 = H

36 R^1 = —, R^2 = R^4 = R^6 = OH, R^3 = R^5 = —O—
37 R^1 = —, R^2 = R^3 = R^5 = —O—, R^4 = R^6 = OH
38 R^1 = —, R^2 = R^6 = OH, R^3 = R^4 = R^5 = —O—
39 R^1 = —, R^2 = R^3 = R^5 = R^6 = —O—, R^4 = OH
40 R^1 = —, R^2 = R^3 = R^4 = R^5 = —O—, R^6 = OH
41 R^1 = —, R^2 = R^3 = R^4 = R^5 = R^6 = —O—

Ter- and quaterphenyl units

42 R^1 = R^3 = —, R^2 = R^4 = R^6 = OH, R^5 = H
43 R^1 = R^3 = —, R^2 = R^6 = OH, R^4 = —O—, R^5 = H

44 R^1 = R^3 = R^5 = —, R^2 = R^4 = R^6 = OH
45 R^1 = R^3 = R^5 = —, R^2 = —O—, R^4 = R^6 = —OH

*"—" represents a direct (carbon–to–carbon) bond between phloroglucinol-based units. OH is replaced by CH_3CO or OCH_3 for the acetoxy or methoxy derivatives.

Glombitza and co-workers to be units of oligophloroglucinols in certain brown algae (although not *F. vesiculosus*). For structures whose chemical shifts were not available from reference compounds or from the literature, expected chemical shifts were calculated as before (7) using chemical shift substitutent effects derived from appropriate reference compounds. Full details are given in the Supplementary Material.[4] In general, no distinctions were made among different aryl (or aryloxy) substitutents for purposes of chemical shift calculations or symmetry considerations; this assumption was justified by the close similarities shown in substituent effects observed from different phloroglucinol-based substituents (Table 1).

Results

^{13}C nuclear magnetic resonance spectra

The ^{1}H-decoupled broadband ^{13}C nmr spectrum of the native polymer from *F. vesiculosus* (Fig. 1) shows three envelopes of signals which will be referred to as the high-frequency (δ_C 151.5–163.5), mid-frequency (126.0–128.5), and low-frequency (96.0–106.0 ppm) envelopes. Analysis of corresponding signals in the calculated or experimentally derived ^{13}C spectra of model structures **1***a*–**45***a* (Supplementary Material) demonstrates that the high-frequency envelope is composed of resonances from ^{13}C nuclei bearing hydroxy or aryloxy substituents and shielded by no more than one *ortho* oxy substituent (generally 149.3–163.9), and from oxy-substituted carbons shielded by two *ortho* and no *para* oxy substituents (141.6–152.4 ppm). Similarly, the mid-frequency envelope arises from the oxy-substituted carbons shielded by a *para* and two *ortho* oxy substituents, and the low-frequency envelope arises from directly bonded (as in C-1,1′ of biphenyl) and methine carbons shielded by a *para* and two *ortho* oxy substituents. The chemical shift ranges from ^{13}C nuclei in these environments in **1**–**45** and in the MW $>10^4$ polymer, both before and after acetylation or methylation (Table 2), are consistent with the hypothesis that the polymer is composed exclusively of phloroglucinol-based units.

This hypothesis also predicts that the combined integrated intensities I of the mid- (I_M) and low-frequency (I_L) envelopes should equal that of the high-frequency envelope (I_H). Analyses of ^{13}C spectra of the polymer and its acetoxy derivative (Table 3) confirmed these expectations: $I_H/(I_M + I_L)$ was 0.99 $\pm$ 0.01 when averaged over seven experiments designed (see Experimental) to minimize problems arising from differences in spin-lattice relaxation times and nOe.

A further test of the above hypothesis was available from the EDIT experiments. Signals in the mid- and high-frequency envelopes were all removed under conditions which suppressed signals from quaternary and methylene carbons, leaving only the methine carbon signals in the low-frequency envelope unaffected. Conversely, conditions which suppressed methyl and methine carbon resonances removed most of the signals in the low-frequency quaternary carbons (Fig. 1) having chemical shifts similar to those of the directly-bonded quaternary carbons (C-1) in **22**–**45** (see below). The completeness of suppression by the EDIT technique was confirmed by the absence of any residual methine carbon resonances in regions where they did not overlap quaternary carbon resonances. This technique permitted the direct measurement of the integrated in-

[4]The tabulated ^{13}C and ^{1}H chemical shifts for **1**–**45**, and full details of calculations, are available at a nominal charge from the Depository of Unpublished Data, CISTI, National Research Council of Canada, Ottawa, Ont., Canada K1A 0S2.

TABLE 1. Influence of differently substituted substituent

From	To	R = H ipso	ortho	meta	para
—H	-2,4,6-tri(OR)phenyl	+4.4	−1.3 to −1.5	0.0 to +0.2	−0.4 to −0.6
—H	-(2,6-di(OR)-4(2,4,6-tri(OR)-phenoxy)phenyl	+4.1 to +4.2	−1.6 to −1.7	+0.1	−0.4
—H	-3,5-di(OR)phenoxy	+28.3	−7.7	+0.6	−3.9
—H	-3,5-di(OR)-4-(2,4,6-tri(OR)-phenyl)phenoxy	+28.3	−7.6	+0.7	−3.9
—OR	-2,4,6-tri(OR)phenoxy	+2.4	−0.8	+0.2	+1.6
—OR	-4,6-di(OR)-2-(2,4,6-tri(OR)-phenoxy)phenoxy	+2.4	−0.6	+0.2	+1.6

[a]Data from refs. 5, 6, 14. For further details of calculations, see Supplementary Material.

TABLE 2. Chemical shift ranges of ^{13}C signals in spectra of model structures **1−45** and in mol. wt. $>10^4$ polymer from *Fucus vesiculosus*. All data in ppm[a]

	1−45*a*	Native polymer	**1−45***b*	Acetoxy polymer	**1−45***c*	Methoxy polymer
High-frequency envelope						
tri- and tetra-*O*-	149.3−163.9	151.5−163.5	142.0−159.5	142.0−159.5	148.7−161.5	151.0−161.5
penta-*O*-	141.6−152.4	N/O	135.9−148.0	N/O	142.3−150.1	N/O
hexa-*O*-	N/A	—	122.3−143.3	N/O	N/A	—
Mid-frequency envelope	122.1−130.6	126.0−128.5	123.8−140.2	129.0−137.0	122.9−135.6	124.0−131.0
Low-frequency envelope	93.8−101.3	96.0−106.0	99.1−117.6	102.5−119.5	90.1−102.6	90.0−98.0

[a]N/A = shifts not available. N/O = not observed. Chemical shift ranges in polymer rounded to nearest 0.5 ppm. Signals in region from 104.0−121.0 ppm in spectrum of methylated polymer arise from *C*-methylated ring carbons.

tensity ratios I_{LQ}, I_{MQ}, and I_{HQ} of quaternary carbons within each envelope (Table 3).

Because the low-frequency quaternary signals arise from directly bonded carbons (C-1 in **22−45**), and because the high-frequency signals arise from exactly half of all ring carbons in the polymer (above), the proportion p_d of directly bonded units in the polymer may be estimated by $p_d = 100 \times 6I_{LQ}/2I_{HQ} = 52.5 \pm 3.3\%$. This estimate is an upper limit which does not take into consideration the presence of hydroxy ter-, quater-, and polyphenyl units. In order to make this correction, it is necessary to assign signals in the spectra of the polymer in much more detail.

Further details of the composition of the polymer were obtained by comparing chemical shifts (Fig. 1) and integrated intensities (Table 3) from the polymer spectra with those of the model units **1−45**. Chemical shift ranges expected for each type of ^{13}C nucleus in **1−45** already contain, in many cases, allowance for prediction error (for details, see Supplementary Material). Based on extensive experience, we estimate the accuracy of chemical shift comparisons between these model units and known model compounds to be ca. ±0.5 ppm. Thus, in the ensuing discussion, absence of a peak within the expected range, extended by 0.5 ppm on either end, is taken to indicate the absence of the corresponding unit from the polymer.

Using these criteria, 25 units may immediately be ruled out as components of the polymer: **3**, **9−20**, **27**, **29−32**, and **35−41** (Table 4). Unit **2** can be also ruled out because its characteristic ^{1}H nmr signal (**2***b* expected at δ_H 6.46−6.47 ppm) is absent, and **25** because the signal expected for C-1 of **25***b* (104.6−106.0 ppm) is absent from the appropriate EDIT spectrum. Seven further units (**1**, **6**, **7**, **23**, **26**, **33**, and **34**) not eliminated under these criteria are expected to exhibit signals in regions of the spectra where very small signals or tails from larger signals are found; these will be discussed individually below. With one exception (below), all remaining signals can be assigned to one or more of the remaining constituent units as described below.

vic-*Trihydroxylated units*

Absence of signals corresponding to C-2 of **10***a* and **10***c* (Table 4) indicates that **10** is not a component of the polymer, in agreement with results from Ca−NH_3 degradation (9). The *vic*-trihydroxylated unit **17** is discussed below with the other penta-*O*-substituted units.

*Penta-*O*-substituted units*

Absence of signals in the 141.6−151.5 ppm region of the polymer, and in the 142.3−150.1 region of its methoxy derivative, rules out the presence of penta-*O*-substituted units **11−17** and **36−41**. Most resonances from C-1, C-3, C-5 of **11−17**, and from C-2, C-4, C-6 of **36−41**, are expected to occur in these regions, and indeed do so in spectra of the corresponding MW $>10^4$ polyphloroglucinols from the brown algae *Chorda filum*, *Chordaria flagelliformis*, and *Dictyosiphon foeniculaceus* (13). The absence of these units was also indicated by the results from Ca−NH_3 degradation (9).

*Hexa-*O*-substituted units*

Absence of characteristic signals rules out the occurrence of hexa-*O*-substituted units **18−20** as constituents of the polymer (Table 4). The six identical carbons of **21***b* are expected at ca. 130.0−131.4 ppm, although this estimate is perhaps less certain than most due to the necessity of a solvent correction (see Supplementary Material). Although a small signal is apparent at 128−130.1 ppm, it is fully assignable to C-2 of **7***b* and (or) groups on substituent effects (all values in ppm)[a]

R = COCH$_3$				R = CH$_3$			
ipso	*ortho*	*meta*	*para*	*ipso*	*ortho*	*meta*	*para*
+2.6 to +3.4	−1.6 to −2.0	+1.0 to +1.2	−0.4 to −0.8	+12.2	−2.5	−1.6	−1.0
+2.6	−2.0	+1.2	−0.8	+12.4 to +12.5	−2.5	−1.4	−1.9
+23.7	−7.5	+2.3	−4.4	+32.8	−7.9	−1.3	3.9
+23.8	−7.4	+2.4	−4.3	+33.3	−7.7	−1.1	−4.1
+6.9 to +7.1	−5.0 to −5.2	+0.4 to +0.6	−1.9 to −2.3	—	—	—	—
+7.5	−5.6	+0.5	−2.6	—	—	—	—

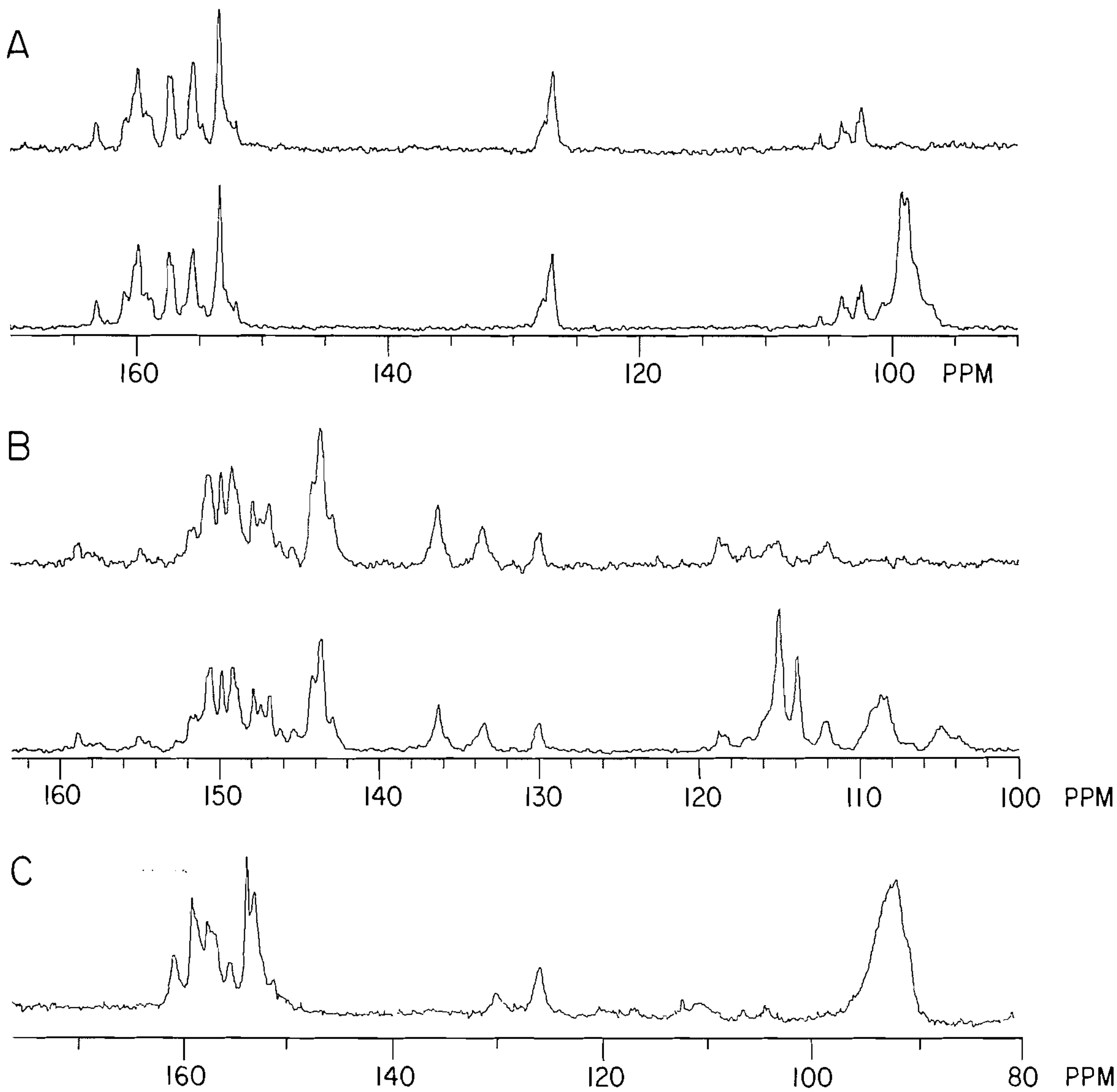

FIG. 1. The ^{13}C nmr spectra of the *Fucus vesiculosus* polymer. (A) Native hydroxy polymer, EDIT: quaternary carbons (above), and full spectrum (below). (B) Acetoxy polymer, EDIT: quaternary carbons (above) and full spectrum (below). (C) Methoxy polymer.

8*b* (below). Better evidence for the absence of **21** comes from integration of the three signal envelopes. The results displayed in Table 1 suggest that all six carbons of **21** will have almost identical chemical shifts, yet the results from signal envelope integration require that half the signals from each unit occur in the high-frequency envelope, and half in the mid- and (or) low-frequency envelopes. Therefore **21** cannot be a significant component of the polymer. This conclusion is reinforced by the absence of penta-*O*-substituted units (above), the lack of evidence from Ca—NH$_3$ degradation for hexa-*O*-substituted units (9), and the absence of precedent among lower-MW oligophloroglucinols for such units (4–7).

TABLE 3. Integrated intensities of ^{13}C spectra of native and acetoxy polymers from *F. vesiculosus*

Native polymer			Acetoxy polymer		
	Average integrated intensity[a]			Average integrated intensity[a]	
δ_C range (ppm)	Broadband decoupled[b]	EDIT[c] (quaternary only)	δ_C range (ppm)	Broadband decoupled[b]	EDIT[c] (quaternary only)
166.0−162.0	0.026	0.022	160.0−157.0	0.023	0.025
162.0−158.0	0.147	0.148	157.0−153.0	0.021	0.021
158.0−156.5	0.074	0.073	153.0−148.3	0.210	0.220
156.5−154.0	0.099	0.088	148.3−145.8	0.093	0.250
154.0−148.0	0.148	0.151	145.8−141.2	0.152	
166.0−148.0	0.494 = I_H	0.482 = I_{HQ}	160.0−141.2	0.499 = I_H	0.516 = I_{HQ}
132.0−122.0	0.099 = I_M	0.111 = I_{MQ}	139.0−134.7	0.040	0.037
			134.7−131.4	0.033	0.027
			131.4−127.5	0.025	0.018
			139.0−127.5	0.098 = I_M	0.082 = I_{MQ}
109.0−104.5	0.006	—	120.0−117.5	0.017	0.018
104.5−103.0	0.028	0.011	117.5−116.2	0.009	0.011
103.0−101.5	0.040	0.030	116.2−114.2	0.131	0.027
101.5− 94.0	0.327	0.046	114.2−112.8	0.057	0.027
109.0− 94.0	0.401 = I_L	0.087 = I_{LQ}	112.8−110.2	0.032	0.005
			110.2−106.1	0.113	—
			106.1−100.0	0.044	—
			120.0−100.0	0.403 = I_L	0.088 = I_{LQ}
Typical error[d]	±0.005	±0.006		±0.005	±0.005
No. of spectra averaged	4	2		3	2

[a]Expressed as a fraction of the total integrated intensity from δ_C 166.0−94.0 (native polymer) or 160.0−100.0 ppm (acetylated polymer). Intensities used in text are from broadband-decoupled spectra, except for low-frequency quaternary signals (from EDIT).
[b]Effects of spin-lattice relaxation and nOe on relative intensity reduced by relaxation reagent (CREN or $Cr(acac)_3$) and use of 2-s delay between acquisitions.
[c]Results scaled so $I_{HQ} + I_{MQ} = I_H + I_M$ for each individual spectrum.
[d]Error shown here is from scatter of results for 2−4 spectra. Error of individual integrations ca. ±0.010 within each range.

Tri-O-substituted units

Units **2**, **3**, and **27** have already been ruled out as possible components of the polymer (Table 4 and above). Signals expected for C-1 and C-4 of **1***b*, and for C-2 of **23***a* and **23***b*, correspond to small peaks or tails of larger peaks which cannot necessarily be attributed to other units. Integration of the 108- to 110.2-ppm region of the EDIT spectrum of the acetoxy polymer (Table 3) indicates a maximum abundance of about 1% for **23** + **26** + **33**. Some indication of the maximum abundance of **1** (plus **2**) may be obtained from the high-frequency region of the spectrum of the methoxy polymer: the signal near 160.9 ppm could arise from C-1, C-3, C-5 of **1***c* and (or) **2***c*, and (or) it could represent C-4 of **22***c* and (or) **24***c*. The signal near 159.0 ppm could arise from twice as many carbons (C-2, C-6) of **22***c* and (or) **24***c*, as well as from C-2 (and perhaps also C-4,6) of the methoxy terphenyl **42***c*. Broadness and confluence of these signals preclude accurate integration, but the 160.9-ppm signal accounts for about 9.5−10% of the integral of the high-frequency envelope, and the 159.0-ppm signal, 22−23%. Correction for the contribution of **42** to the latter (below and Table 5) leaves a minimum of 19−20% corresponding to **22***c* and (or) **24***c*. Thus **22***c* and (or) **24***c* must be responsible for virtually all of the 160.9-ppm signal, and **1***c* and **2***c* must be virtually absent.

With units **1**−**3**, **26**, and **27** absent or negligibly minor, the signal at 163.1 ppm in the spectrum of the native polymer must arise from C-4 of **24***a* (expected: 162.5 ppm), and the signal near 158 ppm in the spectrum of the acetoxy derivative from C-4 of **24***b* (expected: 157.7−158.1 ppm). Repeated integration of these signals indicates an abundance of 14.4 ± 1.1% for **24** (Table 5).

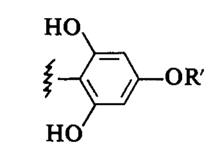

22*a* R′ = H
24*a* R′ = R
(R = phloroglucinol-based unit)

With units **1**, **2**, **23**, **25**, **27** (above), and **43** (below) absent or negligible, the signal at 160.8 ppm in the spectrum of the native polymer must come from C-4 of **22***a* (expected: 160.3 ppm) and most of the integral remaining unaccounted for so far in the 157.9−162.0 ppm region of the spectrum of the methoxy derivative must come from C-4 of **22***c* (expected: 159.8−160.6 ppm); repeated integration and computer-aided deconvolution (using the Nicolet curve-resolution program NMRCAP) of these signals indicate an abundance of 18.6 ± 1.0% for **22** (Table 5).

Several independent checks on these estimates of **22** and **24** are available. The integral of the 158- to 162-ppm region of the spectrum of the methoxy polymer gives an estimate of 28.5−30.0% for **22** + **24** (see above). The integral of the

TABLE 4. Model units ruled out, or demonstrated to be minor constituents, by comparison with polymer spectra. All data in ppm

Unit No.	A. Predicted δ_C incompatible with polymer spectra
2	*b*: C-2 (101.9−102.8); ^{1}H nmr
3	*b*: C-2,4,6 (99.1−100.9)
9	*b*: C-2 (123.8−124.3)
10	*a*: C-1,3 (149.3), C-2 (130.0); *c*: C-2 (134.6)
11	*a*: C-1,5 (148.9−149.2), C-3 (145.0−145.3); *b*: C-1,5 (139.2−139.4), C-2,4 (138.5−139.0); *c*: C-3 (145.9−146.3)
12	*a*: C-1,5 (148.8−149.6), C-3 (147.0−147.7); *b*: C-1,5 (139.6−140.0); *c*: C-3 (143.9−145.5)
13	*a*: C-3 (144.9−145.7), C-4 (128.7−128.9), C-5 (148.8−149.6); *b*: C-5 (139.6−140.0); *c*: C-3 (145.6−146.2)
14	*a*: C-3 (146.9−148.1), C-5 (148.7−150.0); *b*: C-2 (128.1−129.0), C-4 (131.0−132.1), C-5 (140.0−140.6); *c*: C-3 (143.6−145.4)
15	*a*: C-3 (144.8−146.1); *b*: C-2,4 (131.0−132.1); *c*: C-3 (145.3−146.1)
16	*a*: C-3 (146.8−148.5); *b*: C-2,4 (125.8−127.1); *c*: C-3 (143.3−145.3)
17	*a*: C-1 (146.7−146.8), C-2 (125.8), C-3 (141.6), C-4 (130.6), C-5 (145.4); *b*: C-5 (140.0−140.3 or 139.3−139.6); *c*: C-1 (144.6−144.8), C-3 (146.0−146.2)
18	*b*: C-1,3,5 (122.3−123.1)
19	*b*: C-2,6 (137.5−138.3), C-3,5 (122.7−123.7), C-4 (140.4−141.4)
20	*b*: C-3 (123.1−124.3)
21	See text
25	*b*: C-1 (104.6−106.0) (EDIT spectrum), C-2,6 (155.5−157.1)
27	*b*: C-3,5 (100.7−102.1), C-2,6 (155.9−157.7)
29	*b*: C-1 (112.8−113.2)
30	*a*: C-1 (104.8), C-3 (124.3−126.4); *b*: C-3 (131.4−131.7), C-5 (110.6−111.2)
31	*a*: C-3 (128.1−128.4); *b*: C-1 (112.8−113.2), C-3 (134.3−134.8); *c*: C-5 (110.6−111.2)
32	*a*: C-3 (122.1−126.6); *b*: C-1 (110.5−111.3), C-3 (126.2−126.7); *c*: C-2 (149.0−150.6)
35	*b*: C-3 (123.9−124.8), C-6 (152.7−153.4); *c*: C-2 (148.7−150.5)
36	*a*: C-2,6 (147.4−147.9), C-4 (144.4−144.9); *b*: C-1 (119.9−121.0), C-2,6 (137.2−137.8), C-3,5 (139.5−140.2); *c*: C-1 (102.4−103.0), C-2,6 (147.2−147.6), C-3,5 (122.9−123.6), C-4 (144.9−145.3)
37	*a*: C-2 (149.4−150.3), C-4 (144.3−145.3), C-6 (147.3−148.3); *b*: C-5 (137.2−138.3), C-6 (137.6−138.4); *c*: C-2 (145.2−146.8), C-4 (144.6−145.2), C-6 (146.9−147.5)
38	*a*: C-2,6 (147.3−148.3), C-4 (146.4−147.3); *b*: C-2,6 (137.6−138.4); *c*: C-2,6 (146.9−147.5), C-4 (142.9−144.5)
39	*a*: C-2,6 (149.3−150.7), C-4 (144.2−145.7); *c*: C-2,6 (144.9−146.7), C-4 (144.3−145.1)
40	*a*: C-2 (149.3−150.7), C-4 (146.3−147.7), C-6 (147.2−148.7); *b*: C-6 (138.0−139.0); *c*: C-2 (144.9−146.7), C-4 (142.6−144.4), C-6 (146.6−147.4)
41	*a*: C-2,6 (149.2−151.1), C-4 (146.2−148.1); *b*: C-3,5 (126.8−128.3); *c*: C-2,6 (144.6−146.6), C-4 (142.3−144.3)
	B. Predicted δ_C in regions of very small signals, or of tails from larger signals. For individual consideration, see text
1	*b*: C-1 (157.1−158.1), C-4 (110.2−110.5)
23	*a*: C-2 (161.0−161.6); *b*: C-2 (155.1−156.5)
26	*a*: C-2 (161.1−162.2); *b*: C-2 (156.3−157.3), C-4 (157.5−158.7)
33	*b*: C-6 (152.3−152.8); *c*: C-2 (149.0−150.6)
34	*b*: C-1 (110.5−111.3)

TABLE 5. Abundances of constituent units as estimated from ^{13}C nuclear magnetic resonance

Unit(s) No.	Abundance (%)		Number of branching points
1[a]	Trace?		0
4[a] + **6**	13.5 ± 3.8		0
5	19.8 ± 2.0	51.9 ± 3.6[b]	0
7 + **8**	15.0 ± 2.1		1
22[a]	18.6 ± 1.0		0
24	14.4 ± 1.1		0
28	10.5 ± 0.8		0
23 + **26** + **33**	<1		0, 1, 2
34	Trace?		2
42	3.7 ± 1.0		0
44	2.5 ± 0.5		1
43 + **45**	<2		1, 2
Unknown[c]	<2?		?
	(101.6 ± 8.0) + (<5)		

[a]Terminal units.
[b]Mean of four estimates (see text); **4**, maximum 3.4%.
[c]δ_C 105.5 ppm signal in native polymer spectrum (see text).

101.5- to 103.0-ppm region of the EDIT spectrum of the native polymer (Table 3) suggests an abundance of 18.0 ± 4.0% for **22**, although this estimate is complicated by the possible contribution of hydroxy polyphenyl units near this region. Finally, the integral of the 110.2- to 116.2-ppm region of the EDIT spectrum of the acetoxy polymer (Table 3) corresponds to an abundance of 35.4 ± 3.0% for units **22**, **24**, **34**, **43**, and **45**, in good agreement with the above estimate of 33.0 ± 2.1% for **22** + **24** and suggesting that units **34**, **43**, and **45** are at best minor components.

*Directly bonded tetra-*O*-substituted units*

Only one individual tetra-*O*-substituted unit can be readily identified from the ^{13}C nmr spectra: the signal at 118.2–118.5 ppm in the spectrum of the acetoxy polymer is characteristic of **28***b* (C-1 expected: 118.0–118.2 ppm), and integrates (Table 3) for an abundance of 10.5 ± 0.8%. Two other characteristic signals from this unit, those for C-2 of **28***a* (151.9, expected 151.4–151.6 ppm) and C-6 of **28***b* (145.2, expected 145.0–145.1 ppm), are not well resolved from larger neighboring signals, but integrals and computer-aided curve resolution indicate an abundance of 9.2 ± 1.5%.

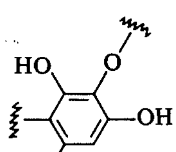

28*a*

All other directly bonded tetra-*O*-substituted units have already been ruled out (**29**–**32** and **35**, above), or have been shown to be present in only trace amounts (**33** and **34**, above). Further confirmation of the low abundance of **33** and **34** may be inferred from the abundances of the corresponding non-phenoxylated units **25** and **26** (zero and <1%, respectively), from the lack of evidence from Ca–NH_3 degradation for **29**–**35** (9), and from the lack of precedent among known lower-MW polyphloroglucinols (4–7) for such structures in brown algae.

Hydroxy polyphenyl units

The ratio $6I_{LQ}/2I_{HQ}$ from EDITed ^{13}C nmr spectra (above) places a maximum (uncorrected) limit of 52.5 ± 3.3% on the abundance of directly bonded units in the polymer. Units **22**, **24**, and **28** have already accounted for 43.5 ± 2.9%, and **23**, **26**, **33**, and **34** for perhaps another 1%, leaving at most ca. 8.0 ± 6.2% (uncorrected) for hydroxyl polyphenyl units such as **42**–**45**. An estimate of **44** can be made from the integral of the small signal at 146.2 ppm in the acetoxy polymer spectrum (C-2,4,6 expected: 146.4–146.8 ppm), which indicates an abundance of 2.5 ± 0.5%, other units with resonances in this region having been eliminated or otherwise accounted for. Unit **42** exhibits only one characteristic ^{13}C nmr signal, at ca.

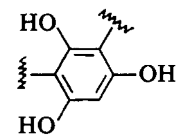

42*a*

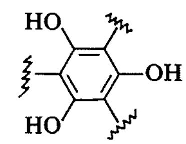

44*a*

117 ppm in the acetoxy polymer EDIT spectrum. Integration and curve resolution yields 3.7 ± 1.0% for **42** (Table 3), but again the poor baseline and small, partially confluent signals in this region make this estimate questionable. These levels of **42** and **44** agree well, however, with the results from Ca–NH_3 degradation (9). Units **43** and **45** therefore probably amount to <2%.

The estimated abundance of directly bonded units can now be corrected for the presence of polyphenyl units: (52.5 ± 3.3) – (4/18)(3.7) – (6/24)(2.5) = 51.1 ± 3.5%. This estimate, which is again an upper limit, stands in good agreement with the sum of **22**, **24**, **28**, **33**, **34**, and **42**–**45** = ca. 49.7 ± 4.4% (Table 5). The difference, if real, may reflect the presence of small quantities of polyphenyl units other than **42**–**45**. In this regard it is interesting that the small signal at 105.5 ppm in the spectrum of the native polymer could not be assigned; it remained after suppression of ^{13}C—H resonances by the EDIT procedure, and presumably arises from C-1 of a minor unit (<2% abundance) having substituents or experiencing deshielding not considered here.

*Remaining tetra-*O*-substituted units*

The ca. 48.9 ± 3.5% of the units of the polymer which so far has not been considered are the tetra-*O*-substituted, entirely ether-linked structures **4**, **5**, **8**, and possibly **6** and **7** (Table 4). Four independent estimates of the abundance of these units are available: two (a and b) are direct, while two (c and d) require the absence of penta- and hexa-*O*-substituted units and supernumerary hydroxylation: (a) the integral of the 156.2- to 157.9-ppm region of the methoxy polymer spectrum (C-5 of **4***c*–**8***c*, corrected for C-2,4,6 of **44***c*) indicates an abundance

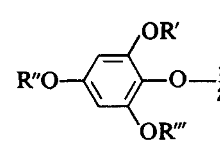

	R′	R″	R‴
4*a*	H	H	H
5*a*	R	H	H
6*a*	H	R	H
7*a*	R	H	R
8*a*	R	R	H

(R = phloroglucinol-based unit)

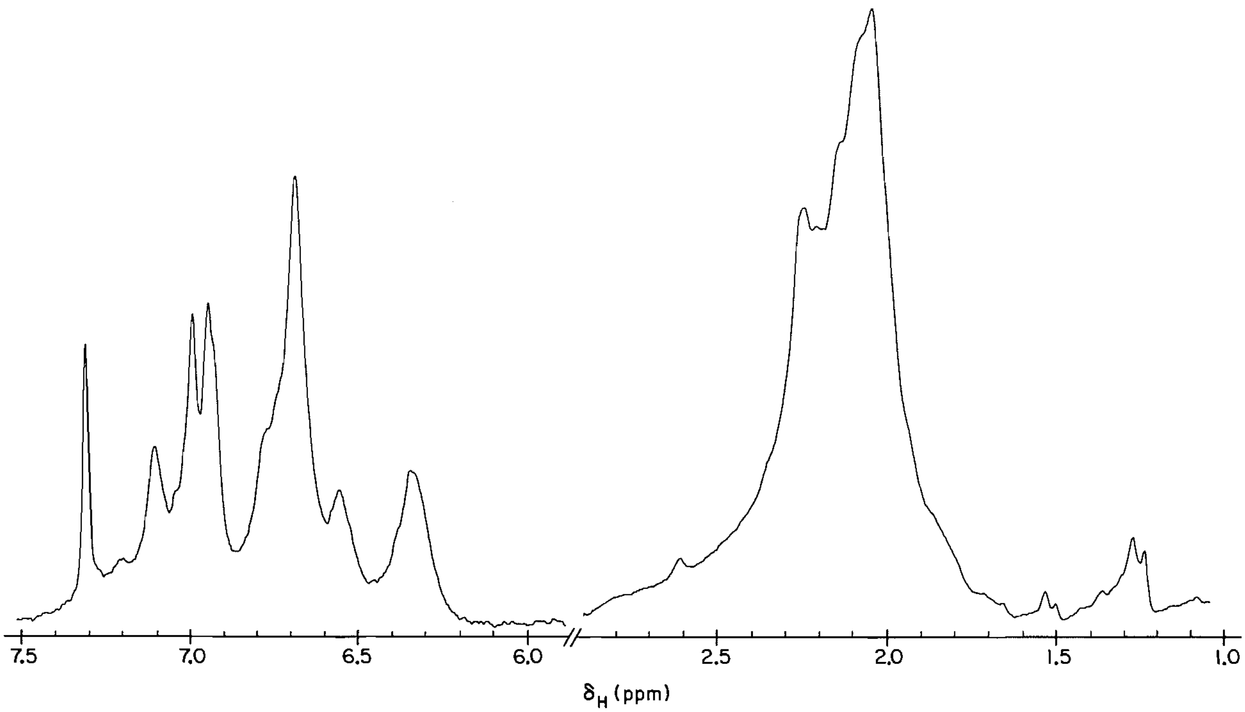

FIG. 2. The ^{1}H nmr spectrum of acetoxy polymer from *Fucus vesiculosus*.

of 53.7 ± 6.0% for **4**–**8**; (b) the integral of the 127.5- to 139.0-ppm region of the broadband-decoupled acetoxy polymer spectrum (Table 3; C-2 of **4***b*–**8***b*, possibly including small amounts of C-3 from **33***b* and **34***b*, and corrected for C-3 of **28***b*) indicates an abundance of 48.3 ± 3.8% for **4**–**8**; (c) from the integrals of the acetoxy methyl, acetoxy carbonyl, and methoxy ^{13}C nuclei in spectra of the acetoxy and methoxy polymer, there are 2.40 ± 0.07 derivatizable hydroxyls per unit in the native polymer, hence (after correction for **28**) 52 ± 7% of entirely ether-linked units; and (d) from the ratio of derivatizable hydroxyls to aromatic protons as determined by ^{1}H nmr, graphical analysis based on model compounds demonstrates that 53.5 ± 2.5% (corrected for **28**) of all units are entirely ether linked. These results (mean, 51.9 ± 3.6%) agree well with abundances of fragments present in the Ca–NH_3 degradation product of the methoxy polymer (9). Consideration of units **4**–**8** will therefore complete the roster of units allowable as components of the polymer.

Accurate assignment of the three signals in the mid-frequency region of the broadband-decoupled spectrum of the acetoxy polymer is crucial to a more detailed quantitative analysis of individual units **4**–**8**. The signal at 129.9 ppm clearly arises from C-2 of **7***b* (expected: 125.8–128.4 ppm) and **8***b* (expected: 129.0–129.3), as these are the only remaining possibilities (C-3 of **33***b* and **34***b*, expected at 129.1–129.8 ppm, may contribute slightly to this signal). The integral of this signal (Table 3) suggests an abundance of 15.0 ± 2.1% for these units; this may be a slight underestimate due to the presence of tails on this signal. The central signal, at 133.3 ppm, arises from C-2 of **5***b* (19.8 ± 2.0%; expected: 131.0–133.4 ppm), while the signal at 136.1 ppm (corresponding to 24.0 ± 3.0%) is due to C-2 of **4***b* (expected: 136.3–136.8 ppm) and C-3 of **28***b* (expected: 136.6–136.7 ppm).

Problems arise with C-2 of **6***b*, if present (Table 4). Its resonance is expected at 134.2–134.6 ppm, between the 133.3 and 136.1 peaks but slightly closer to the former. If it is assumed to be absent or to contribute to the 133.3-ppm signal, the 136.1-ppm peak would therefore arise entirely from **4***b* and **28***b*, and the abundance of **4** could be calculated by difference as 13.5 ± 3.8%. This is not possible for the following reason (see Discussion): in a large polymer, the proportion of terminal units cannot exceed the proportion of branching points. Here, the proportion of branching points (**7**, **8**, **43**–**45**, and perhaps some minor units: Table 5) is only ca. 22% at most, and the terminal unit **22** (18.6 ± 1.0%) already accounts for most of this. Therefore **4** can constitute at most 3.4% of the polymer, requiring that C-2 of **6***b* contribute to the 136.1-ppm signal in the spectrum of the acetoxy polymer and yielding 13.5 ± 3.8% for **4***b* + **6***b*.

With C-2 of **6***b* assigned to the 136.1-ppm signal, the integral of the 133.3-ppm peak, corresponding to 19.8 ± 2.0%, can be assigned entirely to **5***b*, a unit already encountered in a tetrameric phloroglucinol isolated earlier from *F. vesiculosus* (7). Further attempts to estimate **4** independently of **6**, and **7** independently of **8**, are subject to considerable uncertainty.

^{1}H nuclear magnetic resonance spectra

The ^{1}H nmr spectrum of the native polymer was recorded in H_2O (containing a small amount of D_2O) using selective gated saturation to suppress the solvent signal. Aromatic proton resonances appeared as a broad envelope (δ_H ca. 5.65–6.65 ppm) with poorly resolved maxima at ca. 6.11, 6.18–6.21, and 6.28 ppm. No signals attributable to the polymer were observed outside this region. When DMSO-$^2H_6$ was employed as solvent, the signals from the polymer were still very broad, but suggested a ratio of hydroxy to aromatic protons of ca. 1.55:1. After methylation of the polymer, the aromatic protons resonated in a broad envelope between ca. 5.60–6.75 ppm, with poorly resolved maxima at ca. 6.15 and 6.18 ppm; *O*-methyl protons were seen between ca. 3.00 and 4.20, with poorly resolved maxima at 3.63 and 3.74 and with a minor downfield tail extending beyond 4.50 ppm, and with the ratio of *O*-methyl

TABLE 6. Comparison of abundances of constituent units as estimated from ^{1}H and ^{13}C nuclear magnetic resonance

Unit(s) No.[a]	Abundance (^{1}H nmr)[b]	Abundance (^{13}C nmr)[c]
4 + **6** + **22** + **24**	45.7	46.5 ± 5.9
5	18.6	19.8 ± 2.0
7	16.5	<17.1
28	15.1	10.5 ± 0.8
42	4.1	3.7 ± 1.0
	100.0	<97.6 ± 9.7

[a]Units grouped as required by spectra.
[b]Values normalized assuming presence of only **4**–**7**, **22**, **24**, **28**, and **42**. Individual estimates in this column will therefore tend to be overestimates: see text. For estimate of error, see text.
[c]Values from Table 5.

groups to aromatic protons ca. 1.4:1. A small signal probably arising from *C*-methyl protons (introduced during the methylation procedure) occurred at 1.26 ppm. Little other information could be gleaned from these spectra because the resonances were broad and poorly resolved.

Aromatic protons in the acetoxy polymer, however, yielded relatively well-resolved signals (Fig. 2) which could be assigned by comparison with reference compounds (Supplementary Material). Because some units contain no aromatic protons (e.g. **44**, **45**) and because reference spectra were not available for others (most importantly **8***b*), quantitation of constituent units based on ^{1}H nmr could be only approximately (to within perhaps ±15% overall) congruent with quantitation based on ^{13}C nmr. Nonetheless, a similar quantitative picture emerged (Table 6). Tentative assignments are: δ_H 6.34 (**7***b*), 6.56 (H-6 of **5***b*), 6.69 (**6***b* and **24***b*), 6.78 (H-4 of **5***b*), 6.94 (**4***b*), 6.99 (**22***b*), 7.10 (**28***b*), and 7.20 ppm (**42***b*). Unit **2***b* (H-2 expected: 6.46–6.47 ppm) was absent.

Discussion

Some conclusions about the structure of the polymer can be drawn from the proportions of constituent units (Table 5). As mentioned earlier, in a sufficiently large polymer the proportion of terminal units cannot exceed the proportion of branching points. The proportion of branching points in the *F. vesiculosus* polymer cannot be determined exactly, but units contributing one branch point each (**7**, **8**, **26**, **43**, **44**) constitute about 17–18% of the units of the polymer, and units contributing two branch points (**33**, **34**, and **45**) add an indeterminate but small amount (Table 5). Even considering the possibility that the unidentified unit having C-1 at 105.5 ppm in the native polymer spectrum could hypothetically contribute a few percent more branching points, it is difficult to imagine that the total proportion of branching points could exceed about 22% on a per-unit basis. This is almost certainly completely matched by the abundances of the terminal units **22** (18.6 ± 1.0%), **4** (maximum 3.4%), and **1** if present. Physical properties of the polymer in solution make it extremely unlikely that any large interlocking or cross-linked rings of units occur, as there is no indication that the polymer or its derivatives form gels or viscoelastic solutions at any concentration in a variety of solvents; moreover, the native polymer is extremely soluble (>1 g mL^{-1} H_2O).

The 18.6 ± 1.0% abundance of **22** immediately requires that most of the directly bonded units in the polymer occur in

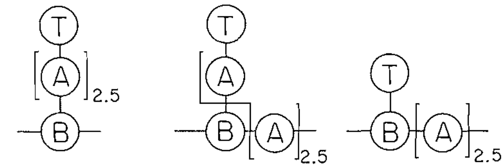

FIG. 3. Three possible average substructures (ignoring minor units) of the *Fucus vesiculosus* polymer. A = **5**, **6**, **24**, **28**, or **42**; B = **7**, **8**, **43**, **44**, or **45**; T = **4** or **22**.

terminal bi- or polyphenyl groups. The minimum proportion of such units would occur if all units **43**–**45** were internal, were directly bonded to a maximum number (**43** and **44**, one; **45**, two) of unit **22** each, and if no **22** was linked to any **42**; the maximum proportion would be found if all **22** and **42** contributed to terminal groups. These estimates, respectively, correspond to 54% to 82% of all directly bonded units being present in terminal bi- or polyphenyl groups, in qualitative agreement with results from Ca–NH_3 degradation (9). The corresponding estimate for terminal ether-linked units (**4**) is ca. 5–10%.

The existence of ca. 22% terminal (T) and ca. 22% branching (B) units (neglecting, for the moment, units **33**, **34**, and **45**) implies that on average there are (100 − 2(22) = 56)/22 = ca. 2.5 non-branching, non-terminal units for every terminus and every branch point. This situation corresponds to the "average" polymer substructures depicted in Fig. 3. If any regularity occurs in the structure of the polymer, it is only over a large scale, as may be deduced from the relatively low intensity of some signals and from the large number (≈65) of distinct aromatic ^{13}C resonances in the high-field (8.45 T) spectrum. The evidence points to the *F. vesiculosus* high-MW polyphloroglucinol fraction containing topologically linear polymers with numerous short branches, many of which terminate in hydroxy bi- or polyphenyl groups.

The occurrence, in approximately equivalent amounts, of directly bonded and exclusively ether-linked units establishes the *F. vesiculosus* polymer as distinct from the entirely ether-linked type found in *Chorda filum*, *Chordaria flagelliformis*, and *Dictyosiphon foeniculaceus*, and equally distinct from the almost exclusively carbon–carbon bonded type in *Pilayella littoralis* and *Spongonema tomentosum* (13). The absence of numerous potential candidate units from all of these polymers, the nonrandom distribution of ether-linked and directly bonded units within the *F. vesiculosus* polymer, the existence of different structural types of polymers within the brown algae, and the apparent correlation of these structural types with taxonomic position (13) strongly suggest that these polymers are produced by a nonrandomly directed assembly of smaller moieties.

Acknowledgements

We thank our colleagues J. S. Craigie, M. Falk, and C. Masson for helpful advice. The 90.80-MHz ^{13}C nmr spectra were recorded on the Nicolet 360 NB spectrometer of the Atlantic Region Magnetic Resonance Centre, Dalhousie University, Halifax.

1. A. HAUG and B. LARSEN. Acta Chem. Scand. **12**, 650 (1958).
2. M. A. RAGAN and A. JENSEN. J. Exp. Mar. Biol. Ecol. **34**, 245 (1978).
3. J. A. GIESELMAN and O. J. MCCONNELL. J. Chem. Ecol. **7**, 1115 (1981).

4. K.-W. GLOMBITZA. *In* Marine algae in pharmaceutical science. *Edited by* H. A. Hoppe, T. Levring, and Y. Tanaka. Walter de Gruyter, Berlin. 1979. pp. 303–342.
5. M. A. RAGAN. Ph.D. thesis, Dalhousie University, Halifax, 1976.
6. M. A. RAGAN and J. S. CRAIGIE. Can. J. Biochem. **54**, 66 (1976).
7. J. S. CRAIGIE, A. G. MCINNES, M. A. RAGAN, and J. A. WALTER. Can. J. Chem. **55**, 1575 (1977).
8. M. A. RAGAN, O. SMIDSRØD, and B. LARSEN. Mar. Chem. **7**, 265 (1979).
9. M. A. RAGAN. Can. J. Chem. **63**, 294 (1985).
10. A. J. FATIADI and W. F. SAGER. Org. Synth. Coll. Vol. 5, 595 (1973).
11. R. FREEMAN, H. D. W. HILL, and R. KAPTEIN. J. Magn. Reson. **7**, 327 (1972).
12. M. R. BENDALL, D. M. DODDRELL, and D. T. PEGG. J. Am. Chem. Soc. **103**, 4603 (1981).
13. A. G. MCINNES, M. A. RAGAN, D. G. SMITH, and J. A. WALTER. Proc. Int. Seaweed Symp. **11**, 597 (1984).
14. M. A. RAGAN. Can. J. Chem. **63**, 291 (1985).

Cyclotetraphosph(III)azanes: donor properties and ylide formation

KEITH D. GALLICANO AND NORMAN L. PADDOCK
Department of Chemistry, University of British Columbia, 2036 Main Mall, Vancouver, B.C., Canada V6T 1Y6

Received March 26, 1984

KEITH D. GALLICANO and NORMAN L. PADDOCK. Can. J. Chem. **63**, 314 (1985).

The ligand $(MeNPMe)_4$ (L) forms complexes $(L.CoCl^+)_2CoCl_4^{2-}$, $(L.CoCl)^+BPh_4^-$, $L.M(CO)_3$ (M = Cr, Mo, W, Mn^+), and a nickel complex $L.Ni_2(CO)_3$, which is easily oxidised to the phosphonimide $[MeNP(O)Me]_4$. Quaternary complexes $[LM(CO)_3R]^+I^-$ have been prepared both by quaternisation of the neutral complex (R = Me, CH_2CN, $CH_2C(O)NH_2$, M = Cr, Mo, W) and (R = Me) by reaction of the simple quaternary with the metal carbonyl. The quaternary complexes have been deprotonated to ylidic complexes, $L.M(CO)_3CH_2$ (M = Mo, W) in which the ylidic group has displaced one phosphine function. Chemical and structural features are discussed in terms of *d*-orbital contraction by acceptor groups. The phosphazane $(MeNPPh)_4$ has been prepared.

KEITH D. GALLICANO et NORMAN L. PADDOCK. Can. J. Chem. **63**, 314 (1985).

Le ligand $(MeNPMe)_4$ (L) forme des complexes $(L.CoCl^+)_2CoCl_4^{2-}$, $(L.CoCl)^+BPh_4^-$, $L.M(CO)_3$ (M = Cr, Mo, W, Mn^+) et un complexe de nickel $L.Ni_2(CO)_3$, qui s'oxyde facilement en phosphonimide de $[MeNP(O)Me]_4$. On a préparé des complexes quaternaires du type $[LM(CO)_3R]^+I^-$ soit par quaternisation du complexe neutre (R = Me, CH_2CN, $CH_2C(O)NH_2$, M = Cr, Mo, W) et (R = Me) ou par réaction du dérivé quaternaire simple avec le métal carbonyle. On a déprotoné les complexes quaternaires afin d'obtenir les complexes d'ylides, $L.M(CO)_3CH_2$ (M = Mo, W) dans lesquels le groupe ylide a remplacé une fonction phosphine. On discute des caractéristiques chimiques et structurales en fonction d'une contraction des orbitales *d* par les groupes accepteurs. On a également préparé le phosphazane $(MeNPPh)_4$.

[Traduit par le journal]

Introduction

The chemistry of the cyclic phosphazanes $(R'NPR)_n$, recently reviewed by Keat (1), was significantly extended in 1977 by the synthesis of the tetrameric phosphazanes **1** (n = 4, R' = Me; *a*, *b*, R = Me, Et) by Zeiss and co-workers (2). The compound **1***a*, which has a crown conformation (2) similar to that of S_8, adds sulphur to give the trisulphide $(MeNPMe)_4S_3$ (3), forms new heterocyclic systems with acetylenes (4), and is quaternised by methyl iodide (**2***a*) (5). All the reactions, like that of **1***a* with $Mo(CO)_6$ (6), have special points of interest. This paper extends the study of the reactions of cyclotetraphosphazanes with acceptors, and describes the formation of ylidic metal carbonyl derivatives. The principal compounds referred to are illustrated in Fig. 1.

Experimental

All reactions and manipulations of air-sensitive products were carried out in an atmosphere of dry nitrogen. Solvents were distilled before use: tetrahydrofuran (THF) and toluene from sodium/benzophenone, acetonitrile from calcium hydride, and dimethylformamide (DMF) from potassium hydroxide.[1] In a typical photolysis experiment, the reaction mixture, in a silica vessel, was irradiated at a distance of 10–13 cm by a 450 W Hanovia mercury vapour lamp placed inside a quartz water-cooled jacket.

Infrared spectra, calibrated against polystyrene, were obtained from Nujol mulls on CsI plates using a Perkin Elmer 457 spectrophotometer. Mass spectra were recorded at 70 eV on a Varian (Atlas) CH4-B mass spectrometer. Nuclear magnetic resonance spectra were run on Varian XL-100 (^1H, 100 MHz; ^{31}P, 40.5 MHz) and Bruker WH-400 (^1H, 400 MHz) spectrometers. Positive chemical shifts are to low field of reference. Conductance measurements were made with a Wayne Kerr bridge Model B221A on solutions in nitromethane or water, concentrations near 10^{-3} *M*. Abbreviations: b, broad; m, medium; sh, sharp; shl, shoulder; st, strong; v, very; w, weak.

N-*Tetramethyl*-P-*tetraphenylcyclotetraphosph(III)azane* (**1***c*)

Phenyldichlorophosphine (10.73 g, 0.06 mol), purified by distillation over $AlCl_3$, was dissolved in 10 mL CH_3CN and added to heptamethyldisilazane (10.5 g, 0.06 mol). The mixture was heated under reflux with stirring for 3 h. Colourless crystals of **1***c* precipitated from the cooled reaction mixture, and were crystallised from chloroform; yield 15%, mp (decom.) 270–275°C. δ_P($CDCl_3$, ext. H_3PO_4) 107.6 ppm; δ_H($CDCl_3$, int. TMS) 3.18 (12H, NMe, multiplet), 7.4–7.7 (20 H PPh, multiplet). Major peaks in the mass spectrum: *m/e* 548 (M^+), 471 $(M - Ph)^+$, 411 $(MeNPPh)_3^+$, 274 $(MeNPPh)_2^+$, 197 $[PhP(NMe)_2P]^+$ (base peak). *Anal.* calcd. for $C_{28}H_{32}N_4P_4$: C 61.3, H 5.9, N 10.2; found: C 60.9, H 5.9, N 10.2.

Quaternisation reactions

Bromoacetophenone (0.131 g, 0.00066 mol) in 5 mL THF was added dropwise to **1***a* (0.097 g, 0.00032 mol) in 15 mL THF. After 1–5 min a heavy white precipitate formed, which was filtered off after stirring for 2 h at room temp. The hygroscopic solid was washed with 2 × 4 mL THF to give analytically pure $[(MeNPMe)_4CH_2C(O)Ph]^+Br^-$ (**2***b*) yield about 50% mp (decom.) 118–125°C under N_2. ν(C═O) 1678 cm^{-1}. *Anal.* calcd. for $C_{10}H_{31}BrN_4OP_4$: C 38.5, H 6.3, N 11.2, Br 16.0; found, C 38.4; H 6.4, N 11.0, Br 15.9. In a similar reaction of **1***a* with iodoacetamide, a 50% yield of $[(MeNPMe)_4CH_2C(O)NH_2]^+I^-$ (**2***c*) was obtained as a very hygroscopic solid, mp (decom.) 140–146°C under N_2 to a yellow liquid. *Anal.* calcd. for $C_{10}H_{28}IN_5OP_4$: C 24.8, H 5.8, N 14.4, I 26.2; found: C 24.9, H 5.8, N 14.2, I 26.0. The quaternary tetraphenylborate, from **2***a* and sodium tetraphenylborate in THF, was hydrolysed in damp air to bis(dimethylamino)dimethylphosphonium tetraphenylborate $[(MeNH)_2PMe_2]^+BPh_4^-$, δ_P($(CD_3)_2CO$, ext. H_3PO_4) + 53.7 ppm.[2] *Anal.* calcd. for $C_{28}H_{34}BN_2P$: C 76.4, H 7.8, N 6.4; found: C 76.1, H 7.8, N 6.4.

Complex formation with Co(II)

If a dilute solution of $CoCl_2$ in CH_3CN is added slowly to **1***a* in CH_3CN, an orange colour develops. If $CoCl_2$: **1***a* > 1.0, the green complex $[(MeNPMe)_4CoCl^+]_2CoCl_4^{2-}$ (**3***a*) is formed. **1***a* (0.115 g, 0.00038 mol) and $CoCl_2$ (0.100 g, 0.00077 mol) were dissolved in 5 mL hot acetonitrile, a green precipitate being formed immediately. The mixture was heated to boiling for 30 min, filtered, and the bright green product **3***a* washed with 2 × 5 mL CH_3CN (0.175 g, 93%, mp (decom.) > 270°C). ν[CoCl(in $CoCl_4^{2-}$)] (cm^{-1}) 311 (st), 298 (m).[3]

---

[1] Nitromethane was purified on an alumina column, dried over P_2O_5, and stored over molecular sieves.

[2] Cf. +54 ppm for $[Me_2N(NH_2)PMe_2]^+Cl^-$ (7).

[3] It is insoluble in organic solvents, but soluble in water, in which the anion (only) is hydrolysed.

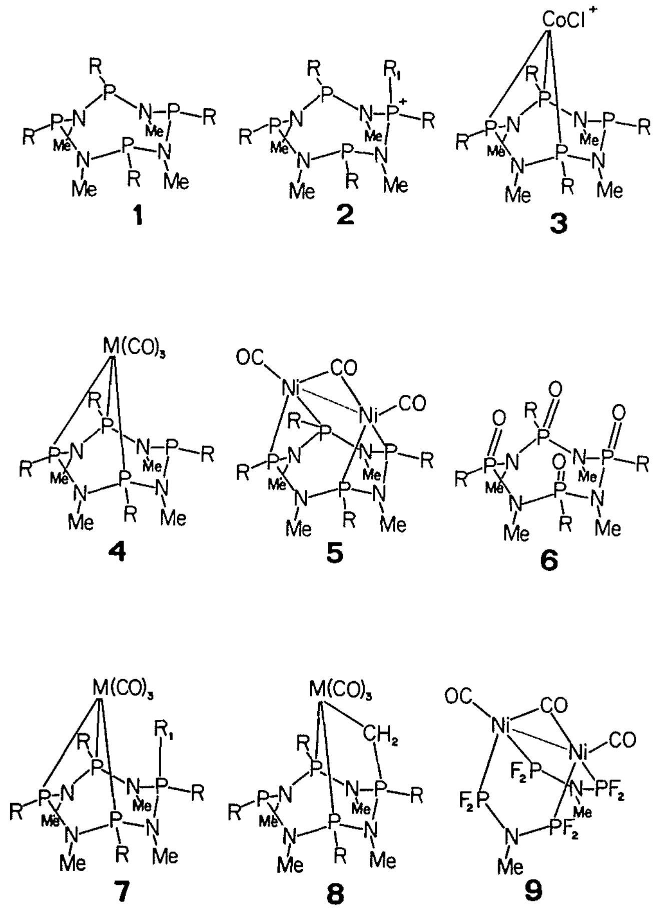

FIG. 1. **1**, *a*, R = Me; *b*, Et; *c*, Ph. **2**. R = Me: *a*, R_1 = Me; *b*, $PhC(O)CH_2$; *c*, $NH_2C(O)CH_2$. Anion I^- except **2***b*, Br^-. **3**, R = Me. **4**, R = Me: *a*, M = Mo; *b*, W; *c*, Cr; *e*, Mn^+ (anion Br^-); *f*, Mn^+ (anion $Mo(CO)_5^-$); *d*, R = Et, M = Mo. **5**, **6**, R = Me. **7**, anion I^-, R = Me for all, R_1 = Me: *a*, M = Mo; *b*, W; *c*, Cr; *d*, R_1 = $NH_2C(O)CH_2$, M = Cr; *e*, R_1 = $NCCH_2$, M = Cr; **8**, R = Me: *a*, M = Mo; *b*, W. **9**, adapted from ref. 16.

Anal. calcd. for $C_{16}H_{48}Cl_6Co_3N_8P_8$: C 19.4, H 4.9, N 11.3, Cl 21.5; found: C 19.7, H 4.9, N 11.3, Cl 21.4. On exposure to air, **3***a* forms a dihydrate. *Anal.* calcd. for $C_{16}H_{52}Cl_6Co_3N_8O_2P_8$: C 18.7, H 5.1, N 10.9; found: C 18.7, H 5.0, N 10.7. The tetraphenylborate $[(MeNPMe)_4CoCl]^+BPh_4^-$ (**3***b*) was precipitated as a lilac–green solid from an aqueous solution of **3***a* by the addition of $NaBPh_4$ and crystallised as needles from CH_3CN, mp (decom.) 225–270°C. It is soluble in DMF and $MeNO_2$; Λ_m ($MeNO_2$, 25°C) 68.8 ohm^{-1} cm^2 mol^{-1}. Its visible spectrum shows a strong charge transfer band at 386 nm (ϵ_{max} ~ 3600) and a broad band centred at ~672 nm. ν(Co—Cl) was not observed. *Anal.* calcd. for $C_{32}H_{44}BClCoN_4P_4$: C 53.8, H 6.2, N 7.9, Cl 5.0; found: C 53.6, H 6.3, N 7.8, Cl 4.8.

Reactions of **1***a*, **1***b with metal carbonyls*

The preparation of $(MeNPMe)_4Mo(CO)_3$ (**4***a*), already described (6), is better done photochemically in either THF or acetonitrile at 65°C (3 h for 200 mg of **1***a*) as described below for the tungsten complex. **1***a* (0.13 g, 0.00043 mol) and $W(CO)_6$ (0.154 g, 0.00044 mol) were dissolved in 15 mL hot, oxygen-free CH_3CN and irradiated at 60°C for 1 h. After a further 30 min at room temperature, yellow crystals appeared. The mixture was cooled to −30°C, and the crystals of $(MeNPMe)_4W(CO)_3$ (**4***b*) filtered off and washed with boiling CH_3CN; mp (decom.) >250°C, ν(C≡O) (cm^{-1}) 1922, sh; 1816 (side bands at 1775, 1848). The mass spectrum shows the parent ion at *m*/*e* 568 and stepwise loss of three CO groups. *Anal.* calcd. for $C_{11}H_{24}N_4O_3P_4W$: C 23.3, H 4.3, N 9.9; found: C 23.2, H 4.3, N 10.0. The chromium complex $(MeNPMe)_4Cr(CO)_3$ (**4***c*) was prepared similarly; mp (decom.) >280°C, ν(C≡O) (cm^{-1}) 1921, sh; 1813, 1824 b. The mass spectrum shows the parent ion at *m*/*e* 436 and stepwise loss of three CO groups. *Anal.* calcd. for $C_{11}H_{24}CrN_4O_3P_4$: C 30.3, H 5.6, N 12.8; found: C 30.1, H 5.4, N 12.9. **4***c* was also prepared in low yield by stirring equimolar quantities of **1***a* and $Cr(CO)_5$.THF in solution in THF for 3 days at room temperature. The complex $(MeNPEt)_4Mo(CO)_3$ (**4***d*) was prepared by heating a solution of **1***b* (0.092 g, 0.00026 mol) and $Mo(CO)_6$ (0.069 g, 0.00026 mol) in 15 mL toluene at 70°C for 1 h. Upon cooling, pale yellow crystals of **4***d* precipitated (0.084 g, 60%), which were recrystallized twice from toluene as tiny pale yellow needles, mp (decom.) 210–260°C; δ_P($CDCl_3$, ext. H_3PO_4) 111.0 ppm; δ_H($CDCl_3$, int. TMS) 2.89 (NMe, 5-line multiplet, J_{PH} 3.1 Hz), 1.96 ($PC\underline{H}_2CH_3$, quartet not split by P), 1.2 ($PCH_2C\underline{H}_3$, b); ν(C≡O) (cm^{-1}) 1921, 1835, 1819; solid state bands at 1941, 1787. The mass spectrum shows the parent ion at *m*/*e* 536 and the stepwise loss of three CO groups. *Anal.* calcd. for $C_{15}H_{32}MoN_4P_4O_3$: C 33.6, H 6.0, N 10.5; found: C 33.5, H 6.0, N 10.4. The manganese carbonyl complex $[(MeNPMe)_4Mn(CO)_3]^+$ Br^- (**4***e*) was prepared from **1***a* (0.162 g, 0.00054 mol) and $Mn(CO)_5Br$ (0.149 g, 0.00054 mol) in 15 mL THF at 60°C. After 2.5 h, the yellow **4***e* was filtered off (0.112 g, 40%) and washed with 3 × 5 mL THF: mp (decom.) 198–209°C. **4***e* soluble in H_2O, EtOH, CH_3CN, and slightly soluble in $CHCl_3$ in which it slowly decomposes. In nitromethane at 25°C, Λ_m = 79.0 ohm^{-1} cm^2 mol^{-1}, ν(C≡O) (cm^{-1}) 2030 (st, sh); 1929, (st, b); 1971 (m). *Anal.* calcd. for $C_{11}H_{24}BrMnN_4O_3P_4$: C 25.5, H 4.7, N 10.8, Br 15.4; found: C 25.3, H 4.8, N 10.5, Br 15.2. **4***e* forms a dihydrate, Λ_m($MeNO_2$, 25°C) 72.1 ohm^{-1} cm^2 mol^{-1}. *Anal.* calcd. for $C_{11}H_{28}BrMnN_4O_5P_4$: C 23.8, H 5.1, N 10.1, Br 14.4; found: C 23.5, H 5.1, N 9.9, Br 14.3. The same complex cation, with a different anion, was prepared by filtering a solution of $Mn_2(CO)_{10}$ (0.130 g, 0.00033 mol) in 5 mL toluene into a solution of **1***a* (0.100 g, 0.00033 mol) in 12 mL toluene. Evolution of CO began within 1 min. The clear yellow solution was stirred at room temperature for 18 h. The pale yellow product $[(MeNPMe)_4Mn(CO)_3]^+Mn(CO)_5^-$ (**4***f*) (0.127 g, 60%; 80% if the reaction is carried out photolytically) was filtered off and washed with toluene; mp (decom.) >250°C. Λ_m($MeNO_2$, 25°C) = 61.9 ohm^{-1} cm^2 mol^{-1}; ν(C≡O) (cm^{-1}) 2032 (st, sh); 1968, 1952 (st); 1899 (st, b), 1851 (st, vb). δ_H($(CD_3)_2CO$, int. TMS) 2.18 (PMe, b), 3.25 (NMe, b). *Anal.* calcd. for $C_{16}H_{24}Mn_2N_4O_8P_4$: C 30.3, H 3.8, N 8.8, O 20.2; found: C 30.2, H 4.0, N 8.9, O 19.9. The nickel complex $(MeNPMe)_4Ni_2(CO)_3$ (**5**) was prepared by filtering a solution of $(Ph_3P)_2Ni(CO)_2$ (0.499 g, 0.00078 mol) in 11 mL THF into a solution of **1***a* (0.117 g, 0.00039 mol) in THF. The yellow solution was irradiated at room temperature for 2 h (silica filter). After about 1 h the solution became orange–brown, and some brownish solid began to precipitate along with the yellow **5**, which was filtered off after a further 18 h in the dark at room temperature. The brown solid was removed by washing the residue with 2 × 15 mL CH_3CN. The bright yellow **5** (0.084 g, 43%, mp (decom.) >250°C) is slightly soluble in CH_3CN and acetone, in which it is relatively stable for short periods and moderately soluble in DMF. It is insoluble in THF and diethyl ether, and decomposes in $CHCl_3$. ν(C≡O) (cm^{-1}) 1972, 1946, 1775 (st, sh); weaker bands 2076 (w, sh), 1992 (m, sh), 1907 (sh, w), 1922 (shl). *Anal.* calcd. for $C_{11}H_{24}N_4Ni_2O_3P_4$: C 26.3, H 4.8, N 11.2, P 24.7, Ni 23.4; found: C 26.6, H 4.9, N 11.3, P 24.8, Ni 23.3. A new compound $[MeNP(O)Me]_4$ (**6**) was precipitated when a solution of **5** in DMF was oxidised in air. Filtration, followed by washing with DMF and pentane left analytically pure **6**, colourless blocks from acetonitrile, mp (decom.) >265°C. It is soluble in water, hot CH_3CN, and hot CH_3OH, insoluble in $CHCl_3$, CH_2Cl_2. Its mass spectrum shows the parent ion at *m*/*e* 364 and peaks arising from the loss of Me, MeN. ν(P=O) 1228 cm^{-1} (br, st). δ_P(CD_3OD, ext. H_3PO_4) +30.5. δ_H(CD_3OD, int. TMS) 1.86 (PMe, J_{PH} 15 Hz, doublet), 3.06 (NMe, J_{PH} 10.8 Hz, triplet). *Anal.* calcd. for $C_8H_{24}N_4O_4P_4$: C 26.4, H 6.6, N 15.4; found: C 26.5, H 6.6, N 15.1. A small yield of **6**, grossly contaminated with hydrolysis products, was obtained by the oxidation of **1***a* in THF with aqueous hydrogen peroxide.

Quaternary carbonyl complexes

The preparation and crystal structure of the complex $[Me(MeNPMe)_4Mo(CO)_3]^+I^-$ (7*a*) is described elsewhere (7). For the tungsten complex, 1*a* (0.115 g, 0.00038 mol) and $W(CO)_6$ (0.134 g, 0.00038 mol) were dissolved in 20 mL THF, and the clear colourless solution was irradiated at 65°C for 2 h. The mixture was cooled to room temperature and a large excess of MeI was added (about 1 mL). The mixture was heated under reflux for 18 h, during which time a pale yellow solid was precipitated from the red solution. It was filtered off and washed with 5 × 2 mL warm MeCN, leaving $[Me(MeNPMe)_4W(CO)_3]^+I^-$ (7*b*) as a very pale yellow solid (0.110 g, 41%, decomposing near 200°C). It is soluble in hot MeOH, DMSO, and pyridine, and can be crystallised as a 1 : 1 adduct from CH_3CN, to which the following results refer. ν(C≡O) (cm^{-1}) 1940 (st, sh); 1850, 1832 (st). δ_H(CD_3OD, ext. TMS) 1.82 (3H, doublet, J_{PH} 6.5 Hz), 2.12 (6H, b), 2.42 (3H, doublet, J_{PH} 12.5 Hz), 2.73 (3H, doublet, J_{PH} 13.2 Hz), 2.92 (6H, quintet, J_{PH} 4.5), 3.25 (6H, doublet split into virtual triplets, J_{PH} 10, 2.2 Hz). The ^1H nmr spectrum in DMSO was very similar, except that the group at lowest field formed a simple doublet. *Anal.* calcd. for $C_{14}H_{30}IN_5O_3P_4W$: C 22.4, H 4.0, N 9.3; found: C 22.3, H 4.1, N 9.2. The chromium complex $[Me(MeNPMe)_4Cr(CO)_3]^+I^-$ was prepared similarly and crystallised from CH_3CN as its hemi-adduct with CH_3CN (7*c*), mp (decom.) ~260°C, ν(C≡O) (cm^{-1}) 1935 (st, sh); 1847, 1829 (shl). *Anal.* calcd. for $C_{26}H_{57}Cr_2I_2N_9O_6P_8$: C 26.1, H 4.8, N 10.5, O 8.0; found: C 26.2, H 4.9, N 10.6, O 8.3. The complexes $[NH_2C(O)CH_2(MeNPMe)_4Cr(CO)_3]^+I^-$ (7*d*) and $[NCCH_2(MeNPMe)_4Cr(CO)_3]^+I^-$ (7*e*) were prepared similarly using iodoacetamide and iodoacetonitrile as quaternising agents. 7*d*, yellow–green crystals, mp (decom.) >250°C; ν(C≡O) (cm^{-1}) 1943, 1933; 1868 (shl), 1824 (st, sh); 1858, 1808 (st, sh). ν(C≡O) 1686 (m). *Anal.* calcd. for $C_{13}H_{28}CrIN_5O_4P_4$: C 25.1, H 4.5, N 11.3; found: C 25.1, H 4.5, N 11.3. 7*e*, pale yellow platelets, dark green ~200°C, mp (decomp.) >260°C; ν(C≡O) (cm^{-1}) 1945 (st, b); 1855 (st), 1828 (split, b). No ν(C≡N) observed. *Anal.* calcd. for $C_{13}H_{26}CrIN_5O_3P_4$: C 25.9, H 4.3, N 11.6; found: C 26.1, H 4.4, N 11.5. The carbonyl stretching bands are broadened in 7*e* and split into two sets in 7*d*, presumably a result of conformational or configurational isomerism caused by the bulky quaternising groups.

Ylides

A molybdenum carbonyl ylide was prepared by the addition of 2.2 equiv. of *n*BuLi (1.6 *M*) to 7*a* (0.135 g, 0.00022 mol) in 6 mL THF, with an immediate decrease in turbidity. The solution became yellow. After stirring for 45 min at room temperature, the mixture was filtered, the solid washed with MeCN until the washings were colourless, and then again with water until the washings were colourless. The residual pale yellow solid product $(MeNPMe)_4Mo(CO)_3CH_2$ (8*a*, 0.015 g, 14%) was recrystallised from hot DMSO; mp (decom.) >170°C. It is very soluble in warm DMF (very pale yellow solution) and in $MeNO_2$ (very bright yellow solution). Its mass spectrum (260°C) shows the parent ion *m/e* 494, the $(M - CH_2)^+$ ion, and the stepwise loss of three CO groups from each ion. ν(C≡O) (cm^{-1}) 1909 (st, sh); 1810, 1785 (st, split). CH_2 frequencies 975, 936 (m) (26). δ_H (DMSO-d_6, ext. TMS) −0.15 (2H, b), 1.48 (3H, doublet, J_{PH} 16.5 Hz), 1.74 (6H, singlet, b), 2.00 (3H, doublet, J_{PH} 12.5 Hz), 2.87 (12H, multiplet). *Anal.* calcd. for $C_{12}H_{26}MoN_4O_3P_4$: C 29.2, H 5.3, N 11.3; found: C 29.2, H 5.3, N 11.1. The tungsten ylide $(MeNPMe)_4W(CO)_3CH_2$ (8*b*) was prepared similarly as a bright yellow solid, mp (decom.) >180°C. It is soluble in hot DMSO (with slow decomposition), slightly soluble in hot MeCN, insoluble in H_2O, CH_2Cl_2, $CHCl_3$, acetone. Its mass spectrum (270°C) is similar to that of 8*a*. ν(C≡O) (cm^{-1}) 1900 (st, sh); 1800, 1775 (st). CH_2 frequencies 980, 934 (m). δ_H (DMSO-d_6, ext. TMS) 0.14 (2H, broad, with possible fine structure), 1.48 (3H, doublet, J_{PH} 16 Hz), 1.85 (6H, singlet, broad), 2.03 (3H, doublet, J_{PH} 12.8 Hz), 2.80 (12H, multiplet). *Anal.* calcd. for $C_{12}H_{26}N_4O_3P_4W$: C 24.8, H 4.5, N 9.6, O 8.3; found: C 24.9, H 4.5, N 9.4, O 8.5.

Results and discussion

The compounds 1*a*, *b* were obtained previously (2). One additional tetraphosphazane, the P-phenyl derivative 1*c*, has been prepared. Its ^{31}P and ^1H nmr spectra show that the phosphorus atoms and *N*-methyl groups are less shielded than they are in 1*a*, *b* (2), and it is possible that 1*c* was obtained in low and irreproducible yield because in $MeN(PhPCl)_2$, the main product in this and other work (8), the phosphorus atoms are weakly nucleophilic. No evidence of larger or smaller rings was obtained in any preparation of 1*a*–*c*. The following discussion is based mainly on the chemistry of 1*a*. Some of the nmr information is illustrated in Fig. 2.

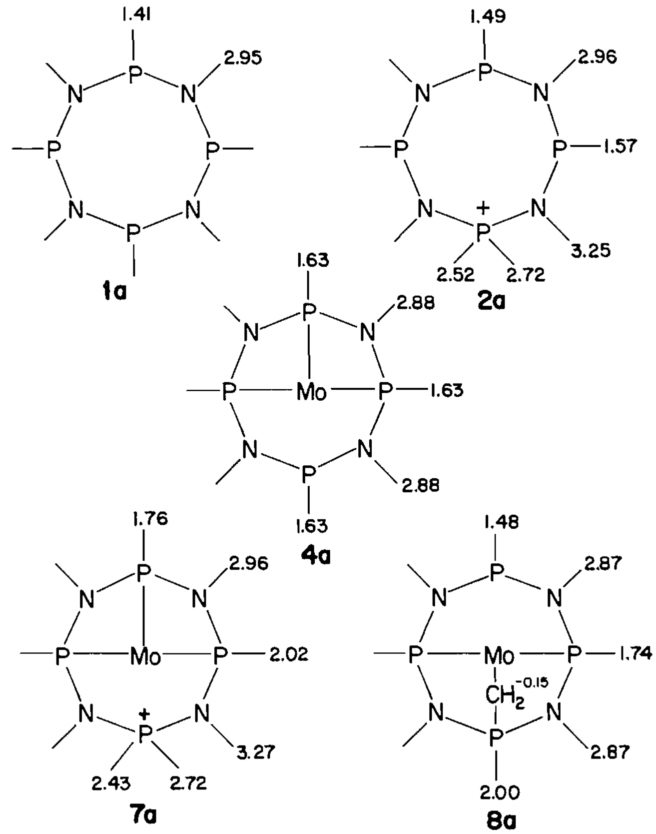

FIG. 2. ^1H chemical shifts of the methyl groups in 1*a* (2), its monomethyl quaternary ion 2*a* (5) (different assignments), its complex with $Mo(CO)_3$ (4*a*) (6), the quaternised complex 7*a* and the ylide 8*a* formed from it.

The electronic structures of the cyclic phosph(III)azanes $(R'NPR)_n$ are different from those of their P(V) isomeric phosphazenes $(NPRR')_n$; their skeletal structure is singly bonded, at least to a first approximation, and the phosphorus and nitrogen atoms each carry both a substituent and a formally unshared pair of electrons. The crown conformation of 1*a*, like that of S_8 (9) and $S_4(NMe)_4$ (10), is qualitatively compatible with the interaction of stereochemically active lone pairs (11), and the importance of steric interactions in other phosph(III)azanes has been stressed elsewhere (12, 13). Keat, especially, has associated conformational stability with the mutual perpendicularity of lone-pair directions at adjacent atoms (12). Important though these interactions are, the suggestion that they are not the whole story (6, 14) is confirmed and made specific by the present work.

The first point, recognised early for aminophosphines (15), is that electron release from nitrogen to phosphorus, indicated by the near-planarity of the groups attached to nitrogen (2), strengthens the donor function, so that the tetraphosphazanes are normally multidentate ligands. As a consequence, they can be expected to form cage complexes with a variety of acceptors. As an example of such complex formation by a transition metal ion, the complex cation **3**, with either $CoCl_4^{2-}$ or BPh_4^- as anion, seems likely to have the structure shown (Fig. 1), in which the phosphazane acts as a tridentate ligand. In the carbonyl complexes, too, the ligand is multidentate; attempts to prepare a derivative $LCr(CO)_5$ by the use of THF.$Cr(CO)_5$ were unsuccessful, leading to L.$Cr(CO)_3$ instead. Similar compounds **4** were obtained with $W(CO)_6$, $Mo(CO)_6$. All are fluxional at room temperature on the nmr time scale, but three carbonyl stretching frequencies are seen, two corresponding to the lifting of the degeneracy of the E band, compatibly with the structure shown.

The nickel carbonyl complex **5** is different. The evidence for the structure shown, in which the ligand is tetradentate, rests on the infrared spectrum, which shows ν(C≡O) corresponding to two terminal groups (1972, 1946 cm^{-1}) and a bridging group (1775 cm^{-1}). In an apparently related complex **9** of the stronger π-acceptor $MeN(PF_2)_2$ (16), the frequencies are higher (2070, 2055, 1891 cm^{-1}). Possibly as a result of smaller back-donation to phosphorus, **5** is sensitive to heat and is hardly stable in solution, in which it is easily oxidised to the oxophosph(V)azane **6**, an *N*-methylimide of methylphosphonic acid. The structure shown is to be expected if the oxidation is stereospecific, and is consistent with the nmr results, although the high symmetry might be attained statistically.

The ligand is also tetradentate in the complex quaternary salts **7**, which can be prepared by quaternisation of the neutral carbonyl complex; details of the crystal structure of **7***a* have been published (14) and are discussed further below.

By contrast, reaction of **1***a* with alkyl halides goes no further than the biquaternary stage. If the quaternising group is methyl, the monoquaternary cation is still a donor, and reacts (slowly) with metal carbonyls to give the quaternary carbonyls **7**. These, in turn, can be deprotonated by butyllithium, the quaternary carbonyl compounds **7***a*, *b*, leading to the ylides **8***a*, *b*, in which the molecule is stabilised by coordination of the ylide group to the metal, at the expense of the weaker phosphine donor.[4] The qualitative structure **8** is indicated by the ^{1}H nmr spectra (Fig. 2). The polar ylidic group, identified unambiguously in the spectrum by its integral, resonates at the highest field. The strong donor properties of the phosphazane are again noticeable, both in the need for two equivalents of base in the deprotonation reaction, and in the formation by the ylide of complexes with lithium salts (presumably through the fourth phosphorus atom), which need to be decomposed before pure **8***a*, *b* can be isolated. It is also likely that the (stereospecific) addition of more than three sulphur atoms to **1***a* (3) is restricted sterically rather than electronically; the three sulphur atoms are spaced out in the distorted ring, but a fourth sulphur atom, on P(4), would be unacceptably close to S(1) (1.9 Å).

Secondly, the donor properties of the phosphazane are likely to be limited by the transmission of electronic effects round the ring. The importance of this feature is shown by the pronounced inequalities in the lengths of the P—N bonds in the biquaternary ion $[(MeNPMe)_4Me_2]^{2+}$ (5) (mean 1.652, 1.749 (σ 0.005 Å) from the quaternary centres).[5] It is seen also in the easy hydrolysis of the $(MeNPMe)_4Me^+$ ion, nucleophilic attack (giving the $[Me_2P(NHMe)_2]^+$ ion) taking place not at the quaternary centre, but at the next nearest phosphorus atom. Again, if **1***a* is quaternised with either of the electron-withdrawing groups $[CH_2C(O)NH_2]^+$ or $[CH_2CN]^+$, no reaction takes place with metal carbonyls, presumably because the lone pairs have been significantly stabilised. In general, we can expect that, as a consequence of the transmission effect, σ-donation, at least, will become weaker as further acceptor molecules are added. If direct electrostatic effects are taken into account, it is not surprising that the quaternisation reaction stops at the second stage.

This view of the reactions is nevertheless incomplete, and the third point is the decisive effect of *d*-orbital occupancy on both the structures and chemistry of phosphazane derivatives. To some extent, the ^{1}H shifts of Fig. 2 can, indeed, be interpreted without explicit consideration of *d*-orbitals. Quaternisation of **1***a* deshields all the methyl groups, decreasingly from the positive centre (mean δ_H, (P)Me 1.97, (N)Me 3.11). Coordination of **1***a* to (fluxional) $Mo(CO)_3$ has a smaller effect (mean δ_H, (P)Me 1.63, (N)Me 2.88); in the quaternary complex **7***a* shielding is least (mean δ_H, (P)Me 2.19, (N)Me 3.12). The influence of the *d*-orbitals on the metal can be seen, possibly, in the smaller effect of $Mo(CO)_3$ compared with Me^+, and the fact that in the ylide **8***a*, in which the methylene group can donate no electrons to phosphorus, the phosphorus atoms are deshielded (mean δ_H, (P)Me 1.74, (N)Me 2.87) relative to those in **4***a*. It is seen convincingly in the properties of the $[L.Mn(CO)_3]^+$ ion (**4***e*) in which the positive charge restricts back-donation to both neighbouring atoms, raising ν(C≡O) and deshielding the ring atoms (fluxional; mean δ_H, (P)Me 2.18, (N)Me 3.25) compared to the $Mo(CO)_3$ complex. In the ylides **8**, the methylene group is unable to accept electrons, and ν(C≡O) is therefore reduced relative to L.$M(CO)_3$; for **8***a*, mean $\delta\nu = -23$ cm^{-1}. As a comparison, even lower frequencies are found in the tri-ylidic complex $(Ph_3PCH(Me))_3$-$Mo(CO)_3$, for which ν(C≡O) = 1898, 1799, 1767 cm^{-1} (19). The ligand is then more nearly a σ-donor, with a small decrease in shielding (mean δ_H, (P)Me 1.74, (N)Me 2.87) relative to **4***a*. Back-donation from the metal to the *d*-orbitals of phosphorus is important, but the net donor properties of the ligand are confirmed by the decrease in shielding of phosphorus on complex formation (δ_P, $(MeNPEt)_4$, 100(2); $(MeNPEt)_4Mo(CO)_3$ (**4***d*) 111.0).

The importance of *d*-orbital interactions is seen most directly in the transmission of electronic influences within the ligand, the energetics of its reactions with acceptors, and the changes in bond length which accompany the reactions. Earlier structural investigations[6] have shown that they are significant for the bonding in phosphazanes; the point of particular importance here is the sensitivity of *d*-orbitals to effective nuclear charge (20). The crystal structure of **7***a* (14) in comparison with those of **1***a* (2) and **4***a* (6), shows that the moderate strengthening of the C≡O bonds on quaternisation (mean $\delta\nu$(C≡O) 22 cm^{-1}) is accompanied by some strengthening of both the P—Mo and the P—N bonds (mean decrease in length 0.041, 0.012 Å). The dominant effect of the positive charge on the ring is therefore to make it, by *d*-orbital contraction, a better π-acceptor, though not as good (on similar evidence) as the PF_2 groups in $P[N(Ph)PF_2]_3Mo(CO)_3$ (21). The additional bond energy so

[4] For a review see ref. 17.

[5] As a comparison, the structural effects, at least, are less pronounced in C—N heterocyclics; protonation of a piperidine derivative (18) causes no significant changes in the lengths of the bonds meeting at N (σ 0.01 Å).

[6] For references, see ref. 14.

obtained makes the quaternary cation (thermodynamically speaking) a better donor than the neutral phosphazane.

We can apply these concepts to two reactions of **1***a* investigated earlier, with methyl iodide (5) and with sulphur (3). In both cases reaction with an acceptor facilitates further reaction; in the first, a monoquaternary salt easily disproportionates to a diquaternary and the neutral compound, in the second, the trisulphide is formed even with a deficit of sulphur. In an effort to reduce the nucleophilicity of a second phosphorus atom, we have quaternised **1***a* with the stronger acceptors phenacyl bromide and iodoacetamide. The monoquaternary derivatives were indeed obtained, even with an excess of these reagents, but their stability may depend on their insolubility, because disproportionation occurs in solution in CD_3OD. The stabilisation by the quaternary group of the formal lone pairs on phosphorus is more than compensated by the strengthening of the ring bonds by *d*-orbital contraction, and the same argument applies to the addition of sulphur atoms to the phosphazane ring. The strengthening is illustrated by the mean ring bond lengths, which decrease from 1.722 Å in $(MeNPMe)_4$ (2) to 1.700 Å in $(MeNPMe)_4Me_2^{2+}$ (5) and 1.701 Å in $(MeNPMe)_4S_3$ (3), comparable to the changes in the formation of **7***a*. Although the contraction effect is decisive here, it is likely that the energies are finely balanced, and disproportionation may not always occur. In carbonyl complexes of the related cyclodiphosph(III)azanes (22, 23) the ligand is apparently monodentate (23),[7] and all four sulphides $P_4(NMe)_6S_n$ ($n = 1-4$) have been obtained (25). Nevertheless, the work reported here shows clearly that the energy changes induced by *d*-orbital contraction have a significant effect on the properties of phosphazanes, and must be taken into account in discussions of their electronic structure.

Acknowledgements

We are grateful to Dr. G. Eigendorf for mass spectra, Dr. S. O. Chan for nmr spectra, Mr. P. Borda for analyses, and the Natural Sciences and Engineering Research Council of Canada for financial support.

[7] A cyclotetraphosphazane ring, complexed by two $M(CO)_5$ groups, is formed in the tetramerisation of a triazaphosphole (24). It is not strictly comparable with the compounds discussed here, because its centrosymmetric structure, forced by four fused triazaphosphole rings, prevents chelate complex formation.

1. R. KEAT. Top. Curr. Chem. **102**, 89 (1982).
2. W. ZEISS, W. SCHWARZ, and H. HESS. Angew. Chem. Int. Ed. Engl. **16**, 407 (1977).
3. W. ZEISS, W. SCHWARZ, and H. HESS. Z. Naturforsch. **35**b, 959 (1980).
4. W. ZEISS and H. HENJES. Chem. Ber. **111**, 1655 (1978).
5. W. ZEISS, T. KUHN, D. LUX, W. SCHWARZ, and H. HESS. Z. Naturforsch. **36**b, 561 (1981).
6. K. D. GALLICANO, N. L. PADDOCK, S. J. RETTIG, and J. TROTTER. Can. J. Chem. **60**, 2415 (1982).
7. D. F. CLEMENS and H. H. SISLER. Inorg. Chem. **4**, 1222 (1965).
8. R. JEFFERSON, J. F. NIXON, T. M. PAINTER, R. KEAT, and L. STOBBS. J. Chem. Soc. Dalton Trans. 1414 (1973).
9. S. C. ABRAHAMS. Acta Crystallogr. **8**, 661 (1955).
10. A. L. MACDONALD and J. TROTTER. Can. J. Chem. **51**, 2504 (1973).
11. L. PAULING. Proc. Nat. Acad. Sci. **35**, 495 (1949).
12. R. KEAT, D. S. RYCROFT, and D. G. THOMPSON. J. Chem. Soc. Dalton Trans. 321 (1980); R. Keat, L. Murray, and D. S. RYCROFT. J. Chem. Soc. Dalton Trans. 1503 (1982); D. A. HARVEY, R. KEAT, and D. S. RYCROFT. J. Chem. Soc. Dalton Trans. 425 (1983).
13. W. ZEISS, A. POINTNER, C. ENGELHARDT, and H. KLEHR. Z. Anorg. Allgem. Chem. **475**, 256 (1981).
14. K. D. GALLICANO, N. L. PADDOCK, S. J. RETTIG, and J. TROTTER. Can. J. Chem. **62**, 1869 (1984).
15. A. B. BURG and P. J. SLOTA. J. Am. Chem. Soc. **80**, 1107 (1958).
16. R. B. KING and J. GIMENO. Inorg. Chem. **17**, 2390 (1978).
17. W. C. KASKA. Coord. Chem. Rev. **48**, 1 (1983).
18. M. H. J. KOCH and G. GERMAIN. Acta Crystallogr. B**28**, 121 (1972).
19. H. BOCK and H. T. DIECK. Z. Naturforsch. **21**b, 739 (1966).
20. D. P. CRAIG, A. MACCOLL, R. S. NYHOLM, L. E. ORGEL, and L. E. SUTTON. J. Chem. Soc. 332 (1954).
21. G. M. BROWN, J. E. FINHOLT, R. B. KING, and T. W. LEE. J. Am. Chem. Soc. **103**, 5249 (1981).
22. L. S. JENKINS and G. R. WILLEY. J. Chem. Soc. Dalton Trans. 777 (1979).
23. J. C. T. R. B. ST. LAURENT, H. E. HOSSEINI, J. SINCLAIR, and J. F. NIXON. Inorg. Chim. Acta, **44**, L17 (1980).
24. A. SCHMIDPETER, H. TAUTZ, J. V. SEYERL, and G. HUTTNER. Angew. Chem. Int. Ed. Engl. **20**, 408 (1981).
25. A. WOLFF and J. G. RIESS. Bull. Soc. Chim. Fr. 1587 (1973).
26. E. KURRAS, U. ROSENTHAL, H. MENNENGA, and G. OEHME. Angew. Chem. Int. Ed. Engl. **12**, 854 (1973).

The preparation, characterization, and crystal and molecular structure of oxobis(ethan-1,2-dithiolato-S,$\mu S'$)technetium(V)oxo(ethan-1,2-dithiolato-S,S')technetium(V) $[(TcO)_2(SCH_2CH_2S)_3]$. A Tc(V) compound containing metal—sulfur—metal bridges

A. DAVISON[1]
Department of Chemistry, Massachusetts Institute of Technology, Cambridge, MA 02139, U.S.A.

B. V. DEPAMPHILIS
Department of Radiology, Harvard Medical School and Brigham and Women's Hospital, Boston, MA 02115, U.S.A.

R. FAGGIANI
Institute for Materials Research, McMaster University, Hamilton, Ont., Canada L8S 4M1

A. G. JONES
Department of Radiology, Harvard Medical School and Brigham and Women's Hospital, Boston, MA 02115, U.S.A.

C. J. L. LOCK[1]
Institute for Materials Research, McMaster University, Hamilton, Ont., Canada L8S 4M1

AND

C. ORVIG
Department of Chemistry, Massachusetts Institute of Technology, Cambridge, MA 02139, U.S.A. and the Institute for Materials Research, McMaster University, Hamilton, Ont., Canada L8S 4M1

Received May 22, 1984

A. DAVISON, B. V. DEPAMPHILIS, R. FAGGIANI, A. G. JONES, C. J. L. LOCK, and C. ORVIG. Can. J. Chem. **63**, 319 (1985).

As a result of an investigation undertaken to evaluate the acetamidomethyl group ($—CH_2NHCOCH_3$) as a water-solubilizing protecting group for thiolate ligands, a new type of oxotechnetium(V) complex was prepared. The compound oxobis(ethan-1,2-dithiolato-S,$\mu S'$)technetium(V)oxo(ethan-1,2-dithiolato-S,S')technetium(V), $[(TcO)_2(SCH_2CH_2S)_3]$, **1**, was synthesized by the reaction of $[TcOCl_4]^-$ with either an excess of bis(acetamidomethyl)ethanedithiol or 1.5 equiv. of ethanedithiol. The complex was characterized by field desorption mass spectrometry (m/e = 505(8), 507(2.8)) and its structure determined by single crystal X-ray diffraction. **1** has a monoclinic space group $P2_1/c$ with cell dimensions a = 8.833(2) Å, b = 15,034(3) Å, c = 11.350(2) Å, and β = 108.17(1)°, and has four formula units in the unit cell. Data were collected with the use of MoKα radiation and a Nicolet P3 diffractometer. The crystal structure was determined by standard methods and refined to R_1 = 0.0366 and R_2 = 0.0455 on the basis of 3312 independent reflections. The compound contains two technetium atoms. Two sulphur atoms of one square pyramidal $TcOS_4$ core are bonded to another $TcOS_2$ unit forming two square pyramids sharing an edge with an angle of 106.0(1) between the basal planes. The Tc—Tc distance is 3.654(1) Å. There are four distinct types of Tc—S bonds (range 2.256(2)—2.418(2) Å) and the Tc—O distances (1.66 Å) are normal.

A. DAVISON, B. V. DEPAMPHILIS, R. FAGGIANI, A. G. JONES, C. J. L. LOCK et C. ORVIG. Can. J. Chem. **63**, 319 (1985).

A la suite d'une étude entreprise dans le but d'évaluer l'utilité du groupe acétamidométhyle ($—CH_2NHCOCH_3$) comme groupe protecteur, soluble dans l'eau, des ligands thiolates, on a préparé un nouveau type de complexe oxotechnétium(V). On a synthétisé le complexe oxobis(éthanedithiolato-1,2-S,$\mu S'$)technétium(V)oxo(éthanedithiolato-1,2-S,S')technétium(V), $[(TcO)_2(SCH_2CH_2S)_3]$, **1**, par réaction du $[TcOCl_4]^-$ avec soit un excès de bis(acétamidométhyl)éthanedithiol ou 1,5 équiv. d'éthanedithiol. On a caractérisé le complexe par spectrométrie de masse par désorbtion de champ (m/e = 505(8), 507(2,8)) et on a déterminé sa structure par diffraction de rayons-X sur un cristal unique. Le composé **1** est monoclinique, groupe d'espace $P2_1/c$, dimensions de la maille unitaire a = 8,833(2), b = 15,034(3) et c = 11,350(2) Å et β = 108,17(1)° et la maille unitaire contient quatre unités. On a recueilli les données en utilisant la radiation MoKα et un diffractomètre Nicolet, modèle P3. La structure cristalline a été determinée par des méthodes standards et on l'a affinée jusqu'à des valeurs de R_1 = 0,0366 et de R_2 = 0,0455 sur la base de 3312 réflexions indépendantes. Le composé contient deux atomes de technétium. Les deux atomes de soufre d'une pyramide carrée de $TcOS_4$ formant le coeur de la structure sont liés à une autre unité de $TcOS_2$ formant deux pyramides carrées partageant un côté avec un angle de 106,0(1)° entre les plans de base. La distance Tc—Tc est égale à 3,654(1) Å. Il y a quatre types distincts de liaisons Tc—S (longueurs allant de 2,256(2) à 2,418(2) Å) et les distances Tc—O sont normales (1,66 Å).

[Traduit par le journal]

Introduction

Widespread use of technetium in the field of nuclear medicine has resulted (1) from the favorable nuclear properties of the metastable isotope ^{99m}Tc (λ = 140 keV, $t_{1/2}$ = 6 h). Concomitantly, a growing number of chemical studies using the readily available, long-lived isotope ^{99}Tc (β^- = 292 keV, $t_{1/2}$ = 2.12×10^5 y) are in the process of outlining the basic chemistry of the element (2). The pentavalent oxidation state (Tc(V), low spin d^2) has emerged as an important species in the reduction chemistry of pertechnetate (TcO_4^-), and the aqueous

[1] To whom correspondence should be addressed.

TABLE 1. Crystal data

Compound	$Tc_2O_2(SCH_2CH_2S)_3$, $C_6H_{12}O_2S_6Tc_2$
fw	506.33
crystal size (mm)	cylinder, r = 0.10, l = 0.38
Systematic absences	$h0l$, $l = 2n + 1$, $0k0$, $k = 2n + 1$
Space group	$P2_1/c$
Unit cell parameters	a = 8.833(2), β = 108.17(1)
(Å and deg)	b = 15.034(3)
	c = 11.350(2)
Volume (Å^3)	1432.1(5)
Z	4
$\rho_{calc.}$ (g cm^{-3})	2.348
$\rho_{obs.}$ (g cm^{-3})	2.35(1)
Linear absorption coef. (cm^{-1})	17.12
Absorp. corr. factors, A*, limits	1.33–1.34
Max 2θ, reflctn collected	55°, h, k, $\pm l$
Standard reflctn. (esd%)	4 1 −5, 1.02; 3 3 −6, 1.06
No. of independent reflctns.	3312
No. with $I > 3\sigma(I)$[a]	2510
$3\sigma(I) > I > 0$, where $F_c > F_o$	246
$3\sigma(I) > I > 0$, where $F_c < F_o$	393
$I < \sigma(I)$, rejected	163
Final R_1[b], R_2[b]	0.0366, 0.0455
Final shift/error max (ave)	0.037, (0.004)
g (secondary extinction)	$1.6(6) \times 10^{-7}$
Final difference map	
Highest peak (e Å^{-3}); location	0.98; 0.10, 0.15, 0.40
Lowest valley (e Å^{-3}); location	−0.68; 0.75, 0.65, 0.40
Weighting	$w = (\sigma^2 + (0.025F_o)^2)^{-1}$
Error in an obs. of unit wt.	1.206

[a]The 0 0 2 reflection was too intense to measure.
[b]$R_1 = (\Sigma||F_o| - |F_c||)/\Sigma|F_o|$; $R_2 = \{\Sigma w(|F_o| - |F_c|)^2/\Sigma wF_o^2\}^{1/2}$.

chemistry of Tc(V) has been dominated by the TcO(3+) core and its affinity for sulfur-containing ligands (3). Sulfur can be used in combination with other ligating atoms and subsequently a series of $TcON_2S_2$ complexes was prepared (4), one of which undergoes rapid renal excretion (5). The fast renal clearance fostered an interest in simplifying the synthesis of this important series of compounds because the thiol-protecting benzoyl groups employed rendered the amide thiolate ligands water-insoluble, necessitating the use of biologically-compatible co-solvent, such as ethanol, in the preparation of the oxotechnetium complexes.

The acetamidomethyl functionality (acm)(—$CH_2NHCOCH_3$) is a useful protecting moiety for sulfhydryl groups in peptide synthesis (6, 7). The protection is particularly useful because acm is stable to acids such as liquid HF and to bases such as hydrazine, yet it is readily removed by the electrophilic attack of reagents such as Hg(II). In addition, water-solubility is imparted to thiols protected with acm. In order to test its effectiveness as a protecting group for thiols in the N_2S_2 system, bis(acetamidomethyl)ethanedithiol (edt(acm)$_2$) was prepared as a model and studied in its reactions with TcO_4^- and $[TcOCl_4]^-$. The desired product was the well-characterized (8, 9) $[TcO(edt)_2]^-$ ion, but, in addition, an apparent intermediate $[(TcO)_2(edt)_3]$ was isolated in the study. The same intermediate was isolated during ligand-exchange studies of oxotechnetium(V) complexes (10). We report here the full chemical and structural characterization of this intermediate.

Experimental section

Technetium as $NH_4{}^{99}TcO_4$ was obtained as a gift from New England Nuclear, Billerica, MA. All manipulations were carried out following precautions which have been detailed elsewhere (9). All reagents were used as received unless otherwise specified. Bis(acetamidomethyl)-ethanedithiol was prepared from ethanedithiol (Eastman) and N-hydroxymethylacetamide (11) in HCl. Literature procedures were followed to prepare [n-Bu_4N][$TcOCl_4$] (9) and [Ph_4As][$TcO(SCH_2CH_2S)_2$] (9). Elemental analyses were performed by Schwarzkopf Microanalytical Laboratories, Woodside, NY. and Spang Microanalytical Laboratory, Eagle Harbor, MI. Melting points were measured with a Mel-Temp apparatus and are uncorrected.

Infrared spectra were recorded with a Perkin-Elmer PE180 grating spectrophotometer from KBr pellets. Optical spectra were obtained in solution with a Cary 17 spectrophotometer. The high field proton nmr spectrum was recorded with a Bruker 250 MHz instrument. The positive ion field desorption mass spectrum was obtained with a Varian MAT 731 described elsewhere (12). Conductivity measurements were made with a Yellow Springs Model 3403 conductivity cell and a Serfass conductivity bridge. The acetonitrile used in this experiment was passed down a column of activated alumina immediately before use. (Woelm Neutral Activity Grade I supplied by ICN.)

Preparation of $[(TcO)_2(edt)_3]$

This orange solid was prepared by the reaction of $TcOCl_4^-$ with an excess of bis(acetamidomethyl)ethanedithiol (Method A) or with 1.5 equiv. of ethanedithiol (Method B). Both methods provide a ca. 80% yield of a microcrystalline orange solid which can be recrystallized in high yield from methylenechloride/hexane at −25°C to form orange blocks.

Method A

To a solution of 0.298 g [n-Bu_4N][$TcOCl_4$] (0.60 mmol) in 20 mL methanol was added a solution of 0.301 g edt(acm)$_2$ (1.27 mmol) in 30 mL methanol with stirring. Within 1 min after the addition, the resulting solution went from pale green to deep orange and became cloudy. This suspension deposited fine orange crystals over a period of 30 min. These were separated by suction filtration and dried *in*

TABLE 2. Atomic positional parameters ($\times 10^4$) and temperature factors ($Å^2 \times 10^3$)

Atom	x	y	z	U_{eq}* or U_{iso}
Tc(1)	3862.6(4)	−954.1(3)	3036.2(3)	20.3(2)*
Tc(2)	988.8(5)	850.6(3)	2670.4(4)	29.3(2)*
S(1)	2557(2)	−2261.9(9)	2567(1)	38.9(8)*
S(2)	4467(2)	−1132.9(9)	1264(1)	32.7(7)*
S(3)	3600(2)	611.4(8)	2598(1)	26.7(6)*
S(4)	471(2)	1332(1)	684(1)	48.2(9)*
S(5)	1744(1)	−480.8(9)	3817(1)	29.2(6)*
S(6)	−1487(2)	231(1)	1988(2)	44.3(8)*
C(1)	3020(7)	−2742(4)	1250(6)	47(1)
C(2)	4469(7)	−2340(4)	1050(6)	46(1)
C(3)	3660(7)	964(4)	1069(5)	41(1)
C(4)	2402(7)	1690(4)	600(6)	48(1)
C(5)	−52(8)	−1176(4)	3460(6)	47(1)
C(6)	−1474(8)	−567(4)	3201(6)	47(1)
O(1)	5508(4)	−1090(2)	4231(3)	35.3(8)
O(2)	977(5)	1694(3)	3610(4)	53(1)

*$U_{eq} = (1/3)(U_{11} + U_{22} + U_{33} + 2U_{13}\cos\beta)$.

vacuo for 4 h. The yield was 0.124 g, 82% based on Tc.

Method B

To a solution of 0.148 g [n-Bu_4N][$TcOCl_4$] (0.30 mmol) in 7 mL methanol was added 37 μL ethanedithiol (0.45 mmol). The green solution turned orange immediately and deposited fine orange crystals within 1 min. After stirring for 1 h, the orange solid was separated and dried as in method A. The yield was 0.060 g, 80% based on Tc. *Anal.* calcd. for $C_6H_{12}O_2S_6Tc_2$: C 14.23, H 2.39, S 37.99; found: C 14.76, H 2.63, S 36.85. Optical spectrum in CH_2Cl_2: 424 nm (ϵ = 6300 L mol^{-1} cm^{-1}), 286 (9600). Ir (KBr): ν(Tc=O) = 953, 946 cm^{-1} (both vs). Conductivity: neutral, 10^{-3} *M*, CH_3CN. FDMS: m/e = 505 (relative intensity 8), 507 (2.8). ^{1}H nmr, 250 MHz in $CDCl_3$: δ 3.22–3.34, δ 3.41–3.53 (total intensity 1, AA′BB′ multiplet); δ 3.53–4.12 (total intensity 2, ABCD multiplet). Mp 205–207°C (dec). The compound is soluble in methylene chloride, acetone, and acetonitrile. It is insoluble in nonpolar organic solvents and alcohols, except methanol in which it is slightly soluble.

Preparation of [TcO(edt)$_2$]$^-$ from edt(acm)$_2$

To a green solution of 0.125 g [n-Bu_4N][$TcOCl_4$] (0.25 mmol) in 10 mL methanol was added a solution of 0.15 g edt(acm)$_2$ (0.63 mmol) in 10 mL methanol, resulting in an orange suspension. To this suspension, 4 mL 1 *M* NaOH were added and the suspension refluxed for 6 h. Traces of $TcO_2 \cdot xH_2O$ were removed by filtration after cooling the orange solution to room temperature. To the orange filtrate was added 0.5 g $Ph_4AsCl \cdot H_2O$ in 10 mL water. This precipitated an orange solid which was redissolved by the addition of 40 mL acetone. The solution was placed aside for 24 h during which time orange needles of [Ph_4As][TcO(edt)$_2$] precipitated. These were separated by suction filtration, washed with 30 mL ether, and dried *in vacuo*. The yield was 0.145 g, 85% based on Tc. The identity of this product was confirmed by comparison of the infrared and optical spectra with those of an authentic sample (9).

Conversion of Tc_2O_2(edt)$_3$ to [TcO(edt)$_2$]$^-$

The compound Tc_2O_2(edt)$_3$ can be converted to [TcO(edt)$_2$]$^-$ by dissolution in acetone and addition of excess ethanedithiol. After stirring for 1 h, addition of $Ph_4AsCl \cdot H_2O$ in water and evaporation of the acetone precipitates [Ph_4As][TcO(edt)$_2$] quantitatively.

Collection of the X-ray data

Precession photographs showed the crystal was monoclinic and unit cell parameters were obtained from a least-squares fit of χ, φ, and 2θ for 15 reflections in the range 23.6° <2θ <34.4° recorded on a Nicolet P3 diffractometer using graphite-monochromated Mo$K\alpha_1$ radiation (λ 0.70926 Å at 22°C). Crystal data and other numbers related to data

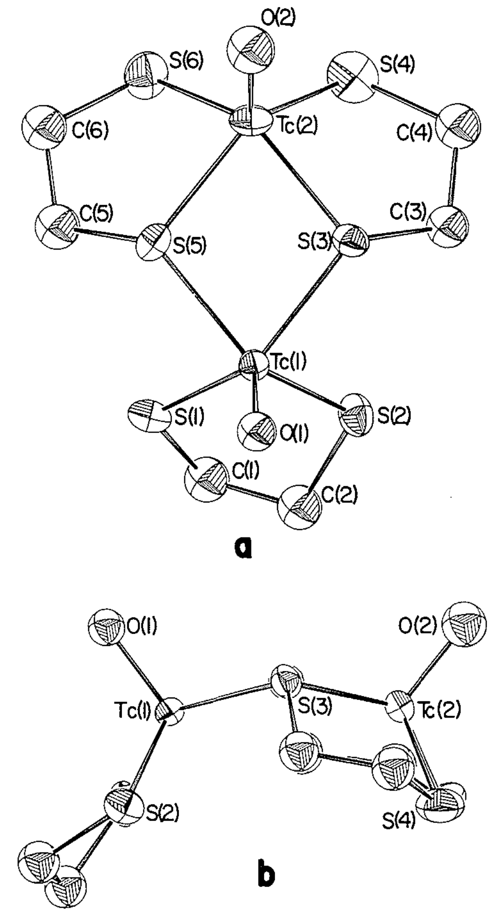

FIG. 1 (*a*) The molecule showing the atom numbering. (*b*) The molecule oriented to show the angle between the two square pyramids.

collection are summarized in Table 1. The density was obtained by flotation in a carbon tetrachloride – dibromoethane mixture. Intensities were measured on the P3 diffractometer using a coupled θ(crystal)–2θ (counter) scan. The methods of selection of scan rates and initial data treatment have been described (13, 14). Corrections were made for Lorentz polarization effects and absorption.

Solution of the structure

The coordinates of the technetium atom were found from a three-dimensional Patterson synthesis and a series of full-matrix least-squares refinements followed by three-dimensional electron density difference syntheses revealed all the atoms. At this stage the temperature factors of the technetium and sulfur atoms were made anisotropic. Tests were made to show the use of increased parameters was justified (15) except in the case of the hydrogen atoms. Further refinement, using full-matrix least-squares minimizing $\Sigma w(|F_o| - |F_c|)^2$, was terminated when the maximum shift/error was <0.04. Only x, y, z of hydrogen atoms were refined; temperature factors were fixed at roughly 50% greater than the atoms to which they were attached. Corrections were made for secondary extinction by the method of Larson (16). Throughout the refinement, the scattering curves were taken from ref. 17 and anomalous dispersion corrections from ref. 18 were applied to the curves for technetium and sulfur. The atom parameters for non-hydrogen atoms are listed in Table 2.[2]

[2] Lists of temperature factors, hydrogen atom positional parameters, best planes, dihedral and torsional angles and a listing of the moduli of the observed and calculated structure factor amplitudes and figure; unit cell packing are available from the Depository of Unpublished Data, CISTI, National Research Council of Canada, Ottawa, Ont., Canada K1A 0S2.

TABLE 3. Selected interatomic distances (Å) and angles (deg)

Atoms	Distance	Atoms	Distance	Atoms	Distance
Tc(1)—S(1)	2.260(1)	Tc(1)—S(2)	2.256(2)	Tc(1)—S(3)	2.404(1)
Tc(2)—S(4)	2.277(2)	Tc(2)—S(6)	2.283(2)	Tc(2)—S(3)	2.365(1)
Tc(1)—S(5)	2.418(2)	Tc(1)—O(1)	1.665(3)	S(3)—C(3)	1.834(7)
Tc(2)—S(5)	2.370(1)	Tc(2)—O(2)	1.661(5)	S(5)—C(5)	1.840(7)
C(3)—C(4)	1.531(8)	C(4)—S(4)	1.822(7)	S(1)—C(1)	1.821(7)
C(5)—C(6)	1.510(9)	C(6)—S(6)	1.825(7)	S(2)—C(2)	1.832(6)
C(1)—C(2)	1.50(1)	Tc(1)...Tc(2)	3.654(1)		

Bonds	Angle	Bonds	Angle	Bonds	Angle
O(1)—Tc(1)—S(1)	109.8(1)	O(1)—Tc(1)—S(2)	108.8(2)	O(1)—Tc(1)—S(3)	107.0(1)
O(1)—Tc(1)—S(5)	108.5(2)	S(1)—Tc(1)—S(2)	86.07(6)	S(1)—Tc(1)—S(3)	142.66(5)
S(1)—Tc(1)—S(5)	86.87(6)	S(2)—Tc(1)—S(3)	88.07(5)	S(2)—Tc(1)—S(5)	142.16(4)
S(3)—Tc(1)—S(5)	75.61(5)	O(2)—Tc(2)—S(3)	109.9(2)	O(2)—Tc(2)—S(4)	110.8(2)
O(2)—Tc(2)—S(5)	110.5(2)	O(2)—Tc(2)—S(6)	109.4(2)	S(3)—Tc(2)—S(4)	84.88(6)
S(3)—Tc(2)—S(5)	77.25(5)	S(3)—Tc(2)—S(6)	140.39(6)	S(4)—Tc(2)—S(5)	138.52(6)
S(4)—Tc(2)—S(6)	85.29(6)	S(5)—Tc(2)—S(6)	85.28(5)	Tc(1)—S(1)—C(1)	108.0(2)
S(1)—C(1)—C(2)	104.3(2)	C(1)—C(2)—S(2)	112.8(5)	C(2)—S(2)—Tc(1)	110.1(5)
Tc(1)—S(3)—Tc(2)	100.03(5)	Tc(1)—S(5)—Tc(2)	99.51(6)	Tc(1)—S(3)—C(3)	116.8(2)
Tc(1)—S(5)—C(5)	117.8(2)	Tc(2)—S(3)—C(3)	107.8(2)	S(3)—C(3)—C(4)	107.7(5)
C(3)—C(4)—S(4)	111.3(5)	C(4)—S(4)—Tc(2)	104.1(2)	Tc(2)—S(5)—C(5)	106.5(2)
S(5)—C(5)—C(6)	107.9(4)	C(5)—C(6)—S(6)	110.8(5)	C(6)—S(6)—Tc(2)	103.4(2)

Results and discussion

The reaction of $[n\text{-}Bu_4N][TcOCl_4]$ with either 1.5 equiv. of ethanedithiol or 2 or more equiv. of bis(acetamidomethyl)-ethanedithiol at room temperature rapidly yields orange crystals of $[(TcO)_2(edt)_3]$, **I**, in high yield. It is possible to synthesize $[TcO(edt)_2]^-$ from $[TcOCl_4]^-$ and excess $edt(acm)_2$ by the addition of NaOH and heating the reaction mixture after **I** has been formed. The base must be added after the formation of **I** because of the tendency of $[TcOCl_4]^-$ to disproportionate (9) in aqueous or basic solution. While it is possible to synthesize $[TcO(edt)_2]^-$ from a preformed suspension of **I** with excess $edt(acm)_2$ in basic solution, it proved impossible to make either this complex or **I** via the reduction of pertechnetate in the presence of $edt(acm)_2$. Attempts were made with several reducing agents upon whose utility we have previously reported (19) in these types of systems.

The positive ion field desorption mass spectrum unequivocally identifies **I** as a 3:2 complex because of the presence of two peaks m/e = 505, 507 (from ^{32}S and ^{34}S, respectively) with appropriate intensities for six sulfur atoms in the molecular unit. Unfortunately, the complicated nmr spectrum does not yield any structural information, therefore a structure determination by single crystal X-ray diffraction was undertaken.

The molecule is shown in Fig. 1 and selected interatomic distances and angles are given in Table 3. The molecule contains two technetium atoms with similar near neighbour environments. Each technetium atom sits in the centre of a square pyramid, the base formed by four sulfur atoms, and the apex occupied by a tightly bonded (Tc—O(1) 1.665(3), Tc—O(2) 1.661(3) Å) oxygen atom. The technetium atoms are 0.7410(3) Å (Tc(1)) and 0.8025(4) Å (Tc(2)) above the sulfur atom planes values similar to those reported for other $TcOS_4$ systems (0.791 Å (20), 0.761 Å (21)) and for the molybdenum atom in corresponding $LMoS_4$ systems (0.66–0.83 Å) (22, 23).

When nearest neighbours are considered, the environments of the two technetium atoms are quite different. Tc(1) is bonded to both the sulfur atoms of one ethan-1,2-dithiolate group, S(1) and S(2), and to one sulfur atom of each of the other two ethan-1,2-dithiolate groups, S(3) and S(5). S(3) and S(5) also bond to Tc(2), acting as bridges. The remaining sulfur atoms, S(4) and S(6), are also bonded to Tc(2). This type of bridging sulfur has been observed previously for the $(NH_2CH_2CH_2S)^-$ ligand in the $[Ni_3(SCH_2CH_2NH_2)_4]^{2+}$ cation (24). The structure of **I** thus has four distinct types of Tc—S bonds. The bonds to the unique ethan-1,2-dithiolate group are quite short (Tc(1)—S(1) 2.260(1), Tc(1)—S(2) 2.256(2) Å), whereas the bridging bonds *trans* to the former are 0.15 Å longer (Tc(1)—S(3) 2.404(1), Tc(1)—S(5) 2.418(1) Å). The differences in the lengths of the two types of Tc—S bonds to the remaining ethan-1,2-dithiolate groups are less, but again the bridging bonds are longer (Tc(2)—S(3) 2.365(1), Tc(2)—S(5) 2.370(1) vs. Tc(2)—S(4) 2.277(2), Tc(2)—S(6) 2.283(2) Å). The Tc—S bonds are generally shorter than Mo—S bonds to the ethan-1,2-dithiolate ligand (edt) in *syn* and *anti*-(edt)MoS-$(\mu\text{-}S)_2$-MoS(edt), **II** and **III**, probably reflecting the stronger *trans* influence of the sulfide ligand (22).

The nearest neighbour S—S distances are in the normal range for transition metal complexes, where weak sulfur–sulfur interactions have been postulated. There are significant differences between these distances, but no consistent pattern of intra-ligand distances being shorter than inter-ligand distances or vice versa. The observed pattern can be explained if it is postulated that the strongest interaction (shortest distance, S(3)—S(5) 2.956(3) Å) between the bridging sulfur atoms causes weaker interactions (S(1)—S(5) 3.218(3), S(2)—S(3) 3.241(3), S(3)—S(4) 3.133(3), S(5)—S(6) 3.153(3) Å) in adjacent S—S systems, with consequent stronger interactions in the next nearest S—S systems (S(1)—S(2) 3.082(3), S(4)—S(6) 3.089(3) Å), regardless of whether they are intra- or inter-ligand.

The two square pyramidal systems are arranged in the *syn* configuration and, as can be seen in Fig. 1*b*, form the previously unknown structure **3** as defined by Bunzey and Enemark (22), where the dihedral angle between the sulfur atom planes, measured round from plane to plane on the oxo side is >180°. The actual value of 206.5(1)° agrees well with the predicted value of 210°. There was some doubt whether a Mo—Mo bond was present in **II** and **III**, but the present structure suggests this was the case. The Tc(1)—Tc(2) distance of 3.654(1) Å is substantially longer than the Mo—Mo distances of 2.79–2.92 Å. This results in much larger M—S—M angles (Tc, 100.03(5), 99.51(6)° vs. Mo, 76.2, 76.6, 77.62°) and consequent smaller S—M—S angles (Tc, 75.61(5), 77.25(5)° vs. Mo, 99.97, 99.72, 103.38°). We considered the possibility that the larger M—S—M angles in our compound might be because the bridging S atoms are three-coordinate, compared to the two-coordinate sulfide ions in **II** and **III**. However, Rh—S—Rh angles of 79.2, 80.2° are found in $Rh_2(SC_6H_5)_2(CO)_4$, where the bridging sulfur atoms are three-coordinate and the smaller values seem to be typical of systems where a metal–metal bond is present (25). The packing of the molecules in the unit cell shows no strong intermolecular interactions; all intermolecular distances are equal to or greater than van der Waals distances. The molecules are packed in a roughly hexagonal closed packed lattice.

The 3:2 complex was first observed spectrophotometrically (10), was subsequently isolated by both procedures described herein, and now has been unequivocally characterized by X-ray crystallography. We have isolated and spectrophotometrically observed the same type of dimer (10) in the reaction of $[TcOCl_4]^-$ with *excess* 1,3-propanedithiol while trying to prepare $[TcO(SCH_2CH_2CH_2S)_2]^-$, which was originally synthesized by Byrne and Smith (8) by $NaBH_4$ reduction of ethanolic TcO_4^- in the presence of propanedithiol. The titration of $[TcOCl_4]^-$ with 3,4-toluenedithiol (10), however, leads directly to the bis(dithiolato) monomer $[TcO(S_2C_6H_3(CH_3))_2]^-$ which we have previously reported (9).

These observations, taken together, raise the possibility of steric factors governing the reaction of $[TcOCl_4]^-$ with various dithiols. Indeed, molecular model studies suggest that steric hindrance prohibits the approach of the protected dithiol at the empty sixth coordination site (*trans* to the *oxo*) (10). The same rationale applies to the extra methylene group in the 1,3-propanedithiolato complex and explains the dimer formation in the presence of excess dithiol.

The electrophilicity of the oxotechnetium(V) core is adequate to remove the acetamidomethyl blocking group from edt(acm)$_2$. Subsequent experiments with a bis(acetamidomethyl) N_2S_2 amide thiolate (26) showed that the group functions in a more predictable manner in that system because TcO has the same electrophilicity, the ligand is much larger and tetradentate, and the final ligand:Tc ratio is 1:1. This allowed the formation of this important class of $TcON_2S_2$ anions in aqueous solution with no evidence for any intermediates.

Acknowledgements

This work was supported by USPHS Grant No. GM 23270 and DOE Contract No. AC0276EV04115 (at M.I.T. and Harvard) and by NSERC of Canada (at McMaster). C.O. acknowledges an NSERC of Canada Predoctoral Fellowship while at M.I.T. (1978–1981).

1. N. D. Heindel, H. D. Burns, T. Honda, and L. W. Brady. The chemistry of radiopharmaceuticals. Masson, New York. 1978.
2. E. Deutsch, K. Libson, S. Jurisson, and L. F. Lindoy. Prog. Inorg. Chem. **20**, 75 (1983).
3. A. Davison and A. G. Jones. Int. J. Appl. Radiat. Isot. **33**, 875 (1982).
4. A. Davison, A. G. Jones, C. Orvig, and M. Sohn. Inorg. Chem. **20**, 1629 (1981).
5. A. G. Jones, A. Davison, M. R. LaTegola, J. W. Brodack, C. Orvig, M. Sohn, A. K. Toothaker, C. J. L. Lock, K. J. Franklin, C. E. Costello, S. A. Carr, K. Biemann, and M. L. Kaplan. J. Nucl. Med. **23**, 801 (1982).
6. D. F. Veber, J. D. Milkowski, R. G. Denkewalter, and R. Hirschman. Tetrahedron Lett. 3057 (1968).
7. D. F. Veber, J. D. Milkowski, S. L. Varga, R. G. Denkewalter, and R. Hirschman. J. Am. Chem. Soc. **94**, 5456 (1972).
8. E. F. Byrne and J. E. Smith. Inorg. Chem. **18**, 1832 (1979).
9. A. Davison, C. Orvig, H. S. Trop, M. Sohn, B. V. DePamphilis, and A. G. Jones. Inorg. Chem. **19**, 1988 (1980).
10. B. V. DePamphilis, A. G. Jones, and A. Davison. Inorg. Chem. **22**, 2292 (1983).
11. A. Einhorn. Justus Liebigs Ann. Chem. **343**, 207 (1905).
12. B. W. Wilson, C. E. Costello, S. A. Carr, K. Biemann, C. Orvig, A. Davison, and A. G. Jones. Anal. Lett. **12**(A3), 303 (1979).
13. B. Lippert, C. J. L. Lock, B. Rosenberg, and M. Zvagulis. Inorg. Chem. **16**, 1525 (1977).
14. R. P. Hughes, N. Krishnamachari, C. J. L. Lock, J. Powell, and G. Turner. Inorg. Chem. **16**, 314 (1977).
15. W. C. Hamilton. Acta Crystallogr. **18**, 502 (1965).
16. A. C. Larson. Acta Crystallogr. **23**, 664 (1967).
17. D. T. Cromer and J. A. Waber. International tables for X-ray crystallography. Vol. IV. *Edited by* J. A. Ibers and W. C. Hamilton. Kynoch Press. Birmingham, England. 1974. Table 2.2B.
18. D. T. Cromer. Reference 18, Table 2.3.1. pp. 149, 150.
19. A. G. Jones, C. Orvig, H. S. Trop, A. Davison, and M. A. Davis. J. Nucl. Med. **21**, 279 (1980).
20. B. V. DePamphilis, A. G. Jones, M. A. Davis, and A. Davison. J. Am. Chem. Soc. **100**, 5570 (1978).
21. J. R. Smith, E. F. Byrne, F. A. Cotton, and J. C. Sekutowski. J. Am. Chem. Soc. **100**, 5571 (1978).
22. G. Bunzey and J. H. Enemark. Inorg. Chem. **17**, 682 (1978).
23. L. Ricard, J. Estienne, P. Karagiannidis, P. Toledano, J. Fischer, A. Mitschler, and R. Weiss. J. Coord. Chem. **3**, 277 (1974).
24. C. H. Wei and L. F. Dahl. Inorg. Chem. **9**, 1878 (1970).
25. J.-J. Bonnet, P. Kalck, and R. Poilbanc. Inorg. Chem. **16**, 1514 (1977).
26. A. Davison, A. G. Jones, C. Orvig, M. Sohn, M. R. LaTegola, and G. Freeman. J. Nucl. Med. **22**, P57 (1981).

IV. Order−disorder transitions: solid state kinetics, thermal analyses, X-ray diffraction and electrical conductivity studies in the $Ag_2SO_4-K_2SO_4$ system

M. SUNITHA KUMARI AND ETALO A. SECCO[1]
Chemistry Department, St. Francis Xavier University, Antigonish, N.S., Canada B2G 1CO

M. SUNITHA KUMARI and ETALO A. SECCO. Can. J. Chem. **63**, 324 (1985).

Order−disorder transitions occurring in the $Ag_2SO_4-K_2SO_4$ system were investigated by reaction kinetics, thermal analyses, X-ray diffraction, and electrical conductivity techniques. Solid−liquid and solid−solid phase diagrams are reported.

The conductivity data in the high temperature phase of the solid resemble superionic conductivity behavior. The higher conductivity of Ag_2SO_4 with K^+ presence relative to pure Ag_2SO_4 and $Ag_{2-x}Na_xSO_4$ compositions support a lattice expansion facilitating higher mobility of ions.

The reaction kinetics, X-ray diffraction, and electroconductivity results suggest a relatively open periodic SO_4^{2-} sublattice in the high-temperature phase of the sulfate-based systems studied in this series.

M. SUNITHA KUMARI et ETALO A. SECCO. Can. J. Chem. **63**, 324 (1985).

Faisant appel aux cinétiques de réaction et aux techniques d'analyse thermique, de diffraction de rayons-X et de conductivité électrique, on a étudié les transitions ordre-désordre qui se produisent dans le système $Ag_2SO_4-K_2SO_4$. On rapporte les diagrammes de phase solide-liquide et solide−solide.

Les donnés de conductivité thermique de la phase à haute température ressemblent à un comportement de conductivité superionique. Le fait que la conductivité du Ag_2SO_4, en présence de K^+, soit plus élevée que celle du Ag_2SO_4 à l'état pur ou de celles des compositions $Ag_{2-x}Na_xSO_4$ milite en faveur d'une expansion du réseau facilitant ainsi une mobilité plus grande des ions.

Les résultats observés avec les cinétiques de réaction, avec la diffraction de rayons-X et avec l'électroconductivité suggèrent la présence d'un sous-réseau périodique d'ions SO_4^{2-} qui est relativement ouvert dans la phase à haute température des systèmes à base de sulfates étudiés dans cette série.

[Traduit par le journal]

Introduction

Binary sulfates containing monovalent cations are members of a group of compounds which exhibit fast-ion or "superionic" conductivity in the high temperature phase (1). Such compounds are referred to as superionic conductors (SIC's) or solid electrolytes and have attracted considerable attention because of (*i*) their promise in applications in high-energy-density batteries and (*ii*) their unusual transport behavior.

The mechanism of fast-ion conduction is not completely understood although proposed models involve basically two structural types, viz. (*i*) layer structure as in β-alumina and (*ii*) channel structure as in α-AgI or in NASICON where an open network or skeleton framework of anions facilitates cation mobility (1). This paper is part of a continuing effort (2−4) to probe the nature of the phase transition, the structure of the high temperature phase and the effects of guest ions relating to the mechanism of fast-ion conductivity in binary sulfate systems.

Our earlier study on Na^+ presence in Ag_2SO_4 lattice revealed a decrease in conductivity in $Ag_{2-x}Na_xSO_4$ compositions attributed to lattice contraction resulting from $r_{Na^+} < r_{Ag^+}$. The interpretation suggested that incorporation of a slightly larger radius cation in the Ag_2SO_4 lattice would effect a higher conductivity. To test this hypothesis, the slightly larger radius K^+ was chosen, $r_{K^+} = 133$ pm versus $r_{Ag^+} = 126$ pm.

The high temperature form of Ag_2SO_4, II-Ag_2SO_4(α), hexagonal and space group $P6_3/mmc$ with unit cell dimensions $a_o = 5.519$ Å, $c_o = 7.504$ Å (5) is isomorphic with the high temperature form of K_2SO_4, α-K_2SO_4, with unit cell dimensions $a_o = 5.90$ Å, $c_o = 8.11$ Å, and $Z = 2$ (6). The structure of α-K_2SO_4 is described as disordered where the anions are evenly distributed among two oppositely directed orientations. Furthermore, the low temperature forms of Ag_2SO_4, I-Ag_2SO_4 (β) (7), and of K_2SO_4, β-K_2SO_4 (8), are isostructural orthorhombic with space groups *Fddd* and *Pnam*, respectively. To our knowledge, the only literature record of the Ag_2SO_4 phase diagram is the early report by Nacken (9) showing the existence of solid solutions and solid−solid phase transitions over the complete composition range.

This paper contains the results of a study on the condensed phase transitions in the $Ag_2SO_4-K_2SO_4$ system, the kinetics of the solid-state reaction between Ag_2SO_4 and K_2SO_4 and the conductivity of selected undoped and doped (Cd^{2+}), $Ag_{2-x}K_xSO_4$ compositions using thermal analyses, DSC, electroconductivity, and X-ray diffractometry techniques.

Experimental

Anhydrous Ag_2SO_4 and anhydrous K_2SO_4 were Alfa Products ultrapure grade; $CdSO_4$ was Fisher Certified grade. All $Ag_2SO_4-K_2SO_4$ samples were prepared by fusing the requisite composition mixture, previously well ground manually, of the respective sulfates in a Pt crucible.

DTA traces were recorded on a duPont 990 Thermal Analyzer in a flowing N_2 (ultrapure) atmosphere using ignited Al_2O_3 as reference material. The precision of a melting temperature was ±5°C whereas the transition temperature measurement was within ±2°C. The enthalpies of transformation were evaluated with the DSC accessory to the 990 DTA module using the heats of fusion or transition for In, Sn, Zn, AgI, CsCl as references; samples were encapsulated in Al containers — identical results within experimental error were obtained using Au containers.

X-ray diffraction patterns were obtained using a Norelco diffractometer with CuK_α radiation. Diffraction patterns at elevated temperatures were recorded with a Model X-86-N high temperature accessory (Materials Research Corp.) attached to the Norelco unit (10).

Electrical conductivity measurements were made on compressed polycrystalline sample in a stainless steel conductivity cell following the procedure described earlier (3, 11). The Ag_2SO_4-rich samples were in the form of a disc, 1 mm thick and 100 m^2 in surface area; other compositions were 1 mm thick and ~75 mm^2 in surface area of the crack-free portion recovered from the compressed disc.

[1]To whom all correspondence should be addressed.

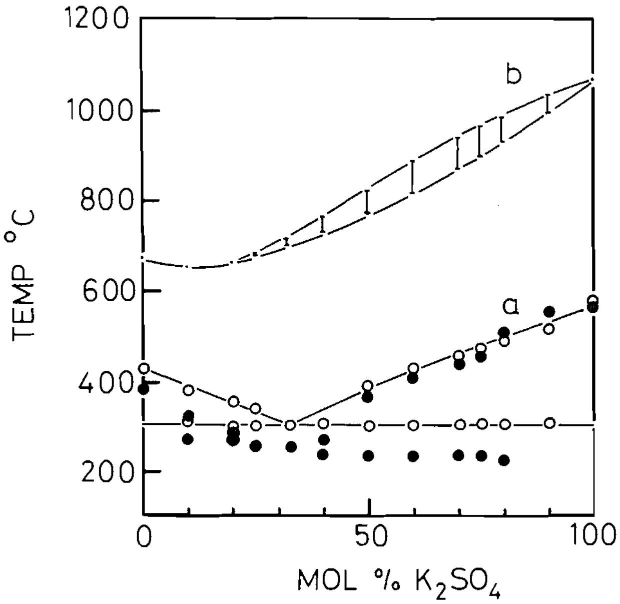

FIG. 1. (*a*) Solid−solid phase diagram of the $Ag_2SO_4-K_2SO_4$ system; ○, heat mode, ●, cool mode. (*b*) Solid−liquid phase diagram $Ag_2SO_4-K_2SO_4$ system, heat mode.

In the solid state kinetics measurements each sample of $Ag_2SO_4-K_2SO_4$ mixture, 2:1 mole ratio, of constant mass was ground manually to a uniform consistency; the sample was maintained at the set temperature in the DTA cell in the isothermal mode for the required time interval. The fraction of reaction of the 2:1 eutectoid, α, was evaluated by comparing the DSC enthalpic areas in the heat mode of the individual transitions for the final eutectoid state. The low degree of crystallinity of the samples did not permit a cross-check of the DSC kinetic data with X-ray diffraction data using the characteristic X-ray peak heights.

Results and discussion

Phase diagram

The transition temperatures recorded on DTA traces are plotted versus composition in Fig. 1 — Fig. 1(*a*) represents the solid−solid phase diagram and Fig. 1(*b*) represents the solid−liquid phase diagram. The Fig. 1(*b*) plot is in agreement with Nacken's report (9) but the Fig. 1(*a*) plot differs significantly from Nacken's — however, the relationship between our Fig. 1(*a*) cool mode data, filled circles, and Nacken's plot is apparent. Figure 2 gives the enthalpy change, ΔH_t, dependence on composition for the solid−solid transition.

The solid−liquid diagram is of the minimum type solid solution normally expected for isostructural binary systems with the noteworthy absence of the liquidus curve in the 80−100% Ag_2SO_4 region. Reisman (12) has done theoretical analyses of minimum type solid solutions using computer-derived models incorporating ΔH_f°, heat of fusion, and T_0, the melting temperature for each component. The minimum involves dimer−monomer transformation or dissociation of one component on melting which is displaced markedly toward the lower melting component when the higher melting component undergoes dissociation and vice versa. The minimum at 85% Ag_2SO_4 in Fig. 1(*b*) supports K_2SO_4 dissociation on melting as was found in the $Na_2SO_4-K_2SO_4$ system (2).

The solid state phase diagram, Fig. 1(*a*), displays solid solution behavior with the existence of an eutectoid at 305°C and 33 mol% K_2SO_4. The cool mode data, filled circles, show

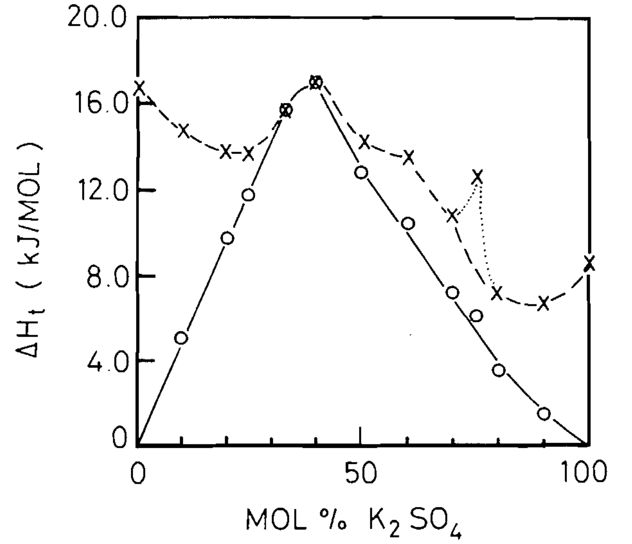

FIG. 2. Plot of enthalpy change for solid−solid phase transitions versus composition in $Ag_2SO_4-K_2SO_4$ system; ○, only 305°C transition value and ×, total sum.

irregular behavior and appreciable hysteresis effects relative to the heat mode data, open circles, for the eutectoid and Ag_2SO_4-rich compositions, i.e. >60%. The eutectoid composition was chosen at 33 mol% instead of 25 or 40% on the basis that a single thermal effect was reproducible on both heat and cool modes. It can be argued that the maximum ΔH_t value, Fig. 2, suggests 40% to be a more justifiable eutectoid composition. On the other hand, the maximum ΔH_t value may result from mixing or relative increased disorder — thus suggesting that 33% is the more ordered state with possible compound characteristics. The abnormal ΔH_t value for 75% K_2SO_4 is reproducible but unexplained — the only distinct feature of this datum being its broad temperature range, 385−485°C, for the solidus line transition. Thermal hysteresis effect, $\Delta T = T_p^f - T_p^r$, where T_p^f refers to the peak temperature on heating and T_p^r to the peak temperature on cooling, has been linked (13) to the co-existence mechanism of continuous transformations, the main factor controlling the hysteresis being the strain energy E_s, where $E_s \propto \Delta T \cdot \Delta S$ and ΔS is the entropy change for the transformation. Another basis for the hysteresis effect may be the disorder → order direction which imposes a configurational requirement of "long-range" order with the ordered migration of ions from one set of sites to another expressed by the relation $\Delta S = R \ln Q$ where Q is the ratio of the numbers of disordered states in the two phases (14).

X-ray diffraction

X-ray diffraction patterns at room temperature and above the transition temperature for Ag_2SO_4, K_2SO_4, 33 mol% K_2SO_4, 50 mol% K_2SO_4, and 70 mol% K_2SO_4 are presented in Fig. 3. The patterns confirm the solid phase structural transformation. The high temperature patterns of all compositions are simpler than their room temperature patterns. The high temperature pattern at 33 mol% K_2SO_4 closely resembles the Ag_2SO_4 high temperature pattern displaced to slightly higher "*d*" spacing. The characteristic high temperature peaks of 50 and 70 mol% K_2SO_4 appear at much higher "*d*" spacing relative to Ag_2SO_4. These patterns suggest that the low temperature structure of the $Ag_2SO_4-K_2SO_4$ solid state system undergoes a transformation to a phase resembling the II-Ag_2SO_4(α) form at high temperature. These results parallel the structural transformation behav-

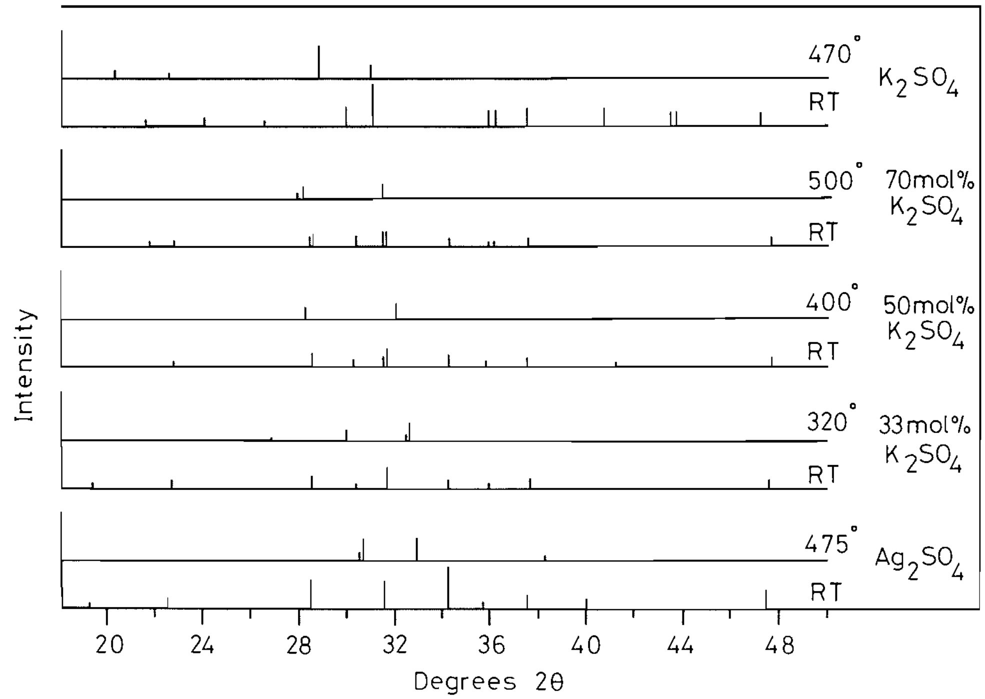

FIG. 3. X-ray diffraction line patterns, converted from diffractogram peaks, of relative intensity versus angle 2θ for Ag_2SO_4, 33, 50, 70 mol% K_2SO_4, and K_2SO_4 at room temperature (RT) and transition temperatures in °C.

ior observed for the $Na_2SO_4-Ag_2SO_4$ solid solution system (4) and $Na_2SO_4-K_2SO_4$ system (17).

Solid state kinetics

The best fit between the experimental results and the known kinetic equations, over the temperature range 323−369°C for reaction fraction α up to 0.8, was obtained for the second-order rate expression by Honig *et al.* (15) which at sufficiently large *t* takes the form

$$[1] \quad (1 - \alpha)^{-1} = 1 + \sigma G N_g t$$

where $(1 - \alpha)$ represents the unreacted fraction, σ is the shape factor, *G* is the lineal growth rate of the new phase, N_g is the initial density of germ nuclei, and *t* is the time. Equation [1] is also recognized as the integrated form of the second-order rate law, where integration of

$$d\alpha/dt = k(1 - \alpha)^2$$

yields

$$[2] \quad (1 - \alpha)^{-1} = 1 + kt$$

Plots of $(1 - \alpha)^{-1}$ versus time give straight lines for 2:1 mole ratio $Ag_2SO_4:K_2SO_4$, Fig. 4(*a*), whose slopes equal the formal rate constant *k* or the composite quantity $\sigma G N_g$, along with the intercept of unity. The slope of the standard Arrhenius plot of log *k* versus $T\,(K)^{-1}$, Fig. 4(*b*), yields an activation energy, E_a, of 96 ± 10 kJ/mol. This value is in contrast to the E_a values of 232 and 165 kJ/mol for $KNaSO_4$ and $K_3Na(SO_4)_2$, respectively.

The second-order rate behavior and the relatively high *k* values, i.e. $\sim 10^{-1}$, involving two solid reactants in solid state reactions is uncommon and the mechanism for such a reaction rate must incorporate highly mobile reacting species. The reaction mechanism is envisaged (2) to involve the cations as the effective reacting species in a sublattice of SO_4^{2-} units and the fundamental reaction step being the ordering of the cations on crystallographically preferential lattice sites which constitute a sublattice of superstructures or incommensurate structures (16). The model might be classified as involving a type of quasi-homogeneous solid state ionic reaction where a simple first-order dependence on the two principal reactants results in the overall second-order rate. The proposed model requires highly mobile cations, implying high ionic conductivity, in agreement with data reported in the following section.

Electrical conductivity

The temperature dependence of the ionic conductivity, σ, is interpreted in terms of the Arrhenius-type equation

$$\sigma = (\sigma_o/T) \exp(-Q_c/RT)$$

where σ_o represents a composite constant $(ne^2\lambda^2\nu/k)$, *n*, the number of ions per unit volume, *e*, the ionic charge, λ, the distance between the two jump positions, ν, the jump frequency, *k*, the Boltzmann constant, and Q_c is the activation energy for ionic motion, assuming the conductivity to be effectively ionic with negligible electronic or hole conductivity.

Plots of log (σ*T*) vs. $T(K)^{-1}$ for pure Ag_2SO_4 along with doped and undoped 33 mol% K_2SO_4 are presented in Fig. 5. In Fig. 6 are given plots of log (σ*T*) vs. $T(K)^{-1}$ for undoped 25 and 60 mol% K_2SO_4. The reproducibility of T_t for the major transition effect for the undoped compositions, 302−305°C, is in excellent agreement with T_t values from heat mode DTA, Fig. 1(*a*); the 2 mol% $CdSO_4$-doped sample (■,□) Fig. 5, shows a lower T_t of 292°C. A pronounced hysteresis effect occurs in all $Ag_2SO_4-K_2SO_4$ compositions plotted. While the 2 mol% $CdSO_4$-doped sample possesses a slightly higher conductivity prior to the transition than its undoped counterpart, the two samples show the same post-transition conductivity values. The predicted enhanced conductivity of Ag_2SO_4 containing K^+ on the basis of lattice expansion due to the larger K^+ radius is observed. On the other hand, the presence of 2 mol% Cd^{2+} with its attendant vacancies in the $Ag_2SO_4-K_2SO_4$ structure did not

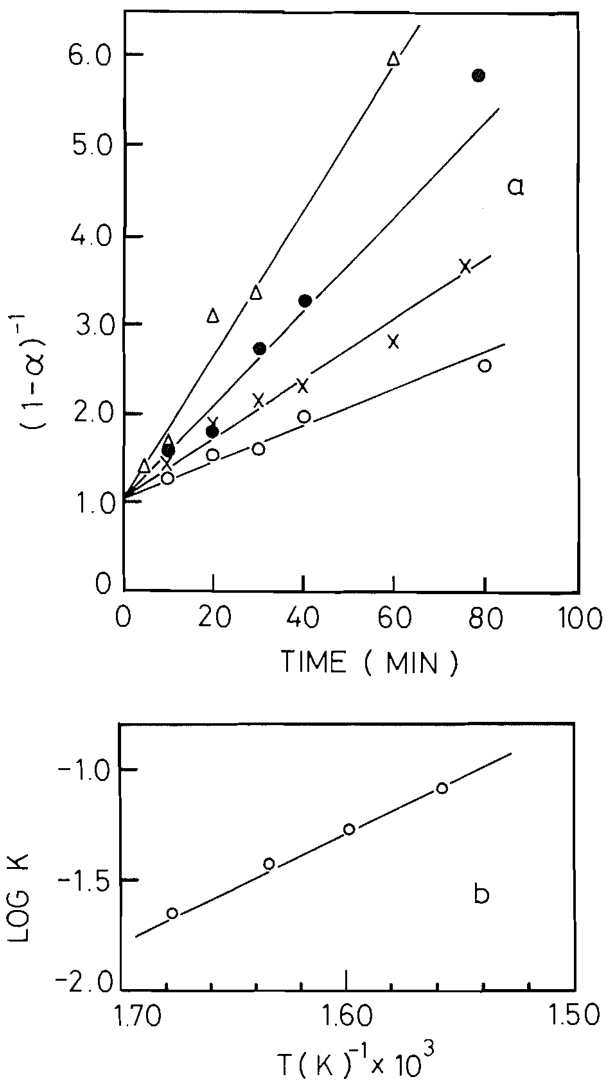

FIG. 4. (*a*) Plot of $(1-\alpha)^{-1}$ versus time, second order rate law; ○ 323°C, × 339°C, ● 353°C, △ 369°C. (*b*) Plot of log *k* versus T^{-1}.

increase the conductivity as expected. However, a counter balancing effect of lattice contraction by the smaller Cd^{2+}, $r_{Cd^{2+}}$ = 100 pm relative to r_{K^+} and r_{Ag^+} ~130 pm, might have militated against the anticipated increase as was found for the Ag_2SO_4–Na_2SO_4 system.

The $\sigma-T$ behavior of 25 and 60 mol% K_2SO_4 reveals along with erratic conductivity behavior in the post-transition region above 440°C. Such a decrease in conductivity versus temperature has been reported for Na_2SO_4 (18) and CsCl (19). The striking feature of such behavior is the recovery of the higher conductivity values and the regain of stability on the cool mode. The conductivity drop is interpreted in terms of collapse of the SO_4 framework, i.e. SO_4^{2-} sublattice, and its subsequent recovery on cooling implies restructuring of that sublattice. Contrast these effects with the "anti-hysteresis" effect observed in CD^{2+}-doped $KNaSO_4$ (3) and undoped 40 mol% Ag_2SO_4–Na_2SO_4 ascribed to vacancy–cation cluster formation analogous to that proposed for anion conductors (20).

The activation energy values for the ionic conductivity Q_c in the temperature region 525–650 K for 25, 33, and 60 mol% are tabulated in Table 1. The constant Q_c value, 41 ± 4 kJ/mol, in the two phases for 25 mol% K_2SO_4 and for doped and

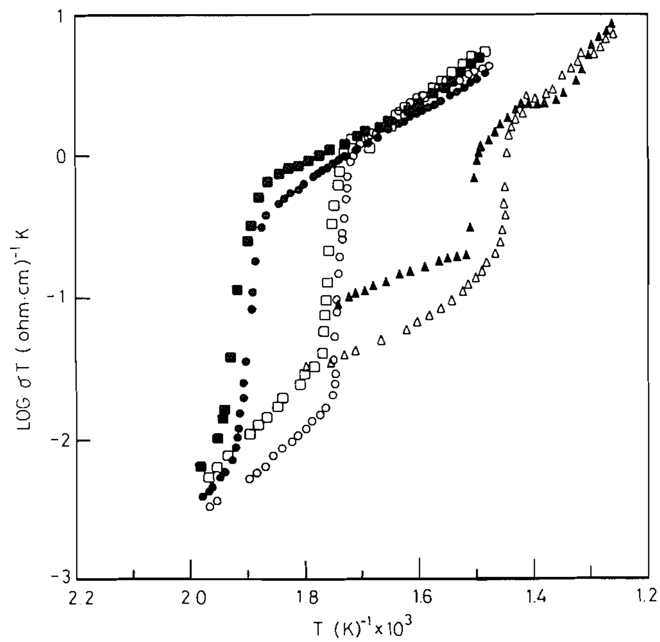

FIG. 5. Plots of log σT versus T^{-1}. Ag_2SO_4, △, ▲, heat and cool modes, respectively; 33 mol% K_2SO_4, ○, ●, heat and cool modes, respectively; 2 mol% Cd^{2+} in 33 mol% K_2SO_4, □, ■ heat and cool modes, respectively.

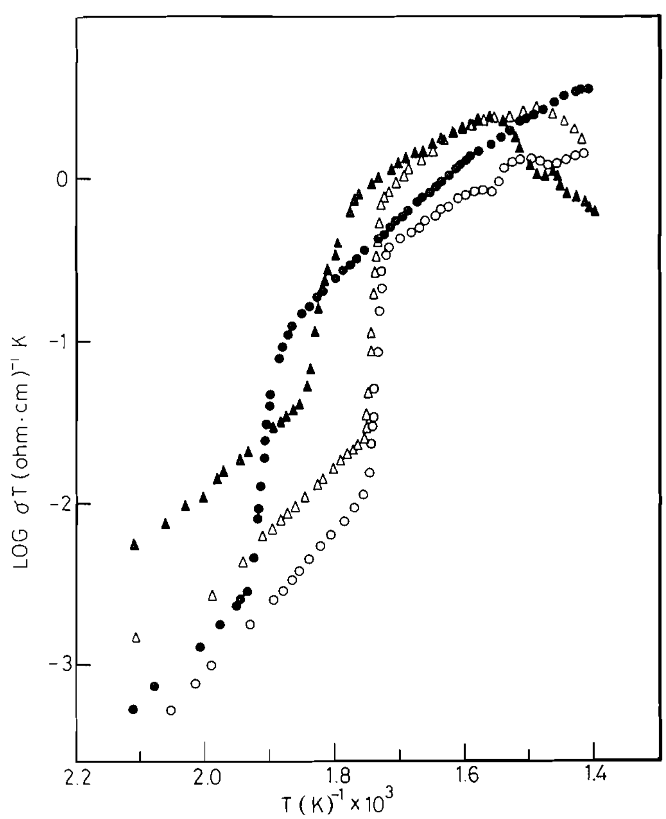

FIG. 6. Plots of log σT versus T^{-1}, 25 mol% K_2SO_4, △, ▲ heat and cool modes, respectively; 60 mol% K_2SO_4, ○, ● heat and cool modes, respectively.

undoped 33 mol% K_2SO_4 suggests a common ionic species, viz. Ag^+ and conductivity mechanism. The higher Q_c and lower relative conductivity values in the two phases of 60 mol% K_2SO_4 suggest a smaller concentration of mobile ions

TABLE 1. Ionic conductivity activation energy values, Q_c, of various samples (% K_2SO_4)

Composition	Temperature region[a]	Q_c (kJ/mol) 25 mol%	33 mol%	60 mol%
Pure	A	76.8 ± 10	41.4 ± 4	90.2 ± 9
	B	1150 ± 100	1015 ± 100	1200 ± 100
	C	45.0 ± 4	44.2 ± 4	97.5 ± 10
2 mol% Cd^{2+}	A	—	36.8 ± 4	—
	B	—	966 ± 100	—
	C	—	46.0 ± 4	—

[a]A, ordered phase; B, transition; C, disordered phase.

or a larger ion, viz. K^+. These Q_c values are within limits of experimental error of the Q_c values observed in $KNaSO_4$ and $K_3Na(SO_4)_2$ (3), pure and doped Na_2SO_4 (4) and 40 mol% $Ag_2SO_4-Na_2SO_4$ system (4). The average Q_c of 1100 ± 100 kJ/mol for the phase transition of all compositions in Table 1 are in contrast with the average Q_c for Ag_2SO_4 and 40 mol% $Ag_2SO_4-Na_2SO_4$ (4) but compares with the Q_c and E_a activation energy values reported for phase transitions in $KNaSO_4$ and $K_3Na(SO_4)_2$ (2), K_2SO_4 (21), ZnS (22), and anthranilic acid (23).

The picture that emerges from the sulfate-based systems studied in this series is that a closely related structure of a relatively open periodic SO_4^{2-} sublattice exists in the high-temperature post-transition region. The open SO_4^{2-} framework facilitates the motion of the mobile cations contributing to the fast-ion or superionic conductivity in these systems. The superionic conductivity can be affected by contraction or expansion of the sublattice, within structural limits, effected by guest cations of different ionic radii relative to the host cation and/or by the presence of vacancies on cation lattice sites. This analysis further suggests that the presence of guest anions of different ionic radii and charges, e.g. WO_4^{2-}, TeO_4^{2-}, PO_4^{3-}, etc. in the SO_4^{2-} sublattice would effect similar or parallel behavior — this study is being considered in this series.

Acknowledgment

The authors are indebted to the Natural Sciences and Engineering Research Council of Canada for financial support.

1. P. VASHISHTA, J. N. MUNDY, and G. K. SHENOY (*Editors*). Fast ion transport in solids. Elsevier North-Holland Inc., New York. 1979.
2. M. S. KUMARI and E. A. SECCO. Can. J. Chem. **61**, 594 (1983).
3. M. S. KUMARI and E. A. SECCO. Can. J. Chem. **61**, 599 (1983).
4. M. S. KUMARI and E. A. SECCO. Can. J. Chem. **61**, 2804 (1983).
5. J. M. NEWSAM, A. K. CHECTHAM and B. C. TOFILED. Fast ion transport in solids. *Edited by* P. Vashishta, J. N. Mundy, and G. K. Shenoy. Elsevier North-Holland Inc., New York. 1979. p. 435.
6. A. J. VAN DEN BERG and F. TUINSTRA. Acta Crystallogr. B**34**, 3177 (1978).
7. ASTM File No. 7-203.
8. J. A. MCGINNETY. Acta Crystallogr. B**28**, 2845 (1972).
9. R. NACKEN. Neues Jahrb. Mineral. Geol. **24**, 55 (1907).
10. E. A. SECCO. Can. J. Chem. **42**, 2143 (1964).
11. M. NATARAJAN and E. A. SECCO. Can. J. Chem. **52**, 712 (1974).
12. A. REISMAN. Phase equilibria. Academic Press, New York. 1970. Chapts. 29, 30.
13. C. N. R. RAO and K. J. RAO. Progress in solid state chemistry. *Edited by* H. Reiss. **4**, 131 (1967).
14. G. B. GUTHRIE and J. P. MCCULLOUGH. J. Phys. Chem. Solids, **18**, 53 (1961).
15. A. W. CZANDERNA, J. M. HONIG, and C. N. R. RAO. Trans. Faraday Soc. **54**, 1069 (1958).
16. E. MAKOVICKY and B. G. HYDE. Structure and bonding. **46**, 101 (1981) (as quoted in Gmelin Newsletter No. 2, 1982, Springer-Verlag New York, Inc.).
17. M. S. KUMARI and E. A. SECCO. Can. J. Chem. **61**, 2804 (1983).
18. R. MACL. MURRAY and E. A. SECCO. Can. J. Chem. **56**, 2616 (1978).
19. M. NATARAJAN. Ph.D. Dissertation. Indian Institute of Technology, Kanpur, India. 1970. Chapt. III.
20. H. SCHMALZRIED. Z. Phys. Chem. **105**, 47 (1977).
21. F. A. I. EL-KABBANY. Phys. Stat. Sol. (a) **58**, 373 (1980).
22. T. BANSAGI, E. A. SECCO, O. K. SRIVASTAVA, and R. R. MARTIN. Can. J. Chem. **46**, 2881 (1968).
23. K. RAJESHWAR and E. A. SECCO. Can. J. Chem. **54**, 2509 (1976).

Halogenodephenylation of triphenyltin(IV) pseudohalides

P. C. SRIVASTAVA,[1] S. K. SRIVASTAVA, AND SUMAN B. SHARMA
Department of Chemistry, University of Lucknow, Lucknow – 226007, India

Received December 20, 1983[2]

P. C. SRIVASTAVA, S. K. SRIVASTAVA, and SUMAN B. SHARMA. Can. J. Chem. **63**, 329 (1985).

The halogenodephenylation of Ph_3SnX (X = NCO, NCS, and N_3) with IX′ (X′ = Cl and/or Br) yielded new $Ph_2Sn(X)X'$ and PhI. The diphenyltin mixed halide pseudohalides have been characterised by elemental analyses, molar conductance, molecular weight, tlc data, ir, and ^1H nmr spectral studies.

$Ph_2Sn(NCS)Br$ with DMSO forms $Ph_2Sn(NCS)Br\cdot 2DMSO$ complex.

P. C. SRIVASTAVA, S. K. SRIVASTAVA et SUMAN B. SHARMA. Can. J. Chem. **63**, 329 (1985).

L'halogénodéphénylation du Ph_3SnX (X = NCO, NCS et N_3) à l'aide de IX′ (X′ = Cl et/ou Br) conduit à du PhI et aux nouveaux composés $Ph_2Sn(X)X'$. On a caractérisé ces nouveaux composés en se basant sur des données d'analyse élémentaire, de conductivité molaire, de poids moléculaire et de C.C.M. ainsi que sur des études des spectres ir et rmn du ^1H.

Le $Ph_2Sn(NCS)Br$ et le DMSO forment le complexe $Ph_2Sn(NCS)Br\cdot 2DMSO$.

[Traduit par le journal]

Introduction

The cleavage reactions of tetraorganotins of the type $ArSnR_3$ (Ar = aryl, R = alkyl) have been extensively studied (1). There seems to be no report on the cleavage reactions of Ar_3SnX (X = pseudohalide). As a part of our studies on $Ph_3Sn(IV)$ pseudohalides (2–6), we report the halogenodephenylation of Ph_3SnX (X = NCO, NCS, and N_3) with ICl and/or IBr which yields hitherto unknown diphenyltin(IV) mixed halide pseudohalides; $Ph_2Sn(X)X'$ (X = NCS, X′ = Cl and Br; X = NCO, X′ = Cl; and X = N_3, X′ = Cl) and PhI. The $Ph_2Sn(X)X'$ have been characterised through elemental analyses, molar conductance, molecular weight, tlc data, ir, and ^1H nmr spectral studies.

$Ph_2Sn(NCS)Br$ with DMSO in acetone gives the complex $Ph_2Sn(NCS)Br\cdot 2DMSO$ which contains oxygen-bonded DMSO (ir evidence) and is non-electrolytic and monomeric in nitrobenzene.

Experimental

Materials and methods

Ph_3SnNCS (7), Ph_3SnNCO (8), Ph_3SnN_3 (9), and IBr (10) were prepared. ICl (Fluka) was procured commercially. The halides (Cl or Br) were estimated volumetrically (11) after decomposing the compounds with alcoholic KOH. All reactions and manipulations were carried out under nitrogen and the physicochemical measurements were done as before (4).

Halogenodephenylation reactions

Ph_3SnNCS with ICl (1:1): A solution of ICl (1.62 g, 0.01 mol) in $CHCl_3$ (25 mL) was added dropwise with vigorous stirring to a 50 mL chloroform solution of Ph_3SnNCS (4.08 g, 0.01 mol) at room temperature. This procedure was followed immediately by decolourisation. After complete addition, the mixture was refluxed for 2 h and concentrated by distilling off the excess of solvents at reduced pressure (10 mm Hg). It was then distilled to give PhI (1.32 g, 64.7%). To the residue 5 mL petroleum ether (40–60°C) was added and kept at 0°C. After 24 h a light yellow solid separated. This solid was washed with petroleum ether (40–60°C) and dried at 20°C/10 mm Hg and identified as $Ph_2Sn(NCS)Cl$ (1.65 g, 45%; mp 162°C).

Ph_3SnNCS with IBr (1:1): Under similar experimental conditions Ph_3SnNCS (4.08 g, 0.01 mol) with IBr (2.07 g, 0.01 mol) yielded PhI (1.45 g, 71.8%) and a light yellow solid, $Ph_2Sn(NCS)Br$ (2.05 g, 49.9%; mp 155°C).

Ph_3SnNCO with ICl (1:1): Reaction of Ph_3SnNCO (3.92 g, 0.01 mol) with ICl (1.62 g, 0.01 mol) in chloroform yielded PhI (1.73 g, 85%) and (1.75 g, 50%; mp 180°C) solid $Ph_2Sn(NCO)Cl$.

Ph_3SnN_3 with ICl (1:1): Reaction of Ph_3SnN_3 (3.92 g, 0.01 mol) with ICl (1.62 g, 0.01 mol) under similar conditions yielded PhI (1.63 g, 80%) and solid $Ph_2Sn(N_3)Cl$ (1.57 g, 45%; mp 167°C).

Preparation of complex $Ph_2Sn(NCS)Br\cdot 2DMSO$: To a solution of $Ph_2Sn(NCS)Br$ (4.11 g, 0.01 mol) in anhydrous acetone (20 mL) was added DMSO (1.56 g, 0.02 mol) ligand in 10 mL acetone. The mixture was refluxed for 3 h and excess solvent was distilled off. Petroleum ether (5 mL) (60–80°C) was added and the solution on concentration and cooling gave white crystalline solid which was washed with petroleum ether (60–80°C) and dried at 20°C/10 mm Hg and was identified as $Ph_2Sn(NCS)Br\cdot 2DMSO$ (3.97 g, 70%; mp 165°C).

Results and discussion

The phenyl group of Ph_3Sn pseudohalides is cleaved in preference to pseudohalide group by ICl and/or IBr and these reactions provide synthetic routes to hitherto unknown $Ph_2Sn(IV)$ mixed halide pseudohalides, $Ph_2Sn(X)X'$ (X = pseudohalide and X′ = Cl or Br). The recrystallisation of these compounds from CCl_4 and dichloromethane separately yielded the same product of same melting points indicating that these were pure compounds. Further, in tlc, the exhibition of a single spot by $Ph_2Sn(NCS)Cl$ (Rf. 0.47, ethyl acetate/*n*-propanol (3:2)), $Ph_2Sn(NCS)Br$ (Rf. 0.40, ethyl acetate/*n*-propanol (3:2)), $Ph_2Sn(NCO)Cl$ (Rf. 0.50, ethyl acetate/*n*-propanol (3:2)), and $Ph_2Sn(N_3)Cl$ (Rf. 0.80, chloroform/methanol (3:2)) and their parent compounds Ph_3SnNCS, Ph_3SnNCO, and Ph_3SnN_3 of Rf. 0.44, 0.64, and 0.60, respectively, in the stated solvent systems confirmed the purity of these compounds obtained after the halogenodephenylation reactions. The objective of complexing $Ph_2Sn(NCS)Br$ with DMSO were two-fold: (*i*) for checking the purity of the compound $Ph_2Sn(NCS)Br$ through ^1H nmr and (*ii*) the ease of formation of the adduct indicated that $Ph_2Sn(NCS)Br$ is as good acceptor as $Ph_2Sn(NCS)_2$, (7, 12). The molar conductance data in nitrobenzene indicate that they are non-electrolytes and molecular weight data in the same solvent show their monomeric character (Table 1). Further cleavage reactions of $Ph_3Sn(IV)$ pseudohalides with IN_3 and BrCN are in progress.

[1] To whom all correspondence should be addressed.
[2] Revision received June 25, 1984.

TABLE 1. Characterisation data for $Ph_2Sn(X)X'$ [¶]

Compound $Ph_2Sn(X)X'$		Elemental analysis (%) obsd. (calcd.)					Molar conductance (10^{-3} M)	Molecular weight obsd.	Infrared (cm^{-1})			^1H nmr (δ) ppm	
X	X′	Sn	C	H	N	X′ [‖]	(ohm^{-1} cm^2 mol^{-1})	(calcd.)	ν_{asy}	ν_{sym}	Solvent	Phenyl protons	Multiplicity
NCO	Cl	33.88 (33.95)	44.50 (44.50)	2.87 (2.85)	3.94 (3.99)	10.06 (10.13)	4.92	315.04 (350.50)	2240m	1320m	$CDCl_3$ + DMSO-d_6	7.64(7)† 7.04(19.8)†	(m)
NCS	Cl	32.43 (32.47)	42.50 (42.56)	2.65 (2.72)	3.75 (3.82)	9.62 (9.68)	4.51	317.25 (366.50)	2085s	840w	$CDCl_3$	7.45(3.8)† 7.14(9.0)†	(m)
NCS	Br	28.88 (28.95)	37.92 (37.95)	2.40 (2.43)	3.36 (3.40)	19.30 (19.46)	6.34	387.52 (411)	2090s	820w	$CDCl_3$	7.35(9)† 7.23(21)†	(m)
*N_3	Cl	33.80 (33.95)	41.05 (41.08)	2.82 (2.85)	11.92 (11.98)	10.10 (10.13)	3.16	320.15 (350.50)	2080s	1330m	$CDCl_3$	7.33(40)† 7.12(100)†	(m)
‡$Ph_2Sn(NCS)$-Br·2DMSO		20.92 (20.98)	35.68 (35.97)	3.82 (3.88)	2.45 (2.46)	14.05 (14.10)	4.48	515 (567)	2050s	840w	DMSO-d_6	7.67(7)† 7.31(19)†	(m)
									ν_{SO} − ν_{SO} DMSO complex (1045s − 948s) = 97			2.48(31.2)†§	(s)

*The ^1H nmr data are at 60 MHz.
†The peak areas are located in parentheses following the ppm values.
‡The peak areas are consistent with the proposed stoichiometry of the complex.
§Methyl protons.
‖Estimated volumetrically by Volhard's method (11).
¶Infrared: s = strong, m = medium, w = weak; ^1H nmr, (m) multiplet, (s) = singlet. (*i*) The characteristic peaks in ir, indicate N-bonded pseudohalide group (12, 13), (*ii*) The ^1H nmr data are at 90 MHz and the position of the multiplet is approximately the centre of the multiplet.

Acknowledgements

Thanks are due to the Head of the Chemistry Department for laboratory facilities and to the Director of C.D.R.I., Lucknow, for elemental and spectral analyses. S.K.S. is thankful for a Post Doctoral Fellowship from C.S.I.R., New Delhi.

1. C. EABORN. J. Organomet. Chem. **100**, 43 (1974) and references therein.
2. T. N. SRIVASTAVA, P. C. SRIVASTAVA, and S. K. SRIVASTAVA. Ind. J. Chem. **20**A, 443 (1981).
3. T. N. SRIVASTAVA, P. C. SRIVASTAVA, S. K. SRIVASTAVA, and O. P. SRIVASTAVA. J. Antibact. Antifung. Agents. **9**, 439 (1981).
4. T. N. SRIVASTAVA, P. C. SRIVASTAVA, and S. K. SRIVASTAVA. Synth. React. Inorg. Met.-Org. Chem. **12**, 533 (1982).
5. T. N. SRIVASTAVA, P. C. SRIVASTAVA, S. K. SRIVASTAVA, O. P. SRIVASTAVA, and B. CHANDRA. J. Antibact. Antifung. Agents. **10**, 429 (1982).
6. P. C. SRIVASTAVA and S. K. SRIVASTAVA. Spectrochim. Acta. **40**A, 607 (1984).
7. J. H. HOLLOWAY, G. P. MCQUILLAN, and D. S. ROSS. J. Chem. Soc. A, 1935 (1971).
8. A. S. MUFTI and R. C. POLLER. J. Chem. Soc. 5055 (1965).
9. J. S. THAYER and R. WEST. Inorg. Chem. **3**, 406 (1964).
10. A. FOLARANMI, R. A. N. MCLEAN, and N. WADIBIA. J. Organomet. Chem. **73**, 59 (1974).
11. A. I. VOGEL. Quantitative inorganic analysis. Longman, London. 1975. p. 267.
12. S. K. SRIVASTAVA. Ph.D. Thesis. University of Lucknow, Lucknow, India. 1981. pp. 165–194.
13. A. H. NORBURY. Adv. Inorg. Chem. Radiochem. **17**, 231 (1975).

The crystal structure of *p*-diethylaminobenzenediazonium hexafluorophosphate

RICHARD G. BALL[1]
Department of Chemistry, University of Alberta, Edmonton, Alta., Canada T6G 2G2

AND

RICHARD MACLEOD ELOFSON
Alberta Research Council, 11315 – 87th Avenue, Edmonton, Alta., Canada T6G 2C2

Recieved May 28, 1984

RICHARD G. BALL and RICHARD MACLEOD ELOFSON. Can. J. Chem. **63**, 332 (1985).

p-Diethylaminobenzenediazonium hexafluorophosphate, $C_{10}H_{14}N_3^+ \cdot PF_6^-$, crystallized in space group $P\bar{1}$ with a = 12.105(4), b = 12.340(5), c = 10.439(4) Å, α = 96.53(3), β = 104.11(3), γ = 64.44(3)°, and Z = 4. The structure was solved using direct methods and refined with full-matrix least-squares techniques on F, to a final R of 0.054 for 1917 reflections with $F^2 > 3\sigma(F^2)$. The mean bond lengths for the diazo group are: N—N 1.096(6); C—N 1.357(7) Å. The geometry of the molecule is discussed in terms of the possible resonance forms and it is shown to be consistent with a form in which the N—N triple bond is essentially intact and the aminobenzene moiety has "quinoidal" character.

RICHARD G. BALL et RICHARD MACLEOD ELOFSON. Can. J. Chem. **63**, 332 (1985).

L'hexafluorophosphate de *p*-diéthylaminobenzènediazonium, $C_{10}H_{14}N_3^+ \cdot PF_6^-$, cristallise dans le groupe d'espace $P\bar{1}$ avec a = 12,105(4), b = 12,340(5), c = 10,439(4) Å, α = 96,53(3), β = 104,11(3), γ = 64,44(3)° et Z = 4. On a résolu la structure par des méthodes directes et on l'a affinée par la méthode des moindres carrés (matrice complète) sur F jusqu'à une valeur finale de R = 0,054 pour 1917 réflexions avec $F^2 > 3\sigma(F^2)$. Les longueurs moyennes des liaisons du groupe diazo sont: N—N = 1,096(6); C—N = 1,357(7) Å. On discute de la géométrie de la molécule en fonction des formes possibles de résonance et on montre qu'elle est en accord avec une forme dans laquelle la triple liaison N—N est essentiellement intacte et l'unité aminobenzène a un caractère "quinoïdal".

[Traduit par le journal]

Introduction

The unusual properties of diazonium salts such as explosive decomposition under certain conditions, reaction with retention of nitrogen to produce industrially important products such as dyes, photochemical decomposition with loss of N_2 (the basis of the industrially important Diazolid process), etc., have fascinated chemists for over one hundred years.

Until 1960, resonance structures "A", "B", and "C" were

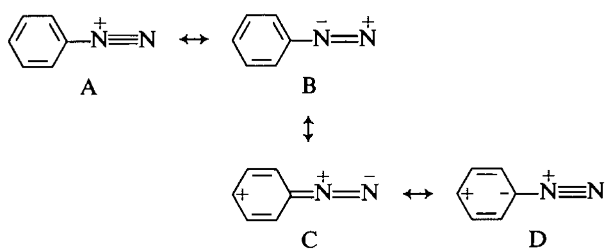

used routinely to accommodate the various properties of benzenediazonium salts. Subsequently, X-ray studies have consistently shown the N—N distance, regardless of substitution patterns or the nature of the anion, remains in the range 1.08 to 1.14 Å, which is indicative, when compared to the dinitrogen distance of 1.097 Å (1), of the N—N triple bond remaining largely intact in the ground state. In recent years ^{13}C and ^{15}N nmr studies (2, 3) have suggested that resonance form "D" is a major contributor to the ground state. An important compound for the purpose of correlating structural parameters and the spectroscopic results would be the salts of the *p*-diethylaminobenzenediazonium ion. This compound has been investigated as the chlorozincate salt (4) but the poor quality of the experimental results and the lack of agreement with other benzendiazonium compounds led us to undertake a re-examination of the crystal structure of *p*-diethylaminobenzenediazonium. Attempts were made to prepare suitable crystals first as the tetrafluoroborate and later as the hexafluorophosphate salts since these anions do not tend to strongly coordinate with the cation. However, success was not obtained until the *p*-diethyl derivative was crystallized as the hexafluorophosphate salt. The results of the structural analysis of this compound are presented herein and these, as expected, correlate closely with those of the similar compound *p*-morpholinobenzenediazonium tetrafluoroborate (5).

Experimental

Yellow crystals of *p*-*N*,*N*-diethylaminobenzenediazonium hexafluorophosphate were prepared by the method of Rutherford *et al.* (6) with the substitution of H_2SO_4 for HCl. Diffraction quality crystals were obtained by recrystallizing from methanol/diethyl ether.

Crystal data:
$C_{10}H_{14}N_3^+ \cdot PF_6^-$ fw = 321.21
Triclinic, $P\bar{1}$, a = 12.105(4), b = 12.340(5), c = 10.439(4) Å; α = 96.53(3), β = 104.11(3), γ = 64.44(3)°, V = 1364.2 Å^3, Z = 4, D_c = 1.56 g cm^{-1}, μ(MoKα) = 2.57 cm^{-1}.

Reflection data were collected at −70°C using an Enraf–Nonius CAD4 diffractometer. Reflections in the range $0 < 2\theta < 50°$ were measured using an $\omega-2\theta$ scan with $\Delta\omega = (0.80 + 0.35 \tan \theta)°$ and scan speeds varying from 1.7 to 5.0 deg min^{-1}. Two crystals, of approximate size 0.02 × 0.06 × 0.12 mm, were needed for data collection since the first crystal was lost when ice build-up on the goniometer head fractured the crystal from its glass fiber. 3873 reflections were measured from crystal 1 and 2175 from crystal 2. Over the course of data collection on both crystals two reflections, chosen as standards, were remeasured every 60 min of exposure time to monitor crystal and diffractometer stability. These intensities did not change by more than 11% for either crystal and no correction was applied to the data.

After correcting each data set separately for Lorentz, polarization, and background effects the two data sets were brought to a common

[1] Author to whom correspondence should be addressed.

TABLE 1. Positional (× 10^4) and thermal (× 10^2) parameters

Atom	x	y	z	U, Å^2	Atom	x	y	z	U, Å^2
P(1)	2704(1)	4702(2)	3366(2)	1.97(6)*	C(1)	4236(5)	−1298(5)	3030(7)	2.3(2)
P(2)	8198(2)	665(2)	2168(2)	2.53(6)*	C(2)	4459(5)	−1994(5)	4138(6)	1.8(2)
F(1)	2595(3)	5660(3)	2376(4)	4.0(1)*	C(3)	3515(5)	−2152(5)	4460(7)	2.4(2)
F(2)	2782(3)	3759(3)	4337(4)	3.4(1)*	C(4)	2310(5)	−1627(5)	3686(6)	2.0(2)
F(3)	1349(3)	5571(3)	3608(4)	3.6(2)*	C(5)	2059(5)	−957(5)	2578(7)	2.5(2)
F(4)	2088(3)	4080(3)	2167(4)	3.6(2)*	C(6)	2990(5)	−788(6)	2258(7)	2.4(2)
F(5)	3304(3)	5324(3)	4551(4)	4.5(2)*	C(7)	6485(6)	−1736(6)	3497(7)	2.8(3)*
F(6)	4054(3)	3840(3)	3107(4)	3.9(2)*	C(8)	6707(6)	−1061(6)	4702(8)	3.7(3)*
F(7)	8969(4)	−698(4)	1890(5)	5.7(2)*	C(9)	4932(6)	−370(6)	1632(6)	3.2(3)*
F(8)	7056(5)	689(5)	1085(6)	10.4(3)*	C(10)	4369(6)	953(6)	1960(7)	3.4(3)*
F(9)	9350(4)	670(4)	3207(6)	8.8(2)*	C(11)	6975(5)	5669(5)	1522(6)	1.8(2)
F(10)	8703(5)	982(5)	1099(5)	11.0(2)*	C(12)	6354(5)	5405(5)	2329(6)	2.1(2)
F(11)	7436(4)	2051(4)	2451(5)	6.9(2)*	C(13)	5081(5)	5733(5)	1960(6)	1.6(2)
F(12)	7697(5)	365(5)	3218(6)	12.4(3)*	C(14)	4425(5)	6348(5)	781(6)	1.7(2)
N(1)	1369(4)	−1786(4)	4015(5)	2.4(1)	C(15)	5009(5)	6599(5)	−65(6)	1.7(2)
N(2)	633(5)	−1931(5)	4287(6)	3.5(2)	C(16)	6280(5)	6259(5)	293(6)	1.5(2)
N(3)	5164(4)	−1150(4)	2722(5)	2.2(1)	C(17)	8937(5)	4900(6)	3215(6)	2.4(2)*
N(4)	3177(4)	6651(4)	409(5)	2.2(1)	C(18)	9550(6)	3540(6)	3212(7)	3.8(3)*
N(5)	2160(4)	6881(4)	143(5)	2.6(1)	C(19)	8911(5)	5536(6)	1033(6)	2.2(2)*
N(6)	8205(4)	5388(4)	1902(5)	1.7(1)	C(20)	8866(5)	6788(6)	1103(7)	2.7(3)*

* Indicates an atom refined anisotropically. The equivalent isotropic thermal parameter is given by: $U = 1/3\,(U_{11} + U_{22} + U_{33} + 2U_{23}\cos\alpha + 2U_{13}\cos\beta + 2U_{12}\cos\gamma)$.

scale and merged to yield 4813 unique reflections. Of these 1917 had $I > 3\sigma(I)$ and were used in the structure refinement.

The structure was solved[2] using the direct methods program SHELX 84 and refined using full-matrix least-squares minimizing $\Sigma\omega(|F_o| - F_c|)^2$ where $\omega = 1/\sigma(I)$. Neutral atom scattering factors were calculated from the analytical expression for the scattering factor curves (8*a*) and the f' and f'' components of anomalous dispersion (8*b*) were included for all non-H atoms. In the final model the two PF_6 groups and the carbons of the four ethyl groups were refined with anisotropic thermal parameters, while the remaining non-H atoms were refined with isotropic thermal parameters for a total of 271 variables. The H atom contributions were included as fixed, isotropic atoms located at their "idealized" positions (C—H 0.95 Å and appropriate sp^2 or sp^3 geometry). No attempt was made to refine the H atom parameters because of the already low observations/variables ratio of 7.1:1.

Refinement converged with $R = 0.054$ ($R_w = 0.059$); the largest shift in any parameter was 0.7 times its esd. The highest peak in a final difference Fourier was 0.60(9) e Å^{-3} and was not considered chemically significant.

Final positional and thermal parameters are presented in Table 1.[3]

Discussion

The crystal structure comprises the two independent cations, depicted in Fig. 1, arranged in approximately parallel planes with the associated anions occupying spots near the cations, Fig. 2. Table 2 lists the interionic distances to 3.2 Å between the N and F atoms. There are six short contacts, <2.9 Å, and these are indicated in Fig. 2.

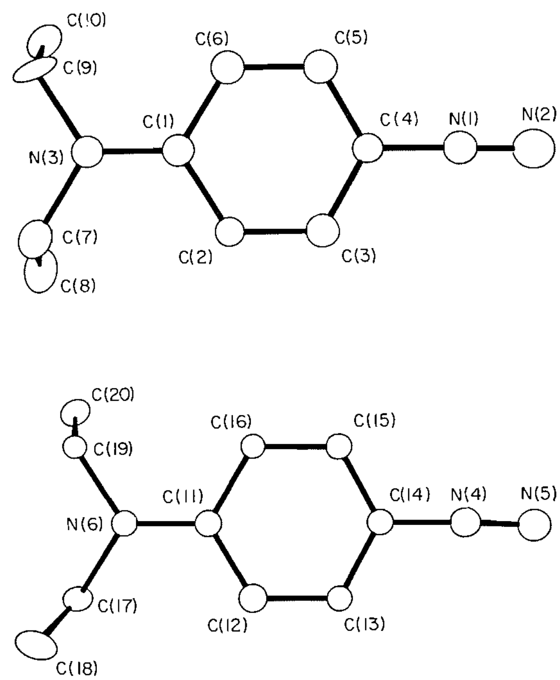

FIG. 1. Perspective view of the two independent cations showing the atom numbering scheme. Atoms are represented by thermal ellipsoids at the 50% probability level. For clarity the H atoms have been omitted.

Bond distances and angles are listed in Tables 3 and 4 respectively. The geometry of the anions is as expected, with P—F distances ranging from 1.573(4) to 1.601(4) Å for the anion based on P(1) and from 1.522(5) to 1.588(5) Å for the second anion. Since the second anion is the one involved in most of the interionic contacts, it is not surprising to see a larger range of P—F distances for this anion.

The two cations have essentially identical bond distances and angles with the only appreciable difference being the

[2] G.M. Sheldrick made available a pre-release version of SHELX 84 during a diffraction methods school in July, 1983. Other computer programs used in this analysis include the Enraf–Nonius Structure Determination Package (7) and several locally written or modified programs.

[3] Tables of anisotropic thermal parameters, derived H atom parameters, torsion angles, least-squares planes, and observed and calculated structure factors are available, at a nominal charge, from the Depository of Unpublished Data, CISTI, National Research Council of Canada, Ottawa, Ont., Canada K1A 0S2.

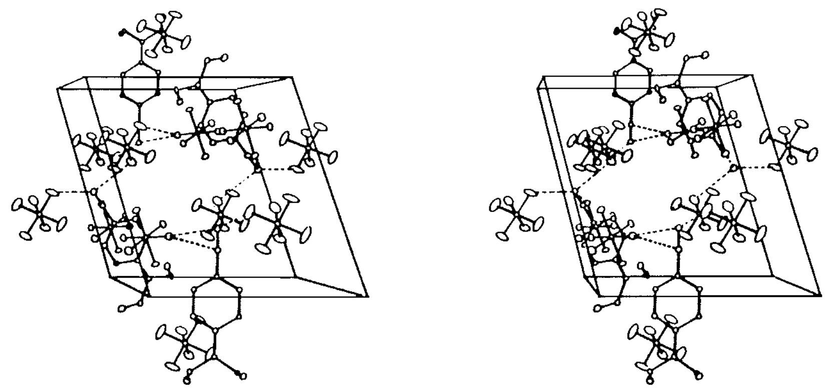

FIG. 2. Stereoview showing the ionic packing. The four cations in the cell are shown with more than one cell of anions. The F···N interionic distances less than 3.0 Å have been drawn as dashed lines. The unit cell has been oriented such that c runs left to right and b points toward the viewer.

TABLE 2. Selected interionic distances to 3.2 Å

Atom	Atom	Symmetry operator	Distance
F(10)	N(5)	$1-x, 1-y, z$	2.733(7)
F(1)	N(4)	x, y, z	2.738(7)
F(1)	N(5)	x, y, z	2.868(7)
F(3)	N(2)	$x, 1+y, z$	2.873(6)
F(9)	N(2)	$1-x, y, 1-z$	2.889(7)
F(7)	N(2)	$1+x, y, z$	2.898(6)
F(9)	N(1)	$1+x, y, z$	3.009(6)
F(7)	N(1)	$1+x, y, z$	3.055(6)
F(9)	N(2)	$1+x, y, z$	3.107(7)
F(10)	N(4)	$1-x, 1-y, z$	3.123(7)

TABLE 3. Bond distances in angstroms*

Atom 1	Atom 2	Distance	Atom 1	Atom 2	Distance
P(1)	F(1)	1.601(4)	N(6)	C(11)	1.339(7)
P(1)	F(2)	1.587(4)	N(6)	C(17)	1.470(7)
P(1)	F(3)	1.589(4)	N(6)	C(19)	1.462(7)
P(1)	F(4)	1.591(4)	C(1)	C(2)	1.422(8)
P(1)	F(5)	1.573(4)	C(1)	C(6)	1.423(8)
P(1)	F(6)	1.588(4)	C(2)	C(3)	1.360(8)
P(2)	F(7)	1.566(4)	C(3)	C(4)	1.389(8)
P(2)	F(8)	1.549(5)	C(4)	C(5)	1.394(8)
P(2)	F(9)	1.546(4)	C(5)	C(6)	1.352(8)
P(2)	F(10)	1.552(5)	C(7)	C(8)	1.462(9)
P(2)	F(11)	1.588(5)	C(9)	C(10)	1.508(9)
P(2)	F(12)	1.522(5)	C(11)	C(12)	1.401(8)
N(1)	N(2)	1.086(6)	C(11)	C(16)	1.429(7)
N(1)	C(4)	1.360(7)	C(12)	C(13)	1.377(7)
N(3)	C(1)	1.329(7)	C(13)	C(14)	1.392(7)
N(3)	C(7)	1.496(7)	C(14)	C(15)	1.389(7)
N(3)	C(9)	1.469(7)	C(15)	C(16)	1.371(7)
N(4)	N(5)	1.105(6)	C(17)	C(18)	1.514(9)
N(4)	C(14)	1.354(7)	C(19)	C(20)	1.517(9)

*Numbers in parentheses are estimated standard deviations in the least significant digits.

C(7)—C(8) bond which is shorter than the other three bonds of the same type. In fact it is the orientation of the ethyl groups which is the only feature distinguishing between the two cations; in one form both methyl groups point to the same side of the phenyl ring, while in the other they point to opposite sides.

The focus of this study is the geometry of the benzenediazonium moiety and how this geometry relates to the contribution of the resonance forms "A"–"D" to the ground state structure. For amino derivatives of benzenediazonium the resonance forms "C" and "D" can be drawn as

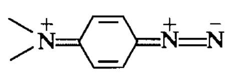

E

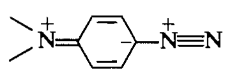

F

At the present time ^{13}C and ^{15}N nmr results (2, 3) indicate "F" should be the favoured structure. Table 5 presents the geometries of six structures, of roughly similar quality, containing benzenediazonium cations. For all the structures the N—N bond distance is essentially invariant and the values observed in the present study are in close agreement with the average value determined from the other structures. This observation is in accord with the conclusion of Sorriso (13*a*) that the N—N triple bond, as measured crystallographically, remains essentially intact in these types of compounds.

It is likely, by comparison with results of studies on C≡N bonds (14), that the mean N—N bond length observed in the X-ray structures is shorter by about 0.02 Å than the true internuclear N—N distance. If this is the case, then the bond order of the N—N interaction is slightly decreased from the full triple bond value and this should be reflected in a concomitant increase in the bond orders of both C(arene)—N bonds. Indeed these two distances (mean distances of 1.334(7) and 1.357(7) Å, for amino and diazo groups respectively) are both somewhat shorter than a usual C_{sp^2}—N single bond distance of approximately 1.42 Å and are in the range expected if there is some degree of double bonding between the ring and the diazo and amino groups. While the difference between these two distances is only just significant, it is interesting that the C(arene)—N(amino) distance is consistently shorter than the C(arene)—N(diazo) distance, which is what would be expected if both forms "E" and "F" contribute to the observed structure. These observations are supported by similar results observed in the structure of the morpholino derivative (5).

Observing the effect of a "quinoidal" form on the C—C distances in the benzene ring is somewhat more difficult due to the small differences involved compared to their associated standard deviations. Examination of the geometries presented in Table 5 shows that compounds **1** to **5**, in which the quinoid resonance forms may not be strong contributors, tend to have nearly equivalent distances around the ring while compounds **6**

TABLE 4. Selected bond angles in degrees*

Atom 1	Atom 2	Atom 3	Angle	Atom 1	Atom 2	Atom 3	Angle
N(2)	N(1)	C(4)	178.7(6)	C(4)	C(5)	C(6)	120.0(6)
C(1)	N(3)	C(7)	121.5(5)	C(1)	C(6)	C(5)	120.9(6)
C(1)	N(3)	C(9)	121.5(5)	N(3)	C(7)	C(8)	112.0(5)
C(7)	N(3)	C(9)	117.0(5)	N(3)	C(9)	C(10)	114.0(5)
N(5)	N(4)	C(14)	177.7(6)	N(6)	C(11)	C(12)	120.6(5)
C(11)	N(6)	C(17)	122.3(5)	N(6)	C(11)	C(16)	120.0(5)
C(11)	N(6)	C(19)	122.1(5)	C(12)	C(11)	C(16)	119.4(5)
C(17)	N(6)	C(19)	115.6(4)	C(11)	C(12)	C(13)	120.6(5)
N(3)	C(1)	C(2)	120.9(5)	C(12)	C(13)	C(14)	118.5(5)
N(3)	C(1)	C(6)	121.6(5)	N(4)	C(14)	C(13)	118.4(5)
C(2)	C(1)	C(6)	117.4(5)	N(4)	C(14)	C(15)	118.7(5)
C(1)	C(2)	C(3)	121.4(5)	C(13)	C(14)	C(15)	122.8(5)
C(2)	C(3)	C(4)	119.3(6)	C(14)	C(15)	C(16)	118.8(5)
N(1)	C(4)	C(3)	119.0(5)	C(11)	C(16)	C(15)	119.9(5)
N(1)	C(4)	C(5)	120.0(5)	N(6)	C(17)	C(18)	112.3(5)
C(3)	C(4)	C(5)	121.0(6)	N(6)	C(19)	C(20)	112.9(5)

*Numbers in parentheses are estimated standard deviations in the least significant digits.

TABLE 5. Selected distances in benzenediazonium structures

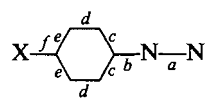

Compound	—X	*a*	*b*	*c*	*d*	*e*	*f*	Reference
1	$—OCH_3$	1.099(2)	1.389(3)	1.389(3)	1.370(3)	1.399(3)	—	9
2	$—SO_3$	1.091(3)	1.410(4)	1.383(4)	1.375(4)	1.384(4)	—	10
3	—	1.093(7)	1.418(6)	1.386(8)	1.358(8)	1.399(10)	—	11
4	—	1.083(3)	1.415(3)	1.377(4)	1.382(4)	1.376(5)	—	12
5	—	1.093(2)	1.410(2)	1.396(2)	1.392(2)	1.395(2)	—	13*b*
6	$—NC_4H_8O$	1.100(1)	1.381(1)	1.395(1)	1.371(1)	1.424(1)	1.352(1)	5
7	$—NC_4H_{10}$	1.086(6)	1.360(7)	1.391(8)	1.356(8)	1.422(8)	1.329(7)	
		1.105(6)	1.354(7)	1.390(7)	1.374(7)	1.420(8)	1.339(7)	

and **7** do display an ordering of distances which is consistent with structures "E" and "F". This is in accord with the observation of greater electrophilicity of compounds **1–5** as compared to **6** and **7**, as measured by redox potentials or by the rate of coupling with suitable substrates (15, 16).

Thus, to date, the structural studies tend to support the spectroscopic evidence for resonance form "F" as an important contributor to the ground state structure of amino derivatives of benzenediazonium compounds. However, they also indicate at least a small contribution from form "E" in order to account for the consistently observed shortening of the arene–diazo bond distance from the usual single bond distance.

Acknowledgement

We wish to thank J.K. Laidler for the preparation of the crystals.

1. B. P. STOICHEFF. Can. J. Phys. **82**, 630 (1954).
2. R. M. ELOFSON, N. CYR, J. K. LAIDLER, K. F. SCHULZ, and F. F. GADALLAH. Can. J. Chem. **62**, 92 (1984).
3. G. A. OLAH and J. L. GRANT. J. Am. Chem. Soc. **97**, 1546 (1975).
4. YA. M. NESTROVA and M. A. PORAI-KOSHITS. Zh. Strukt. Khim. **12**, 108 (1971).
5. N. W. ALCOCK, T. J. GREENHOUGH, D. M. HIRST, T. J. KEMP, and D. R. PAYNE. J. Chem. Soc. Perkin Trans., 8 (1980).
6. K. G. RUTHERFORD, W. REDMOND, and J. RIGAMONTI. J. Org. Chem. **26**, 5149 (1961).
7. B. A. FRENZ. Computing in Crystallography. Delft University Press, Delft, Holland. 1978. pp. 64–71.
8. (*a*) International tables for X-ray crystallography. Vol. IV. Kynoch Press, Birmingham, England. 1974. Table 2.2B; (*b*) Table 2.3.1.
9. P. GROTH. Acta Chem. Scand. Ser. A, **35**, 541 (1981).
10. C. ROMMING. Acta Chem. Scand. **26**, 523 (1972).
11. C. ROMMING and T. TJORNHOM. Acta Chem. Scand. **22**, 2934 (1968).
12. M. CYGLER, M. PRZYBYLSKA, and R. M. ELOFSON. Can. J. Chem. **60**, 2852 (1982).
13. (*a*) S. SORRISO. *In* The chemistry of the diazonium and diazo groups. *Edited by* S. Patai. J. Wiley and Sons, New York. 1978. p. 100; (*b*) p. 98.
14. R. G. LITTLE, D. PAUTLER, and P. COPPENS. Acta Crystallogr. Sect. B, **27**, 1493 (1971).
15. F. HEGERTY. *In* The chemistry of the diazonium and diazo groups. *Edited by* S. Patai. J. Wiley and Sons, New York. 1978. Chapt. 12.
16. R. M. ELOFSON and F. F. GADALLAH. J. Org. Chem. **34**, 854 (1969).

Enthalpies of interaction of ketones with organic solvents

W. KIRK STEPHENSON AND RICHARD FUCHS

Department of Chemistry, University of Houston, Houston, TX 77004, U.S.A.

Received April 17, 1984

W. KIRK STEPHENSON and RICHARD FUCHS. Can. J. Chem. **63**, 336 (1985).

Enthalpies of solution (ΔH_s) of a series of ketones (acetone, 2-butanone, 2-heptanone, 2-nonanone, 5-nonanone, 2,2,4,4-tetramethyl-3-pentanone, cyclohexanone) and alkane model compounds (*n*-heptane, *n*-nonane, 2,2,4,4-tetramethylpentane, cyclohexane) have been determined in 17 organic solvents (*n*-heptane, cyclohexane, CCl_4, α,α,α,-trifluorotoluene, 1,2-dichloroethane, triethylamine, butyl ether, ethyl acetate, DMF, DMSO, benzene, toluene, mesitylene, 1-octanol, methanol, *t*-butyl alcohol, 2,2,2-trifluoroethanol), and combined with heats of vaporization to give enthalpies of transfer from vapor to solvent ($\Delta H(\mathrm{v} \rightarrow \mathrm{S})$). These values have been used to evaluate ketone–solvent polar interactions ($\Delta\Delta H(\mathrm{v} \rightarrow \mathrm{S}) = \Delta H(\mathrm{v} \rightarrow \mathrm{S})(\mathrm{ketone}) - \Delta H(\mathrm{v} \rightarrow \mathrm{S})(\mathrm{alkane})$). The linear relationships between $\Delta\Delta H(\mathrm{v} \rightarrow \mathrm{S})$ and solvent dipolarity-polarizability (Taft-Kamlet π^* parameters) are derived. Based on the deviations from these correlations, ketone–CF_3CH_2OH enthalpies of hydrogen bond formation have been evaluated. The other alcohol solvents show no evidence of exothermic H-bond formation with ketones.

W. KIRK STEPHENSON et RICHARD FUCHS. Can. J. Chem. **63**, 336 (1985).

On a déterminé les enthalpies de solution (ΔH_s) d'une série de cétones (acétone, butanone-2 heptanone-2, nonanone-2, nonanone-5, tétraméthyl-2,2,4,4 pentanone-3, cyclohexanone) ainsi que d'alcanes modèles (*n*-heptane, *n*-nonane, tétraméthyl-2,2,4,4 pentane, cyclohexane) dans 17 solvants organiques (*n*-heptane, cyclohexane, CCl_4, α,α,α,-trifluorotoluène, dichloro-1,2 éthane, triéthylamine, éther butylique, acétate d'éthyle, DMF, DMSO, benzène, toluène, mésitylène, octanol-1, méthanol, alcool *tert*-butylique, trifluoro-2,2,2 éthanol) et on les a combinés avec les chaleurs de vaporisation pour obtenir les enthalpies de transfert de la vapeur au solvant ($\Delta H(\mathrm{v} \rightarrow \mathrm{S})$). On a utilisé ces valeurs pour évaluer les interactions polaires cétone-solvant ($\Delta\Delta H(\mathrm{v} \rightarrow \mathrm{S}) = \Delta H(\mathrm{v} \rightarrow \mathrm{S})(\mathrm{cétone}) - \Delta H(\mathrm{v} \rightarrow \mathrm{S})(\mathrm{alcane})$). On en a déduit la relation linéaire entre $\Delta\Delta H(\mathrm{v} \rightarrow \mathrm{S})$ et la polarité-polarisabilité du solvant (paramètres de π^* de Taft–Kamlet). En se basant sur les déviations par rapport à ces corrélations, on a évalué les enthalpies de formation de la liaison hydrogène cétone–CF_3CH_2OH. Il ne semble pas que les autres alcools étudiés comme solvant forment des liaisons hydrogènes exothermiques avec les cétones.

[Traduit par le journal]

Enthalpies of polar interaction of a series of ketones with methanol (MeOH), dimethylformamide (DMF), benzene, and cyclohexane (c-C_6) have been reported (1) using the solvation enthalpy, or $\Delta\Delta H(\mathrm{v} \rightarrow \mathrm{S})$, method. This method utilizes enthalpies of transfer of a solute from vapor to solvent,

$$[1] \quad \Delta H(\mathrm{v} \rightarrow \mathrm{S}) = \Delta H_s - \Delta H_v$$

where ΔH_s is the enthalpy of solution of the solute and ΔH_v denotes the solute heat of vaporization. $\Delta H(\mathrm{v} \rightarrow \mathrm{S})$ is often referred to as the solvation enthalpy, or the heat of solution of the gas. The enthalpy of polar interaction is taken as the difference in solvation enthalpies of a ketone (K) and an alkane model (M) with the same number of carbon atoms and a similar carbon skeleton:

$$[2] \quad \Delta H_p = \Delta\Delta H(\mathrm{v} \rightarrow \mathrm{S}) = \Delta H(\mathrm{v} \rightarrow \mathrm{S})(\mathrm{K}) - \Delta H(\mathrm{v} \rightarrow \mathrm{S})(\mathrm{M})$$

The model is used to cancel the ketone dispersion interactions and enthalpy of cavity formation within the solvent, thereby isolating the polar interactions,

$$[3] \quad \Delta\Delta H(\mathrm{v} \rightarrow \mathrm{S}) = \Delta\Delta H_c + \Delta\Delta H_d + \Delta H_p$$

where $\Delta\Delta H_c = \Delta H_c(\mathrm{K}) - \Delta H_c(\mathrm{M})$ ("c" denotes cavity) and $\Delta\Delta H_d = \Delta H_d(\mathrm{K}) - \Delta H_d(\mathrm{M})$ ("d" refers to dispersion). It is usually assumed that the $\Delta\Delta H_c$ and $\Delta\Delta H_d$ terms are equal to zero, or that the terms are non-zero but of opposite signs such that their sum is equal to zero, and eq. [3] simplifies to give eq. [2]. Failure of the model to cancel the cavity formation or dispersion interactions will be reflected in the ΔH_p values. In hydrogen-bond-donating (HBD) solvents, the formation of ketone–solvent hydrogen bonds may occur. Enthalpies of H-bond formation will be incorporated into the $\Delta\Delta H(\mathrm{v} \rightarrow \mathrm{S}) = \Delta H_p$ values.

Ketone–solvent polar interactions fall into two main classes: dipole–dipole and dipole – induced dipole. Using the Taft–Kamlet π^* solvatochromic parameters (2, 3) as a measure of solvent dipolarity-polarizability, one can obtain expressions in the form of eq. [4],

$$[4] \quad \Delta\Delta H(\mathrm{v} \rightarrow \mathrm{S})(\text{ketone vs. model}) = s\pi^* + y$$

where s is the π^* coefficient and y is the calculated $\Delta\Delta H(\mathrm{v} \rightarrow \mathrm{S})$ value in a solvent with $\pi^* = 0.00$ (i.e., y-intercept).

To investigate ketone–solvent interactions, $\Delta\Delta H(\mathrm{v} \rightarrow \mathrm{S})$ values for a series of ketones (acetone, 2-butanone, 2-heptanone, 4-heptanone, 2-nonanone, 5-nonanone, 2,2,4,4-tetramethyl-3-pentanone, and cyclohexanone) in 17 organic solvents of varying polarity will be reported. Dependencies of $\Delta\Delta H(\mathrm{v} \rightarrow \mathrm{S})$ on solvent dipolarity-polarizability will be evaluated via solvatochromic equations in π^* (eq. [4]). Ketone hydrogen bonding interactions with alcohol solvents will also be examined.

Experimental

Solutes and solvents were commercial samples in excess of 99% purity, which were dried over 4A molecular sieve, except for methanol and trifluoroethanol, which were dried over 3A sieve. Purities were established by gas chromatography using a Shimadzu Mini 2 gc with a glass-lined system, a 30 m × 0.25 mm id SE-30 silica capillary column, and a Hewlett-Packard 3390A integrator.

The calorimetric procedure and apparatus have previously been described (4). The vacuum jacketed calorimeter was immersed in a water bath at 25.00°C, with regulation to ±0.002°C. Liquid samples were introduced into 65–80 mL of solvent with 10-, 20-, or 50-μL syringes with immersed tips. Heats of solution were corrected (0.01–0.03 kcal/mol less endothermic) to allow for the heat capacity of the samples which were introduced at 21–23°C. The uncertainty intervals in ΔH_s (twice the standard deviation of the mean of three or more determinations) are 0.00–0.09 kcal/mol. No effect of concentration on ΔH_s was observed.

Results and discussion

Heats of vaporization, and heats of solution of acetone, 2-butanone, 2-heptanone, 4-heptanone, 2-nonanone, 5-nonanone, 2,2,4,4-tetramethyl-3-pentanone, and cyclohexanone in 17 solvents are listed in Table 1. Heats of vaporization and solution of *n*-heptane (*n*-C_7), *n*-nonane (*n*-C_9), 2,2,4,4-tetramethylpentane (Me_4C_5), and cyclohexane (*c*-C_6) are given in Table 2. Derived $\Delta\Delta H(\mathrm{v} \rightarrow \mathrm{S})$(ketone vs. alkane) values are shown in Table 3).

Methylene increments

Correlations of $\Delta H(\mathrm{v} \rightarrow \mathrm{S})$(ketone) vs. number of carbon atoms (n_c) for the series of 2-ketones are given in Table 4; correlation slopes (m) correspond to methylene increments. In all solvents, ketone solvation enthalpies increase exothermically with the addition of a methylene group, but the methylene increments are less exothermic for the more polar solvents. It is usually assumed that the dispersion interactions of a methylene (or alkyl) group do not vary significantly from solvent to solvent, so differences in $\Delta H(\mathrm{v} \rightarrow \mathrm{S})(CH_2)$ result from differences in ΔH_c. Since dipolarity-polarizability interactions between solutes and solvents increase with the π^* value of each (5), it is reasonable that solvent–solvent interactions are dependent on π^* of each solvent molecule, and that ΔH_c is primarily a function of $(\pi^*)^2$. The linear relationship of methylene group solvation enthalpies to solvent $(\pi^*)^2$ is:

$$[5] \quad \Delta H(\mathrm{v} \rightarrow \mathrm{S})(CH_2) = 0.443(\pi^*)^2 - 1.14 \text{ kcal/mol}$$

$$n = 17,\ r = 0.912,\ \text{see} = 0.06$$

where n is the number of solvents, r refers to the correlation coefficient, and see is the standard error of the estimate. However, correlation of the methylene increments of a series of *n*-alkanes (5) is considerably better:

$$[6] \quad \Delta H(\mathrm{v} \rightarrow \mathrm{S})(CH_2) = 0.399(\pi^*)^2 - 1.17 \text{ kcal/mol}$$

$$n = 20,\ r = 0.956,\ \text{see} = 0.04$$

The ketone methylene increment is more dependent on solvent $(\pi^*)^2$ because addition of a methylene group to a ketone not only increases dispersion interaction and cavity formation contributions to the solvation process (as is the case for alkanes), but also increases steric hindrance to carbonyl group dispersion interactions (1).

Methylene increments determined for the series of symmetrical ketones (acetone, 4-heptanone, 5-nonanone) are less exothermic than those of the 2-ketone series by 0.00–0.10 kcal/mol. For the symmetrical ketones:

$$[7] \quad \Delta H(\mathrm{v} \rightarrow \mathrm{S})(CH_2) = 0.521(\pi^*)^2 - 1.10 \text{ kcal/mol}$$

$$n = 17,\ r = 0.929,\ \text{see} = 0.06$$

Ketone polar interactions

$\Delta\Delta H(\mathrm{v} \rightarrow \mathrm{S})$(ketone vs. alkane) values, which provide a measure of ketone–solvent dipole–dipole or dipole – induced dipole interactions, are listed in Table 3. The values show a strong dependence on solvent dipolarity-polarizability, as illustrated by the π^* coefficient of the following correlation (ROH solvents omitted) for acetone (vs. *n*-propane) and Fig. 1.

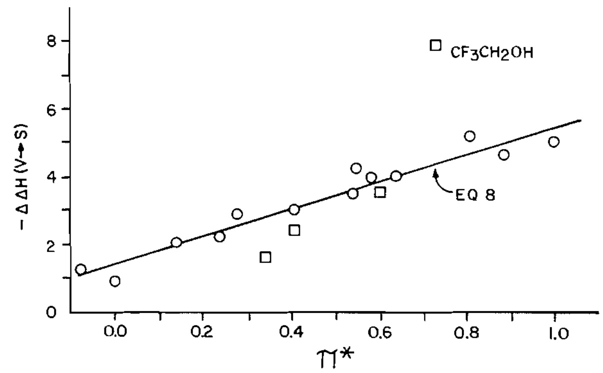

FIG. 1. $-\Delta\Delta H(\mathrm{v} \rightarrow \mathrm{S})$(acetone vs. *n*-propane) vs. solvent π^* for aprotic (○) and alcohol (□) solvents.

$$[8] \quad \Delta\Delta H(\mathrm{v} \rightarrow \mathrm{S})(\text{acetone vs. propane}) = 4.03\pi^* - 1.42 \text{ kcal/mol}$$

$$n = 13,\ r = 0.971,\ \text{see} = 0.35$$

The calculated value for cyclohexane ($\pi^* = 0.00$) is −1.42 kcal/mol (observed, −0.99 kcal/mol), and corresponds to the *y*-intercept. Because acetone (mv = 73.5 mL) is smaller than propane (mv = 88.1 mL), the $\Delta\Delta H_c$ term (eq. [3]) should be more exothermic for the more polar solvents; however, the points corresponding to DMF and DMSO are displaced endothermically from eq. [8] (Fig. 1). This suggests that the *y*-intercept does not result primarily from a solute – model cavity formation mismatch.

$\Delta\Delta H(\mathrm{v} \rightarrow c\text{-}C_6)$(acetone vs. propane) values have been attributed to carbonyl dipole – hydrocarbon solvent induced dipole interactions (6). This is consistent with the smaller $\Delta\Delta H(\mathrm{v} \rightarrow c\text{-}C_6)$(ketone vs. alkane) values of the larger ketones. The variation is fairly small and might be the result of different ketone – model cavity formation and dispersion interaction mismatches. Contrary to this explanation based on ketone–hydrocarbon induction interactions, $\Delta\Delta H(\mathrm{v} \rightarrow \mathrm{S})$ values of 5-nonanone and 2,2,4,4-tetramethyl-3-pentanone in *n*-heptane or in cyclohexane are in good agreement, but agreement is poor for polar solvents (aromatics, haloaliphatics) in which carbonyl dipole – solvent induced dipole interactions are operative. Solomonov and co-workers (7, 8) have estimated $\Delta H(\mathrm{v} \rightarrow c\text{-}C_6)$, usually to within 6% of the experimental value, for a wide variety of solutes based on the assumption that all compounds interact with alkane solvents through dispersion interactions only. It is probable that $\Delta\Delta H(\mathrm{v} \rightarrow c\text{-}C_6)$(acetone vs. propane) values result from larger dispersion interactions by a carbonyl group relative to a methylene group, consistent with the agreement between $\Delta\Delta H(\mathrm{v} \rightarrow \mathrm{S})$ for 5-nonanone and 2,2,4,4-tetramethyl-3-pentanone in the alkane solvents, and with Solomonov's findings. However, small contributions from induction forces or cavity formation mismatches cannot be ruled out.

Because acetone is a hydrogen-bond-accepting (HBA) compound, dissolution in an alcohol might be expected to be more exothermic than dissolution in a comparably polar but aprotic solvent, resulting in an exothermic displacement from eq. [8] (Fig. 1). Of the alcohol solvents used in this study, only CF_3CH_2OH is exothermically displaced; *t*-BuOH, MeOH, and

TABLE 1. Ketone heats of solution and heats of vaporization (kcal/mol)[a]

	ΔH_s							
Solvent[b]	Acetone	2-Butanone	2-Heptanone	4-Heptanone	2-Nonanone	5-Nonanone	2,2,4,4-Me_4-3-pentanone	Cyclohexanone
n-C_7H_{16}	2.32±0.07[c]	1.95±0.06[c]	1.52±0.05[c]	1.18±0.04[c]	1.55±0.05[c]	1.15±0.03[c]	0.77±0.03[c]	1.74±0.05[c]
c-C_6H_{12}	2.69±0.08[c,d]	2.29±0.07[c,d]	2.01±0.06[c,d]	1.69±0.05[c,d]	1.98±0.06[c,d]	1.70±0.05[c,d]	1.00±0.03[c,d]	1.77±0.05[c,d]
CCl_4	0.73±0.01	0.56±0.00	0.24±0.00	0.24±0.00	0.34±0.00	0.11±0.00	0.11±0.01	−0.07±0.01
n-BuCl	—	—	0.02±0.02	—	—	—	—	—
Cl_3CCH_3	—	—	−0.18±0.01	—	—	—	—	—
CF_3Ph	−0.05±0.00[e]	−0.27±0.01	−0.34±0.00[e]	−0.23±0.00[e]	−0.29±0.03	−0.20±0.00	−0.30±0.01[e]	−0.40±0.01[e]
$ClCH_2CH_2Cl$	−0.38±0.02	−0.40±0.01	−0.01±0.01	0.11±0.01	0.36±0.03	0.42±0.02	0.25±0.02	−0.50±0.03
Et_3N	1.46±0.03	1.09±0.05	0.82±0.05	0.61±0.02	0.64±0.03	0.53±0.06	0.31±0.03	0.88±0.02
n-Bu_2O	1.27±0.01	1.00±0.01	0.70±0.01	0.54±0.01	0.59±0.01	0.47±0.00	0.26±0.01	0.84±0.01
CH_3COOEt	0.12±0.01	0.10±0.01	0.36±0.05	0.49±0.02	0.62±0.06	0.76±0.06	0.50±0.05	0.25±0.07
DMF	−0.02±0.02[c,d]	0.10±0.01[c,d]	0.53±0.03[c,d]	0.65±0.03[c,d]	0.97±0.03[c,d]	1.09±0.03[c,d]	0.90±0.03[c,d]	0.34±0.02[c,d]
DMSO	0.34±0.01	0.53±0.02	1.54±0.03	1.58±0.06	2.25±0.05	2.41±0.05	2.44±0.06	0.77±0.05
Mesitylene	0.70±0.01[e]	0.39±0.01	0.00±0.01[e]	−0.11±0.00[e]	−0.04±0.02	0.00±0.01	0.19±0.01[e]	0.19±0.00[e]
Toluene	0.32±0.01[e]	0.11±0.00	−0.10±0.01[e]	−0.09±0.02[e]	−0.10±0.02	−0.05±0.01	0.21±0.06[e]	−0.16±0.00[e]
Benzene	0.29±0.02[c,d]	0.10±0.02[c,d]	0.24±0.02[c,d]	0.15±0.01	0.39±0.02[c,d]	0.37±0.02[c,d]	0.56±0.03[c,d]	−0.26±0.02[c,d]
1-Octanol	2.08±0.05	1.89±0.04	1.60±0.03	1.43±0.01	1.47±0.08	1.46±0.05	1.14±0.08	1.87±0.09
t-BuOH	1.69±0.06	1.55±0.03	1.37±0.03	1.38±0.03	1.37±0.01	1.25±0.03	1.02±0.02	1.37±0.01
MeOH	0.60±0.03[c,d]	0.58±0.03[c,d]	0.75±0.03[c,d]	0.77±0.03[c,d]	1.13±0.03[c,d]	0.94±0.03[c,d]	0.92±0.03[c,d]	0.14±0.02[c,d]
CF_3CH_2OH	−2.65±0.07	−2.34±0.04	−1.68±0.02	−1.61±0.05	−1.10±0.02	−0.98±0.01	−1.53±0.06	−2.58±0.01
ΔH_v	7.48±0.02[f]	8.29±0.02[f]	11.34±0.07[d]	11.10±0.09[g]	13.53±0.14[d]	13.12±0.09[d]	10.84±0.02[f]	10.77±0.05[g]

[a]Me is methyl, Et is ethyl, Ph is phenyl.
[b]Values and uncertainty intervals in kcal/mol.
[c]Uncertainty interval estimated.
[d]Reference 1.
[e]Reference 11.
[f]Reference 12.
[g]Reference 13.

TABLE 2. Alkane heats of solution and heats of vaporization[a,b]

Solvent	n-Heptane	n-Nonanone	2,2,4,4-Tetramethylpentane	Cyclohexane
n-C_7H_{16}	0.00±0.02[c]	0.01±0.02[c]	0.02±0.02[c]	0.19±0.00[c]
c-C_6H_{12}	0.39±0.02[c,d]	0.47±0.02[c]	0.07±0.02[c]	0.00±0.02[c,e]
CCl_4	0.50±0.01	0.63±0.01[f]	0.55±0.01	0.20±0.00
n-BuCl	0.54±0.02	0.68±0.02	0.49±0.02	—
Cl_3CCH_3	0.69±0.01	0.84±0.02	0.62±0.01	—
CF_3Ph	0.91±0.01[f]	1.11±0.00[f]	0.94±0.01[f]	0.97±0.02[f]
$ClCH_2CH_2Cl$	2.39±0.01	2.85±0.02	2.33±0.05	1.77±0.02
Et_3N	0.10±0.02	0.15±0.01	0.09±0.05	0.16±0.02
n-Bu_2O	0.12±0.00	0.17±0.01	0.13±0.00	0.20±0.01
CH_3COOEt	1.60±0.02	2.11±0.01	1.55±0.01	1.36±0.05
DMF	2.22±0.06[c,d]	2.83±0.08[c]	2.64±0.08[c]	1.84±0.06[c,d]
DMSO	3.69±0.04	4.49±0.05	4.05±0.07	2.83±0.10
Mesitylene	0.30±0.01[f]	—	0.38±0.00[f]	0.47±0.01[f]
Toluene	0.69±0.03[f]	0.87±0.02[f]	0.89±0.02[f]	0.60±0.00[f]
Benzene	1.33±0.04[c,d]	1.62±0.05[c,d]	1.46±0.04[c,d]	0.87±0.03[c,d]
1-Octanol	0.30±0.03	0.37±0.01	0.44±0.03	0.45±0.04
t-BuOH	1.21±0.06	1.47±0.02	1.17±0.01	1.03±0.02
MeOH	1.39±0.04[c,d]	1.82±0.05[c,d]	1.39±0.04[c,d]	1.18±0.04[c,d]
CF_3CH_2OH	2.89±0.03	3.61±0.04	2.67±0.06	2.60±0.05
ΔH_v	8.74±0.01[g]	11.10±0.01[g]	9.20±0.01[f]	7.90±0.01[g]

[a]Me is methyl, Et is ethyl, Ph is phenyl.
[b]Values and uncertainty intervals in kcal/mol.
[c]Uncertainty interval estimated.
[d]Reference 14.
[e]Reference 15.
[f]Reference 11.
[g]Reference 12.

TABLE 3. $\Delta\Delta H(\mathrm{v} \rightarrow \mathrm{S})$ (ketone vs. alkane) values[a,b]

Solvent[c]	Acetone[d]	2-Butanone[e]	2-Heptanone	4-Heptanone	2-Nonanone	5-Nonanone	2,2,4,4-Me_4-3-pentanone	Cyclohexanone
n-C_7H_{16}	−1.22	−1.20	−1.08	−1.18	−0.89	−0.88	−0.89	−1.32
c-C_6H_{12}	−0.99	−1.05	−0.98	−1.00	−0.92	−0.79	−0.71	−1.10
CCl_4	−2.93	−2.81	−2.86	−2.62	−2.72	−2.54	−2.08	−3.14
n-BuCl	—	—	−3.12	—	—	—	—	—
Cl_3CCH_3	—	—	−3.47	—	—	—	—	—
CF_3Ph	−4.03	−3.98	−3.85	−3.50	−3.83	−3.33	−2.88	−4.24
$ClCH_2CH_2Cl$	−5.23	−5.12	−4.94	−4.64	−4.92	−4.45	−3.72	−5.14
Et_3N	−2.04	−2.06	−1.88	−1.85	−1.94	−1.64	−1.42	−2.15
n-Bu_2O	−2.25	−2.17	−2.02	−1.94	−2.01	−1.72	−1.51	−2.23
CH_3COOEt	−4.27	−4.10	−3.84	−3.47	−3.92	−3.37	−2.69	−3.98
DMF	−4.69	−4.48	−4.29	−3.93	−4.29	−3.76	−3.38	−4.37
DMSO	−5.03	−4.90	−4.83	−4.45	−4.71	−4.14	−3.18	−4.93
Mesitylene	−3.05	−3.00	−2.90	−2.77	−2.79	−2.34	−1.76	−3.15
Toluene	−3.50	−3.43	−3.39	−3.14	−3.40	−2.94	−2.32	−3.63
Benzene	−4.00	−3.95	−3.69	−3.54	−3.66	−3.27	−2.54	−4.00
1-Octanol	−1.58	−1.44	−1.30	−1.23	−1.33	−0.93	−0.94	−1.45
t-BuOH	−2.38	−2.31	−2.44	−2.19	−2.53	−2.24	−1.79	−2.53
MeOH	−3.53	−3.36	−3.24	−2.98	−3.12	−2.90	−2.11	−3.91
CF_3CH_2OH	−7.92	−7.52	−7.17	−6.95	−7.14	−6.61	−6.09	−8.05

[a]In kcal/mol.
[b]$\Delta\Delta H(\mathrm{v} \rightarrow \mathrm{S})(\text{ketone vs. alkane}) = \Delta H(\mathrm{v} \rightarrow \mathrm{S})(\text{ketone}) - \Delta H(\mathrm{v} \rightarrow \mathrm{S})(\text{alkane})$.
[c]Me is methyl, Bu is butyl, Ph is phenyl.
[d]$\Delta H(\mathrm{v} \rightarrow \mathrm{S})(n\text{-}C_3)$ was estimated.
[e]$\Delta H(\mathrm{v} \rightarrow \mathrm{S})(n\text{-}C_4)$ was estimated.

1-octanol are not. This can be rationalized in terms of the relative hydrogen-bond-accepting basicities of the alcohols and acetone. The Taft–Kamlet β parameter (2, 3) will be used as a measure of HBA basicity. The CF_3CH_2OH oxygen (β = 0.00) is much less basic than the acetone carbonyl oxygen (β = 0.48), and solute–solvent H-bonds are preferred over solvent–solvent H-bonds. The other alcohols have oxygens which are better H-bond acceptors ($0.62 < \beta < 1.01$) than the carbonyl oxygen. Solvent–solvent H-bonds are not broken, and exothermic displacements are not observed. An alternative view is that solvent–solvent H-bonds are broken to form a solute cavity, but reassociate after the cavity is filled (9).

Dependencies on π^* similar to that of acetone are observed for the ketones listed in Table 3. Correlations of ketone $\Delta\Delta H$(v

TABLE 4. $\Delta H(\text{v}\rightarrow\text{S})$ (2-ketone) vs. number of carbon atoms (n_c) correlations and solvent π^* values[a]

Solvent	$\pi^{*\,b,c}$	m^d	b	n^e	r	see
n-C_7H_{16}	−0.08	−1.13	−1.77	4	0.9999	0.06
c-C_6H_{12}	0.00	−1.12	−1.46	4	0.9999	0.04
CCl_4	0.28	−1.08	−3.46	4	0.9998	0.06
CF_3Ph	0.64	−1.04	−4.37	4	>0.9999	0.02
$ClCH_2CH_2Cl$	0.81	−0.88	−5.17	4	0.9999	0.03
Et_3N	0.14	−1.13	−2.61	4	0.9999	0.05
n-Bu_2O	0.24	−1.12	−2.81	4	>0.9999	0.03
CH_3COOEt	0.55	−0.92	−4.52	4	0.9998	0.06
DMF	0.88	−0.85	−4.86	4	0.9996	0.08
DMSO	1.00	−0.68	−5.02	4	0.9996	0.06
Mesitylene	0.41	−1.13	−3.37	4	>0.9999	0.02
Toluene	0.54	−1.08	−3.88	4	>0.9999	0.03
Benzene	0.59	−0.98	−4.22	4	0.9999	0.03
1-Octanol	0.34[f]	−1.11	−2.00	4	0.9998	0.07
t-BuOH	0.41	−1.06	−2.53	4	0.9998	0.06
MeOH	0.60	−0.92	−4.05	4	0.9998	0.05
CF_3CH_2OH	0.73	−0.76	−7.71	4	0.9996	0.13

[a]In kcal/mol
[b]π^* values from ref. 3.
[c]$\pi^*(n\text{-BuCl}) = 0.39$, $\pi^*(Cl_3CCH_3) = 0.49$; used in eq. [10].
[d]Slope (m) represents the methylene increment $[\Delta H(\text{v}\rightarrow\text{S})(CH_2)]$.
[e]Ketones are acetone, 2-butanone, 2-heptanone, and 2-nonanone.
[f]π^* estimated.

$\rightarrow$ S) with π^* of the aprotic solvents are given by eq. [9]−[15].

[9] $\Delta\Delta H(\text{v}\rightarrow\text{S})$(2-butanone vs. n-C_4)

$$= -3.88\pi^* - 1.46 \text{ kcal/mol)}$$

$$n = 13,\ r = 0.971,\ \text{see} = 0.33$$

[10] $\Delta\Delta H(\text{v}\rightarrow\text{S})$(2-heptanone vs. n-C_7)

$$= -3.81\pi^* - 1.40 \text{ kcal/mol}$$

$$n = 15,\ r = 0.970,\ \text{see} = 0.31$$

[11] $\Delta\Delta H(\text{v}\rightarrow\text{S})$(4-heptanone vs. n-C_7)

$$= -3.39\pi^* - 1.36 \text{ kcal/mol}$$

$$n = 13,\ r = 0.971,\ \text{see} = 0.29$$

[12] $\Delta\Delta H(\text{v}\rightarrow\text{S})$(2-nonanone vs. n-C_9)

$$= -3.87\pi^* - 1.29 \text{ kcal/mol}$$

$$n = 13,\ r = 0.971,\ \text{see} = 0.33$$

[13] $\Delta\Delta H(\text{v}\rightarrow\text{S})$(5-nonanone vs. n-C_9)

$$= -3.40\pi^* - 1.14 \text{ kcal/mol}$$

$$n = 13,\ r = 0.964,\ \text{see} = 0.33$$

[14] $\Delta\Delta H(\text{v}\rightarrow\text{S})$(2,2,4,4-tetramethyl-3-pentanone vs.

$$2,2,4,4\text{-}Me_4C_5) = -2.69\pi^* - 1.00 \text{ kcal/mol}$$

$$n = 13,\ r = 0.953,\ \text{see} = 0.30$$

[15] $\Delta\Delta H(\text{v}\rightarrow\text{S})$(cyclohexanone vs. c-C_6)

$$= -3.75\pi^* - 1.60 \text{ kcal/mol}$$

$$n = 13,\ r = 0.963,\ \text{see} = 0.37$$

For all ketones, $\Delta\Delta H(\text{v}\rightarrow\text{S})$ becomes more exothermic with increasing solvent dipolarity-polarizability. Acetone (eq. [8]) shows the strongest dependence on π^*. The symmetrical ketones exhibit s values smaller than those of the corresponding 2-ketones. The carbonyl of 2,2,4,4-tetramethyl-3-pentanone is by far the most sterically hindered, eq. [14] having an s value of only −2.69. The most dipolar of the ketones, cyclohexanone (μ = 3.1 D) has a π^* dependency weaker than the 2-ketones (2.6 D < μ < 2.9 D). This is attributed to the larger π^* of the model compound cyclohexanone (π^* = 0.00) relative to the n-alkane models (π^* = −0.08). It has been found (10) in such cases that the s coefficient of π^* is dependent on the *difference* in π^* values of the polar compound vs. model. More of the polar interaction of cyclohexanone is cancelled by its model than is cancelled for 2-ketones by less polar alkane models.

For a given solvent, $\Delta\Delta H(\text{v}\rightarrow\text{S})$ will be largest for acetone or cyclohexanone (Table 3). Acetone values tend to be largest for the more polar solvents, a consequence of the large s value of eq. [8]. The larger cyclohexanone values in nonpolar or slightly polar solvents probably result from solute−model cavity formation and dispersion interaction mismatches. 2,2,4,4-Tetramethyl-3-pentanone $\Delta\Delta H(\text{v}\rightarrow\text{S})$ values represent minima in all solvents except n-heptane and 1-octanol, in which cases the values are within 0.01 kcal/mol of the minima. The relatively small values reflect the steric requirements of the large t-butyl groups, and the resulting hindrance to approach of solvent molecules to the carbonyl group.

2,2,2-Trifluoroethanol solvent − ketone solute enthalpies of hydrogen bond formation (ΔH_h), as measured by exothermic displacements of CF_3CH_2OH from the $\Delta\Delta H(\text{v}\rightarrow\text{S})$ vs. π^* correlations (Fig. 1), are:

ΔH_h(acetone) = −3.56 kcal/mol
ΔH_h(2-butanone) = −3.23 kcal/mol
ΔH_h(2-heptanone) = −2.99 kcal/mol
ΔH_h(4-heptanone) = −3.03 kcal/mol
ΔH_h(2-nonanone) = −3.02 kcal/mol
ΔH_h(5-nonanone) = −2.99 kcal/mol
ΔH_h(2,2,4,4-tetramethyl-3-pentanone)
= −2.88 kcal/mol
ΔH_h(cyclohexanone) = −3.71 kcal/mol

The values show an expected small dependence on steric factors due to the small size of the solvent hydroxyl group. 2-Heptanone, 4-heptanone, 2-nonanone, and 5-nonanone values are the same within experimental uncertainty (combined $\Delta\Delta H(\text{v}\rightarrow\text{S})$ uncertainty intervals), while the values for 2-butanone and acetone are progressively larger. ΔH_h(2,2,4,4-tetramethyl-3-pentanone) is slightly less exothermic than the isomer values. Hydrogen bonding is strongest with cyclohexanone, the ketone with the largest value of β. The $\Delta\Delta H(\text{v}\rightarrow\text{S})$ vs. π^* correlation see values range from 0.29−0.37 kcal/mol. If these large uncertainties are also considered in the overall uncertainties of the ΔH_h values, one may only conclude that acetone and cyclohexanone are stronger hydrogen-bond-acceptors than the other ketones, which have values within experimental uncertainty of each other.

Acknowledgement

This study was supported by the Robert A. Welch Foundation (Grant E-136).

1. P. P. S. SALUJA, L. A. PEACOCK, and R. FUCHS. J. Am. Chem. Soc. **101**, 1958 (1979).

2. M. J. KAMLET, J. L. M. ABBOUD, and R. W. TAFT. Prog. Phys. Org. Chem. **13**, 485 (1981).
3. M. J. KAMLET, J. L. M. ABBOUD, M. H. ABRAHAM, and R. W. TAFT. J. Org. Chem. **48**, 2877 (1983).
4. R. FUCHS and P. P. S. SALUJA. Can. J. Chem. **54**, 3857 (1976).
5. R. FUCHS and W. K. STEPHENSON. To be published.
6. E. F. MEYER, R. H. WEISS, and T. H. GENS. J. Chem. Thermodyn. **9**, 439 (1977).
7. B. N. SOLOMONOV, J. S. ANTIPIN, V. B. NOVIKOV, and A. I. KONOVALOV. J. Gen. Chem. U.S.S.R. **52**, 2364 (1982).
8. B. N. SOLOMONOV, V. V. GORBACHUK, and A. I. KONOVALOV. J. Gen. Chem. U.S.S.R. **52**, 2370 (1982).
9. M. J. KAMLET, R. DOHERTY, R. W. TAFT, and M. H. ABRAHAM. J. Am. Chem. Soc. **105**, 6741 (1983).
10. R. FUCHS and W. K. STEPHENSON. J. Am. Chem. Soc. **105**, 5159 (1983).
11. R. FUCHS, L. A. PEACOCK, and W. K. STEPHENSON. Can. J. Chem. **60**, 1953 (1982).
12. J. B. PEDLEY and J. RYLANCE. Sussex-N.P.L. computer analysed thermochemical data: organic and organometallic compounds. University of Sussex, Brighton. 1977.
13. R. FUCHS, L. A. PEACOCK, and K. DAS. Can. J. Chem. **58**, 2301 (1980).
14. P. P. S. SALUJA, T. M. YOUNG, R. F. RODEWALD, F. H. FUCHS, D. KOHLI, and R. FUCHS. J. Am. Chem. Soc. **99**, 2949 (1977).
15. R. FUCHS, T. M. YOUNG, and R. F. RODEWALD. J. Am. Chem. Soc. **96**, 4705 (1974).

Enthalpies of hydrogen bond formation of 1-octanol with aprotic organic solvents. A comparison of the solvation enthalpy, pure base, and non-hydrogen-bonding baseline methods

W. KIRK STEPHENSON AND RICHARD FUCHS[1]
Department of Chemistry, University of Houston, Houston, TX 77004, U.S.A.

Received April 30, 1984

W. KIRK STEPHENSON and RICHARD FUCHS. Can. J. Chem. **63**, 342 (1985).

Enthalpies of solution (ΔH_s) of 1-octanol and five model compounds (di-*n*-butyl ether, *n*-heptyl methyl ether, 1-fluorooctane, 1-chlorooctane, and *n*-octane) have been determined in 13 solvents (heptane, cyclohexane, CCl_4, 1,1,1-trichloroethane, 1,2-dichloroethane, triethylamine, butyl ether, ethyl acetate, DMF, DMSO, benzene, toluene, mesitylene), and combined with heats of vaporization to give enthalpies of transfer from vapor to solvent ($\Delta H(\mathrm{v} \rightarrow \mathrm{S})$). These values have been used to calculate the enthalpy of hydrogen bond formation (ΔH_h) of 1-octanol with each solvent, using the pure base (PB), solvation enthalpy (SE), and non-hydrogen-bonding baseline (NHBB) methods. Evidence is presented suggesting that (*a*) the SE method is susceptible to mismatches of the 1-octanol vs. model polar and dispersion interactions, (*b*) the PB method is sensitive to polar interaction mismatches, whereas (*c*) the NHBB method compensates for both polar and dispersion interactions mismatches. The (apparent) ΔH_h values determined by the SE and PB methods may be as much as several kcal/mol (nearly 50%) too large, because of the inclusion of other polar and dispersion interactions. The NHBB method is therefore preferred for determining enthalpies of H-bond formation from calorimetric data. However, apparent ΔH_h values from the SE and PB methods can be incorporated into total solvatochromic equations using Taft–Kamlet π^*, β, and ξ parameters, to provide enthalpies of H-bond formation in good agreement with ΔH_h (NHBB).

W. KIRK STEPHENSON et RICHARD FUCHS. Can. J. Chem. **63**, 342 (1985).

On a déterminé les enthalpies de solution (ΔH_s) de l'octanol-1 et de cinq composés modèles (éther di-*n*-butylique, méthoxy-1 heptane, fluoro-1 octane, chloro-1 octane et *n*-octane) dans treize solvants organiques (heptane, cyclohexane, CCl_4, trichloro-1,1,1 éthane, dichloro-1,2 éthane, triéthylamine, éther butylique, acétate d'éthyle, DMF, DMSO, benzène, toluène, mésitylène) et on a combiné ces valeurs avec les chaleurs de vaporisation afin d'obtenir les enthalpies de transfert de la phase vapeur au solvant ($\Delta H(\mathrm{v} \rightarrow \mathrm{S})$). On a utilisé ces valeurs pour calculer l'enthalpie de formation de la liaison hydrogène (ΔH_h) de l'octanol-1 avec chacun des solvants en utilisant les méthodes de la base pure (BP), de l'enthalpie de solvatation (ES) et de la ligne de base sans liaisons hydrogènes (LBSLH). Les données obtenues suggèrent que: (*a*) la méthode des ES peut être affectée si les interactions soit polaires ou de dispersion de l'octanol-1 sont mal assorties par rapport au composé modèle, (*b*) la méthode de la BP est sensible aux mauvais assortiments qui peuvent être dus aux interactions polaires tandis que (*c*) la méthode de la SLH permet de compenser aussi bien les mauvais assortiments dus aux interactions polaires que ceux dus aux interactions de dispersion. Les valeurs (apparentes) du ΔH_h, telles que déterminées par les méthodes des ES et de la BP, peuvent être surévaluées par plusieurs kcal/mol (presque 50%) à cause de l'inclusion d'autres interactions polaires et de dispersion. On préfère donc la méthode de la LBSLH pour déterminer les enthalpies de formation des liaisons hydrogènes à partir des donnés calorimétriques. Cependant, on peut incorporer les valeurs apparentes du ΔH_h obtenues à partir des méthodes des ES et de la BP dans les équations solvatochromiques totales en utilisant les paramètres π^*, β et ξ de Taft–Kamlet pour obtenir des enthalpies de formation de la liaison hydrogène qui sont en bon accord avec les valeurs de ΔH_h (LBSLH).

[Traduit par le journal]

Enthalpies of hydrogen bond formation of 1-octanol with several aromatic solvents have recently been determined by both the pure base and solvation enthalpy ($\Delta\Delta H(\mathrm{v} \rightarrow \mathrm{S})$) methods (1). In the pure base method (2, 3) the enthalpy of H-bond formation (ΔH_h) is taken as the difference in heats of solution of the alcohol (A) and a similarly polar but non-hydrogen-bond-donating model compound (M), in the "pure base" (H-bond acceptor) solvent (S), minus the difference of the heats of solution of A and M in an "inert" reference solvent (an alkane or CC_4):

$$[1] \quad \Delta H_h(\mathrm{PB}) = (\Delta H_s^A - \Delta H_s^M)_B - (\Delta H_s^A - \Delta H_s^M)_{\mathrm{ref}}$$

where PB refers to the use of the pure base method. The heats of vaporization of A and M need not be known.

The $\Delta\Delta H(\mathrm{v} \rightarrow \mathrm{S})$ method utilizes enthalpies of transfer from vapor to solvent($\Delta H(\mathrm{v} \rightarrow \mathrm{S})$) for each solute,

$$[2] \quad \Delta H(\mathrm{v} \rightarrow \mathrm{S}) = \Delta H_s - \Delta H_v$$

where ΔH_s is the enthalpy of solution of a liquid sample in the solvent at 25°C giving an "infinitely dilute" ($10^{-4}-10^{-2}$ *M*) solution, and ΔH_v is the solute heat of vaporization at 25°C. $\Delta H(\mathrm{v} \rightarrow \mathrm{S})$ is often referred to as the solvation enthalpy, or the heat of solution of the gas. The enthalpy of H-bond formation in a particular solvent is taken as the difference in solvation enthalpies of the alcohol (A) and model (M):

$$[3] \quad \Delta H_h(\mathrm{SE}) = \Delta\Delta H(\mathrm{v} \rightarrow \mathrm{S}) = \Delta H(\mathrm{v} \rightarrow \mathrm{S})^A - \Delta H(\mathrm{v} \rightarrow \mathrm{S})^M$$

where SE denotes the use of the $\Delta\Delta H(\mathrm{v} \rightarrow \mathrm{S})$ method (which utilizes solvation enthalpies).

From eqs. [1]–[3] it can be shown that

$$[4] \quad \Delta H_h(\mathrm{PB}) = \Delta H_h(\mathrm{SE}) - \Delta\Delta H(\mathrm{v} \rightarrow \mathrm{ref})$$

The two methods will be equivalent only when $\Delta\Delta H(\mathrm{v} \rightarrow \mathrm{ref}) = 0$. Typically, however, $\Delta\Delta H(\mathrm{v} \rightarrow \mathrm{ref})$ values range from +1.0 to −0.5 kcal/mol, and the two results differ.

Both methods utilize a model compound to cancel the non-hydrogen-bonding (dispersion and polar) interactions of the H-bond donor with the solvent, and the enthalpy of cavity formation within the solvent, thereby isolating the H-bonding interactions:

[1]Author to whom correspondence may be addressed.

TABLE 1. Enthalpies of solution of 1-octanol and model compounds in organic solvents[a]

Solvent	Solute					
	C_8OH	Bu_2O	$MeOC_7$	FC_8	ClC_8	C_8
n-C_7H_{16}	5.59±0.10[b]	0.11±0.02[b]	0.19±0.02	0.43±0.02	0.36±0.02	0.00[c]
c-C_6H_{12}	5.69±0.10	0.37±0.00	0.59±0.04	0.88±0.02	0.71±0.02	0.44±0.02*b*
CCl_4	4.76±0.12	−0.23±0.02	−0.29±0.02	0.30±0.02	0.20±0.04	0.56[c]
Cl_3CCH_3	4.24±0.06	−0.05±0.02	−0.12±0.02	0.02±0.02	0.12±0.02	0.74±0.02
$ClCH_2CH_2Cl$	4.50±0.02	1.10±0.02	0.79±0.04	1.19±0.02	1.03±0.02	2.69±0.02
Et_3N	−1.21±0.02	−0.06±0.00	0.07±0.02	0.13±0.02	0.00±0.00	0.11±0.02
Bu_2O	1.94±0.02	0.00±0.00	0.06±0.02	0.11±0.02	0.03±0.02	0.13±0.00
CH_3COOEt	2.70±0.04	0.93±0.04	0.85±0.02	0.72±0.04	0.81±0.04	1.83±0.04
DMF	1.73±0.02	1.70±0.06	1.56±0.06	1.41±0.04	1.57±0.04	2.52±0.04[b]
DMSO	2.56±0.10	3.03±0.06	2.90±0.02	2.91±0.06	3.01±0.08	4.16±0.04
Benzene	4.35±0.06	0.60±0.00	0.50±0.02	0.49±0.02	0.48±0.02	1.44±0.02
Toluene	4.02±0.02	0.11±0.02	−0.10±0.02	−0.03±0.02	−0.12±0.02	0.78±0.00
Mesitylene	4.05±0.04	0.02±0.00	−0.12±0.00	−0.26±0.02	−0.35±0.02	0.30±0.00

[a]Values and uncertainty intervals (2 × standard deviation of the mean) in kcal/mol.
[b]Uncertainty interval estimated.
[c]Estimated by interpolation.

$$[5] \quad \Delta H_h(\text{SE}) = \Delta\Delta H_c + \Delta\Delta H_d + \Delta\Delta H_p + \Delta\Delta H_h$$

and

$$[6] \quad \Delta H_h(\text{PB}) = (\Delta\Delta H_c + \Delta\Delta H_d + \Delta\Delta H_p + \Delta\Delta H_h) - (\Delta\Delta H_c' + \Delta\Delta H_d' + \Delta\Delta H_p')$$

where the prime refers to the reference solvent, $\Delta\Delta H_c = \Delta H_c^A - \Delta H_c^M$ ("c" denotes cavity), $\Delta\Delta H_d = \Delta H_d^A - \Delta H^M$ ("d" refers to dispersion), and $\Delta\Delta H_p = \Delta H_p^A - \Delta H_p^M$ ("p" denotes polar). Both methods assume that the $\Delta\Delta H_c$, $\Delta\Delta H_d$, and $\Delta\Delta H_p$ terms are equal to zero (or that $\Delta\Delta H_c + \Delta\Delta H_d$ are non-zero but of opposite sign such that the sum is equal to zero).

The choice of model compound is important because a failure of the model to cancel the non-hydrogen-bonding interactions will be reflected in the ΔH_h(PB) and ΔH_h(SE) values. In order to investigate the influence of the solute–model match and the validity of the usual assumptions, we will determine $\Delta\Delta H_h(\text{v} \rightarrow \text{S})$ values for 1-octanol (C_8OH) in various solvents using five different model compounds: di-n-butyl ether (Bu_2O), n-heptyl methyl ether ($MeOC_7$), 1-fluorooctane (FC_8), 1-chlorooctane (ClC_8), and n-octane (C_8). Two common reference solvents (cyclohexane (c-C_6) and carbon tetrachloride (CCl_4)) will be included in the study. We hope to gain insights into the nature of the $\Delta\Delta H(\text{v} \rightarrow \text{ref})$ term, the distinguishing feature between the pure base and solvation enthalpy methods. Finally, we will examine the use of the non-hydrogen-bonding baseline (NHBB) method (4), which uses correlations with the Taft–Kamlet solvent parameters π^*, β, and ξ, for determining the enthalpy of H-bond formation.

Experimental

n-Heptyl methyl ether was prepared by heating 1-bromoheptane with sodium methoxide in methanol solution. The other solutes and solvents were commercial samples in excess of 99% purity, which were dried over 4A molecular sieve. Heat of vaporization samples were 1-fluorooctane (99.77%) and n-heptyl methyl ether (99.9%). Purities of all solvents and solutes were established by gas chromatography using a Shimadzu Mini 2 gc with a glass lined system, a 30 m × 0.25 mm id SE-30 silica capillary column, and a Hewlett-Packard 3390A integrator.

The calorimetric procedure and apparatus have previously been described (5). The calorimeters were immersed in a water bath at 25.00°C, with regulation to ±0.002°C. Liquid samples were introduced into the calorimeters from 10-, 20-, or 50-μL syringes with immersed tips. Heats of solution were corrected (0.01–0.03 kcal/mol less endothermic) to allow for the heat capacity of the samples which were introduced at 21–23°C. The uncertainty intervals in ΔH_s (twice the standard deviation of the mean of three or more determinations) are 0.00–0.12 kcal/mol. No effect of concentration on ΔH_s was observed.

Heats of vaporization were determined by evaporating 100 μL samples at 6–7 Torr into a slow stream of nitrogen (0.5 mL/min) at 25°C, using the vaporization calorimeter and technique previously reported (1). Determinations were made on four samples. The uncertainties (2 × sdm) are 0.01–0.02 kcal/mol.

Results and discussion

Enthalpies of solution of C_8OH, Bu_2O, $MeOC_7$, FC_8, ClC_8, and C_8 in 13 solvents of varying polarity and hydrogen-bond-accepting (HBA) basicity are listed in Table 1. Solute heats of vaporization, molar volumes, and Hildebrand δ_H parameters (7) are given in Table 2. In Table 3 are listed the Taft–Kamlet π^*, β, and ξ parameters (4, 8), and Hildebrand δ_H values for each solvent (heptane, cyclohexane, CCl_4, 1,1,1-trichloroethane, 1,2-dichlorethane, triethylamine, butyl ether, ethyl acetate, dimethylformamide, dimethyl sulfoxide, benzene, toluene, mesitylene), where π^* is a measure of solvent dipolarity-polarizability, β indicates solvent HBA basicity, and ξ is the solvent coordinate covalency parameter (9). Derived $\Delta\Delta H(\text{v} \rightarrow \text{S})(C_8OH \text{ vs. model})$ values are also in Table 3.

Dependence of ΔH_h *on* C_8OH*-model polar interaction match*

A plot of $\Delta\Delta H(\text{v} \rightarrow \text{S})(C_8OH \text{ vs. } Bu_2O)$ vs. π^* (Fig. 1) illustrates relationship of ΔH_h(SE) and ΔH_h(PB) to solvent dipolarity-polarizability. The baseline for the solvation enthalpy method is the $\Delta\Delta H(\text{v} \rightarrow \text{S}) = 0.00$ kcal/mol line; the baseline for the pure base method (c-C_6 reference solvent) is the $\Delta\Delta H(\text{v} \rightarrow \text{S}) = \Delta\Delta H(\text{v} \rightarrow c\text{-}C_6) = -0.96$ kcal/mol line, as eq. [4] suggests. Both methods assume that exothermic displacements from the respective baselines are due entirely to H-bonding interactions. For example, in DMF solvent

$$[7] \quad \Delta H_h(\text{SE}) = \Delta\Delta H(\text{v} \rightarrow \text{DMF}) = -6.25 \text{ kcal/mol}$$

and

TABLE 2. Solute properties

Solute	ΔH_v[a]	δ_H[b]	mv[c]
C_8OH	16.96±0.10[d]	8.8[e]	157.5
Bu_2O	10.68±0.02[f]	7.72	169.4
$MeOC_7$	11.21±0.01[g]	8.01	165.5
FC_8	11.87±0.02[g]	8.31	163.2
ClC_8	12.52±0.02[h]	8.37	170.2
C_8	9.92±0.01[i]	7.57	162.6

[a]Heat of vaporization, kcal/mol.
[b]Hildebrand solubility parameter.
[c]Molar volume, mL.
[d]Reference 13.
[e]Estimated δ_c value from extrapolation of δ_c values for C_1-C_4 alcohols in ref. 14. This represents δ_H in the absence of H-bond association.
[f]Reference 1.
[g]This study.
[h]Reference 15.
[i]Reference 6.

$$[8] \quad \Delta H_h(\text{PB}) = \Delta\Delta H(\text{v} \rightarrow \text{DMF}) - (-0.96) = 5.29 \text{ kcal/mol}$$

Of particular interest are the correlations of ΔH_h(SE) vs. π^* and ΔH_h(PB) vs. π^* for the non-hydrogen-bonding (NHB) solvents

$$[9] \quad \Delta H_h(\text{SE}) = -2.32\pi^* - 0.89 \text{ kcal/mol}$$

$$[10] \quad \Delta H_h(\text{PB}) = -2.32\pi^* + 0.07 \text{ kcal/mol}$$

where n (number of solvents) = 5, r (correlation coefficient) = 0.985, and see (standard error of the estimate) = 0.17 for both equations. Equations [9], [10], and Fig. 1 show that ΔH_h(SE) and ΔH_h(PB) values reflect not only H-bonding interactions, but also polar interactions, which result from the difference in solute (C_8OH) and model (Bu_2O) dipolarities. (It is noteworthy that monomeric 1-octanol solute appears to be more dipolar than associated 1-octanol solvent). The ΔH_p terms (eqs. [5], [6]) are nonzero (negative) and are incorporated into the ΔH_h(SE) and ΔH_h(PB) values. Correlations of ΔH_h(SE) and ΔH_h(PB) with π^* for the other C_8OH−model pairs are in Table 4. All show a strong dependence of ΔH_h(SE) and ΔH_h(PB) values on solvent polarity. The slope is largest when octane (C_8) is used as the model, because the alkane is completely nonpolar and does not even partially cancel C_8OH polar interactions.

We suggest that more accurate ΔH_h values can be obtained by measuring displacements from the $\Delta\Delta H(\text{v} \rightarrow \text{S})$(solute vs. model) vs. π^* line for the NHB solvents (4) (Fig. 1). This technique of evaluating H-bonding interactions will be referred to as the non-hydrogen-bonding baseline (NHBB) method and the resulting values denoted ΔH_h(NHBB). Use of this non-hydrogen-bonding baseline reduces or eliminates the contribution of the $\Delta\Delta H_p$ term to the ΔH_h(NHBB) value. It should be noted that the NHBB method is conceptually and formally similar to the "stepwise solvatochromic comparison method" for determining H-bonding contributions to uv/visible spectral shifts (10). For 1-octanol (Bu_2O model) in DMF solvent, ΔH_h(NHBB) is −3.32 kcal/mol. This value is much less exothermic than the corresponding ΔH_h(SE) and ΔH_h(PB) values (eqs. [7], [8]) which incorporate significant $\Delta\Delta H_p$ terms.

Dependence of ΔH_h *on* C_8OH*−model dispersion interaction match*

As previously stated (eq. [4]), the pure base and solvation

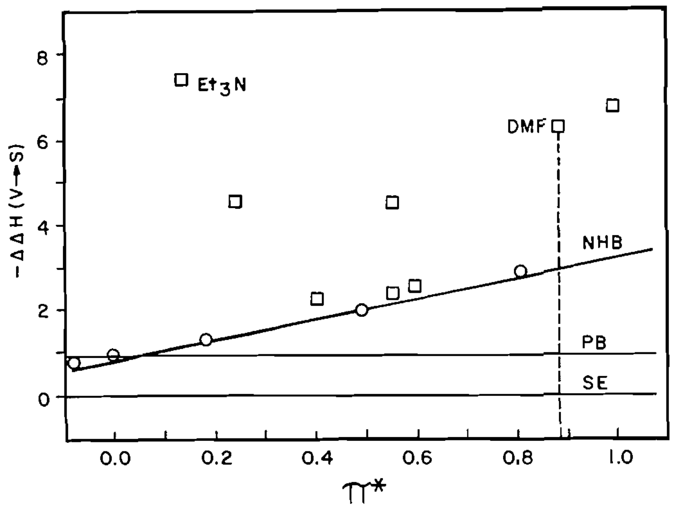

FIG. 1. $-\Delta\Delta H(\text{v} \rightarrow \text{S})$(1-octanol vs. n-Bu_2O) vs. solvent π^* for non-hydrogen-bonding (○) hydrogen-bond-accepting (□) solvents. Baselines for the non-hydrogen-bonding baseline, pure base, and solvation enthalpy methods are denoted NHB, PB, and SE, respectively.

enthalpy methods differ by an amount $\Delta\Delta H(\text{v} \rightarrow \text{ref})$. This $\Delta\Delta H(\text{v} \rightarrow \text{ref})$ term is reflected in the y-intercept values of the ΔH_h(SE) vs. π^* correlations for the NHB solvents in Table 4. The y-intercepts of the ΔH_h(PB) vs. π^* (NHB solvents) correlations are within a standard error of the estimate (see) of the origin. Determination of the factors which give rise to the y-intercept and $\Delta\Delta H(\text{v} \rightarrow \text{ref})$ values is crucial for an evaluation of the two methods.

Because the y-intercept corresponds to a hypothetical nonpolar ($\pi^* = 0$) solvent, it is logical that the y-intercept and $\Delta\Delta H(\text{v} \rightarrow \text{ref})$ are due to a C_8OH−model dispersion interaction or cavity formation mismatch rather than a polar interaction mismatch. To investigate this possibility enthalpies of dispersion interactions and of cavity formation of C_8OH in c-C_6 and CCl_4 have been estimated using the regular solution theory equations of Hildebrand and Scatchard (11, 12),

$$[11] \quad \Delta H_d = 2(\text{mv}_A)\delta_A\delta_S$$

and

$$[12] \quad \Delta H_c = (\text{mv}_A)\delta_S^2$$

where mv_A is the solute molar volume; δ_A, the solute solubility parameter (7) (Table 2); and δ_S, the solvent solubility parameter (Table 3). Calculated $\Delta\Delta H_d$(C_8OH vs. model) and $\Delta\Delta H_c$(C_8OH vs. model) values in c-C_6 and CCl_4 are given in Table 5.

The correlation of $\Delta\Delta H_d$(c-C_6 solvent) values with the y-intercepts of the NHB baselines for the ΔH_h(SE) vs. π^* correlations (Table 4) is

$$[13] \quad \Delta\Delta H_d(c\text{-}C_6 \text{ solvent}) = 1.328(y\text{-int}) - 0.24 \text{ kcal/mol}$$

where n = 5, r = 0.996, and see = 0.12. This excellent correlation suggests that the displacements of the y-intercepts from the origin are due primarily, if not totally, to a C_8OH−model dispersion interaction mismatch, rather than to H-bonding. Correlation of $\Delta\Delta H_d$ with $\Delta\Delta H(\text{v} \rightarrow c\text{-}C_6)$ gives

$$[14] \quad \Delta\Delta H_d(c\text{-}C_6 \text{ solvent}) = 1.350\Delta\Delta H(\text{v} \rightarrow c\text{-}C_6) - 0.09\text{kcal/mol}$$

TABLE 3. $\Delta\Delta H(v \rightarrow S)$ values for 1-octanol[a,b] and solvent solvatochromic parameters

	Model					Parameters			
Solvent	Bu_2O	$MeOC_7$	FC_8	ClC_8	C_8	π^*	β	ξ	δH[c]
n-C_7H_{16}	−0.80	−0.35	0.07	0.79	−1.45	−0.08	0.00	0.00[d]	7.46
c-C_6H_{12}	−0.96	−0.65	−0.28	0.54	−1.79	0.00	0.00	0.00[d]	8.22
CCl_4	−1.29	−0.70	−0.63	0.12	−2.84	0.28	0.00	0.00[d]	8.61
Cl_3CCH_3	−1.99	−1.39	−0.87	−0.32	−3.54	0.49	0.00	0.00[d]	8.49
$ClCH_2CH_2Cl$	−2.88	−2.04	−1.78	−0.97	−5.23	0.81	0.00	0.00[d]	9.31
Et_3N	−7.43	−7.00	−6.40	−5.62	−8.36	0.14	0.71	1.00	7.47
Bu_2O	−4.54	−3.87	−3.26	−2.53	−5.23	0.24	0.46	0.20	7.72
CH_3COOEt	−4.51	−3.90	−3.11	−2.55	−6.17	0.55	0.45	0.00	8.93
DMF	−6.25	−5.58	−4.77	−4.28	−7.83	0.88	0.69	0.00	11.83
DMSO	−6.75	−6.09	−5.44	−4.89	−8.64	1.00	0.76	0.00[d]	13.04
Benzene	−2.53	−1.90	−1.23	−0.57	−4.13	0.59	0.10	0.00[d]	9.19
Toluene	−2.37	−1.63	−1.04	−0.30	−3.80	0.54	0.11	0.00[d]	9.19
Mesitylene	−2.25	−1.58	−0.78	−0.04	−3.29	0.41	0.13[e]	0.00[d]	8.80

[a]In kcal/mol.
[b]$\Delta\Delta H(v \rightarrow S) = \Delta H_h(SE) = \Delta H(v \rightarrow S)(C_8OH) - \Delta H(v \rightarrow S)(\text{model})$.
[c]Hildebrand solubility parameter.
[d]Estimated; ir spectral shifts suggest that $\xi = 0.0-0.1$ (private communication, Dr. M. J. Kamlet).
[e]Estimated.

TABLE 4. Correlations of $\Delta H_h(SE)$ and $\Delta H_h(PB)$ with π^* for NHB solvents

C_8OH model	ΔH_h vs. π^* correlation	n	r	see (kcal/mol)
Bu_2O	$\Delta H_h(SE) = -2.32\pi^* - 0.89$ kcal/mol	5	0.984	0.17
$MeOC_7$	$\Delta H_h(SE) = -1.81\pi^* - 0.48$	5	0.967	0.20
FC_8	$\Delta H_h(SE) = -1.89\pi^* - 0.13$	5	0.981	0.16
ClC_8	$\Delta H_h(SE) = -1.92\pi^* + 0.61$	5	0.998	0.05
C_8	$\Delta H_h(SE) = -4.13\pi^* - 1.73$	5	0.996	0.16
Bu_2O	$\Delta H_h(PB) = -2.32\pi^* + 0.07$	5	0.984	0.17
$MeOC_7$	$\Delta H_h(PB) = -1.81\pi^* + 0.17$	5	0.967	0.20
FC_8	$\Delta H_h(PB) = -1.89\pi^* + 0.15$	5	0.981	0.16
ClC_8	$\Delta H_h(PB) = -1.92\pi^* + 0.17$	5	0.998	0.05
C_8	$\Delta H_h(PB) = -4.13\pi^* + 0.06$	5	0.996	0.16

where $n = 5$, $r = 0.999$, and see $= 0.07$. Equation [14] supports the idea that the $\Delta\Delta H(v \rightarrow c\text{-}C_6)$ terms, the distinguishing feature between the pure base (c-C_6 reference solvent) and solvation enthalpy methods, can also be attributed to a C_8OH–model dispersion interaction mismatch. The $\Delta\Delta H_d$ term contained in the $\Delta H_h(SE)(C_8OH$ vs. model) values is eliminated or reduced in the pure base and NHBB baseline methods.

Comparison of eqs. [5] and [6] indicates that the $\Delta H_h(SE)$ value is composed of only one dispersion term, $\Delta\Delta H_d$, while the $\Delta H_h(PB)$ value is composed of two, $\Delta\Delta H_d$ and $-\Delta\Delta H_d'$ (prime refers to reference solvent). The solute–model dispersion interaction mismatch ($\Delta\Delta H_d$) in a given solvent is cancelled in the pure base method by the analogous term for the reference solvent ($-\Delta\Delta H_d'$). All $\Delta H_h(PB)$ vs. π^* (NHB solvents) correlations have y-intercepts within a standard error of the estimate of the origins. This requires that the solute–model dispersion interaction differences vary little with changing solvent.

The only $\Delta H_h(SE)(C_8OH$ vs. model) vs. π^* (NHB solvents) correlation having a y-intercept within a standard error of the estimate of the origin utilizes FC_8 as the model, suggesting that FC_8 is the best model for C_8OH with respect to dispersion interactions.

The correlation of calculated $\Delta\Delta H_d(CCl_4$ solvent) values with the y-intercepts ($\Delta H_h(SE)$ vs. π^* (NHB solvents)) is

$$[15]\quad \Delta\Delta H_d(CCl_4\ \text{solvent}) = 1.389\ (y\text{-int}) - 0.26\ \text{kcal/mol}$$

where $n = 5$, $r = 0.996$, see $= 0.12$. The correlation with $\Delta\Delta H(v \rightarrow CCl_4)$ is

$$[16]\quad \Delta\Delta H_d(CCl_4\ \text{solvent}) = 1.056\Delta\Delta H(v \rightarrow CCl_4) + 0.14\ \text{kcal/mol}$$

with $n = 5$, $r = 0.965$, and see $= 0.37$. This correlation coefficient is appreciably poorer, and the see value is at least three times larger than those of eq. [13] ($r = 0.996$), [14] ($r = 0.999$), and [15] ($r = 0.996$). This probably results from the difference in polar interaction of C_8OH and model ($\Delta\Delta H_p$) with CCl_4 ($\pi^* = 0.28$). For CCl_4 reference solvent, the C_8OH–model polar interaction mismatch will give rise to a $-\Delta\Delta H_p$ term (eq. [6]), which will cancel part of the $\Delta\Delta H_p$ term observed in solvents more polar than CCl_4 and will overcompensate for the $\Delta\Delta H_p$ term observed in solvents less polar than CCl_4.

Correlations of y-intercept ($\Delta H_h(SE)$ vs. π^* (NHB solvents))

TABLE 5. Calculated $\Delta\Delta H_d$ and $\Delta\Delta H_c$ values for 1-octanol vs. model in cyclohexane and carbon tetrachloride solvents[a]

C_8OH model	c-C_6 solvent		CCl_4 solvent	
	$\Delta\Delta H_d$[b]	$\Delta\Delta H_c$[c]	$\Delta\Delta H_d$[b]	$\Delta\Delta H_c$[c]
Bu_2O	−1.29	−0.81	−1.35	−0.88
$MeOC_7$	−1.00	−0.54	−1.04	−0.59
FC_8	−0.49	−0.39	−0.52	−0.42
ClC_8	+0.63	−0.86	+0.66	−0.94
C_8	−2.55	−0.35	−2.67	−0.37

[a]In kcal/mol.
[b]$\Delta\Delta H_d = \Delta H_d(C_8OH) - \Delta H_d$(model).
[c]$\Delta\Delta H_c = \Delta H_c(C_8OH) - \Delta H_c$(model); based on extrapolated values of $\delta_c(C_8OH)$ (Table 2).

or $\Delta\Delta H$(v → ref) values with calculated $\Delta\Delta H_c$ values are very poor ($r < 0.58$ for all equations), so mismatches in the cavity term ($\Delta\Delta H_c$) do not appear to be a problem in any of the methods.

These conclusions are based on $\Delta\Delta H_d$ and $\Delta\Delta H_c$ values calculated from simple regular solution theory equations. These values should be regarded as rough estimates when polar species are involved.

ΔH_h vs. β and ξ correlations

The relationship of calculated ΔH_h values to solvent H-bond basicity for the C_8OH-Bu_2O system are given in eqs. [17]–[19]

[17] $\Delta H_h(SE) = -6.668\beta - 1.052\xi - 1.58$

$n = 13, r = 0.973$, see $= 0.56$

[18] $\Delta H_h(PB) = -6.668\beta - 1.052\xi - 0.62$

$n = 13, r = 0.973$, see $= 0.56$

[19] $\Delta H_h(NHBB) = -4.929\beta - 2.842\xi + 0.06$

$n = 13, r = 0.996$, see $= 0.20$

where β is a measure of solvent HBA basicity, and ξ is the solvent coordinate covalency parameter, which allows for the "family dependent" nature of enthalpies of H-bond formation (9).

The correlation coefficient and standard error of the estimate for the NHBB method are substantially more favorable than the corresponding values for the solvation enthalpy and pure base methods. The y-intercepts of eqs. [17] and [18] are exothermically displaced from the origins by significant amounts while the intercept of eq. [19] is within a standard error of the estimate of the origin. This leads us to conclude that the NHBB method is superior to the solvation enthalpy and pure base methods for evaluating enthalpies of H-bond formation of 1-octanol, and probably of other H-bond donor solutes as well.

Total solvatochromic equations

Single expressions for the dependence of ΔH_h on π^*, β, and ξ may be determined through multiple parameter least squares correlations (4). The total solvatochromic equations for the C_8OH-Bu_2O solute–model pair are given by eqs. [20]–[22].

[20] $\Delta H_h(SE)$

$= -2.03\pi^* - 5.14\beta - 2.62\xi - 0.92$ kcal/mol

$n = 13, r = 0.997$, see $= 0.19$

TABLE 6. $b\beta + e\xi$ values for C_8OH–model pairs in DMF and Et_3N solvents[a]

Solvent	Model	$b\beta + e\xi$	$\Delta(b\beta + e\xi)$[b]	Overall see[c]
DMF	Bu_2O	−3.55		
	$MeOC_7$	−3.67	0.12	0.28
	FC_8	−3.33	−0.22	0.36
	ClC_8	−3.45	−0.10	0.34
	C_8	−2.93	−0.62	0.38
Et_3N	Bu_2O	−6.27		
	$MeOC_7$	−6.33	0.06	0.28
	FC_8	−6.13	−0.14	0.36
	ClC_8	−6.12	−0.15	0.34
	C_8	−6.15	−0.12	0.38

[a]In kcal/mol.
[b]$\Delta(b\beta + e\xi) = b\beta + e\xi$ (from eq. [22]) $- b\beta + e\xi$ (from eqs. [23], [24], [25], or [26]).
[c]Overall standard error of the estimate of the parent equations.

[21] $\Delta H_h(PB)$

$= -2.03\pi^* - 5.14\beta - 2.62\xi + 0.04$ kcal/mol

$n = 13, r = 0.997$, see $= 0.19$

[22] $\Delta H_h(NHBB)$

$= 0.28\pi^* - 5.14\beta - 2.62\xi - 0.03$ kcal/mol

$n = 13, r = 0.997$, see $= 0.19$

The y-intercepts, which result from the C_8OH-Bu_2O dispersion interaction mismatch ($\Delta\Delta H_d$), are small for eq. [21] and eq. [22] and relatively large for eq. [20]. The large π^* coefficients (s) of eqs. [20] and [21] result from incorporation of the polar interaction mismatch ($\Delta\Delta H_p$) into the ΔH_h(SE) and ΔH_h(PB) values, whereas the small s value of eq. [22] shows that the contribution of the $\Delta\Delta H_p$ term to the ΔH_h(NHBB) values is virtually nil. The β coefficients (b) of eqs. [20]–[22] are identical, as are the ξ coefficients (e). The b (and e) values of eqs. [20]–[22] are in good agreement with the b (and e) value of eq. [19] and in poor agreement with those of eqs. [17] and [18].

Analogous total solvatochromic equations for the other C_8OH–model pairs follow a similar trend. For a given solute–model pair (a) the y-intercepts of the ΔH_h(SE) equations are usually significantly displaced from the origin, while the y-intercepts of the ΔH_h(PB) and ΔH_h(NHBB) equations are not, (b) the π^* coefficients of the ΔH_h(SE) and ΔH_h(PB) equations are identical and much larger than that of the ΔH_h(NHBB) equation, and (c) the β and ξ coefficients are the same, or nearly so, for the ΔH_h(SE), ΔH_h(PB), ΔH_h(NHBB) equations.

Because the $s\pi^*$ and y-intercept terms reflect C_8OH–model polar and dispersion interaction mismatches, it is reasonable that the "true" enthalpy of H-bond formation is more accurately represented by the $b\beta + e\xi$ portion of the total solvatochromic equation, rather than by the entire equation.

Based on eqs. [20]–[22], the $b\beta + e\xi$ values for C_8OH (Bu_2O model) in DMF (β = 0.69, ξ = 0.00) are identical (−3.55 kcal/mol). Previously determined values for the solute–model pair in DMF are $\Delta H_h(SE) = -6.25$, $\Delta H_h(PB) = -5.29$, and $\Delta H_h(NHBB) = -3.32$ kcal/mol. The difference between the ΔH_h(SE) or ΔH_h(PB) and $b\beta + e\xi$ values are 2.70 and 1.74 kcal/mol, respectively, whereas the difference be-

TABLE 7. Average ΔH_h(SE), ΔH_h(PB), and ΔH_h(NHB) values for the five C_8OH–model pairs in organic solvents[a]

Solvent	Mean ΔH_h(SE)	Mean ΔH_h(PB)	Mean ΔH_h(NHBB)
n-C_7H_{16}	−0.35±0.76	0.28±0.07	−0.04±0.04
c-C_6H_{12}	−0.63±0.77	0.00±0.00	−0.10±0.04
CCl_4	−1.07±0.99	−0.44±0.33	0.13±0.12
Cl_3CCH_3	−1.62±1.11	−0.99±0.40	0.09±0.10
$ClCH_2CH_2Cl$	−2.58±1.46	−1.95±0.77	−0.10±0.04
Et_3N	−6.96±0.93	−6.33±0.17	−6.10±0.13
Bu_2O	−3.89±0.95	−3.26±0.22	−2.78±0.21
CH_3COOEt	−4.05±1.25	−3.42±0.54	−2.19±0.18
DMF	−5.74±1.24	−5.11±0.53	−3.09±0.36
DMSO	−6.36±1.30	−5.73±0.59	−3.43±0.35
Benzene	−2.07±1.22	−1.44±0.49	−0.10±0.17
Toluene	−1.83±1.20	−1.20±0.47	−0.05±0.16
Mesitylene	−1.59±1.13	−0.96±0.39	−0.07±0.25

[a]Averages and uncertainty intervals in kcal/mol.

tween the ΔH_h(NHBB) and $b\beta + e\xi$ values (0.23 kcal/mol) is only slightly larger than the standard error of the estimate of eq. [22]. The analogous values in n-C_7 solvent (β = 0.00, ξ = 0.00) are $b\beta + e\xi$ = 0.00, ΔH_h(SE) = −0.76, ΔH_h(PB) = 0.20, and ΔH_h(NHBB) = −0.05 kcal/mol.

The other C_8OH–model pairs give rise to similar results. The agreement between $b\beta + e\xi$ and ΔH_h(SE) values is poor, except for the case of a relatively nonpolar solvent (π^* = small) *and* an unusually good solute–model dispersion interaction match (y-intercept = small). The agreement between $b\beta + e\xi$ and ΔH_h(PB) is poor for highly polar solvents (π^* = large) but improves with decreasing solvent polarity. The agreement between $b\beta + e\xi$ and ΔH_h(NHBB) values is good in all cases.

This demonstrates that C_8OH–solvent H-bonding interactions (i.e., $b\beta + e\xi$ values) can be extracted from the total solvatochromic equations of ΔH_h values calculated with the SE, PB, or NHBB methods, and that the difference between the ΔH_h(NHBB) and $b\beta + e\xi$ values will be small.

The β and ξ coefficients vary with changing model. ΔH_h(NHBB) total solvatochromic equations for the five C_8OH–model pairs are given by eqs. [22]–[26].

[23] ΔH_h(NHBB)(C_8OH vs. $MeOC_7$)

$$= 0.18\pi^* - 5.32\beta - 2.55\xi + 0.03 \text{ kcal/mol}$$

$$n = 13,\ r = 0.997,\ \text{see} = 0.20$$

[24] ΔH_h(NHBB)(C_8OH vs. FC_8)

$$= 0.31\pi^* - 4.82\beta - 2.71\xi + 0.08 \text{ kcal/mol}$$

$$n = 13,\ r = 0.991,\ \text{see} = 0.30$$

[25] ΔH_h(NHBB)(C_8OH vs. ClC_8)

$$= 0.19\pi^* - 5.00\beta - 2.57\xi + 0.12 \text{ kcal/mol}$$

$$n = 13,\ r = 0.993,\ \text{see} = 0.28$$

[26] ΔH_h(NHBB)(C_8OH vs. C_8)

$$= 0.36\pi^* - 4.24\beta - 3.14\xi + 0.04 \text{ kcal/mol}$$

$$n = 13,\ r = 0.989,\ \text{see} = 0.33$$

Comparison of eqs. [22]–[26] reveals that an increase (or decrease) in the β coefficient due to a model change is usually accompanied by a decrease (or increase) in the ξ coefficient. Differences between the $b\beta + e\xi$ value of the C_8OH–Bu_2O pair (eq. [22]) and those of the other pairs (eqs. [23]–[26]) for DMF solvent are shown in Table 6, as are the analogous values for Et_3N (β = 0.71, ξ = 1.00) solvent. The $b\beta + e\xi$ differences are usually within the combined uncertainties.

Average ΔH$_h$ *values*

Average ΔH_h(SE), ΔH_h(PB), and ΔH_h(NHBB) values for the five C_8OH–model pairs in 13 solvents are listed in Table 7. The uncertainty intervals of the average ΔH_h(SE) values for the NHB solvents range from 0.76 to 1.46 kcal/mol, while the uncertainty interval range for the corresponding ΔH_h(PB) averages is 0.00 to 0.77 kcal/mol. This supports the idea that the SE and PB methods are sensitive to the C_8OH–model match. The uncertainty intervals of the ΔH_h(NHBB) averages for the NHB solvents range from 0.04 to 0.12 kcal/mol. The same trend is observed for the HBA solvents; the uncertainty intervals of the ΔH_h(SE) averages are larger than those of the ΔH_h(PB) averages, which are in turn larger than the uncertainty intervals of the ΔH_h(NHBB) averages.

Summary

The solvation enthalpy method is very susceptible to C_8OH–model polar and dispersion interaction mismatches. The pure base method allows for a solute–model dispersion interaction mismatch but not for a polar interaction mismatch. The NHBB method compensates for both polar and dispersion interaction mismatches and is therefore the preferred method for determining enthalpies of hydrogen bond formation of 1-octanol. The NHBB method is the only method showing (within experimental uncertainty) no C_8OH polar or H-bonding interactions with nonpolar (π^* = 0.00) and NHB (β = 0.00) solvents. Also, $b\beta + e\xi$ values, which measure C_8OH–solvent H-bonding interactions and are in good agreement with ΔH_h(NHBB) values, can be extracted from the total solvatochromic equations of ΔH_h values calculated with the SE, PB, or NHBB methods.

Acknowledgements

We thank David Miller for determining several heats of solution. This study was supported by the Robert A. Welch Foundation (Grant E-136).

1. R. FUCHS, L. A. PEACOCK, and W. K. STEPHENSON. Can. J. Chem. **60**, 1953 (1982).
2. E. M. ARNETT, L. JORIS, T. S. S. R. MURTY, T. M. GORRIE, and P. v. R. SCHLEYER. J. Am. Chem. Soc. **92**, 2365 (1970).
3. J. H. SPENCER, J. E. GLELM, C. H. BLERINS, R. C. GARRETT, and F. J. MAYER. J. Phys. Chem. **83**, 1249 (1979).
4. M. J. KAMLET, J. L. M. ABBOUD, and R. W. TAFT. Prog. Phys. Org. Chem. **13**, 485 (1981).
5. R. FUCHS and P. P. S. SALUJA. Can. J. Chem. **54**, 3857 (1976).
6. J. D. COX and G. PILCHER. Thermochemistry of organic and organometallic compounds. Academic Press, New York. 1970. p. 43.
7. A. F. M. BARTON. Chem. Rev. **75**, 731 (1975).
8. M. J. KAMLET, J. L. M. ABBOUD, M. H. ABRAHAM, and R. W. TAFT. J. Org. Chem. **48**, 2877 (1983).
9. R. W. TAFT, T. GRAMSTAD, and M. J. KAMLET. J. Org. Chem. **47**, 4557 (1982).
10. M. J. KAMLET, M. E. JONES, R. W. TAFT, and J. L. ABBOUD. J. Chem. Soc. Perkin Trans. **2**, 342 (1979).
11. C. V. KRISHNAN and H. L. FRIEDMAN. J. Phys. Chem. **75**, 3598 (1971).
12. J. H. HILDEBRAND and R. L. SCOTT. The solubility of non-electrolytes., 3rd ed. Dover Publications, New York. 1964.
13. M. MANSSON, P. SELLERS, G. STRIDH, and S. SUNNER. J. Chem. Thermodyn. **9**, 91 (1977).
14. M. J. KAMLET, R. DOHERTY, R. W. TAFT, and M. H. ABRAHAM. J. Am. Chem. Soc. **105**, 6741 (1983).
15. I. WADSO. Acta Chem. Scand. **22**, 2438 (1968).

Enthalpies of transfer of alkane solutes from the vapor state to organic solvents

RICHARD FUCHS AND W. KIRK STEPHENSON
Department of Chemistry, University of Houston, Houston, TX 77004, U.S.A.

Received June 18, 1984

RICHARD FUCHS and W. KIRK STEPHENSON. Can. J. Chem. **63**, 349 (1985).

Heats of solution of 5–8 C_5–C_{16} alkane liquids have been determined in each of 19 organic solvents covering the Taft–Kamlert π^* (dipolarity-polarizability) range −0.08 to 1.00. Enthalpies of alkane transfer from vapor to solvents have been calculated ($\Delta H(\text{v} \rightarrow \text{S}) = \Delta H_s - \Delta H_v$). The methylene increments in $\Delta H(\text{v} \rightarrow \text{S})$ in the 19 solvents and water (−1.18 to −0.67 kcal/mol) are not well correlated with the Hildebrand solubility parameter δ, but an empirical correlation exists with solvent π^* and polarizability:

$$\Delta H(\text{v} \rightarrow \text{S})(\text{CH}_2) = -0.879 + 0.385(\pi^*)^2 - 1.431((n^2 - 1)/(2n^2 + 1))$$

($n = 20$, $r = 0.977$, see = 0.032). By this criterion the small methylene increment in water appears to be associated with the high dipolarity and low polarizability of water.

RICHARD FUCHS et W. KIRK STEPHENSON. Can. J. Chem. **63**, 349 (1985).

On a déterminé les chaleurs de solution de 5–8 alcanes liquides en C_5–C_{16} dans 19 solvants organiques couvrant des valeurs de polarité/polarisabilité (π^* de Taft–Kamlet) allant de −0,08 à 1,00. On a calculé les enthalpies de transfert ($\Delta H(\text{v} \rightarrow \text{S}) = \Delta H_s - \Delta H_v$). Il n'y a pas de bonne corrélation entre, d'une part, les valeurs des incréments par méthylène pour le $\Delta H(\text{v} \rightarrow \text{S})$ dans les 19 solvants et l'eau (−1,18 à −0,67 kcal/mol) et, d'autre part, le paramètre de solubilité, δ, de Hildebrand; toutefois, il existe une corrélation empirique entre la valeur π^* du solvant et la polarisabilité:

$$\Delta H(\text{v} \rightarrow \text{S})(\text{CH}_2) = -0{,}879 + 0{,}385(\pi^*)^2 - 1{,}431((n^2 - 1)/(2n^2 + 1))$$

(où $n = 20$, $r = 0{,}977$, erreur st. = 0,032). En se basant sur ce critère, il semble que le faible incrément par méthylène dans l'eau soit associé à la polarité élevée et à la faible polarisabilité de l'eau.

[Traduit par le journal]

The free energy of transfer ($\Delta G(\text{v} \rightarrow \text{S})$) of nonpolar solutes from the gas to liquid water is highly unfavorable (endogenic), and this is particularly true of alkane solutes (1). However, for the rare gases, several inorganic gases (H_2, N_2, CO, O_2), and C_1–C_5 alkanes, the enthalpy contribution ($\Delta H(\text{v} \rightarrow \text{S})$) is actually more favorable for transfers to water than for transfers to organic solvents (1). Entropies of transfer ($T\Delta S(\text{v} \rightarrow \text{S})$) of these species to water are particularly unfavorable (negative), leading to the observed endogenic values of $\Delta G(\text{v} \rightarrow \text{S})$, and low solute solubility. Alkane $\Delta G(\text{v} \rightarrow \text{w})$ values reach a minimum at ethane, and become increasingly endogenic with alkane molecular weight (1) (C_2–C_7 methylene increment, 0.16 kcal/mol). The corresponding methylene increment in $\Delta H(\text{v} \rightarrow \text{w})$ is −0.67 kcal/mol, which Abraham (1) regarded as the net result of a "normal" solvent effect (−0.97 kcal/mol), and an unfavorable hydrophobic effect. He concluded that the hydrophobic contribution to the free energy, 0.54 kcal/mol, is more an enthalpic effect (0.30–0.44 kcal/mol) than an entropic effect (0.10–0.24 kcal/mol). The rare gases and inorganic gases were regarded as "normal" solutes in water, and this behavior was used (1, 2) to predict the "normal" solvent effect of alkanes in water. Differences between the "normal" and experimental values of $\Delta H(\text{v} \rightarrow \text{w})$ were attributed to a special (hydrophobic) effect. Calculations of solvent–solute interaction terms and scaled particle theory solvent cavity formation terms (3) also suggested that the enthalpy of methylene–water interaction is less exothermic than expected.

In examining the available enthalpy data on gas to solvent transfers (1) one notes that the C_2–C_5 alkane methylene increments in a given solvent are often quite inconsistent, and in substantial disagreement with increments derived from the higher alkanes. Our previous experience with C_5–C_{16} liquid hydrocarbons (4–6) suggests that increments in this range can be obtained quite precisely, from measured heats of solution of the liquids, and heats of vaporization ($\Delta H(\text{v} \rightarrow \text{S}) = \Delta H_s - \Delta H_v$). We have observed appreciable differences in the methylene increments among the several solvents we have examined previously, with some tendency toward less exothermic increments for the more "polar" solvents.

In the present study we will report the enthalpies of solution of liquid alkanes in polar and nonpolar aprotic and hydroxylic solvents. The objectives are to determine the methylene increments in a variety of solvents, to look for a relationship between the methylene increment and solvent properties, and to observe whether the methylene increment in water appears anomalous according to this relationship.

Experimental

Solutes and solvents were commercial materials in excess of 99% purity, which were dried with 4A molecular sieve, except for methanol and trifluoroethanol for which 3A sieve was used. Purities were established by gas chromatography using a Shimadzu Mini 2 gc with a glass lined system, a 30 m × 0.25 mm id SE-30 silica capillary column, and a Hewlett-Packard 3390A integrator.

The calorimetric procedure and apparatus have been described previously (7). The vacuum jacketed calorimeter was immersed in a 25.0°C water bath regulated to 0.002°C. Liquid samples were introduced with 10-, 20-, or 50-μL syringes at 21–23°C, and corrections were made (0.01–0.03 kcal/mol) for the sample heat capacity. The uncertainty interval in ΔH_s (twice the standard deviation of the mean) are 0.01–0.24 kcal/mol, with most falling in the range of 0.02–0.10 kcal/mol. Published heats of vaporization (4) were used to calculate $\Delta H(\text{v} \rightarrow \text{S})$.

Results and discussion

Enthalpies of solution of the C_5–C_{16} alkane liquids in 19 solvents are reported in Table 1, together with alkane heats of vaporization. These have been used to calculate the enthalpies of transfer from vapor to solvents in Table 2. The methylene

TABLE 1. Enthalpies of solution of alkane liquids in organic solvents at 25°C (kcal/mol)

	Solute							
Solvent	n-C_5H_{12}	n-C_6H_{14}	n-C_7H_{16}	n-C_8H_{18}	n-C_9H_{20}	n-$C_{10}H_{22}$	n-$C_{12}H_{26}$	n-$C_{16}H_{34}$
DMSO		3.33	3.69	4.16	4.49	4.92		
DMF[a]	1.75	2.03	2.22	2.52	2.83	3.23	3.79	5.05
CF_3CH_2OH	2.35	2.57	2.89	3.07	3.61	3.77		
$ClCH_2CH_2Cl$	1.85	2.09	2.39	2.69	2.85	3.07	3.65	4.74
MeOH[a]	1.01	1.20	1.39	1.58	1.82	2.05	2.44	3.20
CH_3COOEt	1.27	1.40	1.60	1.83	2.11	2.28	2.69	3.47
Benzene[a]	1.07	1.17	1.33	1.44	1.62	1.80	2.15	2.70
t-BuOH (30°C)	0.91	1.07	1.21	1.37	1.47	1.61	1.87	2.58
$PhCF_3$[b]		0.80	0.91	1.01	1.11			2.01
Toluene[b]		0.61	0.69	0.78	0.87	0.96		1.48
Cl_3CCH_3		0.60	0.69	0.74	0.84		1.08	
n-BuCl	0.42	0.48	0.54	0.60	0.68	0.74	0.87	
c-C_6H_{12}[a]	0.26	0.27	0.39	0.44	0.47	0.56	0.69	0.97
1-Octanol	0.26	0.29	0.30	0.34	0.37	0.40	0.52	0.76
n-Bu_2O	0.08	0.10	0.12	0.13	0.17		0.28	0.43
Mesitylene[b]		0.30	0.30	0.30		0.34	0.38	0.52
CCl_4	0.34	0.43	0.50		0.63	0.72	0.86	1.11
Et_3N	0.06	0.08	0.10	0.11	0.15	0.18	0.18	0.35
n-C_7C_{16}	0.02	0.00	0.00	0.00	0.01	0.00	0.03	0.11
Solute ΔH_v	6.36	7.54	8.74	9.92	11.10	12.28	14.65	19.45

[a]Reference 6.
[b]Reference 4.

TABLE 2. Enthalpies of transfer of alkanes from vapor to solvents at 25°C (kcal/mol)

	Solute							
Solvent	n-C_5H_{12}	n-C_6H_{14}	n-C_7H_{16}	n-C_8H_{18}	n-C_9H_{20}	n-$C_{10}H_{22}$	n-$C_{12}H_{26}$	n-$C_{16}H_{34}$
Water	−6.5	−7.5	−8.1					
DMSO		−4.21	−5.05	−5.76	−6.61	−7.36		
DMF	−4.61	−5.51	−6.52	−7.40	−8.27	−9.05	−10.86	−14.40
CF_3CH_2OH	−4.01	−4.97	−5.85	−6.85	−7.49	−8.51		
$ClCH_2CH_2Cl$	−4.51	−5.45	−6.35	−7.23	−8.25	−9.21	−11.00	−14.71
MeOH	−5.35	−6.34	−7.35	−8.34	−9.28	−10.23	−12.21	−16.25
CH_3COOEt	−5.09	−6.14	−7.14	−8.09	−8.99	−10.00	−11.96	−15.98
Benzene	−5.29	−6.37	−7.41	−8.48	−9.48	−10.48	−12.50	−16.75
t-BuOH (30°C)	−5.45	−6.47	−7.53	−8.55	−9.63	−10.67	−12.78	−16.87
$PhCF_3$		−6.74	−7.83	−8.91	−9.99			−17.44
Toluene		−6.93	−8.05	−9.14	−10.23	−11.32		−17.97
Cl_3CCH_3		−6.94	−8.05	−9.18	−10.26		−13.57	
n-BuCl	−5.94	−7.06	−8.20	−9.32	−10.42	−11.54	−13.78	
c-C_6H_{12}	−6.10	−7.27	−8.35	−9.48	−10.63	−11.73	−13.96	−18.48
1-Octanol	−6.10	−7.25	−8.44	−9.58	−10.73	−11.88	−14.13	−18.69
n-Bu_2O	−6.28	−7.44	−8.62	−9.79	−10.93		−14.37	−19.02
Mesitylene		−7.24	−8.44	−9.62		−11.94	−14.27	−18.93
CCl_4	−6.02	−7.11	−8.24		−10.47	−11.56	−13.79	−18.34
Et_3N	−6.30	−7.46	−8.64	−9.81	−10.95	−12.10	−14.47	−19.10
n-C_7H_{16}	−6.34	−7.54	−8.74	−9.92	−11.09	−12.28	−14.62	−19.34

increment in $\Delta H(\mathrm{v} \rightarrow \mathrm{S})$, the Taft–Kamlet π^* value (8), and the polarizability function $(n^2 - 1)/(2n^2 + 1)$ are listed for each solvent in Table 3.

Abraham, Kamlet, and Taft (9) have correlated $\Delta G(\mathrm{v} \rightarrow \mathrm{S})$ of nonpolar solutes with δ_H, the Hildebrand solubility parameters (10) of solvents ($\delta_H = ((\Delta H_v - RT)/\text{molar volume})^{1/2}$), and $\Delta G(\mathrm{v} \rightarrow \mathrm{S})$ of polar solutes with combinations of δ_H and the dipolarity–polarizability parameter π^* ($\Delta G(\mathrm{v} \rightarrow \mathrm{S}) = g + h\delta_H\ (+\ s\pi^*)$). The rationale is that π^* describes the solvent–solute dipole–dipole interactions, whereas δ_H is an indication of solvent–solvent interactions and of the energy of cavity formation within the solvent. It was noted that the coefficient h increases with cavity size (solute molar volume), and s tends to become more negative with solute dipolarity (9, 11). This study involved only "select" solvents, which are aliphatic, non-hydrogen-bonded, non-halogenated compounds containing no more than one dipolar functional group, for which π^* is dependent on the dipole moment.

For alcohols δ_H does not properly predict the free energy or enthalpy of cavity formation, presumably because ΔH_v and δ_H reflect the loss of all hydrogen bonding, whereas cavity formation in alcohol solvents does not (12, 13). Correlational

TABLE 3. Methylene increments in $\Delta H(v \rightarrow S)$ for alkanes in organic solvents (kcal/mol)

Solvent	R—H	Methylene increment[a]	Std. error	Correlation coefficient	π^*	$\frac{n^2-1}{2n^2+1}$
Water[b]	6	−0.673	0.147	0.9946	1.09	0.1706
DMSO	5	−0.786	0.036	0.9997	1.00	0.2203
DMF	8	−0.885	0.062	0.9998	0.88	0.2055
CF_3CH_2OH	6	−0.887	0.092	0.9988	0.73	0.1547
$ClCH_2CH_2Cl$	8	−0.929	0.039	0.9999	0.81	0.2102
MeOH	8	−0.987	0.039	0.9999	0.60	0.1690
CH_3COOEt	8	−0.984	0.049	0.9999	0.55	0.1853
Benzene	8	−1.036	0.043	0.9999	0.59	0.2276
t-BuOH	8	−1.041	0.027	0.9999	0.41	0.1908
$PhCF_3$	5	−1.069	0.020	0.9999	0.64	0.2001
Toluene	6	−1.103	0.016	0.9999	0.54	0.2261
Cl_3CCH_3	5	−1.104	0.014	0.9999	0.49	0.2079
n-BuCl	7	−1.119	0.011	0.9999	0.39	0.1958
c-C_6H_{12}	8	−1.123	0.019	0.9999	0.00	0.2042
1-Octanol	8	−1.144	0.027	0.9999	0.34[c]	0.2051
n-Bu_2O	7	−1.157	0.018	0.9999	0.24	0.1948
Mesitylene	6	−1.167	0.017	0.9999	0.41	0.2271
CCl_4	7	−1.119	0.029	0.9999	0.28	0.2150
Et_3N	8	−1.164	0.015	0.9999	0.14	0.1995
n-C_7H_{16}	8	−1.180	0.015	0.9999	−0.08	0.1908

[a]Based on correlations of carbon number vs. $\Delta H(v \rightarrow S)$ for alkanes. The standard error of the estimate and correlation coefficient are also indicated.
[b]Data from ref. 1. Values in addition to those in Table 2 used in determining the CH_2 increment are ethane, −4.72; propane, −5.38; and butane, −6.21 kcal/mol.
[c]π^* estimated by extrapolation of methanol to 1-butanol values in ref. 8.

values of solubility parameters (δ_C) have been proposed (13) for alcohols, which remove the H-bonding contribution to δ_H.

We have previously observed numerous correlations of $\Delta H(v \rightarrow S)$ of polar solutes with solvent π^*, *provided* that the enthalpy term considered is $\Delta H(v \rightarrow S)$ (polar solute) − $\Delta H(v \rightarrow S)$ (nonpolar model) (11). This largely avoids the need to account for cavity formation enthalpies in the various solvents, and the nonpolar solute−solvent forces, both of which are presumed similar for the polar solute and nonpolar model. In considering the methylene increment in $\Delta H(v \rightarrow S)$ for alkanes the situation is quite different. It has recently been stated (14, 15) that alkanes show no appreciable free energy or enthalpy of *polar* interactions with dipolar molecules. Unless a solute methylene group alters solvent structure in an enthalpically significant way, the methylene increment should depend only on ΔH_{cav} (endothermic) and ΔH_{disp} (exothermic). One might expect that ΔH_{cav} should be related to δ_H, and that ΔH_{disp} should depend on a solvent polarizability function such as $(n^2 - 1)/(2n^2 + 1)$. However, we have found only a fair correlation

$$[1] \quad \Delta H(v \rightarrow S)(CH_2) = -1.335 - 2.108((n^2 - 1)/(2n^2 + 1)) + 0.079\delta_H$$

$$n = 15,\ r = 0.934,\ \text{see} = 0.045\ \text{kcal/mol}$$

and this only by omitting alcohols and water from consideration. The hydroxylic solvents are poorly correlated whether δ_H or δ_C is used. The correlation is still poorer if the polarizability term is omitted. On the other hand, we have found an empirical correlation of the methylene increment with solvent π^*

$$[2] \quad \Delta H(v \rightarrow S)(CH_2) = -0.879 + 0.385(\pi^*)^2 - 1.431((n^2 - 1)/(2n^2 + 1))$$

$$n = 20,\ r = 0.977,\ \text{see} = 0.032\ \text{kcal/mol}$$

which includes all 19 organic solvents and water. This seems surprising for a process which presumably does not involve polar solute−solvent interactions. However, the $(\pi^*)^2$ term makes an *endothermic* contribution to the methylene increment. This suggests that the dipolarity and polarizability of a solvent, which cause it to have polar interactions with a polar solute, also tend to lead to enhanced solvent−solvent interactions and greater ΔH_{cav}. For nonpolar media including the gaseous state, perfluoroalkanes, *n*-alkanes, cycloalkanes, aromatic hydrocarbons, and CCl_4 δ_H depends on polarizability

$$[3] \quad \delta_H = 0.01 + 39.48((n^2 - 1)/(2n^2 + 1))$$

$$n = 12,\ r = 0.999,\ \text{see} = 0.14$$

π^* of nonpolar solvents also tends to increase with polarizability. Substantial dipolarity of a solvent leads to dipole−dipole association of the solvent, but does not contribute to methylene group solvation.

We acknowledge that eq. [2] predicts a methylene increment in perfluorodimethylcyclohexane (−1.05 kcal/mol) 0.20 kcal/mol larger than the observed (5). Also, the value of π^* at which the increment becomes zero is −1.50, whereas a mean value of −1.06 ± 0.10 has been reported for the gaseous state (16). The application of eq. [2] is therefore limited to solvents of $\pi^* > \sim 0$. However, such anomalies are far more severe using eq. [1].

It is of interest that eq. [2] predicts a methylene increment in water of −0.66 kcal/mol, compared with the experimental value −0.67 ± 0.15 kcal/mol, from which it appears that water does not have an anomalous increment. Equation [2] suggests that the difference in methylene increments of water and DMSO is due equally to the higher π^* and lower polarizability of water.

We are unable at this time to answer the question of why the methylene increment is not better correlated with the solubility parameter, or to derive a satisfactory theoretical basis for eq. [2]. In view of this we cannot claim that the equation unequivocally refutes Abraham's discussion of the methylene group hydrophobic effect (1).

Acknowledgements

We wish to thank Frederick H. Fuchs for developing the multiple linear regression program. This study was supported by the Robert A. Welch Foundation (Grant E-136). Acknowledgement is made to the donors of the Petroleum Research Fund, administered by the American Chemical Society, for additional support of this research, which provided computing capabilities.

1. M. H. ABRAHAM. J. Am. Chem. Soc. **104**, 2085 (1982).
2. M. H. ABRAHAM. J. Am. Chem. Soc. **101**, 5477 (1979).
3. M. H. ABRAHAM and A. NASEHZADEH. J. Chem. Soc. Faraday Trans. 1, **77**, 321 (1981).
4. R. FUCHS, L. A. PEACOCK, and W. K. STEPHENSON. Can. J. Chem. **60**, 1953 (1982).
5. R. FUCHS, L. A. PEACOCK, and K. DAS. Can. J. Chem. **58**, 230 (1980).
6. P. P. S. SALUJA, T. M. YOUNG, R. F. RODEWALD, F. H. FUCHS, D. KOHLI, and R. FUCHS. J. Am. Chem. Soc. **99**, 2949 (1977).
7. R. FUCHS and P. P. S. SALUJA. Can. J. Chem. **54**, 3857 (1976).
8. M. J. KAMLET, J.-L. M. ABBOUD, and R. W. TAFT. Prog. Phys. Org. Chem. **13**, 485 (1981).
9. M. H. ABRAHAM, M. J. KAMLET, and R. W. TAFT. J. Chem. Soc. Faraday Trans. 2, 923 (1982).
10. J. H. HILDEBRAND and R. L. SCOTT. The solubility of nonelectrolytes. 3rd ed. Dover Publications, New York, NY. 1964.
11. R. FUCHS and W. K. STEPHENSON. J. Am. Chem. Soc. **105**, 5159 (1983).
12. C. V. KRISHNAN and H. L. FRIEDMAN. J. Phys. Chem. **75**, 3598 (1971).
13. M. J. KAMLET, R. DOHERTY, R. W. TAFT, and M. H. ABRAHAM. J. Am. Chem. Soc. **105**, 6741 (1983).
14. M. J. KAMLET, P. W. CARR, R. W. TAFT, and M. H. ABRAHAM. J. Am. Chem. Soc. **103**, 6062 (1981).
15. B. N. SOLOMONOV, V. V. GORBACHUK, and A. I. KONOVALOV. J. Gen. Chem. USSR, **52**, 2370 (1982).
16. M. ESSFAR, G. GUIHENEUF, and J.-L. M. ABBOUD. J. Am. Chem. Soc. **104**, 6786 (1982).

Insertion and other reactions of some hydridoolefin complexes of iridium(I)

MICHEL DROUIN and JOHN F. HARROD
Chemistry Department, McGill University, 801 Sherbrooke Street West, Montreal, P.Q., Canada H3A 2K6

Received May 10, 1984

MICHEL DROUIN and JOHN F. HARROD. Can. J. Chem. **63**, 353 (1985).

A family of complexes $IrH(CO)(Ph_3P)_2(ol)$, where ol is a monosubstituted ethylene, has been synthesized. Under an inert atmosphere the acrylonitrile complex undergoes clean decomposition to produce C_2H_5CN, half of the necessary hydrogen for the ligand reduction apparently being furnished by the phosphine ligand. The first step in the hydrogenation is insertion of the unsaturated ligand into the Ir—H bond. The alkyl product is unstable but may be trapped by O_2, to give the alkyl dioxygen complex, or by excess acrylonitrile to give the α-cyanoethyl acrylonitrile complex. Other ligands, such as CO and phosphines, displace the olefinic ligand more rapidly than insertion occurs. When ol = sytrene, the complex is very unstable with respect to styrene dissociation and very little insertion is observed. Under O_2, the styrene complex gives the first known hydridodioxygen complex $IrH(CO)(PPh_3)_2(O_2)$. The methyl acrylate complex exhibits behavior intermediate between that of the styrene and acrylonitrile analogues.

MICHEL DROUIN et JOHN F. HARROD. Can. J. Chem. **63**, 353 (1985).

On a synthétisé une famille de complexes $IrH(CO)(Ph_3P)_2(ol)$, où ol est un éthylène monosubstitué. Sous atmosphère inerte, le complexe d'acrylonitrile se décompose de façon nette pour produire du C_2H_5CN alors que la moietié de l'hydrogène nécessaire pour la réduction du ligand semble être fournie par le ligand phosphine. La première étape de l'hydrogénation consiste en une insertion du ligand insaturé dans la liaison Ir—H. Le produit alkylé est instable, mais il peut être piégé soit par O_2, pour donner le complexe d'alkyle dioxygéné, soit par de l'acrylonitrile en excès, pour donner le complexe α-cyanoéthyle acrylonitrile. Avec d'autres ligands, tels le CO et les phosphines, le déplacement du ligand oléfinique se produit plus rapidement que l'insertion. Lorsque ol = styrène, le complexe est très instable par rapport à la dissociation du styrène et on observe très peu d'insertion. Sous une atmosphère de O_2, le complexe de styrène conduit au premier complexe hydridodioxygène connu, soit le $IrH(CO)(PPh_3)_2(O_2)$. Le complexe, avec l'acrylate de méthyle, présente un comportement qui est intermédiaire entre celui du styrène et des analogues de l'acrylonitrile.

[Traduit par le journal]

Introduction

The insertion of an olefinic ligand into a metal–hydride bond is a key step in a large number of important catalytic reactions (see, for example, ref. 1). Despite a long history of experimental (2) and theoretical (3) investigations, and the synthesis of a large family of more or less stable hydridoolefin complexes (some representative references to hydridoolefin complexes are given in ref. 4), surprisingly little is known of the intimate mechanism of the hydridoolefin to alkyl transformation.

In the present paper we describe some reactions of a family of complexes: $IrH(CO)(PPh_3)_2(ol)$, where ol is a monosubstituted ethylene ligand. The reactions of these complexes, both in the presence and absence of reagents designed to trap the alkyl products of insertion, illustrate how the relative rates of olefin dissociation, olefin insertion, and trapping of alkyl products can greatly modify the mode of reaction.

Results

Synthesis of $IrH(CO)(PPh_3)_2(ol)$ complexes

Complexes of the type $IrH(CO)(PPh_3)_2(ol)$, where ol is a disubstituted ethylene with strongly electron withdrawing substituents, were first reported by Baddley and Fraser (5). These workers did not prepare any analogues with monosubstituted ethylenes, but tentatively concluded that the product of an attempted synthesis of the acrylonitrile (AN) complex was the compound **2**. In the present study the hydridoacrylonitrile complex was successfully prepared using a slight modification of the synthetic method of Baddley and Fraser (5). In fact, the reaction of $IrH_3(CO)(PPh_3)_2$ with pure olefinic ligand, followed by a stripping of the volatile olefin at low temperature, or by low temperature precipitation of product, proved to be a generally useful synthetic method for preparing the title compounds. In addition to the acrylonitrile complex, **1***a*, the methylacrylate (MA), **1***b*, and styrene (ST), **1***c*, complexes were also pre-

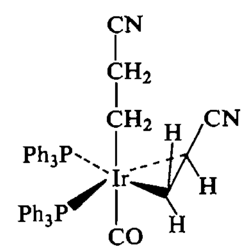

2

pared, isolated in a reasonably pure state and characterized by the usual physical and chemical methods. Other analogous compounds were detected in solution by ^{1}H-nmr, but were too unstable to isolate. All vinyl halide complexes were unstable with respect to transfer of halide to the metal under ambient conditions. However, several were observed at low temperature by nmr (see Table 1). The vinyl acetate complex, **1***d*, showed similar instability, but methyl vinyl ether did not form a complex.

With the exception of the vinyl chloride complex, **1***e*, all of the vinylic complexes observable by nmr showed the presence of two rotameric isomers, as previously observed by Fraser and Baddley for unsymmetrically disubstituted ethylenes (6) (see Table 1). The hydride resonances of the two rotamers (ethylene substituent in either the hydride or the carbonyl hemisphere) each appear as a pair of overlapping doublets due to the inequivalence of the two phosphine ligands.

Stability of the complexes $IrH(CO)(PPh_3)_2(ol)$ with respect to olefin dissociation

The three complexes **1***a*, *b*, *c*, span a range of stability with respect to olefin loss. Dissolution of the ST complex at room temperature rapidly produces free styrene and the products of the disproportionation of $IrH(CO)(PPh_3)_2$, **3** (7). On the other

TABLE 1. ^{1}H-nmr parameters for $IrH(CO)(PPh_3)_2(ol)$ in the hydride region[a]

ol	Chemical shift, (ppm), multiplicity,[b] $J_{H—P}$ (Hz)[c] Less abundant isomer	More abundant isomer	Isomer ratio
AN	−11.14, dd, 17.4 (or 22.4), 17.1 (or 22.1)	−12.07, pseudo t, 19.1 and 19.5	1.6
MA	−11.17, dd, 16.8 (or 22.5), 17.0 (or 22.7)	−12.05, pseudo t, 19.8 and 19.8	3.3
ST	−11.18, dd, 16.3 (or 26.1), 16.7 (or 26.5)	−12.03, pseudo t, 19.1 and 21.5	1.0
CH_2=CHCl[d]	—	−12.14, pseudo t, 19.1 and 20.5	>10
CH_2=C(CN)Cl	−10.35, m, 14.8 (or 22.4) and 15.1 (or 22.7)	−10.97, m, 17.3 (or 20.3) and 17.0 (or 20.0)	2.3
BrCH=CHC_6H_5	−11.2, pseudo t, 19.5	−12.1, pseudo t, 19.0	—[e]

[a] In C_6D_6 at 20°C unless otherwise indicated.
[b] dd = doublet of doublets; pseudo t = dd with central pair fully overlapped; m = pseudo t with observable additional coupling to =CH_2.
[c] Due to the closeness of the two doublets in the dd cases, which resonances were paired was not resolved, hence the two cited $J_{H—P}$ values in the dd cases.
[d] In toluene-d_8 at −25°C.
[e] Not measured.

hand, the AN complex can be easily isolated at room temperature and dissolution of the pure solid at room temperature gives a very slow decomposition which does not produce free acrylonitrile (see below). The MA complex is intermediate between the ST and AN complexes in its behaviour.

The qualitative order of stability described above is confirmed by ^{1}H-nmr observations, of line widths for free and coordinated olefin, and of spin saturation transfer between the hydride resonances of one isomer and the other (9). At −20°C, the ST complex gives reasonably sharp lines for all resonances, but exhibits a strong spin saturation transfer between the hydride resonances of the two isomers. At 0°C, the resonances of this complex, and also those of the free styrene produced by ligand dissociation, are very broad. Both the MA and AN complexes give sharp resonances at room temperature, but spin saturation transfer is evident for both complexes. Quantitative treatment of the spin saturation transfer, using the methods described by Martin *et al.* (9), yielded average lifetimes of 12.5 s (−30°C), 4.3 s (20°C), and 1.5 s (20°C) for the ST, MA, and AN complexes, respectively.

Decomposition of $IrH(CO)(PPh_3)_2(ol)$ under inert atmosphere

Solutions of the AN complex in hydrocarbon solvents at room temperature decompose slowly (ca. 50% in 24 h) in a reaction which transforms all of the AN to propionitrile. Observation of the ^{1}H-nmr spectrum of the solution during this transformation shows that all of the starting hydride complex is eventually consumed and about 0.1 equiv. of $IrH(CO)(PPh_3)_3$, **4**, is produced. The latter product is most likely the result of AN ligand dissociation and disproportionation of the resulting $IrH(CO)(PPh_3)_2$. Deliberate addition of **4** at the beginning has no observable effect on the decomposition reaction. Addition of diphenylpicrylhydrazyl (DPPH) to the reaction led to a very slight increase in rate, while a spin trap (phenyl-*N*-butylnitrone, PBN) had no discernible effect on the rate. No incorporation of deuterium into the propionitrile occurred when the reaction was run in C_6D_6, but the decomposition of $IrD(CO)(PPh_3)_2(AN)$ gave propionitrile with a broad, poorly resolved ^{1}H-nmr spectrum, indicative of partial deuteration at both carbon positions.

The MA complex decomposes more slowly (25 to 30% in 24 h) under the same conditions, mainly by the loss of the ligand. Unlike the case of the AN complex, free olefin builds up in solution and only small amounts of the hydrogenation product, methyl propionate, are observed. Complete decomposition of the ST complex occurs in a few hours, almost entirely by olefin dissociation. Only traces of ethyl benzene are produced and the complex **4** appears rapidly, achieving a final concentration of ca. 30% of the total iridium. The rate of decomposition is reduced by either lowering the temperature, or by inclusion of an excess of olefin in the solution, but in neither case is the hydrogenation reaction increased relative to ligand dissociation. However, the presence of hydrogen in solution does lead to increased hydrogenation. For example, when the MA or ST complexes are prepared *in situ* by reaction of $IrH_3(CO)(PPh_3)_2$ with excess olefin in an nmr tube, the hydrogen liberated in the reaction forming the olefin complex is reconsumed by hydrogenation of free olefin.

The deuterio complexes, $IrD(CO)(PPh_3)_2(ol)$, where ol = AN, MA, and ST, were prepared by reaction of olefin with $IrD_3(CO)(PPh_3)_2$ of 90% isotopic purity. The isotopic purities of the products were found to be 85, 70, and 50%, respectively. The room temperature ^{1}H-nmr spectrum of a freshly prepared solution of $IrD(CO)(PPh_3)_2(AN)$ revealed a progressive increase in the concentration of $IrH(CO)(PPh_3)_2(AN)$. The rate of decomposition of the deuterio complex is considerably slower than that of the hydrido complex under the same conditions (ca. 25% conversion in 24 h).

Decomposition of $IrH(CO)(PPh_3)_2(ol)$ in the presence of dioxygen

The ^{1}H-nmr spectrum of a solution of the AN complex in C_6D_6 under an atmosphere of O_2 showed the disappearance of the reactant complex at about the same rate as under an inert atmosphere. However, instead of propionitrile, the disappearance of coordinated AN produces a new species with a sharp doublet at 1.40 ppm and a complex multiplet at 3.51 ppm. These two resonances are coupled and in the ratio of 3:1 (see Fig. 1). The presence of DPPH or PBN had no apparent effect on the reaction.

A reaction of $IrD(CO)(PPh_3)_2(AN)$ under the same conditions proceeded much more slowly (c.f. reaction under inert atmosphere) to give a product superficially similar to that of the H—Ir—AN reaction, but with changes in the multiplet at 3.51 ppm indicative of deuterium incorporation.

The product of the reaction of **1***a* with O_2 was made on a preparative scale to determine its structure. Although obtained as a crystalline material, the product did not yield to X-ray diffraction methods and its structural assignment rests on spectroscopic and chemical evidence. The conclusion that this compound has the structure **5** is based on the following evidence: (*1*) The ir spectrum of the compound shows bands due

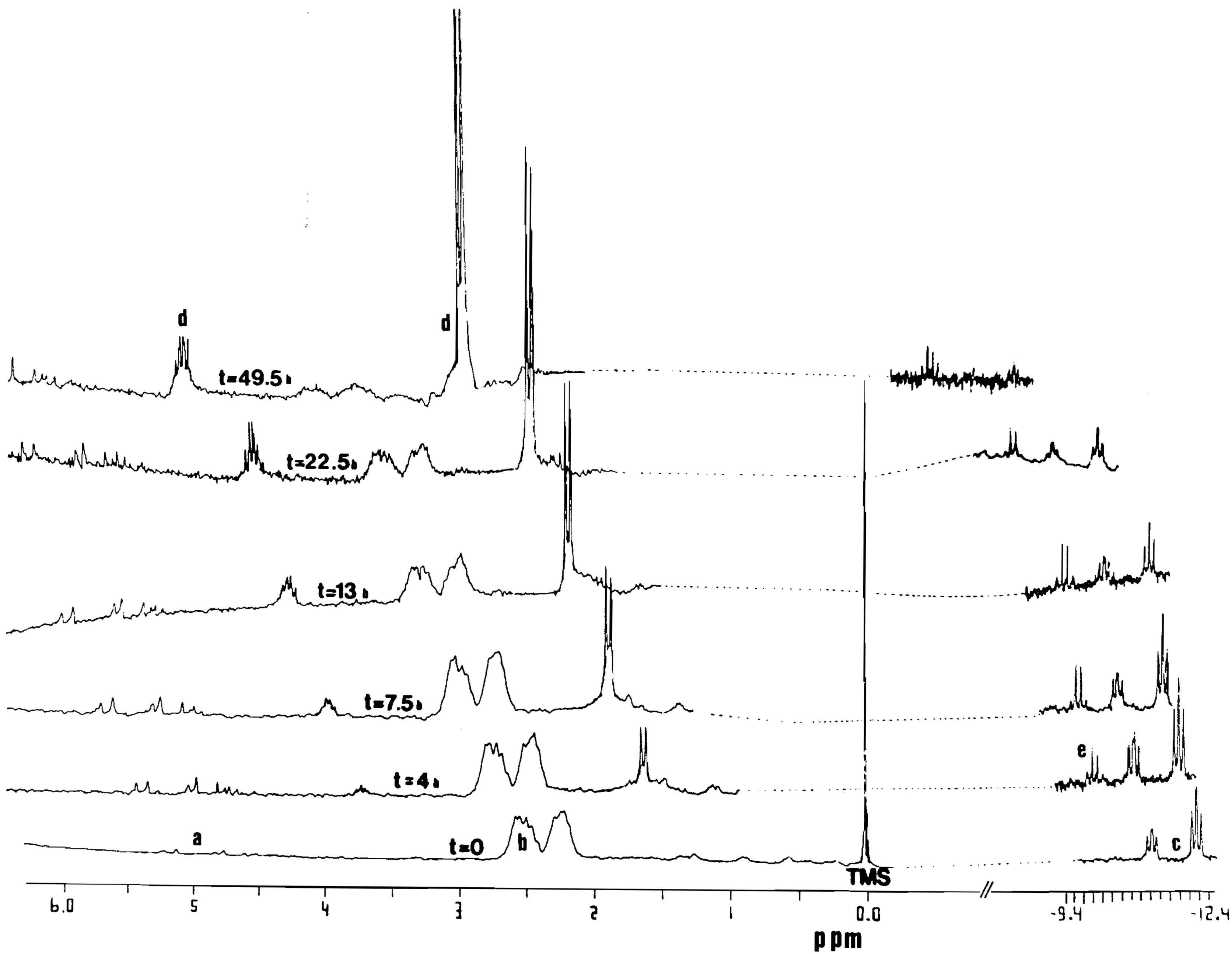

FIG. 1. Reaction of $IrH(CO)(PPh_3)_2(AN)$ with O_2, followed by ^1H-nmr in C_6D_6 at 20°C. Assignments of resonances: (*a*) free AN, (*b*) coordinated AN, (*c*) hydride resonances of reactant isomers, (*d*) —$CH(CN)CH_3$ of product, (*e*) hydride resonance of $IrH(CO)(PPh_3)_3$. The spectrum at $t = 0$ h is on scale, the other spectra are slightly offset for clarity.

TABLE 2. Infrared and nmr data for $Ir(X)(CO)(PPh_3)_2(Y)$[a]

X	Y	ν(CO) (cm^{-1})	ν(Ir(O–O)) (cm^{-1})	^{31}P (ppm)	^{1}H (ppm)	Reference
Cl	O_2	1999	855	6.47	—	10
CH_3	O_2	1968	826	−2.56[b]	0.40(t)	11
CH_2CN	O_2	1989 [2218, ν(CN)]	835	—	1.88(t)[c]	12
$CH(CN)CH_3$	O_2	1997 [2201, ν(CN)]	830	8.22, 7.77 (1:1)	1.4(d) 3.51(m) (3:1)	—
$CH(COOCH_3)CH_3$	O_2	1978 [1695, ν(>C=O)]	830	7.38[e]	1.41(d) 3.39(s) 4.16(m) (3:3:1)	—
H	O_2	1986 [2079, ν(Ir—H)]	823	9.99	−14.5(t) 8.5(m) (1:15)	—
Cl	SO_4	2045[d]	—	−0.78	—	—
$CH(CN)CH_3$	SO_4	2033[d]	—	−0.74	0.98(d) 3.87(m) (3:1)	—

[a]Infrared spectra as Nujol mulls, ^{31}P-nmr in CD_2Cl_2, and ^{1}H-nmr in C_6D_6 unless otherwise noted.
[b]Solvent not reported.
[c]In CD_2Cl_2.
[d]In KBr pellet.
[e]Greater line-width and poorer resolution may have been responsible for the observation of only one line in this case.

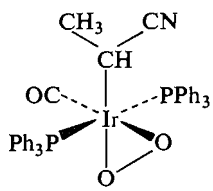

5

to ν_{CN}, ν_{CO}, and ν_{O-O}, with frequencies and intensities comparable to those of analogous compounds (see Table 2). (*2*) The ^{1}H-nmr spectrum conforms to that of an α-cyanoethyl derivative. Decoupling of the methyl resonance simplifies the methine resonance to a pseudotriplet, due to coupling with two near-equivalent phosphorus nuclei. This coupling excludes the possibility that the compound is an alkylperoxo- complex and supports the direct bonding of the alkyl ligand to the metal. (*3*) The observation of two ^{31}P resonances of equal intensity which are attributed to the two diastereotopically inequivalent P ligands. (*4*) The compound reacts rapidly and cleanly with SO_2 to give a product whose ir spectrum shows a remarkable resemblance to the known compound $IrCl(CO)(PPh_3)_2(SO_4)$ (see Fig. 2) (10). The peaks at 1296 and 1160–1170 cm^{-1} (ν_3), 902 and 868 cm^{-1} (ν_1), and 694 cm^{-1} (ν_2) are highly characteristic of the chelating SO_4 group (11). Except for changes in chemical shifts, the ^{1}H-nmr features of the α-cyanoethyl group are the same as for the O_2 complex.

The reaction of the MA complex under oxygen, as under an inert atmosphere, proceeds primarily by olefin dissociation. However, the proton spectrum of a reaction carried out in an nmr tube showed the formation of a $—CH(COOCH_3)(CH_3)$ derivative in about 14% yield. Although this species (see Table 2 for ir and nmr data) is almost certainly the dioxygen complex, its instability and admixture with large amounts of other reaction products precluded its isolation as a pure compound.

The reaction of **1***c* with oxygen yields no detectable alkyl dioxygen compound. Instead, the disappearance of the hydride resonances of the reactant is accompanied by the appearance of a new hydride resonance (triplet, −14.5 ppm, C_6D_6). A preparative scale reaction in benzene afforded a yellow crystalline product whose analysis and spectroscopic properties (see Table 2) corresponded to $IrH(CO)(PPh_3)_2(O_2)$. In particular, the ratio of hydride to phenyl protons (1:29) and the J_{P-H} (18.5 Hz) confirm the presence of a hydride *cis* to two phosphine ligands. The presence of the dioxygen ligand is strongly suggested by the ir band at 823 cm^{-1}. The frequency of this band is very close to that observed for the methyl dioxygen analogue reported by Mason and Ibers (12) and somewhat lower than that of the analogues with more electron withdrawing ligands, such as halogen or α-cyanoethyl. Reaction of this compound with SO_2 led to the immediate disappearance of the hydride, possibly as a result of the insertion of the sulfate intermediate into the Ir—H bond. Resonances due to such an insertion were not observed, perhaps because of the strongly acidic character of the OH groups produced. A reaction of deuterio-**1***c* (about 50% of the hydride replaced by deuterium) with O_2 gave a product with an additional ν_{CO} at 2015 cm^{-1} due to CO *trans* to D.

Trapping of the insertion product by olefin

By heating the trisphosphine complex **4** with AN, Baddley and Fraser obtained an unstable compound to which they assigned the structure **2** on the basis of chemical analysis and ir spectrum (5). In view of the results described above, it appears more likely that an alkyl ligand, if present, would be the α-cyanoalkyl, rather than the β-cyanoalkyl. A second difficulty with the approach of Baddley and Fraser is that the method of synthesis liberates a phosphine ligand which can compete very effectively with the AN for a coordination site.

The problem of the presence of excess phosphine can be avoided by trapping the insertion product from **1***a* in AN as solvent. This reaction goes cleanly and to high conversion (>80%) in about 48 h. However, the ^{1}H-nmr spectrum of the product is very complicated. The source of this complication is evident when the structures of the most likely products **6***a* and **6***b* are considered. Since each of the isomers exists as two diastereomers, it is possible that there will be four sets of resonances for the alkyl and olefin ligands in the nmr spectra. In the proton spectrum there are two clearly identifiable doublets due to CH_3 at 0.50 ppm (J = 7.1 Hz) and 0.83 ppm (J = 7.3 Hz), and a multiplet resembling a pseudo-triplet at 1.5

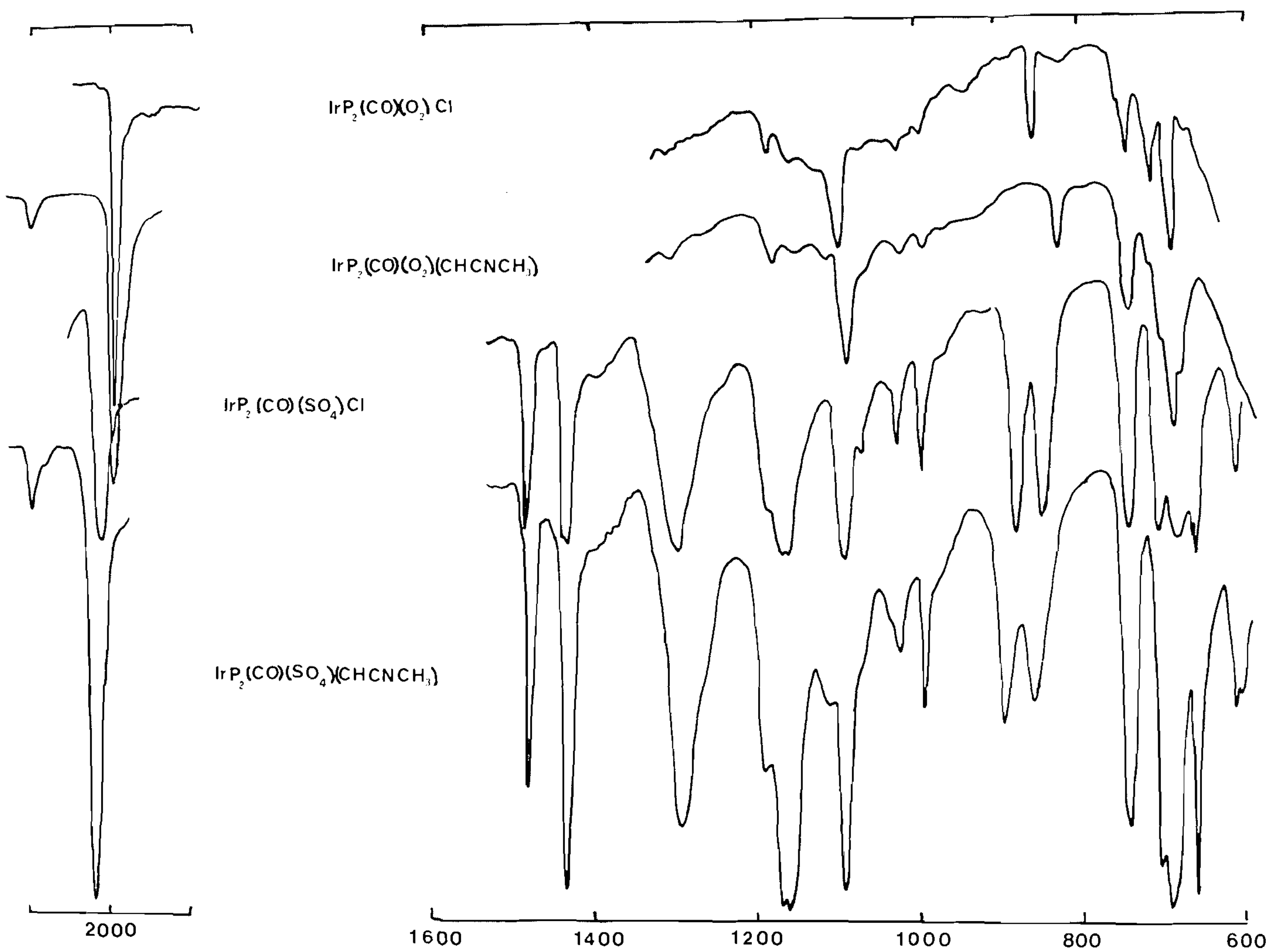

FIG. 2. Infrared spectra of the O_2 complexes $IrX(CO)(PPh_3)_2(O_2)$ (X = Cl and $CH(CN)CH_3$) and of their products of reaction with SO_2.

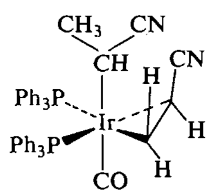

6a

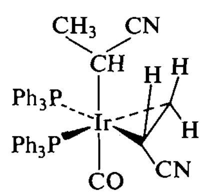

6b

ppm. This latter resonance probably corresponds to two overlapping doublets. In addition there are two broad complex massifs at 2.0–2.3 ppm and 2.4–2.7 ppm due to the coordinated AN. The integrals for the CH_3 resonances and the AN resonances are in a ratio slightly greater than 1:1, most likely because the methine resonances are hidden in the multiplet at 1.5 ppm. The ^{31}P-nmr spectra are insensitive to the presence of diastereomers and, in the proton decoupled spectrum, four doublets at 0.8 and −7.6 ppm (J_{P-P} = 7.3 Hz) and 0.1 and −9.1 ppm (J_{P-P} = 9.8 Hz) were observed, a pattern very similar to that observed for **1***a*.

The proton spectrum, as expected, is simplified by replacement of acrylonitrile by ligands of higher symmetry. Fumaronitrile, which removes the possibility of rotamers, but still gives diastereomers, reacts in solution with **6** and simplifies the spectrum to two overlapping methyl doublets centred at 0.42 ppm, coupled to two methine multiplets at 2.0 and 2.4 ppm. Tetracyanoethylene, which can give neither rotamers nor diastereomers, gives a product with a doublet and multiplet at 0.98 and 3.8 ppm, respectively. Bubbling CO through a solution of **6** rapidly produces a product with two overlapping doublets at 1.93 ppm and a complex multiplet at 2.97 ppm. The presence of two different α-cyanoethyl resonances suggests that if the product is $Ir(CO)_2(PPh_3)_2[CH(CN)CH_3]$, as might be expected, it probably exists as two isomers. The ir spectrum of this product had no bands in the region typical of a metal acyl, excluding the possibility that insertion of CO into the Ir—C bond had occurred. Finally, bubbling O_2 through a solution of **6** under ambient conditions transforms it rapidly and completely to **5**.

Apart from O_2, AN proved to be the only neutral ligand with which the insertion product of **1***a* could be successfully trapped. Reaction of **1***a* with CO and phosphorus-containing ligands led to rapid substitution of the AN ligand. No evidence was obtained for a transformation of **1***b* or **1***c* into analogues of **6**.

Discussion

All of the observations in the present study conform to the widely held view that insertion of an olefin ligand will not occur if the double bond of the olefin is orthogonal to the M—H bond (3). The essentially constant rates of reaction for the AN complex, independent of trapping agent, the insensitivity of the reaction rates to a free radical trap and the appreciably slower rates of the Ir—D relative to Ir—H compounds, all point to the unimolecular insertion reaction as being the rate controlling process. The spectroscopic data are in accord with a structure in which the olefin ligand double bond is coplanar with the two phosphine ligands and perpendicular to the H—Ir—CO unit. This structure was previously demonstrated crystallographically for the fumaronitrile compound (6). It is therefore reasonable to suppose that the rate of insertion is controlled by the rate of the rotation of the olefinic double bond into coplanarity with the Ir—H bond.

Whether or not insertion can be observed in the present systems depends on a delicate balance between the rates of olefin rotation and olefin dissociation. Even though the spin saturation transfer data and the general stability of compounds **1***a* and **1***b* suggest only modest differences in the rates at which they lose olefin, their abilities to give stable trapped insertion products are markedly different. Even without taking the irreversible disproportionation of **3** into account, the kinetic behavior of a system in which reversible olefin dissociation competes with an olefin rotation process, with at least two different potential minima, is very complicated and beyond the scope of the present results.

The relative rates of reaction of **1***a* with such neutral ligands as CO and PPh_3 and with O_2 are very different. In the case of CO and PPh_3 the reaction is complete in less than 1 h and the product results from the trapping of **3**, the product of olefin dissociation. For O_2, the reaction under the same conditions has a half life of about 24 h and the final product results from trapping the insertion product. Thus, in the case of **1***a* it appears that the combined rates of olefin dissociation and the reaction of **3** (present in very low concentration) with O_2 do not compete significantly with insertion. However, for **1***c*, the greater rate of olefin loss and the resulting higher concentration of **3** favours the reaction of **3** with O_2 and leads to the formation of the remarkable hydridodioxygen complex $IrH(CO)(PPh_3)_2(O_2)$. It is likely that this complex has a structure analogous to **1**, with the O_2 occupying the same position as the olefin. The comparative stability of this compound with respect to the insertion of the O_2 into the Ir—H bond is probably also due to the orthogonal disposition of the O—O and Ir—H bonds. This hydridodioxygen complex is also produced in small amounts in reactions of O_2 with other precursors of **3**, e.g. $IrH(CO)(PPh_3)_2$, $IrH(CO)(PPh_3)_3$, and **1***a* and **1***b*, but in these cases the rate of production of the dioxygen complex is comparable to its rate of decomposition in solution.

Only two examples of alkyldioxygen complexes have been previously reported (11, 12). Our attempts to use the method reported by Zecchin *et al.* for the synthesis of $Ir(CH_2CN)(CO)(PPh_3)_2$, were not successful for the higher α-cyanoalkyl derivatives. The presence of a β-hydrogen on the alkyl group, as is often the case, renders the product unstable. The trapping of the insertion products described above by O_2 thus remains a unique method for the synthesis of the higher alkyldioxygen compounds. To our knowledge, the hydridodioxygen complex reported above is the first of its kind. Such species may well participate in many reactions, either stoichiometric or catalytic, involving O_2 and organometallic complexes. The participation of a hydroperoxoiridium complex in a catalytic oxygenation reaction has recently been proposed by Atlay *et al.* (14).

The observed replacement of D by H in the $IrD(CO)(PPh_3)_2(ol)$ complexes is explained by H/D exchange within the transient square planar intermediate **3**. The orthometallation shown in [1] is a likely source of such an exchange and could

[1]

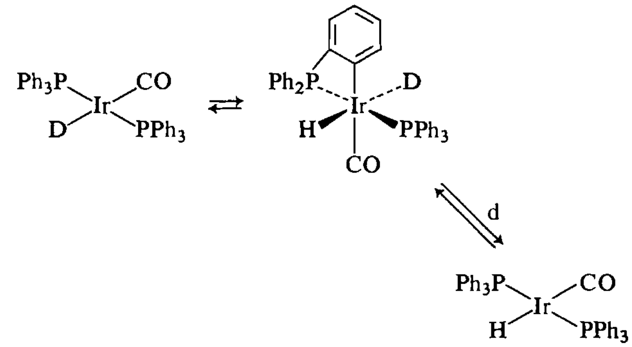

also furnish the additional hydrogen needed to effect complete hydrogenation of the acrylonitrile ligand, as observed. The D/H exchange cannot be attributed to a reversible insertion/β-elimination process since deuterated olefin is not observed until after much longer times than are required for considerable loss of Ir—D. In fact, the rate of H/D exchange is comparable to the rate of replacement of olefin by donor ligands and much faster than the rate of appearance of trapped insertion or hydrogenation products. Since the rate of hydrogenation of AN ligand, which occurs when **1***a* decomposes in solution under inert atmosphere, is very similar to the rate of production of insertion product trapped with O_2 or AN, it is reasonable to conclude that the rate controlling process in each case is the insertion of AN into the Ir—H bond. In the absence of trapping agent, the intermediate $Ir[CHCN(CH_3)](CO)(PPh_3)_2$ undergoes rapid hydrogenolysis, either by an intramolecular metallation analogous to [1] followed by reductive elimination of propionitrile, or by transfer of hydride from some other hydride complex in solution.

Experimental

All solvents were subjected to standard drying procedures and distilled prior to use. Deuterated solvents and $LiAlD_4$ were purchased from Merck, Sharp and Dohme, Canada Limited. Acrylonitrile (Matheson, Coleman and Bell), methyl acrylate (Aldrich Chemical Co.), and styrene (Kodak Chemical Co.) were freshly distilled under reduced pressure immediately before use. The iridium complexes $IrCl(CO)(PPh_3)_2$ (15), $IrH_3(CO)(PPh_3)_2$ (15), $IrD_3(CO)(PPh_3)_2$ (16), and $IrH(CO)(PPh_3)_3$ (17) were prepared by standard procedures.

^{1}H-nmr spectra were measured on a Varian XL-200 instrument operating in the FT mode at 200.06 MHz. ^{31}P spectra were recorded on a Brüker WH-90 instrument at 36.44 MHz. All proton shifts were measured relative to an internal tetramethylsilane standard and ^{31}P shifts were relative to an external 85% phosphoric acid standard. Infrared spectra were recorded on a Nicolet 7000 FT-IR machine at a resolution of 2 cm^{-1}.

Preparation of (η^2-acrylonitrile)carbonylhydridobis(triphenylphosphine)iridium(I)

A suspension of $IrH_3(CO)(PPh_3)_2$ (1.0 g; 1.34 mmol) in acrylonitrile (100 mL) was stirred at room temperature, with passage of a slow stream of nitrogen through the mixture. After several hours the solid had entirely dissolved and the volume of the solution was reduced to 20 mL by vacuum evaporation. Following filtration through celite, 45 mL of hexane was added and the solution was cooled to −20°C for several hours, filtered, and evaporated to dryness. The pale yellow solid was extracted with 12 mL of acrylonitrile and the white insoluble product recovered by centrifugation, washed with a further 8 mL of acrylonitrile and dried under vacuum. Yield: variable, but generally 20–35%. Decomp. 69–70°C. Ir (cm^{-1}): 2233(w), 2202(m), 2080(vs), 1958(vs). Nmr: see Table 1. *Anal.* calcd. for $C_{40}H_{34}IrNOP_2$: C 60.13, H 4.30, N 1.75, P 7.75; found: C 59.78, H 4.27, N 1.82, P 8.01.

(η^2-Methylacrylate)carbonylhydridobis(triphenylphosphine)-iridium(I)

Nitrogen was passed through a solution of $IrH_3(CO)(PPh_3)_2$ (1.33 g; 1.78 mmol) in 100 mL of methylacrylate for several hours. During this time almost all of the solid dissolved and the volume of the solution was reduced to ca. 10 mL. Following filtration through celite, the solution was evaporated to dryness under vacuum. The pale yellow, glassy residue was dissolved in 10 mL of benzene, filtered through celite into 6 mL of pentane, and evaporated to give a light yellow powder. It is essential that these last steps be performed as quickly as possible. The yield of product is variable between 80–90%. An analytically pure sample was obtained from a further recrystallization from methylacrylate at −20°C. Decomp. 72–75°C. Ir (cm^{-1}): 2067(vs), 1967(s), 1680(vs). Nmr: see Table 1. *Anal.* calcd. for $C_{41}H_{37}IrO_3P_2$: C 59.19, H 4.49, P 7.45; found: C 59.42, H 4.99, P 7.58.

(η^2-Styrene)carbonylhydridobis(triphenylphosphine)iridium(I) (18)

A stream of nitrogen was passed through a solution of $IrH_3(CO)(PPh_3)_2$ (0.35 g; 0.47 mmol) in 40 mL styrene, maintained at 40°C for 1 h. The solution volume was reduced to ca. 5.0 mL and, following filtration through celite, 8.0 mL of hexane was added. The solution was refiltered and quickly evaporated to dryness under vacuum. The product was obtained as a pale yellow powder in ca. 90% yield. Low temperature (<−20°C) recrystallization from a styrene/hexane mixture did not change the purity of the product which, from nmr and ir evidence, was greater than 95%. Ir (cm^{-1}): 2060(vs), 1941(vs). Nmr, see Table 1.

Preparation of deuterated analogues

The deuterated analogues of the AN, MA, and ST complexes were prepared by the same methods as the normal compounds, using $IrD_3(CO)(PPh_3)_2$ as reactant. Ir (cm^{-1}): AN complex 2197(w), 1998(sh), 1990(vs), 1513(w); MA complex 1963(vs), 1694(vs), 1496(w); ST complex 1975(vs).

Generation of the vinyl chloride complex

Vinyl chloride was bubbled through a solution of the styrene complex, **1***c*, at −25°C for 10 min. The sample was then left for 2 h at −25°C and the ^{1}H-nmr spectrum was recorded at −25°C (see Table 1). A similar experiment using AN gave the same nmr spectrum as that of an authentic sample of **1***a* prepared at room temperature.

Carbonyl(α-cyanoethyl)dioxygenbis(triphenylphosphine)iridium

The synthesis of the AN complex was followed as described above, up to the first filtration and then the solution was evaporated to dryness and the solid residue taken up in 25 mL of benzene. Oxygen was bubbled through the solution for 30 min and the mixture was stirred under an atmosphere of O_2 for a further 24 h. After periods of 5 and 10 h had elapsed, oxygen was bubbled through the solution for 10 min. The resulting green solution was evaporated to dryness and the product purified by elution as a yellow band from an alumina column with 1:1 acetone/hexane. An analytically pure sample was obtained as a dichloromethane solvate by recrystallization from dichloromethane/pentane. The presence of one molecule of CH_2Cl_2 per mole of complex was verified by ^{1}H-nmr and chemical analysis. Yields are variable between 40 and 50%. Decomp. 159–160°C. Ir and nmr, see Table 2. *Anal.* calcd. for $C_{40}H_{34}IrNO_3P_2.CH_2Cl_2$: C 53.77, H 3.97, P 6.76; found: C 54.17, H 3.92, P 7.06.

Carbonylhydridodioxygenbis(triphenylphosphine)iridium

Nitrogen was bubbled through a solution of $IrH_3(CO)(PPh_3)_2$ (0.40 g; 0.54 mmol) in 25 mL of styrene at 40°C for 1 h and the solution rapidly evaporated to dryness under vacuum. The yellow residue was dissolved in toluene at 0°C and O_2 gently bubbled through the solution for 24 h. During this time a yellow solid precipitated and the solution turned dark blue. The yellow product was filtered, washed several times with toluene at 0°C and dried under vacuum. A sample for analysis was recrystallized from CH_2Cl_2/pentane at −20°C. Yield ca. 30%. Decomp. 118°C. Ir and nmr, see Table 2. *Anal.* calcd. for $C_{37}H_{31}IrO_3P_2$: C 57.13, H 4.03, P 7.96; found: C 57.23, H 4.07, P 7.86.

Trapping experiments

The trapping of the insertion products was followed by ^{1}H-nmr. Such experiments were performed using a concentration of 2% of reactant complex in C_6D_6 and a cavity temperature of 20°C. In the case of the O_2 trapping experiment the solution was purged with pure O_2 for 5 min before the tube was sealed and put in the spectrometer cavity. In the case of AN trapping, the complex solution was treated with a ten-fold molar excess of AN before purging with argon and introduction into the spectrometer. After the reaction was completed the product solution was flash-evaporated to dryness and the solid redissolved in C_6D_6 containing either fumaronitrile or tetracyanoethylene in a two-fold molar excess over the original iridium complex. Under these conditions, the AN of **6** was completely displaced and the more heavily substituted cyanoolefin was fully coordinated.

Acknowledgements

The authors thank the Natural Sciences and Engineering Research Council of Canada and the Fonds FCAC du Québec for scholarships (M.D.) and for financial support of this work.

1. G. W. Parshall. Homogeneous catalysis. J. Wiley and Sons, New York. 1980.
2. H. C. Clark, C. Jablonski, and C. S. Wong. Inorg. Chem. **14**, 1332 (1975); J. W. Byrne, H. V. Blaser, and J. A. Osborn. J. Am. Chem. Soc. **97**, 3871 (1975); J. Werner and R. Feser. Angew. Chem. Int. Eng. Ed. **18**, 157 (1979); J. Organometal. Chem. **233**, 193 (1982); D. J. Cole-Hamilton and G. Wilkinson. Nouv. J. Chim. **1**, 141 (1979); H-F. Klein, R. Hammer, J. Gross, and O. Schiebert. Angew. Chem. Int. Eng. Ed. **19**, 809 (1980); A. H. Deeming, B. F. G. Johnson, and J. Lewis. J. Chem. Soc. Dalton Trans. 1848 (1973).
3. D. L. Thorn and R. Hoffmann. J. Am. Chem. Soc. **100**, 2079 (1978); G. Henrici-Olivé and S. Olivé. Transition Met. Chem. **1**, 109 (1976); A. Dedieu. Inorg. Chem. **20**, 2803 (1981).
4. A. J. Deeming, B. F. G. Johnson, and J. Lewis. J. Chem. Soc. Chem. Commun. 598 (1970); F. N. Tebbe and G. W. Parshall. J. Am. Chem. Soc. **93**, 3794 (1971); M. E. Tully and A. P. Ginsberg. J. Am. Chem. Soc. **95**, 2042 (1973); T. W. S. Benfield and M. L. H. Green. J. Chem. Soc. Dalton Trans. 1324 (1974); A. H. Klazinger and J. H. Teuben. J. Organomet. Chem. **157**, 413 (1978); P. R. Sharp and R. R. Schrock. J. Organomet. Chem. **171**, 43 (1979); H-J. Kablitz and G. Wilke. J. Organomet. Chem. **194**, 309 (1980).
5. W. H. Baddley and M. S. Fraser. J. Am. Chem. Soc. **91**, 3661 (1969).
6. M. S. Fraser and W. H. Baddley. J. Organomet. Chem. **36**, 377 (1972).
7. C. A. Reed and W. J. Roper. J. Chem. Soc. Dalton Trans. 1370 (1973); J. F. Harrod, D. F. R. Gilson, and R. Charles. Can. J. Chem. **47**, 1431 (1969).
8. T. A. Albright, R. Hoffmann, J. C. Thibeault, and D. L. Thorn. J. Am. Chem. Soc. **101**, 3801 (1979) and references therein; T. A. Albright. Acc. Chem. Res. **15**, 149 (1982).
9. M. L. Martin, G. J. Martin, and J. J. Delpuech. Practical NMR spectroscopy. Heyden, London. 1980. p. 315.
10. L. Vaska. Science, **140**, 809 (1963).
11. R. Eskenazi, J. Raskovan, and R. Levitus. J. Inorg. Nucl. Chem. **28**, 521 (1966); W. R. McWhinnie. **26**, 21 (1964); K. Nakomoto. Infrared spectra of inorganic and coordination compounds. John Wiley and Sons, New York. 1970. p. 173.
12. M. G. Mason and J. A. Ibers. J. Am. Chem. Soc. **104**, 5153

(1982).
13. S. ZECCHIN, G. ZOTTI, and G. PILLONI. J. Organomet. Chem. **235**, 353 (1982).
14. M. T. ATLAY, M. PREECE, M. STRUKUL, and B. R. JAMES. J. Chem. Soc. Chem. Commun. 406 (1982).
15. K. VRIEZE, J. P. COLLMAN, C. T. SEARS, and M. KUBOTA. Inorg. Synth. **11**, 101 (1982).
16. L. MALATESTA, G. CAGLIO, and M. ANGOLETTA. J. Chem. Soc. 6974 (1965); C. K. BROWN, W. MOWAT, G. YAGUPSKY, and G. WILKINSON. J. Chem. Soc. A, 850 (1971); J. F. HARROD and W. YORKE. Inorg. Chem. **20**, 1156 (1981).
17. G. YAGUPSKY and G. WILKINSON. Inorg. Synth. **13**, 127 (1972).
18. M. DROUIN and J. F. HARROD. Inorg. Chem. **22**, 999 (1983).

Synthesis of derivatives of isoindole and of pyrazino[2,1-*a*]isoindole

JEAN-MARIE FERLAND,[1] CHRISTOPHER A. DEMERSON,[2] AND LESLIE G. HUMBER[2]
Ayerst Research Laboratories, Montréal, P.Q., Canada H4R 1J6

Received July 5, 1983[3]

JEAN-MARIE FERLAND, CHRISTOPHER A. DEMERSON, and LESLIE G. HUMBER. Can. J. Chem. **63**, 361 (1985).

Amines were reacted with lactones **7** or with unsaturated nitro derivatives **8** to give isoindole and pyrazino[2,1-*a*]isoindole derivatives. The mechanisms of formation, proofs of structure, and stereochemistry are presented.

JEAN-MARIE FERLAND, CHRISTOPHER A. DEMERSON et LESLIE G. HUMBER. Can. J. Chem. **63**, 361 (1985).

La réaction d'amines avec les lactones et les dérivés nitro-insaturés du type **7** et **8** donne accès à des isoindoles et des pyrazino[2,1-*a*]isoindoles. Nous décrivons les mécanismes de formation ainsi que les preuves de structure et de stéréochimie.

The 1,2,3,4-tetrahydropyrazino[2,1-*a*]isoindole-6-one **1** was found to lower blood pressure in spontaneously hypertensive rats. In order to explore the structure–activity relationships in this type of compound, several analogs of the parent structure were synthesized. We envisioned different routes that would not only allow structural variations within the series but also give access to other heterocycles such as isoindole derivatives.

Some 1,2,3,4-tetrahydropyrazino[2,1-*a*]isoindole-6-(2*H*)-ones bearing a hydroxyl group at C-10a have been prepared (1,2,4) and the fully reduced ring system has also been described (3). However, none of those approaches (1–4) was general enough to provide access to the desired products.

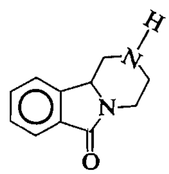

1

An interesting approach to isoindoles (3) has been published by Whelton and Huitric (6) involving the reaction of the nitrolactone **2** with bases (7). However, only weak bases such as aniline can be used (Scheme 1). With other amines the reactions followed a different pathway, leading to 1,3-dihydro-3-methylene-2*H*-isoindol-1-ones (**16**) (Scheme 3).

Kemp and Vellacio (8) have also shown that an amine can add in a Michael-type fashion to the double bond of the nitrostyrene derivative **4** to give **5**. This reaction is then followed by an acyl transfer from the phenol to the amine to give **6** (Scheme 2).

These two syntheses (Schemes 1 and 2) have been incorporated into a pathway that has led to the synthesis of a series of substituted isoindoles (Scheme 3). The nitrolactones **7** were transformed into the nitrostyrenes **8** (dimethyl sulfate/K_2CO_3). The latter reacted with bases such as methylamine, benzylamine, glycine ester, and aminoacetaldehyde diethyl acetal to give the nitroisoindole derivatives **9**. This approach proved to be very general (5).

As shown by nmr spectroscopy (see experimental), the lactone **7***b* exists as a mixture of stereoisomers. When transformed

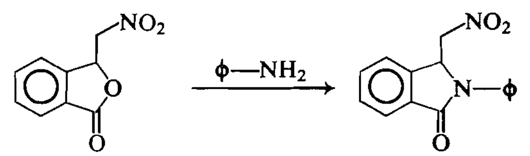

2 **3**

SCHEME 1

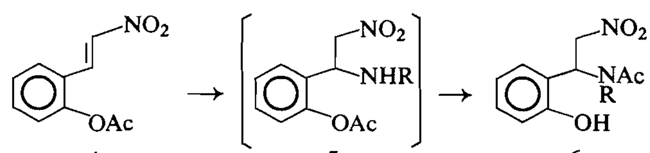

4 **5** **6**

SCHEME 2

to the nitrostyrene **8***b*, a single isomer was obtained. Because of their high electronic densities, the nitro group and the benzene ring should be as far apart as possible, giving rise to a preferred stereochemistry. Only one conformation of the lactone would therefore be capable of displacing the CH_3 group of dimethyl sulfate in a *trans* diaxial or antiperiplanar fashion and the nitro group would end up being *trans* to the aromatic ring. This was confirmed through the examination of the nmr spectrum of **8***a*. Indeed, in this case the benzylic proton is centered at 8.7 ppm with a coupling constant equal to 12 Hz, a value indicative of a *trans* fusion (9).

The nitroisoindole derivatives **9***a* and *b* were then hydrogenated under neutral conditions to the corresponding amino derivatives **10***a* and *b*. Under similar conditions the isomers **9***f* and *g* yielded the amine derivatives **10***f* and *g*, which were separated by chromatography. Each isomer was then rehydrogenated in the presence of palladium under acidic conditions. This led to the generation of a free aldehyde group and subsequent reduction of the intermediate imine to give the 1,2,3,4-tetrahydropyrazino[2,1-*a*]isoindole-6-one derivatives **11** and **12** (Scheme 4). The methyl group of the isoindole derivative **11** appears at 1.53 ppm and must be equatorial to lie in the negative cone of the aromatic ring. The axial methyl of **12** is centered at 0.68 ppm. In **11**, the benzilic protons H_b and H_a are located respectively at 4.16 and 4.41 ppm and the coupling constant of the doublet for H_a is equal to 10 Hz. It agrees with an angle of 130–180°, indicative of a *trans* fusion. For product **12** the same protons are centered at 4.3[4] and 4.85 ppm and H_a appears as a doublet with J = 4 Hz. This is as

[1] Present address: Bio-Méga Inc., 1 Complexe Desjardins, bureau 3804, C.P. 158, Montreal, P.Q., Canada H5B 1B3.
[2] Present address: Ayerst Laboratories Research Inc., 567 Ridgeroad, Monmouth Junction, NJ 08852, U.S.A.
[3] Revision received May 11, 1984.

[4] On the spin decoupling experiment, irradiation of the CH_3 causes a coalescence of H_b at 4.3 ppm.

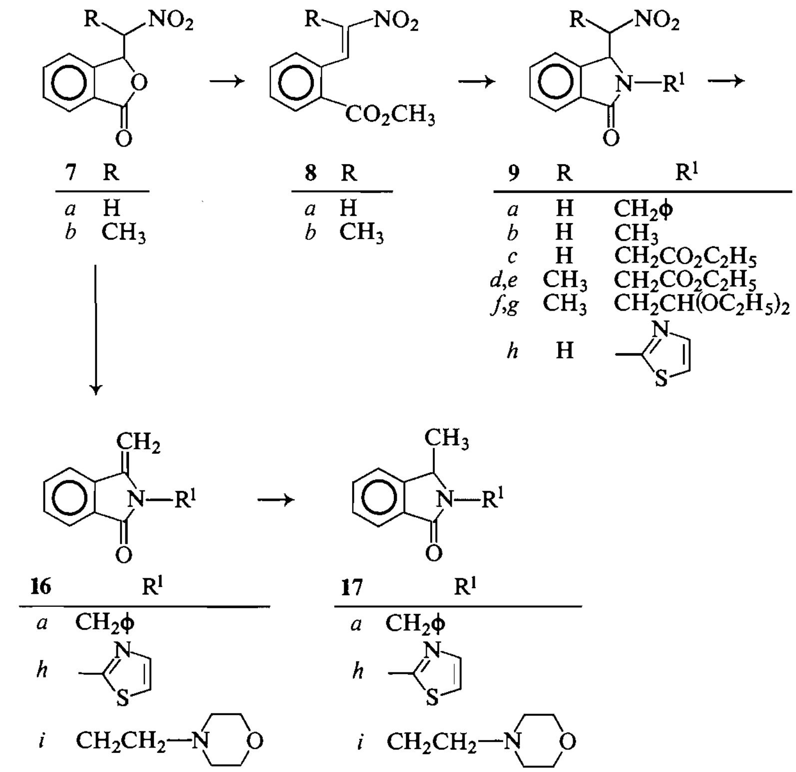

SCHEME 3

expected for a *cis* stereochemistry.

It is important to notice that a difference of 0.44 ppm is found in the location of the H_a of **11** and **12**. Such a difference arises from the anisotropic effect due to the β-substitution. A similar effect has been found in methyl cyclohexane (10). In this study, it was determined that an equatorial CH_3 would shield a β-axial proton by a value of 0.25 ppm while an axial CH_3 would deshield a β-equatorial proton by a value of 0.2 ppm for a total difference of 0.45 ppm. It constitutes an additional proof for the structures proposed for **11** and **12**.

The lactams **11** and **12** were reduced with diborane to the corresponding diamines **14** and **15**. These reactions are shown in Scheme 4.

As mentioned previously, when the nitrolactone **7***a* was treated wih a relatively strong amine such as benzylamine the novel 1,3-dihydro-3-methylene-2-phenylmethyl-2*H*-isoindol-1-one **16** was obtained. This structure was confirmed by nmr spectroscopy (the C=CH_2 appears as two doublets with a coupling constant equal to 2.5 Hz at 4.75 and 5.10 ppm), elemental analysis, and mass spectroscopy. The formation of such a compound can only be explained through the elimination of nitrous acid from the lactam **9***a*. A similar mechanism has already been proposed by Kloetzel (11). The mechanism and structure were further substantiated when **16** was again obtained when **9***a* was heated in the presence of benzylamine at reflux in toluene. The hydrogenation of the *exo* methylene derivative yielded the isoindol-1-one derivative **17***a*. Using another strongly basic amine such as *N*-(aminoethyl) morpholine, we observed the formation of the *exo* methylene derivative **16***i*. However, when a weakly basic amine such as aminothiazolidine was used, the nitrolactone **9***h* was isolated, as observed also by Huitric (6). The *exo* methylene derivative **14***h* was prepared on treatment with benzylamine. Both **16***h* and **16***i* were hydrogenated to yield **17***h* and **17***i*. These reactions are described in Scheme 3.

Some oxomethylene-isoindol-3-one derivatives have been reported in the literature (12). They were, however, obtained through a different pathway.

Experimental

Melting points are uncorrected. The ir spectra were taken on a Perkin–Elmer 225 ir spectrophotometer and nmr spectra were recorded on a Varian CFT-20 spectrophotometer operating at 80 MHz; TMS was used as an internal standard. The mass spectra were obtained on a LKB gc–ms 9000S instrument. Merck silica gel 60 (60–230 mesh) was used.

Preparation of the nitro lactones 7

3-(Nitromethyl)-isobenzofuran-1-(3*H*)-one (**7***a*) or the 3-(nitroethyl)lactone (**7***b*) are known products and were prepared according to methods described in literature (6, 7). Compound **7***a*, ms: 193 $(M)^+$, 132 $(M - HNO_2)^+$, and 133^+. Compound **7***b* exists as a mixture (2:1) of two isomers, the major one having its methyl centered at 1.1 ppm; nmr ($CDCl_3$): 1.1 and 1.63 (CH_3, 2d, J = 7 Hz), 5.8 (CHϕ, 0.66 H, d, J = 5 Hz), and 6.1 (CHϕ, 0.33 H, d, J = 3 Hz) ppm; ms: 207 $(M)^+$, 160 $(M - HNO_2)$, and 133^+.

*2-[(2-Methyl-2-nitro)ethylene]benzoic acid methyl ester (8*b*)*

Under anhydrous conditions a mixture of nitrolactone **7***b* (7) (2.0 g), dimethyl sulfate (1.6 mL), and K_2CO_3 (2.4 g) in acetone (50 mL) was stirred at room temperature for 18 h. The carbonate was removed by filtration and the filtrate evaporated. The residue was chromatographed on silica gel (50 g/g, toluene) to give product **8***b* (1.67 g) in 78% yield; ir ($CHCl_3$): 1715 and 1520 cm^{-1}; nmr ($CDCl_3$): 2.25 (CH_3, 3H), 3.91 (CO_2CH_3, 3H), 7.40 and 7.60 (Ar H, 3H, m), 8.18 (Ar H, 1H), and 8.50 (=CH) ppm; ms: 221 $(M)^+$, 190 $(M - OCH_3)^+$, 175 $(M - NO_2)^+$, 162 $(M - CO_2CH_3)^+$, and 129^+.

In a similar fashion was obtained **8***a* (from **7***a* (6)) in 65% yield, mp 87°C; nmr ($CDCl_3$): 3.8 (OCH_3, 3H, s), 7.0 (5H, m), and 8.7 (1H, d, J = 12 Hz) ppm; ms: 207 $(M)^+$, 176 $(M - OCH_3)^+$, 161 $(M - NO_2)^+$, 148 $(M - CO_2CH_3)$, and 129^+.

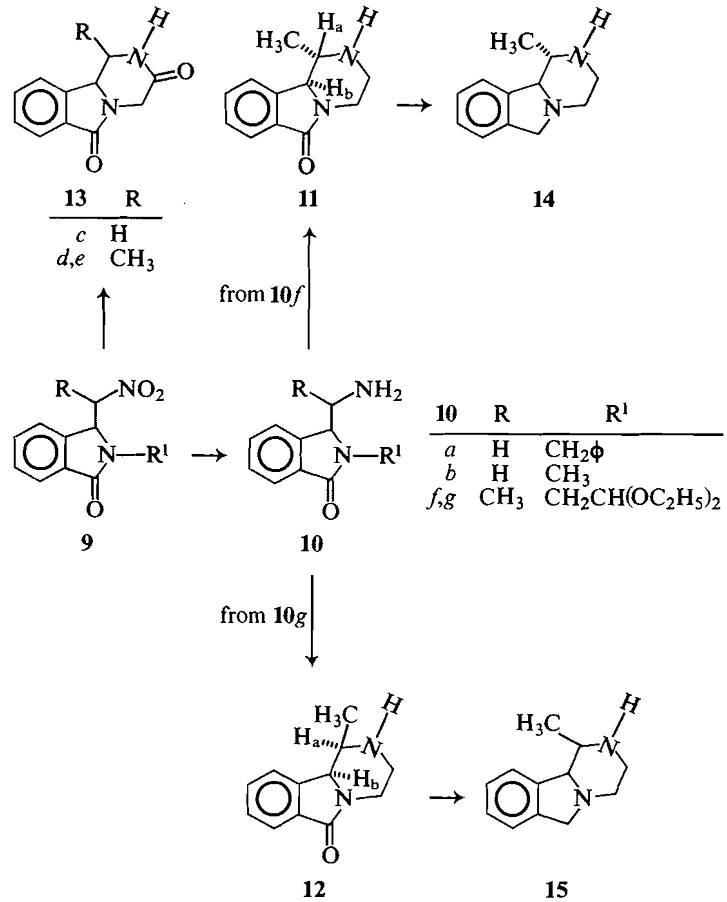

SCHEME 4

Formation of the nitro lactams 9

*2,3-Dihydro-3(nitromethyl)-2-(2-thiazolidinyl)-1*H*-isoindol-1-one (9*h*)*

A mixture of the nitrolactone **7***a* (20 g) and freshly crystallized 2-aminothiazole (20 g) in toluene (100 mL) was heated under reflux for 20 h. The dark orange mixture was diluted with more toluene and the organic solution washed with 10% HCl (3×), brine (4×), dried, and evaporated. The crude product obtained was taken into MeOH (200 mL) and the mixture heated under reflux for 1/2 h. After cooling, the solid obtained was filtered (9.4 g). The solid obtained after evaporation of the mother liquors was taken into EtOAc (100 mL) and heated at reflux for 1/2 h. The mixture was cooled and filtered to give a solid (5.2 g). The combined solids were crystallized from EtOAc/hexane to give the pure title product, in 50% yield, mp 146–147°C; ir ($CHCl_3$): 1715, 1555, and 1365 cm^{-1}; uv (MeOH) λ_{max}: 395, 235 and 228; ϵ: 12 160, 11 725, and 14 470; nmr ($CDCl_3$) 5.3 (CH_2NO_2, 2H, m), 5.9 (ϕCHN, 1H, m), and 7.55 (6 ArH, m) ppm; ms: 275 $(M)^+$, 229 $(M - NO_2)^+$ 215 $(M - CH_2NO_2)^+$. *Anal.* calcd. for $C_{12}H_9N_3O_3S$: C 52.35, H 3.29, N 15.26; found: C 52.19, H 3.15, N 15.25.

*2,3-Dihydro-3-(nitromethyl)-2-phenylmethyl-1*H*-isoindol-1-one (9*a*)*

A mixture of the nitroderivative **8***a* (1.0 g), benzylamine (0.57 g), and sodium acetate (0.45 g) was stirred vigorously in acetonitrile (20 mL) for 4 h. The salt was removed by filtration and the filtrate evaporated (bath temperature < 50°C). The residue was taken into EtOAc and th organic solution washed with 1 *N* HCl, brine, dried, and evaporated. The oil obtained (1.2 g) was used as such for the following reaction; nmr ($CDCl_3$): 4.80 (CH_2NO_2, 2H, d, J = 5 Hz), 5.0 (CH_2ϕ, 2H, s), 5.3 ($CHCH_2NO_2$, 1H, t, J = 5 Hz), 7.3 (5 Ar H), and 7.7 (4 Ar H) ppm. In a similar fashion were obtained the following.

*Compound 9*b

The reaction was carried out with **8***a* and aqueous methyl amine to give an oil in 60% yield; nmr ($CDCl_3$): 3.15 (N—CH_3, 3H, s), 4.80 (CH_2NO_2, 2H, d, J = 5 Hz), 5.18 (ϕCH, t, J = 5 Hz), and 7.7 (4 Ar H) ppm; ms: 206 $(M)^+$, 160 $(M - NO_2)^+$, and 159^+.

*Compounds 9*f *and* g

The reaction was carried out using **8***b* and aminoacetaldehyde diethyl acetal to give a mixture of isomers as an oil. It was used as such for the following reaction; nmr (DMSO): 4.3/4.6 ($CHNO_2$, 1/2H, m) and 5.5/5.8 ppm (CHϕ, 1/2H, m).

*2,3-Dihydro-3-nitromethyl-1-oxo-1*H*-isoindol-2-acetic acid ethyl ester (9*c*)*

To a suspension of glycine ethylester HCl (5.56 g) in acetonitrile (75 mL) was added Et_3N (4.04 g) and the mixture stirred at room temperature for 10 min. The unsaturated nitro derivative (**8***a*) (3.86 g) was added and the mixture stirred at room temperature for 22 h. The solvent was evaporated under reduced pressure (bath temperature < 50°C) and the residue dissolved in EtOAc. The organic solution was washed with 1 *N* HCl (2×), brine, dried, and evaporated. The crude product obtained (4.6 g) was chromatographed on silica gel (50 g/g, EtOAc/toluene 1:9) to give product **9***c* (2.4 g) in 44% yield; ir (Nujol): 1720, 1690, and 1550 cm^{-1}; nmr ($CDCl_3$): 1.3 (CH_3, 3H, t, J = 6 Hz), 4.4 (CH_2—CH_3, 2H, q, J = 6 Hz), 4.85 (CH_2NO_2, 2H, d, J = 5 Hz), 5.48 (CH—CH_2—NO_2, 1H, t, J = 5 Hz), and 7.3, 8.0 (4 Ar H) ppm; ms: 278 $(M)^+$, 232 $(M - NO_2)^+$, 205 $(M - CO_2Et)^+$, 158 $(\phi\overset{\overset{O}{\|}}{C}—N{=}CH_2)^+$. In a similar fashion were obtained the following.

*Compounds 9*d *and* e

The reaction was carried out using **8***b* and the crude product obtained chromatographed on silica gel (75 g/g, EtOAc/toluene, 1:9) to give **9***d* and *e* as a mixture of isomers in 21%/ yield; ir ($CHCl_3$): 1730, 1690, and 1550 cm^{-1}; nmr ($CDCl_3$): 1.2 (CH_3, 3H, m), 5.25 (ϕCH, 1/2H), 5.43 (ϕCH, 1/2H), and 7.1, 7.6 (4 Ar H) ppm; ms: 292 $(M)^+$, 246 $(M - NO_2)^+$, and 219^+.

*3-(Aminomethyl)-2-3-dihydro-2-(phenylmethyl)-1*H*-isoindol-1-one* (***10*****a**)

A solution of the nitro lactam **9***b* (1.2 g) in MeOH (75 mL) was hydrogenated over 10% Pd/C (0.5 g) at room temperature and atmospheric pressure. The catalyst was then removed by filtration and the filtrate evaporated. The crude product obtained was chromatographed on silica gel (50 g/g, $MeOH/CH_2Cl_2$, 1:9) to give 10*a* as an oil (1.0 g); ms: 223^+ and 30 $(CH_2NH_2)^+$.

The maleate was prepared in MeOH and recrystallized in EtOH/ether to give the analytical sample (0.7 g), mp 175–176°C; ir (Nujol): 2800, 1680, 1582, and 1355 cm^{-1}; uv (MeOH) λ_{max}: 277, 238, 228; ε: 1440, 9580, and 14 590; nmr (DMSO): 3.62 (CH_2NH_2, 2H, d, J = 3.5 Hz) 4.35 and 5.12 (ϕCH_2, 2H, 2d, J = 15 Hz), 4.72 (ϕCH, 1H, t, J = 3.5 Hz), 6.07 (=CH, 2H, s), 7.3 (5 Ar H), and 7.7 (4 Ar H) ppm. *Anal.* calcd. for $C_{20}H_{20}N_2O_5$: C 65.20, H 5.47, N 6.71; found: C 65.27, H 5.44, N 7.53.

In a similar fashion was obtained **10***b* as an oil; nmr ($CDCl_3$): 1.15 (NH_2), 3.15 (N—CH_3, 3H, s), 3.3 (CH_2, 2H, d, J = 3.5 Hz), 4.5 (CH, 1H, t, J = 3.5 Hz), and 7.7 (4 Ar H) ppm; ms: 147 $(M - CH_2NH_2)^+$, 146 $(M - CH_3NH_2)^+$, and 30 $(CH_2NH_2)^+$.

The maleate was prepared in MeOH and recrystallized from EtOH/ether to give the analytical sample in 40% from **9***b*; mp 165–167°C; ir (Nujol): 2880, 1660, 1577, and 1362 cm^{-1}; uv (MeOH) λ_{max}: 277, 267, 227; ε: 1350, 2340, 14 350. *Anal.* calcd. for $C_{14}H_{16}N_2O_5$: C 57.53, H 5.52, N 9.58; found: C 57.32, H 5.45, N 9.41.

*1α-Methyl-1,2,3,4,5,10b-hexahydropyrazino[2,1-*a*]isoindol-6-one (**11**) and its 1β-methyl isomer (**12**)*

A solution of the nitro lactam **9***f*, **9***g* (2.5 g) in acetic acid/water (4:1, 50 mL) was hydrogenated over 10% Pd/C, at room temperature and 50 psi (1 psi = 6.89 kPa) for 18 h. The catalyst was removed by filtration on the filtrate evaporated. The residue was taken into 2% HCl and extracted twice with ether. The aqueous solution was made basic (pH 9) with NH_4OH and extracted (3×) with EtOAc. The organic solution was dried and evaporated. The residue was chromatographed on silica gel (100 g/g, acetone/toluene, 2:3) to give isomer **10***f* (1.14 g), ir ($CHCl_3$): 1675, 1120, and 1050 cm^{-1} and isomer **10***g* (0.880 g), ir ($CHCl_3$): as for **10***f*.

A solution of the amine **10***f* (1.13 g) in MeOH (40 mL) and 1 *N* HCl (30 mL) was hydrogenated over 10% Pd/C at room temperature and atmospheric pressure for 48 h. The catalyst was removed by filtration, the filtrate neutralized with concentrated NH_4OH, and the methanol evaporated under reduced pressure. The water solution at pH 9 was salt saturated and extracted with EtOAc (3×). The organic solution was dried and evaporated to give **11** as an oil (0.648 g); ms: 202 $(M)^+$, 159^+, and 146^+.

The maleate salt was prepared in methanol and recrystallized twice from EtOH/ether to give the analytical sample (0.440 g), mp 181–182°C; ir (Nugol): 2800, 1690, 1615, 1575, and 1455 cm^{-1}; uv (MeOH) λ_{max}: 277, 269; ε: 1783, 2387; nmr (DMSO): 1.58 (CH_3, 3H, d, J = 6 Hz), 3.1 (CH_2N, 4H, m), 4.16 (CH_3—*CH*, m), 4.41 (ϕCH, d, J = 10.5 Hz), 5.9 (=CH), 7.4 (4 Ar H), and 11.0 (CO_2H and NH) ppm. *Anal.* calcd. for $C_{16}H_{18}N_2O_6$: C 60.37, H 5.70, N 8.80; found: C 60.25, H 5.68, N 8.79.

In a similar fashion, but hydrogenating the amine derivative **10***g*, was obtained the 1β-methyl isomer **12** as an oil; ms is identical to **11**.

The maleate salt was prepared in methanol and recrystallized twice from EtOH/ether to give the analytical sample in 40% yield from **10***g*, mp 190–191°C; nmr (DMSO): 0.68 (CH_3, 3H, d, J = 7 Hz), 3.2 (CH_2N, 3H, m), 4.3 (CH_3CH and CH_2N, 2H, m), 4.85 (ϕCH, d, J = 4 Hz), 5.9 (=CH), and 7.5 (4 Ar H) ppm; ms: as **11***h*. *Anal.* calcd. for $C_{16}H_{18}N_2O_6$: C 60.37, H 5.70, N 8.80; found: C 60.19, H 5.64, N 8.86.

*1α-Methyl-1,2,3,4,6,10b-hexahydropyrazino[2,1-*a*]isoindole (**14**)*

To a solution of the indolene derivative **11** (0.55 g) in dry THF at 0°C, under nitrogen, a 1 *M* solution of diborane in THF (136 mL) was added dropwise over a period of 10 min. The mixture was then heated under reflux for 18 h. The excess diborane was then destroyed with 10% HCl to pH 2 and the mixture distilled at atmospheric pressure until the distillate temperature reached 90°C. It was then neutralized to pH 12 and extracted (3×) with CH_2Cl_2. The organic solution was dried and evaporated to give **14** as an oil; ms: 188 $(M)^+$, 131^+, 118^+, and 117^+.

The maleate was prepared from the crude **14** and recrystallized twice from EtOH/ether to give the analytical sample (0.26 g), mp 144–145°C; ir (Nujol): 2800, 1620, and 1355 cm^{-1}; nmr (DMSO): 1.42 (CH_3, 3H, d, J = 6 Hz), 3.2 (CH_2N and CHN, 5H, m), 4.0 (ϕCH_2 and ϕCH, 3H, m), 6.1 (=CH, 2H), and 7.35 (4 Ar H) ppm. *Anal.* calcd. for $C_{16}H_{20}N_2O_4$: C 63.14, H 6.62, N 9.21; found: C 63.60, H 6.54, N 9.30.

In a similar fashion but starting from the lactone **12** was obtained the *1β-methyl-1,2,3,4,6,10b-hexahydropyrazino[2,1-*a*]-isoindole* ***15*** as an oil; ms: identical to **14**.

The maleate was prepared in MeOH and recrystallized from EtOH/ether to give the analytical sample in 50% yield from **12**, mp 135–137°C; nmr (DMSO): 1.2 (CH_3, 3H, d, J = 6.5 Hz), 2.7 and 4.4 (CH_2, CH, 8H, m), 6.08 (=CH, 2H), and 7.3 (4 Ar H) ppm. *Anal.* calcd. for $C_{16}H_{20}N_2O_4$: C 63.14, H 6.62, N 9.21; found: C 63.11, H 6.71, N 9.18.

*1,2,3,4,10b-Tetrahydropyrazino[2,1-*a*]isoindol-3,6(3*H*,6*H*)-dione (**13**c)*

A solution of the nitro lactam **9***e* (1.9 g) in methanol (100 mL) was hydrogenated over prehydrogenated PtO_2 (0.5 g) at room temperature and atmospheric pressure. The catalyst was removed by filtration and the filtrate evaporated. The residue was crystallized twice from acetone–water to give the dilactone **13***c* (0.70 g), mp 267–270°C; ir (Nujol): 3220, 3110, and 1680 cm^{-1}; ms: 202 $(M)^+$, 173 $(M - CH_2{=}NH)^+$, 145 $(173 - CO)^+$. *Anal.* calcd. for $C_{11}H_{10}N_2O_2$: C 65.38, H 4.98, N 13.86; found: C 65.47, H 5.16, N 13.76.

In a similar fashion were hydrogenated the nitro derivatives **9***d, e* to yield the dilactone derivatives **13***d* and *e* after chromatography on silica gel (50 g/g, i-propanol/toluene, 3:17). The two isomers were partially separated at a low yield (molecular ion present). However, only **13***e* was partially purified by crystallization from MeOH/ether, in 10% yield, mp 223–224°C; nmr (DMSO): 0.5 (CH_3, 3H, d, J = 6 Hz), 3.70 and 4.25 ($NCH_2C{=}O$, 2H, 2d, J = 17 Hz), 4.82 (ϕCHN, 1H, d, J = 4 Hz), and 7.40 (4 Ar H) ppm; ms: 216 $(M)^+$, 173 $(M - O{=}C{=}NH)^+$. *Anal.* calcd. for $C_{12}H_{12}N_2O_2$: C 66.65, H 5.60, N 12.96; found: C 66.30, H 5.56, N 12.99. (This product is unstable.)

*1,3-Dihydro-3-methylene-2-phenylmethyl-2*H*-isoindol-1-one (**16**a)*

Method A

A solution of the nitro lactone **7***a* (1.3 g) and benzylamine (1.3 mL) in benzene (50 mL) was heated under reflux for 18 h. The solvent was evaporated and the residue was chromatographed on silica gel (30 g/g, ether/hexane, 1:1). The residue was crystallized from ether/hexane to give the pure **16***a* (0.22 g), mp 116–117°C; uv (MeOH) λ_{max}: 305, 262, 254, 223, 217; ε: 7790, 12 940, 14 350, 37 315, 38 185; nmr ($CDCl_3$): 4.75 and 5.10 (=CH_2, 2H, 2d, J = 2.5 Hz), 5.0 ($CH_2\phi$, 2H, s), 7.22 (5 Ar H), and 7.65 (4 Ar H) ppm. *Anal.* calcd. for $C_{16}H_{13}NO$: C 81.68, H 5.57, N 5.95; found: C 81.58, H 5.48, N 5.94.

Method B

A solution of the nitro lactam **9***a* (0.95 g) and benzylamine (1 mL) in benzene (50 mL) was heated under reflux for 18 h. The product was isolated and purified as in Method A to give an identical product, mp 114–116°C (mixture mp 114–116°C), as shown by ir and nmr spectroscopy.

*1,3-Dihydro-3-methyl-2-phenylmethyl-2*H*-isoindole-1-one (**17**a)*

A solution of the *exo* methylene derivative **14***a* (1.5 g) in methanol (200 mL) was hydrogenated over 10% Pd/C (1.0 g) at atmospheric pressure and room temperature. The catalyst was removed by filtration and the filtrate evaporated. The residue was chromatographed on silica gel (30 g/g, ether/hexane, 1:3) to give **17***a* as an oil (1.0 g); nmr ($CDCl_3$): 1.42 (CH_3, 3H, d, J = 7 Hz), 4.25 and 5.32 (CH_2, 2H, 2d, J = 1.5 Hz), 4.35 (CH, 1H, q, J = 7 Hz), and 7.3 (9 Ar H) ppm; ms: 237 $(M)^+$, 146 $(M - CH_2\phi)^+$, 133 $(OCH_2—N{=}CO)^+$. *Anal.* calcd. for $C_{16}H_{15}NO$: C 80.98, H 6.37, N 5.90; found: C 80.88, H 6.37, N 5.84.

*1,3-Dihydro-3-methyl-2[2-(4-morpholinyl)ethyl]-2*H*-isoindol-1-one* ***17****i*

The *exo* methylene derivative **16***i* was obtained as in Method A and the crude product was hydrogenated as for **17***a*. The HCl salt was prepared directly from the crude mixture and crystallized 4 times from i-propanol/hexane to give the analytical sample in 17% yield, mp 208–209°C; nmr (DMSO: 1.45 (CH_3, 3H, d, J = 7 Hz), 3.6 (CH_2, 12H, m), 4.8 (ϕCHN, 1H, q, J = 7 Hz), and 7.6 (4 Ar H) ppm; ms: 260 $(M)^+$, 100^+, and 160^+. *Anal.* calcd. for $C_{15}H_{21}ClN_2O_2$: C 60.70, H 7.13, N 9.44; found: C 60.65, H 7.31, N 9.42.

*3-Methyl-1,3-dihydro-2-(2-thiazolyl)-2*H*-isoindol-1-one (17*h*)*

The *exo* methylene derivative **16***h* was obtained from **9***h* (10 g) as described in Method B. The benzene solution was washed with 2 *N* HCl, brine (3×), dried, and evaporated. The residue (3.5 g) in acetonitrile (300 mL) was hydrogenated over 10% Pd/C (1.75 g) at atmospheric pressure and room temperature. The catalyst was removed by filtration and the filtrate evaporated. The residue was chromatographed on silica gel (100 g/g, ether/hexane, 1:1) to give an oil (1.6 g). It was crystallized from benzene/i-propyl ether to give the pure **17***h*, mp 127–129°C; nmr ($CDCl_3$): 1.78 (CH_3, 3H, d, J = 7 Hz), 5.42 (CH, 1H, q, J = 7 Hz), 7.02 (=CHS, 1H, d, J = 4 Hz), 7.52 (4 Ar H), and 7.93 (1 Ar H) ppm; ms: 230 $(M)^+$, 215 $(M - CH_3)^+$. *Anal.* calcd. for $C_{12}H_{10}N_2OS$: C 62.58, H 4.38, N 12.17; found: C 62.61, H 4.47, N 12.31.

Acknowledgements

The authors wish to thank Dr. G. Schilling and his associates for analytical data and Mrs. C. Chazin and Mr. S. Toutounji for invaluable technical assistance.

1. M. Machida, H. Takechi, and Y. Kanoaka. Heterocycles, 273 (1977).
2. J. D. Coyle and G. L. Newport. Synthesis, 381 (1979).
3. M. Winn and H. E. Zaugg. J. Org. Chem. **34**, 249 (1969).
4. W. M. Welch. J. Org. Chem. **47**, 886 (1982).
5. C. A. Demerson, L. H. Humber, and J. M. Ferland. U.S. patent 4,273,773. June 16, 1981.
6. B. D. Whelton and A. C. Huitric. J. Org. Chem. **35**, 3143 (1970).
7. G. E. Ullyot, J. J. Stehle, C. L. Zirkle, R. L. Shriner, and F. J. Wolf. J. Org. Chem. **10**, 429 (1945).
8. D. S. Kemp and F. Vellacio Jr. J. Org. Chem. **40**, 3464 (1975).
9. N. S. Bhacca and D. H. Williams. Application of NMR spectroscopy in organic chemistry. Holden–Day Inc., New York. 1966. p. 85.
10. F. C. Nachod and J. J. Zucherman. Determination of organic structure by physical methods. Vol. 3. Academic Press, New York. 1971. p. 375.
11. M. C. Kloetzel. J. Am. Chem. Soc. **70**, 3571 (1948).
12. P. S. Anderson, M. E. Christy, C. D. Colton, and K. L. Shepard. J. Org. Chem. **43**, 3720 (1978).

Autoxidation in micelles. Synergism of vitamin C with lipid-soluble vitamin E and water-soluble Trolox

LAWRENCE ROSS COATES BARCLAY,[1] STEVEN JEFFREY LOCKE, AND JOSEPH MARK MACNEIL
Department of Chemistry, Mount Allison University, Sackville, N.B., Canada E0A 3C0

Received May 23, 1984

LAWRENCE ROSS COATES BARCLAY, STEVEN JEFFREY LOCKE, and JOSEPH MARK MACNEIL. Can. J. Chem. **63**, 366 (1985).

A study was made of the effect of the inhibitors ascorbic acid (C), α-tocopherol (E), and 6-hydroxy-2,5,7,8-tetramethylchroman-2-carboxylate (Trolox, T) on the autoxidation of linoleic acid in 0.50 *M* sodium dodecyl sulfate (SDS) micelles at pH 7.0 in phosphate buffer. Reactions were thermally initiated at 30°C in the SDS micelles by a micelle-soluble initiator, di-*tert*-butylhyponitrite (DBHN). Although water-soluble C alone is an inefficient inhibitor, when combined with micelle-soluble E, it acts synergistically with the latter to extend the efficient antioxidant action of E beyond the sum of the induction periods of C and E acting separately. Similarly C acts synergistically with the water-soluble antioxidant, T. Quantitative studies of these effects under controlled rates of initiation (R_i) reveal that C functions to regenerate a mole of E (or T) per mole of C used. Kinetic studies show that the rate of autoxidation is first order in micellar linoleic acid and one-half order in micellar DBHN concentrations. Therefore, the classical rate law, $-dO_2/dt = k_p[R—H]\,(R_i)^{1/2}/(2k_t)^{1/2}$ is followed. The higher oxidizability ($k_p/2k_t^{1/2} = 4.48 \times 10^{-2}\ M^{-1/2}\ s^{-1/2}$) of linoleate in micelles compared to that in homogeneous solution in chlorobenzene ($k_p/2k_t^{1/2} = 2.30 \times 10^{-2}\ M^{-1/2}\ s^{-1/2}$) is interpreted in terms of the effect of the polar interfacial region of the micelles on a dipolar transition state, $R—\overset{-}{O}\overset{-}{O}{:}\ \overset{+}{H}\cdot R$, of the propagation reaction.

LAWRENCE ROSS COATES BARCLAY, STEVEN JEFFREY LOCKE et JOSEPH MARK MACNEIL. Can. J. Chem. **63**, 366 (1985).

On a étudié l'effet de l'acide ascorbique (C), de l'α-tocophérol (E) et de l'hydroxy-6 tétraméthyl-2,5,7,8 chromanecarboxylate-2 (Trolox, T) comme inhibiteurs de l'autoxydation de l'acide linoléique, dans des micelles à 0,50 *M* de dodécylsulfate de sodium (DSS) et dans un tampon de phosphate à un pH de 7,0. A 30°C, les réactions sont induites thermiquement dans les micelles de DSS en faisant appel à un initiateur soluble dans la micelle, le di-*tert*-butylhyponitrite (DBHN). Bien que C, qui est soluble dans l'eau, ne soit pas un inhibiteur efficace lorqu'on l'utilise seul, il agit d'une façon synergique lorsqu'on le combine à l'inhibiteur E, qui est soluble dans la micelle; il en résulte que l'action antioxydante efficace du composé E est prolongée au-delà de la somme des périodes d'induction des composés C et E agissant séparément. De la même manière, le composé C agit de façon synergique avec l'antioxydant qui est soluble dans l'eau. Des études quantitatives de ces effets, utilisant des vitesses d'initiation (R_i) contrôlées, révèlent que C regère une mole de composé E (ou T) par mole de C utilisée. Les études cinétiques montrent que la vitesse d'autoxydation est d'ordre un en acide linéloique micellaire et d'ordre une demie en concentration de DBHN micellaire. Donc, la réaction obéit à la loi classique de vitesse $-dO_2/dt = k_p[R—H]\,(R_i)^{1/2}/(2k_t)^{1/2}$. On interprète le fait que le linoléate dans les micelles est plus oxydable ($k_p/2k_t^{1/2} = 4{,}48 \times 10^{-2}\ M^{-1/2}\ s^{-1/2}$) qu'une solution homogène dans le chlorobenzène ($k_p/2k_t^{1/2} = 2{,}30 \times 10^{-2}\ M^{-1/2}\ s^{-1/2}$) en fonction de l'effet de la région interfaciale polaire des micelles sur un état de transition dipolaire $R—\overset{-}{O}\overset{-}{O}{:}\ \overset{+}{H}\cdot R$ de la réaction de propagation.

[Traduit par le journal]

Introduction

Important structural and functional properties of biomembranes are disrupted by the peroxidation of unsaturated membrane lipids. Autoxidation in biological systems is associated with important pathological events including aging (1, 2) and heart attack (3), and with the action of foreign toxic substances (4).[2]

We have shown that *quantitative* kinetic studies of autoxidation can be made in biologically important microenvironments such as bilayers (5) and micelles (6). Recently we have demonstrated that water-soluble initiators and inhibitors can be used to quantitatively study autoxidations in these systems (7). The kinetic data with aqueous initiator/inhibitor combinations were in agreement with those for lipid-soluble initiators and inhibitors, and with various lipid-soluble and aqueous-soluble initiator/inhibitor combinations. These results led us to extend our preliminary studies of synergism between lipid-soluble α-tocopherol and water-soluble ascorbate (6) to the present study of the interaction between ascorbate and both a lipid-soluble inhibitor (α-tocopherol) and a water-soluble inhibitor, 6-hydroxy-2,5,7,8-tetramethylchroman-2-carboxylate (Trolox).

This study was undertaken to answer two fundamental questions concerning autoxidation in microenvironments.

1. *Are combinations of water-soluble antioxidants (e.g. ascorbate and Trolox) more effective in inhibiting autoxidation than either alone, as was observed for ascorbate and the lipid-soluble α-tocopherol (6) and, if so, what is the quantitative nature of these synergistic effects?*

Recent outstanding publications by Ingold and Burton have finally established the key role of α-tocopherol as an antioxidant (8–10). While ascorbic acid is also implicated in a wide variety of biological phenomena and continues to attract a great deal of interest (11, 12), its role in lipid peroxidation is not well understood. In biological tissue, it is reported to act as either an inhibitor or as a catalyst of lipid peroxidation (13, 14). Quantitative data on its antioxidant activity is lacking. We hope that the present quantitative study on the interaction of ascorbate with other inhibitors will clarify its role as an antioxidant in micellar autoxidation. These results in turn have important implications for autoxidations in biological systems.

2. *Does autoxidation of a substrate solubilized in micelles follow the same classical rate law well known for homogeneous solutions?*

The autoxidation of organic substrates in homogeneous solu-

[1]Author to whom correspondence may be addressed. For a preliminary account of this work, see ref. 6.

[2]Reviews on this subject (4) include the effect of oxygen toxicity (I. Fridovich, Vol. I, Chapt. 6, p. 239), air pollutants (D.B. Menzel, Vol. II, Chapt. 6, p. 181, and J.B. Mudd, Vol. II, Chapt. 7, p. 203), and liver damage (E.S. Reynold and M.T. Moslen, Vol. IV, Chapt. 2, p. 49).

tion at oxygen pressures near 760 Torr (1 Torr = 133.3 Pa) is known to be a free-radical chain process which proceeds by the following reaction sequence (15–18).

[1] Initiation: formation of R· (or ROO·) rate = R_i

[2] Propagation: $R\cdot + O_2 \xrightarrow{\text{fast}} ROO\cdot$

[3] $ROO\cdot + RH \xrightarrow{k_p} ROOH + R\cdot$

[4] Termination: $ROO\cdot + ROO\cdot \xrightarrow{2k_t}$ nonradical products + O_2

The classical rate law for a system which follows these reactions is given by eq. [5]:

$$[5] \quad -\frac{d[O_2]}{dt} = \frac{k_p}{2k_t^{1/2}}[RH]R_i^{1/2}$$

where RH is the organic substrate, R_i the rate of chain initiation, k_p is the propagation rate constant, and k_t the termination rate constant. The ratio $k_p/(2k_t)^{1/2}$ is known as the "oxidizability" of the substrate. For our quantitative autoxidation studies, the rate of chain initiation (R_i) must be known and reproducible. This is accomplished by using azo initiators of known k_i. Because of the solvent "cage effect", the R_i must be determined, usually by the inhibitor method (19), using a phenolic antioxidant which terminates two chains by reacting with two peroxyls. Under these conditions:

$$[6] \quad R_i = 2[ArOH]/\tau$$

$$[7] \quad e = R_i/2k_i[R{-}N{=}N{-}R]$$

where τ is the length of time during which the reaction is inhibited and e is the efficiency of chain initiation.

Micelles (0.50 *M* SDS) were selected as microenvironments for these model quantitative studies for two main reasons: (1) such micelles are optically clear and concentrations of solubilized inhibitor and initiator can be measured directly by absorption spectral methods, and (2) α-tocopherol can be solubilized in micelles and this makes it possible for such micellar α-tocopherol to be transported to the site of autoxidation (6). Thus it should be possible to directly compare the antioxidant activity of lipid-soluble α-tocopherol with water-soluble Trolox and also to compare the effect of a combination of ascorbate with either of these inhibitors.

Results

1. *The antioxidant activity of ascorbate (C), and of combinations of C with α-tocopherol (E) and with Trolox (T)*

The system selected for synergism studies was linoleic acid in 0.50 *M* sodium dodecyl sulphate (SDS) micelles because this system gave convenient rates for our studies and the kinetics followed the classical rate law in the concentration range employed (*vide infra*). Reactions were initiated by using the lipid-soluble initiator, di-*tert*-butylhyponitrite (DBHN).

A new technique was required for quantitative studies using α-tocopherol as an antioxidant to inhibit autoxidation initiated in micelles. Previous sattempts to transport this excellent antioxidant through an aqueous phase were unsuccessful (5). However, for the present work we found that stock solutions of α-tocopherol could be prepared in 0.50 *M* SDS (1.2 × 10^{-2} molar in the micellar volume) by sonication and the concentration determined by ultraviolet spectroscopy. This greatly improved the precision of insertion of known amounts of this

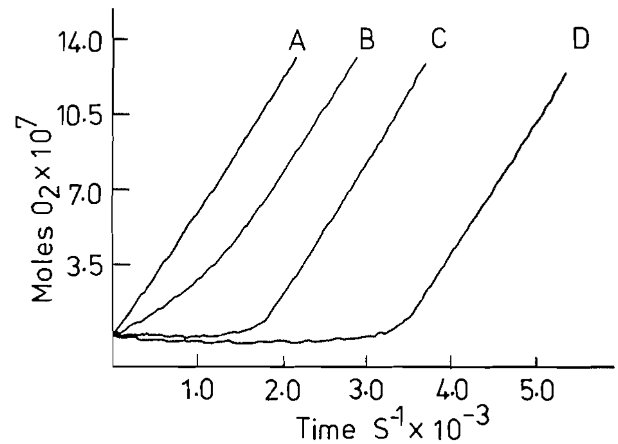

FIG. 1. Autoxidation of linoleic acid (6.43 × 10^{-5} mol) in 2.00 mL 0.50 *M* SDS – phosphate buffer (pH 7.0), initiated with DBHN (1.81 × 10^{-5} mol) at 30°C: A, uninhibited reaction; B, inhibited with ascorbic acid (4.80 × 10^{-8} mol); C, inhibited with α-tocopherol (2.34 × 10^{-8} mol); D, inhibited with ascorbic acid (4.80 × 10^{-8} mol) and α-tocopherol (2.34 × 10^{-8} mol).

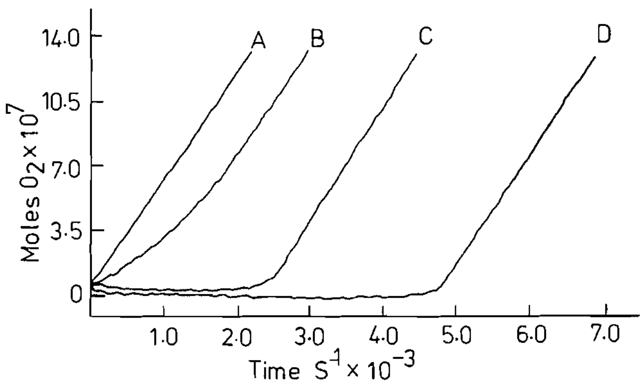

FIG. 2. Autoxidation of linoleic acid (6.43 × 10^{-5} mol) in 2.00 mL 0.50 *M* SDS – phosphate buffer (pH 7.0), initiated with DBHN (1.53 × 10^{-5} mol) at 30°C: A, uninhibited reaction; B, inhibited with ascorbic acid (4.77 × 10^{-8} mol); C, inhibited with Trolox (2.36 × 10^{-8} mol); D, inhibited with ascorbic acid (4.77 × 10^{-8} mol) and Trolox (2.36 × 10^{-8} mol).

antioxidant and it proved to be an effective inhibitor when introduced this way (see Fig. 1).

In the initial experiments, we compared the effect of the inhibitors C and E, and C and T, separately and in combinations, on the autoxidation of linoleic acid in SDS micelles. The results of a typical experiment are illustrated in Fig. 1 for C and E and in Fig. 2 for C and T and the data are summarized in Table 1.

A series of experiments was then conducted in order to *quantitatively* determine the effect of C on the inhibiting effect of E and of T. For this purpose, the ratio of C to E (or C to T) was kept constant in each experiment and the rate of initiation (R_i) determined immediately before and again after the determination of the extended induction period by the combination of these inhibitors. The results of these experiments are given in Tables 2 and 3.

2. *Kinetics of autoxidation in SDS micelles*

In order to use DBHN in our quantitative kinetic studies, it was necessary to have a convenient analytical procedure to determine its concentration in micellar solutions and also a

TABLE 1. Inhibiting effect of ascorbic acid (C), α-tocopherol (E), Trolox (T), and combinations of E + C and T + C on the thermally initiated autoxidation of linoleic acid[a] in 0.50 M SDS at pH 7.0

Initiator[b] (mol × 10^5) DBHN[c]	Inhibitors[b] (mol × 10^8) C	E[c]	Induction periods (s × 10^{-3}) τ_C	τ_E	$\tau_{(E+C)}$	R_i[b] (mol s^{-1} × 10^{11})	$\tau_{(E+C)} - (\tau_E + \tau_C)$ (s × 10^{-3})
1.81	4.80		1.332				
		2.34		1.710		2.74	
	4.80	2.34			3.384		0.342
	4.80		1.341				
		2.34		1.197		2.44	
	4.80	2.34			3.555		0.297
	4.80		1.440				
		2.34		1.971		2.37	
	4.80	2.34			3.708		0.297
	C	T	τ_C	τ_T	$\tau_{(T+C)}$		$\tau_{(T+C)} - (\tau_T + \tau_C)$
1.53	4.77		1.495			2.01	
		2.36		2.410		1.96	
	4.77	2.36			4.770	1.95	0.800
	4.77		1.640				
		2.36		2.575		1.83	
	4.77	2.36			5.185		0.810

[a] 6.43 × 10^{-5} mol of acid and isomolar sodium hydroxide were used in each experiment.
[b] Amounts are given in moles for ease of comparison, since the DBHN, linoleic acid, and E are concentrated in the micelles while the T and C are in the aqueous phase (see text).
[c] Amounts of DBHN and E in the micellar solutions were determined by spectral analyses.

TABLE 2. Effect of inhibitors α-tocopherol (E) and combinations of E with ascorbic acid (C) on the thermally initiated autoxidation of linoleic acid[a] in 0.50 M SDS at pH 7.0

Run No.	Initiator[b] (mol × 10^5) DBHN[c]	Inhibitors[b] (mol × 10^8) E[c]	C	Induction Periods (s × 10^{-3}) τ_E[d]	$\tau_{(E+C)}$	$\tau_{(E+C)} - \tau_C$	R_i[b,d] (mol s^{-1} × 10^{11})	R_i × $[\tau_{(E+C)} - \tau_E]$	R_i × $[\tau_{(E+C)} - \tau_E]/C_{mol}$
48	1.67	3.15	2.36	2.645	3.640	0.995	2.39	2.38	1.01
		3.15	2.36	2.815	3.940	1.125	2.24	2.52	1.07
		3.15	2.36	2.925	3.930	1.005	2.16	2.17	0.920
		3.15	2.36	2.990	4.290	1.300	2.11	2.74	1.16
49	1.60	3.58	7.19	3.330	5.710	2.380	2.16	5.14	0.715
		3.58	7.19	3.635	6.140	2.505	1.97	4.94	0.686
		3.58	7.19	3.725	6.520	2.795	1.92	5.37	0.747
		3.58	7.19	3.760	6.860	3.100	1.90	5.89	0.819
54	1.58	1.98	1.23	1.959	2.592	0.633	2.03	1.28	1.04
		1.98	1.23	2.052	2.520	0.468	1.94	0.908	0.738
56	1.81	2.34	4.80	1.710	3.384	1.674	2.71	4.53	0.946
		2.34	4.80	1.917	3.555	1.638	2.41	3.95	0.823
		2.34	4.80	1.971	3.708	1.737	2.34	4.06	0.846
57	[e]	3.65	4.02	3.197	4.709	1.512	2.29	3.46	0.861
		3.65	4.02	3.384	4.752	1.368	2.16	2.96	0.735
		3.65	4.02	3.615	4.795	1.181	2.02	2.39	0.595
		3.65	4.02	3.802	5.184	1.382	1.92	2.65	0.660

[a] See footnote a, Table 1.
[b] Same as footnote b, Table 1.
[c] Same as footnote c, Table 1.
[d] The average of two induction periods, measured immediately before and after the $\tau_{(E+C)}$ induction period. The R_i is calculated from the average of the two τ_E s.
[e] Not measured.

measure of its rate constant (k_i) for decomposition at 30°C in SDS micelles. The DBHN was dissolved in 0.50 M SDS by vortex stirring. Analyses for DBHN were made spectrophotometrically on aliquots taken from DBHN in micelles and diluted in methanol–water (1:1). The molar absorptivity for DBHN at λ_{max} = 227 nm in methanol–water (ϵ = 5954) and in hexane (ϵ = 6910) is much different than that reported (20) but this value has been corrected.[3] The k_i (3.2 × 10^{-6} s^{-1} at 30°C) in SDS micelles measured by decay of the 227-nm ab-

[3] Dr. T. G. Traylor has recently advised us that the correct ϵ = 7.13 × 10^3, measured in isooctane.

TABLE 3. Effect of inhibitors trolox (T) and combinations of T with ascorbic acid (C) on the thermally initiated autoxidation of linoleic acid[a] in 0.50 M SDS at pH 7.0

Run No.	Initiator[b] (mol × 10^5) DBHN[c]	Inhibitors[b] (mol × 10^8) T	C	Induction Periods (s × 10^{-3}) τ_T[d]	$\tau_{(T+C)}$	$\tau_{(T+C)} - \tau_T$	R_i[b,d] (mol s^{-1} × 10^{11})	R_i × $[\tau_{(T+C)} - \tau_T]$	R_i × $[\tau_{(T+C)} - \tau_T]/C_{mol}$
41	1.03	2.24	2.34	2.930	4.300	1.370	1.54	2.11	0.902
		2.24	2.34	3.160	4.455	1.295	1.42	1.84	0.786
		2.24	2.34	3.225	4.660	1.435	1.39	1.99	0.850
42	1.00	2.42	1.40	3.470	4.590	1.120	1.41	1.56	1.11
		2.42	1.40	3.830	4.895	1.065	1.27	1.35	0.964
		2.42	1.40	3.748	4.645	0.897	1.30	1.17	0.836
		2.42	1.40	4.500	5.910	1.410	1.08	1.52	1.09
43	0.959	2.34	0.617	2.635	2.990	0.355	1.79	0.635	1.03
		2.34	0.617	2.765	3.155	0.390	1.70	0.663	1.07
		2.34	0.617	2.713	3.040	0.327	1.73	0.566	0.917
		2.34	0.617	2.755	3.155	0.400	1.70	0.680	1.10
44	1.36	2.55	4.72	2.708	4.980	2.272	1.89	4.29	0.910
		2.55	4.72	2.993	5.275	2.282	1.71	3.90	0.827
		2.55	4.72	3.100	5.375	2.275	1.65	3.75	0.795
		2.55	4.72	3.033	5.465	2.432	1.68	4.09	0.867
		2.55	4.72	3.020	5.670	2.650	1.69	4.48	0.949
45	1.18	2.40	9.38	3.263	7.325	4.062	1.47	5.97	0.638
		2.40	9.38	3.548	7.865	4.317	1.36	5.87	0.626
		2.40	9.38	3.683	8.210	4.527	1.31	5.93	0.632
		2.40	9.38	3.835	8.480	4.645	1.25	5.81	0.619
58	1.65	2.38	3.58	2.254	3.614	1.360	2.12	2.88	0.804
		2.38	3.58	2.427	4.032	1.605	1.96	3.15	0.880
		2.38	3.58	2.492	4.075	1.583	1.91	3.02	0.844

[a] Same as footnote a, Table 1.
[b] See footnote b, Table 1.
[c] Same as footnote c, Table 1.
[d] See footnote d, Table 2.

sorption agreed with literature values in homogeneous solution (5, 20).

A series of kinetic runs was carried out to measure the dependence of the rate of oxygen absorption on linoleic acid concentration [R—H] and on DBHN concentration.[4] Typically, the micellar substrate concentrations were varied by a factor of four (e.g. 0.0643 to 0.257 M) within a kinetic run by injecting linoleic acid into the reaction from a precision syringe. The DBHN micellar concentrations were varied six-fold (typically 0.86×10^{-2} to 5.08×10^{-2} M) in separate runs. The R_i and efficiency, e, in each experiment were determined by injecting α-tocopherol of known concentration in 0.50 M SDS into the system. A stoichiometric factor (n) of 2 for α-tocopherol was used (5, 8) for calculating the R_i. The results of these studies are outlined in Table 4.

Discussion

1. *Synergistic effects of ascorbate (C) on α-tocopherol (E) and on Trolox (T)*

The combination of inhibitors C with E, and C with T, exhibited two remarkable effects on the micellar autoxidation of linoleate.

(1) Although C is a relatively poor inhibitor when used alone (Fig. 1B), *the combination with E extends the typically efficient induction period observed for E alone* (Figs. 1C and D).

(2) The induction periods observed by combinations of E + C ($\tau_{(E+C)}$) *were longer than the sum of the separate induction periods* ($\tau_E + \tau_C$) for the same amounts of E and C (see Table 1). The amount of synergism observed in these experiments (i.e. as reflected in $\tau_{(E+C)} - (\tau_E + \tau_C)$, last column of Table 1) was typically in the range of 9–11%. Very similar behavior was exhibited when water-soluble inhibitors C and T were added to the aqueous phase. That is, the efficient induction period observed by Trolox was extended when used in combination with ascorbate. Furthermore, the combination of T + C gave induction periods ($\tau_{(T+C)}$) longer than the sum of the separate induction periods ($\tau_T + \tau_C$) (Table 1, last column). The amount of synergism observed here (ca. 20%) was significantly greater than that for C and E.

Two characteristics of the induction period during the combination of C and E clearly indicate that C functions so as to regenerate the E: (1) the *extended* induction period ($\tau_{(E+C)}$) observed for C and E combined exhibited the same efficient inhibition of autoxidation as observed for E (Fig. 1), and (2) high pressure liquid chromatography (hplc) analyses made during a typical $\tau_{(E+C)}$ induction period showed that the amount of E remained unchanged during the first half of the induction period. On the other hand, hplc analysis from a comparable run without C but the same amount of E indicated that the latter was being consumed as expected from the first of the induction period. Thus the interaction of E and C (and presumably T and C) involves a hydrogen transfer equilibrium of the type

$$\dot{E} + \bar{C} \rightleftharpoons E + \dot{\bar{C}} \text{ (or } \dot{T} + \bar{C} \rightleftharpoons T + \dot{\bar{C}}\text{)}$$

[4] A micellar reaction volume of 2.5×10^{-4} liters for 2.00 mL of 0.50 M SDS, estimated from density measurements (6, 21), was used in concentration calculations. The reaction volume calculated from the equation $v = 27.4 + 26.9n$ Å^3 (n = number of carbons) (22) gives a volume of 2.0×10^{-4} liters but this different volume does not change our results significantly.

TABLE 4. Kinetics of autoxidation of linoleic acid at 30°C in 0.50 M SDS micelles at pH 7.0

Run No.	$[RH]^a$ M	$10^2[DBHN]^a$ M	$10^4[\alpha\text{-toc}]^a$ M	$10^{-3}\,\tau$ s	$2k_i[DBHN]$ $\times 10^8\ M\ s^{-1}$	$R_i^b \times 10^8\ M\ s^{-1}$ Meas.	Calcd.	e	$-d[O_2]/dt^c$ $\times 10^7\ M\ s^{-1}$	ν	$-d[O_2]/dt^a$ / $[RH]R_i^{1/2}$ $\times 10^2\ M^{-1/2}\ s^{-1/2}$
48	0.0643	1.88				—	3.81		5.48	14	4.37
	0.129	1.86				—	3.79		11.8	31	4.71
	0.193	1.84				—	3.73		16.8	45	4.51
	0.257	1.81				—	3.67		22.3	61	4.53
		1.68	5.84	34.3	10.8	3.41	—	0.317	—	—	—
51	0.129	2.74				—	5.75		15.1	26	4.88
	0.257	2.72				—	5.71		31.1	55	5.06
	0.387	2.70				—	5.67		41.7	74	4.53
	0.516	2.68				—	5.63		54.1	96	4.42
		2.63	1.75	6.34	16.8	5.52	—	0.328	—	—	—
73	0.0643	1.17				—	2.07		3.57	17	3.86
	0.129	1.15				—	2.03		7.37	36	4.01
	0.193	1.14				—	2.01		10.7	53	3.91
	0.257	1.13				—	2.00		13.7	69	3.77
		1.07	1.65	17.5	6.85	1.89	—	0.276	—	—	—
74	0.0643	5.14				—	8.78		8.10	9	4.25
	0.129	5.03				—	8.60		16.1	19	4.26
	0.193	5.01				—	8.56		27.2	32	4.82
	0.257	4.89				—	8.36		36.3	43	4.89
		4.85	1.24	2.99	31.0	8.29	—	0.267	—	—	—
75	0.0643	2.05				—	3.59		5.98	27	4.91
	0.129	2.03				—	3.56		11.7	54	4.81
	0.193	2.02				—	3.54		17.8	83	4.90
	0.257	1.97				—	3.45		23.0	110	4.82
		1.50	1.89	14.4	9.63	2.63	—	0.274	—	—	—
76	0.0643	0.918				—	1.57		3.80	24	4.72
	0.129	0.912				—	1.56		7.10	46	4.41
	0.193	0.902				—	1.54		9.98	65	4.17
	0.257	0.896				—	1.53		12.8	84	4.03
		0.850	1.89	25.99	5.44	1.45	—	0.267	—	—	—

[a] Concentrations are moles per liter of micelles, using a calculated volume of 2.5×10^{-4} L for 2.00 mL of 0.50 M SDS, and the amounts of DBHN and α-toc were measured spectrally.
[b] The R_i s were calculated using the e values measured for each run and k_i for DBHN = $3.2 \times 10^{-6}\ s^{-1}$.
[c] Corrected for the evolution of nitrogen from the initiator (DBHN).

The synergism observed is therefore analogous to the general type defined by Mahoney and Da Rouge (23, 24).

In our case, the magnitude of the synergistic effects will depend upon the favourable competition of ascorbate ($\dot{\bar{C}}$) with the generated peroxyl radical for the vitamin E radical, $\dot{E}$. That is, the effect observed will depend upon the rate constant ratio for:

$$\dot{E} + \bar{C}/\dot{E} + ROO\cdot$$

The rate constant for the hydrogen transfer reaction involved in $\dot{E} + \bar{C}$ has been measured ($1.55 \pm 0.2 \times 10^6\ M^{-1}\ s^{-1}$) (25), as has the rate constant for the reaction of α-tocopherol with peroxyl radicals ($ArOH + ROO\cdot \rightarrow ROOH + ArO\cdot$) ($3.24 \pm 0.15 \times 10^6\ M^{-1}\ s^{-1}$) (8). 4-Peroxycyclohexadienone adducts have been identified from the addition of peroxyl radicals to the α-tocopheryl radical (i.e. $E + ROO\cdot \rightarrow$ adduct) (26). We are not aware of a rate constant measurement for this reaction but the value is estimated to be approximately $7.3 \times 10^8\ M^{-1}\ s^{-1}$.[5] The successful competition of $\bar{C}$ for $\dot{E}$ observed here is attributed to the relatively high concentration of $\bar{C}$ (approximately 2.4×10^{-5} molar in the aqueous phase) and the probability that the polar phenoxyl head group of $\dot{E}$ is located near the polar micelle–water interface, allowing for effective hydrogen transfer between $\bar{C}$ and $\dot{E}$.

Niki *et al.* have reported electron spin resonance results to show that vitamin C regenerates vitamin E from the α-chromanoxyl radical (27) and, while this current work was in progress, they published an important paper to show that vitamin C and vitamin E are effective antioxidants *when used in combination* during the autoxidation of methyl linoleate (28). However, their results differ from ours in two important respects. Their studies were carried out in homogenous solution, and the inhibition period for C + E was lengthened to *the sum* of the inhibition period when either C or E was used alone; that is, they did not report a synergistic extension.

The results of our quantitative studies on the effects of varying the ratio of C/E and C/T on the induction periods give further insights into the efficiency with which ascorbate in the aqueous phase interacts to regenerate α-tocopherol in the micellar phase and likewise to regenerate Trolox in the aqueous phase. The results in Table 2 illustrate the *extension*, $\tau_{(E+C)} - \tau_E$, of the efficient induction periods ($\tau_{(E+C)}$) due to additions of known amounts of E and C in separate experiments where the rate of chain initiation (R_i) was controlled, by using known amounts of the lipid-soluble initiator DBHN, and monitored throughout each run by the measurement of induction periods (τ_E) with the known amounts of E. The extensions of the

[5] J. A. Howard, private communication.

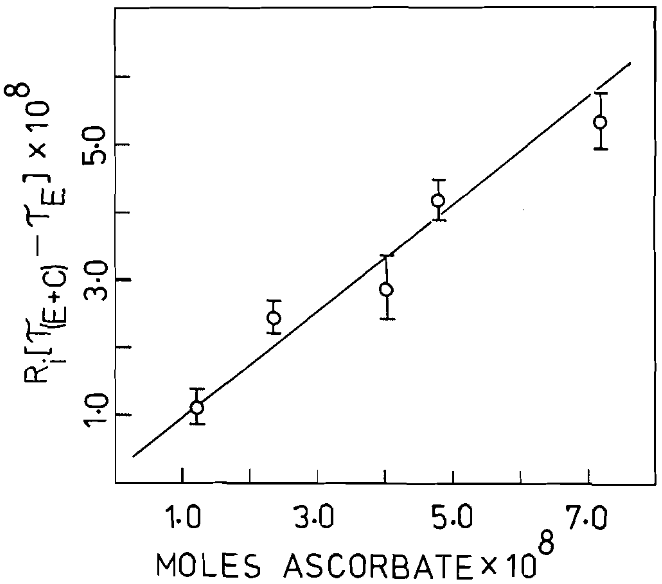

FIG. 3. Autoxidation of linoleic acid (6.43×10^{-5} mol) inhibited with α-tocopherol (E) and with ascorbate (C) in 2.00 mL 0.50 *M* SDS – phosphate buffer (pH 7.0), initiated with DBHN. Plot of the extension of the induction period × R_i versus the moles of ascorbate (see text and Table 2). The error bars represent standard deviations of 3 or 4 measurements.

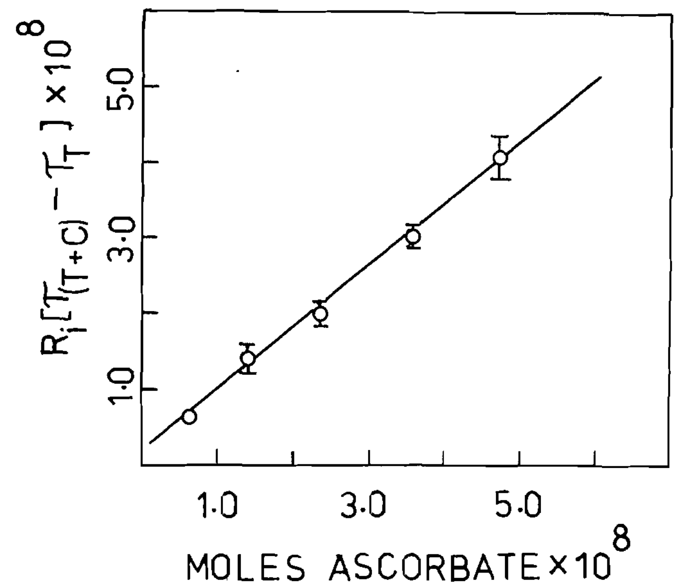

FIG. 4. Autoxidation of linoleic acid (6.43×10^{-5} mol) inhibited with Trolox (T) and with ascorbate (C) in 2.00 mL 0.50 *M* SDS – phosphate buffer (pH 7.0), initiated with DBHN. Plot of the extension of the induction period × R_i versus the moles of ascorbate (see text and Table 3). The error bars represent standard deviations of 3 or 4 measurements.

induction periods can be taken as an indication of the amount of vitamin E regenerated for a particular R_i and the product of R_i $[\tau_{(E+C)} - \tau_E]$ is thus a measure, indirectly obtained, of the amount of radicals trapped by C. When calculated per mole of C, one has a measure of the "stoichiometric factor" (n) for vitamin C *under these conditions*, in other words, a measure of the moles of vitamin E regenerated per mole of C. At lower combined induction periods ($\tau_{(E+C)}$), as in Runs 48, 54, and 56, a maximum stoichiometric factor of approximately one is observed. We find a near constancy of the value of n (the last column of Table 2) as the mole ratio of C to E was varied from 0.62 to 2.1. This is also illustrated in a near linear variation of R_i $[\tau_{(E+C)} - \tau_E]$ with C_{moles} as illustrated in Fig. 3 where the computed slope up to 5×10^{-8} moles of C is 0.78. At longer induction periods, usually corresponding to higher ascorbate, there appears to be a drop in n. This may be due to the loss of C in oxidation processes. Vitamin C does undergo slow oxidation under these conditions, and it is estimated that up to 20% of it would be consumed at higher combined induction periods (i.e. longer $\tau_{(E+C)}$).[6]

Remarkably similar quantitative results were obtained for the interaction of ascorbate with Trolox (T) as summarized in Table 3 and Fig. 4. That is, the stoichiometric factor, n, for the regeneration of T by C was approximately constant as the ratio C/T was varied from 0.264 to ca. 1.9. The value of n was approximately one at low C as in Runs 41, 42, and 43, and the slope of the plot (Fig. 4) of R_i $[\tau_{(T+C)} - \tau_T]$ versus C gives a value of $n = 0.82$ up to $C = 5 \times 10^{-8}$ moles. After longer extended induction periods ($\tau_{(T+C)} = 7.3 \times 10^3$ s), the value of n decreases, probably due to oxidation of C.[7]

2. *The rate law and oxidizability of linoleate in SDS micelles*

In order to determine the oxidizability of linoleate in SDS micelles, it is necessary to demonstrate that the rate of oxygen uptake follows the classical rate law given in eq. [5]. This means that the rate should be first order in substrate concentration in the micelles and one-half order in the R_i or initiator concentration in the micelles. For purposes of the calculations shown in Table 4, the assumption is made that the linoleate and the initiator, DBHN, are both completely partitioned into the micellar phase. This seems reasonable since DBHN is only very slightly soluble in water (5). We have not measured the partition coefficient of linoleic acid between the water–SDS phases, but is reasonable to assume that it is essentially all in the SDS phase, since the mole ratio of SDS to linoleate was never less than approximately 15:1. If the aggregation number of SDS is taken as 62 (30), this means there are, on the average, four linoleate molecules per SDS micelle for the most concentrated linoleate used (0.257 *M* in the micellar phase). The data in Table 4 indicate that the corrected rates follow very closely the classical first-order rate law for order in substrate. The actual value found for the order in [R—H] was 0.970 ± 0.077, averaged over six separate runs where the substrate was varied by a factor of four in each run. Figure 5 illustrates the linear relationships found for the variation of corrected rates with substrate concentration in the micelles for three typical runs with different DBHN concentrations. Correlation coefficients were better than 0.997 for all such runs.

The order with respect to initiator (DBHN) concentration in the micelle was more difficult to determine precisely. It is not possible to vary the DBHN concentration in a single experi-

[6] We have found the self-initiated rate of autoxidation of 5×10^{-3} molar ascorbate in the presence of 0.50 *M* SDS at pH 7.0 to be 1.55×10^{-7} *M* s^{-1} and the rate in the presence of DBHN (1.47×10^{-5} moles) under these conditions to be 2.01×10^{-7} *M* s^{-1}. This is somewhat higher than a reported rate of ca. 10^{-10} *M* s^{-1} (29) for 5×10^{-5} *M* ascorbate, when corrected for the concentration difference.

[7] Under our conditions, the limiting value of n is one for E + C and T + C. We recognize that a larger value might be applicable at lower R_i and high E/C (T/C) ratios. This condition is under investigation.

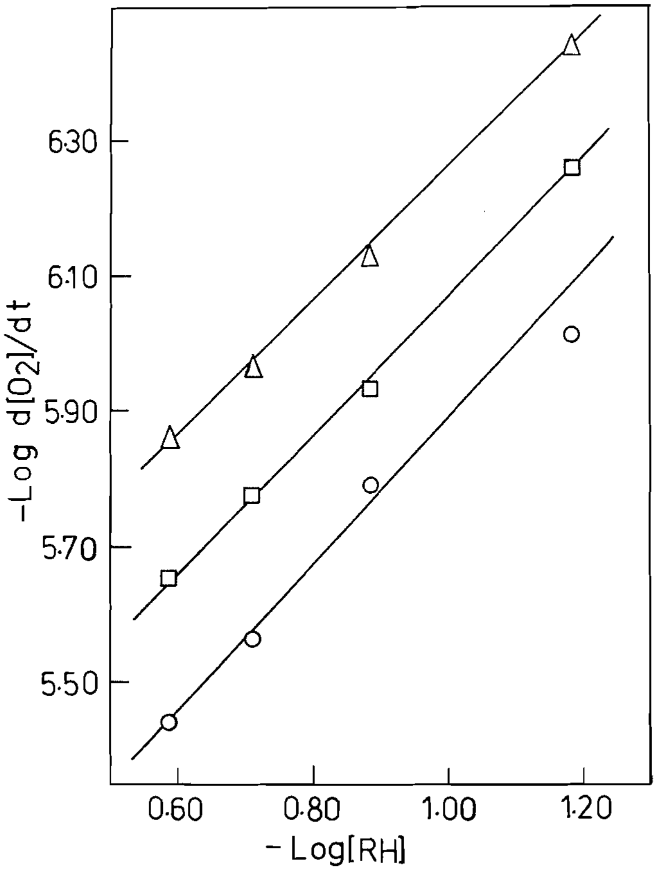

FIG. 5. Plot for the order in substrate for autoxidation of linoleic acid (0.0643 M to 0.257 M) in 2.00 mL 0.50 M SDS – phosphate buffer (pH 7.0): △, [DBHN] = 1.17×10^{-2} M; □, [DBHN] = 1.88 M; ○, [DBHN] = 5.14×10^{-2} M (taken from Table 4).

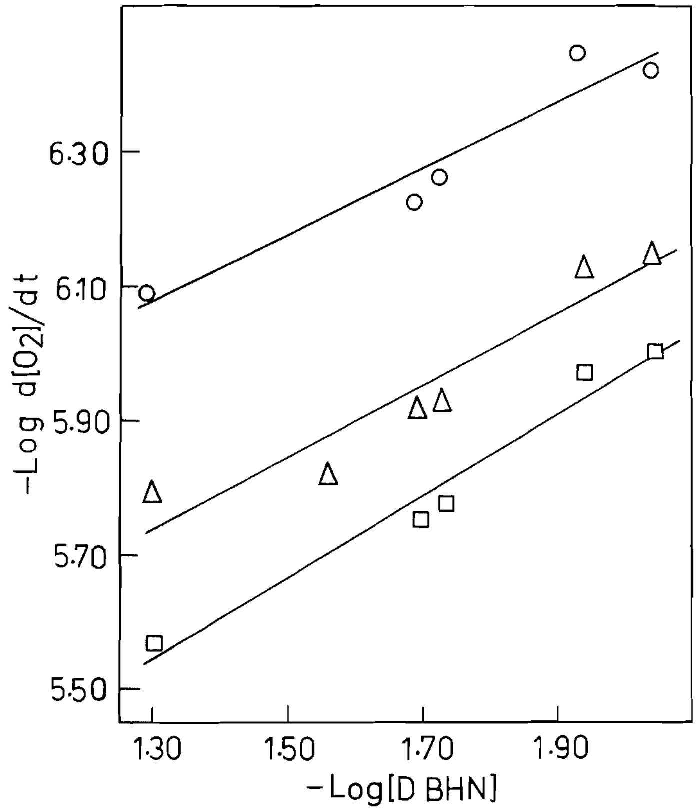

FIG. 6. Plot for the order in initiator (DBHN) for autoxidation of linoleic acid in 2.00 mL 0.50 M SDS – phosphate buffer (pH 7.0): ○, [R—H] = 0.0643 M; △, [R—H] = 0.129 M; □, [R—H] = 0.193 M (taken from table 4).

ment; therefore, measurements of the variation of corrected rates with [DBHN] were taken from separate experimental runs. Furthermore the [DBHN] was measured spectrally on diluted samples from these runs. There was a scatter of the points from plotting corrected rates versus [DBHN] as shown in Fig. 6, where the correlation coefficient was as low as 0.95. Nevertheless, the average order with respect to [DBHN] was 0.547 ± 0.050 and from this we conclude that the reaction is one-half order in [DBHN].

The efficiency, e, of chain initiation by DBHN in these 0.50 M SDS micelles (Table 4), is considerably lower (28.8 ± 2.5%) than that found in homogeneous solution in chlorobenzene (66%) (5). The lower e for DBHN in the micelles compared to that in chlorobenzene is attributed to the higher microviscosity of micelles. A reported microviscosity of 11.5 cP at 25°C (or 10 cP at 40°C) (31) contrasts with the bulk viscosity of 0.73 cP for chlorobenzene (5). Although there is no simple relationship between medium viscosity and initiator efficiencies (32), it is known that e for DBHN decreases as viscosity increases due to a larger proportion of free radical recombination within the solvent cage where they are formed (32). The e for DBHN in autoxidation initiated in bilayers, where the microviscosity is even higher, was further reduced to only 9.1% (5). Thus the lowering of e in micelles is expected and indeed serves to support the idea that these autoxidations are initiated in the micellar phase.

The near constancy of the oxidizability values for linoleate (last column of Table 4) also indicates that the classical rate law is followed for autoxidation in SDS micelles. The value obtained, $4.48 \pm 0.37 \times 10^{-2}$ $M^{-1/2}$ $s^{-1/2}$, is approximately *double* the reported value of 2.10×10^{-2} $M^{-1/2}$ $s^{-1/2}$ (33) measured in chlorobenzene.[8]

The increased substrate oxidizability of linoleate in SDS is attributed to the effect of the polarity of the micelles on the rate-determining step (i.e. the k_p) of the autoxidation. Solvent effects on the autoxidation of hydrocarbons are known to correlate with the dielectric constant of the medium (34, 35), apparently due to a general solvent effect on a transition state with dipolar character of the type

$$\text{R—O—O}\cdot + \text{H—R} \xrightarrow{k_p} [\text{R—O—O:}^- \ \text{H}\cdot\overset{+}{\text{R}}]$$

The local microenvironment can influence the physical and chemical behavior of solubilized species in micelles and even nonpolar hydrocarbons can be concentrated primarily near the micelle–water interface (36). Peroxyl radicals are known to be polar (5, 37) and are expected to reside mainly in or near the polar region at the interface.

The dielectric constant in this region of SDS micelles has been estimated from fluorescence studies (38) to be 45. Dielectric constant changes from 5.6 for chlorobenzene to 36 or 38 for solvents like nitromethane and acetonitrile have been

[8] We have recently determined the oxidizability of methyl linoleate ($2.26 \times 10^{-2} - 9.04 \times 10^{-2}M$) in chlorobenzene initiated by azobisisobutyronitrile to be 2.30 ± 0.30 $M^{-1/2}$ $s^{-1/2}$ (average of six measurements), which is in excellent agreement with the reported (33) result.

shown to approximately double the oxidizability of hydrocarbon substrates such as tetralin (34) and cyclohexene (35). This is in general agreement with the above postulate for an increase in linoleate oxidizability due to the location of the chain propagating free radicals in such a polar region of the micelle.[9]

Conclusions

1. Vitamin C has an important synergistic function in autoxidations and can act from the aqueous phase to regenerate a mole of α-tocopherol in the micellar phase per mole of ascorbate during the inhibited autoxidation of linoleate in a SDS microenvironment at pH 7.0.

2. Vitamin C also acts synergistically with a water-soluble inhibitor (Trolox) to inhibit the autoxidation of linoleate when the autoxidation is initiated in the micellar microenvironment.

3. The autoxidation of linoleate in 0.50 M SDS micelles follows the classical rate law for autoxidation since the rate of oxygen uptake was first order in substrate concentration and one-half order in initiator concentration in the micelles.

4. The higher oxidizability of linoleate in SDS micelles ($4.48 \times 10^{-2}\ M^{-1/2}\ s^{-1/2}$) compared to that in homogeneous solution in chlorobenzene ($2.30 \times 10^{-2}\ M^{-1/2}\ s^{-1/2}$) is attributed to the increased polarity of the micellar microenvironment. The polar peroxyl radicals, involved in the rate-propagating hydrogen abstraction reaction from the substrate, are expected to reside in the polar interface between the micellar core and the water. The higher dielectric of this region would provide a favourable solvent effect on a dipolar transition state for hydrogen abstraction.

These model experiments in micellar microenvironments have important implications for protective mechanisms in biological systems, especially from our findings which show that a water-soluble inhibitor can interact synergistically with a lipid-soluble one. We are currently extending these initial studies to other substrates in micellar systems and other inhibitors that may interact with vitamin E.

Experimental

1. *Materials and preparations*

Phosphate buffer

Solutions were prepared from 0.05 M of each of NaH_2PO_4 and Na_2HPO_4 in glass-distilled water containing 1×10^{-4} M EDTA. Immediately before use, this solution was passed through a Chelex-100 column (Bio-Rad 50–100 mesh) to remove traces of heavy metals (29).

Sodium dodecyl sulfate

The SDS was electrophoresis purity reagent (Bio-Rad).

Linoleic acid

The linoleic acid (Nu-Chek-Prep > 99%) was found to be free of hydroperoxides by tlc analysis on silica gel and testing with a *N,N*-dimethyl-*p*-phenylenediamine spray.

Initiators

DBHN, prepared by the method of Mendenhall (39), was recrystallized from cold methanol and stored as a solid at −30°C. Azobis(2-amidinopropane·HCl) was obtained from Polysciences, Inc. and stored at −30°C. The solutions of DBHN in 0.50 M SDS were prepared for each run by vortex stirring the DBHN (ca. 7 mg) with 5.00 mL of 0.50 M SDS for 20 min. This solution was gravity filtered; 1.00 mL was diluted to 50 mL with 1 : 1 methanol–water and analyzed for DBHN using the λ_{max} at 227 nm.

Inhibitors

α-Tocopherol (Eastman–Kodak) was stored in known concentrations in hexane under argon at −30°C. Solutions in SDS were prepared as follows. A 2.00-mL sample of the hexane solution (8.77×10^{-3} M in α-tocopherol) was evaporated to a thin film on the rotary evaporator under nitrogen. The 0.50 M SDS – phosphate buffer (12.00 mL) was added and this mixture was sonicated under argon in a Bransonic 220 bath sonicator at 20°C for 3 h. This stock solution could be stored under argon at least 1 week without a decrease in α-tocopherol concentration. When used as an inhibitor, the α-tocopherol concentration was checked by diluting a 1.00-mL sample to 50 mL in 1 : 1 methanol–water and measuring the absorbance at 292 nm. The Trolox was a gift from Hoffmann–LaRoche, Nutley, New Jersey. Freshly prepared standard solutions in phosphate buffer (pH 7.0) were used as an inhibitor. The ascorbic acid (L-(+)- from Anachemia) used was freshly prepared in phosphate buffer pH 7.0.

2. *Analyses*

Analyses for DBHN and α-tocopherol concentrations were made on a Varian–Cary 219 spectrophotometer. The hplc analyses were done on a Spectraphysics SP 8000 liquid chromatograph using a 4.6 mm × 25 cm Li Chrosorb NH_2 10-μm column and an ultraviolet detector set at 210 nm. For separation of components from an autoxidation sample, an aliquot was added to an acetanilide solution (internal standard); this was eluted on the column with 45:55 (v/v) acetonitrile – 2.5 mM NaH_2PO_4 buffer (pH 4.75) at 2.0 mL min^{-1} and 20°C for 9 min. The mobile phase was then changed over 2 min to 80:20 v/v acetonitrile–buffer. Under these conditions good resolution of acetanilide (3.4 *m*), DBHN (6.5 *m*), ascorbic acid (13 *m*), and α-tocopherol (24 *m*) was obtained. For identification, the DBHN and α-tocopherol were collected from the column and their ultraviolet spectra recorded.

3. *Autoxidation procedure*

Autoxidations were carried out at 30°C and 760 Torr of O_2 using a sensitive automatic recording gas absorption apparatus similar to that described (5). In a typical run, a 2.00-mL sample of the DBHN – 0.50 M SDS in phosphate buffer was equilibrated at 30°C. Then known amounts of linoleic acid were added from a precision syringe and the rates of oxygen uptake recorded after each addition. The per cent consumption of linoleic acid was generally less than 10%. Induction periods were obtained by adding α-tocopherol – SDS in phosphate buffer and the time was measured on the recorder until the uptake of oxygen resumed its original rate. For induction periods with both α-tocopherol and ascorbate, the solutions were added sequentially from separate syringes and the combined induction periods measured as before. In these cases, the rate of chain initiation (R_i) was followed by measuring the induction period with α-tocopherol alone, immediately before and again immediately after the combined induction periods found for α-tocopherol and ascorbate together.

Acknowledgements

We thank Dr. G. W. Burton and Dr. K. U. Ingold for their continued interested and helpful suggestions. Technical assistance provided by Mr. R. D. Smith and Mr. A. MacDonald is gratefully acknowledged. This research was supported by a grant from the Natural Sciences and Engineering Research Council of Canada.

1. A. L. TAPPEL. *In* Free radicals in biology. Vol. IV. *Edited by* W. A. Pryor. Academic Press, New York. 1980. Chapt. 1. pp. 1–47.
2. C. DE DUVE and O. HAYAISHI (*Editors*). Tocopherol, oxygen and

[9] D. Kong of our laboratory recently found the rate of autoxidation of 6.43×10^{-5} moles of linoleic acid dispersed in phosphate buffer (pH 7.0) and initiated by the water-soluble initiator, azobis(2-amidinopropane·HCl) to be $1.05 \times 10^{-5}\ M\ s^{-1}$. The rate on this same sample dissolved in 0.50 M SDS decreased to $2.40 \times 10^{-7}\ M\ s^{-1}$. This decrease in rate is consistent with a change of environment from the polar ionic buffer to the micellar phase.

biomembranes. Elsevier, North Holland, Amsterdam. 1978.
3. N. A. PORTER. *In* Free radicals in biology. Vol. IV. *Edited by* W. A. Pryor. Academic Press, New York. 1980. Chapt. 8. pp. 261–294.
4. W. A. PRYOR (*Editor*). Free radicals in biology. Academic Press, New York.
5. L. R. C. BARCLAY and K. U. INGOLD. J. Am. Chem. Soc. **103**, 6478 (1981).
6. L. R. C. BARCLAY, S. J. LOCKE, and J. M. MACNEIL. Can. J. Chem. **61**, 1288 (1983).
7. L. R. C. BARCLAY, S. J. LOCKE, J. M. MACNEIL, J. VANKESSEL, G. W. BURTON, and K. U. INGOLD. J. Am. Chem. Soc. **106**, 2479 (1984).
8. G. W. BURTON and K. U. INGOLD. J. Am. Chem. Soc. **103**, 6472 (1981).
9. G. W. BURTON, L. HUGHES, and K. U. INGOLD. J. Am. Chem. Soc. **105**, 5950 (1983).
10. T. DOBA, G. W. BURTON, and K. U. INGOLD. J. Am. Chem. Soc. **105**, 6505 (1983).
11. P. A. SEIB and B. M. TOLBERT (*Editors*). Ascorbic acid: chemistry, metabolism, and uses. Advances in Chemistry Series 200, A. C. S., Washington, D.C. 1982.
12. H. M. SWARTZ and N. J. F. DODD. *In* Oxygen and oxy-radicals in chemistry and biology. *Edited by* M. A. J. Rodgers and E. L. Powers. Academic Press, New York. 1981. p. 161.
13. H. H. DRAPER. *In* Vitamin E. A comprehensive treatise. Basic and clinical nutrition. *Edited by* L. J. Machlin. Marcel Dekker, Inc., New York. 1980. Part 5D. p. 272.
14. J. F. MEAD. *In* Free radicals in biology. Vol. I. *Edited by* W. A. Pryor. Academic Press, New York. 1976. Chapt. 2. p. 51.
15. W. O. LUNDBERG (*Editor*). Autoxidation and antioxidants. Vols. I and II. Interscience, New York. 1961.
16. F. R. MAYO. Acc. Chem. Res. **1**, 193 (1968).
17. K. U. INGOLD. Acc. Chem. Res. **2**, (1969).
18. (*a*) J. A. HOWARD. *In* Free radicals. Vol. II. *Edited by* J. K. Kochi. Wiley, New York. 1973. Chapt. 12. pp. 3–62; (*b*) Adv. Free-Radical Chem. **4**, 49 (1972).
19. C. E. BOOZER, G. S. HAMMOND, C. E. HAMILTON, and J. N. SEN. J. Am. Chem. Soc. **77**, 3233 (1953).
20. H. KIEFER and T. G. TRAYLOR. Tetrahedron Lett. 6163 (1966).
21. G. M. MUSBALLY, G. PERRON, and J. E. DESNOYERS. J. Colloid Interface Sci. **48**, 494 (1974).
22. D. FENNELL EVANS and B. W. NINHAM. J. Phys. Chem. **87**, 5025 (1983).
23. L. R. MAHONEY. Angew. Chem. Int. Ed. Engl. **8**, 547 (1969).
24. L. R. MAHONEY and M. A. DAROOGE. J. Am. Chem. Soc. **89**, 5619 (1967).
25. J. E. PACKER, T. F. SLATER, and R. L. WILLSON. Nature, **278**, 737 (1979).
26. J. S. WINTERLE and T. MILL. Oxygen and oxyradicals in chemistry and biology. *Edited by* M. A. J. Rodgers and E. L. Powers. Academic Press, New York. 1981. p. 779.
27. E. NIKI, J. TSUCHIYA, R. TANIMURA, and Y. KAMIYA. Chem. Lett. 789 (1982).
28. E. NIKI, T. SAITO, and Y. KAMIYA. Chem. Lett. 631 (1983).
29. M. SCARPA, R. STEVANATO, P. VIGLINO, and A. RIGO. J. Biol. Chem. **258**, 6695 (1983).
30. J. H. FENDLER and E. J. FENDLER. Catalysis in micellar and macromolecular systems. Academic Press, New York. 1975.
31. N. J. TURRO and T. OKUBO. J. Am. Chem. Soc. **103**, 7224 (1981).
32. H. KIEFER and T. G. TRAYLOR. J. Am. Chem. Soc. **92**, 2440 (1970).
33. J. A. HOWARD and K. U. INGOLD. Can. J. Chem. **45**, 793 (1967).
34. J. A. HOWARD and K. U. INGOLD. Can. J. Chem. **42**, 1044 (1967); **42**, 1250 (1964).
35. D. G. HENDRY and G. A. RUSSELL. J. Am. Chem. Soc. **86**, 2368 (1964).
36. P. MUKERJEE, J. R. CARDINAL, and N. R. DESAI. *In* Micellization, solubilization and microemulsions. Vol. 1. *Edited by* K. L. Mittal. Plenum, New York. 1977. pp. 241–261.
37. R. W. FESSENDEN, A. HITACHI, and V. NAGARAJAN. J. Phys. Chem. **88**, 107 (1984).
38. K. KALYANASUNDARAM and J. K. THOMAS. J. Phys. Chem. **81**, 2176 (1977).
39. G. D. MENDENHALL. Tetrahedron Lett. **24**, 241 (1983).

Dihydro-9,14(4*H*)tripyrazolo(1,5-*a*:1′,5′-*d*:1″,5″-*g*)triazonine-1,4,7. Synthèse et étude par résonance magnétique nucléaire

ALAIN FRUCHIER,[1] BRIGITTE LUPO ET GEORGES TARRAGO
ERA au CNRS n° 169, Université des Sciences et Techniques du Languedoc, Place Eugène Bataillon, 34060 Montpellier Cedex, France

Reçu le 8 février 1984

ALAIN FRUCHIER, BRIGITTE LUPO et GEORGES TARRAGO. Can. J. Chem. **63**, 375 (1985).

Nous avons réalisé la synthèse selon une voie univoque de la triméthyl-2,7,12 dihydro-9,14(4*H*)tripyrazolo(1,5-*a*:1′,5′-*d*;1″,5″-*g*)triazonine-1,4,7. Une étude rmn de cette nouvelle molécule dans divers solvants a pour la première fois mis en évidence l'existence d'un équilibre conformationnel de type crown ⇌ saddle dans un dérivé du triazacyclononatriène.

ALAIN FRUCHIER, BRIGITTE LUPO, and GEORGES TARRAGO. Can. J. Chem. **63**, 375 (1985).

We have accomplished an unequivocal synthesis of 2,7,12-trimethyl-9,14-dihydro-1,5-*a*;1′,5′-*d*;1″,5″-*g*-(4*H*)tri-pyrazolo-1,4,7-triazonine. An nmr study of this new molecule in different solvents shows, for the first time, the existence of a crown ⇌ saddle conformationl equilibrium in a triazacyclononatriene derivative.

[Journal translation]

Introduction

Dans une publication précédente (1), nous avons montré que le composé obtenu par action du brome sur le sel d'argent du triméthyl-3,4,5 pyrazole ne pouvait avoir la structure **1** qui lui avait été attribuée (2).

Sur la base de la masse moléculaire déterminée par spectrométrie de masse et du spectre de rmn dans le DMSO-d_6 indiquant une symétrie élevée, nous avions suggéré une structure cyclique tripyrazolique **2**. Cependant, étant donnée la méthode d'obtention, une structure de type **3** ne pouvait être absolument exclue.

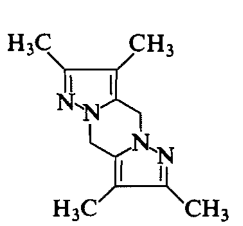

1

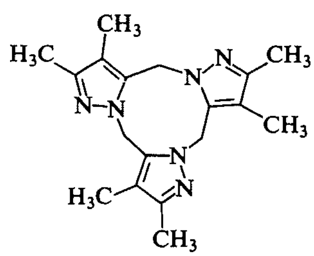

2

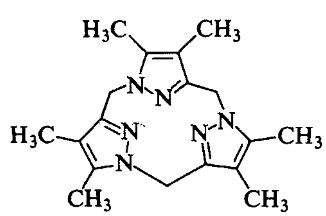

3

Nous présentons dans ce travail la synthèse univoque d'un composé analogue à **2**, la triméthyl-2,7,12 dihydro-9,14-(4*H*)tripyrazolo(1,5-*a*:1′,5′-*d*:1″,5″-*g*)triazonine-1,4,7 **4**, dont l'étude rmn prouve la structure proposée précédemment (1).

Résultats

La synthèse de **4** est effectuée selon le schéma réactionnel suivant:

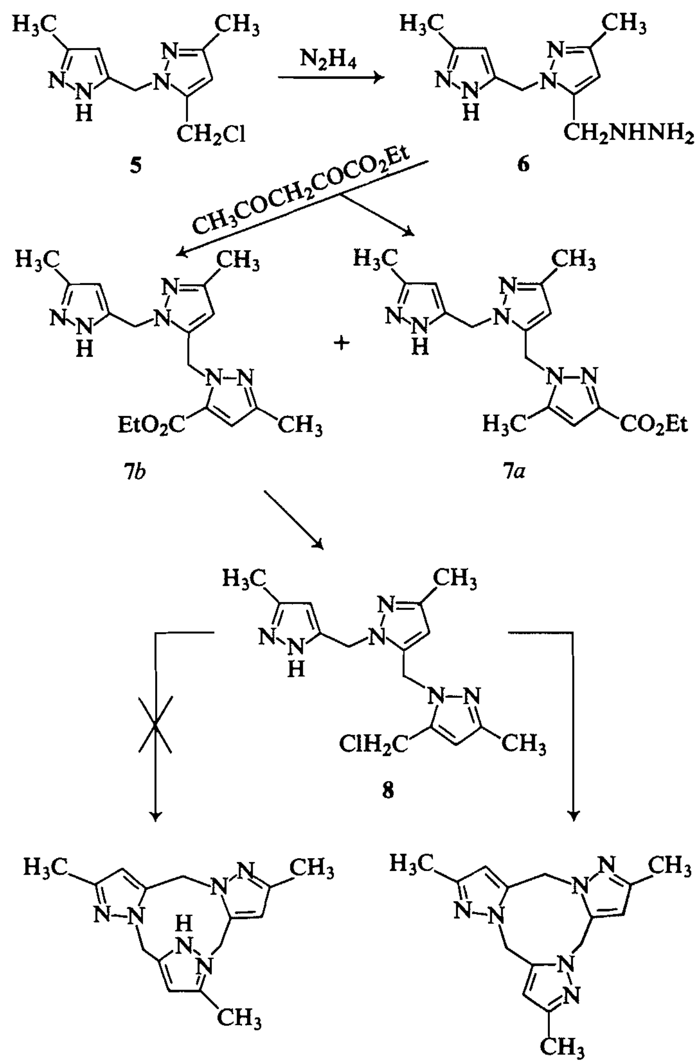

Le composé **5**, dont nous avons déja décrit la synthèse (1), est traité par l'hydrazine pour donner **6**, qui par condensation avec l'acétylpyruvate d'éthyle conduit aux deux isomères **7***a* et **7***b*. Ces derniers sont séparés par chromatographie et identifiés par rmn sur la base du couplage entre les groupes méthyle-3(5) et les protons en position 4 des noyaux pyrazoliques (3). L'es-

[1] Auteur auquel la correspondance doit être adressée.

TABLEAU 1. Effet du solvant sur les déplacements chimiques (δ)

Solvant	DMSO-d_6			C_6D_6		Acétone[a]	CD_3OH[a]	CD_3CN[a]	$CDCl_3$			
Product	2C	4C	12C	2C	4C	4C	4C	4C	2C	2S	4C	4S
Pourcentages	100	100	100	100	100	100	100	100	70	30	80	20
CH_2 4,9,14	5,16[b]	5,23[b]	5,43[b]	4,44[b]	4,36[b]	5,30[b]	5,27[b]	5,28[b]	5,31[b]		5,37[b]	
										4,97		5,07
	5,86[b]	5,93[b]	5,98[b]	5,03[b]	5,02[b]	5,87[b]	5,81[b]	5,59[b]	5,36[b]		5,42[b]	
CH_3 2,7,12	2,01[d]	2,05	2,20	2,14[d]	2,06	2,05	2,15	2,09	2,12[d]	2,15[d]	2,18	2,23
H 3,8,13	—	6,09	—	—	6,11	6,11	6,23	6,12	—	—	6,24	6,12
CH_3 3,8,13	1,97[d]	—	—	2,01[d]	—	—	—	—	2,08[d]	1,98[d]	—	—

[a]Le composé 2 est insoluble dans ce solvant.
[b]J = 16 Hz (résolution digitale: 0,2 Hz).
[c]Anisochronie non mesurable à 100 MHz.
[d]L'attribution des groupes méthvle peut être inversér.

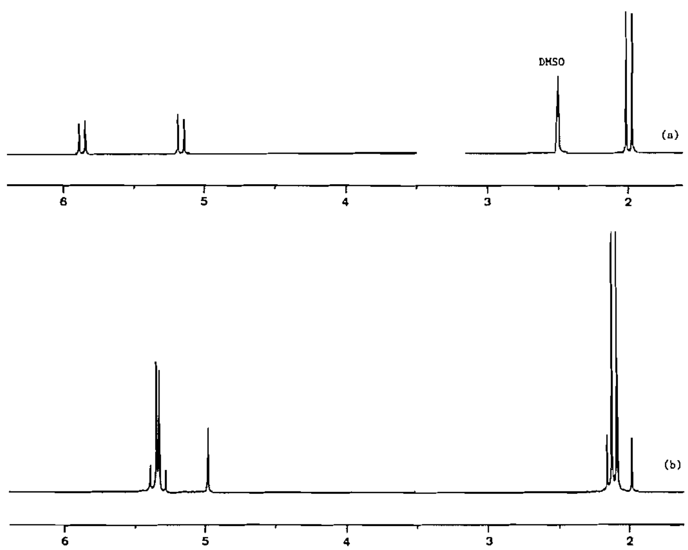

FIG. 1. Spectres en rmn de ¹H à 360 MHz de **2**. (a) DMSO-d_6; (b) $CDCl_3$.

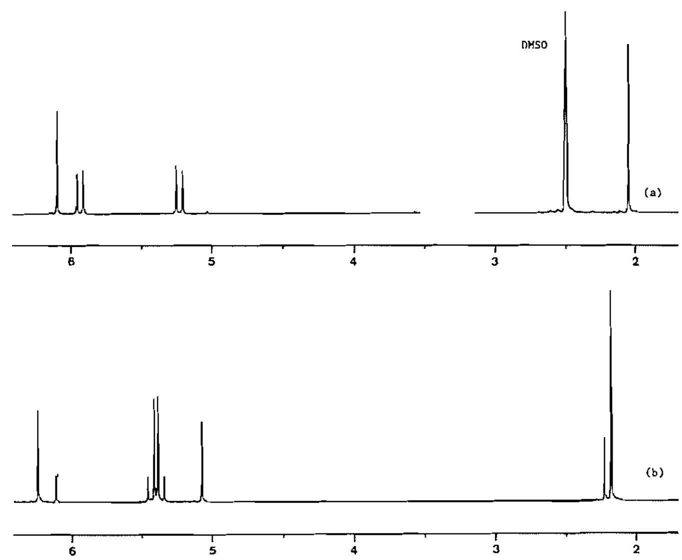

FIG. 2. Spectres en rmn de ¹H à 360 MHz de **4**. (a) DMSO-d_6; (b) $CDCl_3$.

ter **7***b* est ensuite réduit puis traité par le chlorure de thionyle pour donner **8**.

De par la présence de deux atomes d'azote nucléophiles dans le noyau pyrazole non *N*-substitué, la condensation du groupe chlorométhyle de **8** peut s'effectuer de deux façons et conduire à **4** et(ou) **9**. Cependant, soumis à un milieu basique fort dans les conditions de la catalyse par transfert de phase, **8** subit une cyclisation intramoléculaire par attaque du groupe chlorométhyle sur l'azote en β du substituant méthyle et donne le composé **4** avec un rendement de 38%. Si de nombreux autres produits sont formés au cours de la réaction, nous n'avons pu les identifier, le rendement de chacun d'eux étant inférieur à 3%.

Les spectres en rmn du proton de **2** et **4** dans $CDCl_3$ et DMSO-d_6 sont réunis dans les figures 1 et 2 respectivement, et les déplacements chimiques dans le tableau 1.

On notera une grande analogie, d'une part entre les spectres des deux composés dans le même solvant (fig. 1a et 2a, 1b et 2b), d'autre part en ce qui concerne l'effet du solvant sur un composé donné (fig. 1a et 1b, 2a et 2b). Pour chacun d'eux, le spectre dans le DMSO-d_6 est celui d'un composé unique de symétrie C_3 dont les protons méthyléniques sont fortement anisochrones, tandis que celui dans $CDCl_3$ correspond à un mélange de deux espèces en proportions inégales. La plus abondante est celle observée dans le DMSO, la moins abondante a la même symétrie mais ne montre aucune anisochronie des protons méthyléniques à 360 MHz.

Les produits **2** et **4** étant très peu solubles dans les deux solvants (étude de solutions saturées), et bien que chromatographiquement purs, la solubilisation sélective de deux espèces différentes dans les deux solvants ne pouvait être exclue. Cependant, cette hypothèse a pu être rejetée après étude de l'évolution du spectre d'une solution chloroformique lors de l'addition de DMSO-d_6 (fig. 3 et 4). Les composés **2** et **4** ont exactement le même comportement: dans les deux cas, l'addition de DMSO provoque la disparition progressive du produit et les pourcentages de forme C et S des composés **2**, **4** et **12**

		CDBr₃				CD_2Cl_2				$(CCl_3)_2CO$			
12C	12S	2C	2S	4C	4S	2C	2S	4C	4S	2C	2S	4C	4S
50	50	75	25	80	20	90	10	90	10	90	10	90	10
5,38[b]				5,36[b]									
	5,12	5,30[c]	4,93		5,05	5,56[c]	5,44	5,35[c]	5,02	5,25[c]	4,92	5,43[c]	5,03
5,59[b]				5,42[b]									
2,19	2,23	2,08[d]	2,10[d]	2,16	2,21	2,09[d]	2,12[d]	2,12	2,18	2,04[d]	2,07[d]	2,11	2,17
—	—	—	—	6,24	6,12	—	—	6,15	6,05	—	—	6,30	6,06
—	—	2,04[d]	1,96[d]	—	—	2,05[d]	1,95[d]	—	—	1,98[d]	1,93[d]	—	—

mineur, ainsi qu'une augmentation d'anisochronie des protons des méthylènes du produit majeur.

Discussion

La structure **9** pouvant être rejetée à cause de l'absence de symétrie qui conduirait à un spectre rmn plus complexe que celui de la figure 2a, le cycle central à neuf éléments de **4** explique son comportement en rmn.

En effet, il est connu (4) que le cyclononatriène-1,4,7 existe sous deux conformères C (crown) et S (saddle):

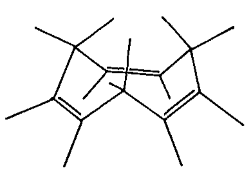

C

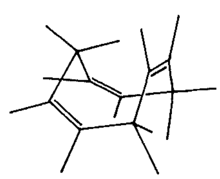

S

En rmn, seule la forme C est observée à basse température, tandis qu'à température ambiante ou élevée, le spectre correspond à un équilibre plus ou moins rapide entre les différentes formes possibles.

Dans le cas du cyclotrivératrylène (CTV) **10**, la forme C est seule observée (5), même à 200°C (absence de coalescence du système AB méthylénique). Dans tous les composés analogues cités (6), soit la forme C est seule présente, soit la forme S. Les

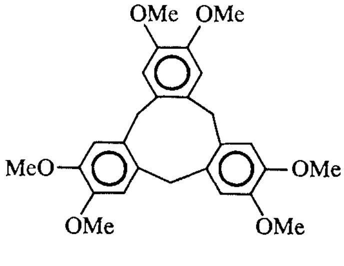

10

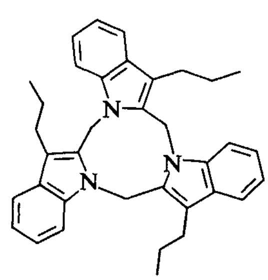

12

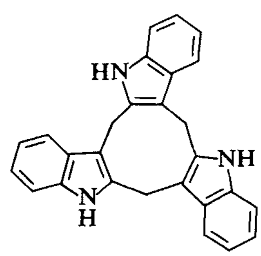

11

deux conformères ont été cependant signalés dans un même spectre rmn pour le produit **11** où le cycle benzénique est remplacé par un cycle à cinq éléments (7).

Le seul triazacyclononatriène-1,4,7 symétrique décrit à notre connaissance est le composé **12** (8) dans lequel les trois méthylènes sont isochrones dans le $CDCl_3$.

Il apparait donc que les spectres dans le DMSO-d_6 de **2** et **4** (fig. 1a et 2a) sont ceux d'une forme C (fig. 5): isochronie des protons situés sur les positions homologues des noyaux pyrazoliques et des groupes méthyléniques, indiquant la symétrie C_3, et anisochronie des protons à l'intérieur de chaque méthylène.

Dans le $CDCl_3$, par contre, si la forme C est encore majoritaire, il est raisonnable d'attribuer à la forme S les signaux du composé minoritaire. Cette structure n'ayant aucun élément de symétrie, conduirait à un spectre rmn complexe si elle n'était en équilibre rapide avec deux autres formes S équivalentes (4, 6, 8, 9).

La preuve que les formes majeure (C) et mineure (S) observées dans le spectre de **4** sont en équilibre conformationnel lent à température ambiante est apportée par l'évolution du spectre de **4** dans l'hexachloroacétone avec la température, montrant une coalescence des signaux des deux formes vers 140°C (fig. 6). La réversibilité du processus a été vérifiée lors du refroidissement.

En utilisant la méthode décrite dans la référence 10 pour les échanges entre sites inégalement peuplés, on peut évaluer le $\Delta G^{\neq}$ de l'équilibre C/S de **4** dans l'hexachloroacétone à 20 ± 1 kcal mol^{-1}. Cette barrière est inférieure à celle du CTV dans le même solvant: ce dernier se décompose à 200°C sans qu'il

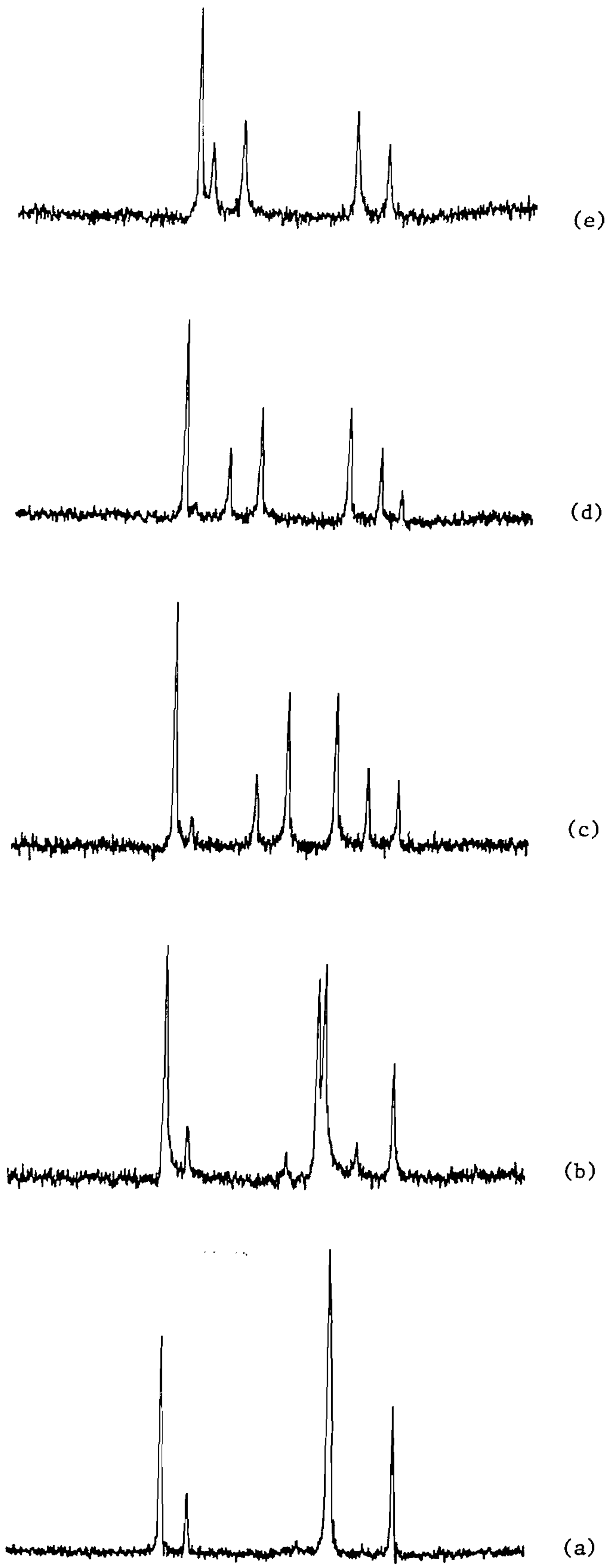

FIG. 3. Etude à 80 MHz de l'évolution du spectre de **4** par addition de DMSO-d_6 à une solution chloroformique (zone comprise entre 5 et 6,5 ppm); pourcentages $CDCl_3$/DMSO-d_6: (a) 100:0; (b) 90:10; (c) 85:15: (d) 80:20; (e) 0:100.

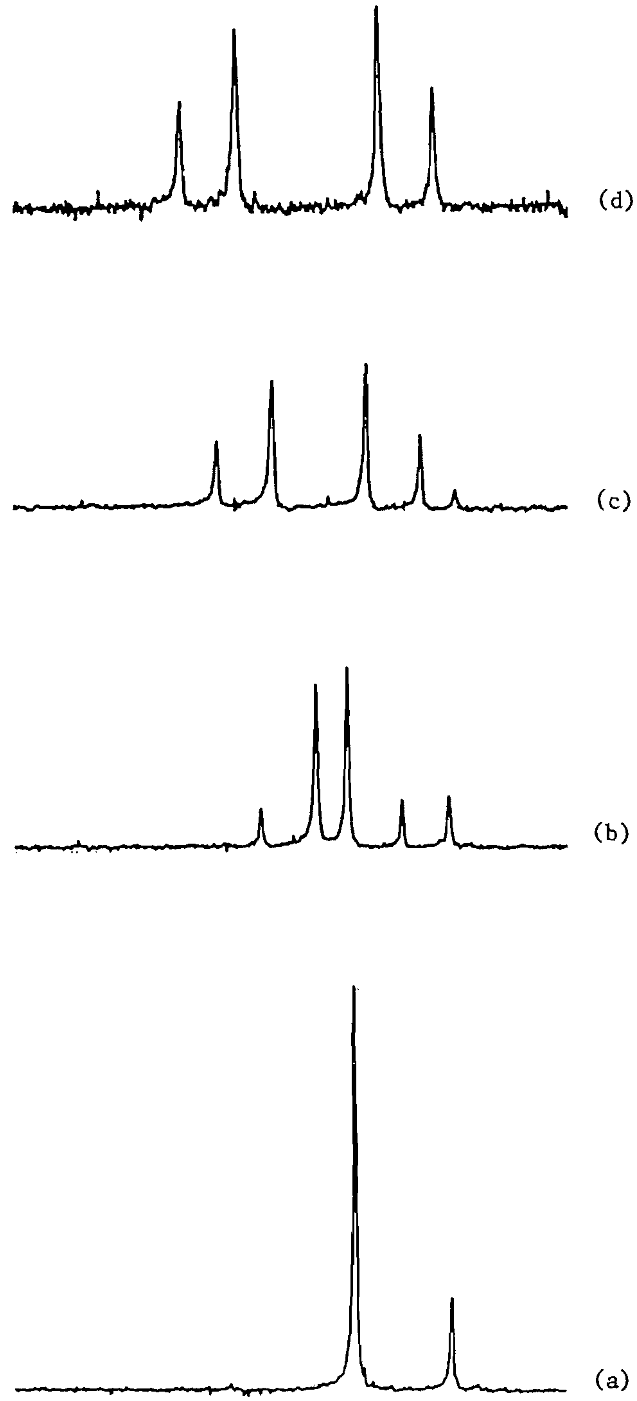

FIG. 4. Etude à 80 MHz de l'évolution du spectre de **2** par addition de DMSO-d_6 à une solution chloroformique (zone comprise entre 5 et 6 ppm); pourcentages $CDCl_3$/DMSO-d_6: (a) 100:0; (b) 84:16; (c) 80:20; (d) 0:100.

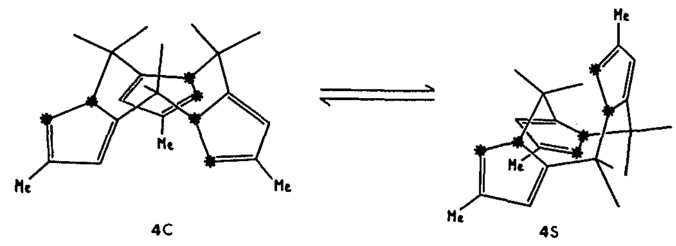

FIG. 5. Equilibre conformationnel crown ⇌ saddle du composé **4**.

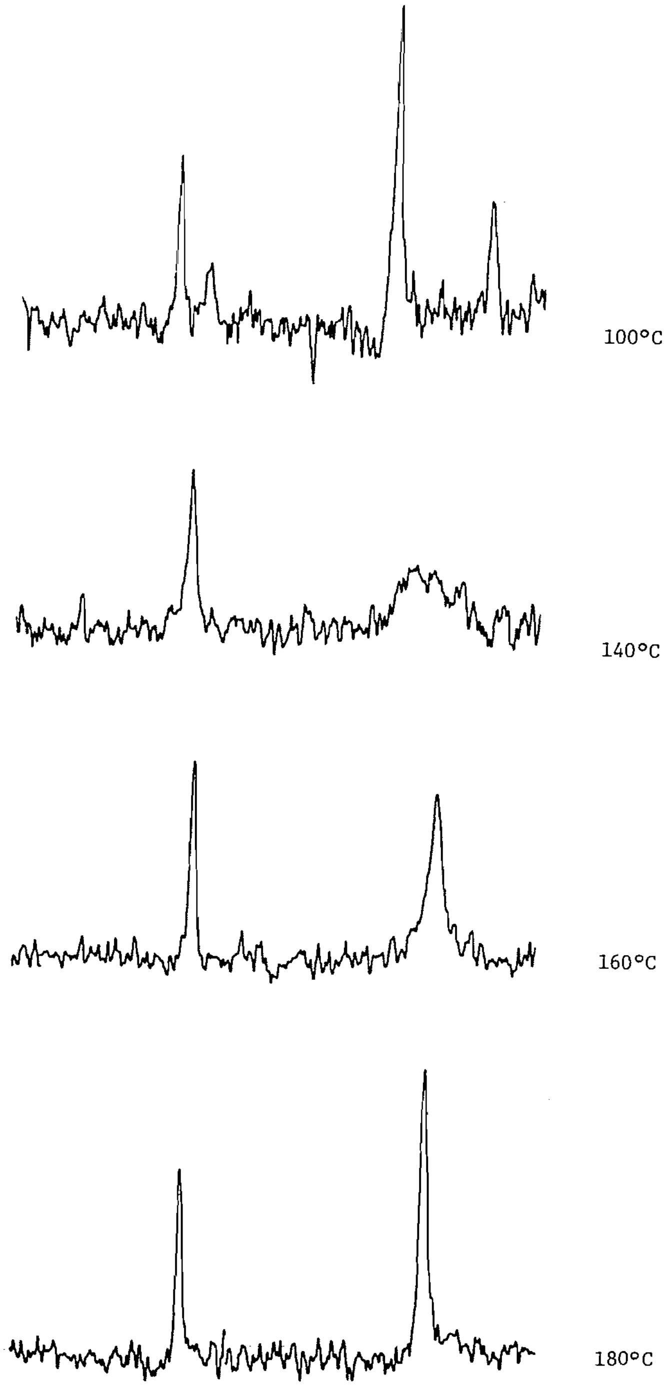

FIG. 6. Etude à 100 MHz de l'évolution avec la température du spectre de **4** dans l'hexachloroacétone (zone comprise entre 5.0 et 6.5 ppm).

y ait eu évolution du système AB méthylénique de la forme C seule visible (5). Par contre, aucun élargissement des signaux de la forme S n'est observé dans CD_2Cl_2 à −95°C. De toute évidence, et malgré que l'étude des deux équilibres ne soit pas possible dans le même solvant, la barrière de l'interconversion S/S est donc très inférieure à celle de l'équilibre C/S. En effet, le rôle du solvant est important. Par exemple, contrairement à ce qui est observé dans l'hexachloroacétone, le spectre de **4** dans le DMSO-d_6 à 140°C est identique à celui observé à température ambiante.

D'autre part, la différence de comportement de **2** et **4** dans $CDCl_3$ et DMSO-d_6 nous a incités à les étudier dans plusieurs autres solvants. Les déplacements chimiques sont réunis dans le tableau 1. On constate que dans les solvants tels que DMSO, benzène, méthanol, acétonitrile, acétone, l'équilibre est totalement déplacé en faveur de la forme C, mais que l'anisochronie des protons méthyléniques ainsi que le centre du système AB sont variables. Par contre, les solvants dans lesquels les deux conformères coexistent sont tous halogénés: chloroforme, dichlorométhane, bromoforme, hexachloroacétone. C'est aussi dans ces solvants que l'anisochronie des protons méthyléniques est la plus faible.

Enfin, des expériences réalisées à partir de mélanges $CDCl_3$/DMSO-d_6 et benzène/DMSO-d_6 ont mis en évidence la sensibilité plus grande d'un des deux protons méthyléniques à l'effet de solvant. Par exemple, lors de l'addition progressive de DMSO à une solution benzénique de **2** ou de **4**, le déplacement du système AB vers les fréquences élevées s'effectue avec croisement des signaux des protons méthyléniques.

Ces différentes observations sont en faveur d'une solvatation spécifique du conformère C, solvatation qui a déja été invoquée dans le cas du CTV (6, 9) pour expliquer la stabilisation de la forme C pourtant plus encombrée que la forme S. Ce dernier point est illustré dans notre série par le pourcentage de forme S qui passe de 20 (produit **4**) à 30 (produit **2**) puis à 50 (produit **12**) quand on remplace l'hydrogène de la position 4 des noyaux pyrazoliques par un méthyle (dans **2**) ou un brome (dans **12**) (tableau 1).

Conclusion

Dans la série du CTV, il a été montré (6) qu'au moins un des carbones sp^3 méthyléniques doit être remplacé par un carbone sp^2 pour qu'il y ait, dans l'échelle des temps de la rmn, équilibre entre conformères C et S. Dans tous les autres cas, c'est soit la forme C seule, soit la forme S seule qui est observé.

Nous venons de voir que cette condition n'est pas nécessaire dans la série de la tripyrazolotriazonine-1,4,7 où les formes C et S sont observées en même temps dans certains solvants.

D'autre part, étant donné que la différence observable entre formes S et C est l'anisochronie des hydrogènes méthyléniques de cette dernière, un spectre à haut-champ au moins sera souhaitable chaque fois que la forme S sera "vue" seule. Nous avons en effet montré que, dans certains solvants, l'anisochronie de la forme C peut être si faible qu'elle n'est pas mesurable à 80 ou 100 MHz.

Partie expérimentale

Les spectres rmn du proton ont été enregistrés sur les spectromètres suivants: Varian HA-100 et Bruker WP-80-DS du Laboratoire de Mesures Physiques de l'U.S.T.L., Bruker WM-250 de la Sadis Bruker à Wissembourg que nous remercions de son aide, Bruker WM-360-WB du Laboratoire de RMN à Haut-Champ de Montpellier. Tous les déplacements chimiques sont donnés en ppm par rapport au TMS pris comme référence interne.

Les spectres de masse ont été obtenus sur un spectromètre JEOL JMS D-100 au Laboratoire de Mesures Physiques de l'U.S.T.L.

Les points de fusion inférieurs à 250°C, non corrigés, ont été déterminés en tubes capillaires avec un appareil Tottoli, et ceux supérieurs à 250°C avec une platine chauffante Leitz.

Les analyses ont été effectuées par le Service Central de Microanalyses du C.N.R.S.

Les rendements indiqués correspondent à des produits ne présentant qu'une seule tache en chromatographie sur couche mince.

Hydrazinométhyl-5 diméthyl-3,5'(3') dipyrazolyl-1,3'(5') méthane **6**

Ce composé très instable a été préparé *in situ* pour éviter toute oxydation éventuelle (11). Un courant d'azote est envoyé sur une solution de 0,10 mol (26 g) du chlorhydrate de **5** (1) dans 500 mL d'éthanol puis 0,80 mol d'hydrate d'hydrazine (40 g) en solution dans 50 mL d'éthanol sont ajoutés. Le mélange est agité à température ambiante pendant 20 min puis refroidi jusqu'à apparition d'un précipité de chlorhydrate d'hydrazine que l'on filtre. Le filtrat est concentré sous atmosphère d'azote. L'huile obtenue est chauffée à 90°C sous 0,1 Torr (1 Torr = 133.3 Pa) afin d'éliminer le maximum d'hydrazine et est utilisée aussitôt pour l'étape suivante.

Carbéthoxy-5 triméthyl-3,3',5"(3") [pyrazole méthylène-3"(5")]-yl-1' dipyrazolyl-1,5' méthane 7b

Un mélange de 0,05 mol de **6** (11 g) et 0,06 mol d'acétylpyruvate d'éthyle (9,5 g) est chauffé à reflux 2 h sous atmosphère d'azote dans 500 mL d'éthanol. Après évaporation du solvant sous pression réduite, le résidu huileux est chromatographié sur alumine (ether/ethanol 98:2). A côté de produits non identifiés, les deux isomères suivants sont isolés.

Composé 7a, R_f = 0,10, avec un rendement de 10%; F = 120°C; spectre de masse (pic moléculaire): m/e = 342; rmn ($CDCl_3$): 6,52 (1H, s), 5,92 (1H, s), 5,67 (1H, s), 5,32 (2H, s), 5,28 (2H, s), 4,36 (2H, q), 2,20 (3H, d, J = 0,6 Hz: CH_3-5"), 2,16 (3H, d, J = 0,7 Hz: CH_3-5), 2,15 (3H, s, CH_3-3'), 1,34 (3H, t); rmn (C_6D_6): 6,43 (1H, s), 6,07 (2H, s), 5,88 (1H, s), 5,47 (1H, s), 5,24 (2H, s), 4,14 (2H, q), 2,06 (3H, s: CH_3-3'), 1,95 (3H, d, J = 0,6 Hz: CH_3-5"), 1,62 (3H, d, J = 0,7 Hz: CH_3-5), 1,03 (3H, t).

Composé 7b, R_f = 0,25, avec un rendement de 24%; F = 138°C; spectre de masse (pic moléculaire): m/e = 342; rmn ($CDCl_3$): 6,59 (1H, s), 5,88 (2H, s), 5,69 (2H, s), 5,42 (2H, s), 4,30 (2H, q), 2,24 (3H, d, J = 0,3 Hz: CH_3-3), 2,19 (3H, d, J = 0,6 Hz: CH_3-5"), 2,16 (3H, d, J = 0,3 Hz: CH_3-3'), 1,30 (3H, t); rmn (C_6D_6): 6,43 (1H, s), 6,03 (1H, s), 5,84 (1H, s), 5,65 (2H, s), 5,42 (2H, s), 3,92 (2H, q), 2,06 (3H, d, J = 0,3 Hz: CH_3-3), 2,03 (3H, d, J = 0.3 Hz: CH_3-3'), 1,83 (3H, d, J = 0,6 Hz: CH_3-5"), 1,02 (3H, t).

Hydroxyméthyl-5 triméthyl-3,3',5"(3") [pyrazole méthylène-3"(5")]-yl-1' dipyrazolyl-1,5' méthane

Cet alcool est obtenu par réduction de l'ester 7*b* par $AlLiH_4$ selon un protocole analogue à celui décrite dans la littérature pour l'homologue inférieur à deux noyaux pyrazole (1). Rendement 75%; F = 118–120°C; spectre de masse (pic moléculaire): m/e = 300; rmn ($CDCl_3$): 5,87 (1H, s), 5,82 (1H, s), 5,70 (1H, s), 5,23 (2H, s), 5,12 (2H, s), 4,42 (2H, s), 2,14 (3H, s: CH_3-3), 2,11 (3H, d, J = 0,6 Hz: CH_3-5"), 2.09 (3H, s: CH_3-3'); rmn (C_6D_6): 5,87 (1H, s), 5,83 (1H, s), 5,82 (1H, s), 5,22 (2H, s), 5,12 (2H, s), 4,38 (2H, s), 2,14 (3H, s: CH_3-3), 2,08 (3H, s: CH_3-3'), 1,81 (3H, d, J = 0,6 Hz: CH_3-5").

Chlorométhyl-5 triméthyl-3,3',5"(3") [pyrazole méthylène-3"(5")]-yl-1' dipyrazolyl-1,5' méthane 8

Ce composé est obtenu par action du chlorure de thionyle sur l'alcool précédent selon le même mode opératoire décrit pour l'homologue inférieur à deux noyaux pyrazoles (1). Rendement 65%; F = 80°C (décomposition); spectre de masse (pic moléculaire): m/e = 318; rmn ($CDCl_3$): 6,01 (1H, s), 5,92 (2H, s), 5,42 (2H, s), 5,34 (2H, s), 4,47 (2H, s), 2,32 (3H, d, J = 0,4 Hz: CH_3-5'), 2,19 (3H, s: CH_3-3), 2,17 (3H, s: CH_3-3'); rmn (C_6D_6): 5,80 (1H, s), 5,73 (1H, s), 5,71 (1H, s), 5,37 (2H, s), 5,23 (2H, s), 4,18 (2H, s), 2,10 (3H, s: CH_3-3), 2,09 (3H, s: CH_3-3'), 1,88 (3H, d, J = 0,4 Hz: CH_3-5").

*Triméthyl-2,7,12 dihydro-9,14 (4*H*)tripyrazolo(1,5-*a*:1',5'-*d*:1",5"-*g*)triazonine-1,4,7 4*

A 4 mL d'une solution de soude à 50% en poids sont ajoutés 2 × 10^{-4} mol de bromure de tétrabutylammonium et 300 mL de benzène en agitant vivement. Une solution de 0,005 mol de **8** dans 300 mL de benzène est alors ajoutée goutte à goutte au mélange précédent et le milieu réactionnel est chauffé au bain-marie à 60°C pendant 2 h.

Très rapidement, un précipité blanc, fin et floconneux apparait. En fin de réaction, ce précipité est filtré, lavé à l'eau puis extrait au chloroforme. La phase organique est séchée sur sulfate de sodium, filtrée puis le solvant évaporé. Le résidu solide est recristallisé dans un mélange eau/éthanol et donne **4** avec un rendement de 38%; F = 310°C; spectre de masse (pic moléculaire): m/e = 282. *Anal.* calc. pour $C_{15}H_{18}N_6$: C 63,89, H 6,43, N 29,80; trouvée: C 63,49, H 6,47, N 29,51; rmn, voir tableau 1.

*Tribromo-3,8,13 triméthyl-2,7,12 dihydro-9,14(4*H*)tripyrazolo-(1,5-*a*:1',5'-*d*:1",5"-*g*)triazonine-1,4,7* **12**

A 0,001 mol de **4** en solution dans le chloroforme est ajouté goutte à goutte 0,003 mol de brome en solution chloroformique. L'addition terminée, le mélange est porté à reflux pendant 1 h. Le bromohydrate de **12**, insoluble dans le chloroforme, précipite et le milieu est neutralisé par une solution aqueuse de Na_2CO_3. La phase organique est séparée, séchée et évaporée. Le solide blanc obtenu est recristallisé dans le chloroforme et conduit à **12** avec un rendement de 67%; F = 300°C; spectre de masse (pic moléculaire): m/e = 522. *Anal.* calc. pour $C_{15}H_{15}Br_3N_6$: C 34,71, H 2,91, N 16,19; trouvée: C 35,50, H 3,11, N 16,23; rmn, voir tableau 1.

*Hexaméthyl-2,3,7,8,12,13 dihydro-9,14 (4*H*)tripyrazolo-(1,5-*a*:1',5'-*d*:1",5"-*g*)triazonine-1,4,7 2*

Ce composé a été préparé selon les indications de la littérature (2). Le produit que nous avons isolé après recristallisation et sublimation possède les même caractéristiques que celles décrites dans la référence 2: Rendement 3% (litt. (2): 6%); F = 320°C (litt. (2): 325°C). *Anal.* calc. pour $C_{18}H_{24}N_6$: C 66,64, H 7,46, N 25,90; trouvée: C 66,59, H 7,38, N 25,58; rmn, voir tableau 1. La seule différence avec la littérature (2) est le pic moléculaire du spectre de masse à m/e = 324.

1. B. LUPO, A. RAMDANI et G. TARRAGO. J. Heterocycl. Chem. **21**, 545 (1984).
2. H. REIMLINGER, A. NOELS et J. JADOT. Chem. Ber. **103**, 1949 (1970).
3. J. ELGUERO et R. JACQUIER. J. Chim. Phys. 1242 (1966).
4. F. A. L. ANET et M. GHIACI. J. Am. Chem. Soc. **102**, 2528 (1980) et références citées.
5. B. MILLER et B. D. GESNER. Tetrahedron Lett. 3351 (1965).
6. J. F. MANVILLE et G. E. TROUGHTON. J. Org. Chem. **38**, 4278 (1973) et références citées.
7. W. D. RAVERTY, R. H. THOMSON et T. J. KING. J. Chem. Soc. Perkin Trans. 1, 1204 (1977).
8. W. R. ROTH. Ann. Chem. **671**, 10 (1964).
9. G. BUEMI, F. ZUCCARELLO et D. GRASSO. J. Mol. Struct. **42**, 195 (1977).
10. M. L. MARTIN, J.-J. DELPUECH et G. J. MARTIN. Practical NMR spectroscopy. Heyden and Son Ltd. 1980.
11. J. FIFANI, A. RAMDANI et G. TARRAGO. Nouv. J. Chim. **1**, 521 (1977).

A simple reason for non-linear mixture rules in chemical kinetics. Part 1. Vibrational relaxation of diatomic molecules

CHRIS CARRUTHERS AND HESHEL TEITELBAUM
Ottawa–Carleton Institute for Research and Graduate Studies in Chemistry, University of Ottawa Campus, Ottawa, Ont., Canada K1N 9B4

Received January 4, 1984[1]

CHRIS CARRUTHERS and HESHEL TEITELBAUM. Can. J. Chem. **63**, 381 (1985).

The generalized rate law for the vibrational relaxation of diatomic molecules is extended to include inert collision partners. V–V energy transfer processes are accounted for explicitly as are thermal effects. The molecules are treated as Morse oscillators as far as energetics are concerned; however, the microscopic rate constants are Landau–Teller type. It is found that the phenomenon of non-linear mixture rules arises when experimental data are forced to fit a first-order rate law. The persistence of V–V processes at times well-advanced into the relaxation zone is responsible for deviations from linearity. The non-linearities are most pronounced at high temperatures, and can be avoided only by using extremely dilute mixtures. Several sources of ambiguity are pointed out. The type of excitation method influences the initial deviation from a Boltzmann distribution and plays a crucial role in determining the importance of V–V processes and hence the degree of non-linearity. Thus, when the initial distribution is Boltzmann as in shock waves, the mixture rule is found to be absolutely linear for the vibrational relaxation of diatomic molecules.

Several examples, heretofore not recognized as such, are pointed out in the literature.

CHRIS CARRUTHERS et HESHEL TEITELBAUM. Can. J. Chem. **63**, 381 (1985).

Dans le but d'inclure des partenaires inertes impliqués dans des collisions, on a étendu la loi généralisée de vitesse des relaxations vibrationnelles des molécules diatomiques. On peut interpréter explicitement tant les effets thermiques que les processus de transferts d'énergie V–V. En autant que les énergies sont concernées, on traite les molécules comme des oscillateurs de Morse; toutefois, les constantes microscopiques de vitesse sont du type Landau–Teller. Lorsqu'on force les données expérimentales à obéir à une loi de vitesse du premier ordre, on observe que le phénomène des règles de mélanges non-linéaires se développe. C'est la persistance des processus V–V, à des temps bien avancés dans la zone de relaxation, qui provoque des déviations de la linéarité. Les non-linéarités sont plus prononcées à hautes températures et on peut les éviter uniquement en utilisant des mélanges extrèmement dilués. On identifie plusieurs sources d'ambiguité. La méthode d'excitation influence la déviation initiale, par rapport à la distribution de Boltzmann, et elle joue un rôle crucial dans la détermination de l'importance des processus V–V et, par conséquent, dans le degré de non-linéarité. Donc, lorsque la distribution initiale est du type Boltzmann, comme dans les ondes de choc, on trouve que la règle des mélanges est absolument linéaire pour la relaxation vibrationnelle des molécules diatomiques.

On a relevé, dans la littérature, plusieurs exemples qui n'avaient pas été reconnus comme tels.

[Traduit par le journal]

A. Introduction

In the last 10 years interest has been aroused among theoreticians concerning the validity of the linear mixture rule for parallel rate processes (1–9). This rule states that if k_1 is the rate coefficient for $A + M_1 \rightarrow B + M_1$ and if k_2 is the rate coefficient for $A + M_2 \rightarrow B + M_2$ where M_1 and M_2 are species not undergoing any chemical change, then the overall rate coefficient, k, for the effective process $A \rightarrow B$ is $k = k_1x_1 + k_2x_2$ where x_1 and x_2 are the mole fractions of species M_1 and M_2, respectively. The above processes may represent vibrational relaxation or diatomic dissociation or unimolecular decomposition/isomerization at the low pressure limit. Even though this study concerns vibrational relaxation, we introduce the mixture rule in terms of familiar chemical kinetics concepts. It has been pointed out (1) that the linear mixture rule does not hold strictly except under very limited conditions. Neglecting complications due to fall-off behaviour, we can distinguish between two effects:

(*a*) *Mixed order kinetics*. The linear mixture rule will hold only if the products of, e.g., dissociation do not recombine, thus avoiding processes which are describable in terms of second-order kinetics. Furthermore, the linear mixture rule will hold only if A is infinitely diluted in a mixture with truly inert collision partners. Otherwise, A must be explicitly included as one of the collision partners. The rate law becomes $d[A]/dt = -k_1[M_1][A] - k_2[M_2][A] - k_A[A]^2$, and then it is clear that non-linearities are inherently built into the kinetics. It is impossible to define a quasi-first order effective rate coefficient. If the attempt is made, then a non-linear mixture rule is a necessary consequence. Unfortunately, the practice is widespread. This study points out the dangers involved.

(*b*) *Non-equilibrium kinetics*. Even when mixed-order kinetics is not in question, the linear mixture rule will hold only when the reaction is beyond the incubation period and only when local thermodynamic equilibrium can be said to exist (9). Clearly, if the above two processes are not elementary ones, but rather involve microscopic detail such as molecular energy transfer processes among vibrational levels which are not infinitely fast, then non-equilibrium kinetics prevail, and much depends on the relative ability of M_1 and M_2 to restore local equilibrium. The question here is whether the overall rate is a linear combination or a holistic combination of the two partial rates.

There are relatively uninteresting occasions when the rates are linearly additive: (*a*) there is only one quantum level in A, i.e., there is an undissociated A, and a product state B; (*b*) there are many levels in A, but the microscopic rate constants describing the energy transfer processes by M_1 and M_2 are all related by a constant factor (3). It is clear that in real systems neither of these criteria can be met absolutely. In general, then, the partial rates add non-linearly. When this happens, two significantly different mechanisms compete, one faster than the other, or one collider more efficient than the other (9). Each

[1] Revision received July 18, 1984.

competing route passes via several intermediates (e.g. vib/rot states), which may or may not be common to both of the routes. When one collision partner chooses one route and the other partner a second route we term this a non-cooperative pair. For example, during steady dissociation the closer a vibrational state is to the dissociation limit, the greater the deviation from Boltzmann population. The weaker the collider, the greater is the inability to restore thermal equilibrium. The extent of non-equilibrium depletion of the states below the dissociation limit depends non-linearly on the mixture composition, particularly if competing colliders are of different strengths. Therefore the rate of reaction (and hence the effective rate coefficient) depends non-linearly on the mixture composition (4). Thus, for non-cooperative routes the nonlinearity arises totally from the failure to additively account for the inability of each partner to restore thermal equilibrium. However, if the two routes communicate, i.e., if intermediates in each route are connected by yet a third process, then the slower of the two routes can be partially shunted. The very presence of an efficient route thus creates intermediates which obviate the need to move along part of the slow route, and thus helps to work around a potential bottleneck. We term this a synergistic system. An example of such a communicative process would be V–V energy transfer connecting two competing T–V routes.

A theoretical treatment by Troe (4) has given quantitative substance to the deviation from linearity of the mixture rule for polyatomic dissociation when the non-equilibrium criterion fails in a non-cooperative way. However, Troe concludes that the effect is barely within the experimentalist's detectability limits. Dove and Raynor (8) have also described non-cooperative effects for diatoms. In the latter study it was shown that non-equilibrium rotational distributions and vibrational distributions influence the additivity of vibrational relaxation and dissociation rates respectively. However, one could say that here cooperative effects are also involved (with V–RT processes acting as communicating routes). Both studies (refs. 4, 8) must be considered as involving A infinitely dilute in a mixture of inert M, since V–V processes are ignored. In this work we concentrate on mixtures containing finite amounts of A, without non-equilibrium phenomena, in which cooperative effects of A–A collisions can be demonstrated unambiguously.

Pritchard has shown that V–V (5) and/ or R–R (6) processes are responsible for non-linear rate laws in mixtures of finite composition. This was accomplished by direct numerical integration of the appropriate master equation. In the present work we demonstrate non-linear rate laws by analytical solution of the master equation for vibrational relaxation. In this way we may investigate the circumstances in which deviations might be observable, and we may suggest how to analyze experimental data in such cases.

Some experiments have come to light showing the non-linear effect markedly. Kiefer has pointed out (3) that H atoms and N atoms (10, 11) do not contribute linearly to the rate of their parent diatomic molecule's dissociation. This may not be too surprising since the atom–molecule interactions may give rise to distinctly different mechanisms than diatom–diatom or rare gas atom–diatom interactions. On the other hand, a systematic test of the mixture rule by Breshears *et al.* (12, 13) for the dissociation of H_2 and O_2 revealed no apparent non-linearities. The reason behind these apparent discrepancies is not known. However, we should note that the two effects (non-equilibrium distributions and mixed order kinetics) are not well separated in these cases. The situation is clearer for studies of vibrational relaxation where there is no complication due to dissociation depleting the vibrational level populations. A systematic test of the mixture rule for the vibrational relaxation of H_2 showed it to be linear (14) within experimental error. On the other hand, the NO/Ar system (15) showed very strong deviations from linearity at very high dilutions. Admittedly, Glänzer's graph is of log k vs. mole fraction. Nevertheless, even if Glänzer's graph is replotted on a linear scale, one would nevertheless be forced to conclude that a linear extrapolation of his data to zero mole fraction of NO leads to an overestimate of the argon contribution by orders of magnitude. Likewise, the only systematic test to date of the linear mixture rule for vibrational relaxation of a polyatomic molecule has shown strong deviations (16). All of these relaxation cases fall into the category of mixed-order kinetics in that the relaxing molecules may actively participate in their own relaxation. Hence they should all display non-linear mixture rules if one attempts to fit first order kinetics to the data. That they do not all do so may simply mean that measurements are not being made at sufficiently high dilutions nor at early enough times nor at high enough temperatures where the effect is most easily observed. This may also apply to the paucity of examples for dissociation (1). However, it is still not clear if the experimental technique itself plays a role. (Some techniques rely on measuring bulk vibrational energy profiles which are basically insensitive to second-order processes involving near-resonant V–V energy transfer steps.) It is also not clear whether there is a basic difference between diatomic molecules and polyatomic molecules due to the difference in vibrational state densities and in the number of vibrational degrees of freedom. For example, it is almost always thought (but not necessarily correctly, in general (17)) that the rate law for the vibrational relaxation of the vibrational energy, E, of a diatomic molecule obeys the rate law $dE/dt = -(E - E_\infty)/\tau$, where $1/\tau$ is an effective quasi-first-order rate constant obeying the linear mixture rule. On the other hand, if a polyatomic molecule is considered to consist of several independent normal oscillating modes, i, each obeying a similar rate law, then $dE/dt = -\Sigma_i(E_i - E_{i,\infty})/\tau_i$. Clearly there is no unique effective rate "constant". A phenomenological rate coefficient for such a system is time-dependent. However, the less dilute the mixture is, the greater the communication between parallel channels, i.e., the greater the influence of independence-destroying intermode-intermolecular V–V energy transfer processes. In the extreme limit of pure polyatomic gas it is conceivable that all τ_i could become identical — at which point a unique effective rate coefficient would exist. Thus, time- and mole-fraction-dependence become enmeshed.

In order to elucidate some of these points, we have carried out a study of the vibrational relaxation of diatomic molecules mixed with inert gases, which is valid for any conceivable type of excitation, and which solves the detailed master equation describing the vibrational level population changes as a function of time. Bimolecular V–V energy transfer steps are explicitly considered, and conditions for the validity of the linear mixture rule are examined. We follow on the model of our previous study which led to a non-exponential rate law for the rate of relaxation of vibrational energy of a pure diatomic gas (17). Here we generalize the model to include finite mixture compositions, and we study the effect of mole fraction on the phenomenological rate coefficient. We further show why some experiments show strictly linear mixture rules, while others must show non-linear mixture rules.

B. Relaxation model

For collisions of N_m diatomic molecules AB(m) in vibrational state m with other molecules in a mixture of AB and inert M molecules, the rate of change of the population, dN_m/dt, can be written in terms of T–V and V–V components

$$[1] \quad -\frac{dN_m}{dt} = -\left.\frac{dN_m}{dt}\right|_{T-V} - \left.\frac{dN_m}{dt}\right|_{V-V}$$

For T–V processes AB(m) may collide with any other AB in vibrational state $m = 0 \rightarrow m_*$, where m_* is the level just below the dissociation limit. AB(m) may also collide with the inert species M. The master equation describing the rate of change of the population of level m with time due to T–V processes is then given by

$$[2] \quad -\left.\frac{dN_m}{dt}\right|_{T-V} = (k^{AB}_{m,m+1}N_m + k^{AB}_{m,m-1}N_m - k^{AB}_{m+1,m}N_{m+1} - k^{AB}_{m-1,m}N_{m-1})\Sigma N_M + (k^{M}_{m,m+1}N_m + k^{M}_{m,m-1}N_m - k^{M}_{m+1,m}N_{m+1} - k^{M}_{m-1,m}N_{m-1})N_M$$

Here, $k^i_{m,n}$ is the rate constant for AB(m) $\rightarrow$ AB(n) upon collision with species i. In our previous study (17) we did not include collisions with the inert species M. The above rate equation assumes that (i) AB(m) can be excited or de-excited by one quantum, (ii) the various AB states are equally efficient at V–T de-excitation of AB(m) (but $k^{AB}_{i,j} \neq k^{M}_{i,j}$), and ($iii$) the rotational sublevels are equilibrated on a very short time scale, so that the rotational substructure need not be included explicitly.

We furthermore assume that the T–V rate constants can be scaled according to symmetrized Landau–Teller rules:

$$k^i_{m+1,m} = k^i_{1,0}(m+1)\, e^{-m\phi}$$

$$k^i_{m,m+1} = k^i_{0,1}(m+1)\, e^{m\phi}$$

where $\phi = h\nu_c\chi_c/kT$, and ν_c and χ_c are the Morse spectroscopic constants. These rate constants obey microscopic reversibility, and ensure the proper relative equilibrium populations. In [2] we gather coefficients of N_m, N_{m+1}, and N_{m-1}. We note that because the rate constants for different collision partners, i, depend in the same way on m, then [2] can be written in terms of $(k^{AB}_{0,1}N_{AB} + k^{M}_{0,1}N_M)$ and $(k^{AB}_{1,0}N_{AB} + k^{M}_{1,0}N_M)$. Since $k^i_{0,1}/k^i_{1,0}$ is just the Boltzmann factor, $\exp[-h\nu_c(1-2\chi_c)/kT]$, and is independent of the collision partner, i, then the concentration dependence in [2] can be written entirely in terms of the factor $(k^{AB}_{1,0}N_{AB} + k^{M}_{1,0}N_M)$. We follow the same procedure as in our previous study (17) and obtain an expression for the contribution of T–V processes to the rate of change of vibrational energy. Wherever $Nk_{1,0}$ appeared in that study involving pure AB it is now replaced by $(N_{AB}k^{AB}_{1,0} + N_M k^{M}_{1,0})$. We obtain, for Morse oscillators,

$$[3] \quad \left.\frac{dE}{dt}\right|_{T-V} = -(E - E_\infty)\,(N_{AB}k^{AB}_{1,0} + N_M k^{M}_{1,0}) \times [1 - \exp\{-h\nu_c(1-3\chi_c)/kT\}]$$

The effective rate constant, k, clearly is a simple linear combination of contributions by AB and M. This result is in perfect agreement with previous findings (9) that linear mixture rules are expected in quasi-first-order kinetic systems whenever the microscopic rate constants for different collision partners are all related by the same constant factor. In this case it is a consequence of the Landau–Teller rules. However, it is by no means guaranteed that even with these unique properties, the inclusion of V–V processes will not modify this conclusion for mixtures of finite mole fraction.

When V–V processes are included, it is only AB–AB collisions that affect $dN_m/dt|_{V-V}$. In our previous study we included all processes AB(m) + AB(n) $\rightleftarrows$ AB($m+1$) + AB($n-1$), and we scaled the individual rate constants according to Landau–Teller-like rules. The contribution of V–V processes to the rate of change of vibrational energy was found to be given by (17)

$$[4] \quad \left.\frac{dE}{dt}\right|_{V-V} = -N^2 k^{2,0}_{1,1}\chi'_c\,[2\bar{E}^2/h\nu' + \bar{E} - \overline{E^2}/h\nu']$$

where $k^{2,0}_{1,1}$ is the rate coefficient for the process

$$2AB(v=1) \rightarrow AB(v=2) + AB(v=0)$$

$\chi'_c = \chi_c/(1-\chi_c)$, $\nu' = \nu_c(1-\chi_c)$, $\bar{E}/h\nu' \equiv \Sigma m N_m/N$, and $\overline{E^2}/(h\nu')^2 \equiv \Sigma m^2 N_m/N$. In the present generalization we must explicitly recognize that only the AB–AB collisions can contribute to V–V processes. Thus N is identified here as N_{AB}. Our final rate law (consisting of two equations, one for $\bar{E}$ and one for $\overline{E^2}$) becomes, on a per molecule basis:

$$[5] \quad \frac{d\bar{E}}{dt} = -\frac{(\bar{E} - \bar{E}_\infty)}{\tau} - N_{AB}k^{2,0}_{1,1}\chi'_c\,[2\bar{E}^2/h\nu' + \bar{E} - \overline{E^2}/h\nu']$$

$$[6] \quad \frac{d\overline{E^2}}{dt} = (N_{AB}k^{AB}_{1,0} + N_M k^{M}_{1,0})\,[e^{\phi-\theta'/T} + (1 + 3e^{\phi-\theta'/T})\bar{E}/h\nu' - 2(1 - e^{\phi-\theta'/T})\overline{E^2}/(h\nu')^2](h\nu')^2 + N_{AB}k^{2,0}_{1,1}[2\bar{E}^2/h\nu' + \bar{E} - \overline{E^2}/h\nu']h\nu'$$

where $\theta' = h\nu'/k$ and $1/\tau = (N_{AB}k^{AB}_{1,0} + N_M k^{M}_{1,0})\,[1 - e^{2\phi-\theta'/T}]$. Therefore, with the following proviso, it would seem that all operations in our previous study (17) can be repeated simply by replacing $Nk_{1,0}$ by $(N_{AB}k^{AB}_{1,0} + N_M k^{M}_{1,0})$ and $Nk^{2,0}_{1,1}$ by $N_{AB}k^{2,0}_{1,1}$. The complication arises from thermal effects: as the vibrational energy changes, the translational–rotational energy changes correspondingly. $\bar{E}_\infty$, which depends on temperature, therefore changes during the relaxation, and $\bar{E}$ appears to approach equilibrium more quickly (18). In order to account for temperature variations we need to relate the vibrational energy to temperature or to translational energy. In other words, we need an expression for the conservation of energy, and then convert our differential equation into one involving temperature. From a practical point of view this is desirable anyway, since in many experiments it is not $\bar{E}$ but rather refractive index gradients which are measured. We consider the energy balance between the translational–rotational and the vibrational degrees of freedom. Shock tube experiments can be considered to be at constant pressure and enthalpy. This is an approximation, and indeed one analyzes data more carefully on a routine basis (12, 13). However, for a first-order determination of the influence of thermal effects on the non-linearity of the mixture rule, the approximation is good. The gas enthalpy

$$\bar{H} = \int_0^{T_e} \bar{C}\,dT$$

is a constant, where T_e is the true final (equilibrium) temperature, and $\bar{C}$ is the molar constant-pressure heat capacity = $\Sigma_i X_i \bar{C}_i$. $\bar{C}_i$ is the molar heat capacity of species i present with mole fraction X_i. This procedure is also valid for laser- or chemically-activated systems if heat loss to the walls of the cell is not significant. Then $\bar{C}$ would be a constant-pressure heat capacity only at relatively high pressures, but a constant-volume heat capacity at low pressures where the excitation energy diffuses over the whole cell. The relaxing molecules, AB, can release or take up heat from an inert buffer gas, depending on the type of experiment. In our previous study we did not include thermal effects because we considered them not to be a major effect, as far as determining the role of V–V processes was concerned. However, here we must consider thermal effects because they depend on mole fraction of the buffering gas.

C. Conservation of energy

The gas enthalpy is composed of translational and rotational contributions denoted by $\int(\bar{C} - \bar{C}_{\text{vib}})\mathrm{d}T$ plus a vibrational term $\bar{E}$ associated only with the diatomic molecule. In our relaxation model we do not exclude polyatomic colliders, M. However, for the sake of simplicity we give a detailed analysis here only for the case M = atom. Thus $\bar{C}_{\text{M}} = 5k/2$ (on a per molecule basis). Then, at constant pressure

$$[7] \quad \bar{C} - \bar{C}_{\text{vib}} = k(X_{\text{AB}} + 5/2)$$

where X_{AB} is the mole fraction of AB in the mixture $\equiv N_{\text{AB}}/(N_{\text{AB}} + N_{\text{M}})$. The conservation equation becomes

$$\bar{H} = \int(\bar{C} - \bar{C}_{\text{vib}})\mathrm{d}T + X_{\text{AB}}\bar{E} = \text{constant} = \int_0^{T_c} \bar{C}\mathrm{d}T$$

In differential form this becomes

$$[8] \quad X_{\text{AB}}\mathrm{d}\bar{E}/\mathrm{d}t = -(\bar{C} - \bar{C}_{\text{vib}})\mathrm{d}T/\mathrm{d}t$$

Phenomenological rate coefficient

Whenever the rate law is not that for pure first-order kinetics, it becomes important to specify the phenomenology, which is otherwise arbitrary. Here, as in ref. 17 the rate of relaxation is not purely exponential, and any arbitrarily defined rate coefficient will be time-dependent. The equivalence in eq. [8] suggests a definition which at least facilitates the comparison between shock tube and fluorescence experiments. One ought to get the same rate "constant" if ln $(\mathrm{d}E/\mathrm{d}T)$ or ln $(\mathrm{d}T/\mathrm{d}t)$ is plotted as a function of time. Thus we define τ'' as

$$[9] \quad -\frac{1}{\tau''} \equiv \frac{\mathrm{d}}{\mathrm{d}t} \ln(|\mathrm{d}\bar{E}/\mathrm{d}t|) \equiv \frac{\mathrm{d}}{\mathrm{d}t} \ln(|\mathrm{d}T/\mathrm{d}t|)$$

D. The generalized rate law for vibrational relaxation of diatomic molecules

Equations [5] and [6] can be combined by differentiating [5], eliminating $\mathrm{d}\overline{E^2}/\mathrm{d}t$, and obtaining an expression for $\overline{E^2}$ in terms of $\mathrm{d}\bar{E}/\mathrm{d}t$, $\mathrm{d}^2\bar{E}/\mathrm{d}t^2$, and $\bar{E}$. This result can then be resubstituted into [5] to obtain the final tractable rate law. Because of thermal effects the first stage in this procedure is not as straightforward as in ref. 17. We consider neither τ nor $k_{1,1}^{2,0}$ to depend strongly on temperature. However, the derivative of $\bar{E}_\infty$ becomes

$$\frac{\mathrm{d}\bar{E}_\infty}{\mathrm{d}t} = \frac{\mathrm{d}\bar{E}_\infty}{\mathrm{d}T}\frac{\mathrm{d}T}{\mathrm{d}t} = -\left(X_{\text{AB}}\frac{\mathrm{d}\bar{E}_\infty}{\mathrm{d}T}\right)\left(\frac{1}{\bar{C} - \bar{C}_{\text{vib}}}\right)\frac{\mathrm{d}\bar{E}}{\mathrm{d}t}$$

where we have used [8] explicitly. We further note that $X_{\text{AB}}\mathrm{d}\bar{E}_\infty/\mathrm{d}T$ is simply the contribution of the vibrational degree of freedom to $\bar{C}$. Thus, $\mathrm{d}\bar{E}_\infty/\mathrm{d}t = -[\bar{C}_{\text{vib}}/(\bar{C} - \bar{C}_{\text{vib}})]\mathrm{d}\bar{E}/\mathrm{d}t$.

Differentiation of [5] leads to

$$\frac{\mathrm{d}^2\bar{E}}{\mathrm{d}t^2} = -\frac{\mathrm{d}\bar{E}}{\mathrm{d}t}\left(\frac{1}{\tau_*} + N_{\text{AB}}k_{1,1}^{2,0}\chi_c'\right) - 4\chi_c'N_{\text{AB}}k_{1,1}^{2,0}\frac{\bar{E}}{h\nu'}\frac{\mathrm{d}\bar{E}}{\mathrm{d}t} + \frac{\chi_c'N_{\text{AB}}k_{1,1}^{2,0}}{h\nu'}\frac{\mathrm{d}\overline{E^2}}{\mathrm{d}t}$$

where

$$[10] \quad \frac{1}{\tau_*} = \frac{1}{\tau}\left(\frac{\bar{C}}{\bar{C} - \bar{C}_{\text{vib}}}\right)$$

Elimination of $\mathrm{d}\overline{E^2}/\mathrm{d}t$ leads to

$$\chi_c'N_{\text{AB}}k_{1,1}^{2,0}\frac{\overline{E^2}}{h\nu'}\left[N_{\text{AB}}k_{1,1}^{2,0} + \frac{2}{\tau}\right] = -\frac{\mathrm{d}\bar{E}}{\mathrm{d}t}\left[\frac{1}{\tau^*} + \chi_c'N_{\text{AB}}k_{1,1}^{2,0}\right] - 4\chi_c'N_{\text{AB}}k_{1,1}^{2,0}\frac{\bar{E}}{h\nu'}\frac{\mathrm{d}\bar{E}}{\mathrm{d}t} - \frac{\mathrm{d}^2\bar{E}}{\mathrm{d}t^2} + \chi_c'N_{\text{AB}}k_{1,1}^{2,0}h\nu' \times \left\{[N_{\text{AB}}k_{1,0}^{\text{AB}} + N_{\text{M}}k_{1,0}^{\text{M}}]\left[\mathrm{e}^{-u} + \frac{\bar{E}}{h\nu'}(1 + 3\mathrm{e}^{-u})\right] + N_{\text{AB}}k_{1,1}^{2,0}\frac{\bar{E}}{h\nu'}\left(1 + \frac{2\bar{E}}{h\nu'}\right)\right\}$$

where $u = h\nu_c(1 - 2\chi_c)/kT$. Substitution of this expression for $\overline{E^2}$ into [5] leads to

$$[11] \quad \frac{\mathrm{d}\bar{E}}{\mathrm{d}t}\left[\frac{N_{\text{AB}}k_{1,1}^{2,0}}{1 - \chi_c} + \frac{2}{\tau} + \frac{1}{\tau_*}\right] = -\frac{(\bar{E} - \bar{E}_\infty)}{\tau}\left[N_{\text{AB}}k_{1,1}^{2,0} + \frac{2}{\tau}\right] - \chi_c'N_{\text{AB}}k_{1,1}^{2,0}\left[\frac{(\bar{E} - \bar{E}_\infty)}{\tau}\left(1 + \frac{4\bar{E}}{h\nu'}\right) + \frac{4\bar{E}}{h\nu'}\frac{\mathrm{d}\bar{E}}{\mathrm{d}t}\right] - \frac{\mathrm{d}^2\bar{E}}{\mathrm{d}t^2}$$

This is the generalized rate law. It can be simplified by supposing a solution of the form

$$[12] \quad \frac{\mathrm{d}\bar{E}}{\mathrm{d}t} = -\frac{(\bar{E} - \bar{E}_\infty)}{\tau} + f(t)$$

Differentiating [12] and using $\mathrm{d}\bar{E}_\infty/\mathrm{d}t = -[\bar{C}_{\text{vib}}/(\bar{C} - \bar{C}_{\text{vib}})]\mathrm{d}\bar{E}/\mathrm{d}t$ we obtain

$$[13] \quad \frac{N_{\text{AB}}k_{1,1}^{2,0}}{1 - \chi_c} + \frac{2}{\tau} = -\chi_c'N_{\text{AB}}k_{1,1}^{2,0}\frac{4\bar{E}}{h\nu'} - \frac{\mathrm{d}\ln f}{\mathrm{d}t}$$

Just as in ref. 17 we are justified in neglecting the term $4\bar{E}\chi_c'/h\nu'$ compared with unity. Therefore

$$[14] \quad f(t) = f(0)\exp\left[-\left(\frac{N_{\text{AB}}k_{1,1}^{2,0}}{1 - \chi_c} + \frac{2}{\tau}\right)t\right]$$

Comparing eq. [12] with [5] we can easily deduce that

$$[15] \quad \left[\frac{2\bar{E}^2}{h\nu'} + \bar{E} - \frac{\overline{E^2}}{h\nu'}\right] = \left[\frac{2\bar{E}^2}{h\nu'} + \bar{E} - \frac{\overline{E^2}}{h\nu'}\right]_0 \exp\left[-\left(\frac{N_{\text{AB}}k_{1,1}^{2,0}}{1 - \chi_c} + \frac{2}{\tau}\right)t\right]$$

and

$$[16] \quad \frac{\mathrm{d}\bar{E}}{\mathrm{d}t} = -\frac{(\bar{E} - \bar{E}_\infty)}{\tau} - N_{\text{AB}}k_{1,1}^{2,0}\chi_c'\left[\frac{2\bar{E}^2}{h\nu'} + \bar{E} - \frac{\overline{E^2}}{h\nu'}\right]_0 \exp\left[-\left(\frac{N_{\text{AB}}k_{1,1}^{2,0}}{1 - \chi_c} + \frac{2}{\tau}\right)t\right]$$

There are some noteworthy features associated with this rate law:

(*a*) Thermal effects do not enter explicitly into [16], although they are implicitly contained in the time-variation of $\bar{E}_\infty$. (Of course, both τ and $k_{1,1}^{2,0}$ depend on temperature, the latter very weakly so. However, the temperature changes are usually only a few degrees K, and so we ignore this aspect.)

(*b*) The rate is not at all the same as supposed by experimentalists. Although $(\bar{E} - \bar{E}_\infty)$ relaxes nearly exponentially with a rate coefficient closely related to $1/\tau$ (see below), a second contribution relaxes somewhat faster. This term represents the effect of V–V processes. Whereas a relatively small amount of energy is associated with this term (the anharmonicity) compared with the main term, $N_{AB}k_{1,1}^{2,0}$ is usually $\gg 1/\tau$, and the amplitude of the V–V rate may be comparable to or even exceed the T–V rate, particularly since $[2\bar{E}^2/h\nu' + \bar{E} - \bar{E}^2/h\nu']_0$, the initial deviation from a Boltzmann distribution, can be arbitrarily large, depending on the type of excitation experiment. The V–V rate decays faster than the T–V rate; however, the large amplitude of the V–V term may contribute significantly to observed rates of relaxation.

(*c*) A unique relaxation time cannot be said to exist. It is only in the extreme limit of $N_{AB} \to 0$, or $k_{1,1}^{2,0} \to 0$ or $\chi_e \to 0$, or $[2\bar{E}^2/h\nu' + \bar{E} - \bar{E}^2/h\nu']_0 \to 0$ that the V–V term drops out and that a unique relaxation time results. In ref. 17 it was shown that $[2\bar{E}^2/h\nu' + \bar{E} - \bar{E}^2/h\nu']_0$ is zero when the initial population distribution is Boltzmann, such as in shock tube experiments. This predicts that the rate of vibrational relaxation of diatomic molecules measured in shock waves is exponential with a unique T–V relaxation time which obeys the linear mixture rule!

(*d*) In the limit that $N_{AB} \to 0$ the V–V term decays according to $e^{-2t/\tau}$. The factor of 2 seems reasonable, since if in the limit of $N_{AB} \to 0$, $\bar{E}$ decays according to $e^{-t/\tau}$, then functions of $\bar{E}^2$ ought to additionally decay according to $e^{-2t/\tau}$. Of course, the amplitude of the V–V term $\to 0$ in this limit. Alternatively, the $N_{AB}k_{1,1}^{2,0}$ term represents the V–V process $2AB(v = 1) \to AB(v = 0) + AB\ (v = 2)$. This can compete with the T–V process $AB(v = 1) \to AB(v = 0)$ only if the $v = 2$ state can also make its way back to $v = 0$. This is efficiently done by the T–V process $AB(v = 2) \to AB(v = 1)$ which is twice as fast as the $v = 1 \to 0$ step in our model (18) at the limit $N_{AB} \to 0$. Therefore $2/\tau$ must appear in conjunction with $N_{AB}k_{1,1}^{2,0}/(1 - \chi_e)$. This function has been known in the literature for many years. Rankin and Light (19), who used a V–V model very similar to ours, showed that the individual vibrational levels decay during early relaxation at more than twice the steady rate. Even the term $[\epsilon_0(1 + 2\epsilon_0) - \langle n^2\rangle_0]$ (essentially part of our pre-exponential term) appeared in their functions. Unfortunately, they neglected the molecular anharmonicity, and their energy rate law therefore reduced to the Bethe–Teller law.

E. Solution of the rate law

1. Shock tubes

As mentioned above, the rate law reduces simply to

$$[17]\quad \frac{d\bar{E}}{dt} = -\frac{(\bar{E} - \bar{E}_\infty)}{\tau}$$

In order to eliminate the time variation of $\bar{E}_\infty$, we differentiate eq. [17] and use $d\bar{E}_\infty/dt = [\bar{C}_{vib}/(\bar{C} - \bar{C}_{vib})]d\bar{E}/dt$ in order to obtain

$$[18]\quad \frac{d^2\bar{E}}{dt^2} = -\frac{1}{\tau_*}\frac{d\bar{E}}{dt}$$

We reintegrate in order to express the rate law in terms of final conditions. At $t \to \infty$; $d\bar{E}/dt \to 0$; $\bar{E}_\infty \to \bar{E}_{\infty,e}$, the true equilibrium energy. Therefore

$$[19]\quad \frac{d\bar{E}}{dt} = -\frac{1}{\tau_*}(\bar{E} - \bar{E}_{\infty,e})$$

The solution is a pure exponential, with time constant τ_*. The phenomenological time constant τ'' defined by [9] is simply $\tau'' = \tau_*$.

2. Laser excitation or chemical activation

At this point we should emphasize that, although this kind of experiment is amenable to monitoring individual vibrational level populations by narrow band fluorescence, in actual practice a broad-band fluorescence signal is measured which is proportional to $\Sigma nh\nu N_n$, i.e., to the total vibrational energy of an approximately harmonic oscillator mode (18). This is certainly the case for the experiments cited below.

In this general case we must integrate [16]. The same procedure is used as in the shock tube case to eliminate the time-dependence of $\bar{E}_\infty$. Setting

$$a = \left(\frac{N_{AB}k_{1,1}^{2,0}}{1 - \chi_e} + \frac{2}{\tau}\right)$$

and

$$b = h\nu_e\chi_e N_{AB}k_{1,1}^{2,0}\left[2\left(\frac{\bar{E}}{h\nu'}\right)^2 + \left(\frac{\bar{E}}{h\nu'}\right) - \frac{\bar{E}^2}{(h\nu')^2}\right]_0$$

and using eq. [9] we obtain

$$[20]\quad \bar{E} - \bar{E}_{\infty,e} = (\bar{E}_0 - \bar{E}_{\infty,e})\,e^{-t/\tau_*} + b(e^{-at} - e^{-t/\tau_*})/(a - 1/\tau_*)$$

and

$$[21]\quad \frac{\tau''}{\tau_*} = \frac{ab\tau_* e^{-at} + [(\bar{E}_0 - \bar{E}_{\infty,e})(a - 1/\tau_*) - b]e^{-t/\tau_*}}{a^2b\tau_*^2 e^{-at} + [(\bar{E}_0 - \bar{E}_{\infty,e})(a - 1/\tau_*) - b]e^{-t/\tau_*}}$$

In this study, we are interested in the dependence of τ'' on mole fraction, $X_{AB} \equiv N_{AB}/(N_{AB} + N_M)$. τ''/τ_* depends on five additional parameters:

$$\gamma \equiv k_{1,1}^{2,0}/(k_{1,0}^{AB} - k_{0,1}^{AB})$$

$$\phi_M \equiv (k_{1,0}^{M} - k_{0,1}^{M})/(k_{1,0}^{AB} - k_{0,1}^{AB})$$

$$\delta \equiv (\bar{E}_0 - \bar{E}_{\infty,e})/\{h\nu_e\chi_e[2(\bar{E}/h\nu')^2 + (\bar{E}/h\nu') - \bar{E}^2/(h\nu')^2]_0\}$$

$\lambda \equiv \bar{C}_{AB}/k$ and χ_e

One may look upon Figs. 1 and 2 as correction factors to be applied to measured relaxation times. Depending on the regime of t/τ_* studied, one measures τ'' which is far removed from the desired T–V τ_*. However, in order to apply these correction factors, one must know γ (the relative importance of V–V and T–V rate constants), ϕ_M (the relative T–V efficiencies of M and AB), δ (the deviation from equilibrium relative to the initial first and second moments of the vibrational energy) as well as λ and χ_e. It is not likely that γ and ϕ_M are known in advance of the measurements, and it is very difficult to measure δ. Therefore, it is unlikely that graphs such as Fig. 1 could ever be useful in this way. Furthermore, an experimentalist would not know unambiguously what his regime of t/τ_* is. If anything, he would measure τ'' and hence he would have an idea only of t/τ''. The dependence of the measured phenom-

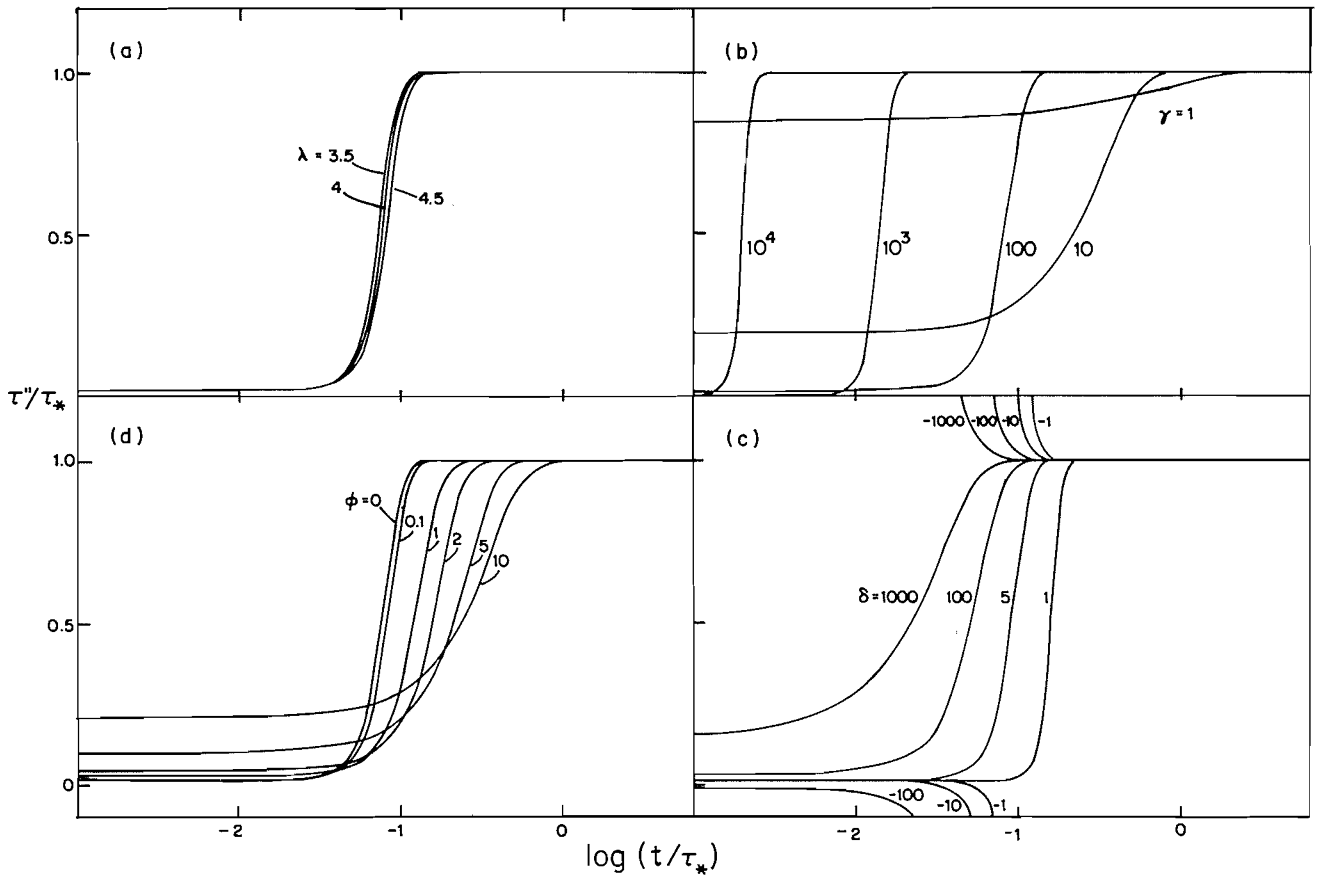

FIG. 1. Phenomenological relaxation times for the vibrational relaxation of diatomic molecules in gas mixtures as a function of reduced time, t/τ_*. (*a*) Effect of λ, i.e., of how nearly classical the oscillator is, for $X_{AB} = 0.5$, $\gamma = 100$, $\delta = 10$, $\chi_e = 0.01$, $\phi_M = 0.1$. For $\lambda = 4.5$, the vibration is classical; (*b*) effect of γ, i.e., of the relative importance of V–V and T–V rate coefficients, for $X_{AB} = 0.5$, $\delta = 10$, $\chi_e = 0.01$, $\phi_M = 0.1$, $\lambda = 4.5$; (*c*) effect of δ, i.e., of the deviation from equilibrium relative to that from a Boltzmann distribution. Here $X_{AB} = 0.5$, $\gamma = 100$, $\chi_e = 0.01$, $\phi_M = 0.1$, $\lambda = 4.5$. The discontinuities correspond to overshoots in energy; (*d*) effect of ϕ_M, i.e., of the relative efficiency of M and AB at equilibrating AB via T–V processes. Here $X_{AB} = 0.5$, $\gamma = 100$, $\delta = 10$, $\chi_e = 0.01$, $\lambda = 4.5$.

enological relaxation time on t/τ'' is even more complicated, as seen in Fig. 2*b*. In view of these difficulties it is advisable that workers report their measured values of $p\tau$ not only at given temperatures but also the measured time intervals of t/τ''. In this way, comparison between the results of different experimental techniques is facilitated.

In Fig. 1*b*, we note that the larger the γ, the earlier the V–V effects are over. However, it is also easy to calculate from [20] the percentage of energy change relaxed at a given time. We find that despite the rapidity of V–V processes, they are nevertheless important in some cases for late time measurements. For example, by the time $\tau'' = 0.95\tau_*$, 20% of the energy has already relaxed if $\gamma = 100$, $\delta = 10$, $\chi_e = 0.01$, $\lambda = 4.5$, $\phi_M = 0,1$, and $X_{AB} = 0.5$. (This might correspond to exciting Na_2 or Li_2 in the range $v = 2–6$ at some suitable temperature.)

When $\delta < 0$ the vibrational energy temporarily surpasses its equilibrium value. As shown in ref. 20 this manifests itself as an apparently negative τ until the maximum energy is reached. Beyond this point in time, the relaxation rate speeds up and approaches that controlled by the V–T processes. In terms of Treanor pumping, it is during this induction period that molecules pile up in high vibrational states. Thereafter, they relax at a relatively slow rate. The experimental conditions required for δ to be < 0 are difficult to obtain in studies designed to measure rate constants; and we therefore ignore this case here. Indeed, ref. 20 shows that for most, if not all laser- or chemically-activated molecules δ lies in the range 10–1000. For $\delta = 1000$, $\gamma = 100$, 6% of the energy change has relaxed by the time $\tau'' = 0.95\tau_*$; even for $\gamma = 10^4$, $\delta = 10$, as much as 10% change has occurred already. It seems that V–V processes make themselves felt on time scales that are up to 20 times greater than what one would have expected from the value of γ, i.e. the relative V–V/T–V rate constants, depending on the size of the perturbation, δ.

For collision partners which are as efficient as AB itself is at T–V excitation ($\phi_M = 1$), 25% of the energy has relaxed by the time $\tau'' = 0.95\tau_*$. The less efficient M is, the more important is V–V relative to T–V, and thus the earlier in time is the V–V effect over.

λ depends on how classical the oscillating molecule is (i.e. on the value of $h\nu/kT$). For a classical diatomic oscillator $\lambda = 9/2$; for the extreme case of a quantum oscillator $\lambda = 7/2$. Nevertheless, the nearness to classical oscillation plays little role in the transient behaviour.

Because the mole fraction, X_{AB}, affects not only the duration of V–V processes but also their amplitude, the dependence of this effect on X_{AB} is somewhat complicated: for $X_{AB} = 1$, $X_{AB} = 0.5$, $X_{AB} = 0.2$, $X_{AB} = 0.1$, $X_{AB} = 0.01$, $X_{AB} = 0.001$, the percentage of the vibrational energy relaxed by the time $\tau'' = 0.95\tau_*$ is 25%, 20%, 21%, 24%, 48%, and 56%, respectively. The mole fraction of AB must be as low as 10^{-4} before less than 5% of the energy has relaxed during the transient period when

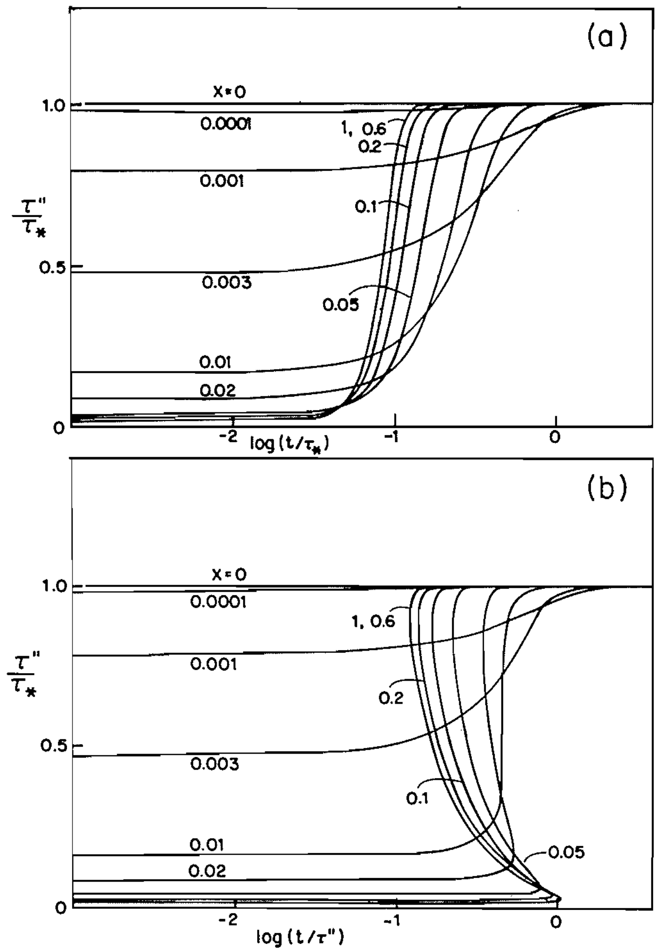

FIG. 2. Phenomenological relaxation times for the vibrational relaxation of diatomic molecules in gas mixtures as a function of reduced time and mole fraction. Here $\gamma = 100$, $\delta = 10$, $\lambda = 4.5$, $\chi_e = 0.01$, and $\phi_M = 0.1$. (*a*) t is normalized by dividing by the effective T–V time constant, τ_*; (*b*) t is normalized by dividing by the experimentally observed time constant, τ''.

$\gamma = 100$, $\delta = 10$. The mole fraction at which V–V effects are most felt is closely related to that at which the mixture rule deviates the most from linearity (see below). Therefore, despite the low mole fractions (10^{-3}) and the anharmonicity (10^{-2}), modest V–V processes ($\gamma = 100$) can have marked effects on measured rate coefficients! Great care is needed in interpreting vibrational relaxation data when $t < \tau_*$.

F. Mixture rules

The aim of this study was to see the effect of mole fraction on measured rate constants for relaxation, i.e., on $1/N\tau''$, or $1/p\tau''$. Using [21], [10], and the definition for τ, we obtain

$$\frac{1}{N\tau''} = \left(\frac{\bar{C}}{\bar{C} - \bar{C}_{\text{vib}}}\right) [X_{AB}(k_{1,0}^{AB} - k_{0,1}^{AB}) + X_M(k_{1,0}^{M} - k_{0,1}^{M})] \left(\frac{\tau_*}{\tau''}\right)$$

We note that the mole-fraction dependence is due to three factors: (*a*) thermal effects; (*b*) a linear dependence on relative efficiency of M; and (*c*) a non-linear factor due to the influence of V–V processes. We do not wish to confuse the issue by including thermal effects as a source of non-linearity, because experimentalists tend to account for them before attempting mixture rule plots. Therefore in Figs. 3 and 4 we include only the second and third factors, and plot the function

$$g = \left(\frac{1}{N\tau''}\right)\left(\frac{1}{k_{1,0}^{AB} - k_{0,1}^{AB}}\right)\left(\frac{\bar{C} - \bar{C}_{\text{vib}}}{\bar{C}}\right)$$

as a function of X_{AB}:

$$[22] \quad g = [X_{AB} + (1 - X_{AB})\phi_M] \times \left\{\frac{a^2 b\tau_*^2 e^{-at} + [(\bar{E}_0 - \bar{E}_{\infty,c})(a - 1/\tau_*) - b]e^{-t/\tau_*}}{ab\tau_* e^{-at} + [(\bar{E}_0 - \bar{E}_{\infty,c})(a - 1/\tau_*) - b]e^{-t/\tau_*}}\right\}$$

Not only does g depend on X_{AB}, but it also depends on time! It is here that we encounter at once both the crux of the matter and the experimentalists' dilemma. There is no unique choice for t/τ_*. Thus there is no unique mixture rule plot! Three reasonable choices are reflected in Figs. 3*a*, *b*, and *c*: (*a*) constant t/τ_*; (*b*) constant t/τ'', which is more readily estimable than t/τ_*; (*c*) constant absolute time, i.e. constant $Nt(k_{1,0}^{M} - k_{0,1}^{M})$, which is the most likely experimental situation (one is likely to measure at the earliest possible time permitted by electronic response regardless of X_{AB}). Of course, if Nt is fixed then t/τ_*, chosen in this way, also depends on X_{AB}: e.g., if we choose $t/\tau_* = n$ when $X_{AB} = 0$, then $Nt(k_{1,0}^{M} - k_{0,1}^{M}) = n$; and for fixed Nt,

$$\frac{t}{\tau_*} = \frac{n}{\phi_M}\{X_{AB} + (1 - X_{AB})\phi_M\}\left(\frac{\bar{C}}{\bar{C} - \bar{C}_{\text{vib}}}\right)$$

In Fig. 3 we have chosen typical parameters $\gamma = 100$, $\delta = 10$, $\chi_e = 0.01$, and $\phi_M = 0.1$. Since g has been normalized to give ϕ_M when $X_{AB} = 0$, i.e., the relative T–V efficiency of M:AB, then a linear mixture rule corresponds to a straight line connecting $g = 1$ (at $X_{AB} = 1$) with $g = 0.1$ (at $X_{AB} = 0$). It is only at or close to equilibrium that a linear mixture rule will be observed. At long times the relatively rapid V–V rate decays leaving only the T–V rates which do obey the linear mixture rule, as can be seen from [3]. At other times non-linearities are very evident. The danger lies in an experimenter's not measuring over the entire concentration range. Over any short range of mole fractions such plots will always appear to be linear — certainly within experimental error. The common procedure of extrapolating to $X_{AB} = 0$ and $X_{AB} = 1$ in order to extract the T–V rate constants for M and AB respectively is apparently wrong, except when measuring at equilibrium. We see that (*1*) linear extrapolations originating from a limited range of X_{AB} can give very large underestimates or overestimates of $k_{1,0}^{AB}$ and $k_{1,0}^{M}$. (*2*) It is only when measurements are made at $X_{AB} \lesssim 1/\gamma$ that linear extrapolations to $X_{AB} = 0$ can give a good estimate of $k_{1,0}^{M}$. In many cases, though, the large value γ (typically as large as 10^6) may make it impossible to properly estimate k_{10}^{M}. On the other hand, for those cases where curvature of the type in Fig. 3*a* can be observed experimentally, one has a good handle on the magnitude of γ. (*3*) When measurements are made in mixtures which are rich in relaxer, the mixture rule plots may be deceptively linear. However, linear extrapolation to $X_{AB} = 1$ will give effective rate constants which depend strongly on time. At earlier and earlier times the rate constants reflect more and more V–V character; but it is wrong to assume that in general they are V–V coefficients. Even at $t = 0$ they are at best a sum of V–V and T–V constants, $k_{1,1}^{2,0}/(1 - \chi_e) + 2(k_{1,0}^{AB} - k_{0,1}^{AB})$. At $t = \infty$, they are the T–V constants, $(k_{1,0}^{AB} - k_{0,1}^{AB})$. (*4*) The curvatures are markedly variable and depend on how the experimenter perceives his

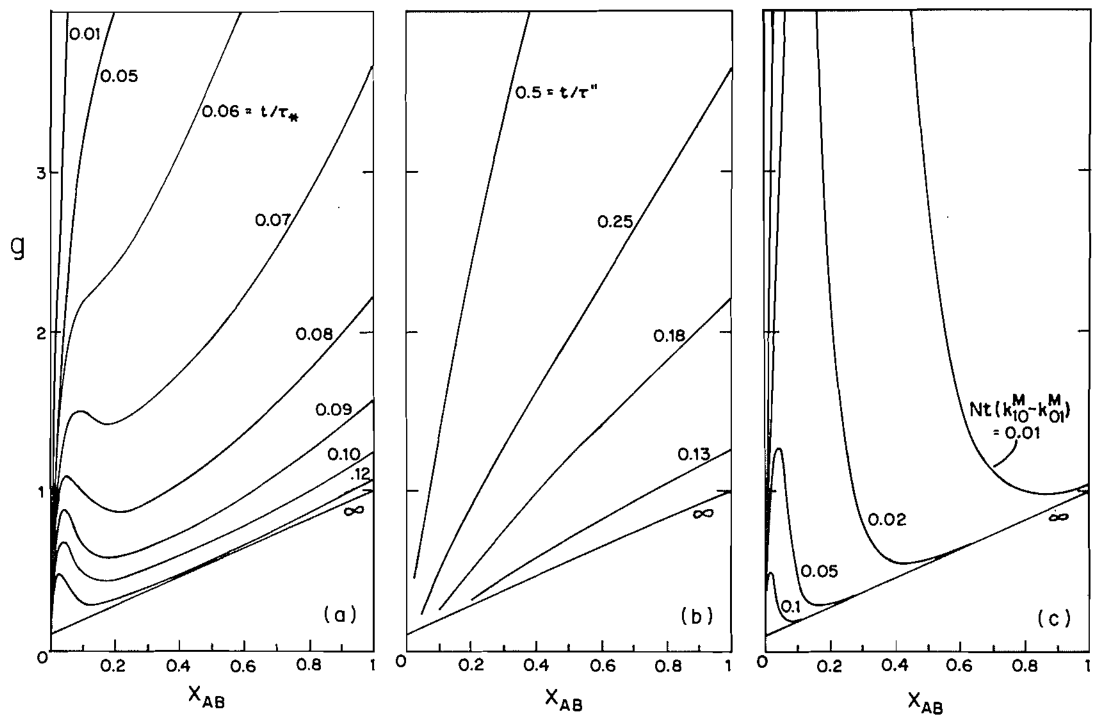

FIG. 3. Effective second order rate constant, g, as a function of mole fraction of the diatomic molecule, AB, undergoing vibrational relaxation. Typical conditions used here are $\gamma = 100$, $\delta = 10$, $\chi_c = 0.01$, $\lambda = 4.5$, and $\phi_M = 0.1$. The non-linearities are shown for three different choices of progress variable: (*a*) time reduced by the effective T–V time-constant; (*b*) time reduced by an effective relaxation time, as perceived by the experimenter; and (*c*) absolute time, or, time reduced by a mole-fraction-independent time-constant.

time scale. In Fig. 3*a* the rate coefficients are measured consistently at a fixed t/τ_*. Deviations from linearity are always present and are always positive. They must be positive when $\delta > 0$ because then V–V processes increase the rate of relaxation over that by T–V processes by introducing alternative mechanistic routes. Deviations are of two types: (*a*) monotonically varying; and (*b*) exhibiting a maximum. At early times only V–V processes are important, and they thus become monotonically more important as X_{AB} increases. The maximum manifests itself at later times even close to equilibrium. It exists because (as can be seen in Fig. 2 and in [16]) the smaller the mole fraction of AB, the smaller the amplitude of the V–V effect but the *longer* it takes relatively for the V–V effect to decay. These two properties compete, producing a maximum. We estimate the X_{AB} for maximum deviation from linearity, below. The X_{AB} at the maximum correlates well with the mole fraction at which the % energy change has relaxed the most by a fixed time via V–V processes. One should also note that an experimenter measuring in the region just beyond the maximum may get the erroneous impression that (since g decreases wih increasing X_{AB} here) AB appears to be *less* efficient than M is as a T–V collider even when it really is not ($\phi_M = 0.1$ here).

As mentioned earlier, if non-linearities are observed then it is because τ'' is not a unique quasi-first order time constant. Measurements are apparently being made in transient zones. Thus, the experimenter does not know the value of t/τ_*, merely that of t/τ''. Using that time scale the experimenter will obtain plots like those in Fig. 3*b* which are mildly curved, but still time-dependent. Note that there are actually three values of g possible for a given t/τ'' (see Fig. 2*b*). The fixed values of t/τ'' ($=[t/\tau_*][\tau_*/\tau'']$) chosen for Fig. 3*b* correspond to the transient zone where t/τ'' actually decreases while t/τ_* increases. Since the range of t/τ'' is restricted, then the range of X_{AB} is also restricted to that which results in transient zones falling within that time-scale window. (At times beyond this transient zone, when $\tau'' \approx \tau_*$, curves such as those in Fig. 3*a* are obtained.) The mildness of the curvature in Fig. 3*b* represents a very subtle danger to the experimenter, since he is then less likely to be aware of ambiguities.

In Fig. 3*c* the time scale has been divided by the characteristic time constant for T–V collisions of M, i.e., by $N(k^M_{10} - k^M_{01})$, which is independent of X_{AB}. This is essentially the same as choosing a fixed absolute time. At different mole fractions this fixed time corresponds to different t/τ_*. For example, measurements at $t = 1$ μs in mixtures with low mole fractions of AB may correspond to relatively early portions of the relaxation zone and hence have significant V–V character. On the other hand, in mixtures having large mole fractions, X_{AB}, which relax relatively faster, 1 μs may correspond to a relaxation very close to equilibrium where the T–V mechanism prevails. This choice of time scale is probably common in the literature, and could provide the most dramatic non-linear mixture effects.

Figure 4 shows the effect of the parameters δ, γ, λ, and ϕ_M on the mixture plots, for a fixed $t/\tau_* = 0.1$. The degree of closeness to classical oscillation, λ, affects only the residual thermal effects (the major thermal effect having been factored out earlier). However, these effects are weak. We also note from [16] and from Fig. 1*b* that the smaller the value of γ the smaller the amplitude of the V–V effects but the longer in time they last. This competition causes the deviation from linearity to be most pronounced at intermediate values of γ. In Fig. 4*c* when $\delta = 10$, the value of γ leading to worst deviation from linearity is for a modest $\gamma \sim 40$. Thus it is by no means certain that the larger the V–V rate constants are relative to the T–V rate constants the greater the non-linearity. In fact, it appears that the more important parameter for determining the degree

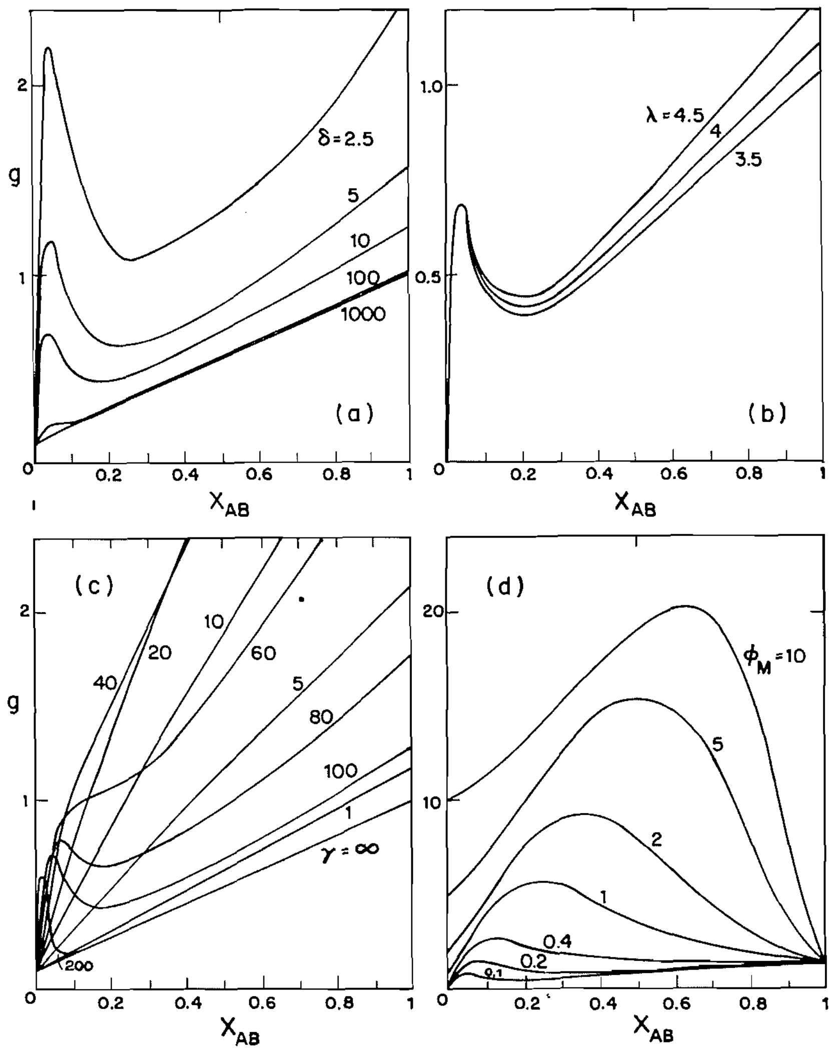

FIG. 4. Effective second order relaxation rate constant, g, as a function of mole fraction of the relaxing diatomic, AB, at $t/\tau_* = 0.1$. (a) Effect of δ, i.e., of the relative deviations from equilibrium and statistical distributions. Here $\gamma = 100$, $\chi_e = 0.01$, $\lambda = 4.5$, $\phi_M = 0.1$; (b) effect of λ, i.e., of how nearly classical the oscillator is. (At $\lambda = 4.5$ the oscillation is purely classical.) Here $\gamma = 100$, $\delta = 10$, $\chi_e = 0.01$, $\phi_M = 0.1$; (c) effect of γ, i.e., of the relative importance of V–V and T–V rate coefficients. Here $\delta = 10$, $\chi_e = 0.01$, $\lambda = 4.5$, $\phi_M = 0.1$; (d) effect of ϕ_M, i.e., of the relative efficiency of M and AB at T–V excitation. Here $\delta = 10$, $\gamma = 100$, $\chi_e = 0.01$, $\lambda = 4.5$.

of V–V character is δ. Figure 4a shows the sensitivity of non-linearity to δ. For $\delta = 1000$, the mixture rule is essentially linear. For $\delta = 10$, it is very non-linear. Reference 20 summarizes typical values of δ. For shock tube excitation (the initial population distribution is Boltzmann), $\delta = \infty$; the energy relaxes exponentially [19]; g is independent of time; $1/\tau'' = 1/\tau_*$, i.e. is a linear combination of T–V rate constants; and the mixture rule is always linear for this special kind of experiment. For laser-or-chemical excitation, $|\delta|$ is in the range 4–100, and we obtain non-linear mixture rules. In some of those cases, δ can also be negative (corresponding to energy overshoots or undershoots). We have not considered such cases in this study: an experimenter noting such overshoots would normally fit his data to a model including V–V and T–V processes.

It is also interesting to deduce the effect of temperature, T, on the non-linear mixture rule for a given experiment. As noted in ref. 20, δ does not seem to depend on temperature significantly. Therefore for fixed λ, δ, and ϕ_M we need only determine the temperature dependence of $\gamma = k_{1,1}^{2,0}/(k_{10}^{AB} - k_{01}^{AB})$. The V–V rate constant empirically is not significantly temperature dependent. If anything, it decreases with T. On the other hand, k_{10}^{AB} increases with T according to exp $(-cT^{-1/3})$ where c is a constant. Thus γ decreases with increasing T. We thus expect that for small $\delta < 100$ and $\gamma \gtrsim 40$, increasing the temperature decreases γ, and hence increases the non-linear effects. If the temperature is increased so much that $\gamma < 40$ then the non-linearities become less serious again. However, such high temperatures are rarely attained.

Finally, we note in Fig. 4d, where $\gamma = 100$, $\delta = 10$, that whereas the deviation from linearity is greatest when there is only 4% AB in the mixture if $\phi_M = 0.1$, the deviation is greatest at 63% AB if $\phi_M = 10$. Apparently, non-linearities manifest themselves in the mole fraction region corresponding to the *least* efficient collider. We also note that Fig. 4d is a way of expressing the use of a variety of different colliders to relax AB. In the mole fraction range $X_{AB} \sim 1$ linear extrapolations to $X_{AB} = 1$ give a common value regardless of the collider, as is reasonable. However, extrapolating from some intermediate range of X_{AB} (even if beyond the maximum) leads to problems.

Mild curvature prevents any two such extrapolations to lead to a common intercept. This should prove to be a useful diagnostic tool for detecting non-linearities when they are mild. The study of Miller and Hancock (21) is a good example, showing the existence of curvature indirectly. Admittedly their colliders were not inert atoms; nevertheless, the same principles are involved. It should be pointed out, however, that this is merely a necessary but insufficient test for linearity. Even if common intercepts are obtained they may not be easily interpretable unless the intercepts are time-independent as well.

It is interesting to investigate when the relaxation rate, $d\bar{E}/d(Nt)$ is least well described by a linear mixture rule. The first term on the right hand side of [16] is constructed from a linear combination of partial T–V rates with contributions from both colliders M and AB. The deviation from this linearity arises entirely from the second (V–V) rate term on the right hand side of [16]. This deviation from $(\bar{E} - \bar{E}_\infty)/N\tau$ is a maximum when

$$\left(\frac{X_{AB}k_{1,1}^{2,0}}{1-\chi_c}\right)\exp\left[-\left(\frac{N_{AB}k_{1,1}^{2,0}\tau}{1-\chi_c}+2\right)\frac{t}{\tau}\right]$$

reaches a maximum. We constrain ourselves to measurements made at fixed t/τ, such as in Figs. 3*a* and 4. Using the definition for τ, γ, and ϕ_M, the mole fraction of relaxer at the maximum, X, is given by

$$[23]\quad \frac{X\gamma(t/\tau)\phi_M}{[X+(1-X)\phi_M]^2(1-\chi_c)} = 1$$

As seen in Fig. 4, X does not depend on λ nor on δ. As an example, we choose the parameters of Fig. 4, where $t/\tau_* = 0.1$. $t/\tau \approx 0.1$ also, particularly when the mixture is dilute in AB. For $\gamma = 100$ (Fig. 4*d*) X varies between 0.012 and 0.404 in the range $\phi_M = 0.1 \to 10$. For $\phi_M = 0.1$ (Fig. 4*c*) X varies between 0 and 0.112 in the range $\gamma = \infty \to 80$. These are in qualitative agreement with the actual maxima in Fig. 4. However, we note that [23] corresponds to the deviations of *rates* from linearity; whereas Fig. 4 correspond to deviations of phenomenological *rate coefficients* from linearity.

Furthermore, in the likely case that $\gamma(t/\tau) \gg 1$, and $\phi_M \lesssim 1$, then $X \approx \phi_M/(\gamma t/\tau)$, i.e.

$$X = \frac{k_{1,0}^M - k_{0,1}^M}{k_{1,1}^{2,0}\,t/\tau}$$

In other words, the mole fraction at which non-linear deviations make themselves most felt is of the order of the relative T–V (collider M) rate constant to V–V rate constant. This is a very small number. However, more importantly the rate *coefficient* approaches to within 5% of the T–V limiting value only when X_{AB} is almost 100 times smaller yet. It puts *very* stringent requirements on an experimenter wishing to extract $k_{1,0}^M$ from data taken at finite mixture composition!

It is also useful to estimate the magnitude of the maximum deviation from linearity. We substitute [23] into an expression for the deviation from linearity divided by the linearly additive rate, i.e.

$$\frac{N_{AB}k_{1,1}^{2,0}h\nu_c\chi_c[2(\bar{E}/h\nu')^2 + (\bar{E}/h\nu') - \overline{E^2}/(h\nu')^2]_0 \exp[-(N_{AB}k_{1,1}^{2,0}\tau/\{1-\chi_c\}+2)t/\tau]}{(\bar{E}-\bar{E}_\infty)/\tau}$$

Noting that at early times $\bar{E} \approx \bar{E}_0$ and $\bar{E}_\infty \simeq \bar{E}_{\infty,c}$, and using the definition for δ, this maximum relative deviation becomes (for small X)

$$\frac{1-\chi_c}{\delta(t/\tau)}\,e^{-(1+2t/\tau)}$$

The relative deviation becomes more pronounced at earlier times and for smaller δ, i.e., the more non-Boltzmann the initial distribution is. For example, when $t/\tau = 0.1$ and $\delta = 5$, the rate of relaxation is more than 60% greater than it would have been without the non-linearities.

If, instead of choosing fixed t/τ, we consider experiments measured at fixed $N(k_{1,0}^M - k_{0,1}^M)t$, as in Fig. 3*c*, then X_{AB} at the maximum is given by

$$X = \frac{\phi_M}{N(k_{1,0}^M - k_{0,1}^M)t}[\gamma/(1-\chi_c) + 2(1-\phi_M)]^{-1}$$

Again, for the usual situation where γ is large, X is a small number,

$$X \approx \frac{(1-\chi_c)\phi_M}{\gamma}\cdot\frac{1}{N(k_{1,0}^M - k_{0,1}^M)t}$$

and the maximum relative deviation from linearly additive rates,

$$\frac{(1-\chi_c)e^{-1}}{\delta N(k_{10}^M - k_{01}^M)t},\ \text{can be} \gg 1$$

G. Suggestions for analyzing data

It appears that the safest experimental procedure (with respect to ambiguous interpretations) is to work as close as possible to equilibrium. In dilute mixtures ($X_{AB} \lesssim 1/\gamma$) linear extrapolation to $X_{AB} = 0$ leads to k_{10}^M. At $X_{AB} = 1$, one obtains k_{10}^{AB}. One should then measure $N\tau''$ as a function of time for $X_{AB} = 1$. Having already determined k_{10}^{AB} one can normalize $(1/N\tau'')$ by dividing by $(k_{10}^{AB} - k_{01}^{AB})$ to obtain g. Then, as can be seen from [22], when $X_{AB} = 1$

$$[24]\quad \frac{g-1}{a\tau_* - g} = a\tau_*\left[\frac{\delta(a\tau_* - 1)\bar{C}}{\gamma(\bar{C} - C_{vib})} - 1\right]^{-1} e^{-(a-1/\tau_*)t}$$

We note that $a\tau_* \sim \gamma$. At times far enough from equilibrium that some time-dependence in g is observable, but near enough to equilibrium that the variation is no more than a factor of 2 (i.e. $g \lesssim 2$), then $a\tau_* \gg g > 1$. Thus, a plot of ln $(g - 1)$ vs. time will give approximately a straight line with $(a - 1/\tau_*)$ as slope, i.e.

$$\frac{N_{AB}k_{1,1}^{2,0}}{1-\chi_c} + \frac{2}{\tau} - \frac{1}{\tau_*}$$

Having already determined k_{10}^{AB} and k_{10}^M (and therefore also τ and τ_*) as described above, $k_{1,1}^{2,0}$ is easily extracted. Alternatively, one can use the procedure given in ref. 20 (again for pure relaxer, AB) to determine $k_{1,0}^{AB}$ and $k_{1,1}^{2,0}$. However, in contradistinction to the above suggestion, where not even a knowledge of δ is required, the method of ref. 20 requires some knowledge of the population distributions. That procedure is based on the exponential decay of the function $2(\Sigma vN_v/N)^2 + \Sigma vN_v/N - \Sigma v^2 N_v/N$, as shown above (eq. [15]). The slope of a log plot of this function vs. time gives

$$\left(\frac{N_{AB}k_{1,1}^{2,0}}{1-\chi_c} + \frac{2}{\tau}\right)$$

Figure 1 shows that if measured at times sufficiently long ($\gtrsim 20\tau_*/\gamma$) then τ'' is just τ_*. Thus $N_{AB}k_{1,1}^{2,0}$ can be extracted by this method.

H. Comparison with experiment

The literature on the vibrational relaxation of molecules, pure or in mixtures with inert gases, is vast. We have not attempted an exhaustive search. Instead, we concentrate on two or three systems.

It appears that non-linearities are the rule rather than the exception for polyatomic molecules. We have observed them in our own laboratory for CH_4 (16), for N_2O and C_2H_2 (22) at mole fractions of the order of 0.01 in shock waves of Ar mixtures. In laser-induced experiments Moore and co-workers (23) have made measurements of the relaxation of H_2O diluted in Ar and in N_2. Slight curvature is evident for the ν_3 mode at mole fractions ~ 0.01. Wittig also (24) has studied the vibrational relaxation of the ν_1 and ν_3 modes of H_2O at mole fractions only as low as 0.05. However, extrapolations of his data to $X = 1$ using two different diluents do not give the same intercept. This is evidence for non-linearity, as discussed above. Since our model does not apply to polyatomics, we shall not discuss them further.

Diatomic molecules can be divided into two classes: according to whether the initial distributions are Boltzmann (shock tube experiments) or not. For the former class, we expect relaxation rates to be linearly additive. Indeed we have not found a single case contradicting this. Of some relevance is Glänzer's study of NO/Ar mixtures (15). In his shock wave experiments the $v = 0$, 1, and 2 vibrational level populations (in contradistinction to the total vibrational energy) did not decay or grow with linearly additive rates. Borrell's studies of CO mixtures with Ne (25) and with the hydrogen halides (26) seem to us to show the same behaviour. In analogy with the present study, the whole effect may be an artifact of the experimenter's imposition of quasi-first order kinetics onto the data, when the mechanism involves rapid second-order processes. Nevertheless, Glänzer's study showed that V–V effects can be eliminated by measuring at extremely low mole fractions $<10^{-4}$. It should serve as a warning to experimenters working far from equilibrium, particularly with molecules in the latter class. Unfortunately, fitting data to pure exponential functions is prevalent in the literature. V–T rate coefficients determined in this way are not likely to be unique rate *constants*, nor necessarily be interpretable as reported, unless $X \lesssim 10^{-4}$, or $\alpha \lesssim 10^{-4}$ (27).

In evaluating the second class of experiments, we concentrate on the hydrogen halides and on CO — molecules which have been the most extensively studied. It is evident to us that in the vast majority of these studies the mole fraction range was not sufficiently well covered, if at all. To complicate matters, in most studies neither the time regime used, t/τ, nor even the absolute time scale is ever cited. It is, moreover, extremely rare for the degree of excitation, α, to be mentioned. All of this is very important for diatomics where γ is expected to be much larger than for polyatomics. We expect that non-linearities should be most pronounced at $X \lesssim 10^{-3}$, as in Glänzer's study, far below the regime usually studied. Thus, very few studies show direct evidence of non-linearities in diatomic mixture rules: Hancock and Saunders discovered very strong non-linearities in their studies of DF relaxation at mole fractions as low as 0.0076. At the low temperatures involved it is probably dimerization which is responsible (28). Linear extrapolations of HF relaxation data, measured at mole fractions as low as 0.001, to $X = 1$ differ very much from the results for pure HF, thus indirectly indicating non-linearities (29). Similarly for H_2 (21). By measuring at very early times and at mole fractions as low as 0.002, Chen saw very strong non-linearities in the relaxation of HBr (30). The non-linearities in all of the above examples are consistently in the same direction as predicted by the present study.

Summarizing, we believe that the few experimental studies of mole-fraction dependence of relaxation times, as published in the literature, confirm the *predictions* of our study. However, it is not clear if experiments (particularly with hydrogen halides) confirm the scaling laws used in our basic model. Data on scaling relationships for V–V energy transfer in pure gases is surprisingly meagre (see ref. 31 for a thorough review). Only HCl and HF and CO have been studied in this respect. The consensus of opinion is that as v increases, the V–V channel becomes less able to compete with the V–T route. The data are considered to be substantially influenced by V–T processes (32), and we cannot conclude very much from this.

The question of the scaling of V–T rate constants is also not yet clear. On the one hand, the "V–T" rate constants are found to depend more strongly on v than linearly (33). On the other hand, our model, which accounts for a stronger variation by including an $e^{\Delta E/kT}$ term, (and presumably any model with "correct" scaling) would predict that the procedures used to draw such conclusions (i.e., treating the rates of population changes according to pure first order kinetics when α is as large as 0.01) are deficient. At the very best, such measurements lead to information on the sum of V–T and V–V rate constants; however, the possibility exists that they are artifacts, just as is the observed non-linear mixture rule. In other words, it is very hard for an experimenter to prove that so-called V–T rate constants are free of V–V character.

Notwithstanding these comments, some key experiments involving CO and DCl seem to confirm the scaling laws we used. Simpson and co-workers have shown that CO and DCl each relax via a continuous sequence of Boltzmann distributions behind shock waves (34, 35). This can only happen when V–T rate constants depend linearly on quantum number. The argument for this involves a discussion of canonical invariance, to which we now turn.

It has been shown by Shuler and co-workers (36, 37) that if the initial distribution of vibrational levels is Boltzmann, as in shock wave experiments, then equilibrium is approached via a continuous series of Boltzmann distributions, on condition that the harmonic oscillator molecules obey the Landau–Teller rules. The converse has also been proven (38, 39). As a corollary, Pritchard has stated that canonical invariance, linear mixture rules, and exponential decay all originate in the uniqueness of Landau–Teller sum rules (40). However, proofs of these properties have been given only for models where T–V are the only processes. There is as yet no satisfactory discussion in the literature on the question of canonical invariance for anharmonic molecules when V–V processes are involved: Osipov showed (41) that with V–V processes included and scaled according to Landau–Teller rules, then after the V–V transient period the distributions approach Boltzmann ones. However, he treated the molecules as harmonic oscillators and did not discuss the special case of an initial Boltzmann distribution. Rankin and Light did find canonical invariance even when V–V processes were considered (19). However, their model also used harmonic oscillators; we have already shown (17) that such a simplification essentially eliminates the influence of V–V processes on bulk measurements. The study which is closest to being satisfactory is Treanor's (42), who showed that, in general, canonical invariance is not valid. However, he used non-Landau–Teller scaling, and his result is thus expected. Moreover, Treanor did not consider the case which interests us here, namely, what happens if the initial distribution is Boltzmann? Therefore we still do not know whether or not the existence of canonical invariance implies Landau–Teller behaviour. Even our own study (20), which proved that energy-changes in a set of anharmonic oscillators decay exponentially when V–V and T–V rate constants scale according to Landau–Teller rules, does not prove canonical invariance (although we suspect that our study is a good starting point for a proof). We do not know whether exponential decay, linear mixture rules (and presumably canonical invariance) are a consequence of the unique sum rules or merely of an *initial* Boltzmann distribution, when V–V processes are involved.

In summary, the indications are that Simpson's experiments (made in a time regime where V–V effects have died out) show that T–V rate constants scale according to Landau–Teller rules.

I. Conclusion

We have shown that non-linear mixture rules can arise for the vibrational relaxation of diatomic molecules. Although we have evaluated the effect in detail for the atomic collision partner, M, the principle is the same for any inert collision partner. We have made a few reasonable approximations, such as isobaric relaxation, and we have neglected the temperature dependence of the microscopic rate constants. Except for thermal effects, it seems that non-linear mixture rules arise entirely as an artefact caused by the insistence of experimentalists on fitting measured data to first order kinetics, whereas a double exponential is more appropriate. The persistence of V–V energy transfer processes to times relatively advanced in the relaxation causes the rate law to be non-exponential and thus injects non-linearities into the analysis of data. Ambiguity is introduced by the experimentalist's conception of the time regime being probed. Some inconsistencies in choosing well-defined fixed or relative times accentuate the problem of the validity of the linear mixture rule. Such inconsistencies may lead to spurious results, e.g., in a plot of log $p\tau$ vs. $T^{-1/3}$, or at least lead to unnecessary scatter in the data. Even if a consistent time scale is chosen, linear extrapolations from curved mixture rule plots lead to wrong values for $k_{1,0}^{AB}$ and $k_{1,0}^{M}$. Furthermore, since the measured relaxation times are phenomenological in nature, different mixture rules may result depending on one's definition. For example, defining $\tau' \equiv -(\bar{E} - \bar{E}_\infty)/(\mathrm{d}\bar{E}/\mathrm{d}t)$ leads to different results than does use of [9] (20). We believe that, if our own suggestions for data analysis are not followed, then using definition [9] at least facilitates comparison between different experimental techniques such as fluorescence and schlieren methods, assuming that the regimes of t/τ'' and the degree of pertubation are reported.

We find that non-linearities are most evident at high temperatures, at early times, and in mixtures rich in the least efficient of the colliders. The larger the anharmonicity and the larger the degree of perturbation of the diatomic molecule the more pronounced the non-linearity becomes. Elimination of these non-linearities requires measurements at times up to 20 times longer and mole fractions up to 100 times smaller than expected on the basis of the magnitude of the V–V rate constant, depending on the initial conditions.

A special case was discovered where linear mixture rules are always expected — namely, shock tube measurements of the rate of vibrational relaxation of diatomic molecules. This results from the property that the initial distribution is Boltzmann. The same molecule at the same temperature using a different excitation method such as laser excitation would have relaxation times which disobey the linear mixture rule. However, we do not know if this result is due to the unique properties of Landau–Teller rate constants, i.e., if other scaling laws, which do not lead to canonical invariance, would also lead to the present result, or whether it is merely a consequence of the unique initial distribution in shock waves. Contrary to Pritchard's conclusion (40), obedience of Landau–Teller rules is now seen not to be sufficient to guarantee linear behaviour.

It is also instructive to interpret our results in terms of the synergism concept mentioned in the Introduction. Here, the two competing routes are (*1*) T–V processes by M, and (*2*) T–V processes by AB, each weighted by X_M and X_{AB}, respectively. The relatively slow T–V routes involve the steps $v = 0 \rightarrow v = 1 \rightarrow v = 2$. Even though in the present model the step $v = 1 \rightarrow v = 2$ is about twice as fast as $v = 0 \rightarrow v = 1$, the mere presence of AB in the mixture which allows for communicating V–V process $(v = 1) + (v = 1) \rightarrow (v = 0) + (v = 2)$ that may be more than 100 times as fast as $v = 0 \rightarrow v = 1$, obviates the need for T–V to accomplish $v = 1 \rightarrow 2$ at all. The role of T–V is relegated to restoring newly created $v = 0$ back to $v = 1$, a role which only T–V can accomplish. This symbiosis extends all the way up the vibrational ladder. However, the higher the vibrational level, the larger the T–V rate constants and the smaller the V–V constants. Thus the V–V route becomes relatively less important as a communicator. The synergism is most pronounced among the lower vibrational states. This idea has two consequences: (*1*) The whole effect depends on the initial conditions. The vibrational level to which the molecules are excited, the actual fraction excited, the closeness to equilibrium and hence need for communication, as well as the direction of relaxation (low $v \rightleftarrows$ high v) *all* determine the value of the all-important parameter δ. What may be an avoided bottleneck from one direction may not be so much of a bottleneck from the other direction, which has a different "average" vibrational quantum number and hence different δ. Indeed, as mentioned earlier, if enough molecules are produced in high vibrational states, δ can become < 0, and Treanor pumping will cause molecules to be trapped in high vibrational states and thus relax more slowly. (*2*) We can make a further prediction concerning the linear mixture rule. If the T–V rate constants depend less strongly on v than in the Landau–Teller model, then communication becomes even more important, and non-linearities become even more pronounced than found in this work. Conversely, if T–V constants depend more strongly on v than the Landau–Teller model, then the linear mixture rule will be better obeyed.

In our analysis, we implied that rotation of the diatomic molecule plays no role, or at least a passive role. Our analysis is valid only when the rotational levels have equilibrated on a much shorter time scale than that in question (43). Whereas this may be true with respect to the relatively improbable T–V processes, it may not be true with respect to the relatively probable V–V processes. A more proper treatment would have to involve the rotational substructure. As mentioned earlier, additional synergism can only lead to even greater nonlinearities. Work is now in progress in this direction.

Finally, we hope that this work will spur studies of vibrational relaxation to cover wide ranges of mole fraction.

Acknowledgements

The authors gratefully acknowledge financial support from the Natural Sciences and Engineering Research Council of Canada. C.C. acknowledges a summer research scholarship from NSERC.

1. R. K. BOYD. Can. J. Chem. **55**, 802 (1977).
2. D. C. TARDY and B. S. RABINOVITCH. J. Chem. Phys. **48**, 1282 (1968).
3. J. H. KIEFER. J. Chem. Phys. **57**, 1938 (1972).
4. J. TROE. Ber. Bunsenges. Phys. Chem. **84**, 829 (1980).
5. D. L. S. MCELWAIN and H. O. PRITCHARD. J. Am. Chem. Soc. **92**, 5027 (1972).
6. H. O. PRITCHARD, N. I. LABIB, and A. LAKSHMI. Can. J. Chem. **57**, 1115 (1979).
7. D. J. KEWLEY. J. Phys. B. Mol. Phys. **8**, 2565 (1975).
8. J. E. DOVE and S. RAYNOR. J. Phys. Chem. **83**, 127 (1979).
9. E. SCHLAG and W. G. VALANCE. J. Chem. Phys. **49**, 605 (1968).
10. S. R. BYRON. J. Chem. Phys. **44**, 1378 (1966).
11. I. R. HURLE, A. JONES, and J. L. J. ROSENFELD. Proc. R. Soc. London, A**310**, 253 (1969).
12. W. D. BRESHEARS, P. F. BIRD, and J. H. KIEFER. J. Chem. Phys. **55**, 4017 (1971).
13. W. D. BRESHEARS and P. F. BIRD. Proc. 14th Symp. (Internat.) on Combustion, Pittsburgh, Combustion Institute. 1975. p. 211.
14. J. E. DOVE and H. TEITELBAUM. Chem. Phys. **6**, 431 (1974).
15. K. GLÄNZER. Chem. Phys. **22**, 367 (1977).
16. H. TEITELBAUM. *In* Shock tubes and waves. Proc. 13th Internat. Shock Tube Symposium. *Edited by* C. E. Treanor. SUNY, Buffalo. 1981. p. 560.
17. H. TEITELBAUM. Can. J. Chem. **61**, 1267 (1983).
18. H. TEITELBAUM. Can. J. Chem. **61**, 1253 (1983).
19. C. C. RANKIN and J. C. LIGHT. J. Chem. Phys. **46**, 1305 (1967).
20. H. TEITELBAUM. Can. J. Chem. **61**, 1276 (1983).
21. R. G. MILLER and J. K. HANCOCK. J. Chem. Phys. **66**, 5150 (1977).
22. Z. BAALBAKI and H. TEITELBAUM. Chem. Phys. To be published.
23. J. FINZI, F. E. HOVIS, V. N. PANFILOV, P. HESS, and C. B. MOORE. J. Chem. Phys. **67**, 4053 (1977).
24. A. HARIRI and C. WITTIG. J. Chem. Phys. **68**, 2109 (1978).
25. P. BORRELL and G. E. MILLWARD. J. Chem. Soc. Faraday II, **69**, 1060 (1973).
26. P. M. BORRELL, P. BORRELL, and R. GUTTERIDGE. J. Chem. Soc. Faraday II, **71**, 571 (1975).
27. H. TEITELBAUM. Chem. Phys. Lett. **106**, 69 (1984).
28. J. K. HANCOCK and A. W. SAUNDERS, JR. J. Chem. Phys. **65**, 1275 (1976).
29. J. K. HANCOCK and W. H. GREEN. J. Chem. Phys. **57**, 4515 (1972).
30. H-L. CHEN. J. Chem. Phys. **55**, 5551 (1971).
31. S. R. LEONE. J. Phys. Chem. Ref. Data, **11**, 953 (1982).
32. L. S. DZELZKALNS and F. KAUFMAN. J. Chem. Phys. **79**, 3836 (1983).
33. T. J. FOSTER and F. F. CRIM. J. Chem. Phys. **75**, 3871 (1981).
34. J. P. MARTIN, M. R. BUCKINGHAM, J. A. CHENERY, and C. J. S. M. SIMPSON. Chem. Phys. **74**, 15 (1983).
35. A. J. AHERNE, J. P. BUXTON, J. A. CHENERY, A FAKHR, and C. J. S. M. SIMPSON. Chem. Phys. Lett. **98**, 93 (1983).
36. E. W. MONTROLL and K. E. SHULER. J. Chem. Phys. **26**, 454 (1957).
37. R. J. RUBIN and K. E. SHULER. J. Chem. Phys. **25**, 59 (1956).
38. K. E. SHULER, G. H. WEISS, and K. ANDERSEN. J. Math. Phys. **3**, 550 (1962).
39. H. C. ANDERSEN, I. OPPENHEIM, K. E. SHULER, and G. H. WEISS. J. Math. Phys. **5**, 522 (1964).
40. A. W. YAU and H. O. PRITCHARD. Can. J. Chem. **55**, 737 (1977).
41. A. I. OSIPOV. Dokl. Akad. Nauk SSSR, **130**, 523 (1960).
42. C. E. TREANOR, J. W. RICH, and R. G. REHM. J. Chem. Phys. **48**, 1798 (1968).
43. P. K. DAVIS and I. OPPENHEIM. J. Chem. Phys. **56**, 86 (1972).

Syntheses and X-ray structural analyses of $[(C_6H_5)_4As][Sn(EC_6H_5)_3]$, E = S and Se

PHILIP A. W. DEAN,[1] JAGADESE J. VITTAL, AND NICHOLAS C. PAYNE[1]
Department of Chemistry, University of Western Ontario, London, Ont., Canada N6A 5B7

Received April 2, 1984

PHILIP A. W. DEAN, JAGADESE J. VITTAL, and NICHOLAS C. PAYNE. Can. J. Chem. **63**, 394 (1985).

Stannous chloride, in solutions containing at least three mole equivalents of $NaEC_6H_5$, E = S and Se, forms triligated anions which crystallize readily as the tetraphenylarsonium salts, $[(C_6H_5)_4As][Sn(SC_6H_5)_3]$, **1**, and $[(C_6H_5)_4As][Sn(SeC_6H_5)_3]$, **2**. The crystals so formed are isomorphous, and their structures have been determined by single crystal X-ray diffractometry techniques. The salts crystallize in the monoclinic space group $P2_1/c$, with four formula units in unit cells of dimensions a = 10.760(1), b = 17.515(2), c = 20.247(3) Å, β = 104.71(1)° for **1**, and a = 10.885(2), b = 17.587(2), c = 20.612(2) Å, β = 105.47(1)°, for **2**. The structures have been refined by full-matrix least-squares techniques on F to agreement factors R = 0.024 (4780 observations with $F_o > 3\sigma(F_o)$) for **1**, and R = 0.030 (3442 observations with $F_o > 3\sigma(F_o)$) for **2**. The discrete $[Sn(EC_6H_5)_3]^-$ anions are isostructural; the three S or Se atoms form the base of a triangular pyramid whose apex is occupied by the Sn atom. Two Sn—S distances in **1** are 2.532(1) and the third 2.552(1) Å, while in **2** the Sn—Se distances are 2.649(1), 2.650(1), and 2.671(1) Å. Angles at the Sn atom are 89.91(3), 90.55(3), and 96.73(3)° in **1**, and 88.74(3), 89.72(3), and 97.27(3)° in **2**. In both anions all three phenyl groups adopt a propeller-like conformation and are disposed in equatorial positions above the basal plane of chalcogen atoms. These salts represent the first thiolato- and selenolatostannates(II) to be characterized structurally. Tin-119 nmr spectra confirm that the $[Sn(EC_6H_5)_3]^-$ ions are the same anionic Sn(II) species recently prepared *in situ* in solution.

PHILIP A. W. DEAN, JAGADESE J. VITTAL et NICHOLAS C. PAYNE. Can. J. Chem. **63**, 394 (1985).

Le chlorure stanneux, dans des solutions qui contiennent au moins trois équivalents molaires de $NaEC_6H_5$, E = S et Se, forme des anions triplement liés qui cristallisent facilement sous forme de sels de tétraphénylarsonium, $[(C_6H_5)_4As]$-$[Sn(SC_6H_5)_3]$ (**1**) et $[(C_6H_5)_4As][Sn(SeC_6H_5)_3]$ (**2**). Les cristaux qui se forment ainsi sont isomorphes et on a déterminé leurs structures par des techniques de diffraction des rayons-X sur des cristaux uniques. Les sels cristallisent sous forme monoclinique dans le groupe d'espace $P2_1/c$, avec quatre unités par unité et les dimensions de la maille sont a = 10,760(1), b = 17,515(2), c = 20,247(3) Å, β = 104,71(1)° pour **1** et a = 10,885(2), b = 17,587(2), c = 20,612(2) Å, β = 105,47(1)° pour **2**. On a affiné les structures par les techniques des moindres carrés (matrices complètes sur F) jusqu'à des facteurs d'accord R = 0,024 (pour 4780 observations avec $F_o > 3\sigma(F_o)$) et R = 0,030 (pour 3442 observations avec $F_o > 3\sigma(F_o)$) respectivement pour **1** et **2**. Les anions individuels $[Sn(EC_6H_5)_3]^-$ sont isostructuraux; les trois atomes de S (ou Se) forment la base d'une pyramide triangulaire dont le sommet est occupé par un atome de Sn. Deux des distances Sn—S dans **1** sont égales à 2,532(1) et la troisième est égale à 2,552(1) Å alors que dans **2** les distances Sn—Se sont égales à 2,649(1), 2,650(1) et 2,671(1) Å. Dans **1**, la valeur des angles au niveau de l'atome de Sn sont 89,91(3), 90,55(3) et 96,73(3)° alors que dans **2** les valeurs sont 88,74(3), 89,72(3) et 97,27(3)°. Dans chacun des anions, les trois groupes phényles adoptent une conformation hélicoïdale et ils occupent des positions équatoriales au-dessus du plan de base des atomes chalcogènes. Ces sels sont les premiers thiolato- et sélénolato-stannates(II) dont la structure a été caractérisée. Les spectres rmn du ^{119}Sn confirment que les ions $[Sn(EC_6H_5)_3]^-$ sont les mêmes espèces ioniques Sn(II) qui ont récemment été préparées *in situ* en solution.

[Traduit par le journal]

Introduction

The structural chemistry of thiolato complexes of the *d*-block elements has been of intense interest in recent years. Thus, for example, complexes of the general type $[M(S\text{-Aryl})_4]^{2-}$ have been characterized structurally for M = Mn(II) (1), Fe(II), Co(II), Ni(II), Zn(II), and Cd(II) (2, 3), and Hg(II) (4). Similarly, the structures of polynuclear thiolato complexes have been described for a wide range of elements including Mn(II) (1), Fe(II) (5–8), Co(II) (9, 10), Zn(II) (11), Cd(II) (12), V(III) (13, 14), Mn(III) (15), Cu(I) (16, 17), and Ag(I) (18). By comparison, thiolato complexes of the *p*-block elements have received little attention. In particular, phenylthiolatostannates(II), together with the analogous selenolatostannates(II), the subject of the present paper, do not seem to have been investigated prior to a recent multinuclear solution nmr study from one of our laboratories (19), though salts of the $[Sn(SC_6F_5)_3]^-$ anion have been synthesized (20) and organometallic tin(IV) thiolates are well known (21).

In the previous nmr study (19), slow exchange ^{119}Sn and ^{77}Se nmr spectra could be obtained at reduced temperature for $C_6H_5S^-/C_6H_5Se^-/Sn(II)$ mixtures in methanol when $L_{total}/M <$ 3, allowing characterization in solution of the all of the species $[Sn(SC_6H_5)_x(SeC_6H_5)_{3-x}]^-$. As no structural data are currently available for either $[Sn(SR)_3]^-$ or $[Sn(SeR)_3]^-$ anions, we thought it desirable to isolate the parent complexes of this series and determine their structures; further we felt that comparison with the corresponding plumbates(II) for which we have recently presented structural data (22) would be of interest. Accordingly we report here the syntheses and X-ray structure analyses of $[(C_6H_5)_4As][Sn(EC_6H_5)_3]$ (E = S and Se). At the outset of our work no X-ray structural data were available for neutral stannous thiolates or selenolates. Very recently, however, the structures of two substituted benzene thiolates of tin(II) have been reported (23).

Experimental

All the chemicals were of reagent grade and used as received. Carbon and hydrogen analyses were performed by Guelph Chemical Laboratories Ltd.

Syntheses of the compounds were carried out under an argon atmosphere in a glove bag, using solvents that had been thoroughly deoxygenated with argon.

Synthesis of $[(C_6H_5)_4As][Sn(SC_6H_5)_3]$

Benzenethiol, 1.18 g (10.7 mmol), was added to 0.248 g (10.7 mmol) of sodium metal dissolved in 10 mL of methanol. The resultant

[1] To whom correspondence should be addressed.

TABLE 1. Crystal data and experimental conditions

Compound	$SnAsS_3C_{42}H_{35}$	$SnAsSe_3C_{42}H_{35}$
Formular weight	829.54	970.23
Unit cell dimensions	a = 10.760(1)	a = 10.885(2)
(Å and deg)	b = 17.515(2)	b = 17.587(2)
	c = 20.247(3)	c = 20.612(2)
	β = 104.71(1)	β = 105.47(1)
Cell volume ($Å^3$)	3690.8	3802.8
Temperature (C)	25	
Z	4	
Density (obsd) (g cm^{-3})	1.505(3)	1.699(6)
(calcd)	1.493	1.695
Crystal dimensions (cm)	0.032 × 0.034 × 0.033	0.030 × 0.026 × 0.027
Crystal faces	{00$\underline{1}$} {100} {01$\underline{1}$} {1$\underline{0}\underline{2}$} {010} (012) (012)	{010} {100} {011}
Space group	$P2_1/c$ C_{2h}^5 No. 4	
Radiation, wavelength (Å)	Mo Kα λ = 0.71073	
Absorption coefficient (cm^{-1})	17.7	44.1
Gaussian grid	16 × 12 × 10	10 × 10 × 14
Transmission factors max.	0.666	0.422
min.	0.582	0.316
Detector aperture vertical (mm)	4.0	
horizontal	4.0 + 1.0 tan θ	
Crystal–detector distance (mm)	205	
Take-off angle (deg)	2.7	
Scan mode	ω–2θ	
Scan width (deg)	0.60 + 0.35 tan θ	0.75 + 0.35 tan θ
Data collected	$+h$, $-k$, $\pm l$	
(deg)	$0.5 < \theta < 25$	

solution of $NaSC_6H_5$ was added to a stirred solution of 0.83 g (3.25 mmol) of $SnCl_2\cdot 2H_2O$ in 10 mL of water, producing a yellow precipitate. A solution containing 1.39 g (3.3 mmol) of tetraphenylarsonium chloride hydrate in 5 mL of methanol was added with stirring to the yellow precipitate followed by 50 mL of acetonitrile. The mixture was warmed to 70°C for 30 min giving a very pale yellow solution, filtered hot, and left to crystallize. The pale yellow crystals of diffraction quality obtained in a few hours were separated by decantation and washed with water, methanol, and carbon tetrachloride, then dried in a stream of argon. Concentration of the mother liquor provided a second crop of crystals. Yield: 500 mg. (18.5%). *Anal.* calcd. for $C_{42}H_{35}AsSnS_3$: C 60.81, H 4.25; found: C 60.63, H 4.36.

Synthesis of $[(C_6H_5)_4As][Sn(SeC_6H_5)_3]$

The preparation of this yellow compound was very similar to that of the sulfur analog but C_6H_5SeH was used instead of C_6H_5SH. The hot solution was sealed and refrigerated for a day to get lemon yellow crystals of diffraction quality. Yield: 150 mg (10%). *Anal.* calcd. for $C_{42}H_{35}AsSnSe_3$: C 51.99, H 3.64; found: C 51.91, H 3.73.

Physical measurements

^{119}Sn nuclear magnetic resonance spectra

The 296 K 149.2 MHz ^{119}Sn nmr spectra were measured and referenced to neat $SnMe_4$ as described previously (19). The samples were prepared in CH_2Cl_2 and were ~0.1 M and ~0.06 M for $[(C_6H_5)_4As][Sn(SC_6H_5)_3]$ and $[(C_6H_5)_4As][Sn(SeC_6H_5)_3]$, respectively.

Collection and reduction of X-ray data

Well developed, pale yellow crystals of equant habit were chosen for each salt. A preliminary photographic examination indicated the monoclinic space group $P2_1/c$ (24), and a careful examination of the films showed that the salts were isomorphous and isostructural. Crystal densities were determined by flotation in mixtures of 1,2-dibromoethane and carbon tetrachloride.

The analyses were carried out on an Enraf-Nonius CAD4F diffractometer using an incident beam monochromator and Mo radiation (25). The thiolate structure **1** was undertaken first. Cell constants and an orientation matrix were determined from reflections recorded on a rotation photograph, and refined using the angular settings for 25 high angle reflections with $40 < 2\theta < 50°$. ω-Scans of intense, low-angle reflections had an average width at the base of 0.80°, a satisfactory value (26). Crystal data for both salts are given in Table 1. Intensity data were recorded at variable scan speeds ranging from 4 to 0.9 deg min^{-1}, values chosen to optimize counting statistics within a maximum time per datum of 75 s. Background estimates were made by extending the scan by 25% on each side. Standard reflections 4 0 0, 0 4 0, and 0 0 10 were monitored every 166 min of X-ray exposure time, and showed an average 4.1% decay over the total period of 133.4 h. In all, 7551 observations were recorded, of which 204 were standards. Corrections were applied for Lorentz, monochromator and crystal polarization, and background radiation effects using the structure determination package (27) running on a PDP 11/23+ computer. Standard deviations were assigned based upon counting statistics, and a value chosen for p of 0.05 to avoid overweighting strong reflections (28). Fourteen crystal faces were identified by optical goniometry, and the crystal dimensions measured on a microscope equipped with a filar eyepiece. The data were corrected for absorption by the Gaussian method. A linear decay correction was applied, and the equivalent forms averaged, leaving 4780 unique data with $F_o > 3\sigma(F_o)$ for solution and refinement of the structure.

The same procedure was followed for the selenolate structure **2**. ω-Scans showed an average width at base of 0.58°. Variable scan speeds ranged from 4.0 to 0.9 deg min^{-1}, with a maximum time per datum of 75 s. A total of 136.7 h was required for recording the intensity data. The crystal chosen had eight faces, and an absorption correction was applied. A preliminary value of 0.04 was chosen for p. No decay correction was applied. In all, 3442 unique data with $F_o > 3\sigma(F_o)$ were available. Details of experimental procedures are given in Table 1 for both **1** and **2**.

TABLE 2(*a*). Positional ($\times 10^4$) and thermal ($\times 10^3$) parameters for **1**

Atom	x	y	z	U_{eq}* (Å^2)
Sn	1568.1(2)	2207.2(1)	−954.1(1)	494.0(5)
As	1885.9(2)	6068.8(2)	7843.3(1)	383.9(7)
S1	1115.5(8)	2811.7(6)	96.7(4)	721(3)
S2	3101.2(8)	3298.7(5)	−1024.1(4)	586(2)
S3	3225.1(9)	1335.1(5)	−211.0(4)	723(3)
C11	−559(3)	2656(2)	−40(1)	46.0(7)
C12	−1335(3)	3269(2)	27(1)	54.4(8)
C13	−2632(3)	3171(2)	−59(2)	72(1)
C14	−3185(3)	2476(3)	−207(2)	85(1)
C15	−2426(4)	1866(2)	−271(2)	89(1)
C16	−1126(3)	1953(2)	−188(2)	68(1)
C21	3230(3)	3164(2)	−1870(1)	49.1(8)
C22	4426(3)	3041(2)	−2001(2)	64(1)
C23	4519(3)	2944(2)	−2660(2)	80(1)
C24	3463(4)	2959(2)	−3196(2)	80(1)
C25	2296(4)	3068(2)	−3076(2)	78(1)
C26	2170(3)	3178(2)	−2425(2)	63(1)
C31	3587(3)	770(2)	−865(2)	58.3(9)
C32	3754(3)	−10(2)	−776(2)	72(1)
C33	4035(4)	−455(2)	−1287(2)	91(1)
C34	4131(4)	−141(2)	−1880(2)	92(1)
C35	3980(3)	624(3)	−1977(2)	81(1)
C36	3726(3)	1074(2)	−1469(2)	70(1)
C41	680(2)	5708(2)	8321(1)	40.3(7)
C42	−508(3)	6054(2)	8233(1)	52.7(8)
C43	−1367(3)	5753(2)	8568(2)	59.3(9)
C44	−1053(3)	5126(2)	8972(2)	59.1(9)
C45	117(3)	4775(2)	9054(2)	56.5(9)
C46	999(3)	5067(2)	8730(1)	47.8(8)
C51	1599(2)	5527(2)	7002(1)	41.7(7)
C52	2620(3)	5340(2)	6735(1)	57.1(9)
C53	2393(3)	4937(2)	6130(2)	67(1)
C54	1176(3)	4735(2)	5796(2)	64(1)
C55	157(3)	4936(2)	6052(2)	60.4(9)
C56	356(3)	5328(2)	6660(1)	49.8(8)
C61	1670(3)	7137(2)	7683(1)	40.9(7)
C62	1439(3)	7611(2)	8188(2)	53.0(8)
C63	1335(3)	8387(2)	8071(2)	67(1)
C64	1460(3)	8683(2)	7460(2)	69(1)
C65	1699(3)	8213(2)	6966(2)	68(1)
C66	1815(3)	7437(2)	7076(1)	53.5(8)
C71	3587(2)	5894(2)	8399(1)	42.6(7)
C72	4093(3)	5166(2)	8476(2)	57.1(9)
C73	5250(3)	5044(2)	8947(2)	69(1)
C74	5882(3)	5638(2)	9329(2)	68(1)
C75	5409(3)	6358(2)	9237(2)	64(1)
C76	4248(3)	6493(2)	8771(1)	51.2(8)

* U_{eq} values for Sn, As, and S have been multiplied by 10^4, $U_{eq} = (1/3) \Sigma_i \Sigma_j U_{ij} a_i^* a_j^* a_i a_j$.

TABLE 2(*b*). Atomic positional ($\times 10^4$) and thermal ($\times 10^3$) parameters for **2**

Atom	x	y	z	U_{eq}^* (Å^2)
Sn	1561.6(4)	2211.1(3)	−968.6(2)	51.1(1)
As	1841.9(5)	6100.1(3)	7833.2(3)	42.9(2)
Se1	1124.3(6)	2834.3(5)	118.5(3)	72.0(2)
Se2	3173.8(6)	3347.0(4)	−999.5(3)	58.9(2)
Se3	3237.1(7)	1278.6(4)	−192.0(3)	69.1(2)
C11	−668(5)	2657(3)	−47(3)	46(2)
C12	−1451(6)	3246(4)	7(3)	61(2)
C13	−2751(6)	3126(5)	−90(3)	82(2)
C14	−3247(7)	2431(5)	−219(4)	95(3)
C15	−2468(7)	1845(5)	−268(4)	95(3)
C16	−1201(6)	1942(4)	−191(3)	68(2)
C21	3306(6)	3178(3)	−1896(3)	50(2)
C22	4467(6)	3045(4)	−2021(3)	67(2)
C23	4557(7)	2942(5)	−2667(4)	85(3)
C24	3503(8)	2959(5)	−3193(3)	85(3)
C25	2365(7)	3099(5)	−3083(3)	81(3)
C26	2258(6)	3210(4)	−2442(3)	69(2)
C31	3637(5)	728(4)	−908(3)	53(2)
C32	3826(6)	−54(4)	−845(3)	70(2)
C33	4107(7)	−469(4)	−1367(4)	85(3)
C34	4196(7)	−113(5)	−1937(3)	85(3)
C35	4035(6)	644(5)	−1996(3)	79(3)
C36	3774(6)	1071(4)	−1484(3)	70(2)
C41	667(5)	5740(3)	8304(2)	39(2)
C42	−523(6)	6067(4)	8203(3)	53(2)
C43	−1364(6)	5772(4)	8534(3)	63(2)
C44	−1035(6)	5155(4)	8950(3)	61(2)
C45	125(6)	4829(4)	9036(3)	59(2)
C46	992(5)	5117(3)	8721(3)	49(2)
C51	1547(5)	5564(3)	7000(3)	45(2)
C52	2542(6)	5384(4)	6733(3)	59(2)
C53	2320(6)	4989(4)	6141(3)	66(2)
C54	1122(7)	4780(4)	5813(3)	68(2)
C55	119(6)	4967(4)	6069(3)	63(2)
C56	327(5)	5354(3)	6667(3)	49(2)
C61	1627(5)	7169(3)	7676(3)	45(2)
C62	1395(6)	7632(4)	8176(3)	61(2)
C63	1295(7)	8403(4)	8053(3)	75(2)
C64	1425(7)	8696(4)	7466(4)	78(3)
C65	1664(7)	8233(4)	6977(3)	71(2)
C66	1763(6)	7466(4)	7082(3)	58(2)
C71	3543(5)	5925(3)	8377(3)	42(2)
C72	4071(6)	5209(4)	8431(3)	57(2)
C73	5235(6)	5094(4)	8880(3)	69(2)
C74	5865(6)	5669(5)	9266(3)	70(2)
C75	5356(6)	6384(4)	9198(3)	65(2)
C76	4197(6)	6520(4)	8750(3)	53(2)

* $U_{eq} = (1/3) \Sigma_i \Sigma_j U_{ij} a_i^* a_j^* a_i a_j$.

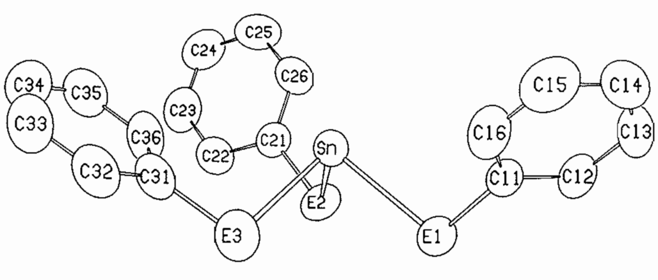

FIG. 1. A perspective view of an anion, showing the atom numbering scheme.

Solution and refinement of the structures

The atom positions for $[(C_6H_5)_4As][Pb(SC_6H_5)_3]$ (22) were used as a starting point for refinement of the structure of **1**. With all non-hydrogen atoms included, minimizing the function $\Sigma w(\|F_o| - |F_c\|)^2$, where F_o and F_c are the observed and calculated structure amplitudes, and the weight w is defined as $4F_o^2/\sigma^2(F_o^2)$, refinement converged at agreement factors $R_1 = \Sigma(\|F_o| - |F_c\|)/\Sigma|F_o|) = 0.037$ and $R_2 = (\Sigma w(|F_o| - |F_c|)^2/\Sigma w F_o^2)^{1/2} = 0.055$. Scattering factors for neutral, non-hydrogen atoms were taken from ref. 24, and real dispersion corrections were included for all atoms (29). A difference Fourier synthesis showed clear evidence for all 35 H atoms on the phenyl rings, at peak heights ranging from 0.65(9) to 0.39(9) e Å^{-3}, so all were included in idealized positions (C—H 0.90 Å, sp^2 hybridization) with fixed isotropic thermal parameters arbitrarily set to 5 Å^2. The

TABLE 3(*a*). Bond distances (Å) for **1** and **2**

Atom 1	Atom 2	Distance* 1	Distance* 2	Atom 1	Atom 2	Distance* 1	Distance* 2	Atom 1	Atom 2	Distance* 1	Distance* 2
Sn	E1	2.532(1)	2.649(1)	C23	C24	1.358(6)	1.352(11)	C53	C54	1.360(5)	1.350(10)
Sn	E2	2.552(1)	2.671(1)	C24	C25	1.352(6)	1.340(11)	C54	C55	1.372(5)	1.374(10)
Sn	E3	2.532(1)	2.650(1)	C25	C26	1.373(5)	1.370(10)	C55	C56	1.379(4)	1.374(8)
E1	C11	1.773(3)	1.914(6)	C26	C21	1.383(4)	1.374(9)	C56	C51	1.385(4)	1.372(8)
E2	C21	1.768(3)	1.914(6)	C31	C32	1.384(5)	1.391(9)	C61	C62	1.389(4)	1.387(8)
E3	C31	1.773(4)	1.911(7)	C32	C33	1.388(6)	1.399(11)	C62	C63	1.379(5)	1.378(10)
As	C41	1.912(3)	1.908(6)	C33	C34	1.350(6)	1.356(11)	C63	C64	1.379(5)	1.357(10)
As	C51	1.904(3)	1.911(6)	C34	C35	1.358(6)	1.344(12)	C64	C65	1.369(5)	1.374(10)
As	C61	1.903(3)	1.911(6)	C35	C36	1.378(5)	1.384(10)	C65	C66	1.379(5)	1.367(9)
As	C71	1.914(3)	1.916(6)	C36	C31	1.376(5)	1.374(9)	C66	C61	1.381(4)	1.374(8)
C11	C12	1.387(4)	1.364(8)	C41	C42	1.384(4)	1.382(8)	C71	C72	1.379(4)	1.376(8)
C12	C13	1.372(5)	1.391(10)	C42	C43	1.382(4)	1.381(9)	C72	C73	1.379(5)	1.371(9)
C13	C14	1.354(6)	1.334(12)	C43	C44	1.360(5)	1.368(9)	C73	C74	1.370(5)	1.353(10)
C14	C15	1.371(6)	1.355(13)	C44	C45	1.373(5)	1.356(9)	C74	C75	1.355(5)	1.366(10)
C15	C16	1.374(5)	1.356(11)	C45	C46	1.382(4)	1.376(8)	C75	C76	1.381(4)	1.371(9)
C16	C11	1.374(5)	1.385(9)	C46	C41	1.385(4)	1.378(8)	C76	C71	1.381(4)	1.381(8)
C21	C22	1.395(4)	1.375(9)	C51	C52	1.381(4)	1.375(8)				
C22	C23	1.375(5)	1.375(10)	C52	C53	1.381(4)	1.369(9)				

*Numbers in parentheses are estimated standard deviations in the least significant digits.

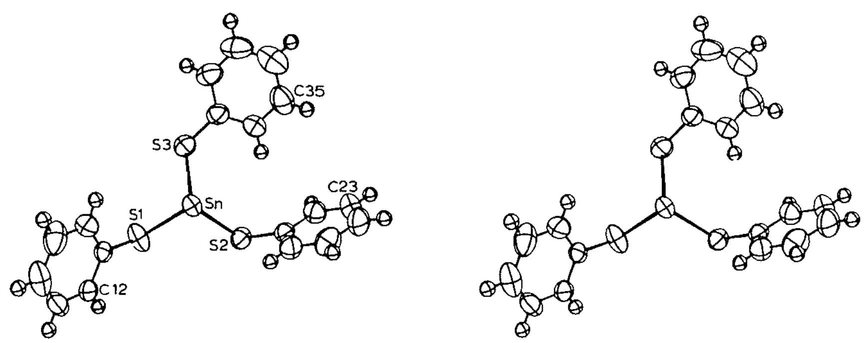

FIG. 2. A stereoview of the $[Sn(SC_6H_5)_3]^-$ anion.

scattering factor values were taken from Stewart *et al.* (30). With all non-hydrogen atoms assigned anisotropic thermal parameters, and hydrogen atom positions recalculated to maintain ideal geometries, refinement of 424 variables converged at $R_1 = 0.024$ and $R_2 = 0.033$ using 4780 observations with $F_o > 3\sigma(F_o)$. In a total difference Fourier synthesis there were eight peaks with electron density greater than 0.21(6) e Å^{-3}; of these, two were associated with the Sn atom, and the remainder were of no chemical significance. The error on an observation of unit weight was 1.022 electrons, and there were no parameter shifts in the final cycle. An analysis of R_2 in terms of F_o, $\lambda^{-1}\sin\theta$ and various combinations of Miller indices showed no unusual trends.

The positions for the thiolate structure were used as a starting point for refinement of the selenolate structure **2**. The 47 non-hydrogen atoms were refined with anisotropic thermal parameters and the refinement converged at agreement factors $R_1 = 0.040$ and $R_2 = 0.048$. Thirty four of the 35 hydrogen atoms were found from a difference Fourier synthesis, at peak heights ranging from 0.56(10) to 0.28(10) e Å^{-3}, so all were included in idealized positions. The refinement converged at $R_1 = 0.032$ and $R_2 = 0.035$. An inspection of F_o and F_c suggested that an extinction parameter should be refined. Employing 3442 observations with $F_o > 3\sigma(F_o)$ and a p factor of 0.05, refinement of 425 variables converged at agreement factors $R_1 = 0.030$ and $R_2 = 0.035$. Again, an analysis of R_2 in terms of F_o, $\lambda^{-1}\sin\theta$ and Miller indices combinations indicated a satisfactory weighting scheme. The error on an observation of unit weight is 1.011 electrons. The extinction parameter refined to $1.08(7) \times 10^{-7}$. In a final difference Fourier synthesis there were three peaks with electron density greater than 0.42(8) e Å^{-3}; these were associated with the tin and selenium atoms.

Positional and U_{eq} thermal parameters are given for the refined atoms of both structures in Table 2. Tables of hydrogen atom parameters, anisotropic thermal parameters, root-mean-square amplitudes of vibration, supplementary dimensions, weighted least-squares planes, torsion angles and structure amplitudes have been deposited.[2]

Results and discussion

General

The anions $[Sn(EC_6H_5)_3]^-$ (E = S or Se) produced by the reaction

$$Sn^{2+} + 3EC_6H_5^- \rightarrow [Sn(EC_6H_5)_3]^-$$

were isolated as their $[(C_6H_5)_4As]^+$ salts. The ^{119}Sn chemical shifts for $[(C_6H_5)_4As][Sn(SC_6H_5)_3]$ and $[(C_6H_5)_4As][Sn(SeC_6H_5)_3]$ in CH_2Cl_2 are 146 and 208 ppm, respectively, at

[2] Anisotropic thermal parameters, hydrogen atom parameters, root-mean-square amplitudes of vibration, additional bond distances and bond angles, weighted least-squares planes, selected torsion angles and structure amplitudes are available at a nominal charge from the Depository of Unpublished Data, CISTI, National Research Council of Canada, Ottawa, Ont., Canada K1A 0S2.

TABLE 3(*b*). Bond angles in degrees for **1** and **2**

			Angle*					Angle*					Angle*	
Atom 1	Atom 2	Atom 3	**1**	**2**	Atom 1	Atom 2	Atom 3	**1**	**2**	Atom 1	Atom 2	Atom 3	**1**	**2**
E1	Sn	E2	89.91(3)	88.74(3)	C21	C22	C23	120.1(3)	120.7(7)	C52	C51	C56	120.4(3)	119.9(6)
E1	Sn	E3	90.55(3)	89.72(3)	C22	C23	C24	121.4(4)	120.6(7)	C51	C52	C53	119.3(3)	120.2(6)
E2	Sn	E3	96.73(3)	97.27(3)	C23	C24	C25	119.1(3)	119.6(7)	C52	C53	C54	120.3(3)	120.1(7)
Sn	E1	C11	102.1(1)	100.8(2)	C24	C25	C26	121.0(3)	120.6(7)	C53	C54	C55	120.4(3)	120.2(6)
Sn	E2	C21	99.5(1)	97.2(2)	C21	C26	C25	121.0(3)	121.3(7)	C54	C55	C56	120.5(3)	120.4(6)
Sn	E3	C31	98.5(1)	96.3(2)	E3	C31	C32	120.0(3)	119.2(5)	C51	C56	C55	118.9(3)	119.2(6)
C41	As	C51	108.1(1)	108.6(3)	E3	C31	C36	122.8(3)	122.9(6)	As	C61	C62	119.9(2)	119.3(5)
C41	As	C61	110.0(1)	110.2(3)	C32	C31	C36	117.2(3)	117.9(7)	As	C61	C66	119.3(2)	119.2(5)
C41	As	C71	108.7(1)	108.9(2)	C31	C32	C33	120.3(4)	120.0(7)	C62	C61	C66	120.7(3)	121.5(6)
C51	As	C61	110.6(1)	110.5(3)	C32	C33	C34	121.0(4)	120.4(7)	C61	C62	C63	118.9(3)	117.5(7)
C51	As	C71	111.1(1)	110.5(3)	C33	C34	C35	119.8(4)	119.9(8)	C62	C63	C64	120.2(3)	121.0(7)
C61	As	C71	108.4(1)	108.3(3)	C34	C35	C36	119.7(4)	121.1(8)	C63	C64	C65	120.5(3)	121.0(7)
E1	C11	C12	118.7(2)	119.4(5)	C31	C36	C35	122.0(4)	120.7(7)	C64	C65	C66	120.1(3)	119.3(7)
E1	C11	C16	123.3(3)	122.4(5)	As	C41	C42	120.9(2)	120.9(5)	C61	C66	C65	119.5(3)	119.6(7)
C12	C11	C16	118.0(3)	118.2(6)	As	C41	C46	118.2(2)	119.0(4)	As	C71	C72	120.4(2)	120.9(5)
C11	C12	C13	120.6(3)	120.5(7)	C42	C41	C46	120.8(3)	120.0(6)	As	C71	C76	118.9(2)	118.6(5)
C12	C13	C14	121.1(4)	120.6(8)	C41	C42	C43	118.7(3)	119.1(6)	C72	C71	C76	120.5(3)	120.4(6)
C13	C14	C15	118.8(4)	118.9(8)	C42	C43	C44	120.6(3)	120.7(6)	C71	C72	C73	118.9(3)	118.7(6)
C14	C15	C16	121.0(4)	122.2(8)	C43	C44	C45	121.0(3)	119.7(6)	C72	C73	C74	120.4(3)	121.3(7)
C11	C16	C15	120.5(3)	119.6(7)	C44	C45	C46	119.7(3)	121.0(6)	C73	C74	C75	120.8(3)	119.9(7)
E2	C21	C22	120.5(3)	121.1(5)	C41	C46	C45	119.2(3)	119.5(6)	C74	C75	C76	119.8(3)	120.4(7)
E2	C21	C26	122.2(3)	121.7(5)	As	C51	C52	120.3(2)	120.8(5)	C71	C76	C75	119.6(3)	119.2(6)
C22	C21	C26	117.3(3)	117.2(6)	As	C51	C56	119.3(2)	119.3(5)					

*Numbers in parentheses are estimated standard deviations in the least significant digits.

296 K. These values can be regarded as identical to those previously attributed to $[Sn(SC_6H_5)_3]^-$ and $[Sn(SeC_6H_5)_3]^-$ prepared *in situ* in methanol (140.0 and 207.0 ppm, respectively) (19), allowing for a small solvent effect on δ_{Sn} (31). Hence the earlier formulation is confirmed.

Description of the structures

The crystal structure of each compound consists of discrete cations and anions, the shortest cation . . anion As . . Sn distances being 5.020(3) and 4.972(1) Å in **1** and **2**, respectively. The shortest interionic distances are 2.54 and 2.55 Å between H44 and H74 in **1** and **2**, respectively. We note particularly that there are no interanionic interactions, the shortest Sn—Sn distances being 9.629(1) and 9.758(1) Å in **1** and **2**, respectively. Figure 1 gives the atom numbering scheme used and shows a perspective view of a $[Sn(EC_6H_5)_3]^-$ anion. Figure 2 shows a stereoview of the anion in **1**, with atoms plotted as 50% probability thermal ellipsoids. Selected bond distances and bond angles in the two compounds are listed in Table 3; those of the cations are unexceptional and are not discussed further.

It can be seen from the figures that the coordination about tin is trigonal pyramidal in both anions, as is commonly observed for $Sn^{II}L_3$ complexes of the VSEPR type AX_3E (see below). Overall, the four compounds $[(C_6H_5)_4As][M(EC_6H_5)_3]$, (M = Sn(II) or Pb(II), E = S or Se) are both isomorphous and isostructural. In contrast the compounds $[M(SAr')_2]_3$ (M = Sn(II) or Pb(II); Ar' = 2,6-diisopropylphenyl) are not isomorphous and are not considered to be isostructural (23).

The $[Sn(SC_6H_5)_3]^-$ anion

In the thiolato-complex the three sulfur atoms form the base of a trigonal pyramidal with the tin atom at the apex. The overall idealized symmetry of the SnS_3 kernel is C_{3v}, but two of the Sn—S distances are equal at 2.532(1) and shorter than the third distance of 2.552(1) Å, while the S—Sn—S angles are 89.91(3), 90.55(3), and 96.73(3)°. The largest angle, S2—Sn—S3, might be a result of repulsive steric interactions between the associated phenyl groups. There are short intramolecular non-bonded distances between H36 and C21 and C22: 2.862(3) and 2.920(4) Å in **1** and 2.913(6) and 2.972(7) in **2**. The Sn—S distances in **1** are intermediate between the short (terminal) Sn—S distance of 2.471(5) and the two longer (bridging) Sn—S distances of 2.643(4) and 2.583(4) Å found for the pyramidally coordinated Sn(II) centres in trimeric $[Sn(SAr')_2]_3$ (see above), but longer than the Sn—S distance of 2.435(1) Å found for monomeric $Sn(SAr)_2$ (Ar = 2,6-diisobutylphenyl) (23). The S—Sn—S angle of 85.4(1)° reported for $Sn(SAr)_2$ is less than any angle found in **1**.

As can be seen from Fig. 1, the phenyl groups all occupy equatorial positions above the three basal sulfur atoms. The dihedral angles Sn—S—CX1—CX6 are 51.9, 58.1, and 41.6° so that the phenyl rings are twisted into a propeller-like arrangement. Within the phenyl rings the C—C—C angles are in the range found in other phenylthiolates (4, 32, 33) and also in triphenylphosphines (34). The S—CX1—CX6 angles of 123.3(3), 122.2(3), and 122.8(3)° are systematically larger than the related S—CX1—CX2 angles of 118.7(2), 120.5(3), and 120.0(3)°; similar canting of the phenyl rings relative to the corresponding S—C vectors has been found in other arylthiolate complexes. At sulfur, M—S—CX1 angles of 102.1(1), 99.5(1), and 95.5(1)° are comparable to the values found for $[Pb(SC_6H_5)_3]^-$ (22), but are smaller than values found for terminal ligands in other arylthiolate complexes (e.g. 107.2(2) and 107.9(2)° in $[(CH_3)_4N]_2[Hg(S(4\text{-}C_6H_4Cl))_4]$ (4), and 107.8(4), 110.2(5), and 114.4(4)° in $[(C_6H_5)_4P]_2$-$[Cu(SC_6H_5)_3]$ (32).

The $[Sn(SeC_6H_5)_3]^-$ anion

This anion is isostructural with its sulfur analog. Two Sn—Se distances are equal at 2.649(1) Å, the third one is 2.671(1) Å and the Se—Sn—Se angles are 88.74(3), 89.72(3), and 97.3(3)°. Little information is available in the literature regarding Sn(II)—Se bond distances. To our knowledge the only previously reported data for Sn(II)—Se species is for tin(II) selenide (35). In SnSe, the tin atom is in a distorted octahedral environment with the three nearest selenium atoms at distances 2.77, 2.82, and 2.82 Å, all longer than the distances found here, though the corresponding Se—Sn—Se bond angles of 89, 89, and 96° are quite comparable to those found for **2**.

Comparison with other pyramidal Sn(II) compounds

Discrete triligated tin(II) species are of the VSEPR type AX_3E and are thus expected to have trigonal pyramidal coordination geometry about Sn(II), as described here for **1** and **2**. In earlier work, a trigonal pyramidal arrangement of the nearest atoms to tin(II) has been found in a variety of stannous compounds including, for example, $CsSnCl_3$, NH_4SnF_3, SnS, SnSe, $SnCl_2$, $SnSO_4$, and $K_3[Sn(HCO_2)_3]$ (21, 35, 36). Quite commonly in these compounds two of the Sn—X (X = F, Cl, S, or O) bonds of the trigonal pyramid are found to be equal or nearly equal in length, while the third one is significantly different, just as we find in the thiolato- and selenolatostannates; also the X—Sn—X angles are irregular as we find here. In many cases, as discussed for SnSe (above), in addition to three close contacts, Sn(II) enjoys additional long contacts to three atoms to complete a distorted octahedral environment. Such longer contacts are not found in either **1** or **2**, where the closest intermolecular Sn—E distances are 8.291(1) and 7.952(1) Å, respectively.

Several generalizations can be made regarding the structures of the two $[Sn(EC_6H_5)_3]^-$ anions. Firstly, they are both discrete and have the trigonal pyramidal coordination geometry expected for species of the VSEPR type AX_3E. Secondly, they both have all three phenyl groups in equatorial positions, and thirdly, they both have one Sn—E bond significantly longer than the other two with no apparent correlation with the angles at sulfur or selenium atoms. Finally, one Sn—E—CX1 angle is much larger than the other two. The same comments were made about the Pb structures (22), and we are inclined at present to attribute the variation in bond angles to packing forces, but we still have no explanation for the disparity in bond lengths.

Acknowledgments

We thank the Natural Sciences and Engineering Research Council of Canada for financial support of this work through grants to P.A.W.D. and N.C.P. High field ^{119}Sn nmr spectra were obtained at the S.W. Ontario NMR Centre, Guelph, funded by a Major Installation Grant from N.S.E.R.C.

1. T. COSTA, J. R. DORFMAN, K. S. HAGEN, and R. H. HOLM. Inorg. Chem. **22**, 4091 (1983).
2. D. COUCOUVANIS, D. SWENSON, N. C. BAENZIGER, D. G. HOLAH, A. KOSTIKAS, A. SIMOPOULOS, and V. PETROULEAS. J. Am. Chem. Soc. **98**, 5721 (1976).
3. D. SWENSON, N. C. BAENZIGER, and D. COUCOUVANIS. J. Am.

Chem. Soc. **100**, 1932 (1978).
4. S. CHOUDHURY, I. G. DANCE, P. J. GUERNEY, and A. D. RAE. Inorg. Chim. Acta, **70**, 227 (1983).
5. M. R. SNOW and J. A. IBERS. Inorg. Chem. **12**, 249 (1973).
6. K. S. HAGEN, D. W. STEPHAN, and R. H. HOLM. Inorg. Chem. **21**, 3928 (1982).
7. G. HENKEL, W. TREMEL, and B. KREBS. Angew. Chem. Int. Ed. Engl. **22**, 319 (1983).
8. K. S. HAGEN and R. H. HOLM. Inorg. Chem. **23**, 418 (1984).
9. I. G. DANCE and J. C. CALABRESE. J. Chem. Soc. Chem. Commun. 762 (1975).
10. I. G. DANCE. J. Am. Chem. Soc. **101**, 6264 (1979).
11. J. L. HENCHER, M. KHAN, F. F. SAID, and D. G. TUCK. Inorg. Nucl. Chem. Lett. **17**, 287 (1981).
12. K. S. HAGEN and R. H. HOLM. Inorg. Chem. **22**, 3171 (1983).
13. J. R. DORFMAN and R. H. HOLM. Inorg. Chem. **22**, 3179 (1983).
14. R. W. WIGGINS, J. C. HUFFMAN, and G. CHRISTOU. J. Chem. Soc. Chem. Commun. 1313 (1983).
15. G. CHRISTOU and J. C. HUFFMAN. J. Chem. Soc. Chem. Commun. 558 (1983).
16. I. G. DANCE. J. Chem. Soc. Chem. Commun. 103 (1976).
17. I. G. DANCE. J. Chem. Soc. Chem. Commun. 68 (1976).
18. I. G. DANCE. Aust. J. Chem. **31**, 2195 (1978).
19. J. J. I. ARSENAULT and P. A. W. DEAN. Can. J. Chem. **61**, 1516 (1983).
20. M. MULLER, R. J. H. CLARK, and R. S. NYHOLM. Transition Met. Chem. **3**, 369 (1978).
21. J. A. ZUBIETA and J. J. ZUCKERMAN. Prog. Inorg. Chem. **24**, 251 (1978).
22. P. A. W. DEAN, J. J. VITTAL, and N. C. PAYNE. Inorg. Chem. To be published.
23. P. B. HITCHCOCK, M. F. LAPPERT, B. J. SAMWAYS, and E. L. WEINBERG. J. Chem. Soc. Chem. Commun. 1492 (1983).
24. International tables of X-ray crystallography, Kynoch Press, Birmingham, England, Vol. I. 1969; Vol. IV. 1974.
25. Enraf-Nonius CAD4F users manual. Enraf-Nonius Delft, Delft, The Netherlands. 1982.
26. T. C. FURNAS. Single crystal orienter instruction manual. G. E. Company, Milwaukee, WI. 1966.
27. Enraf-Nonius structure determination package. SDP-PLUS, Version 1.0. 1982.
28. W. R. BUSING and H. A. LEVY. J. Chem. Phys. **26**, 563 (1957).
29. D. T. CROMER and D. LIBERMAN. J. Chem. Phys. **23**, 1891 (1970).
30. R. F. STEWART, E. R. DAVIDSON, and W. T. SIMPSON. J. Chem. Phys. **42**, 3175 (1965).
31. R. K. HARRIS and R. G. KIDD. *In* NMR and the periodic table. *Edited by* R. K. Harris and B. E. Mann. Academic Press, London. 1978. Chapt. 8.
32. D. COUCOUVANIS, C. N. MURPHY, and S. K. KANODIA. Inorg. Chem. **19**, 2993 (1980).
33. A. C. MCDONELL, T. W. HAMBLEY, M. R. SNOW, and A. G. WEDD. Aust. J. Chem. **36**, 253 (1983).
34. D. H. FARRAR and N. C. PAYNE. Inorg. Chem. **20**, 821 (1981).
35. J. D. DONALDSON. Prog. Inorg. Chem. **8**, 287 (1967).
36. M. VEITH and O. RECKTENWALD. Top. Curr. Chem. **104**, 3 (1982).

Nitrooctaethylporphyrins: synthesis, optical and redox properties

LIANG-CHU GONG AND DAVID DOLPHIN
Department of Chemistry, The University of British Columbia, 2036 Main Mall, Vancouver, B.C., Canada V6T 1Y6

Received April 13, 1984

LIANG-CHU GONG and DAVID DOLPHIN. Can. J. Chem. **63**, 401 (1985).

The reaction of zinc octaethylporphyrin with N_2O_4 in dichloromethane gives, in a stepwise reaction, the zinc complexes of mono-, di-, tri-, and tetra-nitrooctaethylporphyrins. Demetallation, under acidic conditions, gives the corresponding free base porphyrins. The *meso*-nitro groups exert both steric and electronic effects on the porphyrin macrocycle. Thus N-protonation of the nitrated species causes a distortion of the ring and gives an optical spectrum similar to that of protonated *meso*-aryl-substituted porphyrins. In addition, the nitro groups make the oxidation of the porphyrin ring more difficult and at the same time facilitate the ring reductions.

LIANG-CHU GONG et DAVID DOLPHIN. Can. J. Chem. **63**, 401 (1985).

La réaction du sel de zinc de l'octaéthylporphyrine avec le N_2O_4 dans le dichlorométhane conduit, par l'intermédiaire d'une série de réactions, aux complexes de zinc des mono-, di-, tri- et tétra-nitrooctaéthylporphyrines. La démétalation, en utilisant des conditions acides, conduit aux porphyrines correspondantes qui existent sous forme de bases libres. Les groupes nitro en positions *méso* exercent des effets à la fois stériques et électroniques sur le macrocycle de porphyrine. La N-protonation des espèces nitrées provoque donc une distortion du cycle et fournit un spectre optique semblable à celui des porphyrines protonées portant des substituants aryles en position *méso*. De plus, les groupes nitro rendent le cycle porphyrine moins susceptible à l'oxydation et ils facilitent les réductions des cycles.

[Traduit par le journal]

Porphyrins, like most other aromatic systems, undergo electrophilic substitution. However, as with all heteroaromatic systems, the competition between the basicity of the heteroatom and the nucleophilicity of the aromatic π-system can prevent many substitution reactions from occurring. A striking example of this is the faster rate of *meso*-substitution of octaethylporphyrin (OEP) in CH_3CO_2D compared to CF_3CO_2D (1)!

Electrophilic substitution at the porphyrin periphery has been recently reviewed (2) and, while a wide variety of reactions have been described, few high-yield reactions have been reported. The usually large effort that must be expended to prepare any porphyrin, other than the trivially easy reactions to generate *meso*-arylporphyrins (3), requires that further manipulations should be as efficient as possible. We report here on the convenient preparation of the nitrooctaethylporphyrins and the effect the electron-withdrawing groups have on the redox properties of the free bases and some metal complexes.

The direct nitration of OEP in fuming nitric acid/acetic acid gives good yields of 5-nitrooctaethylporphyrin (5-(NO_2)OEP (**1**)) with considerably diminished yields of the dinitroporphyrins 5,10-$(NO)_2$OEP (**2**) and 5,15-(NO_2)OEP (**3**). Under more forcing conditions (HNO_3/H_2SO_4), 20% of the 5,10,15-trinitrooctaethylporphyrin (**4**) can be formed but isolable amounts of the 5,10,15,20-tetranitroporphyrin (**5**) are not observed (4).

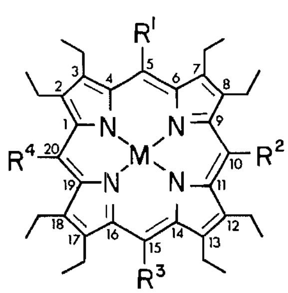

Compound	R^1	R^2	R^3	R^4	M
1	NO_2	H	H	H	H,H
2	NO_2	NO_2	H	H	H,H
3	NO_2	H	NO_2	H	H,H
4	NO_2	NO_2	NO_2	H	H,H
5	NO_2	NO_2	NO_2	NO_2	H,H
7	NO_2	H	H	H	Zn
8	NO_2	H	NO_2	H	Zn
9	NO_2	NO_2	NO_2	H	Zn
10	NO_2	NO_2	NO_2	NO_2	Zn

Metallation of the porphyrin reduces the nitrogen basicity and can allow for preferential attack of an electrophile at the porphyrin periphery. Indeed, the nature of the metal can direct preferential pyrrolic- or *meso*-substitution. An example of the rate difference that may be observed upon metallation is that in neat CF_3CO_2D a half-life of 275 h at 90°C is observed for exchange of the *meso*-protons of OEP while Cu(OEP) undergoes almost complete exchange of the *meso*-protons in 1:1 $CF_3CO_2D/CHCl_3$ at room temperature within 20 min (5). Watanabe *et al.* (6) have shown that the nitration of zinc octaethylporphyrin (ZnOEP) using zinc nitrate in acetic anhydride proceeds in 2 min to give low yields of a mixture of **1**, **3**, and **4**, while after 3 h 57% of **5** is obtained.

Despite the fact that aromatic electrophilic substitution is normally thought to proceed via carbocation intermediates, there is growing evidence that such reactions proceed via an initial electron transfer followed by coupling of the resultant radicals (7). In fact, for the nitration of aromatic compounds, more reactive than toluene, by NO_2^+, electron transfer appears to be the principal route (7). If mesitylene with an oxidation potential of 1.62 V (vs. Ag/Ag^+, in CH_3CN) is nitrated via single electron transfer reactions, then metalloporphyrins with their first oxidation potentials of $\sim$1.0 V(8) must surely be nitrated by mechanisms involving electron transfer. Earlier we showed (9), that treatment of MgOEP with N_2O_4 caused a one-electron oxidation to give the corresponding π-cation radical (**6**) (10), which in the presence of excess NO_2 gives 5-(NO_2)MgOEP. The simplest rationale is that the radical **6** couples with NO_2, itself a radical, to give the isoporphyrin cation yielding a *meso*-nitroporphyrin upon deprotonation.

As each successive *meso* position is nitrated, the rate of further oxidation to a π-cation radical is decreased (due to the increase in redox potential as successive nitro groups are added, see below). Thus the extent of nitration can be conveniently controlled by simply varying the concentration of NO_2. Reaction of ZnOEP with thallium(III) nitrate gives nitroporphyrins (11). These reactions also initially generate the porphyrin π-cation radical, but it was suggested (11) that the radicals might not be the source of the nitroporphyrins. Be that as it may, the reactions of metalloporphyrins with NO_2 provides an excellent route to nitroporphyrins, as detailed below, providing the reaction conditions in the experimental section are carefully followed, since in the presence of dichloromethane (12) nitromethylation may occur.

In the present study we have chosen to use ZnOEP rather than pursue the initial studies (9) with MgOEP since the former is more robust, being less readily demetallated and less susceptible to photochemical decomposition. Care must be taken during demetallation since acid catalyzed *nucleophilic* substitution of the nitro groups can readily occur (24).

Free base porphyrins give unstable π-cation radicals and are thus unsuitable for the nitration studies described here.

TABLE 1. ^{1}H nuclear magnetic resonance spectra[a]

Compound	*meso*-H	—CH_2—[b]	—CH_3[b]
1	10.25 (s, 2H)	4.11 (12H)	1.93 (18H)
	10.10 (s, 1H)	3.75 (4H)	1.69 (6H)
2	10.10 (s, 2H)	4.01 (8H)	1.87 (6H)
		3.70 (4H)	1.85 (6H)
		3.64 (4H)	1.61 (6H)
3	10.36 (s, 2H)	4.10 (8H)	1.94 (12H)
		4.71 (8H)	1.70 (12H)
4	10.08 (s, 1H)	3.96 (4H)	1.81 (6H)
		3.59 (4H)	1.55 (6H)
		3.56 (8H)	1.49 (6H)
			1.43 (6H)
5	—	3.38 (16H)	1.27 (24H)
7	9.84 (s, 2H)	4.08 (4H)	1.91 (6H)
	9.48 (s, 1H)	3.80 (8H)	1.78 (12H)
		3.79 (4H)	1.75 (6H)
8	10.29 (s, 2H)	4.08 (8H)	1.93 (12H)
		3.74 (8H)	1.69 (12H)
9	10.24 (s, 1H)	4.05 (4H)	1.91 (6H)
		3.68 (12H)	1.65 (6H)
			1.61 (6H)
			1.59 (6H)
10	—	3.54 (16H)	1.43 (24H)

[a]Chemical shifts δ (ppm) measured in dilute solutions of $CDCl_3$.
[b]All ethyl groups appeared as a quartet and a triplet with 8-Hz coupling.

Experimental

The nmr spectra were measured on a Varian XL-100 instrument, uv/vis spectra were recorded on a Cary 17 spectrometer, and the cyclic voltammograms were measured using tetra-*n*-propylammonium tetrafluoroborate in a three-electrode system as previously described (13). Oxidations were performed in CH_2Cl_2 (spectroscopic grade, distilled from calcium hydride) and reductions in DMF (reagent grade, dried over solid KOH, then distilled).

Zinc 5-nitrooctaethylporphyrin (**7**)

Octaethylporphyrin (2.34 g, 4.38 mmol) in dichloromethane (2340 mL) was treated with zinc acetate (2.14 g, 11.67 mmol) in methanol (13 mL). The mixture was stirred at room temperature for 1 h by which time metallation was complete (checked by tlc on silica gel using CH_2Cl_2/CCl_4 (1:3 v/v).

Thirty milliliters of a stock solution of 0.32 *N* NO_2 (Matheson Gas Products, Canada) in dichloromethane, determined titrimetrically (14), were diluted to 150 mL with dichloromethane and this dilute solution was added in one portion to the ZnOEP with rapid stirring at room temperature. The progress of the reaction was followed by tlc on silica gel (CH_2Cl_2/CCl_4 (1:3 v/v)). When all of the ZnOEP had been consumed (additional small aliquots of stock solution of NO_2 may need to be added to complete the reaction), the principal product was zinc 5-(NO_2)OEP (**7**). The reaction was stopped by the addition of 500 mL of saturated $NaHCO_3$. The organic phase was separated, washed with water (3 × 200 mL), and taken down to dryness on a rotary evaporator. The product was crystallized from $CHCl_3/CH_3OH$ and collected by filtration to give 1.46 g (52% yield). The filtrate may be used to make further nitrated products. *Anal.* calcd. for $C_{36}H_{43}N_5O_2Zn$: C 67.23, H 6.74, N 10.89; found: C 66.54, H 6.80, N 10.55.

Zinc 5,15-dinitrooctaethylporphyrin (**8**)

The same procedure as for **7**, above, was employed using 70 mL of the stock NO_2 solution to give 2.08 g (69% yield). The reaction was followed on silica gel tlc using CH_2Cl_2/CCl_4 (1:1 v/v). *Anal.* calcd. for $C_{36}H_{42}N_6O_4Zn$: C 62.83, H 6.15, N 12.21; found: C 62.87, H 6.13, N 12.06.

Zinc 5,10,15-trinitrooctaethylporphyrin (**9**)

The same procedure as for **8**, above, was employed using 140 mL of the stock NO_2 solution to give 1.59 g (49% yield). *Anal.* calcd. for $C_{36}H_{41}N_7O_6Zn{:}2CH_3OH$: C 57.25, H 6.20, N 12.30; found: C 56.60, H 6.05, N 12.71. The polar products **9** and **10** (below) crystallize with varying amounts of $CHCl_3$ and CH_3OH of crystallization.

Zinc 5,10,15,20-tetranitrooctaethylporphyrin (**10**)

The same procedure as for **3**, above, was employed using 170 mL of the stock NO_2 solution to give 3.24 g (95% yield). *Anal.* calcd. for $C_{36}H_{40}N_8O_8Zn{:}CH_3OH$: C 54.85, H 5.47, N 13.83; found: C 54.90, H 4.91, N 14.03.

5-Nitrooctraethylporphyrin (**1**)

Zinc 5-nitrooctaethylporphyrin (**7**) (100 mg) in glacial acetic acid (50 mL) was treated with concentrated hydrochloric acid (25 mL; 37%). After stirring at room temperature for half an hour, water (50 mL) was added. The organic layer was separated, washed with water (25 mL), saturated sodium bicarbonate (25 mL), and again with water (25 mL). The solvent was removed on a rotatory evaporator at room temperature and the residue was recrystallized from chloroform/methanol to give 72 mg (80%) of the product (**1**) identical, by electronic and mass spectra, to that previously reported (4).

5,15-Dinitrooctaethylporphyrin (**3**)

Zinc 5,15-dinitrooctaethylporphyrin (**8**) (103 mg) in methylene dichloride (100 mL) was treated with perchloric acid (10 mL, 72%). After stirring at room temperature for half an hour the solution was treated as for **1** above to give 78 mg of the product, **3**, identical, by electronic and mass spectra, to an authentic sample (4).

5,10-Dinitrooctaethylporphyrin (**2**)

The product was obtained from the filtrates, during the preparation of **3** reported above, by preparative tlc on silica gel (200 × 200 × 1 mm) using CH_2Cl_2/CCl_4 (1:3 v/v) to give less than 5% of material identical, by electronic and mass spectra, to an authentic sample (4).

5,10,15-Trinitrooctoethylporphyrin (**4**)

The same procedure as for **2** above gave 76 mg of the product (83%)

TABLE 2. Electronic spectra[a]

Zinc complexes						
ZnOEP		331(4.28),	402(5.63),	490(3.51),	532(4.21),	569(4.39)
7		350(4.36),	401(5.42),	497(3.37sh),	534(4.17),	573(4.30)
8		352(4.43sh),	404(5.29),	503(3.32sh),	539(4.15),	576(4.29)
9	264(4.52),	360(4.61sh),	413(5.15),	510(3.35sh),	547(4.16),	571(4.07)
10	260(4.07),	370(4.69sh),	426(5.09),	520(3.43sh),	561(4.15),	580(4.01)
Free bases						
OEP		397(5.57),	497(4.14),	531(4.04),	566(3.82),	620(3.69)
1	270(3.79),	396(5.08),	502(4.05),	537(3.88),	571(3.74),	624(3.67)
2	273(3.85),	380(5.14),	504(4.10),	538(3.97),	575(3.76),	629(3.82)
3	273(3.70),	381(4.93),	507(3.92),	537(3.64),	578(3.57),	629(3.32)
4	272(4.07),	385(4.99),	512(4.01),	540(3.79),	589(3.64),	637(3.33)
5	268(4.00),	426(4.82),	529(3.97),	572(3.58sh),	611(3.57),	666(3.04)
Protonated derivatives						
OEP		405(5.75),	514(3.23sh),	548(4.19),	591(3.74)	
1		414(5.26),	520(3.33sh),	559(4.05),	609(3.82)	
2		427(5.27),	535(3.43sh),	571(4.03),	621(4.04)	
3		435(5.01),	538(3.23sh),	576(3.89),	622(3.59)	
4	230(4.18),	444(5.09),	550(3.39sh),	588(3.98),	637(3.72)	
5	299(4.10),	458(5.00),	580(3.35sh),	609(3.93),	660(3.66)	

[a] λ_{max} nm (log ϵ).

identical, by electronic and mass spectra, to an authentic sample.

5,10,15,20-Tetranitrooctaethylporphyrin (**5**)

As for **2** above giving 81% of the product identical, by electronic and mass spectra, to an authentic sample (6).

Discussion

The powerfully electron-withdrawing nitro groups can be expected to modify the properties of the substituted porphyrins by decreasing the electron density in the aromatic π-system. However, the electron-withdrawing properties of the nitro group in such a sterically encumbered situation may be less than traditionally measured by the electrophilic substituent constants (σ). Indeed, even though σ_m for the nitro group (0.71) is greater than that of the cyano (0.56; ref. 15), the *meso*-protons of 5-cyano-OEP are more deshielded, as indicated by the ^{1}Hmr spectrum (δ 9.98 and 9.89; ref. 16), than those of **1** (10.25 and 10.10) which in turn are more deshielded than those of the parent OEP. This reflects both electronic and steric effects of the nitro group but it is clear from the nmr data (Table 1) that these effects are small and cannot be readily separated.

The optical spectra on the other hand (Table 2) show dramatic changes as the *meso*-positions are progressively substituted by nitro groups. In every case each additional nitro group causes both a bathochromic shift and weakening in intensity of all of the visible bands. While the Soret bands become weaker and broader with increasing substitution, an initial hypsochromic followed by a bathochromic shift was observed for the free bases. With the diprotonated species a bathochromic shift and decrease in intensity (associated with band broadening) was observed in all cases (Table 2). However, in the case of the zinc complexes the extent of both the bathochromic shifts and band broadening is far less (Table 2). This suggests that the major perturbations in all cases are steric rather than electronic. The zinc complexes, which are required to remain "essentially coplanar", will not allow the π-system of the nitro group to become coplanar with the aromatic π-system. However, with both the free bases and the diprotonated salts considerably more distortion may occur, as reflected by the optical spectra. The same effect is shown by the sterically crowded 2,3,7,8,12,13,17,18-octamethyl-5,10,15,20-tetraphenylporphyrin (**12**) (17) and the corresponding octaethyl derivative (18). Indeed, the optical spectra of **5** and **12** are quite similar (Fig. 1). A

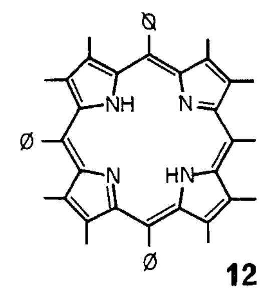

12

major difference between *meso*-tetraarylporphyrins and octaalkyl-like porphyrins is that in the former case the diprotonated salts are green and the latter violet in solution. This dramatic change in color results from quite different optical spectra of the two classes of diprotonated salts. Figure 2 shows the spectra of the protonated forms of **5** and *meso*-tetra-*N*(methyl-4-pyridyl)porphyrin (**14**). The latter two compounds show similar spectra which are quite different from that of protonated OEP (Table 2). There has been much speculation as to the source of this difference upon protonation. But it is clear, from the above results and from an examination of the optical spectra of compounds such as $N_aN_bN_c$-trimethyl-*meso*-tetraphenylporphyrin iodide (19), that the major optical changes that *meso*-aryltetraphenylporphyrins and *meso*-nitrooctaethylporphyrins undergo upon protonations result from the distortion from planarity of the porphyrin macrocyle, aided both by the electrostatic repulsion of the positively charged inner nitrogens and the steric interaction between the *meso*- and β-substituents, a conclusion reached by Meot-Ner and Adler (20) and Bonnett

TABLE 3. Redox potentials[a]

	Half-wave potentials[b,c]			
Compound	$E^{ox}_{1/2}(1)$	$E^{ox}_{1/2}(2)$	$E^{red}_{1/2}(1)$	$E^{red}_{1/2}(2)$
OEP	1.04	1.54	−1.19	−1.66
1	1.23	1.62	−0.85	
3	1.45	1.68	−0.49	
4	1.57		−0.22	
5	1.73		−0.12	
ZnOEP	0.87	1.19	−1.47	−1.86
7	1.01	1.30	−1.02	
8	1.16	1.42	−0.78	
9	1.31	1.50	−0.50	
10	1.49		−0.28	

[a]Potentials were measured against Ag/AgCl at a scan rate of 100 mV/s.
[b]Oxidation was measured in CH_2Cl_2 (dried over CaH_2)/tetra *n*-propylammonium fluoroborate.
[c]Reduction was measured in DMF (distilled from KOH)/ tetra *n*-propylammonium fluoroborate.

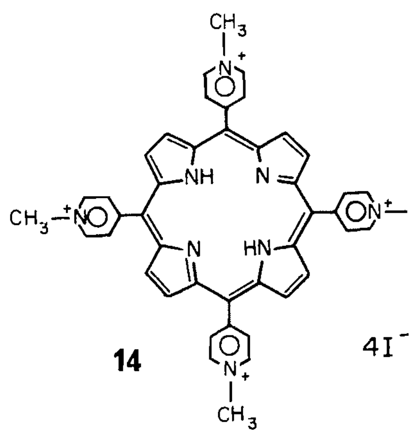

14

and Stephenson (4). A well-characterized example of this phenomenon was shown by the X-ray crystal studies of both protonated and distorted *meso*-tetraphenyl and *meso*-tetra-4-pyridylporphyrins (21).

While the electronic properties of the nitro groups do not have a major influence on the electronic spectra, they exert a major influence on the redox properties of both the free base and zinc complexes. The majority of metalloporphyrins show two sequential and reversible one-electron oxidation and reduction steps. Fuhrhop *et al.* (22) have noted, for a wide range of metallooctaethylporphyrins, that $E^{ox}_{1/2}(2) - E^{ox}_{1/2}(1)$ is roughly constant at about 300 mV for ring oxidations and is similarly constant for porphyrin ring reduction where $E^{red}_{1/2}(2) - E^{red}_{1/2}(1) = 0.4-0.5$ V. Furthermore, when only ring redox processes are involved, $E^{ox}_{1/2}(1) - E^{red}_{1/2}(2)$ is about 2 V. As can be seen from Table 3, all of the redox processes listed are close to these values, suggesting in each case that ring redox processes are being observed. However, the reduction waves in every case correspond to a two-electron process. All of the reductive electrode processes were quasi-reversible as were oxidations of the zinc complexes. But, as is often the case, the oxidation of the free bases was followed by a chemical reaction, making the process irreversible. It is clear that the nitro groups are exerting a considerable electronic effect in these redox processes, as can be seen from the monotonic increase in the oxidation potentials and decrease in the reduction potentials with increasing nitro substitution. The redox potentials of a large number of free-base porphyrins have recently been collected (23). It is interesting to note, for a variety of *meso*- and β-substituents, that the *meso*-tetra(*N*-methyl-4-pyridyl)porphyrin was the most readily reduced ($E^{red}_{1/2}(1) = -1.01$ V) and that, like our systems, it showed only a single two-electron reduction wave unlike the majority of porphyrins which show two one-electron waves.

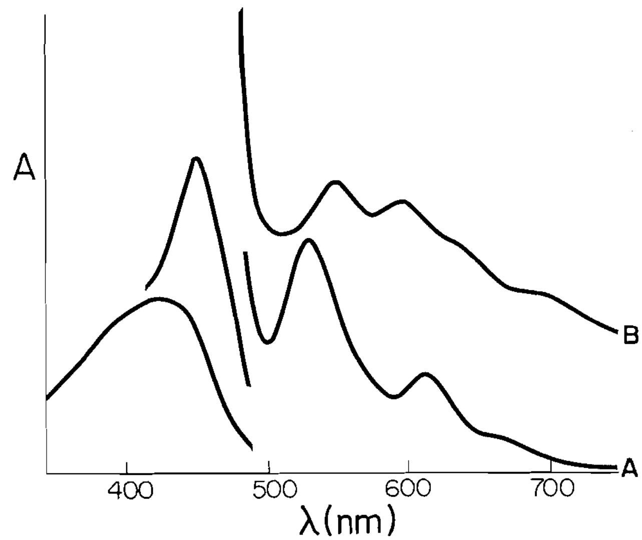

FIG. 1. Optical spectra (CH_2Cl_2) of A, *meso*-tetranitrooctaethylporphyrin (**5**), and B, *meso*-tetraphenyloctamethylporphyrin (**12**). Region below 500 nm was recorded at an attenuation of ten.

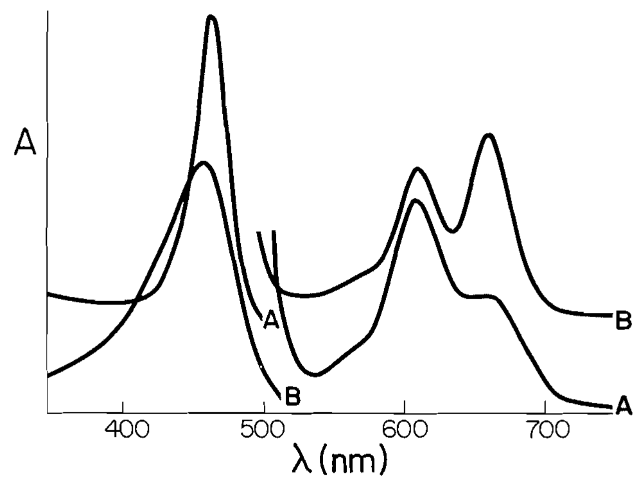

FIG. 2. Optical spectra (CH_2Cl_2, 1% TFA) of protonated **5** and protonated **14**. Region below 500 nm was recorded at an attenuation of ten.

We prepared these variously nitrated porphyrins anticipating that ring oxidations would become more difficult and ring reduction easier. Since this has proved to be the case we expect, for the future, that these systems may be useful for the preparation of metalloporphyrins having metals in unusually high oxidation states.

Acknowledgements

This work was supported by the United States National Institute of Health GM 29198 and the Natural Sciences and Engineering Research Council of Canada. We also gratefully acknowledge the support of the People's Republic of China during Liang-chu Gong's leave of absence from the Chemistry Department of the East China Normal University, Shanghai, while a visiting Chinese Scholar at U.B.C.

1. J. B. PAINE and D. DOLPHIN. J. Am. Chem. Soc. **93**, 4080 (1971).
2. J.-H. FUHRHOP. *In* The porphyrins. Vol. II. *Edited by* D. Dolphin. Academic Press, New York. 1978. pp. 131–159.
3. A. D. ADLER, E. R. LONGO, F. KAMPAS, and J. KIM. J. Inorg. Nucl. Chem. **32**, 2443 (1970).
4. R. BONNETT and G. F. STEPHENSON. J. Org. Chem. **30**, 3282 (1965).
5. R. GRIGG, A. SWEENEY, and A. W. JOHNSON. Chem. Commun. 1237 (1970).
6. E. WATANABE, S. NISHIMURA, H. OGOSHI, and Z. YOSHIDA. Tetrahedron, **31**, 1385 (1975).
7. C. L. PERRIN. J. Am. Chem. Soc. **99**, 5516 (1977).
8. D. G. DAVIS. *In* The Porphyrins. *Edited by* D. Dolphin. Academic Press, New York. 1978. pp. 127–152.
9. E. C. JOHNSON and D. DOLPHIN. Tetrahedron Lett. **26**, 2197 (1976).
10. D. DOLPHIN and R. H. FELTON. Acc. Chem. Res. **7**, 26 (1974).
11. B. EVANS, K. M. SMITH, and J. A. S. CAVALEIRO. J. Chem. Soc. Perkin Trans. **1**, 768 (1978).
12. J. C. FANNING, F. S. MANDEL, and T. L. CRAY. Tetrahedron, **35**, 1251 (1979).
13. D. DOLPHIN, Z. MULJIANI, K. ROUSSEAU, D. C. BORG, J. FAJER, and R. H. FELTON. Ann. N.Y. Acad. Sci. **206**, 177 (1973).
14. C. A. STREULI and P. R. AVERELL. *In* The analytical chemistry of nitrogen and its compounds. Part I. Wiley, New York. 1970. p. 99.
15. H. C. BROWN and Y. OKAMOTO. J. Am. Chem. Soc. **80**, 4979 (1958).
16. H. J. CALLOT, A. LOUATI, and M. CROSS. Tetrahedron Lett. **21**, 3281 (1980).
17. D. DOLPHIN. J. Heterocycl. Chem. **7**, 275 (1970).
18. B. EVANS, K. M. SMITH, and J.-H. FUHRHOP. Tetrahedron Lett. 443 (1977).
19. H. M. G. AL-HAZIMI, A. H. JACKSON, A. W. JOHNSON, and M. WINTER. J. Chem. Soc. Perkin Trans. **1**, 98 (1977).
20. M. MEOT-NER and A. D. ADLER. J. Am. Chem. Soc. **97**, 5107 (1975).
21. A. STONE and E. B. FLEISCHER. J. Am. Chem. Soc. **90**, 2735 (1968).
22. J.-H. FUHRHOP, K. M. KADISH, and D. G. DAVIS. J. Am. Chem. Soc. **95**, 5140 (1973).
23. P. WORTHINGTON, P. HAMBRIGHT, R. F. X. WITHAMS, J. REID, C. BURNHAM, A. SHAMIN, J. TURAY, D. M. BELL, and R. KIRKLAND. J. Inorg. Biochem. **12**, 281 (1980).
24. L.-C. GONG and D. DOLPHIN. Can. J. Chem. **63**, 406 (1985).

Nucleophilic substitution of *meso*-nitrooctaethylporphyrins

LIANG-CHU GONG AND DAVID DOLPHIN

Department of Chemistry, The University of British Columbia, 2036 Main Mall, Vancouver, B.C., Canada V6T 1Y6

Received April 13, 1984

LIANG-CHU GONG and DAVID DOLPHIN. Can. J. Chem. **63**, 406 (1985).

Nitrooctaethylporphyrins readily undergo nucleophilic aromatic substitution in the presence of HCl or HBr. In the presence of methoxide, nucleophilic addition to give a porphodimethane occurs, followed by autoxidation to the methoxyporphyrin. Unlike the nitrated complexes, the chlorosubstituted porphyrins exhibit redox potentials similar to those of unsubstituted analogs. *Meso*-halogenated porphyrins do, however, show steric distortion due to the bulk of the halogen atoms.

LIANG-CHU GONG et DAVID DOLPHIN. Can. J. Chem. **63**, 406 (1985).

En présence de HCl ou de HBr, les nitrooctaéthylporphyrines subissent facilement des réactions de substitutions aromatiques nucléophiles. En présence d'ions méthylates, il se produit une addition nucléophile conduisant à un porphodiméthane; cette réaction est suivie d'une auto-oxydation qui conduit à une méthoxyporphyrine. Contrairement au comportement observé avec les complexes nitrés, les potentiels rédox des chloroporphyrines sont semblables à ceux de leurs analogues qui ne sont pas substitués. Par contre, les porphyrines portant des halogènes dans les positions *méso* présentent une distortion stérique qui est due à l'encombrement des atomes d'halogènes.

[Traduit par le journal]

Introduction

The chemistry of porphyrins, like that of most aromatic systems, is dominated by electrophilic substitution (1) and, like most other aromatic systems nucleophilic substitution is far less frequently observed. Indeed, in porphyrin chemistry only one or two authentic examples of nucleophilic substitution are known and these occur under special circumstances, as with the relief of considerable steric strain (2). We have shown that when the porphyrin HOMO is depleted of both electrons, to give the π-dication, facile nucleophilic substitution occurs to give an intermediate isoporphyrin (3) which will either be stable or lose a proton to give a substituted porphyrin (4). Even when only one electron is removed from the HOMO, to give a porphyrin π-cation radical, nucleophilic substitution occurs but by more complex mechanisms (4–6). We report here on the nucleophilic substitution of free base porphyrins where, as with benzenoid systems, nucleophilic attack is aided by the powerfully electron-withdrawing nitro group.

Experimental

All chemicals were reagent grade; nitrooctaethylporphyrins were prepared as reported earlier (7). The ^{1}H nmr spectra were measured on a Varian XL-100 spectrometer with the exception of that of 5,10-dichloro-15-nitrooctaethylporphyrin, which was measured on a Bruker WH 400 spectrometer. Mass spectra were measured on a Varian MAT CH 4B instrument. Electronic spectra were measured on a Cary 17 spectrometer and the cyclic voltammograms were measured under the conditions previously described (7). Microanalyses were performed by Peter Borda (U.B.C.)

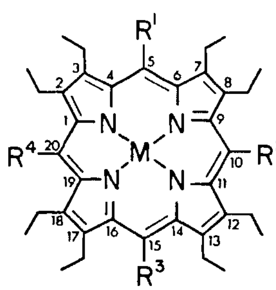

Compound	R¹	R²	R³	R⁴
1	NO_2	NO_2	NO_2	NO_2
2	Cl	NO_2	NO_2	NO_2
4	Cl	Cl	NO_2	NO_2
5	Cl	Cl	Cl	NO_2
6	Cl	Cl	Cl	Cl
7	Cl	Cl	Cl	H
8	NO_2	NO_2	NO_2	H
9	Cl	Cl	NO_2	H
10	Cl	H	NO_2	H
11	NO_2	H	NO_2	H
12	Br	Br	NO_2	NO_2
15	CH_3O	H	NO_2	H

5-Chloro-10,15,20-trinitrooctaethylporphyrin (2)

5,10,15,20-Tetranitrooctaethylporphyrinato zinc (**1**) (7) (100 mg, 0.13 mmol) was placed in glacial acetic acid (100 mL) and dichloromethane (50 mL). The solution was cooled to 10°C and concentrated hydrochloric acid (10 mL, 37%) was added. The mixture was stirred at 10°C for 1 h. Dichloromethane (50 mL) was added and the organic layer was washed with water, saturated sodium bicarbonate, and then water. The organic phase was reduced in volume and the product crystallized by the addition of methanol to give **2** (52 mg, 57%). An analytical sample was recrystallized from dichloromethane/methanol; uv/vis CH_2Cl_2 (log ϵ): 255 sh (3.39), 270 (3.51), 436 (4.69), 538 (3.74), 568 sh (3.51), 617 (3.41), 682 (2.85); CH_2Cl_2/TFA (log ϵ): 268 sh (3.63), 293 (3.29), 467 (4.84), 560 sh (3.19), 615 (3.68), 678 (3.63); ^{1}H nmr: 1.18 (t, 6H), 1.23 (t, 6H), 1.25 (t, 12H), 3.30 (q, 12H), 3.69 (q, 4H); ms: 703 (80), 657 (75), 549 (100). *Anal.* calcd. for $C_{36}H_{42}N_7O_6Cl$: C 61.40, H 6.01, N 13.91, Cl 5.03; found: C 61.01, H 6.27, N 14.11, Cl 5.45.

Reaction of zinc tetranitrooctaethylporphyrin (1) with hydrofluoric acid

5,10,15,20-Tetranitrooctaethylporphyrinato zinc (**1**) (7) (100 mg, 0.13 mmol) was placed in a mixture of glacial acetic acid (100 mL), hydrofluoric acid (15 mL, 48.8%), and dichloromethane (500 mL). The mixture was stirred for 24 h, after which the organic layer was washed with water, saturated sodium bicarbonate, and then water. The organic layer was reduced in volume and chromatographed on a silica column using dichloromethane. The first fraction was unreacted starting material. The second fraction was rechromatographed on silica (200 × 200 × 1 mm) using CH_2Cl_2/CCl_4 (1:3 v/v) to give **2** (9.3 mg, 10%). Finally, elution of the column with methanol gave octaethylxanthoporphyrinogen (**3**) (20 mg, 26%). No fluorine-containing porphyrins were observed.

5,10-Dichloro-15,20-dinitrooctaethylporphyrin (4)

5,10,15,20-Tetranitrooctaethylporphyrinato zinc (**1**) (7) (100 mg) was placed in a mixture of glacial acetic acid (100 mL) and hydrochloric acid (15 mL, 37%). The mixture was stirred at room temperature for 1 h. Dichloromethane (50 mL) was added and the organic phase washed with water, saturated sodium bicarbonate, and then water. The solution was taken to dryness and the residue crystallized from chloroform/petroleum ether (30–60°C) to give 55 mg (55%) of product; uv/vis CH_2Cl_2 (log ε): 270 (3.39), 305 (3.99), 440 (4.84), 546 (3.80), 575 (3.73), 612 (3.65), 685 sh (2.98); CH_2Cl_2/TFA (log ε): 275 (3.98), 300 (3.99), 467 (5.06), 570 sh (3.40), 611 (3.84), 678 (3.84); ^{1}H nmr: 1.18 (t, 6H), 1.21 (t, 6H), 1.42 (t, 6H), 3.22 (q, 8H), 3.54 (q, 4H), 3.63 (q, 4H); ms: 692 (90), 547 (90), 602 (90), 565 (90), 564 (90), 549 (100). *Anal.* calcd. for $C_{36}N_{42}N_6O_4Cl_2$: C 62.33, H 6.10, N 12.12, Cl 10.22; found: C 62.26, H 6.03, N 11.85, Cl 9.90.

5,10,15-Trichloro-20-nitrooctaethylporphyrin (5)

5,10,15,20-Tetranitrooctaethylporphyrinato zinc (**1**) (7) (100 mg) was placed in a mixture of glacial acetic acid (100 mL) and hydrochloric acid (30 mL, 37%). The reaction mixture was stirred for 50 h at room temperature in the dark. Water (300 mL) was added and the mixture filtered. The residue was dissolved in dichloromethane and the organic phase washed with saturated sodium bicarbonate and water. The solvent was removed under reduced pressure and the residue crystallized from chloroform/methanol. This product was then chromatographed on silica (200 × 200 × 1 mm) using benzene/hexane (2:1, v/v). The main (second) band was extracted and crystallized from chloroform/methanol to give 54 mg (62%); uv/vis CH_2Cl_2 (log ε): 274 (4.39), 304 (4.37), 442 (5.29), 548 (4.20), 591 (4.10), 630 sh (3.90), 703 (3.09); CH_2Cl_2/TFA (log ε): 280 (4.36), 307 (4.33), 462 (5.48), 573 sh (3.75), 612 (4.09), 684 (4.42); ^{1}H nmr: 1.17 (t, 6H), 1.42 (t, 12H), 1.46 (t, 6H), 3.18 (q, 4H), 3.52 (q, 8H), 3.60 (q, 4H); ms: 683, 681 (100), 637, 635 (70), 601 (20). *Anal.* calcd. for $C_{36}H_{42}N_5O_2Cl_2\cdot 3H_2O$: C 58.66, H 6.56, N 9.50, Cl 14.43; found: C 58.59, H 6.70, N 9.56, Cl 16.31.

5,10,15,10-Tetrachlorooctaethylporphyrin (6)

5,10,15,20-Tetranitrooctaethylporphyrinato zinc (**1**) (7) (50 mg) was placed in a mixture of glacial acetic acid (50 mL) and hydrochloric acid (15 mL, 37%). The mixture was heated in an oil bath at 100°C for 7 h. After cooling, water (400 mL) was added and the green solid collected by filtration. The filtrate was extracted with ether and the residue dissolved in ether. The combined ether layers were washed with saturated sodium bicarbonate, then water, and dried over Na_2SO_4. The ether was removed and the residue chromatographed on silica (200 × 100 × 1 mm) using dichloromethane/carbon tetrachloride (1:2 v/v). The major (third) green band was removed and crystallized from chloroform/methanol to give 13.7 mg (31%). The product was identical to an authentic sample (8); uv/vis CH_2Cl_2 (log ε): 280 (4.12), 306 (4.06), 356 (4.29), 446 (5.18), 550 (3.92), 593 (3.89), 640 sh (3.44), 714 (3.58); CH_2Cl_2/TFA (log ε): 283 (4.18), 312 (4.07), 401 (4.20), 457 (5.32), 582 sh (3.32), 629 (3.80), 684 (4.36).

5,10,15-Trichlorooctaethylporphyrin (7)

5,10,15,20-Tetranitrooctaethylporphyrinato zinc (**8**) (7) (50 mg) was placed in glacial acetic acid (50 mL) and treated with concentrated hydrochloric acid (15 mL, 37%). The solution was heated at 100°C for 6 h. After cooling, the product was isolated, as above, and purified on silica (200 × 200 × 1 mm) using benzene/hexane (2:1 v/v). The major band, after crystallization from methanol/chloroform, gave 14.8 mg (31%) of the product identical to an authentic sample (8); uv/vis CH_2Cl_2 (log ε): 268 (400), 299 (3.99), 348 sh (4.24), 430 (5.17), 532 (4.03), 572 (3.83), 611 (3.60), 672 (3.21); CH_2Cl_2/TFA (log ε): 273 (4.05), 395 sh (3.58), 443 (5.33), 554 sh (3.49), 595 (3.92), 652 (4.09). An additional 12.2 mg of 5,10-dichloro-15-nitrooctaethylporphyrin (**9**) (see below) was recovered from the tlc plate.

5,10-Dichloro-15-nitrooctaethylporphyrin (9)

5,10,15-Trinitrooctaethylporphyrinato zinc (**8**) (7) (100 mg) was stirred for 1 h at room temperature with a mixture of glacial acetic acid (80 mL) and hydrochloric acid (30 mL, 37%). Dichloromethane (40 mL) and water (200 mL) were added. The organic layer was separated, washed with saturated sodium bicarbonate, water, and then dried over sodium sulphate. After filtration, the solvent was removed and the residue was dissolved in benzene (5 mL); methanol (10 mL) was added and the solution stored at 4°C for 12 h. The precipitate was collected and chromatographed on silica (200 × 200 × 1 mm) using dichloromethane/carbon tetrachloride (1:3 v/v). The major band was recrystallized from chloroform/methanol to give 65 mg (73%) of the product (**9**); uv/vis CH_2Cl_2 (log ε): 263 (3.98), 300 sh (3.99), 423 (5.06), 528 (4.00), 569 (3.76), 604 (3.71), 607 (3.12); CH_2Cl_2/TFA (log ε): 271 (4.02), 447 (5.22), 550 (3.49), 591 (3.98), 6647 (3.99); ^{1}H nmr: 1.25 (t, 3H), 1.41 (t, 3H), 1.46 (t, 3H), 1.53 (t, 3H), 1.61 (t, 3H), 1.63 (t, 3H), 1.64 (t, 3H), 1.66 (t, 3H), 3.37 (9, 2H), 3.39 (q, 2H), 3.66 (q, 2H), 3.71 (q, 2H), 3.72 (q, 2H), 3.77 (q, 2H), 3.79 (q, 2H), 3.92 (q, 2H), 9.44 (s, 1H). *Anal.* calcd. for $C_{36}H_{43}N_5O_2Cl_2$: C 66.66, H 6.68, N 10.30, Cl 10.93; found: C 66.84, H 6.48, N 10.92, Cl 10.77.

5-Chloro-15-nitrooctaethylporphyrin (10)

5,15-Dinitrooctaethylporphyrinato zinc (**11**) (7) (50 mg) was placed in a mixture of glacial acetic acid (50 mL) and hydrochloric acid (15 mL, 37%). The mixture was heated at 100°C for 3.5 h. After cooling and washing with saturated sodium bicarbonate and water the organic phase was taken to dryness and the residue crystallized from chloroform/methanol to give 25.1 mg of **10** (51%); uv/vis CH_2Cl_2 (log ε): 250 sh (3.95), 274 (3.80), 405 (5.15), 510 (4.13), 544 (3.80), 581 (3.77), 634 (3.42); CH_2Cl_2/TFA (log ε): 268 sh (3.85), 429 (5.30), 540 (3.42), 574 (4.07), 621 (3.81); ^{1}H nmr: 1.68 (t, 6H), 1.86 (t, 6H), 1.89 (t, 6H), 1.93 (t, 6H), 3.70 (q, 4H), 4.08 (q, 4H), 4.10 (q, 4H), 4.22 (q, 4H), 10.25 (s, 2H). *Anal.* calcd. for $C_{36}H_{44}N_5O_2Cl$: C 70.40, H 7.22, N 11.40; found: C 70.17, H 7.34, N 11.20.

5,10-Dibromo-15,20-dinitrooctaethylporphyrin (12)

The reaction was carried out in the same way as for the preparation of the corresponding dichloro derivative (**4**) but using 48% HBr; 10% of octaethylxanthoporphyrinogen (**3**) and 20% of the product (**12**) were isolated; ^{1}H nmr: 1.14 (t, 6H), 1.19 (t, 6H), 1.30 (t, 6H), 1.44 (t, 6H), 3.10 (q, 8H), 3.30 (1, 4H), 3.52 (q, 4H). *Anal.* calcd. for $C_{36}H_{442}N_6O_4Br_2$: C 55.25, H 5.41, N 10.74, Br 20.43; found: C 55.27, H 5.82, N 11.10, Br 21.07.

5-Methoxy-15-nitrooctaethylporphyrinato zinc(II) (13)

5-Nitrooctaethylporphyrinato zinc (**14**) (7) (100 mg) was dissolved in dry THF (50 mL) and 8 *M* NaOMe in methanol (5 mL) was added. Solvent was evaporated by a stream of nitrogen until solid sodium methoxide appeared. The mixture was then refluxed and stirred. The progress of the reaction was monitored by tlc on silica gel (CH_2Cl_2/CCl_4 1:3 (v/v)) and the reaction continued until the starting material disappeared. After 6 h the mixture was cooled, dry THF (50 mL) was added, and the mixture was filtered through silica gel. The silica was washed with THF and the combined filtrates were taken down to dryness. The residue was chromatographed on silica gel (200 × 200 × 1 mm) using dichloromethane/carbon tetrachloride 1:3 (v/v). The major band was extracted and crystallized from dichloromethane/hexane to give 39 mg (37%) of product; uv/vis CH_2Cl_2 (log ε): 250 sh (4.07), 346 (4.32), 408 (4.46), 502 sh (3.41), 539 (4.22), 577 (3.92); ^{1}H nmr: 1.70 (t, 6H), 1.86 (t, 6H), 1.90 (t, 6H), 1.94 (t, 6H), 3.73 (q, 4H), 4.10 (q, 12H), 4.41 (s, 3H), 10.20 (s, 2H); ms: 671 (60), 656 (25), 641 (50), 626 (100), 611 (60). *Anal.* calcd. for $C_{37}H_{45}N_5O_3Zn$: C 66.02, H 6.74, N 10.48; found: C 66.11, H 7.02, N 10.40.

5-Methoxy-15-nitrooctaethylporphyrin (15)

5-Methoxy-15-nitrooctaethylporphyrin zinc (30 mg) was dissolved in methylene chloride (25 mL) and then trifluoroacetic acid (1 mL) was added with stirring. After 10 min the solution was washed with water, sodium bicarbonate, and again with water. The organic phase

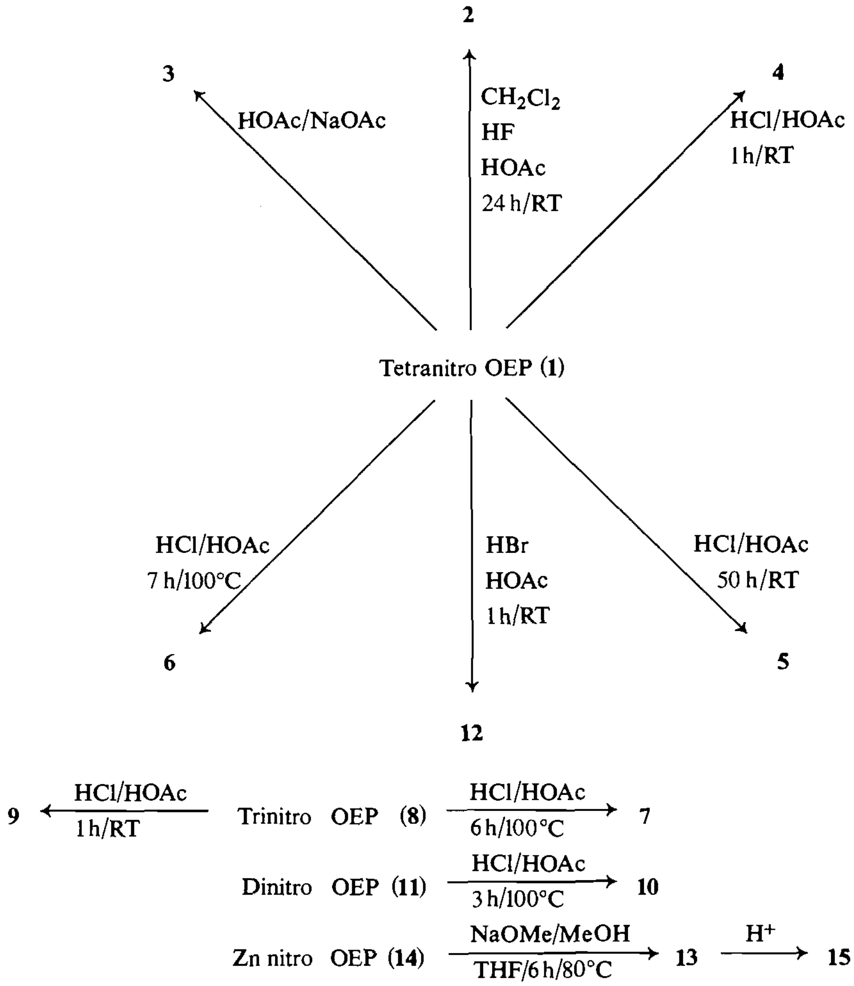

SCHEME 1

was dried over Na_2SO_4, filtered, and the filtrate taken down to dryness. The product was crystallized from chloroform/methanol to give 22.9 mg (84%) of **15**; uv/vis CH_2Cl_2 (log ϵ): 250 (3.99), 275 (3.83), 404 (5.15), 508 (4.19), 542 (3.66), 577 (3.79), 631 (3.09); CH_2Cl_2/TFA (log ϵ): 427 (5.22), 537 (3.47 sh), 573 (4.03), 622 (3.82); ^1H nmr: 1.68 (t, 6H), 1.82 (t, 6H), 1.87 (t, 6H), 1.91 (t, 6H), 3.70 (q, 4H), 4.08 (q, 12H), 4.48 (s, 3H), 10.18 (s, 2H); ms: 609 (100), 594 (25), 579 (35), 564 (60), 548 (20). *Anal.* calcd. for $C_{37}H_{47}N_5O_3$: C 72.87, H 7.77, N 11.49; found: C 73.04, H 7.69, N 11.21.

Results and discussion

Several mechanistic pathways to achieve nucleophilic aromatic substitution are known (9, 10). In general, when the aromatic system bears strongly electron-withdrawing groups (such as nitro) an addition–elimination (activated) mechanism is seen. Formation of Jackson–Meisenheimer complexes is now well established, though in many cases the initially formed (kinetically controlled) complexes are in equilibrium with the thermodynamically more stable complex which leads to product formation. The stability of the delocalized anion of the Meisenheimer complex is the driving force for the reaction and the collapse of the anion and loss of the leaving group gives the net nucleophilic substitution.

The loss of nitro groups during such reactions is well known, and, indeed, the leaving group ability of the nitro group can be about 200 times greater than that of chloride (11). Scheme 1 outlines the nucleophilic substitutions observed in this study. In the presence of HCl, tetranitrooctaethylporphyrin[1] can be made to undergo stepwise replacement of each nitro by a chloro group. As subsequent nitro groups are placed on the porphyrin ring more vigorous conditions must be employed for further substitution, suggesting that the rate-limiting step is indeed the formation of the corresponding Jackson–Meisenheimer complex. The monochloro-trinitro derivative gives only the 5,10-dinitrooctaethylporphyrin and none of the more symmetric "5,15" isomer. Scheme 2 shows some of the canonical resonance structures of intermediates for both of these reactions. Delocalization of the negative charge onto the nitro group, which leaves all atoms with an octet of electrons, is possible on both nitro groups for both intermediates. However, attack at the 10-position generates a symmetric canonical form (favoured) where both halves represent stable dipyrromethenium moieties with the charges, resulting from protonation, distributed one on each "dipyrromethene". On the other hand, attack at the 15-position gives a higher energy canonical form (disfavoured) in which there is a "pyrrolic unit" and a "tripyrromethene" bearing both charges. Thus, formation of the 5,10-dichloro isomer is favoured thermodynamically as well as statistically.

[1] The zinc complex **1** was used in these studies as a matter of convenience. It is, however, immediately demetallated under the acid reaction conditions.

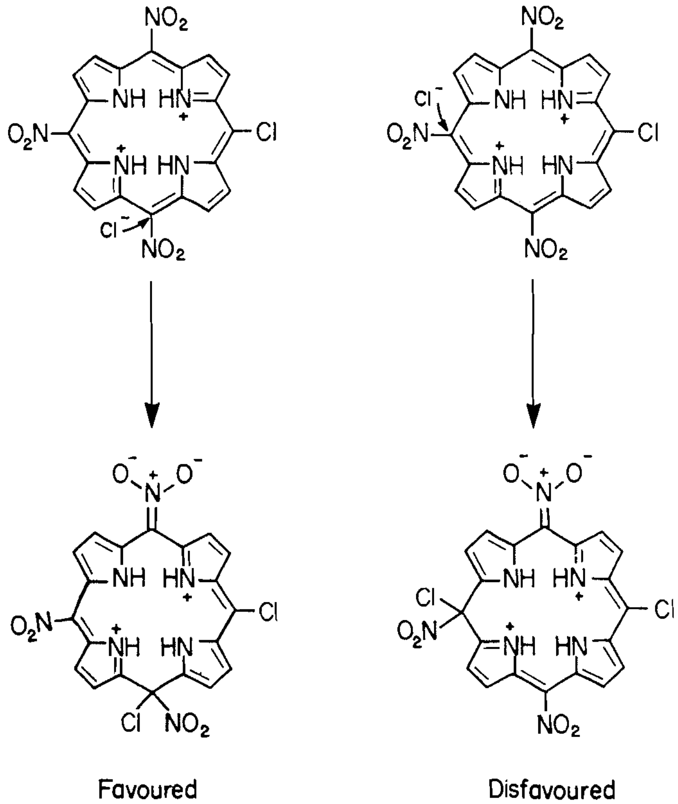

SCHEME 2

The same substitution pattern is observed when HBr is used. In this case substitution is slower, due presumably to the larger covalent radius of bromine and the considerable steric crowding that will ensue in both the transition state and the product (see below). The slow rate for substitution by bromide allows for competing side-reactions to occur with the formation of octaethylxanthoporphyrinogen (**3**). The xanthoporphyrinogen

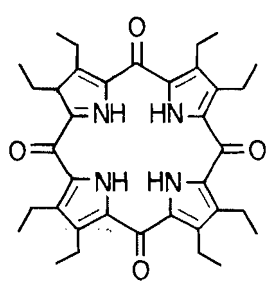

3

was also observed when tetranitrooctaethylporphyrin (or its zinc complex) was reacted with hydrofluoric acid. No fluorine-substituted porphyrins were observed, due presumably to the low nucleophilicity of fluoride under these conditions. However, monochloro trinitrooctaethylporphyrin was produced. The chlorine must be derived from the dichloromethane, possibly during the radical oxidation of the dihydroxanthoporphyrinogen (a hydroquinone-like material). The xanthoporphyrinogen was obtained in high yield when tetranitrooctaethylporphyrin was treated with acetic acid in the presence of sulfuric acid, or with acetic acid and sodium acetate when the only reasonable nucleophile is the acetate ion.

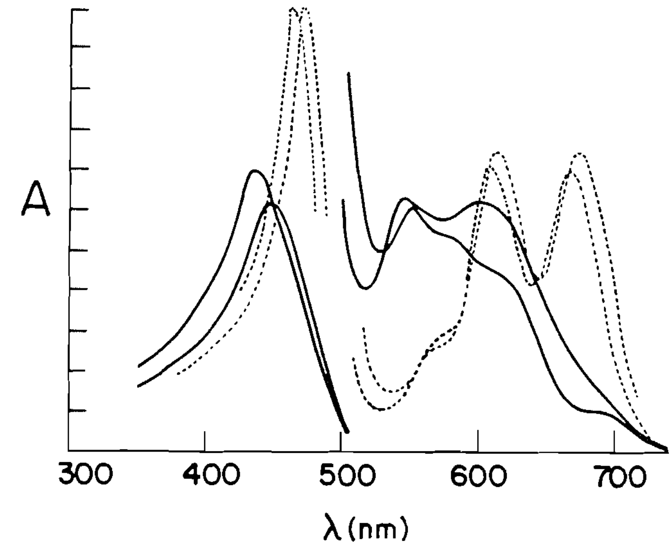

FIG. 1. Optical spectra of 5,10-dichloro- and 5,10-dibromooctaethylporphyrin. Free bases in CH_2Cl_2 (------), protonated species in CH_2Cl_2/1% TFA (------). In each case the bromo derivatives are slightly bathochromically shifted.

The 5,10-dibromo-15,20-dinitrooctaethylporphyrin exhibited (Fig. 1) a visible spectrum which was broader and more diffuse than the corresponding dichloro complex, attesting to the greater distortion from planarity due to the larger bromine atoms. However, upon N-protonation, when even more distortion occurs due to the repulsion of positive charge on the inner nitrogen (7), the dinitro and dichloro show very similar electronic spectra (Fig. 1).

Nucleophilic substitutions under basic conditions gave far more intractable by-products than under acidic conditions, due presumably to the increased electrophilicity of the porphyrin upon N-protonation and the improved leaving-group properties of the nitro group (as nitrous acid) upon protonation. Nevertheless, reaction of mononitrooctaethylporphyrinato zinc with sodium methoxide in THF proved of interest. As the reaction proceeded, the optical spectrum of the starting material was replaced by a spectrum (Scheme 3) in which the porphyrin absorptions were replaced by two weaker bands in the visible region. After several hours at reflux the optical spectrum again resembled a porphyrin and 5-methoxy-15-nitrooctaethylporphyrinato zinc(II) could be isolated at this stage. As outlined in Scheme 3, nucleophilic attack at the *meso*-position of **14** opposite the nitro group will give, upon protonation, the dihydroporphyrin (porphodimethene) **16**. Autoxidation of **16** will give the observed product **13**. Consistent with this interpretation is the observation that α,γ-dimethyl-α,γ-dihydrooctaethylporphyrinato zinc(II) (**17**) shows a qualitatively similar optical

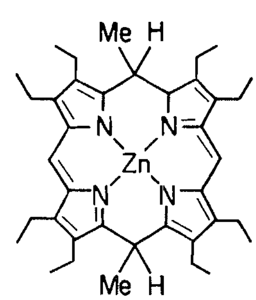

17

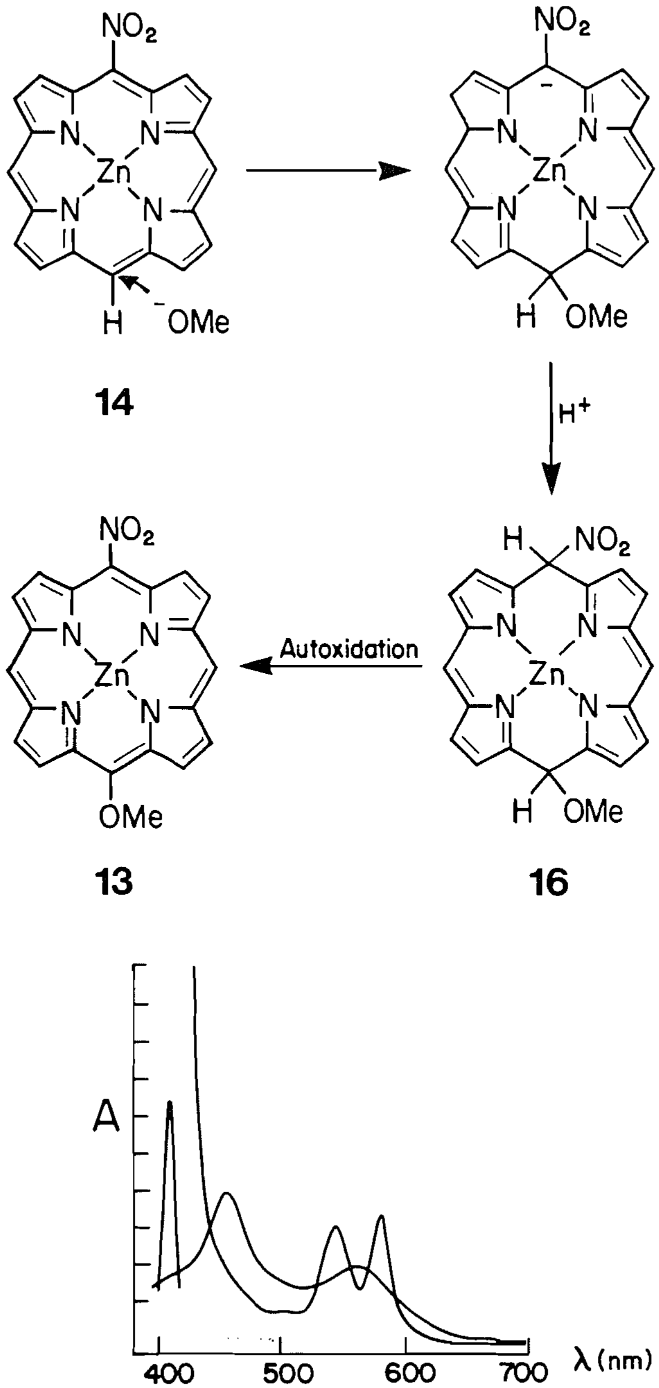

SCHEME 3

spectrum to **16** and undergoes rapid autoxidation to the corresponding 5,15-dimethyloctaethylporphyrin (12).

We have shown (7) that the redox properties of octaethylporphyrin are dramatically changed with successive nitration at the *meso*-positions. For instance, the first ring oxidation of **1** occurs at a potential 620 mV higher than for the corresponding unsubstituted ZnOEP. Similarly tetranitrooctaethylporphyrin oxidizes at 690 mV higher than the parent porphyrin. In addition to more difficult oxidations, the nitro groups allow for more facile reductions; thus **1** reduces at a potential 1190 mV more positive than ZnOEP. Chlorine with a σ_m value of 0.37

TABLE 1. Redox potentials[a]

	Half-wave potentials			
Compound[b]	$E^{ox}_{1/2}$ (1)	$E^{ox}_{1/2}$ (2)	$E^{red}_{1/2}$ (1)	$E^{red}_{1/2}$ (2)
OEP	1.04	1.54	−1.19	−1.66
2	1.45 (1.57)[c]	—	−0.18[d,e] (−0.22)	−0.96[c]
4	1.22 (1.45)	—	−0.32 (−0.49)	—
5	1.10 (1.23)	—	−0.44 (−0.85)	—
6	0.86 (1.04)	1.72	−0.80 (−1.19)	—
7	0.96	1.36	−0.86	—
9	1.17	—	−0.50[d]	
10	1.22	1.42	−0.62	
ZnOEP	0.87	1.19	−1.47	−1.86
13	0.97[d]	1.18[d]	−1.08[d]	−1.16[d]
15	1.12	1.26	−0.85[d]	−0.96[d]

[a]Potentials were measured against Ag/AgCl at a scan rate of 100 mV/s.
[b]Oxidations were measured in CH_2Cl_2 (dried over CaH_2)/tetra-*n*-propylammonium fluoroborate (~0.1 *M*) and reductions in DMF (distilled from solid KOH).
[c]Figures in parentheses refer to the derivative where chlorine is replaced by hydrogen (7).
[d]Reversible or quasi-reversible.
[e]A two-electron process.

(13) would be expected to show a smaller effect than the nitro group. Table 1 lists the redox properties of the halogenated complexes described above and it is apparent that the chlorine atoms have only a minimal effect, with the oxidation potentials being dominated by the nitro substituents. In fact, the electronegative chlorine atoms facilitate the oxidation by approximately 100–200 mV. The reductions are somewhat more affected by chlorine substitution but even the tetrachloro derivative (**6**) is reduced at a potential only 400 mV more negative than OEP.

In the case of the methoxy-nitroporphyrin (**15**), the two electronically opposed groups tend to neutralize each other and only small differences in redox properties are seen compared to OEP.

Acknowledgements

This work was supported by the United States National Institute of Health (GM 29198) and the Natural Sciences and Engineering Research Council of Canada. We also gratefully acknowledge the support of the People's Republic of China during Liang-chu Gong's leave of absence from the Chemistry Department of the East China Normal University, Shanghai, while a visiting Chinese Scholar at U.B.C.

1. J.-H. FUHRHOP. *In* The porphyrins. Vol. II. *Edited by* D. Dolphin. Academic Press, New York. 1978. pp. 131–159.
2. L. WITTE and J.-H. FUHRHOP. Angew. Chem. Int. Ed. Engl. **14**, 361 (1975).
3. D. DOLPHIN, R. H. FELTON, D. C. BORG, and J. FAJER. J. Am. Chem. Soc. **92**, 743 (1970).
4. D. DOLPHIN, D. J. HALKO, E. C. JOHNSON, and K. ROUSSEAU. *In* Porphyrin chemistry advances. *Edited by* F. R. Longo. Ann Arbor Science, Ann Arbor, MI. 1979. pp. 119–141.
5. H. J. SHINE, A. G. PADILLA, and S.-M. WU. J. Org. Chem. **44**, 4069 (1979).
6. K. M. SMITH, G. H. BARNETT, B. EVANS, and Z. MARTYNENKO. J. Am. Chem. Soc. **101**, 5953 (1979).
7. LIANG-CHU GONG and D. DOLPHIN. Can. J. Chem. **63**, 401 (1985).

8. R. BONNETT, I. A. D. GALE, and G. F. STEPHENSON. J. Chem. Soc. (C) 1600 (1966).
9. J. MILLER. Aromatic nucleophilic substitution. Elsevier, Amsterdam. 1968.
10. J. F. BUNNETT. Acc. Chem. Res. **11**, 413 (1978).
11. J. F. BUNNETT, E. W. GARBISCH, and K. M. PRUITT. J. Am. Chem. Soc. **79**, 385 (1957).
12. J. W. BUCHLER and L. PUPPE. Justus Liebigs Ann. Chem. **740**, 142 (1970).
13. H. C. BROWN and Y. O. KAMOTO. J. Am. Chem. Soc. **80**, 4979 (1958).

On the mechanism of disproportionation reactions of 1,2-dihydroquinolines

T. P. Forrest, G. A. Dauphinee, and S. A. Deraniyagala
Chemistry Department, Dalhousie University, Halifax, N.S., Canada, B4H 4J3

Received May 8, 1984

T. P. Forrest, G. A. Dauphinee, and S. A. Deraniyagala. Can. J. Chem. **63**, 412 (1985).

The commonly accepted mechanism for the acid-catalyzed disproportionation of 1,2-dihydroquinolines involves a hydride transfer from C-2 of one dihydroquinoline molecule to C-4 of another molecule which has already been protonated at C-3. This mechanism is shown to be incorrect. The proposed intermediate is shown to react by solvent addition and not by reduction under the conditions of the reaction. Evidence has been obtained which shows that the reaction proceeds by way of a 3,4-dihydroquinoline intermediate. A possible mechanism for the formation of the intermediate is discussed.

T. P. Forrest, G. A. Dauphinee et S. A. Deraniyagala. Can. J. Chem. **63**, 412 (1985).

Le mécanisme communément accepté pour la dimérisation, catalysée par les acides, des dihydro-1,2 quinoléines implique un transfert d'hydrure de la position C-2 d'une molécule de dihydroquinoléine à la position C-4 d'une autre molécule déjà protonée en C-3. On montre que ce mécanisme est inexact. On démontre que, dans les conditions utilisées pour la réaction, l'intermédiaire proposé réagit par addition de solvant et non par réduction. On a obtenu des indications qui indiquent que la réaction se produit via un intermédiaire dihydro-3,4 quinoléine. On discute du mécanisme possible pour la formation de cet intermédiaire.

[Traduit par le journal]

Introduction

The aromatization of an electron-rich dihydroaromatic system by hydride transfer is a well-known reaction typified by the ubiquitous hydride transfer reagents of nature, the reduced pyridine nucleotides. These reduced pyridine nucleotides are commonly considered (1) to function by transfer of a hydride ion directly to the substrate being reduced. Although this mechanism for the reduction step is commonly cited, a controversy regarding its validity has arisen during the past decade (2). Reduced quinolines are frequently used as models in the investigation of these mechanisms because they are more stable under the conditions required for reaction than are the corresponding N-alkyl-1,4-dihydronicotinamides, the other models commonly employed in these studies (3).

The 1,2-dihydroquinoline system is an example of a partially reduced heteroaromatic system which in a formal sense could act as both hydride donor and hydride acceptor, as do the reduced and oxidized pyridine nucleotides respectively. Such a redox reaction of 1,2-dihydroquinolines results in a disproportionation reaction yielding a quinoline and a tetrahydroquinoline. The mechanism of acid-catalyzed disproportionation of 1,2-dihydroquinolines (4), as well as their sulphur (5) (thiachromens) and oxygen (6) (Δ^3-chromens) analogues, has been commonly accepted as a protonation of the 3,4-double bond at C-3, thus creating a carbocation at C-4 which accepts a hydride ion from another molecule of the dihydroquinoline (Scheme 1). We wish to present results of our investigation of the acid-catalyzed disproportionation of 1,2-dihydroquinolines, which revealed that the generally accepted mechanism shown in Scheme 1 cannot be correct, and to indicate an alternate pathway for such a reaction.

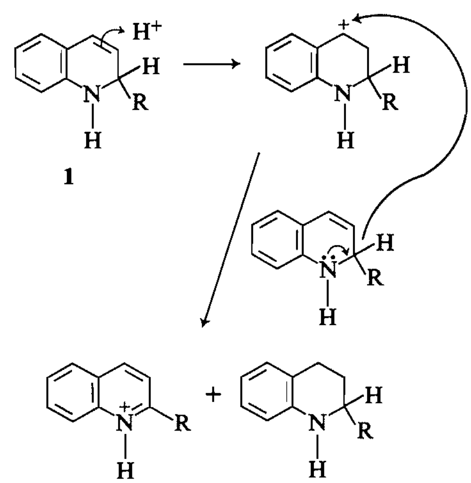

3 *a*: R = CH_3 2
b: R = Ph
c: R = H

Scheme 1

Results and discussion

The commonly accepted intermediate for the disproportionation reactions, a carbocation at C-4, has been shown (7) to be formed by the acid-catalyzed hydrolysis of 4-phenylamino-2,6-dimethyl-1,2,3,4-tetrahydroquinolines. Since this carbocation underwent solvent addition during these hydrolysis reactions we were suspicious of its intermediacy in the disproportionation reactions because no solvent addition products were formed. To show that the intermediate would also add methanol, the solvent used in disproportionation reactions, we investigated the methanolysis of *cis* (**4**) and *trans* (**5**) 4-hydroxy-2,6-dimethyl-1,2,3,4-tetrahydroquinoline under conditions similar to those required by the disproportionation reaction. The kinetic product of methanolysis of 4-hydroxy-2,6-dimethyl-1,2,3,4-tetrahydroquinoline had the same stereochemistry (*trans*), irrespective of whether the starting material was the *cis* or the *trans* isomer (Scheme 2). When the methanolysis reaction was conducted in deuterated media no deuterium was incorporated at the C-3 position of the methoxy product, which indicated the absence of an elimination–addition pathway. When the methanolysis reaction was allowed to remain overnight, an equilibrium mixture of the *cis* and *trans* 4-methoxy-2,6-dimethyl-1,2,3,4-tetrahydroquinoline was obtained with the *trans* isomer in predominance (*trans*/*cis* = 2.5:1). These results are similar to those obtained (7) from the hydrolysis reaction, and support the existence of a C-4 carbocation intermediate during the methanolysis of 4-hydroxy-2,6-dimethyl-1,2,3,4-tetrahydroquinolines. No solvolysis products are observed in the disproportionation reactions of 1,2-dihydro-

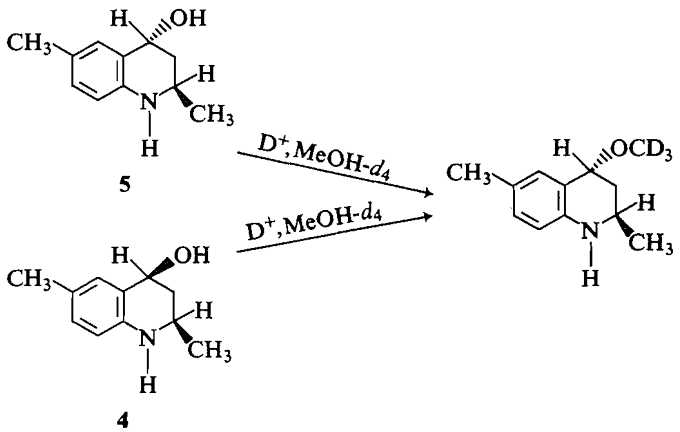

SCHEME 2

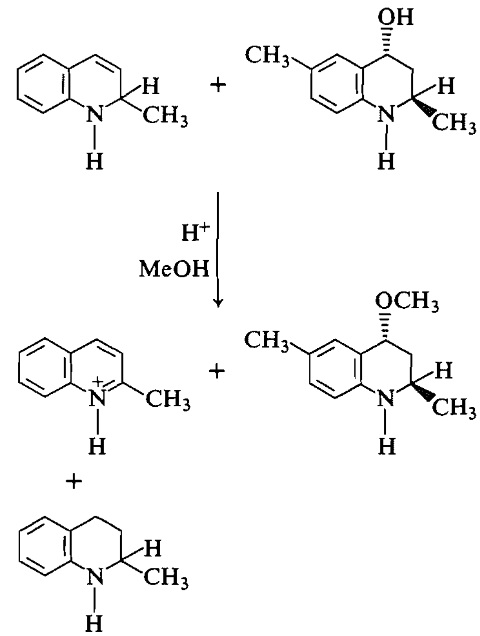

SCHEME 3

quinoline (**1***c*), 2-methyl-1,2-dihydroquinoline (**1***a*), 2,6-dimethyl-1,2-dihydroquinoline (**1***d*), or 2-phenyl-1,2-dihydroquinoline (**1***b*), although, under the conditions employed, they might be expected to be the predominant products.

The lack of solvent addition products from the 1,2-dihydroquinolines might not be inconsistent with the intermediacy of a carbocation in the disproportionation reactions, as the formation of the solvolysis product is reversible (*vide infra*) and, as such, the carbocation is continuously regenerated and could eventually be completely reduced. It was therefore necessary to obtain confirmation of the non-participation of the carbocation in the disproportionation reaction. This was done by conducting a disproportionation reaction in the presence of an independent source of a similar carbocation to determine whether the added carbocation would be reduced. The experiment was performed by conducting the disproportionation of 2-methyl-1,2-dihydroquinoline (**1***a*) in weakly acidic methanol with *trans*-4-hydroxy-2,6-dimethyl-1,2,3,4-tetrahydroquinoline (**5**) added as the source of the additional carbocation (identical to that which would be formed from **1***a* except for the extra methyl group in the 6-position) (Scheme 3). The mixed reaction gave no 2,6-dimethyl-1,2,3,4-tetrahydroquinoline, the reduction product which would have been formed from **5** if the carbonium ion was reduced. The products of the reaction were the normal disproportionation products from **1***a*, and the normal solvolysis product from **5**. By following the progress of the reaction by ^{1}H nmr spectroscopy it could be seen that the disproportionation reaction was only slightly faster (half-life = 50 min) than the solvolysis of **5** (half-life = 70 min), thus indicating that the dihydroquinoline would have been available to carry out the reduction while the carbocation from **1***a* was present. In a similar experiment no 2,6-dimethyl-1,2,3,4-tetrahydroquinoline was obtained when a mixture of 2-phenyl-1,2-dihydroquinoline (**1***b*) and *trans*-4-hydroxy-2,6-dimethyl-1,2,4-tetrahydroquinoline was allowed to react in weakly acidic methanol.

In order to determine the origin of the hydrogens added to the dihydroquinoline, the disproportionation reactions were conducted in deuterated media. 2-Methyl-1,2-dihydroquinoline (**1***a*) yielded 2-methyl-1,2,3,4-tetrahydroqinoline (**2***a*), which had deuterium in position 3, as might be expected from the carbocation mechanism (Scheme 1); however, the labelling pattern was not simply that of one deuterium having been added at carbon-3. Nuclear magnetic resonance (nmr) spectroscopy (^{1}H and ^{2}H) indicated that the *cis* and *trans* hydrogens on carbon-3 each contained about 76% deuterium and that the methyl group was about 22% deuterated.[1] The mass spectrum of the product also showed the presence of monodeuterated, dideuterated, and trideuterated molecules. 2-Methylquinoline (**3***a*), the other product of the disproportionation reaction, also had deuterium in the methyl group (about 21%),[2] but it had no deuterium at carbon-3.

These labelling results may also be used as evidence against the mechanism shown in Scheme 1. The presence of deuterium at C-3 in the tetrahydroquinoline product (**2***a*) is compatible with the reversible protonation of the dihydroquinoline (**1***a*), but if reversible protonation had taken place, the 2-methylquinoline (**3***a*), the oxidized product of the reaction, would also have been labelled at carbon-3. It would appear that in order to explain the difference in the labelling pattern of the two products at C-3 it is necessary to postulate the irreversible formation of an intermediate which can exchange at C-3 and which is converted exclusively to the reduced product. This intermediate could not be the carbocation because it would in the exchange process revert to the starting material, and thus also label the oxidized product.

If the reduction does occur by a hydride transfer, it is necessary to propose the formation of an acceptor species other than the proposed carbocation intermediate.

The 1,2-dihydro species is quite stable to attack by hydride (8) (e.g. $LiAlH_4$), but the 3,4-dihydro species, as the imine tautomer, would be susceptible to attack by hydride (9). This intermediate could exchange at carbon-3 via the enamine–iminium equilibration.

Evidence in support of the 3,4-dihydro species as an intermediate was obtained from the deuterium labelling results of the disproportionation of differently substituted dihydro-

[1] That no deuterium was incorporated into the tetrahydro product after it was formed was shown by allowing 2-methyl-1,2,3,4-tetrahydroquinoline (**2***a*) to equilibrate in acidic methanol under identical conditions.

[2] 2-Methylquinoline (**3***a*), when equilibrated in deuterated acidic methanol under similar conditions to that of the disproportionation reaction, incorporated 26% into the methyl group.

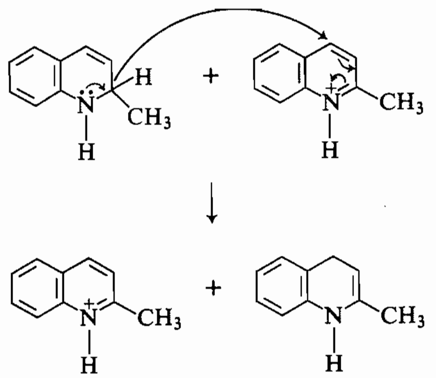

SCHEME 4

quinolines. Disproportionation of 2-phenyl-1,2-dihydroquinoline (**1***b*) in deuterated media gave 2-phenyl-1,2,3,4-tetrahydroquinoline (**2***b*) which was almost completely deuterated at C-3 and 2-phenylquinoline (**3***b*) which contained no deuterium, whereas disproportionation of 1,2-dihydroquinoline (**1***c*) under similar conditions gave 1,2,3,4-tetrahydroquinoline (**2***c*) containing only 50% deuterium at C-3, indicating no exchange. The variation in the percentage of deuterium at C-3 with the change in the substituent at C-2 (phenyl = 100%, CH_3 = 76% (52% exchange), H = 50% (0% exchange)) is consistent with the stability of the proposed exchangeable intermediate. The most stable, longer-lived phenyl intermediate showed full exchange while the least stable intermediate showed only one deuterium at C-3, indicating no exchange had taken place.

The feasibility of reduction of the 3,4-dihydroquinoline intermediate (tautomeric with 1,4-dihydroquinoline) was determined by reacting 1,4-dihydroquinoline (**6**) with an equivalent amount of 2-methyl-1,2-dihydroquinoline (**1***a*) in acidic methanol. The products of the reaction, 1,2,3,4-tetrahydroquinoline and 2-methylquinoline, indicated that the 1,4-dihydroquinoline was completely reduced by the 1,2-dihydroquinoline. The inability of the 1,4-dihydroquinoline intermediate to produce the oxidized product of the reaction is indicated by the lack of formation of quinoline in this reaction. Similar results were obtained for the reaction of 1,4-dihydroquinoline (**6**) and 6-methyl-1,2-dihydroquinoline (**1***f*).

In the disproportionation reaction of 1,2-dihydroquinolines, the 3,4-dihydroquinoline intermediate could conceivably arise from a 1,4-reduction of a quinoline nucleus by a hydride transfer from a 1,2-dihydroquinoline (Scheme 4). The trace amounts of quinoline required for the initiation of the reaction would be unavoidably present in the samples of the 1,2-dihydroquinoline.

The susceptibility of the quinoline nucleus to reduction by 1,2-dihydroquinolines was investigated by reacting 2-methyl-1,2-dihydroquinoline (**1***a*) in different experiments with equimolar amounts of 6-methylquinoline (**3***f*), 2,6-dimethylquinoline (**3***d*), and 6-methyl-2-phenylquinoline (**3***g*). In each case the added quinoline was partially reduced to the respective 1,2,3,4-tetrahydroquinoline. Similarly, 6-methylquinoline (**3***f*), 2,6-dimethylquinoline (**3***d*), and 6-methyl-2-phenylquinoline (**3***g*) were reduced by 2-phenyl-1,2-dihydroquinoline (**1***b*) to the respective 1,2,3,4-tetrahydroquinoline.

Furthermore, when a mixed-label disproportionation was conducted using 2,6-dimethyl-1,2-dihydroquinoline (**1***d*) and 2-deutero-2-methyl-1,2-dihydroquinoline (**1***e*) as reactants, the deuterium labelling pattern of the tetrahydroquinoline products (determined by ^{13}C triple resonance spectroscopy with decoupling of ^{1}H and ^{2}H) showed that 42% of the 2,6-dimethyl-1,2,3,4-tetrahydroquinoline molecules had deuterium at C-2 and 37% had one deuterium at C-4. 2-Methyl-1,2,3,4-tetrahydroquinoline, the other reduced product of the mixed-label disproportionation, had 56% of the molecules with a deuterium on C-2 and 46% with a deuterium on C-4, thus confirming the exchange at C-2. The finding of deuterium at C-2 and C-4 of the tetrahydroquinoline product derived from the non-deuterated dihydroquinoline indicates that the dihydroquinoline had gone through the quinoline stage, being reduced by the deuterated 1,2-dihydroquinoline to the 4-deutero-1,4-dihydroquinoline intermediate followed by reduction of the latter (via its imine tautomer) at C-2 by another molecule of the deuterated 1,2-dihydroquinoline. The presence of ^{1}H at C-2 of the tetrahydroquinoline derived from the deuterated dihydroquinoline verifies this conclusion.

The above results clearly show that a 1,4-dihydroquinoline is an intermediate in the disproportionation reaction, and that this intermediate can be formed by reduction of a quinoline nucleus. Although at this point a mechanism involving a 1,4-reduction of a quinoline nucleus seems the most obvious pathway for the formation of the 1,4-dihydroquinoline intermediate, in the absence of detailed kinetic results such a proposal is unconfirmed and it may well be that the disproportionation of 1,2-dihydroquinolines takes place by somewhat a less obvious pathway; kinetic investigations are in progress.

Experimental

The nmr spectra were recorded on Varian T-60, Varian CFT-20, XL-100, Bruker-250, and Nicolet 360-MHz spectrometers in solvents as indicated. The chemical shifts are delta (δ) values and are given in ppm relative to TMS as internal standard. The "*J*" values reported are in hertz as line separations measured directly from the spectra. Mass spectra were recorded on a DuPont-CEC model 21-104 spectrometer with an ionizing voltage of 70 eV. The melting points were recorded on a Fisher Johns apparatus and are uncorrected.

Materials

Quinoline (Fisher), 6-methylquinoline (Fluka), and 2-methylquinoline (Aldrich) were distilled under reduced pressure and stored under nitrogen away from light. 2,6-Dimethylquinoline (mp 57–59°C) was obtained from Aldrich.

2-D-Quinoline

This was prepared by the reduction of 2-chloro quinoline with tin in D_2O by the method of Metzger *et al.* (10); nmr ($CDCl_3$, 60 MHz) δ: 7.28 (d, $J_{3,4}$ = 8.0, H-3), 7.36–8.20 (m, H-4 – H-8); ms *m/e* (relative intensity): 131(11), 130 (M^+, 100), 129(22), 103(8), 102(7).

1,2-Dihydroquinoline (1c)

A solution of quinoline (2.0 g, 15.5 mmol) in anhydrous ether (5.0 mL) was slowly added with stirring to lithium aluminium hydride (1.2 g, 31.6 mmol) in the same solvent (50.0 mL). The solution was stirred for 1.5 h. It was then cooled and water added dropwise under nitrogen until the solution turned colorless. Filtration, followed by drying the filtrate with anhydrous sodium sulphate and evaporation of the solvent (using minimum heat as necessary), yielded 1,2-dihydroquinoline as a white crystalline solid; mp 66.0–69.5°C (lit. (11) mp 70–72°C); nmr ($CDCl_3$, 60 MHz) δ: 3.50 (br, NH), 4.00 (dd, $J_{2,3}$ = 4.0, $J_{2,4}$ = 2.0, H-2), 5.43 (td, $J_{3,4}$ = 10.0, $J_{3,2}$ = 4.0, H-3), 6.0–6.85 (m, H-4 and aromatic protons); ms *m/e* (relative intensity): 131(100), 130(46), 104(6), 103(7).

6-Methyl-1,2-dihydroquinoline (1f)

This was prepared by a procedure identical to that of 1,2-dihydroquinoline, with the exception that 6-methylquinoline (2.2 g, 15.3 mmol) was used instead of quinoline; mp 57–59°C (lit. (12) mp 61°C); nmr ($CDCl_3$, 60 MHz) δ: 2.10 (s, CH_3), 3.97 (dd, $J_{2,3}$ = 4.0, $J_{2,4}$ = 1.0, H-2), 5.53 (dt, $J_{3,4}$ = 10.0, $J_{3,2}$ = 4.0), 6.40–6.70 (m, aromatic protons).

2-Methyl-1,2-dihydroquinoline (1a)

Methyl lithium (Aldrich, 1.3 *M* in ether, 8.0 mL, 10.4 mmol) was added to quinoline (0.6 g, 4.7 mmol) in anhydrous ether under an atmosphere of nitrogen. After 2 min, water was added dropwise until the yellow solution became colourless. The solution was filtered, dried with anhydrous sodium sulphate, and the solvent evaporated (colourless oil, 87% yield). The nmr and mass spectra are consistent with those reported (13).

2,6-Dimethyl-1,2-dihydroquinoline (1d)

This was prepared using an analogous procedure to that of 2-methyl-1,2-dihydroquinoline, with the exception that 6-methylquinoline was used instead of quinoline. Yield: 94%, mp 65.5–67.0°C (lit. (11) mp 60–63°C). The nmr and mass spectra are consistent with those reported (13).

2-D-2-Methyl-1,2-dihydroquinoline (1e)

Preparative procedure was identical to that of 2-methyl-1,2-dihydroquinoline with the exception that 2-D-quinoline was used instead of quinoline; nmr ($CDCl_3$, 60 MHz) δ: 1.18 (s, CH_3), 3.69 (br NH), 5.43 (d, $J_{3,4}$ = 10.0, H-3), 6.19–7.00 (m, H-4 and aromatic protons).

2-Phenyl-1,2-dihydroquinoline (1b)

Phenyl lithium (Aldrich, 1.8 *M* in cyclohexane–ether, 8.0 mL, 14.4 mmol) was added to quinoline (0.60 g, 4.7 mmol) in anhydrous ether under an atomosphere of nitrogen. After 2 min, water was added dropwise until the solution became colorless. The solution was filtered, the filtrate dried with anhydrous sodium sulphate, and the solvent evaporated. The compound was purified by column chromatography on silica gel (merck 70–230 mesh) using a 60:40 mixture of petroleum ether (30–60°C)/benzene as eluant. Yield: 83%, mp 51–52°C (lit. (14) mp 49–50°C); nmr ($CDCl_3$, 360 MHz) δ: 4.05 (br, NH), 5.39 (dd, $J_{2,4}$ = 1.6, $J_{2,3}$ = 3.9, H-2), 5.57 (dd, $J_{3,4}$ = 9.8, $J_{3,2}$ = 3.9, H-3), 6.34 (d, $J_{8,7}$ = 7.3, H-8), 6.36 (dd, $J_{4,3}$ = 9.8, $J_{4,2}$ = 1.6, H-4), 6.58 (t, $J_{6,7}$ = 7.3, $J_{6,5}$ = 7.3, H-6), 6.87 (d, $J_{5,6}$ = 7.3, H-5), 6.95 (t, $J_{7,8}$ = 7.3, $J_{7,6}$ = 7.3, H-7), 7.27–7.42 (m, phenyl protons); ms *m/e* (relative intensity): 207 (M^+, 20), 206(35), 205(24), 204(16), 130(100).

6-Methyl-2-phenyl-1,2-dihydroquinoline (1g)

The preparative procedure was identical to that of 2-phenyl-1,2-dihydroquinoline with the exception that 6-methylquinoline was used instead of quinoline. Yield: 88%, mp 58.0–60.5°C; nmr ($CDCl_3$, 60 MHz) δ: 2.16 (s, CH_3), 3.50 (br, NH), 5.28 (dd, $J_{2,3}$ = 4.0, $J_{2,4}$ = 2.0, H-2), 5.43 (td, $J_{3,4}$ = 10.0, $J_{3,2}$ = 4.0, H-3), 6.0–6.85 (m, H-4 and aromatic protons); ms *m/e* (relative intensity): 221 (M^+, 43), 220(73), 219(57), 218(19), 144(100).

1,4-Dihydroquinoline (6)

This was prepared by lithium in liquid ammonia reduction of quinoline according to the method of Birch and Lehman (15), mp 45–46°C. The compound was found to polymerize at room temperature, but was relatively stable in ether solution for 24 h under nitrogen at −15°C. The compound polymerized in $CDCl_3$ but was somewhat more stable in deuterobenzene; nmr (C_6D_6, 60 MHz) δ: 3.43 (dd, $J_{4,3}$ = 3.0, $J_{4,2}$ = 1.5, H-4), 4.36 (m, $J_{3,2}$ = 7.0, $J_{3,4}$ = 3.0, $J_{3,1}$ = 1.0, H-3), 4.90 (br, NH), 5.76 (m, $J_{2,4}$ = 1.5, $J_{2,3}$ = 7.0, $J_{2,1}$ = 4.0, H-2), 6.26–7.26 (m, aromatic protons).

2-Phenylquinoline (3b)

To a solution of 2-phenyl-1,2-dihydroquinoline (*1b*) (1.0 g, 4.8 mmol) in 95% ethanol (15.0 mL) was added dropwise with stirring a solution of iodine (15% in ethanol, ca. 12 mL). After ca. 20 min the excess of iodine was destroyed by the dropwise addition of sodium thiosulphate (20% aqueous). Removal of the ethanol, followed by extraction into ether, gave 2-phenylquinoline, which was recrystallized from ethanol/H_2O. Yield: 67%, mp 79.5–81.0°C (lit. (16) mp 84°C); nmr ($CDCl_3$, 60 MHz) δ: 8.3–7.4 (m, aromatic protons); ms *m/e* (relative intensity): 206(17), 205 (M^+, 100), 204(67), 103(9), 102(13).

6-Methyl-2-phenylquinoline (3g)

This was prepared by an analogous procedure to that of 2-phenylquinoline, using 2-phenyl-6-methyl-1,2-dihydroquinoline (*1g*) instead of 2-phenyl-1,2-dihydroquinoline. The compound was recrystallized from ethanol/H_2O. Yield: 70%, mp 64–65.5°C (lit. (17) 67°C); nmr ($CDCl_3$, 60 MHz) δ: 2.53 (s, 6-CH_3), 7.37–8.16 (m, aromatic protons); ms *m/e* (relative intensity): 220(19), 219 (M^+, 100), 218(37), 204(16).

Cis (4) and trans (5) 4-hydroxy-2,6-dimethyl-1,2,3,4-tetrahydroquinoline

This was synthesized according to the procedure of Edwards *et al.* (18) from acetaldehyde and *p*-toluidine; *cis* isomer, mp 164.0–165.0°C (lit. (7) 165°C); *trans* isomer, mp 110.0–111.0°C (lit. (7) 110°C). The spectroscopic data were identical to those reported by Forrest *et al.* (7).

Methanolysis of cis *(4) and* trans *(5) 4-hydroxy-2,6-dimethyl-1,2,3,4-tetrahydroquinoline*

Trans 4-hydroxy-2,6-dimethyl-1,2,3,4-tetrahydroquinoline (5) (200 mg, 1.1 mmol) was allowed to remain overnight in methanolic HCl (25.0 mL of 0.02 *M*), after which it was basified with 10% sodium hydroxide, and the solvent evaporated. The residue was then extracted into ether (2 × 20.0 mL). The ether extracts were washed with water (2 × 20.0 mL), dried over anhydrous sodium sulphate, and the solvent evaporated. The residue was identified as *cis* and *trans* 4-methoxy-2,6-dimethyl-1,2,3,4-tetrahydroquinoline, with the *trans* isomer in predominance (*trans/cis* = 2.5:1).

Cis 4-hydroxy-2,6-dimethyl-1,2,3,4-tetrahydroquinoline, when allowed to remain overnight in acidic methanol under identical conditions to that of the *trans* isomer, yielded the *cis* and *trans* methanolysis products in the same ratio as that observed for the *trans* isomer; nmr ($CDCl_3$, 360 MHz) *trans* isomer, δ: 4.12 (unresolved quartet, $J_{4e,3a}$ = 3.2, $J_{4e,3e}$ = 2.5, H-4e), 3.54 (m, $J_{2a,3e}$ = 2.5, $J_{2a,3a}$ = 12.2, J_{2a,CH_3} = 6.3, H-2) 3.39 (s, OCH_3), 2.22 (s, 6-CH_3), 2.06 (dt, $J_{3e,3a}$ = 13.5, $J_{3e,4e}$ = 2.5, $J_{3e,2a}$ = 2.5, H-3e), 1.45 (m, $J_{3a,4e}$ = 3.2, $J_{3a,3e}$ = 13.5, $J_{3a,2a}$ = 12.2, H-3a), 1.20 (d, $J_{CH_3,2a}$ = 6.3, CH_3). For the *cis* isomer, as obtained from the product mixture, nmr ($CDCl_3$, 360 MHz) δ: 4.55 (dd, $J_{4a,3a}$ = 10.1, $J_{4a,3e}$ = 5.8, H-4), 3.44 (s, OCH_3), 2.22 (s, 6-Me), 1.62 (apparent quartet, $J_{3a,3e}$ = 11.8, $J_{3a,2a}$ = 11.5, $J_{3a,4a}$ = 10.1, H-3a), 1.21 (d, $J_{CH_3,2}$ = 6.3, CH_3).

The progress of the methanolysis reaction was monitored by scanning the nmr spectrum of a reaction mixture containing *trans* 4-hydroxy-2,6-dimethyl-1,2,3,4-tetrahydroquinoline (30.5 mg, 0.17 mmol) in methanol-d_4 (0.50 mL) with DCl/D_2O (2.0 μL, 2.0 *M*) as acid catalyst.

The methanol-d_4 was evaporated from the reaction mixture, the residue basified, extracted into ether, and subjected to mass spectroscopic analysis. Mass spectrum, *m/e* (relative intensity): 195(5.8), 194(42), 161(7.0), 160(50), 158(53), 157(100), 144(94), 145(12).

The formation of the *trans* 4-methoxy-2,6-dimethyl-1,2,3,4-tetrahydroquinoline as the kinetic product of methanolysis from *cis* 4-hydroxy-2,6-dimethyl-1,2,3,4-tetrahydroquinoline (30.0 mg, 0.17 mmol) was observed by following its reaction in methanol-d_4 (0.50 mL) with DCl/D_2O (4.0 μL, 2.0 *M*) as acid catalyst.

Disproportionation reactions of 1,2-dihydroquinolines

All disproportionation reaction mixtures were worked up as follows: the methanol was evaporated from the reaction mixture, and the residue was made basic with 10% sodium hydroxide and extracted into ether (2 × 40.0 mL). The ether extracts were washed with water (2 × 40.0 mL), dried over anhydrous sodium sulphate, and the solvent evaporated.

Disproportionation of 2-methyl-1,2-dihydroquinoline (1a)

2-Methyl-1,2-dihydroquinoline (300 mg, 2.1 mmol) was allowed to remain overnight in methanolic HCl (50 mL, 0.02 *M*) under an atmosphere of nitrogen.

The product mixture after work-up was chromatographed on silica gel (Merck, 70–230 mesh). The 2-methyl-1,2,3,4-tetrahydroquinoline was eluted out with benzene, while the 2-methylquinoline was eluted out with chloroform.

2-Methyl-1,2,3,4-tetrahydroquinoline (2a): nmr ($CDCl_3$, 60 MHz) δ: 1.11 (d, $J_{CH_3,2}$ = 6.0), 1.30–2.16 (m, H-3), 2.30–2.66 (m, H-4), 3.13–3.67 (m, H-2), 3.53 (br, NH), 6.33–7.10 (m, aromatic protons) (lit. (19)). Mass spectrum, *m/e* (relative intensity): 147 (M^+, 34), 132(100), 130(11), 117(10).

2-Methylquinoline (3a): nmr ($CDCl_3$, 60 MHz) δ: 2.67 (s, CH_3), 7.10–8.18 (m, H-3 – H-8). Mass spectrum, *m/e* (relative intensity): 143 (M^+, 100), 128(14), 115(12).

Disproportionation of 1,2-dihydroquinoline (1c)

Methanolic HCl (28.0 mL, 0.02 *M*) was added to 1,2-dihydroquinoline (150 mg, 1.2 mmol) and allowed to remain overnight under an atmosphere of nitrogen. After usual work-up, the products were identified by comparison of the nmr spectrum of the product mixture to that of authentic quinoline and 1,2,3,4-tetrahydroquinoline.

Disproportionation of 2-phenyl-1,2-dihydroquinoline (1b)

2-Phenyl-1,2-dihydroquinoline (300 mg, 1.4 mmol) was allowed to disporportionate in methanolic HCl (35.0 mL, 0.02 *M*) under an atmosphere of nitrogen. Usual work-up gave a product mixture which was chromatographed on silica gel (Merck, 70–230 mesh). The 2-phenyl-1,2,3,4-tetrahydroquinoline was separated from the 2-phenylquinoline with a mixture of light petroleum ether/benzene = 60:40, and the 2-phenylquinoline eluted out with chloroform.

2-Phenyl-1,2,3,4-tetrahydroquinoline (2b): nmr ($CDCl_3$, 60 MHz) δ: 2.37 (m, H-3), 2.73 (m, H-4), 3.70 (bs, NH), 4.29 (dd, $J_{2,3a}$ = 8.0, $J_{2,3e}$ = 5.0, H-2), 6.40–7.30 (m, aromatic protons) (lit. (20)). Mass spectrum, *m/e* (relative intensity): 209 (M^+, 100), 208(41), 132(78), 130(21).

2-Phenylquinoline (3b): nmr ($CDCl_3$, 60 MHz) δ: 7.40–8.31 (m, aromatic protons). Mass spectrum, *m/e* (relative intensity): 206(17), 205 (M^+, 100), 204(68), 103(10), 102(13).

Disproportionation of 2-methyl-1,2-dihydroquinoline (1a) in the presence of trans *4-hydroxy-2,6-dimethyl-1,2,3,4-tetrahydroquninoline (5)*

2-Methyl-1,2-dihydroquinoline (150 mg, 1.0 mmol) and *trans* 4-hydroxy-2,6-dimethyl-1,2,3,4-tetrahydroquinoline (160 mg, 0.90 mmol) were allowed to remain overnight in methanol (6.0 mL, 0.02 *M*) with aqueous ammonium chloride (0.15 mL, 2.0 *M*) as acid catalyst, under an atmosphere of nitrogen. Following work-up, the product mixture was analyzed by mass spectroscopy to determine the presence of 2,6-dimethyl-1,2,3,4-tetrahydroquinoline from its molecular ion expected at *m/e* 161. Mass spectrum, *m/e* (relative intensity): 191(61), 161(12), 160(84), 158(52), 157(15), 147(20), 145(19), 144(100), 143(72), 132(50).

The progress of the reaction was monitored by repeated scanning of the nmr signals of a mixture containing 2-methyl-1,2-dihydroquinoline (10 mg, 0.07 mmol) and *trans* 4-hydroxy-2,6-dimethyl-1,2-dihydroquinoline (12 mg, 0.07 mmol) in methanol-d_4 (0.40 mL), with NH_4Cl in D_2O (0.01 mL, 2.0 *M*) as acid catalyst. The half-life for the methanolysis of *trans* 4-hydroxy-2,6-dimethyl-1,2-dihydroquinoline was obtained by following the integration for the disappearance of the upfield triplet of the C-3 equatorial proton relative to the integration of dioxane as internal standard. The half-life for the disproportionation of 2-methyl-1,2-dihydroquinoline was obtained by monitoring the disappearance of its proton at C-3. $t_{1/2}$ for the methanolysis of 4-hydroxy-2,6-dimethyl-1,2,3,4-tetrahydroquinoline = 70 min; $t_{1/2}$ for the disproportionation of 2-methyl-1,2-dihydroquinoline = 50 min.

Disproportionation of 2-phenyl-1,2-dihydroquinoline in the presence of 4-hydroxy-2,6-dimethyl-1,2,3,4-tetrahydroquinoline

2-Phenyl-1,2-dihydroquinoline (150 mg, 0.72 mmol) and 2,6-dimethyl-4-hydroxy-1,2,3,4-tetrahydroquinoline (130 mg, 0.73 mmol) were allowed to remain overnight in methanolic HCl (18.0 mL, 0.02 *M*) under an atmosphere of nitrogen. Following work-up of the reaction mixture in the usual manner, the mass spectrum of the product mixture was recorded to determine the presence of 2,6-dimethyl-1,2,3,4-tetrahydroquinoline from its molecular ion expected at *m/e* 161. By slowly increasing the source temperature, no peak at 161 was observed until the molecular ion (191) for the methoxy product appeared, and then only at the intensity expected for the isotope (*M* + 1) of the 160 ion. Mass spectrum, *m/e* (relative intensity): 209(4), 205(20), 191(11), 161(4), 160(28), 158(31), 145(13), 144(100), 132(10), 130(16).

Reaction of 2-methyl-1,2-dihydroquinoline (1a) with 1,4-dihydroquinoline (6)

A mixture of 2-methyl-1,2-dihydroquinoline (220 mg, 1.5 mmol) and 1,4-dihydroquinoline (180 mg, 1.4 mmol) as allowed to remain overnight in methanolic HCl (25.0 mL, 0.02 *M*) under an atmosphere of nitrogen. Following work-up, the nmr spectrum of the product mixture was recorded, from which 1,2,3,4-tetrahydroquinoline and 2-methylquinoline were identified as the major products of the reaction. A small amount of 2-methyl-1,2,3,4-tetrahydroquinoline was also present but no quinoline was observed.

Reaction of 6-methyl-1,2-dihydroquinoline (1f) with 1,4-dihydroquinoline (6)

6-Methyl-1,2-dihydroquinoline (200 mg, 1.5 mmol) and 1,4-dihydroquinoline (165 mg, 1.3 mmol) were left overnight in methanolic HCl (25.0 mL, 0.02 *M*) under an atmosphere of nitrogen. Following work-up, the product mixture was analyzed by nmr spectroscopy; the products of the reaction were 1,2,3,4-tetrahydroquinoline, 6-methylquinoline, and small amounts of 6-methyl-1,2,3,4-tetrahydroquinoline. No quinoline was formed.

Disproportionation of 1,2-dihydroquinoline in deuterated media

2-Methyl-1,2-dihydroquinoline (1a)

2-Methyl-1,2-dihydroquinoline (150 mg, 1.0 mmol) was allowed to remain overnight in contact with DCl/methanol-O-*d* (12.0 mL, 0.04 *M*), under an atmosphere of nitrogen. Following work-up in the usual manner, the product mixture was column chromatographed on silica gel (Merck, 70–230 mesh). 2-Methyl-1,2,3,4-tetrahydroquinoline was eluted with benzene, while chloroform was used to elute the 2-methylquinoline.

2-Methyl-1,2,3,4-tetrahydroquinoline (2a): nmr ($CDCl_3$, 250 MHz) δ: 1.23 (d, $J_{CH_3,2}$ = 6.8, 2.35 H), 1.62 (m, H-3a, 0.24H), 1.95 (m, H-3e, 0.23H), 2.81 (m, H-4, 2H), 3.43 (m, H-2, 1H), 3.63 (br, NH, 1H), 6.48–7.05 (m, aromatic protons, 4H); ^2H nmr ($CDCl_3$, 38.4 MHz) δ: 1.15, 1.50, and 1.86. Mass spectrum, *m/e* (relative intensity): 152(4), 151(9), 150(17), 149(30), 148(33), 147(18), 146(9), 145(11), 144(13), 143(9), 135(18), 134(100), 133(91), 132(38), 131(15), 130(9).

2-Methylquinoline (3a): mass spectrum, *m/e* (relative intensity): 145(5.6), 144(37.0), 143(100.0), 142(9.1), 129(1.7), 128(17.0).

2-Phenyl-1,2-dihydroquinoline (1b)

2-Phenyl-1,2-dihydroquinoline (155 mg, 0.75 mmol) was left overnight in DCl/methanol-O-*d* (9.0 mL, 0.04 *M*). Following work-up, the nmr spectrum of the product mixture was recorded; nmr ($CDCl_3$, 60 MHz) δ: 2.70 (s, (AB quartet at 360 MHz), H-4), 3.60 (br, NH), 4.30 (s, H-2), 6.40–8.23 (m, aromatic protons). The product mixture was then chromatographed on silica gel as for the reaction in protic media. Mass spectrum, *m/e* (relative intensity): 206(17.0), 205(100.0, M^+), 204(68.4), 103(10.5), 102(18.5). The mass spectrum was identical to that of authentic 2-phenylquinoline.

1,2-Dihydroquinoline (1c)

A reaction mixture consisting of 1,2-dihydroquinoline (150 mg, 1.1 mmol) in DCl/methanol-O-*d* (14.0 mL, 0.04 *M*) was allowed to remain overnight under an atmosphere of nitrogen. Work-up was carried out in the usual manner; nmr ($CDCl_3$, 60 MHz) δ: 1.86 (m, H-3, 1H), 2.73 (m, H-4, 2H), 3.18 (m, H-2), 3.79 (br, NH, 1H), 6.30–8.16 (m, aromatic protons), 9.80 (dd, *J* = 2.0, 4.5).

Blank experiments

2-Methyl-1,2,3,4-tetrahydroquinoline (**2***a*) isolated from the disproportionation of 2-methyl-1,2-dihydroquinoline (**1***a*) in protic media was allowed to equilibrate overnight in DCl/methanol-O-*d* (20.0 mL, 0.04 *M*), and the product was analyzed by nmr spectroscopy after work-up.

The product mixtures obtained from disproportionation of 1,2-dihydroquinoline (**1***c*) and 2-phenyl-1,2-dihydroquinoline (**1***b*) were similarly allowed to remain in deuterated media and then analyzed by nmr spectroscopy. The nmr spectra obtained in each of these three cases were identical to that of the compounds before equilibration in deuterated media.

2-Methylquinoline was similarly allowed to remain overnight in acidic methanol-O-*d*, and subjected to mass spectroscopic analysis after the usual work-up. Mass spectrum, *m/e* (relative intensity): 145(11), 144(52), 143(100).

Disproportionation of 1,2-dihydroquinolines in the presence of added quinolines

*Reaction of 2-methyl-1,2-dihydroquinoline (1*a*) in the presence of added quinolines*

2-Methyl-1,2-dihydroquinoline (**1***a*) (150 mg, 1.0 mmol) was allowed to remain overnight in methanolic HCl (26.0 mL, 0.02 *M*) under an atmosphere of nitrogen in the presence of each of 6-methylquinoline (**3***f*) (150 mg, 1.0 mmol), 6-methyl-2-phenylquinoline (**3***g*) (225 mg, 1.0 mmol), and 2,6-dimethylquinoline (**3***d*) (165 mg, 1.0 mmol). Following work-up, the relative percentages of the tetrahydroquinolines were calculated by integration of the singlet at δ 2.18 (6-methyl of 6-methyl-2-R-substituted-1,2,3,4-tetrahydroquinoline (R = CH_3, H, Ph)) and the doublet (J = 6.0) at δ 1.12 (2-CH_3 of 2-methyl-1,2,3,4-tetrahydroquinoline) in its nmr spectrum. Percentage of tetrahydroquinoline formed by the reduction of the added quinoline from that of the total tetrahydroquinoline content (relative percentages): 6-methylquinoline (49.1 ± 4.3%), 6-methyl-2-phenylquinoline (52.0 ± 4.8%), 2,6-dimethylquinoline (77.0 ± 2.5%). Errors are the mean deviations obtained from three sets of experiments.

*Reaction of 2-phenyl-1,2-dihydroquinoline (1*b*) in the presence of added quinolines*

2-Phenyl-1,2-dihydroquinoline (**1***b*) (150 mg, 0.7 mmol) was allowed to remain overnight in methanolic HCl (18.0 mL, 0.02 *M*) under an atmosphere of nitrogen in the presence of each of 6-methylquinoline (**3***f*) (103 mg, 0.7 mmol), 2-phenyl-6-methylquinoline (**3***g*) (160 mg, 0.7 mmol), 2,6-dimethylquinoline (**3***d*) (110 mg, 0.7 mmol). Thereafter, product mixtures obtained after usual work-up were analyzed for the relative percentages of the tetrahydroquinolines by integration of the peak at δ 4.29 (dd, 2-H of the 2-phenyl-1,2,3,4-tetrahydroquinoline) and δ 2.18 (s, 6-CH_3 of 6-methyl-2-R-1,2,3,4-tetrahydroquinoline (R = CH_3, H, Ph)) in its nmr spectrum. Percentage of tetrahydroquinoline obtained by reduction of the added quinoline from that of the total tetrahydroquinoline content (relative percentages): 6-methylquinoline (51.3 ± 4.2%), 6-methyl-2-phenylquinoline (72.4 ± 3.9%), 2,6-dimethylquinoline (60.0 ± 7.1%). Errors are the mean deviations obtained from three sets of experiments.

*Mixed labelled disproportionation of 2,6-dimethyl-1,2-dihydroquinoline (1*d*) and 2-d-2-methyl-1,2-dihydroquinoline (1*e*)*

2,6-Dimethyl-1,2-dihydroquinoline (**1***d*) (1.40 g, 8.8 mmol) and 2-*d*-2-methyl-1,2-dihydroquinoline (**1***e*) (1.30 g, 8.9 mmol) were dissolved in ethanol and 2 *M* aqueous ammonium chloride (1.0 cc) was added, and the solution allowed to remain under an atmosphere of nitrogen for 48 h. Following work-up, the product mixture was column chromatographed on silica (Merck, 70–230 mesh). Benzene was used to separate the tetrahydroquinolines from the quinolines and a 50:50 mixture of benzene – petroleum ether (30–60°C) was used to separate the individual tetrahydroquinolines. The ^{13}C nmr spectra, with proton and deuterium decoupling and chromium triacetylacetonate as relaxation reagent, were recorded for both. The product ratio of 2,6-dimethyl-1,2,3,4-tetrahydroquinoline to 2-methyl-1,2,3,4-tetrahydroquinoline was approximately 8:2.

2,6-Dimethyl-1,2,3,4-tetrahydroquinoline: ^{13}C nmr ($CDCl_3$, 25.2 MHz) δ: 47.44, 46.97 (C-2), 30.89 (C-3), 26.82, 26.44 (C-4).

2-Methyl-1,2,3,4-tetrahydroquinoline: ^{13}C nmr ($CDCl_3$, 25.2 MHz) δ: 47.74, 47.27 (C-2), 30.43 (C-3), 27.12, 26.72 (C-4).

Acknowledgements

The authors are grateful for financial assistance from the Natural Sciences and Engineering Research Council of Canada, for the award of an I.W. Killam postgraduate fellowship to S.D., and to the Atlantic Region Magnetic Resonance Centre and to Dr. J. Walter of the Atlantic Research Laboratories for nmr spectral determinations.

1. R. J. KILL and D. A. WIDDOWSON. *In* Bioorganic chemistry. *Edited by* E. E. van Tamelen. Academic Press, New York. 1978 p. 239.
2. (*a*) J. J. STEFFENS and D. M. CHIPMAN. J. Am. Chem. Soc. **93**, 6694 (1970); (*b*) D. J. CREIGHTON, J. HAJDU, G. MOOSER, and D. S. SIGMAN. J. Am. Chem. Soc. **95**, 6855 (1973); (*c*) D. J. CREIGHTON, J. HAJDU, and D. S. SIGMAN. J. Am. Chem. Soc. **98**, 4619 (1976).
3. (*a*) S. SHINKAI, H. HAMADA, Y. KUSANO, and O. MANABE. J. Chem. Soc. Perkin Trans. 2, 699 (1979); (*b*) Tetrahedron Lett. 3511 (1979); (*c*) S. SHINKAI, T. NAKANO, H. HAMADA, T. KUSANO, and O. MANABE. Chem. Lett. 229 (1979).
4. (*a*) Y. OGATA, A. KAWASAKI, and S. SUYAMA. Tetrahedron, **25**, 1361 (1969); (*b*) B. D. TILAK, T. RAVINDRANATHAN, and K. N. SUBBASWAMI. Tetrahedron Lett. **18**, 1959 (1966); (*c*) J. A. JOULE and G. F. SMITH. Heterocyclic Chemistry. Van Nostrand Reinhold Company, London. 1978. p. 95.
5. B. D. TILAK and V. M. VAIDIYA. Tetrahedron Lett. 487 (1963).
6. B. D. TILAK and Z. MULJANI. Tetrahedron, **24**, 949 (1968).
7. T. P. FORREST, G. A. DAUPHINEE, and W. F. MILES. Can. J. Chem. **52**, 884 (1974).
8. R. C. ELDERFIELD and B. H. WARK. J. Org. Chem. **27**, 543 (1962).
9. D. R. COMFORT. Ph.D. thesis. Catholic University of America, 1972.
10. J. METZGER, H. LARIVE, E. J. VINCENT, and R. DENNILAULER. Bull. Soc. Chim. Fr. 46 (1967).
11. G. M. BADGER, H. P. CROCKER, B. C. ENNIS, J. A. GAYLER, W. E. MATTHEWS, W. G. C. RAPER, EVA L. SAMUEL, and T. M. SPOTWOOD. Aust. J. Chem. **16**, 814, (1963).
12. K. W. ROSENMUND, F. ZYMALKOWSKI, and N. SCHWARTE. Ber. **87**, 1229 (1954).
13. G. A. DAUPHINEE and T. P. FORREST. Can. J. Chem. **56**, 632 (1978).
14. C. E. CRAWFORD, O. METH-COHN, and C. A. RUSSEL. J. Chem. Soc. Perkin Trans. 1, 2807 (1972).
15. A. J. BIRCH and P. G. LEHMAN. Tetrahedron Lett. 2395 (1974).
16. W. PFITZINGER. J. Prakt. Chem. **56**, 283 (1897).
17. G. A. EPLING, K. N. AYENGAR, A. LOPES, and U. C. YOON. J. Org. Chem. **43**, 2928 (1978).
18. M. G. EDWARDS, R. E. GARROT, and H. O. JONES. J. Chem. Soc. 1376 (1912).
19. G. H. FISHER and H. P. SCHULTZ. J. Org. Chem. **39**, 635 (1974).
20. R. WEIL and N. COLLIGNON. Bull. Soc. Chim. Fr. 258 (1974).

The preparation and rearrangements of some 8,8-dimethylhomotropylium cations and their iron tricarbonyl complexes

RONALD F. CHILDS[1] AND ARAVAMUTHAN VARADARAJAN
Department of Chemistry, McMaster University, Hamilton, Ont., Canada L8S 4M1

Received June 7, 1984

RONALD F. CHILDS and ARAVAMUTHAN VARADARAJAN. Can. J. Chem. **63**, 418 (1985).

The circumambulatory rearrangements of some 8,8-dimethylhomotropylium cations and their corresponding iron tricarbonyl complexes have been examined. 8,8-Dimethylhomotropylium cation, **4**, has been prepared by protonation of 8,8-dimethylbicyclo[5.1.0]octa-3,5-dien-2-ol in FSO_3H/SO_2ClF. Evidence for homoaromatic delocalization in **4** was found in its characteristic ^1H nmr spectrum, particularly when this was compared to that of the non-cyclically delocalized 8,8-dimethylbicyclo[5.1.0]octadienyliron tricarbonyl complex **7**. Cation **4** was found to be stable at low temperatures but to isomerize to isopropyltropylium ion, **8**, at −50°C, $k = (4.6 \mp 0.2) \times 10^{-4}\ s^{-1}$. The specifically deuterated cation **4D** was prepared and a slow circumambulation of C8 around the basal 7-membered ring of this cation was found to occur at −90°C. The free energy of activation for this circumambulation is 14.5 kcal/mol. Homotropylium cation **4** was also prepared by protonation of 8,8-dimethylbicyclo[3.2.1]octa-3,6-dien-2-ol, **14**, at −120°C. No evidence for the presence of the corresponding bicyclo[3.2.1]octadienyl ion **12** was obtained. The 2,8,8-trimethylhomotropylium cation, **17**, was prepared and shown to undergo a circumambulatory rearrangement to give the 4,8,8-trimethyl substituted cation **20** as the major product. In this trimethyl series it also proved possible to generate the 2,8,8-trimethylbicyclo[3.2.1]octadienyl cation, **18**, and observe its ^1H nmr spectrum at very low temperatures (−116°C). The proton chemical shifts of **18** suggest that the charge is predominantly located on the 3-carbon bridge. Cation **18** isomerized to **17**, **20**, and other products at temperatures above −100°C. The 2,8,8-trimethylbicyclo[5.1.0]octadienyliron tricarbonyl complex **22** was also shown to undergo a circumambulatory rearrangement in which both C8 and the $Fe(CO)_3$ grouping migrate.

RONALD F. CHILDS et ARAVAMUTHAN VARADARAJAN. Can. J. Chem. **63**, 418 (1985).

On a étudié les transpositions circambulatoires des quelques cations diméthyl-8,8 homotropylium et des complexes fer-tricarbonyles correspondants. On a préparé le cation diméthyl-8,8 homotropylium (**4**) par protonation du diméthyl-8,8 bicyclo[5.1.0]octadiène-3,5 ol-2 dans un mélange FSO_3H/SO_2ClF. C'est dans son spectre rmn ^1H caractéristique que l'on a trouvé des indices de l'existence d'une délocalisation homoaromatique dans **4** et particulièrement lorqu'on l'a comparé au spectre rmn du complexe **7**, le diméthyl-8,8 bicyclo[5.1.0]octadiènyl-fer-tricarbonyle, qui n'est pas délocalisé d'une façon cyclique. On a trouvé que le cation **4** est stable à basses températures mais qu'il s'isomérise en ion isopropyltropylium (**8**) à −50°C avec une constante $k = (4{,}6 \mp 0{,}2) \times 10^{-4}\ s^{-1}$. On a préparé le cation **4D** spécifiquement deutéré et on a trouvé que, à −90°C, il se produit une circambulation lente de C8 autour du cycle de base à 7 chaînons de ce cation. L'énergie libre d'activation de cette circambulation est de 14,5 kcal/mol. On a aussi préparé le cation homotropylium **4** par protonation du diméthyl-8,8 bicyclo[3.2.1]octadiène-3,6 ol-2 (**14**) à −120°C. Les résultats obtenus n'ont pas permis de mettre en évidence la présence de l'ion bicyclo[3.2.1]octadiènyle correspondant, **12**. On a préparé le cation triméthyl-2,8,8 homotropylium (**17**) et on a observé qu'il subit une transposition circambulatoire conduisant au cation triméthyl-4,8,8 substitué (**20**) comme produit principal. Dans la série des produits triméthylés, on a aussi pu générer le cation triméthyl-2,8,8 bicyclo[3.2.1]octadiènyle (**18**) et observer son spectre de rmn ^1H à de très basses températures (−116°C). Les déplacements chimiques des protons du composé **18** suggèrent que la charge est localisée principalement sur le pont à trois chaînons. A des températures supérieures à −100°C, le cation **18** s'isomérise pour donner, entre autres, les cations **17** et **20**. On a aussi démontré que le complexe triméthyl-2,8,8 bicyclo[5.1.0]octadiènyl-fer-tricarbonyle (**22**) subit aussi une transposition circambulatoire dans laquelle le C8 ainsi que la $Fe(CO)_3$ migrent tous les deux.

[Traduit par le journal]

The homotropylium cation can potentially undergo a degenerate circumambulatory rearrangement in which the bridging methylene group migrates around the basal carbons that form the "seven-membered ring", eq. [1] (1). As a suprafacial [1,6] sigmatropic shift, this rearrangement would be expected to proceed thermally with retention of configuration at C8. This would lead to an overall interconversion of the *exo* and *endo* substituents at each step.

[1]

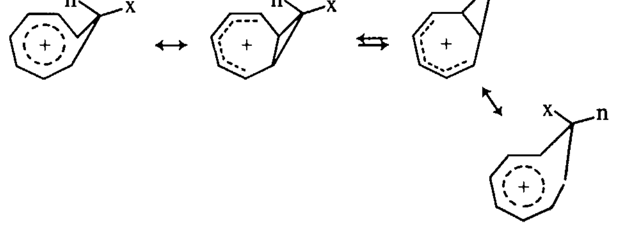

In contrast to the frequent occurrence of comparable circumambulation rearrangements with the analogous bicyclo[3.1.0]-hexenyl cations, there are few reports of such reactions with homotropylium cations. The activation energies required for circumambulation to occur in homotropylium ions appear to be high. For example, the parent cation has been investigated in some detail and it has been shown that the barrier to circumambulation must be at least 26–27 kcal/mol (2).

The high energy barriers associated with thermally induced circumambulation of homotropylium cations would seem to stem from two factors, first, the constraints of orbital symmetry and, second, the thermodynamic stability of these cations. If circumambulation were to occur by a concerted, symmetry-allowed process then the transition state for the reaction would have an unfavourable geometry. Migration with retention of configuration, the thermally allowed process, involves a large twisting motion of C8 and this type of migration would be expected to be difficult on geometric grounds. In contrast, the ground state symmetry-forbidden but photochemically allowed

[1] Author to whom correspondence may be addressed.

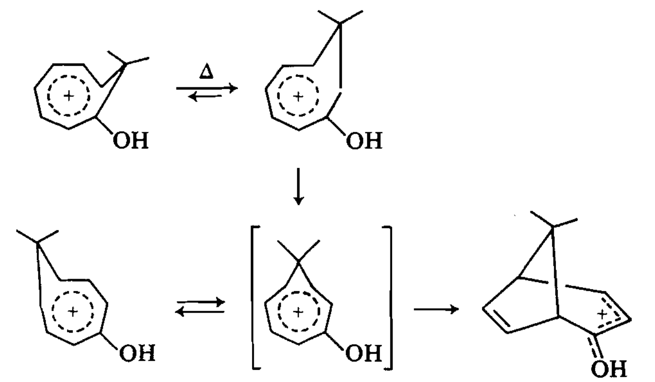

SCHEME 1

migration involving inversion of configuration at the migrating carbon is a least-motion reaction and, indeed, stereoselective circumambulatory rearrangements have been detected on irradiation of 2-hydroxyhomotropylium cations (3, 4).

Compounding these geometrical factors is a thermochemical consideration. Homotropylium cations are homoaromatic and the cyclic delocalization in these cations results in a measurable stabilization (5). For circumambulation to proceed it is necessary to disrupt this cyclic delocalization and this will be reflected in the high activation energies associated with this process. As an increased fraction of the positive charge is transferred onto C8, the migrating carbon in the transition state, the aromatic stabilization of the ground state of these cations can be partly offset by placing charge stabilizing groups at C8. Thus we have shown that 8,8-dimethyl substituted hydroxyhomotropylium cations undergo the series of thermally induced circumambulations shown in Scheme 1 (4, 6, 7).

In this present paper we extend our studies of these perambulating systems to the parent 8,8-dimethylhomotropylium cation. In particular we hoped that circumambulations with this ion might be sufficiently facile to permit observation by dynamic nmr methods and thus enable the stereochemistry of these reactions to be probed. Secondly, it was intended to further explore the nature of the conversion of the homotropylium cations to bicyclo[3.2.1]octodienyl shown in Scheme 1. This intriguing reaction involves the conversion of a homoaromatic cation to what may be considered formally to be an "anti-bis-homoaromatic system", a reaction which at first glance seems to be going in the wrong direction.

Results and discussion

Reduction of homotropone **1** (8) with diisobutylaluminum hydride (9) gave the reactive alcohol **2**. The ^{1}H nmr spectra of **2** were consistent with its assigned structure. In attempting to exchange the OH proton of **2** with deuterium in order to simplify the nmr spectrum using D_2O in $CDCl_3$ at room temperature, it was noted that **2** isomerized to cycloheptatriene **3** (10). The extreme ease of this isomerization precluded storage of **2** for any length of time and this alcohol was used directly in subsequent reactions.

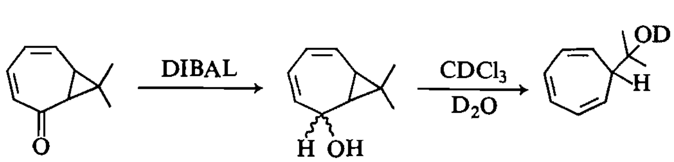

1 **2** **3**

Dissolution of **2** in FSO_3H/SO_2ClF at −78°C led to the formation of **4**. The ^{1}H nmr spectrum of this cation, obtained at −80°C, consisted of four resonances (Table 1), the positions of which were clearly indicative of the formation of the 8,8-dimethylhomotropylium cation. The chemical shift difference between the two methyl groups was large, as would be expected for such a homotropylium cation, and the positions of the resonances of the ring protons show a similar pattern to those of the parent homotropylium cation (11). Interestingly, the bridgehead protons (H1, H7) occur about 1 ppm upfield of the comparable protons of homotropylium cation itself, suggesting perhaps more cyclopropyl character for the C1, C7 bond in **4**. Comparable effects of a *gem*-dimethyl group have been observed with the bridged [10]-annulenes (12). The signal corresponding to the *exo* methyl protons was relatively broad at low temperature (−80°C) but sharpened as the temperature was raised. Similar broadenings of the *exo*-methyl resonances were observed with corresponding neutral compounds and presumably result from restricted rotation of the methyl group at low temperatures.

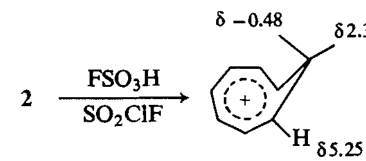

4

As a model for the chemical shifts to be expected for a nonaromatic counterpart of **4**, the corresponding iron complex was prepared. Reduction of **5** (8) gave **6**, which was again found to be unstable. Ionization of **6** in a CF_3COOH/SO_2 mixture gave **7**, which exhibited an ^{1}H nmr spectrum (Table 1) which was completely different from that of **4**. The chemical shift difference between the resonances of the C8 methyl groups was only 0.02 ppm. Apart from the resonance attributed to the methyl groups, the nmr spectrum of **7** was comparable to the corresponding iron complex of the parent system (13).

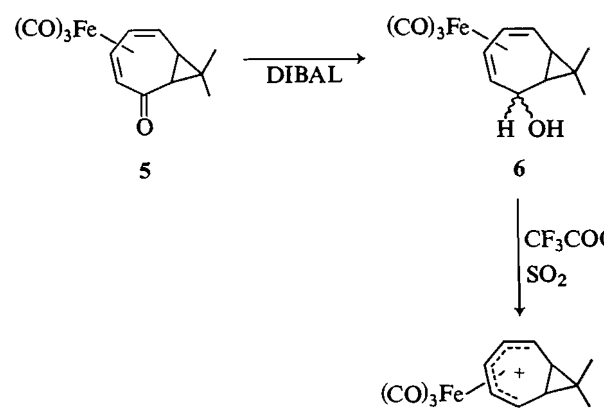

7

In order to determine whether circumambulatory rearrangements occurred with **4**, its ^{1}H nmr spectra were examined at higher temperatures. No evidence for the broadening or averaging of the ring proton resonances in the nmr spectra of **4** was observed at temperatures up to −50°C. Degenerate circumambulatory rearrangements of this cation must therefore be slow on the nmr time scale ($\Delta G^{\neq}$ >12 kcal/mol).

At −50°C, **4** was observed to isomerize irreversibly to iso-

TABLE 1. ^{1}H nuclear magnetic resonance spectra

Compound/ cation	Solvent	Temperature (°C)	Chemical shift (ppm)[a]									Coupling constant (Hz)								
			H1	H2	H3	H4	H5	H6	H7	H8	Other	1,2	2,3	3,4	4,5	5,6	6,7	1,7	1,3	CH_3,H
2	$CDCl_3$	34	1.98dd	4.78dd	5.72m	5.72m	5.72m	6.10m	1.52dd	(1.00) (1.22)	2.0(OH)	5.5					6	10		
6	$CDCl_3$	34	0.85	3.96dd	3.23bd	5.16m	5.16m	3.48dd	1.34dd	(0.78) (1.00)	1.68(OH)		3				7	10		
14	$CDCl_3$	34	2.05bs	3.80bs	5.28dt	5.95dd	2.21dd	6.23dd	5.70dd	(1.07) (1.22)			3	10	5	3	6	3	3	
15	$CDCl_3$	34	1.72m	(1.36)	—	5.53m & 6.00m		—	1.72	(1.10) (1.17)										
16	$CDCl_3$	34	2.10m	(1.34)	5.13dd	5.93dd	2.24dd	6.22dd	5.80dd	(1.04) (1.13)	1.57(OH)			10	6	3	6	3	2	
21	$CDCl_3$	34		(1.36)	3.13d	5.28dd	5.14dd	3.43t		(0.94) (0.97)				9						
28	$CDCl_3$	34	0.63m	(1.47)	3.08bd	5.01m	5.01m	3.78m	1.17m	0.05m (0.96d)										
4	FSO_3H/SO_2ClF	−80	5.26bs			8.17bs			5.26bs	(−0.48) (2.36)										
7	$CF_3COOH/SO_2/CDCl_3$		2.76bs	5.4m	5.4m	7.87bt	5.4m	5.4m	2.76bs	(0.99) (1.01)				6	6					
8	$FSO_3H/SO_2ClF/SO_2F_2$	−30			9.07bs				—	(1.56d)	3.68m									6.5
17	$FSO_3H/SO_2ClF/SO_2F_2$	−80	4.86bs	(2.84)		8.03m			4.86bs	(−0.15) (2.37)										
18	$FSO_3H/SO_2ClF/SO_2F_2$	−120	4.04bs	(3.08)	7.86bd	9.55bt	4.04bs	7.17bs[b]	7.35bs[b]	(1.54) (1.30)										
20	$FSO_3H/SO_2ClF/SO_2F_2$	−70	4.86bs	8.03m		(2.87)	8.03		4.86bs	(−0.27) (2.37)										
22	$CF_3COOH/SO_2/CDCl_3$	−50	2.42d	(2.03)	5.09d	7.65t	5.74dd	4.77dd	2.97dd	(0.99) (1.11)				6	6	11	8	11		
23	$CF_3COOH/SO_2/CDCl_3$	−20	2.7bm	4.87bd	(2.37)	7.64d	5.33m		2.7m	(1.00) (1.09)		8			6					
24	$CF_3COOH/SO_2/CDCl_3$	−20	2.73d	5.22m	5.33d	(3.10)	5.33d	5.22m	2.73d	(1.00) (1.09)		8		11		11	9			
29	$CF_3COOH/SO_2/CDCl_3$	0	2.1m	(2.12)	5.07d	7.60t	5.58q	~5m	2.7q	2.1m (.82)				6	6	10				5

[a] s singlet, d doublet, t triplet, m multiplet, b broad. Values in parentheses represent methyl groups.
[b] Assignments may be reversed.

propyltropylium cation, **8** (14). This cation was identified by its independent synthesis from 7-isopropylcycloheptatriene. The first-order rate constant for the isomerization of **4** to **8** was $(4.6 \mp 0.2) \times 10^{-4}\ s^{-1}$ at −50°C, corresponding to a $\Delta G^{\neq} = 16.3$ kcal/mol.

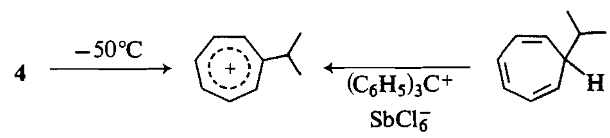

8 9

The occurrence of this irreversible isomerization to **8** precluded the investigation of possible circumambulations of **4** at higher temperatures by dynamic nmr methods. Instead it was decided to label the seven-membered ring with a single deuterium atom at C2. A degenerate circumambulatory rearrangement would distribute the label equally over all the seven carbons. This process will result in an increase in intensity of the signals for the vinyl protons H2–H6 and a decrease in the intensity of the signal for the methine protons H1 and H7, in the ^{1}H nmr spectrum. Thus, the intensity of the signal for the vinyl protons H2–H6 would change from the relative value of 4 in the starting cation before the rearrangement, to 4.29 after complete equilibration, and that of the signal for the methine protons H1 and H7 would change from the starting relative value of 2 to the final value of 1.71. In other words, the ratio of the relative intensities of these two signals would increase from a starting value of 2 to the final value of 2.51 after complete equilibration.

The alcohol **2D** was prepared by the lithium aluminium deuteride reduction of **1** in ether at −78°C. Protonation of this alcohol in $CFCl_3$–SO_2ClF–FSO_3H medium at −116°C led to the formation of **4D**. On warming from −120°C to −70°C in steps of 10°C, the ratio of the integrals for the vinyl and the methine proton signals in the ^{1}H nmr spectrum of **4D** increased from 1.9 to 2.55. At −70°C this value remained constant at 2.45 ∓ 0.09 for several minutes. On the basis of the predictions made earlier, this observation would indicate the occurrence of deuterium scrambling in **4D**, presumably via circumambulation of the C8 group. Continued observation of the same sample at −70°C by nmr showed that the intensities of the signals for all the protons decreased slowly with time. This could be attributed to the slow formation ($k = (3.7 \mp 0.06) \times 10^{-5}\ s^{-1}$) of the isopropyltropylium cation **8D**. As the resonances of the ring protons of **8** occur as a singlet in its ^{1}H nmr spectrum, it was not possible to locate the positions of the deuterium in **8D**.

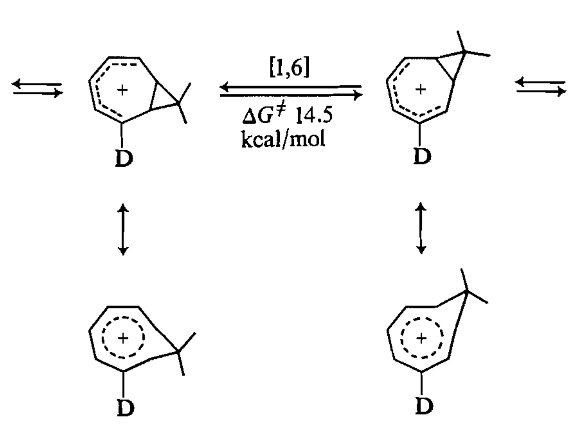

In a further attempt, observations were made on the cation **4D** at −90°C, in order to obtain the rate constant for the circumambulation. Conversion to the isopropyltropylium cation **8D** would be expected to slow down considerably at this temperature. Measurement of the increase in the relative intensity (peak height) of the signal for the vinyl proton with time yielded a rate constant of $(2.0 \mp 1) \times 10^{-5}\ s^{-1}$ corresponding to a free energy of activation of 14.5 kcal/mol.

No stereochemical information could be obtained here about the course of this reaction. Hehre has suggested, on the basis of calculations at the STO-3G level, that the barrier to circumambulation by the symmetry-forbidden inversion process should be 13 kcal/mol while the formally allowed retention mechanism requires 28 kcal/mol (15). The agreement between the calculated and measured barrier for this process is gratifying but it should not be taken as definitely establishing the steric course of circumambulation in these ions.

The conversion of **4** to **8** and analogous isomerization of **2** to **3**, presented earlier, could formally involve a cation such as **10**. A hydride shift from C7 of **10** to the cationic center would lead to **8**, whereas attack by water would yield **3**. The difficulty with such a mechanism is that cycloheptatriene carbinyl cations are known to exist primarily as their norcaradiene valence tautomers, e.g. **11**, which readily collapse to benzenoid species (16). While nucleophilic attack on **11** could still lead to species such as **3**, a hydride shift is unlikely to occur. Alternatively it may be possible, as suggested by Hehre (15), that **10** is stabilized by hydrogen bridging of the proton on C7. For such a bridging to occur the conformation of **10** must be the same as that involved in the transition state from symmetry-allow circumambulation.

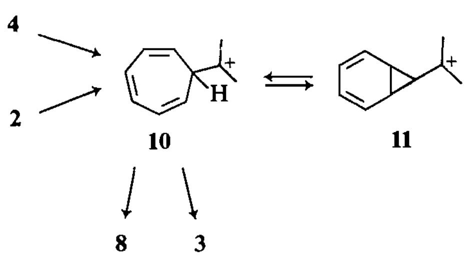

8,8-Dimethylbicyclo[3.2.1]octadienyl cation

Unlike the hydroxy substituted analogues referred to in Scheme 1, homotropylium ion **4** does not appear to rearrange to a bicyclo[3.2.1]octadienyl cation. In order to check the properties of this latter ion, attempts were made to prepare **12**

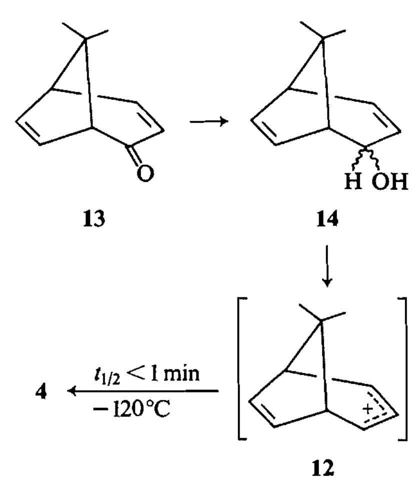

independently by an alternative route.

Reduction of **13** (4) gave **14**, which was subsequently protonated and ionized by dissolution in FSO_3H/SO_2ClF at −120°C. The ^1H nmr spectrum of the solution was recorded at −120°C and only signals attributable to **4** could be detected. By working rapidly and keeping prepared cation samples frozen at liquid nitrogen temperatures, it was possible to obtain a spectrum within 3 min of the initial preparation. Even under these conditions, no resonance other than those of **4** could be detected. The half-life of **12** at −120°C must be less than 1 min. At higher temperatures **4** rearranged to **8** as described before.

The isomerization of **12** to **4** is the reverse of the reaction observed with the hydroxy system, Scheme 1, indicating that the position of the equilibrium between homotropylium and bicyclo[3.2.1]octadienyl cations is delicately balanced. Clearly substituents can alter the position of the equilibrium. Viewing the situation in a simplistic way, there is proportionately less positive charge on each of the seven basal carbons of **4** than there is on C2 or C4 of the allyl portion of **12**. Consequently charge stabilizing substituents will affect the relative energy of **12** more than that of **4**. It is interesting that Hart, in his extensive studies of polymethylated bicyclo[3.2.1]octadienyl cations, uncovered a variety of isomerization pathways but never detected a rearrangement to a substituted homotropylium cation (17). Presumably multiple alkyl substitution pushes the equilibrium constant well in favour of the bicyclo[3.2.1]octadienyl form.

Trimethyl substituted systems

Entry into the trimethyl substituted systems was provided by the reaction of ketones **1** and **13** with methyl lithium to give **15** and **16**, respectively. The low temperature protonation of **15** led to the formation of **17**, which was characterized by the very large chemical shift difference between the C8 methyl resonances and typical positions of the ring protons. This ion was stable at −80°C although it underwent a complex series of rearrangements at higher temperatures.

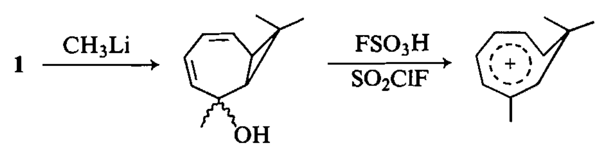

15 **17**

The protonation of **16** was carried out at −120°C using a mixture of $FSO_3H/SO_2ClF/SO_2F_2$. Observation of the resulting solution by ^1H nmr at −116°C suggested that the bicyclic cation **18** was formed.

The ^1H nmr of **18** (Table 1) showed the presence of three methyl groups with one of them occurring at δ 3.08, a relatively low field position for a methyl resonance. In addition, there were four vinyl protons with one being at a very low field position (δ 9.55). The low field methyl and vinyl resonances are very suggestive of the presence of a methyl substituted allyl cation. For example, the 1-methylcyclohexenyl cation exhibits resonances at δ 9.73, 8.08, and 3.36 (H3, H2, and CH_3, respectively) (18). The positions of the other resonances of the cation produced on protonation of **16** are entirely consistent with its formulation as **18**, with the bulk of the positive charge being located on the allyl portion of the molecule. The spectrum of **18** is similar to that of the corresponding protonated

TABLE 2. ^{13}C nuclear magnetic resonance chemical shifts for **17** and **20**[a]

Cation	Chemical shifts (δ)[b]										
	C2	C3	C4	C5	C6	C7	C1	C8	8-CH_3 *exo*	8-CH_3 *endo*	CH_3 (ring)
17	183.0	133.9[c]	158.6	150.7	131.6[c]	93.1[d]	89.8[d]	41.9[e]	27.0	9.9	26.6[e]
20	159.8	135.3	170.3	135.3	159.8	90.5	90.5	43.5[f]	28.1	9.6	26.1[f]

[a] In FSO_3H–SO_2ClF medium at −80°C.
[b] Relative to CD_2Cl_2 internal standard (δ 53.6).
[c–f] Assignments may be reversed.

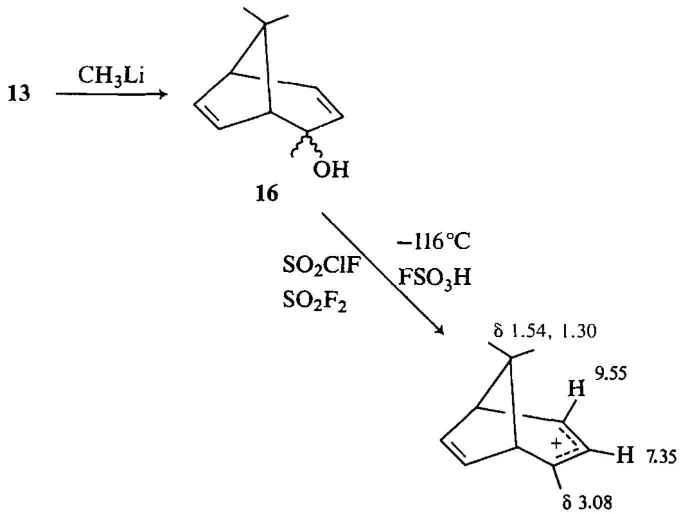

18

ketone **19** but with all the resonances moved somewhat further downfield, as would be expected for an allyl cation lacking the stabilizing effect of a hydroxy substituent.

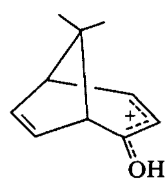

19

Both **17** and **18** are thermally labile and undergo a complex series of rearrangements. A solution of **17** was heated to −70°C for 1 h and an ^1H nmr spectrum obtained, Fig. 1. A very similar spectrum was obtained with a solution of **18** which had been heated to −60°C for 10 min. One or more uncharacterized intermediary cations were observed during the course of this latter isomerization. The major cation present in the final mixtures, in addition to **17**, appeared to be a further homotropylium cation. It exhibited methyl resonances at δ −0.27, 2.37, and 2.87 and ring proton resonances which were very similar to that of **17**. By obtaining ^{13}C nmr spectra of **17** at low temperatures prior to isomerization and of the mixture after the isomerization, and using a spectral subtraction technique, it was possible to obtain the ^{13}C nmr spectra of this additional trimethylhomotropylium cation and show that it had the struture **20**. In particular, the ^{13}C spectra exhibited a symmetry which is only consistent with this structure, Table 2.

The other cations present in these solutions were not identified. At higher temperatures still (−30°C), further isomerizations occurred to give what appeared to be a mixture of isopropylmethyltropylium ions. These reactions were not followed in detail.

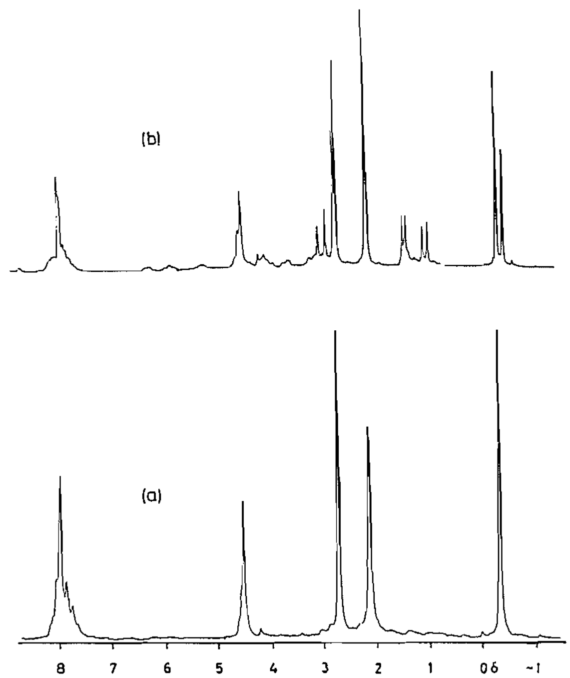

FIG. 1. The ^1H nmr spectrum of **17** in FSO_3H/SO_2ClF (a) at −80°C and (b) after 1 h at −70°C.

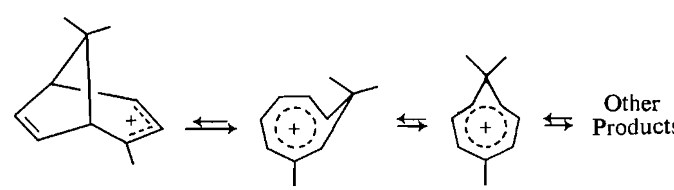

18 (trace) **17** (48%) **20** (29%) (23%)

While it has not been possible to completely characterize all the cations present in these rearrangements, several important points emerge from these rather complex rearrangements of the trimethyl substituted cations **17**, **18**, and **20**. First, it is clear that the bicyclo[3.2.1]octadienyl cation **18** is thermodynamically less stable than the homotropylium cations **17** and **20**. The fact that **18**, in contrast to **10**, can be directly observed by ^1H nmr at low temperatures suggests that the energy difference between these trimethyl substituted bicyclo[3.2.1]octadienyl, homotropylium cations is more closely balanced. Second, the isomerization of **17** to **20** represents a further example of a circumambulation in homotropylium cations. Third, of the four possible methyl substituted 8,8-dimethylhomotropylium cations the 2(6)- and 4-substituted isomers **17** and **20** are the most stable. Bearing in mind entropy factors, the symmetrical isomer **20** is marginally more stable than **17** (~80 cal/mol). The 1(7)- and 3(5)-methyl substituted isomers were present to less than 1%, meaning that they are some 1700 cal/mol less stable than **20**. These results suggest that the greatest fraction of positive charge in the homotropylium cations is at C2, C4, and C6. A similar conclusion was reached in the case of the hydroxy-8,8-dimethylhomotropylium cations (4).

Structure of bicyclo[3.2.1]octadienyl cations

Diaz *et al.* (19) and Shin (20) have concluded on the basis of solvolytic work and nmr studies, respectively, that the bicyclo[3.2.1]octadienyl cations are antihomoaromatic, a conclusion which is at odds with that of Mayr and co-workers (21). It is clear from the results described above that the 8,8-dimethylbicyclo[3.2.1]octadienyl and homotropylium cations are relatively close in energy and this would suggest that there is no large destabilization of the former cations.

The trimethyl substituted cation **18** is the simplest bicyclo-[3.2.1]octadienyl cation which has yet been prepared as a long-lived species in solution, and [1]H nmr chemical shifts of the various protons are informative in terms of the delocalization in this ion. As was mentioned earlier, chemical shifts of the allyl portion of **18** are similar in position to those of other similarly substituted allyl cations. The question, however, is whether there is involvement of the electrons of other double bonds. On protonation, the H6 and H7 resonances of **16** are shifted downfield by 1.13 and 1.37 ppm, respectively (Table 1). The magnitude of this shift is larger than would be expected on the basis of inductive effects alone and is suggestive of a π-type overlap. However, it should be noted that the downfield shift of H4 (2.71 ppm) and H3 (3.62 ppm) is three times as great as those seen for H6 and H7, indicating that **18** can be viewed primarily as an allylic system.

Circumambulations in bicyclo[5.1.0]octadienyliron tricarbonyl complexes

The presence of the iron tricarbonyl group on **7** does not necessarily preclude circumambulations from taking place in this system. While no broadening of the various resonances of the [1]H nmr spectrum of **7** could be detected on heating the acid solutions to −10°C, a slow circumambulation could be occurring with this cation. To examine this, the trimethyl cation **22** was prepared, in which the methyl group can serve as a ring label.

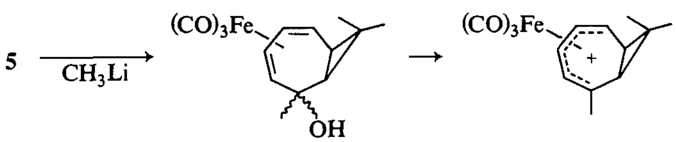

21 **22**

Treatment of **5** with methyl lithium gave **21**, which was subsequently converted to **22** by adding it to a mixture of CF_3COOH and SO_2 at low temperatures. The low temperature (−50°C) [1]H nmr spectrum of **22** (Table 1) was entirely consistent with the indicated structure, it being very similar, apart from the C2-Me signal, to that of **7** and other bicyclo[5.1.0]-octadienyliron tricarbonyl complexes (13). As the acid solution of **22** was warmed to −40°C, it partially isomerized to two additional cations. It was apparent from their [1]H nmr spectra

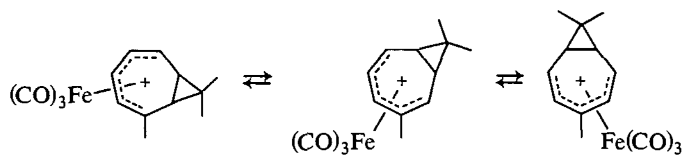

22 (18%) **23** (43%) **24** (29%)

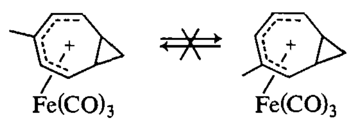

25 **26**

that these ions were similar in structure to **22** and they have been assigned the structures **23** and **24**. The resonances of the various protons of **22** and **23** were assigned on the basis of decoupling experiments and comparison with the shifts of **25** and **26** reported by Brookhart *et al.* (13). An equilibrium was established between these three cations containing **22** (18%), **23** (43%), and **24** (39%).

No comparable interconversions of **25** and **26** have been reported. In order to see if a single methyl group at C8 were sufficient to permit circumambulations in these iron complexes, cation **29** was prepared. This species was unchanged when heated at 0°C for 16 h and seemingly no circumambulatory rearrangements take place in this system ($\Delta G^{\neq} >$ 22.9 kcal/mol).

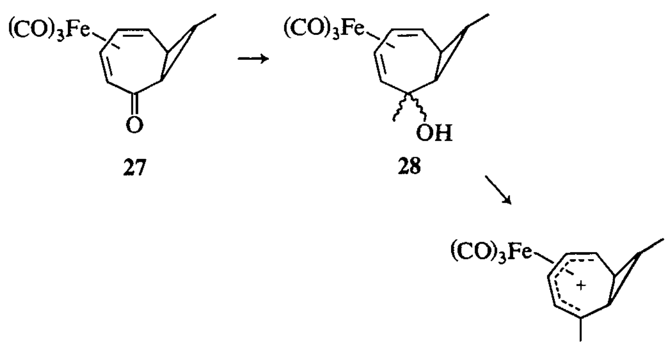

27 **28** **29**

It is clear from these results that circumambulatory rearrangements in these bicyclic iron complexes require the presence of a *gem*-dimethyl grouping at C8, the migrating carbon, indicating that considerable positive charge is localized on this carbon during the migration. The iron tricarbonyl moiety has also to migrate during this unusual type of circumambulation. The timing of the two migrations which are involved in the overall circumambulation, stereochemical considerations, and the possible occurrence of any intermediates remain speculative.

Experimental

General

The [1]H nmr spectra were obtained on Varian EM-390 and HA-100, and Bruker WP-80, WH-90, and WM-250 spectrometers. Probe temperatures were measured using an iron–constantan thermocouple. Chemical shifts of cations are referred to tetramethylammonium tetrafluoroborate taken as δ 3.1 ppm. The ir spectra were obtained on a Perkin–Elmer model 283 spectrometer and mass spectra were run on a VG-7070-F mass spectrometer operating at an ionization potential of

70 eV.

FSO_3H was purified before use by distillation from a small quantity of anhydrous NaF. The distilled acid was stored in glass ampoules. SO_2ClF and SO_2F_2 were used as supplied.

*2-Deutero-8,8-dimethylbicyclo[5.1.0]octa-3,5-dien-2-ol, **2D***

$LiAlD_4$ (29.1 mg) was added to a solution of **1** (85.3 mg) in anhydrous ether (5 mL) kept at −78°C under nitrogen. The resulting heterogeneous mixture was stirred at this temperature, under nitrogen for 1 h, after which time the yellow color of the starting material disappeared. CH_3OH (10 mL) was added, and the solution stirred for 15 min. The solution was warmed to room temperature and filtered twice through Celite to remove the coagulated solid. The solvent was evaporated to give the crude alcohol **2D** as a pale yellow liquid. The product was purified by bulb-to-bulb distillation (110°C/7.5 Torr; 1 Torr = 133.3 Pa), yield: 67.5 (mg).

In the ^1H nmr spectrum of **2D**, the signal at δ 4.78 corresponding to the resonance for H2 in **2** was absent; ms *m/e* (rel. abund.%): 151 (M^+, 81.3), 118 (54.3), 93 (49.6), 92 (100), 91 (56.8), 83 (95.7), 82 (43.5), 80 (64), 79 (71.2), 78 (50.7), 77 (55.8), 68 (47.1), 67 (52.2), 59 (44.6), 51 (42.4).

*8,8-Dimethylbicyclo[5.1.0]octa-3,5-dien-2-ol, **2***

Diisobutylaluminum hydride (0.85 mL of a 25% solution in C_6H_6) was slowly added to **1** (74 mg) in C_6H_6 (3 mL) at 0°C. The solution was sitrred for 2 h at 0°C. CH_3OH (20 mL) was added and the aluminum salts removed by filtration through Celite. The solvent was evaporated *in vacuo* and the residual oil distilled in a short path length bulb-to-bulb apparatus (110°C/5 Torr) to give a colourless oil; ^1H nmr spectrum, Table 1. Alcohol **2** allowed to stand in $CDCl_3$ or CS_2 solutions in contact with D_2O in nmr tubes rearranged to give **3** over a period of several hours; ^1H nmr ($CDCl_3$) of **3**, δ: 7.65 (t, 2H), 6.22 (bd, 2H), 5.35 (q, 2H), 1.32 (s, 6H).

*8,8-Dimethylbicyclo[5.1.0]octa-3,6-dien-2-ol, **14***

A solution of 8,8-dimethylbicyclo[3.2.1]octa-3,6-dien-2-one, **13**, (74 mg) in 3 mL dry benzene was kept stirred under nitrogen at 0°C; 5 mL of a 1 *M* solution of diisobutylaluminum hydride in hexane was added slowly at this temperature. The solution was stirred at this temperature for 2 h. Excess CH_3OH (10–15 mL) was then added and the mixture stirred at room temperature for a further 15 min. It was then filtered through Celite and the solvent evaporated to give a pale yellow oil; ^1H nmr analysis of this product showed that two isomeric compounds were present in an approximate ratio of 2:1. The crude mixture was distilled bulb-to-bulb (100°C/7.5 Torr) and a white solid sublimed over. Yield: 35 mg; mp 81–83°C; ^1H nmr, Table 1; ir (CS_2) cm^{-1}: 3600, 2920, 1020, 780, 735, 700. High res. ms (*m/e*), M^+ calcd.: 162.1045; M^+ found: 162.1029.

*2,8,8-Trimethylbicyclo[5.1.0]octa-3,5-dien-2-ol, **15***

A solution of **1** (101 mg) in dry ether (10 mL), kept under nitrogen, was cooled to −78°C. To this was added a 1.4 *M* solution of CH_3Li in ether (0.7 mL). The reaction mixture was stirred at −78°C for 1 h. After warming at 0°C, ice-cold water (5 mL) was added to quench the reaction. The ether layer was separated from the aqueous layer and the aqueous layer extracted with ether (3 × 10 mL). The combined ether extract was washed with water, dried over anhydrous $MgSO_4$, filtered, and the solvent removed to give a pale-yellow solid. Bulb-to-bulb distillation (110°C/7.5 Torr) resulted in the sublimation of **15** as a colorless solid. Yield: 113.2 mg; mp 61–64°C; ^1H nmr, Table 1; ir (KBr pellet) cm^{-1}: 3300, 2940, 1380, 1105, 975, 970, 730, 690. High res. ms (*m/e*), M^+ calcd.: 164.1201; M^+ found: 164.1207.

*2,8,8-Trimethylbicyclo[3.2.1]octa-3,6-dien-2-ol, **16***

This compound was prepared from **13** (140.9 mg) and a 1.4 *M* solution of CH_3Li in ether (1 mL) by the same method as that described for **15**. The crude product was obtained as a colorless liquid. The product was purified by bulb-to-bulb distillation (100°C/7.5 Torr). The oil solidified to give colorless crystals upon storage in the freezer. Yield: 148.7 mg; mp 38–40°C; ^1H nmr, Table 1; ir (CS_2) cm^{-1}: 3600, 3480, 2925, 1365, 1265, 1105, 1095, 915, 780, 730, 710. High res. ms (*m/e*), M^+ calcd.: 164.1201; M^+ found: 164.1255.

*Isopropyltropylium hexachloroantimonate, **8***

To a solution of 7-methoxycycloheptatriene (300 mg) in 15 mL dry ether, a 2 *M* solution of isopropylmagnesiumchloride in ether (5 mL) was added slowly under nitrogen at 0°C. The solution was stirred at this temperature for 3 h. A solution of NH_4Cl (2 g) in water (15 mL) was added and the solution was stirred at 0°C for 30 min. The ether layer was removed and the aqueous layer was extracted with ether (3 × 10 mL). The combined organic layer was dried over anhydrous $MgSO_4$, filtered, and the solvent evaporated to give a brown oil. Bulb-to-bulb distillation (80°C/7.5 Torr) of this oil yielded the pure 7-isopropylcycloheptatriene **9** (133.8 mg). This product was added to a solution of triphenylmethyl hexachloroantimonate (305 mg) in CH_2Cl_2 (15 mL) at room temperature, under nitrogen. The mixture was kept overnight under nitrogen at room temperature, when a dark solution was obtained. The solvent was evaporated under vacuum and the off-white solid product was washed with dry ether several times to remove triphenylmethane and the excess 7-isopropylcycloheptatriene. The crude product was recrystallized from dry CH_2Cl_2 at −20°C to give isopropyltropylium hexachloroantimonate **8** as colorless crystals. Yield: 230 mg; ^1H nmr, Table 1.

*8,8-Dimethylbicyclo[5.1.0]octa-3,5-dien-2-oliron tricarbonyl, **6***

Diisobutylaluminum hydride (0.5 mL of a 20% solution in hexane) was added to a solution of **5** (70 mg) in C_6H_6 (10 mL) kept at 0°C. The mixture was stirred for 1 h before CH_3OH (20 mL) was added. The aluminium salts were filtered off through Celite and the salts well washed with ether. The combined filtrate and washings were evaporated to dryness. The oily residue was chromatographed rapidly on alumina (activity II), eluting with benzene. The second fraction obtained was **6**, with the first being unreacted **5**. The ^1H nmr spectrum of **6** is given in Table 1. The alcohol **6** was unstable and was used directly for protonation studies.

*2,8,8-Trimethylbicyclo[5.1.0]octa-3,5-dien-2-oliron tricarbonyl, **21***

A solution of **5** (72 mg; 0.25 mmol) in anhydrous ether (2 mL) was cooled to −78°C under argon and treated dropwise with methyl lithium solution (0.31 mmol in ether). The solution was stirred at −78°C for 2 h, allowed to warm to 0°C, and treated with water (3 mL). The organic layer was separated from the aqueous phase and the latter washed with ether (3 × 1 mL). The combined organic fractions were dried over K_2CO_3 and the ether evaporated *in vacuo* to give a brown oil. The material was chromatographed very rapidly on a short (2 in.) alumina column (activity II), eluting with benzene. The second fraction collected was **21**; ^1H nmr spectrum, Table 1. This material was used directly in the protonation studies.

Protonation of the bicyclic alcohols

Each of the alcohols (20 mg) was dissolved in CD_2Cl_2 (a few drops) and cooled to −78°C in a 5.0-mm nmr tube. SO_2ClF (about 0.2 mL) was condensed into the nmr tube at this temperature. The tube was transferred to an ether – liquid nitrogen slush bath (−116°C) and 1 mL of a solution of FSO_3H in SO_2ClF (1:4 v/v) at the same temperature was added to the alcohol solution. The solution was rapidly stirred with a thin quartz rod previously cooled in liquid nitrogen, to effect complete mixing. The tube was quickly transferred to the probe of the nmr spectrometer, kept at −120°C.

*Low temperature protonation of **2D** and kinetics of deuterium scrambling in **4D***

This protonation was carried out exactly in the same way as that reported for the other bicyclic alcohols, except for the use of $CFCl_3$ instead of CD_2Cl_2 as the solvent in this case. Kinetics of deuterium scrambling at −90°C was followed by measuring the increase in the intensity (peak height) of the vinyl proton signal or the decrease in the intensity (peak height) of the bridgehead methine proton signal, with time. The error quoted in the value of *k* is the standard deviation of the individual values from the mean.

Acknowledgement

This work was supported by the Natural Sciences and Engineering Research Council of Canada.

1. R. F. CHILDS. Tetrahedron, **38**, 567 (1982).
2. J. A. BERSON and J. A. JENKINS. J. Am. Chem. Soc. **94**, 8907 (1972).
3. R. F. CHILDS and C. V. ROGERSON. J. Am. Chem. Soc. **98**, 6391 (1976).
4. R. F. CHILDS and C. V. ROGERSON. J. Am. Chem. Soc. **102**, 4159 (1980).
5. R. F. CHILDS, D. L. MULHOLLAND, A. VARADARAJAN, and S. YEROUSHALMI. J. Org. Chem. **48**, 1431 (1983).
6. R. F. CHILDS and C. V. ROGERSON. J. Am. Chem. Soc. **100**, 649 (1978).
7. L. T. SCOTT and W. R. BRUNSVOLD. J. Am. Chem. Soc. **100**, 6535 (1978).
8. M. FRANCK-NEUMANN and D. MARTINA. Tetrahedron Lett. 1759 (1975).
9. K. E. WILSON, R. T. SEIDNER, and S. MASAMUNE. J. Chem. Soc. Chem. Commun. 213 (1970).
10. W. VON E. DOERING and D. W. WILEY. Tetrahedron, **11**, 183 (1960); C. R. GANELLIN and R. PETTIT. J. Chem. Soc. 576 (1958).
11. P. WARNER, D. L. HARRIS, C. H. BRADLEY, and S. WINSTEIN. Tetrahedron Lett. 4013 (1970).
12. R. BIANCHI, G. MOROSI, A. MUGNOLI, and M. SIMONETTA. Acta Crystallogr. Sect. B, **29**, 1196 (1973); H. B. BUNGI, E. SHEFTER, and J. D. DUNITZ. Tetrahedron, **31**, 3089 (1975).
13. M. BROOKHART, E. R. DAVIS, and D. L. HARRIS. J. Am. Chem. Soc. **94**, 7853 (1972); A. DAVISON, M. MCFARLANE, L. PRATT, and G. WILKINSON. Chem. Ind. (London) 553 (1961).
14. T. NOZOE, K. TAKEHASHI, and H. YAMANOTO. Bull. Chem. Soc. Jpn. **42**, 3277 (1969).
15. W. J. HEHRE. J. Am. Chem. Soc. **96**, 5207 (1974).
16. I. PIKULIK and R. F. CHILDS. Can. J. Chem. **53**, 1818 (1975); W. BETZ and J. DAUB. Chem. Ber. **107**, 2095 (1974); G. D. SARGENT, N. LOWRY, and S. D. REICH. J. Am. Chem. Soc. **89**, 5985 (1967); G. L. THOMPSON, W. E. HEYD, and L. A. PAQUETTE. J. Am. Chem. Soc. **95**, 2364 (1973).
17. H. HART and M. KUZUYA. J. Am. Chem. Soc. **98**, 1551 (1976).
18. T. S. SORENSON. Can. J. Chem. **43**, 2744 (1965).
19. A. F. DIAZ, M. SAKAI, and S. WINSTEIN. J. Am. Chem. Soc. **95**, 7477 (1970).
20. J.-H. SHIN. Bull. Korean Chem. Soc. **3**, 66 (1982).
21. E. KAUFMAN, H. MAYR, J. CHANDRASEKHAR, and P. VON R. SCHLEYER. J. Am. Chem. Soc. **103**, 1375 (1981).

Réactions de Wittig et d'Horner–Emmons en série trifluorométhylée : synthèse de nouveaux F-alkyl esters isomères α,β et β,γ-insaturés

HEDI TRABELSI, BRIGITTE BERTAINA ET AIMÉ CAMBON
Laboratoire de Chimie Organique du Fluor, U.E.R. — I.M.S.P., Université de Nice, Parc Valrose, 06034 Nice Cedex, France

Reçu le 8 mai 1984

HEDI TRABELSI, BRIGITTE BERTAINA et AIMÉ CAMBON. Can. J. Chem. **63**, 426 (1985).

Les réactions de Wittig et Horner–Emmons sont réalisées en utilisant la n-butyl trifluorométhyl cétone et la benzyl trifluorométhyl cétone. De nouveaux F-alkyl esters α,β et β,γ-éthyléniques sont obtenus. Le mode de formation de ces derniers est discuté.

HEDI TRABELSI, BRIGITTE BERTAINA, and AIMÉ CAMBON. Can. J. Chem. **63**, 426 (1985).

New F-alkyl α,β and β-γ-unsaturated esters were obtained by Wittig and Horner–Emmons reactions using n-butyl and benzyl trifluoromethyl ketones. A mechanism for formation is discussed.

Introduction

Les réactions de Wittig, Wittig–Horner ou Horner–Emmons, très utilisées en série hydrocarbonée (1–5), se sont également révélées de bonnes méthodes pour synthétiser des alcènes F-alkylés activés par des groupements électro-attracteurs (6–10): la réaction de condensation d'un dérivé carbonylé, d'accès facile (9), sur un ylure de phosphore ou un phosphonate conduit alors, essentiellement à un composé α,β-insaturé et F-alkylé.

(réf. 7)

$R_f = CF_3$
R = Me, Ph...

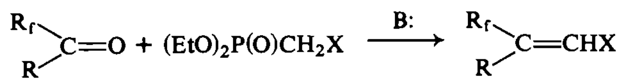

(réf. 9)

$R_f = C_nF_{2n+1}$ ($n = 3,5,7...$)
R = Me, Ph, Et, nPr...
X = COOMe, CN, $COCH_3$...

Nous avons souhaité utiliser ces réactions pour synthétiser des composés du type:

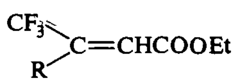

en vue de l'obtention de polymères à bas indice de réfraction utilisables dans l'industrie des fibres optiques (11).

Si la méthode de Wittig a répondu à nos espérances, celle d'Horner–Emmons a conduit majoritairement à des esters β,γ-insaturés.

Résultats et discussion

Dans le cas de la réaction de Wittig, la condensation de la n-butyl trifluorométhyl cétone avec le carboéthoxyméthylène-triphénylphosphorane conduit aux résultats suivants:

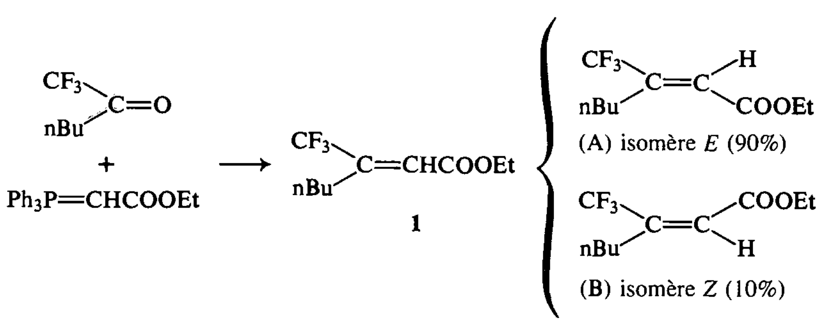

1

(A) isomère *E* (90%)

(B) isomère *Z* (10%)

Dans le cas de la réaction d'Horner–Emmons, la même cétone a été condensée avec le carboéthoxyméthyl diéthyl phosphonate en présence de NaH. Les résultats sont les suivants:

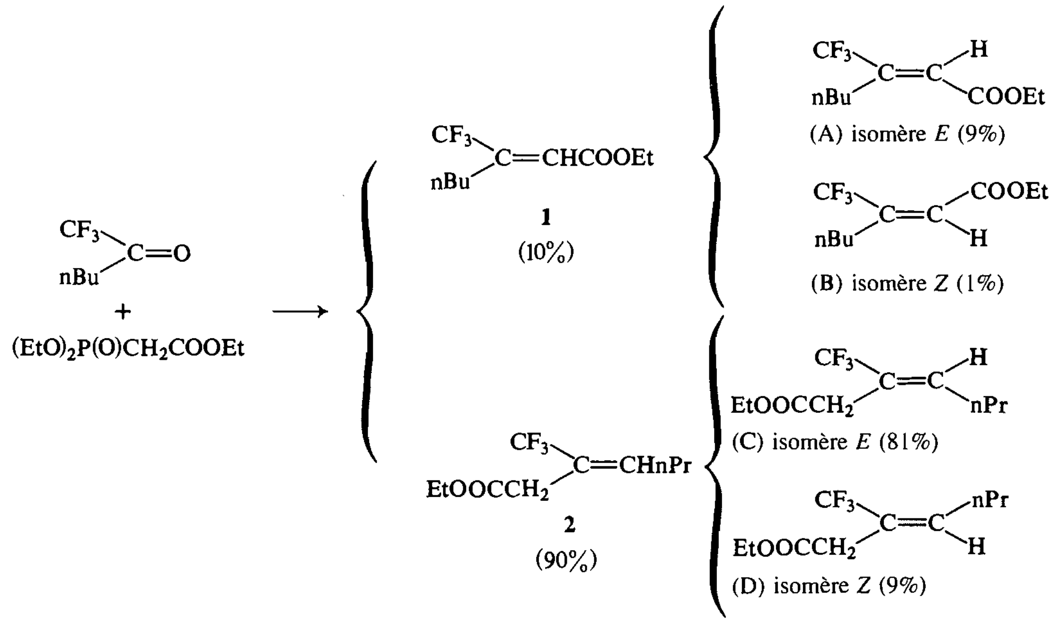

On voit clairement que la réaction d'Horner–Emmons donne un mélange de trifluorométhyl oléfines activées α,β-insaturées (**1**) ((A) + (B) = 10%) et β,γ-insaturées (**2**) ((C) + (D) = 90%).

La formation de **2** peut être envisagée par une isomérisation prototropique en milieu basique de **1** comme cela été montré en série hydrocarbonée (12–17).

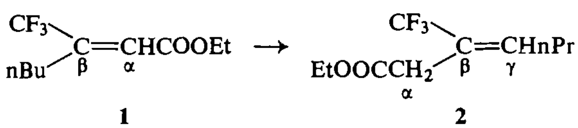

En effet, il est bien connu qu'il existe un équilibre entre les formes α,β et β,γ-insaturées des ions carboxylates, des esters carboxyliques, des cétones et des nitriles.

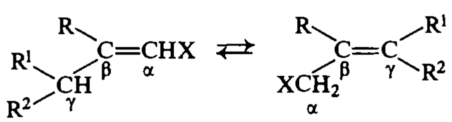

X = COO^-, COOEt, $COCH_3$, CN …

Afin de démontrer l'existence d'une telle prototropie en série trifluorométhylée nous avons procédé aux essais suivants.

(a) Nous avons fait agir sur le mélange (*Z* + *E*) du composé **1** à température ambiante et en milieu THF (conditions de la réaction d'Horner–Emmons).

(b) Nous avons mis le composé **1** au reflux du THF pendant 24 h, afin de déterminer si ce dernier était responsable de l'éventuelle prototropie.

(c) Nous avons fait réagir Ph_3P=CHCOOEt respectivement sur les composés **1** et **2** au reflux du THF pour savoir si l'éventuelle isomérisation se produisait sous l'influence de l'ylure.

(d) Nous avons effectué la même réaction avec le phosphonate $(EtO)_2P(O)CH_2COOEt$.

Les résultats suivants ont été obtenus: les essais (b) et (c) se sont révélés négatifs et les produits de départ ont été intégralement récupérés. Dans les essais (a) et (d), c'est-à-dire en milieu fortement basique (en présence de NaH ou du carbanion dérivé du phosphonate), nous constatons qu'environ 95% des composés **1** (isomères *Z* et *E*) sont réarrangés en composés **2**.

Ceci permet de conclure que les esters β,γ-insaturés obtenus au cours de la réaction d'Horner–Emmons résultent de la prototropie catalysée par le milieu basique des esters α,β-insaturés. Seuls ces derniers sont obtenus par la réaction de Wittig qui ne nécessite pas l'utilisation d'une base.

En série hydrocarbonnée, Kon et Linstead (13, 14) ont montré que l'équilibre entre les formes α,β et γ,β-insaturées dépend peu de la nature de X, mais est très sensible à la nature des groupements sur l'atome de C en position γ.

Ainsi, dans le cas où R^1 = Ph, R^2 = H, l'équilibre est complètement déplacé vers la formation de l'ester β,γ-éthylénique.

Afin de démontrer une éventuelle analogie en série trifluorométhylée, nous avons condensé la benzyl trifluorométhyl cétone avec le carboéthoxyméthyl diéthyl phosphonate dans les conditions d'Horner–Emmons.[1] Les résultats sont les suivants:

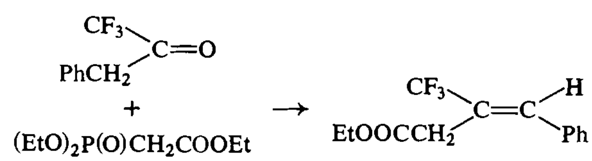

3 isomère *E*

Dans ce cas, seul l'ester β,γ-insaturé est obtenu et la réaction est stéréospécifique (100% *E*).

Nous avons alors synthétisé l'isomère α,β-éthylénique[2] par une réaction de Wittig et nous l'avons soumis aux essais (a), (b), (c) et (d). Nous avons constaté que les essais (b) et (c) sont négatifs comme précédemment alors que (a) et (d) donnent uniquement le composé **3** (isomère *E*). Sous l'effet de la base NaH ou du carbanion dérivé du phosphonate, le benzyl-3

[1]La réaction d'Horner–Emmons avec $(CF_3)C(O)Ph$ est stéréospécifique et conduit au produit $(CF_3)C(Ph)$=CH—COOEt (isomère *E*).

[2]Dans le cas de la réaction de Wittig, cette cétone condensée avec le carboéthoxyméthylènetriphénylphosphorane conduit au benzyl-3 trifluoro-4,4,4 butène-2 oate d'éthyle (isomère *E* (75%); isomère *Z* (25%)).

trifluoro-4, 4, 4 butène-2 oate d'éthyle (*Z* + *E*), s'isomèrise intégralement en un composé unique **3**.

Identification des divers composés obtenus

*(**1**)* (E, Z)

L'analyse élémentaire jointe à la détermination de la masse moléculaire par spectrométrie de masse (M^+ 224), conduit à la formule brute $C_{10}H_{15}F_3O_2$. Le spectre ir montre que nous avons affaire à des oléfines conjuguées avec un groupement ester: $\nu_{(C=O)} = 1709\ cm^{-1}$, $\nu_{(C=C)} = 1653\ cm^{-1}$. On note également $\nu_{(C-F)} = 1100-1250\ cm^{-1}$. Le spectre[3] rmn du ^1H montre: à 6,05 ppm et 6,33 ppm les signaux des H éthyléniques; à 4,21 et 1,3 ppm respectivement un quadruplet et un triplet (OCH_2CH_3); entre 2,66 et 1,5 ppm un large multiplet correspondant aux CH_2 de nBu; et à 0,95 ppm, le CH_3 du groupement n-butyle.

La présence de 2 signaux attribuables aux H éthyléniques, l'un vers 6,33 ppm, l'autre vers 6,05 ppm (moins déblindé et environ 3 fois moins intense), montre l'existence d'un mélange de 2 stéréoisomères.

La configuration (*Z, E*) a été déterminée grâce au couplage allylique du proton éthylénique et du groupement CF_3.

En effet, en rmn du ^{19}F, on observe sur le spectre du mélange, deux groupes de signaux à −63,8 ppm et à −69,6 ppm correspondant aux CF_3. La résolution de ces signaux a permis de déduire les constantes de couplage ^4J allylique de H et CF_3. Le CF_3 résonant à −69,6 ppm se présente sous forme de doublet $^4J_{H-CF_3} = 1{,}6$ Hz. La résolution du signal de CF_3 à −63,8 ppm ne fait apparaître aucun couplage ($^4J_{H-CF_3} = 0$ Hz).

Il est communément admis que la constante de couplage ^4J allylique $H-CF_3$ est pratiquement nulle si H est en *trans* par rapport à CF_3 et peut atteindre 2,1 Hz, si H est *cis*. La confrontation de ces données expérimentales (18−20) avec celles tirées des spectres nous a permis d'attribuer la constante de couplage $^4J = 1{,}6$ Hz au composé *E*. L'absence de couplage

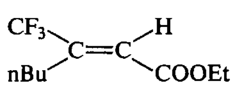

E

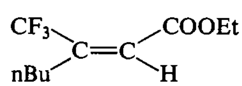

Z

$^4J_{H-CF_3}$ est donc attribuable au composé *Z*. L'intensité relative des signaux nous permet d'attribuer la configuration *E* au produit majoritaire (90%).

*(**2**)* (E, Z)

La caractérisation des composés **2** peut s'opérer à partir des observations suivantes.

Composé majoritaire

L'analyse élémentaire jointe à la masse moléculaire, déterminée par spectrométrie de masse (M^+ 224), conduit à la formule brute $C_{10}H_{15}F_3O_2$. En ir, $\nu_{(C=O)} = 1724\ cm^{-1}$ correspond à un ester éthylique qui est confirmé en rmn du ^1H par le quadruplet à 4,16 ppm d'intensité *2* et un triplet à 1,3 ppm d'intensité *3*. La fréquence de celui-ci est augmentée de 15 cm^{-1} par rapport à la bande $\nu_{(C=O)}$ du composé **1**. Ceci démontre la non conjugaison du groupement ester. Cette situation suggère qu'il existe au moins un groupement méthylénique susceptible de former un écran. Le singulet à 3,18 ppm d'intensité *2* correspond à un CH_2 en α d'un C=O. On a le groupement $—CH_2—C(=O)—O—CH_2CH_3$.

Compte-tenu de la formule brute, il nous reste: $C_6H_8F_3$ avec un centre d'insaturation. L'insaturation peut être une double liaison ou un cycle.

La position de la bande ir à 1669 cm^{-1}, la présence du triplet d'intensité *1* à 6,33 ppm dans la zone des "éthyléniques" et le couplage mis en évidence par ce triplet (*J* = 7,5 Hz), témoignent en faveur d'un système du type:

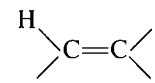

Le couplage H−H est variable selon le schéma envisagé:

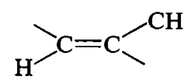

$^4J_{trans} = -0{,}8$ à $-2{,}5$ Hz

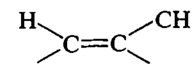

$^4J_{cis} = -0{,}8$ à -2 Hz

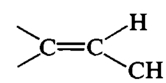

$^3J_{gem} = 4$ à 10 Hz

La valeur expérimentale *J* = 7,5 Hz démontre que H est couplé avec un CH_2 géminé absorbant à 2,66 ppm. Ceci est en accord avec la structure:

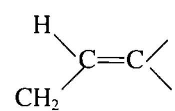

Il reste donc à affecter $C_3H_5F_3$.

L'infra-rouge suggère que l'absorption à 1100−1250 cm^{-1} peut être attribuée à une vibration $\nu_{(C-F)}$ (confirmée en rmn du fluor par un signal à −68,5 ppm, caractéristique d'un groupement CF_3). Il reste donc C_2H_5.

Le triplet à 0,91 ppm (*J* = 7,5 Hz), d'intensité *3* et le multiplet à 1,43 ppm, d'intensité *2* font partie du groupement $CH_3CH_2CH_2$ porté par la double liaison.

Ceci nous conduit à la formule:

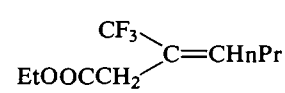

Ce composé peut exister sous deux formes stéréoisomères:

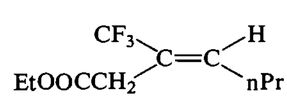

isomère *E*

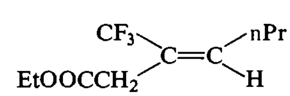

isomère *Z*

Avant d'aborder la détermination de la stéréochimie de ce composé, nous allons voir si le composé minoritaire est l'une de ces deux formes stéréoisomères envisagées.

Composé minoritaire

Un raisonnement analogue au précédent est appliqué.

L'analyse élémentaire associée à la masse moléculaire déterminée par spectrométrie de masse (M^+ 224), conduit à la formule brute $C_{10}H_{15}F_3O_2$. Ce composé présente en ir, les bandes suivantes: à 1728 cm^{-1} $\nu_{(C=O)}$, à 1667 cm^{-1} $\nu_{(C=C)}$ et à

[3]Le spectre rmn a été réalisé sur une fraction enrichie du mélange dans la proportion 75%:25%.

1100–1250 cm^{-1} $\nu_{(C-F)}$. En rmn du ^1H on observe: un triplet à 5,88 ppm, un quadruplet à 4,16 ppm, un singulet à 3,16 ppm, un multiplet à 2,28 ppm, un multiplet à 1,46 ppm, un triplet à 1,23 ppm, un triplet à 0,93 ppm avec un rapport d'intensités relatives *1/2/2/2/2/3/3*. Le spectre rmn du ^{19}F montre un signal à −60,2 ppm caractéristique d'un CF_3.

La seule structure compatible avec les spectres ir, rmn ^1H, ^{19}F, la masse et l'analyse élémentaire (C, H, F, O) est:

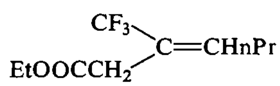

Les deux produits isolés sont donc bien deux stéréoisomères. La configuration correspondante à chaque isomère a été attribuée par étude des constantes de couplage ^4J allylique du proton et du fluor (rmn ^1H, rmn ^{19}F).

En rmn du ^1H, le signal du proton éthylénique, pour le composé majoritaire, résonant à 6,33 ppm, est constitué par un triplet de quadruplet dû à la multiplicité avec le CF_3 $^4J_{H-CF_3}$ = 1,8 Hz. Ce couplage est compatible avec un couplage allylique *cis* $^1H-^{19}F$. La configuration attribuée à ce composé est donc *E*.

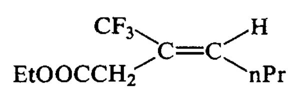

Ceci est confirmé par la rmn du ^{19}F. Le signal correspondant au CF_3 paraît être un quadruplet bien résolu. En réalité, c'est un faux quadruplet. En effet, le CF_3 est couplé d'une part au proton éthylénique et d'autre part au CH_2 (b):

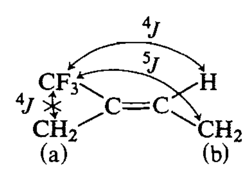

Le couplage $^4J_{CH_2\,(a)-CF_3\,(\text{géminé})}$ n'est pas observable.

On devrait s'attendre à un triplet de doublet. Les composantes des triplets sont séparées par $^5J_{CH_2\,(b)-CF_3\,(trans)}$ = 2 Hz, tandis que le dédoublement correspond à $^4J_{H-CF_3\,(cis)}$ = 2 Hz confirmant une configuration *E* pour ce composé.

Quant au composé minoritaire, en rmn du ^1H la résolution du triplet à 5,88 ppm du proton éthylénique fait apparaître un quadruplet mal résolu $^4J_{H-CF_3}$ = 0,8–0,7 Hz résultant d'un couplage *trans* du H et du CF_3. La configuration attribuée à ce composé est *Z*:

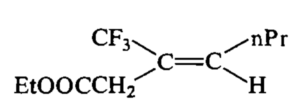

La rmn du ^{19}F est en accord avec cette stéréochimie. En effet, le signal du CF_3 est un triplet très mal résolu et résulte d'un couplage *trans* $^4J_{H-CF_3}$ = 0 Hz.

Seul apparaît le couplage homoallylique $^5J_{CH_2\,(b)-CF_3}$ = 2 Hz.

(3) (E)

L'analyse élémentaire jointe à la masse moléculaire déterminée par spectrométrie de masse (M^+ 258), conduit à la formule brute $C_{13}H_{13}F_3O_2$.

L'infra-rouge montre une bande $\nu_{(C=O)}$ non conjuguée d'ester éthylique à 1724 cm^{-1}. Cette fonction est confirmée en rmn par un quadruplet à 4,2 ppm d'intensité *2* et un triplet à 1,26 ppm d'intensité *3*.

En ir, une bande à 1621 cm^{-1} correspond à $\nu_{(C=C)}$ conjuguée avec un noyau aromatique (bandes fines entre 1450 et 1600 cm^{-1}). La double liaison ainsi mise en évidence n'est pas conjuguée avec la fonction ester éthylique. Nous envisageons entre les deux un groupement CH_2. Cette hypothèse est en accord avec un signal unique rencontré en rmn du ^1H à 3,36 ppm d'intensité *2*.

Par ailleurs, un signal à 7,4 ppm d'intensité *6*, indique que le signal du noyau aromatique se superpose à l'absorption d'un H éthylénique. En rmn du fluor, on observe à −68 ppm un signal attribuable à un groupement CF_3 porté par une double liaison. La résolution de ce signal se présente sous forme d'un doublet, la constante de couplage 1,6 Hz est compatible avec un couplage $^4J_{H-CF_3\,(cis)}$.

Deux structures peuvent être proposées:

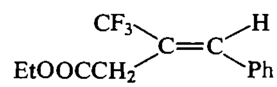

(a)

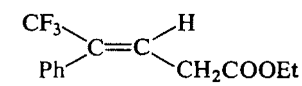

(b)

La structure (b) doit être rejetée à cause de la multiplicité du signal du CH_2 en α du groupement ester qui se présente sous forme d'un singulet.

Le produit obtenu est donc le phényl-4 trifluorométhyl-3 butène-3 oate d'éthyle, de configuration *E*.

Conclusion

Si nous récapitulons les résultats obtenus, nous observons que quelque soit la cétone $(CF_3)C(O)R$ avec R = nBu et $PhCH_2$, la réaction de Wittig conduit toujours aux trifluorométhyl oléfines activées α,β-insaturées. Par contre, la réaction d'Horner–Emmons, réalisée sur les phosphonates en milieu fortement basique, donne un mélange d'esters α,β-éthyléniques (**1**) (*Z* + *E*) et β,γ-éthyléniques (**2**) (*Z* + *E*) majoritaires quand R = nBu ou exclusivement le composé (**3**) (*E*) quand R = $PhCH_2$.

Le produit transposé est dû à une prototropie de l'oléfine attendue sous l'influence de la base.

Donc la réaction d'Horner–Emmons ne permet pas d'obtenir de manière spécifique les trifluorométhyl oléfines activées α,β-insaturées.

Il est à noter également une différence de réactivité des cétones en série hydrocarbonée et fluorée vis-à-vis du phosphorane $Ph_3P{=}CHCOOEt$. Les réactions de condensation avec les trifluorométhyl cétones s'effectuent dans des conditions douces (7) comparativement à celles requises pour les cétones classiques hydrocarbonées. En effet, il est bien connu, en série hydrocarbonée, que les ylures stabilisés par un groupement carbonylé réagissent avec les aldéhydes, mais pas avec les cétones sauf dans des conditions dures, alors que l'utilisation d'un carbanion phosphonate permet une réaction beaucoup plus aisée (21–25).

Partie expérimentale

Les spectres rmn ^1H et ^{19}F ont été enregistrés sur Bruker Spectroscope WH-90-DS (^1H = 90 MHz; ^{19}F = 84,67 MHz). Les spectres ir ont été effectués sur un spectromètre Leitz–Wetzlar, modèle IIIG. Les spectres de masse ont été enregistrés sur un appareil Ribermag R 10-10 couplé à la chromatographie en phase gazeuse. Les analyses élémentaires ont été effectuées par les laboratoires d'analyse du

CNRS à Lyon.

La pureté des produits a été contrôlée sur C.P.V. Girdel (séries 30 et 3000), colonne 1,3 m inox SE30 10% Chromosorb WHMDS 80/100; colonne 1,5 m inox 5% OV 17 Gas-Chrom Q 80/100, colonne capillaire Pyrex SE30 30 m, ϕ = 0,30 mm, et colonne capillaire Carbowax 20M-25 m.

Synthèse des trifluorométhyl cétones

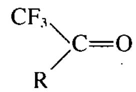

Deux trifluorométhyl cétones (R = nBu, Ph—CH_2) ont été synthétisées par action des organomagnésiens sur les F-acides (26, 27).

1. *n-Butyl trifluorométhyl cétone (trifluoro-1,1,1 hexanone-2)*

Préparation du bromure de n-butyl magnésium (réf. 28)

Dans un ballon rodé de 500 mL équipé d'un agitateur magnétique, d'une ampoule à brome et maintenu sous atmosphère d'azote, on place 6,48 g (0,27 at-g) de Mg en tournure et un petit cristal d'iode. Quinze millilitres d'une solution de 34 g (0,25 mol) de bromobutane dans 100 mL d'éther anhydre sont ajoutés par l'ampoule à brome. Dès que la réaction a démarré, on ajoute le reste de la solution de bromobutane de façon à maintenir un léger reflux. L'addition terminée, le mélange réactionnel est maintenu au reflux de l'éther pendant 30 min.

Synthèse de la cétone

On ajoute 11,4 g (0,1 mol) d'acide trifluoroacétique goutte à goutte à la solution de bromure de n-butyl magnésium agitée et refroidie à 15°C par un bain d'eau thermostaté. L'addition terminée, l'agitation est poursuivie pendant 3 h à température ambiante. Le mélange est hydrolysé à froid par environ 100 mL d'une solution de HCl à 15%. La phase éthérée est séparée par décantation, traitée à l'aide d'une solution saturée de bicarbonate de sodium, lavée à l'eau, séchée sur $MgSO_4$ puis P_2O_5. L'éther est évaporé aux 2/3 puis le résidu est purifié par distillation fractionnée à pression atmosphérique. Nous obtenons 8,47 g de produit, Rt 55%, Eb 89°C (lit. (26) Eb 91°C); ir (CCl_4) ν en cm^{-1}: 1754 (C=O), 1100–1250 (C—F); rmn ^{19}F ($CDCl_3$, référence interne $CFCl_3$) δ en ppm: −79,6 (CF_3).

2. *Benzyl trifluorométhyl cétone (phényl-3 trifluoro-1,1,1 propanone-2)*

Cette cétone est obtenue de la même façon que la trifluoro-1,1,1 hexanone-2. À une solution de chlorure de benzylmagnésium, obtenu à partir de 0,27 at-g de Mg en tournure et 0,25 mol de chlorure de benzyle (refroidie à 15°C par un bain d'eau thermostaté), on ajoute lentement 11,4 g (0,1 mol) d'acide trifluoroacétique. Le mélange est ensuite agité à température ambiante pendant 3 h. Après traitement, l'éther est évaporé et le résidu est distillé sous vide. Nous obtenons 9,4 g de produit, Rt 50%, Eb/160 Torr 120°C (lit. (29) Eb 66/16 Torr) (1 Torr = 133.3 Pa); ir (CCl_4) ν en cm^{-1}: 1754 (C=O), 1100–1250 (C—F); rmn ^{19}F ($CDCl_3$, référence interne $CFCl_3$) δ en ppm: −78,7 (CF_3).

*Synthèse de **1** (E, Z)*

Nous avons utilisé la technique décrite dans la littérature (7). À partir de 0,015 mol de carboéthoxyméthylènetriphénylphosphorane et 0,015 mol de trifluoro-1,1,1 hexanone-2 on obtient un mélange de deux composés avec un rendement global de 90%, Eb/280 Torr 80°C. La composition du mélange a été determinée par cpv (90/10%); ir (CCl_4) ν en cm^{-1}: 1709 (C=O), 1653 (C=C), 1100–1250 (C—F); rmn ^1H ($CDCl_3$, référence interne TMS) δ en ppm: 6,05 et 6,33 (q et s, H, =CH— (**1**) (*E*) et (**1**) (Z), $^4J_{H-CF_3\,(cis)}$ = 1,6 Hz), 4, 21 (9, 2H, —OCH_2—, $^3J_{H-H}$ = 7,5 Hz), 1,3 (t, 3H, —CH_3, $^3J_{H-H}$ = 7,5 Hz), 2,66–1,5 (m, 6H, —$(CH_2)_3$—), 0,95 (t, 3H, —CH_3, $^3J_{H-H}$ = 7,5 Hz); rmn ^{19}F ($CDCl_3$, référence interne $CFCl_3$) δ en ppm: −69,6 et −63,8 (d et s, CF_3 (**1**) (*E*) et (**1**) (Z), $^4J_{H-CF_3\,(cis)}$ = 1,6 Hz); spectrométrie de masse: M^+ = 224. *Anal.* calc. pour $C_{10}H_{15}F_3O_2$: C 53,57, H 6,69, F 25,44; trouvé: C 53,42, H 6,82, F 25,28.

*Synthèse du mélange **1** (E, Z) + **2** (E, Z)*

À 0,96 g de NaH (préalablement lavé deux fois à l'hexane et deux fois au THF) mis en suspension dans 30 mL de THF anhydre, on ajoute goutte à goutte 0,02 mol de carboéthoxyméthyl diéthyl phosphonate. On laisse 1 h sous agitation magnétique et sous courant d'azote, puis on ajoute lentement 0,02 mol de trifluoro-1,1,1 hexanone-2. Après 3 h de réaction, le mélange est porté au reflux du THF pendant 1/2 h. On laisse refroidir, puis le mélange est traité par l'eau et extrait à l'éther. La phase éthérée est lavée à l'eau et séchée. Après évaporation du solvant, le mélange est analysé par un appareil de spectrométrie de masse couplé à la chromatographie en phase vapeur.

Nous avons obtenu un mélange complexe de 2 produits attendus **1** = 10%, déjà caractérisés et 2 produits inattendus **2** dans la proportion 81/9%, Rt 62%; **2** Eb/125 Torr 104°C; **1** Eb/280 Torr 80°C.

Les composés **2** sont séparés par chromatographie en phase liquide, colonne d'alumine d'activité neutre, calibre 0,063–0,200 mm, éluant hexane–éther 9:1 (v/v).

***2** (E, Z)*

Isomère E: ir (CCl_4) ν en cm^{-1}: 1724 (C=O), 1669 (C=C), 1100–1250 (C—F); rmn ^1H ($CDCl_3$, référence interne TMS) δ en ppm: 6,33 (tq, H, =CH—, $^3J_{H-H}$ = 7,5 Hz, $^4J_{H-CF_3\,(cis)}$ = 1,8 Hz), 4,16 (q, 2H, —OCH_2—, $^3J_{H-H}$ = 7,5 Hz), 1,23 (t, 3H, —CH_3, $^3J_{H-H}$ = 7,5 Hz), 3,18 (s, 2H, —CH_2COO—), 2,11–1,43 (m, 4H, —$(CH_2)_2$—), 0,91 (t, 3H, —CH_3, $^3J_{H-H}$ = 7,5 Hz); rmn ^{19}F ($CDCl_3$, référence interne $CFCl_3$) δ en ppm: −68,5 (q, CF_3, $^4J_{H-CF_3\,(cis)}$ = $^5J_{CH_2-CF_3\,(trans)}$ = 2 Hz); spectrométrie de masse: M^+ = 224. *Anal.* calc. pour $C_{10}H_{15}F_3O_2$: C 53,57, H 6,69, F 25,44; trouvé: C 53,48, H 6,72, F 25,31.

Isomère Z: ir (CCl_4) ν en cm^{-1}: 1728 (C=O), 1667 (C=C), 1100–1250 (C—F); rmn ^1H ($CDCl_3$, référence interne TMS) δ en ppm: 5,88 (tq, H, =CH—, $^3J_{H-H}$ = 6,5 Hz, $^4J_{H_3-CF_3\,(trans)}$ = 0,8 Hz), 4,16 (q, 2H, —OCH_2—, $^3J_{H-H}$ = 7,5 Hz), 1,23 (t, 3H, —CH_3, $^3J_{H-H}$ = 7,5 Hz), 3,16 (s, 2H, —CH_2COO—), 2,28–1,46 (m, 4H, —$(CH_2)_2$—), 0,93 (t, 3H, —CH_3, $^3J_{H-H}$ = 7,5 Hz); rmn ^{19}F ($CDCl_3$, référence interne $CFCl_3$) δ en ppm: −60,2 (t, CF_3, $^5J_{H-CF_3}$ = 2 Hz); spectrométrie de masse: M^+ = 224. *Anal.* calc. pour $C_{10}H_{15}F_3O_2$: C 53,57, H 6,69, F 25,44; trouvé: C 53,62, H 6,82, F 25,35.

*Synthèse de **3** (E)*

Les conditions opératoires sont identiques aux précédentes (Horner–Emmons), avec la benzyl trifluorométhyl cétone; Rt 74,5%, Eb/30 Torr 121°C; ir (CCl_4) ν en cm^{-1}: 1724 (C=O), 1621 (C=C), 1100–1250 (C—F); rmn ^1H ($CDCl_3$, référence interne TMS) δ en ppm: 7,4 (s, 6H, protons aromatiques et proton éthylénique), 4,2 (q, 2H, —OCH_2—, $^3J_{H-H}$ = 7,5 Hz), 1,26 (t, 3H, —CH_3, $^3J_{H-H}$ = 7,5 Hz), 3,36 (s, 2H, —CH_2COO—); rmn ^{19}F ($CDCl_3$, référence interne $CFCl_3$) δ en ppm: −67,6 (d, CF_3, $^4J_{H-CF_3\,(cis)}$ = 1,6 Hz); spectrométrie de masse: M^+ = 258. *Anal.* calc. pour $C_{13}H_{13}F_3O_2$: C 60,46, H 5,03, F 22,09; trouvé: C 60,38, H 5,10, F 22,14.

1. G. WITTIG. Experientia, **12**, 41 (1956); Angew. Chem. **68**, 505 (1956).
2. L. HORNER, H. HOFFMANN et H. G. WIPPEL. Chem. Ber. **91**, 61 (1958).
3. L. HORNER, H. HOFFMANN, H. G. WIPPEL et G. KLAHRE. Chem. Ber. **92**, 2499 (1959).
4. W. S. WADSWORTH, JR. et W. D. EMMONS. J. Am. Chem. Soc. **83**, 1732 (1961).
5. A. W. JOHNSON. *Dans* Ylid chemistry. *Edité par* A. T. Blomquist. Academic Press, New York. 1966.
6. I. K. KNUNYANTS, N. P. GAMARYAN et CH'EN CH'ING YUN. Bull. Acad. Sci. U.S.S.R. (Engl. Transl.), 633 (1962).
7. D. L. DULL, I. BAXTER et H. S. MOSHER. J. Org. Chem. **32**, 1622 (1967).
8. H. MOLINES et C. WAKSELMAN. J. Fluorine Chem. **16**, 97 (1980).
9. M. C. CESARETTI. Thèse de 3ème Cycle, Nice (1976).
10. F. CAMP, J. COLL, A. MESSEGUER et A. ROCA. Tetrahedron Lett. **10**, 791 (1976).
11. H. DISLICH. Angew. Chem. Int. Ed. Engl. **18**, 49 (1959).
12. C. K. INGOLD. Structure and mechanism in organic chemistry. Cornell University Press, Ithaca, NY. 1969. p. 823.
13. G. A. R. KON et R. P. LINSTEAD. Ann. Rep. Prog. Chem.

(Chem. Soc. London), **24**, 109 (1927).
14. G. A. R. KON et R. P. LINSTEAD. Ann. Rep. Prog. Chem. (Chem. Soc. London), **25**, 119 (1928).
15. J. W. BAKER. Tautomerism. Routledge, London. 1934. Chap. 9.
16. H. GILMAN. Organic chemistry. Wiley, New York. 1938. p. 819.
17. R. LESPIAU. Bull. Soc. Chim. Fr. 460 (1905).
18. D. J. BURTON, R. L. JOHNSON et R. T. BOGAN. Can. J. Chem. **44**, 635 (1966).
19. W. R. CULLEN et W. R. LEEDER. Inorg. Chem. **5**, 1004 (1966).
20. D. J. BURTON, F. E. HERKES et K. J. KLABUNDE. J. Am. Chem. Soc. **88**, 5042 (1966).
21. S. TRIPPETT et D. M. WALKER. Chem. Ind. 990 (1961).
22. A. MAECHER. Org. React. **14**, 277 (1965).
23. I. GOSNEY et A. G. ROWLEY. *Dans* Organophosphorous reagents in organic synthesis. *Edité par* J. I. G. Cadogan. Academic Press, Londres. 1979. Chap. 2. p. 17.
24. L. A. YANOVSKAYA et V. F. KUCHEROV. Izv. Akad. Nauk S.S.S.R. Ser. Khim. 1341 (1964); Chem. Abstr. **61**, 11887 (1964).
25. M. KIRILOU et G. PETROV. Monatsh. Chem. 1651 (1972).
26. A. SYKES, J. C. TATLOW et R. C. TOHAMAS. J. Chem. Soc. 835 (1956); Chem. Ind. 630 (1955).
27. K. T. DISHART et R. LEVINE. J. Am. Chem. Soc. **78**, 2268 (1956).
28. E. E. DREGER. Org. Synth. **1**, 306 (1967).
29. F. E. HERKES et D. J. BURTON. J. Org. Chem. **32**, 1311 (1967).

The formation of branched-chain deoxypentofuranosides by ring contraction in the reductive desulfonyloxylation of hexopyranoside *p*-toluenesulfonates[1]

HANS H. BAER, DAVID J. ASTLES, HO-CHI CHIN, AND LISA SIEMSEN
Ottawa–Carleton Institute for Research and Graduate Studies in Chemistry, Department of Chemistry, University of Ottawa, Ottawa, Ont., Canada K1N 9B4

Received May 23, 1984

HANS H. BAER, DAVID J. ASTLES, HO-CHI CHIN, and LISA SIEMSEN. Can. J. Chem. **63**, 432 (1985).

Several methyl 6-deoxy-, 6-deoxy-6-halo-, and 6-*O*-*p*-tolylsulfonylhexopyranoside 2- and 4-*p*-toluenesulfonates reacted readily with lithium triethylborohydride in boiling tetrahydrofuran under reductive desulfonyloxylation at C-2 and C-4, respectively, and with reduction at C-6 where applicable. The desulfonyloxylations proceeded with ring contraction to furnish, in 40–60% isolated yields, new branched-chain pentofuranoside derivatives, namely, methyl 2,5-dideoxy-2-*C*-(hydroxymethyl)pentofuranosides having the α-L-*xylo*, α-D-*xylo*, and α-D-*ribo* configurations (from 2-tosylates), and methyl 3,5-dideoxy-3-*C*-(hydroxymethyl)pentofuranosides having the α-D-*arabino* and α-D-*ribo* configurations (from 4-tosylates). In some of the reactions, reductively desulfonyloxylated but unrearranged products were formed in addition. Methyl 4,6-*O*-benzylidene-2,3-di-*O*-*p*-tolylsulfonyl-α-D-galactopyranoside reacted by partial de-*O*-sulfonylation and partial desulfonyloxylation, with and without ring contraction, to give methyl 3,5-*O*-benzylidene-2-deoxy-2-*C*-(hydroxymethyl)-α-D-*lyxo*-pentofuranoside, methyl 4,6-*O*-benzylidene-3-deoxy-α-D-*lyxo*-hexopyranoside, and the parent 2,3-diol.

HANS H. BAER, DAVID J. ASTLES, HO-CHI CHIN et LISA SIEMSEN. Can. J. Chem. **63**, 432 (1985).

Plusieurs méthyl-6-désoxy-, 6-désoxy-6-halo- et 6-*O*-*p*-tolylsulfonylhexopyranosides 2- et 4-*p*-toluènesulfonates donnent lieu à désulfonyloxylation réductive en C-2 et C-4 respectivement, ainsi qu'à réduction en C-6 s'il y a lieu, sous l'action du triéthylborohydrure de lithium dans le tétrahydrofuranne à reflux. La désulfonyloxylation s'accompagne de contraction de cycle et conduit, avec des rendements de 40–60% en produits isolés, à des nouveaux dérivés pentofuranosides ramifiés, les méthyl-2,5-didésoxy-2-*C*-(hydroxyméthyl)pentofuranosides de configuration α-L-*xylo*, α-D-*xylo* et α-D-*ribo* partant du sulfonate en C-2, ou encore méthyl-3,5-didésoxy-3-*C*-(hydroxymethyl)pentofuranosides de configuration α-D-*arabino* et α-D-*ribo* partant du sulfonate en C-4. Dans quelques cas, une désulfonyloxylation réductive sans réarrangement est également observée. Le méthyl-4,6-*O*-benzylidène-2,3-di-*O*-*p*-tolylsulfonyl-α-D-galactopyranoside donne ainsi lieu, à la fois à dé-*O*-sulfonylation et désulfonyloxylation avec, et sans contraction de cycle respectivement, pour conduire aux méthyl-3,5-*O*-benzylidène-2-*C*-(hydroxyméthyl)-α-D-*lyxo*-pentofuranoside, méthyl-4,6-*O*-benzylidène-3-désoxy-α-D-*lyxo*-hexopyranoside ainsi que au diol en C-2, C-3 correspondant.

Introduction

Recently we reported on the reductive desulfonyloxylation of methyl 4,6-*O*-benzylidene-α- and -β-D-glucopyranoside *p*-toluenesulfonates by means of lithium triethylborohydride (LTBH), which permitted the convenient preparation of certain 2- and 3-deoxyhexopyranoside derivatives in high yields (1). The method has also been applied to various tosylates of the analogous bisacetal from the disaccharide α,α-trehalose (2). A structural prerequisite for facile desulfonyloxylation appeared to be the presence of a free, or potentially free, hydroxyl group adjacent and *trans* to the sulfonate ester, and it was established that the reaction proceeds through intermediary epoxides, the formation and subsequent reductive ring-opening of which is governed by well-known stereochemical prinicples. One of the factors promoting high regioselectivity in the sense of the Fürst–Plattner rule doubtless was the conformational rigidity imparted to the intermediates by their *trans*-fused, cyclic acetal structures. It became of interest, therefore, to examine the degree to which this structural constraint contributed to the stereochemical outcome of the reaction, and it was decided to study the action of LTBH upon a number of simple, non-acetalated hexopyranoside tosylates, particularly of the 6-deoxy type. Appropriate derivatives of the latter class of sugars are readily available and it was considered that, stereochemical interest apart, LTBH reduction might offer practical advantages for the preparation of 2,6- and 3,6-dideoxyhexoses. Such sugars have great biological importance as they occur widespread in nature, in the form of plant glycosides (e.g., digitoxose in *Digitalis*), as components of antibiotics (e.g., chromose and oleandrose in chromomycins and oleandomycin), and as bacterial constituents (e.g., abequose, paratose, and tyvelose in *Salmonella* polysaccharides).

Results and discussion

Ring contraction effected by lithium triethylborohydride

Reaction of methyl 2-*O*-tosyl-α-L-fucopyranoside (**1**) with LTBH was expected to lead to internal displacement of the ester group, followed by reductive opening of the resulting 2,3-epoxide, to give one or both of the dideoxyhexopyranosides which this sequence of events can provide. However, no such product was detected upon treatment of **1** with an excess of the reductant in boiling oxolane, although all of **1** was consumed within 30 min and desulfonyloxylation did take place. Instead, ring contraction occurred and the branched-chain glycoside **10**, methyl 2,5-dideoxy-2-*C*-(hydroxymethyl)-α-L-*xylo*-pentofuranoside, was isolated crystalline in ca. 60% yield. Evidently the loss of the tosyloxy group was coupled with a skeletal rearrangement by migration of the C-3—C-4 bond. Performance of the reaction with the D enantiomer **2** provided the D enantiomer **11**, likewise in crystalline form. When methyl 4-*O*-benzoyl-6-bromo-6-deoxy-2-*O*-tosyl-α-D-glucopyranoside (**3**) or methyl 6-deoxy-6-iodo-2-*O*-tosyl-α-D-glucopyranoside (**4**) were used as substrates, the crystalline α-D-*ribo* isomer of the foregoing 2,5-dideoxy-2-*C*-(hydroxymethyl)pentofuranosides was obtained.

[1] The essential results of this work were included in preliminary form in the communication (I-37) presented by H. H. Baer, H. R. Hanna, and D. J. Astles at the XIth International Carbohydrate Symposium, Vancouver, B.C., August 22–28, 1982.

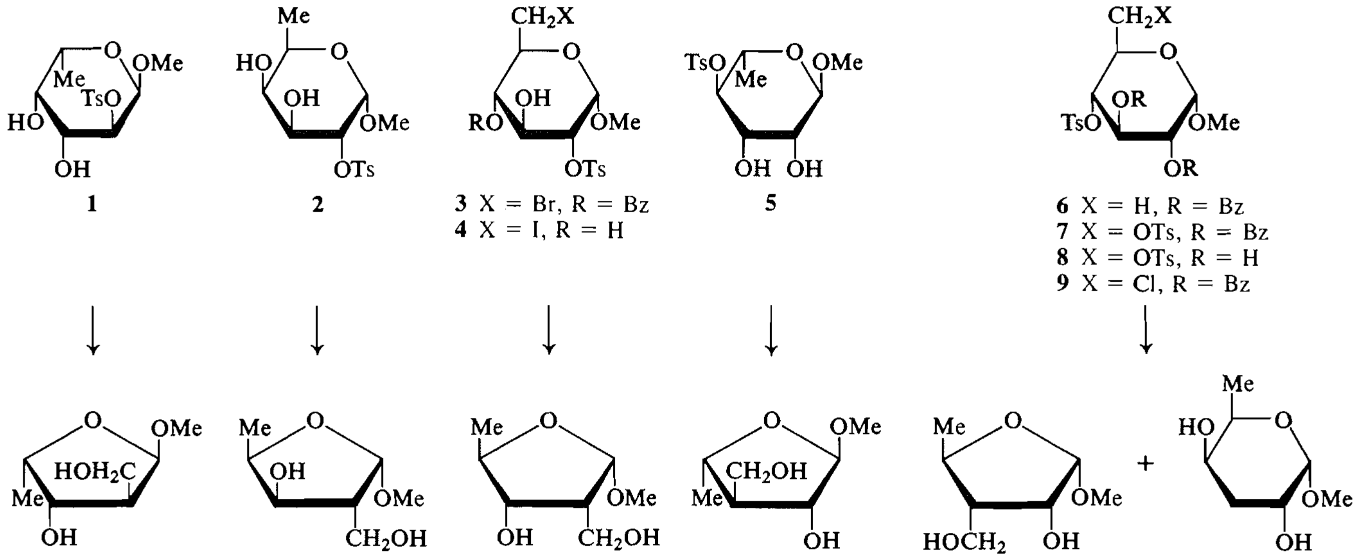

1, 2, 3 X = Br, R = Bz; 4 X = I, R = H; 5; 6 X = H, R = Bz; 7 X = OTs, R = Bz; 8 X = OTs, R = H; 9 X = Cl, R = Bz

10, 11, 12, 13, 14, 15

In corresponding hexopyranoside 4-tosylates, ring contraction took place in the opposite direction, i.e., by migration of the C-2—C-3 bond, furnishing isomeric 3,5-dideoxy-3-*C*-(hydroxymethyl)pentofuranosides. Thus, methyl 4-*O*-tosyl-α-L-rhamnopyranoside (**5**) produced the crystalline α-L-*arabino* isomer (**13**), and methyl 2,3-di-*O*-benzoyl-4-*O*-tosyl-α-D-quinovoside (**6**) gave the α-D-*ribo* isomer **14**, which failed to crystallize but was isolated chromatographically in pure condition. In all of these experiments, the starting tosylates reacted rapidly and completely (provided a sufficient excess of hydride reagent, normally 8 mol. equiv., was employed), and no unrearranged dideoxyhexopyranosides were detected, although traces of unidentified by-products were usually seen in tlc. The crude reaction mixtures apparently contained the product glycosides as alkali-stable organoboron complexes, and because of a high (and not unexpected) acid-sensitivity of the dideoxyfuranosides the products tended to behave somewhat capriciously in processing and during isolation. Isolated yields of chromatographically pure products generally were in the 40–60% range.[2]

In contrast to the 6-deoxy sugar **6**, the analogous methyl 2,3-di-*O*-benzoyl-4,6-di-*O*-tosyl-α-D-glucopyranoside (**7**) gave the ring-contracted product (**14**) *and* the unrearranged hexopyranoside **15**, in a ratio of ~3:2. Although complete chromatographic separation was difficult to achieve and the reaction was therefore of limited preparative value, the isomers were obtained sufficiently pure for unambiguous spectroscopic identification, and **15** was identified as methyl 3,6-dideoxy-α-D-*xylo*-hexopyranoside (methyl α-abequoside) by comparison with an independently-prepared (3) sample. The de-*O*-benzoylated 4,6-ditosylate[3] **8** and the 6-chloro-6-deoxyglycoside **9** on treatment with LTBH gave mixtures of **14** and **15** in approximately equal proportions.

The exclusive or predominant occurrence of ring contraction here reported stands in sharp contrast to the desulfonyloxylations that had been performed (1) in 4,6-*O*-benzylidenated glucopyranoside tosylates. In the latter, an analogous rearrangement would require the formation of a highly strained system comprising a six-membered acetal ring *trans*-fused to a five-membered furanose ring, and presumably is disfavored for this reason. To test this hypothesis, methyl 4,6-*O*-benzylidene-2,3-di-*O*-tosyl-α-D-galactopyranoside (**16**) was subjected to reduction with LTBH, the surmise being that a *cis*-fused acetal might not interdict furanoside formation. Indeed, ring-contracted methyl 3,5-*O*-benzylidene-2-deoxy-2-*C*-(hydroxymethyl)-α-D-*lyxo*-pentofuranoside (**17**) was isolated crystalline (38%), although methyl 4,6-*O*-benzylidene-3-deoxy-α-D-*lyxo*-hexopyranoside (**18**) was a second, major product (22%), and a significant proportion (18%) of the diol **19** was formed by

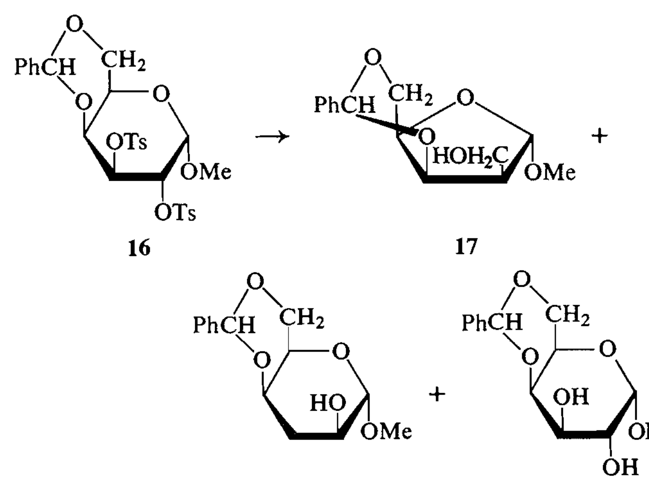

16, 17, 18, 19

[2] The crude reaction products showed in tlc a slow-moving spot that corresponded to that given by the isolated, rearranged glycoside, and an additional strong spot (fast moving, but slightly slower than the starting tosylate) which was invisible under uv light and therefore represented tosyl-free material also. Upon chromatographic isolation, this fast-moving material showed the same ^{1}H nmr features as the rearranged glycoside but additionally gave strong resonances near δ 0.9, presumably attributable to alkylboron moieties. Treatment of the alkaline reaction mixtures with hydrogen peroxide diminished the proportion of these products whose more-detailed characterization must await further study. So far it seems that the primary hydroxyl group present in the glycosides formed must be involved in the occurrence of this complication, which was not encountered in the LTBH reductions previously (1) studied.

[3] Obtained from **7** by deacylation with methanolic ammonia. For complex results obtained on attempted deacylation with sodium methoxide, see the experimental section.

TABLE 1. ^{1}H Magnetic resonance data for methyl dideoxy-*C*-(hydroxymethyl)pentofuranosides[a]

	Chemical shifts[b] (δ)									
Compound	H-1	H-2	H-2′a	H-2′b	H-3	H-3′a	H-3′b	H-4	*C*-CH_3	*O*-CH_3
11	5.04d	2.32m[c]	3.86cm (2H)		4.33ddd[d]			4.20qn	1.25d	3.37s
12	5.00d	2.39cm[e]	3.99cm[f,g]	3.86cm[f,h]	~3.9[f]			4.16qd	1.25d	3.39s
13	4.84d[i]	4.10nm[j]			1.86dddd	~3.70m (2H)		3.94dq	1.37d	3.35s
14	4.96	4.43m[k]			1.95tdd	3.77 (2H)[l]		4.05dq[m]	1.29d	3.49s
14[n]	5.05d	5.13dd			2.29dddd	4.28dd	4.11dd	4.06qn	1.33d	3.37s

	Coupling constants (Hz)									
Compound	$J_{1,2}$	$J_{2,3}$	$J_{2,2'a}$	$J_{2,2'b}$	$J_{2'a,2'b}$	$J_{3,4}$	$J_{3,3'a}$	$J_{3,3'b}$	$J_{3'a,3'b}$	$J_{4,5}$
11	5.6	5.0	4.5	5.2	11.5	6.2				6.3
12	4.7	6.7	6.7	5.8	11.6	2.7				6.5
13	1.0	4.0				8.0	~6	~7		6.3
14	4.65	8.1				8.0	7	4.6	11.4	6.1
14[n]	4.3	9.0				6.25	6.6	8.3	11.2	6.25

[a]From 200-MHz spectra of solutions in $CDCl_3$ containing tetramethylsilane as the standard. Spectra with spin–spin decoupling by double irradiation and spectra with D_2O exchange were additionally obtained for all compounds.
[b]Signal multiplicities are indicated as cm (complex multiplet), d (doublet), nm (narrow multiplet), m (multiplet), q (quartet), qn (quintet), s (singlet), and t (triplet). Values refer to signal midpoints.
[c]Apparent qn; width 20.3 Hz, compatible with dddd having splittings of 4.5, 5.0, 5.2, and 5.6 Hz; collapsing to q, width 14.7 Hz, on H-1 irradiation.
[d]Giving on D_2O exchange an apparent t, width 11.2 Hz, by removal of a 3.8-Hz splitting.
[e]Width, 23.8 Hz; reduced to td on H-1 irradiation, with remaining splittings of 5.8, 6.7, and 6.7 Hz.
[f]The signals for H-2′a, -2′b, and -3 were poorly resolved in the regular spectrum.
[g]Sharp dd on D_2O exchange, and d (with broadened lines because of coupling with OH) on irradiation of H-2.
[h]Upon D_2O exchange, a clearly visible dd superimposed on the H-3 multiplet; without exchange, but with irradiation of H-2, a dd due to coupling with H-2′a and OH was seen.
[i]In the presence of D_2O, a singlet was observed, probably due to a slight change in overall conformation related to hydrogen bonding.
[j]Simplified to d in the presence of D_2O, due to coupling with H-3 only; see also *i*.
[k]Simplified to dd on D_2O exchange, and further to d upon subsequent irradiation of H-3.
[l]After D_2O exchange, the signal was an AB-q, as part of an ABX system.
[m]Collapsing to q on irradiation of H-3.
[n]Spectrum of the di-*O*-acetyl derivative. The acetyl singlets were at δ 2.05 and 2.11.

TABLE 2. ^{13}C Chemical shifts (ppm) for methyl dideoxy-*C*-(hydroxymethyl)pentofuranosides[a]

Compound	C-1	C-2	C-3	C-4	C-5	CH_2OH	OCH_3	Σ
11	104.6	54.2	76.1	73.5	14.4	59.8	55.1	437.7
12	105.4	48.2	77.2	83.1	19.4	58.1	54.9	446.3
13	109.5	80.1	54.7	76.0	20.5	61.9	56.9	459.6
14	102.6	73.5	50.1	74.5	20.0	60.1	55.2	436.0

[a]From 20-MHz spectra, obtained with a Varian FT-80 spectrometer, for solutions in $CDCl_3$ containing TMS as the internal standard.

twofold S—O cleavage (desulfonylation) of **16**. The last-mentioned side reaction was markedly more pronounced than in the *gluco* series (1).[4]

Structure of the branched glycosides

The constitutions of the methyl 2,5(or 3,5)-dideoxy-2(or 3)-*C*-(hydroxymethyl)pentofuranosides **10–14** followed from elemental analysis (excepting **14**) and nuclear magnetic resonance data. The 200-MHz ^{1}H nmr spectra (Table 1) showed the appropriate substituent resonances, and the ring proton signals were for the most part well resolved. In particular, there was in each case a *single* proton resonating at high field, indicating a methine, rather than methylene, structure for C-2 or C-3 and, therefore, chain branching. The position of the branch was confirmed by spin decoupling, which proved the methine proton to be vicinal to the anomeric proton in **10–12**, and vicinal to H-2 and H-4 in **13** and **14**. Isomeric 2- and 3-deoxyhexopyranosides, by contrast, show at high field two proton signals, sometimes well resolved as, for example, in **15** (7). The ^{13}C nmr data (Table 2) clearly supported the constitutions. The proton-coupled spectra each contained two quartets (for *C*-methyl and *O*-methyl), a triplet (for hydroxymethyl), a doublet at relatively high field for the branch-point carbon, and three doublets for the remaining ring carbon atoms in the usual shift ranges. Spectral data establishing the structures of the benzylidene acetals **17** and **18** are listed in the experimental section.

The question of configuration at the branch point was somewhat more difficult to decide. The vicinal ^{1}H—^{1}H coupling constants (Table 1) were all in accord with the assigned config-

[4]A similar difference in sulfonate ester stability between **16** and its α-D-*gluco* epimer had been noted in their reactions with lithium aluminum hydride, in which **16** suffered far-reaching O—S fission at both O-2 and O-3 (4), whereas the *gluco* epimer was more stable toward this type of cleavage, particularly in position 3 (1, 5, 6).

urations, but, for some of the compounds, the alternative branch-point configuration could not be excluded with any certainty on this basis alone. Such difficulty was not unexpected for conformationally flexible, furanoid systems where reasonable models accommodating spectral data can often be constructed for more than one configuration. Comparisons with known conformational preferences in unbranched furanosides (8, 9) were helpful, but the possibility of bias associated with the *C*-hydroxymethyl branch had to be borne in mind. The assignments indicated were arrived at on the basis of the discussion that follows, which considers both ^{1}H and ^{13}C nmr parameters and is predicated on the assumption that only the branch-point configuration is at issue, with the other chiral centers not having been involved in the reaction and having, therefore, retained their original stereochemistry. (See also the subsequent section on the mechanism.)

Beginning with the C-3 branched isomers, the α-L-*arabino* configuration of **13** can be regarded as secure. The $^3J_{H,H}$ values (Table 1) demand dihedral angles of $\phi_{1,2} > 90° < 120°$, and $\phi_{3,4} \leq 180°$, corresponding to a conformation in the $E_0 \rightleftharpoons {}^4T_0 \rightleftharpoons {}^4E$ segment of the pseudorotational itinerary for this configuration. This is in good agreement with Perlin's (8) and Angyal's (9) deduction of E_0 as the favored conformation of methyl α-L-arabinofuranoside. A shift towards $^4T_0$, as suggested by the particularly large $J_{3,4}$ value (8 Hz) in **13**, appears reasonable because it permits the hydroxymethyl group to become quasi-equatorial without sacrificing the quasi-axial orientation of the anomeric methoxyl group.[5] The ^{13}C chemical shifts (Table 2) indicate for **13** the largest overall deshielding (Σ = 459.6 ppm) among all the isomers, signifying the least amount of crowding in harmony with the all-*trans* substituent pattern (10). In the stereoisomer **14**, markedly increased shielding is experienced by C-1, C-2, and C-3 while C-4 and C-5 are affected little, which strongly suggests a *cis,cis,trans* substituent pattern, i.e., the α-D-*ribo* configuration. The $^3J_{H,H}$ data fit the $^0E \rightleftharpoons {}^0T_4$ conformation thereof, which has $\phi_{1,2}$ ~30°, $\phi_{2,3}$ ~0°, and $\phi_{3,4}$ ~160°, and in which the bulky C-3 substituent occupies a somewhat more outward position than does OH-3 in methyl α-D-ribofuranoside for which the adjacent segment $E_1 \rightleftharpoons {}^0T_1 \rightleftharpoons {}^0E$ has been proposed (8, 9). Although the ^{1}H couplings are equally consistent with the α-D-*xylo* ($^2E \rightleftharpoons {}^2T_3$) arrangement, we prefer the α-D-*ribo* assignment for **14** in view of the ^{13}C data just mentioned.

Turning now to the C-2 branched isomers **11** and **12**, we note their closely similar ^{13}C shifts for C-1, upfield in comparison with **13**, and therefore assume an identical, 1,2-*cis* arrangement. (The shielding effect of a *cis*-2-(hydroxymethyl) upon C-1 appears smaller than that of a *cis*-2-hydroxyl, cf. **14**.) This is borne out by the remaining shift data. The C-2 is shielded in **12**, relative to **11**, by the *cis*-vicinal OH-3. Conversely, C-4 in **11** is shielded, relative to **12**, due to the 3,4-*cis* arrangement which, incidentally, has also a marked effect on C-5, moving this signal upfield by 5–6 ppm from the resonance position in all the other isomers. The C-3 shifts are similar for **11** and **12**, as either compound possesses one *cis* and one *trans* pattern surrounding that carbon atom. The assignments resulting from these considerations are α-D-*xylo* for **11** and α-D-*ribo* for **12**. The $^3J_{H,H}$ values for **12** are in excellent accord therewith, fitting the $E_1 \rightleftharpoons {}^0T_1$ conformation ($\phi_{1,2}$ ~30°, $\phi_{2,3}$ ~25°, $\phi_{3,4}$ ~120°) that has been suggested (8, 9) for methyl α-D-ribofuranoside, and they are inconsistent with the 2-epimeric, α-D-*arabino* configuration.[6] The $^3J_{H,H}$ data for **11** allow no distinction, as they agree with both the α-D-*xylo* and the α-D-*lyxo* configuration in the respective conformations ^2E ($\phi_{1,2}$ ~30°, $\phi_{2,3}$ ~150°, $\phi_{3,4}$ ~30°) and ^3E ($\phi_{1,2}$ ~150°, $\phi_{2,3}$ and $\phi_{3,4}$ ~30°) or close pseudorotational variants. Our decision in favor of the former therefore rests solely on the foregoing interpretation of the ^{13}C data. However, it receives support from mechanistic considerations (see below). Compound **10**, being the enantiomer of **11**, requires no extra discussion.

The acetal **17** shows $J_{3,4}$ = 2.1 Hz as expected for the *gauche* orientation of the protons situated at the ring junctions, and $J_{1,2} = J_{2,3}$ = 4.8 Hz. The size of $J_{2,3}$ requires H-2 and H-3 to be *cis* ($\phi_{2,3}$ <60°); if they were *trans* ($\phi_{2,3}$ ~90°), a very small coupling would result. Clearly, the α-D-*lyxo* configuration is indicated. Compound **18** gave a two-proton multiplet at δ 2.13 attributable to a ring methylene group. The anomeric proton signal occurring at δ 4.79 was a slightly broadened singlet as is normal, in benzylidenated hexopyranosides, for a 1,2-diequatorial proton arrangement and is indicative of absence of a 1,2 axial–equatorial proton relationship. Double irradiation at δ 2.13 caused spin decoupling in the signal (δ 3.58) which was due to the ring proton at the hydroxylated position, and in the H-4 signal (δ 4.12). These features, whose interpretation was corroborated by comparison with data from several related isomers (1), established the structure shown.

Preliminary mechanistic considerations

While this work was in progress, we became aware of a precedent for LTBH-induced ring contraction in pyranosides. Pozsgay and Neszmélyi (12) obtained from benzyl 2,4-di-*O*-benzyl-3-*O*-trifluoromethylsulfonyl-α-L-rhamnopyranoside (**20**)

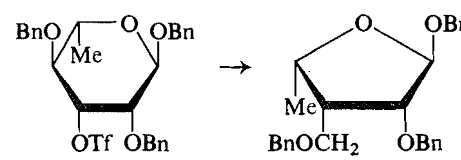

20 **21**

in 40% yield the ring-contracted product **21**. They interpreted the reaction as being initiated by departure of the sulfonyloxy group, to generate a pyranosid-3-yl carbocation that would rearrange by migration of the C-4,5 bond (which is antiparallel to the leaving group), and the rearranged ion would then accept hydride ion at the branch carbon atom, giving the 3-*C*-(benzyloxymethyl)-3-deoxypentofuranoside **21**. Whereas such a mechanism, which is supported by similar rearrangements occurring in solvolyses of pyranoside 3-sulfonates and in nitrous acid deamination of 3-amino sugars (13), may well apply for **20**, its operation in the present context could not be confidently presumed, for two main reasons. First, for the 2- and

[5] For a discussion of the factors which govern furanoside conformation, see ref. 9. The $^3J_{H,H}$ values for **13** would also be compatible with the 3-epimeric, α-L-*lyxo* glycoside, but only for a conformation close to ^1E. This is a highly unlikely form as it has three contiguous, *cis*-oriented substituents severely eclipsed; it is avoided by methyl α-L-lyxofuranoside (8, 9) and should be favored even less by the C-3 branched analog.

[6] For a series of 10 diversely substituted, C-2 branched α-L-arabinofuranosides, structurally related to our compounds but obtained in a different way, Jarý and co-workers (11) reported $J_{1,2}$ values in the range of 1.3–3.8 Hz (average, 2.1 Hz), and $J_{3,4}$ values in the range of 5.1–7.5 Hz (average, 6.5 Hz).

4-sulfonates **1–9**, it would imply the development of positive charge on C-2 or C-4, respectively. Although examples of pyranoside ring contraction involving incipient carbonium ions at those sites are in fact known in the domains of solvolysis and deamination mentioned (13), the dominant course of rearrangement in these cases is by participation of the ring oxygen atom, and alternative migrations of a carbon atom (C-2 to $^{+}$C-4, or C-4 to $^{+}$C-2) have been encountered as subordinate events only (14). In the present study, no evidence for the formation of products originating from ring oxygen migration was found. Secondly, in contrast to **20** the glycosides considered here all contain a free or potentially free (i.e., esterified) hydroxyl group positioned *trans*-vicinal to the sulfonate function, a feature which should play a key role in the observed transformations. Alcohols, including sugar hydroxyls, react instantly with alkali metal trialkylborohydrides to give hydrogen and alkoxytrialkylboronates (15). As we have seen earlier (1, 2), such boronates formed from tosylated sugars and LTBH can undergo internal displacement to produce epoxides, provided the proper geometry exists. Although in the previous examples (1, 2) the epoxides incurred ring opening with excess reductant as expected (16), giving deoxyhexopyranosides, an intermediacy of epoxides in the ring contractions now observed could not a priori be ruled out. Epoxide → carbonyl rearrangements, including instances with alkyl migration, are known and are, relevantly, catalyzed by lithium salts (halides or perchlorate) (17). Lithium salt produced in the epoxide-forming step (and by C-6 reduction, where applicable) might have induced rearrangement. In fact, when the ditosylate **7** was treated with an amount of LTBH insufficient for its complete conversion into the final products **14** and **15**, the 3,4-anhydrohexopyranoside **22** could be isolated from the reaction mixture. However, independently-synthesized **22** was rapidly (within 5 min) and almost quantitatively converted into **15** (isolated yield, 94%) under the same conditions, and no trace

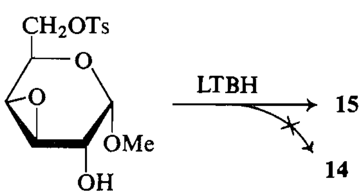

22

of **14** was detected (7). Similarly, the 3,4-anhydrohexopyranoside **23**, obtainable from **5** by action of base, reacted (7) with LTBH in the same way, to give methyl 3,6-dideoxy-α-L-*lyxo*-hexopyranoside (**24**) in the same yield and without any **13**. There was no discernible difference between the reductions of **22** and **23**, and lithium tosylate engendered during the reaction

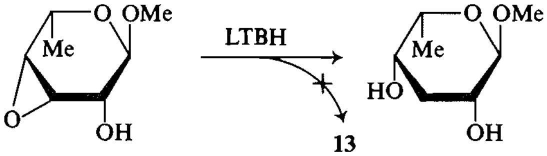

23 **24**

of the former appeared without influence. We therefore conclude that epoxides, where they do arise, are precursors for the unrearranged, minor products (**15**, **18**, and possibly others which may have escaped detection), but *not* for the ring-

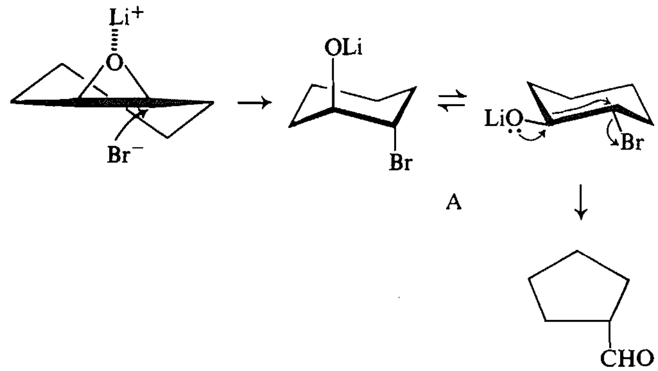

SCHEME 1

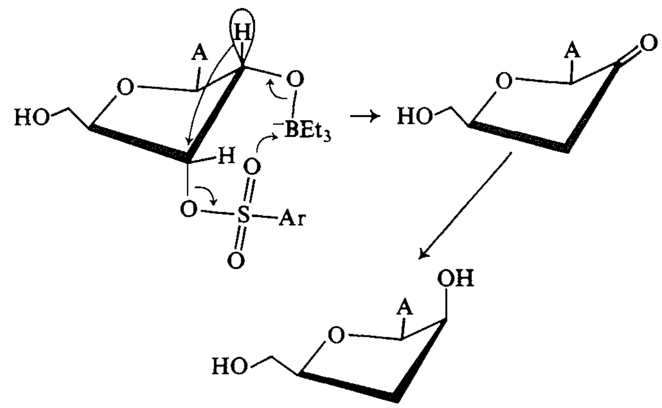

SCHEME 2

contracted furanosides, the formation of which must be due to some other mechanism.

One plausible mechanism would nevertheless be akin to the lithium salt-catalyzed epoxide → carbonyl rearrangement (17) just considered. It is assumed in the latter that intermediary halohydrin salts (A) arise from epoxides and react as shown in Scheme 1. Ring contraction as in A could well occur in the lithium alkoxytriethylboronates formed from glycoside tosylates; it would of course be followed by reduction of the carbonyl species primarily formed. The configurations assigned to our branched products would in every case accord with this process, the stereochemistry of which is determined by migration of a C—C bond that is antiparallel to the leaving group and gives retention of configuration. Support for the idea is provided by recent work of Hansske and Robins (18), who have deoxygenated ribonucleoside monotosylates with LTBH. Understandably there was no carbon migration in their furanosidic substrates, but hydride shifts following the same principle were demonstrated to occur (Scheme 2).

It appeared puzzling at first sight that the galactoside **16** gave a ring-contracted product (**17**) having the *lyxo* configuration and thus appeared to have incurred inversion at C-2. However, this is readily explained (see Scheme 3) by initial, partial desulfonylation (with little discrimination between O-2 and O-3) to produce monosulfonates. The 3-sulfonate **25** is then seen as the precursor for **17**, which is formed by migration of the C-1,2 bond, and retention at the original C-3 (that becomes C-2) is seen to hold. The 2-sulfonate **26**, on the other hand, reacting in this instance not by ring contraction but through the *talo* epoxide **27**, is the source of the 3-deoxyhexopyranoside derivative **18** which was obtained.

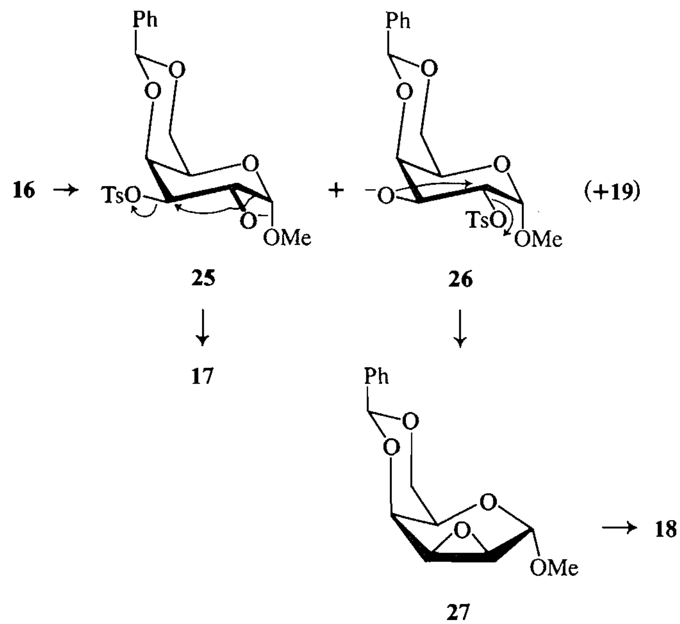

SCHEME 3

Although the mechanistic hypothesis outlined in this section appears attractive at the present time, it will probably require refinement in the light of additional observations which are being made in our currently continuing studies, and which are not fully understood as yet. One intriguing point is that the use of other metal trialkylborohydrides instead of LTBH apparently leads to quite different results. It is hoped that the investigations in progress will throw more light on the nature and scope of these interesting and synthetically useful desulfonyloxylations.

Experimental

Apparatus, materials, and methods

Lithium triethylborohydride (Super Hydride[R], LTBH) was purchased from Aldrich Chemical Co. as an *M* solution in oxolane (THF). Optical rotations were measured at ~25°C with a Perkin–Elmer 241 polarimeter and refer to chloroform solutions. Melting points were determined with a Gallenkamp apparatus and are uncorrected. Thin layer chromatography (tlc) was performed on precoated plates of silica gel SIL-25UV$_{254}$ (Macherey–Nagel & Co., Germany). Spots were made visible by spraying the plates with 5% sulfuric acid in ethanol, and heating them briefly on a hot plate. Column chromatography was performed on Merck Silica Gel 60, 230–400 mesh, or on basic aluminum oxide suitable for chromatography (Shawinigan), as referred to by SiO_2 and Al_2O_3, respectively. Unless otherwise indicated, the following solvent mixtures (v/v) were employed for chromatography: A, ethyl acetate – hexane, 1:2; B, the same solvents, but 1:1; C, the same, but 2:1, and D, ethyl acetate.

Preparation of the starting glycosides

(a) *Known compounds*

Published procedures were employed, occasionally with minor technical modifications, for the preparation of **1** (19), **5** (20), **6** (21), **7** (22), **9** (22), and **16** (23). Compound **2** (mp 156–157°C, $[\alpha]_D$ +86.3°) was obtained from its known (24) 3,4-*O*-isopropylidene derivative as described (19) for **1** (mp 157–158°C, $[\alpha]_D$ −85°). The ir and nmr spectra of **1** and **2** were identical.

(b) *Methyl 4-O-benzoyl-6-bromo-6-deoxy-2-O-p-tolylsulfonyl-α-D-glucopyranoside (3)*

Pure (1) methyl 4,6-*O*-benzylidene-2-*O*-*p*-tolylsulfonyl-α-D-glucopyranoside (9.1 g) was heated for 2.5 h with *N*-bromosuccinimide (4.72 g) and barium carbonate (10 g) in refluxing carbon tetrachloride (350 mL). Processing as for the analogous 2-*O*-mesyl compound (25) gave **3** (5.1 g, 47.5%) after crystallization from a small volume of CCl_4; mp 50–51°C, $[\alpha]_D$ +48.7° (*c* 0.25). The ^{1}H nmr data (200 MHz, $CDCl_3$) δ: 8.04–7.26 (9H, arom.), 5.05 (dd, $J_{3,4}$ = 9, $J_{4,5}$ = 9.9 Hz, H-4), 4.87 (d, $J_{1,2}$ = 3.7 Hz, H-1), 4.34 (dd, $J_{2,3}$ = 9.5 Hz, H-2), 4.19 (dt, $J_{3\text{-}OH}$ = 13.7 Hz; t upon D_2O exchange, $J_{2,3}$ = $J_{3,4}$ = 9.3 Hz, H-3), 4.06 (ddd, $J_{4,5}$ = 10, $J_{5,6}$ = 2.8, $J_{5,6'}$ = 7.2 Hz, H-5), 3.44 (m, 2H, H-6,6′), 3.42 (s, *O*-Me), and 2.44 (s, *Ar*Me); *m/z* (DCI mode): 515, 517 (*M* + 1), 483, 485 (M + 1 − OCH_3), 405 (M + 1 − OCH_3 − Br). *Anal.* calcd. for $C_{21}H_{23}BrO_8S$ (515.4): C 48.93, H 4.50, Br 15.51; found: C 49.01, H 4.60, Br 15.4.

(c) *Methyl 6-deoxy-6-iodo-2-O-p-tolylsulfonyl-α-D-glucopyranoside (4)*

Crystalline (mp 119.5–121°C, from ethyl acetate – hexane) 3,4-di-*O*-acetyl derivative (26) of **4** (5.42 g, 10.6 mmol) was deacetylated by treatment with sodium methoxide (2 mL of a 2 *M* solution) in a mixture of chloroform (50 mL) and methanol (10 mL), at room temperature during 1 h. Complete saponification of the diacetate (R_f 0.65) to **4** (R_f 0.5) was indicated by tlc (solvent B), and pilot runs had shown that **4** is stable for several hours under these conditions, with only minute traces of a faster-moving by-product arising. The solvents were removed at low temperature, and 3 portions of added THF were evaporated from the residue, which was obtained as a slightly yellowish foam and used without purification, after drying in a desiccator.

(d) *Methyl 4,6-di-O-p-tolylsulfonyl-α-D-glucopyranoside (8) by ammonolysis of 7*

Methanolic ammonia (160 mL, saturated at 0°C) and a solution of **7** (4.11 g) in methanol (160 mL) were mixed and stored in a refrigerator for 3 days; tlc with solvent A revealed clean replacement of the fast-moving **7** by slow-moving **8**. The solvent was removed at low temperature and the residue chromatographed on a short column of SiO_2 by means of solvent B. Compound **8** was obtained as a colorless syrup (2.37 g, 82%), $[\alpha]_D$ +102° (*c* 1.1). A 60-MHz nmr spectrum indicated complete removal of the benzoate and retention of the tosyl groups.

(e) *Attempted Zemplén deacylation of 7*

Although **7** is known to give the anhydro sugar **22** on heating with sodium methoxide in methanol solution (21), we attempted to prepare the presumed intermediate, **8**, by employing milder conditions. In spite of its failure in this regard, the experiment is recorded because of unexpected results concerning relative stabilities of different ester functions.

To a solution of **7** (3.55 g, 5 mmol) in 1:1 chloroform–methanol (50 mL) was added at 0°C an *M* sodium methoxide solution (1 mL). After standing for 4 h at 0°C, the mixture showed a complex pattern in tlc (solvent B), which changed little during another hour and after addition of another 0.5 mL of methoxide. There were 5 spots, R_f 0.8, 0.6, 0.35, 0.1, and 0.0. Work-up included neutralization with Dry Ice, evaporation, deionization in methanolic medium with cation and anion exchange resins, and evaporation of added toluene from the material which was obtained as a syrup. Trituration of the syrup with toluene and refrigeration (2 days) caused crystallization of the immobile component (R_f 0.0), which evidently was the major reaction product (1.735 g). Recrystallized from a small amount of ethyl acetate, it had mp 103–104°C, whereas from chloroform it gave long needles of mp 122–123.5°C. From a small amount of water a hydrate (mp 55–56°C) crystallized readily. These data, together with ir and ^{1}H nmr data showing absence of benzoyl and presence of only one tosyl group besides hydroxyl, identified the product as methyl 6-*O*-*p*-tolylsulfonyl-α-D-glucopyranoside (lit. (27) mp 124°C (anhydrous) and 56–58°C (hydrate)). Addition of a little hexane to the above toluene mother liquor gave a gummy deposit containing some of the same product together with the component of R_f 0.1. The latter probably was ditosylate **8**, but the amount was small and it could not be isolated pure. The three faster-moving components, contained in the toluene–hexane solution that was decanted from the gum, were separated on a column (16 × 1 cm) of SiO_2 (solvent B). There was obtained some unchanged **7**, R_f 0.8, mp 132°C (from methanol); a small amount of crystalline product R_f 0.6, mp 145.5°C (from ethanol), whose ir and ^{1}H nmr spectra suggested that it was the 3-monobenzoate of **8**; and methyl 3,4-anhydro-6-*O*-*p*-tolylsulfonyl-α-D-galactopyranoside (**22**), R_f 0.3, needles upon trituration with water and a few drops of ethanol on a steam bath, mp 95–96°C (lit. (21) mp 94–95°C). The extensive de-*O*-sulfonylation at the 4-position, to give the major product (R_f 0.0) under conditions where even debenzoylation was incomplete, appears rather remarkable.

General procedure for reactions of glycoside tosylates with LTBH

The starting sugar derivative was dissolved in reagent-grade THF that had been dried, immediately before use, by refluxing it over, and distilling it from, potassium metal in the presence of benzophenone. All operations were carried out under a nitrogen atmosphere. The *M* LTBH solution was introduced by syringe into the magnetically stirred and chilled (ice-water bath) solution of the substrate. Cooling was then discontinued and the mixture was boiled under reflux, with periodic monitoring of the progress of reaction by tlc. Amounts of materials and reaction times are given for each individual experiment. For processing, the reaction mixture was chilled to 0°C, and methanol was added dropwise in slight excess to ensure the complete decomposition of remnant hydride. The solution was then concentrated on the rotary evaporator at 35°C to a small volume (one-quarter to one-fifth) and poured into 10 volumes of ice water. The mixture was stirred at ambient temperature for several hours (or overnight). An amount of 30% hydrogen peroxide as specified was diluted with water and added cautiously and dropwise to the mixture, preferably with cooling. (**Violent reaction may occur if this addition is done too rapidly**.) After 1 h, the solution was carefully neutralized to pH 7 with aqueous sodium hydrogen sulfate solution unless otherwise indicated; any excess of acid must be avoided. The solution was then evaporated to about one-third its volume, and exhaustively extracted with chloroform or ethyl acetate as specified. Finally, the aqueous phase was evaporated to dryness, and the residue was checked by tlc. If it still contained a significant amount of organic material, it was extracted with ethyl acetate or chloroform. The combined extracts were dried ($MgSO_4$ or Na_2SO_4), and evaporated to give the crude reaction product.

*Methyl 2,5-dideoxy-2-C-(hydroxymethyl)-α-L-*xylo*-pentofuranoside (10)*

The reaction was performed with **1** (4.10 g, 12.35 mmol) in THF (100 mL) and LTBH solution (100 mL, 8.1 mol. equiv.) during 30 min, after which tlc (solvent D) showed absence of **1** (R_f 0.7) and presence of a new spot, R_f 0.35. The oxidative treatment was performed with 33 mL of 30% hydrogen peroxide. Extraction of the aqueous phase with ethyl acetate, and of the residue of evaporation with chloroform, gave a combined yield of 1.27 g (63.5%) of crude **10** which crystallized in part from ethyl acetate – hexane; mp 73°C. Chromatography of the mother liquor material on Al_2O_3, using solvent B followed by solvent D as eluants, furnished additional, crystalline **10**. The combined crops were recrystallized from chloroform, affording 1.06 g (53%) of analytically pure **10**, mp 74–74.5°C, $[\alpha]_D$ −174.5° (*c* 2.2). *Anal.* calcd. for $C_7H_{14}O_4$ (162.2): C 51.84, H 8.70; found: C 51.60, H 8.67.

*Methyl 2,5-dideoxy-2-C-(hydroxymethyl)-α-D-*xylo*-pentofuranoside (11)*

Compound **11** was obtained from **2** in 61% crude yield, as described for the enantiomer **10**. After purification by chromatography and crystallization, it showed mp 73–75°C and $[\alpha]_D$ +173° (*c* 0.9). Its ir, ^{1}H nmr, and ^{13}C nmr spectra were superposable on those of **10**.

*Methyl 2,5-dideoxy-2-C-(hydroxymethyl)-α-D-*ribo*-pentofuranoside (12)*

(a) *From the 6-bromo glycoside 3*

Compound **3** (5.15 g, 10 mmol) in THF (60 mL) and LTBH solution (100 mL) were allowed to react for 2 h. Processing included a peroxide treatment with 35 mL of 30% reagent, and was performed as described before, except that neutralization with $NaHSO_4$ was dispensed with. Chloroform extraction of the partially evaporated, aqueous solution afforded crude **12** (868 mg, 53.6%) as a solid after solvent evaporation. Recrystallized from 1:1 carbon tetrachloride – hexane, it had mp 41–42°C and $[\alpha]_D$ +133° (*c* 2.2). *Anal.* calcd. for $C_7H_{14}O_4$ (162.2): C 51.84, H 8.70; found: C 51.91, H 8.48.

(b) *From the 6-iodo glycoside 4*

The crude **4** obtained in the aforedescribed saponification of 5.42 g (10.6 mmol) of its diacetate was dissolved in THF (60 mL) and allowed to react with LTBH solution (80 mL) during 1.75 h. In this instance, the treatment with 30% hydrogen peroxide (26 mL) included in the work-up was followed by neutralization of the reaction mixture with $NaHSO_4$, and the partially evaporated solution was extracted with ethyl acetate. There was obtained crude **12** (1.27 g, 62%) as a yellow syrup. Column chromatography on Al_2O_3 using solvent C as the eluant gave, from chromatographically homogeneous fractions, compound **12** as a colorless syrup that crystallized on refrigeration but proved difficult to recrystallize; mp 34–35°C and $[\alpha]_D$ +118° (*c* 4.4). Although the physical constants were somewhat lower than in **12** prepared under (a), the ir, ^{1}H nmr, and ^{13}C nmr spectra of the two preparations were identical.

*Methyl 3,5-dideoxy-3-C-(hydroxymethyl)-α-D-*arabino*-pentofuranoside (13)*

Compound **5** (3.40 g, 10.23 mmol) in THF (80 mL) and LTBH solution (82 mL) were allowed to react for 30 min, after which all of the **5** was consumed (tlc with solvent D). In this and similar, preceding experiments with **5** no peroxide treatment was included in the work-up procedure as the studies were performed at an early stage before the beneficial effect of such treatment on yields was realized. The yield of pure **13** (506 mg, 30.5%) obtained upon chloroform extraction and column chromatography on Al_2O_3 with solvent B followed by solvent D, and recrystallization from ether – petroleum ether (bp 30–60°C). was therefore low, and a considerable proportion of product emerged from the column as a fast-moving organoboron conjugate. Crystalline **13** showed R_f 0.35 (solvent D), mp 64°C, $[\alpha]_D$ −112° (*c* 2.3). *Anal.* calcd. for $C_7H_{14}O_4$ (162.2): C 51.84, H 8.70; found: C 51.67, H 8.47.

*Methyl 3,5-dideoxy-3-C-(hydroxymethyl)-α-D-*ribo*-pentofuranoside (14)*

(a) *From the 6-deoxy glycoside 6*

Compound **6** (4.32 g, 8.0 mmol) in THF (32 mL) was allowed to react with LTBH solution (64 mL, 8 mol. equiv.) during 45 min. Normal processing, but with addition of potassium carbonate in the treatment with hydrogen peroxide (22 mL), and prolongation of this treatment overnight, furnished 1.00 g (77%) of **14**, R_f 0.34 (solvent D), by chloroform extraction. Compound **15** (R_f 0.40, see below) was not detected. Compound **14** resisted all attempts at crystallization. After chromatography on SiO_2 with solvent A (recovery, 74%) it showed $[\alpha]_D$ +162.2° (*c* 1.2). To corroborate the structure, a sample of **14** was acetylated in the conventional manner (acetic anhydride – pyridine), and the 200-Mz nmr data of the diacetate are included in Table 1.

(b) *From the 4,6-ditosylate 7*

Compound **7** (3.70 g, 5.21 mmol) in THF (40 mL) and LTBH solution (37 mL) was boiled for 2 h, after which time another 7 mL of LTBH was added (for a total of 8.4 mol. equiv.), and boiling was continued for 1 h. Work-up included oxidation with 15 mL of 30% H_2O_2, and chloroform extraction. It gave a syrupy glycoside mixture (470 mg, 56%) that showed two partially overlapping spots, R_f 0.40 and 0.35, in tlc with solvent D. The ^{1}H nmr spectral features of **14** were superposed on those of methyl α-abequoside (**15**), as was ascertained by comparison with the spectra of pure **14** and independently prepared (7), pure **15**. A ratio of 3:2 was found by signal integration for H-1, *O*-CH_3, and *C*-CH_3 at δ 4.96, 3.49, and 1.29 (for **14**), and 4.68, 3.45 and 1.21 (for **15**), respectively.

Several similar experiments were carried out using 10 mol. equiv. of LTBH and reaction times of 2–6 h, and results were always similar. However, in a 30-min reaction, desulfonyloxylation was incomplete, and from the mixture of products a small proportion of the 3,4-epoxide

22 was chromatographically isolated crystalline (mp 93°C). It was identified by comparison with an authentic sample (21).

Separation of **14** and **15** was difficult to achieve and required multiple chromatography. While it was possible to isolate part of **14** in spectroscopically homogeneous form, the abequoside **15** was never obtained free from small proportions of **14**. Nevertheless, its identity was established beyond doubt as the 200-MHz ^{1}H nmr data matched those published (7).

(c) *From the 4,6-ditosylate 8 and the 6-chloro glycoside 9*

A 40-min reaction performed with **8** (2.3 g, 4.58 mmol) and 13.5 mol. equiv. of LTBH gave, after standard processing, a mixture of **14** and **15** (yield not recorded), for which the nmr spectrum indicated an approximate 1:1 ratio. A 60-min reaction of **9** (1.49 g, 2.6 mmol) with 10 mol. equiv. of LTBH gave a similar, 1:1 mixture (200 mg, 47%).

*Methyl 3,5-*O*-benzylidene-2-deoxy-2-*C*-(hydroxymethyl)-α-*D*-*lyxo*-pentofuranoside (17) and methyl 4,6-*O*-benzylidene-3-deoxy-α-*D*-*lyxo*-hexopyranoside (18)*

To a solution of **16** (1.00 g, 1.75 mmol) in THF (10 mL) was added LTBH solution (10 mL), followed after 30 min of refluxing by another 10 mL of the same. After 20 h of boiling, the solution showed 3 spots, at R_f 0.57, 0.22, and ~0.1 (tlc with 1:4 ethyl acetate – chloroform). Processing was unproblematic and was performed as in the work (1) with benzylidenated glucosides. It included addition of methanol to the chilled reaction mixture followed by dilution with water, evaporation to remove most of the THF, and extraction of the products by ethyl acetate. Peroxide treatment was not required. The product mixture was chromatographed on a silica gel column by use of 1:4 ethyl acetate – chloroform. The component emerging first (R_f 0.57) proved to be the pyranoside **18**; yield, 100 mg (21.5%); mp 88.5–89°C; $[\alpha]_D$ +56.8° (*c* 0.9); ^{1}H nmr (200 MHz, $CDCl_3$) δ: 7.52–7.26 (m, 5H, Ph), 5.49 (s, *Ph*-CH), 4.79 (s, slightly broadened, H-1), 4.30 (dd, $J_{5,6}$ = 1.6, $J_{6,6'}$ = 12.5 Hz, H-6), 4.12 (nm, W_H = 3.2 Hz, H-4), 4.075 (dd, J = 1.6 and 12.5 Hz, H-6′), 3.70 (d, $J_{2,OH}$ = 11.5 Hz, OH-2, strongly hydrogen-bonded with O-4), 3.69 (nm, $J_{4,5}$ ~1.5 Hz, H-5), 3.58 (d of nm; on double irradiation at δ 2.13: dd, $J_{2,OH}$ = 11.5, $J_{2,4}$ = 1.6 Hz, H-2), 3.44 (s, 3H, OMe), and 2.13 (nm, 2H, H-3,3′); *m/z* (FAB mode): 267 (*M* + 1) and 235 (M − OCH_3). *Anal.* calcd. for $C_{14}H_{18}O_5$ (266.3): C 63.14, H 6.81; found: C 63.00, H 6.75.

The second product (R_f 0.22) eluted from the column was the furanoside **17**; yield, 177 mg (38%); mp 121–122°C, $[\alpha]_D$ +51.4° (*c* 0.9); ^{1}H nmr (200 MHz, $CDCl_3$) δ: 7.49–7.34 (m, 5H, Ph), 5.47 (s, *Ph*-CH), 5.30 (d, $J_{1,2}$ = 4.8 Hz, H-1), 4.63 (dd, $J_{2,3}$ = 5.0, $J_{3,4}$ = 2.1 Hz, H-3), 4.46 (d, $J_{5,5'}$ = 13.2 Hz, H-5), 4.16 (dd, $J_{4,5'}$ = 2.2, $J_{5,5'}$ = 13.2 Hz, H-5′), 4.00 (m, 3H, H-4 and H-2′,2″ (hydroxymethyl)), 3.47 (s, 3H, OMe), and 2.46 (ddt, $J_{1,2} \approx J_{2,3} \approx$ 4.8, $J_{2,2'}$ = 4.5, $J_{2,2''}$ = 6.2 Hz, H-2); *m/z* (FAB mode): 267 (*M* + 1) and 235 (M − OCH_3). *Anal.* calcd. for $C_{14}H_{18}O_5$ (266.3): C 63.14, H 6.81; found: C 63.14, H 6.73.

The third component (R_f ~0.1) eluted from the column amounted to 90 mg (18%) and was identified as the diol **19** by spectral comparison with an authentic sample.

Acknowledgments

We acknowledge gratefully the financial support of this work by the Natural Sciences and Engineering Research Council of Canada. Professor A. S. Perlin, Montreal, is thanked for valuable discussion concerning the interpretation of nuclear magnetic resonance data. Professor R. Köster, Mülheim/Ruhr, provided stimulating suggestions relating to problems associated with organoboron reactions. Ms. Cristine Lajeunesse and Mr. Fabio Zanetti have skilfully participated in the preparation of starting compounds and the performance of preliminary experiments.

1. H. H. BAER and H. R. HANNA. Carbohydr. Res. **110**, 19 (1982).
2. H. H. BAER, M. MEKARSKA, and F. BOUCHER. Carbohydr. Res. In press.
3. G. SIEWERT and O. WESTPHAL. Justus Liebigs Ann. Chem. **720**, 171 (1968).
4. V. HEŘMÁNKOVÁ, A. ZOBÁČOVÁ, and J. JARÝ. Collect. Czech. Chem. Commun. **36**, 303 (1971).
5. A. ZOBÁČOVÁ, V. HEŘMÁNKOVÁ, and J. JARÝ. Collect. Czech. Chem. Commun. **35**, 327 (1970).
6. S. UMEZAWA, T. TSUCHIYA, and H. HINENO. Bull. Chem. Soc. Jpn. **43**, 1212 (1970).
7. H. H. BAER and D. J. ASTLES. Carbohydr. Res. **126**, 343 (1984).
8. N. CYR and A. S. PERLIN. Can. J. Chem. **57**, 2504 (1979).
9. S. J. ANGYAL. Carbohydr. Res. **77**, 37 (1979).
10. A. S. PERLIN. Int. Rev. Sci. Org. Chem. Ser. 2, **7**, 1 (1975).
11. K. ČAPEK, J. JARÝ, and Z. SAMEK. Collect. Czech. Chem. Commun. **40**, 149 (1975).
12. V. POZSGAY and A. NESZMÉLYI. Tetrahedron Lett. 211 (1980).
13. J. M. WILLIAMS. Adv. Carbohydr. Chem. Biochem. **31**, 9 (1975); J. DEFAYE. Adv. Carbohydr. Chem. Biochem. **25**, 181 (1970); D. H. BALL and F. PARRISH. Adv. Carbohydr. Chem. Biochem. **24**, 167 (1969); J. S. BRIMACOMBE. Fortschr. Chem. Forsch. **14**, 367 (1970); D. HORTON and J. D. WANDER. *In* The carbohydrates. Vol. IB. *Edited by* W. Pigman and D. Horton. Academic Press, New York. 1980. pp. 702–710.
14. C. ERBING, B. LINDBERG, and S. SVENSSON. Acta Chem. Scand. **27**, 3699 (1973); N. M. K. NG YING KIN, J. M. WILLIAMS, and A. HORSINGTON. J. Che. Soc. (C) 1578 (1971); G. O. ASPINALL, E. PRZYBYLSKI, R. G. S. RITCHIE, and C. O. WONG. Carbohydr. Res. **66**, 225 (1978).
15. R. KÖSTER. *In* Houben-Weyl. Methoden der organischen Chemie. Vol. XIII/3b. Georg Thieme Verlag, Stuttgart. 1983. pp. 838–839.
16. H. C. BROWN, S. C. KIM, and S. KRISHNAMURTHY. J. Org. Chem. **45**, 1 (1980); H. C. BROWN, S. NARASIMHAN, and V. SOMAYAJI. J. Org. Chem. **48**, 3091 (1983).
17. B. RICKBORN and R. M. GERKIN. J. Am. Chem. Soc. **93**, 1693 (1971).
18. F. HANSSKE and M. R. ROBINS. J. Am. Chem. Soc. **105**, 6736 (1983).
19. E. E. PERCIVAL and E. G. V. PERCIVAL. J. Chem. Soc. 690 (1950).
20. J. JARÝ, K. ČAPEK, and J. KOVÁŘ. Collect. Czech. Chem. Commun. **28**, 2171 (1963).
21. G. SIEWERT and O. WESTPHAL. Justus Liebigs Ann. Chem. **720**, 171 (1968).
22. G. SIEWERT and O. WESTPHAL. Justus Liebigs Ann. Chem. **720**, 161 (1968).
23. E. SORKIN and T. REICHSTEIN. Helv. Chim. Acta, **28**, 1 (1945).
24. B. ISELIN and T. REICHSTEIN. Helv. Chim. Acta, **29**, 508 (1946).
25. S. HANESSIAN and N. R. PLESSAS. J. Org. Chem. **34**, 1035 (1969).
26. J. JARÝ, K. ČAPEK, and J. KOVÁŘ. Collect. Czech. Chem. Commun. **29**, 930 (1964).
27. F. CRAMER, H. OTTERBACH, and H. SPRINGMANN. Chem. Ber. **92**, 384 (1959).

A new synthesis of 3-amino-3-deoxy-α-D-mannopyranosyl 3-amino-3-deoxy-α-D-mannopyranoside, a potential antituberculous agent

HANS H. BAER[1] AND BRUNO RADATUS

Ottawa–Carleton Institute for Research and Graduate Studies in Chemistry, Department of Chemistry, University of Ottawa, Ottawa, Ont., Canada K1N 9B4

AND

JACQUES DEFAYE

Centre de Recherches sur les Macromolécules Végétales, C.N.R.S. Grenoble, 68X-38402 Saint-Martin-d'Hères, France

Received June 1, 1984

HANS H. BAER, BRUNO RADATUS, and JACQUES DEFAYE. Can. J. Chem. **63**, 440 (1985).

A practical, four-step synthesis of the title compound starting from 2-*O*-benzyl-4,6-*O*-benzylidene-α-D-altropyranosyl 2-*O*-benzyl-4,6-*O*-benzylidene-α-D-altropyranoside is described. Trifluoromethylsulfonylation followed by azide displacement furnished the corresponding α-D-*manno*,α-D-*manno* 3,3′-diazido-3,3′-dideoxy derivative, and subsequent hydrolytic deacetalation, followed by catalytic transfer hydrogenolysis to simultaneously reduce the azido groups and cleave the benzyl ether groups, gave the title disaccharide in 30% overall yield. As preceding work had provided the blocked starting disaccharide in a sequence of four facile operations departing from commercial α,α-trehalose (overall yield, 53%), the title compound can now be prepared conveniently on a multigram scale.

HANS H. BAER, BRUNO RADATUS et JACQUES DEFAYE. Can. J. Chem. **63**, 440 (1985).

Le 3-amino-3-désoxy-α-D-mannopyranosyl-3-amino-3-désoxy-α-D-mannopyranoside est obtenu commodément en quatre étapes partant du 2-*O*-benzyl-4,6-*O*-benzylidène-α-D-altropyranosyl-2-*O*-benzyl-4,6-*O*-benzylidène-α-D-altropyranoside. Une trifluorométhylsulfonylation suivie de déplacement par l'ion azide conduit au dérivé α-D-*manno*,α-D-*manno* 3,3′-diazido-3,3′-didésoxy qui, par hydrolyse des groupes protecteurs acétaliques, puis hydrogènolyse catalytique simultanée par transfert, des groupes azide et des groupes protecteurs benzyle, permet d'obtenir le disaccharide aminé attendu avec un rendement global de 30%. L'altroside de départ étant lui-même obtenu en quatre étapes commodes et un rendement global de 53% partant de l'α,α-tréhalose commercial, ce disaccharide aminé est donc désormais accessible à l'échelle préparative.

Introduction

Some years ago, we undertook chemical syntheses of several new, nitrogenous disaccharides structurally related to the important natural sugar α-D-glucopyranosyl α-D-glucopyranoside (α,α-trehalose, **1**). They included 3-amino-3-deoxy-α,α-trehalose (1) as well as 3,3′-diamino-3,3′-dideoxy-α,α-trehalose and its stereoisomers having the α-D-*gluco*,α-D-*manno* and α-D-*manno*,α-D-*manno* configurations (2). One point of interest attaching to these compounds relates to their use as substrate analogs for studies of the specificity and mechanism of action of the enzyme trehalase (3). Furthermore, the synthetic work was prompted by the fact that some naturally occurring amino disaccharides related to α,α-trehalose, which are produced as metabolites by certain *Streptomyces* species, had been found to show antibiotic activity (4). These were the 2-amino-2-deoxy (5) and 4-amino-4-deoxy (6) derivatives of **1**, and 2-amino-2-deoxy-α-D-glucopyranosyl α-D-mannopyranoside (7). It has subsequently been determined that one of the disaccharides obtained by us (2), namely 3-amino-3-deoxy-α-D-mannopyranosyl 3-amino-3-deoxy-α-D-mannopyranoside dihydrochloride (**11**), possesses a remarkable inhibitory activity (at 10 μg/mL in vitro) against *Mycobacterium tuberculosis* (human strain H37RV) and *Mycobacterium avium*, whereas the two stereoisomers mentioned showed no significant activity.[2] Unfortunately, the reported synthesis (2), based on the nitromethane cyclization methodology, had furnished chiefly the inactive isomers while **11** was formed as a minor product only, and was rather tedious to isolate. A more efficient procedure was therefore required in order to provide **11** conveniently in quantities which would enable detailed, pharmacological evaluation to be undertaken.

Several possible approaches were devised. One of them involved osmium tetraoxide-catalyzed *cis*-oxyamination, with chloramine-T, of a 2,2′-bis-enoside related to α,α-trehalose. This approach, expected to lead to diaminated disaccharides having the D-*manno*,D-*manno* configuration, did in fact afford **11** but, once again, in low yield, with the 2,3′- and 2,2′-diamino regioisomers constituting the major products (8). Although these latter disaccharides, which were previously unknown and have not thus far been evaluated biologically, command interest of their own, the problem of rendering **11** more readily available remained unsolved until an alternative synthesis, to be reported here, could be achieved.

Results

The synthesis departs from commercially available α,α,-trehalose (**1**), which is readily converted, in three high-yielding steps involving known procedures, into the bis-benzylidenated diepoxide **2**. As already reported (9), the latter reacted with sodium benzoxide in benzyl alcohol by predominantly diaxial opening of the oxirane ring, in accord with the Fürst–Plattner rule, affording the key intermediate **3**, 2-*O*-benzyl-4,6-*O*-benzylidene-α-D-altropyranosyl 2-*O*-benzyl-4,6-*O*-benzylidene-α-D-altropyranoside. The overall yield of **3** from **1** was 53% (9).

From **3**, the crystalline ditriflate **4** was obtained in 94% yield. The next step consisted of nucleophilic displacement with azide ion, to give the *manno,manno* diazide **5**. This crucial reaction was the only somewhat problematical point in the sequence of operations. The difficulty arose from a strong tendency for elimination to compete with substitution, resulting in the formation of the unwanted mono- and di-alkenes **6** and

[1] Author to whom inquiries may be directed.

[2] The authors are indebted to Dr. H. L. David, Chef du Service de la Tuberculose à l'Institut Pasteur, Paris, for performing the assays. (Private communication, October 1979).

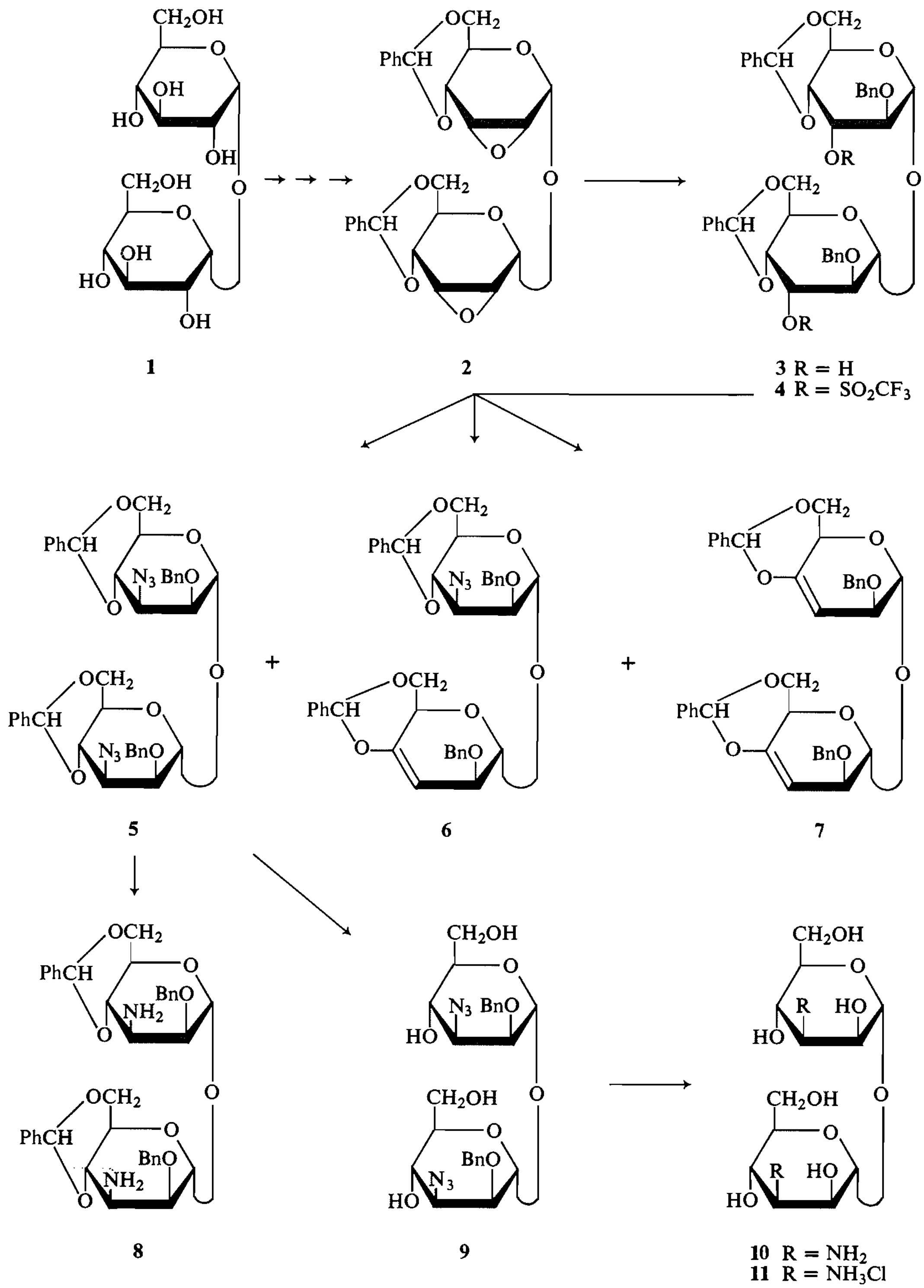

7. In an analogous operation previously executed (1), a trehalose-derived 3-triflate had been very easily displaced at ambient to slightly elevated temperature, giving an 80% yield of the desired product and showing no evidence for elimination,[3] and that experience encouraged us in our present endeavor. However, the analogous substrate in question had possessed the D-*allo* configuration, with an equatorial benzoate ester function at C-2, and it was understandable that, in **4**, the axial benzyl ether group in that position would be apt to interfere seriously in the transition state of a parallel approach of nucleophile to C-3. We investigated the azide displacement in **4** under a wide variety of conditions, and invariably obtained mixtures of **5**, **6**, and **7**, generally with the desired diazide **5** present in an unsatisfactory proportion. However, we eventually succeeded in specifying conditions under which **5** was the main product. On a multigram scale, the reaction was best performed with sodium azide in a refluxing mixture of benzene

[3] The reaction was performed with lithium azide in a mixture of DMF and DMSO. The corresponding 3-mesylate reacted much more sluggishly (12 h at 105°C in DMSO–HMPA), and did suffer partial elimination.

and water, in the presence of tetrabutylammonium hydrogen sulfate as a phase transfer catalyst. The slow process was essentially complete after five days, and chromatographic separation of the products afforded crystalline **5** in 51.5% yield, and the unsymmetrical azidoalkene **6** and the dialkene **7**, both crystalline, in 40 and ~2% yield, respectively.

In order to convert **5** most efficiently into the target compound, several possibilities for sequential or simultaneous operations to reduce the azido functions and remove the protecting groups were considered, and tested in pilot experiments. Catalytic hydrogenation of **5**, or reduction with lithium aluminum hydride, gave the blocked diamino sugar **8**, but difficulties experienced in its complete deprotection caused us not to pursue this route any further. Instead, **5** was first debenzylidenated by hydrolysis with 80% acetic acid, affording the partially deprotected diazide **9**, crystalline in 91% yield. This product was then subjected to catalytic transfer hydrogenolysis (10) with cyclohexene in the presence of palladium on charcoal, which effected rapid reduction of the azido groups and simultaneously, although more slowly, cleavage of the benzyl ethers (11). The 3,3′diamino-3,3′-dideoxy disaccharide (**10**) was obtained as a crystalline monohydrate in 61% yield after purification. The crude **10** contained a small proportion of a by-product which was removed by recrystallization, and was judged to be a mono-*N*-ethyl derivative of **10**, on the basis of its ^{1}H nmr spectrum.[4] The free base **10** was converted into its dihydrochloride **11** that proved in every respect identical with previously synthesized (2, 8) material.

In summary, the present synthesis allows the convenient preparation of the title compound in four steps with ~30% overall yield from the intermediate (9) disaccharide **3**, or in eight steps from commercial trehalose with ~16% overall yield. The reactions can be performed on a multigram scale and require only common reagents and standard operations.

NOTE ADDED IN PROOF. The base **10** was submitted for testing to Dr. H. L. David, Institut Pasteur, Paris, and Dr. A. Laszlo, National Reference Centre of Tuberculosis, Ottawa. Neither laboratory was able to observe antimycobacterial activity as previously found[2] for the dihydrochloride **11** prepared by our first (2) method. The reason for this apparent discrepancy is being investigated.

Experimental

Instruments and general methods

Optical rotations were measured at ~25°C with a Perkin–Elmer 241 polarimeter. The ^{1}H nmr data refer to 300-MHz spectra recorded on a Varian XL-300 instrument, unless otherwise indicated. Melting points were determined with a Gallenkamp apparatus, and are uncorrected. Column chromatography was performed on Silica Gel 60, 230–400 mesh (E. Merck AG, West Germany), and the medium-pressure technique was usually employed for separations on a multigram scale. For tlc, precoated silica gel plates were used, and components were made visible by spraying the plates with 5% sulfuric acid in ethanol, and heating them briefly on a hot plate. Frequently used solvent combinations were ethyl acetate and hexane in the proportions (v/v) 1:9 (solvent A), 1:4 (solvent B), and 1:1 (solvent C).

[4] It may be assumed that ethanol, which was employed as a co-solvent, acted to some extent as a hydrogen donor (10) in the system, producing acetaldehyde that, with **10**, formed an imine whose hydrogenation gave the by-product. To optimize the transfer hydrogenation, it may be worthwhile to try modified conditions such as, for example, the use of 1,4-cyclohexadiene, which has been recommended (12) for the efficient debenzylation of protected peptides.

2-O-Benzyl-4,6-O-benzylidene-3-O-trifluoromethylsulfonyl-α-D-altropyranosyl 2-O-benzyl-4,6-O-benzylidene-3-O-trifluoromethylsulfonyl-α-D-altropyranoside (4)

Trifluoromethanesulfonic anhydride (7.3 mL, 43 mmol) in dry dichloromethane (200 mL) was added dropwise over a period of 30 min to a chilled (−17°C) solution of the diol (9) **3** (7.0 g, 10 mmol) in dry dichloromethane (70 mL) and pyridine (6 mL). After the end of the addition, spots of about equal strength were seen for starting **4** and what appeared to be its monotriflated derivative (tlc with chloroform). The triflation was then allowed to continue at room temperature and was complete after 2.5 h. The mixture was shaken with added water and, after phase separation, the organic layer was washed twice with sodium hydrogen carbonate solution and once with water. The combined aqueous phase and washings were extracted twice with dichloromethane. The combined organic phases were dried (Na_2SO_4), and evaporated (bath temperature, 35°C), and remnant pyridine was removed by two coevaporations with toluene. The residue was eventually obtained as a syrupy foam. Trituration of the material with ethanol (20 mL) gave a first crop (8.157 g) of slightly yellowish crystals, which were collected and washed with cold ethanol; mp 97–98.5°C, with decomposition starting at 91°C. The ethanolic mother liquor was diluted with several volumes of benzene, washed with aqueous $NaHCO_3$ solution, dried (Na_2SO_4), and evaporated, to give a thin syrup from which a second crop of **4** (0.644 g) was obtained by crystallization from ethanol. The combined crops were recrystallized by dissolution in benzene, evaporation of the solvent, and trituration of the residue with ethanol (20 mL), to give 8.61 g of pure **4**. The mother liquor of recrystallization was combined with the original mother liquor, and the solute was chromatographed on a short column of silica gel, with solvent A followed by solvent B as eluants, yielding another crop of crystalline **4** (0.246 g). The mother liquor therefrom was evaporated, and the residue was treated with triflic anhydride as described before (with appropriate proportions of reagents). Similar processing gave a final crop of **4** (0.239 g), for a total of 9.092 g (94.4%) of chromatographically homogeneous product.

An analytical sample was recrystallized twice more as described; mp 98–102°C, $[\alpha]_D$ +80.0° (*c* 0.5, chloroform); δ ($CDCl_3$): 7.44 (m, Ph), 5.64 (s, *Ph*-CH), 5.12 (narrow t, H-3), 4.66 (s, H-1), 4.82 and 4.57 (AB-q, J_{gem} = 12.0 Hz, *Ph*-CH_2), 4.13 (dd, $J_{5,6e}$ = 5.0, $J_{6a,6e}$ = 10.0 Hz, H-6e), 4.08 (dd, $J_{3,4}$ = 2.7, $J_{4,5}$ = 9.7 Hz, H-4), 3.91 (d, $J_{2,3}$ = 3.0 Hz, H-2), 3.72 (t, $J_{5,6a}$ = $J_{6a,6e}$ = 10.0 Hz, H-6a), 3.58 (dt, $J_{4,5}$ = 9.7, $J_{5,6a}$ = 10.0, $J_{5,6e}$ = 5.0 Hz, H-5). *Anal.* calcd. for $C_{42}H_{40}F_6O_{15}S_2$ (962.8): C 52.39, H 4.19, S 6.66; found: C 52.58, H 4.25, S 6.81.

*3-Azido-2-O-benzyl-4,6-O-benzylidene-3-deoxy-α-D-mannopyranosyl 3-azido-2-O-benzyl-4,6-O-benzylidene-3-deoxy-α-D-mannopyranoside (5), 3-azido-2-O-benzyl-4,6-O-benzylidene-3-deoxy-α-D-mannopyranosyl 2-O-benzyl-4,6-O-benzylidene-3-deoxy-α-D-*threo*-hex-3-enopyranoside (6), and 2-O-benzyl-4,6-O-benzylidene-3-deoxy-α-D-*threo*-hex-3-enopyranosyl 2-O-benzyl-4,6-O-benzylidene-3-deoxy-α-D-*threo*-hex-3-enopyranoside (7)*

A solution of **4** (8.158 g) in benzene (1.6 L) and a solution of sodium azide (10.0 g) and tetrabutylammonium hydrogen sulfate (3.0 g) in water (200 mL) were mixed with efficient stirring and heated under reflux for 2 days. (Smaller volumes of solvent tended to lead to decreased yields of **5**.) Additional sodium azide (10.0 g) and tetrabutylammonium salt (3.0 g), suspended in 25 mL of water, were introduced and refluxing continued for 3 more days. Progress of the reaction was monitored by two-dimensional tlc using solvent B in the first direction, and double irrigation with chloroform in the second. For processing, solvent was distilled from the reaction mixture until 1250 mL of distillate (~1075 mL of benzene and 175 mL of water) had been collected. The remaining mixture was cooled, the phases were separated, and the benzene phase was washed 4 times with water. The aqueous phase and washings were back-extracted with benzene. The combined benzene solutions were again washed repeatedly with water (as nmr spectroscopy had revealed the presence of remnant tetrabutylammonium salt), then dried with Na_2SO_4, and evaporated to give a mixture of carbohydrate material (7.34 g). The mixture was applied to a column of silica gel (58 × 4.5 cm) with the aid of a small amount of benzene, and chromatographed with solvent A. The effluent fractions were examined by tlc with solvent B. Appropriate fractions were combined and gave 3.278 g (51.5%) of the diazide **5** (R_f 0.4) as an amorphous material, 2.575 g of a mixture containing chiefly the azidoalkene **6** (R_f 0.3), and 0.295 g of a mixture rich in the dialkene **7** (R_f 0.25).

For analysis, a sample of **5** was dissolved in a large proportion of methanol and recovered as a white, gummy precipitate by partial evaporation of the solvent. The gum was washed with a little methanol, and dried under high vacuum with occasional rubbing by spatula to give a brittle solid that melted to a glass at 78–87°C; $[\alpha]_D$ +42.4° (*c* 0.7, chloroform); ν_{max} neat: 2115 (azide) cm^{-1}; δ ($CDCl_3$): 7.43 (m, Ph), 5.67 (s, *Ph*-CH), 4.85 (d, $J_{1,2}$ = 1.4 Hz, H-1), 4.86 and 4.63 (AB-q, J_{gem} 12.0 Hz, *Ph*-CH_2), 4.21 (dd, $J_{4,5}$ = 9.5, $J_{3,4}$ = 10.5 Hz, H-4), 4.09 (dd, $J_{5,6e}$ = 5.0, $J_{6a,6e}$ = 10.5 Hz, H-6e), 3.81 (t, $J_{5,6a} \approx J_{6a,6e}$ = 10.5 Hz, H-6a), 3.76 (dd, $J_{2,3}$ = 3.4, $J_{3,4}$ = 10.5 Hz, H-3), 3.69 ($J_{1,2}$ = 1.4, $J_{2,3}$ = 3.3 Hz, H-2), 3.46 (~dt, *J* = 5.0, 9.5, and 10.5 Hz, H-5). *Anal.* calcd. for $C_{40}H_{40}N_6O_9$ (748.8): C 64.16, H 5.38, N 11.22; found: C 64.29, H 5.44, N 11.31.

The aforementioned column eluate (2.575 g) containing **6** (R_f 0.3) was crystallized from hot methanol (200 mL), yielding pure **6** (1.852 g, plus 0.53 g by concentration of the mother liquor; 39.7%); mp 110–112°C, unchanged after recrystallization; $[\alpha]_D$ +118° (*c* 0.5, chloroform); ν_{max}: 2111 (azide) and 1694 (vinyl ether) cm^{-1}; δ ($CDCl_3$) for the azido moiety: 5.71 (s, *Ph*-CH), 4.93 (s, H-1), 4.92 and 4.67 (AB-q, J_{gem} 12.0 Hz, *Ph*-CH_2), 4.25 (H-4, not separated from H-6e and H-6′e), and 3.81 (dd, $J_{2,3}$ = 3.4, $J_{3,4}$ = 11.0 Hz, H-3); δ for the alkenic moiety: 5.63 (s, *Ph*-CH), 5.46 (d, $J_{2,3}$ = 5.5 Hz, H-3), 5.17 (s, H-1), 4.64 (AB-q having the inner lines at 4.66 and 4.62; *Ph*-CH_2); δ for both moieties: 7.45 (m, Ph), 4.27 (m, H-6e and H-6′e), 3.90 and 3.77 (2 m, H-2,2′, 5,5′, 6a,6′a). (The assignments were made by comparison with the data for the symmetrical derivatives **5** and **7**). *Anal.* calcd. for $C_{40}H_{39}N_3O_9$ (705.7): C 68.07, H 5.57, N 5.95; found: C 67.94, H 5.43, N 5.89.

The column eluate (0.295 g) containing **7** (R_f 0.25) was chromatographed again on silica gel, using 1% ethyl acetate in dichloromethane as the eluant, and fractions further enriched in **7** were eluted. The syrupy material obtained from these was crystallized in part, from ethanol, by inoculation with seed crystals of **7** that had formed in a previous, syrupy preparation after storage for several months. The mother liquor of crystallization was combined with the less-pure fractions from the column, and preparative tlc (3 irrigations with dichloromethane) furnished additional **7** that was recrystallized from ethanol, for a total yield of 116 mg (2%). The crystals still contained an impurity (R_f 0.2) even after several subsequent recrystallizations, and the entire material was therefore purified once more by ptlc (solvent B), to give 87 mg (1.5%) of pure **7**; mp 106–108°C; $[\alpha]_D$ +176.7° (*c* 0.5, chloroform); ν_{max}: 1692 (vinyl ether; azide band absent) cm^{-1}; δ ($CDCl_3$): 7.43 (m, Ph), 5.67 (s, *Ph*-CH), 5.49 (d, $J_{2,3}$ = 5.4 Hz, H-3), 5.28 (s, H-1), 4.72 and 4.65 (AB-q, J_{gem} = 12.0 Hz, *Ph*-CH_2), 4.40 (dd, $J_{5,6e}$ = 6.6, $J_{6a,6e}$ = 10.8 Hz, H-6e), 4.14 (m, H-5), 3.97 (dd, $J_{2,3}$ = 5.4, $J_{2,5}$ = 1.8 Hz, H-2), 3.89 (t, $J_{6a,6e}$ = $J_{5,6a}$ = 10.8 Hz, H-6a). *Anal.* calcd. for $C_{40}H_{38}O_9$ (662.7): C 72.49, H 5.78; found: C 72.36, H 5.71.

By-product

The methanolic mother liquor from the crystallization of **6** showed a spot at R_f 0.52 in addition to one for residual **6** (tlc with CH_2Cl_2). After standing for several days at room temperature, partial decomposition was noticed (appearance of an immobile spot, and smell of benzaldehyde), but the component R_f 0.52 was still visible. The methanol was evaporated and the residue dissolved in dichloromethane, washed with aqueous $NaHCO_3$, dried, and subjected to ptlc, with CH_2Cl_2 as irrigant. About 20 mg of the fast-moving compound was isolated. Its ir spectrum was similar to that of the ditriflate **4** in the 1550–600 cm^{-1} region but also showed a strong azide band at 2112 cm^{-1}. The 300-MHz nmr spectrum revealed the structure of an unsymmetrically substituted disaccharide, showing the essential features of both **4** and **5**, with a narrow, one-proton triplet at δ 5.1 characteristic for the 3-triflate moiety. Evidently, the substance was the monoazidomonotriflate intermediate of the reaction **4** → **5**.

3-Amino-2-O-benzyl-4,6-O-benzylidene-3-deoxy-α-D-mannopyranosyl 3-amino-2-O-benzyl-4,6-O-benzylidene-3-deoxy-α-D-mannopyranoside (8)

Compound **5** (140 mg) in ethanol (25 mL) was hydrogenated with 10% palladium on charcoal (200 mg) for 17 h at room temperature, in a Parr flask under 400 kPa of hydrogen pressure. The solution thereafter showed one major product spot, R_f 0.24, in tlc using 95:5 ethyl acetate – ethanol. Isolation of the product by ptlc with the same solvents, but 98:2, gave ~100 mg of **8**. The ir spectrum showed no azido-group absorption. The [1]H nmr data (200 MHz, $CDCl_3$), δ: 7.41 (m, Ph), 5.56 (s, *Ph*-CH), 5.05 (s, H-1), 4.69 (s, *Ph*-CH_2), 4.12 (dd, $J_{6a,6e}$ = 10.0, $J_{5,6e}$ = 4.5 Hz, H-6e), 3.84–3.63 (m, H-2,4,6a), 3.55 (m, $J_{4,5}$ = $J_{5,6a}$ = 10, $J_{5,6e}$ = 4.5 Hz, H-5), 3.18 (dd, $J_{2,3}$ = 3.7, $J_{3,4}$ = 10.0 Hz, H-3), and 1.70 (broad s, removable by D_2O exchange, NH_2).

The same product was obtained by treatment of **5** in ether with lithium aluminum hydride for 15 min.

3-Azido-2-O-benzyl-3-deoxy-α-D-mannopyranosyl 3-azido-2-O-benzyl-3-deoxy-α-D-mannopyranoside (9)

A suspension of **5** (3.73 g) in 80% acetic acid (50 mL) was agitated on a steam bath, whereby the initially formed oil dissolved within 10 min. The debenzylidenation was complete after 30 min, as judged by tlc (solvent C). The solution was cooled, and evaporated repeatedly with added portions of ethanol until the smell of acetic acid was no longer noticeable, and a dry foam was obtained (~2.94 g). The foam crystallized on treatment with dichloromethane (20 mL), giving 2.167 g of **9** (R_f 0.17), mp 140–142°C, contaminated by a trace of a product having R_f 0.34. The mother liquor showed components having R_f 0.17, 0.34, and 0.43 (solvent C). Upon removal of the solvent, this mixture was subjected to hydrolysis as previously described, using 10 mL of 80% acetic acid, which caused disappearance of the component having R_f 0.43. After processing as before, the material was heated on the steam bath for 15 min in a mixture (10 mL) of methanol–water–triethylamine (5:3.5:1.5). Evaporation, followed by crystallization from dichloromethane, gave an additional 308 mg of **9**, plus 153 mg from the mother liquor after its passage through a short column of silica gel (solvent C). The combined crops (2.628 g, 92.5% yield) were recrystallized as described, by treating with dichloromethane the dry foam obtained on evaporation of an ethanolic solution of the compound. Pure **9** so prepared (2.589 g, 91.1%) had mp 141–143°C; $[\alpha]_D$ +83.2° (*c* 0.5, ethanol); ν_{max}: 3350 (OH) and 2111 (N_3) cm^{-1}; δ (CD_3COCD_3): 7.46 (m, Ph), 5.18 (d, $J_{1,2}$ = 1.8 Hz, H-1), 4.78 (d, $J_{4,OH}$ = 6.4 Hz, OH-4), 4.76 (s, 4H, 2 *Ph*-CH_2), 4.17 (dt, $J_{4,OH}$ = 6.4, $J_{3,4} \approx J_{4,5}$ = 10.2 Hz, H-4), 4.03 (dd, $J_{1,2}$ = 1.8, $J_{2,3}$ = 3.2 Hz, H-2), 4.00–3.90 (m, 6H, H-6, H-6′, and OH-6), 3.85 (dd, $J_{2,3}$ = 3.2, $J_{3,4}$ = 10.4 Hz, H-3), and 3.78 (octet, H-5). When D_2O was added to the solution, the OH-4 signal disappeared, H-4 gave a clear triplet, the *Ph*-CH_2 singlet became an AB quartet (J_{gem} = 12.6 Hz), the δ 4.0–3.9 region was resolved and revealed H-6 at δ 4.00 (dd, $J_{5,6}$ = 2.6, $J_{6,6'}$ = 12 Hz) as well as H-6′ at δ 3.88 (dd, $J_{5,6'}$ = 5.6 Hz). All assignments were verified by spin decoupling experiments. *Anal.* calcd. for $C_{26}H_{30}N_6O_9$ (570.5): C 54.73, H 5.30, N 14.73; found: C 54.58, H 5.40, N 14.88.

3-Amino-3-deoxy-α-D-mannopyranosyl 3-amino-3-deoxy-α-D-mannopyranoside (10) and its dihydrochloride (11)

A solution of **9** (2.567 g) in 95% ethanol (40 mL) together with 10% palladium on charcoal (2.5 g) was heated with magnetic stirring, and cyclohexene (20 mL) was added when refluxing started. Progress of the reaction was monitored by tlc using 5:4:1 methanol–chloroform – ammonium hydroxide (concentrated, aqueous) as the irrigant. After 6 min, the presence of 5 products was indicated: R_f 0.10 (**10**), 0.34 (diaminomonobenzyl derivative), 0.44 (weak; monoaminomonoazidomonobenzyl derivative), 0.73 (diaminodibenzyl derivative), and 0.86 (**9**). After 12 min, the product having R_f 0.44 was no longer detectable. To promote the reaction, the following was added to the boiling mixture: cyclohexene (10 mL, after 45 min), water (2 mL, after 1 h), and Pd catalyst (0.5 g, after 2 h). About 140 min after the start of the reaction only a trace of **9** had remained, and after 3 h there were intense spots for **10** (R_f 0.1) and a by-product (R_f 0.2), accompanied only by weak spots of more-mobile intermediates. Refluxing was stopped, the mixture was filtered, and the catalyst was washed with hot 95% ethanol followed by hot 90% ethanol (100 mL each). Evaporation of the filtrate and washings gave ~1.6 g of a material, which was dissolved in a methanol–water mixture. The solution was evaporated to a thin syrup to which some fresh methanol was added, and scratching with a glass rod then initiated crystallization of **10** (1.045 g) contaminated by a trace of the compound having R_f 0.2. Twice recrystallized from methanol, the substance (988 mg, 61.3%) was chromatographically homogeneous (R_f 0.11), but faintly yellowish. The coloration was removed by vacuum filtration of the compound, in concentrated aqueous solution (3 mL of water), through a plug of activated carbon and Celite. The recovered, colorless compound (874 mg, plus 95 mg from the mother liquor; see below) had mp 177–180°C; $[\alpha]_D$ +105.7° (*c* 0.7, water); δ (D_2O, acetone lock signal): 4.95 (d, $J_{1,2}$ = 2.0 Hz, H-1), 3.74 (narrow m, H-2), 3.72 (dd, $J_{5,6}$ = 2.0, $J_{6,6'}$ = 12.0 Hz, H-6), 3.56 (dd, $J_{5,6'}$ = 7.0, $J_{6,6'}$ = 12 Hz, H-6′), 3.47 (m, J = 2.0, 7.0, and 10.0 Hz, H-5), 3.29 (t, $J_{3,4}$ = $J_{4,5}$ = 10 Hz, H-4), 3.15 (dd, $J_{2,3}$ = 3.0, $J_{3,4}$ = 10.0 Hz, H-3). All assignments were confirmed by spin decoupling; ^{13}C nmr data, δ (H_2O, with acetone lock signal 29.8 ppm from TMS): 94.5 (C-1), 73.2, 69.5, and 67.3 (C-2, -4, and -5), 60.6 (C-6), and 51.5 (C-3). *Anal.* calcd. for $C_{12}H_{24}N_2O_9 \cdot H_2O$ (358.3): C 40.22, H 7.31, N 7.82; found: C 40.20, H 7.18, N 7.66.

A sample of **10** was converted into its dihydrochloride **11** by precipitation from methanolic solution with ether containing anhydrous hydrogen chloride (2); mp 199.5°C (dec.), $[\alpha]_D$ + 84.2°, in excellent agreement with the reported (2, 8) values. The ^{13}C chemical shift data, differing slightly from those of the free base, above, completely matched those reported (8) for **11**.

The N-*ethyl derivative as by-product*

The mother liquors from the isolation and purification of **10** were combined and evaporated. The residue was chromatographed on a column of powdered cellulose by means of 85:13:2 ethanol–water–ammonium hydroxide (concentrated, aqueous) as the eluant. The fractions containing the faster-moving (R_f ~0.25) by-product were inhomogeneous, whereas from subsequent fractions some additional **10** was obtained in crystalline form (95 mg). The inhomogeneous fractions were passed through the same column again, with a 90:8:2 mixture of the previous solvents, and 45 mg of the compound showing R_f 0.25 could thereby be isolated pure. The ^1H nmr spectrum (D_2O, acetone lock signal) indicated unequal substitution of the disaccharide due to the presence of one *N*-ethyl group; δ: 5.05 and 5.02 (two d, J = 2 Hz, H-1 and H-1′), 4.12 and 3.98 (two narrow dd, H-2 and H-2′), 3.8–3.5 (unresolved m, 8H, H-4,4′, 5,5′, 6a,6a′, 6b,6b′), 3.38 and 3.32 (two dd, $J_{2,3}$ and $J_{2',3'}$ = 3.5 Hz, $J_{3,4}$ and $J_{3',4'}$ = 10.5 Hz, H-3 and H-3′), 3.04 (complex symm. multiplet, 2H, CH_2 of Et), and 1.14 (t, 3H, CH_3 of Et). The assignments were verified by spin decoupling.

Acknowledgments

Financial support of this work by the Medical Research Council of Canada is gratefully acknowledged. H. H. B. thanks the Ministère de l'Education Nationale, France, and the Université de Grenoble I for a Visiting Professorship (1983–1984).

1. H. H. BAER and A. J. BELL. Carbohydr. Res. **75**, 175 (1979); **78**, C19 (1980).
2. H. H. BAER and A. J. BELL. Can. J. Chem. **56**, 2872 (1978).
3. J. DEFAYE, H. DRIGUEZ, B. HENRISSAT, and E. BAR-GUILLOUX. *In* Mechanism of saccharide polymerization and depolymerization. *Edited by* J. J. Marshall. Academic Press, New York. 1980. pp. 331–353; J. DEFAYE, H. DRIGUEZ, B. HENRISSAT, and E. BAR-GUILLOUX. Nouveau J. Chim. **4**, 59 (1980); Carbohydr. Res. **124**, 265 (1983); and references cited therein.
4. S. UMEZAWA. Adv. Carbohydr. Chem. Biochem. **30**, 111 (1974).
5. M. GHIONE, A. MINGHETTI, and A. SANFILIPPO. Giorn. Microbiol. **7**, 94 (1959); F. ARCAMONE and F. BIZIOLI. Gazz. Chim. Ital. **87**, 896 (1957).
6. H. NAGANAWA, N. USUI, T. TAKITA, M. HANADA, K. MAEDA, and H. UMEZAWA. J. Antibiot. Ser. A, **27**, 145 (1974).
7. M. URAMOTO, N. OTAKE, and H. YONEHARA. J. Antibiot. Ser. A, **20**, 236 (1967).
8. H. H. BAER, L. SIEMSEN, J. DEFAYE, and K. BURAK. Carbohydr. Res. In press.
9. H. H. BAER and B. RADATUS. Carbohydr. Res. **128**, 165 (1984).
10. G. BRIEGER and T. J. NESTRICK. Chem. Rev. **74**, 567 (1974).
11. A. E. JACKSON and R. A. W. JOHNSTONE. Synthesis, 685 (1976); G. M. ANANTHARAMAIAH and K. M. SIVANANDAIAH. J. Chem. Soc. Perkin Trans. 1, 490 (1977).
12. A. M. FELIX, E. P. HEIMER, T. J. LAMBROS, C. TZOUGRAKI, and J. MEIENHOFER. J. Org. Chem. **43**, 4194 (1978).

Kinetics and mechanism of oxidation of *N,N'*-dimethyl-9,9'-biacridanyl by some π acceptors and a one-electron oxidant

ALLAN K. COLTER, CHARLES C. LAI, A. GREGG PARSONS, N. BRUCE RAMSEY, AND GUNZI SAITO
Guelph–Waterloo Centre for Graduate Work in Chemistry, Department of Chemistry, University of Guelph, Guelph, Ont., Canada N1G 2W1

Received June 21, 1984

ALLAN K. COLTER, CHARLES C. LAI, A. GREGG PARSONS, N. BRUCE RAMSAY, and GUNZI SAITO. Can. J. Chem. **63**, 445 (1985).

Oxidation of *N,N'*-dimethyl-9,9'-biacridanyl (DD) has been investigated as a model for single electron transfer (SET)-initiated oxidation of NADH coenzyme models such as *N*-methylacridan (DH). Oxidants investigated cover a 10^{10}-fold range of reactivity in acetonitrile and include the π acceptors 1,4-benzoquinone (BQ), 2,6-dichloro-1,4-benzoquinone (DClBQ), *p*-chloranil (CA), 2,3-dicyanobenzoquinone (DCBQ), 2,3-dicyano-1,4-naphthoquinone (DCNQ), 2,3-dicyano-5-nitro-1,4-naphthoquinone (DCNNQ), 9-dicyanomethylene-2,4,7-trinitrofluorene (DCMTNF), 9-dicyanomethylene-2,4,5,7-tetranitrofluorene (DCMTENF), 7,7,8,8-tetracyanoquinodimethane (TCNQ), and tetracyanoethylene (TCNE), and the one-electron oxidant *tris*(2,2'-bipyridyl)cobalt(III), $Co(bipy)_3^{3+}$. The oxidation product is, in every case, *N*-methylacridinium ion (D^+). A mechanism involving a rate-determining electron transfer with simultaneous fragmentation to D^+ and *N*-methyl-9-acridanyl radical (D·) is proposed. This mechanism is supported by the observed dependence of the rate on oxidant reduction potential, by spin-trapping experiments, by kinetic isotope effects in oxidation of 9,9'-dideuterio-DD, and by substituent effects in oxidation of 2,2'- and 3,3'-dimethoxy-DD. The rate of oxidation of DD relative to that of DH is 3.4×10^2 with $Co(bipy)_3^{3+}$, and with the π acceptors varies from ca. 0.3 (BQ) to 8.1×10^4 (DCMTENF). The results rule out a SET-initiated mechanism for oxidation of DH by all of the oxidants studied except TCNQ and DCMTENF.

ALLAN K. COLTER, CHARLES C. LAI, A. GREGG PARSONS, N. BRUCE RAMSAY et GUNZI SAITO. Can. J. Chem. **63**, 445 (1985).

On a étudié l'oxydation du *N,N'*-diméthylbiacridanyl-9,9' (DD), un modèle pour l'oxydation, initiée par le transfert d'un seul électron (TSE), de modèles de la coenzyme NADH, comme le *N*-méthylacridan (DH). Avec les oxydants étudiés dans l'acétonitrile, on couvre dix ordres de grandeur de réactivité et les oxydants comprennent des accepteurs π comme la benzoquinone-1,4 (BQ), la dichloro-2,6 benzoquinone-1,4 (DClBQ), le *p*-chloranil (CA), la dicyano-2,3 benzoquinone (DCBQ), la dicyano-2,3 naphtoquinone-1,4 (DCNQ), la dicyano-2,3 nitro-5 naphtoquinone (DCNNQ), le dicyanométhylène-9 trinitro-2,4,7 fluorène (DCMTNF), le dicyanométhylène-9 tétranitro-2,4,5,7 fluorène (DCMTENF), le tétracyano-7,7,8,8 quinodiméthane (TCNQ) et le tétracyanoéthylène (TCNE) ainsi que l'oxydant à un électron, *tris*(bipyridyl-2,2')cobalt(III), $Co(bipy)_3^{3+}$. Dans tous les cas, le produit de l'oxydation est l'ion *N*-méthylacridinium (D^+). On propose un mécanisme impliquant, dans l'étape qui détermine la vitesse de la réaction, un transfert d'un électron avec une fragmentation simultanée conduisant à D^+ et au radical *N*-méthylacridanyl-9 (D·). Ce mécanisme est en accord avec le fait que la vitesse de la réaction dépend du potentiel de réduction de l'oxydant, avec des expériences de trappage de spin, avec les effets isotopiques cinétiques du dideutéro-9,9' DD et avec les effets des substituants sur l'oxydation des diméthoxy-2,2' (et 3,3') DD. Les vitesses d'oxydation du produit DD par rapport à celles du produit DH sont égales à $3,4 \times 10^2$ avec le $Co(bipy)_3^{3+}$ et, avec les accepteurs π, elles varient d'environ 0,1 (BQ) à $8,1 \times 10^4$ (DCMTENF). On discute des implications de ces résultats en relation avec les mécanismes d'oxydation du composé DH.

[Traduit par le journal]

Introduction

The mechanisms of hydride transfer reactions of nicotinamide coenzyme models continue to attract considerable attention (1, 2 and references cited). Much of this interest has focused on the experimental distinction between a one-step hydride transfer mechanism and stepwise mechanisms involving an initial single electron transfer (SET). This distinction has proven to be very elusive for oxidants, such as quinones and carbonyl compounds, that are capable of reacting either as hydride or one-electron acceptors. One of the difficulties lies in the fact that the responses of the rate to changes in structure or solvent predicted by the stepwise and one-step mechanisms are very similar. For this reason, it would be instructive to examine model oxidation reactions that could be guaranteed to occur via an initial SET.

In principle, two approaches to the investigation of oxidation of NADH models by SET-initiated pathways are possible. The first is to investigate oxidants capable of reaction as one-electron acceptors only (3–5). A second approach is to design NADH models in which oxidation by hydride transfer either cannot occur or is strongly inhibited. We were encouraged to examine the oxidation of *N,N'*-dimethyl-9,9'-biacridanyl (DD)

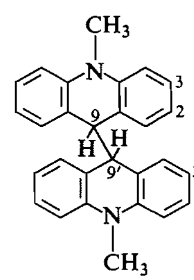

1, DD

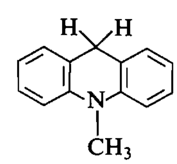

2, DH

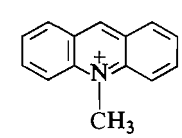

3, D^+

as a model for SET-initiated oxidation of *N*-methylacridan (DH) to *N*-methylacridinium ion (D^+) (5, 6) for the following reasons. DD is reported to be oxidized by iodine to D^+ (7), a reaction corresponding to removal of 2 electrons (and no protons) from DD, with fragmentation. In contrast, removal of hydride from DD would lead to the known (8) conjugate acid of *N,N'*-dimethyl-9,9'-biacridylidene which, after the loss of a proton, would be further oxidized to *N,N'*-dimethyl-9,9'-biacridinium ion (luzigenin) (9). The dimeric dihydronicotinamides analogous to DD are similarly oxidized by methyl-

TABLE 1. Charge-transfer absorption maxima for complexes of π acceptors with DD, DH, and pyrene[a]

Acceptor	$10^{-3}\ \bar{\nu}$, cm^{-1} DD	DH	Pyrene
2-Methyl-1,4-benzoquinone	19.7	20.8	23.5
BQ	18.4	19.8	22.6
1,3,5-Trinitrobenzene	17.9 (16.4,[b] 17.5[c])	19.7	22.2
2,3-Dichloro-1,4-naphthoquinone	16.0	17.9	19.5
DClBQ	14.7	17.7	19.2

[a]Benzene solution.
[b]2,2′-Dimethoxy-DD.
[c]3,3′-Dimethoxy-DD.

viologen and 2,6-dichloroindophenol (10) as well as electrochemically (11, 12) to the corresponding monomeric nicotinamide salts. The electrochemical oxidations of the dimeric dihydronicotinamides occur at lower positive potentials than the oxidations of the corresponding monomeric dihydronicotinamides (11, 12).

Results

The biacridanyls investigated included DD as well as 2,2′- and 3,3′-dimethoxy-*N*,*N*′-dimethyl-9,9′-biacridanyl (2,2′-dimethoxy-DD and 3,3′-dimethoxy-DD), the last two as diastereomeric mixtures. DD and 2,2′-dimethoxy-DD were obtained by reduction of the corresponding *N*-methylacridinium salts (D^+ and 2-methoxy-D^+, respectively) by phenylhydrazine (13), Raney Nickel (14), or various Grignard reagents (15), while 3,3′-dimethoxy-DD was obtained by the last two methods only. The oxidants investigated kinetically included four benzoquinones (**4–7**), two naphthoquinones (**8–9**), four dicyanomethylene π acceptors (**10–13**), and the one-electron oxidant *tris*(2,2′-bipyridyl)Co(III) ($Co(bipy)_3^{3+}$).

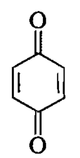

4, BQ

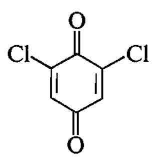

5, DClBQ

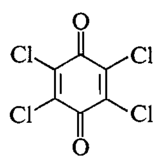

6, CA

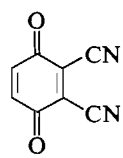

7, DCBQ

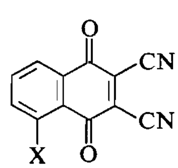

8, X = H, DCNQ
9, X = NO_2, DCNNQ

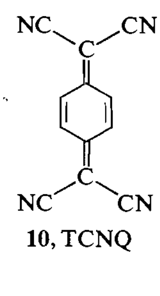

10, TCNQ

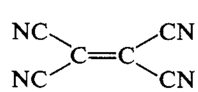

11, TCNE

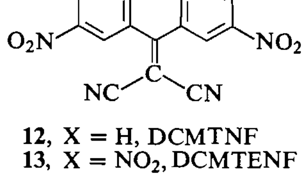

12, X = H, DCMTNF
13, X = NO_2, DCMTENF

The oxidation product in reaction of DD with oxidants **4–13**, 2,3-dicyano-5,6-dichloro-1,4-benzoquinone (DDQ), and triphenylmethyl fluoborate, all in acetonitrile (AN), was identified by uv–visible spectral examination of reaction solutions or of product isolated as the perchlorate salt. In every case the only detectable oxidation product was *N*-methylacridinium cation (D^+). The uv–visible spectrum of D^+ (λ_{max} = 356 nm in AN) is easily distinguishable from that of *N*,*N*′-dimethyl-9,9′-biacridinium ion (λ_{max} = 367 nm in AN), the oxidation product expected from initial hydride transfer (above), even though they are very similar. Quantitative formation of $2D^+$ from each DD was confirmed by absorbance measurements on reaction mixtures with the oxidants BQ, CA, TCNE, and $Co(bipy)_3^{3+}$ at 356 nm, and with DClBQ at 420 nm. With DCNQ, DCNNQ, TCNQ, DCMTNF, and DCMTENF the spectrum of D^+ is masked by that of the radical anion reduction product. In oxidations with these five oxidants, plus CA, DCBQ, TCNE, and DDQ, the oxidation product was isolated as $D^+ClO_4^-$ in yields greater than 90%. With DCNQ, DCNNQ, TCNQ, DCMTNF, and DCMTENF, formation of 2 mol of acceptor radical anion (i.e., $DCNQ^{\dot{-}}$, etc.) was confirmed by absorbance measurements on reaction solutions. Finally, the stoichiometry of oxidation of DD with CA was investigated by measuring the absorbance due to D^+ (356 nm) in a series of experiments involving reaction of CA with excess DD. All of the product and stoichiometry studies are consistent with the stoichiometry represented by reaction [1].

$$[1]\quad DD + 2A \rightarrow 2D^+ + 2A^{\dot{-}}$$

The complete oxidation of DD by BQ in AN requires a proton source such as acetic acid, presumably because of the instability of $BQ^{\dot{-}}$. For example, in one experiment in pure AN, oxidation of DD (3.4×10^{-5} *M*) by BQ (6.6×10^{-2} *M*) occurred to the extent of roughly 20%.

In earlier work (6) transient charge-transfer (CT) absorptions were observed in solutions containing DH and any of several π acceptors. In order to compare the π donor properties of DD and DH, the positions of their CT maxima with several π acceptors were measured (Table 1). These measurements in general require much higher concentrations of both DD and π acceptor than those used in the kinetic studies (below) and are limited to less reactive π acceptors because of interference from formation and precipitation of product. To conform that the measured maxima are due to CT absorption pyrene was also included in the comparison. A plot of $\bar{\nu}_{max}$(DD) vs. $\bar{\nu}_{max}$(pyrene) is reasonably linear (r = 0.979) with a slope close to unity (1.01 ± 0.09) as required (16). A similar plot for DH vs. pyrene including data for two additional acceptors reported earlier (6) has a slope of 0.94 ± 0.07, r = 0.982.

TABLE 2. Rates of oxidation of DD[a]

Oxidant	$E°$, V[b]	[Oxidant], M	k (M^{-1} s^{-1})[c]
BQ[d]	−0.51[e]	(0.493–3.36) × 10^{-1}	5.0 × 10^{-5}
DClBQ[d]	−0.18[e]	(2.46–6.61) × 10^{-2}	7.62 × 10^{-3}
DCMTNF	−0.100[f]	(1.73–3.45) × 10^{-3}	3.47
CA	0.01[e]	(1.54–13.9) × 10^{-4}	4.77
DCNQ	0.05[g]	(1.14–3.18) × 10^{-3}	2.05 × 10^{3}
TCNQ	0.19[h]	(1.00–550) × 10^{-5}	4.04 × 10^{3}
TCNE	0.24[h]	(0.917–535) × 10^{-3}	6.16 × 10^{3}
DCMTENF	0.115[f]	(0.919–3.13) × 10^{-3}	1.50 × 10^{4}
DCBQ	0.31[i]	(3.56–5.40) × 10^{-3}	1.17 × 10^{5}
DCNNQ	0.30[g]	(1.67–2.25) × 10^{-3}	1.60 × 10^{6}
$Co(bipy)_3^{3+}$	0.235[j]	(0.877–2.00) × 10^{-3}	8.50 × 10
D^+I^-	—	(3.82, 4.88) × 10^{-3}	1.3 × 10^{-4}

[a] AN solvent, 25°C. [DD] = 1.11–5.92 × 10^{-5} M except with D^+I^-, where [DD] = 7.52 × 10^{-5} M and 9.27 × 10^{-5} M.
[b] Standard one-electron reduction potential in AN vs. SCE.
[c] Number of measurements averaged: 2 with D^+I^-, 3 with BQ, and 6–15 with the other oxidants. Estimated uncertainties ±20% for BQ, ±10% for D^+I^- and DClBQ, and ±4% for the other oxidants.
[d] 0.01 M acetic acid added.
[e] Reference 21, 0.1 M tetraethylammonium perchlorate.
[f] Reference 22, 0.1 M $Li^+ClO_4^-$.
[g] Reference 23, 0.1 M tetrapropylammonium perchlorate.
[h] Reference 24, 0.1 M tetraethylammonium perchlorate.
[i] Reference 25, 0.1 M $Li^+ClO_4^-$.
[j] Reference 26, 5 × 10^{-3} M tetraethylammonium perchlorate.

The most important observation is that the CT maximum for DD consistently appears at lower energy than that for DH with the same acceptor, indicating that DD should undergo one-electron oxidation more easily than DH (16, 17). This difference, for two compounds having identical π electron systems, is consistent with the predictions of current theory on orbital interactions through σ bonds (18). The interaction of π orbitals through three σ bonds is possibly enhanced by the elongated (1.58 Å) (19) C_9—$C_{9'}$ bond (20). Secondly, the results of the comparison of DD, 2,2′- and 3,3′-dimethoxy-DD with 1,3,5-trinitrobenzene (Table 1) parallel those obtained with the corresponding *N*-methylacridans (5) and indicate that the HOMO energies lie in the order 2,2′-dimethoxy-DD > 3,3′-dimethoxy-DD > DD.

The results of a kinetic investigation of oxidation of DD with oxidants **4**–**13** are summarized in Table 2. Rate measurements were carried out under pseudo first-order conditions using a 30-fold or greater molar excess of oxidant over DD for all oxidants. Pseudo first-order rate constants so obtained are proportional to acceptor concentration within experimental error. Complex formation between DD and π acceptor oxidants could, in principle, cause some error in calculated second-order rate constants if the association constants are large enough (6). However, judging from the intensities of the CT absorptions in benzene solution, the equilibrium constants for complexation of DD and DH with the same acceptor are of similar magnitude, and hence too small to produce significant errors at the concentrations of the rate measurements (6). With CA, TCNQ, and TCNE lower ratios of oxidant to DD were investigated as well, and the rate constant obtained by a second-order analysis.

N-Methylacridinium ion (D^+) was also examined as an oxidant by measuring the rate of reaction of D^+ with DD (reaction [2]) using DD labelled with $^{14}CH_3$.

[2] $D^+ + {}^*DD \rightleftharpoons {}^*D^+ + DD$

In order to assist in the characterization of the oxidation transition state, rates of oxidation of 9,9′-dideuterio-DD with CA, and of DD, 2,2′- and 3,3′-dimethoxy-DD with CA and $Co(bipy)_3^{3+}$ were measured. These results are summarized in Table 3. The dimethoxybiacridanyls were obtained as a mixture of the *meso* and *dl* diastereomers. First-order plots were strictly linear through 90% reaction indicating that the two diastereomers do not differ significantly in oxidation rate for the two oxidants investigated.

TABLE 3. Kinetic isotope effects and substituent effects in oxidation of *N,N′*-dimethyl-9,9′-biacridanyls[a]

Biacridanyl	Oxidant	k (M^{-1} s^{-1})	Relative rate[b]
DD	CA	4.77	(1)
9,9′-Dideuterio-DD	CA	4.25	0.89 ± 0.03[c]
2,2′-Dimethoxy-DD	CA	5.79 × 10^{2}	1.2 × 10^{2}
3,3′-Dimethoxy-DD	CA	1.05 × 10^{2}	2.2 × 10
DD	$Co(bipy)_3^{3+}$	8.50 × 10	(1)
2,2′-Dimethoxy-DD	$Co(bipy)_3^{3+}$	6.69 × 10^{3}	7.9 × 10
3,3′-Dimethoxy-DD	$Co(bipy)_3^{3+}$	5.57 × 10^{2}	6.8

[a] Acetonitrile solvent, 25°C.
[b] Relative to rate constant for reaction of DD with the same oxidant.
[c] Based on four independent determinations of $k_{DD} \div k_{DD\text{-}9,9'\text{-}d_2}$.

To test for the occurrence of C_9—$C_{9'}$ bond fission in DD (reaction [3]) under the conditions of the kinetic measurements,

[3] $DD \rightleftharpoons 2D^{\bullet}$

spin-trapping experiments (27) were carried out using the spin trap 2-nitroso-2-methylpropane (NtB). A solution of DD (5.2 × 10^{-4} mol) and NtB (2.0 × 10^{-4} mol) in acetonitrile was mixed with a solution of DCBQ (2.6 × 10^{-4} mol) in acetonitrile under nitrogen, and the solid D^+ $DCBQ^{\bar{\cdot}}$ product removed by filtration through a cotton plug. The esr spectrum of the filtrate showed a clean persistent triplet of doublets characteristic of *t*-butyl 9-acridanyl nitroxide, the spin adduct of $D^{\bullet}$ (**14**) and NtB (28). In contrast, solutions containing

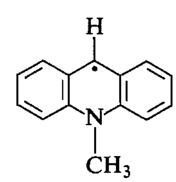

14, D·

DD and NtB alone in acetonitrile (in the dark) showed no detectable esr signal.

Because one of the objectives of this work was to compare reactivity patterns in oxidations of DH and DD, we have extended earlier (5, 6) kinetic measurements of oxidation of DH to the acceptors DCNQ, DCNNQ, DCMTNF, and DCMTENF. The stoichiometry of oxidation of DH by the four new acceptors is identical to that previously determined for **7**, **10**, and **11** (6). These rates were measured under pseudo first-order conditions following the progress of the reaction as with the corresponding oxidation of DD. These rates, along with earlier rates of oxidation of DH by the oxidants investigated in this study, and the relative reactivites of DD and DH toward each oxidant, are listed in Table 4.

Discussion

Mechanism of oxidation of DD

The possibility of mechanisms in which C_9—$C_{9'}$ bond fis-

TABLE 4. Relative rates of oxidation of DD and DH[a]

Oxidant[b]	k (M^{-1} s^{-1})[c]	k_{DD}/k_{DH}	Reference
$Co(bipy)_3^{3+}$	2.47×10^{-1}	3.4×10^2	5
	Benzoquinones		
BQ	5.67×10^{-4}	0.1	5
CA	1.18×10	0.40	5
DCBQ	1.15×10^4	1.0×10	5
	Naphthoquinones		
DCNQ	3.09×10^2	6.6	This work
DCNNQ	1.23×10^4	1.3×10^2	This work
	Dicyanomethylenes		
DCMTNF	4.50×10^{-2}	7.7×10	This work
DCMTENF	1.86×10^{-1}	8.1×10^4	This work
TCNQ	2.35×10^{-1}	1.7×10^4	5
TCNE	1.09×10^2	5.7×10	5

[a] Acetonitrile solvent, 25°C.
[b] Concentrations: [DCNQ] = 1.03×10^{-2} M, [DCNNQ] = $(1.46–7.21) \times 10^{-3}$ M. [DCMTNF] = $(2.76–4.91) \times 10^{-2}$; [DCMTENF] = $(4.37–6.04) \times 10^{-3}$ M.
[c] Estimated errors ±10% with DCNQ and DCNNQ; ±5% with DCMTNF and DCMTENF.

sion occurs prior to oxidation must be considered. A mechanism analogous to [4] with $k_2[D^\cdot][A] \gg k_{-1}[D^\cdot]^2$ is observed in oxidations of 3,5,5-trimethyl-2-morpholinon-3-yl radical dimer (**15**) investigated by Koch and co-workers (29). Such a

$$[4] \quad DD \underset{k_{-1}}{\overset{k_1}{\rightleftharpoons}} 2D^\cdot \qquad D^\cdot + A \xrightarrow{k_2} D^+ + A^{\overline{\cdot}}$$

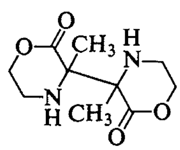

15

mechanism is excluded for the oxidations of DD in this work by the strong dependence of the rate on acceptor structure and by the first-order dependence of the rate on oxidant concentration over the full range of oxidant reactivity. Mechanism [4] with $k_{-1}[D^\cdot]^2 \gg k_2[D^\cdot][A^{\overline{\cdot}}]$ is likewise excluded because it would lead to a 0.5-order dependence on DD concentration. All mechanisms involving formation of free $D^\cdot$ prior to oxidation are also inconsistent with the observation that $D^\cdot$ can be trapped in oxidation of DD with DCBQ but not in the absence of oxidant.

Reversible formation of N-methylacridanyl π-*mer* (30), $(D^\cdot)_2$, which reforms DD more rapidly than it is oxidized is consistent with the rate law. However, for the D^+ + DD exchange reaction, the electron-transfer step in such a mechanism ($*D^+ + D^\cdot D^\cdot \rightarrow *D^\cdot D^\cdot + D^+$) would have $\Delta G^0 = 0$ and should therefore have a very small activation barrier. The electron transfer from $(D^\cdot)_2$ would then be exoergic for all of the other oxidants except BQ. It is then impossible to account for the 13.6 kcal mol^{-1} decrease in $\Delta G^\ddagger$ (corresponding to a 2.1×10^8-fold increase in rate) observed between DClBQ and DCNNQ.

A plot of log k vs. oxidant reduction potential, which is essentially a plot of $\Delta G^\ddagger$ for oxidation vs. ΔG^0 for electron

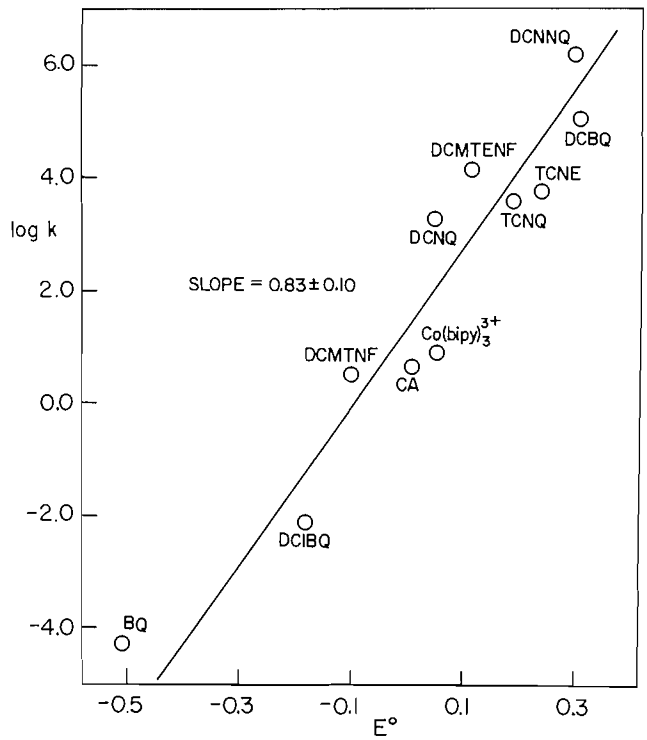

FIG. 1. Plot of log k for oxidation of DD vs. oxidant reduction potential.

transfer from the species oxidized to the oxidant, is shown in Fig. 1. To compare $Co(bipy)_3^{3+}$ with the electrically-neutral oxidants it is necessary to correct either ΔG^0 or E^0 for differences in coulombic stabilization of the product, i.e., $DD^{\dagger}A^{\overline{\cdot}}$ or $DD^{\dagger}$ $Co(bipy)_3^{2+}$ (31). For $DD^{\dagger}A^{\overline{\cdot}}$ we estimate this stabilization to be about 0.06 eV (1, 32). Taking the stabilization in $DD^{\dagger}$ $Co(bipy)_3^{2+}$ to be about -2×0.06 eV we have subtracted 0.18 V from the reduction potential of $Co(bipy)_3^{3+}$ in plotting Fig. 1.

Allowing for the considerable variation in oxidant structure as well as some spread in reported E^0 values for certain acceptors it is clear that a reasonable linear relationship exists between log k and E^0. The slope is strongly influenced by the BQ point, for which the rate constant has a substantial uncertainty. Expressed as a plot of $\Delta G^\ddagger$ vs. ΔG^0 (i.e., observed slope × RT/F) the slope is 0.75 sd 0.07 (r = 0.960) (all points, 3.2×10^{10}-fold range of reactivity) or 0.83 sd 0.10 (r = 0.936) (BQ excluded, 2.1×10^8-fold range of reactivity). Omission of the $Co(bipy)_3^{3+}$ point does not affect the slope significantly. Some regularities in the deviations from the best fit straight line in Fig. 1 are evident. The naphthoquinones are 1 to 2 powers of 10 more reactive than benzoquinones of similar reduction potential. Similarly, the 9-dicyanomethylenefluorenes are 1 to 2 powers of 10 more reactive than expected. These deviations are in the direction expected if the transition state resembles a π–π complex since complex stabilities typically increase with increasing area of donor–acceptor contact (33). For the three benzoquinones DClBQ, CA, and DCBQ, the slope (as defined above) is 0.87 sd 0.00 (r = 1.00).

A mechanism involving an initial reversible and strongly-endothermic electron transfer followed by a slow step in which the C—C bond is broken at a rate independent of the oxidant should lead to a plot of $\Delta G^\ddagger$ vs. ΔG^0 that is linear, with a slope of 1.0 (31, 34) and with very little scatter. The slope of ca.

0.80, together with the kind of regular scatter observed is best accommodated by a mechanism such as [5] in which electron-transfer within a reversibly-formed charge-transfer complex, DDA, occurs with simultaneous C—C bond fission.

$$[5]\quad \begin{aligned} &\mathrm{DD + A} \overset{K}{\rightleftharpoons} \mathrm{DDA} \\ &\mathrm{DDA} \xrightarrow{\text{slow}} \mathrm{D^+ + D^{\cdot} + A^{\cdot-}} \\ &\mathrm{D^{\cdot} + A} \xrightarrow{\text{fast}} \mathrm{D^+ + A^{\cdot-}} \end{aligned}$$

In principle the extent of C—C bond fission in the transition state should be reflected in the secondary deuterium kinetic isotope effect (Table 3). However, in the absence of a reliable estimate of the isotope effect for complete bond fission, the observed value (k_H/k_D = 1.12 or 1.06 per deuterium) provides little quantitative information. By comparison, secondary 9-deuterium kinetic isotope effects in oxidation of DH are in the neighborhood of 1.1 ± 0.05 (6) and α-deuterium isotope effects in E2 reactions range from 1.0 to 1.15 (50°C) (35). The results in oxidation of DD by CA therefore suggest a transition state in which the C—C bond is less than half broken.

A second measure of the extent of C—C bond fission in the transition state is provided by the substituent effects. In oxidation of 2- and 3-methoxy-*N*-methylacridans (2- and 3-methoxy-DH) with BQ, CA, and DCBQ, 2-methoxy-DH is 1/3.9, 1/5.4, and 1/9.2 times as reactive, respectively, as 3-methoxy-DH (5). The greater rate of oxidation of 3-methoxy-DH with quinones reflects the greater stability (relative to the corresponding acridan) of 3-methoxy-D^+. In contrast, in oxidation by $Co(bipy)_3^{3+}$, a reaction believed to occur by rate-determining SET, 2-methoxy-DH is 56 times as reactive as 3-methoxy-DH, reflecting the greater relative stability of 2-methoxy-$DH^{\cdot+}$. In the present work 2,2′-dimethoxy-DD is more reactive than 3,3′-dimethoxy-DD by factors of 5.5 (CA) and 12 ($Co(bipy)_3^{3+}$). Consequently, assuming that the substituent effects on the stability of $D^{\cdot}$ (relative to DD) are negligible, these results indicate that the transition state resembles $DD^{\cdot+}$ more closely than $D^+ + D^{\cdot}$.

Implications concerning the mechanisms of oxidation of DH with π acceptors

In earlier papers (1, 6) we have considered the possibility that oxidation of *N*-methylacridan (DH) and related compounds occurs via a mechanism in which a reversible SET is followed by a slow proton transfer [6]. The agreement between deuterium isotope effects determined kinetically and by isotope partitioning ratios

$$[6]\quad \begin{aligned} &\mathrm{DH + A} \underset{k_{-1}}{\overset{k_1}{\rightleftharpoons}} \mathrm{DH^{\cdot+}\,A^{\cdot-}} \\ &\mathrm{DH^{\cdot+}\,A^{\cdot-}} \xrightarrow[\text{slow}]{k_2} \mathrm{D^{\cdot}AH^{\cdot}} \\ &\mathrm{D^{\cdot}AH^{\cdot}} \xrightarrow{\text{fast}} \mathrm{D^+ + AH^-} \end{aligned}$$

for π acceptors covering a 10^7-fold range of reactivity (BQ to DCBQ) (6) requires that for any such mechanism k_{-1} be much larger than k_2. We have presented arguments based on the estimated standard free energy of formation of $DH^{\cdot+}\,A^{\cdot-}$ to rule out this species as an intermediate in oxidation of DH by BQ or CA (1). However, it was not possible using these arguments to exclude $DH^{\cdot+}\,A^{\cdot-}$ as an intermediate in oxidation of DH by TCNE, TCNQ, or DCBQ. Indeed, we have shown that the *N*-methyl-9-acridanyl radical, $D^{\cdot}$, can be trapped in oxidation of DH with DCBQ (28).

The results of our studies of the oxidation of DH with $Co(bipy)_3^{3+}$ are consistent with a mechanism involving an initial irreversible SET with concurrent or rapid subsequent loss of H^+ (5). If, in the corresponding oxidation of DD, each electron transfer leads to bond fission, the observed rates of oxidation of DD and DH by $Co(bipy)_3^{3+}$ provide a measure of the relative rates of SET from DD and DH (Table 4). The greater ease of one-electron oxidation of DD is consistent with the charge-transfer maxima (Table 1), and parallels the greater ease of oxidation of the dimeric reduced nicotinamides than the corresponding dihydronicotinamides by one-electron oxidants (10) and electrochemically (11, 12).

Because oxidation of DH with π acceptors via a mechanism such as [6] necessarily involves a *reversible* electron transfer (above), such a mechanism requires that for the π acceptors $k_{DD} \div k_{DH}$ (Table 4) be substantially (perhaps 5 to 10 ×) larger than 3.4×10^2, the ratio for $Co(bipy)_3^{3+}$. Consequently any value of $k_{DD} \div k_{DH}$ less than about 1.5×10^3 would exclude a stepwise mechanism involving an initial SET for the DH oxidation. On this basis, an electron–proton–electron mechanism can be excluded for all of the quinones investigated, as well as for DCMTNF and TCNE. For oxidation of DH by these π acceptors electron and hydrogen transfer must be strongly coupled. Only for TCNQ and DCMTENF does mechanism [6] remain a possibility. This conclusion would seem to be at odds with the successful trapping of $D^{\cdot}$ in oxidation of DH by DCBQ (28). We are presently uncertain as to how to interpret this result. Possibly the formation of $D^{\cdot}$ in reaction of DH with DCBQ is unrelated to the major pathway leading to D^+.

Experimental

Melting points were measured in open capillary tubes and are uncorrected. Proton nmr spectra were measured using a Varian EM-360 spectrometer. Chemical shifts are reported in δ units, with tetramethylsilane as internal standard. Ultraviolet-visible spectra were obtained using Beckman 24 or Cary 118C spectrophotometers. Electron spin resonance spectra were recorded at room temperature on a Varian E-104 spectrometer. Radioactivity measurements utilized Beckman LS-255 and LS-7000 liquid scintillation counters. Elemental microanalyses were performed by Guelph Chemical Laboratories, Guelph, Ontario.

Reagents and solvents

BQ, CA, TCNE, TCNQ, DCBQ, and $Co(bipy)_3(ClO_4)_3 \cdot 3H_2O$ were obtained and purified as previously described (5, 6). Eastman Kodak White Label DClBQ was crystallized twice from 30–60°C petroleum ether and sublimed under vacuum. DCMTNF, prepared following Mukherjee (36) and purified by recrystallizing twice from AN, had mp 263–264°C (lit. (36) mp 266–268°C). DCMTENF (37) was prepared from 2,4,5,7-tetranitrofluorenone and malononitrile following the procedure used to prepare DCMTNF (36) and purified by recrystallizing twice from AN, mp ca. 380–382°C (dec.) (lit. (37) mp > 400°C (dec.)). DCNQ was prepared from 2,3-dichloro-1,4-naphthoquinone (Aldrich) following the procedure of Reynolds (38) and purified by vacuum sublimation, recrystallization from benzene–toluene and from AN, mp 268–272°C (lit. (38) mp 274–275°C). DCNNQ was prepared from 2,3-dichloro-5-nitro-1,4-naphthoquinone (6) following Wallenfels (39) and purified by recrystallizing three times from methylene chloride – heptane. *Anal.* calcd. for $C_{12}H_3N_3O_5$: C 56.93, H 1.19, N 16.60; found: C 56.86, H 1.60, N 16.46. 2-Methyl-1,4-benzoquinone and 1,3,5-trinitrobenzene were obtained from commercial sources and were purified by sublimation or recrystallization before use. *N,N′*-Dimethyl-9,9′-biacridinium nitrate, for spectral comparison with D^+ salts, was obtained from K & K Laboratories. $^{14}CH_3$-labelled $D^+ClO_4^-$ was prepared by methylation of acridine (6) using ^{14}C-enriched methyl iodide. The preparation of *N*-methylacridan (DH) has been described (6). AN was Fisher Certified ACS grade further purified by distillation over phosphorus pentoxide followed by distillation over calcium hydride. 2-Nitroso-2-methylpropane was prepared by the procedure of Calder *et al.* (40).

N,N-*Dimethyl-9,9'-biacridanyl* (DD) was synthesized in 82% yield from *N*-methylacridinium iodide (D^+I^-) (6) and phenylhydrazine following Chupakhin (13) and recrystallized from dimethylformamide, mp 261–263°C (lit. (13) mp 280–281°C, (41) 270–271°C). ^1H nmr ($CDCl_3$) δ: 2.97 (s, 6H, N—CH_3), 3.88 (s, 2H, 9-H), 6.27–7.21 (m, 16H, aromatic). *Anal.* calcd. for $C_{28}H_{24}N_2$: C 86.56, H 6.23, N 7.21; found: C 86.54, H 6.06, N 7.21. This compound was also obtained in 41% yield by reduction of D^+I^- with Raney Nickel (14) and as a minor product in addition of several Grignard reagents to D^+I^- (15) as described below for 3,3'-dimethoxy-DD. 9,9'-Dideuterio-DD was prepared from 9-deuterio-D^+I^- (6) by Chupakhin's method (13).

*2,2'-Dimethoxy-*N,N'*-dimethyl-9,9'-biacridanyl* (2,2'-dimethoxy-DD) was obtained in 62% yield from 2-methoxy-D^+I^- (5) using Chupakhin's procedure (13). Recrystallization from pyridine–methanol afforded white crystals, mp 231–233°C. ^1H nmr ($CDCl_3$) δ: 3.27 (s, 6H, N—CH_3), 3.71 (s, 6H, OCH_3), 3.82 (s, 2H, 9-H), 6.57–7.33 (m, 14H, aromatic). In C_6D_6 solvent the two high-field peaks appear as a pair of peaks of relative intensity 48:52, respectively, at δ 2.58 and 2.62, and at 3.25 and 3.27, showing that the *meso* and *dl* diastereomers are produced in almost equal amounts. *Anal.* calcd. for $C_{30}H_{29}N_2O_2$: C 80.33, H 6.29, N 6.25; found: C 80.78, H 6.50, N 6.38. This compound was also obtained by treatment of 2-methoxy-D^+I^- with Raney Nickel (14) and as a byproduct in the treatment of 2-methoxy-D^+I^- with various Grignard reagents (15) as described below for 3,3'-dimethoxy-DD.

*3,3'-Dimethoxy-*N,N'*-dimethyl-9,9'-biacridanyl* (3,3'-dimethoxy-DD) was prepared from 3-methoxy-D^+I^- by a procedure modeled after that described by Grigorovskii and Simeonov for DD (14). 3-Methoxy-D^+I^- (0.28 g (8.0×10^{-4} mol)) was added to a slurry of 1 g of Raney Nickel W2 (42) that had been stirred for 15 min. The mixture was heated under reflux for 15 min during which time the solution turned yellow to colorless and a white precipitate appeared. The methanol suspension was separated from the Raney Nickel by decantation and the methanol removed under reduced pressure. Recrystallization from dimethylformamide led to 0.82 g (46%) of yellow crystalline product, mp 220–224°C. ^1H nmr ($CDCl_3$) δ: 2.91 (s, 6H, N—CH_3), 3.74 (s, 6H, OCH_3), 3.81 (s, 2H, 9-H), 6.0–7.2 (m, 14H, aromatic). In C_6D_6 the two high field peaks were again shifted upfield (to δ 2.53 and 3.35, respectively) but peaks due to the two diastereomers, if present, were not resolved. *Anal.* calcd. for $C_{30}H_{29}N_2O_2$: C 80.33, H 6.29, N 6.25; found: C 80.39, H 6.21, N 6.21. This compound was also obtained as a byproduct in the reaction of 3-methoxy-D^+I^- with several Grignard reagents. The following preparation is typical. To a suspension of 0.47 g (1.3×10^{-3} mol) of 3-methoxy-D^+I^- in 15 mL of dry ether was added 2 mL of a 2 *M* solution of *t*-butylmagnesium chloride in ether (4.0×10^{-3} mol) (Aldrich). After stirring for 4 h the excess Grignard reagent was decomposed with water, the ether solution washed with water, dried (K_2CO_3), filtered, and the ether evaporated. The solid was heated with 10 mL of absolute ethanol, dissolving the 9-*t*-butyl-3-methoxy-*N*-methylacridan and leaving the biacridanyl as a residue. Filtration and recrystallization from pyridine–methanol led to 0.080 g (27%) of 3,3'-dimethoxy-DD. All attempts to prepare this compound by reduction of 3-methoxy-D^+I^- with phenylhydrazine failed.

Kinetic measurements

Kinetics of oxidation were measured spectrophotometrically using methods and instrumentation described earlier (1, 6). Stopped flow methods were used with acceptors more reactive than CA. In reaction of DD with six of the oxidants the formation of D^+ was followed at 357 nm (BQ, CA, TCNE, DCBQ, $Co(bipy)_3^{3+}$) or at 420 nm (DClBQ, CA, DCBQ, $Co(bipy)_3^{3+}$). The formation of the acceptor radical anion was followed for DCMTNF (440, 550, or 600 nm) (36, 43), DCNQ (520 nm) (44), DCMTENF (550 nm) (45), TCNQ (680 nm) (46) and DCNNQ (520 nm) (47). Oxidation of 2,2'- and 3,3'-dimethoxy-DD by CA and $Co(bipy)_3^{3+}$) was followed at the 2- and 3-methoxy-D^+ absorption at 367 nm. Measurements were carried out under pseudo first-order conditions using a 30-fold or greater excess of oxidant over DD, except with some of the CA, TCNE, and TCNQ rates where a second-order analysis (1) was used. Both first-order and second-order plots were linear through at least 85% reaction. Final absorbances were constant for 10–20 half-lives with all acceptors except DCMTNF and DClBQ. The absorbance due to $DCMTNF^{\cdot-}$ reached a maximum after 6 to 8 half-lives, thereafter decreasing approximately linearly with time. Experimental final absorbance readings were corrected for this decrease; these corrections led to an increase of 0–2% in k. With DClBQ final absorbances continued to increase slowly after 10 half-lives due to instability of the acceptor and possibly its reduction product. While uncertainties in final absorbances (±1–3%) due to this source contributed to some of the scatter in the rate constants for DClBQ, we do not believe this to be the sole source of error.

Rates of radiochemical exchange of D^+ with DD were measured using DD labeled at the N—CH_3 position with ^{14}C. A 25.0 mL volume of solution containing D^+I^- (ca. 4×10^{-3} *M*) and labeled DD (ca. 8×10^{-5} *M*) in dry AN was maintained at 25°C. Aliquots (1.0 mL) were withdrawn at measured intervals and quenched by addition to a separatory funnel containing 8.0 mL of toluene and 50 mL of water. The toluene layer was extracted three times with 50 mL portions of water to remove D^+I^- and AN and then dried over K_2CO_3. A 5.0 mL aliquot of the dried toluene solution was mixed with 10.0 mL of PPO/POPOP scintillation cocktail (Fisher ScintiPrep 2 diluted 24:1 with toluene) and counted. The sample radioactivity decreased with time. The reported second-order rate constant is the pseudo first-order rate constant obtained in the usual way divided by the D^+I^- concentration.

Product isolations

$D^+ClO_4^-$ was isolated in yields of 90% or greater in oxidation of DD with CA, DCBQ, DDQ, DCNQ, DCNNQ, TCNE, TCNQ, DCMTNF, and DCMTENF as described earlier (1, 6).

Acknowledgements

Financial support from the Natural Sciences and Engineering Research Council of Canada is gratefully acknowledged. We wish to thank R. J. Balahura for use of stopped flow equipment.

1. A. K. Colter, C. C. Lai, T. W. Williamson, and R. E. Berry. Can. J. Chem. **61**, 2544 (1983).
2. M. F. Powell and T. C. Bruice. J. Am. Chem. Soc. **105**, 7139 (1983).
3. T. Okamoto, A. Ohno, and S. Oka. Bull. Chem. Soc. Jpn. **53**, 330 (1980).
4. B. W. Carlson and L. L. Miller. J. Am. Chem. Soc. **105**, 7453 (1983).
5. A. K. Colter, P. Plank, J. P. Bergsma, R. Lahti, A. A. Quesnel, and A. G. Parsons. Can. J. Chem. **62**, 1780 (1984).
6. A. K. Colter, G. Saito, and F. J. Sharom. Can. J. Chem. **55**, 2741 (1977).
7. A. Albert and G. Catterall. J. Chem. Soc. 4657 (1965).
8. H. Decker and W. Petsch. J. Prakt. Chem. **143**, 211 (1935).
9. (*a*) H. Decker and G. Dunant. Chem. Ber. 1176 (1909); (*b*) A. Albert. The acridines. Edward Arnold, Inc., London. 1966. p. 394.
10. K. Wallenfels and M. Gellrich. Chem. Ber. **92**, 1406 (1959).
11. A. L. Underwood and R. W. Burnett. *In* Electroanalytical Chemistry. *Edited by* A. J. Bard. Marcel Dekker, Inc., New York, NY. 1973. p. 1.
12. C. O. Schmakel, K. S. V. Santhanam, and P. J. Elving. J. Am. Chem. Soc. **97**, 5083 (1975).
13. O. N. Chupakhin, V. L. Rusinov, and I. Ya. Postovskii.

Khim. Geterotsikl. Soedin. 284 (1972). Chem. Abstr. **76**, 140463x (1972).
14. A. M. GRIGOROVSKII and A. SIMEONOV. Zhur. Obschchei Khim. **21**, 589 (1951).
15. W. L. SEMON and D. CRAIG. J. Am. Chem. Soc. **58**, 1278 (1936).
16. R. FOSTER. Organic charge-transfer complexes. Academic Press, New York, NY. 1969. Chapt. 3.
17. E. S. PYSH and N. C. YANG. J. Am. Chem. Soc. **85**, 2124 (1963).
18. (*a*) J. W. VERHOEVEN and P. PASMAN. Tetrahedron, **37**, 943 (1981); (*b*) M. N. PADDON-ROW. Acc. Chem. Res. **15**, 245 (1982).
19. J. PREUSS, A. GIEREN, W. HOPPE, and V. ZANKER. Ann. 221 (1973).
20. (*a*) D. A. DOUGHERTY, H. B. SCHLEGEL, and K. MISLOW. Tetrahedron, **34**, 1441 (1978); (*b*) E. OSAWA, P. M. IVANOV, and C. JAIME. J. Org. Chem. **48**, 3990 (1983).
21. M. E. PEOVER. J. Chem. Soc. 4540 (1962).
22. T. P. MUKHERJEE. Tetrahedron, **24**, 721 (1968).
23. S. CHATTERJEE. J. Chem. Soc. B, 2194 (1971).
24. M. E. PEOVER. Trans. Faraday Soc. **58**, 2370 (1962).
25. R. M. SCRIBNER. J. Org. Chem. **31**, 3671 (1966).
26. N. TANAKA and Y. SATO. Bull. Chem. Soc. Jpn. **41**, 2059 (1968).
27. E. G. JANZEN. Acc. Chem. Res. **4**, 31 (1971).
28. C. C. LAI and A. K. COLTER. J. Chem. Soc. Chem. Commun. 1115 (1980).
29. R. W. BENNETT, D. L. WHARRY, and T. H. KOCH. J. Am. Chem. Soc. **102**, 2345 (1980).
30. J. HERNOLIN, M. LEVIN, and E. M. KOSOWER. J. Am. Chem. Soc. **103**, 4801 (1981).
31. L. EBERSON. *In* Advances in physical-organic chemistry. *Edited by* V. Gold and D. Bethell. Academic Press, Inc., London. 1982. p. 79.
32. D. REHM and A. WELLER. Ber. Bunsenges. Phys. Chem. **73**, 834 (1969).
33. (*a*) K. A. CONNORS, M. H. INFELD, and B. J. KLINE. J. Am. Chem. Soc. **91**, 3597 (1969); (*b*) A. K. COLTER, A. L. MCKENNA, III, and M. A. KASEM. Can. J. Chem. **52**, 3748 (1974).
34. F. SCANDOLA, V. BALZANI, and G. B. SCHUSTER. J. Am. Chem. Soc. **103**, 2519 (1981).
35. W. H. SAUNDERS, JR., and A. F. COCKERILL. Mechanisms of elimination reactions. John Wiley and Sons, New York, NY. 1972. p. 85.
36. T. K. MUKHERJEE and L. A. LEVASSEUR. J. Org. Chem. **30**, 644 (1965).
37. T. K. MUKHERJEE. J. Phys. Chem. **70**, 3848 (1966).
38. G. A. REYNOLDS and J. A. VAN ALLAN. J. Org. Chem. **29**, 3591 (1964).
39. K. WALLENFELS, G. BACHMANN, D. HOFMANN, and R. KERN. Tetrahedron, **21**, 2239 (1965).
40. A. CALDER, A. R. FORRESTER, and S. P. HEPBURN. Org. Synth. **52**, 77 (1972).
41. F. MADER and V. ZANKER. Chem. Ber. **97**, 2418 (1964).
42. R. MOZINGO. Org. Synth. Coll. Vol. III, 183 (1955).
43. Y. MATSUNAGA and Y. YOSHIDA. Bull. Chem. Soc. Jpn. **51**, 1547 (1978).
44. Y. IIDA. Bull. Chem. Soc. Jpn. **45**, 624 (1972).
45. J. DUPUIS and J. NÉEL. C. R. Acad. Sci., Paris, Ser. C. **265**, 557 (1969).
46. A. YAMAGISHI and M. SAKAMOTO. Bull. Chem. Soc. Jpn. **47**, 2152 (1974).
47. G. SAITO and A. K. COLTER. Tetrahedron Lett. 3325 (1977).

Enzymes in organic synthesis. 33.[1] Stereoselective pig liver esterase-catalyzed hydrolyses of *meso* cyclopentyl-, tetrahydrofuranyl-, and tetrahydrothiophenyl-1,3-diesters

J. BRYAN JONES, R. SCOTT HINKS, AND PHILIP G. HULTIN
Department of Chemistry, University of Toronto, Toronto, Ont., Canada M5S 1A1

Received May 15, 1984

This paper is dedicated to Professor Adrian G. Brook on the occasion of his 60th birthday

J. BRYAN JONES, R. SCOTT HINKS, and PHILIP G. HULTIN. Can. J. Chem. **63**, 452 (1985).

Preparative-scale pig liver esterase-catalyzed hydrolyses of five-membered ring *meso*-1,3-diesters are enantiotopically selective. While pro-*S* enantiotopic selectivity is exhibited in each case, the absolute configuration sense of the hydrolysis in the cyclopentyl series is opposite to that of both the tetrahydrofuranyl and tetrahydrothiophenyl diesters. The enantiomeric excess levels induced are in the 34–46% range.

J. BRYAN JONES, R. SCOTT HINKS et PHILIP G. HULTIN. Can. J. Chem. **63**, 452 (1985).

Les hydrolyses préparatives, catalysées par l'estérase du foie de cochon, de *méso*-diesters-1,3 incorporés dans des cycles à cinq chaînons sont énantiosélectives. Même si on observe une énantiosélectivité pro-*S* dans chaque cas, le sens de la configuration absolue de l'hydrolyse obtenu en série cyclopentanique est l'inverse de celui observé avec des diesters tant tétrahydrofurannique que tétrahydrothiophénique. Les niveaux d'excès énantiomériques induits sont de l'ordre de 34 à 46%.

[Traduit par le journal]

The asymmetric synthetic opportunities provided by the abilities of enzymes to discriminate between enantiotopic groups of symmetrical substrates such as *meso* compounds are now widely recognized (2). Alcohol dehydrogenases (3) and esterases (4) have already proven particularly valuable in this regard. Of these two enzyme groups, esterases are the more convenient to use because they do not require expensive coenzymes.

One of the synthetically most useful hydrolytic enzymes reported so far is pig liver esterase (PLE). PLE is a commercially available enzyme that is capable of effecting stereospecific hydrolyses on a broad structural range of ester substrates (4, 5). Its asymmetric synthetic potential is receiving increasing attention and recently several stereospecific PLE-mediated transformations of acyclic and cyclic 1,2-diesters to useful chiral synthons have been documented (4). We now report that PLE-catalyzed hydrolyses of the monocyclic *meso*-1,3-diesters **1–3** also proceed with considerable enantiotopic stereoselectivity.

Results

The *cis* diester substrates **1–3** were prepared by Fischer esterification of the corresponding anhydrides, obtained by literature methods (6, 7*a*, 8). In the case of **1** and **2**, a methanol esterification procedure was used to give the acid-esters (±)-**4** and (±)-**5**. These were then transformed into **1** and **2** respectively by treatment with diazomethane. For **3**, direct Fischer esterification of the anhydride was performed.

Each of the *cis* diesters was a substrate of the enzyme. The rates of PLE-catalyzed hydrolyses were assayed using ethyl butyrate as the reference substrate (9). Diesters **1** and **3** were excellent substrates, with rates of hydrolysis 51% and 35% respectively of that of the ethyl butyrate standard. Although **2** was hydrolyzed more slowly, with a rate of 3% that of the standard, it remained an excellent candidate for a preparative-scale reaction.[2]

Preparative-scale hydrolyses of **1–3** were performed in aqueous solution at room temperature (20°C) on up to 20 mmole of substrate using up to 100 units of PLE per mmole of substrate. The pH was maintained at 7.0 by pH-stat-controlled addition of 0.4 *M* sodium hydroxide. The reactions were terminated after the addition of 1 equivalent of base. The acid-esters **4–6** were isolated without difficulty. Their reductions to the corresponding hydroxyesters **7–9** also proceeded smoothly. The results are summarized in Scheme 1. On treatment with acid, the alcohol esters **7** and **8** lactonized readily to give **10** and **11** respectively. In contrast, the thiophenyl derivative **9** could not be induced to form the corresponding lactone.

The enantiomeric excesses(ee's) of the chiral products in the carbocyclic and tetrahydrofuranyl series were determined on the hydroxyesters **7** and **8**. Treatment of **7** and **8** with (+)-(*R*,*R*)-2,3-butanediol afforded the orthoesters **12** and **13**,

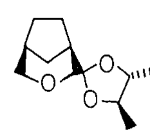

12

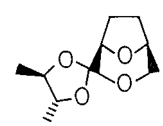

13

whose diastereomeric ratios were determined by glc analysis (10). The orthoesters obtained from (±)-**7** and (±)-**8** were used as reference standards. For the tetrahydrothiophenyl compounds, it was found more convenient to establish the enantiomeric excess of the series by ^{1}H nmr spectroscopic examination of the methoxyl protons of the acid ester **6** in the presence of (−)-(*S*)-1-methylbenzylamine (4*e*). For the (+)-**6** sample used as the reference, a $\Delta\Delta\delta$ value of 0.018 ppm was observed at 200 MHz. The ee values obtained are recorded in Scheme 1.

The absolute configurations of the Scheme 1 compounds were established by their conversions to known compounds. In the carbocyclic series, the (+)-enantiomer of **10** was available for direct comparison (3*a*). The furanyl hydroxyester (−)-**8** and the thiophenyl acid ester (+)-**6** were converted to the known (12) (+)-*trans* diol **14** and diacid **16** respectively, as summarized in Scheme 2. The *meso* diol **15** and *meso* diacid **17**

[1] For Part 32, see ref. 1.
[2] We currently consider that any substrate hydrolyzed at a rate ≤ 0.02% of that of ethyl butyrate will give good results in preparative-scale hydrolyses.

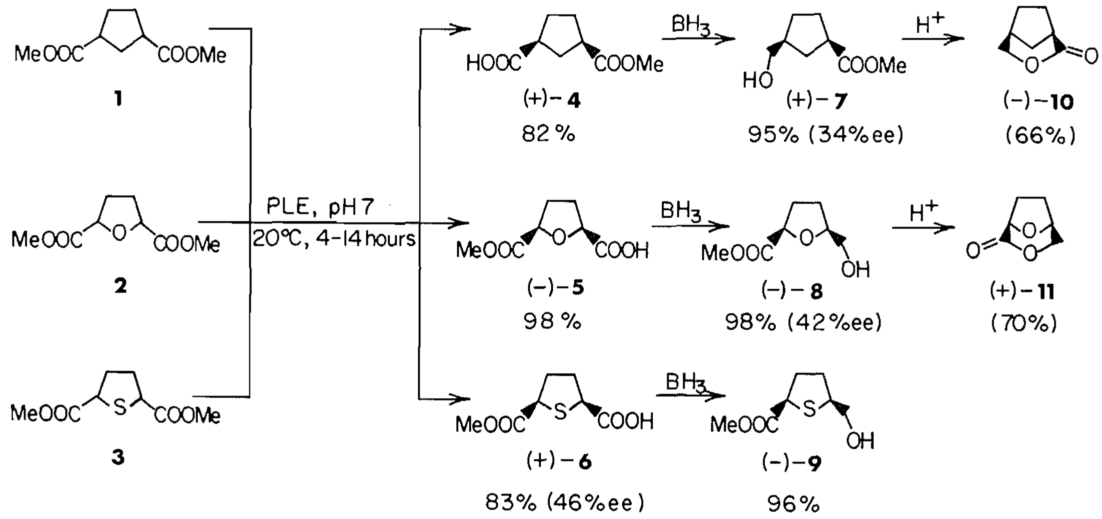

SCHEME 1

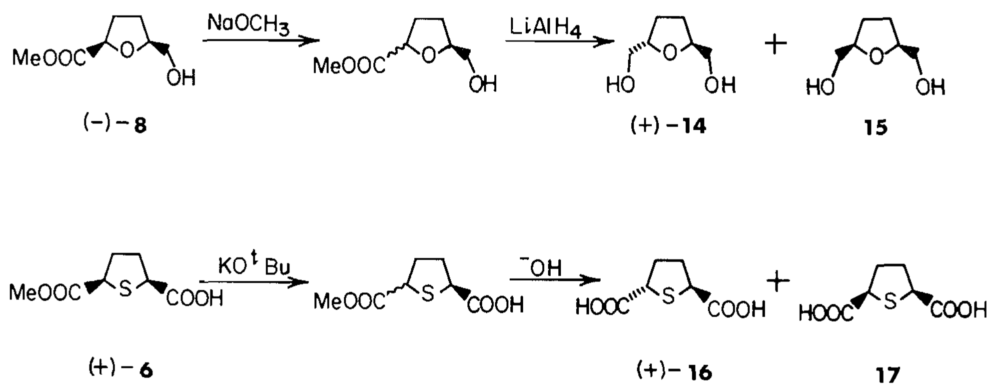

SCHEME 2

by-products of the correlation reactions do not affect the absolute configuration assignments since they are optically inactive.

Discussion

The preparations of the substrates **1–3** and of the racemic reference compounds (±)-**4–9** were straightforward. While use of a pH-stat is convenient for assaying the relative rates of hydrolysis of **1–3**, pH-stat control of the preparative-scale reactions is not essential. The use of a buffer, or of pH control via periodic burette-addition of base, is quite satisfactory. The reaction has a built-in fail-safe control in that the pH falls as the hydrolysis proceeds, thereby automatically switching off the reaction if it is left unattended for too long.

The hydrolyses were performed at pH 7. At this pH, the concurrent chemical hydrolysis that can reduce the ee levels in pH 8 reactions (4, 5) is avoided. The enzyme also appears to be intrinsically more stereospecific at lower pH (5*d*) and the ee levels of the Scheme 1 reactions could be significantly higher for pH <7 reactions.

Also, since one enantiotopic group is hydrolyzed faster than the other, allowing the reaction to proceed beyond the point at which one ester equivalent is hydrolyzed should progressively increase the ee of the acid ester that remains (13). The fact that the pH-stat curves for the hydrolyses of **1–3** show a sharp reduction in rate after one ester equivalent has been hydrolyzed augurs well for this approach. These aspects are being evaluated.

Chiral acid-ester products such as **4–6** are valuable synthetic intermediates since they may be converted to either enantiomer of hydroxyesters **7–9** or lactones **10** and **11** by appropriate choice of reducing agent. In this study, only the borane-mediated carboxyl reductions were performed. Preparations of the opposite enantiomeric series via the complementary selective lithium borohydride reductions of the carbomethoxy functions of **4–6** should present no problem (4, 5).

The reluctance of the thiophenyl hydroxyester **9** to undergo lactonization under a variety of acidic conditions was surprising, particularly since the corresponding anhydride required for the synthesis of **3** was readily formed.[3] The sulfur atom is clearly exerting an unusual effect here, since sulfur is easily accommodated in other bridged bicyclic structures (14).

As Scheme 1 shows, the absolute configuration sense of the enantiotopically selective PLE-catalyzed hydrolyses of **1–3** changes, with that of the **1** → (−)-**4** reaction being opposite to those of the **2** → (−)-**5** and **3** → (+)-**6** hydrolyses.[4] A reversal of enzymic stereospecificity dictated only by the presence or

[3] Reduction of the anhydride with sodium borohydride afforded the expected acid-alcohol, but this also failed to lactonize under a variety of acidic conditions.

[4] Due to the selection rules of the Cahn–Ingold–Prelog system, while (−)-**5** and (+)-**6** are of opposite absolute configuration type to (+)-**4**, the hydrolyses of each of **1–3** proceed with a pro-*S* ester preference.

absence of a heteroatom has not, to our knowledge, been observed before. PLE is clearly remarkable with regard to its penchant for inducing unusual switches of stereospecificity within related series of substrates (4*g*). The factors controlling such reversals are being investigated. The substrate orientation model proposed recently (4*d*) does not enable such stereospecificity reversals to be interpreted.

Experimental

Pig liver esterase (EC 3.1.1.1, Sigma Type I) was obtained from Sigma Chemical Co. All enzymic reactions were monitored using a Radiometer RTS 822 pH-stat. The ^{1}H nmr spectra were recorded on Varian T60 or XL 200 instruments and ^{13}C nmr spectra on a Varian CFT-20 spectrometer. The ir spectra were recorded on a Nicolet 5DX FT-IR system, optical rotations on a Perkin–Elmer 141 polarimeter, and glc analyses on a Hewlett–Packard HP 57/019 chromatograph using a methylsilicone capillary column at 11 psi (1 psi = 6.9 kPa) and 100°C.

cis-1,3-Dicarbomethoxycyclopentane (1)

cis-Cyclopentane-1,3-dicarboxylic acid anhydride (0.34 g, 2.5 mmol, prepared by the method of Carleer *et al.* (6)) was refluxed in dry MeOH (20 mL) for 3 h and then rotoevaporated. Kugelrohr distillation yielded (±)-*cis*-carbomethoxycyclopentane carboxylic acid ((±)-**4**, 0.42 g, 99% yield), bp 80°C/0.05 Torr (1 Torr = 133.3 Pa); ir (film) ν: 1735, 1705 cm^{-1}; ^{1}H nmr ($CDCl_3$) δ: 1.87–2.40 (6H, m), 2.50–3.10 (2H, m), 3.72 (3H, s), and 11.76 (1H, s) ppm. This monoester (0.41 g, 2.4 mmol) in ether (20 mL) was esterified with diazomethane to give *cis*-1,3-dicarbomethoxycyclopentane (**1**, 0.46 g, 97% yield), bp 70°C/0.05 Torr (lit. (6) bp 130°C/25 Torr); ir (film) ν: 1732 cm^{-1}; ^{1}H nmr ($CDCl_3$) (lit. (15)) δ: 1.90–2.32 (6H, m), 2.60–3.10 (2H, m), and 3.70 (6H, s) ppm; ^{13}C nmr ($CDCl_3$) δ: 28.60 (t), 32.83 (t), 43.21 (d), 51.05 (q), and 174.94 (s) ppm.

cis-2,5-Dicarbomethoxytetrahydrofuran (2)

cis-Tetrahydrofuran-2,6-dicarboxylic acid anhydride (3.03 g, 21.3 mmol, prepared by the method of Moore and Kelly (7*a*)) was refluxed in dry MeOH (10 mL) for 1 min and rotoevaporated to give (±)-*cis*-5-carbomethoxytetrahydrofuran-2-carboxylic acid ((±)-**5**, 3.71 g, 99%), bp 100°/0.15 Torr; ir (film) ν: 1761, 1720 cm^{-1}; ^{1}H nmr ($CDCl_3$) δ: 2.0–2.6 (4H, m), 3.86 (3H, s), 4.5–4.9 (2H, m), and 10.42 (1H, br s) ppm; ^{13}C nmr ($CDCl_3$) δ: 29.00 (t), 29.67 (t), 52.52 (q), 77.76 (d), 172.79 (s), and 175.76 (s) ppm. This monoester (3.94 g, 22.6 mmol) was esterified with diazomethane as above to give *cis*-2,5-dicarbomethoxytetrahydrofuran (**2**, 4.16 g, 98% yield), bp 70°C/0.05 Torr (lit. (16) bp 81–83°C/0.1 Torr); ir (film) ν: 1738 cm^{-1}; ^{1}H nmr ($CDCl_3$) δ: 2.23 (4H, m), 3.76 (6H, s), and 4.56 (2H, m); ^{13}C nmr δ: 28.10 ($CDCl_3$) δ: (t), 50.87 (q), 77.20 (d), and 171.09 (s) ppm.

cis-2,5-Dicarbomethoxytetrahydrothiophene (3)

cis-Tetrahydrothiophene-2,5-dicarboxylic acid anhydride (1.5 g, 9.5 mmol, prepared by the method of Horak (17)) was esterified for 21 h at 20°C with HCl-saturated MeOH (125 mL) containing triethyl orthoformate (1 mL, 9 mmol). The solution was rotoevaporated and saturated aqueous $NaHCO_3$ (100 mL) added. Extraction with CH_2Cl_2 (6 × 150 mL) followed by rotoevaporation of the dried ($MgSO_4$) extracts and Kugelrohr distillation afforded *cis*-2,5-dicarbomethoxytetrahydrothiophene (**3**, 1.34 g, 69% yield), bp 90°C/0.03 Torr (lit. (18) bp 70°C/0.1 Torr); ir (film) ν: 1740 cm^{-1}; ^{1}H nmr ($CDCl_3$) δ: 1.83–2.80 (4H, m), 3.70 (6H, s), and 4.03 (2H, m) ppm; ^{13}C nmr ($CDCl_3$) δ: 33.10 (t), 48.89 (d), 52.47 (q), and 172.55 (s) ppm.

(±)-cis-5-Carbomethoxytetrahydrothiophene-2-carboxylic acid ((±)-6)

This reference compound was prepared as described for (±)-**4** and -**5** above from *cis*-tetrahydrothiophene-2,6-dicarboxylic acid anhydride (103 mg, 0.65 mmol, obtained by the method of Della and Kendall (18)). The acid-ester (±)-**6** (105 mg, 85% yield) had bp 95°C/0.1 Torr, mp 61–63°C (lit. (18) mp 50–53°C); ir (film) ν: 3500–2400, 1739, 1712 cm^{-1}; ^{1}H nmr ($CDCl_3$) δ: 2.00–2.85 (4H, m), 3.75 (3H, s), 4.00–4.20 (2H, m), and 11.28 (1H, s) ppm.

Relative rates of PLE-catalyzed hydrolyses of meso *diesters 1–3*

The assays were performed at pH 7.0 at 20°C on 10-mL aliquots of 0.1 *M* aqueous KCl 1–2 m*M* in substrate diester. The reaction was initiated by the addition of 1 unit of PLE. The uptake of 0.02 *M* aqueous NaOH as each hydrolysis proceeded was monitored using a pH-stat. As a standard reference, the rate of ethyl butyrate hydrolysis under the same conditions was performed for each substrate. The initial rates of hydrolyses of **1**, **2**, and **3**, relative to ethyl butyrate = 100, were found to be 51, 3, and 35 respectively.

Preparative-scale PLE-catalyzed hydrolyses of meso *diesters 1–3*

(a) *Of* cis-*1,3-dicarbomethoxycyclopentane (1)*

The diester **1** (0.56 g, 3 mmol) was suspended in 0.1 *M* aqueous KCl (50 mL) at room temperature (20°C) and the mixture adjusted to pH 7.0. PLE (90 units) was added and the pH maintained at 7.0 by the addition of 0.4 *M* aqueous NaOH (via a burette or pH-stat). The reaction slowed down, but did not stop, after the addition of 1 equiv. of base and was terminated after 1.06 equiv. of NaOH had been added (4 h). The mixture was first extracted at pH 7.0 with ether (75 mL) to remove unchanged diester and then acidified to pH 2.0 with 12 *M* hydrochloric acid. Re-extraction with ether (5 × 75 mL) followed by rotoevaporation of the dried ($MgSO_4$) ether extracts afforded an oil (0.5 g) which was Kugelrohr-distilled twice to remove diacid and yielded (+)-*cis*-(1*S*,3*R*)-3-carbomethoxycyclopentane carboxylic acid ((±)-**4**, 0.43 g, 82% yield), bp 80°C/0.06 Torr; $[\alpha]_D^{25}$ +0.2° (*c* 3.5, $CHCl_3$); ir and ^{1}H nmr spectra identical with those of (±)-material above.

(b) *Of* cis-*2,5-dicarbomethoxytetrahydrofuran (2)*

The above procedure was followed using diester **2** (3.54 g, 18.8 mmol) and PLE (1050 units). The reaction was terminated after the addition of 1.1 equiv. of base (12 h). In this case the product was extracted from the pH 2 solution with CH_2Cl_2 (10 × 75 mL). The (−)-(2*S*,5*R*)-*cis*-5-carbomethoxytetrahydrofuran-2-carboxylic acid ((−)-**5**, 2.77 g, 85% yield) obtained had bp 100°C/0.15 Torr; $[\alpha]_D^{25}$ −20.3° (*c* 1.4, $CHCl_3$) and ir and ^{1}H nmr spectra identical with the (±)-monoester.

(c) *Of* cis-*2,5-dicarbomethoxytetrahydrothiophene (3)*

With diester **3** (1.01 g, 4.9 mmol) and PLE (262 units) 1.03 equiv. of base was consumed in 8 h. Work-up using ether extraction gave (+)-(2*S*,5*R*)-*cis*-5-carbomethoxytetrahydrothiophene-2-carboxylic acid ((+)-**7**, 0.8 g, 83% yield, 46% ee) as a solidifying oil, bp 80°C/0.1 Torr; $[\alpha]_D^{25}$ +6.34° (*c* 1.4, $CHCl_3$); ^{1}H nmr as for (±)-**6**, ^{13}C nmr ($CDCl_3$) δ: 34.41, 34.76, 50.51, 54.05, 174.35, and 179.05 ppm.

Reductions of acid-esters 4–6 to the hydroxyesters 7–9

(a) *Of (+)-1S,3R)-cis-3-carbomethoxycyclopentanecarboxylic acid ((+)-4)*

The acid-ester ((±)-**4**, 0.31 g, 1.8 mmol) was dissolved in dry THF (5 mL) under N_2 and $BH_3 \cdot Me_2S$ (1.5 mL of 2 *M* THF solution, 3.0 mmol) added at −78°C to the stirred solution. The mixture was allowed to warm to 20°C during the 30 min and then stirred for a further 3 h at 20°C. The mixture was then cooled to −20°C and quenched slowly with stirring with 1 *M* aqueous KH_2PO_4 (5 mL). After rewarming to 20°C and stirring for 20 min more, the mixture was extracted with ether (4 × 50 mL) and the dried ($MgSO_4$) ether solution rotoevaporated. MeOH (25 mL) was added and the solution re-evaporated. The residual oil was then Kugelrohr-distilled to give (+)-*cis*-(1*R*,3*S*)-3-hydroxymethyl-1-carbomethoxycyclopentane ((±)-**7**, 0.271 g, 95% yield, 34% ee), bp 70°C/0.05 Torr; $[\alpha]_D^{25}$ +0.2° (*c* 1.6, $CHCl_3$); ir (film) ν: 3393, 1732 cm^{-1}; ^{1}H nmr ($CDCl_3$) δ: 1.3–2.4 (7H, m), 2.47 (1H, br s, OH), 2.92 (1H, m), 3.70 (3H, s), and 3.50–3.75 (2H, m); ^{13}C nmr ($CDCl_3$) δ: 28.28 (t), 29.01 (t), 32.91 (t), 42.04 (d), 43.54 (d), 51.39 (q), 66.12 (t), and 179.79 (s) ppm.

The hydroxyester (+)-**7** (150 mg, 0.9 mmol) in dry benzene (5 mL) containing toluene-*p*-sulfonic acid (5 mg) was refluxed for 2.5 h. The cooled solution was then filtered through a silica plug (5 g), and the solvent rotoevaporated. Kugelrohr distillation yielded (−)-(1*R*,5*S*)-3-oxabicyclo[3.2.1]octan-2-one ((−)-**10**, 81 mg, 66% yield), bp 80°C/0.25 Torr; $[\alpha]_D^{25}$ −1.9° (*c* 1.3, $CHCl_3$) (lit. (3*a*) (1*S*,5*R*)-enantiomer $[\alpha]_D^{25}$ +4.33° (*c* 1.5, $CHCl_3$)); ir and ^{1}H nmr spectral data identical with literature values (3*a*).

(b) *Of (−)-(2*S,5R*)-cis-5-carbomethoxytetrahydrofuran-2-carboxylic acid ((−)-5)*

The acid-ester (−)-**5** (1.33 g, 7.1 mmol) in dry THF (8 mL) was reduced with $BH_3 \cdot Me_2S$ (5.3 mL of 2 *M* THF solution, 7.1 mmol) as described above except that the reaction mixture was worked up by the dropwise addition of MeOH (5 mL) in place of KH_2PO_4.[5] The (−)-(2*R*,5*S*)-*cis*-5-hydroxymethyl-2-carbomethoxytetrahydrofuran ((−)-**8**, 1.21 g, 98% yield, 42% ee) isolated had bp 80°C/0.06 Torr (lit. (7*b*) (±) bp 50°C/0.2 Torr); $[\alpha]_D^{25}$ −9.4° (*c* 1.8, $CHCl_3$); ir (film) ν: 2463, 1734 cm^{-1}; ^{1}H nmr ($CDCl_3$) δ: 1.70–2.50 (4H, m), 3.79 (3H, s), and 3.3–4.7 (5H, m) ppm; ^{13}C nmr ($CDCl_3$) δ: 25.24 (t), 30.36 (t), 51.55 (q), 63.08 (t), 76.15 (d), 81.41 (d), and 174.50 (s) ppm. *Anal.* calcd. for $C_7H_{12}O_4$: C 52.50, H 7.55%; found: C 52.38, H 7.55%.

The hydroxyester (−)-**8** (219 mg, 1.37 mmol) was lactonized as described above for (−)-**10** to give (+)-(1*R*,5*S*)-3,8-dioxabicyclo-[3.2.1]octan-2-one ((±)-**11**, 124 mg, 70% yield), bp 80°C/0.4 Torr (lit. (7*b*) bp 45°C/0.2 Torr); $[\alpha]_D^{25}$ +1.7° (*c* 1.1, $CHCl_3$); ir (film) ν: 1755 cm^{-1}; ^{1}H nmr ($CDCl_3$) δ: 2.13 (4H, m) and 4.00–4.61 (4H, m) ppm; ^{13}C nmr ($CDCl_3$) δ: 26.03 (t), 29.96 (t), 71.29 (d), 73.74 (t), 75.19 (d), and 168.56 (s) ppm.

(c) *Of (+)-(2*S,5R*)-cis-5-carbomethoxytetrahydrothiophene-2-carboxylic acid ((+)-6)*

The acid-ester (+)-**6** (193 mg, 1.01 mmol) in dry THF (5 mL) was reduced with $BH_3 \cdot Me_2S$ (0.8 mL of 2 *M* THF solution, 1.62 mmol) as for (−)-**5** above to give (−)-(2*R*,5*S*)-*cis*-5-hydroxymethyl-2-carbomethoxytetrahydrothiophene ((−)-**9**, 172 mg, 96% yield), bp 60°C/0.05 Torr; $[\alpha]_D^{25}$ −14.5° (*c* 1, $CHCl_3$); ir (film) ν: 3416, 1733 cm^{-1}; ^{1}H nmr ($CDCl_3$) δ: 2.0–2.6 (4H, m), 3.63 (3H, m), 3.70 (3H, s), and 3.9 (2H, m) ppm; ^{13}C nmr ($CDCl_3$) δ: 32.27, 32.86, 47.81, 51.95, 52.18, 65.27, and 173.97 ppm. *Anal.* calcd. for $C_7H_{12}O_3S$: C 47.71, H 6.86; found: C 47.92, H 7.00%.

Enantiomeric excess determinations

For the cyclopentyl and tetrahydrofuran series, the ees were established by capillary column glc analysis (10) of the orthoesters **12** and **13** derived from (+)-**7** and (−)-**8** respectively, using the orthoesters from (±)-**7** and (±)-**8** as reference standards.[6]

The hydroxyester (+)-**7** (32 mg, 0.21 mmol) in benzene (15 mL) containing toluene-*p*-sulfonic acid (2 mg) and (+)-(2*R*,3*R*)-butane-2,3-diol (41 mg, 0.45 mmol) was refluxed for 12 h to give, after Kugelrohr distillation, orthoester **12** (29 mg, 72% yield), bp 70°C/0.05 Torr; ^{1}H nmr ($CDCl_3$) δ: 1.28 (6H, d, J = 6 Hz), 1.40–2.33 (8H, m), and 3.30–43.0 (4H, m) ppm; glc retention times: 7.33 min (33%), 7.52 min (67%); 34% ee.

The hydroxyester (−)-**8** (41 mg, 0.26 mmol) was similarly converted to orthoester **13** (46 mg, 88% yield), bp 70°C/0.05 Torr; ^{1}H nmr ($CDCl_3$) δ: 1.26 (3H, d, J = 6 Hz), 1.33 (3H, d, J = Hz), 2.03 (4H, m), and 3.40–4.40 (6H, m) ppm; glc retention times: 9.56 min (71%), 9.85 min (29%); 42% ee.

For the tetrahydrothiophene series, the ee was established by 200-MHz ^{1}H nmr examination of the acid-ester (+)-**6** (15 mg, 0.077 mmol) and (−)-(*S*)-1-methylbenzylamine (12 mg, 0.1 mmol) in $CDCl_3$ (0.5 mL) (4*e*). The diastereomeric methyl peaks were cleanly resolved with ΔΔδ 0.018 ppm. Integration, using the (±)-**6** spectrum as the reference standard, showed the ee to be 46 ± 4%.

Absolute configuration determinations

(a) *Of* cis-*(1*R*,3*S*)-3-hydroxymethyl-1-carbomethoxycyclopentane ((±)-7)*

The absolute configuration assignment of this compound was accomplished by its conversion to the known (3*a*) (1*R*,5*S*)-3-oxabicyclo[3.2.1]octan-2-one ((−)-**10**) described above.

(b) *Of* cis-*(2*R*,5*S*)-5-hydroxymethyl-2-carbomethoxytetrahydrofuran ((−)-8)*

The hydroxyester (−)-**8** (0.8 g, 5 mmol) in MeOH (50 mL) containing NaOMe (from Na 1.78 g, 77 mmol in MeOH (100 mL)) was refluxed for 4 h (20). The cooled mixture was then poured into 1 *M* hydrochloric acid at 0°C, and the pH adjusted to 7.0 with 1 *M* aqueous NaOH. The solution was then saturated with NaCl and extracted with ether (7 × 50 mL). The dried ($MgSO_4$) ether extracts were rotoevaporated and the residual oil Kugelrohr-distilled to give a 1 : 1 mixture of the (2*R*/*S*,5*S*)-diastereomers of **8** (0.46 g, 57% yield), bp 72°C/0.05 Torr; glc retention times: 4.65 min (55%, *cis*) and 5.10 min (45%, *trans*); ir (film) ν: 3464 (br) and 1736 cm^{-1}; ^{1}H nmr ($CDCl_3$) δ: 1.8–2.4 (4H, m), 3.76 (3H, narrowly split "singlet"), and 3.4–4.7 (5H, m) ppm; ^{13}C nmr ($CDCl_3$) *cis*-isomer, δ: 25.23, 30.57, 51.75, 63.16, 76.25, 81.57, and 174.74; *trans*-isomers, δ: 26.30, 27.75, 51.45, 63.90, 76.75, 80.57, and 173.28 ppm. This *cis*–*trans* mixture of **8** (207 mg, 1.3 mmol) in dry THF (10 mL) was added dropwise during 5 min to a refluxing suspension of $LiAlH_4$ (202 mg, 5.3 mmol) in dry THF (30 mL) under N_2. After refluxing for 1 h, the reaction was quenched with saturated aqueous Na–K tartrate (Rochelle salt, ref. 21). The mixture was then refluxed for 30 min, filtered, and the residue washed with hot THF (2 × 15 mL). The combined THF solutions were dried ($MgSO_4$), rotoevaporated, and Kugelrohr-distilled to give a mixture of the *trans*-((+)-**14**) and *cis*-(**15**)-isomers of 2,5-bis(hydroxymethyl)tetrahydrofuran (144 mg, 84% yield), bp 75°C/0.05 Torr; glc retention times: 3.04 min (45%, *trans*) and 3.20 min (55% *cis*); $[\alpha]_D^{25}$ +13.6° (*c* 1, $CHCl_3$) (lit. (11) $[\alpha]_D^{22}$ +42° (*c* 1.1, $CHCl_3$) for (+)-**14**); ir (film) ν: 3368 (br); ^{1}H nmr ($CDCl_3$) δ: 1.6–2.2 (4H, m) and 3.4–4.4 (8H, m) ppm; ^{13}C nmr ($CDCl_3$) *cis*-isomer, δ: 26.76, 64.37, and 79.93; *trans*-isomer, δ: 27.25, 64.37, and 76.92 ppm.

(c) *Of cis-(2*S,5R*)-5-carbomethoxytetrahydrothiophene-2-carboxylic acid ((+)-6)*

To the acid-ester (+)-**6** (91 mg, 0.48 mmol) and 18-crown-6 (16 mg, 0.06 mmol) in THF (5 mL) at 0°C under N_2 was added potassium *tert*-butoxide (108 mg, 0.96 mmol). The yellow suspension was stirred for 15 min at 0°C, and then for 24 h at 20°C. The mixture was then acidified to pH 2 with 1 *M* hydrochloric acid and the solvent rotoevaporated. 5% Aqueous $NaHCO_3$ (10 mL) was added and the mixture washed with CH_2Cl_2 (2 × 10 mL). The aqueous layer was acidified to pH 2 with 6 *M* hydrochloric acid and extracted with ethyl acetate (5 × 10 mL). Evaporation of the dried ($MgSO_4$) extracts gave an oil (85 mg, a mixture of methyl and *tert*-butyl acid-esters) which was refluxed with 15% aqueous NaOH (10 mL) for 30 min. Water (10 mL) was then added and the cooled solution washed with ethyl acetate (2 × 10 mL). The aqueous layer was acidified to pH 2 with 6 *M* hydrochloric acid and extracted with ethyl acetate (4 × 10 mL). Evaporation of the dried ($MgSO_4$) ethyl acetate solutions yielded (after decolorization with Norite) a mixture of *cis*-(**17**) and *trans*-((+)-**16**) 2,5-dicarboxytetrahydrothiophene (45 mg, 53% yield) as a solid, $[\alpha]_D^{25}$ +2.3° (*c* 0.9, EtOH) (lit. (12) $[\alpha]_D^{25}$ +258.5° (EtOH) for (+)-**16**).[7] A *cis*/*trans* ratio of 0.72 : 1 in this diacid was estimated by its conversion to the diester with diazomethane and examination of the 50.3-MHz ^{13}C nmr spectrum in $CDCl_3$; *cis*-isomer, δ: 32.93, 48.71, 52.46, and 172.51; *trans*-isomer, δ: 32.75, 48.28, 52.41, and 173.18 ppm.

Acknowledgements

The generous support of the Natural Sciences and En-

[5] Work-up of the (+)-**4** reduction mixture with methanol afforded a mixture of the hydroxyester (+)-**7** and the lactone (−)-**10**.

[6] ^{13}C nmr analysis (19) of **12** and **13** gave ees within 4% of th glc results.

[7] The low rotation of our sample of (+)-**16** is due to double epimerization. Less vigorous basic conditions are recommended in any future conversions of (+)-**6** to (+)-**16**.

gineering Research Council of Canada for operating funds and the award of a Scholarship (to P.G.H.), and of University of Toronto and Ontario Graduate Scholarship awards (to R.S.H.) are gratefully acknowledged.

1. J. B. JONES and C. J. FRANCIS. Can. J. Chem. **62**, 2578 (1984).
2. (*a*) A. FISCHLI. *In* Modern synthetic methods. *Edited by* R. Scheffold. Salle/Sauerlander, Frankfurt. 1980. pp. 269 *et seq.*; (*b*) J. B. JONES. *In* Enzymic and non-enzymic catalysis. *Edited by* P. Dunnill, A. Wiseman, and N. Blakeborough. Ellis Horwood/Wiley, Chichester/New York. 1980. pp. 54–83; *In* Asymmetric synthesis. Vol. 5. *Edited by* J. A. Morrison. Academic Press, New York. 1985. In press; (*c*) C.-H. WONG and G. M. WHITESIDES. Aldrichimica Acta, **16**, 27 (1983); M. A. FINDEIS and G. M. WHITESIDES. Annu. Rep. Med. Chem. **19**, 263 (1984).
3. (*a*) A. J. BRIDGES, P. S. RAMAN, G. S. Y. NG, and J. B. JONES. J. Am. Chem. Soc. **106**, 1461 (1984), and references therein; (*b*) D. R. DODDS and J. B. JONES. J. Chem. Soc. Chem. Commun. 1080 (1982); (*c*) M. NAKAZAKI, H. CHIKAMATSU, and M. TANIGUCHI. Chem. Lett. 1762 (1982).
4. (*a*) C.-S. CHEN, Y. FUJIMOTO, and C. J. SIH. J. Am. Chem. Soc. **103**, 3580 (1981); (*b*) Y. ITO, T. SHIBATA, M. ARITA, H. SAWAI, and M. OHNO. J. Am. Chem. Soc. **103**, 6739 (1981); (*c*) S. IRIUCHIJIMA, K. HASEGAWA, and G. TSUCHIHASHI. Agric. Biol. Chem. **46**, 1907 (1982); (*d*) P. MOHR, N. W.-SARCEVIC, C. TAMM, K. GAWRONSKA, and J. C. GOWRONSKI. Helv. Chim. Acta, **66**, 2501 (1983); (*e*) M. SCHNEIDER, N. ENGEL, P. HONICKE, G. HEINEMANN, and H. GORISCH. Angew. Chem. Int. Ed. Engl. **23**, 67 (1984); (*f*) H. J. GAIS and T. LIED. Angew. Chem. **96**, 143 (1984); (*g*) G. SABBIONI, M. L. SHEA, and J. B. JONES. J. Chem. Soc. Chem. Commun. 236 (1984).
5. (*a*) F.-C. HUANG, L. F. H. LEE, R. S. D. MITTAL, P. R. RAVIKUMAR, J. A. CHAN, C. J. SIH, E. CASPI, and C. R. ECK. J. Am. Chem. Soc. **97**, 4144 (1975); (*b*) M. OHNO, S. KOBAYASHI, T. IIMORI, Y.-F. WANG, and T. IZAWA. J. Am. Chem. Soc. **103**, 2405 (1981); Y.-F. WANG, T. IZAWA, S. KOBAYASHI, and M. OHNO. J. Am. Chem. Soc. **104**, 6465 (1982); (*c*) W. K. WILSON, S. B. BACA, Y. J. BARBER, T. J. SCALLEN, and C. J. MORROW. J. Org. Chem. **48**, 3960 (1983); (*d*) D. W. BROOKS and J. T. PALMER. Tetrahedron Lett. **24**, 3059 (1983); (*e*) M. SCHNEIDER, N. ENGEL, and H. BOENSMANN. Angew. Chem. Int. Ed. Engl. **23**, 66 (1984); (*f*) C. J. FRANCIS and J. B. JONES. J. Chem. Soc. Chem. Commun. 579 (1984).
6. R. CARLEER, N. HOSTEN, and M. J. O. ANTAUNIS. Bull. Soc. Chim. Belg. **87**, 709 (1978).
7. (*a*) J. A. MOORE and J. E. KELLY. Org. Prep. Proc. Int. **4**, 289 (1972); **6**, 255 (1974); (*b*) J. Polym. Sci. Polym. Lett. Ed. **13**, 333 (1975).
8. E. A. FEHNEL and G. C. OPPENLANDER. J. Am. Chem. Soc. **75**, 4660 (1953).
9. J. K. STOOPS, S. E. HAMILTON, and B. ZERNER. Can. J. Biochem. **53**, 565 (1975).
10. G. SAUCY, R. BORER, D. P. TRULLINGER, J. B. JONES, and K. P. LOK. J. Org. Chem. **42**, 3206 (1977).
11. M. NAKAZAKI, K. NAEMURA, M. MAKIMURA, T. KAWANO, and Y. OHTA. J. Org. Chem. **47**, 2429 (1982).
12. A. FREDGA. J. Prakt. Chem. **150**, 124 (1938).
13. C.-S. CHEN, Y. FUJIMOTO, G. GIRDAUKAS, and C. J. SIH. J. Am. Chem. Soc. **104**, 7294 (1982).
14. J. OHISHI, K. TSUNEOKA, S. IKEGAMI, and S. AKABOSHI. J. Org. Chem. **43**, 4013 (1978).
15. D. E. JAMES and J. K. STILLE. J. Am. Chem. Soc. **98**, 1810 (1976).
16. A. C. COPE and W. N. BAXTER. J. Am. Chem. Soc. **77**, 393 (1955).
17. V. HORAK. Chem. Listy, **44**, 34 (1950).
18. E. W. DELLA and M. KENDALL. J. Chem. Soc. Perkin Trans. 1, 2729 (1973).
19. H. HIEMSTRA and H. WYNBERG. Tetrahedron Lett. 2183 (1977).
20. G. J. FONKEN and S. SHIENTHONG. J. Org. Chem. **28**, 3435 (1963).
21. B. P. MUNDY and J. J. THEODORE. J. Am. Chem. Soc. **102**, 2005 (1980).

Experimental and theoretical shakeup studies. VI. The fluoromethanes[1]

JOHN S. TSE[2]
Chemistry Division, National Research Council of Canada, Ottawa, Ont., Canada K1A 0R9

AND

EMMANUEL PELLACH[3] AND G. MICHAEL BANCROFT
Department of Chemistry and Centre for Chemical Physics, The University of Western Ontario, London, Ont., Canada N6A 5B7

Received January 19, 1984[4]

JOHN S. TSE, EMMANUEL PELLACH, and G. MICHAEL BANCROFT. Can. J. Chem. **63**, 457 (1985).

We report the observation of satellite structures associated with the core C 1*s* and F 1*s* levels in the photoelectron spectra of CH_3F, CF_3H, and CF_4. These structures are attributed to monopole "shakeup" excitations. Qualitative assignments aided by theoretical Xα-SW calculations are presented. We found shakeup intensities in the C 1*s* spectrum of CF_4 are enhanced by barrier created by the fluorine lone pair electrons. However, this effect is less apparent in the F 1*s* core hole photoelectron spectra.

JOHN S. TSE, EMMANUEL PELLACH et G. MICHAEL BANCROFT. Can. J. Chem. **63**, 457 (1985).

Dans les spectres photoélectroniques du CH_3F, du CF_3H et du CF_4, on a observé des structures satellites associées avec les niveaux 1*s* tant du C que du F. On attribue ces structures à des excitations de "secousse". On présente des attributions qualitatives faites à l'aide de calculs théoriques Xα-SW. On a trouvé que, dans les spectres 1*s* du C du CF_4, les intensités des "secousses" sont augmentées par la barrière créée par la paire d'électrons libres de fluor. Toutefois, cet effet est moins apparent dans les spectres photoélectroniques des électrons 1*s* du F.

[Traduit par le journal]

I. Introduction

Apart from the usefulness of X-ray photoelectron spectra in providing chemical shift information on the core levels of molecules which can be correlated to their ground state electronic properties, recent studies on the satellites often associated with the core photoionization reveal the possibility of extracting information on the excited ionic states and the mode of bonding of the molecules (1). To advance the understanding of this interesting phenomenon, considerable effort has been devoted to improve experimental instrumentation and theoretical models in the last few years (2, 3). The prevailing theory suggests that these satellites are the result of many-electron relaxation processes accompanying the creation of the core hole during photoionization (1). In the photoelectron spectra, these structures usually appear as satellite bands situated on the higher binding energy region of the intense core hole photoelectron peak. For molecules with no low lying excited states (e.g. main group compounds), the satellite structure can be ascribed as simple secondary electron processes such as double ionization (shakeoff) and simultaneous monopole excitations (shakeup). A detailed description of the theory is given in a recent review article (1). Our previous experimental and theoretical studies on this subject (4−10) demonstrate that for simple molecules such as the ten-electron hydrides (5) CH_4, NH_3, and H_2O, when the valence and virtual orbitals are dominated by one central atom, the core hole spectra can be interpreted on the basis of a simple "atomic" model. Our results suggest the effect of the bonding hydrogen on the shakeup spectra is minimal. In the present work, we sought to investigate the perturbation of the shakeup pattern by systematically substituting hydrogen atoms in methane by the heavier fluorine atoms. There are several reasons for selecting the fluoromethanes in our studies. First, for neutral monomeric gas phase molecules, the complication due to intermolecular interactions on the shakeup transitions can be eliminated (3). Second, the shakeup spectrum of the parent molecule methane is well documented and any changes in the spectral pattern of fluoromethanes can be correlated with it. Third, the electronic structure of the fluoromethanes is relatively simple and theoretical molecular orbital calculations can be used to assist the assignment. Finally, substitution of hydrogen by fluorine in methane will establish a potential barrier (11, 12). This "potential wall" helps to localize the lower energy Rydberg orbitals and may, therefore, enhance shakeup transitions of these orbitals. We wish to observe this phenomenon through the analysis of intensity distributions in the core hole spectra within the fluoromethanes.

In this paper we report the results of a study on shakeup satellites on the C 1*s* and F 1*s* core level spectra of CH_3F, CHF_3, and CF_4 in the gaseous phase. In Section II, we present the details of the experimental procedure and the theoretical model. The electronic structures of the fluoromethanes are examined in Section III. Finally, in Section IV assignments of the core hole spectra are made and discussed.

II. Experimental and theoretical model

(A) Experimental

Tetrafluoromethane (Freon 14) was purchased from Matheson (99.7%) purity, trifluoromethane was purchased from PCR (99% purity), and methylfluoride from Calions Inc., (99% purity). All samples have been used directly without further purification. Core level spectra of the above mentioned compounds were measured in the gas phase on a McPherson ESCA-36 spectrometer. Duplicate spectra were obtained with MgKα and AlKα radiation sources. The observed satellite structures were found to be independent of the source of ionization used. Owing to the low intensity of the satellite structures, we had to accumulate a large number of scans covering the appropriate energy region in order to achieve good statistics. Typically 110−150 scans (~10 min per scan) were taken for the C 1*s* core level spectra and 50−70 scans were sufficient for F 1*s* core level spectra. The operating

[1]NRCC No. 23710.
[2]To whom all correspondence should be addressed.
[3]Present address: Solid State Division, Technion, Israel Institute of Technology, Haifa, Israel.
[4]Received August 15, 1984.

TABLE 1. Parameters used in Xα-SW calculations[a] (au)

Molecule	Symmetry	α_{out}[b]	R_C	R_F	R_H	R_{out}
CH_4	T_d	0.76826	1.2701	—	0.7898	2.8500
CH_3F	C_{3v}	0.75215	1.2862	1.3311	0.8095	3.9484
CHF_3	C_{3v}	0.74223	1.1942	1.3230	0.8807	3.8401
CF_4	C_{3v}	0.74171	1.1720	1.3281	—	3.8282

[a]Geometry of molecules from ref. 34.
[b]Exchange parameters for atoms from ref. 35.

pressure in the ionization chamber of the spectrometer is ca. $1-5 \times 10^{-5}$ Torr. We found that the F 1s shakeup was slightly pressure dependent indicating inelastic scattering (13). However, this pressure dependence is small compared to the reported spectra of HF and therefore should not hamper our discussion.

The photoelectron spectra were fitted with a combination Lorentzian–Gaussian function (14). The weak satellite structure was analyzed separately so that the intense main photoelectron line would not dominate the fitting procedure. For the weaker satellite peaks, in particular those at higher binding energy, there exists a significant uncertainty on the fitted peak energy and intensity.

(B) Theoretical model

To interpret the satellite structures observed in the core level spectra, it is essential to understand the electronic structure of both the ground and excited states of the molecule. We employed the Xα-SW (15) method to generate the wavefunctions of the molecules (16). The merit and accuracy of this theoretical method have been discussed in several publications (4–10). Within the sudden approximation (17), the shakeup excitation energy is given by the difference in total energy of the excited hole state with the neutral ground state (ΔSCF). An alternative method is to use Slater's "transition-state" (TS) procedure (15). The intensity of a shakeup transition is determined by the matrix element (18).

$$[1] \quad I_{n\to 1} \propto \left| \langle \Psi^{N-1}_{n \to 1} \left| a_k \right| \Psi^{N}_{0} \rangle \right|^2$$

where $\Psi^{N-1}_{n\to 1}$ is the $(n \to 1)$ shakeup state of the ion and Ψ^{N}_{0} is the ground state of the neutral molecule and a_k is the electron annihilation operator that creates a core hole in orbital k. This matrix element can be easily evaluated within the Xα-SW formalism once the wavefunctions of the ground and excited state are known (10, 19).

In the calculations of the F 1s hole states in CF_4 and CHF_3, a localized core hole scheme was adopted. In principle, the calculation of the final ionic states of a symmetrical molecule is formally equivalent within the localized (symmetry unrestricted) or delocalized (symmetry restricted) core hole approximation (20–22). The fluctuation of the core hole between symmetry equivalent atoms through scattering processes breaks the symmetry of the final state. This symmetry breaking lessens the restrictions governing monopole and dipole shakeup transitions. The summation over all possible excitations simply represents the response of the system to a hole localization on symmetry equivalent nuclei (23–25). However, the calculation of the relaxation shift of a delocalized hole requires a larger basis set with extensive configuration interaction. Earlier calculations on the shakeup spectra of dialkyl metal compounds showed the core hole localization scheme gave reasonably good agreement with experiments (6).

We have performed Xα-SW calculations using the touching spheres approximation on the ground and hole excited states for CH_4, CH_3F, CHF_3, and CF_4. Table 1 summarizes the symmetries and sphere parameters employed in the calculations. Partial wave expansions are truncated at l_{max} = 1(sp), 2(spd), and 3($spdf$) for the hydrogen, heavy atoms (carbon and fluorine) and outersphere, respectively. Core orbitals were never frozen during the SCF interactions. The convergence criteria used required the difference in constant potential between successive cycles be less than 0.001 Ryd.

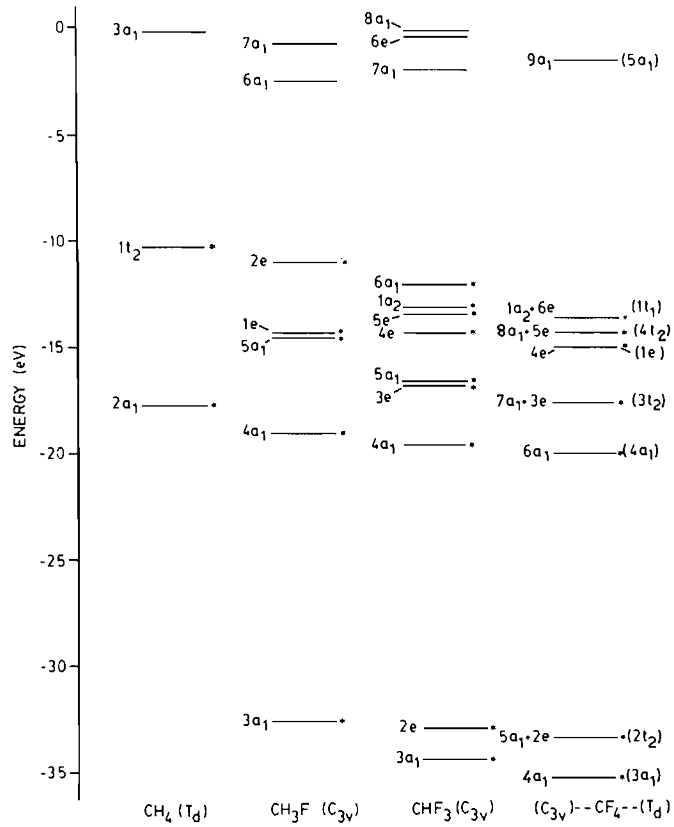

FIG. 1. Molecular orbital diagrams for CH_4, CH_3F, CHF_3, and CF_4; * indicates occupied orbitals.

III. Electronic properties of the fluoromethanes

(A) Ground state

To facilitate the discussion, we present the molecular-orbital (MO) diagram for CH_4, CH_3F, and CF_3H in the ground electronic state in Fig. 1.

We observe from the diagrams that the valence orbital energies stabilize gradually with the degree of fluorination. Our results agree very well with both the *ab initio* (27) and an earlier Xα calculation (26). The slight discrepancy between the present results and the previous calculation is due to the different parameters employed in the computations. It is gratifying that the sequence of the valence orbitals is consistent with the experimental assignments (28).

In Fig. 1 we also display the bound unoccupied orbitals found from an energy search up to −0.01 Rydberg. In contrast to our previous studies on the ten-electron hydrides (5) (e.g., CH_4), where the LUMO is mostly 3s Rydberg in character, the fluoromethanes showed a significant shift of the electron density from the outersphere region into the intersphere. However, we do not observe a concerted electron migration into the atomic sphere regions. A careful examination of the individual wavefunctions reveals the predominantly Rydberg nature of the orbitals with only a slight admixture of C—F antibonding character. The accumulation of charge inside the intersphere region in the fluoromethanes is probably an artifact owing to the larger size of the outersphere used in the calculations. We can assign the first symmetry allowed electronic transition in the partly fluorinated molecules as the σ(C—H) → 3s excitation. In the case of CF_4, this transition corresponds to the σ(C—F) → 3s excitation. The small hypsochromic shift observed experimentally (29) substantiates this assignment. In

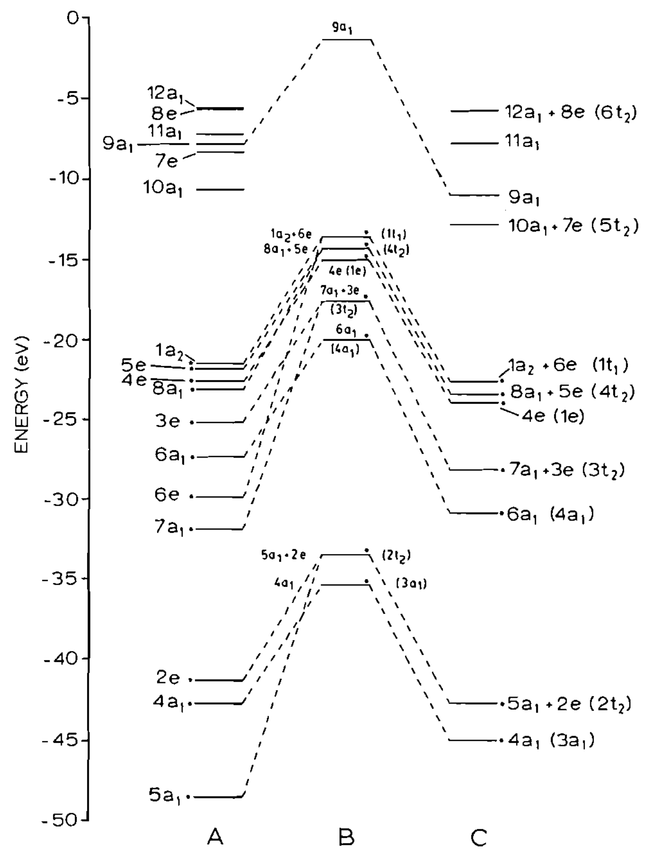

FIG. 2. Molecular orbital diagrams for CF_4: (*A*) F 3*s* hole state, (*B*) ground state, (*C*) C 1*s* hole state.

addition, the predicted order for the transition energies: CF_4 $(1t_1 \rightarrow 4a_1) > CHF_3\ (6a_1 \rightarrow 7a_1) > CH_4\ (1t_2 \rightarrow 3a_1) > CH_3F$ $(2e \rightarrow 6a_1)$ complies with the observed sequence. It is noteworthy that a HOMO-LUMO separation of ca. 8 eV in the fluoromethanes precludes the possibility of any "shakedown" processes. Therefore the most intense photoelectron line can be regarded as the primary hole state.

(B) Primary hole states

The carbon and fluorine core ionized states of the fluoromethanes were generated by removing one electron from the core 1*s* orbital from the respective atom in the molecule. Removal of the core electron from the central carbon atom retains the symmetry of the neutral molecule and therefore the carbon hole state MO diagram is relatively simple and resembles that of the ground state molecule. In the calculations of the F 1*s* hole state, we lower the molecular symmetry of CF_4 from T_d to C_{3v}, and C_{3v} to C_s in the CHF_3. Owing to computation restriction we are not able to perform calculation on the F 1*s* hole state of CF_3H. Instead, a schematic MO diagram was constructed from information obtained in CF_4 and CH_3F (for details, see Section IV). The energy of the molecular orbitals in the hole states are compared with the ground state values in Figs. 2–4 for CF_4, CHF_3, and CH_3F, respectively.

In the case of C 1*s* ionizations, we observe that there is a uniform shift (ca. 11 eV) to higher binding energies for all the valence orbitals. This shift is the result of decreased screening when an electron is removed from the core. This observation is of practical significance. Since the energy intervals between valence orbitals of a molecule do not change appreciably from the neutral ground state to the hole state, therefore, within the

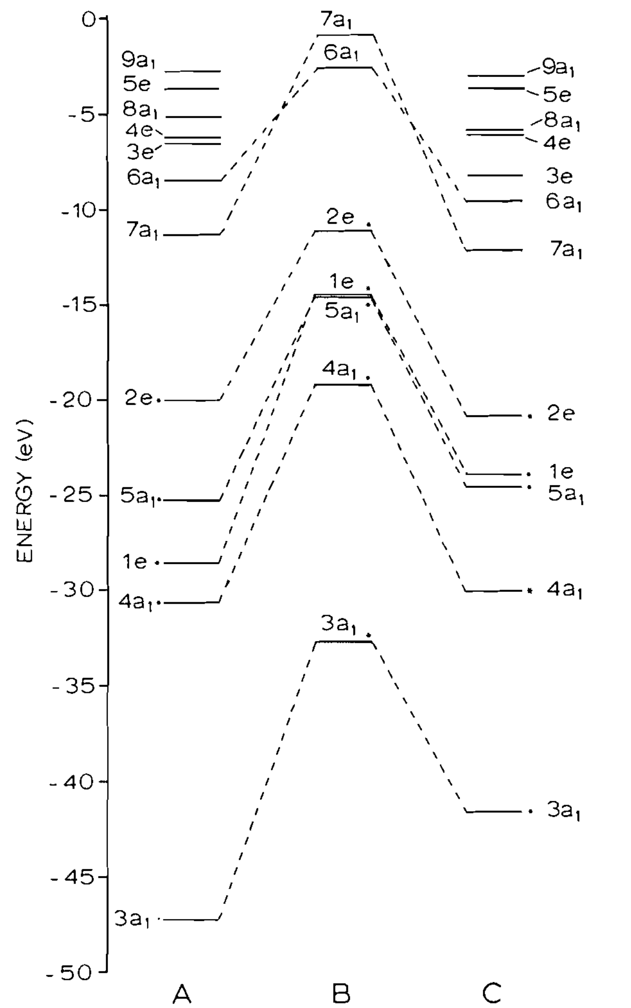

FIG. 3. Molecular orbital diagrams for CF_3H: (*A*) F 1*s* hole state, (*B*) ground state, (*C*) C 1*s* hole state.

one-electron approximation, we can correlate the shakeup transitions with the optical electron transitions (28, 29).

The lowering of molecular symmetry in the F 1*s* hole state lifts the degeneracy of the generate levels. For illustration, let us analyze the $2t_2$ orbital in CF_4 in more detail. The $2t_2$ orbital splits into the $5a_1$ and $2e$ representations in the C_{3v} symmetry of the hypothetical CF_3F^* molecule. On symmetry grounds, the charge distribution inside the fluorine spheres of each representation need not be the same anymore. In fact, the charge density of the axial fluorine (F^*) atom is concentrated in the $5a_1$ orbital and the other three equatorial fluorines atoms are evenly distributed in the $2e$ orbital (Table 2). Removal of a core electron from the axial fluorine atom produces a much larger shift of binding energy for the $5a_1$ orbital (15.2 eV) than the more remote fluorine $2e$ orbital (7.9 eV). (See Fig. 2.)

The seemingly complicated F 1*s* hole state MO diagrams can now be interpreted in a more systematic manner. For each fluorine atom in the molecule, there should be three valence orbitals associated with the lone pairs and the C—F bond pair. These orbitals will be most affected by the creation of a core hole. Electrons localized on the other atoms in the molecule will be perturbed to a lesser degree. Furthermore, if we assume the interaction between the electrons with the ionized fluorine atom is entirely electrostatic in nature, we would then expect a fairly uniform shift to higher binding energies for these or-

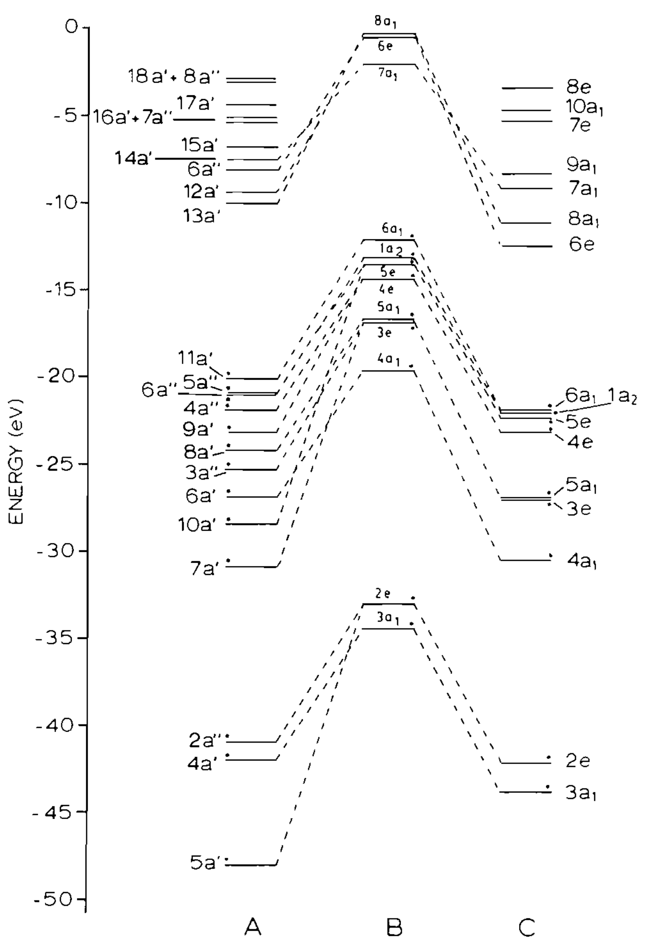

FIG. 4. Molecular orbital diagrams for CH_3F: (*A*) 1*s* hole state, (*B*) ground state, (*C*) C 1*s* hole state.

TABLE 2. Charge density distribution in the $2t_2$ orbital of CF_4 in the ground state

Orbital	Q_{out}	Q_{int}	Q_C	Q_{F^*}[a]	Q_{3F}
$5a_1$	0.039	0.331	0.054	1.180	0.395
$2e$	0.079	0.662	0.108	0.002	3.149
$2t_2$	0.118	0.993	0.162	1.182	3.544

[a]Axial fluorine.

bitals. This anticipation is in full accord with our theoretical calculations. It is quite clear from the MO diagrams, that the energy shift of the orbitals with majority F* character, such as $1e$, $7a_1$, in CH_3F, $5a'$, $7a'$, $10a'$ in CHF_3 and the $6e$ and $7a_1$, orbital in CF_4 are the most significant.

(C) The hole state unoccupied orbitals

Unlike the unoccupied orbitals in the ten electron hydrides, it was found that in fluoromethanes there is a tendency of electron migration from the outersphere region into the intersphere and atomic sphere region. Although as we have explained earlier this may be an artifact due to the larger size of the outersphere, the increase of charge density inside the atomic region cannot be overlooked. It is generally understood that the size of an antibonding orbital is not much larger than the molecular core (30). On the contrary, Rydberg type orbitals are diffuse and in most cases essentially nonbonding. Unfor-

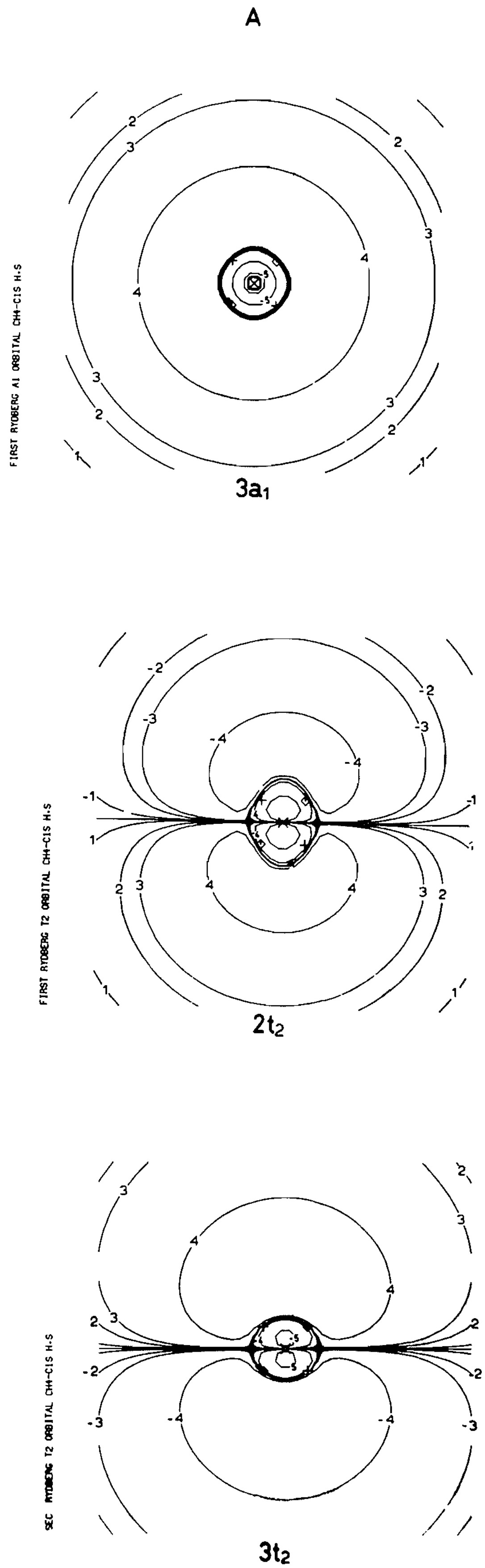

FIG. 5. Contour diagrams for the unoccupied orbitals of CH_4 in the C 1*s* hole state.

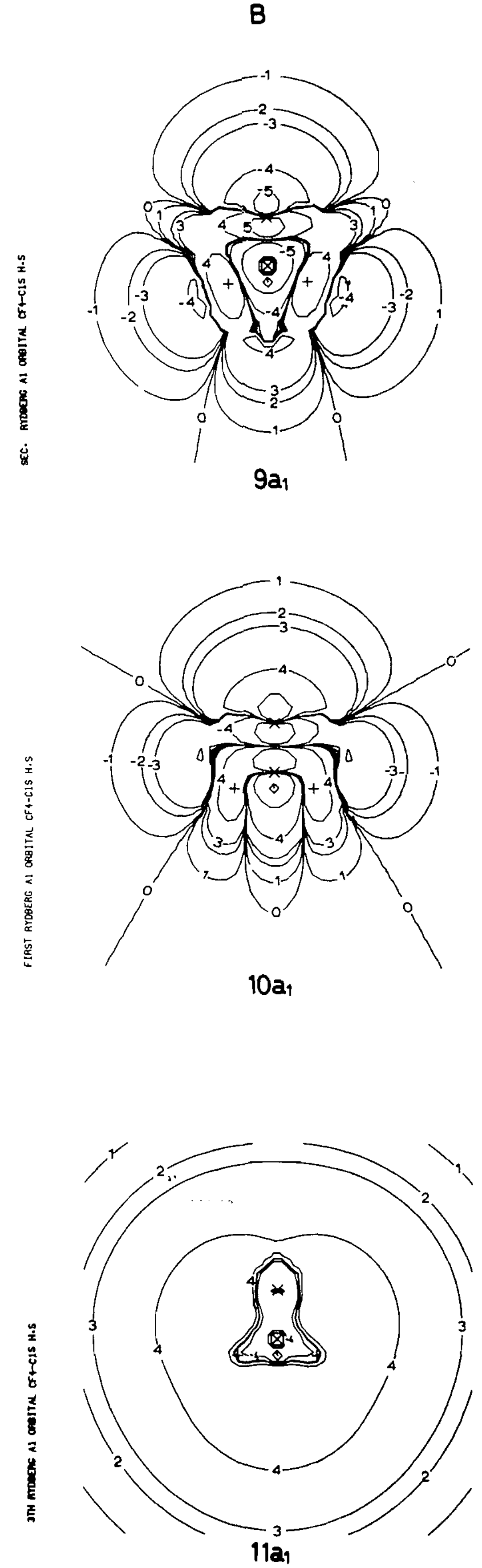

FIG. 6. Contour diagrams for the unoccupied orbitals of CF_4 in the C 1*s* hole state.

tunately, in some cases, the distinction is not so clear-cut. To avoid confusion, we define our terminology according to the orbital charge distribution in spheres as determined by the Xα-SW calculation. We define a Rydberg orbital if 50% or more of the orbital electrons are located outside the outersphere region. An orbital is regarded as having mixed Rydberg–valence character if the majority of the electrons reside within the intersphere region. Concentration of charge density inside the atomic sphere regions indicates an antibonding orbital. This way of defining orbital character of course is subject to the arbitrariness of the sphere sizes used in the calculations. To this end we present the contour drawings for some unoccupied orbitals of CH_4 and CF_4 in the C 1*s* hole state in Figs. 5 and 6. Several interesting observations emerge from this comparison. First, all the unoccupied orbitals of CH_4 retain their Rydberg character even in the core hole state. This is in contrast to the $9a_1$ and $10a_1$ orbitals of CF_4, which are obviously C—F antibonding in character in the hole state. This is also reflected in the large charge localization in the atomic spheres as tabulated in Table 3. The Rydberg character of the unoccupied orbital is more apparent as the term value of the orbital decreases.

The behaviour of the unoccupied orbitals in the fluoromethanes substantiates the presence of an inner–outer potential wall (11). The positive hole from the central carbon atom pulls the unoccupied orbitals to lower energies. These orbitals become more contracted, thus losing their diffuse character. The localization process is reinforced by the effective potential created by the peripheral nonbonding fluorine electrons which act as a repulsive barrier on the outer rim of the molecule enhancing the stability of the inner empty orbitals (12, 31, 32). Therefore, as the number of fluorine atoms increases, the orbitals become more tightly bound. The charge densities reported in Table 3 for the fluoromethanes clearly show this trend. Another important point from our calculations is that there is a change in the MO sequence of the virtual orbitals in the hole states with the exception of the CH_4 molecule. The "*p*-type" unoccupied orbitals involving strong (C—F) σ antibonding character are lowered in energy more than the "*s*-type" Rydberg orbital. This is another indication of the existence of the effective potential barrier which confines the antibonding orbitals. This interchanging of the MO order is reflected in the gradual merging of absorption peaks observed in the soft X-ray absorption carbon K-edge spectra of the fluoromethanes (33).

IV. The core-hole spectra of the fluoromethanes

The redistribution of molecular charges following the removal of a core electron is related to the core-hole relaxation and correlation. We have demonstrated previously (8) for main group compounds that the individual orbital contribution to the relaxation energy accompanying photoionization is proportional to the amount of charge reorganization within that molecular orbital, and intense shakeup transitions are expected to originate from these orbitals. In Tables 4 and 5 we tabulate the charge transfer within each orbital of the fluoromethanes when an electron is removed from the 1*s* core of the carbon atom and the fluorine atom respectively. For the C 1*s* hole states except for CF_4, the core hole is more than totally screened (total charge transfer more than one electron). We find that the $1t_2$ orbital in CH_4, the $1e$ and $2e$ orbitals in CH_3F, the $3e$ and $5a_1$ in CHF_3, and the $3t_2$ ($7a_1$ + $3e$) and $6a_1$ orbitals in CF_4 constitute most of the screening electrons. The F 1*s* core holes in the fluoromethanes are slightly less than totally screened. The most involved molecular orbitals are the $1e$ in CH_3F and $6e$ in CF_4.

TABLE 3. Charge distribution in the unoccupied orbitals of the fluoromethanes in the C 1s hole state (%)

Molecule	Orbital	Q_{out}	Q_{int}	Q_C	Q_F or Q_H	Orbital character[a]	Energy (eV)
CH_4	$3a_1$	68(s)	15	15(s)	2	Rydberg	6.87
	$2t_1$	45(d)	26	17(p)	12	Ryd. - a.b.	5.59
	$3t_2$	80(p)	14	4	1	Rydberg	4.16
CF_4	$5t_2$ { $10a_1$	2	15	42(p)	41(p)	a.b.	12.74
	$5t_2$ { $7e$	2	15	42(p)	41(p)	a.b.	12.74
	$9a_1$	2	13	32(s)	52(p)	a.b.	11.04
	$11a_1$	48(s)	47	0	5	Ryd. - a.b.	7.74
	$6t_2$ { $12a_1$	52(p)	39	1	8	Rydberg	5.79
	$6t_2$ { $8e$	52(p)	39	1	8	Rydberg	5.79

Molecule	Orbital	Q_{out}	Q_{int}	Q_C	Q_F	Q_H	Orbital character	Energy (eV)
CH_3F	$7a_1$	4	26	37(p)	33(p)	0	a.b.	11.98
	$6a_1$	28(s)	49	15(s)	3	5	Ryd. - a.b.	9.44
	$3e$	24(p)	44	21(p)	0	11	Ryd. - a.b.	8.09
	$4e$	40(p)	54	1	3	4	Ryd. - a.b.	5.94
	$8a_1$	45(p)	40	9(p)	2	3	Ryd. - a.b.	5.71
	$5e$	55(d)	39	2	3	2	Rydberg	3.56
	$9a_1$	79(s)	17	2	1	2	Rydberg	2.91
CHF_3	$6e$	2	18	41(p)	38(p)	0	a.b.	12.38
	$8a_1$	3	15	37(p)	45(p)	1	a.b.	11.03
	$7a_1$	30(s)	43	13(s)	5	8	Ryd. -a.b.	9.03
	$9a_1$	35(p)	44	8	5	8	Ryd. -a.b.	8.20
	$7e$	58(p)	35	2	6	0	Rydberg	5.20
	$10a_1$	57(s)	35	0	4	4	Rydberg	4.56
	$8e$	64(d)	31	1	3	0	Rydberg	2.32

[a]a.b. = antibonding.

(A) The C 1s satellite spectra

The satellite structures associated with the C 1s core hole spectra of the fluoromethanes are enlarged in Fig. 7. The general spectral features are very similar within this series of compounds. The satellite bands started at ca. 12.5 eV on the higher binding energy side of the primary photoline. Several prominent peaks can be resolved with the aid of computer deconvolution. Above ca. 25 eV, the satellite spectra extend into a structureless tail.

Within the independent electron model we have adopted here, the intensity of the monopole excitation is determined primarily by the overlap integral between the originating and terminating orbital. To a first approximation we expect strong satellite bands only from those orbitals having similar spatial arrangement. Examining the character of the occupied and unoccupied orbitals given in Tables 3 and 4 we anticipate the following monopole excitations, $3t_2 \rightarrow 5t_2$ in CF_4; $2e \rightarrow 3e$ and $1e \rightarrow 3e$ in CH_3F; and $3e \rightarrow 6e$ and $5a_1 \rightarrow 8a_1$ in CF_3H will be mainly responsible for the satellites. These transitions are responsible for transferring electrons from the C—F and the C—H bonds to the antibonding orbitals which are localized on the carbon centre, thus, shielding the core hole. The experimental and theoretical Xα-SW results for the C 1s hole states of the fluoromethanes are summarized in Table 6.

Because of the low resolution of the satellite spectra it is impossible for us to give an unambiguous individual assignment to each excitation. We simply group the calculated monopole transitions into bands and identify them with the structure observed in the spectra. Our assignments are mainly based on the theoretical predicted order.

The CF_4 hole state spectrum is the simplest among the fluoromethanes. The first band exists as a weak structure situated 12.26 eV from the higher binding energy side of the primary photoline. According to our calculation, this band can be assigned to the non-bonding fluorine to antibonding C—F orbital, $4t_2 \rightarrow 5t_2$ transition. Since the lone pair electrons localized on the fluorine atoms are less mobile, the amount of charge transfer will be small. The second band having a significantly larger intensity is assigned to the bonding–antibonding $3t_2 \rightarrow 5t_2$ transition which represents the major screening mechanism. The calculated intensity of 9.8% is higher than the observed value of 4.7% and the predicted energy is off by 3.0 eV. The third band centered at 23.65 eV is assigned to a combination of $5e \rightarrow 8e$ and $6a_1 \rightarrow 9a_1$ transition. The band at 26.26 eV probably is the onset of the shake off processes. The double ionization of the valence orbitals starts at 23.5 eV, and this may explain the unexpected high intensity of the bands. It should be emphasized that the calculated intensities and energies are only approximate since configuration interaction between shakeup states of the same symmetry has been ignored completely (3).

The satellite spectra of CH_3F and CF_3H are assigned in a similar fashion. The results are given in Table 6. Once again, the calculated transition energies are not in good agreement with experiments especially for the higher energy excitations in which the theory underestimates the transition energies by ca. 3 eV. Despite the complexity of the spectra and the inherent deficiency of the independent electron model, the theoretical

TABLE 4. Electronic charge distribution in the ground state and changes in the C 1s hole state of CH_4, CH_3F, CHF_3, and CF_4

(*a*) CH_4

Symmetry	Q_{out}	Q_{int}	Q_C	Q_H
$2a_1$	0.066(−0.054)	0.672(−0.102)	0.972(0.213)	0.288(−0.056)
$1t_2$	0.360(−0.353)	1.890(−0.295)	2.682(0.883)	1.072(−0.236)
Total	0.427(−0.408)	2.561(−0.398)	3.652(1.096)	1.360(−0.292)

(*b*) CF_4

Symmetry	Q_{out}	Q_{int}	Q_C	Q_{3F+F^*}
$4a_1$	0.023 (−0.007)	0.449(−0.001)	0.207 (0.078)	1.322(−0.074)
$5a_1$	0.033 (−0.006)	0.033(−0.298)	0.087 (0.033)	1.555(−0.20)
$6a_1$	0.068 (−0.017)	0.414(−0.033)	0.486 (0.129)	1.032(−0.080)
$7a_1$	0.054 (−0.017)	0.441(−0.053)	0.512 (0.238)	0.993(−0.168)
$8a_1$	0.044 (−0.018)	0.435 (0.004)	0.034(−0.010)	1.487 (0.025)
$1a_2$	0.036 (−0.009)	0.375(−0.023)	0.000 (0.0)	1.589 (0.032)
$2e$	0.0666(−0.013)	0.651(−0.011)	0.173 (0.065)	3.110(−0.040)
$3e$	0.108 (−0.035)	0.882(−0.106)	1.024 (0.476)	1.986(−0.335)
$4e$	0.086 (−0.026)	0.975(−0.072)	0.008 (0.000)	2.930 (0.098)
$5e$	0.088 (−0.036)	0.869 (0.007)	0.068(−0.020)	2.974 (0.049)
$6e$	0.072 (−0.018)	0.748(−0.047)	0.000 (0.0)	3.180 (0.065)
Total	0.678 (−0.203)	6.564(−0.336)	2.599 (0.988)	22.158(−0.448)

(*c*) CH_3F

Symmetry	Q_{out}	Q_{int}	Q_C	Q_F	Q_H
$3a_1$	0.006(−0.001)	0.384(−0.008)	0.100 (0.033)	1.508(−0.24)	0.002(−0.001)
$4a_1$	0.013(−0.012)	0.719(−0.092)	0.824 (0.213)	0.278(−0.091)	0.166(−0.018)
$5a_1$	0.024(−0.020)	0.518(−0.087)	0.572 (0.190)	0.812(−0.042)	0.073(−0.042)
$1e$	0.038(−0.025)	1.445(−0.014)	1.179 (0.785)	1.018(−0.922)	0.319 (0.147)
$2e$	0.042(−0.068)	1.053(−0.473)	0.670(−0.135)	1.972 (1.006)	0.262(−0.331)
Total	0.123(−0.126)	4.120(−0.645)	3.346 (1.087)	5.588(−0.074)	0.823(−0.242)

(*d*) CHF_3

Symmetry	Q_{out}	Q_{int}	Q_C	Q_F	Q_H
$3a_1$	0.018 (−0.005)	0.433 (0.001)	0.182 (0.068)	1.365 (0.065)	0.002 (0.001)
$4a_1$	0.043 (−0.018)	0.529(−0.029)	0.582 (0.168)	0.770(−0.129)	0.075 (0.009)
$5a_1$	0.039 (−0.023)	0.632(−0.076)	0.615 (0.337)	0.571(−0.263)	0.143 (0.025)
$6a_1$	0.039 (−0.040)	0.473(−0.107)	0.205(−0.046)	1.170 (0.342)	0.113(−0.150)
$1a_2$	0.035 (−0.009)	0.373(−0.020)	0.000 (0.00)	1.592 (0.030)	0.00 (0.00)
$2e$	0.047 (−0.009)	0.673(−0.016)	0.156 (0.054)	3.124(−0.029)	0.000 (0.000)
$3e$	0.079 (−0.029)	0.892(−0.084)	0.999 (0.448)	2.028(−0.336)	0.001 (0.000)
$4e$	0.068 (−0.023)	0.971(−0.046)	0.028(−0.009)	2.933 (0.077)	0.000 (0.000)
$5e$	0.081 (−0.030)	0.807(−0.022)	0.024(−0.008)	3.088 (0.060)	0.000 (0.000)
Total	0.499(−0.186)	5.784(−0.399)	2.791 (1.012)	16.641(−0.313)	0.334(−0.115)

predicted intensity distributions are in qualitative agreement with the experiments. Assignments above 25 eV are even more difficult and perhaps will not be too useful as the spectra are probably dominated by double ionization processes. The onset of the ionization limit for the valence electrons is predicted to occur at ca. 23 eV. The featureless tail extending from ca. 25 eV to 50 eV can be attributed to these shakeoff processes. Electron shakeoffs are the dominant relaxation processes accompanying the photoionization of a core electron (1).

The satellite spectrum of the CF_4 molecule possesses several features that are distinct from the other fluoromethanes. First, the main satellite peaks observed in CF_4 are more closely packed and their line widths are relatively smaller than in the other fluoromethanes. Second, the intensity of the extended high energy structures shakeoff tail in CF_4 is much weaker than in CH_3F and CF_3H. These two points suggests that the potential barrier concept is important in CF_4. The potential wall confines the CF_4 antibonding and low-lying Rydberg orbitals therefore reducing the energy separation between orbitals and enhancing the intensity of the excitations. By the same token, the repulsive potential restrains electron transitions to the outer diffuse Rydberg and continuum orbitals, thereby decreasing the

TABLE 5. Electron charge distribution in the ground state and changes in the F 1s hole state of CH_3F and CF_4

Symmetry	Q_{out}	Q_{int}	Q_C	Q_F^*	Q_H
			CH_3F		
$3a_1$	0.004(−0.003)	0.289(−0.103)	0.037(−0.030)	1.670 (0.138)	0.000(−0.001)
$4a_1$	0.011(−0.014)	0.423(−0.388)	0.279(−0.332)	1.258 (0.889)	0.029(−0.155)
$5a_1$	0.028(−0.016)	0.817 (0.212)	0.620 (0.238)	0.276(−0.578)	0.259 (0.144)
$1e$	0.013(−0.050)	0.705(−0.726)	0.037(−0.357)	3.238 (1.298)	0.007(−0.165)
$2e$	0.089(−0.021)	1.795 (0.269)	1.277 (0.472)	0.108(−0.858)	0.731 (0.142)
Total	0.145(−0.104)	4.029(−0.736)	2.249(−0.010)	6.550 (0.889)	1.026(−0.039)

Symmetry	Q_{out}	Q_{int}	Q_C	Q_F	Q_F^*
			CF_4		
$4a_1$	0.030 (0.000)	0.408(−0.037)	0.116(−0.013)	0.037(−0.312)	1.410 (0.362)
$5a_1$	0.025(−0.014)	0.279(−0.052)	0.049(−0.005)	1.633 (0.453)	0.014(−0.381)
$6a_1$	0.071(−0.014)	0.429(−0.018)	0.349(−0.007)	0.102(−0.176)	1.049 (0.215)
$7a_1$	0.051(−0.020)	0.314(−0.180)	0.216(−0.058)	1.320 (0.743)	0.099(−0.485)
$8a_1$	0.045(−0.017)	0.522 (0.091)	0.028(−0.016)	0.098(−0.286)	1.307 (0.229)
$1a_2$	0.040(−0.005)	0.391(−0.007)	0.0 (0.0)	0.0 (0.0)	1.570 (0.013)
$2e$	0.073(−0.006)	0.659(−0.003)	0.118 (0.010)	0.004 (0.002)	3.146(−0.003)
$3e$	0.124(+0.019)	0.858(−0.130)	0.588 (0.040)	0.146(−0.148)	2.284 (0.256)
$4e$	0.101(−0.011)	0.864(−0.183)	0.047 (0.038)	0.013(−0.695)	2.976 (0.852)
$5e$	0.090 (0.034)	0.834(−0.028)	0.024(−0.064)	0.010(−0.703)	3.042 (0.829)
$6e$	0.045(−0.045)	0.674(−0.121)	0.046 (0.046)	3.155 (1.987)	0.081(−1.866)
Total	0.694(−0.187)	6.230(−0.670)	1.580(−0.031)	6.518 (0.866)	16.977 (0.021)

TABLE 6. C 1s-shakeup energies (eV) and intensities[a] for the fluoromethanes

Molecule	Assignment	Experimental ΔE	Experimental F.W.H.M.	Experimental Int. %	Theoretical-Xα-SW $\Delta E(\Delta SCF)$	Theoretical-Xα-SW ΔE(TS)	Theoretical-Xα-SW Int. %
CH_4	$1t_2 \rightarrow 3a_1$	15.66	4.0	4			
	$1t_2 \rightarrow 2t_2$	18.91	2.3	10	16.13		15.2
	$1t_2 \rightarrow 3t_2$	22.01	3.2	2	18.17		5.9
	$1t_2 \rightarrow nt_2$	26.50					
	$2a_1 \rightarrow 3a_1$	26.89	6.0	10	22.91		3.2
	$2a_1 \rightarrow 4a_1$	34.84	6.8	5			
CH_3F	$5a_1 \rightarrow 7a_1$	13.76	4.7	8.8	12.56	12.55	2.0
	$2e \rightarrow 3e$				13.18	13.21	10.5
	$5a_1 \rightarrow 6a_1$				15.63	15.62	0.9
							13.4
	$1e \rightarrow 3e$	19.62	4.9	10.0	16.30	16.11	2.1
	$2e \rightarrow 5e$				17.99	17.99	0.9
	$4a_1 \rightarrow 7a_1$				18.10	18.09	0.8
	$1e \rightarrow 4e$				18.50	—	0.7
	$5a_1 \rightarrow 8a_1$				19.46	—	0.5
							5.0
	$4a_1 \rightarrow 6a_1$	25.58	4.0	6.4	20.72	20.71	2.5
	$5a_1 \rightarrow 9a_1$				22.71		0.3
	$4a_1 \rightarrow 8a_1$				24.58		0.1
	$2e \rightarrow \infty$[b]					>22.50	
	$1e \rightarrow \infty$					>25.0	
	$5a_1 \rightarrow \infty$					>26.0	
							2.9
	$4a_1 \rightarrow \infty$	30.14	7.3	5.2		>31.0	
	$3a_1 \rightarrow \infty$	39.39	14.2	11.0		>43.0	
CHF_3	$5e \rightarrow 6e$	12.35	2.9	3.1	10.45		0.2
	$6a_1 \rightarrow 8a_1$				10.99		0.79
	$4e \rightarrow 6e$				11.26		0.15
	$6a_1 \rightarrow 7a_1$				13.13		2.58
							3.72

TABLE 6. (*Concluded*)

Molecule	Assignment	Experimental ΔE	Experimental F.W.H.M.	Experimental Int. %	Theoretical-Xα-SW $\Delta E(\Delta SCF)$	Theoretical-Xα-SW ΔE(TS)	Theoretical-Xα-SW Int. %
	$6a_1 \to 9a_1$	17.39	5.9	8.9	14.00		0.19
	$3e \to 6e$				14.78		6.28
	$5a_1 \to 8a_1$				16.02		2.98
							9.45
	$5a_1 \to 7a_1$	21.31	2.1	4.1	18.17		1.80
	$5a_1 \to 9a_1$				19.16		0.73
							2.53
	$4a_1 \to 8a_1$	25.68	4.9	12.1	19.57		0.76
	$4a_1 \to 7a_1$				21.80		1.26
	$4a_1 \to 9a_1$				22.73		0.33
	$6a_1 \to \infty$					>23.0	
	$1a_2 \to \infty$					>23.0	
	$5e \to \infty$					>23.50	
	$4e \to \infty$					>24.0	
							2.35
	$5a_1 \to \infty$	33.43	12.0	11.1		>29.0	
	$3e_1 \to \infty$					>29.0	
	$4a_1 \to \infty$					>32.50	
	$2e \to \infty$	43.17	9.0	6.4		44.0	
	$3a_1 \to \infty$					45.50	
CF_4	$4t_2\,\{5e \to 7e$	12.26	3.0	0.7	11.13	11.05	0.8
	$8a_1 \to 10a_1\}\,5t_2$				11.20	11.17	0.8
							1.6
	$3t_2\,\{7a_1 \to 10a_1$	18.55	4.9	4.7	15.44	15.40	3.3
	$3e \to 7e\}\,5t_2$				15.44	15.40	6.5
							9.8
	$5e \to 8e$	23.65	2.5	8.7	18.00	17.96	0.7
	$6a_1 \to 9a_1$				19.78	—	2.6
							3.3
	$3e \to 8e$	26.26	3.0	7.3	22.91	22.88	0.3
	$6a_1 \to 11a_1$				23.62		0.1
	$6a_1 \to 12a_1$				25.54	25.51	0.1
	$1t_1\,\{1a_2 \to \infty$					>23.50	
	$6e \to \infty\}$					>23.50	
	$4t_2\,\{5e \to \infty$					>24.50	
	$8a_1 \to \infty$					>24.50	
	$4e \to \infty\}$					>25.0	
	$3t_2\,\{7a_1 \to \infty$					>29.5	
	$3e \to \infty$					>29.5	
	$6a_1 \to \infty\}$					>32.0	

[a]Relative to the main peak after orthogonality correction.
[b]Shake off transition.

probability of double ionizations. Furthermore, the higher molecular symmetry of the CF_4 molecule restricts the number of monopole allowed transitions resulting in a relatively simple satellite pattern as compared to CH_3F and CF_3H.

(*B*) *the F 1*s *satellite spectra*

The satellite spectra accompanying the F 1*s* core ionization of the fluoromethanes are displayed in Fig. 8. At first glance, the observed features are much simpler than in the corresponding C 1*s* hole spectra. However, this does not necessarily make the assignments easier. The lowering of molecular symmetry in the F 1*s* hole state relaxes the symmetry selection rules and more monopole transitions become allowed. The charge reorganization accompanying photoionization of a F 1*s* electron calculated in the localized hole approximation for CF_4 and CH_3F is depicted in Table 5. The screening process is not as effective as for photoionization at the carbon site. In both cases, the fluorine spheres only gain ca. 0.9 e in the relaxed hole states. A majority of the screening electrons are derived from the intersphere region indicating the C—F and C—H bonding orbitals are strongly involved in the relaxation mechanism. It is quite surprising to note that the net change in electron population in the carbon and unionized fluorine spheres does not vary appreciably. As explained above, owing to computer limitations we are not able to perform calculations on the F 1*s* hole state of CF_3H in C_s symmetry. The spectrum of this molecule was assigned by extrapolating the MO diagrams in Fig. 3 and inferring from the assignments of CF_4 and CH_3F. The theoretical and experimental results with the proposed assignments are given in Table 7.

As one might expect from the arguments presented earlier, the excitations originating from the C—H and C—F bonding

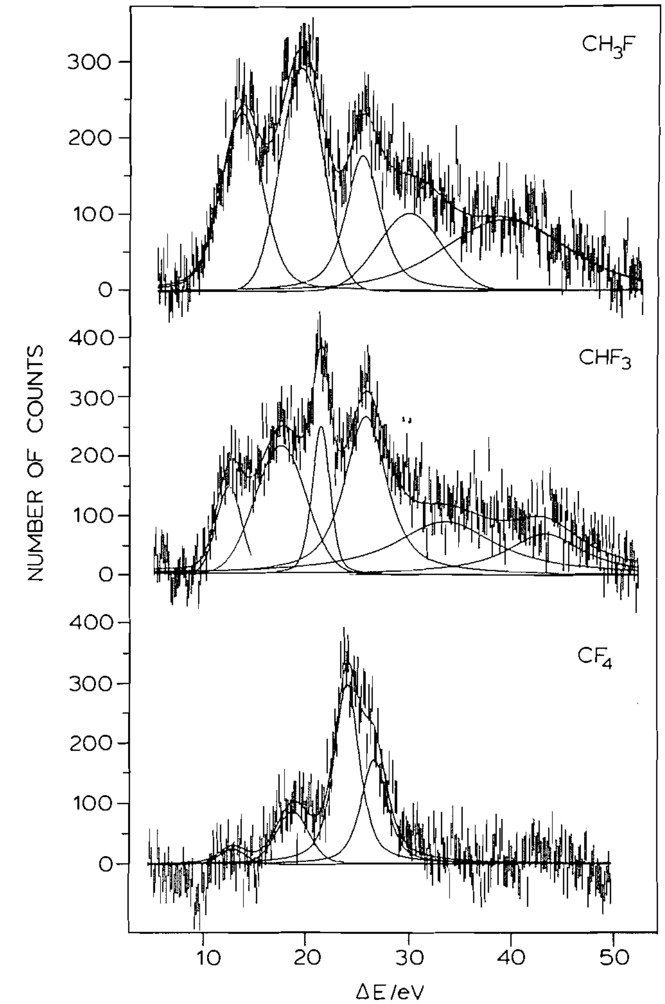

FIG. 7. C 1s satellite photoelectron spectra for CH_3F, CHF_3, and CF_4.

orbitals will give the most intense shakeups. In the case of CH_3F, the transitions from the $4a_1$ and $5a_1$ orbitals dominate the spectrum. The calculated mean excitation energy ($5a_1 \rightarrow 7a_1$ and $4a_1 \rightarrow 7a_1$) is 17.50 eV with a total intensity of 10.4% relative to the main photoline. These are in good agreement with observed band maximum at 17.10 and a relative intensity of 13.4%. Excitation out of the $1e$ orbital is largely responsible for the intensity of the second band located at 25.92 eV. The theory predicts a total intensity of 4.8% for this band centered at about 25.5 eV. The profile above 30 eV is dominated by shakeoff transitions, although the calculation puts the $1e \rightarrow 5e$ transition at 28.02 eV with relative intensity of 2.4% which is, fortuitously, in good agreement with the peak at 30.07 eV.

The first satellite band in CF_4 is observed at 14.20 eV. We assign this to a combination of the $8a_1 \rightarrow 10a_1$ and $6a_1 \rightarrow 10a_1$ transitions. By far the most intense shakeup is the $7a_1 \rightarrow 10a_1$ transition. This transition removes electrons from the C—F bonding region into the F* sphere. The calculated energy and intensity of 22.59 eV and 12.2% are in fair agreement with experiment. Once again the band observed at 30.80 eV can be attributed to the overlap of discrete shakeup transitions and shakeoff. Excitations out of the $6e$ orbital fall into this region and the calculated intensities seem to justify the assignment.

The shakeup in CHF_3 can be estimated from the theoretical data obtained for CHF_3 and CF_4. To construct the F 1s hole

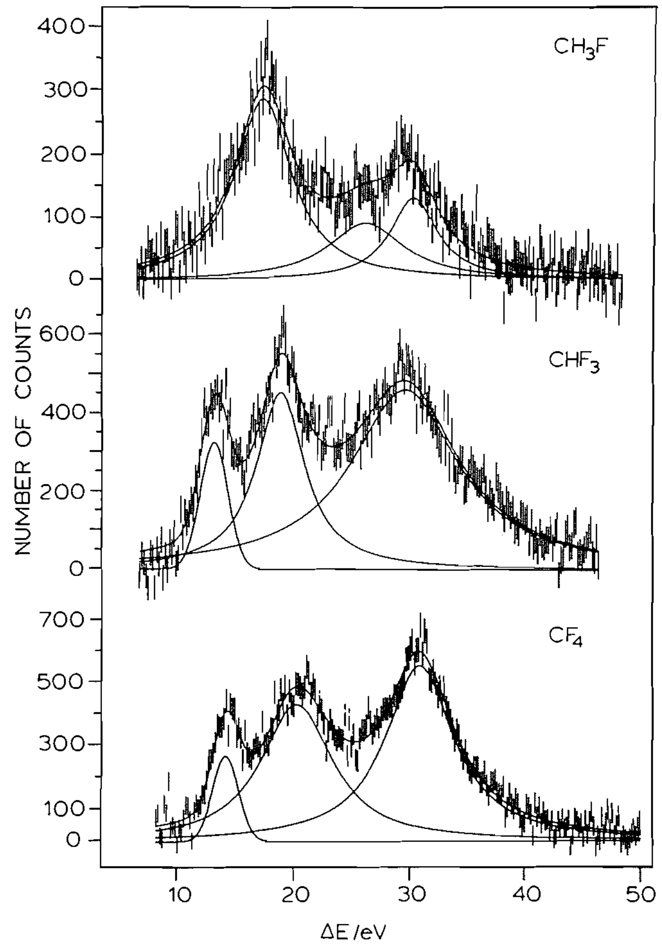

FIG. 8. F 1s satellite photoelectron spectra for CH_3F, CHF_3, and CF_4.

state molecular orbital diagram we shifted the C—H bonding orbitals and the unionized fluorine atoms from their ground state values by 7.9 eV and the ionized fluorine orbitals by 15.2 eV (*vide supra*). The unoccupied $6e$ and $8a_1$ orbitals are shifted down by 6.5 eV. Assuming intense shakeup only occurs for transitions to the antibonding orbitals we can then estimate the shakeup energies from the energy difference of the terminating and originating orbitals (Fig. 3). The results are presented in Table 7. We made no attempt here to rationalize our results any further due to the lack of intensity information. However, the assignments seem to be quite reasonable.

Conclusion

We have shown that by counting to high statistics, satellite structures of relatively low intensities can be observed in the core level photoelectron spectra of the fluoromethanes. The structures can be reasonably attributed to monopole $\sigma \rightarrow \sigma^*$ excitations (shakeup). The intense transitions observed in the C 1s core hole spectrum of CF_4 support the prevailing belief of the existence of a potential wall created by the fluorine lone pair electrons in this molecule. The effect of the potential barrier is less apparent in the F 1s core hole photoelectron spectra. Although the physics of the relaxation mechanism can be understood within the simple independent electron model, the actual calculations of the spectra should include the effect of electron correlation and spin couplings. For molecules of the size studied here, the Xα-SW method is still a very useful and

TABLE 7. F 1s-shakeup energies (eV) and intensities[a] for the fluoromethanes

Molecule	Assignment	ΔE	F.W.H.M.	Int.%	$\Delta E(\Delta SCF)$	Δe(T S)	Int.%
CH_3F	$2e \rightarrow 3e$	17.10	5.9	13.4	13.61	13.57	0.9
	$5a_1 \rightarrow 7a_1$				14.00	14.01	2.2
	$2e \rightarrow 5e$				16.80	16.76	0.8
	$5a_1 \rightarrow 6a_1$				16.98	16.96	0.9
	$4a_1 \rightarrow 7a_1$				21.05	20.71	5.6
							10.4
	$1e \rightarrow 3e$	25.92	8.0	5.7	25.48	25.31	1.5
	$1e \rightarrow 4e$				25.62	25.43	3.3
	$2e \rightarrow \infty$					>22.0	
							4.8
	$4a_1 \rightarrow 8a_1$	30.07	5.0	5.1	27.87	—	0.6
	$1e \rightarrow 5e$				28.20	28.02	2.4
	$5a_1 \rightarrow \infty$					>27	
	$1e \rightarrow \infty$					>32.50	
	$4a_1 \rightarrow \infty$					>33.50	
							3.0
CHF_3[b]	$11a' \rightarrow 14a'$					13.50	
	$9a' \rightarrow 13a'$	13.10	2.8	1.7		14.00	
	$9a' \rightarrow 12a'$					14.70	
	$6a' \rightarrow 13a'$	18.76	5.0	6.2		17.50	
	$6a' \rightarrow 12a'$					18.20	
	$10a' \rightarrow 12a'$					19.70	
	$7a' \rightarrow 13a'$					21.50	
	$10a' \rightarrow 14a'$					21.50	
	$7a' \rightarrow 12a'$					22.20	
	$10a' \rightarrow 16a'$					23.80	
	$7a' \rightarrow 14a'$					24.00	
	$7a' \rightarrow 16a'$	29.47	11.2	14.4		26.50	
	$7a' \rightarrow 17a'$					27.50	
	$7a' \rightarrow 18a'$					28.50	
CF_4	$8a_1 \rightarrow 10a_1$	14.20	2.6	1.5	13.37	—	1.0
	$6a_1 \rightarrow 10a_1$				17.08	—	1.2
							2.2
	$7a_1 \rightarrow 10a_1$	20.20	7.4	9.3	22.94	22.59	12.2
	$5e \rightarrow \infty$					>22.50	
	$4e \rightarrow \infty$					>23.50	
	$8a_1 \rightarrow \infty$					>24.00	
	$6e \rightarrow 7e$	30.80	7.2	11.8	25.0		7.7
	$6e \rightarrow 8e$				27.39	27.19	4.0
	$7a_1 \rightarrow 11a_1$				27.39	—	0.5
	$3e \rightarrow \infty$					>26.50	
	$6a_1 \rightarrow \infty$					>30	
	$6e \rightarrow \infty$					>33.50	
	$7a_1 \rightarrow \infty$					>35.0	
							12.2

[a]See footnote to Table 6.
[b]Energies are estimated using MO diagram (Fig. 3).

reliable technique to assist our understanding on both ground state and hole state electronic structures; even though in most cases the calculated shakeup transition energies and relative intensities are only in rough agreement with the experiments.

1. G. WENDIN. Photoelectron spectra. Springer-Verlag, New York. 1981.
2. (*a*) S. SVENSSON, H. ÅGREN, and U. I. WAHLGREN. Chem. Phys. Lett. **38**, 1 (1976); (*b*) H. ÅGREN, B. O. ROOS, P. S. BAGUS, U. GELIUS, P. Å. MALMQUIST, S. SVENSSON, R. MARIPUU, and K. SEIGBAHN. J. Chem. Phys. **77**, 3893 (1982).
3. H. J. FREUND and E. W. PLUMMER. Phys. Rev. B**23**, 4859 (1981).
4. J. S. TSE, D. J. BRISTOW, G. M. BANCROFT, and G. SCHROBILGEN. Inorg. Chem. **18**, 1766 (1979).
5. D. K. CREBER, J. S. TSE, and G. M. BANCROFT. J. Chem. Phys. **74**, 2097 (1981).
6. J. S. TSE, D. K. CREBER, and G. M. BANCROFT. J. Chem. Phys. **74**, 2097 (1981).
7. D. J. BRISTOW, J. S. TSE, and G. M. BANCROFT. Phys. Rev. A**25**, 1 (1982).
8. J. S. TSE. J. Chem. Phys. **73**, 3015 (1980).
9. J. S. TSE. J. Chem. Phys. **73**, 5734 (1980).
10. J. S. TSE and G. LOUBRIEL. J. Chem. Phys. **74**, 5190 (1981).
11. J. L. DEHMER. J. Chem. Phys. **56**, 4496 (1972).
12. A. GUPTA and J. A. TOSSELL. J. Elect. Spectrosc. Relat. Phenom. **26**, 223 (1982).
13. K. SEIGBAHN, C. NORDLING, G. JOHANNSON, J. HEDMAN, P. F. HEDEN, K. HAMRIN, U. GELIUS, T. BERMARK, L. O. WERME, R. MANNE, and Y. BAER. ESCA applied to free molecules. North-

Holland. 1971.
14. G. M. BANCROFT, I. ADAMS, L. L. COATSWORTH, C. D. BENNETWITZ, J. D. BROWN, and W. D. WESTWOOD. Anal. Chem. **47**, 586 (1975).
15. (*a*) J. C. SLATER. The self-consistent field for molecules and solids. Vol. 4. McGraw-Hill, New York. 1974; (*b*) J. C. SLATER. The calculation of molecular orbitals. Wiley. 1980.
16. K. H. JOHNSON. Adv. Quant. Chem. **7**, 143 (1973).
17. (*a*) T. ABERG. Phys. Rev. (*a*) **156**, 35 (1967); (*b*) A**2**, 1726 (1970).
18. R. L. MARTIN and D. A. SHIRLEY. J. Chem. Phys. **64**, 3685 (1976).
19. G. LOUBRIEL. Phys. Rev. B**20**, 5339 (1979).
20. (*a*) L. C. CEDERBAUM and W. DOMCKE. J. Chem. Phys. **66**, 5084 (1977); (*b*) G. A. SAWATSKY and A. LENSELINK. J. Chem. Phys. **72**, 3748 (1980).
21. L. C. SNYDER. J. Chem. Phys. **55**, 95 (1971).
22. P. S. BAGUS and H. F. SCHAEFER, III. J. Chem. Phys. **56**, 224 (1972).
23. H. T. JONKMAN. Ph.D. These. University Görigen, Netherland.
24. L. E. NITZSCHE and E. R. DAVIDSON. Chem. Phys. **64**, 159 (1982).
25. L. NOODLEMAN, D. POST, and E. J. BAERENDS. Chem. Phys. **64**, 159 (1982).
26. (*a*) G. D. ALTI, P. DECLEVA, and A. SGAMELLOTTI. Chem. Phys. Lett. **50**, 476 (1977); (*b*) G. D. ALTI, P. DECLEVA, and A. SGAMELLOTTI. J. Elect. Spectrosc. Relat. Phenom. **12**, 249 (1977).
27. (*a*) C. R. BUNDLE, M. B. ROBIN, and H. BASCH. J. Chem. Phys. **53**, 2196 (1970); (*b*) J. MUELLER, E. POULAIN, O. GOSCINSKI, and L. KARLSSON. J. Chem. Phys. **72**, 2587 (1980).
28. (*a*) W. R. HARSHBARGER and E. N. LASSETTRE. J. Chem. Phys. **58**, 1505 (1973); (*b*) G. R. WRIGHT and C. E. BRION. J. Elect. Spectrosc. Relat Phenom, 327 (1974); (*c*) M. TRONC, G. C. KING, and F. H. READ. J. Phys. B**12**, 137 (1979).
29. M. B. ROBIN. Higher excited states of polyatomic molecules. Vol. II. Academic Press, New York. 1975.
30. R. S. MULLIKEN. Acc. Chem. Res. **9**, 7 (1976).
31. J. R. SWANSON, D. DILL, and J. L. DEHMER. J. Chem. Phys. **75**, 619 (1981).
32. P. S. BAGUS, M. KRAUSS, and R. E. LAVILLA. Chem. Phys. Lett. **23**, 13 (1973).
33. F. C. BROWN, R. Z. BACHRACH, and A. BIANCONI. Chem. Phys. Lett. **54**, 425 (1978).
34. L. C. SNYDER and H. BASCH. Molecular wave functions and properties. Wiley, Interscience, New York. 1972.
35. K. SCHWARZ. Phys. Rev. B**5**, 2466 (1972).

Photochemistry of halogenated benzene derivatives. Part VI.[1] Photoreactions of tetra- and pentachlorophenols in water–acetonitrile mixtures

GHULAM GHAUS CHOUDHRY
Pesticide Research Laboratory, Department of Soil Science, The University of Manitoba, Winnipeg, Man., Canada R3T 2N2

FRANS W. M. VAN DER WIELEN
Laboratory of Environmental and Toxicological Chemistry, University of Amsterdam, Nieuwe Achtergracht 166, 1018 VW Amsterdam, The Netherlands

G. R. BARRIE WEBSTER[2]
Pesticide Research Laboratory, Department of Soil Science, The University of Manitoba, Winnipeg, Man., Canada R3T 2N2

AND

OTTO HUTZINGER
The Chair of Ecological Chemistry and Geochemistry, University of Bayreuth, D-8580 Bayreuth, Germany

Received May 14, 1984

GHULAM GHAUS CHOUDHRY, FRANS W. M. VAN DER WIELEN, G. R. BARRIE WEBSTER, and OTTO HUTZINGER. Can. J. Chem. **63**, 469 (1985).

Laboratory photochemical studies of aqueous acetonitrile solutions of some polychlorinated phenols (PCPs) such as 2,3,4,5-tetrachlorophenol (2,3,4,5-Cl_4-Pn) (**1**), 2,3,4,6-Cl_4-Pn (**2**), 2,3,5,6-Cl_4-Pn (**3**), and pentachlorophenol (Cl_5-Pn) (**4**) at $\lambda > 285$ nm have been carried out for 6 and 24 h exposure times. All the investigated PCPs underwent reductive dechlorination. This process was dependent not only upon the position of OH group but also upon the relative positions of the Cl substituents on the benzene ring. The Cl_4-Pn **2** (and **3**) and Cl_5-Pn (**4**) also yielded photoproducts of molecular formulae $C_8H_4Cl_3NO$ ($M^{+\cdot}$ = 235) and $C_8H_3Cl_4NO$ ($M^{+\cdot}$ = 269), respectively. Furthermore, phenol **3** is unique amongst the investigated PCPs; in addition to the above mentioned photoproducts, it yielded hexa-, hepta-, and octachlorodihydroxybiphenyl(s) as well as heptachlorohydroxydiphenyl ether.

GHULAM GHAUS CHOUDHRY, FRANS W. M. VAN DER WIELEN, G. R. BARRIE WEBSTER et OTTO HUTZINGER. Can. J. Chem. **63**, 469 (1985).

Opérant à des $\lambda > 285$ nm et pour des temps d'exposition de 6 et de 24 h, on a effectué des études photochimiques en laboratoire de quelques phénols polychlorés (PPC), comme le tétrachloro-2,3,4,5 phénol (Cl_4-2,3,4,5 Pn) (**1**), Cl_4-2,3,4,6 Pn (**2**), Cl_4-2,3,5,6 Pn (**3**) et le pentachlorophénol (Cl_5Pn) (**4**). Tous les PPC étudiés subissent des déchlorations réductives. Ce processus ne dépend pas seulement de la position du groupement OH mais aussi des positions relatives des substituants Cl sur le noyau benzénique. Les composés Cl_4-Pn (**2** et **3**) et Cl_5-Pn (**4**) fournissent aussi respectivement des photoproduits de formules moléculaires $C_8H_4Cl_3NO$ ($M^{+\cdot}$ = 235) et $C_8H_3Cl_4NO$ ($M^{+\cdot}$ = 269). De plus, le phénol **3** est unique parmi les PPC étudiés: en plus des photoproduits mentionnés plus haut, il fournit aussi des hexa-, hepta- et octa-chlorodihydroxybiphényles ainsi que de l'heptachlorohydroxydiphényl éther.

[Traduit par le journal]

Introduction

Polychlorophenols (PCPs) are ubiquitous environmental contaminants which have been found in several aquatic environments around the world. For instance, Wegman and his associates have reported the occurrence of 19 individual PCPs in surface waters (2) and in river sediments (3) located in The Netherlands. Likewise PCPs are known to occur in mussels, pike, and sediments in the lakes of central Finland (4). Chlorophenolic pollutants originate from pulp bleaching and the disinfection of waters, but are also contaminants and degradation products of pesticides (4). Furthermore, pentachlorophenol (Cl_5-Pn) itself has been widely used in agriculture and industry as a fungicide, bactericide, herbicide, molluscicide, algicide, and insecticide (5, 6). Currently, Cl_5-Pn is utilized mainly as a wood preservative, which has led to its widespread presence in the environment (5). A large number of organic compounds including PCPs have also been identified in the flue gas and fly ash from some municipal and industrial incinerators (7).

In the past, several publications have reported photoconversions and photodegradations of (poly)chlorinated phenols. Photolyses of basic aqueous solutions of all three monochlorophenols at wavelengths of 254 nm and ≥290 nm are well known (8–10). Photoreactions (11) of 2,5-dichlorophenol (2,5-Cl_2-Pn), 2,6-Cl_2-Pn, 3,4-Cl_2-Pn, and 3,5-Cl_3-Bz in deuteriated methanol at λ = 254 nm as well as riboflavin photosensitized oxidation (12) of 2,4-Cl_2-Pn at $\lambda \geq 280$ nm in aqueous solution have been described. Furthermore, several authors have reported photolyses of pentachlorophenol in organic solvents such as hexane, cyclohexane, acetone, and 95% ethanol at 254 nm (13) and on wood (14). Photolysis of the sodium salt of Cl_5-Pn in water using natural sunlight and sunlamps has also been documented (14).

Previously, we have observed that, in addition to reductively dechlorinated products (major), polychlorobiphenyls (PCBs) appear as photoproducts in the case of irradiation of solutions of 1,3,5-trichlorobenzene (1,3,5-Cl_3-Bz) (15), tetrachlorobenzenes (16), and pentachlorobenzene (16) in various water–acetonitrile mixtures. Under such photochemical circumstances, 1,2,3-Cl_3-Bz (15), 1,3,5-Cl_3-Bz (15), and all three isomers of tetrachlorobenzene (1, 16) undergo photoconversions, eventually giving rise to the production of photoisomerized chlorobenzenes. More recently, we have reported

[1]For Part V, see ref. 1.
[2]To whom all correspondence should be addressed.

that laboratory irradiation (at $\lambda \geqslant 285$ nm) of tetra-, penta-, and hexachlorobenzenes in aqueous acetonitrile containing phenol yields polychlorinated dibenzofurans (PCDFs) possessing two Cl atoms less than the starting chlorobenzenes (17). It was concluded that, during these photochemical reactions, products such as PCBs (15, 16) and PCDFs (17) are apparently formed through the intermediate involvement of some polychlorophenyl radical species which are circumstantially longer surviving. In view of our interest in the photochemical fate of pollutants such as halogenated benzene derivatives in the environment (1, 15–18), we decided to investigate the photochemistry of polychlorophenols (PCPs). The present paper is concerned with the results of our laboratory photochemical studies on some PCPs, viz., three tetrachlorophenols and pentachlorophenol in different acetonitrile–water mixtures using radiation of wavelength $\geqslant$285 nm with special emphasis on reductive dechlorination and formation of dihydroxypolychlorobiphenyls, hydroxypolychlorodiphenyl ethers, and other products.

Experimental

Substrates and standards

All chemicals were purchased from Aldrich Chemical Co., Inc.

Solvents and procedures for the preparation of solutions and irradiation experiments

Solvents and procedures utilized have been described previously (16).

Extraction procedures

One millilitre of aqueous solution of 0.589 *M* NaOH was added to a photolyzed sample and shaken well, the pH value of the resulting solution being $\geqslant$11. Subsequently, 2 mL of *n*-hexane containing pentachlorobenzene (0.108×10^{-3} *M*) as an internal standard (IS) were added. After shaking well, the *n*-hexane layer was separated from the water–acetonitrile layer. To the *n*-hexane fraction, a few drops of *n*-nonane were added; the solution was then reduced in volume to ca. 0.2 mL under a stream of dry nitrogen. One millilitre of 1.080–1.400 *M* HCl in water was added to the water–acetonitrile fraction to adjust the pH to $\leqslant$1. The *n*-hexane extract (ca. 0.2 mL) containing the IS was prepared by following the method described above. An unphotolyzed sample solution was also subjected to the extraction procedure as cited.

Gas chromatography

Qualitative and quantitative analyses of the *n*-hexane extracts were carried out on a Hewlett-Packard 5830A instrument equipped with a flame ionization detector (FID) and an 18850 GC terminal.

Column A: Glass column (2 m × 0.2 cm) containing 3% SE 52 on 160–180 Mesh Chromosorb WAW; temperature 1 (T_1) = 60°C, time 1 (t_1) = 2 min, rate 8°/min, temperature 2 (T_2) = 240°C, time 2 (t_2) = 20 min, carrier gas (N_2) flow = 30 mL/min, injector temperature = 250°C and FID temperature = 300°C.

Column B: Glass column (2 m × 0.2 cm) containing 3% FFAP/SP 1000 on 160–180 mesh Chromosorb WAW; T_1 = 60°C, t_1 = 2 min, rate 8°/min, T_2 = 240°C, t_2 = 25 min, carrier gas (N_2) flow = 26 mL/min, injector temperature = 250°C and FID temperature = 300°C.

Gas chromatography – mass spectrometry

A Hewlett-Packard 5894 A gas chromatograph mass spectrometer (gc–ms) was used in the electron-impact mode at 70 eV. All photoproducts (documented in Table 1) were identified using a fused silica capillary column (25 m × 0.25 mm i.d.) coated with 0.4 μm CP-SIL 5 (Chrompack). The procedure of Grob and Grob (19) was followed for operating the capillary injection system. The gc conditions for this capillary system were T_1 = 70°C, t_1 = 0 min, rate = 32°/min; after 2 min rate being 8°/min, T_2 = 300°, t_2 = 30 min. The mass (*M*)

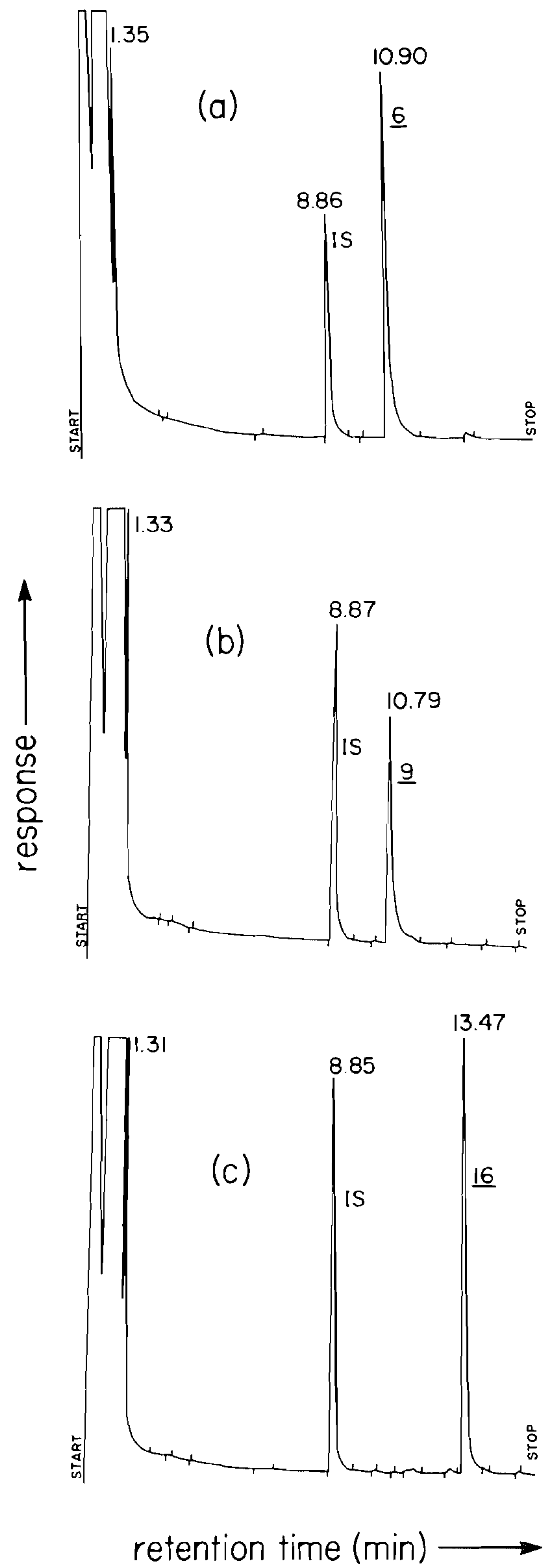

FIG. 1. Typical gas chromatograms of the *n*-hexane extracts at pH $\geqslant$ 11 of the 6 h photolyzates of (*a*) 2,3,4,6-tetrachlorophenol (**2**), (*b*) 2,3,5,6-tetrachlorophenol (**3**), and (*c*) 2,3,4,5,6-pentachlorophenol (**4**). The peaks labelled with numbers and "IS" indicate the photoproducts and internal standard (pentachlorobenzene), respectively; 4 μL were injected. (Mass spectra are described in Fig. 2, and other conditions are given in Table 1 and Experimental.)

TABLE 1. Photolyses[a] of polychlorophenols (PCPs) in water–acetonitrile mixtures

No.	Substrate, -chlorophenol	$H_2O:CH_3CN$ (v/v)	Concentration (in 10^{-3} *M*)	Irradiation time (h)	Percentage disappearance of the starting phenol[b,c,g] (%)	Photoproducts identified[d] in the *n*-hexane extracts; when the pH value of the photolyzed sample was changed to: >11[c,e,f]	<1[b,c,g,h,i]
1	2,3,4,5-Tetra-	1:1	5.00	6	30	—	2,3,5-Cl_3-Pn (**5**) (10%)
1	2,3,4,5-Tetra-	1:1	5.00	24	73	—	2,3,5-Cl_3-Pn (**5**) (9%)
2	2,3,4,6-Tetra-	1:1	5.00	6	51	$C_8H_4Cl_3NO$, $M^{+\cdot}$=235 (**6**) (8%)	2,3,4-Cl_3-Pn (**7**) (0.4%); 2,3,6-Cl_3-Pn (**8**) (1.8%)
2	2,3,4,6-Tetra-	1:1	5.00	24	89	—	2,3,4-Cl_3-Pn (**7**) (0.3%); 2,3,6-Cl_3-Pn (**8**) (1.5%)
3	2,3,5,6-Tetra-	1:1	5.09	6	19	$C_8H_4Cl_3NO$, $M^{+\cdot}$=235 (**9**) (10%)	2,3,5-Cl_3-Pn (**5**) (13%) Cl_7-$(OH)_2$-BP (**10**) (4%)
3	2,3,5,6-Tetra-	1:1	5.09	24	69	—	2,3,5-Cl_3-Pn (**5**) (9%); (**11**) (0.5%)[j]; Cl_6-$(OH)_2$-BP (**12**) (0.5%); Cl_7-$(OH)_2$-BP (**10**) (1.5%); Cl_7-(OH)-DPE (**13**) (0.2%); Cl_7-$(OH)_2$-BP (**14**) (0.2%); Cl_8-$(OH)_2$-BP (**15**) (1.0%)
4	2,3,4,5,6-Penta-	4:6	4.11	6	30	$C_8H_3Cl_4NO$, $M^{+\cdot}$=269 (**16**) (11%)	2,3,4,5-Cl_4-Pn (**1**) (3%); 2,3,4,6-Cl_4-Pn (**2**) and/or 2,3,5,6-Cl_4-Pn (**3**) (5%)
4	2,3,4,5,6-Penta-	4:6	4.11	24	52	$C_8H_3Cl_4NO$, $M^{+\cdot}$=269 (**16**) (3%)	2,3,4,5-Cl_4-Pn (**1**) (7%); 2,3,4,6-Cl_4-Pn (**2**) and/or 2,3,5,6-Cl_4-Pn (**3**) (8%)

[a]Sample solutions in Pyrex tubes which transmit less than 1% of the radiation below 287 nm were irradiated in a Rayonet Photoreactor, equipped with RPR 3000 Å uv lamps, having an energy output of 90% between 290 and 310 nm.
[b]*n*-Hexane extracts were treated with diazomethane.
[c]Quantifications were carried out by fid-gc utilizing pentachlorobenzene as the internal standard.
[d]Percentages in the parentheses represent chemical yields calculated from the amount of photoconverted starting material.
[e]Quantitative analyses were performed by gc equipped with Column A (see Experimental).
[f]Typical gas chromatograms and mass spectra of the photoproducts **6**, **9**, and **16** are shown in Figs. 1 and 2, respectively.
[g]Quantitative analyses of chlorophenols were conducted by gc equipped with Column B (see Experimental), whilst those of other compounds were performed as described in the footnote *e*.
[h]Typical total ion chromatograms (TICs) of *n*-hexane extract of photolyzates of the substrate **3** subjected to halogen test computer program (20) are given in Fig. 3.
[i]Structures: 2,3,5-Cl_3-Pn = 2,3,5-trichlorophenol; Cl_6-$(OH)_2$-BP = hexachlorodihydroxybiphenyl; Cl_7-(OH)-DPE = heptachlorohydroxydiphenyl ether; etc.
[j]Typical mass spectrum of this product is shown in Fig. 4.

ranges were: $100 \leqslant M \leqslant 500$. To identify chlorine-containing photoproducts in the photolyzate, the computer programme for specific detection of organochlorine and organobromine compounds (20) was used.

Identification of photoproducts

n-Hexane extracts (at pH $\leqslant$ 1) of the sample solutions were treated with diazomethane in ether. Methylated photoproducts such as PCPs were identified by comparing their retention times (Column B) and mass spectra with those of authentic chlorophenols treated with CH_2N_2. Identification of all other photoproducts (recorded in Table 1) are tentative pending availability of standards. Structures of such compounds were ascribed from their mass spectra.

Results

Table 1 lists the photoproducts of PCPs (**1**–**4**) after 6 and 24 h irradiation. The 6 h photolyses of **2** and **3** yield photoproducts of molecular formula $C_8H_4Cl_3NO$; whereas **4** following 6 and 24 h exposure times provide 11 and 3% of $C_8H_3Cl_4NO$, respectively. Typical gas chromatograms and mass fragmentation pattern of these products yielded from 6 h photochemical reactions of PCPs **2**, **3**, and **4** are shown in Figs. 1 and 2, respectively.

The last column of Table 1 records phenolic products identified in the *n*-hexane extracts of the photolyzates after changing their pH value of >11 to <1. Such photoproducts were derivatized with CH_2N_2 prior to gc and gc–ms analysis. With the exceptional case of 2,3,5,6-tetrachlorophenol (2,3,5,6-Cl_4-Pn) (**3**), the *n*-hexane extracts (at pH < 1) of all other photolysed PCPs contain only reductively dechlorinated photoproducts; e.g., on irradiating **1** for 6 and 24 h, 10 and 9% of the disappeared starting compound **1** are photoconverted into **5**. But in the case of photoreaction of **3** for 24 h, in addition to the usual reductively dechlorinated photoproduct **5** (9%), hexachlorodihydroxybiphenyl (**12**), heptachlorodihydroxybiphenyl (**10**), heptachlorohydroxydiphenyl ether (**13**), another isomer of biphenyl **10** (**14**), and octachlorodihydroxybiphenyl (**15**) at yields 0.5, 1.5, 0.2, 0.2, and 1.0%, respectively, together with an unidentified photoproduct **11** (0.5%) are seen. It is noteworthy that the biphenyl **10** (4% yield) is also produced during the 6 h exposure of **3**. Using the Olie and Hutzinger computer search technique to locate chlorinated organic compounds (20), typical total ion chromatograms (TICs) of the methylated *n*-hexane extracts of the unphotolysed and photolysed aqueous acetonitrile solutions of the tetrachlorophenol **3** are given in

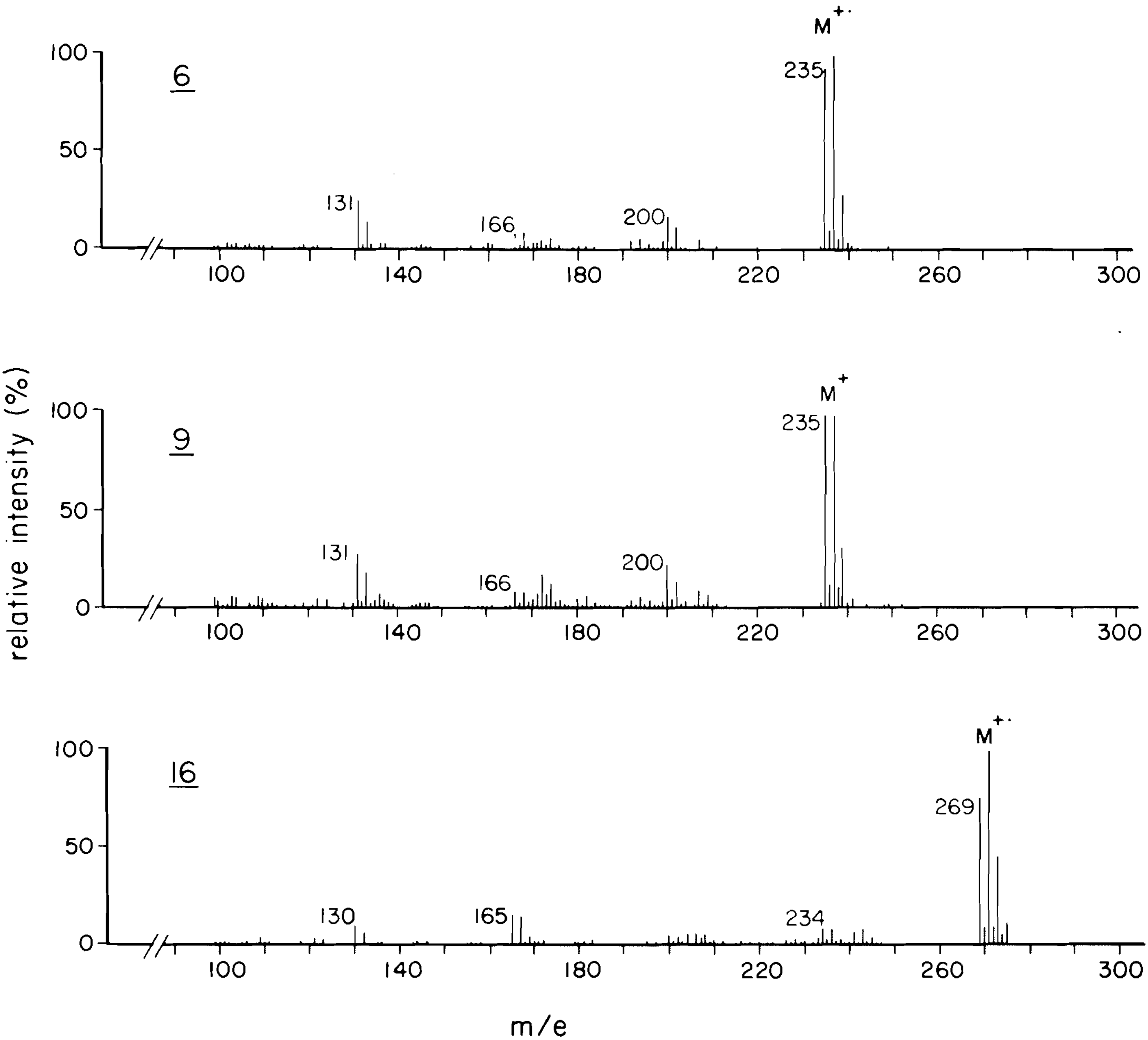

FIG. 2. Mass spectra of the peaks labelled with numbers **6**, **9**, and **16** in the gas chromatograms shown in Fig. 1. (See Experimental and Table 1 for further details.)

Fig. 3. The mass fragmentation pattern of the unidentified product **11** is described in Fig. 4. Finally, when pentachlorophenol **4** in water–acetontrile (4:6 v/v) is exposed to uv radiation for 24 h, besides the above mentioned non-phenolic product **16**, 7% **1** and 8% **2** and/or **3** are formed (Table 1). We and other researchers (21) did not succeed in separating 2,3,4,6- and 2,3,5,6-tetrachloroanisole by gc or gc–ms.

Discussion

It is evident (Table 1) that the photoreactions of the Cl_4-Pns **1–3** in water–acetonitrile (1:1 v/v) produce photoproducts through reductive dechlorination dependent on the relative positions of the hydroxyl (OH) and chlorine substituent groups on the benzene ring. In the case of all tetrachlorophenols, the Cl atom(s) present at the *meta* position(s) (relative to the OH group) do *not* undergo photoreaction. 2,3,4,5-Tetrachlorophenol (**1**) yields only 2,3,5-Cl_3-Pn (**5**) (for both exposure times) via the reduction of the *para* Cl substituent; whilst the product of **3** is also **5**, formed by reductive dechlorination at the *ortho* position (Table 1). So far as photochemical reductive dechlorination is concerned, **2** is unique amongst the three isomers of tetrachlorophenol giving (**7**) and (**8**) through the reduction of the *ortho* and *para* substituents, respectively. It is worth noting that 2,4,5-trichlorophenol (expected from photolysis at the ortho chlorine) is *not* detected amongst the reductively dechlorinated photoproducts of **2**, thereby indicating that, in the case of the photolyses of polychlorinated phenols, isomeric distribution of the photoreductively dechlorinated products is dependent not only upon the position of the OH group but also upon the relative positions of the chlorine substituents. As cited in the previous section, because of our failure to separate 2,3,4,6-tetrachlorophenol (**2**) from its

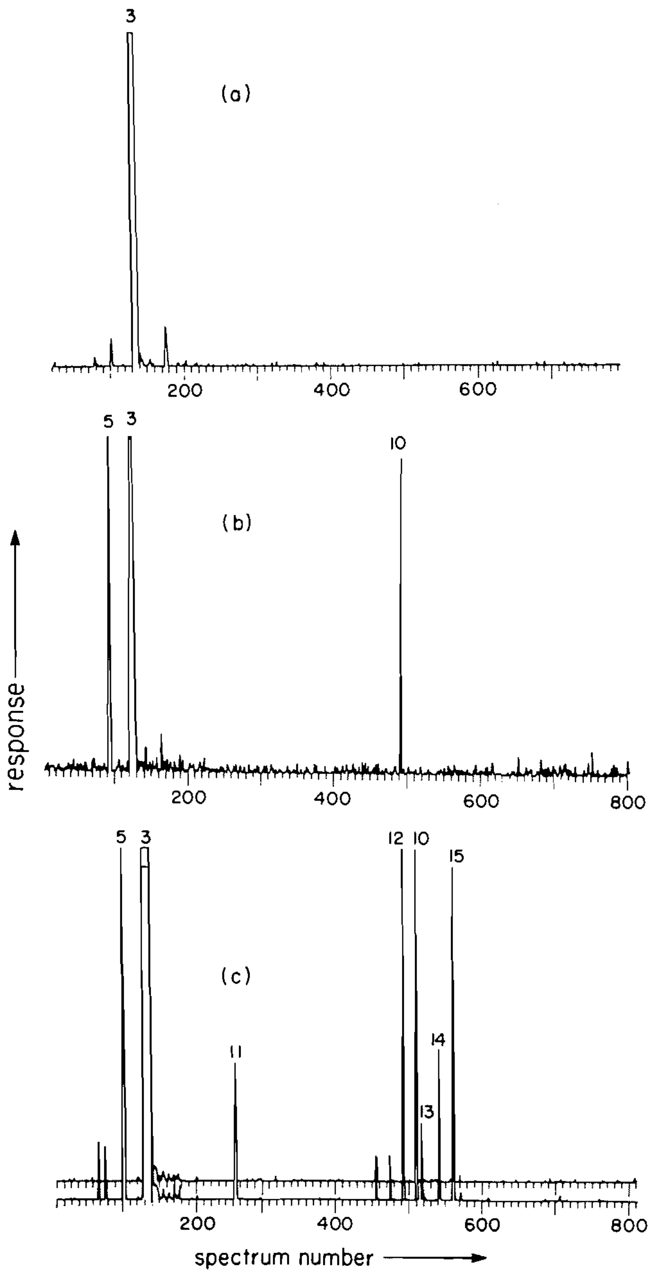

FIG. 3. Plots of the total ion chromatograms (TICs) of the methylated n-hexane extracts at pH $\leq$ 1 of the sample solutions of unirradiated (a), and irradiated 2,3,5,6-tetrachlorophenol (3) for 6 h (b) and 24 h (c) subjected to the halogen test computer program (20) for locating chlorine containing compounds. The peaks with numbers exhibit the compounds which have been identified (Table 1). (For conditions of gc–ms, see Experimental.)

isomer **3**, we are unable to conclude whether *meta* or *para* Cl substituent(s) or both is (are) photolabile in case of photoreductive dechlorination of pentachlorophenol (**4**). It is interesting to mention that, under the present circumstances, on irradiating Cl_5-Pn (**4**) for 6 and 24 h, Cl_4-Pns namely **1** and **2** and/or **3** in the ratios of ca. 1:1.5 and 1:1, respectively, appear as photoproducts. Our findings differ from those of Crosby and Hamadmad (13) who report that irradiation (λ = 254 nm) of **4** for 32 h in organic solvents yields **3** (30%) as the major decomposition product accompanied by a minor product, ca. 10% assumed to be an isomeric tetrachlorophenol.

In order to account for the products arising from the irradiation of **3**, the following postulated scheme can be considered: A molecule of 2,3,5,6-Cl_4-Pn (**3**) in the ground state absorbs a photon, yielding the excited state of **3**. Homolytic scission of the C—Cl bond at position 2 (or position 6) of **3** in the excited state gives 2,4,5-trichloro-6-hydroxyphenyl radicals (**17**). Radical species **17** abstracts hydrogen atoms from the solvent to provide 2,3,5-Cl_3-Pn (**5**). Likewise, attack of intermediate radicals **17** on the ground state molecules of the starting substance **3** results in the formation of σ-complex species **18**, which lose hydrogen atoms leading to the eventual generation of 2,2′,3,4′,5,5′,6-heptachloro-4,6′-dihydroxybiphenyl (**G**). The structure **G** may be ascribed to the photoproduct **10** or **14** (Table 1 and Fig. 3b and c). Due to the unavailability of an authentic standard, structure **G** is tentative. However, it is well known that under the similar photochemical circumstances, the intermediate polychlorophenyl radicals such as 3,5-dichlorophenyl radicals (15) and all trichorophenyl radicals (16) and tetrachlorophenyl radicals (16), produced via the homolytic cleavage of the C—Cl bond on the polychlorobenzenes (PCBzs), interact with the corresponding starting PCBz to provide the corresponding polychlorobiphenyl(s) (PCB(s)). The alternative structure 2,2′,3,4′,5,5′,6-heptachloro-3′,4-dihydroxybiphenyl (not shown in Scheme 1), possibly attributable to the product **10** or **14** formed by the arylation of **3** by 2,4,5-trichloro-3-hydroxyphenyl radicals can be ruled out due to the fact that 2,3,6-trichlorophenol, which is likely to be generated by the abstraction of H atoms from solvents by these anticipated trichlorohydroxyphenyl radicals, has not been identified amongst the photoproducts of **3**. Furthermore, some of the photoexcited molecules of **3** provide 2,3,5,6-tetrachlorophenoxy radicals (**19**) generated through the photohomolysis of the OH bond on **3**. In addition, phenoxy radicals **19** may also be yielded by a process involving the abstraction of the H atom of the hydroxyl group on **3** by radical species like Cl, CH_2CN and **17**. The phenoxy radicals **19** combine with 2,4,5-trichloro-3-hydroxyphenyl radicals and/or isomeric radicals (**17**), thereby forming heptachlorohydroxydiphenyl ether (Cl_7-(OH)-DPE) (**13**). The involvement of the former trichlorohydroxyphenyl radicals in the production of the DPE **13** seems highly unlikely, as discussed above. Moreover, the unpaired electron on the oxygen atom of the phenoxy species **19** is delocalized over the benzene nucleus as depicted by resonance structures **20** and **21**. The radicals **20** dimerize giving rise possibly to the generation of intermediate compound **22**. The substance **22** aromatizes to give 2,2′,3,3′,5,5′,6,6′-octachloro-4,4′-dihydroxybiphenyl (**15**). Although this structure designated to the photoproduct Cl_8-$(OH)_2$-BP (**15**) (Table 1 and Fig. 3c) is again tentative, no other logical structure for product **15** can be considered. Furthermore, photodegradation of biphenyl **15** may yield heptachlorodihydroxybiphenyl (Cl_7-$(OH)_2$-BP) (product **10** or **14**) (structure **H** given in Scheme 1). The absence of an expected product, Cl_8-(OH)-DPE (a likely structure being 2,2′,3,3′,5,5′,6,6′-octachloro-4-hydroxydiphenyl ether), in the photolyzate of **3** (Table 1) evidently reflects that (i) 2,3,5,6-tetrachlorophenoxy radicals (**19**) do not attack at the position 4 of ground state molecules of **3** and (ii) radical **19** does not interact with radical **20**. It can be inferred from this fact that reactions of the sort **20** + **3** $\twoheadrightarrow$ **15**, another possible route for the production of the photoproduct **15**, do not take place in the present solvent system. Likewise, reaction **20** + **21** $\twoheadrightarrow$ **G** does not occur. However, **20** + **17** $\twoheadrightarrow$ **G** may contribute in the generation of photoproduct **G**, because tri-

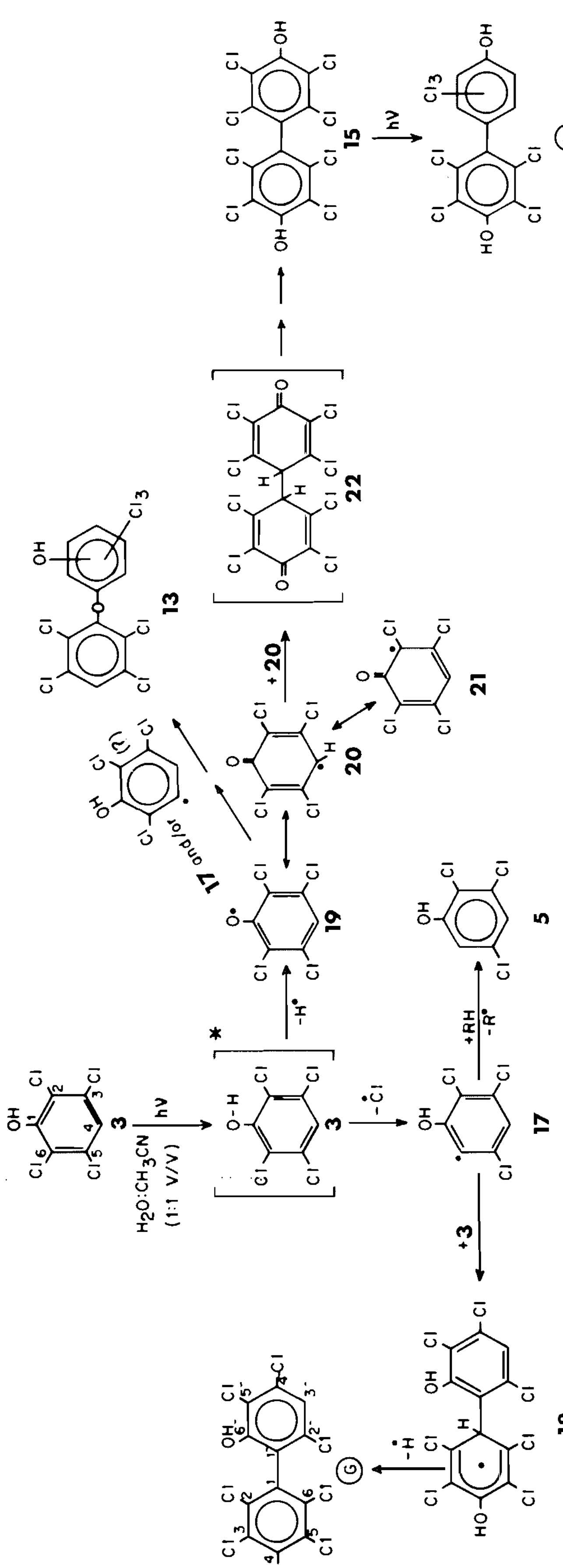

SCHEME 1. Proposed mechanism.

chlorohydroxyphenyl radicals **17** are more reactive (less stable) compared to the phenoxy radical **19** and its mesomeric structures **20** and **21**. Finally, the discussion presented above leads one to conclude that, in the $H_2O:CH_3CN$ solvent system, in the context of replacement of a H atom of a (chlorinated) benzene nucleus by a phenoxy radical, the intermediate phenoxy species are less reactive and are unable to undergo such reaction. Therefore, the scheme showing the mechanism of formation of 2,3-dichlorodibenzofuran during the irradiation of solution of 1,2,4,5-tetrachlorobenzene in $H_2O:CH_3CN$ (4:6 v/v) containing phenol, previously postulated by Choudhry *et al.* (17), can be modified by including phenoxy radicals bearing full (instead of partial) radical character on the oxygen atom which interact with photochemically generated 2,4,5-trichlorophenyl radicals.

For instance, the photoproduct **16** of **4** (Figs. 1 and 2) has molecular ion ($M^{+\bullet}$) *m/e* 269 and the molecular formula $C_8H_3Cl_4NO$ has been assigned by interpreting its mass spectrum. Structure **I**, namely hydroxytetrachlorophenylacetonitrile, can be considered for compound **16**, formed presumably through the coupling between $\dot{C}H_2CN$ (which may

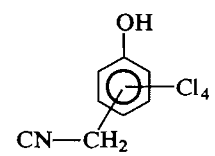

I

have been generated via abstraction of hydrogen atoms from the cosolvent acetonitrile by intermediate free radical species) and photolytically produced hydroxytetrachlorophenyl radical. Because the product **16** has been detected in the *n*-hexane extract at pH $\geqslant$ 11 and because the phenolic compound **I** at such a high pH is expected to remain in the $H_2O:CH_3CN$ layer as is the case of the starting phenol **4**, the structure **I** proposed for **16** is ruled out. The rejection of structure **I** is supported by the lower retention time and the shape of the gc peak for product **16** (Fig. 1*c*). It should be mentioned that Lemaire and co-workers (9, 10), during their photochemical investigations on 2-chlorophenol (in the anionic form), have suggested the intermediary of 1,2-ketocarbene and its contraction to a five member ring ketene. With the aid of our present experimental data, we are unable to conclude whether such a ring contraction also occurs during the photolyses of tetra- and pentachlorophenols. However, it is interesting to note that **1** does not provide a photoproduct of molecular formula $C_8H_4Cl_3NO$. In addition, during the irradiation of **1** 3,4,5-Cl_3-Pn, expected via the homolysis of the 2-Cl, is not seen. These two facts lead to the conclusion that products such as $C_8H_3Cl_4NO$ and $C_8H_4Cl_3NO$ are possibly produced through the intermediate involvement of tetrachloro- and trichloro-2-hydroxyphenyl radicals, respectively. It is notable that Choudhry and Hutzinger (16) have recently reported the photoformation of $C_8H_5Cl_2NO$ from 1,2,3,4- and 1,2,3,5-tetrachlorobenzene as well as $C_8H_4Cl_3NO$ from pentachlorobenzene, water–acetonitrile being used as the solvent. Similar products (viz. $C_8H_5Cl_2NO$) may be formed during the photolysis of appropriate trichlorophenols. The full characterisation of these reaction pathways and the compounds so yielded will be the subject of another paper.

Conclusions

Our laboratory photochemical investigations at $\lambda \geqslant 285$ nm

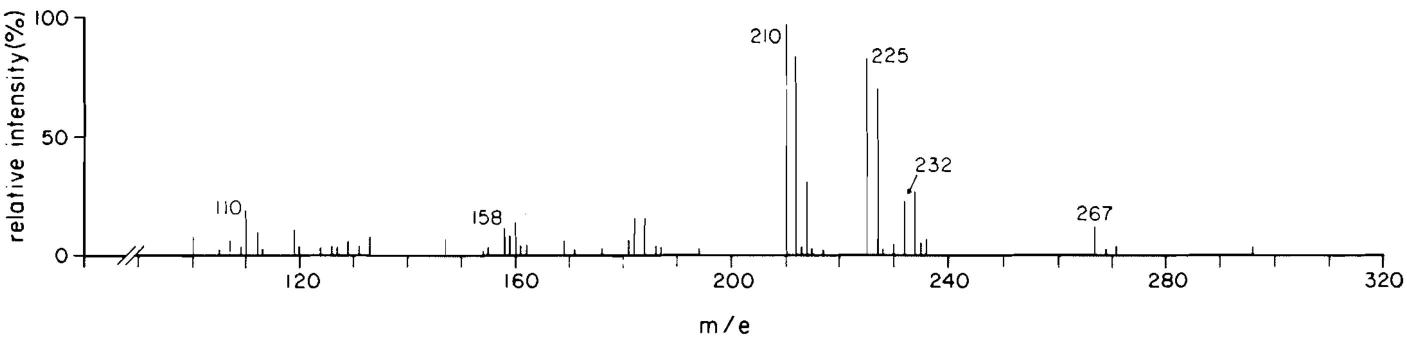

FIG. 4. Mass spectrum of peak No. 11 in the total ion chromatogram (TIC) shown in Fig. 3(*c*).

on 4–5 × 10^{-3} *M* solutions of tetra- and pentachlorophenols in water–acetonitrile mixtures lead us to conclude that, in the context of reductive dechlorination of tetrachlorophenols (Cl_4-Pns), the 4-Cl substituent of 2,3,4,5-Cl_4-Pn (**1**); 4-Cl and 6-Cl substituent of 2,3,4,6-Cl_4-Pn (**2**); and 2-Cl (6-Cl) substituent of 2,3,5,6-Cl_4-Pn are photolabile, whilst 3-Cl (and 5-Cl) substituent(s) on this substrate(s) is (are) not photochemically reactive. In the case of pentachlorophenol **4**, it can be concluded that the C—Cl bond at position 2 (and 6) is labile to homolytic cleavage, but the question whether the C—Cl bond at position 3 (and 5) or 4 or at both positions undergoes such a photoreaction remains unanswered. Failure to yield $C_8H_4Cl_3NO$ ($M^{+\cdot}$ = 235) from **1** stresses that similar products observed in the case of other PCPs **2**–**4** are formed through the intermediacy of hydroxypolychlorophenyl radicals generated via the homolytic cleavage of a C—Cl bond *ortho* to the OH group (Scheme 1). Likewise, among the Cl_4-Pns, only the irradiation of 2,3,5,6-tetrachlorophenol (**3**) provides the relatively longer surviving trichlorohydroxyphenyl radicals in addition to (possibly) tetrachlorophenoxy radicals (and their mesomeric form bearing unpaired electron at the *para* position), which act as sources of photoproducts such as hexa-, hepta-, octa-chlorodihydroxybiphenyl(s) and heptachlorohydroxydiphenyl ether. Finally, contrary to our previous observations in the case of irradiation of polychlorobenzenes (PCBzs), namely, 1,2,3-, 1,3,5-trichlorobenzene (15), all three tetrachlorobenzenes (1, 16) and 2,4,5-trichlorodiphenyl ether (17), it is very unlikely that photoisomerization occurs during the photolyses of tetrachlorophenols in $H_2O:CH_3CN$.

1. G. G. CHOUDHRY and G. R. B. WEBSTER. Toxicol. Environ. Chem. In press.
2. R. C. C. WEGMAN and A. W. M. HOFSTEE. Water Res. **13**, 651 (1979).
3. R. C. C. WEGMAN and H. H. VAN DEN BROEK. Water Res. **17**, 227 (1983).
4. M. T. VIRTANEN and M.-L. HATTULA. Chemosphere, **11**, 641 (1982) and references therein.
5. U. M. WEISS, P. MOZA, I. SCHEUNERT, A.-UL HAQUE, and F. KORTE. J. Agric. Food Chem. **30**, 1186 (1982).
6. U. M. WEISS, I. SCHEUNERT, W. KLEIN, and F. KORTE. J. Agric. Food Chem. **30**, 1191 (1982).
7. J. W. A. LUSTENHOUWER, K. OLIE, and O. HUTZINGER. Chemosphere, **9**, 501 (1980).
8. K. OMURA and T. MATSUURA. Tetrahedron, **27**, 3103 (1971).
9. P. BOULE, C. GUYON, and J. LEMAIRE. Chemosphere, **11**, 1179 (1982).
10. C. GUYON, P. BOULE, and J. LEMAIRE. Tetrahedron Lett. **23**, 1581 (1982).
11. M. MANSOUR, H. PARLAR, and F. KORTE. Chemosphere, **9**, 59 (1980).
12. J. R. PLIMMER and U. I. KLINGEBIEL. Science, **174**, 407 (1971).
13. D. G. CROSBY and N. HAMADMAD. J. Agric. Food Chem. **19**, 1171 (1971).
14. G. G. CHOUDHRY and O. HUTZINGER. Residue Rev. **84**, 113 (1982) and references therein.
15. G. G. CHOUDHRY, A. A. M. ROOF, and O. HUTZINGER. Tetrahedron Lett. 2059 (1979).
16. G. G. CHOUDHRY and O. HUTZINGER. Environ. Sci. Technol. **18** 235 (1984).
17. G. G. CHOUDHRY, J. A. VAN DEN BROECKE, and O. HUTZINGER. Chemosphere, **12**, 487 (1983).
18. G. G. CHOUDHRY, A. A. M. ROOF, and O. HUTZINGER. J. Chem. Soc. Perkin Trans. I, 2957 (1982).
19. K. GROB and G. GROB. Chromatographia, **5**, 3 (1972).
20. K. OLIE and O. HUTZINGER. *In* Recent developments in: mass spectrometry in biochemistry and medicine. Vol. 1. *Edited by* A. Frigerio, Plenum Press, New York and London. 1978. pp. 555–562.
21. R. ENGST, R. M. MACHOLZ, and M. KUJAWA. Chemosphere, **6**, 401 (1977) and references therein.

An eigenvalue method for determination of multicomponent diffusion coefficients. Application to NaOH + NaCl + H_2O mixtures

DEREK G. LEAIST[1] AND ROBERT A. NOULTY
Department of Chemistry, University of Western Ontario, London, Ont., Canada N6A 5B7

Received June 25, 1984

DEREK G. LEAIST and ROBERT A. NOULTY. Can. J. Chem. **63**, 476 (1985).

A general method for the determination of multicomponent diffusion coefficients is developed using the algebraic technique of matrix diagonalization. When linear combinations of measurements from several multicomponent diffusion experiments performed with different initial concentration gradients (but with the same final composition) are analyzed as simple binary data, particular combinations may be found that transform the multicomponent diffusion coefficient matrix **D** to diagonal form and thus yield time-invariant, pseudo-binary diffusion coefficients: the eigenvalues of **D**. Since the matrix that diagonalizes **D** is given by the coefficients used to form the linear combinations, **D** is easily recovered by the inverse transformation. The advantages of the eigenvalue method are briefly discussed. For testing purposes, ternary diffusion coefficients are determined from conductance measurements for dilute aqueous NaOH + NaCl mixtures. Diffusion of NaOH in aqueous NaCl is significantly more rapid than in pure water, and large coupled flows of NaCl are observed. The results are in close agreement with behavior predicted by Onsager–Fuoss theory.

DEREK G. LEAIST et ROBERT A. NOULTY. Can. J. Chem. **63**, 476 (1985).

Faisant appel à une technique algébrique de diagonalisation des matrices, on a développé une méthode générale permettant de déterminer les coefficients de diffusion à plusieurs composantes. Lorsqu'on analyse, sous forme de données binaires simples, des combinaisons linéaires de mesures provenant de plusieurs expériences de diffusion à plusieurs composantes, réalisées avec des gradients différents de concentrations initiales (mais avec la même composition finale), on peut trouver des combinaisons particulières qui permettent de transformer en une forme diagonale la matrice **D** du coefficient de diffusion à plusieurs composantes; on peut ainsi obtenir des coefficients de diffusion peudo-binaires qui ne varient pas avec le temps. Puisque la matrice qui diagonalise **D** est obtenue à partir des combinaisons utilisées pour former les combinaisons linéaires, on peut facilement récupérer **D** par la transformation inverse. On discute brièvement des avantages de la méthode des valeurs de eigen. Pour fins de vérification, on a déterminé les coefficients de diffusion ternaires à partir de mesures de conductivité sur des solutions aqueuses diluées de mélanges de NaOH + NaCl. La diffusion du NaOH dans le NaCl aqueux est beaucoup plus rapide que dans l'eau pure et on observe d'importantes migrations couplées de NaCl. Les résultats obtenus sont en bon accord avec le comportement prédit par la théorie de Onsager–Fuoss.

[Traduit par le journal]

1. Introduction

Multicomponent diffusion is of theoretical interest and considerable practical importance (1, 2). In many cases the diffusivity of a solute in a multicomponent mixture is significantly different from its binary diffusivity, especially if the solutes are electrolytes or they react chemically (3–8). Moreover, because diffusional flows interact, multicomponent diffusion of a component produces countercurrent or cocurrent flows of other components in the mixture. If the interaction is strong, a gradient in concentration of one component can effectively control transport of a second component.

Multicomponent diffusion is measured by classical gradient techniques (8–16). Typically, a system is prepared with initial concentration differences across a sharp boundary. As the system relaxes toward thermodynamic equilibrium, changes in a concentration-dependent property (such as the refractive index) are measured along the diffusion path. Diffusion coefficients are then obtained by fitting mathematical solutions of the multicomponent diffusion equations to the measurements. Because these solutions are complicated functions which contain the diffusion coefficients as non-linear parameters, determination of diffusivities for multicomponent systems by this procedure is substantially more difficult than for binary systems (17).

The purpose of this work is to develop a simpler method for the analysis of multicomponent diffusion data. Rather than fit solutions of the diffusion equations to measurements from individual experiments, we propose to treat linear combinations of measurements from experiments performed with different initial conditions as simple binary diffusion data. Particular combinations diagonalize (18, 19) the multicomponent diffusion equations and yield time-invariant, pseudo-binary diffusion coefficients — the eigenvalues of the multicomponent diffusion coefficient matrix **D**. The eigenvalues provide **D** in diagonal form. We show that the coefficients used to form the linear combinations define the matrix that diagonalizes **D**, and that **D** is easily reconstructed by the inverse transformation using matrix inversion and multiplication.

To evaluate the eigenvalue method, ternary diffusion coefficients have been determined for NaOH + NaCl + H_2O mixtures. This system was chosen in order to test recent predictions (21) that aqueous hydroxides diffuse much more rapidly in supporting electrolytes than in pure water. Another purpose of the study was to determine whether or not pH gradients produced by hydroxide gradients, like pH gradients produced by acid gradients (6–8), can generate large coupled flows of salts. Coupled transport driven by pH gradients has applications to separation technology and plays vital roles in biological systems (22–24).

2. Theory

n + 1 components

Provided the concentration gradients are not too large, isothermal diffusion in a system containing $n + 1$ components may be described by n coupled equations (25)

$$[1] \qquad \partial c_i/\partial t = \sum_{k=1}^{n} D_{ik}\nabla^2 c_k \qquad i = 1, 2, \ldots, n$$

where c_i is the concentration of component i in moles per unit

[1] To whom all correspondence should be addressed.

volume, t is the time, and ∇^2 denotes the Laplacian operator. Multicomponent diffusion coefficient D_{ik} measures the flux of component i produced per unit concentration gradient in component k. In matrix notation

$$[2] \quad \partial \boldsymbol{c}/\partial t = \mathbf{D}\nabla^2\boldsymbol{c}$$

where $\boldsymbol{c}$ denotes the column vector of n component concentrations and $\mathbf{D}$ is the $n \times n$ matrix of diffusion coefficients.

Consider linear combinations (18, 19) u_i of the component concentrations defined by

$$[3] \quad c_i = \sum_{k=1}^{n} A_{ik}u_k$$

Upon substitution of $\boldsymbol{c} = \mathbf{A}\boldsymbol{u}$ into eq. [2] and multiplying by $\mathbf{A}^{-1}$, the diffusion equations may be rewritten as

$$[4] \quad \partial \boldsymbol{u}/\partial t = (\mathbf{A}^{-1}\mathbf{D}\mathbf{A})\, \nabla^2\boldsymbol{u}$$

If coefficients A_{ik} are chosen so that the columns of $\mathbf{A}$ are eigenvectors of $\mathbf{D}$, the transform of $\mathbf{D}$ is diagonal (20)

$$[5] \quad \mathbf{A}^{-1}\mathbf{D}\mathbf{A} = \begin{pmatrix} D_1 & & & \\ & D_2 & & 0 \\ & & \ddots & \\ 0 & & & D_n \end{pmatrix}$$

and the transformed diffusion equations

$$[6] \quad \partial u_i/\partial t = D_i\nabla^2 u_i$$

are de-coupled. D_i are eigenvalues of $\mathbf{D}$ and u_i are solutions of the binary diffusion equations.

Reduction to diagonal form is a powerful technique (18, 19) that is frequently used to *solve* coupled differential equations. Can the same technique be used to *measure* multicomponent diffusion coefficients? Consider n diffusion experiments run at the same final composition of the system but with different initial concentration gradients. The idea is to use measurements from these runs as a "basis set" of data from which suitable linear combinations may be taken that diagonalize $\mathbf{D}$ and thus simplify the analysis.

Let Y represent the refractive index (4–6, 8–13), conductance (14, 21), density (26), optical absorbance (27), or another concentration-dependent property measured along the path of diffusion during an experiment. For initial concentration differences $\Delta c_i(0)$ across a sharp diffusion boundary, the corresponding difference in Y is

$$[7] \quad \Delta Y(0) = \sum_{i=1}^{n} S_i \Delta c_i(0)$$

where S_i are derivatives

$$[8] \quad S_i = \partial Y/\partial c_i$$

evaluated at the final composition of the system. X_i will be used to denote the fraction of $\Delta Y(0)$ contributed by component i.

$$[9] \quad X_i = S_i\Delta c_i(0)/\sum_{k=1}^{n} S_k\Delta c_k(0)$$

Apparent binary diffusion coefficients $D_a(t)$ may be obtained from multicomponent experiments by analyzing measured values of Y as if they were from a binary experiment (8, 11, 21, 28, 29). Apparent diffusion coefficients obtained in this manner usually vary with time. For example, if an experiment is performed with initial concentration gradients in solutes 1 and 2, and 1 diffuses rapidly compared to 2, values of $D_a(t)$ will be large initially but will decrease toward the end of the experiment as the initial gradient in 1 decays rapidly and diffusion of slower solute 2 predominates.

Although apparent diffusion coefficients are generally time-dependent, consider an experiment with particular initial conditions $X_i^{(k)}$ such that the column vector of initial concentration differences $\Delta c^{(k)}$ (0) is an eigenvector of $\mathbf{D}$

$$[10] \quad \mathbf{D}\begin{pmatrix} \Delta c_1^{(k)}(0) \\ \Delta c_2^{(k)}(0) \\ \vdots \\ \Delta c_n^{(k)}(0) \end{pmatrix} = D_k \begin{pmatrix} \Delta c_1^{(k)}(0) \\ \Delta c_2^{(k)}(0) \\ \vdots \\ \Delta c_n^{(k)}(0) \end{pmatrix}$$

Under these conditions

$$[11] \quad \partial c_i^{(k)}/\partial t = D_k\nabla^2 c_i^{(k)}$$

and hence

$$[12] \quad \partial Y^{(k)}/\partial t = D_k\nabla^2 Y^{(k)}$$

Consequently, the experiment behaves as a simple binary diffusion experiment with time-invariant, pseudo-binary diffusion coefficient equal to eigenvalue D_k. Once values of $X_i^{(k)}$ and D_k are established, the multicomponent diffusion coefficients are easily determined using

$$[13] \quad A_{ik} = X_i^{(k)}/S_i$$

and the inverse transformation

$$[14] \quad \mathbf{D} = \mathbf{A}^{-1}\begin{pmatrix} D_1 & & & \\ & D_2 & & 0 \\ & & \ddots & \\ 0 & & & D_n \end{pmatrix}\mathbf{A}$$

Since $\mathbf{D}$ is unknown at the start of the experiments, it is of course virtually impossible to choose the exact initial conditions that diagonalize $\mathbf{D}$. Nevertheless, by taking linear combinations of data from experiments with different (specifically, linearly independent values of $\Delta c(0)$) initial conditions, measurements corresponding to arbitrary initial conditions may be obtained. For instance, if $\Delta Y_i(t)/\Delta Y_i(0)$ symbolizes normalized measurements of property Y for an experiment in which the initial concentration gradient is entirely in component i ($X_i = 1$), measurements corresponding to arbitrary initial conditions X_i may be constructed from

$$[15] \quad \Delta Y(t)/\Delta Y(0) = \sum_{i=1}^{n} X_i\Delta Y_i(t)/\Delta Y_i(0)$$

A detailed example is given later.

In order to establish the initial conditions that reduce the diffusion equations to diagonal form, the standard deviation of measured values of the apparent diffusion coefficient

$$[16] \quad \sigma_D = \left[(N-1)^{-1}\sum_{i=1}^{N}(D_a(t_i) - \bar{D}_a)^2\right]^{1/2}$$

may be evaluated as a function of X_i. $\bar{D}_a$ is the mean apparent diffusion coefficient

$$[17] \quad \bar{D}_a = N^{-1}\sum_{i=1}^{N}\bar{D}_a(t_i)$$

For the particular initial conditions $X_i^{(k)}$, the apparent diffusion coefficient is effectively constant over the duration of a run, and hence σ_D is minimized. Therefore, values of $X_i^{(k)}$ may be obtained from the positions of the minima in σ_D. Eigenvalue D_k is obtained from the mean value of the apparent diffusion coefficient evaluated at $X_i^{(k)}$.

Ternary diffusion (n = 2)

When the standard deviation of the apparent diffusion coefficient for a ternary system is plotted against X_1, minima are found at $X_1^{(1)}$ and $X_1^{(2)}$. Since $X_1 + X_2 = 1$, we have

$$[18] \quad \mathbf{A} = \begin{pmatrix} X_1^{(1)}/S_1 & X_1^{(2)}/S_1 \\ (1-X_1^{(1)})/S_2 & (1-X_1^{(2)})/S_2 \end{pmatrix}$$

The mean diffusion coefficients evaluated at $X_1^{(1)}$ and $X_1^{(2)}$ equal eigenvalues D_1 and D_2, respectively. The ternary diffusion coefficients are evaluated from eq. [14].

$$[19] \quad \begin{pmatrix} D_{11} & D_{12} \\ D_{21} & D_{22} \end{pmatrix} = \mathbf{A}^{-1} \begin{pmatrix} D_1 & 0 \\ 0 & D_2 \end{pmatrix} \mathbf{A}$$

3. Experimental

Ternary diffusion coefficients of dilute aqueous NaOH + NaCl mixtures were measured at 25°C using a simplified version (14) of Harned's conductimetric procedure (30). In this technique, initial concentration gradients are formed by introducing a small volume of electrolyte into the bottom of a column of solution. The rate of diffusion is followed by monitoring changes in electrical conductance measured near the top and bottom of the column.

Because Harned's technique employs very small concentration gradients, changes in the transport coefficients due to compositional changes along the diffusion column are negligible, and the measured diffusion coefficients correspond to differential values defined by eq. [1]. (For diaphragm cell results (31), and to a lesser extent for optical results (32, 33), small but troublesome corrections are required to allow for the concentration-dependence of the diffusion coefficients.) Moreover, the conductimetric technique is reliable at low ionic strength where the transport coefficients can be estimated from limiting ionic conductances (14). Comparison of measured diffusion coefficients with theoretical predictions will provide a check on the reliability of the proposed eigenvalue method.

Equipment and procedure

The diffusion cells used in this work had cylindrical diffusion channels (height 0.04560 m, diameter 0.0126 m). The cells were constructed from high density polyethylene rather than glass in order to resist leaching by hydroxide. Pairs of circular platinum electrodes (diameter 10^{-3} m, cell constant $k \sim 10^3$ m^{-1}) were positioned at levels one-sixth of the distance from the top and bottom of the channel. At the start of each experiment, 0.1–0.3 mL of electrolyte was carefully injected with a calibrated syringe into the bottom of each solution-filled chamber. Initial concentration differences across the diffusion boundary were 0.05–0.2 mol L^{-1}. Conductances were measured six times per day for four consecutive days beginning one day after injection of electrolyte. Further details of the equipment and procedure have been reported (14, 34). Cell constants were obtained by calibration with 0.01 mol L^{-1} aqueous KCl (conductance 0.01413 m^2 S mol^{-1} (35)). Values of S_1 and S_2 were determined using an auxiliary conductance cell.

Reagents

Reagent grade NaCl was dried in a vacuum oven at 140°C and used without further purification. Stock solutions of NaOH were prepared by diluting saturated solutions that had been filtered to remove insoluble carbonate. The NaOH solutions were stored in polyethylene bottles and protected from the atmosphere. Concentrations of NaOH were determined by titration against potassium hydrogen pthalate. Winkler analyses (36) before and after the experiments indicated that the solutions contained less than 0.05% carbonate based on total alkali. Water used to make up the solutions was doubly-distilled and deionized (conductivity 0.8 × 10^{-4} ohm^{-1} m^{-1}). Corrections for solvent conductance were negligible.

Data analysis

For binary diffusion in a Harned cell, the difference in electrolyte concentration between the top (T) and bottom (B) electrode positions is given by (30)

$$[20] \quad \Delta c(t) = c_B(t) - c_T(t) = C \exp(-\pi^2 Dt/a^2)$$

where C is a constant, D is the binary diffusion coefficient, t is the time elapsed since introduction of electrolyte, and a is the height of the diffusion channel. For strong electrolytes, $\Delta c(t)$ is directly proportional to the conductance difference defined by (14, 21, 30)

$$[21] \quad \Delta K(t) = (k_B/k_T)K_B(t) - K_T(t)$$

where k_B/k_T denotes the ratio of cell constants of the top and bottom electrode pairs. Values of D are conveniently determined from the difference equation

$$[22] \quad D = -\frac{a^2}{\pi^2}\frac{\Delta \ln \Delta K(t)}{\Delta t}$$

by pairing each conductance reading with the corresponding reading taken on the following day.

In order to determine ternary diffusion coefficients, conductance differences $\Delta K_1(t)$ and $\Delta K_2(t)$ were measured for experiments run with the initial concentration gradient entirely in NaOH ($X_1 = 1$) or NaCl ($X_1 = 0$), respectively. Apparent diffusion coefficients for initial condition X_1 were calculated using the difference equation

$$[23] \quad D_a\left(\frac{t'+t''}{2}\right) = -\frac{a}{\pi^2}\frac{\ln \Delta K(t'') - \ln \Delta K(t')}{t''-t'}$$

wherein

$$[24] \quad \Delta K(t) = X_1 \frac{\Delta K_1(t)}{S_1 \Delta c_1(0)} + (1 - X_1)\frac{\Delta K_2(t)}{S_2 \Delta c_2(0)}$$

4. Results and discussion

Diffusion coefficients for NaOH(c_1) + NaCl(c_2) + H_2O mixtures were measured at a total electrolyte concentration of 0.020 mol L^{-1} for ratios of $c_1:c_2$ equal to 1:3, 1:1, and 3:1. Paired experiments with the initial concentration gradient in NaOH or NaCl were carried out in triplicate at each of the three compositions studied.

Typical results for a pair of experiments for $c_1 = 0.0150$ and $c_2 = 0.0050$ mol L^{-1} are shown in Figs. 1 and 2. In Fig. 1, values of the apparent diffusion coefficient computed from eq. [23] are plotted against t for various initial conditions. It is evident from the figure that the apparent diffusion coefficient varies substantially over the duration of a run when the initial concentration gradient is entirely in NaOH or NaCl ($X_1 = 1$ and $X_1 = 0$, respectively). It may be noted, however, that values of $D_a(t)$ are essentially constant for values of X_1 near 0.6 and 1.2. The "stationary" values of $D_a(t)$ (the eigenvalues of **D**) were found by plotting the standard deviation of the apparent diffusion coefficients against X_1, the fraction of the conductance difference across the initial diffusion boundary due to NaOH. From the two minima in σ_D shown in Fig. 2, initial conditions $X_1^{(1)} = 1.21$ and $X_1^{(2)} = 0.64$ that diagonalize **D** were obtained. From the mean apparent diffusion coefficients evaluated at these two values of X_1, eigenvalues $D_1 = 2.58 \times 10^{-9}$ and $D_2 = 1.71 \times 10^{-9}$ m^2 s^{-1} were obtained.

The results of the experiments are summarized in Tables 1 and 2. As shown in Table 2, values of D_{11}, the ternary dif-

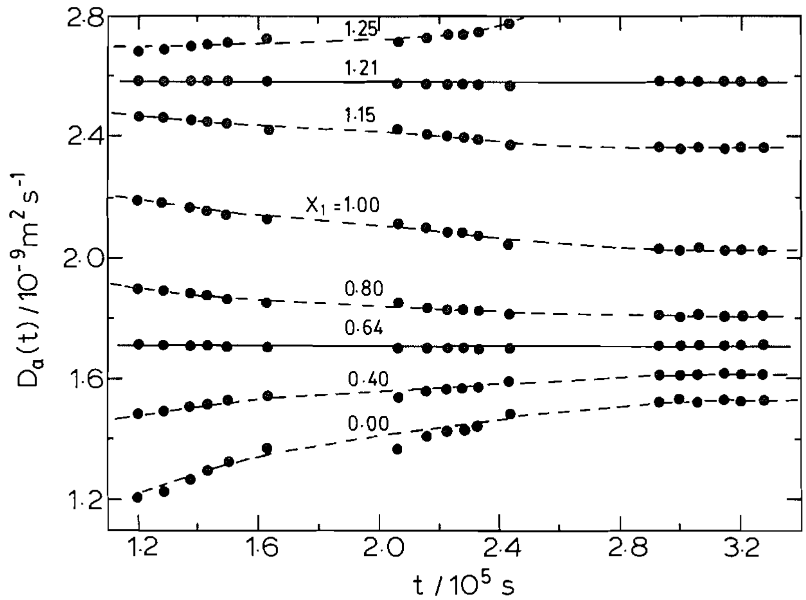

FIG. 1. Apparent binary diffusion coefficients of aqueous NaOH(1) + NaCl(2) for c_1 = 0.015 mol L^{-1} and c_2 = 0.005 mol L^{-1} for selected initial conditions. For the experiment with the initial concentration gradient entirely in NaCl (X_1 = 0), 0.32 mL of solution containing 0.015 mol L^{-1} NaOH and 0.0712 mol L^{-1} NaCl was injected into a cell filled with solution containing 0.015 mol L^{-1} NaOH and 0.001 mol L^{-1} NaCl. For the experiment with the initial gradient in NaOH (X_1 = 1), 0.32 mL of solution containing 0.254 mol L^{-1} NaOH and 0.005 mol L^{-1} NaCl was injected into the same cell filled with 0.001 mol L^{-1} NaOH and 0.005 mol L^{-1} NaCl. The curves for X_1 = 0.4, 0.64, 0.80, 1.15, 1.21, and 1.25 were obtained by analysis of linear combinations of data from the two experiments run with X_1 = 0.00 and X_1 = 1.00. The volume of the cell was 5.78 mL.

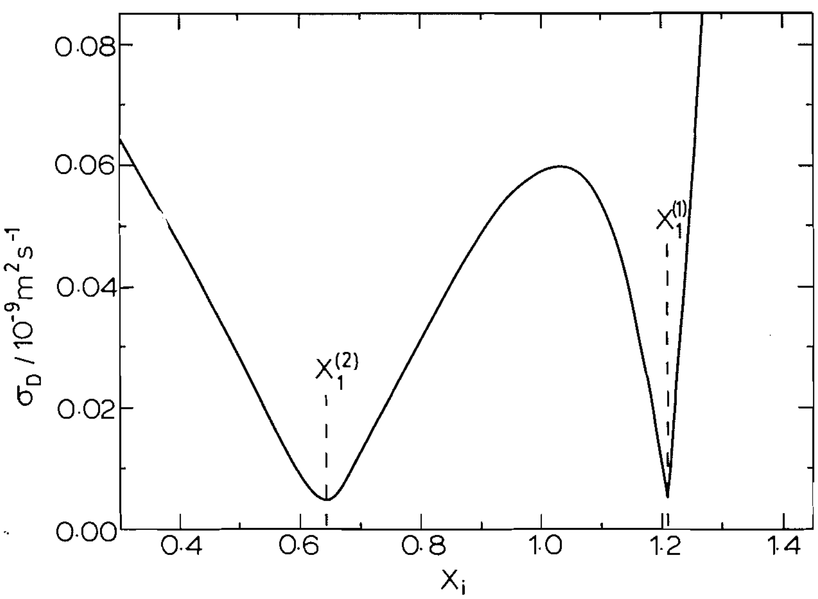

FIG. 2. Standard deviation of the apparent diffusion coefficient of aqueous NaOH(1) + NaCl(2) for c_1 = 0.015 mol L^{-1} and c_2 = 0.005 mol L^{-1}. See caption of Fig. 1 for details.

fusivity of NaOH in aqueous NaCl, increase steadily as the system becomes richer in NaCl. At the same ionic strength, in contrast, the binary diffusivity of aqueous NaOH is only 1.99 $\times 10^{-9}$ m^2 s^{-1} (34). In binary solutions of NaOH, however, the condition of electroneutrality requires that Na^+ and OH^- diffuse at the same rate, even though OH^- has approximately four times the mobility of Na^+ (35); the electric field produced by flow of the electrolyte slows down OH^- and speeds up Na^+ so that they travel at the same rate and the electric current is zero. In ternary NaOH(1) + NaCl(2) + H_2O mixtures, on the other hand, the electric field along the NaOH gradient which slows down OH^- also generates counterflow of Cl^-. Highly mobile OH^- can thus diffuse down the NaOH gradient more rapidly than Na^+ while still maintaining electroneutrality. This mechanism accounts for the increased diffusivity of the NaOH component in aqueous NaCl as well as the large negative values of D_{21} (the cross-diffusion coefficient measuring coupled flow of NaCl produced per unit concentration gradient in NaOH). Similar diffusional behavior has been observed for HCl + NaCl + H_2O and other acid-containing mixed electrolytes (6, 8, 21). In those systems, the electric field generated by diffusion of highly mobile protons produces counterflow of cations.

TABLE 1. Parameters used to calculate experimental diffusion coefficients for NaOH(1) + NaCl(2) + H_2O at 25°C

c_1[a]	c_2[a]	S_1/S_2	$X_1^{(1)}$	$X_1^{(2)}$	D_1[b]	D_2[b]
5.0	15.0	2.12	1.42 (±0.05)	0.23 (±0.03)	3.91 (±0.02)	1.58 (±0.02)
10.0	10.0	1.90	1.36 (±0.09)	0.31 (±0.06)	3.12 (±0.23)	1.54 (±0.06)
15.0	5.0	2.29	1.23 (±0.05)	0.62 (±0.04)	2.64 (±0.11)	1.69 (±0.03)

[a] In 10^{-3} mol L^{-1}.
[b] In 10^{-9} m^2 s^{-1}.

TABLE 2. Observed and predicted ternary diffusion coefficients for NaOH(1) + NaCl(2) + H_2O at 25°C

c_1[a]	c_2[a]	D_{11}[b]	D_{12}[b]	D_{21}[b]	D_{22}[b]
5.0	15.0	Obsd. 3.72 (±0.02)	−0.30 (±0.04)	−1.34 (±0.13)	1.76 (±0.03)
		Calcd. 3.70	−0.23	−1.29	1.71
10.0	10.0	Obsd. 2.95 (±0.19)	−0.33 (±0.07)	−0.71 (±0.21)	1.70 (±0.10)
		Calcd. 2.93	−0.37	−0.71	1.82
15.0	5.0	Obsd. 2.42 (±0.07)	−0.52 (±0.01)	−0.31 (±0.10)	1.90 (±0.01)
		Calcd. 2.39	−0.47	−0.30	1.89

[a] In 10^{-3} mol L^{-1}.
[b] In 10^{-9} m^2 s^{-1}.

TABLE 3. Comparison of observed and predicted L_{ik} coefficients

c_1[a]	c_2[a]	RTL_{11}[b]	RTL_{12}[b]	RTL_{21}[b]	RTL_{22}[b]
5.0	15.0	Obsd. 1.69 (±0.02)	−0.94 (±0.04)	−0.90 ±0	1.94 (±0.05)
		Calcd. 1.67	−0.87	−0.87	1.89
10.0	10.0	Obsd. 2.18 (±0.16)	−0.94 (±0.09)	−0.94 (±0.18)	1.47 (±0.12)
		Calcd. 2.33	−0.97	−0.97	1.55
15.0	5.0	Obsd. 2.27 (±0.09)	−0.65 (±0.05)	−0.64 (±0.10)	0.89 (±0.02)
		Calcd. 2.41	−0.625	−0.625	0.89

[a] In 10^{-3} mol L^{-1}.
[b] In 10^{-9} mol m^{-1} s^{-1}.

The difference in mobility between Na^+ and Cl^- is not as great as the difference in mobility between Na^+ and OH^-: Cl^- is about 50% more mobile than Na^+ (35). The electric field per unit concentration gradient in NaCl is therefore weaker than for NaOH, and values of D_{12} for aqueous NaOH(1) + NaCl(2) are proportionally smaller than for D_{21}. Also, the increase in the diffusivity D_{22} of NaCl in NaOH-rich mixtures is not as dramatic as for D_{11} in NaCl-rich mixtures.

Onsager's equations (25)

$$[25] \quad J_i = -\sum_{k=1}^{n} L_{ik} \nabla \mu_k$$

relate molar fluxes, J_i, of components to gradients in the chemical potentials of the components. Conveniently, values for the L_{ik} phenomenological coefficients can be estimated (14) for dilute mixed electrolytes from limiting ionic conductances and Onsager–Fuoss theory (37, 38) of the electrophoretic and relaxation effects. Details of the calculations have been reported (14). Given L_{ik} values, diffusion coefficients are calculated from (25)

$$[26] \quad D_{ik} = \sum_{m=1}^{n} L_{im} \partial \mu_m / \partial c_k$$

The parameters used to predict the transport coefficients of aqueous NaOH(1) + NaCl(2) are listed in Table 4. Values of $\partial \mu_m / \partial c_k$ were calculated by differentiation of expressions

TABLE 4. Molar ionic conductances and other parameters[a] used to calculate theoretical values for the transport coefficients

Electrolyte	Λ°_{+m}[d]	Λ°_{-m}[d]	β[e]
NaOH	50.10	198.3	0.08[b]
NaCl	50.10	76.35	0.16[c]

[a] Ion size parameter (14) $a = 4 \times 10^{-10}$ m; solvent viscosity (35) $\eta = 8.90 \times 10^{-4}$ kg m^{-1} s^{-1}; solvent dielectric constant (35) $\epsilon = 78.4$; Debye–Hückel constant (35) $\alpha = 1.17$.
[b] Reference 34.
[c] Reference 39.
[d] In 10^{-4} m^2 s mol^{-1}.
[e] In L mol^{-1}.

$$[27] \quad \mu_1 = \mu_1^0 + RT \ln [c_1(c_1 + c_2) y_{\pm 1}^2]$$

$$[28] \quad \mu_2 = \mu_2^0 + RT \ln [c_2(c_1 + c_2) y_{\pm 2}^2]$$

for the chemical potentials of the solutes. Mean ionic activity coefficients (on the molar concentration scale) were evaluated using Guggenheim's expression (39)

$$[29] \quad \ln y_{\pm i} = -\alpha \frac{\sqrt{c_1 + c_2}}{1 + \sqrt{c_1 + c_2}} + \beta_1 c_1 + \beta_2 c_2 + \beta_i (c_1 + c_2)$$

where α is the Debye–Hückel constant and β_i are small empir-

TABLE 5. Experimental diffusion coefficients for NaOH(1) + NaCl(2) + H_2O at 25°C determined by non-linear least squares

$c_1{}^a$	$c_2{}^a$	$D_{11}{}^b$	$D_{12}{}^b$	$D_{21}{}^b$	$D_{22}{}^b$
5.0	15.0	3.77 (±0.15)	−0.27 (±0.04)	−1.35 (±0.19)	1.72 (±0.05)
10.0	10.0	3.02 (±0.02)	−0.35 (±0.08)	−0.75 (±0.14)	1.75 (±0.08)
15.0	5.0	2.45 (±0.07)	−0.55 (±0.08)	−0.33 (±0.08)	1.93 (±0.02)

[a]In 10^{-3} mol L^{-1}.
[b]In 10^{-9} m^2 s^{-1}.

ical constants which allow for specific ion interactions.

Experimental transport coefficients are compared with predicted values in Tables 2 and 3. Agreement is very good. The observed values of the L_{ik} coefficients are consistent with the Onsager reciprocal relation (2, 25) $L_{12} = L_{21}$ which lends further confidence to the reliability of the eigenvalue method.

A general procedure for the determination of ternary diffusion coefficients from conductance measurements using non-linear least squares has been reported (40). In practice, we found that the eigenvalue method was much easier to use. The non-linear least-squares procedure, for instance, requires lengthy computations in order to simultaneously optimize values of the four diffusion coefficients. Experimental diffusion coefficients determined for NaOH + NaCl mixtures by the non-linear least-squares method are given in Table 5. Comparison of Tables 2 and 5 indicates that the eigenvalue and non-linear least-squares procedures give essentially identical results. With the eigenvalue method, however, the problem of locating the minimum in the variance in four dimensions is replaced by the more manageable problem of locating two minima in one dimension (i.e. minima in σ_D as a function of X_1).

In effect, the eigenvalue method reduces the analysis of coupled, multicomponent transport equations to an analysis based on de-coupled, well-understood binary equations. This transformation enables the determination of ternary diffusivities without explicitly solving multicomponent diffusion equations or resorting to non-linear curve fitting procedures.

The eigenvalue method holds especial promise for the measurement of quaternary diffusion (17). For those systems, the non-linear least-squares method requires simultaneous optimization of nine parameters (a formidable task), while the eigenvalue method would involve searching for three minima in only two dimensions.

The present study has employed time invariance of the apparent diffusion coefficient to locate the eigenvalues of **D**. This criterion is well suited to the Harned technique and other restricted diffusion experiments (1, 41) in which the concentrations are measured at two positions along the path of diffusion. On the other hand, optical methods (4–6, 8–13) such as Rayleigh or Gouy experiments employ free diffusion boundary conditions. In those experiments the position of interference fringes is followed as a function of time. The apparent diffusion coefficient obtained by analysis of the position of a single fringe will generally vary from fringe to fringe. By locating the minimum in σ_D as a function of fringe number the eigenvalue technique can also be used to analyze multicomponent optical data.

Acknowledgement

This work was supported by the Natural Sciences and Engineering Research Council of Canada.

1. E. L. CUSSLER. Multicomponent diffusion. Elsevier, Amsterdam. 1976.
2. L. ONSAGER. Ann. N. Y. Acad. Sci. **46**, 241 (1945).
3. V. VITAGLIANO and R. SARTORIO. J. Phys. Chem. **74**, 2949 (1970).
4. R. P. WENDT. J. Phys. Chem. **69**, 1227 (1965).
5. P. J. DUNLOP. J. Phys. Chem. **63**, 612 (1959).
6. H. KIM, G. REINFELDS, and L. J. GOSTING. J. Phys. Chem. **77**, 934 (1973).
7. D. G. LEAIST. J. Chem. Soc. Faraday Trans. 1. **78**, 3069 (1982).
8. A. REVZIN. J. Phys. Chem. **76**, 3419 (1972).
9. Ref. 1, Chapt. 4.
10. P. J. DUNLOP, B. J. STEEL, and J. E. LANE. Experimental methods studying diffusion in liquids, gases, and solids. *In* Physical methods of chemistry. Vol. 1. *Edited by* A. Weissberger and B. W. Rossiter. Wiley, New York. 1972. p. 205.
11. H. FUJITA and L. J. GOSTING. J. Phys. Chem. **64**, 1256 (1960).
12. J. G. ALBRIGHT and B. C. SHERRIL. J. Solution Chem. **8**, 201 (1979).
13. D. G. MILLER. J. Solution Chem. **10**, 831 (1981).
14. D. G. LEAIST and P. A. LYONS. Aust. J. Chem. **33**, 1869 (1980).
15. E. L. CUSSLER and P. J. DUNLOP. J. Phys. Chem. **70**, 1880 (1966).
16. G. KOSANOVICH and H. T. CULLINAN. Can. J. Chem. Eng. **49**, 753 (1971).
17. H. KIM. J. Phys. Chem. **73**, 1716 (1969).
18. H. L. TOOR. A. I. Ch. E. J. **10**, 448 (1964); **10**, 460 (1964).
19. W. E. STEWART and R. PROBER. Ind. Eng. Chem. Fundam. **3**, 224 (1964).
20. H. MARGENAU and G. M. MURPHY. The mathematics of physics and chemistry. 2nd ed. Van Nostrand, New York. 1956. p. 320.
21. D. G. LEAIST and P. A. LYONS. J. Phys. Chem. **86**, 564 (1982).
22. E. M. CHOY, D. F. EVANS, and E. L. CUSSLER. J. Am. Chem. Soc. **96**, 7085 (1974).
23. R. M. IZATT, D. V. DEARDEN, D. W. MCBRIDE, J. L. OSCARSON, J. D. LAMB, and J. J. CHRISTENSEN. Sep. Sci. Technol. **18**, 1113 (1983).
24. N. N. LI and A. L. SHRIER. *In* Recent advances in separation science. CRC Press, Cleveland. 1972. p. 163.
25. S. R. DE GROOT and P. MAZUR. Non-equilibrium thermodynamics. North-Holland, Amsterdam. 1962.
26. F. T. WALL, P. F. GRIEGER, and C. W. CHILDERS. J. Am. Chem. Soc. **74**, 3562 (1952).
27. M. TANIGAKI, K. KONDO, M. HARADA, and W. EGUCHL. J. Phys. Chem. **87**, 586 (1983).
28. E. L. CUSSLER. Ph.D. Thesis. University of Wisconsin. 1965.
29. E. L. CUSSLER and E. N. LIGHTFOOT. J. Phys. Chem. **69**, 736 (1965).
30. H. S. HARNED and R. L. NUTTAL. J. Am. Chem. Soc. **69**, 736 (1947).
31. R. H. STOKES. J. Am. Chem. Soc. **72**, 2243 (1950).
32. J. A. RARD and D. G. MILLER. J. Solution Chem. **8**, 701 (1979).
33. J. G. ALBRIGHT and D. G. MILLER. J. Phys. Chem. **79**, 2061 (1975).
34. R. A. NOULTY and D. G. LEAIST. J. Solution Chem. **13**, 767 (1984).
35. R. A. ROBINSON and R. H. STOKES. Electrolyte solutions. 2nd

ed. Academic Press, New York. 1959. App. 6.1, 6.2.
36. W. C. PIERCE and E. L. HAENISCH. Quantitative analysis. Wiley, New York. 1948. p. 136.
37. L. ONSAGER and R. M. FUOSS. J. Phys. Chem. **36**, 2689 (1932).
38. M. CHEN and L. ONSAGER. J. Phys. Chem. **81**, 2017 (1977).
39. E. A. GUGGENHEIM and J. C. TURGEON. Trans. Faraday Soc. **51**, 747 (1955).
40. D. G. LEAIST and P. A. LYONS. J. Phys. Chem. **85**, 1756 (1981).
41. A. F. COLLINGS, D. C. HALL, R. MILLS, and L. A. WOOLF. J. Phys. E. Sci. Instr. **4**, 425 (1971).

An evaluation of high resolution nuclear magnetic resonance experiments and protocols in the structure elucidation of organic molecules. I. A relatively simple system, brucine[1]

MICHAEL A. BERNSTEIN[2] AND LAURANCE D. HALL
Department of Chemistry, University of British Columbia, Vancouver, B.C., Canada V6T 1W5

Received April 5, 1984

MICHAEL A. BERNSTEIN and LAURANCE D. HALL. Can. J. Chem. **63**, 483 (1985).

Using a *combination* of one-dimensional (1D) and two-dimensional (2D) high resolution nmr methods, the ^{1}H nmr spectrum of brucine was fully assigned. The 2D *J*-resolved and homonuclear chemical shift correlated (COSY) experiments provided assignments without full structural information; this was obtained from nuclear Overhauser effect (nOe) enhancement experiments (1D and 2D). With the proton spectrum fully assigned, proton-bearing carbons in the ^{13}C nmr spectrum were easily assigned using the 2D heteronuclear chemical shift correlation map (CSCM) experiment.

MICHAEL A. BERNSTEIN et LAURANCE D. HALL. Can. J. Chem. **63**, 483 (1985).

Faisant appel à une *combinaison* de méthodes rmn à haute résolution en une dimension (1D) et en deux dimensions (2D), on a fait une attribution complète de tout le spectre rmn ^{1}H de la brucine. Grâce à des expériences en 2D résolues pour *J* impliquant une corrélation des déplacements chimiques homonucléaires (COSY), on a pu obtenir des attributions sans avoir d'informations structurales complètes; on a obtenu ceci à l'aide d'expériences de rehaussement d'effet nucléaire Overhauser tant en 1D qu'en 2D. L'ensemble du spectre du proton étant attribué, on a pu facilement faire une attribution des carbones portant des protons dans le spectre rmn du ^{13}C en utilisant l'expérience de la carte de corrélation des déplacements chimiques hétéronucléaires en 2D (CCDC).

[Traduit par le journal]

Introduction

It is already obvious from the literature that modern nmr methods used singly can have very high information content, and that *synergistic combinations* of these can result in a further dramatic increase in chemical insight. This laboratory has reported the combination of 2D *J*-resolved spectroscopy with homonuclear chemical shift correlated spectroscopy as part of a sequence for oligosaccharide sequence determination (1, 2), and related approaches have been utilized with protein studies (3, 4). An exhaustive survey of all such combined experiments is not in order, but a report by Kessler and Eierman (5) on the combined use of homo- and heteronuclear correlated 2D nmr with cyclic peptides merits mention. The purpose of this study is to evaluate the combined use and sequence of high resolution 2D nmr methods for molecular structure and conformation determination in the natural products area. Given the exploratory nature of this work, we have chosen the well-known alkaloid brucine (**2**), which is very similar to strychnine (**1**), as an exemplar.

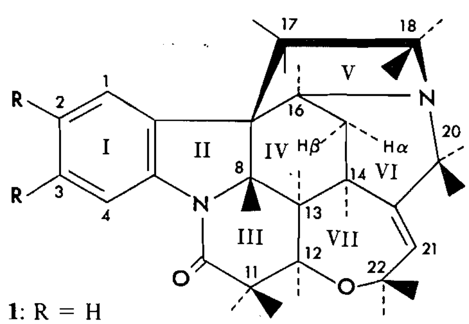

1: R = H
2: R = OCH_3

We shall not discuss in detail individual experiments since all have been adequately reviewed (1, 6); however, some brief comments are pertinent. The 2D *J*-resolved experiment has been widely applied to organic molecules (see, for example, ref. 7) since it efficiently simplifies spectra that have a complex, overlapping set of resonances. Projection of the tilted data matrix onto the F_2 axis yields one line at the chemical shift of each proton; "slices" (F_1 traces) taken at each chemical shift give a "*J*-spectrum" for that proton – its coupling pattern, with high resolution (due to the removal of magnetic inhomogeneity contributions to line-width). That information which the 2D *J*-resolved experiment does not provide is the coupling pathway. A quick and convenient 2D experiment that does this (8) is homonuclear 2D spectroscopy[3] (COSY). Normally viewed "from above," along the signal intensity axis and represented as a contour plot, this experiment shows a series of peaks along the "diagonal" where $F_1 = F_2$. *J*-coupling is encoded in "off diagonal" correlation peaks whose positions exactly indicate the frequencies of the coupled protons (9).

It is well known that dipolar relaxation effects occur "through space" and their observation, either as the nuclear Overhauser enhancement effect (nOe) or in relaxation rates, is invaluable for molecular structure elucidation and the measurement of precise interproton distances (10). We have found the nOe experiment particularly useful, especially when performed in the difference mode (SSNOEDS ≡ steady state nOe difference spectroscopy). A "control" spectrum with the decoupler placed well out of the spectral region is digitally subtracted from an "experiment" where a set of resonances is *selectively* irradiated for a number of T_1 periods prior to an observation pulse and signal acquisition (11 and 12 for a recent review). In the difference mode, only protons experiencing an nOe (plus the proton irradiated) will appear and all other resonances will exactly cancel; this experiment can reproducibly measure nOe's of <1% even for an overlapping multiplet.

Although the SSNOEDS experiment is extremely powerful and relatively quick to perform, it suffers from the sometimes

[1]Abstracted in part from ref. 1.
[2]Present address: Merck Frosst Canada Inc., P.O. Box 1005, Pointe Claire – Dorval, Quebec, Canada H9R 4P8.

[3]An analogous experiment with identical information content is SECSY–spin-echo correlation spectroscopy.

important limitation that it is impossible to perform without ambiguity due to the nonselectivity of irradiation which is inescapable when the signal of a proton overlaps with that of another. Here, the 2D experiment, NOESY (2D nOe spectroscopy) can be useful (13). The output from this experiment is identical to that of the COSY experiment, but off-diagonal peaks now correlate protons relaxing one another via the dipole–dipole mechanism (in the extreme-narrowing limit and in the absence of chemical exchange). Correlation peaks are relatively small for molecules in the fast-tumbling regime and this has probably deterred many experimenters from using this experiment with this chemical system. However, in our limited experience with the experiment, we have found it to be quite tractible.

Given adequate quantities of a substance and its fully assigned ^{1}H nmr spectrum, it is now almost a trivial matter to assign all proton-bearing carbons in the ^{13}C nmr spectrum without recourse to selective irradiation experiments. Initially, it is helpful to know the number of protons attached to each carbon. Classically, this is achieved by single frequency off-resonance decoupling (SFORD), but this experiment (14) is not without difficulties, (a) in a spectrally crowded region and (b) when a carbon bears magnetically inequivalent protons. A number of multi-pulse methods provide the necessary information very efficiently, and we have found utility for one, dubbed DEPT (distortionless enhancement and polarization transfer) (15). Now, the proton chemical shift may be correlated with carbons in a "single" 2D experiment termed CSCM – the heteronuclear chemical shift correlation map (16). The experiment is designed to show a proton multiplet at the coordinates defined by the respective chemical shifts of a carbon nucleus and its attached proton or protons. The ability to differentiate between spectrally close carbons and define proton multiplets is limited by the data storage capability of the spectrometer and the amount of time available for collection and processing of what are invariably very large data matrices. Usually, ^{1}H multiplet detail is forsaken in the interest of conserving experimental time; this is no great sacrifice since those details are most efficiently derived from the 2D *J*-resolved experiment.

Experimental

Our experience with the above experiments suggested that there are two levels of structure elucidation, one requiring a modest investment of instrument time and the other somewhat more. The statements below on the ^{1}H nmr experiments pertain to the user with access to a modern high-field nmr instrument, and ca. 5 mg of organic material of mol. wt. <1000. Obviously this should be used as a guide, as it does not exclude, for example, the protocol being applied to smaller amounts of material with appropriate allowances made for additional signal-averaging.

The proton nmr spectrum is readily assigned to the point of identifying coupling pathways, chemical shifts, and coupling constants by a combination of the 2D *J*-resolved experiment (yielding δ and *J* information) and the COSY experiment (providing coupling pathways). In fortunate circumstances this information may be sufficient to assign the spectrum fully and determine the structure. In some instances, however, as is the case with brucine, this level of analysis does not necessarily answer all questions since it may fail to distinguish axial and equatorial geminal protons,[4] and may leave unanswered questions on conformation.

These latter points are amply covered with selected nOe experiments, which report on the local environment of the saturated spin(s), often with the added bonus of a confirmation of previous assignments from the two, 2D nmr experiments mentioned above. It should be stressed that SSNOEDS experiments are time consuming, and the experimenter is advised to construct a molecular model of the compound, consider the available data, and establish which nOe experiments will have unambiguous conformational implications. Although it is, in principle, possible to calculate accurate *inter*-proton distances with such methods (10), we point out the utility of a qualitative inspection of the results, and the possibility for an unambiguous structural assignment with this non-mathematical approach. This approach has the further advantage that the conditions for data collection are relaxed, in that saturation of a multiplet need not be complete,[5] and relaxation delays and saturation times may be trimmed to speed up signal acquisition.

In certain instances a key SSNOEDS experiment may not be accessible; such is the case when several proton signals overlap and none can be selectively irradiated without ambiguity. Here the NOESY experiment is useful, since no irradiations are performed, *per se*.

Given sufficient sample, it is possible now to proceed with the assignment of protonated carbons in the molecule. A spectral editing sequence such as DEPT will not only serve to identify the number of protons attached to each carbon, but also usefully determine the pulse lengths necessary for the execution of the heteronuclear CSCM experiment. These two experiments, along with the assigned proton spectrum, should expedite the assignment of the carbon resonances.

Results

The overall strategy chosen was first to fully assign the proton nmr spectrum and then use this to assign the nonquaternary signals in the carbon-13 spectrum. The former was achieved primarily using COSY, with some assistance from 2D *J*-resolved spectroscopy, and 1D and 2D nOe experiments and chemical shift arguments. With this completed, the ^{13}C nmr spectrum was easily assigned using the CSCM experiment, with spectral editing performed using DEPT.

Portions of the ^{1}H nmr spectrum of brucine are presented in Fig. 1. Two singlets in the aromatic region are omitted, and the multiplet in the vinyl region is shown in an inset. Analysis at 360 MHz began with the COSY spectrum. The experiment was performed with coherence transfer echo selection, on a ca. 0.01 *M* solution in $CDCl_3$. A relaxation delay of only 0.2 s and the minimum of 4 acquisitions per t_1 interval meant that 20 min was required for the collection of a 512 * 1K data set; the sweep-width was 10 ppm in both frequency dimensions. Next, a 2D *J*-resolved experiment was set up, and this experiment required ca. 54 min for collection of the data; this was somewhat longer than that for the COSY due to the necessarily longer relaxation delay and the need for more scans. Whilst these *J*-resolved data were being collected, the COSY data set was processed and plotted. By this time, acquisition of the 2D *J*-resolved data set was complete, and data processing was performed. All the above operations were performed automatically in a MACRO program on the Nicolet system.[6] Minimal operator intervention was required, except at the plotting stage, where decisions were made to expand certain spectral regions for clarification. Details of these "survey-condition" parameters are in Table 1.

The COSY spectrum of brucine is shown in Fig. 2. Only the

[4]This is especially a problem in distorted ring systems, where coupling constants may not unambiguously assign a proton's orientation.

[5]This point takes on special significance in crowded spectra, where frequency selectivity may only be possible under sub-saturating conditions.

[6]All experiments at 360 MHz were performed at Nicolet Magnetics Corp., Fremont, CA, U.S.A.

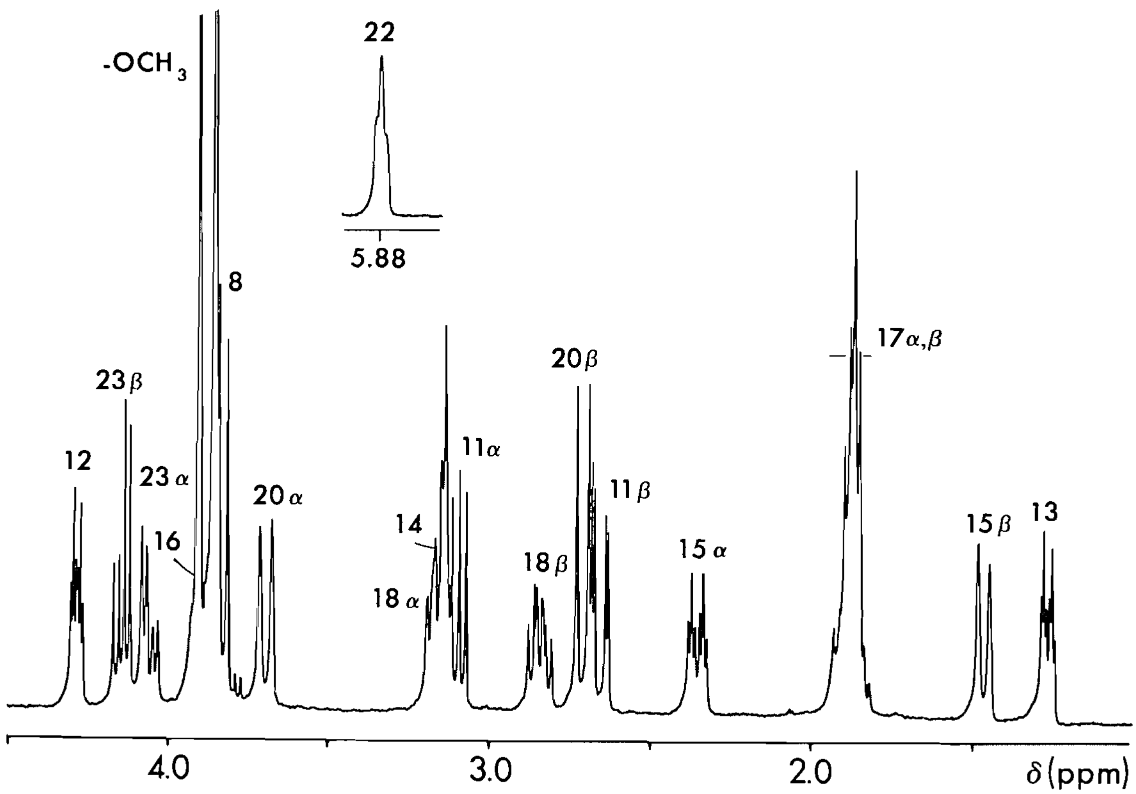

FIG. 1. 400-MHz ^{1}H nmr spectrum of brucine (ca. 0.02 M in $CDCl_3$), showing the assignment of non-aromatic protons.

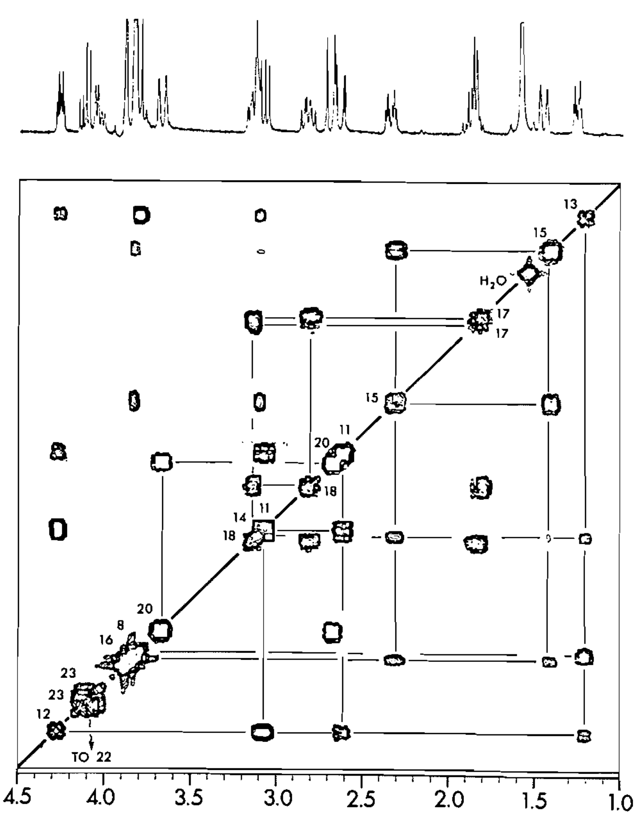

FIG. 2. 360-MHz COSY spectrum of brucine in the region δ 4.5 and 1.0. Connectivities to the vinylic proton are indicated, though they are not on the diagram.

region between δ 4.5 and 1.0 is plotted here, for the sake of clarity. The analysis began with the realization that four "pockets" of coupled spins exist in the molecule, with little or no coupling between them: namely (a) H-20α and H-20β; (b) H-17α, H-17β, H-18α, and H-18β; (c) H-22, H-23α, and H-23β; and (d) H-11α, H-11β, H-12, H-13, H-8, H-14, H-15α, H-15β, and H-16. COSY succeeded in assigning all protons in spin sets (a), (c), and (d). With the H-17 and H-18 protons it was necessary to invoke a chemical shift argument, namely that the protons on C-18 are relatively deshielded by the ring nitrogen atom. Herewith, the protons in spin set (b) were assigned in the COSY spectrum. However, it was not possible at this stage to differentiate α from β geminal protons.[7] The connectivities are indicated along with the assignments in the figure; these were made without ambiguity. The large —OCH_3 peaks that resonate very close to H-8 and H-16 could have hindered the assignment had H-8 and H-16 been scalar coupled to each other, as they might then have obscured a set of cross peaks; this was not the case. Special considerations were required for the tightly coupled geminal protons, which were assigned to the H-23 and H-17 pairs. Distortion of peak intensities indicated tight coupling, especially in the case of the H-17 pair. To assess the reliability of the COSY spectrum, it is interesting to consider H-15β (ca. δ 1.4), which shows one large splitting and several smaller (≤1.5 Hz) ones. In the COSY spectrum, the expected three connectivities are clear, even though the digitization is less than 7 Hz per point.

[7]The molecule is not planar and hence an upper (β) and lower (α) face is not clear. For this reason, geminal protons are defined (see **1** and **2**) for the purpose of this study.

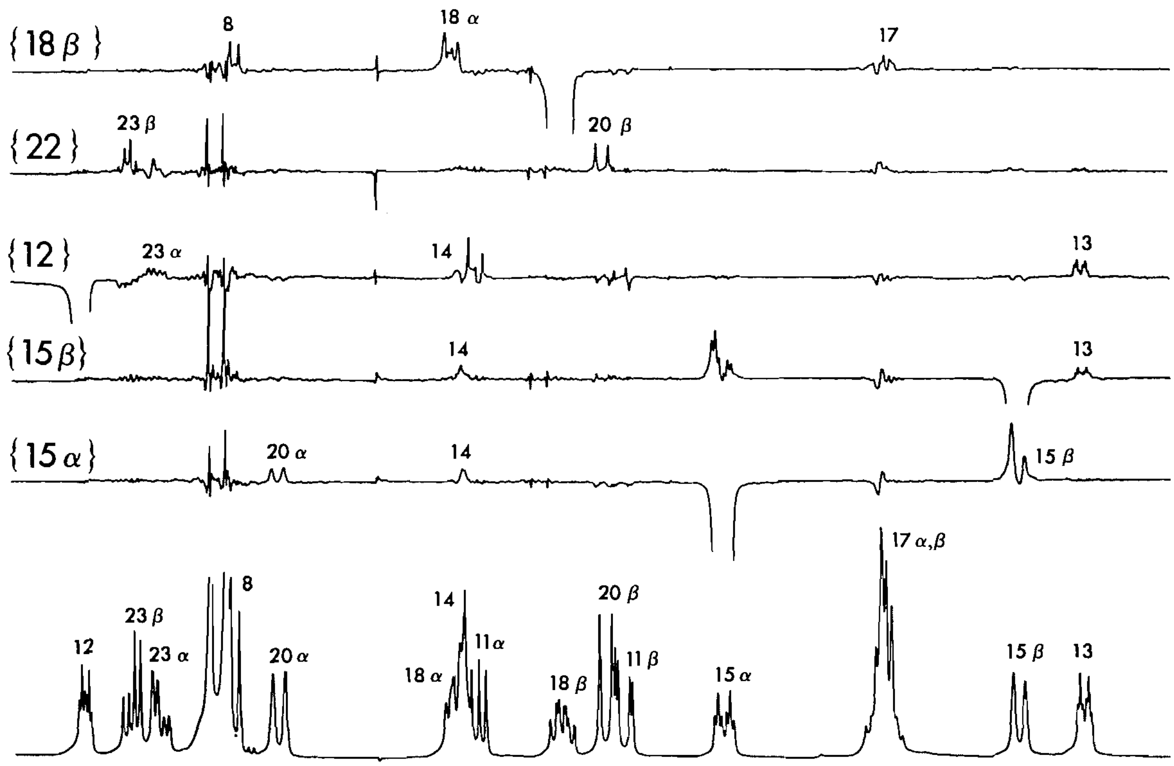

FIG. 3. SSNOEDS experiments performed on brucine at 400 MHz. At the bottom is the "control" spectrum and, next to each difference spectrum, the irradiated proton is indicated. Since the analysis was only qualitative, the sample was not degassed.

TABLE 1. Parameters used in automated "survey conditions" collection and processing of ^{1}H COSY and 2D J-resolved experiments at 360 MHz

Total time (min)		Sweep width[a] F_2	Sweep width[a] F_1	Block size[b] F_2	Block size[b] F_1	Relax. delay[c]	No. scans per t_1	Apodization[d] t_1	Apodization[d] t_2	Zerofill t_1	Symm.[e]
—	Begin collecting COSY data			16K							
—	Calibrate pulse widths										
0	Begin collecting COSY data	3,600	3,600	1,024	512	0.2	4				
20	Begin collecting 2D J-resolved data	3,600	29	4,096	64	1.0	16				
—	Process and plot COSY							MS	MS	No	Yes
65	Commence processing and plotting of 2D J-resolved experiment							EM DM	DM MS	Yes	No
120	End										

[a]Full-sweep width (Hz).
[b]Block sizes (words).
[c]Relaxation delay (s).
[d]Apodization function: EM = exponential multiplier; DM = double exponential multiplier; MS = sinebell multiplier. With the J-resolved experiment, the strongest resolution enhancement function is chosen for t_2 which the signal-to-noise permits.
[e]Symmetrization was not possible with the 2D J-resolved data, but would be recommended where the software is available.

The 2D J-resolved experiment did not prove very useful and these data are not included here. It would have been particularly useful in the —OCH$_3$ signal region. However, the overlapping H-16 resonance remained obscured by the familiar "tailing" in F_1 from the intense —OCH_3 singlets. The partial J-spectrum of the hidden H-18 resonance was not useful, since it suffered from the same virtual coupling effects as the other H-18 resonance at δ 2.83, making the extraction of accurate coupling constant data impossible without spectral simulation. (The geminal H-17 protons, to which they are vicinal, are tightly coupled.) The solid-state conformation determined by X-ray crystallography (18) was used to build a molecular model having the correct configuration. This was found to be a rigid structure, suggesting that the solution conformation might be very similar to that in the solid state. The experiments required to complete these ^{1}H assignments also served to corroborate this postulated solution conformation.

In the determination of conformation, techniques relying on "through-space" phenomena (e.g., T_1, nOe) prove very useful, often in conjunction with (through-bond) coupling-constant information. Axial protons taken on unusual importance in an nOe experiment. The 1,3 diaxial interaction provides important information in a six-membered ring and, with a boat conformation, the "flagpole" protons are close to one another in

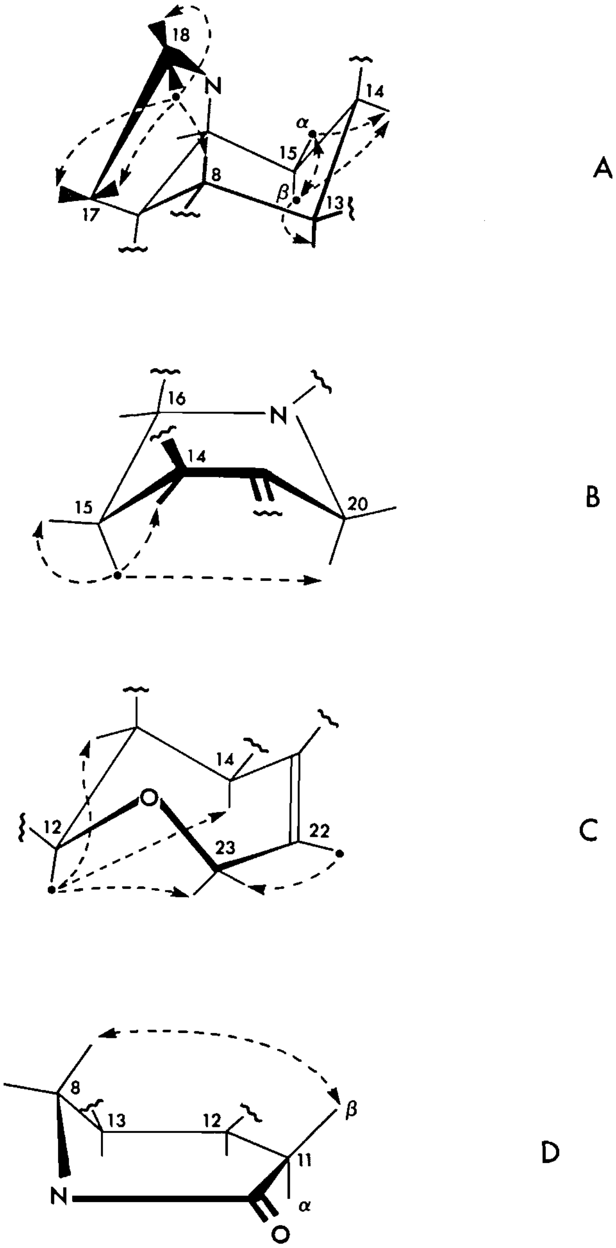

FIG. 4. Conformations of rings IV and V (A), VI (B), VII (C), and III (D) in brucine, indicating some of the results from the SSNOEDS experiments. The irradiated proton is indicated with (●) and nOe's (---).

spite of their being 5 bonds removed; an nOe experiment will also detect this.

The SSNOEDS results are presented in Fig. 3. No special effort was made to optimize the experiment and the data were collected in approximately 3 hours. A single decoupler power setting was used (which resulted in 40–80% saturation, depending on the total multiplet width). In all cases a check was made for decoupler power leakage into neighbouring resonances ("spillover"), and was found to be absent. The irradiation time was set at 0.5 s,[8] and the experiments "interleaved" by collecting scans in blocks of 16, repeated 30 times.

Let us consider ring IV, which is in a chair conformation in the solid state (Fig. 4A). Evidence for this also being so in solution comes from a consideration of coupling constants, and nOe experiments. J (8, 18) = 10.5 Hz, which indicates a *trans* or *cis* arrangement of the two protons. In keeping with the chair conformation, H-14 and H-16 are judged to be roughly coplanar since J (14, 15α) ≈ J (16, 15α), and J (14, 15β) ≈ J (16, 15β).[9] Strong confirmatory evidence for the proposed conformation[9] comes from the SSNOEDS experiment where H-15 (δ 1.46) was irradiated, inducing an nOe in H-13; the two protons must assume axial orientations in a ring having a chair conformation, and the irradiated proton is accordingly assigned to H-15β. Irradiation of the higher field of the two H-18 protons induced an nOe in H-8, thereby identifying the proton irradiated as H-18β, and H-8 to be axial, as depicted in Fig. 4A. Consider now ring VI. Since the H-20 protons have no vicinal neighbours, no conformational information can be sought from arguments based on vicinal coupling constants. The nOe experiment where H-15α was irradiated induced a strong nOe in the lower field of the two H-20 resonances. This confirms the approximate "boat" conformation of this ring (Fig. 4B), which placed the "flagpole" protons, H-15β and H-20α, close to one another; this is a "bowsprit–flagpole" interaction. Hence, this single experiment confirms the expected conformation of ring VI, and identifies H-20α (and H-20β, by default).

The analysis of ring VII was complicated somewhat by the fact that it is a seven-membered ring, with a double bond and ring hetero-atom.[10] Two nOe experiments were performed to support the structure shown in Fig. 4C. Irradiation of the vinylic H-22 induces an nOe into the pseudo-equatorial proton H-23β, the lower field of the two H-23 protons. Additionally, an nOe is induced in H-20β. Although not depicted in this diagram, H-22 and H-20β are close to one another and this confirms the assignment of the geminal H-20 protons based on the irradiation of H-15α. Irradiation of H-12 induces an nOe into other axial or axial-like protons: H-14 and H-23α.[11] The assignment of the H-23 protons is now confirmed.

The conformational analysis of ring III is more complex. Here the H-11α and H-11β protons must be assigned. The molecular model favours a boat-like conformation. A pure boat conformation would make H-12 and H-11β *trans* diaxial, and one would anticipate a large vicinal coupling constant here on the basis of the Karplus relationship; using this argument, the lower field of the two H-11 protons would be assigned to H-11β. The geminal coupling constant J (11α, 11β) is, at 17.4 Hz, unusually large. This suggests that the carbonyl on C-10 roughly bisects the angle between the geminal protons and C-11 (19), and this would *not* be the case if ring III were to be in the pure boat conformation considered above. Satisfying the condition of the relationship between the carbonyl and geminal protons "flattens" one end of the boat, placing N-9, C-10, C-11, C-12, and C-13 approximately co-planar. In this situation H-12 and H-11α have a small dihedral angle (ca. 10°), and, hence, a large vicinal coupling constant would be antici-

[8]This is far less than the time usually used for nOe build-up (ca. 3* T_1), and was chosen to minimize the experimental acquisition time and "three spin effects," without jeopardizing the observation of "direct" interactions.

[9]The H-15 protons are assigned here to allow the reader to check the statement with the reported data in Table 2, but the absolute assignment of the H-15 protons is not necessary at this stage.

[10]This is a tetrahydro-oxepin ring.

[11]Here, a negative nOe is induced in H-23β due to the "three-spin effect" (12).

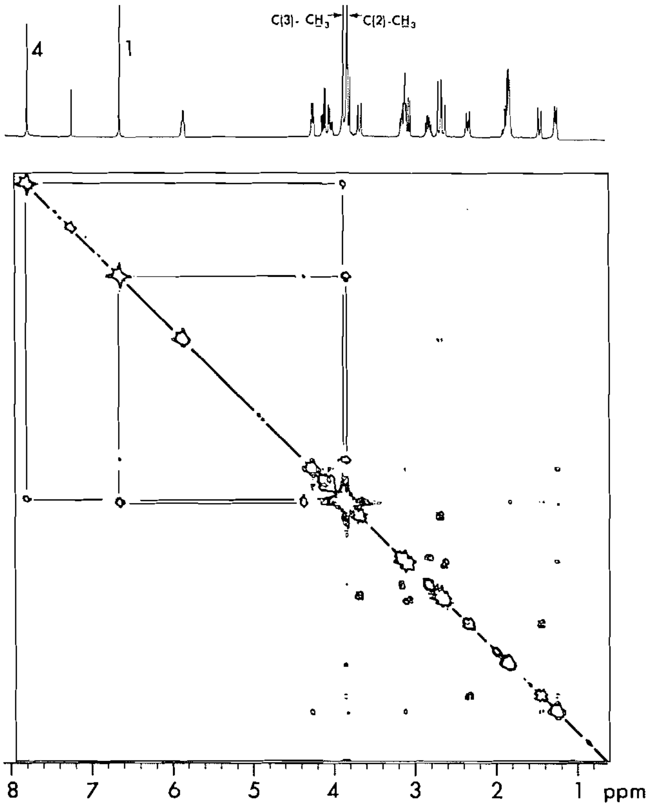

FIG. 5. 400-MHz NOESY spectrum of brucine. The 256 * 1K data matrix was collected in ca. 8 h, with relaxation delay 3.0 s, mixing time 0.6 s ± 10% and 32 scans per t_1 interval. The data were processed and plotted using a Nicolet 1280 computer and Zeta 8 recorder. The final digitization was 5.8 Hz pt^{-1} in both dimensions, after zero-fitting in F_1; the "sinebell" multiplier was used in both dimensions, and magnitude spectra calculated.

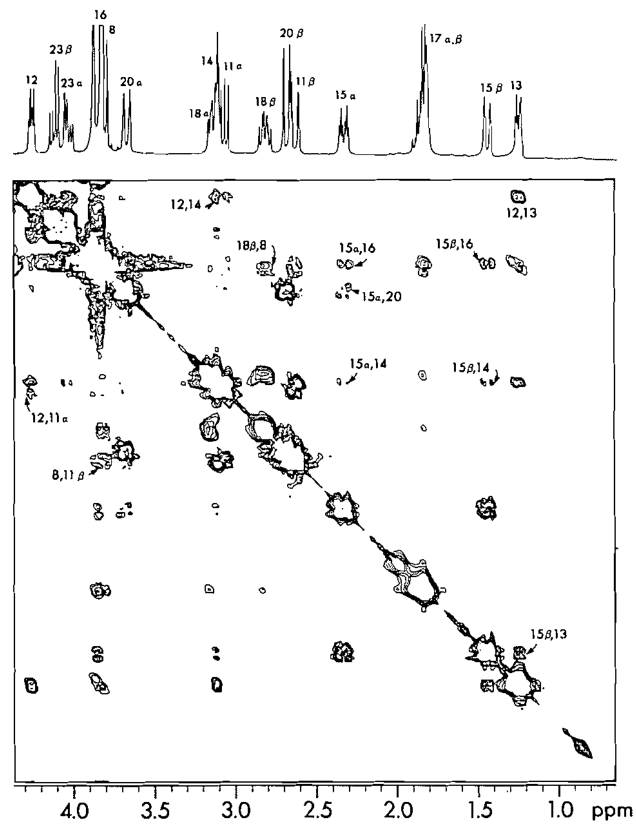

FIG. 6. The high-field region of the NOESY spectrum in Fig. 5.

pated. This argument assigns the *lower field* of the two H-11 protons as H-11β — a reversal of assignment. It is clear that in both cases H-8 and H-11β are close in space, and an nOe experiment would not suffer from these ambiguities. The H-11 protons could be assigned, and on this basis the ring conformation determined from the coupling-constant arguments.

The SSNOEDS experiment (*vide supra*) was not possible here, since all three protons — H-8, H-11α, and H-11β — overlap with other resonances, precluding decoupler irradiation selectivity. A 2D NOESY experiment was performed, and the resultant data are given in Figs. 5 and 6. Figure 5 shows the NOESY spectrum over the entire spectral width, and Fig. 6 shows the high-field portion of this data in more detail; we concentrate on the latter, for the moment. Before searching for the 8-11β nOe, it is worth checking the experiment by looking for the nOe's determined previously using SSNOEDS. These are all clearly discernable and are indicated in the upper half of Fig. 6. A number of nOe's with H-16 are clear here that were not in the 1D experiments, as a result of being obscured by subtraction errors with the overlapping sharp $O\text{-}CH_3$ singlets.

The 8-11β nOe correlation is discernable, assigning H-11β as the higher field of the H-11 resonances. This is in accord with the second argument above using vicinal and geminal *J*-coupling magnitudes and suggests a boat-like conformation, flattened at C-11 (see Fig. 4D). This is confirmed by the observation of a larger nOe between H-12 and H-11α than H-12 and H-11β.

The NOESY spectrum also provides the means for the assignment of the aromatic and *O*-methyl signals. The relaxation of H-4 would likely be dominated by the $O\text{-}CH_3$ protons on C-3, and H-1 by those on C-2. H-1 has additional relaxation contributions from H-16 and H-17α. Figure 5 shows the nOe between the aromatic and the *O*-methyl protons. Correlations between an aromatic proton and protons on ring V are below the contour threshold; slices taken at each aromatic proton's chemical shift (not shown) identify the higher field of the two aromatic resonances as that of H-1, by the above reasoning. The nOe with H-17 is not clear, as its cross peak overlaps with the strong corelation to the *O*-methyl resonance. Further, the *O*-methyl resonances are easily assigned; the higher field of the two singlets corresponds to the *O*-methyl on C-2 and the lower field to that on C-3.

The final assignments of the ^1H nmr spectrum of brucine are compiled in Table 2. These data are in complete accord with recent reports for strychnine (17, 20).

We have seen that the COSY experiment was sufficient to perform the bulk of the analysis of the ^1H nmr spectrum of brucine. The 1D and 2D nOe experiments assigned individual geminal protons and provided valuable conformational information.

Now, the ^{13}C spectrum was analysed. A ca. 0.3 *M* solution of brucine in $CDCl_3/CD_3OD$ (10:1) was prepared.[12] First, the number of protons attached to each carbon was determined using DEPT. This might have been redundant because a CSCM experiment was planned; however, in this case not all methylene protons have very different chemical shifts (*vide infra*).

[12]The proton nmr spectrum was essentially identical to the one for the more dilute $CDCl_3$ solution, used for the ^1H nmr experiments.

TABLE 2. Summarized ^1H nuclear magnetic resonance chemical shift assignments and coupling constants of brucine in $CDCl_3$ (ca. 0.02 *M*)[a]

Proton	δ (ppm)	*J* (Hz)
1	6.66	—
4	7.80	—
8	3.83	(8, 18) = 10.5
11α	3.09	(11α, 11β) = 17.4 (11α, 12) = 8.5
11β	2.64	(11β, 12) = 3.3
12	4.27	(12, 13) = 3.3
13	1.26	(13, 14) = 3.2
14	3.14	(14, 15α) = 4.0 (14, 15β) = 1.0
15α	2.34	(15α, 15β) = 14.2 (15α, 16) = ca. 4.9
15β	1.46	(15β, 16) = 2.1
16	3.9	
17α, β[b]	1.9, 1.8	(17α, 17β) = ca. 12.0
18α[c]	3.15	
18β[c]	2.83	
20α	3.68	(20α, 20β) = 14.8 (20α, 22) = 1.6
20β	2.70	
23α	4.05	(23α, 23β) = 13.8 (23α, 22) = 6.3
23β	4.13	(23β, 22) = 6.9
(C-2)-OCH_3	3.85	—
(C-3)-OCH_3	3.89	—

[a]The coupling constant signs were not determined and geminal coupling constants would most likely be negative.
[b]Strong coupling.
[c]Coupling pattern complicated by second order effects.

TABLE 3. Table of assigned ^{13}C chemical shifts for brucine, compared with the literature. Chemical shifts are referenced to the central transition of $CDCl_3$ (δ 77.0). The solution was ca. 0.3 *M* in $CDCl_3$/CD_3OD (10:1) and the instrument a Bruker WH-400, operating at 100.6 MHz for ^{13}C

Carbon	^{13}C shifts: Ref. 21	Ref. 22	This study
1	105.78	105.7	106.4
4	101.00	101.1	101.5
8	59.84	60.3	60.2[a]
11	50.09	42.3	42.2[b]
12	77.64	77.8	77.5
13	48.18	48.3	48.1
14	31.50	31.5	31.4
15	26.73	26.8	26.5
16	60.28	59.9	59.6[a]
17	42.28	42.3	41.9[b]
18	52.57	50.1	49.9
20	42.28	52.7	52.4
22	127.14	127.2	127.6
23	64.47	64.6	64.4
OCH_3	56.43; 56.08	56.4; 56.2	56.6; 56.0

[a,b]May be interchanged.

The CSCM experiment required 45–60 min for data collection. The CSCM spectrum of the interesting regions of δ_C 22–80 and δ_H 1.0–4.5 is shown in Fig. 7. (All assignments outside this region are unambiguous.) The DEPT information is included. Knowing the proton assignments, the indicated carbon assignments were made. In only two cases was there any uncertainty. H-8 and H-16 resonate very close to one another, making the assignment of the carbon signals around δ 59 difficult. The carbon signals around δ 41 are very close and

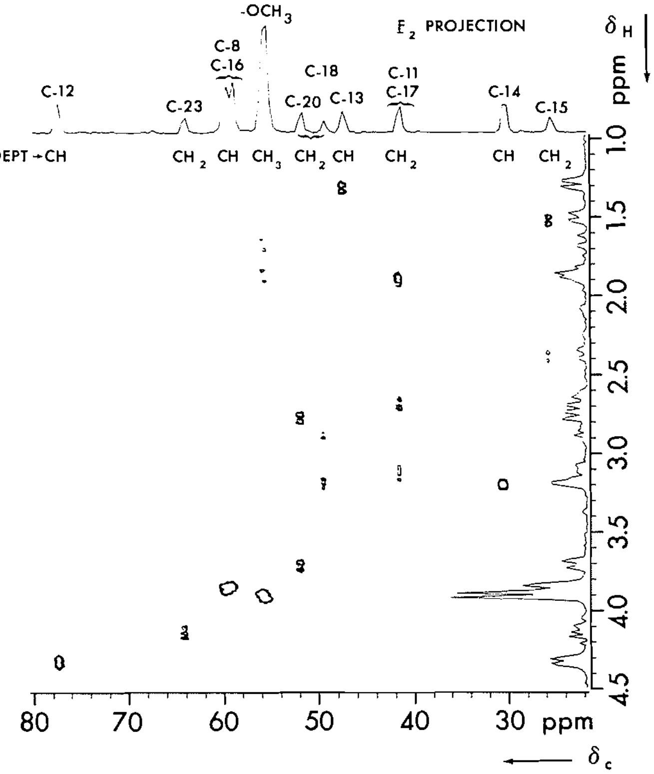

FIG. 7. 360-MHz ^1H CSCM experiment with brucine (ca. 0.3 *M* in C_6D_6/CD_3OD, 10:1). δ_C 22–80 and δ_H 1.0–4.5 is plotted in the contour mode. F_1 and F_2 projections are on the abscissa and ordinate, respectively. The results from the DEPT experiments are indicated under each ^{13}C peak.

insufficiently digitized in this case. Hence, C-11 and C-16 cannot be distinguished.

No attempt was made to assign quaternary carbons since this would not fall within the scope of the present design protocol. The data from the CSCM is compared with that of Srinivasan and Lichter (21) – that referred to whilst the work was in progress – and the now accepted assignments of Verpoorte (22). Our results are in complete agreement with the latter. These data are compiled in Table 3.

Summary

Several conclusions can be drawn from this study. First, only modest amounts of spectrometer time are necessary for the partial assignment of the ^1H nmr spectrum of a medium sized molecule such as brucine; in this case a total of ca. 2 h for the 2D *J*-resolved and COSY experiments and an additional 3–8 h for the complete spectroscopic and conformational assignment. Additional conformational information plus the assignment of individual geminal protons result from nOe experiments. Where the selective irradiation experiments can be performed, the SSNOEDS experiment is probably the most expeditious route. In the case of signal overlap, the 2D NOESY experiment will provide all the necessary relaxation pathway information in a single experiment, but with greater demands on spectrometer time. This investment of time is offset by the fact that all possible nOe experiments are "simultaneously" performed, resulting in a high return being realized in terms of information yield.

With the proton spectrum assigned at least to the point before nOe experiments are performed, non-quaternary resonances in the ^{13}C nmr spectrum can be routinely assigned providing they are not too close (ca. > 0.1 ppm) and the attached proton resonances are not badly overlapping. The ability to distinguish resonances with small chemical shift differences is limited by the intrinsic line width, the spectrometer's data storage capability, and the available spectrometer and data processing time. Within these restrictions, the data presented in Fig. 7 were acquired under conditions where the digitization in the ^{13}C frequency domain was less than optimal and resonances <0.7 ppm apart were not resolved.

We believe that the 2D *J*-resolved and COSY experimental data can be collected and processed in a highly efficient, integrated fashion, without the prior knowledge of the chemical system. The nOe data might require some educated guesswork in the selection of an irradiation time (SSNOEDS experiment) or the mixing time (NOESY), or a series of exploratory experiments could be performed. All the experiments described in this study provided the required information from the data collected the first time it was performed.

Hurd (23) has independently reported on the utility of the combination of COSY with the CSCM experiment. It is advantageous to use a ^{13}C probe to measure both the ^{13}C and ^{1}H spectra (the latter via the ^{1}H decoupler coil). In this way the COSY assignment (and NOESY, if required) is for the molecule at the same concentration as for the CSCM experiment and no time is expended changing probes. This approach has the further merit that with automated changeover of the probe circuits, it is possible to automate the acquisition and processing of all ^{1}H and ^{13}C data into a single (overnight) run. Given its high efficiency, it seems probable that the mode of analysis described in this study will find a place for those organic structural investigations that warrant more than a few, disrelated nmr measurements.

Acknowledgments

This work was supported by operating grants from the Natural Sciences and Engineering Research Council of Canada (A 1905 to LDH). Many of the measurements were made using a 360-MHz spectrometer located in the Nicolet applications laboratory; we are indebted to Nicolet for their generous hospitality and in particular wish to thank Dr. Ralph Hurd and Dr. L.F. Johnson for numerous stimulating discussions.

1. M. A. BERNSTEIN. Ph.D. Thesis, University of British Columbia, 1983.
2. M. A. BERNSTEIN and L. D. HALL. J. Am. Chem. Soc. **104**, 5553 (1982).
3. K. WÜTHRICH, G. WIDER, G. WAGNER, and W. BRAUN. J. Mol. Biol. **155**, 311 (1982).
4. H. KESSLER, W. BERMEL, A. FRIEDRICH, G. KRACK, and W. E. HULL. J. Am. Chem. Soc. **104**, 6297 (1982).
5. H. KESSLER and V. EIERMAN. Tetrahedron Lett. **23**, 4689 (1982).
6. R. BENN and H. GÜNTHER. Angew. Chem. Int. Ed. Engl. **22**, 350 (1983).
7. L. D. HALL and J. K. M. SANDERS. J. Am. Chem. Soc. **102**, 5703 (1980).
8. A. BAX and R. FREEMAN. J. Magn. Reson. **44**, 542 (1981).
9. M. A. BERNSTEIN and L. D. HALL. Carbohydr. Res. **103**, C1 (1982).
10. K. F. WONG. Ph.D. Thesis, University of British Columbia, 1979.
11. L. D. HALL and J. K. M. SANDERS. J. Chem. Soc. Chem. Commun. 368 (1980).
12. J. K. M. SANDERS and J. D. MERSH. Prog. Nucl. Magn. Reson. **15**, 353 (1982), and references therein.
13. J. JEENER, B. H. MEIER, P. BACHMAN, and R. R. ERNST. J. Chem. Phys. **71**, 4546 (1979).
14. R. R. ERNST. J. Chem. Phys. **45**, 3845 (1966).
15. D. T. PEGG, D. M. DODDRELL, W. M. BROOKS, and M. R. BENDALL. J. Magn. Reson. **44**, 32 (1981).
16. A. BAX and G. A. MORRIS. J. Magn. Reson. **42**, 501 (1981).
17. W. J. CHAZIN, J. T. EDWARD, and L. D. COLEBROOK. Can. J. Chem. **61**, 1749 (1983).
18. L. H. BRIGGS, H. T. OPENSHAW, and R. ROBINSON. J. Chem. Soc. 903 (1946), and others in the series.
19. R. R. FRASER and B. F. RABY. J. Am. Chem. Soc. **94**, 3458 (1972).
20. E. WENKERT, H. T. A. CHEUNG, H. E. GOTTIEB, M. C. KOCH, A. RABARON, and M. M. PLAT. J. Org. Chem. **43**, 1099 (1978).
21. P. R. SRINIVASAN and R. L. LICHTER. Org. Magn. Reson. **8**, 198 (1976).
22. R. VERPOORTE. J. Pharm. Sci. **69**, 865 (1980).
23. R. E. HURD. Relaxation times. An in-house publication of Nicolet Magnetic Corp., Fremont, California, U.S.A. January 1982.

Étude structurale d'un *C*-glycoside insaturé; le tri-*O*-acétyl-3,4,6-désoxy-2-α-D-*thréo*-hexéno-2-pyrannosyle benzène

HÉLÈNE GILLIER-PANDRAUD ET RACHID BRAHMI

Laboratoire de Chimie Structurale Biomoléculaire, Université Paris-Nord, 74 rue Marcel Cachin, 93000-Bobigny, France

ET

VÉRONIQUE BELLOSTA-DECHAVANNE ET STANISLAS CZERNECKI

Laboratoire de Cinétique et Mécanismes de Réactions Organiques, Université Pierre et Marie Curie, CNRS ER 84, 4 place Jussieu, Paris, France

Reçu le 24 février 1984

HÉLÈNE GILLIER-PANDRAUD, RACHID BRAHMI, VÉRONIQUE BELLOSTA-DECHAVANNE et STANISLAS CZERNECKI. Can. J. Chem. **63**, 491 (1985).

La structure du tri-*O*-acétyl-3,4,6-désoxy-2-α-D-*thréo*-hexéno-2-pyrannosyle benzène **1** a été déterminée par diffraction des rayons X. Les cristaux de **1** sont orthorhombiques et appartiennent au groupe d'espace $P2_12_12_1$ avec a = 22,946(10), b = 10,319(6), c = 7,684(4) Å, V = 1819,42 Å^3, Z = 4, ρ_c = 1,27 g cm^{-3}. La conformation du cycle glucidique est demi-chaise $^0H_5$ dans laquelle le noyau aromatique est quasi-axial. Le carbone anomère possède la configuration α. La comparaison des données de rmn ^{1}H avec les données cristallographiques a permis d'établir que la conformation de **1** en solution est très vite voisine de celle adoptée à l'état cristallin.

HÉLÈNE GILLIER-PANDRAUD, RACHID BRAHMI, VÉRONIQUE BELLOSTA-DECHAVANNE, and STANISLAS CZERNECKI. Can. J. Chem. **63**, 491 (1985).

The structure of 3,4,6-tri-*O*-acetyl-2-deoxy-α-D-*threo*-hexeno-pyranosyl benzene **1** has been determined by X-ray diffraction methods. Crystals of **1** are orthorhombic, space group $P2_12_12_1$ with a = 22.946(10), b = 10.319(6), c = 7.684(4) Å, V = 1819.42 Å^3, Z = 4, ρ_c = 1.27 g cm^{-3}. The sugar moiety exhibits a half-chair $^0H_5$ conformation in which the aromatic ring is quasi-axial. The anomeric carbon has the α configuration. The comparison of the ^{1}H nmr data with the crystallographic data established that, in solution, the conformation of **1** is very similar to that in the crystalline state.

L'arylation des glycals peracétylés catalysée par les sels de palladium constitue une nouvelle méthode de synthèse de *C*-glycosides (1). Appliquée au tri-*O*-acétyl-3,4,6-anhydro-1,5-désoxy-2-D-*lyxo*-hexène-1-itol (tri-*O*-acétyl-D-galactal), elle conduit à des *C*-glycosides insaturés, selon la réaction:

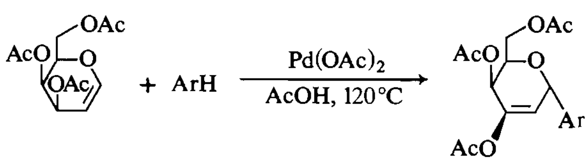

La structure de ces composés a été déterminée par les méthodes spectroscopiques classiques (1) exceptée la configuration du carbone anomère. En effet, à cause de la présence d'une double liaison entre les carbones C-2 et C-3, l'examen du spectre de rmn ^{1}H ne permet pas de trancher, car le couplage $^3J_{1,2}$ se fait à travers un carbone hybridé sp^2 et la valeur observée (3,9 Hz) est compatible avec les deux configurations, sans préjuger de la conformation. D'autre part, comme la réaction est stéréospécifique, nous ne possèdons qu'un seul des anomères, et, de ce fait, l'utilisation du pouvoir rotatoire ne peut être que spéculative. En effet, si les *C*-glycosides pyranniques suivent, en général, les règles de Hudson (2), des exceptions concernant des composés à cycle pyrannique insaturé ont été cependant signalées (3).

Aussi la structure du tri-*O*-acétyl-3,4,6-désoxy-2-α-D-*thréo*-hexèno-2-pyrannosyle benzène, **1** (Ar = Ph), a-t-elle été déterminée par diffraction des rayons X et corrélée avec les données de rmn ^{1}H pour écarter toute ambiguité en ce qui concerne la stéréochimie de la réaction.

Partie expérimentale

Les cristaux, obtenus par recristallisation dans l'éthanol 95% se présentent sous l'aspect de petites plaquettes transparentes allongées. Les paramètres de la maille orthorhombique ont été déterminés sur diffractomètre automatique Philips PW 1100 à partir de 24 réflexions telles que $20 < \theta < 50°$ pour λCu Kα.

Les données de diffraction, enregistrées en premier lieu avec le rayonnement MoKα, ont été mesurées à nouveau avec celui du cuivre en raison du pouvoir diffractant limité des cristaux, dans les conditions suivantes: λCuKα monochromatisée, $2\theta_{max}$ = 138°, $-27 < h < 27$, $0 \le k < 12$, $0 \le l < 9$, balayage θ/2θ, μ = 8,36 cm^{-1}. Sur les 3989 intensités mesurées, 1964 étaient indépendantes. Parmi celles-ci 1786, telles que $I > 2\sigma(I)$, ont été déclarées observées.

La mise en oeuvre de la chaîne de programmes MULTAN (4) a fourni les positions des atomes de carbone et d'oxygène qui ont été affinées par moindres carrés dans l'hypothèse d'une agitation thermique isotrope puis anisotrope (X RAY (5)). Les atomes d'hydrogènes ont été localisés sur des séries de Fourier différence et pris en compte dans les derniers cycles d'affinement, leurs paramètres restant toutefois bloqués. Le facteur R final non pondéré est de 0,08 (valeurs maximale et moyenne du rapport déplacement/erreur: 0,9 et 0,3), S = $[\Sigma W(F_o - F_c)^2/(m - n)]^{1/2}$: 10,2. La densité électronique résiduelle est de l'ordre de 0,3 e Å^{-3}.

Les coordonnées et le B équivalent[1] des atomes de carbone et d'oxygène sont donnés dans le tableau 1.

Le spectre de rmn a été enregistré dans $CDCl_3$ à 250 MHz sur un appareil Brücker en utilisant le tétraméthylsilane comme référence interne: 7,3–7,5 (5H, s, H aromatiques), 5,54 (H-1, d, J_{1-2} = 3,9

[1] Les valeurs des six coefficients d'agitation thermique anisotrope de chacun de ces atomes et les coordonnées des atomes d'hydrogène ont été déposées et peuvent être obtenues à un prix nominal, en s'adressant au Dépôt de données non publiées, ICIST, Conseil national de recherches du Canada, Ottawa, Ont., Canada K1A 0S2.

TABLEAU 1. Coordonnées réduites des atomes de carbone et d'oxygène. Paramètre d'agitation thermique isotrope

Atome	x	y	z	B_{iso}
C(1)	0,3805(3)	0,5483(7)	−0,5108(9)	3,8
C(2)	0,3342(3)	0,4478(7)	−0,5281(9)	3,9
C(3)	0,3215(3)	0,3693(6)	−0,3999(10)	3,6
C(4)	0,3502(3)	0,3722(7)	−0,2265(9)	3,3
C(5)	0,3858(3)	0,4964(7)	−0,2114(9)	3,1
C(6)	0,4286(3)	0,4920(7)	−0,0620(10)	4,0
C(7)	0,3585(3)	0,6850(7)	−0,4965(10)	3,6
C(8)	0,3977(4)	0,7874(8)	−0,5220(12)	5,2
C(9)	0,3795(5)	0,9128(8)	−0,5040(16)	6,9
C(10)	0,3222(5)	0,9428(8)	−0,4626(16)	6,9
C(11)	0,2833(4)	0,8440(9)	−0,4375(15)	6,0
C(12)	0,3013(3)	0,7139(8)	−0,4544(12)	4,4
C(13)	0,2220(3)	0,3036(7)	−0,4179(10)	3,8
C(14)	0,1849(4)	0,1881(8)	−0,4435(13)	5,2
C(15)	0,3885(4)	0,1916(8)	−0,0656(13)	5,0
C(16)	0,4293(4)	0,0778(8)	−0,0825(14)	5,9
C(17)	0,4884(3)	0,6391(7)	0,0903(10)	3,8
C(18)	0,5151(4)	0,7714(8)	0,0896(13)	5,4
O(3)	0,2798(2)	0,2688(4)	−0,4161(8)	3,9
O(4)	0,3874(2)	0,2576(4)	−0,2183(6)	3,5
O(5)	0,4186(2)	0,5170(5)	−0,3640(6)	3,2
O(6)	0,4531(2)	0,6205(5)	−0,0505(7)	4,4
O(7)	0,2070(2)	0,4125(5)	−0,4039(8)	4,9
O(8)	0,3613(3)	0,2244(8)	0,0637(9)	7,2
O(9)	0,4971(3)	0,5574(6)	0,1932(7)	5,8

Hz), 6,07 (H-2, d), 5,44 (H-4, d, J_{4-5} = 1,5 Hz), 4,19 (H-6, dd, J_{5-6} = 9 Hz), massif centré à 4,07 (H-5 et H-6'), 1,96–2,14 et 2,18 (3s, 3 × $OCOCH_3$).

Résultats et discussion

La figure 1 donne la représentation de la molécule, dessinée à l'aide du programme ORTEP (6), et précise le numérotage adopté pour les atomes. Les valeurs des distances interatomiques et lès angles de valence sont présentées dans les tableaux 2 et 3 respectivement.

Conformation dans le cristal

Le cycle du composé étudié, **1**, adopte la conformation demi-chaise $^{0}H_5$ dans laquelle les atomes C(1), C(2), C(3) et C(4) déterminent un plan (π) de part et d'autre duquel se situent les atomes C(5) et O(5) aux distances respectives de 0,32(1) et de 0,44(1) Å (fig. 2 et tableau 4). Cette conformation de cycle se retrouve dans les composés analogues suivants qui peuvent être comparés à **1**: le tri-*O*-acétyl-1,4,6-*N*-acétylacétamido-2-didésoxy-2,3-α-D-*thréo*-hexéno-2-pyrannose **2** (7*a*), le di-*O*-acétyl-4,6-didésoxy-2,3-α-D-*thréo*-hexéno-2-pyrannoside de méthyle **3** (7*b*), le (methyl *N*-acétylamino-2-*O*-acétyl-6-tri-désoxy-2,3,4-β-D-*thréo*-hexéno-2-pyrannosidyle-4)-7 théophylline **4** (7*c*) et le (*O*-acétyl-4-didésoxy-2,3-β-L-*glycéro*-pentèno-2-pyrannosyl)-2-dichloro-5,6-benzotriazole **5** (7*d*).

Pour le composé **1**, la configuration de l'atome C(1) est telle que le noyau benzénique qui lui est lié se situe de l'autre côté du plan moyen π par rapport à C(6): elle correspond donc à l'anomère α qui, du fait de la conformation du cycle éno-pyrannique, impose la position axiale au noyau benzénique.

Le plan π et celui du benzène sont proches de l'orthogonalité (81, 7(7)°). Cette valeur est en bon accord avec celle trouvée pour les éno-2-pyrannosides **4** et **5** qui sont liés à un hétérocycle en α de la double liaison (7*c*, *d*). L'orientation du noyau aromatique autour de la liaison hétérocyclique C(1)—C(7) (fig. 3) l'amène à s'engager sous le cycle éno-pyrannique du côté où la coplanéité de C(1), C(2), H(2), C(3) et C(4) résultant de la présence de la double liaison occasionne une répulsion moindre. Ce phénomène est encore plus prononcé dans le cas de **5** (7*d*), car le cycle triazole est moins volumineux qu'un noyau aromatique.

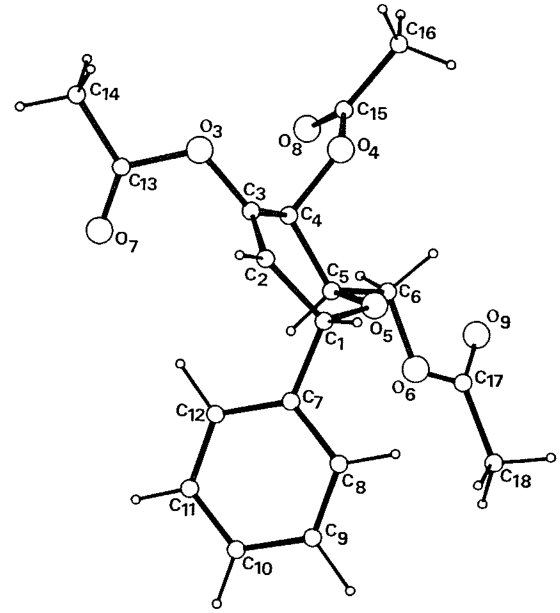

FIG. 1. Représentation en perspective de la molécule.

TABLEAU 2. Distances interatomiques

Liaison	Distance (Å)	Liaison	Distance (Å)
C(1)—C(2)	1,494(8)	C(1)—C(7)	1,503(9)
C(2)—C(3)	1,308(8)	C(7)—C(8)	1,401(11)
C(3)—C(4)	1,488(8)	C(8)—C(9)	1,366(12)
C(4)—C(5)	1,523(8)	C(9)—C(10)	1,388(16)
C(5)—O(5)	1,409(8)	C(10)—C(11)	1,368(16)
C(1)—O(5)	1,459(8)	C(11)—C(12)	1,409(12)
C(5)—C(6)	1,511(16)	C(12)—C(7)	1,385(10)
C(3)—O(3)	1,415(8)	C(4)—O(4)	1,458(8)
O(3)—C(13)	1,375(9)	O(4)—C(15)	1,357(11)
C(13)—C(14)	1,476(11)	C(15)—C(16)	1,506(12)
C(13)—O(7)	1,180(9)	C(15)—O(8)	1,222(12)
C(6)—O(6)	1,442(9)	C(17)—C(18)	1,495(11)
O(6)—C(17)	1,366(9)	C(17)—O(9)	1,173(10)

La conjugaison entre la double liaison cyclique et le groupe acétyle porté par l'atome C(3) devrait assurer la coplanéité entre ce groupe et le plan π. Il n'en est rien, puisque l'angle entre les deux plans est de 74(7)°. Une situation analogue se présente avec le dérivé **2** dont l'atome C(2) est porteur d'un groupe *N*-acétyl-acétamide. Dans ce cas, l'absence de co-planéité (angles dièdres de 79,3 et 74,7°) se justifie par un encombrement stérique très important.

La configuration de l'atome C(4) met en position axiale le groupe acétyle qui lui est lié. L'épimérisation qui était à craindre pour un acétate allylique en présence de sel de palladium ne s'est donc pas produite. Le plan de ce groupe acétyle est quasi-orthogonal au plan π (85(7)°). L'augmentation de cette valeur par rapport à celle observée pour les dérivés désoxy-3, **2** et **3** qui possèdent également un acétoxy en

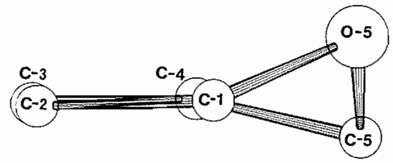

FIG. 2. Vue du cycle énopyrannique suivant la direction de C(2)—C(3).

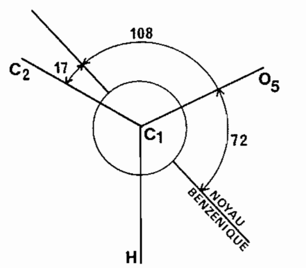

FIG. 3. Représentation de Newman relative à la liaison C(1)—C(7). Ecart-type sur les angles dièdres: 0,7°.

TABLEAU 3. Angles de valence

	Angle (deg)		Angle (deg)
O(5) C(1) C(2)	109,9(5)	C(12) C(7) C(8)	118,6(7)
C(1) C(2) C(3)	121,4(6)	C(7) C(8) C(9)	120,2(8)
C(2) C(3) C(4)	124,3(6)	C(8) C(9) C(10)	121,6(9)
C(3) C(4) C(5)	108,8(5)	C(9) C(10) C(11)	119,0(8)
C(4) C(5) O(5)	110,5(5)	C(10) C(11) C(12)	120,3(8)
C(5) O(5) C(1)	111,1(5)	C(11) C(12) C(7)	120,2(7)
C(2) C(1) C(7)	114,5(6)	C(1) C(7) C(8)	118,7(6)
O(5) C(1) C(7)	110,6(5)	C(1) C(7) C(12)	122,7(6)
C(2) C(3) O(3)	122,5(7)	C(3) C(4) O(4)	106,4(5)
C(4) C(3) O(3)	113,1(6)	C(5) C(4) O(4)	111,4(5)
C(3) O(3) C(13)	117,5(5)	C(4) O(4) C(15)	117,1(5)
O(3) C(13) C(14)	110,3(6)	O(4) C(15) C(16)	109,2(7)
O(3) C(13) O(7)	121,9(7)	O(4) C(15) O(8)	123,7(8)
C(14) C(13) O(7)	127,7(7)	C(16) C(15) O(8)	127,1(9)
C(4) C(5) C(6)	112,4(6)	O(6) C(17) C(18)	111,6(6)
O(5) C(5) C(6)	106,9(5)	O(6) C(17) O(9)	122,3(7)
C(5) C(6) O(6)	105,8(6)	C(18) C(17) O(9)	126,1(7)
C(6) O(6) C(17)	114,2(6)		

position allylique (7*a*, *b*) est attribuable à la répulsion entre les groupements acétoxy en C(4) et C(3) dans le composé **1**.

La conformation autour de la liaison C(5)—C(6) qui met O(6) en position *gauche-trans* respectivement par rapport à O(5) et C(4) pour les trois composés **1**, **2** et **3**, a été signalée comme la plus probable pour les résidus galactopyrannosyles (8).

Conformation en solution

L'examen des données de rmn ^{1}H à 250 MHz du composé **1** permet de conclure que celui-ci adopte également la conformation demi-chaise $^0H_5$ en solution. En effet, il existe un bon accord entre les valeurs expérimentales des constantes de couplages ^3J et les valeurs calculées à partir des angles dièdres mesurés dans le cristal. De plus, nous n'avons pas observé de modifications notables du spectre à basse température (90 MHz, −60°C) ce qui montre que la molécule n'est pas en équilibre conformationnel rapide.

TABLEAU 4. Angles de torsion énopyranniques

	Angle (deg)
O(5) C(1) C(2) C(3)	17,7 (5)
C(1) C(2) C(3) C(4)	1,1 (5)
C(2) C(3) C(4) C(5)	12,1 (5)
C(3) C(4) C(5) O(5)	−45,7 (5)
C(4) C(5) O(5) C(1)	68,7 (5)
C(5) O(5) C(1) C(2)	−52,5 (5)

Pour les constantes de couplage des protons H-4, H-5, H-6 et H-6′, mis à part $^3J_{5,6'}$ que nous n'avons pas pu déterminer car H-5 et H-6′ ont des déplacements chimiques très voisins, les valeurs expérimentales ($^3J_{4,5}$ = 1,5 Hz et $^3J_{5,6}$ = 9 Hz) sont en bon accord avec les valeurs calculées ($^3J_{4,5}$ = 0,8 Hz, $^3J_{5,6}$ = 9 Hz et $^3J_{5,6'}$ = 3,1 Hz) à l'aide de la relation de Altona et Haasnoot (9) pour la conformation décrite.

Le couplage $^3J_{1,2}$ se faisant à travers un carbone hybridé sp^2 mérite un commentaire particulier. En effet, dans ce cas, la relation la plus utilisée pour calculer la constante de couplage en fonction de l'angle dièdre ψ est celle de Garbisch (10) ($^3J = 4\cos^2\psi + 2{,}6$; $0 \le \psi \le 90°$). En l'appliquant au composé **1** avec la valeur de ψ mesurée dans le cristal (ψ = 42°), on trouve $^3J_{1,2}$ calc. = 4,8 Hz ± 0,15 en tenant compte de la valeur de l'écart type sur l'angle ψ, alors que la valeur mesurée est plus faible ($^3J_{1,2}$ exp. = 3,9 Hz). Avant de conclure à des déformations de la molécule, il faut remarquer que Baer et Hanna (11) et Anet (12) avaient déjà noté que la constante 2,6 était vraisemblablement trop grande dans cette relation. De plus, celle-ci a été établie pour des hydrocarbures et, ne prenant pas en compte la nature des groupements fixés sur la double liaison, elle ne convient pas pour calculer des valeurs de constante de couplage dans le cas des énopyrannosides.

En revanche, en utilisant la relation publiée plus récemment (13) dans laquelle un terme correctif a été introduit pour essayer de tenir compte de l'environnement chimique, on trouve une valeur ($^3J_{1,2}$ = 3,6 Hz ± 0,05) qui est en bon accord avec la valeur expérimentale.

1. S. CZERNECKI et V. DECHAVANNE. Can. J. Chem. **61**, 533 (1983).
2. (*a*) S. HANESSIAN et A. G. PERNET. Can. J. Chem. **52**, 1266 (1974); (*b*) D. L. WALKER, B. FRASER-REID et J. K. SAUNDERS. J. Chem. Soc. Chem. Commun. 319 (1974); (*c*) B. FRASER-REID, R. D. DAWE et D. B. TULSHIAN. Can. J. Chem. **57**, 1746 (1979) et références citées; (*d*) J. R. POUGNY, M. A. M. NASSR et P. SINAŸ. J. Chem. Soc. Chem. Commun. 375 (1981).
3. (*a*) R. U. LEMIEUX, K. A. WATANABE et A. A. PAVIA. Can. J. Chem. **47**, 4413 (1969); (*b*) B. FRASER-REID, B. J. CARTHY, N. L. HOLDER et M. YUNKER. Can. J. Chem. **49**, 3038 (1971); (*c*) R. D. DAWE et B. FRASER-REID. J. Chem. Soc. Chem. Commun. 1180 (1981).
4. P. MAIN, S. E. HULL, L. LESSINGER, G. GERMAIN, J. P. DECLERCQ et N. M. WOOLFSON. MULTAN 78. A system of computer programs for the automatic solution of crystal structures from X-ray diffraction data. Univ. of York, Angleterre et Louvain, Belgique. 1978.
5. J. M. STEWART, G. J. KRUGER, H. L. AMMON, C. DICKINSON et S. R. HALL. The X-RAY system version of June 1972. Techn. Rep. TR 192. Computer Science Center, Univ. of Maryland, College Park, Maryland. 1972.
6. C. K. JOHNSON. Report ORNL-3794. Oak Ridge National Laboratory, Tennessee. 1965.
7. (*a*) B. KOJIĆ-PRODIĆ, V. ROGIĆ et Z. RUŽIĆ-TOROŠ. Acta Crys-

tallogr. Sect. B, **32**, 1833 (1976); (*b*) J. W. KRAJEWSKI, Z. URBAŃCZYK-LIPKOWSKA, P. GLUZIŃSKI, J. BLEIDELIS et A. KEMME. Acta Crystallogr. Sect. B, **35**, 2625 (1979); (*c*) B. KOJIĆ-PRODIĆ. Acta Crystallogr. Sect. B, **35**, 1162 (1979); (*d*) J. LOPEZ DE LERMA, S. MARTINEZ-CARRERA et S. GARCIA-BLANCO. Acta Crystallogr. Sect. B, **29**, 537 (1973).
8. D. AVENEL, J. OHANESSIAN et H. GILLIER-PANDRAUD. Acta Crystallogr. Sect. B, **38**, 225 (1982).
9. C. ALTONA et C. A. G. HAASNOOT. Org. Magn. Reson. **13**, 417 (1980).
10. E. W. GARBISCH, JR. J. Am. Chem. Soc. **86**, 5561 (1964).
11. H. H. BAER et Z. S. HANNA. Can. J. Chem. **59**, 889 (1981).
12. E. F. L. J. ANET. Carbohydr. Res. **1**, 348 (1966).
13. K. JANKOWSKI, J. BELANGER, F. SÖLER et A. ZAMOJSKI. Org. Magn. Reson. **12**, 544 (1979).

On the structure of rubrifacine[1]

Gottfried Feistner[2] and Herbert Budzikiewicz
Institut für Organische Chemie, Universität zu Köln, Greinstr. 4, 5000 Köln 41, West Germany

Received January 9, 1984

Gottfried Feistner and Herbert Budzikiewicz. Can. J. Chem. **63**, 495 (1985).

Evidence is presented that rubrifacine, the red pigment of *Erwinia rubrifaciens*, is 3-(3-carboxymethyl-4,5-dihydro-4,5-dioxo-2-pyrrolyl)-4,5,6-trihydroxypyridine-2-acetic acid, based on mass spectrometric and nmr data of rubrifacine, its hydrolysis and reduction products as well as their methyl derivatives.

Gottfried Feistner et Herbert Budzikiewicz. Can. J. Chem. **63**, 495 (1985).

En se basant sur des données de spectrométrie de masse et de rmn obtenues avec la rubrifacine et ses dérivés méthylés, sur la nature de leurs produits d'hydrolyse et de réduction, on présente des données qui permettent d'affirmer que la rubrifacine, le pigment rouge de la *Erwinia rubrifaciens*, est l'acide (carboxyméthyl-3 dihydro-4,5 dioxo-4,5 pyrrolyl-2)-3 trihydroxy-4,5,6 pyridineacétique-2.

[Traduit par le journal]

Recently we reported on the isolation and characterization of rubrifacine, a red pigment of *Erwinia rubrifaciens* (1). Mass spectrometric analysis had established a molecular weight of 338 u and nmr measurements had shown that the compound contained thirteen carbon atoms two of which were in isolated methylene groups (Table 1). Here we want to present further analytical results which led us to assign formula **1** to rubrifacine.

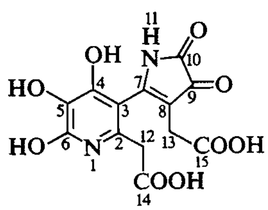

1

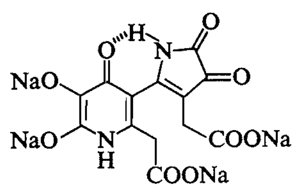

1*a*

Results

Determination of the empirical formula

Permethylation of rubrifacine with CH_2N_2 yielded two colorless, uv-active compounds which according to high resolution mass spectrometry (HMS) possess the elemental compositions $C_{21}H_{26}N_2O_9$ (**2**) (m/z 450) and $C_{20}H_{24}N_2O_9$ (**3**) (m/z 436), respectively. Comparison with the molecular weight of **1** (m/z 338) showed that seven and eight CH_2 units, respectively, had been introduced. From this it was possible to calculate an empirical formula $C_{13}H_{10}N_2O_9$ for the parent compound **1**. Taking into account that four hydrogen atoms are contained in the two methylene groups (v. supra), only six acidic hydrogens can be present in **1**. Therefore the seventh methylene unit must have been inserted into the chromophore, most likely in the pyrrolindione ring which undergoes expansion to a 3-hydroxy-2-pyridone and further derivatization to a 3-methoxy-2-pyridone. Such reaction sequences have been established for isatin **4** and coumarandione **5** (4).

Determination of functional groups

By incomplete methylation with CH_2N_2 a tetramethyl derivative **6** was obtained with a still intact chromophore. The electron impact mass spectrum (EI-MS) of **6** showed (besides some loss of $CH_3^{\cdot}$) twice the loss of $CH_3O^{\cdot}/CH_3OH$ (31/32 u) followed by the loss of CO (28 u) typical for carbomethoxy groups. No other fragmentation of importance was observed, especially none which yielded N_1-products. This excluded structural formulas with a nitrogen atom in a peripheral functional group. The two nitrogens had to be elements of a conjugated ring system and the methylene groups could only be incorporated in side chains probably terminated by the aforementioned carbomethoxy groups. The existence of —CH_2—COONa groups in the sodium salt of rubrifacine **1*a*** was supported by the ^{13}C chemical shifts of 181.3 and 181.4 ppm (Table 1) close to that of tetramethylammonium acetate (181.4 ppm (5)).

Table 1. Tentative assignment of ^{13}C chemical shifts of rubrifacine **1*a*** (sodium salt) and its hydrolysis product **7*a*** (sodium salt), both in H_2O (reference CD_3OD δ 49.0)

C[c]	1*a*	7*a*
2	151.3 (t, 4.3 Hz)	131.8
3	112.7 (t, 6.1 Hz)	111.5
4	170.8 (s)	174.0 (s)
5	116.0 (s)	118.6 (s)
6	168.6 (s)	169.1 (s)
7	146.9 (t, 5.5 Hz)	192.2
8	102.1 (t, 6.7 Hz)	35.9 (T, broad)
9	182.1 (t, 4.9 Hz)	
10	167.6 (t, 4.5 Hz)	
12	32.7[a] (T, 128.5 Hz)	33.11 (T)
13	31.3[a] (T, 127.3 Hz)	33.05 (T, broad)
14	181.3[b] (t, 6.7 Hz)	181.8
15	181.4[b] (t, 7.3 Hz)	182.5

[a,b] Interchangeable.
[c] For numbering see formulas **1** and **7**.

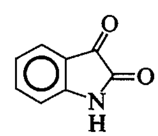

4

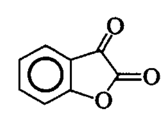

5

Hydrolysis of rubrifacine

Rubrifacine **1** was easily hydrolyzed with discoloration by

[1] Part XIX of the series "Bacterial constituents". For Part XVIII see ref. 1, Part XVII ref. 2, Part XVI ref. 3.

[2] To whom all correspondence should be addressed. Present address: Department of Bacteriology, University of California, Davis, CA 95616, USA.

1 *N* KOH whereby two carbon atoms were lost. This could directly be seen from the ^{13}C-nmr spectrum of the product **7** (Table 3; for **7***a*, sodium salt of **7** see Table 1). Correspondingly, HMS of its tetramethyl derivative **8** gave the elemental composition $C_{15}H_{19}NO_8$ which also indicated the loss of one nitrogen. By HMS only one nitrogen-free fragment ion with a mass > 100 u could be identified, viz. *m/z* 115, which will be discussed below. From this we concluded that the remaining nitrogen had to be part of an aromatic ring. For the ^{13}C signals of this heteroaromate, except for that of C-2, one can easily find a pendant among those of the intact pigment. Apparently this aromatic ring is little effected by hydrolysis. The elemental composition as well as the mass spectrometric and chemical behavior made the presence of a trihydroxy pyridine ring very likely, which has been substantiated (v. infra) by comparison with an authentic compound. As a recent ^{13}C-nmr investigation of nicotine metabolites (6) shows, the difference in the chemical shifts of C-2 cannot be accounted for by the newly generated carbonyl group per se. However, **1***a* and **7***a* do not exist necessarily in the same tautomeric form. ^{13}C data of various isomeric hydroxy and methoxy pyridines have been published (7), but too little is known about the influence of two negative charges on the ^{13}C chemical shifts of such heterocycles to allow assignment of definitive tautomeric structures for **1***a* and **7***a*.

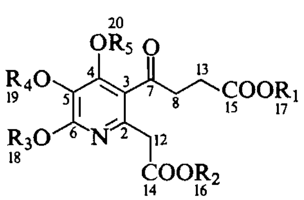

7, R_{1-5} = H
8, R_{1-4} = Me, R_5 = H
13, R_{1-5} = Me

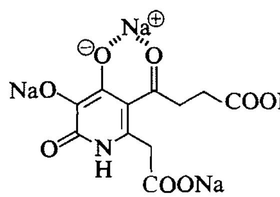

7a

The side chains of 7

Whereas rubrifacine (**1***a*) showed ^{13}C signals for two isolated methylene groups, only one was retained as such in its hydrolysis product **7** while the other one had become part of a —CH_2—CH_2— unit. This was concluded from the presence of an AA′BB′-system in the ^1H-nmr spectrum as well as from the ^{13}C-nmr spectrum (Tables 1–3). The ^{13}C-nmr spectrum also showed the generation of an α,β-unsaturated carbonyl function (192 ppm). Altogether this led to a partial structure Ar—CO—CH_2—CH_2—CO_2H which was confirmed by mass spectrometric comparison of **7**-dimethylester **9** with two differently deuterated derivatives, **10** and **11**. α-Cleavage of the side chain led to CH_3O_2C—CH_2—CH_2—CO^+ (*m/z* 115), CH_3O_2C—CH_2—C^2H_2—CO^+ (*m/z* 117), and $C^2H_3O_2C$—CH_2—CH_2—CO^+ (*m/z* 118), respectively. If one assumes that the aromatic portion of **7** is a trihydroxy pyridine ring the other —CH_2—COOH group postulated has to be attached directly to the ring.

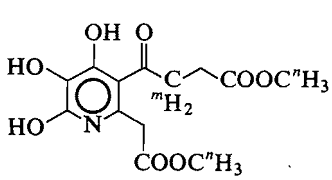

9, *m* = *n* = 1
10, *m* = 2, *n* = 1
11, *m* = 1, *n* = 2

TABLE 2. ^1H chemical shifts of **8** (tetramethyl derivative of **7**), **13** (pentamethyl derivative of **7**), and piericidins **12** (10), all in $CDCl_3$

H[a]	**8**	**13**	**12**
18	3.90	3.82	3.85–3.90
19	3.87	3.80	3.78–3.84
20		4.07	
16,17	3.73, 3.70	3.70, 3.68	
12	3.81	3.67	
8,13	2.7–3.4	2.7–3.3	

[a] For numbering, see formula **7**.

TABLE 3. Tentative assignment of the ^{13}C chemical shifts of rubrifacine hydrolysis product **7** in CD_3OD, its tetramethyl derivative **8** in $CDCl_3$ (δ 77.0), piericidins **12** (10) in $CDCl_3$, and 2,3,4-trihydroxy-6-methylpyridine **15** in H_2O (reference: CD_3CN δ 1.2)

C[c]	**7**	**8**	**12**	**15**
2	151.1	150.6	150.7–150.8	154.9
3	111.8	116.1	112.1–112.2	102.9
4	124.6 (s)	123.0	154.2–154.3	139.1
5	120.5 (s)	121.9	127.9–128.0	127.9
6	164.0 (s)	160.7	153.6–153.7	159.3
7	192.6	173.4		
8	34.8 (T, broad)	34.5		
12	29.2 (T)	29.3		18.4
13	28.7 (T, broad)	27.8		
14	177.5[a]	171.6[a]		
15	176.0[a]	170.8[a]		
16		52.2[b]		
17		52.0[b]		
18		51.9	52.9–53.0	
19		63.2	60.4–60.5	

[a,b] Interchangeable.
[c] For numbering, see formula **7**.

Substitution pattern of 7

Three hydroxy groups can be placed in six different arrangements around the pyridine ring (two of which are symmetrical) which would give ten (4 × 2 and 2 × 1) possible isomeric structures for the hydrolysis product. Of these only one, viz. **7**, is in accordance with the observed splitting pattern in the ^1H coupled ^{13}C-nmr spectrum which shows three non-coupling carbon atoms. Since the $^2J(C_{py}—CH_2)$ and the $^3J(C_{py}—C_{py}—CH_2)$ coupling constants are both to be expected in the range of 4–7 Hz (8) the —CH_2—COOH group cannot be located in a β- or γ-position because in either case only two non-coupling carbons should be observed. The four-carbon side chain has to be in the β-position neighboring the acetic acid group: in any other position $^3J(C_{py}—CO—CH_2)$ coupling would result in the splitting of a further ring carbon.

Comparison of 7 with piericidins (9, 10) of known structure

Piericidins (**12**) and our tetramethyl derivative (**8**) possess the same 2,3-dimethoxy-4-hydroxypyridine partial structure. The ^1H chemical shifts for the methoxy groups of **12** and **8** are in good agreement (Table 2). That indeed the 2,3-dimethoxy derivative **8** and not the 2,4- or 3,4-dimethoxy derivative had been obtained upon methylation can be seen from the chemical shift (4.07 ppm) of the γ-methoxy group in the pentamethyl derivative **13** caused by the anisotropy of the side chain carbonyl function. The ^{13}C data (Table 3) exclude any *N*-methylation as no δ($N\text{-}CH_3$) ≤ 50 ppm is observed (7). Moreover, the ^{13}C data of **8** are in good agreement with those for **12** except for differences for the γ-C-atom which must be the result of hydrogen bridging with the exocyclic carbonyl function. In order to study the interaction of the underivatized phenolic functions in **7** and its influence on the ^{13}C chemical shifts of the trihydroxy pyridine ring, we have synthesized 2,3,4-trihydroxy-6-methyl-pyridine **15** according to the procedure of Lapworth and Collie (11) which has recently been repeated by Findlay *et al.* (12). However, we encountered difficulties in converting 3-amino-2,4-dihydroxy-6-methylpyridine **14** to 2,3,4-trihydroxy-6-methylpyridine **15**, as we obtained mainly the dimerization product mentioned in the literature (11) and only a few milligrams of **15** which did not allow us to obtain a $^{13}C-^{1}H$ coupled ^{13}C-nmr spectrum needed to unambiguously assign δ = 139.1 ppm to C-4 of **15**. This will be the subject of further investigations.

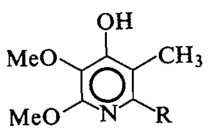

12, R = modified isoprenyl side chains

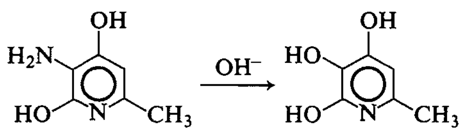

14 **15**

The nature of the second ring

The exocyclic carbonyl function of the hydrolysis product **7** probably stems from an imino function in **1**. The —CH_2— group neighboring the carbonyl function is most likely the one which has been generated during hydrolysis. This could result from a retro-Claisen cleavage of a β-diketone. Taking into account the chemical composition of **1** and the atoms contained in the established partial structures, there remains a difference of only one carbonyl function which suggests for the second ring a pyrrolindione structure.

The presence of a pyrrolindione ring is strongly supported by comparison of **1** with known 2,3-dihydro-2,3-dioxo-5-phenyl-pyrroles: (*a*) 2,3-dihydro-2,3-dioxo-4,5-diphenyl pyrrole (**16**) has a VIS absorption of 483 nm (13), close to that of rubrifacine in the free-acid form (490 nm). (*b*) In strong alkali 2,3-dihydro-2,3-dioxo-5-phenylpyrrole (**17**) undergoes ring opening to **18** and further to acetophenone **19** (14–17). (*c*) Both **17** (17) and rubrifacine give colorless addition products with $NaHSO_3$ from which the colored starting compounds can be regenerated by acidification and passage of air. (*d*) A pyrrolindione ring is likely to undergo ring expansion upon derivatization with diazomethane (4).

Catalytic reduction of rubrifacine

Rubrifacine has been hydrogenated catalytically. Thereby the high field (^1H-nmr) methylene signal split up to the same AB-system at 3.5 ppm both on reduction with H_2 and D_2. The two hydrogens of the methylene group obviously were now diastereotopic because C-7 became chiral upon reduction of the

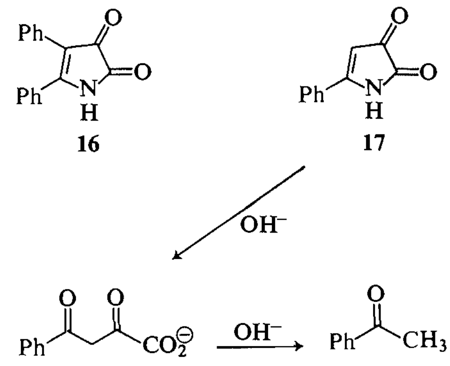

16 **17** **18** **19**

$\Delta^{7,8}$ double bond (for numbering see formula **1**). The additional hydrogen at C-7 gave rise to a ^1H-nmr signal at about 5.6 ppm whereas no signal was observed for the hydrogen at C-8 due to enol formation of the C-9 carbonyl. The pyridine ring was not reduced under these conditions (18). On standing in air the reduced pigment **20** is reoxidized, as is known for pyrrolindiones (19).

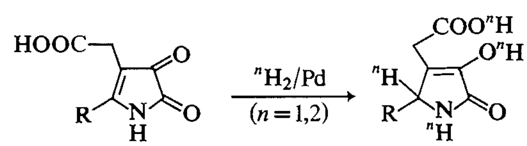

1 **20**

R = 2-carboxymethyl-4,5,6-trihydroxy-3-pyridyl

Experimental

Material

Cation exchange: Dowex AG 50 WX8, Serva; Reversed phase TLC (RP-TLC): KC_{18}, Whatman; Normal phase HPLC: LiChrosorb Si 100, 10 μ, 25 cm × 9.2 mm, Knauer; Reversed phase HPLC: Zorbax ODS, 10 μ, 25 cm × 4.6 mm, Du Pont; Polyamide (<0.07): Macherey Nagel & Co. Düren, FRG.

Instrumental analysis

EI-MS: CH7A, Varian MAT; HMS and field desorption mass spectrometry (FD-MS): MAT 731, Varian MAT; both connected to a Finnigan-MAT SS200 data system; ir: Perkin-Elmer model 720; uv: Beckman model 25; nmr: Varian EM 390, Bruker WP-60, WP-80, WM-300.

Microanalysis of rubrifacine 1a

For a microanalysis 30 mg **1***a* have again been produced in a 12 L culture and purified according to ref. 1. The ^1H-nmr signals of this batch showed slightly different chemical shifts for the two methylene groups than reported: δ = 3.48 and 3.20 compared to δ = 3.32 and 3.22 according to ref. 1 thereby indicating a different pH of the solution. Acetone was used as reference (2.09 ppm) in both cases. *Anal.* calcd. for $C_{13}H_6N_2(Na_{3.5}H_{0.5})O_9 \cdot 4H_2O$: C 32.05, H 3.00, N 5.75, Na 16.5; found: C 32.15, H 3.01, N 5.79, Na 16.4. This analysis confirms the result from fast atom bombardment mass spectrometry (1) which showed that **1***a* exists as a tetrasodium salt.

Thermolability of rubrifacine 1a

The chromophore of **1***a* will be destroyed at about 50°C. **1***a* was therefore stored in a frozen aqueous stock solution at −30°C, solvents were evaporated i.v. at 35°C, and all reactions were performed at room temperature (23°C).

Methylation of rubrifacine 1

In a preliminary investigation a few milligrams crude rubrifacine **1** in dilute hydrochloric acid (pH 2) were treated with excess diazomethane in glyme (20). Derivatives **2** and **3** were separated on LiChrosorb (hexan: *i*-PrOH = 9:1, flow 4 mL/min, retention time 6.4 min (**2**) and 8.4 min (**3**)) in microgram quantities for EI-MS: **2**: *m/z* 450.1651 (100%, calcd. for $C_{21}H_{26}N_2O_9$: 450.1638, M^+) 419 (10%) 391.1517 (30%, calcd. for $C_{19}H_{23}N_2O_7$: 391.1505) 375.1188 (63%, calcd. for $C_{18}H_{19}N_2O_7$: 375.1192); **3**: *m/z* 436.1480 (100%, calcd. for $C_{20}H_{24}N_2O_9$: 436.1482, M^+) 404.1210 (11%, calcd. for $C_{19}H_{20}N_2O_8$: 404.1220) 377.1342 (13%, calcd. for $C_{18}H_{21}N_2O_7$: 377.1348) 361.1034 (31%, calcd. for $C_{17}H_{17}N_2O_7$: 361.1036) 329.0775 (23%, calcd. for $C_{16}H_{13}N_2O_6$: 329.0773) 317.1140 (23%, calcd. for $C_{16}H_{17}N_2O_5$: 317.1137) 299.1032 (18%, calcd. for $C_{16}H_{15}N_2O_4$: 299.1034). To obtain the tetramethyl-derivative **6** 30 mg rubrifacine **1***a* were converted into the free acid form (Dowex, 33 cm high, 3.5 cm in diameter, H^+-form) and dissolved in 3 mL methanol. The methylation (6 mL diazomethane in glyme) was controlled by RP-TLC (KC_{18}, MeOH:H_2O = 3:2) on which **6** had R_f = 0.5. The reaction was stopped at the maximum yield of **6**, which was then chromatographed on Zorbax ODS (MeOH:H_2O = 1:1, flow 1.75 mL/min, retention time 13 min) to give 6 mg pure **6**. ^{1}H-nmr ($CDCl_3$, TMS): 4.30 (s, 3H), 3.95 (s, 3H), 3.80 (s, 3H), 3.69 (s, 3H), 3.62 (s, 2H), 3.57 (s, 2H). EI-MS: *m/z* 394.1008 (100% calcd. for $C_{17}H_{18}N_2O_9$: 394.1012) 379.0821 (10%) 363 (13%) 362 (12%) 335 (15%) 334.0802 (18%, calcd. for $C_{15}H_{14}N_2O_7$: 334.0801), 319.0569 (21%, calcd. for $C_{14}H_{11}N_2O_7$: 319.0566) 303 (28%) 302.0557 (70%, calcd. for $C_{14}H_{10}N_2O_6$: 302.0539) 287.0310 (32%, calcd. for $C_{13}H_7N_2O_6$: 287.0304) 275.0656 (48%, calcd. for $C_{13}H_{11}N_2O_5$: 275.0668) 259.0343 (16%, calcd. for $C_{12}H_7N_2O_5$: 259.0355) 231.0417 (7%, calcd. for $C_{11}H_7N_2O_4$: 231.0406).

Hydrolysis of rubrifacine

To a solution of 10 mg rubrifacine **1***a* in 3 mL H_2O a few milliliter 1 *N* KOH were added drop-wise until discoloration occurred (5 min). The solution was then neutralized with Dowex (22.5 cm high, 2 cm in diameter, H^+-form) to give **7**. ^{1}H-nmr (D_2O, $(CH_3)_2CO$ 2.09 ppm): 3.69 (s, 2H), 2.5–3.2 (AA′BB′, 4H); FD-MS: $[M + H]^+$ 286; EI-MS: *m/z* 285 (1.2%, M^+) 267 (1.7%) 249 (1.9%) 239 (1.6%) 223 (5%) 221 (6%) 205 (2%) 203 (3%) 193 (4%) 177 (5%) 166 (10%) 148 (9%) 122 (4%) 44 (100%); uv: λ_{max} 370, 305 (pH 12), 295, 230 (pH 2). **7***a* was obtained by cation exchange (Dowex, Na^+-form). When the hydrolysis was carried out in D_2O H/D exchange at C-8 occurred and yielded compound **10** after esterification.

Tetra- 8 and pentamethyl- 13 derivatives of 7

1*a* (30 mg) was converted into **7** as described above and dissolved in 25 mL methanol. Gaseous diazomethane (21) was passed through this solution until a maximum yield of **8** was obtained (checked by mass spectrometry). **8** (4 mg) could be separated on LiChrosorb (Hexan, 5% *i*-PrOH, flow 3 mL/min, retention time 4 min). Ir (KBr): ν_{max} 3275 (OH), 2962, 2930, 1743, 1723, 1714, 1651, 1315, 1269; uv (MeOH): λ_{max} 295; EI-MS: *m/z* 341.1114 (41%, calcd. for $C_{15}H_{19}NO_8$: 341.111, M^+) 310.0935 (21%, calcd. for $C_{14}H_{16}NO_7$: 310.0927) 282.0972 (22%, calcd. for $C_{13}H_{16}NO_6$: 282.0978) 281 (16%) 254.0674 (18%, calcd. for $C_{11}H_{12}NO_6$: 254.0665) 250.0722 (28%, calcd. for $C_{12}H_{12}NO_5$: 250.0715) 222.0752 (32%, calcd. for $C_{11}H_{12}NO_4$: 222.0766) 194.0457 (100%, calcd. for $C_{10}H_8NO_4$: 194.0453) 190.0507 (18%, calcd. for $C_{10}H_8NO_3$: 190.0505) 115.0393 (10%, calcd. for $C_5H_7O_3$: 115.0395). **8** was converted into **13** by permethylation and chromatography in the same system like **8** (retention time 2.8 min); uv (MeOH): λ_{max} 294; EI-MS: *m/z* 355.1263 (100%, calcd. for $C_{16}H_{21}NO_8$: 355.1267, M^+) 324 (36%) 323 (20%) 296 (57%) 268 (81%) 264 (20%) 241 (19%) 236 (31%) 194 (46%) 182 (22%) 180 (23%) 115 (31%).

Dimethylesters of 7

The carboxyl function could be esterified with methanol under acidic catalysis or by autocatalysis on standing in methanolic solution for several days. The dimethylester could be separated from the monoesters by chromatography on Zorbax (H_2O:MeOH = 7:3, flow 1.4 mL/min, retention time: monoesters 7.5 and 9 min, diester 22 min). 0.01% acetic acid was added to reduce dissociation but this had the disadvantage that the ester was partially saponified on concentrating the eluate. Therefore, the following procedure was applied to obtain mass spectra of pure dimethylesters: **7** was precipitated on Dowex (H^+-form) by evaporating to dryness a solution of **7** (5 mg) in 10 mL H_2O together with 1 g wet cation exchange resin. This was then suspended in 5 mL methanol or methanol-d_3, respectively, in which only the di- but not the monoester is soluble. After 3 h a few μL of these solutions were directly used for mass spectrometric investigations.

EI-MS: **7**: *m/z* 313 (54%, M^+) 282 (26%) 281 (31%) 254 (24%) 253 (30%) 249 (28%) 226 (20%) 222 (43%) 221 (75%) 203 (28%) 194 (39%) 193 (31%) 180 (22%) 176 (50%) 167 (28%) 166 (40%) 148 (60%) 115 (53%) 55 (100%); **8**: *m/z* 315 (100%, M^+) 284 (44%) 283 (62%) 256 (32%) 255 (45%) 251 (41%) 226 (40%) 223 (95%) 205 (34%) 204 (36%) 194 (63%) 178 (61%) 166 (63%) 148 (75%) 117.0518 (52%, calcd. for $C_5H_5D_2O_3$: 117.0520); **9**: *m/z* 319 (50%, M^+) 285 (25%) 284 (31%) 257 (20%) 256 (24%) 249 (30%) 222 (41%) 221 (70%) 203 (24%) 194 (35%) 193 (23%) 185 (28%) 176 (33%) 166 (29%) 148 (36%) 118 (41%) 55 (100%).

Reduction of rubrifacine

1*a* (5 mg) in 15 mL dilute hydrochloric acid (pH 2) were catalytically reduced at atmospheric pressure for 10 min using 2 mg Pd/C which had been prehydrogenated for 15 min. The catalyst was centrifuged off, the solution evaporated to dryness, and the residue dissolved in D_2O for ^{1}H-nmr measurement. In case of reduction with D_2 in D_2O/DCl the probe was ready for nmr-measurement after centrifugation and concentration to 1 mL.

2,3,4-Trihydroxy-6-methyl-pyridine 15

The final purification of **15** (ca. 10 mg) was achieved by chromatography on polyamide (50 cm long, 1 cm in diameter) in 0.2% acetic acid. EI-MS: *m/z* 141.0426 (100%, calcd. for $C_6H_7NO_3$: 141.0426, M^+) 112 (13%) 95 (4%) 84 (7%) 68 (12%) 57 (8%); uv (H_2O): λ_{max} 289 (E 67700); uv (KOH): λ_{max} 318 (E 19700); ^{1}H-nmr (D_2O, MeOH δ 3.39): 6.10 (s, 1H) 2.25 (s, 3H); ir (KBr) ν_{max} 3520 (sharp), 3700–2400 (broad), 1670 (shoulder), 1660 (shoulder), 1640, 1590, 1460, 1400.

Acknowledgments

We wish to thank Professor Dr. E. Breitmaier (Univ. Bonn), Dr. H. Schmickler, Dipl.-Chem. C. Schnieders, and Dipl.-Chem. H. Unterberg for the nmr measurements, and G. Briskot for the synthesis of 2,3,4-trihydroxy-6-methyl-pyridine.

1. G. Feistner, H. Korth, H. Budzikiewicz, and G. Pulverer. Curr. Microbiol. **10**, 169 (1984).
2. G. Feistner, H. Korth, H. Ko, G. Pulverer, and H. Budzikiewicz. Curr. Microbiol. **8**, 239 (1983).
3. H. Budzikiewicz, U. Hildebrand, W. Ockels, M. Reiche, and K. Taraz. Z. Naturforschg. **38**b, 516 (1983).
4. R. Gompper. Adv. Heterocycl. Chem. **2**, 245 (1963).
5. E. Breitmaier and W. Voelter. ^{13}C NMR spectroscopy. 1st ed. Weinheim: Verlag Chemie. 1978. p. 162.
6. N. Toshiaki, A. Pilotti, and C. R. Enzell. Org. Magn. Res. **13**, 434 (1980).
7. U. Vögeli and W. von Philipsborn. Org. Magn. Res. **5**, 551 (1973).
8. Y. Takeuchi. Org. Magn. Res. **7**, 181 (1975).
9. S. Yoshida, S. Shiraishi, and N. Takahashi. Agric. Biol. Chem. **41**, 587 (1977).
10. S. Yoshida, K. Yoneyama, S. Shiraishi, A. Watanabe, and N. Takahashi. Agric. Biol. Chem. **41**, 855 (1977).
11. A. Lapworth and J. N. Collie. J. Chem. Soc. **71**, 838 (1897).
12. J. A. Findlay, J. Krepinsky, A. Schum, C. G. Casinovi, and

L. RADICS. Can. J. Chem. **55**, 600 (1977).
13. T. EICHER and G. FRANKE. Liebigs Ann. Chem. 1337 (1981).
14. O. MUMM and C. BERGELL. Chem. Ber. **45**, 3040 (1912).
15. O. MUMM and G. MÜNCHMEYER. Chem. Ber. **43**, 3334 (1910).
16. L. HORWITZ. J. Am. Chem. Soc. **75**, 4060 (1953).
17. O. MUMM and G. MÜNCHMEYER. Chem. Ber. **43**, 3345 (1910).
18. E. MEDINA and G. SPITELLER. Chem. Ber. **112**, 376 (1979).
19. O. MUMM and H. HORNHARDT. Chem. Ber. **70**, 1930 (1937).
20. M. J. ROBINS, S. R. NAIK, and A. S. K. LEE. J. Org. Chem. **39**, 1891 (1974).
21. T. H. BLACK. Aldrichim. Acta, **16**, 3 (1983).

Identification, par spectroscopie optique, des dihydrodiols formés lors de la métabolisation des hydrocarbures polybenzéniques. Application dans le cas de la métabolisation in vitro du dibenzo[a,e]pyrène

ODILON CHALVET
Centre de Mécanique Ondulatoire Appliquée, 23, rue du Maroc, F-75019 Paris, France

ET

JEAN-FRANÇOIS GOURVEST, HÉLÈNE STRAPELIAS ET MAURICE DUQUESNE
LA 198 CNRS, Institut Curie, Section de Physique et Chimie, 11, rue Pierre et Marie Curie, F-75231 Paris Cedex 05, France

Reçu le 11 avril 1984

ODILON CHALVET, JEAN-FRANÇOIS GOURVEST, HÉLÈNE STRAPELIAS et MAURICE DUQUESNE. Can. J. Chem. **63**, 500 (1985).

La première étape de la métabolisation d'une molécule d'hydrocarbure polybenzénique est la saturation d'une double liaison et la formation d'un époxyde puis d'un dihydrodiol. Après séparation par chromatographie, les spectres d'absorption de ces dihydrodiols peuvent être établis et comparés directement aux prévisions théoriques qui, pour des molécules planes, sont très aisées à établir. Une identification du site de la première attaque enzymatique est alors possible sans avoir recours à des molécules modèles.

ODILON CHALVET, JEAN-FRANÇOIS GOURVEST, HÉLÈNE STRAPELIAS, and MAURICE DUQUESNE. Can. J. Chem. **63**, 500 (1985).

The first step in the metabolization of a polycyclic hydrocarbon molecule is the saturation of a double bond, the formation of an epoxide, then of a dihydrodiol. Once separation has been achieved by chromatography, the absorption spectra of these dihydrodiols can be established and directly compared with theoretical predictions which are reasonably easy to elaborate in the case of plane molecules. The initial site of enzyme attack can then be identified without using model molecules.

Introduction

Dans une précédente publication (1), l'un de nous, au moyen d'une méthode de "reconnaissance de formes", a montré que la forme des molécules d'hydrocarbures polybenzéniques est corrélée à leur pouvoir cancérogène.

Pour éprouver, sur le plan expérimental, la validité de certains concepts suggérés par cette étude, il était intéressant de considérer en premier lieu le rôle de la topologie de ce type de molécule au niveau de l'acte de métabolisation de la molécule.

La métabolisation des benzo[*a*]pyrène et benzo[*e*]pyrène a été particulièrement étudiée ces dernières années (2, 3). Il nous a donc paru intéressant d'étudier la métabolisation du dibenzo[*a,e*]pyrène (DB[*a,e*]P), molécule qui présente dans sa structure à la fois la topologie du benzo[*a*]pyrène (B[*a*]P), cancérogène, et celle du benzo[*e*]pyrène (B[*e*]P), non cancérogène (Fig. 1).

Généralement, l'identification d'une espèce chimique se fait à l'aide de molécules modèles synthétisées spécialement pour cette identification. Celle-ci se fait soit à partir des paramètres de chromatographie, soit à partir des propriétés spectroscopiques (absorption, fluorescence, excitation de fluorescence . . .). Cette méthode est extrêmement lourde et coûteuse, surtout lorsque l'objectif de la recherche est de comparer la métabolisation de plusieurs molécules d'une même famille comme les dibenzopyrènes.

Compte tenu des propriétés particulières liées à la structure des molécules d'hydrocarbures polybenzéniques, il nous est apparu qu'il était possible de faire cette identification du site de la première attaque enzymatique, à partir des données spectroscopiques, c'est-à-dire d'une manière directe, sans avoir recours à la synthèse de molécules modèles.

Bases expérimentales et discussions

Métabolisation

Dans nos expériences, la métabolisation in vitro est effectuée en plaçant l'hydrocarbure dans un milieu incubateur comprenant le système enzymatique (4). Les métabolites qui retiennent notre attention sont les dihydrodiols, eux-mêmes formés à partir des époxydes par l'action de l'époxyde hydrolase. Ces dihydrodiols sont identifiés dans l'ensemble des pics du profil de chromatographie par le fait que certains pics de ce profil disparaissent lorsque l'on ajoute au milieu d'incubation un oxyde stable (TCPO)[1] qui inhibe l'action de l'époxyde hydrolase.

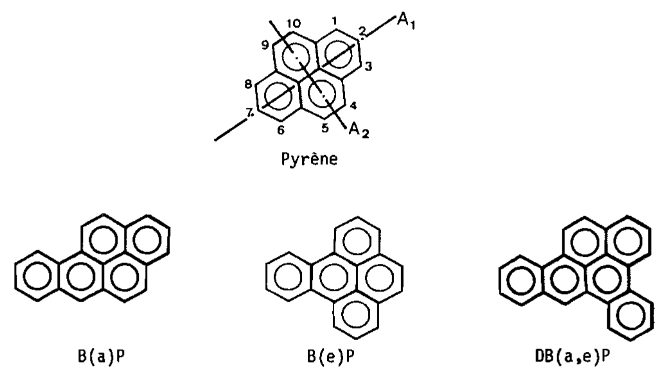

FIG. 1. Topologie de la molécule de pyrène et des trois molécules qui en dérivent par adjonction d'un ou deux noyaux benzéniques.

L'identification des molécules du type "dihydrodiol" informe sur la position du site de la première attaque enzymatique qui sature une double liaison pour former un époxyde. L'utilisation de molécules marquées permet de connaître en plus l'importance de cette attaque.

La quantité de métabolites extraite par chromatographie hplc étant souvent inférieure à 10 µg, l'identification par rmn est pratiquement impossible. Par contre, la sensibilité de la fluorescence et le rendement quantique élevé des hydrocarbures polybenzéniques rendent souvent possible l'identification de la double liaison attaquée.

[1]Epoxy-1,2 trichloro-3,3,3 propane.

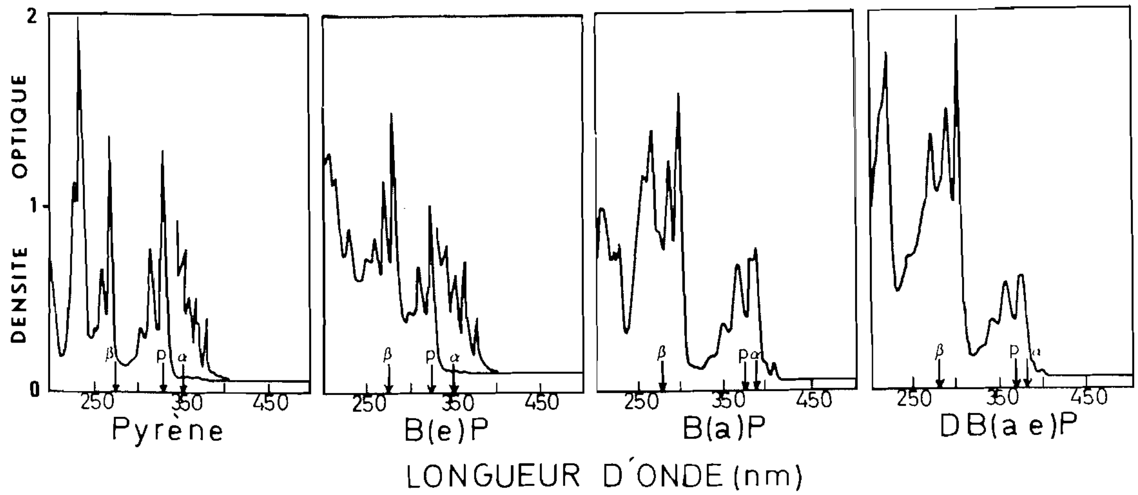

FIG. 2. Spectres d'absorption des 4 molécules: pyrène, benzo[*e*]pyrène, benzo[*a*]pyrène et dibenzo[*a,e*]pyrène. Les positions des bandes α, *p* et β, qui sont indiquées sur l'échelle des longueurs d'ondes exprimées en nanomètres, résultent de calculs effectués par la méthode CNDO/S.

Spectroscopie

Les spectres d'absorption et d'excitation de fluorescence des 3 molécules B[*a*]P, B[*e*]P et DB[*a,e*]P présentent une grande analogie avec ceux du pyrène (Fig. 2).

En effet, en parcourant le spectre d'absorption du rouge vers l'ultraviolet, on rencontre, pour ces 4 molécules, suivant la nomenclature de E. Clar (5), une bande de très faible intensité (bande α) et une bande d'intensité moyenne (bande *p*). Les énergies relatives attachées à ces bandes permettent de séparer ces 4 molécules en 2 groupes: le pyrène et le B[*e*]P d'une part, le B[*a*]P et le DB[*a,e*]P d'autre part (Fig. 2).

Pour les deux molécules du premier groupe, les différences d'énergie entre les bandes α et *p* sont nettement plus importantes que pour celles du second groupe. Il faut noter en outre un déplacement vers les grandes longueurs d'onde de la bande *p* lorsqu'on passe du premier au second groupe, alors que la position de la bande α est sensiblement stable. En raison de la loi d'annelation (5), si le déplacement bathochrome de la bande *p* paraît normal dans la série pyrène, B[*a*]P, DB[*a,e*]P, par contre l'absence de déplacement dans le cas du B[*e*]P apparaît comme une exception (Fig. 2). C'est cette exception que nous exploiterons pour l'identification des métabolites du type "dihydrodiol".

Il convient toutefois de noter que cette loi d'annelation n'est valable que pour la série des hydrocarbures polybenzéniques plans, sans substituants ni hétéroatomes.

Cette absence de déplacement bathochrome peut être constatée pour d'autres polybenzéniques dérivés du pyrène. Le pyrène possède, entre autres éléments de symétrie, deux axes binaires, l'un (A_1) passant par les carbones 2 et 7, et l'autre (A_2) bissecteur des liaisons 4−5 et 9−10 (Fig. 1). On vérifie aisément que toute adjonction de cycles benzéniques respectant la symétrie de la molécule par rapport à l'axe A_2 perturbe peu la position de la bande *p* (5). Au niveau des métabolites, la formation d'un dihydrodiol revient, en première approximation, à rompre le système conjugué de la molécule. Ainsi le 7,8 dihydrodiol et le 9,10 dihydrodiol du B[*a*]P peuvent être, dans une approximation raisonnable, assimilés au 8 vinyl pyrène et au 7 vinyl pyrène supposés plans (Fig. 3). Les spectres d'absorption et d'excitation de fluorescence des deux premiers composés montrent une situation relative des bandes α et *p* différente (Fig. 3). Pour le 7,8 dihydrodiol, la bande *p* est déplacée vers le rouge et recouvre en partie les bandes α. Pour le 9,10 dihydrodiol au contraire, la bande *p* n'est pas déplacée, laissant visibles les bandes α.

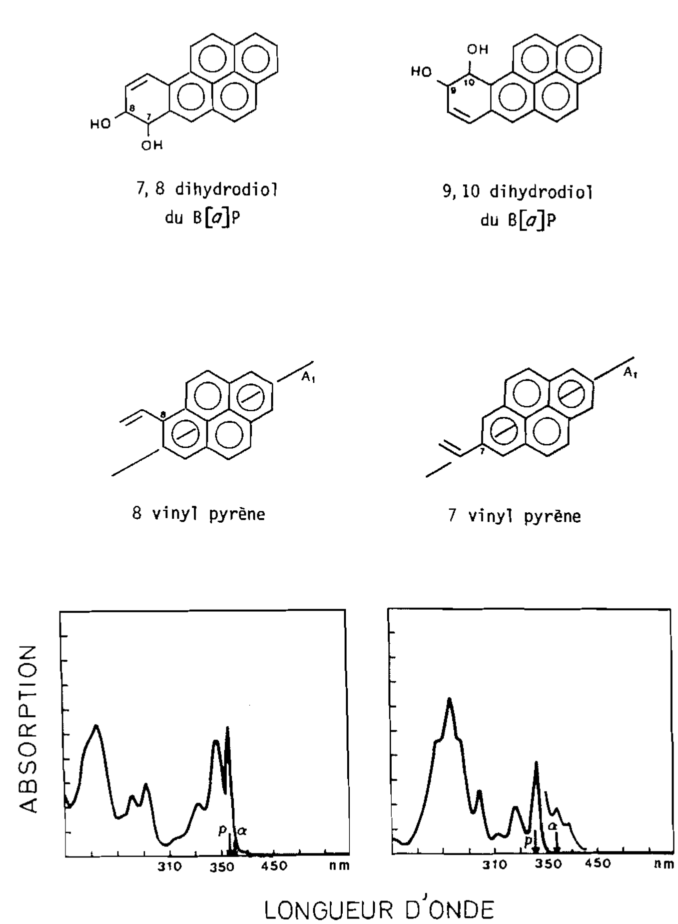

FIG. 3. Deux des hydrodiols du benzo[*a*]pyrène et leurs spectres d'absorption. Le déplacement vers les grandes longueurs d'ondes de la bande *p* du 7,8 dihydrodiol du benzo[*a*]pyrène est nettement visible (d'après la réf. 6 et nos propres résultats).

D'une manière générale, la conjugaison d'un groupe vinylique, bien que faible, est plus importante lorsque la partie vinylique est liée à un carbone situé hors de l'axe de symétrie (A_1) du pyrène. Dans le 9,10 dihydrodiol, cette partie vinylique du système conjugué est liée à un carbone situé sur l'axe de

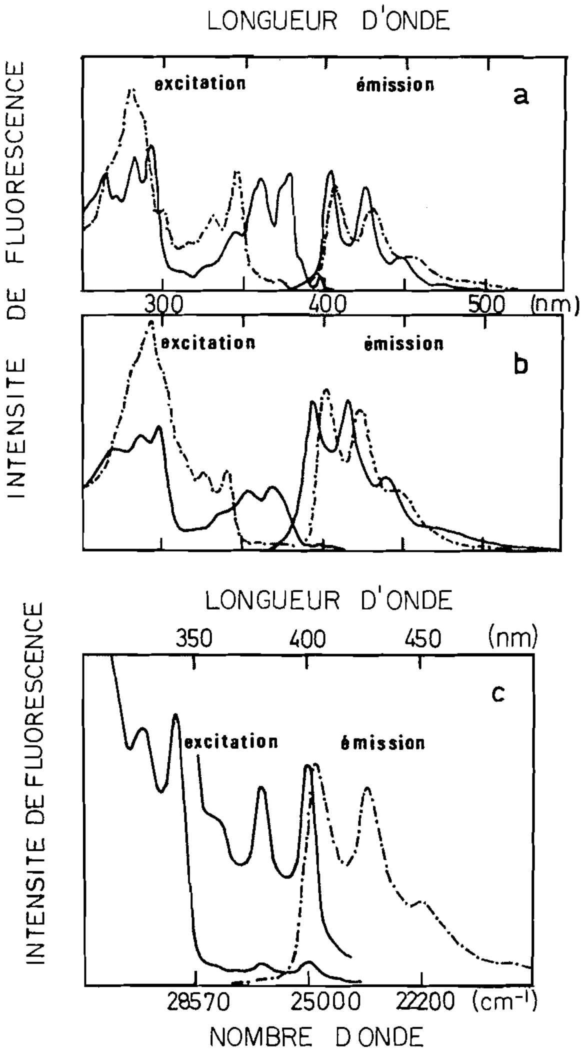

FIG. 4. (*a*) Spectres d'émission et d'excitation de fluorescence des B[*a*]P (—) et 9,10 dihydrodiol B[*a*]P (------).

	Spectre d'émission	Spectre d'excitation
B[*a*]P	$\lambda_{exc.}$ = 380 nm	$\lambda_{analyse}$ = 400 nm
9,10 dihydrodiol B[*a*]P	$\lambda_{exc.}$ = 342 nm	$\lambda_{analyse}$ = 405 nm

(b) Spectres d'émission et d'excitation de fluorescence du DB[*a*,*e*]P (—) et du dihydrodiol majoritaire de cet hydrocarbure (------).

	Spectre d'émission	Spectre d'excitation
DB[*a*,*e*]P	$\lambda_{exc.}$ = 372,5 nm	$\lambda_{analyse}$ = 395 nm
Dihydrodiol majoritaire du DB[*a*,*e*]P	$\lambda_{exc.}$ = 342 nm	$\lambda_{analyse}$ = 405 nm

(c) Spectres détaillés d'émission ($\lambda_{exc.}$ = 342 nm) et d'excitation de fluorescence ($\lambda_{analyse}$ = 405 nm) du métabolite majoritaire du DB[*a*,*e*]P, le 11,12 dihydrodiol du DB[*a*,*e*]P.

symétrie (A_1) du pyrène et le déplacement est beaucoup moins important que dans le cas du 7,8 dihydrodiol.

Conclusion

Pour le métabolite majoritaire (12,5%) correspondant à un dihydrodiol du DB[*a*,*e*]P, son spectre d'excitation montre sans ambiguité une bande *p* située dans la zone d'énergie de celle du 9,10 dihydrodiol du B[*a*]P (Fig. 4). Forts de notre remarque sur l'adjonction d'un cycle benzénique en position [*e*] du pyrène, nous pouvons conclure que le dihydrodiol majoritaire de la métabolisation du DB[*a*,*e*]P correspond à une saturation de la liaison 11–12 de cette molécule. Nous avons par ailleurs vérifié que le spectre d'émission de fluorescence est bien l'effet miroir d'une bande α nettement séparée de la bande *p* comme c'est le cas pour le B[*e*]P.

1. M. DUQUESNE et J. SALLANTIN. C. R. Acad. Sci. Paris, Sér. III, **292**, 495 (1981).
2. J. K. SELKIRK et M. C. MCLEOD. *Dans* Polynuclear aromatic hydrocarbons. *Edité par* P. W. Jones et P. Leber. Ann Arbor Science Publishers, Ann Arbor, MI. 1979. p. 21.
3. D. M. JERINA et J. W. DALY. Science, **185**, 573 (1974).
4. B. N. AMES, J. MCCANN et E. YAMASAKI. Mutat. Res., **31**, 347 (1975).
5. E. CLAR. Polycyclic hydrocarbons. Vol. 1. Academic Press – Springer Verlag, New York. 1964.
6. D. J. MCCAUSTLAND *ET AL*. Polycyclic aromatic hydrocarbon derivatives. Synthesis and physicochemical characterization, carcinogenesis. Vol. 1. Polynuclear aromatic hydrocarbons. Raven Press, New York. p. 408.

Synthesis and characterization of $[Me_2Ga(3,5\text{-}Me_2pz)_2]Rh(CO)PPh_3$ and the X-ray structure of its toluene solvate

BRENDA M. LOUIE, STEVEN J. RETTIG, ALAN STORR, AND JAMES TROTTER
Department of Chemistry, University of British Columbia, 2036 Main Mall, Vancouver, B.C., Canada V6T 1Y6

Received May 4, 1984

BRENDA M. LOUIE, STEVEN J. RETTIG, ALAN STORR, and JAMES TROTTER. Can. J. Chem. **63**, 503 (1985).

Details of the synthesis and physical properties of $[Me_2Ga(3,5\text{-}Me_2pz)_2]Rh(CO)PPh_3$ are given. Crystals of [dimethylbis(3,5-dimethyl-1-pyrazolyl)gallato-N,N'](triphenylphosphine)carbonylrhodium(I) − toluene (1:1) are triclinic, a = 10.690(2), b = 12.928(2), c = 13.998(2) Å, α = 77.44(1), β = 83.50(1), γ = 72.70(1)°, Z = 2, space group $P\bar{1}$. The structure was solved by conventional heavy-atom methods and was refined by full-matrix least-squares procedures to R = 0.039 and R_w = 0.048 for 5987 reflections with $I \geq 3\sigma(I)$. The Rh(I) is in a distorted square planar environment with Rh—N = 2.090(3) and 2.097(2), Rh—CO = 1.815(4), and Rh—P = 2.2700(8) Å. The central six-membered $RhGaN_4$ ring has a steep boat conformation with a Rh···Ga separation of 3.3819(4) Å.

BRENDA M. LOUIE, STEVEN J. RETTIG, ALAN STORR et JAMES TROTTER. Can. J. Chem. **63**, 503 (1985).

On rapporte les détails relatifs à la synthèse et aux propriétés physiques du $[Me_2Ga(Me_2\text{-}3,5\ pz)_2]Rh(CO)PPh_3$. Les cristaux du [diméthyl bis(diméthyl-3,5 pyrazolyl-1) gallato-N,N'](triphénylphosphine) carbonyl rhodium(I) − toluène (1:1) sont tricliniques, a = 10,690(2), b = 12,928(2), c = 13,998(2) Å, α = 77,44(1), β = 83,50(1), γ = 72,70(1)°, Z = 2, groupe d'espace $P\bar{1}$. On a résolu la structure par des méthodes conventionnelles avec des atomes lourds et on l'a affinée par la méthode des moindres carrés (matrice entière) jusqu'à des valeurs de R = 0,039 et R_w = 0,048 pour 5987 réflexions avec $I \geq 3\sigma(I)$. Le Rh(I) se trouve dans un environnement plan carré déformé avec Rh—N = 2,090(3) et 2,097(2), Rh—CO = 1,815(4) et Rh—P = 2,2700(8) Å. Le cycle central à six chaînons, $RhGaN_4$, existe dans une conformation bateau et la séparation entre Rh···Ga est égale à 3,3819 Å.

[Traduit par le journal]

Introduction

An earlier paper (1) has described the synthesis and characterization of a number of Rh(I) square planar complexes incorporating the chelating gallate ligand $Me_2Gapz_2^-$ (where pz = pyrazolyl, $N_2C_3H_3$). Attempts to synthesize analogous complexes containing the ligand $Me_2Ga(3,5\text{-}Me_2pz)_2^-$ (where 3,5-Me_2pz = 3,5-dimethylpyrazolyl, $N_2C_5H_7$) were thwarted by the ready formation of the Rh(I) dimer species, e.g. $[Rh(\mu\text{-}3,5\text{-}Me_2pz)(CO)_2]_2$. Recently our perseverance in this area has been rewarded with the isolation and structural characterization of the complex $[Me_2Ga(3,5\text{-}Me_2pz)_2]Rh(CO)PPh_3$, the subject of this report.

Experimental

Air-sensitive materials were handled in oxygen-free dry nitrogen. Tetrahydrofuran (THF) was dried by refluxing over sodium benzophenone and used immediately following distillation. Methylene chloride was dried by refluxing over P_2O_5 prior to distillation and n-hexane by distillation from $CaSO_4$. $[Rh(CO)_2Cl]_2$ (Strem Chemicals) was sublimed *in vacuo* before use. PPh_3 (MCB) was used as supplied and the sodium salt of the gallate ligand $[Me_2Ga(3,5\text{-}Me_2pz)_2]$- was prepared as a THF solution as described earlier (2).

Preparation of $[Me_2Ga(3,5\text{-}Me_2pz)_2]Rh(CO)PPh_3$

$Na^+[Me_2Ga(3,5\text{-}Me_2pz)_2]^-$ (0.941 mmol in 50 mL THF) was added dropwise to a stirred solution of $[Rh(CO)_2Cl]_2$ (0.183 g, 0.471 mmol) and PPh_3 (0.247 g, 0.943 mmol) in 100 mL THF at −78°C. The resultant solution was allowed to warm gradually to room temperature. Approximately 100 mL of n-hexane was then added to the mixture and the lemon−yellow solution subsequently filtered. Removal of the solvents from the filtrate *in vacuo* left a yellow−orange residue. Recrystallization of this residue from CH_2Cl_2/n-hexane yielded lemon−yellow prisms of $[Me_2Ga(3,5\text{-}Me_2pz)_2]Rh(CO)PPh_3$ in approximately 35% yield, together with needles of $[Rh(\mu\text{-}3,5\text{-}Me_2pz)(CO)PPh_3]_2$. *Anal.* calcd. for $[Me_2Ga(3,5\text{-}Me_2pz)_2]Rh(CO)PPh_3$: C 54.50, H 5.16, N 8.20; found: C 54.43, H 5.10, N 8.19. ^{1}H nmr (C_6D_6, τ values refer to $\tau(C_6H_6)$ = 2.84 ppm): 9.28 s, 9.73 s ($GaMe_2$); 7.35 s, 7.85 s, 7.86 s, 8.14 s (pz—Me); 4.24 s, 4.71 s (pz—H^4); 2.42 m, 3.01 m (PPh_3). Ir (cyclohexane) ν_{co} = 1985 s. The mass spectrum of the compound displayed a weak signal due to the parent ion, P^+ (1%), with major signals arising from the P − Me^+ (93%), P − Me − CO^+ (34%), and P − Me − CO − $(3,5\text{-}Me_2pzH)^+$ (100%) ions.

Spectra

The ir spectrum was recorded on a Perkin-Elmer 598 spectrometer, the ^{1}H nmr spectrum on a Varian XL 100 instrument using FT techniques, and the mass spectrum on a Varian MAT CH4B spectrometer at 70 eV and 200°C.

X-ray crystallographic analysis of $[Me_2Ga(3,5\text{-}Me_2pz)_2]Rh(CO)PPh_3\cdot CH_3C_6H_5$

The crystal used for the X-ray analysis was obtained by recrystallization from benzene (later shown by mass spectrometry to be contaminated by toluene) and sealed in a Lindemann glass capillary. A crystal ca. 0.40 × 0.45 × 0.55 mm in size was mounted in a general orientation. Unit-cell parameters were refined by least-squares on 2 sin θ/λ values for 25 reflections (2θ = 35−40°) measured on a diffractometer with Mo-$K\alpha$ Radiation ($\lambda(K\alpha_1)$ = 0.70930, $\lambda(K\alpha_2)$ = 0.71359 Å). Crystal data at 22°C are:

$C_{31}H_{35}GaN_4OPRh\cdot C_7H_8$ fw = 775.38
Triclinic, a = 10.690(2), b = 12.928(2), c = 13.998(2) Å, α = 77.44(1), β = 83.50(1), γ = 72.70(1)°, V = 1800.5(6) Å^3, Z = 2, ρ_c = 1.430 Mg m^{-3}, $F(000)$ = 796, μ(Mo-$K\alpha$) = 12.74 cm^{-1}. Absent reflections: none, space group $P\bar{1}$ (C_i^1, No. 2, reduced cell) from structure analysis.

Intensities were measured with graphite-monochromated Mo-$K\alpha$ radiation on an Enraf-Nonius CAD4-F diffractometer. An ω−2θ scan at 1.26−10.06° min^{-1} over a range of (0.75 + 0.35 tan θ) degrees in ω (extended by 25% on both sides for background measurement) was employed. Data were measured to 2θ = 55°. The intensities of three check reflections, measured every 3600 s throughout the data collection, decreased uniformly by approximately 30%, the data being scaled accordingly. After data reduction,[1] an absorption correction

[1]The computer programs used include locally written programs for data processing and locally modified versions of the following: ORFLS, full-matrix least-squares, and ORFFE, function and errors, by W. R. Busing, K. O. Martin and H. A. Levy; FORDAP, Patterson and Fourier syntheses, by A. Zalkin; ORTEP II, illustrations, by C. K. Johnson.

was applied using the Gaussian integration method (3, 4). Transmission factors ranged from 0.574 to 0.654 for 148 integration points. Of the 8254 independent reflections measured, 5987 (72.5%) had intensities greater than $3\sigma(I)$ above background where $\sigma^2(I) = S + 2B + (0.04(S - B))^2$ with S = scan count and B = normalized background count.

The centrosymmetric space group $P\bar{1}$ was indicated by both the Patterson function and the E-statistics. The structure was solved by conventional heavy-atom methods; the coordinates of the Rh, Ga, and P atoms being determined from the Patterson function and those of the remaining non-hydrogen atoms from a subsequent difference map. There was no indication of disordering of the toluene methyl carbon atom (C(38)). This is substantiated by comparison of the equivalent isotropic thermal parameters obtained for the toluene ring atoms (C(32–37), mean U = 0.215 Å^2) with the value of 0.298 for the methyl carbon, the latter expected to be somewhat larger. In the final stages of refinement all non-hydrogen atoms were refined with anisotropic thermal parameters and hydrogen atoms were included as fixed contributors in idealized positions (C(sp^3)—H = 0.98, C(sp^2)—H = 0.97 Å). The scattering factors of ref. 5 were used for non-hydrogen atoms and those of ref. 6 for hydrogen atoms. Anomalous scattering factors from ref. 7 were used for the Rh, Ga, and P atoms. The weighting scheme $w = 1/\sigma^2(F)$, where $\sigma^2(F)$ is derived from the previously defined $\sigma^2(I)$, gave uniform average values $w(|F_o| - |F_c|)^2$ over ranges of both $|F_o|$ and $\sin\theta/\lambda$ and was employed in the final stages of refinement. Reflections with $I < 3\sigma(I)$ were not included in the refinement. Convergence was reached at R = 0.039 and R_w = 0.048 for 5987 reflections with $I \geq 3\sigma(I)$. For all 8254 reflections R = 0.071. The function minimized was $\Sigma w(|F_o| - |F_c|)^2$, $R = \Sigma||F_o| - |F_c||/\Sigma|F_o|$ and $R_w = (\Sigma w(|F_o| - |F_c|)^2/\Sigma w|F_o|^2)^{1/2}$.

On the final cycle of refinement the mean and maximum parameter shifts corresponded to 0.05 and 1.26σ, respectively. The maximum parameter shift was associated with the U_{33} parameter of the toluene atom C(34), all shifts for the complex molecule were less than 0.08σ. The mean error in an observation of unit weight was 1.800. A final difference map showed maximum fluctuations of −1.94 to +0.57 e Å^{-3} near Rh and was essentially featureless away from the heavy atoms. The final positional and thermal parameters appear in Tables 1 and 5,[2] respectively. Measured and calculated structure factors have been placed in the Depository of Unpublished Data.[2]

The ellipsoids of thermal motion for the non-hydrogen atoms are shown in Fig. 1. The thermal motion has been analysed in terms of the rigid-body modes of translation, libration, and screw motion (8). The rms standard error in the temperature factors σU_{ij} (derived from the least-squares analysis) is 0.0065 Å^2. Analysis of the entire molecule indicated significant independent motion of several structural subunits. The following fragments were analysed separately: 3PPh, 2Me$_2$pz, GaC$_2$N$_2$, and RhGaPN$_4$C(1) (rms ΔU_{ij} = 21, 25, 19, 16, 14, 16, and 27 × 10^{-4} Å^2, respectively). The appropriate bond distances have been corrected for libration (8, 9), using shape parameters q^2 of 0.08 for all atoms involved. Corrected bond lengths appear in Table 2 along with the uncorrected values; corrected bond angles do not differ by more than 1σ from the uncorrected values given in Table 3. Intra-annular torsion angles defining the conformation of the central RhGaN$_4$ ring are listed in Table 4. Calculated hydrogen coordinates and thermal parameters (Table 6 and 7) are included as supplementary material.[2]

TABLE 1. Final positional (fractional × 10^4; Rh, Ga, and P × 10^5) and isotropic thermal parameters (U × 10^3 Å^2) with estimated standard deviations in parentheses

Atom	x	y	z	U_{eq}
Rh	41453(2)	31835(2)	25382(2)	36
Ga	54082(4)	20760(3)	47632(3)	43
P	29424(8)	23578(7)	18822(5)	36
O	5877(4)	3209(4)	736(2)	94
N(1)	5238(3)	3948(2)	3150(2)	43
N(2)	5785(3)	3475(2)	4044(2)	43
N(3)	2970(3)	3284(2)	3835(2)	39
N(4)	3465(3)	2655(2)	4711(2)	39
C(1)	5197(4)	3190(4)	1429(3)	57
C(2)	6066(4)	911(3)	3971(3)	56
C(3)	5975(4)	1702(4)	6107(3)	68
C(4)	5518(4)	4919(3)	2836(3)	51
C(5)	6238(4)	5070(4)	3510(3)	62
C(6)	6391(3)	4167(3)	4264(3)	50
C(7)	1724(3)	3836(3)	4008(2)	43
C(8)	1379(3)	3553(3)	4996(3)	50
C(9)	2491(4)	2817(3)	5416(2)	47
C(10)	4996(5)	5670(4)	1910(4)	74
C(11)	7094(5)	3947(4)	5181(3)	72
C(12)	913(4)	4644(4)	3228(3)	61
C(13)	2651(5)	2246(4)	6459(3)	62
C(14)	3744(3)	979(3)	1625(2)	39
C(15)	5106(3)	599(3)	1526(2)	48
C(16)	5701(4)	−438(3)	1294(3)	58
C(17)	4958(5)	−1087(3)	1155(3)	59
C(18)	3624(4)	−730(3)	1267(3)	58
C(19)	3020(4)	284(3)	1509(3)	49
C(20)	1489(3)	2128(3)	2612(2)	41
C(21)	1684(4)	1457(3)	3541(3)	52
C(22)	625(5)	1286(4)	4146(3)	67
C(23)	−622(5)	1775(5)	3847(4)	80
C(24)	−835(4)	2433(5)	2948(4)	79
C(25)	219(4)	2599(3)	2312(3)	57
C(26)	2336(3)	3168(3)	686(2)	41
C(27)	2239(4)	4289(3)	483(3)	55
C(28)	1826(5)	4932(4)	−416(3)	69
C(29)	1534(4)	4466(4)	−1113(3)	66
C(30)	1631(5)	3372(4)	−925(3)	67
C(31)	2036(4)	2713(3)	−19(3)	57
C(32)	−705(16)	1941(16)	−1453(13)	211
C(33)	−1106(12)	2160(12)	−2377(9)	147
C(34)	−501(14)	1399(17)	−2778(21)	287
C(35)	437(22)	459(19)	−2624(18)	242
C(36)	842(19)	247(20)	−1674(12)	237
C(37)	313(11)	959(9)	−1044(12)	168
C(38)	−1290(13)	2549(14)	−835(13)	298

Results and discussion

In a recent paper (1) we discussed the preparation and characterization of a number of Rh(I) complexes containing the ligand Me$_2$Gapz$_2^-$ and compared these new complexes with Rh(I) complexes containing pyrazolyl borate ligands (10–18). At that time we were unable to isolate compounds of the type [Me$_2$Ga(3,5-Me$_2$pz)$_2$]Rh(L—L) (where L—L = (CO)$_2$ or COD, COD = 1,5-cyclooctadiene), postulating that facile disproportionation of the Me$_2$Ga(3,5-Me$_2$pz)$_2^-$ ligand led to the formation of stable Rh(I) dimers of the formulation [Rh-(μ-3,5-Me$_2$pz)L—L]$_2$. However, the complex [Me$_2$Ga(3,5-Me$_2$pz)$_2$]Rh(CO)PPh$_3$, has now been isolated as an air-stable lemon−yellow crystalline material, albeit in low yield, together with two dimer species, viz.

$$4Na^+[Me_2Ga(3,5\text{-}Me_2pz)_2]^- + 2[Rh(CO)_2Cl]_2 + 4PPh_3 \rightarrow 2[Me_2Ga(3,5\text{-}Me_2pz)_2]Rh(CO)PPh_3 + [Rh(\mu\text{-}3,5\text{-}Me_2pz)(CO)PPh_3]_2 + [Me_2Ga(\mu\text{-}3,5\text{-}Me_2pz)]_2 + 4NaCl + 4CO$$

[2]The structure factor table, Table 5 (anisotropic thermal parameters), and other material mentioned in the text are available, at a nominal charge, from the Depository of Unpublished Data, CISTI, National Research Council of Canada, Ottawa, Ont., Canada K1A 0S2.

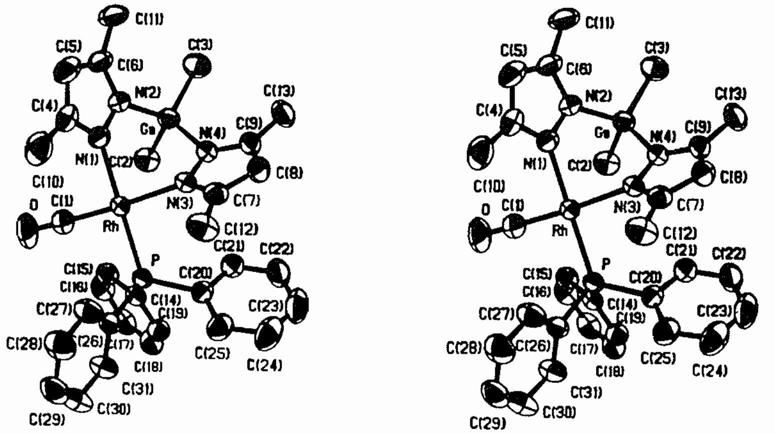

FIG. 1. Stereoscopic view of the $[Me_2Ga(3,5\text{-}Me_2pz)_2]Rh(CO)PPh_3$ molecule; 50% probability thermal ellipsoids are shown. Hydrogen atoms are omitted for clarity.

TABLE 2. Bond lengths (Å) with estimated standard deviations in parentheses

	Length			Length	
Bond	Uncorr.	Corr.	Bond	Uncorr.	Corr.
Rh —P	2.2686(8)	2.2700	C(14)—C(15)	1.393(5)	1.400
Rh —N(1)	2.088(3)	2.090	C(14)—C(19)	1.392(5)	1.397
Rh —N(3)	2.093(2)	2.097	C(15)—C(16)	1.393(5)	1.396
Rh —C(1)	1.812(4)	1.815	C(16)—C(17)	1.371(6)	1.376
Ga —N(2)	1.999(3)	2.006	C(17)—C(18)	1.364(6)	1.371
Ga —N(4)	1.991(3)	1.997	C(18)—C(19)	1.375(5)	1.378
Ga —C(2)	1.978(4)	1.984	C(20)—C(21)	1.396(5)	1.403
Ga —C(3)	1.957(4)	1.963	C(20)—C(25)	1.384(5)	1.393
P —C(14)	1.828(3)	1.831	C(21)—C(22)	1.378(5)	1.383
P —C(20)	1.825(3)	1.830	C(22)—C(23)	1.364(7)	1.373
P —C(26)	1.844(3)	1.848	C(23)—C(24)	1.358(7)	1.364
O —C(1)	1.144(5)	1.145	C(24)—C(25)	1.394(6)	1.399
N(1)—N(2)	1.379(4)	1.385	C(26)—C(27)	1.388(5)	1.401
N(1)—C(4)	1.346(4)	1.358	C(26)—C(31)	1.364(5)	1.374
N(2)—C(6)	1.350(4)	1.361	C(27)—C(28)	1.386(5)	1.390
N(3)—N(4)	1.380(3)	1.385	C(28)—C(29)	1.359(6)	1.369
N(3)—C(7)	1.333(4)	1.341	C(29)—C(30)	1.355(6)	1.368
N(4)—C(9)	1.353(4)	1.361	C(30)—C(31)	1.399(5)	1.402
C(4)—C(5)	1.362(6)	1.370	C(32)—C(33)	1.35(2)	
C(4)—C(10)	1.493(6)	1.498	C(32)—C(37)	1.46(2)	
C(5)—C(6)	1.376(6)	1.385	C(32)—C(38)	1.281(14)	
C(6)—C(11)	1.493(5)	1.498	C(33)—C(34)	1.22(2)	
C(7)—C(8)	1.388(5)	1.395	C(34)—C(35)	1.32(3)	
C(7)—C(12)	1.488(5)	1.493	C(35)—C(36)	1.39(3)	
C(8)—C(9)	1.381(5)	1.388	C(36)—C(37)	1.37(2)	
C(9)—C(13)	1.489(5)	1.493			

The ir spectrum of the title complex in cyclohexane solution displays a single, strong, carbonyl stretching frequency at 1985 cm^{-1}, slightly lower than the corresponding ν_{CO} band at 1995 cm^{-1} reported for $[Me_2Gapz_2]Rh(CO)PPh_3$ (1). This shift to lower ν_{CO} frequencies with methyl substitution on the pyrazolyl rings of the ligands reflects the enhanced electron donating power of the substituted ligands, which in turn leads to increased $d\pi-\pi^*$ interaction with the ancillary carbonyl ligands.

It is of interest to compare the room temperature ^1H nmr spectra of the two analogous complexes $[Me_2Ga(3,5\text{-}Me_2pz)_2]$-$Rh(CO)PPh_3$ (Fig. 2) and $[Me_2Gapz_2]Rh(CO)PPh_3$ (1). The spectrum of the latter compound exhibits one sharp singlet in the "$GaMe_2$" region of the spectrum whilst the title complex displays two sharp singlets in this region. Indeed it is not until −65°C that the unsubstituted pyrazolyl complex gives two sharp "GaMe" singlets comparable to those observed at room temperature for the title complex. Evidently the fluxional process proposed for the Rh(I) complexes incorporating the $Me_2Gapz_2^-$ ligand (1) is considerably less facile for the $[Me_2Ga(3,5\text{-}Me_2pz)_2]Rh(CO)PPh_3$ compound. Rapid inversion of the Ga—$(N—N)_2$—Rh boat conformation predicted for this complex, **1**, would be severely hindered by steric interactions in a planar intermediate, particularly between the bulky PPh_3 ligand and the pz—Me group. The boat conformation of the title complex, in addition to two singlets for the $GaMe_2$ protons, gives rise to four pz—Me singlets and two pz—H^4 singlets in its ^1H nmr spectrum (Fig. 2).

The crystal structure of [dimethylbis(3,5-dimethyl-1-pyra-

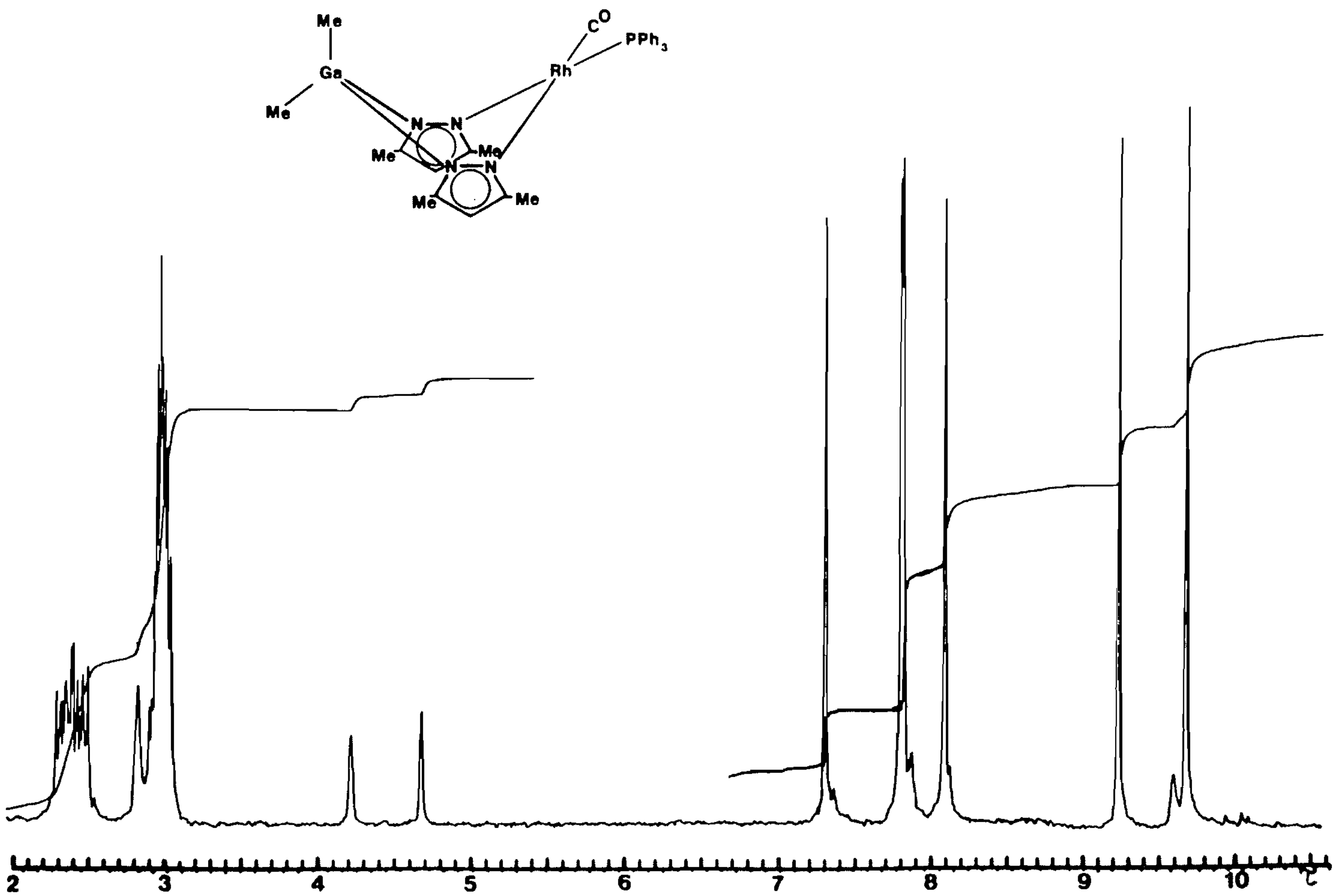

FIG. 2. Room temperature 100 MHz ¹H nmr spectrum of $[Me_2Ga(3,5\text{-}Me_2pz)_2]Rh(CO)PPh_3$ in C_6D_6.

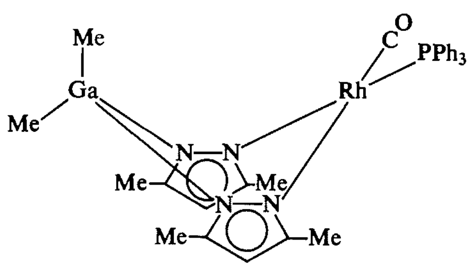

1

zolyl)gallato-*N*,*N′*](triphenylphosphine)carbonylrhodium(I) − toluene (1:1) consists of discrete molecules of $[Me_2Ga(3,5\text{-}Me_2pz)_2]Rh(CO)PPh_3$ and toluene, separated by normal van der Waals distances. The Rh(I) atom is in a distorted square planar environment with Rh—N = 2.090(3) and 2.097(2), Rh—CO = 1.815(4), and Rh—P = 2.2700(8) Å. These distances are similar to those reported for related molecules (1, 16, 19, and references therein). The Rh—N distances are slightly longer than the corresponding mean values of 2.087(2), 2.063(6), and 2.084(1) Å reported for $[Me_2Gapz_2]Rh(COD)$, $[Rh(\mu\text{-}3,5\text{-}Me_2pz)(CO)_2]_2$, and $[Rh(\mu\text{-}3,5\text{-}Me_2pz)(COD)]_2$, respectively (1). The Rh—CO distance is shorter than the mean value of 1.852(9) Å reported for $[Rh(\mu\text{-}3,5\text{-}Me_2pz)(CO)_2]_2$. The N(1)—pyrazolyl and C(26)—phenyl rings are planar within experimental error (χ^2 = 1.9 and 2.8) while the N(3)—pyrazolyl and the two remaining phenyl rings are slightly but significantly nonplanar (χ^2 = 15.3−41.0, maximum deviation from the mean plane 0.014(5) Å). The geometry of the toluene molecule (Tables 2 and 3) is far from ideal, probably a result of the relatively large degree of thermal motion undergone by the solvate molecule and/or some form of minor disordering.

As a result of steric interaction between the PPh_3 ligand and the *cis* Me_2pz group, the central six-membered $RhGaN_4$ ring has a steeper boat conformation than that observed in the less strained μ-pz_2 molecule $[Me_2Gapz_2]Rh(COD)$. This leads to a significant shortening of the cross-ring Rh···Ga distance, from 3.5527(5) in $[Me_2Gapz_2]Rh(COD)$ to 3.3819(4) Å in the present structure. The dependence of ring folding and the associated M···M′ distance in M—(μ-$R_2pz)_2$—M systems upon intramolecular steric requirements has been discussed in ref. 1. The PPh_3−Me_2pz interaction manifests itself as a marked torsional twist about the N(3)—N(4) bond (see Table 4) and may also be responsible for the nonplanarity of the N(3)—pz and C(20)—phenyl rings. The Rh and Ga atoms are displaced by 0.1299(3) and −0.4993(4) Å, respectively, from the mean plane of the N(3)—pyrazolyl ring, compared to corresponding values of −0.0544(3) and −0.1546(4) Å for the N(1)—pyrazolyl ring.

TABLE 3. Bond angles (deg) with estimated standard deviations in parentheses

Bonds	Angle (deg)	Bonds	Angle (deg)
P —Rh —N(1)	179.49(8)	N(3)—C(7)—C(12)	122.4(3)
P —Rh —N(3)	95.08(7)	C(8)—C(7)—C(12)	128.3(3)
P —Rh —C(1)	88.90(13)	C(7)—C(8)—C(9)	105.9(3)
N(1)—Rh —N(3)	84.44(10)	N(4)—C(9)—C(8)	108.8(3)
N(1)—Rh —C(1)	91.57(14)	N(4)—C(9)—C(13)	123.2(4)
N(3)—Rh —C(1)	175.52(15)	C(8)—C(9)—C(13)	128.0(3)
N(2)—Ga —N(4)	95.71(11)	P —C(14)—C(15)	120.6(3)
N(2)—Ga —C(2)	110.16(15)	P —C(14)—C(19)	121.4(3)
N(2)—Ga —C(3)	110.9(2)	C(15)—C(14)—C(19)	117.9(3)
N(4)—Ga —C(2)	109.58(14)	C(14)—C(15)—C(16)	119.9(3)
N(4)—Ga —C(3)	112.0(2)	C(15)—C(16)—C(17)	120.6(4)
C(2)—Ga —C(3)	116.6(2)	C(16)—C(17)—C(18)	119.9(4)
Rh —P —C(14)	117.94(11)	C(17)—C(18)—C(19)	120.3(4)
Rh —P —C(20)	116.06(11)	C(14)—C(19)—C(18)	121.3(4)
Rh —P —C(26)	111.73(12)	P —C(20)—C(21)	117.2(3)
C(14)—P —C(20)	100.93(15)	P —C(20)—C(25)	124.1(3)
C(14)—P —C(26)	103.37(14)	C(21)—C(20)—C(25)	118.7(3)
C(20)—P —C(26)	105.17(15)	C(20)—C(21)—C(22)	120.2(4)
Rh —N(1)—N(2)	121.1(2)	C(21)—C(22)—C(23)	120.4(4)
Rh —N(1)—C(4)	131.1(2)	C(22)—C(23)—C(24)	120.5(4)
N(2)—N(1)—C(4)	107.8(3)	C(23)—C(24)—C(25)	120.3(4)
Ga —N(2)—N(1)	117.5(2)	C(20)—C(25)—C(24)	119.9(4)
Ga —N(2)—C(6)	134.4(2)	P —C(26)—C(27)	117.9(3)
N(1)—N(2)—C(6)	107.8(3)	P —C(26)—C(31)	123.3(3)
Rh —N(3)—N(4)	119.6(2)	C(27)—C(26)—C(31)	118.8(3)
Rh —N(3)—C(7)	132.1(2)	C(26)—C(27)—C(28)	120.4(4)
N(4)—N(3)—C(7)	108.3(3)	C(27)—C(28)—C(29)	120.2(4)
Ga —N(4)—N(3)	117.3(2)	C(28)—C(29)—C(30)	119.9(4)
Ga —N(4)—C(9)	132.5(2)	C(29)—C(30)—C(31)	120.6(4)
N(3)—N(4)—C(9)	107.8(3)	C(26)—C(31)—C(30)	120.1(4)
Rh —C(1)—O	178.3(4)	C(33)—C(32)—C(37)	124.2(13)
N(1)—C(4)—C(5)	109.0(3)	C(33)—C(32)—C(38)	121(2)
N(1)—C(4)—C(10)	121.1(4)	C(37)—C(32)—C(38)	114(2)
C(5)—C(4)—C(10)	129.8(4)	C(32)—C(33)—C(34)	109(2)
C(4)—C(5)—C(6)	107.0(3)	C(33)—C(34)—C(35)	141(3)
N(2)—C(6)—C(5)	108.4(3)	C(34)—C(35)—C(36)	109.5(15)
N(2)—C(6)—C(11)	123.9(4)	C(35)—C(36)—C(37)	122(2)
C(5)—C(6)—C(11)	127.7(4)	C(32)—C(37)—C(36)	114(2)
N(3)—C(7)—C(8)	109.2(3)		

TABLE 4. Intra-annular torsion angles (deg) standard deviations in parentheses

Atoms	Value (deg)
N(3)—Rh —N(1)—N(2)	58.1(2)
Rh —N(1)—N(2)—Ga	−3.3(3)
N(4)—Ga —N(2)—N(1)	−52.7(2)
N(2)—Ga —N(4)—N(3)	43.3(2)
Rh —N(3)—N(4)—Ga	19.5(3)
N(1)—Rh —N(3)—N(4)	−68.2(2)

Acknowledgments

We thank the Natural Sciences and Engineering Research Council of Canada for financial support and the University of British Columbia Computing Centre for assistance.

1. B. M. LOUIE, S. J. RETTIG, A. STORR, and J. TROTTER. Can. J. Chem. **62**, 1057 (1984).
2. K. R. BREAKELL, D. J. PATMORE, and A. STORR. J. Chem. Soc. Dalton Trans. 749 (1975).
3. P. COPPENS, L. LEISEROWITZ, and D. RABINOVICH. Acta Crystallogr. **18**, 1035 (1965).
4. W. R. BUSING and H. A. LEVY. Acta Crystallogr. **22**, 457 (1967).
5. D. T. CROMER and J. B. MANN. Acta Crystallogr. Sect. A, **24**, 321 (1968).
6. R. F. STEWART, E. R. DAVIDSON, and W. T. SIMPSON. J. Chem. Phys. **42**, 3175 (1965).
7. D. T. CROMER and D. LIBERMAN. J. Chem. Phys. **53**, 1891 (1970).
8. V. SCHOMAKER and K. N. TRUEBLOOD. Acta Crystallogr. Sect. B, **24**, 63 (1968).
9. D. W. J. CRUICKSHANK. Acta Crystallogr. **9**, 747 (1956); **9**, 754 (1956); **14**, 896 (1961).
10. S. TROFIMENKO. Inorg. Chem. **10**, 1372 (1971).
11. R. B. KING and A. BOND. J. Organomet. Chem. **73**, 115 (1974).
12. F. BONATI, G. MINGHETTI, and G. BANDITELLI. J. Organomet. Chem. **87**, 365 (1975).
13. H. C. CLARK and S. GOEL. J. Organomet. Chem. **165**, 383 (1979).
14. M. COCIVERA, T. J. DESMOND, G. FERGUSON, B. KAITNER, F. J. LALOR, and D. J. O'SULLIVAN. Organometallics, **1**, 1125 (1982).
15. M. COCIVERA, G. FERGUSON, B. KAITNER, F. J. LALOR, D. J.

O'SULLIVAN, M. PARVEZ, and B. RUHL. Organometallics, **1**, 1132 (1982).
16. M. COCIVERA, G. FERGUSON, F. J. LALOR, and P. SZCZECINSKIVAN. Organometallics, **1**, 1139 (1982).
17. N. F. BORKETT and M. I. BRUCE. J. Organomet. Chem. **65**, C51 (1974).
18. S. MAY, P. REINSALU, and J. POWELL. Inorg. Chem. **19**, 1582 (1980).
19. R. USON, L. A. ORO, M. A. CIRIANO, M. T. PINILLOS, A. TIRIPICCHIO, and M. CARMELLINI. J. Organomet. Chem. **205**, 247 (1981).

Structural studies of organoboron compounds. XXI.[1] Crystal and molecular structures of 3-(phenylmethylidene)-4-methyl-1-phenyl-2,6,7-trioxa-3-azonia-1-boratabicyclo-[2.2.2]octane and *N*-(4-nitrophenylmethylidene)-5-methyl-2-phenyl-1,3-dioxa-2-bora-5-cyclohexaneamine *N*-oxide

W. KLIEGEL AND L. PREU

Institut für Pharmazeutische Chemie, der Technischen Universität Braunschweig, 3300 Braunschweig, Beethovenstraße 55, Bundesrepublik Deutschland

AND

STEVEN J. RETTIG AND JAMES TROTTER

Department of Chemistry, University of British Columbia, 2036 Main Mall, Vancouver, B.C., Canada V6T 1Y6

Received July 16, 1984

W. KLIEGEL, L. PREU, STEVEN J. RETTIG, and JAMES TROTTER. Can. J. Chem. **63**, 509 (1985).

Crystals of 3-(phenylmethylidene)-4-methyl-1-phenyl-2,6,7-trioxa-3-azonia-1-boratabicyclo[2.2.2]octane are orthorhombic, a = 8.0732(7), b = 11.8499(10), c = 31.679(2) Å, Z = 8, space group *Pbca*, and those of *N*-(4-nitrophenylmethylidene)-5-methyl-2-phenyl-1,3-dioxa-2-bora-5-cyclohexaneamine *N*-oxide are monoclinic, a = 6.1873(6), b = 23.206(2), c = 11.3081(11) Å, β = 92.326(5)°, Z = 4, space group $P2_1/n$. Both structures were solved by direct methods and were refined by full-matrix least-squares procedures to final R values of 0.041 and 0.036 for 943 and 1679 reflections with $I \geq 3\sigma(I)$, respectively. Both compounds are condensation products of bis(hydroxyalkyl)nitrones and phenylboronic acid. 3-(Phenylmethylidene)-4-methyl-1-phenyl-2,6,7-trioxa-3-azonia-1-boratabicyclo[2.2.2]octane was found to possess a bicyclic structure resulting from intramolecular O→B coordination (O—B = 1.604(7) Å) and is the first such bicyclic boron compound to be structurally characterized. In *N*-(4-nitrophenylmethylidene)-5-methyl-2-phenyl-1,3-dioxa-2-bora-5-cyclohexaneamine *N*-oxide, which has weakened nitrone basicity, the O→B interaction does not occur, resulting in a monocyclic system incorporating a trigonal planar boron atom.

W. KLIEGEL, L. PREU, STEVEN J. RETTIG et JAMES TROTTER. Can. J. Chem. **63**, 509 (1985).

Les cristaux du (phénylméthylidène)-3 méthyl-4 phényl-1 trioxa-2,6,7 azonia-3 borata-1 bicyclo [2.2.2] octane sont orthorhombiques avec a = 8,0732(7), b = 11,8499(10), c = 31,679(2) Å, Z = 8 et groupe d'espace *Pbca* alors que ceux du *N*-oxyde de la *N*-(nitro-4 phénylméthylidène) méthyl-5 phényl-2 dioxa-1,3 bora-2 cyclohexylamine-5 sont monocliniques avec a = 6,1873(6), b = 23,206(2), c = 11,3081(11) Å, β = 92,326(5)°, Z = 4 et groupe d'espace $P2_1/n$. On a résolu les deux structures par des méthodes directes et on les a affinées par la méthode des moindres carrés (matrice entière) jusqu'à des valeurs finales de R de 0,041 et 0,036 respectivement pour 943 et 1679 réflexions avec $I \geq 3\sigma(I)$. Les deux composés sont des produits de condensation de bis(hydroxyalkyl)nitrones et de l'acide phénylboronique. On a trouvé que le (phénylméthylidène)-3 méthyl-4 phényl-1 trioxa-2,6,7 azonia-3 borata-1 bicyclo [2.2.2] octane possède une structure bicyclique qui résulte d'une coordination O→B intramoléculaire (O—B = 1,604(7) Å) et il s'agit du premier composé bicyclique de ce type et contenant du bore à être caractérisé du point de vue de la structure. Dans le *N*-oxyde de la *N*-(nitro-4 phénylméthylidène) méthyl-5 phényl-2 dioxa-1,3 cyclohexylamine, pour laquelle la basicité de la nitrone est plus faible, l'interaction O→B ne se produit pas et il en résulte que le composé est un système monocyclique comportant un atome de bore plan et trigonal.

[Traduit par le journal]

Introduction

The condensation products of bis(hydroxyalkyl)nitrones such as **1** and phenylboronic acid can generally have an intramolecularly coordinated bicyclo[2.2.2]octane structure **2** and/or a simple monocyclic diester structure **3** (1). Sufficient electron density at the nitrone oxygen atom should qualify the nitrone **1** as a tridentate ligand and should result in the formation of a bicyclic chelate of the type **2**. A comparable "cage" structure has been postulated for similar trialkylamine-*N*-oxide chelates (2). On the other hand, weakening of the nitrone basicity by *para*-nitro substitution of the arylaldehyde moiety, generally attainable for *C*-arylnitrones (3), should favor the monocyclic ester structure **3** which could be stabilized by $pp(\pi)$ back-donation from both oxygens of the boronate ester function into the vacant *p*-orbital of the trigonal planar boron atom.

From a series of various arylboronates, synthesized from nitrones of the type **1** (1), we chose the phenylboronates of benzaldehyde nitrone (**1***a*) and of 4-nitrobenzaldehyde nitrone (**1***b*) on the basis of their distinct ^{1}H nmr spectra which suggested different structures for the boronate ring systems of the two compounds. For the benzaldehyde derivative (Ar = C_6H_5) the "cage" structure **2** was postulated, whereas the monocyclic boronate structure **3** was ascribed to the 4-nitrobenzaldehyde derivative (Ar = 4-$NO_2C_6H_4$) (1). To prove unambiguously the intramolecular O→B coordination in **2** and the noncoordination in **3**, X-ray crystallographic analyses of both compounds were undertaken.

Experimental

Compounds **2** (Ar = C_6H_5) and **3** (Ar = 4-$NO_2C_6H_4$) were prepared by refluxing solutions of 1 mmol of phenylboronic acid and 1 mmol of *N*-benzylidene-1,3-dihydroxy-2-methyl-2-propanamine *N*-oxide (**1***a*) (1, 4) or 1 mmol of 1,3-dihydroxy-2-methyl-*N*-(4-nitrophenylmethylidene)-2-propanamine *N*-oxide (**1***b*) (1), respectively, in 60 mL ethanol for 15 min. After evaporation of the solution the residue is crystallized, if necessary, by addition of ether.

3-(Phenylmethylidene)-4-methyl-1-phenyl-2,6,7-trioxa-3-azonia-1-boratabicyclo[2.2.2]octane (**2**, Ar = C_6H_5). *Anal.* calcd.: C 69.17, H 6.16, N 4.75; found: C 69.22, H 6.15, N 4.84. Mp 178–180°C (from benzene or ethylene chloride). Crystals suitable for X-ray analysis

[1]Previous paper in this series: see ref. 25

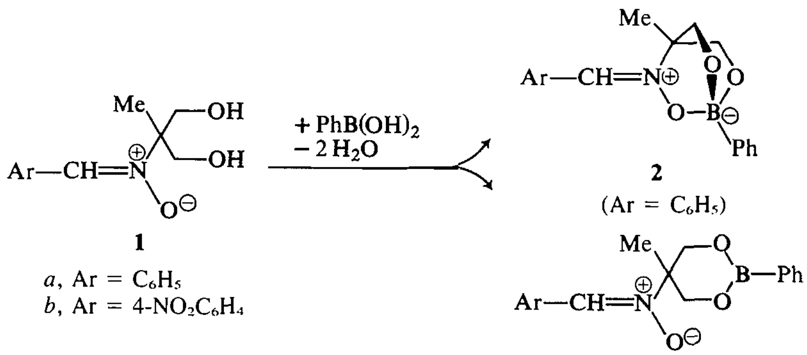

1

a, Ar = C_6H_5
b, Ar = 4-$NO_2C_6H_4$

2 (Ar = C_6H_5)

3 (Ar = 4-$NO_2C_6H_4$)

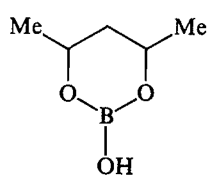

4

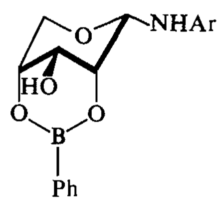

5 (Ar = 4-BrC_6H_4)

were obtained by recrystallization from ethylene chloride.

N-*(4-nitrophenylmethylidene)-5-methyl-2-phenyl-1,3-dioxa-2-bora-5-cyclohexaneamine* N-*oxide* (**3**, Ar = 4-$NO_2C_6H_4$). *Anal.* calcd.: C 60.02, H 5.05, N 8.24; found: C 59.87, H 5.04, N 8.13. Mp 193–194°C (from benzene). Crystals suitable for X-ray analysis were obtained by recrystallization from benzene. Spectroscopic data for both compounds are compiled in ref. 1.

X-ray crystallographic analyses

3-(Phenylmethylidene)-4-methyl-1-phenyl-2,6,7-trioxa-3-azonia-1-boratabicyclo[2.2.2]octane (2, Ar = C_6H_5)

A crystal bounded by the six faces (followed by their distances in mm from a common origin): ±(0 0 1), 0.053 ±(1 0 0), 0.188, ±(0 1 0), 0.265 was mounted in a general orientation. Unit-cell parameters were refined by least-squares on 2 sin θ/λ values for 25 reflections (2θ = 25–36°) measured on a diffractometer with Mo-$K\alpha$ Radiation ($\lambda(K\alpha_1)$ = 0.70930, $\lambda(K\alpha_2)$ = 0.71359 Å). Crystal data at 22°C are:

$C_{17}H_{18}BNO_3$ fw = 295.17
Orthorhombic, a = 8.0732(7), b = 11.8499(10), c = 31.679(2) Å, V = 3030.6(4) Å^3, Z = 8, ρ_c = 1.294 g cm^{-3} $F(000)$ = 1248, μ(Mo-$K\alpha$) = 0.82 cm^{-1}. Absent reflections: $0kl$, k odd, $h0l$, l odd, and $hk0$, h odd uniquely indicate the space group *Pbca* (D^{15}_{2h}, No. 61).

Intensities were measured with graphite-monochromated Mo-$K\alpha$ radiation on an Enraf-Nonius CAD4-F diffractometer. An ω–2θ scan at 0.67–6.71° min^{-1} over a range of (0.85 + 0.35 tan θ) degrees in ω (extended by 25% on both sides for background measurement) was employed. Data were measured to 2θ = 52°. The intensities of three check reflections, measured every 3600 s throughout the data collection, remained constant to within 1.5%. Of the 2959 independent reflections measured and processed[2], 943(32%) had intensities greater than $3\sigma(I)$ above background where $\sigma^2(I) = S + 2B + (0.04(S - B))^2$ with S = scan count and B = normalized background count. The crystals were poor scatterers, most of the "observed" data having θ < 18°. Higher angle data, a few of which had significant intensities, were collected in order to maximize the number of observations. Using a 2σ cutoff would only have increased the total by 35.

The structure was solved by direct methods, the positions of the non-hydrogen atoms being determined from an E-map. After full-matrix least-squares refinement of the non-hydrogen atoms with anisotropic thermal parameters to R = 0.088, a difference map gave the positions of the hydrogen atoms. Refinement of the structure with fixed hydrogen atoms (idealized geometry) reduced R to 0.058. In the final stages of refinement the hydrogen atoms were refined with isotropic thermal parameters in spite of the small number of observations. This action may be justified by the better residuals eventually obtained, the esd's of derived parameters being essentially the same for the refinements with fixed and varied hydrogen parameters (the smaller m/n ratio being balanced by the better agreement between observed and calculated structure factors). The scattering factors of ref. 5 were used for non-hydrogen atoms and those of ref. 6 for hydrogen atoms. The weighting scheme, $w = 1/\sigma^2(F)$ where $\sigma^2(F)$ is derived from the previously defined $\sigma^2(I)$, gave uniform average values of $w(|F_o| - |F_c|)^2$ over ranges of both $|F_o|$ and sin θ/λ and was employed in the final stages of refinement. Reflections with $I < 3\sigma(I)$ were not included in the refinement. Convergence was reached at R = 0.041 and R_w = 0.049 for 943 reflections with $I \geq 3\sigma(I)$. The function minimized was $\Sigma w(|F_o| - |F_c|)^2$, $R = \Sigma||F_o| - |F_c||/\Sigma|F_o|$ and $R_w = (\Sigma w(|F_o| - |F_c|)^2/\Sigma w|F_o|^2)^{1/2}$.

On the final cycle of refinement the mean and maximum parameter shifts corresponded to 0.03 and 0.19σ, respectively. The mean error in an observation of unit weight was 1.993. A final difference map showed no unusual features, residual densities ranging from −0.22 to +0.20 e Å^{-3}. The final positional and thermal parameters appear in Tables 1 and 5,[3] respectively. Measured and calculated structure factors have been placed in the Depository of Unpublished Data.[3]

[2]The computer programs used include locally written programs for data processing and locally modified versions of the following: MULTAN 80, multisolution program by P. Main, S. J. Fiske, S. E. Hull, L. Lessinger, G. Germain, J. P. Declercq, and M. M. Woolfson; ORFLS, full-matrix least-squares, and ORFFE, function and errors, by W. R. Busing, K. O. Martin and H. A. Levy; FORDAP, Patterson and Fourier syntheses, by A. Zalkin; ORTEP II, illustrations, by C. K. Johnson.

[3]The structure factor table, Table 5 (anisotropic thermal parameters) and other material mentioned in the text are available, at a nominal charge, from the Depository of Unpublished Data, CISTI, National Research Council of Canada, Ottawa, Canada K1A 0S2.

TABLE 1. Final positional (fractional) and isotropic thermal parameters ($U \times 10^3$ Å^2) with estimated standard deviations in parentheses

Atom	x	y	z	U_{eq}/U_{iso}	Atom	x	y	z	U_{eq}/U_{iso}
		2 (× 10^4, H × 10^3)					**3**		
O(1)	6109(4)	6856(3)	1154(1)	46	O(1)	6703(3)	710(1)	5381(2)	67
O(2)	5973(5)	8350(3)	637(1)	52	O(2)	11503(3)	3043(1)	3034(2)	73
O(3)	4677(4)	6554(3)	491(1)	51	O(3)	14535(3)	2992(1)	4015(2)	73
N	7447(5)	6358(3)	978(1)	40	O(4)	8258(2)	429(1)	8985(1)	50
C(1)	7665(6)	6675(4)	521(1)	44	O(5)	4655(2)	468(1)	8137(1)	49
C(2)	7531(9)	7951(5)	499(2)	50	N(1)	7990(3)	638(1)	6292(2)	43
C(3)	6163(8)	6169(5)	297(2)	49	N(2)	12661(4)	2841(1)	3828(2)	53
C(4)	8378(7)	5705(4)	1197(2)	44	C(1)	10203(3)	1485(1)	5893(2)	39
C(5)	9295(8)	6239(6)	346(2)	54	C(2)	8924(4)	1750(1)	5005(2)	46
C(6)	8186(6)	5416(5)	1641(2)	43	C(3)	9692(4)	2204(1)	4362(2)	48
C(7)	7292(8)	6042(6)	1932(2)	59	C(4)	11785(4)	2391(1)	4588(2)	40
C(8)	7274(9)	5706(7)	2346(2)	81	C(5)	13082(4)	2152(1)	5485(2)	51
C(9)	8089(9)	4748(7)	2476(2)	74	C(6)	12282(4)	1709(1)	6133(2)	49
C(10)	8986(9)	4142(6)	2191(2)	69	C(7)	9585(4)	988(1)	6570(2)	41
C(11)	9051(8)	4468(5)	1781(2)	55	C(8)	7587(4)	79(1)	6955(2)	45
C(12)	3354(6)	7835(4)	1038(2)	40	C(9)	8889(4)	29(1)	8111(2)	48
C(13)	2545(8)	8839(5)	928(2)	54	C(10)	5195(4)	65(1)	7232(3)	50
C(14)	1136(9)	9212(6)	1143(2)	65	C(11)	8124(6)	−414(1)	6128(3)	66
C(15)	476(8)	8550(6)	1467(2)	64	C(12)	5543(4)	1001(1)	10055(2)	43
C(16)	1260(8)	7604(6)	1581(2)	62	C(13)	7109(5)	1125(1)	10940(2)	54
C(17)	2665(8)	7243(5)	1368(2)	55	C(14)	6667(6)	1455(1)	11906(3)	71
B	4982(8)	7440(6)	800(2)	46	C(15)	4627(6)	1678(1)	12004(3)	73
H(2a)	828(5)	829(4)	65(1)	33(17)	C(16)	3040(5)	1568(1)	11156(3)	66
H(2b)	766(6)	803(4)	16(2)	59(15)	C(17)	3487(4)	1227(1)	10183(2)	52
H(3a)	617(6)	531(6)	29(2)	87(21)	B	6159(4)	613(1)	8994(2)	42
H(3b)	623(5)	639(4)	−3(1)	40(12)	H(2)	760(4)	162(1)	478(2)	59(7)
H(4)	922(8)	546(6)	102(2)	102(26)	H(3)	884(4)	240(1)	371(2)	46(6)
H(5a)	1022(6)	650(4)	52(1)	46(15)	H(5)	1447(4)	230(1)	562(2)	60(8)
H(5b)	932(6)	650(5)	3(2)	83(20)	H(6)	1302(4)	153(1)	679(2)	70(8)
H(5c)	921(6)	539(6)	33(2)	82(22)	H(7)	1034(4)	89(1)	729(2)	55(7)
H(7)	664(6)	657(4)	183(1)	35(15)	H(9a)	867(4)	−39(1)	841(2)	59(7)
H(8)	658(6)	611(4)	253(2)	67(19)	H(9b)	1041(4)	7(1)	800(2)	44(6)
H(9)	799(5)	462(4)	278(2)	46(14)	H(10a)	487(4)	−35(1)	750(2)	59(7)
H(10)	950(7)	337(5)	231(2)	100(21)	H(10b)	444(4)	14(1)	651(2)	59(8)
H(11)	962(5)	413(4)	158(1)	27(15)	H(11a)	728(7)	−40(2)	540(4)	131(16)
H(13)	289(6)	936(4)	68(2)	61(17)	H(11b)	959(6)	−44(1)	603(3)	89(10)
H(14)	58(6)	984(4)	103(1)	53(17)	H(11c)	777(5)	−77(2)	655(3)	109(12)
H(15)	−53(8)	909(5)	162(2)	110(23)	H(13)	849(5)	99(1)	1087(2)	72(9)
H(16)	87(8)	737(6)	182(2)	109(29)	H(14)	784(5)	152(1)	1254(3)	90(10)
H(17)	319(6)	645(5)	146(1)	64(17)	H(15)	431(5)	190(1)	1268(3)	96(10)
					H(16)	158(5)	176(1)	1117(2)	79(9)
					H(17)	240(4)	118(1)	956(3)	72(9)

*U_{eq} = (1/3) trace U(diag).

N-(4-nitrophenylmethylidene)-5-methyl-2-phenyl-1,3-dioxa-2-bora-5-cyclohexaneamine N-oxide (3, Ar = 4-$NO_2C_6H_4$)

Experimental details are as above except where noted. The bounding planes of the crystal used for data collection were ±(0 2 −1), 0.100, ±(0 2 1), 0.148, ±(1 0 0), 0.310 mm. Reflections employed in the refinement of the unit-cell constants had 2θ = 30−37°. Crystal data:

$C_{17}H_{17}BN_2O_5$ fw = 340.17

Monoclinic, a = 6.1873(6), b = 23.206(2), c = 11.3081(11) Å, β = 92.326(5)°, V = 1622.3(3) Å^3, Z = 4, ρ_c = 1.393 g cm^{-3}, $F(000)$ = 712, μ(Mo-$K\alpha$) = 0.96 cm^{-3}. Absent reflections: 0k0, k odd, and h0l, $h + l$ odd uniquely indicate the space group $P2_1/n$ (non-standard setting of $P2_1/c$, C^5_{2h}, No. 14 with equivalent positions ±(x, y, z; 1/2 − x, 1/2 + y, 1/2 − z)).

An ω − 2θ scan at 1.06−10.06° min^{-1} over a range of (0.65 + 0.35 tan θ)° in ω was employed. Of 3698 independent reflections measured (to 2θ = 55°), 1679 had intensities greater than 3σ(I) above background. The intensities of the standard reflections remained constant to within 1.5%.

The structure was solved by direct methods, all non-hydrogen atoms being positioned from an E-map. After refinement of the non-hydrogen atoms with anisotropic thermal parameters to R = 0.076, all 17 hydrogen atoms were located on a difference map and were refined with isotropic thermal parameters in subsequent least-squares cycles. Convergence was reached at R = 0.036 and R_w = 0.044 for 1679 reflections. The mean and maximum parameter shifts on the final cycle of refinement were 0.05 and 0.6σ (H(17), y coordinate) and the mean error in an observation of unit weight was 1.950. A final difference map showed fluctuations in the range −0.22 to +0.16 e Å^{-3}.

Analysis of thermal motion

The thermal motion in the two molecules (Fig. 1) has been analysed in terms of the rigid-body modes of translation, libration, and screw-motion (TLS model) (7). The rms errors in the U_{ij} (derived from the least-squares analyses) are 0.0037 and 0.0014 Å^2, respectively, for **2** and **3**. Analyses of the entire molecules indicated significant independent motion of the phenyl rings in each case. Fragments of each molecule were separately analysed. In the case of **2** these were PhB,

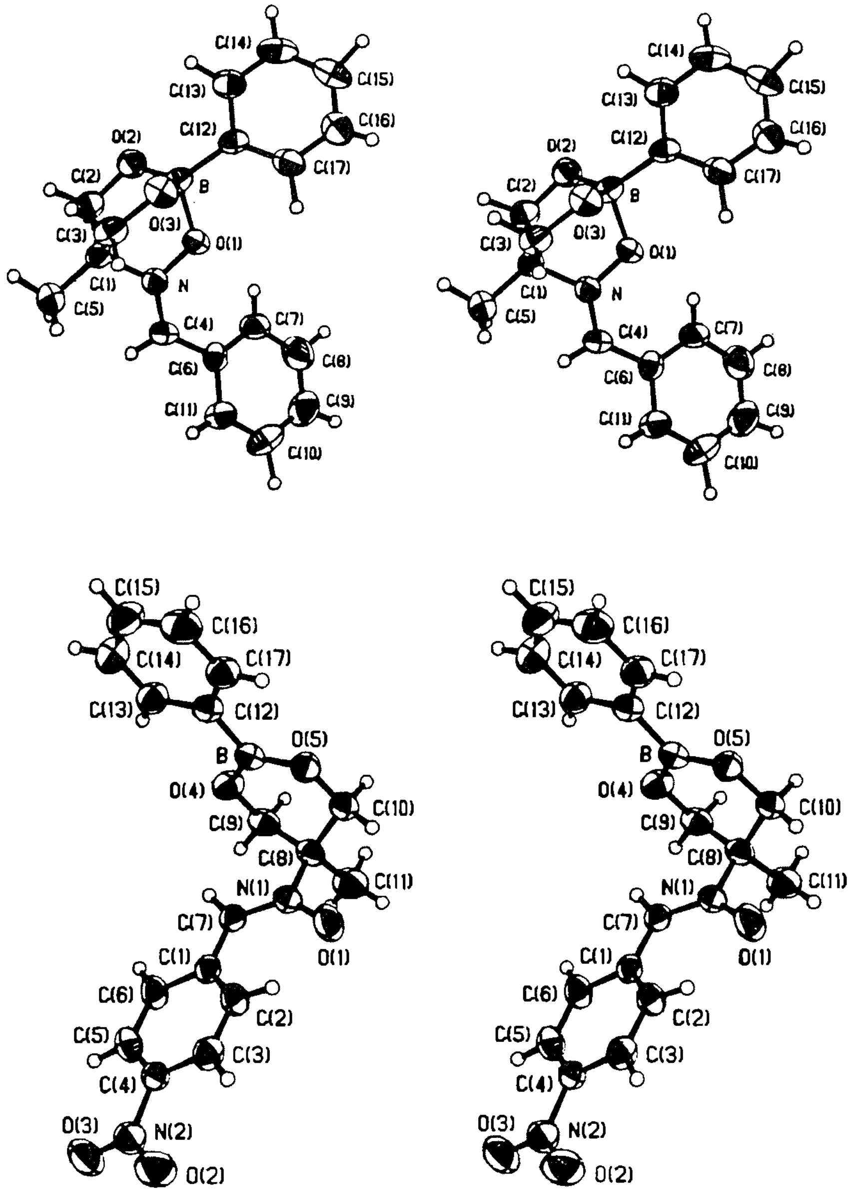

FIG. 1. Stereoscopic views of 3-(phenylmethylidene)-4-methyl-1-phenyl-2,6,7-trioxa-3-azonia-1-boratabicyclo[2.2.2]octane (top) and *N*-(4-nitrophenylmethylidene)-5-methyl-2-phenyl-1,3-dioxa-2-bora-5-cyclohexaneamine *N*-oxide bottom) molecules; 50% probability thermal ellipsoids are shown. Hydrogen atoms are assigned arbitrarily small thermal parameters for clarity.

PhC(4), and the bicyclic system plus C(4) and C(5) (rms ΔU_{ij} = 52, 33, and 43 × 10^{-4} Å^2) and for **3**, PhB, O_2NArC(7), and the six-membered heterocycle plus C(7)N(1)C(11) (rms ΔU_{ij} = 23, 31, and 36 × 10^{-4} Å^2). The appropriate bond distances have been corrected for libration (7, 8), using shape parameters q^2 of 0.08 for all atoms involved. Corrected bond lengths appear in Table 2 along with the uncorrected values; corrected bond angles do not differ by more than 1σ from the uncorrected values given in Table 3. Intra-annular torsion angles defining the conformations of the heterocyclic rings are listed in Table 4. Bond lengths and angles involving hydrogen and a complete listing of torsion angles (Tables 6–8) are included as supplementary material.[3]

Results and discussion

Both compounds **2** and **3** show the expected structures which are consistent with the predictions made on the basis of the electronic influence of the *C*-aryl moiety of the nitrone group (1). In compound **2**, with a tetrahedral sp^3-boron, the 1,3-dioxa-2-boracyclohexane ring system is forced into a slightly distorted boat conformation by coordinative acceptance of the Lewis-base nitrone oxygen atom. This is the first report of the structural dimensions of a bicyclic boron complex of this type. In compound **3**, with a trigonal planar sp^2-boron atom, the 1,3-dioxa-2-boracyclohexane ring has a "semi-planar" (9, 10) (envelope) conformation in which C(8) deviates from the approximate plane formed by the five remaining ring atoms. Very similar conformations have been reported for the 1,3-dioxa-2-boracyclohexane rings in the borate of *meso*-2,4-pentanediol **4** (11) and the 2,4-phenylboronate of *N*-(4-bromophenyl)-α-*D*-ribopyranosylamine **5** (12).

The mean[4] B—O bond length in the boronate ester grouping of **3** (1.367(4) Å) is significantly shorter than in **2** (1.453(9) Å),

[4]Here and elsewhere in this report mean values refer to weighted means with rms deviations from the mean in parentheses.

TABLE 2. Bond lengths (Å) with estimated standard deviations in parentheses

Bond	Length Uncorr.	Length Corr.	Bond	Length Uncorr.	Length Corr.
			2		
O(1)—N	1.352(5)	1.355	C(6)—C(11)	1.394(8)	1.404
O(1)—B	1.601(7)	1.604	C(7)—C(8)	1.370(8)	1.375
O(2)—C(2)	1.413(6)	1.417	C(8)—C(9)	1.376(9)	1.385
O(2)—B	1.438(7)	1.444	C(9)—C(10)	1.362(9)	1.377
O(3)—C(3)	1.423(6)	1.427	C(10)—C(11)	1.359(8)	1.364
O(3)—B	1.455(7)	1.462	C(12)—C(13)	1.402(7)	1.413
N —C(1)	1.504(5)	1.511	C(12)—C(17)	1.374(7)	1.381
N —C(4)	1.284(6)	1.286	C(12)—B	1.587(8)	1.591
C(1)—C(2)	1.517(7)	1.523	C(13)—C(14)	1.398(8)	1.402
C(1)—C(3)	1.528(7)	1.533	C(14)—C(15)	1.396(9)	1.403
C(1)—C(5)	1.519(7)	1.523	C(15)—C(16)	1.339(9)	1.349
C(4)—C(6)	1.456(7)	1.462	C(16)—C(17)	1.388(8)	1.393
C(6)—C(7)	1.386(7)	1.400			
			3		
O(1)—N(1)	1.287(2)	1.291	C(3)—C(4)	1.380(3)	1.391
O(2)—N(2)	1.219(3)	1.229	C(4)—C(5)	1.383(3)	1.395
O(3)—N(2)	1.221(3)	1.232	C(5)—C(6)	1.367(4)	1.370
O(4)—C(9)	1.422(3)	1.425	C(8)—C(9)	1.512(3)	1.517
O(4)—B	1.367(3)	1.371	C(8)—C(10)	1.525(3)	1.529
O(5)—C(10)	1.436(3)	1.439	C(8)—C(11)	1.522(4)	1.526
O(5)—B	1.358(3)	1.363	C(12)—C(13)	1.395(3)	1.403
N(1)—C(7)	1.307(3)	1.311	C(12)—C(17)	1.389(3)	1.396
N(1)—C(8)	1.523(3)	1.528	C(12)—B	1.559(4)	1.564
N(2)—C(4)	1.470(3)	1.473	C(13)—C(14)	1.370(4)	1.374
C(1)—C(2)	1.396(3)	1.408	C(14)—C(15)	1.373(4)	1.380
C(1)—C(6)	1.404(3)	1.414	C(15)—C(16)	1.368(4)	1.376
C(1)—C(7)	1.445(3)	1.447	C(16)—C(17)	1.391(4)	1.396
C(2)—C(3)	1.375(3)	1.378			

demonstrating the partial π-bond character which results from $pp(\pi)$ back-donation in the trigonal planar boronate ester group of **3**. Similar values were found for the mean B(sp^2)—O distances in **4** (11) and **5** (12) (1.362(8) and 1.396(2) Å, both uncorrected), and in free boronic acids such as 4-$BrC_6H_4B(OH)_2$ (13) (1.36 Å, uncorrected) and $C_6H_5B(OH)_2$ (14) (1.371(6) Å). The approximate coplanarity of the B-phenyl ring and the COBOC plane of the 1,3-dioxa-2-boracyclohexane ring in **3** (the dihedral angle between normals to the mean planes being 1.8(2)°) enables a π-interaction between the aromatic system and the boronate group. The B—C bond length of 1.564(4) Å in **3** is nearly identical to the corresponding distance of 1.565(3) Å in phenylboronic acid (14). The B—C distance of 1.591(8) Å in **2** is longer, indicating little or no π-interaction with the sp^3-boron atom. Comparable bond distances ranging from 1.582 to 1.613 Å have been observed in various tetracoordinated phenylboronates (15–18). The coordinative B—O bond between the nitrone and boronate groups in **2** (B—O(1) = 1.604(7) Å) is very long. Even longer bonds of this type, however, have been observed in boron complexes with weak interactions between B and O atoms of an amide group (1.621 Å, uncorrected) (19) and of a sulphone group (1.710(3) Å, uncorrected) (20).

The nitrone group in **3** has a longer C=N bond than in **2**, and shorter N—O and C—C(aryl) distances (in the latter case this difference, although not statistically significant, is in the expected direction). This indicates a lesser degree of double bond character for the C=N bond and a cetain π-bond contribution to the N—O and C—C(aryl) bonds as demonstrated by the following resonance hybrid:

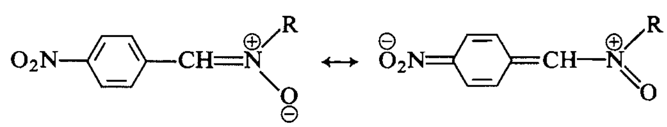

The C=N and N—O bond lengths in **3** (1.311(3) and 1.291(2) Å, respectively) may be compared to those reported for other free nitrones of various structure: 1.309(7) and 1.284(6) (21), 1.299(6) and 1.298(6) (22), 1.309(8) and 1.284(8) (22), 1.327(5) and 1.300(5) Å (23). The nitrone chelate **2** has shorter C=N (1.286(6) Å) and longer N—O (1.355(5) Å) distances, indicating a more pronounced iminium salt character for the B,N-betaine complex.

Both crystal structures consist of discrete molecules separated by normal van der Waals distances, the only notable intermolecular contact occurring in **2** where H(5b)···O(2) ($1/2 + x$, $3/2 - y$, $-z$) = 2.50(6) Å. The nitrone O atoms and the phenyl groups are *cis* with respect to the C=N double bond in both molecules, the phenyl groups being rotated out of the nitrone group mean planes by 19.7(5) and 21.4(2)° for **2** and **3**, respectively. The formation of six-membered NO···HCCC rings via intramolecular C—H···O hydrogen bonds (H···O = 2.22(5) and 2.29(2), C···O = 2.816(7) and 2.819(3) Å, C—H···O = 125(3) and 117(2)°, respectively, for the two compounds) may be responsible for this near coplanarity of nitrone and phenyl groups. In **2** the nitrone group is planar within experimental error while both phenyl rings are slightly but significantly nonplanar (χ^2 = 11.7 and 15.6, maximum deviation from the mean plane 0.019(7) Å). In **3** the nitro, the B-phenyl, and B-coordination groups are all planar to within

TABLE 3. Bond angles (deg) with estimated standard deviations in parentheses

Bonds	Angle (deg)	Bonds	Angle (deg)	Bonds	Angle (deg)
		2			
N —O(1)—B	110.8(4)	O(2)—C(2)—C(1)	112.5(5)	C(17)—C(12)—B	123.1(5)
C(2)—O(2)—B	110.8(4)	O(3)—C(3)—C(1)	110.0(4)	C(12)—C(13)—C(14)	121.7(6)
C(3)—O(3)—B	112.3(4)	N —C(4)—C(6)	127.2(6)	C(13)—C(14)—C(15)	119.4(6)
O(1)—N —C(1)	112.4(4)	C(4)—C(6)—C(7)	124.8(5)	C(14)—C(15)—C(16)	119.3(7)
O(1)—N —C(4)	120.5(4)	C(4)—C(6)—C(11)	116.2(5)	C(15)—C(16)—C(17)	120.8(7)
C(1)—N —C(4)	127.1(5)	C(7)—C(6)—C(11)	118.8(6)	C(12)—C(17)—C(16)	122.9(6)
N —C(1)—C(2)	106.5(4)	C(6)—C(7)—C(8)	119.1(7)	O(1)—B —O(2)	104.9(4)
N —C(1)—C(3)	104.8(4)	C(7)—C(8)—C(9)	121.5(7)	O(1)—B —O(3)	104.8(4)
N —C(1)—C(5)	111.6(5)	C(8)—C(9)—C(10)	119.4(7)	O(1)—B —C(12)	105.3(4)
C(2)—C(1)—C(3)	108.3(5)	C(9)—C(10)—C(11)	120.4(7)	O(2)—B —O(3)	113.2(5)
C(2)—C(1)—C(5)	112.5(5)	C(6)—C(11)—C(10)	120.8(7)	O(2)—B —C(12)	114.2(5)
C(3)—C(1)—C(5)	112.5(5)	C(13)—C(12)—C(17)	115.8(5)	O(3)—B —C(12)	113.1(5)
		C(13)—C(12)—B	121.1(5)		
		3			
C(9)—O(4)—B	119.8(2)	N(2)—C(4)—C(3)	118.8(2)	O(4)—C(9)—C(8)	113.6(2)
C(10)—O(5)—B	119.8(2)	N(2)—C(4)—C(5)	119.8(2)	O(5)—C(10)—C(8)	112.9(2)
O(1)—N(1)—C(7)	123.2(2)	C(3)—C(4)—C(5)	121.4(2)	C(13)—C(12)—C(17)	117.3(2)
O(1)—N(1)—C(8)	113.3(2)	C(4)—C(5)—C(6)	118.9(2)	C(13)—C(12)—B	119.2(2)
C(7)—N(1)—C(8)	123.3(2)	C(1)—C(6)—C(5)	121.6(2)	C(17)—C(12)—B	123.5(2)
O(2)—N(2)—O(3)	122.9(2)	N(1)—C(7)—C(1)	125.7(2)	C(12)—C(13)—C(14)	122.2(3)
O(2)—N(2)—C(4)	118.9(2)	N(1)—C(8)—C(9)	113.4(2)	C(13)—C(14)—C(15)	119.2(3)
O(3)—N(2)—C(4)	118.2(2)	N(1)—C(8)—C(10)	107.4(2)	C(14)—C(15)—C(16)	120.6(3)
C(2)—C(1)—C(6)	117.6(2)	N(1)—C(8)—C(11)	107.1(2)	C(15)—C(16)—C(17)	120.0(3)
C(2)—C(1)—C(7)	125.3(2)	C(9)—C(8)—C(10)	107.9(2)	C(12)—C(17)—C(16)	120.6(3)
C(6)—C(1)—C(7)	117.0(2)	C(9)—C(8)—C(11)	110.6(2)	O(4)—B —O(5)	122.8(2)
C(1)—C(2)—C(3)	121.3(2)	C(10)—C(8)—C(11)	110.4(2)	O(4)—B —C(12)	116.6(2)
C(2)—C(3)—C(4)	119.1(2)			O(5)—B —C(12)	120.7(2)

TABLE 4. Intra-annular torsion angles (deg) standard deviations in parentheses

Atoms	Value (deg)
2	
B —O(1)—N —C(1)	10.8(5)
O(1)—N —C(1)—C(2)	49.0(5)
N —C(1)—C(2)—O(2)	−61.2(6)
B —O(2)—C(2)—C(1)	5.4(7)
C(2)—O(2)—B —O(1)	54.4(6)
N —O(1)—B —O(2)	−66.8(5)
B —O(1)—N —C(1)	10.8(5)
O(1)—N —C(1)—C(3)	−65.6(5)
N —C(1)—C(3)—O(3)	55.0(5)
B —O(3)—C(3)—C(1)	8.8(6)
C(3)—O(3)—B —O(1)	−62.6(5)
N —O(1)—B —O(3)	52.7(5)
B —O(2)—C(2)—C(1)	5.4(7)
C(3)—C(1)—C(2)—O(2)	51.1(6)
C(2)—C(1)—C(3)—O(3)	−58.4(6)
B —O(3)—C(3)—C(1)	8.8(6)
C(3)—O(3)—B —O(2)	51.2(6)
C(2)—O(2)—B —O(3)	−59.2(6)
3	
B —O(4)—C(9)—C(8)	30.1(3)
C(10)—C(8)—C(9)—O(4)	−51.0(3)
C(9)—C(8)—C(10)—O(5)	50.7(3)
B —O(5)—C(10)—C(8)	−29.8(3)
C(10)—O(5)—B —O(4)	5.8(3)
C(9)—O(4)—B —O(5)	−5.8(3)

experimental error while the nitrone and C(1)-phenyl groups are significantly non-planar (χ^2 = 223 and 222, maximum deviations 0.025(2) and 0.019(2) Å, respectively). The nitro group in **3** is rotated out of the C(1)-ring plane by 5.2(3)°. The substituent-induced geometrical distortions of the aromatic rings in both **2** and **3** are as expected (ref. 24 and references therein).

Acknowledgments

We thank the Natural Sciences and Engineering Research Council of Canada and the Fonds der Chemischen Industrie, Frankfurt am Main, for financial support and the University of British Columbia Computing Centre for assistance.

1. W. KLIEGEL and L. PREU. To be published.
2. W. KLIEGEL and E. AHLENSTIEL. Chem. Ber. **110**, 1623 (1977).
3. (*a*) V. A. BREN', E. A. MEDYANTSEVA, I. M. ANDREEVA, and V. I. MINKIN. J. Org. Chem. USSR. **9**, 790 (1973); (*b*) W. KLIEGEL and H. BECKER. Chem. Ber. **110**, 2067 (1977).
4. E. G. JANZEN and R. C. ZAWALSKI. J. Org. Chem. **43**, 1900 (1978).
5. D. T. CROMER and J. B. MANN. Acta Crystallogr. Sect. A, **24**, 321 (1968).
6. R. F. STEWART, E. R. DAVIDSON, and W. T. SIMPSON. J. Chem. Phys. **42**, 3175 (1965).
7. V. SCHOMAKER and K. N. TRUEBLOOD. Acta Crystallogr. Sect. B, **24**, 63 (1968).
8. D. W. J. CRUICKSHANK. Acta Crystallogr. **9**, 747 (1956); **9**, 754 (1956); **14**, 896 (1961).
9. T. URBANSKI, D. GÜRNE, R. KOLINSKI, H. PIOTROWSKA, A. JONCZYK, B. SERAFIN, M. SZRETTER-SZMID, and M. WITA-

NOWSKI. Tetrahedron, **20** (Suppl. 1), 195 (1964).
10. V. V. KUZNETSOV, A. I. GREN', A. V. BOGATSKII, S. P. ERGOROVA, and V. I. SIDOROV. Khim. Geterotsikl. Soedin. 26 (1978); Chem. Heterocycl. Comp. 19 (1978).
11. S. KURIBAYASHI. Bull. Chem. Soc. Jpn. **46**, 1045 (1973).
12. H. SHIMANOUCHI, N. SAITO, and Y. SASADA. Bull. Chem. Soc. Jpn. **42**, 1239 (1969).
13. Z. V. ZVONKOVA and V. P. GLUSHKOVA. Kristallografija, **3**, 559 (1958); Sov. Phys. (Crystallography) **3**, 564 (1958).
14. S. J. RETTIG and J. TROTTER. Can. J. Chem. **55**, 3071 (1977).
15. S. J. RETTIG and J. TROTTER. Can. J. Chem. **53**, 1393 (1975).
16. S. J. RETTIG, J. TROTTER, W. KLIEGEL, and H. BECKER. Can. J. Chem. **54**, 3142 (1976).
17. W. KLIEGEL, D. NANNINGA, S. J. RETTIG, and J. TROTTER. Can. J. Chem. **62**, 845 (1984).
18. W. KLIEGEL, S. J. RETTIG, and J. TROTTER. Can. J. Chem. **62**, 515 (1984).
19. P. R. MALLINSON, D. N. J. WHITE, A. PELTER, K. ROWE, and K. SMITH. J. Chem. Res (S), 234 (1978).
20. J. H. NOORDIK and T. E. M. VAN DEN HARK. Cryst. Struct. Commun. **7**, 287 (1978).
21. K. FOLTING, W. N. LIPSCOMB, and B. JERSLEV. Acta Crystallogr. **17**, 1263 (1964).
22. K. G. JENSEN and B. JERSLEV. Acta Crystallogr. Sect. B, **25**, 916 (1969).
23. J. N. BROWN and L. M. TREFONAS. Acta Crystallogr. Sect. B, **29**, 237 (1973).
24. A. DOMENICANO, P. MURRAY-RUST, and A. VACIAGO. Acta Crystallogr. Sect. B, **39**, 457 (1983).
25. W. KLIEGEL, S. J. RETTIG, and J. TROTTER. Can. J. Chem. **62**, 1363 (1984).

Infrared spectra of the ammonium ion in crystals. Part XIII. Crystal structure of $(NH_4)_2[AlF_5(H_2O)]$ and NH_3D^+ probe-ion spectra in $(NH_4)_2[AlF_5(H_2O)]$, NH_4AlF_4, and $(NH_4)_3ZnCl_5$, with remarks on structural filiation of AMF_4 fluorides[1,2]

OSVALD KNOP, T. STANLEY CAMERON, S. P. DERANIYAGALA, AND D. ADHIKESAVALU
Department of Chemistry, Dalhousie University, Halifax, N.S., Canada B3H 4J3

AND

MICHAEL FALK
Atlantic Research Laboratory, National Research Council of Canada, Halifax, N.S., Canada B3H 3Z1

Received May 25, 1984

OSVALD KNOP, T. STANLEY CAMERON, S. P. DERANIYAGALA, D. ADHIKESAVALU, and MICHAEL FALK. Can. J. Chem. **63**, 516 (1985).

The crystal structure of $(NH_4)_2AlF_5 \cdot H_2O$ = $(NH_4)_2[AlF_5(H_2O)]$ (*Pbcn*, a = 10.192(4) Å, b = 8.037(2) Å, c = 7.844(1) Å, Z = 4) consists of isolated $[AlF_5(H_2O)]^{2-}$ octahedra and NH_4^+ ions. The octahedra are linked by F···H—O—H···F bonds to form zigzag chains parallel to c and the chains are cross-linked by normal N—H···F hydrogen bonds to the NH_4^+ ions. The ir characteristics of the hydrogen bonds in this and the other two title compounds were probed with the NH_3D^+ ion between 10 and 293 K. The probe-ion spectra confirm the C_1 symmetry of the ammonium ion in $(NH_4)_2[AlF_5(H_2O)]$ and point to N—H···F bonding of moderate strength. For NH_4AlF_4 the spectra agree with the expectation from the known crystal structure of both the ordered and the disordered phase, but the transition at ~150 K is not evident in the evolution of the spectra with temperature. Detailed assignment of the ND stretching and bending component absorptions of NH_3D^+ is not possible for $(NH_4)_3ZnCl_5$ = $(NH_4)_3(ZnCl_4)Cl$. However, the unusually low frequencies of two of the components of the ND stretching absorptions in this crystal indicate the existence of N—H···Cl^- bonds stronger than those in NH_4Cl. The filiation of the known AMF_4 structures deriving from $TlAlF_4$ is presented in terms of two-colour space groups.

OSVALD KNOP, T. STANLEY CAMERON, S. P. DERANIYAGALA, D. ADHIKESAVALU et MICHAEL FALK. Can. J. Chem. **63**, 516 (1985).

La structure cristalline du $(NH_4)_2AlF_5 \cdot H_2O$ = $(NH_4)_2[AlF_5(H_2O)]$ (*Pbcn*, a = 10,192(4) Å, b = 8,037(2) Å, c = 7,844(1) Å, Z = 4) est formée d'ions NH_4^+ et d'ions $[AlF_5(H_2O)]^{2-}$ octaédriques isolés. Les octaèdres sont reliés par des liaisons F···H—O—H···F qui forment des chaînes en zigzag le long de l'axe c alors que les chaînes sont réticulées par des liaisons hydrogènes N—H···F normales avec les ions NH_4^+. Opérant entre 10 et 293 K et utilisant l'ion NH_3D^+ comme sonde, on a étudié les caractéristiques infrarouges de ces liaisons hydrogènes ainsi que celles des deux autres composés mentionnés dans le titre. Le spectre de l'ion sonde confirme la symétrie C_1 de l'ion ammonium dans le produit $(NH_4)_2[AlF_5(H_2O)]$ et suggère que la force de la liaison N—H···F est modérée. Dans le cas du NH_4AlF_4, le spectre correspond à ce que l'on aurait pu escompter sur la base de ce que l'on connait de la structure cristalline des phases tant ordonnée que désordonnée; toutefois, la transition autour de 150 K n'est pas évidente si l'on examine l'évolution du spectre avec la température. Dans le cas du $(NH_4)_3ZnCl_5$ = $(NH_4)_3(ZnCl_4)Cl$, on ne peut pas faire d'attributions détaillées aux absorptions dues aux composantes d'élongation et de déformation angulaire de la liaison ND du NH_3D^+. Toutefois, les fréquences anormalement basses de deux des composantes des absorptions dues aux élongations de la liaison ND dans ce cristal suggèrent l'existence de liaisons N—H···Cl^- qui sont plus fortes que celles que l'on observe dans le NH_4Cl. On présente la filiation des structures connues de AMF_4 dérivant du $TlAlF_4$ en fonction de groupes d'espace en deux couleurs.

[Traduit par le journal]

In the course of our recent investigation of ammonium cryolites, $(NH_4)_3MF_6$, we had occasion to prepare two related compounds, $(NH_4)_2AlF_5 \cdot H_2O$ and NH_4AlF_4. The very good quality of exploratory ir spectra of the NH_3D^+ probe ion in both these compounds at 10 K encouraged us to undertake a systematic study of the spectra between 10 K and room temperature. Although the $\nu_1(NH_3D^+)$ and $\nu_{4bc}(NH_3D^+)$ frequencies in NH_4AlF_4 at liquid-nitrogen temperature had been recorded earlier (2), the recently reported (3) transition in this compound, in the vicinity of 150 K, made a more thorough investigation desirable. Neither a structural nor a spectroscopic study of $(NH_4)_2AlF_5 \cdot H_2O$ seems to have been published previously. In view of the crystallographic diversity of known $A_2MF_5 \cdot H_2O$ compounds[3] it did not seem safe to interpret the spectra of $(NH_4)_2AlF_5 \cdot H_2O$ on a presumed structural analogy with one of the other monohydrates, and we have therefore determined the crystal structure of this fluoride. In addition, to test the potential of the probe-ion method realizable with an FT ir spectrometer, we have obtained NH_3D^+ spectra, between 10 and 293 K, of $(NH_4)_3ZnCl_5$ = $(NH_4)_3(ZnCl_4)Cl$, which has been

[1] For Part XII, see ref. 1.
[2] NRCC No. 23854.

[3] The $A_2MF_5 \cdot H_2O$ fluorides reported to date fall in two classes, $A_2[MF_5(H_2O)]$ and $A_2[MF_4F_{2/2}] \cdot H_2O$. The structures in the first class contain isolated $[MF_5(H_2O)]$ octahedra and have symmetry *Cmcm* (CsFe, ref. 4) or *Fm3m* (TlV and RbCr, refs. 5 and 6). The structures in the second class are characterized by *trans*-linked chains of $[MF_6]$ octahedra. The following symmetries are represented: $P2_1/m$ — KMn (7); *Cmcm* — KAl (8, 9), RbAl (10), TlAl (10), RbMn (11), RbFe (10); *Cmmm* — CsMn (12).

reported (13) to contain two types of ammonium ions at sites of low symmetry.

Experimental

Preparation

According to Novoselova (14) the three compounds that exist in the system $NH_4F-AlF_3-H_2O$ at 25°C are $(NH_4)_3AlF_6$, $(NH_4)_2AlF_5\cdot H_2O$, and NH_4AlF_4. The hydrate has not been investigated previously. The structural aspects of the two anhydrous salts were studied by Brosset (8, 9); that of NH_4AlF_4 also by Thilo (15). Brosset prepared NH_4AlF_4 by neutralizing a strongly HF-acid solution of AlF_3 with concentrated NH_4OH, whereas Thilo decomposed $(NH_4)_3AlF_6$ thermally at temperatures below 350°C. Both authors reported NH_4AlF_4 to be tetragonal, $a \sim 3.59$ Å, $c \sim 6.35$ Å, with a structure of the same type as that proposed for $TlAlF_4$ by Brosset (16).

We prepared NH_4AlF_4 by slowly adding a stoichiometric amount of solid NH_4F to a hot solution of AlF_3 obtained by dissolving Al in 48% HF. The precipitate was digested for 1/2 h on a steam bath, filtered, washed with weak HF followed by EtOH, and dried over P_2O_5. Because of its slight solubility in weak HF the salt could not be deuterated by recrystallization from H_2O-D_2O; partially deuterated samples were obtained by repeating the preparation from aqueous HF containing D_2O.

$(NH_4)_2AlF_5\cdot H_2O$ was prepared in a similar manner using an NH_4F/AlF_3 ratio of 2.5/1. The precipitate was filtered and washed etc., as under NH_4AlF_4. It was deuterated by repeating the procedure with solutions containing D_2O.

$(NH_4)_2ZnCl_4$ and $(NH_4)_3ZnCl_5$ are reported to be the only two compounds in the system $NH_4Cl-ZnCl_2-H_2O$ between 0 and 30°C (cf. ref. 13). $(NH_4)_3ZnCl_5$ was prepared by slow evaporation over $CaCl_2$, at room temperature, of a 3/1 molar aqueous solution of NH_4Cl and $ZnCl_2$ (13, 17). It was deuterated by repeating the preparation with H_2O-D_2O solutions. Unlike $(NH_4)_2ZnCl_4$ (18, 19), crystals of $(NH_4)_3ZnCl_5$ are not deliquescent under ordinary atmospheric conditions.

The identity of NH_4AlF_4 and $(NH_4)_3ZnCl_5$ was confirmed by internal evidence from the ir spectra and for NH_4AlF_4 also by comparison with a published spectrum (20). The authenticity of $(NH_4)_2AlF_5\cdot H_2O$ was guaranteed by the crystal-structure determination. However, the reported narrowness of the stability range of this phase in the $NH_4F-AlF_3-H_2O$ system (14) invited caution as to the homogeneity of the bulk sample. Of particular concern was the absence of typical H_2O absorptions in the ir spectra (see below). To prove that the products did contain H_2O, samples of separately prepared material with zero, low and high D contents were heated in a mass spectrometer and the low-resolution spectra were recorded at increasing sample temperatures. The intensity vs. temperature plots for these dynamic thermolysis conditions indicated clearly that water was present and that it was given off over a temperature range below ~100°C, the bulk of it at ca. 70°C and in any case before the liberation and dissociation of NH_4F.

Infrared spectra

Finely ground sample powders were mulled in Nujol or fluorolube and the mulls were supported between CaF_2 plates. The spectra were obtained with a Fourier-transform ir spectrometer (Bomem DA3.02) fitted with a closed-cycle He refrigerator (Displex model 202, Air Products and Chemicals Co.). The variable-temperature spectral runs were made in the heating mode.

$(NH_4)_2AlF_5\cdot H_2O$: crystal data

$AlF_5H_{10}N_2O$ fw = 176.07

Orthorhombic, *Pbcn* (no. 60) (systematic absences: $hk0$, $h + k = 2n + 1$; $h0l$, $l = 2n + 1$; $0kl$, $k = 2n + 1$); $a = 10.192(4)$ Å, $b = 8.037(2)$ Å, $c = 7.844(1)$ Å, $V = 642.5(5)$ Å^3, $Z = 4$, $\rho_c = 1.820$ g/cm^3; Mo $K\alpha_1$, $\lambda = 0.70926$ Å (graphite monochromator), $\mu_{Mo} = 2.89$ cm^{-1}, $F(000) = 360$ e.

$(NH_4)_2AlF_5\cdot H_2O$: structure determination

A CAD-4 four-circle diffractometer was used in the determination of the unit cell dimensions and to collect intensities (θ = 2–25°). The intensities were reduced by routine procedures (21). Corrections for Lorentz and polarization factors were applied but not for absorption or extinction. The scattering factors for neutral atoms were taken from ref. 22. The structure was solved from 344 unique reflections by Patterson and Fourier methods using the SHELX system (23). Full-matrix least-squares ($w\Delta F^2$ = minimum) refinements were carried out with isotropic temperature factors on the heavy atoms until R was reduced to a suitably low value. The hydrogen atoms were located from a difference map. The N—H, O—H, and H—H distances were appropriately constrained to ensure convergence. The final refinement, with anisotropic temperature factors on the nonhydrogen atoms and isotropic factors on the hydrogens gave $R = 4.6\%$, $R_w = 4.4\%$. Least-squares weights were calculated from the expression $0.5267w^{-1} = \sigma^2|F_o| + 0.000500F_o^2$, where σ is the weight for an individual reflection derived from the diffractometer counting statistics. The anisotropic temperature factor is defined as $T = \exp[-2\pi^2(U_{11}h^2a^{*2} + U_{22}k^2b^{*2} + U_{33}l^2c^{*2} + 2U_{23}klb^*c^* + 2U_{13}hla^*c^* + 2U_{12}hka^*b^*)]$.

The positional and thermal parameters are listed in Table 1, structure factors in Table 2,[4] and interatomic distances and bond angles in Table 3.

TABLE 1. $(NH_4)_2[AlF_5(H_2O)]$: positional and thermal parameters (× 10^4)

Atom	x / y / z	U_{11} / U_{22} / U_{33}	U_{12} / U_{13} / U_{23}
Al	0	274(12)	0
	1996(3)	238(12)	−10(9)
	$\frac{1}{4}$	122(10)	0
F(1)	0	353(25)	0
	4226(5)	223(22)	43(22)
	$\frac{1}{4}$	231(22)	0
F(2)	0400(3)	572(21)	−11(16)
	1966(4)	297(16)	45(13)
	0288(3)	162(16)	−37(15)
F(3)	1713(3)	295(19)	94(18)
	1975(4)	503(21)	−84(14)
	3012(4)	436(20)	−85(18)
O	0	1123(59)	0
	−0412(7)	209(32)	−214(38)
	$\frac{1}{4}$	245(31)	0
H_w	0052(107)	1012(311)*	
	−1179(49)		
	3490(27)		
N	2997(4)	285(22)	27(22)
	0230(6)	318(26)	22(21)
	0265(6)	272(25)	41(23)
H(1)	2554(44)	356(152)*	
	−0681(45)		
	−0439(51)		
H(2)	2339(42)	603(212)*	
	0741(64)		
	1136(53)		
H(3)	3285(56)	936(292)*	
	1183(51)		
	−0567(58)		
H(4)	3805(36)	737(249)*	
	−0200(65)		
	0916(61)		

* U_{iso}.

[4] This table has been deposited. Complete set of data is available, at a nominal charge, from the Depository of Unpublished Data, CISTI, National Research Council of Canada, Ottawa, Ont., Canada K1A 0S2.

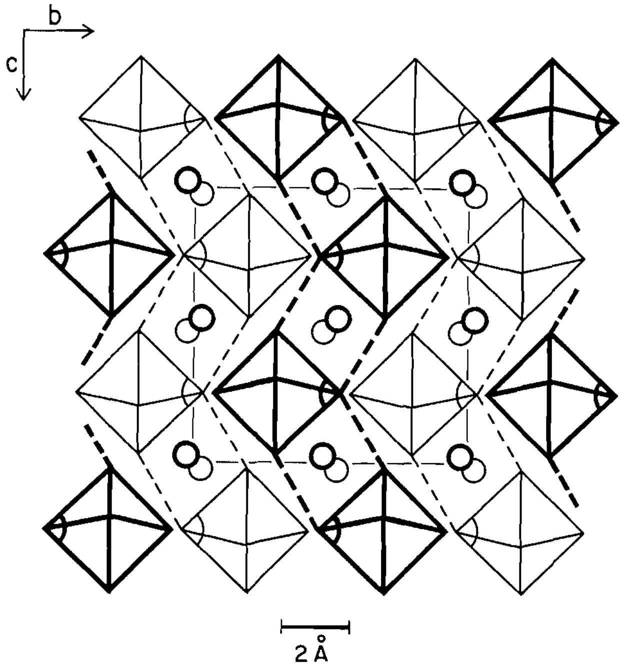

FIG. 1. $(NH_4)_2[AlF_5(H_2O)]$: projection of the structure on (100) displaying the distorted antifluorite packing of the ions and the O—H_w···F bonding scheme. In the heavily outlined $[AlF_5(H_2O)]$ octahedra $x(\mathrm{Al}) = \frac{1}{2}$, in the lightly outlined ones, $x(\mathrm{Al}) = 0$. Only the N atoms of the ammonium ions are shown.

TABLE 3. $(NH_4)_2[AlF_5(H_2O)]$: interatomic distances (Å) and bond angles (deg)

Atoms	Distance*	Atoms	Angle
Al—F(1)	1.792(2)	F(1)—Al—F(2)	90.8(1)
Al—F(2)	1.783(3)	F(1)—Al—F(3)	90.5(1)
Al—F(3)	1.791(2)	F(2)—Al—F(3)	89.7(1)
Al—O	1.936(2)	O—Al—F(2)	89.2(1)
N—H(1)	1.02(4)	O—Al—F(3)	89.5(1)
N—H(2)	1.04(5)	N(C)—H(1C)—F(3D)	169(4)
N—H(3)	1.05(5)	N(C)—H(2C)—F(3C)	159(4)
N—H(4)	1.03(5)	N(C)—H(3C)—F(3B)	164(4)
N(C)···F(1A)	2.810(5)	N(C)—H(4C)—F(1A)	166(4)
N(C)···F(3D)	2.826(6)	O(C)—H_w(C)—F(2D)	163(5)
N(C)···F(3B)	2.873(6)	F(2)—O—F(2′)	121.4(2)
N(C)···F(3C)	2.884(6)		
H(1C)···F(3D)	1.82(4)	Symmetry code:	
H(2C)···F(3C)	1.89(5)	A x y z	
H(3C)···F(3B)	1.85(5)	B x $\bar{y}$ $z-\frac{1}{2}$	
H(4C)···F(1A)	1.80(5)		
O—H_w	0.99(6)	C $\frac{1}{2}-x$ $\frac{1}{2}+y$ z	
O(C)···F(2D)	2.551(3)		
H_w(C)···F(2D)	1.59(6)	D $\frac{1}{2}-x$ $\frac{1}{2}-y$ $z-\frac{1}{2}$	

* Mean d(Al—F) = 1.789(6) Å.

Results and discussion

$(NH_4)_2AlF_5 \cdot H_2O$: crystal structure

The structure consists of isolated $[AlF_5(H_2O)]$ octahedra (of symmetry C_2) and NH_4^+ ions arranged in a distorted antifluorite packing (Fig. 1). In each layer of $[AlF_5(H_2O)]$ octahedra parallel to (001) all the Al—O bonds are oriented in the same direction; the directions alternate from plane to plane in an "antiferro" manner. In layers parallel to (100) the octahedra are linked by F(2)···H—O—H···F(2) hydrogen bonds to form zigzag chains parallel to the c-axis. These chains in turn are cross-linked within *and* between these layers by normal, somewhat bent N—H···F(1) and N—H···F(3) hydrogen bonds (Figs. 2 and 3). Each ammonium ion is surrounded by four $[AlF_5(H_2O)]$ octahedra, each N-hydrogen being bonded to a fluorine in a different octahedron.

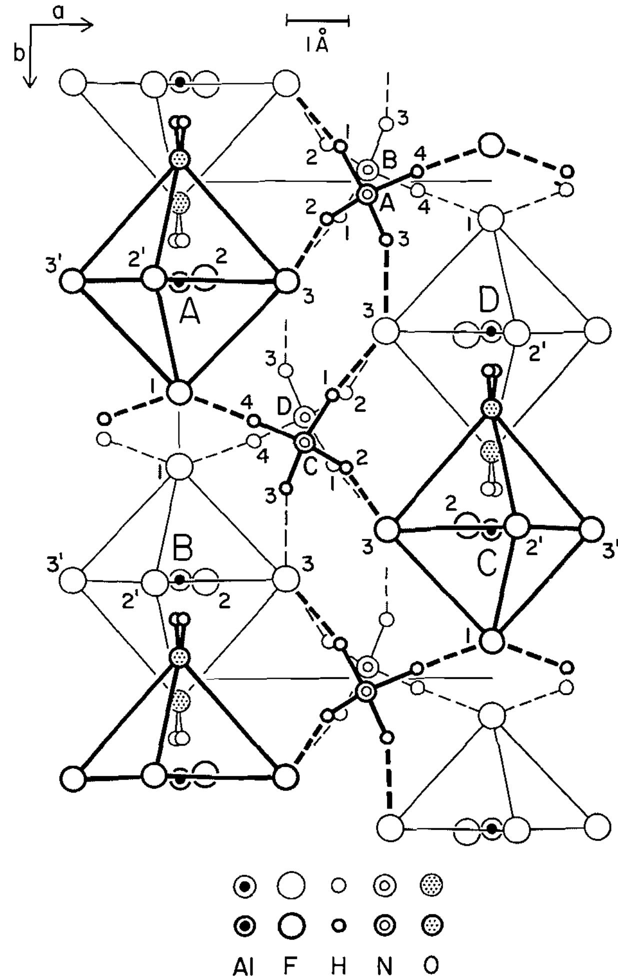

FIG. 2. $(NH_4)_2[AlF_5(H_2O)]$: projection of the unit cell on (001) displaying the N—H···F bonding scheme. The H_w···F bonds are not shown. For symmetry code, interatomic distances and bond angles see Table 3.

The F(2) atoms are hydrogen-bonded exclusively to the water molecules. Each F(1) atom is symmetrically bonded to two H(4) hydrogens (H···F, 1.80 Å), and each F(3) atom is bonded to three H atoms, H(1), H(2), and H(3) (mean H···F distance, 1.85(3) Å). The four H···F distances are quite similar (mean H···F, 1.84(4) Å) and would be classified as moderately strong. The O···F(2) and H_w···F(2) distances, however, are quite short, 2.551(3) and 1.59(6) Å, respectively. The O···F(2) distance, which compares with the corresponding distance in $RbVF_4 \cdot 2H_2O$, 2.56 Å (24), $ZnF_2 \cdot 4H_2O$, 2.57 Å (25), and $Cs_2[FeF_5(H_2O)]$, 2.61 Å (4), is at the lower limit of the O···F range in metal fluoride hydrates (26), as also is the $OH_wF(2)$ angle of 163(5)°.

The filiation of the $(NH_4)_2[AlF_5(H_2O)]$ and related structures from the $Fm3m$ antifluorite aristotype will be discussed elsewhere. It is, however, interesting to note that $Rb_2AlF_5 \cdot H_2O$, which contains a cation dimensionally similar to NH_4^+, has a structure built of chains of $[AlF_6]$ octahedra sharing opposite

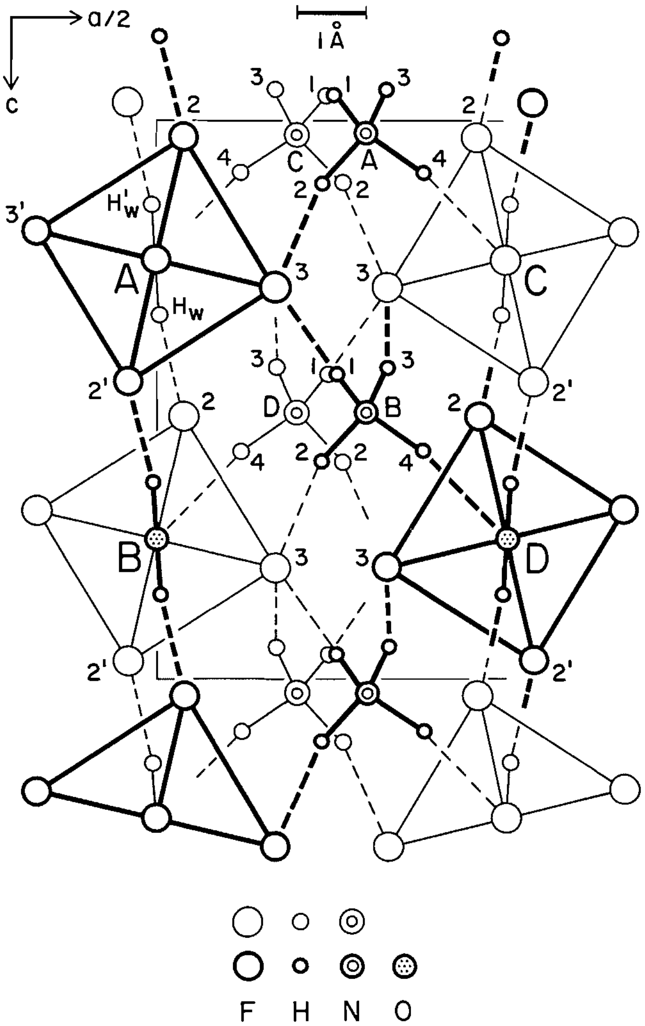

FIG. 3. $(NH_4)_2[AlF_5(H_2O)]$: projection of a portion of the unit cell on (010) displaying details of the O—H_w···F and N—H···F hydrogen-bonding scheme. For symmetry code, interatomic distances and bond angles see Table 3. The following values have been added to the coordinates of Table 1: ammonium ions, B + (0, 0, 1), C + (0, −1, 0), D + (0, −1, 1); anions, B + (0, 0, 1), C + (0, −1, 0), D + (0, 0, 1).

corners, $Rb_2[AlF_4F_{2/2}]\cdot H_2O$, and not of isolated $[AlF_5(H_2O)]^{2-}$ ions (10). It is not clear to what extent this difference is attributable to the hydrogen bonding of the ammonium ions. The volume per formula unit V_1 of $(NH_4)_2[FeCl_5(H_2O)]$ is smaller than the V_1 of $Rb_2[FeCl_5(H_2O)]$; this and spectroscopic evidence (2, 27) indicate that N—H···Cl bonding is present in the ammonium compound. Yet these two compounds, and similarly $(NH_4)_2[VCl_5(H_2O)]$ and $Rb_2[VCl_5(H_2O)]$, form isostructural pairs.[5] This lack of structural distinction may of course arise from the relative weakness of the N—H···Cl bonding compared with the N—H···F bonding. On the other hand, $Cs_2FeF_5\cdot H_2O$, though not isostructural with $(NH_4)_2AlF_5\cdot H_2O$, contains isolated $[FeF_5(H_2O)]$ ions despite the absence of N—H···F bonding (4); and as the following list shows, ionic size may not be a strong determining factor either (**A**, $A_2[MF_5(H_2O)]$; **B**, $A_2[MF_4F_{2/2}]\cdot H_2O$):

[5] In fact, all the known $A_2MCl_5\cdot H_2O$ chlorides contain isolated $[MCl_5(H_2O)]$ ions (cf. ref. 27).

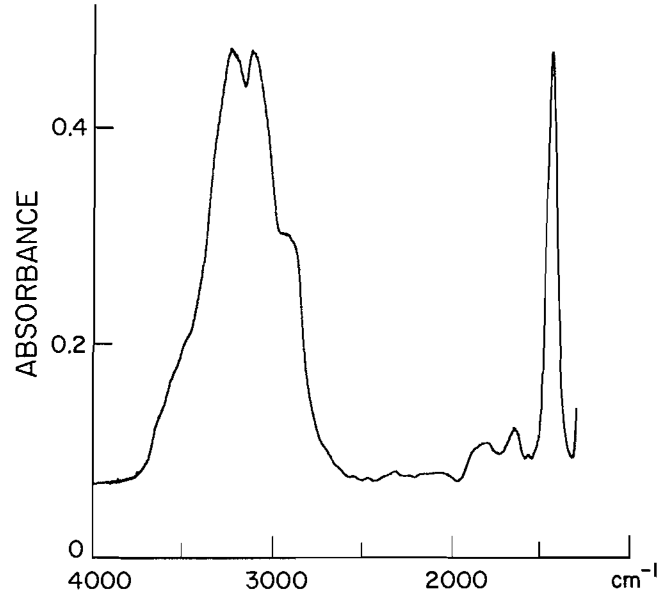

FIG. 4. $(NH_4)_2[AlF_5(H_2O)]$: the ND stretching and bending regions of the NH_3D^+ probe-ion spectrum at different temperatures (~2% D).

	A = K	Rb	Cs
M = Al	**B** (8, 9)	**B** (10)	
Cr		A? (6)	
Mn	**B** (7)	**B** (11)	**B** (12)
Fe		**B** (10)	**A** (4)

$(NH_4)_2AlF_5\cdot H_2O$: probe-ion spectra

The expectation for a single type of ammonium ion at sites of symmetry C_1 ideally would be a ν_1 quartet and a ν_{4bc} octet, each with all the components of equal weight. From ν(ND) vs. d(N···F) or d(H···F) and ν_{4bc} vs. ν_1 plots (cf. ref. 2 and updated versions to be published) the mean $\bar{\nu}_1$ and $\bar{\nu}_{4bc}$ frequencies at room temperature would be predicted as ~2370 and ~1285 cm^{-1} respectively, and since they correspond to somewhat bent but normal (i.e. to a single acceptor atom) N—H···F bonds, the $\bar{\nu}_1$ frequency would be expected to increase and the $\bar{\nu}_{4bc}$ frequency to decrease with increasing temperature.

The 10 K spectrum indeed contained a well-resolved ν_1 quartet, with components at 2313, 2333, 2346, and 2364 cm^{-1} ($\bar{\nu}_1$ (10) = 2339 cm^{-1}, total range = 51 cm^{-1}); the ν_{4bc} absorption consisted of six resolved components, with frequencies between 1273 and 1307 cm^{-1} ($\bar{\nu}_{4bc}$ (10) = 1288 cm^{-1}, total range = 34 cm^{-1}) (Fig. 4). The halfwidths were 6–10 cm^{-1}.

With increasing temperature the components of the ν_1 as well as the ν_{4bc} absorption gradually broadened and coalesced, with no apparent discontinuities in the evolution with temperature. By 220 K the ν_1 absorptions had collapsed to a single broad band centred at 2350 cm^{-1}. The centre of gravity kept moving to higher frequencies and went over smoothly into the peak of the broad band, ending up at 2356 cm^{-1} at room temperature (a total shift of +16 cm^{-1}). The halfwidth at room temperature was about 46 cm^{-1}, corresponding roughly to the spread of the component frequencies at low temperature.

The ν_{4bc} components also coalesced with increasing temperature but only partially: even at room temperature three components could still be discerned. At the same time the $\bar{\nu}_{4bc}$ frequency shifted to lower values, about 1280 cm^{-1} at room

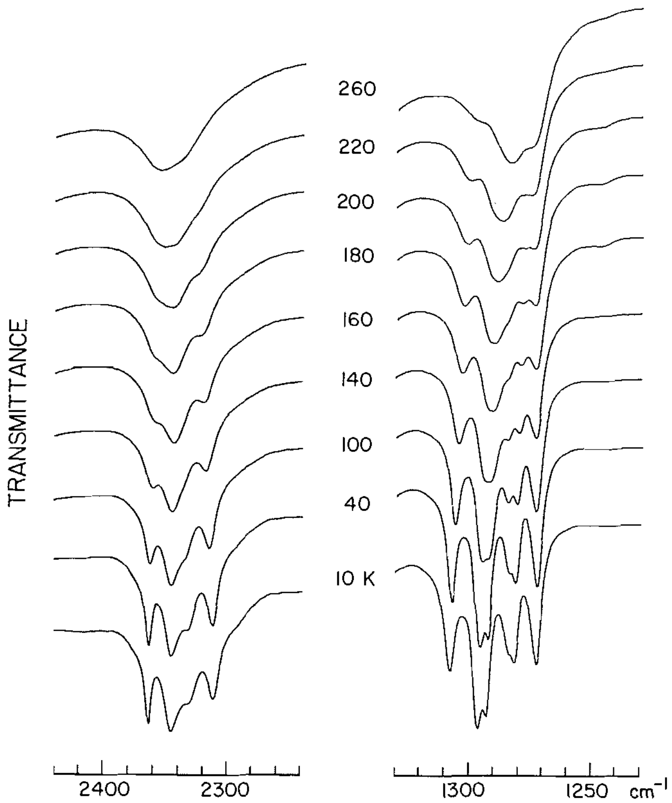

FIG. 5. $(NH_4)_2[AlF_5(H_2O)]$: survey spectrum at room temperature (fluorolube mull).

temperature, which corresponds to a total shift of ca. -8 cm^{-1}. The above prediction is thus seen to be quite successful.

As the observed ν_1 and ν_{4bc} frequencies indicate, the N—H···F bonding in $(NH_4)_2[AlF_5(H_2O)]$ is moderately strong.

The absence of typical H_2O absorptions in the room-temperature spectrum of this hydrate (Fig. 5) was puzzling. While the small band at ~1641 cm^{-1} *may* arise from the HOH bending fundamental, the spectrum contained no obvious features that could be assigned to the OH stretching fundamental — and this in spite of the fact that, in the ir spectra of crystalline hydrates, the absorption due to the OH stretching mode is generally many times more intense than the bending absorption (20, 28). At the same time, however, there are almost no hydrate spectra in the literature that could usefully serve as precedents for the absorptions of an H_2O molecule as strongly bonded as that in $(NH_4)_2[AlF_5(H_2O)]$, with an O···F distance of only 2.55 Å. The nearest comparison would be with $(NH_4)_2[Cr(H_2O)_6]F_5$, which we have also studied recently (results to be published). In this fluoride the O···F distances are similarly short, 2.53–2.57 Å (29), and the OH stretching fundamental is found as an extremely broad absorption extending from 2000 to 3800 cm^{-1} and centred at ~2900 cm^{-1}. We should then expect a similar band in the spectrum of $(NH_4)_2[AlF_5(H_2O)]$ if allowance is made for the difference of stoichiometry, which would make the intensity of the band about six times weaker relative to the NH stretching bands in this region. It is concluded that the OH stretching absorption in Fig. 5 underlies the group of peaks at 3223, 3105, and 2915 cm^{-1} originating in $\nu_3(NH_4^+)$ and $2\nu_2(NH_4^+)$ and complicated by factor-group splitting and Fermi resonance.

The corresponding OD stretching absorptions of HDO and D_2O, expected in the 2800–1500 cm^{-1} region, are probably also very broad. In any event they could not be located in our spectra of the partially deuterated compound.

The untypical nature of the H_2O molecule in $(NH_4)_2[AlF_5(H_2O)]$ is undoubtedly also reflected in the very strong anisotropy of the U_{ii} thermal parameters of the oxygen atom (Table 1): $U_{22} \sim U_{33}$, $2U_{11}/(U_{22} + U_{33}) = 5(1)$, where U_{11} refers to a direction perpendicular to the Al—O bond and almost perpendicular to the HOH plane (Fig. 3).

If a low-temperature transition in $(NH_4)_2[AlF_5(H_2O)]$ exists, there was no evidence of it in the probe-ion spectra.

NH_4AlF_4

A recent X-ray powder and single-crystal diffraction study by Fourquet *et al.* (30) gave a tetragonal cell four times larger than that originally proposed (cf. Experimental): $a' = a\sqrt{2} = 5.078(2)$ Å, $c' = 2c = 12.715(4)$ Å, $Z' = 4$. With the H atoms not included the space group was $I4/mcm$, with N in $4(b)$-$0\frac{1}{2}\frac{1}{4}$ etc., Al in $4(c)$-000 etc., F_{ax} in $8(f)$-$00z$ etc., and F_{eq} in $8(h)$-$x, \frac{1}{2}+x, 0$ etc. These authors further proposed that inclusion of the hydrogens would yield a noncentrosymmetric space group (consistent with the observed generation of the second harmonic) and settled on $I\bar{4}c2$, with the H atoms in $16(i)$-xyz etc. Re-investigation by neutron diffraction from a single crystal (31) and from a powder profile refinement (3) led to a revision of the space group to $I4/mcm$, with the hydrogens distributed over the $32(m)$-xyz etc. equipoint in a way consistent with a statistical distribution of the ammonium ions over two possible orientations. In this structure the site symmetry at N is D_{2d}. No evidence of a transition between room temperature and 350°C was observed either by dta or ^{1}H nmr (30).

An X-ray investigation between 80 and 300 K did not reveal any noticeable departure from tetragonal symmetry or from the body-centering (3). However, an esr study of NH_4AlF_4:Fe^{3+} and NH_4AlF_4:Cr^{3+} indicated the existence of a structural phase transition in the vicinity of 150 K (31, 32). Neutron powder diffraction at 5 K (3) led to $P4_2/mbc$ as the space group of the low-temperature phase (N in $4(b)$-$00\frac{1}{4}$ etc., Al in $4(c)$-$0\frac{1}{2}0$ etc., F_{ax} in $8(f)$-$0\frac{1}{2}z$ etc., F_{eq} in $8(h)$-$xy0$ etc. ($x \sim y$), and H in $16(i)$-xyz etc.), and to S_4 as the site symmetry at N. The ammonium ions in this structure are orientationally ordered; the ordering is described by the authors as "ferro" within the ammonium layers ‖(001) and "antiferro" between these layers. The intra-layer ordering is present already at temperatures more than 100° above T_{tr}, whereas the inter-layer ordering sets in only at T_{tr} (33). The shortest H···F distances (to F_{ax}) are 1.898(4) Å at 300 K and 1.852(3) Å at 5 K; the corresponding N···F_{ax} distances are 2.900(1) Å and 2.893(1) Å, and the NHF_{ax} angles are 171.2(5)° and 170.8(1)° (N—H = 1.010(4) and 1.043(2) Å). These distances and angles are unchanged on passage through T_{tr}.

The expectation for the NH_3D^+ probe-ion spectrum is a single ν_1 absorption and a ν_{4bc} 1:1 doublet for both $S = D_{2d}$ and $S = S_4$ (Table 1, ref. 34). Consequently there should be no change in the number of the ν_1 and ν_{4bc} absorptions on passage through T_{tr}, though the ordering might affect the linewidths and frequencies of these absorptions.

The 10 K spectrum (Fig. 6) contained a single ND stretching absorption ν_1, at 2347 cm^{-1} ($\Delta\nu_{1/2}$ = 12 cm^{-1}). The ND bending ν_{4bc} was an approximately 3:2 doublet at 1287 and 1303 cm^{-1}, also with a ca. 12 cm^{-1} component halfwidth. With increasing temperature the frequency of the ν_1 band increased, the shift between 10 and 293 K amounting to +9(3) cm^{-1}, while the ν_{4bc} doublet partially collapsed and shifted to 1283.5 and 1294 cm^{-1} at 293 K, i.e. a total shift of −6(1) cm^{-1}. These results are in agreement with those reported earlier (2) for liquid-nitrogen temperature (probably ~100 K). At room temperature the halfwidths were about 45 cm^{-1} for ν_1 and ca. 36 cm^{-1} for the ν_{4bc} components.

The observed number of ν_1 and ν_{4bc} bands is consistent with a single type of ammonium ion in the structure, of effective symmetry D_{2d}, S_4, or D_2 and at a site of nonpolar tetragonal or D_{2h} or D_2 symmetry. This confirms the site symmetries reported in ref. 3. The signs of the temperature coefficients of the ν_1 and ν_{4bc} frequencies indicate (35) that the N—H···F bonds are normal, i.e. essentially straight. This too is consistent with the reported crystal structures. The observed ν_1 frequency points to a hydrogen bonding substantially weaker than that in NH_4F and even NH_4HF_2 (2); this would be expected in view of the relatively long H···F distance (cf. Fig. 1 of ref. 2). The smallness of the ν_1 frequency shift on cooling from room temperature to 10 K indicates that the hydrogen bonding does not strengthen appreciably, and this again is consistent with the constancy of the N···F_{ax} distance, although the change in the reported H···F distance, ca. 0.05 Å, might suggest a larger ν_1 shift.

The changes, with temperature, in the probe-ion spectra were gradual. There was no evidence of the transition in the vicinity of 150 K, nor of changes in the degree of the intra-layer ordering above 150 K. This lack of sensitivity to the orientation of the ammonium ion is paralleled in the Raman spectrum of neat NH_4AlF_4 (36): of the observed features the only ones that were found to respond to the ordering below 150 K were those due to the E_g translatory (~150 cm^{-1}) and rotatory (~250 cm^{-1}) modes of NH_4^+.

The nature of the ordering in NH_4AlF_4 is most directly described by the use of two-colour space-group symmetry. In the (fully ordered) intermediate phase the [AlF_6] octahedra in layers ‖(001) are rotated about their tetragyres and the rotational displacements are "antiferro" ordered; the orientations of these "antiferro" nets in adjacent layers alternate.[6] This arrangement is derived from the arrangement of the octahedra in the highest-symmetry ($P4/mmm$) aristotype structure[7] by the dichromatic Bravais translation $(\mathbf{a}_1' + \mathbf{a}_2)/2$ of the Shubnikov group Sh_{140}^{550}-I_c4/mcm: four unit cells of the aristotype structure (a_0, c_0, $Z = 1$) combine to generate the intermediate structure ($a_0\sqrt{2}$, $2c_0$, $Z = 4$),[8] and the chromatic component of the translation, interpreted as orientation reversal, assures the "antiferro" intralayer ordering of the [AlF_6] octahedra and the alternation of the orientations of the octahedra in adjacent layers. In this structure, describable in terms of $I4/mcm$, the ammonium ions are in a twofold orientational disorder. The ordering process, which sets in at T_{tr}, results in an ordered arrangement of the ammonium ions, leaving the rest of the structure essentially unchanged. This orientational order of NH_4^+ is derivable from the intermediate structure by the dichromatic Bravais translation $(\mathbf{a}_1' + \mathbf{a}_2' + \mathbf{c}')/2$ of the Shubnikov group

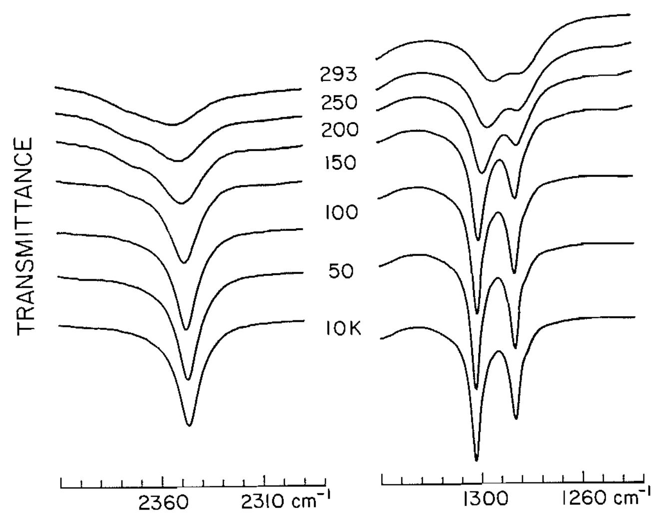

FIG. 6. NH_4AlF_4: the ND stretching and bending regions of the NH_3D^+ probe-ion spectrum at different temperatures (~5% D).

Sh_{135}^{494}-P_I4_2/mbc. This translation, again associated with orientation reversal, generates a "ferro" ordering of the ammonium ions *within* the NH_4^+ layers ‖(001) but an "antiferro" stacking arrangement of these layers. The low-temperature structure, describable in terms of $P4_2/mbc$, can thus be regarded as doubly ordered relative to the $P4/mmm$ aristotype (cf. Figs. 4 and 5 of ref. 33, and Figs. 3 and 5 of ref. 3).

The presence of the ammonium ion does not appear to lead, apart from the orientational effects on the space-group symmetry, to specific types of AMF_4 structure: NH_4AlF_4(HT) (3, 33) and $TlAlF_4$(RT) (33) appear to be isostructural, and so do NH_4CrF_4(HT) (37) and $CsFeF_4$(LT) (38, 39). On the other hand, NH_4MnF_4 (2/2/1) is triclinic (40), and the symmetry of NH_4FeF_4 has been reported as $P2_12_12$ (ref. 41; cf. also refs. 42 and 43).

Structural filiation of AMF_4 fluorides

In spite of their simple stoichiometry and M coordination the $A[MF_2F_{4/2}]$ fluorides deriving from the tetragonal $TlAlF_4$ (1/1/1) aristotype exhibit a remarkable variety of structural detail. Of the many compounds reported in the literature those with known crystal structures are included in Fig. 7. The formal symmetry relationship between a higher- (H) and a lower-symmetry (L) space group SG(H)|SG(L) is presented in terms of a two-colour (Shubnikov) space group. While ultimately not different from considerations of "zellengleiche" and "klassengleiche" subgroups, this formulation has the advantage that the type of ordering of the [MF_6] orientations within and between MF_6 layers ‖(001) is immediately evident. When a dichromatic Bravais translation is present in the Shubnikov group (type IV, cf. ref. 44), the [MF_6] orientations in the L structure must be "antiferro" ordered with respect to the H structure, and the type of order follows from the chromatic operations of the group. The symmetry elements lost on going from H to L are the chromatic symmetry elements of the Shubnikov group, the essential of which are identified in the group symbol. Composite cations are affected in a similar manner, as are also [MF_6] distortions without "tilt", i.e. without rotational [MF_6] displacement.

The relevant Shubnikov groups Sh_p^q are the following:

---

[6] If the axial fluorines in NH_4AlF_4(HT) were shared by adjacent AlF_6 layers, the structure would be analogous to $KCuF_3$.

[7] The highest-symmetry phase does not appear to be accessible because of the thermal instability of NH_4AlF_4 (cf. ref. 30).

[8] In the following the unit-cell size will be indicated by $\sqrt{2}/\sqrt{2}/2$ etc.: a (or a_1) ~ $a_0\sqrt{2}$, b (or a_2) ~ $a_0\sqrt{2}$, c ~ $2c_0$.

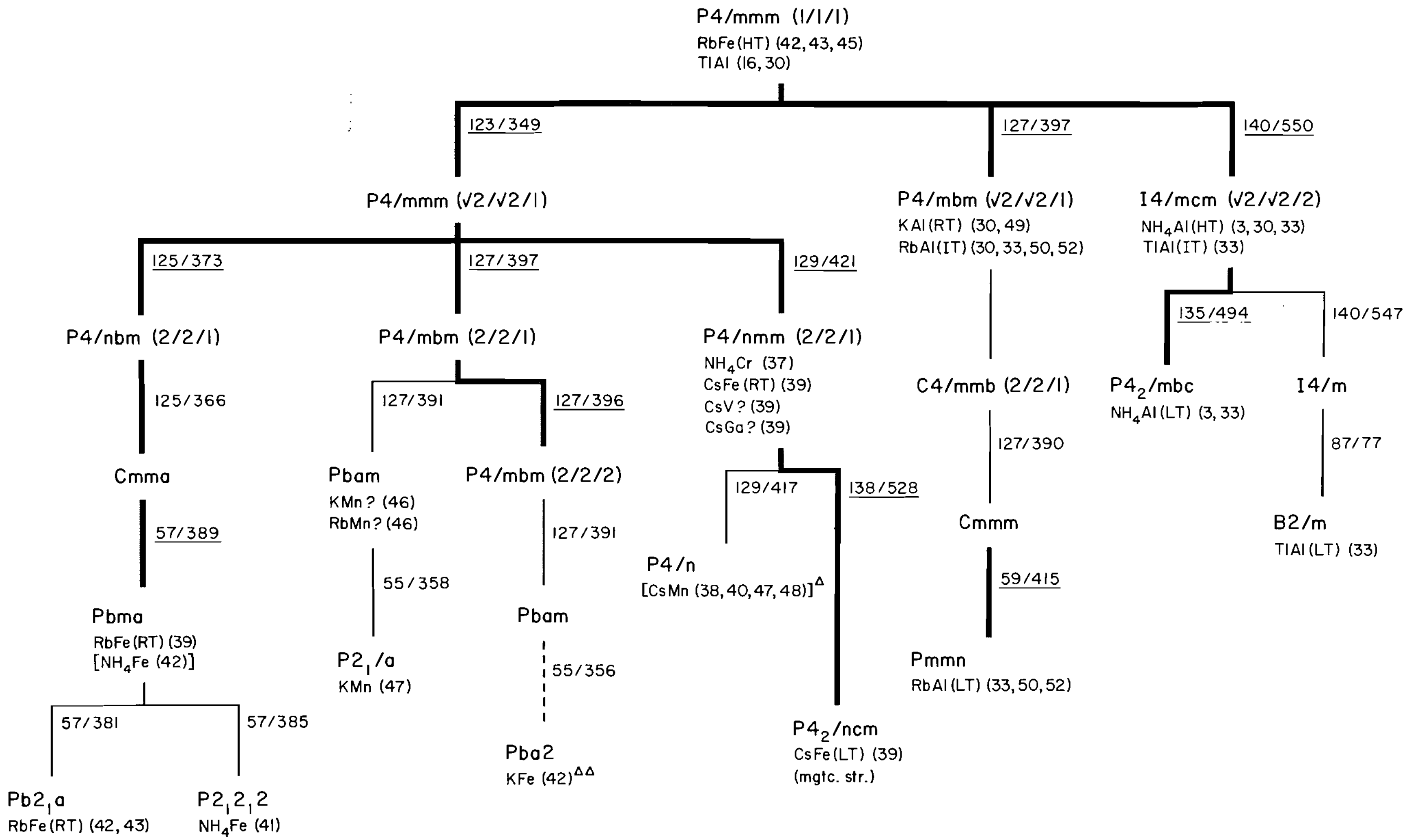

FIG. 7. Filiation of AMF_4 structures deriving from the $TlAlF_4$ aristotype. HT high, IT intermediate, LT low-temperature phase. 123/349 stands for Sh_{123}^{349} etc. (see text); heavy connecting lines and underlining refer to dichromatic Bravais translations. For the meaning of $\sqrt{2}/\sqrt{2}/2$ etc. (shown only when Z changes) see footnote[8]. —$^{\Delta}$ A Jahn–Teller structure; symmetry actually observed, *P*4/*nmm*. —$^{\Delta\Delta}$ According to ref. 51 the structure of $KFeF_4$ (and probably also KVF_4) can be described adequately in terms of a 2/1/2 pseudocell of symmetry *Amma*; the magnetic structure with a 2/2/4 cell (Fig. 5 of ref. 51) appears to be of Sh_{60}^{427} symmetry, P_bbcn-2$Pmca|Pbcn$.

	Dichromatic Bravais translation is present
p/q	
57/389	$P_C bma\text{-}Cmma|Pbma$
59/415	$P_C mmn\text{-}Cmmm|Pmmn$
123/349	$P_C 4/mmm\text{-}2P4/mmm|P4/mmm$
125/373	$P_C 4/nbm\text{-}2P4/mmm|P4/nbm$
127/396	$P_c 4/mbm\text{-}2P4/mbm|P4/mbm$
127/397	$P_C 4/mbm\text{-}2P4/mmm|P4/mbm$
129/421	$P_C 4/nmm\text{-}2P4/mmm|P4/nmm$
135/494	$P_I 4_2/mbc\text{-}I4/mcm|P4_2/mbc$
138/528	$P_c 4_2/ncm\text{-}2P4/nmm|P4_2/ncm$
140/550	$I_c 4/mcm\text{-}4P4/mmm|I4/mcm$
	absent
p/q	
55/356	$Pbam'\text{-}Pbam|Pba2$
55/358	$Pb'am'\text{-}Pbam|P2_1/a$
57/381	$Pbm'a\text{-}Pbma|Pb2_1a$
57/385	$Pb'm'a'\text{-}Pbma|P2_12_12$
87/77	$I4'/m\text{-}I4/m|B2/m$
125/366	$P4'/nb'm\text{-}P4/nbm|Cmma$
127/390	$C4'/mmb'\text{-}C4/mmb|Cmmm$
127/391	$P4'/mbm'\text{-}P4/mbm|Pbam$
129/417	$P4/nm'm'\text{-}P4/nmm|P4/n$
140/547	$I4/mc'm'\text{-}I4/mcm|I4/m$

For the sake of brevity, in Fig. 7 the groups are denoted by p/q, with those involving a dichromatic Bravais translation underlined.

Some doubt seems to exist about the symmetry of the room-temperature form of $RbFeF_4$. In ref. 45 it (and $RbVF_4$) is reported to be tetragonal, 2/2/1. Tressaud *et al.* (42, 43) concluded that the space group was *Pbma* or $Pb2_1a \subset Pbma$ and opted for the latter, while Babel *et al.* (39), on re-refining the structure from the data of ref. 43, favoured the centrosymmetric group. Of the $TlMF_4$ fluorides investigated by powder diffraction, those with M = V, Fe, Ga (39), and Mn (46) are reported to be orthorhombic, $\sqrt{2}/\sqrt{2}/2$, and that with M = Cr (39) tetragonal, 2/2/2. No definite conclusion has yet been arrived at for $CsCrF_4$ (39).

It is possible that examples of actual structures will be found for the intermediate formal symmetries in Fig. 7; additional theoretical possibilities exist for generating derivative structures from the *P4/mmm* aristotype.

$(NH_4)_3ZnCl_5$

The structure determination by Klug and Alexander (13) shows that this compound should be formulated $(NH_4)_3(ZnCl_4)Cl$. The orthorhombic *Pnma* unit cell contains four $NH_4^+(1)$ ions at sites of symmetry C_s and eight $NH_4^+(2)$ ions at sites of symmetry C_1. The coordination figures of the ammonium ion are irregular and their description depends to some extent on what N···Cl distance is assumed to represent the limit of hydrogen-bonding interaction between the two atoms.

The Cl environments of $NH_4^+(1)$ and $NH_4^+(2)$ are shown in Fig. 8. The eight N(1)···Cl distances range from 3.14 to 3.69 Å (Table 4). If we assume (somewhat arbitrarily) N···Cl = 3.4 Å as the limit of effective N—H···Cl bonding, the Cl atoms within this bound form a distorted octahedron round N(1). Although the H positions are not known, it is highly probable that one of the hydrogens forms a normal N—H···Cl^- bond to the Cl^- ion involved in the shortest N···Cl distance, 3.14 Å, in which case at least one of the three other bonds would be bifurcated or trifurcated.

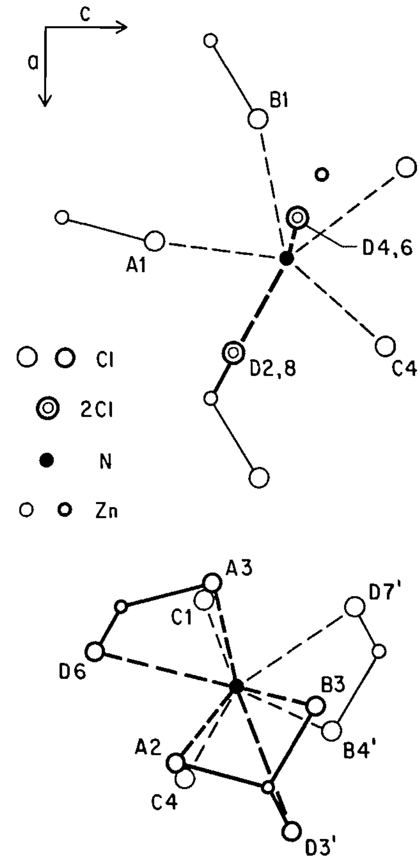

FIG. 8. $(NH_4)_3(ZnCl_4)Cl$: environments of the N(1) (*top*) and N(2) (*bottom*) atoms (after ref. 13). The chloride atoms are C1 and C4, the other Cl atoms belong to $ZnCl_4^{2-}$ ions. The N(1) atom is in the plane of reflection at $y = \frac{1}{4}$ and the N(2) is at $y = \frac{1}{2}$. For N···Cl distances see Table 4.

TABLE 4. N···Cl distances (Å) in $(NH_4)_3(ZnCl_4)Cl$*

Cl	N(1)···Cl	Cl	N(2)···Cl
C(4)	3.14†	B(3)	3.24
D(4), D(6)	3.20	A(2)	3.33
		C(1)	3.35†
D(2), D(8)	3.28	D(6)	3.40
A(1)	3.30	C(4)	3.48†
B(1)	3.49	A(3)	3.56
C(1)	3.69†	B(4')	3.66
		D(7')	3.68
		D(3')	3.82

*Calculated from the data of ref. 13. See Fig. 8 for identification of Cl atoms. The designating letters follow Table 1 of ref. 13.
†N···Cl^- distance.

The nine Cl neighbours of $NH_4^+(2)$ correspond to N···Cl distances from 3.24 to 3.82 Å (Table 4). Klug and Alexander describe the coordination figure as an augmented trigonal prism, but in view of the limited accuracy of the determination and of the uncertainty of the N···Cl cut-off it is impossible at

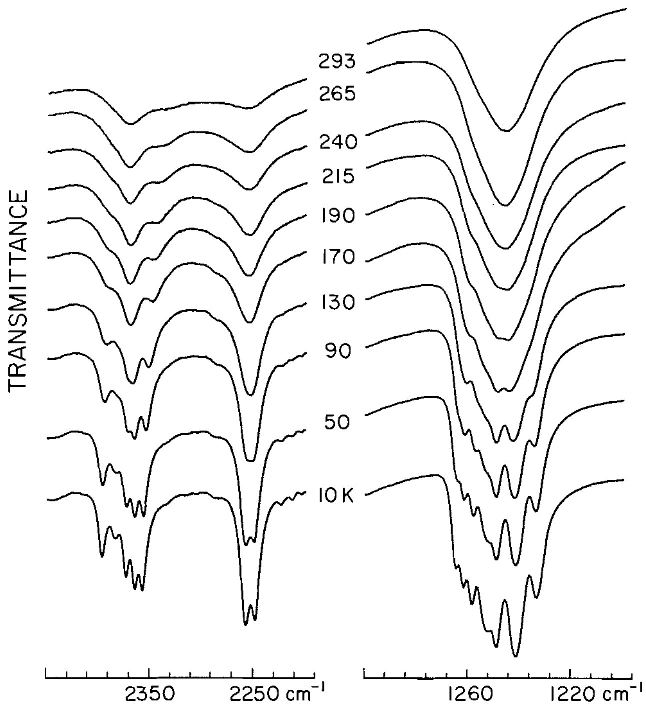

FIG. 9. $(NH_4)_3(ZnCl_4)Cl$: the ND stretching and bending regions of the NH_3D^+ probe-ion spectrum at different temperatures (~5% D).

present to say what the N(2) coordination figure relevant to hydrogen bonding really is.

The spectroscopic expectation from this structure ideally would be a 1:1:2 ν_1 triplet and a 1:1:1:1:2:2 ν_{4bc} sextet for $NH_4^+(1)$, and an equiponderant ν_1 quartet and an equiponderant ν_{4bc} octet for $NH_4^+(2)$. Allowing for the 2:1 abundance ratio of the two ions the expected overall spectrum would be a 1:1:2:2:2:2:2 ν_1 septet and a 14-line ν_{4bc} absorption consisting of four components of single and ten components of double weight. Furthermore, if the assumption of a normal N(1)—H···Cl⁻ bond corresponding to N···Cl = 3.14 Å is correct, at least one of the single-weight ν_1 components would have a significantly lower frequency than the rest.

The ν_1 spectrum at 10 K consisted of seven components arranged in two groups, a quintet at 2397.1, 2384.2, 2373.7, 2365.1, and 2357.7 cm^{-1}, and an approximately 1:1 doublet, of higher intensity, at the much lower frequencies of 2258 and 2249 cm^{-1} (Fig. 9). The component halfwidths were about 8 cm^{-1}. The ν_{4bc} absorption at 10 K consisted of seven *resolved* components covering the range from 1264.9 to 1233.7 cm^{-1}, with halfwidths of 4–6 cm^{-1}.

Increasing temperature produced a gradual coalescence of the ν_1 components, maintaining, however, the separation of the two groups (Fig. 9). At room temperature only three broad bands remained, at 2370, 2332, and 2260 cm^{-1}. The ν_{4bc} components gradually coalesced into a single broad band at room temperature.

There was no evidence in either ND absorption of abrupt changes pointing to the existence of a transition between 10 and 293 K. The 10 K spectrum can therefore be regarded as a resolved version of the room-temperature spectrum and interpreted from the room temperature crystal structure. The seven ν_1 components correspond to the expectation in number though not in relative intensity. However, the higher intensity of the lower-frequency bands (corresponding to stronger hydrogen bonding) is not surprising (cf. ref. 53). The appearance of *two* rather than one lower-frequency components points to a second N—H···Cl⁻ bond, almost certainly involving N(2). A more detailed interpretation of the NH_3D^+ probe-ion spectrum in this compound cannot be offered at present.

The relative strength of the N—H···Cl bonding in $(NH_4)_3(ZnCl_4)Cl$ can be estimated from the ν_{4bc} vs. ν_1 plot of Fig. 3 of ref. 2 (or from its updated version, to be published). Combining the highest ν_1 component frequency with the lowest ν_{4bc} component frequency yields a point falling in the region of the plot typical of trifurcated N—H···3Cl bonds, e.g. in $(NH_4)_2PdCl_6$ and $(NH_4)_2PtCl_6$. The point corresponding to the combination of the lowest ν_1 and highest ν_{4bc} component frequency falls in an unpopulated region which may be characterized as representing strong normal N—H···Cl⁻ bonds, stronger than those in NH_4Cl. The two ν_1 absorptions with the lowest frequencies, 2258 and 2249 cm^{-1}, are in fact among the lowest-lying ND stretching absorptions encountered with N—H···Cl bonds, comparable to similar absorptions in alkylammonium halides, e.g. in Et_3NHCl and $(n\text{-}Pr_2NH_2)_3(SnCl_6)Cl$ (54, 55), but unlike the latter they are unencumbered by the extensive Fermi resonance. The probable reason for the much stronger N—H···Cl bonding in these crystals is the possibility of formation of privileged normal N—H···Cl⁻ bonds to the chloride ions, which exists where the Cl coordination figure of the cation consists of isolated Cl⁻ ions *and* the weaker Cl acceptors of MCl_n^{m-} anions, but not with homogeneous, more symmetric NH_4^+ or $R_nNH_{4-n}^+$ chlorine environments, such as those in NH_4Cl of $(NH_4)_2MCl_6$.

NOTES ADDED IN PROOF. The existence of a transition in NH_4AlF_4 has been confirmed in a recent ^1H and ^{19}F nmr investigation (56); the transition is described as continuous in nature, with T_{tr} = 147 K. The results of further esr studies of NH_4AlF_4: Fe^{3+}, undertaken to elucidate the nature of the ordering process in NH_4AlF_4, have also been reported (57–59), and a rigid-ion model has been proposed (and tested on $RbAlF_4$) to describe the lattice dynamics of $AAlF_4$ (60). The redetermination of the crystal structure of $(NH_4)_3ZnCl_5$ (61) has confirmed the essential correctness of Klug and Alexander's structure, but it has not provided a direct clarification of the hydrogen-bonding scheme. An abstract of ref. 62 has only just come to our attention. The crystal data given there (original paper not seen at proof time) would suggest that $(NH_4)_2[GaF_5(H_2O)]$ is isostructural with $(NH_4)_2[AlF_5(H_2O)]$.

Acknowledgments

We are indebted to Dr. J. S. Grossert for the mass spectra of $(NH_4)_2AlF_5 \cdot H_2O$. Research grants from the Natural Sciences and Engineering Research Council of Canada to O.K. and T.S.C. are acknowledged.

1. G. KERESZTURY, O. KNOP, and M. FALK. Can. J. Chem. **60**, 1972 (1982).
2. O. KNOP, I. A. OXTON, and M. FALK. Can. J. Chem. **57**, 404 (1979); **57**, 2003 (1979).
3. A. BULOU, A. LEBLÉ, A. W. HEWAT, and J.-L. FOURQUET. Mater. Res. Bull. **17**, 391 (1982).
4. N. V. BELOV, N. I. GOLOVASTIKOV, A. N. IVASHCHENKO, B. YA. KOTYUZHANSKII, O. K. MEL'NIKOV, and V. I. FILIPPOV. Kristallogr. **27**, 511 (1982); Sov. Phys.- Crystallogr. **27**, 309 (1982).
5. L. PASSERINI and R. PIRANI. Gazz. Chim. Ital. **62**, 279 (1932).
6. L. PASSERINI and R. PIRANI. Gazz. Chim. Ital. **62**, 289 (1932).
7. A. J. EDWARDS. J. Chem. Soc. A, 2653 (1971).

8. C. BROSSET. Z. Anorg. Allg. Chem. **239**, 301 (1938).
9. C. BROSSET. Doctoral dissertation. University of Stockholm. 1942.
10. J.-L. FOURQUET, F. PLET, and R. DE PAPE. Rev. Chim. Miner. **18**, 19 (1981).
11. P. BUKOVEC and V. KAUČIČ. Acta Crystallogr. B, **34**, 3339 (1978).
12. V. KAUČIČ and P. BUKOVEC. Acta Crystallogr. B, **34**, 3337 (1978).
13. H. P. KLUG and L. ALEXANDER. J. Amer. Chem. Soc. **66**, 1056 (1944).
14. A. V. NOVOSELOVA. Zh. Obshch. Khim. **10**, 1547 (1940).
15. E. THILO. Naturwiss. **26**, 529 (1938).
16. C. BROSSET. Z. Anorg. Allg. Chem. **235**, 139 (1937).
17. M. C. MORRIS, H. F. MCMURDIE, E. H. EVANS, B. PARETZKIN, J. H. DE GROOT, B. S. WEEKS, and R. J. NEWBERRY. NBS Monogr. 25, **15**, 12 (1978).
18. I. MIKHAIL. Acta Crystallogr. B, **36**, 2126 (1980).
19. H. MATSUNAGA, K. ITOH, and E. NAKAMURA. Acta Crystallogr. B, **38**, 898 (1982).
20. R. A. NYQUIST and R. O. KAGEL. Infrared spectra of inorganic compounds. Academic Press, New York and London. 1971.
21. T. S. CAMERON and R. E. CORDES. Acta Crystallogr. B, **35**, 748 (1979).
22. International tables for X-ray crystallography. Vol. IV. The Kynoch Press, Birmingham, England. 1974.
23. G. M. SHELDRICK. SHELX system report. University Chemical Laboratories, Lensfield Road, Cambridge, England. 1976.
24. B. V. BUKVETSKY, L. A. MURADYAN, R. L. DAVIDOVICH, and V. I. SIMONOV. Sov. J. Coord. Chem. **2**, 869 (1976).
25. B. V. BUKVETSKY, S. A. POLISHCHUK, and V. I. SIMONOV. Kristallogr. **18**, 956 (1973).
26. V. I. SIMONOV and B. V. BUKVETSKY. Acta Crystallogr. B, **34**, 355 (1978).
27. M. FALK, C.-H. HUANG, and O. KNOP. Can. J. Chem. **53**, 51 (1975).
28. M. FALK and O. KNOP. Water: a comprehensive treatise. Vol. 2. *Edited by* F. Franks. Plenum Press, New York. 1973. Chapt. 2.
29. W. MASSA. Z. Anorg. Allg. Chem. **436**, 29 (1977).
30. J.-L. FOURQUET, F. PLET, G. COURBION, A. BULOU, and R. DE PAPE. Rev. Chim. Miner. **16**, 490 (1979).
31. A. LEBLÉ, J. J. ROUSSEAU, J. C. FAYET, J. PANNETIER, J.-L. FOURQUET, and R. DE PAPE. Phys. Status Sol. (a) **69**, 249 (1982).
32. A. LEBLÉ, J. J. ROUSSEAU, J. C. FAYET, J.-L. FOURQUET, and R. DE PAPE. Ferroelectrics, **36**, 323 (1981).
33. A. BULOU, J.-L. FOURQUET, A. LEBLÉ, J. NOUET, R. DE PAPE, and F. PLET. Studies in Inorg. Chem. **3**, 679 (1982). (Proc. 2nd Eur. Conf. Solid State Chem., Veldhoven, 7–9 June 1982. *Edited by* R. Metselaar, H. J. M. Heiligers, and J. Schoonman.) Elsevier, Amsterdam. 1983.
34. O. KNOP, I. A. OXTON, W. J. WESTERHAUS, and M. FALK. J. Chem. Soc. Faraday 2, **77**, 309 (1981).
35. O. KNOP, W. J. WESTERHAUS, and M. FALK. Can. J. Chem. **58**, 867 (1980).
36. M. COUZI, P. L. LOYZANCE, R. MOKHLISSE, A. BULOU, and J.-L. FOURQUET. Ber. Bunsenges. Phys. Chem. **87**, 232 (1983).
37. G. KNOKE, D. BABEL, and T. HINRICHSEN. Z. Naturforsch. **34**b, 934 (1979).
38. W. MASSA and M. STEINER. J. Solid State Chem. **32**, 137 (1980).
39. D. BABEL, F. WALL, and G. HEGER. Z. Naturforsch. **29**b, 139 (1974).
40. W. MASSA. Inorg. Nucl. Chem. Lett. **13**, 253 (1977).
41. G. FEREY, M. LEBLANC, R. DE PAPE, M. PASSARET, and M. BOTHOREL-RAZAZI. J. Cryst. Growth, **29**, 209 (1975).
42. A. TRESSAUD, J. PORTIER, R. DE PAPE, and P. HAGENMULLER. J. Solid State Chem. **2**, 269 (1970).
43. A. TRESSAUD, J. GALY, and J. PORTIER. Bull. Soc. Fr. Miner. Crist. **92**, 335 (1969).
44. C. J. BRADLEY and A. P. CRACKNELL. The mathematical theory of symmetry in solids. Clarendon Press, Oxford. 1972.
45. D. BABEL. Z. Naturforsch. **23**a, 1417 (1968).
46. P. KÖHLER, W. MASSA, D. REINEN, B. HOFMANN, and R. HOPPE. Z. Anorg. Allg. Chem. **446**, 131 (1978).
47. W. MASSA. Habilitationsschrift. Philipps-Universität Marburg. 1982.
48. E. DUBLER, L. LINOWSKY, J.-P. MATHIEU, and H. R. OSWALD. Helv. Chim. Acta, **60**, 1589 (1977).
49. J. NOUET, J. PANNETIER, and J.-L. FOURQUET. Acta Crystallogr. B, **37**, 32 (1981).
50. A. BULOU and J. NOUET. J. Phys. C: Solid State Phys. **15**, 183 (1982).
51. G. HEGER, R. GELLER, and D. BABEL. Solid State Commun. **9**, 335 (1971).
52. A. BULOU, M. ROUSSEAU, J. NOUET, P. L. LOYZANCE, R. MOKHLISSE, and M. COUZI. J. Phys. C: Solid State Phys. **16**, 4527 (1983).
53. M. FALK and M. J. WÓJCIK. Spectrochim. Acta, **35**A, 1117 (1979).
54. O. KNOP, T. S. CAMERON, M. A. JAMES, and M. FALK. Can. J. Chem. **61**, 1620 (1983).
55. T. S. CAMERON, M. A. JAMES, O. KNOP, and M. FALK. Can. J. Chem. **61**, 2192 (1983).
56. M. MACKOWIAK and R. J. C. BROWN. Mat. Res. Bull. **19**, 249 (1984).
57. A. LEBLÉ, Y. DAGORN, J. J. ROUSSEAU, and J. C. FAYET. Proc. XXIIth Ampère Congress, Zürich. 1984. p. 36.
58. Y. DAGORN, A. LEBLÉ, J. J. ROUSSEAU, and J. C. FAYET. Proc. XXIIth Ampère Congress, Zürich. 1984. p. 38.
59. Y. DAGORN, A. LEBLÉ, J. J. ROUSSEAU, J. C. FAYET, and J.-L. FOURQUET. Ferroelectrics, **54**, 609 (1984).
60. A. BULOU, J. M. LAUNAY, M. ROUSSEAU, C. RIDOU, and J. NOUET. Ferroelectrics, **54**, 249 (1984).
61. D. SCHMITZ. Acta Crystallogr. B, **37**, 518 (1981).
62. E. A. SOLDATOV, E. A. KUZ'MIN, V. V. ILYUKHIN, and N. V. BELOV. Dokl. AN SSSR, **254**, 363 (1980); Chem. Abstr. **93**, 248581*z* (1980).

Homoenolization of 1,3,3-trimethylbicyclo[2.2.1]heptan-2-one in perdeuterated *tert*-butyl alcohol. Evidence that the medium potassium *tert*-butoxide – *tert*-butyl alcohol is unstable at elevated temperatures

NICK HENRY WERSTIUK AND GEORGE TIMMINS

Department of Chemistry, McMaster University, Hamilton, Ont., Canada, L8S 4M1

Received May 9, 1984

NICK HENRY WERSTIUK and GEORGE TIMMINS. Can. J. Chem. **63**, 526 (1985).

Homoenolization of 1,3,3-trimethylbicyclo[2.2.1]heptan-2-one (**1**) (fenchone) in potassium *tert*-butoxide – *tert*-butyl alcohol-O-*d* and perdeuterated potassium *tert*-butoxide – *tert*-butyl alcohol at 220°C established that there is significant deterioration of the medium and dilution of the deuterium pool. We show that the major pathway of deterioration of the medium and dilution of the pool involves formation of isobutene by elimination of water from the alcohol. Exchange data already accumulated in the literature are used to support our view that the elimination also occurs at 185°C, the temperature commonly used to homoenolize ketones.

NICK HENRY WERSTIUK et GEORGE TIMMINS. Can. J. Chem. **63**, 526 (1985).

L'homoénolisation, à 220°C, de la triméthyl-1,2,3 bicyclo[2.2.1]heptanone-2 (**1**) (fenchone) en présence de *tert*-butylate de potassium/*tert*-butanol O-*d* ou de *tert*-butylate de potassium/*tert*-butanol perdeutéré montre qu'il se produit une détérioration importante du milieu et une dilution de la quantité de deutérium. Nous démontrons que la voie principale de la détérioration du milieu et de la dilution de la quantité de deutérium implique une élimination d'eau de l'alcool conduisant à de l'isobutène. On a utilisé les données d'échange déjà accumulées dans la littérature pour appuyer notre conclusion selon laquelle l'élimination se produit également à 185°C, la température couramment utilisés pour provoquer l'homoénolisation des cétones.

[Traduit par le journal]

Introduction

Potassium *tert*-butoxide in *tert*-butyl alcohol-O-*d* has been used routinely to study hydrogen isotope exchange of carbon acids at elevated temperatures (1, 2). In fact, it has been the medium of choice for homoenolizing ketones (3–5). Although it was suggested by Cram *et al.* that alkoxide bases react with glass (6) during exchange reactions at elevated temperatures, and recycling has been used by Nickon, Stothers, and co-workers in homoenolization studies (7, 8) to increase deuterium incorporation, no definitive information was available as regards the stability of *t*-BuOK – *t*-BuOH(D) solutions. In this paper we show, through homoenolization of 1,3,3-trimethylbicyclo[2.2.1]heptan-2-one (fenchone) (**1**) at 220°C, that the solution definitely is unstable at elevated temperatures, determine the major pathway of its deterioration, and establish that perdeuterated *tert*-butyl alcohol should be used as a solvent to improve the stability of the medium and maximize deuterium incorporation.

Results

Homoenolizations of fenchone (**1**) were carried out in Pyrex tubes at 220 ± 3°C for 300–330 h. To equalize pressure and reduce the possibility of tube rupture, the tubes were placed in a 600-mL Parr reaction vessel that contained water. Base solutions were freshly prepared by dissolving clean potassium in the appropriate alcohol in a glove bag pressurized with dry nitrogen. Recoveries of deuterated **1** ranged between 70 and 80% and the other minor products reported by Stothers and co-workers (8) also were observed. Total deuterium content was determined mass spectrometrically at low ionizing voltage and the distribution was established by computerized curve fitting of 38.4-MHz ^{2}H nmr spectra to Lorentzian curves. Figure 1(A) shows the 250-MHz ^{1}H nmr spectrum of **1** and the assignments that were established by double irradiation experiments at 400 MHz, consideration of the ^{1}H nmr spectrum (Fig. 1(B)) of deuterated **1**-$d_{3.75}$ (Table 1, entry 3), comparison with the ^{1}H nmr spectrum of 3,3,6,6-tetramethylbicyclo-[2.2.1]heptan-2-one (9), and the shift of the ^{2}H signals of **1**-$d_{3.52}$ in the presence of 0.25 equivalents of Eu(fod)$_3$. The signal at 1.75 ppm assigned to *syn*-7-D was shifted downfield, essentially to the same extent (0.34 ppm) as the *exo*-methyl at C-3 (0.33 ppm) and the bridgehead methyl (0.43 ppm). If the signal at 1.75 ppm was due to deuterium located at the *anti*-7 position, the shift would not be as large as the methyl shifts.

The results of homoenolizations of **1** at 220 ± 3°C in $C(CH_3)_3OD$ and $C(CD_3)_3OD$ are given in Table 1. As is indicated in entries 1 and 2, heating **1** for 304 h at 220 ± 3°C leads to the incorporation of 1.5–1.6 deuterium atoms. Figure 1(C) shows the 38.4-MHz ^{2}H nmr spectrum of deuterated **1**-$d_{1.52}$ along with the deuterium distribution. While there is an increase in incorporation to 2.51 deuterons per molecule after recycling once (entry 2), there is no significant increase in the amount of deuterium located *exo* and *endo* at C-6. Clearly, in both cases the *exo* and *endo* positions are equilibrated with a deuterium pool that has been diluted by 150%. That this is the case is seen from the data listed in entries 3 and 4. When **1** is exchanged in $C(CD_3)_3OD$, twice as much deuterium is incorporated and the equilibrated *exo* and *endo* positions at C-6 each contain nearly one atom of deuterium. The difference between the homoenolizations described in entries 3 and 4 results from temperature variations and the fact that it is difficult to reproduce homoenolization solutions exactly. Figure 1(D) shows the ^{2}H nmr spectrum of **1**-$d_{3.75}$ (entry 3). The results of this study are also in keeping with our recent findings that *syn*-7 exchange is preferred over *anti*-7 exchange (9). Significant incorporation occurs at the *syn*-7 position. Since the *exo*-6 and *endo*-6 resonances are equal in area within experimental error and the anti-7 resonance overlaps with the *exo*-6 resonance, it is clear that *anti* exchange must be substantially slower than *syn* exchange.

When 0.3 *M* *t*-BuOK – *t*-BuOH was heated for 300 h at 220 ± 3°C in the absence of ketone and an ^{1}H nmr spectrum of the solution was obtained, resonances at 1.65 (t) and 4.63 (m) ppm in addition to the resonances due to $C(CH_3)_3OH$ were observed. The relative areas, chemical shifts, and couplings correspond to those reported for isobutene (10), thereby establishing that

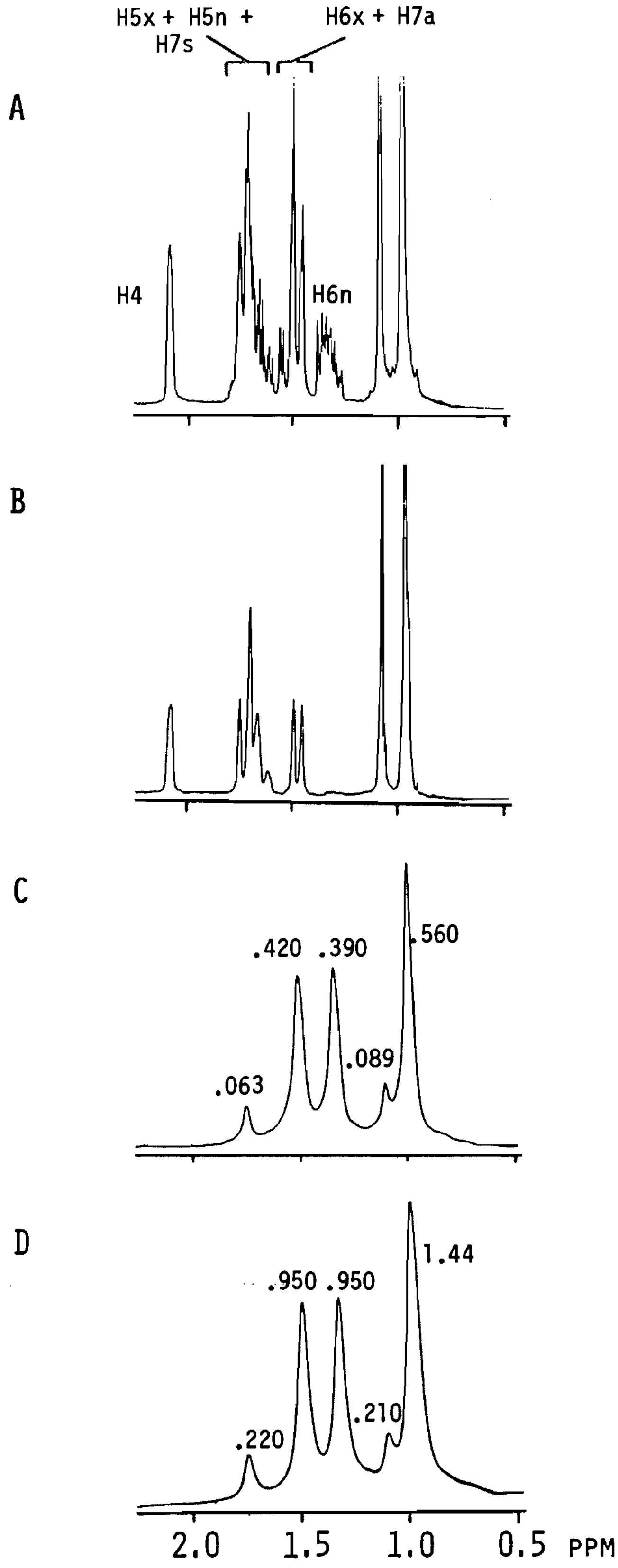

FIG. 1. (A) High-field (250-MHz) ^{1}H nmr spectrum of fenchone (**1**) in $CDCl_3$. (B) High-field (250-MHz) ^{1}H nmr spectrum of deuterated fenchone (**1**-$d_{3.75}$) in $CDCl_3$. (C) High-field (38.4-MHz) ^{2}H nmr spectrum of deuterated fenchone (**1**-$d_{1.52}$) in $CHCl_3$. (D) High-field (38.4-MHz) ^{2}H nmr spectrum of deuterated fenchone (**1**-$d_{3.75}$) in $CHCl_3$.

H_2O is eliminated from *t*-BuOH at elevated temperatures. Integration established that 5−7% of the mixture consisted of isobutene. To work up the reactions the tubes were cooled in liquid N_2, opened, and allowed to warm to ambient temperature. When the solid reaction mixture, with or without ketone, began to melt, bubbling occurred and an hydrocarbon odor was detected. Since isobutene boils at −6.6°C, a substantial amount is lost during work-up and nmr analysis.

When 0.3 *M* *t*-BuOK − *t*-BuOD was heated for 300 h at 220 ± 3°C and an ^{2}H nmr spectrum was obtained of the solution, in addition to a resonance at 4.32 ppm that corresponded to the deuteroxyl group, signals at 1.65 and 4.63 ppm with relative intensities of 3:1 indicated that the hydrogens of isobutene were equilibrated with the deuterium pool. An additional resonance at 1.21 indicated that deuterium was located in the methyls of *t*-BuOD as well. The relative areas of O—D and methyl resonances established that there was approximately 3.5% exchange of the methyl groups. Whether the exchange occurs by deprotonation−deuteronation or by nucleophilic addition of $^-$OD to isobutene presently is unknown.

Gas chromatographic (gc) analysis of the concentrated pentane extracts obtained from the homoenolization of **1** showed that three minor components (~5%) of shorter retention time than **1** were present in a ratio of 6:1:5. The same compounds were formed when *t*-BuOK was heated in *t*-BuOH and *t*-BuOD in the absence of ketone. The gc−ms analysis of the mixture obtained from heating *t*-BuOK − *t*-BuOH established molecular ions at *m/z* 136 ($C_{10}H_{16}$) for the major components. Analysis of the mixture obtained from an homoenolization in *t*-BuOD (entry 1) established that the components were highly deuterated. Comparison of the ms fragmentation patterns with standard spectra of a number of unsaturated hydrocarbons of molecular formula $C_{10}H_{16}$ revealed common features. It is conceivable that the C_{10} hydrocarbons are derived from the dehydration of an alcohol formed by the addition of methide to an enone derived from the trimerization of acetone, methide and acetone being derived from *t*-BuO$^-$. However, due to the small amount of the products, further studies were not undertaken.

To establish whether dehydration of *t*-BuOH occurs in the absence of base, *t*-BuOH was heated for 240 h at 220°C. The ^{1}H nmr spectrum showed resonances at 1.61 and 4.63 ppm characteristic of isobutene. Integration establshed that ~5% of the mixture consisted of isobutene.

Discussion and conclusions

This work clearly establishes the instability of *t*-BuOK − *t*-BuOH(D) solutions at elevated temperatures and the major source of deterioration of the medium. Based on the degree of dilution of the deuterium pool observed in the exchange reactions in $C(CH_3)_3OD$ (entries 1 and 2), if dilution occurs primarily by exchange of isobutene, then a maximum of 16% elimination occurs after 300 h at 220 ± 3°C. But the small amount of elimination has an enormous impact on the medium; the deuterium pool is diluted by 150%, the base concentration is reduced, and the water produced by elimination most likely significantly reduces the basicity of the medium (11, 12). While Herndon and Reid (13) established that *t*-BuOH dehydrates at 300°C,[1] this study establishes that elimination occurs slowly at temperatures around 200°C.

A number of studies have been reported in which *t*-BuOK −

[1]We thank a referee for bringing this work to our attention.

TABLE 1. H−D exchange of fenchone at 220 ± 3°C

Entry	[Ketone] (wt, g)	[t-BuOK] (vol, mL)[a]	Solvent	Time (h)	Excess D per molecule[b]	Distribution of deuterium[c] C-6x	C-6n	C-7s	Bridge-head methyl	Other methyls
1	0.33(0.250)	1.3(5)	$(CH_3)_3COD$	304	1.52	0.420	0.390	0.063	0.089	0.560
2	0.33(0.256)	1.2(5)	$(CH_3)_3COD$	304	1.62	[e]	—	—	—	—
	0.32(0.137)[d]	1.3(2.8)	$(CH_3)_3COD$	330	2.51	0.390	0.390	0.120	0.240	1.370
3	0.29(0.176)	1.3(4)	$(CD_3)_3COD$	304	3.75	0.950	0.950	0.220	0.210	1.410
4	0.32(0.250)	1.2(5)	$(CD_3)_3COD$	300	3.52	0.930	0.930	0.130	0.130	1.390

[a]The base solutions were prepared in a glove bag under N_2.
[b]Determined mass spectrometrically at low voltage. Recoveries of the ketone usually were 70−80%.
[c]Determined by ^2H nmr at 38.4 MHz. Incorporations were determined by computerized curve-fitting of the spectra to Lorentzian line shapes. Multiple fittings established that the average errors for fitting large peaks were <5% and for fitting small peaks 10−20%.
[d]The deuterated ketone was isolated and recycled.
[e]Not determined.

t-BuOH(D) was used at temperatures >200°C. Cram *et al.* (6) studied base-catalyzed exchange and racemization of 2-phenylbutane and 1-phenyl methoxyethane in t-BuOK − t-BuOH(D) and $KO(CH_2)_2O(CH_2)_2OH(D)/((D)HOCH_2CH_2)_2O$ at temperatures ranging from 215 to 260°C for periods up to 240 h. The authors reported that a tremendous pressure build-up occurred when potassium diethylene glycolate − diethylene glycol was heated at 260°C and stated that the base was completely destroyed by reaction with the glass. It is conceivable that elimination occurred to yield volatile divinyl ether and acetaldehyde. In the presence of base, divinyl ether could yield acetylene and acetaldehyde which could decarbonylate (13).

A number of homoenolizations have been carried out in t-BuOK − t-BuOH(D) at temperatures above 200°C where deterioration of the medium is expected to be significant. Nickon *et al.* (7) studied the homoenolization of camphenilone at 250°C and after two cycles at 216 and 215 h observed incorporation of 3.8 deuterium atoms, but the location of the deuterium was not established. Coates and Chen (14) have documented the partial homoenolate rearrangement of longicamphenilone after 14 h at 275°C. Hunter, Stothers, Nickon and co-workers (15) reported on the homoenolate rearrangement of fenchone and the *exo*- and *endo*-isocamphanones at 220−250°C. Nickon *et al.* (16) studied the rearrangement and exchange of camphor and the *exo*- and *endo*-isocamphanones at 220−250°C.

While it is evident that dehydration of t-BuOH is a major problem at temperatures above 200°C, it must also lead to deterioration of the medium even at 185°C, especially if long reaction periods (>100 h) are used − a common practice in homoenolization studies. Data (Table 2) for exchange of fenchone at C-6, accumulated by Stothers and co-workers (8), support our view.

It is clear from this study that $C(CD_3)_3OD$ should be used for hydrogen isotope exchange studies at elevated temperatures to maximize the deuterium incorporation and improve the stability of the medium, since we expect that primary and secondary KIEs should slow the rate of elimination. It may be useful to develop a medium − perhaps adamantanol-O-d and its alcoholate in DMSO-d_6 − where elimination of water is not possible (17).

Finally, we now wonder about the source of carboxylic acids − the products of Haller−Bauer cleavage − produced in quantity in some reactions. Although it has been postulated that nucleophilic attack by t-BuO$^-$ at the carbonyl group leads to ring opening which is followed by base-promoted elimination of the acid from the *tert*-butyl ester (18), it is conceivable that ring opening is initiated by attack of the smaller nucleophile hydroxide (deuteroxide).

TABLE 2. H−D exchange of fenchone at C-6 in t-BuOK − t-BuOD at 185°C[a]

Time (h)	Deuterium incorporation *exo*-6	*endo*-6
10	0.26	0.08
20	0.34	0.12
40	0.70	0.38
100	0.75	0.58
200	0.68	0.68
300	0.65	0.64

[a]Taken from ref. 8.

Experimental

General

The ^1H and ^2H nmr spectra were obtained on a Bruker WM-250 spectrometer. Resonances are reported as ppm downfield form TMS. Mass spectral deuterium analyses were carried out at low voltage (12−15 eV) on a Micromass VG 7070 mass spectrometer. A Tracor 560 gas chromatograph with 6 ft × 4 mm id 3% OV-1 on 100−120 mesh Chromosorb W was used for analysis of reaction mixtures, and preparative collection of fenchone was carried out with a 5 ft × 1/4 in. 15% SE-30 on 80−100 mesh Chromasorb W in a Varian A-700 gas chromatograph. Perdeuterated *tert*-butyl alcohol was obtained from Aldrich Chemical Co. and distilled from potassium prior to use in the experiments.

Homoenolization reactions

In a typical reaction, in a glove bag pressurized with dry nitrogen, clean potassium (0.207 g) was added to dry $(CD_3)_3COD$ (4 mL) and reaction carried out to completion by heating. To the base solution was added fenchone (0.176 g) and the tube was sealed under vacuum after three freeze/pump/thaw cycles for degassing. The reaction tube was heated at 220 ± 3°C for 304 h in a 600-mL Parr pressure apparatus that contained water to equalize pressure. The reaction mixtures were worked up by adding saturated aqueous NaCl (10 mL) and extracting with pentane (5 × 10 mL); extracts were washed with saturated aqueous NaCl (5 mL), dried over anhydrous Na_2SO_4, and filtered. Solvent was removed by distillation through a 12-cm glass helices column. Analytical gc showed that fenchone was 73.5% of the product mixture and collection by preparative gc gave 0.115 g (88.9%).

Medium-deterioration reactions

Reactions to study the deterioration of the basic medium were carried out as above with 0.3 *M* *t*-BuOK − *t*-BuOH(D) for 300 h at 220 ± 3°C. A small amount of the reaction mixture was added to benzene-d_6 (benzene) for ^{1}H (^{2}H) nmr studies. The ^{1}H nmr spectrum showed, in addition to the resonances for $(CH_3)_3COH(D)$, resonances at 1.65(t) and 4.63(m) ppm corresponding to chemical shift, coupling, and area with those reported for isobutene (10).

The ^{2}H nmr spectrum of deuterated reaction medium had resonances at 4.32 ppm (deuteroxyl group), 1.65 and 4.63 ppm (area ratio 3:1 − isobutene equilibrated with the deuterium pool), and an additional resonance at 1.21 ppm (deuterium in the methyl of *t*-BuOD). Comparison of the area of this resonance with that for O—D indicated ~3.5% exchange of the methyl groups in *t*-BuOD.

Acknowledgement

We thank the Natural Sciences and Engineering Research Council of Canada for financial support.

1. D. H. HUNTER. *In* Isotopes in organic chemistry., Vol. 1. *Edited by* E. Buncel and C. C. Lee. Elsevier, Amsterdam. 1975. pp. 141−204.
2. O. A. REUTOV, I. P. BELETSKAYA, and K. P. BUTIN. *In* CH-Acids. *Translation Editor* T. R. Crompton. Pergamon Press, Oxford. 1978. pp. 78−125.
3. E. BUNCEL. Reaction mechanisms in organic chemistry. Monograph 9. Elsevier, Amsterdam. 1975. pp. 116−121 and 161−167.
4. D. H. HUNTER, J. B. STOTHERS, and E. W. WARNHOFF. *In* Rearrangements in ground and excited states. Vol. 1. *Edited by* P. de Mayo. Academic Press, New York. 1980. pp. 393−461.
5. N. H. WERSTIUK. Tetrahedron, **39**, 205 (1983).
6. D. J. CRAM, C. A. KINGSBURY, and B. RICKBORN. J. Am. Chem. Soc. **83**, 3688 (1961).
7. A. NICKON, J. L. LAMBERT, and S. J. OLIVER. J. Am. Chem. Soc. **88**, 2787 (1966).
8. A. L. JOHNSON, J. B. STOTHERS, and C. T. TAN. Can. J. Chem. **53**, 212 (1975).
9. N. H. WERSTIUK, S. YEROUSHALMI, and G. TIMMINS. Can. J. Chem. **61**, 1945 (1983).
10. R. K. HARRISON and B. R. HOWES. J. Mol. Spectrosc. **28**, 191 (1968).
11. D. J. CRAM, B. RICKBORN, C. A. KINGSBURY, and P. HABERFIELD. J. Am. Chem. Soc. **83**, 3678 (1961).
12. J. B. STOTHERS and C. T. TAN. J. Chem. Soc. Chem. Commun. 738 (1974).
13. L. R. HERNDON and E. E. REID. J. Am. Chem. Soc. **50**, 3066 (1928).
14. R. M. COATES and J. P. CHEN. Chem. Commun. 1481 (1970).
15. D. H. HUNTER, A. L. JOHNSON, J. B. STOTHERS, A. NICKON, J. L. LAMBERT, and D. F. COVEY. J. Am. Chem. Soc. **94**, 8582 (1972).
16. A. NICKON, J. L. LAMBERT, J. E. OLIVER, D. F. COVEY, and J. MORGAN. J. Am. Chem. Soc. **98**, 2593 (1976).
17. G. A. CRAZE and I. WATT. J. Chem. Soc. Perkin Trans. 2, 175 (1981).
18. A. NICKON and J. L. LAMBERT, S. J. J. Am. Chem. Soc. **88**, 1905 (1966).

Protium–deuterium exchange of cyclic and acyclic alkenes in dilute acid medium at elevated temperatures

NICK HENRY WERSTIUK AND GEORGE TIMMINS
Department of Chemistry, McMaster University, Hamilton, Ont., Canada L8S 4M1

Received May 14, 1984

NICK HENRY WERSTIUK and GEORGE TIMMINS. Can. J. Chem. **63**, 530 (1985).

A modification of the high temperature – dilute acid (HTDA) method for deuterium labelling of aromatic compounds has been applied to the H–D exchange of a number of cyclic and acyclic alkenes. Cyclopentene, cyclohexene, cyclododecene, and tetramethylethylene have been completely exchanged in excellent yield. 1-Methylcyclopentene and 1-methylcyclohexene have also been perdeuterated and cycloheptene and cyclooctene partially labelled but require spinning band distillation or preparative glpc for separation from rearrangement products. A variety of C5–C8 acyclic alkenes have also been treated under HTDA conditions.

NICK HENRY WERSTIUK et GEORGE TIMMINS. Can. J. Chem. **63**, 530 (1985).

On a appliqué une modification de la méthode à haute température en milieu acide dilué, développée pour marquer des composés aromatiques avec du deutérium, à l'échange H–D d'un certain nombre d'alcènes cycliques et acycliques. Le cyclopentène, le cyclohexène, le cyclodécène et le tétraméthyléthylène s'échangent tous complètement avec d'excellents rendements. Le méthyl-1 cyclopentène et le méthyl-1 cyclohexène sont aussi perdeutérés alors que le cycloheptène et le cyclooctène ne sont que partiellement marqués; toutefois, dans ces cas, il faut faire appel soit à des distillations à l'aide de bande tournante soit à la cpg préparative pour séparer les produits désirés des produits de transposition. On a aussi traité de la même manière un certain nombre d'alcènes acycliques comptant de 5 à 8 C.

[Traduit par le journal]

Introduction

In an attempt to develop high temperature – dilute acid exchange (HTDA) (1–6) into a general technique for preparing deuterated (or tritiated) organic compounds we have extended our studies from aromatic compounds to alkenes.

Early attempts to label alkenes using heterogeneous platinum catalysis resulted in extensive (up to 100%) disproportionation with only low levels of deuterium incorporation (7). Also, radiation induced methods such as the Wilzbach technique for tritium labelling lead to addition products in preference to substitution (8). In attempting to avoid some of these problems, Calf *et al.* (9) carried out exchange reactions in dilute DCl/D_2O at temperatures of 110–130°C. They were successful in achieving incorporations of up to 35 at.% D.

In this paper we describe deuterium labelling of alkenes using a modification of the HTDA method (1–5). Exchange reactions were carried out with dilute DCl/D_2O in sealed Pyrex tubes at elevated temperatures (165–280°C) in the presence and absence of decalin as a cosolvent and with or without mixing by shaking. In general, reactions were run to near equilibration (92–95 at.% D) with the deuterium pool in one cycle. For example, cyclopentene was labelled with 7.38 D atoms of deuterium per molecule (92.2 at.%; entry 5, Table 1) in one cycle, whereas, Calf *et al.* (9) reported the incorporation of only 2.39 D atoms at 130°C.

Results and discussion

The results of application of the modified high temperature – dilute acid (HDTA) protium–deuterium exchange method to cyclopentene (**1**), cyclohexene (**2**), cycloheptene (**3**), cyclooctene (**4**), cyclododecene (**5**), cyclohexanol (**6**), *E*-2-pentene (**7**), 1-hexene (**8**), 1-heptene (**9**), 1-octene (**10**), 1-pentanol (**11**), 1-hexanol (**12**), 1-heptanol (**13**), 1-octanol (**14**), and tetramethylethylene (**15**) are given in Tables 1 and 2. Reactions in deuterated and nondeuterated medium were carried out concurrently in a Parr pressure vessel. Products were identified by isolating the components from the reactions in nondeuterated medium by preparative glpc or distillation, in some cases as mixtures, and using high field (250 and 400 MHz) ^1H nmr spectroscopy. Spectra were compared with spectra of standards or spectra obtained from the Sadtler NMR Index. In the case of the acyclic alkenes it was necessary to use a 10-m, SP1700 (Supelco) column formulated specifically for gc separation of low molecular weight alkenes. The relative yields of products were determined using gc and ^1H nmr data and the E/Z ratio of 2.8 for the 2-pentenes was used to confirm the assignment of the E/Z ratios for the hexenes, heptenes, and octenes. It was noted that more rearrangement occurred in DCl/D_2O than in HCl/H_2O.

That alcohols **6**, **11**, **12**, **13**, and **14** yield the same products as alkenes **2**, **7**, **8**, **9**, and **10**, respectively, indicates that any substrate which yields a carbocation under HTDA conditions and has β-hydrogens, in principle, can undergo exchange. In fact alcohols **6**, **11**, **12**, **13**, and **14** yielded greater than 95% of elimination products.[1]

Initial attempts to deuterate by simply heating the alkenes in the presence of dilute acid produced large amounts of higher molecular weight products (shown by mass spectrometry to be dimers and trimers) which were not further examined (for example see Table 1, entry 1). In an attempt to reduce the extent of addition, decalin was added in order to dilute the substrate and, as documented in Table 1, entries 1 and 2, this was successful; the proportion of higher molecular weight products was greatly reduced. In our initial study of cyclododecene using decalin as cosolvent we observed an unusual saddle-shaped pattern of deuterium incorporation which ranged from 17.5% d_0 and 7% d_1 species down to 0.9% d_{10} and then increased to 11.7% d_{21} and 6.5% of d_{22} species. This distribution was attributed to the fact that phase transfer rather than exchange was rate determining for large molecules. The reactions were repeated in an apparatus which agitated the reaction mixtures by a rocking motion. This modification allowed the use of lower reaction temperatures and (or) shorter reaction times

[1]Calf *et al.* (9) reported that up to 80°C, hydrogen halides add to alkenes, but at approximately 110°C elimination of HX occurs.

TABLE 1. Protium–deuterium exchange and rearrangement of cyclic alkenes

Entry	Substrate	Conditions[a]	Products[b] (relative % yield)	% Exchange (excess D atoms/ molecule)
1	**6**	225°C, 24 h[c]	**1***b* + **1***c* (5.0), **1***a* (8.6), **2** (18.4), other (68.0)[g]	
2	**6**	225°C, 24 h[d]	**1***b* + **1***c* (3.3), **1***a* (10.1), **2** (77.2), other (9.4)[g]	
3	**5**	280°C, 70 h[d]	**5** (62.7), other (37.3)	**5**, 58.3 (12.8)
4	**5**	240°C, 72 h[e]	**5** (92.3), other (7.7)	**5**, 92.5 (20.4)
5	**1**	200°C, 83 h[e]	**1** (99.1), other (0.9)[g]	**2**, 92.2 (7.38)
6	**2**	225°C, 49 h[e]	**1***b* + **1***c* (6.7), other (1.2),[f] **1***a* (45.4), **2** (36.1), other (10.6)[g]	**1***a*, 94.9 (9.49), **2**, 94.9 (9.49)
7	**3**	225°C, 49 h[e]	Other (4.3),[f] other (2.9),[f] **2***b* + **2***c* (17.2), **1***d* + **1***e* (16.1), **2***a* (54.9), other (4.6)[g]	**2***b* + **2***c*, 95.4 (11.4) **2***a*, 94.9 (11.4)
8	**4**	225°C, 49 h[e]	Other (5.6),[f] **1***f* + **1***g* + **1***h* (15.4), **2***f* + **2***g* (25.4), **2***d* + **2***e* (49.7), other (3.9)[g]	**1***f* + **1***g* + **1***h*, 94.6 (13.2), **2***f* + **2***g*, 93.2 (13.1), **2***d* + **2***e*, 93.6 (13.1)
9	**2**	175°C, 24 h[e]	**2** (95.4), **1***a* (1.6), other (2.8)[g]	**2**, 92.5 (9.3)
10	**3**	175°C, 24 h	Rearrangement products (31.8), **3** (60.6), other (7.6)[g]	**3**, 77.3 (9.27)
11	**4**	175°C, 24 h[e]	Rearrangement products (18), **4** (79), other (3)[g]	**4**, 54.1 (7.57)

[a]Reactions were carried out in 1% w/v DCl/D_2O or for product identification in 1% w/v HCl/H_2O. Temperature control was ±3°C. Equilibration corresponded to 94–95% deuterium incorporation.
[b]Values were obtained from gc analysis using electronic integration. The products are listed in order of increasing retention time.
[c]Without decalin and without mixing.
[d]With decalin, without mixing.
[e]With decalin, with mixing.
[f]Unidentified minor products.
[g]Unidentified higher molecular weight products; total.

and in general led to cleaner reactions and a normal deuterium distribution in cyclododecene (**5**) (Table 1, entries 3 and 4). While decalin is a good inert cosolvent for exchange of low molecular weight alkenes, it would be a simple matter to replace decalin with a lower boiling solvent if the substrate had a boiling point close to decalin.

Examination of Table 1 shows that all products were perdeuterated and usually equilibrated with the deuterium pool. The incorporation of 22 deuterium atoms into cyclododecene in a single reaction is remarkable. Calf *et al.* (9) observed no incorporation of deuterium into **5** at 130°C.

For the cycloalkenes (except cyclopentene and cyclododecene) the product mixtures consisted largely or solely of ring-contracted isomers of the parent substrate as shown in Table 1, entries 5–8. Involvement of corner-protonated cyclopropanes (Scheme 1) can lead to ring-contracted and rearrangement products and consecutive protonation–deprotonations can produce all products. Ring contraction of the cyclohexyl, cycloheptyl, and cyclooctyl cations to tertiary species is exactly what is observed for the species in strongly acidic media (10, 11). Rings smaller than C_5 were not observed, presumably because of their lower stability. That the medium-sized rings cascade to cyclopentenes and cyclohexenes while cyclododecene rearranges only slowly is in keeping with the degree of ring strain in the series of cycloalkenes.

Formation of 1-ethylcyclopentene (**1***e*) and 1-ethylcyclohexene (**2***d*) from cycloheptene and cyclooctene, respectively, is easily rationalized by invoking involvement of methyl-substituted protonated cyclopropanes as indicated in Scheme 1.

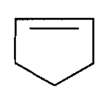

1

1*a* 1-Me
b 3-Me
c 4-Me
d 1,2-di-Me
e 1-Et
f 1-Et - 2-Me
g 2-Me - 3-Et
h 2-Et - 3-Me

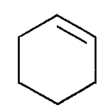

2

2*a* 1-Me
b 3-Me
c 4-Me
d 1-Et
e 1,2-di-Me
f 2,3-di-Me
g 3,4-di-Me

Cyclopentene (**1**), cyclohexene (**2**), cyclododecene (**5**), 1-methylcyclopentene (**1***a*), 1-methylcyclohexene (**2***a*), 1-ethylcyclohexene (**2***d*) (containing ~10% other products), and a variety of other alkylated C-5 and C-6 cycloalkenes can be perlabelled. While cycloheptene and cyclooctene undergo facile ring contraction even at 200°C, reactions carried out at 175°C yield partially labelled substrates (entries 10 and 11, Table 1). These products may be obtained in pure form by spinning band distillation or preparative gas chromatography.

Acyclic alkenes also undergo exchange and extensive rearrangement. *E*-2-pentene (**7**) can be perlabelled (entry 1, Table 2) with little rearrangement. At higher temperatures substantial rearrangement occurs and perdeuterated 2-methyl-2-butene and 2-methyl-1-butene are obtained. As expected, 1-pentanol (entry 5, Table 2) yields a similar mixture of al-

TABLE 2. Protium–deuterium exchange and rearrangement of acyclic alkenes

Entry	Substrate	Conditions[a]	Products[a,b]	% Exchange[a] (excess D atoms/molecule)
1	**7**	198°C, 24 h	1-Pentene (4.9), **7** (65.6), *Z*-2-pentene (23.6), 2-methyl-2-butene (5.9)	89.3 (8.93)[i]
2	**8**	200°C, 24 h	Other (1.3),[c] **8** (<5), *E*-3-hexene (23.6), *E*-2-hexene (46.5), *Z*-3-hexene (8.4), *Z*-2-hexene (19.3)	78.3 (9.40)[i,j]
3	**9**	198°C, 24 h	Other (2),[c] *E*-3-heptene (37), **9** (3), *E*-2-heptene (33), *Z*-3-heptene (13), *Z*-2-heptene (13)	54.2 (7.59)[i]
4	**10**	200°C, 24 h	Other (4),[c] *E*+*Z*-4-octenes (~18), *E*+*Z*-3-octenes (~36), **10** (<2), *E*+*Z*-2-octenes (~42)	35.2 (5.62)[i]
5	**11**	200°C, 83 h	1-Pentene (~2), 2-pentenes (~65), 2-methyl-2-butene (~25), 2-methyl-1-butene (~5) other (~3)[g,h,k]	89.6 (8.96)[i]
6	**12**	210°C, 84 h	**8** (~2), 2+3-hexenes (~90), rearrangement products (~8)[h]	83.2 (9.96)[i]
7	**13**	210°C, 84 h	**9** (<5), 2+3-heptenes (~85), rearrangement products (~10)[h]	87.7 (12.28)[i]
8	**14**	210°C, 84 h	**10** (~5), 2-, 3-, and 4-octenes (~85), rearrangement products (~10)[h]	65.5 (10.48)[i]
9	**15**	165°C, 20 h	**16** (20.1), **15** (79.9)	**15**, 95.7 (11.48) **16**, 95.7 (11.48)

[a]Exchange reactions were carried out in 1% w/v DCl/D_2O or for product identification in 1% w/v HCl/D_2O. Temperature control was ±3°C. Equilibration corresponded to 94–95% exchange. All reactions were carried out with decalin mixing.
[b]Values were obtained from gc analysis using electronic integrations and nmr integration. The products are listed in order of increasing retention time unless otherwise stated.
[c]Unidentified minor shorter-retention-time products.
[d]Peaks due to *E*-2-hexene and *Z*-3-hexene overlapped.
[e]Peaks due to *E*-2-heptene and *Z*-3-heptene overlapped.
[f]Peaks due to *E*-4-, *Z*-4-, and *E*-3-octenes overlapped. Peaks due to *Z*-3- and *E*-4-octenes overlapped.
[g]Unidentified minor longer-retention-time products.
[h]Products not listed in order of increasing retention time.
[i]Mass spectral analysis was carried out on the mixture of deuterated alkenes isolated by preparative gc.
[j]Deuterium analysis at 70 eV using gc–ms established that the components did not exhibit vastly different deuterium incorporations.
[k]Product analysis obtained from a run carried out at 203°C for 77 h. Exchange was carried out at 200°C for 83 h.

kenes. Similar results are observed for 1-hexene, 1-heptene, 1-octene, and the corresponding alcohols **12**, **13**, and **14** (entries 2, 3, 4, 6, 7, and 8, Table 2). At 205°C 1-hexene, 1-heptene, and 1-octene are isomerized mainly to the 2- and 3-alkenes and the deuterium incorporation decreases as the chain length increases. When 1-hexene, 1-heptene, and 1-octene are heated at 215°C to increase deuterium incorporation, extensive rearrangement occurs. The corresponding primary alcohols (entries 6, 7, and 8, Table 2) yield similar results. Although acyclic alkenes may be perdeuterated by the HTDA technique, the considerable rearrangement occurring in most cases necessitates that reactions be carried out on a fairly large scale and spinning band distillation or preparative gas chromatography equipment used to separate the components. In some cases, products may only be obtainable as mixtures. As documented in entry 9, Table 2, tetramethylethylene (**15**) is easily perdeuterated in good yield and perlabelled 2,3-dimethyl-1-butene also is formed. Perhaps methyl groups can be used generally to anchor double bonds and minimize rearrangement.

Since the yields are quite good (65–85%) and alkenes can easily be converted into other classes of compounds, HTDA exchange is established as a valuable route to a wide range of deuterated cyclic compounds. Certain deuterated acyclic compounds may also be prepared, but with the limitations expressed above. Since D_2O can be replaced by THO after exchange conditions have been determined, the method, in principle, can be used to tritiate organic compounds with the added advantage that the degree of exchange and the location of the label can be inferred from the studies in deuterated medium.

Experimental

General

Proton and deuteron magnetic resonance spectra were recorded on Bruker WP-250 and 400 spectrometers with $CDCl_3$ as internal standard. Samples were dissolved in chloroform or chloroform-*d*. Chemical shifts are expressed in parts per million downfield from tetramethylsilane. Deuterium assay analyses were performed on a VG Micromass 7070 mass spectrometer at low ionization voltage (12–

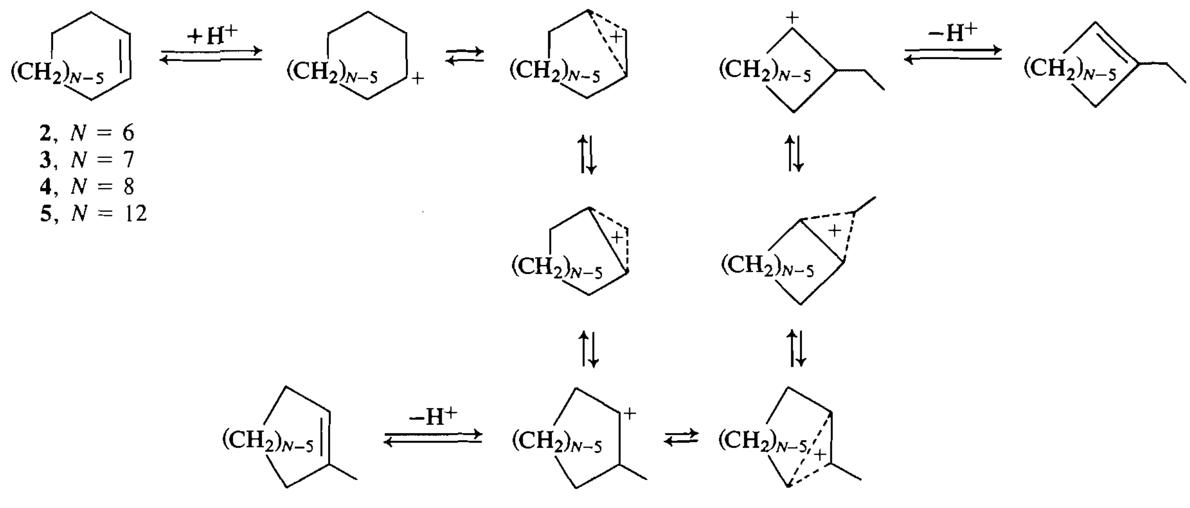

SCHEME 1

15 eV) and are expressed as atoms of deuterium per molecule in excess of natural abundance deuterium. Analytical gas−liquid partition chromatography was performed on a Tracor 560 dual column analytical gas chromatograph equipped with flame ionization detectors using helium as the carrier gas. Flow rate was usually 20−30 mL/min. Columns used were 6 ft × 4 mm id 3% OV-1 on 100−120 mesh Chromosorb W and 30 ft × 1/8 in. 23% SP-1700 on 80−100 mesh Chromosorb PAW (Supelco, Inc.). Preparative gas−liquid partition chromatography was carried out on a Varian Aerograph Model A-700 gas chromatograph with a thermal conductivity detector at a helium flow rate of 50−60 mL/min with a 5 ft × 1/4 in. 15% SE-30 on 60−80 mesh Chromosorb W column.

Exchange reactions

In a typical exchange reaction, substrate (0.20 g) was added to 1% w/v DCl/D_2O (5 mL) in a medium-walled glass tube, the mixture was degassed via three freeze−pump−thaw cycles and sealed under vacuum. The tube was placed in a 600-mL Parr pressure vessel which contained water to equalize pressure and heated at the desired temperature for an appropriate period.

For later reactions the procedure was slightly modified. Decalin (1 mL) was added as a cosolvent and reaction was carried out in a 600-mL Parr pressure apparatus which was heated in an apparatus which agitated the reaction mixture by a rocking motion. After reaction, the decalin layer was decanted from the frozen aqueous solution and analysed by gc and in some cases by gc−ms. The deuterium content of samples isolated by preparative gc was determined mass spectrometrically at low ionizing voltage (12−15 eV).

Structure elucidation of products

In a typical reaction, substrate (0.20 g) was added to 1% w/v HCl/H_2O (5 mL) and decalin (1 mL) in a medium-walled glass tube, the mixture was degassed via three freeze−pump−thaw cycles and sealed under vacuum. The tube was placed in a 600-mL Parr pressure vessel which contained water to equalize pressure and heated with agitation at the desired temperature for an appropriate period. The decalin layer was decanted from the frozen aqueous layer and analyzed by analytical gc. The products were isolated by preparative gc, in some cases as mixtures, and analyzed by high-field ^{1}H nmr (250 and 400 MHz).

Large scale reactions

Preparation of deuterated cyclopentene

Three tubes, each containing cyclopentene (0.32 g), 1% w/v DCl/D_2O (8 mL), and decalin (1.6 mL), prepared in the usual manner, were heated at 200°C for 24 h with agitation. The deuterated cyclopentene was isolated from the combined decalin solutions by flash distillation through a 9-cm Vigreux column. The yield was 0.58 g (60%) of cyclopentane with deuterium incorporation of 87.0% (6.96 excess D atoms/molecule).

Preparation of deuterated pentenes

Three tubes, each containing *E*-2-pentene (0.30 g), 1% w/v DCl/D_2O (8 mL), and decalin (1.5 mL) were heated for 24 h at 198°C with agitation. The deuterated pentenes (see entry 1, Table 2) were isolated from the combined decalin layers by flash distillation through a 9-cm Vigreux column. The yield was 0.58 g (64%). See entry 1, Table 2 for the approximate product composition.

Preparation of deuterated hexenes

Eight tubes, each containing 1-hexanol (0.32 g), decalin (1.6 mL), and 1% w/v DCl/D_2O (8 mL) were rocked for 72 h at 205°C. The organic layer was separated from the combined reaction mixtures and the deuterated *E*-2- and *E*-3-hexenes (2.76 g, 73.7%) were flash distilled from the decalin at atmospheric pressure through a 9-cm vacuum-jacketed Vigreux column. Mass spectrometric analysis established that exchange was 91.4% complete, corresponding to an incorporation of 10.97 deuterium atoms per molecule.

Preparation of octenes

Four tubes each containing 1-octene (0.30 g) 1% w/v HCl/H_2O (8 mL) and decalin (1.5 mL) were prepared in the usual manner and heated for 24 h at 200°C with agitation. The octenes (1.00 g, 83%) were isolated from the combined decalin layers by flash distillation through a 9-cm Vigreux column; see entry 4, Table 2 for the approximate product composition.

Acknowledgement

We thank the Natural Sciences and Engineering Research Council of Canada for financial support.

1. N. H. WERSTIUK and T. KADAI. Can. J. Chem. **51**, 1485 (1973).
2. N. H. WERSTIUK and T. KADAI. Can. J. Chem. **52**, 2169 (1974).
3. N. H. WERSTIUK and T. KADAI. U.S. Patent 3,989,705. 1976.
4. N. H. WERSTIUK and T. KADAI. Canadian Patent 1048556. 1979.
5. N. H. WERSTIUK and G. TIMMINS. Can. J. Chem. **59**, 1022 (1981).
6. N. H. WERSTIUK and G. TIMMINS. Can. J. Chem. **59**, 3218 (1981).
7. S. J. THOMSON and T. F. WALTON. Trans. Faraday Soc. **33**, 821 (1957).
8. H. J. DUTTON and R. F. NYSTROM. Adv. Tracer Methodol. **1**, 18 (1962).
9. G. E. CALF, D. B. FISHER, and J. L. GARNETT. Aust. J. Chem. **21**, 947 (1968).
10. G. A. OLAH, J. M. BOLLINGER, J. LUKAS, and C. CUPAS. J. Am. Chem. Soc. **89**, 2692 (1967).
11. G. A. OLAH, D. P. KELLY, and R. G. JOHANSON. J. Am. Chem. Soc. **92**, 4137 (1970).

Towards a complete account of the mechanism of hydrogen isotope exchange of diastereotopic protons of carbon acids. II. Acid- and base-catalyzed enolization of bicyclo[2.2.1]heptan-2-ones. Evidence for exchange by inversion

NICK HENRY WERSTIUK AND SUJIT BANERJEE[1]
Department of Chemistry, McMaster University, Hamilton, Ont., Canada L8S 4M1

Received January 30, 1984[2]

NICK HENRY WERSTIUK and SUJIT BANERJEE. Can. J. Chem. **63**, 534 (1985).

A study of acid- and base-catalyzed hydrogen isotope exchange of bicyclo[2.2.1]heptan-2-one (**1***a*) and its 3-deuteriated analogs has been carried out. We find that the k_{exo}/k_{endo} ratio (658 ± 66) for deuteroxide-catalyzed H → D exchange of **1***a* at C-3 is 7.2 ± 1.5 times greater than the k_{exo}/k_{endo} ratio (91 ± 9) for hydroxide-catalyzed D → H exchange of **1***b*. For acid-catalyzed exchange in $CH_3COOD(H)-D(H)Cl$ the rate ratios are 156 ± 20 and 29 ± 2 for H → D and D → H exchange, respectively. Equations which relate the observed selectivity k_{exo}/k_{endo} (k_{fast}/k_{slow}) to the intrinsic selectivity and the primary, secondary, and solvent KIEs are developed. The differences between the rate ratios for H → D and D → H exchange are interpreted on the basis of a significant contribution of an inversion pathway to exchange of the slow proton (deuteron). The significance of our study – it relates to the mechanism of hydrogen isotope exchange of diastereotopic protons (deuterons, tritons) of any carbon acid – is discussed.

NICK HENRY WERSTIUK et SUJIT BANERJEE. Can. J. Chem. **63**, 534 (1985).

On a effectué une étude de l'échange d'isotopes d'hydrogène, catalysé soit par les acides ou par les bases, de la bicyclo[2.2.1]heptanone-2 (**1***a*) et de ses analogues deutérés en position 3. On trouve que le rapport (658 ± 66) des vitesses k_{exo}/k_{endo} pour l'échange H → D, catalysé par l'ion deutéroxyde, en C-3 de **1***a* est 7,2 ± 1,5 fois plus grand que le rapport (91 ± 9) des vitesses k_{exo}/k_{endo} pour l'échange D → H, catalysé par l'ion hydroxyde, de **1***b*. Pour l'échange catalysé par les acides, $CH_3COOD(H)/D(H)Cl$, les rapports de vitesse sont respectivement 156 ± 20 et 29 ± 2 pour les échanges H → D et D → H. On a développé des équations qui permettent de relier la sélectivité observée k_{exo}/k_{endo} (k_{rapide}/k_{lent}) avec la sélectivité intrinsèque et les EIC primaire, secondaire et du solvant. On interprète les différences observées entre les rapports de vitesses pour les échanges H → D et D → H en fonction d'une contribution importante d'une voie d'inversion pour l'échange du proton lent (deutéron). On discute de l'importance de notre travail dans sa relation avec le mécanisme d'échange isotopique de protons diastéréotopes (deutérons et tritons) d'acides carboxyliques.

[Traduit par le journal]

Introduction

Acid- and base-catalyzed enolizations of carbonyl compounds are two of the most important organic reactions, and, in keeping with that fact, have been the focus of considerable research designed to establish mechanistic details (1–3). Hydrogen isotope exchange, in particular, has played an important role in many mechanistic studies (2, 3). It was clear to us, however, from a review of the literature, that there was a paucity of mechanistic information in the area of hydrogen isotope exchange (enolization) of polycyclic monoketones and diketones. In fact, prior to 1970 there were no accurate rate data for base-catalyzed exchange of diastereotopic protons of ketones even though there were reports (4–7) of the preparation of 80–90% stereochemically pure 3-monodeuterated bicyclo[2.2.1]heptan-2-ones. Of particular interest to us was the possibility of exchange of diastereotopic protons by an inversion mechanism, which had been recognized, but not quantified (8). A research program was initiated at that time to detail the mechanistic intricacies of hydrogen isotope exchange (enolization) of bicyclic ketones and determine the effect of groups located remote (β or γ) from an α enolizable site. A number of papers documenting our work have been published (9–16). We noted, most importantly, from a study of the stereoselectivity of H → D and D → H exchange of **1***a* and its 3,3-dideuteriated analog **1***b*, that the k_{exo}/k_{endo} (k_{fast}/k_{slow}) ratio decreased from 660 for exchange of **1***a* in deuteriated medium to 72 for exchange of **1***b* in nondeuteriated medium. We published a preliminary account (10) of an analysis that established that the difference was due to involvement of an inversion pathway for exchange of the *endo* (slow) proton (deuteron) at C-3. In this paper we give a complete account of our work on bicycloheptanones **1***a*, **1***b*, **1***c*, and **1***d*, develop equations including primary, secondary, and solvent KIEs (kinetic isotope effects) which relate the observed selectivity to the intrinsic selectivity *S*, and interpret the difference between $(k_{exo}/k_{endo})^{H\to D}$ and $(k_{exo}/k_{endo})^{D\to H}$ on the basis of a significant contribution of an inversion pathway to exchange of the slow proton (deuteron) of a diastereotopic pair. The importance of our study – it details the mechanism of hydrogen isotope exchange of diastereotopic protons, deuterons, or tritons of any carbon acid – is discussed.

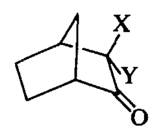

1

a, X = Y = H
b, X = Y = D
c, X = Cl; Y = H
d, X = Cl; Y = D

Results

Hydrogen isotope exchange of bicyclo[2.2.1]heptan-2-ones

The rates of NaOD(H)-catalyzed H → D and D → H exchange of **1***a* and **1***b* were measured at 30°C in 60% dioxane – 40% D_2O or H_2O by following the uptake or loss of deuterium mass spectrometrically at low voltage (12–15 eV) (13).

[1] Present address: Safety and Environmental Protection Division, Brookhaven National Laboratory, Upton, New York 11973.
[2] Revision received August 1, 1984.

TABLE 1. Second-order rate constants for hydrogen isotope exchange of bicyclo[2.2.1]heptan-2-ones at 30.00 ± 0.05°C

				$k(M^{-1}\ s^{-1})^c$		
Entry	Substrate	Medium	[$^-$OH(D)]	*exo* × 10^2	*endo* × 10^5	k_f/k_s
1	**1***a*	D[a]	0.045	5.89 ± 0.26		
2	**1***a*	D	0.045		9.07 ± 0.55	
3	**1***a*	D	0.045		8.83 ± 0.43	658 ± 66[d]
4	**1***b*	H[b]	0.008	0.721 ± 0.021		
5	**1***b*	H	0.020	0.704 ± 0.033		
6	**1***b*	H	0.040	0.658 ± 0.007		
7	**1***b*	H	0.200	0.594 ± 0.008		
8	**1***b*	H	0.020		7.89 ± 0.28	
9	**1***b*	H	0.040		7.22 ± 0.69	
10	**1***b*	H	0.100		6.72 ± 0.28	91 ± 9[e]

[a]The medium was composed of 60% dioxane – 40% D_2O (v/v).
[b]The medium was composed of 60% dioxane – 40% H_2O (v/v).
[c]Errors quoted are the standard deviations.
[d]Obtained as a ratio of k_{exo} (entry 1) and k_{endo} (average of entries 2 and 3).
[e]Obtained as a ratio of k_{exo} (entry 6) and k_{endo} (entry 9).

The pseudo-first-order rate constants were obtained by computerized analysis of the kinetic data and the second-order rate constants, obtained by dividing the first-order rate constants by the base concentration, are given in Table 1. A correction for dilution of the deuterium pool was not made in these studies because a previous study (13) showed that the corrected and uncorrected rate constants usually differed by less than 10%. A computer generated plot of the kinetic data for a typical run on **1***b* is given in Fig. 1(A).

Since it was not possible to determine the primary KIE for *endo* exchange of **1***a* directly, **1***c* and **1***d* were prepared and the rates of exchange were determined by monitoring the rates of isomerization in deuteriated and nondeuteriated medium as described previously (13). The second-order rate constants for isomerization of **1***c* and **1***d* obtained by computer analysis of isomerization data are listed in Table 2. A computer generated plot of the kinetic data for a typical run is given in Fig. 1(B).

The rates of acid-catalyzed H → D and D → H exchange of **1***a* and **1***b* were measured at 100°C in 90% CH_3COOD – 10% 2.08 *N* DCl and 90% CH_3COOH – 10% 2.00 *N* HCl, respectively. The pseudo-first-order rate constants uncorrected for dilution of the deuterium pool and obtained by computer analysis of the data are listed in Table 3. A computer generated plot of the kinetic data obtained from a typical run is given in Fig. 1(C).

Determination of the secondary KIE for exo *proton abstraction in deuterated medium*

A competition method was used to determine the secondary KIE (ν_D) for *exo* exchange of **1***a* in deuteriated medium. Mixtures (~50:50) of **1***a* and its *endo*-3-*d* analog **1***f* of known composition were reacted in 60% dioxane – 40% NaOD/D_2O for periods ranging from 0.9 to 2.8 half-lives, quenched by a buffer, and analyzed by mass spectrometry. If the processes shown in Scheme 1 are considered, then eqs. [1]–[5] are obtained and the secondary KIE for *exo* deprotonation = $1/\alpha$. Since eq. [1] describes α and $[\mathbf{1}a]_0 = [d_0]_0$, $[\mathbf{1}a]_t = [d_0]_t$, and $[\mathbf{1}f] = [d_1]_0$, eqs. [2], [3], [4], and [5] are obtained.

$$[1] \quad \alpha = \frac{\ln([\mathbf{1}f]_t/[\mathbf{1}f]_0)}{\ln([\mathbf{1}a]_t/[\mathbf{1}a]_0)}$$

$$[2] \quad [\mathbf{1}f]_t = [d_1]_t - [\mathbf{1}e]_t$$

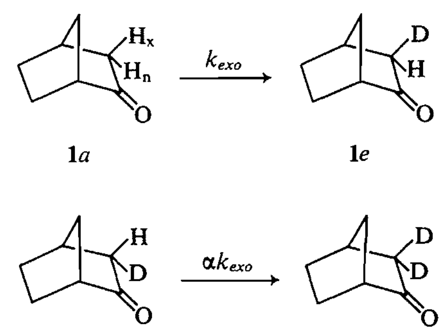

1*a* **1***e* **1***f* **1***e*

SCHEME 1

TABLE 2. Second-order rate constants for hydrogen isotope exchange of *exo*-3-chlorobicyclo[2.2.1]heptan-2-ones at 30.00 ± 0.05°C

Entry	Substrate	Medium	[$^-$OH(D)]	$k(M^{-1}\ s^{-1}) \times 10^{3\,c}$
1	**1***c*	H[a]	0.024	6.93 ± 0.10
2	**1***c*	H	0.024	7.23 ± 0.16
3	**1***c*	D[b]	0.061	11.10 ± 0.07
4	**1***c*	D	0.061	11.60 ± 0.13
5	**1***d*	H	0.024	1.02 ± 0.06
6	**1***d*	D	0.061	1.79 ± 0.06
7	**1***d*	D	0.061	1.64 ± 0.05

[a]The medium was composed of 60% dioxane – 40% H_2O (v/v).
[b]The medium was composed of 60% dioxane – 40% D_2O (v/v).
[c]Errors quoted are the standard deviations.

$$[3] \quad [\mathbf{1}f]_t = [d_1]_t - ([\mathbf{1}a]_0 - [\mathbf{1}a]_t)$$

$$[4] \quad [\mathbf{1}f]_t = [d_1]_t - [d_0]_0 + [d_0]_t$$

$$[5] \quad \alpha = \frac{\ln[([d_1]_t - [d_0]_0 + [d_0]_t)/[d_1]_0]}{\ln([d_0]_t/[d_0]_0)}$$

The results of our study are given in Table 4 and the secondary KIE for *exo* proton abstraction $\nu_D = 1/\alpha = 1.12 \pm 0.03$. It is interesting to note that Tidwell and co-workers (8) obtained a value of 1.064 ± 0.047 for exchange of bicyclo[2.2.2]octan-2-one by using a fitting routine. While the competition method

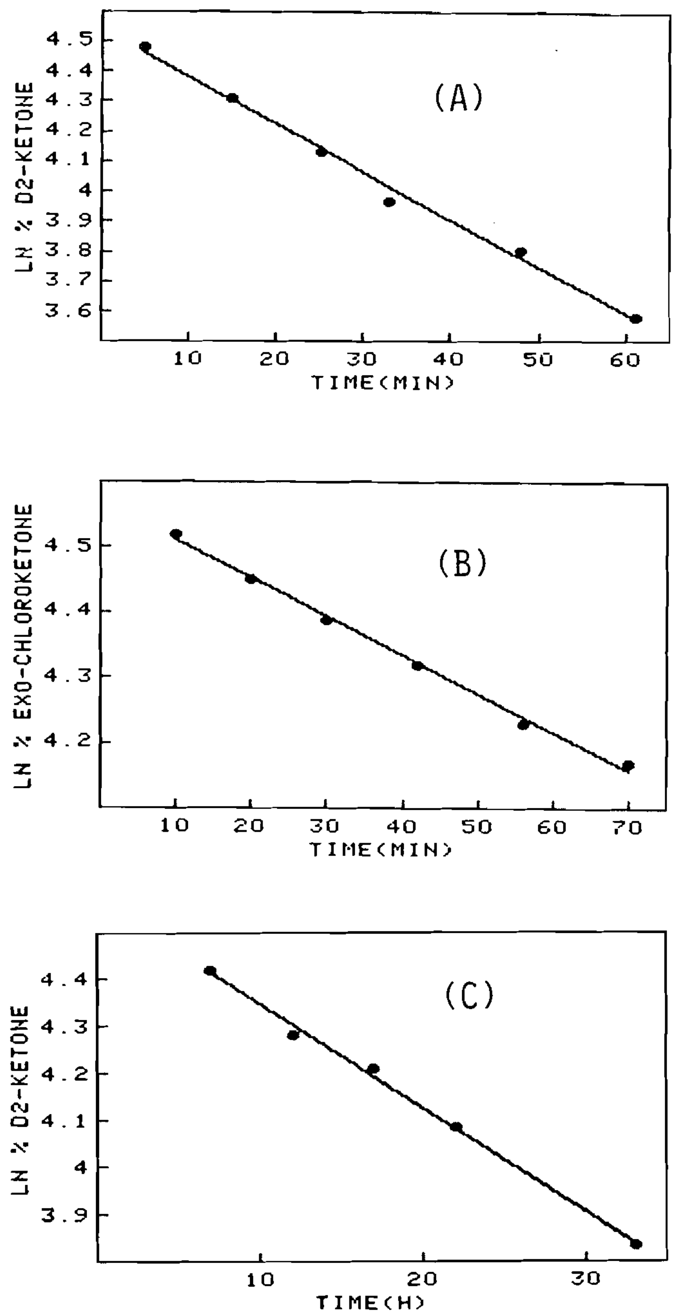

FIG. 1. (A). Plot of ln % bicyclo[2.2.1]heptan-2-one-*exo,endo*-3,3-d_2 versus time (min) for D → H exchange in 60% dioxane – 40% 0.040 *M* NaOH at 30.00 ± 0.05°C (entry 6, Table 1). (B). Plot of ln % *exo*-3-chlorobicyclo[2.2.1]heptan-2-one-*endo*-3-*d* versus time (min) for D → H exchange in 60% dioxane – 40% 0.061 *M* NaOD at 30.00 ± 0.05°C (entry 7, Table 2). (C). Plot of ln % bicyclo[2.2.1]-heptan-2-one-*exo,endo*-3,3-d_2 versus time (h) for D → H exchange in 90% HOAc – 10% 2 *M* HCl at 100.0 ± 0.5°C.

described here is useful for determining secondary KIEs, there are several sources of error which must be considered. Dilution of the deuterium pool must be negligible. In this study, since 2 mg of a mixture of ketones were used in 1 mL of 60% dioxane – 40% $NaOD/D_2O$, the dilution was ~0.1%. The stereoselectivity of exchange (k_f/k_s) is important as well – d_0-ketone is converted to d_1-ketone by *exo* and *endo* deprotonations and *endo*-3-*d* ketone can be isomerized to the *exo*-3-*d* species. A computerized simulation was carried out to probe the effects of the magnitude of k_f/k_s, the reaction period, and the $[d_0]/[d_1]$ ratio on the observed secondary KIE. The results are given in Table 5. It is clear that for high selectivities the observed KIE is a good measure of the intrinsic KIE. This is not the case when the selectivity is low, an initial $[d_0]/[d_1]$ ratio > 1 is used, and the reaction is allowed to proceed for more than one half-life.

Discussion and conclusions

It is seen from the data listed in Table 1 that $(k_f/k_s)^{D\to H}$ is considerably smaller than $(k_f/k_s)^{H\to D}$ for base-catalyzed hydrogen isotope exchange of the diastereotopic protons and deuterons of **1***a* and **1***b*, respectively. The $(k_f/k_s)^{H\to D}/(k_f/k_s)^{D\to H}$ ratio is 7.2 ± 1.5.[3] As is documented in Table 3, $(k_f/k_s)^{D\to H}$ is considerably less than $(k_f/k_s)^{H\to D}$ for acid-catalyzed exchange as well and the ratio is 5.4 ± 1.1. Since $k_f >> k_s$, in our view Scheme 2 is an adequate representation of the exchange of diastereotopic protons α to a carbonyl group. Since a common enolate is undoubtedly involved,[4] a steady-state treatment involving *E* and *S'* leads to eq. [6] as the expression for the rate constant for slow H → D exchange.[5]

[3] The ratio of 7.2 is somewhat smaller than the ratio of 9.1 reported in our preliminary communication (10). The difference arises from the fact that the ratios were obtained in a slightly different manner. As is seen in Table 1, there is a significant medium effect on the fast and slow exchanges. In our earlier account, $k_f^{D\to H}$ and $k_s^{D\to H}$ were obtained from plots of k_f (obs) and k_s (obs) versus $[OH^-]$. In the present analysis the $(k_f/k_s)^{H\to D}$ and $(k_f/k_s)^{D\to H}$ ratios were obtained by using second-order rate constants obtained at similar base concentrations since a study of the variation of $k_{exo}^{H\to D}$ and $k_{endo}^{H\to D}$ with $[OH^-]$ was not carried out.

[4] Warkentin and Tee (17), through a study of the hydrogen isotope exchange of 2-butanone, have supported earlier suggestions that base-catalyzed enolization of ketones in aqueous medium involves concerted formation of enols rather than enolates. However, if hydroxide-catalyzed enolization occurs to generate enols directly, then it is difficult to account for the fact that solvent KIEs for base-catalyzed enolization of ketones ((k_{D_2O}/k_{H_2O}) for acetone × 1.47) (18) are very similar to the solvent KIEs for H–D exchange of other carbon acids; 9-fluorenylmethanol 1.49 (19), 1,4-dicyano-2-butene 1.39 (20), and phenylacetylene 1.33 (21). In fact, a recent study by Kresge and co-workers (22) has established that acetone yields the enolate in dilute aqueous NaOH. However, whether enolates or enols are involved is immaterial to our analysis.

[5] We thank a referee for pointing out an alternative, perhaps more quantitative, analysis that involves Scheme A (for H → D exchange), development of differential equations for the change in concentrations of various species, and utilization of a steady-state analysis based on enolates E and E'. Following a solution of the resulting differential equations using the Carson–Laplace transformation, the k_f/k_s ratios could be obtained by fitting isotopic composition–time data to theoretical curves generated from different k_f/k_s values. While this approach would probably lead to a "final" general solution, the calculations are difficult and the fitting of the experimental data would not be a simple matter. It is noteworthy that Ohnishi (23) utilized a scheme similar to the one referred to above to discuss the kinetics of $^-$OD-catalyzed H → D exchange of 6,6-dimethylbicyclo[3.1.1]-heptan-2-one (nopinone), but used a different analysis of the rate equation. In our view, our approach, which uses experimentally determined parameters – k_f/k_s, primary and secondary KIEs and SIEs – which have been documented and discussed in the literature, is a viable account of the acid- or base-catalyzed exchange of diasterotopic protons (deuterons or tritons) in cases where $k_f >> k_s$.

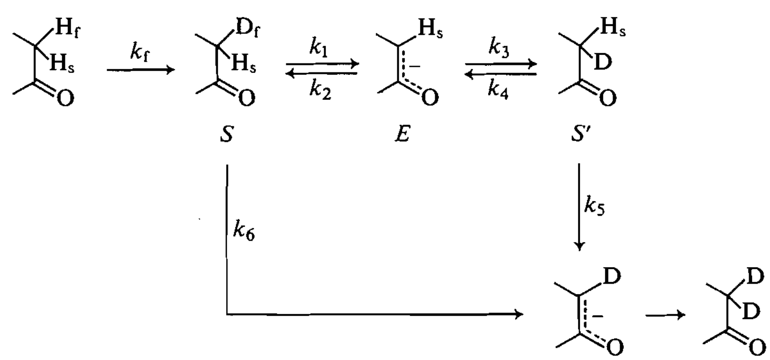

SCHEME 2

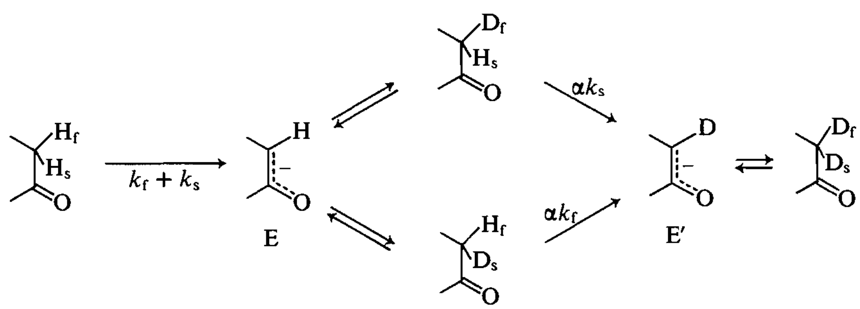

SCHEME A

TABLE 3. Pseudo-first-order rate constants for acid-catalyzed hydrogen isotope exchange of bicyclo[2.2.1]heptan-2-ones at 100.0 ± 0.5°C

Substrate	Medium	$k(\mathrm{s}^{-1}) \times 10^3$ *exo* (fast)	$k(\mathrm{s}^{-1}) \times 10^3$ *endo* (slow)	k_f/k_s
1*a*	D[a]	3.86 ± 0.28[c,d]	0.0247 ± 0.0013[c]	156 ± 20
1*b*	H[b]	0.362 ± 0.018[e]	0.0124 ± 0.0002[c]	29 ± 2

[a] D = 90% CH_3COOD – 10% 2.08 *N* DCl.
[b] H = 90% CH_3COOH – 10% 2.00 *N* HCl.
[c] Errors quoted are the standard deviations obtained from linear least-squares analysis.
[d] Obtained by multiplying the rate constant (4.48×10^{-4} s^{-1} ± 7.4%) determined at 75.0 ± 0.1°C by a factor of 8.61 that was obtained by dividing $k_f^{D\to H}$ (3.62×10^{-4} s^{-1} ± 10.1%) obtained at 100.0 ± 0.5°C by $k_f^{D\to H}$ (4.20×10^{-5} s^{-1} ± 5.8%) obtained at 75.0 ± 0.1°C.
[e] Average of two determinations; average deviation ≤ 10%.

TABLE 4. Secondary KIEs for *exo* proton exchange of bicyclo[2.2.1]-heptan-2-one in 60% dioxane – 40% D_2O at 30.00 ± 0.05°C

Initial[a] $[d_0]/[d_1]$	[NaOD]	Approximate number of half-lives	α
$\frac{53.59 \pm 0.60}{44.69 \pm 0.40}$	0.064	1.3	0.89 ± 0.02[b]
$\frac{53.59 \pm 0.60}{44.69 \pm 0.40}$	0.064	1.4	0.90 ± 0.02[c]
$\frac{59.89 \pm 0.27}{38.54 \pm 0.30}$	0.064	2.8	0.90 ± 0.02[d]
$\frac{59.89 \pm 0.27}{38.54 \pm 0.30}$	0.023	0.9	0.88 ± 0.02[e]
			Avg. 0.89 ± 0.02

[a] Obtained mass spectrometrically as an average of 10 scans at low voltage.
[b] Obtaned as an average of 14 determinations of α from 14-ms scans.
[c] Obtaned as an average of 14 determinations of α from 14-ms scans.
[d] Obtaned as an average of 13 determinations of α from 13-ms scans.
[e] Obtaned as an average of 12 determinations of α from 12-ms scans.

$$[6] \quad k_{s_{obs}}^{H\to D} \simeq k_6 + k_1\left[1 - \frac{k_2(k_4 + k_5)}{(k_2 + k_3)(k_4 + k_5) - k_3k_4}\right]$$

Since $(k_2 + k_3)(k_4 + k_5) >> k_3k_4$ in cases where $k_f > k_s$, eq. [6] can be approximated by eq. [7]. Although k_2 is greater

$$[7] \quad k_{s_{obs}}^{H\to D} \simeq k_6 + k_1\left(1 - \frac{k_2}{k_2 + k_3}\right)$$

than k_3, if $k_f > k_s$ and $k_2/(k_2 + k_3)$ approaches unity, because $k_1 >> k_6$ the $k_1(1 - (k_2/k_2 + k_3))$ term – basically a measure of the contribution of inversion to exchange of the slow proton – can make a significant contribution to $(k_s)_{obs}^{H\to D}$. If S_D = intrinsic selectivity in deuteriated medium, V_D and L_D are the primary KIEs for fast and slow deprotonation, V_D' and L_D' are the isotope effects for fast and slow protonation, and v_D and l_D are the secondary KIEs for fast and slow proton exchange in deuteriated medium, then $S_D \simeq k_1V_D/k_6l_D \simeq k_2 V_D'/k_3 L_D'$, $k_3/k_2 \simeq V_D'/S_DL_D'$, and $k_6 \simeq k_1V_D/S_Dl_D \simeq k_{f_{obs}}/S_Dl_D$. By mak-

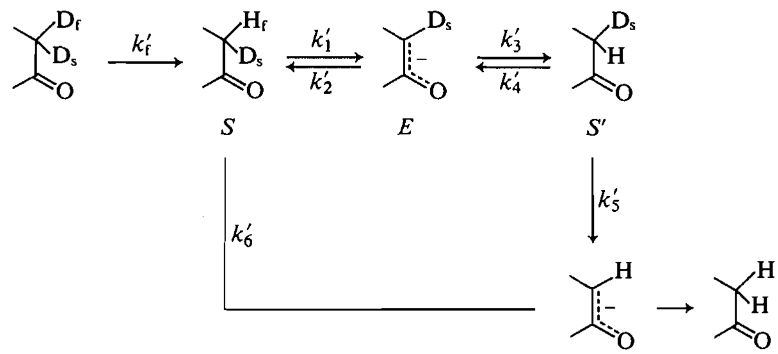

SCHEME 3

TABLE 5. Variation of secondary KIEs for base-catalyzed enolization

k_f/k_s	Actual k_H/k_D	Initial d_0/d_1 ratio	Number of half-lives (calcd. k_H/k_D)		
750	1.11	25:75	1(1.11)	2(1.11)	3(1.11)
750	1.11	50:50	1(1.11)	2(1.11)	3(1.10)
750	1.11	75:25	1(1.11)	2(1.10)	3(1.09)
250	1.11	50:50	1(1.11)	2(1.10)	3(1.09)
50	1.11	25:75	1(1.13)	2(1.11)	3(1.09)
50	1.11	50:50	1(1.11)	2(1.07)	3(1.00)
50	1.11	75:25	1(1.07)	2(0.96)	3(0.73)

ing the appropriate substitution into eq [7],[6] eq. [8] is obtained.

$$[8] \quad (k_f/k_s)_{\text{obs}}^{\text{H}\to\text{D}} \simeq \frac{(S_DV_Dl_D)(S_DL_D' + V_D')}{V_D\left(\dfrac{S_DV_D'l_D}{V_D} + S_DL_D' + V_D'\right)}$$

If $S_D >> V_D$ or V_D', then eq. [9] is obtained

$$[9] \quad (k_f/k_s)_{\text{obs}}^{\text{H}\to\text{D}} \simeq \frac{S_DL_D'l_D}{\left(L_D' + \dfrac{V_D'}{V_D}l_D\right)}$$

and the intrinsic selectivity is given by eq [10].

$$[10] \quad S_D \simeq \frac{(k_f/k_s)_{\text{obs}}^{\text{H}\to\text{D}}\left(L_D' + \dfrac{V_D'}{V_D}l_D\right)}{L_D'l_D}$$

If the assumption is made that the protonation isotope effects are approximately equal to the deprotonation isotope effects, then eq. [11] is obtained.

$$[11] \quad (k_f/k_s)_{\text{obs}}^{\text{H}\to\text{D}} \simeq \frac{S_DL_D'l_D}{L_D' + l_D}$$

Presently there is little information available on the relative magnitudes of the deprotonation and protonation isotope effects and it is difficult to make predictions.[7] From the limited data available it appears that the protonation KIE is less than the deprotonation KIE. Pocker (24) has shown that the protonation KIE for acetone enolate (enol) in basic aqueous medium is ~5.5 while the deprotonation KIE, neglecting secondary effects, is 7.5. Long and Watson (25) have established that the primary KIE for protonation of methylacetylacetone enolate by $CH_3COOH(D)$ in aqueous medium is 5.6. The acetate-catalyzed enolization of the ketone is characterized by a primary KIE of 5.8 in H_2O.

If a further assumption is made that $V_D \simeq V_D' \simeq L_D \simeq L_D' = i$ and the secondary KIEs v_D and l_D are set equal to 1, then eq. [11] can be approximated by eq. [12]. That l_D is small,

$$[12] \quad (k_f/k_s)_{\text{obs}}^{\text{H}\to\text{D}} \simeq \frac{S_Di}{i+1}$$

1.12 ± 0.03 according to our studies, indicates that the assumption regarding v_D and l_D is reasonable.

If an analogous mechanism for D → H exchange in nondeuteriated medium is considered (Scheme 3), then a steady-state treatement using E and S' yields eq. [13]. If S_H is the intrinsic selectivity in nondeuteriated medium, V_H and L_H are

$$[13] \quad (k_s)_{\text{obs}}^{\text{D}\to\text{H}} \simeq k_6' + k_1'\left(1 - \frac{k_2'}{k_2' + k_3'}\right)$$

the primary KIEs in fast and slow exchange, respectively, in nondeuteriated medium, and v_H and l_H are the respective α-secondary KIEs, then $S_H \simeq k_2'l_H/k_3'v_H \simeq k_f^{\text{H}\to\text{H}}/k_s^{\text{H}\to\text{H}}$, $k_1 \simeq k_f^{\text{H}\to\text{H}}/V_H$, $k_6' \simeq k_s^{\text{H}\to\text{H}}/L_H$, and $k_f^{\text{D}\to\text{H}} \simeq k_f^{\text{H}\to\text{H}}/V_Hv_H$. By making the appropriate substitutions into eq. [13] and since $S_H >> v_H$ and l_4, eq. [14] is obtained. If v_H and l_H are set equal to 1 and $V_H \simeq L_H = i$ then eq. [14] is reduced to eq. [15].

$$[14] \quad (k_f/k_s)_{\text{obs}}^{\text{D}\to\text{H}} \simeq \frac{S_HL_Hv_H}{V_H(L_Hl_H + v_H^2)}$$

That $V_D \simeq V_H \simeq L_D \simeq L_H = i$ is reasonable since the protonation

$$[15] \quad (k_f/k_s)_{\text{obs}}^{\text{D}\to\text{H}} \simeq \frac{S_H}{i+1}$$

KIE is expected to be similar in magnitude to the deprotonation KIE and primary KIEs measured in nondeuteriated and deuteriated medium are very similar. Pocker (24) studied the hydroxide (deuteroxide) bromination of actone and perdeuteroacetone and established that $(k_H/k_D)_{H_2O} = (k_H/k_D)_{D_2O} = 7.5$. Jones (18), in a more recent study of the rates of abstraction of hydrogen, deuterium, and tritium from acetone by OH^- (OD^-),

[6] Even though $(k_f)_{\text{obs}}$ is actually equal to $k_f + k_s$, the assumption that $(k_f)_{\text{obs}} \simeq k_1V_D$ is valid because $k_f \simeq 650 \times k_s$.

[7] If the ZPEs (zero point energies) for C—H and C—D of substrate and the transition state are considered and a common intermediate is generated, then if ΔZPE in the transition state is ½ ΔZPE for substrate, k_H/k_D for protonation ≃ k_H/k_D for deprotonation.

TABLE 6. Kinetic isotope effects for hydrogen isotope exchange of *exo*-3-chlorobicyclo[2.2.1]heptan-2-ones

Entry	KIE	
1	SIE^{H}	1.60 ± 0.04[a]
2	SIE^{D}	1.68 ± 0.16[b]
3	$(k_H/k_D)_{H_2O}$	6.9 ± 0.5[c]
4	$(k_H/k_D)_{D_2O}$	6.6 ± 0.3

[a] A ratio of the averages of entries 1 and 2 and 3 and 4 of Table 2.
[b] A ratio of entry 5 and the average of entries 6 and 7 of Table 2.
[c] A ratio of the averages of entries 1 and 2 and entry 5 of Table 2.
[d] A ratio of the averages of entries 3 and 4 and 6 and 7 of Table 2.

established that $(k_H/k_D)_{H_2O} = 9.8 \pm 0.5$ and $(k_H/k_D)_{D_2O} = 11.2 \pm 0.4$. The secondary KIE for 5 deuterium atoms was shown to be 1.067. The reason for the difference between Pocker's and Jones' findings is not clear. It is interesting to note that the solvent KIEs for acetone and perdeuterated acetone were 1.47 ± 0.07 and 1.28 ± 0.05, respectively. Long and Watson (25) studied the acetate-catalyzed bromination of methylacetylacetone in H_2O and D_2O and found $(k_H/k_D)_{H_2O} = 5.8$ and $(k_H/k_D)_{D_2O} = 5.6$. As is seen from the data in Table 6, the primary KIEs for *endo*-proton abstraction of **1***c* and **1***d*, perhaps a better model for exchange of **1***a*, in H_2O and D_2O are 6.9 ± 0.5 and 6.6 ± 0.3, respectively. The solvent KIEs for *endo*-proton abstraction from **1***c* and *endo*-deuteron abstraction from **1***d* are 1.60 ± 0.04 and 1.68 ± 0.16, respectively. The data establish that the primary KIEs are not substantially different in nondeuteriated and deuteriated medium. The same surely holds for the secondary KIEs as well. Consequently, we predict that if exchange by inversion contributes significantly to exchange of the slow proton of a diastereotopic pair, then $(k_f/k_s)_{obs}^{H\to D}$ should differ substantially from $(k_f/k_s)_{obs}^{D\to H}$. The ratio of eqs. [12] and [15] yields eq. [16]

$$[16] \quad (k_f/k_s)_{obs}^{H\to D}/(k_f/k_s)_{obs}^{D\to H} \simeq \frac{S_D i}{i+1} \Big/ \frac{S_H}{i+1} \simeq i$$

and i should range between $4 \to 8$. A number of examples where this is the case have now been documented and are listed in Table 7. It is interesting to note that Lamaty and co-workers (30) have corroborated our findings for exchange of **1***a*. It is clear that our prediction is supported in every case where the intrinsic selectivity is greater than the primary isotope effects. If exchange occurred only with retention, then, neglecting solvent isotopic effects, the ratios of the rate constants for $H \to D$ and $D \to H$ exchange yield eq. [17]

$$[17] \quad \frac{(k_f/k_s)_{obs}^{H\to D}}{(k_f/k_s)_{obs}^{D\to H}} \simeq \frac{S_D l_D}{\dfrac{L_H S_H}{V_H \nu_H}} \simeq \frac{V_H l_D \nu_H}{L_H}$$

since $S_H = S_D$. It can be argued that vastly different primary KIEs for $D \to H$ exchange, especially for the cases where k_f and k_s are substantially different, could, coupled with secondary KIEs, account for the observed difference between $(k_f/k_s)_{obs}^{H\to D}$ and $(k_f/k_s)_{obs}^{D\to H}$. Since the secondary KIEs are small ($\simeq 1.1$) and the primary KIEs are expected not to be vastly different, certainly not by a factor of 4 or more, especially for exchange of camphor (**3**), the experimental results are not in accord with exchange by retention only. From Table 6 it is seen that k_H/k_D for *endo* abstraction in **1***c* in H_2O is 6.9 ± 0.5. Bell and Grainger (31), by a study of the mutarotation of *endo*-3-bromo-(+)-camphor and its *exo-d* analog, established that k_H/k_D for *exo* abstraction was 6.9 in 15% DMSO/H_2O at 25°C. Since k_H was 0.54 M^{-1} s^{-1} and 0.49 M^{-1} s^{-1} in 15% DMSO/H_2O and 45% dioxane/H_2O, respectively, the primary KIE is expected to be similar in dioxane/H_2O. Since *endo*-3-bromo-camphor should be a reasonably good model for *exo* exchange of *endo*-3-chlorobicyclo[2.2.2]heptan-2-one, the data suggest that the *exo* and *endo* KIEs for exchange of [2.2.1]-ketones should not be vastly different. Tidwell and co-workers have shown that the primary KIE for *exo* abstraction of **1***a* is 5 in 2:1 dioxane/NaOD/D_2O (8). If solvent isotope effects (SIEs) are included for $H \to D$ exchange (Scheme 2) then with

$$S_D \simeq \frac{k_1 V_D SIE_6}{k_6 l_D SIE_1} \simeq \frac{k_2 V_D' SIE_2}{k_3 L_D' SIE_3},$$

$$k_6 \simeq \frac{k_1 V_D SIE_6}{S_D l_D SIE_1} \simeq \frac{k_f SIE_6}{S_D l_D SIE_1}$$

appropriate substitution into eq. [7] yields eq. [18]. A ratio of eqs. [18] and [14] yields eq. [19].

$$[18] \quad (k_f/k_s)_{obs}^{H\to D} \simeq \frac{S_D L_D' l_D SIE_1}{\left[L_D' + \dfrac{SIE_1 SIE_3}{SIE_6 SIE_2}\left(\dfrac{V_D' l_D}{V_D}\right)\right] SIE_6}$$

$$[19] \quad \frac{(k_f/k_s)_{obs}^{H\to D}}{(k_f/k_s)_{obs}^{D\to H}} \simeq \frac{(V_H L_D' l_D)(L_H l_H + \nu_H^2) SIE_1}{\left[L_D' + \dfrac{SIE_1 SIE_3}{SIE_6 SIE_2}\left(\dfrac{V_D' l_D}{V_D}\right)\right] SIE_6} \left(\frac{1}{L_H \nu_H}\right)$$

If ν_H and l_H are set equal to 1 and V_D, V_D', V_H, L_H, and L_D' are set equal to i, then in the case where exchange of the slow proton occurs by inversion, eq. [20] is obtained.

$$[20] \quad \frac{(k_f/k_s)_{obs}^{H\to D}}{(k_f/k_s)_{obs}^{D\to H}} \simeq \left[\frac{i(i+1)}{i + \left(\dfrac{SIE_1 SIE_3}{SIE_6 SIE_2}\right)}\right] \frac{SIE_1}{SIE_6}$$

For the case where exchange occurs by retention only, inclusion of SIEs into eq. [17] yields eq. [21].

$$[21] \quad \frac{(k_f/k_s)_{obs}^{H\to D}}{(k_f/k_s)_{obs}^{D\to H}} \simeq \frac{V_H l_D \nu_H SIE_1}{L_H SIE_6}$$

Thus, if SIE_1 was substantially greater than SIE_6 and $V_H > L_H$, the difference between $(k_f/k_s)_{obs}^{H\to D}$ and $(k_f/k_s)_{obs}^{D\to H}$ could be indicative of a mechanism which involves exchange only by retention. Unfortunately there are no data available in the literature on the relative magnitudes of the SIEs for exchange of diastereotopic protons. However, there is no reason to expect the SIEs to be substantially different, especially in the cases, i.e. camphor, where k_f and k_s are not vastly different. It is interesting to note that on the basis of our proposal, using eqs. [9] and [14], given eq. [22], and assuming that $SIE_1 \simeq SIE_6$ and $SIE_2 \simeq SIE_3$,

TABLE 7. Ratios of rate constants for base-catalyzed hydrogen isotope exchange of ketones

	$(k_f/k_s)^{H \to D}$	$(k_f/k_s)^{D \to H}$	$(k_f/k_s)^{T \to H}$
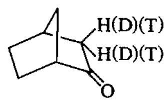	658 ± 66 (this work) 700 (ref. 30)	91 ± 9 (this work) 100 (ref. 30)	81 (ref. 28)
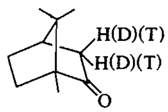	18 (ref. 26) 21 (ref. 27)	2 (ref. 26)	4 (ref. 28)
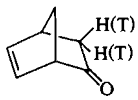	120 (ref. 27)		19 (ref. 28)
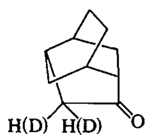	293 ± 20 (ref. 29)	63 ± 5 (ref. 29)	

$$[22] \quad \frac{k_f^{H \to D}}{k_f^{D \to H}} \simeq V_H \nu_H \mathrm{SIE}_I$$

eq. [23] is obtained and rearranged into eq. [24].

$$[23] \quad (k_s/k_f)_{obs}^{H \to D} \times (k_f/k_s)_{obs}^{D \to H} \simeq \left[\frac{L_D' + \dfrac{V_D'}{V_D} l_D}{S_D L_D' l_D}\right]\left[\frac{S_H L_H \nu_H}{V_H(L_H l_H + \nu_H^2)}\right]$$

$$[24] \quad \left(\frac{k_s^{H \to D}}{k_s^{D \to H}}\right)_{obs} \simeq \left[\frac{L_D' + \dfrac{V_D' l_D}{V_D}}{S_D L_D' l_D}\right]\left[\frac{S_H L_H \nu_H}{V_H(L_H l_H + \nu_H^2)}\right][V_H \nu_H \mathrm{SIE}_I]$$

If $S_D = S_H$, $L_D \simeq L_D' \simeq L_H$, $V_D \simeq V_D'$, and $l_D = l_H = \nu_H = 1$ then eq. [24] is reduced to eq. [25].

$$[25] \quad \left(\frac{k_s^{H \to D}}{k_s^{D \to H}}\right)_{obs} \simeq \mathrm{SIE}_I$$

If exchange of the slow proton occurs by retention only, then eq. [21] is rearranged into eq. [26]

$$[26] \quad \left(\frac{k_f}{k_s}\right)_{obs}^{H \to D}\left(\frac{k_s}{k_f}\right)_{obs}^{D \to H} \simeq \frac{V_H l_D \nu_H \mathrm{SIE}_I}{L_H \mathrm{SIE}_6}$$

that yields eq. [27] using eq. [22] and assuming $l_D \simeq 1$.

$$[27] \quad \left(\frac{k_s^{H \to D}}{k_s^{D \to H}}\right)_{obs} \simeq L_H \mathrm{SIE}_6$$

It is seen from the data in Table 1 (entries 2, 3, and 9) that $(k_s^{H \to D}/k_s^{D \to H})_{obs} = 1.24 \pm 0.19$, in accord with our proposal, but not with the latter case, since L_H is expected to be ≥ 5.

While our analysis[8] is based on hydrogen isotope exchange α to a carbonyl group, it must also hold for exchange of diastereotopic protons for all carbon acids such as sulfoxides (32–35), sulfones (35), sulfonium salts (36), and *N*-nitrosoamines (37)[9] where a common intermediate is generated or the barrier to inversion of the incipient diastereomeric anions is less than the barrier to protonation. Although the barriers to inversion of carbanions appear to be quite low (38), we expect that in the case where diastereomeric anions are formed and the inversion barrier is high, provided the primary, secondary, and SIEs are not vastly different for the fast and slow protons, $(k_f/k_s)^{H \to D} \simeq (k_f/k_s)^{D \to H}$.

Presently, we are studying H → D and D → H exchange in several sulfoxides and plan to report our findings in the near future.

Experimental

Bicyclo[2.2.1]heptan-2-one (**1**) was obtained from Aldrich Chemical Co. and was purified by preparative gas chromotagraphy prior to use. *exo*-3-Chlorobicyclo[2.2.1]heptan-2-one and its deuteriated analog were prepared by the chlorination of **1***a* and **1***b*, respectively, according to the method of Tobler *et al.* (39) and were separated and purified by preparative gas chromatography.

Kinetic methods

Base-catalyzed exchange

(a) *Ketones* **1**a *and* **1**b

The method described in a previous publication (14) was used to determine the rates of H → D and D → H exchange of the diastereotopic protons and deuterons of **1***a* and **1***b*, respectively.

(b) *Chloroketones* **1**c *and* **1**d

The method described previously (13) was used to determine the rates of H → D and D → H exchange of **1***c* and **1***d*, respectively.

[8] All the derivations of equations have been deposited as Supplementary Material. Copies may be obtained at a nominal charge, from the Depository of Unpublished Data, CISTI, National Research Council of Canada, Ottawa, Ont., Canada, K1A 0S2.

[9] The references listed are only representative of the systems which have been studied. Many other examples have been documented.

Acid-catalyzed exchange

Stock solutions of 2.00 *N* HCl and 2.08 *N* DCl were prepared by diluting concentrated HCl and DCl in H_2O and D_2O, respectively. In a typical run, ketone (0.020–0.030 g) was dissolved in 1–2 mL of CH_3COOH/2.00 *N* HCl or CH_3COOD/2.08 *N* DCl and aliquots (~0.1 mL) were sealed in thick-walled tubes and placed in a fluidized sand bath maintained at 100.0 ± 0.5°C. The tubes were withdrawn at appropriate intervals, quenched with liquid nitrogen, and stored in a freezer. Mass spectrometric analyses were carried out on a Hitachi–Perkin–Elmer RMU6A mass spectrometer at low voltage by simply subliming the volatile ketone into the spectrometer inlet system.

Bicyclo[2.2.1]heptan-2-one-3,3-d_2 *(1*b*)*

Ketone **1***a* (3 g) was heated in a sealed tube with 20 mL of 0.5 *N* NaOD/D_2O for 16 h at 140°C. The aqueous layer was extracted with purified pentane (3 × 20 mL), the combined pentane extracts were dried over Na_2SO_4, and most of the pentane was distilled off through a 30-cm Vigreux column. The final traces of solvent were removed under vacuum to yield 2.6 g (87%) of deuterated ketone. Mass spectrometric analysis established that the ketone was composed of 94.30% d_2, 3.91% d_1, and 1.83% d_0 species. The ketone was purified by preparative gas chromatography prior to its use in kinetic runs.

Bicyclo[2.2.1]heptan-2-one-endo-*3*-d *(1*f*)*

The 3,3-dideuterated ketone (0.2 g) was heated in 60% dioxane – 40% aqueous NaOH and was monitored periodically by mass spectrometry until <1% dideuterated ketone was present. The solution was worked up as described above to yield the desired monodeuterio substrate.

Acknowledgements

We thank the Natural Sciences and Engineering Research Council of Canada for financial support.

1. S. FORSÉN and N. M. NILSSON. *In* The chemistry of the carbonyl group. Vol II. *Edited by* S. Patai. John Wiley and Sons, Inc., New York, NY. 1970. pp. 157–240.
2. E. BUNCEL. *In* Carbanions: mechanistic and isotopic aspects. Monograph 9. *Edited by* C. Eaborn and N. B. Chapman. Elsevier Scientific Publishing Col., Amsterdam. 1975. pp. 69–93.
3. J. TOULLEC. *In* Advances in physical organic chemistry. Vol. 18. *Edited by* V. Gold and D. Bethell. Academic Press, London. 1932. pp. 1–77.
4. A. F. THOMAS and B. WILLHALM. Tetrahedron Lett. 1309 (1965).
5. J. M. JERKUNICA, S. BORČIĆ, and D. E. SUNKO. Tetrahedron Lett. 4465 (1965).
6. A. F. THOMAS, R. A. SCHNEIDER, and J. MEINWALD. J. Am. Chem. Soc. **89**, 68 (1967).
7. P. BARRACLOUGH and D. W. YOUNG. Tetrahedron Lett. 2293 (1970).
8. G. A. ABAD, S. P. JINDAL, and T. T. TIDWELL. J. Am. Chem. Soc. **95**, 6326 (1973).
9. N. H. WERSTIUK and R. J. TAILLEFER. Can. J. Chem. **48**, 3966 (1970).
10. S. BANERJEE and N. H. WERSTIUK. Can. J. Chem. **53**, 1099 (1975).
11. S. BANERJEE and N. H. WERSTIUK. Can. J. Chem. **54**, 678 (1976).
12. N. H. WERSTIUK and S. BANERJEE. Can. J. Chem. **55**, 173 (1977).
13. N. H. WERSTIUK, R. J. TAILLEFER, and S. BANERJEE. Can. J. Chem. **56**, 1140 (1978).
14. N. H. WERSTIUK, R. J. TAILLEFER, and S. BANERJEE. Can. J. Chem. **56**, 1148 (1978).
15. N. H. WERSTIUK and P. ANDREWS. Can. J. Chem. **56**, 2605 (1978).
16. N. H. WERSTIUK and S. BANERJEE. J. Org. Chem. **46**, 470 (1981).
17. J. WARKENTIN and D. S. TEE. J. Am. Chem. Soc. **88**, 5540 (1966).
18. J. R. JONES. Trans. Faraday Soc. **61**, 95 (1965).
19. R. A. MORE O'FERRALL and S. SLAE. J. Chem. Soc. (B), 260 (1970).
20. E. A. WALTERS and F. A. LONG. J. Phys. Chem. **76**, 362 (1972).
21. E. A. HALEVI and F. A. LONG. J. Am. Chem. Soc. **83**, 2809 (1961).
22. Y. CHIANG, A. J. KRESGE, Y. S. TANGE, and J. WIRTZ. J. Am. Chem. Soc. **106**, 460 (1984).
23. R. OHNISHI. J. Chem. Soc. Perkin Trans. 2, 530 (1980).
24. Y. POCKER. Chem. Ind. (London) 1383 (1959).
25. F. A. LONG and D. WATSON. J. Chem. Soc. 2019 (1958).
26. W. O. CRAIN. Ph.D. Thesis, Indiana University. 1969.
27. T. T. TIDWELL. J. Am. Chem. Soc. **92**, 1448 (1970).
28. M. LAJUNEN and H. PILBACKA. Acta. Chem. Scand. **30**, 391 (1976).
29. R. R. FRASER and P. J. CHAMPAGNE. J. Am. Chem. Soc. **100**, 657 (1978).
30. G. LAMATY. *In* Isotopes in organic chemistry. Vol. 2. *Edited by* E. Buncell and C. C. Lee. Elsevier, Amsterdam. 1976. p. 33.
31. R. P. BELL and S. GRAINGER. J. Chem. Soc. Perkin Trans. 2, 1606 (1976).
32. B. J. HUTCHINSON, K. K. ANDERSON, and A. K. KATRITZKY. J. Am. Chem. Soc. **91**, 3839 (1969).
33. R. R. FRASER, F. J. SCHUBER, and Y. Y. WIGFIELD. J. Am. Chem. Soc. **94**, 8795 (1972).
34. J. F. KING and J. R. DU MANOIR. Can. J. Chem. **51**, 4082 (1973).
35. U. FOLLI, D. IAROSSI, I. MORETTI, F. TADDEI, and G. TORRE. J. Chem. Soc. Perkin Trans. 2, 1655 (1974).
36. G. BARBARELLA, A. GARBESI, A. BOICELLI, and A. FAVA. J. Am. Chem. Soc. **95**, 8051 (1973).
37. R. R. FRASER and Y. Y. WIGFIELD. Tetrahedron Lett. **27**, 2505 (1971).
38. P. R. PEOPLES and J. B. GRUTZNER. J. Am. Chem. Soc. **102**, 4709 (1980).
39. E. TOBLER, D. E. BATTIN, and D. J. FOSTER. J. Org. Chem. **29**, 2834 (1964).

The gas-phase photochemistry and thermal decomposition of glyoxylic acid[1]

R. A. BACK AND S. YAMAMOTO[2]

Division of Chemistry, National Research Council of Canada, 100 Sussex Drive, Ottawa, Ont., Canada K1A 0R6

Received April 24, 1984

R. A. BACK and S. YAMAMOTO. Can. J. Chem. **63**, 542 (1985).

The photolysis of glyoxylic acid vapour has been studied at five wavelengths, 382, 366, 346, 275, and 239 nm, and pressures from about 1 to 6 Torr, at a temperature of 355 K. Major products were CO_2 and CH_2O, initially formed in almost equal amounts, while minor products were CO and H_2. Except at 382 nm, the system was complicated by the rapid secondary photolysis of CH_2O. Three primary processes are suggested, each involving internal H-atom transfer followed by dissociation.

The absorption spectrum is reported and shows the three distinct absorption systems. A finely-structured spectrum from about 320 to 400 nm is attributed to a transition to the first excited $\pi^* \leftarrow n_+$ singlet state; a more diffuse absorption ranging from about 290 nm to a maximum at 239 nm is assigned to the $\pi^* \leftarrow n_-$ state, while a much stronger absorption beginning below 230 nm is attributed to the $\pi^* \leftarrow \pi$ transition. Product ratios vary with wavelength and depend on which excited state is involved.

The thermal decomposition was studied briefly in a static system at temperatures from 470 to 710 K and pressures from 0.4 to 8 Torr. Major products were again CO_2 and CH_2O, but the latter was always less than stoichiometric. First-order rate constants for the apparently homogeneous formation of CO_2 are described by Arrhenius parameters log A (s^{-1}) = 7.80 and E = 30.8 kcal/mol. Carbon monoxide and H_2 were minor products, and the CO/CO_2 ratio increased with increasing temperature and showed some surface enhancement at lower temperatures. The SF_6-sensitized thermal decomposition of glyoxylic acid, induced by a pulsed CO_2 laser, was briefly studied, with temperatures estimated to be in the 1100−1600 K range, and the CO/CO_2 ratio increased with increasing temperature, continuing the trend observed in the static system.

R. A. BACK et S. YAMAMOTO. Can. J. Chem. **63**, 542 (1985).

Opérant à des pressions allant de 1 à 6 Torr et à une température de 355 K, on a étudié la photolyse de l'acide glyoxylique en phase vapeur aux cinq longueurs d'onde suivantes: 382, 366, 346, 275 et 239 nm. Les produits principaux sont le CO_2 et le CH_2O qui se forment initialement en quantités pratiquement égales; il se forme aussi du CO et du H_2 comme produits mineurs. Excepté à 382 nm, le système est compliqué par la photolyse secondaire rapide du CH_2O. On suggère l'existence de trois processus primaires qui impliquent tous un transfert interne d'un atome d'hydrogène qui serait suivi par une dissociation.

On rapporte le spectre d'absorption qui présente trois systèmes distincts d'absorption. On attribue le spectre à structure fine, qui s'étale de 320 à 400 nm, à une transition vers le premier état singulet excité $\pi + \leftarrow n_+$; on attribue une absorption plus diffuse, qui va de 290 nm jusqu'à un maximum à 239 nm, à l'état $\pi^* \leftarrow n_-$ alors que l'absorption beaucoup plus forte qui commence en dessous de 239 nm serait due à la transition $\pi^* \leftarrow \pi$. Les rapports des quantités de produits obtenus varient avec la longueur d'onde utilisée pour provoquer la photolyse et ils dépendent de l'état excité impliqué.

Opérant à des températures allant de 470 à 710 K et à des pressions allant de 0,4 à 8 Torr, on a brièvement étudié la décomposition thermique dans un système statique. De nouveau, les produits majeurs sont le CO_2 et le CH_2O; toutefois, la quantité formée de ce dernier composé est toujours inférieure à la stoïchiométrie. Les constantes de vitesse du premier ordre, pour la formation apparement homogène de CO_2, est décrite par les paramètres d'Arrhénius suivants: log A (s^{-1}) = 7,80 et E = 30,8 kcal/mol. Le CO et le H_2 sont formés comme produits mineurs; le rapport CO/CO_2 augmente avec une augmentation de la température et, à basse température, il est rehaussé par la présence de surfaces. On a brièvement étudié la décomposition thermique de l'acide glyoxylique, sensibilisée par du SF_6 et induite par un laser pulsé au CO_2; on a évalué que les températures se situaient entre 1100 et 1600 K et, comme dans le système statique, le rapport CO/CO_2 augmente avec une augmentation de la température.

[Traduit par le journal]

Introduction

The photolysis and spectroscopy of glyoxal and biacetyl have been the subjects of much investigation and interest, but few other α-dicarbonyl compounds have been studied in the gas phase. We have recently completed studies of the spectroscopy (1) and photochemistry (2) of oxalic acid vapour, and the present paper describes the extension of this work to glyoxylic acid, H—C(=O)—C(=O)—O—H. The thermal decomposition and the decomposition induced by a pulsed infrared laser were also studied for comparison with the photolysis.

Experimental

The apparatus and techniques were similar to those used with oxalic acid (2). Photolyses were done in a cylindrical quartz vessel, 10 cm long and 5 cm in diameter, with the vessel and gas-handling manifold kept at a temperature of 355 K, high enough to permit an adequate vapour pressure but low enough so that thermal dark reaction was minimal, and no correction was needed. The thermal decomposition was studied in a static system, a cylindrical quartz vessel 11 cm long and 3 cm in diameter heated in a tube furnace. The laser-induced pyrolysis was done in a cylindrical Pyrex vessel, 10 cm long and 4 cm in diameter, fitted with NaCl windows, also held at 355 K.

The light source for the ultraviolet photolysis was a 1000 W Hg-Xe high pressure arc lamp with matching monochromator that gave a band width of about 20 nm. For the laser-induced decomposition, a Lumonics Model 203 pulsed CO_2 TEA laser was used, as previously described (2, 3).

Glyoxylic acid (98% pure) was obtained from Aldrich as the hydrate, and was dehydrated by judicious heating and pumping until a constant vapour pressure was attained; it was thoroughly pumped to remove any decomposition products before each experiment. Propylene was Phillips Research grade.

[1]NRCC 23762.

[2]NRCC Research Associate, 1981−1983. Present address: Department of Chemistry, Okayama University, Tsushima, Okayama 700, Japan.

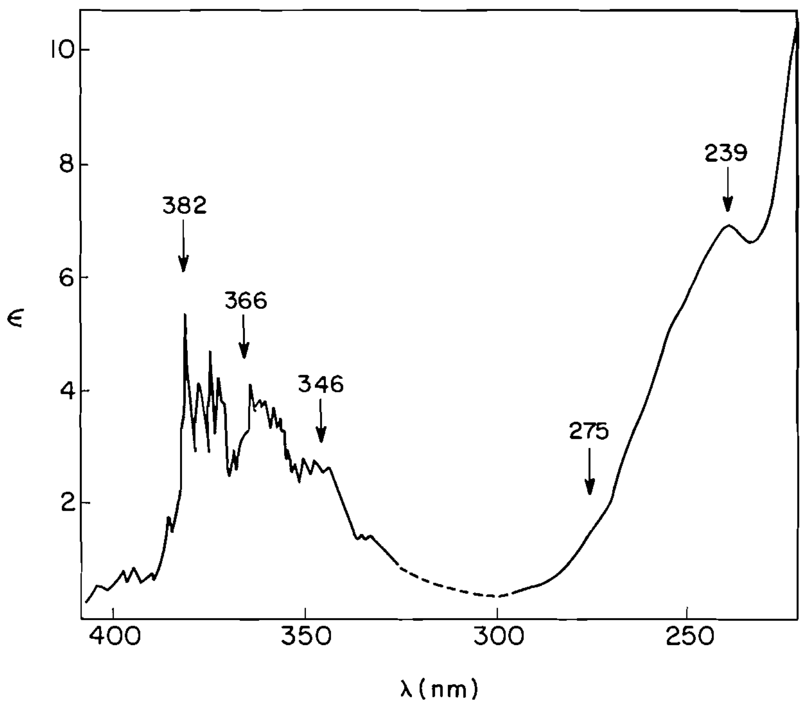

FIG. 1. Low-resolution absorption spectrum of glyoxylic acid vapour. ε = molar decadic extinction coefficient.

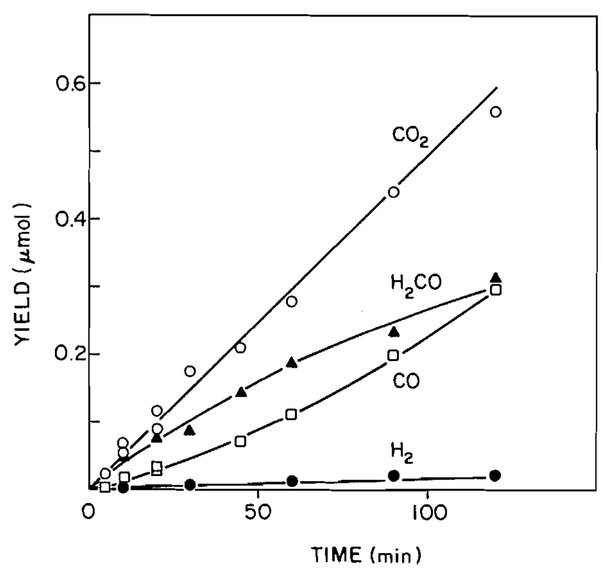

FIG. 2. Time dependence of products in the photolysis of glyoxylic acid at 366 nm and a pressure of 4 Torr.

Results

Absorption spectrum

The absorption spectrum of glyoxylic acid vapour, previously unreported, was measured in a modified Heath spectrophotometer fitted with a 4 m heated cell, and is shown in Fig. 1. Three absorption systems are evident. The highly structured spectrum extending from about 320 to 400 nm undoubtedly corresponds to excitation of the $\pi^* \leftarrow n_+$ first excited singlet state. The absorption beginning at about 290 nm and extending to a maximum at 239 nm, with broad diffuse vibrational features, is probably due to the $\pi^* \leftarrow n_-$ excitation, while the much stronger absorption setting in below about 230 nm is most probably from a $\pi^* \leftarrow \pi$ excited state. The photolysis was studied at the five wavelengths indicated in Fig. 1, three in the first absorption system and two in the second. A more detailed account and analysis of this spectrum will be published elsewhere (4).

Ultraviolet photolysis

Major primary products of the photolysis were CO_2 and formaldehyde, with much smaller amounts of H_2 and CO. The time dependence of products at 366 nm is shown in Fig. 2. Production of CO_2 was linear with time at this and all other wavelengths. Yields of H_2CO, however, fell with increasing time, and those of CO increased, and similar behaviour was observed at 346, 275, and 239 nm. In the photolysis at 382 nm, however, both CO_2 and CO were linear functions of time; yields of H_2CO could not be measured accurately because the amounts were quite small at this wavelength.

Experiments at 366 nm with added air or propylene at pressures up to 50 Torr showed no difference in the production of CO_2, indicating that neither free radicals nor triplet states were involved in its formation.

Some light emission was observed on excitation between 340 and 380 nm, but the excitation spectrum was almost exactly that of formaldehyde and thus the emission was very probably from excitation of formaldehyde product; there may have been some weak underlying emission from glyoxylic acid itself.

Thermal decomposition

The thermal decomposition was studied in a static system at pressures from 0.4 to 8 Torr and temperatures from 470 to 710 K. Products observed and measured were those observed in the photolysis, CO_2, H_2CO, CO, and H_2, all volatile at dry-ice temperature. No systematic search was made for higher products. Figure 3 shows an Arrhenius plot of the first-order rate-constant for the formation of CO_2. No trend with pressure was observed between 2.5 and 8 Torr, and all the data shown were obtained in this range. At lower pressures the rate constant decreased substantially (Fig. 4). Formaldehyde was always less than CO_2, with the ratio reaching a constant value of about 0.8

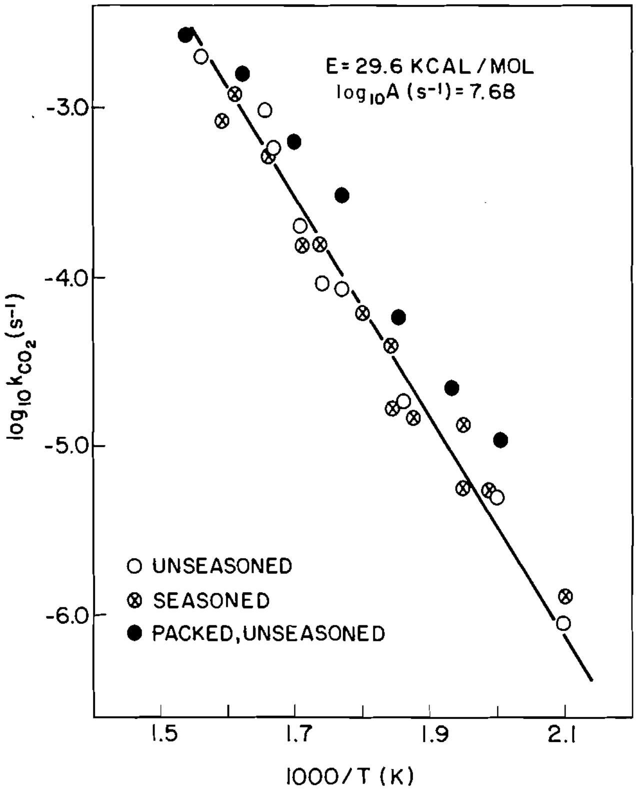

FIG. 3. Arrhenius plot for the first-order rate constant for the formation of CO_2 in the thermal decomposition of glyoxylic acid.

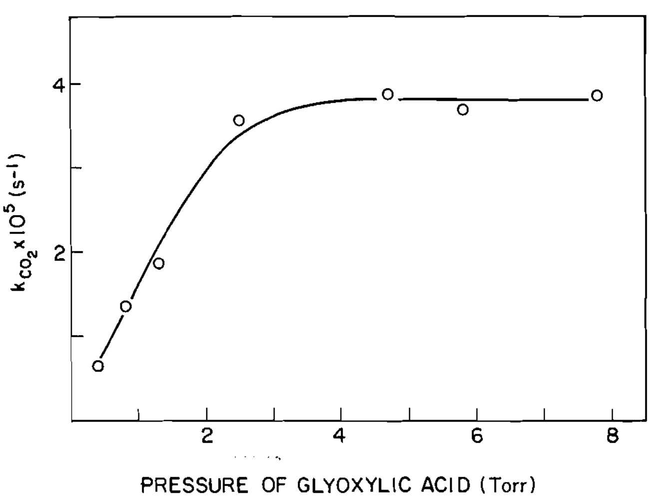

FIG. 4. Pressure dependence of the first-order rate constant for the formation of CO_2.

above 625 K, and falling markedly at lower temperatures (Fig. 5). Yields of CO and H_2 were each less than 10% of the CO_2 and decreased with decreasing temperature (Fig. 6). All products were linear functions of time at the low conversions attained in the experiments.

Decomposition induced by a pulsed infrared laser

Glyoxylic acid did not itself absorb infrared radiation at the wavelengths of the CO_2 laser, but its decomposition was easily sensitized by a small pressure of SF_6, which is a strong absorber. Two sets of experiments were done, one with a constant pressure of 1.2 Torr of SF_6 and varying pressures of glyoxylic acid, the other with a constant pressure of 2.8 Torr of glyoxylic acid and variable SF_6 pressure. Results are shown in Figs. 7 and 8. Although the extent of decomposition of the reagent in the laser beam (1.2 cm diameter) was quite high in some of these experiments, product yields were proportional to the number of pulses up to about four pulses, with the reagent in the beam presumably replenished in the 2 s between pulses by diffusion and convection. All the data shown were obtained with two pulses per experiment.

The probability of decomposition, P, and the CO/CO_2 ratio, behaved in a parallel manner (Figs. 7 and 8), reflecting changes in the effective temperature of the system with changing gas composition. The major effect is that caused by dilution of the absorbing SF_6 by non-absorbing glyoxylic acid with consequent decrease in temperature. The decrease in P in Fig. 7 is less than expected, however, and the increase in P in Fig. 8 more than expected on this basis, as shown more clearly in a plot of P vs. mole fraction of SF_6 (Fig. 9). The explanation probably lies in a pressure dependence of the multiphoton absorption by SF_6, evident from the dependence of P on total pressure (indicated on Fig. 9 beside each experimental point). There is also probably an additional increase in P with pressure due to an increase in reaction time, as the hot gas cools more slowly after the pulse at higher pressure. A reaction time of the order of 1 ms can be estimated, and if the decomposition follows the Arrhenius parameters found in the static thermal decomposition (Fig. 3), reaction temperatures between about 1100 and 1500 K are indicated for the experiments shown in Figs. 7 and 8.

Figure 10 shows the effect of added air on the laser-induced decomposition. The decrease in P and in the CO/CO_2 ratio are again less than expected from simple dilution, and countervailing effects of total pressure on energy absorption and reaction time are again probably responsible. Figure 11 shows the effect of laser fluence (varied by means of a long-focus lens (4)) on the CO/CO_2 ratio.

Discussion

The photolysis products, their time dependence, and the lack of effect of O_2 and propylene, suggests strongly that the major primary process at all wavelengths is a simple photodissociation into CO_2 and formaldehyde. The increase in CO and the decrease in H_2CO production with increasing time points to a secondary photolysis of formaldehyde, a conclusion supported by the absence of this behaviour at 382 nm where formaldehyde is almost transparent. The secondary CO was not accompanied by H_2 in comparable amounts, and it appears that disproportionation reactions involving excited H_2CO and HCO, similar to those invoked in the photolysis of formaldehyde alone (5), are probably involved in CO formation. There were also smaller yields of CO and H_2 formed as primary products, and the following set of reactions accounts for our observations.

$$[1]\quad \mathrm{H{-}\overset{\overset{\displaystyle O}{\|}}{C}{-}\underset{\underset{\displaystyle O}{\|}}{C}{-}O{-}H} + h\nu \rightarrow CO_2 + H_2CO$$

$$[2]\quad \rightarrow CO_2 + CO + H_2$$

$$[3]\quad \rightarrow CO + HCOOH \text{ (or } 2CO + H_2O)$$

$$[4]\quad H_2CO + h\nu \rightarrow H_2CO^*$$

$$[5]\quad H_2CO^* \rightarrow CO + ?$$

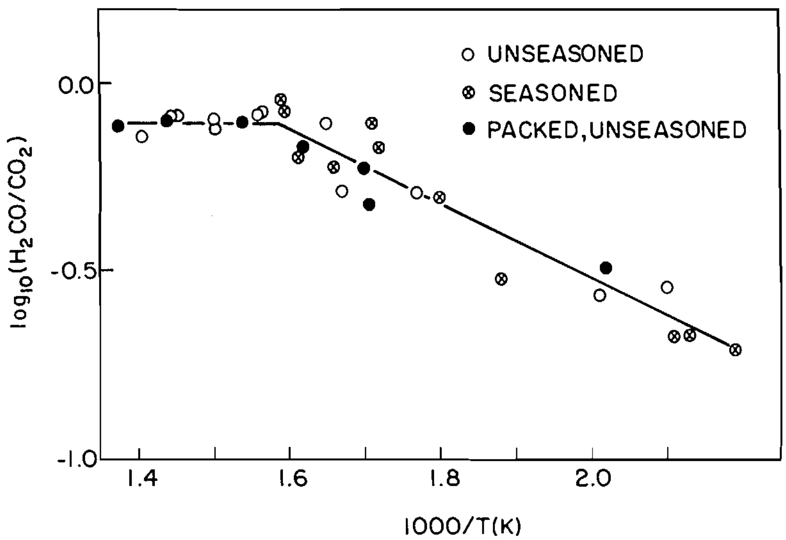

FIG. 5. Arrhenius plot of the ratio of formaldehyde to CO_2 from the thermal decomposition of glyoxylic acid.

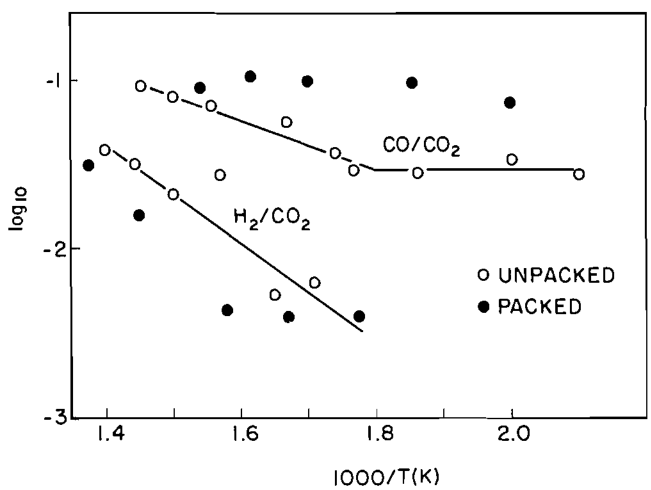

FIG. 6. Arrhenius plot of product ratios CO/CO_2 and H_2/CO_2 from the thermal decomposition of glyoxylic acid.

[6] $H_2CO^* \rightarrow$ other products

Reaction [1] was the predominant primary process at all wavelengths, while reaction [2], measured by the yield of H_2, was consistently about 3% of reaction [1] under all conditions. Reaction [3] is suggested to account for the primary production of CO unaccompanied by H_2. This process was clearly evident at 382 nm and easily measured directly. At 366 and 346 nm it was obscured by secondary production of CO via reaction [5] (Fig. 2). Reactions [5] and [6] are not elementary reactions, but simply represent formally the photochemical loss of formaldehyde with and without formation of CO. A simple mathematical modelling of reactions [1] to [6] to give the best fit to the time dependence of the CO/CO_2 ratio (Fig. 12) led to estimates of reaction [3] at these two wavelengths by extrapolation to zero time. At 275 and 239 nm a simple empirical extrapolation was used. Values for the yields of reactions [2] and [3], relative to that of [1], are shown in Table 1. Values of ϕ_3 are based on formation of CO + HCOOH; if 2CO + H_2O are formed instead, these would be halved. Neither HCOOH nor H_2O was measured in these systems, as the absolute amounts were small and easily lost by adsorption in the vacuum

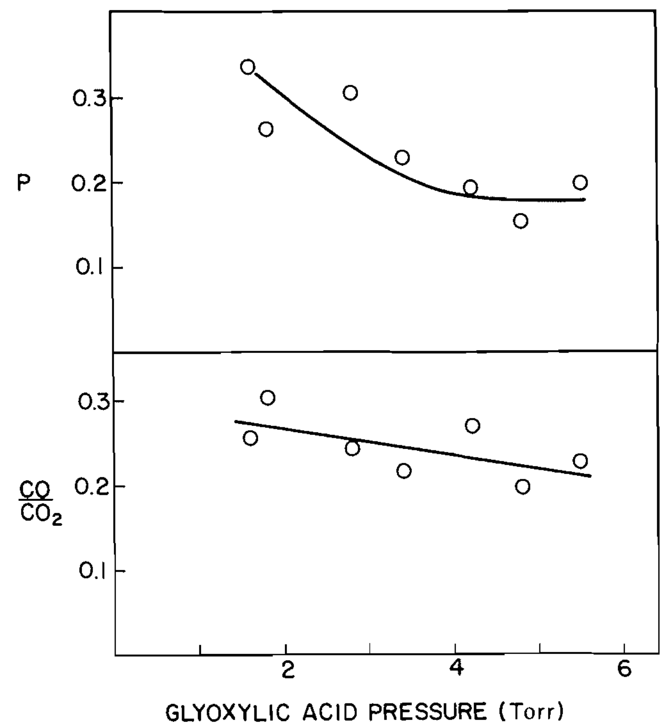

FIG. 7. Probability, P, decomposition of glyoxylic acid in the laser beam in a single pulse, and the CO/CO_2 product ratio, for the SF_6-sensitized thermal decomposition induced by a pulsed CO_2 laser. Pressure of SF_6 = 1.2 Torr.

line.

Absolute quantum yields of CO_2 were estimated at the three longest wavelengths using azomethane as an actinometer, and values of 0.08, 0.66, and 0.76 were obtained at 382, 366, and 346 nm, respectively. The trend with wavelength is probably real, but absolute values are rather uncertain, especially at 382 nm, because of the difficulty in estimating the light absorbed by the glyoxylic acid. Absorption was too weak to be measured directly in the 10-cm photolysis cell (the spectrum in Fig. 1 was obtained in a 4-m cell), and the sharp structure of the spectrum, especially at the longest wavelengths, made it hard to estimate effective extinction coefficients for the photolytic light. There

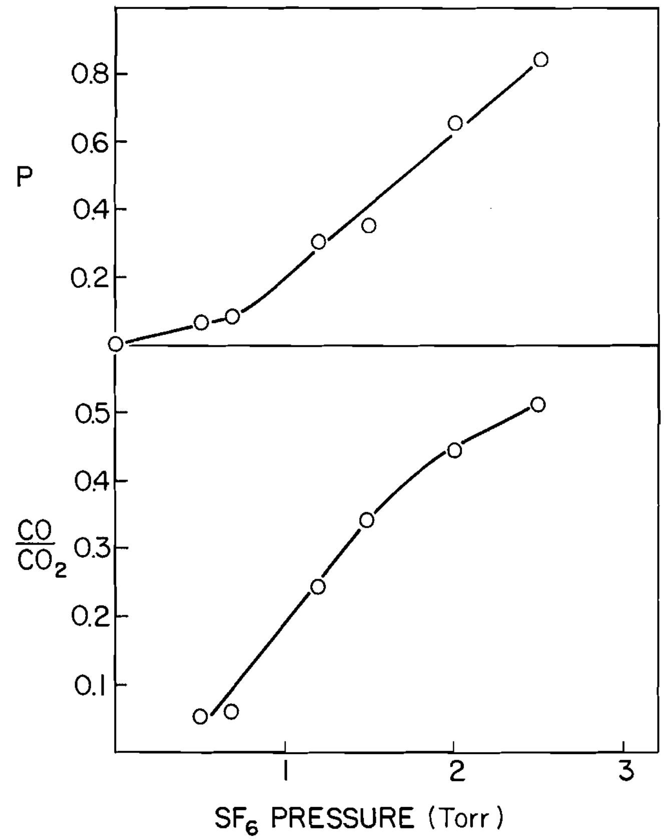

FIG. 8. Dependence of P and CO/CO_2 product ratio on pressure of added SF_6 in the laser-induced thermal decomposition of 2.8 Torr of glyoxylic acid.

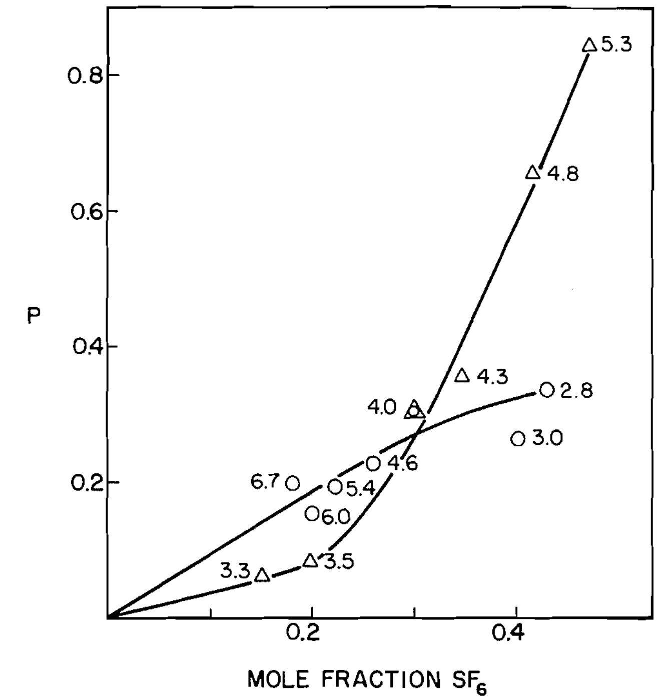

FIG. 9. Probability, P, of decomposition of glyoxylic acid vs. mole fraction of SF_6. Numbers show total pressure in Torr for each experiment.

was no evidence for collisional quenching of the photodissociation by added gas (air or propylene) up to 50 Torr at 366 nm, and no strong fluorescence was seen, so it seems probable that the absolute quantum yield at 366 nm and shorter wavelengths may have been close to unity; the lower value at 382 nm is probably real.

The photochemistry of glyoxylic acid differs from that of oxalic acid (2) in that the ratio Φ_1/Φ_3, and thence the CO/CO_2 ratio, depends strongly on wavelength (Table 1). At the three longest wavelengths, the CO/CO_2 ratio *decreases* with increasing photon energy, although in the thermal decomposition the same ratio *increases* with increasing temperature (see below). This indicates that the photolysis does not proceed through internal conversion and dissociation of the vibrationally-excited ground state, but probably occurs directly from the $\pi^* \leftarrow n_+$ singlet state or perhaps a short-lived triplet. As in oxalic acid, internal transfer of H to the carbonyl oxygen may be involved, with rearrangement of the resulting carbenes leading to H_2CO and HCOOH.

[7] 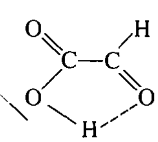 $\rightarrow CO_2 + \text{H}\ddot{\text{C}}\text{OH}$

[8] 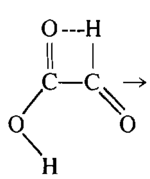 $\rightarrow CO + \text{HO}\ddot{\text{C}}\text{OH}$

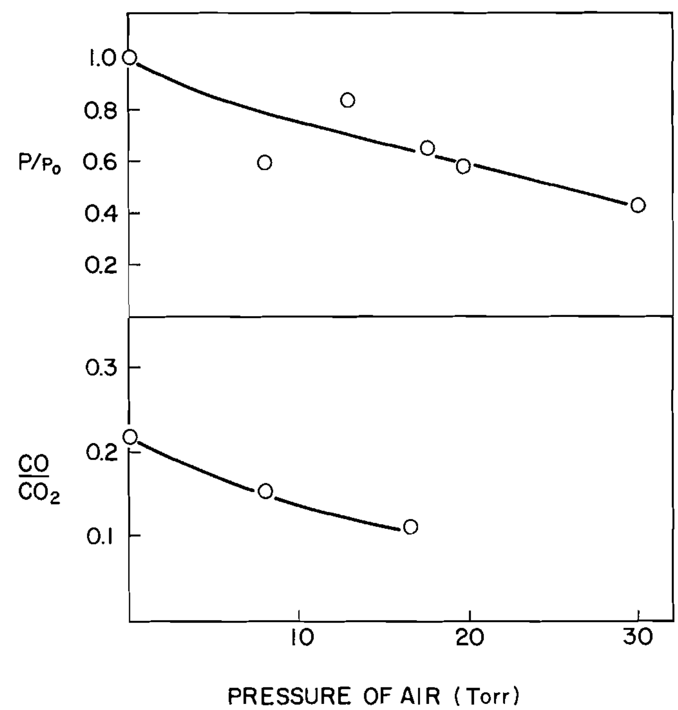

FIG. 10. Effect of added air on P and on the product ratio CO/CO_2 in the laser-induced thermal decomposition of glyoxylic acid. Glyoxylic acid = 2.8 Torr, SF_6 = 1.2 Torr, P_0 = probability of decomposition in the absence of air.

The observed minor formation of H_2 (reaction [2]) might arise from an alternative decomposition of HCOH into H_2 and CO. At the two shortest wavelengths, the CO/CO_2 ratio *increases* with increasing photon energy. It is clear from the absorption spectrum (Fig. 1) that the excitation here involves the second

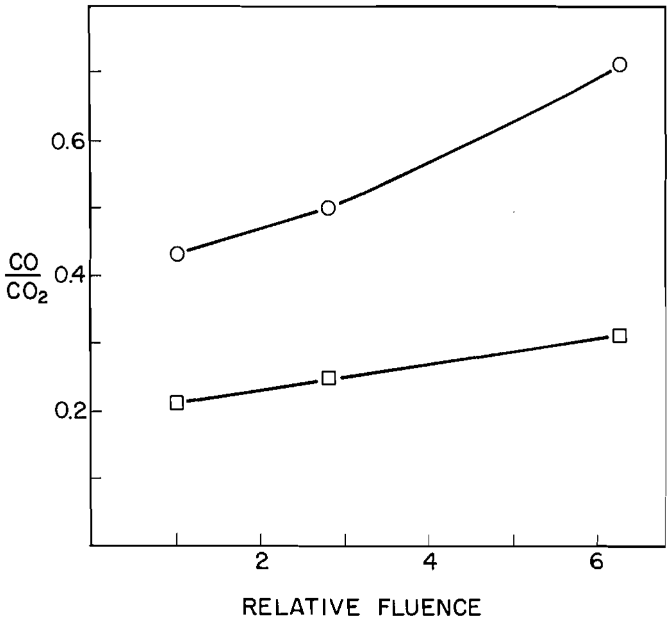

FIG. 11. Effect of laser fluence on CO/CO_2 product ratio in the laser-induced thermal decomposition of glyoxylic acid. Relative fluence is in arbitrary units. □ = 2.8 Torr glyoxylic acid, 1.2 Torr SF_6, ○ = 2.8 Torr glyoxylic acid, 2.6 Torr SF_6.

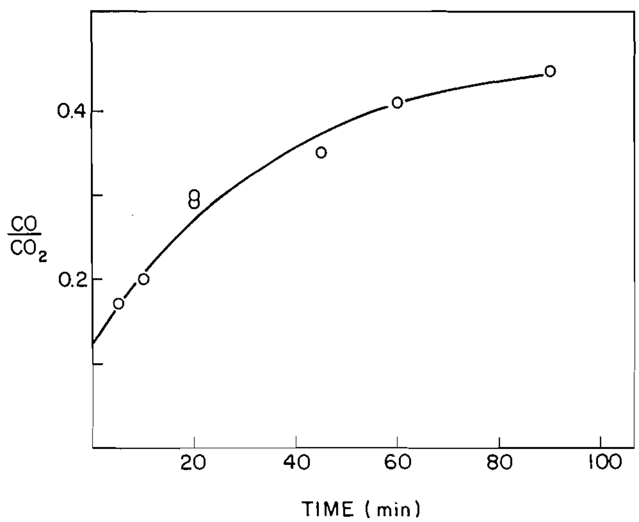

FIG. 12. Time dependence of the CO/CO_2 product ratio from the photolysis of glyoxylic acid at 366 nm. Curve is calculated from model based on mechanism in text. Points are experimental.

excited singlet state, $\pi^* \leftarrow n_-$, and perhaps the $\pi^* \leftarrow \pi$ state, which probably has a strong absorption tail underlying the former. A different decomposition mechanism, perhaps through the vibrationally excited ground state, is probably operative at these wavelengths.

The thermal decomposition is more complicated than the photolysis, although there seems to be no secondary decomposition of products as all yields were linear with time. At the higher temperatures, the major process is again the formation of CO_2 and H_2CO, but the latter remains at only 80% of its stoichiometric yield; at lower temperatures much more is missing (Fig. 5), perhaps lost through polymerization or reaction with glyoxylic acid to give higher products. Production of CO_2 showed some enhancement in the packed vessel, in which the

TABLE 1. Relative quantum yields of primary processes in the photolysis of glyoxylic acid

λ (nm)	ϕ_1	ϕ_2	ϕ_3
382	1.0	0.03	0.69
366	1.0	0.03	0.09
346	1.0	0.03	0.01
275	1.0	0.03	0.16
239	1.0	0.03	0.37

surface/volume ratio was increased by a factor of 4 (Fig. 3). A correction for surface reaction, assuming simple additivity with the gas-phase decomposition, led to corrected Arrhenius parameters of log A (s^{-1}) = 7.80 and E = 30.8 kcal/mol, not much changed from the values obtained before correction (Fig. 3). If these parameters can be ascribed to a simple homogeneous process,

[9] 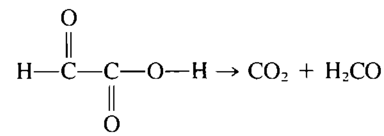

they may be compared with those for the similar formation of CO_2 and HCOOH from oxalic acid (6). The activation energies are almost the same (30.8 vs. 30 kcal/mol) but the frequency factor for glyoxylic acid is four orders of magnitude smaller. This is much too low for a normal simple unimolecular reaction. As with the corresponding decomposition of oxalic acid (2), one might expect reaction [9] to proceed by internal transfer of the O—H hydrogen through a four-membered transition state:[3]

[10] 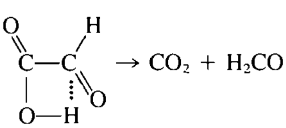

It is difficult to see why this should be a factor of 10^4 slower in glyoxylic acid, or in simpler terms, why glyoxylic acid should be so much more stable towards thermal decomposition than oxalic acid.

Formation of CO, at least at the lower temperatures, showed a strong surface enhancement while H_2, a very minor product, was somewhat reduced (Fig. 6). Carbon monoxide was not a product of the thermolysis of oxalic acid, which suggests that in glyoxylic acid it is formed by transfer of the aldehydic hydrogen:

[11] 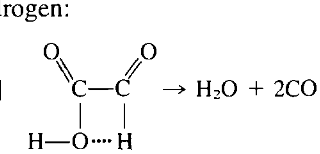

[12] 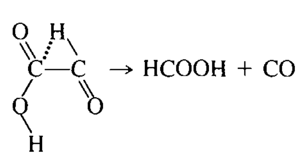

[3]Transfer of H to the carbonyl oxygen as in reaction [7] is unlikely in the thermal reaction because of the expected high energy required to form hydroxymethylene.

Neither H_2O nor HCOOH was detected, but their analysis in this system in the amounts expected is difficult, and either reaction [11] or [12] may have occurred. The upward trend in the CO/CO_2 ratio with increasing temperature evident in Fig. 6 continues in the laser-induced pyrolysis, reaching values as high as 0.71 at the highest fluence (Fig. 11).

It has been shown (7) that the most stable structure of glyoxylic acid in the gas phase is planar, with the two carbonyl groups in a *trans* configuration maintained by strong hydrogen bonding. All the processes we have suggested, both in the thermal and the photochemical decomposition, proceed from this configuration except for reaction [11] which would require a *cis* structure. The barrier to isomerization is probably less than 10 kcal/mol, and would not hinder the occurrence of reaction [11] in the thermal decomposition.

1. R. A. BACK. Can. J. Chem. **62**, 1414 (1984).
2. S. YAMAMOTO and R. A. BACK. J. Phys. Chem. In press.
3. R. A. BACK. Can. J. Chem. **60**, 2542 (1982).
4. R. A. BACK and J. M. PARSONS. To be published.
5. H. OKABE. Photochemistry of small molecules. Wiley, New York. 1978.
6. G. LAPIDUS, D. BARTON, and P. E. YANKWICH. J. Phys. Chem. **68**, 1863 (1964).
7. I. CHRISTIANSEN, K.-M. MARSTOKK, and H. MOLLENDAL. J. Mol. Struct. **30**, 137 (1976).

The photolysis and thermal decomposition of pyruvic acid in the gas phase[1]

S. YAMAMOTO[2] AND R. A. BACK
Division of Chemistry, National Research Council of Canada, 100 Sussex Drive, Ottawa, Ont., Canada K1A 0R6

Received May 30, 1984

S. YAMAMOTO and R. A. BACK. Can. J. Chem. **63**, 549 (1985).

The photolysis of pyruvic acid vapour has been studied at wavelengths of 366, 345, and 320 nm, at a temperature of 340 K and pressures from about 1 to 10 Torr. Products observed were CO_2 and CH_3CHO, with the former always in excess, and a quantum yield of CO_2 of 0.9 ± 0.1 at 366 nm. Light emission was also observed, and from the effect of added O_2 it was concluded that emission occurred from both singlet and triplet states. It is suggested that the primary process in the photolysis is an internal hydrogen-atom transfer followed by dissociation into CO_2 and CH_3—C—OH, with the latter then rearranging to give CH_3CHO and other products.

The absorption spectrum is reported; the first system begins at about 380 nm, rising to a maximum at about 350 nm, with $\epsilon_{max} \approx 10\ M^{-1}\ cm^{-1}$, and is attributed to the first excited $\pi^* \leftarrow n_+$ singlet state. Weak absorption below 300 nm is probably due to the $\pi^* \leftarrow n_-$ state and much stronger absorption below 220 nm to the $\pi^* \leftarrow \pi$ state.

The thermal decomposition was studied briefly at temperatures from 455 to 584 K and pressures from about 0.8 to 7 Torr. Products were the same as in the photolysis, and Arrhenius parameters of log A (s^{-1}) = 7.19 and E = 27.7 kcal/mol were obtained, based on the formation of CO_2, which was apparently a simple, homogeneous unimolecular process.

S. YAMAMOTO et R. A. BACK. Can. J. Chem. **63**, 549 (1985).

Opérant à une température de 340 K et à des pressions allant de 1 à 10 Torr, on a étudié la photolyse de l'acide pyruvique en phase vapeur à des longueurs d'onde de 366, 345 et 320 nm. Parmi les produits observés, on note le CO_2 et le CH_3CHO et le premier est toujours présent en excès; à 366 nm, le rendement quantique en CO_2 est égal à 0,9 ± 0,1. On a aussi observé une émission de lumière et, sur la base des résultats obtenus par addition de O_2, on en conclut que l'émission se fait tant de l'état singulet que de l'état triplet. On suggère que le processus primaire de la photolyse est un transfert interne d'un atome d'hydrogène qui est suivi par une dissociation en CO_2 et en CH_3—C—OH et éventuellement par une transposition de cette dernière entité en CH_3CHO et en d'autres produits.

On rapporte le spectre d'absorption; le premier système commence à 380 nm, il augmente pour atteindre un maximum à environ 350 nm, avec un $\epsilon_{max} = 10\ M^{-1}\ cm^{-1}$, et on l'attribue au premier état singulet excité $\pi^* \leftarrow n_+$. L'absorption faible que l'on observe à une longueur d'onde inférieure à 300 nm est probablement due à l'état $\pi \leftarrow n_-$ alors que l'absorption beaucoup plus forte apparaissant à une longueur d'onde inférieure à 220 nm est attribuée à l'état $\pi^* \leftarrow \pi$.

Opérant à des températures allant de 455 à 584 K et à des pressions allant de 0,8 à 7 Torr, on a brièvement étudié la décomposition thermique. Les produits sont les mêmes que ceux obtenus par photolyse; sur la base de la formation du CO_2, qui est apparemment un processus unimoléculaire simple et homogène, on a aussi obtenue les paramètres d'Arrhénius qui sont: log A (s^{-1}) = 7,19 et E = 27,7 kcal/mol.

[Traduit par le journal]

Introduction

With the exception of glyoxal and biacetyl, the photochemistry of α-dicarbonyl compounds in the gas phase has largely been neglected. Recently, the photolyses of oxalic acid (1) and glyoxylic acid (2) have been studied in this laboratory, and the present paper describes an investigation of the gas-phase photochemistry of pyruvic acid,

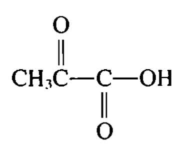

which was studied only very briefly before by Vesley and Leermakers (3) in 1964. A brief examination of the thermal decomposition, apparently not studied previously, is also reported.

Experimental

Techniques and apparatus were very similar to those used and described before (1, 2). The light source was a Hg-Xe high-pressure arc lamp with matching monochromator, and the cylindrical quartz photolysis vessel was 10 cm long and 5 cm in diameter. Light emission was measured with a photomultiplier in a traditional T-shaped fluorescence cell 5 cm in diameter with a Wood's horn light trap and filters to remove scattered exciting light. All experiments were done at a temperature of 340 K. The thermal decomposition was studied in a static quartz cylindrical reaction vessel, 10 cm long and 3 cm in diameter, mounted in a tube furnace. Pyruvic acid (>98% pure) was obtained from Kodak.

Results

Ultraviolet absorption spectrum

This is shown in Fig. 1, with the arrows showing wavelengths used for photolysis. By analogy with glyoxylic and oxalic acids (1, 2, 4) and other α-dicarbonyl compounds, the first absorption system, beginning at about 385 nm and reaching a maximum ($\epsilon \approx 10\ M^{-1}\ cm^{-1}$) at 350.6 nm, can be assigned to a $\pi^* \leftarrow n_+$ transition, the first excited singlet state. Some vibrational structure is evident at the longer wavelengths, and the sharp feature at 369.8 nm probably marks the (0, 0) band, since no further bands could be seen to the red even at four times higher pressures. A second weak absorption system with broad vibrational features begins below 300 nm, probably the $\pi^* \leftarrow n_-$ transition, which disappears beneath a much stronger absorption setting in about 220 nm (not shown), probably the $\pi^* \leftarrow \pi$ transition. The three wavelengths used in the photolysis experiments all fall within the $\pi^* \leftarrow n_+$ system (Fig. 1).

---

[1]NRCC 23761.

[2]NRCC Research Associate, 1981–1983. Present address: Department of Chemistry, Okayama University, Tsushima, Okayama 700, Japan.

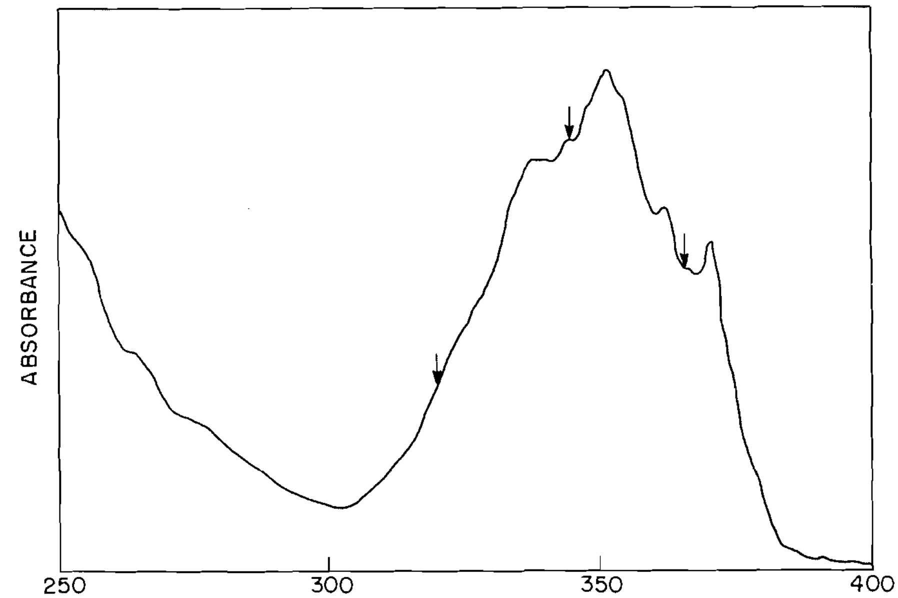

FIG. 1. Absorption spectrum of pyruvic acid vapour, measured in a 4-m tube at a pressure of 4.85 Torr at 85°C. Absorbance is in arbitrary units.

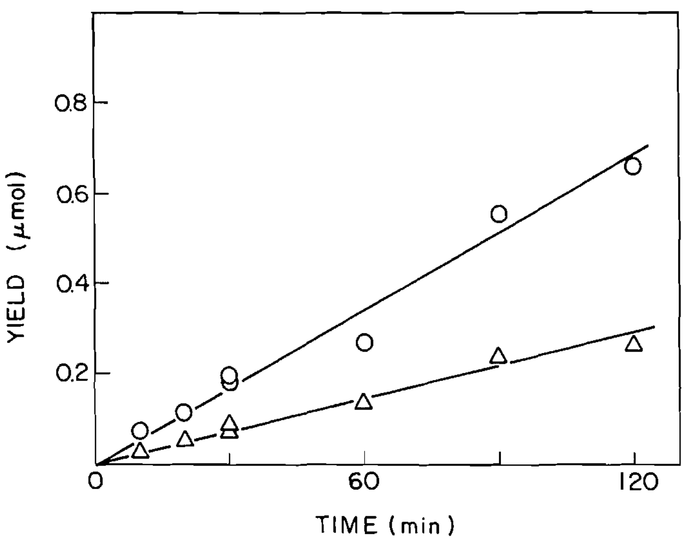

FIG. 2. Time dependence of photolysis products at 366 nm and pressure of 5 Torr. ○ = CO_2, △ = CH_3CHO.

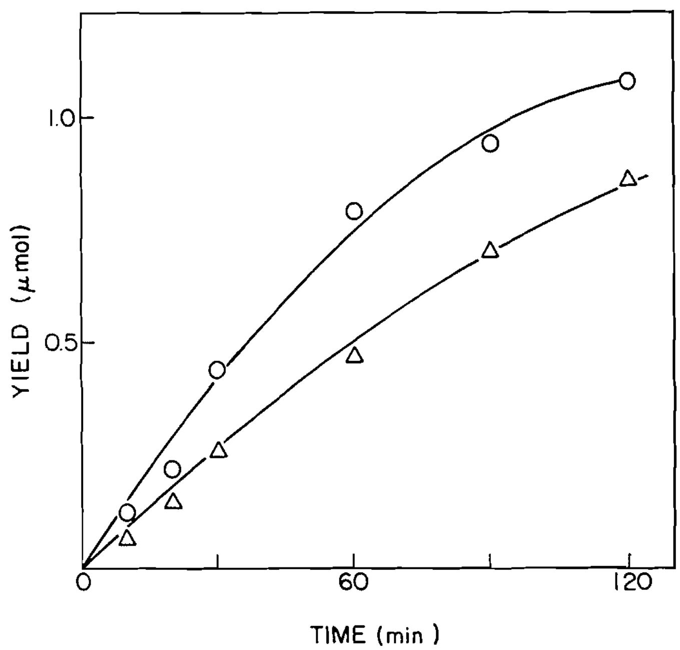

FIG. 3. Time dependence of photolysis products at 345 nm and pressure of 5 Torr. ○ = CO_2, △ = CH_3CHO.

Photolysis

At all wavelengths, the only products of the photolysis volatile at room temperature were CO_2 and CH_3CHO. These were measured by gas chromatography, and their time dependence is shown in Figs. 2–4. Both products were linear with time at 366 nm, but at the shorter wavelengths, yields of one or both products fell off with time; the cause of this behaviour is not clear. Yields of acetaldehyde were always much less than those of CO_2, 45% of the CO_2 at 366 nm, and varying between about 30 and 80%, and increasing with time, at 345 and 320 nm (Figs. 3, 4). Figure 5 shows the pressure dependence of product yields at 345 nm; similar linear dependence was found at the other two wavelengths, and as the light absorption was small, quantum yields must have been independent of pressure, at least up to about 10 Torr. The absolute quantum yield of CO_2 at 366 nm was measured using azomethane actinometry to be 0.9 ± 0.1; this may be compared with the value of 1.02 ± 0.06 reported by Vesley and Leermakers (3) at the same wavelength. Realistically, both these values are indistinguishable from unity within experimental uncertainty. Figure 6 shows the effect of air on the photolysis product ratio at 345 and 366 nm; CO_2 was unaffected, but CH_3CHO fell steadily to a constant value of about 10% of the CO_2 above 100 Torr.

Light emission

Light was emitted upon irradiation between 335 and 390 nm. An excitation spectrum is shown in Fig. 7, normalized to constant incident light intensity. Comparison with the absorption spectrum (also shown) makes it clear that the strongest emission came from the first vibrational band at 369.6 nm (probably

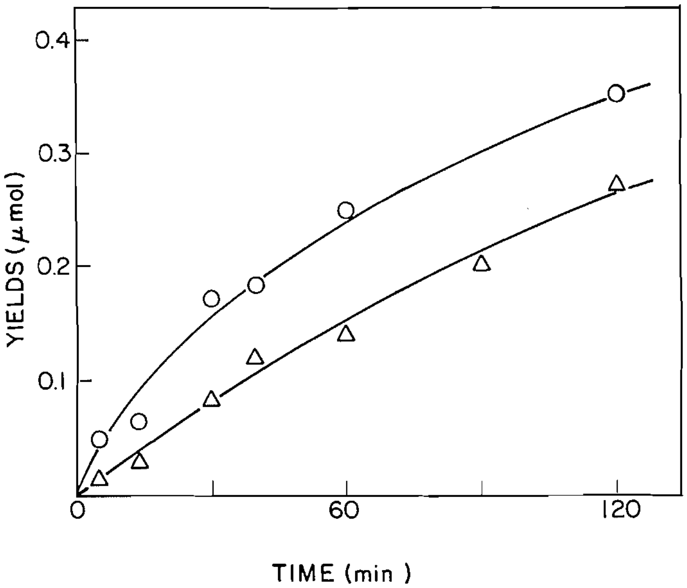

FIG. 4. Time dependence of photolysis products at 320 nm and pressure of 5 Torr. ○ = CO_2, △ = CH_3CHO.

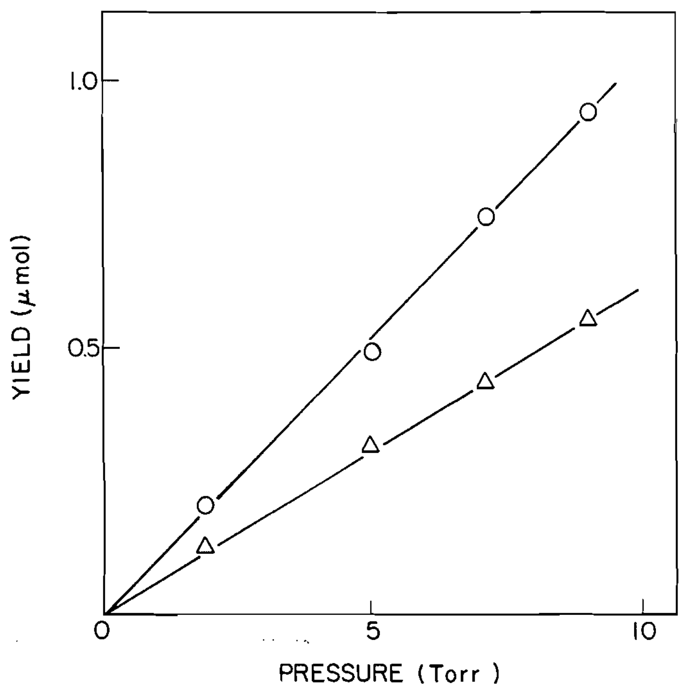

FIG. 5. Pressure dependence of photolysis products at 345 nm. ○ = CO_2, △ = CH_3CHO.

the (0,0) band) at the long-wavelength end of the spectrum. Emission on excitation at the maximum absorption around 350 nm was much less, probably reflecting more rapid loss of excited molecules by dissociation at the shorter wavelengths (*vide infra*). Figure 8 shows the effect of air on the emission excited at 366 and 350 nm. It appears that at both wavelengths the emission consisted of two components, one air-sensitive (presumably triplet emission) and one not affected (presumable singlet fluorescence). Figure 9 shows the effect of cyclohexane vapour on the emission intensity excited at 350, 366, and 380 nm.

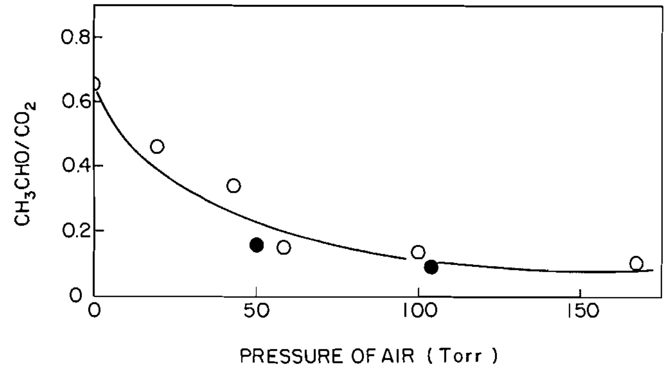

FIG. 6. Effect of air on photolysis product ratio at a pressure of 5 Torr of pyruvic acid. ○ = 345 nm, ● = 366 nm.

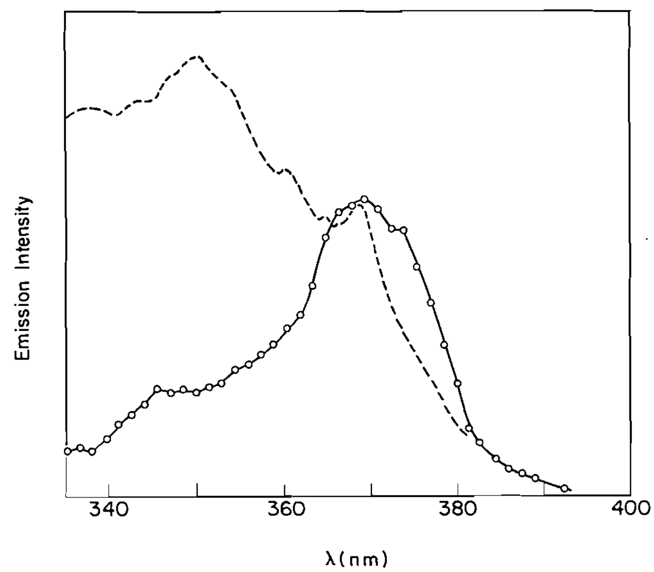

FIG. 7. Excitation spectrum of emission normalized to constant lamp intensity. Dashed curve is the absorption spectrum.

Thermal decomposition

The decomposition was studied at temperatures from 455 to 584 K and pressures between 0.8 and 7 Torr. Products again were CO_2 and CH_3CHO, and Fig. 10 shows that yields of both were linear with time. The positive intercept in the CO_2 plot is apparently due to CO_2 formed during the vaporization of the liquid pyruvic acid; when this was subtracted,[3] the ratio CH_3CHO/CO_2 was unity at 1 Torr but fell significantly with increasing pressure (Fig. 11). Figure 12 shows an Arrhenius plot of the first-order rate constant based on CO_2 formation, with the straight line corresponding to log A (s^{-1}) = 7.19 and E = 27.7 kcal/mol. Values of k showed no effect of pressure between 0.8 and 8 Torr, and no significant enhancement in the packed vessel, in which the surface/volume ratio was increased by a factor of 4.

Discussion

The mechanism of the photolysis

The simplicity of the volatile products, and the absence of products such as CH_4, C_2H_6, and CO, argue against a free-radical mechanism, although there is probably enough energy

[3]A similar correction was made in the photolysis experiments.

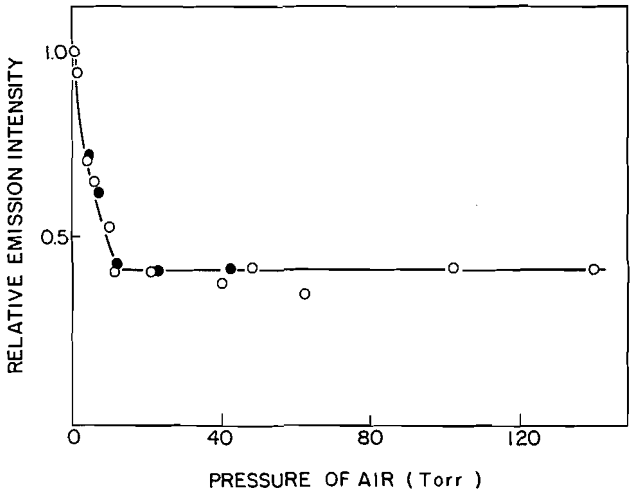

FIG. 8. Effect of air on light emission. ○ = 366 nm, ● = 350 nm.

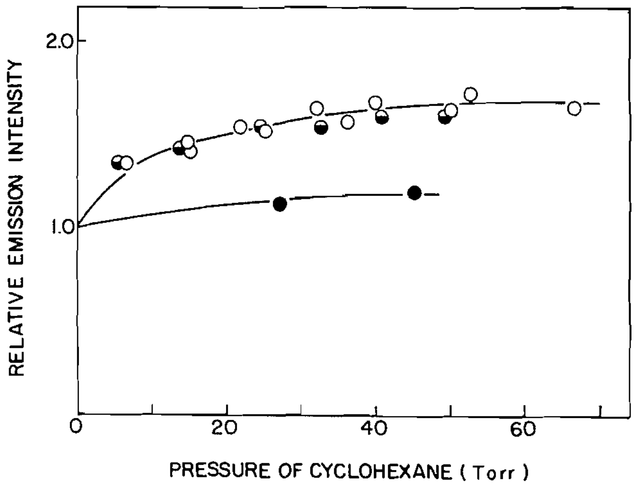

FIG. 9. Effect of cyclohexane on light emission ○ = 350, ◒ = 366 nm, ● = 380 nm.

even at 366 nm (78 kcal/mol) to break the CH_3—C bond. The deficit of CH_3CHO relative to CO_2 (Figs. 2–5), and the selective effect of air on the yield of CH_3CHO (Fig. 6) also rule out a simple molecular dissociation into CO_2 and CH_3CHO, while the emission of light indicates appreciable lifetimes for excited singlet and triplet states. The following mechanism is suggested:

[1] $PY + h\nu \rightarrow PY_s^*$

[2] $PY_s^* \rightarrow CO_2 + CH_3\text{—}\ddot{C}\text{—}OH$

[3] $\rightarrow PY + h\nu_f$

[4] $\rightarrow PY_t^*$

[5] $PY_t^* \rightarrow PY + h\nu_p$

[6] $PY_t^* + O_2 \rightarrow$ quenching

[7] $CH_3\text{—}\ddot{C}\text{—}OH \rightarrow CH_3CHO$

[8] $\rightarrow$ other products

[9] $O_2 + CH_3\text{—}\ddot{C}\text{—}OH \rightarrow$ other products

where PY, PY_s^*, and PY_t^* represent the ground state, the first excited singlet, and the first excited triplet states of pyruvic acid.

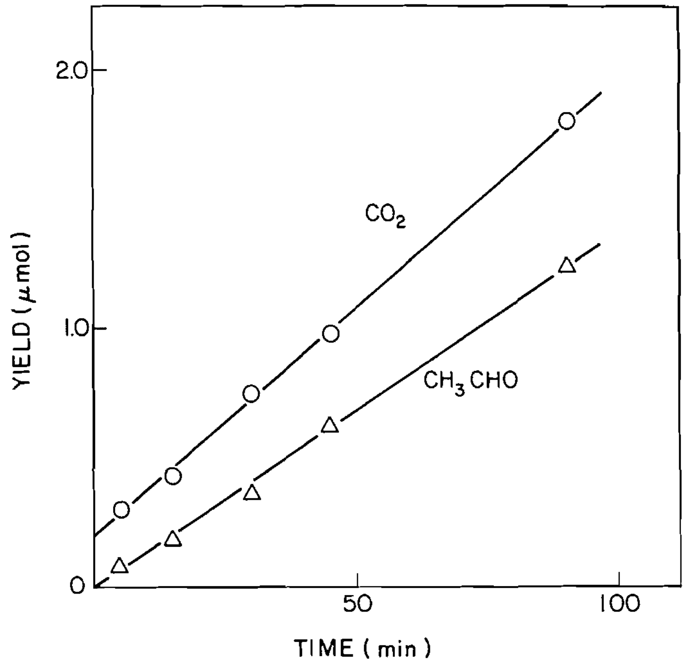

FIG. 10. Product yields vs. time in the thermal decomposition at 3.6 Torr and T = 522 K.

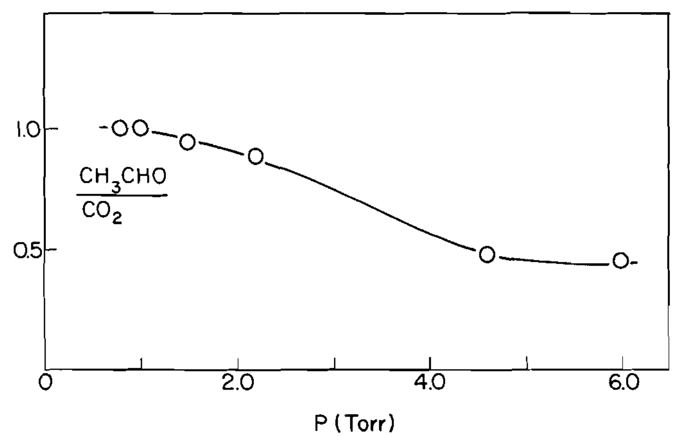

FIG. 11. Dependence of the product ratio on the pressure of pyruvic acid in the thermal decomposition at 540 K.

Direct dissociation of the excited singlet state (reaction [2]) following hydrogen-atom transfer through a five-membered transition state,

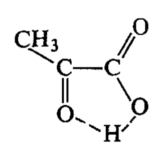

is suggested as the source of CO_2. The lack of effect of 160 Torr of air on the yield of CO_2 would appear to rule out both the triplet state and a vibrationally excited ground state as precursors. With the quantum yield of CO_2 close to unity, and the fluorescence and phosphorescence weak, reaction [2] appears to be the only important loss process for the initially-formed singlet state.

The effect of air on the light emission (Fig. 8) suggests that both fluorescence (unaffected by O_2) and phosphorescence

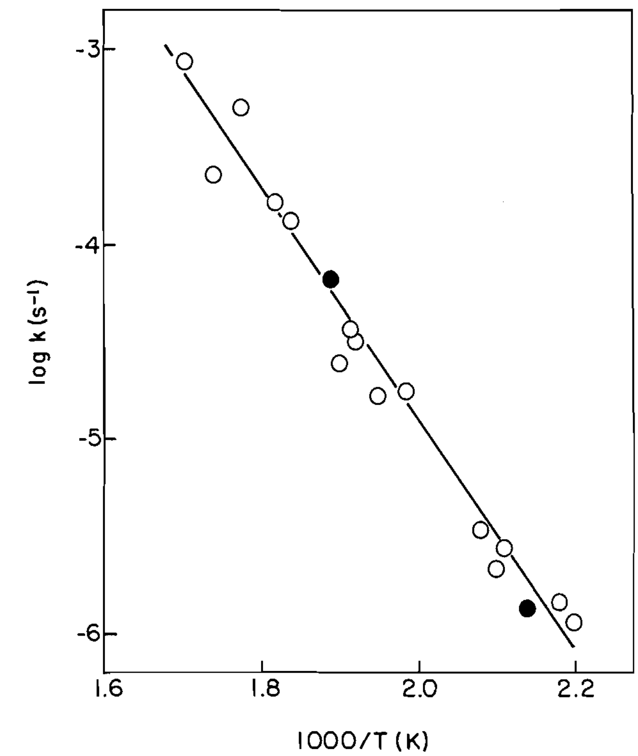

FIG. 12. Arrhenius plot of first-order rate constant for the thermal decomposition of pyruvic acid, based on the formation of CO_2. Filled circles are for packed vessel.

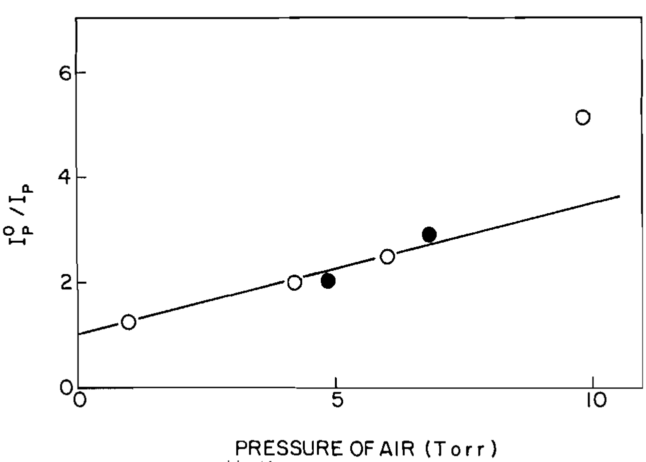

FIG. 13. Stern–Volmer plot for quenching of emission by air. ○ = 366 nm, ● = 350 nm.

(quenched by O_2) were occurring. The constant emission intensity at pressures of air above 15 Torr shows that there was little collisional electronic deactivation of the excited singlet state in these experiments. In fact, the addition of cyclohexane *enhanced* the emission appreciably at 350 and 366 nm, and perhaps slightly at 380 nm (Fig. 9). The most probable explanation of this behaviour is vibrational deactivation of PY_s^*, which would decrease the rate of dissociation via reaction [2], and hence increase its lifetime and the probability of emission (reaction [3]). Similar anomalous pressure dependence of fluorescence in biacetyl has been explained in a similar way (5). The excitation spectrum (Fig. 7) supports this view, with the yield of emission falling markedly with increasing photon energy and consequent increased vibrational excitation of PY_s^*. The relative lack of effect of cyclohexane on excitation at 380 nm (Fig. 9) similarly reflects the lesser vibrational excitation at this wavelength, probably not far from the (0,0) band of the transition (Fig. 1). The data in Fig. 8 may also be somewhat affected by vibrational deexcitation superimposed on the effect of O_2 on the triplet emission, although the effect would be small since air should be much less efficient than cyclohexane for vibrational relaxation. The triplet quenching in Fig. 8 follows simple Stern–Volmer kinetics (Fig. 13), and from the slope a half-quenching pressure of 0.78 Torr was obtained for O_2, not untypical for triplet quenching.

The fate of the $CH_3\ddot{C}$—OH carbene formed in reaction [2] requires some comment. Reaction [7], a simple rearrangement to CH_3CHO, is suggested as the source of this product, and because the latter was always less than the CO_2, reaction [8] is suggested. Because the CH_3CHO/CO_2 ratio was independent of the pressure of pyruvic acid (Fig. 5, text), loss of CH_3—$\ddot{C}$—OH by reaction with pyruvic acid is ruled out. One possibility for reaction [8] is the formation of vinyl alcohol, CH_2=CHOH, which would probably have been lost by polymerization before or during analysis (6). Although vinyl alcohol is about 20 kcal/mol less stable thermodynamically than CH_3CHO (6), formation of either compound from the carbene should be considerably exothermic; both would require hydrogen transfer through three-membered transition states which might be about equally probable:

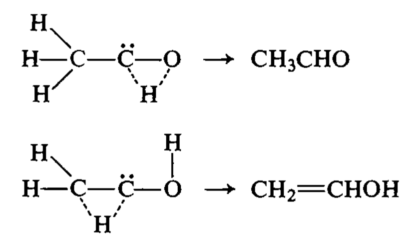

Reaction [9] is suggested to explain the reduction in CH_3CHO on the addition of air (Fig. 6), although it is unusual for a carbene of this type to have a lifetime long enough to permit removal by chemical reaction with an additive.

The mechanism of the thermal decomposition

As with oxalic and glyoxylic acid, if the activation energy measured for the decomposition of pyruvic acid can be ascribed to a simple homogeneous unimolecular reaction, the energy is too low to permit access to the carbene postulated as an intermediate in the photolysis. The only alternative appears to be hydrogen transfer through a four-membered transition state, forming CH_3CHO directly:

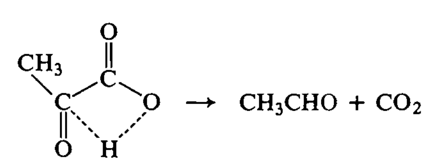

Again, there was a deficit of CH_3CHO, although the product ratio now showed a pressure dependence and at low pressures approached unity (Fig. 11). The mechanism of loss of CH_3CHO is not clear. Simple secondary reactions can be ruled out as formation of both products was linear with time. The pressure dependence (Fig. 11) suggests a bimolecular reaction yielding CO_2 and higher products, not detected, although pro-

TABLE 1. The gas-phase thermal decomposition of α-carbonyl acids

Acid	Structure	Products	k_{450} (s^{-1})	log A (s^{-1})	E (kcal/mol)
Oxalic (7)	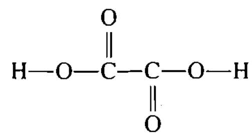	$HCOOH + CO_2$	1.9×10^{-3}	11.9	30
Glyoxylic (2)	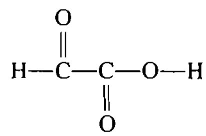	$H_2CO + CO_2$	6.2×10^{-8}	7.8	30.8
Pyruvic	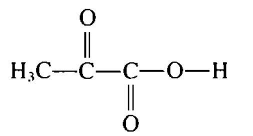	$CH_3CHO + CO_2$	4.9×10^{-7}	7.2	27.7

duction of CO_2 was always approximately first-order.

Table 1 summarizes the results of the three α-carbonyl acids that have been studied. The decompositions all appear to proceed by homogeneous unimolecular internal hydrogen-atom transfer through four-membered transition states, and have similar activation energies. Oxalic acid, however, is much less stable than the other two (note $k_{450\,K}$ values), with most of the difference arising from the frequency factors. Values of the latter for glyoxylic and pyruvic acid are much too low for a normal unimolecular reaction. Both decompositions *appear* to be simple, largely homogeneous, first-order reactions, and the cause of the low frequency factors is not clear; quantum mechanical tunnelling is perhaps one possibility. It is also not clear why oxalic acid should be so much less stable than the other two.

Acknowledgement

We are grateful to John Parsons for measuring the spectrum shown in Fig. 1.

1. S. YAMAMOTO and R. A. BACK. J. Phys. Chem. In press.
2. R. A. BACK and S. YAMAMOTO. Can. J. Chem. **63**, 542 (1985).
3. G. F. VESLEY and P. A. LEERMAKERS. J. Phys. Chem. **68**, 2364 (1964).
4. R. A. BACK. Can. J. Chem. **62**, 1414 (1984).
5. W. A. NOYES, JR., G. B. PORTER, and J. E. JOLLEY. Chem. Rev. **56**, 49 (1956).
6. R. A. BACK. Can. J. Chem. **60**, 2537 (1982).
7. G. LAPIDUS, D. BARTON, and P. E. YANKWICH. J. Phys. Chem. **68**, 1863 (1964).

COMMUNICATION

Thermolysis of unsymmetrically substituted vinylcyclopropanes. Regarding the effect of oxygen substituents on the site-selectivity of homo-[1,5]-sigmatropic hydrogen migrations

EDWARD PIERS, ANDERSON RICHARD MAXWELL, AND NEIL MOSS
Department of Chemistry, University of British Columbia, 2036 Main Mall, University Campus, Vancouver, B.C., Canada V6T 1Y6

Received September 19, 1984

EDWARD PIERS, ANDERSON RICHARD MAXWELL, and NEIL MOSS. Can. J. Chem. **63**, 555 (1985).

Thermal rearrangement of compounds **1**, **8–11**, and **20** results, in each case, in the exclusive migration of the hydrogen (H_A) not associated with the oxygen substituent. On the other hand, thermolysis of **19**, **22**, and **23** provides, in each case, a mixture of the two possible sigmatropic rearrangement products. Similar bond reorganization of the hydrocarbon **21** affords the dienes **27** and **28** (98:2, respectively). On the basis of these results, along with those reported earlier, it is proposed that in the transition states for these rearrangements (a) there is an accumulation of electron density at the carbon from which the hydrogen migrates, and (b) this carbon center has a planar or nearly planar geometry.

EDWARD PIERS, ANDERSON RICHARD MAXWELL et NEIL MOSS. Can. J. Chem. **63**, 555 (1985).

La transposition thermique des composés **1**, **8–11** et **20** conduit, dans chaque cas, à la migration exclusive de l'hydrogène (H_A) qui n'est pas associé avec le substituant de l'oxygène. Par ailleurs, la thermolyse des composés **19**, **22** et **23** conduit, dans chaque cas, à un mélange des deux produits possibles de transposition sigmatropique. Une répartition semblable des liaisons de l'hydrocarbure **21** conduit aux diènes **27** et **28** dans des proportions respectives de 98 et 2. En se basant sur ces résultats, ainsi que ceux rapportés antérieurement, on croit que dans les états de transition de ces transpositions: (a) il y a une accumulation de la densité électronique au niveau du carbone à partir duquel l'hydrogène migre et (b) que ce carbone possède une géométrie plane ou presque plane.

[Traduit par le journal]

In a previous communication (1), we reported that in the thermal rearrangement of a number of unsymmetrically substituted vinylcyclopropane systems, there is an impressive substituent effect on the site-selectivity of homo-[1,5]-sigmatropic hydrogen migrations. For example, while thermolysis of *trans*-2-methoxy-*endo*-7-vinylbicyclo[4.1.0]heptane (**1**) afforded exclusively the product **4** resulting from migration of H_A,[1] similar rearrangement of the trimethylsilyl-containing substrate **2** gave only substance **5** (H_X migration). On the other hand, a methyl substituent was shown to have only a small rate-retarding effect on hydrogen migration, since thermolysis of compound **3** provided products **6** (H_A shift) and **7** (H_X shift) in a ratio of 3:2, respectively. Furthermore, with respect to the effect of OR substituents on the site-selectivity of the process, it was found that thermolysis of the substrates **8–11** produced, in each case, only the product resulting from migration of H_A.

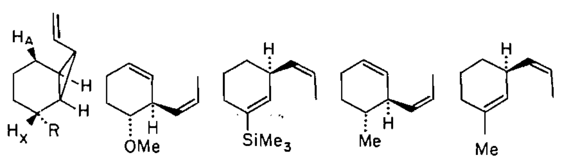

1 R = OMe 4 5 6 7
2 R = $SiMe_3$
3 R = Me

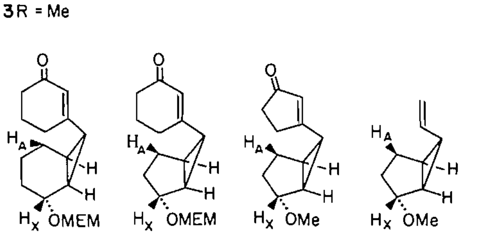

8 9 10 11
MEM = $CH_2OCH_2CH_2OMe$

In each of compounds **1** and **8–11**, the OR substituent is external to the ring from which the hydrogen H_X would have migrated. Although, in these substances, there is free rotation about the C—O bonds, the carbocycles are conformationally quite rigid. As an extension to this study, it was of interest to obtain information that would answer the following question. Would thermolysis of substrates in which the structural relationship between an oxygen substituent and the adjacent H_X is quite different from that in **1** and **8–11** produce products resulting from H_X migration? We report herein some results which relate to this question and which provide a clue regarding the geometry of the transition state for hydrogen migration.

Reduction (n-Bu_3SnH, neat, room temperature) of 7,7-dibromo-3-oxabicyclo[4.1.0]heptane (**12**)[2] (2) gave a mixture of the *endo* bromide **13** and the corresponding *exo* isomer (ratio 2.2:1, respectively), which were separated by chromatography (41% isolated yield of **13**). Conversion of the latter substance into the bicyclic vinylcyclopropane **19** (59% overall) was accomplished via a series of standard reactions: 2.4 equiv. t-BuLi, Et_2O, −78°C; dimethylformamide, −78°C → room temperature, 7.5 h; Ph_3P=CH_2, tetrahydrofuran. A similar sequence of reactions was employed to convert the dibromocyclopropane **14** (obtained by dibromocyclopropanation (3) of *cis*-2-oxabicyclo[3.3.0]oct-7-ene (4)) into the tricyclic alkene **20**.

[1] Throughout this communication, hydrogens migrating from carbons bearing no substituent and those migrating from carbons containing a substituent are designated H_A and H_X, respectively.

[2] All compounds reported herein gave spectral data consistent with assigned structures. New compounds provided satisfactory molecular mass determinations (high resolution mass spectrometry).

TABLE 1. Thermal rearrangement of vinylcyclopropanes **19–23**[a]

Experiment	Substrate	Product(s) (ratio)	Yield (%)[b]
1	**19**	**24** + **25** (66:34)	98
2	**20**	**26**	89
3	**21**	**27** + **28** (98:2)	96
4	**22**	**29** + **30** (15:85)	96
5	**23**	**31** + **32** (64:36)	94

[a]Thermolysis of each of the substrates was performed in benzene solution (230–240°C, 4.5–8 h) in sealed, base-washed silylated glass tubes. In each case, the cooled reaction mixture was analyzed directly by gas–liquid chromatography (glc). The benzene was removed, the product (s) was (were) distilled and subjected again to analysis (glc, ^{1}H nmr spectroscopy).

[b]Yield of isolated, distilled product(s).

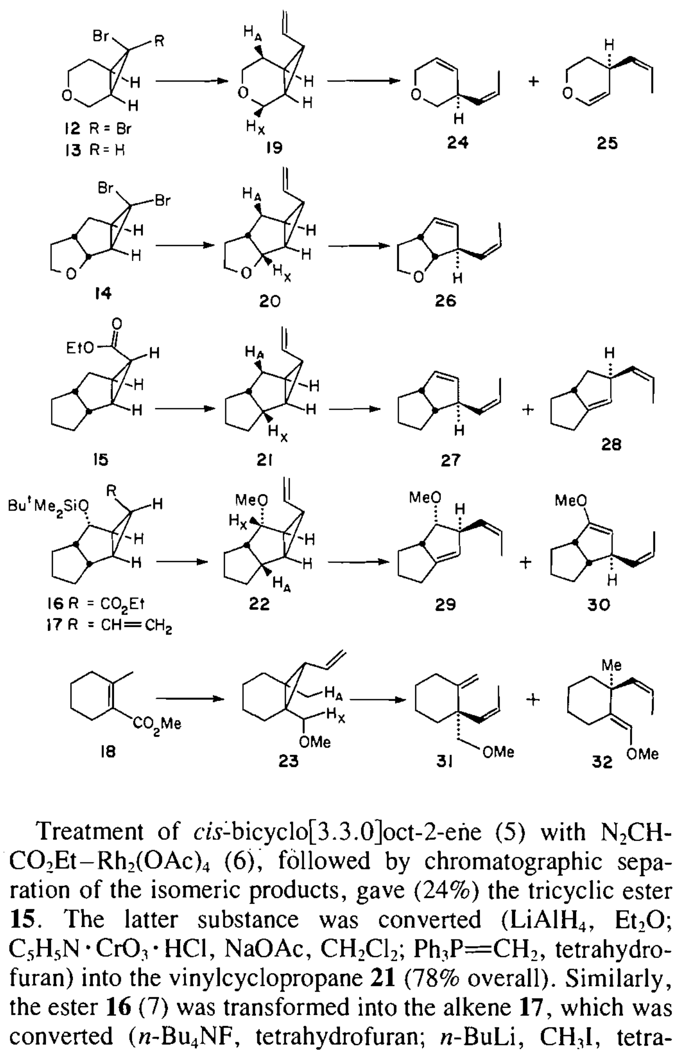

Treatment of *cis*-bicyclo[3.3.0]oct-2-ene (5) with N_2CH-CO_2Et–$Rh_2(OAc)_4$ (6), followed by chromatographic separation of the isomeric products, gave (24%) the tricyclic ester **15**. The latter substance was converted ($LiAlH_4$, Et_2O; $C_5H_5N \cdot CrO_3 \cdot HCl$, NaOAc, CH_2Cl_2; $Ph_3P{=}CH_2$, tetrahydrofuran) into the vinylcyclopropane **21** (78% overall). Similarly, the ester **16** (7) was transformed into the alkene **17**, which was converted (n-Bu_4NF, tetrahydrofuran; n-BuLi, CH_3I, tetrahydrofuran) into the methyl ether **22** (61% from **16**).

Methyl 2-methylcyclohexene-1-carboxylate (**18**) (8) was transformed into the substrate **23** as follows: i-Bu_2AlH, Et_2O; NaH, CH_3I; N_2CHCO_2Et, copper bronze, heat; $LiAlH_4$, Et_2O; $C_5H_5N \cdot CrO_3 \cdot HCl$, NaOAc, CH_2Cl_2; $Ph_3P{=}CH_2$, tetrahydrofuran; separation of *endo* and *exo* vinyl isomers (ratio 1:2) by preparative thin-layer chromatography.

The results obtained from thermolysis of compounds **19–23** are summarized in Table 1. As was the case for the previously reported thermolyses (1), the reactions were very clean. In experiment 2, we were unable to detect any of the product which would have resulted from migration of H_X in substrate **20**. Each of the product pairs from experiments 1, 4, and 5 were separated and all six substances (**24**, **25**, **29–32**) were individually characterized. Although a pure sample of the minor product from experiment 3 was not obtained, a ^{1}H nmr study (including decoupling experiments) of a 2:1 mixture of **27** and **28**, obtained by partial chromatographic separation of the thermolysis products, showed clearly that the minor rearrangement product was the diene **28**.

In the thermolysis of substrates **1**, **8–11**, **19**, **20**, **22**, and **23**, only three (**19**, **22**, **23**) produced products resulting from migration of H_X. For two of these (**19**, **23**) the major product was that derived from a H_A shift. Indeed, of the number of oxygen-containing substrates that we have studied, the only one which exhibited predominant H_X migration was substance **22**. Interestingly, the structural relationship between H_X and the OMe substituent in the latter substrate is very similar to that in other compounds (e.g. **10**, **11**) which exhibited no H_X migration. Furthermore, since a previous result (1) (thermolysis of **3**) had shown that the effect of an alkyl group on site-selectivity is small, the result derived from rearrangement of **21** (Table 1, experiment 3) indicates that other molecular characteristics affect the magnitude of the site-selectivity. In any case, it is clear that (a) the site-selectivity of the sigmatropic rearrangement does vary with the structural relationship between an oxygen substituent and the adjacent H_X (compare, for example, substrates **1**, **19**, and **23**), and (b) other structural features are important as well (compare substrates **3**, **21**; **11**, **22**).

In the earlier communication (1), we had postulated tentatively that, in the transition states for these sigmatropic rearrangements, electron density accumulates at the carbon from which the hydrogen migrates.[3] Although the effect of an oxygen atom on the stability of an adjacent negative charge has been the subject of considerable recent discussion,[4] it appears that an OR group stabilizes the charge when the latter is associated with an sp^3 orbital (pyramidal geometry) and destabilizes the charge when it is associated with a p orbital (planar geometry) (9, 10). Thus, it is possible to suggest that not only do the transition states for these reactions have a "partial negative charge" on the carbon from which the hydrogen shift occurs, but that the carbon has an sp^2-like geometry (double bond character in the transition state). On this basis, the results derived from the thermolyses of substrates **20–23** are particularly interesting. In each case, the transition state for migration of the bridgehead hydrogen (H_X in **20** and **21**, H_A in **22**) would be (would have been) destabilized by the fact that a strained double bond (bridgehead in a bicyclo[3.3.0]octane system (11)) is being introduced into the molecule. In **20**, further transition state destabilization by the oxygen atom excludes H_X migration and, thus, **26** is the only product. In the absence of an oxygen atom (substrate **21**), a small amount of H_X migration does occur. Introduction of a methoxy group (substrate **22**)

[3] An alternative rationale, suggested by one of the referees, involves the postulate that in the transition states for these rearrangements there is a build-up of *positive* charge at the carbon center where fragmentation of the cyclopropane ring takes place, i.e. at the cyclopropyl carbon adjacent to the H_A- or H_X-bearing carbons in substrates **1–3**, **8–11**, and **19–23**. This electron-deficient center would be stabilized by a β-trimethylsilyl group (substrate **2**) and destabilized (via an inductive effect) by oxygen-containing substituents.

[4] See citations in ref. 1. For a very recent pertinent report, see ref. 9.

would be expected to disfavor H_X migration and thus increase (relatively) the amount of bridgehead alkene **29**. This expectation was observed, although the extent of the increase (2% **28** to 15% **29**) was quite small.

Acknowledgements

We are grateful to (a) the Natural Sciences and Engineering Research Council of Canada for financial support and for a Postgraduate Scholarship (to N.M.), (b) MacMillan Bloedel Limited and the University of British Columbia for Graduate Fellowships (to A.R.M.), and (c) the Alberta Heritage Scholarship Fund for the Sir James Lougheed Award for Distinction (to N.M.).

1. E. PIERS and A. R. MAXWELL. Can. J. Chem. **62**, 2392 (1984).
2. K. G. TAYLOR, W. E. HOBBS, and M. SAQUET. J. Org. Chem. **36**, 369 (1971).
3. M. MAKOSZA and M. FEDORYNSKI. Synth. Commun. **3**, 305 (1973).
4. K. C. NICOLAOU, R. L. MAGOLDA, W. J. SIPIO, W. E. BARNETTE, Z. LYSENKO, and M. M. JOULLIÉ. J. Am. Chem. Soc. **102**, 3784 (1980).
5. H. C. BROWN and W. J. HAMMAR. Tetrahedron, **34**, 3405 (1978).
6. M. P. DOYLE, D. VAN LEUSEN, and W. H. TAMBLYN. Synthesis, 787 (1981).
7. E. PIERS, G. L. JUNG, and N. MOSS. Tetrahedron Lett. **25**, 3959 (1984).
8. F. W. SUM and L. WEILER. Can. J. Chem. **57**, 1431 (1979); M. ALDERDICE, F. W. SUM, and L. WEILER. Org. Synth. **62**, 14 (1984).
9. J. S. SAWYER, T. L. MACDONALD, and G. J. MCGARVEY. J. Am. Chem. Soc. **106**, 3376 (1984).
10. J. M. LEHN and G. WIPFF. J. Am. Chem. Soc. **98**, 7498 (1976).
11. W. C. AGOSTA and S. WOLFF. J. Org. Chem. **40**, 1699 (1975).

Synthesis of heterocyclic 1,4-dihydropyridylacetic acid derivatives of 6-aminopenicillanic acid and D-α-aminobenzylpenicillin with antibacterial activity

SUSHIL K. DUBEY AND EDWARD E. KNAUS[1]

Faculty of Pharmacy and Pharmaceutical Sciences, University of Alberta, Edmonton, Alta., Canada T6G 2N8

Received April 2, 1984

SUSHIL K. DUBEY and EDWARD E. KNAUS. Can. J. Chem. **62**, 559 (1984).

Condensation of 4-substituted 3-(4,4-dimethyloxazolin-2-yl)-1,4-dihydropyridylacetic acids **3** with the C-2 *p*-bromophenacyl esters of 6-aminopenicillanic acid salt **4** and D-α-aminobenzylpenicillin **8** afforded the respective 1,4-dihydropyridylacetic acid analogs **6** and **10** which exhibited moderate antibacterial activity toward Gram-positive strains. The 6-APA derivatives **6** exhibited dual ^{1}H nmr resonances for H2′, H2, H5, and one of the C3-Me groups, suggesting the presence of two rotamers which differ in configuration at the carbonyl-to-nitrogen bond. The D-aminobenzylpenicillin derivatives **9** may exist in more than one conformation, one of which may be an intramolecular hydrogen bonded species such as **11**.

SUSHIL K. DUBEY et EDWARD E. KNAUS. Can. J. Chem. **62**, 559 (1984).

La condensation d'acides X-4 (diméthyl-4,4 oxazolinyl-2)-3 dihydro-1,4 pyridylacétiques (**3**) avec les esters *p*-bromophénacyles en C-2 du sel de l'acide amino-6 pénicillanique **4** et de la D-α-aminobenzylpénicilline **8** fournissent respectivement les analogues **6** et **10** de l'acide dihydro-1,4 pyridylacétique qui présentent une activité antibactérienne modérée contre les souches Gram-positives. Les spectres rmn ^{1}H des dérivés **6** de l'acide amino-6 pénicillanique présentent des résonances doubles pour H2′, H2, H5 et pour l'un des groupes C3-Me et ces résultats suggèrent la présence de deux rotamères qui diffèrent de configuration au niveau de la liaison carbonyl−azote. Les dérivés **9** de la D-α-aminobenzylpénicilline peuvent exister sous plus d'une conformation et l'une d'elle pourrait être une espèce comportant une liaison hydrogène intramoléculaire, comme dans **11**.

[Traduit par le journal]

The β-lactam antibiotics are the most widely used class of antimicrobial agents. However, the bacterial development of β-lactamase enzymes which decrease the effectiveness of β-lactam antibiotics has prompted a continued search for structurally modified antibiotics (1). A variety of 2- and 4-pyridone derivatives have been used for the preparation of some penicillin and cephalosporin analogs (2, 3). It was therefore of interest to investigate the utility of stabilized 1,4-dihydropyridines (4) as medicinal synthons (5). The 3-(4,4-dimethyloxazolin-2-yl) substituent of **3** could serve the dual role of stabilizing the 1,4-dihydropyridine ring system and provide increased penicillinase resistance due to electronic and steric effects, respectively. We now describe the synthesis and antibacterial activity of some novel 1,4-dihydropyridyl derivatives of 6-aminopenicillanic acid (6-APA) and D-α-aminobenzylpenicillin (Ampicillin).

The reaction of 3-(4,4-dimethyloxazolin-2-yl)pyridine (**1**) with organolithium reagents in tetrahydrofuran at −78°C afforded the *N*-lithio-1,4-dihydropyridyl intermediates **2***a*−*c* (4*b*, 5). The *in situ* reaction of **2***a*−*c* with lithium bromoacetate gave the required 4-substituted 1,4-dihydropyridyl acetic acids **3***a*−*c* in 65−80% yield (Scheme 1). Condensation of **3***a*−*c* with the *p*-bromophenacyl penicillate benzenesulfonic acid salt **4** (6) under a variety of reaction conditions (*N*,*N*′-dicyclohexylcarbodiimide (DCC), $MeOCOCl/Et_3N$) yielded **5***a*−*c*. However, the products **5***a*−*c* were obtained in optimum yield (69−72%) and highest purity when trimethylacetyl chloride (Me_3COCl/Et_3N) was employed as the condensation reagent. Reaction of **5***a*−*c* with potassium thiophenoxide afforded the desired 1,4-dihydropyridyl acetic acid derivatives **6***a*−*c* in 51−57% yield (Scheme 2).

In a similar sequence of reactions, treatment of D-α-aminobenzylpenicillin (**7**) with α,*p*-dibromoacetophenone afforded **8**, which was used immediately in subsequent reactions since it was unstable upon storage. Condensation of **8** with the 1,4-dihydropyridyl acetic acids **3***a*−*c* in the presence of DCC yielded **9***a*−*c* in 60−80% yield. Reaction of **9***a*−*c* with potassium thiophenoxide afforded the target compounds **10***a*−*c* in 45−68% yield, as illustrated in Scheme 3. The use of DCC for the conversion of **8** to **9** in the D-α-aminobenzylpenicillin series provided higher yields than trimethylacetyl chloride or methoxycarbonyl chloride − triethylamine reagents.

The ^{1}H nmr spectra of **6***a*−*c* and **9***a*−*c* displayed some interesting conformational characteristics which are worthy of

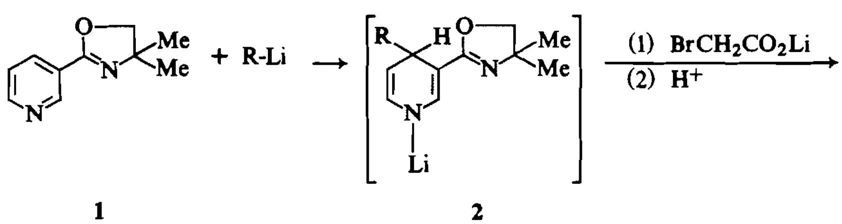

1 **2** **3**

a R = Ph
b R = Me
c R = n-Bu

SCHEME 1

[1]Author to whom correspondence may be addressed.

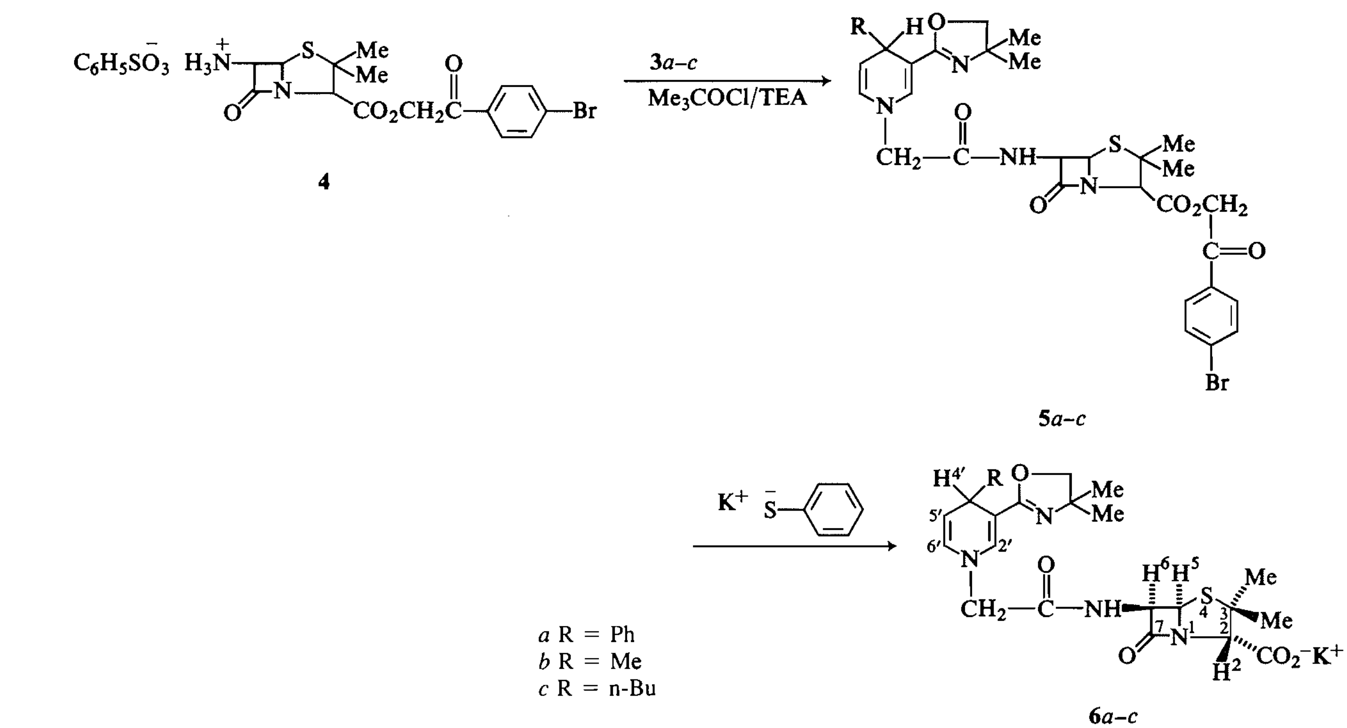

SCHEME 2

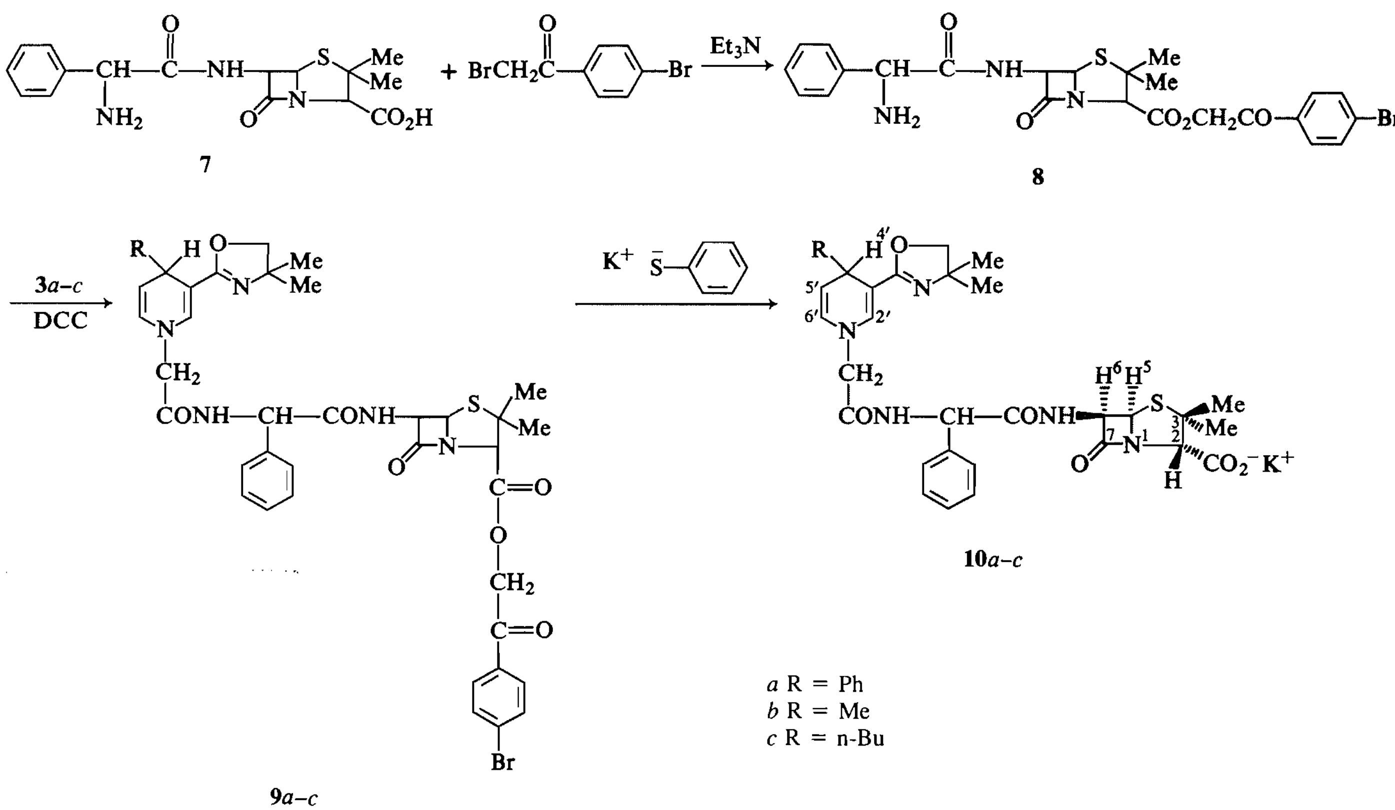

SCHEME 3

discussion. The assignments were confirmed by extensive double irradiation experiments. The ^{1}H nmr spectrum of **6***c* exhibited the following spectral data (D_2O), δ: 6.88 and 6.92 (two doublets, $J_{2',6'}$ = 1.15 Hz, 1H, H2′), 6.0 (d, $J_{5',6'}$ = 8 Hz of d, $J_{2',6'}$ = 1.15 Hz, 1H, H6′), 5.62 (d, $J_{5,6}$ = 4 Hz, 1H, H6), 5.54 and 5.56 (two overlapping doublets, $J_{5,6}$ = 4 Hz, 1H, H5), 4.88 (d, $J_{5',6'}$ = 8 Hz of d, $J_{4',5'}$ = 5 Hz, 1H, H5′), 4.26 and 4.28 (two s, 1H, H2), 1.63 and 1.66 (two s, 3H, C3-βMe), and 1.57 (s, 3H, C3-αMe). The ^{1}H nmr spectra of the structurally related **6***a*–*b* also exhibited dual absorptions for H2′, H2, H5, and the C-3 β-methyl substituent. In contrast, the ^{1}H nmr spectrum (D_2O) of potassium benzylpenicillin exhibited single resonances for H2, H5, and each of the C3-Me substituents. The possibility that epimerization at the C-6 position of the penicillin moiety occurred during the reaction has been excluded since epimerization would provide for two sets of doublets for the C5-H and C6-H, having different coupling constants due to different dihedral angles between H5 and H6 in the two epimers. The possibility that long range coupling between H2 and H5 was present was excluded since irradiation of the H2 resonances at δ 4.26 and 4.28 did not influence the resonances for the H5 proton at δ 5.54 and 5.56. A similar irradiation at δ 5.54 had no effect on the resonances at δ 4.26 and 4.28. Therefore, the existence of two conformers is most likely due to restricted rotation about the carbonyl-to-amide bond, in which the two rotamers are somehow stabilized by the dihydropyridyl moiety. The dual absorptions observed for H2′, H2, H5, and the C-3 β-methyl substituent indicate that these atoms are located in significantly different molecular environments in the two rotamers. The observation that the NH proton of **5***a* appears as two overlapping doublets ($J_{NH,C6\text{-}H}$ = 6 Hz) at δ 8.86 and 8.88 when the ^{1}H nmr spectrum was determined in DMSO-d_6 also supports the presence of two rotamers.

The ^{1}H nmr spectra of the D-α-aminobenzylpenicillin derivatives **9***a*–*c* were more complex than those of **6***a*–*c* since there are two amide groups. The conformational effects for **9***a*–*c* were more evident for the dihydropyridyl moiety than for the penicillin moiety since H2, H5, and the C3-Me_2 substituents appear as single resonances. The ^{1}H nmr spectra were different in deuteriochloroform and dimethylsulfoxide-d_6 since the latter solvent disrupts hydrogen bonding. The ^{1}H nmr spectrum of **9***a* ($CDCl_3$) exhibited dual resonances for H2′ at δ 6.88 and 7.0 and for H6′ at δ 5.91 and 5.96. Decoupling experiments indicated that the absorption for H2′ of one conformer at 7.0 is related to the absorption at δ 5.91, while the resonance for H2′ of the other conformer at 6.88 is coupled to the H6′ proton at δ 5.96. On the other hand, the dual absorptions observed for H2′ and H6′ in $CDCl_3$ appear as singlets in DMSO-d_6 at δ 6.92 and 6.04. This observation suggests that one of the preferred conformations in $CDCl_3$ has a strong hydrogen bond, as illustrated by **11**, in which case the H2′ and H6′ would be located

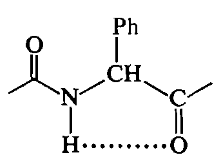

11

in either a deshielding or shielding zone of the —CH_2CO— or phenyl ring attached to the —CH— moiety of **11**, resulting in dual absorptions. Further double irradiation studies for **9***a*–*c* indicated that there are at least two stable conformations present. For example, in DMSO-d_6 the —C*H*-Ph resonance of **9***a* appears at δ 5.76 as two closely overlapped doublets while the NH moiety attached to it appears at δ 8.74 and 8.76 as two partially overlapped doublets. Irradiation of the C*H*-Ph resonances at 5.76 resulted in the appearance of two single peaks at δ 8.74 and 8.76, which suggests that these two peaks for the CH_2CONH moiety are due to two different conformers. The fact that the C6—N*H*CO moiety also appears as two overlapping doublets ($J_{NH,6}$ = 7.5 Hz each) further supports the presence of two different stable conformations for compounds **9**.

A variable temperature ^{1}H nmr study for **9***a* in DMSO-d_6 was performed to determine if the dual absorptions observed for *CH*Ph, *NH*CHPh, and CO*NH*—C6 were due to rotamers as described or to a mixture of two diastereomers. When a sample of **9***a* in DMSO-d_6 was heated to +100°C, the two sets of doublets assigned to CO*NH*—C6 coalesced to one doublet whereas the two sets of doublets due to *CH*-Ph partially coalesced and the resonances for *NH*CHPh became more broad. At +120°C complete coalescence of the two sets of doublets for *CH*Ph occurred to give one doublet at δ 5.76. This study shows that the dual resonances observed for **9** are not due to the presence of two diastereomers but to the presence of conformational isomers as described. The derivatives of 6-aminopenicillanic acid **6** do not have an asymmetric carbon in the C-6 side chain. There is, however, a chiral center at the C-4′ position of the 1,4-dihydropyridyl ring. It is difficult to visualize how this remote chiral center could cause H-2, H-5, and one of the C-3 methyl groups to appear as dual resonances. The dual resonances observed for H-2′ of **6** are most likely due to the effect of rotamers rather than a mixture of diastereomers since H-2 of **3** appear as single resonances. The low solubility of **6***c* in DMSO-d_6 and the low boiling point of deuterium oxide precluded a ^{1}H nmr variable temperature study to determine the coalescence temperature. However, it is not known if these different conformations influence the antibacterial activity of these compounds.

The antibacterial activity of some selected compounds has been investigated (Table 1). All of the compounds tested showed reasonable activity against Gram-positive strains (Organisms 1–5) with the exception of a β-lactamase producing strain of *Staphylococcus aureus* (Organism 6). In contrast, their antibacterial activity toward Gram-negative strains (Organisms 7–9) was poor. The best overall spectrum of activity was shown by the D-α-aminobenzyl analog **10***c*, although it was not better than D-α-aminobenzylpenicillin (Ampicillin®).

Experimental

Infrared spectra (potassium bromide unless otherwise noted) were taken on a Unicam SP 1000 or Perkin–Elmer 267 spectrometer. Nuclear magnetic resonance spectra were determined with a Bruker WH-200, AM-300, or Varian EM-360A spectrometer. The purity of the bio-assay samples was determined to be greater than 95% by the absence of extraneous peaks in the ^{1}H nmr spectra. Mass spectra were measured on a AEI-MS 50 mass spectrometer. The antibacterial screen was performed by Bristol–Myers, Syracuse, New York.

1-[4-n-Butyl-3-(4,4-dimethyloxazolin-2-yl)-1,4-dihydropyridyl]acetic acid (3c)

A solution of n-butyllithium (1.28 g, 0.02 mol) in 5 mL dry tetrahydrofuran was added dropwise to a solution of **1** (4*a*) (3.52 g, 0.02 mol) in 50 mL dry tetrahydrofuran at −78°C with stirring under an atmosphere of nitrogen. The reaction mixture was stirred at −78°C for 30 min and then lithium bromoacetate (2.9 g, 0.02 mol) was added. The reaction mixture was allowed to warm to 25°C and stirring was continued for 12 h. The reaction mixture was cooled to 0°C, water (10 mL) was added, and the pH was adjusted to 4 using 5% aqueous hydrochloric acid. Extraction with chloroform–methanol (9:1 v/v; 10 × 20 mL), washing the combined organic extracts with 10 mL water, drying (Na_2SO_4), and removal of the solvent *in vacuo* afforded **3***c* as a foam. Repeated washing with ether gave pure **3***c* (4.6 g, 78.7%); ir: 1740 (CO); nmr ($CDCl_3$) δ: 12.1 (br, s, 1H, COO*H*, exchanges with deuterium oxide), 7.9 (s, 1H, H2), 5.94 (d, $J_{5,6}$ = 8 Hz, 1H, H6), 5.06 (d, $J_{5,6}$ = 8 Hz of d, $J_{4,5}$ = 5 Hz, 1H, H5), 4.34 (s, 2H, NCH_2—), 4.02 (s, 2H, OCH_2), 3.34–3.64 (m, 1H, H4), 1.06–1.7 (m, 12H, C—$(CH_3)_2$, —$(CH_2)_3CH_3$), 0.86 (t, J = 7 Hz, —$(CH_2)_3$—CH_3). *Exact Mass* calcd. for $C_{16}H_{24}N_2O_3$: 292.1787; found (high resolution ms): 292.1783.

Compounds **3***a* and **3***b* were prepared using a similar procedure.

TABLE 1. Some antibacterial activities of **6***a*–*c* and **10***a*–*c*

Organism	Bristol A No.	Compound, MIC (μg/mL)[a]						
		6*a*	**6***b*	**6***c*	**10***a*	**10***b*	**10***c*	Sodium Ampicillin[b]
1. *Streptococcus pneumoniae*[c]	9585	0.13	0.13	0.13	0.06	0.06	0.03	0.008
2. *Streptococcus pyogenes*[c]	9604	0.13	0.13	0.13	0.06	0.06	0.03	0.004
3. *Streptococcus faecalis*	20688	8	16	4	8	8	4	0.25
4. *Staphylococcus aureus*	9537	0.25	0.06	0.06	0.06	0.06	0.06	0.03
5. *Staphylococcus aureus* + 50% serum	9537	8	4	8	8	4	1	0.13
6. *Staphylococcus aureus*[d]	9606	>125	>125	>125	>125	>125	>125	>125
7. *Escherichia coli*	15119	>125	63	63	63	63	8	2
8. *Escherichia coli*	20341-1	>125	>125	>125	>125	>125	>125	125
9. *Klebsiella pneumoniae*	9664	>125	>125	>125	125	>125	>125	63
10. *Klebsiella pneumoniae*	20468	>125	>125	>125	>125	>125	>125	>125
11. *Enterobacter chloacae*	9659	>125	>125	>125	63	63	32	16
12. *Enterobacter chloacae*	9656	>125	>125	>125	63	63	63	125
13. *Proteus mirabilis*	9900	125	32	125	32	16	1	0.13
14. *Proteus vulgaris*	21559	>125	>125	>125	125	>125	>125	63
15. *Morganella morganii*	15153	125	125	125	63	63	63	63
16. *Providencia rettgeri*	22424	>125	>125	>125	125	>125	>125	>125
17. *Serratia marcesens*	20019	>125	>125	>125	63	63	32	16
18. *Pseudomonas aeruginosa*	9843A	>125	125	125	63	63	63	125
19. *Pseudomonas aeruginosa*[e]	21213	125	125	125	63	63	63	125

[a]The minimal inhibitory concentration (MIC) of the compound in μg/mL required to inhibit growth in a media of nutrient broth unless otherwise indicated.
[b]Sodium salt of D-α-aminobenzylpenicillin (Ampicillin) was used as a reference standard.
[c]The media was comprised of 45% antibiotic assay broth, 5% human serum, and 50% nutrient broth.
[d]Penicillin resistant strain.
[e]Carbenicillin (α-carboxybenzylpenicillin) resistant strain.

1-[4-Phenyl-3-(4,4-dimethyloxazolin-2-yl)-1,4-dihydropyridyl]acetic acid (3a)

Yield 80%; ir: 1737(CO); nmr ($CDCl_3$) δ: 8.75 (br s, 1H, COO*H*, exchanges with deterium oxide), 8.3 (s, 1H, H2), 7.24 (m, 5H, Ph), 5.96 (d, $J_{5,6}$ = 8 Hz, 1H, H6), 5.15 (d, $J_{5,6}$ = 8 Hz of d, $J_{4,5}$ = 4.5 Hz, 1H, H5), 4.55 (d, $J_{4,5}$ = 4.5 Hz, 1H, H4), 4.3 (br s, 4H, NCH_2, OCH_2), 1.45 (s, 6H, C—$(CH_3)_2$). *Exact Mass* calcd. for $C_{18}H_{20}N_2O_3$: 312.1474; found (high resolution ms): 312.1472.

1-[4-Methyl-3-(4,4-dimethyloxazolin-2-yl)-1,4-dihydropyridyl]acetic acid (3b)

Yield 65%; ir: 1740(CO); nmr ($CDCl_3$ and DMSO-d_6) δ: 10.8 (br s, 1H, COO*H*, exchanges with deuterium oxide), 8.0 (s, 1H, H2), 5.9 (d, $J_{5,6}$ = 8 Hz, 1H, H6), 5.18 (d, $J_{5,6}$ = 8 Hz of d, $J_{4,5}$ = 5 Hz, 1H, H5), 4.46 (s, 2H, NCH_2), 4.2 (s, 2H, OCH_2), 3.5 (m, 1H, H4), 1.6 (s, 6H, C—$(CH_3)_2$), 1.18 (d, *J* = 7 Hz, 3H, CH—CH_3). *Exact Mass* calcd. for $C_{13}H_{18}N_2O_3$: 250.1317; found: (high resolution ms): 250.1308.

p-*Bromophenacyl-6-β-[{4-phenyl-3-(4,4-dimethyloxazolin-2-yl)-1,4-dihydropyridylacetyl}amino]-3,3-dimethyl-7-oxo-4-thia-1-azabicyclo[3.2.0]heptane-2-carboxylate (5a)*

A solution of trimethylacetyl chloride (0.96 mL, 8 mmol) in dry tetrahydrofuran (10 mL) was added dropwise to a solution of **3***a* (2.8 g, 9 mmol) and triethylamine (2.88 mL, 20 mmol) in 150 mL dry tetrahydrofuran at −78°C with stirring. The reaction was allowed to proceed at −78°C for 30 min and then **4** (6) (2.28 g, 4 mmol) was added. The reaction was allowed to proceed at 0°C for 8 h with stirring and water (20 mL) was added. The reaction mixture was extracted with ethyl acetate (5 × 20 mL) and the combined extracts were washed successively with a saturated aqueous sodium bicarbonate solution, a solution of 4% aqueous hydrochloric acid, and water. The organic layer was dried (Na_2SO_4) and the solvent removed *in vacuo* to yield impure **5***a*. This product was then triturated with hexane and washed repeatedly with ether to give **5***a* as a foam (3.5 g, 70%); ir: 3300–3400 (NH), 1785 (β-lactam CO), 1755 (CO_2), 1705 (CH_2CO), 1675 (CONH); nmr (DMSO-d_6) δ: 8.86 and 8.88 (two overlapping d, J_{NH,C_6H} = 6 Hz, 1H, NH, exchanges with deuterium oxide), 7.8 and 7.9 (d, *J* = 8 Hz, 2H each, —C_6H_4-Br), 7.08–7.42 (m, 5H, Ph), 6.92 (s, 1H, H2′), 6.0–6.1 (d, $J_{5',6'}$ = 8 Hz, 1H, H6′), 5.4–5.8 (m, 4H, H5, H6, OCH_2CO), 4.74 (d, $J_{5',6'}$ = 7.6 Hz of d, $J_{4',5'}$ = 4.6 Hz, 1H, H5′), 4.52 (s, 1H, H2), 4.4 (d, $J_{4',5'}$ = 4.6 Hz, 1H, H4′), 4.06 (s, 2H, NCH_2CO), 3.75 (s, 2H, O$CH_2$$CMe_2$), 1.66 and 1.70 (two s, 3H, C3-Me), 1.6 (s, 3H, C3-Me), 1.12 and 1.14 (two s, 3H each, OCH_2C*Me*$_2$). Mass, FAB (positive), $(M + 1)^+$: 707 and 709, $(M + 2H)^+$: 708 and 710.

Compounds **5***b* and **5***c* were prepared using a similar procedure.

p-*Bromophenacyl-6-β-[{4-methyl-3-(4,4,-dimethyloxazolin-2-yl)-1,4-dihydropyridylacetyl}amino]-3,3-dimethyl-7-oxo-4-thia-1-azabicyclo[3.2.0]heptane-2-carboxylate (5b)*

Yield 69%; ir: 3300–3400 (NH), 1780 (β-lactam CO), 1760 (CO_2), 1705 ($CH_2COC_6H_4Br$), 1675 (NHCO); nmr (DMSO-d_6) δ: 8.76 and 8.78 (overlapping d, J_{NH,C_6H} = 6 Hz, 1H, NH, exchanges with deuterium oxide), 7.8 and 7.9 (d, *J* = 8 Hz, 2H each, —C_6H_4-Br), 6.7 (s, 1H, H2′), 5.85 (d, $J_{5',6'}$ = 8 Hz, 1H, H6′), 5.42–5.8 (m, 4H, H5, H6, OCH_2CO), 4.6 (d, $J_{5',6'}$ = 8 Hz of d, $J_{4',5'}$ = 5 Hz, 1H, H5′), 4.38 (s, 1H, H2), 3.84 and 3.96 (two s, 2H each, NCH_2CO and O$CH_2$$CMe_2$), 3.2–3.34 (m, 1H, H4′), 1.64 and 1.67 (two s, 3H, C3-Me), 1.58 (s, 3H, C3-Me), 1.02–1.22 (m, 9H, OCH_2C*Me*$_2$, C4′-Me). Mass, FAB (positive), $(M + 1)^+$: 645 and 647, $(M + 2H)^+$: 646 and 648.

p-*Bromophenacyl-6-β-[{4-n-butyl-3-(4,4-dimethyloxazolin-2-yl)-1,4-dihydropyridylacetyl}amino]-3,3-dimethyl-7-oxo-4-thia-1-azabicyclo[3.2.0]heptane-2-carboxylate (5c)*

Yield 72%; ir: 3360 (NH), 1790 (β-lactam CO), 1760 (CO_2), 1710 ($CH_2COC_6H_4Br$), 1680 (CONH); nmr (DMSO-d_6) δ: 8.64 and 8.67 (overlapping d, J_{NH,C_6H} = 6 Hz, 1H, NH, exchanges with deuterium oxide), 7.8 and 7.9 (d, *J* = 8 Hz, 2H each, C_6H_4-Br), 6.74 (s, 1H, H2′), 5.9 (d, $J_{5',6'}$ = 8 Hz, 1H, H6′), 5.42–5.72 (m, 4H, H5, H6, OCH_2CO), 4.52–4.64 (m, 1H, H5′), 4.5 (s, 1H, H2), 3.92 (br s, 4H, NCH_2CO, O$CH_2$$CMe_2$), 3.74–3.86 (m, 1H, H4′), 1.58 (s, 3H, C3-Me), 1.65 and 1.68 (two s, 3H, C3-Me), 1.1–1.4 (m, 12H, OCH_2C*Me*$_2$, —$(CH_2)_3$Me), 0.82 (t, *J* = 7 Hz, 3H, $(CH_2)_3$—CH_3).

Mass, FAB (positive), $(M + 1)^+$: 687 and 689, $(M + 2H)^+$: 688 and 690.

6-β-[{4-n-Butyl-3-(4,4-dimethyloxazolin-2-yl)-1,4-dihydropyridylacetyl}amino]-3,3-dimethyl-7-oxo-4-thia-1-azabicyclo[3.2.0]-heptane-2-carboxylic acid potassium salt (6c)

A mixture of **5c** (0.755 g, 1.1 mmol) and potassium thiophenoxide (0.148 g, 1 mmol) in 5 mL dry DMF was stirred at 0°C for 1 h. Ether (25 mL) was added and the solid which precipitated was filtered. The residue was washed repeatedly with dry ether and acetone to yield **6c** (0.3 g, 56.8%); ir: 3400 (NH), 1780 (β-lactam CO), 1685 (CONH), 1610−1635 (CO_2); nmr (D_2O) δ: 6.88 and 6.92 (two d, $J_{2',6'}$ = 1.15 Hz, 1H, H2′), 6.0 (d, $J_{5',6'}$ = 8 Hz of d, $J_{2',6'}$ = 1.15 Hz, 1H, H6′), 5.62 (d, $J_{5,6}$ = 4 Hz, 1H, H6), 5.54 and 5.56 (overlapping d, $J_{5,6}$ = 4 Hz, 1H, H5), 4.88 (d, $J_{5',6'}$ = 8 Hz of d, $J_{4',5'}$ = 5 Hz, 1H, H5′), 4.26 and 4.28 (two s, 1H, H2), 4.05 (br s, 4H, OCH_2, NCH_2), 3.3−3.44 (m, 1H, H4′), 1.63 and 1.66 (two s, 3H, C3-Me), 1.57 (s, 3H, C3-Me), 1.1−1.4 (m, 12H, CH_2CMe_2, —$(CH_2)_3$—CH_3), 0.86 (t, J = 7 Hz, 3H, —$(CH_2)_3$—CH_3). Mass, FAB (negative), $(M - 1)^+$: 527.

Compounds **6a** and **6b** were prepared from **5a** and **5b** respectively using a similar procedure.

6-β-[{4-Phenyl-3-(4,4-dimethyloxazolin-2-yl)-1,4-dihydropyridylacetyl}amino]-3,3-dimethyl-7-oxo-4-thia-1-azabicyclo[3.2.0]-heptane-2-carboxylic acid potassium salt (6)

Yield 54%; ir: 3380−3440 (NH), 1765 (β-lactam CO), 1685 (CONH), 1610 (CO_2); nmr (D_2O) δ: 7.32−7.42 (m, 5H, Ph), 7.12 and 7.14 (overlapping d, $J_{2',6'}$ = 1.15 Hz, 1H, H2′), 6.0 (d, $J_{5',6'}$ = 8 Hz, 1H, H6′), 5.6 (d, $J_{5,6}$ = 4 Hz, 1H, H6), 5.48 and 5.52 (two d, $J_{5,6}$ = 4 Hz, 1H, H5), 5.03 (d, $J_{5',6'}$ = 8 Hz of d, $J_{4',5'}$ = 5 Hz, 1H, H5′), 4.5 and 4.52 (two overlapping d, $J_{4',5'}$ = 5 Hz, 1H, H4′), 4.24 and 4.26 (two s, 1H, H2), 4.1 (s, 2H, NCH_2CO), 3.9 (s, 2H, OCH_2), 1.56 and 1.59 (two s, 3H, C3-Me), 1.48 (s, 3H, C3-Me), 1.18 (s, 3H, OCH_2CMe), 1.0 (s, 3H, OCH_2CMe). Mass, FAB (negative), $(M - 1)^+$: 547.

6-β-[{4-Methyl-3-(4,4-dimethyloxazolin-2-yl)-1,4-dihydropyridylacetyl}amino]-3,3-dimethyl-7-oxo-4-thia-1-azabicyclo[3.2.0]-heptane-2-carboxylic acid potassium salt (6b)

Yield 51%; ir: 3380−3440 (NH), 1765 (β-lactam CO), 1685 (NHCO), 1605 (CO_2); nmr (D_2O) δ: 6.87 and 6.89 (overlapping d, $J_{2',6'}$ = 1.15 Hz, 1H, H2′), 5.92 (d, $J_{5',6'}$ = 8 Hz, 1H, H6′), 5.4−5.66 (m, 2H, H5, H6), 4.94 (d, $J_{5',6'}$ = 8 Hz of d, $J_{4',5'}$ = 5 Hz, 1H, H5′), 4.26 and 4.28 (two s, 1H, H2), 4.04 (br s, 4H, NCH_2, OCH_2), 3.3 (m, 1H, H4′), 1.58 and 1.62 (two s, 3H, C3-Me), 1.5 (s, 3H, C3-Me), 1.04−1.3 (m, 9H, C4′*Me*, OCH_2CMe_2). Mass, FAB (negative), $(M - 1)^+$: 485.

p-Bromophenacyl-6-β-[(aminophenylacetyl)amino]-3,3-dimethyl-7-oxo-4-thia-1-azabicyclo[3.2.0]heptane-2-carboxylate (8)

A suspension of Ampicillin (6.98 g, 20 mmol) and triethylamine (5.76 mL, 40 mmol) was stirred at 0°C in dry methylene chloride (300 mL) for 30 min to give a clear solution, after which α,*p*-dibromoacetophenone (5.56 g, 20 mmol) in 50 mL dry methylene chloride was added dropwise. The reaction mixture was stirred at 0°C for 4 h and then 25 mL water was added. The organic layer was separated and washed in succession with a saturated solution of sodium bicarbonate and then water (2 × 20 mL). The organic layer was dried (Na_2SO_4) and the solvent removed *in vacuo* to yield **8** as a viscous oil which under vacuum for 1 h afforded a foam (6.0 g, 58.8%); ir: 3300−3380 (NH_2, CONH), 1790 (β-lactam CO), 1760 (CO_2), 1680−1705 (CH_2CO—C_6H_4-Br, CONH); nmr ($CDCl_3$) δ: 8.07 (d, J_{NH,C_6H} = 9 Hz, 1H, NH exchanges with deuterium oxide), 7.55 and 7.68 (d, J = 8 Hz, 2H each, C_6H_4-Br), 7.28−7.44 (m, 5H, Ph), 5.7 (d, $J_{5,6}$ = 4.12 Hz of d, J_{NH,C_6H} = 9 Hz, 1H, H6), 5.56 (d, $J_{5,6}$ = 4.12 Hz, 1H, H5), 5.5 (d, J_{gem} = 16.48 Hz, 1H, O—*CH*—CO), 5.28 (d, J_{gem} = 16.48 Hz, 1H, O*CH*CO), 4.58 and 4.59 (two s, 2H, *CH*-Ph and H2), 1.84 (br s, 2H, NH_2, exchanges with deuterium oxide), 1.7 and 1.75 (two s, 6H, C3-Me_2).

p-Bromophenacyl-6-β-[{4-phenyl-3-(4,4-dimethyloxazolin-2-yl)-1,4-dihydropyridylmethylcarbonylaminophenylacetyl}amino]-3,3-dimethyl-7-oxo-4-thia-1-azabicyclo[3.2.0]heptane-2-carboxylate (9a)

A solution of DCC (0.824 g, 4 mmol) in 10 mL dry methylene chloride was added dropwise with stirring to a solution of **3a** (1.56 g, 5 mmol) and **7** (2.176 g, 4 mmol) in 50 mL dry methylene chloride. The reaction was allowed to proceed for 12 h at 25°C with stirring prior to filtration. The filtrate was washed successively with a saturated solution of sodium bicarbonate (2 × 10 mL), 2% aqueous hydrochloric acid (2 × 5 mL), and then water (2 × 10 mL). The organic fraction was dried (Na_2SO_4) and the solvent removed *in vacuo* to afford impure **9a**. Trituration of this material with hexane and extensive washing with ether yielded **9a** (2.7 g, 80%); ir: 3340 (NH), 1795 (β-lactam CO), 1770 (CO_2), 1710 ($CH_2COC_6H_4Br$), 1675−1690 (CONH); nmr (DMSO-d_6) δ: 9.37 (two overlapping d, J_{NH,C_6H} = 7.5 Hz, 1H, CHCO*NH*, exchanges with deuterium oxide), 8.74 and 8.76 (two overlapping d, J_{NHCH} = 7.5 Hz, 1H, $CH_2CONHCH$, exchanges with deuterium oxide), 7.8 and 7.92 (d, J = 8 Hz, 2H each, COC_6H_4-Br), 7.04−7.56 (m, 10H, Ph, CH-*Ph*), 6.92 (s, 1H, H2′), 6.04 (d, $J_{5',6'}$ = 7.5 Hz, 1H, H6′), 5.76 (br d, J_{NHCH} = 7.5 Hz, 1H, *CH*-Ph), 5.54−5.7 (m, J_{NH,C_6H} = 7.5 Hz, $J_{5,6}$ = 4 Hz, 3H, H6 and $CH_2COC_6H_4Br$), 5.48 (d, $J_{5,6}$ = 4 Hz, 1H, H5), 4.7 (d, $J_{5',6'}$ = 8 Hz of d, $J_{4',5'}$ = 5 Hz, 1H, H5′), 4.44 (s, 1H, H2), 4.38 (d, $J_{4',5'}$ = 5 Hz, 1H, H4′), 4.1 (s, 2H, NCH_2CO), 3.72 (s, 2H, OCH_2CMe_2), 1.5 and 1.61 (two s, 6H, C3-Me_2), 1.0 (s, 3H, OCH_2-*Me*), 0.98 (s, 3H, OCH_2CMe); nmr ($CDCl_3$) δ: 7.63 and 7.73 (two d, J = 8 Hz, 2H each, C_6H_4Br), 7.08−7.56 (m, 12H, $CH_2CONHCH$, CHCO*NH*, CH-*Ph*, C4′-*Ph*, NH exchanges with deuterium oxide), 6.88 and 7.0 (two s, 1H, H2′), 5.91 and 5.96 (two d, $J_{5',6'}$ = 7.6 Hz, 1H, H6′), 5.6−5.8 (m, 2H, *CH*-Ph, H6), 5.33−5.4 (m, J_{CH_2gem} = 16 Hz, 2H, $CH_2COC_6H_4Br$), 5.26 (d, $J_{5,6}$ = 4 Hz, 1H, H5), 4.98 (d, $J_{5',6'}$ = 8 Hz of d, $J_{4',5'}$ = 5 Hz, 1H, H5′), 4.66 (d, $J_{4',5'}$ = 5 Hz, 2H, H4′), 4.5 (s, 1H, H2), 3.66−4.0 (m, 4H, NCH_2CO, OCH_2CMe_2), 1.63 (s, 6H, C3-Me_2), 1.08 and 1.23 (two s, 3H each, OCH_2CMe_2). Mass, FAB (positive) $(M + 1)^+$: 840 and 842; $(M + 2H)^+$: 841 and 843.

Compounds **9b** and **9c** were prepared by the respective reaction of **3b** and **3c** with **8**.

p-Bromophenacyl-6-β-[{4-methyl-3-(4,4-dimethyloxazolin-2-yl)-1,4-dihydropyridylmethylcarbonylaminophenylacetyl}amino]-3,3-dimethyl-7-oxo-4-thia-1-azabicyclo[3.2.0]heptane-2-carboxylate (9b)

Yield 80%; ir: 3340−3400 (NH), 1800 (β-lactam CO), 1770 (CO_2), 1715 ($CH_2COC_6H_4Br$), 1680 (CONH); nmr (DMSO-d_6) δ: 9.3 and 9.32 (two overlapping d, J_{NH,C_6H} = 7.5 Hz, 1H, CO*NH*-C_6), 8.6 and 8.64 (two overlapping d, $J_{CONHCH\text{-}Ph}$ = 7.5 Hz, 1H, CO*NH*CH-Ph, exchanges with deuterium oxide), 7.8 and 7.9 (d, J = 8 Hz, 2H each, COC_6H_4-Br), 7.24−7.5 (m, 5H, CH-*Ph*), 6.7 (s, 1H, H2′), 5.88 (d, $J_{5',6'}$ = 8 Hz, 1H, H6′), 5.72 (two overlapping d, J_{CHNH} = 7.5 Hz, 1H, *CH*Ph), 5.52−5.7 (m, 3H, $OCH_2C_6H_4Br$ and H6), 5.47 (d, $J_{5,6}$ = 4.4 Hz, 1H, H5), 4.61 (d, $J_{5',6'}$ = 8 Hz of d, $J_{4',5'}$ = 5 Hz, 1H, H5′), 4.46 (s, 1H, H2), 3.98 (two s, 2H, NCH_2CO), 3.83 (s, 2H, OCH_2CMe_2), 3.4 (m, 1H, H4′), 1.54 and 1.65 (two s, 3H each, C3-Me_2), 1.1−1.3 (m, 9H, C4′-Me, OCH_2CMe_2); nmr ($CDCl_3$) δ: 7.64 and 7.74 (d, J = 8 Hz, 2H each, C_6H_4Br), 7.36 (m, 5H, Ph), 6.84 (two d, 2H, CO*NH*CHCO*NH*), 6.67 and 6.7 (two d, $J_{2',6'}$ = 1.15 Hz, 1H, H2′), 5.74 and 5.78 (two overlapping d, $J_{5',6'}$ = 8 Hz of d, $J_{2',6'}$ = 1.15 Hz, 1H, H6′), 5.54−5.56 (m, 2H, *CH*Ph, H6), 5.38−5.5 (m, J_{CH_2gem} = 16 Hz, 2H, $CH_2C_6H_4Br$), 5.26 (d, $J_{5,6}$ = 4.5 Hz, 1H, H5), 4.98 (d, $J_{5',6'}$ = 8 Hz of d, $J_{4',5'}$ = 5 Hz, 1H, H5′), 4.47 (s, 1H, H2), 3.86−3.90 (m, 4H, NCH_2CO, OCH_2CMe_2), 3.4−3.55 (m, 1H, H4′), 1.6 (s, 6H, C3-Me_2), 1.2−1.34 (m, 9H, C4′-*Me*, OCH_2CMe_2). Mass, FAB (positive) $(M + 1)^+$: 778 and 780; $(M + 2H)^+$: 779 and 781.

p-Bromophenacyl-6-β-[{4-n-butyl-3-(4,4-dimethyloxazolin-2-yl)-1,4-dihydropyridylmethylcarbonylaminophenylacetyl}amino]-3,3-dimethyl-7-oxo-4-thia-1-azabicyclo-[3.2.0]heptane-2-carboxylate (9c)

Yield 60%; ir: 3300−3400 (NH), 1800 (β-lactam CO), 1765

(CO_2), 1710 ($CH_2COC_6H_4Br$), 1680–1690 (CONH); nmr (DMSO-d_6) δ: 9.4 (br d, J_{NH,C_6H} = 7.6 Hz, 1H, CHCO*NH*C_6H, exchanges with deuterium oxide), 8.66 and 8.7 (two overlapping d, $J_{NH,CH}$ = 8.3 Hz, 1H, CH_2CO*NH*CH), 7.8 and 7.9 (two d, J = 8 Hz, 2H each, C_6H_4Br), 7.18–7.64 (m, 5H, *Ph*), 6.76 (br s, 1H, H2′), 5.95 (d, $J_{5',6'}$ = 8 Hz, 1H, H6′), 5.43–5.9 (m, 5H, *CH*-Ph, H5, H6, CH_2CO-C_6H_4Br, $J_{5,6}$ = 4.4 Hz), 4.58 (d, $J_{5',6'}$ = 8 Hz of d, $J_{4',5'}$ = 5 Hz, 1H, H5′), 4.45 (s, 1H, H2), 3.98 (br s, 2H, NCH_2CO), 3.7–3.94 (m, 3H, H4′, OCH_2CMe$_2$), 1.0–1.85 (m, 18H, —$(CH_2)_3CH_3$, OCH$_2$CMe_2, C3-Me_2), 0.84 (t, J = 7 Hz, 3H, $(CH_2)_3CH_3$); nmr ($CDCl_3$) δ: 7.65 and 7.75 (d, J = 8 Hz, 2H each, C_6H_4Br), 7.38 (m, 5H, CH-*Ph*), 6.9–7.06 (m, 2H, CH_2CO*NH*CHCO*NH*, exchanges with deterium oxide), 6.76 and 6.78 (two s, 1H, H2′), 5.82 and 5.86 (two overlapping d, $J_{5',6'}$ = 8 Hz, 1H, H6′), 5.2–5.78 (m, 5H, *CH*Ph, H5, H6, $CH_2COC_6H_4Br$), 4.86 (d, $J_{5',6'}$ = 8 Hz of d, $J_{4',5'}$ = 5 Hz, 1H, H5′), 4.5 (s, 1H, H2), 3.6–4.0 (m, 5H, OCH_2CMe$_2$, NCH_2CO, H4′), 1.1–1.9 (m, 18H, $(CH_2)_3CH_3$), OCH$_2$CMe_2, C3-Me_2), 0.9 (t, J = 7 Hz, 3H, $(CH_2)_3CH_3$). Mass, FAB (postitive), $(M + 1)^+$: 820 and 822; $(M + 2H)^+$: 821 and 823.

The potassium salts **10**$a-c$ were prepared from the reaction of **9**$a-c$ with potassium thiophenoxide as outlined previously in the procedure for the preparation of **6**c.

*6-β-[{4-Phenyl-3-(4,4-dimethyloxazolin-2-yl)-1,4-dihydropyridylmethylcarbonylaminophenylacetyl}amino]-3,3-dimethyl-7-oxo-4-thia-1-azabicyclo[3.2.0]heptane-2-carboxylic acid potassium salt (**10**a)*

Yield 68%; ir: 3200–3400 (NH), 1780 (β-lactam CO), 1680 (CONH), 1630 (CO_2). Mass, FAB (negative), $(M - 1)^+$: 680.

*6-β-[{4-Methyl-3-(4,4-dimethyloxazolin-2-yl)-1,4-dihydropyridylmethylcarbonylaminophenylacetyl}amino]-3,3-dimethyl-7-oxo-4-thia-1-azabicyclo[3.2.0]heptane-2-carboxylic acid potassium salt (**10**b)*

Yield 45%; ir: 3200–3400 (NH), 1770–1780 (β-lactam CO), 1680 (CONH), 1620 (CO_2). Mass, FAB (negative), $(M - 1)^+$: 618.

*6-β-[{4-n-Butyl-3-(4,4-dimethyloxazolin-2-yl)-1,4-dihydropyridylmethylcarbonylaminophenylacetyl}amino]-3,3-dimethyl-7-oxo-4-thia-1-azabicyclo[3.2.0]heptane-2-carboxylic acid potassium salt (**10**c)*

Yield 47%; ir: 3400 (NH), 1775 (β-lactam CO), 1680 (CONH), 1610 (CO_2). Mass, FAB (negative), $(M - 1)^+$: 660.

Acknowledgements

We are grateful to the Medical Research of Council (MT-4888) for financial support of this research and to the Alberta Heritage Foundation for Medical Research for providing a fellowship to one of us (S.K.D.). We also thank Bristol–Myers for the antibacterial screening results.

1. R. B. MORIN and M. GORMAN. Chemistry and biology of β-lactam antibiotics. Academic Press, New York. 1982.
2. D. PERLMAN. Structure–activity relationships among the semisynthetic antibiotics. Academic Press, New York. 1977. p. 217.
3. (*a*) M. L. EDWARDS, R. E. BAMBURY, and H. W. RITTER. J. Med. Chem. **20**, 560 (1977); (*b*) M. L. EDWARDS and R. C. ERICKSON. J. Med. Chem. **22**, 1416 (1979).
4. (*a*) A. E. HAUCK and C. S. GIAM. J. Chem. Soc. Perkin Trans. 1, 2070 (1980); (*b*) A. I. MEYERS and R. A. GABEL. J. Org. Chem. **47**, 2633 (1982).
5. S. K. DUBEY, E. KNAUS, and C. S. GIAM. Heterocycles, **22**, 1091 (1984).
6. P. BAMBERG, B. EKSTROM, and B. SJOBERG. Acta Chem. Scand. **21**, 2210 (1967).

Propriétés volumiques du nitrate d'éthylammonium fondu à 298 K et de ses mélanges avec l'eau

M. HADDED, M. BIQUARD, P. LETELLIER ET R. SCHAAL
Laboratoire de Physicochimie des Solutions, Université P. et M. Curie, E.N.S.C.P. 11 Rue P. et M. Curie, 75231 Paris Cedex 05

Reçu le 16 mars 1984

M. HADDED, M. BIQUARD, P. LETELLIER et R. SCHAAL. Can. J. Chem. **63**, 565 (1985).

Les volumes molaires partiels de l'eau et du nitrate d'éthylammonium ont été déterminés avec précision dans leurs différents mélanges entre l'eau pure et le sel fondu pur à 298 K. Il est montré dans cette étude que le volume molaire partiel de l'eau suit une loi linéaire avec la fraction molaire x du sel dès que x devient supérieur à 0,04. Les lois décrivant les variations des principales grandeurs thermodynamiques relatives aux volumes sont établies pour le sel, l'eau et la solution. Il est également montré que le volume intrinsèque du sel dans les solutions salines concentrées ($x > 0{,}04$) s'identifie en première approximation au volume molaire du sel fondu pur, et que la valeur du volume molaire apparent de l'eau correspond à une estimation convenable du volume effectif moyen attribuable à chaque molécule d'eau dans la solution.

M. HADDED, M. BIQUARD, P. LETELLIER, and R. SCHAAL. Can. J. Chem. **63**, 565 (1985).

Partial molar volumes of water and ethylammonium nitrate EAN are determined accurately in all water–EAN mixtures, between pure water and pure fused salt at 298 K. It has been found that the partial molar volume of water decreases linearly with molar fraction of salt, x, in concentrated solution of EAN ($C > 2$ mol L^{-1}, $x > 0.04$). The main thermodynamic relations are established to describe the volumetric behaviour of salt, water, and solution. It has been shown that the intrinsic volume of salt can be identified roughly with the molar volume of the pure fused salt and the value of apparent molar volume of water with the actual volume of water in solution.

L'étude des propriétés volumiques des mélanges eau – sel fondu, à des températures très supérieures à l'ambiante a permis de proposer et de discuter différents modèles de solvatation pour les espèces ioniques, particulièrement pour les milieux les plus riches en sel (1, 2, 20).

Toutefois, la difficulté de mesurer avec une très grande précision les masses volumiques de solutions à des températures éloignées des conditions standard ne permet généralement pas une détermination suffisamment précise des propriétés individuelles de l'eau et du sel dans leurs différents mélanges, pour pouvoir vérifier l'intégralité des conséquences impliquées par les modèles.

L'utilisation d'un sel à bas point de fusion (14°C), le nitrate d'éthylammonium (NEA), miscible à l'eau en toutes proportions, nous a permis en revanche d'effectuer ce type d'étude. Le but de cet article est donc, tout d'abord de présenter une technique expérimentale donnant accès à des valeurs précises des volumes molaires partiels de l'eau et du NEA à 298 K dans leurs différents mélanges, puis d'examiner les valeurs expérimentales à l'aide d'un formalisme développé dans une publication antérieure (3).

I. Technique expérimentale

I-1. *Le nitrate d'éthylammonium* pur a été préparé par une technique proche de celle proposée par Evans *et al.* (4): une solution d'éthylamine à 33% (Prolabo) a été neutralisée par de l'acide nitrique de densité égale à 1,33 (Prolabo) dans un bécher refroidi dans un bain de glace. La solution saline a été concentrée à l'évaporateur rotatif à 60°C pendant 3 h. L'eau, de la solution concentrée, a été éliminée par séchage sous vide pendant 3 jours, en présence de P_2O_5. Le point de fusion du sel a été trouvé égal à 14°C.

L'eau utilisée pour réaliser les différents mélanges a été bidistillée. Sa masse volumique a été prise égale à 0,997047 g/cm^3 pour les calculs de volumes molaires partiels.

Les mesures de masses volumiques ont été effectuées au moyen d'un densimètre vibratomètre Picker modèle 03D régulé à 298 ± 2 × 10^{-3} K par un thermostat Setaram.

I-2. *Détermination des volumes molaires partiels de l'eau et du sel dans les différents mélanges eau–NEA*

La technique classique de détermination du volume molaire partiel d'un constituant 1 dans un mélange binaire 1–2 consiste généralement à mesurer le volume molaire apparent de 1, ϕ_1, pour différentes fractions molaires x de 2 et d'en déduire le volume molaire partiel $\bar{V}_1$ par la relation:

$$[1] \quad \bar{V}_1 = \phi_1 - x(1-x)\left[\frac{\partial \phi_1}{\partial x}\right]_{(n_1+n_2)}$$

ce qui nécessite l'estimation toujours délicate d'une grandeur dérivée.[1] L'utilisation d'une telle technique ne conduit généralement qu'à des valeurs approchées des volumes molaires partiels de 1 et de 2. Afin d'obtenir des valeurs précises (incertitudes inférieures à 0,1 cm^3 mol^{-1}) des volumes molaires partiels de l'eau et du nitrate d'éthylammonium, notés respectivement 1 et 2 par la suite dans le texte, dans leurs melanges nous avons utilisé une technique de *détermination directe*, exposée en détail dans un précédent travail (3). Cette technique fait appel à une "méthode d'ajouts" dont les principes sont rappelés brièvement ci-dessous.

"Méthode d'ajouts"

Le volume d'une solution contenant n_1 moles d'eau et n_2 moles de sel est égal à:

$$V = n_1\bar{V}_1 + n_2\bar{V}_2$$

Si l'on ajoute à cette solution *une très faible quantité* ϵ de l'un des deux constituants, le volume change et devient V'. On peut caractériser la variation du volume total de la solution en la ramenant à une mole de soluté additionné.

On aurait, par exemple, pour un ajout ϵ_1 d'eau dans un mélange eau–NEA

$$P_1 = \frac{V' - V}{\epsilon_1}$$

[1]Lorsque l'on connaît sans ambiguité les volumes molaires des composés 1 et 2 respectivement V_1^0 et V_2^0 on peut également déterminer $\bar{V}_1$ à partir du volume d'excès, V_{ex}, par la relation:

$$\bar{V}_1 = V_1^0 + V_{ex} - x\left[\frac{\partial V_{ex}}{\partial x}\right]_{(n_1+n_2)}$$

Là également l'estimation de $\left[\frac{\partial V_{ex}}{\partial x}\right]_{(n_1+n_2)}$ est particulièrement délicate et peut conduire à d'importantes incertitudes près des bornes ($x = 0$ et $x = 1$) (5).

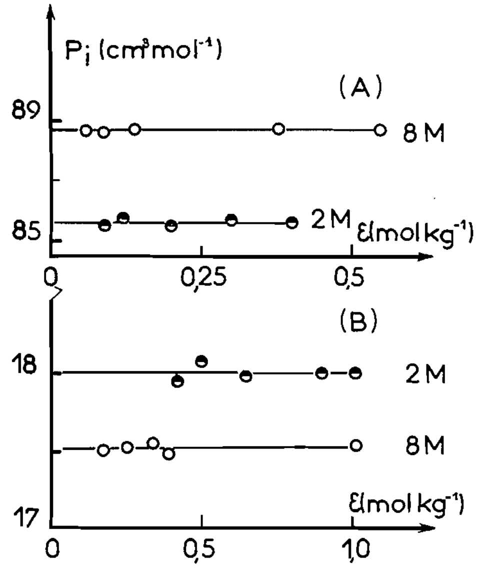

FIG. 1. Exemple d'extrapolation à "ajout nul" ($\epsilon = 0$) des grandeurs P_i pour le sel (A) et pour l'eau (B) dans les solutions 2 et 8 mol L^{-1} en NEA.

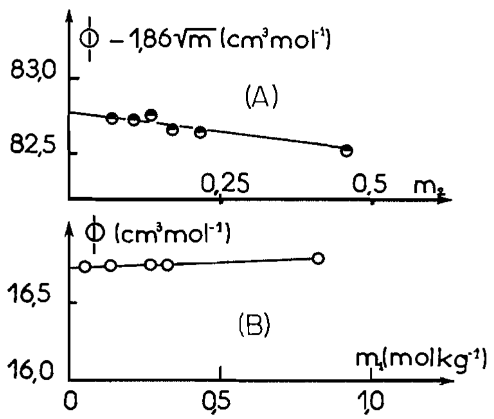

FIG. 2. (A) Détermination du volume molaire partiel à "dilution infinie" du nitrate d'éthylammonium dans l'eau à partir de la technique d'extrapolation proposée par Redlich et Rosenfeld. (B) Détermination du volume molaire partiel à "dilution infinie" de l'eau dans le sel fondu.

Par définition de la grandeur molaire partielle, la grandeur P_1 admet pour limite $\bar{V}_1$, lorsque l'ajout ϵ_1 tend vers zéro

$$[2] \quad \lim_{\epsilon_1 \to 0} P_1 = \bar{V}_1$$

On aurait bien évidemment pour un ajout ϵ_2 de sel dans le même mélange

$$[2a] \quad \lim_{\epsilon_2 \to 0} P_2 = \bar{V}_2$$

Dans la pratique, on détermine les volumes molaires partiels de l'eau et du sel en utilisant la procèdure suivante.

(*a*) On prépare par *volumétrie* le mélange eau−sel désiré.

(*b*) On effectue dans ce mélange 4 à 6 additions d'eau puis de sel. Les quantités ajoutées sont déterminées avec précision *par gravimétrie*.

(*c*) On calcule les quantités P_i correspondant aux ajouts du constituant i par la relation

$$[3] \quad P_i = \frac{1000}{\epsilon_i}\left(\frac{1}{\rho_i} - \frac{1}{\rho_M}\right) + \frac{M_i}{\rho_i}$$

où ρ_M et ρ_i sont respectivement les masses volumiques du mélange avant et après l'ajout; ϵ_i est le nombre de moles du constituant i ajouté à 1000 g de mélange.

(*d*) On extrapole ensuite les valeurs de P_i linéairement avec ϵ_i à "ajout nul" ($\epsilon_i = 0$). La justification de cette technique d'extrapolation a été exposée précédemment (3). Les volumes molaires partiels de l'eau et du NEA ont été déterminés pour 7 mélanges eau−sel régulièrement répartis sur l'échelle des fractions molaires.

Plusieurs exemples d'extrapolation à "ajout nul" sont reportés sur la fig. 1. Les droites obtenues possèdent toutes des pentes faibles conduisant à des valeurs extrapolées à $\pm 0,1$ cm³ mol⁻¹.

TABLEAU 1. Exemple des variations de P_1 et P_2 obtenues pour différents ajouts d'eau (ϵ_1) et de sel (ϵ_2) dans un mélange eau−NEA ($x = 0,625$). Les valeurs de $\bar{V}_2$ et $\bar{V}_1$ sont reportées en correspondance de $\epsilon = 0$

Nitrate d'éthylammonium		
ϵ_2 (mol kg⁻¹)	ρ (g/cm³)	P_2 (cm³ mol⁻¹)
0	1,19 2587	89,1
0,066	1,19 2734	89,08
0,093	1,19 2766	89,12
0,117	1,19 2828	89,17
0,178	1,19 2953	89,17
0,366	1,19 3309	89,20
Eau		
ϵ_1 (mol kg⁻¹)	ρ (g/cm³)	P_1 (cm³ mol⁻¹)
0	1,19 2587	17,1
0,179	1,19 2068	17,15
0,471	1,19 1201	17,19
0,541	1,19 0993	17,20
1,042	1,18 9534	17,21
2,384	1,18 5702	17,23

II. Résultats expérimentaux

À titre d'exemple, les résultats expérimentaux obtenus pour le milieu $x = 0,625$ sont reportés dans le tableau 1.

La valeur du volume molaire partiel du nitrate d'éthyl ammonium à dilution infinie dans l'eau a été obtenu par extrapolation selon la méthode proposée par Redlich et Rosenfeld (6) (fig. 2(A)). Cette valeur (82,9 cm³ mol⁻¹) est sensiblement supérieure à celle que l'on peut calculer à partir de la valeur de $\bar{V}^0$ publiée pour le bromure d'éthylammonium (81,9 cm³ mol⁻¹) (7), en supposant l'additivité des $\bar{V}^0$ individuels des ions (8).

La valeur du volume molaire partiel de l'eau à dilution infinie dans le sel pur a été obtenue par extrapolation linéaire avec la molalité de l'eau dans la solution (fig. 2(B)). Les valeurs des volumes molaires partiels de l'eau et du nitrate d'éthylammonium sont regroupées dans le tableau 2. Les variations des volumes molaires partiels de l'eau et du sel dans leurs différents mélanges sont reportées sur la fig. 3.

La masse volumique du sel pur a été trouvée égale à:

$$\rho_{NEA} = 1,21062 \text{ g/cm}^3 \text{ à } 298 \text{ K}$$

ce qui correspond à une concentration de 11, 2 moles par litre de sel. La valeur de la masse volumique est supérieure à celle que l'on peut calculer à partir de la relation proposée par Sugden et Wilkins (9).

TABLEAU 2. Valeurs des volumes molaires partiels de l'eau $\bar{V}_1$ et du nitrate d'éthylammonium $\bar{V}_2$ pour les différents mélanges eau–NEA à 298 K

C (mol L^{-1})	0	2,02	4,04	6,02	8,08	8,96	10,03	10,75	11,2
x	0	$4{,}22\times10^{-2}$	0,100	0,186	0,336	0,441	0,625	0,819	1
$\bar{V}_1$ (cm^3 mol^{-1})	18,07	18,0	17,9	17,8	17,5$_5$	17,4	17,2	16,9	16,7
$\bar{V}_2$ (cm^3 mol^{-1})	82,8	85,6	87,2	88,1	88,7	89,0	89,2	89,3	89,3
$\bar{V}_2$ (cm^3 mol^{-1}) calculé	—	86,11	87,29	88,06	88,70	88,94	89,18	89,29	89,32

III. Discussion des résultats

Comme le montre la fig. 3, le volume molaire partiel de l'eau varie linéairement avec la fraction molaire, x, du sel entre ses deux valeurs limites V_1^0 et $\bar{V}_1^0$ (volume molaire et volume molaire partiel à dilution infinie de l'eau dans le sel pur).

À partir de cette simple représentation graphique, on serait donc tenté d'adopter pour rendre compte des variations de $\bar{V}_1$, la relation suivante:

$$[4] \quad \bar{V}_1 = V_1^0 - x\,(V_1^0 - \bar{V}_1^0)$$

sur l'intervalle des fractions molaires comprises entre 0 et 1, bornes incluses. Or ce choix conduirait à une description tout à fait incorrecte des propriétés du sel dans le domaine des solutions diluées en électrolyte.

En effet, on peut montrer que la description des variations du volume molaire partiel du constituant 1 dans le binaire 1–2, au moyen d'une équation polynomiale en x (x = fraction molaire du constituant 2) ne peut *au minimum* débuter qu'à l'ordre 2, l'ordre unité conduisant à une valeur infinie pour $\bar{V}_2$ lorsque x tend vers zéro (5).

Le domaine correspondant aux solutions diluées doit donc être impérativement exclu de l'intervalle de définition de la reaction 4, ce qui conduit à envisager deux intervalles d'étude: (*a*) un premier intervalle très étroit, correspondant aux solutions salines diluées, pour des fractions molaires inférieures à 4×10^{-2} (la valeur choisie pour cette borne sera justifiée ultérieurement); (*b*) un second intervalle beaucoup plus large, correspondant aux solutions concentrées en NEA pour x supérieur à 4×10^{-2} dans lequel le comportement des deux constituants de la solution sera entièrement déterminé, par les conséquences de la relation [4].

III-1. *Solutions concentrées en NEA dans l'intervalle $4 \times 10^{-2} < x \leq 1$*

III-1-1. *Volumes molaires partiels du sel*

L'utilisation conjointe de la relation de Gibbs–Duhem et de la relation [4] permet d'établir une loi de variation pour le volume molaire partiel du NEA en fonction de x:

$$d\bar{V}_2 = \frac{1-x}{x}\,(V_1^0 - \bar{V}_1^0)\,dx$$

Cette équation différentielle peut être intégrée entre la borne limite correspondant au sel pur (x = 1) et une autre borne caractéristique de l'une des solutions appartenant à l'intervalle de définition de l'équation [4].

On obtient alors, pour décrire les variations de $\bar{V}_2$, l'expression suivante:

$$[5] \quad \bar{V}_2 = V_2^0 + (V_1^0 - \bar{V}_1^0)\,(\ln x + 1 - x)$$

Les valeurs de $\bar{V}_2$ calculées au moyen de la relation [5] sont reportées dans le tableau 2 en regard des valeurs expérimentales.

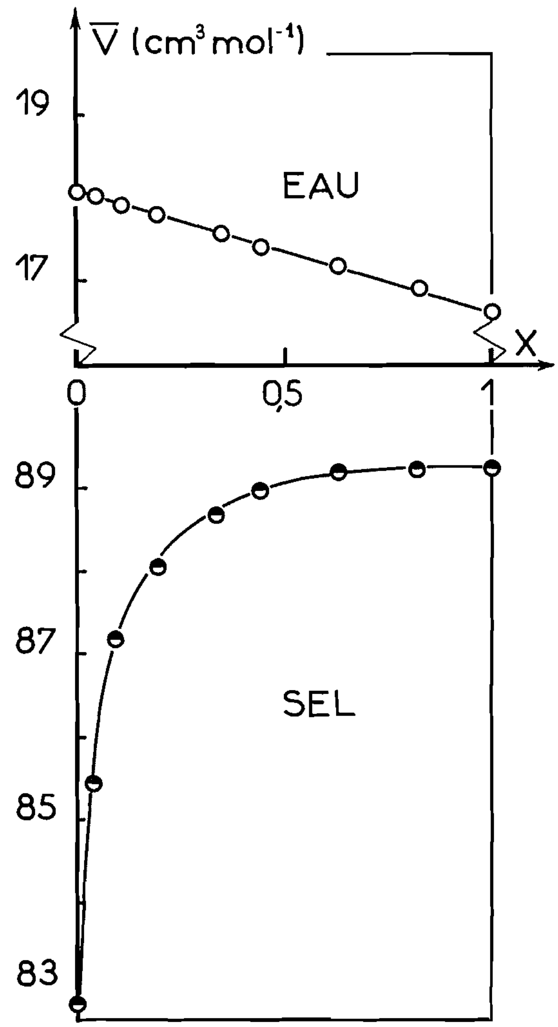

FIG. 3. Volumes molaires partiels de l'eau et du sel à 298 K dans leurs différents mélanges en fonction de la fraction molaire du NEA.

Les valeurs calculées sont en excellent accord avec les valeurs expérimentales pour l 'ensemble des mélanges étudiés ce qui justifie la forme polynomiale au premier ordre adoptée pour décrire les variations de $\bar{V}_1$. Le système d'équation choisi est auto-cohérent.

Les expressions de $\bar{V}_1$ et $\bar{V}_2$ étant établies en fonction de la fraction molaire du NEA, on peut compléter la description du binaire au moyen des autres grandeurs molaires. Certaines d'entre elles seront utiles lors de la discussion concernant les différents modèles pouvant rendre compte des résultats expérimentaux.

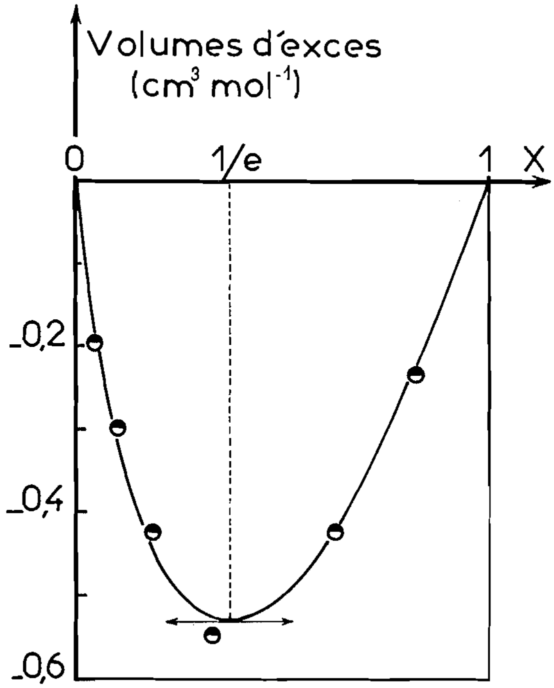

FIG. 4. Volumes d'excès des mélanges eau–NEA. La courbe représentative a été tracée à partir des valeurs calculées au moyen de la relation [9].

III-1-2. *Autres grandeurs molaires du sel et de l'eau dans leurs mélanges*

(a) *Volumes molaires apparents du NEA*

Par définition le volume molaire apparent ϕ_2 du sel s'écrit

$$\phi_2 = \bar{V}_2 + \frac{1-x}{x}(\bar{V}_1 - V_1^0)$$

soit en substituant $\bar{V}_2$ par son expression

$$[6] \quad \phi_2 = V_2^0 + (V_1^0 - \bar{V}_1^0) \ln x$$

(b) *Volumes molaires apparents de l'eau*

Les volumes molaires apparents de l'eau ϕ_1 et du sel ϕ_2 sont reliés par:

$$\phi_1 = V_1^0 + \frac{x}{1-x}(\phi_2 - V_2^0)$$

soit

$$[7] \quad \phi_1 = V_1^0 + (V_1^0 - \bar{V}_1^0)\frac{x}{1-x} \ln x$$

(c) *Volumes réduits et volumes d'excès*

Par définition le volume réduit, V_R, représente le volume du mélange ramené à 1 mole de constituants, soit

$$V_R = x\bar{V}_2 + (1-x)\bar{V}_1$$

$$[8] \quad V_R = xV_2^0 + (1-x)V_1^0 + (V_1^0 - \bar{V}_1^0)x \ln x$$

Conventionnellement le volume d'excès, V_{ex}, rend compte de l'écart entre les propriétés réelles de la solution et celles du système modèle que constitue la solution idéale.

$$V_{ex} = V_R - x V_2^0 - (1-x) V_1^0$$

$$[9] \quad V_{ex} = (V_1^0 - \bar{V}_1^0)x \ln x$$

Les variations du volume d'excès sont représentées sur la fig. 4; le maximum de la courbe se situe à $x = 1/e$.

III-2. *Solutions diluées en NEA dans l'intervalle* $0 \leqslant x \leqslant 4 \times 10^{-2}$

Loi limite de Debye–Hückel

Lorsque les solutions salines sont suffisamment diluées le volume molaire partiel du sel peut être décrit au moyen de la relation

$$[10] \quad \bar{V}_2 = \bar{V}_2^0 + 2{,}8\sqrt{m}$$

dans laquelle m est la molalité du sel. La valeur 2,8 est celle que l'on obtient de manière théorique par dérivation de l'expression proposée par Debye et Hückel pour décrire les variations du coefficient d'activité du sel (6) référé à la solution infiniment diluée.

Les variations de $\bar{V}_2$ peuvent être aisément exprimées en fonction de la fraction molaire. La molalité m et x sont reliées par:

$$m = \frac{x}{1-x}\frac{1}{M_1}$$

où M_1 est la masse molaire de l'eau exprimée en kg mol^{-1}. Dans le domaine des solutions salines diluées, la fraction molaire x reste toujours très petite devant l'unité.

La relation [10] peut donc encore être écrite:

$$[11] \quad \bar{V}_2 = \bar{V}_2^0 + 20{,}8\sqrt{x}$$

soit pour la grandeur molaire apparente

$$[12] \quad \phi_2 = \bar{V}_2^0 + 13{,}87\sqrt{x}$$

Le volume molaire partiel de l'eau obéit alors à la loi limite

$$[13] \quad \bar{V}_1 = V_1^0 - 6{,}93\, x^{3/2}$$

Dans le domaine de validité de la loi limite de Debye–Hückel les variations du volume molaire partiel de l'eau sont inférieures à l'erreur expérimentale et ne peuvent de ce fait être mises en évidence, tout au moins par la technique qui a été utilisée.

Le changement de comportement du sel lorsque l'on passe des solutions très diluées aux solutions concentrées apparaît sur la fig. 5 où sont reportées, en traits pointillés les deux lois limites correspondant aux relations [6] et [12], et en trait plein la courbe expérimentale.

Pour une concentration en NEA supérieure à 2 moles par litre soit $x > 4 \times 10^{-2}$, le comportement de la solution peut être décrit au moyen de la relation [4]. Cette valeur a donc été adoptée comme borne inférieure de son intervalle de définition.

IV. Interprétation des résultats

L'analyse des résultats expérimentaux peut être effectuée au moyen d'un formalisme, développé dans une étude antérieure concernant les mélanges eau–KCl (3,19) qui suppose qu'à l'échelle macroscopique toutes les molécules d'eau de la solution sont perturbées d'une manière identique par la présence du sel (10–12). Il a été ainsi montré que le volume intrinsèque V_i^{I} d'un électrolyte est directement proportionnel à son volume cristallin V_i^{c} calculé à partir des rayons de Pauling.

$$[14] \quad V_i^{\mathrm{I}} = 1{,}92\, V_i^{\mathrm{c}}$$

La validité de cette relation a été vérifiée pour de nombreux électrolytes pour toutes les solutions concentrées en KCl comprises entre 0,5 mol L^{-1} et la saturation.

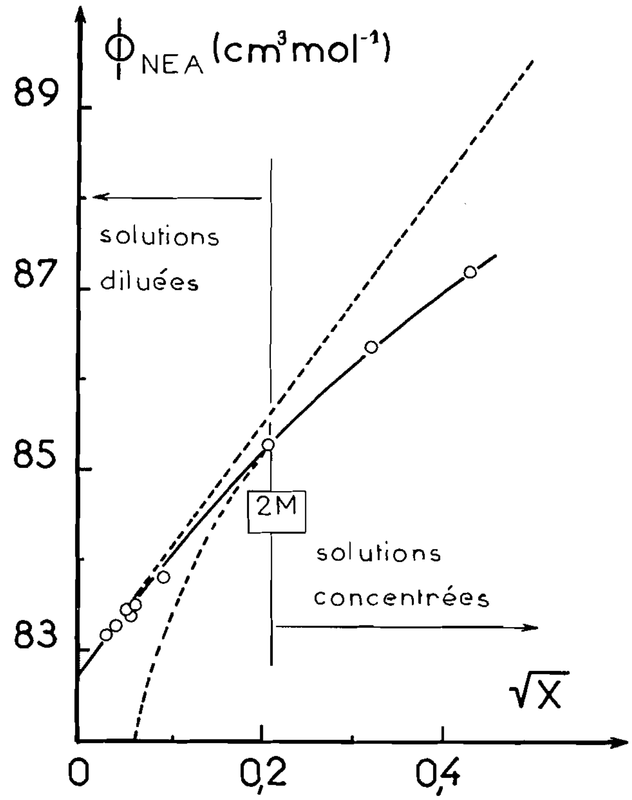

FIG. 5. Variation des volumes molaires apparents du NEA reportée en fonction de $x^{1/2}$. Pour les solutions les plus diluées en sel le comportement du NEA peut être décrit au moyen de la loi limite de Debye et Hückel. Pour les solutions concentrées de molarité supérieure à 2 mol L^{-1} ($x = 4 \times 10^{-2}$) le comportement de la solution est décrit au moyen de la relation [4].

Le volume de la solution saline concentrée s'écrit alors en gardant les notations habituelles (indice 1 pour l'eau et 2 pour le sel)

$$[15]\quad V = n_1 V_{\phi_1} + 1{,}92\, n_2 V_2^c$$

V_{ϕ_1} est une grandeur molaire qui caractérise le volume effectif moyen attribuable à chaque molécule d'eau dans le milieu salin. L'avantage de ce formalisme est de faire apparaître d'une manière explicite l'intervention des propriétés de l'eau dans l'expression du volume molaire partiel de l'électrolyte

$$[16]\quad \bar{V}_2 = 1{,}92\, V_2^c + (1 - x)^2 \left[\frac{\partial V_{\phi_1}}{\partial x}\right]_{(n_1 + n_2)}$$

Dans le cas des mélanges eau–NEA le calcul du volume intrinsèque du sel peut être effectué à partir d'une évaluation des volumes cristallins individuels des ions nitrate et éthylammonium, obtenue par une technique de corrélation exposée en détail dans un article précédent (13). Les valeurs des volumes cristallins des deux ions sont données avec une incertitude de l'ordre de 1%:

$$V^c_{NO_3^-} = 19{,}9 \text{ cm}^3 \text{ mol}^{-1}$$

$$V^c_{EtNH_3^+} = 27{,}0 \text{ cm}^3 \text{ mol}^{-1}$$

soit pour le sel

$$V^c_{NEA} = 46{,}9 \pm 0{,}5 \text{ cm}^3 \text{ mol}^{-1}$$

Si l'on admet que le coefficient de proportionnalité intervenant dans la relation [14] reste du même ordre pour les mélanges eau–NEA, le volume intrinsèque du sel peut être estimé à:

$$V^I_{NEA} = 90 \text{ cm}^3 \text{ mol}^{-1}$$

Cette valeur, tout à fait comparable à celle du volume molaire V^0_{NEA} du sel fondu (89, 3 cm^3 mol^{-1}), laisse supposer que le *volume intrinsèque du nitrate d'éthylammonium dans les mélanges eau–NEA s'identifie en première approximation à son volume molaire*

$$[17]\quad V^0_{NEA} \simeq V^I_{NEA} = 89{,}3 \text{ cm}^3 \text{ mol}^{-1}$$

et que le sel en solution garde "l'empreinte" de sa structure lorsqu'il est pur à l'état liquide.

Cette particularité des mélanges eau–NEA permet d'écrire la relation [15] sous la forme:

$$V = n_1 V_{\phi_1} + n_2 V_2^0$$

V_{ϕ_1} s'identifie alors au volume molaire apparent de l'eau ϕ_1 dans le mélange et ses variations avec la composition peuvent être décrites au moyen de la relation [7].

Comme on peut le remarquer (fig. 6), la variation du volume effectif moyen de l'eau est maximum dans les milieux les plus aqueux et s'atténue pour atteindre une valeur limite pour les solutions les plus riches en sel. Cette limite est liée à la valeur du volume molaire partiel à dilution infinie $\bar{V}_1^0$ de l'eau dans le sel fondu.

$$\lim_{x\to 1} \left|\frac{\partial \phi_1}{\partial x}\right| = -\frac{1}{2}(V_1^0 - \bar{V}_1^0) = \left|\frac{\partial \phi_1}{\partial x}\right|^L$$

soit

$$[18]\quad \bar{V}_1^0 = V_1^0 + 2\left|\frac{\partial \phi_1}{\partial x}\right|^L$$

$\bar{V}_1^0$ représente alors le volume molaire effectif attribuable à une mole d'eau infiniment diluée dans le sel pur.

Sa valeur reste supérieure aux estimations faites par Millero *et al.* (14) et Shimizu (15) pour le volume de l'eau participant à la solvatation directe des ions dans le cas des solutions diluées.

L'utilisation du volume molaire apparent de l'eau pour analyser les propriétés des solutions salines concentrées avait déjà été signalée par Kodejš et Slama (16) qui ont proposé de décrire ses variations par la relation:

$$[19]\quad \phi_1 = x V_1^0 + \left[A + C\frac{1 - x}{1 + x(D - 1)}\right](1 - x)$$

A, C, D sont des paramètres empiriques.

Sacchetto et Kodejš (2) supposent que cette relation est définie sur tout l'intervalle des fractions molaires, *bornes comprises*, et simplifient cette expression en:

$$[20]\quad \phi_1 = V_1^0 + (\bar{V}_1^0 - V_1^0)\, D\, \frac{x}{1 + x(D - 1)}$$

Par un calcul de mécanique statistique, ils relient la valeur de D à l'enthalpie de dilution de l'eau à dilution infinie dans le sel pur (2).

Bien que la forme mathématique proposée par ces auteurs pour décrire les variations de ϕ_1 avec la fraction molaire du sel diffère de celle présentée par la relation [7], nous avons tenté l'examen de nos résultats expérimentaux à l'aide de cette formulation.

La relation [20] ayant été établie en supposant que les bornes $x = 0$ et $x = 1$ appartenaient au domaine de définition de l'éq. [19], il est licite de calculer la valeur de D à partir des

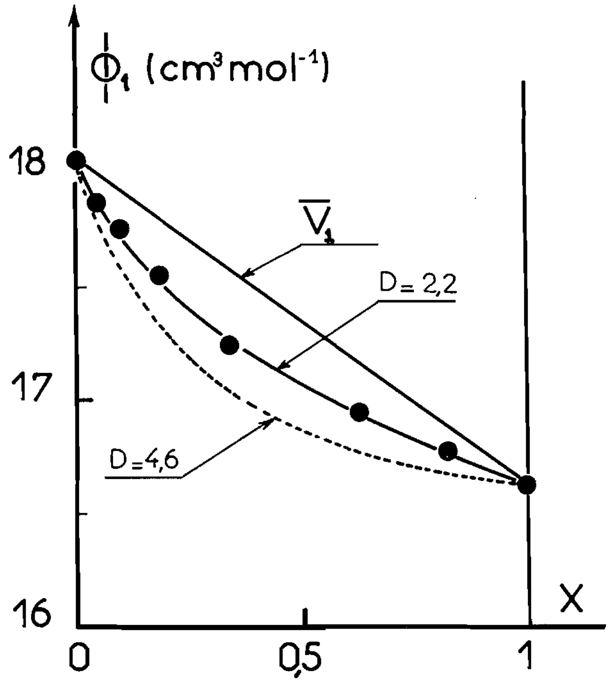

FIG. 6. Variation du volume molaire apparent de l'eau en fonction de la fraction molaire du sel. Les courbes calculées à partir de la relation [19] pour les valeurs D = 2,2 et D = 4,6 sont reportées sur le graphe.

différentes valeurs limites.

Le volume molaire apparent ϕ_2 du sel peut être écrit:

$$\phi_2 = V_2^0 + \frac{1-x}{x}(\phi_1 - V_1^0)$$

soit encore

$$[21]\quad \phi_2 = V_2^0 + [\bar{V}_1^0 - V_1^0]D\,\frac{1-x}{1+x(D-1)}$$

Le volume molaire apparent du sel s'identifie à son volume molaire partiel $\bar{V}_2^0$ lorsque x tend vers zéro soit:

$$\lim_{x\to 0} \phi_2 = \bar{V}_2^0 = V_2^0 + D(\bar{V}_1^0 - V_1^0)$$

La valeur de D est donc égale à

$$[22]\quad D = \frac{V_2^0 - \bar{V}_2^0}{V_1^0 - \bar{V}_1^0}$$

Dans le cas des mélanges eau−NEA, la valeur de D serait donc égale à 4,6. La description des variations de ϕ_1 à l'aide de cette valeur est pour le moins imparfaite (fig. 6).

Toutefois, la similitude de formes entre les courbes expérimentale et calculée nous a incités à tenter cette exploitation avec d'autres valeurs de D, *empiriques cette fois-ci.*

La valeur D = 2,2 conduit à une excellente description des valeurs de ϕ_1 sur toute la gamme des fractions molaires (fig. 6). On peut également vérifier, au moyen des relations suivantes déduites de l'éq. [20], que cette valeur de D permet de retrouver avec précision les résultats expérimentaux pour $\bar{V}_1$ et $\bar{V}_2$, en excluant cependant le domaine des solutions diluées.

$$[23]\quad \bar{V}_1 = V_1^0 - (V_1^0 - \bar{V}_1^0)\left[\frac{Dx}{1+x(D-1)}\right]^2$$

$$[23a]\quad \bar{V}_2 = V_2^0 - (V_1^0 - \bar{V}_1^0)\,D\left[\frac{1-x}{1+x(D-1)}\right]^2$$

$$D = 2{,}2$$

L'utilisation de la relation [20] proposée par Sacchetto et Kodejš conduit à une description précise des résultats expérimentaux à la condition toutefois d'exclure la borne $x = 0$ de son domaine de validité, ce qui paraît contradictoire avec le traitement de l'éq. [19] à l'origine de la relation [20].

Conclusion

L'étude volumétrique des mélanges eau − nitrate d'éthylammonium à 298 K montre que le volume intrinsèque du sel dans ses solutions aqueuses s'identifie à son volume molaire.

La description des comportements individuels de l'eau et du NEA dans leurs différents mélanges a pu être effectuée à partir d'un système d'équations basé sur l'existence d'une relation linéaire entre le volume molaire partiel de l'eau et la fraction molaire du sel. Toutefois ce système d'équations n'est pas unique, et il a été montré que les relations proposées par Kodejš et Sacchetto permettaient également une excellente description des comportements des constituants de la solution à condition d'exclure la borne $x = 0$ de leur domaine de validité. Plus généralement, les mélanges entre l'eau et le nitrate d'éthylammonium apparaissent comme des milieux très particuliers, le sel pur ayant par ses propriétés de nombreuses similitudes avec l'eau pure (17, 18). À titre d'exemple, il a été observé, dans le sel fondu pur, des phénomènes de micellisation comparables à ceux mis en évidence dans l'eau par les composés tensio-actifs.

1. P. CLAES, G. Y. LOIX et J. GLIBERT. Electrochim. Acta, **28**, 421 (1981); M. MICHIELSEN, G. Y. LOIX, J. GLIBERT et P. CLAES. J. Chim. Phys. **79**, 247 (1982).
2. G. A. SACCHETTO et Z. KODEJŠ. J. Chem. Soc. Faraday Trans. 1, **78**, 3519 (1982); Z. KODEJŠ et G. A. SACCHETTO. J. Chem. Soc. Faraday Trans. 1, **78**, 3529 (1982).
3. S. BOUGUERRA et P. LETELLIER. J. Chim. Phys. **79**, 845 (1982).
4. D. F. EVANS, A. YAMAUCHI, R. ROMAN et E. Z. CASASSA. J. Colloid Interface Sci. **88**, 89 (1982).
5. P. LETELLIER et M. BIQUARD. Can. J. Chem. **60**, 1155 (1982).
6. O. REDLICH et P. ROSENFELD. Z. Electrochem. **37**, 705 (1931).
7. J. E. DESNOYERS et M. AREL. Can. J. Chem. **45**, 359 (1967).
8. F. J. MILLERO. Chem. Rev. **71**, 147 (1971).
9. S. SUGDEN et H. WILKINS. J. Chem. Soc. 1291 (1929).
10. F. FRANKS. Water, a comprehensive treatise. Vol. 4. Plenum Press, New York, London. 1974. pp. 1−94; W. J. WEN. *Dans* Water and aqueous solutions. *Edité par* R. A. Horne. Wiley−Interscience, New York. 1972. pp. 613−661; J. O'M. BOCKRISS et A. K. N. REDDY. Modern electrochemistry. Vol. 1. Plenum Rosetta, New York, London. 1973.
11. J. H. ENDERBY et G. W. NEILSON. Adv. Phys. **29**, 323 (1980).
12. R. L. FROST et D. W. JAMES. J. Chem. Soc. Faraday Trans. **78**, 3223 (1982).
13. P. LETELLIER et R. GABORIAUD. J. Chim. Phys. **78**, 829 (1981).
14. F. J. MILLERO, A. LO SURO et C. SHIN. J. Phys. Chem. **82**, 784 (1978).
15. K. SHIMIZU. Bull. Chem. Soc. Jpn. **52**, 2429 (1979).
16. Z. KODEJŠ et I. SLAMA. Collect. Czech. Chem. Commun. **45**, 17 (1980).
17. D. F. EVANS, A. YAMAUCHI, G. J. WEL et V. A. BLOOMFELD. J. Phys. Chem. **87**, 3537 (1983).
18. D. F. EVANS, E. W. KALER et W. J. BENTON. J. Phys. Chem. **87**, 533 (1983).
19. S. BOUGUERRA et P. LETELLIER. J. Chim. Phys. **81**, 55 (1984).
20. M. ABRAHAM. J. Chim. Phys. **81**, 207 (1984).

Five-coordinate dicarbonyl complexes of rhodium(I): $[RhX(CO)_2(PPh_3)_2]$ (X = Cl, Br, I)

ALAN R. SANGER

Alberta Research Council, 11315-87 Avenue, Edmonton, Alta., Canada T6G 2C2

Received July 23, 1984

ALAN R. SANGER. Can. J. Chem. **63**, 571 (1985).

The complexes *trans*-$[RhX(CO)PPh_3)_2]$ (**1**, X = Cl, Br, I) react with CO to form $[RhX(CO)_2(PPh_3)_2]$ (**2**), and not to form *cis*-$[RhX(CO)(PPh_3)_2]$. Complexes **2** contain equivalent axial carbonyl ligands. It is proposed that a series of dicarbonyl complexes, including **2**, is formed during decarbonylation reactions catalyzed by **1**.

ALAN R. SANGER. Can. J. Chem. **63**, 571 (1985).

La réaction des complexes $[RhX(CO)(PPh_3)_2]$-*trans* (**1**, X = Cl, Br, I) avec le CO conduit aux complexes $[RhX(CO)_2(PPh_3)_2]$ (**2**) et il ne se forme pas de complexe $[RhX(CO)(PPh_3)_2]$-*cis*. Les complexes **2** contiennent des ligands carbonyles axiaux équivalents. On suggère l'hypothèse qu'il y a formation d'une série de complexes dicarbonyles, y compris **2**, lors des réactions de décarbonylations catalysées par **1**.

[Traduit par le journal]

Introduction

The complexes *trans*-$[RhX(CO)(PPh_3)_2]$ (**1***a*, X = Cl; **1***c*, X = I) were first synthesized by Vallarino (1), **1***a* from $[Rh_2Cl_2(CO)_4]$, and **1***c* by halogen ligand exchange. Recrystallization of each from various solvents gave unchanged material. Solutions of **1***c* were unstable under the conditions reported, becoming progressively darker. Synthesis of **1***a*, **1***b* (X = Br), or **1***c* under various conditions yields in most cases a product with a single obvious carbonyl band and one rhodium–halogen stretching band in the ir spectrum. However, the reported positions of the bands vary. For products described as **1***a* the carbonyl bands fall into the range 1961 to 1989 cm^{-1}, for **1***b*, 1968 to 1980 cm^{-1}, and for **1***c*, 1968 to 1985 cm^{-1} (e.g. refs. 1–8). For both **1***a* and **1***c*, it has been observed that the materials giving rise to these disparate bands may be formed in mixtures, and it has been assumed that the mixtures were of *cis*- and *trans*-isomers (6, 7). For **1***a* the mixture arose from the decarbonylation of aroyl chlorides catalyzed by $[RhCl(PPh_3)_3]$ (7). For **1***c* the mixture and each component were formed in separate experiments in which halogen exchange of **1***a* with iodide ion was attempted under various conditions (6). It has been reported that *cis*-$[RhI(CO)(PPh_3)_2]$ isomerizes to **1***c* in the solid state within one month (6).

Because the assignment of a "*cis*-$[RhX(CO)(PR_3)_2]$" structure has been made only because of the observation of an extra or displaced CO band in the spectra of such materials, and because the mechanism of decarbonylation catalysed by **1***a* is not fully understood, it was considered appropriate to reinvestigate these materials. A convenient probe is the ^{13}C nucleus, and consequently both the ^{12}CO and ^{13}CO (90% enriched) complexes **1***a*, **1***b*, and **1***c* have been prepared using literature methods (1–6) under either ^{12}CO or ^{13}CO (90% enriched), respectively. Complexes **1***a* and **1***b* enriched with ^{13}CO have previously been described (8, 9). Herein, reactions of **1***a*, **1***b*, and **1***c* (enriched with 90% ^{13}CO) with additional ^{13}CO to give $[RhX(^{13}CO)_2(PPh_3)_2]$ (**2***a*, X = Cl; **2***b*, X = Br; **2***c*, X = I) are reported. Materials previously described as "*cis*-$[RhX(CO)(PPh_3)_2]$" are now considered to be **2***a* and **2***c*, similar to the complex $[RhCl(CO)_2(Ph_2PC_4H_3S)_2]$, reported earlier (10). The complex **2***a* has previously been postulated as an intermediate in the S_N2 exchange of labelled CO with **1***a* (11).

Experimental

All reactions were performed under dry, oxygen-free N_2 or CO. Reagents were either commercially available or prepared by standard literature methods; ^{13}CO (90% ^{13}C-enriched) was purchased from Merck, Sharp, and Dohme Canada Limited, and used as supplied.

Microanalyses were performed at the Microanalytical Laboratory, Department of Chemistry, University of Alberta. Molecular weights were determined osmometrically. Spectra were obtained using the following instruments: ir, Perkin–Elmer 283; ^{13}C and ^{31}P nmr, Bruker WP80. The nmr spectra were obtained from solutions in either dichloromethane-d_2 or toluene-d_8 at +30 to −80°C; at room temperature rapid exchange of ligands prevented observation of coupling.

Reaction of $[Rh_2Cl_2(CO)_4]$ with PPh_3 in CH_2Cl_2

Addition of 4 equiv. of PPh_3 to a solution of $[Rh_2Cl_2(CO)_4]$ in dichloromethane under an atmosphere of CO gave a yellow solution which, after stirring for a few minutes, yielded pale yellow microcrystals. The ir spectrum of the product exhibited carbonyl bands at 1990 (vs) and 1967 (m) cm^{-1}. All attempts to recrystallize this material from benzene or dichloromethane under CO gave similar materials, the ir spectra of which showed the band at 1990 with reduced intensity and the band at 1967 with increased intensity.

Successive recrystallizations of the above material from dichloromethane under an atmosphere of N_2 gave *trans*-$[RhCl(CO)(PPh_3)_2]$ (ν(CO) 1967 cm^{-1}). (*Anal.* calcd.: C 64.3, H 4.4, Cl 5.1; found: C 64.3, H 4.6, Cl 5.25.) Recrystallization from benzene gave the 1 : 1 solvated complex. (*Anal.* calcd.: C 67.2, H 4.7, Cl 4.6; found: C 66.9, H 4.85, Cl 4.7.)

The ^{13}CO (90% ^{13}C-enriched) complexes were prepared under ^{13}CO.

Preparation of the bromo complexes

A solution of $[Rh_2Cl_2(cod)_2]$ in ethanol was stirred with a large excess of KBr under an atmosphere of CO for 4 h. Subsequently 4 equiv. of PPh_3 were added and the mixture was stirred overnight. The mixture was then filtered, and the precipitate was washed with successively water, ethanol, and diethyl ether to give, as a yellow powder, *trans*-$[RhBr(CO)(PPh_3)_2]$ (ν(CO) 1974 cm^{-1}). (*Anal.* calcd.: C 60.4, H 4.1, Br 10.9; found: C 60.4, H 4.1, Br 11.1.)

When the original product was recrystallized from dichloromethane under an atmosphere of N_2, the product was unchanged (ir).

When the original product was recrystallized very slowly from benzene under CO the product was $[RhBr(CO)_2(PPh_3)_2]\cdot C_6H_6$ (ν(CO) 1984 cm^{-1}) (*Anal.* calcd.: C 62.8, H 4.3, Br 9.5, mw 842; found: C 62.4, H 4.4, Br 10.4, mw 879.)

Recrystallization of the latter complex under an atmosphere of N_2

regenerated the original product.

The ^{13}CO complexes were prepared by the same reactions.

Preparation of the iodo complexes

A solution of $[Rh_2Cl_2(cod)_2]$ in ethanol was stirred with a large excess of KI under an atmosphere of CO for 4 h. Then 4 equiv. of PPh_3 were added and the mixture was stirred to form a yellow solution which rapidly gave a yellow precipitate. The mixture was filtered, and the precipitate was washed with successively water, ethanol, and diethyl ether to give, as an orange–yellow powder, $[RhI(CO)_2(PPh_3)_2]$ (ν(CO) 1965 cm^{-1}). (*Anal.* calcd.: C 56.3, H 3.7, I 15.7; found: C 56.1, H 3.8, I 15.4).

Recrystallization of the above product from benzene under an atmosphere of N_2 readily gave *trans*-$[RhI(CO)(PPh_3)_2]\cdot C_6H_6$ (ν(CO) 1989 cm^{-1}). (*Anal.* calcd.: C 60.0, H 4.2, I 14.75; found: C 59.75, H 4.3, I 15.0.) Prolonged stirring of a solution under a stream of N_2 gave $[RhI(PPh_3)_2]_2$ (see also ref. 6).

Recrystallization of the latter product from either benzene or dichloromethane under an atmosphere of CO readily gave large, soft crystals of the original product.

The ^{13}CO complexes were also prepared.

Results and discussion

Reactions of trans-*[RhX(CO)(PPh$_3$)$_2$] with CO*

When preparation of **1***a* was attempted under an atmosphere of CO, a mixture of products was apparently obtained. The carbonyl bands in the ir spectrum were very similar to those reported for what was assumed to be a mixture of the *cis* and *trans* isomers. The complex giving rise to the band at 1990 cm^{-1} was unresolvable, but recrystallization of the mixture under N_2 readily gave the *trans* complex (ν(CO) 1967 cm^{-1}). When a solution of **1***b* in benzene was treated with CO the material isolated was of a different shade of yellow from **1***b*, and the ir spectrum also differed from that of **1***b*. Similarly, attempted preparation of **1***c* under CO, or treatment of **1***c* with CO, gave in each case a novel material, the carbonyl band in the ir spectrum of which coincides with that reported for "*cis*-$[RhI(CO)(PPh_3)_2]$".

The chloro complex giving rise to the ir band at 1990 cm^{-1}, and the new materials obtained by treating **1***b* or **1***c* with CO, are all stable in solution if maintained under an atmosphere of CO. They are assigned the structure $[RhX(CO)_2(PPh_3)_2]$ on the basis of elemental analyses, the following ^{13}C and ^{31}P nmr spectroscopic evidence, and by comparison of the spectroscopic parameters of complexes **1***a* and **2***a* with those of *trans*-$[RhCl(CO)(Ph_2PC_4H_3S)_2]$ and $[RhCl(CO)_2(Ph_2PC_4H_3S)_2]$, respectively (Table 1), which have each been isolated as pure crystals (10).

Solutions of **1***a*, **1***b*, and **1***c* under N_2 were each of a darker hue than the same solutions after treatment with CO, significantly so for **1***c* but only slightly so for **1***a*. The ^{31}P or ^{13}C nmr spectra in each case showed only one environment for either ^{31}P or ^{13}C. In no case was free PPh_3 observed in the ^{31}P nmr spectra of the solutions. Only in the spectrum of **1***c* was a byproduct complex of rhodium observed, which is probably $[RhI(PPh_3)_2]_2$ (6). The ^{31}P nmr spectra of the ^{12}CO complexes **1***a*, **1***b*, or **1***c* in each case showed, as expected, a doublet due to coupling of equivalent ^{31}P nuclei to ^{103}Rh. The spectra of the corresponding ^{13}CO complexes at -50°C each showed a doublet of doublets, due to ^{31}P coupling also to one ^{13}C nucleus. The ^{13}C nmr spectra of **1***a*, **1***b*, or **1***c* each showed a doublet of triplets, confirming that each ^{13}C was coupled to one ^{103}Rh and two equivalent ^{31}P nuclei. The values for **1***a* are consistent with literature values (8).

The ^{31}P nmr spectra of solutions prepared by treatment of solutions of complexes **1***a*, **1***b*, or **1***c* with CO showed that novel complexes **2***a*, **2***b*, or **2***c*, respectively, are formed. The ^{31}P nuclei are in each case chemically equivalent, but the chemical shift and coupling constant to ^{103}Rh of each complex **2** are greatly changed from those of the corresponding complex **1**. For solutions under ^{13}CO each ^{31}P nucleus couples to two equivalent ^{13}C nuclei, observable at -50°C for **2***c*, and at -80°C for **2***b*. For **2***a* broadening of the doublet occurs below -70°C, but coupling to ^{13}C is not resolved. At $+30$°C couplings are not observed due to rapid exchange of ligands. The ^{31}P and ^{13}C nmr spectra of $[RhCl(CO)_2(Ph_2PC_4H_3S)_2]$ differ in a similar manner from those of *trans*-$[RhCl(CO)(Ph_2PC_4H_3S)_2]$ (10) (see Table 1). The ^{13}C nmr spectra of the ^{13}CO-enriched complexes **2***a*, **2***b*, and **2***c* differ from those of **1***a*, **1***b*, and **1***c*. For **2***b* and **2***c* coupling of each ^{13}C nucleus to ^{103}Rh and to two ^{31}P nuclei is resolved. The ^{13}C nmr spectrum of **2***a* remains a singlet to -70°C due to rapid exchange of ligands, but is broad (17.5 Hz) at this temperature. The complexes **2***a*, **2***b*, and **2***c* must be $[RhX(CO)_2(PPh_3)_2]$ because (*i*) the solutions are nonconducting, (*ii*) no free PPh_3 is detected in the ^{31}P nmr spectra, (*iii*) for **2***b* and **2***c* two equivalent ^{31}P nuclei are seen to couple to two equivalent ^{13}C nuclei, and (*iv*) the ^{31}P nmr spectra in no way resemble that of $[RhCl(CO)(Ph_2PCH_2CH_2PPh_2)]$ (P_A: δ_P 97.8 ppm; $^1J_{RhP}$ 158 Hz; P_B: δ_P 76.6 ppm, $^1J_{RhP}$ 124 Hz; $^2J_{P_AB_B}$ 34 Hz) (12).

Large crystals of complex **2***c* are very soft, and light orange–yellow. On standing under an atmosphere other than CO they darken rapidly and steadily to first form yellow–brown **1***c*. Under air **2***c* readily oxidizes within days (c.f. ref. 6). Complex **2***b* is a light yellow, microcrystalline material which appears to be more stable than **2***c* in the solid state. However, in solution it also readily loses 1 mol of CO to form **1***b*. The apparent isomerization of "*cis*-[RhI((CO)-$(PPh_3)_2]$" to **1***c* (6) is now readily understood as loss of CO from **2***c* to form **1***c*.

The ir spectra of complexes **2** are very similar in character to those of **1**, except that the carbonyl and rhodium-ligand bands (Table 2) differ in position and intensity.

The structure of complexes **2** differs from that of the iridium analogs. The complex $[IrCl(CO)_2(PPh_3)_2]$ exhibits two carbonyl bands of similar intensity in the ir spectrum, at 1976 and 1923 cm^{-1} (13), arising from two equatorial carbonyl ligands (14). If complexes **2** were of similar structure, with axial PPh_3 ligands, two carbonyl bands of similar intensity (A_1 and B_2) should also have been observed. Instead, Nujol mulls of complexes **2***a*, **2***b*, and **2***c* each exhibit a single very strong carbonyl band. However, in solution the carbonyl band appears to be an envelope (**2***a*, **2***b*) or broader band (**2***c*). For either a trigonal-bipyramidal structure (Fig. 1), or a *trans*-square-pyramidal structure (Fig. 2), two stretching bands ($A_1 + B_1$) should be ir active, but, for two colinear carbonyl ligands, one stretching band will be weaker than the other. Rapid exchange of ligands (nmr) may include a facile rearrangement between the possible structures. Interconversion of trigonal-bipyramidal

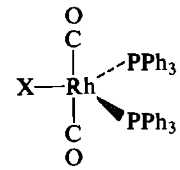

FIG. 1. Trigonal-bypyramidal structure.

TABLE 1. Spectroscopic data for *trans*-[$RhX(CO)(PPh_3)_2$] and [$RhX(CO)_2(PPh_3)_2$]

Complex	Previous formulation	Infrared spectra[a]: Nujol mull $\nu(^{12}CO)$	Nujol mull $\nu(^{13}CO)$	CH_2Cl_2 solution $\nu(^{12}CO)$	CH_2Cl_2 solution $\nu(^{13}CO)$	C_6H_6 solution $\nu(^{12}CO)$	C_6H_6 solution $\nu(^{13}CO)$	Nuclear magnetic resonance spectra[b]: δ_P	δ_C	$^1J_{RhP}$	$^1J_{RhC}$	$^2J_{PC}$
trans-$RhCl(CO)(PPh_3)_2$	Same	1967	1924	1980	1915	1982		28.7		128		16[c]
								(28.7)	(183.4[c])	(127)	(73[c])	(16[c])
$RhCl(CO)_2(PPh_3)_2$	*cis*-$RhCl(CO)(PPh_3)_2$	1990	1941	1982	1922	1980		31.1		116	n.o.	n.o.
				1978(sh)	(sh?)	1960(sh)		(25.2)	(185.9[d])	(96)	(n.o.[d])	(n.o.[d])
trans-$RhBr(CO)(PPh_3)_2$	Same	1974	1926	1985	1936		1933	30.0		124		16.5
								(23.7)	(182.8)	(126)	(76[c])	(15.3)
$RhBr(CO)_2(PPh_3)_2$	—	1984	1937	1980(vs)	1934	1981(vs)		36.5[e]	191.0[e]	90[e]	72[e]	16[e]
				1966(sh)		1964(s, sh)		(35.5)	(187.6)	(88)	(70)	(16)
trans-$RhI(CO)(PPh_3)_2$	Same	1989	1940	1986	1939			28.5	191.2	121.5	70	15
								(27.6)	(186.5)	(123)	(76)	(15)
$RhI(CO)_2(PPh_3)_2$	*cis*-$RhI(CO)(PPh_3)_2$	1965 (vs, b)	1935	1965(vs, b)	1935			34.0	191.1	91	70	16
								(33.1)	(193.6)	(90)	(70)	(15.5)
trans-$RhCl(CO)(Ph_2PC_4H_3S)_2$	(ref. 10)	1974	1925					18.6	187	126	74.5	16.5
$RhCl(CO)_2(Ph_2PC_4H_3S)_2$	(ref. 10)	1990	1944					20.0	187	117	n.o.	n.o.

[a]Values in wavenumbers (±2).
[b]Solutions in dichloromethane-d_2 at −50°C, ^1H decoupled; chemical shifts in ppm downfield from 85% H_3PO_4 (^{31}P) or $Si(CH_3)_4$ (^{13}C), and coupling constants in Hertz. (Values in parentheses are for solutions in toluene-d_8 at −70°C.)
[c]See also ref. 8.
[d]See also ref. 19*a*; peak width at half-height 17.5 Hz at −70°C.
[e]At −80°C.

TABLE 2. Infrared spectra (250–800 cm^{-1}) of complexes **1** and **2**[a]

1*a*	**2***a*[b]	**1***b*	**2***b*·C_6H_6	**1***c*·C_6H_6	**2***c*
	758 (m)				
752 (sh)	754 (m)	752 (sh)			760 (w)
746 (vs)	745 (s)	747 (s)	748 (s)	744 (s)	746 (s)
	721 (w)		722 (vw)	721 (vw)	
705 (s)	705 (s)	707 (s)	704 (sh)	703 (s)	710 (s)
692 (vs)	692 (vs)	693 (vs)	696 (vs)	693 (vs)	692 (vs)
			681 (vs)	674 (s)	
618 (vw)	617 (vw)	618 (vw)			619 (vw)
	570 (w)				
570 (s)	562 (m)	562 (m)	559 (m)	553 (m-w)	
				545 (w-m)	
544 (w)	540 (vw)	540 (w)	538 (w)	539 (w)	
525 (m)	524 (sh)	524 (sh)	521 (s)		
514 (vs)	514 (vs)	516 (vs)	513 (vs)	514 (vs)	514 (vs)
501 (vs)	505 (sh)	501 (s)	504 (s)	506 (sh)	508 (vs)
492 (s)	493 (m)	494 (s)	492 (m)	491 (m)	490 (sh)
				461 (vw)	
450 (w)	450 (w)	451 (w)	449 (vw)	451 (vw)	450 (m-w)
					440 (sh)
431 (w)	430 (vw)	432 (w)	427 (w)	431 (w)	422 (w)
417 (w)	418 (w)	414 (w)			
					344 (w)
308 (w)	308 (sh)				
	297 (w)				

[a]Nujol mulls; values in wavenumbers.
[b]Contaminated with **1***a* (see text).

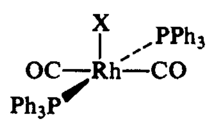

FIG. 2. Square-pyramidal structure.

and square-pyramidal structures occurs for $[RhCl_2(COR)(PPh_3)_2]$ (R = CH_3, CH_2CH_2Ph) (15). Nevertheless, the nmr data for **2** indicate that the trigonal-bipyramidal is the most probable structure, based on a comparison of coupling constants between complexes **1** and **2**. The Rh—C coupling constants for complexes **2** are less than for complexes **1** by 5 to 8%. The Rh—P coupling constants for **2** are less than for **1** by 9 to 27%. For a trigonal-bipyramidal structure with equatorial phosphine ligands and axial carbonyl ligands (Fig. 1) the degree of *s*-character in the equatorial bonds would be expected to drop more in comparison to the corresponding *trans*-square-planar complex than would the *s*-character of the axial bonds. Consequently the Rh—P coupling constant is more greatly reduced than the Rh—C coupling constant.

The existence of complexes **2** has implications for various reactions catalysed by phosphine complexes of rhodium, especially carbonylation and decarbonylation reactions. Under mild conditions $[RhCl(PPh_3)_3]$ is an effective reagent for the stoichiometric decarbonylation of aldehydes and aryl or aroyl halides, but complex **1***a* (which is formed) is not (5, 7, 15, 18). Under more rigorous conditions each material is an effective *catalyst* for such decarbonylation reactions, and intermediates are formed which contain alkyl and hydrido or halogen ligands (15–21). Although the mechanism of the stoichiometric reaction is well understood, the subsequent reactions of **1***a* in the catalytic process, especially elimination of CO, have remained subject to speculation. Catalytic activity is inhibited by the presence of excess PPh_3 (22), and loss of CO from **1***a* is far from facile (23). Consequently it is proposed that catalytic decarbonylation occurs by initial loss of a PPh_3 ligand from **1***a*. Oxidative addition and ligand migration reactions similar to those of the stoichiometric reaction will subsequently afford dicarbonyl complexes, including **2***a*. Elimination of CO from the dicarbonyl complexes will be facile.

Acknowledgement

It is a pleasure to acknowledge the assistance of Mrs. W. Wade in obtaining the nmr spectra.

1. L. VALLARINO. J. Chem. Soc. 2287 (1957).
2. D. EVANS, J. A. OSBORN, and G. WILKINSON. Inorg. Synth. **11**, 99 (1968).
3. J. CHATT and B. L. SHAW. J. Chem. Soc. A, 1437 (1966).
4. A. WINZER and R. GRIEBEL. Z. Chem. **12**, 181 (1972).
5. J. TSUJI and K. OHNO. Tetrahedron Lett. 3969 (1965); 4713 (1966).
6. F. R. HARTLEY, S. G. MURRAY, and D. M. POTTER. J. Organomet. Chem. **254**, 119 (1983).
7. J. BLUM, E. OPPENHEIMER, and E. D. BERGMANN. J. Am. Chem. Soc. **89**, 2338 (1967).
8. L. S. BRESLER, N. A. BUZINA, Y. S. VARSHAVSKY, N. V. KIESELEVA, and T. G. CHERKASOVA. J. Organomet. Chem. **171**, 229 (1979).
9. P. E. GARROU and G. E. HARTWELL. Inorg. Chem. **15**, 646 (1976).
10. A. R. SANGER. Can. J. Chem. **62**, 2168 (1984).
11. A. WOJCICKI and F. BASOLO. J. Am. Chem. Soc. **83**, 524 (1961).
12. A. R. SANGER. J. Chem. Soc. Dalton Trans. 120 (1977); W. HIEBER and R. KUMMER. Chem. Ber. **100**, 148 (1967).
13. L. VASKA. Science, **152**, 769 (1966).
14. N. C. PAYNE and J. A. IBERS. Inorg. Chem. **8**, 2714 (1969).
15. D. L. EGGLESTONE, M. C. BAIRD, C. J. L. LOCK, and G. TURNER. J. Chem. Soc. Dalton Trans. 1576 (1977).

16. J. P. COLLMAN and L. S. HEGEDUS. Principles and applications of organotransition metal chemistry. University Science Books, Mill Valley, CA. 1980. p. 496 *et. seq*.
17. G. W. PARSHALL. Homogeneous catalysis. Wiley, New York. 1980. pp. 90–92.
18. D. H. DOUGHTY and L. H. PIGNOLET. *In* Homogeneous catalysis with metal phosphine complexes. *Edited by* L. H. Pignolet. 1983. Chapt. 11.
19. (*a*) J. A. KAMPMEIER and S. MAHALINGAM. Organometallics, **3**, 489 (1984); (*b*) J. A. KAMPMEIER, S. H. HARRIS, and I. MERGELSBERG. J. Org. Chem. **49**, 621 (1984).
20. J. K. STILLE and M. T. REGAN. J. Am. Chem. Soc. **96**, 1508 (1974); J. K. STILLE and R. W. FRIES. J. Am. Chem. Soc. **96**, 1514 (1974); J. K. STILLE, F. HUANG, and M. T. REGAN. J. Am. Chem. Soc. **96**, 1518 (1974).
21. K. S. Y. LAU, Y. BECKER, F. HUANG, N. BAENZIGER, and J. K. STILLE. J. Am. Chem. Soc. **99**, 5664 (1977).
22. J. B. PHILIP, JR. Ph.D. Thesis, University of Rochester, 1980.
23. G. L. GEOFFROY, D. A. DENTON, M. E. KEENEY, and R. R. BUCKS. Inorg. Chem. **15**, 2382 (1976).

The kinetics, isotope effects, and mechanism of the reaction of 2,2-di(4-nitrophenyl)-1,1,1-trifluoroethane with alkoxide bases in alcohol solvents

ARNOLD JARCZEWSKI, GRZEGORZ SCHROEDER, AND WLODZIMIERZ GALEZOWSKI
Department of Chemistry, Adam Mickiewicz University, 60-780 Poznan, Poland

AND

KENNETH T. LEFFEK AND URSZULA MACIEJEWSKA[1]
Department of Chemistry, Dalhousie University, Halifax, N.S., Canada B3H 4H6

Received May 22, 1984

ARNOLD JARCZEWSKI, GRZEGORZ SCHROEDER, WLODZIMIERZ GALEZOWSKI, KENNETH T. LEFFEK, and URSZULA MACIEJEWSKA. Can. J. Chem. **63**: 576 (1985).

The reaction between 2,2-di(4-nitrophenyl)-1,1,1-trifluoroethane and the alkoxide bases $\bar{O}CH_3$, $\bar{O}C_2H_5$, $\bar{O}nC_4H_9$, $\bar{O}CH(CH_3)_2$, and $\bar{O}C(CH_3)_3$ in their corresponding alcohol solvents is a multistep reaction with several intermediates: 2,2-di(4-nitrophenyl)-1,1-difluoro-1-alkoxyethane (A), 2,2-di(4-nitrophenyl)-1-fluoro-1-alkoxyethene (B), 2,2-di(4-nitrophenyl)-1,1-dialkoxyethene (C), 2,2-di(4-nitrophenyl)-1,1-difluoroethene (D), and 4,4′-dinitrobenzophenone (E). Rate constants and activation parameters have been measured for the appearance of the two stable products B and C. The kinetic deuterium isotope effects for the appearance of B fell in the range of k_H/k_D = 1 to 2 at 25°C for the primary and secondary alkoxides, whereas k_H/k_D = 5.4 at 30°C for the appearance of D with *tert*-butoxide. Exchange experiments showed that H/D exchange took place between the substrate and solvent to the extent of 100% with methoxide, 50% with ethoxide and isopropoxide, and 0% with *tert*-butoxide. It is concluded the HF elimination from the substrate follows an $(E1cB)_R$ mechanism with methoxide/methanol, changing to $(E1cB)_I$ or E2 with *tert*-butoxide/*tert*-butanol.

ARNOLD JARCZEWSKI, GRZEGORZ SCHROEDER, WLODZIMIERZ GALEZOWSKI, KENNETH T. LEFFEK et URSZULA MACIEJEWSKA. Can. J. Chem. **63**: 576 (1985).

La réaction du di(nitro-4 phényl)-2,2 trifluoro-1,1,1 éthane avec les alcoolates $CH_3\bar{O}$, $C_2H_5\bar{O}$, $nC_4H_9\bar{O}$, $(CH_3)_2CH\bar{O}$ et $(CH_3)_3\bar{O}$, dans leurs alcools agissant comme solvants, est un processus en plusieurs étapes impliquant plusieurs intermédiaires: di(nitro-4 phényl)-2,2 difluoro-1,1 alkoxy-1 éthane (A), di(nitro-4 phényl)-2,2 fluoro-1 alkoxy-1 éthène (B), di(nitro-4 phényl)-2,2 dialkoxy-1,1 éthène (C), di(nitro-4 phényl)-2,2 difluoro-1,1 éthène (D) et dinitro-4,4′ benzophénone (E). On a mesuré les constantes de vitesse et les paramètres d'activation pour l'apparition des deux produits stables B et C. Pour les alcoolates primaires et secondaires, à 25°C, les effets isotopiques cinétiques du deutérium, k_H/k_D, varient entre un et deux alors que, pour l'apparition de D sous l'influence du *tert*-butylate à 30°C, k_H/k_D = 5,4. Des expériences d'échange ont permis de démontrer qu'il se produit des échanges H/D entre le substrat et le solvant qui vont jusqu'à 100% avec le méthylate, 50% avec l'éthylate et 0% avec le *tert*-butylate. On en conclut que l'élimination du HF à partir du substrat se fait par un mécanisme $(E1cB)_R$ avec le méthylate/méthanol et que le mécanisme évolue vers un mécanisme $(E1cB)_I$ ou E2 avec le *tert*-butylate/*tert*-butanol.

[Traduit par le journal]

Introduction

The reaction between 2,2-di(4-nitrophenyl)-1,1,1-trifluoroethane and alkoxide bases has already been examined (1–4) and found to be a multistep process with several intermediates which exhibit different reactivity.

The reaction between the substrate and methoxide ion in methanol (1) was found to have a product absorbing at λ_{max} = 325 nm which was assigned to the olefin $(O_2NC_6H_4)_2C{=}CF_2$. From the rate of formation of the product and the absence of a primary kinetic isotope effect, a preequilibrium carbanion $(E1cB)_R$ mechanism was proposed.

The reaction of the substrate with *tert*-butoxide in tertiary butanol was found to be a more complex reaction (2) yielding four different products by sequential reactions. The first product, absorbing at λ_{max} = 525 nm, was thought to be the anion produced by proton removal from the substrate, which then decomposed to the difluoroolefin and subsequently to two additional products absorbing at λ_{max} 530 and 625, and 267 nm. However, the isotope effect, k_H/k_D = 1.42 at 26°C on the appearance of the 525 peak was very low for a proton transfer reaction.

The dissimilarity of the reactions with the two bases led to a further study of the methoxide reaction (3) in which it was found that the first product did react further in a slow reaction to give a substituted product di(4-nitrophenyl)ketene dimethyl acetal with λ_{max} = 350 nm.

Since the mechanism of the reaction of the substrate with the alkoxide bases appeared to take place by a set of sequential reactions which differ with the alkoxide/alcohol system, the present study was initiated of the reaction of the substrate with a series of alkoxides in their corresponding alcohols in order to obtain a clear and self-consistent understanding of the mechanism of the whole set of reactions.

Results and discussion

Product analysis

The reaction of the substrate was carried out with the alkoxide bases in the corresponding alcohol solvent with the base in large excess over the substrate. The products were isolated by preparative scale thin-layer chromatography. Each reaction gave several different products, which are summarized in Table 1.

The major features of the mass spectra and nmr spectra for these products for the ethoxide/ethanol reaction are given in Table 2, together with the structures assigned to them.

The product $(O_2NC_6H_4)_2C{=}CF(OR)$, B in Table 2, formed as an intermediate with all the alkoxide bases except *tert*-butoxide, absorbs at λ_{max} = 332 nm. This material was previ-

[1]Postdoctoral Fellow 1983–1984.

$$(O_2NC_6H_4)_2CHCF_3 \xrightarrow{\bar{O}AlK} (O_2NC_6H_4)_2C{=}CF_2 \rightarrow (O_2NC_6H_4)_2CHCF_2(OR)$$

D $\qquad$ A

$$(O_2NC_6H_4)_2CHCF_2(OR) \xrightarrow{} (O_2NC_6H_4)_2C{=}CF(OR) \rightarrow\rightarrow (O_2NC_6H_4)_2C{=}C(OR)_2$$

B $\qquad$ C

SCHEME 1

TABLE 1. Products of the reaction of 2,2-di(4-nitrophenyl)-1,1,1-trifluoroethane with alkoxide bases

Alkoxide base/solvent	No. of products	Product designation
Methoxide/methanol	3	A, B, C
Ethoxide/ethanol	4	A(trace), B, C, D
n-Butoxide/n-butanol	3	B, C, D
iso-Propoxide/isopropanol	4	B, C, D, E(trace)
tert-Butoxide/*tert*-butanol	2	D, E

ously erroneously thought to be the olefin D (1). This intermediate B undergoes further reaction in a slow step with an excess of alkoxide base giving product C, $(O_2NC_6H_4)_2C{=}C(OR)_2$, absorbing at λ_{max} = 358 nm. This is the final product for the methoxide reaction (2). For the other alkoxides, however, the olefin D, $(O_2NC_6H_4)_2C{=}CF_2$ was formed and the amount of this product increased with decreasing dielectric constant of the solvent alcohol used. Thus, the reaction of the substrate with *tert*-butoxide in *tert*-butanol gives the largest amount of olefin D together with the product E, 4,4′-dinitrobenzophenone.

When the olefin D was treated with small amounts of methoxide or ethoxide, the monosubstituted compound B was again obtained.

The complete reaction sequence is shown in Scheme 1.

Kinetic study

The reaction of the substrate to yield B is much faster than the conversion B to C; therefore, it was possible to measure the kinetics of these two processes separately. Pseudo first-order rate constants were determined by measuring the rate of appearance of B by monitoring the growth of the absorption at 325 nm. These rate constants and the derived second-order rate constants for the normal and deuterated substrate with several alkoxide bases are given in Table 3.

In general, the second-order rate constants increase with the chain length of the normal alkoxide/alcohol systems and the secondary systems show larger k_2 values than the primary ones. However, except for the 140-fold change between methoxide (2) and ethoxide, the rate changes are rather modest.

The isotopic rate ratios k_H/k_D for all the systems were small, confirming the k_H/k_D = 1 previously observed for methoxide (1). Thus, for the ethoxide and n-propoxide reactions, where k_H/k_D is unity or very slightly above unity, the elimination of the HF step proceeds by an $(E1cB)_R$ mechanism. For the other alkoxide bases k_H/k_D ranges up to a value of 2, indicating that proton transfer is partially rate determining.

The activation parameters calculated from the second-order rate constants in Table 3 are given in Table 4, together with those previously measured for methoxide. The enthalpy of activation values show a clear differentiation between the primary and secondary alkoxides, and the entropy of activation values are similarly differentiated in a compensating manner so that the free energy of activation shows little variation.

The rate constants for the appearance of the absorption at about 355 nm corresponding to the product C are given in Table 5. The k_2 values are larger for the primary alkoxides than for the secondary ones. The activation parameters derived from these rate constants, given in Table 6, show compensating behaviour and give rise to free energies of activation 1 to 2 kcal mol^{-1} larger for the secondary systems than for the primary.

In order to verify that the olefin D is an intermediate in all the reactions studied, the substrate was reacted with alkoxide bases with the substrate in large excess. It was determined by mass spectroscopy that under these conditions the olefin D is the main product. Therefore, it is assumed that the olefin D is an intermediate under the conditions of an excess of base. Also, the olefin D was isolated and purified, then used to follow the reaction kinetically from D to product B by again monitoring the appearance of the absorption at 325 nm. The rate constants are shown in Table 7 for the reaction with methoxide, ethoxide, and isopropoxide bases. The second-order rate constants are at least three times larger than the corresponding rate constant for the trifluoro substrate so that the rate constants and activation parameters in Tables 3 and 4 must refer to the elimination of the HF step from the substrate to form the olefin D. In the case of methoxide, the rate of reaction of the olefin D is 2000 times that of the trifluoro substrate, so that in this reaction no D product was observed (Table 1).

In a previous paper (1) it was concluded from the isotope effect of unity and from exchange experiments that the trifluoro substrate reacts with methoxide in methanol by an $(E1cB)_R$ mechanism. The exchange experiment was repeated with methoxide, ethoxide, isopropoxide, and *tert*-butoxide. The reaction of deuterated substrate was carried out with a 10-fold molar excess over the alkoxide base and the degree of deuteration remaining in the substrate was determined by mass spectroscopy. The substrate was completely exchanged in the methoxide reaction, about 50% exchanged in the ethoxide and isopropoxide reactions, and almost completely deuterated in the *tert*-butoxide reaction.

Therefore, the mechanism of the HF elimination from the trifluoro substrate is $(E1cB)_R$ for methoxide/methanol and gradually becomes more $(E1cB)_I$ or E2 with secondary and tertiary bases. The activation parameters in Table 4 show characteristically high $\Delta H^{\neq}$ values for the removal of F^- for the primary alkoxides and much smaller $\Delta H^{\neq}$ values for the secondary bases characteristic of proton abstraction reactions (5).

The solvent isotope effects for the reaction of the substrate leading to the product B were measured in methanol-*d* and ethanol-*d*. At 25°C, k_{2H} in methanol-*d* is 0.97 dm^3 mol^{-1} s^{-1}, which, when combined with the previous measurement (4) of 0.30 for the normal solvent, gives $k_{2H}(CH_3OD)/k_{2H}(CH_3OH)$ = 3.2. For ethanol at 20°C the K_{2H} value from Table 3 is 30.8 and the corresponding value in ethanol-*d* was measured as 31.0,

TABLE 2. Spectral characteristics and assigned structures of the products of the reaction of 2,2-di(4-nitrophenyl)-1,1,1-trifluoroethane with sodium ethoxide in ethanol

Product	Structure	λ_{max} in ethanol	Mass spectral peaks (relative intensity)	Nuclear magnetic resonance in $CDCl_3$
A	Ar_2CHCF_2OEt	Not determined	Detected as a molecular peak 352[M^+]	Not determined
B	$Ar_2C{=}C(F)(OEt)$	332	332(38.0) [M^+], 304(19.7), 284(19.3), 257(14.0), 230(13.0), 229(13.4), 183(39.0), 165(19.7), 164(18.2), 163(25.0), 29(100.0)	δ = 4.25 (q 2H), 1.25 (t 3H), 7.2–8.4 (8H)
C	$Ar_2C{=}C(OEt)(OEt)$	358	358(15.5) [M^+], 302(13.1), 301(8.4), 284(8.7), 152(7.9), 147(37.9), 119(11.4), 91(42.4), 63(35.4), 46(86.6), 32(100.0), 29(79.4)	δ = 3.75 (q 4H), 1.05 (t 6H), 7.2–8.4 (8H)
D	$Ar_2C{=}CF_2$	290	306(100.0) [M^+], 276(12.1), 214(39.6), 213(18.6), 212(11.7), 202(14.6), 201(22.5), 164(8.5), 163(14.7), 45(23.1), 30(13.8)	δ = 7.2–8.5
E*	$Ar_2C{=}O$*	275	272(24.1) [M^+], 150(100.0), 104(27.6), 76(25.9)	δ = 7.2–8.5

*Not obtained with $\bar{O}C_2H_5/C_2H_5OH$, but isolated from the t-$C_4H_9\bar{O}/t$-C_4H_9OH reaction.

TABLE 3. Rate constants and isotope effects of the reaction of $(O_2NC_6H_4)_2CHCF_3$ to give $(O_2NC_6H_4)_2C{=}CF(OR)$

Temperature (°C)	[AlkONa] $\times 10^4$ (M)	10^2k_{1H} (s^{-1})	10^2k_{1D} (s^{-1})	k_{2H} ($dm^3\ mol^{-1}\ s^{-1}$)	k_{2D} ($dm^3\ mol^{-1}\ s^{-1}$)	k_{2H}/k_{2D}
(a) Sodium ethoxide in ethanol solvent						
10	3.0–6.0	0.125–0.411	0.102–0.340	9.5±0.5	8.0±0.2	1.19±0.07
15	3.0–6.0	0.234–0.724	0.206–0.612	16.4±0.3	13.5±0.2	1.21±0.03
20	3.0–6.0	0.444–1.36	0.310–1.09	30.9±0.9	26.5±2.3	1.17±0.10
25	3.0–6.0	0.705–2.24	0.750–2.01	51.2±0.2	42.5±2.0	1.20±0.06
30	3.0–6.0	1.57–4.56	1.39–3.95	98.9±2.9	85.4±0.1	1.16±0.03
(b) Sodium n-propoxide in n-propanol						
10	13–330	3.94–30.1	2.29–29.5	8.5±0.5	8.6±0.7	0.99±0.10
15	13–330	4.72–56.5	3.50–54.8	16.3±0.2	16.4±0.5	0.99±0.03
20	13–330	10.1–95.2	6.92–89.4	26.1±1.5	25.4±1.2	1.03±0.08
25	13–330	13.4–156	8.8–148	44.8±0.3	44.3±1.9	1.01±0.04
30	13–330	26.4–254	11.8–226	71.6±0.8	67.5±1.2	1.06±0.02
35	13–330	26.5–385	12.9–337	112.1±2.1	104.6±5.5	1.07±0.06
(c) Sodium isopropoxide in isopropanol						
10	14–350	16.3–165	7.4–84.4	44.2±0.1	23.4±1.5	1.89±0.04
15	14–350	24.8–249	11.4–129	66.5±1.0	34.8±0.4	1.91±0.07
20	14–350	26.7–290	16.4–157	78.5±0.8	41.9±0.4	1.87±0.03
25	14–350	33.6–397	22.7–210	111±6	55.8±1.3	1.99±0.11
30	14–350	40.8–507	27.6–285	137±5	76.5±0.2	1.79±0.06
35	14–350	53.6–585	35.9–337	159±11	90.8±2.5	1.75±0.13
(d) Sodium n-butoxide in n-butanol						
10	40–460	18.6–83.8	5.9–50.3	15.2±1.1	10.8±0.8	1.41±0.14
15	40–460	27.5–112	9.3–70.4	20.2±0.2	14.4±0.4	1.40±0.04
20	40–460	33.6–203	16.7–149	40.2±0.3	31.8±0.8	1.26±0.03
25	40–460	53.5–404	21.7–289	82.0±7.1	62.9±3.5	1.30±0.13
30	40–460	60.1–496	44.6–369	105±3	77.4±2.0	1.36±0.05
35	40–460	165–720	77.1–522	133±4	107±4.0	1.24±0.06
(e) Sodium *sec*-butoxide in *sec*-butanol						
10	50–390	49.0–240	24.4–152	56.6±1.4	37.5±0.1	1.51±0.04
15	50–390	67.6–335	33.8–204	78.6±0.1	50.0±1.1	1.57±0.03
20	50–390	97.6–406	35.6–245	90.4±2.0	61.2±4.0	1.48±0.10
25	50–390	105–460	40.6–287	104.3±1.3	72.5±0.1	1.44±0.02
30	50–390	147–557	48.6–344	120.4±2.7	86.7±2.3	1.39±0.05
35	50–390	163–764	50.6–470	176.6±0.5	123.4±0.1	1.43±0.01

TABLE 4. Activation parameters for the reaction of $(O_2NC_6H_4)_2CHCF_3$ with alkoxide bases in the corresponding alcohols to give $(O_2NC_6H_4)_2C{=}CF(OR)$

Activation parameters	Methoxide*	Ethoxide	n-Propoxide	iso-Propoxide	n-Butoxide	*sec*-Butoxide
$\Delta H^{\ddagger}_{H}$ kcal mol^{-1}	19.6±0.7	19.2±0.6	17.0±0.4	8.2±0.5	15.8±1.5	6.5±1.0
$\Delta H^{\ddagger}_{D}$ kcal mol^{-1}	20.0±0.5	19.5±0.8	16.6±0.4	8.8±0.4	16.5±1.6	7.1±0.5
$\Delta S^{\ddagger}_{H}$ cal mol^{-1}deg^{-1}	5.0±2.3	13.9±1.8	6.1±1.3	−21.8±1.8	2.7±5.0	−27.6±2.4
$\Delta S^{\ddagger}_{D}$ cal mol^{-1}deg^{-1}	6.4±1.7	14.3±2.8	4.6±1.4	−21.1±1.4	4.5±5.2	−26.1±1.6
$\Delta G^{\ddagger}_{H}$ kcal mol^{-1}	18.1±0.9	15.1±0.8	15.2±0.5	14.7±0.8	15.0±2.1	14.7±1.0

*References 1, 2, and 4.

TABLE 5. Rate constants of the reaction of $(O_2NC_6H_4)_2C{=}CF(OR)$ to yield $(O_2NC_6H_4)_2C{=}C(OR)_2$

Temperature (°C)	10^3[AlkONa] (M)	10^4k_1 (s^{-1})	10^2k_2 (dm^3 mol^{-1} s^{-1})
(a) Sodium ethoxide in ethanol solvent			
15	45−227	10.5−34.4	1.33±0.04
20	45−227	14.6−50.9	2.06−0.13
25	45−227	15.7−85.1	3.66±0.21
30	45−227	38.5−124	4.69±0.04
35	45−227	39.8−155	6.32±0.02
(b) Sodium n-propoxide in n-propanol			
15	18−70	6.0−19.0	2.60±0.24
20	18−70	9.9−37.3	5.23±0.08
25	18−70	10.1−46.2	6.94±0.02
30	18−70	12.0−68.7	10.9±0.1
35	18−70	19.9−126	20.3±0.2
(c) Sodium isoproproxide in isopropanol			
20	15−73	8.4−47.8	6.78±0.11
25	15−73	15.0−73.3	10.1±0.5
30	15−73	36.2−111	13.3±1.0
35	15−73	109−225	20.4±1.0
40	15−73	197−352	27.2±1.8
(d) Sodium n-butoxide in n-butanol			
15	42−210	16.4−59.3	2.67±0.34
20	42−210	20.7−83.6	3.67±0.27
25	42−210	25.4−101	4.56±0.40
30	42−210	47.7−166	7.00±0.94
35	42−210	87.0−288	11.6±3
(e) Sodium *sec*-butoxide in *sec*-butanol			
25	11−78	0.81−2.31	0.223±0.003
30	11−78	1.67−4.39	0.396±0.041
35	11−78	2.77−7.18	0.665±0.025
40	11−78	3.30−8.73	0.801±0.039
45	11−78	4.00−12.2	1.26±0.11

giving $k_{2H}(C_2H_5OD)/k_{2H}(C_2H_5OH) = 1.0$. These results are also consistent with an $(E1cB)_R$ mechanism for methoxide and $(E1cB)_I$ or E2 for ethoxide.

The tert-*butoxide*/tert-*butanol reaction*

The reaction of the substrate with *tert*-butoxide in *tert*-butanol gives markedly different products from the other systems in that no significant amount of substituted olefins are produced. It was previously reported (3) that the *tert*-butoxide reaction goes via a stable carbanion to olefin D and then to butoxy substituted compounds.

It has now been discovered that the products of the reaction with *tert*-butoxide in *tert*-butanol are very dependent on the purity of the solvent. In particular a very small amount of secondary or primary alcohol as impurity causes the reaction of the olefin D to produce the substituted olefins B and C.

When very carefully purified *tert*-butanol was used, the only products which could be detected by thin-layer chromatography were the olefin D and 4,4′-dinitrobenzophenone. With the *tert*-butoxide in large excess over the substrate, this reaction gave a violet colour with a broad absorption band with maxima at 525 nm and 430 nm. No maxima at 332 or 358 nm were observed, but upon the addition of a small amount of either primary or secondary alcohol the 332-nm peak developed rapidly. The larger the excess of *tert*-butoxide used, the greater was the proportion of 4,4′-dinitrobenzophenone in the product.

The rate of the elimination reaction of the substrate with *tert*-butoxide to yield the olefin D was measured by following the appearance of the absorption at 290 nm. This fast reaction was measured with the stopped-flow spectrophotometer at five different base concentrations and yielded $k_2 = 2.51 \pm 0.07 \times 10^3$ dm^3 mol^{-1} s^{-1} at 30°C.

The rate of reaction of the olefin D with *tert*-butoxide was determined using a pure sample of D and monitoring the disappearance of the absorption at 290 nm. This reaction is considerably slower and gave $k_2 = 49$ dm^3 mol^{-1} s^{-1} at 30°C.

The rate of appearance of the coloured species (λ_{max} 525 nm) from the trifluoro substrate was measured previously (3) and the value of k_2 as 25 dm^3 mol^{-1} s^{-1} at 30°C was confirmed in this work.

Thus, the trifluoro compound undergoes a fast elimination reaction to yield the difluoro-olefin D, which subsequently reacts with the excess *tert*-butoxide in slower processes to yield violet-coloured species which are eventually oxidized to 4,4-dinitrobenzophenone.

If the elimination mechanism is $(E1cB)_I$ or E2 as concluded above, the rate of appearance of the olefin D at 290 nm should show a primary deuterium isotope effect. The deuterated substrate gave a k_{2D} of 464 ± 9 dm^3 mol^{-1} s^{-1} at 30°C to yield a primary isotope effect $k_H/k_D = 5.4 \pm 0.2$ at 30°C. Thus,

TABLE 6. Activation parameters for the reaction of $(O_2NC_6H_4)_2CHCF_3$ with alkoxide bases in the corresponding alcohols to give $(O_2NC_6H_4)_2C{=}C(OR)_2$

Parameter	Methoxide*	Ethoxide	n-Propoxide	iso-Propoxide	n-Butoxide	*sec*-Butoxide
$\Delta H^{\neq}$	9.0±0.9	13.4±1.1	16.5±1.3	12.1±0.5	13.1±2.3	15.2±1.3
$\Delta S^{\neq}$ [cal mol^{-1}deg^{-1}]	−35.0±3.0	−20.5±3.7	−8.2±4.3	−26.9±1.7	−20.5±7.8	−19.6±4.2
$\Delta G^{\neq}$ [kcal mol^{-1}]	19.4±1.2	19.5±1.6	19.9±1.8	20.3±0.7	19.2±3.3	21.0±1.8

*References 1, 2, and 4.

TABLE 7. Rate constants for the reaction of olefin D, $(O_2NC_6H_4)_2C{=}CF_2$, with alkoxide bases to yield the substituted olefin $(O_2NC_6H_4)_2C{=}CF(OR)$

Temperature (°C)	[AlkONa] × 10^3 (M)	k_{obs} (s^{-1})	k_2 ($dm^3\ mol^{-1}\ s^{-1}$)
(a) Sodium methoxide in methanol			
25	1.0−5.0	0.732−3.24	637±79
35	1.0−5.0	0.981−6.19	1274±77
(b) Sodium ethoxide in ethanol			
25	1.0−4.0	0.229−0.869	216±6
40	1.0−4.0	0.456−1.78	438±25
(c) Sodium isopropoxide in isopropanol			
15	14−350	0.279−6.80	19.8±2.3
25	14−350	0.416−9.42	28.2±2.9
35	14−350	0.628−15.7	46.3±2.9

the primary deuterium isotope effects and the deuterium exchange experiments indicate that the HF elimination mechanism for 2,2-di(4-nitrophenyl)-1,1,1-trifluoroethane is $(E1cB)_R$ with methoxide/methanol, changing to $(E1cB)_I$ or E2 with *tert*-butoxide/*tert*-butanol.

Experimental

Materials

2,2-Di(4-nitrophenyl)-1,1,1-trifluoroethane and its deuterated analogue were prepared by reduction of α,α,α-trifluoroacetophenone (Aldrich, bp 165−155°C) in dry ether by $LiAlH_4$ or $LiAlD_4$ (6) to yield the carbinol, which was dissolved in a four-fold molar excess of benzene and cooled to 0°C. Then 102% oleum was added dropwise with vigorous stirring, and the product 2,2-di(phenyl)-1,1,1-trifluoroethane was isolated.

The nitration of the phenyl groups was accomplished according to the method of Skerrett and Woodcock (7) using fuming nitric acid at −30°C. The raw 2,2-di(4-nitrophenyl)-1,1,1-trifluoroethane was recrystallized from methanol to yield light yellow crystals of mp 117°C.

The alcohols were purified by standard methods using fractional distillation under oxygen-free dry nitrogen. The *tert*-butanol was purified as above and only the middle fraction distilling at 82.4°C was collected.

The olefin $(O_2NC_6H_4)_2C{=}CF_2$ (D) was prepared by the reaction of 2,2-di(4-nitrophenyl)-1,1,1-trifluoroethane with a three molar excess of t-BuO̅ in t-BuOH. The products of the reaction were purified by thin-layer chromatography using benzene as the eluent. The mass spectra and λ_{max} data are given in Table 2.

Kinetic measurements

The reaction rates were measured using a Specord uv-vis and a stopped-flow spectrophotometer, fitted with a temperature controlled cell block.

The technique and calculations were as previously described (1,8).

Acknowledgement

The authors are grateful for financial support by the Natural Sciences and Engineering Research Council of Canada.

1. J. KURZAWA and K. T. LEFFEK. Can. J. Chem. **55**, 1696 (1977).
2. K. T. LEFFEK and G. SCHROEDER. Can. J. Chem. **60**, 1696 (1982).
3. A. JARCZEWSKI and K. T. LEFFEK. Can. J. Chem. **58**, 1979 (1980).
4. K. T. LEFFEK and G. SCHROEDER. Can. J. Chem. **60**, 3077 (1982).
5. D. J. MCLENNAN and R. J. WONG. J. Chem. Soc. Perkin Trans. 2, 526 (1974).
6. F. BERGMANN and A. KALMUS. J. Am. Chem. Soc. **76**, 4137 (1954).
7. E. J. SKERRETT and D. WOODCOCK. J. Chem. Soc. 2807 (1952).
8. A. JARCZEWSKI and K. T. LEFFEK. Can. J. Chem. **50**, 24 (1972).

Crystal and molecular structure of 3-ethyl-4-hydroxy-1,2,3(4*H*)-benzotriazine and 6-chloro-4-hydroxy-3-methyl-4-phenyl-1,2,3-benzotriazine[1]

KWONG KHEE LAI AND CARL H. SCHWALBE
Department of Pharmacy, University of Aston in Birmingham, Gosta Green, Birmingham B47ET, England

KEITH VAUGHAN[2] AND RONALD J. LAFRANCE
Department of Chemistry, Saint Mary's University, Halifax, N.S., Canada B3H 3C3

AND

CLIVE D. WHISTON
Department of Physical Sciences, The Polytechnic, Wolverhampton, WV1 1LY, England

Received January 4, 1984[3]

KWONG KHEE LAI, CARL H. SCHWALBE, KEITH VAUGHAN, RONALD J. LAFRANCE, and CLIVE D. WHISTON. Can. J. Chem. **63**, 581 (1985).

The crystal structures of the title compounds have been determined from X-ray data collected on a four-circle diffractometer and refined by the full-matrix least-squares method. The former compound crystallizes in the orthorhombic system, space group *Pbcn*, with a = 14.346(8), b = 7.239(1), c = 17.276(2) Å, and has been refined to a conventional R factor of 0.043 for 890 observed reflections. Corresponding results for the latter compound are monoclinic, $P2_1/n$, a = 12.222(4), b = 7.482(2), c = 14.170(8) Å, β = 94.06(4)°, R = 0.060 for 2128 observed data. The triazine rings of both compounds exhibit short N(1)—N(2) bonds and tetrahedral geometry at C(4); however, the ring is puckered in the first compound but flat in the second. Molecules in both crystals are linked by O(4)—H···N(1) hydrogen bonds.

KWONG KHEE LAI, CARL H. SCHWALBE, KEITH VAUGHAN, RONALD J. LAFRANCE et CLIVE D. WHISTON. Can. J. Chem. **63**, 581 (1985).

Faisant appel à des données de rayons-x obtenues à l'aide d'un diffractomètre à quatre cercles et affinées par la méthode des moindres carrés (matrice complète), on a déterminé les structures cristallines des composés mentionnés dans le titre. Le premier composé cristallise dans le système orthorhombique, groupe d'espace *Pbcn*, avec a = 14,346(8), b = 7,239(1), c = 17,276(2) Å et on a affiné sa structure jusqu'à un facteur R de 0,043 pour 890 réflexions observées. Les résultats correspondants pour le dernier composé sont: monoclinique, $P2_1/n$, a = 12,222(4), b = 7,482(2), c = 14,170(8) Å, β = 94,06(4)°, R = 0,060 pour 2128 réflexions observées. Les cycles triazines des deux composés sont caractérisées par des liaisons N(1)—N(2) qui sont courtes et une géométrie tétraédrique en C(4); toutefois, alors que le cycle du premier composé est plissé, celui du deuxième est plan. Dans chacun des cristaux, les molécules sont rellées par des liaisons hydrogènes O(4)—H···N(1).

[Traduit par le journal]

Introduction

This paper describes the X-ray crystal structure determination of 3-ethyl-4-hydroxy-1,2,3(4*H*)-benzotriazine (**1**) and 6-chloro-4-hydroxy-3-methyl-4-phenyl-1,2,3-benzotriazine (**2**).

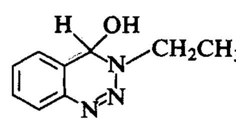

1

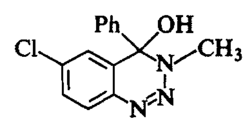

2

Interest in the chemistry of the 4-hydroxy-1,2,3-triazines was stimulated by the study of Fong and Vaughan (1) in which the diazonium salt (**3**) from *o*-aminoacetophenone was coupled with an excess of aqueous methylamine. The initial coupling product, the monomethyltriazene (**4**), could not be isolated due to the facility of the cyclodehydration of **4** to give the novel methylenetriazine (**6**). The intermediate 4-hydroxy-1,2,3-benzotriazine (**5**), itself a novel heterocyclic structure, could not be isolated from this reaction. An alternative route to **6**, via the reaction of methyl magnesium bromide with 3-methyl-4-oxo-1,2,3(4*H*)-benzotriazine, likewise proceeds directly without isolation of **5** (2).

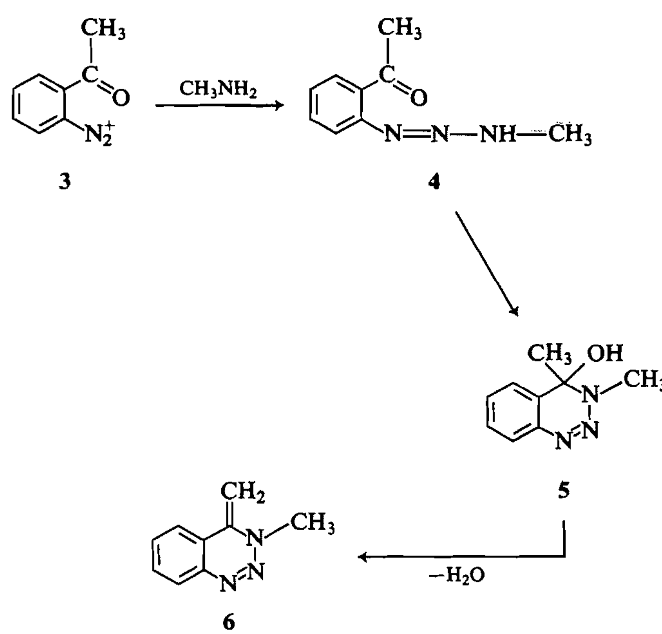

3 **4** **5** **6**

Stable 4-hydroxytriazines should be available from analogous reactions with diazonium salts in which the *o*-acyl group is lacking the α-hydrogen necessary for the dehydration step **5** → **6**. Indeed it has now been shown (3) that coupling the diazonium salt from *o*-aminobenzaldehyde (**7***a*) or *o*-aminobenzophenone (**7***b*) with alkylamines leads to stable

[1]Contribution from the Joint Crystallography Unit, Universities of Aston and Birmingham.
[2]To whom all correspondence should be addressed.
[3]Revision received August 21, 1984.

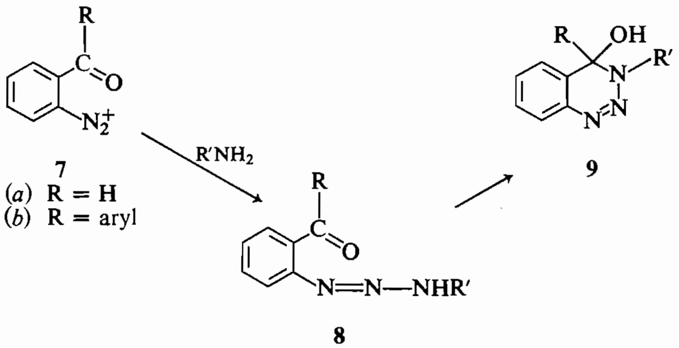

crystalline 4-hydroxytriazines (**9**) via the apparently unstable monoalkyltriazene (**8**). The spectroscopic characteristics of these products definitely point to the cyclic structure **9**, rather than the valence tautomer **8**. The elucidation of the crystal structures of representative examples of both types of triazine, **1** and **2**, was undertaken (*a*) to verify the heterocyclic structure of the molecules, (*b*) to ascertain the nature of the stereochemistry at the C-4 chiral centre of molecules of type **9**, and (*c*) to compare with the structures of other benzo-1,2,3-triazines.

Experimental

The title compounds **1** and **2** were prepared and recrystallized as in ref. 3. The specimen of **1** chosen for crystallographic analysis was a laterally elongated hexagonal prism $0.9 \times 0.3 \times 0.25$ mm^3, and that of **2** was a tabular crystal $1.0 \times 0.6 \times 0.25$ mm^3. Unit cell dimensions were obtained by least-squares analysis of the setting angles of 25 reflections measured on an Enraf-Nonius CAD4 diffractometer.

Crystal data for 1
$C_9H_{11}N_3O$ fw = 177.21
Orthorhombic, space group *Pbcn* (D_{2h}^{14}, No. 60), $a = 14.346(8)$, $b = 7.239(1)$, $c = 17.276(2)$ Å, $V = 1794.1$ Å^3, $Z = 8$, $\rho_c = 1.31$ g cm^{-3}, $\mu(\text{MoK}\alpha) = 0.54$ cm^{-1}, $\lambda = 0.71069$ Å, $t = 20$°C.

Crystal data for 2
$C_{14}H_{12}ClN_3O$ fw = 273.73
Monoclinic, space group $P2_1/n$ (C_{2h}^5, No. 14), $a = 12.222(4)$, $b = 7.482(2)$, $c = 14.170(8)$ Å, $\beta = 94.06(4)$°, $V = 1292.5$ Å^3, $Z = 4$, $\rho_c = 1.41$ g cm^{-3}, $\mu(\text{MoK}\alpha) = 2.43$ cm^{-1}, $\lambda = 0.71069$ Å, $t = 18$°C.

Intensity data for both structures were measured by the $\omega-2\theta$ scan method between $2° \le \theta \le 25°$ with graphite-monochromated MoKα radiation. Data for **2** were collected under conditions of minimum absorption by using the Enraf-Nonius option "FLAT" (for paths parallel to a crystal edge the maximum and minimum transmission factors for *F* are 0.970 and 0.886). The ω scan angle was $(1.0 + 0.35 \tan\theta)°$ for **1** and $(1.2 + 0.35 \tan\theta)°$ for **2** extended on each side by 25% for background measurement. The scan rate was set from 0.8 to 3.3 deg min^{-1} for **1** and 1.3 to 4.0 deg min^{-1} for **2**, depending on the intensity of a particular reflection. Two standard reflections were remeasured every 3600 s; for **1** these changed negligibly with time. However, for **2** they declined by about one-quarter during data collection, and a linear correction factor for intensity versus time was derived from them and applied to all reflections. Data were corrected for Lorentz and polarization effects but not for absorption or extinction. Estimated standard deviations σ were assigned on the basis of counting statistics and an allowance of $0.02F_o$ for the minimum expected instability of the diffractometer. For **1**, 1580 unique reflections were measured, of which 890 were considered observed ($F > 3\sigma$). For **2** 3349 reflections were collected, of which 2828 were unique ($R_{int} = 0.091$) and 2128 observed.

Structure determination and refinement

Both structures were solved by direct methods: **1** by the EEES routine in SHELX (4) and **2** by MULTAN (5). All the non-hydrogen atoms of **1** and all but one phenyl carbon atom of **2** were located in *E*-maps; this missing atom was found after calculation of structure factors and an electron density map. Least-squares refinement ensued under the following conditions: SHELX system, scattering factors stored therein, refinement to minimize $\Sigma w(|F_o| - |F_c|)^2$. Positions and isotropic temperature factors were first refined for the non-hydrogen atoms with unit weights for all observed reflections. All hydrogen atoms of **1** and some hydrogen atoms of **2** (including the hydroxyl hydrogen atom) were revealed by difference electron density maps. In the final refinement cycles for both structures the parameters were refined until no shift exceeded 0.195 esd and the observed reflections were weighted by $w = k/[\sigma^2(F_o) + gF_o^2]$, where *k* converged to 1.4946 for **1** and 3.2435 for **2** and *g*, representing unexpected additional instrument instability, refined to 0.000213 for **1** and 0.000248 for **2**. For **1** the parameters refined included a scale factor, coordinates and anisotropic thermal parameters for non-hydrogen atoms, and coordinates and isotropic temperature factors for hydrogen atoms. Similar parameters were refined in **2**, but all benzene ring hydrogen atoms were assumed to ride on their attached carbon atom at a distance of 1.080 Å, and the hydrogen atoms of the 3-methyl group were subjected to constraints on their C—H, H···H, and N(3)···H distances. The 1 7 8 reflection was eliminated from the data set of **2** because F_o was only 40% of F_c, a discrepancy of 17σ, and impairment of the measurement due to temporary loss of beam intensity or physical obstruction is suspected. The final discrepancy indices were $R = \Sigma||F_o| - |F_c||/\Sigma|F_o| = 0.043$ for **1** and 0.058 for **2**, and $R_g = [\Sigma w(|F_o| - |F_c|)^2/\Sigma w|F_o|^2]^{1/2} = 0.046$ for **1** and 0.081 for **2**.

No peak on a final difference Fourier synthesis for **1** exceeded 0.15 e Å^{-3}. Although a similar map of **2** contained residual peaks as high as 0.56 e Å^{-3}, these were near the chlorine atom and elsewhere no peak exceeded 0.27 e Å^{-3}. Final atomic coordinates are given in Tables 1 and 2. The molecules are displayed in Figs. 1 and 2. Measured and calculated structure factors, anisotropic thermal parameters for non-hydrogen atoms, and parameters for phenyl and alkyl hydrogen atoms have been deposited.[4]

TABLE 1. Coordinates and equivalent isotropic temperature factors ($\times 10^4$) for non-hydrogen atoms of **1** with esd in parentheses*

Atom	*x*	*y*	*z*	U_{eq}
N(1)	4981(2)	1967(3)	10382(1)	528(15)
N(2)	5028(2)	2561(3)	9693(2)	561(15)
N(3)	4262(2)	2675(3)	9259(1)	572(16)
C(4)	3416(2)	1609(4)	9406(2)	511(18)
C(4A)	3312(2)	1418(4)	10251(2)	457(15)
C(5)	2459(3)	1065(4)	10604(2)	594(19)
C(6)	2417(3)	766(5)	11380(2)	723(24)
C(7)	3218(3)	788(5)	11829(2)	736(25)
C(8)	4063(3)	1162(5)	11491(2)	633(23)
C(8A)	4108(2)	1493(4)	10704(2)	487(18)
C(31)	4430(3)	3351(7)	8472(3)	772(28)
C(32)	3893(3)	5040(7)	8295(2)	780(27)
O(4)	3436(1)	−103(4)	9010(1)	611(13)

*Equivalent isotropic temperature factors are calculated from anisotropic thermal parameters by the equation $U_{eq} = (1/3)(U_{11} + U_{22} + U_{33})$.

Discussion

The 4-hydroxybenzotriazine structure for **1** and **2** established from spectra (3) is confirmed here. These molecules may be

[4]These tables are available at a nominal charge, from the Depository of Unpublished Data, CISTI, National Research Council of Canada, Ottawa, Ont., Canada K1A 0S2.

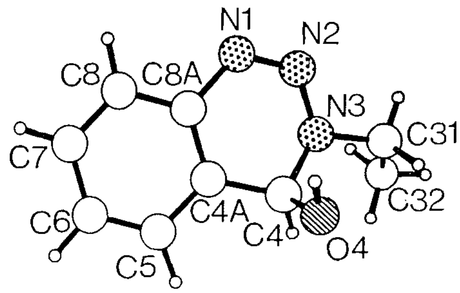

FIG. 1. The molecule of 3-ethyl-4-hydroxy-1,2,3(4*H*)-benzotriazine projected onto its least-squares plane, showing the numbering scheme. Nitrogen atoms are stippled and oxygen atoms hatched.

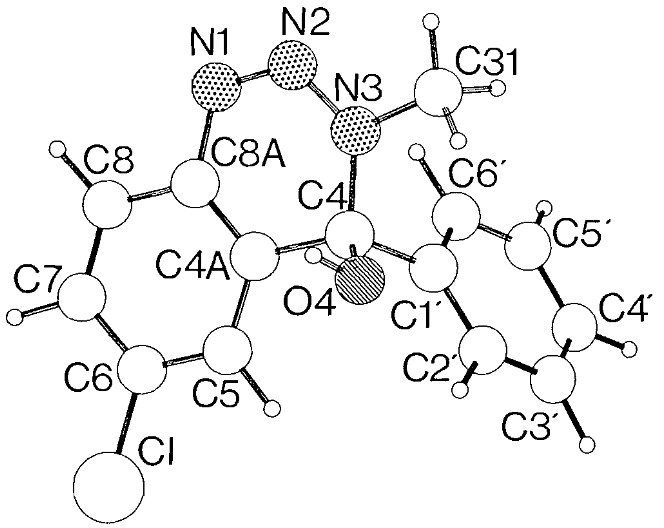

FIG. 2. The molecule of 6-chloro-4-hydroxy-3-methyl-4-phenyl-1,2,3-benzotriazine in projection onto its least-squares plane. Nitrogen atoms are stippled and oxygen atoms hatched.

regarded as 1-aryl-3,3-dialkyltriazenes, one of whose 3-alkyl groups has been tied back to the ring. Bond distances (Table 3) and bond angles (Table 4) can be compared with those in a series of open-chain triazenes: 1-*p*-tolyl-3-methyltriazene (6), 1-(4-carbethoxyphenyl)-3-hydroxymethyl-3-methyltriazene (7), 2-(3,3-dimethyl-1-triazeno)phenyl-1-carboxamide (8), and two independent tautomers of 5-(3,3-dimethyl-1-triazenyl)imidazole-4-carboxamide (9) and its hydrochloride (10). The title compounds may also be regarded as reduced forms of 1,2,3-benzotriazin-4(3*H*)-ones (henceforth abbreviated triazinones), for which crystal structure determinations exist on 1,2,3-benzotriazin-4(3*H*)-one (11), 3-hydroxy-1,2,3-benzotriazin-4(3*H*)-one (12), and *O*,*O*-dimethyl-*S*-(4-oxo-1,2,3-benzotriazin-3-yl) methyl phosphorodithioate (13).

The N(1)—N(2) bond remains very strong across this entire series of compounds: 1.268(3) Å in **1**, 1.263(3) Å in **2**, an average of 1.281 Å over the independent molecules of the triazenes, and an average of 1.255 Å in the triazinones. The N(2)—N(3) bond is affected little by ring closure: 1.333(3) Å in **1**, 1.316(3) Å in **2**, and 1.325 Å in the triazenes. However, introduction of conjugation at C(4) considerably weakens this bond; for N(2)—N(3) is 1.385 Å in the triazinones. The "natural" bond angles averaging 112.1° at N(1) and 113.8° at N(2) in the unrestrained triazenes are increased by ring closure to 120.0(2)° and 119.3(2)° at N(1) and 120.3(2)° and 122.3(2)° at N(2) in **1** and **2** respectively. Oxidation at C(4) has little effect on these angles: they are 120.3° at N(1) and 118.6° at N(2) in the triazinones.

In both **1** and **2** carbon atom C(4) shows the expected tetrahedral geometry. In the relatively uncrowded **1** the OH group is able to avoid both the 3-ethyl substituent and the fused ring by increasing the O—C(4)—N(3) and O—C(4)—C(4A) angles above tetrahedral values to 111.3(2)° and 113.4(3)°. The requirement to accommodate a phenyl group in **2** and the dim-

TABLE 2. Coordinates and equivalent isotropic temperature factors ($\times 10^4$) for non-hydrogen atoms of **2** with esd in parentheses

Atom	x	y	z	U_{eq}
N(1)	2190(2)	4738(4)	2053(2)	528(15)
N(2)	2410(2)	4706(3)	2937(2)	502(15)
N(3)	3375(2)	4204(3)	3318(2)	458(13)
C(4)	4328(2)	3577(3)	2832(2)	351(13)
C(4A)	3990(2)	3539(3)	1788(2)	351(13)
C(5)	4711(2)	2879(4)	1163(2)	417(14)
C(6)	4408(3)	2869(4)	213(2)	490(16)
C(7)	3398(3)	3495(4)	−137(2)	566(19)
C(8)	2675(3)	4126(4)	472(2)	564(19)
C(8A)	2972(2)	4135(4)	1455(2)	409(14)
C(31)	3468(3)	4233(6)	4350(2)	677(23)
O(4)	4657(1)	1899(2)	3183(1)	417(11)
C(1′)	5284(2)	4868(3)	3049(2)	345(13)
C(2′)	6341(2)	4243(4)	3243(2)	407(15)
C(3′)	7194(2)	5454(4)	3406(2)	480(17)
C(4′)	7002(3)	7250(4)	3379(2)	503(17)
C(5′)	5956(3)	7876(4)	3187(2)	563(19)
C(6′)	5098(2)	6684(4)	3016(2)	487(17)
Cl	5318(1)	2053(1)	−564(1)	747(6)

*Equivalent isotropic temperature factors are calculated from anisotropic thermal parameters by the equation $U_{eq} = (1/3)(U_{11} + U_{22} + U_{33} + 2U_{13}\cos\beta)$.

TABLE 3. Bond distances (Å) for non-hydrogen atoms with esd in parentheses

Bond	Distance 1	Distance 2
N(1)—N(2)	1.268(3)	1.263(3)
N(2)—N(3)	1.333(3)	1.316(3)
N(3)—C(4)	1.460(3)	1.472(3)
C(4)—C(4A)	1.475(4)	1.507(3)
C(4A)—C(5)	1.391(4)	1.384(4)
C(5)—C(6)	1.360(4)	1.371(4)
C(6)—C(7)	1.388(5)	1.379(4)
C(7)—C(8)	1.372(5)	1.362(5)
C(8)—C(8A)	1.383(4)	1.414(4)
C(4A)—C(8A)	1.384(4)	1.374(3)
N(1)—C(8A)	1.413(3)	1.396(4)
N(3)—C(31)	1.464(4)	1.458(4)
C(31)—C(32)	1.477(6)	
C(4)—O(4)	1.414(4)	1.399(3)
C(4)—C(1′)		1.530(3)
C(1′)—C(2′)		1.383(3)
C(2′)—C(3′)		1.389(4)
C(3′)—C(4′)		1.364(4)
C(4′)—C(5′)		1.371(5)
C(5′)—C(6′)		1.385(4)
C(1′)—C(6′)		1.377(4)
C(6)—Cl		1.731(3)

TABLE 4. Bond angles (deg) for non-hydrogen atoms with esd in parentheses

Bonds	Angle 1	Angle 2
N(2)—N(1)—C(8A)	120.0(2)	119.3(2)
N(3)—N(2)—N(1)	120.3(2)	122.3(2)
C(4)—N(3)—N(2)	123.7(2)	127.9(2)
C(4A)—C(4)—N(3)	107.8(2)	107.1(2)
C(5)—C(4A)—C(4)	122.7(3)	119.5(2)
C(8A)—C(4A)—C(4)	118.1(3)	120.7(2)
C(8A)—C(4A)—C(5)	119.1(3)	119.9(2)
C(6)—C(5)—C(4A)	120.0(4)	119.4(3)
C(7)—C(6)—C(5)	120.9(4)	121.5(3)
C(8)—C(7)—C(6)	119.7(3)	119.6(3)
C(8A)—C(8)—C(7)	119.7(3)	119.6(3)
N(1)—C(8A)—C(8)	118.1(3)	117.5(3)
N(1)—C(8A)—C(4A)	121.2(3)	122.5(3)
C(4A)—C(8A)—C(8)	120.6(3)	120.0(3)
C(31)—N(3)—N(2)	114.0(3)	114.3(2)
C(31)—N(3)—C(4)	118.3(3)	117.8(2)
C(32)—C(31)—N(3)	112.6(3)	
O(4)—C(4)—N(3)	111.3(2)	109.7(2)
O(4)—C(4)—C(4A)	113.4(3)	112.6(2)
C(1′)—C(4)—N(3)		108.8(2)
C(1′)—C(4)—C(4A)		111.2(2)
C(1′)—C(4)—O(4)		107.4(2)
C(2′)—C(1′)—C(4)		121.0(2)
C(6′)—C(1′)—C(4)		119.6(2)
C(2′)—C(1′)—C(6′)		119.4(2)

TABLE 5. Selected torsion angles (deg)

Bonds	Angle 1	Angle 2
C(8A)—N(1)—N(2)—N(3)	−2.6	3.4
N(1)—N(2)—N(3)—C(4)	−21.7	−1.5
N(1)—N(2)—N(3)—C(31)	−178.8	−179.2
N(2)—N(3)—C(4)—C(4A)	35.0	−2.1
C(31)—N(3)—C(4)—C(4A)	−168.8	175.6
N(3)—C(4)—C(4A)—C(8A)	−26.4	3.7
C(4)—C(4A)—C(8A)—N(1)	7.8	−2.4
C(4A)—C(8A)—N(1)—N(2)	9.0	−1.5
N(3)—C(4)—C(1′)—C(2′)		138.5
N(3)—C(4)—C(1′)—C(6′)		−44.0
C(4A)—C(4)—C(1′)—C(2′)		−103.7
C(4A)—C(4)—C(1′)—C(6′)		73.8
O(4)—C(4)—C(1′)—C(2′)		19.8
O(4)—C(4)—C(1′)—C(6′)		−162.6

inution of the 3-substituent to methyl allow the OH group to move closer to N(3): O—C(4)—N(3) is 109.7(2)° while O—C(4)—C(4A), Ph—C(4)—N(3), and Ph—C(4)—C(4A) are 112.6(2)°, 108.8(2)°, and 111.2(2)°, respectively. In **1** the single bond C(4)—C(4A) is only 1.475(4) Å long; in **2** this increases to 1.507(3) Å.

Torsion angles (Table 5) show that the degree of planarity is quite different in these two molecules. In the triazine ring of **1** there are deviations from pure *cis* geometry of 22° about N(2)—N(3) and 35° about N(3)—C(4). In **2** these alterations are only 2°. Apparently the unconjugated triazine ring in these systems is flexible. In **1** it distorts, allowing the C(31)···O(4) contact to reach 3.025(4) Å. The distortion is not simply a

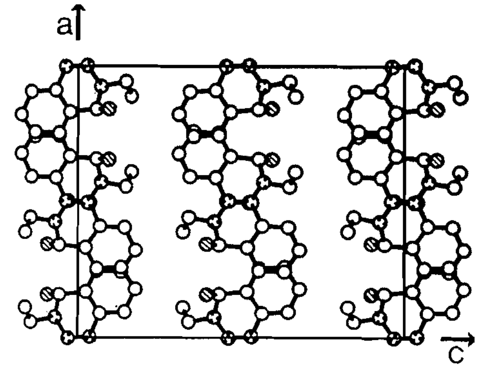

FIG. 3. Packing of molecules of 3-ethyl-4-hydroxy-1,2,3(4*H*)-benzotriazine in the unit cell viewed down b with hydrogen atoms omitted for clarity.

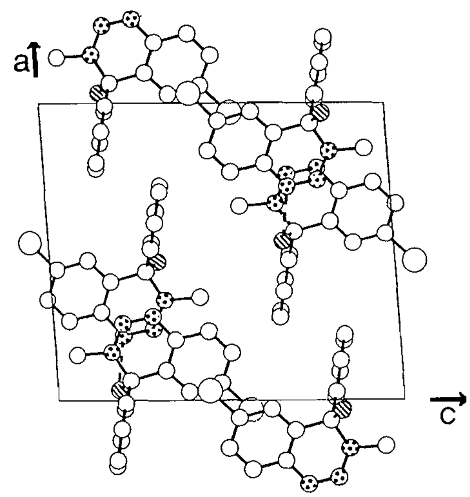

FIG. 4. Packing of molecules of 6-chloro-4-hydroxy-3-methyl-4-phenyl-1,2,3-benzotriazine in the unit cell viewed down b. The O(4)—H···N(1) hydrogen bonds are shown by dashed lines. All hydrogen atoms have been omitted for clarity.

twisting of bonds N(2)—N(3) and N(3)—C(4); some pyramidalization of N(3) is also involved since the deviation of N(3) from the plane of N(2), C(4), and C(31), the atoms bonded to it, is 0.164(4) Å. However, in **2** the 3-substituent is sandwiched between the 4-hydroxyl and 4-phenyl moieties at C(31)···O(4) and C(31)···C(1′) contact distances of 2.870(4) and 3.022(4) Å. Apparently there is no energy gain from distorting the ring since one contact would be relieved only at the expense of the other. The deviation of N(3) from the plane of the atoms bonded to it is only 0.015(4) Å in **2**.

As expected, the OH group in each molecule acts as a proton donor in an intermolecular hydrogen bond. Of the various proton acceptors available, N(1) plays this role in both molecules. The OH···N distance and O—H···N angle are 2.842(4) Å and 169° in **1**, 2.778(3) Å and 180° in **2**. Although these hydrogen bonds are similar in **1** and **2**, the mode of association is quite different (Figs. 3 and 4). Molecules of **1** dimerize about a center of symmetry with the heterocyclic rings resembling two treads of a staircase and the N(1)···N(1)′ contact being only 3.139(3) Å. The hydroxyl group of each molecule is turned back over its own ring so that it can associate with N(1) of the other ring. In **2** the hydrogen-bonded contact is generated by the action of a screw axis, thereby producing chains of molecules. The presence of centers of symmetry within the unit cells of both **1** and **2** guarantees that the populations of these chiral molecules are equal.

Acknowledgement

The financial assistance (to K.V.) of the Natural Sciences and Engineering Research Council of Canada is gratefully acknowledged.

1. H. FONG and K. VAUGHAN. Can. J. Chem. **53**, 3714 (1975).
2. J. A. CAMPBELL, S. J. NOYCE, and R. C. STORR. Chem. Commun. 1344 (1983).
3. P. L. FAYE, K. VAUGHAN, and D. L. HOOPER. Can. J. Chem. **61**, 179 (1983).
4. G. M. SHELDRICK. SHELX-76. Program for crystal structure determination. University of Cambridge, England. 1976.
5. G. GERMAIN, P. MAIN, and M. M. WOOLFSON. Acta Crystallogr. A**27**, 368 (1971).
6. A. J. RANDALL, C. H. SCHWALBE, and K. VAUGHAN. J. Chem. Soc. Perkin Trans. II, 251 (1984).
7. R. J. SIMMONDS and C. H. SCHWALBE. Unpublished results.
8. S. L. EDWARDS, G. CHAPUIS, D. H. TEMPLETON, and A. ZALKIN. Acta Crystallogr. B**33**, 276 (1977).
9. H. C. FREEMAN and N. D. HUTCHINSON. Acta Crystallogr. B**35**, 2051 (1979).
10. S. L. EDWARDS, J. S. SHERFINSKI, and R. E. MARSH. J. Am. Chem. Soc. **96**, 2593 (1974).
11. J. HJORTÅS. Acta Crystallogr. B**29**, 1916 (1973).
12. W. E. HUNT, C. H. SCHWALBE, and K. VAUGHAN. Acta Crystallogr. C**39**, 738 (1983).
13. W. J. ROHRBAUGH, E. K. MEYERS, and R. A. JACOBSON. J. Agric. Food Chem. **24**, 713 (1976).

Crystal structures of tetrakis(ammoniomethyl)methane tetrachloride, $C(CH_2NH_3)_4Cl_4$, and disulfate, $C(CH_2NH_3)_4(SO_4)_2$

T. STANLEY CAMERON, WALTER J. CHUTE, AND OSVALD KNOP[1]
Department of Chemistry, Dalhousie University, Halifax, N.S., Canada B3H 4J3

Received April 18, 1984

T. STANLEY CAMERON, WALTER J. CHUTE, and OSVALD KNOP. Can. J. Chem. **63**, 586 (1985).

The crystal structures of $C(CH_2NH_3)_4Cl_4$ ($P4_2/n$, a = 9.503(1) Å, c = 6.549(1) Å, Z = 2) and $C(CH_2NH_3)_4(SO_4)_2$ ($P2_12_12_1$, a = 8.382(2) Å, b = 10.508(3) Å, c = 14.400(3) Å, Z = 4) have been determined. Both crystals contain strong N—H···X bonds; in the sulfate the hydrogen-bonding network is particularly extensive. The thermal motion of the cation can be described satisfactorily as a rigid-body motion.

T. STANLEY CAMERON, WALTER J. CHUTE et OSVALD KNOP. Can. J. Chem. **63**, 586 (1985).

On a déterminé les structures cristallines du $C(CH_2NH_3)_4Cl_4$ ($P4_2/n$, a = 9,503(1), c = 6,549(1) Å, Z = 2) et du $C(CH_2NH_3)_4(SO_4)_2$ ($P2_12_12_1$, a = 8,382(2), b = 10,508(3), c = 14,400(3) Å, Z = 4). Les deux cristaux contiennent de fortes liaisons N—H···X; dans le sulfate, le réseau des liaisons hydrogènes est particulièrement étendu. Utilisant le mouvement d'un corps rigide comme modèle, on peut décrire adéquatement le mouvement thermique du cation.

[Traduit par le journal]

The high symmetry of "globular" $C(CH_2X)_4$ molecules and the regular tetrahedral configuration at the central carbon atom have made pentaerythritol and its derivatives and cognates the subjects of numerous structural and other investigations (cf. ref. 1 and Table 1). Most of the crystals listed in Table 1 are molecular, and easy molecular reorientation and the occurrence of plastic phases in these compounds are not surprising. What would be less expected is the existence (5) of a plastic phase in pentaerythritol itself (X = OH), where at room temperature the molecules are bonded to sheets parallel to (001) by strong, only weakly bent O—H···O bonds, d(O···O) ~ 2.71 Å, d(H···O) ~ 1.9 Å, OHO ~ 163° (9–15). At 457 K the ordered crystal goes over into a plastic phase of cubic symmetry; the volume per formula unit of this phase is about the same as for neopentane (X = H), but the strong resistance to thermal breakdown of the order in the pentaerythritol crystal is reflected in the much higher T_{tr} (Table 1).

In view of the possibility that other, not purely molecular (and in particular ionic) crystals containing globular units of this type may exhibit unusual behaviour, we have undertaken an exploratory survey of several such compounds. The crystal structures of the first two, $C(CH_2NH_3)_4Cl_4$ and $C(CH_2NH_3)_4(SO_4)_2$, are reported in the following. The hydrogen bonding in both crystals is of interest in its own right, particularly as it involves a compact quadruply-charged cation.

The chloride was investigated crystallographically as early as 1938 by Cox, whose preliminary report (24) stated it correctly to be tetragonal, a = 9.44 Å, c = 6.53 Å, space group $P4_2/n$, with the central carbon on an S_4 axis. However, no mention of a completed structure determination could be found in the literature. The sulfate does not appear to have been investigated previously.

Experimental

The title compounds were prepared by the method described by Litherland and Mann (ref. 25; cf. also ref. 26). The chloride was recrystallized by dissolving it in a minimum volume of distilled water and allowing HCl from 36% aqueous acid to diffuse into the filtered solution.

The sulfate is only slightly soluble in water, but it dissolves in concentrated sulfuric acid (25). In an early attempt to obtain crystals suitable for X-ray studies H_2O + EtOH vapour was allowed to diffuse into a solution of the sulfate in 80% sulfuric acid placed in a desiccator. The crystals that formed were of inferior quality and crystallization by slow evaporation at room temperature of a hot-saturated aqueous solution of the sulfate was eventually resorted to, yielding gem-like crystals. Surprisingly, the material obtained from the sulfuric solution led to a tetragonal unit cell, a = 7.549(6) Å, c = 26.87(2) Å, c/a = 3.56, V = 1521(4) Å^3. The identity of this compound was not investigated further.

According to ref. 25, the chloride appears to remain unaffected up to 300°C when heated rapidly; on slow heating it decomposes above ca. 260°C. The mp of the sulfate is reported to be 303°C (dec.).

Crystal data

(Mo Kα_1, λ = 0.70926 Å (graphite monochromator); θ-range, 2–25°).

$C_5H_{20}Cl_4N_4$ fw = 278.06
Tetragonal, $P4_2/n$ (No. 86; systematic absences, $hk0$ for $h + k = 2n + 1$, $00l$ for $l = 2n + 1$); a = 9.503(2) Å, c = 6.549(1) Å, V = 591.4(2) Å^3, Z = 2, ρ_c = 1.562 g/cm^3; μ_{Mo} = 8.90 cm^{-1}, $F(000)$ = 292 e. Total reflections measured, 950; unique reflections, 615 (of which 465 with $I \geq 3\sigma(I)$). Final $R = R_w$ = 0.0392 (R = 0.0583 for full data).

$C_5H_{20}N_4O_8S_2$ fw = 328.36
Orthorhombic, $P2_12_12_1$ (No. 19; systematic absences, $h00$ for $h = 2n + 1$, $0k0$ for $k = 2n + 1$, $00l$ for $l = 2n + 1$); a = 8.382(2) Å, b = 10.508(3) Å, c = 14.400(3) Å, V = 1268.3(9) Å^3, Z = 4, ρ_c = 1.720 g/cm^3; μ_{Mo} = 4.00 cm^{-1}, $F(000)$ = 696 e. Total reflections measured, 1049; unique reflections, 1035 (of which 908 with $I \geq 3\sigma(I)$). Final R = 0.056, R_w = 0.060 (R = 0.060 for full data).

Structure determination

A CAD-4 four-circle diffractometer was used in the determination of the unit-cell dimensions and to collect intensities. The intensities were reduced by routine procedures (27). Corrections for Lorentz and polarization factors were applied but not for absorption or extinction. The scattering factors for neutral atoms were taken from ref. 28. The structures were solved by Patterson and Fourier methods using the SHELX system (29). Full-matrix least-squares ($w\Delta F^2$ = min.) refinements were carried out with isotropic temperature factors on the heavy atoms until R was reduced to a suitably low value. The locations of the hydrogen atoms were determined according to their geometric requirements: the C—H, N—H, and H—H distances were appropriately constrained (29) to ensure convergence (C—H to 1.08 Å, N—H to 1.02 Å, and H—H to ~1.66 Å), and the NH_3 groups were refined as rigid groups rotationally adjustable about the C—N axis.

The final refinement was with anisotropic temperature factors on the nonhydrogen atoms and isotropic factors on the hydrogens. Least-

[1]To whom all correspondence may be addressed.

TABLE 1. Crystallographic and caloric data of $C(CH_2X)_4$ crystals*‡

X	T	S.G.	Z	V_1	T_{tr}	$\Delta S_{tr}/R$	T_f	$\Delta S_f/R$	References
H	118	Hexagonal	12	130	140.0λ	2.21	256.5	1.53	2, 3; 4
	140	fcc	4	159					
	233	fcc	4	172					
	?	$Fd3m$?	8	178?					
CH_3							240.1		
F					249.4F	6.39	367.4	1.69	—; 5
Cl	RT	$P2/m$	48	222	235λ	0.13	368.2	7.30	6, 7; 8
Br	RT	$P2/m$	1†	240	320λ	0.53	433.5	7.79	6; 8
I	RT	$P2/m$	1†	(272)	385λ	0.21	~490d		6; 8
OH	RT	$I\bar{4}$	2	161.4	457	11.5	539	1.59	9–15; 1, 5
	503	fcc	4	180.0					
ONO_2 (I)	RT	$P\bar{4}2_1c$	2	295			416.1	12–14	16–18; 19
(II)	409	$Pcnb$	4	306			416.3		18; 19
OC(O)H	RT	$Pbca$	8	287			330		20; —
$OC(O)CH_3$	RT	$P4_2/n$	2	396			356–357		21; —
OPh	RT	$I\bar{4}$	2	640			387		22, 23; —

*Temperatures in K; S.G., space group; V_1, volume per formula unit, Å^3; λ, λ-point; F, first-order transition. The first set of references concerns crystallographic and the second, caloric data.

†Z = 1 cannot be correct for an ordered crystal. A preliminary re-examination of the bromide at room temperature has indicated a monoclinic unit cell with double the c-dimension reported in ref. 6 (a = 7.127 Å, b = 6.287 Å, c = 10.796 Å, β = 104.23°, Z = 2; probable space group, $P2_1/n$), but even this may be a subcell of the real unit cell.

‡ADDENDUM TO TABLE 1. The structure of $C(CH_2ONO_2)_4$ was recently re-refined from the data of ref. 17 (36). The $\bar{4}$ molecular symmetry is not retained in the structure of pentaerythrityl tetracinnamate: $P\bar{1}$, Z = 2, V_1 = 987 Å^3 (37).

TABLE 2. $C(CH_2NH_3)_4Cl_4$: positional and thermal parameters (×10^4)

Atom	x / y / z	U_{11} / U_{22} / U_{33}	U_{12} / U_{13} / U_{23}
C(1)	$\frac{1}{2}$	148(15)	0
	$\frac{1}{2}$	148(15)	0
	0	175(27)	0
C(2)	3791(3)	179(12)	0(10)
	4602(3)	204(13)	−56(11)
	−1453(5)	218(13)	−20(12)
H(21)	4176(3)	289(116)*	
	3809(3)		
	−2495(5)		
H(22)	3497(3)	289(108)*	
	5531(3)		
	−2301(5)		
N	2508(3)	176(11)	−25(10)
	4041(3)	241(12)	−20(12)
	−0449(5)	385(17)	−44(13)
H(1)	2686(3)	768(163*)	
	3004(3)		
	−0136(5)		
H(2)	1633(3)	1416(212)*	
	4131(3)		
	−1345(5)		
H(3)	2356(3)	1277(215)*	
	4575(3)		
	0880(5)		
Cl	1907(1)	260(4)	−18(3)
	4161(1)	233(4)	−15(3)
	4407(1)	284(3)	−8(3)

*U_{iso}. The NH_3 group was refined as a rigid body.

squares weights were calculated from expressions of the type $w^{-1} = k_1\sigma^2|F_o| + k_2F_o^2$, where σ is the weight for an individual reflection derived from the diffractometer counting statistics. The anisotropic temperature factor is defined as $T = \exp[-2\pi^2(U_{11}h^2a^{*2} + U_{22}k^2b^{*2} + U_{33}l^2c^{*2} + 2U_{23}klb^*c^* + 2U_{13}hla^*c^* + 2U_{12}hka^*b^*)]$.

The positional and thermal parameters are listed in Tables 2, 6, and 7[2], structure factors in Tables 3[2] and 8[2], and interatomic distances and bond angles in Tables 4, 5, 9, and 10.

Results and discussion

$C(CH_2NH_3)_4Cl_4$

A projection of the structure is shown in Fig. 1. Like in pentaerythritol at room temperature and in some of its derivatives (Table 1), the high symmetry of the central tetrahedral group of the cation is reflected in the symmetry of the crystal: the space group contains the element $\bar{4}$ characteristic of the maximum-symmetry conformation of the $C(CH_2X)_4$ molecule, and the cation is on this axis.

The cations and anions are arranged in layers ∥ (001). The side chains of the cations are folded flat and inward in such a way (Fig. 2) that the thickness of each cation/anion slab (as defined by the atomic coordinates of C and N) does not exceed 2 Å. The slabs are separated by vertical gaps, a little over 1 Å wide, which contain the CH_2 hydrogens.

Each N-hydrogen is involved in H···Cl bonding to one or more Cl^- ions (Fig. 2, top; Table 5). The shortest of these hydrogen bonds, H(1)···Cl = 2.15(3) Å, is almost straight and not much longer than the H···Cl bond in $Et_3NH^+Cl^-$, 2.08 Å (30), where the N—H···Cl group is linear by symmetry.

The H(2)···Cl bond is asymmetrically trifurcated and the H(3)···Cl bond, asymmetrically bifurcated. However, one of the NHCl angles in the trifurcated and one in the bifurcated bond are only 100°, and the H···Cl distances corresponding to these angles are about 2.8 Å. The N—H(2)···Cl bond may then equally well be regarded as an asymmetrically bifurcated, nonplanar N—H(2)···2 Cl bond, and the N—H(3)···Cl bond

[2]These tables have been deposited. Complete set of data is available, at a nominal charge, from the Depository of Unpublished data, CISTI, National Research Council of Canada, Ottawa, Ont., Canada K1A 0S2.

TABLE 4. $C(CH_2NH_3)_4Cl_4$: interatomic distances (Å) and bond angles (deg)

Atoms	Distance	Atoms	Angle
C(1)—C(2)	1.539(3)	C(2A)—C(1A)—C(2B)	103.6(2)
C(2)—N	1.485(4)	C(2A)—C(1A)—C(2C)	112.5(1)
C(2A)···C(2B)	2.419(5)	C(1A)—C(2A)—N(A)	115.3(2)
C(2A)···C(2C)	2.559(5)		
Cl(F)···Cl(Ec)	3.961(1)	Symmetry code:	
Cl(F)···Cl(A)	4.180(1)	A x y z	
Cl(F)···Cl(Ca)	4.309(1)	B $1-x$ $1-y$ z	
Cl(F)···Cl(Dd)	4.309(1)	C $1-y$ x $-z$	
Cl(F)···Cl(Hb)	4.375(1)	D y $1-x$ $-z$	
		E $\frac{1}{2}+x$ $\frac{1}{2}+y$ $\frac{1}{2}-z$	
a X + (0, 0, −1)		F $\frac{1}{2}-x$ $\frac{1}{2}-y$ $\frac{1}{2}-z$	
b X + (−1, 0, 0)		G $\frac{1}{2}-y$ $\frac{1}{2}+x$ $z-\frac{1}{2}$	
c X + (0, −1, 0)		H $\frac{1}{2}+y$ $\frac{1}{2}-x$ $z-\frac{1}{2}$	
d X + (0, −1, −1)			

TABLE 5. $C(CH_2NH_3)_4Cl_4$: N—H···Cl bond lengths (Å) and NHCl angles (deg)*

Cl	H	N	N···Cl†	H···Cl‡	NHCl§
Environment of a Cl atom:					
F	3C	C	3.153	2.81	100
	2C			2.79	101
F	1A	A	3.168	2.15	176
F	3F	F	3.233	2.38	141
F	2Dc	Dc	3.307	2.59	127
F	2Fa	Fa	3.419	2.79	120
Environment of an N atom:					
F	1A	A	3.168	2.15	176
Hb	2A	A	3.307	2.59	127
Aa			3.419	2.79	120
C			3.153	2.79	101
A	3A	A	3.233	2.38	141
G			3.153	2.81	100

*For symmetry code see Table 4.
†esd = 0.003 Å.
‡esd = 0.03 Å (rigid-body refinement of NH_3).
§esd = 3° (rigid-body refinement of NH_3).

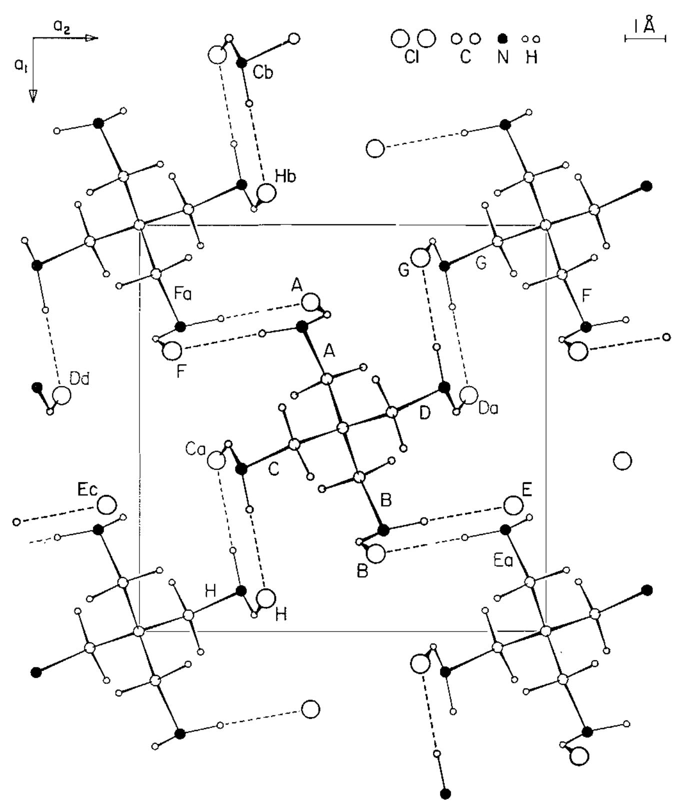

FIG. 1. Projection of the $C(CH_2NH_3)_4Cl_4$ structure on (001). The H(2) N-hydrogens are not shown. The shortest hydrogen bonds, H(1)···Cl, are indicated by broken lines; because of their shortness in the projection the H(3)···Cl bonds are shown as solid lines or not at all. For symmetry code see Table 4.

could similarly be described as a highly-bent hydrogen bond to a single acceptor atom.

Each Cl^- ion is surrounded by six N-hydrogens, with Cl···H distances ranging from 2.15 to ~2.8 Å (Fig. 2, bottom). The cations and the Cl^- ions in the cation/anion slabs ‖ (001) are connected by the N—H(1)···Cl bonds, with participation of the much longer N—H(2)···Cl bonds. The slabs are cross-linked vertically by the N—H(3)···Cl bonds, which are more or less parallel to the c-axis.

The overall cation/anion packing scheme and the organization of this $A^{4+}X^-_4$ structure can be visualized more directly by considering the structure to be composed of tetragonally compressed Cl_{12} cuboctahedra packed in such a way that each Cl atom is shared by three adjacent cuboctahedra (Fig. 3). The centre of each cuboctahedron is occupied by the central carbon C(1), and the N atoms are slightly inward of the centres of the vertical faces. The N—H(1)···Cl bonds are then approximately parallel to the (001) plane and the N—H(3)···Cl are roughly parallel to the c-axis.

$C(CH_2NH_3)_4(SO_4)_2$

In this chiral $A^{4+}X^{2-}_2$ structure (Fig. 4) the cation does not display its characteristic tetragonal symmetry. The cation/anion packing can be described as being of a very distorted fluorite type. There are two nonequivalent sets of SO_4^{2-} ions in the structure; the mean uncorrected S—O bond length is 1.465(6) Å (Table 9).

The cations and the sulfate groups are interconnected by an exhaustive three-dimensional system of hydrogen bonds (Fig. 5). Every N-hydrogen forms a H···O bond to a single acceptor, the H···O distances ranging from 1.74(10) to 2.14(10) Å, and the NHO angles from 126(5)° to 170(5)° (Table 10). The two shortest H···O distances, H(21)···O(3)

TABLE 6. $C(CH_2NH_3)_4(SO_4)_2$: positional parameters ($\times 10^4$)*

Atom	x	y	z
C(1)	4960(6)	4830(4)	5716(3)
C(2)	5274(6)	5464(5)	4778(3)
C(3)	5277(6)	3395(4)	5640(3)
C(4)	6045(5)	5455(5)	6444(4)
C(5)	3209(5)	4982(4)	6056(4)
N(2)	4195(5)	5049(4)	4017(3)
N(3)	4829(6)	2658(4)	6493(3)
N(4)	7790(5)	5207(5)	6317(3)
N(5)	2596(5)	6309(4)	6097(3)
S(1)	4764(2)	7278(1)	2117(1)
S(2)	−0143(2)	0789(1)	1074(1)
O(1)	4850(5)	7896(4)	3032(3)
O(2)	3443(5)	7828(4)	1583(3)
O(3)	4549(5)	5912(3)	2249(3)
O(4)	6256(5)	7501(4)	1605(3)
O(5)	0870(7)	0170(7)	0392(4)
O(6)	−1359(7)	1609(4)	0653(3)
O(7)	0790(6)	1550(4)	1729(3)
O(8)	−0960(5)	−0220(8)	1592(3)
H(21)	6483(6)	5244(5)	4573(3)
H(22)	5150(6)	6480(5)	4865(3)
H(31)	6536(6)	3257(4)	5515(3)
H(32)	4605(6)	3023(4)	5060(3)
H(41)	5697(5)	5105(5)	7120(4)
H(42)	5854(5)	6471(5)	6414(4)
H(51)	3125(5)	4574(4)	6743(4)
H(52)	2455(5)	4455(4)	5585(4)
HN(21)	4489(5)	5516(4)	3420(3)
HN(22)	3045(5)	5259(4)	4192(3)
HN(23)	4304(5)	4092(4)	3917(3)
HN(31)	5073(6)	1715(4)	6399(3)
HN(32)	3639(6)	2773(4)	6616(3)
HN(33)	5463(6)	2994(4)	7046(3)
HN(41)	8410(5)	5659(5)	6829(3)
HN(42)	8149(5)	5543(5)	5686(3)
HN(43)	8001(5)	4153(5)	6352(3)
HN(51)	1442(5)	6308(4)	6323(3)
HN(52)	2650(5)	6707(4)	5453(3)
HN(53)	3283(5)	6822(4)	6546(3)

*CH_2 and HN_3 groups refined as rigid bodies.

= 1.74(10) Å and H(31)···O(8) = 1.76(11) Å, are significantly shorter than the H···O distances in pentaerythritol, 1.983(23) Å (14), while the corresponding NHO angles, ~160°, are comparable to the OHO angle in pentaerythritol, 163°.

All the oxygens are hydrogen-bonded, but there being more N-hydrogens than sulfate oxygens, three of the oxygen atoms, O(1), O(4), and O(7), are involved in two hydrogen bonds each.

Infrared spectra

The strength of the N—H···Cl and N—H···O bonding in the title compounds is reflected in the very broad, unresolved NH (+ CH) stretching absorptions between ~3300 and ~2200 cm^{-1}. The spectra of the two compounds in this region are quite similar, with visually estimated centres of gravity near 2900 cm^{-1} for the chloride and near 2800 cm^{-1} for the sulfate. The broad absorption in the chloride spectrum showed somewhat more structure, in particular in the NH bending region.

Since the NH stretching absorptions in the ir spectra of ammonium and alkylammonium salts are also quite complex (cf. refs. 31−33), numerical frequency comparisons bearing on relative strength of the hydrogen bonding are difficult to make. However, the frequency of the centroid of the NH stretching absorption in the sulfate is roughly 200 cm^{-1} lower

TABLE 9. $C(CH_2NH_3)_4(SO_4)_2$: interatomic distances (Å) and bond angles (deg)

Atoms	Distance	Atoms	Angle
C(1)—C(2)	1.529(7)	C(2)—C(1)—C(3)	109.5(4)
C(1)—C(3)	1.535(7)	C(2)—C(1)—C(4)	108.3(4)
C(1)—C(4)	1.535(7)	C(2)—C(1)—C(5)	113.3(4)
C(1)—C(5)	1.556(7)	C(3)—C(1)—C(4)	111.6(4)
		C(3)—C(1)—C(5)	106.6(4)
C(2)—N(2)	1.486(6)	C(4)—C(1)—C(5)	107.5(4)
C(3)—N(3)	1.500(7)		
C(4)—N(4)	1.497(7)	C(1)—C(2)—N(2)	114.8(4)
C(5)—N(5)	1.487(6)	C(1)—C(3)—N(3)	113.9(4)
		C(1)—C(4)—N(4)	114.8(4)
S(1)—O(1)	1.471(10)	C(1)—C(5)—N(5)	115.8(4)
S(1)—O(2)	1.467(11)		
S(1)—O(3)	1.459(9)	O(1)—S(1)—O(2)	109.4(6)
S(1)—O(4)	1.471(11)	O(1)—S(1)—O(3)	108.9(6)
		O(1)—S(1)—O(4)	109.7(6)
S(2)—O(5)	1.452(15)	O(2)—S(1)—O(3)	111.3(6)
S(2)—O(6)	1.466(12)	O(2)—S(1)—O(4)	108.4(6)
S(2)—O(7)	1.463(11)	O(3)—S(1)—O(4)	109.1(6)
S(2)—O(8)	1.467(10)		
		O(5)—S(2)—O(6)	113.0(8)
		O(5)—S(2)—O(7)	111.6(7)
		O(5)—S(2)—O(8)	107.0(7)
		O(6)—S(2)—O(7)	108.5(6)
		O(6)—S(2)—O(8)	108.1(6)
		O(7)—S(2)—O(8)	108.4(6)

Symmetry code:
A x y z
B $\frac{1}{2} - x$ $1 - y$ $\frac{1}{2} + z$
C $\frac{1}{2} + x$ $\frac{1}{2} - y$ $1 - z$
D $1 - x$ $\frac{1}{2} + y$ $\frac{1}{2} - z$

a X + (1, 0, 0)
b X + (0, 1, 0)
c X + (0, 0, 1)
d X + (−1, 0, 0)
e X + (0, −1, 0)
f X + (0, 0, −1)
g X + (1, −1, 0)
h X + (−1, 1, 0)
i X + (1, 0, −1)
k X + (0, −1, 1)
m X + (−1, −1, 0)
n X + (0, −1, −1)

TABLE 10. $C(CH_2NH_3)_4(SO_4)_2$: N—H···O bond lengths (Å) and NHO angles (deg)*

N	HN	O	N···O	H···O	NHO
2A	21A	3A	2.719(10)	1.74(10)	160(5)
	23A	4De	2.848(11)	1.89(11)	155(5)
	22A	8Dd	2.864(10)	2.14(10)	126(5)
3A	31A	8Be	2.735(11)	1.76(11)	159(5)
	32A	2B	2.793(11)	1.86(11)	151(6)
	33A	7C	2.810(11)	1.85(11)	156(5)
4A	42A	5D	2.705(16)	1.80(16)	146(7)
	41A	1Cb	2.799(11)	1.95(11)	139(5)
	43A	4Ba	2.916(11)	1.90(11)	170(5)
5A	52A	6Dd	2.743(12)	1.93(12)	135(5)
	51A	1Ch	2.751(11)	1.83(11)	149(5)
	53A	7B	2.778(11)	1.90(11)	143(5)

*For coordinate transformations see Table 9. NH_3 groups refined as rigid bodies.

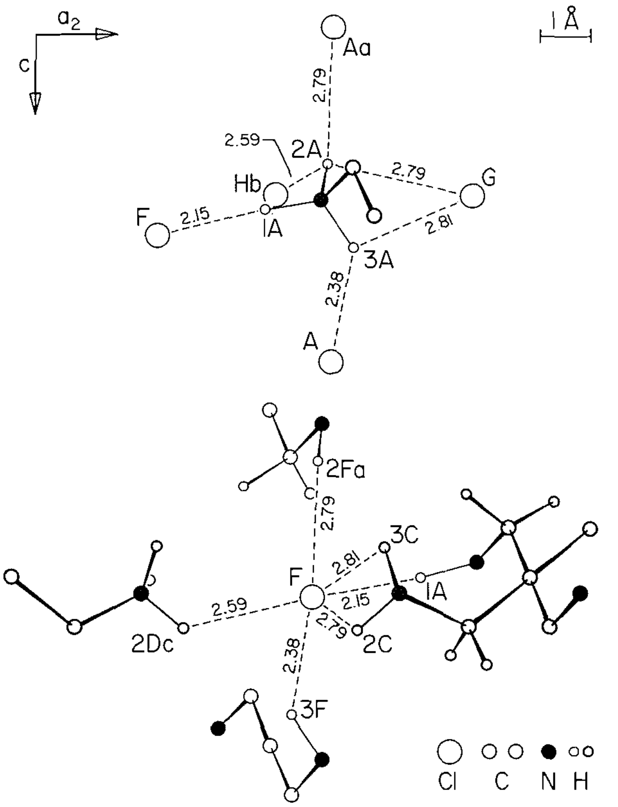

FIG. 2. Hydrogen bonding in $C(CH_2NH_3)_4Cl_4$ (projection on (100)). (*Top*) Environment of a nitrogen atom. (*Bottom*) Environment of a chlorine atom. For symmetry code and NHCl angles see Tables 4 and 5.

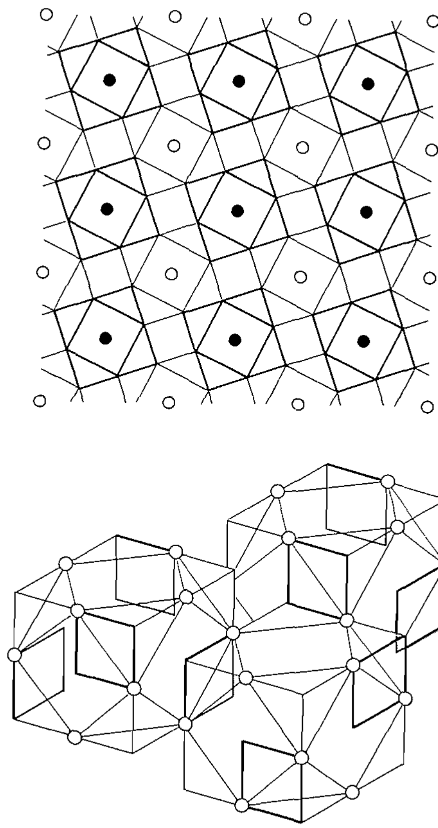

FIG. 3. (*Top*) Schematic representation of the packing of the $[C(CH_2NH_3)_4]Cl_{12}$ coordination cuboctahedra (projection on (001)). The C(1) atoms are at the centres of the cuboctahedra (filled circles, $z = 0$; open circles, $z = 1/2$). Each Cl (at a vertex of a cuboctahedron) is shared by three cuboctahedra. (*Bottom*) Representation of the hydrogen-bonding scheme. The corners and the centres of the vertical faces of the cubes correspond approximately to the positions of the NH_3 groups; the cuboctahedra inscribed in the cubes are the Cl_{12} groupings. The C(1) atoms are located at the cube centres. The two shortest N—H···Cl bonds are indicated by heavy lines: horizontal, H(1)···Cl ~ 2.15 Å; vertical, H(3)···Cl ~ 2.33 Å.

than the corresponding value in $(NH_4)_2SO_4$ (34) and in fact comparable to the corresponding frequency in NH_4F, which is the lowest so far reported for ammonium-containing halides. The strength of the N—H···O bonding in $C(CH_2NH_3)_4(SO_4)_2$ is undoubtedly intensified by the high ionic-charge combination and may well be, together with the extent of the hydrogen bonding in this crystal, responsible for the unexpected slight solubility of this salt in water.

Rigid-body motion of the cation

In view of the significant motion reported for the molecule in the pentaerythritol crystal (14), the refined parameters of the $C(CH_2NH_3)_4^{4+}$ cation in the chloride and sulfate were analysed for rigid-body translation and libration.[3] The results for the chloride indicated that the cation indeed acts as a rigid body. The rms amplitudes of translation were essentially isotropic, 0.12(2) Å along the two equivalent axes and 0.13(2) Å along c. These values are about 20% lower than the corresponding values in pentaerythritol, where some anisotropy is observed. The rms librational amplitudes were 3.3(10)° about a_1 and a_2 and 2.2(6)° about the c-axis, i.e. in each case about half the value in pentaerythritol. These results are compatible with the existence of the two short N—H···Cl bonds in the structure and point to a greater restraining potential in the ionic chloride crystal compared with the molecular pentaerythritol crystal.

In the sulfate the rigid-body motion hypothesis is satisfactory but less so than in the chloride, and the cation motion is less simple to interpret. The translation tensor **T** (in Å^2), the libration tensor **L** (in deg^2) and other relevant details of the analysis are given in Table 11.[2] The rms amplitudes relative to the crystallographic axes were 0.12(4), 0.14(4), and 0.14(4) Å for the translation and 2.7(15)°, 2.8(13)°, and 2.4(13)° for the libration components, i.e. essentially isotropic. Referred to the principal axes of the translation motion the rms amplitudes remained much the same, 0.15, 0.14, and 0.12 Å. However, with respect to the principal axes the ratio L_{11}/L_{33} of the elements of **L** was 4.8 and the corresponding rms amplitudes were 3.2(12)°, 2.9(11)° and 1.5(6)°, pointing to the existence of anisotropy of the librational motion. The L_3 axis is displaced by ~3 Å from the centre-of-gravity origin and its direction is roughly perpendicular to the N(2A)—N(3A) line (Figs. 4 and 5). These two N atoms are involved in the very short N(2)—H(21)···O(3) and N(3)—H(31)···O(8) bonds, and it is this involvement that seems to be responsible for the small libration amplitude about L_3.

In neither of the title compounds are the librational amplitudes at room temperature of a magnitude comparable to that in known precursors of plastic phases. If a transition to a plastic crystal exists, one would expect the T_{tr} to be quite high, probably higher than in pentaerythritol (Table 1). An investigation of the thermal behaviour of both salts is planned.

[3]The MGTLS program of Schomaker and Trueblood (35) was used in this analysis.

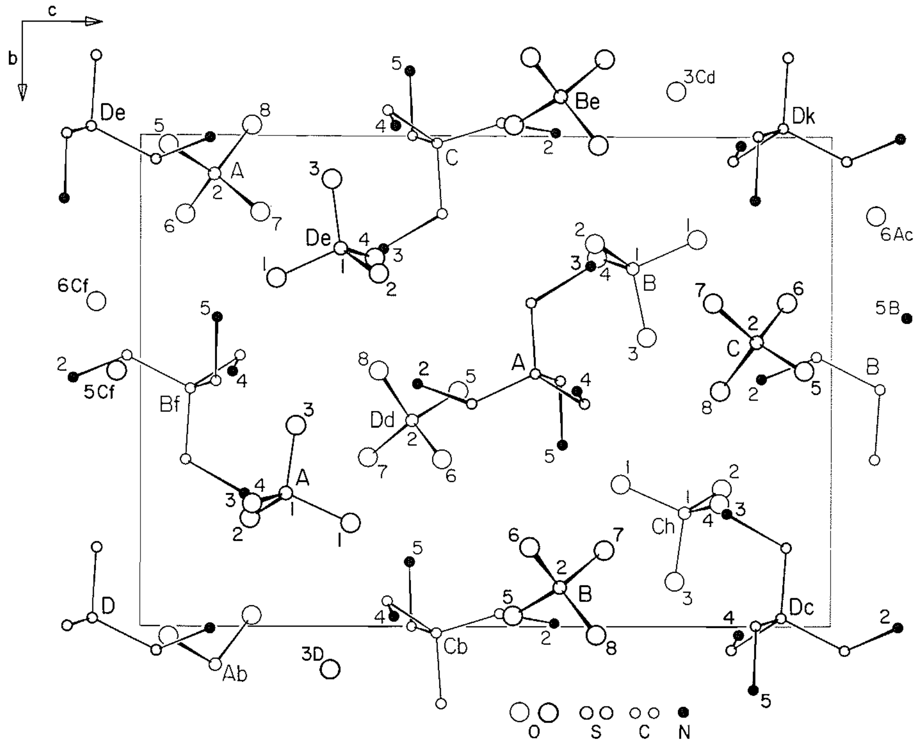

FIG. 4. Projection of the $C(CH_2NH_3)_4(SO_4)_2$ structure on (100). The hydrogen atoms have been omitted for clarity. For interatomic distances, bond angles and symmetry code see Tables 9 and 10.

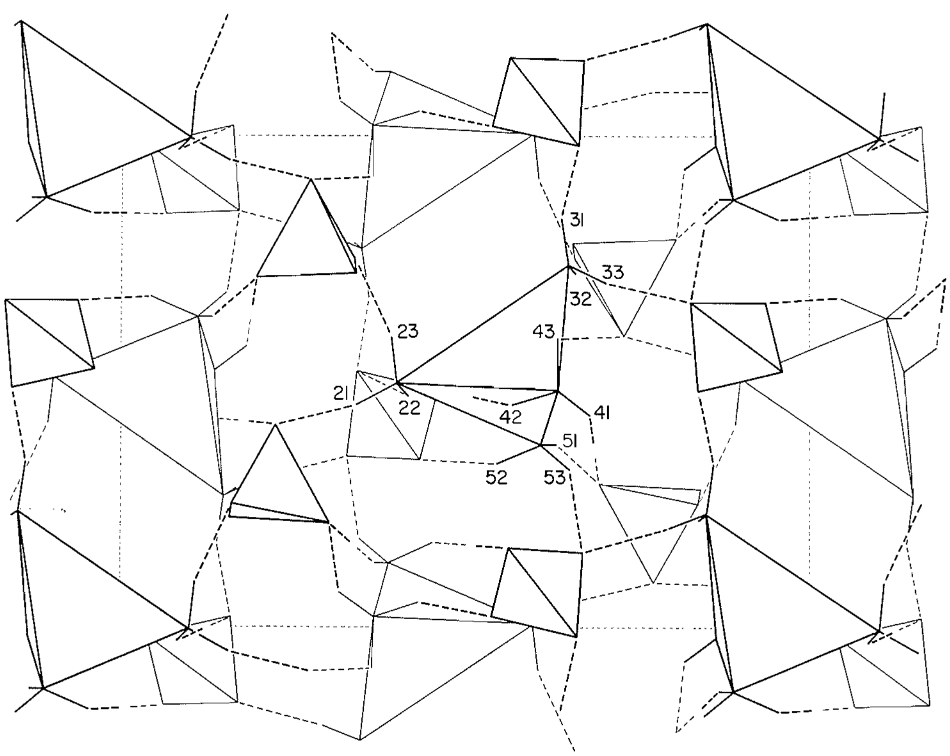

FIG. 5. Hydrogen bonding in $C(CH_2NH_3)_4(SO_4)_2$ (projection on (100), as in Fig. 4). The small tetrahedra represent the SO_4 groups. Each large tetrahedron is defined by the N atoms of a cation; the NH bonds are represented by the solid lines radiating from the vertices. H···O bonds are shown as broken lines. The H(32)···O(2) bonds project awkwardly on (100) and are not included in the drawing.

Geometry of the $C(CH_2NH_3)_4^{4+}$ cation

The bond lengths and angles obtained for the cation are listed in Table 12. They are the same in the chloride and the sulfate, whether corrected or uncorrected, and the corrected C(1)—C distances are statistically indistinguishable from the corresponding corrected distance in pentaerythritol. Corrections to the bond angles were insignificant.

The two C—C(1)—C angles in the chloride differ by

TABLE 12. Bond lengths (Å) and angles (deg) in the $C(CH_2X)_4$ ion or molecule*

Bond length or angle	X = NH_3 Chloride	X = NH_3 Sulfate	X = OH (14)	X = ONO_2(*I*) (18)
C(1)—C	1.539(3) (1.543)	1.539(12)† (1.542)†	1.527(1) (1.548)	1.536
C—N	1.485(4) (1.487)	1.493(7)† (1.495)†		
C(1)—C—N	115.3(2)	114.8(8)†		
C—C(1)—C	{103.6(2) 112.5(1)	106.6(4)‡ 113.3(4)§	107.33(9) 110.55(5)	109.2 109.9

*Values corrected for rigid-body motion are in parentheses.
†Mean value.
‡Smallest angle.
§Largest angle.

8.9(3)°, as against 6.7(6)° between the largest and the smallest angle in the sulfate and 3.2(1)° in pentaerythritol.

Acknowledgments

We wish to thank Mrs. Wanda Tacreiter for technical assistance, Dr. C. P. Huber for performing the rigid-body motion analyses, and Dr. M. Falk for the ir spectra. Financial support through research grants from the Natural Sciences and Engineering Research Council of Canada to two of the authors (T.S.C. and O.K.) is acknowledged.

1. N. G. PARSONAGE and L. A. K. STAVELEY. Disorder in crystals. Clarendon Press, Oxford. 1978.
2. R. RUDMAN and B. POST. Mol. Cryst. **5**, 95 (1968).
3. A. MONES and B. POST. J. Chem. Phys. **20**, 755 (1952).
4. J. E. ASTON and G. MESSERLY. J. Am. Chem. Soc. **58**, 2354 (1936).
5. J. C. TROWBRIDGE and E. F. WESTRUM, JR. J. Phys. Chem. **68**, 255 (1964).
6. G. WAGNER and G. DENGEL. Z. Physik. Chem. B, **16**, 382 (1932).
7. O. HASSEL and L. C. STRØMME. Strukturber. **5**, 156 (1937).
8. H. L. CLEVER, W.-K. WONG, and E. F. WESTRUM, JR. J. Phys. Chem. **69**, 1209 (1965).
9. I. NITTA and T. WATANABÉ. Bull. Chem. Soc. Jpn. **13**, 28 (1938).
10. J. HVOSLEF. Acta Crystallogr. **11**, 383 (1958).
11. R. SHIONO, D. W. J. CRUICKSHANK, and E. G. COX. Acta Crystallogr. **11**, 389 (1958).
12. G. W. SMITH. J. Chem. Phys. **50**, 3595 (1969).
13. M. F. C. LADD. Acta Crystallogr. B, **35**, 2375 (1979).
14. D. EILERMAN and R. RUDMAN. Acta Crystallogr. B, **35**, 2458 (1979).
15. H. HOPE and B. G. NICHOLS. Acta Crystallogr. A, **37**, C136 (1981).
16. A. D. BOOTH and F. J. LLEWELLYN. J. Chem. Soc. 837 (1947).
17. J. TROTTER. Acta Crystallogr. **16**, 698 (1963).
18. H. H. CADY and A. C. LARSON. Acta Crystallogr. B, **31**, 1864 (1975).
19. A. T. BLOMQUIST and J. F. RYAN, JR. Cited in ref. 18.
20. M. A. BREDIG. Z. Kristallogr. **74**, 49 (1930).
21. T. H. GOODWIN and R. HARDY. Proc. Roy. Soc. London, **164**A, 369 (1938).
22. J. BEINTEMA, P. TERPSTRA, and W. J. VAN WEERDEN. Rec. Trav. Chim. **54**, 627 (1935).
23. H. J. BACKER and G. DIJKEN. Rec. Trav. Chim. **55**, 22 (1936).
24. E. G. COX. Cited in ref. 25.
25. A. LITHERLAND and F. G. MANN. J. Chem. Soc. 1588 (1938).
26. L. J. ZOMPA and R. F. BOGUCKI. J. Am. Chem. Soc. **88**, 5186 (1966).
27. T. S. CAMERON and R. E. CORDES. Acta Crystallogr. B, **35**, 748 (1979).
28. International tables for X-ray crystallography. Vol. IV. The Kynoch Press, Birmingham, England. 1974.
29. G. M. SHELDRICK. X-ray system report. University Chemical Laboratories, Lensfield Road, Cambridge, England. 1976.
30. F. GENET. Bull. Soc. Fr. Min. Crist. **88**, 463 (1965).
31. O. KNOP, I. A. OXTON, and M. FALK. Can. J. Chem. **57**, 404, 2003 (1979).
32. O. KNOP, I. A. OXTON, W. J. WESTERHAUS, and M. FALK. J. Chem. Soc. Faraday 2, **77**, 309 (1981).
33. O. KNOP, T. S. CAMERON, M. A. JAMES, and M. FALK. Can. J. Chem. **61**, 1620 (1983); errata, Can. J. Chem. **62**, 1227 (1984).
34. R. A. NYQUIST and R. O. KAGEL. Infrared spectra of inorganic compounds. Academic Press, New York and London. 1971.
35. V. SCHOMAKER and K. N. TRUEBLOOD. Acta Crystallogr. B, **24**, 63 (1968).
36. A. D. BOOTH and I. J. BOOTH. Phys. Can. **40**, 57 (1984).
37. G. TIEGHI and M. ZOCCHI. Cryst. Struct. Commun. **1**, 167 (1972).

Électrochimie dans l'oxydipropionitrile. Étude des systèmes du mercure en milieu complexant et non complexant

M. PERSIN
Laboratoire de Chimie et Electrochimie Analytique, E.N.S.C.M., 8, rue de l'Ecole Normale, 34000 Montpellier, France

ET

J. Y. GAL
Laboratoire de Chimie Analytique de l'U.S.T.L., Place Eugène Bataillon, 34000 Montpellier, France

Reçu le 28 février 1984

M. PERSIN et J. Y. GAL. Can. J. Chem. **63**, 593 (1985).

L'ensemble des résultats obtenus montre qu'en milieu fortement complexant le mercure s'oxyde en mercure(II) avec formation des complexes supérieurs HgX_4^{2-}, HgX_3^-. Il n'en est plus de même en milieu peu complexant ou l'on doit envisager la formation de complexes avec le Hg(I). Ceci complique l'exploitation des courbes de titrage par suite de la transformation progressive des complexes du mercure II en complexes du mercure I au contact du mercure métallique. Les systèmes du mercure ne montrent cependant pas un comportement fondamentalement différent de celui observé dans de nombreux solvants organiques.

M. PERSIN and J. Y. GAL. Can. J. Chem. **63**, 593 (1985).

The results obtained show that, in a strongly complexing medium, mercury is oxidized to mercury(II) with the concomitant formation of more highly oxidized complexes like HgX_4^{2-} and HgX_3^-. When the reactional medium is less strongly complexing, however, the formation of complexes with Hg(I) can be considered. This complicates the exploitation of titration curves resulting from the progressive transformation of the complexes of mercury(II) into complexes of mercury(I) by contact with metallic mercury. Compared to the behavior observed in numerous organic solvents, the behavior of these systems is not fundamentally different.

[Journal translation]

Introduction

Au cours de nos travaux antérieurs (1–4) nous avons déjà décrit l'étude des propriétés acide base et de divers complexes avec les ions argent dans l'oxydipropionitrile. Nous avons pensé qu'il était souhaitable de compléter ceci en nous intéressant au comportement des systèmes des ions du mercure dans ce solvant.

Le mercure présente habituellement trois degrès d'oxydation (0, 1 et 2). La stabilité de l'espèce intermédiaire correspondant au degré +(I) dépend du milieu considéré. L'ion mercureux existe ainsi dans l'eau avec un taux de dismutation voisin de 1% (5); la dismutation est également partielle dans le DMF (6), la *N*-méthylpyrrolidone (7) et le DMSO (8). Par contre dans l'éthanolamine (9), l'éthylène diamine (10), la *N*-méthylacétamide (11) la dismutation du mercure(I) est totale.

En milieu complexant on assiste souvent à la dismutation totale du degré intermédiaire par suite de la formation de complexes supérieurs plus stables avec le degré d'oxydation (II) du mercure. Ainsi généralement en milieu halogénure rencontre-t-on les complexes HgX_2, HgX_4^{2-} comme le montrent les résultats publiés dans le DMF (12), le DMSO (8), l'acétonitrile (13), le HMPT (14).

Au cours de ce travail nous avons étudié par polarographie et titrages potentiométriques les complexes du mercure avec les ions halogénures et observé que les résultats obtenus sont compatibles avec ceux déjà publiés pour d'autres solvants.

Partie expérimentale

Synthèse et purification du solvant

Nous avons repris la synthèse et la purification du solvant mises au point au laboratoire et déjà décrites (3, 4).

Réactifs

Les sels de mercure utilisés proviennent des établissements K et K, de même que le perchlorate de tétrabutyl ammonium et les halogénures de tétrabutylammonium. Les chlorure, bromure et iodure mercuriques sont des produits pour analyse Prolabo.

Réalisation des mesures

Le tracé des courbes intensité–potentiel a été réalisé à l'aide d'un montage à 3 électrodes comprenant un enregistreur Tacussel EPL 2 couplé à un tiroir Typol. Le potentiel de l'électrode de travail était contrôlé par un millivoltmètre S6 Tacussel.

Les titrages potentiométriques à courant nul ont été effectués à l'aide d'un millivoltmètre Tacussel S6, la température d'exécution des mesures était régulée à 25°C par un thermostat à circulation.

Les potentiels rapportés dans le texte sont donnés par rapport à une électrode de référence Ag/Ag^+ dans le solvant qui a déjà été décrite par ailleurs (1).

Résultats expérimentaux

1. *Etude des systèmes du mercure en milieu non complexant*

1-1. *Etude à l'électrode à goutte de mercure*

Le perchlorate mercureux est soluble dans l'oxydipropionitrile en milieu acide. Les tracés des polarogrammes pour des concentrations variables d'ions Hg_2^{2+} sont très déformés par des maximums polarographiques que nous n'avons pu éliminer, néanmoins la hauteur du palier est proportionnelle à la concentration des ions Hg_2^{2+}.

La réduction des ions mercuriques dans les mêmes conditions conduit à des résultats analogues et en particulier la hauteur des vagues est identique pour des concentrations égales en ions Hg^{2+} ou Hg_2^{2+}; ce qui est compatible avec l'existence du dimère Hg_2^{2+}. La position des vagues observées laisse penser qu'en réalité on réduit toujours le mercure(I) par suite de la réduction chimique du mercure(II) par le mercure métallique de l'électrode selon:

$$Hg^{2+} + Hg \rightleftharpoons Hg_2^{2+}$$

1-2. *Etude à l'électrode de platine poli*

Les résultats obtenus à l'électrode à goutte s'avérant inexploitables, une étude des systèmes du mercure sur électrode de platine poli a été entreprise.

Cas des ions Hg_2^{2+}

La figure 1 montre que les ions mercureux sont réductibles

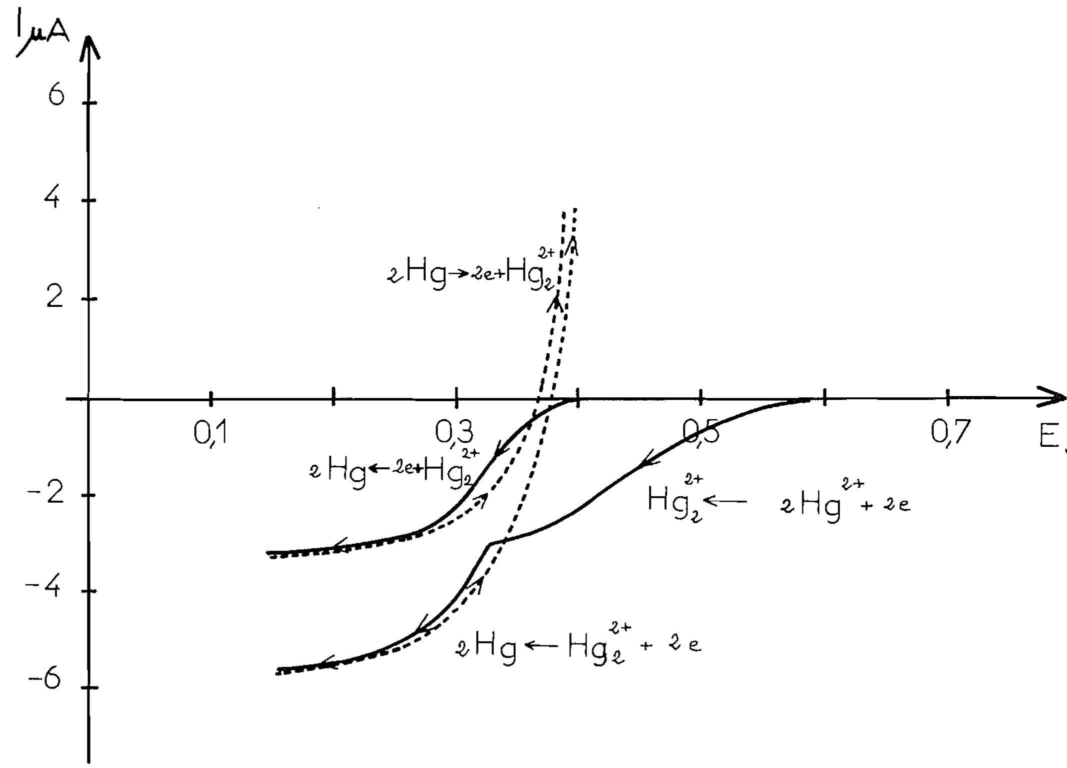

FIG. 1. Courbe voltamperométrique des systèmes $Hg/Hg_2^{2+}/Hg^{2+}$ à l'électrode de platine poli ($[Hg_2(ClO_4)_2] = 3 \times 10^{-3}$ M; $[Hg(ClO_4)_2] = 1,5 \times 10^{-3}$ M).

à l'électrode de platine poli; par ailleurs il est possible d'observer la redissolution du mercure déposé sur l'électrode lors du balayage retour des potentiels. La transformée logarithmique de la courbe intensité–potentiel obtenue en portant log ($I_l - i$) en fonction de E confirme l'irréversibilité partielle du système (pente de 80 mV au lieu des 29 mV attendus). On observe que le potentiel mesuré à courant nul au cours de la redissolution du film du mercure répond à la loi de Nernst avec une pente de 29 mV conformément à la relation

$$E = E^0 + \frac{0,06}{2} \log [Hg_2^{2+}]$$

L'extrapolation à log $[Hg_2^{2+}] = 0$ permet de déterminer le potentiel normal apparent[1] du couple Hg_2^{2+}/Hg soit 0,450 V ± 0,005 V. Ces données confirment l'existence dans l'oxydipropionitrile du dimère Hg_2^{2+}. Comme dans les autres solvants organiques (6–8) les ions Hg_2^{2+} ne sont pas électroactifs en oxydation contrairement à ce qui est observé dans l'eau; ce qui implique la non réversibilité du couple Hg^{2+}/Hg_2^{2+}.

cas des ions Hg^{2+}

La courbe intensité–potentiel de réduction des ions Hg^{2+} présente deux vagues de hauteur égale qui correspondent aux deux étapes:

$$2\,Hg^{2+} + 2e \rightleftharpoons Hg_2^{2+}$$
$$Hg_2^{2+} + 2e \rightleftharpoons 2\,Hg \downarrow$$

Le balayage retour effectué à partir du second palier de réduction montre que le mercure s'oxyde bien en ions mercureux Hg_2^{2+} et non en ion Hg^{2+}.

[1] En milieu $HClO_4$ 10^{-2} M.

Tentative d'évaluation de la constante de dismutation des ions Hg_2^{2+}

Dans la mesure où après une oxydation coulométrique d'une nappe de mercure, on observe uniquement à l'électrode de platine poli la vague de réduction des ions Hg_2^{2+}, on peut dire que ceux-ci sont peu dismutés, il s'en suit que les potentiels normaux apparents des couples Hg_2^{2+}/Hg et Hg^{2+}/Hg_2^{2+} sont tels que:

$$E^0_{Hg^{2+}/Hg_2^{2+}} > E^0_{Hg_2^{2+}/Hg}$$

Si l'on agite du mercure métallique en presence d'une solution d'ion Hg^{2+}, pour déterminer la constante de dismutation il faut pouvoir connaître le rapport des concentrations Hg^{2+}/Hg_2^{2+} à l'équilibre. M. Breant (6) a mis a profit le fait que l'ion Hg_2^{2+} est oxydable dans l'eau pour déterminer la concentration en ion Hg_2^{2+} dans le DMF par dilution aqueuse. Connaissant la concentration initiale en ions Hg^{2+} introduits on en déduit la concentration en ion Hg^{2+} restante. Cette méthode n'est valable que dans la mesure où les ions Hg_2^{2+} sont moins dismutés dans l'eau que dans le solvant étudié. Par ailleurs J. Courtot Coupez a proposé une méthode indirecte de détermination potentiométrique du potentiel normal du couple Hg^{2+}/Hg (8).

L'ordre de grandeur de cette constante de dismutation dans l'oxydipropionitrile a été obtenue en évaluant les concentrations en ions Hg^{2+} et Hg_2^{2+} après agitation d'une solution d'ions Hg^{2+} en présence de mercure métallique, à partir des hauteurs des vagues de réduction observées sur platine poli. Avant agitation on observe une vague de réduction des ions Hg^{2+} de hauteur h, après celle-ci on constante une forte diminution de la hauteur de la vague de réduction de ces derniers et l'augmentation de la vague de réduction des ions Hg_2^{2+}. On peut observer que la hauteur totale des deux vagues est constante conformément au bilan:

$[Hg^{2+}]_i = [Hg^{2+}]_r + [Hg_2^{2+}]_r$

Dans ces conditions $K_D = [Hg^{2+}]/[Hg_2^{2+}] = 10^{-1,3}$. On peut observer que la dismutation des ions Hg_2^{2+} dans l'oxydipropionitrile apparaît légèrement plus importante que dans l'eau où K_D est égale à 10^{-2}. Compte tenu de la méthode utilisée cette valeur reste un ordre de grandeur que nous avons utilisé pour calculer le potentiel normal du couple Hg^{2+}/Hg nécessaire à la détermination des constantes de stabilité des complexes mercuriques. On obtient aisèment

$$E^0_{Hg^{2+}/Hg_2^{2+}} = E^0_{Hg_2^{2+}/Hg} - 0,06 \log K_D = 0,530 \text{ V} \pm 0,010 \text{ V}$$

et

$$E^0_{Hg^{2+}/Hg} = \frac{E^0_{Hg^{2+}/Hg_2^{2+}} + E^0_{Hg_2^{2+}/Hg}}{2} = 0,490 \text{ V} \pm 0,010 \text{ V}$$

2. *Etude des systèmes du mercure en milieu halogénures complexant*

Le présent travail est consacré à l'étude du comportement des systèmes du mercure en présence de chlorure, bromure et iodure. Comme nous l'avons précédemment indiqué la présence d'un complexant stabilise généralement l'un des dégrés d'oxydation (I) ou (II) du mercure et par conséquent favorise ou défavorise la dismutation du degré intermédiaire.

2-1. *Etude polarographique*

2-1.1. *Etude des complexes Hg(II) iodure*

L'oxydation polarographique du mercure en présence d'iodure à concentration variable s'effectue en deux étapes, la première vague étant trois fois plus haute que la seconde. Cela est compatible avec les mécanismes d'oxydation suivants:

$$Hg\downarrow + 4I^- \rightleftharpoons HgI_4^{2-} + 2e$$

$$Hg\downarrow + 3\,HgI_4^{2-} \rightleftharpoons 4\,HgI_3^- + 2e$$

La hauteur des deux vagues est proportionnelle à la concentration d'iodure mais l'analyse mathématique des courbes $I = f(E)$ conduit à des droites de pente très supérieure à 30 mV confirmant l'irréversibilité des systèmes mis en jeu. Il est donc impossible d'atteindre les constantes de stabilité de ces complexes directement par le traitement des courbes $I = f(E)$.

2-1.2. *Etude des complexes Hg(II) chlorure et bromure*

L'oxydation polarographique du mercure en présence de ces deux halogénures conduit à des résultats identiques, on observe la présence de deux vagues de hauteurs égales proportionnelles à la concentration d'halogénures. On peut proposer le mécanisme

$$Hg\downarrow + 4X^- \rightleftharpoons HgX_4^{2-} + 2e$$

$$HgX_4^{2-} + Hg\downarrow \rightleftharpoons 2\,HgX_2 + 2e$$

Tout comme dans le cas de l'iodure l'analyse mathématique des vagues obtenues ne conduit à aucun résultat satisfaisant par suite de l'irréversibilité des systèmes mis en jeu.

2-2 *Etude potentiométrique*

2-2.1. *Cas de l'iodure*

La figure 2 montre que la courbe de titrage potentiométrique à l'électrode de mercure d'une solution d'iodure par les ions mercuriques présente trois points singuliers correspondant respectivement à la formation des complexes HgI_4^{2-}, HgI_3^- et HgI_2.

Cette hypothèse est confirmée par l'analyse mathématique

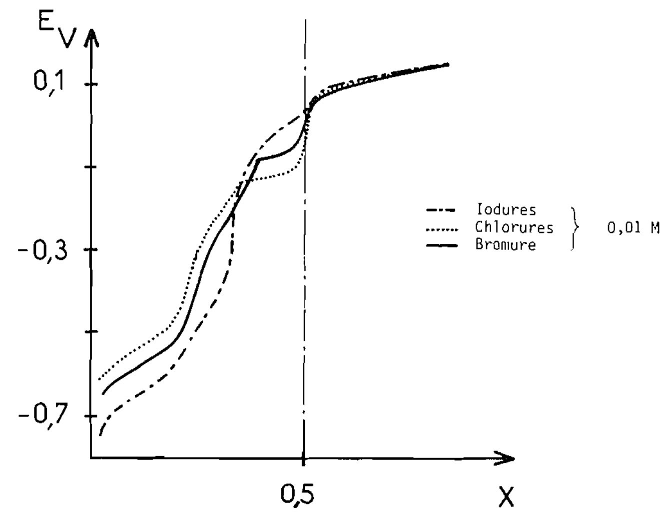

FIG. 2. Titrage potentiométrique des ions halogénures par le perchlorate mercurique (milieu Bu_4NClO_4 0,1 *M*; électrode indicatrice de mercure).

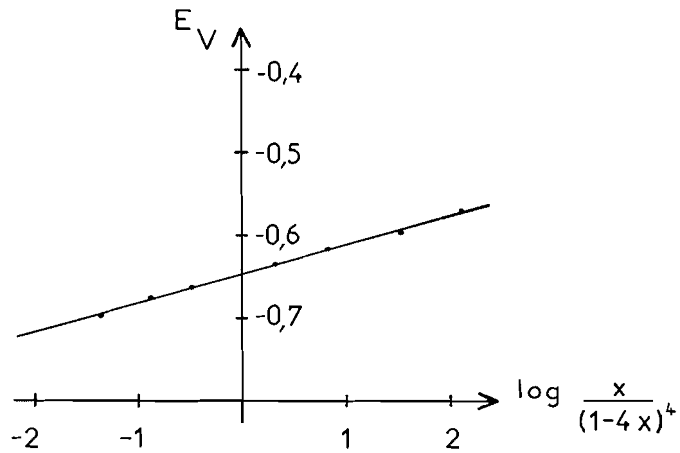

FIG. 3. Transformée logarithmique de la première partie de la courbe de titrage de l'iodure par le cation Hg^{2+} ($x < 0,25$).

de la courbe de titrage. Pour une fraction titrée x telle que $0 < x < 0,15$ on observe une variation linéaire du potentiel en fonction de $\log x/(1-4x)^4$ avec une pente de 31 mV au lieu des 29 mV théoriques attendus. L'ordonnée à l'origine de la droite obtenue (fig. 3) reliée à la constante β_{41} de formation du complexe HgI_4^{2-} par la relation:

$$H_1 = E^0_{Hg/Hg^{2+}} - 0,03 \log \beta_{41} - 0,03 \log C_0^3$$

permet connaissant $E^0_{Hg/Hg^{2+}}$ et la concentration C_0 de l'espèce titrée, de déterminer $\log \beta_{41}$.

Pour une fraction titrée $0,25 < x < 0,30$ la réaction de titrage mise en jeu est:

$$3HgI_4^{2-} + Hg^{2+} \rightleftharpoons 4HgI_3^-$$

de constante

$$K = \frac{[HgI_3^-]^4}{[HgI_4^{2-}]^3[Hg^{2+}]}$$

La transformée logarithmique de la courbe de titrage obtenue est une droite de pente 28 mV et d'ordonnée à l'origine:

$$H_2 = E^0_{Hg/Hg^{2+}} - 0,03 \log K - 0,03 \log C_0$$

TABLEAU 1. Constantes d'équilibre des complexes Hg(II) halogénures (chlorure, bromure, iodure)

Halogénures	HgX_4^{2-} log β_{41} ± 0,2	HgX_3^- log β_{31} ± 0,2	Équilibre $HgX_4^{2-} \rightleftharpoons HgX_3^- + X^-$ log K
Iodure	43,8	39,3	4,5
Bromure	41,6	37	4,6
Chlorure	40,2	35,5	4,7

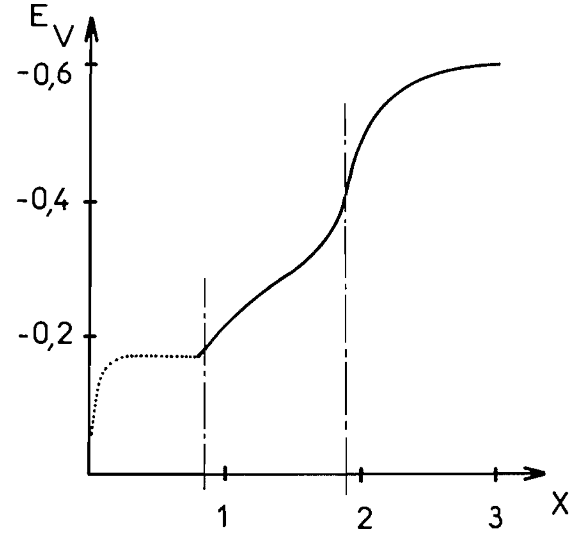

FIG. 4. Titrage potentiométrique de $HgBr_2$ par les ions Br^- (milieu Bu_4NClO_4 0,1 M; électrode indicatrice de mercure).

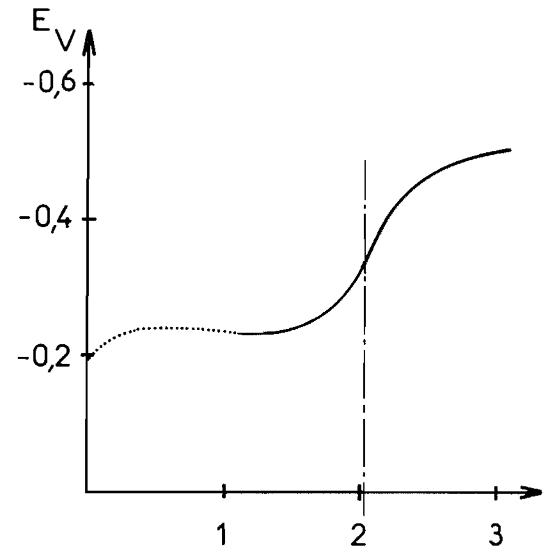

FIG. 5. Titrage potentiométrique de $HgCl_2$ par les ions Cl^- (milieu Bu_4NClO_4 0,1 M; électrode indicatrice de mercure).

on déduit aisèment

$$\beta_{31} = \frac{[HgI_3^-]}{[Hg^{2+}][I^-]^3} = \sqrt[4]{\beta_{41}^3\ K}$$

Au delà du deuxième point équivalent l'analyse de la courbe de titrage ne conduit à aucun résultat satisfaisant tendant à confirmer la formation de HgI_2 et l'on observe l'apparition d'un précipité jaune vert tandis que le mercure de l'électrode s'oxyde. Ces observations permettent de penser que le milieu n'est plus assez complexant pour dismuter totalement le mercure mercureux, celui-ci apparaît alors selon la réaction:

$$2HgI_3^- + Hg^{2+} + 3Hg \rightleftharpoons 3Hg_2I_2\downarrow$$

2-2.2 *Cas des chlorures et bromures*

Les résultats obtenus sont identiques et en milieu fortement concentré en halogénures nous avons bien l'existence de HgX_4^{2-}. La poursuite du titrage laisse apparaître un point équivalent pour $x = 0{,}33$ correspondant à la formation de HgX_3^- cependant moins net que dans le cas de l'iodure (fig. 2). Le point équivalent observé pour $x = 0{,}5$ correspond à l'apparition d'un précipité qui ne peut être attribué à la formation de HgX_2 car les chlorures et bromures mercuriques sont solubles dans l'oxydipropionitrile. Comme dans le cas de l'iodure nous pensons avoir formation des complexes Hg_2Br_2 et Hg_2Cl_2 tout deux insolubles dans l'oxydipropionitrile. Il y a de nouveau oxydation du mercure au niveau de l'électrode selon:

$$2\ HgX_3^- + 3Hg + Hg^{2+} \rightleftharpoons 3Hg_2X_2\downarrow$$

Le tableau 1 rassemble les différentes constantes d'équilibre des complexes déterminées.

2-2.3 *Titrage potentiométrique de $HgCl_2$ et $HgBr_2$ par les ions Cl^- et Br^-*

Le début du titrage est caractérisé par des potentiels mesurés peu stables qui proviennent en fait de la réaction de HgX_2 sur le mercure de l'électrode, on observe en effet l'apparition au contact du mercure d'un précipité qui ne peut qu'être attribué à Hg_2X_2:

$$HgX_2 + Hg\downarrow \rightleftharpoons Hg_2X_2\downarrow$$

La poursuite de l'ajout d'halogénure indique que le potentiel devient stable pour une quantité d'halogénure ajoutée identique à la quantité de HgX_2 présent. On observe un saut de potentiel dans le cas du titrage par les ions bromures (fig. 4). Ceci indique qu'en milieu de plus en plus complexant l'oxydation du mercure par le mercure (II) cesse et par conséquent le degré (I) du mercure est de plus en plus dismuté. Un second saut de potentiel est observé pour une quantité double d'halogénures versée (figs. 4, 5). Les réactions de titrages mises en jeu sont:

$$HgX_2 + X^- \rightleftharpoons HgX_3^-$$

$$HgX_3^- + X^- \rightleftharpoons HgX_4^{2-}$$

Entre les deux sauts de potentiel on peut écrire la variation du potentiel de l'électrode à l'aide du couple oxydoréducteur:

$$3HgX_4^{2-} + Hg\downarrow \rightleftharpoons 4HgX_3^- + 2e$$

$$E = E^0_{HgX_4^{2-}/HgX_3^-} + \frac{0{,}06}{2}\log\frac{[HgX_3^-]^4}{[HgX_4^{2-}]^3}$$

On vérifie que la pente de la droite obtenue est de 31 mV dans les conditions expérimentales, l'ordonnée à l'origine conduit à

TABLEAU 2. Constantes d'équilibre des complexes Hg(II) halogénures dans quelques solvants

	HgX_4^{2-} log β_{41}			HgX_3^- log β_{31}			$HgX_4^{2-} \rightleftharpoons HgX_3^- + X^-$ log K		
Solvant	I	Br	Cl	I	Br	Cl	I	Br	Cl
Eau	29,8	21	15,1	27,6	19,7	14,1	2,2	1,3	1
Acétonitrile[a]	48,7	46,7	45,5	44,5	42,9	42,7	4,2	3,8	2,8
DMSO[b]	32,6	30,4	26,9	30,4	28	23,5	2,2	2,4	3,4
ODPN	43,8	41,6	40,2	39,3	37	35,5	4,5	4,6	4,7

[a]D'après réf. 13.
[b]D'après réf. 8.

$E^0_{HgX_4^{2-}/HgX_3^-}$.

Au delà du point équivalent l'électrode répond selon

$$E = E^0_{HgX_4^{2-}/X^-} + \frac{0,06}{2}\log\frac{[HgX_4^{2-}]}{[X^-]^4}$$

La transformée logarithmique présente également une pente voisine de 30 mV et permet de calculer $E^0_{HgX_4^{2-}/X^-}$. Un simple calcul montre que:

$$K = \frac{[HgX_4^{2-}]}{[HgX_3^-][X^-]} = \frac{\beta_{41}}{\beta_{31}} = 10^{\Delta E^0/0.12}$$

Nous avons pu vérifier tout au moins dans le cas du titrage du complexe $HgBr_2$ que la valeur de K trouvée est très voisine de celle déterminée précédemment.

Conclusion

L'ensemble des résultats obtenus montre qu'en milieu fortement complexant le mercure s'oxyde en mercure(II) avec formation des complexes supérieurs HgX_4^{2-}, HgX_3^-. Il n'en est plus de même en milieu peu complexant ou l'on doit envisager la formation de complexes avec le Hg(I). Ceci complique l'exploitation des courbes de titrage par suite de la transformation progressive des complexes du mercure (II) en complexes du mercure (I) au contact du mercure métallique. Les systèmes du mercure ne montrent cependant pas un comportement fondamentalement différent de celui observé dans de nombreux solvants organiques (Tableau 2).

1. J. Y. GAL et M. PERSIN. J. Electroanal. Chem. **77**, 361 (1977).
2. J. Y. GAL, D. DE BARROS, M. PERSIN et F. PERSIN. J. Electroanal. Chem. **99**, 347 (1979).
3. J. Y. GAL et M. PERSIN. Can. J. Chem. **59**, 2491 (1981).
4. J. Y. GAL, M. PERSIN et B. CASTELAS. Can. J. Chem. **61**, 1189 (1983).
5. I. M. KOLTHOFF et C. S. MILLER. J. Am. Chem. Soc. **63**, 2732 (1941).
6. NGUYEN VAN KIET et M. BREANT. C. R. Acad. Sci. Paris Sér. C-t, **264**, 1042 (1967).
7. M. BREANT. Bull. Soc. Chim. Fr. 725 (1971).
8. A. FOLL, M. LE DEMEZET et J. COURTOT COUPEZ. Bull. Soc. Chim. Fr. 1207 (1972).
9. M. GRALL. Rapport CEA R, 2902 (1966).
10. M. BIGOIS, J. C. TOULLER et B. TREMILLON. Bull. Soc. Chim. Fr. 1847 (1965).
11. L. B. AGURTO-CID et M. MACHTINGER. Bull. Soc. Chim. Fr. 1915 (1965).
12. M. BREANT et NGUYEN VAN KIET. CR. Acad. Sci. Paris Sér. C-t, **262**, 955 (1966).
13. J. F. COETZEE, J. J. CAMPION, and D. R. LIBERMAN. Anal. Chem. **45**, 343 (1973).
14. J. Y. GAL et F. PERSIN. Bull. Soc. Chim. Fr. 1005 (1977).

Reaction of hydroxide ion with 1,3,5-trinitrobenzene in cationic micelles: evidence of variable counterion binding to micellar head groups

LEONG-HUAT GAN
Department of Chemistry, University of Malaya, Pantai Valley, Kuala Lumpur, Malaysia

Received March 30, 1984

LEONG-HUAT GAN. Can. J. Chem. **63**, 598 (1985).

Cationic micelles of hexadecyltrimethylammonium bromide, chloride, and hydroxide (CTABr, CTACl, and CTAOH) greatly enhance the stability of anionic σ-complex formed by hydroxide ion and 1,3,5-trinitrobenzene (TNB). The counterion binding to the micellar head groups is assumed to vary but is governed by a distribution constant. Different distribution constants are used for different types of counterion. Using this treatment, the rate constant − surfactant concentration profiles for the reactions of TNB with hydroxide ion in CTAOH, CTABr, and CTACl can all be satisfactorily accounted for, yielding consistent results in various conditions. The ion distribution constants, $K_{OH} = 55$ mol^{-1} dm^3, $K_{Br} = 1800$ mol^{-1} dm^3, and $K_{Cl} = 420$ mol^{-1} dm^3 and the rate constant $k_M = 3600$ s^{-1} are obtained. In view of the success of this treatment, the assumption of a constant β value associated with the pseudophase model at best could only be viewed as an approximation, valid only for micellar systems with tightly bound counterions such as those in the micelles of CTABr.

LEONG-HUAT GAN. Can. J. Chem. **63**, 598 (1985).

Les micelles cationiques des bromure, chlorure et hydroxyde de l'hexadécyltriméthylammonium (CTABr, CTACl et CTAOH) augmentent considérablement la stabilité des complexes anioniques σ formés par l'ion hydroxyde et le trinitro-1,3,5 benzène (TNB). On fait l'hypothèse que la fixation de l'ion complémentaire sur les groupes de têtes de la micelle varie; toutefois, cette fixation est gouvernée par une constante de distribution. On utiise des constantes de distribution différentes pour différents types d'ions complémentaires. Utilisant cette approche, on peut expliquer d'une façon satisfaisante les profils de constantes de vitesse/concentration d'agents tensioactifs pour les réactions du TNB avec l'ion hydroxyde dans des micelles cationiques de CTABr, de CTACl et de CTAOH; les résultats sont cohérents sous diverses conditions. On a obtenu les constantes de distribution des ions, $K_{OH} = 55$ mol^{-3} dm^3, $K_{Br} = 1800$ mol^{-3} dm^3 et $K_{Cl} = 420$ mol^{-3} dm^3 ainsi que la constante de vitesse $K_M = 3600$ s^{-1}. Compte tenu des résultats excellents obtenus en faisant appel à notre approche, il apparait que, dans le meilleur des cas, on ne doit considérer l'hypothèse suivant laquelle il faut associer une constante de valeur β avec le modèle de la pseudophase que comme une approximation qui ne serait valide que pour des systèmes micellaires comportant des ions complémentaires intimement liés comme ceux présents dans les micelles de CTABr.

[Traduit par le journal]

Introduction

Micellar catalysis in water for unimolecular reaction and bimolecular reaction between two uncharged reactants can generally be interpreted in accordance with the pseudophase model (1−3). The rate enhancements or inhibitions are rationalized in terms of medium effect or concentration effect or both (3, 4). For reactions in ionic micelles, it is generally assumed that the extent of charge neutralization at the micellar headgroups, β, remains constant once the micelle is formed. This assumption, widely used in kinetic analysis, has been found to be satisfactory for a large number of reactions between hydrophilic ions and neutral substrates, especially in micelles of CTABr (4−8). More recently, however, this kinetic treatment has been shown to have failed for micelles with more hydrophilic counterions, specifically micelles of CTAOH and CTAF (9). While several possible reasons for the failure of this simple kinetic model in these systems have been discussed (9), it is believed that the assumption of a constant β value could be a major cause. By discarding the constraint of this invariance in β value and assuming instead that the binding of the counterions to the micellar phase be represented by an equilibrium process similar to that for the distribution of an organic substrate, Bunton *et al.* (10) have shown that many observed "anomalous" rate−surfactant profiles can be satisfactorily accounted for. This treatment has recently been applied to an alkoxide functionalized micellar system (11). To furnish further evidence for the support of this approach, a reversible reaction between OH^- and TNB is now reported.

Experimental

Materials

Hexadecyltrimethylammonium bromide and chloride (CTABr and CTACl) were obtained from Tokyo Kasei, Japan and were purified by repeated recrystallization from Et_2O−EtOH. The purities of these surfactants were checked by surface tension measurements. Solutions of hexadecyltrimethylammonium hydroxide (CTAOH) were prepared by the method described previously (10). Eastman 1,3,5-trinitrobenzene (TNB) was recrystallized several times from ethanol.

Binding of TNB to micelles of CTABr

The binding constant of TNB, K_S, defined by eq. [1]

$$[1] \quad K_S = \frac{[\text{TNB.D}_n]}{[\text{TNB}_W][\text{D}_n]}$$

where TNB.D_n denotes TNB in micellar phase, in micelles of CTABr, was determined by the solubility method. A Cary 17 spectrophotometer was used to determine the concentrations of TNB. Saturated solutions of TNB in various concentrations of CTABr at 25°C were diluted to ~5 × 10^{-5} mol dm^{-3} by isopropanol. Suitable amounts of NaOH were then added so that the NaOH concentrations of the final solutions were ~5 × 10^{-3} mol dm^{-3}. Essentially all the TNB would be reacted to form anionic σ-complexes. This method is sensitive, as both the equilibrium constant and the molar extinction coefficient of the complex in isopropanol are high (12). The binding constant thus obtained is $K_S = 46 \pm 2$[1] mol^{-1} dm^3 with the solubility of TNB in water being 1.9 × 10^{-3} mol dm^{-3} at 25°C.

[1]Least-square errors from five determinations in various CTABr concentrations.

Equilibrium and kinetic studies

A Durrum–Gibson (new name: Dionex) D-110 stopped-flow spectrophotometer connected with a Tektronix R5103N oscilloscope was used for both the kinetic and equilibrium studies. The cuvette has an optical path length of 2 cm. All the reactions were carried out at a thermostated temperature of 25 ± 0.1°C. Reactions were followed at λ = 500 nm. The concentrations of the substrate solutions were ~3 × 10^{-5} mol dm^{-3}, and the observed first-order rate constants k_ψ are in s^{-1}. A much faster reaction was observed to precede the formation of the TNB–OH^- complex. They were found in all the micellar systems studied, i.e., CTABr, CTACl, $CTANO_3$, CTACN, and CTAOH, hence unlikely to have resulted from the impurities in the surfactants.

While it is regrettable that the nature of this fast reaction has yet to be identified, its existence should not have had any effect on the values of k_ψ. This is because the slower formation of the TNB–OH^- complex begins only well after this fast reaction has been completed, and good first-order reactions are observed throughout. Furthermore, in most cases, especially those at lower hydroxide ion concentrations, the absorbances due to these fast reactions were small relative to those of the TNB–OH^- complexes. Due to the extremely low equilibrium constant of TNB–OH^- in water as compared to that in the micelles (see results and discussion), the observed absorbances were attributed solely to the TNB–OH^- complexes in the micellar phase.

Results and discussion

Hydroxide ion reacts reversibly with TNB to form an anionic σ-complex. The equilibrium constant in water is low, K = 2.7 mol^{-1} dm^3 at 25°C with the forward and reverse rate constants being 25.3 mol^{-1} dm^3 s^{-1} and 13.4 s^{-1} respectively (12). Micellar effects on the rate and equilibrium constants of anionic σ-complexes have been reported (13, 14). It is found that the formation of the TNB–OH^- complex is affected by the presence of cationic micelles of CTABr, CTACl, and CTAOH. Quantitative kinetic analyses for the reactions in these systems are now presented.

Kinetics

Reaction of OH^- with TNB in micelles is assumed to follow the pathways outlined in Scheme 1.

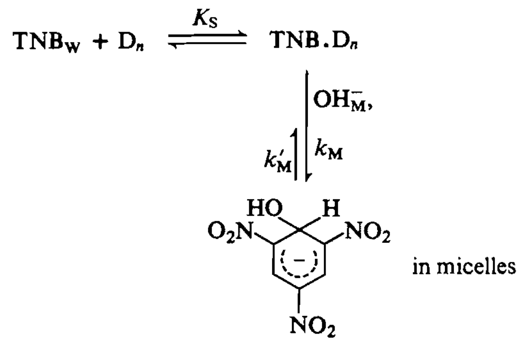

I

SCHEME 1

Reaction in water is neglected because of its low equilibrium constant. The observed first-order rate constant is given by

$$[2] \quad k_\psi = \frac{K_S k_M [OH_M^-]}{1 + K_S [D_n]}$$

Here the reverse rate constant of complex **I** is again omitted (see discussion later for justification of its omission).

Reactions in micelles of CTAOH

Reactions of TNB in CTAOH with and without the addition of NaOH are shown in Figs. 1 and 2. These results do not conform to the pseudophase model with a constant value of β as have been found for the reactions with other substrates such as 2,4-dinitrochlorobenzene (DNCB), 2,4-dinitrochloronapthalene (DNCN), and p-nitrophenyldiphenylphosphate (pNPDPP) (10). The concentration of hydroxide ion in the micellar phase $[OH_M^-]$ is assumed to be governed by a distribution constant and is calculated from eq. [3].

$$[3] \quad K_{OH} = \frac{[OH_M^-]}{[OH_W^-]([D_n] - [OH_M^-])}$$

where the micellized surfactant $[D_n]$ = C_D = CMC (CMC is critical micelle concentration). Reasonably good fits are obtained by using K_{OH} = 55 mol^{-1} dm^3, k_M = 3600 s^{-1}, and the

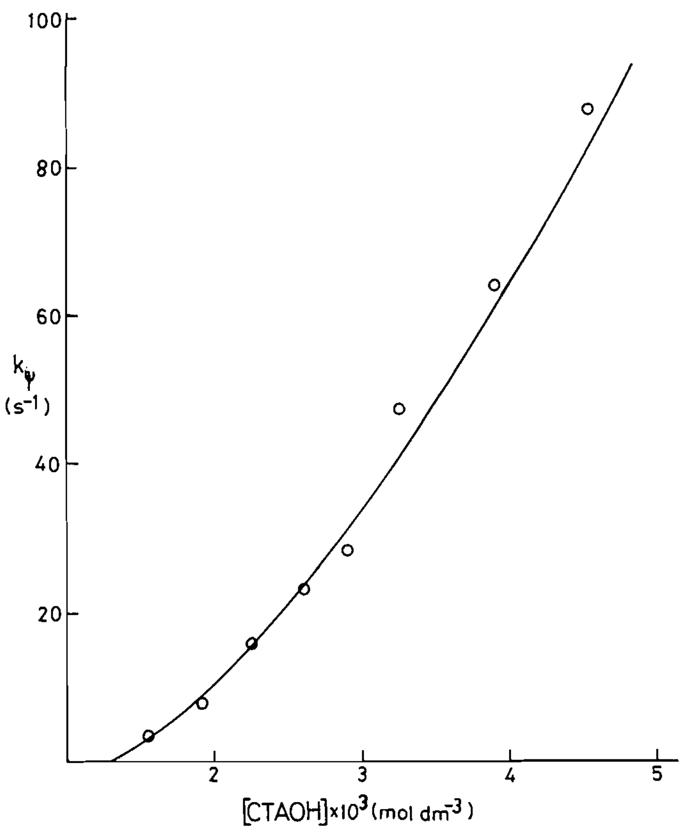

FIG. 1. Rate constant – surfactant profile for the reaction of TNB in CTAOH. Calculated k_ψ values are shown by the solid line.

experimentally determined K_S = 46 mol^{-1} dm^3.

Reactions in micelles of CTABr and CTACl at constant [NaOH]

The values of k_ψ for the formation of **I** as a function of surfactant concentrations are shown in Fig. 3. The competition between OH^- and X^- (X = Br or Cl) is assumed to be governed by two equilibra with equilibrium constants K_X and K_{OH} as given in eqs. [4] and [5].

$$[4] \quad K_X = \frac{[X_M^-]}{[X_W^-]([D_n] - [X_M^-] - [OH_M^-])}$$

$$[5] \quad K_{OH} = \frac{[OH_M^-]}{[OH_M^-]([D_n] - [OH_M^-] - [X_M^-])}$$

Expanding eqs. [4] and [5] yields eqs. [6] and [7] respectively.

TABLE 1. Parameters used to calculate k_ψ for reaction of TNB with OH^- in CTABr

10^3[NaOH] (mol dm^{-3})	10^4 CMC (mol dm^{-3})	k_M (s^{-1})	K_{OH} (mol^{-1} dm^3)	K_{Br} (mol^{-1} dm^3)	K_S (mol^{-1} dm^3)
0.788	6	3600	55	1800	75
1.97	5	3600	55	1800	92

TABLE 2. Parameters used to calculate k_ψ for reaction of TNB with OH^- in CTACl

10^3[NaOH] (mol dm^{-3})	10^3 CMC (mol dm^{-3})	k_M (s^{-1})	K_{OH} (mol^{-1} dm^3)	K_{Cl} (mol^{-1} dm^3)	K_S (mol^{-1} dm^3)
0.788	1	3600	55	420	83

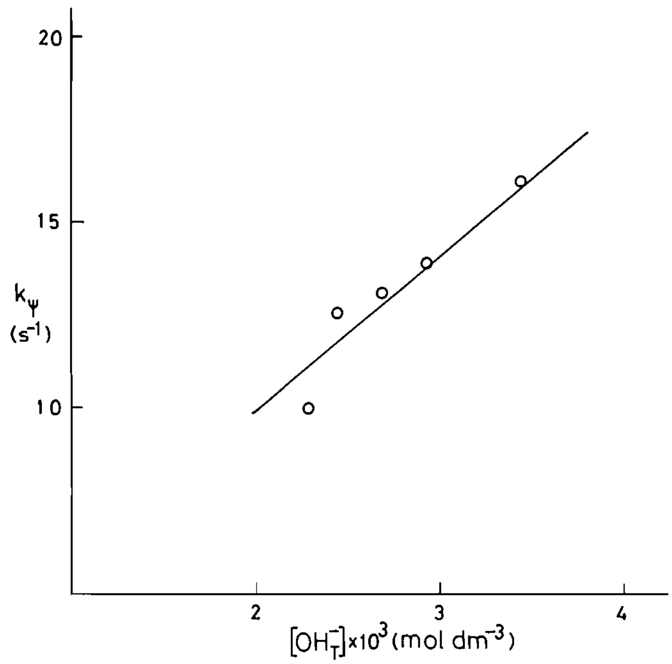

FIG. 2. Reaction of TNB in CTAOH with added NaOH. The line is predicted.

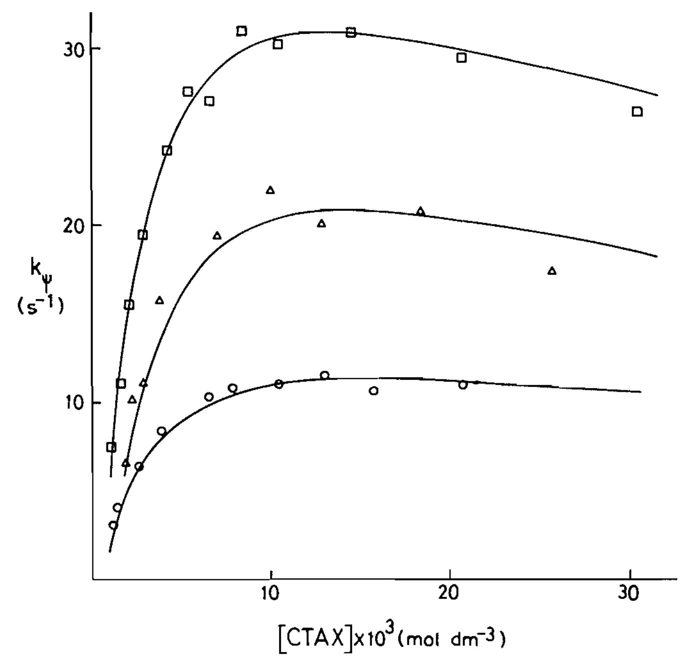

FIG. 3. Reactions of TNB with OH^- in CTAX (X = Br and Cl). X = Br; ○, [NaOH] = 7.88 × 10^{-4} mol dm^{-3}; □, [NaOH] = 1.97 × 10^{-3} mol dm^{-3}; X = Cl; △, [NaOH] = 7.88 × 10^{-4} mol dm^{-3}. The lines are predicted.

$$[6] \quad K_X[X_M^-]^2 - [X_M^-](1 + K_X[D_n] + K_X[X^-]_0) + K_X[OH_M^-][X_M^-] - K_X[X^-]_0(OH_M^-] + K_X[D_n][X^-]_0 = 0$$

$$[7] \quad K_{OH}[OH_M^-]^2 - [OH_M^-](1 + K_{OH}[D_n] + K_{OH}[OH^-]_0) + K_{OH}[X_M^-][OH_M^-] - K_{OH}[OH^-]_0[X_M^-] + K_{OH}[D_n][OH_0^-] = 0$$

Values of $[OH_M^-]$ and $[X_M^-]$ are obtained by iterative methods using a computer. The sets of parameters that give reasonably good fits to the rate – surfactant concentration profiles (Fig. 3) are listed in Tables 1 and 2. It is noted that while maintaining constant values for K_{OH}, K_X, and k_M, a slightly different value of K_S at different [NaOH] is used in order to give a good fit to the experimental data. The fact that K_S varies with [NaOH] is, however, not unusual for a substrate which does not bind strongly to micelles. A similar effect was observed for another more hydrophilic substrate, DNCB in CTABr (K_S = 75 mol^{-1} dm^3) (10).

Effect of NaOH on k_ψ *at constant [CTABr]*

At constant surfactant concentration, increasing NaOH concentration increases $[OH_M^-]$, hence increases k_ψ (Fig. 4). Using the method described earlier, $[OH_M^-]$ are obtained. It is, however, more difficult to predict an accurate value for k_ψ because K_S may vary slightly as the concentration of NaOH changes. Nevertheless, with the same set of values for K_{OH}, K_{Br}, and k_M listed in Table 1, the calculated k_ψ values agree reasonably well with the experimental data if an average value of K_S = 82 mol^{-1} dm^3 is assumed (Fig. 4).

*Equilibrium constant of complex **I** in CTABr*

In a fixed concentration of CTABr, the absorbance of complex **I** increases with increasing [NaOH] (Table 3). Referring to Scheme 1, the equilibrium constant for complex **I** in the micelles is

$$[8] \quad K_I = \frac{[\mathbf{I}_M]}{[OH_M^-][TNB.D_n]}$$

Combining eq. [8] with eq. [1] for K_S yields

$$[9] \quad K_S \cdot K_I = \frac{[\mathbf{I}_M]}{[OH_M^-][TNB_W][D_n]}$$

and

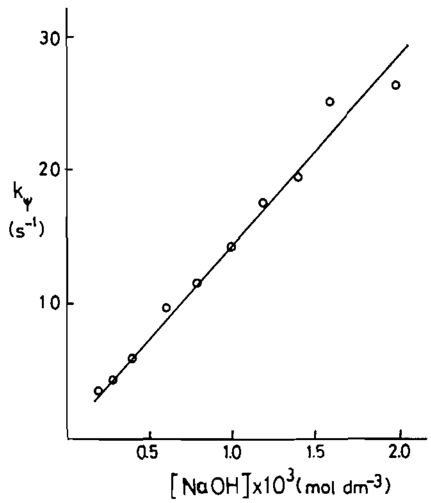

FIG. 4. Reaction of TNB with OH^- at constant [CTABr]. The line is predicted.

TABLE 3. Absorbance (A_∞) of complex **I** for reaction of TNB with OH^- in CTABr[a]

10^3[NaOH] (mol dm^{-3})	$10^4[OH_M^-]$ (mol dm^{-3})	A_∞
0.2	0.166	0.3893
0.3	0.248	0.4584
0.4	0.330	0.5258
0.6	0.493	0.5654
0.8	0.653	0.5784
1.0	0.813	0.6055
1.2	0.970	0.6234
1.4	1.130	0.6345
1.6	1.286	0.6421
2.0	1.593	0.6491

[a][CTABr] = 8.560×10^{-3} mol dm^{-3}; [TNB] = 2.179×10^{-5} mol dm^{-3}; λ = 500 nm.

$$[10] \quad [TNB_W] = [TNB]_0 - [TNB \cdot D_n] - [\mathbf{I}_M] \approx [TNB]_0 - [\mathbf{I}_M]$$

$[TNB \cdot D_n]$ is neglected in eq. [10] because K_I is large. By rearranging eq. [10], ones gets

$$[11] \quad \frac{1}{[OH_M^-]} = [D_n] \cdot K_I \cdot K_S \frac{[TNB]_0}{[I_M]} - K_I \cdot K_S [D_n] = [D_n] \cdot K_I \cdot K_S \frac{[TNB]_0 \epsilon l}{A_\infty} - K_I \cdot K_S [D_n]$$

Using the same values of K_{OH} and K_{Br}, the calculated values of $[OH_M^-]$ are also shown in Table 3. A plot of $[OH_M^-]^{-1}$ versus A_∞^{-1} gives a straight line as expected if eq. [11] were to be followed. From the slope and intercept of the plot, $\epsilon = 1.65 \times 10^4$ mol^{-1} dm^3 cm^{-1} is obtained. This agrees very well with those of other anionic σ-complexes of TNB (12). To obtain K_I, however, requires a knowledge of K_S. If K_S = 82 mol^{-1} dm^3 is used, $K_I = 1.09 \times 10^5$ mol^{-1} dm^3.

The second-order rate constant calculated by eq. [12] (9)

$$[12] \quad k_2^m \approx 0.14\, k_M$$

is k_2^m = 504 mol^{-1} dm^3 s^{-1}. This in turn yields the reverse rate constant $k'_M = 4.6 \times 10^{-3}$ s^{-1}. The very low value of k'_M thus justifies its omission in the treatment of the rate data described earlier. When the rate constants for the formation of complex **I** in water and those in micelles are compared, it can be seen that the high K_I value is a result of a marked increase in forward rate constant and an even larger decrease in reverse rate constant for the reactions in micelles. These can be rationalized in terms of stabilization of the transition state and the complex **I** in the presence of the positively charged micellar head groups.

While the inadequacies of the pseudophase model with a constant β value have been demonstrated in many systems involving hydroxide ions (9, 15), the equilibrium model for the binding of counterions on the other hand, as has been shown here, has more success as far as kinetic treatment is concerned. A very low value of β (0.3) for the micelles of CTAOH reported recently by Lianos and Zana (16) is in agreement with the finding that K_{OH} is much lower than K_{Br}, thus augmenting the validity of this equilibrium model.

Acknowledgements

The author is grateful to Prof. C. A. Bunton for making this work possible. The author also wishes to thank the University of Malaya for financial support, Vote F33/81 to this study.

1. J. H. FENDLER and E. J. FENDLER. Catalysis in micellar and macromolecular solutions. Academic Press, New York. 1975.
2. E. H. CORDES. Pure Appl. Chem. **50**, 617 (1978).
3. C. A. BUNTON. Catal. Rev. Sci.-Eng. **20**, 1 (1979).
4. C. A. BUNTON and L. S. ROMSTED. *In* Solution behavior of surfactants. *Edited by* E. J. Fendler and K. L. Mittal. Plenum Press, New York. 1981.
5. L. S. ROMSTED. Ph.D. Thesis, Indiana University, 1975.
6. L. S. ROMSTED. *In* Micellization, solubilization and microemulsions. *Edited by* K. L. Mittal. Plenum Press, New York. 1977.
7. C. A. BUNTON, L. S. ROMSTED, and C. THAMAVIT. J. Am. Chem. Soc. **102**, 3900 (1980).
8. H. A. AL-LOHEDAN, C. A. BUNTON, and L. S. ROMSTED. J. Org. Chem. **47**, 3528 (1982).
9. C. A. BUNTON, L. S. ROMSTED, and G. SAVELLI. J. Am. Chem. Soc. **101**, 1253 (1979).
10. C. A. BUNTON, L. H. GAN, J. R. MOFFAT, L. S. ROMSTED, and G. SAVELLI. J. Phys. Chem. **85**, 4118 (1981).
11. C. A. BUNTON, L. H. GAN, and G. SAVELLI. J. Phys. Chem. **87**, 5491 (1983).
12. L. H. GAN and A. R. NORRIS. Can. J. Chem. **49**, 2490 (1971).
13. E. J. FENDLER and J. H. FENDLER. Chem. Commun. 816 (1970).
14. J. H. FENDLER, E. J. FENDLER, and M. V. MERRITT. J. Org. Chem. **36**, 2172 (1971).
15. F. NOME, A. F. RUBLRA, C. FRANCO, and L. G. IONESCU. J. Phys. Chem. **86**, 1881 (1982).
16. P. LIANOS and R. ZANA. J. Phys. Chem. **87**, 1289 (1983).

Preparation and properties of a linked porphyrin–cyclodextrin[1]

MONICA C. GONZALEZ[2] AND ALAN C. WEEDON[3]

Photochemistry Unit, Department of Chemistry, University of Western Ontario, London, Ont., Canada N6A 5B7

Received June 28, 1984

MONICA C. GONZALEZ and ALAN C. WEEDON. Can. J. Chem. **63**, 602 (1985).

The synthesis of the linked porphyrin–cyclodextrin **3** and its zinc complex **4** is described and their characterization by ^{1}H nmr, ^{13}C nmr, circular dichroism, ultraviolet, and infrared spectroscopy is reported. The linked porphyrin–cyclodextrin compounds exhibited perturbed electronic absorption and emission spectra which are consistent with their adopting two conformations, one extended with little interaction between the porphyrin and cyclodextrin, and the other folded with the cyclodextrin weakly complexed to the porphyrin. Quenching of the porphyrin excited state of **3** by benzoquinone was examined by measurement of the fluorescence lifetime as a function of quinone concentration; the results suggest that the porphyrin excited state can be quenched intermolecularly by benzoquinone and also intramolecularly by quinone complexed within the cyclodextrin cavity.

MONICA C. GONZALEZ et ALAN C. WEEDON. Can. J. Chem. **63**, 602 (1985).

On décrit la synthèse du composé **3** (cyclodextrine–porphyrine liées) et de son complexe de zinc (**4**) ainsi que leur caractérisation par les spectroscopies infrarouge, ultraviolette et rmn ^{1}H et ^{13}C ainsi que par leur dichroïsme circulaire. Les composés liés de cyclodextrine–porphyrine présentent des spectres d'absorption et d'émission électronique qui sont perturbés et qui sont en accord avec le fait qu'ils adoptent deux conformations: une étendue, dans laquelle il n'existe que peu d'interactions entre la cyclodextrine et la porphyrine, et une autre repliée, dans laquelle la cyclodextrine est faiblement complexée par la porphyrine. En mesurant le temps de vie de la fluorescence en fonction de la concentration de quinone, on a examiné la réaction de piégeage, par la benzoquinone, de l'état excité de la porphyrine présente dans **3**; les résultats suggèrent que l'état excité de la porphyrine peut être piégé d'une façon intermoléculaire par la benzoquinone et aussi d'une façon intramoléculaire par de la quinone qui est complexée dans la cavité de la cyclodextrine.

[Traduit par le journal]

Introduction

The primary event in the reaction centre of photosynthesis is believed to involve the transfer of an electron from a visible light excited porphyrin chromophore to a nearby acceptor, and there has been considerable recent interest in the synthesis and study of molecules which mimic this photosynthetic reaction (1). These artificial electron transfer systems consist of a donor (usually also the light absorber) chemically linked to an electron acceptor such as a benzoquinone derivative. These compounds have been prepared with the aim of elucidating the effect of degree of separation of donor and acceptor upon the efficiency of the light-induced electron transfer reaction and subsequent back electron transfer (1). Another parameter which would be expected to have an important effect upon this process is the relationship between the oxidation potential of the donor and the reduction potential of the acceptor.

To examine the effect of variation of redox potentials would require the synthesis of a series of compounds in which the oxidation potential of the donor or the reduction potential of the acceptor is systematically varied. The lengthy synthetic effort involved in such a study could be avoided by constructing a system consisting of a donor linked to a moiety capable of complexing potential acceptors; in this way a single molecule could be prepared and the electron transfer efficiency to a large number of acceptors examined. Such a system is shown in structure **3**, which can also be represented as shown in Fig. 1. Structure **3** consists of a tetra-aryl porphyrin chemically linked to a β-cyclodextrin; in Fig. 1 the porphyrin is shown as a disc and the β-cyclodextrin as a truncated hollow cone.

The β-cyclodextrin consists of seven glucose rings joined by α-(1,4)-linkages to form a cylindrical molecule. From one end of the cylinder project the primary hydroxyl groups of the six position of glucose. The secondary hydroxyl groups of the two and three positions of the glucose rings project from the other end of the cylinder. The interior cavity of the β-cyclodextrin ring has been shown capable of complexing a variety of different types of molecule (2).

3 Y=Z=H
4 Y,Z=Zn

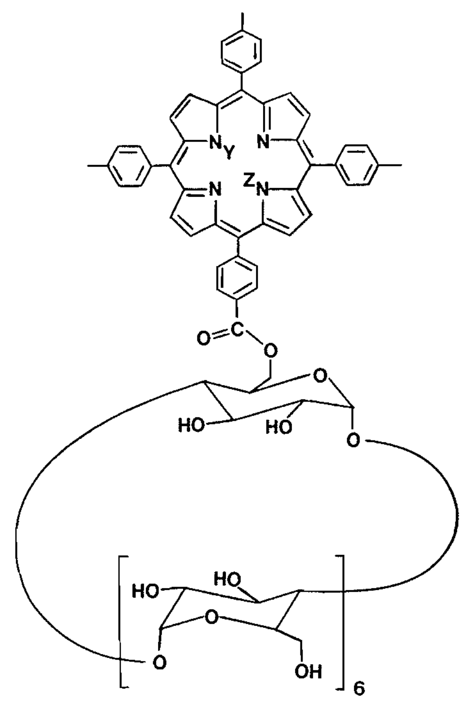

Many functional derivatives of β-cyclodextrin have been described (3), including some involving the attachment of porphyrins (4, 5), but these have not all been well characterized. Described here are the details of the preparation and

[1]Contribution Number 325, The Photochemistry Unit, University of Western Ontario.

[2]Institutio de Investigationes Fisicoquimica Teoricas y Aplicadas, La Plata, Argentina.

[3]Author to whom correspondence may be addressed.

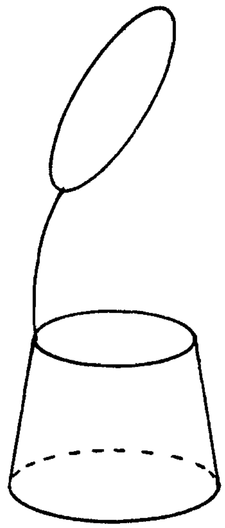

FIG. 1. Schematic representation of structures 3 and 4. The cyclodextrin is shown as a truncated cone, the interior of which is hydrophobic, and the porphyrin is as shown as a disc.

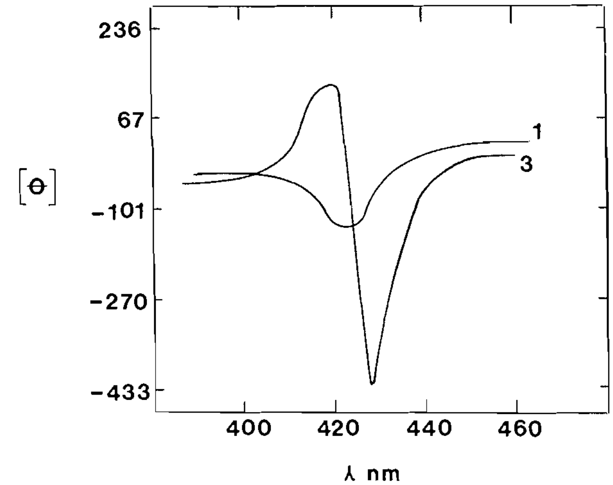

FIG. 2. Circular dichroism spectra of 3 and of 1 in the presence of a 25-fold excess of β-cyclodextrin. The cd spectrum of 1 was unchanged by further addition of β-cyclodextrin. Concentration of 3; 4.65×10^{-6} *M*, concentration of 1; 5.3×10^{-6} *M*.

characterization of the linked porphyrin–cyclodextrin 3 and its zinc derivative **4**.

Results and discussion

Preparation of 3

The linked porphyrin–cyclodextrin 3 was prepared by reaction of excess β-cyclodextrin with the acid chloride 2 in pyridine solution. In order to avoid hydrolysis of 2 under the reaction conditions it was found to be necessary to ensure that the β-cyclodextrin was completely free of water; the β-cyclo-

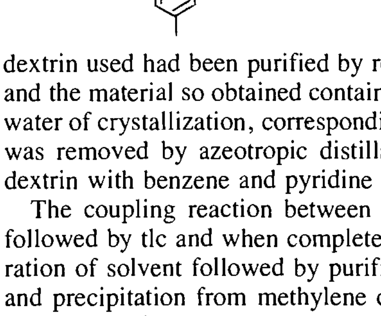

1 X=OH, Y=Z=H
2 X=Cl, Y=Z=H
5 X=OH Y,Z = Zn

dextrin used had been purified by recrystallization from water and the material so obtained contained up to 14% by weight of water of crystallization, corresponding to 90 mol% water. This was removed by azeotropic distillation of predried β-cyclodextrin with benzene and pyridine (see Experimental).

The coupling reaction between **2** and β-cyclodextrin was followed by tlc and when complete was worked up by evaporation of solvent followed by purification by chromatography and precipitation from methylene chloride and pyridine. The product obtained was homogeneous by tlc and gave a satisfactory combustion analysis; as expected for a free base (as opposed to protonated or metallated) porphyrin, it was purple in colour.

The linked compound **3** was completely converted to its zinc complex **4** by treatment with zinc acetate in pyridine, and was isolated by addition of water and purified by precipitation from pyridine–acetonitrile.

Confirmation of structures of 3 and 4

That coupling had occurred between the β-cyclodextrin and the porphyrin was confirmed by infrared spectroscopy. A spectrum of **3** recorded as a KBr disc exhibited bands due to both the β-cyclodextrin and the porphyrin, along with extra peaks at 1720 and 1275 cm^{-1} assignable to the ester function. These usually strong peaks were of only moderate intensity, the major bands being cyclodextrin derived (broad hydroxyl band around 3400 cm^{-1} and several bands assignable to carbon–oxygen single bonds in the 1000–1100 cm^{-1} region). These relative intensities are consistent with the structure of **3** which possesses seven glucose rings (along with their associated hydroxyl groups and ether linkages) for each ester linkage.

The circular dichroism (cd) spectrum of **3** was also recorded. The spectrum is shown in Fig. 2. As might be expected, the inherently achiral porphyrin ring is found to give rise to a weak cd spectrum when chemically attached to a β-cyclodextrin (the latter is constructed from *d*-glucose and so is optically active). This effect could simply be due to the formation of complexes between unlinked β-cyclodextrin and porphyrin; that this was not so was demonstrated by comparing the spectrum obtained from a solution of an unlinked porphyrin (the mono-acid **1**) and a large excess of free β-cyclodextrin (see Fig. 2). In this case no cd spectrum was seen unless large amounts of β-cyclodextrin were present, and even then it was extremely weak and different in appearance compared with the spectrum obtained from **3**. Cyclodextrin-induced circular dichroism has previously been observed for a linked porphyrin–cyclodextrin (4) and also in solutions of porphyrins containing β-cyclodextrin as a cosolute (6).

Benzoylation of β-cyclodextrin, as in the preparation of **3**, could in principle occur either at one of the primary hydroxyl groups or at one of the secondary hydroxyl groups. The primary hydroxyl function would normally be favoured on steric grounds; however, it has been shown that cyclodextrins can undergo selective esterification at a secondary site when esters are used as acyl transfer agents (2, 3). Esterification at a secondary site is thought to proceed by complexation of the alcohol-derived portion of an ester into the cyclodextrin cavity, followed by acyl transfer to one of the cyclodextrin hydroxyls and release of the alcohol produced. This yields the product linked through a secondary alcohol of the cyclodextrin, since the ester is complexed by entry into the opening of the

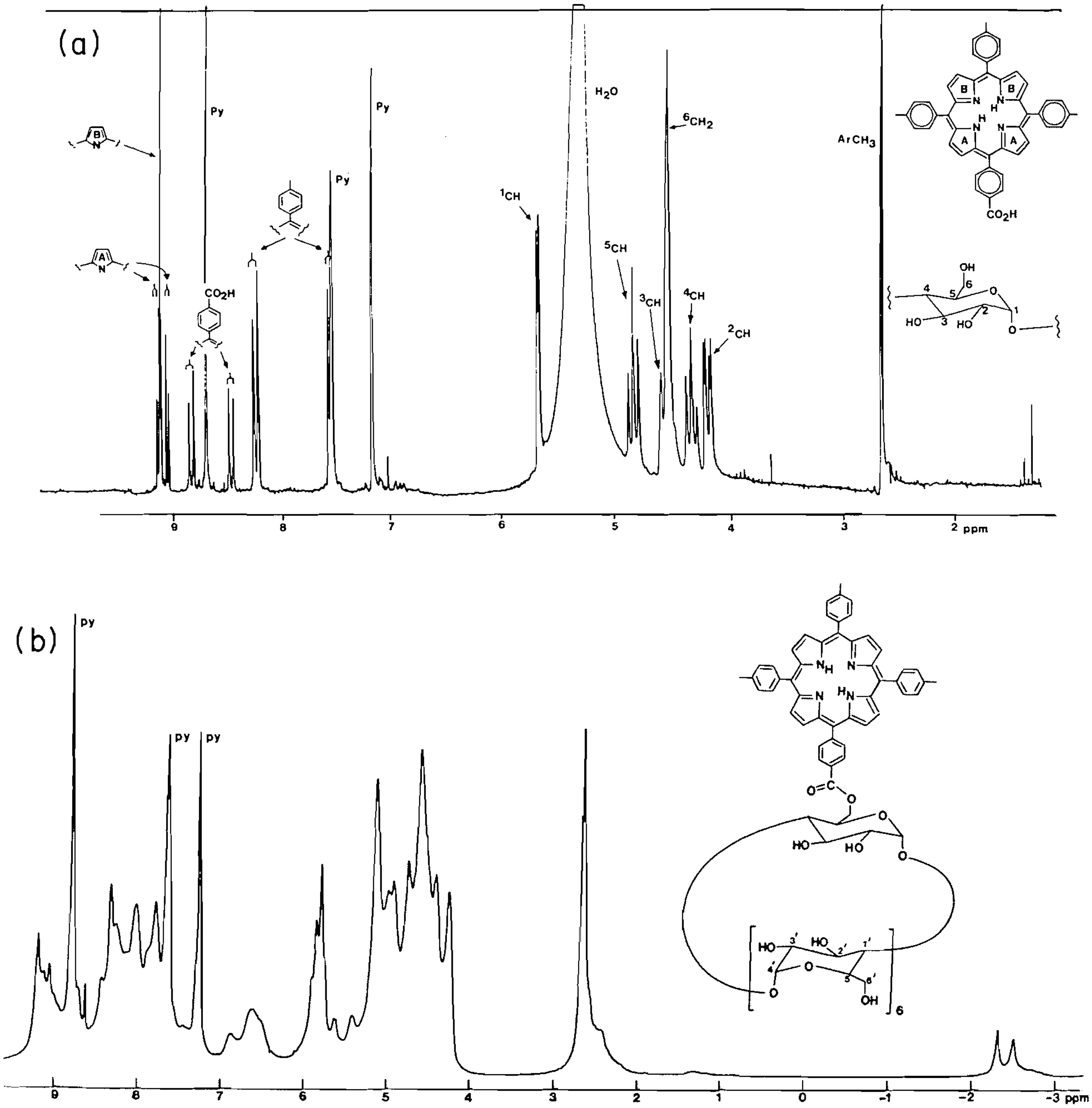

FIG. 3. (a) The [1]H nmr spectrum (200 MHz) of an equimolar mixture of β-cyclodextrin and the porphyrin **1** in pyridine-d_5. (b) The [1]H nmr spectrum (400 MHz) of the linked porpyrin–cyclodextrin **3** in pyridine-d_5.

cyclodextrin cavity bearing the secondary alcohol functions; the primary alcohol functions block the other end of the cyclodextrin (2, 3).

If a complex were formed between cyclodextrin and **2** during the benzoylation reaction, it would be expected to involve insertion of one of the tolyl groups into the cyclodextrin cavity. Under these circumstances the acid chloride function of the porphyrin would be held at a considerable distance from the cyclodextrin hydroxyls and "intramolecular" esterification could not occur. Consequently reaction of the acid chloride **2** with β-cyclodextrin would be expected to yield the product derived from reaction of one of the primary hydroxyl groups. Attempts were made to confirm this by examination of the [1]H nmr spectrum of **3**.

The [1]H nmr spectrum of **3** was compared with that of an equimolar mixture of β-cyclodextrin and **1**. In Fig. 3*a* is shown the spectrum of the mixture of **1** and predried β-cyclodextrin recorded at 200 MHz in pyridine-d_5. Despite the complexity of the molecules, most of the signals can be identified and assignments are made in Fig. 3*a*. The spectrum of β-cyclodextrin has been reported previously (7). In Fig. 3*b* is shown the spectrum of **3** recorded in pyridine-d_5 at 400 MHz, and it is seen to be considerably broadened, presumably because of the non-equivalence of the seven glucose rings of β-cyclodextrin, which in β-cyclodextrin itself are all equivalent. This broadening precludes assignment of the signals to different protons in **3**, particularly those at either C-6 or C-2 and C-3, which would be adjacent to the new ester function were it on a primary or secondary hydroxyl function, respectively.

The site of esterification was eventually determined un-

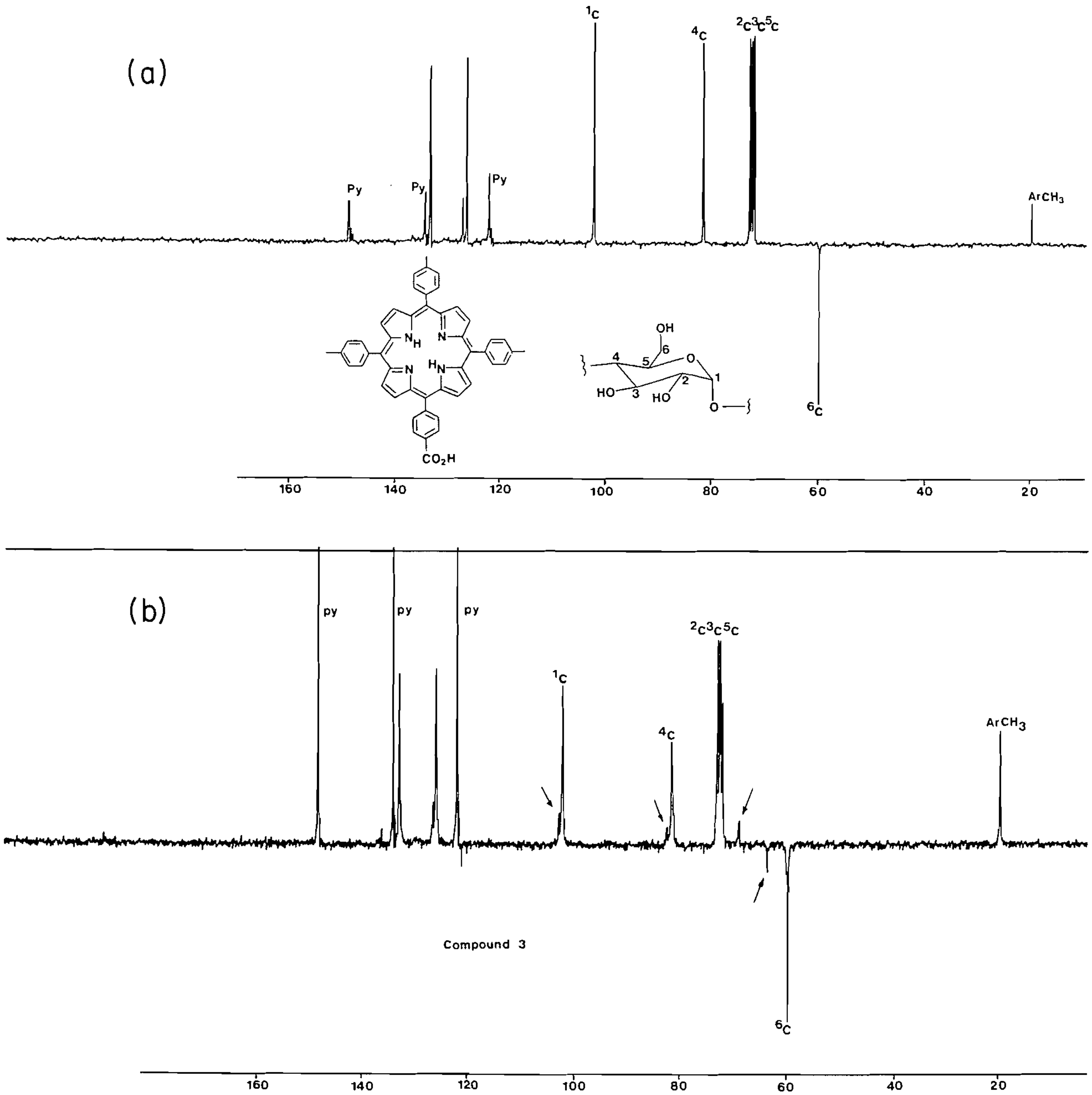

FIG. 4. (a) The ^{13}C nmr spectrum of an equimolar mixture of β-cyclodextrin and porphyrin **1** in pyridine-d_5. (b) The ^{13}C nmr spectrum of the linked porphyrin–cyclodextrin **3** in pyridine-d_5. The signals due to the carbon atoms in the esterified ring of the cyclodextrin are arrowed. The spectra were recorded in the DEPT mode so that methylene signals appear inverted.

ambiguously by the use of ^{13}C nmr spectroscopy. The spectrum of an equimolar mixture of β-cyclodextrin and **1** in pyridine-d_5 is shown in Fig. 4*a*, and that of **3** in Fig. 4*b*. These spectra were recorded using cross polarization so that the quaternary carbons do not appear. As was the case in the ^{1}H nmr spectrum of **3**, slight broadening of some of the signals has occurred due to the nonequivalence of the seven glucose rings of the cyclodextrin. Also, peaks can be seen at 70.7 and 65.4 ppm, of smaller intensity than the rest, corresponding to shifted carbons on the single esterified glucose ring. These signals can be assigned unambiguously to a downfield shifted C-6 carbon and an upfield shifted C-5 carbon respectively, indicating that esterification of the cyclodextrin ring has occurred at the C-6 position. Very slightly downfield shifted peaks corresponding to the C-1 and C-4 carbons of the esterified glucose ring can also be seen. If the benzoylation had occurred at either C-2 or C-3, then no change in C-6 would have been expected and the new signals would have corresponded to shifted C-2 and C-3 carbons. Similar arguments have been used previously to distinguish between 6-tosyl cyclodextrin and the 2-tosyl isomer (8).

Properties of 3 and 4

Neutral free base tetra-aryl porphyrins are usually readily soluble in moderately polar organic solvents such as methylene chloride and insoluble in water, whilst β-cyclodextrin is fairly soluble in water (ca. 3 g/100 mL (2)), dimethylsulphoxide, and pyridine but is insoluble in less polar organic solvents, including methylene chloride. The linked porphyrin–cyclodextrin **3** was totally insoluble in water and methylene chloride

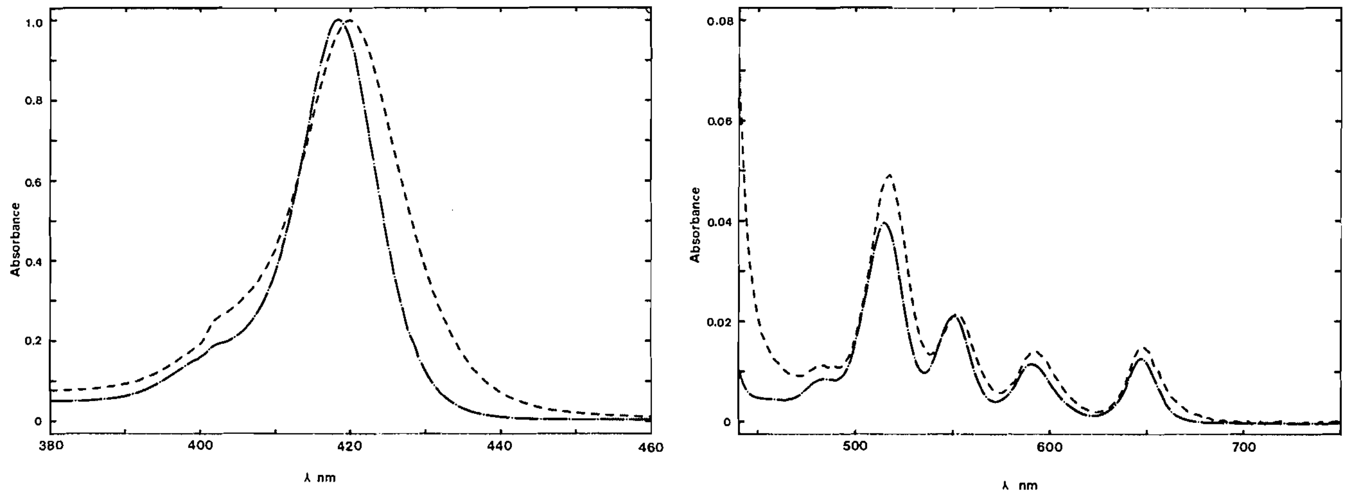

FIG. 5. Ultraviolet/visible absorption spectra of the unlinked porphyrin **1** and the linked porphyrin–cyclodextrin **3** in DMSO. The spectra are normalized at the Soret band maxima (418 nm for **1** and 420 nm for **3**). –•–•–•–• **1**, ----- **3**.

TABLE 1. Fluorescence lifetimes for the linked porphyrin–cyclodextrin **3** and the unlinked porphyrin **1**, and their zinc derivatives **4** and **5**

λ_{ex}[a]	Compound	Lifetime[b]	Ratio[c]
420	3	3.66, 11.0	1.71
440	3	3.29, 10.5	2.9
420, 430	1	11.6	—
420, 430	4	1.89	—
420, 430	5	1.92	—

[a]Excitation wavelengths (nm).
[b]Fluorescence lifetime (ns ± 3%) recorded in dimethylsulphoxide.
[c]Ratio of amplitudes of fluorescence of the short and long lived fluorescent species (A_S/A_L).

but did dissolve quite readily in polar solvents such as dimethylsulphoxide and pyridine.

The electronic absorption spectra of **3** and **4** were recorded and compared with those of the unlinked porphyrin **1** and its zinc derivative **5**. The linked derivative **3** exhibited normal porphyrin absorption bands in the near uv and visible regions, namely the Soret band at 420 nm and the less intense Q bands at 518, 552, 592, and 648 nm. However, these were all slightly red shifted compared with the corresponding bands in the spectrum of the unlinked compound **1** (see Fig. 5). A similar red shift was observed in the spectra of the zinc derivatives of **1** and **3**. Such red shifts have been observed previously in porphyrins attached to benzoquinones and hydroquinones through flexible linkages (1) and were there ascribed to folded conformations of the molecules in which the porphyrin was interacting with the linked species. A similar effect may be occurring in **3** and **4**, and the following results of steady-state fluorescence and fluorescence lifetime measurements support this hypothesis.

Porphyrins fluoresce from the first excited singlet state with moderate efficiency and **1** and **3** were found to be no exception. The spectrum of **1** was independent of the excitation wavelength, whereas that of **3** was not. Excitation at the red end of the Soret band of **3** yielded an emission spectrum which was slightly shifted and broadened relative to the spectrum obtained when excitation was performed at the blue end of the Soret band. The spectrum obtained by excitation of the blue end of the Soret band is similar to that obtained from the unlinked porphyrin **1**. These observations are consistent with the existence of two conformations (or families of conformations) for **3**, one in which the molecule is extended and there is no interaction between the porphyrin chromophore and the cyclodextrin during the excited state lifetime, and one in which the porphyrin and cyclodextrin are interacting in the ground state, resulting in shifted absorption and emission spectra as compared with the unlinked porphyrin **1**.

The fluorescence lifetimes of **1** and **3** reflect this situation (Table 1). When excited by irradiation of the Soret band the unlinked porphyrin **1** exhibited a single fluorescent decay of 11 ns, whereas **3** showed two decays, one of similar magnitude and one much shorter. The contribution of the latter was enlarged as the excitation wavelength was moved to the red edge of the Soret band. It would therefore appear that in the postulated interacting species the interaction results in a shortening of the singlet excited state lifetime, due either to enhancement of the rate of radiationless decay to the ground state or to an increase in the rate of intersystem crossing to the triplet excited state.

Whilst comparison of the absorption and emission spectra of **4** and **5** suggested the same type of interaction as in **3**, the fluorescence lifetimes of **4** and **5** were similar (ca. 2 ns)[4] and no shorter component was seen for **4**, although this may have been present but hidden by the excitation flash.

Inclusion complexes of 3 with benzoquinone

Cyclodextrins form inclusion complexes with hydrophobic compounds in polar media (2). The preferred solvent is water, where the polarity of the solvent and the driving force for complexation in the hydrophobic cavity of the cyclodextrin are maximized. Because of the insolubility of **3** in water, dimethylsulphoxide was chosen as the solvent for studies of the ability of **3** to include benzoquinone. Complexes are known to form between cyclodextrins and hydrophobic compounds in this solvent although the equilibrium constants for complexation are less favourable than when water is the solvent (11).

It had been hoped to study the ability of the linked por-

[4]The shortening of the singlet lifetime resulting from insertion of zinc into the porphyrin may arise from an enhancement of the rate of intersystem crossing. Such a decrease in lifetime is commonly observed when porphyrins are metallated (1).

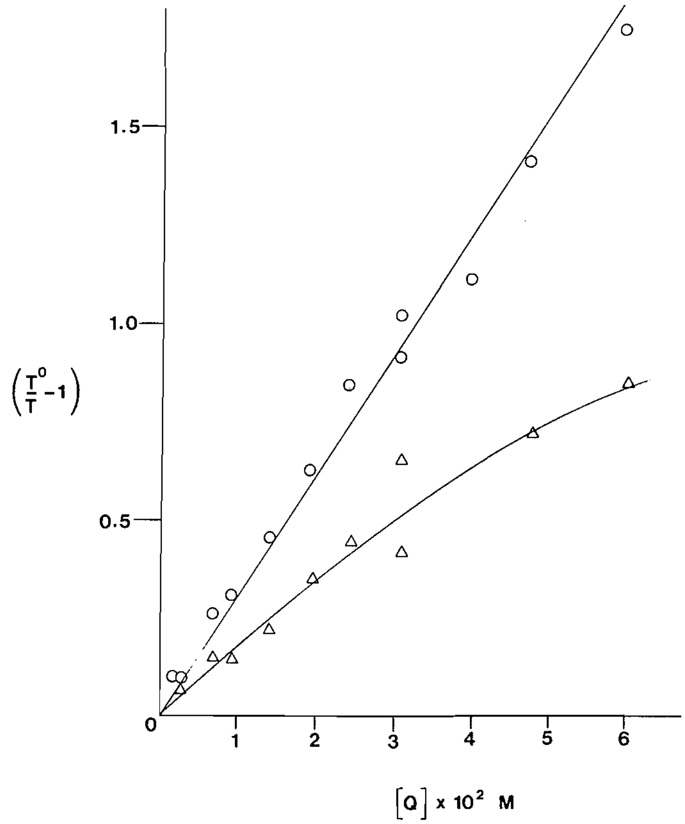

FIG. 6. Stern–Volmer plots for the quenching of the two fluorescent states of **3** by benzoquinone in dimethylsulphoxide at room temperature. [Q] = concentration of benzoquinone; τ = fluorescent lifetime in the presence of quencher; τ^0 = lifetime in the absence of quencher; ○ = long lifetime; △ = short lifetime.

phyrin–cyclodextrin **3** to complex benzoquinone by observation of the ^{1}H nmr and electronic absorption spectra of solutions of the two compounds. However, the complexity and broadness of the nmr spectrum precluded this. When the electronic absorption spectrum of **3** was recorded in the presence of benzoquinone it was found that charge transfer complexation of benzoquinone by the porphyrin was competitive with complexation by the cyclodextrin.[5] This prevents analysis of the complexing ability of the cyclodextrin moiety in **3** by this method. The ability of **3** to complex benzoquinone was, however, successfully demonstrated by observation of the kinetics of electron transfer quenching of porphyrin fluorescence by quinones.

The two fluorescence lifetimes exhibited by **3** were measured in dimethylsulphoxide in the presence of varying amounts of benzoquinone.[6] The results are shown in Fig. 6, where they are plotted to fit the Stern–Volmer expression:

$$\frac{\tau^0}{\tau} - 1 = k_q\tau^0[Q]$$

where τ^0 is the unquenched lifetime, τ is the lifetime in the presence of quencher Q, and k_q is the quenching rate constant. It can be seen that the species giving rise to the longer-lived emission apparently undergoes normal Stern–Volmer quenching. The slope of the line corresponds to the Stern–Volmer constant $k_q\tau$, and taking an unquenched lifetime of 11 ns indicates a quenching rate constant of 2.7×10^9 L M^{-1} s^{-1}. This suggests that quenching of the long-lived porphyrin fluorescence is proceeding intermolecularly at close to the diffusion controlled rate which can be calculated as 3.3×10^9 L M^{-1} s^{-1} in this solvent.[7] The quenching of the species giving rise to the shorter-lived fluorescence appears to occur at a rate of 5×10^9 L M^{-1} s^{-1} (assuming an unquenched lifetime of 3.5 ns) at lower benzoquinone concentrations, but becomes less efficient at benzoquinone concentrations greater than 3×10^{-2} M, causing the line shown in Fig. 6 to depart from linearity. A similar experiment performed with **1** and benzoquinone showed Stern–Volmer quenching of the single emitting species with a rate similar to that of the longer-lived component of **3**, corresponding to normal diffusion controlled intermolecular quenching.

These observations can be understood in terms of different modes of quenching of the two conformations postulated for **3**: in the extended conformation of **3** the porphyrin fluorescent state undergoes diffusional intermolecular quenching only, whereas the interacting conformer (i.e. that in which it is postulated that the porphyrin is folded over the cyclodextrin cavity, resulting in a shorter-lived fluorescence) can undergo intermolecular quenching and, if a benzoquinone molecule is in the cyclodextrin cavity, competitive intramolecular quenching. At high benzoquinone concentrations the cyclodextrin cavity always contains a quinone molecule and subsequent increase in quinone concentration increases the efficiency of intermolecular quenching only, without affecting the efficiency of intramolecular quenching. Consequently the line for quenching the shorter fluorescent state of **3** in Fig. 6 shows downward curvature at high benzoquinone concentrations and the apparent rate constant for diffusional quenching at lower benzoquinone concentrations is greater than the maximum possible rate, viz. the rate of diffusion in this solvent.

The departure from linearity in the quenching of the shorter-lived component shown in Fig. 6 commences when the benzoquinone concentration reaches approximately 3×10^{-2} M; if it is assumed that at this point 90% of **3** contains a quinone in the cyclodextrin cavity, then a very approximate equilibrium constant for complexation of benzoquinone by **3** in dimethylsulphoxide can be calculated, and is found to be of the order of 10 L M^{-1}. This value is comparable to the constants reported elsewhere (11) for complexation by β-cyclodextrin in dimethylsulphoxide.

The quenching of **3** by benzoquinone presumably occurs by an electron transfer process since the alternative process, energy transfer, is endothermic.[8] Studies of the efficiency of the quenching reaction in the presence of quinones of different reduction potential are being made to confirm this and to determine the effect of variation of acceptor reduction potential upon the light-induced electron transfer reaction.

[5]M. C. Gonzalez, J. R. Bolton, and A. C. Weedon, unpublished work.

[6]The ground state complexes referred to in the citation to footnote 4 were non-emissive and so do not interfere with this analysis.

[7]Calculated from the Debye equation, $k = 8RT/3000\eta$, taking the viscosity η of dimethylsulphoxide as 1.996 centipoise at 25°C.

[8]From the absorption spectra of benzoquinone and tetratolyl porphyrin the singlet excited state energies of these compounds can be estimated as approximately 60 kcal/mol and 44 kcal/mol, respectively. This corrsponds to a endothermicity for energy transfer from the singlet excited porphyrin to the quinone of 16 kcal/mol.

TABLE 2. R_f values for the linked porphyrin–cyclodextrin **3** and 5-(*p*-carboxyphenyl)-10,15,20-*p*-tolylporphyrin, **1**, on fluorescor-free silica gel

Compound	Solvent[a] A	B	C
1	0.6	1.0	0.5
3	0.0	0.9	0.3

[a]A: Benzene/pyridine, 1:1; B: 100% pyridine; C: aq. NH_3/nPrOH/EtOAc, 1:1:1.

Experimental

Preparation of the linked porphyrin–cyclodextrin 3

The porphyrin acid chloride, **2**, was prepared from the free acid **1** and thionyl chloride using the published procedure (9). It was found to be important to ensure complete removal of all traces of excess thionyl chloride from the porphyrin **1** for the subsequent reaction with β-cyclodextrin. Failure to do so resulted in the formation of unidentified by-products when **1** was dissolved in pyridine.

β-Cyclodextrin was purchased from the Aldrich Chemical Company, and also from the Sigma Chemical Company, and was dried before use to prevent hydrolysis of the porphyrin acid chloride, **2**, during the coupling reaction. The β-cyclodextrin was purified and dried by the reported methods (10) which required recrystallization from water and drying at 70°C/1 Torr (1 Torr = 133.3 Pa) overnight. The β-cyclodextrin was further dried by distilling a solution of the cyclodextrin in a mixture of dry pyridine and benzene under a nitrogen atmosphere until all of the benzene had been removed and the temperature of the distilling vapours had reached the boiling point of pyridine. The resulting solution was used for the reaction with the porphyrin acid choride **2**.

The porphyrin acid chloride **2** (263 mg) and β-cyclodextrin (a three-fold excess) were stirred together in pyridine under dry nitrogen for 15 h after which time tlc (fluorescor-free silica gel; benzene–pyridine, 1:1) of a sample of the reaction mixture treated with methanol indicated that the acid chloride **2** (observed as the methyl ester) was ca. 95% converted to products. The greater part of the pyridine solvent was removed by distillation under vacuum at 40°C until the product began to precipitate. At this point all porphyrin-containing products were precipitated by addition of water. The solids were washed with water (to remove excess β-cyclodextrin) and dried under vacuum at 40°C.

The dried precipitate was redissolved in a small volume of pyridine and the linked porphyrin–cyclodextrin was precipitated and so separated from other porphyrins by addition of methylene chloride. The precipitated linked compound was chromatographed on a column of silica gel using pyridine was eluent. The major fraction was filtered and concentrated under vacuum; addition of methylene chloride gave a purple precipitate of the linked porphyrin–cyclodextrin **3** which was dried under vacuum at room temperature. The yields obtained by this route were 40–50%.

The linked compound was homogeneous by tlc on fluorescor-free silica gel (see Table 2); however, attempts to obtain a satisfactory combustion analysis were frustrated by the apparent ability of **3** to complex solvent into the cyclodextrin cavity. Analyses were obtained corresponding to **3** containing non-integral numbers of pyridine molecules. Eventually, prolonged drying under vacuum at room temperature gave a sample which had C 59.23%, H 5.48%: $C_{90}H_{104}N_4O_{36}$ requires C 59.47, H 5.77%. The linked compound **3** had: ir (KBr disc): 3400 (s, br), 2920 (m), 1720 (m), 1635 (w), 1610 (w), 1275 (m), 1160 (s), 1080 (s), 1030 (vs), 800 (m), 700 (m) cm^{-1}; uv/vis (DMSO): 420 ($\epsilon = 3.08 \times 10^5$), 518 ($\epsilon = 1.63 \times 10^4$), 552 ($\epsilon = 7.51 \times 10^3$), 592 ($\epsilon = 4.94 \times 10^3$), 648 ($\epsilon = 4.97 \times 10^3$) (see Fig. 5). The ^1H nmr spectrum of **3** is shown in Fig. 3; ^{13}C nmr (pyridine-d_5): 21.3 (CH_3), 61.5 (CH_2), 65.4 (CH_2, approximately 1/6 the intensity of the signal at 61.5 ppm), 70.7 (CH, approximately 1/6 the intensity of the signal at 73.9 ppm), 73.9 (CH), 74.3 (CH), 74.7 (CH), 83.3 (CH), 104.0 (CH), 128.0 (CH), 134.9 (CH) ppm (see Fig. 4); cd ($c = 4.65 \times 10^{-6}$ *M*, DMSO, 25°C): $[\theta]_{445}$ 0, $[\theta]_{427}$ −438.4, $[\theta]_{421}$ 0, $[\theta]_{416}$ +168, $[\theta]_{400}$ 0 (see Fig. 2).

Preparation of the zinc complex of 3 (4)

The linked porphyrin–cyclodextrin **3** (50 mg) was dissolved in pyridine (10 mL) along with a 50% excess of anhydrous zinc acetate and the mixture was stirred at room temperature in the dark. The electronic absorption spectra of aliquots of the mixture were monitored to follow the reaction (upon metallation the free porphyrin absorption at 518 nm is shifted to 562 nm) and this indicated complete conversion after 20 h. The major part of the pyridine was removed under vacuum at room temperature and excess water was added to the residue to precipitate the porphyrin-containing products. The solid obtained was vacuum dried and redissolved in the minimum of pyridine; addition of acetonitrile induced deposition of **4**, which was homogeneous by tlc (benzene/pyridine, 1:3). For **4**: uv/vis, (DMSO): 430 ($\epsilon = 3.8 \times 10^5$), 522 ($\epsilon = 3.9 \times 10^3$), 562 ($\epsilon = 1.61 \times 10^4$), 602 ($\epsilon = 8.5 \times 10^3$) nm (see Fig. 5); cd ($c = 2.88 \times 10^{-6}$ *M*, DMSO, 25°C): $[\theta]_{450}$ 0, $[\theta]_{434}$ −253, $[\theta]_{420}$ 0; Γ = 12 nm.

Fluorescence lifetime measurements

Fluorescence lifetime measurements were performed on a Photochemical Research Associates Model 300 nanosecond lifetime fluorimeter by the method of time-correlated single photon counting. The measurements were made at room temperature on solutions of concentration $10^{-5} - 10^{-6}$ *M*; the fluorescence lifetimes were independent of concentration over the range $10^{-4} - 10^{-7}$ *M*.

Acknowledgements

Financial support for this project was received from the Natural Sciences and Engineering Research Council of Canada through a Strategic Grant in Energy to A.C.W. (with J. R. Bolton). The government of Argentina is thanked for a fellowship (to M.C.G.). We also thank Mr. David Wong and Mr. John Coccimiglio for technical assistance during the early part of the work, and Dr. J. B. Stothers for recording the ^{13}C nmr spectra. The cd spectra were recorded with the assistance of Dr. M. J. Stillman and his group.

1. T.-F. Ho, A. R. McIntosh, and A. C. Weedon. Can. J. Chem. **62**, 967 (1984); A. R. McIntosh, A. Siemiarczuk, J. R. Bolton, M. J. Stillman, T.-F. Ho, and A. C. Weedon. J. Am. Chem. Soc. **105**, 7215 (1983); A. Siemiarczuk, A. R. McIntosh, T.-F. Ho, M. J. Stillman, K. J. Roach, A. C. Weedon, J. R. Bolton, and J. S. Connolly. J. Am. Chem. Soc. **105**, 7224 (1983), and references therein.
2. M. L. Bender, and M. Komiyama. Cyclodextrin chemistry. Springer, Berlin. 1978; J. Szejtli. Cyclodextrins and their inclusion complexes. Akademiai Kiado, Budapest. 1982.
3. A. P. Croft and R. A. Bartsch. Tetrahedron Report Number 147, Tetrahedron, **39**, 1417 (1983).
4. N. Kobayashi, U. Akiba, K. Takatori, A. Ueno, and T. Osa. Heterocycles, **19**, 2011 (1982).
5. R. L. Wife, D. E. Creed, and H. C. Volger. Cyclodextrin derivatisation: directed reaction of silylated intermediates. *In* Proceedings of the First International Symposium on Cyclodextrins. *Edited by* J. Szejtli. Reidel Publishing Co., Dordrecht. 1981. p. 289.
6. H. Hirai, N. Toshima, S. Hayashi, and Y. Fujuii. Chem. Lett. 643 (1983).
7. M. Vincendon. Bull. Soc. Chim. Fr. II-129 (1981).
8. A. Ueno and R. Breslow. Tetrahedron Lett. **23**, 3451 (1982).
9. J. L. Y. Kong and P. A. Loach. J. Heterocycl. Chem. **17**, 737 (1980).
10. D. French, M. L. Levine, J. H. Pazur, and E. Norberg. J. Am. Chem. Soc. **71**, 353 (1949).
11. B. Siegel and R. Breslow. J. Am. Chem. Soc. **97**, 6869 (1975).

Structure and fragmentation of $C_5H_{11}O^+$ ions formed by chemical ionization

JOHN V. HEADLEY[1] AND ALEX. G. HARRISON
Department of Chemistry, University of Toronto, Toronto, Ont., Canada M5S 1A1

Received May 30, 1984

JOHN V. HEADLEY and ALEX. G. HARRISON. Can. J. Chem. **63**, 609 (1985).

The proton transfer chemical ionization mass spectra of eleven $C_5H_{10}O$ isomers have been obtained using H_3^+, N_2H^+, HCO^+, and D_3^+ as reagent ions. The chemical ionization mass spectra in combination with isotopic labelling and metastable ion studies have made it possible to elucidate the major fragmentation reaction channels of the $C_5H_{11}O^+$ ions formed and their dependence on precursor structure. From collision induced dissociation studies nine stable distinct $C_5H_{11}O^+$ ion structures have been identified; protonated 3-methylbutanone and protonated 2,2-dimethylpropanal readily interconvert by a pinacolic – retro-pinacolic rearrangement.

JOHN V. HEADLEY et ALEX. G. HARRISON. Can. J. Chem. **63**, 609 (1985).

Utilisant les ions H_3^+, N_2H^+, HCO^+ et D_3^+ comme ions réactifs, on a examiné les spectres de masse par ionisation chimique des transferts de protons de onze isomères $C_5H_{10}O$. En combinant les spectres de masse par ionisation chimique avec des études de marquage isotopique et d'ions métastables, on a pu élucider les principales voies de fragmentations des ions $C_5H_{11}O^+$ formés ainsi que leurs dépendances sur la structure de leurs précurseurs. En se basant sur des études de dissociations induites par des collisions, on a pu identifier neuf structures stables distinctes de l'ion $C_5H_{11}O^+$; la méthyl-3 butanone protonée et le diméthyl-2,2 propanal protoné se transforment facilement l'un dans l'autre par le biais d'une transposition pinacolique/rétropinacolique.

[Traduit par le journal]

Introduction

The $C_nH_{2n+1}O^+$ ions are abundant fragment ions in the electron impact mass spectra of aliphatic alcohols and ethers (1) and, because of their widespread occurrence, have received extensive study with respect to their thermochemistry, structures, and unimolecular fragmentation reactions. The thermochemistry of the lower members of the series (up to C_4) is well established as a result of the elegant work of Lossing (2). The structures and low energy (metastable) unimolecular fragmentation reactions of the $C_2H_5O^+$, $C_3H_7O^+$, and $C_4H_9O^+$ ions formed by electron impact have been studied exhaustively by many groups and are now well understood (for a review and summary of these studies see ref. 3). Indeed, the study of these systems played a large role in the development of the potential energy profile approach (4–6) to the interpretation of the low energy unimolecular chemistry of isolated gaseous organic ions. The $C_nH_{2n+1}O^+$ ions also can be prepared by proton transfer chemical ionization of carbonyl compounds and cyclic ethers and, recently, the chemistry of the $C_3H_7O^+$ ions (7, 8) and $C_4H_9O^+$ ions (9) formed by proton transfer chemical ionization have been studied in detail and interpreted in terms of the potential energy profiles established from the earlier EI studies. In this chemical ionization approach a number of structures, such as protonated cyclic ethers inaccessible by electron impact methods, become available for study.

In contrast to the extensive studies of the lower members of the series, the higher members of the $C_nH_{2n+1}O^+$ series have received much less attention. McLafferty and Sakai (10) have reported the collision-induced dissociation (CID) mass spectra of a few $C_5H_{11}O^+$ ions, while Zahorszky (11) has surveyed briefly the unimolecular ion chemistry of higher members of the series. The most extensive study has been that of Audier *et al.* (12) of the $C_5H_{11}O^+$ ions of nominal structures **1** to **7** (Scheme 1) prepared by electron impact methods. They studied not only the unimolecular metastable ion chemistry but also the CID mass spectra, and were able to show that all the ions

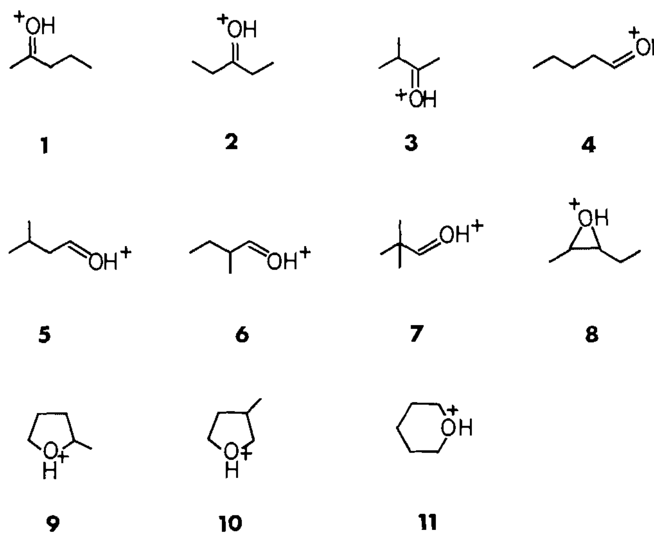

SCHEME 1

except **3** and **7** gave distinct CID mass spectra indicating single structures or mixtures of structures; structures prepared initially as **3** and **7** gave identical CID mass spectra and it was concluded that these two ions interconverted freely by way of pinacolic – retro-pinacolic rearrangements. Using deuterium isotopic labelling for a number of the species, they delineated a number of the metastable isomerization and fragmentation mechanisms and proposed detailed reaction pathways. Their work will be discussed later in relation to the results obtained in the present study, which reports an extensive investigation of the $C_5H_{11}O^+$ ions of nominal structures **1** to **11** (Scheme 1) prepared by proton transfer chemical ionization. The present study consisted of three parts: first, a study of the proton transfer chemical ionization (CI) mass spectra using H_3^+, N_2H^+, and HCO^+ as reagent ions to examine the higher energy fragmentation reactions of $C_5H_{11}O^+$ ions and their dependence on internal energy; second, collision-induced dissociation (CID) studies to characterize the structures of non-decomposing $C_5H_{11}O^+$ ions; and, third, the use of isotopic labelling in conjunction

[1] Present Address: Alberta Environment Centre, Vegreville, Alberta.

TABLE 1. H_2 chemical ionization mass spectra of $C_5H_{10}O$ isomers

Isomer		m/z 87 $C_5H_{11}O^+$	85 $C_5H_9O^+$	71 $C_4H_7O^+$	69 $C_5H_9^+$	57 $C_3H_5O^+/C_4H_9^+$	45 $C_2H_5O^+$	43 $C_2H_3O^+/C_3H_7^+$	41 $C_3H_5^+$
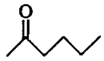	**1**	35	8	9	13	7	100	64	10
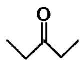	**2**	10	2	—	22	30	100	18	14
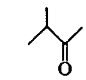	**3**	35	2	8	100	6	44	53	22
	**4**	9	11	2	79	35	18	43	100
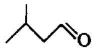	**5**	17	7	6	43	28	41	100	25
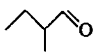	**6**	17	4	—	38	37	100	35	26
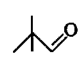	**7**	18	2	6	100	30	46	23	31
	**8**	9	2	2	11	15	100	27	32
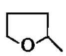	**9**	18	57	46	85	28	20	42	100
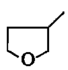	**10**	18	100	6	53	54	47	36	95
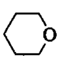	**11**	16	79	1	62	43	21	21	100

with CI mass spectra and metastable ion studies to obtain information on detailed fragmentation reaction pathways. In part, the present study serves to confirm and extend the results obtained in the earlier EI study (12) and, in part, it provides the opportunity to compare the metastable reactions of ions prepared by chemical ionization and electron impact methods. As Holmes and Terlouw (13) have pointed out, there have been relatively few studies of metastable ion fragmentation reactions following chemical ionization.

Experimental

The chemical ionization mass spectra were obtained using a DuPont 21-490 mass spectrometer equipped with a high pressure chemical ionization source. The source temperature was ~100°C and the ionizing electron energy 70 eV, with the repellers at cage potential. The liquid samples were introduced through a heated inlet system held at ~100°C. Reagent gas pressures were not measured directly but were estimated to be 0.2 to 0.3 Torr (1 Torr = 133.3 Pa). The H_3^+ and D_3^+ reactant ions were produced by electron impact ionization of H_2 and D_2, respectively, at high pressure, while the N_2H^+ and HCO^+ reagent ions were prepared by electron impact ionization of the appropriate gas X (10%) in H_2 as described previously (7, 14).

Unimolecular (metastable) fragmentation reactions of the $C_5H_{11}O^+$ ions and deuterated analogues (formed by CH_4 or CD_4 chemical ionization) were recorded for fragmentation reactions occurring in the second drift region (between the magnetic and electric sectors) of a ZAB-2F mass spectrometer (University of Ottawa) using the MIKES (mass analyzed ion kinetic energy spectroscopy) technique. In this technique the ion of interest is selected by adjusting the magnetic field and undergoes fragmentation in the drift region (either unimolecular or, on addition of a collision gas, collision induced) with the fragmentation products being selected and identified according to their kinetic energy by scanning the voltage on the electric sector. The kinetic energy releases associated with the metastable fragmentation reactions, evaluated as $T_{1/2}$, were obtained from the peak widths after correction for the main beam width according to the relation (13): $\omega_{corr} = (\omega^2_{met} - \omega^2_{main\ beam})^{1/2}$. The collision-induced dissociation (CID) mass spectra were obtained by the MIKES technique with the ZAB-2F instrument using helium gas; the helium was admitted to the collision cell to reduce the main beam intensity to 50%. Source temperatures for the ZAB experiments were ~150°C and the ion accelerating potential was 8 keV.

Chemical ionization reagent gases were of the highest possible purity while the $C_5H_{10}O$ compounds were commercial samples of high purity. The majority of the labelled compounds were prepared by base-catalyzed exchange of the appropriate carbonyl compound with D_2O. The syntheses of 2-pentanone-1,1,1-d_3 and 2-pentanone-5,5,5-d_3 have been described previously (15). Final purification was by gas chromatography.

Results and discussion

Unimolecular ion chemistry

The proton transfer chemical ionization mass spectra of the eleven $C_5H_{10}O$ isomers studied are presented in Tables 1 to 4 for the reagent ions H_3^+, N_2H^+, HCO^+, and D_3^+ respectively. The results clearly indicate that the following fragmentation reactions of the $C_5H_{11}O^+$ ion are occurring:

$$[1]\quad C_5H_{11}O^+ \xrightarrow{-CH_4} C_4H_7O^+\ (m/z\ 71)$$

$$[2]\quad \xrightarrow{-H_2O} C_5H_9^+\ (m/z\ 69)$$

$$[3]\quad \xrightarrow{-C_2H_4} C_3H_5^+\ (m/z\ 41)$$

TABLE 2. N_2/H_2 chemical ionization mass spectra of $C_5H_{10}O$ isomers

Isomer		*m/z* 87 $C_5H_{11}O^+$	85 $C_5H_9O^+$	71 $C_4H_7O^+$	69 $C_5H_9^+$	57 $C_3H_5O^+/C_4H_9^+$	45 $C_2H_5O^+$	43 $C_2H_3O^+/C_3H_7^+$	41 $C_3H_5^+$
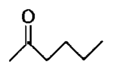	**1**	38	1	4	18	4	100	46	10
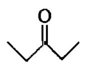	**2**	36	1	—	33	28	100	11	4
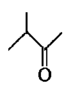	**3**	100	—	5	78	3	32	56	18
	**4**	6	4	1	100	5	8	13	24
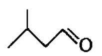	**5**	17	4	5	54	11	43	100	30
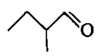	**6**	23	2	1	36	19	100	18	9
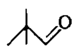	**7**	53	3	1	100	40	62	12	12
	**8**	10	2	3	2	11	100	19	17
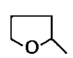	**9**	7	18	23	100	9	12	15	37
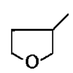	**10**	9	34	4	100	30	24	17	52
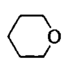	**11**	5	37	—	100	17	12	6	41

[4] $\xrightarrow{-CH_2O/C_2H_6} C_4H_9^+/C_3H_5O^+$ (*m/z* 57)

[5] $\xrightarrow{-C_3H_6} C_2H_5O^+$ (*m/z* 45)

[6] $\xrightarrow{-C_3H_8/C_2H_4O} C_2H_3O^+/C_3H_7^+$ (*m/z* 43)

In two cases, reactions [4] and [6], we cannot distinguish between two possible compositions of the fragment ion observed and it appears that the elemental composition of these ions depends on the molecule involved. The CI mass spectrum of $CH_3CD_2COCD_2CH_3$ showed that the *m/z* 57 ion (reaction [4]) shifted cleanly to *m/z* 59, while the D_2CI mass spectrum (Table 4) showed that the added proton was not contained in the ion. Thus we conclude that in this case the ion is the acyl ion $C_2H_5C{\equiv}O^+$; on the other hand, it is possible that for 2,2-dimethyl propanal (ion **7**) the *m/z* 57 fragment is $C_4H_9^+$. Similarily the CI mass spectra of $CD_3COCH_2CH_2CH_3$ and $CD_3COCH(CH_3)_2$ showed that the *m/z* 43 fragment (reaction [6]) largely incorporated the Cl methyl and is the acyl ion $CH_3{-}C{\equiv}O^+$, while for 3-methyl pentanal (ion **5**) the ion appears to be largely $C_3H_7^+$ (essentially no shift in the CI mass spectrum of $(CH_3)_2CHCD_2CHO$ or in the D_2CI mass spectrum). In other cases the elemental composition of these ions is not known. Reaction [1] and that part of reaction [4] leading to formation of $C_3H_5O^+$ may occur either by elimination of CH_4 or C_2H_6, respectively, from MH^+ or may occur by direct alkide ion abstraction; the CID spectra (see below) indicate that elimination of neutral alkanes is a significant reaction channel for decomposition of activated $C_5H_{11}O^+$ ions. The $(M - H)^+$ ion (*m/z* 85) is of low abundance except for the cyclic ethers where it becomes a major ion in the CI mass spectra. This product does not contain the added proton (see the D_2 CI mass spectra) and may arise primarily by direct hydride abstraction. The $C_3H_5^+$ ion is assumed to arise by fragmentation of $C_5H_9^+$ (*m/z* 69, $MH^+ - H_2O$); interestingly, this fragmentation reaction seems to be much more facile for the $C_5H_9^+$ ions arising from **4**, **9**, **10**, and **11** than for the $C_5H_9^+$ ions arising from **3** and **7**.

The H_2 CI mass spectra permit a distinction to be made between the eleven compounds studied, with the possible exception of 3-methyl tetrahydrofuran and tetrahydropyran (ions **10** and **11**) where the CI mass spectra are quite similar. Ions **1**, **2**, **6**, and **8** show reaction [5] as the major fragmentation channel while ions **3**, **4**, **7**, **9**, **10**, and **11** show $C_5H_9^+$ as the dominant fragment ion. In the H_2 CI mass spectrum, ion **5** shows $C_3H_7^+$ as the base peak (reaction [6]) although reaction [2] becomes the major reaction channel as the protonation exothermicity decreases from H_3^+ to CHO^+. As expected, the total extent of fragmentation decreases as the protonation exothermicity decreases.

In agreement with the EI study of ions **1** to **7** (12), only two metastable fragmentation reactions of $C_5H_{11}O^+$ ions were observed, corresponding to elimination of H_2O (reaction [2]) and elimination of C_3H_6 (reaction [5]). Table 5 records the intensity ratio $(C_5H_9^+ + C_3H_5^+)/C_2H_5O^+$ observed in the CI mass spectra and in the metastable ion mass spectra following both CI and EI ionization; this ratio represents the relative importance of fragmentation reactions [2] and [5] for the ions studied. The enthalpy of formation of $C_5H_9^+ + H_2O$ (~527 kJ mol^{-1}) is

TABLE 3. CO/H_2 chemical ionization mass spectra of $C_5H_{10}O$ isomers

Isomer		87 $C_5H_{11}O^+$	85 $C_5H_9O^+$	71 $C_4H_7O^+$	69 $C_5H_9^+$	57 $C_3H_5O^+/C_4H_9^+$	45 $C_2H_5O^+$	43 $C_2H_3O^+/C_3H_7^+$	41 $C_3H_5^+$
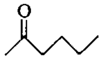	**1**	100	1	4	5	2	24	39	1
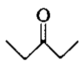	**2**	100	—	—	6	32	16	2	1
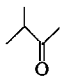	**3**	100	—	3	6	1	2	31	3
	**4**	20	2	1	100	7	4	6	9
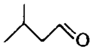	**5**	29	3	4	100	9	23	30	12
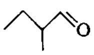	**6**	76	3	2	47	15	100	12	8
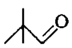	**7**	100	1	1	24	17	10	10	9
	**8**	80	1	2	24	5	100	14	12
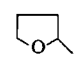	**9**	12	11	13	100	2	5	14	12
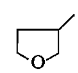	**10**	24	21	2	100	15	8	5	37
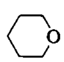	**11**	25	20	—	100	6	7	3	27

(Column values are m/z.)

TABLE 4. D_2 Chemical ionization mass spectra of $C_5H_{10}O$ isomers

m/z	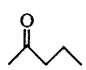 **1**	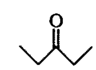 **2**	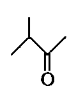 **3**	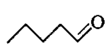 **4**	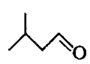 **5**	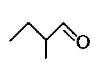 **6**	 **7**	 **8**	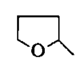 **9**	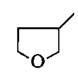 **10**	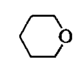 **11**
88	12	13	23	4	5	21	26	2	3	5	5
87	7	5	6	9	11	37	25	3	7	13	14
85	1	1	2	13	6	3	1	2	62	97	95
71	9	—	7	3	6	—	2	2	51	5	2
70	3	9	15	15	11	6	11	—	19	13	12
69	17	33	100	100	26	31	100	9	95	66	74
58	6	16	4	23	12	21	5	9	24	33	26
57	1	29	3	12	10	14	17	8	12	32	19
46	100	100	37	14	30	100	47	100	14	30	9
45	20	22	7	5	9	32	9	32	10	6	11
44	8	10	5	16	21	10	6	8	10	8	4
43	43	11	35	37	100	25	20	25	30	31	15
42	2	4	3	9	3	4	5	10	25	15	12
41	8	12	15	72	16	23	30	32	100	100	100

significantly less than that of $CH_3CHOH^+ + C_3H_6$ (~602 kJ mol^{-1}) yet both fragmentation reactions are observed as metastable ions (for the thermochemical data, see the Appendix). On the other hand $\Sigma\Delta H_f^0(CH_3C{\equiv}O^+ + C_3H_8) \approx 557$ kJ mol^{-1}, yet this reaction is not observed as a metastable fragmentation reaction even for ions such as **1** and **3** where the ion is observed in the CI mass spectra. Presumably the critical reaction energy for formation of $CH_3C{\equiv}O^+ + C_3H_8$ must be considerably higher than the reaction endothermicity. The fact that both reactions [2] and [5] are observed for metastable ions must mean that the critical reaction energies are similar despite the lower reaction endothermicity for reaction [2]. The ratio $(C_5H_9^+ + C_3H_5^+)/C_2H_5O^+$ increases with decreasing mean internal energy (Table 5), particularly for those ions which show reaction [2] as the major reaction channel. This is consistent with reaction [2] having both a lower critical reaction energy and a lower frequency factor. It should also be noted that the intensity ratio is larger for the metastable ions gener-

TABLE 5. Ratio of H_2O vs. C_3H_6 loss from $C_5H_{11}O^+$ ions

Ion	H_2 CI	N_2/H_2 CI	CO/H_2 CI	m^* (CI)	m^* (EI)[a]
1	0.23	0.28	0.25	0.48	0.63
2	0.36	0.37	0.44	0.76	1.05
3	2.8	3.0	4.5	5.6	7.1
4	9.9	15.5	27.3	22.2	~100
5	1.7	2.0	4.9	3.2	~10
6	0.64	0.45	0.55	1.4	2.5
7	2.9	1.8	3.3	4.8	6.7
8	0.43	0.19	0.36	0.69	—
9	9.3	11.4	22.4	100	—
10	3.2	6.3	17.1	20	—
11	7.7	11.8	18.1	100	—

[a] From ref. 12.

ated by EI than for the ions generated by CI. This is in agreement with earlier conclusions (8) that metastable ions generated by CI have a higher mean internal energy than the same ions generated by EI methods. The kinetic energy releases ($T_{1/2}$) for metastable loss of H_2O were essentially invariant (26 ± 5 meV) for all $C_5H_{11}O^+$ structures, as were the $T_{1/2}$ values (22 ± 4 meV) for metastable elimination of C_3H_6. No distinction between ion structures can be made on this basis. In passing, we would note that our $T_{1/2}$ results for **1** to **7** are in reasonable agreement with the $T_{22\%}$ data of Audier *et al.* (12) but not in agreement with their $T_{50\%}$ data, which are more than two times larger.

Characterization of $C_5H_{11}O^+$ ion structures

The comparison of the collision-induced dissociation (CID) mass spectra of gaseous ions has proven (16, 17) to be an extremely useful method for characterizing and comparing the structures of such ions. Accordingly we have obtained the CID mass spectra of the ions of nominal structures **1** to **11** with the results tabulated in Tables 6 and 7 (m/z 69 and m/z 45, which may have unimolecular contributions, are not included in this tabulation). The results obtained for **1** to **7** are in good agreement with those reported earlier (12).

The $C_5H_{11}O^+$ ions can be classified in terms of the base peak observed in the CID mass spectrum. Thus, the ions **1**, **3**, **5**, **7**, and **8** (the first five entries in Table 6) have m/z 43 as the base peak, while **2** (entry six, Table 6) has m/z 57 as the base peak and **6** (entry seven, Table 6) shows m/z 43 and m/z 57 at almost equal intensity. The remaining ions **4**, **9**, **10**, and **11** (Table 7) show m/z 41 as the base peak in the CID mass spectra.

Within the first group (m/z 43 base peak) **1** and **8** are clearly distinguishable from **3**, **5**, and **7** by the relative intensities at m/z 58, while **1** and **8** are distinguishable from each other by the m/z 59, 57, and 42 ion intensities. Structure **5** is distinguished from **3** and **7** by the relative intensities of the ion signals at m/z 71, 57, 44, and 42. On the other hand, **3** and **7** have very similar CID mass spectra and cannot be distinguished. This similarity has been interpreted by Audier *et al.* (12) in terms of a facile interconversion of **3** and **7** by the pinacolic – retro-pinacolic rearrangment outlined in Scheme 2. Thus, in this case, the collisional activation process samples the same mixture of ion structures whether we start with **3** or **7**. (Further evidence for this interchange comes from the isotopic labelling results discussed below.)

A similar type of rearrangement could lead to interconversion of **1**, **2**, and **6** (Scheme 3). However, it is clear from

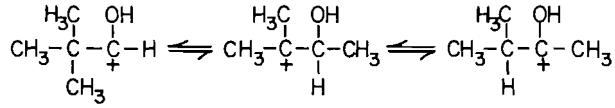

7 **3**

SCHEME 2

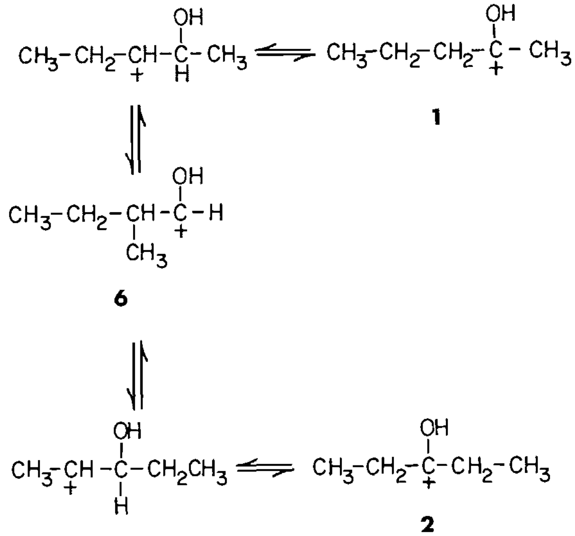

SCHEME 3

the results in Table 6 that the collisional activation process is not sampling the same (equilibrium) mixture of structures in the three systems; in particular, the CID spectrum of **6** cannot be reproduced by a linear combination of the spectra of **1** and **2**. We conclude that **1**, **2**, and **6** are stable species existing in potential wells, although we cannot discount some interconversion. The fragmentation reactions of **6**, particularly the formation of CH_3CHOH^+, are more readily rationalized if we allow the isomerizations of Scheme 3. Similarly, the formation of $CH_3CH{=}OH^+$ from **2** obviously requires skeletal isomerization which may occur as outlined in Scheme 3.

Alternatively, it is possible that the ions of nominal structures **1**, **2**, and **8** interconvert through the rearrangements outlined in Scheme 4. However, once again the results indicate that we are not dealing with the same mixture of structures in the CID process and, in particular, that the spectrum of **8** is not a linear combination of the spectra of **1** and **2**. Consequently, we conclude that **8** also erpresents a stable ion, although rearrangement to **1** or **2** probably occurs prior to fragmentation.

The ions **4**, **9**, **10**, and **11** all show m/z 41 ($C_3H_5^+$) as the base peak in their CID mass spectra (Table 7). The structure **4** is clearly distinct from **9** to **11** while the latter three show substantial differences in the m/z 67–72 and m/z 56–59 regions which indicate different structures for the three ions.

In summary, the CID results indicate that the ions of nominal structures **3** and **7** freely interconvert and cannot be distinguished from each other. The remaining ions appear to be structurally distinct although in a number of cases some limited interconversions may be occurring.

Mechanistic considerations

Deuterium isotopic labelling both in the EI study (12) and in the present CI study have provided some insight into the mech-

TABLE 6. Collision-induced dissociation (CID) mass spectra of $C_5H_{11}O^+$ ions with m/z 43 or m/z 57 as base peak

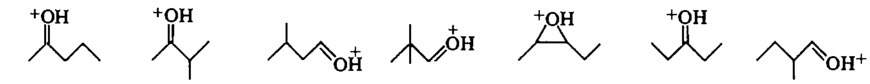

m/z	1	3	5	7	8	2	6
86	9	8	7	7	7	25	13
85	1	2	—	2	5	2	6
72	6	11	4	5	5	6	6
71	31	52	22	20	28	8	35
70	—	—	—	—	—	—	—
68	—	—	—	—	—	—	—
67	3	3	4	3	4	3	6
59	4	2	2	3	14	3	7
58	47	2	8	10	36	7	37
57	18	14	29	18	47	100	100
56	—	—	—	—	—	6	—
55	8	6	7	6	10	13	19
54	—	—	—	—	—	—	—
53	5	9	8	10	8	4	13
51	2	5	4	—	7	2	6
44	—	—	32	—	—	—	—
43	100	100	100	100	100	50	100
42	—	—	13	—	18	11	—
41	39	66	55	77	51	40	78
39	26	31	32	34	30	21	50
31	11	6	10	7	16	19	31
29	23	14	20	16	37	52	71
28	—	—	—	—	—	11	—
27	27	31	30	34	37	35	56

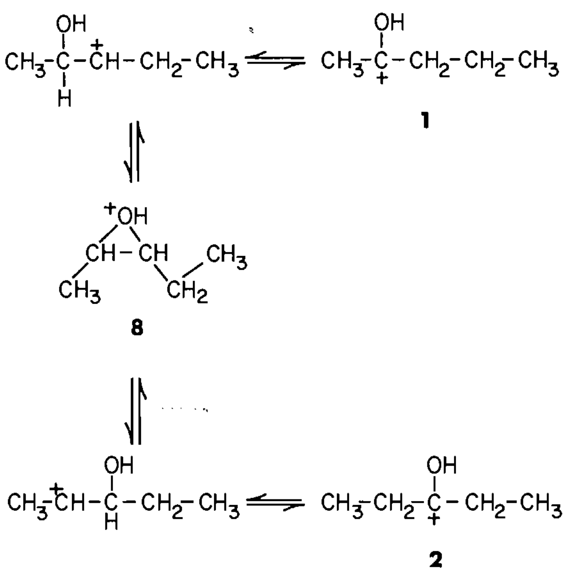

SCHEME 4

anisms of reactions [2] and [5] in particular. These results are discussed in the following.

$C_5H_{11}O^+ \rightarrow C_5H_9^+ + H_2O$

Table 8 records the relative intensities resulting from H_2O and HDO loss from the O-*d* forms of **1** to **11** as recorded in the metastable ion spectra and in the D_2 CI mass spectra. The results given in parentheses come from the earlier EI study (12) and it is clear that the results obtained by the two methods of

TABLE 7. Collision-induced dissociation (CID) mass spectra of $C_5H_{11}O^+$ ions with m/z 41 as the base peak

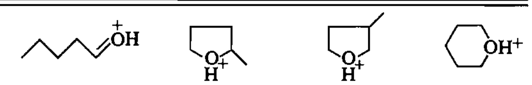

m/z	4	9	10	11
86	11	6	5	24
85	—	—	3	8
72	7	10	1	—
71	15	18	8	7
70	—	12	13	10
68	—	34	16	34
67	7	14	13	16
59	4	—	5	—
58	10	17	15	5
57	70	18	44	44
56	—	11	28	12
55	12	12	15	15
54	—	—	5	7
53	8	9	10	10
51	4	5	5	5
44	40	27	19	13
43	51	38	33	20
42	16	19	16	10
41	100	100	100	100
39	40	35	40	32
31	24	26	36	34
29	53	23	31	25
28	14	10	10	14
27	56	26	28	27

TABLE 8. Elimination of $(H,D)_2O$ from oxygen-deuterated ions[a]

Ion		m* −H_2O	m* −HDO	D_2 CI −H_2O	D_2 CI −HDO
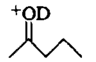	1-O-*d*	17 (21)	83 (79)	15	85
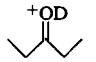	2-O-*d*	21	79	21	79
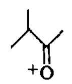	3-O-*d*	3 (3)	97 (97)	13	87
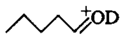	4-O-*d*	30	70	13	87
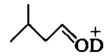	5-O-*d*	60 (67)	40 (33)	30	70
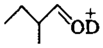	6-O-*d*	(49)	(51)	16	84
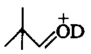	7-O-*d*	3	97	10	90
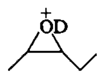	8-O-*d*	37	63	0	~100
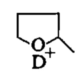	9-O-*d*	47	53	17	83
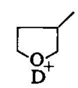	10-O-*d*	38	62	16	84
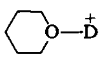	11-O-*d*	32	68	14	86

[a] Data in parentheses from metastable EI studies of ref. 12.

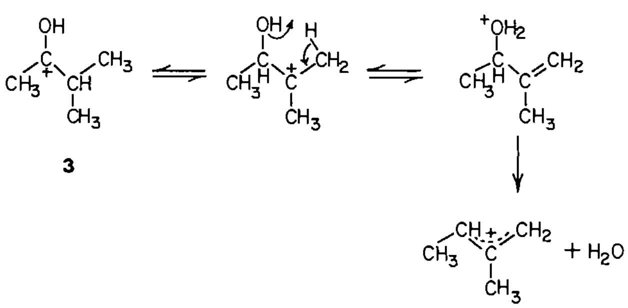

SCHEME 5

ion production are very similar. The most notable feature of these results is that, with few exceptions, the added hydrogen (oxygen-bonded hydrogen) is not always lost with the neutral water but undergoes interchange with carbon-bonded hydrogens. In general, the extent of this interchange decreases with increasing internal energy (decreasing lifetime) as shown by the results from the D_2 CI mass spectra. The extent of interchange is particularly pronounced in the metastable fragmentation of the protonated aldehydes **4–6** and cyclic ethers **8–11**, but is significant even in the D_2 CI mass spectra. Similar results have been reported earlier in chemical ionization studies (18–20).

Further information concerning the water elimination comes from deuterium labelling on the carbon skeleton. Thus **4**-2,2-d_2 and **5**-2,2-d_2 showed loss of H_2O only in metastable ion fragmentation reactions, although 10–15% HDO elimination was

TABLE 9. Metastable elimination of $(H,D)_2O$ from labelled **3** ions[a]

Ion		% Loss of H_2O	% Loss of HDO	% Loss of D_2O
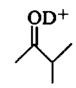	3-O-*d*	3 (3)	97 (97)	—
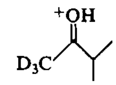	3-1,1,1-d_3	83 (81)	17 (18)	(1)
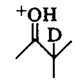	3-3-d_1	(100)	—	—
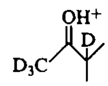	3-1,1,1,3-d_4	83	17	—
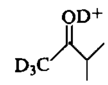	3-1,1,1,O-d_4	2	83	15
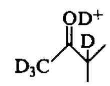	3-1,1,1,3,O-d_5	2	82	16

[a] Data in parentheses from metastable EI studies of ref. 12.

TABLE 10. Metastable elimination of $(H,D)_2O$ from labelled **1** ions[a]

Ion		% Loss of H_2O	% Loss of HDO	% Loss of D_2O
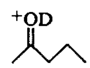	1-O-*d*	17 (21)	83 (79)	—
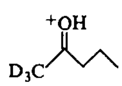	1-1,1,1-d_3	73 (82)	24 (17)	3 (1)
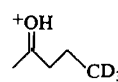	1-5,5,5-d_3	39	58	3
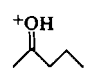	1-3,3-d_2	(97)	(3)	—
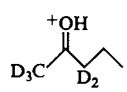	1-1,1,1,3,3-d_5	70 (69)	27 (30)	3 (1)
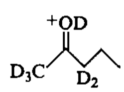	1-1,1,1,3,3,O-d_6	4	76	20

[a] Data in parentheses from metastable EI study of ref. 12.

observed in the CI mass spectra. Audier *et al.* (12) have shown that only H_2O is eliminated from **5**-1-*d* and **6**-1-*d* metastable ions. These results are in agreement with the labelling results of Fales *et al.* (18) who showed that water elimination from protonated n-heptanal involved only the added proton and hydrogens on C3 to C7.

The metastable ion intensities for loss of $(H,D)_2O$ from labelled **3** ions are recorded in Table 9. Again the CI and EI results are in good agreement. The results can be readily rationalized in terms of Scheme 5 after equilibration of the methyl groups by the retro-pinacolic rearrangement of Scheme 2. The

TABLE 11. Metastable formation of $C_2(H,D)_5O^+$ ions from labelled **3** ions[a]

Ion		% Formation of					
		$C_2H_5O^+$	$C_2H_4DO^+$	$C_2H_3D_2O^+$	$C_2H_2D_3O^+$	$C_2HD_4O^+$	$C_2D_5O^+$
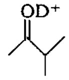	**3**-O-*d*	48 (40)	52 (60)	—	—	—	—
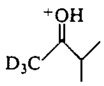	**3**-1,1,1-d_3	30 (28)	30 (32)	3 (3)	37 (37)	—	—
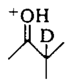	**3**-3-d_1	(81)	(19)	—	—	—	—
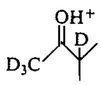	**3**-1,1,1,3-d_4	18	40	9	27	6	—
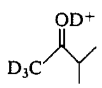	**3**-1,1,1,O-d_4	6	40	17	14	24	—
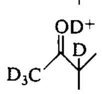	**3**-1,1,1,3,O-d_5	4	33	29	11	21	3

[a]Data in parentheses from metastable EI study of ref. 12.

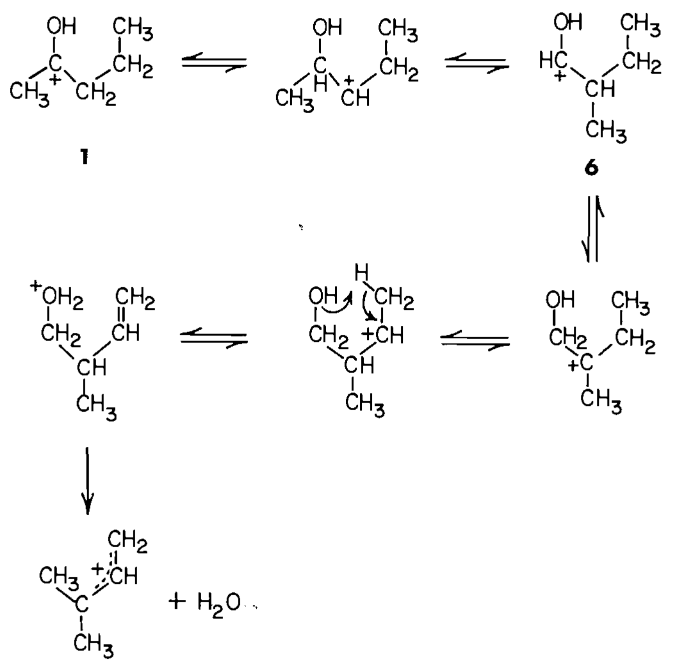

SCHEME 6

equilibration of methyl groups also occurs prior to the higher energy fragmentation in the CI mass spectra; **3**-1,1,1,3-d_4 showed ~26% HDO loss and 74% H_2O in the H_2, N_2/H_2, and CO/H_2 CI mass spectra.

The metastable ion intensities for loss of $(H,D)_2O$ from labelled **1** ions are recorded in Table 10 for EI and CI studies. It is clear from these results that the oxygen-bonded hydrogen and the hydrogens of C1 and C5 are the major origins of the hydrogens lost as H_2O, with extremely minor participation of the C3 hydrogens; the extent of participation of the C4 hydrogens is not clearly established but appears to be relatively minor. A possible mechanism for H_2O loss which rationalizes the important participation of the C5 hydrogens, involving isomerization to **6**, is presented in Scheme 6. The participation of the C1 hydrogens can be rationalized by a migration of the hydroxyl function from C2 to C4 prior to the sequence shown in Scheme 6; evidence for this hydroxy migration comes from the study of the propylene elimination reaction discussed below.

Finally, the study of **2**-2,2,4,4-d_4 showed that the hydrogens in the 2 and 4 positions are involved in H_2O elimination only to a minor extent.

$C_5H_{11}O^+ \rightarrow CH_2CH{=}OH^+ + C_3H_6$

The relative metastable ion intensities for formation of $C_2(H,D)_5O^+$ ions from isotopically labelled **3** ions are presented in Table 11. The results for **3**-O-*d* show that in metastable ions approximately half have interchanged the oxygen-bonded deuterium with a carbon-bonded hydrogen prior to fragmentation. By contrast, in the D_2 CI mass spectrum ~84% of the fragment ions contain the added deuteron; clearly the extent of interchange is lifetime dependent. The metastable ion spectrum of **3**-1,1,1-d_3 shows that only ~37% of the fragment ions contain the C1 methyl group. This is consistent with the facile interchange of methyl groups indicated in Scheme 2. The origin of the other two hydrogens in the fragment ion obviously is complex, as indicated by the distribution of metastable ion signals. Unfortunately, a large signal for $CD_3C{\equiv}O^+$ in the CI mass spectra of the compounds labelled at C1 made complete evaluation of the relative $C_2(H,D)_5O^+$ intensities in the mass spectra impossible. However, for **3**-1,1,1,3-d_4 the relative intensities in the H_2 CI mass spectrum were $C_2H_5O^+/C_2H_3D_2O^+/C_2H_2D_3O^+/C_2HD_4O^+$ = 1.0:0.35:1.0:0.4 compared to 0.67:0.33:1.0:0.22 in the metastable ion spectrum. Similarly for **3**-1,1,1,3,0-d_5 the relative intensities were $C_2H_5O^+/C_2H_3D_2O^+/C_2H_2D_3O/C_2HD_4O^+/C_2D_5O^+$ = 0.18:1.0:0.23:0.63:0.24 compared to 0.14:1.0:0.38:0.72:0.10 in the metastable ion spectrum. Clearly, even in the higher energy CI system, the methyl groups are equilibrating and the origin of the remaining hydrogens is complex; detailed mechanisms would only be speculative.

TABLE 12. Metastable formation of $C_2(H,D)_5O^+$ ions from labelled **1** ions[a]

Ion		% Formation of					
		$C_2H_5O^+$	$C_2H_4DO^+$	$C_2H_3D_2O^+$	$C_2H_2D_3O^+$	$C_2HD_4O^+$	$C_2D_5O^+$
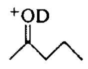	**1**-O-*d*	51 (59)	49 (41)	—	—	—	—
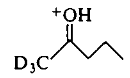	**1**-1,1,1-d_3	12 (12)	8 (8)	—	80 (80)	—	—
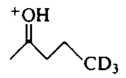	**1**-5,5,5-d_3	50	29	1	20		
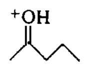	**1**-3,3-d_2	(22)	(68)	(10)			
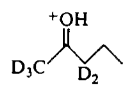	**1**-1,1,1,3,3-d_5	6 (5)	11 (10)	3 (2)	11 (11)	61 (64)	8 (8)
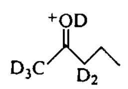	**1**-1,1,1,3,3,O-d_6	2	12	6	5	36	40

[a] Data in parentheses from metastable EI study of ref. 12.

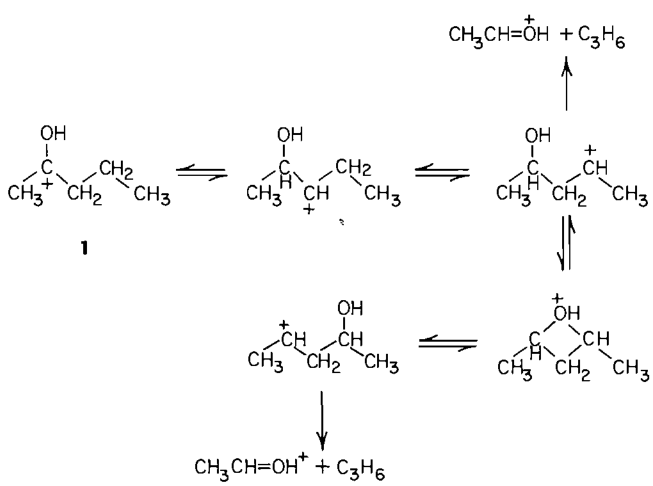

SCHEME 7

The relative metastable ion intensities for formation of $C_2(H,D)_5O^+$ ions from labelled **1** ions are presented in Table 12. Again there is good agreement between EI and CI results. The results for **1**-O-*d* show that in metastable ions approximately half have exchanged the oxygen-bonded hydrogen prior to fragmentation. By contrast, in the D_2 CI mass spectrum (Table 4) only ~17% of the ions have exchanged the oxygen-bonded hydrogen with a carbon-bonded hydrogen prior to fragmentation. The most interesting result, indicated most clearly by the results for **1**-5,5,5,-d_3, is the significant specific inclusion of the C5 methyl group in the $CH_3CH{=}OH^+$ fragment ion. This is true not only for metastable ions but also for ions which fragment in the ion source, since in the H_2 CI mass spectrum **1**-5,5,5-d_3 gave the relative intensities $C_2H_5O^+/C_2H_4DO^+/C_2H_3D_2O^+/C_2H_2D_3O^+ = 67:18:2:13$, very similar to the distribution observed in the metastable ion spectrum. Clearly the oxygen function must migrate ~20% of the time to C4 prior to fragmentation. This could occur through the sequence of interchanges outlined in Scheme 4 or may involve the mechanism of Scheme 7, proposed by Audier *et al.* (12). The origin of the remaining hydrogens clearly is complex.

Acknowledgements

The authors are indebted to the Natural Sciences and Engineering Research Council of Canada for financial support and to Professor J. L. Holmes for providing access to the ZAB-2F mass spectrometer.

1. (*a*) F. W. McLAFFERTY. Interpretation of mass spectra. 3rd ed. Univ. Science Books, Mill Valley, California. 1980; (*b*) H. BUDZIKIEWICZ, C. DJERASSI, and D. H. WILLIAMS. Mass spectrometry of organic compounds. Holden-Day Inc., San Francisco. 1967.
2. F. P. LOSSING. J. Am. Chem. Soc. **99**, 7526 (1977).
3. K. LEVSEN. Fundamental aspects of mass spectrometry. Verlag Chemie, New York. 1978.
4. D. H. WILLIAMS. Acc. Chem. Res. **10**, 280 (1970).
5. R. D. BOWEN, D. H. WILLIAMS, and H. SCHWARZ. Angew. Chem. Int. Ed. Engl. **14**, 451 (1979).
6. R. D. BOWEN and D. H. WILLIAMS. *In* Rearrangements in ground and excited states. Vol. 1. *Edited by* P. DeMayo. Academic Press, New York. 1980. Chapt. 2.
7. R. D. BOWEN and A. G. HARRISON. Org. Mass Spectrom. **16**, 159 (1981).
8. A. G. HARRISON, T. GÄUMANN, and D. STAHL. Org. Mass Spectrom. **18**, 517 (1983).
9. R. D. BOWEN and A. G. HARRISON. J. Chem. Soc. Perkin Trans. 1, 1544 (1981).
10. F. W. McLAFFERTY and I. SAKAI. Org. Mass Spectrom. **7**, 971 (1973).
11. U. I. ZAHORSZKY. Org. Mass Spectrom. **17**, 253 (1982).
12. H. E. AUDIER, R. FLAMMANG, A. MAQUESTIAU, and A. MILLIET. Nouv. J. Chem. **4**, 531 (1980).
13. J. L. HOLMES and J. K. TERLOUW. Org. Mass Spectrom. **15**, 383 (1980).
14. J. A. HERMAN and A. G. HARRISON. Can. J. Chem. **59**, 2125 (1981).

15. K. R. LADEROUTE, J. J. ZWINSELMAN, and A. G. HARRISON. Org. Mass Spectrom. In press.
16. K. LEVSEN and H. SCHWARZ. Mass Spectrom. Rev. **2**, 77 (1983).
17. K. LEVSEN. *In* Tandem mass spectrometry. *Edited by* F. W. McLafferty. John Wiley and Sons, New York. 1983.
18. H. M. FALES, C. FENSELAU, and J. H. DUNCAN. Org. Mass Spectrom. **11**, 669 (1976).
19. H. E. AUDIER, A. MILLIET, C. PERRET, and P. VARENNE. Org. Mass Spectrom. **14**, 129 (1979).
20. H. E. AUDIER, A. MILLIET, C. PERRET, and P. VARENNE. Org. Mass Spectrom. **14**, 132 (1979).
21. F. P. LOSSING and J. C. TRAEGER. Int. J. Mass Spectrom. Ion Phys. **19**, 9 (1976).
22. R. H. STALEY, R. D. WIETING, and J. L. BEAUCHAMP. J. Am. Chem. Soc. **99**, 5964 (1977).
23. J. D. COX and G. PILCHER. Thermochemistry of organic and organometallic compounds. Academic Press, New York. 1970.

Appendix

The heat of formation of the most stable $C_5H_9^+$ structure is 770 kJ mol^{-1} (21) while $\Delta H_f(CH_3CH{=}OH^+)$ = 582 kJ mol^{-1} (2) and ΔH_f $(CH_3C{\equiv}O^+)$ = 661 kJ mol^{-1} (22). The neutral heats of formation (H_2O = −243 kJ mol^{-1}, C_3H_6 = 19.7 kJ mol^{-1}, C_3H_8 = −104 kJ mol^{-1}) were taken from Cox and Pilcher (23).

Synthesis and thermolysis of 2-(phenylthio)ethanesulfonyl chloride. The absence of a reported "rearrangement of radicals with migration of the chlorine atom from sulfur to carbon"[1]

JAMES FREDERICK KING AND KISHAN CHAND KHEMANI

Department of Chemistry, University of Western Ontario, London, Ont., Canada N6A 5B7

Received July 3, 1984

JAMES FREDERICK KING and KISHAN CHAND KHEMANI. Can. J. Chem. **63**, 619 (1985).

2-(Phenylthio)ethanesulfonyl chloride (**1**) is the major product of the reaction of (a) lithium 2-(phenylthio)ethanesulfinate (**6**) and chlorine, and, notwithstanding contrary reports, also of (b) benzenethiol (**3**) and ethenesulfonyl chloride (**4**), and (c) sodium 2-(phenylthio)ethanesulfonate (**5**) and phosphorus pentachloride. The rearrangement referred to in the title, which was proposed to account for the isolation of 2-(phenylthio)ethyl chloride (**2**) rather than **1** from **3** and **4**, therefore does not occur. Desulfonylation of **1** to form **2**, however, readily takes place thermally and, in accord with a rate-determining internal displacement of the chlorosulfonyl group with formation of the episulfonium ion, shows a substantial increase in rate with increase in solvent polarity.

JAMES FREDERICK KING et KISHAN CHAND KHEMANI. Can. J. Chem. **63**, 619 (1985).

Le chlorure de (phénylthio)-2 éthanesulfonyle (**1**) est le produit majeur de la réaction du (a) (phénylthio)-2 éthanesulfinate de lithium (**6**) et du chlore et, malgré les rapports qui énoncent le contraire, c'est aussi le produit principal lors des réactions du (b) benzènethiol (**3**) et du chlorure d'éthène sulfonyle (**4**) et du (c) (phénylthio)-2 éthanesulfonate de sodium (**5**) avec le pentachlorure de phosphore. La transposition à laquelle il est fait allusion dans le titre, qui a été proposée pour expliquer le fait que la réaction (b) conduirait au chlorure de (phénylthio)-2 éthyle plutôt qu'au produit **1**, ne se produit donc pas. La désulfonylation de **1** conduisant à **2** se produit toutefois facilement sous l'influence de la chaleur et, en accord avec un mécanisme impliquant un déplacement interne du groupe chlorosulfonyle comme étape déterminant la vitesse de la réaction qui conduit à la formation d'un ion épisulfonium, la vitesse de cette réaction augmente considérablement avec une augmentation de la polarité du solvant.

[Traduit par le journal]

One focus of recent work in this laboratory has been the investigation of the effect that other functional groups have on the reactions and reactivity of sulfonyl-containing species.[2] It was therefore with considerable interest that we noted two reports of two quite different reactions which in each case might reasonably have been expected to yield 2-(phenylthio)-ethanesulfonyl chloride (**1**), but which describe instead only the identification of the formal desulfonylation product, 2-(phenylthio)ethyl chloride (**2**). In the first of these papers Kandror and Freidlina reported that reaction of benzenethiol (**3**) and ethenesulfonyl chloride (**4**) gives **2**, and, to account for this product, put forward a free radical rearrangement mechanism involving migration of a chlorine atom from sulfur to carbon followed by loss of sulfur dioxide (7). In the second paper McManus *et al.* describe the formation of **2** instead of **1** by the reaction of sodium 2-(phenylthio)ethanesulfonate (**5**) with phosphorus pentachloride or other inorganic acid chlorides (8). Significantly, both of these accounts describe the product only after it had been subjected to heating (glc analysis at 135°C or higher, and distillation at 97°C/2 Torr, respectively) (1 Torr = 133.3 Pa) and it seemed reasonable to hope that milder conditions of reaction and work-up might well enable us to obtain **1**. We wish to report (a) that with appropriate work-up these two reactions, and another route as well, all yield **1** as the major product (see Scheme 1), and (b) that **1** is readily thermally desulfonylated to **2**, probably by way of the episulfonium ion (**7**) as initially suggested by McManus *et al.* (8).

To obtain **1** under gentle conditions, lithium 2-(phenylthio)-ethanesulfinate (**6**), prepared by the method of Vilsmaier and Becker (9), was treated with an equimolar amount of chlorine in chloroform for a short time and the solvent evaporated. The product showed appropriate ^{1}Hmr and ^{13}Cmr spectra (see Experimental) and strong ir bands at 1375 and 1165 cm^{-1} characteristic of the chlorosulfonyl group; the ir and ^{13}Cmr spectra of **1** are readily distinguished from those of **2** but the ^{1}Hmr spectra of **1** and **2** are quite similar and easily confused. All attempts to obtain pure **1** by distillation proved fruitless (see below) and **1** was characterized by conversion to the amide **8** with ammonia.

Reaction of benzenethiol (**3**) and ethenesulfonyl chloride (**4**) following the procedure of Kandror and Freidlina (4 mmol of **3** and 2 mmol of **4** under argon at room temperature for 2.5 h) gave a product which, from its ^{13}Cmr spectrum, contained mostly unreacted **3** and **4** along with a small amount (~7%) of **1**. With a much longer reaction time (144 h) at room temperature the product consisted of **1** (~75%, based on **4**), diphenyl disulfide (~25%, based on **3**), an unidentified material (~15%), and unreacted **3** (27%) and **4** (7%). In our hands the best yield of **1** was obtained by reaction of **3** (3 mmol) and **4** (2 mmol) at 3°C (in air) for 20 days; this gave **1** (~85%), PhSSPh (~16%), a reduced amount of the unidentified product (~5%), plus unreacted **3** (22%) and **4** (8%). The presence of **1** in the product from **3** and **4** was confirmed by isolation of crystalline **8** in good yield by reaction with ammonia. Since **1** and not **2** is clearly the primary product of the reaction of **3** with **4**, it is obvious that the unprecedented "rearrangement of radicals with migration of the chlorine atom from sulfur to carbon" simply does not occur. Reaction of **3** and **4** to form **1** was unaffected by (a) replacing argon by air, (b) bubbling in oxygen, or (c) irradiation with visible light. It would seem reasonable, therefore, to regard the reaction not as a free radical

---

[1] Part 28 in the series Organic Sulfur Mechanisms; for part 27 see ref. 1.

[2] e.g. (a) 1-alkene-1-sulfonyl chlorides (2); (b) "betylates" and "*S*-betylates" (ammonio- and sulfonio-alkanesulfonate esters, respectively) (3, 4); (c) hydroxyalkanesulfonyl chlorides (ref. 5, and unpublished work in this laboratory by M.R. Webster, N. Chiba, K. J. M. Parker, J. K. Allen, and S. Skonieczny); and (d) 2-substituted alkanesulfonyl chlorides (6).

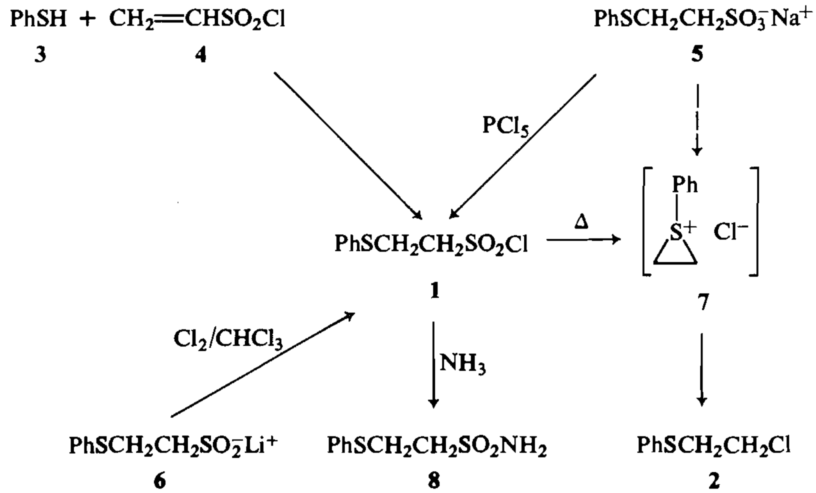

SCHEME 1

process but rather as an ionic addition possibly proceeding by way of a carbanionic or zwitterionic intermediate. As precedent for such an ionic reaction of **4**, we recall the formation of *N*-(2-chlorosulfonylethyl)pyridinium chloride ($C_5H_5N^+CH_2CH_2$-$SO_2Cl\ Cl^-$) on treatment with pyridinium chloride and a trace of pyridine (2).

Following McManus *et al.* (8), sodium 2-(phenylthio)-ethanesulfonate (**5**) was treated with equimolar phosphorus pentachloride to yield **1** in 70% yield (>95% pure as judged by ^{1}Hmr and ^{13}Cmr spectra), with its identity again confirmed by conversion to crystalline **8** as before. In view of the purity of the product relative to that from **3** and **4**, and the ease with which **5** is obtained as compared to **6**, the reaction of **5** with PCl_5 is the current method of choice for preparing **1**. Use of a larger proportion of PCl_5 gave a higher yield of crude product which was, however, contaminated with another compound: the latter material was not isolated but its ^{1}Hmr and ^{13}Cmr spectra suggested that it might be 2-chloro-2-(phenylthio)-ethanesulfonyl chloride. Reaction of **5** with thionyl chloride – *N,N*-dimethylformamide also led to **1**, but the reaction at room temperature was relatively slow and gave the same unidentified second product; at the temperature of refluxing thionyl chloride some **2** was formed as well.

Since mild reaction and work-up conditions give **1**, it seemed likely that the **2** reported by previous workers arose as a result of subsequent thermal conversion. This was confirmed by simple heating of neat **1**, which was cleanly transformed at 135°C into **2** with a half-life of about 4 min. In our hands all attempts to distil **1** gave only **2** in the distillate; by contrast Krutak *et al.* (10) report that 2-(phenylthio)ethanesulfonyl fluoride distils without apparent decomposition under normal conditions (96°C, 0.5 Torr).[3] Precedent for nucleophilic displacement of the chlorosulfonyl group (perhaps in a concerted fragmentation to sulfur dioxide and chloride ion) may be found elsewhere (12–14) and evidence for the intermediacy of the episulfonium ion (**7**), as shown in Scheme 1, has already been presented by McManus *et al.* (8), though for a different starting material and somewhat different reaction conditions. Also in agreement with this picture is the comparative stability of the next homologue of **1**, 3-(phenylthio)-1-propanesulfonyl chloride ($PhSCH_2CH_2CH_2SO_2Cl$) (4), which distils at ~100°C (0.1 Torr) without decomposition (S. Skonieczny, unpublished observation); the much lower reactivity of 3-(phenylthio)-propyl systems, presumably because of the comparative slowness of the formation of the four-membered ring sulfonium ion, is well known from the work of Bordwell and Brannen (15). To shed further light on the mechanism, the rate of thermolysis of **1** in acetophenone solution was examined and found to show first-order behavior to >80% reaction. The following approximate rate constants for the reaction at 114°C were estimated for a range of solvents: sulfolane 4×10^{-3}, acetophenone 4×10^{-4}, tetrachloroethylene 4×10^{-6}, and cyclohexane $5 \times 10^{-7}\ s^{-1}$. A plot of log k against Hildebrand's solubility parameter, δ, gave a rough straight line (r = 0.955) corresponding to $\log k = 0.84\delta - 12.9$. This, when taken with the correlation of δ with the Grunwald–Winstein Y value (16), corresponds to an m value of about 1.6. This, though much too inaccurate for any detailed mechanistic discussion, does, however, provide a clear indication of substantial charge development in the transition state, in full accord with a rate-determining formation of **7** as shown in Scheme 1.

Experimental

Reagent grade chemicals and solvents were used without additional purification unless otherwise noted. Melting points were determined on a Kofler Hot Stage and are uncorrected. Infrared spectra were obtained with a Beckman 4250 spectrophotometer and refer to chloroform solutions. The ^{1}Hmr spectra were obtained using Varian T60 and XL100 spectrometers, with all reported chemical shifts from the latter instrument; ^{13}Cmr spectra were determined on Varian XL200 and XL300 instruments using a sweep width of 15 K with 65 K transforms. Mass spectra were run on a Varian MAT-311A spectrometer. Solvent evaporation on work-up was carried out using a Büchi rotary evaporator connected to a water aspirator. Except as otherwise noted, organic starting materials were supplied by Aldrich Chemical Co. (Milwaukee). An authentic specimen of 2-(phenylthio)ethyl chloride (**2**) was made by the reaction of 2-(phenylthio)ethanol with thionyl chloride (17); the distilled product (**2**) gave the following spectra: ir

[3] The preparation of the sulfonyl fluoride given by these authors prescribes the addition of **3** to $CH_2{=}CHSO_2F$ with tributylphosphine as catalyst; such catalysis of the addition of **3** to **4** is precluded by the rapid reaction of tertiary phosphines with sulfonyl chlorides (11). Both this preparation and the observed stability of the sulfonyl fluoride to distillation serve to point up the low reactivity of sulfonyl fluorides as compared to sulfonyl chlorides; as with alkyl fluorides vs. alkyl chlorides, the behavior of one is not a reliable guide to that of the other.

ν_{max}: 3060 (w), 1585 (w), 1470 (m), 1440 (m), 1200 (w) cm^{-1}; ^{1}Hmr ($CDCl_3$) δ: 7.38–7.16 (m, 5H), 3.65–3.48 and 3.23–3.06 (symmetrical A_2B_2 pattern, 4H); ^{13}Cmr ($CDCl_3$) δ: 134.1, 130.2, 129.0, 126.8, 42.4, 35.9.

Chlorination of lithium 2-(phenylthio)ethanesulfinate (6)

Chlorine gas was bubbled into dry, alcohol-free chloroform at room temperature for 10 min, and the chlorine concentration determined by treating an aliquot with excess KI and titrating the liberated iodine against standard sodium thiosulfate solution using starch as indicator: the Cl_2–$CHCl_3$ solution was used immediately. Lithium 2-(phenylthio)ethanesulfinate (**6**) (9) (42 mg, 0.20 mmol) was suspended in dry, alcohol-free chloroform (1 mL) in a round-bottom flask at 0°C. An equimolar amount of Cl_2–$CHCl_3$ solution was added with stirring. Filtration and evaporation of the solvent after 5 min gave **1** as a colorless liquid (38 mg, 0.18 mmol, 90%); ir ν_{max}: 3000 (w), 2920 (w), 1585 (w), 1480 (m), 1440 (m), 1375 (vs), 1165 (vs), 1020 (w), 905 (m), and 685 (m) cm^{-1}; ^{1}Hmr ($CDCl_3$) δ: 7.47–7.29 (m, 5H), 3.91–3.75 and 3.49–3.33 (symmetrical A_2B_2 pattern, 4H); ^{13}Cmr ($CDCl_3$) δ: 132.3, 131.2, 129.7, 128.1, 64.3, and 28.1.

Compound **1** (38 mg, 0.18 mmol) was dissolved in anhydrous ether (30 mL) and anhydrous NH_3 bubbled in for 15 min at 25°C. The precipitated white solid was removed by filtration and washed with more ether. The filtrate and washings were all combined, dried with $MgSO_4$, and evaporated to yield **8** as a white solid which was purified by flash chromatography (Kieselgel 60, 35:65 (v/v), ethyl acetate – petroleum ether) and recrystallized from chloroform (30 mg, 0.14 mmol, 77%); mp 104–105°C; ir ν_{max}: 3345 (s), 3245 (s), 1318 (vs), 1134 (vs), and 1120 (vs) cm^{-1}; ^{1}Hmr ($CDCl_3$) δ: 7.35–7.26 (m, 5H), 4.79 (s, br, 2H), and 3.32 (s, 4H); ^{13}Cmr ($CDCl_3$) δ: 133.5, 130.5, 129.4, 127.4, 54.6, and 27.8. *Exact Mass* calcd. for $C_8H_{11}NO_2S_2$: 217.0231; found: 217.0238.

Reaction of benzenethiol (3) with ethenesulfonyl chloride (4)

Neat **3** and **4** (both freshly distilled) in a 5-mL round-bottom flask were stirred together using the quantities and conditions as specified in the main text; the irradiation experiment was carried out using a 400-W medium pressure Hg lamp (high intensity discharge. Canadian General Electric) encased in a Pyrex envelope with fluorescer. Reaction products were determined from ^{13}Cmr spectra of dilute solutions ($CDCl_3$) and the relative amounts of various compounds present in the reaction mixture estimated; integrations have an estimated precision of ±5%.

In a typical run, **3** (440 mg, 4 mmol) and **4** (253 mg, 2 mmol) were stirred together in an argon atmosphere at room temperature in a 5-mL round-bottom flask for 144 h. The reaction mixture was dissolved in anhydrous ether (30 mL) and anhydrous ammonia was bubbled in for 15 min at room temperature. Work-up, followed by purification by chromatography and recrystallization as described previously, gave pure crystalline **8** (213 mg, 0.98 mmol, 49% based on **4**) with mp, ir, ^{1}Hmr, and ^{13}Cmr identical to those reported above.

Reaction of sodium 2-(phenylthio)ethanesulfonate (5) with phosphorus pentachloride

Sodium 2-(phenylthio)ethanesulfonate (**5**) (8) (1.115 g, 4.65 mmol) was ground with PCl_5 (0.96 g, 4.65 mmol) in a dry mortar. Reaction occurred after a few seconds to yield a pasty liquid, to which water (10 mL) was added. The mixture was extracted with pentane (4 × 50 mL) in a separatory funnel, all organic extracts were combined, dried with $MgSO_4$, and the solvent evaporated to yield **1** (0.765 g, 3.19 mmol, 69%). A portion of this product (200 mg, 0.85 mmol) was treated with anhydrous ammonia in anhydrous ether (30 mL) and the mixture worked up by the procedure described above to yield pure crystalline **8** (141 mg, 0.65 mmol, 76%) with mp, ir, ^{1}Hmr, and ^{13}Cmr identical to those reported above.

In another experiment, **5** (2.5 g, 10.4 mmol) was treated with excess PCl_5 (4.0 g, 19.2 mmol) in a dry mortar and worked up as above to yield a colorless liquid (2.153 g, crude yield 88%) which showed, in addition to the characteristic signals due to **1**, an apparent ABX pattern (δ 5.68, 1H, dd, J = 6 and 7.5 Hz, plus a multiplet at 4.5–4.1) in the ^{1}Hmr spectrum and ^{13}Cmr absorptions at 134.9, 130.2, 71.4, and 59.6 ppm, evidently derived from a $PhSCHCH_2$-system, perhaps as in $PhSCHClCH_2SO_2Cl$. From ^{1}Hmr integrals the relative amounts of **1** and the second material were estimated as 87 and 13% respectively.

Reaction of 5 with thionyl chloride – N,N*-dimethylformamide*

(a) *At room temperature*

Compound **5** (104 mg, 0.433 mmol) was stirred with 3 mL of freshly distilled $SOCl_2$ and 4 drops of DMF at room temperature for 24 h. Ice-water (10 mL) was then added and the mixture extracted with CH_2Cl_2 (4 × 50 mL) in a separatory funnel; all organic extracts were combined, dried with $MgSO_4$, and evaporated to yield a colorless liquid (120 mg), which showed major peaks in ^{13}Cmr at δ ($CDCl_3$): 164.1, 134.9, 132.1, 130.8, 130.2, 129.3, 127.8, 71.4, 64.1, 59.7, 38.6, 33.2, and 27.9. The peaks were assigned to **1** (132.1, 130.8, 129.3, 127.8, 64.1, and 27.9 ppm), DMF (164.1, 38.6, and 33.2 ppm), and the unidentified product (134.9, 130.2, 71.4, and 59.7 ppm) with the ratio of the peak areas corresponding to approximate relative proportions of 57, 30, and 10% respectively. No sign of any **2** was seen in the ^{13}Cmr spectrum.

(b) *At reflux*

Compound **5** (205 mg, 0.85 mmol) was refluxed with stirring for 11 h with 5 mL of freshly distilled $SOCl_2$ containing 1 drop of DMF in a round-bottom flask and the mixture worked up as above yielding a colorless liquid (215 mg) which by ^{13}Cmr ($CDCl_3$) was found to contain peaks at δ: 134.9, 134.0, 132.1, 130.8, 130.2, 129.3, 129.0, 127.8, 126.8, 71.3, 64.1, 59.7, 42.3, 35.9, and 27.9. The peaks were assigned to **1** (132.1, 130.8, 129.3, 127.8, 64.1, and 27.9 ppm), **2** (134.0, 130.2, 129.0, 126.8, 42.3, and 35.9 ppm), and the unidentified product (134.9, 130.2, 71.3, and 59.7 ppm) with the ratio of the peak areas corresponding to approximate relative proportions of 79, 11, and 10% respectively.

Thermolysis of 2-(phenylthio)ethanesulfonyl chloride (1)

Conventional as well as flash distillation of compound **1** was attempted at various temperatures (80°, 95°, 110°, 120°, and 135°C) and under reduced pressure (0.2 Torr). The ^{13}Cmr spectra of the distillate (in $CDCl_3$) showed the presence of only **2** (>95% pure), with no trace of any **1**.

Neat **1** (33 mg, 0.14 mmol) was sealed under nitrogen in an nmr tube and thermolysed for 2 min in a preheated oil bath (135°C). The ^{13}Cmr spectrum in $CDCl_3$ solution gave the relative amounts of **1** and **2** as 78 and 22% respectively. Chloroform was driven off by blowing nitrogen over the surface and the liquid obtained sealed under nitrogen as before and thermolysed further for 6 min at the same temperature. The ^{13}Cmr spectra in $CDCl_3$ solution gave the relative amounts of **1** and **2** as 31 and 69% respectively (integrations have an estimated precision of ±5%). No sign of any other side products was seen in the ^{13}Cmr spectra. The above data give an approximate half-life of 4 min for the above conversion.

2-(Phenylthio)ethanesulfonyl chloride (**1**) (130.5 mg, 0.55 mmol) was dissolved in freshly distilled acetophenone (3 mL) in a 5-mL round-bottom flask containing a magnetic stirring bar and flushed with dry nitrogen gas. The flask was lowered into a preheated oil bath (114°C) mounted on a stirring base, and the timer started. Aliquots (0.5 mL each) of the acetophenone solution were removed after 5, 15, 30, 60, and 120 min and ^{13}Cmr spectra run immediately. The relative amounts of **1** and **2** in the reaction mixtures were determined by monitoring the high-field peaks; integrations have an estimated precision of ±5%. A plot of ln ($[\mathbf{1}]_0/[\mathbf{1}]$) vs. t gave a straight line passing through the origin (r = 0.999); the slope of the line gave a rate constant of 4.2×10^{-4} s^{-1}.

Solutions of compound **1** (25–50 mg) in freshly distilled sulfolane, acetophenone, tetrachloroethylene, and cyclohexane solvents (0.4 mL each) were sealed under nitrogen atmosphere in different nmr tubes and thermolysed for various times (3 min, 5 min, 2974 min, and 3560 min respectively) in a preheated oil bath (114°C). At the end of these times, the rate constants for the conversion of **1** to **2** were calculated from relative amounts as given by the [13]Cmr spectra using the first-order rate equation.

Acknowledgement

We thank the Natural Sciences and Engineering Research Council for financial support of this work.

1. J. F. KING, J. H. HILLHOUSE, and K. C. KHEMANI. Can. J. Chem. **63**, 1 (1985).
2. J. F. KING, J. H. HILLHOUSE, and S. SKONIECZNY. Can. J. Chem. **62**, 1977 (1984).
3. J. F. KING, S. M. LOOSMORE, M. ASLAM, J. D. LOCK, and M. J. MCGARRITY. J. Am. Chem. Soc. **104**, 7108 (1982).
4. J. F. KING, S. SKONIECZNY, and G. A. POOLE. Can. J. Chem. **61**, 235 (1983).
5. J. F. KING and J. H. HILLHOUSE. Can. J. Chem. **61**, 1583 (1983).
6. J. H. HILLHOUSE. Ph.D. thesis, University of Western Ontario. 1982. Chapt. 3.
7. I. I. KANDROR and R. KH. FREIDLINA. Izv. Akad. Nauk SSSR, Ser. Khim. 1890 (1974).
8. S. P. MCMANUS, M. R. SMITH, F. T. HERRMANN, and R. A. ABRAMOVITCH. J. Org. Chem. **43**, 647 (1978).
9. E. VILSMAIER and G. BECKER. Synthesis, 55 (1975).
10. J. J. KRUTAK, R. D. BURPITT, W. H. MOORE, and J. A. HYATT. J. Org. Chem. **44**, 3847 (1979).
11. L. HORNER and H. NICKEL. Justus Liebigs Ann. Chem. **597**, 20 (1955).
12. J. F. KING and D. J. H. SMITH. J. Am. Chem. Soc. **89**, 4803 (1967).
13. H. O. FONG, W. R. HARDSTAFF, D. G. KAY, R. F. LANGLER, R. H. MORSE, and D. N. SANDOVAL. Can. J. Chem. **57**, 1206 (1979).
14. J. F. KING and M. ASLAM. Can. J. Chem. **57**, 3278 (1979).
15. F. G. BORDWELL and W. T. BRANNEN, JR. J. Am. Chem. Soc. **86**, 4645 (1964).
16. H. F. HERBRANDSON and F. R. NEUFELD. J. Org. Chem. **31**, 1140 (1966).
17. A. H. FORD-MOORE, R. E. PETERS, and R. W. WAKELIN. J. Chem. Soc. 1754 (1949).

Metallophthalocyanine dimers incorporating five-atom covalent bridges

CLIFFORD C. LEZNOFF,[1] SEBASTIAN M. MARCUCCIO, SHAFRIRA GREENBERG, AND A. B. P. LEVER
Department of Chemistry, York University, Downsview (Toronto), Ont., Canada M3J 1P3

AND

KENNETH B. TOMER
Midwest Center for Mass Spectrometry, University of Nebraska–Lincoln, Lincoln, NE 68588, U.S.A.

Received June 4, 1984

CLIFFORD C. LEZNOFF, SEBASTIAN M. MARCUCCIO, SHAFRIRA GREENBERG, A. B. P. LEVER, and KENNETH B. TOMER. Can. J. Chem. **63**, 623 (1985).

Metal-free copper and cobalt(II) binuclear phthalocyanines, in which the two phthalocyanine nuclei are covalently linked through five-atom bridges, have been prepared and characterized. Some new metal-free, copper, cobalt(II), and zinc 2,9,16,23-tetraalkoxyphthalocyanines, some of which are extremely soluble in organic solvents, are described.

CLIFFORD C. LEZNOFF, SEBASTIAN M. MARCUCCIO, SHAFRIRA GREENBERG, A. B. P. LEVER et KENNETH B. TOMER. Can. J. Chem. **63**, 623 (1985).

On a préparé et caractérisé une série de phtalocyanines, libres ou complexées par du cuivre ou du cobalt(II), dans lesquelles les deux noyaux de phtalocyanines sont liés d'une manière covalente par des ponts de cinq atomes. On décrit quelques nouvelles tétraalkoxy-2,9,16,23 phtalocyanines, libres ou complexées avec du cuivre, du cobalt(II) ou du zinc, qui sont extrèmement solubles dans les solvants organiques.

[Traduit par le journal]

The use of cobalt phthalocyanine as a catalyst for the electroreduction of oxygen has been known for some time (1) and extensive research efforts have shown that porphyrins and phthalocyanines can act as potential catalysts for energy conversion processes (2–4). It is well known that iron(II) porphyrins decompose oxygen through a mechanism involving two porphyrins acting on one oxygen molecule (5). Binuclear porphyrins (6–9) have been prepared and used in the 4-electron reduction of molecular oxygen to water. Under operating conditions, however, binuclear porphyrins lose catalytic activity with time (7) and it may be that the porphyrin nucleus itself is not sufficiently stable to be used as a long term photocatalyst. For this reason, we envisioned that binuclear photocatalysts based on the thermally (10) and photochemically stable phthalocyanine nucleus would be worthwhile molecules to synthesize and examine in electrochemical and photocatalytic studies.

Using a solid phase method of synthesis we have recently prepared some unsymmetrical phthalocyanines which are very soluble in organic solvents (11, 12), compared with most phthalocyanines which are notoriously insoluble. These soluble, unsymmetrical, mononuclear phthalocyanines contained the necessary handle, a hydroxy functional group, which could be used to attach the phthalocyanine to electrodes (13, 14). The synthesis of a very soluble mononuclear phthalocyanine in our earlier studies (11, 12) and the development of chromatographic methods for the separation of phthalocyanines in general (12) has enabled us to contemplate the syntheses of the hitherto unknown binuclear phthalocyanines.

Although we believed that a solid phase approach could be advantageously used in the synthesis of binuclear phthalocyanines, as a first experiment, prior to adopting solid phase methodology, we tried to synthesize a binuclear phthalocyanine in solution. As shown below, binuclear phthalocyanines *can* be separated chromatographically from mononuclear phthalocyanines using our unusual eluting solvent mixture (12), and hence the more elaborate scheme using polymer supports was unnecessary.

Synthesis of mononuclear phthalocyanines, soluble in organic solvents

Treatment of 4-nitrophthalonitrile (**1**) with 2-propanol (**2**), 2-methyl-1-propanol (**3**), and 2,2-dimethyl-1-propanol (**4**) with potassium carbonate in dimethylformamide (DMF) in a useful modification (15) of published procedures (16, 17) gave in some instances at high temperatures the unwanted by-products 4-hydroxyphthalonitrile (**5**) (18) and bis(3,4-dicyanophenyl)-ether (**6**), but at room temperature (15) the desired 4-isopropoxyphthalonitrile (**7**) (11, 15), 4-isobutoxyphthalonitrile (**8**), and 4-neopentoxyphthalonitrile (**9**) respectively in 69 to 87% yield. Phthalonitriles **7–9** were readily converted, using gaseous ammonia and sodium methoxide in methanol (19, 20), to 5-isopropoxy-1,3-diiminoisoindoline (**10**), 5-isobutoxy-1,3-diiminoisoindoline (**11**), and 5-neopentoxy-1,3-diiminoisoindoline (**12**) respectively. The solvent was evaporated and compounds **10–12** were next used without further purification. We have previously reported the condensation of **10** in 2-*N*,*N*-dimethylaminoethanol (Method A) (19) to give the metal-free 2,9,16,23-tetraisopropoxyphthalocyanine (**13***a*) (12), but had not described any metallated derivatives of **13***a*. In fact, several methods exist for the direct condensation of phthalonitriles to metallated phthalocyanines without the necessity of forming isoindolines. Thus, treatment of **7** with CuCN in DMF (Method B) (20) or with $CuCl_2$ and diazabicyclononane (DBN) in ethanol (Method C) (21) gave 2,9,16,23-tetraisopropoxyphthalocyaninato copper (**13***b*) in 34 and 49% yield respectively (Table 1). Compound **7** was similarly converted to 2,9,16,23-tetraisopropoxyphthalocyaninato cobalt(II) (**13***c*) and 2,9,16,23-tetraisopropoxyphthalocyaninato zinc (**13***d*) using Methods B and C (Table 1; Scheme 1).

Isoindoline **11** was converted to the metal-free 2,9,16,23-tetraisobutoxyphthalocyanine (**14***a*) by Method A and **14***a* was converted to 2,9,16,23-tetraisobutoxyphthalocyaninato copper (**14***b*) by simple treatment of **14***a* with cupric acetate in toluene (Method D) (19), in this example (Table 1). Similarly, isoin-

[1]Author to whom correspondence may be addressed.

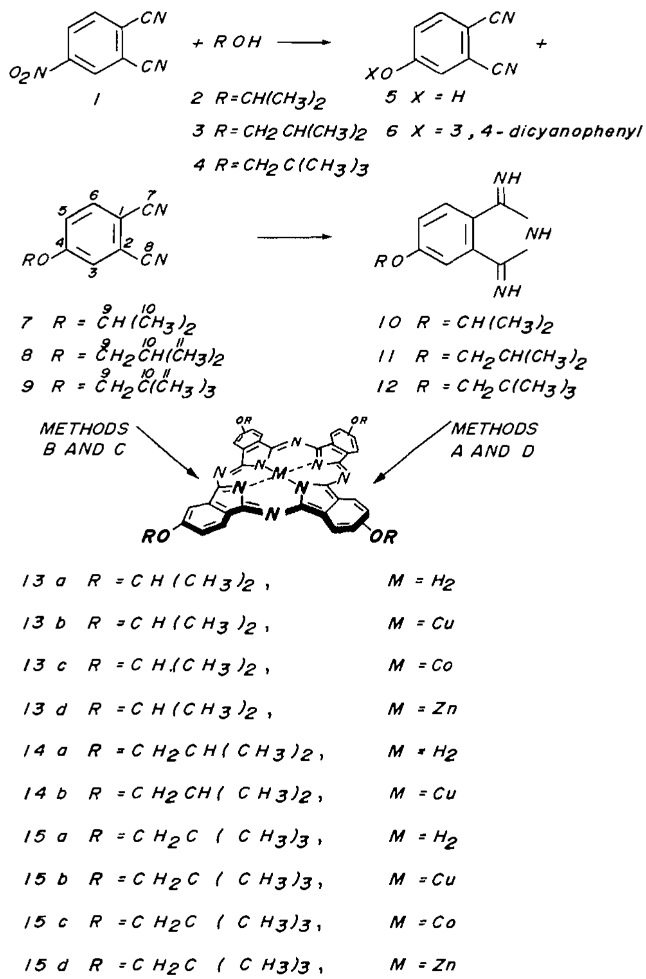

SCHEME 1

doline **12** was converted to 2,9,16,23-tetraneopentoxyphthalocyanine (**15***a*) (Method A) and subsequently to 2,9,16,23-tetraneopentoxyphthalocyaninato copper (**15***b*) and 2,9,16,23-tetraneopentoxyphthalocyaninato cobalt(II) (**15***c*) (Method D). Treatment of phthalonitrile **9** under the conditions of Method B using copper, cobalt, and zinc salts yielded **15***b*, **15***c*, and 2,9,16,23-tetraneopentoxyphthalocyaninato zinc (**15***d*) in varying yields (Table 1; Scheme 1). The structures of **13***a*–*d*, **14***a*–*b*, and **15***a*–*d* were confirmed by spectroscopic and elemental analysis (see experimental section and Table 2).

A comparison of the yields of metallophthalocyanines by three different routes (Table 1) shows that a combination of Methods A and D, i.e. formation of metal-free phthalocyanines followed by metal insertion, or Method C, using DBN as a condensing agent, is superior to Method B. In fact, in our hands, organic soluble metallophthalocyanines are most conveniently prepared in the purest state, and in the highest yield, by metal insertion into metal-free phthalocyanines (Methods A and D). Direct preparation of metallophthalocyanines by Method C gives metallophthalocyanines contaminated by impurities difficult to remove by chromatographic methods.

The selection of the 4-isopropoxy group as a substituent of a phthalonitrile and hence of its isoindoline was predicated on the fact that a bulky isopropoxy group in **7** and **10** similar to the less accessible 4-*tert*-butylphthalonitrile (22) would inhibit aggregation processes and lead to organic solvent soluble phthalocyanines. Indeed, **13***a* proved to be exceedingly soluble (Table 2) in organic solvents and hence was readily separable from polymer-supported phthalocyanines (11, 12) and, as shown below, separable from a binuclear phthalocyanine. Although **13***a*–*d* were prepared as pure compounds, it was noted that some deterioration occurred with age and, indeed, old samples had to be rechromatographed before their use in electrochemical studies. Since the phthalocyanine nucleus is reputed to be extremely stable to decomposition, we believed for two reasons that the isopropoxy group was responsible for this instability. Firstly, isopropyl ethers are known to readily form peroxides and, secondly, base catalyzed elimination of the isopropyl group may occur as shown in Scheme 2.

TABLE 1. Yields of monomeric metallophthalocyanines by different synthetic methods

Starting material	Method[a]	Salt	Product	Yield (%)
7	A	[b]	**13***a*	38
7	B	CuCN	**13***b*	34
7	B	$CoCl_2$	**13***c*	20
7	B	$Co(CN)_2$	[c]	—
7	B	$Co(OAc)_2$	**13***c*	37
7	B	$ZnCl_2$	**13***d*	35
7	C	$CuCl_2$	**13***b*	49
7	C	$CoCl_2$	**13***c*	46
7	C	$Co(OAc)_2$	**13***c*	35
7	C	$ZnCl_2$	**13***d*	31
9	A	[b]	**15***a*	45
9	B	CuCN	**15***b*	17
9	B	$Co(OAc)_2$	**15***c*	29
9	B	$ZnCl_2$	**15***d*	2
9	B	$Zn(OAc)_2$	**15***d*	27
14*a*	D	$Cu(OAc)_2$	**14***b*	74
15*a*	D	$CuCl_2$	**15***b*	94[d]
15*a*	D	$CoCl_2$	**15***c*	94[d]

[a]See text for reaction conditions and references for Methods A–D.
[b]Method A gives metal-free phthalocyanines and no salt is used.
[c]No reaction.
[d]The overall yield, which is a combination of Methods A and D, is 42%.

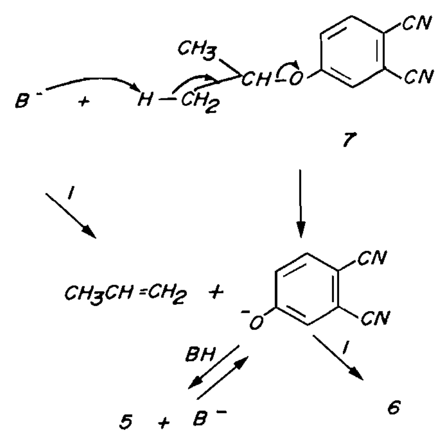

SCHEME 2

The formation of **6** in the preparation of **7** at temperatures higher than room temperature shows that the mechanistic scheme shown in Scheme 2 is at least partially operative. We have shown that pure **7** on reaction with K_2CO_3 or KNO_2 at 80°C does liberate, upon protonation, **5** without concomitant formation of **6**, since no **1** is available. Some earlier studies (23) on the formation of *tert*-butyl aryl ethers have shown that

TABLE 2. Absorption spectra of mononuclear and binuclear phthalocyanines and their solubilities in CH_2Cl_2 at 24°C

Phthalocyanine	λ max (nm) (ε log)						Solubility (mol/L)
13*a*	342 (4.40)	388 (4.09)	608 (3.98)	640 (4.19)	670 (4.58)	706 (4.64)	0.78
13*b*	338 (4.74)	384 (4.37)	614 (4.47)	638 (4.48)	677 (4.93)		0.62
13*c*	328 (4.72)	386 (4.32)	608 (4.40)		674 (4.92)		0.84
13*d*	342 (4.67)	384 (4.26)	614 (4.32)		682 (4.96)		0.30
14*a*	343 (4.98)	390 (4.54)	610 (4.47)	642 (4.66)	670 (4.97)	706 (5.02)	0.013
14*b*	337 (4.76)	384 (4.40)	620 (4.59)		682 (4.89)		0.018
15*a*	341 (4.57)	390 (4.27)	608 (4.17)	642 (4.36)	670 (4.73)	705 (4.79)	1.10
15*b*	338 (4.82)	380 (4.42)	614 (4.57)		680 (5.09)		0.26
15*c*	335 (4.74)	390 (4.31)	620 (4.52)		680 (4.97)		0.15
15*d*	344 (4.91)	384 (4.57)	614 (4.60)		680 (5.18)		0.43
25		384 (4.10)	618 (4.57)		682 (4.99)		—
26*a*	336 (4.99)	384 (4.69)	612 (4.80)	636 (4.90)	668 (4.84)	700 (4.69)	0.0057
26*b*	336 (5.08)	384 (4.72)		628 (5.06)	676 (5.03)		0.00028
26*c*	320 (4.95)	386 (4.56)		626 (4.92)	670 (4.88)		0.00071
27*a*	332 (5.00)	384 (4.66)	610 (4.76)	638 (4.90)	670 (4.81)	700 (4.66)	0.35
27*b*	320 (4.95)	380 (4.37)		626 (4.77)	668 (4.76)		0.039

eliminative processes as described above do occur but also that elimination more likely occurs through an alternate pathway involving the initial nucleophilic addition adduct. In any case, it became apparent that the 4-isopropoxy group of **7** and **10** was not ideally suited to subsequent use as a "partner" in the synthesis of binuclear phthalocyanines. It was for these reasons that the isobutoxy derivatives **8** and **11** were prepared. The isobutoxy group is not a secondary ether and hence is less susceptible to peroxide formation, and in addition only contains one hindered β-hydrogen for participation in possible elimination reactions. It was subsequently shown, however, that the isobutoxyphthalocyanines, **14***a* and **14***b*, prepared from **11**, were considerably less soluble than their isopropoxy analogs, **13***a* and **13***b* (Table 2). The 4-neopentoxy derivatives, **9** and **12**, are primary hindered ethers and contain no β-hydrogens for possible elimination reactions. Most importantly, the neopentoxyphthalocyanine, **15***a*, derived from **12**, proved to be exceedingly soluble in organic solvents (Table 2) and ultimately exhibited little decomposition with age. The formation of **9** at room temperature using the standard procedure (15) gave **9** in 86% yield in 84 h in a small scale reaction. On a large scale, the reaction was only completed after 144 h. Since **9** could not undergo β-elimination processes such as **7**, an evaluation of the yield of **9** at different temperatures was undertaken and it was shown that **9** should be prepared in optimal yield in reasonable times at 60°C (Table 3). At higher temperatures, the formation of **5** by the displacement of the nitro group by carbonate or nitrite becomes important (18).

TABLE 3. Yields of **9** from **1** at different temperatures and reaction times

Temperature (°C)	Time (h)[a]	Yield (%)
22	84	86
60	18	82
70	10	76
80	5	66

[a]Starting material **1** was completely consumed after the given reaction times.

The syntheses of binuclear phthalocyanines

A straightforward route to binuclear phthalocyanines would involve a *mixed* condensation of a bisphthalonitrile or its isoindoline derivatives with a simple phthalonitrile or isoindoline in solution. Since phthalocyanines are so insoluble, the above simple approach would give insoluble, inseparable mixtures of mononuclear phthalocyanines, binuclear phthalocyanines, and by-products, as even good preparations of mononuclear phthalocyanines occur in less than 50% yield. The development (11, 12) of exceedingly soluble mononuclear phthalocyanines and particularly **15***a* described above indicated that even binuclear phthalocyanines may be soluble and separable by chromatography (12).

Initially, we had been interested in preparing not only binuclear phthalocyanines but also one containing a "handle" suitable for attachment to electrodes (13), polymers (24), or micelles (25). In addition, we wished to prepare binuclear phthalocyanines, incorporating five-, four-, or three-atom covalent bridges, as these bridges seemed most likely to yield phthalocyanine dimers having electrocatalytic and photocatalytic activity. Bisphthalonitriles can be readily prepared (16) by treatment of symmetrical diols with **1**. The goal of obtaining binuclear phthalocyanines incorporating a five-atom bridge thus requires a bisphthalonitrile incorporating a five-atom bridge. The symmetrical diol forming this bridge should not have hydrogen atoms available for β-elimination. Treatment of excess 2-hydroxymethyl-2-methyl-1,3-propanediol (**16**) with triphenylmethyl chloride (trityl chloride) in pyridine yielded upon column chromatography 68% (based on trityl chloride) of 2-methyl-2-trityloxymethyl-1,3-propanediol (**17**).

Symmetrical diols **17**, 2,2-dimethyl-1,3-propanediol (**18**), and 2-ethyl-2-methyl-1,3-propanediol (**19**), reacted with more than two equivalents of **1** and K_2CO_3 in dimethylsulfoxide (DMSO) (16) to give 1,3-bis(3′,4′-dicyanophenoxy)-2-methyl-2-trityloxymethylpropane (**20**), 1,3-bis(3′,4′-dicyanophenoxy)-2,2-dimethylpropane (**21**), and 1,3-bis(3′,4′-dicyanophenoxy)-2-ethyl-2-methylpropane (**22**) respectively. Bisnitriles **21** and **22** were converted to their bisisoindolines **23** and **24** as before and used in subsequent condensations without further purification. For our first mixed condensation for the preparation of binuclear phthalocyanines we decided to try the direct route of reacting bisphthalonitrile **20** with 4-isopropoxyphthalonitrile

(7) using cuprous cyanide in DMF (Method B), as Method C was known to generate many by-products. Flash chromatography (26) using 2-methoxyethanol − toluene (5:200) as eluant removed the mononuclear copper phthalocyanine **13***b*, formed by self-condensation of **7**. Further elution gave the binuclear phthalocyanine, 1,3-bis-2′-(9′,16′,23′-triisopropoxyphthalocyaninato copper)-2-methyl-2-trityloxymethylpropane (**25**), in 1% yield (Scheme 3). Characterization of **25** was based on elemental and spectroscopic analysis and its method of synthesis. Elemental analysis of **25**, which still contains the trityl blocking group, is more meaningful than elemental analysis of any detritylated dimer, as **25** exhibits a more considerable difference in its calculated analysis than the related monomer **13***b*. Indeed, the close but not perfect analysis indicates the structure **25**, rather than a monomeric species. The mass spectrum of **25** was most informative and, after much effort using the FAB techniques (27) and using thioglycerol as solvent, a parent ion with m/z centered at 1859.5 amu was observed. A major fragment ion at 1816 ($M^+ - 43$) was indicative of loss of an isopropyl group, consistent with structure **25**. The much slower chromatographic mobility of **25** compared to **13***b* further suggested **25** as the most likely structure. The infrared spectrum of **25** gives us an indication of the purity of our compounds, as by-product impurities exhibit absorptions in the nitrile or carbonyl regions of the spectra which are absent in both pure mononuclear and binuclear phthalocyanines. The ultraviolet spectrum of **25** and all mononuclear and binuclear phthalocyanines are given in Table 2 for comparison purposes, as small but significant differences are apparent between metal-free and metallophthalocyanines and between mononuclear and binuclear phthalocyanines.

Although the synthesis of the first binuclear phthalocyanine **25** was achieved using Method B and **7** as the "partner" in the condensation, the yield was very low. For this reason the formation of binuclear phthalocyanines using Method A (via diiminoisoindolines) and using 5-neopentoxy-1,3-diiminoisoindoline (**12**) as the "partner" was attempted. Heating the bis-isoindolines **23** or **24** at 150°C with a large excess of **12** in 2-*N*,*N*-dimethylaminoethanol for 24 h (Method A) under argon yielded a dark blue solution which was diluted with water giving blue coloured residues. Flash chromatography of solutions of these residues separated the mononuclear phthalocyanine **15***a* from the desired binuclear phthalocyanines 1,3-bis-2′-(9′,16′,23′-trineopentoxyphthalocyaninoxy)-2,2-dimethylpropane (**26***a*) and 1,3-bis-2′-(9′,16′,23′-trineopentoxyphthalocyaninoxy)-2-ethyl-2-methylpropane (**27***a*) respectively. The relatively high yields of **26***a* (17%) and **27***a* (10%) achieved by Method A as compared to Method B for **25** (1%) more than compensated for the extra effort of making the isoindolines. Simple treatment of **26***a* with anhydrous cupric acetate in toluene at 100°C for 17 h gave the binuclear phthalocyaninato dicopper derivative **26***b* in 54% yield, while similar reactions of **26***a* or **27***a* with anhydrous cobaltous chloride gave the binuclear phthalocyaninato dicobalt(II) derivatives **26***c* and **27***b* in 60 and 74% yields respectively. Binuclear phthalocyanines, **26***a*–*c* and **27***a*–*b*, exhibited parent ions in their mass spectra using the FAB system and *o*-nitrophenyl octyl ether (ONPOE) as solvent. The infrared spectra of **26***a* and **27***a* exhibit characteristic N—H absorptions at 3300 and 1020 cm^{-1} (28), similar to metal-free mononuclear phthalocyanines **13***a*, **14***a*, and **15***a*. The ^{1}H nmr spectra of **26***a* and **27***a* show a characteristic broad N—H absorption peak at approximately −6.0 ppm as do **13***a*, **14***a*, and **15***a* at high concentrations.

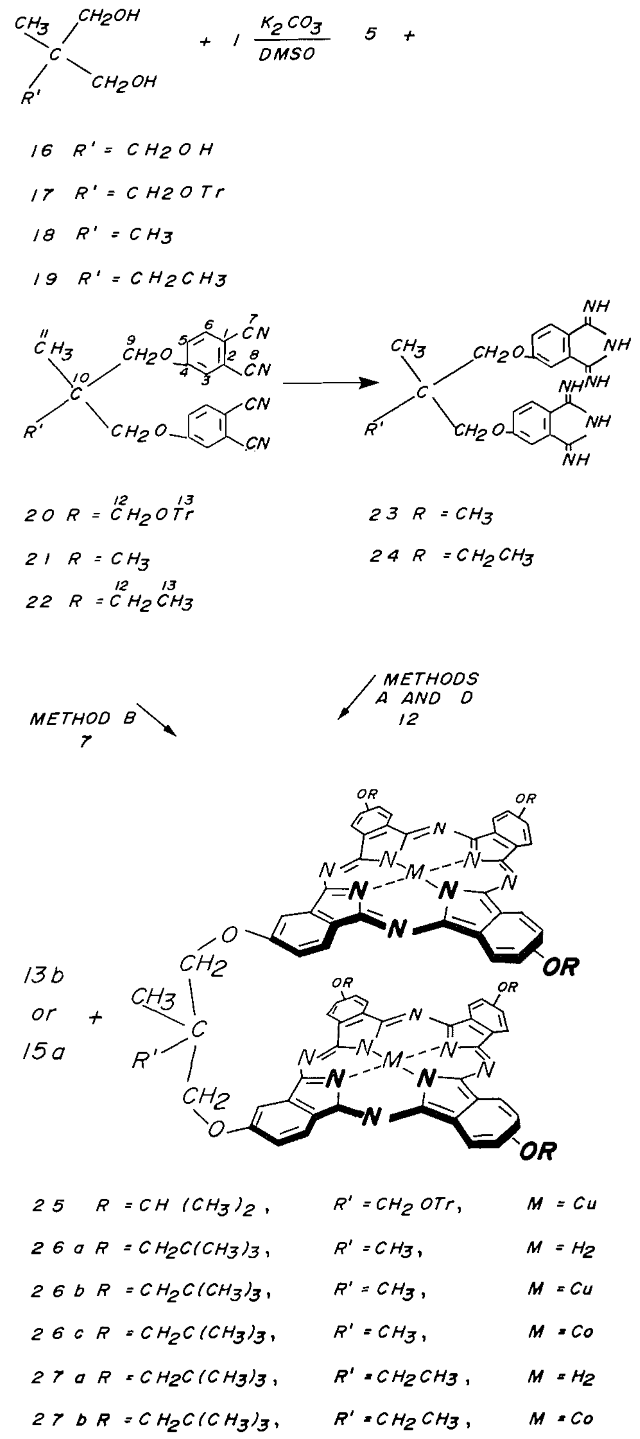

SCHEME 3

Other peaks in the ^{1}H nmr spectra, however, are also very broad, which renders ^{1}H nmr spectroscopy less useful for characterization of phthalocyanines, both monomeric and dimeric. It is likely that the ^{1}H nmr signals are broad due to both aggregation effects and the fact that all the mononuclear and binuclear phthalocyanines described herein are a mixture of a large number of possible positional isomers. Even using a high field instrument and multiple scans, a dilute solution of **15***a* yielded a spectrum showing broad absorptions, and hence the multiplicity of positional isomers is the likely primary cause of this effect. The ^{13}C nmr spectra (see Experimental), of **13***a*,

TABLE 4. ^{13}C Chemical shifts of **7–9** and **20–22**

	δ ppm					
Carbon[a]	**7**	**8**	**9**	**20**	**21**	**22**
1	106.3	106.1	106.7	107.1	107.7	107.4
2	117.1	116.5	117.2	117.0	117.6	117.4
3	119.9[b]	119.2	119.5[b]	119.2[b]	119.8[b]	119.5[b]
4	161.1	161.9	162.6	161.5	162.4	162.0
5	120.3[b]	119.2	119.8[b]	119.5[b]	120.0[b]	119.7[b]
6	135.1	135.1	135.3	135.1	135.6	135.3
7	115.3[c]	115.1[c]	115.9	115.1[c]	115.7[c]	115.2[c]
8	115.7[c]	115.6[c]	115.9	115.5[c]	116.1[c]	115.7[c]
9	71.6	75.0	78.9	70.5	74.1	72.0
10	21.5[d]	27.6	31.9	40.4	36.1	38.3
11	—	18.5	26.4	17.3	21.8	18.3
12	—	—	—	63.5	—	26.6
13	—	—	—	86.4[e]	—	7.3

[a]The numbering of the carbon atoms in **7–9** and **20–22** follows that given for these structures in Schemes 1 and 2 and does not follow from the names of these compounds. All compounds were run in $CDCl_3$ except **21**, which was run in CD_2Cl_2.
[b]These assignments may be interchanged.
[c]These assignments may be interchanged.
[d]This value is typical of methyl carbon atoms and correlates well with carbon 11 for other compounds in the table.
[e]This assignment is for the quaternary carbon of the trityl group. The phenyl groups absorb at 143.3, 128.4, 127.7, and 127.0, consistent with previous assignments (30).

13*d*, **14***a*, **15***a*, **15***d*, **26***a*, and **27***a* give sharp absorbancies, characteristic of the given structures. The reduced solubilities of **26***a* and **27***a* compared to **13***a* and **15***a* meant that even overnight scans of these samples on a Bruker 400-MHz nmr spectrometer could not show most of the quaternary carbon atoms. The ^{13}C nmr of **7–9** and **20–22** have been assigned using standard correlations (29) (Table 4). The absorption spectra of all mononuclear and binuclear phthalocyanines reported herein are reported in Table 2. Mononuclear metal-free and metallophthalocyanines give well-known characteristic absorption spectra (10) and the present availability of binuclear metal-free and metallophthalocyanines shows that these dimeric phthalocyanines are different from the monomeric phthalocyanines and from each other. Both mononuclear and binuclear metal-free phthalocyanines exhibit absorption maxima between 700 and 706 nm with the binuclear ones absorbing near 700 nm. Metallophthalocyanines do not give absorption maxima at this wavelength. Other differences, especially between monomers and dimers, are reflected in intensity changes which in tabular form appear minor, but in graphic form (Fig. 1) of one example of each class show that simple inspection can often identify the phthalocyanine as mononuclear or binuclear, and metal-free or containing metal.

The successful syntheses of the first characterized binuclear phthalocyanines rest largely on the preparation of monomeric phthalocyanines, which are exceedingly soluble in organic solvents, and their subsequent separation from binuclear phthalocyanines which still exhibit significant solubility in organic solvents. From Table 2 one can see that metallophthalocyanines are generally less soluble than metal-free phthalocyanines, and binuclear phthalocyanines are understandably less soluble than mononuclear phthalocyanines. Thus the difference in solubility of metal-free mononuclear phthalocyanine (**15***a*) and a binuclear metallophthalocyanine (**26***c*) is over three orders of magnitude, but **26***c* and other

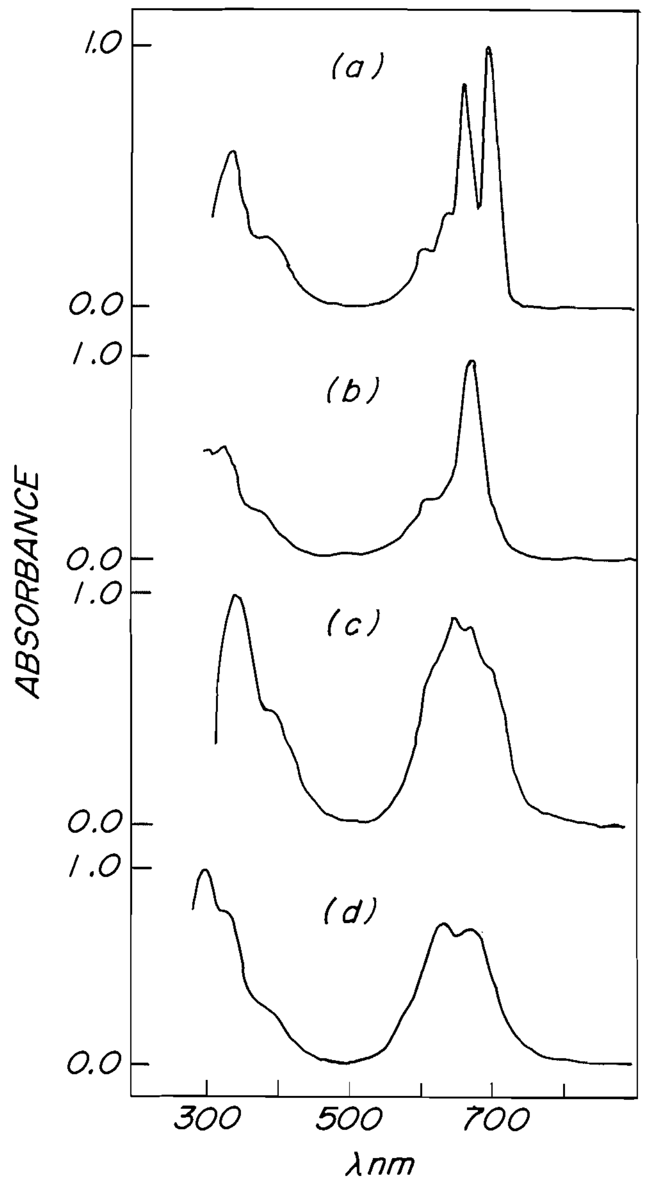

FIG. 1. The λ (nm) visible spectra in CH_2Cl_2 at room temperature of (a) a mononuclear metal-free phthalocyanine, **13***a*, (b) a mononuclear metallophthalocyanine, **13***c*, (c) a binuclear metal-free phthalocyanine, **27***a*, (d) a binuclear metallophthalocyanine, **27***b*.

phthalocyanine dimers are still sufficiently soluble to purify and characterize. A full analysis of **26***a–c* and **27***a–b* by visible spectroscopy and electrochemical methods under a variety of conditions has been undertaken and a preliminary report has appeared (31).

Experimental

Matheson high purity argon was used to maintain inert atmosphere conditions. Infrared (ir) spectra were recorded on a Pye Unicam SP1000 infrared spectrophotometer using KBr discs for solids or as neat films between NaCl discs. Nuclear magnetic resonance (nmr) spectra for protons were recorded on a Varian LM 360 spectrometer using deuterochloroform as solvent and tetramethylsilane as the internal standard. The positions of the signals are reported in δ units. (The splittings of the signals are described as singlets (s), doublets (d), triplets (t), quartets (q), or multiplets (m).) A Bruker WH250 or WH400 spectrometer was used for all ^{13}C nmr spectra and for ^{1}H nmr spectra of **13***a*, **13***d*, **14***a*, **15***a*, **15***d*, **26***a*, and **27***a* at 10^{-2} to 10^{-1} *M*.

The visible–ultraviolet spectra (uv) were recorded on a Perkin–Elmer–Hitachi 340 spectrometer. Mass spectra (ms) were recorded at 70 eV on a VG Micromass 16F mass spectrometer in the EI mode.

The FAB spectra were obtained with a Kratos MS-50 triple analyzer mass spectrometer equipped with a FAB ion source of standard Kratos design and an Ion Tech atom gun. The sample was dissolved in chloroform and a microliter of the resulting solution added to a microliter of *o*-nitrophenyloctylether on the probe tip. The spectra of the molecular ions of the binuclear phthalocyanines were obtained by signal averaging up to 256 scans over the appropriate mass range. The number in parentheses after the indicated ion shows the percentage of the base peak represented by that ion. Melting points (mp) were determined using a Kofler hot stage melting point apparatus and are uncorrected. Thin-layer chromatography (tlc) was performed using silica gel G as the adsorbent. All reactions were stirred with a magnetic stirrer. All solvents were freshly distilled before use. Microanalyses were performed by Guelph Chemical Laboratories Ltd., Guelph, Ont.

*Bis-(3,4-dicyanophenyl)ether (**6**) and 4-isopropoxyphthalonitrile (**7**)*

At room temperature

In a minor modification of Siegl's procedure (15) 4-nitrophthalonitrile (1.64 g, 9.49 mmol), isopropanol (2.0 mL, 26 mmol), and anhydrous potassium carbonate (2.94 g, 21.3 mmol) were stirred at room temperature under an argon atmosphere in 10 mL of dry DMF for 43 h. The potassium carbonate was added in three portions. The crude reaction mixture was poured into water (300 mL). The precipitate was collected by filtration, washed thoroughly with water, and dried. The crude product was purified by silica gel column chromatography using ether – petroleum ether (2:3) as the eluting solvent. It was then recrystallized from a mixture of ether–hexanes to give 1.21 g of slightly yellow crystals of 4-isopropoxyphthalonitrile (**7**), mp 58–59°C (lit. (11, 15) mp 56–57°C) in 69% yield.

At 50–60°C

In another experiment, 17.3 g of 4-nitrophthalonitrile (0.10 mol) reacted with 24 mL of isopropanol (0.31 mol) and 32 g of anhydrous potassium carbonate (0.23 mol) in 120 mL of dry DMF and the mixture *was heated at 50–60°C* under Ar for 93 h. Under these conditions and using an identical work-up as before, a mixture of bis(3,4-dicyanophenyl)ether (**6**) (15) and (**7**) was obtained. Compound **7** was separated from the insoluble **6** by extraction with ether. The 4-isopropoxyphthalonitrile (**7**) was further purified by column chromatography, followed by recrystallization as before to yield 6.10 g of (**7**) in 33% yield.

Further purification of **6** by recrystallization from acetonitrile gave in 44% yield 6.0 g of **6**, mp 256–257°C (lit. (15) mp 254–256°C).

*4-Isobutoxyphthalonitrile (**8**)*

Treatment of 5.19 g (30 mmol) of **1** with 4.44 g (60 mmol) of isobutyl alcohol (**3**) in DMF for 240 h at room temperature as described above for the preparation of **7** yielded after distillation in a Kugelrohr apparatus 5.3 g of 4-isobutoxyphthalonitrile (**8**) in 87% yield. Thin-layer chromatography of the crude reaction mixture indicated the presence of a small amount of 4-hydroxyphthalonitrile (**5**) (18) but this product was not isolated. Crystallization of a small sample of **8** from ethyl acetate – petroleum ether gave colourless crystals of **8**, mp 49–49.5°C; ir (cm^{-1}): 2240 (CN), 1600 (C=C), 1562 (C=C); ^{1}H nmr ($CDCl_3$) δ: 7.9–7.2 (m, 3H, aromatic), 3.9 (d, 2H, CH_2O, J = 6 Hz), 2.2 (m, 1H, CH), 1.1 (d, 6H, $(CH_3)_2C$, J = 6.0 Hz); ms, m/z: 200 (M$^+$, 29), 142 (42), 144 (40), 127 (21), 57 (100), 56 (70), 55 (21), 43 (24), 41 (43), 39 (56). *Anal.* calcd. for $C_{12}H_{12}N_2O$: C 71.98, H 6.04, N 13.99; found: C 72.08, H 5.84, N 13.98.

*4-Neopentoxyphthalonitrile (**9**)*

A solution of 1.73 g (10 mmol) of **1**, 2.30 g (26 mmol) of neopentyl alcohol, and 3.4 g (25 mmol) of potassium carbonate was stirred *at 60°C* (Table 3) as described for the preparation of **7** above. Column chromatography of the reaction product on silica using ethyl acetate – petroleum ether (1:19) gave in 82% yield 1.60 g of 4-neopentoxyphthalonitrile (**9**), mp 61.5–62°C; ir (cm^{-1}): 2230 (CN), 1590 (C=C), 1562 (C=C); ^{1}H nmr ($CDCl_3$) δ: 7.9–7.2 (m, 3H, aromatic), 3.75 (s, 2H, CH_2O), 1.05 (s, 9H, CH_3C); ms, m/z: 214 (M$^+$, 9), 199 (16), 157 (2), 145 (3), 72 (7), 71 (91), 70 (14), 57 (31), 55 (22), 43 (100), 41 (11). *Anal.* calcd. for $C_{13}H_{14}N_2O$: C 72.87, H 6.58, N 13.07; found: C 72.89, H 6.66, N 12.89.

Thin-layer chromatography of the crude reaction product indicated the presence of a small amount of **5** (18) but this product was not isolated.

*Preparation of 5-isopropoxy-1,3-diiminoisoindoline (**10**), 5-isobutoxy-1,3-diiminoisoindoline (**11**), and 5-neopentoxy-1,3-diiminoisoindoline (**12**)*

All diiminoisoindolines were prepared as previously described (19). In a typical example 246 mg (1.15 mmol) of **9** was converted to 297 mg of **12** which was used directly in condensation reactions without further purification. Compounds **10**–**12** did not exhibit nitrile absorptions in their ir spectra.

*Preparation of 2,9,16,23-tetraisopropoxyphthalocyanine (**13**a), 2,9,16,23-tetraisobutoxyphthalocyanine (**14**a), and 2,9,16,23-tetraneopentoxyphthalocyanine (**15**a) (Method A)*

Compound **13***a* was previously prepared in our laboratory (11, 12) from **10** using the procedure of Beach *et al.* (19) and purified by column chromatography using ether – petroleum ether as eluant.

A solution of **11** derived from 600 mg of **8** in 2-*N*,*N*-dimethylaminoethanol underwent self-condensation as for the preparation of **13***a* to give 285 mg of a crude reaction product. Flash chromatography (26) of this product using 2-methoxyethanol – toluene (1:40) as eluant gave upon evaporation of the solvent a purer product, still containing a trace of fluorescent material on examination by tlc. Further purification by flash chromatography yielded upon evaporation of the solvent 163 mg of very pure 2,9,16,23-tetraisobutoxyphthalocyanine (**14***a*) as a shiny blue solid in 27% yield; ir (cm^{-1}): 3300 (NH), 1630 (C=C), 1245, 1100, 1015 (NH), 750; ^{1}H nmr (CD_2Cl_2, 400 MHz) δ: 7.5–6.6 (m, 12H, aromatic), 3.7 (br s, 8H, CH_2O), 2.2 (m, 4H, CH), 1.2 (br s, 24H, CH_3), −5.8 (very br s, 2H); ^{13}C nmr (CD_2Cl_2, 400 MHz) δ: 159.9 (aromatic C—O), 121.9, 121.7, 117.2, 103.6, 74.5 (CH_2—O), 28.6 ($CHCH_2$), 19.3 (CH_3); ms m/z: 804 (M$^+$, 54), 803 (100), 802 (82), 746 (17). *Anal.* calcd. for $C_{48}H_{50}N_8O_4$: C 71.79, H 6.29, N 13.95; found: C 72.02, H 5.84, N 13.98.

Similarly, the isoindoline **12**, derived from 246 mg of phthalonitrile **9**, yielded on condensation a crude product. Flash chromatography using freshly distilled toluene as eluant gave upon evaporation of the solvent 112 mg of a dark blue, shining solid in 45% yield; ir (cm^{-1}): 3290 (NH), 1620 (C=C), 1240, 1100, 1060, 1015 (NH), 750; ^{1}H nmr (CD_2Cl_2, 250 MHz) δ: 7.6–6.0 (m, 12H, aromatic), 3.8 (s, 8H, CH_2O), 1.5 (s, 36H, CH_3), −6.5 (br, 2H, NH); ^{13}C nmr (CD_2Cl_2, 250 MHz) δ: 160.6 (aromatic C—O), 122.1, 117.4, 117.2, 78.6 (CH_2—O), 78.4 (CH_2O), 32.5 (CH_3C), 27.3 (CH_3C); ms, m/z: 859 (M$^+$, 100), 858 (62), 801 (2), 789 (23). *Anal.* calcd. for $C_{52}H_{58}N_8O_4$: C 72.70, H 6.80, N 13.04; found: C 72.78, H 6.86, N 13.00.

General procedures for the preparation of mononuclear metallophthalocyanines (Methods B and C)

Mononuclear metallophthalocyanines were prepared in varying yields (Table 1) according to the procedures of Pawlowski and Hanack (20) (Method B) and Tomoda *et al.* (21) (Method C) from the corresponding phthalonitriles. The metallophthalocyanines were isolated from the reaction mixture by dilution with water, filtration, and thorough washing with water, except for the case in which cuprous cyanide was used as the salt, in which the reaction mixture was treated with aqueous ammonia prior to washing with water. The metallophthalocyanines were purified by flash chromatography (26) using 2-methoxyethanol – toluene 1:40 as the eluting solvent.

*2,9,16,23-Tetraisopropoxyphthalocyaninatocopper (**13**b)*

In a typical procedure (Method B) (20), 0.21 g (1.15 mmol) of 4-isopropoxyphthalonitrile (**7**) reacted with 0.15 g (1.66 mmol) of cuprous cyanide in 2 mL of DMF at 145°C for 20 h to give, after the standard work-up described above, 0.080 g of 2,9,16,23-tetraisopropoxyphthalocyaninatocopper (**13***b*) in 34% yield as a dark blue solid; ir (cm^{-1}): 1610 (C=C), 1245, 1100, 1055, 750; ms, *m/z*: 809 (100), 808 (M$^+$, 55), 807 (67), 765 (36), 724 (16). *Anal.* calcd. for $C_{44}H_{40}N_8O_4Cu$: C 65.37, H 4.99, N 13.86, Cu 7.86; found: C 65.00, H 5.24, N 13.53, Cu 7.47.

In a typical procedure using Method C (21), 0.38 g (2.0 mmol) of **7** reacted with 0.14 g (1.0 mmol) of cupric chloride and 0.62 g (5 mmol) of diazabicyclononane (DBN) in 10 mL of absolute alcohol at reflux temperatures for 24 h to give, after the standard work-up, 0.20 g of **13***b* in 49% yield. Although Method C gave **13***b* in higher yields than Method B, repetitive flash chromatography of the reaction product was necessary to remove some fluorescent impurities and hence, in general, Method B or Method D (see below) is preferred.

*2,9,16,23-Tetraisopropoxyphthalocyaninatocobalt(II) (13*c*)*

Using Methods B and C, **7** was readily converted (Table 1) into 2,9,16,23-tetraisopropoxyphthalocyaninatocobalt(II) (**13***c*), isolated as a shining dark blue solid; ir (cm^{-1}): 1615 (C=C), 1245, 1100, 1060, 755; ms, *m/z*: 804 (M$^+$, 100), 803 (49), 762 (19). *Anal.* calcd. for $C_{44}H_{40}N_8O_4Co$: C 65.75, H 5.02, N 13.94, Co 7.33; found: C 65.73, H 4.99, N 13.63, Co 7.49.

*2,9,16,23-Tetraisopropoxyphthalocyaninatozinc (13*d*)*

Using methods B and C, **7** was converted (Table 1) into 2,9,16,23-tetraisopropoxyphthalocyaninatozinc (**13***d*), isolated as a shining, dark blue solid; ir (cm^{-1}): 1610 (C=C), 1240, 1100, 1050, 750; ^{13}C nmr (CD_2Cl_2, 400 MHz) δ: 159.3 (aromatic C—O), 125.4, 121.7, 109.4, 71.5 (CH_2—O), 70.6 (CH_2—O), 22.7 (CH_3), 21.8 (CH_3); ms, *m/z*: 813 (64), 812 (79), 811 (96), 810 (M$^+$, 95), 809 (100), 808 (70), 767 (31). *Anal.* calcd. for $C_{44}H_{40}N_8O_4Zn$: C 65.23, H 4.98, N 13.83, Zn 8.07; found: C 65.41, H 5.00, N 13.76, Zn 7.76.

*Metal insertion reactions on metal-free phthalocyanines. 2,9,16,23-Tetraisobutoxyphthalocyaninatocopper (14*b*) (Method D in toluene)*

To a solution of 100 mg (0.12 mmol) of 2,9,16,23-tetraisobutoxyphthalocyanine (**14***a*) in 10 mL of toluene was added 150 mg (0.83 mmol) of cupric acetate. The solution was stirred at 100°C under an argon atmosphere for 3 h. The crude reaction mixture was applied to 3 tlc preparative plates, and eluted 3 times with 2-methoxyethanol − toluene (1:100) to give a dark green band which was extracted with toluene in a Soxhlet extractor. Further purification by flash chromatography using 2-methoxyethanol − toluene (1:20) gave in 74% yield 80 mg of 2,9,16,23-tetraisobutoxyphthalocyaninatocopper (**14***b*) as a dark blue, shining solid; ir (cm^{-1}): 1620 (C=C), 1250, 1105, 1065, 755; ms, *m/z*: 867 (28), 866 (M$^+$, 56), 865 (71), 864 (100), 863 (59), 808 (25). *Anal.* calcd. for $C_{48}H_{48}N_8O_4Cu$: C 66.53, H 5.60, N 12.77, Cu 7.02; found: C 66.68, H 5.61, N 12.96, Cu 7.35.

*2,9,16,23-Tetraneopentoxyphthalocyaninatocopper (15*b*) and 2,9,16,23-tetraneopentoxyphthalocyaninatocobalt(II) (15*c*) (Method D, in DMF and 2-*N,N*-dimethylaminoethanol)*

To a solution of 41 mg (0.048 mmol) of **15***a* in 3 mL of a 1:2 mixture of dry DMF and 2-*N,N*-dimethylaminoethanol was added 10 mg (0.074 mmol) of anhydrous cupric chloride. The mixture was heated for 1 h under an argon atmosphere using an oil bath heated to 110°C. The mixture was cooled to room temperature and directly subjected to flash chromatography using freshly distilled toluene as the eluting solvent to give in 94% yield (Table 1) 41 mg of 2,9,16,23-tetraneopentoxyphthalocyaninatocopper (**15***b*) as a dark blue, shining solid; ir (cm^{-1}): 1615 (C=C), 1240, 1100, 1060, 745; ms, *m/z*: 922 (78), 921 (M$^+$, 81), 920 (100), 864 (4), 850 (9). *Anal.* calcd. for $C_{52}H_{56}N_8O_4Cu$: C 67.84, H 6.13, N 12.17, Cu 6.90; found: C 68.10, H 6.24, N 11.89, Cu 6.97.

Similarly, 33 mg of **15***a* gave in 94% yield (Table 1) 33 mg of 2,9,16,23-tetraneopentoxyphthalocyaninocobalt(II) (**15***c*) as a dark blue, shining solid; ir (cm^{-1}): 1615 (C=C), 1240, 1100, 1065, 750; ms, *m/z*: 916 (M$^+$, 100), 915 (47), 859 (7), 846 (19). *Anal.* calcd. for $C_{52}H_{56}N_8O_4Co$: C 68.18, H 6.16, N 12.23, Co 6.43; found: C 68.22, H 6.14, N 12.07, Co 6.94.

Compounds **15***b* and **15***c* were also prepared directly from **9** by the methods of Pawlowski and Hanack (20) (Method B, Table 1).

*2,9,16,23-tetraneopentoxypthalocyaninatozinc (15*d*)*

Using a modification of the procedure of Pawloski and Hanack (20) (Method B), 394 mg (1.84 mmol) of 4-neopentoxyphthalonitrile (**9**) was suspended in 2 mL of dry DMF. Zinc acetate (1.04 g, 5.66 mmol) was added and the mixture heated using an oil bath at 155°C under argon. The clear reaction mixture turned yellow after 1 h and dark green after an additional 1 h. After heating for 20 h at 155°C, the mixture was cooled to room temperature, diluted with water, filtered, and washed thoroughly with water. The crude product was purified by flash chromatography using petroleum ether − ether (6:1) as the eluting solvent to give in 27% yield (Table 1) 114 mg of 2,9,16,23-tetraneopentoxyphthalocyaninatozinc (**15***d*) as a dark blue, shining solid; ir (cm^{-1}): 1610 (C=C), 1240, 1100, 1060, 750; ^{1}H nmr (CD_2Cl_2, 250 MHz) δ: 7.7−6.1 (m, 12H, aromatic), 3.5 (s, 8H, CH_2O), 1.3 (s, 36H, CH_3); ^{13}C nmr (CD_2Cl_2, 250 MHz) δ: 160.1 (aromatic C—O), 149.5, 121.7, 121.3, 116.9, 116.6, 104.2, 103.9, 78.2 (CH_2O), 78.1 (CH_2O), 32.2 (CH_3C), 27.1 (CH_3C), 26.8 (CH_3C), 26.5 (CH_3C); ms, *m/z*: 925 (52), 924 (84), 923 (91), 922 (M$^+$, 97), 921 (100), 868 (2), 853 (40). *Anal.* calcd. for $C_{52}H_{56}N_8O_4Zn$: C 67.71, H 6.12, N 12.15, Zn 7.07; found: C 67.80, H 6.39, N 11.85, Zn 6.94.

2-Methyl-2-trityloxymethyl-1,3-propanediol (17)

To a solution of 1,1,1-tris(hydroxymethyl)ethane (**16**) (6.48 g, 54.00 mmol) in 15 mL of dry pyridine, triphenylmethyl chloride (2.60 g, 9.32 mmol) was added and the mixture was stirred for 22 h at room temperature under exclusion of moisture ($CaCl_2$ drying tube). The mixture was then poured into 180 mL of ice-water and extracted 4 times with ether. The combined ether extracts were washed six times with water, dried over anhydrous $MgSO_4$, and evaporated to give a viscous oil which was dried under high vacuum for 4 h. The crude product was purified by column chromatography on silica gel using a mixture of chloroform−hexane (3:1) as the eluting solvent. Evaporation of the solvent yielded a product which was recrystallized from a mixture of ether−hexane to give in 68% yield 2.18 g of white crystals, mp 127−128°C; ir (cm^{-1}): 3360 (OH), 1600 (C=C), 1500, 1495, 1050, 770, 710, 705; ^{1}H nmr ($CDCl_3$, 60 MHz) δ: 7.6−7.2 (m, 15H, aromatic), 3.65 (d, 4H, CH_2O, J = 6 Hz), 3.2 (s, 2H, CH_2O), 2.4 (t, 2H, OH, J = 6 Hz), 0.8 (s, 3H, CH_3); ^{13}C nmr ($CDCl_3$, 400 MHz) δ: 143.7 (aromatic C-1′), 128.6 and 127.9 (aromatic C-2′, C-6′, C-3′, C-5′), 127.1 (aromatic C-4′), 86.7 (PhC), 67.8 (CH_2OC), 67.0 (CH_2OH), 41.1 (CCH$_2$), 17.3 (CH_3); ms, *m/z*: 362 (M$^+$, 3), 285 (20), 259 (50), 239 (100), 183 (80), 105 (75), 77 (23). *Anal.* calcd. for $C_{24}H_{26}O_3$: C 79.53, H 7.23; found: C 79.58, H 7.19.

1,3-Bis(3′,4′-dicyanophenoxy)-2-methyl-2-trityloxymethylpropane (20) 1,3-bis(3′,4′-dicyanophenoxy)-2,2-dimethylpropane (21), and 1,3-bis(3′,4′-dicyanophenyl)-2-ethyl-2-methylpropane (22)

A solution of 1.09 g (3.01 mmol) of **17**, 1.07 g (6.18 mmol) of **1**, and 1.75 g (12.68 mmol) of anhydrous potassium carbonate was heated at 65°C in 7 mL of dry DMSO by the method of Keller *et al.* (16). The reaction mixture was filtered and washed with methylene chloride (CH_2Cl_2). The filtrate was diluted with CH_2Cl_2 and washed thoroughly 6 times with water and finally with saturated sodium chloride. After drying over anhydrous magnesium sulfate ($MgSO_4$), the solvent was evaporated to give 1.77 g of a light brown solid. The crude product was purified by flash chromatography using chloroform−hexane (3:1) as the eluting solvent. Evaporation of the solvent yielded an oil which was dissolved in warm methanol and rapidly cooled to −35°C (but not lower) to give in 56% yield 1.02 g of 1,3-bis(3′,4′-dicyanophenyl)-2-methyl-2-trityloxymethylpropane (**20**) as light yellow crystals, mp 89−92°C; ir (cm^{-1}): 2240 (CN), 1600 (C=C), 1495, 1255, 1090, 1030, 710, 700; ^{1}H nmr ($CDCl_3$, 60 MHz) δ: 7.80−7.05 (m, 21H, aromatic), 4.03 (s, 4H, CH_2O), 3.30 (s, 2H, CH_2O), 1.30 (s, 3H, CH_3); ms, *m/z*: 614 (M$^+$, 18), 537 (20), 283 (10), 243 (65), 240 (100), 183 (48), 144 (19), 105 (58). *Anal.* calcd. for $C_{40}H_{30}N_4O_3$: C 78.16, H 4.92, N 9.11; found: C 78.18, H 4.72, N 8.92.

Similarly, a solution of 1.04 g (10.0 mmol) of 2,2-dimethyl-1,3-propanediol (**18**), 3.81 g (22 mmol) of **1**, and 6.7 g (48.6 mmol) of anhydrous K_2CO_3 in 10 mL of dry DMSO gave a crude reaction product. The reaction mixture was filtered and washed with ethyl acetate. The filtrate was diluted with ethyl acetate, thoroughly washed with water until the aqueous layer was clear, and finally washed with a saturated sodium chloride solution. After drying over anhydrous $MgSO_4$, the solvent was evaporated to give a dark brown solid. The crude product was purified by column chromatography on silica gel using benzene–acetonitrile (9:1) as the eluting solvent. Evaporation of the solvent and recrystallization of the residue from acetonitrile–water gave 1.36 g (38%) of 1,3-bis(3′,4′-dicyanophenoxy)-2,2-dimethylpropane (**21**) as creamy crystals, mp 168–169°C; ir (cm^{-1}): 2240 (CN), 1600 (C═C), 1260, 1100, 1040, 845; ^{1}H nmr (acetone-d_6, 60 MHz) δ: 8.10–7.42 (m, 6H, aromatic), 4.27 (s, 4H, CH_2OC), 1.27 (s, 6H, CH_3); ms, *m/z*: 356 (M$^+$, 11), 213 (30), 171 (88), 127 (43). *Anal.* calcd. for $C_{21}H_{16}N_4O_2$: C 70.78, H 4.52, N 15.72; found: C 70.74, H 4.37, N 15.43.

In a manner similar to that described above for the preparation of **21**, 1.60 g of 2-ethyl-2-methyl-1,3-propanediol (**19**) yielded a crude reaction product. Thin-layer chromatography of this product using benzene–acetonitrile (9:1) as eluant exhibited the presence of a minor amount of 4-hydroxyphthalonitrile (**5**). Thus, the ethyl acetate filtrate was washed several times with water, followed by 0.5 *M* cold NaOH, water, and finally saturated NaCl solution. The ethyl acetate solution yielded upon the normal work-up a dark brown solid. The aqueous layer was acidified with dilute HCl and the organic material was extracted into ethyl acetate. The ethyl acetate was dried over anhydrous $MgSO_4$, filtered, and evaporated to give 560 mg of **5** (18) which was not further purified. Purification of the dark brown solid, obtained from the original ethyl acetate extract above, yielded, upon recrystallization from ethyl acetate – hexanes, 1.84 g (37%) of 1,3-bis-(3′,4′-dicyanophenoxy)-2-ethyl-2-methylpropane (**22**) as creamy crystals, mp 157–158°C; ir (cm^{-1}): 2240 (CN), 1600 (C═C), 1260, 1095, 1025, 845; ^{1}H nmr ($CDCl_3$, 60 MHz) δ: 7.87–7.18 (m, 6H, aromatic), 4.03 (s, 4H, CH_2O), 1.62 (q, 2H, CH_2C, *J* = 7 Hz), 1.18 (s, 3H, CH_3C), 1.10 (t, 3H, CH_3CH$_2$, *J* = 7 Hz); ms, *m/z*: 370 (M$^+$, 23), 227 (46), 185 (60), 171 (65), 127 (52). *Anal.* calcd. for $C_{22}H_{18}N_4O_2$: C 71.34, H 4.90, N 15.12; found: C 71.30, H 5.03, N 15.09.

Preparation of the bis-1,3-diiminoisoindolines **23** *and* **24**

Compounds **23** and **24** were prepared from **21** and **22** respectively as described above for **10**–**12** with one minor exception. As **21** and **22** were only slightly soluble in methanol at room temperature, these compounds were dissolved in a solution of sodium methoxide in methanol at 65°C and ammonia was bubbled into this solution for 1 h at 65°C and for 3 h under reflux conditions.

1,3-Bis-2′-(9′,16′,23′-triisopropoxyphthalocyaninoxycopper)-2-methyl-2-trityloxymethylpropane (25)

A mixture of 0.14 g (0.23 mmol) of **20**, 1.0 g (5.4 mmol) of **7**, and 1.54 g (17.23 mmol) of cuprous cyanide was heated at 130°C (oil bath) in 7.5 mL of dry DMF for 20 h under argon atmosphere (Method B) (20). After dilution with ammonia, the product was filtered and washed with water. The dark blue-green residue was dissolved in toluene and chromatographed under argon using the flash chromatography technique. Elution with 2-methoxyethanol – toluene (1:40) gave, upon solvent evaporation, 340 mg of 2,9,16,23-tetraisopropoxyphthalocyaninatocopper (**13***b*) in 31% yield. Elution with 2-methoxyethanol – toluene (1:4) gave a slightly impure product. Thin-layer chromatography of this product exhibited a major blue spot and slightly faster moving green impurity (2-methoxyethanol – toluene, 1:4 as eluant). Further purification by flash chromatography using a small diameter column (1 cm) gave in 1% yield 6 mg of the pure dimer, 1,3-bis-2′-(9′,16′,23′-triisopropoxyphthalocyaninatocopper)-2-methyl-2-trityloxymethylpropane (**25**) as a dark blue, shining solid; ir (cm^{-1}: 1615 (C═C), 1250, 1120, 1105, 1060, 755; ms, *m/z*: 1859.5 (M$^+$), 1816 (*M*$^+$ – 43). *Anal.* calcd. for $C_{106}H_{90}N_{16}O_9Cu_2$: C 68.48, H 4.88, N 12.05; found: C 67.85, H 5.34, N 12.53.

*1,3-Bis-2′-(9′,16′,23′-trineopentoxyphthalocyaninoxy)-2,2-dimethylpropane (26*a*) and 1,3-bis-2′-(9′,16′,23′-trineopentoxyphthalocyaninoxy)-2-ethyl-2-methylpropane (27*a*)*

The two crude diiminoisoindolines **12** and **23** obtained from 4.2 g (19.6 mmol) of 4-neopentoxyphthalonitrile (**9**) and 249 mg (0.7 mmol) of 1,3-bis-(3′,4′-dicyanophenoxy)-2,2-dimethylpropane (**21**), respectively, were heated at 150°C (oil bath) in 30 mL of 2-*N*,*N*-dimethylaminoethanol for 23 h under an argon atmosphere. The mixture gradually changed colour from yellow to dark blue. After cooling to room temperature, the mixture was diluted with water and the blue coloured residue was filtered and washed thoroughly with water until the filtrate was colourless. The crude product was purified in two separate batches by flash chromatography using a 5 cm wide column packed with silica gel 9 cm high. The dark blue-green product was preadsorbed on silica and eluted with 1500 mL of freshly distilled toluene to give 1.92 g of the monomeric 2,9,16,23-tetraneopentoxyphthalocyanine (**15***a*) in 46% yield. Further elution with 2-methoxyethanol – toluene in ratios of 1:40 and 1:10 yielded, after solvent evaporation, 340 mg of a purified product, containing traces of monomer **15***a* and some green material (fluorescent under uv) which moved closely behind the desired product when examined by tlc (2-methoxyethanol – toluene, 1:40 as eluting solvent). Flash chromatography of this purified material on a smaller column 3 cm wide removed, on elution with toluene and 2-methoxyethanol – toluene (1:100), all traces of monomer **15***a*. Further elution with 2-methoxyethanol – toluene (1:20) yielded some fractions of a very pure, dark blue product. Other fractions were still contaminated with the green material. Purification of these fractions was achieved using preparative tlc and 2-methoxyethanol – toluene (1:20) as eluting solvent. Finally, the product was purified by flash chromatography as above to give in 17% yield 195 mg of 1,3-bis-2′-(9′,16′,23′-trineopentoxyphthalocyaninoxy)-2,2-dimethylpropane (**26***a*) as a very pure, dark blue, shining solid; ir (cm^{-1}): 3300 (NH), 1615 (C═C), 1240, 1100, 1055, 1020 (NH), 750; ^{1}H nmr (CD_2Cl_2, 400 MHz) δ: 8.21–7.12 (br), 4.05–3.65 (br), 1.42 (br), –6.12 (br); ^{13}C nmr (CD_2Cl_2, 400 MHz) δ: 32.35 (CH_3*C*), 27.20 (*C*H_3C); ms, *m/z*: 1645 (100), 1644 (M$^+$, 84). *Anal.* calcd. For $C_{99}H_{104}N_{16}O_8$: C 72.24, H 6.37, N 13.61; found: C 72.47, H 6.27, N 13.49.

Similarly, the two crude isoindolines **12** and **24** obtained from 5.6 g (26.2 mmol) of **9** and 0.4 g (1.08 mmol) of **22**, respectively, yielded 1.72 g of **15***a* in 31% yield and 184 mg in 10% yield of 1,3-bis-2′-(9′,16′,23′-trineopentoxyphthalocyaninoxy)-2-ethyl-2-methylpropane (**27***a*) as a dark blue, shining solid; ir (cm^{-1}): 3310 (NH), 1618 (C═C), 1240, 1100, 1058, 1020 (NH), 750; ^{1}H nmr ($CDCl_3$, 400 MHz) δ: 9.4–6.8 (br), 4.2–3.6 (br), 1.8–0.8 (br), –5.8 – (–6.4) (br); ^{13}C nmr (CD_2Cl_2, 400 MHz) δ: 78.6 (*C*H_2O), 32.4 (*C*CH$_3$), 30.1 (*C*CH$_2$), 27.2 (*C*H$_3$C), 26.6 (CCH$_2$*C*H$_3$); ms, *m/z*: 1662 (100), 1660 (M$^+$, 41), 1658 (30). *Anal.* calcd. for $C_{100}H_{106}N_{16}O_8$: C 72.35, H 6.44, N 13.50; found: C 72.51, H 6.77, N 13.56.

*1,3-Bis-2′-(9′,16′,23′-trineopentoxyphthalocyaninoxycopper)-2,2-dimethylpropane (26*b*), 1,3-bis-2′-(9′,16′,23′-trineopentoxyphthalocyaninoxycobaltII)-2,2-dimethylpropane (26*c*), and 1,3-bis-2′-(9′,16′,23′-trineopentoxyphthalocyaninoxycobaltII)-2-ethyl-2-methylpropane (27*b*)*

A mixture of 50 mg (0.03 mmol) of **26***a*, 23 mg (0.13 mmol) of anhydrous cupric acetate, and 10 mL of freshly distilled toluene was heated at 100°C for 17 h under an argon atmosphere. The solution was cooled and purified by flash chromatography (26) by direct application of the crude reaction product to the column. Elution with 2-methoxyethanol – toluene (7:200) gave, after solvent evaporation, 29 mg (54% yield) of a dark blue, shining product which was washed with anhydrous ether to remove very minor fluorescent impurities (detected by tlc) leaving 28 mg of very pure 1,3-bis-2′-(9,16,23-trineopentoxyphthalocyaninoxycopper)-2,2-dimethylpropane (**26***b*); ir (cm^{-1}): 1615 (C=C), 1240, 1100, 1060, 750; ms, m/z: 1772, 1771, 1770, 1769, 1768 (M^+), 1767. *Anal.* calcd. for $C_{99}H_{100}N_{16}O_8Cu_2$: C 67.22, H 5.70, N 12.67, Cu 7.18; found: C 67.41, H 5.52, N 12.40, Cu 6.83.

Similarly, 50 mg (0.03 mmol) of **26*a*** and 105 mg (0.81 mmol) of anhydrous cobaltic chloride in 15 mL of a 1:2 mixture of 2-methoxyethanol − toluene was heated at 100°C for 20 h to give, after purification as above, 32 mg (60% yield) of 1,3-bis-2′-(9′,16′,23′-trineopentoxyphthalocyaninoxycobaltII)-2,2-dimethylpropane (**26*c***) as a dark blue, shining solid: ir (cm^{-1}): 1615 (C=C), 1240, 1100, 1068, 755; ms, m/z: 1761 (61), 1760 (M^+, 100), 1759. *Anal.* calcd. for $C_{99}H_{100}N_{16}O_8Co_2$: C 67.57, H 5.73, N 12.73, Co 6.70; found: C 67.92, H 5.88, N 12.84, Co 6.25.

Similarly, 70 mg (0.04 mmol) of **27*a*** and 57 mg (0.44 mmol) of anhydrous cobaltic chloride in 10 mL of a 3:7 mixture of 2-methoxyethanol − toluene were heated at 110°C for 24 h under an argon atmosphere. Purification as above gave 55 mg (74% yield) of pure 1,3-bis-2′-(9′,16′,23′-trineopentoxyphthalocyaninatocobaltII)-2-ethyl-2-methylpropane (**27*b***) as a dark blue, shining solid; ir (cm^{-1}): 1620 (C=C), 1245, 1100, 1068, 758; ms, m/z: 1774 (M^+, 100). *Anal.* calcd. for $C_{100}H_{102}N_{16}O_8Co_2$: C 67.71, H 5.80, N 12.63, Co 6.64; found: C 68.14, H 6.21, N 12.61, Co 6.64.

Acknowledgements

We are grateful to the Natural Sciences and Engineering Research Council of Canada for financial support of this research. This work was also partially funded by the Office of Naval Research (Washington) and by the Midwest Center for Mass Spectrometry, a National Science Foundation Regional Instrumentation Facility (Grant No. CHE 8211164). We thank Dr. Jack Martin Miller of Brock University for providing the mass spectra of the mononuclear metallophthalocyanines, **15*b*−*d***.

1. R. JASINSKI. Nature, **201**, 1212 (1964); J. Electrochem. Soc. **112**, 526 (1965).
2. P. SAYER, M. GOUTERMAN, and C. R. CONNELL. Acc. Chem. Res. **15**, 73 (1982).
3. M. R. TARASEVITCH and RADYSHKINA. Usp. Khim. **49**, 1498 (1980); Russ. Chem. Rev. **49**, 718 (1980).
4. F. VAN DEN BRINK, E. BARENDRECHT, and W. VISSCHER. Recl. Trav. Chim. Pays-Bas, **99**, 253 (1980).
5. J. P. COLLMAN. Acc. Chem. Res. **10**, 265 (1977).
6. F. P. SCHWARZ, M. GOUTERMAN, Z. MULJIANI, and D. H. DOLPHIN. Bioinorg. Chem. **2**, 1 (1972); J. HIOM, J. B. PAINE III, V. ZAPF, and D. DOLPHIN. Can. J. Chem. **61**, 2220 (1983).
7. J. P. COLLMAN, F. C. ANSON, S. BENCOSME, A. CHONG, T. COLLINS, P. DENISEVICH, E. EVITT, T. GEIGER, J. A. IBERS, G. JAMESON, Y. KONAI, C. KOVAL, K. MEIER, P. OAKLEY, R. B. PETTMAN, E. SCHMITTOV, and J. SESSLER. *In* Organic synthesis today and tomorrow. *Edited by* B. M. Trost and C. R. Hutchinson. Pergamon, Oxford. 1981.
8. J. P. COLLMAN, F. C. ANSON, C. E. BARNES, C. S. BENCOSME, T. GEIGER, E. R. EVITT, R. P. KRCH, K. MEIER, and R. B. PETTMAN. J. Am. Chem. Soc. **105**, 2694 (1983).
9. C. K. CHANG. J. Am. Chem. Soc. **99**, 2819 (1977); N. E. KAGAN, D. MAUZERALL, and R. B. MERRIFIELD. J. Am. Chem. Soc. **99**, 5484 (1977); J. E. BALDWIN, M. J. CROSSLEY, T. KLOSE, E. A. O'REAR, and M. K. PETERS. Tetrahedron, **38**, 27 (1982); I. TABUSHI and T. SASAKI. J. Am. Chem. Soc. **105**, 2901 (1983).
10. A. B. P. LEVER. Adv. Inorg. Chem. Radiochem. **7**, 27 (1965).
11. C. C. LEZNOFF and T. W. HALL. Tetrahedron Lett. **23**, 3023 (1982).
12. T. W. HALL, S. GREENBERG, C. R. MCARTHUR, B. KHOUW, and C. C. LEZNOFF. Nouv. J. Chim. **6**, 653 (1982).
13. R. W. MURRAY. Acc. Chem. Res. **13**, 135 (1980).
14. P. SAYER, M. GOUTERMAN, and C. R. CONNELL. Acc. Chem. Res. **15**, 73 (1982).
15. W. O. SIEGL. J. Hetereocycl. Chem. **18**, 1613 (1981).
16. T. M. KELLER, T. R. PRICE, and J. R. GRIFFITH. Synthesis, 613 (1980); T. M. KELLER and J. R. GRIFFITH. U.S. Patent No. 4, 226, 801 (1980).
17. N. P. MARULLO and A. W. SNOW. ACS Symposium Series, **14**, 325 (1982).
18. V. A. USTINOV, V. V. PLAKHTINSKII, G. S. MIRONOV, and N. S. RYABUKHINA. J. Org. Chem. USSR, **15**, 1595 (1979); Zh. Org. Khim. **15**, 1775 (1979).
19. P. J. BEACH, S. J. GRAMMATICA, O. A. OSSANNA, and L. WEINBERGER. J. Heterocycl. Chem. **7**, 1403 (1970).
20. G. PAWLOWSKI and M. HANACK. Synthesis, 287 (1980).
21. H. TOMADA, S. SAITO, S. OGAWA, and S. SHIRAISHI. Chem. Lett. 1277 (1980).
22. M. HANACK, J. METZ, and G. PAWLOSKI. Chem. Ber. **115**, 2836 (1982).
23. J. S. BRADSHAW and RICHARD H. HALES. J. Org. Chem. **36**, 318 (1971); J. S. BRADSHAW, E. Y. CHEN, R. H. HALES, and J. A. SOUTH. J. Org. Chem. **37**, 2051 (1972); F. DELCLIMA, G. BIGGI, and F. PIETRO. J. Chem. Soc. Perkin Trans. 2, 55 (1973).
24. H. SHIRAI, S. HIGAKI, K. HANABUSA, N. HOJO, and O. HIRABARU. J. Chem. Soc. Chem. Commun. 751 (1983).
25. J. H. FENDLER. Acc. Chem. Res. **13**, 7 (1980).
26. W. C. STILL, M. KAHN, and A. MITRA. J. Org. Chem. **43**, 2923 (1978).
27. M. L. GROSS, E. K. CHESS, P. A. LYON, F. W. CROW, S. EVANS, and H. TUDGE. Int. J. Spectrom. Ion. Phys. **42**, 243 (1982).
28. H. F. SHURVELL and L. PINZUTI. Can. J. Chem. **44**, 125 (1966); M. P. SAMMES. J. Chem. Soc. Perkin Trans. 2, 160 (1972).
29. J. T. CLERC, E. PRETSCH, and J. SEIBL. Structural analysis of organic compounds. Elsevier, New York. 1981. p. 277.
30. G. J. RAY, R. J. KURLAND, and A. K. COLTER. Tetrahedron, **27**, 735 (1971); A. J. JONES, C. C. LEZNOFF, and P. I. SVIRSKAYA. Org. Magn. Reson. **18**, 236 (1982).
31. C. C. LEZNOFF, S. GREENBERG, S. M. MARCUCCIO, P. C. MINOR, P. SEYMOUR, A. B. P. LEVER, and K. B. TOMER. Inorg. Chim. Acta, **89**, L35 (1984).

Analogs of cannabinoids: synthesis of some 7*H*-indolo-, 5*H*-imidazolo, 7*H*-benzimidazolo[1,2-*c*] [1,3]benzoxazines – novel ring systems

V. K. MAHESH, MAMTA MAHESWARI, RAKESH SHARMA, AND RASHMI SHARMA
Department of Chemistry, University of Roorkee, Roorkee (U.P.) 247667, India

Received August 13, 1984

V. K. MAHESH, MAMTA MAHESWARI, RAKESH SHARMA, and RASHMI SHARMA. Can. J. Chem. **63**, 632 (1985).

Tetrahydrocannabinol **1**, the active constituent of *Cannabis sativa Linn*, is a well-known CNS-active compound and introduction of a nitrogen atom at the ring junction of the pyran and alicyclic ring is of considerable interest. This prompted the synthesis of 7*H*-indolo[1,2-*c*] [1,3]-, 5*H*-imidazolo[1,2-C] [1,3],- and 7*H*-benzimidazolo[1,2-*c*] [1,3]-benzoxazine, a novel heterocyclic system. 2-(2′-Hydroxyphenyl) indoles, 2-(2′-hydroxyphenyl) imidazoles, and 2-(2′-hydroxyphenyl) benzimidazoles are suitable intermediates for the preparation of this type of benzoxazines, as the second heterocycle (ring B) can then be constructed by introduction of a methylene bridge between the hydroxyl of the 2′-hydroxy phenyl substituent and the imino group of the heterocyclic system.

V. K. MAHESH, MAMTA MAHESWARI, RAKESH SHARMA et RASHMI SHARMA. Can. J. Chem. **63**, 632 (1985).

Le tétrahydrocannabinol (**1**), le constituant actif du *Cannabis sativa Linn* est un composé dont l'activité sur le CNS est bien connue et l'introduction d'un atome d'hydrogène à la jonction entre le cycle pyranne et l'alicycle présente beaucoup d'intérêt. Ceci nous a conduit à réaliser la synthèse des 7*H*-indolo[1,2-*c*], 5*H*-imidazolo[1,2-*c*] et 7*H*-benzimidazolo[1,2-*c*] [1,3]benzoxazines, un nouveau système hétérocyclique. Les (hydroxy-2 phényl)-2 indoles, (hydroxy-2 phényl)-2 imidazoles et (hydroxy-2 phényl)-2 benzimidazoles sont des intermédiaires bien adaptés à la préparation de ce type de benzoxazines puisque le deuxième hétérocycle (cycle B) peut alors être construit par l'introduction d'un pont méthylène entre l'hydroxyle du substituant hydroxy-2′ phényle et le groupe imino du système hétérocyclique.

[Traduit par le journal]

Introduction

Tetrahydrocannabinols **1**, active constituents of *Cannabis sativa Linn*, are among a very small number of non-nitrogenous compounds which are central nervous active. To bring about a suitable modification in the activity, several nitrogen-containing analogs have been synthesized; some of these compounds showed CNS activity, but no separation of biological activities could be achieved (1–6). Introduction of a nitrogen atom at the ring junction of the pyran ring (ring B) and the alicyclic ring (ring C) of THC appears to be of considerable interest in studying the structure–activity relationship among this class of compounds. 9,10,11,11a-Tetrahydro 6*H*,8*H*-pyrido[1,2-*c*] [1,3]benzoxazine **2** has been prepared as a model compound containing a nitrogen atom at the ring junction (7).

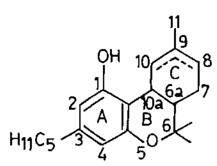

1

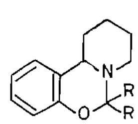

2

Some well-known CNS-active agents are reported to have indole, imidazole, and benzimidazole in their structural makeup (8–10); therefore it was thought that molecules having mixed features of cannabinoids (ring A and B) and substituted pyrrole and imidazole as ring C, with a nitrogen atom as a part of both ring B and C, would be of great pharmacological interest. Such heterocyclic systems would be novel and have not been prepared before. In this paper we wish to report on the preparation and studies of 7,7-dimethyl-7*H*-indolo[1,2-*c*] [1,3]benzoxazines, 5*H*-imidazolo[1,2-*c*] [1,3]benzoxazines, and 7*H*-benzimidazolo[1,2-*c*] [1,3]benzoxazine.

Discussion

For the preparation of the benzoxazine systems an ingenious method has been developed. A methylene bridge has been constructed between the hydroxyl group of the 2′-hydroxy-

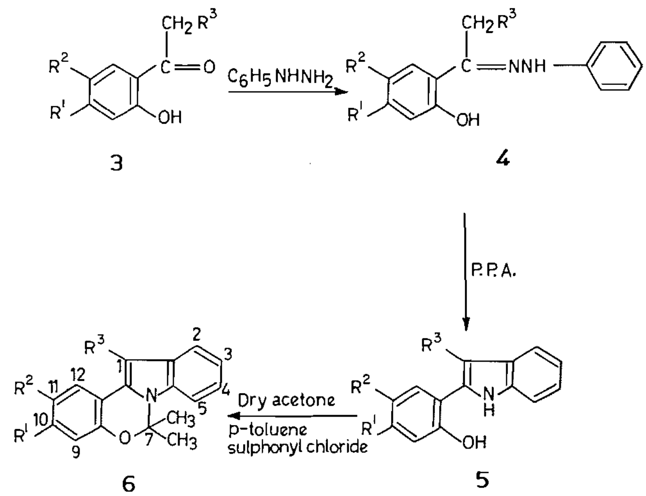

SCHEME 1

phenyl substituent and the imino group of the heterocyclic system – indole, imidazolo, or benzimidazole. This is achieved by boiling the properly substituted heterocyclic compound with either (a) dry acetone in presence of *p*-toluene sulphonyl chloride (11) or (b) methylene dibromide in potassium carbonate – dimethylformamide mixture. 2-(2′-Hydroxyphenyl) indoles, on refluxing in dry acetone in presence of *p*-toluene sulphonyl chloride, gave the expected product, 7,7-dimethyl-7*H*-indolo[1,2-*c*] [1,3]benzoxazines, in good yields. The use of methylene dibromide, however, resulted in a number of compounds, from which the expected 7*H*-indolo[1,2-*c*] [1,3]benzoxazine could not be isolated (12). Condensation of 2-(2′hydroxyphenyl) imidazoles and 2-(2′-hydroxyphenyl) benzimidazoles with methylene dibromide in K_2CO_3–DMF gave 5*H*-imidazolo[1,2-*c*] [1,3]benzoxazines and 7*H*-benzimidazolo[1,2-*c*] [1,3]benzoxazines. It has also been noted that the phenolic group in ring A is essential for the biological activity (13, 14).

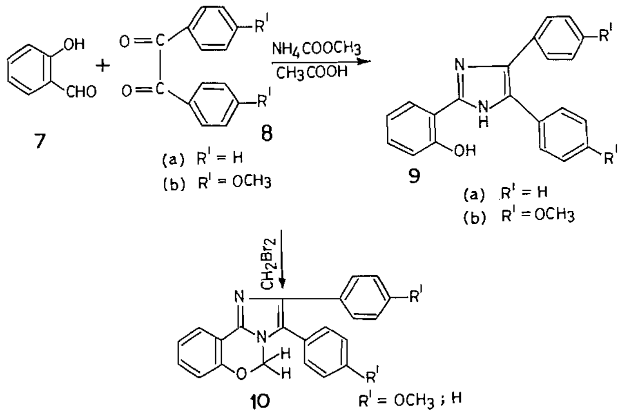

SCHEME 2

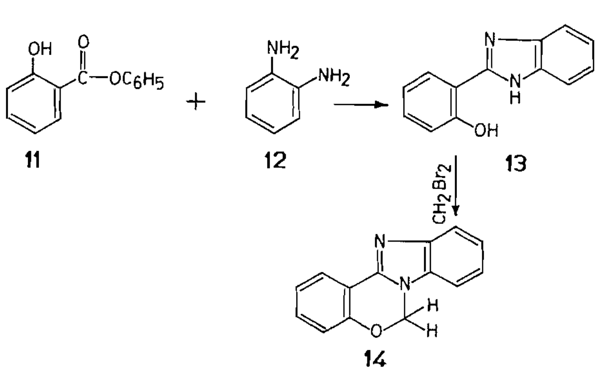

SCHEME 3

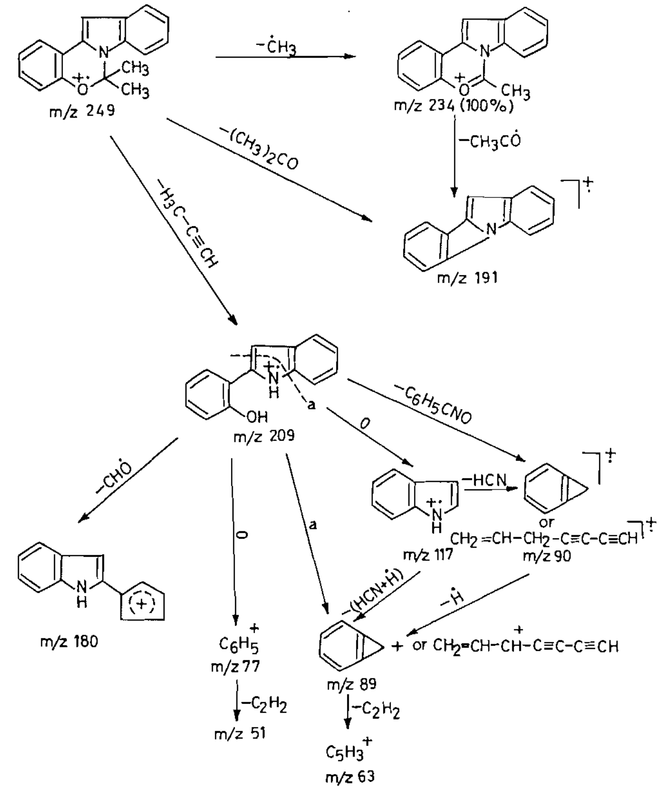

CHART 1

Nuclear magnetic resonance studies

The nmr spectrum of 7,7-dimethyl-7*H*-indolo[1,2-*c*] [1,3]-benzoxazine **6***a* showed a sharp singlet at δ 1.81 for the *gem*-dimethyl at the 7 position. The other protons of benzoxazine are at comparable values to the 2-(2′-hydroxyphenyl indole) protons. In the case of the imidazolo benzoxazines, in addition to the signals for aromatic protons, a singlet at δ 5.67 integrating for two protons which can be assigned to methylene protons at position 5 in the molecule has been observed.

Mass spectral analyses

The molecular ions in the mass spectra of compounds 7,7-dimethyl-7*H*-indolo[1,2-*c*] [1,3]benzoxazine **6***a* and its 10-hydroxy derivative **6***g* appeared at *m/z* 249 to 265 respectively. Loss of one methyl radical from molecular ion **6***a* at position 7 resulted in the predominant fragment at *m/z* 234 which is the base peak. The molecular ions undergo a loss of propyne molecule to yield an ion at *m/z* 209 which corresponds to the molecular weight of the 2-(2′-hydroxyphenyl) indole ion. These ions split into further fragments which are common in 2-phenyl indoles (15), shown in Chart 1. However, a peak at *m/z* 117 which corresponds to unsubstituted indoles definitely results by a rearrangement process. The ion displays all the characteristic fragmentations reported for indoles (16).

The molecular ion of compound **6***a* also suffers a loss of acetone molecule resulting in an ion at *m/z* 191. An alternative pathway to this ion, *m/z* 191, involves the loss of acetyl radical from the peak cation appearing at *m/z* 234 (Chart I). The most intense peaks in the mass spectra of the compound **6***a* are *m/z* 249, 234(100%), 209, 191, 180, 117, 90, 89, 77, 63, and 51. Spectral peaks *m/z* 265, 250(100%), 225, 196, 117, 89, 77, 63, and 51 in the case of the 10-hydroxy derivative can be explained in a similar way.

Experimental

All melting points reported are uncorrected. Infrared spectra were reported on a Beckman IR-20 spectrophotometer (λ_{max} in cm^{-1}) and nmr spectra were recorded on Varian A-60D and Brucker WH-270 spectrometers with TMS as an internal standard. The mass spectra were scanned on a spectrophotometer equipped with a direct inlet system at 70 eV and at filament current 100 μA. Compounds were routinely checked for their homogeneity by tlc on silica gel-G plates and spots were visualized by exposure to iodine vapours.

Corresponding phenylhydrazones were prepared by condensation of phenylhydrazine with respective acetophenones, propiophenones, and butrophenones (17), which in turn were prepared by condensation of phenols or resorcinols with the corresponding carboxylic acids.

2-(2′-Hydroxyphenyl) indole (*5*)

A mixture of 2-hydroxyacetophenone phenylhydrazone (8.4 g, 0.04 mol) and polyphosphoric acid (60 g, prepared from 40 g phosphorous pentoxide and 20 g orthophosphoric acid) was heated on an oil bath at 120°C for 1 h and left overnight at room temperature. The reaction mixture was poured into ice-cold water. The precipitated product was filtered, washed with water, and dried. It was crystallized from methanol to yield 5.0 g (68%) of the title compound, mp 162–164°C; ir (KBr): 3445, 3440 (OH and NH) cm^{-1}; nmr (DSS) (NaOD): 6.68 (t, 1, H-3′), 6.82 (m, 1, H-5′), 7.18–7.35 (m, 4, H-3, H-4, H-4′, H-6′), 7.54 (d, *J* = 6.7 Hz, 1, H-5), 7.65 (d, *J* = 6.7 Hz, 1, H-6), 7.70 (d, *J* = 6.7 Hz, 1, H-7).

*7,7-Dimethyl-7*H*-indolo[1,2-c] [1,3]benzoxazine* (*6a*)

A mixture of 2-(2′-hydroxyphenyl) indole (**5**) (3.0 g, 0.015 mol), *p*-toluene sulphonyl chloride (0.05 g), and dry acetone (50 mL) was refluxed on a steam bath for 50 h. The solvent was removed *in vacuo*. The residue was taken up in chloroform and washed with water, dried (Na_2SO_4), filtered, and concentrated to yield 2 g (56%) of the title compound which, after recrystallization from ethanol/ethyl acetate (1:1), had mp 110–112°C; nmr: ($CDCl_3$): 6.00 (s, 2H, $2CH_3$), 6.88–7.97 (m, 9H, ArH); ms *m/e* (%): 249(55), 234(100), 209(27), 180(19), 117(48), 90(20), 89(26), 77(25), 63(32), 51(28), 191(31).

TABLE 1. Physical data of 7,7-dimethyl-7*H*-indolo[1,2-*c*] [1,3]benzoxazines (**6**)

Compound No.	R^1	R^2	R^3	Yield (%)	Melting point (°C)	Molecular formula	Analysis (%) Calculated	Found
a	H	H	H	60	111	$C_{17}H_{15}NO$	C: 81.92	81.64
							H: 6.02	5.92
							N: 5.62	5.36
b	CH_3	H	H	55	105	$C_{18}H_{17}NO$	C: 82.13	82.00
							H: 6.46	6.35
							N: 5.32	5.20
c	Cl	CH_3	H	65	135	$C_{18}H_{16}ClNO$	C: 72.60	72.50
							H: 5.38	5.25
							N: 4.70	4.44
d	CH_3	H	CH_3	50	Viscous oil	$C_{19}H_{19}NO$	C: 82.31	82.09
							H: 6.86	6.85
							N: 5.05	4.80
e	H	CH_3	H	50	93	$C_{18}H_{17}NO$	C: 82.13	81.92
							H: 6.46	6.32
							N: 5.32	5.27
f	H	OCH_3	H	55	110	$C_{18}N_{17}NO_2$	C: 77.42	77.35
							H: 6.09	5.85
							N: 5.01	4.85
g	OH	H	H	55	173	$C_{17}H_{15}NO_2$	C: 76.98	76.82
							H: 5.66	5.48
							N: 5.28	5.02
h	OH	H	CH_3	48	86	$C_{18}N_{17}NO_2$	C: 77.42	77.38
							H: 6.09	5.75
							N: 5.01	4.86
i	OH	H	C_2H_5	53	72	$C_{19}H_{19}NO_2$	C: 77.81	77.60
							H: 6.48	6.32
							N: 4.78	4.56
j	H	CH_3	CH_3	56	115	$C_{19}H_{19}NO$	C: 82.31	82.20
							H: 6.86	6.80
							N: 5.03	4.85
k	OH	C_2H_5	H	50	144	$C_{19}H_{19}NO_2$	C: 77.81	77.80
							H: 6.48	6.30
							N: 4.78	4.75
l	H	H	CH_3	46	50	$C_{18}H_{17}NO$	C: 82.13	82.00
							H: 6.46	6.35
							N: 5.32	5.25

*11-Methoxy-7,7-dimethyl-7*H*-indolo[1,2-*c*] [1,3]benzoxazine (***6**b*)*

Condensation of 2(2′-hydroxy-5-methoxyphenyl) indole (2.4 g, 0.01 mol) in a similar way with dry acetone and *p*-toluene sulphonyl chloride yielded the 11-methoxy derivative (**6***b*). It was crystallized from ethanol/ethyl acetate (1:1) to give 1.28 g (55%) of the title compound, mp 110–111°C; nmr ($CDCl_3$): 1:818 (6H, $(CH_3)_2$), 2:22 (s, 3H, CH_3), 6.81–7.59 (m, 8H, ArH).

*10-Hydroxy-7,7-dimethyl-7*H*-indolo[1,2-*c*] [1,3]benzoxazine (***6**g*)*

By the same procedure used for the preparation of **6***a*, 2-(2′,4′-dihydroxyphenyl) indole (2.25 g, 0.01 mol) was converted to 1.3 g (55%) of the title compound, mp 170–173°C; nmr ($CDCl_3$ + DMSO-d_6): 1.75 (s, 6H, $(CH_3)_2$), 4.83 (m, 1H, OH), 6.83–7.71 (m, 8H, ArH).

*2-(2′-Hydroxyphenyl)-4,5-diphenyl imidazole (***9**a*)*

A mixture of salicylaldehyde (6.1 g, 0.05 mol), benzil (10.5 g, 0.05 mol), ammonium acetate (30 g), and glacial acetic acid (150 mL) was refluxed for a period of 2 h, cooled, and treated with ice-cold water to give 10 g (64%) of the title compound which, after recrystallization from methanol/ether, had mp 238–240°C; ir(KBr): 3435, 3250 (OH and NH) cm^{-1}. *Anal.* calcd. for $C_{21}H_{16}N_2O$: C 80.76, H 5.13, N 8.9; found: C 80.45, H 5.00, N 8.87.

*2,3-Diphenyl-5*H*-imidazolo[1,2-*c*] [1,3]benzoxazine (***10***)*

A mixture of 2-(2′-hydroxyphenyl)-4,5-diphenyl imidazole (**9***a*) (3.12 g, 0.01 mol), anhydrous potassium carbonate (10 g), methylene bromide (7 mL), and dry dimethylformamide (40 mL) was heated on a steam bath for 16 h. It was filtered to remove the inorganic salts and the filtrate was concentrated under vacuum. The residue was triturated with water to yield 2.4 g (74%) of the title compound, mp 60–62°C; nmr ($CDCl_3$): 7.60–7.03 (m, 14, ArH), 1.67 (s, 2, H-5).

*2-(2′-Hydroxyphenyl)-4,5-bis(*p*-methoxyphenyl) imidazole (***9**b*, $R' = OCH_3$)*

This compound was prepared in a similar way as **9** from 4,4′-dimethoxy benzil (**8***b*) (2.7 g, 0.01 mol) and salicylaldehyde (**7**) (1.22 g, 0.01 mol) to yield 2.38 g (70%) of the title compound, mp 92–95°C; nmr (TFA): 3.90 (s, 6, $(OCH_3)_2$, 6.65–7.45 (m, 12, ArH), 3.16 sweep of set 500 Hz (m, 2, NH, OH). *Anal.* calcd. for $C_{23}H_{20}N_2O$: N 8.23; found: N 8.00.

*2,3-Bis(*p*-methoxyphenyl)-5*H*-imidazolo[1,2-*c*] [1,3]benzoxazine (***10***, $R' = OCH_3$)*

This compound was prepared by condensation of 2-(2′-hydroxyphenyl)-4,5-bis(*p*-methoxyphenyl) imidazole (**9***b*) (1.7 g, 0.005 mol) with methylene bromide, as in the method described above for **9***a* (R′ = H) to yield 1.23 g (70%) of the title compound, mp 80°C; nmr($CDCl_3$): 3.97 (s, 6, $(OCH_3)_2$), 5.80 (s, 2, H-5), 7.10–8.30 (m, 12, ArH). *Anal.* calcd. for $C_{24}H_{20}N_2O$: C 81.82, H 5.68, N 7.95; found: C 81.65, H 5.50, N 7.72.

*2-(2′-Hydroxyphenyl) benzimidazole (***13***)*

A mixture of phenyl salicylate (8.56 g, 0.04 mol) and *O*-

phenylenediamine (4.32 g, 0.04 mol) was heated at 180°C in an oil bath for 5 h; the reaction mixture was cooled and then dissolved in 10% sodium hydroxide solution. It was acidified with ice-cold acetic acid to give 6.0 g (71%) of the title compound, mp 240–241°C (lit. (18) mp 238°C); ir(KBr): 3430, 3320 (OH and NH) cm^{-1}.

7H-Benzimidazolo[1,2-c] [1,3]benzoxazine (14)

To a solution of 2-(2′-hydroxyphenyl) benzimidazole (4.2 g, 0.02 mol) in dry dimethylformamide (40 mL) in the presence of anhydrous potassium carbonate (5 g), methylene bromide (7 mL) was added and the reaction mixture was filtered and concentrated under vacuum. The residue was treated with chilled water to yield 3.1 g (70%) of the title compound, mp 151–153°C; nmr ($CDCl_3$): 6.00 (s, 2H, —CH_2), 7.10–8.17 (m, 8H, ArH); *m/e* (%) ms: 222(100), 221(100), 220(10), 194(83), 193(100), 169(53), 168(100), 167(67), 140(34), 113(100), 104(41), 103(50), 98(71), 93(35), 91(34), 85(41), 79(100).

Acknowledgement

One of the authors (R.S.) thanks the C.S.I.R., New Delhi for financial assistance.

1. R. M. Anker and A. H. Cook. J. Chem. Soc. 58 (1946).
2. H. G. Pars, F. E. Ganehelli, J. K. Keller, and R. K. Razadan. J. Am. Chem. Soc. **88**, 3664 (1966).
3. H. G. Pars and R. K. Razdan. Ann. N.Y. Acad. Sci. **191**, 15 (1971).
4. W. L. Dewey, L. S. Harris, J. F. Howes, J. S. Kennedy, F. E. Caranehelli, H. G. Pars, and R. K. Razdan. Nature (London) **226**, 1267 (1970).
5. M. Cushman and N. Castagnolli, Jr. J. Org. Chem. **38**, 440 (1973).
6. M. Cushman and N. Castagnolli, Jr. J. Org. Chem. **39**, 1546 (1974).
7. O. P. Malik, R. S. Kapil, and N. Ananand. Indian J. Chem. **14B**, 975 (1976).
8. M. N. Rapport. J. Biol. Chem. **180**, 961 (1949).
9. P. Millee, J. P. Malrian, J. Beniam, J. Y. Lallemand, and M. Julia. J. Med. Chem. **11**, 207 (1968).
10. H. H. Pennes and P. H. Hock. Am. J. Psychiat. **113**, 887 (1957).
11. A. W. D. Avisor, A. L. Morrison, and M. W. Parkes. J. Chem. Soc. 952 (1949).
12. E. C. Taylor, K. Lenard, and B. Loev. Tetrahedron, **23**, 77 (1967).
13. A. Calvaire and R. Palloud. C. R. Acad. Sci. **250**, 3194 (1960).
14. V. K. Mahesh, M. Maheshwari, and R. Sharma. Chem. Ind. 200 (1980).
15. J. C. Powers. J. Org. Chem. **33**, 2044 (1968).
16. Catalog of Mass Spectra Data, American Petroleum Institute Research Project 44, Carnegie Institute of Technology, Pittsburgh Pa. Spectra No. 623.
17. C. M. Brewester and J. C. Harris. J. Am. Chem. Soc. **52**, 4869 (1930).
18. I. S. Ioffe and D. N. Glebovskii. Zh. Obshch. Khim. **30**, 1158 (1960).

Hétérocycles organiques de l'arsenic. Synthèse d'arsinimines hétérocycliques par la "réaction de Staudinger." Mécanisme de la réaction

PIERRE MARONI, YVES MADAULE, TULA SEMINARIO ET JEAN-GÉRARD WOLF

Laboratoire de Synthèse et Physicochimie Organique, Unité Associée au Centre National de la Recherche Scientifique n° 471, Université Paul Sabatier, 118, route de Narbonne, F 31062 Toulouse Cedex, France

Reçu le 24 février 1984

PIERRE MARONI, YVES MADAULE, TULA SEMINARIO et JEAN-GÉRARD WOLF. Can. J. Chem. **63**, 636 (1985).

La réaction de Staudinger a été appliquée à des hétérocycles arséniés. L'action des azotures de picryle et de para-toluènesulfonyle sur une série d'arsatranes tétracoordinés conduit à des arsinimines originales pentacoordinées, avec maintien de la liaison atrane N → As. Ces arsinimines se dimérisent pour donner des diarsadiazacyclobutanes comportant des atomes d'arsenic hexacoordinés. La réactivité des arsanes est plus faible. Seul l'azoture de picryle donne lieu à réaction. Les arsinimines obtenues se dimérisent plus ou moins rapidement dans pratiquement tous les cas, sauf un où l'arsinimine reste sous forme monomère. L'étude de la réaction en ultraviolet permet de mettre en évidence un complexe intermédiaire, différent de celui de la réaction "classique" des homologues phosphorés.

PIERRE MARONI, YVES MADAULE, TULA SEMINARIO, and JEAN-GÉRARD WOLF. Can. J. Chem. **63**, 636 (1985).

Staudinger's reaction is applied on arsenic heterocycles. Picryl and tosyl azides lead, by action on tetracoordinated arsatranes, to previously unknown pentacoordinated arsinimines with an "atran" bond (N → As). In a second step, they dimerize to diarsadiazacyclobutanes, bearing hexacoordinated arsenic atoms. Heterocyclic arsanes react only with picryl azide. All imines were obtained as dimers or oligomers, with the single exception of **8A**. Ultraviolet studies give evidence for an intermediate complex different from the one demonstrated in the "classical" Staudinger's reaction with phosphorus compounds.

La réaction de Staudinger, synthèse de phosphinimines par action d'azotures sur les phosphanes tertiaires, connue dès 1919 (1) a été depuis largement étendue (2). Cadogan et Gosney (3) ont été parmi les premiers à l'utiliser dans la chimie de l'arsenic, à partir d'arylazotures contenant des groupes attracteurs d'électrons. Cependant, les arsinimines sont obtenues le plus souvent par action d'arsanes sur des chloramines (4, 5) ou par condensation d'oxydes de triarylarsane avec des isocyanates et des N-sulfinylamides (6, 7).

Pour notre part nous avons appliqué la réaction de Staudinger à la synthèse d'arsinimines hétérocycliques originales, en faisant agir des azotures sur des hétérocycles organiques de l'arsenic appartenant à deux grandes séries: (*i*) des arsatranes, composés originaux stables de l'arsenic tétracoordiné synthétisés au laboratoire (8)

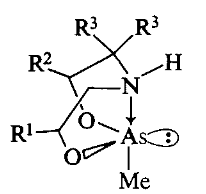

1 {R¹ = R² = Me; R³ = H}
2 {R¹ = Ph, R² = H; R³ = Me}

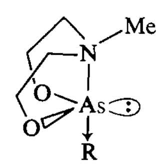

3 R = Me
4 R = Ph

(*ii*) des arsanes tricoordinés dérivant du pinacol (**5**, **6**), du pyrocatéchol (**7**, **8**) et de la (−) éphédrine (**9**)

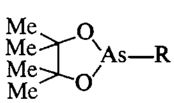

R = {Me **5**; Cl **6**}

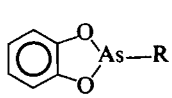

R = {Me **7**; Cl **8**}

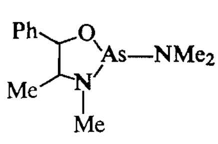

9

Ces hétérocycles possèdent sur l'arsenic une paire électronique libre. La disponibilité de ce doublet, déjà montrée sur les arsatranes (8), permet d'envisager une bonne réactivité vis à vis des azotures.

Pour obtenir ces nouvelles arsinimines hétérocycliques, pour lesquelles l'arsenic est relié à d'autres hétéroatomes (N, O) nous avons opéré par voie thermique et photochimique.

La gamme des azotures utilisables est relativement large. Nous en avons essayé six: d'abord

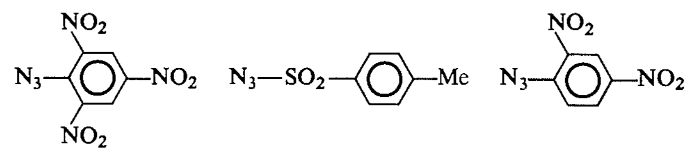

A **B** **C**

tous porteurs de groupements attracteurs et qui se sont révélés au moins partiellement réactifs sur tous les composés arséniés; puis N_3COPh, N_3Ph et N_3SiMe_3 qui n'ont pas réagi.

I. Action des azotures sur les arsatranes

A. *Résultats*

La réaction entre les composés **1** et **A** est un bon modèle: elle pourra conduire à l'arsinimine **1A**, possédant ou non une structure atrane.

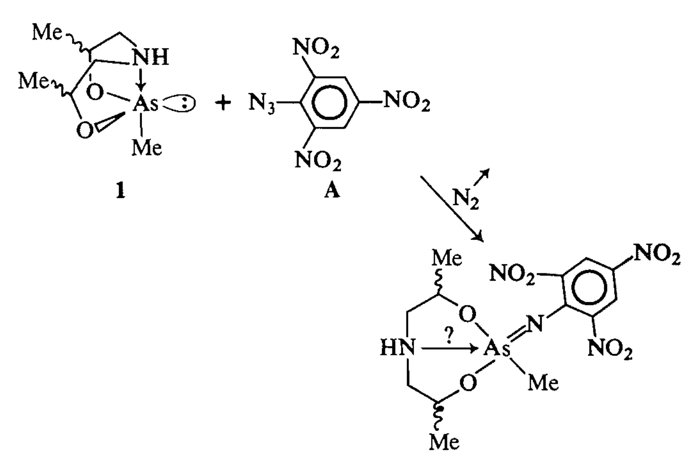

1A

Dans tous les cas, les composés obtenus à partir de **C** sont très instables et n'ont pu être étudiés de manière satisfaisante. Par contre, les réactions ont lieu dès la température ordinaire à partir de **A** et **B**. La vitesse de la réaction est fortement augmentée par voie photochimique mais les résultats et les rendements sont les mêmes que pour la voie thermique. Les composés obtenus à partir de **A** et **B** se décomposent très rapidement une fois isolés, et ont été étudiés principalement en solution. Leur structure a été déterminée par spectrométrie de masse, infrarouge et rmn.

1. *Spectrométrie de masse*

Nous avons entièrement dépouillé les spectres de masse de quatre composés, qui présentent tous des modes de rupture comparables:

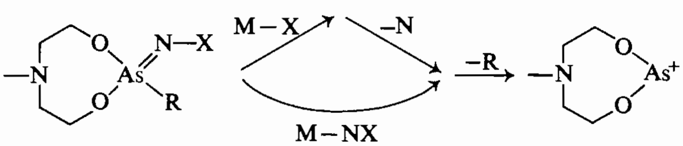

Pour **1B**, **3A**, **3B** et **4A**, respectivement: pic moléculaire faible (1 à 3%) (m/z = 390, 433, 376, 495), M − X (235, 221, 221, 283), M − NX (221, 209, 207, 269) de l'ordre de 70% et l'ion arsénium M − NX − R (206, 192, 192, 192). On relève ensuite pour **1B** deux pics à m/z = 178 (100%) et 149 (60%) qui correspondent vraisemblablement à la rupture du cycle arsénium et la perte succesive de CHMe et $NHCH_2$. Pour **3A**, **3B** et **4A**, le fragment à m/z = 177 (50%) est dû à la perte par l'ion arsénium du substituant méthyle de l'azote cyclique. Le pic de base à 147 pour ces 3 composés correspond à la rupture du cycle et la perte supplémentaire de OCH_2.

2. *Infrarouge*

L'infrarouge montre la disparition progressive de la bande ν_{N_3} de l'azoture (2120 et 2110 cm^{-1} respectivement pour **A** et **B**), et l'apparition d'une bande dans la région des $\nu_{As{=}N}$ que nous avons comparée à la vibration correspondante du composé $Ph_3As{=}N{-}SO_2$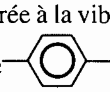Me (1250 cm^{-1} d'après la référence 3) (tableau 1). La valeur de ces fréquences pour les composés obtenus à partir de l'azoture de paratoluènesulfonyle **B** est bien en concordance avec celle du composé de référence (1250 cm^{-1}). Les dérivés de l'azoture de picryle **A** présentent un déplacement de 30 à 40 cm^{-1} attribuable à l'effet des groupes NO_2. En outre, les spectres infrarouge d'une solution enregistrés à intervalles régulier et pendant 24 h après la fin de la synthèse montrent un phénomène supplémentaire: la bande As=N disparaît progressivement, alors qu'apparaît une nouvelle vibration vers les fréquences plus basses, dans la région des $\nu_{As{-}N}$, par exemple pour les composés **3A** (1290 → 1010 cm^{-1}) et **3B** (1250 → 1130 cm^{-1}).

3. *Résonance magnétique nucléaire*

La rmn ^1H (60 et 90 MHz) confirme la formule brute des composés. En outre, elle permet de suivre une évolution identique à celle révélée par l'infrarouge: on observe, dès la fin de la synthèse, la présence de deux entités, (m) et (d), dans des proportions relatives 40−60% (tableau 2), qui présentent les mêmes types de signaux. Ceux attribués à (m) disparaissent en 24 h en même temps que la bande As=N en infrarouge.

B. *Interprétation*

La disparition de la vibration $\nu_{As{=}N}$ et l'apparition d'une bande $\nu_{As{-}N}$ peuvent être dues pour **1A**, **1B**, **2A** et **2B** à une tautomérie prototropique donnant un arsorane

TABLEAU 1. Fréquences des vibrations $\nu_{As{=}N}$ (cm^{-1}), solutions $M/20$ dans CCl_4

		Arsatrane			
	Azoture	1	2	3	4
A	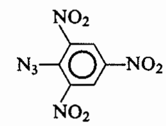	1280	1290	1290	1285
B	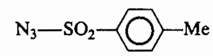	1255	1260	1250	1250

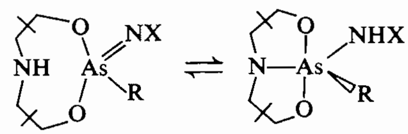

Mais ce type de passage à la pentacoordination, connu à partir des phosphinimines comportant un groupe à hydrogène mobile (NH ou OH) (9, 10), n'a jamais pu être mis en évidence dans le cas de composés arséniés.[1]

Dans notre cas, la présence initiale dans tous les composés d'une bande As=N infirme la structure arsorane pour (m). La transformation (m) → (d) qui s'accompagne de l'apparition d'une bande dans la région des $\nu_{As{-}N}$ et de la disparition de la vibration $\nu_{As{=}N}$ ne conduit pas non plus à l'arsorane à groupement NH: le phénomène est identique quel que soit le substituant sur l'azote du cycle (H ou Me). Pour tous les composés, l'apparition de (d) pourrait correspondre à une dimérisation (ou une oligomérisation) des formes arsinimines, souvent observée pour les phosphinimines (11).

Cette hypothèse est étayée par une cryométrie dans le benzène qui montre, au bout de 24 h, que l'on est en présence du dimère, la bonne résolution des spectres rmn permettant d'autre part d'exclure la présence en proportions notables d'oligomères de rang supérieur. On peut donc considérer que (m) et (d) correspondent à la structure globale:

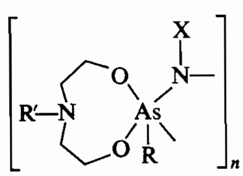

n = 1 (m)
n = 2 (d)

L'atome d'azote du cycle à huit chaînons se trouvant en position 5 on peut envisager qu'il va former une liaison "atrane" avec l'atome d'arsenic.

Pour démontrer cette structure atrane éventuelle, nous avons comparé les composés **3A** et **3B** avec l'atrane tétracoordiné **3** et l'atrane hexacoordiné **3**^{VI}, préparés antérieurement au laboratoire. La structure de **3**^{VI} a été déterminée par RX (8a).

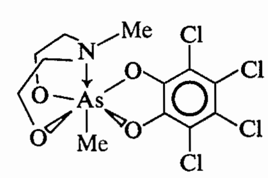

3^{VI}

[1]Voir la référence 26.

TABLEAU 2. Spectres en résonance magnétique nucléaire du ^1H de **3A** et **3B** (60 MHz, $CDCl_3$) δ (ppm)

Composé		AsMe singulet	NMe singulet	NCH_2 multiplet	OCH_2 multiplet	Picryle $C_6H_2(NO_2)_3$	Tosyle Me	Tosyle C_6H_4
3A	(d)	1,65	2,60	2,82	4,10	9,33		
	(m)	1,85	2,25	2,84	4,12	8,40		
3B	(d)	1,60	2,52	2,80	4,00		2,40	7,50
	(m)	1,70	2,40	2,82	4,02		2,38	7,35

TABLEAU 3. Déplacement chimique en résonance magnétique nucléaire du ^1H des parties NCH_2 et OCH_2 de l'entité (d) ($CDCl_3$, 60 MHz)

	Composé 3	3A*	3B*	3^{VI}	Mor-Me†
NCH_2	2,72	2,82	2,80	3,05	2,28
OCH_2	3,65	4,10	4,00	4,20	3,58

*Entité (d). Les signaux de (m) sont tous déblindés de 0,02 ppm.

†Mor = morpholino 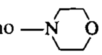

TABLEAU 4. Effet de solvant aromatique en résonance magnétique nucléaire du ^1H (ASIS) $\Delta\delta = \delta_{CDCl_3} - \delta_{C_6H_6}$

	Composé 3	3A*	3B*	3^{VI}
AsMe	−0,25	+0,15	+0,15	+0,12
NMe	+0,30	+0,38	+0,35	+0,85
NCH_2	+0,30	+0,72	+0,73	+1,23
OCH_2	0	+0,50	+0,55	+0,73

*Entité (d). Les valeurs de Δδ de (m) sont identiques à 0,02 près.

Nous avons rapporté les résultats de rmn dans les tableaux 3 à 5: déplacement chimique des protons de cycle, comparés à ceux de la N-méthyl-morpholine (tableau 3); effet de solvant (tableau 4); déplacements chimiques des carbones (tableau 5). On observe dans tous les cas un comportement de **3A** et **3B** intermédiaire entre celui des arsatranes tétra- et hexacoordinés. Les tableaux 3 et 4 montrent de plus une forte similitude au niveau du cycle entre les entités (m) et (d). D'autres remarques sont en faveur de la structure atrane: (*i*) les protons du cycle sont nettement déblindés par rapport à la N-méthylmorpholine; (*ii*) le fort effet de solvant aromatique (effet ASIS), comparable pour (m) et (d) lorsque l'on passe de $CDCl_3$ à C_6D_6 ne peut s'expliquer que si ces deux composés ont des structures et donc des sites de complexation identiques, qui pourraient être proches de celui trouvé pour $\mathbf{3}^{VI}$ (8); (*iii*) en rmn ^{13}C, l'écart entre

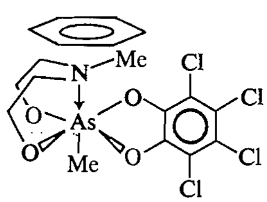

les signaux N—CH_2 et OCH_2, de l'ordre de 4 ppm pour **3A** et **3B** est plus faible que pour la morpholine (21 ppm), la N-éthyl morpholine (14,4 ppm) et le tris-morpholino-arsane (20,3 ppm) (12) (dans ce dernier composé l'azote est directement lié à l'arsenic par une liaison covalente). Cette diminution est en particulier dûe au déblindage de N—CH_2. Elle peut s'expliquer par un affaiblissement de la densité électronique sur l'azote compatible avec la présence d'une liaison de coordination N → As.

Les observations sont identiques pour les autres composés, bien que les spectres rmn soient généralement plus complexes et que les vibrations caractéristiques ν_{SO_2} ne permettent pas d'attribuer la bande $\nu_{As—N}$ en infrarouge pour **1B**, **2B** et **4B**.

Le phénomène de dimérisation, observé pour **3A** et **3B** semble cependant général: la cryométrie des composés indique dans tous les cas la présence de dimères; l'infrarouge montre la disparition progressive de la bande $\nu_{As=N}$ et l'apparition d'une vibration $\nu_{As—N}$; les spectres rmn ^1H révèlent dans la plupart des cas la présence initiale de deux entités qui évoluent au cours du temps.

Les modifications les plus caractéristiques se situent au niveau des signaux: AsMe pour **1B** et **2B** (deux pics vers 1,80 et 1,90 ppm; $CDCl_3$) et SO_2—⟨◯⟩—Me pour **1B**, **2B** et **4B** (deux pics méthyle vers 2,40, $CDCl_3$) et superposition de deux systèmes phényle *para* disubstitués vers 7,50 ppm ($CDCl_3$).

Pour les composés obtenus à partir de l'azoture de picryle, nous avons observé particulièrement la position des protons du cycle picryle: les spectres rmn ^1H du composé **3A** montrent en effet que la transformation monomère−dimère se traduit par un net déblindage de ces protons (de 8,40 à 9,33 ppm dans $CDCl_3$, de 8,35 à 8,77 ppm dans C_6D_6).

Les spectres de **4A** présentent deux pics à 8,47 et 9,26 ppm ($CDCl_3$) le premier disparaissant au bout de 30 h. Nous n'avons pas relevé le pic aux champs forts pour **1A** et **2A**, mais un seul signal (à respectivement 9,31 et 9,21 ppm; $CDCl_3$) qui correspond à l'apparition rapide du dimère. Le maintien de la structure atrane des monomères et des dimères est corroboré par un fort effet ASIS, comparable à celui relevé pour **3A** et **3B**. On peut donc conclure que l'action d'azotures sur les arsatranes conduit dans une première étape à des arsinimines pentacoordinées possédant une structure atrane, et ne donnant pas lieu à la tautomérie prototropique. Ces arsinimines se dupliquent ensuite pour conduire à un dimère possédant deux atomes d'arsenic hexacoordiné de structure atrane.

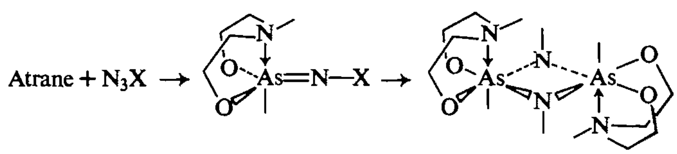

TABLEAU 5. Résonance magnétique nucléaire du ^{13}C ($CDCl_3$, 15,08 MHz)

	Composé							
	3	3A*	3B*	3^{VI}	MorH†	Mor-Me	Mor-Et	Mor_3As
AsMe	25,7	20,0	19,0	22,8				
NMe	41,3	42,5	42,2	45,3				
NCH_2	61,9	57,8	57,3	55,3	47,1		53,4	48,3‡
OCH_2	66,7	61,5	61,4	57,4	68,1		67,9	68,6‡

*Entité (d).

†Mor = morpholino 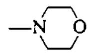

‡Dans C_6D_6 (12).

II. Synthèse d'arsinimines à partir d'arsanes

Pour connaître l'influence de la structure atrane sur le phénomène de dimérisation observé, nous avons tenté d'effectuer la synthèse d'arsinimines à partir de modèles plus simples, les arsanes **5** à **9** et des azotures de picryle **A** et de tosyle **B**, qui se sont révélés les plus réactifs sur les arsatranes.

On observe des différences notables: (*i*) l'azoture de tosyle **B** ne conduit ni à l'arsinimine ni au dimère: il se décompose sans réagir avec **5** et **8** et n'est pas modifié par action sur **6**, **7** et **9**; (*ii*) la réactivité de l'azoture de picryle **A** est moins importante que celle observée à partir des arsatranes. Alors que la réaction sur ces derniers composés se fait à la température ambiante, elle nécessite dans tous les cas un long chauffage à reflux. D'une manière générale, les rendements observés sont plus faibles et les réactions parfois incomplètes (persistance d'azoture).

Enfin, la synthèse par voie photochimique ne donne pas lieu à réaction ou conduit à des résultats non exploitables (formation de goudrons).

Pour interpréter les résultats, nous nous sommes intéressés au déplacement chimique des protons du cycle picryle dont le blindage ou déblindage relatifs indique la présence de monomère ou de dimère.

La position de ces protons révèle la formation directe du dimère à partir de **5** (9,38 ppm) et **6** (9,40 ppm) bien que les vibrations caractéristiques du cycle pinacolique ne permettent de distinguer que la bande $\nu_{As—N}$ de **6A** (1165 cm^{-1}; CCl_4). Inversement, le blindage des protons picryle (8,15 ppm) et la présence d'une bande $\nu_{As=N}$ à 1230 cm^{-1} indiquent que **8A** est une arsinimine monomère stable, la seule obtenue. Notons que la valeur de la fréquence infrarouge est différente de celle des As=N picryle relevée pour les arsatranes (~1280 cm^{-1}).

Nous avons constaté que, si l'azoture **A** se décompose en présence de **7**, la réaction ne conduit pas au monomère ou au dimère.

Les spectres rmn ^1H du composé **9A** enregistrés dans un mélange C_7D_8 − DMSO-d_6 car peu soluble dans $CDCl_3$, montrent la transformation progressive du monomère (8,36 ppm) en dimère (8,83 ppm) (à comparer avec le déplacement de 8,35 à 8,77 ppm observée pour **3A** dans C_6D_6).

Nous constatons donc que, dans la plupart des cas, la dimérisation est prépondérante.

Si l'on considère les différences observées entre les atranes et les arsanes tricoordinés (réactivité plus faible de ces derniers, pas de réaction par voie photochimique), on peut penser qu'elles sont dues à l'originalité de l'environnement de l'arsenic dans les arsatranes par rapport aux arsanes rendant le doublet plus réactif:

III. Synthèse des arsinimines: mise en évidence d'un intermédiaire de réaction

Nous pouvons formuler deux hypothèses quant au comportement de l'azoture vis à vis du composé arsénié.

1. *La formation préalable de nitrène*

$$X—N_3 \longrightarrow X—N\!: + N_2\uparrow$$

qui s'additionnerait sur l'atome d'arsenic.

La synthèse d'arsinimines par photochimie n'a pas été réalisée avant nous. Horner et Christmann (13) ont cependant synthétisé par cette voie des sulfonylimines, ce qui peut laisser supposer que l'irradiation des azotures engendre des nitrènes. Cadogan et Gosney (3) effectuent la synthèse d'arsinimines à haute température, ou font intervenir un catalyseur: ils considèrent l'attaque sous forme de nitrène, le catalyseur abaissant la température de décomposition de l'azoture.

Nous ne pouvons passer sous silence cette hypothèse, au vu des synthèses sous irradiation. Nous pouvons cependant l'écarter dès maintenant, pour deux raisons. Les synthèses par voie thermique ont lieu à la température ordinaire pour les atranes. Et surtout (*vide infra*) nous avons mis en évidence un intermédiaire réactionnel.

2. *Une addition de l'azoture sous forme non décomposée* sur l'atome d'arsenic, comme cela a déjà été montré dans le cas de l'action des azotures aromatiques sur la triphénylphosphine (14) (intermédiaire dit de Staudinger):

$$Ph_3P + ArN_3 \longrightarrow Ph_3P=N—N=N—Ar \xrightarrow{-N_2\uparrow} Ph_3P=N—Ar$$

Goldwhite *et al.* ont isolé un intermédiaire de ce type lors de la réaction entre l'azoture de phényle et $(Me_2N)_3P$ (15). Ils présentent un arrangement linéaire:

$$(Me_2N)_3P=N—N=N—Ph$$

Généralement instable, cet intermédiaire conduit aux phosphinimines par libération d'une mole d'azote, suivant un processus décrit par Leffler et Temple (16), mettant en jeu deux états de transition équiénergétiques. Le phosphore se charge

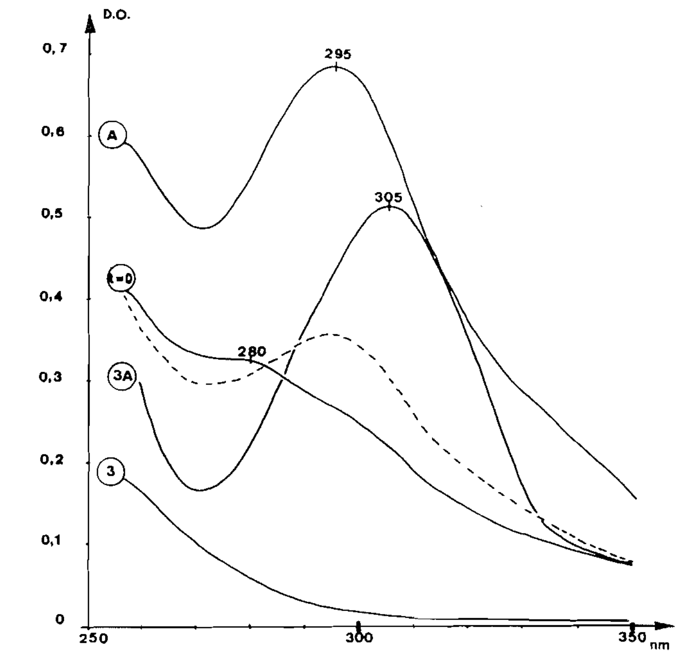

FIG. 1. Spectres ultraviolet (CCl_4). **A** et **3**: produits de départ ($0{,}66 \times 10^{-4}$ *M*); $t = 0$: spectre initial du mélange **A** + **3** $\left(\text{en pointillé } \sum \frac{DO}{2}\right)$; **3A**: spectre du produit final isolé ($0{,}66 \times 10^{-4}$ *M*).

positivement, l'azote en γ négativement, la neutralisation de ces charges conduisant à la formation d'une liaison

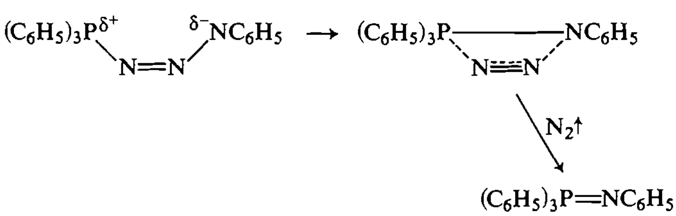

Nous avons suivi par ultraviolet l'action de l'azoture de picryle **A** sur **3** et **5** en mélangeant les réactifs à 10^{-2} *M* et en enregistrant les spectres de prélèvements successifs dilués à $0{,}66 \times 10^{-4}$ *M* (fig. 1). Le spectre initial ($t = 0$) est différent de la somme des densités optiques des composés de départ (en pointillé) et révèle la présence d'une entité possédant un maximum d'absorption vers 280 nm pour **3** + **A** et 285 nm pour **5** + **A**. Le spectre évolue ensuite progressivement pour aboutir au produit final (λ_{max} = 305 nm, ϵ = 7800 pour **3A** et **5A**).

Ces résultats montrent l'apparition, comme dans le cas du phosphore d'un intermédiaire réactionnel. La comparaison des bandes d'absorption uv de l'azoture (λ_1 = 295 nm; ϵ = 10 300 pour **A**), de l'intermédiaire réactionnel (λ_i) et de l'imine (λ_2) pour les deux composés étudiés avec les résultats rapportés par Goldwhite dans la chimie du phosphore (15) (intermédiaire réactionnel isolé) montre que, dans les trois cas, $\lambda_2 - \lambda_1$ est de l'ordre de 10 nm. Mais, alors que dans le cas du phosphore, l'intermédiaire réactionnel est déplacé vers les grandes longueurs d'ondes (+51 nm par rapport à l'azoture initial) on observe un phénomène inverse pour **3A** et **5A** (respectivement −15 et −10 nm) (fig. 2).

Un intermédiaire de type Staudinger (I.S.) possédant un

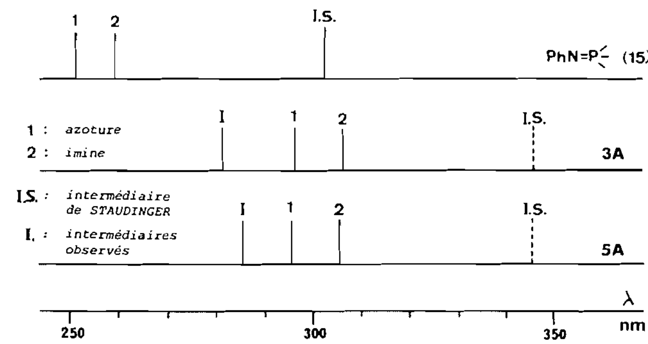

FIG. 2. Spectres ultraviolet de **3A** et **5A**, comparaison avec le phosphore.

enchaînement linéaire $>As{=}N{-}N{=}N{-}X$ aurait présenté une bande vers 345 nm (en pointillé sur la fig. 2) par extension de la conjugaison du cycle picryle. Nous avons donc été conduits à envisager un complexe par transfert de charge As^{IV} — azoture.

A l'appui de cette hypothèse, nous avons noté pour **3A** que les spectres infrarouge enregistrés en cours de synthèse présentent une bande à 1320 cm^{-1}, absente des spectres des réactifs et du produit final, qui pourrait correspondre au complexe.

En outre, en isolant au cours du temps des fractions du mélange réactionnel et en les concentrant par évaporation, nous n'observons en infrarouge et en rmn que les produits initiaux et le produit final: on aurait brisé le complexe qui se trouvait en équilibre avec les composés de départ.

A partir des atranes, cet intermédiaire serait le même par voie "thermique" et par voie "photochimique", l'utilisation des deux méthodes conduisant au même produit final, avec le même rendement. La grande différence de vitesse observée (la voie photochimique est environ dix fois plus rapide dans nos conditions expérimentales) pourrait être due à l'accélération de la destruction du complexe par photolyse.

En résumé, il semble raisonnable d'admettre, pour les réaction entre nos composés et les azotures **A** et **B**, un mécanisme réactionnel en deux étapes: la première comportant, comme dans le cas du phosphore, un intermédiaire réactionnel, mais de nature différente, la second conduisant à l'arsinimine par départ d'azote.

IV. Conclusion

Les travaux réalisés au cours de ce mémoire nous ont permis de faire les constatations qui suivent.

1. La gamme des azotures réactifs pour l'arsenic est plus restreinte que pour les dérivés phosphorés (11). La réactivité des arsatranes est cependant très supérieure à celle des arsanes.

2. Nous n'avons jamais observé de tautomérie $As^{IV} \rightleftharpoons As^{V}$ conduisant à un arsorane homologue des dérivés phosphorés (9, 10) lorsqu'elle est théoriquement envisageable (atranes à groupement NH: **1A**, **1B**, **2A** et **2B**). La structure atrane s'est toujours révélée la plus stable.

3. Les phosphinimines peuvent soit exister sous la forme monomère, soit donner par dimérisation, un cycle diazadiphosphacyclobutane (17). Nous n'avons obtenu une forme monomère stable que dans un seul cas (**8A**). Pour le reste, on obtient la forme dimère, soit directement sans observer le monomère, soit par transformation progressive du monomère en dimère.

Une explication de cette prépondérance à la dimérisation est possible à partir des résultats infrarouge. Nous avons noté une grande dispersion dans la position des $\nu_{As=N}$ et ν_{As-N}, qui doit traduire une variation du caractère π de ces liaisons, comme cela a été noté pour la liaison P=N des phosphinimines (18).

Il est connu par ailleurs que, si l'azote est plan dans les aminophosphanes, il est pyramidal pour $>$As—N$<$ (19) ce qui indique que la liaison As—N est moins proche d'une double liaison que P—N.

Enfin, l'écart entre les $\nu_{M=N}$ et ν_{M-N} est de l'ordre de 250 cm^{-1} pour nos composés (M = As) alors qu'il est de 600 cm^{-1} lorsque M = P (20).

Ces observations dénotent un faible caractère π de la liaison As=N, et donc une plus grande polarité $As^{+}—N^{-}$. Or, on sait que la frontière dimère $(P)^{V} \leftrightarrow$ monomère $(P)^{IV}$ est très sensible à la polarisation de la liaison P=N (11), dont l'accentuation favorise la dimérisation.

Partie expérimentale

I. *Synthèse*

Les réactifs

Les azotures peuvent se décomposer par action de la lumière, et ont été utilisés fraîchement préparés, selon la référence 21 pour **A** (ν_{N_3} = 2120 cm^{-1}, CCl_4; rmn ^1H: singulet à 8,90 ppm, $CDCl_3$, 60 MHz) et la référence 22 pour **B** (ν_{N_3} = 2110 cm^{-1}, CCl_4; rmn ^1H: singulet à 2,33 ppm, quadruplet autour de 7,50 ppm, $CDCl_3$, 60 MHz).

Les arsatranes **1** à **4** ont été préparés suivant la référence 8, ainsi que les arsanes **5** (δ_{AsMe} = 1,04 ppm, δ_{Me_2C} = 1,17 ppm, C_6D_6, 60 MHz) et **7** (δ_{AsMe} = 0,78 ppm, C_6D_6; 1,30 ppm, CCl_4, 60 MHz).

Les autres arsanes ont été préparés selon les références 23, 24 et 25 pour **6**, **8** et **9** respectivement.

Les arsinimines. Voie thermique

Synthèse de **3A**

On dissout dans 200 cm^3 de solvant (CCl_4 ou C_6H_6) 2,07 g (0,01 mol) de l'atrane **3** et 2,54 g (0,01 mol) de l'azoture de picryle (**A**). On agite pendant 6 h à la température ambiante. On mesure le rendement par le dégagement d'azote (90%).

La même procédure est utilisée pour tous les arsatranes, le temps de réaction variant de 6 à 8 h. Les rendements varient de 70% (**2A** et **3B**) à 85% (**1A**, **1B**, **2B**) (légèrement supérieurs dans C_6H_6). Les composés sont isolés par évaporation du solvant, mais se dégradent rapidement même conservés sous azote sec.

Les mesures physicochimiques sont effectués sur des échantillons préparés "*in situ*", la fin de la synthèse étant indiquée par la disparition de la bande azoture en infrarouge.

Synthèse de **5A**

On place 2,06 g (0,01 mol) de **5** dilués dans 100 cm^3 de toluène dans un erlenmeyer à deux voies; 2,54 g (0,01 mol) d'azoture dissous dans 100 cm^3 du même solvant sont introduits goutte à goutte. On chauffe à reflux du solvant pendant 3 h. Le composé est isolé par distillation du toluène sous vide, et recristallisé dans le minimum de benzène. Le rendement massique est de 80%.

A partir des autres arsanes, le temps de chauffage varie entre 3 et 12 h. Les rendements massiques sont compris entre 50% (**9A**) et 80% (**5A**).

Voie photochimique

Les réactifs dissous en quantités stoechiométriques (0,02 mol) dans 250 cm^3 de solvant (CCl_4 ou C_6H_6) sont placés dans un réacteur en quartz équipé d'une lampe Hanovia 450 W. La réaction a lieu en moins de 40 min. Les rendements à partir des arsatranes sont identiques à ceux observés par voie chimique.

Analyse élémentaire

Elle n'a pu être effectuée que pour les produits **5A** à **9A**. Les autres composés ne sont en effet stables qu'en solution.

	Calc.			Tr.		
Composé	C	H	N	C	H	N
5A	36,13	3,96	13,28	34,42	4,32	12,69
6A	31,84	3,18	12,38	31,72	3,07	12,08
8A	32,42	1,36	12,60	33,55	1,65	12,91
9A*	42,53	4,16	16,74	38,94	4,23	17,23

* Composé comportant de l'azoture en excès.

II. *Physicochimie*

Cryométrie: elles ont été réalisées "*in situ*" à l'aide d'un cryostat différentiel réalisé au laboratoire (1 cm^3 de benzène pour 40 mg de soluté environ). Les réactifs (arsatrane et azoture) sont dissous en quantité stoechiométrique dans C_6H_6. L'évolution du mélange réactionnel est suivie régulièrement.

Les mesures physicochimiques sont effectuées sur les appareils suivants: spectrographe de masse Riber QSM à 70 eV; spectrographe de masse Varian MAT; spectromètres Varian T 60, Perkin Elmer R 32 (90 MHz) pour la rmn ^1H; spectromètre rmn ^{13}C WP 60 Bruker 15,08 MHz; spectromètre ir: Beckman IR 20 – IR 9; spectromètre uv Cary 15.

1. H. STAUDINGER et J. MEYER. Helv. Chim. Acta, **2**, 635 (1919).
2. YU. G. GOLOLOBOV, I. N. ZHMUROVA et L. F. KASUKHIN. Tetrahedron Report n° 102, Tetrahedron, **37**, 437 (1981).
3. J. I. G. CADOGAN et I. GOSNEY. J. Chem. Soc. Perkin Trans. I, 466 (1964).
4. F. G. MANN et E. J. CHAPLIN. J. Chem. Soc. 527 (1937).
5. G. WITTIG et D. HELLWINKEL. Chem. Ber. **97**, 769 (1964).
6. J. J. MONAGLE. J. Org. Chem. **27**, 3851 (1962).
7. P. FRØYEN. Acta Chem. Scand. **23**, 2935 (1969); **25**, 983 (1971).
8. (*a*) P. MARONI, M. HOLEMAN, J. G. WOLF, L. RICARD et J. FISCHER. Tetrahedron Lett. 1193 (1976); (*b*) P. MARONI, M. HOLEMAN et J. G. WOLF. Bull. Soc. Chim. Belg. **86**, 199 (1977); (*c*) **86**, 209 (1977).
9. M. SANCHEZ, J. F. BRAZIER, D. HOUALLA, A. MUÑOZ et R. WOLF. J. Chem. Soc. Chem. Commun. 730 (1976).
10. H. B. STEGMANN, G. BAUER, E. BREITMAIER, E. HERMANN et K. SCHEFFLER. Phosphorus **5**, 207 (1975); J. I. G. CADOGAN, N. J. STEWART et N. J. TWEDDLE. J. Chem. Soc. Chem. Commun. 182 (1978); J. I. G. CADOGAN, I. GOSNEY, E. HENRY, T. NAISBY, B. NAY, N. J. STEWART et N. J. TWEDDLE. J. Chem. Soc. Chem. Commun. 189 (1979).
11. M. R. MARRE, M. SANCHEZ, J. F. BRAZIER, R. WOLF et R. BELLAN. Can. J. Chem. **60**, 456 (1982).
12. K. BERGESEN, B. PEDERSEN et J. SONGSTAD. Acta Chem. Scand. Ser. A, **35**, 147 (1981).
13. L. HORNER et A. CHRISTMANN. Chem. Ber. **96**, 389 (1963).
14. H. STAUDINGER et E. HAUSER. Helv. Chim. Acta, **4**, 861 (1921).
15. H. GOLDWHITE, P. GYSEGEM, S. SCHOW et C. SWYKE. J. Chem. Soc. Dalton Trans. 16 (1975).
16. J. E. LEFFLER et R. D. TEMPLE. J. Am. Chem. Soc. **89**, 5235 (1967).
17. A. F. GRAPOV, N. N. MELNIKOV et L. V. RAZVODOVSKAIA. Russ. Chem. Rev. **39**, 20 (1970); V. P. KUKHAR et V. A. GILYAROV. Pure Appl. Chem. **52**, 891 (1980); V. P. KUKHAR, E. V. GRISHKUN, V. P. RUDAVSKII et V. A. GILYAROV. Zh. Obshch. Khim. **50**, 1477 (1980).
18. J. EMSLEY et D. HALL. The chemistry of phosphorus. Harper and Row, Londres. 1976. Chap. X, p. 393; R. MATHIS, N. ZENATI, N. AYED et M. SANCHEZ. Spectrochim. Acta, Part A, **38**, 1181 (1982).
19. N. AYED, M. HADDAD, B. BACCAR, R. MATHIS et F. MATHIS. C. R. Acad. Sci. Paris, Ser. B, **283**, 449 (1976).
20. G. SINGH et H. ZIMMER. Organomet. Chem. Rev. **2**, 279 (1967) et réf. incluses.

21. E. SCHRADER. Ber. **50**, 777 (1917).
22. W. VON E. DOERING et C. H. DE PUY. J. Am. Chem. Soc. **75**, 5955 (1953).
23. G. KAMAI et Z. L. KHISAMOVA. Zh. Obshch. Khim. **24**, 816 (1954).
24. H. FUNK et H. KÖHLER. J. Prakt. Chem. **13**, 322 (1961).
25. P. MARONI, Y. MADAULE et J. G. WOLF. Bull. Soc. Chim. Fr. 668 (1973).
26. Y. MADAULE. Thèse d'Etat n° 1058, Toulouse, France, Octobre 1982; J. G. WOLF, Y. MADAULE et G. TRINQUIER. Communication au GECOM XI, Angers, France, Avril 1983; G. TRINQUIER, J. DAUDEY, G. CARUANA et Y. MADAULE. J. Am. Chem. Soc. **106**, 4794 (1984).

Studies of medium effects on the DPASV determination of Cu in natural waters using conventional and flow-through electrodes[1]

IBRAHIM K. ALZAND AND COOPER H. LANGFORD[2]

Department of Chemistry, Concordia University, Montreal, P.Q., Canada H3G 1M8 and Department of Chemistry, Carleton University, Ottawa, Ont., Canada K1S 5B6

Received November 18, 1983

IBRAHIM K. ALZAND and COOPER H. LANGFORD. Can. J. Chem. **63**, 643 (1985).

A survey of DPASV signals for Cu in a variety of media and under varying conditions has been undertaken. It is possible to identify the circumstances associated with two distinct problems in Cu determination which have not been clearly distinguished in earlier literature. The role of Cl^- in influencing the Hg wave form (which in turn affects the relative apparent peak heights and widths of the two Cu signals arising from Cu(Hg) amalgam and undissolved Cu(solid)) is distinguished from the role of Cl^- as a complexing agent in solution at higher Cl^- concentration. Effects of dissolved organic matter in natural waters are shown to resemble Cl^- effects. Data are also presented on two related matters: (*1*) some factors in a natural water sample that confuse the use of DPASV as a tool for Cu species identification, and (*2*) the effects of high Cl^- concentration on Cd, Pb, and Cu signals.

Following the study of medium effects and interferences influencing DPASV signals, a fresh water sample has been examined at the conventional hanging Hg drop electrode, thin Hg films on graphite and Hg thin films on a novel reticulated vitreous carbon flow-through electrode. Hg thin film electrodes deposited *in situ* are confirmed to be very sensitive for analysis of river water samples. The flow-through electrode has excellent sensitivity. Promising storage characteristics of the flow-through electrode are evaluated with a view to suggesting an ASV system using a simple electronic unit for field sampling.

IBRAHIM K. ALZAND et COOPER H. LANGFORD. Can. J. Chem. **63**, 643 (1985).

On a entrepris un relevé des signaux DPASV du cuivre dans divers solvants et sous des conditions variées. Il est possible d'identifier deux problèmes distincts associés à la détermination du Cu qui n'avaient pas été relevés antérieurement. On établit une distinction entre le rôle du Cl^- lorsqu'il influence la forme de la vague du Hg (qui affect à son tour les hauteurs et les largeurs relatives apparentes des pics des deux signaux provenant de l'amalgame Cu(Hg) et du Cu(solide) qui n'est pas dissous) et le rôle du chlore agissant comme agent complexant dans des solutions contenant des concentrations plus élevées de Cl^-. On démontre que les effets des matières organiques dissoutes dans les eaux naturelles ressemblent à ceux des ions Cl^-. On présente aussi des données relatives à deux sujets apparentés: (*1*) quelques facteurs dans un échantillon d'eau naturelle qui provoque de la confusion lors de l'utilisation du DPASV comme méthode d'identification des espèces Cu et (*2*) les effets de concentrations élevées en Cl^- sur les signaux du Cd, Pb et Cu.

A la suite de l'étude sur les effets du milieu et sur les facteurs influençant les signaux DPASV, on a examiné un échantillon d'eau fraîche à l'aide d'une électrode conventionnelle à goutte de mercure tombante, de films fins de Hg sur du graphite et de films fins de Hg sur une nouvelle électrode poreuse de carbone vitreux réticulé. On a confirmé que les électrodes utilisant des films fins de Hg déposés *in situ* sont très sensibles pour l'analyse d'échantillons d'eau de rivières. La sensibilité de l'électrode poreuse est excellente. Dans le but de suggérer un système ASV qui utiliserait une unité électronique pour des études dans le champ, on a évalué des caractéristiques de storage prometteuses de l'électrode poreuse.

[Traduit par le journal]

Introduction

This report was motivated by the effort to develop a flow-through electrode using reticulated vitreous carbon. The purpose is to evaluate its possible usefulness in a field sampling device which would allow a simple electronic unit to be exploited in the field with the sample returned to the laboratory for anodic stripping. However, the evaluation of this electrode requires first examination of the electrode in comparison to various electrodes used in anodic stripping voltammetry (ASV). This has led us to explore some of the problems shared by all these electrodes. The work emphasizes the effects that occur in the mercury film and at the interface, and some observations on the use of ASV data for "speciation" studies in natural water systems. The report is organized around studies of Cu^{2+}.

A number of papers have discussed the application of DPASV to the differentiation of various trace metal species in natural water samples (1–4). The idea is sufficiently accepted that it has appeared in a review for the reader of general chemistry (5). The basis is to associate changes in peak position, peak multiplicities, and peak widths with changing speciation in the natural water. Unfortunately, these parameters are also influenced by speciation in the Hg phase of the electrode, the electrochemistry of Hg at the electrode, and interfacial phenomena. The presence of Cl^- causes problems in the determination of Cu by anodic stripping voltammetry (6–8). This has not yet been completely elucidated. Two different factors have been established; copper complexing by Cl^- (7) and the limited solubility of Cu in Hg (8). It is important to resolve any ambiguities because the widespread use of ASV to study speciation (3) requires that effects due to speciation in the Hg phase be distinguished from effects due to speciation in the aqueous sample. There is a third problem as well. Cl^- alters the Hg wave in such a way that the peak heights and widths for nearby Cu peaks are affected (Hg_2Cl_2).

In Part A of this paper the chloride interference is studied in depth. Part B deals with the effects of natural water organic matter. They are shown to be very similar to Cl^- effects. The final goal of this study is the characterization of a flow through electrode for differential pulse anodic stripping voltammetry (DPASV) of natural waters which might be used in an electron-

[1]Supported by the Natural Sciences and Engineering Research Council of Canada. I.K.A acknowledges a scholarship from the government of Iraq. We thank J. Alfheim for discussion and editorial assistance.

[2]To whom correspondence should be addressed at Concordia University.

ically simple field device to collect samples which could be analyzed later in the laboratory.

Experimental

Apparatus

Differential pulse anodic stripping voltammetry (DPASV) was carried out in a conventional manner using a PAR 264 Polarographic Analyzer equipped with a standard PAR cell for three electrodes and an N_2 purge. Instrumental parameters were a 5 mV s^{-1} scan rate, and a 50 mV modulation amplitude. Most commonly, deposition was carried out at -1.00 (vs. sce) with a deposition time of 5 min. Specific conditions are mentioned below. The reference electrode was sce connected to the cell via a salt bridge filled with either 1 *M* KNO_3 or 0.5 *M* $NaNO_3$ and terminated at a vycor frit sealed into a length of heat shrinkable Teflon tubing. The counter electrode was a Pt wire coil. pH was measured with an Orion model 701A digital analyzer.

Four types of electrodes were employed: (*i*) a hanging mercury drop (HMDE, PAR model 9323), (*ii*) a mercury thin film electrode with *in situ* mercury deposition (MTFE *in situ*), (*iii*) a MTFE predeposited (MTFE *predep.*), and (*iv*) a mercury-coated reticulated vitreous carbon flow-through electrode (MCRVCE). The films were deposited on a wax-impregnated graphite electrode supplied by PAR instruments (Model 9319). This electrode had a diameter of 0.625 cm. The end was polished and the remainder of the lower half of the rod was covered with a tight-fitting Teflon tube pressed on from the polished end. The electrode was polished before each use with fine emery paper washed with ethanol and wiped with lens tissue.

The reticulated vitreous carbon electrode was fabricated from 100 pore per inch RVS (Chemtronics International Inc., Ann Arbor, MI). The configuration is shown in Fig. 1. The electrochemical cell consisted of two sections connected by polyethylene tubing to allow easy replacement and storage of the RVC electrodes. The upper section, constructed from a Pyrex tube 7 mm id housed the reference electrode salt bridge and the Pt counter electrode. The lower Pyrex section was 1 mm id at the upper end and 2 mm id at the lower, and housed the 7 mm by 5 mm RVC disc. Electrical contact was made by a Pt wire sealed from the outside by epoxy glue. The sce was connected to the cell via a 1 *M* $NaNO_3$ salt bridge.

A peristaltic pump (Markson Scientific) was placed downstream from the cell to pull solution through the RVC electrode and recirculate it to a sample reservoir which was deoxygenated with purified N_2. Acetate buffer (100 mL of 0.012 *M*) containing 1 mL of 0.01 *M* Hg^{2+} was introduced into the reservoir.

Materials

Mercury was triply distilled and was transferred only with a clean dry siliconized capillary. Hydrochloric acid and nitric acid were Ultrex grade (J. T. Baker). KCl, KNO_3, and sodium acetate were reagent grade. All solutions were prepared from water purified from "tap" distilled water by passing through a high efficiency mixed bed ion exchanger followed by distillation from alkaline permanganate in all glass apparatus. Solutions were stored in preleached linear polyethylene bottles. The Hg(II) plating solution was prepared by dissolution of triply distilled Hg in a minimum amount of Ultrex HNO_3 and dilution with distilled water to give a 0.010 *M* $Hg(NO_3)_2$ stock solution. Stock standard solutions of metals were prepared by dissolution of 1 g of pure metal (99.9%, previously cleaned with acid and dried) in a minimum amount of 8 *M* Ultrex HNO_3 followed by dilution with 1% v/v HNO_3 to 1000 μg mL^{-1}. More dilute secondary stock solutions were prepared by diluting these solutions just prior to use. N_2 gas was scrubbed of residual O_2 by passage through a gas washing bottle containing V(II) and a second containing the supporting electrolyte of the experiment in question.

Procedure

Part A: Small aliquots of solutions were transferred to the cell using Eppendorf 500−100 and 20−200 μL pipettes with disposable tips. Initial deaeration was by N_2 purging for 10 min. During the deposition period the solution was stirred with a magnetic stirrer and a slow N_2

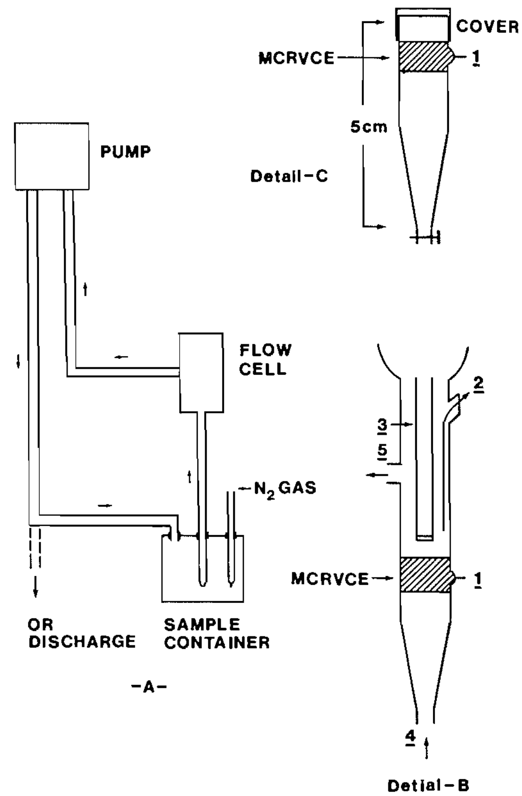

FIG. 1. The flow-through MCRCVE system. Parts are (*1*) the RCVE, (*2*) the counter electrode, (*3*) the reference electrode chamber, (*4*) the input from the reservoir, (*5*) the output to the peristaltic pump. The arrows indicate flow direction.

flow passed over the solution during deposition and stripping. All glassware was leached with 5 *M* HNO_3 between uses.

Part B: To coat the MCRVCE the Hg film was deposited by holding the potential at -0.8 V and passing the deaerated mercury solution through the electrode at 4.8 mL min^{-1} for 20 min. After plating, the flow was stopped and the reservoir was replaced with a blank solution. Holding the MCRVCE at $+0.05$ V for 10 min followed by 2 min at -1.0 V and stripping anodically to 0.0 V removed any co-deposited contaminants. Finally, the sample solution was buffered and placed in the reservoir. During dearation, the MCRVCE was held at 0.0 V. As with the previous experiments (Part A) deposition of Cd, Pb, and Cu was at -1.0 V and DPASV was preformed with a 5 mV s^{-1} scan rate and a 50 mV modulation amplitude. The scan was stopped at 0.0 V and the electrode was held for 1 min at this potential after which it was ready for the next determination.

For the storage experiments, the stability during storage of the MCRVCE's was evaluated by first rinsing the electrode with circulating deareated blank immediately after plating. During this flow, potential was held at -1.0 V. The unit containing the MCRVCE and 2 mL of blank was closed and stored for a period of up to 96 h.

The natural water samples used in the analyses were collected from the Rideau River adjoining the Carleton University Campus at an Environment Canada gauging station.

The collection containers were high density polyethylene bottles which had been leached with 3 *M* HNO_3 for at least 2 weeks and then rinsed with doubly distilled water followed by river water. River water was allowed to stand in the bottle for 1/2 h before a fresh sample was collected. Samples were filtered through acid washed millipore 0.45 μm membrane filters. Analyses were normally completed on the same day.

Procedure for "uv digestion" involved addition of 50 μL of 80% H_2O_2 to a 25 mL aliquot of sample which had been acidified to pH = 2 with 2 *M* Ultrex HNO_3. The irradiation was carried out with a 1 kW medium pressure mercury vapour lamp for 4 h with stirring. A final

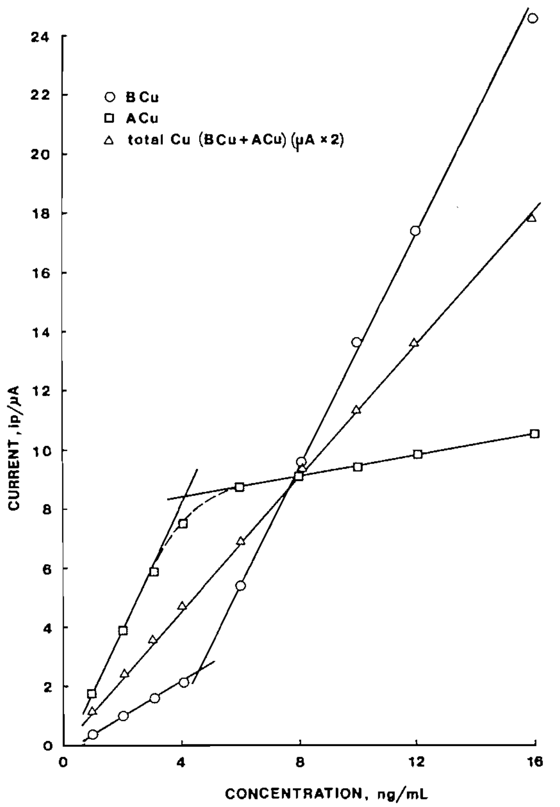

FIG. 2. Analytical curves for standard Cu solutions showing the response of total Cu (A + B) to the total concentration. Note that for total Cu the current axis is to be multiplied by two. Films were "preformed" so that Hg film thickness is independent of Cu plating time.

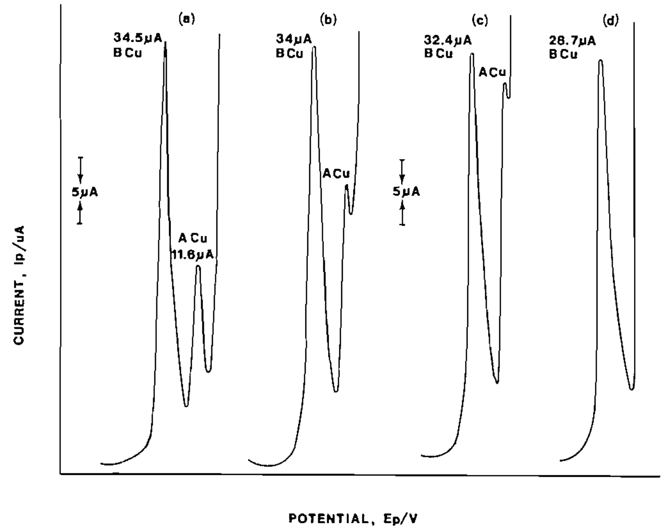

FIG. 3. ASV voltammograms demonstrating the effect of chloride concentration on the peak currents of A-type Cu and B-type Cu. (*a*) ASV obtained from 20 ng mL^{-1} Cu and 4 × 10^{-5} *M* Hg^{2+} on a MTFE *in situ* with a 5 min plating time at −1.0 V; (*b*), (*c*), and (*d*) were recorded after the addition of 5 × 10^{-4}, 1 × 10^{-3}, and 2 × 10^{-3} *M* KCl, respectively.

5 min irradiation with purified N_2 bubbling removed residual peroxide.

Acid digestion of samples was carried out as follows. Aliquots (25 mL) of filtered river water were acidified to pH = 0.7 and reduced to 1 mL on a hot plate (without boiling). This residual sample was diluted with doubly distilled water and brought to pH = 5.0.

Insoluble particles retained on the millipore filters from 1.00 L of river water were dissolved for analysis by wet ashing. Filters plus 10 mL of 2 *M* Ultrex HNO_3 were heated for 1/2 h at 70°C. The solutions were filtered through new membrane filters and the filters were washed with doubly distilled water and the resulting solutions finally diluted to 50.0 mL. Aliquots (1.25 mL) were transferred to the electrolysis cell and diluted with doubly distilled water and acetate buffer to give 25.0 mL at pH = 5.0. The fractionation and treatments just described is used below to classify metal ions into "bound", "labile", and "particulate" fractions. These terms have the operational meaning given by this procedure.

Results

Part A

In preliminary experiments, KCl was used in the salt bridge. A change from saturated KCl to 1 *M* KNO_3 or 0.5 $NaNO_3$ affected the Cu signal MTFE's. In the absence of Cl^-, two Cu peaks appeared; the first (cathodic side) at −0.21 V in these experiments had a half width, $b_{1/2}$, of 55 mV; the second at a more anodic potential of −0.08 V had a half width of 45 mV. The height of each of these two Cu peaks and their relation to each other proved to be a function of the thickness of the Hg film, the plating time for *in situ* electrodes, deposition potential, the chloride concentration, and the Cu^{2+} concentration.

The more anodic peak (called A-Cu) dominates at low (1 ng mL^{-1}) concentration but that the more cathodic peak (called B-Cu below) grows in faster as the concentration rises. (Behaviour at the HMDE was quite similar.) An analysis of the contribution to the total Cu signal from each peak as Cu concentration increases is given in Fig. 2. (A quite similar analysis can be derived from the HMDE experiments.) The *sum* of peak currents, i_p, for the two peaks is linear in added Cu.

Mercury film thickness in MTFE's was also a parameter. This report follows the equations of Stojek and co-workers to estimate film thickness (8, 9). When Cu at 1.00 μg mL^{-1} is deposited for 5.0 min at −1.0 V a preformed MTFE of 77 Å thickness results. The peaks for B-Cu and A-Cu have i_p values of 0.80 and 1.3 μA, respectively. As the film thickness was increased to 500 Å in four steps between 50 and 200 Å each, the height of the B-Cu peak decreased reaching "zero" at 500 Å. Conversely, the A-Cu peak height increased to a maximum value of 2.30 μA. (The sum increased slowly from 2.10 to 2.30 μA.) When *in situ* film formation is used, films become thicker at the same time as the quantity of Cu plated increases. The second factor ultimately dominates. The change in peak height with plating time for 1.00 ng mL^{-1} of Cu is similar to the change of peak height with Cu concentration. (Long plating times can deplete the Cu. Non-linearity was observed beyond 60 min.)

From this, the effect of Cl^- ion can now be examined in the case of *in situ* MTFE analysis. The most revealing experiment is presented in Fig. 3 where the effects on Cu peaks of 0.50 × 10^{-4} *M*, 1.0 × 10^{-3} *M*, and 2.0 × 10^{-3} *M* KCl are recorded. The B-Cu peak is affected slightly at most. The A-Cu peak "disappears". Careful inspection of the figure, however, reveals that it is disappearing into the large Hg wave which is advancing cathodically with increasing Cl^- concentration. There is no evidence available for a change in the A-Cu peak height because that peak cannot be resolved clearly from the chloro Hg peak at Cl^- concentration 5 × 10^{-4} *M*. In this concentration range, there is little literature precedent for Cl^- complexing of Cu unless the cuprous state is involved (note the nearly constant B-Cu peak height). There appears to be loss of

TABLE 1. Summary of the effects of increasing chloride concentration on a 25 mL solution containing 10 ng mL^{-1} of Zn, Cd, and Pb and 15 ng mL^{-1} of Cu deposited on a HMDE*

KCl conc. (mol/L)	Cd E_p/V	Pb E_p/V	A-Cu i_p/μA	A-Cu E_p/V	A-Cu $b_{1/2}$/mV	B-Cu i_p/μA	B-Cu E_p/V	B-Cu $b_{1/2}$/mV
0.00	0.672	0.520	0.160	0.16	80	0.135	0.08	55
2×10^{-4}	0.672	0.520	0.165	0.16	80	0.135	0.08	
4×10^{-4}	0.672	0.520	0.163	0.16			0.08	
6×10^{-4}	0.672	0.520	0.161	0.16			0.08	
8×10^{-4}	0.672	0.520	0.163	0.16				
1.2×10^{-3}	0.672	0.520	0.145	0.165				
1.5×10^{-3}	0.672	0.520	0.130	0.17				
5×10^{-3}	0.675	0.520	0.10	0.18				
1×10^{-2}	0.680	0.520	0.09	0.21				
5×10^{-2}	0.685	0.520	0.11	0.26	120			
0.10	0.693	0.524	0.12	0.275	115			
0.50	0.710	0.540	0.14	0.320	115			
1.00	0.720	0.550	0.14	0.340	115			

*HMDE: 25 mL solution contains 10 ng mL^{-1} Zn, Cd, and Pb and 15 ng mL^{-1} copper deposition time 3 min. Scan rates 5 mV s^{-1}. In all cases where HMDE was used, 0.03 cm drop area was used.

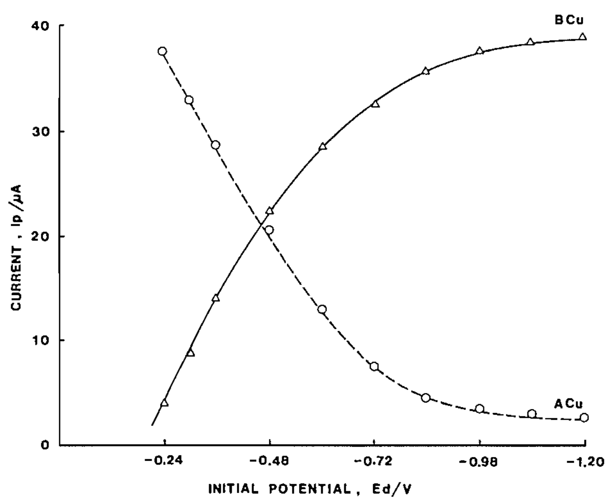

FIG. 4. Relationship between the varying peak currents of both A-Cu and B-Cu and the initial plating potential in the absence of chloride.

information concerning the probably nearly constant A-Cu peak which is a consequence of Cl$^-$ "complexing" Hg not Cu.

These observations do not deny the effect that Cl$^-$ complexation can exert on voltammograms. At higher Cl$^-$ concentration both peak potential, E_p, and peak current, i_p, for the well resolved B-Cu signal become a function of Cl$^-$ ion concentrations. Relevant results, in this case at an HMDE, are collected in Table 1. Results involving Cd, and Pb are also included. The effect of Cl$^-$ on E_p and i_p of the B-Cu band begins to be significant at $1.2-1.5\times10^{-3}$ M KCl. In the Cd peak, the effect is observable at 5×10^{-3} M KCl and for Pb it emerges at 0.10 M KCl.

Finally, for Part A, the two Cu peaks, A and B, can be altered relative to each other absolutely by the choice of plating potential in the absence of Cl$^-$. An example of this is shown in Fig. 4 which refers to an experiment conducted on an Ottawa drinking water buffered at pH = 5.0 with sodium acetate/acetic acid and which utilized a preformed MTFE of 1500 Å thickness. It is seen that the B-Cu peak is strongly favoured by more cathodic deposition potential.

Part B

Two preliminary experiments were performed in which a DPASV was run on an untreated river water sample. The first experiment used a HMDE and it was observed that the background signal could be reduced and the Cu signal enhanced. This was done by cycling the pH down to 2 and then back to pH = 5. Schonberger (4) has reported similar pH effects.

The intermetallic effect of Zn on the Cu signal which has been discussed elsewhere (10) was seen when a DPASV was run on the same untreated river water using a MTFE.

Table 2 is a summary of the analytical results for the analysis of river water by various methods and with various methods of sample treatment. Little difference among the three types of electrodes (HMDE, MTFE (*in situ*), MTFE (predep.)) is seen from the tabulated results. The problems encountered with one of the electrodes is shared by all. The results show that sample pretreatment is clearly critical. This is reinforced by Table 3 which indicates how the sample divides in percentage terms, what is the total concentration identified by each method, and the sensitivity of each of the three types of electrodes.

While previous figures and tables record the data on performance of conventional DPASV electrodes and the explanation of some Cu "pecularities" the remaining results concern synthetic samples and river water samples studied with the new electrode, the MCRVCE. The first results involve immediate analysis of synthetic samples, which were prepared in the same manner as samples used in Part A. Analytical calibration curves for Cd, Pb, and Cu using 2 min deposition times are linear. Linear regression gave with R^2 values in excess of 0.999 except for B-Cu where R^2 is 0.957. (Total Cu has an R^2 0.999.) All intercepts (blanks) are 0.5 μA and slopes (sensitivities) range from 1.93 ± 0.2 to 2.30 ± 0.2 μA/ng mL^{-1}. These are good and analyte quantities near 0.1 ng mL^{-1} require deposition times of only about 10 min. The enhanced sensitivity compared to stationary systems is one advantage of the flow through electrode. The peak potentials are: Cd, −0.73 V; Pb, −0.57 V; A-Cu, −0.21 V; and B-Cu, −0.11 V.

Characteristic DPASV's recorded with river water samples (buffered to pH = 5.5) using MCRVC's are shown in Fig. 5. Peak potentials at natural levels are: Cd^{2+}, −0.73 V; Pb −0.59 V; A-Cu, −0.30 V; B-Cu, −0.11 V. The concentrations are

TABLE 2. Analytical results of the Rideau river samples by DPASV with HMDE, preformed MTFE and MTFE prepared *in situ* with various methods of sample treatment*

Sample treatment	HMDE†				Preformed MTFE (600 Å)†				MTFE prepared *in situ* (170 Å)			
	Zn	Cd	Pb	Cu	Zn	Cd	Pb	Cu	Zn	Cd	Pb	Cu
Filtered river water	2.79	0.12	0.27	0.11	2.80	0.11	0.30	0.20	3.08	0.12	0.31	0.20
Acidified filtered river water	3.45	0.15	0.36	0.37	3.20	0.15	0.38	0.32	3.50	0.16	0.37	0.29
River water digested by uv	3.64	0.19	0.43	1.60	3.90	0.20	0.42	1.79	4.80	0.25	0.49	1.55
River water digested in strong acid	4.30	0.20	0.46	1.80	4.50	0.23	0.48	1.87	4.90	0.28	0.53	1.64
Metals in particulate	2.10	0.18	0.32	1.00	2.25	0.22	0.32	1.08	2.40	0.23	0.37	1.07

*Relative standard deviation ranging from 2 to 5% in all the three modes.
†Concentrations in ng mL^{-1}.

TABLE 3. Distribution of metal ions in Rideau river samples*

Method	Zinc					Cadmium				
	Total conc. (ng mL^{-1})	Percentage distribution: Filtered sample, Labile	Filtered sample, Bound	In particulate	Average sensitivity (nA/n*M* min)	Total conc. (ng mL^{-1})	Percentage distribution: Filtered sample, Labile	Filtered sample, Bound	In particulate	Average sensitivity (nA/m*M* min)
HMDE	6.40	43.6	24.1	32.3	0.63	0.38	31.4	21.5	47.1	0.46
Preformed MTFE 600 Å thickness	6.75	42.8	25.2	32.0	40.0	0.45	25.0	27.2	47.8	38.0
MTFE prepared *in situ* 170 Å thickness	7.30	42.2	25.0	32.8	50.0	0.51	24.3	25.4	50.3	48.0

Method	Lead					Copper				
	Total conc. (ng mL^{-1})	Percentage distribution: Filtered sample, Labile	Filtered sample, Bound	In particulate	Average sensitivity (nA/n*M* min)	Total conc. (ng mL^{-1})	Percentage distribution: Filtered sample, Labile	Filtered sample, Bound	In particulate	Average sensitivity (nA/m*M* min)
HMDE	0.78	35.0	24.4	40.60	0.40	2.82	4.3	59.9	36.8	0.36
Preformed MTFE 600 Å thickness	0.80	36.9	23.1	40.0	31.0	2.95	6.3	57.6	36.1	9.5
MTFE prepared *in situ* 170 Å thickness	0.89	34.8	24.0	41.2	44.0	2.71	7.3	53.1	39.6	13.0

*For fraction definition see procedures at the end of the Experimental section.

estimated from spiking results.

The peaks for Pb and Cu are reduced and difficult to resolve because of the cathodic shift of the Hg oxidation wave background *similar to that seen above induced by* Cl^- *in Part A*. Cl^- cannot be the cause here. The interference becomes more severe in repeated runs on a sample, probably because of adsorption following exposure of the surface to a larger volume of river water. The magnitude of the interference with Pb and Cu is documented by the spiking experiments shown in Fig. 6. That the effect arises from organic matter and from the adsorption on the electrode and not complexing in the solution is shown, because, first uv digestion improves the signals and second the inteference can be reintroduced by treating the unpolarized electrode with untreated river water that has not been uv-digested, rinsing the electrode, and only then carrying out plating and DPASV on a solution which had *been uv-digested*.

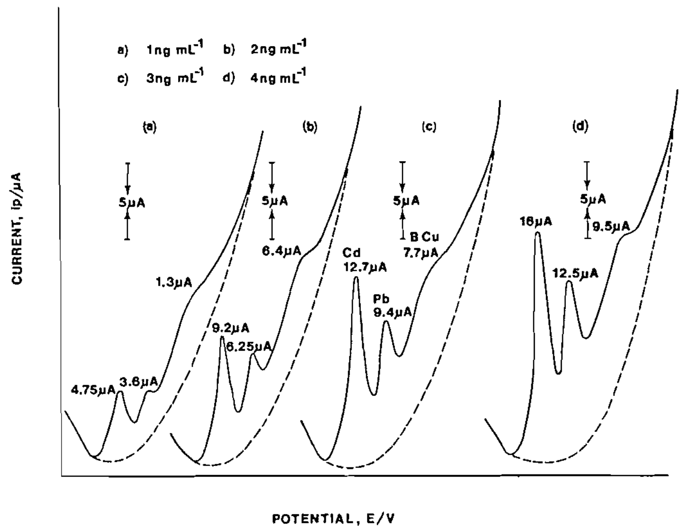

FIG. 5. Analysis by spiking of river water using the MCRVCE. (Plating −2 min at −1.0 V; 5 mV s^{-1} scan rate and 4.8 mL min^{-1} flow rate).

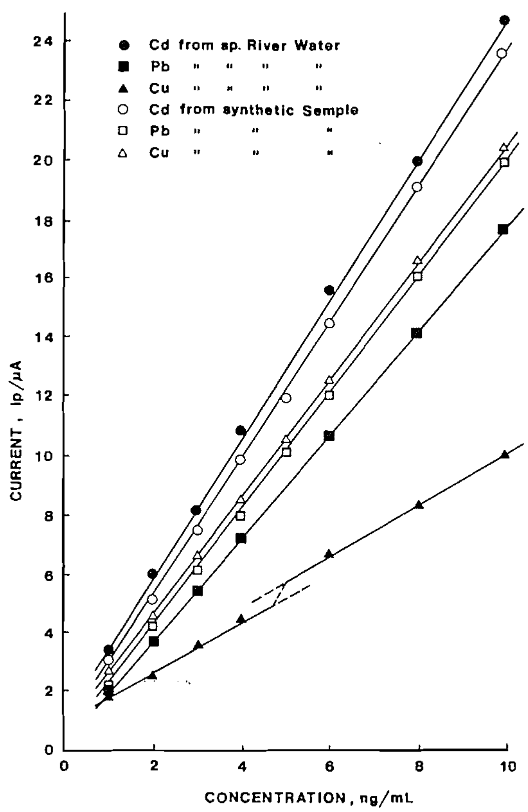

FIG. 6. Comparison of analytical curves obtained by the MCRVCE of synthetic and spiked river water samples.

Some of the adsorbed film survives the rinsing and produces the cathodic shift of the Hg wave! In a related experiment it was demonstrated that the background interference was additive. An electrode that had been through six successive runs involving 6 min deposition times was compared to a fresh electrode with a mercury film deposited from an entirely synthetic solution. The fresh electrode was found to have a substantially lower background interference. This experiment was also intended to test the role of irreversible adsorption on the electrode

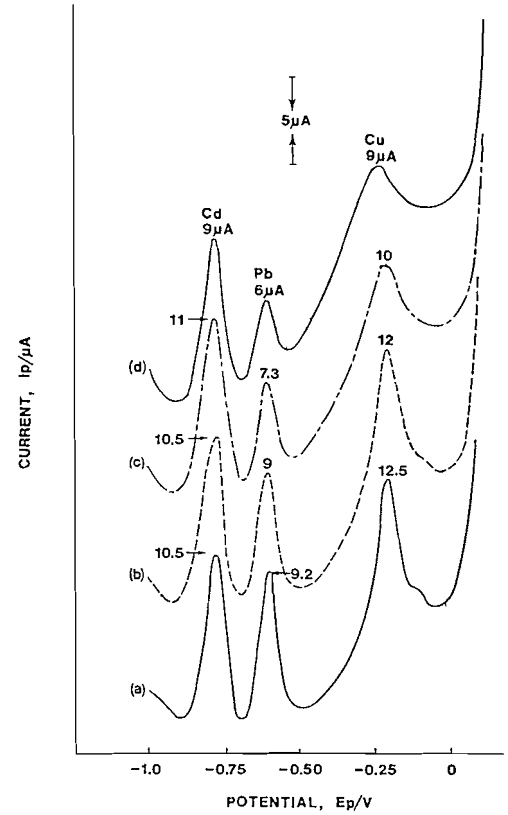

FIG. 7. ASV voltammograms demonstrating the effect of fulvic acid concentration on the peak currents of metal species in a synthetic river water sample. (*a*) ASV obtained from 1 ng mL^{-1} of Cd and Pb and 1.5 ng μL^{-1} Cu; (*b*), (*c*), and (*d*) were recorded after the addition of 1, 4, and 8 μg mL^{-1} of fulvic acid.

as opposed to complexation in the solution.

Finally, an effort was made to model the inteference effect in river water with a purified sample of a soil organic acid (fulvic acid) which has been characterized extensively (11). The results appear in Fig. 7. As fulvic acid concentration increases, Cu peaks decrease and broaden in a manner similar to that observed in river water samples. However, for this low molecular weight relatively hydrophilic soil organic, the Hg wave cathodic shift is not as pronounced as it is in river water where typical organic colloids would be expected to be of greater molecular weight and more hydrophobic.

On balance, the MCRVCE is fully competitive with other ASV electrodes for analysis of trace metals in water samples such as drinking water or Rideau river water.

In the interest of testing the idea of using the MCRVCE for plating in a simple field sampler to be followed by stripping using a more sophisticated laboratory polarograph, MCRVCE electrodes were rinsed with blank and stored closed with air free blank inside after plating. After storage for 12 to 96 h the unit was remounted in the flow system and 8 mL additional blank (total volume 10.0 mL) was circulated while potential was held at −1.0 V for 5 min to replate any oxidized metal. At the end of this period the DPASV scan was recorded.

Typical results of analysis of stored electrodes are shown in Fig. 8. There is evidence of loss of each of the metal ions, especially in the case of Cd. The mechanism is not clear. One aspect, however, is encouraging. The calibration curves for all metals remain linear after up to 96 h. The scatter of points in Fig. 8 also show results from independent runs which suggest

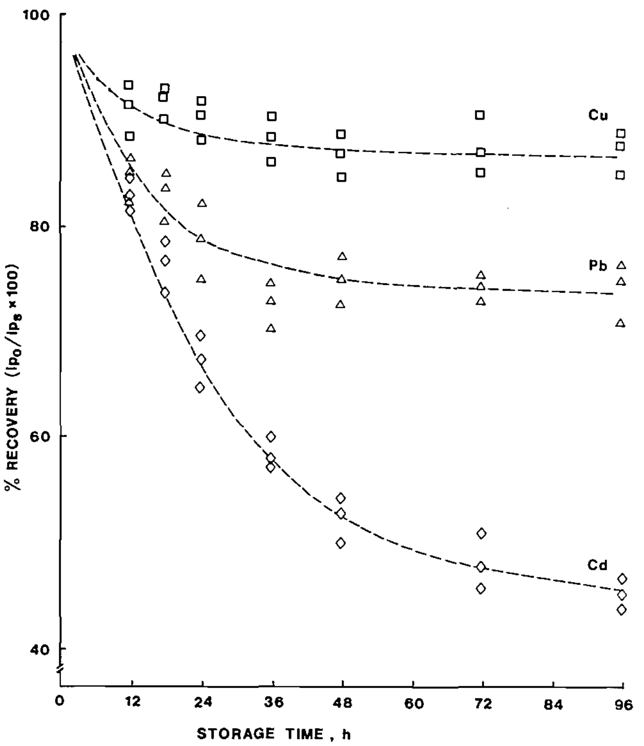

FIG. 8. Effect of storage on percentage recovery from the MCRVCE.

that losses are fairly reproducible. One experiment tends to reveal the nature of the losses. Dissolving of stored metal ions in 10 mL of blank solution followed by replating the dissolved metal ions for 20 min on freshly prepared MCRVCE followed by stripping improves the sensitivity for Cd and Pb.

Discussion

Part A

The results presented first cannot be associated with complex formation and clearly reflect the ASV consequences of the limited solubility of Cu in Hg (first demonstrated in ref. 8). The B-Cu peak is that for particles of solid Cu suspended in, or plated on, the Hg electrode. The A-Cu peak is the peak for a Cu amalgam. The results presented are selected to give a clear idea of a cross section of our many experiments. Double peaks for Cu on all four electrode types were observed, with the Cu (solid) peak being most prominent at low Hg film thickness as would be expected. The conclusion is reinforced by data in Fig. 4. There it is obvious that "fast" deposition of Cu at highly cathodic voltages favours precipitation of Cu where as "slow" deposition at voltages much nearer the reversible values favours Cu atom formation and amalgamation.

A confusion appears to have infected some earlier discussions with respect to the role of Cl^-. It is apparent that Cl^- complexing of Cu is not the only way Cl^- can affect Cu signals. Rather, Fig. 5 shows that the major effect at low concentration can be on Hg as the relative interaction energy with Cu and Hg would imply. Since ASV studies are frequently directed to identification of speciation in the sample (3), it is especially important to be aware of which circumstances affect properties of Hg and not the analyte. Chloride can mask "labile" Cu by the shift of the Hg wave which is subtle and easily overlooked. This is the effect reported in ref. 6.

An analogy to this "masking" can be drawn from the studies done by Forsmann (12). In his studies of the cathodic stripping voltammetry of Penicillamine he reported that the measurement of the Penicillamine amalgam peak was interferred with by the presence of cupric ions. This is the inverse of what we discuss.

Two general points may be made. First, effects of Cl^- will follow usual inorganic chemical complexity constant sequences. Second, the effect of Cl^- appears only at relatively high Cl^- concentrations *except* for the case of the one metal present at high concentration, Hg.

Part B

In Part A it was shown that interferences in DPASV of simple inorganic species like Cl^- arise not only from complexation of the analyte ions in solution but also from interactions at the interface and in the Hg phase which affect *inter alia* the Hg background wave. In Part B we first observed that very similar effects arise in natural fresh waters which are low in Cl^-. The emphasis on interfacial effects was confirmed by the variation of interferences on pH cycling. Moreover, the effects which resemble Cl^- effects are reduced by procedures which are expected to destroy organic matter. Synthetic solutions containing organic matter do exhibit similar interferences. The clearest demonstration that the effects arise from adsorption is the fact that they survive the removal of carbon electrodes and light rinsing. Since the shape and scale of the anodic stripping voltammogram is very sensitive to effects connected to the interface and the Hg phase, it seems unlikely that the voltammograms can be reliably interpreted in terms of speciation of metals in the solution phase.

Turning to the new electrode, Trojanek and Opekar (13) in a paper describing a flow-through electrode for ASV point out that flow through electrodes in general have the advantages of permitting treatment of large solution volumes and attaining high sensitivity. Furthermore, Batley (14) notes the problem of possible contamination during trace metal analysis in natural waters. Techniques that require sample handling and multiple reagent additions are prone to errors whereas the use of the *in situ* preconcentration methods forego these problems. For these reasons, the results obtained with our electrode (MCRVCE) imply a potential for trace metal analyses in natural waters. The ageing studies indicate that the use in an electronically simple field device for plating with the transport of the electrode to the laboratory for stripping at an electronically sophisticated device is plausible. The interferences discussed here suggest that photochemical H_2O_2 treatment in the reservoir chamber would be needed in the field for river water but perhaps not for drinking water.

1. R. ERNST, H. E. ALLEN, and K. H. MANCY. Water Res. **9**, 317 (1975).
2. S. A. WILSON, T. C. HUTH, R. E. AMDTAND, and R. K. SKOGERBOE. Anal. Chem. **52**, 1515 (1980).
3. G. E. BATLEY and F. M. FLORENCE. Marine Chem. **4**, 317 (1976).
4. E. A. SCHONBERGER and W. F. PICKERING. Talanta, **27**, 11 (1980).
5. R. M. HARRISON and O. P. H. LAXEN. Chem. Br. **16**, 316 (1980).
6. T. M. FLORENCE and G. E. BATLEY. J. Electroanal. Chem. **75**, 791 (1977).
7. M. J. PINCHIN and J. NEWHAM. Anal. Chim. Acta, **90**, 91 (1977).
8. Z. STOJEK, B. STEPNICK, and Z. KUBLIC. J. Electroanal. Chem. **74**, 277 (1976).

9. Z. STOJEK and Z. KUBLIC. J. Electroanal. Chem. **105**, 247 (1979).
10. J. WANG and H. D. DEWALD. Anal. Chem. **55**, 933 (1983).
11. A. W. UNDERDOWN, C. H. LANGFORD, and D. S. GAMBLE. Anal. Chem. **53**, 2139 (1981).
12. U. FORSMANN. J. Electroanal. Chem. **11**, 325 (1980).
13. A. TROJANEK and F. OPEKAR. Anal. Chim. Acta, **126**, 15 (1981).
14. G. E. BATLEY. Anal. Chim. Acta, **124**, 121 (1981).

Synthesis and resolution of $R(-)$-5-hexyn-3-ol

BERNARD L. ROY[1] AND PIERRE DESLONGCHAMPS
Laboratoire de synthèse organique, Département de chimie, Faculté des Sciences, Université de Sherbrooke, Sherbrooke (Qué.), Canada J1K 2R1

Received June 26, 1984

BERNARD L. ROY and PIERRE DESLONGCHAMPS. Can. J. Chem. **63**, 651 (1985).

The resolution of (±)-5-hexyn-3-ol (**1**) was effected by high performance chromatography of its *O*-methyl mandelic esters **3** and **4**. The absolute configuration of (−) and (+)-5-hexyn-3-ol were determined by comparison with an authentic sample prepared from D(+)-glucose.

BERNARD L. ROY et PIERRE DESLONGCHAMPS. Can. J. Chem. **63**, 651 (1985).

La résolution du (±)-hexyne-5 ol-3 (**1**) fut réalisée grâce à la chromatographie à haute performance de ses esters *O*-méthyl mandélique **3** et **4**. La configuration absolue du (−) et (+)-hexyne-5 ol-3 fut déterminée par comparaison avec un échantillon préparé à partir du D(+)-glucose.

As part of our work on the total synthesis of erythromycin *A*,[2] the *R* enantiomer of 5-hexyn-3-ol (**1***R*) was required as starting material. We have obtained this compound by resolution and wish to report this work.

The racemic form of **1** (Scheme 1), which is readily available from the condensation of propargyl magnesium bromide on propionaldehyde (3), was transformed into the corresponding diasteroisomeric *O*-methyl mandelic esters **3** and **4** by reaction with optically active acid chloride **2** (4). The separation of diastereoisomers **3** and **4** was carried out by high performance chromatography using toluene − ethyl acetate (99.5:0.5) as the solvent. After separation, the more polar compound had an $[\alpha]_D^{25}$ +86° (*c* 1.1, $CHCl_3$) and the less polar had an $[\alpha]_D^{25}$ +28° (*c* 1.9, $CHCl_3$).

Referring to Mosher's work (4) on the anisotropic effect of the phenyl ring on proton chemical shifts, we were able to predict that the more polar diastereoisomer would correspond to **3** and the less polar to **4**, having respectively the *SR* and the *SS* absolute configuration. This assignment is based on the fact that (a) the protons at C1 and C2 in **3** (Table 1) absorb at a higher field than those in **4**, and (b) the protons at C4 and C6 in **3** absorb at a lower field than those in **4**.

Hydrolysis of the more polar diastereoisomer **3** gave an alcohol ($[\alpha]_D^{25}$ −4° (*c* 1.1, $CHCl_3$)) which must therefore have the *R* absolute configuration, whereas the less polar diastereoisomer **4** yielded an alcohol ($[\alpha]_D^{25}$ +4° (*c* 2.1, $CHCl_3$)) having the *S* configuration.

This configurational assignment based on Mosher's work (4), was rigorously established by preparing a sample of alcohol **1***R* starting from D-glucose using the method described in Scheme 2. The known compound **5** (5, 6) was prepared in four steps from D-glucose. The alcohol **1***R* obtained from compound **11** was levorotatory ($[\alpha]_D^{25}$ −4° (*c* 1.1, $CHCl_3$)), so our original assignment was correct. The alcohol **1***S* can also be transformed into the benzoate **12** of alcohol **1***R* using the Mitsunobu inversion procedure (7). The benzoate **12** obtained had a rotation ($[\alpha]_D^{25}$ +28° (*c* 1.6, $CHCl_3$)) essentially identical to that of an authentic sample of **12** ($[\alpha]_D^{25}$ +29° (*c* 1.2, $CHCl_3$)) prepared by benzoylation of alcohol **1***R*.

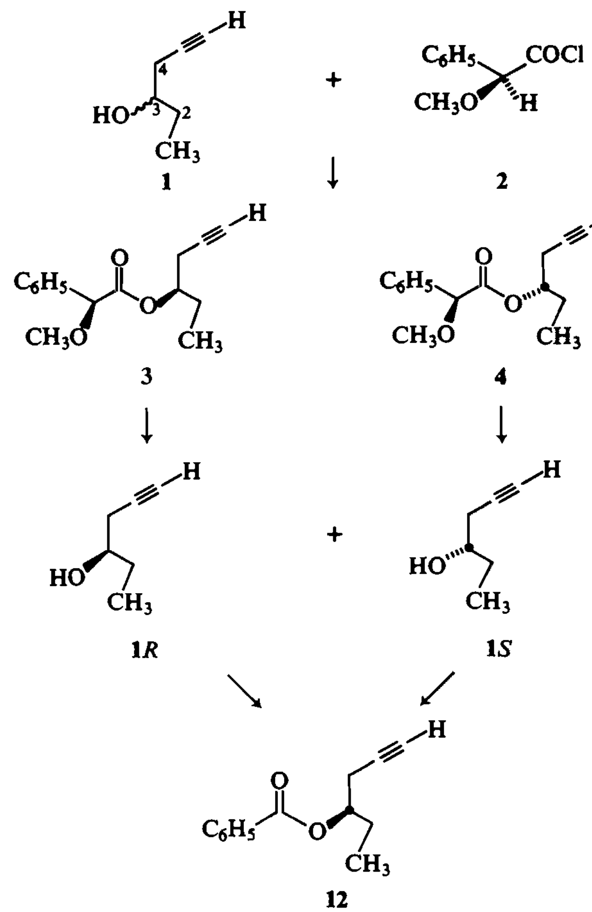

SCHEME 1

Experimental

The infrared (ir) spectra were taken on a Perkin−Elmer 681 spectrophotometer. Proton nmr spectra were recorded on a Bruker WP-60 or a Bruker WP-250 instrument. The following abbreviations have been used: s, singlet; d, doublet; dd, doublet of doublet; t, triplet; q, quadruplet; m, multiplet. Chemical shifts are reported in δ values relative to tetramethylsilane as internal standard. A Waters prep LC/System 500 A chromatograph was used for separation of **3** from **4**. The mass spectra (ms) were recorded on a VG Micromass ZAB-1F mass spectrometer.

Reactions were carried out under argon. Anhydrous magnesium sulfate was used as the drying agent in work-up of reactions.

R(−)-5-hexyn-3-ol (1R) from 3

Ester **3** (5 g, 20.3 mmol) and an aqueous sodium hydroxide solution (15 mL, 1 *N*) were stirred at room temperature for 40 h. The solution was extracted with ether (3 × 100 mL) and the ethereal extracts were

[1]NSERCC and FCAC predoctoral fellowships, 1980−1984.

[2]For a discussion of this synthetic approach, see pp. 330−333 in ref. 1. See also ref. 2 for a model study.

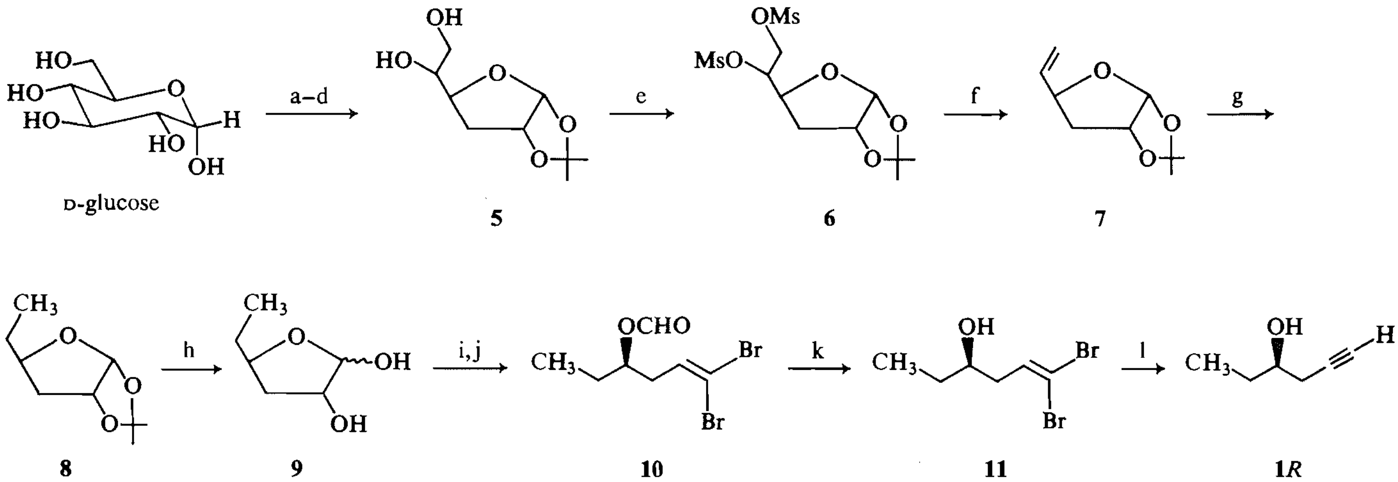

(a) H_2SO_4, acetone, 70% yield (8)
(b) NaH, CS_2, CH_3I, THF, 95% yield (5, 6)
(c) n-Bu_3SnH, xylene, reflux, 80% yield (5, 6)
(d) HCl, THF, CH_3OH, 73% yield (6)
(e) CH_3SO_2Cl, $(C_2H_5)_3N$, CH_2Cl_2, 98% yield
(f) Zn, NaI, DME, reflux, 89% yield (9)
(g) H_2, PtO_2, $CH_3CO_2C_2H_5$, 99%
(h) H_2SO_4, dioxane, H_2O, reflux, 82% yield (10)
(i) $NaIO_4$, $(C_2H_5)_2O$, H_2O
(j) CBr_4, $(C_6H_5)_3P$, CH_2Cl_2, 37% yield from **9** (11)
(k) $KHCO_3$, CH_3OH, 96% yield
(l) n-BuLi, $(C_2H_5)_2O$, −78°C, 80% yield (11)

SCHEME 2

dried. The ether was distilled off at atmospheric pressure and the residue was distilled (75–80°C, 45 Torr (1 Torr = 133.3 Pa)) to afford $R(-)$-5-hexyn-3-ol (**1*R***) (1.53 g, 76%); ir ($CHCl_3$): 3580, 3460, 3310, and 2100 cm^{-1}; nmr ($CDCl_3$) δ: 3.65 (1H, quintuplet, —C*H*—OH), 2.40 (3H, m, —*CH*$_2$—C≡C—H, O*H*), 2.05 (1H, t, —C≡C—*H*), 1.58 (2H, m, CH_3—*CH*$_2$—CHOH—), 0.96 (3H, t, J = 6.3 Hz, *CH*$_3$—CH_2—); ms m/e: 98 (M^+); $[\alpha]_D^{25}$ −4° (c 1.1, $CHCl_3$).

$S(+)$-5-hexyn-3-ol (**1*S***) was prepared in the same manner from **4**; $[\alpha]_D^{25}$ +4° (c 2.1, $CHCl_3$).

*R(−)-5-hexyn-3-ol (1*r*) from 11*

n-Butyllithium (1.6 M in hexane, 712 μL, 1.14 mmol) was added to a solution of dibromoolefin **11** (94.8 mg, 0.367 mmol) in ether (8 mL) at −78°C. The mixture was stirred for 5 min and then quenched by the addition of a saturated aqueous solution of ammonium chloride (5 mL). The organic layer was separated and the aqueous layer extracted twice with ether (2 × 10 mL); the combined organic phase was dried and distilled at atmospheric pressure. Microdistillation *in vacuo* afforded $R(-)$5-hexyn-3-ol (**1*R***) (29 mg, 80%); $[\alpha]_D^{25}$ −4° (c 1.1, $CHCl_3$).

Esters 3, 4

Oxalyl chloride (50.1 g, 386 mmol) was added to $S(+)$-O-methyl mandelic acid (42.8 g, 258 mmol) and the solution was allowed to stir for 2 h at room temperature. The excess oxalyl chloride was pumped off and the residue pumped under vacuum for 1 h. Benzene (150 mL) was added to the residue and to this solution was added (±)-5-hexyn-3-ol (22.7 g, 232 mmol) in benzene (50 mL) and pyridine (21 mL). After addition, water (100 mL) was added and the reaction mixture was extracted with ether (2 × 200 mL). The ethereal extracts were washed successively with hydrochloric acid (1 N, 50 mL), saturated aqueous sodium chloride solution (100 mL), dried, and evaporated to give a 1:1 mixture of diastereoisomers **3** asnd **4** (54.5 g, 95%).

TABLE 1. Chemical shifts of diastereoisomers **3** and **4**

	CH_3 (C1)	CH_2 (C2)	*CH*$_2$C≡C (C4)	C≡C*H* (C6)
3	0.61	1.60	2.45	1.95
4	0.87	1.68	2.33	1.73

Chromatographic separation of 3 and 4

The separations were done on a Waters prep LC/System 500 A chromatograph with two 500-mL cartridges. The average run was as follows: the columns were charged with 6 g of esters **3** and **4**; as the compounds started to elute, the mixed fractions were recycled and the pure ones were collected. This way it was possible to collect 2 g of **3**, 2 g of **4**, and 2 g of a mixture which was rechromatographed. After extensive chromatography of the "mixed fractions" the esters **3** and **4** were completely separated.

Ester **3**: ir ($CHCl_3$): 3310, 3020, 2990, 1750, 1460, 1260, and 1180 cm^{-1}; nmr ($CDCl_3$) δ: 7.45 (5H, m, phenyl), 4.89 (1H, quintuplet, J = 5.9 Hz, —*CH*—CH_2—C≡C—H), 4.77 (1H, s, —*CH*—OCH_3), 3.41 (3H, s, CH_3O—), 2.45 (2H, dd, J = 2.7 Hz, 5.9 Hz, —*CH*$_2$—C≡C—H), 1.95 (1H, t, J = 2.7 Hz, —C≡C—*H*), 1.60 (2H, m, CH_3—*CH*$_2$—), 0.61 (3H, t, J = 7.4 Hz, *CH*$_3$—CH_2—). *Mol. Wt.* (ms) calcd.: 246.1256; found: 246.1255; $[\alpha]_D^{25}$ + 86° (c 1.1, $CHCl_3$).

Ester **4**: ir ($CHCl_3$): 3310, 3020, 2990, 1750, 1460, 1260, and 1180 cm^{-1}; nmr ($CDCl_3$) δ: 7.45 (5H, m, phenyl), 4.92 (1H, quintuplet, J = 5.9 Hz, —*CH*—CH_2—C≡CH), 4.78 (1H, s, —*CH*—OCH_3), 3.43 (3H, s, *CH*$_3$O—), 2.33 (2H, dd, J = 2.6 Hz, 5.9 Hz, —CH—*CH*$_2$—C≡CH), 1.73 (1H, t, J = 2.6 Hz, —C≡C*H*), 1.68 (2H, m, CH_3*CH*$_2$—), 0.87 (3H, t, J = 7.4 Hz, *CH*$_3$—CH_2—). *Mol. Wt.* calcd.: 246.1256; found: 246.1255; $[\alpha]_D^{25}$ +28° (c 1.9, $CHCl_3$).

Dimesylate 6

Methanesulfonyl chloride (4 g, 35 mmol) was added to a solution of diol **5** (1.43 g, 7 mmol) in methylene chloride (50 mL) containing triethylamine (7.08 g, 40 mmol) at 0°C. The reaction was complete after the addition of the mesyl chloride. Water was added and the layers were separated, the organic layer was washed with an aqueous solution of saturated sodium bicarbonate (30 mL), dried, and evaporated. Dimesylate **6** (2.5 g, 98%) could be used in the next step without purification; ir ($CHCl_3$): 2990, 1370, and 1180 cm^{-1}; nmr ($CDCl_3$) δ: 5.84 (1H, d, J = 3.2 Hz, anomeric proton), 4.85 (2H, m, H-C2, H-C3), 4.51 (3H, m, MsO*CH*$_2$—*CH*(OMs)—), 3.12 (3H, s, *CH*$_3$—SO_3—), 3.09 (3H, s, *CH*$_3$—SO_3—), 2.15 (2H, m, H2-C3), 1.53 (3H, s, CH_3—), 1.33 (3H, s, CH_3—); ms m/e: 345 (M^+ − 15). *Mol. Wt.* (ms) calcd.: 345.0314; found: 345.0314; $[\alpha]_D^{25}$ −1.6° (c 3.3, $CHCl_3$).

Olefin 7

Sodium iodide (2.2 g, 33.4 mmol) and zinc (5.0 g, 33.4 mmol) were added to a solution of dimesylate **6** (2.4 g, 6.68 mmol) in dimethoxyethane (50 mL). The mixture was allowed to reflux for 2h, after which the solution was filtered, hexane was added (100 mL), and the hexane solution was washed once with water (50 mL) and once with an aqueous solution of saturated sodium thiosulfate. The organic phase was then dried and evaporated to afford olefin **7** (1.0 g, 89%) as an oil which could be used in the next step without purification; ir ($CHCl_3$): 2980 and 1375 cm^{-1}; nmr ($CDCl_3$) δ: 5.83 (1H, d, J = 3.4 Hz, anomeric proton), 5.5−5.0 (3H, m, CH_2=CH—), 4.72 (2H, m, H-C2, H-C4), 2.03 (2H, m, H2-C3), 1.52 (3H, s, CH_3—), 1.31 (3H, s, CH_3—); ms m/e: 155 (M^+ − 15). *Mol. Wt.* (ms) calcd.: 155.0708; found: 155.0708; $[\alpha]_D^{25}$ −38° (c 1.1, $CHCl_3$).

Acetonide 8

Olefin **7** (462 mg, 2.72 mmol) was dissolved in ethyl acetate (3 mL). This solution was added to a suspension of platinum(IV) oxide (50 mg) in ethyl acetate (3 mL) and shaken under hydrogen atmosphere (45 psi (1 psi = 6.9 kPa)) for 30 min. The solution was filtered and evaporated to afford acetonide **8** (463 mg, 99%) as an oil which could be used in the next step without purification; ir ($CHCl_3$): 1375, 1460, 1385, and 1240 cm^{-1}; nmr ($CDCl_3$) δ: 5.81 (1H, d, J = 3.8 Hz, anomeric proton), 4.70 (1H, t, J = 4.1 Hz, H1-C2), 4.17 (1H, sextuplet, J = 6.4 Hz, H-C4), 2.17 (2H, m, H2-C3), 1.75 (2H, m, CH_3—*CH*$_2$—), 1.50 (3H, s, CH_3—), 1.30 (3H, s, CH_3—), 0.93 (3H, t, J = 7.0 Hz, *CH*$_3$—CH_2—); ms m/e: 157 (M^+ − 15). *Mol. Wt.* (ms) calcd.: 157.0865; found: 157.0865; $[\alpha]_D^{25}$ −5.5° (c 1.2, $CHCl_3$).

Hemiketal alcohol 9

To a solution of acetonide **8** (500 mg, 2.9 mmol) dissolved in dioxane (15 mL) was added a 4% aqueous sulfuric acid solution (15 mL); the resulting mixture was stirred under reflux for 1 h. The reaction was cooled to 25°C and carefully neutralized with solid sodium carbonate. The layers were separated and the aqueous layer was extracted with dioxane (25 mL). The dioxane was evaporated and the residue was taken up in ethyl acetate, the layers were separated, and the aqueous layer was extracted twice with ethyl acetate (2 × 50 mL). The combined organic layers were dried and evaporated to give hemiketal alcohol **9** (313 mg, 82%) which could be used without purification; ir ($CHCl_3$): 3610, 3400, and 1250 cm^{-1}; nmr ($CDCl_3$) δ: 5.33 (1H, t, J = 4.0 Hz, anomeric proton), 4.26 (3H, m, 2 × OH, CH_3—CH_2—*CH*—O—), 3.73 (1H, m, H-C2), 1.97 (2H, m, H2-C3), 1.4 (2H, m, CH_3—*CH*$_2$—), 0.90 (3H, t, J = 7.6 Hz, *CH*$_3$—CH_2—); ms m/e: 114 (M^+ − 18).

Dibromoolefin 10

Sodium periodate (369 mg, 1.72 mmol) was added to a solution of hemiketal alcohol **9** (136 mg, 1.03 mmol) in ether (5 mL) and water (1 mL). The reaction mixture was stirred for 1 min, water (3 mL) was then added, the layers were separated, and the aqueous layer was extracted with ether (2 × 10 mL). The combined ethereal extracts were dried and distilled off at atmospheric pressure. The crude compound was dissolved in dry ether (2 mL) and added to a solution of carbon tetrabromide (689 mg, 2.07 mmol) and triphenylphosphine (1.06 g, 4.04 mmol) in methylene chloride (15 mL). The reaction mixture was stirred for 10 min, after which pentane was added to precipitate the phosphine oxide. The mixture was then filtered and the solvent evaporated. Pentane was added to the residue to precipitate out additional phosphine oxide, the mixture was then filtered, and the solvent was evaporated; this was repeated until no more precipitate was formed. The residue was distilled (84−86°C, 0.4 Torr) to afford pure compound **10** (110 mg, 37%). The distillation residue contained a very small quantity of deformylated compound **11** mixed with some other impurities (76.7 mg). Compound **10**: ir ($CHCl_3$): 2920, 1720, 1625, 1470, and 1180 cm^{-1}; nmr ($CDCl_3$) δ: 8.09 (1H, s, H—C(O)—), 6.42 (1H, t, J = 7.2 Hz, —*H*C=CBr_2), 5.03 (1H, quintuplet, J = 5.9 Hz, —*CH*—O—CHO), 2.43 (2H, t, J = 5.9 Hz, —CH—*CH*$_2$—CH=CBr_2), 1.64 (2H, q, J = 6.3 Hz, CH_3—*CH*$_2$—), 0.94 (3H, t, J = 6.3 Hz, *CH*$_3$—CH_2—); ms m/e: 240 (M^+ − 46). *Mol. wt.* (ms) calcd.: 239.8974; found: 239.8974; $[\alpha]_D^{25}$ +26° (c 3.0, $CHCl_3$).

Dibromoolefin alcohol 11

Potassium bicarbonate (200 mg, 2 mmol) was added to a solution of formate olefin **10** (110 mg, 0.385 mmol) in methanol (5 mL) and was allowed to stir for 1.5 h. The methanol was then evaporated and water (5 mL) was added to the residue. The aqueous phase was extracted with ethyl acetate (3 × 10 mL) and the combined organic layer was dried and evaporated to afford pure dibromoolefin alcohol **11** (94.8 mg, 96%); ir ($CHCl_3$): 3600, 3485, and 1650 cm^{-1}; nmr ($CDCl_3$) δ: 6.54 (1H, t, J = 7.0 Hz, —*CH*=CBr_2), 3.69 (1H, quintuplet, J = 6.1 Hz, *CH*—OH), 2.28 (2H, m, —*CH*$_2$—CH=CBr_2), 1.45 (3H, q, J = 5.7 Hz, CH_3*CH*$_2$—, OH), 0.97 (3H, t, J = 5.7 Hz, *CH*$_3$—CH_2—); $[\alpha]_D^{25}$ −8.7° (c 0.9, $CHCl_3$).

*Benzoate 12 from 1*R

Benzoyl chloride (88.8 mg, 0.58 mmol) was added to a solution of R(−)-5-hexyn-3-ol (**1***R*) (56.3 mg, 0.574 mmol) in pyridine (3 mL). The reaction mixture was stirred at room temperature for 10 h. Methylene chloride (10 mL) was then added and the solution washed with hydrochloric acid (2 N, 10 mL), dried, and evaporated to give pure benzoate **12** (113 mg, 98%); ir ($CHCl_3$): 3310, 3020, 2990, 1720, and 1280 cm^{-1}; nmr ($CDCl_3$) δ: 8.13−7.20 (5H, m, phenyl), 5.25 (1H, quintuplet, J = 6.3 Hz, —*CH*—OBz), 2.60 (2H, dd, J = 3.0 Hz, 6.3 Hz, —*CH*$_2$—C≡CH), 2.01 (1H, t, J = 3.0 Hz, —C≡C—*H*), 1.88 (2H, m, CH_3—*CH*—), 1.00 (3H, t, J = 6.9 Hz, *CH*$_3$—CH_2—); ms m/e: 202 (M^+). *Mol. Wt.* (ms) calcd.: 202.0994; found: 202.0979; $[\alpha]_D^{25}$ +28° (c 1.6, $CHCl_3$).

*Benzoate 12 from 1*S

Benzoic acid (165 mg, 1.35 mmol) was added to a solution of S(+)-5-hexyn-3-ol (**1***S*) (121 mg, 1.23 mmol) and triphenylphosphine (354 mg, 1.35 mmol) in tetrahydrofuran (5 mL). To this mixture was added diethyl azodicarboxylate (234 mg, 1.35 mmol) in tetrahydrofuran (2 mL); the reaction mixture was allowed to stir overnight. Water (5 mL) was then added and the mixture extracted with ether (3 × 20 mL); the ethereal extracts were dried and evaporated. The crude residue was purified on silica gel with hexane − ethyl acetate (6:1) as the eluent to afford pure benzoate **12** (114 mg, 46%); $[\alpha]_D^{25}$ +29° (c 1.2, $CHCl_3$).

Acknowledgements

This research was supported by the Natural Sciences and Engineering Research Council of Canada (NSERCC) and by the "Ministère de l'éducation (F.C.A.C.) du Québec". Financial assistance in the form of an unrestricted grant from Merck Frosst Canada Inc. is also appreciated.

1. P. DESLONGCHAMPS. *In* Stereoelectronic effects in organic chemistry. Organic Chemistry Series. Vol. I. *Edited by* J. E. Baldwin. Pergamon Press, Oxford. 1983.
2. G. SAUVÉ, D. A. SCHWARTZ, L. RUEST, and P. DESLONGCHAMPS. Can. J. Chem. In press.
3. A. VIOLO. J. Am. Chem. Soc. **93**, 6967 (1971).

4. J. A. DALE and H. S. MOSHER. J. Am. Chem. Soc. **95**, 512 (1973).
5. G. JUST and C. LUTHE. Can. J. Chem. **58**, 1799 (1980).
6. D. H. R. BARTON and S. W. MCCOMBIE. J. Chem. Soc., Perkin Trans. 1, 1574 (1975).
7. O. MITSUNOBU. Synthesis, 1 (1981).
8. R. L. WHISTLER and M. J. WOLFROM. Methods in carbohydrate chemistry. Vol. II. Academic Press, New York. 1963.
9. R. S. TIPSON and A. COHEN. Carbohydr. Res. **1**, 338 (1965).
10. F. E. ZIEGLER and P. J. GILLIGAN. J. Org. Chem. **46**, 3874 (1981).
11. E. J. COREY and P. L. FUCHS. Tetrahedron Lett. **36**, 3769 (1972).

Kinetics of the reduction of 1-methylquinolinium cations by 1-benzyl-1,4-dihydronicotinamide

JOHN W. BUNTING AND NORMAN P. FITZGERALD
Department of Chemistry, University of Toronto, Toronto, Ont., Canada M5S 1A1

Received November 3, 1983[1]

JOHN W. BUNTING and NORMAN P. FITZGERALD. Can. J. Chem. **63**, 655 (1985).

The reduction of a series of 3-W-1-methylquinolinium cations (**1**: W = H, Br, $CONH_2$, CO_2CH_3, CN, NO_2) by 1-benzyl-1,4-dihydronicotinamide has been investigated. In all cases the kinetically controlled product from these reactions is the appropriate 3-W-1,4-dihydro-1-methylquinoline. Only for W = Br is any significant amount of the 1,2-dihydro isomer obtained (15% in this case). This kinetic preference for C-4 attack over C-2 attack in dihydronicotinamide reductions contrasts with the kinetically preferred attack at C-2 by hydroxide ion and in borohydride reductions. Rates of reduction were measured for each **1** and also 1,2-dimethyl- and 1,4-dimethylquinolinium cations in 20% CH_3CN – 80% H_2O, ionic strength 1.0 at 25°C, under pseudo-first-order conditions. Kinetic saturation due to nonproductive 1 : 1 complex formation was observed for several cations at high concentrations (>0.1 *M*). Second-order rate constants (k_2^H) were evaluated for each W, and also kinetic isotope effects from second-order rate constants (k_2^D) for reduction by 1-benzyl-4,4-dideuterio-1,4-dihydronicotinamide. Second-order rate constants are correlated with σ_p^- for W with $\rho = 4.5$, and are also closely correlated with pK_{R^+} for pseudobase formation at C-4 of these quinolinium cations by: $\log k_2^H = -0.56\ pK_{R^+} + 7.3$. Values of k_2^H/k_2^D vs. pK_{R^+} describe a Westheimer curve reaching a maximum of 5.8 for W = Br and falling to 1.5 for W = NO_2 and 4.2 for W = H. These data are consistent with an intrinsic barrier of 2.9 ± 0.5 kcal/mol for hydride transfer between this 1,4-dihydronicotinamide and quinolinium cations. However, quinolinium cations display a dramatically enhanced rate of dihydronicotinamide reduction relative to hydroxide ion attack when compared with isoquinolinium cations. This observation, and the predominance of C-4 rather than C-2 reduction, suggests that these reactions may not be simple one-step hydride transfer processes.

JOHN W. BUNTING et NORMAN P. FITZGERALD. Can. J. Chem. **63**, 655 (1985).

On a étudié la réaction de réduction d'une série d'ions W-3 méthyl-1 quinolinium (W = H, Br, $CONH_2$, CO_2CH_3, CN et NO_2) par la benzyl-1 dihydro-1,4 nicotinamide. Dans tous les cas, le produit de contrôle cinétique de ces réactions est la W-3 dihydro-1,4 méthyl-1 quinoléine appropriée. Ce n'est que dans le cas où W = Br que l'on obtient des quantités significatives de l'isomére dihydro-1,2 (15% dans ce cas). Cette préférence pour une attaque en C-4 par opposition à une attaque en C-2 lors de réductions par la dihydronicotinamide est en opposition avec les résultats obtenus lors de réactions avec l'ion hydroxyde ou avec le borohydrure alors que l'attaque cinétique préférentielle se fait en position C-2. Opérant à 25°C, à une force ionique de 1,0, sous des conditions de pseudo-premier ordre et dans des solutions contenant 20% de CH_3CN et 80% de H_2O, on a mesuré les vitesses de réduction de tous les ions **1** ainsi que celles des cations diméthyl-1,2 ainsi que diméthyl-1,4 quinolinium. Dans les cas de plusieurs cations, à des concentrations élevées (>0,1 *M*), on a observé une saturation cinétique due à la formation non productive de complexes 1 : 1. Pour chacun des W, on a évalué les constantes de vitesse du deuxième ordre (k_2^H) ainsi que les effets isotopiques cinétiques, évalués à partir des constantes de vitesse du deuxième ordre (k_2^D), pour la réduction par la benzyl-1 dideutéro-4,4 dihydro-1,4 nicotinamide. On a pu établir une corrélation entre les constantes de vitesse du deuxième ordre et les valeurs σ_p^- des substituants W et la valeur de $\rho = 4{,}5$; il existe aussi une bonne corrélation avec les valeurs de pK_{R^+} pour la formation de la pseudobase en C-4 de ces cations quinolinium et cette corrélation est définie par l'équation $\log k_2^H = -0{,}56\ pK_{R^+} + 7{,}3$. Les valeurs de k_2^H/k_2^D vs. pK_{R^+} décrivent une courbe de Westheimer qui atteint un maximun de 5,8 pour W = Br et qui tombe à 1,5 pour W = NO_2 et à 4,2 pour W = H. Ces valeurs sont en accord avec la présence d'une barrière intrinsèque de 2,9 ± 0,5 kcal/mol pour le transfert d'hydrure entre la dihydro-1,4 nicotinamide et les cations quinolinium. Toutefois, si l'on compare les cations quinolinium aux cations isoquinolinium, on observe que dans le premier cas les vitesses de réduction par la dihydronicotinamide sont de beaucoup augmentées par rapport aux vitesses d'attaque par l'ion hydroxyde. Cette observation et le fait que la réduction se fait de préférence en C-4 plutôt qu'en C-2 suggèrent que ces réactions ne sont peut-être pas des transferts simples d'hydrures qui se produiraient en une étape.

[Traduit par le journal]

There has been considerable recent interest in kinetic studies as mechanistic probes of the reductions of nitrogen heteroaromatic cations by 1,4-dihydronicotinamide derivatives. Isoquinolinium cations (1–3) and acridinium cations (4–16) have been extensively investigated as acceptors in what are formally hydride transfer reactions. Extensive substituent and kinetic isotope effect data indicate that the mechanisms of the reductions of isoquinolinium cations by 1,4-dihydronicotinamides are best represented as simple one-step hydride transfer processes in aqueous reaction media (1, 2). Reductions of acridinium cations by 1,4-dihydronicotinamides have been the subjects of considerable mechanistic controversy. However, the recent elegant work of Powell and Bruice (14, 15) has considerably clarified the situation in this area, and these workers have concluded that the reduction of the 10-methylacridinium cation by 1,4-dihydronicotinamides in acetonitrile solution is also best represented as a direct hydride transfer process. On the other hand, kinetic data for the reductions of acridinium cations in predominantly aqueous solvents cannot be readily rationalized in the same way, and we have recently suggested (16) that the two-step $e^- + H^\cdot$ mechanism occurs in these latter solvent systems.

Comparisons of relative rates of 1,4-dihydronicotinamide reduction of isoquinolinium and acridinium cations with relative rates of hydroxide ion attack upon these cations indicate that acridinium cations are unusually reactive (approximately 40,000-fold) towards dihydronicotinamide reductants (16). This observation also supports a mechanism other than simple nucleophilic ("hydride") attack occurring in acridinium cation reductions in aqueous solutions. Furthermore, isoquinolinium and acridinium cations differ in that the former formally generate 1,2-dihydropyridine derivatives upon reduction whereas the

[1] Revision received September 5, 1984.

latter formally give 1,4-dihydropyridines.

In the light of these observations, we felt that a detailed kinetic study of the 1,4-dihydronicotinamide reduction of quinolinium cations would be very appropriate, since these cations are readily susceptible to attack at either C-2 or C-4 to give 1,2-dihydro- and 1,4-dihydroquinolines respectively. Our initial investigation in this area has concentrated upon the reduction of 3-W-1-methylquinolinium cations (**1**) by 1-benzyl-1,4-dihydronicotinamide, since detailed quantitative data are now available (17) upon the relative rates of nucleophilic (hydroxide ion) attack at C-2 and C-4 of these cations, and also upon the relative thermodynamic stabilities of the isomeric dihydroquinoline products (**3** and **4**). The current paper reports kinetic studies of these reductions, and also upon the assignment of the structures of the reaction products.

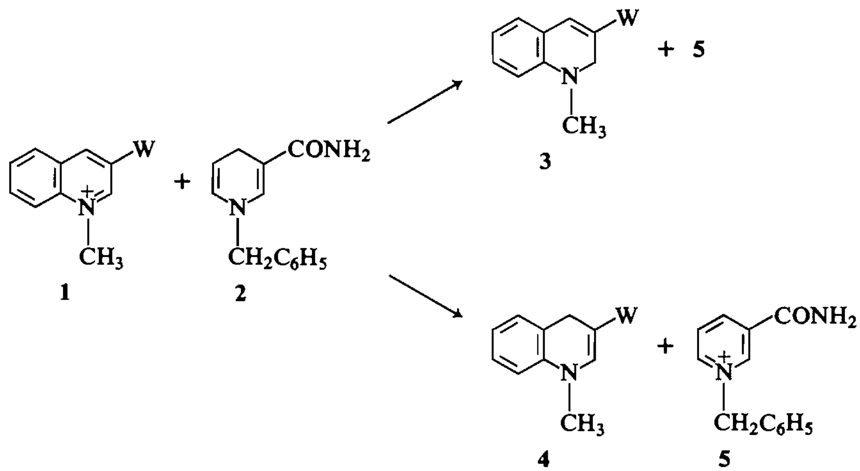

Experimental

Most 3-W-1-methylquinolinium cations **1** were available from the accompanying study (17). Salts of the 1-methyl-3-nitro-,1,2-dimethyl-, and 1,4-dimethyl-quinolinium cations, which were also available from other work in our laboratories, were recrystallized several times before use. 1-Benzyl-1,4-dihydronicotinamide and its 4,4-dideuterio derivative (using 5 oxidation–reduction cycles) were prepared as previously described (1).

3-Bromo-1,2-dihydro-1-methylquinoline

3-Bromo-1-methylquinolinium bromide (0.5 g) was treated with lithium aluminum hydride (0.02 g) in anhydrous ether for 5 min. Saturated aqueous ammonium chloride was added at 0°C, and the inorganic salts were removed by filtration. The filtrate was dried over magnesium sulfate, and the solvent removed on the rotary evaporator; ^{1}Hmr ($CDCl_3$) δ: 2.78 (3H, s), 4.20 (2H, d), 6.3–7.2 (5H, m).

Isolation of reduction products

An acetonitrile solution (2 mL) of 1-benzyl-1,4-dihydronicotinamide (0.1 *M*) was mixed with a buffered aqueous solution (5 mL) of the 3-W-1-methylquinolinium cation (0.04 *M*) and water was added to a final volume of 10 mL. This reaction mixture was stirred for 20 min after which the organic product was extracted into chloroform. After drying with magnesium sulfate, the solvent was removed on the rotary evaporator and the product was characterized by ^{1}Hmr and uv–visible spectroscopy.

Kinetic studies

All reactions excepting **1**:W = NO_2 were studied spectrophotometrically with the quinolinium cations in 20- to 10,000-fold excesses over the 1-benzyl-1,4-dihydronicotinamide (0.1 m*M*) in 20% CH_3CN – 80% H_2O (v/v) buffered at pH 7 (0.005 *M* phosphate), ionic strength 1.0 (quinolinium salt + KCl) at 25°C. Absorbance changes due to the consumption of the reductant were monitored at 390 nm. This method was not applicable to **1**:W = NO_2 since its reduction product absorbs strongly in the vicinity of 400 nm. In this case, formation of this product was monitored at 450 nm for reactions containing 20- to 200-fold excesses of reductant over the 1-methyl-3-nitroquinolinium cation. It was also necessary to study this cation (pK_{R^+} 6.82 (18)) at pH 4 (acetate buffer) since it exists significantly in the form of its C-4 pseudobase at pH 7. Control studies using **1**:W = CN indicated that rates of reduction were identical at pH 4 and pH 7.

Kinetic data were collected on either a Varian Cary 219 spectrophotometer or Durrum Gibson stopped-flow instrument (for W = CN and NO_2). All reactions proved to be kinetically strictly first order in dihydronicotinamide (or quinolinium cation, in the case of W = NO_2). Pseudo-first-order rate constants were calculated from absorbance vs. time data by standard methods.

Results

Reaction products

1-Benzyl-1,4-dihydronicotinamide reacted with each of the 1-methylquinolinium cations **1**:W = H, Br, $CONH_2$, CO_2CH_3, CN, and NO_2 in aqueous acetonitrile solution at room temperature at rates that were strongly influenced by the nature of W. For W = NO_2 the reaction is essentially instantaneous, although amenable to investigation by stopped-flow methods, while for W = H significant reaction rates are only observed when at least one of the reactants is present at relatively high concentration (0.1–1 *M*). As shown below, these reaction rates are quantitatively correlated with the electron-withdrawing effects of W.

For each substituent, the reaction products have been isolated and(or) characterized spectroscopically. After the completion of this work, Roberts *et al.* reported (19) extensive ^{1}Hmr spectral characterization of the reaction products from the reduction of **1**:W = Br, $CONH_2$, and CN by 1-benzyl-1,4-dihydronicotinamide. Since our results, including the observation of a 6:1 product ratio of **4** and **3** for W = Br, are in exact agreement with these observations, we will not detail our own ^{1}Hmr spectral study. Apart from the 3-bromo derivative, all reduction products appear to be exclusively the 1,4-dihydroquinolines (**4**) rather than their 1,2-dihydro isomers (**3**).

TABLE 1. Absorption spectra of products from the reduction of 1 by 1-benzyl-1,4-dihydronicotinamide

	λ_{max} (nm)		
W	Reduction product[a]	3	4
H	(303)	345 (21)[b]	303 (20)[b]
Br	328 (318)	344	
$CONH_2$	346 (344)		337 (23)[c]
CO_2CH_3	346	422 (23)[d]	348 (23)[d]
CN	335 (332)	410 (23)	333 (24)
NO_2	435	510 (25)	420 (25)

[a] Data in 20% CH_3CN – 80% H_2O; data in parentheses in chloroform.
[b] Literature references in parentheses; unreferenced data from current work.
[c] Data for 3-aminocarbonyl-1,4-dihydroquinoline.
[d] Data for ethyl ester.

These conclusions are confirmed by the electronic absorption spectra listed in Table 1 for the reaction products, both in the aqueous acetonitrile reaction solvent and also in chloroform extracts of these solutions. 3-Bromo-1,2-dihydro-1-methylquinoline was prepared by lithium aluminum hydride reduction of the 3-bromoquinolinium cation, and its long wavelength absorption maximum at 344 nm in chloroform solution confirms that the predominant 1,4-dihydronicotinamide reduction product (λ_{max} = 318 nm) is the 1,4-dihydro isomer as suggested by the ¹Hmr spectral data.

We have been unable to obtain a clean ¹Hmr spectrum for the product from the reduction of the parent 1-methylquinolinium cation by 1-benzyl-1,4-dihydronicotinamide. The ¹Hmr spectra of chloroform extracts of these reactant solutions indicate complex mixtures. Ultraviolet spectra of chloroform extracts from more dilute solutions of these reactants have λ_{max} = 303 nm, which is essentially identical with the absorption maximum reported (20) for 1,4-dihydro-1-methylquinoline, and quite different from λ_{max} = 345 nm for the 1,2-dihydro isomer (21). However, we note that **4**:W = H is an enamine and would be expected to undergo hydration of the C(2)—C(3) double bond in aqueous solution to give **6**, which would also be expected to

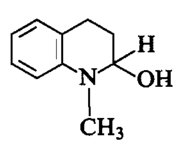

6

absorb in the vicinity of 300 nm (e.g. 1-methyl-1,2,3,4-tetrahydroquinoline has λ_{max} 305 nm (22)). Thus while we cannot be sure of the identity of the species absorbing at 303 nm, it nevertheless seems to indicate that the primary reduction product is the 1,4-dihydro derivative **4**:W = H. This species is known to be relatively unstable towards decomposition (20), and this fact is consistent with our inability to obtain clean ¹Hmr spectra of this reaction product. Reduction at C-4 rather than at C-2 of the 1-methylquinolinium cation is also consistent with the relative rates of reduction reported below for the 1,2-dimethyl- and 1,4-dimethylquinolinium cations, and with the overall substituent effects observed for W on the rates of reduction of **1** at C-4.

Kinetic studies

Rates of reduction of the 3-W-1-methylquinolinium cations (**1**) by 1-benzyl-1,4-dihydronicotinamide were measured in 20% CH_3CN – 80% H_2O (v/v), ionic strength 1.0, at 25°C. Time-dependent electronic absorption spectra with reactants in stoichiometric ratio (excepting W = H which reacts too slowly, and W = NO_2 which reacts too rapidly, to study in this way) contain several clean isosbestic points. All reactions proved to be strictly first order kinetically for at least three reaction half-lives. Pseudo-first-order rate constants (k_{obs}) for W = H and Br display kinetic saturation effects at high concentrations of **1**. For all other W, solubility considerations only allow the use of lower concentrations of **1**. In these cases the pseudo-first-order rate constants are strictly proportional to the concentration of **1** over at least a tenfold concentration range of these cations. Second-order rate constants (k_2) evaluated from $k_2 = k_{obs}/[\mathbf{1}]$ are listed in Table 2.

For W = H and Br, plots of $1/k_{obs}$ vs. $1/[\mathbf{1}]$ are linear in the range where kinetic saturation is found. This situation is similar to that reported previously for the reduction of isoquinolinium cations (1, 2), and indicates the presence of a 1:1 complex between the quinolinium cation and 1-benzyl-1,4-dihydronicotinamide. The assumption that this complex is nonproductive, as was previously established for isoquinolinium cations, allows the evaluation of the second-order rate constants and association constants reported in Table 2.

Similar rate measurements were also made for the reduction of each quinolinium cation by 1-benzyl-4,4-dideuterio-1,4-dihydronicotinamide. These second-order rate constants are also included in Table 2, along with the (predominantly) primary kinetic isotope effects calculated from these data.

Rates of reduction were also measured for the reaction of the 1,2-dimethylquinolinium and 1,4-dimethylquinolinium cations with 1-benzyl-1,4-dihydronicotinamide. Kinetic saturation was observed for the former cation; however, solubility considerations prevented the investigation of this phenomenon for the latter cation. Kinetic parameters for these two cations are also included in Table 2.

Discussion

Reaction products

The above spectral data are consistent with the products of reduction of 3-W-1-methylquinolinium cations by 1-benzyl-1,4-dihydronicotinamide being predominantly (and possibly exclusively for most W) the corresponding 3-W-1,4-dihydro-1-methylquinolines. The 3-bromo derivative is the only case where any significant amount (15%) of the 1,2-dihydro isomer can be detected spectroscopically. These product distributions contrast with those observed for the borohydride ion reductions of these same cations (19, 23); such reductions give the 1,2-dihydro derivatives as the major kinetic products, although significant amounts of the 1,4-dihydro isomers are also usually present in the initial product mixture.

Roberts *et al.* (19) have shown that 3-cyano-1,2-dihydro-1-methylquinoline isomerizes to its 1,4-dihydro isomer with the equilibrium between these two species favouring the latter isomer by about 20:1 in 80% 2-propanol – 20% water. This ratio is consistent with the observation that the thermodynamic mixture of pseudobases derived from the 3-cyano-1-methylquinolinium cation favours the C-4 hydroxide adduct over the C-2 adduct in a 26:1 ratio (17). Studies of pseudobase formation indicate the greater thermodynamic stability of the 1,4-dihydroquinoline over its 1,2-dihydro isomer for 3-W-quinolines having W = NO_2, CN, CO_2CH_3, and $CONH_2$, whereas the 1,2-dihydroquinolines are the thermodynamically more stable pseudobases for W = H and Br (17). On the

TABLE 2. Kinetic parameters for the reduction of **1** by 1-benzyl-1,4-dihydronicotinamide[a]

W	k_2^H (M^{-1} s^{-1})	K (M)	k_2^D (M^{-1} s^{-1})	K (M)	k_2^H/k_2^D
H	$5 (\pm 0.5) \times 10^{-3}$	1.9 ± 0.2	$1.2 (\pm 0.1) \times 10^{-3}$	2.1 ± 0.1	4.2 ± 0.7
Br	0.38 ± 0.01[b]	0.70 ± 0.05	0.065 ± 0.005[b]		5.8 ± 0.5
$CONH_2$	2.8 ± 0.1		0.54 ± 0.04		5.2 ± 0.4
CO_2CH_3	14.3 ± 0.3		3.6 ± 0.1		4.0 ± 0.2
CN	121 ± 2		67 ± 2		1.8 ± 0.1
NO_2	$6.5 (\pm 0.2) \times 10^3$		$4.4 (\pm 0.1) \times 10^3$		1.5 ± 0.1
1,2-Dimethylquinolinium	$1.3 (\pm 0.2) \times 10^{-3}$	1.9 ± 0.2			
1,4-Dimethylquinolinium	$2.8 (\pm 0.5) \times 10^{-4}$				

[a]Data in 20% CH_3CN – 80% H_2O (v/v), ionic strength 1.0 at 25°C.
[b]Combined rate constant for reduction at C-2 and C-4.

assumption that these relative thermodynamic stabilities of pseudobases are also applicable to the corresponding dihydroquinolines, it becomes clear that the reduction of **1** by 1-benzyl-1,4-dihydronicotinamide gives the thermodynamically more stable products for W = $CONH_2$, CO_2CH_3, CN, and NO_2 but the less stable products for W = H and Br.

The 1,4-dihydroquinolines can be established to be the products of kinetic control for these four strongly electron-withdrawing W substituents in the following way. The clean isosbestic points observed for stoichiometric ratios of reactants does not allow the presence of any significant buildup of an intermediate species during the course of these reactions. If any significant amount of the 1,2-dihydro isomer were initially produced in these reductions its presence would become quite obvious from its characteristic electronic absorption spectrum (Table 1), and the fact that its isomerization to the 1,4-dihydro isomer is expected to be much slower than the observed rates of reduction. For instance, Roberts *et al.* (19) report the second-order rate constant to be 0.05 M^{-1} s^{-1} for the reaction of 3-cyano-1,2-dihydro-1-methylquinoline with the 3-cyano-1-methylquinolinium cation to give the 1,4-dihydro isomer in 80% 2-propanol – 20% water at room temperature. This reaction, which represents the most probable mechanism for all such isomerizations, is over 2000-fold slower than the measured second-order rate constant (Table 2) for the reaction of **1**:W = CN with 1-benzyl-1,4-dihydronicotinamide. Thus in this case, and presumably for other W substituents too, the 1,2-dihydro species can be ruled out as an intermediate in these reductions, and there can be little doubt that the observed products are also the predominant products of kinetic control.

Our spectroscopic observations also give no evidence for covalent adduct formation between C-5 of the 1,4-dihydronicotinamide and either C-2 or C-4 of the quinolinium cation, as has been speculated upon (13, 51), but never established, for acridinium cations. We note that Roberts *et al.* (19) also did not observe such adducts in their studies of the reduction of quinolinium cations, and we can conclude that if such species do exist, they can only be present in insignificant concentrations under the current reaction conditions.

This preponderance of C-4 attack in the reduction of **1** by 1-benzyl-1,4-dihydronicotinamide contrasts with the somewhat greater rate of attack at C-2 than at C-4 in the borohydride ion reduction of these cations (19), and with the much greater rate of hydroxide ion attack at C-2 than at C-4 in pseudobase formation (17). 4-Cyano-1,4-dihydro-1-methylquinoline is the sole product isolated from reaction of cyanide ion with **1**:W = H (26–28). It is not clear, however, whether this is the product of kinetic control, thermodynamic control, or simply the species which has the lowest aqueous solubility.

TABLE 3. Comparison of relative rates of attack at C-2 and C-4 of the 3-bromo-1-methylquinolinium cation[a]

Reagent	k^4/k^2	Rel. k^4/k^2
1-Benzyl-1,4-dihydronicotinamide[b]	6	9000
Borohydride ion[c]	<0.05	<70
Hydroxide ion[d]	7×10^{-4}	1

[a]k^4/k^2 represents the ratio of the second-order rate constants for attack at C-4 and C-2 by the indicated reagent.
[b]Data from current work.
[c]Data from ref. 19.
[d]Data from ref. 17.

The only quantitative measure that we can obtain of the relative rates of 1-benzyl-1,4-dihydronicotinamide reduction at C-2 and C-4 is for the case of **1**:W = Br. We feel that the 6:1 product ratio observed in this case probably represents kinetic control, since this ratio proved to be independent of whether the quinolinium cation or the reductant was in excess. This ratio should vary for such differences in reactant excess if an isomerization involving the quinolinium cation is occurring at any significant rate. The overall second-order rate constant for reduction of **3**:W = Br has therefore been partitioned in this ratio. Table 3 compares the relative rates of dihydronicotinamide reduction and borohydride ion and hydroxide ion attack at C-2 and C-4 for the 3-bromo-1-methylquinolinium cation. These data indicate that although the product ratio is only 6:1 in this reduction, this ratio actually represents a kinetic preference for C-4 over C-2 of 9000-fold in dihydronicotinamide reduction relative to hydroxide ion attack, and of at least 120-fold relative to borohydride ion.

This pronounced difference in kinetic preferences for attack at C-2 and C-4 in borohydride and dihydronicotinamide reductions of quinolinium cations requires that, whatever the mechanistic details of these reactions may be, they cannot both be represented by rate-determining transition states which formally involve hydride migration without a further role for either the nicotinamide or boron-containing species. If one accepts that cyanide ion does show a kinetic preference for C-4, then one might suggest that soft nucleophiles (29) such as this preferentially attack C-4, whereas harder nucleophiles such as hydroxide ion show a kinetic preference for C-2. In this light, at the very least it must be concluded that the transition states for borohydride and dihydronicotinamide reductions differ in having a much "harder" hydridic nucleophile in the former case than in the latter.

Lithium aluminum hydride also reduces both the 1-methylquinolinium cation (20, 30) and its 3-bromo derivative (current work) cleanly at C-2. Reduction of 3-W-1-methylquinolinium cations (W = $CONH_2$, CO_2CH_3, or CN) with triethylammonium formate gives the 1,4-dihydro derivatives (24, 31, 48) which are also expected to be the thermodynamically more stable dihydro isomers. Labelling experiments using DCO_2^- suggest that these 1,4-dihydro derivatives are also the products of kinetic control (48). Thus formate and 1,4-dihydronicotinamide reductions of quinolinium cations seem to show a kinetic preference for C-4 reduction in contrast to the preference for C-2 shown by complex metal hydride reductants. Dithionite reduction of **1**: W = Br or $CONH_2$ gives exclusively the 1,4-dihydro isomer (19, 32); however, the product from this reaction depends upon the relative reactivities of the C-2 and C-4 dithionite ion adducts. Interestingly, a transient orange species is reported as an intermediate in the dithionite reduction of **1**: W = $CONH_2$ (32). Although this intermediate has been assumed to be a charge-transfer complex, it seems equally possible that it is a 1,2-dihydroquinoline derivative as the product of kinetic control.

Sodium amalgam reduction of the 1-methylquinolinium cation does give the 1,4-dihydro derivative without any evidence for the presence of the more stable 1,2-dihydro isomer (20). This reaction, like other sodium amalgam reductions (33), probably proceeds through radical intermediates. It is also known that alkyl radicals show about equal reactivities at C-2 and C-4 of quinolinium cations (34, 35), and this contrasts with the specific addition at C-2 observed for dialkyl cadmiums and Grignard reagents (36).

These examples seem to suggest that reactions of quinolinium cations which occur via radical intermediates show a more pronounced kinetic preference for C-4 over C-2 relative to what is observed for direct nucleophilic attack on these cations. Thus the observation of exclusively C-4 reduction products from the kinetic control of dihydronicotinamide reduction of quinolinium cations is consistent with expectations for reaction via one of the one-electron mechanisms ($e^- + H^{\bullet}$ or $e^- + H^+ + e^-$) that are often considered for these reductions. This possibility is considered further below.

Kinetic studies

The kinetic saturation effects observed for the pseudo-first-order rate constants for reduction of several quinolinium cations are similar to those observed previously for the reduction of a number of isoquinolinium cations (1–3). It has been concluded that this phenomenon arises from the formation of nonproductive 1:1 complexes between the isoquinolinium cation and dihydronicotinamide, with complexation involving an interaction between the dihydronicotinamide and the homocyclic ring of the isoquinoline. A similar interpretation seems reasonable for the quinolinium cations of the current study since the association constants reported in Table 2 are essentially identical to those found for the 2-methylisoquinolinium (K = 2.1 M^{-1} (2)) and 2-methyl-3,4-dihydroisoquinolinium (K = 1.4 M^{-1} (3)) cations. This interpretation allows evaluation of second-order rate constants for reduction, and is supported by the clean substituent effects upon k_2 discussed below.

The second-order rate constants given in Table 2 for reduction at C-4 of **1** are correlated with the Hammett σ constants for the substituents W as indicated in eqs. [1] and [1a] for k_2^H and [2] and [2a] for k_2^D.

[1] $\log k_2^H = 4.5\ (\pm 0.3)\ \sigma_p^- - 2.1\ (\pm 0.2)$ (corr. coeff. = 0.991)

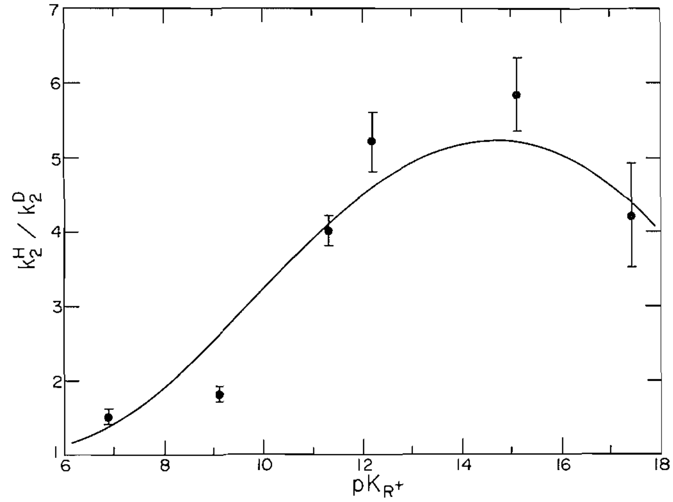

FIG. 1. Dependence of the primary kinetic isotope effects for the reduction of **1** by 1-benzyl-1,4-dihydronicotinamide (and its 4,4-dideuterio derivative) on pK_{R^+} for **1**. The curve is calculated from eq. [6] using the parameters given in the text.

[1a] $\log k_2^H = 7.5\ (\pm 0.5)\ \sigma_p - 2.3\ (\pm 0.3)$ (corr. coeff. = 0.990)

[2] $\log k_2^D = 4.9\ (\pm 0.3)\ \sigma_p^- - 2.9\ (\pm 0.2)$ (corr. coeff. = 0.992)

[2a] $\log k_2^D = 8.2\ (\pm 0.6)\ \sigma_p - 3.2\ (\pm 0.3)$ (corr. coeff. = 0.990)

The correlations with either of the *para* substituent constants are quite acceptable, while correlations with σ_m are much poorer (correlation coefficients of 0.931 and 0.930 for k_2^H and k_2^D respectively). In each case the use of σ_p^- rather than σ_p gives a correlation that is marginally better. Alternatively these rate constants may be correlated with the pK_{R^+} values for pseudobase formation at C-4 of these quinolinium cations (17):

[3] $\log k_2^H = -0.54\ (\pm 0.04)\ pK_{R^+} + 7.3\ (\pm 0.4)$ (corr. coeff. = 0.991)

[4] $\log k_2^D = -0.59\ (\pm 0.04)\ pK_{R^+} + 7.4\ (\pm 0.5)$ (corr. coeff. = 0.992)

Equations [3] and [4] imply that positive charge neutralization is 55–60% complete in the rate-determing transition state for the dihydronicotinamide reduction of these quinolinium cations. This implication, that charge development in the transition state is similar for all W, is difficult to rationalize, however, in view of the pronounced substituent dependence of the primary kinetic isotope effects in Table 2. These isotope effects imply significant variations in the extent of C—H bond-breaking at C-4 of the dihydronicotinamide species in the transition state, and also presumably signal variations in the extent of C—H bond-making at C-4 of the quinolines. It seems unlikely that significant differences in C—H bond formation at C-4 of these quinolines can be achieved without influencing the effective charge on the quinoline moiety as a whole in the transition state.

The overall dependence of k_2^H/k_2^D in Table 2 appears to vary smoothly with the electronic effect of W, and to pass through a maximum value in the vicinity of W = Br. This relationship is illustrated in Fig. 1, in which the substituent effect is quantitated in terms of pK_{R^+} for pseudobase formation at C-4 of **1**.

Although eqs. [3] and [4] individually give quite reasonable fits to the experimental data, the combination of these equations cannot predict the maximum observed for k_2^H/k_2^D. The maximum four-fold variation in isotope effect is hidden in the greater that 10^6-fold variation in k_2^H and k_2^D individually. Stewart and Toone (37) have studied substituent effects upon the reduction of triphenylmethyl cations by formate ion and found these data to be well correlated with a quadratic equation of the form of eq. [5]:

$$[5] \quad \log k_2 = a\,(pK_{R^+})^2 + b\,pK_{R^+} + c$$

We have attempted to fit both k_2^H and k_2^D to eq. [5]. Although we are able to obtain reasonable fits of our experimental data, the uncertainties in the values of the parameters a, b, and c are quite large because of the very shallow curvature required to fit the data.

The data of Fig. 1 may be fitted to eq. [6]. An iterative curve-fitting routine allowed evaluation of the parameters as: $d = 1.66 \pm 0.13$; $e = 14.6 \pm 0.2$; $f = 8.4 \pm 1.4$.

$$[6] \quad \ln (k_2^H/k_2^D) = d\,(1 - ((pK_{R^+} - e)/f)^2)$$

Equation [6] has the form of the Marcus relationship in eq. [7] (38, 39), with $d = \ln (k_2^H/k_2^D)^{max}$, $\Delta G^0 = -2.3RT\,(pK_{R^+} - e)$, and $f = 4\Delta G_0^{\ddagger}/2.3RT$.

$$[7] \quad \ln (k_2^H/k_2^D) = \ln (k_2^H/k_2^D)^{max}\,(1 - (\Delta G^0/4\Delta G_0^{\ddagger})^2)$$

These relationships allow the evaluation of $(k_2^H/k_2^D)^{max} = 5.3 \pm 0.7$ and $\Delta G_0^{\ddagger} = 2.9 \pm 0.5$ kcal/mol. This latter value is similar to the intrinsic barrier reported for other reactions which are formal hydride transfer processes. Thus Bethel *et al.* (40) report 3.5 kcal/mol for hydride transfer between di- or triarylmethanes and 9-arylfluorenyl cations, while Stewart and Toone's data for the reduction of triphenylmethyl cations by formate anions yield an intrinsic barrier of 2.5 kcal/mol (37, 40). To the best of our knowledge, these latter two reactions represent the only previous examples of "Westheimer maxima" (41) for primary kinetic isotope effects in reactions which formally involve hydride transfer.

The maximum isotope effect of 5.3 found in the present study is considerably larger than the maxima of 3.9 and 2.8 reported in these earlier two investigations of hydride transfer reactions. It is therefore much closer to the theoretical maximum of 6.9 at 25°C for a symmetrical transition state for a one-step hydrogen transfer process (42). The e parameter in eq. [6] represents the pK_{R^+} for the quinolinium cation for which the maximum value of k_2^H/k_2^D is achieved (i.e. $\Delta G^0 = 0$). Thus $pK_{R^+} = 14.6$ should correspond to a transition state which most closely approximates equivalent bond-breaking at C-4 of the nicotinamide moiety and bond-formation at C-4 of the quinoline species. On the assumption that these reactions do involve one-step hydride migration processes, one would predict that such a symmetrical transition state would occur for that quinolinium cation that most closely matches the 1-benzylnicotinamide cation in its susceptibility to nucleophilic attack.

This then suggests that, to a first approximation, one might assign $pK_{R^+} = 14.6$ to the 1-benzylnicotinamide cation. Several linear free energy relationships between rate and equilibrium constants for hydroxide ion attack are available for quinolinium and isoquinolinium cations (17, 43), although analogous data are not readily obtainable for pyridinium cations. For nicotinamide cations, pK_{R^+} values are not directly measurable because of the ionization of the amide proton in basic solution rather than hydroxide ion attack (44). For the 3-acetyl-1-methylpyridinium cation a value of $pK_{R^+} = 13.3$ has been measured (44). If one assumes that the known substituent effects upon equilibrium constants for cyanide ion addition at C-4 of pyridinium cations exactly parallel substituent effects for hydroxide ion addition, one might attempt to predict pK_{R^+} for the 1-benzylnicotinamide cation using $\Delta pK_{R^+} = +2.2$ for $CONH_2$ vs. $COCH_3$ (45), and $\Delta pK_{R^+} = -1.1$ for benzyl vs. methyl (46). Thus $pK_{R^+} = 13.3 + 2.2 - 1.1 = 14.4$, which is remarkably close to the value of e obtained for eq. [6].

This analysis makes it clear that the maximum in the curve in Fig. 1 occurs at, or close to, $\Delta pK_{R^+} = 0$, i.e. an equilibrium constant of 1 for hydride transfer in the reaction

$$\mathbf{1} + \mathbf{2} \rightleftharpoons \mathbf{4} + \mathbf{5}$$

This observation is consistent with theoretical considerations.

The substitution of $pK_{R^+} = 14.6$ into eq. [3] leads to $k_2^H = 0.26\,M^{-1}\,s^{-1}$ at the maximum on the curve in Fig. 1. This value is six-fold larger than the largest of the range of second-order rate constants $((6.5 \times 10^{-4}) - (4.3 \times 10^{-2})\,M^{-1}\,s^{-1})$ reported by Roberts *et al.* (49) for a series of degenerate hydride transfers in 80% 2-propanol – 20% water at 25°C. However, in view of the 66-fold variation in the second-order rate constant for these degenerate hydride transfers, and the small solvent change, it would not be unreasonable to suggest that the current value represents a member of this class of one-step hydride transfers having $K = 1$.

The elucidation of the dramatically enhanced susceptibility towards dihydronicotinamide reduction of acridinium cations relative to isoquinolinium cations (16) was one of the major considerations in our undertaking the current study. Our product studies clearly indicate that the dihydronicotinamide reduction of quinolinium cations shows a pronounced kinetic preference for the formation of the 1,4-dihydroquinoline products over their 1,2-dihydro isomers, despite the inherently greater susceptibility of C-2 to nucleophilic attack. As indicated above, attack at C-4 of quinolinium cations seems to be more readily attributable to a mechanism involving a radical intermediate than to a direct hydride transfer. We have recently argued for an $e^- + H^\bullet$ mechanism in the case of the acridinium cations (16) and so a consideration of this possibility in the case of the quinolinium cations seems necessary.

Assuming that eq. [3] may also be applicable to acridinium cations, one would predict a second-order rate constant of 80 $M^{-1}\,s^{-1}$ for the reduction of the 10-methylacridinium cation ($pK_{R^+} = 10.01$ (47)) by 1-benzyl-1,4-dihydronicotinamide. This value is five-fold smaller than the experimental value of 400 $M^{-1}\,s^{-1}$ (16) under the current experimental conditions. Equation [6] predicts $k_2^H/k_2^D = 3.2$ for the reduction of the 10-methylacridinium cation. This value is somewhat larger than the experimental isotope effect of 1.56 (16). However, if k_2^H/k_2^D is considered as function of $\log k_2^H$ (Fig. 2) rather than of pK_{R^+} as in Fig. 1, then the acridinium cation does appear to conform to the data for these substituted quinolinium cations.

We previously attributed (16) this relatively small isotope effect in the reduction of the 10-methylacridinium cation to the fact that the electron transfer and the hydrogen atom transfer occur at similar rates and thus neither step is clearly rate determining. The isotope effects for W = CN and NO_2 in Table 2 are similar in magnitude to those observed for the acridinium cation, and may possibly arise in this same way. However, for the other W substituents in Table 2 the much larger isotope effects seem to imply that hydrogen atom transfer is rate deter-

TABLE 4. Comparison of relative rates of 1-benzyl-1,4-dihydronicotinamide reduction (k_2) and hydroxide ion attack (k_{OH}) on heterocyclic cations of $pK_{R^+} = 10.0$

Cation	$k_2(M^{-1}\ s^{-1})$	$k_{OH}(M^{-1}\ s^{-1})$	k_2/k_{OH}	$(k_2/k_{OH})^{rel}$
10-Methylacridinium	400[a]	550[b]	0.7	9×10^4
Quinolinium	80[c]	5000[d]	0.016	2×10^3
Isoquinolinium	1.3[e]	1.7×10^5[f]	8×10^{-6}	1.0

[a]From ref. 16.
[b]From ref. 47.
[c]Calculated from eq. [3] for $pK_{R^+} = 10.0$.
[d]Calculated from $\log k_{OH} = -0.46\ pK_{R^+} + 8.3$ (ref. 17) for hydroxide attack at C-4 with $pK_{R^+} = 10.0$.
[e]Calculated from $\log k_2 = -0.50\ pK_{R^+} + 4.9$ (ref. 2) for $pK_{R^+} = 10.0$.
[f]Calculated from $\log k_{OH} = -0.36\ pK_{R^+} + 8.84$ (ref. 43) for $pK_{R^+} = 10.0$.

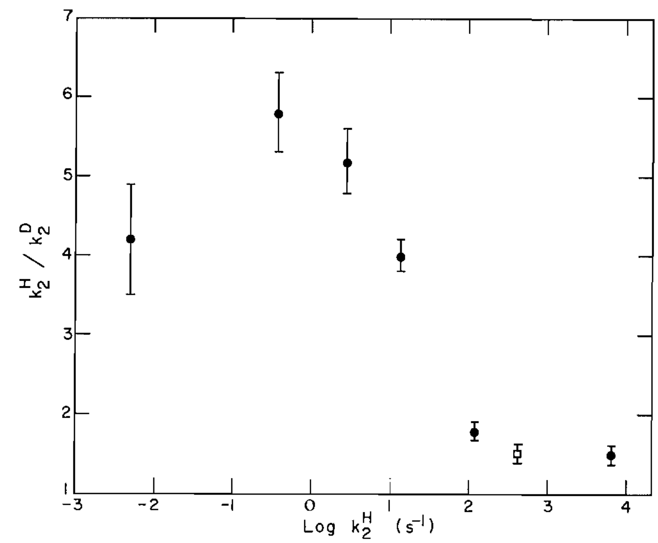

FIG. 2. Dependence of the primary kinetic isotope effects for the reduction of quinolinium cations **1** (●) and the 10-methylacridinium cation (□) by 1-benzyl-1,4-dihydronicotinamide (and its 4,4-dideuterio derivative) upon $\log k_2^H$.

mining. It is difficult to accommodate this within the $e^- + H^{\bullet}$ mechanism since this would require that complete positive charge neutralization should occur on the quinoline prior to hydrogen atom transfer. Equation [3] implies that such does not seem to be the case.

A quantitative comparison of the relative susceptibilities of acridinium, quinolinium, and isoquinolinium cations to dihydronicotinamide reduction and hydroxide ion attack is given in Table 4. From the linear free energy relationships that are available for the rates of both dihydronicotinamide reduction and hydroxide ion attack upon quinolinium and isoquinolinium cations it is possible to estimate rate constants for each of these processes for quinolinium (at C-4) and isoquinolinium cations of $pK_{R^+} = 10.0$. Because the 10-methylacridinium cation also has $pK_{R^+} = 10.0$, the kinetic data in Table 4 are uncomplicated by thermodynamic effects, since the equilibrium constants are identical in each of these three heterocyclic systems for each of these reactions. From Table 4 it is clear that while the isoquinolinium cation is much more reactive towards hydroxide ion than the other two heterocyclic cations, it is much less reactive in dihydronicotinamide reductions. The relative reactivities of these cations indicate that the quinolinium and acridinium cations are 2×10^3 and 9×10^4 respectively more reactive in dihydronicotinamide reductions than expected on the basis of relative reactivities to nucleophilic attack as exemplified by hydroxide ion as the nucleophile.

Dihydronicotinamide reductions of isoquinolinium cations have been established to involve a transition state in which the attacking hydride species bears a significant fractional negative charge (1, 3). The dramatically enhanced rates of dihydronicotinamide reduction in the quinolinium and acridinium series argue against such an "hydridic" transition state in these cases. We have previously argued in favour (16) of the $e^- + H^{\bullet}$ two-step mechanism for acridinium cation reduction.

The primary kinetic isotope effects observed for the 3-cyano- and 3-nitro-1-methylquinolinium cations and the 10-methylacridinium cations are significantly smaller than the range $k_2^H/k_2^D = 4.42-5.95$ reported by Ostovic *et al.* (50) for a series of analogous reactions which are believed to be one-step hydride transfer processes to various nitrogen heterocyclic cations. This in itself is suggestive of a mechanism other than direct hydride transfer in these three cases. On the other hand, reduction of the quinolinium cations **1**:W = H, Br, $CONH_2$, and CO_2CH_3 does give k_2^H/k_2^D values in the range associated with one-step hydride transfers (50), and, as indicated above, the Marcus fit in eq. [7] does give an intrinsic barrier similar to that observed in two other classes of reactions which have been interpreted as direct hydride transfers. At the present time we cannot definitively rule out the possibility of a change in mechanism between these two groups of substituents in **1**.

We have then a situation in which C-4 attack in the dihydronicotinamide reduction of these quinolinium cations seems to be too rapid to be consistent with an "hydridic" transition state such as is indicated in the corresponding isoquinolinium cation reductions. However, the alternative $e^- + H^{\bullet}$ mechanism attributed to the acridinium cations does not seem to be suitable for all W in **1**. We are currently pursuing the electronic structure of the transition state in these reactions via further substituent effect studies in the hope that such data will further clarify the mechanisms of these reactions.

Acknowledgement

We appreciate the continued support of this work by the Natural Sciences and Engineering Research Council of Canada.

1. J. W. BUNTING and S. SINDHUATMADJA. J. Org. Chem. **46**, 4211 (1981).
2. J. W. BUNTING, V. S. F. CHEW, and G. CHU. J. Org. Chem. **47**, 2303 (1982).
3. J. W. BUNTING, V. S. F. CHEW, and G. CHU. J. Org. Chem. **47**, 2308 (1982).

4. D. J. CREIGHTON, J. HAJDU, G. MOOSER, and D. S. SIGMAN. J. Am. Chem. Soc. **95**, 6855 (1973).
5. J. HAJDU and D. S. SIGMAN. J. Am. Chem. Soc. **97**, 3524 (1975).
6. J. HAJDU and D. S. SIGMAN. J. Am. Chem. Soc. **98**, 6060 (1976).
7. J. HAJDU and D. S. SIGMAN. Biochemistry, **16**, 2841 (1977).
8. S. SHINKAI, T. IDE, H. HAMADA, O. MANABE, and T. KUNITAKE. J. Chem. Soc. Chem. Commun. 848 (1977).
10. S. SHINKAI, T. IDE, and O. MANABE. Bull. Chem. Soc. Jpn. **51**, 3655 (1978).
11. S. SHINKAI, T. TSUNO, and O. MANABE. Chem. Lett. 1203 (1981).
12. A. OHNO, T. SHIO, H. YAMAMOTO, and S. OKA. J. Am. Chem. Soc. **103**, 2045 (1981).
13. A. VAN LAAR, H. J. VAN RAMESDONK, and J. W. VERHOEVEN. Recl. Trav. Chim. Pays-Bas, **102**, 157 (1983).
14. M. F. POWELL and T. C. BRUICE. J. Am. Chem. Soc. **104**, 5834 (1982).
15. M. F. POWELL and T. C. BRUICE. J. Am. Chem. Soc. **105**, 7139 (1983).
16. J. W. BUNTING, V. S. F. CHEW, G. CHU, N. P. FITZGERALD, A. GUNASEKARA, and H. T. P. OH. Bioorg. Chem. **12**, 141 (1984).
17. J. W. BUNTING and N. P. FITZGERALD. Can. J. Chem. **62**, 1301 (1984).
18. J. W. BUNTING and W. G. MEATHREL. Can. J. Chem. **52**, 303 (1974).
19. R. M. G. ROBERTS, D. OSTOVIC, and M. M. KREEVOY. J. Org. Chem. **48**, 2053 (1983).
20. J. W. BUNTING and W. G. MEATHREL. Tetrahedron Lett. 133 (1971).
21. J. W. BUNTING and W. G. MEATHREL. Can. J. Chem. **50**, 917 (1972).
22. J. METZGER, H. LARIVE, R. DENNILAULER, R. BARALLE, and C. GAURAT. Bull. Soc. Chim. Fr. 30 (1967).
23. Y. KIKUGAWA, M. KURAMOTO, I. SAITO, and S. YAMADA. Chem. Pharm. Bull. **21**, 1914 (1973).
24. M. FERLES and O. KOCIAN. Collect. Czech. Chem. Commun. **44**, 2238 (1979).
25. T. SEVERIN, D. BATZ, and H. LERCHE. Chem. Ber. **101**, 2731 (1968).
26. A. KAUFMANN and A. ALBERTINI. Chem. Ber. **42**, 3776 (1909).
27. A. D. AINLEY and H. KING. Proc. R. Soc. B, **125**, 60 (1938).
28. R. BRAMLEY and M. D. JOHNSON. J. Chem. Soc. 1372 (1965).
29. R. G. PEARSON and J. SONGSTAD. J. Am. Chem. Soc. **89**, 1827 (1967).
30. E. A. BRAUDE, J. HANNAH, and R. P. LINSTEAD. J. Chem. Soc. 3249 (1960).
31. M. FERLES and O. KOCIAN. Collect. Czech. Chem. Commun. **44**, 3141 (1979).
32. J. F. MUNSHI and M. M. JOUILLIE. Tetrahedron, **24**, 1923 (1968).
33. Y. IKEGAMI, S. KUBOTA, and H. WATANABE. Bull. Chem. Soc. Jpn. **52**, 1563 (1979).
34. G. P. GARDINI and F. MINISCI. Ann. Chim. (Rome), **60**, 746 (1970).
35. T. CARONNA, G. FRONZA, F. MINISCI, and O. PORTA. J. Chem. Soc. Perkin Trans. 2, 2035 (1972).
36. W. BRADLEY and S. JEFFREY. J. Chem. Soc. 2770 (1954).
37. R. STEWART and T. W. TOONE. J. Chem. Soc. Perkin Trans. 2, 1243 (1978).
38. R. A. MARCUS. J. Phys. Chem. **72**, 891 (1968).
39. A. O. COHEN and R. A. MARCUS. J. Phys. Chem. **72**, 4249 (1968).
40. D. BETHEL, G. J. HARE, and P. A. KEARNEY. J. Chem. Soc. Perkin Trans. 2, 684 (1981).
41. F. H. WESTHEIMER. Chem. Rev. **61**, 265 (1961).
42. L. MELANDER and W. H. SAUNDERS, JR. Reaction rates of isotopic molecules. John Wiley and Sons, New York. 1980. p. 26.
43. J. W. BUNTING and D. J. NORRIS. J. Am. Chem. Soc. **99**, 1189 (1977).
44. R. B. MARTIN and J. G. HULL. J. Biol. Chem. **239**, 1237 (1964).
45. K. WALLENFELS and M. GELLRICH. Justus Liebigs Ann. Chem. **621**, 149 (1959).
46. R. N. LINDQUIST and E. H. CORDES. J. Am. Chem. Soc. **90**, 1269 (1968).
47. J. W. BUNTING and W. G. MEATHREL. Can. J. Chem. **51**, 1965 (1973).
48. L. R. GIZZI and M. M. JOULLIE. Tetrahedron Lett. 3117 (1969).
49. R. M. G. ROBERTS, D. OSTOVIC, and M. M. KREEVOY. Faraday Discuss. Chem. Soc. **74**, 257 (1982).
50. D. OSTOVIC, R. M. G. ROBERTS, and M. M. KREEVOY. J. Am. Chem. Soc. **105**, 7629 (1983).
51. P. VAN EIKEREN, D. L. GRIER, and J. ELIASON. J. Am. Chem. Soc. **101**, 7406 (1979).

Kinetics and mechanisms of oxidations by metal ions. Part IV.[1] Oxidation of phenylphosphinic acid by aquavanadium(V) ions

RAJ NARAIN MEHROTRA
Department of Chemistry, University of Jodhpur, Jodhpur 342 001, India

Received January 16, 1984[2]

RAJ NARAIN MEHROTRA. Can. J. Chem. **63**, 663 (1985).

The kinetics of the oxidation of phenylphosphinic acid by quinquevalent vanadium ion have been investigated in aqueous perchlorate media under pseudo-first order conditions (phenylphosphinic acid in excess). The reaction has a first order dependence in [V(V)] and [phenylphosphinic acid] and the observed pseudo-first order rate constant k_{obs} is given by $k_{obs} = a + b[H^+]$.

The acid-independent path is considered to be due to the reaction between VO_2^+ (aq.) and $C_6H_5P:(OH)_2$, the active form of phenylphosphinic acid, while the reaction between $V(OH)_3^{2+}$ (aq.) and $C_6H_5P(O)(OH)H$, the inactive form of phenylphosphinic acid, is considered to explain the acid-dependent path. Phenylphosphinic acid in aqueous acidic solution is known to exist as an equilibrium mixture of the active and inactive forms. The composite activation and thermodynamic parameters associated with the constants a and b are reported.

RAJ NARAIN MEHROTRA. Can. J. Chem. **63**, 663 (1985).

Opérant dans un milieu aqueux d'acide perchlorique et sous des conditions de pseudo-premier ordre (acide phénylphosphinique en excès), on a étudié l'oxydation de l'acide phénylphosphinique par l'ion vanadium pentavalent. La réaction est du premier ordre en vanadium(V) et en acide phénylphosphinique et la constante de vitesse du pseudo-premier ordre qui est observée (k_{obs}) est définie par l'équation $k_{obs} = a + b[H^+]$.

On croit que la voie d'oxydation qui n'est pas influencée par la présence d'acide est due à la réaction du VO_2^+ (aq.) avec le $C_6H_5P:(OH)_2$, la forme active de l'acide phénylphosphinique; par ailleurs, on croit que la voie d'oxydation qui est influencée par les acides peut être expliquée en faisant appel à une réaction entre l'ion $V(OH)_3^{2+}$ (aq.) et la forme inactive de l'acide phénylphosphinique, $C_6H_5P(O)(OH)H$. Il est connu que l'acide phénylphosphinique, en milieu acide aqueux, existe sous la forme d'un mélange à l'équilibre entre les formes active et inactive. On rapporte les valeurs observées pour les paramètres thermodynamiques et d'activation associés avec les constantes a et b.

[Traduit par le journal]

Introduction

The structure of phenylphosphinic acid in form **A** has been confirmed by nuclear magnetic resonance and infrared spectroscopy (2). However, on the basis of chemical evidence a suggestion was made (3) about the existence of the tautomer **B** too, with tautomer **A** as the overwhelming predominant species. The tautomer **A** is known as the inactive form and the tautomer **B** is known as the active form.

[1] 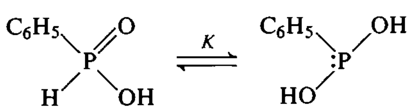

Form A Form B

The oxidation of phenylphosphinic acid by quinquevalent vanadium ion in 3.5–6.0 mol dm^{-3} perchloric acid has been reported (4). This study (4) suggested that the form **B** predominated in aqueous acidic solution and therefore it was considered to be the reactive species. Assuming that the equilibrium constant for [1] is not appreciably different from the equilibrium constant for the similar equilibrium in hypophosphorous acid for which K is of the order of 10^{-12} (2), the assumption that form **B** predominated seemed to be erroneous. The formation of phosphonium ion, $Ph\overset{+}{P}O_2H$, in the rate-limiting step was also suggested, which by implication meant that vanadium(V) underwent a two-electron change. Since the reaction was studied in perchloric acid solution > 3.5 mol dm^{-3}, nothing is known about the nature of the reaction at lower acid concentration, particularly the dependence of k_{obs} on lower [H$^+$]. Hence a reinvestigation became desirable to gain the insight about the reactive form of phenylphosphinic acid and other parameters.

The reinvestigation was therefore carried out at lower concentrations of perchloric acid, 0.5–3.0 mol dm^{-3}, at constant ionic strength of 3.0 mol dm^{-3}. The results thus obtained have indicated a different dependence of k_{obs} on [H$^+$], the formation of a free radical in the rate-limiting step indicating vanadium(V) to be a one-electron oxidant and that both of forms **A** and **B** are reactive.

Experimental

Reagents

The stock vanadium(V) solution was prepared from ammonium trioxovanadate(V) (Hopkin and Williams, GPR grade). The perchloric acid (E. Merck, GR) concentration present in the stock solution was taken as the difference between the known amount added minus the amount neutralised by the standard aqueous vanadium(V) solution according to the relation [2]. Hence an extrapolation of the rate to zero concentration of perchloric acid would mean that vanadium(V) species present in the system is VO_2^+(aq.).

[2] $VO_3^- + 2H^+ \rightarrow VO_2^+ + H_2O$

Phenylphosphinic acid (Fluka) was twice recrystallised from hot water, mp 70–71°C (lit. 5, 71°C). Solutions were prepared by direct weighing of the recrystallised sample and strength determined against a standard alkali. Because of its limited solubility, values of k_{obs} at high concentrations of phenylphosphinic acid could not be determined.

Perchloric acid was suitably diluted and standardised against a standard alkali. Sodium perchlorate, used to maintain the ionic strength at 3.0 mol dm^{-3}, was prepared by the neutralisation of sodium carbonate by perchloric acid.

All other chemicals were of standard grade and used as supplied.

[1]For Part III, see ref. 1.

[2]Revision received September 6, 1984.

Distilled water was once redistilled from alkaline permanganate using an all-glass still.

Kinetic studies

The kinetic experiments were carried out under pseudo-first order conditions where excess concentration of phenylphosphinic acid over vanadium(V) was present in the reaction mixtures. The disappearance of vanadium(V) was followed by using a volumetric method described elsewhere (6). However, in adopting the method it was ensured that the presence of phenylphosphinic acid in a concentration present in the reaction mixtures did not change the titre value of ferrous ammonium sulphate solution, in which the reaction mixture was quenched, with vanadium(V). Barium *N*,*N*-diphenylsulphamate in the presence of phosphoric acid was used as indicator. The runs were studied until the reaction was 80–90% complete. The pseudo-first order rate constant k_{obs} was calculated from the gradient of the linear plots obtained between ln [V(V)] and time. Such plots were linear for three half-lives and beyond. The k_{obs} values from replicate runs were reproducible within ±3% and the mean values are in the tables.

Stoichiometry

A series of determination carried out in reaction mixtures having [V(V)] > [PPA] (PPA is the abbreviated form of phenylphosphinic acid) at different acidities indicated that $\Delta[V(V)]/\Delta[PPA] = 1.93 \pm 0.1$. That phenylphosphonic acid, the reaction product, was not further oxidised was confirmed by the failure of an authentic sample to reduce vanadium(V). Hence the stoichiometric equation of the reaction is given by [3].

$$[3]\quad C_6H_5P(O)(OH)H + 2V(V) + H_2O \rightarrow C_6H_5P(O)(OH)_2 + 2V(IV) + 2H^+$$

Results

The invariance of k_{obs} with varying [V(V)] is indicative of the first-order dependence of the reaction in vanadium(V). The order with respect to phenylphosphinic acid, Table 1, was one. The plot between k_{obs} and [PPA] was linear and passed through the origin. The effect of $[H^+]$ on k_{obs} was investigated at different temperatures. The results are reported in Table 2. The plot between k_{obs} and $[H^+]$, Fig. 1, was linear for all the five temperatures with an intercept on the rate ordinate. The k_{obs} at constant [PPA] and $[H^+]$ was independent of ionic strength (Table 3). Thus the previous observations (4) about the order of the reaction with respect to the oxidant and substrate are confirmed.

Mechanism and discussion

The hydrogen atom attached to phosphorous in phenylphosphinic acid undergoes isotopic exchange with deuterium in H_2O/D_2O solution, probably via the formation of an intermediate having structure **B**. The rate of the acid catalysed hydrogen exchange in 50% ethanol-*d*–D_2O(v/v) solution has been studied (7) and the following mechanism with reaction [5] as the rate determining was suggested.

[4] 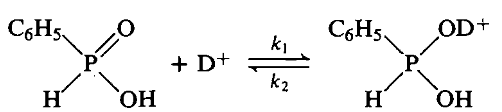

[5] 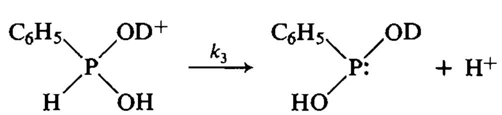

[6] 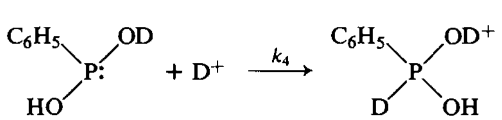

[7] 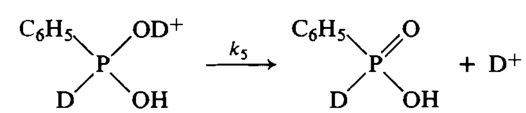

The above mechanism yields the rate law given in eq. [8] which is consistent with the observed first-order dependence in phenylphosphinic acid.

[8] 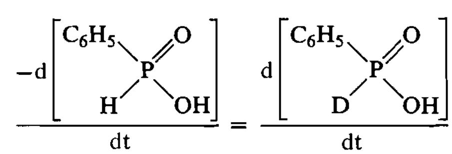

$$= \frac{k_1k_3[C_6H_5P(O)(OH)H][D^+]}{k_2 + k_3}$$

Since the plot between observed first order exchange rate constant k_{ex} for hydrogen exchange, with respect to phenylphosphinic acid, and [DCl] had an intercept on the rate ordinate, it was suggested (7) that

$$[9]\quad k_{ex} = k_H[D^+] + k_w$$

where k_H is the catalysis constant for the hydrogen (deuterium) ion and k_w is the specific rate of acid-independent exchange of the unprotonated pentacovalent species in the stated solvent. The value of k_H is 3.5×10^{-4} dm^3 mol^{-1} s^{-1} and $k_w = 2.0 \times$

TABLE 1. The dependence of k_{obs} (s^{-1}) on [phenylphosphinic acid] at 45°C; 10^2[V(V)] = 1.0, [$HClO_4$] = 2.0, and I = 3.0 mol dm^{-3}*

10^2[PPA] (mol dm^{-3})	$10^5 k_{obs}$ (s^{-1})	10^2[PPA] (mol dm^{-3})	$10^5 k_{obs}$ (s^{-1})
2.9	1.1	16.4	6.4
4.2	1.6	28.7	11.2
8.2	3.2	34.2	13.5

*Average $10^4 k_{obs}/[C_6H_5P(O)(OH)H] = 3.9 \pm 0.1$ dm^3 mol^{-1} s^{-1}.

TABLE 2. The effect of $[H^+]$ on k_{obs} at different temperatures; 10^2[V(V)] = 1.0, [$C_6H_5P(O)(OH)H$] = 0.08, and I = 3.0 mol dm^{-3}

$[H^+]$ (mol dm^{-3})	$10^5 k_{obs}$ (s^{-1}) at T = 40°C	45°C	50°C	55°C	60°C
0.5	0.62	1.4	3.2	9.1	24.3
1.0	1.0	2.1	4.2	10.7	27.4
1.5	1.3	2.6	5.2	12.4	29.8
2.0	1.7	3.1	6.2	14.1	33.3
2.5	2.1	3.8	7.1	15.7	36.1
3.0	2.4	4.4	8.2	16.9	38.8

TABLE 3. The dependence of k_{obs} on the ionic strength at 45°C; 10^2[V(V)] = 2.0, [$HClO_4$] = 2.0, 10^2[$C_6H_5P(O)(OH)H$] = 3.2 mol dm^{-3}

[$NaClO_4$] (mol dm^{-3})	$10^5 k_{obs}$ (s^{-1})	[$NaClO_4$] (mol dm^{-3})	$10^5 k_{obs}$ (s^{-1})
0.0	1.3	0.8	1.3
0.2	1.2	1.0	1.3
0.4	1.3	1.2	1.2

10^{-4} s^{-1}, both at 23°C (7).

The k_H and k_w values for aqueous solution from the data (7) could not be determined. However, an assumption that could be made without any serious error is that the order ($\sim 10^{-4}$) of the k_H and k_w values will not be changed for the aqueous solution. The correlation between k_H and k_1, k_2, and k_3, deduced from eq. [8] and [9] is given in [10].

$$[10] \quad k_H = \frac{k_1 k_3}{k_2 + k_3}$$

where in view of the reactions [4]–[7] it is understood that $k_1 > k_2$, $k_3 > k_2$, and k_4, $k_5 \gg k_3$.

The pK_a value of monobasic phenylphosphinic acid is 1.75 at 25°C (8). Hence it is clear that almost all of it will exist in the undissociated state in the presence of [$HClO_4$] used in the study which will be therefore the reactive species. It might be mentioned here that if the phenylphosphinate ion were to be the reactive species a retardation in the k_{obs} was expected with increasing [H^+] which is not the case.

In view of the dependence of k_{obs} on [H^+], Fig. 1, the following reactions are considered for the mechanism of the reaction and the justification for the same is deferred to a later stage of discussion.

The rate of disappearance of vanadium(V) in terms of reactions [1] and [11]–[14] with reactions [12] and [13] as rate

[1] 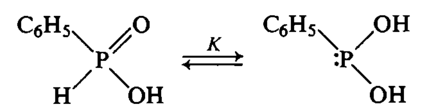

$$[11] \quad VO_2^+(aq.) + H_3O^+ \overset{K_1}{\rightleftharpoons} V(OH)_3^{2+}(aq.)$$

[12] 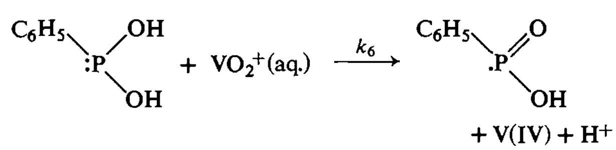

[13] 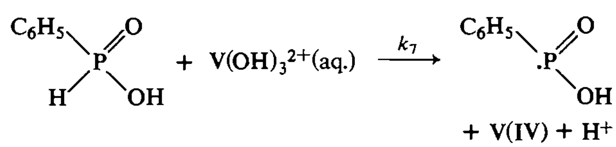

[14] 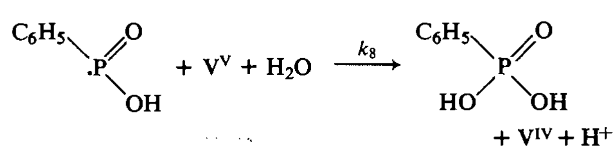

determining is given by eq. [15] because $1 \gg K_1[H^+]$ in the range 1–5 mol dm^{-3} perchloric acid (9–13), and $1 \gg K$ because K for phenylphosphinic acid is considered to be not much different from K for hypophosphorous acid for which it has a value of the order of 10^{-12} (2, 14).

$$[15] \quad k_{obs} = 2(k_6K + k_7K_1[H^+])[C_6H_5P(O)(OH)H]$$

The above mechanism thus differs from that proposed by earlier workers (4) in the sense that (*a*) VO_2^+(aq.) and $V(OH)_3^{2+}$(aq.) ions are reactive where VO_2^+(aq.) is written for $(VO_2.2H_2O)^+$ (15), (*b*) both inactive **A** and active **B** forms of phenylphosphinic acid are reactive, (*c*) k_{obs} is the sum total of two components, one independent and the other is dependent on [H^+], and (*d*) the rate-controlling step is the formation of a free radical instead of phosphonium ion (4).

The formation of the free radical was checked by the induced

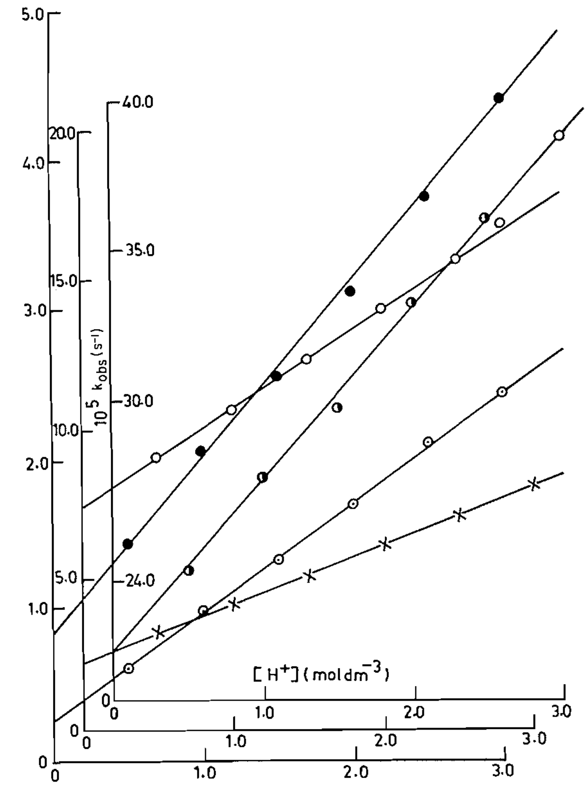

FIG. 1. Dependence of k_{obs} on [H^+] in the reaction with 10^2 [V(V)] = 1.0, 10^2 [PPA] = 8.0, and I = 3.0 mol dm^{-3} at 40°C (⊙), 45°C (●), 50°C (×), 55°C (○), and 60°C (◑).

polymerisation of acrylonitrile by the partially oxidised reaction mixtures previously degassed with nitrogen. No such polymerisation of the monomer was observed when it was added under similar conditions to the solutions of vanadium(V), or phenylphosphinic acid taken separately. It might be noted that the previous workers (4) too noted the induced polymerisation of the monomer in reaction mixtures prepared in sulphuric acid. The induced polymerisation of the monomer established vanadium(V) to be a one-electron oxidant. Sengupta and co-workers (4) claimed vanadium(V) to be a two-electron equivalent oxidant in perchloric acid solution and one equivalent in sulphuric acid solution. These authors, however, did not explain how a change from one mineral acid to another changed the very character of the oxidant.

It is known that in the reaction [16] the rate law has a strong dependence upon $[H^+]^{-1}$ (16). This prompted Kustin and Toppen (17) to suggest that the possibility of the formation of V(IV) through the reaction between V(V) and V(III) can be safely ruled out in any reaction if its rate law is independent of $[H^+]^{-1}$ term. The application of this criterion to the present reaction reinforces the view that vanadium(V) acted as a one-electron equivalent oxidant.

$$[16] \quad V(V) + V(III) \rightarrow 2V(IV)$$

The slope of the linear plots (0.61 at 40°C, 0.49 at 45°C, 0.47 at 50°C, 0.33 at 55°C, and 0.25 at 60°C) between log k_{obs} and $-H_0$ is not unusual primarily because the ideal slope of the unity is expected for the protonation of the amide bases and, secondly, it is known (18) that groups of indicators with different structures specially with different basic sites often show significant deviations from ideal value of unity. The H_0 is the Hammett acidity function (19) and the values used are those of Day and Wyatt (20). The decreasing slope value with tem-

TABLE 4. The values of k_6K and k_7K_1 at different temperatures; $10^2[V(V)] = 1.0$ mol dm^{-3}

T (°C)	$10^5 k_6K$ (dm^3 mol^{-1} s^{-1})	$10^5 k_7K_1$ (dm^6 mol^{-2} s^{-1})
23	0.025	0.625
40	1.59	4.60
45	5.24	7.35
50	14.0	12.3
55	46.1	20.9
60	133	36.7
	$\Delta H(k_6K) = 187 \pm 5$ kJ mol^{-1}	$\Delta H(k_7K_1) = 100 \pm 6$ kJ mol^{-1}
	$\Delta S(k_6K) = -33 \pm 4$ J K^{-1} mol^{-1}	$\Delta S(k_7K_1) = -151 \pm 4$ J K^{-1} mol^{-1}

perature is considered due to possible changes of H_0 values with temperature. The H_0 values are, unfortunately, known only at one temperature.

Active vs. inactive form

The problem which of the two forms, present in equilibrium with each other in an acidic solution, are reactive is attempted to be answered by comparing k_{ex} [9] and k_{redox} [18]. The need for deriving eq. [18] is that k_{ex} [9] and k_{obs} [15] cannot be directly compared because the former is derived with respect to phenylphosphinic acid whereas the latter is derived with respect to vanadium(V). Hence it is essential that k_{obs} is first converted to a rate constant k_{redox} which is the first-order rate constant with respect to phenylphosphinic acid itself. The correlation between k_{obs} and k_{redox} is given in eq. [17] which is derived on the basis of stoichiometry of the reaction.

[17] $k_{obs}[V(V)] = 2k_{redox}[C_6H_5P(O)(OH)H]$

[18] $k_{redox} = (k_7K_1[H^+] + k_6K)[V(V)]$

Equation [18] is obtained by substituting the k_{obs} value given in [15] into [17]. The comparison of equations [9] and [18] makes it apparent that k_H has to be compared with $k_7K_1[V(V)]$ and k_w with $k_6K[V(V)]$.

The values of k_7K_1 (dm^6 mol^{-2} s^{-1}) and k_6K (dm^3 mol^{-1} s^{-1}) computed from the slope and intercept of the linear plots between $k_{redox}/[V(V)]$ and $[H^+]$ at each temperature are given in Table 4. The values at 23°C were obtained by extrapolating the linear plots between $\log k_7K_1$ or $\log k_6K$ against T^{-1} because k_H is known at 23°C only (9). The $k_H/k_7K_1[V(V)]$ thus obtained is 5.6×10^3 and $k_w/k_6K[V(V)]$ is 8.0×10^4 both at 23°C, indicating that the rate of transformation of inactive form into active form is much higher than the rate of oxidation of phenylphosphinic acid. Thus the oxidation may apparently involve selectively either form of phenylphosphinic acid or both of them.

The next approach to the problem was therefore to compare k_7 with k_1, and k_6 with k_4 to give a firm support to the proposed mechanism. Unfortunately neither k_1 nor k_4 are known. Nevertheless, an approximate estimate of k_1 value with relation to the known value of k_H is possible on the basis of the two following plausible assumptions ($k_2 \gg k_3$ is improbable): (*i*) $k_2 \sim k_3$, whence $k_H = k_1/2$; (*ii*) $k_2 \ll k_3$, whence $k_H = k_1$.

Similarly k_7 can be estimated if K_1 is known. Unfortunately, K_1 is not known. Nevertheless, the inequality $1 \gg K_1[H^+]$, valid in several studies (9–13) in the range 1–5 mol dm^{-3} perchloric acid will be rendered invalid if $K_1 \geqslant 10^{-2}$ dm^3 mol^{-1}. Hence the inequality is valid only for any value of $K_1 \leqslant 10^{-3}$ dm^3 mol^{-1}. Since $k_7K_1 \sim 10^{-6}$ dm^6 mol^{-2} s^{-1} at 23°C, k_7 is estimated to be $\sim 10^{-3}$ dm^3 mol^{-1} s^{-1} when $K_1 \sim 10^{-3}$ dm^3 mol^{-1}, which is its maximum permitted value. Thus k_7 (dm^3 mol^{-1} s^{-1}) is one order greater than the value of $k_1 \sim 10^{-4}$ dm^3 mol^{-1} s^{-1}. The consequence of this result is that the form **B** cannot be involved in the oxidation. It must be noted that the ratio k_7/k_1 will be much greater for K_1 values $< 10^{-3}$ dm^3 mol^{-1} which will further strengthen the conclusion.

Again k_6 is found to be $\sim 10^5$ dm^3 mol^{-1} s^{-1} with the assumption that $K \sim 10^{-12}$. This high value of k_6 exceeds the k_4 value, which is not exactly known though it may not be of this high order. Considering the values of the constants k_1, k_2, and k_3, all of which are necessarily of the order of 10^{-4}, there will be no difficulty in justifying the inclusion of reaction [12] in the proposed mechanism.

Acknowledgement

Thanks are due to CSIR and UGC, New Delhi, for the financial support, and to Professor R. C. Kapoor for laboratory facilities.

1. RAJ N. MEHROTRA. Indian J. Chem. **22A**, 169 (1983).
2. J. R. VAN WAZER. Phosphorous and its compounds. Interscience, New York. 1958. p. 368.
3. A. W. FRANK. J. Org. Chem. **26**, 850 (1961).
4. K. K. SENGUPTA, J. K. CHAKLADAR, B. B. PAL, and D. C. MUKHERJI. J. Chem. Soc. Perkin Trans. II, 926 (1973).
5. V. M. PLETS. Zh. Obsheh Khim. **6**, 1198 (1936).
6. A. KUMAR and RAJ N. MEHROTRA. J. Org. Chem. **40**, 1248 (1975).
7. J. REUBEN, D. SAMUEL, and B. L. SILVER. J. Am. Chem. Soc. **85**, 3093 (1963).
8. L. D. QUIN and M. R. DYSART. J. Org. Chem. **27**, 1012 (1962).
9. C. F. WELLS and L. V. KURITSYN. J. Chem. Soc. A, 1372 (1970).
10. C. F. WELLS and A. F. M. NAZER. J. Chem. Soc. Faraday Trans. **72**, 910 (1976).
11. A. F. M. NAZER and C. F. WELLS. J. Chem. Soc. Dalton Trans. 1532 (1980); 2143 (1980).
12. Z. AMJAD and A. MCAULEY. Inorg. Chim. Acta, **25**, 127 (1977).
13. RAJ N. MEHROTRA. J. Chem. Soc. Dalton Trans. 681 (1978).
14. H. A. J. CHAMP. Hypophosphorous acid and the hypophosphites. *In* Comprehensive treatise on inorganic and theoretical chemistry. Vol. VIII. Supplement III. Wiley Interscience, New York. 1971. p. 615.
15. RAJ N. MEHROTRA. J. Chem. Soc. B, 642 (1968).
16. N. A. DAUGHERTY and T. W. NEWTON. J. Phys. Chem. **68**, 612 (1964).
17. K. KUSTIN and D. L. TOPPEN. Inorg. Chem. **12**, 1404 (1973).
18. C. H. ROCHESTER. Acidity functions. Academic Press, London. 1970. p. 21.
19. L. P. HAMMETT and A. J. DEYRUP. J. Am. Chem. Soc. **54**, 2721 (1932).
20. J. S. DAY and P. A. H. WYATT. J. Chem. Soc. B, 343 (1966).

The reactions of sulfur atoms with propadiene and 1,2-butadiene

MARTINA GREEN[1], BELA VERKOCZY[2], ELIZABETH M. LOWN, AND OTTO P. STRAUSZ
Department of Chemistry, University of Alberta, Edmonton, Alta., Canada, T6G 2G2

Received March 26, 1984

MARTINA GREEN, BELA VERKOCZY, ELIZABETH M. LOWN, and OTTO P. STRAUSZ. Can. J. Chem. **63**, 667 (1985).

The gas phase reactions of both $S(^1D)$ and $S(^3P)$ atoms with propadiene afford methylenethiirane in nearly quantitative yields at high pressure. With 1,2-butadiene the three novel unsaturated isomeric thiirane products, resulting from addition to the 2,3 double bond and *cis*- and *trans*-addition to the 1,2 double bond, have been characterized. The yields are pressure and exposure-time dependent and, at zero conversion and high pressures, comprise ~94% of the C_4H_6S adducts, the remainder being two thiol insertion products. The ratio of 2,3-addition to 1,2-addition is ~1.3 for $S(^1D)$ atoms and ~2.1 for $S(^3P)$ atoms. Rate parameters for the $S(^3P)$ + 1,2-butadiene reaction were determined in competition with the $S(^3P)$ + 1-C_4H_8 reaction and found to be $A = 6.4 \pm 1.1 \times 10^{10}\ M^{-1}\ s^{-1}$ and $E_a = 1.4 \pm 0.2$ kcal mol^{-1}. The E_a's associated with 1,2- and 2,3-addition are comparable but the preexponential factors are slightly different.

MARTINA GREEN, BELA VERKOCZY, ELIZABETH M. LOWN et OTTO P. STRAUSZ. Can. J. Chem. **63**, 667 (1985).

A des pressions élevées, les réactions en phase gazeuse des atomes de $S(^1D)$ et de $S(^3P)$ avec le propadiène fournissent le méthylènethiiranne avec un rendement pratiquement quantitatif. Lors des mêmes réactions avec le butadiène-1,2, on a pu caractériser les trois nouveaux thiirannes insaturés isomères qui proviennent de l'addition sur la double liaison en 2,3 et des additions *cis* et *trans* sur la double liaison en 1,2. Les rendements dépendent de la pression et du temps d'exposition et, à des pressions élevées et à des conversions nulles, ils sont composés d'environ 94% d'adduits C_4H_6S alors que le reste correspond à deux produits d'insertion des thiols. Les rapports des additions en position 2,3/position 1,2 sont d'environ 1,3 et 2,1 respectivement pour les atomes $S(^1D)$ et les atomes $S(^3P)$. On a déterminé les paramètres de vitesse pour la réaction du $S(^3P)$ + butadiène-1,2 par compétition avec la réaction du $S(^3P)$ + butène-1 et on a trouvé que $A = 6{,}4 \pm 1{,}1 \times 10^{10}\ M^{-1}\ s^{-1}$ et $E_a = 1{,}4 \pm 0{,}2$ kcal mol^{-1}. Les valeurs de E_a associées avec les additions en 1,2 ou en 2,3 sont comparables; toutefois, les facteurs préexponentiaux sont légèrement différents.

[Traduit par le journal]

Introduction

The chemistry of sulfur atoms has been explored for over two decades (1). In most studies the source of sulfur atoms was the uv photolysis of carbonyl sulfide (1, 2):

[1] $\quad COS + h\nu\ (240\ nm) \rightarrow CO + S(^1D_2)\ (67\%),\ S(^3P_J)\ (33\%),\ \phi = 0.91$

The ensuing reactions are:

[2*a*] $\quad S(^1D) + COS \rightarrow S_2 + CO$

[2*b*] $\quad \rightarrow S(^3P) + COS^*$

[3] $\quad S(^3P) + COS \rightarrow S_2 + CO$

A lower limit $k_{2a} \geq 4.0 \times 10^{10}$ L mol^{-1} s^{-1} has been reported from flash photolysis experiments (3) and the abstraction/deactivation rate constant ratio, k_{2a}/k_{2b}, is estimated to be $\simeq 2$ (2). Step [3] has been studied using flash photolysis – resonance fluorescence techniques, from which $k_3 = 2 \times 10^6$ L mol^{-1} s^{-1} (4). In the presence of >ca. 15-fold excess of CO_2 nearly all the initially produced $S(^1D)$ atoms are collisionally deactivated to the ground state and thus this system can be used to study the reactions of $S(^3P)$ atoms exclusively.

The reactions of ground (^3P_J) and metastable ($^1D_2$) excited sulfur atoms have been extensively studied (5) with alkenes. $S(^1D)$ atoms add to the double bond in a spin and symmetry allowed reaction to yield a vibrationally excited ground state thiirane molecule as shown by the example of propylene:

$$S(^1D) + CH_3CH{=}CH_2 \rightarrow CH_3\overline{CH{-}CH_2S}\ (S_0)^\dagger$$

Parallel, and in competition with addition, C—H insertion can also take place (5, 6):

$$S(^1D) + CH_3CH{=}CH_2 \rightarrow HSCH_2CH{=}CH_2,\ CH_3C(SH){=}CH_2,\ CH_3CH{=}CHSH$$

The rates of addition and insertion are rapid, being close to the gas kinetic collision frequencies. $S(^3P)$ atoms, on the other hand, do not insert into C—H bonds and the primary adduct is the vibrationally excited lowest triplet state thiirane (7) which is subsequently collisionally deactivated to the ground state:

$$S(^3P) + CH_3CH{=}CH_2 \rightarrow CH_3\overline{CH{-}CH_2S}\ (T_1)^\dagger \xrightarrow{M} CH_3\overline{CH{-}CH_2S}\ (S_0)$$

Absolute rate constants and Arrhenius parameters have been reported for a variety of alkenes (8, 9) and the room temperature values range from 8×10^8 to 4.3×10^{10} L mol^{-1} s^{-1} on going from ethylene to tetramethylethylene. The activation energies decrease, eventually becoming negative, with increasing alkyl substitution, and are linearly related to the ionization potential of the alkene. With the exception of vinylthiols, all the reaction products are reasonably stable and under suitable experimental conditions essentially quantitative product recoveries can be achieved.

The reactions of S-atoms with only one diene substrate, namely 1,3-butadiene, have been investigated (10). The major product is vinylthiirane and the rate of the $S(^3P)$ + 1,3-C_4H_6 reaction is, as expected, somewhat (about fourfold) faster than that with the butenes (5). Cumulated double bonds might be expected to exhibit a somewhat different chemical reactivity from that of conjugated dienes. For this reason we have undertaken the first study of the reactions of S-atoms with the cumulated dienes propadiene and 1,2-butadiene, the results of which are reported here.

---

[1]Present Address: Department of Chemistry, University of Saskatchewan, Saskatoon, Saskatchewan S7N 0W0.
[2]Present Address: Saskatchewan Oil and Gas Corporation, 1500 Chateau Tower, 1920 Broad Street, Regina, Saskatchewan S4P 3V2.

Experimental

Photolyses were carried out in 10 × 5 cm cylindrical quartz cells, one of which (for the study of the S + 1,2-C_4H_6 reaction) was equipped with Suprasil windows. The latter was enclosed in a cylindrical aluminium block furnance, 16 cm long, 12.5 cm od, and 6 cm id, covered at both ends by 2 mm thick quartz plates and around the sides by 1-in. fibreglass. Heating was achieved by four 10 cm long 150-W pencil heaters inserted axially into the block. Temperatures were maintained by an API 2-mode temperature controller and measured by standard iron–constantan thermocouples.

The light source was a Harovia medium pressure mercury arc equipped with three 2 mm thick Vycor 7910 filters to limit the effective wavelength to >240 nm.

COS (Matheson) was purified as described previously (11). CO_2 (Airco, >99.9% pure) was used as such. C_3H_4 (Matheson, teaching grade, 99%) was degassed at −186°C and distilled at −132°C; <0.5% C_3H_6 remained. 1-C_4H_8 (Linde, research grade) was degassed at −196°C and distilled at −115°C. 1,2-C_4H_6 (Chemical Sample Co., 99%) was degassed at −139°C and distilled at −105°C.

Non-condensable products were collected and measured in a gas burette and, for the S + 1,2-C_4H_6 reaction, analyzed on a 3 ft × 2 mm 80/100 mesh molecular sieve 5 A column at 27°C. The sulfur-containing products were isolated following low pressure distillations of the reaction mixtures and analyzed by gc as follows: 305 cm × 3.2 mm Teflon column, 60/80 mesh Chromosorb W.A. coated with 10% tricresylphosphate (C_3H_4S); 7 ft × 2 mm quartz column, 5% Ucon polar 50 HB 2000 on 80/100 mesh Chromosorb P, AW-DMCS (C_4H_6S).

The nmr, ir, uv, and mass spectra were obtained using either a Bruker 200 or 400 MHz, a Nicolet 7199 FTIR, a Unicam SP-1700 spectrophotometer, and an AEI MS-12 spectrometer, respectively.

Results

Because propadiene and 1,2-butadiene exhibit small but measurable absorptions at λ 240 nm, at least a fourfold excess of COS was used throughout in order to ensure that at least 95% of the incident radiation would be absorbed by COS.

1. *The S + C_3H_4 reaction*

Photolysis of COS in the presence of C_3H_4 led to the formation of methylenethiirane as the major product, identified on the basis of its mass, nmr, and ir spectra (12). Smaller amounts of CS_2 and methylthiirane were also detected, the latter as a result of S-atom addition to C_3H_6, an unresolvable impurity in the substrate.

In the gas phase, methylenethiirane is somewhat more stable than claimed before (13); the rate of disappearance (0.9 Torr at 25°C, in a 10 × 1.6 cm quartz vessel) (1 Torr = 133.3 Pa) of its large uv absorption band at 231 nm appeared to be a second-order process with a half-life of about 12 h, without producing any new uv absorptions. This compound is, however, very sensitive to Pyrex and metal surfaces, polymerizing upon prolonged storage at −196°C.

The effects of exposure time and total pressure on the product yields are listed in Table 1. C_3H_4S is photolabile, its rate of formation declining by a factor of 2 over the course of a 7-min photolysis in the two pressure regimes examined. A twofold increase in the total pressure (for COS/C_3H_4 ~10) results in a significant enhancement in the product recoveries, in terms of the amount of S-atoms reacting with C_3H_4, and at short conversions the reaction is nearly quantitative.

The presence of 600 Torr CO_2, which quenches a large proportion of the $S(^1D)$ atoms to the ground (^3P) state, has little discernible effect on the product yields (Table 1).

2. *The S + 1,2-C_4H_6 reaction*

Photolysis of COS in the presence of 1,2-C_4H_6 led to the formation of five isomeric products (**1–5**) of molecular weight 86, corresponding to the adduct C_4H_6S. A gc/ms analysis using a mass-86 cross-scan showed the presence of two additional mass-86 peaks, **6** and **7**, but because these were formed in only trace quantities their structural identification was not attempted. Mass spectral data for the C_4H_6S products are summarized in Table 2.

TABLE 1. Effects of exposure time and total pressure on the product yields from the S + C_3H_4 reaction

Time (min)	Yields (μmol) CO	C_3H_4S	CS_2	C_3H_6S	% Product recovery[a]
P(COS) = 545, *P*(C_3H_4) = 55 Torr					
1	2.19	0.59	0.06	0.02	77
1[b]	2.17[b]	0.57[b]	0.03[b]	0.02[b]	67[b]
3	6.23	1.55	0.02	0.07	52
5	10.44	1.86	0.12	0.07	41
7	14.37	2.01	0.26	0.12	35
P(COS) = 1090, *P*(C_3H_4) = 109 Torr					
1	2.73	1.19	0.10	0.04	100
3	7.99	2.81	0.49	0.11	87
5	13.20	3.37	0.30	0.10	56
7	18.32	3.94	0.43	0.11	49

[a] % Recovery = $[\Sigma(C_3H_4S + 2CS_2 + C_3H_6S)/(CO^0 - CO)] \times 100$. For *P*(COS) = 545 Torr, R^0(CO) = 3.14 μmol min^{-1}. For *P*(COS) = 1090 Torr, R^0(CO) = 4.15 μmol min^{-1} for the first 4 min, then 3.90 μmol min^{-1}.
[b] In the presence of 600 Torr CO_2.

The structures of the C_4H_6S adducts **1–5** were identified on the basis of their nmr spectral characteristics, summarized in Table 3, and, for the cases of **1**, **4**, and **5**, supportive ir spectra. Moreover, the resonance shifts and coupling constants reported for 2-isopropylidine-3,3-dimethylthiirane (14) and methylenethiirane (12) are very similar to those assigned to the isomeric vinylidenethiiranes **1**, **3**, and **4**. Assignment of the *Z* and *E* isomers to **3** and **4**, respectively, is based on the relative chemical shifts of the ethylenic proton H_A. According to the literature (15), an *RS*-group in a substituted ethylene shifts a proton *cis* to it by about 0.24 ppm to higher field, whereas a *trans* proton will be shifted by only 0.04 ppm to higher field, relative to the unsubstituted ethylene. Consequently, **3** (δ_{H_A} = 6.05) is assigned to the *Z* isomer and **4** (δ_{H_A} = 5.62) to the *E* isomer. Not surprisingly, the ir spectra of **1** and **4** were very similar, both featuring strong C—H out-of-plane deformations at 840 and 895 cm^{-1}, C=C(st) at 1715 and 1700 cm^{-1}, and vinyl C—H(st) around 3060 cm^{-1}. The 1,3-butadiene skeleton structure was assigned to **2** because it is a C_4H_6S isomer that has five protons in the vinyl region of the nmr spectrum but no methyl absorptions. The allene structure of compound **5** is assigned on the basis of the typical C=C=C(st) absorption at 1960 cm^{-1}, clearly evident in the ir spectrum, and its nmr spectrum, Table 3.

Products **1–5** are all sensitive to Pyrex surfaces and when kept in Pyrex vessels decompose completely at room temperature over a period of ~12–15 h; under the same conditions, storage in a quartz cell effected ~50% loss. Mercury accelerates the rate of decomposition.

The results in Table 4 show that **1** and **4** are sensitive with respect to photodecomposition, whereas the rates of formation of **2**, **3**, and **5** are relatively constant. The rate of formation of CH_4 increases with exposure time, suggesting that at least part

TABLE 2. Mass spectral data[a] for the C_4H_6S isomers

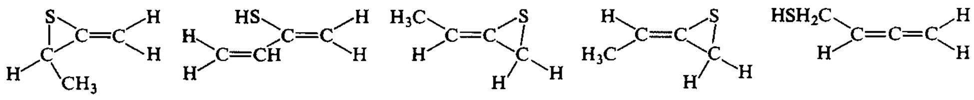

1	2	3	4	5	6	7
86(66.3)	86(100)	86(70.3)	86(71.6)	86(83.7)	86(100)	86(61.8)
85(19.6)	85(12.5)	85(23.4)	85(22.9)	85(45.3)	85(18.4)	85(100)
71(100)	71(83.1)	(71(100)	71(100)	71(100)	71(78.4)	71(19.8)
59(14.7)	59(44.6)	59(19.8)	59(15.4)	53(67.2)	59(49.8)	59(10.5)
58(26.3)	58(16.8)	58(26.4)	58(24.9)	52(20.3)	58(17.7)	53(65.9)
53(14.3)	53(22.3)	53(17.2)	53(15.4)	51(33.6)	53(48.8)	52(14.1)
50(9.0)	51(12.5)	51(14.3)	51(9.0)	50(28.4)	51(23.9)	51(23.1)
46(10.0)	50(12.2)	46(15.8)	46(17.4)	47(33.0)	50(19.3)	50(19.5)
45(33.3)	45(31.5)	45(41.4)	45(37.3)	45(47.6)	45(41.2)	45(33.5)
39(12.9)	39(13.0)	39(21.6)	39(15.5)	39(20.3)	39(66.0)	39(15.2)

[a] m/e (relative intensity) at 70 eV for the 10 most intense peaks.

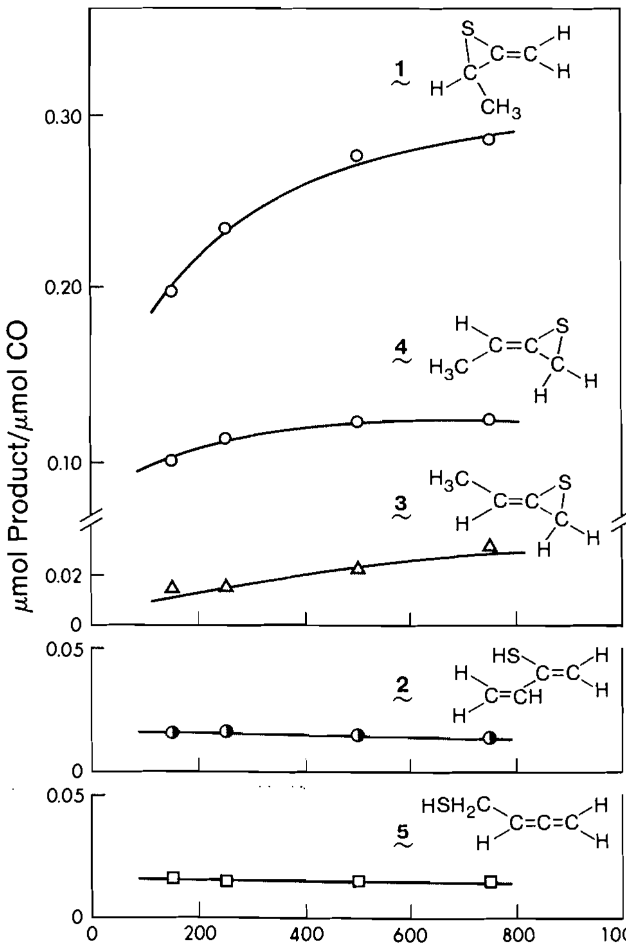

FIG. 1. Rates of product formation versus total pressure for the S + $CH_3CH{=}C{=}CH_2$ system. $P(COS)/P(C_4H_6) = 4$. Rates of **1** and **4** have been corrected to zero time.

of the CH_4 is formed in a secondary process. It is seen that the product yields, in terms of S atoms reaction with 1,2-C_4H_6, are low, even at low conversions; using the extrapolated zero time rates for **1** and **4** (0.235 and 0.115 μmol/μmol CO, respectively), the zero time extrapolated total product recovery is only marginally better, ~63%.

The effects of total pressure (at a constant COS/1,2-C_4H_6 ratio) are illustrated in Fig. 1. It is seen that the yields of thiiranes **3**, **4**, and particularly those of **1**, are markedly enhanced with increasing pressure. In order to minimize the effects of secondary photodecomposition, all the experiments were carried out at constant conversion (~5.2 μmol CO) and the rates of formation of thiiranes **1** and **4** were corrected to zero time values, assuming that their temporal behaviour at 250 Torr, Table 4, was the same over the entire pressure range studied. The overall product recoveries exhibit a similar trend, increasing from 64% at 150 Torr to 81% (corrected to zero time) at 750 Torr. These results parallel those observed for the S + C_3H_4 reaction, Table 1.

Photolysis of 100-Torr COS in the presence of 50-Torr 1,2-C_4H_6 and 1216-Torr CO_2 led to enhanced yields of **1**, **3**, and **4**, and the complete suppression of **5** and **2**; CH_4 was formed in barely detectable amounts. The rates of formation of **1**, **3**, and **4** were 0.542, 0.036, and 0.227 μmol/μmol CO, respectively, **1** and **4** being corrected to zero time.

Rate parameters for the $S(^3P)$ + 1,2-C_4H_6 reaction were determined in competitive experiments in the presence of 1-C_4H_8. The latter substrate was chosen for the reason that its vapour pressure is similar to that of 1,2-C_4H_6, thus allowing facile separation of the products from the reactants by distillation and because the rate parameters for the $S(^3P)$ + 1-C_4H_8 reaction, which affords ethylthiirane in nearly quantitative yields, have been measured directly (8, 9). For this system, then, the two competing reactions are:

$$S(^3P) + 1\text{-}C_4H_8 \xrightarrow{a} C_4H_8S$$

$$S(^3P) + 1,2\text{-}C_4H_6 \xrightarrow{b} C_4H_6S$$

If A_0 and A, and CO_0 and CO, represent the amounts of C_4H_8S and CO formed in the absence and presence of 1,2-C_4H_6, respectively, then it can be shown that

$$\frac{A_0/CO_0 - A/CO}{A/CO} = \frac{k_b}{k_a}\frac{[1,2\text{-}C_4H_6]}{[1\text{-}C_4H_8]}$$

where division of A's by the corresponding measured CO yield corrects for random fluctuations of the lamp intensity. Sources of error include the following: (a) incomplete quenching of $S(^1D)$ atoms by CO_2; (b) secondary decomposition of C_4H_8S; (c) some minor free radical reactions producing CO from COS

TABLE 3. Nuclear magnetic resonance data for the C_4H_6S isomers **1–5**

Structure	Proton A	Proton B	Proton C	Proton D	Proton E	Proton F
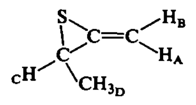 **1**	5.62 (1H, t) $J_{AB} \simeq J_{AC} \simeq 1.6$	5.21 (1H, t) $J_{BA} \simeq J_{BC} \simeq 1.8$	3.26 (1H, q of t) $J_{AB-C} = 1.7$ $J_{CD} = 5.8$	1.55 (3H, d) $J_{CD} = 5.8$		
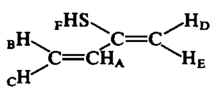 **2**	6.48 (1H, d of d) $J_{AB} = 16.8$ $J_{AC} = 10.4$	5.41 (1H, d) $J_{BA} = 16.8$	5.26 (1H, bd) $J_{CA} = 10.4$	5.36 (1H, bs) $J_{DC} = 1.2^a$ $J_{DA} < 0.5$	5.31 (1H, s) $J_{DE} < 0.5^a$	2.96 (1H, s)
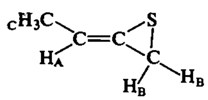 **3**	6.05 (1H, q of t) $J_{AC} = 6.5$ $J_{AB} = 1.6$	2.77 (2H, m) $J = 1.5$	1.89 (3H, d of t) $J_{CA} = 6.5$ J_{CB} 1.5			
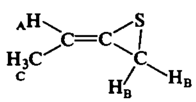 **4**	5.62 (1H, q of t) $J_{AC} = 6.8$ $J_{AB} = 1.8$	2.66 (2H, m)	1.82 (3H, d of t) $J_{CA} = 6.9$ $J_{CB} = 1.0$			
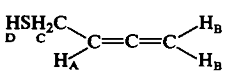 **5**	5.28 (1H, t of t) $J_{AC} = 7.4$ $J_{AB} = 6.6$	4.80 (2H, d of t) $J_{BA} = 6.6$ $J_{BC} = 2.7$	3.10 (2H, q of t) $J_{CA} = 7.4$ $J_{CB} = 2.7$	1.58 (1H, t) $J_{DC} = 7.9$		

[a] Determined in decoupling experiments.

TABLE 4. Effect of exposure time on the product yields in the COS – 1,2-C_4H_6 system[a]

Time (min)	Products (μmol) and rates (μmol/μmol CO in brackets)							% Recovery[b]
	CO	**1**	**2**	**3**	**4**	**5**	CH_4	
3.5	1.23	0.255 (0.207)	0.020 (0.016)	0.016 (0.013)	0.119 (0.097)	0.020 (0.016)	0.006 (0.005)	57
5.0	1.79	0.334 (0.187)	0.036 (0.020)	0.036 (0.020)	0.152 (0.085)	0.015 (0.009)	0.010 (0.006)	55
10	3.42	0.600 (0.175)	0.052 (0.015)	0.065 (0.019)	0.255 (0.074)	0.061 (0.018)	0.024 (0.007)	46
15	5.13	0.788 (0.154)	0.083 (0.016)	0.081 (0.016)	0.350 (0.068)	0.075 (0.015)	0.037 (0.007)	42
20	6.54	0.911 (0.139)	0.096 (0.015)	0.115 (0.018)	0.400 (0.061)	0.108 (0.016)	0.077 (0.012)	35

[a] $P(1,2\text{-}C_4H_8)$ = 51 Torr, P(COS) = 200 Torr.
[b] % Recovery = $[R\,(\mathbf{1} + \mathbf{2} + \mathbf{3} + \mathbf{4} + \mathbf{5} + CH_4)/R(CO^0 - CO)] \times 100$ where $R^0(CO) = 0.569\ \mu\text{mol min}^{-1}$.

TABLE 5. Product yields as a function of temperature and methylallene/1-butene ratio[a]

$P(C_4H_6)$	$\frac{[C_4H_6]}{[C_4H_8]}$	Products (μmol) CO	C_4H_8S	$\frac{A_0/CO_0 - A/CO}{A/CO} \cdot \frac{[C_4H_8]}{[C_4H_6]}$
27°C, 500 s				
0	0	1.61	1.122	0.0
10.81	0.165	1.60	0.993	0.742
21.53	0.328	1.60	0.895	0.737
32.01	0.489	1.55	0.790	0.748
42.29	0.647	1.51	0.708	0.748
60°C, 470 s				
0	0	1.63	1.163	0.0
14.70	0.212	1.62	0.977	0.868
22.41	0.324	1.64	0.907	0.890
29.74	0.430	1.61	0.831	0.880
38.55	0.558	1.59	0.755	0.889
90°C, 435 s				
0	0	1.69	1.208	0.0
14.62	0.214	1.68	0.979	1.04
21.98	0.322	1.72	0.919	1.06
29.28	0.429	1.68	0.831	1.03
37.37	0.549	1.68	0.764	1.04
120°C, 410 s				
0	0	1.69	1.301	0.0
14.46	0.209	1.80	1.037	1.18
22.11	0.320	1.76	0.914	1.21
29.85	0.433	1.76	0.834	1.19
37.83	0.549	1.72	0.750	1.18
150°C, 350 s				
0	0	1.78	1.244	0.0
14.46	0.209	1.73	0.945	1.34
21.87	0.318	1.76	0.860	1.36
29.60	0.432	1.74	0.777	1.33
37.32	0.545	1.67	0.680	1.33

[a] P(COS) = 100 Torr, $P(CO_2)$ ~1300 Torr, $P(1\text{-}C_4H_8)$ = 69 Torr.

via unknown mechanisms. It is assumed that these complicating factors do not affect the *relative* yields of C_4H_8S measured.

Product yields as a function of the $[1,2\text{-}C_4H_6]/[1\text{-}C_4H_8]$ ratio at 27°, 60°, 90°, 120°, and 150°C are summarized in Table 5, and the corresponding plots of $(A_0/CO_0 - A/CO)/A/CO$ versus $[1,2\text{-}C_4H_6]/[C_4H_8]$ are illustrated in Fig. 2. The slopes of these plots, summarized in Table 6, are plotted in the Arrhenius form in Fig. 3, from which:

$$A_{1,2\text{-}C_4H_6}/A_{1\text{-}C_4H_8} = 5.31 \pm 0.26$$

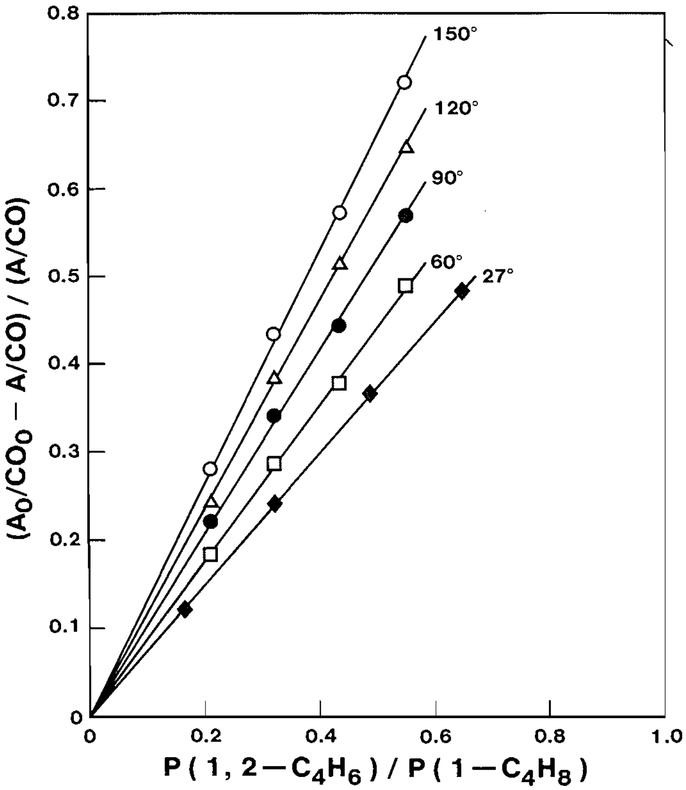

FIG. 2. $(A_0/CO_0 - A/CO)/A/CO$ versus $[CH_3CH{=}C{=}CH_2]/[CH_3CH_2CH{=}CH_2]$ at 27 (○), 60 (●), 90 (△), 120 (▲), and 150 (□) °C.

and

$$E_{1\text{-}C_4H_8} - E_{1,2\text{-}C_4H_6} = (1.17 \pm 0.03) \text{ kcal mol}^{-1}$$

Discussion

Since $S(^1D)$ atoms insert into C—H and add to alkenic double bonds, the following reactions can be considered for propadiene:

[4*a*] $S(^1D) + H_2C{=}C{=}CH_2 \longrightarrow H_2C{=}C{=}CHSH$

[4*b*] 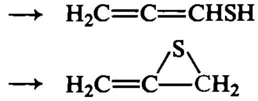

For 1,2-butadiene, three cycloaddition products can be formed,

[5*a*] $S(^1D) + CH_3CH{=}C{=}CH_2$

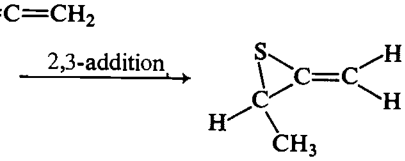

1

[5*b*] 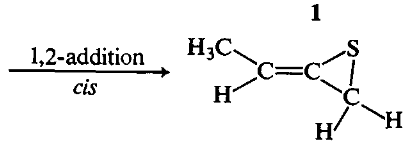

3

[5*c*] 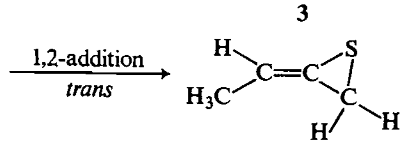

4

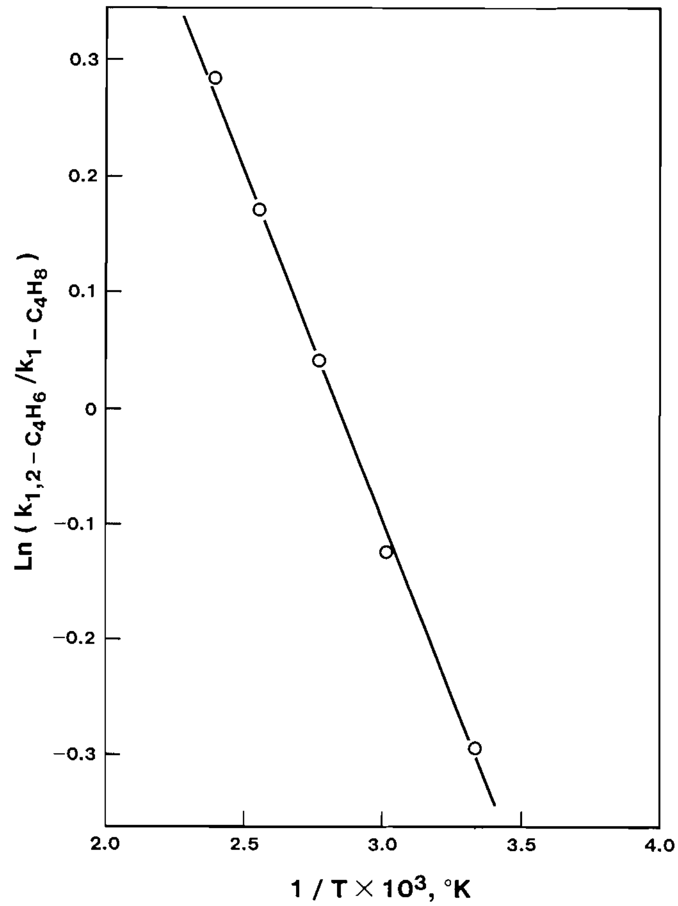

FIG. 3. Arrhenius plot for the $S(^3P) + CH_3CH{=}C{=}CH_2$ reaction.

TABLE 6. Slopes of the plots in Fig. 2

Temperature (°C)	Slope[a] $(k_{S+C_4H_6}/k_{S+C_4H_8})$
27	0.747 ± 0.019
60	0.886 ± 0.033
90	1.042 ± 0.042
120	1.188 ± 0.059
150	1.330 ± 0.069

[a]The errors are standard deviations. The correlation coefficients are ≥0.997.

and there are three possible sites for C—H insertion:

[5*d*] $S(^1D) + CH_3CH{=}C{=}CH_2 \longrightarrow$ 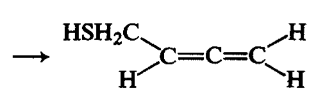

5

[5*e*] 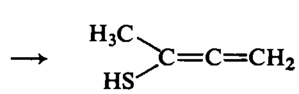

6

[5*f*] $\longrightarrow CH_3CH{=}C{=}CHSH$

7

For the case of propadiene the thiol insertion product was not detected. By analogy to vinylthiol and 1,3-butadiene-3-thiol

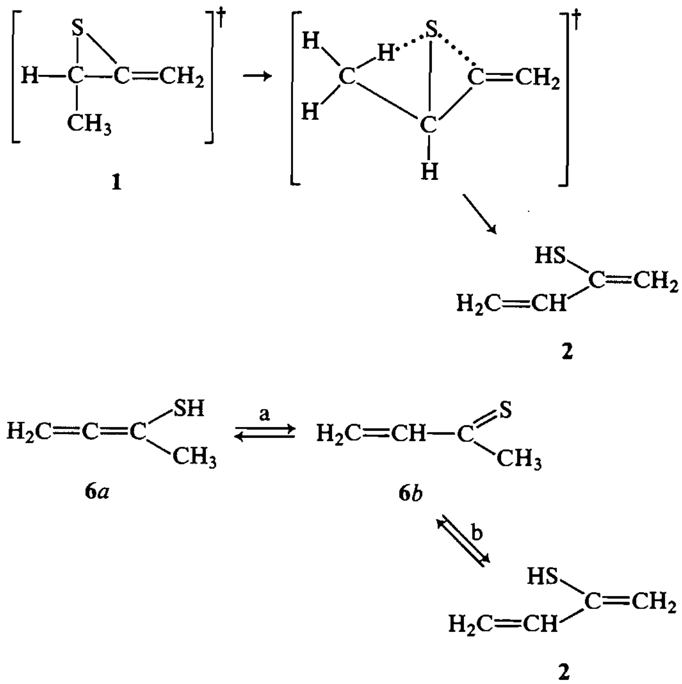

SCHEME 1

(*vide infra*), propadienethiol is expected to be prone to surface catalyzed polymerization and the fact that it was not detected in the present investigation may be due to the conditions employed; the high product yields observed at high pressures, however (Table 1), strongly suggest that insertion, if it occurs, is of very minor importance compared to cycloaddition.

In contrast, in the case of the analogous O-atom reaction $O(^3P) + C_3H_4$, methyleneoxirane, the expected cycloaddition product, was not detected and instead CO(57%), C_2H_4(38%), and acrolein(1%) were reported to be the major products (16). Since cyclopropanone was calculated to be ~21 kcal mol^{-1} more stable than methyleneoxirane (17), it appears that the major reaction path consists of isomerization of the initial biradical adduct to cyclopropanone, which subsequently decomposes. The relative stabilities of the C_3H_4S analogues, on the other hand, are reversed, i.e. cyclopropanethione is less stable than methylenethiirane, by ~7 kcal mol^{-1} (13), and thus the latter is the end product of the $S(^3P) + C_3H_4$ reaction.

For the $S(^1D) + CH_2{=}C{=}CHCH_3$ reaction all three cycloaddition products were detected, as well as the thiol formed from insertion into the —CH_3 group. 1,3-Butadiene-3-thiol **2** was also a product, and it definitely does not arise from the reactions of $S(^1D)$ atoms with any 1,3-C_4H_6 impurity. It may, however, be formed either from a "hot" thiirane–thiol rearrangement involving thiirane **1** or via an enethiol–thioketene–enethiol tautomerization of 1,2-butadiene-3-thiol **6** formed in step [5*e*], Scheme 1. The occurrence of a hot thiirane–thiol rearrangement **1**–**2** is, however, unlikely since in chemically activated methylthiirane, which has fewer degrees of freedom than the C_4H_6S adduct, this process is of very minor importance even at low pressures (2). On the other hand, the existence of enethiol–thioketone rearrangements is well documented (18) and moreover, of the three species involved in the tautomerization of **6**, the most stable, by virtue of carbon–carbon conjugation, is expected to be 1,3-butadiene-2-thiol, **2**. The intermediate thioketone $H_2C{=}CH{-}C({=}S)CH_3$ has been synthesized by flash thermolysis techniques (19); it reportedly dimerizes at −60°C, and undergoes spontaneous polymerization at room temperature. In the present system, however, it is generated in the gas phase at high dilution, thus allowing tautomerization to compete effectively with bimolecular reactions. Tautomerization of the hypothetical thiol **7** would lead to methylthioacrolein which, like the thioketone analogs, is expected to be inherently unstable. It is therefore concluded that insertion into the =CH— and =CH_2 moieties of 1,2-C_4H_6 does occur and that tautomerization can then take place, but only in the former case can tautomerization lead to a stable product. The trace C_4H_6S adducts detected in the gc/ms cross scan may be the initial =CH— and =CH_2 insertion products **6** and **7**.

The primary adducts for the case of the $S(^1D)$ reaction are likely the ground, vibrationally excited singlet state thiiranes and thiols, and, for the case of $S(^3P)$ addition, vibrationally excited triplet state thiiranes (7). From Benson's group additivity method (20), the heats of formation of the ground state C_3H_4S and C_4H_6S adducts are estimated to be:

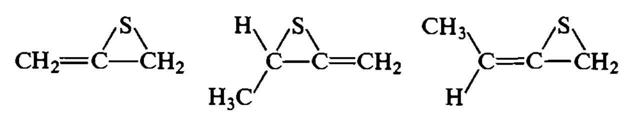

ΔH: 38.4 32.02 32.34 kcal mol^{-1}

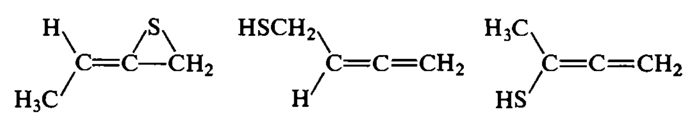

ΔH: 31.34 47.02 45.81 kcal mol^{-1}

from which the thiirane-forming reactions with $S(^1D)$ atoms are computed to be exothermic by ~100–101 kcal mol^{-1} and the thiol-forming reactions, by ~85–86 kcal mol^{-1}. For C_2–C_4 alkenes, on the other hand, the corresponding cycloaddition reactions are only ~85–88 kcal mol^{-1} exothermic. Thus the enhancing effect of pressure on the thiirane yields from the $S(^1D) + C_3H_4$/1,2-C_4H_6 reactions is probably a result of collisional deactivation of the hot primary cycloadducts.

From the high pressure (750 Torr) rates of formation of **1**–**5** (Fig. 1) and the corrected zero time rates of **1** and **4** (0.283 and 0.122 μmol/μmol CO, respectively), assuming that the temporal variations of **1** and **4** at 750 Torr are the same as at 250 Torr (Table 4), the total product recovery is estimated to be 81% at zero time, of which the thiiranes comprise 94%.[3] This is high, in comparison with alkene reactions (e.g. the reaction with 1-butene affords 59% thiirane, 12% methallylthiol, and 29% alkenyl type thiols), and it may be concluded that insertion into the C—H bonds of 1,2-C_4H_6 is a very minor process compared to cycloaddition. Similarly, the S + C_3H_4 reaction at low conversions and high pressures, affords only methylenethiirane up to 100% yield (Table 1).

The high ratio of thiirane to thiols in the diene reactions is partly due to molecular structural effects and partly to the experimental conditions employed.

As was shown above, the preexponential factors for the

[3]The mass imbalance is probably due to the combined thermal and photochemical instabilities of 1–5 rather than to exclusive loss of insertion products.

$S(^3P)$ + 1,2-C_4H_6 reaction are 5.13 times higher than for the $S(^3P)$ + 1-C_4H_8 reaction owing to the presence of the elongated, orthogonal π-system. It may be assumed that the pre-exponential factors for the $S(^1D)$ + diene $\rightarrow$ thiirane reactions, [4*b*] and [5*a*–*c*], are also somewhat higher than for the $S(^1D)$ + monoalkene reactions, resulting in higher ratios for the thiirane to thiol products.

Also, the higher [COS]/[alkene] ratios used in the diene as compared to the monoalkene reactions tend to increase the ratio of $S(^3P)$ to $S(^1D)$ atom reactions with the substrate. Thus, a crude approximation of the relative proportions of (^1D) and (^3P) atoms in the system can be calculated on the basis of the experimental CO yields in the absence (CO^0) and presence (CO) of a reactive substrate, the branching ratio for step [1], and the abstraction/deactivation ratio k_{2a}/k_{2b} (cf. Introduction). For the reaction mixture consisting of 200-Torr COS and 51-Torr 1,2-C_4H_6 (Table 4) the total yield of S-atoms generated in step [1] is $CO^0/2 = 0.285$ μmol, of which 0.191 and 0.094 are in the (^1D) and (^3P) states, respectively. Step [3], abstraction from COS by $S(^3P)$, is slow compared to addition to 1,2-C_4H_6 (*vide infra*) and can be neglected. Hence, the yield of the abstraction reaction [2*a*] is $CO - CO^0/2 = 0.066$ μmol. Since $k_{2a}/k_{2b} \sim 2$, the yield of $S(^3P)$ atoms formed from deactivation, step [2*b*], is $0.066/2 = 0.033$ μmol and the combined amount of $S(^3P)$ atoms available for reaction with 1,2-C_4H_6 is $0.094 + 0.033 = 0.127$ μmol. Now the total amount of S-atoms reacting with C_4H_6 is equal to the total sulfur produced in step [1] less the yield of the abstraction reaction [2*a*], $0.285 - 0.066 = 0.219$ μmol. Hence, only 42% of the S-atoms reacting with C_4H_6 are in the $S(^1D)$ state. For the COS–C_3H_4 system where higher relative concentrations of COS were employed, only 29% of the S-atoms reacting with the substrate were in the $S(^1D)$ state. Thus, the low yields (or absence) of insertion products in these systems may also be a consequence of the fact that most of the $S(^1D)$ atoms generated in step [1] had been deactivated to the ground (^3P) state prior to reaction. It should be noted, however, that the branching ratio for step [1] and the abstraction/deactivation rate constant ratio for step [2] are indirect estimates only, and a more quantitative assessment of the relative concentrations of (^1D) and (^3P) atoms awaits our studies on direct rate measurements of these reactions.

From the data in Table 4 and Fig. 1, it can be shown that at zero time and high pressure, ($k_{2,3\text{-addition}}/k_{1,2\text{-addition}}$) is ~2.1 for the case of $S(^3P)$ addition and ~1.3 for $S(^1D)$ addition. Surprisingly few studies on the orientation of radical addition to 1,2-dienes have been reported in the literature. For EtS (21) and $(CH_3)_3Sn$ (22) radical addition to 1,2-butadiene, end product analyses show that 48.2% and 86.5% of the attack, respectively, occurs at the C2 position and addition of these radicals to 3-methyl-1,2-butadiene takes place exclusively at C2. Since the former is an electrophilic, and the latter, a nucleophilic species, it appears that polar effects do not influence the orientation of addition and, rather, that methyl substitution favours the formation of the more stable allylic radical. Subsequent hydrogen abstraction by the allylic radical takes place exclusively at the C1 position for the case of the RS adduct. The $(CH_3)_3Sn$ adduct, however, abstracts preferentially at C1, but C3 abstraction products are also formed. Thus, the final products correspond to 1,2-addition. Recently, Creary (23) has studied the regioselectivities of the additions of a variety of singlet and triplet carbenes to 3-methyl-1,2-butadiene. Singlet state carbenes led to a predominance of 2,3-addition products whereas for triplet carbenes, which add in a stepwise manner and thus more closely resemble monoradicals, 1,2-addition was favoured. The reaction was suggested to be useful as a new probe for the determination of carbene multiplicity.

As shown above, however, both $S(^3P)$ and $S(^1D)$ atoms add predominantly to the 2,3-double bond of 1,2-butadiene and the somewhat higher selectivity exhibited by $S(^3P)$ atoms might be due to their lower (by 26 kcal mol^{-1}) energy content. This result was not unexpected since our earlier results showed that $S(^3P)$ atoms, like $S(^1D)$ atoms and singlet carbenes, add to double bonds in a concerted fashion (10).

Addition to the 1,2 double bond leads to the formation of two isomers, ***E*4** and ***Z*3** in extrapolated (1200 Torr, zero time) ratios of 1.4 and 6.2 for (^1D) and (^3P) atom addition, respectively. The reason for the high stereoselectivity observed in the triplet case is not immediately apparent.

The reactions of $O(^3P)$ atoms with 1,2-butadiene, as with 1,2-propadiene, afford fragmentation products – CO (64%) and propylene (43%) – together with only small amounts (3.1%) of oxygenated material (16). The involvement of excited cyclopropanone intermediates appears to be a common feature of the $O(^3P)$ + 1,2-diene reactions.

Rate parameters for the $S(^3P)$ + 1-butene reaction have been measured by flash photolysis – kinetic absorption and flash photolysis – resonance fluorescence methods and are reported to be $k = (8.2 \pm 0.6) \times 10^9 \exp(-200 \pm 200/RT)$ (8) and $(2.4 \pm 0.2) \times 10^9 \exp(-400 \pm 100/RT)\ M^{-1}\ s^{-1}$ (9), respectively. For all the $S(^3P)$ + alkene (8, 9) and $O(^3P)$ + alkene (24) reactions studied to date, the latter method yields *A*-factors which are consistently lower than those obtained by other techniques. For the time being, we prefer to use van Roodselaar *et al.*'s data for the reference reaction and thus $k_{S(^3P)+1,2\text{-}C_4H_6} = (6.4 \pm 1.1) \times 10^{10} \exp[(-1.4 \pm 0.2)/RT]\ M^{-1}\ s^{-1}$. Experimentally, it was observed that the ratio of the 2,3- and 1,2-addition products, i.e. **1**/(**3** + **4**), was relatively constant (~2.2) in the temperature range 27–150°C. Thus, the E_a's associated with 1,2- and 2,3-addition are comparable but the *A*-factors are slightly different: $A_{1,2\text{-addition}} \simeq 4 \times 10^{10}$ and $A_{2,3\text{-addition}} \simeq 8.8 \times 10^{10}\ M^{-1}\ s^{-1}$. The corresponding entropies of activation are $\Delta S^{\ddagger}_{1,2} = -22.33$ and $\Delta S^{\ddagger}_{2,3} = -20.77$ eu. These high values reflect the newly created rotational contributions to the activated complex upon going from a linear C═C═C molecule to a bent 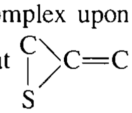 skeleton.

Arrhenius parameters for the reactions of $S(^3P)$, $O(^3P)$, and $OH(^2\Pi)$ with simple dienes are listed in Table 7, along with those reported for reactions with some alkenes for the sake of comparison. For $S(^3P)$ and $O(^3P)$ atoms, the reactions with dienes feature higher *A*-factors than those associated with their monounsaturated analogues, and conjugation lowers the activation energy. Not unexpectedly, the E_a's for the S + C_4H_6 and O + C_3H_4 reactions deviate from the linear E_a versus ionization potential relationships observed for the reactions with alkenes. Relative rate data (at 25°C) for the reactions of $O(^3P)$ with a number of 1,2-dienes (16) show that the rate constant increases with increasing alkyl substitution in much the same way as for the $O(^3P)$ + alkene case and therefore it is likely that there is also a linear relationship between E_a and I_p for the $S(^3P)$ and $O(^3P)$ reactions with dienes, but displaced to the left of the corresponding alkene plots. In contrast, the E_a's associated with the reactions of $OH(^2\Pi)$ with alkenes and propadiene are all negative and neither the *A*-factors nor the E_a's exhibit any

TABLE 7. Arrhenius parameters[a] for the reactions of $S(^3P)$, $O(^3P)$ and $OH(^2\Pi)$ with dienes and alkenes

Substrate	$S(^3P)$ A	$S(^3P)$ E_a	$O(^3P)$ A	$O(^3P)$ E_a	$OH(^2\Pi)$ A	$OH(^2\Pi)$ E_a
$H_2C{=}C{=}CH_2$	—	—	1.8[b]	1.9[b]	0.34[c]	−0.31[c]
$H_3CCH{=}C{=}CH_2$	6.4[d]	1.4[d]	—	—	—	—
$H_2C{=}CC{=}CH_2$	~2.8[e]	~−0.4[e]	1.2[b]	0[b]	0.87[c]	−0.93[c]
$CH_3CH{=}CH_2$	1.3[f]	0.5[f]	0.76[g]	0.72[g]	0.25[c]	−1.1[c]
$C_2H_5{-}CH{=}CH_2$	1.2[f]	0.2[f]	0.72[g]	0.66[g]	0.46[c]	−0.93[c]

[a] A, $\times 10^{-10}$ M^{-1} s^{-1}; E_a, kcal mol^{-1}.
[b] Reference 25.
[c] Reference 26.
[d] This work.
[e] Calculated from the relative data reported in ref. 5.
[f] Reference 8.
[g] Reference 27.

obvious trend. Relative rate data (at 25°C) for OH reactions with propadiene, 1,2-pentadiene, and 3-methyl-1,2-butadiene, however, indicate that the overall rate constant increases with alkyl substitution; it was also shown that the rate constants for reaction with conjugated and isolated dienes follow empirical relationships based on additivities of double bond contributions, but those for reactions with cumulated dienes do not follow either trend (28).

To conclude, we would like to point out the synthetic utility of S + diene reactions in general. The unsaturated thiol and thiirane products are relatively unstable and difficult to prepare by conventional techniques and the reactions of sulfur atoms with dienes offer a convenient alternative route to their synthesis.

Acknowledgments

The authors thank the Natural Sciences and Engineering Research Council of Canada for continuing financial support. We are also grateful to Dr. M. Torres for his assistance in the interpretation of the nmr and ir spectra, and to Dr. I. Safarik for many helpful discussions.

1. H. E. GUNNING and O. P. STRAUSZ. Adv. Photochem. **4**, 143 (1966).
2. A. G. SHERWOOD, I. SAFARIK, B. VERKOCZY, G. ALMADI, H. A. WIEBE, and O. P. STRAUSZ. J. Am. Chem. Soc. **101**, 3000 (1979).
3. R. J. DONOVAN, L. J. KIRSCH, and D. HUSAIN. Nature, **222**, 1164 (1969).
4. R. B. KLEMM and D. D. DAVIS. J. Phys. Chem. **78**, 1137 (1974).
5. O. P. STRAUSZ. Pure Appl. Chem. **4**, 165 (1971).
6. P. M. RAO, I. SAFARIK, and O. P. STRAUSZ. To be published.
7. E. M. LOWN, K. S. SIDHU, A. W. JACKSON, A. JODHAN, M. GREEN, and O. P. STRAUSZ. J. Phys. Chem. **85**, 1089 (1981).
8. A. VAN ROODSELAAR, I. SAFARIK, and O. P. STRAUSZ. To be published.
9. D. D. DAVIS and R. B. KLEMM. Int. J. Chem. Kinet. **5**, 841 (1973).
10. K. S. SIDHU, E. M. LOWN, O. P. STRAUSZ, and H. E. GUNNING. J. Am. Chem. Soc. **88**, 254 (1966).
11. H. A. WIEBE, A. R. KNIGHT, O. P. STRAUSZ, and H. E. GUNNING. J. Am. Chem. Soc. **87**, 1443 (1965).
12. E. JONGEJAN, TH. S. V. BUYS, H. STEINBERG, and TH. J. BOER. Recl. Trav. Chim. Pays-Bas, **97**, 214 (1978).
13. E. BLOCK, R. E. PENN, M. D. ENNIS, T. A. OWENS, and S.-L. YU. J. Am. Chem. Soc. **100**, 7436 (1978).
14. A. G. HORTMAN and A. BHATTACHARJYA. J. Am. Chem. Soc. **98**, 7081 (1976).
15. H. M. MCNAIR and E. J. BONELLI. Basic gas chromatography. 5th ed. Varian, Palo Alto, CA. 1969.
16. J. J. HAVEL. J. Am. Chem. Soc. **96**, 530 (1974).
17. A. LIBERLES, A. GREENBERG, and A. LESK. J. Am. Chem. Soc. **94**, 8686 (1972).
18. D. PAQUER. Int. J. Sulfur Chem. B, **7**, 269 (1972); R. MAYER. *In* Sulfur in organic and inorganic chemistry. Vol. 3. *Edited by* A. Senning. M. Dekker, N.Y. 1972.
19. W. J. BAILY and M. ISOGAWA. ACS Polymer Chem. Poly. Prep. **14**, 300 (1973); P. BESLIN, D. LAGAIN, and J. VAILLE. Tetrahedron Lett. 2677 (1979).
20. S. W. BENSON. Thermochemical kinetics. 2nd ed. Wiley, New York. 1976.
21. T. L. JACOBS and G. E. ILLINGWORTH. J. Org. Chem. **28**, 2692 (1963); K. GRIESBAUM, A. A. OSWALD, E. R. QUIRAM, and W. NAEGELE. J. Org. Chem. **28**, 1952 (1963).
22. H. G. KUIVILA, W. RAHMAN, and R. H. FISH. J. Am. Chem. Soc. **87**, 2835 (1965).
23. X. CREARY. J. Am. Chem. Soc. **102**, 1611 (1980).
24. R. J. CVETANOVIC and D. L. SINGLETON. Rev. Chem. Intermed. **5**, 183 (1984).
25. W. S. NIP, D. L. SINGLETON, and R. J. CVETANOVIC. Can. J. Chem. **57**, 949 (1979).
26. R. ATKINSON, K. R. DARNALL, A. C. LLOYD, A. M. WINER, and J. N. PITTS, JR. Adv. Photochem. **11**, 375 (1979).
27. D. L. SINGLETON and R. J. CVETANOVIC. J. Am. Chem. Soc. **98**, 6812 (1976).
28. T. OHTA. J. Phys. Chem. **87**, 1209 (1983).

On the infrared spectrum and dipole moment of dichloroketene

M. C. L. GERRY, W. LEWIS-BEVAN, AND N. P. C. WESTWOOD
Department of Chemistry, The University of British Columbia, 2036 Main Mall, Vancouver, B.C., Canada V6T 1Y6

Received July 23, 1984

M. C. L. GERRY, W. LEWIS-BEVAN, and N. P. C. WESTWOOD. Can. J. Chem. **63**, 676 (1985).

The failure to observe a microwave spectrum of dichloroketene prepared in a low temperature flow system is contrasted with the successful observation of its Fourier Transform infrared spectrum under the same conditions. It is concluded that the lack of a microwave spectrum is a result of a near-zero dipole moment for dichloroketene.

M. C. L. GERRY, W. LEWIS-BEVAN et N. P. C. WESTWOOD. Can. J. Chem. **63**, 676 (1985).

Dans un système continu, on ne peut observer de spectres microondes du dichlorocétène préparé à basse température; ce résultat est en opposition avec le fait que, dans les mêmes conditions, on peut observer son spectre ir par transformation de Fourier. On en conclut que l'absence de spectres microondes provient d'un moment dipôlaire pratiquement nul pour le dichlorocétène.

[Traduit par le journal]

Although dichloroketene, Cl_2CCO, has long been postulated as a reactive intermediate involved in certain organic cycloaddition reactions in solution (1, 2), there are only three unambiguous reports of its detection in isolation. Colbourne *et al.* (3) and Bock *et al.* (4) have measured the gas phase photoelectron spectrum, and Torres *et al.* (5) have reported the infrared spectrum in an argon matrix at 8 K, following photolysis of dichlorovinylene carbonate.

As part of a program to measure the microwave spectra of unstable molecules, we have attempted to observe such a spectrum for dichloroketene, since we had already shown that the spectrum of monochloroketene can be observed relatively easily following generation and continuous flow through a waveguide. The preparation method used in the current experiments involved the dechlorination of trichloroacetyl chloride over zinc metal at 300°C:

[1] 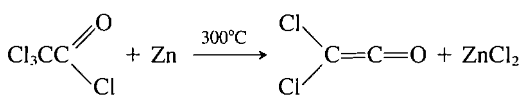

The products were passed at low pressure through a 2 m copper X band Stark cell; the frequency range studied was 26.5–40 GHz. This reaction is known to produce dichloroketene in excellent yield (3), and the reaction and cell conditions were the same as those used to observe microwave spectra of both chloroketene (6) and bromoketene (M.C.L. Gerry, W. Lewis-Bevan, and N.P.C. Westwood, to be published). Although there is no *a priori* reason to suppose that dichloroketene is any less stable than the other two molecules observed under these conditions, no microwave spectrum was found, even when the cell length was reduced to 1 m, and additional pumping was employed.

To check the success of the preparative technique, and to obviate the possibility of decomposition of the product in the metal cell, we have carried out identical experiments to measure the gas phase infrared spectrum. The reaction products from [1] were passed through the long (~45 cm) metal inlet port of a commercial multipass cell attached to a Bomem DA3.002 Fourier Transform infrared spectrometer. The pressures employed (30–100 mTorr) were similar to those used in the microwave experiments. The results are summarized in Fig. 1. Scans were made between 700–3100 cm^{-1} at 1 cm^{-1} resolution. Initially the spectrum of the starting material was obtained (Fig. 1(*a*)), but when this material was passed over zinc at 300°C, its spectrum diminished drastically, and that of

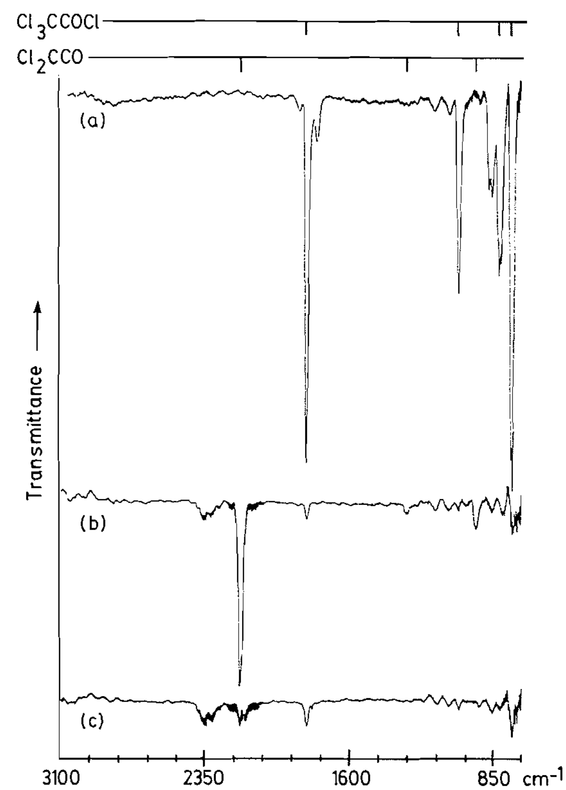

FIG. 1. The gas phase infrared spectrum of dichloroketene between 700 and 3100 cm^{-1}: (*a*) the precursor Cl_3CCOCl, (*b*) the products of the reaction of Cl_3CCOCl with zinc at 300°C (taken to be dichloroketene), (*c*) the spectrum of the reaction products after the cell had been isolated for 30 min; the lines at ~2150 cm^{-1} and ~2350 cm^{-1} are due to CO and CO_2, respectively. The transmittance scale is the same for all three spectra.

a new species appeared, with bands at 2160.3 cm^{-1} (s), 1291 cm^{-1} (w), and 935 cm^{-1} (w) (Fig. 1(*b*)). These are the same as the wavenumber values observed for dichloroketene by Torres *et al.* (5); indeed, the strong band at 2160 cm^{-1}, attributable to the CO stretching frequency, provides a unique fingerprint for ketene-like molecules (7), and in similar experiments we have observed such a band for monochloroketene. When the reaction products were isolated in the cell these bands disappeared over the space of about 30 min, leaving bands attributable to CO and CO_2 (Fig. 1(*c*)). Clearly the reaction product of Fig.

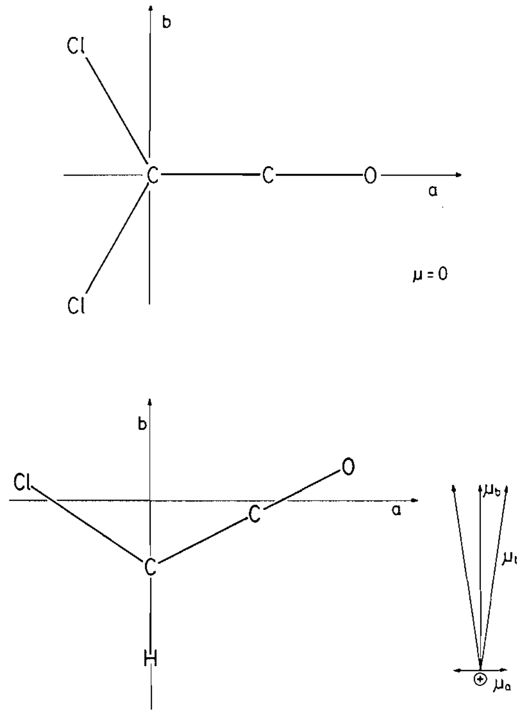

FIG. 2. Comparison of the dipole moments of dichloroketene and chloroketene (6).

1(*b*) is an unstable species, which from the infrared spectrum and the chemistry we take to be dichloroketene.

Since in both the microwave and infrared experiments the preparation conditions were identical (cf. also the photoelectron spectrum (3)) and since in both experiments the reaction products had to pass similar distances, contacting similar materials before reaching the cell, it is highly probable that dichloroketene was indeed prepared in the microwave experiment, and that it has at best an extremely weak microwave spectrum. Because the microwave spectrum is a rotational spectrum, requiring the molecule to have a permanent dipole moment, this implies that the dipole moment of dichloroketene is very small, certainly less than 0.3 D, and probably less than 0.1 D.

This result is consistent with our findings for the dipole moment of monochloroketene (6). As is shown in Fig. 2, the dipole moment of the latter molecule is almost exactly along the CH bond, implying that the C—Cl and C=C=O parts of the molecule have the same moments. Replacement of H by Cl would thus give complete cancellation, leading to a near-zero dipole moment for dichloroketene.

Acknowledgments

M.C.L.G. thanks the Natural Sciences and Engineering Research Council of Canada for support in the form of Research Grants. W.L.-B. acknowledges gratefully the Izaak Walton Killam Foundation for the award of a Postdoctoral Fellowship.

1. W. T. BRADY. Synthesis, 415 (1971).
2. R. S. WARD. *In* The chemistry of ketenes, allenes and related compounds, part 1. *Edited by* S. Patai. Wiley, Chichester. 1980. pp. 223–277.
3. D. COLBOURNE, D. C. FROST, C. A. MCDOWELL, and N. P. C. WESTWOOD. Chem. Commun. 250 (1980).
4. H. BOCK, T. HIRABAYASHI, and S. MOHMAND. Chem. Ber. **114**, 2595 (1981).
5. M. TORRES, J. RIBO, A. CLEMENT, and O. P. STRAUSZ. Nouv. J. Chim. **5**, 351 (1981).
6. M. C. L. GERRY, W. LEWIS-BEVAN, and N. P. C. WESTWOOD. J. Chem. Phys. **79**, 4655 (1983).
7. W. F. ARENDALE and W. H. FLETCHER. J. Chem. Phys. **26**, 793 (1957).

Régiosélectivité et stéréosélectivité de l'hydroxylation homolytique des hydrocarbures par le peracide benzoïque

JACQUES FOSSEY, DANIEL LEFORT, MASSOUD MASSOUDI, JEAN-YVES NEDELEC ET JEANINE SORBA
C.N.R.S., G.R. 12, 2, rue Henri-Dunant, 94320 Thiais, France

Reçu le 27 février 1984

JACQUES FOSSEY, DANIEL LEFORT, MASSOUD MASSOUDI, JEAN-YVES NEDELEC et JEANINE SORBA. Can. J. Chem. **63**, 678 (1985).

Des hydrocarbures cyclohexane, Me-cyclohexane et adamantane sont hydroxylés par le peracide benzoïque selon un processus radicalaire. La régiosélectivité en faveur des alcools tertiaires atteint 60 à 90%. Pour les décalines *cis* et *trans*, la stéréosélectivité des décalols-9 peut atteindre 97%. Une très bonne stéréosélectivité d'hydroxylation par un peracide ne signifie pas obligatoirement que la réaction n'est pas radicalaire.

JACQUES FOSSEY, DANIEL LEFORT, MASSOUD MASSOUDI, JEAN-YVES NEDELEC, and JEANINE SORBA. Can. J. Chem. **63**, 678 (1985).

Cyclohexane, methylcyclohexane, and adamantane are hydroxylated by a radical process using perbenzoic acid. A regioselectivity of 60–90% in favour of tertiary alcohols is noted. In the case of *cis* and *trans* decalins, stereoselection leading to 9-decalols can reach 97%. Such a stereoselectivity for hydroxylation by use of a peracid does not necessarily indicate lack of a radical pathway.

[Journal translation]

L'hydroxylation directe des liaisons C—H non activées par les peroxyacides est une réaction d'intérêt général en synthèse (1–9), dont l'aspect régio- et stéréosélectif recueille une attention particulière. On sait également que le cytochrome P450 (10–13) ou les porphyrines métalliques (14, 15) catalysent cette réaction en utilisant les hydroperoxydes ou les peracides comme source d'oxygène.

Cette réaction d'hydroxylation par les peracides peut être décrite par un mécanisme de type soit oxénoïde, soit radicalaire. Dans le premier cas on observe une très bonne régio- et stéréosélectivité (6–8); par contre dans le second cas, les résultats sont de ce point de vue, beaucoup moins explicites (2–4). Pourtant les résultats de sélectivité sont souvent utilisés pour remonter au type de mécanisme mis en jeu: en clair, si une réaction est très régio- et surtout très stéréosélective, on en conclut en général que la réaction n'est pas radicalaire.

Nous nous sommes donc proposé d'apporter des réponses précises sur la régio- et stéréosélectivité d'hydroxylation d'un certain nombre d'hydrocarbures saturés cycliques par le peracide benzoïque, dans des conditions expérimentales où le mécanisme est, sans ambiguité, radicalaire.

En effet, au cours des travaux que nous avons effectués sur la réactivité homolytique des peracides, nous avons montré (16) que la décomposition du peracide benzoïque en solution, à ébullition, conduit à l'hydroxylation du solvant, dans la mesure où celui-ci est un donneur d'hydrogène, selon le mécanisme en chaîne décrit dans la fig. 1.

Quand on utilise le cyclohexane comme solvant (R—H) on obtient une mole de cyclohexanol (R—OH) par mole de peracide mis en oeuvre, montrant ainsi l'efficacité du processus.

Comme hydrocarbures saturés nous avons utilisé le cyclohexane, dont les résultats servent de références, le méthylcyclohexane et l'adamantane, pour déterminer la régiosélectivité, et les décalines *cis* et *trans* pour obtenir des informations sur la stéréosélectivité.

Résultats

Le peracide benzoïque (réf. 22) et l'hydrocarbure à étudier sont dissous dans le benzène, solvant inerte vis-à-vis des radicaux formés. On utilise toujours un excès d'hydrocarbure par rapport au peracide afin de privilégier la réaction [3] de

[1] $\phi CO_3H \rightarrow \phi CO_2^{\cdot} + HO^{\cdot}$

[2] $\phi CO_2^{\cdot} \rightarrow \phi^{\cdot} + CO_2$

[3] $\phi^{\cdot}$ (ou $\phi CO_2^{\cdot}$) + HR $\rightarrow$ ϕH (ou ϕCO_2H) + $R^{\cdot}$

[4] $R^{\cdot} + \phi CO_3H \rightarrow ROH + \phi CO_2^{\cdot}$

[5] $2\phi^{\cdot} \rightarrow \phi - \phi$

FIG. 1

formation du radical $R^{\cdot}$.

Les résultats exprimant la quantité totale d'alcools formés, secondaires et tertiaires, ainsi que la régiosélectivité observée pour le cyclohexane, le méthyl-cyclohexane et l'adamantane sont donnés dans le tableau 1. Les alcools secondaires ne sont oxydés en cétones qu'en très faibles partie (1 à 2%) comme nous l'avions montré précédemment (16) et ces données ne figurent pas dans le tableau.

En présence d'hydroquinone (0,02 *M*), une solution d'adamantane (1 *M*) et de peracide benzoïque (0,1 *M*) donne 9% d'adamantanols secondaire et tertiaire, au lieu des 60% observés sans hydroquinone. Ceci montre bien le caractère radicalaire de l'hydroxylation.

Par rapport à la solution témoin du peracide seul dans le benzène, l'addition d'un hydrocarbure a deux conséquences: (*i*) une diminution de la quantité d'acide benzoïque du fait de la réaction de décarboxylation suivie des réactions [3] et [4]; celles-ci n'ayant pas lieu dans le benzène, le peracide se décompose en acide selon un mécanisme radicalaire mettant en jeu d'autres intermédiaires (16) et plus lent; et (*ii*) une accélération de la vitesse de réaction due précisément aux étapes [3] et [4], sauf dans le cas de méthyl-cyclohexane. Celui-ci, d'ailleurs, joue un rôle inhibiteur pour la décomposition du peracide en solution dans le *cyclohexane* au lieu du benzène ($t_{1/2}$ respectivement de 5 et 100 min pour des solutions 0,1 *M* de peracide benzoïque dans le cyclohexane et dans le cyclohexane contenant 1 *M* de méthyl-cyclohexane).

Ce résultat pose le problème de la réactivité du radical méthyl-cyclohexyle tertiaire comparée à celle du radical cyclohexyle secondaire.

Quelques expériences ont été faites avec des peracides ayant des pK_a différents de celui du peracide benzoïque, tels que les

TABLEAU 1. Hydroxylation des hydrocarbures saturés par le peracide benzoïque, en solution dans le benzène*

	Produits formés			
		Hydrocarbure		
Paramètres	Témoin (sans hydrocarbure)	Cyclohexane	Me-cyclohexane	Adamantane
k s^{-1} × 10^4†	2,4	6,8	2,4	6,8
ϕCO_2H‡	98	80	60	60
Alcools ROH‡		23	37	60
Alcool tertiaire§		—	64	88
Alcools secondaires§		—	36	12
ϕ–ϕ		0,15	0,08	0,10

*ϕCO_3H = 0,1 M; hydrocarbure (RH) = 1 M; T (bain) = 100 ± 1°C.
†Exprimé en 1er ordre.
‡Acide et somme des alcools (*sec* + *tert*) exprimés en mol%.
§Alcool tertiaire + alcool secondaire = 100.

TABLEAU 2. Hydroxylation des décalines *cis* et *trans* par le peracide benzoïque, en solution dans le benzène*

	Peracide M	k s^{-1} × 10^4†	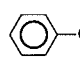—CO_2H	Décalols tertiaires‡	Décalol-9 *trans* / Décalol-9 *cis*
Décaline-*cis*	0,1	7,2	73	56	36:64
	0,2		77	80	16:84
	0,5		89	70	3:97
Décaline-*trans*	0,1	4,5	90	65	97:3
	0,2		80	40	95:5
	0,5		85	44	95:5

*ϕCO_3H = 0,1 M; décaline = 1 M; T (bain) = 100 ± 1°C.
†Exprimé en 1er ordre.
‡En mol% par rapport au peracide.

peracides *m*-chloro et *tert*-butyl-4 benzoïques. Dans le cas du cyclohexane nous avons obtenu sensiblement les mêmes quantités de cyclohexanol quelle que soit la nature du peracide.

La stéréosélectivité de l'hydroxylation a été étudiée dans le cas des décalines *cis* et *trans* (cf. Tableau 2).

Comme dans le cas des autres hydrocarbures, cf. Tableau 2, on observe une accélération de la vitesse de disparition du peracide. Mais surtout le résultat stéréochimique est intéressant: le rapport *trans*/*cis* diminue, dans le cas de la décaline *cis*, quand la concentration en peracide augmente alors qu'il reste constant pour la décaline *trans*. Dans chaque cas l'analyse du mélange réactionnel révèle la présence de diphényle, en très faible quantité, et que nous n'avons pas fait figurer dans le tableau 2.

Discussion

Nos travaux antérieurs (16, 17) ont montré que dans les conditions expérimentales décrites, c'est-à-dire en prenant soin d'éliminer efficacement l'oxygène, le peracide réagit effectivement selon le processus radicalaire.

La régiosélectivité en faveur des C—H tertiaires est déterminée par la réaction [3]; elle est exothermique de 10 à 20 kcal/mol (18) selon que l'on considère les radicaux $Ph^{\cdot}$, ou $PhCO_2^{\cdot}$ et on sait que la vitesse d'arrachement d'un H tertiaire est plus grande que celle d'un H secondaire (19). Ensuite la réaction [4] est également très exothermique et les résultats obtenus précédemment (17) montrent que la réactivité d'un radical vis-à-vis de la liaison O—O d'un peracide est d'autant plus grande que son caractère nucléophile est plus marqué; c'est-à-dire qu'un radical tertiaire est plus réactif qu'un radical secondaire. Les caractéristiques de ces deux réactions [3] et [4] expliquent pourquoi l'hydroxylation a lieu préférentiellement sur les liaisons C—H tertiaires et pourquoi le rendement en alcool croît quand on passe du méthyl-cyclohexane à l'adamantane compte tenu du nombre relatif d'atomes d'hydrogène H tertiaires dans la molécule.

Les résultats stéréochimiques des décalines *cis* et *trans* donnés dans le tableau 2 sont en accord avec ce que l'on sait sur la stéréosélectivité des radicaux décalyle-9 (20, 21). Un précurseur de radical *trans* donne toujours lieu à un maintien de configuration alors que dans le cas d'un précurseur de radical *cis* il faut opérer avec un substrat très réactif, comme l'oxygène ou un hypochlorite, et à forte concentration pour obtenir le produit de réaction *cis*. Nos résultats montrent que la réaction [4] est suffisamment rapide pour être compétitive avec l'isomérisation du radical *cis* en *trans*.

Conclusion

Les liaisons C—H, non activées, des hydrocarbures cycloaliphatiques sont hydroxylées par le peracide benzoïque, selon un processus radicalaire, avec une régiosélectivité de 70% et 80% en faveur des liaisons C—H tertiaires pour le méthylcyclohexane et l'adamantane. Dans le cas des décalines *cis* et *trans*, la stéréosélectivité des décalols-9 peut atteindre 97%.

Ces résultats montrent donc qu'une très bonne stéréosélectivité pour la réaction d'hydroxylation par un peracide ne signifie pas obligatoirement que le processus ne soit pas radicalaire.

Partie expérimentale

Le peracide benzoïque est préparé selon la méthode de Swern[1] (22) par action de H_2O_2 85% sur l'acide benzoïque dans CH_3SO_3H à 95%. La pureté est déterminée par indice de peroxyde (I.P.) (23). Il est nécessaire d'utiliser du peracide fraîchement préparé si on veut obtenir une bonne reproductibilité des résultats.

Les hydrocarbures et le benzène utilisés sont des produits commerciaux dont la pureté a été contrôlée par cpg.

Les analyses sont effectuées par cpg sur un appareil Girdel équipé d'un intégrateur Autolab.

Expérience type

Un ballon de 50 cm^3, surmonté d'un réfrigérant, contenant 10 cm^3 d'une solution à 1 *M* en hydrocarbure et 0,1–0,2 ou 0,5 *M* en peracide benzoïque, est plongé dans un bain thermostaté dont la température est fixée à 100°C. Il est indispensable d'opérer à ébullition vigoureuse pour éliminer l'oxygène dissous, ou se formant au cours de la réaction, sinon on amorce un processus de décomposition du peracide en acide (16). Pour cette raison la température du bain est fixée à 20°C au dessus de celle de l'ébullition du benzène.

On effectue deux expériences simultanées destinées l'une à suivre la vitesse de disparition du peracide par détermination de I.P. au cours du temps, l'autre à effectuer l'analyse quantitative du mélange réactionnel. Les constantes de vitesse (tableau 1) sont exprimées en ordre 1 expérimental. Après 2–3 h d'ébullition il reste seulement 1–2% de peracide. Après estérification par CH_2N_2, l'analyse des produits formés est effectuée par cpg sur deux colonnes (Carbowax 20M, 15%, 2 m ou SE 30, 30%, 4 m) en utilisant des échantillons authentiques et un témoin interne pour le dosage.

[1] L'hydroxylation peut être aussi réalisée en utilisant le peracide dodécanoïque; dans ce cas il y a compétition entre une réaction en chaîne de décarboxylation du peracide en n-undécanol-1 (16, 17) et un transfert sur l'hydrocarbure (réactions [3] et [4]); de ce fait le taux d'hydroxylation de ce dernier est moins bon mais les résultats confirment le caractère radicalaire du processus.

1. G. Olah, D. Parker et N. Yoneda. Angew. Chem. Int. Ed. Engl. **17**, 909 (1978).
2. A. Rotman et Y. Mazur. J. Am. Chem. Soc. **94**, 6228 (1972).
3. P. Schleyer et R. Nicholas. J. Am. Chem. Soc. **83**, 182 (1961).
4. D. Heywood, B. Phillips et H. Stanbury. J. Org. Chem. **22**, 281 (1961).
5. N. Deno, E. Jedziniak, L. Messer, M. Meyer, S. Stroud et E. Tomezsko. Tetrahedron, **33**, 2503 (1977).
6. W. Muller et H. Schneider. Angew. Chem. Int. Ed. Engl. **18**, 407 (1979).
7. H. Schneider, N. Becker et K. Philippi. Chem. Ber. **114**, 1562 (1981).
8. H. Schneider et W. Muller. Angew. Chem. Int. Ed. Engl. **21**, 146 (1982).
9. N. Takaishi, Y. Fujikura et Y. Inamoto. Synthesis, 293 (1983).
10. V. Ullrich. Top. Curr. Chem. **83**, 67 (1978).
11. R. White et M. Coon. Ann. Rev. Biochem. **49**, 315 (1980).
12. R. Blake et M. Coon. J. Biol. Chem. **256**, 12127 (1981).
13. R. White, S. Sligar et M. Coon. J. Biol. Chem. **255**, 11108 (1980).
14. D. Mansuy, J. F. Bartoli, J. C. Chotard et M. Lange. Angew. Chem. Int. Ed. Engl. **19**, 909 (1980).
15. D. Mansuy, J. F. Bartoli et M. Momenteau. Tetrahedron Lett. **23**, 2781 (1982).
16. J. Sorba, J. Fossey, J. Y. Nedelec et D. Lefort. Tetrahedron, **35**, 1509 (1979).
17. J. Fossey et D. Lefort. Tetrahedron, **36**, 1023 (1980).
18. J. Kerr. Chem. Rev. **66**, 465 (1966).
19. K. U. Ingold. *Dans* Free radicals. Vol. I. *Edité par* J. Kochi. Wiley, New-York. 1973. p. 37.
20. P. Bartlett, R. Pincock, J. Rolston, W. Schinidel et L. Singer. J. Am. Chem. Soc. **87**, 2590 (1965).
21. F. Greene et N. Lowry. J. Org. Chem. **32**, 875 (1967).
22. L. Silbert, E. Siegel et D. Swern. J. Org. Chem. **27**, 1336 (1962).
23. R. Johnson et J. Siddiqui. The determination of organic peroxides. Pergamon Press, Oxford. 1970.

Some isotopic scrambling studies with singly or doubly labeled triphenylvinyl bromide[1]

CHOI CHUCK LEE AND CHARLES Y. FIAKPUI

Department of Chemistry, University of Saskatchewan, Saskatoon, Sask., Canada S7N 0W0

Received August 10, 1984

CHOI CHUCK LEE and CHARLES Y. FIAKPUI. Can. J. Chem. **63**, 681 (1985).

The solvolysis of triphenyl[2-^{14}C]vinyl bromide (**1**-Br-2-^{14}C) in 70% HOAc − 30% H_2O or in 2,2,2-trifluoroethanol (TFE) carried out in the presence of an excess of *p*-$CH_3C_6H_4SNa$ gave the triphenylvinyl *p*-tolyl thioether (**1**-STol) with a greatly decreased extent of scrambling of the ^{14}C-label from C-2 to C-1 when compared with analogous reactions without the presence of the *p*-toluenethiolate anion. For example, the **1**-STol product from the reaction of **1**-Br-2-^{14}C in 70% HOAc − *p*-$CH_3C_6H_4SNa$ showed only 0.5−0.9% scrambling, while previous studies on the reaction of **1**-Br-2-^{14}C in 70% HOAc − NaOAc gave 14.7 ± 0.7% scrambling. Previous work on the solvolysis of 1,2-diphenyl-2-[$^2H_5$]phenyl[2-^{13}C]vinyl bromide (**1**-Br-2-^{13}C-2-Ph-d_5) in 70% HOAc, as well as the present results from the solvolysis of **1**-Br-2-^{13}C-2-Ph-d_5 in TFE − 2,6-lutidine, gave products derived from all 4 possible isotopomeric triphenylvinyl cations **3**, **4**, **5**, and **6** arising from successive 1,2-phenyl shifts. On the other hand, solvolysis of **1**-Br-2-^{13}C-2-Ph-d_5 in 70% HOAc or TFE containing an excess of *p*-$CH_3C_6H_4SNa$ gave **1**-STol in which the isotopically rearranged product was derived only from ion **5** arising from a 1,2-shift of the unlabeled phenyl group with no detectable amount of production derived from a 1,2-shift of the perdeuterophenyl group. These results are interpreted by the rapid trapping of the triphenylvinyl cation by the highly nucleophilic *p*-toluenethiolate anion.

CHOI CHUCK LEE et CHARLES Y. FIAKPUI. Can. J. Chem. **63**, 681 (1985).

La solvolyse du bromure de triphényl [^{14}C-2]-vinyle (**1**-Br-^{14}C-2), en solution dans un mélange à 70% AcOH − 30% H_2O ou dans du trifluoro-2,2,2 éthanol (TFE) et en présence d'un excès de *p*-$CH_3C_6H_4SNa$, conduit au triphénylvinyl *p*-tolyl thioéther (**1**-STol); comparés aux résultats obtenus lors de réactions analogues effectuées en l'absence de l'anion *p*-toluènethiolate, le taux de brouillage du marqueur ^{14}C de la position C-2 vers la position C-1 est de beaucoup diminué. Par exemple, le taux de brouillage, observé dans le produit **1**-STol obtenu par réaction du **1**-Br ^{14}C-2 dans AcOH à 70%/*p*-$CH_3C_6H_4SNa$, n'est que de 0,5 à 0,9% alors que celui observé antérieurement, lors de la réaction du **1**-Br ^{14}C-2 dans AcOH à 70%/AcONa, s'élève à 14,7 ± 0,7%. Les résultats obtenus antérieurement, lors de la solvolyse du bromure de diphényl-1,2 [$^2H_5$]-phényl-2 [^{13}C-2]-vinyle (**1**-Br ^{13}C-2 d_5-Ph-2) dans AcOH à 70%, ainsi que les résultats obtenus dans le présent travail, lors de la solvolyse du produit **1**-Br ^{13}C-2 d_5-Ph-2 dans un mélange de TFE/lutidine-2,6, conduisent dans chaque cas aux quatre cations triphénylvinyles isotopomères possibles (**3**, **4**, **5** et **6**) provenant de déplacements 1,2 successifs des groupements phényles. Par ailleurs, la solvolyse du produit **1**-Br ^{13}C-2 d_5-Ph-2, dans AcOH à 70% ou dans le TFE contenant un excès de *p*-$CH_3C_6H_4SNa$, conduit au produit **1**-STol dans lequel le seul produit de transposition isotopique provient de l'ion **5** par le biais d'une transposition-1,2 du groupe phényle qui n'est pas marqué; on n'a pas pu déceler de produit provenant d'une transposition-1,2 du groupement phényle perdeutéré. On interprète ces résultats en invoquant un piégeage rapide du cation triphénylvinyle par l'anion *p*-toluènethiolate qui est hautement nucléophile.

[Traduit par le journal]

Introduction

In the solvolysis of triphenyl[2-^{14}C]vinyl bromide (**1**-Br-2-^{14}C) in 70% HOAc − 30% H_2O (to be called 70% HOAc), it was found that the presence of added NaOAc did not significantly affect the extent of isotopic scrambling, 14.7 ± 0.7% scrambling of the label from C-2 to C-1 arising from 1,2-phenyl shifts in the triphenylvinyl cation being observed in the reaction product, 1,2,2-triphenylethanone, when the reaction was carried out with up to 30 molar equivalents of added NaOAc (2). On the other hand, similar solvolyses of trianisyl-[2-^{14}C]vinyl bromide (**2**-Br-2-^{14}C) in 70% HOAc showed decreasing amounts of scrambling with increasing amounts of added NaOAc and the possibility was considered that 1,2-shifts in the solvolysis of **2**-Br-2-^{14}C may occur in the dissociated, free trianisylvinyl cation which may be competitively captured by different nucleophiles, while 1,2-phenyl shifts in the solvolysis of **1**-Br-2-^{14}C may take place in the ion-pair which may be insensitive to the presence of added acetate ions (2). However, subsequent studies (3) have shown that solvolyses of **1**-Br or **2**-Br in 70% HOAc both showed common ion rate depression and exchange with added ^{82}Br-labeled bromide, findings that are diagnostic of the formation of dissociated cations (4). It was, therefore, suggested that the solvolyses of **1**-Br or **2**-Br in 70% HOAc both gave rise to dissociated ions, but the triphenylvinyl cation, being less stable than the trianisylvinyl cation, would react rapidly once it is formed and would show a low selectivity or low ability to discriminate between different nucleophiles, thus resulting in no significant effect of added NaOAc on the extent of scrambling (3). It is of interest to find out if the presence of anion with stronger nucleophilic character than the acetate ion would be able to trap the triphenylvinyl cation and show a lesser extent of scrambling. The *p*-toluenethiolate anion has been used to trap triarylvinyl cations (5). The initial experiments in the present work thus involved a study on the solvolysis of **1**-Br-2-^{14}C in 70% HOAc carried out in the presence of an excess of sodium *p*-toluenethiolate.

$(C_6H_5)_2{}^{14}C{=}C(Br)C_6H_5$ — **1**-Br-2-^{14}C

$(p\text{-}CH_3OC_6H_4)_2{}^{14}C{=}C(Br)C_6H_4OCH_3\text{-}p$ — **2**-Br-2-^{14}C

[1]Rearrangement studies with ^{14}C. XLIX; for part 48, see ref. 1.

TABLE 1. Data on isotopic scramblings in the solvolysis of triphenyl[2-^{14}C]vinyl bromide (**1**-Br-2-^{14}C)

			Specific activity (dpm/mmol)				Scrambling from C-2 to C-1 (%)	
			Reaction product[d]		Benzophenone[e]			
Expt.	Solvent	Added salt	Run 1	Run 2	Run 1	Run 2	Run 1	Run 2
1[a]	70% HOAc	p-$CH_3C_6H_4SNa$	564 000	325 000	561 000	322 000	0.5	0.9
2[b]	TFE	p-$CH_3C_6H_4SNa$	165 000	367 000	158 000	353 000	4.2	3.8
3[c]	70% HOAc	$LiClO_4$	845 000	698 000	717 000	589 000	15.1	15.6

[a]Solvolysis of 60 mM **1**-Br-2-^{14}C in 70% HOAc – 30% H_2O containing 600 mM p-$CH_3C_6H_4SNa$ at 150 ± 2°C for 8 days.
[b]Solvolysis of 0.12 M **1**-Br-2-^{14}C in TFE containing 1.2 M p-$CH_3C_6H_4SNa$ at 150 ± 2°C for 15 days.
[c]Solvolysis of 15 mM **1**-Br-2-^{14}C in 70% HOAc – 30% H_2O containing 75 mM $LiClO_4$ at 150 ± 2°C for 8 days.
[d]The product from Expts. 1 and 2 was triphenylvinyl p-tolyl thioether (**1**-STol-^{14}C) which was degraded by ozonolysis to benzophenone; the product from Expt. 3 was 1,2,2-triphenylethanone which was oxidized by $KMnO_4$ to benzophenone.
[e]Analyzed as the oxime.

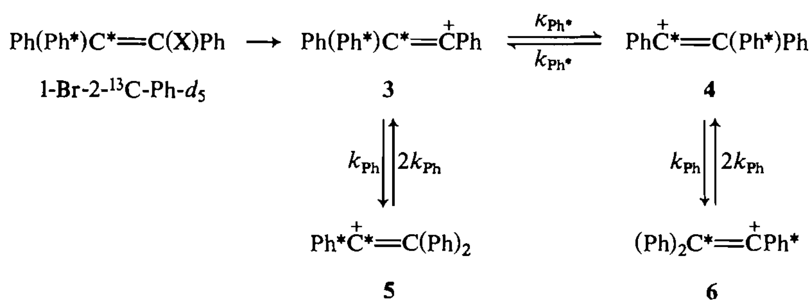

SCHEME 1

Recently, we have investigated the possibility of successive 1,2-shifts in the triphenylvinyl cation using the doubly labeled 1,2-diphenyl-2-[$^2H_5$]phenyl[2-^{13}C]vinyl bromide (**1**-Br-2-^{13}C-2-Ph-d_5) as substrate (6, 7). The present work also included a study on the solvolysis of **1**-Br-2-^{13}C-2-Ph-d_5 in 70% HOAc containing sodium p-toluenethiolate. Due to a combination of its high polarity and low nucleophilicity (8–10), 2,2,2-trifluoroethanol (TFE) is a good solvent for the observation of 1,2-shifts in solvolytic studies. The solvolysis of **1**-Br-2-^{14}C in TFE has been reported (11) and, in the present work, the solvolysis of **1**-Br-2-^{14}C in TFE containing sodium p-toluenethiolate as well as solvolyses of **1**-Br-2-^{13}C-2-Ph-d_5 in TFE with or without added sodium p-toluenethiolate were carried out.

Results and discussion

When **1**-Br-2-^{14}C was solvolyzed in 70% HOAc or in TFE with the presence of 10 molar equivalents of p-$CH_3C_6H_4SNa$, triphenylvinyl p-tolyl thioether (**1**-STol-^{14}C) was obtained as reaction product. Degradation of this thioether by ozonolysis gave benzophenone, the specific activity of which, when compared with that of the thioether from which the benzophenone was obtained, gave the extent of scrambling of the ^{14}C-label from C-2 to C-1. The results are summarized in Table 1. It is seen from Table 1 that the **1**-STol-^{14}C product from the reaction in 70% HOAc showed only 0.5–0.9% scrambling, while similar solvolyses in 70% HOAc containing various amounts of NaOAc gave 14.7 ± 0.7% scrambling (2). For the reaction in TFE, the 3.8–4.2% scrambling observed in the **1**-STol-^{14}C is also much lower than the average value of 44.1% scrambling after complete reaction in the solvolysis of **1**-Br-2-^{14}C in TFE-2,6-lutidine (11). These greatly decreased extents of scrambling, when compared with analogous reactions without the presence of added p-$CH_3C_6H_4SNa$, thus gave conformation of the expectation that the highly nucleophilic p-toluenethiolate anion could trap the triphenylvinyl cation to give **1**-STol-^{14}C and effectively compete and reduce the extent of the 1,2-shift processes.

It is also of interest to note that when **1**-Br-2-^{14}C was solvolyzed in 70% HOAc in the presence of 1, 5, or 10 molar equivalents of added $LiClO_4$, the scramblings observed were 15.3 ± 0.5%, a typical set of data being included in Table 1. This extent of scrambling is essentially the same as the 14.7 ± 0.7% scrambling found for similar solvolyses carried out with different amounts of added NaOAc (2). While $LiClO_4$ was the salt used in the classical work of Winstein showing the occurrence of a special salt effect through interactions with solvent-separated ion-pairs in systems such as the acetolysis of 3-anisyl-2-butyl brosylate (4, 12), $LiClO_4$ was found to give only a normal salt effect, and no special salt effect, in the solvolysis of **1**-Br in 70% HOAc (3). Hence the solvolysis of **1**-Br-2-^{14}C in 70% HOAc with the presence of the poorly nucleophilic perchlorate ion would show no preferential trapping of the triphenylvinyl cation and the extent of scrambling is essentially the same whether $LiClO_4$ or NaOAc is present as an added salt.

In solvolytic reactions with the doubly labeled **1**-Br-2-^{13}C-2-Ph-d_5, 4 isotopomeric triphenylvinyl cations, **3**, **4**, **5**, and **6**, derived from successive 1,2-phenyl shifts, are possible as shown in Scheme 1 (6, 7). From a steady-state treatment, assuming that $k_{Ph} = k_{Ph^*}$, eq. [1] was derived for the ratio of products formed from ions **3**–**6** in terms of α, with $\alpha = k_{SOH}/k_{Ph}$, the ratio of the rate of capture of the cations to give product (k_{SOH}) to the rate of rearrangement from 1,2-phenyl shifts (k_{Ph}) (7).

$$[1] \quad \mathbf{3}:\mathbf{4}:\mathbf{5}:\mathbf{6} = 1.0:(2+\alpha)/[(2+\alpha)^2-2]:1/(2+\alpha):1/[(2+\alpha)^2-2]$$

When a 0.12 M solution of **1**-Br-2-^{13}C-2-Ph-d_5, which was 90% enriched with ^{13}C and essentially completely deuterated (6), was solvolyzed in TFE containing 3 equivalents of 2,6-lutidine under the same conditions as those used to give complete reaction in the trifluoroethanolysis of **1**-Br-2-^{14}C (11), the product obtained was a mixture of isotopomeric triphenylvinyl 2,2,2-trifluoroethyl ethers (**1**-OTFE). Its degradation to benzophenone and analysis by mass spectrometry using the chemical ionization technique as previously described (6) gave the distribution of products derived from the precursor ions **3**, **4**, **5**, and **6** as summarized in Table 2. It has already been indicated that the analogous trifluoroethanolysis of **1**-Br-2-^{14}C gave a mean value of 44.1% scrambling of the ^{14}C-label from C-2 to C-1 (11). Using eq. [2], which has previously been employed in the treatment of such ^{14}C scrambling data (13), k_{SOH}/k_{Ph} or α is calculated to be 0.54. Using this value of α and eq. [1], the distribution of products from ions **3**–**6** in the

$$[2] \quad [\text{unrearranged product}]/[\text{rearranged product}] = 1 + (k_{SOH}/2k_{Ph})$$

trifluoroethanolysis of **1**-Br-2-^{13}C-2-Ph-d_5 was calculated and the results are also given in Table 2. For comparison, the previous data from solvolyses of **1**-Br-2-^{13}C-2-Ph-d_5 in 70% HOAc containing different amounts of added NaOAc are also included in Table 2. The finding that products are derived from all 4 possible isotopomeric triphenylvinyl cations **3**–**6** and the reasonably good agreement between the observed and calculated product distributions from these cations suggest that, under the solvolytic conditions as employed in Expts. 4 and 5 of Table 2, successive 1,2-phenyl shifts as shown in Scheme 1 do occur in the solvolysis of **1**-Br-2-^{13}C-2-Ph-d_5, and the direct demonstration of such successive 1,2-shifts would not have been possible without the use of double labeling.

When **1**-Br-2-^{13}C-2-Ph-d_5 was solvolyzed in 70% HOAc or TFE in the presence of added p-$CH_3C_6H_4SNa$ in the same way as was done earlier with **1**-Br-2-^{14}C, the thioether product, **1**-STol, that was obtained was degraded to benzophenone, analyzed by mass spectrometry (6), and the results are given as Expts. 6 and 7 in Table 2. It may be noted that the 0.5–0.9% and 3.8–4.2% scramblings of the ^{14}C label (Table 1) observed in the solvolysis of **1**-Br-2-^{14}C in 70% HOAc – p-$CH_3C_6H_4SNa$ and in TFE-p-$CH_3C_6H_4SNa$, respectively, are in fair agreement with the 1.0–1.7% and 2.4–3.6% scramblings, respectively, in the analogous solvolyses using **1**-Br-2-^{13}C-2-Ph-d_5 (Table 2). Interestingly, the rearranged **1**-STol products in Expts. 6 and 7 (Table 2) were derived only from ion **5**, with no detectable amount of rearranged products from ions **4** and **6**. These results indicate that the relatively small extent of rearrangement in the product trapped by the p-toluenethiolate anion was formed after 1,2-shifts of the unlabeled phenyl group, with essentially no trapping of any product arising from 1,2-shifts of the perdeuterated phenyl group which would give rise to ions **4** and **6** as shown in Scheme 1. Apparently, when **1**-Br-2-^{13}C-2-Ph-d_5 was solvolyzed in 70% HOAc – NaOAc or in TFE – 2,6-lutidine, the triphenylvinyl cation formed under these conditions would have a sufficiently long lifetime to allow for the occurrence of repeated cycles of successive 1,2-shifts, and even when the assumption was made that the magnitude of any isotope effect was small and $k_{Ph} = k_{Ph^*}$, the

TABLE 2. Distribution of products derived from isotopomeric triphenylvinyl cations **3**–**6** in reactions with **1**-Br-2-^{13}C-2-Ph-d_5

		Product from precursor ion (%)											
		3			**4**			**5**			**6**		
Expt.	Reaction medium	Run 1	Run 2	Calcd.[e]	Run 1	Run 2	Calcd.[e]	Run 1	Run 2	Calcd.[e]	Run 1	Run 2	Calcd.[e]
4[a]	TFE – 2,6-lutidine	47.8	46.3	45.7	24.9	23.3	26.1	17.2	16.2	18.0	10.1	14.2	10.3
5[b]	70% HOAc – NaOAc	84.7 ± 2.2		84.2	7.3 ± 1.2		7.6	6.6 ± 1.2		7.5	1.5 ± 0.5		0.7
6[c]	70% HOAc – p-$CH_3C_6H_4SNa$	98.3	99.0		—	—		1.7	1.0		—	—	
7[d]	TFE – p-$CH_3C_6H_4SNa$	96.4	97.6		—	—		3.6	2.4		—	—	

[a]Solvolysis of 0.12 M **1**-Br-2-^{13}C-2-Ph-d_5 in TFE containing 0.36 M 2,6-lutidine at 150 ± 2°C for 20 days.
[b]Mean values from solvolyses of 60 mM **1**-Br-2-^{13}C-2-Ph-d_5 in 70% HOAc containing 0, 5, or 10 equivalents of NaOAc to 150 ± 2°C for 2 or 10 days (6, 7).
[c]Same as Expt. 1 of Table 1 except that **1**-Br-2-^{13}C-2-Ph-d_5 instead of **1**-Br-2-^{14}C was the substrate.
[d]Same as Expt. 2 of Table 1 except that **1**-Br-2-^{13}C-2-Ph-d_5 instead of **1**-Br-2-^{14}C was the substrate.
[e]Calculated using eq. [1].

calculated distribution of products from **3**–**6** was in reasonably good agreement with the observed data. On the other hand, for the analogous solvolyses carried out in the presence of the highly nucleophilic *p*-toluenethiolate anion, the triphenylvinyl cation that was formed would be trapped rapidly to give the thioether with essentially no cycles of successive 1,2-shifts. Under such conditions, the isotope effect favoring a 1,2-shift of the unlabeled phenyl over the perdeuterophenyl group is more apparent, resulting in the mass spectral detection of only the isotopically rearranged product derived from ion **5**.

Experimental

Previously reported methods were used to prepare the required reactants, **1**-Br-2-^{14}C (14), **1**-Br-2-^{13}C-2-Ph-d_5 (6), and sodium *p*-toluenethiolate (5). Illustrations of typical experimental procedures are given below.

Reactions with 1-Br-2-^{13}C-2-Ph-d$_5$

A mixture of 400 mg (1.2 mol) of **1**-Br-2-^{13}C-2-Ph-d_5 and 1.8 g (12 mmol) of *p*-$CH_3C_6H_4SNa$ in 10 mL of TFE in a sealed tube was heated at 150 ± 2°C for 15 days. The resulting material was poured into H_2O and extracted with $CHCl_3$ (3 × 25 mL). The liberated bromide ions in the aqueous layer were titrated with $AgNO_3$ (3), showing essentially complete reaction. The $CHCl_3$ extract was washed with 10% NaOH and with H_2O, dried over $MgSO_4$, and then the $CHCl_3$ was removed by evaporation. The residue was purified by passage through an alumina column with elution by an 8:1 mixture of petroleum ether (bp 40–60°C) and ether. After removal of the solvent from the eluted product, crystallization from ethanol gave 320 mg (69%) of the isotopomeric triphenylvinyl *p*-tolyl thioethers (**1**-STol) which were degraded by ozonolysis (15) to benzophenone and analyzed by mass spectrometry (6) to give the distribution of products from the isotopomeric triphenylvinyl cations **3**–**6**. From the same reaction using non-labeled materials, the recrystallized **1**-STol melted at 134–135°C. *Anal.* calcd. for $C_{27}H_{22}S$: C 85.71, H 5.82; found: C 85.60, H 6.01.

Similarly, the solvolysis of 400 mg (1.2 mmol) of **1**-Br-2-^{13}C-2-Ph-d_5 in 20 mL of 70% HOAc – 30% H_2O (by volume) containing 1.8 g (12 mmol) of *p*-$CH_3C_6H_4SNa$ in a sealed tube at 150 ± 2°C for 8 days gave a 56% yield of the isotopomeric **1**-STol.

The solvolysis of 400 mg (1.2 mmol) of **1**-Br-2-^{13}C-2-Ph-d_5 in 10 mL of TFE containing 390 mg (3.6 mmol) of 2,6-lutidine was carried out at 150 ± 2°C for 20 days and worked up as previously described (11) to give the isotopomeric triphenylvinyl 2,2,2-trifluoroethyl ethers for degradation to benzophenone and analysis by mass spectrometry.

Reactions with 1-Br-2-^{14}C

The solvolyses of **1**-Br-2-^{14}C in TFE or in 70% HOAc containing 10 molar equivalents of added *p*-$CH_3C_6H_4SNa$ were carried out as described above for the analogous reactions with **1**-Br-2-^{13}C-2-Ph-d_5, except that the product was isolated with the addition of 200–300 mg of unlabeled **1**-STol as carrier. Ozonolysis of each sample of **1**-STol-^{14}C to benzophenone and comparison of their specific activities gave the extents of scrambling as summarized in Table 1.

Solvolyses of **1**-Br-2-^{14}C in 70% HOAc in the presence of 1, 5, or 10 molar equivalents of added $LiClO_4$ (3) were also carried out. Typically, a solution of 100 mg (0.30 mmol) of **1**-Br-2-^{14}C and 160 mg (1.5 mmol) of $LiClO_4$ in 20 mL of 70% HOAc in a sealed tube was heated at 150 ± 2°C for 8 days. The mixture was worked up, with the aid of added carrier, to give 1,2,2-triphenylethanone and degraded to benzophenone to give the extent of scrambling as previously described for the solvolysis of **1**-Br-2-^{14}C in 70% HOAc containing added NaOAc (2).

Acknowledgment

The financial support given by the Natural Sciences and Engineering Research Council of Canada is sincerely acknowledged.

1. D. Wanigasekera, C. C. Lee, Y. Houminer, M. Aviv, and Z. Rappoport. J. Org. Chem. **49**, 4367 (1984).
2. C. C. Lee, E. C. F. Ko, and Z. Rappoport. Can. J. Chem. **58**, 2369 (1980).
3. C. C. Lee, C. A. Obafemi, and Z. Rappoport. Can. J. Chem. **60**, 3019 (1982).
4. D. J. Raber, J. M. Harris, and P. v. R. Schleyer. *In* Ions and ion pairs in organic reactions. Vol. 2. *Edited by* M. Szwarc. John Wiley and Sons, New York. 1974. Chapt. 3.
5. Z. Rappoport and Y. Apeloig. J. Am. Chem. Soc. **91**, 6734 (1969).
6. C. C. Lee, C. Y. Fiakpui, and K. K. Midha. J. Org. Chem. **48**, 1025 (1983).
7. Z. Rappoport, C. Y. Fiakpui, X.-D. Yu, and C. C. Lee. J. Org. Chem. **49**, 570 (1984).
8. C. Reichardt. Solvent effects in organic chemistry. Verlag Chemie, New York. 1979. p. 233.
9. G. W. Klumpp. Reactivity in organic chemistry. Wiley–Interscience, New York. 1982. p. 200.
10. F. L. Schadt, T. W. Bentley, and P. v. R. Schleyer. J. Am. Chem. Soc. **98**, 7667 (1976).
11. C. C. Lee and E. C. F. Ko. Can. J. Chem. **56**, 2459 (1978).
12. S. Winstein, E. Clippinger, A. H. Fainberg, and G. C. Robinson. J. Am. Chem. Soc. **76**, 2597 (1954).
13. C. C. Lee, A. J. Cessna, B. A. Davis, and M. Oka. Can. J. Chem. **52**, 2679 (1974).
15. C. C. Lee, U. Weber, and C. A. Obafemi. Can. J. Chem. **57**, 1384 (1979).

Stereochemical assignment by X-ray crystallography to the product of trapping by solvent of the intermediate zwitterion on irradiation of a 2,5-cyclohexadienone

ANGELO C. BRISIMITZAKIS AND DAVID I. SCHUSTER[1]
Department of Chemistry, New York University, New York, NY 10003, U.S.A.

AND

JAMES M. VAN DER VEEN
Department of Chemistry, Stevens Institute of Technology, Hoboken, NJ 07030, U.S.A.

Received January 24, 1984[2]

ANGELO C. BRISIMITZAKIS, DAVID I. SCHUSTER, and JAMES M. VAN DER VEEN. Can. J. Chem. **63**, 685 (1985).

Ultraviolet irradiation of 4-methyl-4-trichloromethylcyclohexa-2,5-dienone in acidic methanol resulted in the stereospecific generation of a solvent adduct, whose structure has been determined by X-ray crystallography, and whose carbon skeleton can be identified with that of the previously postulated zwitterion intermediate. It is concluded that the photochemical rearrangement of this dienone to the corresponding lumiketone proceeds with inversion of configuration at the migratory carbon.

ANGELO C. BRISIMITZAKIS, DAVID I. SCHUSTER et JAMES M. VAN DER VEEN. Can. J. Chem. **63**, 685 (1985).

L'irradiation ultraviolette de la méthyl-4 trichlorométhyl-4 cyclohexadiène-2,5 one, dans du méthanol acidulé, conduit à la génération stéréospécifique d'un adduit de solvant dont on a déterminé la structure par diffraction des rayons-X et dont la structure carbonée peut être identifiée avec celle qui avait été postulée antérieurement pour l'intermédiaire zwitterionique. On en conclut que la transposition photochimique de cette diénone, en lumicétone correspondante, se produit avec une inversion de configuration au niveau du carbone qui migre.

[Traduit par le journal]

Mechanistic interpretations regarding the photochemistry of cross-conjugated cyclohexadienones have centered around a bicyclic zwitterionic intermediate (1). Indirect evidence for the intermediacy of such a species came from thermal generation of such zwitterions from appropriate precursors (2), as well as trapping of such species by cycloaddition reactions with cyclopentadiene and furan (3). Molecular and stereochemical characterization of these adducts relied on analysis of spectral data.

The first direct evidence for the intermediacy of a zwitterion in the photochemistry of dienone **1** involved the isolation of solvent adduct **3**, in which the carbon skeleton of the postulated zwitterion intermediate was preserved (4). Although the report established the overall structure of **3**, the *exo/endo* configuration of the methyl and CCl_3 groups, as well as the relative orientation of substituents to the carbonyl group, were not established.

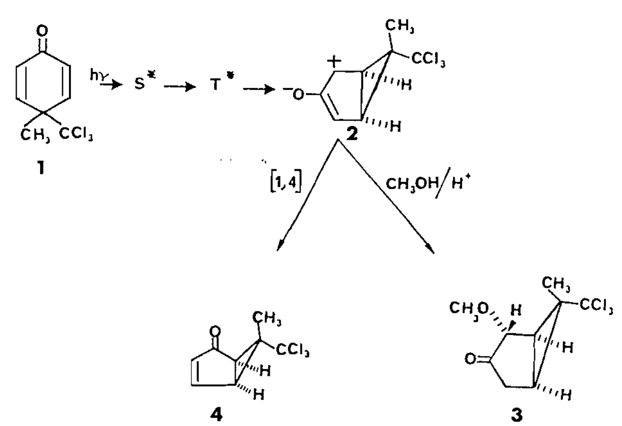

We now report the complete structure including stereochemistry of **3** based on single crystal X-ray analysis, and its mechanistic implications with respect to the photorearrangement of **1** to lumiketone **4** (5), whose stereochemistry has been established previously (6).

Solvent adduct **3** was prepared by ultraviolet irradiation of dienone **1** in acidic methanol. Careful chromatographic separation on Florisil afforded a pure crystalline sample of **3**, which had previously been isolated only as a colorless oil (4). Spectral data of **3** (^{13}C and ^{1}H nmr, ir, ms) matched those previously reported (4) for the oily adduct, and are consistent with the proposed assignment.

Crystal data

$C_9H_{11}O_2Cl_3$ fw = 257.55

The space group was determined to be triclinic, $P\bar{1}$, with $a = 5.963(3)$, $b = 9.958(4)$, $c = 10.106(4)$ Å, $\alpha = 105.47(3)$, $\beta = 105.52(3)°$, $\gamma = 81.91(3)°$, $Z = 2$, $d_{calc} = 1.54$ g/cm³; $\lambda = 0.7107$ Å. Data was collected on a Nicolet Four-Circle Auto diffractometer using Mo-Kα radiation, a graphite monochromator, and ω-scans with a scan range of 1°. The ratio of background counting time to net scanning time was 0.50. Data were collected in two shells with a scan rate of 6.00°/min for $2\theta = 3.00° - 43.00°$ and 4.00°/min for $2\theta = 43.00° - 55.00°$. Six check reflections were monitored every three hundred reflections and showed no decay during the data collection. Of the 2546 reflections collected, 1905 with $F > 2\sigma(F)$ were treated as observed.

The structure was solved using Multan-80 (7). In the first *E*-map the three chlorine atoms and eight other atoms were located. The remaining three atoms were found in a difference map following a structure Fourier factor calculation. Isotropic refinement[3] resulted in an *R*-factor[4] of 0.192 after six least-square cycles. Three anisotropic refinement cycles reduced *R* to 0.090. All the hydrogen atoms were apparent in a difference map at this point. Six cycles of weighted least-squares refine-

[1]Author to whom correspondence may be addressed.
[2]Revision received August 16, 1984.

[3]The X-Ray-System-Version of 1976 was used. J. M. Stewart, Editor, Technical Report TR-446 of the Computer Science Center, University of Maryland, College Park, Maryland.

[4]$$R = \frac{\Sigma |F_o| - |F_c||}{\Sigma |F_o|}$$

TABLE 1. Fractional coordinates (esd's are in parentheses)

Atom	x	y	z
C(1)	0.6261(8)	−0.5520(4)	0.3065(4)
O(1)	0.6265(7)	−0.6277(3)	0.3828(4)
C(2)	0.4209(7)	−0.4583(4)	0.2511(5)
H(2A)	0.312(7)	−0.519(4)	0.175(4)
H(2B)	0.334(8)	−0.416(5)	0.323(5)
C(3)	0.5128(6)	−0.3657(4)	0.1846(4)
H(3)	0.420(6)	−0.340(4)	0.106(4)
C(4)	0.7064(6)	−0.2758(3)	0.2795(4)
C(5)	0.7665(6)	−0.4141(3)	0.1861(4)
H(5)	0.834(7)	−0.415(4)	0.113(4)
C(6)	0.8359(7)	−0.5389(3)	0.2503(4)
H(6)	0.981(7)	−0.530(4)	0.330(4)
O(6)	0.8582(5)	−0.6573(2)	0.1367(3)
C(7)	0.7647(12)	−0.2527(5)	0.4395(5)
H(7A)	0.718(9)	−0.333(5)	0.467(5)
H(7B)	0.917(13)	−0.244(7)	0.472(8)
H(7C)	0.665(12)	−0.177(7)	0.485(7)
C(8)	0.7420(7)	−0.1487(4)	0.2324(4)
Cl(8A)	0.5762(2)	0.0021(1)	0.3087(1)
Cl(8B)	1.0400(2)	−0.1128(1)	0.2895(1)
Cl(8C)	0.6565(2)	−0.1665(1)	0.0469(1)
C(9)	0.9572(12)	−0.7817(5)	0.1809(6)
H(9A)	1.126(10)	−0.773(5)	0.230(5)
H(9B)	0.842(11)	−0.799(6)	0.223(6)
H(9C)	0.958(9)	−0.852(6)	0.090(6)

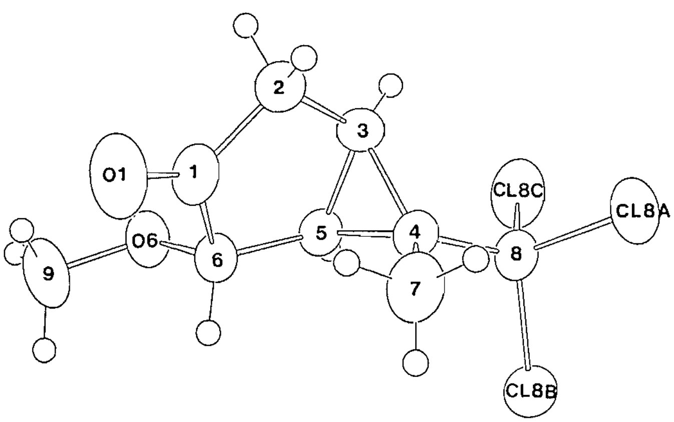

FIG. 1. Crystal structure of **3**.

ment[5] resulted in an R-factor of 0.074. Fractional coordinates, bond distances, and bond angles are shown in Tables 1, 3, and 4, while thermal factors and structure factors are reported in Tables 2 and 5 which are published as supplemental material.[6] An ORTEP (8) drawing of the molecule is shown in Fig. 1. At this point the largest peak in a difference map was 0.44 e/Å^3. None of the peaks in the difference map could be explained in terms of a disordered structure or a solvent molecule. The compound was sensitive to light and this may have contributed to the relatively high R factor, although no crystal deterioration was apparent in the intensities of the check reflections.

The X-ray structure of **3** reveals that attack of methanol occurs, as previously postulated, on the less hindered side of zwitterion **2** opposite to the three-membered ring, on which the C-6 methyl group occupies an *endo* orientation. This structure requires the zwitterion precursor to have the configuration

TABLE 3. Bond distances in angstroms (esd's are given in parentheses)

Bond	Distance
C(1)—O(1)	1.213(7)
C(1)—C(2)	1.507(6)
C(1)—C(6)	1.540(7)
C(2)—H(2A)	0.99(3)
C(2)—H(2B)	0.98(5)
C(2)—C(3)	1.507(7)
C(3)—H(3)	0.92(4)
C(3)—C(4)	1.515(5)
C(3)—C(5)	1.519(5)
C(4)—C(5)	1.505(5)
C(4)—C(7)	1.521(6)
C(4)—C(8)	1.525(6)
C(5)—H(5)	0.93(5)
C(5)—C(6)	1.509(6)
C(6)—H(6)	1.01(3)
C(6)—O(6)	1.429(4)
O(6)—C(9)	1.425(6)
C(7)—H(7A)	1.01(6)
C(7)—H(7B)	0.89(7)
C(7)—H(7C)	0.98(7)
C(8)—Cl(8A)	1.789(4)
C(8)—Cl(8B)	1.772(4)
C(8)—Cl(8C)	1.772(5)
C(9)—H(9A)	1.00(5)
C(9)—H(9B)	0.95(7)
C(9)—H(9C)	0.99(5)

TABLE 4. Bond angles (esd's are given in parentheses)

Angle	Degrees
O(1)—C(1)—C(2)	125.4(5)
O(1)—C(1)—C(6)	124.8(4)
C(2)—C(1)—C(6)	109.8(4)
C(1)—C(2)—C(3)	106.5(3)
C(2)—C(3)—C(4)	116.7(3)
C(2)—C(3)—C(5)	108.2(3)
C(4)—C(3)—C(5)	59.5(2)
C(3)—C(4)—C(5)	60.4(2)
C(3)—C(4)—C(7)	121.5(4)
C(3)—C(4)—C(8)	116.7(3)
C(5)—C(4)—C(7)	121.3(3)
C(5)—C(4)—C(8)	114.6(3)
C(7)—C(4)—C(8)	112.8(3)
C(3)—C(5)—C(4)	60.1(2)
C(3)—C(5)—C(6)	109.5(3)
C(4)—C(5)—C(6)	118.2(3)
C(1)—C(6)—C(5)	104.7(3)
C(1)—C(6)—O(6)	109.2(3)
C(5)—C(6)—O(6)	106.4(3)
C(6)—O(6)—C(9)	114.1(3)
C(4)—C(8)—Cl(8A)	110.5(3)
C(4)—C(8)—Cl(8B)	110.0(2)
C(4)—C(8)—Cl(8C)	114.3(2)
Cl(8A)—C(8)—Cl(8B)	107.8(2)
Cl(8A)—C(8)—Cl(8C)	106.4(2)
Cl(8B)—C(8)—Cl(8C)	107.5(2)

[5]The weighting scheme used in the least-squares minimization of the function $w(|F_o| - |F_c|)^2$ is defined as $w = 1/(\sigma_F^2 + 0.0025(F)^2)$.

[6]Complete tables of thermal parameters and structure factors are available, at a nominal charge, upon request from the Depository of Unpublished Data, CISTI, National Research Council of Canada, Ottawa, Ontario, Canada K1A 0S2.

shown in **2**. Therefore, the [1,4]-sigmatropic shift necessary to proceed from zwitterion **2** to lumiketone **4** must involve retention of the *exo/endo* orientation of the substituents at C-6. This results in an overall inversion of configuration at the migrating carbon of **2**, consistent with Woodward–Hoffmann predictions (9) for a concerted ground state [1,4]-sigmatropic shift originating from zwitterions such as **2**.

Acknowledgment

This study was supported in part by grant CHE-7819750 from the National Science Foundation.

1. H. E. ZIMMERMAN and D. I. SCHUSTER. J. Am. Chem. Soc. **84**, 4527 (1962); D. I. SCHUSTER. Acc. Chem. Res. **11**, 65 (1978).
2. H. E. ZIMMERMAN, D. S. CRUMRINE, and D. DOPP. J. Am. Chem. Soc. **90**, 2990 (1968).
3. C. J. SAMUEL. J. Chem. Soc. Chem. Commun. 275 (1979); J. Chem. Soc. Perkin Trans. 2, 736 (1981).
4. D. I. SCHUSTER and V. Y. ABRAITYS. J. Chem. Soc. Chem. Commun. 419 (1969).
5. D. J. PATEL and D. I. SCHUSTER. J. Am. Chem. Soc. **90**, 5137 (1968).
6. D. I. SCHUSTER and K. V. PRABHU. J. Am. Chem. Soc. **96**, 3511 (1974).
7. P. MAIN, S. J. FISKE, S. E. HULL, L. LESSINGER, G. GERMAIN, J. P. DECLERQ, and M. M. WOOLFSON. MULTAN 80. A system of computer programs for the automatic solution of crystal structures from X-ray diffraction data. Universities of York, England and Louvain, Belgium.
8. C. K. JOHNSON. ORTEP-II. ORNL-5138, Oak Ridge National Laboratory, Oak Ridge, Tennessee.
9. R. B. WOODWARD and R. HOFFMANN. The conservation of orbital symmetry. Academic Press, New York. 1970. p. 89 ff.

Crystal and molecular structure of the binuclear Rh(I) complex (μ-Cl)(μ-pz)[Rh(CO)$_2$]$_2$ (pz = pyrazolyl, $N_2C_3H_3$). An example of molecular stacking via weak intermolecular Rh···Rh interactions

BRENDA M. LOUIE, STEVEN J. RETTIG, ALAN STORR, AND JAMES TROTTER
Department of Chemistry, University of British Columbia, 2036 Main Mall, Vancouver, B.C., Canada V6T 1Y6

Received May 22, 1984

BRENDA M. LOUIE, STEVEN J. RETTIG, ALAN STORR, and JAMES TROTTER. Can. J. Chem. **63**, 688 (1985).

Details of the synthesis and physical properties of (μ-Cl)(μ-pz)[Rh(CO)$_2$]$_2$ are given. Crystals of (μ-chloro) (μ-pyrazolyl)-bis(dicarbonylrhodium(I)) are monoclinic, a = 7.0970(8), b =20.5184(10), c = 15.808(2) Å, β = 94.695(6)°, Z = 8, space group $P2_1/c$. The structure was solved by conventional heavy-atom methods and was refined by full-matrix least-squares procedures to R = 0.035 and R_w = 0.038 for 2949 reflections with $I \geq 3\sigma(I)$. The complex provides a rare example of molecular stacking in a binuclear transition metal complex with Rh···Rh distances of 3.5107(8) and 3.6201(8) Å.

BRENDA M. LOUIE, STEVEN J. RETTIG, ALAN STORR et JAMES TROTTER. Can. J. Chem. **63**, 688 (1985).

On rapporte des détails relatifs à la synthèse et aux propriétés physiques du (μ-Cl)(μ-pz)[Rh(CO)$_2$]$_2$. Les cristaux du (μ-chloro)(μ-pyrazolyl) bis(dicarbonylrhodium(I)) sont monocliniques, a = 7,0970(8), b = 20,5184(10), c = 15,808(2) Å, β = 94,695(6)°, Z = 8, groupe d'espace $P2_1/c$. On a résolu la structure par les méthodes conventionnelles avec des atomes lourds et on l'a affiné par la méthode des moindres carrés (matrice entière) jusqu'à des valeurs de R = 0,035 et R_w = 0,038 pour 2949 réflexions avec $I \geq 3\sigma(I)$. Le complexe correspond à un rare exemple d'empilement moléculaire dans un complexe binucléaire d'un métal de transition avec des distances Rh···Rh égales à 3,5107(8) et 3,6201·Å.

[Traduit par le journal]

Introduction

A recent publication (1) described a series of monomeric Rh(I) complexes involving the bidentate pyrazolyl gallate ligands, $Me_2Gapz_2^-$. In addition, the structural characterization of two binuclear Rh(I) species [Rh(μ-3,5-Me$_2$pz)L—L]$_2$ (where L—L = (CO)$_2$ or COD; 3,5-Me$_2$pz = 3,5-dimethylpyrazolyl, $N_2C_5H_7$) was reported. Our investigations in this area have subsequently produced a mixed-bridge binuclear species, namely (μ-Cl)(μ-pz)[Rh(CO)$_2$]$_2$, which we have structurally characterized and which is a rare example of molecular stacking via weak intermolecular Rh···Rh interactions in zig-zag chains.

Experimental

(μ-Chloro)(μ-pyrazolyl)bis(dicarbonylrhodium(I)) was isolated in low yield as an orange crystalline material from the benzene extract of the products from the reaction:

$$[Rh(\mu\text{-}Cl)(CO)_2]_2 + 2\ Napz \rightarrow [Rh(\mu\text{-}pz)(CO)_2]_2 + 2\ NaCl$$

The compound is readily volatile and air stable. *Anal.* calcd. for (μ-Cl)(μ-pz)[Rh(CO)$_2$]$_2$: C 20.00, H 0.71, N 6.66; found: C 20.08, H 0.70, N 6.42. ^{1}H nmr (C_6D_6, τ values refer to $\tau(C_6D_6)$ = 2.84 ppm): 2.88 d (J ~ 2 Hz, pz-H^3 and pz-H^5), 4.14 t (J ~ 2 Hz, pz-H^4). Infrared ν_{CO} (cyclohexane) 2020, 2075, and 2090 cm^{-1}. The mass spectrum displayed the parent ion grouping (P$^+$) as its strongest signal (100%) with the P − CO$^+$ (65%), P − 2CO$^+$ (75%), P − 3CO$^+$ (75%), P − 4CO$^+$ (70%), P − 4CO − pzH$^+$ (65%), and Rh$^+$ (70%) ions giving rise to other prominent signals in the spectrum.

Spectra

The ^{1}H nmr spectrum was recorded on a Varian XL 100 instrument, the ir spectrum on a Perkin-Elmer 598 spectrometer and the mass spectrum on a Varian MAT CH4B spectrometer at 70 eV and 25°C.

X-ray crystallographic analysis

A crystal bounded by the six faces (followed by their distances in mm from a common origin): ±(1 0 0), 0.345, ±(0 1 0), 0.100, ±(0 0 1), 0.025 was mounted in a general orientation. Unit-cell parameters were refined by least-squares on 2 sin θ/λ values for 25 reflections (2θ = 26–40°) measured on a diffractometer with Mo-$K\alpha$ Radiation ($\lambda(K\alpha_1)$ = 0.70930, $\lambda(K\alpha_2)$ = 0.71359 Å). Crystal data at 22°C are:

$C_7H_3ClN_2O_4Rh_2$ fw = 420.38
Monoclinic, a = 7.0970(8), b = 20.5184(10), c = 15.808(2) Å, β = 94.695(6)°, V = 2294.2(4) Å^3, Z = 8, ρ_c = 2.434 g cm^{-3}, $F(000)$ = 1584, μ(Mo-$K\alpha$) = 30.67 cm^{-1}. Absent reflections: $h0l$, l odd, and $0k0$, k odd, uniquely indicate the space group $P2_1/c$ (C^5_{2h}, No. 14).

Intensities were measured with graphite-monochromated Mo-$K\alpha$ radiation on an Enraf-Nonius CAD4-F diffractometer. An $\omega-2\theta$ scan at 1.12–10.06° min^{-1} over a range of (0.70 + 0.35 tan θ) degrees in ω (extended by 25% on both sides for background measurement) was employed. Data were measured to 2θ = 55°. The intensities of three check reflections, measured every 3600 s throughout the data collection, decreased uniformly to values of approximately 80% of the initial values, the data being scaled accordingly. After data reduction,[1] an absorption correction was applied using the analytical method (2, 3). Transmission factors ranged from 0.537 to 0.856. Of the 5255 crystallographically unique reflections measured, 2949 (56.1%) had intensities greater than $3\sigma(I)$ above background where $\sigma^2(I) = S + 2B + (0.04(S - B))^2$ with S = scan count and B = normalized background count.

The structure was solved by conventional heavy atom methods, the coordinates of the Rh and Cl atoms being determined from the Patterson function and those of the remaining atoms from subsequent difference maps. In the final stages of the full-matrix least-squares refinement, the non-hydrogen atoms were refined with anisotropic and the H atoms with isotropic thermal parameters. The scattering factors of ref. 4 were used for non-hydrogen atoms and those of ref. 5 for hydrogen atoms. Anomalous scattering factors from ref. 6 were used for the Rh and Cl atoms. The weighting scheme $w = 1/\sigma^2(F)$, where $\sigma^2(F)$ is derived from the previously defined $\sigma^2(I)$, gave uniform average values of $w(|F_o| - |F_c|)^2$ over ranges of both $|F_o|$ and sin θ/λ and was employed in the final stages of refinement. Reflections with $I < 3\sigma(I)$ were not included in the refinement. Convergence was reached at R = 0.035 and R_w = 0.038 for 2949 reflections with $I \geq 3\sigma(I)$. For all 5255 reflections R = 0.111. The function minimized was $\Sigma w(|F_o| - |F_c|)^2$, $R = \Sigma||F_o| - |F_c||/\Sigma|F_o|$ and $R_w = (\Sigma w(|F_o| - |F_c|)^2/\Sigma w|F_o|^2)^{1/2}$.

[1]The computer programs used include locally written programs for data processing and locally modified versions of the following: ORFLS, full-matrix least-squares, and ORFFE, function and errors, by W. R. Busing, K. O. Martin and H. A. Levy; FORDAP, Patterson and Fourier syntheses, by A. Zalkin; ORTEP II, illustrations, by C. K. Johnson.

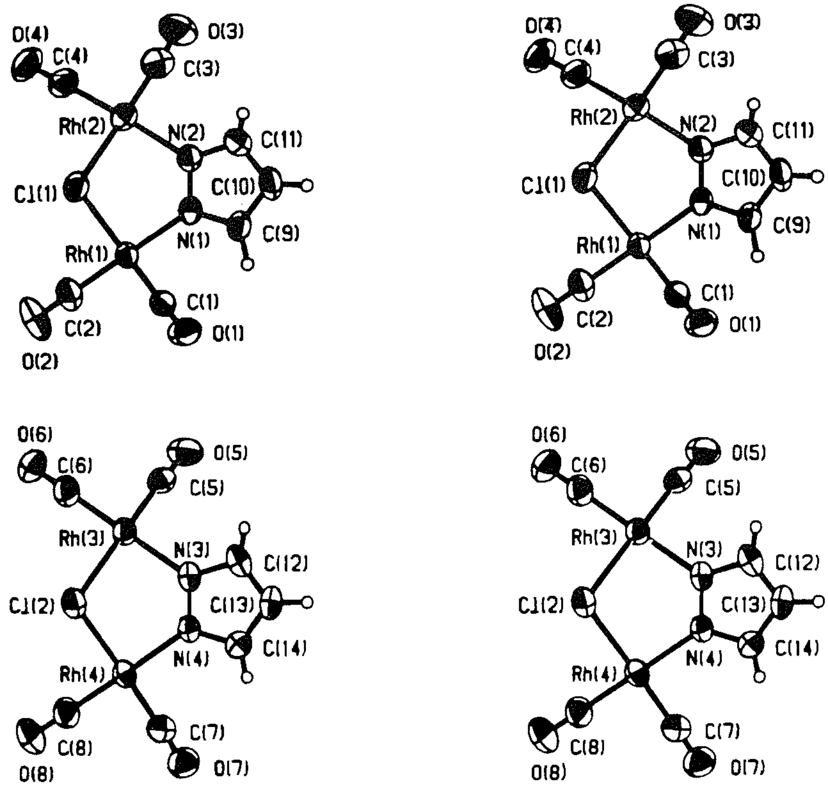

FIG. 1. Stereoscopic views of the two independent (μ-Cl)(μ-pz)[Rh(CO)$_2$]$_2$ molecules; 50% probability thermal ellipsoids are shown. Hydrogen atoms are assigned arbitrarily small thermal parameters for clarity.

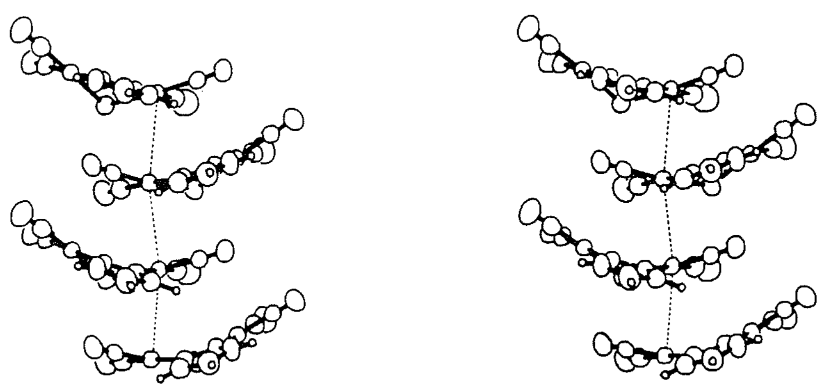

FIG. 2. Stereoscopic view of the stacking of (μ-Cl)(μ-pz)[Rh(CO)$_2$]$_2$ molecules; dotted lines indicate intermolecular Rh···Rh interactions.

On the final cycle of refinement the mean and maximum parameter shifts corresponded to 0.01 and 0.10σ, respectively. The mean error in an observation of unit weight was 1.438. A final difference map showed maximum fluctuations of -1.56 to $+0.97$ e Å^{-3} near Rh and was essentially featureless elsewhere. The final positional and thermal parameters appear in Tables 1 and 5,[2] respectively. Measured and calculated structure factors have been placed in the Depository of Unpublished Data.[2]

The ellipsoids of thermal motion for the non-hydrogen atoms are shown in Fig. 1. The thermal motion has been analysed in terms of the rigid-body modes of translation, libration, and screw motion (7). The rms standard error in the temperature factors σU_{ij} (derived from the least-squares analysis) is 0.0037 Å^2. Each of the two independent molecules behaved reasonably well as a rigid body (rms ΔU_{ij} = 0.0080 and 0.0066 Å^2). The appropriate bond distances have been corrected for libration (7, 8), using shape parameters q^2 of 0.08 for all atoms involved. Corrected bond lengths appear in Table 2 along with the uncorrected values; corrected bond angles do not differ by more than 1σ from the uncorrected values given in Table 3. Intra-annular torsion angles defining the conformations of five-membered chelate rings are listed in Table 4. Bond lengths and angles involving hydrogen and a complete listing of torsion angles (Tables 6–8) are included as supplementary material.[2]

Results and discussion

To our knowledge only one previous example of a binuclear transition metal species bridged by both an exobidentate pyrazolyl and a single atom ligand has been structurally characterized. Johnson and co-workers (9) recently reported the

[2]The structure factor table, Table 5 (anisotropic thermal parameters) and other material mentioned in the text are available, at a nominal charge, from the Depository of Unpublished Data, CISTI, National Research Council of Canada, Ottawa, Ont., Canada K1A 0S2.

TABLE 1. Final positional (fractional × 10^4, Rh and Cl × 10^5, H × 10^3) and isotropic thermal parameters ($U \times 10^3$ Å^2) with estimated standard deviations in parentheses

Atom	x	y	z	U_{eq}/U_{iso}
Rh(1)	78486(7)	38705(3)	28215(3)	45
Rh(2)	88632(7)	21558(3)	25329(3)	49
Rh(3)	27634(8)	37047(3)	27789(3)	48
Rh(4)	41398(7)	54327(3)	28438(3)	48
Cl(1)	74870(26)	28538(9)	35000(10)	59
Cl(2)	27016(27)	46406(9)	36551(10)	63
O(1)	8658(8)	5123(3)	1986(3)	76
O(2)	8169(10)	4531(3)	4511(4)	109
O(3)	10511(10)	1222(3)	1357(4)	98
O(4)	10302(9)	1352(3)	4027(4)	89
O(5)	3309(8)	2553(3)	1686(4)	83
O(6)	2743(9)	2831(3)	4295(4)	87
O(7)	5878(8)	6473(3)	1870(4)	76
O(8)	5287(10)	6146(3)	4452(4)	96
N(1)	7472(7)	3400(3)	1670(3)	43
N(2)	7893(7)	2757(3)	1558(3)	47
N(3)	2651(7)	4310(3)	1735(3)	47
N(4)	3281(7)	4934(3)	1749(3)	48
C(1)	8302(9)	4643(4)	2312(4)	51
C(2)	8079(11)	4283(4)	3877(5)	66
C(3)	9851(11)	1583(4)	1808(6)	68
C(4)	9761(11)	1642(4)	3456(5)	63
C(5)	3059(10)	2981(4)	2113(5)	54
C(6)	2754(11)	3161(4)	3729(5)	64
C(7)	5222(10)	6073(4)	2239(5)	55
C(8)	4881(11)	5878(4)	3837(5)	64
C(9)	6740(10)	3642(4)	928(4)	53
C(10)	6659(12)	3160(4)	324(4)	68
C(11)	7410(13)	2625(4)	742(5)	62
C(12)	2060(11)	4172(4)	926(4)	60
C(13)	2289(12)	4690(4)	420(5)	66
C(14)	3082(12)	5155(4)	950(5)	63
H(9)	625(8)	411(3)	89(3)	40(16)
H(10)	625(10)	323(3)	−25(4)	69(22)
H(11)	751(9)	228(3)	59(4)	39(19)
H(12)	150(8)	380(3)	83(4)	36(18)
H(13)	212(8)	470(3)	−17(4)	53(18)
H(14)	341(10)	554(3)	82(4)	68(24)

structure of the Pt(II) species $(Pt(\mu\text{-pz})(\mu\text{-Cl})(Cl)(C_2H_4))_2$ in which π-bonding between the pyrazolyl moiety and the Pt(II) centres was invoked to explain the planarity of the five-membered Pt_2N_2Cl ring. The title compound does not display this planarity but rather the expected puckered arrangement for the Rh_2N_2Cl rings which have conformations best described as Cl-envelopes (see Fig. 1 and Table 4). This imparts an overall bowed shape to each of the two crystallographically independent molecules, the angles between normals to the mean metal coordination planes being 41.4(2) and 34.2(2)°. The pyrazolyl rings (planar to within experimental error) are rotated out of the metal coordination planes by an average of 24.9°, individual values ranging from 17.9(2) to 29.7(2)°. The coordination about Rh is distorted square planar, each of the four indepenent RhC_2NCl groupings being significantly non-planar (maximum deviation from the mean plane 0.077(7) Å). The mean[3] structural parameters: Rh—Cl = 2.371(8), Rh—N = 2.065(6), Rh—C(*trans* to Cl) = 1.833(11), Rh—C(*trans* to N) = 1.869(8), C—O(*trans* to Cl) = 1.142(13), C—O(*trans* to N) = 1.127(8) Å, and Rh—Cl—Rh = 101.1(11)° are normal.

The structure of $(\mu\text{-Cl})(\mu\text{-pz})[Rh(CO)_2]_2$ does, however, offer a different type of rarity in that the molecules in the crystal lattice form one-dimensional stacks with alternate Rh atoms in the binuclear units interacting intermolecularly in a zig-zag chain arrangement (Fig. 2). Recently Stobart and co-workers (10) reported a similarly rare example of molecular stacking involving interactions between Rh atoms in adjacent mononuclear molecular units $Rh(CO)_2(Cl)(pzH)$, with Rh···Rh separations in the zig-zag chains of 3.4522(4) Å. The Rh···Rh distances in the present complex alternate between 3.5107(8) [Rh(1)···Rh(3) (1 + *x*, *y*, *z*)] and 3.6201(8) Å [Rh(1)···Rh(3)] with individual stacks being separated by normal van der Waals distances. A possible explanation for the longer distances in $(\mu\text{-Cl})(\mu\text{-pz})[Rh(CO)_2]_2$ is the marked non-planarity of the molecules which can be clearly seen in Fig. 2. At each Rh atom involved, one of the Rh···Rh interactions is

[3]Here and elsewhere in this report mean values refer to weighted means with rms deviations from the mean in parentheses.

TABLE 2. Bond lengths (Å) with estimated standard deviations in parentheses

Bond	Length Uncorr.	Length Corr.	Bond	Length Uncorr.	Length Corr.
Rh(1)—Cl(1)	2.369(2)	2.376	O(2)—C(2)	1.120(8)	1.121
Rh(1)—N(1)	2.058(5)	2.066	O(3)—C(3)	1.153(9)	1.155
Rh(1)—C(1)	1.818(7)	1.823	O(4)—C(4)	1.122(8)	1.126
Rh(1)—C(2)	1.867(8)	1.872	O(5)—C(5)	1.130(8)	1.132
Rh(2)—Cl(1)	2.364(2)	2.372	O(6)—C(6)	1.122(8)	1.123
Rh(2)—N(2)	2.050(5)	2.056	O(7)—C(7)	1.128(8)	1.130
Rh(2)—C(3)	1.822(9)	1.827	O(8)—C(8)	1.134(8)	1.138
Rh(2)—C(4)	1.869(8)	1.872	N(1)—N(2)	1.367(7)	1.371
Rh(3)—Cl(2)	2.370(2)	2.376	N(1)—C(9)	1.339(8)	1.341
Rh(3)—N(3)	2.062(5)	2.069	N(2)—C(11)	1.334(9)	1.335
Rh(3)—C(5)	1.843(8)	1.848	N(3)—N(4)	1.355(7)	1.357
Rh(3)—C(6)	1.871(8)	1.876	N(3)—C(12)	1.343(8)	1.344
Rh(4)—Cl(2)	2.354(2)	2.359	N(4)—C(14)	1.340(8)	1.341
Rh(4)—N(4)	2.060(5)	2.067	C(9)—C(10)	1.373(10)	1.374
Rh(4)—C(7)	1.831(8)	1.834	C(10)—C(11)	1.366(11)	1.369
Rh(4)—C(8)	1.855(8)	1.857	C(12)—C(13)	1.347(11)	1.349
O(1)—C(1)	1.150(8)	1.152	C(13)—C(14)	1.360(10)	1.362

TABLE 3. Bond angles (deg) with estimated standard deviations in parentheses

Bonds	Angle (deg)	Bonds	Angle (deg)
Cl(1)—Rh(1)—N(1)	88.65(15)	Rh(1)—N(1)—N(2)	123.6(4)
Cl(1)—Rh(1)—C(1)	176.0(2)	Rh(1)—N(1)—C(9)	127.9(5)
Cl(1)—Rh(1)—C(2)	90.0(2)	N(2)—N(1)—C(9)	108.4(5)
N(1)—Rh(1)—C(1)	91.8(2)	Rh(2)—N(2)—N(1)	123.1(4)
N(1)—Rh(1)—C(2)	177.3(3)	Rh(2)—N(2)—C(11)	130.4(5)
C(1)—Rh(1)—C(2)	89.7(3)	N(1)—N(2)—C(11)	106.3(6)
Cl(1)—Rh(2)—N(2)	89.45(15)	Rh(3)—N(3)—N(4)	124.3(4)
Cl(1)—Rh(2)—C(3)	177.0(3)	Rh(3)—N(3)—C(12)	128.6(5)
Cl(1)—Rh(2)—C(4)	88.2(2)	N(4)—N(3)—C(12)	107.0(6)
N(2)—Rh(2)—C(3)	92.2(3)	Rh(4)—N(4)—N(3)	124.0(4)
N(2)—Rh(2)—C(4)	177.2(3)	Rh(4)—N(4)—C(14)	128.7(5)
C(3)—Rh(2)—C(4)	90.2(3)	N(3)—N(4)—C(14)	107.1(5)
Cl(2)—Rh(3)—N(3)	88.76(15)	Rh(1)—C(1)—O(1)	177.4(6)
Cl(2)—Rh(3)—C(5)	174.5(2)	Rh(1)—C(2)—O(2)	178.3(8)
Cl(2)—Rh(3)—C(6)	90.7(2)	Rh(2)—C(3)—O(3)	178.7(7)
N(3)—Rh(3)—C(5)	91.5(3)	Rh(2)—C(4)—O(4)	177.8(7)
N(3)—Rh(3)—C(6)	177.5(3)	Rh(3)—C(5)—O(5)	176.6(6)
C(5)—Rh(3)—C(6)	89.2(3)	Rh(3)—C(6)—O(6)	179.4(7)
Cl(2)—Rh(4)—N(4)	90.16(15)	Rh(4)—C(7)—O(7)	179.3(7)
Cl(2)—Rh(4)—C(7)	177.7(2)	Rh(4)—C(8)—O(8)	178.1(7)
Cl(2)—Rh(4)—C(8)	89.1(2)	N(1)—C(9)—C(10)	109.5(7)
N(4)—Rh(4)—C(7)	91.5(3)	C(9)—C(10)—C(11)	104.5(7)
N(4)—Rh(4)—C(8)	179.1(3)	N(2)—C(11)—C(10)	111.2(7)
C(7)—Rh(4)—C(8)	89.2(3)	N(3)—C(12)—C(13)	110.8(7)
Rh(1)—Cl(1)—Rh(2)	100.07(6)	C(12)—C(13)—C(14)	104.6(7)
Rh(3)—Cl(2)—Rh(4)	102.20(7)	N(4)—C(14)—C(13)	110.5(7)

TABLE 4. Intra-annular torsion angles (deg) standard deviations in parentheses

Atoms	Torsion angle (deg)
N(1)—Rh(1)—Cl(1)—Rh(2)	33.44(15)
N(2)—Rh(2)—Cl(1)—Rh(1)	−32.9(2)
Cl(1)—Rh(2)—N(2)—N(1)	23.2(4)
Rh(1)—N(1)—N(2)—Rh(2)	2.6(6)
Cl(1)—Rh(1)—N(1)—N(2)	−26.6(4)
N(3)—Rh(3)—Cl(2)—Rh(4)	−28.68(15)
N(4)—Rh(4)—Cl(2)—Rh(3)	26.3(2)
Cl(2)—Rh(4)—N(4)—N(3)	−15.0(5)
Rh(3)—N(3)—N(4)—Rh(4)	−8.5(7)
Cl(2)—Rh(3)—N(3)—N(4)	26.2(5)

more nearly perpendicular to the Rh coordination plane than the other (deviations from perpendicularity are 5.6 and 15.1° at Rh(1), 4.8 and 11.1° at Rh(2)). It is noteworthy that these intermolecular distances, involving only one metal atom of each binuclear species, are shorter than the intramolecular distances Rh(1)···Rh(2) = 3.6274(8) and Rh(3)···Rh(4) = 3.6770(8) Å. The intermolecular distances, whilst longer than those reported by Stobart and co-workers (10), are nevertheless still close to the Rh···Rh distances of 3.253 and 3.271 Å in $Rh(CO)_2(acac)$ (11) for which intrinsic semi-conductor behavior has been suggested on the basis of conductivity measurements (12). Similar ground state non-zero Rh···Rh bond orders have recently been suggested for related face-to-face Rh(I) dimers on the basis of spectroscopic evidence by Gray and co-workers (13, 14). Interestingly Ferraro and Mertes in their recent review (15) mention that in the transition metal area efforts to achieve one-dimensional chains using binuclear complexes have not been successful. It appears that the present complex provides an example in this category.

Acknowledgments

We thank the Natural Sciences and Engineering Research Council of Canada for financial support and the University of British Columbia Computing Centre for assistance.

1. B. M. LOUIE, S. J. RETTIG, A. STORR, and J. TROTTER. Can. J. Chem. **62**, 1057 (1984).
2. P. COPPENS, L. LEISEROWITZ, and D. RABINOVICH. Acta Crystallogr. **18**, 1035 (1965).
3. J. DE MEULENAER and H. TOMPA. Acta Crystallogr. **19**, 1014 (1965).
4. D. T. CROMER and J. B. MANN. Acta Crystallogr. Sect. A, **24**, 321 (1968).
5. R. F. STEWART, E. R. DAVIDSON, and W. T. SIMPSON. J. Chem. Phys. **42**, 3175 (1965).
6. D. T. CROMER and D. LIBERMAN. J. Chem. Phys. **53**, 1891 (1970).
7. V. SCHOMAKER and K. N. TRUEBLOOD. Acta Crystallogr. Sect. B, **24**, 63 (1968).
8. D. W. J. CRUICKSHANK. Acta Crystallogr. **9**, 747 (1956); **9**, 754 (1956); **14**, 896 (1961).
9. W. C. DEESE, D. A. JOHNSON, and A. W. CORDES. Inorg. Chem. **20**, 1519 (1981).
10. M. J. DECKER, D. O. FJELDSTED, S. R. STOBART, and M. J. ZAWOROTKO. J. Chem. Soc. Chem. Commun. 1525 (1983).
11. F. HUG and A. C. SKAPSKI. J. Cryst. Mol. Struct. **4**, 411 (1974).
12. C. G. PITT, L. K. MONTEITH, L. F. BALLARD, J. P. COLLMANN, J. C. MORROW, W. R. ROPER, and D. ULKII. J. Am. Chem. Soc. **88**, 4286 (1966).
13. S. F. RICE and H. B. GRAY. J. Am. Chem. Soc. **103**, 1593 (1981).
14. R. F. DALLINGER, V. M. MISKOWSKI, H. B. GRAY, and W. H. WOODRUFF. J. Am. Chem. Soc. **103**, 1595 (1981).
15. J. R. FERRARO and K. B. MERTES. Coord. Chem. Rev. **36**, 357 (1981).

Iridium(I) complexes containing bidentate pyrazolylgallate ligands. X-ray crystal structures of [Me_2Gapz_2]Ir(COD), [Ir(μ-pz)$(CO)_2$]$_2$, and [Ir(μ-3,5-Me_2pz)$(CO)_2$]$_2$

SOPHIA NUSSBAUM, STEVEN J. RETTIG, ALAN STORR, AND JAMES TROTTER
Department of Chemistry, University of British Columbia, 2036 Main Mall, Vancouver, B.C., Canada V6T 1Y6

Received June 25, 1984

SOPHIA NUSSBAUM, STEVEN J. RETTIG, ALAN STORR, and JAMES TROTTER. Can. J. Chem. **63**, 692 (1985).

The synthesis and characterization of a number of Ir(I) complexes incorporating bidentate, chelating, pyrazolylgallate ligands are described. Non-rigidity for some of the complexes in solution has been demonstrated by variable temperature ^{1}H nmr studies. Crystal structures of three complexes, [Me_2Gapz_2]Ir(COD), [Ir(μ-pz)$(CO)_2$]$_2$, and [Ir(μ-3,5-Me_2pz)$(CO)_2$]$_2$ are reported and confirm the expected boat conformations for the six-membered M—(N—N)$_2$—Ir rings (where M = Ir or Ga) in the compounds. One of the complexes studied has exhibited measurable activity as a catalyst in the hydrogenation reaction of cyclohexene.

SOPHIA NUSSBAUM, STEVEN J. RETTIG, ALAN STORR et JAMES TROTTER. Can. J. Chem. **63**, 692 (1985).

On décrit le synthèse et la caractérisation d'un certain nombre de complexes de Ir(I) incorporant des ligands bidentates et chélatants du type pyrazolylgallate. Faisant appel à des études de rmn du ^{1}H à températures variables, on a démontré que, en solution, quelques uns de ces complexes ne sont pas rigides. On rapporte les structures de trois complexes, soit le [Me_2Gapz_2]Ir(COD), le [Ir(μ-pz)$(CO)_2$]$_2$ et le [Ir(μ-Me_2-3,5pz)$(CO)_2$]$_2$ et on confirme que, dans ces composés, les cycles à six chaînons M—(N—N)$_2$—Ir (où M = Ir ou Ga) existent sous les conformations bateaux que l'on avait prévues. Un des complexes étudiés présente une activité mesurable comme catalyseur pour l'hydrogénation du cyclohexène.

[Traduit par le journal]

Introduction

Recently we reported a series of Rh(I) complexes involving the bidentate chelating pyrazolylgallate ligands, [Me_2Gapz_2]$^-$ and [$Me_2Ga(3,5\text{-}Me_2pz)_2$]$^-$ (where pz = pyrazolyl, $N_2C_3H_3$ and 3,5-Me_2pz = 3,5-dimethylpyrazolyl, $N_2C_5H_7$) (1, 2). We have extended our investigations in this area and now report the synthesis and characterization of a number of Ir(I) complexes, [Me_2Gapz_2]Ir(COD), [Me_2Gapz_2]Ir$(CO)_2$, [Me_2Gapz_2]Ir(CO)(PPh_3), and [$Me_2Ga(3,5\text{-}Me_2pz)_2$]Ir(CO)($PPh_3$). The X-ray crystal structures of the three complexes [Me_2Gapz_2]Ir(COD), [Ir(μ-pz)$(CO)_2$]$_2$, and [Ir(μ-3,5-Me_2pz)$(CO)_2$]$_2$ are reported.

Experimental

All reactions and purifications were performed under a nitrogen atmosphere using Schlenk glassware or a glove-box. Tetrahydrofuran (THF) was dried by refluxing over sodium/benzophenone and distilled prior to use. Benzene was dried by refluxing over molten potassium. Hexane was distilled from calcium sulphate. [Ir(COD)Cl]$_2$ (Strem Chemicals) was used as supplied or prepared according to a literature method (3). Ir(CO)Cl$(PPh_3)_2$ (Strem Chemicals) and PPh_3 (MCB) were used as supplied. Ir$(CO)_2$Cl(p-$NH_2C_6H_4CH_3$) was prepared as described in the literature (4). The sodium salts of the gallium ligands [Me_2Gapz_2]$^-$, [$Me_2Ga(3,5\text{-}Me_2pz)_2$]$^-$, and [$MeGapz_3$]$^-$ were prepared as THF solutions as described earlier (5).

Preparation of [Me_2Gapz_2]Ir(COD)

[Ir(COD)Cl]$_2$ (0.200 g, 0.30 mmol) was dissolved in 50 mL THF and cooled to −78°C. Na[Me_2Gapz_2] (8.2 mL, 0.61 mmol) was added dropwise with stirring. The dark orange mixture was stirred for an additional 1.5 h at −78°C and the solvent was then removed under vacuum at 0°C. The residue was extracted into hexane and yielded large, air-stable, crystals in ~70% yield. Mp 112°C. *Anal.* calcd. for [Me_2Gapz_2]Ir(COD): C 35.96, H 4.50, N 10.49; found: C 36.02, H 4.55, N 10.31. ^{1}H nmr and ir data are reported in Table 1. The mass spectrum of the complex shows a weak signal (1.2%) due to the parent ion P$^+$ at m/e 534 (based on ^{193}Ir and ^{69}Ga), the most intense peak (100%) being due to the P − Me$^+$ ion.

From the hexane-insoluble materials [Ir(μ-pz)(COD)]$_2$ was obtained in ~23% yield by recrystallization from benzene.

Preparation of [Me_2Gapz_2]Ir$(CO)_2$

Method 1: from [Me_2Gapz_2]Ir(COD)

CO gas was passed through a solution of [Me_2Gapz_2]Ir(COD) in hexane at −78°C. The color of the solution turned instantly from orange to pale yellow. An ir spectrum of the solution showed two strong ν_{CO} stretching vibrations at 2074 and 2005 cm^{-1}. Evaporation of the solvent under vacuum at low temperature (−78 to −30°C) resulted in the appearance of the starting material whilst evaporation of the solvent at 0°C gave a mixture of [Ir(μ-pz)$(CO)_2$]$_2$ and [Me_2Gapz_2]Ir$(CO)_2$. Samples of the latter complex were also prepared by passing CO through solutions of [Me_2Gapz_2]Ir(COD) in C_6D_6 and d_6-acetone in nmr tubes. The ^{1}H nmr spectra (Fig. 1) were recorded immediately and revealed the presence of [Me_2Gapz_2]Ir$(CO)_2$ as the main product together with up to ~25% of the corresponding Ir carbonyl dimer [Ir(μ-pz)$(CO)_2$]$_2$. The latter complex exhibits three strong bands in the ν_{CO} region of the ir spectrum at 2083, 2070, and 2011 cm^{-1}. Its ^{1}H nmr in C_6D_6 consists of a triplet at τ = 4.03 (H^4) and a doublet at τ = 2.68 ppm (H^3, H^5).

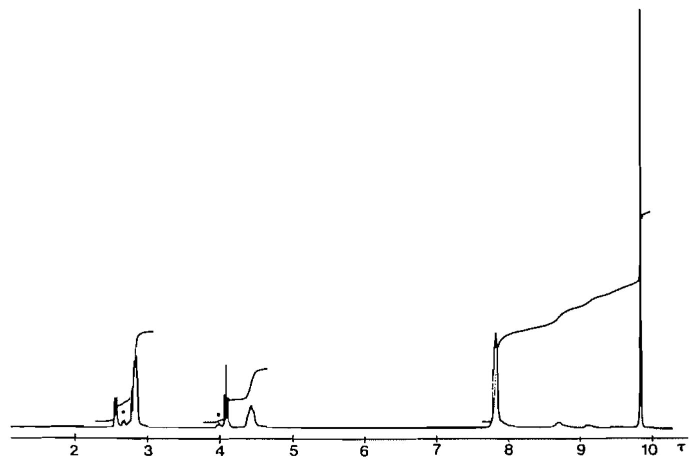

FIG. 1. Room temperature 80 MHz ^{1}H nmr spectrum of [Me_2Gapz_2]Ir$(CO)_2$ in C_6D_6 prepared directly in the nmr tube. Small peaks marked with an asterisk show the presence of the dimer species [Ir(μ-pz)(COD)]$_2$ whilst peaks at 4.4 and 7.8 τ are due to free COD.

Method 2: from Ir$(CO)_2$Cl(p-$NH_2C_6H_4CH_3$)

Ir$(CO)_2$Cl(p-$NH_2C_6H_4CH_3$) (0.100 g, 0.256 mmol) was dissolved in 20 mL THF and the solution was cooled to −78°C. Na[Me_2Gapz_2] (4.0 mL, 0.3 mmol) was added dropwise with stirring. The color turned from brown to dark yellow immediately. The solution was stirred for 30 min at low temperature and then the solvent was re-

TABLE 1. ^{1}H nmr and ir data for the complexes

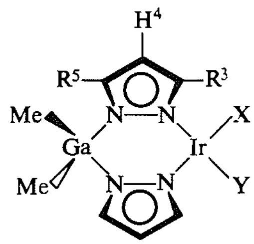

X	Y	GaMe	H^4	$R^3 = H$	$R^5 = H$	$R^3 = Me$	$R^5 = Me$	Other	Infrared $\nu_{CO}(cm^{-1})$(*n*-hexane)
		^{1}H nmr τ(ppm)*							
COD		9.58s	3.69t	2.60d	2.68d	—	—	6.30m, 7.84m 8.54m (COD)	—
CO	CO	9.81s	4.09t	2.56d	2.79d	—	—	—	2005, 2074
CO	PPh_3	9.48s	3.86t	1.96d	2.61d	—	—	2.30m (PPh_3)	1980
			4.33t	2.50d	3.05d	—	—	2.97m	
CO	PPh_3	9.24s	4.25s	—	—	7.31s	7.90s	2.34m (PPh_3)	1974
		9.73s	4.76s			7.87s	8.08s	2.99m	

*τ values refer to $\tau_{C_6H_6} = 2.84$ ppm, s = singlet, d = doublet, t = triplet, m = multiplet; $J_{HCCH} \approx 2$ Hz for pz protons. Assignment of pz-R^3 and pz-R^5 follows from assignment of other pyrazolyl complexes (34, 35).

moved *in vacuo* at −20°C to yield a black residue. This residue was extracted with hexane and the mixture filtered. On removal of hexane from the filtrate a dark yellow oily material, $[Me_2Gapz_2]Ir(CO)_2$, contaminated with canary-yellow crystals of $[Ir(\mu\text{-pz})(CO)_2]_2$, was obtained.

Preparation of $[Me_2Gapz_2]Ir(CO)(PPh_3)$

Method 1: from $[Me_2Gapz_2]Ir(COD)$

$[Me_2Gapz_2]Ir(COD)$ (0.0625 g, 0.117 mmol) was dissolved in about 10 mL THF and the solution was cooled to −78°C. CO gas was passed through the solution for ~45 min and then PPh_3 (0.028 g, 0.117 mmol) was added to the cold solution and the mixture stirred for an additional 30 min. The color changed from pale yellow to orange on the addition of the phosphine ligand. The solvent was evaporated *in vacuo* and the residue washed with hexane and then dissolved in benzene. The benzene solution yielded a slightly impure orange solid product (contaminated with traces of $[Ir(\mu\text{-pz})(CO)(PPh_3)]_2$) on slow evaporation of the solvent. *Anal.* calcd. for $[Me_2Gapz_2]Ir(CO)(PPh_3)$: C 45.26, H 3.77, N 7.82; found: C 45.34, H 4.09, N 6.50. The mass spectrum of the orange product gave a weak parent ion signal P^+ (0.3%) with the strongest signal being due to the $P - Me^+$ ion. In addition strong signals due to the ions $P - Me - pzH^+$ (15%) and $P - Me - CO - pzH^+$ (64%) were also observed. The hexane washings contained mainly the red dimer $[Ir(\mu\text{-pz})(CO)(PPh_3)]_2$.

Method 2: from $Ir(CO)Cl(PPh_3)_2$

$Ir(CO)Cl(PPh_3)_2$ (0.200 g, 0.256 mmol) was dissolved in ~100 mL THF and $Na[Me_2Gapz_2]$ (3.9 mL, 0.29 mmol) was added dropwise with stirring. The solution was then refluxed for 20 h. After evaporation of the solvent, the residue was washed with hexane and then dissolved in benzene. An oily orange material was again obtained upon evaporation of the benzene solvent.

Method 3: from $Ir(CO)_2Cl(p\text{-}NH_2C_6H_4CH_3)$

$Ir(CO)_2Cl(p\text{-}NH_2C_6H_4CH_3)$ (0.025 g, 0.064 mmol) and PPh_3 (0.017 g, 0.064 mmol) were dissolved in THF and $Na[Me_2Gapz_2]$ (1.0 mL, 0.074 mmol) was added dropwise with stirring. An orange solution resulted. The removal of the THF solvent yielded an orange residue which was extracted with benzene. The benzene solution on evaporation of solvent yielded an oily orange product.

In all three experiments it was found impossible to obtain analytically pure product but in all cases spectroscopic evidence and close analytical figures suggest that the oily orange material is predominantly the desired complex, $[Me_2Gapz_2]Ir(CO)(PPh_3)$.

Reaction of $[Ir(COD)Cl]_2$ with $Na[Me_2Ga(3,5\text{-}Me_2pz)_2]$

$[Ir(COD)Cl]_2$ (0.100 g, 0.15 mmol) was dissolved in ~50 mL THF and the solution cooled to −78°C. $Na[Me_2Ga(3,5\text{-}Me_2pz)_2]$ (3.6 mL, 0.32 mmol) was added dropwise with stirring. The initial light orange color darkened slowly during the addition of the gallate ligand. The solution was stirred for an additional hour at −78°C after the addition of the ligand, and then the solvent was removed under vacuum at −50°C. During the removal of the solvent the color changed gradually to purple. Although mass spectral evidence was obtained for the presence of the compound $[Me_2Ga(3,5\text{-}Me_2pz)_2]Ir(COD)$ in the solid obtained from the reaction, the main Ir-containing product isolated was the dimer $[Ir(\mu\text{-}3,5\text{-}Me_2pz)(COD)]_2$.

Preparation of $[Me_2Ga(3,5\text{-}Me_2pz)_2]Ir(CO)(PPh_3)$

$Ir(CO)Cl(PPh_3)_2$ (0.100 g, 0.125 mmol) was dissolved in ~25 mL THF and the solution cooled to −78°C. $Na[Me_2Ga(3,5\text{-}Me_2pz)_2]$ (1.5 mL, 0.14 mmol) was added dropwise with stirring. The mixture was stirred at −78°C for an additional 90 min. The solvent was then removed *in vacuo* and the residue extracted with hexane. The filtrate gave a yellow product in ~70% yield on slow evaporation of the solvent. This was recrystallized from benzene. *Anal.* calcd. for $[Me_2Ga(3,5\text{-}Me_2pz)_2]Ir(CO)(PPh_3).C_6H_6$: C 51.85, H 4.80, N 6.50; found: C 51.95, H 4.97, N 6.40. Ir and ^{1}H nmr data for the complex are reported in Table 1. The mass spectrum did not show a parent ion signal but did display the $P - Me^+$ ion signal as the strongest in the spectrum. The $P - Me - CO^+$ and $P - Me - CO - (3,5\text{-}Me_2pzH)^+$ ion signals were also observed. The hexane insoluble product was also recrystallized from benzene and proved to be a mixture of the Ir starting material and the dimer $[Ir(\mu\text{-}3,5\text{-}Me_2pz)(CO)(PPh_3)]_2$.

Reaction of $[Ir(COD)Cl]_2$ with $Na[Me_2Ga(3,5\text{-}Me_2pz)_2]$ and CO

$[Ir(COD)Cl]_2$ (0.030 g, 0.045 mmol) was dissolved in ~20 mL THF and the solution cooled to −78°C. $Na[Me_2Ga(3,5\text{-}Me_2pz)_2]$ (1.2 mL, 0.10 mmol) was added dropwise and CO gas passed slowly through the solution which was stirred at −78°C for ~2 h. The solvent was then removed at −78°C to yield an orange residue which was recrystallized from hexane to give orange crystals of $[Ir(\mu\text{-}3,5\text{-}Me_2pz)(CO)_2]_2$. *Anal.* calcd. for $[Ir(\mu\text{-}3,5\text{-}Me_2pz)(CO)_2]_2$: C 24.47, H 2.04, N 8.16; found: C 24.10, H 2.08, N 7.79. ν_{CO} (hexane) 2079, 2060, 2004 cm^{-1}. ^{1}H nmr (C_6D_6), τ = 4.25 s (H^4) and 7.75 s (pz—Me) ppm. The mass spectrum (Fig. 2*b*) displayed the parent ion signal P^+ as the strongest signal in the spectrum, other signals arising from the ions $P - CO^+$, $P - 2CO^+$, $P - 3CO^+$, $P - 3CO - MeCN^+$,

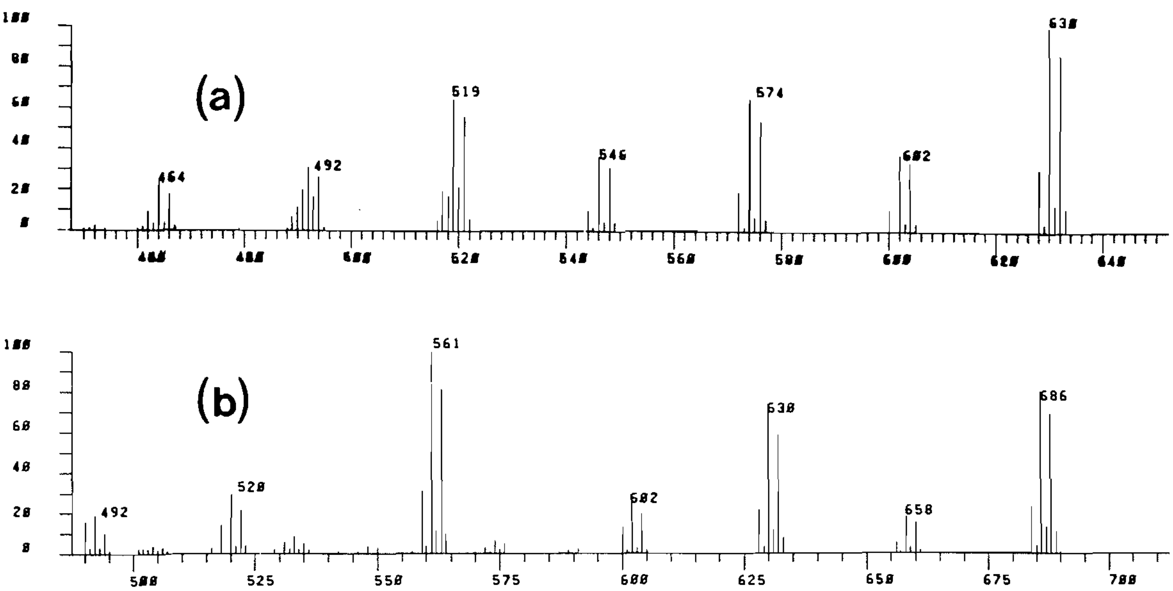

FIG. 2. Partial mass spectra of (*a*) $[Ir(\mu\text{-pz})(CO)_2]_2$ and (*b*) $[Ir(\mu\text{-}3,5\text{-}Me_2pz)(CO)_2]_2$ at 70 eV and 240°C.

and $P - 4CO - 2MeCN^+$. In this reaction, no evidence was obtained for the formation of the desired gallate complex $[Me_2Ga(3,5\text{-}Me_2pz)_2]Ir(CO)_2$.

Reaction of $[Ir(COD)Cl]_2$ with $Na[Me_2Ga(3,5\text{-}Me_2pz)_2]$, CO, and PPh_3

This reaction was identical to the one described above but after the CO had been bubbled through the solution an equimolar amount of PPh_3 was added. No signals corresponding to the gallate complex $[Me_2Ga(3,5\text{-}Me_2pz)_2]Ir(CO)(PPh_3)$ were detected by ^1H nmr spectroscopy of the product. The mass spectrum of the product corresponded to the dimer $[Ir(\mu\text{-}3,5\text{-}Me_2pz)(CO)(PPh_3)]_2$ with the strongest signal due to the parent ion P^+ (100%) and other prominent signals due to the ions $P - CO^+$, $P - CO - (3,5\text{-}Me_2pzH)^+$, and $P - 2CO - (3,5\text{-}Me_2pzH)^+$.

Reaction of $Ir(CO)_2Cl(p\text{-}NH_2C_6H_4CH_3)$ with $Na[Me_2Ga(3,5\text{-}Me_2pz)_2]$

$Ir(CO)_2Cl(p\text{-}NH_2C_6H_4CH_3)$ (0.100 g, 0.26 mmol) was dissolved in 50 mL THF and cooled to −78°C. $Na[Me_2Ga(3,5\text{-}Me_2pz)_2]$ (3.0 mL, 0.29 mmol) was added dropwise with stirring. The color of the solution changed instantly from brown to orange. The solvent was removed *in vacuo* at −50°C to yield an orange residue. This was extracted with hexane. On removal of solvent from the hexane solution orange crystals of the dimer $[Ir(\mu\text{-}3,5\text{-}Me_2pz)(CO)_2]_2$ formed together with a small amount of a yellow solid identified by mass spectral analysis to be the complex $[Me_2Ga(3,5\text{-}Me_2pz)_2]Ir(CO)_2$ (mass spectral signals observed were due to the ions $P - Me^+$ (100%), $P - Me - CO^+$ (56%), $P - Me - 2CO^+$ (19%), and $P - Me - 2CO - (3,5\text{-}Me_2pzH)^+$ (13%)).

Preparation of $[Ir(\mu\text{-pz})(CO)_2]_2$

$[Ir(\mu\text{-pz})(COD)]_2$ (0.020 g, 0.03 mmol) was dissolved in acetone and the solution cooled to −78°C. CO gas was bubbled through the solution for 2 h. The initial purple color first changed to yellow, then to bright green, and finally to dark blue. The cooling bath was then removed and the color of the solution changed back to yellow. The solvent was then allowed to evaporate slowly leaving the product as a mixture of mainly yellow crystals together with a small amount of black solid. Both materials gave virtually identical analytical results. *Anal.* calcd. for $[Ir(\mu\text{-pz})(CO)_2]_2$: C 19.03, H 0.95, N 8.88; found: C 19.05, H 1.03, N 8.74. ν_{CO}(hexane) 2083, 2070, and 2011 cm^{-1}. ^1H nmr (C_6D_6), τ = 4.03 t (H^4) and 2.68 d (H^3, H^5) ppm. The mass spectrum (Fig. 2*a*) of the complex displayed the parent ion signal P^+ as the strongest signal in the spectrum, with other strong signals arising from the ions $P - CO^+$, $P - 2CO^+$, $P - 3CO^+$, $P - 3CO - HCN^+$, $P - 3CO - 2HCN^+$, and $P - 4CO - 2HCN^+$, the latter three ions arising from partial fragmentation of the bridging pyrazolyl moieties.

Spectra

Ir spectra were recorded on a Perkin-Elmer model 598 spectrometer. ^1H nmr spectra were recorded on a Bruker WP-80, a Varian XL-100, or a Bruker WM-400 instrument. Mass spectra were recorded on an AEI MS50 spectrometer at 70 eV and 150 or 240°C. GC/GCMS measurements were performed using 12 m carbowax-20 capillary columns.

X-ray crystallographic analyses

[Dimethylbis(1-pyrazolyl)gallato-N^2,N$^{2\prime}$](cyclooctadiene)iridium(I)

A crystal bounded by the 10 faces (followed by their distances in mm from a common origin): ±(2 1 0), 0.15, ±(2 −1 0), 0.15, ±(1 0 0), 0.16, ±(0 1 0), 0.11, ±(0 1 1), 0.30 was mounted in a general orientation. Unit-cell parameters were refined by least-squares on 2 sin θ/λ values for 25 reflections (2θ = 45−51°) measured on a diffractometer with Mo-$K\alpha$ Radiation ($\lambda(K\alpha_1)$ = 0.70930, $\lambda(K\alpha_2)$ = 0.71359 Å). Crystal data at 22°C are:

$C_{16}H_{24}GaIrN_4$ fw = 534.33
Orthorhombic, a = 22.8123(10), b = 11.9595(5), c = 6.4497(3) Å, V = 1759.6(1) Å^3, Z = 4, ρ_c = 2.017 Mg m^{-3}, $F(000)$ = 1024, μ(Mo-$K\alpha$) = 90.58 cm^{-1}. Absent reflections: $0kl$, $k + l$ odd, and $hk0$, h odd, space group *Pnma* (D_{2h}^{16}, No. 62) from structure analysis.

Intensities were measured with graphite-monochromated Mo-$K\alpha$ radiation on an Enraf-Nonius CAD4-F diffractometer. An ω−2θ scan at 1.18−10.06° min^{-1} over a range of (0.75 + 0.35 tan θ) degrees in ω (extended by 25% on both sides for background measurement) was employed. Data were measured to 2θ = 65°. The intensities of three check reflections, measured every 3600 s throughout the data collection, showed only minor random fluctuations. After data reduction,[1] an absorption correction was applied using the analytical method (6, 7). Transmission factors ranged from 0.092 to 0.188. Of the 3298 independent reflections measured, 2205 (66.9%) had intensities

[1]The computer programs used include locally written programs for data processing and locally modified versions of the following: ORFLS, full-matrix least-squares, and ORFFE, function and errors, by W. R. Busing, K. O. Martin and H. A. Levy; FORDAP, Patterson and Fourier synthesis, by A. Zalkin; ORTEP II, illustrations, by C. K. Johnson.

greater than or equal to $3\sigma(I)$ above background where $\sigma^2(I) = S + 2B + (0.04(S - B))^2$ with S = scan count and B = normalized background count.

The structure is isomorphous with that of the Rh(I) analog (1), the refinement being initiated with the non-hydrogen atom coordinates from the Rh(I) complex. After full-matrix least-squares refinement of the non-hydrogen atoms with anisotropic thermal parameters to R = 0.042, a difference map gave positions for all H atoms. Attempts to refine the hydrogen atoms with isotropic thermal parameters were not successful. In the final stages of refinement the five trigonal planar H atoms were refined with isotropic thermal parameters while the remaining H atoms were included as fixed contributors in idealized positions (C—H = 0.98 Å). The scattering factors of ref. 8 were used for non-hydrogen atoms and those of ref. 9 for hydrogen atoms. Anomalous scattering factors from ref. 10 were used for the Ir and Ga atoms. The weighting scheme $w = 1/\sigma^2(F)$, where $\sigma^2(F)$ is derived from the previously defined $\sigma^2(I)$, gave uniform average values of $w(|F_o| - |F_c|)^2$ over ranges of both $|F_o|$ and $\sin\theta/\lambda$ and was employed in the final stages of full-matrix refinement of variables. Reflections with $I < 3\sigma(I)$ were not included in the refinement. Convergence was reached at R = 0.040 and R_w = 0.046 for 2205 reflections with $I \geq 3\sigma(I)$. For all 3298 reflections R = 0.076. The function minimized was $\Sigma w(|F_o| - |F_c|)^2$, $R = \Sigma||F_o| - |F_c||/\Sigma|F_o|$ and $R_w = (\Sigma w(|F_o| - |F_c|)^2/\Sigma w|F_o|^2)^{1/2}$.

On the final cycle of refinement the mean and maximum parameter shifts corresponded to 0.009 and 0.07σ, respectively. The mean error in an observation of unit weight was 1.724. A final difference map showed maximum fluctuations of −7.5 to +4.0 e Å^{-3} near Ir and ±0.5 e Å^{-3} away from the heavy atoms. The final positional and thermal parameters appear in Tables 2 and 8,[2] respectively. Measured and calculated structure factors have been placed in the Depository of Unpublished Data.[2]

Bis(μ-pyrazolyl)bis[dicarbonyliridium(I)]

Experimental details are as above except where noted. Crystals of this compound were of poor quality, that eventually used for data collection being very irregular in shape with dimensions of approximately 0.30 × 0.45 × 0.45 mm. Unit-cell parameters were determined from least-squares on 2 sin θ/λ values for 25 reflections with 2θ = 30−37°. Crystal data:

$C_{10}H_6Ir_2N_4O_4$ fw = 630.62

Monoclinic, a = 7.270(2), b = 16.1062(13), c = 11.918(3) Å, β = 94.54(1)°, V = 1391.2(5) Å^3, Z = 4, ρ_c = 3.011 Mg m^{-3}, $F(000)$ = 1120, μ(Mo-$K\alpha$) = 190.7 cm^{-1}. Absent reflections: hkl, $h + k + l$ odd, space group $I2/m$ (non-standard setting of $C2/m$, C^3_{2h}, No. 12, equivalent positions: (0, 0, 0), (1/2, 1/2, 1/2) ±(x, y, z; x −y, z)) from structure analysis.

An ω-2θ scan at 2.24−10.06° min^{-1} over a range of (1.1 + 0.35 tan θ)° in ω was employed. Of 1655 independent reflections measured (to 2θ = 55°), 1098 (66.3%) had intensities greater than or equal to $3\sigma(I)$ above background. The intensities of the three standard reflections displayed non-uniform behaviour, one intensity decreasing (by 7%) while the other two increased (by 10 and 15%). The crystal itself, initially yellow, turned dark brown by the end of the data collection. A correction for non-uniform crystal decay was applied (11), but the irregularity of the crystal surface precluded the application of an absorption correction.

The centrosymmetric space group $I2/m$ was indicated by the Patterson function, from which the position of the Ir atom was determined. The remaining non-hydrogen atoms were positioned from subsequent difference maps and the hydrogen atom positions were calculated. In the final stages of refinement only the Ir atom was refined with anisotropic thermal parameters. Attempts to refine the O, N, and C atoms with anisotropic thermal parameters resulted in non-

[2]The structure factor table, Table 8 (anisotropic thermal parameters) and other material mentioned in the text are available, at a nominal charge, from the Depository of Unpublished Data, CISTI, National Research Council of Canada, Ottawa, Canada K1A 0S2.

TABLE 2. Final positional (fractional × 10^4, Ir and Ga × 10^5, H × 10^3) and isotropic thermal parameters (U × 10^3 Å^2) with estimated standard deviations in parentheses

Atom	x	y	z	U_{eq}/U_{iso}
		$[Me_2Gapz_2]Ir(COD)$		
Ir	32645(1)	25000	41338(4)	30
Ga	48027(4)	25000	51256(16)	41
N(1)	3834(2)	1272(4)	3061(8)	37
N(2)	4423(2)	1280(5)	3491(8)	41
C(1)	4490(5)	2500	7974(15)	53
C(2)	5626(5)	2500	4278(18)	64
C(3)	1978(3)	1909(7)	3915(16)	70
C(4)	2557(3)	1339(5)	4276(11)	42
C(5)	2855(3)	1351(5)	6167(10)	44
C(6)	2644(4)	1893(6)	8126(13)	73
C(7)	3728(3)	368(5)	1887(11)	49
C(8)	4249(3)	−225(6)	1578(13)	54
C(9)	4663(3)	384(6)	2603(12)	49
H(4)	265(3)	82(5)	346(10)	35(17)
H(5)	319(3)	80(7)	617(10)	44(20)
H(7)	330(2)	21(6)	117(10)	32(17)
H(8)	432(3)	−74(7)	93(10)	45(21)
H(9)	518(4)	36(6)	241(17)	95(29)
		$[Ir(\mu\text{-}pz)(CO)_2]_2$ (O, N, C × 10^4)		
Ir	22338(32)	10885(12)	23278(16)	33
O(1)	−92(8)	205(4)	311(5)	75(15)
O(2)	208(7)	209(4)	21(4)	67(14)
N(1)	438(5)	39(3)	184(3)	28(9)
N(2)	242(6)	39(3)	381(3)	35(10)
C(1)	22(7)	169(3)	285(4)	28(10)
C(2)	205(9)	165(5)	106(5)	50(15)
C(3)	598(9)	67(4)	143(6)	45(15)
C(4)	705(12)	0	120(7)	48(22)
C(5)	230(8)	69(4)	488(5)	42(14)
C(6)	267(12)	0	554(7)	43(20)
		$[Ir(\mu\text{-}3,5\text{-}Me_2pz)(CO)_2]_2.0.5(p\text{-}Me_2C_6H_4)$		
Ir(1)	28933(3)	31882(3)	39032(5)	40
Ir(2)	21913(3)	33593(3)	74669(4)	36
O(1)	3697(8)	5416(8)	2510(12)	77
O(2)	2357(8)	5647(7)	9099(10)	68
O(3)	5614(8)	3159(9)	3714(12)	82
O(4)	4351(9)	3438(10)	10037(11)	86
N(1)	2206(8)	1631(7)	4856(10)	46
N(2)	1934(7)	1729(7)	6359(10)	41
N(3)	1000(7)	3159(7)	4113(8)	38
N(4)	727(7)	3262(7)	5612(9)	41
C(1)	3398(10)	4568(10)	3070(12)	49
C(2)	2308(9)	4783(9)	8462(12)	45
C(3)	4559(11)	3182(10)	3765(13)	54
C(4)	3504(10)	3416(9)	9060(13)	51
C(5)	2002(10)	529(9)	4380(12)	46
C(6)	1622(12)	−141(9)	5589(17)	65
C(7)	1594(10)	641(9)	6794(13)	48
C(8)	−21(9)	3158(8)	3123(12)	41
C(9)	−958(9)	3273(9)	3946(13)	46
C(10)	−461(9)	3349(8)	5532(11)	38
C(11)	2256(15)	115(14)	2802(16)	79
C(12)	1275(13)	447(12)	8431(17)	69
C(13)	−51(11)	3042(11)	1375(14)	59
C(14)	−1092(11)	3468(10)	6991(15)	55
C(15)	5097(12)	706(12)	8755(25)	93
C(16)	5776(13)	1186(12)	10368(25)	94
C(17)	5706(14)	510(13)	11543(22)	95
C(18)	5243(14)	1424(14)	7578(23)	95

positive definite temperature factors. Convergence was reached at $R = 0.119$ and $R_w = 0.148$ for 1098 reflections with $I \geq 3\sigma(I)$, for all 1655 reflections $R = 0.159$. The use of standard errors weights resulted in no unusual trends in average values of $w(|F_o| - |F_c|)^2$ over ranges of both $|F_o|$ and $\sin\theta/\lambda$. The mean and maximum parameter shifts on the final cycle of refinement corresponded to 0.01 and 0.10 σ, respectively. The mean error in an observation of unit weight was 5.564. An isotropic Type I extinction correction (Thornley-Nelmes definition of mosaic anisotropy with a Lorentzian distribution) was applied (12–14). The final value of g was $0.87(17) \times 10^4$.

Bis(μ-3,5-dimethylpyrazolyl)bis[dicarbonyliridium(I)]xylene (2:1)

The bounding faces of the crystal (followed by their distances in mm from a common origin) were: ±(1 0 −2), 0.03, ±(1 0 −4), 0.06, ±(1 0 0), 0.20, ±(1 −1 0), 0.27, (0 −1 0), 0.27, (2 0 3), 0.07. Crystal data:

$C_{14}H_{14}Ir_2N_4O_4 \cdot 0.5C_8H_{10}$ fw = 739.81

Triclinic, a = 10.877(3), b = 12.532(3), c = 8.591(4) Å, α = 96.02(2), β = 96.55(2), γ = 114.12(1)°, V = 1046.9(6) Å^3, Z = 2, ρ_c = 2.347 Mg m^{-3}, $F(000)$ = 682, μ(Mo-$K\alpha$) = 126.86 cm^{-1}. Absent reflections: none, space group $P\bar{1}$ (C_i^1, No. 2, reduced cell) from structure analysis.

An $\omega-2\theta$ scan at 1.18–10.06° min^{-1} over a range of $(0.80 + 0.35 \tan\theta)°$ in ω was employed. Of 4776 independent reflections measured (to 2θ = 55°), 3437 had intensities greater than or equal to $3\sigma(I)$ above background. The intensities of the standard reflections showed only small random fluctuations. An absorption correction was applied using the Gaussian integration method (6, 15), transmission factors ranging from 0.048 to 0.467 for 364 sampling points.

The centrosymmetric space group $P\bar{1}$ was indicated by both the E-statistics and the Patterson function, from which the coordinates of the Ir atoms were determined. The positions of the remaining non-hydrogen atoms (including those associated with a centrosymmetric xylene solvate) were determined from a subsequent difference map. In the final stages of refinement all non-hydrogen atoms were refined with anisotropic thermal parameters and H atoms were included as fixed contributors in idealized positions. Convergence was reached at $R = 0.039$ and $R_w = 0.049$ for 3437 reflections with $I \geq 3\sigma(I)$; for all 4776 reflections, $R = 0.064$. The mean and maximum parameter shifts on the final cycle of refinement corresponded to 0.06 and 0.25 σ and the mean error in an observation of unit weight was 2.136. Maximum fluctuations on the final difference map corresponded to −4.4 to +3.1 e Å^{-3} near the Ir atoms with no unusual features noted elsewhere.

Bond lengths and angles appear in Tables 3 and 4, respectively and intra-annular torsion angles in Table 5. Calculated hydrogen parameters are given in Table 7.[2] Bond lengths and angles involving H atoms for $[Me_2Gapz_2]Ir(COD)$ (Tables 9 and 10) are included as supplementary material.

TABLE 3. Bond lengths (Å) with estimated standard deviations in parentheses

Bond	Length (Å)	Bond	Length (Å)
	$[Me_2Gapz_2]Ir(COD)$		
Ir —N(1)	2.080(5)	N(1)—C(7)	1.342(8)
Ir —C(4)	2.130(6)	N(2)—C(9)	1.333(8)
Ir —C(5)	2.117(6)	C(3)—C(4)	1.506(10)
Ga —N(2)	1.998(5)	C(4)—C(5)	1.395(10)
Ga —C(1)	1.971(10)	C(5)—C(6)	1.499(10)
Ga —C(2)	1.956(11)	C(7)—C(8)	1.398(9)
N(1)—N(2)	1.371(7)	C(8)—C(9)	1.363(10)
	$[Ir(\mu\text{-pz})(CO)_2]_2$		
Ir —N(1)	2.05(4)	N(1)—C(3)	1.37(7)
Ir —N(2)	2.10(4)	N(1)—N(1)′	1.24(9)
Ir —C(1)	1.90(5)	N(2)—C(5)	1.37(7)
Ir —C(2)	1.76(7)	N(2)—N(2)′	1.25(10)
O(1)—C(1)	1.08(7)	C(3)—C(4)	1.37(8)
O(2)—C(2)	1.24(8)	C(5)—C(6)	1.37(7)
	$[Ir(\mu\text{-3,5-}Me_2pz)(CO)_2]_2.0.5(p\text{-}Me_2C_6H_4)$		
Ir(1)—N(1)	2.079(8)	N(3)—N(4)	1.359(11)
Ir(1)—N(3)	2.074(7)	N(3)—C(8)	1.319(10)
Ir(1)—C(1)	1.838(11)	N(4)—C(10)	1.334(11)
Ir(1)—C(3)	1.832(11)	C(5)—C(6)	1.40(2)
Ir(2)—N(2)	2.055(8)	C(5)—C(11)	1.50(2)
Ir(2)—N(4)	2.077(7)	C(6)—C(7)	1.36(2)
Ir(2)—C(2)	1.844(10)	C(7)—C(12)	1.51(2)
Ir(2)—C(4)	1.835(10)	C(8)—C(9)	1.351(14)
O(1)—C(1)	1.152(13)	C(8)—C(13)	1.49(2)
O(2)—C(2)	1.138(12)	C(9)—C(10)	1.386(14)
O(3)—C(3)	1.165(12)	C(10)—C(14)	1.519(14)
O(4)—C(4)	1.162(12)	C(15)—C(16)	1.43(2)
N(1)—N(2)	1.361(11)	C(15)—C(18)	1.40(2)
N(1)—C(5)	1.317(12)	C(15)—C(17)′	1.39(2)
N(2)—C(7)	1.364(12)	C(16)—C(17)	1.37(2)

Results and discussion

There have been but few reports in the literature dealing with Ir complexes containing polypyrazolylborate ligands. Thus Powell and co-workers (16) reported briefly on a "few" Ir(III) complexes incorporating the $[HB(3,5\text{-}Me_2pz)_3]^-$ ligand and while Bonati *et al.* (17) were successful in isolating the complexes $[H_2Bpz_2]Ir(CO)_2$ and $[H_2Bpz_2]Ir(CO)PPh_3$, King and Bond (18) were unable to isolate any "tractable" products from their experiments in this area. This dearth of information is to be contrasted with the wealth of material available in the area of polypyrazolylborate Rh chemistry (16–24). More recently a considerable effort has focussed on pyrazolyl-bridged Ir dimers (25–29) and Bonati and co-workers (30) have reported the structure of a unique Ir(I) complex containing a monodentate pyrazolyl ligand. As part of an ongoing study of pyrazolylgallate ligands we reported recently our findings in the area of Rh(I) complexes (1, 2, 31). The present paper presents our findings in the related area of Ir(I) chemistry. Thus the two bidentate chelating gallate ligands $[Me_2Gapz_2]^-$ and $[Me_2Ga(3,5\text{-}Me_2pz)_2]^-$ have been used to prepare a number of Ir(I) complexes. In most of the reactions investigated, in addition to the pyrazolylgallate iridium complexes formed, pyrazolyl iridium dimer species were also produced and in a few of the reactions these dimers were the only isolable Ir products. The reactions performed are summarized in Schemes 1 and 2. In addition, the reactivity of some Ir(I) species towards the tridentate pyrazolylgallate ligand $[MeGapz_3]^-$ were also investigated, but in these experiments only pyrazolyl iridium dimers were obtained. The new Ir compounds prepared have been characterized by ir, ^{1}H nmr, mass spectra, and elemental analyses. In addition definitive X-ray structural analyses are presented for the three complexes $[Me_2Gapz_2]Ir(COD)$, $[Ir(\mu\text{-pz})(CO)_2]_2$, and $[Ir(\mu\text{-3,5-}Me_2pz)(CO)_2]_2$.

The complex $[Me_2Gapz_2]Ir(COD)$ was prepared in ~70% yield from $[Ir(COD)Cl]_2$ and $Na[Me_2Gapz_2]$ at low temperature in THF solution. At higher temperatures the yield of the gallate iridium complex is considerably reduced and the pyrazolyl iridium dimer $[Ir(\mu\text{-pz})(COD)]_2$ becomes the predominant product. The complex $[Me_2Gapz_2]Ir(COD)$ can be recrystallized from hexane at room temperature, yielding orange air-stable crystals. The ^{1}H nmr of the complex at room temperature in d_6-acetone displays but one singlet for the "$GaMe_2$" protons and also indicates equivalent pyrazolyl groups in the compound. However, on lowering the temperature (see Fig. 3)

TABLE 4. Bond angles (deg) with estimated standard deviations in parentheses*

Bonds	Angle (deg)	Bonds	Angle (deg)
	$[Me_2Gapz_2]Ir(COD)$		
N(1)—Ir —C(4)	91.6(2)	N(2)—N(1)—C(7)	107.2(5)
N(1)—Ir —C(5)	91.4(2)	Ga —N(2)—N(1)	122.5(4)
N(1)—Ir —N(1)′	89.9(3)	Ga —N(2)—C(9)	129.5(5)
N(1)—Ir —C(4)′	161.4(2)	N(1)—N(2)—C(9)	108.0(5)
N(1)—Ir —C(5)′	160.1(2)	Ir —C(4)—C(3)	111.3(5)
C(4)—Ir —C(5)	38.4(3)	Ir —C(4)—C(5)	70.3(4)
C(4)—Ir —C(4)′	81.3(3)	C(3)—C(4)—C(5)	123.9(7)
C(4)—Ir —C(5)′	93.5(3)	Ir —C(5)—C(4)	71.3(3)
C(5)—Ir —C(5)′	80.9(4)	Ir —C(5)—C(6)	112.5(4)
N(2)—Ga —C(1)	109.6(2)	C(4)—C(5)—C(6)	125.9(7)
N(2)—Ga —C(2)	105.6(3)	C(5)—C(6)—C(6)′	115.6(4)
N(2)—Ga —N(2)′	93.8(3)	N(1)—C(7)—C(8)	109.7(6)
C(1)—Ga —C(2)	127.4(5)	C(7)—C(8)—C(9)	104.3(6)
Ir —N(1)—N(2)	122.6(4)	N(2)—C(9)—C(8)	110.7(6)
Ir —N(1)—C(7)	130.1(4)		
	$[Ir(\mu\text{-pz})(CO)_2]_2$		
N(1)—Ir —N(2)	87(2)	Ir —N(2)—C(5)	126(4)
N(1)—Ir —C(1)	176(2)	Ir —N(2)—N(2)′	122.6(13)
N(1)—Ir —C(2)	93(2)	C(5)—N(2)—N(2)′	111(3)
N(2)—Ir —C(1)	90(2)	Ir —C(1)—O(1)	177(5)
N(2)—Ir —C(2)	178(2)	Ir —C(2)—O(2)	174(6)
C(1)—Ir —C(2)	90(3)	N(1)—C(3)—C(4)	109(5)
Ir —N(1)—C(3)	127(4)	C(3)—C(4)—C(1)′	78(4)
Ir —N(1)—N(1)′	123.5(12)	N(2)—C(5)—C(6)	102(6)
C(3)—N(1)—N(1)′	109(3)	C(5)—C(6)—C(2)′	82(4)
	$[Ir(\mu\text{-}3,5\text{-}Me_2pz)(CO)_2]_2.0.5(p\text{-}Me_2C_6H_4)$		
N(1)—Ir(1)—N(3)	85.3(3)	Ir(1)—C(1)—O(1)	178.2(10)
N(1)—Ir(1)—C(1)	176.4(3)	Ir(2)—C(2)—O(2)	178.3(10)
N(1)—Ir(1)—C(3)	93.0(4)	Ir(1)—C(3)—O(3)	178.0(11)
N(3)—Ir(1)—C(1)	91.1(4)	Ir(2)—C(4)—O(4)	178.0(10)
N(3)—Ir(1)—C(3)	178.1(4)	N(1)—C(5)—C(6)	110.3(10)
C(1)—Ir(1)—C(3)	90.6(5)	N(1)—C(5)—C(11)	123.2(11)
N(2)—Ir(2)—N(4)	86.1(3)	C(6)—C(5)—C(11)	126.3(11)
N(2)—Ir(2)—C(2)	176.5(3)	C(5)—C(6)—C(7)	103.8(9)
N(2)—Ir(2)—C(4)	92.3(4)	N(2)—C(7)—C(6)	110.6(10)
N(4)—Ir(2)—C(2)	91.9(3)	N(2)—C(7)—C(12)	120.4(10)
N(4)—Ir(2)—C(4)	178.1(4)	C(6)—C(7)—C(12)	129.0(10)
C(2)—Ir(2)—C(4)	89.8(4)	N(3)—C(8)—C(9)	109.6(9)
Ir(1)—N(1)—N(2)	115.8(6)	N(3)—C(8)—C(13)	122.1(9)
Ir(1)—N(1)—C(5)	135.4(8)	C(9)—C(8)—C(13)	128.3(8)
N(2)—N(1)—C(5)	108.8(8)	C(8)—C(9)—C(10)	106.1(8)
Ir(2)—N(2)—N(1)	118.4(6)	N(4)—C(10)—C(9)	107.8(9)
Ir(2)—N(2)—C(7)	135.0(7)	N(4)—C(10)—C(14)	122.7(8)
N(1)—N(2)—C(7)	106.4(8)	C(9)—C(10)—C(14)	129.5(8)
Ir(1)—N(3)—N(4)	116.4(5)	C(16)—C(15)—C(18)	121.8(15)
Ir(1)—N(3)—C(8)	135.0(7)	C(16)—C(15)—C(17)′	115(2)
N(4)—N(3)—C(8)	108.3(7)	C(18)—C(15)—C(17)′	123(2)
Ir(2)—N(4)—N(3)	117.6(5)	C(15)—C(16)—C(17)	123.7(13)
Ir(2)—N(4)—C(10)	134.1(7)	C(16)—C(17)—C(15)′	121(2)
N(3)—N(4)—C(10)	108.2(7)		

*Here and elsewhere primed atoms have coordinates related to those in Table 2 by the symmetry operations x, $1/2 - y$, z; x, $-y$, z; and $1 - x$, $-y$, $2 - z$ respectively for the three compounds.

the "$GaMe_2$" singlet gradually broadens and eventually splits into two distinct singlets. In addition, a splitting of the olefinic protons on the COD ligand at ~6 τ is very noticeable at lower temperatures. A single crystal X-ray structure of the complex shows the expected boat conformation for the Ga—(N—N)$_2$—Ir six-membered ring (see Fig. 4) in agreement with the low temperature ^{1}H nmr results. Evidently, at room temperature in solution, a rapid inversion of this six-membered ring is taking place to give equivalent Ga—Me groups and olefinic protons in the spectrum, viz.

A similar phenomenon has been observed for the analogous Rh(I) species, $[Me_2Gapz_2]Rh(COD)$ (1). One distinction between the two complexes is that the iridium compound retains its fluxionality to a temperature about 10°C lower than that observed for the corresponding rhodium compound.

The COD ligand in the complex $[Me_2Gapz_2]Ir(COD)$ is

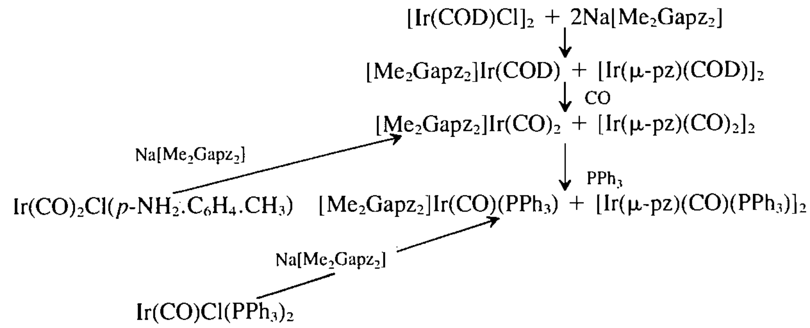

SCHEME 1. Reactions of Ir(I) species with Na[Me_2Gapz_2]

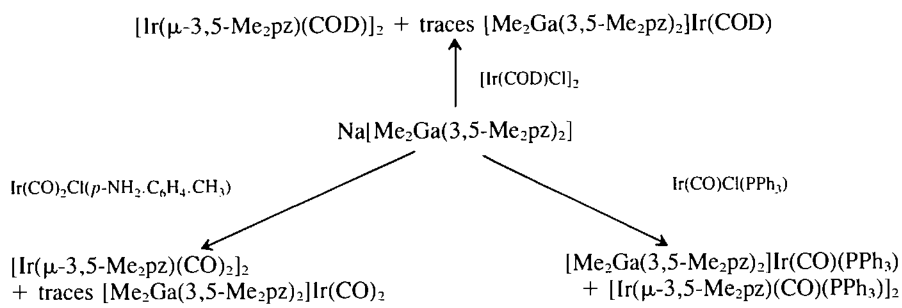

SCHEME 2. Reactions of Ir(I) species with Na[$Me_2Ga(3,5\text{-}Me_2pz)_2$]

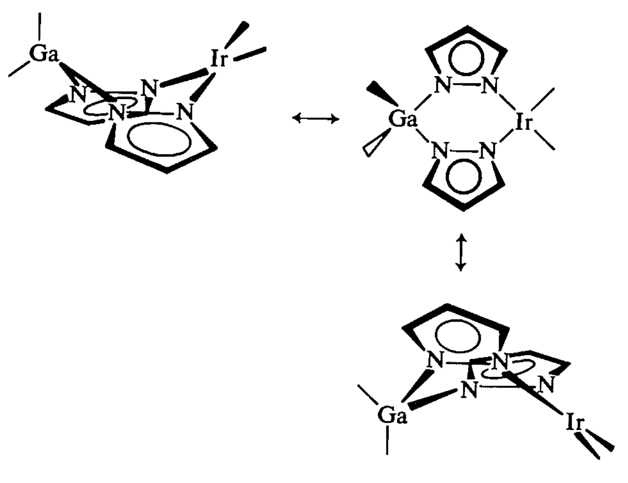

TABLE 5. Intra-annular torsion angles (deg) standard deviations in parentheses*

Atoms	Value (deg)
[Me_2Gapz_2]Ir(COD)	
N(1)′—Ir —N(1)—N(2)	49.4(5)
N(2)′—Ga —N(2)—N(1)	−48.1(5)
Ir —N(1)—N(2)—Ga	−1.9(6)
C(3)′—C(3)—C(4)—C(5)	69.2(7)
C(3)—C(4)—C(5)—C(6)	1.8(10)
C(4)—C(5)—C(6)—C(6)′	−70.6(7)
[Ir(μ-pz)$(CO)_2$]$_2$	
N(2)—Ir —N(1)—N(1)′	52.4(14)
Ir —N(1)—N(1)′—Ir′	0
N(1)—Ir —N(2)—N(2)′	−51.6(14)
Ir —N(2)—N(2)′—Ir′	0
[Ir(μ-3,5-Me_2pz)$(CO)_2$]$_2$.0.5(p-$Me_2C_6H_4$)	
N(3)—Ir(1)—N(1)—N(2)	−63.1(6)
Ir(1)—N(1)—N(2)—Ir(2)	1.2(8)
N(4)—Ir(2)—N(2)—N(1)	60.4(6)
N(2)—Ir(2)—N(4)—N(3)	−59.4(7)
Ir(1)—N(3)—N(4)—Ir(2)	−2.7(9)
N(1)—Ir(1)—N(3)—N(4)	63.8(7)

*Mirror-related torsion angles have the opposite sign.

easily replaced by two CO groups when a stream of CO is passed through a solution of the compound in a variety of solvents. At low temperatures the conversion is quantitative, as indicated by two sharp bands in the ν_{CO} region of the ir spectrum in positions expected for a *cis* square planar dicarbonyl iridium complex (32). Infrared signals due to the presence of the dimer species [Ir(μ-pz)$(CO)_2$]$_2$ were not detected. Unfortunately, the [Me_2Gapz_2]Ir$(CO)_2$ complex cannot be isolated from the product solution by simple evaporation of the solvent. Even at −78°C removal of solvent results in the conversion of the [Me_2Gapz_2]Ir$(CO)_2$ complex back to the starting COD complex [Me_2Gapz_2]Ir(COD). If the solvent is removed at higher temperatures some [Ir(μ-pz)$(CO)_2$]$_2$ is formed immediately as evidenced by a more intense yellow coloration and the appearance of new signals in the ν_{CO} region of the ir spectrum. Complete evaporation of the solvent at higher temperatures results in a mixture of two Ir products, [Me_2Gapz_2]Ir$(CO)_2$ and [Ir(μ-pz)$(CO)_2$]$_2$, the latter predominating. An ^{1}H nmr spectrum (Fig. 1) of almost pure [Me_2Gapz_2]Ir$(CO)_2$ can be obtained by preparing the compound directly in an nmr tube. In this spectrum the two methyl groups on the gallium atom give rise to one singlet and this singlet, even at −90°C, broadens only slightly. This suggests either a planar conformation for the Ga—(N—N)$_2$—Ir six-membered ring in this complex, or, more likely, a very facile inversion of the boat conformation in solution. Our inability to isolate pure [Me_2Gapz_2]Ir$(CO)_2$ precluded the collection of accurate elemental analysis data but a good mass spectrum was obtained for the complex. A signal

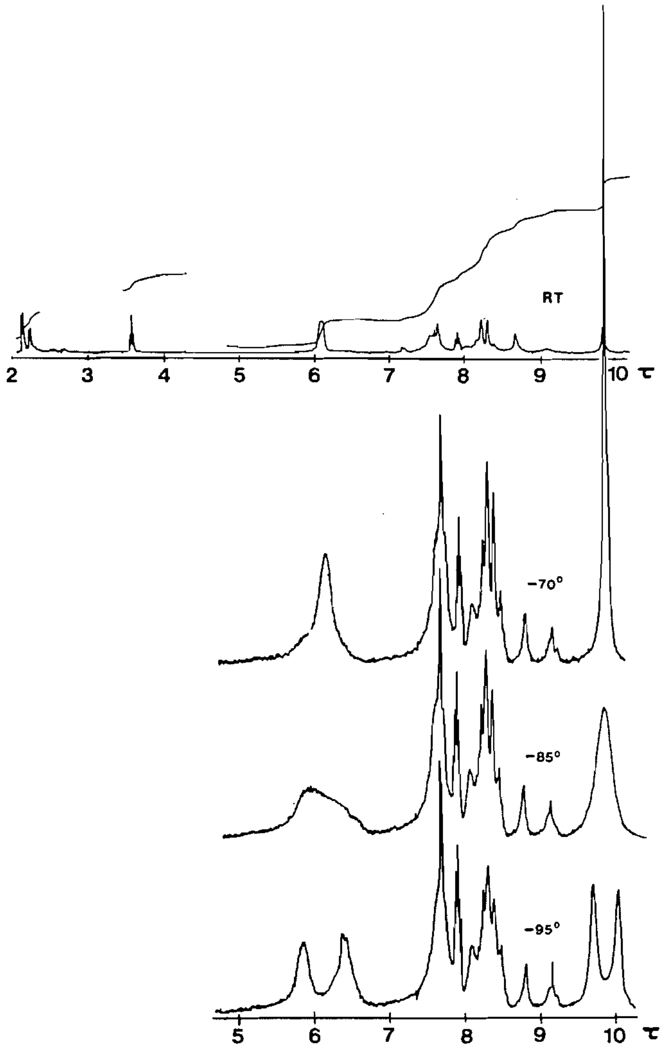

FIG. 3. Room temperature and partial low temperature 80 MHz ^{1}H nmr spectra of $[Me_2Gapz_2]Ir(COD)$ in d_6-acetone solution.

due to the parent ion itself, P^+, was not observed but the strongest signal arose from the $P - Me^+$ ion. The fragmentation pattern also shows strong signals due to the ions resulting from the consecutive loss of two carbonyl groups, $P - Me - CO^+$ and $P - Me - 2CO^+$, and characteristically a strong peak corresponding to an ion where partial loss of a pyrazolyl ring has occurred, $P - Me - 2CO - HCN^+$. The complex $[Me_2Gapz_2]Ir(CO)_2$ can also be prepared by the reaction of $Ir(CO)_2Cl(p\text{-}NH_2C_6H_4CH_3)$ with the gallium ligand. However, the $[Ir(\mu\text{-pz})(CO)_2]_2$ dimer was also produced in quantities varying with the reaction temperature but usually ~50% at −78°C. From this latter reaction the $[Ir(\mu\text{-pz})(CO)_2]_2$ dimer has been crystallized from hexane as yellow air-stable crystals. These have been fully characterized and the predicted boat structure confirmed by X-ray structural analysis (Fig. 5). A previous report (29) mentions this Ir dimer as being unstable. We have found that evaporation of solvent from solutions of the dimer yields, in addition to a yellow crystalline material, a black compound which gave identical ir, nmr, mass spectral and elemental analysis. Interestingly, a biimidazole dicarbonyl iridium complex was also reported as a black solid (33), the color being attributed to some type of weak metal−metal interactions. The black form of $[Ir(\mu\text{-pz})(CO)_2]_2$ can be recrystallized from acetone to give the yellow crystalline form. Solutions of the complex in acetone or benzene change color with temperature, from black up to −50°C through purple to yellow at 0°C and above. The $[Ir(\mu\text{-pz})(CO)_2]_2$ dimer has been prepared also from $[Ir(\mu\text{-pz})(COD)_2]$ and CO, the product having identical properties to those described above.

The $[Me_2Gapz_2]Ir(CO)(PPh_3)$ complex has been prepared via a number of routes (Scheme 1). Its ir spectrum consists of one strong band in the ν_{CO} region of the spectrum at 1980 cm^{-1}. The ^{1}H nmr spectrum of the complex indicates non-equivalence of the bridging pyrazolyl groups as expected and displays a sharp singlet for both methyl groups on the Ga atom at rt. On cooling a d_6-acetone solution of the complex "$GaMe_2$" singlet eventually collapses and is replaced by two singlets at low temperature (Fig. 6) consistent with a boat conformation for the Ga—(N—N)$_2$—Ir six-membered ring. Obviously a fluxional behaviour in solution is again responsible for these observations. The mass spectrum of this complex shows a weak molecular ion peak, P^+, and again the most intense peak is due to the $P - Me^+$ ion, followed by peaks due to the ions $P - Me - CO^+$ and $P - Me - CO - Hpz^+$. The $[Me_2Gapz_2]Ir(CO)(PPh_3)$ compound is unstable in air and, even under an inert atmosphere, decomposes slowly. This instability precluded the collection of good elemental analysis data for the complex.

Reactions involving the $Na[Me_2Ga(3,5\text{-}Me_2pz)_2]$ ligand and various Ir(I) species (Scheme 2) were less productive in terms of producing pyrazolylgallate iridium(I) complexes. Thus the $[Me_2Ga(3,5\text{-}Me_2pz)_2]Ir(CO)(PPh_3)$ complex was the only compound of the series that could be isolated. Both the COD and the dicarbonyl derivatives were unstable with respect to the corresponding iridium dimers, which were the dominant products. Traces of the dicarbonyl complex $[Me_2Ga(3,5\text{-}Me_2pz)_2]Ir(CO)_2$ and the COD complex $[Me_2Ga(3,5\text{-}Me_2pz)_2]Ir(COD)$ were identified by mass spectral analysis of reaction products, the fragmentation patterns of the complexes being similar to those of the $[Me_2Gapz_2]Ir(CO)_2$ and $[Me_2Gapz_2]Ir(COD)$ compounds, respectively.

Crystals of the $[Ir(\mu\text{-}3,5\text{-}Me_2pz)(CO)_2]_2$ dimer were found to be air-stable and have been fully characterized. The ir spectrum of this complex gives three strong ν_{CO} bands and is very similar in appearance to the spectrum of the unsubstituted analog $[Ir(\mu\text{-pz})(CO)_2]_2$. The ^{1}H nmr spectrum of the compound is consistent with the presence of two equivalent 3,5-dimethylpyrazolyl groups and consists of two singlets in the ratio of 1:6 due to the H^4 and pz-Me protons, respectively. A single crystal X-ray analysis (see below) of this dimer has again demonstrated the boat conformation for the compound in the solid state (Fig. 7) with the six-membered Ir—(N—N)$_2$—Ir ring being more puckered than in the structure of $[Ir(\mu\text{-pz})(CO)_2]_2$ (Fig. 5), presumably to relieve steric interactions between the carbonyl groups on the iridium atoms and the methyl groups on the pyrazolyl rings.

The complex $[Me_2Ga(3,5\text{-}Me_2pz)_2]Ir(CO)(PPh_3)$ could be obtained via only one route, from Vaska's complex $Ir(CO)Cl(PPh_3)_2$ and the gallate ligand. It was obtained in good yield if the reaction was performed at low temperature. The complex was recrystallized from benzene to yield yellow air-stable crystals. The ir spectrum of the compound gave one strong ν_{CO} band at 1974 cm^{-1} and the ^{1}H nmr (Fig. 8), even at room temperature, was consistent with a static boat conformation for the Ir—(N—N)$_2$—Ga six-membered ring, the $GaMe_2$ group giving two sharp singlets. Presumably steric interactions between the pz-Me groups and the PPh_3 substituent

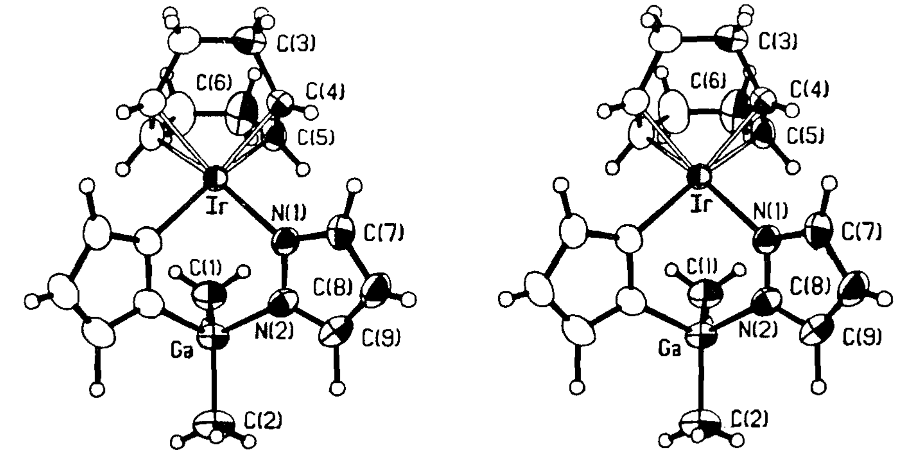

FIG. 4. Stereoview of $[Me_2Gapz_2]Ir(COD)$; 50% probability thermal ellipsoids are shown for the non-hydrogen atoms.

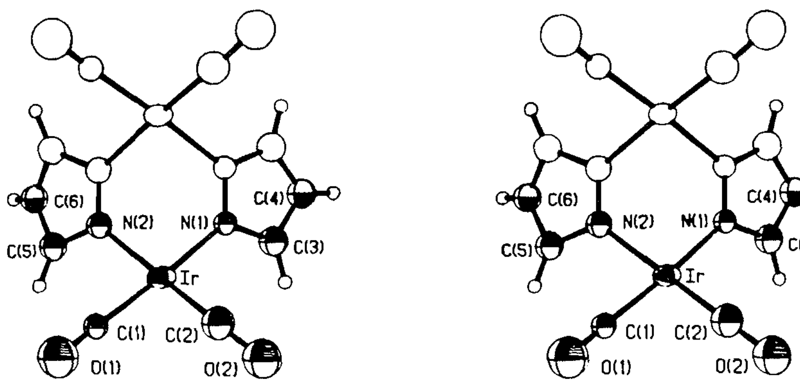

FIG. 5. Stereoview of $[Ir(\mu\text{-}pz)(CO)_2]_2$; 50% probability thermal ellipsoids are shown for the non-hydrogen atoms.

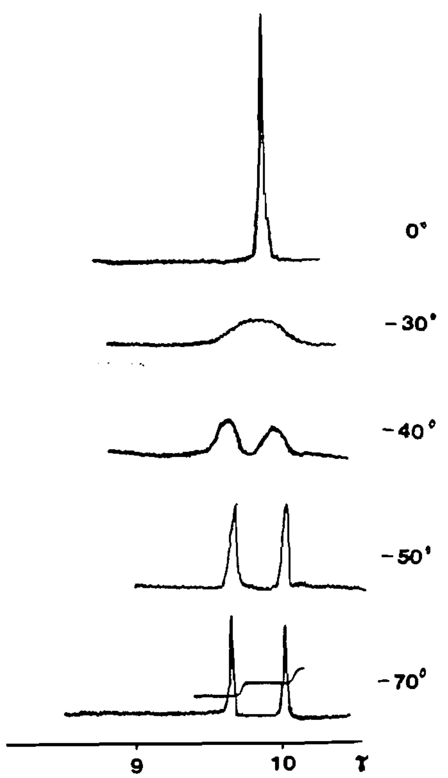

FIG. 6. Variable temperature 80 MHz ^1H nmr spectra of the complex $[Me_2Gapz_2]Ir(CO)(PPh_3)$ in d_6-acetone solution ($GaMe_2$ region only).

on Ir severely hinder any rapid ring inversion process such as that above proposed for the compounds containing the "Me_2Gapz_2" moiety. The mass spectrum of $[Me_2Ga(3,5\text{-}Me_2pz)_2]Ir(CO)(PPh_3)$ displays a fragmentation pattern similar to that of the unsubstituted pyrazolyl derivative $[Me_2Gapz_2]$-$Ir(CO)(PPh_3)$, the strongest signal again corresponding to the P − Me^+ ion.

A number of the complexes described above were tested as potential hydrogenation catalysts for 1-hexene and cyclohexene. In general, the reactions in benzene solution were very slow and hydrogen uptake was minimal. However, in the case of $[Ir(\mu\text{-}3,5\text{-}Me_2pz)(CO)_2]_2$ as a catalyst, some conversion of cyclohexene to cyclohexane did occur over a 5 day period using 1 atm of hydrogen at 45°C. The reaction was still proceeding after this period and the catalyst was recovered unchanged from the reaction mixture. Investigations in this area are continuing.

Crystal structures of $[Me_2Gapz_2]Ir(COD)$, $(Ir(\mu\text{-}pz)(CO)_2]_2$, and $[Ir(\mu\text{-}3,5\text{-}Me_2pz)(CO_2)]_2$

All three crystal structures consist of discrete molecules (Fig. 4, 5, and 7), and in the case of $[Ir(\mu\text{-}3,5\text{-}Me_2pz)(CO)_2]_2$, a centrosymmetric xylene of crystallization. Intermolecular distances correspond to normal van der Waals interactions. The structure of $[Me_2Gapz_2]Ir(COD)$ is isomorphous with that of the Rh(I) analog (1), the molecule possessing exact mirror symmetry. The complexes $[Ir(\mu\text{-}pz)(CO)_2]_2$ and $[Ir(\mu\text{-}3,5\text{-}Me_2pz)(CO)_2]_2$ both have approximate C_{2v} symmetry, the former having crystallographic mirror symmetry with the mirror plane perpendicular to the Ir···Ir vector.

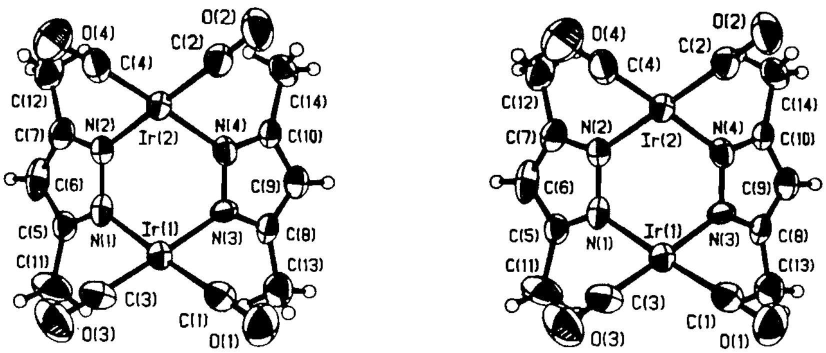

FIG. 7. Stereoview of $[Ir(\mu\text{-}3,5\text{-}Me_2pz)(CO)_2]_2$; 50% probability thermal ellipsoids are shown for the non-hydrogen atoms.

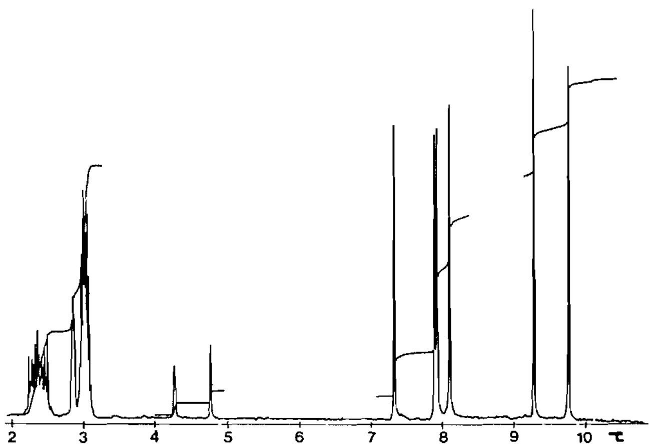

FIG. 8. Room temperature 80 MHz ^1H nmr spectrum of $[Me_2Ga(3,5\text{-}Me_2pz)_2]Ir(CO)(PPh_3)$ in C_6D_6 solution.

TABLE 6. M···M distances in compounds of the type

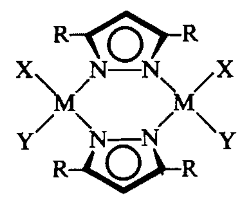

M	X	Y	R	M···M (Å)	Reference
Ir		COD	H	3.216	27, 29
Rh		COD	H	3.267	29
Ir		COD	CF_3	3.073	29
Ir		COD	CH_3, CF_3	3.066	29
Rh		COD	CH_3	3.154	1
Ir	CO	PPh_3	H	3.162	26
Ir	CO	CO	H	3.506	This paper
Ir	CO	CO	CH_3	3.245	This paper
Rh	CO	CO	CH_3	3.262	1
Rh	CO	$P(OPh)_3$	H	3.568	36

The Ir(I) atoms in all three structures have distorted square planar coordination geometry, the mean[3] bond lengths involving Ir (Ir—C = 2.124(7) and Ir—N = 2.080(5) Å in $[Me_2Gapz_2]Ir(COD)$; Ir—CO = 1.83(7) and Ir—N = 2.08(3) Å in $[Ir(\mu\text{-}pz)(CO)_2]_2$; Ir—CO = 1.837(5) and Ir—N = 2.071(11) Å in $[Ir(\mu\text{-}3,5\text{-}Me_2pz)(CO)_2]_2$) being both internally consistent and in good agreement with those reported for closely related Ir(I) complexes (26, 27, 29). It is noteworthy that the Ir—N distances in these three molecules are equal within experimental error while the Rh—N distances in the carbonyl complex $[Rh(\mu\text{-}3,5\text{-}Me_2pz)(CO)_2]_2$ were significantly shorter than those in the COD complexes $[Me_2Gapz_2]Rh(COD)$ and $[Rh(\mu\text{-}3,5\text{-}Me_2pz)(COD)]_2$ (1) (2.063(6) vs. 2.087(2) and 2.084(1) Å). Other bond lengths and angles in the three molecules (Tables 3 and 4) assume normal values.

The most important structural features of these molecules is the degree of folding of the central $M—(N—N)_2—M$ six-membered rings and the associated cross-ring M···M distances, the latter being compared for a number of homobinuclear Ir(I) and Rh(I) complexes in Table 6. The M···M distances are influenced most by steric interactions (discussed in refs. 1, 2, 26, 27, 29, 36), being significantly shortened by substitution at the 3- and 5-positions of the bridging pyrazolyl groups or by the introduction of bulky terminal ligands. The M···M distances are similar for Ir and Rh, those involving Rh being longer as shown in Table 6. For the heterobinuclear species $[Me_2Gapz_2]Ir(COD)$ and its Rh analog (1), Ga···Ir = 3.567(1) and Ga···Rh = 3.5527(5) Å while in the sterically hindered complex $[Me_2Ga(3,5\text{-}Me_2pz)_2]Rh(CO)(PPh_3)$ (2) the Ga···Rh distance is shortened to 3.3819(4) Å.

The pyrazolyl groups are planar within experimental error in all three structures, the metal atoms being significantly displaced from the N_2C_3 mean planes in each case. These deviations are greatest in the case of $[Ir(\mu\text{-}3,5\text{-}Me_2pz)(CO)_2]_2$ where the mean deviation from the mean plane is 0.114 Å. The Ir coordination groups are all slightly but significantly nonplanar, the maximum deviation from the ML_4 mean plane being 0.024(2) Å for $[Ir(\mu\text{-}pz)(CO)_2]_2$.

[3]Here and elsewhere in this report mean values refer to weighted means with rms deviations from the mean in parentheses.

Acknowledgments

We thank the Natural Sciences and Engineering Research Council of Canada for financial support and the University of British Columbia Computing Centre for assistance. We are grateful to Mr. P. Borda for elemental analyses, Ms. M. Austria for ^1H nmr spectra, and Mr. M. Lapawa for mass spectra.

1. B. M. LOUIE, S. J. RETTIG, A. STORR, and J. TROTTER. Can. J. Chem. **62**, 1057 (1984).
2. B. M. LOUIE, S. J. RETTIG, A. STORR, and J. TROTTER. Can. J. Chem. **63**, 503 (1985).
3. J. L. HERDE, J. C. LAMBERT, and C. V. SENOFF. Inorg. Synth.

15, 18 (1974).
4. U. KLABUNDE, D. FORSTER, and W. O. WEINREIS. Inorg. Synth. **15**, 82 (1974).
5. K. R. BREAKELL, D. J. PATMORE, and A. STORR. J. Chem. Soc. Dalton Trans. 749 (1975).
6. P. COPPENS, L. LEISEROWITZ, and D. RABINOVICH. Acta Crystallogr. **18**, 1035 (1965).
7. J. DE MEULENAER and H. TOMPA. Acta Crystallogr. **19**, 1014 (1965).
8. D. T. CROMER and J. B. MANN. Acta Crystallogr. Sect. A, **24**, 321 (1968).
9. R. F. STEWART, E. R. DAVIDSON, and W. T. SIMPSON. J. Chem. Phys. **42**, 3175 (1965).
10. D. T. CROMER and D. LIBERMAN. J. Chem. Phys. **53**, 1891 (1970).
11. J. A. IBERS. Acta Crystallogr. Sect. B, **25**, 1667 (1969).
12. P. J. BECKER and P. COPPENS. Acta Crystallogr. Sect. A, **30**, 129 (1974); **30**, 148 (1974); **31**, 417 (1975).
13. P. COPPENS and W. C. HAMILTON. Acta Crystallogr. Sect. A, **26**, 71 (1970).
14. F. R. THORNLEY and R. J. NELMES. Acta Crystallogr. Sect. A, **30**, 748 (1974).
15. W. R. BUSING and H. A. LEVY. Acta Crystallogr. **22**, 457 (1967).
16. S. MAY, P. REINSALU, and J. POWELL. Inorg. Chem. **19**, 1582 (1980).
17. F. BONATI, G. MINGHETTI, and G. BANDITELLI. J. Organomet. Chem. **87**, 365 (1975).
18. R. B. KING and A. BOND. J. Organomet. Chem. **73**, 115 (1974).
19. S. TROFIMENKO. Inorg. Chem. **10**, 1372 (1971).
20. H. C. CLARK and S. GOEL. J. Organomet. Chem. **165**, 383 (1979).
21. M. COCIVERA, T. J. DESMOND, G. FERGUSON, B. KAITNER, F. J. LALOR, and D. J. O'SULLIVAN. Organometallics, **1**, 1125 (1982).
22. M. COCIVERA, G. FERGUSON, B. KAITNER, F. J. LALOR, D. J. O'SULLIVAN, M. PARVEZ, and B. RUHL. Organometallics, **1**, 1132 (1982).
23. M. COCIVERA, G. FERGUSON, F. J. LALOR, and P. SZCZECINSKIVAN. Organometallics, **1**, 1139 (1982).
24. N. F. BORKETT and M. I. BRUCE. J. Organomet. Chem. **65**, C51 (1974).
25. J. POWELL, A. KUKSIS, S. C. NYBURG, and W. W. NG. Inorg. Chim. Acta **64**, L211 (1982).
26. K. A. BEVERIDGE, G. W. BUSHNELL, K. R. DIXON, D. T. EADIE, S. R. STOBART, J. L. ATWOOD, and M. J. ZAWOROTKO. J. Am. Chem. Soc. **104**, 920 (1982).
27. A. W. COLEMAN, D. T. EADIE, S. R. STOBART, M. J. ZAWOROTKO, and J. L. ATWOOD. J. Am. Chem. Soc. **104**, 922 (1982).
28. G. W. BUSHNELL, D. O. K. FJELDSTED, S. R. STOBART, and M. J. ZAWOROTKO. J. Chem. Soc. Chem. Commun. 580 (1983).
29. K. A. BEVERIDGE, G. W. BUSHNELL, S. R. STOBART, J. L. ATWOOD, and M. J. ZAWOROTKO. Organometallics, **2**, 1447 (1983).
30. A. L. BANDINI, G. BANDITELLI, F. BONATI, F. DEMARTIN, M. MANASSERO, and G. MINGHETTI. J. Organomet. Chem. **238**, C9 (1982).
31. B. M. LOUIE, S. J. RETTIG, A. STORR, and J. TROTTER. Can. J. Chem. **62**, 633 (1984).
32. D. M. ADAMS. Metal ligand and related vibrations. Edward Arnold Ltd., London. 1967. p. 154.
33. S. W. KAISER, A. B. SAILLANT, W. M. BUTLER, and P. G. RASMUSSEN. Inorg. Chem. **15**, 2681 (1976).
34. K. R. BREAKELL, S. J. RETTIG, D. L. SINGBEIL, A. STORR, and J. TROTTER. Can. J. Chem. **56**, 2099 (1978).
35. P. MEAKIN, S. TROFIMENKO, and J. P. JESSON. J. Am. Chem. Soc. **94**, 5677 (1972).
36. R. USON, L. A. ORO, M. A. CIRIANO, M. T. PINILLOS, A. TIRIPICCHIO, and M. CARMELLINI. J. Organomet. Chem. **205**, 247 (1981).

Crystal and molecular structure of *fac*-[dimethylbis(1-pyrazolyl)gallato-N,N']-(triphenylphosphine)tricarbonylrhenium(I)

BRENDA M. LOUIE, STEVEN J. RETTIG, ALAN STORR, AND JAMES TROTTER
Department of Chemistry, University of British Columbia, 2036 Main Mall, Vancouver, B.C., Canada V6T 1Y6

Received August 3, 1984

BRENDA M. LOUIE, STEVEN J. RETTIG, ALAN STORR, and JAMES TROTTER. Can. J. Chem. **63**, 703 (1985).

Crystals of *fac*-[dimethylbis(1-pyrazolyl)gallato-N,N'](triphenylphosphine)tricarbonylrhenium(I) are triclinic, $a = 9.479(2)$, $b = 16.258(4)$, $c = 20.412(6)$ Å, $\alpha = 110.06(1)$, $\beta = 95.46(1)$, $\gamma = 92.65(2)°$, $Z = 4$, space group $P\bar{1}$. The structure was solved by conventional heavy-atom methods and was refined by full-matrix least-squares procedures to $R = 0.027$ and $R_w = 0.031$ for 5965 reflections with $I \geq 3\sigma(I)$. The two crystallographically independent molecules have nearly identical structures. The coordination about Re is distorted *fac*-octahedral with mean bond lengths: Re—P = 2.538(4), Re—N = 2.201(5), Re—CO(*trans* to P) = 1.931(1), and Re—CO(*trans* to N) = 1.913(9) Å. The $ReGaN_4$ chelate rings have twisted boat conformations with cross-ring Re···Ga separations of 3.9396(7) and 3.8981(8) Å.

BRENDA M. LOUIE, STEVEN J. RETTIG, ALAN STORR et JAMES TROTTER. Can. J. Chem. **63**, 703 (1985).

Les cristaux du *fac*-[diméthyl bis(pyrazolyl-1) gallato N, N'] -(triphénylphosphine) tricarbonyl rhénium(I) sont tricliniques avec $a = 9{,}479(2)$, $b = 16{,}258(4)$, $c = 20{,}412(6)$ Å, $\alpha = 110{,}06(1)$, $\beta = 95{,}46(1)$, $\gamma = 92{,}65(2)°$, $Z = 4$, groupe d'espace $P\bar{1}$. On a résolu la structure par les méthodes conventionnelles aux atomes lourds et on l'a affinée par le méthode des moindres carrés (matrice entière) jusqu'à des valeurs respectives de R et R_w de 0,027 et 0,031 pour 5965 réflexions avec $I \geq 3\sigma(I)$. Les deux molécules qui sont indépendantes du point de vue cristallographique ont des structures qui sont pratiquement identiques. La coordination autour du Re est du type *fac*-octaèdre déformé avec des longueurs moyennes de liaisons de: Re—P = 2,538(4), Re—N = 2,201(5), Re—CO (*trans* par rapport au P) = 1,931(1) et Re—CO (*trans* par rapport au N) = 1,913(9) Å. Les cycles du chélate $ReGaN_4$ adoptent des conformations bateau-croisés dans lesquels les séparations Re···Ga sont égales à 3,9396(7) et 3,8981(8) Å.

[Traduit par le journal]

Introduction

Earlier publications have reported the synthesis and characterization of a number of manganese (1) and rhenium (2) carbonyl derivatives incorporating the bidentate chelating pyrazolyl gallate ligand $Me_2Gapz_2^-$ or $Me_2Ga(3,5\text{-}Me_2pz)_2^-$ (where pz = pyrazolyl, $N_2C_3H_3$, and 3,5-Me_2pz = 3,5-dimethylpyrazolyl, $N_2C_5H_7$). These ligands are each uninegative, four-electron donors, analogous to the well-known 1,3-diketonate anions. However, unlike many of their diketonate analogs, transition metal complexes containing the bispyrazolylgallate ligands are invariably monomeric and exhibit a puckered boat conformation as their central structural feature. Thus, in the complex $[Me_2Gapz_2]Re(CO)_4$, the central Ga—(N—N)$_2$—Re six-membered ring was proposed to adopt a boat conformation primarily on the basis of ^{1}H nmr evidence (2). Furthermore one of the carbonyl groups in this tetracarbonyl complex was found to be labile and easily replaced by other neutral two-electron donor species. Based upon steric arguments and spectral data, the favored site for this ligand substitution reaction was predicted (2). Since that time we have been fortunate enough to obtain crystals, suitable for X-ray study, of one such complex, namely $[Me_2Ga(N_2C_3H_3)_2](PPh_3)Re(CO)_3$. The present paper describes the solid state structure of this complex and confirms our earlier prediction.

Experimental

fac-[Dimethylbis(1-pyrazolyl)gallato-N,N'] (triphenylphosphine)-tricarbonylrhenium(I) was prepared as described previously (2) and crystals suitable for X-ray analysis were obtained by slow sublimation in a sealed tube under vacuum. A crystal bounded by the 6 faces (followed by their distances in mm from a common origin): ±(1 0 0), 0.138, ±(0 0 1), 0.050, (0 1 −1), 0.138, (0 −1 −1), 0.113 was mounted in a general orientation. Unit-cell parameters were refined by least-squares on 2 sin θ/λ values for 25 reflections (2θ = 30−40°) measured on a diffractometer with Mo-$K\alpha$ Radiation ($\lambda(K\alpha_1)$ = 0.70930, $\lambda(K\alpha_2)$ = 0.71359 Å). Crystal data at 22°C are:

$C_{29}H_{27}GaN_4O_3PRe$ fw = 766.45
Triclinic, $a = 9.479(2)$, $b = 16.258(4)$, $c = 20.412(6)$ Å, $\alpha = 110.06(1)$, $\beta = 95.46(1)$, $\gamma = 92.65(2)°$, $V = 2931(1)$ Å^3, $Z = 4$, $\rho_c = 1.737$ Mg m^{-3}, $F(000) = 1496$, μ(Mo-$K\alpha$) = 51.9 cm^{-1}. Absent reflections: none, space group $P\bar{1}$ (C_i^1, No. 2, reduced cell) from structure analysis.

Intensities were measured with graphite-monochromated Mo-$K\alpha$ radiation on an Enraf-Nonius CAD4-F diffractometer. An ω−2θ scan at 1.34−10.06° min^{-1} over a range of (0.60 + 0.35 tan θ) degrees in ω (extended by 25% on both sides for background measurement) was employed. Data were measured to 2θ = 50°. The intensities of three check reflections, measured every 3600 s throughout the data collection, showed only small random fluctuations. After data reduction,[1] an absorption correction was applied using the analytical method (3,4). Transmission factors ranged from 0.266 to 0.632. Of the 9155 independent reflections measured, 5965 (65%) had intensities greater than $3\sigma(I)$ above background where $\sigma^2(I) = S + 2B + (0.04(S - B))^2$ with S = scan count and B = normalized background count.

The centrosymmetric space group $P\bar{1}$ was suggested by the Patterson function, from which the coordinates of the Re, Ga, and P atoms of both independent molecules in the asymmetric unit were determined. The remaining non-hydrogen atoms were positioned from a subsequent difference map. In the final stages of refinement all non-hydrogen atoms were refined with anisotropic thermal parameters and hydrogen atoms were fixed in idealized positions (based on observed positions with C(sp^3)—H = 0.98 and C(sp^2)—H = 0.97 Å). The scattering factors of ref. 5 were used for non-hydrogen atoms and those of ref. 6 for hydrogen atoms. Anomalous scattering factors from ref. 7 were used for the Re, Ga, and P atoms. The weighting scheme $w = 1/\sigma^2(F)$, where $\sigma^2(F)$ is derived from the previously defined $\sigma^2(I)$, gave uniform average values of $w(|F_o| - |F_c|)^2$ over ranges of both $|F_o|$ and sin θ/λ and was employed in the final stages of full-

[1]The computer programs used include locally written programs for data processing and locally modified versions of the following: ORFLS, full-matrix least-squares, and ORFFE, function and errors, by W. R. Busing, K. O. Martin and H. A. Levy; FORDAP, Patterson and Fourier syntheses, by A. Zalkin; ORTEP II, illustrations, by C. K. Johnson.

TABLE 1. Final positional (fractional × 10^4; Re, Ga, and P × 10^5) and isotropic thermal parameters ($U \times 10^3$ Å^2)* with estimated standard deviations in parentheses

Atom	x	y	z	U_{eq}	Atom	x	y	z	U_{eq}
Re	26081(2)	9223(2)	28828(1)	32	C(20)	2487(9)	−1979(6)	765(4)	65
Re′	39110(2)	54446(2)	20566(1)	31	C(21)	1173(11)	−2423(6)	497(5)	72
Ga	−4902(8)	11234(5)	40715(4)	48	C(22)	−21(9)	−1987(6)	508(4)	65
Ga′	71520(7)	48672(5)	9901(4)	46	C(23)	62(7)	−1065(5)	830(4)	53
P	15711(17)	5724(12)	16170(9)	35	C(24)	−214(6)	929(4)	1536(3)	39
P′	48975(16)	62847(11)	33272(9)	34	C(25)	−1203(7)	720(5)	1921(4)	50
O(1)	3919(6)	1446(4)	4422(3)	63	C(26)	−2566(7)	960(6)	1877(4)	60
O(2)	4895(6)	2304(4)	2867(3)	70	C(27)	−2990(8)	1413(6)	1431(4)	61
O(3)	4827(5)	−425(4)	2519(3)	68	C(28)	−2026(9)	1611(6)	1031(4)	63
O(1′)	2624(5)	4403(4)	539(3)	68	C(29)	−645(8)	1375(5)	1082(4)	50
O(2′)	1631(5)	4251(4)	2338(3)	69	C(1′)	3168(7)	4796(5)	1092(4)	43
O(3′)	1682(5)	6747(4)	2027(3)	65	C(2′)	2519(8)	4709(5)	2260(4)	47
N(1)	1040(5)	−89(3)	2936(3)	33	C(3′)	2515(7)	6267(5)	2049(4)	41
N(2)	−94(6)	48(4)	3314(3)	44	C(4′)	9220(8)	5019(6)	994(5)	70
N(3)	1117(5)	1948(4)	3209(3)	38	C(5′)	5964(8)	4048(5)	167(4)	59
N(4)	122(5)	1991(4)	3649(3)	44	C(6′)	5335(7)	7170(5)	1907(4)	44
N(1′)	5389(5)	6300(4)	1754(3)	33	C(7′)	6397(8)	7504(5)	1621(4)	55
N(2′)	6487(5)	6064(4)	1364(3)	37	C(8′)	7090(8)	6771(5)	1286(4)	54
N(3′)	5572(5)	4563(3)	2099(3)	35	C(9′)	5650(8)	4060(5)	2495(4)	52
N(4′)	6807(6)	4515(4)	1806(3)	50	C(10′)	6910(8)	3683(5)	2460(5)	61
C(1)	3385(7)	1228(4)	3854(4)	40	C(11′)	7633(8)	3982(6)	2030(5)	64
C(2)	4003(7)	1783(5)	2845(3)	40	C(12′)	4152(6)	6017(4)	4032(3)	36
C(3)	3972(7)	71(5)	2649(4)	42	C(13′)	3509(7)	5206(5)	3947(4)	47
C(4)	−2553(8)	1141(6)	4039(5)	77	C(14′)	3012(8)	5010(5)	4501(4)	56
C(5)	706(10)	1233(7)	4940(5)	80	C(15′)	3165(8)	5651(6)	5158(4)	61
C(6)	974(7)	−948(5)	2577(4)	44	C(16′)	3788(10)	6454(6)	5255(4)	66
C(7)	−190(8)	−1377(5)	2693(4)	52	C(17′)	4274(8)	6647(5)	4702(4)	54
C(8)	−839(8)	740(5)	3161(4)	57	C(18′)	4638(7)	7446(4)	3610(3)	40
C(9)	1128(8)	2694(5)	3066(4)	48	C(19′)	5740(9)	8098(5)	3822(4)	55
C(10)	166(8)	3222(5)	3405(5)	55	C(20′)	5477(13)	8973(7)	4063(5)	86
C(11)	−478(8)	2760(5)	3759(5)	64	C(21′)	4100(16)	9191(6)	4113(5)	86
C(12)	2551(7)	1046(5)	1083(4)	39	C(22′)	2978(11)	8569(7)	3893(5)	75
C(13)	2936(8)	1939(5)	1310(4)	50	C(23′)	3264(8)	7700(5)	3646(4)	60
C(14)	3643(9)	2313(5)	909(5)	62	C(24′)	6825(6)	6237(4)	3532(4)	39
C(15)	3956(8)	1817(6)	264(4)	59	C(25′)	7753(7)	6396(6)	3093(4)	62
C(16)	3613(8)	924(6)	28(4)	65	C(26′)	9199(8)	6360(7)	3235(5)	76
C(17)	2893(7)	537(5)	427(4)	48	C(27′)	9727(8)	6162(6)	3815(6)	78
C(18)	1364(7)	−604(5)	1116(3)	40	C(28′)	8823(10)	6004(7)	4223(6)	87
C(19)	2588(7)	−1081(5)	1068(4)	49	C(29′)	7376(8)	6054(6)	4110(5)	66

*U_{eq} = (1/3)trace(U_{diag}).

matrix refinement of 703 variables. Reflections with $I < 3\sigma(I)$ were not included in the refinement. Convergence was reached at R = 0.027 and R_w = 0.031 for 5965 reflections with $I \geq 3\sigma(I)$. For all 9155 reflections R = 0.067. The function minimized was $\Sigma w(|F_o| - |F_c|)^2$, $R = \Sigma||F_o| - |F_c||/\Sigma|F_o|$ and $R_w = (\Sigma w(|F_o| - |F_c|)^2/\Sigma w|F_o|^2)^{1/2}$.

On the final cycle of refinement the mean and maximum parameter shifts corresponded to 0.02 and 0.10σ, respectively. The mean error in an observation of unit weight was 1.232. A final difference map showed maximum fluctuations of ±1.65 e Å^{-3} near Re and was essentially featureless elsewhere. The final positional and thermal parameters appear in Tables 1 and 6,[2] respectively. Measured and calculated structure factors have been placed in the Depository of Unpublished Data.[2] Calculated parameters for the hydrogen atoms appear in Table 5.[2] Bond distances, bond angles, and intra-annular torsion angles for the chelate rings are listed in Tables 2–4, respectively.

Results and discussion

The crystal structure of *fac*-[dimethylbis(1-pyrazolyl)gallato-*N*,*N′*](triphenylphosphine)tricarbonylrhenium(I) consists of discrete molecules, the most significant intermolecular contacts being the C(17′)—H(17′)···O(1) (1 − *x*, 1 − *y*, 1 − *z*) interaction (H···O = 2.43, C···O = 3.296(9) Å, C—H···O = 149°) and the contacts H(20)···H(5′c) (1 − *x*, −*y*, −*z*) = 2.10 and H(5′b)···H(5′b) (1 − *x*, 1 − *y*, −*z*) = 2.23 Å. All other intermolecular distances correspond to normal van der Waals interactions. The two crystallographically independent molecules (Fig. 1) are very similar, the most significant difference between the two involving the chelate ring conformation (see Table 4). These and other small but statistically significant structural differences between the two independent molecules are most likely the result of packing effects.

The coordination about Re is distorted *fac*-octahedral with mean[3] bond lengths: Re—P = 2.538(4), Re—N = 2.201(5),

[2]The structure factor table, Table 6 (anisotropic thermal parameters) and other material mentioned in the text are available, at a nominal charge, from the Depository of Unpublished Data, CISTI, National Research Council of Canada, Ottawa, Ont., Canada K1A 0S2.

[3]Here and elsewhere in this report mean values refer to weighted means with rms deviations from the mean in parentheses.

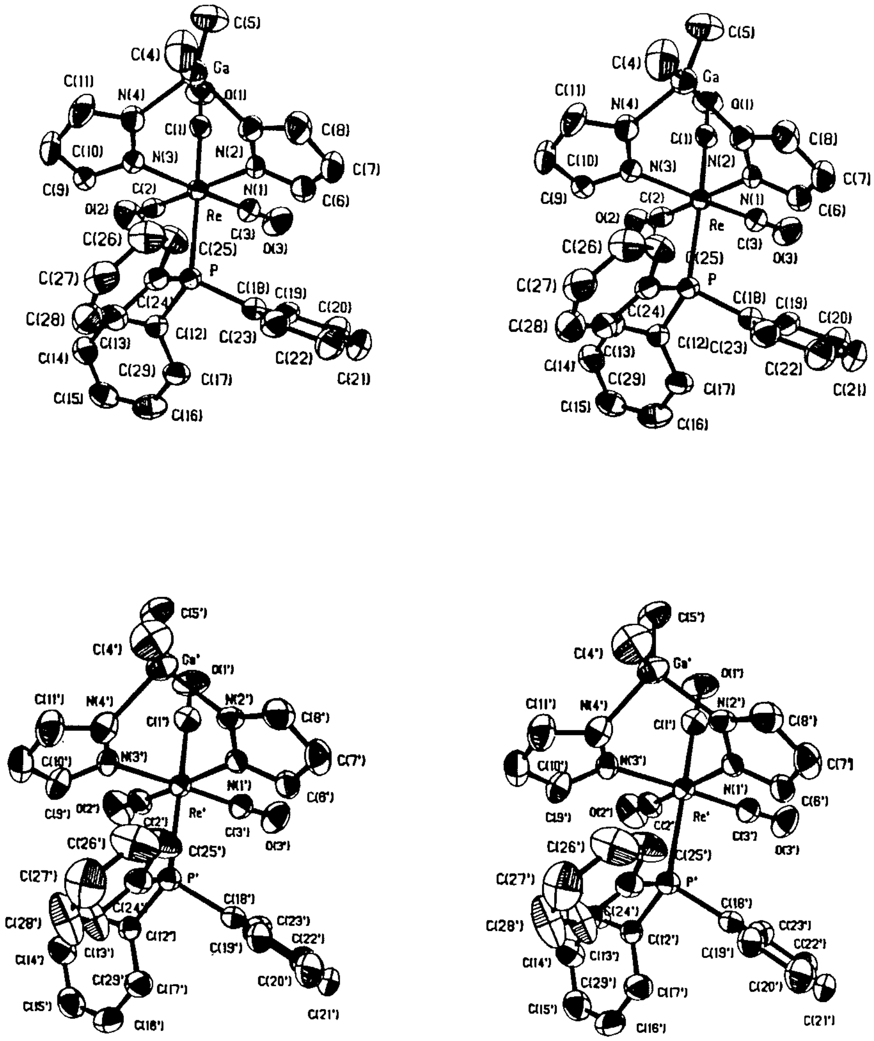

FIG. 1. Stereoscopic views of the two independent $[Me_2Ga(N_2C_3H_3)_2](PPh_3)Re(CO)_3$ molecules; 50% probability thermal ellipsoids are shown.

TABLE 2. Bond lengths (Å) with estimated standard deviations in parentheses

Bond	Length (Å)	Bond	Length (Å)	Bond	Length (Å)	Bond	Length (Å)
Re—P	2.534(2)	P—C(24)	1.825(6)	C(6)—C(7)	1.361(9)	C(6′)—C(7′)	1.389(9)
Re—N(1)	2.202(5)	P′—C(12′)	1.830(6)	C(7)—C(8)	1.363(10)	C(7′)—C(8′)	1.385(11)
Re—N(3)	2.204(5)	P′—C(18′)	1.812(7)	C(9)—C(10)	1.353(9)	C(9′)—C(10′)	1.364(10)
Re—C(1)	1.931(7)	P′—C(24′)	1.846(6)	C(10)—C(11)	1.369(11)	C(10′)—C(11′)	1.363(11)
Re—C(2)	1.907(7)	O(1)—C(1)	1.148(8)	C(12)—C(13)	1.383(10)	C(12′)—C(13′)	1.374(9)
Re—C(3)	1.909(7)	O(2)—C(2)	1.155(8)	C(12)—C(17)	1.389(9)	C(12′)—C(17′)	1.389(9)
Re′—P′	2.541(2)	O(3)—C(3)	1.154(8)	C(13)—C(14)	1.378(10)	C(13′)—C(14′)	1.392(10)
Re′—N(1′)	2.203(5)	O(1′)—C(1′)	1.145(8)	C(14)—C(15)	1.356(11)	C(14′)—C(15′)	1.378(11)
Re′—N(3′)	2.193(5)	O(2′)—C(2′)	1.156(8)	C(15)—C(16)	1.376(11)	C(15′)—C(16′)	1.350(11)
Re′—C(1′)	1.931(8)	O(3′)—C(3′)	1.144(8)	C(16)—C(17)	1.393(10)	C(16′)—C(17′)	1.385(10)
Re′—C(2′)	1.909(8)	N(1)—N(2)	1.364(7)	C(18)—C(19)	1.417(9)	C(18′)—C(19′)	1.378(9)
Re′—C(3′)	1.927(7)	N(1)—C(6)	1.332(9)	C(18)—C(23)	1.379(9)	C(18′)—C(23′)	1.385(10)
Ga—N(2)	1.977(6)	N(2)—C(8)	1.356(9)	C(19)—C(20)	1.371(11)	C(19′)—C(20′)	1.380(13)
Ga—N(4)	1.982(6)	N(3)—N(4)	1.351(7)	C(20)—C(21)	1.374(12)	C(20′)—C(21′)	1.371(14)
Ga—C(4)	1.951(7)	N(3)—C(9)	1.341(9)	C(21)—C(22)	1.361(12)	C(21′)—C(22′)	1.362(14)
Ga—C(5)	1.961(9)	N(4)—C(11)	1.354(9)	C(22)—C(23)	1.411(11)	C(22′)—C(23′)	1.377(12)
Ga′—N(2′)	1.989(5)	N(1′)—N(2′)	1.359(7)	C(24)—C(25)	1.382(9)	C(24′)—C(25′)	1.390(9)
Ga′—N(4′)	1.987(6)	N(1′)—C(6′)	1.344(9)	C(24)—C(29)	1.402(9)	C(24′)—C(29′)	1.376(10)
Ga′—C(4′)	1.963(7)	N(2′)—C(8′)	1.325(9)	C(25)—C(26)	1.370(10)	C(25′)—C(26′)	1.382(10)
Ga′—C(5′)	1.958(7)	N(3′)—N(4′)	1.357(7)	C(26)—C(27)	1.397(11)	C(26′)—C(27′)	1.385(13)
P—C(12)	1.829(7)	N(3′)—C(9′)	1.333(9)	C(27)—C(28)	1.379(11)	C(27′)—C(28′)	1.324(12)
P—C(18)	1.825(7)	N(4′)—C(11′)	1.355(9)	C(28)—C(29)	1.386(10)	C(28′)—C(29′)	1.379(11)

TABLE 3. Bond angles (deg) with estimated standard deviations in parentheses

Bonds	Angle (deg)	Bonds	Angle (deg)	Bonds	Angle (deg)
P—Re—N(1)	87.81(14)	Re′—P′—C(12′)	119.6(2)	P—C(18)—C(23)	123.2(5)
P—Re—N(3)	89.16(15)	Re′—P′—C(18′)	113.5(2)	C(19)—C(18)—C(23)	118.3(7)
P—Re—C(1)	178.1(2)	Re′—P′—C(24′)	114.7(2)	C(18)—C(19)—C(20)	121.3(7)
P—Re—C(2)	93.0(2)	C(12′)—P′—C(18′)	99.3(3)	C(19)—C(20)—C(21)	119.2(8)
P—Re—C(3)	93.9(2)	C(12′)—P′—C(24′)	102.7(3)	C(20)—C(21)—C(22)	121.3(8)
N(1)—Re—N(3)	91.6(2)	C(18′)—P′—C(24′)	104.9(3)	C(21)—C(22)—C(23)	120.1(8)
N(1)—Re—C(1)	93.2(2)	Re—N(1)—N(2)	126.7(4)	C(18)—C(23)—C(22)	119.7(7)
N(1)—Re—C(2)	178.6(2)	Re—N(1)—C(6)	126.5(4)	P—C(24)—C(25)	118.2(5)
N(1)—Re—C(3)	89.9(2)	N(2)—N(1)—C(6)	106.7(5)	P—C(24)—C(29)	123.2(5)
N(3)—Re—C(1)	89.2(2)	Ga—N(2)—N(1)	128.6(4)	C(25)—C(24)—C(29)	118.5(6)
N(3)—Re—C(2)	89.5(2)	Ga—N(2)—C(8)	123.1(5)	C(24)—C(25)—C(26)	121.1(7)
N(3)—Re—C(3)	176.6(2)	N(1)—N(2)—C(8)	107.7(5)	C(25)—C(26)—C(27)	120.4(7)
C(1)—Re—C(2)	86.0(3)	Re—N(3)—N(4)	126.6(4)	C(26)—C(27)—C(28)	119.3(7)
C(1)—Re—C(3)	87.7(3)	Re—N(3)—C(9)	126.2(4)	C(27)—C(28)—C(29)	120.1(8)
C(2)—Re—C(3)	88.8(3)	N(4)—N(3)—C(9)	106.9(5)	C(24)—C(29)—C(28)	120.6(7)
P′—Re′—N(1′)	87.76(14)	Ga—N(4)—N(3)	129.6(4)	Re′—C(1′)—O(1′)	174.5(6)
P′—Re′—N(3′)	84.46(14)	Ga—N(4)—C(11)	122.5(5)	Re′—C(2′)—O(2′)	175.3(6)
P′—Re′—C(1′)	179.5(2)	N(3)—N(4)—C(11)	107.9(6)	Re′—C(3′)—O(3′)	178.4(6)
P′—Re′—C(2′)	95.9(2)	Re′—N(1′)—N(2′)	127.9(4)	N(1′)—C(6′)—C(7′)	110.8(7)
P′—Re′—C(3′)	93.3(2)	Re′—N(1′)—C(6′)	125.5(4)	C(6′)—C(7′)—C(8′)	103.3(7)
N(1′)—Re′—N(3′)	91.3(2)	N(2′)—N(1′)—C(6′)	106.6(5)	N(2′)—C(8′)—C(7′)	110.3(6)
N(1′)—Re′—C(1′)	92.5(2)	Ga′—N(2′)—N(1′)	126.4(4)	N(3′)—C(9′)—C(10′)	110.5(7)
N(1′)—Re′—C(2′)	175.4(2)	Ga′—N(2′)—C(8′)	124.5(5)	C(9′)—C(10′)—C(11′)	105.8(7)
N(1′)—Re′—C(3′)	86.9(2)	N(1′)—N(2′)—C(8′)	109.1(6)	N(4′)—C(11′)—C(10′)	108.2(7)
N(3′)—Re′—C(1′)	95.0(2)	Re′—N(3′)—N(4′)	126.6(4)	P′—C(12′)—C(13′)	123.7(5)
N(3′)—Re′—C(2′)	91.9(3)	Re′—N(3′)—C(9′)	126.1(4)	P′—C(12′)—C(17′)	119.4(5)
N(3′)—Re′—C(3′)	177.2(2)	N(4′)—N(3′)—C(9′)	106.8(5)	C(13′)—C(12′)—C(17′)	116.8(6)
C(1′)—Re′—C(2′)	83.9(3)	Ga′—N(4′)—N(3′)	125.9(4)	C(12′)—C(13′)—C(14′)	122.4(7)
C(1′)—Re′—C(3′)	87.2(3)	Ga′—N(4′)—C(11′)	123.4(5)	C(13′)—C(14′)—C(15′)	119.0(7)
C(2′)—Re′—C(3′)	90.0(3)	N(3′)—N(4′)—C(11′)	108.7(6)	C(14′)—C(15′)—C(16′)	119.8(7)
N(2)—Ga—N(4)	98.0(2)	Re—C(1)—O(1)	175.3(6)	C(15′)—C(16′)—C(17′)	121.0(8)
N(2)—Ga—C(4)	107.3(3)	Re—C(2)—O(2)	175.1(6)	C(12′)—C(17′)—C(16′)	121.0(7)
N(2)—Ga—C(5)	109.3(3)	Re—C(3)—O(3)	178.0(6)	P′—C(18′)—C(19′)	123.5(6)
N(4)—Ga—C(4)	105.4(3)	N(1)—C(6)—C(7)	111.3(6)	P′—C(18′)—C(23′)	118.7(5)
N(4)—Ga—C(5)	112.9(3)	C(6)—C(7)—C(8)	104.8(6)	C(19′)—C(18′)—C(23′)	117.8(7)
C(4)—Ga—C(5)	121.4(4)	N(2)—C(8)—C(7)	109.5(6)	C(18′)—C(19′)—C(20′)	120.8(8)
N(2′)—Ga′—N(4′)	96.7(2)	N(3)—C(9)—C(10)	111.1(6)	C(19′)—C(20′)—C(21′)	119.2(9)
N(2′)—Ga′—C(4′)	106.8(3)	C(9)—C(10)—C(11)	104.8(7)	C(20′)—C(21′)—C(22′)	121.8(9)
N(2′)—Ga′—C(5′)	115.1(3)	N(4)—C(11)—C(10)	109.3(6)	C(21′)—C(22′)—C(23′)	117.9(9)
N(4′)—Ga′—C(4′)	107.3(3)	P—C(12)—C(13)	120.8(5)	C(18′)—C(23′)—C(22′)	122.4(8)
N(4′)—Ga′—C(5′)	107.3(3)	P—C(12)—C(17)	122.0(5)	P′—C(24′)—C(25′)	119.2(5)
C(4′)—Ga′—C(5′)	120.6(3)	C(13)—C(12)—C(17)	117.2(6)	P′—C(24′)—C(29′)	122.0(5)
Re—P—C(12)	117.2(2)	C(12)—C(13)—C(14)	121.8(7)	C(25′)—C(24′)—C(29′)	118.8(6)
Re—P—C(18)	112.8(2)	C(13)—C(14)—C(15)	120.9(8)	C(24′)—C(25′)—C(26′)	120.1(8)
Re—P—C(24)	112.8(2)	C(14)—C(15)—C(16)	118.8(7)	C(25′)—C(26′)—C(27′)	120.0(8)
C(12)—P—C(18)	104.3(3)	C(15)—C(16)—C(17)	120.9(7)	C(26′)—C(27′)—C(28′)	118.8(8)
C(12)—P—C(24)	104.0(3)	C(12)—C(17)—C(16)	120.3(7)	C(27′)—C(28′)—C(29′)	123.1(8)
C(18)—P—C(24)	104.3(3)	P—C(18)—C(19)	118.3(5)	C(24′)—C(29′)—C(28′)	119.1(7)

Re—CO(*trans* to P) = 1.931(1), and Re—CO(*trans* to N) = 1.913(9) Å. The central six-membered $ReGaN_4$ rings have relatively shallow, asymmetrically twisted, boat conformations with cross-ring Re···Ga distances of 3.9396(7) and 3.8981(8) Å and dihedral angles of 144.9(3) and 138.0(3)° between the normals to the pyrazolyl mean planes (180° for a planar chelate ring). This structure is similar to those observed (1) for $(MeGapz_2)Mn(pzH)(CO)_3$ and $[(Me_2Gapz_2)Mo(pzH)(CO)_3]^-$ which have the same *fac*-octahedral coordination geometry, M···Ga distances of 3.818 and 3.929 Å, and dihedral angles of 139.8 and 128.1° between the pyrazolyl mean planes. The conformations of M—$(N—N)_2$—M′ rings and the highly correlated cross-ring M···M′ distances in compounds of this type depend primarily on steric factors which have been discussed in a number of recent publications (refs. 8, 9, and references therein).

Both of the independent molecules of $[Me_2Ga(N_2C_3H_3)_2](PPh_3)Re(CO)_3$ contain an interesting intramolecular interaction between a phenyl hydrogen atom and the π-electron system of a pyrazolyl ring (C(25)—H(25)···(N(1)—N(2)), mean geometrical parameters: H···N = 2.54(5), H···(N—N midpoint) = 2.45(3), C···N = 3.42(7) Å, C—H···N = 152(7)°). The pyrazolyl and phenyl rings are all planar to within experimental error with the exception of the C(18) phenyl ring (χ^2 = 11.4; mean and maximum deviations from the C_6 plane, 0.010 and 0.016(9) Å).

TABLE 4. Intra-annular torsion angles (deg) with standard deviations in parentheses

Atoms	Value (deg)
N(3) —Re —N(1) —N(2)	−22.2(5)
Re —N(1) —N(2) —Ga	−13.8(8)
N(4) —Ga —N(2) —N(1)	40.8(6)
N(2) —Ga —N(4) —N(3)	−29.5(6)
Re —N(3) —N(4) —Ga	−6.9(8)
N(1) —Re —N(3) —N(4)	32.7(5)
N(3′)—Re′ —N(1′)—N(2′)	32.2(5)
Re′ —N(1′)—N(2′)—Ga′	−3.5(7)
N(4′)—Ga′ —N(2′)—N(1′)	−36.3(5)
N(2′)—Ga′ —N(4′)—N(3′)	52.0(5)
Re′ —N(3′)—N(4′)—Ga′	−24.5(8)
N(1′)—Re′ —N(3′)—N(4′)	−17.4(5)

Acknowledgments

We thank the Natural Sciences and Engineering Research Council of Canada for financial support and the University of British Columbia Computing Centre for assistance.

1. S. E. ANSLOW, K. S. CHONG, S. J. RETTIG, A. STORR, and J. TROTTER. Can. J. Chem. **59**, 3123 (1981).
2. B. M. LOUIE and A. STORR. Can. J. Chem. **62**, 1334 (1984).
3. P. COPPENS, L. LEISEROWITZ, and D. RABINOVICH. Acta Crystallogr. **18**, 1035 (1965).
4. J. DE MEULENAER and H. TOMPA. Acta Crystallogr. **19**, 1014 (1965).
5. D. T. CROMER and J. B. MANN. Acta Crystallogr. Sect. A, **24**, 321 (1968).
6. R. F. STEWART, E. R. DAVIDSON, and W. T. SIMPSON. J. Chem. Phys. **42**, 3175 (1965).
7. D. T. CROMER and D. LIBERMAN. J. Chem. Phys. **53**, 1891 (1970).
8. B. M. LOUIE, S. J. RETTIG, A. STORR, and J. TROTTER. Can. J. Chem. **62**, 1057 (1984).
9. S. NUSSBAUM, S. J. RETTIG, A. STORR, and J. TROTTER. Can. J. Chem. **63**, 692 (1985).

The anomalous gas phase acidity of ethyl fluoride. An *ab initio* investigation of the importance of hydrogen bonding between F^- and sp^2 and sp C—H bonds

M. ROY AND T. B. MCMAHON[1]

Department of Chemistry, University of New Brunswick, Fredericton, N.B. Canada E3B 6E2

Received May 16, 1984

M. ROY and T. B. MCMAHON. Can. J. Chem. **63**, 708 (1985).

Ab initio quantum chemical techniques have been used to investigate the structures and energetics of a number of hydrogen bonded adducts of F^- and C—H bonds associated with unsaturated systems as well as their structural isomers. Examination of the possible species of molecular formula $C_2H_4F^-$ reveals that the most stable isomer is a hydrogen bonded adduct of F^- and ethylene, while the classical β-fluoroethyl carbanion is found not to be bound with respect to dissociation into $F^- + C_2H_4$. Similar examination of $C_2H_2F^-$ isomers shows that a hydrogen bonded F^-–acetylene adduct is the most stable structure, however, the remaining α and β-fluorovinyl carbanions are found to be bound with respect to $F^- + C_2H_2$. These results are used to explain the unusual gas phase acidities of ethylfluoride and vinylfluoride. Calculations on $C_3H_4F^-$ isomers show the hydrogen bonded adduct of F^- and allene to be more stable than the classical 2-fluoropropenyl anion and on $C_2H_2FO^-$ isomers show the enolate of acetyl fluoride to be more stable than the hydrogen bonded adduct of F^- and ketene. These latter results are used to explain the gas phase ion molecule reactivities of $C_3H_4F^-$ (predominantly F^- transfer) and $C_2H_2FO^-$ (proton abstraction).

M. ROY et T. B. MCMAHON. Can. J. Chem. **63**, 708 (1985).

On fait appel aux techniques de la chimie quantique *ab initio* pour étudier les structures et les énergies d'un certain nombre d'adduits, liés par des liaisons hydrogènes, du F^- et de liaisons C—H associées à des systèmes insaturés ainsi que leurs isomères de structure. L'étude des espèces possibles, de formule moléculaire $C_2H_4F^-$, révèle que l'isomère le plus stable est un adduit dans lequel le F^- et l'éthylène sont liés par des liaisons hydrogènes; par ailleurs le carbanion classique β-fluoroéthyle n'est pas lié par rapport à la dissociation en F^- et C_2H_4. Une étude semblable des isomères du $C_2H_2F^-$ montre que l'adduit F^-–acétylène, qui est lié par des liaisons hydrogènes, constitue la structure la plus stable; toutefois, on a trouvé que les carbanions α et β fluorovinyles résiduels sont liés par rapport à la dissociation $F^- + C_2H_2$. On utilise ces résultats pour expliquer les acidités inhabituelles en phase gazeuse du fluorure d'éthyle et du fluorure de vinyle. Les calculs faits avec les isomères du $C_3H_4F^-$ révèlent que l'adduit de F^- et de l'allène, qui est lié par des liaisons hydrogènes, est plus stable que l'anion classique fluoro-2 propényle alors que les mêmes calculs faits sur les isomères du $C_2H_2FO^-$ montrent que l'énolate du fluorure d'acétyle est plus stable que l'adduit de F^- et du cétène, qui sont liés par des liaisons hydrogènes. On utilise ces derniers résultats pour expliquer les réactivités ion-molécule en phase gazeuse du $C_3H_4F^-$ (transfert prédominant de F^-) et du $C_2H_2FO^-$ (enlèvement d'un proton).

[Traduit par le journal]

Introduction

Fluorine substituents have been abundantly demonstrated to exhibit pronounced, and frequently ambiguous, effects on the stabilities of both positive and negative gas phase ions (1–8). However, no fluorine substituent effect is perhaps as bizarre as that found for the gas phase acidities of fluoroethanes (2). Sullivan and Beauchamp, using ion cyclotron resonance (ICR) techniques, have shown that ethyl fluoride is intermediate in gas phase acidity between ethanol and 2-propanol. With the aid of deuterium labelling experiments, they have further shown that the only proton removed in reaction with strong anionic bases is β to the fluorine. Assuming a nearly constant C—H bond strength for ethane and the β C—H bonds of ethyl fluoride, these experiments imply a stabilization of β fluoroethyl carbanion of some 30 kcal mol^{-1} relative to ethyl carbanion. This magnitude of remote inductive substituent effect is unprecedented in studies of relative stabilities of gas phase ions. Equally surprising are the effects of multiple fluorine substitution on the relative stabilities of the series of fluoroethyl carbanions. After the first large increase in gas phase acidity of 30 kcal mol^{-1} in proceeding from ethane to ethyl fluoride, no further appreciable increase is observed in successively adding up to 5 fluorines. For example, pentafluoroethane is observed to be only 3 kcal mol^{-1} more acidic in the gas phase than ethyl fluoride. All other fluoroethanes show gas phase acidities between those of ethyl fluoride and pentafluoroethane. In their discussion of these unusual substituent effects, Sullivan and Beauchamp concluded only that "simple electrostatic arguments are inappropriate to explain the order of acidities".

Recent ICR investigations in our laboratory (9, 10) of quantitative fluoride binding energies to Brønsted acids have suggested to us that hydrogen bonding of F^- to organic molecules may be a far more energetically favourable and ubiquitous phenomenon than previously supposed. In particular our studies of fluoride binding energies to fluoroethylenes suggested that the resulting anions are more likely planar hydrogen bonded adducts than pyramidal sp^3 hybridized carbanions, implying that the former species are likely the more stable. It thus seems reasonable to infer that the attack of strong anionic bases on ethyl fluoride may not lead to simple deprotonation but rather to a process of elimination in which the departing F^- remains hydrogen bonded to a proton of a newly formed ethylene group. If this is indeed the case, then the gas phase acidity measurements will not yield a measure of carbanion stability and the need to explain an unusually large substituent effect is avoided.

Recently Bach *et al.* (11) and Schleyer and Kos (12) have examined the β-fluoroethyl carbanion using *ab initio* quantum chemical techniques and have found, in the course of geometry optimization, that this carbanion is not bound with respect to $F^- + C_2H_4$. In addition, Schleyer and Kos have investigated a hydrogen bonded structure of ethylene and F^- and have found

[1] Present address: Department of Chemistry and Guelph–Waterloo Centre for Graduate Work in Chemistry, University of Waterloo, Waterloo, Ont., Canada N2L 3G1.

that this hydrogen bonded adduct of $F^- + C_2H_4$ is bound, thus supporting the conjecture above regarding the anion derived from the gas phase deprotonation of C_2H_5F.

In addition to β-fluoroethyl carbanion, Schleyer and Kos have also examined the β-fluorovinyl carbanion and the isomeric F^-–acetylene hydrogen bonded adduct. As in the fluoroethyl carbanion case the β-fluorovinyl carbanion is found to be unbound with respect to $F^- + C_2H_2$ while the hydrogen bonded complex is bound by some 20 kcal mol^{-1}.

In the course of ongoing studies in our laboratory of gas phase acidities of organo-fluorine compounds and of hydrogen bond energetics of F^- to organic acids (10) we have discovered several fluorinated species which upon deprotonation act as facile F^- transfer reagents. In order to ascertain the most probable structures of these fluorinated anions we have undertaken the present *ab initio* quantum chemical study of several fluorine containing anions. The first of these is a complete investigation of the fluoroethyl system since although Schleyer and Kos have studied β-fluoroethyl carbanion and the F^-–C_2H_4 hydrogen bonded adduct, the potentially stable α-fluoroethyl carbanion has not been investigated. Similarly the fluorovinyl system has been studied completely including the F^-–C_2H_2 hydrogen bonded adduct, both *cis* and *trans* β-fluorovinyl carbanions and α-fluorovinyl carbanion. Two possible isomers of the chemically important $C_3H_4F^-$ anion derived from deprotonation of 2-fluoropropene have been studied — the 2-fluoropropenyl anion and a hydrogen bonded adduct of F^- and allene. Finally, two possible isomers of the isoelectronic analogue, $C_2H_2FO^-$, derived from deprotonation of acetyl fluoride have also been investigated — the acetyl fluoride enolate ion and a hydrogen bonded adduct of F^- and ketene.

Computational method

Ab initio molecular orbital calculations were carried out using the Gaussian 80 (13) and Hondo 5 (14) program packages. All structures were fully optimized using the 4-31G basis set employing an analytical gradient technique (15). In several cases single point total energy calculations were carried out for the 4-31G optimized geometry using the 4-31+G basis set (16, 17). This latter basis set, incorporating additional flat *s* and *p* Gaussian functions on all heavy atoms has been demonstrated by Schleyer to provide a much more accurate description of the energetics of anions than other split valence basis sets. In the present case flat function exponents of 0.090 for fluorine 0.040 for carbon and 0.068 for oxygen were used. In the few cases where diffuse function augmented basis sets calculations were not carried out the conclusions drawn are probably valid since energy differences between isomeric ions rather than absolute energies are being considered. In all cases where 4-31G and 4-31+G calculations were carried out the order of stabilities of isomeric ions was invariant with basis set.

Results

A. Geometries

1. $C_2H_4F^-$: As noted above the β-fluoroethyl carbanion has been shown originally by Bach *et al.* (11) to dissociate without activation energy to $F^- + C_2H_4$ at the 4-31G level. Following his example, for purposes of discussion, we have used an "artificial" $CH_2FCH_2^-$ structure which was obtained from the structure optimized at the STO-3G level where it was found to be stable with respect to dissociation. Further refinement was then carried out at the 4-31G level by holding the C—F and C—H bonds constant and optimizing the C—C bond length

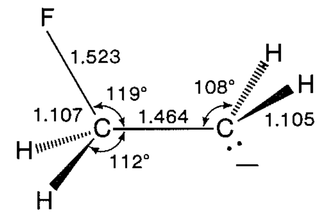

I

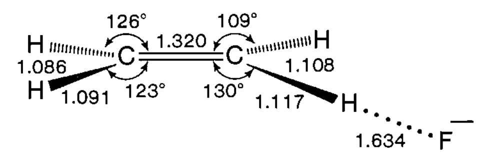

II

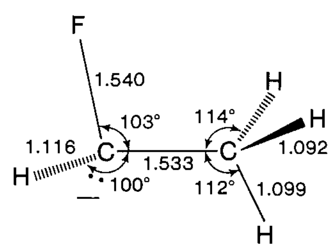

III

FIG. 1. Geometries of the isomers of $C_2H_4F^-$.

and bond angles. The geometry for this isomer (**I**) as well as those obtained for the α-fluoroethyl carbanion, CH_3CHF^- (**III**), and the hydrogen bonded F^-–ethylene complex, $C_2H_4\cdots F^-$ (**II**), are detailed in Fig. 1.

2. $C_2H_2F^-$: There are four possible stable isomers for anions of this formula. The *cis* (**IV**) and *trans* (**V**) β-fluorovinyl carbanions, $CHFCH^-$, and the hydrogen bonded complex of F^- and acetylene, $C_2H_2\cdots F^-$ (**IV**) have been investigated previously by Schleyer and Kos (12). To this we add in the present study the α-fluorovinyl carbanion, CH_2CF^- (**VII**). Geometries for these four species are outlined in Fig. 2.

3. $C_3H_4F^-$: Although there are probably several stable isomers of this molecular formula only those two deemed to be mechanistically feasible from deprotonation of 2-fluoropropene were investigated. The geometries of 2-fluoropropenyl carbanion, $CH_2CFCH_2^-$ (**VIII**), and the hydrogen bonded complex of F^- and allene $C_3H_4\cdots F^-$ (**IX**) are summarized in Fig. 3.

4. $C_2H_2FO^-$: Analogous to the case of $C_3H_4F^-$, only the two possible isomers of the isoelectronic $C_2H_2FO^-$ deemed to be mechanistically feasible from deprotonation of acetyl fluoride were investigated. The geometries of acetyl fluoride enolate, CH_2COF^- (**X**), and the hydrogen bonded complex of F^- and ketene, CH_2COF^- (**XI**), are detailed in Fig. 4.

B. Energies

Total energies of all relevant anionic and neutral species obtained using the 4-31G basis set are summarized in Table 1. In selected cases it was important to determine relative energies of anionic isomers somewhat more accurately and in such cases

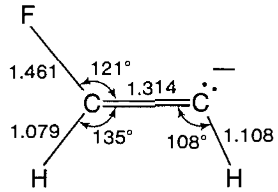

IV

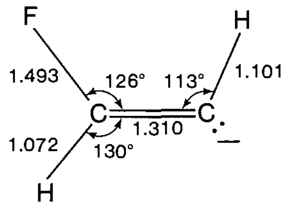

V

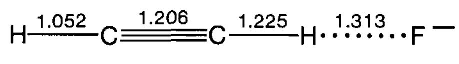

VI

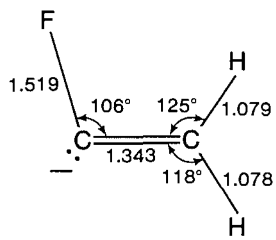

VII

FIG. 2. Geometries of the isomers of $C_2H_2F^-$.

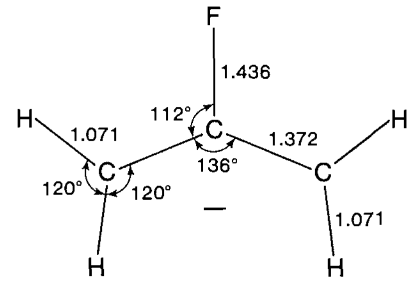

VIII

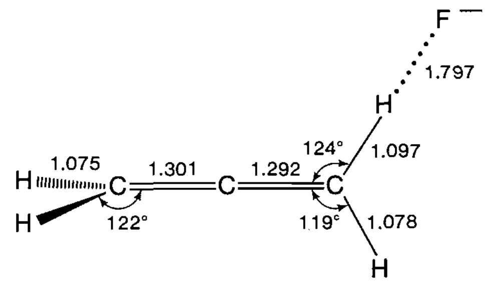

IX

FIG. 3. Geometries of the isomers of $C_3H_4F^-$.

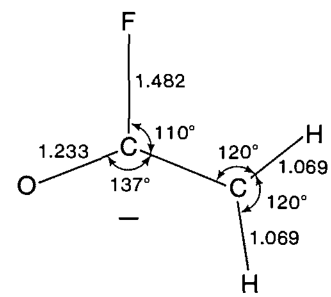

X

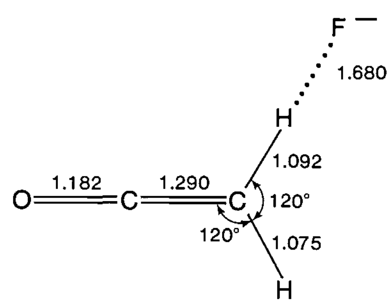

XI

FIG. 4. Geometries of the isomers of $C_2H_2FO^-$.

total energies were calculated at the 4-31G optimized geometry using the 4-31+G basis set described above. Their energy values are given in parentheses in Table 1.

Discussion

$C_2H_4F^-$

It is readily apparent from the data of Table 1 that the most stable of the three possible $C_2H_4F^-$ isomers is the hydrogen bonded adduct, **II**. Even though the hypothetical structure for β-fluoroethyl carbanion, **I**, is known to dissociate at the 4-31G level to F^- + C_2H_4 this artificial structure is still found to be more stable than the α-fluoroethyl carbanion, **III**. It is noteworthy that at the 4-31G level **III** is a minimum on the potential energy surface revealing its stability toward dissociation to F^- and methyl carbene, CH_3CH:. The greater stability of **I** relative to **III** reveals a further example of the partially destabilizing nature of fluorine substituted α to negative charge centers. Further support for the destabilizing nature of the α fluorine may be found in an examination of the geometry of **III**. The C—C bond length in the α carbanion, **III** is a normal C—C single bond length, being within 0.02 Å of those in C_2H_6 and C_2H_5F. However, the C—F bond length is unusually long at 1.54 Å compared to those of 1.38 Å in CH_3F and 1.43 Å in *t*-C_4H_9F. Similar bond lengths have been found for the analogous fluoromethyl carbanion, CH_2F^-, by other investigators (16–19) and in fluorocyclohexadienyl anions (20). Such abnormally long C—F bonds appear to be readily attributable to strong electron–electron repulsions between lone pairs on fluorine and the filled $2p$ orbital on carbon in the carbanion. These effects have frequently been invoked to explain unusual stability orderings of fluorine substituted sp^2 carbanions both in the gas phase (5) and solution (21).

TABLE 1. Calculated total energies of anions and related neutral molecules

Species	Total energy[a] (hartree)
F^-	−99.24782[b] (−99.32621)[c]
$CH_2FCH_2:^-$ (I)	−177.15313
$C_2H_4 \ldots F^-$ (II)	−177.19788 (−177.25720)
$CH_3CHF:^-$ (III)	(−177.14459)
C_2H_4	−77.92216[d] (−77.92780)
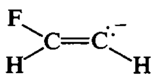 (IV)	−175.97392 (−175.31665)[e]
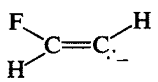 (V)	−175.97878 (−175.32205)[e]
$C_2H_2 \cdots F^-$ (VI)	−176.01330 (−175.37048)[e]
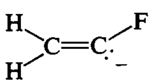 (VII)	−175.99210
C_2H_2	−76.71140[d]
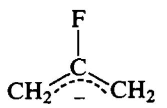 (VIII)	−214.98582 (−215.02580)
$CH_2{=}C{=}CH_2 \cdots F^-$ (IX)	−214.98530 (−215.04001)
$CH_2{=}C{=}CH_2$	−115.69836[f]
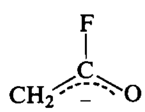 (X)	−250.84189 (−250.87387)
$O{=}C{=}CH_2 \cdots F^-$ (XI)	−250.79571 (−250.85489)
$O{=}C{=}CH_2$	−151.49493[g]

[a] Energies given are calculated using 4-31G optimizations and 4-31G energy calculations. Values in parenthesis are obtained from 4-31G optimizations and 4-31+G single point energy calculations unless otherwise noted.
[b] Reference 30.
[c] Reference 16.
[d] Reference 31.
[e] 3-21+G optimization/3-21+G energy calculation; ref. 12.
[f] Reference 32.
[g] Reference 33.

With the advantage of hindsight it is possible to rationalize the instability of the β-fluoroethyl carbanion toward dissociation to F^- and C_2H_4 and the greater stability of the hydrogen bonded complex on purely thermochemical grounds. From the thermochemical cycle shown in Scheme 1 it is possible to use known data or to make accurate predictions for the individual steps involved and to predict the exothermicity of dissociation of **I**, ΔH^0_{diss}.

The electron affinity of $CH_2FCH_2^{\bullet}$ is estimated as 8 ± 5 kcal mol^{-1} based on the approximate electron affinity of C_2H_5[2] of 0 ± 5 kcal mol^{-1} and an approximate expected inductive effect of the β fluorine of 8 kcal mol^{-1}.[3] The C—F bond strength in $CH_2FCH_2^{\bullet}$ is expected to be the same as that in C_2H_5F, 106 kcal mol^{-1} (24). The π bond energy in C_2H_4 is known to be 60 kcal mol^{-1} (25) and the electron affinity of fluorine atom to be 78 kcal mol^{-1} (26). Thus the overall dissociation enthalpy for **I** may be calculated from eq. [1].

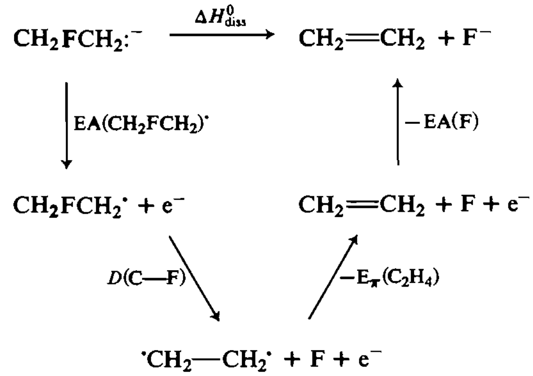

SCHEME 1

$$[1] \quad \Delta H^0_{\text{diss}} = EA(CH_2FCH_2^{\bullet}) + D(C{-}F) - E_\pi(C_2H_4) - EA(F)$$

to be −24 kcal mol^{-1}. The driving force for this dissociation can readily be seen to be the π bond formation and the exothermic electron transfer from carbon to fluorine. Based on recent correlations of fluoride binding energy and gas phase acidity from our laboratory (10) it is possible to estimate a hydrogen bond energy for F^- and C_2H_4 of 5 kcal mol^{-1}. This further exothermic step, eq. [2],

[2] $F^- + C_2H_4 \rightarrow$ 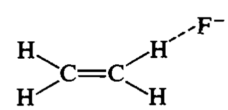

therefore reveals the greatest stability of **II** relative to other $C_2H_4F^-$ isomers. Using the 4-31+G energy data from Table 1 a fluoride binding energy of F^- to C_2H_4 for the hydrogen bonded structure of 2 kcal mol^{-1} is obtained in good agreement with the qualitative prediction above.

The much greater predicted stability of the hydrogen bonded form of $C_2H_4F^-$ has important implications for the stability of fluoroethyl anions inferred from the gas phase acidity measurements and for the mechanism of deprotonation of fluo-

[2] $EA(CH_3CH_2)$ is estimated at 0 ± 5 kcal mol^{-1} based on the assumption that the replacement of H by CH_3 in CH_4 could lead to either an increase or decrease in electron affinity. Calculations at the 4-31+G level (16, 17) show a destabilization by CH_3 for H substitution of 5.6 kcal mol^{-1}; however, at the same level, the calculations fail to reproduce the relative experimental order of stabilities of NH_2^- and CH_3NH^- and fail to indicate the large stabilization of CH_3O^- relative to OH^-. Thus we feel that relative to the experimental $EA(CH_3)$ of 2 kcal mol^{-1} (29) an estimate of $EA(CH_3CH_2)$ of 0 ± 5 kcal mol^{-1} is in order.

[3] The inductive effect of β fluorine on an anionic center is estimated from an average of $EA(CH_2COF) - EA(CH_2CHO)$ = 10.5 kcal mol^{-1} (22), $EA(FCO_2) - EA(HCO_2)$ = 13 kcal mol^{-1} (23) and $EA(CH_2CFCH_2) - EA(CH_2CHCH_2)$ = 9.3 kcal mol^{-1} (T. B. McMahon, unpublished results).

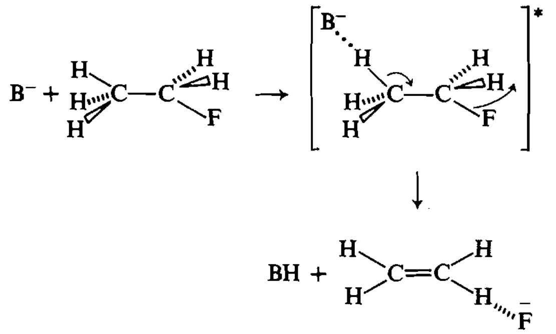

SCHEME 2

roethanes. Prior to the gas phase acidity work on fluoroethanes the acidity of ethyl fluoride might have been predicted to be 398 kcal mol^{-1} and thus deprotonation by even such strong bases as OH^- and CH_3O^- would not have been expected. The fact that an apparent deprotonation is observed suggests to us that rather than participating in a simple proton abstraction reaction, strong anionic bases react with ethyl fluoride in a concerted addition–elimination type of reaction in which the leaving group, F^-, remains hydrogen bonded to ethylene, C_2H_4. Such a mechanism is depicted in Scheme 2. Since this mechanism does not yield the true conjugate base of ethyl fluoride, the reaction cannot be regarded as a true deprotonation and an erroneous gas phase acidity determination would result. The reactions of strongly basic anions with ethyl fluoride might then be interpreted simply as HO^- and CH_3O^- binding sufficiently strongly to C_2H_5F to activate the intermediate towards elimination, whereas $C_2H_5O^-$ and more weakly basic alkoxides do not activate the intermediate to an extent sufficient for elimination to occur.

Additionally it is significant to note that our conclusion, that a hydrogen bonded form of $C_2H_4F^-$ is the most stable one and that this is the species most likely produced in deprotonation of ethyl fluoride, is supported by our experimental observations of fluoride transfer reactions (10). The anions derived from "deprotonation" of ethyl fluoride and other fluoroethanes are found *not* to readily abstract a proton from stronger gas phase acids as would be expected of a carbanion but rather readily transfer F^-, a result quite reasonable for a hydrogen bonded F^- adduct. A similar observation is made for experiments in which F^- donors transfer F^- to fluoroethylenes. For example, the anion derived from addition of F^- to trifluoroethylene, reaction [3], is found to react with strong acids by F^- donation, reaction [4*a*] rather than proton abstraction, reaction [4*b*]. This

[3] $MF^- + C_2HF_3 \rightarrow C_2HF_4^- + M$

[4*a*] $C_2HF_4^- + AH \rightarrow AHF^- + C_2HF_3$

[4*b*] $C_2HF_4^- + AH \not\rightarrow A^- + C_2H_2F_4$

result again supports a hydrogen bonded structure for $C_2HF_4^-$ rather than an sp^3 carbanion. The notable exceptions to the above observations involve reaction of pentafluoroethane, C_2F_5H, and tetrafluoroethylene. The anion derived from deprotonation of C_2F_5H is found to readily abstract protons from stronger gas phase acids and to transfer F^- only at a very slow rate, primarily to Lewis acids. Similarly, in reactions of F^- donors with C_2F_4, F^- transfer occurs very slowly. In these cases the $C_2F_5^-$ anion must have an sp^3 carbanion structure rather than a hydrogen bonded one and the chemical behaviour is completely different.

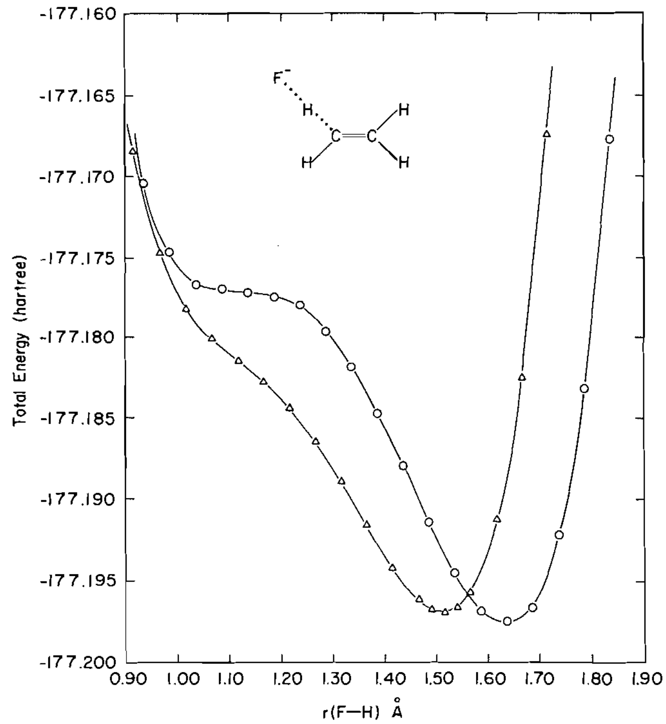

FIG. 5. Plot of potential energy surface for motion of the proton in the F^-—C_2H_4 hydrogen bonded adduct, **III**. ○, total C—F distance of 2.75 Å; △, total C—F distance of 2.63 Å.

It is of considerable interest to consider the nature of the potential for proton motion within the hydrogen bond in **II**. Quite frequently double minima potential wells are postulated for hydrogen bonded species (27). In the present case a double minimum potential well could be envisioned as having one minimum associated with a $C_2H_4\cdots F^-$ structure, **II**, and a possible second minimum of higher total energy associated with a vinyl anion – HF hydrogen bonded complex, $C_2H_3^-\cdots HF$. In order to investigate this possibility a series of calculations was undertaken in which the total C—F distance was held constant and the C—H distance was varied. The results of these calculations are shown in Fig. 5. In one case a total C—F distance of 2.75 Å was used corresponding to the global energy minimum. In addition to this a second series of calculations was carried out at a total C—F distance of 2.63 Å. The plot for the structure with the longer total C—F distance corresponding to the minimum overall geometry shows no barrier to proton motion between F and C and reveals a plateau at short F—H and long C—H distance corresponding to a structure, $C_2H_3^-\cdots HF$ only an inflection point results. This second plot, however, even though having a higher minimum than the previous one, has an overall lower potential for proton motion. This would thus suggest that during vibration about the hydrogen bond the C—H distance remains relatively constant and the F^- position would appear to oscillate.

$C_2H_2F^-$

As in the case of the $C_2H_4F^-$ anions, the most stable structure of molecular formula $C_2H_2F^-$ is a hydrogen bonded adduct, in this case the F^-–acetylene complex (**VI**). The geometry given in Fig. 2 for **VI** shows a —C≡C— bond only slightly elongated from that in acetylene (1.19 Å). Consistent with the substantially greater gas phase acidity of acetylene relative to ethylene the hydrogen bond energy is significantly increased in the F^- adduct and the overall F^-—H distance is appreciably reduced to 1.31 Å from 1.63 Å in the olefinic case. The corresponding C—H distance in the hydrogen bond is increased from the value of 1.05 Å in acetylene to 1.22 Å in **VI**.

The next most stable structure of $C_2H_2F^-$ is the α-fluorovinyl carbanion, **VII**. This species has a C—F bond length of 1.52 Å, similar to that of the α-fluoroethyl carbanion, **III**. In addition, this C—F bond is somewhat longer than that in either the *cis* or *trans* β-fluorovinyl carbanions, **IV** and **V**, while the —C=C— bond length of 1.34 Å is slightly greater than in **IV** and **V**. These bond length differences and the fact that the C—C bonds are all very close in length to that in ethylene indicate that very little delocalization of negative charge is occurring from the nominal carbanion site to the β carbon. Since the charge is localized on the α carbon in **VII** the fluorine atom may undergo a repulsive interaction with the charge center just as occurred in **III**, leading to the lengthened C—F bond.

The geometries of the *cis* and *trans* β-fluorovinyl carbanions, **IV** and **V**, have been investigated previously by Schleyer using the 3-21+G basis set (12). The geometry results obtained in the present study employing the 4-31G basis set are in good agreement with those using the diffuse function augmented basis set with all bond distances lying within 0.02 Å and all bond angles within 1°.

Both the 4-31G and 3-21+G results place the hydrogen bonded structure of $C_2H_2F^-$ as the most stable. However, while the 4-31G results show all of the anions **IV**–**VII** to be stable with respect to dissociation to F^- + C_2H_2 the 3-21+G results find only the hydrogen bonded structure to be energetically lower than the separated species. The 3-21+G results do, however, yield **IV** and **V** as local minima; that is, there is some activation energy associated with their dissociation to F^- + C_2H_2. Our previous correlations of gas phase acidity and hydrogen bond energy to F^- (10) allow a prediction of some 15–20 kcal mol^{-1} for the hydrogen bond energy in **VI** in good agreement with the value of 20 kcal mol^{-1} obtained using the 3-21+G basis set.

The relative energetics of these $C_2H_2F^-$ isomers thus lead to the question of the nature of the anion obtained from deprotonation of fluoroethylene. Gas phase acidity determinations carried out by Beauchamp and Sullivan (2) place the enthalpy of dissociation of C_2H_3F into H^+ + $C_2H_2F^-$ as 380 kcal mol^{-1}. This result then allows $\Delta H_f^0(C_2H_2F^-)$ to be calculated as −18.9 kcal mol^{-1} which further yields a binding energy of F^- to C_2H_2 in the anion of 12.8 kcal mol^{-1}. Since at the 3-21+G level only the hydrogen bonded complex VI is stable with respect to F^- + C_2H_2 the gas phase acidity measurements are strongly suggestive that the hydrogen bonded species is the anion generated upon deprotonation of vinylfluoride.

The reaction of the strongly basic anions such as CH_3O^-, with vinylfluoride yields predominantly the elimination product CH_3OHF^- (81%) with $C_2H_2F^-$ (12%) and F^- (7%) as minor products. Production of CH_3OHF^- and a hydrogen bonded $C_2H_2F^-$ product can be rationalized mechanistically through Scheme 3 involving a common "disolvated" F^- intermediate. Since F^- is known to bind more strongly to CH_3OH than to C_2H_2 this would explain the 4:1 relative abundance of the hydrogen bonded F^-–methanol product. No other alkoxide ions, RO^-, undergo any reaction with vinyl fluoride even though production of ROH···F^- is quite exothermic. Thus it would seem that a partial proton transfer such as that outlined in Scheme 3 is a necessary initial step in the mechanism for ROH···F^- product. In the case of the more weakly basic alkoxide ions this initial partial proton transfer must then not be sufficiently energetically favorable to proceed.

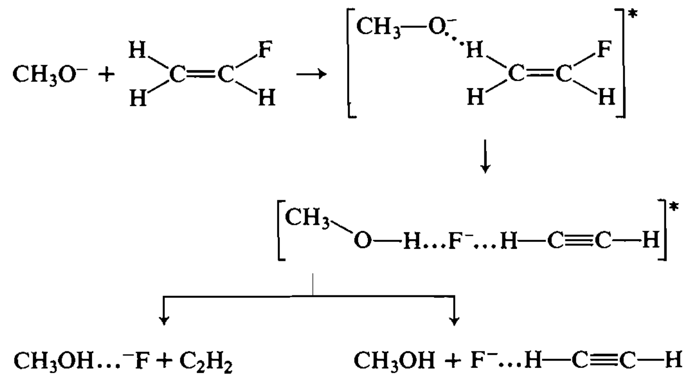

SCHEME 3

$C_3H_4F^-$

The $C_3H_4F^-$ anion derived from deprotonation of 2-fluoropropene, reaction [5], has played an extremely important role in our previous determinations of fluoride binding energies to

[5] A^- + 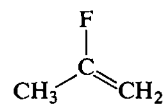 → $C_3H_4F^-$ + AH

Bronsted acids. From a study employing anions, A^-, of known basicity and observation of which would and would not produce $C_3H_4F^-$ a value for $\Delta H_f^0(C_3H_4F^-)$ was obtained which allowed a calculation of the binding energy of F^- to allene, C_3H_4, of 15 kcal mol^{-1} (28). This anion was employed to act as a facile fluoride transfer reagent to species which bind F^- more weakly than H_2O, such as t-C_4H_9F, reaction [6], which may have the structure of a captured S_N2 transition state (10).

[6] $C_3H_4F^-$ + t-$C_4H_9F \rightarrow C_4H_9F_2^-$ + C_3H_4

In view of the preceding results for $C_2H_4F^-$ and $C_2H_2F^-$ isomers two probable structures for the $C_3H_4F^-$ anion were investigated: the 2-fluoropropenyl anion, **VIII**, and a hydrogen bonded complex, **IX**.

Geometry optimization and calculation of energies at the 4-31G level gave nearly identical total energies for the two $C_3H_4F^-$ isomers. However, employing the 4-31+G basis set, previously determined to give a superior description of anions, the hydrogen bonded structure **IX** was found to be more stable by 8.8 kcal mol^{-1}. At this level the hydrogen bond energy of F^- to allene obtained from the data of Table 1 is 10 kcal mol^{-1} in good agreement with the experimentally determined value of 15 kcal mol^{-1}.

The H—F^- bond distance found in **IX** of 1.80 Å is significantly longer than that in $C_2H_2F^-$, indicative of the somewhat weaker hydrogen bond strength in the allenic system. Consistent with this is the substantially shorter C—H bond in the hydrogen bond of **IX** relative to that in **VI**. The C—C distances in **IX** are very similar to those found in neutral allene.

The 2-fluoropropenyl anion, **VIII**, has a C—F bond distance of 1.44 Å. This is only slightly longer than that found in neutral olefinic fluorides indicating that to a small extent repulsive interaction between the fluorine lone pair electrons and the allyl π system may be occurring. The C—C distances found are similar to those obtained for unsubstituted allyl anion.

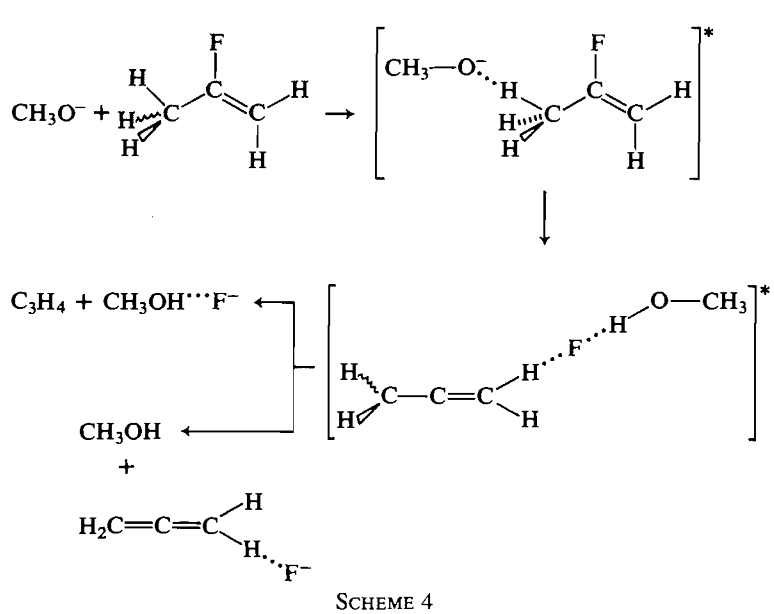

SCHEME 4

The slightly greater stability of the hydrogen bonded complex **IX**, relative to the allylic anion, **VIII**, has significant implications for the anion observed by deprotonation of 2-fluoropropene in ion cyclotron resonance experiments (28). The anion thus obtained, as noted above, is observed to act as a facile fluoride donor, while no tendency for reaction via proton abstraction was observed. These reactivity results are more consistent with a hydrogen bonded structure since even though the 2-fluoropropenyl anion might be expected to react via F^- transfer, some tendency for reaction by proton abstraction with species of high gas phase acidity but low fluoride binding energy, such as cyclopentadiene, would have been anticipated.

The formation of the hydrogen bonded F^-–allene adduct by reaction of strong bases such as CH_3O^- with 2-fluoropropene might then be considered to be analogous to that proposed above for formation of **VI** in vinyl fluoride. Scheme 4 which illustrates such a mechanism can be seen to also lead to formation of $CH_3OH\cdots F^-$ as in the case for reaction of CH_3O^- with C_2H_3F. Consistent with this $CH_3OH\cdots F^-$ is indeed observed in reactions of CH_3O^- with 2-fluoropropene.

$C_2H_2FO^-$

The $C_2H_2FO^-$ anion derived from deprotonation of acetylfluoride (6) has also played an extremely valuable role in our recent determinations of absolute fluoride ion binding energetics. From equilibrium proton transfer determinations of the gas phase acidity of acetyl fluoride, reaction [7], the heat of formation of CH_2COF^- had been

[7] $A^- + CH_3COF \rightleftarrows CH_2COF^- + AH$

accurately established and thus a theoretical fluoride binding energy to ketene obtained of 35.7 kcal mol^{-1} (10). By carrying out equilibrium fluoride transfer measurements between ketene and Lewis acids, reaction [8], an absolute anchor point for the fluoride binding energy scale of relative fluoride exchange equilibria was established.

[8] $LF^- + CH_2{=}C{=}O \rightleftarrows CH_2COF^- + L$

It was therefore of some interest to establish whether the fluoride adduct of ketene had enolate structure, **X**, or a hydrogen bonded structure with F^- bound to the sp^2 hydrogens of the ketene, **XI**. The data of Table 1 reveal that in this case the "classical" enolate structure is the more stable at both the 4-31G and 4-31+G levels of calculation. Significantly, however, both structures are found to be stable with respect to dissociation to F^- + ketene.

The available experimental evidence strongly suggests that the $C_2H_2FO^-$ ions derived from both deprotonation of acetyl fluoride and addition of F^- to ketene have the same structure, presumably **X**. The ions formed in both ways react with Lewis acids such as SO_2F_2 via exothermic fluoride transfer, reaction [9], and with Brønsted acids such as CF_3CH_2OH via exothermic proton transfer, reaction [10]. This latter

[9] $CH_2COF^- - SO_2F_2 \rightleftarrows SO_2F_3^- + CH_2CO$

[10] $CH_2COF^- + CF_3CH_2OH \rightleftarrows CF_3CH_2O^- + CH_2CO + HF$

reaction, in particular, is strongly suggestive of an enolate type structure for this anion since exothermic F^- transfer to CF_3CH_2OH could also occur. Thus both *ab initio* calculation and gas phase reactivity results support an enolate structure for $C_2H_2FO^-$ as the most stable and most probable form of ions derived from either deprotonation of acetyl fluoride or F^- addition to ketene.

Conclusion

The *ab initio* calculations described in the present work demonstrate that the most stable forms of $C_2H_4F^-$, $C_2H_2F^-$, and $C_3H_4F^-$ anions are hydrogen bonded adducts of ethylene, acetylene, and allene, respectively. By contrast, examination of the isoelectronic analogue to the F^-–allene adduct containing an electronegative oxygen atom, $C_2H_2FO^-$, reveals that a "classical" enolate structure is more stable than a hydrogen bonded adduct of F^- and ketene. Consideration of experimental data for gas phase ion molecule reactions of strong anionic bases with ethyl fluoride, vinyl fluoride and 2-fluoropropene show that the hydrogen bonded anions **II**, **VI**, and **IX** are the most probable reaction products. The implications of this finding for gas phase acidities of the parent species and for fluoride binding energies to unsaturated hydrocarbons have been discussed.

The results obtained also suggest that similar hydrogen bonded species might arise from other gas phase deprotonation experiments. For example, it is possible that deprotonation of ethyldimethylamine or methylethylether by strong bases such as H^- or NH_2^- could lead to novel hydrogen bond adducts, reactions [11] and [12]. Investigations of these and related systems will be the subject of future contributions from this laboratory.

[11] 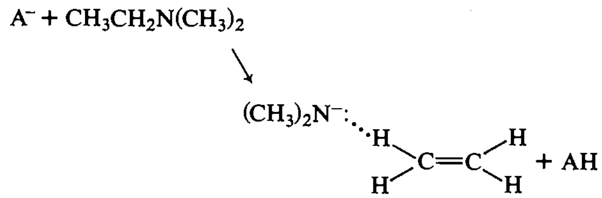

[12] 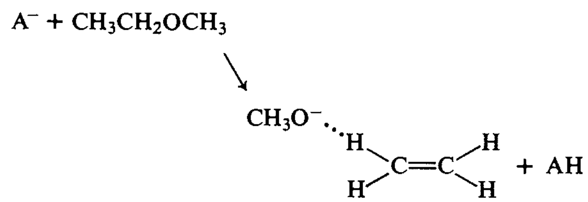

Acknowledgements

Financial support of the Natural Sciences and Engineering Research Council of Canada (NSERC) and the University of New Brunswick is gratefully acknowledged. The considerable assistance of Dr. F. Grein and Mr. U. Sishta is also acknowledged.

1. T. B. McMahon, R. J. Blint, D. P. Ridge, and J. L. Beauchamp. J. Am. Chem. Soc. **94**, 8934 (1972).
2. S. A. Sullivan and J. L. Beauchamp. J. Am. Chem. Soc. **98**, 1160 (1976).
3. S. A. Sullivan and J. L. Beauchamp. J. Am. Chem. Soc. **99**, 5017 (1977).
4. J. H. J. Dawson and K. R. Jennings. Int. J. Mass. Spectrom. Ion Phys. **25**, 47 (1977).
5. R. L. Clair and T. B. McMahon. Int. J. Mass Spectrom. Ion Phys. **33**, 21 (1980).
6. R. Farid and T. B. McMahon. Can. J. Chem. **58**, 2307 (1980).
7. C. E. Doiron and T. B. McMahon. Can. J. Chem. **59**, 2689 (1981).
8. D. F. Drummond and T. B. McMahon. J. Phys. Chem. **85**, 3746 (1981).
9. J. W. Larson and T. B. McMahon. J. Am. Chem. Soc. **104**, 6255 (1982).
10. J. W. Larson and T. B. McMahon. J. Am. Chem. Soc. **105**, 2944 (1983).
11. R. D. Bach, R. C. Badger, and T. J. Lang. J. Am. Chem. Soc. **101**, 2845 (1979).
12. P. V. R. Schleyer and A. J. Kos. Tetrahedron, **39**, 1141 (1983).
13. J. S. Binkley, R. A. Whitesides, R. Krishnan, R. Seeger, D. J. DeFrees, H. B. Schlegel, S. Topiol, L. R. Kahn, and J. A. Pople. Q.C.P.E. **13**, 406 (1981).
14. M. Dupuis, J. Rys, and H. F. King. J. Chem. Phys. **64**, 111 (1976).
15. H. B. Schlegel. J. Comput. Chem. **3**, 214 (1982).
16. J. Chandrasekhar, J. G. Andrade, and P. V. R. Schleyer. J. Am. Chem. Soc. **103**, 5609 (1981).
17. G. W. Sptiznagel, T. Clark, J. Chandrasekhar, and P. V. R. Schleyer. J. Comput. Chem. **3**, 363 (1982).
18. J. Burdon, D. W. Davies, and G. delConde. J. Chem. Soc. Perkin II, 1205 (1979).
19. A. Pross, D. J. DeFrees, B. A. Levi, S. K. Pollack, L. Radom, and W. J. Hehre. J. Org. Chem. **46**, 1693 (1981).
20. J. Burdon, I. W. Parsons, and E. J. Avradmides. J. Chem. Soc. Perkin II, 1210 (1979).
21. D. Holtz. Prog. Phys. Org. Chem. **8**, 1 (1971).
22. A. H. Zimmerman, K. J. Reed, and J. I. Brauman. J. Am. Chem. Soc. **99**, 7203 (1977).
23. T. B. McMahon and C. J. Northcott. Can. J. Chem. **56**, 1069 (1978).
24. J. R. Skinner and H. A. Lacher. J. Chem. Soc. A, 1034 (1968).
25. S. W. Benson. Thermochemical kinetics. 2nd ed. J. Wiley, New York, NY. 1968.
26. H. M. Rosenstock, K. Draxl, B. W. Steiner, and J. T. Herron. J. Phys. Chem. Ref. Data Suppl. No. 1, **6**, 1977.
27. M. D. Joesten and L. J. Schaad. Hydrogen bonding. Marcel Dekker, New York, NY. 1974.
28. C. Northcott and T. B. McMahon. Can. J. Chem. **56**, 1069 (1978).
29. G. B. Ellison, P. C. Engelking, and W. C. Lineberger. J. Am. Chem. Soc. **100**, 2556 (1978).
30. A. L. Hinde, A. Pross, and L. Radom. J. Comput. Chem. **4**, 118 (1980).
31. A. C. Hopkinson, M. H. Lien, K. Yates, P. Mezey, and I. G. Csizmadia. J. Chem. Phys. **67**, 517 (1977).
32. L. Radom, W. A. Lathan, W. J. Hehre, and J. A. Pople. J. Am. Chem. Soc. **93**, 5339 (1971).
33. W. J. Bouma, R. H. Nobes, L. Radom, and C. E. Woodward. J. Org. Chem. **47**, 1869 (1982).

Lactams of sparteine

W. MAREK GOLEBIEWSKI AND IAN D. SPENSER
Department of Chemistry, McMaster University, Hamilton, Ont., Canada L8S 4M1

Received May 18, 1984

W. MAREK GOLEBIEWSKI and IAN D. SPENSER. Can. J. Chem. **63**, 716 (1985).

(2,2-$^2H_2$)Sparteine, (6-^{2}H)sparteine, (10,10-$^2H_2$)sparteine, (15,15-$^2H_2$)sparteine, (17α-^{2}H)sparteine, (17β-^{2}H)sparteine, (17,17-$^2H_2$)sparteine, (17α-^{2}H)lupanine, and (17β-^{2}H)lupanine were prepared and employed to assign the ^{1}H nmr spectrum of sparteine. Contrary to a published report, photochemical oxidation of sparteine does not lead to 15-oxosparteine but to 17-oxosparteine.

W. MAREK GOLEBIEWSKI and IAN D. SPENSER. Can. J. Chem. **63**, 716 (1985).

On a préparé les ($^2H_2$-2,2)-, (^{2}H-6)-, ($^2H_2$-10,10)-, ($^2H_2$-15,15)-, (^{2}H-17α)- et (^{2}H-17β)-spartéines ainsi que les (^{2}H-17α)- et (^{2}H-17β)-lupanines et on les a utilisées pour faire une attribution du spectre rmn ^{1}H de la spartéine. Contrairement à ce qui a été rapporté antérieurment, l'oxydation photochimique de la spartéine ne conduit pas à l'oxo-15 spartéine mais plutôt à l'oxo-17 spartéine.

[Traduit par le journal]

In connection with our studies of the biosynthesis of the lupine alkaloids (1–3), and, in particular, of the incorporation of bond-labelled samples of ^{13}C,^{15}N-lysine and cadaverine (2), and of the prochirality (3) of the reactions leading to the incorporation of lysine and cadaverine into sparteine (**1**) and lupanine (**2**), it was essential to obtain reliable assignments of the nmr signals of the protons on the chiral and prochiral C-atoms adjacent to the nitrogen atoms of the alkaloids, as well as of the ^{13}C nmr signals of these C-atoms.

To facilitate assignment of ^{1}H nmr signals, deuteriated samples of the alkaloids were prepared by adaptation of known reactions.

The samples of sparteine, labelled at the prochiral centres adjacent to nitrogen, were prepared from the corresponding oxosparteine derivatives by reduction with lithium aluminium deuteride (4–6). Thus, 2-oxosparteine (lupanine) (**2**) yielded (2,2-$^2H_2$)sparteine (4–6), 10-oxosparteine (aphylline) gave (10,10-$^2H_2$)sparteine (5), and 15-oxosparteine (**9**) and 17-oxosparteine (**7**) gave (15,15-$^2H_2$)- and (17,17-$^2H_2$)sparteine (4–6), respectively.

Diastereotopically singly deuteriated samples of (17α-^{2}H)-lupanine (17-^{2}H-*si*, pseudo-axial) and (17β-^{2}H)lupanine (17-^{2}H-*re*, pseudo-equatorial) were obtained from 16,17-dehydrolupaninium perchlorate by methods described by Wiewiórowski *et al.* (7). Lithium aluminium hydride reduction at C-2 of these diastereotopically deuteriated lupanines gave (17α-^{2}H)sparteine (17-^{2}H-*si*, pseudo-axial) and (17β-^{2}H)-sparteine (17-^{2}H-*re*, pseudo-equatorial), respectively. As predicted (8), the ^{2}H nmr signal of the equatorially deuteriated samples (δ: (17β-^{2}H)sparteine, 2.63; (17β-^{2}H)lupanine, 2.53 ppm) appears downfield in relation to the signal of the axially deuteriated samples (δ: (17α-^{2}H)sparteine, 2.44; (17α-^{2}H)-lupanine, 1.79 ppm).

The two signals in the ^{2}H nmr spectra of (2,2-$^2H_2$)-, (10,10-$^2H_2$)-, and (15,15-$^2H_2$)sparteine can be assigned on a similar basis. The upfield signal is assigned to the axial deuteron, the downfield signal to the equatorial deuteron (δ: (2,2-$^2H_2$)sparteine, 1.84 (β-^{2}H, axial), 2.58 (α-^{2}H, equatorial); (10,10-$^2H_2$)sparteine, 1.92 (β-^{2}H, axial), 2.43 (α-^{2}H, equatorial); (15,15-$^2H_2$)sparteine, 1.97 (α-^{2}H, axial), 2.73 (β-^{2}H, equatorial)).

The sample of (6-^{2}H)sparteine, deuteriated at the chiral centre, C-6 (δ 1.63 ppm), was prepared (4,5) by sodium borodeuteride reduction of the 1,6-dehydro derivative (**4**) of sparteine, by adaptation of a reaction sequence reported by N. J. Lenoard *et al.* (9). Since reduction of the 1,6:11,16-didehydro derivative (**5**) of sparteine does not yield sparteine (**1**) but α-isosparteine (**8**), which differs from sparteine at the C-11 ring junction, (11-^{2}H)sparteine cannot be prepared by this method.

Assignment of the signal for the proton at C-11 of sparteine was made from the ^{1}H-COSY nmr spectrum of sparteine (10), on the basis of the observed coupling to the proton at C-9 and the β-proton at C-12.

The assignments of the ^{1}H nmr signals in the spectra of sparteine and some of its oxo derivatives are summarized in Table 1.

Since, until recently, lupanine perchlorate was commercially available (Fluka, Koch-Light), most of the starting materials for this study were readily accessible. The one exception is 15-oxosparteine (**9**). It has been reported (11) that this compound can be prepared in 20% yield, together with a small quantity of lupanine (**2**) and some dimeric products, by photochemical oxidation of sparteine (**1**). We have now found that photochemical oxidation of sparteine, as described (11), does not yield either 15-oxosparteine or 2-oxosparteine. The ^{13}C nmr spectrum of the crude lactam fraction isolated from the reaction mixture appeared to indicate the presence of a single lactam carbonyl signal, and the only oxo derivative that was isolated was 17-oxosparteine, identical (^{1}H nmr, ^{13}C nmr, mp, mixture mp, mp of perchlorate salt) with an authentic specimen, prepared by ferricyanide oxidation of sparteine (12, 13).

15-Oxosparteine can be obtained from sparteine by a two-step process, devised by Wiewiórowski.[1] Oxidation of the alkaloid with mercuric acetate, complexed with ethylenediaminetetraacetic acid (Hg^{2+}/EDTA), yields a mixture of 1,6:11,16-didehydrosparteinium (**5**) and 1,6-dehydro-15-oxosparteinium (**10**) ions. Subsequent borohydride reduction leads to a mixture of α-isosparteine (**8**) (from **5**) and 15-oxosparteine (**9**) (from **10**).

The ^{13}C nmr spectrum of 15-oxosparteine (**9**) was tentatively assigned on the basis of the off-resonance spectrum and by comparison with the assignments in the published (6) spectra of sparteine and its 2- and 17-oxo derivatives. The signal of C-17 in the spectrum of 15-oxosparteine is shifted upfield by 13.3 ppm (compared to sparteine) due to the shielding effect of the 15-oxo group on its peri neighbour (15). Upfield shifts are also

[1] M. Wiewiórowski. Personal communication. See also ref. 14.

TABLE 1. ^1H nuclear magnetic resonance spectra of sparteine and its lactams in benzene (δ 7.19 ppm). Chemical shifts (ppm) of the protons on the carbon atoms adjacent to nitrogen

H atom	Sparteine[a]	2-Oxosparteine (lupanine)[b]	15-Oxosparteine[c]	17-Oxosparteine[d]	2,17-Dioxo sparteine (17-oxolupanine)[e]
2-α, *re* (eq)	2.62	—	2.55	2.61	—
2-β, *si* (ax)	1.88	—	1.79	1.75	—
6-β *R* (ax)	1.62	2.74	1.50	1.67	2.78
10-α, *si* (eq)	2.47	4.80	2.22	2.47	4.98
10-β, *re* (ax)	1.96	2.31	1.77	1.93	2.14
11-α *S* (ax)	2.11	1.70	3.28	2.93	2.96
15-α, *re* (ax)	2.04	1.85	—	2.23	2.26
15-β, *si* (eq)	2.76	2.66	—	5.11	4.92
17-α, *si* (ps.ax)	2.47	1.83	2.98	—	—
17-β, *re* (ps.eq)	2.67	2.55	4.95	—	—

[a] Cf. refs. 19–21.
[b] Cf. refs. 7, 20, 22.
[c] Cf. ref. 7.
[d] Cf. refs. 7, 22.
[e] Cf. ref. 22.

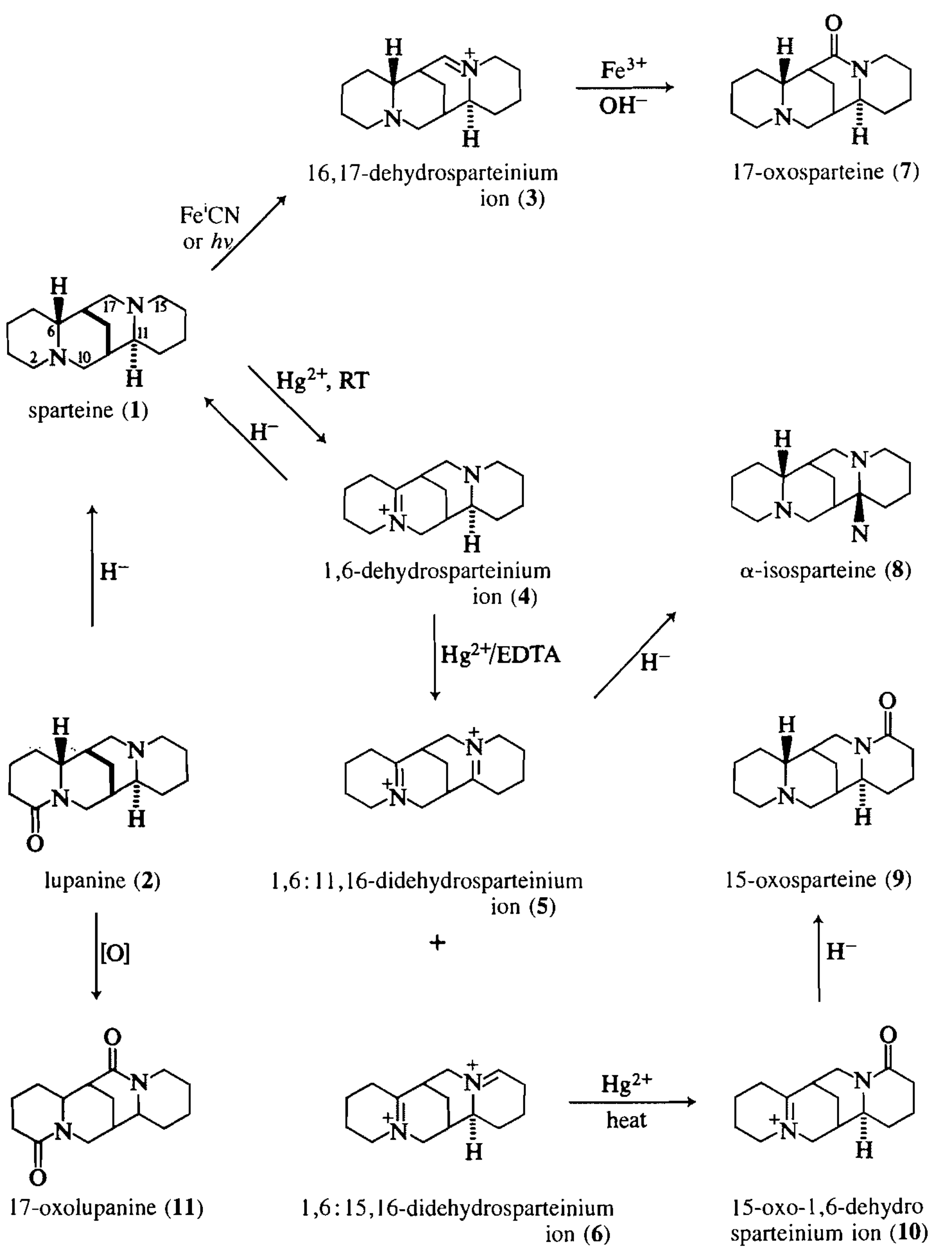

TABLE 2. ^{13}C nuclear magnetic resonance spectra of sparteine and its lactams

Atom	Sparteine[a]	Sparteine sulfate	2-Oxo sparteine (lupanine)[b]	2-Oxo 13α-hydroxy sparteine (13α-hydroxy lupanine)[b]	15-Oxo sparteine	17-Oxo sparteine[b]	2,17-Dioxo sparteine (17-oxo lupanine)
C-2	56.4	57.4	171.4	171.2	56.2	57.0	171.0
C-3	26.0	23.3	33.1	33.7	25.8	25.5	33.2
C-4	24.8	22.7	19.7	20.3	24.6	24.7	19.5
C-5	29.5	27.6	26.8	27.2	29.5	30.3	32.9
C-6	66.6	67.4	61.0	61.1	65.8	65.1	59.0
C-7	33.2	30.0	32.4	32.6	32.1	44.2	43.7
C-8	27.7	23.5	27.5	27.8	27.3	27.3	27.1
C-9	36.2	32.8	34.9	35.3	36.5	35.1	33.9
C-10	62.1	58.0	46.8	47.3	61.5	63.1	48.1
C-11	64.6	64.1	64.2	57.7	58.6	61.4	61.2
C-12	34.4	32.1	33.5	40.6	32.1	33.7	33.5
C-13	24.9	22.4	24.5	64.5	20.0	25.5	25.1
C-14	25.8	23.5	25.2	33.2	32.7	25.5	25.3
C-15	55.5	55.9	55.6	49.9	170.6	42.5	43.1
C-17	53.5	49.9	52.9	52.8	40.2	169.7	167.0
	In $CDCl_3$	In D_2O	In $CDCl_3$	In C_5D_5N	In $CDCl_3$	In $CDCl_3$	In $CDCl_3$

[a]Cf. refs. 6, 23.
[b]Cf. ref. 6.

observed for C-11 (6 ppm), C-13 (4.9 ppm, β to CO), and C-12 (2.3 ppm, γ to CO). A downfield shift (6.7 ppm) is observed in the case of C-14 (α to CO).

Table 2 summarizes the assignments of the ^{13}C nmr signals in the spectra of sparteine and a number of related compounds.

Experimental

Lactams of sparteine

17-Oxosparteine (7) (12, 13)

Sparteine (**1**) (2.9 g, freshly prepared from sparteine sulfate, Fluka) was dissolved in dilute hydrochloric acid (0.4 *M*, 54 mL). The solution was cooled and basified with sodium hydroxide solution (10%, w/v, 81 mL), and a solution of potassium ferricyanide (17.9 g) in water (67 mL) was added. The mixture was shaken for 40 min, acidified with dilute hydrochloric acid (0.4 *M*, 48 mL), and extracted with ether (3 × 80 mL). The water layer was basified with aqueous sodium hydroxide (10% w/v) and extracted with ether. The ether solution was dried (sodium sulfate) and evaporated to dryness. The residue was recrystallized from petroleum ether (40–60°C), yielding 17-oxosparteine (2.7 g), mp 85–87°C (lit. (13) mp 86–87°C).

A sample was converted into the perchlorate salt, mp 240–41°C (lit. (16) mp 241°C).

15-Oxosparteine (9)[1]

A solution of Hg^{2+}/EDTA complex (3.4 g) in water (30 mL) was added to sparteine (0.4 g) and the mixture was shaken 2 h at room temperature in an atmosphere of argon and was then kept at 60°C for 24 h. The resulting mixture of dehydrobases was allowed to cool to room temperature and was reacted with sodium borohydride (0.4 g) which was added in small portions over 1.5 h. The pH of the mixture was adjusted to pH 3 by addition of hydrochloric acid (2 *M*), and the precipitate of mercury salts was filtered off. The solution was basified with sodium hydroxide pellets and was then extracted with ether. The ether solution was dried (KOH pellets) and the solvent evaporated. The oily residue was dissolved in methanol (2 mL), 30% hydrogen peroxide (0.15 mL) was added, and the mixture was kept for 1 h. Excess hydrogen peroxide was destroyed with 10% palladium on charcoal. The mixture was filtered through Celite and the filtrate was concentrated, dissolved in water, and extracted with ether. Evaporation of the ether solution gave a colorless oil (80 mg) which was composed of 15-oxosparteine (major product) and several other minor products whose structure is under investigation. 15-Oxosparteine was purified by column chromatography on alumina (Fisher, activity I). Elution with a mixture of benzene–chloroform 2:1 yielded 15-oxosparteine (50 mg) as a colorless oil which was converted into the perchlorate, mp 150–151°C (lit. (14) mp 152°C). The ^{1}H and ^{13}C nmr spectra of 15-oxosparteine were different from the spectra of lupanine (2-oxosparteine) and of 17-oxosparteine.

Photochemical oxidation of sparteine (11)

A solution of sparteine (390 mg) in methanol (20 mL) was placed in a Pyrex tube and irradiated 14 h with a Philips 5P 500 lamp in the presence of methylene blue (39 mg) as sensitizer, while a stream of oxygen was bubbled through the solution. Methanol was added twice to maintain the volume of the solution. After 14 h, thin-layer chromatography (silica gel, CH_2Cl_2–CH_3OH – 0.880 NH_3, 9:0.9:0.1) of a sample of the reaction mixture showed only traces of sparteine. The solvent was removed *in vacuo*, and the residue applied to a silica gel column (20 g, 70–230 mesh, BDH). The column was washed with methylene chloride (50 mL) and with a solution of methanol (10 mL) in methylene chloride (490 mL) containing 0.880 ammonia (0.6 mL). The product was then eluted with a solution of methanol (25 mL) in methylene chloride (400 mL) containing 0.880 ammonia (3 mL) and was obtained as an oil (70 mg) which crystallized on standing. The ^{1}H and ^{13}C nmr spectra of the reaction product were identical with those of 17-oxosparteine (6) and different from the spectra of 2-oxosparteine (lupanine) (6) and of 15-oxosparteine (Tables 1 and 2). Melting point (from pet. ether 40–60°C) and mixture melting point with an authentic sample of 17-oxosparteine were 85–87°C (lit. (13) mp of 17-oxosparteine 86–87°C).

17-Oxolupanine (17) (i.e., 2,17-dioxosparteine) (**11**) was prepared by permanganate oxidation of lupanine; *13-hydroxylupanine* and *methyl aphyllate* were obtained from the alkaloid collection of the late Léo Marion, National Research Council Laboratories, Ottawa.

Deuteriated samples of sparteine and lupanine

(17,17-$^2H_2$)Sparteine (4–6)

17-Oxosparteine (**7**) (70 mg) in tetrahydrofuran (2.5 mL, freshly distilled from $LiAlH_4$) was added to a stirred suspension of lithium aluminium deuteride (98 at.%, MSD Isotopes, Montreal) (27 mg) in tetrahydrofuran (0.5 mL). The mixture was refluxed with stirring for 1 h and allowed to cool. Excess of reagent was decomposed by successive addition of water (30 μL), sodium hydroxide (15% w/v, 30 μL), and water (90 μL) and the reaction mixture was filtered and the residue washed with benzene (3 × 1 mL). Water (2 mL) was added to the filtrate, the organic phase was separated, and the aqueous phase was extracted with benzene (3 × 1 mL). Evaporation of the solvent yielded (17,17-$^2H_2$)sparteine (46 mg) which was purified via the monobisulfate (79 mg); ^{2}H nmr (C_6H_6) of the free base δ: 2.63 (17β-^{2}H pseudo-equatorial), 2.44 (17α-^{2}H, pseudo-axial). The corresponding peaks were missing in the ^{1}H nmr spectrum (dd of the 17β-H partially superimposed on a doublet of multiplets of the 2α-H; multiplet of the 17α-H superimposed on dt of the 10α-H); 95% deuteriation (by ms); ^{13}C nmr (D_2O) of the sulfate: signal at δ 50.2 ppm (C-17) not discernible.

(2,2-$^2H_2$)Sparteine (4–6) was prepared similarly by lithium aluminium deuteride reduction of lupanine (**2**) (79 mg). Yield 50 mg; ^{2}H nmr (C_6H_6) δ: 2.58 (2α-^{2}H, equatorial), 1.84 (2β-^{2}H, axial); ^{13}C nmr (D_2O) of the sulfate: signal at δ 57.7 ppm (C-2) not discernible.

(10,10-$^2H_2$)Sparteine (5) (5 mg) was obtained by reduction with $LiAlD_4$ from aphylline (11 mg) (10-oxosparteine) which, in turn, had been prepared from methyl aphyllate via the corresponding amino acid (18); ^{2}H nmr (C_6H_6) δ: 2.43 (10α-^{2}H, equatorial), 1.92 (10β-^{2}H, axial); ^{13}C nmr (D_2O) of the sulfate: signal at δ 58.4 ppm (C-10) not discernible.

(15,15-$^2H_2$)Sparteine (5) (8 mg) was prepared by $LiAlD_4$ (20 mg) reduction in tetrahydrofuran (2 mL) of 15-oxosparteine (**9**) (16 mg); ^{2}H nmr (C_6H_6) δ: 2.73 (15β-^{2}H, equatorial), 1.97 (15α-^{2}H, axial); ^{13}C nmr (D_2O) of the sulfate: signal at δ 56.2 ppm (C-15) not discernible.

(6-^{2}H)Sparteine (4, 5) (12 mg) was prepared (cf. ref. 9) by reduction with sodium borodeuteride (98 at.%, MSD isotopes) of 1,6-dehydrosparteinium diperchlorate (24 mg) in methanol; ^{2}H nmr (C_6H_6) δ: 1.63 ppm; ^{13}C nmr (D_2O) of the sulfate: signal at δ 67.7 ppm (C-6) not discernible.

(17α-^{2}H)Lupanine and (17β-^{2}H)Lupanine (5, 7)

These two deuteriated derivatives of lupanine were prepared by reduction of 16,17-dehydrolupaninium perchlorate (**3**) (7). Direct reduction of the dehydrolupanine derivative (42 mg) with sodium borodeuteride (9 mg) in deuterium oxide (1 mL) gave (17β-^{2}H)lupanine (17 mg) (17-^{2}H-*re*, pseudo-equatorial); ^{2}H nmr (C_6H_6) δ: 2.53 ppm. The epimeric (17α-^{2}H)lupanine (17-^{2}H-*si*, pseudo-axial) (36 mg) was obtained by exchange of the proton at C-17 of the dehydrolupanine derivative (55 mg) by deuterium supplied by deuterium oxide (2 mL) in the presence of sodium deuteroxide (0.16 mmol), followed by reduction with sodium borohydride; ^{2}H nmr (C_6H_6) δ: 1.79 ppm.

(17α-^{2}H)Sparteine and (17β-^{2}H)sparteine, respectively, were prepared by lithium aluminum hydride reduction of the corresponding deuteriated lupanine; ^{2}H nmr (C_6H_6) δ: 2.44 (17α-^{2}H, pseudo-axial); 2.63 (17β-^{2}H, pseudo-equatorial).

Instrumental methods

The *^{1}H nmr spectra* were recorded in the Fourier mode on a Bruker WM 250 spectrometer, in 5-mm tubes, in C_6D_6 solution.

The *^{2}H nmr spectra* were recorded in the Fourier mode on a Bruker WM 250 spectrometer, in 10-mm tubes. The spectra of the deuteriated samples of sparteine and lupanine were recorded in benzene solution.

The *^{13}C nmr spectra* were recorded at 20.15 MHz in the Fourier mode on a Bruker WP 80 spectrometer, in 10-mm tubes. For solvents see Table 2.

Acknowledgments

This work was supported by the Natural Sciences and Engineering Research Council of Canada. We are grateful to Professor Dr. Maciej Wiewiórowski for informing us of his unpublished improved procedure for the preparation of 15-oxosparteine, and to Dr. O. E. Edwards for authentic samples from the lupine alkaloid collection of the late Léo Marion, National Research Council of Canada Laboratories, Ottawa.

We thank Brian G. Sayer for recording the ^{1}H- and ^{2}H nmr spectra and J. Ian A. Thompson for the ^{13}C nmr spectra. We are greatly indebted to Dr. R. E. Lenkinski, South Western Ontario NMR facility, University of Guelph, for determining COSY and 2-D *J* resolved spectra.

1. W. M. GOLEBIEWSKI and I. D. SPENSER. J. Am. Chem. Soc. **98**, 6726 (1976).
2. W. M. GOLEBIEWSKI and I. D. SPENSER. J. Chem. Soc. Chem. Commun. 1509 (1983).
3. W. M. GOLEBIEWSKI and I. D. SPENSER. J. Am. Chem. Soc. **106**, 1441 (1984); **106**, 7925 (1984).
4. F. BOHLMANN. Chem. Ber. **91**, 2157 (1958).
5. J. SKOLIK, P. J. KRUEGER, and M. WIEWIÓROWSKI. Tetrahedron, **24**, 5439 (1968).
6. F. BOHLMANN and R. ZEISBERG. Chem. Ber. **108**, 1043 (1975).
7. M. WIEWIÓROWSKI, O. E. EDWARDS, and M. D. BRATEK-WIEWIÓROWSKA. Can. J. Chem. **45**, 1447 (1967).
8. L. JACKMAN and S. STERNHELL. Application of nuclear magnetic resonance spectroscopy in organic chemistry. 2nd ed. Pergamon Press, Oxford. 1969. p. 238.
9. N. J. LEONARD, P. D. THOMAS, and V. W. GASH. J. Am. Chem. Soc. **77**, 1552 (1955).
10. W. M. GOLEBIEWSKI. To be published.
11. D. HERLEM, Y. HUBERT-BRIERRE, F. KHUONG-HUU, and R. GOUTAREL. Tetrahedron, **29**, 2195 (1973).
12. F. GALINOVSKY and E. STERN. Ber. **77**, 132 (1944).
13. H. R. SCHÜTTE, F. BOHLMANN, and W. REUSCHE. Arch. Pharm. (Weinheim) **294**, 610 (1961).
14. M. WIEWIÓROWSKI, A. B. LEGOCKI, and M. D. BRATEK-WIEWIÓROWSKA. Bull. Acad. Polon. Sci. Ser. Sci. Chim. **15**, 385 (1967).
15. E. WENKERT, B. CHAUNCY, K. J. DAVE, A. R. JEFFCOAT, F. M. SCHELL, and H. P. SCHENK. J. Am. Chem. Soc. **95**, 8427 (1973).
16. A. PERKOWSKA and M. WIEWIÓROWSKI. Bull. Acad. Polon. Sci. Ser. Sci. Chim. **28**, 249 (1980).
17. O. E. EDWARDS, F. H. CLARKE, and B. DOUGLAS. Can. J. Chem. **32**, 235 (1954).
18. F. BOHLMANN, W. WEISE, H. SANDER, H.-G. HANKE, and E. WINTERFELDT. Chem. Ber. **90**, 653 (1957).
19. F. BOHLMANN, D. SCHUMANN, and C. ARNDT. Tetrahedron Lett. No. 31, 2705 (1965).
20. A. S. SADYKOV, F. G. KAMAYEV, V. A. KORENEVSKY, V. B. LEONT'EV, and YU. A. USTYNYUK. Org. Magn. Reson. **4**, 837 (1972).
21. J. SKOLIK, V. MAJCHRZAK-KUCZYNSKA, and M. WIEWIÓROWSKI. Bull. Acad. Polon. Sci. Ser. Sci. Chim. **26**, 741 (1978).
22. F. BOHLMANN and D. SCHUMANN. Tetrahedron Lett. No. 28, 2435 (1965).
23. A. J. SHAKA and R. FREEMAN. J. Magn. Reson. **50**, 502 (1982).

Influence of temperature on copper bromide formation and dissolution

R. L. Brossard and G. M. Raynaud
Institut de Recherche d'Hydro-Québec (IREQ), P.O. Box 1000, Varennes (Qué.), Canada J0L 2P0

Received April 24, 1984

R. L. Brossard and G. M. Raynaud. Can. J. Chem. **63**, 720 (1985).

The influence of temperature on copper bromide formation and dissolution has been investigated in deaerated aqueous solutions of 0.2 *M* NaBr at pH 4. The morphology of CuBr accumulated on the copper anode supports the idea that CuBr precipitates in the vicinity of the electrode. Under a constant potential of $-70\ mV_{sce}$, very large flat platelets of CuBr are observed at 71°C compared to grains at 22°C. In addition, irregular current variations are noted on the current time curves at 71°C when large cracks are present in the film. It is deduced that the irregular current variations are due to the formation and repair of the cracks in the film. The current of the anode eventually reaches a steady value equal to the dissolution rate of the copper bromide precipitate formed on the electrode.

The influence of the temperature on the dissolution rate of CuBr may be entirely predicted assuming that the rate-determining step for the dissolution of this compound is the mass transfer of intermediates, e.g., $CuBr_2^-$ from the electrode surface to the bulk electrolyte.

R. L. Brossard et G. M. Raynaud. Can. J. Chem. **63**, 720 (1985).

Opérant à un pH de 4 et sur des solutions aqueuses de NaBr à 0,2 *M* desquelles on a enlevé l'air, on a étudié l'influence de la température sur la formation et sur la dissolution du bromure cuivreux. La morphologie du CuBr qui s'accumule sur l'anode de cuivre supporte l'idée que le CuBr précipite à la proximité de l'électrode. Si on opère à un potentiel constant de $-70\ mV_{sce}$, il se forme de très grandes plaquettes de CuBr à 71°C alors que, à 22°C, le produit précipite sous forme de grains. A 71°C, alors que de grandes fissures apparaissent sur le film, on observe de plus des variations irrégulières de courant sur les courbes courant–temps. On en déduit que les variations irrégulières du courant sont dues à la formation et à la réparation des fissures dans le film. Le courant de l'anode atteint éventuellement une valeur constante qui est égale à la vitesse de dissolution du précipité de bromure cuivreux qui se forme sur l'électrode.

On peut prédire complètement l'influence de la température sur la dissolution en faisant l'hypothèse que l'étape qui détermine la vitesse de la dissolution de ce composé est le transfert de masse des intermédiaires, comme le $CuBr_2^-$, de la surface de l'électrode vers le courde de l'électrolyte.

[Traduit par le journal]

Introduction

The formation of CuBr is observed on copper surfaces (1–3) at potential values larger than the reversible potential (4, 5) for the reaction

$$[1]\quad Cu + Br^- = CuBr + e$$

Two peaks of oxidation are present on the $E-i$ curves and the dissolution current results mainly in the accumulation of copper bromide. The limitation of the current in the peaks region was ascribed to the diffusion of ions in the solution (3). Eventually, an additional current limitation is created by the presence of CuBr on the electrode surface.

Copper bromide compound is slightly soluble in aqueous bromide solution (6). The dissolution of copper bromide formed by the electrochemical oxidation of copper in aqueous sodium bromide was reported for solutions between 0.1 *M* and 1.2 *M* NaBr concentration at 22°C (2). The complete dissolution of the anodically-formed CuBr coincides with a rapid drop in potential which allows a transition time τ to be defined. The dissolution rate of CuBr can then be calculated from the value of τ.

The aim of the present work is to investigate the influence of the temperature on the formation and the dissolution of copper bromide in 0.2 *M* NaBr aqueous solution.

Experimental

The electrochemical cells, their accessories, and the test procedures have been described in detail in previous papers (2, 7). In the present investigation, the copper electrode (Ventron Corporation, 99.99%) consisted of a vertical 0.64 mm diameter wire or of a horizontal 5 mm diameter disk, which gave a sample surface area of 0.5 cm^2 and 0.196 cm^2, respectively.

The solution contained between 0.1 and 0.4 *M* of dissolved NaBr at pH = 4. A potassium-phthalate buffer, 0.05 *M*, was used to stabilize the pH. The solution was carefully deaerated by nitrogen bubbling, which was discontinued prior to the experiments.

The current–time curves were obtained on the copper wire electrode at a constant potential of $-70\ mV_{sce}$ in the temperature range of 22°C to 71°C. The value of the electrode potential was $-400\ mV_{sce}$ prior to the experiment.

The experimental technique to measure the dissolution rate of copper bromide, v, was identical to that recently developed (2). Unless otherwise noted, all electrode potential values are given in relation to the saturated calomel electrode. Dissolution rates were measured on stationary and rotating disk electrodes.

Results and discussion

Formation of copper bromide

The anodic current density is plotted against time in Fig. 1 as the copper wire electrode is maintained at a constant potential of −70 mV, in a quiescent solution of 0.2 *M* NaBr. At this potential value, the current of dissolution results in the accumulation of copper bromide on the electrode surface (2, 3).

The limitation of the current is tentatively attributed to the diffusion (3) and migration of Br^- ions in the solution while an additional current limitation is created by the accumulation of a sufficient amount of copper bromide on the surface (Fig. 2*a*, 2*b*, 2*c*). The electrode surface is entirely covered by the corrosion product after 40 s of oxidation (Fig. 2*c*). Its morphology suggests that CuBr precipitates in the vicinity of the electrode. It is expected that the solution will easily penetrate through the film since the film is relatively porous. The film tends to become more compact with the increase in the duration of the oxidation (Fig. 2*d*). The CuBr grains on the surface grew from

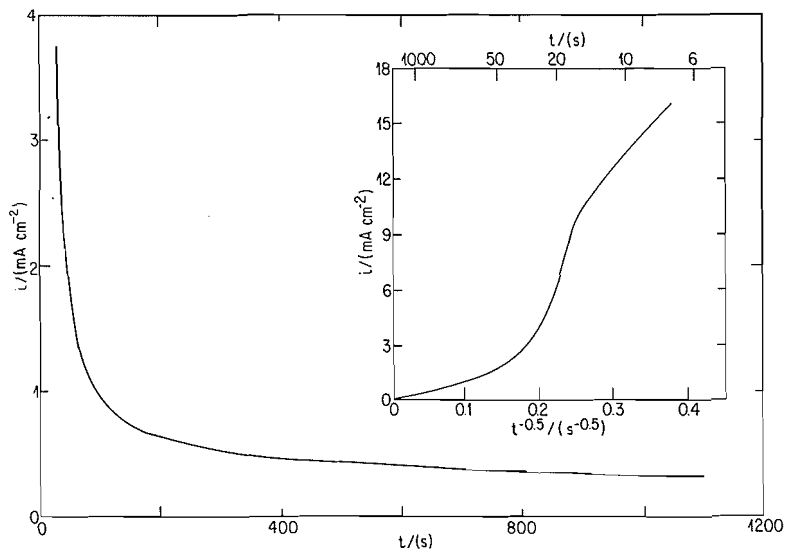

FIG. 1. Current versus time on a copper wire electrode at a constant potential of −70 mV. Just prior to oxidation, the applied potential was −400 mV. The solution is quiescent and the electrode is stationary. T = 22°C, 0.2 M NaBr. The inset shows current density versus (time)$^{-0.5}$.

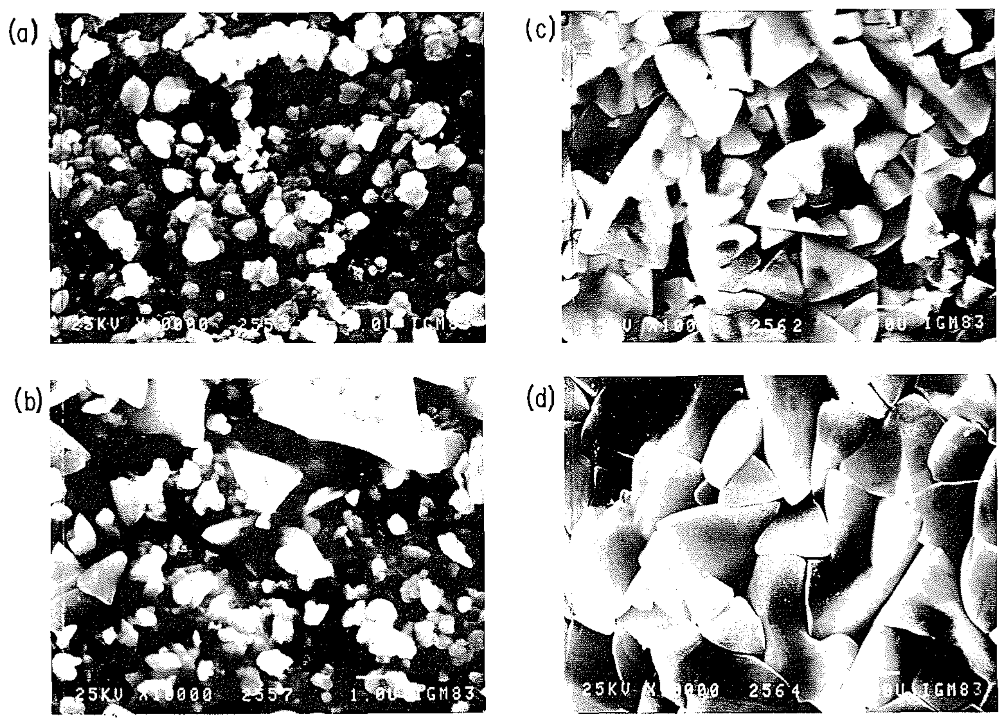

FIG. 2. Surface of copper electrode during oxidation at −70 mV and 22°C. The current–time curve is given in Fig. 1. Times of removal are (a) 5 s, (b) 20 s, (c) 40 s, (d) 5400 s.

an average size of 0.5 μm after 5 s (Fig. 2a) to 3 μm after 5400 s (Fig. 2d).

The shape of the i–t curve and the morphology of CuBr change as the temperature is increased from 22°C to 71°C (Fig. 3, Fig. 4). At 58°C, the current reaches a minimum after 300 s to 400 s while a slight increase of current with time is observed for t larger than 400 s (Fig. 3). In addition, irregular current variations suddenly appear after approximately 120 s. The anodic current and the magnitude of the current oscillations are significantly higher as the temperature is increased from 58°C to 71°C.

It is observed that the morphology of the corrosion product is quite different at 71°C. The copper electrode is partially covered with very large flat platelets of CuBr (Fig. 4a) in the region where the variation of current versus time is regular. The irregular current variations begin near the completion of the surface coverage by CuBr and large cracks are present in the film (Fig. 4b, 4c). It is deduced that the irregular current variations are due to the formation and repair of the cracks in the film.

Dissolution of copper bromide

The copper electrode becomes covered by a CuBr precipitate during the oxidation stage when polarized at potential anodic to the peak potential of the first wave of oxidation (1, 3). It was established that the dissolution rate (v) of the precipitate is

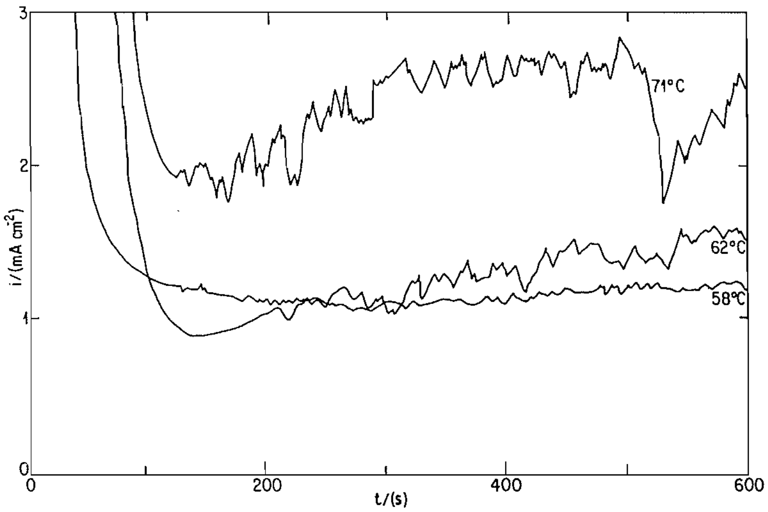

FIG. 3. Current versus time at three different temperatures. Except for temperature, the experimental conditions are those of Fig. 1.

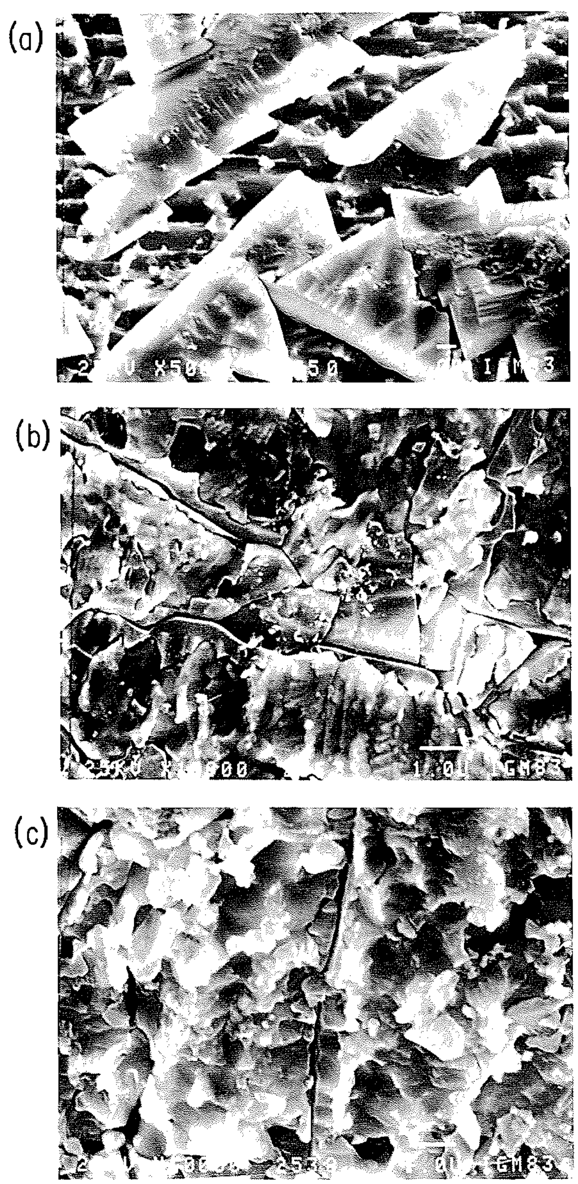

FIG. 4. Surface of copper electrode during oxidation at −70 mV and 71°C. The current–time curve is given in Fig. 3. Times of removal are (*a*) 100 s, (*b*) 200 s, (*c*) 1000 s.

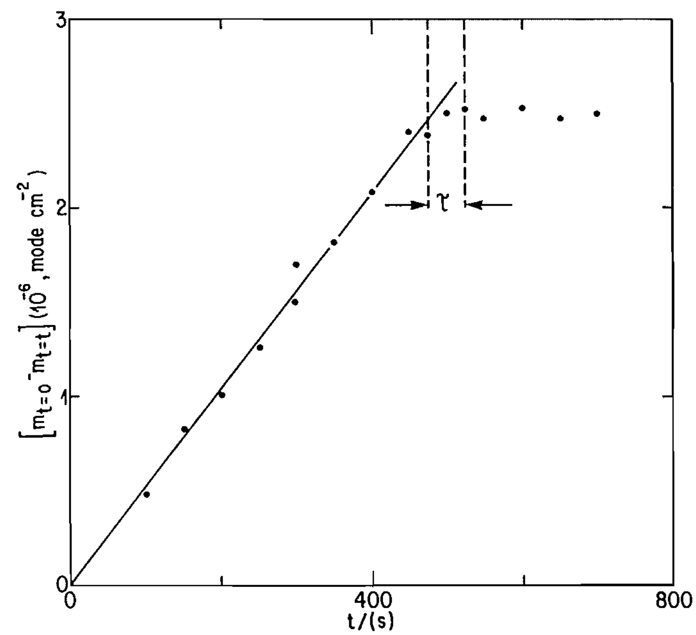

FIG. 5. The amount of precipitate dissolved from the electrode surface (m) after contact with 0.2 M NaBr solution. $m_{t=0}$: at $t = 0$. $m_{t=t}$: m at $t = t$. τ: duration of transient. No stirring in the solution. The electrode is a copper wire.

constant until the completion of its dissolution at 22°C (2). The constant value of v during the dissolution of CuBr at 50°C was confirmed from the reduction of the precipitate at −450 mV after different periods of contact with the solution (Fig. 5). The difference between the charge required for complete film reduction at $t = 0$ and at $t = t$ is ascribed to the dissolution of CuBr during time t. It was assumed that a cathodic charge of 96 500 C is required to decompose 1 g/molecule of this compound because copper ions have a valency of +1 in this compound. The slope of the curve in Fig. 5 corresponds to v; its value is 0.52×10^{-8} mol cm^{-2} s^{-1} in 0.2 M NaBr. The amount of CuBr on the electrode surface is zero as soon as $t = \tau$ where v becomes zero.

The main characteristics of the behavior of the copper electrode covered by CuBr on its surface are the following. (*i*) The open circuit potential (E_{oc}) obtained immediately after ox-

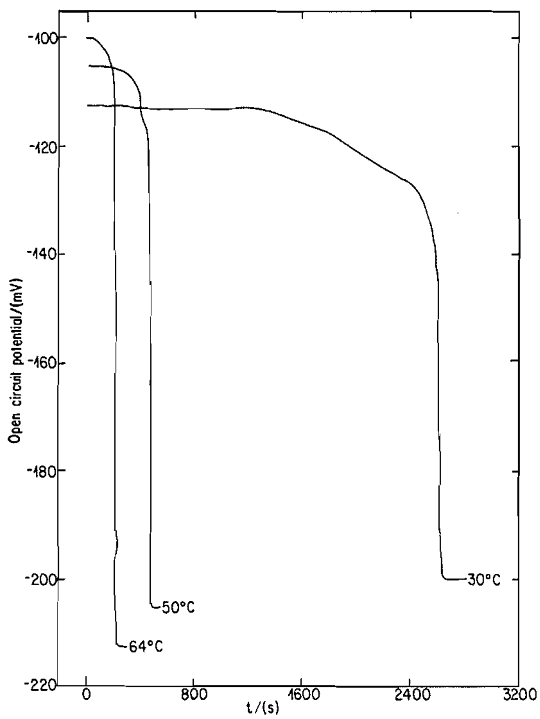

FIG. 6. The open-circuit potential of the copper wire electrode after oxidation at three different temperatures. Oxidation: linear sweep voltammetry from −450 mV to +50 mV at a rate of 5 mV s^{-1}. $m_{t=0}$ is 2.1 × 10^{-6} mol cm^{-2} at 64°C; 2.8 × 10^{-6} mol cm^{-2} at 50°C; 3.1 × 10^{-6} mol cm^{-2} at 30°C.

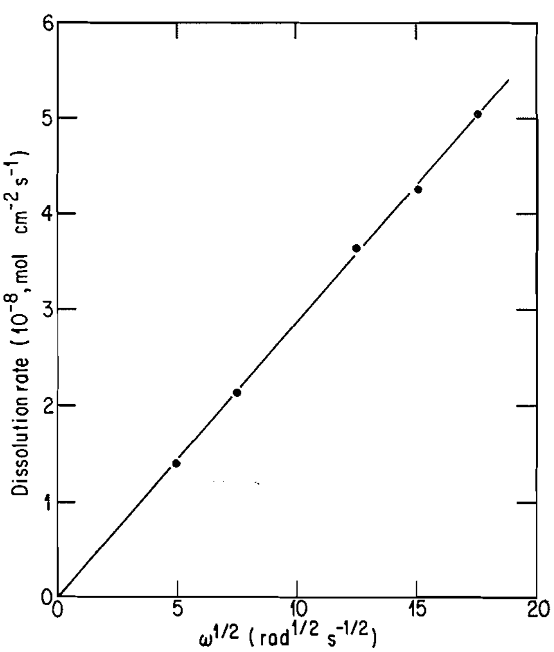

FIG. 7. Dependence of the dissolution rate of a rotating electrode on the angular velocity. Solution: 0.2 *M* NaBr, *T* = 49°C.

idation is higher while τ is considerably reduced as the temperature is increased (Fig. 6). (*ii*) The dissolution rate of copper bromide obeys a $\omega^{1/2}$ law for rotating disk electrode and v is close to zero when ω = 0 (Fig. 7). In this illustration, the solution is 0.2 *M* NaBr. (*iii*) The order of the reaction (ξ) with respect to Br^- ion concentration is 1.1 ± 0.05 (Fig. 8).

The features observed in Figs. 5, 6, and 7 are similar to characteristics previously found concerning the dissolution of

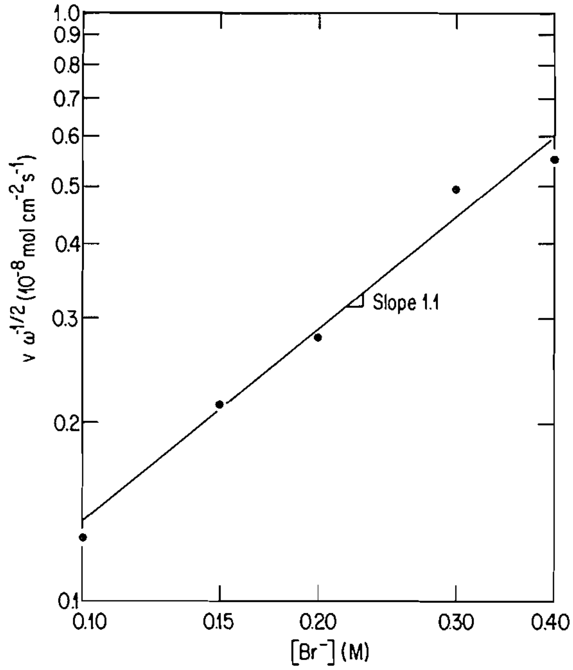

FIG. 8. $v\omega^{-1/2}$ vs. Br^- concentration at 49°C.

copper bromide solutions with up to 1.2 *M* Br^- concentration at 22°C (2). Accordingly, the dissolution process is[1]

$$[2]\quad CuBr + xBr^- = (CuBr_{1+x}^{x-})_i$$

$$[3]\quad (CuBr_{1+x}^{x-})_i \rightarrow (CuBr_{1+x}^{x-})_s \qquad \text{(rds)}$$

where the subscripts i and s refer to concentrations at the electrode solution interface and the bulk solution, respectively. The rate-determining step [3] is the diffusion transport of complexes, as $CuBr_2^-$ and $CuBr_3^{2-}$, from the interface to the bulk solution. The first step [2], the oxidation of CuBr to both $CuBr_2^-$ and $CuBr_3^{2-}$, is assumed to be in equilibrium. The dissolution rate of a rotating electrode should be given by the following application of the Levich equation

$$[4]\quad v = 0.62n\nu^{-1/6}D_{CuBr_{1+x}^{x-}}^{2/3}\ \omega^{1/2}[CuBr_{1+x}^{x-}]_i$$

In this equation, v is in mol cm^{-2} s^{-1}; n is the charge of the diffusing species which is between 1 and 2, ν the kinematic viscosity of the solution, $D_{CuBr_{1+x}^{x-}}$ the diffusion coefficient of the intermediates, ω the angular velocity of the electrode and $[CuBr_{1+x}^{x-}]_i$ is the concentration of copper in the vicinity of the electrode surface.

It is expected that the diffusing species is mainly $CuBr_2^-$ or Br^- since ξ is very close to 1 (Fig. 8). For both species, n is equal to 1. For Br^- ions as the diffusing species, the Levich equation becomes

$$[5]\quad v = 0.62\nu^{-1/6}\ D_{Br^-}^{2/3}\ \omega^{1/2}\ [Br^-]$$

In this equation, D_{Br^-} is the diffusion coefficient of the Br^- ions and [Br^-] is the concentration of Br^- ions in the bulk of the solution. The theoretical values $v\omega^{-1/2}$ calculated from eq. [4], $v\omega_{CuBr_2^-}^{-1/2}$, and [5], $v\omega_{Br^-}^{-1/2}$, are represented in Table 1 for three different temperatures.

The values of $D_{CuBr_2^-}$ and D_{Br^-} at different solution temperatures were calculated from the equation (9):

[1] $(CuBr_{1+x}^{x-})_i$ represents a mixture of $CuBr_2^-$ and $CuBr_3^{2-}$ complexes.

TABLE 1. Experimental and theoretical values of $\nu\omega^{-1/2}$ at 40°C, 49°C, and 68°C in 0.2 *M* NaBr solution

T (°C)	$[CuBr_{1+x}^{x-}]$[a] (mol cm^{-3})	$\nu\omega^{-1/2}_{CuBr_2^-}$[b] ($10^{-8}$ mol cm^{-2} s$^{-1/2}$)	$\nu\omega^{-1/2}_{Br^-}$[c]	$\nu\omega^{-1/2}_{exp}$[d] (10^{-8} mol cm^{-2} s$^{-1/2}$)
40	1.9×10^{-6}	0.20	26.2	0.18
49	2.2×10^{-6}	0.27	30.8	0.28
68	3.1×10^{-6}	0.50	80.1	0.52

[a] $[CuBr_{1+x}^{x-}]$ was determined experimentally using the experimental technique described in ref. 2.
[b] The theoretical values of $\nu\omega^{-1/2}$ were calculated from eq. [4]. ν of water (8) was used and the diffusion coefficient was calculated from eq. [6].
[c] The experimental values of $\nu\omega^{-1/2}$ were calculated from eq. [5]. ν of water (8) was used and the diffusion coefficient was calculated from eq. [6].
[d] The experimental values of $\nu\omega^{-1/2}$ were determined from ν vs. $\omega^{1/2}$ curves (Fig. 7).

TABLE 2. Influence of temperature on ν and i_{an} for a stationary electrode in a quiescent 0.2 *M* NaBr solution

T (°C)	i_{an}[a] (mA cm^{-2})	ν[b] (mA cm^{-2})
50	0.65	0.70
57	0.93	0.86
66	1.5	1.35

[a] The measured current on the copper wire anode for t larger than 8800 s at a constant applied potential of −70 mV.
[b] It is assumed that the decomposition of 1 g/molecule of CuBr corresponds to a charge of 96 500 C since the valency of copper is +1 in this compound.

$$[6] \quad \frac{D\mu}{T} = \text{constant}$$

where μ is the viscosity of the solution, given in ref. 10. It is assumed that $D_{CuBr_2^-}$ and D_{Br^-} are equal to 1.3×10^{-5} cm^2 s^{-1} (2) and 1.8×10^{-5} cm^2 s^{-1} (3), respectively, at 22°C.

The experimental values of $\nu\omega^{-1/2}$, determined from ν vs. $\omega^{1/2}$ curves (Fig. 7), are close to the theoretical values $\nu\omega^{-1/2}_{CuBr_2^-}$ and are far away from the theoretical values $\nu\omega^{-1/2}_{Br^-}$ (Table 1). Therefore, the dissolution model formed by steps [2] and [3] is applicable up to 68°C.

Table 2 contains the values of the measured current on the copper wire anode (i_{an}) when the current reaches a steady value in temperatures ranging from 50°C to 66°C. The experimental values of ν, expressed in mA cm^{-2}, are also illustrated.

The comparison between ν and i_{an} supports the idea that the current of the copper anode decreases to eventually reach a steady value equal to the dissolution rate of the copper bromide precipitate formed on the electrode.

Conclusions

The morphology of copper bromide accumulated on the copper anode suggests that CuBr precipitates in the vicinity of the electrode. Its morphology and characteristics are quite different as the temperature is shifted from 22°C to 71°C while the irregular current variations observed on the i–t curves at 71°C are ascribed to the formation and repair of the cracks in the film. The current of the anode eventually reaches a steady value equal to the dissolution rate of the copper bromide precipitate formed on the electrode. The rate-determining step for the dissolution of CuBr from 22°C to 71°C can be entirely attributed to the mass transfer of intermediates ($CuBr_2^-$, $CuBr_3^{2-}$) from the electrode surface to the bulk electrolyte.

1. L. BROSSARD. Can. J. Chem. **62**, 36 (1984).
2. L. BROSSARD. Can. J. Chem. **62**, 1112 (1984).
3. L. BROSSARD. J. Electrochem. Soc. **131**, 1847 (1984).
4. W. LATIMER. Oxidation potentials. 2nd ed. Prentice-Hall, New York. 1952.
5. C. E. WICKS and F. E. BLOCK. Bulletin 605, U.S. Bureau of Mines, Washington. p. 43.
6. K.-TH. WILKE. Krist. Tech. **3** (3), K53 (1968).
7. L. BROSSARD. Can. J. Chem. **60**, 616 (1982).
8. R. B. BIRD, W. E. STEWART, and E. N. LIGHTFOOT. Transport phenomena. John Wiley and Sons, New York. 1960. p. 8.
9. J. G. PERRY. Chemical engineering handbook. 4th ed. McGraw-Hill, New York. 1963.
10. R. C. WEAST. Handbook of chemistry and physics, The Chemical Rubber Co. 51st ed. Cleveland, OH. 1970–71. p. F36.

Deprotonation de *N*-oxydes d'amines aliphatiques: schéma réactionnel général et nouvelle synthèse de pyrrolidines

RENÉ BEUGELMANS, LEÏLA BENADJILA-IGUERTSIRA, JACQUELINE CHASTANET, GUILLERMO NEGRON ET GEORGES ROUSSI[1]

Institut de Chimie des Substances Naturelles, C.N.R.S., 91190 Gif-sur-Yvette, France

Reçu le 25 janvier 1984

Ce memoire est dédié au Professeur Paul de Mayo à l'occasion de son 60ᵉ anniversaire

RENÉ BEUGELMANS, LEÏLA BENADJILA-IGUERTSIRA, JACQUELINE CHASTANET, GUILLERMO NEGRON et GEORGES ROUSSI. Can. J. Chem. **63**, 725 (1985).

Sous l'action du diisopropyl amidure de lithium, les *N*-oxydes d'amines aliphatiques de structures diverses **1**, **5**, **10**, **15**, **21**, **23** sont déprotonés. La monodéprotonation livre des amines secondaires et du benzaldéhyde résultant de l'hydrolyse d'un imonium (I), ou des hydroxylamines issues d'un réarrangement de type Stevens observé pour la première fois à partir d'un N-oxyde. La double déprotonation livre un intermédiaire ylure d'imonium (Y) pouvant évoluer en fonction de la structure de l'amine tertiaire initiale soit vers des pipérazines "tête–tête" (comportement de radical double (DD)), soit vers des aziridines. L'ylure d'imonium (Y5) dérivant du *N*-oxyde de triméthylamine dont la formation et la réactivité sont décrites pour la première fois possède la propriété remarquable d'entrer dans des réactions de cycloaddition avec des oléfines non activées, permettant ainsi une synthèse originale et efficace de pyrrolidines diverses.

RENÉ BEUGELMANS, LEÏLA BENADJILA-IGUERTSIRA, JACQUELINE CHASTANET, GUILLERMO NEGRON, and GEORGES ROUSSI. Can. J. Chem. **63**, 725 (1985).

Amine oxides, **1**, **5**, **10**, **15**, **21**, **23**, when treated by lithium diisopropylamide undergo deprotonation. Monodeprotonation gives rise either to secondary amines and benzaldehyde resulting from the hydrolysis of an intermediate immonium (I) or to hydroxylamines via a Stevens-like rearrangement observed for the first time on an amine oxide. Double deprotonation gives an immonium ylid (Y) which, depending upon the structure of the initial tertiary amine yields either "head to head" piperazines (biradical-like behavior of (DD)) or aziridines. The immonium ylid (Y5) derived from trimethylamine oxide, whose formation and reactivity are reported for the first time, has the remarkable property of undergoing cycloaddition reactions with unactivated olefins, leading to a new and efficient synthesis of various pyrrolidines.

La déprotonation des ammoniums quaternaires est une propriété bien connue (Réactions de Stevens, de Sommelet–Hauser), mais celle des *N*-oxydes d'amines aliphatiques tertiaires, structuralement proches restait inexplorée.[2] Cette constation fut à l'origine de l'étude systématique (2) présentée ici, dont quelques résultats préliminaires furent publiés (3, 4).

Résultats

Le *N*-oxyde de benzyldiméthylamine **1**, en présence d'un équivalent de BuLi conduit au benzaldéhyde **2**, à la benzylamine **3** et au mélange de pipérazines *cis* + *trans* **4** (15%). Le rendement en pipérazine **4** atteint 30% en présence de 2 équivalents ou plus de cette base. La nature de la base est importante et nous avons constaté que seules les bases lithiées RLi (R = CH_3, *n*-Bu, *t*-Bu, Ph, NH_2, $N(Et)_2$, $N(i\text{-prop})_2$, tétraméthylpiperidine) sont actives et que, parmi elles, le diisopropyl amidure de lithium (DAL) a permis le rendement en pipérazine **4** le plus élevé (61%), dans des conditions reproductibles (exp. 1).

C'est donc cette base qui a été utilisée pour traiter les *N*-oxydes benzyliques **1**, **5**, **10** (tableau 1).

Le *N*-oxyde **5** livre une hydroxylamine **7** (exp. 3) qui ne se forme pas à partir de **1** tandis que la quantité de pipérazine décroît comparativement à l'exp. 1. Cette tendance est plus accentuée pour le *N*-oxyde **10** dont la réaction ne livre plus de pipérazine, l'hydroxylamine **13** étant le produit majoritaire (exp. 5). Selon une publication récente, due à H. Takayama et T. Nomoto (5) qui ont étudié la réactivité de *N*-oxydes tribenzyliques différemment substitués en présence de DAL, les aziridines seraient les seuls produits formés à 0°C. En particulier, les auteurs rapportent la formation de **14** (41%) à partir de **10**. Nous avons donc pratiqué les expériences nº 2, 4 et 6 dans le but d'examiner la réactivité de **1**, **5**, **10** à 0°C. Pour le *N*-oxyde **1**, nous n'avons pas constaté de différence significative entre les expériences nº 1 et 2. Par contre, l'aziridine **9** est formée à partir de **5** traité à 0°C (exp. 4), alors qu'elle ne l'était pas à −78°C (exp. 3). En ce qui concerne la réactivité de **10** à 0°C (exp. 6), nous avons bien retrouvé **14**, avec le rendement

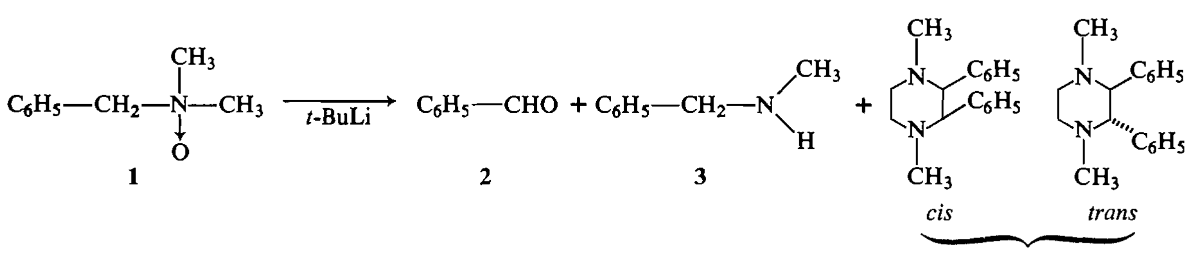

SCHÉMA 1

[1]Auteur à qui toute correspondance doit être adressée.
[2]Une brève revue récente de la réactivité des *N*-oxydes est contenue dans la réf. 1.

TABLEAU 1. Réactivité des *N*-oxydes benzyliques **1**, **5**, **10** en présence de DAL

Expérience n°	Produit de départ	Produits obtenus				
	$R^1CH_2—N(R^3)(O^-)—CH_2R^2$	R^1CHO	$R^1CH_2—N(R^3)—H$	$R^1CH(CH_2—R^2)—N(R^3)OH$	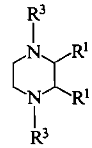	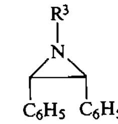
1[a]	**1** $R^1 = C_6H_5$; $R^2 = H$; $R^3 = CH_3$	**2**[b]	**3**[b]	0	**4** 61%[c]	0
2[d]	**1** $R^1 = C_6H_5$; $R^2 = H$; $R^3 = CH_3$	**2** 9%	**3**[b]	0	**4** 66%[c]	0
3[a]	**5** $R^1 = R^2 = C_6H_5$; $R^3 = CH_3$	**2**[b]	**6** 15%[e]	**7** 27%[c]	**8** 27%[c]	0
4[d]	**5** $R^1 = R^2 = C_6H_5$; $R^3 = CH_3$	**2** 8%[e]	**6** 6%	**7** 27%[c]	**8** 31%	**9** 3%
5[a]	**10** $R^1 = R^2 = C_6H_5$; $R^3 = CH_2C_6H_5$	**2**[b]	**12** 29%[e]	**13** 47%[c]	0	0
6[d]	**10** $R^1 = R^2 = C_6H_5$; $R^3 = CH_2C_6H_5$	**2**[b]	**12** 12%	**13** 20%	0	**14** 41%[c]

[a] $t = -78°C$.
[b] Produit pur (cpg ou cm) dont la structure est prouvée par des méthodes spectrales, mais obtenu en quantité trop faible pour qu'un rendement significatif puisse être indiqué.
[c] Rendement déterminé par pesée du produit isolé et pur.
[d] $t = 0°C$.
[e] Identifié par comparaison avec un échantillon authentique.

TABLEAU 2. Réactivité de *N*-oxydes dérivés de la diméthylaniline et de la triméthylamine à −78°C

Expérience n°	Produit de départ	Produits obtenus			
	$R^1CH_2—N(R^3)(O^-)—CH_2R^2$	$R^1CH_2NHR^3$	$R^1CH_2—N(R^3)—CH_2R^4$	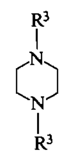	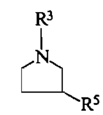
7[a]	**15** $R^1 = R^2 = H$; $R^3 = C_6H_5$	**16**[b,c]	**17** $R^4 = t\text{-}C_4H_9$[b,c]	0	**19** $R^5 = H$[b,c]
8[a]	**15**	**16**[e]	**17**[e]	0	**18**[d,e]
9[b]	**15**	**16**[b]	**19** $R^4 = n\text{-}C_4H_9$[f,g]	0	**20** $R^5 = n\text{-}C_4H_9$ 18%[g,h]
10[i]	**21** $R^1 = R^2 = H$; $R^3 = C_6H_2(CH_3)_3$			**22** 22%[j]	
11[i]	**23** $R^1 = R^2 = H$; $R^3 = CH_3$	0	0	**24** 12%[j]	
12[i,k]	**23**	0	0		**25** $R^5 = C_6H_5$ 57%[l]

[a] *t*-BuLi.
[b] Produit pur (cpg ou cm, dont la structure est prouvée par des méthodes spectrales, mais obtenu en quantité trop faible pour qu'un rendement significatif soit indiqué.
[c] **17**, **18** et **16** sont dans le rapport 7,2:1,7:1 (cpg).
[d] Avec barbottage d'éthylène.
[e] **17**, **18** et **16** sont dans le rapport 3,6:0,85:1 (cpg).
[f] *n*-BuLi.
[g] Évalué par cpg.
[h] Réaction en présence de l'hexène.
[i] DAL.
[j] Pesée de picrate.
[k] Réaction effectuée en présence de styrène.
[l] Pesée du produit purifié.

annoncé par Takayama et Nomoto, mais de plus, nous avons isolé la dibenzylamine **12** (12%) et l'hydroxylamine **13** (20%). C'est pour **10** que le contraste est le plus net puisqu'à 0°C (exp. 6) l'aziridine **14** est le produit majoritaire tandis que les quantités d'hydroxylamine **13** et de dibenzylamine **12** sont réduites de plus de la moitié par rapport à l'expérience 5. Le benzaldéhyde **2** est toujours présent, en quantités plus notables à 0°C qu'à −78°C.

Le *N*-oxyde de diméthylaniline **15** traité par le *t*-BuLi présente une réactivité différente de celle des *N*-oxydes benzyliques puisque les produits obtenus (exp. 7) (tableau 2) sont la *N*-méthylaniline **16**, l'amine tertiaire **17**, la phényl-1-pyrrolidine **18**. Le *t*-BuLi est manifestement la source des 4 atomes de carbone fixés sur **17** et par ailleurs, la formation de la pyrrolidine **18** implique la fixation de 2 atomes de carbone sur **15**. Or, le *t*-BuLi est une base suffisamment puissante pour décomposer le tétrahydrofuranne et donner de l'éthylène (6), source des deux atomes de carbone requis pour la formation de **18**. Un barbottage d'éthylène (exp. 8) provoque le doublement de la quantité de pyrrolidine et vient appuyer cette hypothèse. L'obtention de butyl-3 pyrrolidine **20** en présence de l'hexène-1 (exp. 9) confirme bien que les 2 atomes de carbone nécessaires à la formation des pyrrolidines **18** ou **19** proviennent d'un enchaînement —CH=CH—. Le *N*-oxyde de mésidine **21**

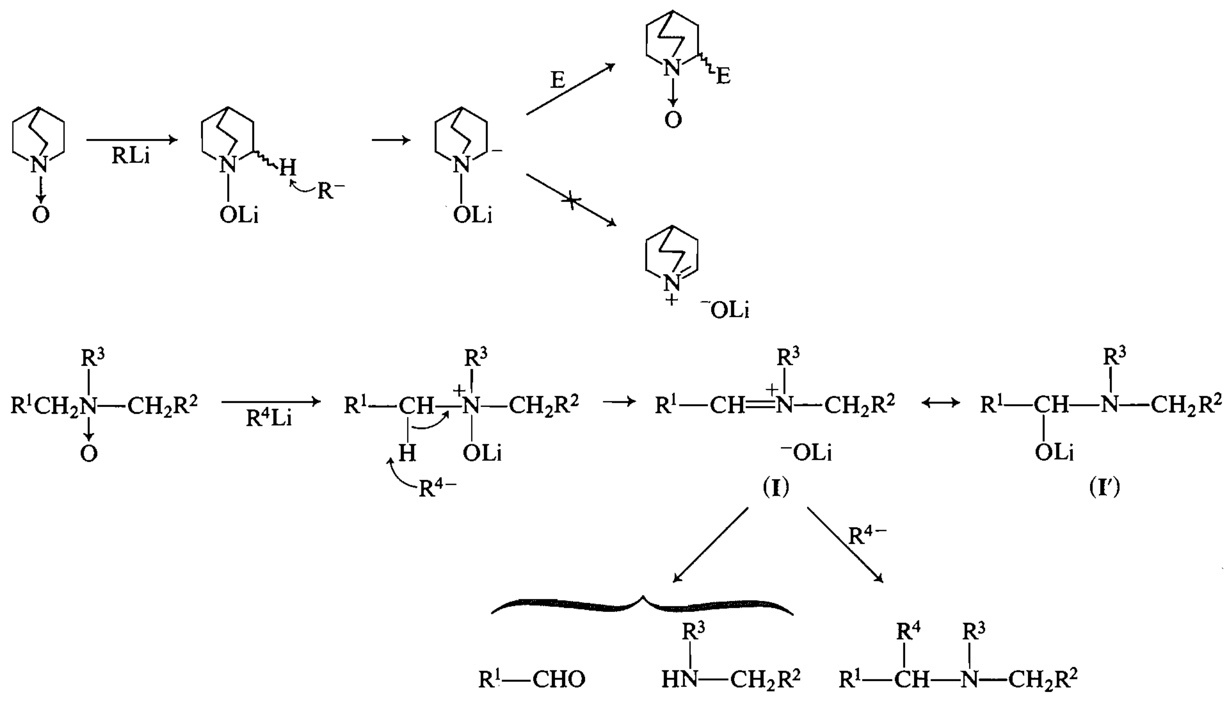

2 R[1] = C_6H_5 **3**; **6**; **12**; **16**   **17** R^4 = t-C_4H_9; R^1 = R^2 = H; R^3 = C_6H_5
19 R^4 = n-C_4H_9; R^1 = R^2 = H; R^3 = C_6H_5

SCHÉMA 2. Produits derivés de l'imonium (I).

TABLEAU 3. Fonctionnalisation α et α,α′ des *N*-oxydes

R^1CH_2—N(R^3)(O^-)—CH_2R^2				Fonctionnalisation α			Fonctionnalisation α,α′		
				Benzaldehyde	Amines	Hydroxylamines	Pipérazines	Aziridines	Pyrrolidines
	R^1	R^2	R^3	**2**					
1	C_6H_5	H	CH_3	+	**3**	—	**4**	—	—
5	C_6H_5	C_6H_5	CH_3	+	**6**	**7**	**8**	**9**	—
10	C_6H_5	C_6H_5	$CH_2C_6H_5$	+	**12**	**13**	—	—[a]	—
					12	**13**	—	**14**[b]	—
15	H	H	C_6H_5		**16**	—		—	**18**, **20**
21	H	H	$C_6H_2(CH_3)_3$		?	—	**22**	—	
23	H	H	CH_3		?		**24**	—	**25**

[a]À −78°C.
[b]À 0°C.

comporte un cycle benzènique stériquement encombré sur les positions 2 et 6, et ne donne lieu qu'à la formation du produit **22**. Le *N*-oxyde de triméthylamine **23** livre la pipérazine **24** (exp. 11) et la pyrrolidine **25** en présence de styrène (exp. 12).

Discussion

La formation des produits obtenus à partir des *N*-oxydes **1**, **5**, **10**, **15**, **21**, **23** implique la déprotonation d'un ou de deux carbones adjacent(s) à la fonction *N*-oxyde (tableau 3).

Monodeprotonation

Le premier cas clairement défini de réactivité anionique du carbone situé en α de la fonction *N*-oxyde est celui rapporté par nous en 1977, qui concerne le *N*-oxyde de quinuclidine (7).

La structure des amines tertiaires d'où dérivent les *N*-oxydes **1**, **5**, **10**, **15**, **21** et **23** permet contrairement à celle de la quinuclidine l'existence d'une liaison imonium $C{=}\overset{+}{N}{=}$ attestée par l'obtention de produits d'hydrolyse et d'attaque par un réactif nucléophile. En effet, l'intermédiaire formulé soit par $(I)^+$ OLi (sel d'imonium) soit par (I′) (amino alcoolate de Li) est hydrolysé en aldéhyde R^1—CHO et en amine secondaire HN (R^3)—CH_2R^2, tout comme dans les cas où il a été engendré à partir de la *N*-diméthylbenzylamine par d'autres voies (oxydation chimique ou électrochimique de l'amine, réduction ou décomposition catalysée par les métaux, du *N*-oxyde[3]) (schéma 2).

L'imonium (I) est également formé en série aniline et est caractérisé non seulement par l'obtention de l'amine secondaire

[3]Une discussion de ces réactions est donnée dans une révue récente (8).

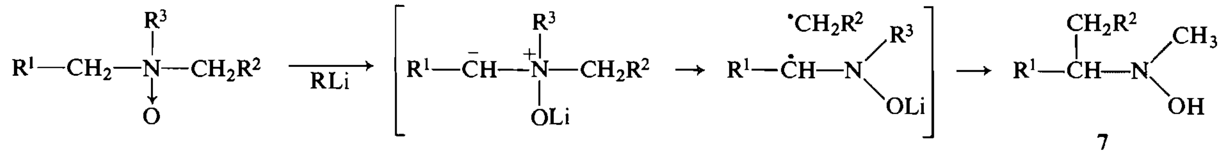

7
13

5 $R^1 = R^2 = C_6H_5$; $R^3 = CH_3$
10 $R^1 = R^2 = C_6H_5$; $R^3 = CH_2C_6H_5$

SCHÉMA 3. Formation des hydroxylamines.

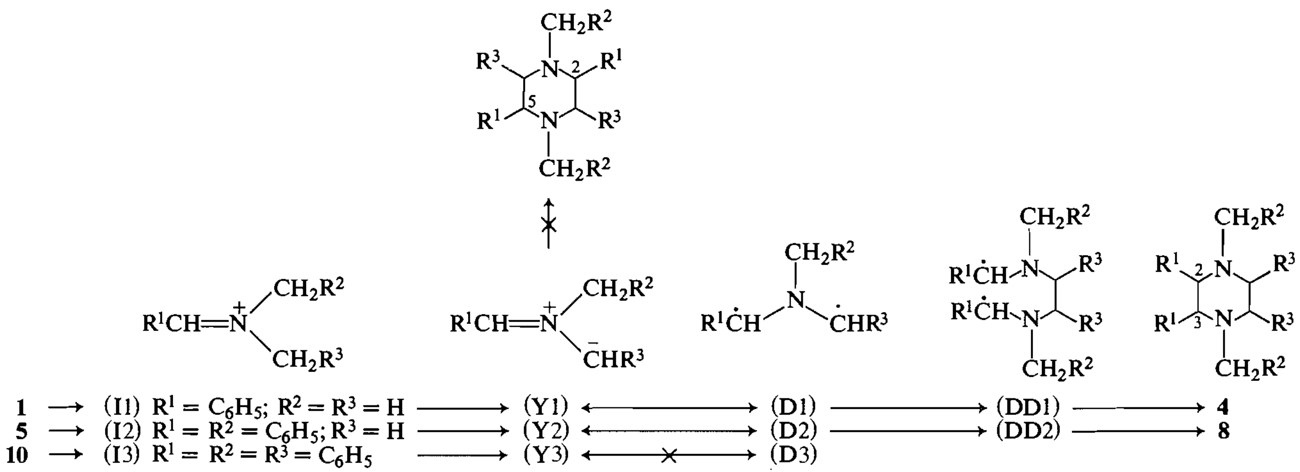

SCHÉMA 4. Formation des pipérazines tête–tête.

16 provenant de l'hydrolyse, mais aussi par celle des amines tertiaires **17** et **19** résultant de l'attaque nucléophile de t-$C_4H_9^-$ ou n-$C_4H_9^-$ sur C_6H_5—$\overset{+}{N}(CH_3)$=CH_2.

Le réarrangement en hydrolyxamines **7** (à partir de **5**) et **13** (à partir de **10**) observé pour la première fois sur des N-oxydes serait dû à un mécanisme radicalaire analogue à celui intervenant sur les sels d'ammonium quaternaires soumis à l'action des bases (Réaction de Stevens) (9, 10).

Parmi les N-oxydes étudiés ici, seuls **5** et **10** engendrent des anions pouvant subir la rupture homolytique nécessaire, avec formation de $\cdot CH_2C_6H_5$ (schéma 3).

Dans le cas du N-oxyde **10**, le processus radicalaire menant à l'hydroxylamine est plus efficace à −78°C qu'à 0°C, ce qui indique qu'il y a compétition entre la migration du radical $\cdot CH_2C_6H_5$ et la seconde déprotonation discutée plus loin.

Deprotonation double

Comme le montre le tableau 3, la monodéprotonation des N-oxydes qui est à l'origine de la formation de l'aldéhyde, des amines primaires et des hydroxylamines n'est pas sélective, puisque des pipérazines, des aziridines, des pyrrolidines sont formées également, même dans les réactions effectuées avec un seul équivalent de base. Cette seconde série de produits a pour origine une entité réactionnelle intermédiaire *difonctionnalisée*.

La déprotonation des sels d'imonium par les bases fortes a déjà été rapportée dans des cas particuliers et les produits, aziridines (11) ou pipérazines (12) selon la structure des imoniums initiaux, proviennent d'un ylure d'imonium qui a pu être piégé par le norbornène. Nous obtenons également des aziridines (**9**, **14**) et des pipérazines (**4**, **8**) à partir des N-oxydes benzyliques **5**, **10**, et de ceux dérivées de l'aniline **21** ou de la triméthylamine **23**. De plus, les pyrrolidines **18**, **20**, **25**, sont formées en présence d'une oléfine. L'origine de tous ces produits peut être rationalisée en invoquant l'existence d'un ylure d'imonium (Y) intermédiaire formé par déprotonation de (I).

Formation des pipérazines

Les pipérazines obtenues par duplication d'ylures d'imonium engendrés selon différentes voies possèdent toutes une structure "tête–queue" (substituants en positions 2 et 5) résultant d'une cycloaddition (3 + 3) (12–14).

Or, les pipérazines **4** et **8** que nous obtenons à partir des N-oxydes respectifs possèdent des structures "tête–tête" (substituants en positions 2 et 3), excluant un couplage d'ylures (Y1) ou (Y2). Cependant, ces ylures sont isoélectroniques de diradicaux (D1) et (D2) où le site benzylique ($C_6H_5\dot{C}H$—N serait stabilisé par l'effet captodatif défini par H. Viehe et coll. (15). Le radical méthylènique N—$CH_2^{\cdot}$ plus réactif réagirait donc le premier en se dupliquant, donnant ainsi un radical double (DD1) (DD2) précurseur des pipérazines "tête–tête" finales. L'interconversion photochimique **4** *cis* → **4** *trans* par l'intermédiaire d'un état excité menant à un radical double fournit un argument important en faveur de l'existence de (DD1) (16). Selon cette hypothèse, seuls les ylures d'imonium, générés à partir de N-oxydes d'amines portant au moins un substituant méthyle, *précurseur du radical méthylène* devraient donner des pipérazines, ce qui est vérifié.

Formation des aziridines

Nous avons vérifié que l'aziridine **26** est stable dans les conditions réactionnelles utilisées pour le traitement du N-oxyde **5** et qu'elle n'est donc pas à l'origine de la pipérazine **8**. L'espèce monodéprotonée (I) issue de **5** se déprotonne une seconde fois pour mener à (Y2) isoélectronique de (D2). Celle issue de **13** subit à −78°C une réaction compétitive menant à l'hydroxylamine **13** (exp. 5), la seconde déprotonation n'intervenant qu'à température plus élevée (exp. 6). La géométrie *cis* des phényles 2 et 3 portés par les aziridines **9** et **14** est conforme

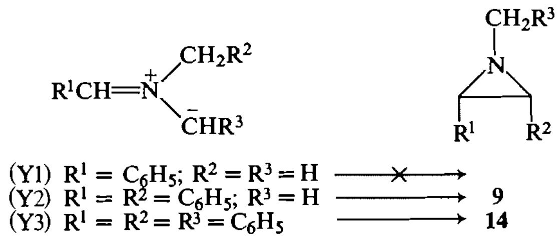

SCHÉMA 5. Formation des aziridines.

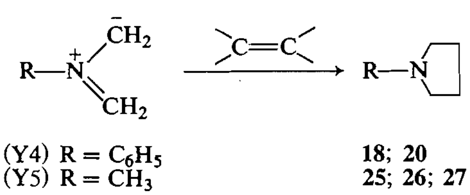

SCHÉMA 6. Formation des pyrrolidines.

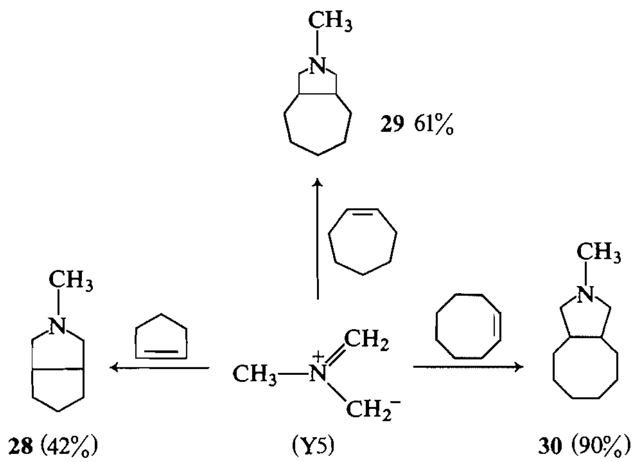

SCHÉMA 7. Réactivité de (Y5) vis-à-vis d'oléfines simples.

à celle attendue pour la cyclisation conrotatoire d'un intermédiaire ionique (Y2) ou (Y3) de conformation *trans*.

Formation des pyrrolidines

La déprotonation de l'imonium provenant du *N*-oxyde **15** livre un ylure (Y4), suffisamment réactif pour s'additionner à des oléfines simples (éthylène ou hexène-1). L'ylure d'imonium (Y5) est formé à partir du *N*-oxyde **23**, sans que l'existence d'un intermédiaire imonium soit étayée comme précédemment par l'obtention de l'amine secondaire $HN(CH_3)_2$ que nous avons recherchée sans succès. Ceci laisse penser que, en l'absence d'un substituant phényle porté sur le carbone (*N*-oxydes **1**, **5**, **10**) ou sur l'azote (*N*-oxyde **15**), l'imonium initial très réactif est déprotoné (de manière synchrone?) pour donner l'ylure (Y5).

Le styrène ajouté dans le milieu réactionnel ne se polymérise pas et livre **25** (50%), indiquant que l'intermédiaire n'est pas de nature radicalaire. D'autre part, l'addition de (Y5) au *cis* ou au *trans* stilbène livre la méthyl-1 diphényl-3,4 pyrrolidine *cis* **26** ou *trans* **27**, en conformité avec le processus de cycloaddition (3 + 2) (pour des révues récentes voir la réf. 17) (schéma 6). En l'absence d'oléfine, le seul produit isolable[4] à partir de **23** est la pipérazine **24**, qui n'étant pas substituée sur le cycle, ne peut fournir d'indice quant à la nature de l'intermédiaire mis en jeu.

Parmi les divers produits rapportés dans le tableau 3, les plus intéressants du point de vue de la synthèse sont ceux résultant de la double fonctionnalisation en α et α': pipérazines, aziridines et pyrrolidines. La réaction de cycloaddition (3 + 2) entre (Y5), *premier terme de la série des ylures d'imonium* ne portant aucun substituant et donc non stabilisé et des dipolarophiles non ou très peu activés par des groupes attracteurs d'électrons est *nouvelle* et nous semble être susceptible de développements synthétiques importants dont nous présentons ici quelques éléments.

Réactivité de (Y5) vis-à-vis d'oléfines simples

La réactivité de (Y5) est importante puisqu'il entre, à basse température, dans des réactions de cycloaddition avec des oléfines simples, ainsi qu'avec des cycloalcènes de taille variée:[5] cyclopentène, cycloheptène, cyclooctène, pour donner les systèmes hétérobicycliques **28**, **29**, **30**.

Réactivité de (Y5) vis-à-vis d'oléfins fonctionnalisées

Les possibilités synthétiques de la cycloaddition de (Y5) sont en fait plus vastes que celles montrées dans le schéma 7 puisque la double liaison de l'alcool allylique ou celle de la cyclopentenone dont la fonction carbonyle est protégée, la subissent pour donner **31** et **32**. La double liaison de la 3-pipéridéine est moins réactive et le rendement en système hétérobicyclique **33** est moindre.

Réactivité de (Y5) vis-à-vis de diènes

Les diènes conjugués cyclooctadiène, diphényl-1,4 butadiène livrent des mélanges de produits résultant d'une cycloaddition simple (**34**, **36**) ou double (**35**, **37**). Alors que **34** est instable, la pyrrolidine insaturée **36** isolée et traitée une seconde fois avec le *N*-oxyde **23** livre la bipyrrolidine **37**; aucun produit résultant d'une cycloaddition en 1,4 sur le système diénique n'a été obtenu. L'hexadiène-1,5 et l'hexadiène-1,5 3-ol se comportent de la même manière que les diènes conjugués, c'est-à-dire qu'ils subissent une ou deux cycloadditions avec (Y5) pour donner respectivement le mélange **38** + **39** et **40**.

Limites de la réaction de cycloaddition

La réaction s'avère sensible à l'encombrement stérique du dipolarophile comme nous l'avons observé à propos du comportement de (Y5) vis-à-vis du méthyl-1 cyclopentène et de l'alcool méthyl-2-allylique contrastant avec l'addition facile sur les homologues inférieurs.

Par ailleurs, (Y4) issu de **15** via (14) possède une réactivité satisfaisante vis-à-vis de l'éthylène et de l'hexène-1 et en ce qui concerne l'addition au norbornène, une expérience préliminaire conduit au produit attendu **41** dont la stéréochimie n'a pas été déterminée.

Conclusion

Les résultats de ce travail permettent de proposer pour la première fois un schéma réactionnel rendant compte de l'ensemble des données actuellement connues concernant la réactivité des *N*-oxydes d'amines aliphatiques traités par les bases fortes; ce schéma est susceptible, selon nous, de servir de fil

[4]La *N*-méthyl aziridine dont nous avons préparé un échantillon au laboratoire n'a pas été trouvée dans les produits issus de cette expérience.

[5]La faible réactivité du cyclohexène est actuellement étudié plus en détail au laboratoire, et peut, selon la remarque de l'un des rapporteurs, avoir des implications concernant le mécanisme réactionnel mis en jeu.

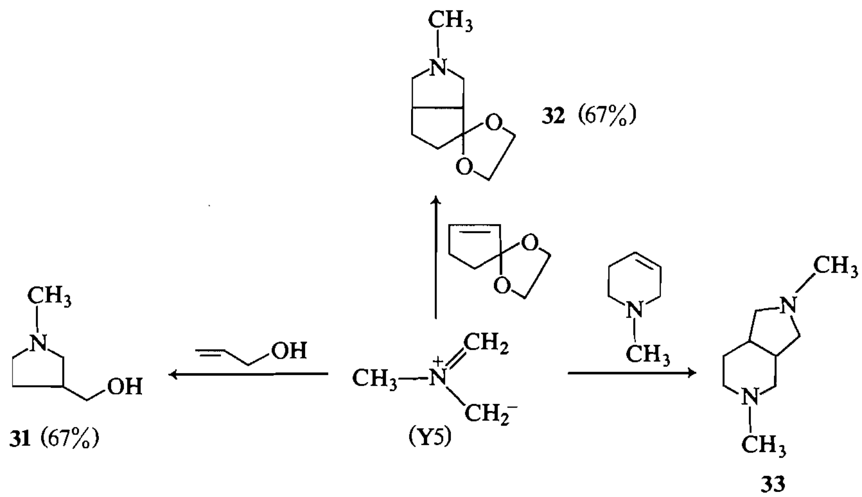

SCHÉMA 8. Réactivité de (Y5) vis-à-vis d'oléfins fonctionnalisées.

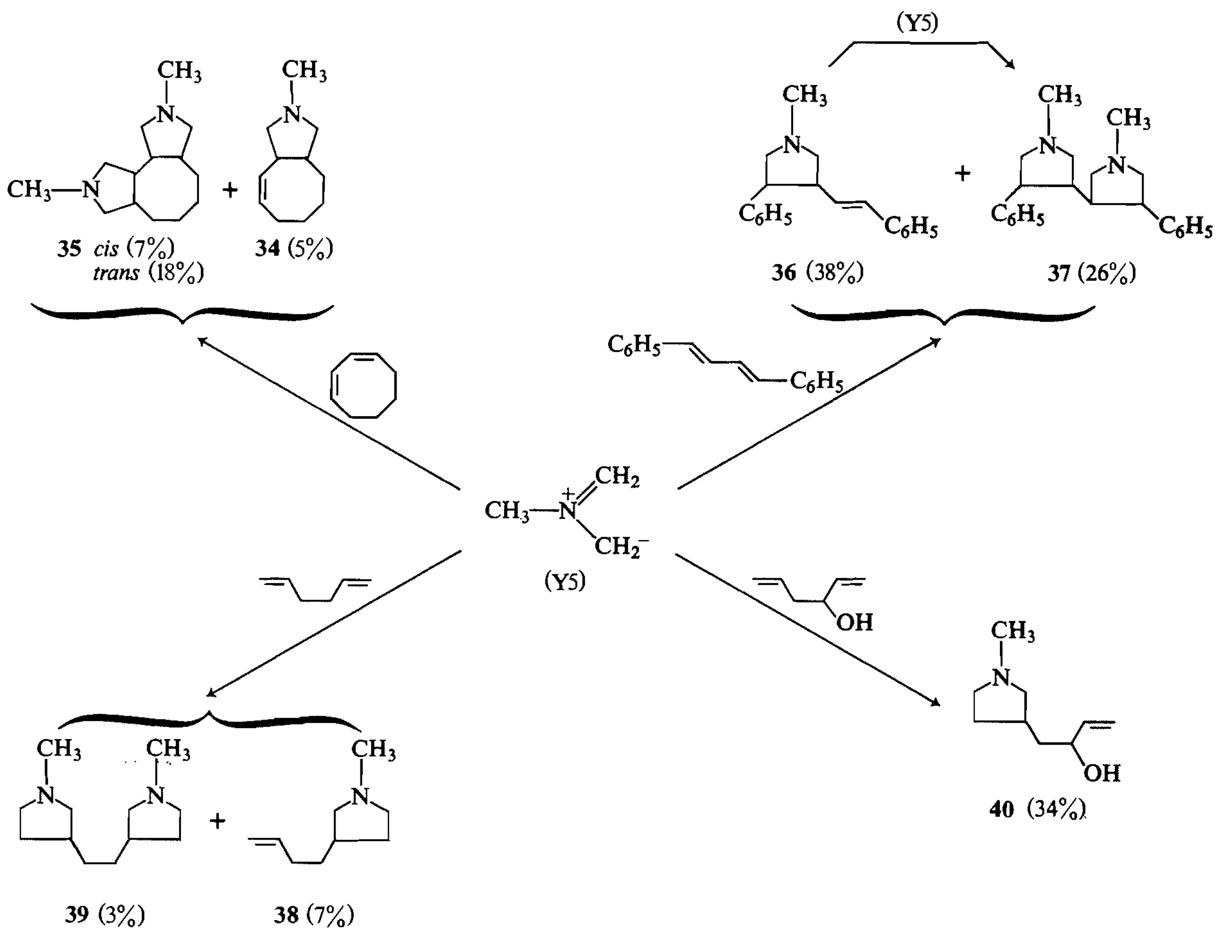

SCHÉMA 9. Réactivité de (Y5) vis-à-vis de diènes.

conducteur pour développer de nouvelles applications synthétiques. En ce qui concerne celles-ci notre méthode de synthèse de pyrrolidines substituées en 3 ou disubstituées en 3 et 4 complète de manière appréciable les méthodes connues fondées sur diverses réactions (18, 19) et particulièrement sur la cycloaddition (3 + 2) d'ylures d'azométhines stabilisés (12, 20, 21), masqués (22) ou diversement protégés (23, 24) avec des oléfines qui dans tous les cas sont activées (25).

Partie expérimentale

L'analyse des mélanges réactionnels et la séparation des composés ont été effectuées par chromatographie: en phase liquide sur colonne d'alumine alcaline (AA), de Florisil 60 Mesh (F), ou de gel de silice (S); sur couche mince de gel de silice Merck HF 254 + 366 neutre ou alcaline (ccm). Les proportions des solvants d'élution ont été exprimées en volume; en phase gazeuse (cpg) à l'aide d'un chromatographe Girdel série 300. Les analyses et dosages ont été réalisés sur une

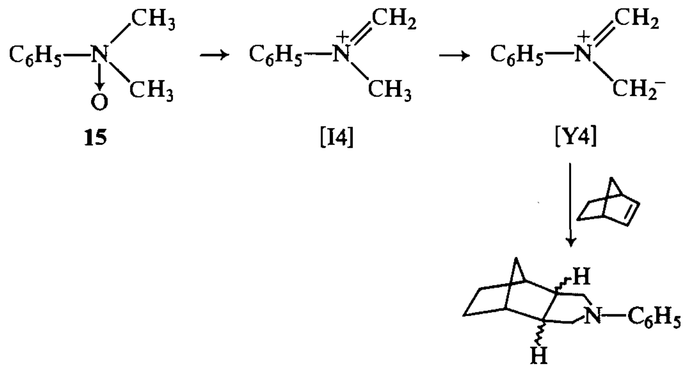

41

SCHÉMA 10

colonne A: OVI 5% (phényl méthyl-silicone 300 × 0,3); B: OVI 10% (300 × 0,3); C: Pennwalt 323 (28%, KOH 4%, 300 × 0,3); D: SE30 QFI 8% (300 × 0,3) ou E: Craig−Polyester 20% (300 × 0,3). L'identification par cpg des produits obtenus a été effectuée par comparaison de leur temps de rétention (tr) avec ceux des produits de référence.

Les spectres infra-rouge (ir) ont été enregistrés sur un appareil Perkin−Elmer 297, en utilisant le chloroforme comme solvant. Les spectres ultra-violet (uv) ont été réalisés en solution dans le méthanol, à l'aide d'un spectromètre Jobin−Yvon. Les spectres de résonance magnétique nucléaire du proton (rmn) ont été enregistrés sur un appareil Perkin−Elmer R12 à 60 MHz ou Bruker WM400 à 400 MHz. Le chloroforme deutérié a été utilisé comme solvant et le TMS comme référence interne. Les spectres de masse (ms) ont été enregistrés sur un spectromètre AEI, MS 50 our sur un appareil couplé avec un chromatographe gc/ms Hewlett Packard 5992A. Les points de fusion (*F*) des composés cristallisés ont été mesurés au banc Kofler ou sur un appareil Büchi.

Les organolithiens utilisés (*n*-BuLi dans l'hexane, PhLi dans l'éther ou *t*-BuLi dans le pentane) sont des préparations commerciales qui ont été titrées avant emploi par une solution 1 *M* d'isobutanol dans le toluène en présence de phénantroline-1,10. Le tétrahydrofuranne (THF) employé a été traité par passage sur colonne d'alumine alcaline puis distillé sur sodium en présence de benzophénone, avant chaque usage.

Toutes les oléfines et les diènes sont des produits commerciaux ainsi que le *N*-oxyde de triméthylamine qui a été utilisé soit après séchage prolongé sous un vide poussé, soit après sublimation.

Préparation des N-*oxydes*

N-*oxyde de diméthylbenzylamine 1*

La diméthylbenzylamine commerciale (10 g, 66 mmol) dissoute dans le méthanol distillé (60 mL) est traitée pendant une nuit par 110 mL d'eau oxygénée à 110 volumes, selon la méthode de Cope et Towle (26). L'excès d'eau oxygénée est détruit par du palladium sur charbon activé à 10%. Un séchage poussé à 60°C sous 10^{-2} Torr (1 Torr = 133.3 Pa) livre le *N*-oxyde **1** (9,8 g, 65 mmol), Rdt = 98%; *F* = 62°C (acétate d'éthyle) (litt. (26) *F* = 64,5°−67°C); *F* picrate = 162°C (litt. (26) *F* = 158−160°C); ir ν_{N-O}: 975 cm^{-1}; rmn: 3,1 (s, 6H), 4.4 (s, 2H), 7,4−7,6 (m, 5H).

N-*oxyde de dibenzylméthylamine 5*

L'oxydation de la dibenzylméthylamine (10 g, 44 mmol) dans les conditions décrites ci-dessus, conduit après séchage prolongé à 8 g (35,2 mmol, 75%) de *N*-oxyde **5**; *F* = 150°C (acétate d'éthyle) (litt. (26) *F* = 150°C).

N-*oxyde de tribenzylamine 10*

L'oxydation de la tribenzylamine (10 g, 35 mmol) en solution dans 30 mL de chloroforme par l'acide *m*-chloroperbenzoïque (12 g, 69 mmol) conduit après purification sur colonne AA ($CHCl_3$−MeOH 3:1) à 10,3 g (33,9 mmol, 97%) de *N*-oxyde **10**; *F* = 138°C (hexane−acétone) (litt. (27) *F* = 133°C).

N-*oxyde de diméthylaniline 15*

L'oxydation par l'eau oxygénée de la diméthylaniline commerciale (3 g, 24,7 mmol) conduit à 1,5 g (11 mmol, 44%) de *N*-oxyde **15**; *F* = 150°C (méthanol) (litt. (27) *F* = 150°C).

N-*oxyde de diméthylmésidine 21*

La diméthylmésidine (2,89 g, 17,73 mmol) préparée par méthylation de la mésidine par le sulfate de méthyle (28), et oxydée par l'acide *m*-chloroperbenzoïque (2,93 g, 18,7 mmol), conduit après chromatographie sur colonne AA au *N*-oxyde **21** (364 mg, 2,01 mmol), Rdt = 11%, amorphe; rmn: 2,2 (s, 3H), 2,7 (s, 6H), 3,7 (s, 6H), 6,9 (s, 2H).

Action du DAL sur les N-*oxydes benzyliques à −78°C* et *à 0°C*

Expérience type

Toutes les réactions sont effectuées sous azote. Le DAL (3,5 mmol) en solution dans le THF est ajouté à l'aide d'une seringue, à 1 mmol de *N*-oxyde en suspension dans 25 mL de THF à −78°C. L'évolution de la réaction est suivie par des prélèvements analysés en ccm ($MeOH/CH_2Cl_2$ 1:99). Après disparition du produit de départ (environ 4 h) l'hydrolyse et l'extraction (CH_2Cl_2) conduisent à un mélange qui est séparé par chromatographie sur colonne.

A 0°C les conditions expérimentales sont identiques à celles décrites dans le cas de réactions effectuées à −78°C, seuls les rapports des concentrations *N*-oxyde/base changent (1:3, 5 à −78°C; 1:1,2 à 0°C).

Action du DAL sur le N-*oxyde de diméthylbenzylamine 1*

(a) *Expérience n° 1 (−78°C)*

Le *N*-oxyde **1** (306 mg, 2,02 mmol) traité dans les conditions décrites ci-dessus, par le DAL (13,5 mmol) donne 310 mg de produit brut qui est chromatographié sur colonne AA. L'élution (pentane) livre des traces de benzaldéhyde identifié par cpg et par ccm analytique. L'élution (pentane/chlorure de méthylène: 90:10) livre un mélange de pipérazines-2,3 diphényl *N*,*N*-diméthyl *cis* (**4***c*) et *trans* (**4***t*) dont l'analyse par cpg sur colonne A indique un rapport **4***c*/**4***t* = 2,4 (tr **4***t* = 20 min; **4***c* = 28 min à 195°C sous 1,1 atm) (1 atm = 101,3 kPa). La cpg préparative sur colonne E permet d'obtenir **4***t* (25 mg) et **4***c* (60 mg), identifiés à des échantillons authentiques.

Pipérazine **4** *trans*: *F* = 263°C (cyclohexane) (litt. (29) *F* = 263−264°C); rmn: 2 (s, 6H), 2,5−3,1 (système AA'BB', 4H), 2,82 (s, 2H), 7−7,5 (m, 10H arom); ^{13}C: 43,54 (*c*, C1 et C4), 54,78 (t, C5 et C6), 75,06 (d, C2 et C3), 128,16 (d, C3*, C4* et C5*), 130,69 (d, C2* et C6*), 138,03 (s, C1*); sm *m*/*e*: 266 (M^+), 146, 118.

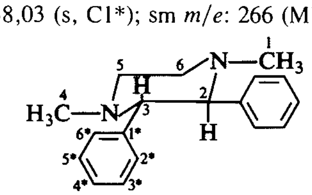

Pipérazine **4** *cis*: *F* = 90°C (cyclohexane) (non décrit dans la litt.); rmn: 2,1 (s, 6H), 2,5−3,2 (système AA'BB', 4H), 3,7 (s, 2H), 6,9−7,5 (m, 10H, arom); ^{13}C: 43,54 (q, C1 et C4), 52,85 (t, C5 et C6), 71,81 (d, C2 et C3), 127,12 (d, C4*), 127,4 (d, C3* et C5*), 130,6 (d, C2* et C6*), 136,9 (s, C1*); sm: identique à **4** *trans*.

*Synthèse de 4*c *et 4*b

*Synthèse de la diphényl-2,3 dihydro-5,6 pyrazine (*a*)*

Le benzil (10 g, 47 mmol) est mis à réagir avec de l'éthylènediamine (2,8 g , 47 mmol) dans 250 mL d'éthanol distillé. Une recristallisation dans l'éthanol livre *a* (9 g, 38 mmol), Rdt = 81%; *F* = 161°C (litt. (29) *F* = 161°C); rmn: 3,7 (s, 4H), 7,2−7,7 (m, 10H arom).

*Obtention des diphényl-2,3 pipérazines (*b cis *et* b trans*)*

Le traitement de *a* (3,5 g, 15 mmol) par le sodium (7 g, 300 mmol) dans l'éthanol à reflux livre, après une première extraction des eaux mères en milieu alcalin, le composé *b* (3 g, 13 mmol) sous forme de mélange d'isomères *b cis* et *b trans* (Rdt = 85%), séparés par cristallisation des tartrates dont l'extraction en milieu alcalin conduit à *b trans* (1 g, 4,2 mmol) et *b cis* (1,8 g, 7,6 mmol).

Composé *b trans*: *F* = 123°C (litt. (30) *F* = 123−124°C); rmn:

3,15 (s, 4H), 3,75 (s, 2H), 7,15 (s large, 10H arom).

Composé *b cis*: F = 112°C (litt. (30) F = 108–109°C); rmn: 2,7–3,5 (système $A_2A'_2$, 4H), 4,3 (s, 2H), 7–7,6 (m, 10H arom).

Un autre mode de réduction de *a* par l'hydrure de lithium et d'aluminium dans l'éther anhydre, permet d'obtenir *b cis* et *b trans* avec un rendement de 37%.

Méthylation de b cis *et* b trans

L'action d'un excès d'iodure de méthyle distillé sur *b trans* (0,5 g, 2,2 mmol) dans l'éthanol à chaud livre **4** *trans* (0,55 g, 2 mmol), Rdt = 97%, cristallisant après chromatographie sur colonne F (élution: éther/pentane, 50:50 jusqu'à 70:30). Un traitement analogue livre **4** *cis* (0,47 g, 1,7 mmol), Rdt = 84%, à partir de *b cis* (0,5 g, 2,2 mmol). Ces produits sont identiques (ir, rmn) à ceux issus de la réaction du *N*-oxyde **1**.

(b) *Expérience n° 2 (0°C)*

Le *N*-oxyde **1** (906 mg, 6 mmol) traité par le DAL (7,2 mmol) livre après chromatographie sur colonne S (élution: chlorure de méthylène/hexane, 5:95): (*i*) les pipérazines **4***c* et **4***t* (530 mg, 1,99 mmol), Rdt = 66%, *c*/*t* = 1,4; (*ii*) le benzaldéhyde **2** (60 mg, 0,56 mmol), Rdt = 9%; (*iii*) le *N*-oxyde **1** (élution: méthanol/chlorure de méthylène, 3:97) (35 mg) contenant de la benzylméthylamine **3**.

Action du DAL sur le N-*oxyde de dibenzylméthylamine* **5**

(a) *Expérience n° 3 (−78°C)*

Le *N*-oxyde **5** (908 mg, 4 mmol) traité par le DAL (14 mmol) livre après chromatographie sur colonne S: (*i*) la pipérazine **8** (229 mg, 0,55 mmol), éluée par CH_2Cl_2/hexane, 5:95), Rdt = 27%, F = 185°C (CH_2Cl_2/hexane); rmn (400 MHz): 2,3 (d, 2H, J = 8 Hz) 2,7–2,9 (d, 2H, J = 8 Hz et d, 2H, J = 14 Hz), 3,35 (s, 2H), 3,6–3,8 (d, 2H, J = 14 Hz), 7–7,3 (m, 20H arom); sm m/e: 417 ($M^+ - 1$), 327, 210; sm (ionisation chimique): 419 $(M + 1)^+$. (*ii*) Le composé **8**, non décrit dans la littérature, est identique (ir, rmn) à un échantillon de référence préparé par le traitement de *b trans* avec le

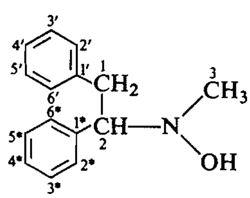

bromure de benzyle. (*iii*) L'hydroxylamine **7** (250 mg, 1,1 mmol, éluée par MeOH/CH_2Cl_2, 1:99), F = 104–105°C (éther), Rdt = 27%; ir ν_{OH}: 3580 cm^{-1}; rmn (400 MHz): 2,5 (s, 3H), 3 (2d, 1H, J = 1 Hz), 3,4–3,8 (2H), 6,7–7,3 (m, 10H arom); ^{13}C: 40,358 (t, C1), 46,40 (q, C3), 76,62 (d, C2), 125,8 (d, C4), 127,5 (d, C4), 127,9 (d, C3C5*), 128,2 (d, C5*C3*), 128,7 (d, C2'C6'), 129,4 (d, C2*C6*), 138,6 (s, C1'), 139,4 (s, C1*); sm m/e: 226 ($M^+ - 1$), 181, 136, 118. *Anal.* calc. pour $C_{15}H_{17}NO$: C 79,20, H 7,48, N 6,16, O 7,04; tr: C 79,18, H 7,52, N 5,90, O 7,45%.

(b) *Expérience n° 4 (0°C)*

Le *N*-oxyde **5** (908 mg, 4 mmol) traité par le DAL (4,8 mmol) livre après chromatographie sur colonne F: (*i*) le benzaldéhyde **2** (30 mg, 0,28 mmol), Rdt = 7% (élution: CH_2Cl_2/hexane, 30:70); (*ii*) la pipérazine **8** (260 mg, 0,62 mmol), Rdt = 31%, (élution: CH_2Cl_2/hexane, 30:70); (*iii*) l'aziridine **9** (23 mg, 0,12 mmol), Rdt = 3% (élution: CH_2/Cl_2 30:70); rmn: 2,7 (3H, s), 2,8 (2H, s), 7,15 (10H, s élargi); M^+ 209, m/e 194; (*iv*) l'hydroxylamine **7** (250 mg, 1,1 mmol), Rdt = 27% (élution: CH_2Cl_2/hexane, 50:50); (*v*) la méthylbenzylamine **6** (30 mg, 0,24 mmol), Rdt = 6% (élution: CH_2Cl_2); (*vi*) le *N*-oxyde **5** (90 mg, 0,4 mmol), Rdt = 10% (élution: CH_2Cl_2/MeOH 90:10).

Action du DAL sur le N-*oxyde de tribenzylamine* **10**

(a) *Expérience n° 5 (−78°C)*

Le *N*-oxyde **10** (909 mg, 3 mmol), traité par le DAL (10,5 mmol) livre après chromatographie sur colonne S: (*i*) l'hydroxylamine **13** (430 mg, 1,42 mmol), Rdt = 47% (élution: CH_2Cl_2/hexane, 50:50); F = 115°C (CH_2Cl_2/hexane); ir: 3580 cm^{-1} (OH); rmn (400 MHz): 3 (2d, 1H, J = 7 Hz), 3,6 (2d, 2H, J = 7 Hz; 1d, J = 13 Hz), 3,8 (d, 1H, J = 13 Hz), 3,9 (2d, 1H, J = 7 Hz), 6,9–7,4 (m, 10H); sm m/e: 304 ($M^+ - 1$), 196, 122, 106. *Anal.* calc. pour $C_{21}H_{21}NO$: C 83,13, H 6,98, N 4,62, O 5,27; tr.: C 82,98, H 6,90, N 4,83, O 5,21%; (*ii*) la dibenzylamine **12** (109 mg, 0,86 mmol), Rdt = 29% (élution: CH_2Cl_2/hexane, 30:70); (*iii*) le *N*-oxyde **10** (60 mg, 0,2 mmol), Rdt = 6% (élution: CH_2Cl_2/MeOH, 90:10).

(b) *Expérience n° 6 (0°C)*

Le *N*-oxyde **10** (900 mg, 3 mmol) traité par le DAL (3,6 mmol) livre après chromatographie sur colonne S: (*i*) l'aziridine **14** (350 mg, 1,22 mmol), Rdt = 42% (élution: CH_2Cl_2/hexane, 40:60); rmn identique à celle décrite (5). (*ii*) l'hydroxylamine **13** (175 mg, 0,58 mmol), Rdt = 20% (élution: CH_2Cl_2/hexane, 50:50); (*iii*) la dibenzylamine **12** (75 mg, 0,38 mmol), Rdt = 12% (élution: CH_2Cl_2/MeOH, 99:1); (*iv*) le *N*-oxyde **10** (45 mg, 0,15 mmol), Rdt = 5% (élution: CH_2Cl_2/MeOH, 90:10).

Action du t-*BuLi sur le* N-*oxyde de diméthylaniline*

Expérience n° 7

Le *N*-oxyde **15** (1,25 g, 9 mmol) traité par le *t*-BuLi (30 mmol) en solution dans le THF livre un mélange (0,600 g), analysé par cpg (colonne A, t = 100°C). Trois composés **17**, **18** et **16** dans le rapport 7,2:1,7:1 sont identifiés et la cpg préparative permet d'obtenir des échantillons pour la spectroscopie de masse. *N*-méthyl aniline **16**: (cpg: (tr) = 11 min), sm m/e: 107 (M$^+$). *N*-phénylpyrrolidine **18**: (cpg: (tr) = 7 min), sm m/e: 147 (M$^+$) 119, 104, identique à un échantillon de référence préparé selon la littérature (31). *N*-méthyl *N*-isopentyl aniline **17**: (cpg: (tr) = 4,8 min) sm m/e: 177 (M$^+$) 162, 120.

Réaction de **15** *en présence d'éthylène*

Expérience n° 8

De l'éthylène est mis à barboter à −78°C dans une solution de **15** (400 mg, 2,9 mmol) dans le THF. Le traitement par le *t*-BuLi (3,9 mL, 6 mmol) conduit à un mélange (0,2 g) analysé par comparaison (cpg, colonne A, t four = 170°C) à un essai témoin ne contenant pas d'éthylène. Les calculs à partir des chromatogrammes montrent que la quantité de **18** est doublée par rapport à l'expérience n° 7.

Réaction de **15** *en présence d'hexène-1*

Expérience n° 9

De l'hexène-1 (500 mg, 6 mmol) est ajouté à **15** (400 mg, 2,9 mmol) en solution dans le THF à −78°C. Le tout est traité par du *n*-BuLi (4,5 mL, 7,3 mmol) puis hydrolysé à basse température. Une première extraction (chlorure de méthylène) suivie d'une deuxième extraction (butanol) livre 0,26 g d'un mélange chromatographié sur colonne AA. L'élution (pentane/éther, 50:50) conduit à la *N*-méthyl *N*-pentyl aniline **19**, Rdt = 10% (cpg); sm m/e: 177 (M$^+$), 120, (M^+ − 57, C_4H_9), 106; l'élution par l'éther conduit à la *N*-phényl butyl-3 pyrrolidine **20**, Rdt = 18% (cpg); rmn: 0,8–1,6 (m, 9H), 1,9–2,4 (m, 2H), 2,6–3 (m, 1H), 3,1–3,6 (m, 4H), 6,5–7 (m, 3H arom), 7–7.5 (m, 2H arom); sm m/e: 203 (M$^+$), 119, 104.

Action du t-*BuLi sur* **21**

Expérience n° 10

Le *N*-oxyde de diméthylmésidine **21** (181 mg, 1,52 mmol) en solution dans 25 mL de THF traité à −78°C par 4 mmol de *t*-BuLi pendant 30 min livre après chromatographie (colonne S) la pipérazine **22** (54 mg, 0,17 mmol), Rdt = 22%, F = 190–191°C (EtOH) (litt. (32) F = 190–191°C).

Action du DAL sur le N-*oxyde de triméthylamine* **23**

Expérience n° 11

Le *N*-oxyde **23** (345 mg, 4,6 mmol) traité par le DAL (16 mmol) à −78°C, conduit après hydrolyse et extraction au CH_2Cl_2 à un mélange brut (72 mg) qui, sous l'action d'une solution alcoolique saturée d'acide picrique, donne le dipicrate de diméthylpipérazine **24** (86 mg, 0,26 mmol), Rdt = 12%, F = 277°C (EtOH). Une solution aqueuse de soude 10% libère la pipérazine **23** identique (cpg, rmn) au produit commercial.

Méthyl-1 phényl-3 pyrrolidine ***25***

Expérience n° 12

Le *N*-oxyde de triméthylamine **23** (91 mg, 1,21 mmol) et du styrène (138 mg, 1,33 mmol) en solution dans 25 mL de THF traité à −78°C par le DAL (4,2 mmol), conduit à la pyrrolidine **25** (111 mg, 0,60 mmol), Rdt = 50%. Picrate: *F* = 158−160°C (EtOH) (litt. (33) *F* = 155−158°C).

Méthyl-1 diphényl-3,4 pyrrolidine cis ***26***

Le *N*-oxyde de triméthylamine **23** (85 mg, 1,13 mmol) et le *cis* stilbène (211 mg, 1,17 mmol) en solution dans 25 mL de THF traité à −78°C par le DAL (3,9 mmol) livre la pyrrolidine **26** (165 mg, 0,70 mmol), Rdt = 62%; *F* = 67−69°C (EtOH); rmn: 2,55 (s, 3H), 2,93−3,33 (m, 4H), 2,73−4,0 (m, 2H), 7,1 (s élargi, 10H); sm *m/e*: 237 (M^+), 180, 57. *Anal.* calc. pour $C_{17}H_{19}N$: C 86,00, H 8,07, N 5,93; tr.: C 85,86, H 8,08, N 5,94%.

Méthyl-1 diphényl-3,4 pyrrolidine trans ***27***

Le *N*-oxyde de triméthylamine **23** (106 mg, 1,42 mmol) et le *trans* stilbène (295 mg, 1,55 mmol) en solution dans 25 mL de THF traité à −78°C par le DAL (4,9 mmol), livre la pyrrolidine **27** (241 mg, 1,01 mmol), Rdt = 72%; rmn: 2,45 (s, 3H), 2,7−3,8 (m, 6H), 7,2 (s élargi, 10H). sm *m/e*: 237 (M^+), 180, 57. Picrate: *F* = 186−187°C (EtOH). *Anal.* calc. pour $C_{23}H_{22}N_4O_8$: C 59,22, H 4,75, N 12,02, O 24,01; tr.: C 58,97, H 4,72, N 12,00, O 23,73%.

Méthyl-3 aza-3 bicyclo[3.3.0]octane ***28***

Le *N*-oxyde de triméthylamine **23** (92 mg, 1,23 mmol) et du cyclopentène (92 mg, 1,35 mmol) en solution dans 25 mL de THF traité à −78°C par le DAL (4,4 mmol) conduit à la pyrrolidine **28** (34) (65 mg, 0,52 mmol), Rdt = 42%; rmn: 1,3−1,8 (m, 6H), 1,8−2,3 (m, 2H), 2,3 (s, 3H), 2,4−2,9 (m, 4H); sm *m/e*: 237 (M^+). Picrate: *F* = 203−205°C (EtOH).

Méthyl-3 aza-3 bicyclo[5.3.0]décane ***29***

Le *N*-oxyde de triméthylamine **23** (161 mg, 2,14 mmol) et du cycloheptène (235 mg, 2,35 mmol) en solution dans 25 mL de THF traité à −78°C par le DAL (5,5 mmol) conduit à la pyrrolidine **31** (201 mg, 1,31 mmol), Rdt = 61%; rmn: 1−2 (m, 12H), 2−2,6 (m + 1s, 5H), 2,6−3 (m, 2H); sm *m/e*: 153 (M^+), 57. Picrate: *F* = 238−240°C (EtOH). *Anal.* calc. pour $C_{16}H_{22}N_4O_7$: C 50,25, H 5,80, N 14,66, O 29,29; tr.: C 50,37, H 5,87, N 14,64, O 29,32%.

Méthyl-3 bicyclo[6.3.0]undécane ***30***

Le *N*-oxyde de triméthylamine **23** (80 mg, 1,06 mmol) et du cyclooctène (129 mg, 1,16 mmol) en solution dans 25 mL de THF traité à −78°C par le DAL (4,2 mmol) livre la pyrrolidine **30** (159 mg, 0,95 mmol), Rdt = 90%; rmn: 1−1,2 (m, 14H), 1,9−2,4 (m, 3H), 2,25 (s, 3H), 2,8−3,2 (m, 2H); sm *m/e*: 167 (M^+), 57. Picrate: *F* = 218−219°C (EtOH); *Anal.* calc. pour $C_{17}H_{24}N_4O_7$: C 51,51, H 6,10, N 14,14, O 28,25; tr.: C 51,44, H 6,09, N 13,96, O 28,14%.

Méthyl-1 méthanol-3 pyrrolidine ***31***

Le *N*-oxyde de triméthylamine **23** (115 mg, 1,52 mmol) et du propen-2 ol (192 mg, 1,67 mmol) en solution dans 25 mL de THF traité à −78°C par le DAL (4,2 mmol) livre la pyrrolidine **31** (106 mg, 0,92 mmol), Rdt = 60%; rmn: 1−2 (m, 3H), 2−3 (m, 7H), 2,35 (s, 3H), 3,6 (d, 2H), 4,2 (s élargi, 1H); sm *m/e*: 115 (M^+), 57.

Méthyl-1 aza-1 (dioxolane-1,3)-4 bicyclo[3.3.0]heptane ***32***

Le *N*-oxyde de triméthylamine **23** (96 mg, 1,24 mmol) et du dioxolane de la cyclopenten-2 one (171 mg, 1,36 mmol) en solution dans 25 mL de THF traité à −78°C par le DAL (4,3 mmol) livre la pyrrolidine **32** (152 mg, 0,83 mmol), Rdt = 67%; rmn: 1,4−2,3 (m, 6H), 2,3 (s, 3H), 2,4−3 (m, 4H), 3,9 (s, 4H); sm *m/e*: 183 (M^+), 99, 57. Picrate: *F* = 171−172°C (EtOH). *Anal.* calc. pour $C_{16}H_{20}N_4O_9$: C 46,60, H 4,89, N 13,59, O 34,92; tr.: C 46,10, H 4,86, N 13,43, O 34,27%.

Diméthyl-3,8 diaza-3,8 bicyclo[4.3.0]nonane ***33***

Le *N*-oxyde de triméthylamine **23** (281 mg, 3,75 mmol) et de la méthyl-1 tétrahydro-1,2,3,6 pyridine (400 mg, 4,12 mmol) en solution dans 25 mL de THF traité à −78°C par le DAL (13 mmol) livre un mélange de produits (209 mg) dont le spectre de masse indique qu'il est constitué de diméthylpipérazine **24** (M^+ 114) et de pyrrolidine **33** (M^+ 154).

Méthyl-1 aza-1 bicyclo[6.3.0.(3.10)]undecene-4 ***34*** *et diméthyl-1,6 diaza-1,6 tricyclo[4.3.0.(3.10)(4.8)]tétradecène* cis ***35***c *et* trans ***35***t

Le *N*-oxyde de triméthylamine **23** (415 mg, 5,53 mmol) et du cyclooctadiène-1,3 (330 mg, 3,06 mmol) en solution dans 50 mL de THF traité à −78°C par le DAL (19 mmol) livre un mélange dont la chromatographie sur colonne donne la pyrrolidine instable **34** (46 mg, 0,27 mmol), Rdt = 5%, la dipyrrolidine *cis* **35***c* (40 mg, 0,18 mmol), Rdt = 7%, et la dipyrrolidine *trans* **35***t* (108 mg, 0,48 mmol), Rdt = 18%, séparées sous forme de picrates:

34 (46 mg, 0,27 mmol) instable, Rdt = 5%; sm *m/e*: 165 (M^+), 57.

35*c* (40 mg, 0,18 mmol), Rdt = 7%; rmn: 1−1,8 (m, 8H), 1,8−2,7 (m, 8H), 2,45 (s, 6H), 2,7−3,5 (m, 4H); sm *m/e*: 222 (M^+), 57. Dipicrate: *F* = 178−180°C (EtOH).

35*t* (106 mg, 0,48 mmol), Rdt = 18%; rmn: 1−1,7 (m, 8H), 1,7−2,7 (m, 8H), 2,3 (s, 6H), 2,7−3,5 (m, 4H); sm *m/e*: 222 (M^+), 57. Dipicrate: *F* = 108−110°C (EtOH). *Anal.* calc. pour $C_{26}H_{32}N_8O_{14}$: C 45,88, H 4,74, N 16,46, O 32,91; tr.: C 45,71, H 4,76, N 16,28, O 32,84%.

Méthyl-1 phényl-3 (phényl-2′ ethene-1′yl)−4 pyrrolidine ***36*** *et bis-(méthyl-1 phényl-3 pyrolidine)-4,4* ***37***

Le *N*-oxyde de triméthylamine **23** (243 mg, 3,34 mmol) et du 1,4-diphényl-1,3-butadiène (350 mg, 1,7 mmol) en solution dans 50 mL de THF traité à −78°C par le DAL (11 mmol) conduit à un mélange dont la chromatographie sur colonne AA permet de séparer:

36 (327 mg, 1,22 mmol), Rdt = 38%; uv λ_{max}: 257 nm (ϵ = 20 200), 285 nm (ϵ = 800), 294 nm (ϵ = 400); rmn: 2,4 (s, 3H), 2,5−3,2 (m, 6H), 6,3 (s élargi, 1H); 7,35 (s élargi, 11H); sm *m/e*: 263 (M^+), 57. Picrate: *F* = 130−131°C (EtOH). *Anal.* calc. pour $C_{25}H_{24}N_4O_7$: C 60,97, H 4,91, N 11,38, O 22,74; tr.: C 60.73, H 4,80, N 11,60, O 22,66%.

37 (131 mg, 0,43 mmol), Rdt = 26%; rmn: 2,1−3,2 (m, 9H), 2,4 (s, 3H), 7,25 (s élargi, 10H); sm *m/e*: 320 (M^+). Dipicrate: *F* = 240−242°C (EtOH). *Anal.* calc. pour $C_{34}H_{44}N_8O_{14}$: C 52,44, H 4,40, N 14,39, O 28,77; tr.: C 52,65, H 4,59, N 14,33, O 28,52%.

Traité par un excès de *N*-oxyde de triméthylamine **23**, la pyrrolidine **36** a conduit, quantitativement, en présence de DAL, au composé disubstitué **37**.

Méthyl-1(butène-2′yl)-3 pyrrolidine ***38*** *et bis(méthyl-1 pyrrolidine)-3 éthane-1,2* ***39***

Le *N*-oxyde de triméthylamine **23** (216 mg, 2,88 mmol) et l'hexadiène-1,5 (131 mg, 1,60 mmol) en solution dans 50 mL de THF traité à −78°C par le DAL (10,1 mmol) conduit, après chromatographie (AA) à:

38 (28 mg, 0,20 mmol), Rdt = 7%; sm *m/e*: 139 (M^+), 57.

39 (18 mg, 0,09 mmol), Rdt = 3%; rmn: 0,9−1,5 (m, 8H), 1,5−3 (m, 10H), 2,3 (s, 6H); sm *m/e*: 196 (M^+), 57.

Méthyl-1(butène-2′ yl ol-1′)-3 pyrrolidine ***40***

Le *N*-oxyde de triméthylamine **23** (245 mg, 3,26 mmol) et l'hexadiène-1,5 ol-3 (176 mg, 1,79 mmol) traités à −78°C par le DAL (16,4 mmol) conduisent à la pyrrolidine **40** (170 mg, 1,09 mmol), Rdt = 34%; ir: 3350, 1625, 920 cm^{-1}; rmn: 1−2 (m, 4H), 2−3 (m, 5H), 2,35 (s, 3H), 3,2−3,7 (m, 1H), 4,5−6,2 (m, 3H); sm *m/e*: 155 (M^+), 57.

N-*phényl-perhydro méthanoisoindole* ***41***

Le *N*-oxyde de diméthylaniline **15** (274 mg, 2 mmol) et du norbornène (198 mg, 2 mmol) en solution dans 25 mL de THF traité à −78°C par le DAL (4 mmol) pendant 30 min, conduit après chromatographie (ccm) à la pyrrolidine **41** (29 mg, 0,13 mmol), Rdt = 7%; rmn: 1−1,18 (m, 6H), 1,8−2,5 (m, 4H), 2,6−3,1 (m, 2H), 3,1−3,7 (m, 2H), 6,2−6,8 (m, 3H), 6,8−7,5 (m, 2H); sm *m/e*: 213 (M^+), 119.

1. S. OAE et K. OGINO. Heterocycles, **6**, 583 (1977); P. A. S. SMITH. *Dans* Open chain nitrogen compounds: Vol. 2. Benjamin, New York. 1966. Chap 8. p. 21.
2. L. BENADJILA-IGUERTSIRA (1980); G. NEGRON (1983). Thèses de spécialité, Université de Paris-Sud, Orsay, France.
3. R. BEUGELMANS, L. BENADJILA-IGUERTSIRA et G. ROUSSI. J. Chem. Soc. Chem. Commun. 544 (1982).
4. R. BEUGELMANS, G. NEGRON et G. ROUSSI. J. Chem. Soc. Chem. Commun. 31 (1983).
5. H. TAKAYAMA et T. NOMOTO. J. Chem. Soc. Chem. Commun. 408 (1982).
6. M. E. JUNG et R. B. BLUM. Tetrahedron Lett. 3791 (1977).
7. D. H. R. BARTON, R. BEUGELMANS et R. N. YOUNG. Nouv. J. Chim. **2**, 363 (1977).
8. Y. L. CHOW, W. C. DANEN, S. F. NELSEN et D. H. ROSENBLATT. Chem. Rev. 243 (1978).
9. A. R. LEPLEY. J. Am. Chem. Soc. **91**, 1237 (1969).
10. C. L. BUMGARDNER, H. B. HSU, F. AFGHAHI, W. L. ROBERTS et S. T. PURRINGTON. J. Org. Chem. **44**, 2348 (1979).
11. J. A. DEYRUP et W. A. SZABO. J. Org. Chem. **40**, 2048 (1975).
12. J. A. DEYRUP et G. S. KUTA. J. Org. Chem. **43**, 501 (1978).
13. R. HUISGEN. J. Org. Chem. **33**, 2291 (1968) et références citées.
14. M. S. OUALI, M. VAULTIER et R. CARRIE. Bull. Soc. Chim. Fr. 633 (1979) et références citées.
15. L. STELLA, Z. JANOUSEK, R. MERENYI et H. G. VIEHE. Angew. Chem. Int. Ed. Engl. **17**, 691 (1978).
16. L. BENADJILA-IGUERTSIRA, J. CHASTANET et G. ROUSSI. Heterocycles, **19**, 213 (1982).
17. R. HUISGEN. Angew. Chem. Int. Ed. Engl. **19**, 497 (1980); R. M. KELLOGG. Tetrahedron, Report n° 20, **32**, 2165 (1976).
18. R. LIVINGSTON. *Dans* Rodd's chemistry of carbon compounds. Vol. IV A. 2ème éd. *Edité par* S. Coffey. Elsevier, Amsterdam. 1973. p. 379.
19. J. BARLUENGA, C. NAJERA et M. YUS. J. Heterocycl. Chem. **18**, 1297 (1981).
20. R. HUISGEN. Angew. Chem. Int. Ed. Engl. **2**, 565 (1963).
21. M. VAULTIER, R. DANION-BOUGOT, D. DANION, J. HAMELIN et R. CARRIE. J. Org. Chem. **40**, 2990 (1975).
22. G. A. KRAUS et J. O. NAGY. Tetrahedron Lett. **22**, 2727 (1981).
23. T. LIVINGHOUSE et R. SMITH. J. Chem. Soc. Chem. Commun. 210 (1983).
24. K. AKIWA et M. SEKIYA. Tetrahedron Lett. **23**, 2589 (1982).
25. C. BIANCHI, C. DE MICHELI et R. GANDOLAHI. The chemistry of double bonded functional groups. Suppl. A. *Edité par* S. Patai. John Wiley and Sons, New York. 1977.
26. A. C. COPE et P. H. TOWLE. J. Am. Chem. Soc. **71**, 3423 (1949).
27. J. CYMERMAN CRAIG et K. K. PURUSHOTHAMAN. J. Org. Chem. **35**, 1721 (1970).
28. C. E. INGHAM et G. C. HAMPSON. J. Chem. Soc. 981 (1939).
29. A. J. MASON. J. Chem. Soc. **55**, 101 (1889).
30. T. HAYASHI. Sci. Papers Inst. Phys. Chem. Res. **38**, 446 (1941).
31. J. VON BRAUN et G. LEMKE. Ber. **55**, 3556 (1922).
32. A. LATTES et A. VERDIER. Bull. Soc. Chim. Fr. 2044 (1965).
33. F. BERGEL, N. C. HINDLEY, A. L. MORRISON et R. RINDERKNECHT. J. Chem. Soc. 269 (1944).
34. R. GRIOT. Helv. Chim. Acta, **42**, 67 (1959).

The Diels–Alder reaction of 4-methoxy-7-hydroxyisobenzofuran with methyl vinyl ketone; a general method for identification of some regioisomeric α-naphthols

B. A. KEAY AND R. RODRIGO[1]

Guelph–Waterloo Centre for Graduate Work in Chemistry, Department of Chemistry, University of Waterloo, Waterloo, Ont., Canada N2L 3G1

Received June 25, 1984

B. A. KEAY and R. RODRIGO. Can. J. Chem. **63**, 735 (1985).

Two regioisomeric α-naphthols **14** and **15** obtained by aromatization of the methyl vinyl ketone adducts of an unsymmetrical isobenzofuran **9** are differentiated from each other by the observation of significant upfield shifts of the *peri* proton resonances in the ^{1}H nmr spectra of their acetates **16** and **17**. Such upfield shifts of 0.3–0.6 ppm appear to be a general phenomenon and are probably due to the anisotropic effect of the acetate carbonyl group.

B. A. KEAY et R. RODRIGO. Can. J. Chem. **63**, 735 (1985).

L'aromatisation des produits de la réaction de la méthylvinylcétone avec l'isobenzofuranne non-symétrique **9** conduit aux deux α-naphtols régioisomères **14** et **15**. On peut les différencier en faisant appel à la rmn du^{1}H et aux glissements marqués vers les champs forts des résonances des protons *péri* de leurs acétates **16** et **17**. Il semble que de tels glissements de 0,3 à 0,6 ppm constituent un phénomène général et ils sont probablement dus à l'effet anisotropique du groupement carbonyle de l'acétate.

[Traduit par le journal]

In a recent publication (1) we described a short synthesis of the AB segment of daunomycinone **1** and its use in a convergent route to this anticancer antibiotic aglycone (for recent reviews, see ref. 2). Diels–Alder reaction of 4,7-dimethoxyisobenzofuran **2** (generated *in situ* (3) from the lactol **3**) with methyl vinyl ketone (MVK) provided adduct **4** which suffered reverse-Michael cleavage (4) to the enone **5**. The latter, suitably modified, was attached to the CD segment in a regiocontrolled annelation and eventually elaborated into the aglycone **1**.

In recent years a group of "second generation" anthracyclinones with reduced cardiotoxicity have been recognized. Prominent among these are aklavinone (2, 5) and some 11-deoxy analogues (2, 6) (e.g. **6**) both of which lack the C-11 hydroxyl group and thus pose an additional regiochemical challenge to the synthetic chemist attempting to assemble these molecules from constituent fragments. To adapt our procedure to a synthesis of the AB half of such compounds it is necessary to differentiate the substituents at C-4 and C-7 of **2** and to control the regiochemistry of the Diels–Alder reaction of the unsymmetrical isobenzofuran thereby resulting.

Since the phthalide **7** was available for our earlier work (1), exploratory experiments were begun with this compound. Reduction of the carbonyl group with DIBAL-H provided the lactol **8** (70% average yield) and Diels–Alder reaction of the unsymmetrical isobenzofuran **9** with MVK a mixture of regioisomeric adducts **10** and **11** in a 3.5:1 proportion by ^{1}H nmr estimation (55% total). Although some of the major isomer crystallized out from this mixture it was more convenient to subject the mixture to reverse-Michael cleavage (90%) and separate the enones **12** (major) and **13** (minor) by column chromatography. These were isolated in the same ratio and individually dehydrated with dilute hydrochloric acid to naphthols **14** and **15** respectively, whose structures must now be unambiguously assigned. This paper describes a simple, general ^{1}H nmr method for the differentiation of isomeric α-naphthols like **14** and **15**.

The spectra of **14** and **15** were very similar and unexceptional. In both compounds H-1 was a doublet, *meta* cou-

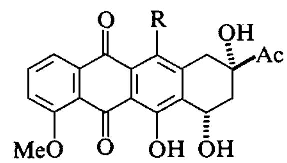

1 (R = OH)
6 (R = H)

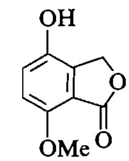

7

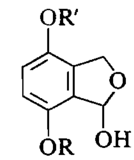

3 (R = R′ = Me)
8 (R = Me, R′ = H)

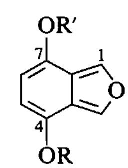

2 (R = R′ = Me)
9 (R = Me, R′ = H)

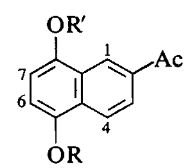

14 (R = Me, R′ = H)
15 (R = H, R′ = Me)
16 (R = Me, R′ = Ac)
17 (R = Ac, R′ = Me)

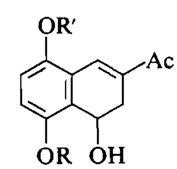

5 (R = R′ = Me)
12 (R = Me, R′ = H)
13 (R = H, R′ = Me)

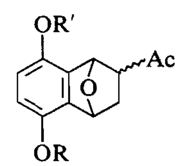

4 (R = R′ = Me)
10 (R = Me, R′ = H)
11 (R = H, R′ = Me)

pled to H-3 ($J_{1,3}$ = 1.70 and 1.76 Hz) at 8.82 ppm. Slight *para* coupling ($J_{1,4}$ = 0.71 Hz) was observed in one isomer. A well-separated AB quartet (J_{AB} = 9 Hz) was present with H-3 at 8.0 ppm and H-4 at 8.26 ppm, assignments that are secured by the *meta*-coupling observed for H-3. Slight differences in the absorptions of H-6, H-7, methoxy, and acetyl signals in the two isomers were not of any diagnostic value. Acetylation provided the α-naphthyl acetates **16** and **17**, respectively, with consequent changes in the spectra. New three-proton singlets at 2.43 and 2.50 ppm and the expected downfield shifts of the aromatic proton *ortho* to the acetate (7) by ca. 0.3–0.4 ppm, in each case, signified the presence of the acetate moiety. The

[1]Author to whom correspondence may be addressed.

changes observed in the absorptions of H-1 and H-4 were of much greater significance to the problem at hand. In one acetate the *meta*-coupled doublet (H-1) was shifted *upfield* by 0.41 ppm (8.82→8.41) while in the other one-half of the AB quartet (H-3, H-4) shifted upfield again, this time by 0.32 ppm (8.26→7.94). Assignment of this signal to H-4 was supported by the lack of *meta*-coupling observed for the H-3 half of the AB quartet ($J_{1,3}$ = 1.46 Hz). Thus a tentative assignment of structure can be made as follows for the α-naphthols and their acetates: acetate **16** is that regioisomer in which the H-1 *meta*-coupled doublet (proton *peri* to the acetate) shifts upfield by 0.41 ppm in comparison to naphthol **14**, and acetate **17** is the other isomer in which H-4 (proton *peri* to the acetate) shifts upfield by 0.32 ppm in comparison to the parent naphthol **15**. Since naphthol **14** was obtained from the major isomer of the Diels–Alder adduct mixture this establishes the structure of adducts **10** (major) and **11** (major) and enones **12** (major) and **13** (minor) as shown. These conclusions received independent support from an X-ray structure determination[2] of the major crystalline adduct **10**.

These upfield acetylation shifts of the *peri*-proton of α-naphthols were investigated in five more examples to determine whether this was a general phenomenon. In the first instance, naphthol **18** obtained by aromatization of a known (3) Diels–Alder adduct was converted to its acetate **19**. Again, one of the aromatic singlets (at 7.19 and 7.67 ppm in **18**) was shifted upfield by 0.3 ppm (7.18 and 7.37 in **19**). The obvious question of whether this signal was due to H-1 or H-4 was answered by observation of a 20% nOe enhancement of the signal at 7.19 ppm of **18** when the C-5 methyl resonance at 2.39 ppm was irradiated. A group of aryl substituted α-naphthols (8) (**20**, **22**, **24**, and **26**) was examined next. In these compounds the two aromatic protons at C-1 and C-4 are easily differentiated because H-4, subjected to the shielding influence of

TABLE 1. Chemical shifts of *peri*-protons in α-naphthols and their acetates

Compound		*peri*-Proton, H-1 (δ) ppm		
α-Naphthol	Acetate	α-Naphthol	Acetate	Δδ (ppm)
14	**16**	8.82	8.41	−0.41
15	**17**	8.26	7.94	−0.32
18	**19**	7.67	7.37	−0.30
20	**21**	7.74	7.22	−0.52
22	**23**	7.74	7.21	−0.53
24	**25**	7.74	7.21	−0.53
26	**27**	7.74	7.16	−0.58

the pendant aryl ring (not coplanar with the naphthalene), always resonates at a higher field than H-1. Thus in all these naphthols H-1 appears as singlet at 7.74 ppm and H-4 at 6.81–6.89 ppm. Upon acetylation H-1 is observed to shift upfield by 0.52–0.58 ppm while H-4 is relatively unaffected. Thus in all seven examples we have studied, a substantial upfield shift of ca. 0.3–0.6 ppm is observed in the *peri*-proton of an α-naphthol upon acetylation (Table 1).

A recent X-ray structure (9) of the α-naphthyl diacetate **28** indicates that the O—C bond of the acetate is at an angle of 82.3° to the plane of the naphthalene ring with the carbonyl double bond directed back over the ring as shown in Fig. 1. This diagram, generated[3] from data reported in that paper, shows that in the crystal of **28** the *peri*-proton lies in the shielding zone of the acetate carbonyl group and is 2.45 Å distant from the carbonyl oxygen atom. Progressively greater shielding of the *peri*-proton in a series of 1-acyl 4-methoxy naphthalenes **29** was observed (10) as the size of the group R is increased (from hydrogen to *tert*-butyl) and the suggestion made that the increasing bulkiness of the substituent forces the

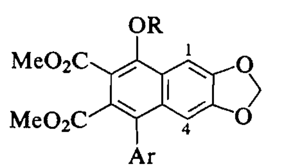

20 (R = H, Ar = 3,4,5-trimethoxyphenyl)
21 (R = Ac, Ar = 3,4,5-trimethoxyphenyl)
22 (R = H, Ar = 3,4-dimethoxyphenyl)
23 (R = Ac, Ar = 3,4-dimethoxyphenyl)
24 (R = H, Ar = 3,4-methylenedioxyphenyl)
25 (R = Ac, Ar = 3,4-methylenedioxyphenyl)

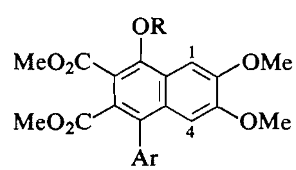

26 (R = H, Ar = 3,4-methylenedioxyphenyl)
27 (R = Ac, Ar = 3,4-methylenedioxyphenyl)

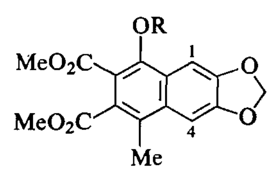

18 (R = H)
19 (R = Ac)

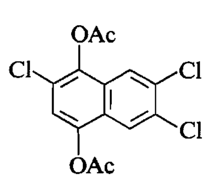

28

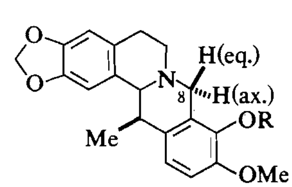

30 (R = H)
31 (R = Ac)

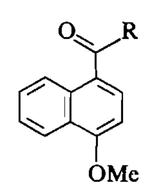

29

[2]N. J. Taylor, B. A. Keay, and R. Rodrigo. Unpublished data.
[3]This computer generated diagram was prepared by Dr. N. J. Taylor of this department from the data reported in ref. 9. We thank Dr. Taylor for his assistance.

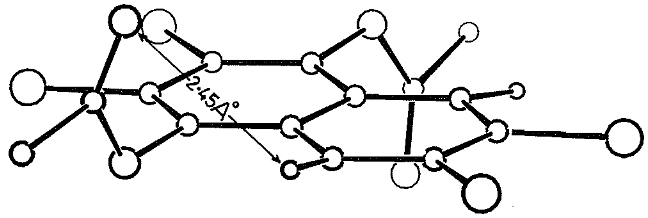

FIG. 1. The crystal structure of **28** (see footnote 3).

carbonyl group to adopt a conformation perpendicular to the plane of the naphthalene ring. This shielding effect is not confined to naphthalenes. It has been reported (11) that acetylation of the tetrahydroprotoberberine **30** causes unequal upfield shifts of the protons at C-8 of the resulting acetate **31**. The H-8 equatorial proton of this *trans*-quinolizidine (12) is shifted upfield by 0.2 ppm, while the H-8 axial proton is only slightly affected ($\Delta\delta = -0.06$ ppm) by acetylation. The inequality of the upfield shifts implies a dependence on geometry and supports the operation of an anisotropic effect. It has been convincingly demonstrated (13) that none of the simple theories of magnetic shielding provide acceptable quantitative predictions of the chemical shifts of all the protons in 1-substituted naphthalenes, but the qualitative trends described in this paper might be of value in the assignment of structures to some α-naphthols.

The 3.5:1 regioselectivity observed in the Diels–Alder reaction of **9** with MVK deserves a brief comment. Previous investigators have established that 1-substituted isobenzofurans show a preference for "*ortho*" addition with unsymmetrical dienophiles (4, 14) which depends neither on the nature of the substituent nor on the dienophile. No studies exist of the influence of substituents on the regiochemistry of the reaction when such substituents are located on the cyclohexadiene ring (i.e. C4–C7 substituted isobenzofurans) except for one example where 4-methoxyisobenzofuran provided a 1:1 mixture of adducts with a quinone (15). The present example of differential substitution on this ring (the Diels–Alder reaction of **9** with MVK), and the regioselectivity observed therein, suggests that this may well be a fruitful area for further exploration. It is possible that the formation of the major adduct **10** is favoured by hydrogen bonding between the 7-hydroxy group of **8** and the carbonyl group of the dienophile in the *endo* transition state of the reaction. We are engaged in the preparation of 4- and 5-hydroxy and methoxy isobenzofurans and in the study of the Diels–Alder reactions of these dienes with unsymmetrical dienophiles. A meaningful discussion of the problem as well as further progress towards the 11-deoxy anthracyclinones will have to await the outcome of such work.

Experimental

Melting points were determined on a Buchi model SMP-20 apparatus and are uncorrected. Elemental analyses were performed by the Guelph Chemical Laboratories, Guelph, Ontario. Proton magnetic resonance spectra were determined, unless otherwise stated, in deuteriochloroform on a BrukerWP-80 spectrometer. Coupling constants were measured directly and confirmed by decoupling where necessary. Spectra are reported in the following manner: chemical shift (δ) in ppm (multiplicity, number of protons, assignment, coupling constants in Hz). Infrared spectra were obtained on a Beckmann model IR 10 or Acculab 10 spectrophotometer in the manner specified in each case. Mass spectra were determined on a Varian VG 7070F instrument and are reported as follows: ion (relative intensity, assignment). Column chromatography was performed with silica gel (Merck, 0.063–0.20 mm, 70–230 mesh ASTM) in the specified solvent system.

4-Methoxy-1,3-dihydroisobenzofuran-3,7-diol 8

The phthalide **7** (ref. 1) (0.25 g) dissolved in dry methylene chloride (20 mL) was cooled to −60°C and diisobutyl aluminum hydride (3.5 mL of 25% solution in toluene) added. After stirring for 70 min, aqueous sodium hydroxide (7 mL, 10%) was added and the solution allowed to warm to room temperature. The methylene chloride was removed, water added, and carbon dioxide bubbled through until the solution was neutral. The aqueous mixture was extracted with ethyl acetate (3 × 10 mL). The extracts were dried (Na_2SO_4) and the solvent removed *in vacuo* at room temperature. The residue was crystallized from chloroform (175 mg, 70%), mp 113°C (dec.); ir (KBr): 3250 (br) cm^{-1}; ^1H nmr (acetone-d_6): 3.76 (s, 3H, OMe), 4.81 (d, 1H, J_{gem} = 12.9, >C*H*—O), 5.09 (dd, 1H, J_{gem} = 12.9, $J_{1,3}$ *trans* = 2.15, CH—O), 5.31 (d, 1H, J = 7.8 disappears with D_2O, OH), 6.42 (dd, 1H, $J_{H,OH}$ = 7.8, >$J_{1,3}$ = 2.15, collapses to doublet with D_2O), 6.73 (s, 2H, H-5 and H-6), 8.0 (s, 1H, phenolic H, disappears with D_2O); ms: 182 (100, $M^{\cdot+}$), 165 (75, $M^{\cdot+}$ − OH), 164 (68, $M^{\cdot+}$ − H_2O). *Anal.* calcd. for $C_9H_{10}O_4$: C 59.34, H 5.53; found: C 60.01, H 5.73.[4]

2-endo-*Acetyl-5methoxy-8-hydroxy-1,4-epoxy-1,2,3,4-tetrahydronaphthalene 10*

The hydroxyphthalan **8** (240 mg) in carbon tetrachloride (8 mL) was refluxed for 19 h with glacial acetic acid (0.5 mL) and methyl vinyl ketone (0.82 mL). Aqueous sodium bicarbonate was added to neutralize the acid and the organic phase separated, dried (Na_2SO_4), and the solvent removed. A ^1H nmr spectrum of the residual oil showed the presence of the two regioisomers **10** and **11** in the ratio of ca. 3.5:1 and a third compound identified as 4-carbomethoxy-2-butanone (2.0 (s, 3H), 2.2 (s, 3H), 2.78 (t, 2H), and 4.35 (t, 2H)) resulting from Michael addition of acetic acid to methyl vinyl ketone. The ratio of **10** to **11** in this mixture was estimated by comparison of the two proton aromatic singlets and methoxy singlets of **10** (at 6.62 and 3.78 ppm) and **11** (at 6.55 and 3.72 ppm). Column chromatography of the crude mixture (ethyl acetate − ligroin, 5:6) and removal of the solvents provided an oil (55% yield) whose ^1H nmr spectrum indicated the presence of **10** and **11** in the same ratio. Other absorptions of the minor regiosomer **11** were clearly discernible in this spectrum but were not separated sufficiently from the corresponding absorptions of **10** to be used for reliable ^1H nmr estimation of the ratio. Crystals formed upon addition of benzene to the mixture (**10**/**11**) were separated, subjected to X-ray analysis, and found to be the *endo*-isomer of **10**.

10 (*endo*-isomer); mp 153–155°C; ir (KBr): 3300, 1710 cm^{-1}; ^1H nmr: 1.67 (dd, 1H, H-3α, J_{gem} = 11.4, $J_{2,3\alpha}$ = 4.82), 2.11 (s, 3H, $COCH_3$), 2.48 (ddd, 1H H-3β, J_{gem} = 11.4, $J_{3\beta,4}$ = 3.5, $J_{2,3\beta}$ = 12.04), 3.42 (ddd, 1H, H-2, $J_{1,2}$ = 3.9, $J_{2,3\beta}$ = 12.04, $J_{2,3\alpha}$ = 4.82), 3.78 (s, 3H, OMe), 5.58 (d, 1H, H-4, $J_{3\beta,4}$ = 3.5), 5.63 (d, 1H, H-1, $J_{1,2}$ = 3.9), 5.72 (s, 1H, OH, disappears with D_2O), 6.62 (s, 2H, H-6 and H-7); ms: 234 (17, $M^{\cdot+}$), 164 (100, $M^{\cdot+}$ − $CH_3COCH{=}CH_2$ retro Diels–Alder). *Anal.* calcd. for $C_{13}H_{14}O_4$: C 66.66, H 6.02; found: C 66.43, H 5.93.

2-Acetyl-4,8-dihydroxy-5-methoxy-3,4-dihydronaphthalene 12 and 2-acetyl-4,5-dihydroxy-8-methoxy-3,4-dihydronaphthalene 13

The mixture of adducts **10** and **11** (600 mg) was suspended in dry methanol (10 mL) under a nitrogen atmosphere and cooled to 0°C. Sodium methoxide (0.5 g sodium in 10 mL of absolute methanol) was added slowly over 20 min. The solution was warmed to room temperature and stirred for 4 h. Water was added and carbon dioxide bubbled through until neutral to litmus. The solution was poured into saturated brine (100 mL) and extracted into chloroform (5 × 20 mL). The extracts were dried (Na_2SO_4) and the solvent removed *in vacuo* to leave a solid (90%) which was chromatographed on a column of silica gel in ethyl acetate − ligroin (8:2) and the two regioisomers of

[4]The somewhat high result obtained for carbon may be due to the dehydration of some of the lactol during combustion. Its physical and chemical properties are consistent with several similar compounds prepared and studied earlier (ref. 3).

12 and **13** obtained[5] in the ratio of ca. 3.5:1.

12; R_f 0.2; mp 116–117°C (ether); ir (KBr): 3500, 3310 (br), 1640, 1620 cm^{-1}; ^{1}H nmr (acetone-d_6): 2–2.4 (m, 1H, H-3β), 2.40 (s, 3H, $COCH_3$), 3.16 (dd, 1H, H-3α, J_{gem} = 18.2, $J_{3\alpha,4}$ = 2.0), 3.55 (d, 1H, C4-OH, J = 8.0, disappears with D_2O), 3.80 (s, 3H, OMe), 5.20 (dd, after D_2O, 1H, H-4, $J_{3\alpha,4}$ = 2.0, $J_{3\beta,4}$ = 6.6), 6.87, 6.94 (AB q, 2H, H-6 and H-7, $J_{6,7}$ = 8.7), 7.92 (d, 1H, H-1, $J_{1,3\beta}$ = 2.7), 8.40 (br s, 1H, C8-OH, disappears with D_2O); ms: 234 (0.5, $M^{\cdot+}$), 216 (100, $M^{\cdot+}$ – H_2O), 201 (84, $M^{\cdot+}$ – H_2O – CH_3). *Mol. Wt.* (hrms) (base peak mass-matched), calcd. for $C_{13}H_{12}O_3$: 216.0786; found: 216.0797.

13; R_f 0.3; mp 199–200°C (methylene chloride); ir (KBr): 3200 (br), 1640, 1615 cm^{-1}; ^{1}H nmr: 2.46 (s, 3H, $COCH_3$), 2.55 (ddd, 1H, H-3β, J_{gem} = 16.6, $J_{3\beta,4}$ = 11.1, $J_{1,3\beta}$ = 2.15), 3.11 (dd, 1H, H-3α, J_{gem} = 16.6, $J_{3\alpha,4}$ = 6.64), 3.84 (s, 3H, OMe), 5.38 (dd, 1H, H-4, after D_2O), 6.78, 6.91 (AB q, H-6 and H-7, $J_{6,7}$ = 9.0), 7.81 (d, 1H, H-1, $J_{1,3\beta}$ = 2.15), 7.92 (br s, 2H, 2 × OH, exchanges with D_2O); ms: 234 (2, $M^{\cdot+}$)0, 216 (100, $M^{\cdot+}$ – H_2O), 201 (78, $M^{\cdot+}$ – H_2O – CH_3). *Mol. Wt.* (hrms) (base peak mass-matched), calcd. for $C_{13}H_{12}O_3$: 216.0786; found: 216.0789.

2-Acetyl-5-methoxy-8-hydroxynaphthalene ***14***

The enone **12** (25 mg) dissolved in chloroform was stirred vigorously with aqueous 2 *N* hydrochloric acid (5 mL) for 4 h. The chloroform layer was separated, washed with water, dried (Na_2SO_4), and the solvent removed. The residual solid was crystallized from ether (85%); mp 155–157°C; ir (KBr): 3310 (br) 1660 cm^{-1}; ^{1}H nmr: 2.75 (s, 3H, $COCH_3$), 3.95 (s, 3H, OMe), 6.79 (s, 2H, H-6 and H-7), 8.0 (dd, 1H, H-3, $J_{3,4}$ = 9.0, $J_{1,3}$ = 1.76), 8.26 (dd, 1H, H-4, $J_{3,4}$ = 9.0, $J_{1,4}$ = 0.71), 8.82 (dd, 1H, H-1, $J_{1,3}$ = 1.76, $J_{1,4}$ = 0.71); ms: 216 (64, $M^{\cdot+}$), 201 (45, $M^{\cdot+}$ – CH_3). *Mol. Wt.* (hrms) calcd. for $C_{13}H_{12}O_3$: 216.0786; found: 216.0782.

2-Acetyl-5-hydroxy-8-methoxynaphthalene ***15***

The enone **13** (25 mg) treated with 2 *N* HCl as above provided the naphthalene **15** which was crystallized from chloroform (85%); mp 195–197°C; ir (KBr): 3200 cm^{-1} (br), 1645 cm^{-1}; ^{1}H nmr (acetone-d_6): 2.71 (s, 3H, $COCH_3$), 4.0 (s, 3H, OMe), 6.84, 7.03 (AB q, 2H, H-6 and H-7, $J_{6,7}$ = 8.06), 8.0 (dd, 1H, H-3, $J_{3,4}$ = 9.0, $J_{1,3}$ = 1.7), 8.26 (d, 1H, H-4, $J_{3,4}$ = 9.0), 8.82 (d, 1H, H-1, $J_{1,3}$ = 1.7); ms: 216 (100, $M^{\cdot+}$), 201 (84 $M^{\cdot+}$ – CH_3). *Mol. Wt.* (hrms) calcd. for $C_{13}H_{12}O_3$: 216.0786; found: 216.0791.

2,3-Methylenedioxy-5-methyl-6,7-dicarbomethoxy-8-hydroxynaphthalene ***18***

The dimethyl acetylene dicarboxylate adduct of 1-methyl-5,6-methylenedioxyisobenzofuran (3) (0.21 g) was refluxed in benzene (15 mL) with a few crystals of *p*-toluene sulfonic acid for 12 h. The benzene solution was washed with dilute aqueous ammonia and the naphthol **18** extracted into aqueous sodium hydroxide. The alkaline extracts were combined, acidified with dilute hydrochloric acid, and extracted into methylene chloride. The organic extracts were washed with water, dried (Na_2SO_4), and the methylene chloride removed. The residual solid was crystallized from ethanol (43%); mp 185–186°C; ^{1}H nmr: 2.4 (s, 3H, CH_3), 3.9 (s, 6H, 2 × CO_2Me), 6.08 (s, 2H, OCH_2O), 7.19 (s, 1H, H-4), 7.67 (s, 1H, H-1), 12.0 (s, 1H, OH); ms: 318 ($M^{\cdot+}$) 287 ($M^{\cdot+}$ – OMe). *Mol. Wt.* (hrms) calcd. for $C_{16}H_{14}O_7$: 318.0739; found: 318.0713.

General procedure for the preparation of α-naphthyl acetates

The naphthol dissolved in dry methylene chloride was treated with excess acetic anhydride and dimethylamino pyridine (1.5 equiv.) and stirred at room temperature for 4 h. Water was added and stirring continued for a further 12 h. The organic phase was separated, washed with aqueous sodium bicarbonate and water, the methylene chloride layer dried (Na_2SO_4), and the solvent removed. Yields varied from 65–90%.

16; mp 119–121°C (methylene chloride); ^{1}H nmr: 2.50 (s, 3H, $OCOCH_3$), 2.77 (s, 3H, $COCH_3$), 4.06 (s, 3H, OCH_3), 6.90 and 7.23 (AB q, 2H, H-6 and H-7, $J_{6,7}$ = 8.3), 8.04 (dd, 1H, H-3, $J_{3,4}$ = 8.8, $J_{1,3}$ = 1.71), 8.34 (d, 1H, H-4, $J_{3,4}$ = 8.8), 8.41 (d, 1H, H-1, $J_{1,3}$ = 1.71); ms: 258 (10, $M^{\cdot+}$), 216 (100, $M^{\cdot+}$ – CH_2CO), 201 (46, $M^{\cdot+}$ – CH_2CO – CH_3).

17; mp 151–152°C (methylene chloride); ^{1}H nmr (acetone-d_6): 2.43 (s, 3H, $OCOCH_3$), 2.74 (s, 3H, $COCH_3$), 4.10 (s, 3H, OCH_3), 7.03 and 7.35 (AB q, 2H, H-6 and H-7, $J_{6,7}$ = 8.3), 7.94 (d, 1H, H-4, $J_{3,4}$ = 9.03), 8.09 (dd, 1H, H-3, $J_{3,4}$ = 9.03, $J_{1,3}$ = 1.46), 8.9 (d, 1H, H-1, $J_{1,3}$ = 1.46); ms: 258 (23, $M^{\cdot+}$), 216 (100, $M^{\cdot+}$ – CH_2O), 201 (89, $M^{\cdot+}$ – CH_2CO – CH_3).

19; mp 165°C (methylene chloride); ^{1}H nmr: 2.4 (3H, CH_3), 2.6 (s, 3H, $OCOCH_3$), 3.88 and 3.92 (s, 3H each, 2 × CO_2Me), 6.12 (s, 2H, OCH_2O), 7.18 (s, 1H, H-4), 7.37 (s, 1H, H-1); ms: 360 (6, $M^{\cdot+}$) 318 (56, $M^{\cdot+}$ – CH_2CO), 2.86 (100, $M^{\cdot+}$ – CH_2CO – MeOH).

21; mp 180–181°C (methylene chloride – ethyl acetate); ^{1}H nmr: 7.22 (s, 1H, H-1), 6.94 (s, 1H, H-4); ms: 512 (23, $M^{\cdot+}$), 470 (63, $M^{\cdot+}$ – CH_2CO).

23; mp 216–217°C (methylene chloride); ^{1}H nmr: 7.21 (s, 1H, H-1), 6.92 (s, 1H, H-4); ms: 482 (17, $M^{\cdot+}$), 440 (61, $M^{\cdot+}$ – CH_2CO).

25; mp 213–214°C (methylene chloride – ethyl acetate); ^{1}H nmr: 7.21 (s, 1H, H-1), 6.90 (s, 1H, H-4); ms: 466 (13, $M^{\cdot+}$), 424 (50, $M^{\cdot+}$ – CH_2CO).

27; mp 184–185°C (methylene chloride – ethyl acetate); ^{1}H nmr: 7.16 (s, 1H, H-1), 6.89 (s, 1H, H-4); ms: 482 (13, $M^{\cdot+}$), 440 (52, $M^{\cdot+}$ – CH_2CO).

Acknowledgement

We thank the Natural Sciences and Engineering Research Council of Canada for support of this work.

1. B. A. KEAY and R. RODRIGO. Can. J. Chem. **61**, 637 (1983); Tetrahedron, **40**, 4597 (1984).
2. F. ARCAMONE. Doxorubicin anticancer antibiotics. Medicinal chemistry. Vol. 17. Academic Press, New York. 1981; H. S. EL KHADEM (*Editor*). Anthracycline antibiotics. Academic Press, New York. 1982.
3. B. A. KEAY, H. P. PLAUMANN, D. RAJAPAKSA, and R. RODRIGO. Can. J. Chem. **61**, 1987 (1983).
4. B. A. KEAY, D. RAJAPAKSA, and R. RODRIGO. Can. J. Chem. **62**, 1093 (1984).
5. J. M. MCNAMARA and Y. KISHI. J. Am. Chem. Soc. **104**, 7371 (1982).
6. J-P. GESSON and M. MONDON. J. Chem. Soc. Chem. Commun. 421 (1982); M. SEKIZAKI, M. JUNG, J. M. MCNAMARA, and Y. KISHI. J. Am. Chem. Soc. **104**, 7372 (1982).
7. R. J. HIGHET and P. F. HIGHET. J. Org. Chem. **30**, 902 (1965).
8. H. P. PLAUMANN, J. G. SMITH, and R. RODRIGO. J. Chem. Soc. Chem. Commun. 354 (1980).
9. J. G. RODRIGUEZ, J. VILCHES, P. SMITH-VERDIER, and S. GARCIA-BLANCO. Tetrahedron, **39**, 199 (1983).
10. W. B. SMITH, D. L. DEAVENPORT, and A. M. IHRIG. J. Am. Chem. Soc. **94**, 1959 (1972).
11. R. H. F. MANSKE, R. RODRIGO, D. B. MACLEAN, and L. BACZYNSKJ. Quimica, **68**, 689 (1972).
12. C. K. YU, D. B. MACLEAN, R. RODRIGO, and R. H. F. MANSKE. Can. J. Chem. **48**, 3673 (1970).
13. J. W. EMSLEY, J. C. LINDON, S. R. SALMAN, and D. T. CLARK. J. Chem. Soc. Perkin Trans. 2, 611 (1973).
14. M. AM. MAKHLOUF and B. RICKBORN. J. Org. Chem. **46**, 2734 (1981); R. N. WARRENER, B. C. HAMER, and R. A. RUSSELL. J. Chem. Soc. Chem. Commun. 942 (1981); L. CONTRERAS and D. B. MACLEAN. Can. J. Chem. **58**, 2573 (1980); J. G. SMITH, S. S. WELANKIWAR, B. S. SHANTZ, E. H. LAI, and N. G. CHU. J. Org. Chem. **45**, 1817 (1980).
15. A. S. KENDE, D. P. CURRAN, Y. G. TSAY, and J. E. MILLS. Tetrahedron Lett. 3537 (1977).

[5]It is unlikely that the reverse-Michael reaction of the **10/11** mixture is responsible for the 3.5:1 ratio observed. An overall yield of 90% was obtained in this step and no selectivity or rearrangements had been encountered in a previous study of this reaction (ref. 4).

Conformation of methyl 3,6-dideoxy-α-D-*arabino*-hexopyranoside, the immunodominant sugar of *Salmonella* serogroup D_1: crystal structure, ^1H nmr analysis, and semi-empirical calculations[1]

GEORGE I. BIRNBAUM AND DAVID R. BUNDLE

Division of Biological Sciences, National Research Council of Canada, Ottawa, Ont., Canada K1A 0R6

Received June 25, 1984

GEORGE I. BIRNBAUM and DAVID R. BUNDLE. Can. J. Chem. **63**, 739 (1985).

Methyl 3,6-dideoxy-α-D-*arabino*-hexopyranoside (methyl tyveloside) crystallizes in the orthorhombic space group $P2_12_12_1$ and the cell dimensions are a = 7.478(1), b = 7.933(1), c = 14.064(1) Å. X-ray intensity data were measured with a diffractometer and the structure was solved by direct methods. Least-squares refinement, which included all hydrogen atoms, converged at R = 0.038. The pyranose ring exists as an almost perfect $^4C_1$ chair and the conformation adopted by the glycosidic methyl group is in agreement with the requirements of the *exo*-anomeric effect. Both acetal oxygen atoms act as hydrogen-bond acceptors, and the H···O bond distances are in agreement with this feature. The ^1H nmr spectrum shows that the conformation of the pyranose ring in aqueous solution is indistinguishable from that in the crystal. The minimum energy conformation of a pentasaccharide fragment of a *Salmonella* O-antigen, calculated with tyvelose coordinates obtained by bond modification, is in good agreement with the conformation which was calculated with tyvelose coordinates obtained from the X-ray analysis.

GEORGE I. BIRNBAUM et DAVID R. BUNDLE. Can. J. Chem. **63**, 739 (1985).

Le didésoxy-3,6 α-D-*arabino*-hexopyrannoside de méthyle (tyveloside de méthyle) cristallise sous forme orthorhombique, groupe d'espace $P2_12_12_1$ avec a = 7,478(1), b = 7,933(1) et c = 14,064(1) Å. On a mesuré les intensités à l'aide d'un diffractomètre et on a résolu la structure par des méthodes directes. L'affinement par la méthode des moindres carrés, que inclut tous les atomes d'hydrogènes, converge vers une valeur de R = 0,038. Le cycle pyrannose existe sous la forme d'une chaise $^4C_1$ qui est presque parfaite et la conformation du groupement méthyle glycosidique est en accord avec ce qui est prévu sur la base des exigences de l'effet anomère *exo*. Les deux atomes d'oxygène de l'acétal agissent comme accepteurs de liaisons hydrogènes; les distances H···O sont en accord avec cette caractéristique. Le spectre rmn ^1H démontre que, en solution dans l'eau, la conformation du cycle pyrannose ne peut pas être distinguée de celle qui existe dans le cristal. La conformation d'un pentasaccharide qui est un fragment d'un O-antigène de la *Salmonella* fut calculé à l'aide de coordonnées du tyvelose obtenues par la modification de liaisons. Cette conformation, représentant une énergie minimale, est en bon accord avec la conformation calculée en utilisant les coordonnées du tyvelose obtenues à l'aide de la diffraction des rayons-X.

[Traduit par le journal]

Introduction

The 3,6-dideoxyhexoses are naturally occurring sugars found in the lipopolysaccharides (LPS) of Gram-negative bacterial cell walls (1). In these structures they play a major role as immunodominant sugars (2). This implies that one bacterial species may be distinguished from another possessing a lipopolysaccharide structurally identical in all respects except for the presence of an isomeric but chirally unique 3,6-dideoxyhexose (1). Three isomers exist in the D-series and these differ from each other by the configuration of the hydroxyl groups at carbon atoms C(2) or C(4) (3). The presence of these 3,6-dideoxyhexoses in otherwise identical *Salmonella* LPSs distinguishes, and serologically defines, the A, B, and D_1 serogroups (1, 2). This differentiation is achieved by antibody molecules, the combining sites of which must be capable of recognising the fine stereochemical differences of 3,6-dideoxy-*arabino*-, *xylo*-, and *ribo*-hexopyranosides (4). In order to further understanding of such fine specificity it is desirable to build reliable models which accurately describe the topography of these important antigens. Molecular modelling of related lipopolysaccharides has been carried out for *Shigella flexneri* (5) but, in order to extend the approach to *Salmonella* LPS, reliable X-ray data for the constituent monosaccharides are desirable. Accurate atomic coordinates for galactopyranose (6), mannopyranose (7), and rhamnopyranose (8) have been available but until recently no experimental data for the 3,6-dideoxyhexoses were reported.

We reported the first such X-ray structure for methyl 3,6-dideoxy-β-D-*ribo*-hexopyranoside (9), but this structure differed from the naturally occurring 3,6-dideoxyhexosides which possess the α-D or α-L configuration. In this paper we report the crystal structure of methyl 3,6-dideoxy-α-D-*arabino*-hexopyranoside (methyl tyveloside) and we use the coordinates obtained from it to calculate the conformation of an oligosaccharide by the HSEA method (10). We compare this conformation with that derived with tyvelose coordinates generated by bond modification of D-mannopyranose. This procedure has been employed when X-ray data for a specific sugar are unavailable, and in such cases closely related monosaccharides for which X-ray structures have been determined are used to construct a set of calculated atomic coordinates (11).

Results and discussion

Molecular dimensions

The final atomic parameters are listed in Table 1. The C—C bond lengths (Fig. 1) in the pyranose ring range from 1.517(2) to 1.530(2) Å. These distances as well as differences of up to ~0.01 Å are characteristic for C—C bonds in pyranose rings. The shorter C(5)—C(6) bond can be ascribed to the relatively larger thermal motion of the methyl group. It is interesting to compare the bond lengths in the sequence C(5)—O(5)—C(1)—O(1)—C(7) with values obtained from X-ray analyses of other methyl α-pyranosides and from *ab initio* molecular orbital calculations (12). The C(5)—O(5) bond in the present structure is 0.012 Å (8σ) longer than the experimental mean derived from eight other molecules. However, in manno- and altropyranoside, in which the 2-OH and 4-OH are axial and equatorial, respectively, as in the present structure, the

[1]Issued as NRCC No. 23669.

TABLE 1. Final atomic parameters and their standard deviations[a]

Atom	x	y	z	B_{eq}/B
C(1)	64637(17)	49546(18)	45340(9)	2.3
O(1)	58288(15)	34156(13)	41744(8)	2.7
C(2)	51238(18)	63185(19)	42808(11)	2.8
O(2)	57055(21)	78071(18)	47619(12)	4.5
C(3)	51009(18)	66064(20)	32052(12)	2.9
C(4)	69885(18)	69427(18)	28446(9)	2.4
O(4)	70801(19)	69916(22)	18346(9)	4.0
C(5)	82488(17)	55344(16)	31500(8)	2.1
O(5)	81866(12)	53371(12)	41724(6)	2.2
C(6)	101771(20)	58742(27)	29001(13)	3.5
C(7)	68069(30)	19812(21)	44967(14)	3.8
H(1)	669(3)	483(3)	517(2)	2.9(4)
H(2)	402(4)	593(4)	447(2)	3.9(5)
H(O2)	482(6)	822(6)	505(3)	5.7(7)
H(3e)	440(5)	754(5)	305(2)	4.6(6)
H(3a)	466(4)	563(4)	289(2)	3.7(5)
H(4)	743(3)	799(3)	306(2)	2.4(3)
H(O4)	621(6)	749(6)	159(3)	5.8(8)
H(5)	789(3)	455(3)	285(2)	2.3(3)
H(61)	1091(6)	507(5)	313(3)	5.7(7)
H(62)	1045(5)	680(5)	316(3)	5.1(7)
H(63)	1042(6)	598(6)	225(3)	6.1(8)
H(71)	622(7)	111(7)	424(4)	6.6(9)
H(72)	677(7)	192(7)	514(3)	6.3(9)
H(73)	795(6)	214(6)	429(3)	5.7(7)

[a]The coordinates of nonhydrogen atoms were multiplied by 10^5, those of the hydrogen atoms by 10^3.

C(5)—O(5) bond lengths are 1.450 and 1.440 Å, respectively, and thus closer to the value we observed. Furthermore, our value of 1.447 Å is in excellent agreement with the theoretical value of 1.444 Å (12). The other three bond lengths in the acetal group are within 2σ of the mean values from previous experiments (1.416, 1.404, 1.430 Å).

The average bond angles in pyranose rings have been found to be 110.2° at C atoms and 113.4° at the O atom (13). In the present structure (Fig. 1) the angles at O(5) and C(1) are significantly larger than these averages. In the acetal group, the O(5)—C(1)—O(1) angle is 0.9° (9σ) smaller than the reported average (13), while C(1)—O(1)—C(7) is larger than previously reported values from X-ray analyses (113.0–113.5°). The bond angles at C(5) are in excellent agreement with the angles in methyl paratoside in which there is also an equatorial methyl group in that position (9). On the other hand, the angles involving the exocyclic -OH groups vary greatly from structure to structure, presumably in order to optimize the geometry of the hydrogen bonds in which they are involved.

Molecular conformation

The conformation of the molecule is shown in Figs. 2 and 3. The pyranose ring can be described by the Cremer and Pople (14) puckering parameters: $\theta = 0.9$, $\phi = 270.5°$, $Q = 0.559$. The low value of θ indicates that the ring is an almost perfect $^4C_1$ (D) chair. The substituents at C(1) and C(2) are axial while those at C(4) and C(5) are equatorial. The endocyclic torsion angles (Fig. 1) show the usual approximate mirror plane normal to the mean plane of the ring and passing through O(5) and C(3). Also as usual, the ring is most puckered at O(5) and least at C(3). The differences between mirror-related torsion angles are all <1°; in methyl paratoside these differences ranged up to 8.5° (9). The range of the absolute values of the torsion angles (53.1–59.0°) is relatively small. This is in line with the recent

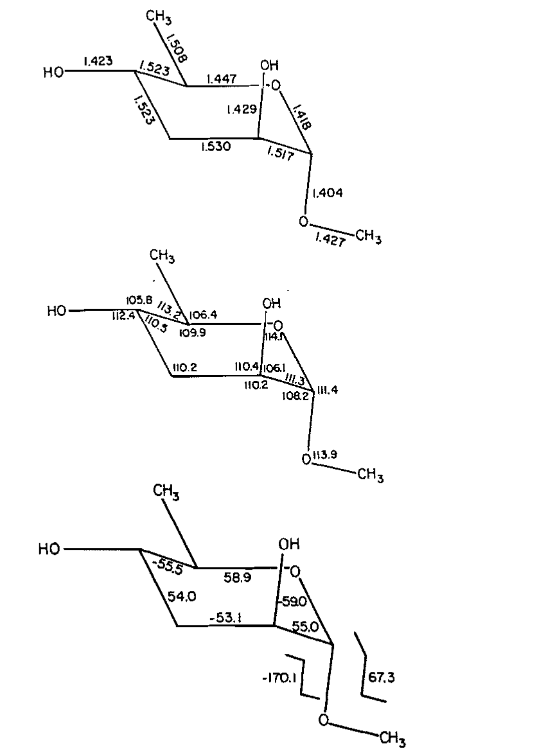

FIG. 1. Molecular geometry; (top) bond lengths, esd's are 0.0014–0.0023 Å; (center) bond angles, esd's are 0.09–0.13°; (bottom) endocyclic torsion angles, esd's are 0.13–0.15°.

observation by Jeffrey and Taylor (15) that the mean range is smaller (53.3–60.3°) in methyl pyranosides with an axial anomeric group and larger (52.7–64.2°) in those with an equatorial anomeric group.

The conformation of the exocyclic methoxy group is consistent with the *exo*-anomeric effect (16), i.e. C(7)—O(1) is *gauche* with respect to C(1)—O(5) and *trans* with respect to C(1)—C(2). The anomeric torsion angle (O(5)—C(1)—O(1)—C(7)) is 67.3°, in excellent agreement with the value (67.0°) obtained from molecular mechanics calculations for 2-methoxytetrahydropyran with an axial methoxy group (15). The experimentally observed values in methyl pyranosides range from 60.5 to 70.5°.

In view of the preceding discussion, one can conclude that the absence of an -OH group at C(3) does not give rise to any distortion of the molecule.

Hydrogen bonding and packing

Both hydroxyl groups donate their protons to symmetry related molecules and in each case an acetal oxygen acts as an acceptor. This is one of the hydrogen-bonding schemes (type II) observed in methyl pyranosides and recently described by Jeffrey and Mitra (17). Both the absence of the "cooperative effect" (···O—H···) and the involvement of chain stoppers as acceptors are expected to result in relatively weaker hydrogen bonds, with H···O distances of ~1.86 Å. Table 2 shows the geometry of the hydrogen bonds in the present structure. The corrected H···O distances were obtained by making the covalent O—H bonds 0.97 Å long, the mean neutron diffraction value. These distances show the hydrogen bonds to have the expected strength. The packing of the molecules is shown in Fig. 4. Each molecule is hydrogen-bonded to four adjacent ones. All other contacts are longer than the sums of van der Waals radii.

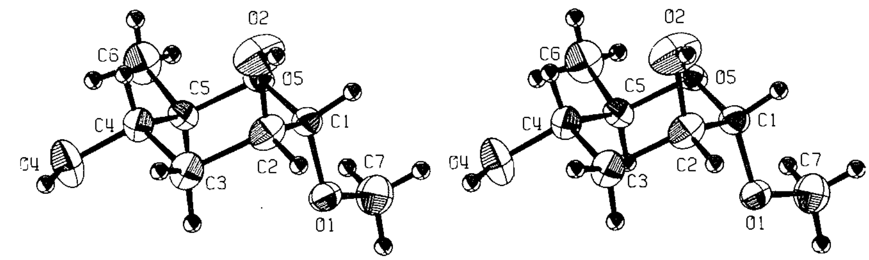

FIG. 2. Stereoscopic view of methyl tyveloside; the ellipsoids include 50% probability.

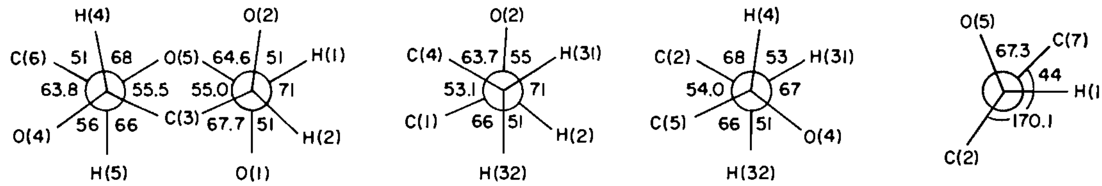

FIG. 3. Newman projections along C(4)—C(5), C(1)—C(2), C(2)—C(3), C(3)—C(4), and C(1)—O(1).

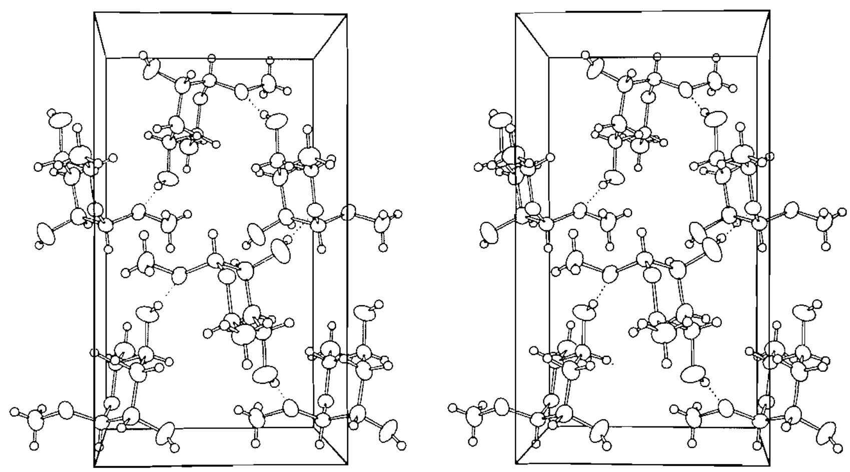

FIG. 4. Stereoscopic view along *a* of the molecular packing in the crystal.

TABLE 2. Geometry of hydrogen bonds

Bonds			Distances, Å			Angles, deg
D	*A*	*A* at	O···O	H···O	H···O$_{corr}$	O—H···O
O(2)—H	···O(5)	$-1/2 + x, 3/2 - y, 1 - z$	2.822	2.00	1.88	165
O(4)—H	···O(1)	$1 - x, 1/2 + y, 1/2 - z$	2.832	2.00	1.87	171

Nuclear magnetic resonance analysis

Proton nmr provides coupling constant data for methyl tyveloside which, via the Karplus equation (18), permits the solution conformation to be compared with that in the crystal. Since little variation was anticipated between the conformations in solution and in the solid state and none was found, it was of interest to correlate recent treatments of the Karplus equation. Altona and Haasnoot presented a simple additivity rule for pyranose rings which permits the coupling constants of the $^4C_1$ or $^1C_4$ chair conformations to be predicted to within ±0.6 Hz in the majority of cases (19). A second paper by Haasnoot *et al.* presented a quantitative analysis of the Karplus equation and an empirical generalization was presented (20). Both approaches were used here to calculate the ^3J coupling constants of methyl tyveloside on the assumption that the solution conformation was indistinguishable from that determined by the X-ray analysis. These coupling constants are presented in Table 3 together with the chemical shifts and coupling constants observed for methyl tyveloside in deuterium oxide solution.

The ^{1}H nmr spectrum was recorded at 500 MHz and spin-decoupling experiments confirmed the assignments. Later a two-dimensional homonuclear shift-correlated (COSY-90) experiment was performed. This not only confirmed the assignment of chemical shifts but also indicated a fairly extensive network of ^4J coupling constants. Inspection of a resolution-enhanced spectrum showed these to be ≤1.0 Hz in all cases. In order to properly assess the effect of these additional coupling constants, overlaid upon an already complex multiplicity resulting from the presence of two deoxy centres in the sugar, an

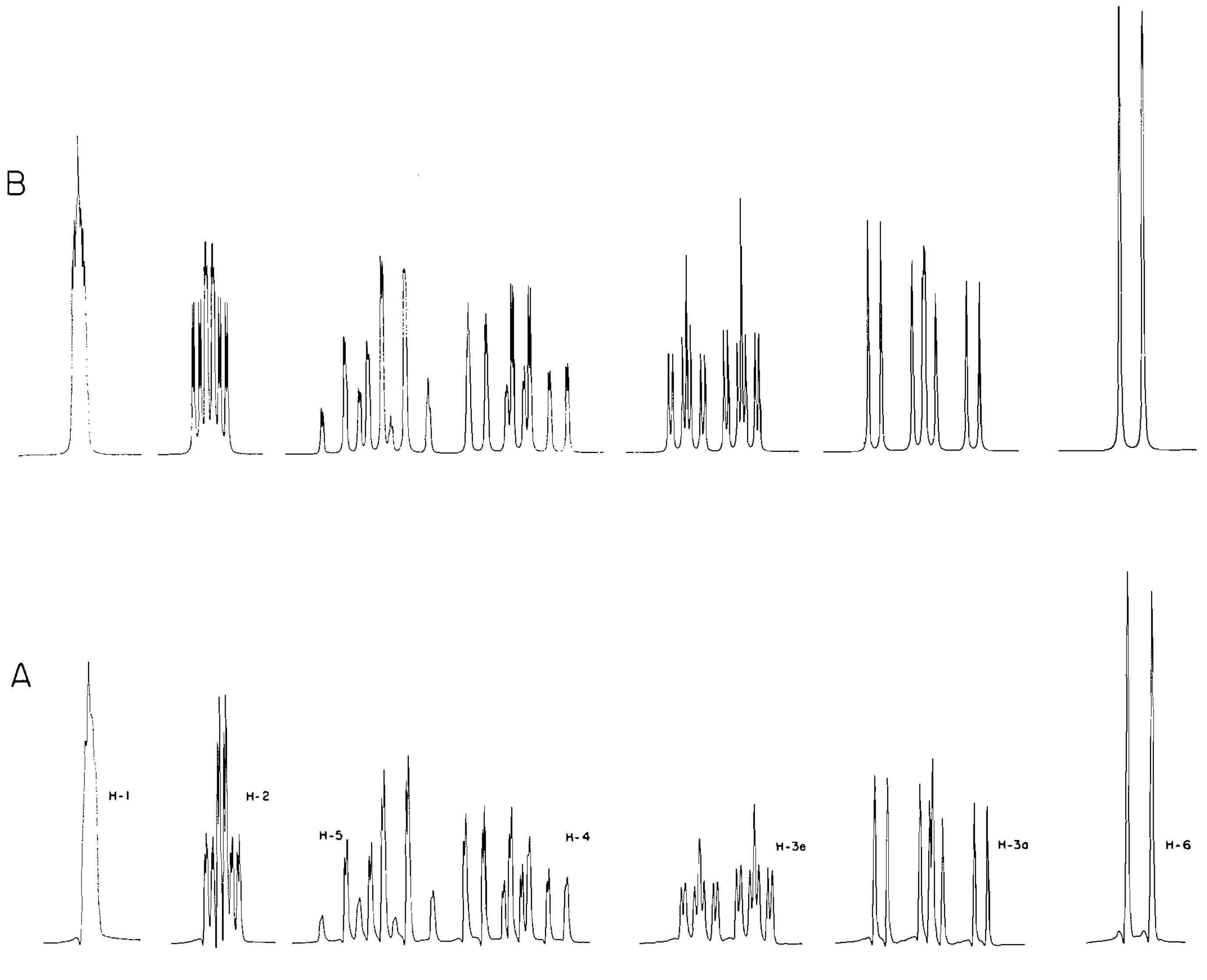

FIG. 5. Observed (A) and simulated (B) ^{1}H nmr spectra of methyl 3,6-dideoxy-α-D-*arabino*-hexopyranoside. The FID acquired in 32K data points was resolution enhanced prior to Fourier transformation by the Lorentz-to-Gauss line shape transformation of Ernst (30). The parameters LB = −0.7 and GB = 0.4 were chosen by trial to give the best compromise for signal-to-noise and resolution. The simulated spectrum (B) was calculated for Lorentzian line shape with 0.2 Hz line width. The spectra are displayed as discontinuous plots at a scale of 10 Hz/division.

iterative analysis of the spin system H1−H6 was performed. The first-order ^3J values and chemical shifts were used initially but the simulated spectrum did not reproduce the observed spectrum. Examination of a resolution-enhanced spectrum (A, Fig. 5) revealed several small, previously unresolved coupling constants. The H(3e) resonance prior to resolution enhancement appeared as two triplets separated by the geminal H(3e)/H(3a) coupling of 13.6 Hz. This now showed the largest ^4J coupling, ca. 1.0 Hz, which collapsed when the H(1) signal was irradiated. The fine detail of the H(2) and H(4) multiplets revealed a ^4J coupling between these protons of 0.5 Hz. The COSY experiment also indicated coupling between H(1)/H(5) and H(1)/H(6); however, these were barely discernible even with resolution enhancement, which failed to show significant fine structure on the H(1) resonance. Particularly interesting was the simulation incorporating the three ^4J values H(1)/H(3e) ≈ −1.0 Hz, H(1)/H(5) ≈ 0.5 Hz, and H(2)/H(4) ≈ −0.5 Hz, which showed H(1) as a broad doublet. Only after incorporation of the H(1)/H(6) ^5J coupling did the H(1) resonance assume its observed broad singlet character. Incorporation of these three ^4J and one ^5J coupling constants in the simulation gave a spectrum (B, Fig. 5) which faithfully reproduced the observed multiplicity and fine splitting of the experimental spectrum, A.

Inspection of the calculated ^3J values obtained by the methods of Altona, Haasnoot, and de Leeuw (19, 20) shows that, although these methods provide a good estimate of the observed ^3J values, the deviations are larger than for those structures upon which the authors based their estimates of accuracy. In this regard it should be noted that trisubstituted fragments such as —CH_2CHX— were observed by them to show systematic differences. Consistent with this, the largest variation between observed and calculated coupling constants occurs for $J_{2,3e}$, $J_{2,3a}$, and $J_{3e,4}$, all of which constitute trisubstituted —CH_2CHX— fragments. These variations in no way affect the interpretation of the nmr data as supporting a $^4C_1$ chair for methyl tyveloside in solution. The diaxial dispositions of H(5), H(4), and H(3a) are all consistent with the large $J_{4,5}$

TABLE 3. Chemical shifts and first-order coupling constants for methyl 3,6-dideoxy-α-D-*arabino*-hexopyranoside in D_2O

Chemical shifts (ppm)[a]		Coupling constants (Hz)			
H	δ(H)	H,H	$^3J_{obs}$	$^3J_{calc}$[b]	$^3J_{calc}$[c]
1	4.491	1,2	1.7	1.8	2.1
2	3.872	2,3e	3.4	3.1	2.5
3a	1.712	2,3a	3.2	2.6	3.0
3e	1.993	3a,3e	13.6	—	—
4	3.549	3e,4	4.5	4.9	5.2
5	3.614	3a,4	11.1	12.0	11.0
6	1.222	4,5	9.4	9.9	9.0
		5,6	5.9		

[a]Measured relative to internal acetone (δ 2.225 ppm).
[b]Based on a $^4C_1$ chair and additivity rules (ref. 19).
[c]Based on a $^4C_1$ chair and generalized Karplus equation (ref. 20).

TABLE 4. Results of HSEA calculations of α-D-Tyv*p*-(1→3)-α-D-Man*p*[a] with tyvelose coordinates obtained from X-ray analysis and from bond modification

	X-ray coords.	Bond-modification coords.
ϕ_H (deg)[b]	312	308
ψ_H (deg)[b]	348	348
E (kcal/mol)[c]	−3.61	−3.83

[a]The disaccharide segment of the pentasaccharide α-D-Gal*p*-(1→2)[α-D-Tyv*p*-(1→3)-α-D-Man*p*-(1→4)-α-L-Rha*p*-(1→3)-α-D-Gal*p*.
[b]ϕ_H and ψ_H are the torsion angles H(1)—C(1)—O(1)—C(3′) and C(1)—O(1)—C(3′)—H(3′), respectively.
[c]Absolute potential energy of the pentasaccharide described in footnote *a*.

and $J_{3a,4}$ values, which serve to fix the ring conformation as $^4C_1$. The small $J_{2,3e}$ and $J_{2,3a}$ values are also consistent with this conformation. The solution conformation of methyl tyveloside is therefore closely related to that in the crystal and since the nmr data may only be extrapolated to torsional angles varying by ca. 10° (9), the agreement with the X-ray results cannot be more accurately tested.

HSEA calculations

Semi-empirical calculations were recently performed for the repeating units of the *Salmonella* LPSs which contain the 3,6-dideoxyhexoses paratose, abequose, and tyvelose (21). For the LPS of serogroup D_1, containing tyvelose, Bock *et al.* used in those calculations a coordinate set for this saccharide derived by bond modification (11) from the neutron diffraction structure of methyl-α-D-mannopyranoside (7) to provide deoxy functions at C(3) and C(6). Since X-ray results for methyl tyveloside are now available, this provides us with an opportunity to compare the use of coordinate sets derived from bond modification with those obtained from crystal structures. In order to make this comparison, a linear tetrasaccharide α-D-Gal*p*-(1→2)-α-D-Man*p*-(1→4)-α-L-Rha*p*-(1→3)-α-D-Gal*p* was constructed according to published work (21). The dideoxyhexopyranose, α-tyvelose, was then introduced at O(3) of the α-D-mannopyranose unit and the minimum energy of the molecule was computed by the HSEA method (10, 11). The torsion angles ϕ_H (H(1)—C(1)—O(1)—C(3′)) and ψ_H (C(1)—O(1)—C(3′)—H(3′)) were obtained simultaneously for the new glycosidic linkage. It was found that the absolute potential energies of the two pentasaccharides, obtained with the tyvelose atomic coordinate set generated either by bond modification or X-ray analysis, were within 0.2 kcal/mol of each other (Table 4). It should be noted that the C—H bond lengths were normalized to 1.10 Å, the usual value obtained from neutron diffraction analyses. The two sets of ϕ_H,ψ_H values fell in a ±2° range (Table 4). Semi-empirical calculations contain many assumptions and approximations, and conformations corresponding to energy minima differing by less than 0.5 kcal/mol are considered as equally probable (10, 11). With the exception of X-ray or neutron diffraction, experimental methods could not detect such small differences. Thus, for practical purposes the bond modification procedure for generating coordinate sets is shown to offer a good approximation, in the absence of crystal structures.

Experimental

Preparation of methyl tyveloside

Methyl -2,4-di-*O*-benzoyl-3,6-dideoxy-α-D-*arabino*-hexopyranoside was synthesized from methyl α-D-glucopyranoside by the published procedure (22) and debenzoylated in absolute methanol containing a catalytic amount of sodium methoxide. The resultant solution was de-ionized with Rexyn 101 H^+ resin (Fisher Scientific), concentrated to a syrup, and chromatographed on silica gel with ethyl acetate, methanol, and water (85:10:5) as eluant. Methyl tyveloside was obtained as a homogeneous syrup which crystallized from ethyl acetate and hexane; mp 87.5–88.5°, $[\alpha]_D^{21}$ 116.2° (*c* 1.2, water). Detailed descriptions of synthetic manipulations and chromatography are to be found in other publications from this laboratory (22, 23).

X-ray analysis of methyl tyveloside

A colorless, prismatic crystal was cut to give a fragment measuring 0.30 × 0.40 × 0.50 mm. Precession photographs showed systematic absences corresponding to the space group $P2_12_12_1$. The crystal was mounted on a CAD4 diffractometer and the following data were obtained:

$C_7H_{14}O_4$ mw = 162.18
Orthorhombic, a = 7.478(1), b = 7.933(1), c = 14.064(1) Å, V = 834.32 Å^3, ρ_c = 1.291 g cm^{-3}, Z = 4 (21°C, CuKα_1, λ = 1.54056 Å), $F(000)$ = 352, μ(CuKα) = 8.5 cm^{-1}.

Unit cell dimensions were determined from a least-squares refinement of the angular settings of 22 high-order ($46 < \theta < 74°$) reflections. Intensities were measured with Ni-filtered CuKα radiation, using ω/2θ scans. Three standard reflections were monitored at regular intervals; their intensities varied by <1%. Of the 1017 unique reflections with $\theta \le 75°$ there were 998 with $I \ge 3\sigma(I)$ which were considered observed. The intensities were corrected for Lorentz and polarization factors; absorption corrections were unnecessary.

The structure was determined by direct methods with the aid of the MULTAN program (24). Refinement was carried out by the block-diagonal least-squares procedure. Anisotropic temperature parameters were used for nonhydrogen atoms, while hydrogen atoms, located on difference Fourier maps, were refined with isotropic parameters. The scattering factors were taken from the "International Tables for X-Ray Crystallography" (25) and the oxygen curve was corrected for anomalous dispersion. Throughout the refinement the function $\Sigma w(|F_o| - |F_c|)^2$ was minimized and a factor of 0.8 was applied to all shifts. The following weighting scheme was used during the final stages: $w = w_1 \cdot w_2$, where $w_1 = 1$ for $|F_o| < 7$, $w_1 = 7/|F_o|$ for $|F_o| \ge 7$, $w_2 = \sin^4\theta/0.9$ for $\sin^2\theta \le 0.9$, and $w_2 = 1$ for $\sin^2\theta > 0.9$. This scheme made the average values of $w(\Delta F^2)$ independent of $|F_o|$ and $\sin^2\theta$. After the final cycle the average parameter shift equalled 0.1σ and the largest 0.25σ. Thirteen strong, low-angle reflections suffered from extinction effects and were given zero weights. The final conventional residual index R is 0.038 and the weighted index R_w is 0.037. Lists of anisotropic temperature parameters and of observed and calculated structure factors are available.[2]

Nuclear magnetic resonance analysis of methyl tyveloside

The ^{1}H nmr spectra were recorded with a Bruker AM-500 instrument at 310K. Spectra were recorded for a 10-mM solution in deuterium oxide using 90° pulses (8 μs) and a digital resolution of ±0.12 Hz. Acetone (1%) was used as an internal reference (δ 2.225 ppm). Two-dimensional homonuclear shift-correlated, COSY-90, experiments were performed without (26) and with a delay period $\approx 0.25/J$ between 90° pulses in order to maximize correlation peaks with small couplings (J) (26). Spectrum simulation was performed with the Bruker software "PANIC", a minicomputer version of the LAOCOON type program. The seven spins H(1)−H(6), with the three H(6) protons treated as a magnetically equivalent spin system, were simulated first with the observed parameters for chemical shift and ^{3}J coupling constants. Subsequently long-range ^{4}J coupling between H(1)/H(3e) −1.0 Hz, H(1)/H(5) 0.5 Hz (27), and H(2)/H(4) −0.5 Hz were incorporated into the simulation and finally together with a ^{5}J H(1)/H(6) 0.5 Hz (27) coupling.

Semi-empirical potential energy calculations, HSEA method (10, 11), were used to compute the minimum energy for a pentasaccharide corresponding to the *Salmonella typhi* O-antigen according to published procedures (21). The atomic coordinates for α-D-mannopyranose (7), α-D-galactopyranose (6), and α-L-rhamnopyranose (8) were taken from published neutron diffraction data. The atomic coordinates of α-D-tyvelopyranose were generated by bond modification of α-D-mannopyranose according to published procedures (11) and from the X-ray analysis reported in this paper.

Acknowledgements

Apart from the MULTAN program (24), all crystallographic computations were carried out with programs written by Ahmed *et al.* (28). Figures 2 and 4 were drawn with the ORTEP program of Johnson (29). The authors would like to thank Dr. Charles Roger, Bruker Spectrospin (Canada) Ltd., for assistance in performing spin simulation and two-dimensional nmr experiments.

1. O. LÜDERITZ, O. WESTPHAL, A. M. STAUB, and H. NIKAIDO. *In* Microbial toxins. Vol. 4. *Edited by* S. J. Ajl, G. Weinbaum, and S. Kadis. Academic Press, New York. 1971. pp. 145–233.
2. O. LÜDERITZ, A. M. STAUB, and O. WESTPHAL. Bacteriol. Rev. **30**, 192 (1966).
3. G. ASHWELL and J. HICKMAN. *In* Microbial toxins. Vol. 4. *Edited by* S. J. Ajl, G. Weinbaum, and S. Kadis. Academic Press, New York. 1971. pp. 235–266.
4. K. JANN and O. WESTPHAL. *In* The antigens. Vol. 5. *Edited by* M. Sela. Academic Press, New York. 1975. pp. 1–125.
5. K. BOCK, S. JOSEPHSON, and D. R. BUNDLE. J. Chem. Soc. Perkin Trans. 2, 59 (1982).
6. S. TAKAGI and G. A. JEFFREY. Acta Crystallogr. Sect. B, **35**, 902 (1979).
7. G. A. JEFFREY, R. K. McMULLAN, and S. TAKAGI. Acta Crystallogr. Sect. B, **33**, 728 (1977).
8. S. TAKAGI and G. A. JEFFREY. Acta Crystallogr. Sect. B, **34**, 2551 (1978).
9. D. R. BUNDLE and G. I. BIRNBAUM. Biochim. Biophys. Acta, **582**, 515 (1979).
10. H. THØGERSEN, R. U. LEMIEUX, K. BOCK, and B. MEYER. Can. J. Chem. **60**, 44 (1982).
11. K. BOCK. Pure Appl. Chem. **55**, 605 (1983).
12. G. A. JEFFREY, J. A. POPLE, J. S. BINKLEY, and S. VISHVESHWARA. J. Am. Chem. Soc. **100**, 373 (1978).
13. B. SHELDRICK and D. AKRIGG. Acta Crystallogr. Sect. B, **36**, 1615 (1980).
14. D. CREMER and J. A. POPLE. J. Am. Chem. Soc. **97**, 1354 (1975).
15. G. A. JEFFREY and R. TAYLOR. J. Comput. Chem. **1**, 99 (1980).
16. R. U. LEMIEUX. Pure Appl. Chem. **25**, 527 (1971).
17. G. A. JEFFREY and J. MITRA. Acta Crystallogr. Sect. B, **39**, 469 (1983).
18. M. KARPLUS. J. Chem. Phys. **30**, 11 (1959).
19. C. ALTONA and C. A. G. HAASNOOT. Org. Magn. Reson. **13**, 417 (1980).
20. C. A. G. HAASNOOT, F. A. A. M. DE LEEUW, and C. ALTONA. Tetrahedron, **36**, 2785 (1980).
21. K. BOCK, M. MELDAL, D. R. BUNDLE, T. IVERSEN, P. GAREGG, T. NORBERG, A. A. LINDBERG, and S. B. SVENSON. Carbohydr. Res. **130**, 23 (1984).
22. T. IVERSEN and D. R. BUNDLE. Carbohydr. Res. **103**, 29 (1982).
23. D. R. BUNDLE and S. JOSEPHSON. Can. J. Chem. **56**, 2686 (1978).
24. P. MAIN, S. E. HULL, L. LESSINGER, G. GERMAIN, J.-P. DECLERCQ, and M. M. WOOLFSON. MULTAN 78, University of York, England, and University of Louvain, Belgium. 1978.
25. J. A. IBERS and W. C. HAMILTON (*Editors*). International tables for X-ray crystallography. Vol. IV. Kynoch Press, Birmingham, England. 1974.
26. A. BAX and R. FREEMAN. J. Magn. Reson. **44**, 542 (1981).
27. G. BATTA and A. LIPTÁK. J. Am. Chem. Soc. **106**, 248 (1984).
28. F. R. AHMED, S. R. HALL, M. E. PIPPY, and C. P. HUBER. J. Appl. Crystallogr. **6**, 309 (1973).
29. C. K. JOHNSON. ORTEP II Report ORNL-5138, Oak Ridge National Laboratory, Oak Ridge, TN. 1976.
30. R. R. ERNST. Adv. Magn. Reson. **2**, 1 (1966).

[2]These tables may be obtained, at a nominal charge, from the Depository of Unpublished Data, CISTI, National Research Council of Canada, Ottawa, Ont., Canada K1A 0S2.

A formal [1,3] sigmatropic reaction involving free radical intermediates: a mechanistic investigation

GORDON S. BATES[1] AND S. RAMASWAMY
Department of Chemistry, 2036 Main Mall, University of British Columbia, Vancouver, B.C., Canada V6T 1Y6

Received June 14, 1984

GORDON S. BATES and S. RAMASWAMY. Can. J. Chem. **63**, 745 (1985).

The quantitative isomerization of 2,2-bis(ethylthio)-3,3-dimethylpent-4-enal to 2,2-bis(ethylthio)-5-methylhex-4-enal was studied over the temperature range 130–170°C. An investigation of the generality and specific mechanism of this formal [1,3] sigmatropic shift was conducted with six related compounds. The rearrangements were found to obey first-order kinetics, and on the basis of significant positive entropies of activation (52–106 J deg^{-1} mol^{-1}), crossover and trapping experiments, and the lack of a solvent effect (decane vs. DMF), an intermolecular, free-radical chain pathway has been proposed for the isomerization. During the rearrangement of several of the compounds esr signals were observed that were consistent with the presence of the proposed free-radical intermediates. These esr signals have been computer simulated.

GORDON S. BATES et S. RAMASWAMY. Can. J. Chem. **63**, 745 (1985).

Opérant à des températures allant de 130 à 170°C, on a étudié l'isomérization quantitative du bis(éthylthio)-2,2 diméthyl-3,3 pentène-4 al en bis(éthylthio)-2,2 méthyl-5 hexène-4 al. Utilisant six composés apparentés, on a déterminé la généralité et le mécanisme spécifique de cette transposition qui est, d'un point de vue formel, du type sigmatropique [1,3]. On a trouvé que la cinétique de ces transpositions est du premier ordre et, sur la base d'entropies d'activation qui sont assez positives (52–106 J deg^{-1} mol^{-1}), d'expériences d'échanges et de piégeages ainsi que sur le fait qu'il n'y a pratiquement pas d'effet de solvant (décane vs. DMF), on suggère que cette isomérisation se produit par le biais d'un processus radicalaire intermoléculaire. Au cours des transpositions de plusieurs composés, on a pu observer des signaux de rpe qui sont en accord avec la présence des intermédiaires radicalaires proposés. Utilisant un ordinateur, on a simulé ces signaux de rpe.

[Traduit par le journal]

Although the chemical literature contains many examples of [1,3] alkyl shifts in cyclic systems, their occurrence in acyclic analogues is relatively rare (1). Cookson and Kemp (2) have reported a benzyl migration in the thermal conversion of 3,3-dicyano-2-methyl-4-phenylpent-1-ene to 1,1-dicyano-2-methyl-4-phenylpent-1-ene which occurs with retention of configuration. Baldwin *et al.* have evidence for the presence of a radical pathway in the [1,3] sigmatropic rearrangements of a number of systems (3). More recently, Ollis and co-workers (4) have reported rearrangements of various dimethylaminobutenes that again can formally be regarded as [1,3] alkyl shifts. These authors speculate that, although a stereoselective transformation involving a concerted pathway is a likely possibility in the case of several of the compounds, a process involving a weakly interacting radical pair is not unlikely.

We recently observed[2] a high yielding[3] thermal rearrangement of 2,2-bis(ethylthio)-3,3-dimethylpent-4-enal **1** into compound **2**. This rearrangement, which is an example of a [1,3] carbon–carbon shift in an acyclic system, should be favoured since the transformation would be accompanied by relief of the steric strain associated with the two adjacent quaternary centres in **1**, as well as by formation of the more highly substituted alkene in **2**. The observation of the transformation of **1** into **2** prompted us to investigate the generality, as well as the specific mechanism, of this rearrangement. Accordingly, aldehydes **3–7** were prepared in order to investigate the steric demands of the reaction, and compounds **8** and **9** as a probe of the electronic requirements of the rearrangement.

The isomerization of **1** into **2** may be rationalized in terms of the several different reaction mechanisms shown in Fig. 1.

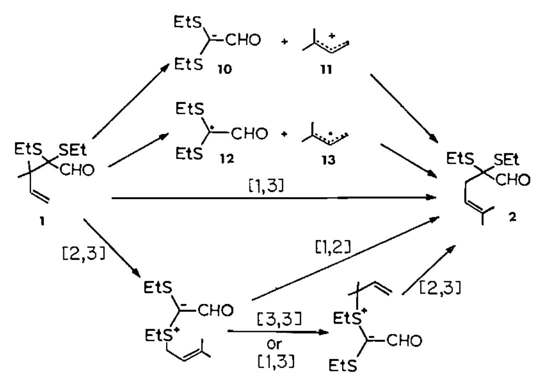

FIG. 1. Possible pathways for [1,3]-alkyl migration in the rearrangement of **1** into **2**.

A heterolytic cleavage of **1** to provide the bis(ethylthio)-ethanal anion **10** and a tertiary allylic carbonium ion **11**, followed by recombination of the ions at the less hindered site of the allylic group, could produce compound **2**. The required dimethylallyl carbonium ion is stabilized both by hyperconjugation as well as by allylic resonance. The anion also is doubly stabilized. Both the electron-withdrawing aldehyde group and the two sulphur atoms flanking the anion have a large stabilizing effect. The stability of anion **10** is easily seen from the fact that the conjugate acid of this anion, 2,2-bis-(ethylthio)ethanal, can be readily extracted into aqueous sodium hydroxide (6).

A homolytic bond cleavage of **1** would give rise to two radicals that could also recombine to provide **2** in a fashion similar to the heterolytic pathway described above. The dimethylallyl radical **13** that would be formed is stabilized by resonance. In addition to the effects due to the electron-withdrawing aldehyde, the bis(ethylthio)ethanal radical **12** is further stabilized by another factor. Stabilization of radicals by

[1]Author to whom correspondence should be addressed.

[2]Portions of this work have appeared as a preliminary communication (5).

[3]Compound **2** has been isolated in 87% yield after the thermal rearrangement of 0.50 g of **1**. The proton magnetic resonance (^{1}H nmr) spectrum of the crude reaction mixture indicated a quantitative conversion.

TABLE 1. Predicted mechanistic features

Mechanism	Solvent effect	Crossover products	Entropy of activation
Concerted	No	No	Negative
Ionic (intermolecular)	Yes	Yes	Positive or negative
Ionic (intramolecular)	Yes	No	Positive or negative
Radical (intermolecular)	No	Yes	Positive
Radical (intramolecular)	No	No	Positive

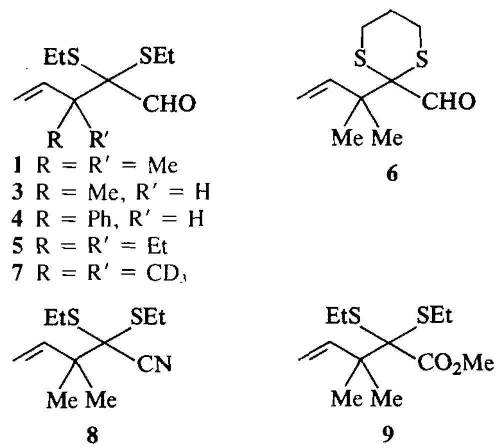

SCHEME 1

heteroatoms such as sulphur is well documented (7, 8) and involves participation of a lone pair of electrons on the heteroatom in delocalization of the radical. If a radical is substituted by these two electronically complementary groups, the stability of the radical is greatly enhanced since the unpaired electron is delocalized over both the donor and the acceptor groups. This phenomenon has been designated as capto-dative stabilization (9).

Finally, the rearrangement may proceed by a concerted pathway (10). The migration of the dimethylallyl group may take place via a symmetry-allowed [1,3] suprafacial pathway, provided inversion of configuration of the migrating group occurs. Alternatively, the rearrangement may in principle occur with retention of configuration at the migrating centre but via a geometrically disfavoured antarafacial process. In addition to a direct [1,3] sigmatropic pathway, the rearrangement could occur via a series of alternate symmetry-allowed sigmatropic migrations as shown in Fig. 1, which result in the overall appearance of a [1,3] shift.

Any of the concerted processes must involve ordered transition states that should be reflected in a relatively large negative entropy of activation ($\Delta S^{\#}$).[4] For example, the well-known Cope rearrangement has $\Delta S^{\#}$'s ranging from −46.4 to −58.6 J deg^{-1} mol^{-1} (11–13). The $\Delta S^{\#}$ for the diradical process should be positive (14). On the other hand, the $\Delta S^{\#}$ for the ionic pathway could vary greatly. If there is considerable freedom in the transition state, then $\Delta S^{\#}$ would be positive. However, a negative $\Delta S^{\#}$ is also possible due to electrostriction of the solvent around the ions produced (15). Any of the proposed concerted processes must be intramolecular in nature. However, both the ionic and radical modes could follow either an intramolecular or an intermolecular pathway. A crossover experiment using isotopically labelled substrates should be sufficient to differentiate the intra- vs. the intermolecular character of the rearrangement. If the rearrangement proceeds by way of an ionic pathway, or indeed, via any process that involves significant charge development in the transition state, there should be a significant solvent effect. On the other hand, the rate of a concerted or of a radical process should be relatively independent of solvent (16). The crossover experiment, analysed in conjunction with the results of changing the solvent on the rate of the reaction, could be used to differentiate an intermolecular radical pathway from an ionic route. Thus a determination of the activation parameters of the reaction, as well as the presence or absence of a solvent effect, and the results of a crossover experiment will allow a mechanistic choice to be made. Table 1 summarizes these various mechanistic requirements.

The compounds required for the kinetic studies that will be used to determine the activation parameters for the rearrangement were prepared by a route that presumably involves a [2,3] sigmatropic rearrangement of an allylic sulphonium ylide (17). Aldehydes **1** and **3–7** were prepared by stirring the required allylic bromide and dithioketal with lithium or potassium carbonate in *N,N*-dimethylformamide overnight at room temperature. Nitrile **8** was prepared by a similar procedure; however, the reaction was incomplete even after prolonged stirring (6 days). Using the above method to form ester **9** always resulted in a mixture of desired material **9** (S_N2' product) and its isomer **14** (S_N2 product). A pure sample of **9**, uncontaminated with **14**, could be obtained by preforming the necessary sulphonium salt followed by an *in situ* deprotonation of this salt and a concomitant [2,3] sigmatropic rearrangement of the resulting ylide.

One mechanism that could account for the exclusive formation of the S_N2' products **1** and **3–8** involves an initial S_N2 attack of sulphur on the allylic halide to generate a sulphonium salt. The acidity of the proton α to the sulphur is enhanced by this salt formation and even a weak base such as lithium or potassium carbonate is strong enough to deprotonate this site. The resulting ylide then rearranges to give the observed S_N2' product. This explanation is similar to that proposed by Ogura *et al.* (18) to account for the product distribution in a related system. An alternate mechanism would be the alkylation of the preformed carbanion (19) to generate the same intermediate ylide described above, which then undergoes the sigmatropic rearrangement. If the former mechanism is the only operating pathway, then the S_N2' product **16** rather than **17** (S_N2) should always be obtained irrespective of the nature of the Z group in compound **15** or of the base used in the deprotonation step. If the alternate mechanism is operative, the product distribution would be expected to exhibit some dependence on both of the parameters mentioned above. In this context it is pertinent to present some of our observations regarding this reaction. As can be seen from Table 2, there is indeed a variation in product

[4] The enthalpy of activation ($\Delta H^{\#}$) for all of the proposed routes would be expected to be positive.

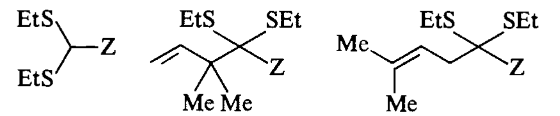

15 16 (S_N2') 17 (S_N2)

SCHEME 2

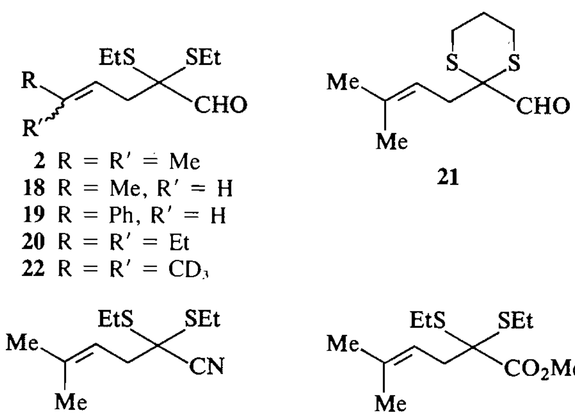

2 R = R′ = Me
18 R = Me, R′ = H
19 R = Ph, R′ = H
20 R = R′ = Et
22 R = R′ = CD_3

21

23 14

SCHEME 3

distribution with both the change in functional group (Z) and the base used in the reaction. We believe that this is consistent with the fact that *S*-alkylation of a preformed carbanion followed by a [2,3] rearrangement of the intermediate ylide is a significant pathway in the reactions leading to the S_N2' products.[5]

Authentic samples of the potential rearrangement products also were prepared. Aldehydes **2** and **18**–**22** were prepared via a metalloenamine alkylation (6) and nitrile **23** by the alkylation of the potassium salt of 2,2-bis(ethylthio)ethanenitrile (20). A sample of ester **14** was obtained by repeated thin-layer chromatographic separation of the mixture of **9** and **14** described above.

The rearrangement of aldehydes **1** and **3**–**6** was effected in decane or tetradecane solution. The solvents were freshly distilled and the samples degassed with argon before the thermolysis. The aldehyde resonances in the ^{1}H nmr spectrum of the starting materials and the products generally differ by ca. 0.1 ppm. Thus the progress of the reactions could be conveniently monitored by following the change in the relative areas of the aldehydic resonances. Neither nitrile **8** nor ester **9** contains a convenient ^{1}H nmr reference signal by which the rearrangement could be monitored. Gas chromatographic analysis therefore was used to determine the relative amounts of starting material and the rearranged product as the reaction proceeded. The rearrangements were carried out in degassed tetradecane. Control experiments were conducted to determine the relative detector responses of the starting materials and the products as well as to establish that no significant amount of rearrangement was occurring during the gas chromatographic analysis of the reaction mixture.

Figures 2–6 clearly indicate that the rarrangements of compounds **1**, **4**, **6**, **8**, and **9**, respectively, follow first-order reaction kinetics.[6] The rate constant at 150°C for the rearrangement of the more compact and less sterically demanding 1,3-dithiane derivative **6** was considerably (ca. 20-fold) lower than that for the rearrangement of the more sterically crowded analogue **1**. On the basis of a simple steric argument it was expected that **3** would rearrange more slowly than **1**, and **5** more rapidly.[7] Compound **3** was indeed less prone to rearrange and in fact no reaction was observed even after prolonged heating at 220°C. It was anticipated that **5**, in which the steric congestion at the adjacent quaternary centres was further accentuated, would show a dramatic increase in the rate of rearrangement as com-

TABLE 2. Product variation in the reaction of $(EtS)_2CHZ$ and 2-methyl-4-bromobut-2-ene

		Relative amounts	
Base and solvent	Z	**16** (S_N2')	**17** (S_N2)
Li_2CO_3/DMF	CHO	100	0
K_2CO_3/DMF	CN	Major	Minor
Li_2CO_3/DMF	CN	100	0
KH/THF	CN	0	100
KH/THF	$CH{=}NC_6H_{11}$	0	100
Li_2CO_3/DMF	CO_2Me	Major	Minor
K_2CO_3/DMF	CO_2Me	Minor	Major

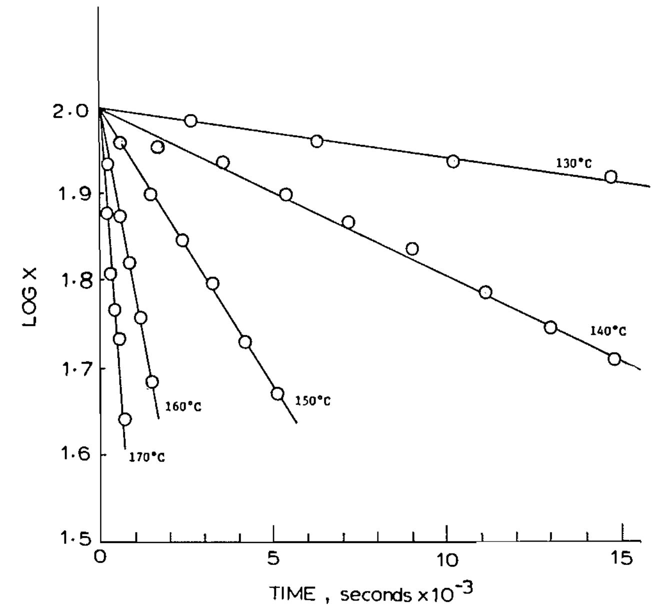

FIG. 2. Rate of rearrangement of **1**: X = 100([**1**]/[**1** + **2**]) as determined by ^{1}H nmr spectroscopy. t = 170°C, $k = 1.08 \times 10^{-3}$ s^{-1}; t = 160°C, $k = 4.70 \times 10^{-4}$ s^{-1}; t = 150°C, $k = 1.43 \times 10^{-4}$ s^{-1}; t = 140°C, $k = 4.51 \times 10^{-5}$ s^{-1}; t = 130°C, $k = 1.19 \times 10^{-5}$ s^{-1}.

[5]The products are also consistent with a one-electron transfer mechanism.

[6]The figures display typical data for the average of a minimum of three rearrangement experiments at each temperature. In each case, the kinetic data were found to agree, within 10%, with those of previous experiments. Photocopies of the kinetic data may be obtained at a nominal charge from the Depository of Unpublished Data, CISTI, National Research Council of Canada, Ottawa, Ont., Canada, K1A 0S2.

[7]Compound **4** would be expected to have two opposing forces, electronic acceleration vs. steric decrease, affecting its rearrangement. Aldehyde **4** rearranges at approximately 1.6 times the rate of **1** over the temperature range studied, indicating that the electronic effect is dominant.

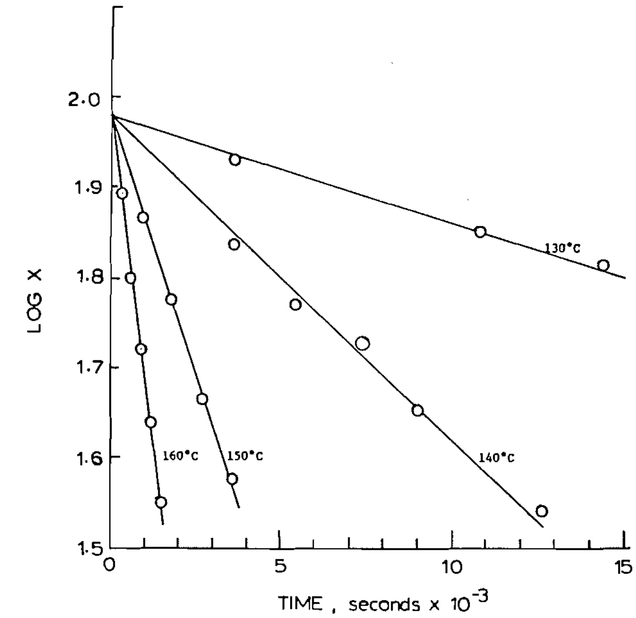

FIG. 3. Rate of rearrangement of **4**: X = 100([**4**]/[**4** + **19**]) as determined by ^{1}H nmr spectroscopy. t = 170°C, $k = 1.57 \times 10^{-3}\ s^{-1}$; t = 160°C, $k = 6.69 \times 10^{-4}\ s^{-1}$; t = 150°C, $k = 2.44 \times 10^{-4}\ s^{-1}$; t = 140°C, $k = 7.53 \times 10^{-5}\ s^{-1}$; t = 130°C, $k = 2.14 \times 10^{-5}\ s^{-1}$.

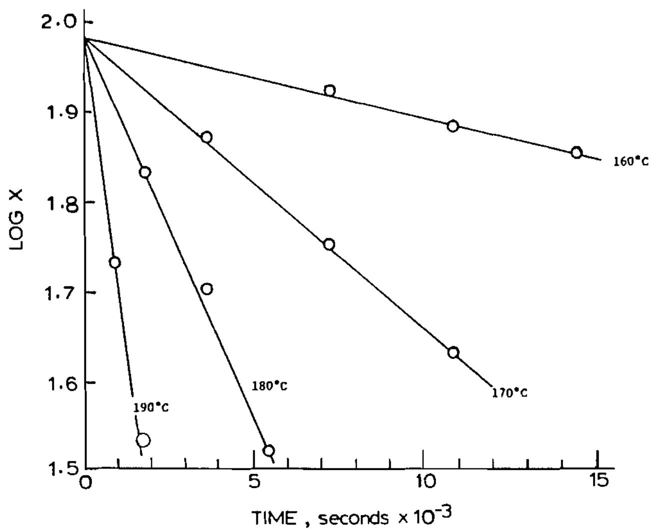

FIG. 4. Rate of rearrangement of **6**: X = 100([**6**])/[**6** + **21**]) as determined by ^{1}H nmr spectroscopy. t = 190°C, $k = 6.42 \times 10^{-4}\ s^{-1}$; t = 180°C, $k = 2.08 \times 10^{-4}\ s^{-1}$; t = 170°C, $k = 7.1 \times 10^{-5}\ s^{-1}$; t = 160°C, $k = 1.9 \times 10^{-5}\ s^{-1}$; t = 150°C, $k = 7.5 \times 10^{-6}\ s^{-1}$.

pared to **1**. Unfortunately, the thermolysis of **5** was accompanied by side reactions and hence a systematic investigation of the rearrangement kinetics could not be achieved. However, a qualitative indication of the expected greater reativity of **5** was obtained. The ^{1}H nmr spectrum of a solution of **5** that had been heated to 160°C for 4 min showed a complete absence of the signal for the aldehydic proton of **5**, whereas at the same temperature **1** has a half-life of approximately 25 min. The rearrangement thus shows a definite steric dependence. Changing the degree of steric congestion at the two adjacent quaternary centres dramatically affects the rate of the rearrangement.

The enthalpy and entropy of activation for the rearrange-

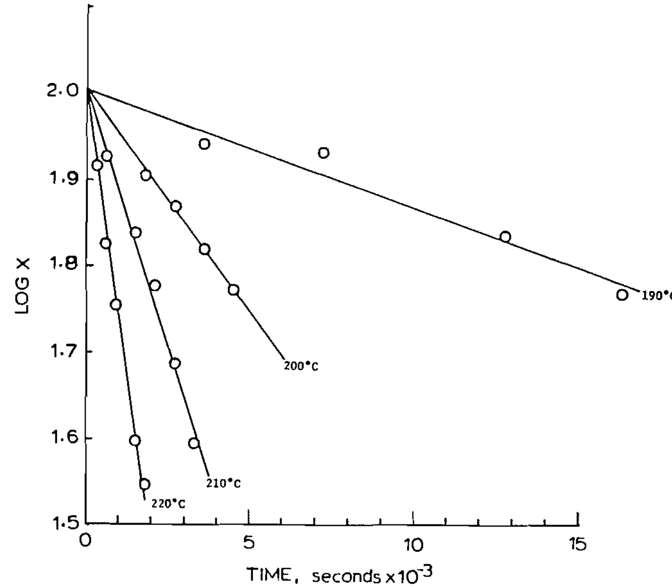

FIG. 5. Rate of rearrangement of **8**: X = 100([**8**]/[**8** + **23**]) as determined by glc analysis. t = 220°C, $k = 6.60 \times 10^{-4}\ s^{-1}$; t = 210°C, $k = 2.82 \times 10^{-4}\ s^{-1}$; t = 200°C, $k = 9.47 \times 10^{-5}\ s^{-1}$; t = 190°C, $k = 3.17 \times 10^{-5}\ s^{-1}$.

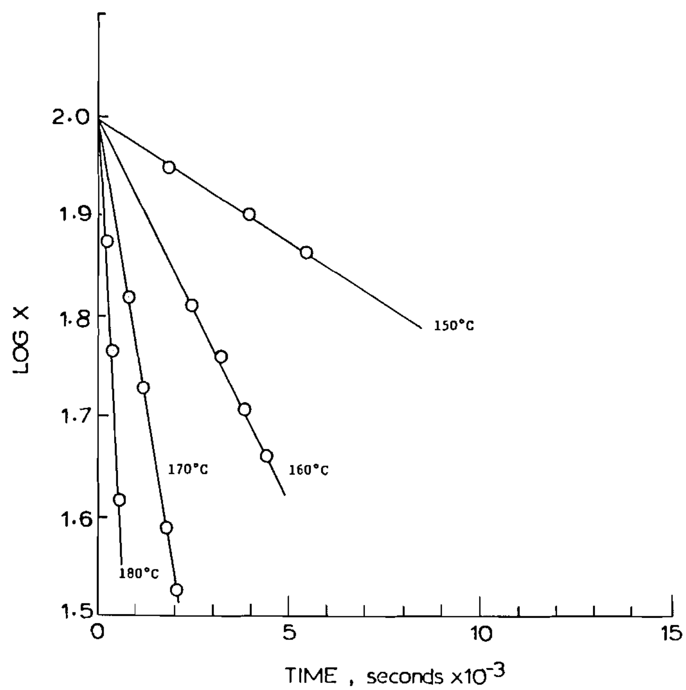

FIG. 6. Rate of rearrangement of **9**: X = 100([**9**]/[**9** + **14**]) as determined by glc analysis. t = 180°C, $k = 1.89 \times 10^{-3}\ s^{-1}$; t = 170°C, $k = 5.15 \times 10^{-4}\ s^{-1}$; t = 160°C, $k = 1.90 \times 10^{-4}\ s^{-1}$; t = 150°C, $k = 5.23 \times 10^{-5}\ s^{-1}$.

ments of **1**, **4**, **6**, **8**, and **9** were calculated from the Eyring equation (21) using the data obtained from Fig. 7 and are summarized in Table 3. The substantial positive values of $\Delta S^{\#}$ in the systems studied appear to be inconsistent with the various concerted mechanisms proposed for the rearrangement. However, it is not yet possible to absolutely preclude either an ionic or radical pathway.

The nitrile and ester functional groups are essentially equal in their ability to stabilize an adjacent negative charge, as

TABLE 3. Rearrangement activation parameters

Compound	Temperature range (°C)	$\Delta H^{\#}$ (kJ mol^{-1})	$\Delta S^{\#}$ (J deg^{-1} mol^{-1})
1	130–170	165	69
4	130–160	157	52
6	150–190	180	79
8	190–220	190	75
9*	150–180	184	106

*The kinetics used to obtain these activation parameters are uncorrected for small (<3%) amounts of methyl 2,2-bis(ethylthio)acetate formed during the rearrangement.

evidenced by their similar acidities. Both compounds have pK_a's of approximately 25 (22). An aldehyde (pK_a ~17) can stabilize an adjacent negative charge even more efficiently than either of these groups. Thus, if the rearrangements are ionic in nature, both **8** and **9** might be expected to rearrange at comparable rates, which in turn would be significantly slower than the rate of rearrangement for aldehyde **1**. In contrast, if a radical process is involved, rate differences between all three compounds might be expected. Recently Dust and Arnold (23) have shown that nitriles are less able to stabilize an adjacent radical site than are esters. It has further been shown that a methyl ketone, and thus by implication an aldehyde, is superior to either a nitrile or an ester in this stabilizing effect. Thus compounds **1**, **8**, and **9** would be expected to rearrange at different rates if a radical process is operating. Indeed, as can be seen in Figs. 2, 5, and 6, the rate of rearrangement of ester **9** is less than half that of aldehyde **1** over the temperature range studied, and the nitrile **8** is even slower. For example, at 180°C, **8** did not rearrange to any significant extent, whereas the half-life of ester **9** at this temperature is approximately 6 min. This observation of a rate difference with functional group substitution is more consistent with a radical pathway than the ionic scheme.[8]

A crossover experiment then was conducted in order to determine whether the rearrangements were proceeding via an inter- or an intramolecular pathway. A 2:1 mixture of ester **9** and deuterated aldehyde **7** was thermolyzed in degassed tetradecane at 160°C for 4 h to ensure complete rearrangement of the starting materials. The reaction mixture was separated into its rearranged ester and aldehyde components using preparative thin-layer chromatography, and the purified products analyzed by mass spectrometry in order to assess the extent of deuterium incorporation in the reaction products. The ratio of the parent ion of the protiated (m/e 262) and deuterated (m/e 268) esters was found to be 22.0:5.6. This ratio is consistent wth 20% deuteration of the vinyl methyl groups of **14**.

A similar analysis of the rearranged aldehyde established that the vinyl methyl groups of **2** were now 37% deuterated. Control experiments were performed in order to ensure that the observed scrambling was a result of only the primary fragmentation process. A mixture of deuterated aldehyde **7** and rearranged ester **14** was thermalized at 160°C for 4 h. In a second experiment a mixture of rearranged deuterated aldehyde **22** and protiated ester **14** was also thermolyzed under the same conditions. Analysis of the products of both control reactions by mass spectrometry revealed that no crossover products had been formed in either case.

[8]The above conclusion is based on the assumption that there is no secondary steric influence (linear nitrile vs. bent aldehyde and ester substituents) on the rates of rearrangements of these compounds.

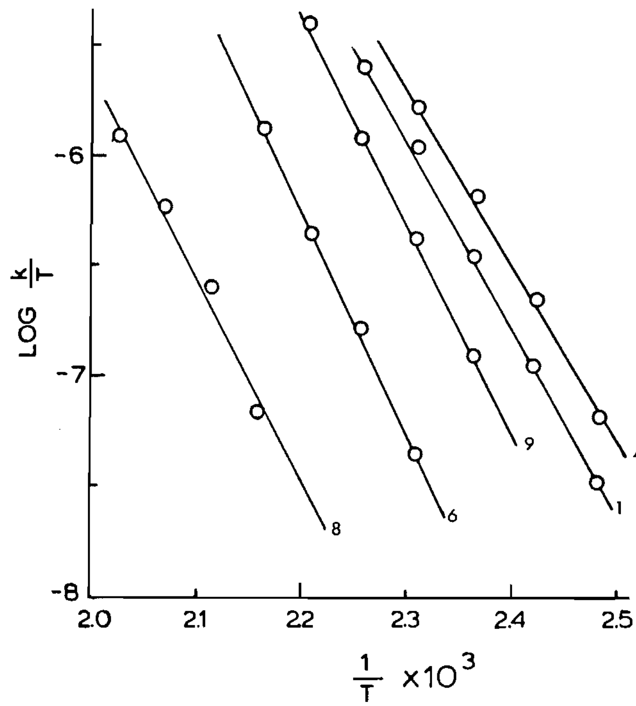

FIG. 7. Dependence of temperature of the rate constants for the rearrangements of **1**, **4**, **6**, **8**, and **9**.

The rearrangement of aldehyde **1** was also carried out in perdeuterio *N*,*N*-dimethylformamide (DMF-d_7). The rate of rearrangement of **1** was found to change by a factor of less than 1.5 with this drastic change in solvent from decane to DMF-d_7. The demonstrated intermolecular nature of the rearrangement, combined with the lack of any significant solvent effect, is clearly inconsistent with the rearrangement being accompanied by any charge separation in the transition state and thus the ionic process may be ruled out.[9] In order to confirm the proposed intermediacy of free-radical intermediates in the rearrangement, further evidence (both chemical and spectroscopic) was sought. It had been noted that the reaction product following thermolysis of ester **9** often contained a small (<3%) amount of methyl 2,2-bis(ethylthio)acetate. The formation of this compound is consistent with hydrogen atom abstraction from the solvent or other source by the proposed radical intermediate. Thermolysis of the more readily available aldehyde **1** was accordingly carried out in the presence of cumene in an attempt to intercept any radical intermediates. Although the rearrangement proceeded as usual, no evidence of hydrogen abstraction products was observed. However, when a superior

[9]See ref. 24 for an alternate view of the mechanistic significance of the lack of a solvent effect on the rate of a reaction.

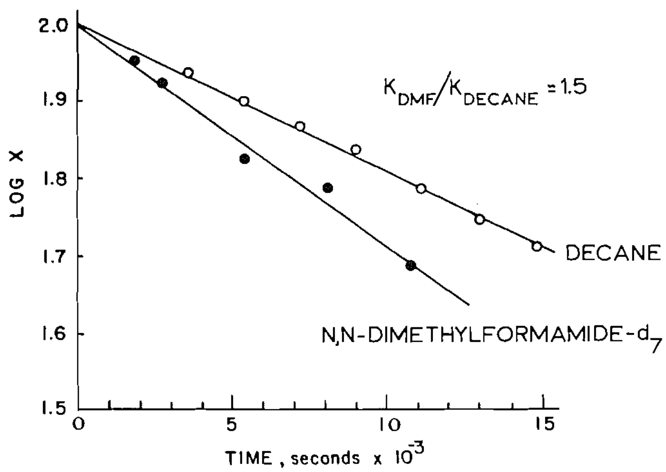

FIG. 8. Solvent effect on the rate of rearrangement of **1** at 140°C. k (decane) = 4.51×10^{-5} s^{-1}; k(DMF-d_7) = 6.52×10^{-5} s^{-1}.

hydrogen atom donor, 1,4-cyclohexadiene, was substituted for cumene the reaction mixture (2.5 h, 145°C, ca. one half-life) contained approximately 45% unreacted starting material, 25% rearranged aldehyde **2**, and 30% 2,2-bis(ethylthio)ethanal. Thus more than half of the proposed radical intermediate **12** had been trapped by the hydrogen donor solvent. This result is consistent therefore both with the free-radical as well as the intermolecular nature of the rearrangement.

Two of the most widely used techniques for the spectroscopic detection of free radicals are Chemically Induced Dynamic Nuclear Polarization (CIDNP) and electron spin resonance (esr) spectroscopy (25). Both techniques were employed in an attempt to further confirm the radical nature of the rearrangement process.

The CIDNP technique is based on the perturbation of the ^{1}H nmr signal intensity by free radicals in the system. No enhancement of any ^{1}H nmr signals was observed when a solution of **1** in decahydronaphthalene-d_{18} was heated at 170°C in the probe of an ^{1}H nmr spectrometer. However, lack of CIDNP enhancement does not rule out the possibility of radical intermediates being involved in the rearrangement.

When a solution of **1** in tetradecane was heated at 150°C in the cavity of an esr spectrometer a strong esr signal was observed (Fig. 9). This signal consisted of an apparent six-line spectrum with a hyperfine coupling of approximately 1.7 G. The line shape and hyperfine coupling were clearly inconsistent with a signal arising from the dimethylallyl radical **13** (26). However, the four hydrogens of the methylene groups and the aldehydic hydrogen of the radical **12** would be expected to couple to the free radical to produce the observed spectrum. The methylene hydrogens can interact with the free radical since considerable delocalization of the free radical onto the sulfur atom through a $p\pi - d\pi$ interaction is expected. The observed hyperfine coupling constant (1.7 G) is within the range expected for such a system. For example, the methyl protons of the methyl sulphide free radical have a hyperfine coupling constant of 3.25 G (27) and the aldehydic hydrogen of the ethanal free radical experiences a hyperfine coupling of ca. 0.5 G (28). Several unsuccessful attempts were made to record an esr spectrum of radical **13** during the rearrangement of aldehyde **1**.

Indeed, a computer simulation of the observed spectrum, assuming two pairs of diastereotopic methylene hydrogens with hyperfine couplings of 1.80 and 1.60 G, respectively, and an aldehydic hydrogen (1.90 G) coupled to a radical, produces a spectrum virtually identical to that observed experimentally. Electron spin resonance signals were also observed during the thermolyses of nitrile **8** (Fig. 10) and ester **9** (Fig. 11). Computer simulation of these signals (nitrile: methylene hyperfine couplings of 1.17 and 1.55 G, nitrogen hyperfine coupling of 2.50 G; ester: methylene hyperfine couplings of 1.50 and 1.70 G, methyl hyperfine coupling of 0.80 G) also yielded excellent agreement with the experimentally obtained spectra.

The lack of observation of an esr signal for the dimethylallyl radical **13** as well as the cleanness, i.e., no random coupling products, of this clearly intermolecular rearrangement is inconsistent with the formation of a *large* number of radical pairs via homolysis of **1**. However, the initial homolytic cleavage of a *small* number of molecules, followed by attack of the thioketal radical **12** on a molecule of **1** at the vinyl position in a *chain reaction*, is consistent with all of the available data. The reaction between **12** and **1** would result in the release of a fresh chain-carrying radical **12** as well as the concomitant inversion of the alkene side chain during the formation of the rearrangement product **2** (Fig. 12).

On the basis of the sign and magnitude of the entropy of activation for the reaction, the lack of any significant solvent effect, the trends arising from electronic perturbation of the system, and the spectroscopic observations, we propose that the compounds under study undergo a thermally induced homolytic cleavage to form two stabilized radicals, a tertiary allylic fragment and a capto-dative stabilized fragment. This latter radical then initiates a smooth, intermolecular chain reaction, which results in the formation of the product of an apparent [1,3] sigmatropic rearrangement.

Experimental

General

All reactions were carried out under an argon or nitrogen atmosphere. Stirring was accomplished using Teflon-coated magnetic stirring bars. Tetrahydrofuran was freshly distilled from sodium benzophenone ketal under a nitrogen atmosphere. All extraction, chromatography, and reaction solvents were distilled before use. Petroleum ether refers to the 30–60°C boiling fraction.

All temperatures are stated in degrees Celsius. Molecular distillations were performed by means of a Büchi Kugelrohr apparatus. Proton magnetic resonance (^{1}H nmr) spectra were obtained on one or more of the following instruments: Varian Associates T-60, EM-360L, and HA-100. Spectra were recorded in deuteriochloroform or carbon tetrachloride solution with tetramethylsilane as an internal reference. Chemical shifts are reported on the δ scale. The multiplicity, integrated peak area, and coupling constants in Hertz (Hz) (if observable) are indicated in parentheses after each signal. Infrared spectra were recorded as liquid films using a Perkin–Elmer 700 spectrometer, and were calibrated with the 1601 cm^{-1} band of polystyrene. High resolution mass spectra were obtained using an AEI MS-50 mass spectrometer. Electron spin resonance (esr) spectra were recorded on an instrument that consisted of a variable temperature 30-cm Varian magnet with an Mk II field-dial control, a Hewlett–Packard Klystron power supply and sweep unit, and a home-built AFC and 100-kHz modulation unit with an Ithanco 391A phase-lock amplifier, which was typically operated at 3210.0 ± 12.5 G, 2–5 mW microwave power, and 0.5 G modulation at 100 kHz. Computer simulations were executed using techniques described in ref. 29. Elemental analyses were performed at the Microanalytical Laboratory, University of British Columbia.

Merck Silica Gel HF-254 was used for preparative thin-layer chromatography while Merck pre-coated tlc sheets Silica Gel 60F-254 were used for analytical thin-layer chromatography. Florisil

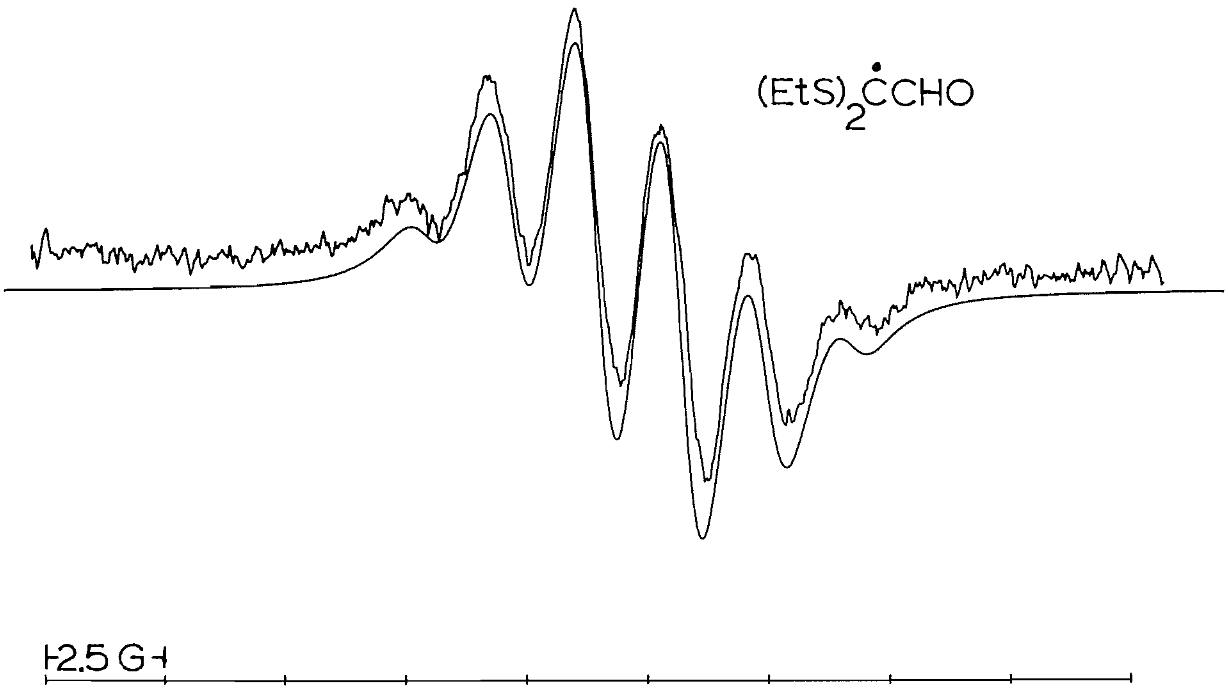

FIG. 9. The esr spectrum recorded during thermolysis of **1** (150°C) (smooth curve = simulated spectrum).

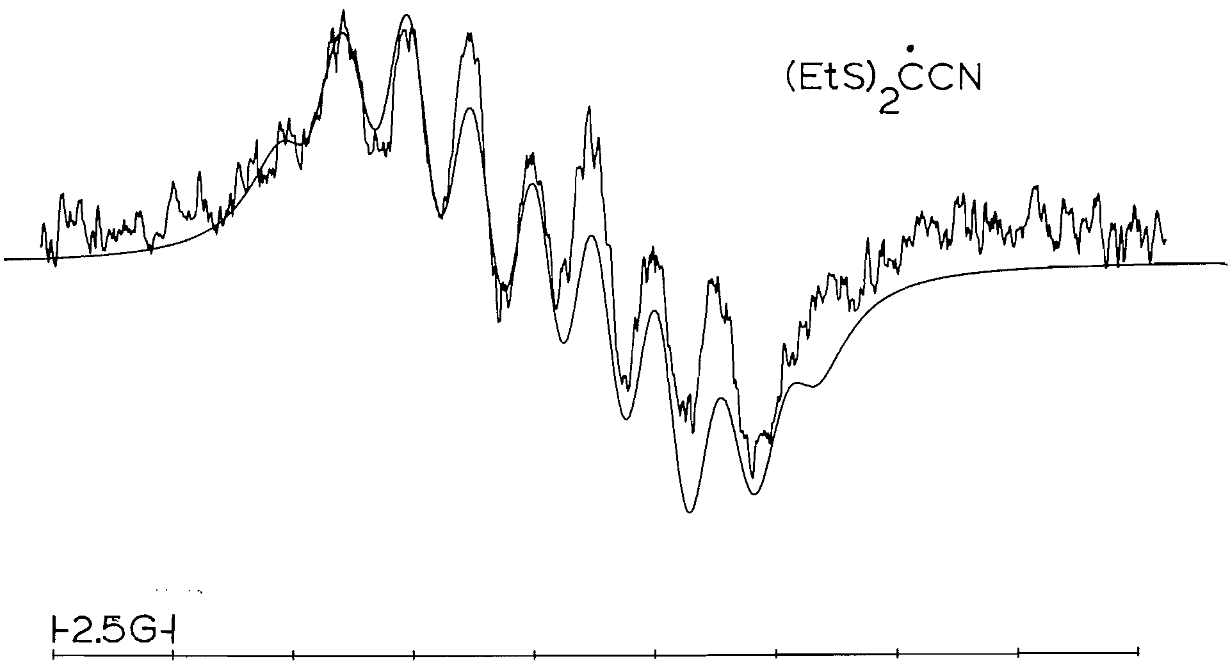

FIG. 10. The esr spectrum recorded during thermolysis of **8** (160°C) (smooth curve = simulated spectrum).

(100–200 mesh) and Merck Silica Gel 60 (230–400 mesh) were used for column chromatography. All chromatography solvent systems are expressed in ratios by volume.

Analytical gas chromatography was carried out on a Hewlett–Packard model 5830-A chromatograph equipped with 1.8 m × 0.3 cm columns packed with 3% OV-17 or 3% OV-101 or 5% Carbowax.

Thermolyses were conducted in ^{1}H nmr tubes or small ampoules heated in an insulated, stirred oil bath that was heated by means of an immersed Nichrome heater. Temperature control was achieved using an I^{2}R Thermowatch controller model L7-1100B that had been modified for use with a 0–300°C mercury contact thermometer supplied by SGA Scientific, Inc. The temperature control is estimated to be ±1°C.

The following abbreviations are used in the description of the multiplicity of each signal in the ^{1}H nmr spectrum: s = singlet, d = doublet, t = triplet, q = quartet, sept = septet, m = multiplet, dd = doublet of doublets, dt = doublet of triplets, dm = doublet of multiplets, b = broad.

The following experimental description illustrates the general procedure that was used to prepare the non-commercially available allylic bromides required for the synthesis of the rearrangement precursors and their products.

1-Bromo-3-ethylpent-2-ene

Magnesium turnings, 5 g (208 mmol), stirred in 10 mL of tetrahydrofuran were activated by the addition of a few drops of 1,2-

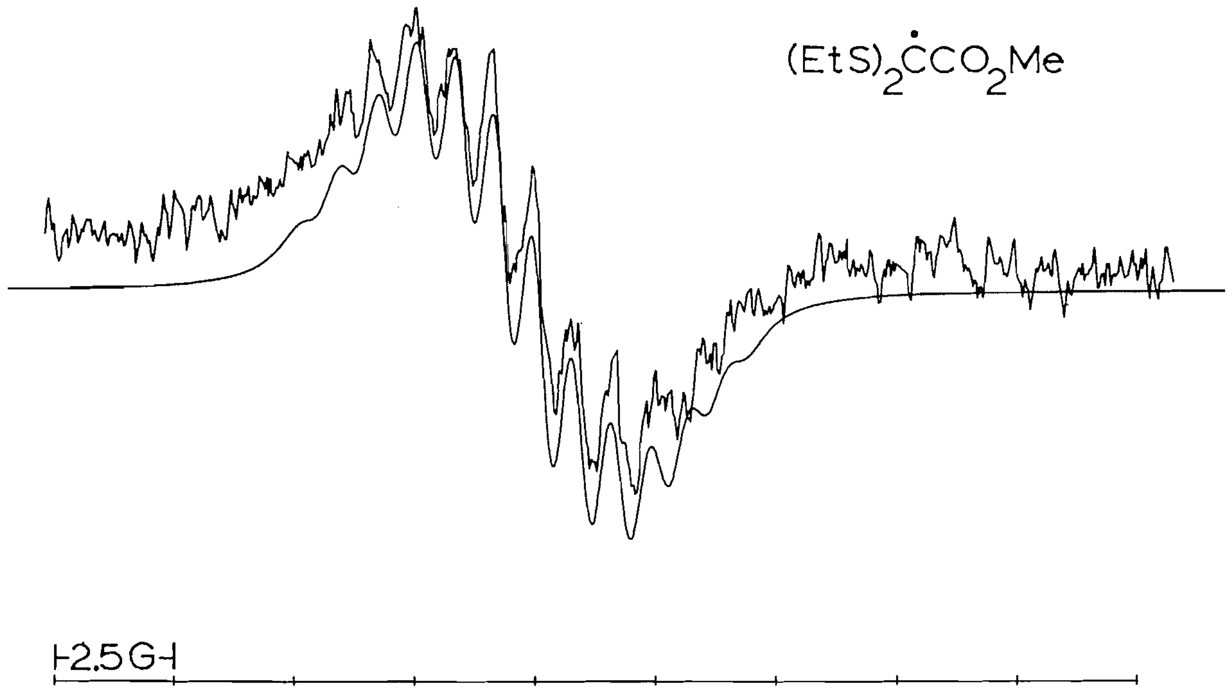

FIG. 11. The esr spectrum recorded during thermolysis of **9** (160°C) (smooth curve = simulated spectrum).

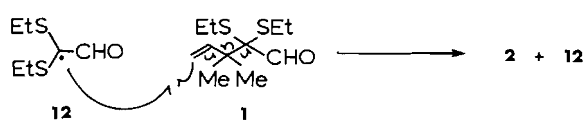

FIG. 12. Proposed free radical chain mechanism for the rearrangement of **1** into **2**.

dibromoethane. Then 15 g (127 mmol) of bromoethene was added over 0.5 h at such a rate as to maintain a gentle reflux. An additional 50 mL of tetrahydrofuran were added when the reaction was proceeding well. It was necessary to occasionally cool the reaction mixture in an ice bath in order to moderate the reaction. After the addition of the bromoethene was complete the reaction mixture was stirred for a further 1 h before an additional 50 mL of tetrahydrofuran were added. The reaction mixture was cooled to 0°C, and 15 g (104 mmol) of 3-pentanone were added over 0.5 h. The reaction mixture was stirred for an additional 1 h and then quenched with aqueous saturated NH_4Cl. The reaction mixture was diluted with 200 mL of ethyl ether, washed with 2 × 40 mL of H_2O, and dried ($MgSO_4$). The solvent was evaporated under reduced pressure to afford 10.5 g (92%) of 3-ethyl-4-penten-3-ol.

A mixture of 5.7 g (50 mmol) of the 3-ethyl-4-penten-3-ol prepared above and 8 g (ca. 100 mmol) of aqueous 48% HBr in 100 mL of pentane was stirred vigorously for 2 h. The reaction mixture was transferred to a separatory funnel and the aqueous phase was removed. The organic phase was washed with 2 × 25 mL of H_2O and dried ($MgSO_4$). The solvent was evaporated under reduced pressure at 0°C and the residual oil molecularly distilled to afford 5.9 g (66%) of 1-bromo-3-ethylpent-2-ene as a colourless liquid that was stored at −15°C until further use; bp (molecular distillation) 60°C/10 Torr (1 Torr = 133.3 Pa); infrared: 1650 cm^{-1}; ^1H nmr ($CDCl_3$) δ: 1.00 (t, 3, J = 7), 1.03 (t, 3, J = 7), 2.13 (m, 4), 4.05 (d, 2, J = 8), 5.48 (bt, 1, J = 8). *Mol. Wt.* calcd. for $C_7H_{13}Br^{81}$: 178.0162; found: 178.0160.

*Standard procedure for the preparation of compounds **1** and **3**–**8***

These compounds were prepared by a modification of the procedure of Ogura *et al.* (18).

A mixture of 10 mmol of the diethylthioketal, 10 mmol of the allylic bromide, and 15 mmol of Li_2CO_3 in 5 mL of *N*,*N*-dimethylformamide was stirred for 1–6 days under a nitrogen atmosphere. The reaction mixture was diluted with petroleum ether, washed several times with H_2O, and dried ($MgSO_4$). The solvent was evaporated under reduced pressure and the product purified by flash chromatography on silica gel using 10% ethyl acetate in petroleum ether (v/v) as the eluting solvent.

*2,2-Bis(ethylthio)-3,3-dimethylpent-4-enal (**1**)*: bp (molecular distillation) 80°C/0.1 Torr; infrared: 1710 cm^{-1}; ^1H nmr (CCl_4) δ: 1.20 (t, 6, J = 7), 1.25 (s, 6), 2.49 (dq, 2, J = 11.5, 7), 2.64 (dq, 2, J = 11.6, 7), 5.00 (dd, 1, J = 18, 1.5), 5.02 (dd, 1, J = 10, 1.5), 6.10 (dd, 1, J = 18, 10), 9.20 (s, 1). *Anal.* calcd. for $C_{11}H_{20}OS_2$ (232.410): C 56.85, H 8.67, S 27.59; found: C 56.55, H 8.65, S 27.33. *Mol. Wt.* calcd. for $C_{11}H_{20}OS_2$: 232.0956; found: 232.0944.

*2,2-Bis(ethylthio)-3-methylpent-4-enal (**3**)*: bp (molecular distillation) 80°C/0.1 Torr; infrared: 1710 cm^{-1}; ^1H nmr (CCl_4) δ: 1.18 (d, 3, J = 7), 1.2 (t, 6, J = 7), 2.5 (m, 4), 2.67 (m,1), 4.98 (m, 1), 5.00 (m, 1), 5.9 (m, 1), 9.0 (s, 1). *Anal.* calcd. for $C_{11}H_{18}OS_2$ (218.381): C 55.00, H 8.31, S 29.36; found: C 55.26, H 8.50, S 29.15. *Mol. Wt.* calcd. for $C_{10}H_{18}OS_2$: 218.0799; found: 218.0801.

*2,2-Bis(ethylthio)-3-phenylpent-4-enal (**4**)*: bp (molecular distillation) 80°C/0.1 Torr; infrared: 1715 cm^{-1}; ^1H nmr (CCl_4) δ: 1.1 (t, 3, J = 7), 1.17 (t, 3, J = 7), 2.37 (m, 4), 4.9 (d, 1 J = 8), 5.03 (dd, 1, J = 17, 1.5), 5.17 (dd, 1, J = 11, 1.5), 6.33 (ddd, 1, J = 17, 11, 8), 7.17 (m, 5), 9.00 (s, 1). *Anal.* calcd. for $C_{15}H_{20}OS_2$ (280.453): C 64.24, H 7.19, S 22.86; found: C 64.06, H 7.09, S 22.63. *Mol. Wt.* calcd. for $C_{15}H_{20}OS_2$: 280.0955; found: 280.0962.

*2,2-Bis(ethylthio)-3,3-diethylpent-4-enal (**5**)*: infrared: 1705 cm^{-1}; ^1H nmr ($CDCl_3$) δ: 0.75 (t, 6, J = 6.5), 1.15 (t, 6, J = 7), 1.73 (dq, 2, J = 14, 6.5), 1.88 (dq, 2, J = 14, 6.5), 2.40 (dq, 2, J = 13.7), 2.59 (dq, 1, J = 13.7), 5.02 (dd, 1, J = 18, 1.5), 5.21 (dd, 1, J = 11, 1.5), 5.91 (dd, 1, J = 18, 11), 9.34 (s, 1). *Anal.* calcd. for $C_{13}H_{24}OS_2$ (260.464): C 59.95, H 9.29, S 24.62; found: C 59.38, H 9.38, S 24.90. *Mol. Wt.* calcd. for $C_{13}H_{24}OS_2$: 260.1269; found: 260.1267.

*2,2-(1′,3′-Propanedithio)-3,3-dimethylpent-4-enal (**6**)*: bp 90°C/0.1 Torr (lit. (30) bp 123°C/1 Torr); infrared: 1710 cm^{-1}; ^1H nmr ($CDCl_3$) δ: 1.3 (s, 6), 1.5–2.1 (m, 2), 2.3–3.2 (m 4), 5.01 (dd, 1, J = 17, 1.5), 5.05 (dd, 1, J = 10, 1.5), 6.1 (m, 1), 9.3 (s, 1).

2,2-Bis(ethylthio)-3,3-bis(trideuteriomethyl)pent-4-enal (7): bp (molecular distillation) 80°C/0.1 Torr; infrared: 1710 cm^{-1}; ^{1}H nmr ($CDCl_3$) δ: 1.22 (t, 6, J = 7), 2.6 (m, 4), 5.08 (dd, 1, J = 18, 1.5), 5.13 (dd, 1, J = 10.5, 1.5), 6.08 (m, 1), 9.35 (s, 1). *Mol. Wt.* calcd. for $C_{11}H_{14}D_6OS_2$: 238.1328; found: 238.1330.

2,2-Bis(ethylthio)-3,3-dimethylpent-4-enenitrile (8): bp (molecular distillation) 80°C/0.1 Torr; infrared: 2240 cm^{-1} ^{1}H nmr ($CDCl_3$): δ: 1.31 (t, 6, J = 7), 1.36 (s, 6), 2.87 (q, 4, J = 7), 5.22 (dd, 1, J = 18, 1), 5.22 (dd, J = 10, 1), 6.14 (dd, 1, J = 18, 10). *Anal.* calcd. for $C_{11}H_{19}NS_2$ (229.41): C 57.59, H 8.35, N 6.11; found: C 57.90, H 8.40 N 6.00. *Mol. Wt.* calcd. for $C_{11}H_{19}NS_2$: 229.0959; found: 229.0959.

Methyl 2,2-bis(ethylthio)-3,3-dimethylpent-4-enoate (9)

To a solution of 0.292 g (ca. 1.5 mmol) of $AgBF_4$ in acetonitrile was added 0.30 g (1.55 mmol) of methyl 2,2-bis(ethylthio)acetate (31) followed by 0.19 g (1.25 mmol) of 1-bromo-3-methylbut-2-ene. An immediate yellow precipitate resulted. The reaction mixture was stirred for 3 h at room temperature and then 0.300 g (ca. 2 mmol) of diazabicyclo[3.3.0]undecene was added and the reaction mixture was stirred for an additional 3 h. The reaction mixture was diluted with petroleum ether and centrifuged. The clear organic phase was washed with 2 × 2 mL of aqueous 2 N HCl, 2 mL of H_2O, and dried ($MgSO_4$). The solvent was evaporated under reduced pressure to afford a pale yellow oil, which upon flash chromatography on silica gel using 5% ethyl acetate in petroleum ether (v/v) as the eluting solvent afforded 0.117 g (42%) of compound **9**; bp (molecular distillation) 80°C/0.1 Torr infrared: 1727 cm^{-1}; ^{1}H nmr ($CDCl_3$): δ: 1.18 (t, 6, J = 7), 1.24 (s, 6), 2.63 (q, 4, J = 7), 3.72 (s, 3), 5.02 (dd, 1, J = 18, 1), 5.02 (dd, 1, J = 10, 1), 6.17 (dd, 1, J = 18, 10). *Anal.* calcd. for $C_{12}H_{22}O_2S_2$ (262.437): C 54.92, H 8.45, S 24.44; found: C 54.67, H 8.55, S 24.17. *Mol. Wt.* calcd. for $C_{12}H_{22}O_2S_2$: 262.1061; found: 262.1066.

The reference standards for the products of the rearrangement were prepared according to procedures developed in this laboratory and published previously (aldehydes, ref. 6; nitrile, ref. 20). The following data are for previously unreported compounds.

2,2-Bis(ethylthio)-5-methyl-d$_3$-hex-4-enal-6-d$_3$ (22): bp (molecular distillation) 70°C/0.1 Torr infrared: 1715 cm^{-1}; ^{1}H nmr ($CDCl_3$): δ: 1.23 (t, 6, J = 7), 2.55 (q, 4, J = 7), 2.58 (d, 2, J = 6.5), 5.28 (t, 1, J = 6.5), 9.05 (s, 1). *Mol. Wt.* calcd. for $C_{11}H_{14}OD_6S_2$: 238.1332; found: 238.1332.

Methyl 2,2-bis(ethylthio)-5-methylhex-4-enoate (14): bp (molecular distillation) 80°C/0.1 Torr; infrared: 1730 cm^{-1}; ^{1}H nmr ($CDCl_3$): δ: 1.25 (t, 6, J = 7), 1.66 (s, 3), 1.74 (d, 3, J = 1), 2.66 (q, 4, J = 7), 2.70 (d, 2, J = 7), 3.78 (s, 3), 5.23 (tm, 1, J = 7, 1). *Anal.* calcd. for $C_{20}H_{22}O_2S_2$ (262.437): C 54.92, H 8.45, S 24.44; found: C 55.20, H 8.49, S 24.22. *Mol. Wt.* calcd. for $C_{20}H_{22}O_2S_2$: 262.1061; found 262.1067.

2,2-(1′,3′-Propanedithio)-5-methylhex-4-enal (21)

This compound was prepared in 64% overall yield by modification of the metalloenamine procedure (6) usine 2,2-(1′,3′-propanedithio)-ethanal (32) as the starting material; bp (molecular distillation) 80°C/0.1 Torr; infrared: 1715 cm^{-1}; ^{1}H nmr ($CDCl_3$): δ: 1.61 (s, 3), 1.66 (d, 3, J = 1.5), 2.02 (m, 2), 2.54 (m, 4), 3 (m, 2), 5.12 (tm, 1), 9.04 (s, 1). *Anal.* calcd. for $C_{10}H_{16}O_2$ (216.367): C 55.51, H 7.45, S 29.64; found: C 55.77, H 7.55, S 29.38. *Mol. Wt.* calcd. for $C_{10}H_{16}OS_2$: 216.0643; found: 216.0641.

*Kinetic studies on the rearrangements of **1**, **4**, **6**, **8**, and **9***

*Aldehydes **1**, **4**, and **6***

A solution of 0.04 g of freshly purified aldehyde in 0.300 mL of freshly distilled tetradecane (or decane or N, N-dimethylformamide-d_7) in a ^{1}H nmr tube, which has been dried at 120°C and cooled in a stream of argon, was degassed by bubbling argon through the solution for 0.5 h. The tube was capped with a rubber serum cap carrying an inlet needle for argon and the tube was placed in a constant-temperature oil bath. The tube was periodically removed from the oil bath and immersed immediately in an ice-water bath to quench the reaction. The reaction progress was analyzed by ^{1}H nmr spectroscopy.

*Nitrile **8** and ester **9***

The relative gas chromatographic detector responses of the starting materials and the products were established by injecting aliquots of known mixtures of the starting material and products.

A solution of 0.005 g of the compound in 0.100 mL of tetradecane in a 4 cm × 0.5 cm tapered ampoule, which had been dried at 120°C and cooled in a stream of argon, was degassed by bubbling argon through the solution for 0.5 h. The ampoule was fitted with a rubber serum cap carrying an inlet needle for argon and the ampoule was immersed in a constant temperature oil bath. Sample aliquots were removed peridically using a microsyringe and the samples analyzed by gas chromatography to determine the progress of the reaction.

Crossover experiments

A solution of 0.012 g (0.05 mmol) of aldehyde **7** and 0.026 g (0.1 mmol) of ester **9** in 0.300 mL of freshly distilled tetradecane in a tube was degassed by bubbling argon through the solution for 0.5 h. The tube was fitted with a rubber serum cap fitted with an inlet needle for argon and was heated at 160°C for 4 h. The reaction mixture was cooled and then transferred onto a 10-g column of Florisil. Initial elution of the column was performed with 50 mL of petroleum ether in order to elute the hydrocarbon solvent. Then elution with 5% ethyl acetate in petroleum ether (v/v) provided a mixture of the reaction products. The mixture was separated by preparative thin-layer chromatography on silica gel using 10% ethyl acetate in petroleum ether (v/v) as the eluting solvent to provide 0.007 g of the rearranged aldehydes, and 0.012 g of the rearranged esters.

Aldehyde mixture

High resolution mass spectrometry:

m/e	% Intensity
238.1327 ($C_{11}H_{14}OS_2D_6$)(M^{*+})	9.0
232.0957 ($C_{11}H_{20}OS_2$)(M^+)	5.2

Ester mixture

High resolution mass spectrometry:

m/e	% Intensity
268.1434 ($C_{12}H_{16}O_2S_2D_6$)(M^{*+})	5.6
262.1061 ($C_{12}H_{22}O_2S_2$)(M^+)	22.0

Control experiments

1. A solution of 0.012 g (0.05 mmol) of aldehyde **7** and 0.026 g (0.1 mmol) of ester **14** in tetradecane was heated at 160°C for 4 h and worked up as above to provide 0.08 g of aldehyde **22** and 0.018 g of ester **14**.

2. The above experiment was repeated with 0.012 g (0.05 mmol) of aldehyde **22** and ester **14**.

In neither case were any crossover products observed by ^{1}H nmr or mass spectral analysis.

Trapping experiment

A solution of 0.232 g (1.0 mmol) of aldehyde **1** in 2.0 mL of 1,4-cyclohexadiene and 2.0 mL of freshly distilled decane in a thick-walled glass tube was degassed with argon and sealed. The tube was heated at 145°C for 2.5 h, cooled to 0°C, and opened. The reaction mixture was concentrated by evaporation at water aspirator pressure to remove the 1,4-cyclohexadiene and any benzene formed in the reaction. An ^{1}H nmr spectrum (δ 3.0−11.0) of the reaction mixture indicated that it consisted of a clean mixture of starting aldehyde **1** (45%), rearranged aldehyde **2** (25%), and 2,2-bis(ethylthio)ethanal (30%).

Acknowledgements

This work was supported by the Natural Sciences and Engineering Research Council of Canada and in part by a

Cottrell Research Grant provided by the Research Corporation. The authors wish to thank Professor F. G. Herring, University of British Columbia, for recording and simulating the esr spectra reported herein, and Professor J. E. Baldwin, Oxford University, for helpful discussions regarding the proposed chain reaction nature of the rearrangement.

1. C. W. SPANGLER. Chem. Rev. 187 (1976).
2. R. C. COOKSON and J. E. KEMP. J. Chem. Soc. Chem. Commun. 385 (1971).
3. J. E. BALDWIN and R. E. HACKLER. J. Am. Chem. Soc. **91**, 3646 (1969); J. E. BALDWIN and J. E. BROWN. J. Am. Chem. Soc. **91**, 3647 (1969); J. E. BALDWIN, J. E. BROWN, and R. W. CORDELL. J. Chem. Soc. D, 31 (1970); J. E. BALDWIN and C. H. ARMSTRONG. J. Chem. Soc. D, 631 (1970); J. E. BALDWIN, W. F. ERICKSON, R. E. HACKLER, and R. M. SCOTT. J. Chem. Soc. D, 576 (1970); J. E. BALDWIN, J. DEBERNARDIS, and J. E. PATRICK. Tetrahedron Lett. 353 (1970); J. E. BALDWIN and J. A. WALKER. J. Am. Chem. Soc. **96**, 596 (1974).
4. R. W. JEMISON, T. LAIRD, W. D. OLLIS, and I. O. SUTHERLAND. J. Chem. Soc. Perkin Trans. 1, 1450 (1980).
5. G. S. BATES and S. RAMASWAMY. Can. J. Chem. **59**, 3120 (1981).
6. G. S. BATES and S. RAMASWAMY. Can. J. Chem. **61**, 2466 (1983).
7. J. W. TIMBERLAKE, A. W. GARNER, and M. L. HODGE. Tetrahedron Lett. 309 (1973).
8. A. OHNO and Y. OHNISHI. Tetrahedron Lett. 4405 (1969).
9. H. G. VIEHE, R. MURENHI, L. STELLA, and Z. JANOUSEK. Angew. Chem. Int. Ed. Eng. **18**, 917 (1979).
10. R. B. WOODWARD and R. HOFFMANN. The conservation of orbital symmetry. Academic Press, New York, NY. 1970.
11. E. G. FOSTER, A. C. COPE and F. DANIELS. J. Am. Chem. Soc. **69**, 1893 (1947).
12. G. R. ALDRIDGE and G. W. MURPHY. J. Am. Chem. Soc. **73**, 1158 (1951).
13. H. M. FREY and R. K. SOLLY. Trans. Faraday Soc. **64**, 1858 (1968).
14. W. VON E. DOERING and E. K. G. SCHMIDT. Tetrahedron, **27**, 2005 (1971).
15. R. STEWART. The investigation of organic reactions. Prentice—Hall, Inc., Englewood Cliffs, NJ. 1966. pp. 74–76.
16. D. C. WIGFIELD and S. FEINER. Can. J. Chem. **48**, 855 (1970).
17. J. E. BALDWIN, R. E. HECKLER and D. P. KELLY. Chem. Commun. 537 (1968); 538 (1968).
18. K. OGURA, S. FURUKAWA, and G. TSUCHIHASHI. J. Am. Chem. Soc. **102**, 2125 (1980).
19. H. REICH and M. L. COHEN. J. Am. Chem. Soc. **101**, 1307 (1979).
20. G. S. BATES and S. RAMASWAMY. Can. J. Chem. **61**, 2006 (1983).
21. H. EYRING. J. Chem. Phys. **3**, 107 (1935); W. F. K. WYNNE-JONES and H. EYRING. J. Chem. Phys. 492 (1935); A. J. GORDON and R. A. FORD. The chemist's companion. John Wiley and Sons, Inc., New York, NY. 1972. p. 136.
22. A. STREITWIESER, JR., and C. H. HEATHCOCK. Introduction to organic chemistry. 2nd ed. Macmillan Publishing Company, Inc., New York, NY. 1981. p. 558.
23. J. M. DUST and D. R. ARNOLD. J. Am. Chem. Soc. **105**, 1221 (1983) and subsequent corrections; J. Am. Chem. Soc. **105**, 6531 (1983).
24. D. C. WIGFIELD and B. LEM. Tetrahedron, **31**, 9 (1975).
25. T. H. LOWRY and K. S. RICHARDSON. Mechanism and theory in organic chemistry. Harper Row, New York, NY. 1976. Chapt. 9.
26. R. E. LINDER, D. L. WINTERS, and A. C. LING. Can. J. Chem. **54**, 1405 (1976).
27. P. J. KRUSIC and J. K. KOCHI. J. Am. Chem. Soc. **93**, 846 (1971).
28. R. LIVINGSTON and H. ZELDES. J. Am. Chem. Soc. **88**, 433 (1966).
29. P. S. PHILLIPS and F. G. HERRING. J. Magn. Reson. **57**, 43 (1984).
30. S. R. WILSON and J. MATHEW. Synthesis, 625 (1980).
31. L. M. LERNER. J. Org. Chem. **41**, 2228 (1976).
32. A. I. MEYERS and R. C. STRICKLAND. J. Org. Chem. **37**, 2579 (1972).

Indium(III) compounds with the 2-[(dimethylamino)methyl]phenyl ligand

RICHARD S. STEEVENSZ AND DENNIS G. TUCK
Department of Chemistry, University of Windsor, Windsor, Ont., Canada N9B 3P4

AND

HARRY A. MEINEMA AND JAN G. NOLTES
Institute of Applied Chemistry, TNO, P.O. Box 5009, 3502 JA Utrecht, The Netherlands

Received May 9, 1984

RICHARD S. STEEVENSZ, DENNIS G. TUCK, HARRY A. MEINEMA, and JAN G. NOLTES. Can. J. Chem. **63**, 755 (1985).

The syntheses of the arylindium compounds L_2InX (X = Cl, I), L_2InR (R = CH_3, C_6H_5), L_3In and $L_2InSnPh_3$ (L = 2-[(dimethylamino)methyl]phenyl) are reported. The pathway of the redistribution reactions involving $InCl_3$ and L_3In are discussed. Mass and ^1H nmr spectra are reported.

RICHARD S. STEEVENSZ, DENNIS G. TUCK, HARRY A. MEINEMA et JAN G. NOLTES. Can. J. Chem. **63**, 755 (1985).

On rapporte la synthèse de composés arylindium des types L_2InX (X = Cl, I), L_2InR (R = CH_3, C_6H_5), L_3In et $L_2InSnPh_3$ (L = [(diméthylamino)méthyl]-2 phényle). On discute des voies des réactions de redistribution impliquant le $InCl_3$ et le L_3In. On rapporte les spectres de masse et de rmn du ^1H.

[Traduit par le journal]

Introduction

This paper, and those published earlier (1, 2), represent the intersection of studies of complexes with the bidentate 2−[(dimethylamino)methyl]phenyl ligand (= L) on the one hand, and investigations of the chemistry of indium on the other. The coordination chemistry of organoindium(III) compounds and their complexes has been of considerable recent interest, and four-, five-, and six-coordinate species are now known (3). We have recently reported the preparation and X-ray crystallographic study of the five coordinate L_2InCl (1), and nmr investigations have established the fluxional behaviour of this and related molecules in solution (2).

The present investigation has focussed on the preparation of L_3In, L_2InR (R = CH_3, C_6H_5), and the use of L_2InCl as a starting point in the synthesis of In—M bonds.

Experimental

General

All solvents were purified and dried over sodium. Reactions were carried out under dry nitrogen. Nuclear magnetic resonance spectra were obtained on JEOL C6OHL, Varian EM360, or Bruker CXP-100 spectrometers, using tetramethylsilane as internal standard. Infrared spectra were run on a Beckman IR-12 spectrometer, using KBr or CsI cells, and mass spectra on a Varian MAT CH-5DF instrument operating in the field desorption (FD) or electron impact (EI) modes. The lithiation of (dimethylamino)methylbenzene (HL) followed the procedure described elsewhere (4, 5).

Preparation of tris{2-[(dimethylamino)methyl]phenyl}indium (L_3In)

Indium(III) chloride (1 g, 5.0 mmol) was added to a fresh preparation of LiL (22 mmol) in 60 mL diethyl ether. The reaction mixture was stirred for a period of 3 h, after which the white suspension was filtered and the ether solution evaporated to dryness. The sticky solid residue was redissolved in benzene, filtered, and the solution concentrated to give a quantitative yield of $In[C_6H_4CH_2N(CH_3)_2\text{-}2]_3$ as colourless crystals which were washed with cold petroleum ether (30−60°C) and dried *in vacuo*. *Anal.* Calcd.: In 22.2; found: In 21.9. Nuclear magnetic resonance results are given in Table 1.

Preparation of bis{2-[(dimethylamino)methyl]phenyl}indium chloride (L_2InCl) (I)

(*a*) Freshly prepared LiL (0.22 mol) was added dropwise over 45 min to a suspension of indium(III) chloride (24.0 g, 0.11 mol) in 100 mL of diethyl ether. An exothermic reaction was observed during the addition, resulting in a brown suspension. The mixture was stirred

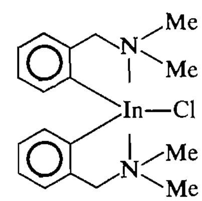

I

for 24 h at room temperature, after which the light brown mixture was filtered and the residue washed with benzene (3 × 100 mL). The volume of the agglomerated benzene phase was reduced to 50 mL, and the white solids which formed were collected, washed with cold petroleum ether (30−60°C), and dried *in vacuo*. The benzene filtrate was further reduced in volume and again treated with petroleum ether, resulting in additional solid. A total yield of 32.0 g (74%) of $ClIn[C_6H_4CH_2N(CH_3)_2]_2$ was obtained. Melting point 190−191°C. *Anal.* calcd.: In 27.4, Cl 8.48; found: In 27.6, Cl 8.39. The nmr spectrum is tabulated in Table 1.

(*b*) Solid $InCl_3$ was added to a solution containing InL_3 in 30 mL diethyl ether. In the initial stage of the reaction, $InCl_3$ was seen to dissolve but after 24 h at room temperature, L_2InCl was present as a suspended crystalline product which was separated by vacuum filtration and dried *in vacuo*. When the quantities of $InCl_3$ (0.37 g, 1.7 mmol) and L_3In (1.7 g, 3.3 mmol) corresponded to those required for the process $InCl_3 + 2L_3In \rightarrow 3L_2InCl$, the yield of L_2InCl was essentially quantitative. In a later experiment, $InCl_3$ (1.50 g, 6.8 mmol) was used in excess over L_3In (1.09 g, 2.1 mmol), but L_2InCl was the only product isolated and no evidence was obtained for the presence of $LInCl_2$ in the reaction mixture.

Preparation of bis{2-[(dimethylamino)methyl]phenyl} indium iodide (L_2InI)

A solution of InI_3 (5.0 g, 2.0 mmol) in diethyl ether (30 mL) was treated with 2 equiv. of freshly prepared LiL in the same solvent (24 h, room temperature). The colour of the InI_3 solution underwent a series of changes following the addition of LiL, from light yellow through red and then brown to a final colourless solution. The final isolation of L_2InI followed the method used for L_2InCl. *Anal.* calcd. for $C_{20}H_{24}NInI$: In 22.1, I 24.4; found: In 22.2, I 23.8.

Preparation of bis{2-[(dimethylamino)methyl]phenyl}methyl indium (L_2InMe)

A suspension of L_2InCl (0.46 g, 1.10 mmol) in 50 mL diethyl ether was treated with methyllithium (1.2 mmol) in diethyl ether, added in one operation at room temperature. The solid L_2InCl immediately

TABLE 1. [1]H nmr spectra of indium complexes and related compounds at 35°C (ppm from TMS)

Compound	Solvent	$N(CH_3)_2$[a]	CH_2[a]	*ortho*-C_6H_4	Other phenyl protons[b]	Other
LH	$CDCl_3$	2.26	3.45	[c]	7.3	
1,3-$C_6H_4(CH_2Br)_2$	$CDCl_3$	—	4.43	[c]	7.3	
1,3-$C_6H_4[N(CH_3)_2]_2$	$CDCl_3$	2.24	3.42	[c]	7.3	
L_2InCl	$CDCl_3$	2.60	3.75	7.60	7.15	
	C_6D_6	2.20	3.50	7.70	7.25	
L_2InCH_3	$CDCl_3$[d]	2.50	3.70	7.7	7.2	−0.03(In—CH_3)
	C_6D_6[e]	2.10(2)	3.30(12)	7.8(2)	7.25(7)	−0.05(3)
L_3In	$CDCl_3$	2.10	3.45	7.8	7.1	
	C_6D_6	1.90	3.33	7.88	7.25	

[a]All sharp singlets.
[b]Mid-point of multiplet.
[c]Not observed as separate resonance.
[d]Freshly prepared solution.
[e]Relative intensities in parentheses.

TABLE 2. Mass spectra of indium complexes

Compound	Method of ionisation[a]	Principle ion[b] m/e	Principle ion[b] Formula	Other important ions, and tentative identification
LBr	EI	170, 172	$C_7H_7Br^+$	86 ($C_5H_{12}N^+$); 84 ($C_5H_{10}N^+$); 28 ($C_2H_4^+$)
L_2InCl	EI	28	$C_2H_4^+$	85 ($C_5H_{11}N^+$); 83 ($C_5H_9N^+$); 79, 78 ($InNC_2H_5^{2+}$); 78, 77 ($InNC_2H_3^{2+}$); 44 ($NC_2H_6^+$)
L_2InCl	FD	417	$[L_2InCl - H]^+$	800 ($L_4In_2Cl^+$); 452 ($L_2InCl_2^+$); 382 ($[L_2In-H]^+$)
L_2InCH_3	FD	383	L_2In^+	531 ($L_3InCH_2^+$); 517 (L_3In^+); 398 ($L_2InCH_3^+$)
$L_2InC_6H_5$	FD	383	L_2In^+	919 ($[L_4In_2(C_6H_5)_2-H]^+$); 421 ($L_2InC_3H_2$); 77 ($C_6H_5^+$)
$Li[L_2In(CH_3)_2]$	FD	383	L_2In^+	517 (L_3In^+); 134 (L^+)

[a]EI = electron impact, FD = field desorption.
[b]All masses quoted as nearest integers; identification based on most abundant isotope of each atom.

dissolved, but after less than 30 s fine white particles of LiCl began to appear. After 24 h, LiCl was removed by filtration and ether was evaporated off, leaving a colourless crystalline solid. The crude material was redissolved in benzene, filtered, and concentrated. Subsequent trituration of the sticky solids with cold petroleum ether (0°C), produced $[C_6H_4CH_2N(CH_3)_2\text{-}2]_2InCH_3$ as a white powder which was dried *in vacuo*. Yield 0.35 g (77.0%). Alternatively, the initial solid was dissolved in benzene, and the solution cooled *in vacuo* to precipitate any residual solids which were removed by filtration. After repeating this sequence a number of times, the final product was obtained by crystallizing from cold (0°C) petroleum ether. *Anal.* calcd. for $C_{19}H_{27}N_2In$: In 28.9; found: In 29.4. This compound reacts with deuterated chloroform/TMS, apparently undergoing complete decomposition in ca. 10 min, but nmr spectra confirming the structure were obtained in C_6D_6 (see Table 2).

Preparation of bis{2-[(dimethylamino)methyl]phenyl}indium tin triphenyl ($L_2InSnPh_3$)

Triphenyltin chloride (1.9 g, 4.8 mmol) was added to a solution of sodium (0.22 g, 9.7 mmol) in 70 mL liquid ammonia at −78°C. The mixture was stirred for 30 min and then allowed to reach room temperature. The yellow−brown residue (Ph_3SnNa) was taken up in diethyl ether, the solution cooled to −78°C and L_2InCl (2.0 g, 4.8 mmol) added, as a solution in diethyl ether (15 mL), plus 5 mmol of pyridine. During a period of 3 h stirring, the yellow colour faded, giving a colourless mixture. The mixture was allowed to reach room temperature, solvent was removed by evaporation, and the resultant residue extracted with petroleum ether (30−60°C). The material obtained on evaporation of the filtrate was recrystallised from petroleum ether/diethyl ether mixtures to give $L_2InSnPh_3$ in 62% yield. *Anal.* calcd. for $C_{36}H_{39}N_2InSn$: In 15.7, Sn 16.2; found: In 16.1, Sn 16.6. Mass, vibrational, and [1]H nmr spectra, discussed below, confirm the identity of this compound.

When Ph_3SnLi was used instead of Ph_3SnNa in this preparation, the products included a tin compound (Sn content 55.7%) containing only aromatic groups ([1]H nmr), plus a metallic deposit and a compound shown to be L_2InPh. *Anal.* calcd. for $C_{24}H_{29}N_2In$: In 24.9, found: In 25.0. See below for mass spectrum.

Results and discussion

Preparative

A number of points concerning the synthesis of L_3In and L_2InCl require discussion. The selective formation of either L_2InCl or L_3In is affected both by the mode of addition and by the concentration. The slow addition of 2-[(dimethylamino)-methyl]phenyl lithium (LiL) to indium trichloride produces an exothermic reaction, in which the initial tan coloured precipitate slowly turns brown. Under these conditions (LiL:$InCl_3$ mole ratio 2:1) the predominant product is L_2InCl, with little or no by-products present. Reversal of this order, that is the addition of $InCl_3$ to LiL, produces a less selective reaction, in that both L_3In and L_2InCl are formed. We also found that the rapid addition of LiL to indium trichloride (overall mole ratio LiL:$InCl_3$ = 4:1) resulted in the formation of L_2InCl and L_3In in a 2:3 ratio after 6 h, but that after 24 h, the intermediary L_2InCl complex was totally converted to L_3In. Conversely, when $InCl_3$ was added to LiL (same overall mole ratio) the reaction was complete within 3 h at room temperature, with no L_2InCl being identified.

The course of these processes, and the relative ratios of L_2InCl and L_3In in the reaction mixture, are readily estimated by utilizing the differences in the ^1H nmr spectra of the two compounds in the 2−4 ppm region (see Table 1). The isolation and purification of the complexes is facilitated by their solubilities; both are soluble in ether, but L_2InCl is only slightly soluble in benzene, and even less so in petroleum ether (30−60°C). The less polar L_3In complex is very soluble in diethyl ether and only partially soluble in petroleum ether. Both compounds are relatively stable in dry air for several hours, but readily decompose in the presence of moisture.

An interesting feature of the redistribution reactions between L_3In and $InCl_3$ is that the potentially four-coordinate compound $LInCl_2$ could not be isolated. In contrast, the reaction of triphenylindium and indium trichloride (1:2 mole ratio) gives a quantitative yield of $PhInCl_2$, as does the reaction of Ph_2InCl and $InCl_3$ (1:1 mole ratio) (6, 7). The inability of L_2InCl to react with $InCl_3$ is presumably due to the stable five-coordination of the former in both solid (1) and solution (2) states. The presence of the internal $—CH_2NMe_2$ group in L_2InCl may also be important, since its coordinating properties have been shown to influence product formation in the redistribution reactions of aryltin compounds (8).

The reaction between L_2InCl and MeLi gives L_2InMe in reasonably good yield, but side-products, which on the evidence of ^1H nmr spectra may include $LInMe_2$, are also formed. The reaction pathway presumably involves the intermediate $Li[L_2In(Cl)Me]$, and in this context we note that the addition of MeLi to InL_3 in diethyl ether at room temperature produces a variety of compounds, including the analogous $Li[L_2InMe_2]$. *Anal.* calcd. for $C_{20}H_{30}N_2InLi$: In 27.3, Li 1.65; found: In 26.9, Li 2.02.

Hydrogenolysis reactions of metal−carbon bonds (alkane elimination) have been widely used in the synthesis of organometallic compounds containing metal−metal bonds. An appropriate example in Main Group chemistry is the preparation in high yield of compounds containing Group II (Zn, Cd) − Group IV (Ge, Sn) bonds by the reaction of dialkylzinc or cadmium compounds with triphenylgermanium (or tin) hydride (9). The reaction of L_2InMe with an organometal hydride appeared to offer a useful route to In—M bonded species, but methane elimination was not observed when L_2InMe was treated under various conditions with Ph_3SnH, Ph_3GeH, or Ph_3SiH. The compound $L_2InSnPh_3$ was eventually synthesized via the reaction between L_2InCl and Ph_3SnNa. The ^1H nmr spectrum of this material ($CDCl_3$/TMS) consisted of complex aromatic multiplets plus singlet CH_2 and $N(CH_3)_2$ resonances in the integrated ratio 6.1:1:2.7 (calcd. 5.75:1:3). The Raman spectrum has an intense band at 205 cm^{-1}, with a corresponding absorption at 206 cm^{-1} in the far infrared, assigned to ν(In—Sn). An interesting feature of the reaction is that as noted earlier the use of Ph_3SnLi gives rise inter alia to L_2InPh and aryl tin species. We suggest that the reaction intermediate **II** is of the form

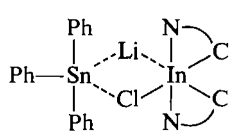

II

which undergoes slow decomposition by phenyl group transfer to L_2InPh and hexaphenylditin, probably via $(Ph_2Sn)_n$. The use of $NaSnPh_3$ apparently allows rapid elimination of NaCl and formation of the stable $L_2InSnPh_3$ species. The phenyl transfer process observed in the lithium case is not unusual; the organotin−zinc compound $Ph_3SnZnCl$ decomposes to PhZnCl and $(Ph_2Sn)_n$ in an apparently analogous manner (10).

Since compounds containing In—In bonds are now known (11−13), we made (unsuccessful) attempts under a wide range of conditions to synthesize L_2InInL_2 by treating L_2InCl with sodium in liquid ammonia. The blue colour of the sodium solution discharged and the mixture turned black; after ca. 10 h the ammonia was removed and the resultant solids extracted with metal were recovered in each case, along with unreacted L_2InCl, and L_3In. A related series of reactions involving sodium and L_2InI in refluxing benzene or toluene gave essentially identical results.

Finally, we note that despite extensive efforts, we were unable to reduce L_2InCl or L_2InI to L_2InH, with none of the reducing agents investigated ($LiAlH_4$, $NaBH_4$, NaH) producing any evidence of reduction of the In—X bond. Negative results were also obtained in attempts to synthesize salts of L_2In^+, for example by the reaction of L_2InCl with $NaClO_4$ or $NaBF_4$ under a variety of solvent and temperature conditions. The molar conductivity of L_2InCl in nitromethane was found to be 19 ohm^{-1} cm^2 (cf. 120−130 for 1:1 electrolytes in this solvent (14)), showing that there is essentially no spontaneous dissociation into L_2In^+ and Cl^- ions in this solvent. The mass spectral results (see below) also demonstrate quite clearly that fragmentation of L_2InCl does not give rise to L_2In^+ ions in the gas phase, as do L_2InMe and L_2InPh, but rather undergoes hydrogen chloride abstraction to $[L_2In - H]^+$. These results are in keeping with the failure to generate L_2In^+ derivatives by solution phase reactions, and we conclude that this ion is unstable. The previously reported lability of the corresponding isoelectronic L_2Cd compound in solution (5) emphasizes the inherent instability of such L_2M species.

Nuclear magnetic resonance spectroscopy

The ^1H and ^{13}C nmr spectra of L_2InCl have been discussed in detail elsewhere (2) and are noted here only for purposes of comparison. Table 1 gives the ^1H nmr spectra of this and related compounds in $CDCl_3$ and C_6D_6 solution at room temperature. The $N(CH_3)_2$ and NCH_2 protons in L_3In are at significantly higher field than for the corresponding atoms in L_2InCl and L_2InMe. Change of solvent from $CDCl_3$ to C_6D_6 results in an upfield shift for these same protons; similar results have been previously reported for 2-[(dimethylamino)methyl]-phenyl compounds of tin (8), and cadmium (5), and it seems probable that in such systems the benzene solvent molecule is oriented at the CH_2NMe_2 site in such a way that these protons are in the diamagnetic region. We have also recorded ^{13}C spectra for some of these molecules, and again the results are similar to those for L_2InCl (2).

The ^1H nmr spectrum of L_3In at 223 K shows only small differences from that at 297 K. Both $N(CH_3)_2$ and NCH_2 resonances are significantly broadened, with half-widths of 7 and 5 Hz, respectively, and a slight assymetry is observed on the high frequency side of both bands, but the effects are much less pronounced than for L_2InCl under comparable conditions. It therefore appears that the fluxional behaviour of L_3In persists even at −50°C, in keeping with the properties of other six-coordinate indium(III) compounds, for which coordination number changes $6 \rightarrow 5 \rightarrow 6$ occur easily even at low temperatures (refs. 2, 15, and references therein).

Mass spectra

Table 2 records the important features of the mass spectra of compounds prepared in this work.

The electron impact (EI) mass spectrum of LBr, taken from an earlier publication (5) shows that the principal ion is $C_7H_7Br^+$, with $C_5H_{12}N^+$, $C_5H_{10}N^+$, and $C_2H_4^+$ as the other important species. The spectrum of L_2InCl in the same mode is quite different, with $C_2H_4^+$ as the principal ion. There are no important peaks with $m/e > 85$, although many low abundant species were recorded up to $m/e \sim 300$. No simple L_nIn^+ ions were detected; the ions at $m/e = 85$ and 83 are clearly different from those at m/e and 84 from LBr. A group of ions at m/e 77−79 are tentatively assigned to doubly charged ions containing indium, as indicated by the isotopic intensities.

The field desorption (FD) spectra of L_2InCH_3, $L_2InC_6H_5$, and $Li[L_2In(CH_3)_2]$ all show L_2In^+ as the principal ion. Weak molecular ions were detected for $L_2InCH_3^+$ and $L_2InC_6H_5^+$, and $LInCH_3^+$ and $LInC_6H_5^+$ ions are also present in low but significant abundance. The formation of such singly charged MX_2^+ ions is usual for indium(III) compounds (16, 17). The FD spectrum of L_2InCl is quite different from those just discussed. The predominant ion is at $m/e = 417$, corresponding to the loss of hydrogen, and instead of L_2In^+ one finds $[L_2In - H]^+$, indicating loss of HCl. These results are in agreement with those reported above, emphasising that L_2InCl does not readily lose chlorine to yield the L_2In^+ ion. One other important feature of the spectrum of L_2InCl is the formation of oligomeric ions (e.g. $L_2In_2Cl^+$), or the formation of ions indicating ligand transfer (e.g. L_3In^+ from L_2InCH_3). Such processes are not uncommon in FD mass spectrometry, and are to be understood in terms of ionization of a condensed phase.

The FD mass spectrum of $L_2InSnPh_3$ had the predominant ion at $m/e = 308$ (InL_2^+), with other intense peaks at 346−351 arising from the isotopic $SnPh_3$ ions. The heaviest ion had $m/e = 702$, corresponding to the loss of two methyl groups from the parent molecule.

Acknowledgement

J.G.N. and D.G.T. gratefully acknowledge financial support of this work by NATO (Grant No. 1247).

1. M. A. Khan, R. S. Steevensz, D. G. Tuck, J. G. Noltes, and P. W. R. Corfield. Inorg. Chem. **19**, 3407 (1980).
2. J. T. B. H. Jastrzebski, G. van Koten, D. G. Tuck, H. A. Meinema, and J. G. Noltes. Organometallics, **1**, 1492 (1982).
3. D. G. Tuck. Comprehensive organometallic chemistry. Vol. 1 *Edited by* G. Wilkinson. Pergamon Press, London. 1982. p. 683.
4. N. Muller and A. L. Otermat. Inorg. Chem. **2**, 1075 (1963).
5. A. Osman, R. S. Steevensz, D. G. Tuck, H. A. Meinema, and J. G. Noltes. Can. J. Chem. **62**, 1698 (1984).
6. H. A. Meinema and J. G. Noltes. Unpublished results.
7. S. B. Miller, B. L. Jelus, and T. B. Brill. J. Organomet. Chem. **96**, 1 (1975).
8. G. van Koten, C. A. Schaap, and J. G. Noltes. J. Organomet. Chem. **99**, 157 (1975).
9. F. J. A. des Tombe, G. J. M. van der Kerk, H. M. J. C. Creemers, N. A. D. Carey, and J. G. Noltes. J. Organomet. Chem. **44**, 247 (1972).
10. F. J. A. des Tombe, G. J. M. van der Kerk, and J. G. Noltes. J. Organomet. Chem. **43**, 323 (1972).
11. M. J. Taylor, D. G. Tuck, and L. Victoriano. Can. J.Chem. **60**, 691 (1982).
12. I. Sinclair and I. J. Worral. Can. J. Chem. **60**, 695 (1982).
13. M. A. Khan, C. Peppe, and D. G. Tuck. Can. J. Chem. **62**, 601 (1984).
14. W. J. Geary. Coord. Chem. Rev. **7**, 81 (1971).
15. A. J. Carty and D. G. Tuck. Prog. Inorg. Chem. **19**, 245 (1975).
16. P. Dobud and D. G. Tuck. Unpublished results.
17. D. G. Tuck, G. W. Wood, and S. Zhandhire. Can. J. Chem. **58**, 833 (1980).

Crystal structure of di-μ-hydroxobis[*fac*-trichloroaquotin(IV)] tetrahydrate, $[Cl_3(H_2O)Sn—OH—]_2 \cdot 4H_2O$, with observations on O···O distances and MOM angles in di-μ-oxygen bridges

T. STANLEY CAMERON, OSVALD KNOP, AND BEVERLY R. VINCENT[1]

Department of Chemistry, Dalhousie University, Halifax, N.S., Canada B3H 4J3

Received August 13, 1984

T. STANLEY CAMERON, OSVALD KNOP, and BEVERLY R. VINCENT. Can. J. Chem. **63**, 759 (1985).

The present redetermination of the crystal structure of the title compound agrees well with a previous determination by Barnes *et al.*, which it supplements by providing details of the hydrogen-bonding scheme. Scrutiny of the O···O distances in homonuclear di-μ-oxygen M_2O_2 bridges in well over a hundred compounds shows that the lower limit for this distance is ~2.3 Å, and that the corresponding distance in the title compound, 2.44(1) Å, is closer to this limit than the O···O distances in the majority of the compounds surveyed. Appreciably shorter nonbonded O···O distances are found only in oxyanions, in particular those acting as bidentate ligands of metal atoms and thus forming heteronuclear di-μ-oxo bridges; an O···O distance as short as ~2.0 Å has been reported and may constitute the limit of such nonbonded O···O distances in general.

T. STANLEY CAMERON, OSVALD KNOP et BEVERLY R. VINCENT. Can. J. Chem. **63**, 759 (1985).

La redétermination de la structure cristalline du composé mentionné dans le titre est en bon accord avec celle qui a été faite antérieurement par Barnes et ses collaborateurs; le présent travail sert de complément au travail rapporté antérieurement en fournissant des détails sur le réseau des liaisons hydrogènes. Un examen minutieux des distances O···O dans des ponts homonucléaires di-μ-oxygène M_2O_2, dans plus de cent composés, montre que la limite inférieure pour cette distance se situe autour de 2,3 Å et que la distance correspondante dans le composé mentionné dans le titre, 2,44(1) Å, est plus proche de cette limite que les distances O···O dans la majorité des composés examinés. Des distances O···O relativement plus courtes ne se retrouvent que dans des oxyanions; en particulier, on en retrouve dans ceux qui agissent comme ligands bidentates d'atomes métalliques et qui forment donc des ponts hétéronucléaires di-μ-oxo. Dans un cas particulier, une distance O···O aussi courte que 2,0 Å a été rapportée et cette valeur peut constituer la limite pour de telles distances O···O non liées.

[Traduit par le journal]

In a recent attempt to crystallize piperidinium hexachlorostannate(IV) from a concentrated, strongly HCl-acid aqueous solution of the amine and H_2SnCl_6, we obtained a small quantity of well-formed crystals the ir spectra of which, unexpectedly, contained no features attributable to CH_2 absorptions (Fig. 1). The sharp bands at 3586, 3528, 3499, 1630(sh), and 1599 cm^{-1} and the two very broad bands centering at 2930 and 2320 cm^{-1}, respectively, all disappeared after the crystals had been heated to 150°C, leaving the 4000−1400 cm^{-1} region completely featureless. This and the frequencies of the sharp bands pointed to strongly held water of hydration, possibly also to OH^- ions. The clear, colourless crystals were too few for a meaningful chemical analysis, but their good quality and their stability in air rendered them suitable for single-crystal X-ray diffraction. The crystal data obtained from a 0.2 × 0.2 × 0.2 mm^3 crystal with a CAD-4 four-circle diffractometer ($MoK\alpha_1$, λ = 0.70926 Å, graphite monochromator; θ-range, 2−27°) are summarized as follows:[2]

Monoclinic, $P2_1/n$ (No. 14); a = 9.676(8) Å, b = 6.518 (13) Å, c = 12.531(15) Å, β = 92.98(9)°, V = 789.2(32) Å^3. Total reflections measured, 1529; unique reflections, 1191 (of which 1053 with $I \geq 3\sigma(I)$, corrected for extinction but not for absorption, were used in the refinement).

A straightforward interpretation of the strong Patterson maxima and of subsequent Fourier maps, together with consideration of the ir spectra and chemical reasonability, established the

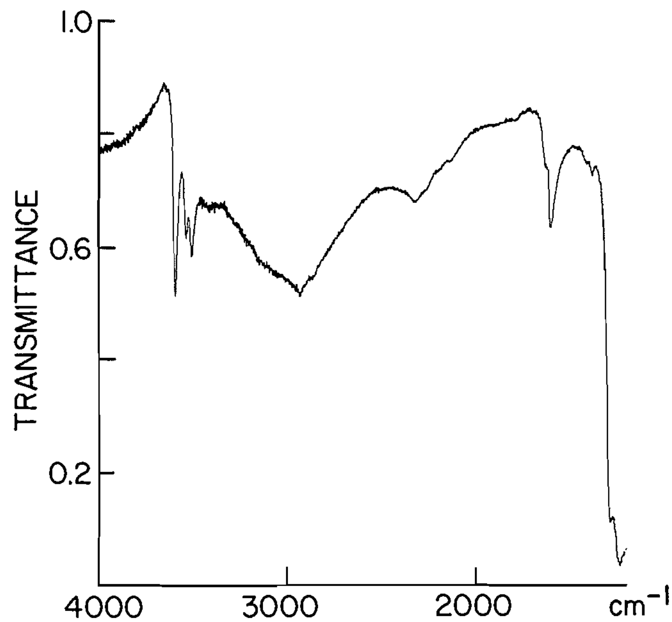

FIG. 1. Infrared spectrum of $[Cl_3(H_2O)Sn—OH—]_2 \cdot 4H_2O$ (fluorolube mull between CaF_2 plates).

minimum formula unit as $SnCl_3O_4$ (all atoms in general positions), for which Z = 4. A Mössbauer ^{119}Sn spectrum (10 mCi $CaSnO_3$ source and absorber at room temperature; single unsplit absorption, δ = +0.12(1) mm/s relative to $BaSnO_3$, FWHH = 0.54(5) mm/s) showed the tin to be exclusively Sn(IV).[3] Refinement with anisotropic temperature factors resulted in R = 0.038 and R_w = 0.039 (Table 1).

The dominant feature of the structure turned out to be a centrosymmetric binuclear di-μ-oxygen Sn(IV) complex. Its skeleton consisted of two *fac*-$SnCl_3O_3$ octahedra sharing the

[1]Holder of NSERC (1983−1985) and Killam (1984−1985) graduate fellowships.

[2]For the composition $[Cl_3(H_2O)SnOH]_2 \cdot 4H_2O$ (see below) these data can be supplemented as follows: fw for $H_{14}Cl_6O_8Sn_2$ = 592.20, Z = 2, μ_{Mo} = 39.0 cm^{-1}, $F(000)$ = 560.

[3]For $[Cl_3(H_2O)SnOH]_2 \cdot 4H_2O$ ref. 1 quotes δ = +0.30 mm/s, and ref. 2 gives δ = +0.30 mm/s for $Ag(PPh_3)_4OH \cdot [Cl_3(H_2O)SnOH]_2$, both with Δ = 0 and relative to $BaSnO_3$.

TABLE 1. Positional parameters ($\times 10^4$) of the title compound*

Atom	x		y		z	
Sn	1722(0)	2(1)	5369(1)	4(2)	4986(0)	−1(1)
Cl(1) axial	2140(2)	5(5)	4007(3)	−2(8)	6734(1)	1(4)
Cl(2)	2877(2)	−5(5)	8522(3)	−2(7)	5348(1)	4(4)
Cl(3)	3474(2)	15(5)	3456(3)	7(7)	4229(1)	−5(5)
O(1) OH	0158(4)	20(13)	3268(6)	−2(17)	4659(3)	1(10)
H(11)	0168(95)		2187(103)		4116(58)	
O(2) H_2O coord.	1354(5)	12(13)	6558(7)	50(21)	3403(3)	16(10)
H(21)	1081(62)		5590(71)		2832(34)	
H(22)	0518(66)		7382(150)		3499(92)	
O(3) H_2O hydr.	0061(5)	−12(20)	0166(8)	−30(20)	3179(4)	12(13)
H(31)	−0879(40)		−0296(137)		2973(58)	
H(32)	0346(67)		0960(121)		2563(40)	
O(4) H_2O hydr.	0468(6)	2(18)	3746(9)	−11(25)	1913(4)	−10(12)
H(41)	1092(45)		4105(178)		1341(46)	
H(42)	−0460(27)		3717(112)		1542(41)	

*The difference in the parameter value between this work and ref. 4 is given, together with the original esd of the parameter, next to the parameter value. The parameters of ref. 4 are obtained from ours as follows: $\bar{x}$, $\frac{1}{2} - y$, $\frac{1}{2} - z$ for O(1), O(3), and O(4); x, $y - \frac{1}{2}$, $z - \frac{1}{2}$ for all the other atoms. The thermal parameters (Table 2) and structure factors (Table 3) have been deposited (see footnote 4).

TABLE 4. Interatomic distances (Å) and bond angles (deg) in the title compound*

Atoms	Distance		Atoms	Angle	
Sn—Cl(1)	2.379(1)	0(4)	Cl(1)—Sn—Cl(2)	95.3(1)	0(2)
Sn—Cl(2)	2.372(2)	−6(4)	Cl(1)—Sn—Cl(3)	94.7(1)	−1(2)
Sn—Cl(3)	2.344(1)	8(6)	Cl(1)—Sn—O(1)	91.3(1)	−26(3)
Sn—O(1)	2.064(4)	−13(14)	Cl(1)—Sn—O(1B)	94.1(1)	(3)
Sn—O(1B)	2.093(6)	15(14)	Cl(1)—Sn—O(2)	179.2(1)	8(4)
Sn—O(2)	2.138(4)	−20(11)	Cl(2)—Sn—Cl(3)	101.2(1)	0(2)
Sn···Sn(B)	3.368(0)	0(2)	Cl(2)—Sn—O(1)	161.0(1)	−43(3)
O(1)···O(1B)	2.437(8)	4	Cl(2)—Sn—O(1B)	89.9(1)	(3)
			Cl(2)—Sn—O(2)	85.3(1)	−8(4)
			Cl(3)—Sn—O(1)	96.0(1)	62(3)
			Cl(3)—Sn—O(1B)	165.2(1)	(4)
Symmetry code:			Cl(3)—Sn—O(2)	84.6(1)	4(4)
A x y z	a X + (010)		O(1)—Sn—O(1B)	71.8(2)	(10)
B $\bar{x}$ $1-y$ $1-z$	b X + $(0\bar{1}0)$		O(1)—Sn—O(2)	88.4(1)	15(5)
C $\frac{1}{2}-x$ $\frac{1}{2}+y$ $\frac{1}{2}-z$	c X + $(\bar{1}0\bar{1})$		O(1B)—Sn—O(2)	86.6(2)	(3)
D $\frac{1}{2}+x$ $\frac{1}{2}-y$ $\frac{1}{2}+z$	d X + $(\bar{1}1\bar{1})$		Sn—O(1)—Sn(B)	108.2(2)	(10)

*The coordinates of all the atoms are as in Table 1 except where stated otherwise. The difference between the present distance and that of ref. 4 is given, with the original esd in parentheses, next to the present value.

bridging O(1)···O(1′) edge to form $[Cl_3O(2)Sn—O(1)—]_2$. The remaining oxygens, O(3) and O(4), were not closer than O(3, 4)···O(1, 2) ~2.67 Å and O(3, 4)···Cl ~3.32 Å. The compound was thus a hydrolysis product of $SnCl_6^{2-}$, but the nature of the oxygens was at this stage not clear, since the H atoms known from the ir spectrum to be present could not be located with confidence in the difference Fourier map.

Search of the literature revealed that the skeleton must belong to the $[Cl_3(H_2O)Sn—OH—]_2$ complex which has been reported in a number of adduct with various organic species (3, 4) as well as in the hydrate $[Cl_3(H_2O)Sn—OH—]_2 \cdot 4H_2O$ (4), and that moreover the serendipitous crystals must be those of the last-named compound. The unit-cell dimensions were all within twice the stated esd's of ref. 4, and the positional parameters of the non-hydrogen atoms were, except for y[O(2)], within 2σ of ref. 4 (Table 1). A similarly gratifying agreement exists for the interatomic distances and bond angles of the $[Cl_3OSn—O—]_2$ skeleton (Table 4).

Hydrogen bonding

Barnes *et al.* (4) report that their difference syntheses gave no clear indication of hydrogen atom positions. This was on the whole also the case with our difference map, but since the esd's of our Sn, Cl, and O positional parameters were 2–4 times smaller and the R was significantly lower than in ref. 4 (3.8% as against 8.4%), an attempt to include the hydrogens in the refinement seemed worthwhile. The O—H bond lengths were constrained to 0.98(2) Å, the H···H distances in the H_2O molecules to 1.55(1) Å, and the OH and H_2O groups were treated as rigid bodies. The resulting H positions (Table 1 and Fig. 2) all fall between the O,O and O,Cl pairs of atoms indicated in Fig. 4 of ref. 4 as involved in O—H···O and O—H···Cl bonds. The relevant H···O and H···Cl distances and OHO and OHCl angles are listed in Table 5.

In the overall hydrogen-bonding scheme in this crystal every H atom is involved in a hydrogen bond (Fig. 2 and Table 5). The hydrogen of the OH group and one of the hydrogens of the

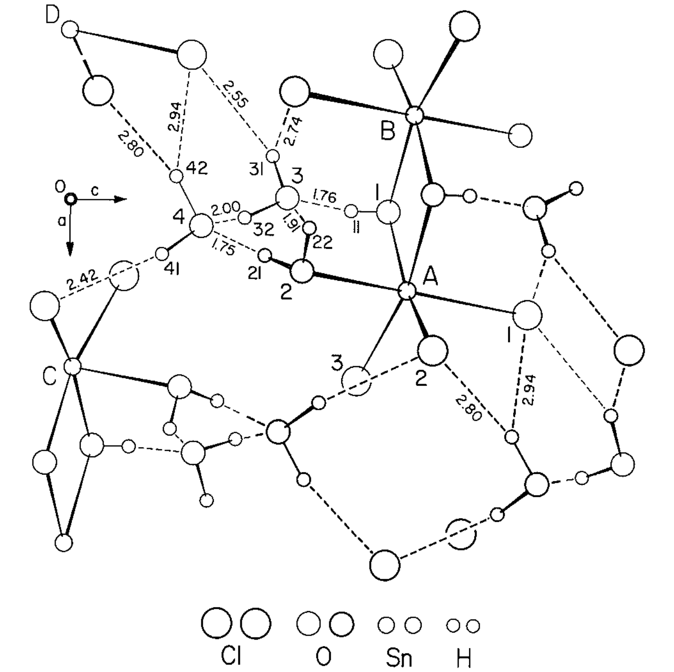

FIG. 2. Details of the hydrogen-bonding scheme in $[Cl_3(H_2O)Sn—OH—]_2 \cdot 4H_2O$. For symmetry code, interatomic distances, and bond angles see Tables 4 and 5.

water molecule of coordination participate in short, almost straight O—H···O bonds to the water molecules of hydration, $H_2O(3)$ and $H_2O(4)$. The second hydrogen of $H_2O(2)$ engages in an O(2)—H···O(3) bond of unfavourable geometry, as the longer H···O distance and the small OHO angle indicate. The hydrogens of $H_2O(3)$ and $H_2O(4)$ have, with the exception of H(32), Cl atoms as acceptors.

The H···Cl distances in the O—H···Cl bonds are on the whole long. The H(31) atom is involved in an unsymmetrically bifurcated H···2 Cl bond. The shortest H···Cl distance is H(41A)···Cl(2C), 2.42(8) Å; a second Cl atom, Cl(3C), is at 2.96(9) Å from H(41A) and at an OHCl angle of 120°, so that the O(4A)—H(41A)···Cl(2C) bond may be regarded as bent but not bifurcated. The H(42) atom, on the other hand, has two Cl neighbours at comparable H···Cl distances and OHCl angles, but the H(42)···Cl(2) and H(42)···Cl(1) distances are quite long, 2.80(5) and 2.94(3) Å, respectively, and the hydrogen-bonding interaction must be very weak.

The oxygens O(3) and O(4) act as acceptors to hydrogens bound to O atoms only: O(3) to H(11) and H(22), O(4) to H(21) and H(32). the Cl(1) atom engages H(31Bb), H(31D) and probably H(42D); Cl(2) engages H(41C) and H(42Da). The nearest H neighbour of Cl(3) is H(41C), which is only marginally eligible for hydrogen bonding (see above).

Given this wide range of O—H···O and O—H···Cl bonds in the crystal, extensive vibrational coupling must be expected, and the complexity and the lack of sharp features of the spectrum of Fig. 1 should come as no surprise.

Dimensions and symmetry of the $[Cl_3OSn—O—]_2$ skeleton

The skeletal bond lengths and angles are listed in Table 4. The Sn—Cl bonds are shorter than in the $SnCl_6^{2-}$ ion: the mean of uncorrected d(Sn—Cl) is 2.365(15) Å in the title compound, 2.427(12) Å in $(H_9O_4)_2SnCl_6 \cdot 2H_2O$ (5), and 2.425(12) Å in alkylammonium hexachlorostannates(IV) (6). The shortening, 0.06(2) Å, reflects the absence of ionic charge. The

TABLE 5. Hydrogen bonds in the title compound: interatomic distances (Å) and bond angles (deg)*

X	H	Y	X···Y	H···Y	X—H—Y
O(1A)	11A	O(3A)	2.742(1)	1.76(1)	175(2)
O(2A)	21A	O(4A)	2.723(1)	1.75(1)	174(1)
	22A	O(3Aa)	2.672(1)	1.91(2)	129(2)
O(3A)	31A	Cl(1Dc)	3.320(1)	2.55(6)	136(6)
	31A	Cl(1Bb)	3.460(2)	2.74(3)	131(6)
	32A	O(4A)	2.860(1)	2.00(1)	145(2)
O(4A)	41A	Cl(2C)	3.329(3)	2.42(8)	153(8)
	41A	Cl(3C)	3.560(6)	2.96(7)	120(7)
	42A	Cl(2Dd)	3.576(6)	2.80(9)	136(5)
	42A	Cl(1Dc)	3.683(8)	2.94(7)	132(5)

*For symmetry code see Table 4.

mean of the uncorrected Sn—OH distances is 0.059(16) Å smaller than the uncorrected $Sn—OH_2$ distance.

The geometry of this skeleton is remarkably constant. Table 6 lists the deviations from our values of bond lengths and angles for the dimer in a number of adducts and related dimers as well as in *cis*-$[SnCl_4(H_2O)_2]$ in $SnCl_4 \cdot 5H_2O$. The deviations are generally consistent with the stated esd's, with one conspicuous exception: the $Sn—OH_2$ bond reported for $[Cl_2Et(H_2O)Sn—OH—]_2$ (7) is about 0.2 Å longer than the $Sn—OH_2$ distance in the title compound and appreciably longer than all the other $Sn—OH_2$ distances in Table 6.

The actual symmetry of the complex, C_i, derives by only a slight distortion from the idealized symmetry of the skeleton, C_{2h}. This symmetry lowering is probably as much a consequence of the packing exigencies as of the strong O—H···O bonding in certain directions. The C_{2h} symmetry does not appear to be reported for Sn(IV) di-μ-oxygen complexes, though it is observed in the related binuclear species $[(OH)O_3Te—O—]_2^{6-}$ (8). In general the C_i symmetry in such complexes prevails: $[(H_2O)_4Al—OH—]_2^{4+}$ (9), $[(OH)_4Al—OH—]_2^{4-}$ (10), $[(OH)_2O_2Te—O—]_2^{4-}$ (11), and $[(OH)O_3I—O—]_2^{4-}$ (12) are typical examples.

The O···O distance in di-μ-oxygen bridges

The shortness of the O···O′ distance and the smallness of the OSnO′ angle raise the question of what is the limit of the effective size of the oxygen atom in M_2O_2 rings in general. To investigate this matter we have plotted the OSnO′ angle against d(O···O′) in Sn(IV) compounds containing Sn_2O_2 rings (Fig. 3). The compositions and code numbers of the compounds are listed in Table 7. We have also prepared a similar plot, MOM′ vs. d(O···O′) (Fig. 4), for a more or less random selection of well over a hundred compounds, all of which contain M_2O_2 rings, either as isolated di-μ bridges or as component groupings in larger units, e.g. tri-μ M_2O_3 binuclear complexes or multiply bridged M_3O_2 and M_3O_4 trimers and M_4O_4 tetramers. These compounds (**101**−**226**) are grouped according to M in Table 8; their compositions, together with references, will be found in Table 9.[4] Three heteronuclear (M ≠ M′) rings (**224**−**226**) are included in this set.

The sample presented in Fig. 3 is small and to some extent repetitious, and the uncertainty in d(O···O′) or the OSnO′

[4]This table has been deposited. Complete set of data is available, at a nominal charge, from the Depository of Unpublished Data, CISTI, National Research Council of Canada, Ottawa, Ont., Canada K1A OS2.

TABLE 6. Bond lengths (Å) and angles (deg) in the *trans*-[*fac*-$Cl_3(H_2O)Sn—OH—]_2$ and related dimers*

Atoms	**1**	**2**	**3**	**4**	**5**	**6**	**8**	**9**	†
Sn···Sn	3.368(0)	0(2)	10(2)	−42	50(3)	22(3)	−70(2)	−22(2)	—
Sn—Cl_{ax}	2.379(1)	0(4)	16(6)	89(20)	25(5)		−41(8)	−21(7)	−4(5)
Sn—Cl_{eq}	2.372(2)	−6(4)	1(4)	−48(20)	37(6)		−77(8)¶	−3(6)	−51(4)¶
	2.344(1)	8(6)	−12(4)	−66(20)	22(5)			21(7)	
Sn—OH_2 (ax.)	2.138(4)	−20(11)	8(12)	78(30)	35(14)	−18(16)	−209(20)	[−42(20)]	40(14)
Sn—OH (bridge)	2.064(4)	−13(14)	8(10)	14(30)	22(10)	36(12)	−3(11)	[−16(10)]	—
	2.093(4)	15(14)	7(11)	−7(30)	49(10)	17(12)	−60(11)	[−17(10)]	—
O···O (bridge)	2.437(8)	4	12	87	52	61	−13(22)	[−23(20)]	[−204]
O—Sn—O′	71.8(2)	1(10)	1(5)	26(13)	4(8)	1(8)	9(6)	−1(6)	−63(8)
Sn—O—Sn′	108.2(2)	−1(10)	−1(5)	−26(16)	−4(8)	−1(8)	−9(7)	1(7)	—

*The bold face numbers refer to the corresponding entries in Table 7. The distances and angles other than those from this work are given, with their original esd's in parentheses, as the differences Δ = *d*(this work) − *d*(literature).
†*cis*-$[SnCl_4(H_2O)_2]$ in $SnCl_4 \cdot 5H_2O$ (4).
¶Weighted mean.

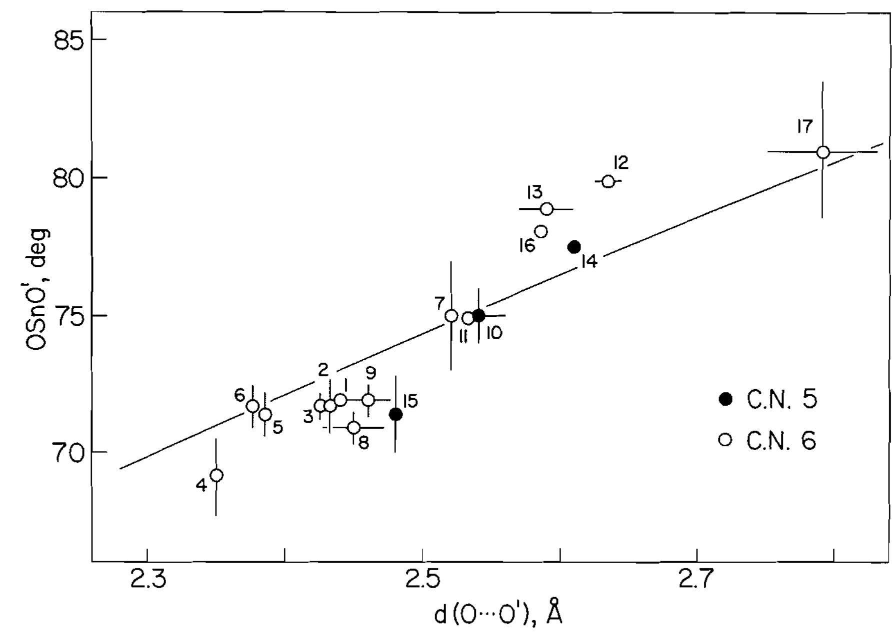

FIG. 3. Plot of the OSnO′ angle against the O···O′ distance in Sn_2O_2 rings. The curved line refers to $d(Sn \cdots Sn') = 3.3$ Å and D_{2h} ring symmetry. The esd's of the angles and distances are indicated wherever they are stated in the original reference. For code numbers see Table 7.

angle or both for some of the determinations is quite large. Within these limitations one can conclude that the C.N. of the Sn atom and the nature of the *exo*-ligand on the bridging oxygen are not significant differentiating factors, and that the relationship between $d(O \cdots O')$ and OSnO′ is largely determined by the nearly constant Sn···Sn′ distance of 3.3 Å (solid line in Fig 3; see text below) and the geometric requirements for an Sn_2O_2 ring of D_{2h} symmetry. The title compound is at the low end of the $d(O \cdots O')$ and OSnO′ ranges, though the point for the dioxan adduct **4** is almost cetainly too low.

Points **16** and **17** refer, not to *discrete* di-μ-oxygen bridges but to three-dimensional —Sn—O— networks containing Sn_2O_2 groups that can be regarded as local di-μ-oxygen bridges corresponding to the smallest O···O separation in the structure. In spite of this difference **16** and **17** conform to the rest of the sample.

The $d(O \cdots O')$ range in this reasonably homogeneous set is ~2.4 to 2.8 Å, and the SnOSn′ angle ranges from ~100° to ~110°, i.e. at short O···O′ distances it approaches the tetrahedral angle.

TABLE 7. Sn(IV) compounds included in Fig. 3

No.	Compound	Reference
1	$[Cl_3(H_2O)Sn—OH—]_2 \cdot 4H_2O$	This work
2	$[Cl_3(H_2O)Sn—OH—]_2 \cdot 4H_2O$	4
3	$[Cl_3(H_2O)Sn—OH—]_2 \cdot$(1,4-dioxan)$_3$	4
4	$[Cl_3(H_2O)Sn—OH—]_2 \cdot$(1,4-dioxan)$_3$	3
5	$[Cl_3(H_2O)Sn—OH—]_2 \cdot$(1,8-cineole)$_4$	4
6	$[Br_3(H_2O)Sn—OH—]_2 \cdot$(1,8-cineole)$_4$	4
7	$[Me_2SnNCS)_2O]_2$	13
8	$[Cl_2Et(H_2O)Sn—OH—]_2$	7
9	$[Cl_3(EtO)Sn—OEt—]_2$	14
10	$[(Bu_2SnOOCCCl_3)_2O]_2$	15
11	$[Me_2ClSnOSnMe_2Cl]_2$	16
12	$[Sn^{II}Sn^{IV}(o\text{-}OOC.C_6H_4NO_2)_4O \cdot (thf)]_2$	17
13	$[Sn^{II}Sn^{IV}O(OOCCF_3)_4]_2 \cdot C_6H_6$	18
14	$\{[Me_2Sn(OOCCF_3)]_2O\}_2$	19
15	$\{(O_2NO)Me_2Sn—OH—]_2$	20
16	SnO_2	24
17	Ca_2SnO_4	21

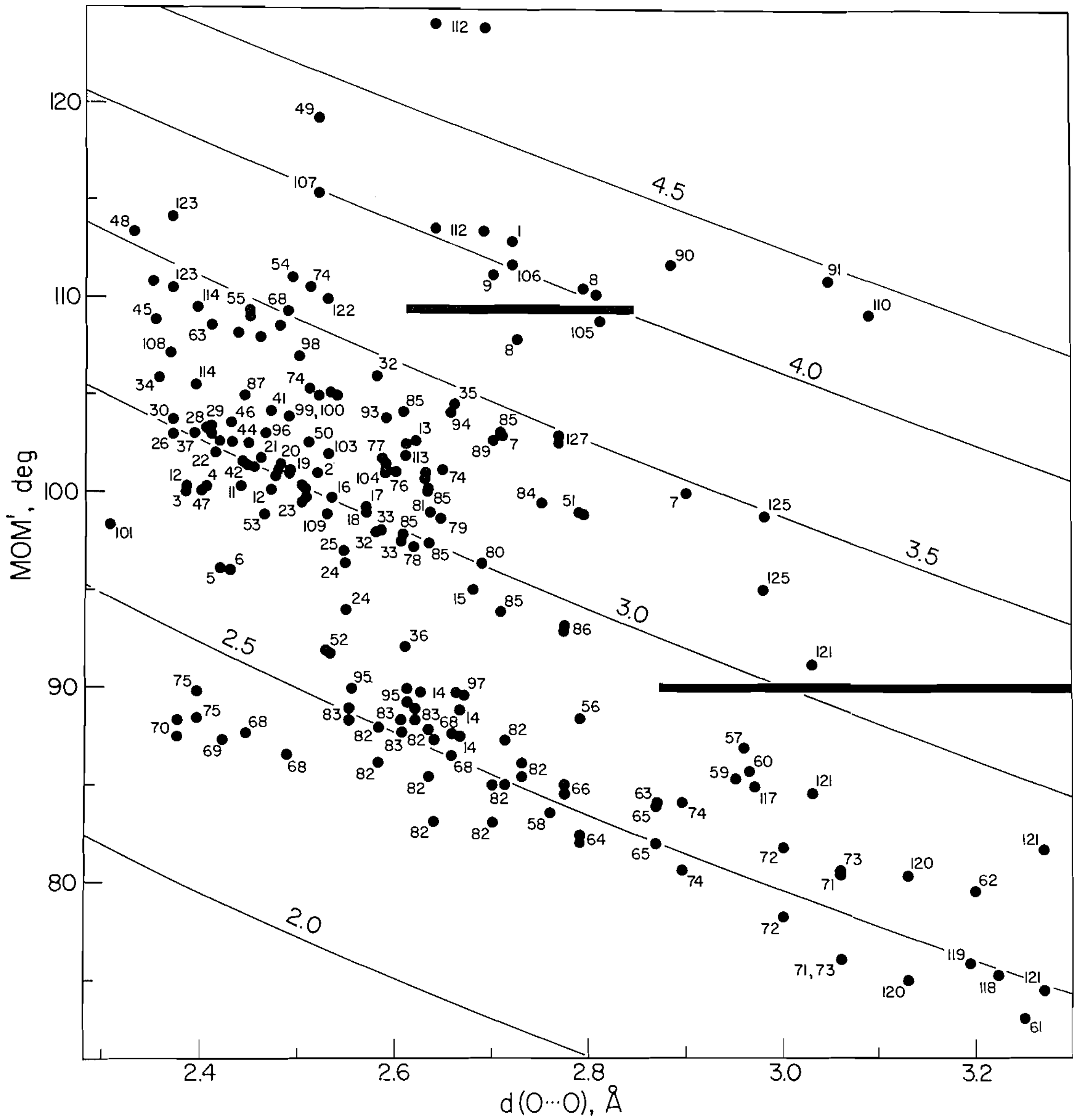

FIG. 4. Plot of the MOM' angle(s) against the O···O' distance(s) in M_2O_2 rings. To reduce crowding, 100 has been subtracted from the code numbers listed in Tables 8 and 9; even so some of the points (and all the M = Sn points) remain unlabelled. The esd's of the angles and distances are not indicated; the uncertainties in the angles may be as high as 2–3°. The heavy bars represent the d(O···O') ranges in the MO (NaCl type, **188** and **216**) and MO_2 (CaF_2, type, **110**, **192**, **202**, and **211**) oxides; the range for MO extends up to d(O···O') = 3.49 Å (PaO, **188**). The curves refer to constant d(M···M') (in Å) in M_2O_2 rings of D_{2h} symmetry.

When the set of points for Sn_2O_2 is embedded in the much larger, and presumably representative, M_2O_2 set of Fig. 4, it is seen that it covers only a small portion of the total d(O···O') and MOM' range, but the low d(O···O') end of the Sn sample comes close to the lower limit of the d(O···O') range of Fig. 4.

For a centrosymmetric MOM'O' ring with the dimensions d(M—O) ≥ d(M—O'), d(M···M'), d(O···O') and the angles MOM' and OMO' = 180° − MOM', we have

$$[1] \quad \cos \mathrm{MOM}' = -\frac{1}{2}(r + r^{-1})(R^2 - 1)/(R^2 + 1)$$

where $r = d(\mathrm{M—O})/d(\mathrm{M—O'})$ and $R = d(\mathrm{M\cdots M'})/d(\mathrm{O\cdots O'})$. The $\frac{1}{2}(r + r^{-1}) = K$ term may be regarded as an asymmetry parameter measuring the extent of distortion of the planar ring from D_{2h} ($K = 1$) to C_{2h} ($K > 1$) symmetry. When the intra-ring distances and angles for the compounds included in Fig. 4 are replotted as cos MOM' vs. R (Fig. 5), all the points corresponding to D_{2h} ring symmetry fall on the $K = 1$ straight line. Within realistic limits the effect of r on K is insignificant; it is quite unlikely that $r > 2$. If $r = 2$, $K = 1.25$, but the lines for $K = 1$ and $K = 1.25$ are so close that in practice the difference between D_{2h} and merely centrosymmetric rings is absorbed in the experimental uncertainty in MOM' and R. In compounds with points outside the two lines the MOM'O' ring is either planar but noncentrosymmetric or nonplanar.

This plot shows clearly that (a) in the majority of the compounds in our sample R is between ~1.1 and ~1.4, and MOM' is between ~95° and the tetrahedral angle; (b) R values exceeding 1.4 and MOM' angles larger than tetrahedral are observed in compounds where M is large though not necessarily having either a high C.N. or unusually bulky ligands; (c) R values smaller than unity and MOM' angles between 70° and 90° occur only in compounds containing single or multiple

TABLE 8. Elements represented in the compounds included in Fig. 4*

M	Compounds	M	Compounds
Ag	**101**	Pa	**188***
Al	**102–104**	Pb	**189***, **190**, **191**
As	**105**, **106**	Po	**192***
Au	**107**	Pt	**193**
Cd	**108***	Re	M_4O_4, **194**
Ce	**109**, **110***	Rh	M_2O_3, **195**
Co	**111–113**; M_2O_3, **114**	Ru	**196***, **197**
Cr	**115***, **116–124**	Sb	**198–200**
Cu	**125–145**	Si	**201***
Fe	**146**	Tb	**202***
Ge	**147***	Te	**203**, **204**
Hf	**148**	Th	**205–207**
Hg	**149**	Ti	**208**, **209***
I	**150**	Tl	**210**
In	**151***	U	**211***
Ir	M_2O_3, **152**	V	**212–215**, **216***
Mn	**153***; other, **154**	W	**217–219**; M_3O_4, **220**; other, **221**
Mo	**155–167**; M_2O_3, **168**; M_3O_2, **169**, **170**; M_3O_4, **171–173**; other, **174**	Yb	**222**
		Zr	**223**
Nb	M_3O_2, **175**	CoCu	**224**
Ni	**176–181**; M_2O_3, **182–184**; M_3O_4, **185**; M_4O_4, **186**	CuHg	**225**
		NiU	**226**
Os	**187***		

*M_2O_2 rings in three-dimensionally connected —M—O— structures. For Sn compounds see Table 7.

M—M′ bonds. For M = Sn the upper limit of R appears to be ~1.4 and the SnOSn′ angles approach the tetrahedral angle.

The shortest O···O′ distance in Fig. 4, ~2.31 Å, is encountered in stishovite (**201**), the rutile-type variety of SiO_2 containing six-coordinated Si. This prompts the question of how this presumably shortest d(O···O′) separation in an M_2O_2 ring compares with the shortest observed nonbonded O···O distance, and what in fact is this distance.

What is the minimum d*(O···O) for nonbonded oxygens in general?*

The shortest nonbonded O···O contact in α-O_2 is ~3.2 Å (22), i.e. greater than twice the van der Waals radius of oxygen, 2.8 Å; this distance does not decrease appreciably with increasing pressure (23). In the ozone molecule the nonbonded O···O distance is 2.18 Å. In tetrahedral varieties of SiO_2 the corresponding distance ranges from ~2.57 to ~2.67 Å; in β-Be$(OH)_2$ it is ~2.52 (24). With the exception of stishovite the minimum nonbonded O···O distance in Si^V and Si^{VI} oxygen compounds is 2.42–2.46 Å (e.g. in SiP_2O_7 (25), $[Ca_3Si(OH)_6(H_2O)_{12}](SO_4)(CO_3)$ (26), $(Me_4N)[C_6H_5Si(O_2C_6H_4)_2]$ (27)). For distances shorter than ~2.3 Å one thus has to look among oxyanions and complexes containing oxyanions as bidentate ligands; the latter may be regarded as heteronuclear di-μ-oxo bridges.

The minimum d(O···O) in XO_3^{n-} and XO_4^{n-} ions does not appear to fall below ~2.1 Å: for example, it is 2.11 Å in $NaNO_3$ (28) and 2.14 Å in $Na_2CO_3 \cdot NaHCO_3 \cdot 2H_2O$ (29, 30). This seems to be true also of the free molecular X_mO_n species, e.g. NO_2 (2.19 Å) or the cyclic $H_2B_2O_3$ (intra-ring d(O···O) = 2.29 Å) (31).

For the nitrate ion in bidentate coordination, i.e. in MO_2N rings, the approximate range is 2.08(5)–2.16 Å (**18–23**, Table 10); the corresponding MOX angles range from ~48° to ~68°. Values lower than ~2.10 Å have so far been found only in NO_2^- ions: ~2.09 Å in $NaNO_2$ (40). The shortest nonbonded

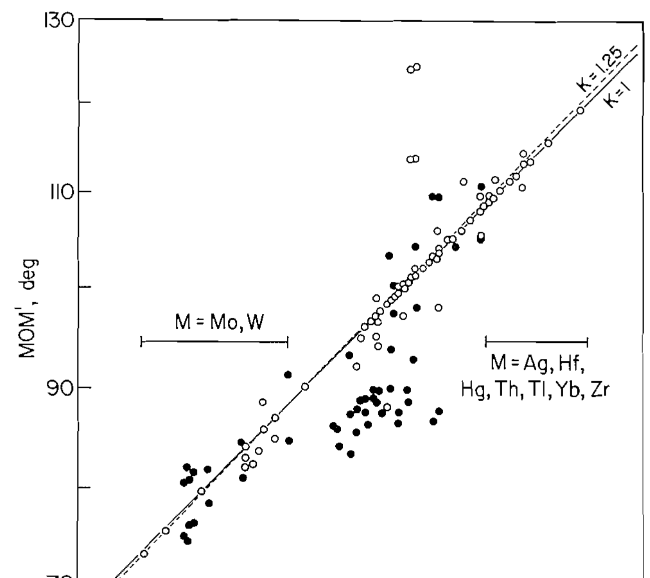

FIG. 5. Plot of MOM′ against R = d(M···M′)/d(O···O′) according to eq. [1]. The open circles refer to isolated M_2O_2 rings, the full circles to M_2O_2 rings of M_2O_3, M_3O_2, M_3O_4, and M_4O_4 bridged groupings. For the meaning of K see text. The points for R < 1 refer exclusively to Mo and W compounds; those for R greater than ~1.4 refer to compounds in which M is a large atom. The Sn compounds of Table 7 and Fig. 3 fall between R ~ 1.3 and ~1.4.

O···O distance reported to date is ~2.02 Å in the di-μ-oxo CuO_2N hetero bridge in $[Cu(bipy)_2(ONO)]NO_3$ (**25**). In contrast, in a similar bridge in Cu(bipy) $(ONO)_2$ (**24**) the distance is ~2.10 Å.

A closer comparison of the nonbonded O···O distances is

TABLE 10. The O···O bridging distance in NO_3^- and NO_2^- ions acting as bidentate ligands

No.	Compound	d(O···O), Å	Reference
18	$Co(NO_3)_3$	2.12	32
19	$Ti(NO_3)_4$	2.13(1)	33
20	$Sn(NO_3)_4$	2.14(1)	34
21	$(Ph_3P)_2CuNO_3$	2.14(1)	35
22	$Rb(UO_2)(NO_3)_3$	2.16	36
23	$MgTh(NO_3)_6 \cdot 8H_2O$	2.08(5)	37
24	$Cu(bipy)(ONO)_2$	2.10	38
25	$[Cu(bipy)_2(ONO]NO_3$	2.02	39

not warranted at present, nor are distinctions between X-ray, neutron, and spectroscopic results (i.e. between internuclear distances and separations of electron-density maxima) or between distances corrected or uncorrected for thermal motion. The accuracy quoted is rarely better than ±0.01 Å and often much poorer. Our survey of the very short O···O distances is by no means exhaustive and it does not differentiate between oxygen atoms of different types. However, it presents what must be essentially the correct picture of the situation in regard of the lower limit of O···O contacts: in M_2O_2 rings the lower d(O···O′) limit appears to be ~2.3 Å unless one of the nonoxygen atoms is B, C, or N. In that case the nonbonded O···O distance can be short as ~2.0 Å, which seems to be also the *overall* lower limit for non-σ-bonded O···O distances.

Acknowledgments

We thank Dr. M. Falk for the ir spectrum and Dr. R. A. Dunlap for the Mössbauer spectrum of the title compound. This work was supported by research grants from the Natural Sciences and Engineering Research Council of Canada to the two first-named authors.

1. P. A. CUSACK. Cited in ref. 2.
2. D. V. SANGHANI, P. J. SMITH, D. W. ALLEN, and B. F. TAYLOR. Inorg. Chim. Acta, **59**, 203 (1982).
3. N. G. BOKII and YU. T. STRUCHKOV. Zh. Strukt. Khim. **12**, 277 (1971).
4. J. C. BARNES, H. A. SAMPSON, and T. J. R. WEAKLEY. J. Chem. Soc. Dalton, 949 (1980).
5. H. HENKE. Acta Crystallogr. B, **38**, 920 (1982).
6. O. KNOP, T. S. CAMERON, M. A. JAMES, and M. FALK. Can. J. Chem. **61**, 1620 (1983); (errata) **62**, 1227 (1984).
7. C. LECOMTE, J. PROTAS, and M. DEVAUD. Acta Crystallogr. B, **32**, 923 (1976).
8. O. LINDQVIST. Acta Chem. Scand. **23**, 3062 (1969).
9. G. JOHANSSON. Acta Chem. Scand. **16**, 403 (1962).
10. A. H. MOINUDDIN AHMED and L. S. DENT GLASSER. Acta Crystallogr. B, **26**, 867 (1970).
11. O. LINDQVIST and G. LUNDGREN. Acta Chem. Scand. **20**, 2138 (1966).
12. A. FERRARI, A. BRAIBANTI, and A. TIRIPICCHIO. Acta Crystallogr. **19**, 629 (1965).
13. Y. M. CHOW. Inorg. Chem. **10**, 673 (1971).
14. M. WEBSTER and P. H. COLLINS. Inorg. Chim. Acta, **9**, 157 (1974).
15. R. GRAZIANI, G. BOMBIERI, E. FORSELLINI, P. FURLAN, V. PERUZZO, and G. TAGLIAVINI. J. Organomet. Chem. **125**, 43 (1977).
16. P. G. HARRISON, M. J. BEGLEY, and K. C. MOLLOY. J. Organomet. Chem. **186**, 213 (1980).
17. P. F. R. EWINGS, P. G. HARRISON, A. MORRIS, and T. J. KING. J. Chem. Soc. Dalton, 1602 (1976).
18. T. BIRCHALL and J. P. JOHNSON. J. Chem. Soc. Dalton, 69 (1981).
19. R. FAGGIANI, J. P. JOHNSON, I. D. BROWN, and T. BIRCHALL. Acta Crystallogr. B, **34**, 3743 (1978).
20. A. M. DOMINGOS and G. M. SHELDRICK. J. Chem. Soc. Dalton, 475 (1974).
21. M. TRÖMEL. Naturwiss. **54**, 17 (1967).
22. C. S. BARRETT, L. MEYER, and J. WASSERMAN. J. Chem. Phys. **47**, 592 (1967).
23. A. HELMY, K. KOBASHI, and R. D. ETTERS. J. Chem. Phys. **80**, 2782 (1984).
24. R. W. G. WYCKOFF. Crystal structures. 2nd ed. Vols. 1–5. Interscience, New York. 1963–1966.
25. G. BISSERT and F. LIEBAU. Acta Crystallogr. B, **26**, 233 (1970).
26. R. A. EDGE and H. F. W. TAYLOR. Acta Crystallogr. B, **27**, 594 (1971).
27. F. P. BOER, J. J. FLYNN, and J. W. TURLEY. J. Am. Chem. Soc. **90**, 6973 (1968).
28. R. L. SASS, R. VIDALE, and J. DONOHUE. Acta Crystallogr. **10**, 567 (1957).
29. C. J. BROWN, H. S. PEISER, and A. TURNER-JONES. Acta Crystallogr. **2**, 167 (1949).
30. G. E. BACON and N. A. CURRY. Acta Crystallogr. **9**, 82 (1956).
31. C. A. COULSON. Acta Crystallogr. B, **25**, 807 (1969).
32. J. HILTON and S. C. WALLWORK. J. Chem. Soc. Chem. Commun. 871 (1968).
33. C. D. GARNER and S. C. WALLWORK. J. Chem. Soc. A, 1496 (1966).
34. C. D. GARNER, D. SUTTON, and S. C. WALLWORK. J. Chem. Soc. A, 1949 (1967).
35. G. G. MESSMER and G. J. PALENIK. Inorg. Chem. **8**, 2750 (1969).
36. G. A. BARCLAY, T. M. SABINE, and J. C. TAYLOR. Acta Crystallogr. **19**, 205 (1965).
37. S. ŠĆAVNIČAR and B. PRODIĆ. Acta Crystallogr. **18**, 698 (1965).
38. F. S. STEPHENS. J. Chem. Soc. A, 2081 (1969).
39. I. M. PROCTER and F. S. STEPHENS. J. Chem. Soc. A, 1248 (1969).
40. M. I. KAY and B. C. FRAZER. Acta Crystallogr. **14**, 56 (1961).

Steroids and related products. LII.[1] 11-Aza steroids. Part IV.[2] The synthesis of 11-aza 9α-steroids. II.[3] The synthesis of 11-aza-4,5α-dihydrotestosterone[4,5]

MARIA GUMULKA, IBRAHIM HALIM IBRAHIM, ZBIGNIEW BOŃCZA-TOMASZEWSKI, AND CH. R. ENGEL
Department of Chemistry, Université Laval, Quebec (Que.), Canada G1K 7P4

Received September 24, 1984

MARIA GUMULKA, IBRAHIM HALIM IBRAHIM, ZBIGNIEW BOŃCZA-TOMASZEWSKI, and CH. R. ENGEL. Can. J. Chem. **63**, 766 (1985).

An efficient synthesis from adrenosterone or 11α-hydroxytestosterone of 17β-hydroxy-11-aza-5α-androstan-3-one, the 11-aza analogue of dihydrotestosterone, is described. For the elaboration of the 11-aza structure, a pathway implying a Curtius-type rearrangement of a 9,11-seco 9-oxo 11-acid was employed.

MARIA GUMULKA, IBRAHIM HALIM IBRAHIM, ZBIGNIEW BOŃCZA-TOMASZEWSKI et CH. R. ENGEL. Can. J. Chem. **63**, 766 (1985).

On rapporte une synthèse efficace de l'hydroxy-17β aza-11 (5α)androstanone-3, l'analogue 11-aza de la dihydrotestostérone, à partir de l'adrénostérone, ou de l'hydroxy-11α testostérone. Pour l'élaboration de la structure 11-aza, une méthode impliquant une réaction du type Curtius sur un 9,11-seco 9-oxo 11-acide fut employée.

In the framework of our program on the synthesis of new steroid hormone analogues, on their biological evaluation, and on the establishment of structure–activity relationships in that field, and in particular in connection with our investigations of steroids modified in position 11, such as 11-hetero steroids, we decided to synthesize 17β-hydroxy-11-aza-5α-androstan-3-one (**1**), the 11-aza analogue of 4,5α-dihydrotestosterone. This

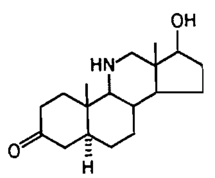

1

androgenically highly active testosterone metabolite is indeed regarded to be the steroid whose binding to the appropriate receptors is mainly responsible for androgenic activity. The study of the androgen agonistic or antagonistic properties of its 11-aza analogue, as well as of other biological activities this product may possess – such as its effect on spermatogenesis – should thus have considerable interest. We here report the synthesis of this new hormone analogue.

We have previously shown (2, 3) that 11-aza steroids of the 9α-series are synthetically accessible, particularly in the A/B-*trans* series, by ozonolysis of 9,11-unsaturated 12-ketones, by ammonolysis of the resulting 9,12-seco 11-nor 9-oxo 12-acids, the reduction of the 8,9-unsaturated lactams thus formed to the 8,9-unsaturated cyclic amines, and by hydrogenation of the latter, for instance via iminium salts (cf. Scheme 1) (cf. also ref. 4). This pathway suffers, however, from the fact that the ammonolysis of the keto acid has to be carried out under pressure, as well as from the low yield of the reduction of the double bond of 8,9-unsaturated 11-aza steroids (2, 4).[6] Therefore, for the synthesis of 11-azadihydrotestosterone (**1**) described here, we investigated an alternate approach implying a Curtius-type rearrangement of a 9,11-seco 9-oxo 11-acid azide, in analogy with reactions described by Lettré and Knof (5) pertaining to B-seco derivatives and which had led to 6-aza steroids.

As starting material, we chose 5α-androstane-3,11,17-trione (**3**), readily available (cf. ref. 6) by Birch reduction of adrenosterone (4-androstene-3,11,17-trione) (**2**) or of 11α-hydroxytestosterone (**2***a*), followed by Jones' oxidation (cf. Experimental). The triketone **3** was transformed in 90% yield with ethylene glycol and *p*-toluenesulfonic acid into its 3,17-diketal **4** which was reduced in 87–89% yield with lithium aluminum hydride or sodium borohydride to the 11β-hydroxy 3,17-diketal **7**. This product was dehydrated in 86% yield with thionyl chloride to 3,17-bisethylenedioxy-5α-androst-9,11-ene (**6***a*) which gave in 72% yield, upon treatment with acetone and *p*-toluenesulfonic acid, 5α-androst-9,11-ene-3,17-dione (**6**), already prepared by Shoppee (7) from 3β-acetoxy-5α-androst-9,11-en-17-one, which was obtained in turn by degradation of Reichstein's Substance A (8). Better yields (90%) in the deketalization were realized by the method of Conia and coworkers (9), consisting in reaction with silica gel, pretreated with dilute hydrochloric acid. Ozonolysis of the androstenedione **6** and oxidation with hydrogen peroxide gave in 75–81% yield the seco keto aldehyde **5**, accompanied by the diketo acid **5***a* (isolated in approximately 20% yield). The oxidation of aldehyde **5** with Jones' reagent to the diketo acid **5***a* proceeded in approximately 75% yield, but the product was unstable. In a first set of experiments it was therefore transformed without purification with oxalyl chloride (cf. ref. 10) into the acid chloride, which was converted with sodium azide to the acid azide **8** which, in turn, was subjected to a Curtius-type rearrangement, leading via the isocyanate **9** to the imine **10**; as side product, the diketo acid **5***a* was recovered. The yield of this

[1]For paper LI, cf. ref. 1.
[2]For part III, cf. ref. 2.
[3]For paper I, cf. ref. 2.
[4]The salient features of this publication were part of a paper presented at the 29th International (IUPAC) Congress of Pure and Applied Chemistry, Cologne, Federal Republic of Germany, June 5–10, 1983 (Abstracts of Papers, p. 216).
[5]Abbreviated from part of the doctoral thesis of I. H. Ibrahim, to be presented to the School of Graduate Studies, Université Laval, Quebec.
[6]Although we were able to improve the yield of this reduction which we originally reported (2), the total yield of the transformation of an 8,9-unsaturated 12-oxo 11-aza steroid into the 12-deoxygenated 8,9-saturated derivative hardly exceeded 16%. Catalytic reduction of an 8,9-unsaturated N-acylated 11-aza steroid under pressure, in the presence of perchloric acid, gave the saturated 11-aza steroid in approximately 50% yield, but under these conditions ester groups present in the molecule may be simultaneously reduced (2).

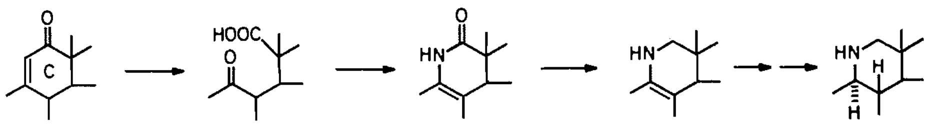

SCHEME 1

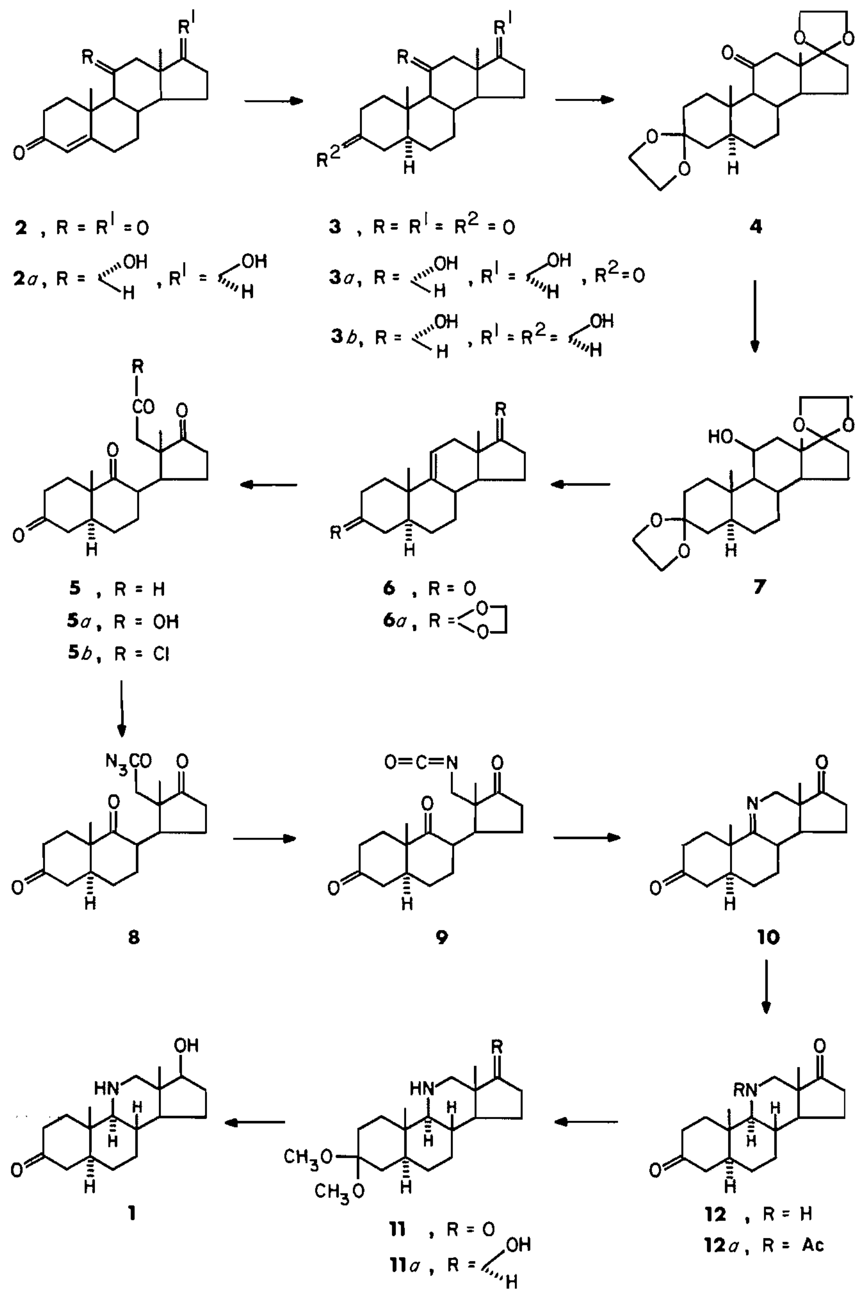

sequence of reactions depends on the conditions employed (cf. Experimental). The best results — a 68% yield, considering the recovery of acid *5a* — were obtained when the acid chloride *5b* was treated in dry benzene with activated sodium azide (11) at reflux temperature and the resulting product with concentrated hydrochloric acid. Significantly better yields (82%) in the preparation of imine **10** were realized in a second set of experiments in which the diketo acid *5a* was transformed without the intermediacy of its chloride *5b*, according to the method of Grouillier *et al.* (12), with triethylamine and ethyl chloroformate in acetone, into the isocyanate **9** which was treated with hydrochloric acid.[7]

Reduction of the imine **10** via its hydrochloride, according to the procedure of Borch *et al.* (13), and reoxidation with Jones'

[7]It is not improbable that, under the mild conditions of certain procedures employed for the conversion of the isocyanate to the imine, this product is not formed (at least not entirely) by cyclization of a 9,11-seco 9-oxo 11-amine but by a direct reaction of the isocyanate group with the keto function (cf. Scheme 2).

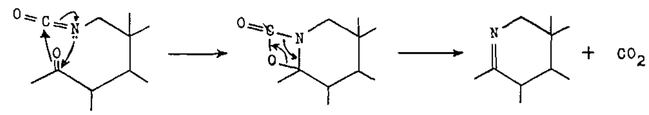

SCHEME 2

reagent, led in 65% yield to 11-aza-5α-androstane-3,17-dione (**12**), further characterized as the acetyl derivative **12***a*. The "natural" 9α-configuration was confirmed by the coupling constants (J = 11 Hz) of the 9α and 8β protons in the nmr spectra of compounds **12** and **12***a*. The 3-monoketal **11** was now formed in 80% yield by treatment of the amine **12** with methanol and oxalic acid, according to the method of Narwid *et al.* (14), the 17-keto function was reduced in over 90% yield with lithium aluminum hydride, and the 3-ketone liberated with acetone and *p*-toluenesulfonic acid, to afford in 69% yield the desired 11-aza analogue **1** of 4,5α-dihydrotestosterone.[8] The biological properties of the new hormone analogue will be reported elsewhere.

In summary, we report the synthesis of 11-aza-4,5α-dihydrotestosterone from readily available starting materials by an efficient and simple method, significantly superior to our previously described route to 11-aza steroids.

Experimental

Melting points were taken in evacuated capillaries and the temperatures were corrected. For elution chromatography, Davison's silica gel 923, and for thin-layer chromatography, Merck silica gel GF-254 and "DC-Alufolien Kieselgel 60" were employed. The ir spectra were recorded on a Beckman IR-12 instrument, the nmr spectra at 60 MHz on a Varian EM 360A spectrometer and at 90 MHz on a Bruker HFX-90 instrument, if not otherwise stated, in deuteriochloroform, tetramethylsilane serving as internal standard. The microanalyses and mass spectroscopies were performed by Dr. G. Schilling, Ayerst Laboratories, Montreal, to whom we express our sincere appreciation.

5α-Androstane-3,11,17-trione (3)

(a) From 4-androstene-3,11,17-trione (adrenosterone, 2)

According to the procedure of Bowers and Denot (6), 1.8 g of adrenosterone (**2**), mp 221–222°C, was transformed into 1.67 g of crude 5α-androstane-3,11,17-trione (**3**) which was absorbed on 60 g of silica gel. Elutions with benzene – ethyl acetate (8:2) afforded 1.497 g (83% yield) of pure trione **3**, mp 174–176°C; $[\alpha]_D^{26}$ +162 ($CHCl_3$) (lit. (17) mp 174.5–176°C; $[\alpha]_D^{23}$ +160 ($CHCl_3$)); ir ν_{max} (KBr): 1740 (17-ketone), 1700 (3- and 11-ketones) cm^{-1}.

(b) From 11α-hydroxytestosterone (2a)

Under stirring, a solution of 5 g of 11α-hydroxytestosterone (**2***a*), mp 175–177°C, in 100 mL of absolute tetrahydrofuran was added to a solution of 3 g of lithium wire, flattened and cut into small pieces, in 200 mL of anhydrous liquid ammonia over a period of 20 min. The mixture was stirred for another 40 min and the blue colour was discharged by addition of approximately 3 g of solid ammonium chloride; subsequently, the ammonia was allowed to evaporate in a nitrogen atmosphere. Water was added carefully to the residue, the product was extracted with methylene chloride, and the organic extract was washed with water and dried over sodium sulfate. Removal of the solvents gave 5 g of an amorphous product which upon crystallization from methanol afforded 3.963 g of *11α,17β-dihydroxy-5α-androstan-3-one* (**3***a*), mp 181–183°C. The mother liquors were subjected to flash chromatography on 100 g of silica gel, chloroform–methanol (98:2) eluting another 126 mg of the same product of the same purity (total yield: 81%). A sample was recrystallized twice from methanol; colourless prisms, mp 182–183°C (lit. (19) mp 183–185°C); $[\alpha]_D^{25}$ −2.2 (c 0.900, dioxane); ir ν_{max} (KBr): 3230 (hydroxyls), 1715 (3-ketone) cm^{-1}; nmr δ (DMSO, 90 Hz): 0.77 (s, 3H, 18-CH_3), 1.14 (s, 3H, 19-CH_3), 3.8 (m, 2H, 11β- and 17α-H). Mass (ms) calcd. for $C_{19}H_{30}O_3$: 306; found: 306.

From the above-mentioned chromatogram, the same solvent mixture eluted 511 mg of a more polar, amorphous product, representing *5α-androstane-3β,11α,17β-triol* (**3***b*). Crystallization from methanol gave 500 mg (9.7%) of crystalline triol **3***b*, mp 239–241°C. A sample was recrystallized twice from methanol; colourless prisms, mp 240–241°C (lit. (19) mp 241–243°C); $[\alpha]_D^{25}$ −8.4 (c 0.95, dioxane); ir ν_{max} (KBr): 3235 (hydroxyls) cm^{-1}; nmr δ (DMSO, 90 MHz): 0.72 (s, 3H, 18-CH_3), 0.94 (s, 3H, 19-CH_3), 3.8 (m, 3H, 3α-, 11β-, 17α-H). Mass (ms) calcd. for $C_{19}H_{32}O_3$: 308; found: 308.

To a solution of 3 g of the 11α,17β-dihydroxy-5α-androstan-3-one (**3***a*) described above, mp 181–183°C, in 100 mL of acetone, 15 mL of Jones' reagent (18) was added at 5°C, dropwise and with stirring, within 10 min. The mixture was left for another 3 h, and isopropyl alcohol (3 mL) and, subsequently, water were added. The product was extracted with dichloromethane, the organic solution was washed with water and dried over sodium sulfate, and the solvent was evaporated. Thus 2.548 g of an oily product was obtained which was chromatographed on 100 g of silica gel, benzene – ethyl acetate (8:2) eluting 2.378 g (80% yield) of authentic *5α-androstane-3,11,17-trione* (**3**), mp 174–176°C.

Under identical conditions, 500 mg of 5α-androstane-3β,11α,17β-triol (**3***b*), mp 239–241°C, was oxidized with Jones' reagent. By chromatography of the crude reaction product (421 mg) on 60 g of silica gel, 406 mg (81% yield) of pure *5α-androstane-3,11,17-trione* (**3**), mp 174–176°C, was obtained.

In another experiment, 5.5 g of 11α-hydroxytestosterone (**2***a*), mp 175–177°C, was reduced as described above to afford 5.318 g of an amorphous product. This material was oxidized directly, without separations or purifications, in 100 mL of acetone with 15 mL of Jones' reagent, as described above. Thus, 5.096 g of a crude product was obtained which was chromatographed on 150 g of silica gel to afford 4.666 g (85% yield) of pure *5α-androstane-3,11,17-trione* (**3**), mp 174–176°C.

3,17-Bisethylenedioxy-5α-androstan-11-one (4)

From a solution of 3 g of 5α-androstane-3,11,17-trione (**3**), mp 174–176°C, and 15 mL of ethylene glycol in 160 mL of dry benzene, some 50 mL was distilled off through a Dean–Stark separator and 100 mg of *p*-toluenesulfonic acid was added. The solution was refluxed with the exclusion of moisture and with a water separator for 18 h and, after cooling, the product was extracted with dichloromethane. The organic solution was washed with a saturated sodium bicarbonate solution and with water, a few drops of pyridine were added, and the mixture was dried over sodium sulfate. Removal of the solvents gave 3.619 g of a product which was crystallized from methanol to give 3.482 g (90% yield) of 3,17-bisethylenedioxy-5α-androstan-11-one (**4**), mp 164–166°C. A sample was recrystallized twice from methanol for analysis; mp 163–165°C; $[\alpha]_D^{26}$ +23 (c 0.950, $CHCl_3$);

[8]This synthesis represents a development of experiments connected with the problem of the preparation of 17-aza steroids.[9] Independently, and subsequently to the beginning of our investigations, Pivnitskiĭ and co-workers (15) used a similar approach for the formation of 11-aza-estradiol and 11-aza-19-nortestosterone derivatives (cf. also ref. 16).[10]

[9]Ch. R. Engel and N. N. Saha. Unpublished results.

[10]When using the procedure followed by Badanova and Pivinitskiĭ (15*b*) for the transformation, via the acid chloride **5***b*, of acid **5***a* into imine **10**, the yield amounted to 64%, considering the recovery of acid **5***a*; this yield is significantly lower than the one we realized (82%) when forming the isocyanate **9** without the intermediacy of acid chloride **5***b*.

ir ν_{max} (KBr): 1700 (11-ketone), 1168, 1095 (ketals) cm^{-1}; nmr δ (90 MHz): 0.77 (s, 3H) and 1.00 (s, 3H) (18- and 19-CH_3), 1.99 (d, 1H, J = 11.5 Hz, 12α-H), 2.47 (d, 1H, J = 11.5 Hz, 12β-H), 3.77 (s, 8H, 3- and 17-OCH_2CH_2O); ms m/e: 390 (M^+), 125, 112, 99 (ethylene ketal fragmentations). *Anal.* calcd. for $C_{23}H_{34}O_5$: C 70.74, H 8.78; found: C 70.43, H 8.56.

3,17-Bisethylenedioxy-5α-androstan-11β-ol (7)

(a) Under vigorous stirring, a solution of 1.2 g of 3,17-bisethylenedioxy-5α-androstan-11-one (**4**), mp 164–166°C, in 30 mL of absolute tetrahydrofuran was added dropwise, at 0°C, to a suspension of 160 mg of $LiAlH_4$ in 100 mL of absolute tetrahydrofuran. The reaction was monitored by tlc analysis; after 5 h, ethyl acetate was added and, subsequently, a saturated aqueous ammonium chloride solution. The tetrahydrofuran solution was separated, the residue was extracted with chloroform, and the extracts were dried over sodium sulfate. Evaporation of the solvents gave 1.052 g (87% yield) of crystals, mp 201–203°C. A sample was recrystallized twice from acetone–hexane for analysis; mp 195–203°C; $[\alpha]_D^{25}$ +32 (c 0.900, $CHCl_3$); ir ν_{max} (KBr): 3520 (OH), 1160, 1082 (ketals) cm^{-1}; nmr δ (90 MHz): 1.02 (s, 3H) and 1.05 (s, 3H) (18- and 19-CH_3), 3.77 (8H, 3- and 17-OCH_2CH_2O), 4.20 (m, 1H, 11α-H); ms m/e: 392 (M^+), 125, 112, 99 (ketal fragmentations). *Anal.* calcd. for $C_{23}H_{36}O_5$: C 70.37, H 9.24; found: C 70.11, H 9.07.

(b) To a solution of 1 g of the diketal **4**, mp 164–166°C, in 80 mL of methanol, 800 mg of sodium borohydride was added with stirring, at room temperature. The solution was refluxed for 3 h, cooled, and poured into 1 L of ice water. The precipitate was filtered, washed, and dried, and the resulting product (1 g, mp 197–202°C) was recrystallized from acetone–hexane to give 900 mg (89% yield) of the 11β-hydroxy diketal **7**, mp 200–203°C. The identity of the product with the one described under *(a)* was established in the usual fashion by spectral comparisons and by the determination of a mixture melting point.

3,17-Bisethylenedioxy-5α-androst-9,11-ene (6a)

A solution of 2.2 g of 3,17-bisethylenedioxy-5α-androstan-11β-ol (**7**) in 6 mL of dry pyridine was left at 0°C for 2.5 h with 20 drops of distilled $SOCl_2$. Crushed ice and water were added, the precipitate was filtered on Celite, washed with water, and dissolved in chloroform. The organic solution was dried with sodium sulfate and taken to dryness to give 2.00 g of a residue which, upon two crystallizations from ether – petroleum ether, gave 1.86 g (88.6%) of 3,17-bisethylenedioxy-5α-androst-9,11-ene (**6*a***), mp 144–147°C. A sample was recrystallized once from ether – petroleum ether for analysis; mp 145–147°C; $[\alpha]_D^{26}$ +51 (c 1.200, $CHCl_3$) ir ν_{max} (KBr): 1635 (double bond), 1170, 1100 (ketals) cm^{-1}; nmr δ (60 MHz): 0.85 (s, 3H, 18-CH_3), 0.95 (s, 3H, 19-CH_3), 3.95 (8H, bisethylene-ketal), 5.35 (d, 1H, 11-H); ms m/e: 374 (M^+), 125, 99 (ketal fragmentations). *Anal.* calcd. for $C_{23}H_{34}O_4$: C 73.76, H 9.15; found: C 73.69, H 9.06.

5α-Androst-9,11-ene-3,17-dione (6)

(a) By transketalization (ref. 20)

To a solution of 7 g of diketal **6*a*** in 150 mL of absolute acetone, 150 mg of p-toluenesulfonic acid was added and the mixture was stirred at room temperature for 4.5 h. The product was diluted with water and was extracted with dichloromethane. The organic solution was washed with a saturated sodium bicarbonate solution and with water and was dried over sodium sulfate. Evaporation of the solvent gave 5 g of a crude product which was chromatographed on silica gel, using hexane–benzene (9:1) as eluent. Thus 3.17 g (72%) of the androstenedione **6** was obtained, mp 146–148°C. A sample was recrystallized from acetone–ether–hexane for analysis; mp 146–148°C (lit. (7) mp 154°C); $[\alpha]_D^{26}$ +153 (c 0.900, $CHCl_3$) (lit. (7) $[\alpha]_D^{14}$ +156); ir ν_{max} (KBr): 1740 (17-ketone), 1715 (3-ketone), 1630 (double bond) cm^{-1}; nmr δ (60 MHz): 0.90 (s, 3H, 18-CH_3), 1.24 (s, 3H, 19-CH_3), 5.55 (br, 1H, 11-H); ms m/e: 286 (M^+), 271 (M – CH_3), 243 (M – CH_3CO), 228 (1,4-seco-2,3,19-trinorandrostra-1(10),4(5),9(11)-trien-17-one). *Anal.* calcd. for $C_{19}H_{26}O_2$: C 79.68, H 9.15; found: C 79.24, H 9.00.

From the above-described chromatogram there was also obtained 1.1 g (18%) of the 3-monoethylenedioxy derivastive of diketone **6**.

(b) By deketalization with humidified, acidic silica gel (ref. 9)

To a suspension of 18 g of silica gel (Merck 60 for column chromatography, 32–63 mesh) in 80 mL of dichloromethane, 1.8 mL of 15% sulfuric acid was added with stirring. After 2–3 min, the aqueous phase disappeared and a solution of 2 g of diketal **6*a***, mp 144–147°C, in 10 mL of dichloromethane was added and the mixture was further stirred at room temperature for 22 h. The product was neutralized with solid sodium carbonate, the mixture was filtered through a fritted glass funnel, and the solid was washed several times with dichloromethane. Evaporation of the solvent from the filtrate gave 1.5 g of an oily product which, upon crystallization from acetone–ether–hexane, gave 1.385 g (90% yield) of the androstenedione **6**, mp 146–148°C, identified by comparison of its infrared spectrum with that of the product described under *(a)* and by the determination of a mixture melting point.

3,9,17-Trioxo-9,11-seco-5α-androstan-11-al (5) and 3,9,17-trioxo-9,11-seco-5α-androstan-11-oic acid (5a) by ozonolysis of the androstenedione 6

Through a solution of 1.193 g of the androstenedione **6**, mp 146–148°C, in 60 mL of dry ethyl acetate there was passed, at –10°C, for 3 h, a stream of oxygen containing 1.75% of ozone, at a flow rate of 220 L/h. The product was treated for 18 h with 1 mL of 30% H_2O_2 and 2 mL of water. Subsequently, 150 mL of water was added and the mixture was extracted with dichloromethane. The organic phase was washed with a cold 2 N aqueous sodium hydroxide solution and with water. After drying over sodium sulfate, the solvent was evaporated to afford 1.083 g of an oily product which gave, upon crystallization from ether–hexane, 1 g (75%) of *3,9,11-trioxo-9,11-seco-5α-androstan-11-al* (**5**), mp 172–175°C. For analysis a sample was recrystallized once more from ether–hexane; mp 171–175°C; $[\alpha]_D^{26}$ +32 (c 0.900, $CHCl_3$); ir ν_{max} (KBr): 2740 (aldehyde), 1735 (17-ketone), 1720 (aldehyde), 1700 (3-ketone) cm^{-1}; nmr δ (90 MHz): 0.79 (s, 3H) and 1.36 (s, 3H) (18- and 19-CH_3), 2.78 (q-AB, 2H, J = 18 Hz, 12-H_2, superimposed on m, 1H, C8β-H), 9.60 (s, 1H, aldehyde); ms m/e: 318 (M^+), 290 (M – CO), 276 (11,12-bisnor-9,13-seco-5α-androstane-3,9,17-trione), 180 (1-methylbicyclo[4.3.0]nonane-4,9-dione$^+$), 97. *Anal.* calcd. for $C_{19}H_{26}O_4$: C 71.67, H 8.23; found: C 71.51, H 8.11.

The aqueous alkaline extract of the dichloromethane solution was acidified with sulfuric acid to the Congo blue reaction and the product was extracted with chloroform. The organic layer was washed with water to neutral, dried over sodium sulfate, and evaporated to afford 305 mg of an oily product which, upon crystallization from benzene, gave 232 mg of *3,9,17-trioxo-9,11-seco-5α-androstan-11-oic acid* (**5*a***), mp 105–106°C, identified by comparison of the infrared and nmr spectra with those of the product described below and by the determination of a mixture melting point.

3,9,17-Trioxo-9,11-seco-5α-androstan-11-oic acid (5a) from aldehyde 5

A solution of 1.2 g of aldehyde **5**, mp 172–175°C, in 60 mL of acetone was treated for 2 h (until the disappearance, on tlc, of the neutral product) with an excess (1.3 mL) of Jones' reagent (18). Isopropyl alcohol (1 mL) and 200 mL of water were added and the product was extracted with dichloromethane. The organic layer was extracted with aqueous 2 N sodium hydroxide, the alkaline extract was acidified to the Congo blue reaction with 2 N H_2SO_4, and the mixture was extracted with chloroform. The organic layer was washed with water and was dried over sodium sulfate. Removal of the solvent gave 1.087 g of crude, oily acid **5*a*** which afforded upon crystallization from benzene 955 mg (76%) of purified acid **5*a***, mp 106–111°C; $[\alpha]_D^{26}$ +22 (c 2.050, $CHCl_3$); ir ν_{max} (KBr): 3400–3000 (acid), 1740 (17-ketone), 1700 (3-ketone and acid) cm^{-1}; nmr δ (90 MHz): 0.77 (s, 3H) and 1.35 (s, 3H) (18- and 19-CH_3), 2.69 (q-AB, outer peaks ill defined, 2H, 12-H_2), 2.86 (m, 8β-H); ms m/e: 335 $(M + 1)^+$, 307, 290 (M – CO_2), 275 (M – CO_2 – CH_3), 231, 180 (8a-methyldecaline-1,6-dione).

Since acid **5***a* decomposes readily, no microanalysis could be performed and the following reactions were carried out without further purifying the product.

The neutral extract of the oxidation reaction (198 mg) was composed of a mixture which was not further investigated.

The total yield of acid **5***a* from the androstenedione **6** amounted to 78%.

11-Aza-5α-androst-9,11-ene-3,20-dione (**10**)

(*a*) *Via the acid chloride 5b, without isolation of the 3,9,17-trioxo seco acid azide 8 and the isocyanate 9*

(*i*) At 0°C, 1.5 mL of oxalyl chloride, dissolved in 10 mL of absolute benzene, was added with repeated shaking to a suspension of 1.193 g of purified acid **5***a*, mp 106–111°C, in 60 mL of absolute benzene. The mixture was allowed to warm to room temperature and was stirred for 12 h, the progress of the reaction being followed by infrared analysis of samples of the reaction mixture. The product was taken to dryness *in vacuo* at room temperature and the residue was redissolved in absolute benzene and taken again to dryness under reduced pressure. This operation was repeated another time. Thus, 1.262 g of crude, solid, *3,9,17-trioxo-9,11-seco-5α-androstan-11-oic acid chloride* (**5***b*) was obtained; ir ν_{max} (KBr): 1800 (acid chloride), 1740 (17-ketone), 1700 (3-ketone) cm^{-1}. This product was used without further purification in the following reaction.

The crude acid chloride **5***b* (1.26 g) was dissolved in 50 mL of acetone and was treated with a paste made up of 500 mg of sodium azide and 0.5 mL of water. The reaction mixture was refluxed for 30 min and a few drops of water were added until the solution became clear. Within 15 min, 50 mL of water were added and the mixture was extracted with chloroform. The organic solution was dried over sodium sulfate and the solvents were evaporated. The crude product (987 mg) did not only contain *3,9,17-trioxo-9,11-seco-5α-androstan-11-oic acid azide* (**8**) but also some rearranged product: *3,9,17-trioxo-9,12-seco-11-nor-5α-androstan-12-yl isocyanate* (**9**); ir ν_{max} (KBr): 2250 (N=C=O), 2130 (N_3), 1800, 1740, and 1700 cm^{-1}. This solid mixture was not separated but dissolved in 3 mL of acetic acid. After addition of 1.1 mL of water the product was warmed and an evolution of N_2 was observed. After the gas evolution had ceased, the mixture was cooled and an aqueous 2 *N* NaOH solution was added until it became alkaline and was then extracted with chloroform. The organic solution was extracted with 10% aqueous hydrochloric acid, the acidic extract was made alkaline with 2 *N* sodium hydroxide, and the product was again extracted with dichloromethane. The organic solution was dried over sodium sulfate and the solvent was evaporated. Thus, 302 mg of an oily product was obtained. It gave upon crystallization from ether–hexane 284 mg (28% yield) of *11-aza-5α-androst-9,11-ene-3,17-dione* (**10**), mp 173–176°C. For analysis, a sample was recrystallized twice from ether–hexane; mp 176–178°C; $[\alpha]_D^{28}$ +165.4 (*c* 1.010, $CHCl_3$); ir ν_{max} (KBr): 1740 (17-ketone), 1715 (3-ketone), 1635 (C=N) cm^{-1}; nmr δ (90 MHz): 0.83 (s, 3H) and 1.25 (s, 3H) (18- and 19-CH_3), 3.41 (d, 1H, J = 13.5 Hz) and 3.79 (d, 1H, J = 13.5 Hz) (12-H_2); ms *m/e*: 287 (M^+), 273 (M − CH_3), 260 (M − HCN), 245, 231. *Anal.* calcd. for $C_{18}H_{25}NO_2$: C 75.22, H 8.77, N 4.87; found: C 75.10, H 8.73, N 4.86.

The original aqueous alkaline solution which had been extracted with hydrochloric acid and the aqueous alkaline solution from which the imine **10** had been extracted with dichloromethane were combined and acidified with 2 *N* sulfuric acid to the Congo blue reaction. The product was extracted with dichloromethane. The organic solution was washed with water and dried over sodium sulfate. Evaporation of the solvent gave 462 mg of an oily product which afforded upon crystallization from benzene 438 mg (37%) of *3,9,17-trioxo-9,11-seco-5α-androstan-11-oic acid* (**5***a*), mp 105–110°C. Its identity was established by the comparison of its infrared spectrum with that of an authentic sample (cf. above) and by the determination of a mixture melting point. Considering the recovery of this starting material, the yield of imine **10** amounted to 44%.

(*ii*) A suspension of 232 mg of freshly activated sodium azide (11, cf. also ref. 21) in a solution in 20 mL of absolute benzene of 502 mg of acid chloride **5***b*, prepared from 500 mg of acid **5***a* as described above under (*i*), was refluxed for 20 h with exclusion of moisture. The product was cooled and filtered. To the filtrate, 5 mL of concentrated hydrochloric acid was added and the mixture was refluxed for 2.5 h. After cooling, the acid layer was separated and the benzene solution was washed with water. The acidic layer and the water washings were combined and made alkaline with 2 *N* sodium hydroxide, and the product was extracted with dichloromethane. The organic solution was washed with water and dried over sodium sulfate. Evaporation of the solvent gave 168 mg (39%) of an oily product which afforded upon crystallization from ether–hexane 146 mg (34%) of *11-aza-5α-androst-9,11-ene-3,17-dione* (**10**), mp 173–176°C. The identity of the product was established by comparison of its infrared spectrum with that of the product described under (*i*), and by the determination of a mixture melting point.

The benzene solution which had been extracted with sodium hydroxide and washed with water (cf. above) was dried over sodium sulfate and the solvent was removed. The oily residue (272 mg) gave upon crystallization from benzene 250 mg (50%) of *3,9,17-trioxo-9,11-seco-5α-androstan-11-oic acid* (**5***a*), mp 105–110°C, identified in the usual manner with an authentic sample. Considering this recovery of starting material, the yield of the imine **10** amounted to 68%.

(*b*) *Via the acid chloride 5b, with isolation of the acid azide 8 and the isocyanate 9*

(*i*) To a solution in 35 mL of acetone of 640 mg of crude acid chloride **5***b*, prepared from 680 mg of acid **5***a* as described above (*a*, *i*), a solution of a 410 mg of sodium azide in 15 mL of water was added at room temperature, with vigorous stirring. The mixture was left at room temperature for another 20 h and 200 mL of water was added. The product was extracted with dichloromethane, and the organic solution was washed with water and dried over sodium sulfate. Removal of the solvent gave 600 mg of a solid, representing crude *3,9,17-trioxo-9,11-seco-5α-androstan-11-oic acid azide* (**8**); ir ν_{max} (KBr): 2128 (C≡N), 1740 (17-ketone), 1700 (3- and 9-ketones) cm^{-1}. This product was used without further purification in the next step.

The crude azide **8** described above was dissolved in 50 mL of benzene and the solution was refluxed for 2 h, at which time gas evolution had ceased. Removal of the solvent under reduced pressure gave 580 mg of crude *3,9,17-trioxo-9,12-seco-11-nor-5α-androstan-12-yl isocyanate* (**9**); ir ν_{max} (KBr): 2250 (N=C=O), 1738 (17-ketone), 1705 (3- and 9-ketones) cm^{-1}. This product was not purified prior to the next step.

The crude isocyanate **9** described above was dissolved in 50 mL of dioxane and there was added, with vigorous stirring and dropwise, 2 mL of concentrated hydrochloric acid. The mixture was left for 20 h at room temperature and was subsequently made alkaline by the addition of 2 *N* sodium hydroxide. The product was extracted with dichloromethane, the organic layer was extracted in turn with 20% aqueous hydrochloric acid, and the acidic extract was made alkaline with 2 *N* sodium hydroxide. The resulting mixture was extracted with dichloromethane, and the organic solution was washed with water and dried over sodium sulfate. Removal of the solvent gave 320 mg of crude, amorphous, *11-aza-5α-androst-9,11-ene-3,17-dione* (**10**) which upon crystallization from ether–hexane gave 291 mg (50%) of pure *azide* **10**, mp 173–176°C, identified in the usual fashion.

The two aqueous alkaline solutions that had been extracted with dichloromethane were combined and were acidified with 2 *N* sulfuric acid to the Congo blue reaction. The mixture was extracted with dichloromethane, and the organic layer was washed with water and dried over sodium sulfate. Removal of the solvent afforded 172 mg (25%) of an oily product which gave upon crystallization from benzene 151 mg (22%) of the *trioxo seco acid* **5***a*, mp 105–110°C, identified in the usual manner. Considering this recovery of starting material, the yield of imine **10** amounted to 64%.

(*ii*) When the procedure employed by Badanova and Pivinitskii (15*b*) in the synthesis of 11-aza-estradiol was used for the transformation of 529 mg of crude acid chloride *5b*, prepared from 562 mg of acid *5a*, into *imine* **10**, 242 mg (50%) of this product, mp 173–176°C, and 120 mg (21%) of *acid* *5a*, mp 105–110°C, were obtained. Considering the recovery of starting material, the yield of imine **10** amounted to 64%.

(*c*) *Without the intermediacy of acid chloride 5b, by direct transformation of the seco acid 5a into the isocyanate 9 and thence into imine 10*

According to the procedure of Grouillier *et al.* (12), there was added, dropwise and with stirring, at −5°C, to a solution of 400 mg of purified 3,9,17-trioxo-9,11-seco-5α-androstan-11-oic acid (*5a*), mp 106–111°C, in 35 mL of acetone, a solution of 0.83 mL of triethylamine in 1 mL of acetone, subsequently a solution of 0.67 mL of ethyl chloroformate in 1 mL of acetone, and, finally, a solution of 0.78 mg of sodium azide in 3 mL of water. The mixture was stirred for 1.5 h at −5°C and then allowed to warm to room temperture, stirring being continued for another 2 h. Ice water (100 mL) was added and the product was extracted with dichloromethane. The organic solution was washed with water and was dried over sodium sulfate. Removal of the solvent gave 388 mg of solid *3,9,17-trioxo-9,12-seco-11-nor-5α-androstan-12-yl isocyanate* (**9**); ir ν_{max} (KBr): 2250 (N=C=O), 1739 (17-ketone), 1705 (3- and 9-ketones) cm^{-1}. This product was used without purification in the next step.

The crude isocyanate **9** described above was dissolved in 30 mL of dioxane and to this solution was added, dropwise and with vigorous stirring, 2 mL of concentrated hydrochloric acid. The mixture was left for 18 h at room temperature and subsequently treated with 2 *N* sodium hydroxide until it became alkaline. The product was extracted with dichloromethane, the organic layer was extracted in turn with 10% aqueous hydrochloric acid, the acidic extract was made alkaline with 2 *N* sodium hydroxide, and the product was again extracted with dichloromethane. The organic solution was washed with water and dried over sodium sulfate. Removal of the solvent gave 270 mg (79%) of an oily product which, upon crystallization from ether–hexane, gave 233 mg (68%) of *11-aza-5α-androst-9,11-ene-3,17-dione* (**10**), mp 173–176°C. The identity of the product was established by comparison of its infrared spectrum with that of an authentic sample (cf. above) and by the determination of a mixture melting point. The aqueous alkaline solutions on which dichloromethane extractions had been performed were combined and acidified with 2 *N* sulfuric acid to the Congo blue reaction. The mixture was extracted with dichloromethane, and the organic layer was washed with water and dried over sodium sulfate. Removal of the solvent afforded 87 mg of an oily product which, upon crystallization from benzene, gave 69 mg (17%) of *3,9,17-trioxo-9,11-seco-5α-androstan-11-oic acid* (**5a**), mp 106–111°C, the identity of which was established in the usual fashion. Considering this recovery of starting material, the yield of imine **10** amounted to 82%.

11-Aza-5α-androstane-3,17-dione (12)

To a solution of 200 mg of the imine **10** in 10 mL of methanol, 2 mL of a 2% HCl solution in methanol was added and, subsequently, with stirring, 100 mg of cyanosodiumborohydride. The reaction was continued for 4 h, the product was made alkaline with an aqueous 2 *N* NaOH solution, and the mixture was extracted with dichloromethane. After washing with water and drying over magnesium sulfate, the solvents were evaporated and the crude product, the keto group of which had been, according to its infrared spectrum (weak carbonyl and OH absorptions), partly reduced, was dissolved in 10 mL of acetone and reoxidized at 0°C in the usual fashion with Jones' reagent (18). After 1 h, the solution was made alkaline with 2 *N* aqueous NaOH and the product was extracted with dichloromethane. The organic solution was washed with water and was dried over magnesium sulfate, and the solvents were removed *in vacuo*. The crystalline residue (200 mg) was recrystallized from ether – petroleum ether to afford 130 mg (65%) of pure 11-aza androstanedione **12**, mp 128–132°C. For analysis a sample was recrystallized twice from ether–hexane; mp 128–132°C; $[\alpha]_D^{26}$ +132.5 (*c* 0.800, $CHCl_3$); ir ν_{max} (KBr): 3360, 3440 (NH), 1740 (17-ketone), 1710 (3-ketone) cm^{-1}; nmr δ (90 MHz): 0.99 (s, 3H) and 1.00 (s, 3H) (18- and 19-CH_3), 2.43 (d, 1H, *J* = 11 Hz) and 2.45 (d, 1H, *J* = 11 Hz) (9α- and 12α-H), 2.91 (d, 1H, *J* = 11 Hz, 12β-H); ms *m/e*: 289 (M^+), 274 (M − CH_3), 261 (M − CO), 232. *Anal.* calcd. for $C_{18}H_{27}NO_2$: C 74.70, H 9.40, N 4.84; found: C 74.78, H 9.32, N 4.81.

N-Acetyl-11-aza-5α-androstane-3,17-dione (12a)

A solution of 180 mg of the 11-aza androstanedione **12** in 0.3 mL of pyridine was heated for 5 min with 0.3 mL of acetic anhydride and subsequently the mixture was left overnight at room temperature. Methanol was added, the product was taken to dryness *in vacuo*, redissolved in benzene, and again taken to dryness; this operation was repeated once. The oily residue (186 mg) was chromatographed on silica gel with benzene–acetone (95:5) as eluent. Thus 90 mg (43% yield) of the crystalline N-acetyl derivative **12***a* was obtained. After two recrystallizations from ether – petroleum ether the product (55 mg) melted at 185–187°C. From the mother liquors, 50 mg of starting material (**12**) was isolated. Thus the effective yield of pure amide **12** corresponded to 45%. A sample of the product was recrystallized once from ether – petroleum ether for analysis; mp 185–187°C; ir ν_{max} (KBr): 1740 (17-ketone), 1710 (3-ketone), 1640 (amide); nmr δ (90 MHz): 0.91 (s, 3H) and 1.10 (s, 3H) (18- and 19-CH_3), 1.99 (s, 3H, CH_3CO), 2.82 (d, 1H, *J* = 13 Hz, 12α-H), 3.85 (d, 1H, *J* = 11 Hz, 9α-H), 4.14 (d, 1H, *J* = 13 Hz, 12β-H); ms *m/e*: 331 (M^+), 316 (M − CH_3), 288 (M − NHCO). *Anal.* calcd. for $C_{20}H_{29}NO_3$: C 72.47, H 8.82, N 4.23; found: C 72.47, H 8.79, N 4.24.

3,3-Dimethoxy-11-aza-5α-androstan-17-one (11)

A solution of 60 mg of 11-aza-5α-androstane-3,17-dione (**12**) in 10 mL of absolute methanol was kept at room temperature with 20 mg of oxalic acid and a few beads of 4A molecular sieves for 20 h. Potassium carbonate and water were added and the product was extracted with dichloromethane. The organic solution was washed with water, a few crystals of potassium carbonate were added, and the mixture was dried over magnesium sulfate. Evaporation of the solvent gave 54 mg (80%) of the crystalline ketal **11**; mp 113–115°C. For analysis the product was recrystallized four times from hexane; mp 114–115°C; $[\alpha]_D^{28}$ +26 (*c* 0.830, $CHCl_3$); ir ν_{max} (KBr): 3360 and 3440 (NH), 1735 (17-ketone), 1128, 1100, and 1049 (ketal) cm^{-1}; nmr δ (90 MHz): 0.88 (s, 3H) and 0.98 (s, 3H) (18- and 19-CH_3), 2.47 (d, 1H, *J* = 13 Hz, 12α-H), 2.91 (d, 1H, *J* = 13 Hz, 12β-H), 3.01 (s, 3H, OCH_3), 3.06 (s, 3H, OCH_3); ms *m/e*: 335 (M^+), 303 (M − CH_3OH), 289. *Anal.* calcd. for $C_{20}H_{33}NO_3$: C 71.60, H 9.92, N 4.18; found: C 71.25, H 9.74, N 4.17.

17β-Hydroxy-11-aza-5α-androstan-3-one (11-aza-4,5α-dihydrotestosterone) (1)

At 0°C, a solution of 370 mg of crude ketal **11** in 30 mL of absolute tetrahydrofuran was added dropwise and with stirring, in the course of 20 min, to a suspension of 100 mg of lithium aluminum hydride in 30 mL of absolute tetrahydrofuran. After 20 min ethyl acetate and, subsequently, a saturated aqueous ammonium chloride solution were added and the organic layer was separated. The aqueous layer was extracted with chloroform and both organic solutions were combined, washed with water, and dried over magnesium sulfate. Evaporation of the solvents gave 340 mg (92%) of crude *3,3-dimethoxy-11-aza-5α-androstan-17β-ol* (**11***a*), melting after two recrystallizations from acetone– ether at 162–164°C; ir ν_{max} (KBr): 3400–3280 (broad OH and NH band), 1114, 1100, 1046 (OCH_3) cm^{-1}; nmr δ (90 MHz): 0.83 (s, 3H) and 0.87 (s, 3H) (18- and 19-CH_3), 2.31 (d, 1H, *J* = 13 Hz, 12α-H), 2.97 (d, 1H, *J* = 13 Hz, 12β-H), 3.02 (s, 3H, OCH_3), 3.06 (s, 3H, OCH_3), 3.55 (1H, br, 17α-H). According to tlc analysis, this product contained an impurity even after purification, and was used in the crude state in the deprotection reaction of the 3-ketone. A quantity of 300 mg of crude ketal **11***a* was dissolved in 30 mL of absolute acetone and treated for 48 h at room temperature with 30 mg of *p*-toluenesulfonic acid. Subsequently, water, a few crystals of sodium hydrogen carbonate, and a few drops of an aqueous NaOH solution were added, the mixture was extracted with dichloromethane, and the organic solution was washed with water and dried over magnesium sulfate. Evaporation of the solvents gave 180 mg (69%) of *17β-hydroxy-11-aza-5α-androstan-3-one (11-aza-4,5α-dihydrotestosterone)* (**1**). The analytical sample was prepared by four recrystallizations from acetone − petroleum ether − hexane; mp 159−160°C; $[\alpha]_D^{26}$ +142 (c 0.500, $CHCl_3$); ir ν_{max} (KBr): 3400−3260 (broad band, OH, NH), 1715 (3-ketone) cm^{-1}; nmr δ (90 MHz): 0.88 (s, 3H) and 1.08 (s, 3H) (18- and 19-CH_3), 2.37 (d, 1H, J = 13 Hz, 12α-H), 3.00 (d, 1H, J = 13 Hz, 12β-H), 3.59 (t, 1H, 17α-H); ms m/e: 291 (M^+), 276 ($M - CH_3$), 166 (1-methyl-5-methylene-9-hydroxy-3-azabicyclo[4.3.0]nonane$^+$), 153 (1-methyl-9-hydroxy-3-azabicyclo-[4.3.0]non-4,5-ene). *Anal.* calcd. for $C_{18}H_{29}NO_2$: C 74.18, H 10.03, N 4.81; found: C 74.24, H 10.01, N 4.73.

Acknowledgements

We remember with deep gratitude the late Mrs. J. Capitaine who cooperated in some of the experiments described here, and we sincerely thank Mrs. M. M. Lourdusamy for her cooperation in some other experiments, as we express our appreciation to Mrs. D. Thibeault for technical assistance. This study was performed pursuant to contract No. N01-HD-8-2815 with the National Institutes of Health, U.S. Department of Health, Education, and Welfare. We express our gratitude for this support and for the cooperation of the National Institute of Child Health and Human Development, especially to Dr. H. K. Kim. We also acknowledge with sincere thanks financial assistance and support from the National Research Council of Canada, the Natural Sciences and Engineering Research Council of Canada, the Ministère de l'Education du Québec, and Ayerst Laboratories, Montréal.

1. CH. R. ENGEL, P. LACHANCE, J. CAPITAINE, J. ZEE, D. MUKHERJEE, and Y. MÉRAND. J. Org. Chem. **48**, 1954 (1983).
2. M. N. ROY CHOWDHURY, V. S. SALVI, R. C. RASTOGI, S. RAKHIT, and CH. R. ENGEL. Steroids, **21**, 361 (1973).
3. CH. R. ENGEL and S. RAKHIT. Can. J. Chem. **40**, 2153 (1962).
4. J. P. KUTNEY and I. J. VLATTAS. Steroids, **4**, 595 (1964).
5. H. LETTRÉ and L. KNOF. Chem. Ber. **93**, 2860 (1960).
6. A. BOWERS and E. DENOT. J. Am. Chem. Soc. **82**, 4956 (1962).
7. C. W. SHOPPEE. J. Chem. Soc. 1134 (1946).
8. C. W. SHOPPEE. Helv. Chim. Acta, **23**, 740 (1940).
9. (*a*) F. HUET, A. LECHEVALLIER, and J. M. CONIA. Tetrahedron Lett. 2521 (1977); (*b*) F. HUET, A. LECHEVALLIER, M. PELLET, and J. M. CONIA. Synthesis, 63 (1978).
10. (*a*) F. REBER, A. LARDON, and T. REICHSTEIN. Helv. Chim. Acta, **37**, 45 (1954); (*b*) A. LARDON and T. REICHSTEIN. Helv. Chim. Acta, **37**, 388 (1954), 443 (1954); (*c*) cf. also R. ADAMS and L. H. ULICH. J. Am. Chem. Soc. **42**, 599 (1920); A. L. WILDS and C. H. SHUNK. J. Am. Chem. Soc. **70**, 2427 (1948).
11. J. NELLES. Ber. Dtsch. Chem. Ges. **65**, 1345 (1932).
12. A. GROUILLIER, J.-Y. NIOCHE, J. BARAILLER, M. ROCHE, and H. PUCHEO. J. Eur. Med. Chem.-Chimica Therapeutica, **15**, 139 (1980).
13. R. F. BORCH, M. D. BERNSTEIN, and H. D. DURST. J. Am. Chem. Soc. **93**, 2897 (1971).
14. TH. A. NARWID, J. F. BLOUNT, J. A. IACOBELLI, and M. R. USKOKOVIĆ. Helv. Chim. Acta, **57**, 781 (1974).
15. (*a*) YU. P. BADANOVA and K. K. PIVINITSKIÍ. Zh. Obshch. Khim. **41**, 242 (1971); (*b*) YU. P. BADANOVA and K. K. PIVINITSKIÍ. Zh. Obshch. Khim. **45**, 2546 (1975); (*c*) K. K. PIVINITSKIÍ and YU. P. BADANOVA. Zh. Obshch. Khim. **48**, 1669 (1978); (*d*) cf. also I. I. IVANENKO, K. K. PIVINITSKIÍ, and N. FEDOTOV. Probl. Endokrinol. **25**, 62 (1979).
16. D. NASIPURI and S. K. GOSH. J. Chem. Soc. Perkin Trans. 1, 1889 (1976).
17. H. HEUSSER, K. HEUSLER, K. EICHENBERGER, C. G. HONEGGER, and O. JEGER. Helv. Chim. Acta, **35**, 295 (1952).
18. (*a*) K. BOWDEN, J. M. HEILBRON, E. R. H. JONES, and B. C. L. WEEDON. J. Chem. Soc. 39 (1946); (*b*) A. BOWERS, T. G. HALSALL, E. R. H. JONES, and A. J. LEMIN. J. Chem. Soc. 2548 (1953).
19. J. P. GUTHRIE and Y. VEDA. Can. J. Chem. **51**, 3936 (1973).
20. H. SCHINZ and G. SCHÄPPI. Helv. Chim. Acta, **30**, 1483 (1947).
21. A. S. SMITH. The Curtius reaction. *In* Organic reactions. Vol. 3. *Edited by* R. ADAMS, L. F. FIESER, J. R. JOHNSON, and H. R. SNYDER. John Wiley and Sons, Inc., New York. 1946. p. 382.

Concerning $^5J_o^{OH,CH_3}$ in 2-methylphenol and its derivatives. A proximate coupling

TED SCHAEFER, TIMOTHY A. WILDMAN, AND RUDY SEBASTIAN

Department of Chemistry, University of Manitoba, Winnipeg, Man., Canada R3T 2N2

Received July 6, 1984

TED SCHAEFER, TIMOTHY A. WILDMAN, and RUDY SEBASTIAN. Can. J. Chem. **63**, 773 (1985).

In 2-chloro-6-methylphenol in CCl_4 solution, $^5J_o^{OH,CH_3}$, the spin–spin coupling between the hydroxyl and methyl protons, is +68(3) mHz. In this compound, the hydroxyl group lies *trans* to the methyl group. If the coupling becomes −120 ± 60 mHz in a *cis* orientation of these two groups, then the apparent vanishing of $^5J_o^{OH,CH_3}$ in some derivatives of 2-methylphenol is understandable, as well as its presence in other derivatives. Computations of this coupling imply its proximate mechanism and can rationalize its value of −220 ± 20 mHz in 2-*tert*-butyl-6-methylphenol. Analogies are noted with $^5J_o^{OH,CF_3}$ in 2-trifluoromethyl phenol and with a coupling in styrene, which also appears to vanish in certain orientations of the vinyl group.

TED SCHAEFER, TIMOTHY A. WILDMAN et RUDY SEBASTIAN. Can. J. Chem. **63**, 773 (1985).

Dans le chloro-2-méthyl-o phénol en solution dans le CCl_4, la constante de couplage spin–spin, $^5J_o^{OH,CH_3}$, entre les protons de l'hydroxyle et du groupement méthyle est égale à +68(3) mHz. Dans ce composé, le groupement hydroxyle occupe une position *trans* par rapport au groupement méthyle. Si la valeur de ce couplage devient égale à −120 ± 60 mHz pour une orientation *cis* de ces deux groupes, on peut alors facilement comprendre l'apparente disparition du $^5J_o^{OH,CH_3}$ dans quelques dérivés du méthyl-2 phénol ainsi que sa présence dans d'autres dérivés. Des calculs de ce couplage suggèrent son mécanisme par proximité et peuvent rationaliser sa valeur de −220 ± 20 dans le *tert*-butyl-2 méthyl-6 phénol. On note un certain nombre d'analogies avec les valeurs de $^5J_o^{OH,CF_3}$ dans le trifluorométhyl-2 phénol ainsi qu'avec un couplage dans le styrène qui semble aussi disparaître avec certaines orientations du groupement vinyle.

[Traduit par le journal]

Introduction

Negative proton spin–spin coupling constants over five formal bonds are usually attributable to proximate interactions involving a close approach of the bonds or atoms carrying the protons in question (1–10). An example is $^5J_o^{H,CH}$ in 2,5-dichlorostyrene (1), involving an *ortho* ring proton and that β-proton which, in a planar conformation, lies very near the ring C—H bond. Other examples are $^5J_o^{H,CH_3}$ in anisole (2, 3, 8–10) and thioanisole derivatives (5–7). The magnitude of $^5J_o^{H,CH_3}$ drops off rapidly as the OCH_3 or SCH_3 moieties move away from the benzene plane (6, 8–10). Indeed, $^5J_o^{H,CH_3}$ is a useful conformational indicator (5–10) and a detailed theoretical study for anisole indicates its mechanism and conformational dependence (10).

If the methyl group in anisole is relocated to form 2-methylphenol, then models suggest that the corresponding proximate coupling, $^5J_o^{OH,CH_3} \equiv {}^5J$, should be observable, at least in a *cis* orientation of the hydroxyl and methyl groups. Because the barrier to rotation about the Csp^2—O bond in phenol is high relative to kT at ambient temperatures, discussion in terms of *cis* and *trans* planar orientations of the hydroxyl group is adequate for 2-methylphenol (11–15).

In the following brief discussion, some peculiar observations on ^5J in 2-methylphenol and its derivatives are rationalized via an experiment on 2-chloro-6-methylphenol. $^5J_{cis} \equiv {}^5J_c$ is established as a proximate coupling, is compared with some analogous couplings in other compounds, and is used to assess the reliability of some molecular orbital calculations of the stabilities of certain conformers of 2-methylphenol.

Discussion

In a number of 2-methylphenol derivatives, ^5J sometimes but not always leads to a broadening of the hydroxyl ^1H nmr peaks. In 2-methylphenol itself in CCl_4 solution at 305 K (15), this coupling must be very small, say ≤20 mHz in magnitude, judging from the spectrum of the hydroxyl proton in ref. 15, where the linewidth at half-height is ≤70 mHz and seven peaks are cleanly resolved in a spectral range of less than 1 Hz. ^5J

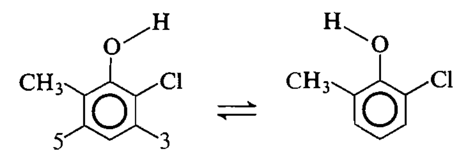

a trans   *b cis*

must also be very small in 2-allyl-6-methylphenol (11). Yet it clearly exists in 2-isopropyl-6-methylphenol (16), and in 2-*tert*-butyl-6-methylphenol ^5J is −220 ± 20 mHz (17). An interpretation of this apparent inconsistency is reached as follows.

In 2-chloro-6-methylphenol, no coupling between the hydroxyl proton and H-3 is detectable (see Experimental and Table 1). As established in a variety of experiments (11–15), this observation is consistent with the virtual exclusion of the *cis* conformer, *b*, in the *a*–*b* equilibrium. A recent ranking of *ortho* substituents as hydrogen bond accepters or repellers in *ortho* substituted phenol derivatives (18) implies that 2-chloro-6-methylphenol exists as the *trans* form, *a*, to the extent of 99% in CCl_4 solution at 305 K. This internally consistent ranking for twelve *ortho* substituents implies that the free energy difference favoring *a* over *b* is 11.5 kJ/mol at 305 K. The presence of as much as 5% of *b* should have been detectable by decoupling experiments, if in no other way, because it would entail a coupling of about 30 mHz between H-3 and the hydroxyl proton. In fact, the linewidths of the peaks due to H-3 and H-5 were identical to within experimental error at ca. 0.05 Hz (at 300 MHz), fully consistent with a negligible quantity of *b*.

Another assumption used below is that nonplanar conformations of the hydroxyl group can be neglected. In the gas phase, the internal barrier to rotation in phenol is 14.6 kJ/mol (19–21), quite large compared to thermal energies of 2.5 kJ/mol at 305 K. In pentachlorophenol the internal barrier rises to 26.4 kJ/mol, no doubt due to internal hydrogen bonding (22). In form *a* the barrier to internal rotation is therefore very likely rather larger than in phenol. The presence of significant nonplanar conformations should also have been reflected in a measurable $^6J_p^{H,OH}$. Yet the peaks due to H-4 are at least as

TABLE 1. ^{1}H nuclear magnetic resonance spectral parameters for a 4.7 mol% solution of 2-chloro-6-methylphenol in CCl_4 at 100.001 MHz and 305 K

Parameter	Value	Parameter	Value
δ_{OH}	5.4672[a]	$^5J_o^{OH,CH_3}$	+0.068(3)[d]
δ_{CH_3}	2.2493	$^5J_m^{H,CH_3}$	0.322(2)
δ_3	7.0643	$^6J_p^{OH,H}$	*c*
δ_4	6.6660	$^6J_p^{H,CH_3}$	−0.594(1)
δ_5	6.9331	$^4J_o^{H,CH_3}$	−0.784(2)
$^3J_{34}$	8.052(2)[b]	rms deviation	0.009
$^3J_{45}$	7.526(2)	Largest deviation	0.028
$^4J_{35}$	1.564(2)	Peaks observed	64
$^5J_m^{OH,3}$	*c*	Transitions assigned	141
$^5J_m^{OH,5}$	0.640(3)	Transitions calculated	208

[a]Delta (δ) values known to higher accuracy than this.
[b]Numbers in parentheses are the standard deviations in Hz of the last significant figure in the couplings.
[c]No evidence for its presence.
[d]Sign and magnitude determined at 300 MHz, see Fig. 1 and Experimental.

narrow as those arising from the other ring protons. $^6J_p^{H,OH}$ is no doubt a σ−π coupling and, as such, should vary as $\sin^2\theta$, where θ is the out-of-plane twist about the C—O bond (in thiophenol, with a low barrier to internal rotation, the analogous coupling is −0.33 Hz (23, 24)). It is also possible that the barrier in phenol is larger in solution than in the vapor, as found for anisole, for example (25). The assumption of a planar *a* appears reasonable.

Furthermore, because $^6J_p^{H,OH}$ has not been observed in any of the other phenol derivatives mentioned below, the discussion for all of them assumes *cis–trans* equilibria of planar conformations. As summarized previously (17), a variety of physical methods are all consistent with coplanar conformations of the hydroxyl group even in a highly hindered molecule like 2,6-di-*tert*-butylphenol. Again, the spin–spin coupling data on 2-isopropyl-6-methylphenol (16) are consistent with correlated conformations of the hydroxyl and isopropyl groups and no nonplanar conformations of the hydroxyl moiety were needed to interpret the experimental results.

Figure 1 shows that ^5J is +68(3) mHz. If ^5J is to be zero or very nearly zero in 2-methylphenol, then the precise coupling data (15) and the concomitant conformational deductions imply the expression $(0.65 \pm 0.01)\ ^5J_t + (0.35 \pm 0.01)\ ^5J_c = \pm 20$ mHz, assuming 20 mHz as a possible error. In this expression, 0.65 is the fraction of the *trans* form in 2-methylphenol, anologous to *a* above, ^5J_t and ^5J_c are the OH,CH_3 couplings for the *trans* and *cis* conformers, respectively. Taking ^5J_t as +68 mHz, ^5J_c follows as −126 ± 57 mHz.

Because 2-allyl-6-methylphenol has the same *cis* and *trans* populations (11) as 2-methylphenol, the apparent vanishing of ^5J in the former is also understandable.

However, in 2-isopropyl-6-methylphenol the population of the *cis* form is 62%. The expression above then yields ^5J as −52 ± 25 mHz, sufficient to account for the observed broadening (16) of the hydroxyl proton resonance. In this compound the methyl protons couple to the methine proton of the isopropyl group, as well as to the ring and hydroxyl protons, disallowing clean experiments of the kind displayed for 2-chloro-6-methylphenol in Fig. 1.

In 2-*tert*-butyl-6-methylphenol, the *cis* conformer, analogous to *b*, has a fractional population of 0.85 in CCl_4 at 305 K (17). The values for ^5J_c and ^5J_t deduced above would yield a ^5J of

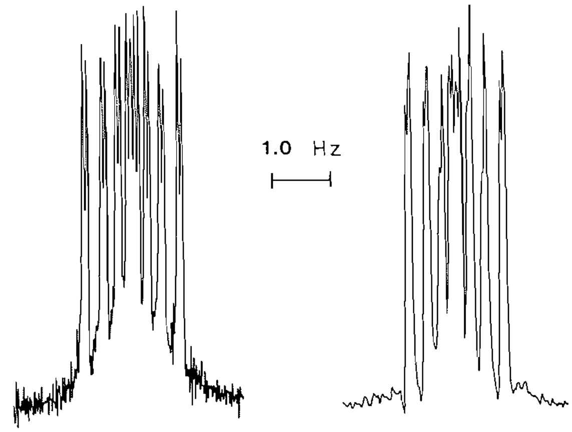

FIG. 1. The methyl group ^{1}H nmr spectrum of 2-chloro-6-methylphenol in CCl_4 at 293 K and 300.135 MHz is shown at the left. Sixteen peaks arise from spin–spin coupling to the four other protons in the molecule. The smallest splitting is 0.068(3) Hz or 68(3) mHz in magnitude. The sign of this coupling was established by double resonance experiments, in which selected peaks from H-5 were weakly irradiated. One such experiment is shown at the right, where the methyl peaks are displayed under conditions in which the H-5 peak at lowest field is being irradiated. In short, low-field peak perturbations observed in the methyl resonance established that $^5J^{OH,CH_3}$ has the same sign as $^5J_m^{OH,H-5}$. The latter is positive. In order to obtain high digital resolution, the methyl bond in the single resonance experiment was isolated using a narrow sweepwidth (100 Hz) and a data area of 8 k (zero-filled to 16 k). For double resonance experiments the sweepwidth had to be increased to include both ring and methyl resonance (1800 Hz). In order to obtain comparable digital resolution, 64 k of data area was used (zero-filled to 128 k). In both cases, 4 scans were acquired using quadrature detection.

−97 ± 48 mHz. The observed value is −220 ± 20 mHz (17). This discrepancy can be rationalized. A substantial distortion of the geometry at the hydroxyl group is indicated by other spin–spin couplings in 2-*tert*-butylphenol, but must be rather less severe in 2-*tert*-butyl-6-methylphenol (17). As argued below, because ^5J_c is a proximate coupling small angle changes can lead to changes in the average distance between the C—H and O—H bonds sufficient to account for the excess magnitude of about 100 mHz in ^5J_c in this compound.

INDO MO FPT computations of $^5J_o^{H,CH_3}$ in anisole yield realistic values for this proximate coupling (10). By analogy, such computations for $^5J_o^{OH,CH_3}$ in 2-methylphenol may well

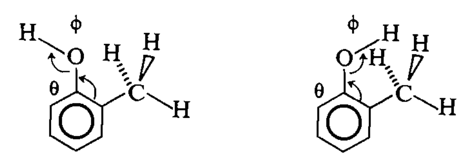

c *d*

prove enlightening. For standard geometries (26), other than the angles θ and ϕ defined in *c* and *d*, the computed ^5J_t varies between −2 and +15 mHz for $120° \le \theta \le 122°$ and $108° \le \theta \le 112°$ in the *trans* form, *c*. In phenol itself θ and ϕ are 122.1 and 108.8°, respectively (27). For the *cis* form, *d* ^5J_c is calculated as −660 mHz for θ = 120°, ϕ = 108° and as −470 mHz for θ = 122°, ϕ = 108°. Similarly, for θ = 120°, ϕ = 112°, ^5J_c becomes −520 mHz and is −370 mHz at θ = 122°, ϕ = 112°. Examination of ^5J_c for the grid of θ,ϕ angles shows that an increase of 1° in θ or 2° in ϕ causes a change of 100 mHz in the computed ^5J_c, the magnitude decreasing as the hydroxyl proton moves away from the methyl group. In other words, small geometrical changes in 2-*tert*-butyl-6-methylphenol, plausibly caused by the bulky *tert*-butyl group and leading to a small decrease in the average distance between the hydroxyl and 6-methyl groups, can lead to the observed −220 mHz for ${}^5J$ in this compound, only about 100 mHz of this value being needed as the result of geometry distortion.

The almost quantitative agreement between computed and observed ${}^5J_o^{\mathrm{H,CH_3}}$ in anisole (9, 10) is not repeated for ${}^5J_c$ in 2-methylphenol. The geometry of the latter is not known nearly as well as that of anisole, probably accounting for at least part of the discrepancy in a computed parameter so sensitive to actual geometry. Nevertheless, the computed values of ${}^5J_c$ strongly imply ${}^5J_c$ as a proximate coupling, in agreement with the available experimental data.

It may be noted that in 2-trifluoromethylphenol, ${}^5J_o^{\mathrm{OH,CF_3}}$ is -4.7 ± 0.2 Hz and ${}^5J_o^{\mathrm{OH,CF_3}}$ is +0.3 Hz (13). The former is certainly a proximate coupling (28) and the latter has the same sign as ${}^5J_t$ in 2-methylphenol.

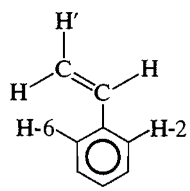

e

The vanishing ${}^5J_o^{\mathrm{H,CH}}$ in styrene, *e* (29) and in 3,5-dibromostyrene (unpublished work in this laboratory), and its value of −150 mHz in 2,5-dichlorostyrene (1), indicate that its value is about +150 mHz in a *trans* orientation of the *ortho* C—H (H-2 in *e*) and sidechain C—H bonds. In styrene the observed coupling is the mean of the *cis* and *trans* couplings, those to H-2 and H-6. It is interesting, therefore, that ${}^5J_o^{\mathrm{H,CH'}}$ is +158 mHz in styrene and +157 mHz in 3,5-dibromostyrene. On the assumption that this coupling is a measure of the normally positive σ and (or) σ−π electron contribution to ${}^5J_o^{\mathrm{H,CH}}$, then it is cancelled by the negative proximate component to yield the approximately zero observed value of ${}^5J_o^{\mathrm{H,CH}}$ in styrene.

Finally, the present dscussion of ${}^5J^{\mathrm{OH,CH_3}}$ in 2-methylphenol and its derivatives is consistent with our previous, and the only direct, determination (15) of the $a-b$ equilibrium in 2-methylphenol. This equilibrium has been discussed extensively from various viewpoints (30−32), estimates of the *trans* population ranging from 93% to 17% near 300 K. Some MO computations (31) imply that the *trans* form, *c*, and a closely related *trans* conformer in which a C—H bond of the methyl group eclipses the C—O bond are nearly isoenergetic. Our computations of ${}^5J_t$ for the latter structure imply values as negative as −50 mHz. Comparison with the positive values computed and observed for *c*, as discussed above, suggests only minor populations of the eclipsed *trans* conformer.

Experimental

A 4.7 mol% solution of 2-chloro-6-methylphenol (Aldrich) in CCl_4 solution, containing ca. 3 mol% tetramethylsilane, was transferred to a 5-mm od nmr sample tube. The sample tube contained beads of previously dried molecular sieve from Fisher (4−8 mesh with 3 Å pore size) and the transfer took place in a dry box. The sample was degassed by eight cycles of a freeze−pump−thaw procedure and was then flame-sealed.

The ^{1}H nmr spectrum was calibrated on an HA100 nmr spectrometer at a probe temperature of 305 K by a method already described in detail (33). The peak frequencies were determined with a typical standard deviation of less than 0.015 Hz. The spectrum was analyzed with the computer program LAME (34, 35) and the spectral parameters appear in Table 1.

The assignment of H-3 and H-5 follows umambiguously from the magnitudes of their couplings to the methyl protons, ${}^4J_o^{\mathrm{H,CH_3}}$ always being larger than ${}^6J_p^{\mathrm{H,CH_3}}$ in toluene derivatives (36−38). Furthermore, ${}^3J_{34}$ is larger than ${}^3J_{45}$, as expected from known substituent effects on vicinal coupling constants in benzene derivatives (39, 40).

The crucial parameter, ${}^5J^{\mathrm{OH,CH_3}}$, could not be obtained to sufficient accuracy from the spectrum at 100 MHz. The latter was not first order and led to severe overlap in the resonance of the methyl protons. Its magnitude was 0.08 ± 0.02 Hz. However, at 300 MHz the ^{1}H nmr spectrum is essentially first order. Figure 1 displays the 16 peaks expected from the methyl protons. The smallest splitting, 0.068(3) Hz, turns out to be positive and represents ${}^5J^{\mathrm{OH,CH_3}}$. This spectrum was recorded on a Bruker AM300 spectrometer in a manner described in the caption to Fig. 1. The weak irradiation experiments for relative sign determinations (41) showed that ${}^5J^{\mathrm{OH,CH_3}}$ has the same sign as ${}^5J_m^{\mathrm{OH,H\text{-}5}}$. The latter is positive (42).

INDO MO FPT (43) computations were done on an Amdahl 470/V8 system.

Acknowledgements

We are grateful to the Natural Sciences and Engineering Research Council of Canada for financial assistance and to the referees for cogent comment.

1. M. BARFIELD, C. J. MACDONALD, I. R. PEAT, and W. F. REYNOLDS. J. Am. Chem. Soc. **93**, 4195 (1971).
2. T. SCHAEFER, H. D. GESSER, and J. B. ROWBOTHAM. Can. J. Chem. **54**, 2235 (1976).
3. H. A. GAUR, J. VRIEND, and W. G. B. HUYSMANS. Tetrahedron Lett. 1999 (1969).
4. T. SCHAEFER and W. J. E. PARR. Can. J. Chem. **55**, 2835 (1977).
5. T. SCHAEFER, R. SEBASTIAN, and S. R. SALMAN. J. Magn. Reson. **46**, 325 (1982).
6. T. SCHAEFER, S. R. SALMAN, T. A. WILDMAN, and P. D. CLARK. Can. J. Chem. **60**, 342 (1982).
7. T. SCHAEFER and R. SEBASTIAN. Can. J. Chem. **61**, 26 (1983).
8. R. LAATIKAINEN. J. Magn. Reson. **52**, 293 (1983).
9. T. SCHAEFER, T. A. WILDMAN, and J. PEELING. J. Magn. Reson. **56**, 144 (1984).
10. T. SCHAEFER and R. SEBASTIAN, and T. A. WILDMAN. Can. J. Chem. **61**, 224 (1983).
11. T. SCHAEFER, R. SEBASIAN, and T. A. WILDMAN. Can. J. Chem. **57**, 3005 (1979).
12. J. B. ROWBOTHAM, M. SMITH, and T. SCHAEFER. Can. J. Chem. **53**, 986 (1975).
13. T. SCHAEFER and J. B. ROWBOTHAM. Can. J. Chem. **54**, 2243 (1976).
14. T. SCHAEFER, J. B. ROWBOTHAM, and K. CHUM. Can. J. Chem. **54**, 3666 (1976).
15. T. SCHAEFER and K. CHUM. Can. J. Chem **56**, 1788 (1978).
16. T. SCHAEFER, B. M. ADDISON, R. SEBASTIAN, and T. A. WILDMAN. Can. J. Chem. **59** 1656 (1981).
17. T. SCHAEFER, R. SEBASTIAN, and S. R. SALMAN. Can. J. Chem. **62**, 113 (1984).
18. T. SCHAEFER, T. A. WILDMAN, R. SEBASTIAN, and D. M. MCKINNON. Can. J. Chem. **62**, 2692 (1984).
19. E. MAHTIER, D. WELTI, A. BAUDER, and HS. H. GÜNTHARD. J. Mol. Spectrosc. **37**, 63 (1971).
20. H. D. BIST, J. C. D. BRAND, and D. R. WILLIAMS. J. Mol. Spectrosc. **24**, 402 (1967).
21. N. W. LARSEN and F. M. NICOLAISEN. J. Mol. Struct. **22**, 29 (1974).

22. J. H. S. GREEN, D. J. HARRISON, and C. P. STOCKLEY. J. Mol. Struct. **33**, 307 (1976).
23. T. SCHAEFER and W. J. E. PARR. Can. J. Chem. **55**, 552 (1977).
24. T. SCHAEFER and T. A. WILDMAN. Can. Phys. Lett. **80**, 280 (1981).
25. T. SCHAEFER, R. LAATIKAINEN, T. A. WILDMAN, J. PEELING, G. H. PENNER, J. BALEJA, and K. MARAT. Can. J. Chem. **62**, 1592 (1984).
26. J. A. POPLE and M. GORDON. J. Am. Chem. Soc. **89**, 4254 (1967).
27. N. W. LARSEN. J. Mol. Struct. **51**, 175 (1979).
28. T. SCHAEFER and J. B. ROWBOTHAM. Chem. Phys. Lett. **29**, 633 (1974).
29. H. NIES, H. BAUER, K. ROTH, and D. REWICKI. J. Magn. Reson. **39**, 521 (1980).
30. S. W. DIETRICH, E. C. JORGENSEN, P. A. KOLLMAN, and S. ROTHENBERG. J. Am. Chem. Soc. **98**, 8310 (1976), and references therein.
31. S. A. KUDCHADKER, R. M. HEDGES, and B. J. ZWOLINSKI. J. Mol. Struct. **43**, 259 (1978).
32. S. A. KUDCHADKER, R. C. WILHOIT, and B. J. ZWOLINSKI. J. Phys. Chem. **82**, 245 (1978).
33. T. SCHAEFER and R. SEBASTIAN. J. Magn. Reson. **41**, 395 (1980).
34. S. CASTELLANO and A. A. BOTHNER-BY. J. Chem. Phys. **41**, 3843 (1964).
35. C. W. HAIGH. Annu. Rep. NMR Spectrosc. **4**, 311 (1971).
36. G. KOTOWYCZ and T. SCHAEFER. Can. J. Chem. **44**, 2743 (1966).
37. M. P. WILLIAMSON, R. KOSTELNIK, and S. M. CASTELLANO. J. Chem. Phys. **49**, 2218 (1968).
38. T. SCHAEFER, R. SEBASTIAN, R. P. VEREGIN, and R. LAATIKAINEN. Can. J. Chem. **61**, 29 (1983).
39. A. D. COHEN and T. SCHAEFER. Mol. Phys. **10**, 209 (1966).
40. T. SCHAEFER, G. KOTOWYCZ, H. M. HUTTON, and J. W. S. LEE. Can. J. Chem. **46**, 2531 (1968).
41. R. FREEMAN and W. A. ANDERSON. J. Chem. Phys. **37**, 2053 (1962).
42. S. FORSEN and R. A. HOFFMAN. J. Mol. Spectrosc. **20**, 168 (1966).
43. P. A. DOBOSH. Quantum Chemistry Program Exchange, **11**, 141 (1979).

Control of the orientation of the aldehyde group in 2-(alkylthio)benzaldehydes by the directional lone-pair on sulfur

TED SCHAEFER, GLENN H. PENNER, KERRY J. DAVIE, AND RUDY SEBASTIAN
Department of Chemistry, University of Manitoba, Winnipeg, Man., Canada R3T 2N2

Received June 14, 1984

TED SCHAEFER, GLENN H. PENNER, KERRY J. DAVIE, and RUDY SEBASTIAN. Can. J. Chem. **63**, 777 (1985).

The [1]H nmr spectral parameters for 2-alkylthio derivatives benzaldehyde (alkyl = CH_3, CH_2CH_3, $CH(CH_3)_2$, $C(CH_3)_3$) are used to show that the O-*syn* conformation of the aldehyde group decreases from 40% for the methyl to zero for the *tert*-butyl compound in CCl_4 solution at about 300 K. It appears that the alkylthio groups twist out of the benzene plane to the same extent as in the alkyl phenyl sulfides and that it is the concomitant approaches of the $3p$ lone-pairs on sulfur into the ring plane which, by repulsive interactions with the C=O bond, determine the conformations of the aldehyde group. The spectral parameters display interesting changes as the size of the alkyl group increases. For example, the chemical shift of the aldehydic proton is larger than that reported for any other benzaldehyde derivative in CCl_4 solution.

TED SCHAEFER, GLENN H. PENNER, KERRY J. DAVIE et RUDY SEBASTIAN. Can. J. Chem. **63**, 777 (1985).

On utilise les paramètres des spectres de la rmn du [1]H d'alkylthio-2 benzaldéhydes (alkyl = CH_3, CH_2CH_3, $CH(CH_3)_2$ et $C(CH_3)_3$) pour démontrer que, en solution dans le CCl_4 et à environ 300 K, le pourcentage du groupement aldéhyde existant sous la conformation O-*syn* diminue de 40% dans le cas du méthyle à zéro pour le composé *tert*-butylé. Il semble que le taux de déplacement des groupements alkylthio hors du plan du benzène est semblable à celui que l'on observe dans les alkyl phényl sulfures et que ce soit l'approche concomitante des paires libres $3p$ du soufre dans le plan du cycle qui, par des interactions répulsives avec la liaison C=O, détermine les conformations du groupement aldéhyde. Les paramètres spectraux présentent des changements intéressants lorsque la taille des groupements alkyles augmente. Par exemple, le déplacement chimique du proton aldéhydique est plus grand que ceux rapportés pour tout autre dérivé du benzaldéhyde en solution dans le CCl_4.

[Traduit par le journal]

Introduction

A recent study of 2-(methylthio)benzaldehyde demonstrated that, contrary to previous investigations, a planar heavy-atom structure is preferred and that the O-*syn*, 1*a*, and O-*anti*, 1*b*, forms are present in similar proportions in CCl_4 solution at 305 K (1). These conclusions depended on the interpretation of the long-range spin–spin coupling constants between side-chain and ring protons and of the proton chemical shifts.

1 R = CH_3
2 R = CH_2CH_3
3 R = $CH(CH_3)_2$
4 R = $C(CH_3)_3$

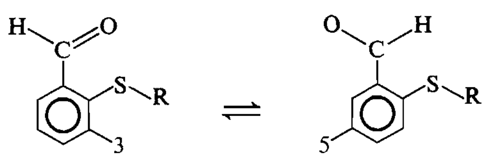

a O-*syn* ⇌ *b* O-*anti*

It is interesting that the populations of *a* and *b* in **1** are not drastically different from those in 2-methylbenzaldehyde in the same solvent (2, 3), whereas 2-chloro and 2-methoxybenzaldehydes exist almost completely as the O-*anti* forms (4, 5). Perhaps favorable dipole–dipole interactions between the C=O and C—S bonds occur in 2-methylthiobenzaldehyde. It is also true that, as the size of alkyl group increases in the 2-alkylbenzaldehydes, the population of the O-*anti* conformer increases, reaching 100% in 2-*tert*-butylbenzaldehyde (3).

Now, for alkylphenylsulfides, ultraviolet, infrared, photoelectron, [13]C nmr, and [1]H nmr spectroscopies all agree that the alkyl group twists out-of-plane as the size of the alkyl group increases, perhaps reaching a twist angle of near 90° in *tert*-butylphenylsulfide (6–12). The preferred conformation of thioanisole is planar, but with a lower internal barrier than anisole, the $3p\cdots\pi$ conjugation favoring planarity being substantially weaker than the $2p\cdots\pi$ conjugation in anisole.

It is of interest whether the steric repulsions favoring nonplanar conformations for SR (R = CH_2CH_3, $CH(CH_3)_2$, $C(CH_3)_3$) dominate in the 2-(alkylthio)benzaldehydes or whether the enhanced conjugation caused by the π-electron accepting aldehyde function, together with its steric property, causes increased planar tendencies in the S-alkyl groups. Further, from the viewpoint of steric repulsions, the O-*syn* and O-*anti* populations need not change much as the size of R increases, even for perpendicular conformers; formally, the interaction between the C=O group and the thioalkyl substituent is dominated by the sulfur atom (interatomic distances). However, the occupied $3p$ orbital is twisted into the benzene plane in perpendicular conformations and therefore the $C{=}O\cdots S$ interaction should now be repulsive (Pauli), causing increased O-*anti* populations relative to the essentially planar 2-methylthiobenzaldehyde.

This paper reports on the resolution of these possibilities.

Experimental

The 2-(*tert*-butylthio)benzaldehyde, **4**, was obtained from Maybridge Chemical Co. The ethyl- and isopropylthiobenzaldehydes were prepared by alkylation of 2-mercaptobenzyl alcohol (Fairfield Chemical Co.) with the iodide, followed by oxidation to the benzaldehyde derivatives with pyridinium chlorochromate (13). Solutions in CCl_4 contained enough tetramethylsilane for an internal lock at 100 MHz, or cyclohexane-d_{12} at 90 MHz and 300 MHz. These were transferred to 5-mm od nmr sample tubes, were degassed by the freeze–pump–thaw procedure, and the tubes were then flame-sealed. The [1]H nmr spectra in the CW or FT mode were accumulated by the methods recently described in detail (14).

Results and discussion

Spectral analyses

The [1]H nmr spectra were analyzed with the computer programs LAME (15, 16) and NUMARIT (17). Table 1 contains the [1]H nmr spectral parameters. Those for 2-(methylthio)-benzaldehyde and for benzaldehyde itself are included because they are needed in the subsequent discussion. The chemical shifts are only quoted to an accuracy of 1 ppb for the sulfur

TABLE 1. ^{1}H nmr nuclear magnetic resonance spectral parameters for 2-(alkylthio)benzaldehydes in CCl_4 solution

Parameter	H[a]	S—Me[b] 1	S—Et[c] 2	S—i-Prop[d] 3	S—*t*-Bu[e] 4
$\delta^{f}_{CH_3}$	—	2.450	—	1.295	1.285
$\delta_{CH(2)}$	—	—	2.450	3.292	—
δ_{CHO}	9.94	10.267	10.414	10.559	10.697
δ_3	7.45	7.276	7.371	7.469	7.565
δ_4	7.54	7.431	7.406	7.420	7.499
δ_5	7.45	7.201	7.230	7.295	7.467
δ_6	7.81	7.739	7.782	7.839	7.927
$^3J_{34}{}^{g}$	7.47	8.026(4)	7.972(6)	7.866(1)	7.729(6)
$^3J_{45}$	7.47	7.323(4)	7.332(5)	7.315(2)	7.365(7)
$^3J_{56}$	7.74	7.674(4)	7.727(2)	7.759(2)	7.747(11)
$^4J_{35}$	1.26	1.078(3)	1.113(6)	1.188(2)	1.253(8)
$^4J_{46}$	1.32	1.614(4)	1.624(4)	1.626(2)	1.668(16)
$^5J_{36}$	0.65	0.476(4)	0.488(3)	0.506(2)	0.502(9)
$^4J_6^{H,CHO}$	−0.10	−0.175(3)	−0.152(2)	−0.103(2)	−0.048(5)
$^5J_3^{H,CHO}$	0.38	0.335(4)	0.199(4)	0.075(5)	0.002(8)[h]
$^5J_5^{H,CHO}$	0.38	0.486(3)	0.652(2)	0.789(2)	0.911(8)
$^6J_4^{H,CHO}$	−0.04	−0.032(4)[h]	−0.038(4)[h]	−0.009(2)[h]	−0.062(11)[i]
$^5J_3^{H,SCH}$	—	−0.341	(−)0.229(5)[j]	(−)0.191(2)[j]	—
Transitions above 0.05	—	84	311	128	89
Transitions assigned	—	80	188	126	78
Peaks observed	—	63	53	59	58
rms deviation	—	0.008	0.010	0.006	0.014

[a]From ref. 43, 10 v/v%.
[b]From ref. 1, 4 mol% at 305 K and 100.00 MHz.
[c]5.0 mol% at 305 K and 90.024 MHz.
[d]4.5 mol% at 295 K and 300.135 MHz.
[e]4.0 mol% at 305 K and 100.00 MHz.
[f]Delta (δ) values given to a precision of 1 ppb, although they are known to higher precision.
[g]Numbers in parentheses are the standard deviations in the last significant figure for the coupling constants in Hz.
[h]No evidence for the existence of these couplings was observed in the spectra.
[i]See text and note that in C_6D_6 solution this coupling drops in magnitude.
[j]The sign could not be determined but is taken as negative in analogy to other such couplings.

compounds. They are known to considerably higher precision but, of course, are concentration dependent and therefore no purpose is served by quotation to higher precision. The footnotes to Table 1 assess the reliability of coupling constants below 0.1 Hz in magnitude. Figure 1 displays part of the ^1H nmr spectrum of H-6 in 2-(isopropylthio)benzaldehyde, demonstrating resolution of a coupling whose magnitude is 0.10 Hz.

*Populations of the O-*syn *and O-*anti *forms*

The sum of $^5J_m^{H,CHO}$ increases monotonically from 0.76 Hz in benzaldehyde to 0.91 Hz in its 2-*tert*butylthio derivative (Table 1). All available data (4, 5, 18–20) imply that $^5J_3$ in the O-*anti* form, *b*, and $^5J_5$ in the O-*syn* form, *a*, are too small to detect. In 2-fluorobenzaldehyde, the sum of the $^5J_m^{H,CHO}$ values is 0.86 Hz (19). For this compound CNDO MO FPT computations imply that $^5J_3$ in the O-*syn* form increases by 0.03 Hz relative to its computed value of 0.90 Hz in benzaldehyde and that $^5J_5$ in the O-*anti* form decreases by 0.02 Hz. This result is in disagreement with the ^5J values in Table 1, where $^5J_5$ in the O-*anti* form is largest (see the 2-*tert*butylthio derivative).

If both ^5J values increase by the same amount on substitution, then the population ratio of the O-*syn* to O-*anti* conformers is simply given by $^5J_3/^5J_5$, yielding 41:59, 23:77, 9:91, and 0:100 for R = CH_3, CH_2CH_3, $CH(CH_3)_2$, and $C(CH_3)_3$, respectively. If $^5J_3$ in the O-*syn* form remains unchanged from its value in benzaldehyde and the increase occurs in $^5J_5$ in the O-*anti* form, the populations of the former increase by 3% for R = CH_3, 4% for R = CH_2CH_3, and 2% for R = $CH(CH_3)_3$. Conversely, these increases turn into comparable decreases if the opposite perturbation of the ^5J values is assumed. It seems safe to conclude that the populations are known to a few percent.

Furthermore, the values of $^6J_p^{H,CHO}$ for these compounds imply very small deviations of the aldehyde group from the ring plane, so that discussion in terms of an *a*−*b* equilibrium is adequate. Thus, in the presence of two sizeable *ortho* substituents $^6J_p^{H,CHO}$ becomes significant in magnitude, reflecting its σ−π mechanism and an out-of-plane twist of the CHO moiety (21). Only $^6J_p^{H,CHO}$ for R = $C(CH_3)_3$ appears at first sight to be significant, being −0.06(1) Hz (Table 1). However, H-3, H-4, and H-5 are very tightly coupled at 100 MHz, the shift range being only 0.1 ppm, so that the precision of the analysis is rather poor (Table 1). Accordingly, a sample was prepared in benzene-d_6 solution. Here the shift range is 0.36 ppm and $^6J_p^{H,CHO}$ is given as −0.045(5) Hz by an analysis, much the same as for most of the other compounds in Table 1. It should be noted that no splittings due to this coupling were actually

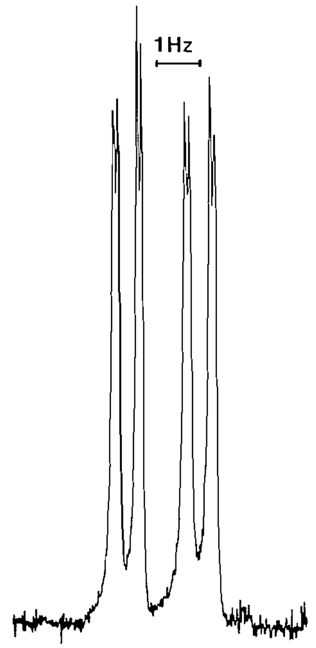

FIG. 1. Part of the ^{1}H nmr spectrum at 300 MHz and 295 K of H-6 in 2-(isopropylthio)benzaldehyde as a 4.5 mol% solution in CCl_4. The smallest splitting is 0.10 Hz and represents the coupling to the aldehyde proton, $^4J_6^{H,CHO}$

observed and that the best analysis, that at 300 MHz for R = $CH(CH_3)_2$, gave −0.009(2) Hz for $^6J_p^{H,CHO}$. Accordingly, it is concluded that, as for benzaldehyde, nonplanarity of the aldehyde group is insignificant. The barrier to rotation about the C—C bond in benzaldehyde is about 31 kJ/mol, much larger than *kT* (22).

The conformations of the —SR groups

(i) Ring proton shifts

The SCH_3 group is a π electron donor, causing an upfield shift for H-4 of about 0.21 ppm relative to benzene (23) in thioanisole. As the size of the alkyl group increases, H-4 shifts to low field, indicating a preferred perpendicular conformation for R = $C(CH_3)_3$, as does the C-4 chemical shift (6–8, 11). Now a plot of δ_5 for the 2-(alkylthio)benzaldehydes from Table 1 versus δ_4 in the alkylthiobenzenes (6) is linear within experimental error and has a slope near unity, implying that the conformation of the alkylthio group in the former is very similar to that in the latter. Note also that in 2-(*tert*-butylthio)-benzaldehyde, 7.467 for δ_5 is very close to that in benzaldehyde, 7.45; this is evidence for negligible π electron donation in the former.

The simplest explanation of these shift correlations is that the alkylthio group conformational preference is very much the same in the two sets of compounds and that the conformation of the aldehydic function is determined by repulsive forces from the directional 3*p* lone-pair of sulfur. This lone-pair lies predominantly perpendicular to the benzene plane in the SCH_3 compounds but lies mainly in the plane in the $SC(CH_3)_3$ compound. In the latter the C=O···3*p* repulsion is so large that only the O-*anti* form exists at 305 K.

δ_4 in **1** to **4** increases by 0.07 as does the corresponding δ in the alkylthiobenzenes, confirming the conclusions above. On the other hand, δ_6 in going from **1** to **4** increases by 0.19 ppm. This result may be rationalized as follows. In benzaldehyde, δ_6 consists of equal contributions from the *cis* orientations of the C=O and C—H bonds of the aldehyde group. In **4**, the C=O bond lies exclusively *cis* to H-6. Correction by 0.07 ppm for the $SC(CH_3)_3$ group (the shift change at H-4) then yields δ_6 (C=O, *cis*) as 7.86 and δ_6 (C—H, *cis*) as 7.76. In other words, the electrical and (or) the magnetic anisotropy of the C—O dipole causes only a 0.1-ppm low-field bias in δ_6 in the O-*anti* conformation. The magnitude of the bias will decrease rapidly with distance, accounting for the success of the arguments above concerning δ_4 and δ_5 in **1** to **4**.

δ_3 increases to 7.565 from 7.276 in moving from **1** to **4**, being only 7.45 in benzaldehyde. Part of this excess shift to low field in the series is due to the increasing proximity of the 3*p* lone-pair, as noted previously for 2-hydroxythiophenol (24) and 2-hydroxythioanisole (25), in which the stereospecific hydroxyl hydrogen bond to the 3*p* lone-pair forces the latter into the benzene plane.

(ii) The shift of the aldehyde proton

δ_{CHO} in **4** is 10.697 relative to 9.94 in benzaldehyde itself, and is larger than that for any reported 2-substituted benzaldehydes (2, 4, 5, 19, 20, 26). In 2-chloro and 2-methoxy-benzaldehyde δ_{CHO} is 10.42 and 10.38, respectively (4, 5). The O-*anti* conformation is the only detected form in these compounds, just as in **4**. The large low-field shift in **4** is again attributed to the predominantly in-plane 3*p* orbital in **4**, leading perhaps to 1*s*,3*p* interference and therefore to a deshielding of the aldehyde proton. Of course, there is no strong argument for a linear relationship between δ_{CHO} and the O-*syn*/O-*anti* ratio in **1** to **4** because, at least for **2** and **3**, it appears that the 3*p* lone-pair takes on a conformation intermediate between planar and perpendicular. A monotonic increase of δ_{CHO} in **1** to **4** is reasonable, however, and is observed.

(iii) The ring proton coupling constants

As the S-alkyl substituent twist out-of-plane, all the couplings but $^4J_{46}$ move towards their values in benzaldehyde. $^3J_{56}$ and $^4J_{35}$ become equal to the values for benzaldehyde. The magnitude of ^3J within the ring depends somewhat on the double bond character of the intervening C—C bond (27, 28), but also on the electronegativity of the substituent (29, 30). Thus, it is tempting to attribute the decrease in $^3J_{34}$ from **1** to **4** to a decreased contribution from resonance structure **5**. The

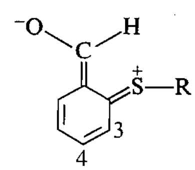

5

double bond character of the C3−C4 bond is least in **4** and therefore $^3J_{34}$ should be smallest in **4**, as observed. A similar argument would hold for $^3J_{56}$.

It is interesting that $^4J_{35}$ in **4** becomes equal to $^4J_{35}$ in benzaldehyde, whereas $^4J_{46}$ varies relatively little between **1** and **4**.

The observed changes of the couplings within the ring are consistent with the conformational changes of the S-alkyl group discussed above. Some of the couplings for the phenylalkyl sulfides have been discussed (6).

(iv) Long-range couplings to the side-chain protons

$^5J_m^{H,CHO}$ values were used above to determine the O-*syn* and O-*anti* populations. $^4J_o^{H,CHO}$ decreases monotonically in magnitude, from 0.175 Hz in **1** to 0.05 Hz in **4**. For *para*-substituted benzaldehyde derivatives (31), the magnitude increases for

π-electron donors, presumably because the C—C bond shortens at the aldehyde group (32); see structure **5**. Consequently, the observed trend in $^4J_o^{H,CHO}$ in **1** to **4** is in agreement with decreasing π conjugation of the $3p$ orbital of sulfur as the S-alkyl group twists out of plane.

Finally, consider the long-range coupling over five formal bonds between H-3 and the alkyl protons, $^5J_3^{H,SCH}$. Its value is −0.34 Hz in 2-methylthiobenzaldehyde (Table 1) and −0.35 Hz in 2,5-dichlorothioanisole (33). This coupling is through-space and drops off rapidly in magnitude as the alkyl group twists away from the ring. The analogous coupling in anisole has been studied in detail (34−37). In the S-methyl compound the coupling to the two methyl protons in the C—H bonds nearest H-3, taking the methyl conformation as staggered about the *ortho* C—H bond, is expected to have a larger magnitude than to the other, distant methyl proton pointing away from the ring (34). Accordingly, the decrease in the magnitude of $^5J_3^{H,SCH}$ in going from the S-methyl to the S-ethyl compound is consistent with an out-of-plane twist of the latter. A further decrease in the size of the coupling occurs for the S-isopropyl derivative.

In 2-hydroxythioanisole, where the S—CH_3 group prefers a plane roughly orthogonal to the benzene plane, $^5J^{H,SCH}$ is not observed (25). By analogy to $^5J^{H,OCH}$ in anisole, the coupling is probably negligible when the twist angle, θ, reaches 60°.

A very rough estimate of the twist angle is obtainable as follows. Assume that δ_5 depends on $\sin^2\theta$ because electron densities at the *para* position are calculated by MO methods to vary in this way. Assume that θ is 90° for **4** and 0° for **1**. It follows that $\sin^2\theta$ is 0.11 for S-ethyl and 0.35 for S-isopropyl, corresponding to values of 19° and 36° for the two compounds. These numbers are to be taken as indicative only, of course, because δ_5 will depend on the expectation value of $\sin^2\theta$, the angle varying as the molecule undergoes internal torsion, and because $\langle\sin^2\theta\rangle$ is not exactly unity in **4** and zero in **1**.

However, $^5J^{H,SCH}$ in **1** to **3** is consistent with the conformational deductions based on the other spectral parameters.

No coupling over six formal bonds between methyl protons and *ortho* ring protons in **2** to **4** could be observed by careful decoupling experiments. Such a coupling is also dependent on the distance between bonds carrying the protons and is observable, for example, in 2-isopropylphenol (38) and 2-*tert*-butylphenol (39). From models it is clear that in **4**, for example, θ must be appreciable if the *tert*-butyl C—H bonds are not to approach the *ortho* C—H bonds sufficiently closely for coupling to occur.

Conclusions

All the ^{1}H nmr spectral parameters in the 2-S-alkyl (CH_3, CH_2CH_3, $CH(CH_3)_2$, $C(CH_3)_3$) derivatives of benzaldehyde are consistent with a description in which the conformation of the S-alkyl groups is approximately that of the alkylphenyl sulfide. As the S-alkyl group rotates about the benzene plane, its sulfur $3p$ orbital twists into this plane and repels the C═O bond of the aldehyde group. In consequence, the O-*anti* conformation increases from 60% to 100% as the size of the alkyl group increases from CH_3 to $C(CH_3)_3$.

The steric requirements of the $3p$ orbital on sulfur have been previously used in simple descriptions of the conformations of 2-hydroxythiophenol (24), and of some phenyl sulfides and disulfides (25). Its directional character also serves as the simplest description of the perpendicular structure of the hydrogen bonded dimer of H_2S and HF (40), but see also refs. 41 and 42.

Acknowledgments

We are grateful to the Natural Sciences and Engineering Research Council of Canada for financial support.

1. T. SCHAEFER and R. SEBASTIAN. Can. J. Chem. **61**, 26 (1983).
2. T. SCHAEFER, S. R. SALMAN, and T. A. WILDMAN. Can. J. Chem. **58**, 2364 (1980).
3. L. LUNAZZI, A. TICCA, D. MACCIANTELLI, and G. SPUNTA. J. Chem. Soc. Perkin Trans. 2, 1121 (1976).
4. D. G. KOWALEWSKI and S. CASTELLANO. Mol. Phys. **16**, 567 (1969).
5. W. B. SMITH, D. L. DEAVENPORT, and A. M. IHRIG. J. Am. Chem. Soc. **94**, 1959 (1972).
6. L. B. KRIVDIN, G. A. KALABIN, and B. A. TROFIMOV. Izv. Akad. Nauk SSSR, Ser. Khim. 565 (1982).
7. G. V. RATOVSKII, A. M. PANOV, V. I. GLUKHIKH, G. A. KALABIN, V. I. DMITRIEV, and I. A. ALIEV. Zhur. Obschch. Khim. **51**, 1504 (1981).
8. V. M. BZHEZOVSKII, G. A. KALABIN, I. A. ALIEV, V. I. DONSKIKH, and B. A. TROFIMOV. Isv. Akad. Nauk SSSR, Ser. Khim. 1525 (1981).
9. I. W. JONES and J. C. TEBBY. J. Chem. Soc. Perkin Trans. **2**, 217 (1979).
10. A. R. KATRITZKY, R. F. PINZELLI, and R. D. TOPSOM. Tetrahedron, **28**, 3441 (1972).
11. M. MOHRAZ, W. JIAN-QU, E. HEILBROMER, A. SOLLADIÉ-CAVALLO, and F. MATLOUBI-MOGHADAM. Helv. Chim. Acta, **64**, 97 (1981).
12. E. HONEGGER and E. HEILBRONNER. Chem. Phys. Lett. **81**, 615 (1981).
13. E. J. COREY and J. W. SUGGS. Tetrahedron Lett. 2647 (1975).
14. T. SCHAEFER and R. SEBASTIAN. J. Magn. Reson. **41**, 395 (1980).
15. S. CASTELLANO and A. A. BOTHNER-BY. J. Chem. Phys. **41**, 3863 (1964).
16. C. W. HAIGH. Annu. Rep. NMR Spectrosc. **4**, 311 (1971).
17. A. R. QUIRT and J. S. MARTIN. J. Magn. Reson. **5**, 318 (1971); J. S. MARTIN, A. R. QUIRT, and K. E. WORVILL. The nmr program library, Daresbury Laboratory, Daresbury, U.K.
18. G. J. KARABATSOS and F. M. VANE. J. Am. Chem. Soc. **85**, 3886 (1963).
19. R. WASYLISHEN and T. SCHAEFER. Can. J. Chem. **49**, 3216 (1971).
20. T. SCHAEFER, S. R. SALMAN, and T. A. WILDMAN. Can. J. Chem. **58**, 2364 (1980).
21. C. L. BELL, S. S. DANYLUK, and T. SCHAEFER. Can. J. Chem. **47**, 3529 (1969).
22. F. A. L. ANET and M. AHMAD. J. Am. Chem. Soc. **86**, 119 (194).
23. G. LLABRÈS, M. BAIWIR, L. CHRISTIAENS, J. DENOEL, L. LAITEM, and J.-L. PIETTE. Can. J. Chem. **56**, 2008 (1978).
24. T. SCHAEFER, T. A. WILDMAN, and S. R. SALMAN. J. Am. Chem. Soc. **102**, 107 (1980).
25. T. SCHAEFER, S. R. SALMAN, T. A. WILDMAN, and P. D. CLARK. Can. J. Chem. **60**, 342 (1982).
26. G. LLABRES, M. BAIWIR, J.-L. PIETTE and L. CHRISTIAENS. Org. Magn. Reson. **15**, 152 (1981).
27. W. B. SMITH, A. M. IHRIG, and J. W. ROARK. J. Phys. Chem. **74**, 812 (1970).
28. H. GÜNTHER, H. SCHMICKLER, M.-E. GÜNTHER, and D. CREMER. Org. Magn. Reson. **9**, 420 (1977).
29. A. D. COHEN and T. SCHAEFER. Mol. Phys., **10**, 209 (1965).
30. S. CASTELLANO and C. SUN. J. Am. Chem. Soc. **88**, 4741 (1966).
31. S. S. DANYLUK, C. L. BELL, and T. SCHAEFER. Can. J. Chem. **47**, 4005 (1969).
32. W. F. REYNOLDS, I. R. PEAT, and G. K. HAMER. Can. J. Chem. **52**, 3415 (1974).

33. T. SCHAEFER, R. SEBASTIAN, and S. R. SALMAN. J. Magn. Reson. **46**, 325 (1982).
34. T. SCHAEFER, and R. LAATIKAINEN. Can. J. Chem. **61**, 224 (1983).
35. T. SCHAEFER, T. A. WILDMAN and J. PEELING. J. Magn. Reson. **56**, 144 (1984).
36. R. W. CRECELY, K. W. MCCRACKEN, and J. H. GOLDSTEIN. Tetrahedron, **25**, 877 (1969).
37. H. A. GAUER, J. VRIEND, and W. G. B. HYUSMANS. Tetrahedron Lett. 1999 (1969).
38. T. SCHAEFER, B. M. ADDISON, R. SEBASTIAN, and T. A. WILDMAN. Can. J. Chem. **59**, 1656 (1981).
39. T. SCHAEFER, R. SEBASTIAN, and S. R. SALMAN. Can. J. Chem. **62**, 113 (1984).
40. R. VISWANATHAN and T. R. DYKE. J. Chem. Phys. **77**, 1166 (1982).
41. A. D. BUCKINGHAM and P. W. FOLWER. J. Chem. Phys. **79**, 6426 (1983).
42. F. A. BAIOCCHI, W. REIHER, and W. KLEMPERER. J. Chem. Phys. **79**, 6428 (1983).
43. S. CASTELLANO. *Quoted in* Handbook of nmr spectral parameters. W. Brugel. Heyden and Son Ltd., London. 1979.

The range of $^5J_o^{H,CH_3}$ in anisole derivatives. An indicator of torsion and compression of the methoxy group

TED SCHAEFER, SALMAN R. SALMAN,[1] TIMOTHY A. WILDMAN, AND GLENN H. PENNER
Department of Chemistry, University of Manitoba, Winnipeg, Man., Canada R3T 2N2

Received May 23, 1984

TED SCHAEFER, SALMAN R. SALMAN, TIMOTHY A. WILDMAN, and GLENN H. PENNER. Can. J. Chem. **63**, 782 (1985).

In a series of anisole derivatives, $^5J_o^{H,CH_3} \equiv {}^5J$, the spin–spin coupling constant between the methyl protons and the ring proton in the *ortho* position, ranges from −0.23 to −0.38 Hz when the methyl group lies *cis* to the *ortho* C—H bond. ^5J, as a proximate coupling, is sensitive to the average distance between the coupled protons. Its variation with substituent can be rationalized in terms of torsion about the Csp^2—O bond and changes in the bond angles near the methoxy moiety. The theoretical ^5J numbers can be empirically reproduced by a $\cos^4 \psi$ function, where ψ is the angle by which the methoxy group twists out of the benzene plane. In general, large *ortho* substituents cause an increase in the magnitude of ^5J (bond angle changes), strong π electron donors in the *para* position cause a decrease in the magnitude of ^5J (increased torsional freedom), and π electron acceptors do the opposite (decreased torsions).

TED SCHAEFER, SALMAN R. SALMAN, TIMOTHY A. WILDMAN et GLENN H. PENNER. Can. J. Chem. **63**, 782 (1985).

Dans une série de dérivés de l'anisole dans lesquels le groupement méthyle se trouve *cis* par rapport à la liaison C—H *ortho*, la valeur de la constante de couplage spin–spin $^5J_o^{H,CH_3} \equiv {}^5J$, entre les protons du groupe méthyle et le proton situé en position *ortho* du cycle, varie entre −0,23 et −0,38 Hz. Le couplage ^5J, qui est un couplage par proximité, est sensible à la distance moyennė entre les protons qui sont couplés. Sa variation avec la nature des substituants peut être rationalisée en fonction d'une torsion autour de la liaison Csp^2—O et des changements dans les angles des liaisons près de la portion méthoxylée. On peut reproduire empiriquement les valeurs théoriques de ^5J en utilisant une fonction $\cos^4 \psi$ dans laquelle ψ est égal à l'angle de torsion du groupement méthoxy en dehors du plan du benzène. D'une façon générale, des substituants volumineux en *ortho* provoquent une augmentation dans l'amplitude de ^5J (changements dans les angles de liaisons), la présence en position *para* de groupements fortement donneurs d'électrons π provoque une diminution dans l'amplitude de ^5J (augmentation de la liberté de torsion) alors que la présence de groupements accepteurs d'électrons π provoque un effet inverse (diminution des torsions).

[Traduit par le journal]

Introduction

A detailed set (1) of INDO MO FPT computations of $^5J_o^{H,CH_3} \equiv {}^5J$, the spin–spin coupling constant between methyl protons and the *ortho* ring proton in anisole, is consistent with the properties of a "through-space" or proximate coupling mechanism (1–4). As a proximate coupling, the magnitude of ^5J is calculated to decrease rapidly as the methoxy group twists out of the benzene plane, being −0.29 Hz for a planar *cis* conformation, **1**, and effectively zero as the out-of-plane twist, ψ, approaches 60°. A coupling of about 0.04 Hz is computed for ψ values between 90 and 180°.

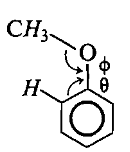

$\psi = 0$

1

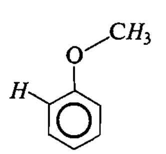

$\psi = 180°$

2

In fact, ^5J in anisole is −0.141(2) Hz (5), which could be taken to mean that ^5J is −0.28 Hz in **1** ($\psi \sim 0$) and 0.00 Hz in **2** ($\psi \sim 180°$). Or, since ^5J is calculated as −0.29 Hz at $\psi = 0$ and as −0.28 Hz at $\psi = 7.5°$, one might loosely interpret the observed value as corresponding to an expectation value of about 7° for ψ. Amusingly, the torsion about the Csp^2—O bond in a crystal of 4-nitroanisole (6) is given as 5.9(6)°. Of course, such an interpretation is best treated with circumspection, although it is true that in solution the barrier to rotation about the Csp^2—O bond in anisole is probably greater than 5 kcal/mol (1 cal ≡ 4.184 J); so that a small average torsion angle can be assumed at 305 K, usually approximated as a planar conformation. At 305 K rapid interconversion between **1** and **2** occurs, leading to the identical ^5J values for the *ortho* protons in anisole.

Early measurements of ^5J in some *ortho*-X-substituted anisoles (X = Cl, Br, I, NO_2) found a magnitude of 0.30 ± 0.03 Hz (7), the sign being determined as negative in 2,4-dibromoanisole (8). In other such compounds (X = OH, OCH_3, F) smaller magnitudes were indicated, the coupling leading to broadening only of ^{1}H nmr peaks. Later work for X = OH, OCH_3 at higher frequencies and different solvents, causing increased ring dispersion, found ^5J as −0.28(1) Hz (1, 9). In fact, for 1,2-dimethoxybenzene in benzene-d_6 solution (1) this result was taken to mean an essentially planar preferred conformation, a point of controversy (10–14). The argument for coplanarity is in agreement with ^{13}C nmr chemical shifts and spin-lattice relaxation times (12), but not with recent measurements of the temperature dependence of the dipole moment of 1,2-dimethoxybenzene, also in benzene solution (13). The conformation of the methoxy group can have important chemical and biological consequences (14, 15).

Although ^5J has been considered as proximate, some modified INDO MO FPT computations and measurements on 2,4-diaminoanisole, for example (16), have indicated substantial π electron transmitted couplings, $^6J_m^{H,CH_3}$, involving the *meta* protons in the compound. In that event, π electron contributions to ^5J can also be imagined, so that the use of ^5J as a conformational indicator would become more complicated.

Of course, if the *ortho* substituent is bulky enough, it might cause an increase in the magnitude of ^5J as steric compression gives rise to smaller average distances between the methyl protons and the *ortho* C—H bond, particularly as a proximate coupling is in principle very sensitive to the distance between

[1]Now at the Department of Chemistry, University of Bhagdad, Bhagdad, Iraq.

TABLE 1. Nuclear magnetic resonance spectral parameters for 3-fluoro-4-methoxybenzaldehyde as a 15 mol% solution in CS_2 at 305 K

Parameter	Value	Parameter	Value
ν_2[a]	741.084(1)	${}^5J_m^{H,CHO}$	0.344(2)
ν_5	701.022(1)	${}^5J_m^{F,CHO}$	2.200(2)
ν_6	750.760(2)		
ν_{CH}	388.384(1)	${}^5J_o^{H,CH_3}$	−0.299(1)
ν_{CHO}	973.665(1)	${}^6J_m^{H,CH_3}$	<0.05
${}^3J_o^{H,H}$	8.359(2)[b]	${}^5J_o^{F,CH_3}$	+0.208(2)
${}^3J_o^{H,F}$	10.911(3)	Root mean square deviation	0.010
${}^4J_m^{H,H}$	1.976(2)	Transitions calculated	525[c]
${}^4J_m^{H,F}$	7.842(2)	Peaks assigned	459[c]
${}^5J_p^{H,H}$	0.233(2)		
${}^5J_p^{H,F}$	−1.124(3)		
${}^4J_o^{H,CHO}$	<0.1		

[a]In Hz at 100.001 MHz to low field of internal TMS.
[b]Coupling constants in Hz; numbers in parentheses are the standard deviations in the last significant figure.
[c]Above a relative intensity of 0.01.

the coupled protons. If literature values of ${}^5J$ are taken at face value, ${}^5J$ varies between essentially zero and about −0.30 Hz. Accordingly, a careful set of analyses in this laboratory, accumulated over some years, was examined for regularities in ${}^5J$ and the results are reported and discussed here. Complete analyses are usually necessary because ${}^5J$ can often be obtained reliably only from the ring proton spectrum.

Experimental

All samples, at concentration indicated in the tables, were transferred to 5-mm od nmr sample tubes and were degassed by the freeze–pump–thaw procedure. All ${}^1H$ nmr spectra were recorded at 305 K, the majority on an HA100 spectrometer in the frequency sweep mode. Calibrations of spectral peak positions were done as described recently (17). Some ${}^1H$ nmr spectra were accumulated on a WH 90 FFT spectrometer, again by procedures previously described (17). The compounds came from Aldrich or were prepared from obvious starting materials.

Results and discussion

Spectral analyses

Performed with the program LAME (18, 19), the spectral data of interest are given in Table 2. Table 1 presents the results of an analysis of the ${}^1H$ nmr spectrum of 3-fluoro-4-methoxybenzaldehyde, illustrating the precision attainable. Table 2 collects some 40 values of ${}^5J_o^{H,CH_3}$ determined for anisole and a variety of its derivatives. The numbers for anisole and a few of its derivatives have been previously published and a few have been discussed in some detail, notably that for 2-methoxyanisole (1). They are included here as reference numbers and for completeness sake.

The ψ, θ, ϕ dependence of ^{5}J*; a model*

In anisole, ${}^5J$ is −0.14 Hz and the sums of the two values of ${}^5J$ in the 3-chloro, 3-bromo, and the 3-amino derivatives lie within experimental error of twice this value, at −0.29, −0.28, and −0.27 Hz, respectively. On the assumption that the barrier to rotation about the Csp^2—O bond in anisole in solution is large compared to kT (20), about 6 kcal/mol, then these numbers are consistent with ${}^5J_{cis} = -0.28$ Hz, ${}^5J_{trans} = 0.00$ Hz, and with a negligible decrease in the barrier for these three *meta* derivatives.

TABLE 2. Some ${}^5J_o^{H,CH_3}$ values in anisole and its derivatives, standard deviations in parentheses

Compound	$-{}^5J_o^{H,CH_3}$	Compound	$-{}^5J_o^{H,CH_3}$
Anisole	0.141(2)[a,p]	2-OCH_3-4-CHO[f]	0.292(15)[s]
			0.308(5)
2-OH[b]	0.288(1)		
		2-Cl-4-OCH_3[d]	0.258(4)
2-SH[c]	0.280(10)		0.240(4)[q]
2-SCH_3[d]	0.282(2)	2,4-diNH_2[l]	0.270(3)
2-OCH_3[e]	0.280(10)	2,4-diNO_2[m]	0.295(11)
2-CH_2OH[f]	0.285(8)	2-I-5-NO_2[n]	0.341(10)
2-CH_2OCH_3[f]	0.270(10)	2-CF_3-4-NO_2[b]	0.341(1)
2-C(O)CH_3[g]	0.28(2)	2,6-diOCH_3[f]	0.250(20)
3-Cl[h]	0.291(9)[q]	2-OCH-3-OH[f]	0.247(5)
		2-OH-3-CHO[d]	0.271(1)
3-Br[h]	0.284(8)[q]	2,3,4-triCl[d]	0.303(3)
3-NH_2[h]	0.273(6)[q]	2-Cl-4-OCH_3-5-NO_2[n]	0.320(1)[u]
			0.327(1)
3,5-diCl[f]	0.158(7)[r]		
	0.144		
		2-Cl-4-NO_2-5-OCH_3[o]	0.379(7)[u]
			0.383(14)
2-F-4-Br[i]	0.271(2)[i]		
	0.281(3)[j]		
		2-Cl-4-I-5-OCH_3[n]	0.348(8)[u]
			0.346(4)
2-F-4-CHO[k]	0.299(1)		
2,4-diOCH_3[f]	0.281(5)[s]	4-SCH_3[d]	0.118(7)
	0.270(40)[q]		
	0.232(5)[t]	2-OH-3-OCH_3-4-CHO	0.27(1)[v]

[a]4.4 mol% in acetone-d_6.
[b]5 mol% in benzene-d_6.
[c]4.6 mol% in CCl_4.
[d]3 mol% in CCl_4.
[e]10 mol% in benzene-d_6.
[f]5 mol% in CCl_4.
[g]10 mol% in CCl_4.
[h]5 mol% in acetone-d_6.
[i]3 mol% in acetone-d_6.
[j]4.5 mol% in CCl_4.
[k]15 mol% in CS_2.
[l]Saturated solution in benzene-d_6, ca. 1.5 mol%.
[m]4 mol% in benzene-d_6.
[n]3 mol% in chloroform-*d*. ${}^5J_o^{H,CH_3}$ correlates by 0.36 with ${}^3J_o^{H,H}$ and ${}^5J_p^{H,H}$.
[o]3 mol% in benzene-d_6.
[p]The *mean* of the *cis* and *trans* couplings.
[q]The *sum* of the *cis* and *trans* couplings.
[r]Adjusted for overlap of Lorentzian lines, the observed splitting being 0.144 Hz.
[s]From the 2-OCH_3 protons to H-3.
[t]From the 1-OCH_3 protons to H-6.
[u]Assignment uncertain, but perhaps immaterial.
[v]Unanalyzed spectrum, ${}^5J_o^{H,CH_3}$ estimated from spacings.

Two causes for a significant change in ${}^5J$ can be hypothesized. First, a substituent may increase or decrease the double bond character of the Csp^2—O bond, thereby decreasing or increasing the bond length *and* the barrier to rotation. Because ${}^5J$ is proximate and sensitive to internuclear distances, a decrease in barrier will lead to larger torsional amplitudes about the Csp^2—O bond and to smaller ${}^5J$ magnitudes. In other words, the expectation value of ψ increases from its value in anisole, causing a decrease in the magnitude of ${}^5J$. Thus, a ψ of 30° yields a calculated ${}^5J$ of −0.17 Hz in anisole, whereas at a ψ of 15° the magnitude of ^5J has dropped by only 0.03 Hz from the 0.29 Hz computed for $\theta = 0$. Second, a large *ortho* substituent may cause bond angle changes in the region of the methoxy group, leading to a smaller average distance between the methyl protons and the *ortho* protons than in anisole, and therefore to a larger magnitude of ^5J.

The computed (1) values of ^5J can be reproduced by an empirical $\cos^4 \psi$ function (see **1**) in the region of 0 to 60°.

ψ (deg)	$-^5J$ (INDO) (Hz)	$0.292 \cos^4 \psi$ (Hz)
0	0.292	0.292
7.5	0.283	0.282
15	0.257	0.254
30	0.167	0.164
45	0.064	0.073
60	0.010	0.018

Furthermore, the INDO MO FPT computations have it that a decrease of 1° in ϕ in **1** causes ^5J to decrease by 0.031 Hz, whereas a decrease of 1° in θ entails a decrease of 0.018 Hz; that is, the magnitude of ^5J increases as the geometry is compressed. Thus a decrease of only 2° in each of θ and ϕ might well lead to a decrease of 0.1 Hz in ^5J. Finally, a change of 0.01 Å in the C—O or O—C(H$_3$) bond lengths entails only a $\leq$0.005 Hz change in ^5J.

The ^5J values in Table 2 can be rationalized by intuitively sensible combinations of average $\Delta\psi$, $\Delta\theta$, $\Delta\phi$ numbers and are discussed further below.

Application of the model

In those 2-X-anisoles where X = OH, SH, SCH_3, OCH_3, CH_2OH, CH_2OCH_3, or CH_3—C=O, no significant variation in ^5J is apparent. It ranges from −0.288(1) Hz for X = OH to −0.270(10) for X = CH_2OCH_3. Apparently, these substituents do not cause appreciable geometrical distortions of the methoxy group.

Turning to 2-X-4-Y-anisoles, consider 2-fluoro-4-bromoanisole and 2-fluoro-4-carboxaldehyde-anisole. In the former, ^5J is −0.271(2) Hz in acetone-d_6 solution and is −0.281(3) Hz in CCl_4 solution, implying negligible perturbations of the conformational preferences of the methoxy groups. In the latter, ^5J is −0.299(1) Hz. It is tempting to attribute the increase of 0.02 Hz in magnitude to an enhanced barrier to torsion about the C$_1$—O bond, arising from conjugation with the CHO group in the *para* position. However, in 2,4-dinitroanisole, ^5J is −0.295(11) Hz and one might have expected somewhat larger conjugative perturbations from two nitro substituents than from a CHO group. The *ortho* nitro group, of course, may well twist out-of-plane itself to relive steric crowding, as it does in many other compounds including those with a methyl group placed *ortho* to the nitro substituent (21).

Again, in 2-methoxy-4-carboxaldehyde-anisole,[2] ^5J is −0.292(15) Hz for H-3 and −0.308(5) Hz for H-6. A tendency towards an increased magnitude of ^5J relative to its value in 2-methoxyanisole is apparent. If the *para* substituent is now replaced by a π electron donor, as in 2,4-dimethoxyanisole, the coupling to H-6 becomes −0.232(5) Hz. A larger amplitude of oscillation of the 1-methoxy group is implied by this result. The ψ dependence calculated above suggests ^5J as −0.23 Hz at $\psi = 20°$.

In a rigorous approach the observed ^5J should be related to the expectation value of ψ, that is $\langle\psi\rangle$. To find the latter, the potential function for the rotation about the Csp^2—O bond is needed. For a simple n-fold potential, and for low-amplitude oscillations (barrier large compared to kT), a classical averaging procedure (22) yields $\langle\psi^2\rangle$ as $2kT/Bn^2$, where ψ^2 is in rad^2. If $n = 2$, then $\langle\psi^2\rangle^{1/2}$ becomes about 13° for a barrier, B, of 6 kcal/mol at 305 K. If $n = 4$, then $\langle\psi^2\rangle^{1/2}$ is about 5°. The Csp^2—O barrier is apparently a mixture of twofold and fourfold components (23, 24). Accordingly, $\langle\psi^2\rangle^{1/2}$ may be about 10° for anisole in this model.

If the barrier to rotation about the Csp^2—O bond in anisole were zero, a simple average over all angles would yield ^5J as about −0.06 Hz according to the computed numbers. A decrease in the barrier from that in anisole leads to a decrease in the magnitude of ^5J, as indicated by the ^5J of −0.118(7) in 4-thiomethylanisole, that is, $^5J_{cis}$ is −0.236(14) Hz.

Now, or an *ortho* derivative of anisole, a large onefold component in the rotational potential must also be present. A naive two-site model with $\psi = 0$ and some value between 60° and 180°, for which ^5J is presumably zero, is in the spirit of numerous conformational discussions of various molecules in the literature. Such a model would have $^5J = -0.232$ Hz $= -0.292\,P(\psi = 0) - 0.00\,(1 - P)$, where P is the fractional population of the planar conformer. It would yield 80% as the population of the planar conformer of the 1-OCH_3 group in 2,4-dimethoxyanisole.

However, it is probably more satisfactory to interpret the above ψ of 20° in 2,4-dimethoxyanisole as a change in the rms amplitude of about 10° from its value in anisole. In other words, the 4-methoxy substituent, being a π donor, induces a smaller double-bond character in the Csp^2—O bond of the 1-methoxy group and therefore a larger $\langle\psi^2\rangle^{1/2}$ number. This does not happen for the 2-methoxy substituent, judging by its ^5J of −0.281(5) Hz. Unfortunately, large uncertainty in the sum of the ^5J values for the 4-methoxy group preempts discussion of its amplitude of oscillation.

However, in 2-chloro-4-methoxyanisole this sum for the 4-methoxy protons is −0.240(4) Hz, consistent with a substantially larger $\langle\psi^2\rangle^{1/2}$ than in anisole. For the other methoxy group, ^5J is −0.258(4) Hz (previously reported as −0.18 Hz (16)) compared to −0.232(5) Hz in 2,4-dimethoxyanisole. The larger magnitude is reasonably attributed to a change in θ and (or) ϕ. In 2,3,4-trichloroanisole, ^5J is −0.303(3) Hz.

Addition of a 5-nitro substituent to 2-chloro-4-methoxyanisole entails a ^5J of −0.320(1) or −0.327(1) Hz for each methoxy group (assignment uncertain). Decreased torsion amplitudes of both methoxy groups and somewhat smaller θ and ψ angles than in anisole are indicated. Interchange of the 5-nitro and 4-methoxy substituents to give 2-chloro-4-nitro-5-methoxyanisole yields the largest magnitudes of ^5J in Table 2, ^5J being −0.38 Hz for both methoxy groups. Neither of these groups now has a π electron donor as a *para* substituent and both are flanked by sizeable substituents. If the nitro group is replaced by an iodo substituent, ^5J drops to 0.35 Hz in magnitude, presumably because a π electron acceptor is no longer present. This magnitude is much the same as the 0.34 Hz in 2-iodo-5-nitroanisole. Clearly, an *ortho* substituent as large as iodine must cause decreases in θ, perhaps as large as 2°.

An apparent exception to the trends discussed above is 2,4-diaminoanisole, for which ^5J is −0.270(3) Hz, rather large in magnitude considering the ^5J of −0.232(5) Hz in 2,4-dimethoxyanisole. A possible reason is the presence of an

[2] The naming is unconventional in this discussion, but permits facile perceptions of coupling patterns.

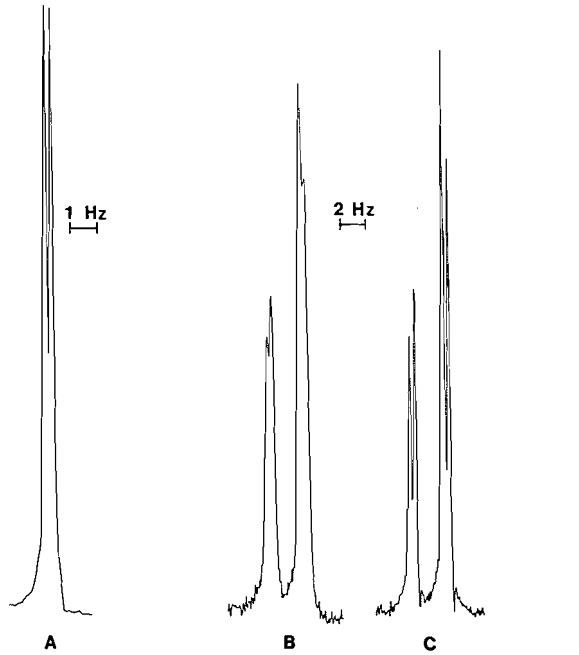

FIG. 1. In Fig. 1A the ^1H nmr spectrum of the methoxy protons in 2,4-diaminoanisole as a 2 mol% solution in acetonitrile-d_3 is displayed at 90 MHz and 305 K. $^5J_o^{H,CH_3}$ is −0.250(5) Hz. Some residual coupling to H-5 occurs, apparent here only as a slight broadening of the two peaks. In 1B the ^1H nmr peaks of H-3 are displayed. The peaks are rather broad due to unresolved coupling to the amino protons of one or two amino groups, intermolecular proton exchange being partially retarded by the presence of some basic alumina. In 1C the decoupling field, set at δ 3.68, the value for the methoxy protons, has an amplitude of 22 Hz, sufficient to decouple the amino protons with δ values of 3.88 and 3.62. Only for a large amplitude of the decoupling field do these peaks become sharp. A field amplitude sufficient to decouple the methoxy protons does not lead to such a spectrum. The line width at half height is 0.10 ± 0.01 Hz for these peaks in 1C.

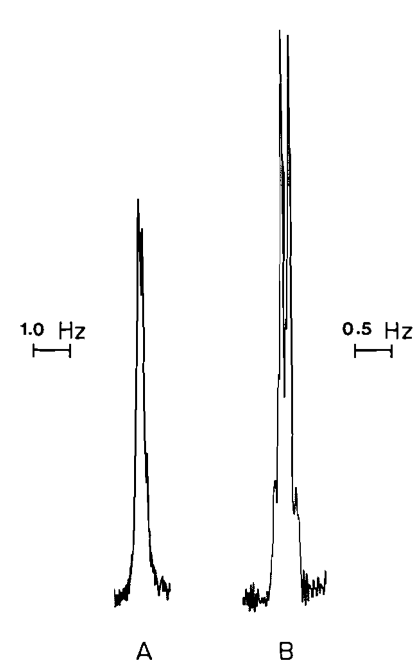

FIG. 2. In A one of the ^1H nmr bands of H-5 in 2,3,4-trichloroanisole as a 3 mol% solution in CCl_4 is displayed at 100 MHz and 305 K. The splitting represents $^6J_m^{H,OCH_3}$ and is given as 0.096(7) Hz from a LAME analysis. In B the same band is shown for a very dilute solution in acetone-d_6 at 295 K and 300.13 MHz. Considerable resolution enhancement has been applied and accounts for distortion. The splitting is 0.095(14) Hz.

N—H . . . O intramolecular hydrogen bond, which could conceivably inhibit wide excursions in ψ. The amino derivative is peculiar for another reason, as is now discussed.

Concerning ^{5}J *and* ^{6}J *in 2,4-diaminoanisole*

In a saturated benzene-d_6 solution ^5J is −0.270(3) Hz at 305 K and ^6J is 0.05(1) Hz to H-5. In view of the reported $|^6J_m^{H,CH_3}|$ values of 0.20 and 0.15 Hz to H-3 and H-5, respectively (16), the following experiments were performed on a Bruker WH90 spectrometer at 305 K. A 2 mol% solution of the compound in CD_3CN gave an ^1H nmr spectrum consistent with δ_{CH}, δ_3, δ_5, and δ_6 as 3.68172(2), 6.02880(2), 5.90970(2), and 6.55290(2), respectively. In addition, $^3J_{56}$, $^4J_{35}$, and $^5J_{36}$ were 8.405(3), 2.662(2), and 0.275(3) Hz, respectively. Figure 1 displays the doublet observed for the methyl protons; the splitting[3] of 0.250(5) Hz represents $|^5J_o^{H,CH_3}|$.

Now, the amino protons give rise to broad bands, as expected, and are centered at about 3.88 and 3.62 ppm relative to internal TMS in a solution in which intermolecular proton exchange is at least partly restricted by treatment with basic alumina. Under these conditions the ring proton peaks display a broadening which we attribute to unresolved coupling to amino protons, known to occur in aniline itself (25). Figure 1 displays the ^1H nmr spectra of H-3 for different decoupling fields centered on δ_{CH_3} at 3.68. As the amplitude of the decoupling field increases from zero to 22 Hz, the coupling from H-6 becomes clearly resolved (the small splitting). The latter decoupling amplitude, $\gamma H_2/2\pi$ = 22 Hz, is large enough at 90 MHz to decouple the amino protons at δ values of 3.9 and 3.6. Similar observations were made for H-5 and H-6. It seems possible that coupling phenomena of this kind are responsible for the literature values of $^6J_m^{H,OCH_3}$.

Other estimates of torsional amplitudes

A harmonic model has been employed in the estimation of force constants for the torsional motions in crystals of a variety of molecules, including anisole derivatives (22). The force constants given for the latter translate into $\langle\psi^2\rangle^{1/2}$ values ranging from 6° to 17°. Of course, intermolecular perturbations of the librational motions will be somewhat larger in the solid than in the solutions studied here. Nevertheless, the torsional amplitudes indicated by ^5J appear reasonable when compared to those implied by atomic vibration tensors obtained from X-ray or neutron diffraction data (22).

Concerning $^6J_m^{H,OCH_3} \equiv {}^6J$

This coupling, when observed, occurs for the *meta* proton in a *cis* arrangement to the methoxy group. Its existence was first reported for 2,4-dibromoanisole (8), and was determined as +0.06(1) Hz in 2-methoxyanisole (1). For the compounds in Table 2, ^6J ranges from 0.02 to 0.09 Hz. Splittings due to ^6J were not always resolved and were then estimated by simulations of ring proton spectra in the presence and absence of decoupling fields applied to the methyl proton peaks. Figure 2 displays splittings arising from ^6J, the analytical value at 100 MHz being confirmed at 300 MHz.

[3]This value is slightly smaller than in benzene-d_6, consistent with a smaller degree of N—H . . . O interaction in CD_3CN.

Conclusion

${}^5J_o^{H,CH_3}$ (*cis*) in anisole and its derivatives can vary from about −0.23 Hz to −0.38 Hz. A value of −0.28 Hz is typical of anisole and those of its 2-X derivatives in which X is not larger than chlorine or is a substituent presenting a similar size to the methoxy moiety. An electron donor, particularly when placed *para* to the methoxy group, reduces the magnitude of ${}^5J_o^{H,CH_3}$, probably because an increased torsional amplitude about the Csp^2—O bond leads to a larger average distance between the *ortho* C—H bond and the methoxyl protons. Large *ortho* substituents cause steric compression of the geometry of the methoxy group, thereby causing an increase in the magnitude of ${}^5J_o^{H,CH_3}$. This increase can be further enhanced in the presence of π electron withdrawing substituents.

${}^6J_m^{H,CH_3}$ is less than +0.1 Hz and appears for the C_m—H bond arranged *cis* to the methoxy group.

It appears that changes in the length of the Csp^2—O bond are a minor cause of changes in ${}^5J$ because an STO 3G optimization computes a decrease of only 0.007 Å in 4-nitroanisole, and the computed ${}^5J$ changes by rather less than 0.005 Hz for such a perturbation. Excursions in the torsion and bond angles are the important determinants of the observed ${}^5J$ in the present model.

Acknowledgments

We are grateful to the Natural Sciences and Engineering Research Council of Canada for financial support.

1. T. SCHAEFER and R. LAATIKAINEN. Can. J. Chem. **61**, 224 (1983).
2. T. SCHAEFER, H. D. GESSER, and J. B. ROWBOTHAM. Can. J. Chem. **54**, 2235 (1976).
3. J. HILTON and L. H. SUTCLIFFE. Prog. Nucl. Magn. Reson. Spectrosc. *Edited by* J. W. Emsley, J. Feeney, and L. H. Sutscliffe. Pergamon Press, Oxford. **10**, 27 (1975).
4. R. LAATIKAINEN. J. Magn. Reson. **52**, 293 (1983).
5. T. SCHAEFER, T. A. WILDMAN, and J. PEELING. J. Magn. Reson. **56**, 144 (1984).
6. H. J. TALBERG. Acta. Chem. Scand. Part A, **32**, 373 (1978).
7. R. W. CRECELY, K. W. MCCRACKEN, and J. H. GOLDSTEIN. Tetrahedron, **25**, 877 (1969).
8. H. A. GAUR, J. VRIEND, and W. G. B. HUYSMANS. Tetrahedron Lett. 1999 (1969).
9. T. SCHAEFER and T. A. WILDMAN. Can. J. Chem. **57**, 450 (1979).
10. G. M. ANDERSON III, P. A. KOLLMAN, L. H. DOMELSMITH, and K. N. HOUK. J. Am. Chem. Soc. **101**, 2344 (1979).
11. J. CAILLET. Acta Crystallogr. Sect. B, **38**, 1786 (1982).
12. A. MAKRIYANNIS and S. FESIK. J. Am. Chem. Soc. **104**, 6462 (1982).
13. O. EXNER and V. JEHLIVKA. Collect. Czech. Chem. Commun. **48**, 1030 (1983).
14. L. N. DOMMELSMITH, T. A. EATON, K. N. HOUK, G. M. ANDERSON, R. A. GLENNON, A. T. SHULGIN, N. CASTAGNOLI, JR., and P. A. KOLLMAN. J. Med. Chem. **24**, 1414 (1981).
15. G. W. BURTON and K. U. INGOLD. J. Am. Chem. Soc. **103**, 6472 (1981).
16. D. G. DE KOWALEWSKI, R. H. CONTRERAS, A. R. ENGLEMANN, J. C. FACELLI, and J. C. DURAN. Org. Magn. Reson. **17**, 199 (1981).
17. T. SCHAEFER and R. SEBASTIAN. J. Magn. Reson. **41**, 395 (1980).
18. C. CASTELLANO and A. A. BOTHNER-BY. J. Chem. Phys. **41**, 3863 (1964).
19. C. W. HAIGH. Annu. Repts. NMR Spectrosc. **4**, 311 (1971).
20. N. L. OWEN and R. E. HESTER. Spectrochim. Acta, Part A, **25**, 343 (1969).
21. B. A. ARBUZOV, A. P. TIMOSHEVA, S. G. VUL'FSON, and A. N. VERESKCHAGIN. Isv. Akad. Nauk SSSR. Ser. Khim. **9**, 2007 (1976).
22. K. N. TRUEBLOOD and J. N. DUNITZ. Acta Crystallogr. Sect. B, **39**, 120 (1983).
23. T. A. WILDMAN. Ph.D. Thesis, University of Manitoba, 1982.
24. M. KLESSINGER and A. ZYWIETZ. J. Mol. Struct. (Theochem), **90**, 341 (1982).
25. R. WASYLISHEN, J. B. ROWBOTHAM, L. ERNST, and T. SCHAEFER. Can. J. Chem. **50**, 2710 (1972).

The distribution of branched octanols between dodecane and water[1]

NORMAN H. SAGERT AND DANNY W. P. LAU

Research Chemistry Branch, Atomic Energy of Canada Limited, Whiteshell Nuclear Research Establishment, Pinawa, Man., Canada R0E 1L0

Received July 19, 1984

NORMAN H. SAGERT and DANNY W. P. LAU. Can. J. Chem. **63**, 789 (1985).

The distribution of four branched chain octanols, 3-ethyl-3-hexanol, 4-ethyl-3-hexanol, 2-ethyl-4-methylpentanol, and 4-octanol, has been measured between dodecane and water. Measurements were made at alcohol concentrations in the dodecane of less than 0.1 mol/dm^3, and as a function of temperature from 10°C to 35°C. From these distribution data, standard thermodynamic functions for transfer were calculated. Standard Gibbs energies of transfer from water to dodecane at 25°C were in the range −14.1 to −15.1 kJ/mol, whereas the standard enthalpies of transfer at 25°C varied from 29 to 39 kJ/mol. Thus, the change in the standard enthalpy tends to inhibit transfer, but a large standard entropy of transfer results in dodecane being the favoured phase.

NORMAN H. SAGERT et DANNY W. P. LAU. Can. J. Chem. **63**, 789 (1985).

On a mesuré la distribution de quatre octanols ramifiés (éthyl-3 hexanol-3 éthyl-4 hexanol-3, éthyl-2 méthyl-4 pentanol et octanol-4) entre le dodécane et l'eau. On a effectué les mesures à des concentrations en alcools dans le dodécane qui étaient inférieures à 0,1 mol/dm^3 et à des températures allant de 10 à 35°C. A l'aide de ces données sur la distribution, on a pu calculer les fonctions thermodynamiques standards pour le transfert. A 25°C, les énergies standards de Gibbs pour le transfert de l'eau au dodécane varient de −14,1 à −15,1 kJ/mol alors que, à 25°C, les enthalpies standards de transfert varient de 29 à 39 kJ/mol. Donc, alors que la variation dans l'enthalpie standard a pour effet d'inhiber le transfert, l'existence d'une entropie standard de transfert élevée fait que le dodécane est la phase favorisée.

[Traduit par le journal]

Introduction

We are presently engaged in a program to study interfacial properties relevant to the solvent extraction systems used in the nuclear industry (1, 2). As an adjunct to that program, we have measured the adsorption of the branched chain octanols, 3-ethyl-3-hexanol and 4-octanol, at the dodecane−water interface. These alcohols were chosen because of their different shapes. To interpret this adsorption data, the thermodynamics of the complete transfer of the alcohol from water to dodecane must be known. The transfer of branched alcohols from water to dodecane is also of interest in the study of lipid membranes (3), and in studies of the microemulsions used in tertiary oil recovery (4).

Standard thermodynamic functions for transfer are often calculated from the thermodynamics of solution of the solute in each of the two solvents (5, 6). The thermodynamics of solution of lower alcohols in alkanes and water are reasonably well known (5, 6). However, octanols are only sparingly soluble in water, so accurate calorimetric data on their heats of solution in water are not available. Recently, Goffredi and co-workers (7−9) have used a direct calorimetric method to obtain the thermodynamics of transfer of smaller alcohols from water to octane. However, they did not report data for octanols.

This work is a short study of the distribution of four branched-chain octanols between water and dodecane, carried out at low solute concentrations so that standard Gibbs energies of transfer at infinite dilution can be obtained. These alcohols, 3-ethyl-3-hexanol, 4-octanol, 4-ethyl-3-hexanol, and 2-ethyl-4-methylpentanol, represent a range of shapes and are available commercially. From the temperature dependence of these standard Gibbs energies of transfer, standard enthalpies of transfer are calculated, although they are less precise than those obtained calorimetrically. The data also give some information about the aggregation of these alcohols at low concentrations in dodecane.

[1]Issued as AECL-8435.

Experimental

The general procedures have been described previously (10). Analyses of alcohol concentrations were done, as previously, using gas chromatography, but the column used was 3% OV-1 on Chromosorb W at a temperature of 120°C.

The 3-ethyl-3-hexanol was obtained from ICN Pharmaceuticals, and the other alcohols from Pfaltz and Bauer. The alcohols were passed through an activated silica gel column until their purity was better than 99%, as determined by gas chromatography. The sources and purification of the water and dodecane have been described previously (11).

Results and discussion

The distribution of 4-octanol, 3-ethyl-3-hexanol, 4-ethyl-3-hexanol, and 2-ethyl-4-methylpentanol between dodecane and water was measured at concentrations up to 0.1 mol/dm^3 in the dodecane and at temperatures from 10°C to 35°C. In some cases a slightly wider temperature range was used. Figure 1 shows the results[2] for 2-ethyl-4-methylpentanol, where D, the distribution ratio, is defined as the concentration of alcohol in the dodecane divided by that in the water. Distribution ratios for this alcohol do increase as the concentration of alcohol increases, at least at lower temperatures, but the ratios are easily extrapolated to zero concentration to give the infinite dilution distribution coefficients, K_D. For reasons that will be discussed later, we actually used a plot of D against the cube of the alcohol concentration in the aqueous phase as the appropriate extrapolation procedure.

Table 1 shows the measured infinite dilution distribution coefficients, K_D. Since the errors in the individual distribution ratios are of the order of ±15%, the errors in the distribution coefficients are likely of the same order. Table 1 also gives the distribution coefficients calculated on a mole-fraction basis, K_D^X. Traditionally (12, 13), mole-fraction standard states have

[2]All the measured distribution ratios are available, at a nominal charge, from the Depository of Unpublished Data, CISTI, National Research Council of Canada, Ottawa, Ont., Canada K1A 0S2.

TABLE 1. Distribution coefficients for the transfer of octanols from water to dodecane

T (°C)	3-Ethyl-3-hexanol K_D	3-Ethyl-3-hexanol K_D^X	4-Ethyl-3-hexanol K_D	4-Ethyl-3-hexanol K_D^X	4-Octanol K_D	4-Octanol K_D^X	2-Ethyl-4-methylpentanol K_D	2-Ethyl-4-methylpentanol K_D^X
5	—	—	—	—	9.9	124	—	—
10	9.6	120	11.5	142	12.7	157	11.4	141
15	12.3	154	14.5	181	18.4	230	16.9	211
20	18.5	233	17.8	225	25.8	327	21.8	276
25	22.4	283	23.4	296	35.3	445	25.9	328
30	31.1	395	27.7	350	43.3	547	33.0	418
35	36.4	464	32.6	415	45.7	580	40.4	514
40	—	—	36.7	465	56.5	716	44.0	557
45	—	—	—	—	—	—	50.4	640

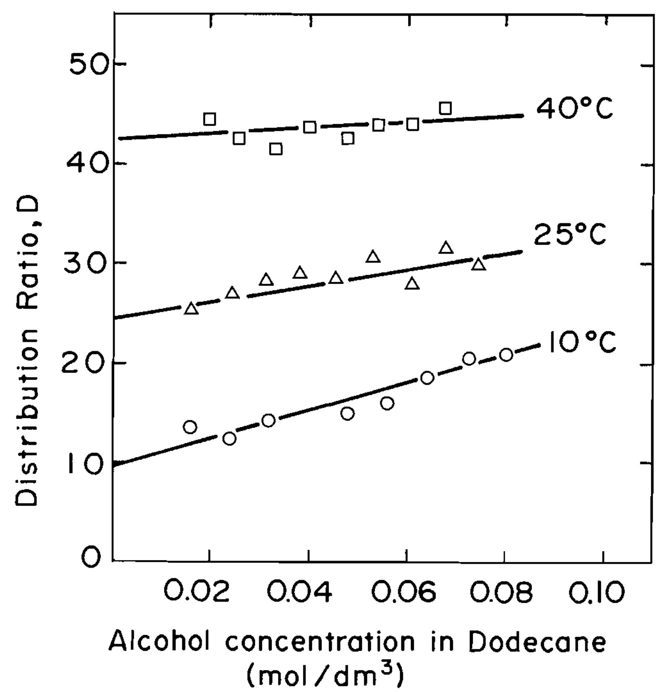

FIG. 1. Distribution ratios, D, for 2-ethyl-4-methylhexanol as a function of 2-ethyl-4-methylhexanol concentration in dodecane at three temperatures.

been used for calculating the thermodynamics of transfer, and we will use them here. Such standard states have the advantage that the reference states are temperature independent. Since both K_D and K_D^X refer to infinite dilution, their ratio is simply given by the ratio of the molar volumes of the two solvents (10, 14).

The standard Gibbs energies of transfer of alcohols from water to dodecane at infinite dilution, $\Delta_\alpha^\beta \bar{G}_1^\theta$, are calculated in the usual way (10, 14) using eq. [1]:

$$[1] \quad \Delta_\alpha^\beta \bar{G}_1^\theta = -RT \ln K_D^X$$

The alcohol is designated component 1, while the α phase is water and the β phase is dodecane. The standard states are the hypothetical standard states of ideal unit solute mole fraction. Thus, the activity coefficients implied are those that approach unity as the mole fraction of the solute approaches zero.

When standard Gibbs energies of transfer are known as a function of temperature, standard enthalpies of transfer can be calculated from eq. [2]:

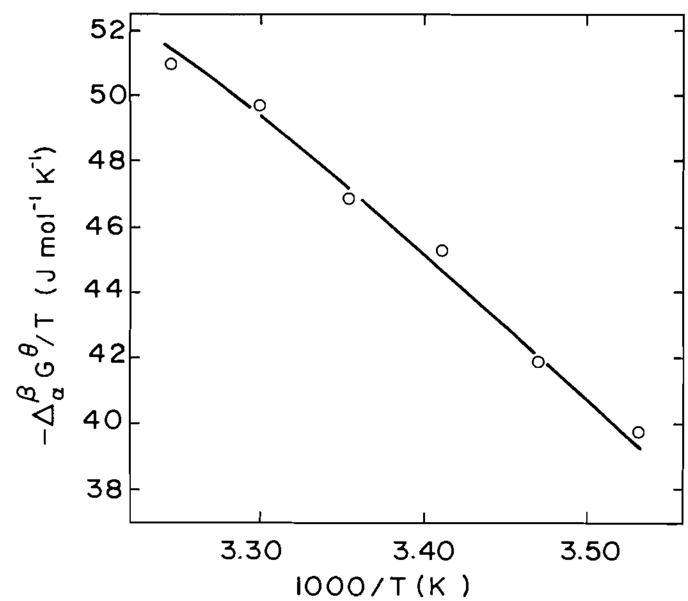

FIG. 2. Enthalpy of transfer plot of the standard Gibbs energy of transfer divided by the temperature plotted against reciprocal temperature. This plot is for 3-ethyl-3-hexanol.

$$[2] \quad \Delta_\alpha^\beta H_1^\theta = \partial(\Delta_\alpha^\beta \bar{G}_1^\theta/T)/\partial(1/T)$$

A plot of the standard Gibbs energy of transfer divided by the temperature, as a function of the reciprocal of the temperature, is shown in Fig. 2 for 3-ethyl-3-hexanol. Even over the small temperature range used, a slight curvature was noted. Thus, the standard enthalpy of transfer varies with temperature, and there is a measurable standard heat capacity of transfer:

$$[3] \quad \Delta_\alpha^\beta C_p^\theta = \partial \Delta_\alpha^\beta H_1^\theta/\partial T$$

Values of the standard Gibbs energies, enthalpies, entropies, and heat capacities of transfer, all of 25°C, are given in Table 2. The errors in the standard functions shown represent 90% confidence limits.

The standard Gibbs energies of transfer are, as expected, a little less than the value for 1-octanol obtained by extrapolating the data of Goffredi and Liveri (8) for lower alcohols up to octanol, and closer to their value for 2-octanol (9). Their data, with concentrations expressed as mole fractions, give values of −15.4 kJ/mol and −14.3 kJ/mol for transfer of 1-octanol and 2-octanol, respectively, from water to n-octanol at 25°C. Aveyard and Mitchell (14) have shown that the mole-fraction distribution coefficients do not change drastically as the solvent

TABLE 2. Standard thermodynamic functions for the transfer of octanols from water to dodecane at 25°C

Solute	$-\Delta_\alpha^\beta G_1^0$ (kJ/mol)	$\Delta_\alpha^\beta H_1^0$ (kJ/mol)	$\Delta_\alpha^\beta S_1^0$ (J K^{-1} mol^{-1})	$-\Delta_\alpha^\beta C_p^0$ (J K^{-1} mol^{-1})
3-Ethyl-3-hexanol	13.99±0.20	39.1±2.0	178±7	600±700
4-Ethyl-3-hexanol	14.10±0.04	29.4±2.0	146±3	730±140
4-Octanol	15.12±0.07	34.4±2.0	166±7	1200±200
4-Ethyl-2-methylpentanol	14.47±0.04	35.8±2.0	158±4	900±150

alkane changes, although in going from n-octanol to dodecane they become ~500 J/mol more negative for hexanol and heptanol. Thus, the Gibbs energies of transfer of Goffredi and Liveri should be approximately valid for transfer to dodecane as well, although it is possible that for transfer to dodecane they could be 400 to 600 J/mol more negative. Our standard Gibbs energies of transfer for the branched chain octanols examined here are in the range −15.1 to −14.1 kJ/mol. Unfortunately, the transfer of 1-octanol and 2-octanol proved difficult to measure accurately using our techniques, because the solubility in water at suitable concentrations in dodecane was lower than we could measure accurately. However, our results seem to bear out Goffredi and Liveri's conclusion that the more branched alcohols have a less negative standard Gibbs energy of transfer than the normal alcohols. Earlier data by Aveyard and Mitchell (14) on the transfer of lower normal alcohols is in good agreement with that of Goffredi and Liveri (8). When the data of Aveyard and Mitchell are extrapolated to 1-octanol at 25°C, one obtains a standard Gibbs energy of transfer of −15.0 kJ/mol, which is still more negative than those of the branched chain alcohols examined here, with the exception of 4-octanol.

The standard enthalpies of transfer of the alcohols from water to dodecane are all positive, so the transfer is opposed enthalpically and only takes place because of the large standard entropy of transfer. The standard enthalpy change at 25°C is, perhaps, equivalent to the breaking of about one or two hydrogen bonds, although the actual processes are unlikely to be that simple, since enthalpy changes in the hydration of the hydrocarbon chain must be considered. It is possible, in principle, to compare the standard enthalpies of transfer obtained here with those calculated from calorimetric data, since the enthalpy of transfer is simply the difference between the enthalpies of solution in the two phases. Standard enthalpies of solution and transfer of smaller linear and branched chain alcohols have been reviewed recently by Kertes and Lai (5). Standard enthalpies of solution in aliphatic hydrocarbons are endothermic and quite constant, at 23 to 24 kJ/mol (5, 15). On the other hand, standard enthalpies of solution in water are exothermic and variable (5, 6). They range from −4.6 kJ/mol for 1-hexanol (16) to −18.3 kJ/mol for 2-methyl-2-butanol (6, 17). The least negative enthalpies are for the longer, straight chain alcohols, and they become more negative as the chain length shortens. Branched chain alcohols, and especially tertiary alcohols, have very negative standard enthalpies of solution; strong hydrogen bonding with water is thought to play a role (18), but differences in the hydration of the hydrocarbon chains are also likely to be quite important here. This hydration seems to be stronger (i.e. more negative) for the branched alcohols.

Thus, standard enthalpies of transfer from water to dodecane measured calorimetrically vary from 28 kJ/mol for 1-hexanol to 41.6 kJ/mol for 2-methyl-2-butanol. Primary alcohols have smaller standard enthalpies of transfer, as a result of their less negative standard enthalpies of solution in water, as discussed above. The standard enthalpies of transfer observed with the octanols studied here are consistent with those observed for smaller branched chain alcohols, with the exception of 4-ethyl-3-hexanol, which is rather low. Also to be noted is that the standard enthalpy of transfer for 2-ethyl-4-methylpentanol is fairly large even though it is, stricty speaking, a primary alcohol.

Our measurements of standard heat capacities of transfer are very crude, being based on the curvature of plots like Fig. 2. The values obtained were compared with the apparent molal heat capacity of the alcohols in water, calculated from the additivity relationships of Jolicoeur and Lacroix (19). If the molal heat capacities of the alcohols in dodecane are small, then our standard heat capacities of transfer should be the negative of the heat capacities in water. The calculated values are in the range 750−780 J K^{-1} mol^{-1}. Our observed value for 3-ethyl-3-hexanol is less negative than predicted and our values for 2-ethyl-4-methylpentanol and 4-octanol are somewhat more negative than predicted. However, our values are subject to large errors and are consistent with the relationships of Jolicoeur and Lacroix (19), with the possible exception of 4-octanol. Thus, the standard heat capacities of transfer can be accounted for by the loss in hydrational heat capacity as the hydrocarbon chains are transferred from water to dodecane.

Finally, with respect to all comparisons with calorimetric data, it must be noted that thermodynamic functions of solution are measured for solution in pure solvents, whereas, when measuring transfer directly, we are dealing with mutually saturated phases. The small solubility of dodecane in water is unlikely to be a problem, but there is evidence that alcohols take complexed water with them into the dodecane (20).

Attempts were made to predict the standard Gibbs energies and enthalpies of transfer from scaled particle theory, using equations developed by Pierotti (21). Molecular parameters for dodecane were taken from the work of Wilhelm and Battino (22). However, all reasonable values of the molecular parameters of the alcohols gave standard Gibbs energies of transfer that were much too positive and standard enthalpies of transfer that were too large.

The concentration dependence of our distribution ratios gives some information about the aggregation of these alcohols in dodecane. From Wooley *et al.* (23) a general association can be written for the alcohols in dodecane:

$$[4] \quad nA \overset{K_n}{\rightleftharpoons} A_n$$

provided that the monomer is assumed to be the predominant species in the aqueous phase. The distribution ratio, D (Fig. 1), is the total alcohol concentration in the dodecane divided by that in the water. At infinite dilution, where by definition D becomes K_D, only monomers would be present in the dodecane as well. Thus, K_D gives the ratio of alcohol monomers in the dodecane to the total alcohol (largely monomers) in the aqueous phase. Branched chain alcohols are thought to associate in alkane phases primarily as the tetramer (24). Any change in the chemical potential of the alcohol monomers due to solute–solute interaction is ignored. Thus, following Woolley *et al* (23), we obtain:

$$[5] \quad D = K_D + 4K_4K_D^4[\text{alcohol}]_{aq}^3$$

Both ethylhexanols showed essentially no variation of D with alcohol concentration. Thus, in the low concentration range used here, these alcohols did not aggregate measurably in the dodecane. With 2-ethyl-4-methylpentanol and 4-octanol, appreciable slopes were noted, although only at lower temperatures for the former. At 25°C, K_4 values were 280 ± 100 and 900 ± 200 dm^9/mol^3, respectively. These can be compared with 230 dm^9/mol^3 obtained by Rytting *et al.* (24) for 2-methylpropanol-2 at 25°C by vapor-pressure methods. When the logarithm of these association constants was plotted against reciprocal temperature, association enthalpies of 85 ± 20 and 65 ± 15 kJ/mol, respectively, were obtained. These enthalpies correspond roughly to the enthalpies required to form the four hydrogen bonds of a tetramer. Thus, our association constants are consistent with those reported in the literature. As these experiments were not designed primarily to measure association, that is probably as much as should be said.

Acknowledgements

We thank our colleagues at the Whiteshell Nuclear Research Establishment, in particular R. J. Lemire, J. Paquette, M. J. Quinn, and P. P. S. Saluja, for aid and advice. R. J. Lemire is thanked especially for his help with the numerical analysis of the raw data.

1. N. H. Sagert and W. Lee. Can. J. Chem. **58**, 2789 (1980).
2. N. H. Sagert, W. Lee, and M. J. Quinn. Can. J. Chem. **60**, 1244 (1982).
3. C. Tanford. The hydrophobic effect: formation of micelles and biological membranes. 2nd ed., John Wiley, New York. 1980.
4. R. A. MacKay and C. Hermansky. J. Colloid Interface Sci. **73**, 324 (1979).
5. A. S. Kertes and W-C. Lai. Colloids Surf. **1**, 197 (1980).
6. A. C. Rouw and G. Somsen. J. Chem. Thermodyn. **13**, 67 (1981).
7. R. de Lisi, M. Goffredi, and V. T. Liveri. J. Chem. Soc. Chem. Commun. 381 (1980).
8. M Goffredi and V. T. Liveri. J. Solution Chem. **10**, 693 (1981).
9. M. Goffredi and V. T. Liveri. J. Phys. Chem. **86**, 2455 (1982).
10. N. H. Sagert and W. Lee. Can. J. Chem. **58**, 1463 (1980).
11. N. H. Sagert, W. Lee, and M. J. Quinn. Can. J. Chem. **57**, 1218 (1979).
12. C. Tanford. J. Phys. Chem. **83**, 1802 (1979).
13. A. Ben-Naim. J. Phys. Chem. **83**, 1803 (1979).
14. R. Aveyard and R. W. Mitchell. Trans. Faraday Soc. **65**, 2645 (1969).
15. F. Smith. Aust. J. Chem. **30**, 23 (1977); **30**, 43 (1977).
16. J. W. Larsen and L. B. Tepley. J. Colloid Interface Sci. **53**, 332 (1975).
17. C. V. Krishnan and H. L. Friedman. J. Phys. Chem. **73**, 1572 (1969).
18. N. Muller. J. Magn. Reson. **28**, 203 (1977).
19. C. Jolicoeur and G. Lacroix. Can. J. Chem. **54**, 624 (1976).
20. P. L. Huyskens, M. C. L. Haulait-Pirson, I. Hanssens, and J. Mullens. J. Phys. Chem. **84**, 28 (1980).
21. R. A. Pierotti. Chem. Rev. **76**, 717 (1976).
22. E. Wilhelm and R. Battino. J. Chem. Phys. **55**, 4012 (1971).
23. E. M. Woolley, J. G. Travers, B. P. Erno, and L. G. Hepler. J. Phys. Chem. **75**, 3591 (1971).
24. J. H. Rytting, B. D. Anderson, and T. Higuchi. J. Phys. Chem. **82**, 2240 (1978).

The reaction of the hexacyanoferrate(III) ion with hydrogen peroxide

DONALD R. EATON[1] AND MARIANNE PANKRATZ
Department of Chemistry, McMaster University, Hamilton, Ont., Canada L8S 4M1

Received June 19, 1984

DONALD R. EATON and MARIANNE PANKRATZ. Can. J. Chem. **63**, 793 (1985).

In basic solution hydrogen peroxide reduces the hexacyanoferrate(III) ion to the Fe(II) complex. The stoichiometry and kinetics of this reaction have been examined. Both a stoichiometric reduction and a catalytic reaction leading to decomposition of the hydrogen peroxide occur. The latter is largely, but not completely, photochemical in origin. The data are consistent with the involvement of a common intermediate for the stoichiometric and the thermal catalytic reactions. It is suggested that this intermediate is formed by nucleophilic attack of the hydroperoxide ion or the superoxide radical on the carbon of a cyanide ligand.

DONALD R. EATON et MARIANNE PANKRATZ. Can. J. Chem. **63**, 793 (1985).

En solution basique, le peroxyde d'hydrogène réduit l'ion hexacyanoferrate(III) en un complexe de Fe(II). On a étudié la stoïchiométrie et la cinétique de cette réaction. Il se produit une réduction stoïchiométrique et une réaction catalytique conduisant à une décomposition du peroxyde d'hydrogène. Cette dernière réaction serait principalement, mais non exclusivement, d'origine photochimique. Les données sont en accord avec l'implication d'un intermédiaire commun pour les réactions stoïchiométriques ainsi que catalytiques thermiques. On suggère que cet intermédiaire se forme par une attaque nucléophile de l'ion hydroperoxyde ou du radical hydroperoxyde sur le carbone d'un ligand cyanure.

[Traduit par le journal]

Introduction

Hydrogen peroxide represents an oxidation state of oxygen intermediate between water and molecular oxygen. As such it can behave either as an oxidising agent or a reducing agent. A well known example of this dual behaviour is the observation that in acid solution hydrogen peroxide will oxidise the ferrocyanide ion to ferricyanide, but in basic solution ferricyanide is reduced to ferrocyanide. This reversal is associated with the pH dependence of the oxidising properties of hydrogen peroxide. Thus O'M. Bockris and Oldfield (1) have measured the potential (E) of hydrogen peroxide at a platinum electrode as a function of pH and find

$$E = 0.84 - 0.0509 \text{ pH Volts}$$

This variation suffices to change the direction of the ferricyanide/ferrocyanide reaction (standard oxidation potential 0.36 V) over the range pH 7 to pH 9. These authors also consider the possible oxidation/reduction and protonation reactions occurring at the electrode. The superoxide ion and its protonation product can both result from the one electron oxidation of peroxide. These electrode reactions have been discussed more recently by Morrison *et al.* (2). The mechanism of the oxidation of ferrocyanide to ferricyanide by hydrogen peroxide is reasonably well understood. It is of the inner sphere type and replacement of a cyanide ligand by a water molecule, either by photolysis or thermolysis, is a necessary first step. The thermal reaction is quite slow. Earlier studies have been reviewed by Baxendale (3) and Davies and Garafalo (4) have examined the mechanism of the reaction of the pentacyanoquo complex with hydrogen peroxide in some detail. The reduction of ferricyanide to ferrocyanide is less well understood. It is a relatively rapid reaction. To our knowledge there have been two reports of kinetic studies of the reduction of ferricyanide by peroxide. Sobkowski (5) describes the reaction in 0.1 M NaOH as being first order in peroxide and first order in ferricyanide and suggests that "one of the rate determining steps is the displacement of cyanide ion by hydroxide ion in the ferricyanide complex". Girdhar (6) agrees on the order of the reaction, but postulates an outer sphere one electron transfer rate determining step to give superoxide radicals.

There are two complications. Ferricyanide may act as a catalyst for the decomposition of hydrogen peroxide. There are many precedents for the catalysis of this reaction by Fe(III) complexes (7–9). Girdhar and Jain (10) indeed report catalysis by the ferricyanide ion. Secondly, photochemical reactions are possible. The photochemistry of complex cyanides has been studied by Asperger (11) and by MacDiarmid and Hall (12). Both ferrocyanide and ferricyanide are photoaquated relatively rapidly in light of moderate intensity. The resultant aquo compounds are considerably more reactive than the parent hexacyanides. It is clear (10) that catalysis of the decomposition of hydrogen peroxide in the presence of hexacyanoferrates occurs by a photochemical reaction. Thermal catalysis is less well established.

There are objections to both mechanisms suggested for the reduction of ferricyanide ions by hydrogen peroxide. An inner sphere mechanism requires prior dissociation of cyanide ligand. The exchange of cyanide ligands has been studied by radiochemical methods and found to be very slow. Thus Adamson, Welker, and Volpe (13) reported that in the absence of light only 12% of the ligands of ferricyanide ion had exchanged after 115 h at high pH. MacDiarmid and Hall (14) found no exchange in the dark at pH 10. These results clearly rule out an inner sphere mechanism for the relatively rapid thermal reduction process. The outer sphere electron transfer mechanism is less easy to eliminate. On this mechanism ferricyanide and peroxide react to give ferrocyanide and superoxide. The superoxide must then react rapidly with a further molecule of ferricyanide to complete the reaction. Brown and Higginson (15) have discussed mechanisms for the reduction of metal complexes involving free radical intermediates and have concluded that they are energetically unfavourable if the metal complex is a weak oxidant. Bennett (16) has discussed the oxidation/reduction potentials in the molecular oxygen/peroxide/water system and has pointed out the advantages of two electron reductions of molecular oxygen in avoiding superoxide intermediates. Similar considerations apply to the two electron oxidation of peroxide to molecular

[1]To whom all correspondence should be addressed.

oxygen. Considerations of this type have been used to explain the catalysis of hemoglobin (17) and myoglobin (18) autoxidations by reducing agents.

The present paper reports a kinetic study of the reaction between ferricyanide and hydrogen peroxide in the pH range 11–12. At these pH's reduction to ferrocyanide is complete.

Experimental

BDH Analar $K_3Fe(CN)_6$ and Anachemia 30% H_2O_2 were used in all experiments. Three types of experiment are reported.

In the first type, progress of the reaction was monitored by measuring the evolution of oxygen. The oxygen given off was measured by displacing water in a gas burette. Solutions of $K_3Fe(CN)_6$ in 0.1 *M* NaOH were placed in a three-necked flask equipped with a serum cap and outlet to the gas burette. H_2O_2 (30%) was added by syringe in quantities sufficient to give the desired concentration of peroxide and the O_2 collected was measured at timed intervals. The pH of the solution was greater than 12 and did not change during the reaction. Blank runs of H_2O_2 in 0.1 *N* NaOH were used to correct for H_2O_2 decomposition due to other factors. Dark reactions were run with aluminum foil around the reaction flask. The objectives of these experiments were to establish the stoichiometry of the reaction and to assess the importance of the photochemical and catalytic reactions.

The reaction was examined spectroscopically using a Tracor Northern spectrophotometer equipped with a photo-diode array detector. It was possible to obtain a spectrum of the reacting mixture 2 to 3 s after mixing the reactants. It was hoped that in this way an intermediate of the type reported by Lancaster and Murray (19, 28) for the sulphite/ferricyanide reaction could be detected. The spectrum obtained in this manner was, however, identical to that of the final ferrocyanide product. We infer that the intermediate, if it exists, is much shorter-lived than that observed in the sulphite reaction.

Stopped-flow experiments were run in a Durrum D110 spectrophotometer equipped with a Nicolet 1170 signal averager. All solutions were made up in phosphate buffer (Na_2HPO_4), with ionic strength corrected to 1.0 *M* with NaCl. Concentrations of dilute H_2O_2 solutions were determined by titration with $KMnO_4$ solution, which had been standardized with sodium oxalate. Temperature was controlled by a water bath maintained at 25 ± 0.2°C. The disappearance of ferricyanide was monitored at 420 nm. The concentrations of hydrogen peroxide used in the present experiments are approximately one order of magnitude greater than those used by Girdhar (6) or by Sobkowski (5). This was partly due to the desire to maintain pseudo first order conditions in the stopped flow experiments and partly with the intent of testing for first order dependence of the rate at higher peroxide concentrations, since the theory predicts that the dependence will become zero order at high peroxide concentrations if the catalytic reaction is important. These experiments have also been carried out at pH values much higher than those reported by Girdhar (6) to ensure that the reaction proceeded to completion and to investigate the pH dependence of the rate in the sensitive region close to the pK_a of hydrogen peroxide. As a result of this choice of conditions the rate of evolution of oxygen is quite rapid and bubbles in the stopped flow observation cuvette limit the accuracy of the data. This is especially true at the higher peroxide concentrations.

Results

In agreement with the previous reports we find that at pH's greater than 11 ferricyanide is completely reduced to ferrocyanide by any amount of hydrogen peroxide equal to or greater than that required by the equation:

$$2Fe(CN)_6^{3-} + H_2O_2 = 2Fe(CN)_6^{4-} + O_2 + 2H^+$$

The results of the oxygen evolution experiments are illustrated in Figs. 1 and 2. Figure 1 shows results obtained for the dark reaction and Fig. 2 for the reaction in laboratory light. It is clear from a comparison of the two figures that a photolytic reaction is occurring. In these experiments the concentration of ferricyanide was 0.022 *M* and that of hydrogen peroxide varied from 0.004 *M* to 0.34 *M*. If the reaction is stoichiometric, the maximum value of the ratio moles O_2/moles $Fe(CN)_6^{3-}$ plotted in Figs. 1 and 2 should be 0.5 if the concentration of peroxide is greater than 0.011 *M*. If the concentration of peroxide is less than 0.011 *M* the ratio should be peroxide concentration/0.022. Ratios greater than these demonstrate a catalytic

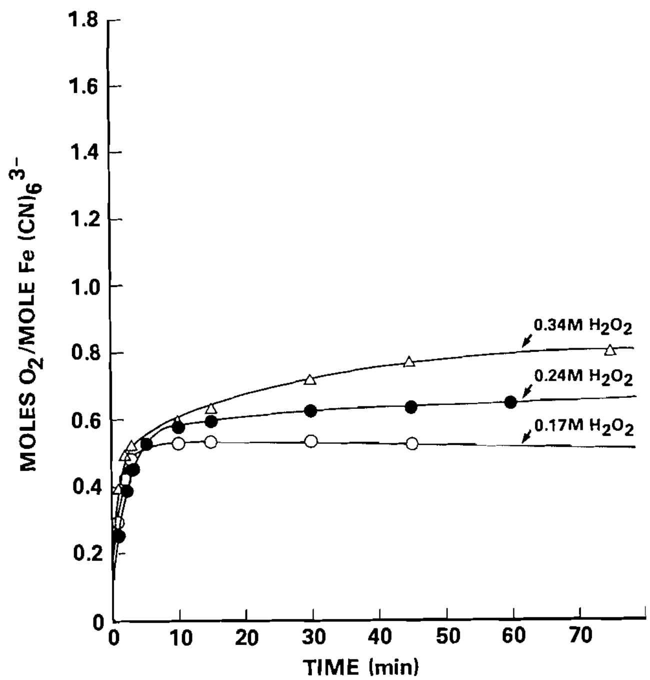

FIG. 1. Oxygen evolution in the dark reaction between $Fe(CN)_6^{3-}$ and H_2O_2. The concentration of $Fe(CN)_6^{3-}$ is 0.022 *M* throughout. The stoichiometric reaction leads to production of 0.5 mol of oxygen per mol of $Fe(CN)_6^{3-}$.

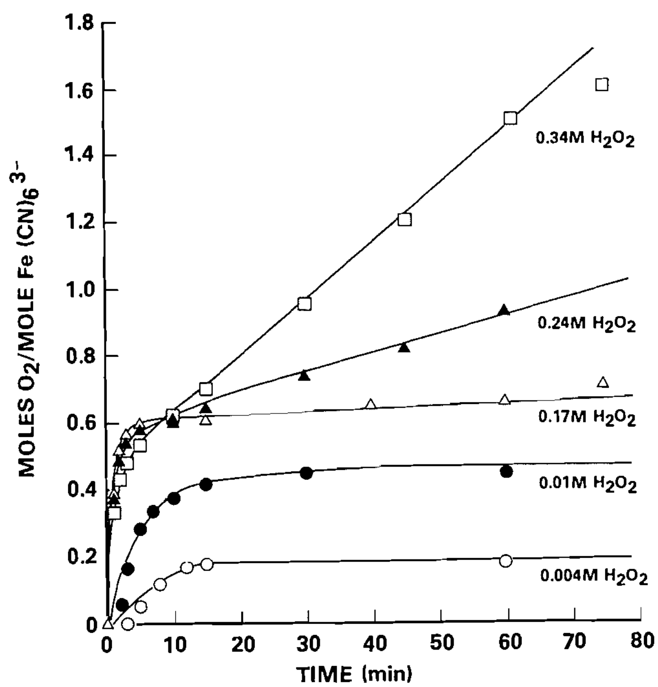

FIG. 2. Oxygen evolution in the reaction between $Fe(CN)_6^{3-}$ and H_2O_2 carried out in laboratory light. Conditions the same as Fig. 1.

TABLE 1. Kinetic data for the reaction of $K_3Fe(CN)_6$[a] with H_2O_2

μ (M)	pH	$[H_2O_2]$ (M)	k_{obs} (s^{-1})	k_{app} (s^{-1} M^{-1})
1.0	11.2	7.08×10^{-3}	0.050	7.06
		14.2×10^{-3}	0.093	6.55
		22.9×10^{-3}	0.101	4.41
		32.2×10^{-3}	0.096	2.98
		45.8×10^{-3}	0.068	1.48
1.0	11.6	6.5×10^{-3}	0.116	17.8
		13.5×10^{-3}	0.132	9.8
		20.4×10^{-3}	0.259	12.7
		29.6×10^{-3}	0.324	10.9
		40.9×10^{-3}	0.395	9.66
1.0	11.8	6.7×10^{-3}	0.394	58.8
		13.2×10^{-3}	0.316	23.9
		21.8×10^{-3}	0.297	13.6
		30.5×10^{-3}	0.325	10.7
		46.0×10^{-3}	0.377	8.20
1.0	12.0	6.7×10^{-3}	0.512	76.4
		14.1×10^{-3}	0.468	33.2
		22.2×10^{-3}	0.518	23.3
		30.5×10^{-3}	0.408	13.4
		44.3×10^{-3}	0.372	8.4
0.5	12.0	37.2×10^{-3}	0.541	14.5
1.0		44.3×10^{-3}	0.372	8.4
1.5		45.35×10^{-3}	0.352	7.76
2.0		46.11×10^{-3}	0.263	5.70
	7.0			0.42[b]
	8.0			4.6[b]
0.01	12.0			1.32[c]
0.10	13.0			4.7[c]
1.0	14.0			8.9[c]

[a]Concentration $K_3Fe(CN)_6^{3-}$ = 5×10^{-4} M.
[b]Data from ref. 6.
[c]Data from ref. 5.

reaction. It is apparent that at low concentrations of hydrogen peroxide the reaction is predominantly stoichiometric but at higher concentrations the catalytic reaction becomes more important. The initial parts of the curves of Figs. 1 and 2 are very similar, terminating at a ratio close to that expected for the stoichiometric reaction. This indicates that the latter reaction is thermal rather than photochemical and is rapid compared to the subsequent reaction. The stopped-flow results reported below therefore reflect only the thermal reaction. Comparison of Figs. 1 and 2 shows that the slower catalytic reaction is predominantly, but not exclusively, photochemical. Even in the dark more oxygen is produced at high peroxide concentrations than can be accounted for by a purely stoichiometric reaction.

The earlier portion of the reaction can be monitored by using stopped-flow spectrophotometry. Reactions were carried out under pseudo first order conditions with hydrogen peroxide in excess. These experiments were carried out in the pH range 11–12. In each case good exponential decays were observed indicating that the reaction is first order in ferricyanide. Table 1 presents the kinetic data obtained in these experiments. The accuracy of the data is limited by the experimental problems caused by oxygen bubbles, but the increase in rate with pH is quite clear. This increase is consistent with the suggestion of Girdhar (6) that HO_2^- is the reacting species. The present data do not indicate that the reaction is first order in hydrogen peroxide. This is shown by the variability of the calculated second order rate constants given in Table 1. Some of this variation could result from the rather poor quality of the data at high peroxide concentrations but the trend to less than first order dependence is consistent and statistically meaningful. The data of Girdhar (6) also show some decrease in apparent second order rate constants at higher peroxide concentrations. Sobkowski (5) did not investigate the peroxide dependence of the rate. A few experiments to investigate the effect of ionic strength on the rate were also carried out and these results are included in Table 1.

Discussion

The results described above have demonstrated the following features of the ferricyanide/hydrogen peroxide reaction. (*1*) Both thermal and photolytic reactions are important. The photolytic reaction leads to the catalytic decomposition of the peroxide and, at least under conditions of normal illumination, is much slower than the thermal stoichiometric reaction. The latter results in the reduction of ferricyanide to ferrocyanide. It seems reasonable to suppose that the photolytic reaction proceeds via a pentacyano-aquo species. Since ferrocyanide is present as the product of the stoichiometric reaction photochemical catalytic decomposition is to be expected (4). (*2*) The thermal reaction is predominantly stoichiometric at low concentrations of hydrogen peroxide but becomes partly catalytic at higher concentrations. (*3*) We were unable to detect an intermediate of the type reported by Lancaster and Murray (19) for the ferricyanide/sulphite reaction. This does not imply that such an intermediate does not exist but places an upper limit of 1–2 s on its lifetime. (*4*) The rate of the thermal reaction is first order in ferricyanide but less than first order in peroxide. (*5*) The rate of the reaction increases with pH. The increase is consistent with the hydroperoxide ion being the reactive species. Since the order of the reaction with respect to peroxide is not well defined it is a little difficult to quantify the pH dependence. However, if the average first order rate constant at a given pH is plotted against the fractional concentration of hydroperoxide ion (calculated assuming a value of 11.62 for the pK_a of hydrogen peroxide) the straight line 0.19 + $1.164[HO_2^-]$ is obtained with a correlation coefficient of 0.996. Although some reactivity for the neutral peroxide molecule is not ruled out, this result clearly indicates that the hydroperoxide ion is the principal reacting species.

Any mechanism for the reaction must be consistent with these observations. The reports that cyanide ligand exchange is very slow (13, 14) would seem to preclude an inner sphere mechanism for the thermal reduction of ferricyanide. For such a mechanism the overall rate could not be greater than the rate of dissociation of cyanide ligands and this rate is clearly insufficient to account for the stopped-flow data. We note that for the ferricyanide/sulphite reaction Wiberg *et al.* (20) have eliminated the inner sphere mechanism by a direct radiochemical exchange experiment. An inner sphere mechanism remains a very plausible path for the photochemical reaction since photodissociation of cyanide is well established.

The mechanism suggested by Girdhar (6), namely,

$$Fe(CN)_6^{3-} + HO_2^- \rightarrow Fe(CN)_6^{4-} + HO_2 \text{ (rate determining)}$$

$$Fe(CN)_6^{3-} + HO_2 \rightarrow Fe(CN)_6^{4-} + O_2 + H^+ \text{ (fast)}$$

does not readily account for the low order dependence of the rate on peroxide at high peroxide concentrations.

We would like to suggest an alternative mechanism based on the interpretation of the ferricyanide/sulphite reaction proposed by Lancaster and Murray (19, 21). These authors demonstrated the existence of an intermediate and originally postulated $Fe(CN)_5(CNSO_3)^{5-}$ formed by nucleophilic attack of sulphite on the carbon of a cyanide group. They subsequently concluded (28) that the intermediate was correctly formulated as $[Fe(CN)_5(CNSO_3)]^{4-}$ and was formed by the nucleophilic attack of a sulphite radical on a ferricyanide ion. This type of reaction is well documented in nitroprusside chemistry (22, 23). An intermediate of this kind could well play a part in the peroxide chemistry. The simplest scheme, based on Lancaster and Murray's original formulation of the intermediate, would be:

$$[1]\quad Fe(CN)_6^{3-} + HO_2^- \underset{k_{-1}}{\overset{k_1}{\rightleftharpoons}} Fe(CN)_5(CNO_2H)^{4-}$$

$$[2]\quad Fe(CN)_5(CNO_2H)^{4-} + Fe(CN)_6^{3-} \xrightarrow{k_2} 2Fe(CN)_6^{4-} + O_2 + H^+$$

$$[3]\quad Fe(CN)_5(CNO_2H)^{4-} + H_2O_2 \xrightarrow{k_3} Fe(CN)_6^{3-} + O_2 + OH^-$$

With the condition that $k_{-1} \ll k_2[Fe(CN)_6^{3-}]$ this scheme leads to the rate equation:

$$\frac{-d[FE(CN)_6^{3-}]}{dt} = \frac{2k_1k_2[FE(CN)_6^{3-}]^2[HO_2^-]}{k_2[Fe(CN)_6^{3-}] + k_3[H_2O_2]}$$

This equation correctly predicts that the catalytic reactions [3] will become more important at high peroxide concentrations and that under these conditions the rate tends to zero order in peroxide. However, it also predicts that at high peroxide concentrations the rate will become second order in ferricyanide and a careful inspection of the stopped-flow traces does not confirm this prediction. A modification of the reaction scheme is to replace reactions [2] and [3] with [4], [5], and [6].

$$[4]\quad Fe(CN)_5(CNO_2H)^{4-} + Fe(CN)_6^{3-} \xrightarrow{k_2}$$

$$[(CN)_5Fe\overset{\overset{\textstyle N}{\|}}{C}{-}OOH\cdots NCFe(CN)_5]^{7-}$$

Int 2

$$[5]\quad \text{Int 2} \xrightarrow{k_3} 2Fe(CN)_6^{4-} + O_2 + H^+$$

$$[6]\quad \text{Int 2} + H_2O_2 \xrightarrow{k_4} 2Fe(CN)_6^{4-} + O_2 + H_2O + OH^-$$

In this modified scheme a further intermediate is formed by reaction with the second ferricyanide molecule and this can either decompose to give the stoichiometric reaction products or react with more peroxide to give the catalytic reaction. This type of intermediate can equally well be formed by the sequence

$$Fe(CN)_6^{3-} + HO_2^- \xrightarrow{k_1} Fe(CN)_6^{4-} + HO_2$$

$$Fe(CN)_6^{4-} + HO_2 + Fe(CN)_6^{3-} \xrightarrow{k_2}$$

$$[(CN)_5Fe\overset{\overset{\textstyle N}{\|}}{C}{-}OOH\cdots NCFe(CN)_5]^{7-}$$

which corresponds to Murray's second suggestion for the intermediate, namely attack of the radical on ferricyanide. The two routes are kinetically indistinguishable. In the first case k_1 is the rate of nucleophilic attack on the cyanide ligand and in the second case it corresponds to an outer sphere electron transfer reaction. They lead to the rate equation

$$\frac{-d[Fe(CN)_6^{3-}]}{dt} = \frac{2k_1k_2k_3[Fe(CN)_6^{3-}]^2[HO_2^-]}{(k_{-1} + k_2[Fe(CN)_6^{3-}])(k_3 + k_4[H_2O_2])}$$

which further simplifies to

$$\frac{-d[Fe(CN)_6^{3-}]}{dt} = \frac{2k_1k_3[Fe(CN)_6^{3-}][HO_2^-]}{k_3 + k_4[H_2O_2]}$$

if $k_{-1} \ll k_2[Fe(CN)_6^{3-}]$. This rate equation is compatible with all the experimental data. A little rearrangement gives

$$\frac{K}{k_{obs}([H^+] + K)} = \frac{k_4}{2k_1k_3} + \frac{1}{2k_1[H_2O_2]}$$

where K is the acid dissociation constant of hydrogen peroxide (taken as 2.4×10^{-12}). Plots of the left-hand side of this equation versus $1/[H_2O_2]$ show a great deal of scatter, which we attribute to the relatively poor quality of the data caused by oxygen bubble problems, but yield values of 58 M^{-1} s^{-1} for k_1 and 0.016 for the ratio k_4/k_3. The former value agrees reasonably well with the value of 99 M^{-1} s^{-1} for the second order rate constant obtained by Girdhar (6) for the rate-determining step of the stoichiometric reaction at much lower concentrations of peroxide and lower pH's. The data of Sobkowski (5) give a second order rate constant approximately one order of magnitude lower than that found above (average 5.2 M^{-1} s^{-1}) but it is difficult to evaluate this data since no peroxide concentration or ionic strength dependence is reported. These literature data are given at the end of Table 1. The value obtained for the ratio k_4/k_3 clearly indicates that the stoichiometric reaction will predominate except at high peroxide concentrations. The results displayed in Fig. 1 show that this is indeed the case. Also included in Table 1 are some data showing the variation of rate with ionic strength. Swinehart (24) and others have reported large variations of rate with alkali metal ion concentration for reactions of this type. This is clearly true for the present reaction with the rate diminishing with increasing metal ion concentration. This effect might perhaps arise from ion pairing with the hydroperoxide ion.

To summarize, the present results show that the reducing agent in the ferricyanide/hydrogen peroxide reaction is the hydroperoxide ion. At low peroxide concentrations the reaction is predominantly stoichiometric. At higher concentrations a catalytic component is apparent. It is suggested that the key intermediate in both the stoichiometric and the catalytic reactions is formed by nucleophilic attack of the hydroperoxide ion or radical on the carbon of a cyanide ligand. We prefer the former mechanism since HO_2^- will certainly be a better nucleophile than HO_2 but the second mechanism cannot be eliminated on kinetic grounds. There is evidence for a similar mechanism in the reduction of met-myoglobin cyanide by dithionite (25, 26). This occurs by attack of the SO_2^- ion without dissociation of the cyanide ligand. A very similar mechanism has been suggested for the reduction of imidazole derivatives of met-myoglobin by dithionite (27). In this case the nucleophilic attack occurs at the 2 position of the imidazole ligand and the electron is then transferred through the ligand π system. This type of mechanism avoids the energetic problems pointed out by Brown and Higginson (15) for outer sphere reactions in which an unstable free radical is formed by a weak oxidizing agent. Either no free radical is formed or if one is formed in an initial electron transfer reaction it is stabilized by complexation.

Acknowledgements

We wish to thank Ms. Kathy Peycha for obtaining some of the preliminary stopped-flow data and the Natural Sciences and Engineering Research Council of Canada for financial support of this research.

1. J. O'M. BOCKRIS and L. F. OLDFIELD. Trans. Faraday Soc. **51**, 249 (1955).
2. M. M. MORRISON, J. L. ROBERTS, and D. T. SAWYER. Inorg. Chem. **18**, 1971 (1979).
3. J. H. BAXENDALE. Adv. Catal. **4**, 67 (1952).
4. G. DAVIES and A. R. GARAFALO. Inorg. Chem. **15**, 1101 (1976).
5. J. SOBKOWSKI. Ann. Soc. Chim. Polonorum. **43**, 1729 (1969).
6. K. K. GIRDHAR. Chemical Era, 21 Oct. (1975).
7. M. BARTERI, M. FARINELLA, B. PISPIA, and L. SPLENDORINA. Inorg. Chem. **17**, 3366 (1978).
8. A. C. MELNYK, N. K. KILDAHL, A. R. RENDINA, and D. H. BUSCH. J. Am. Chem. Soc. **101**, 3232 (1979).
9. P. WALDMEIER and H. SIGEL. Inorg. Chim. Acta, **5**, 659 (1971).
10. K. K. GIRDHAR and D. V. S. JAIN. J. Inorg. Nucl. Chem. **27**, 2653 (1965).
11. S. ASPERGER. Trans. Faraday Soc. **48**, 617 (1952).
12. A. G. MACDIARMID and N. F. HALL. J. Am. Chem. Soc. **75**, 5204 (1953).
13. A. W. ADAMSON, J. P. WELKER, and M. VOLPE. J. Am. Chem. Soc. **72**, 4030 (1950).
14. A. G. MACDIARMID and N. F. HALL. J. Am. Chem. Soc. **76**, 4222 (1954).
15. A. BROWN and W. C. E. HIGGINSON. Chem. Commun. 725 (1967).
16. L. E. BENNETT. Prog. Inorg. Chem. **18**, 1 (1973).
17. W. J. WALLACE and W. S. CAUGHEY. Biochem. Biophys. Res. Commun. **62**, 561 (1975).
18. D. R. EATON and K. M. WILSON. J. Inorg. Biochem. **10**, 195 (1979).
19. J. M. LANCASTER and R. S. MURRAY. J. Chem. Soc. A, 2755 (1971).
20. K. B. WIBERG, H. MALTZ, and A. G. FOGG. Inorg. Chem. **7**, 830 (1968).
21. R. S. MURRAY. Chem. Commun. 824 (1968).
22. J. A. MCLEVERTY. Chem. Rev. **79**, 53 (1979).
23. J. H. SWINEHART and P. A. ROCK. Inorg. Chem. **5**, 573 (1966).
24. J. H. SWINEHART. J. Inorg. Nucl. Chem. **27**, 2313 (1967).
25. R. P. COX and M. R. HOLLAWAY. Eur. J. Biochem. **74**, 575 (1977).
26. E. OLIVAS, D. J. A. DEWAAL, and R. G. WILKINS. J. Biol. Chem. **252**, 4038 (1977).
27. D. R. EATON and R. G. WILKINS. J. Biol. Chem. **253**, 908 (1978).
28. R. S. MURRAY. J. Chem. Soc. Dalton, 2381 (1974).

Free energies and entropies of transfer of hydrogen halides from water to aqueous 2-methoxy ethanol and structuredness of the solvents

PRABIR K. GUHA[1] AND KIRON K. KUNDU[2]
Physical Chemistry Laboratories, Jadavpur University, Calcutta — 700 032, India

Received April 6, 1984

PRABIR K. GUHA and KIRON K. KUNDU. Can. J. Chem. **63**, 798 (1985).

Standard free energies (ΔG_t^0) and entropies (ΔS_t^0) of transfer of HBr and HI from water to some aqueous solutions of 2-methoxy ethanol (ME) have been determined from emf measurements of the cells: Pt, H_2 (g, 1 atm)/HBr (m), solvent/AgBr−Ag and Pt, H_2 (g, 1 atm)/KOH (m_1), KI (m_2), solvent/AgI−Ag, respectively, at seven equidistant temperatures ranging from 15 to 45°C. ΔG_t^0 values of HBr and HI as well as of HCl obtained from literature, and particularly that of the individual ions obtained by tetraphenylarsonium tetraphenylboron (TATB) assumption, suggest that while H^+ is increasingly stabilized by cosolvent-induced larger "basicity", halide ions (X^-) are increasingly destabilized by cosolvent-induced decreased "acidity" and the dielectric constant of the mixed solvents compared to that of water. Analysis of the variation of the observed $T\Delta S_t^0$(HX) and particularly of ΔY (= $T\Delta S_t^0(H^+) + T\Delta S_{t,ch}^0(X^-)$), with composition, in the light of Kundu *et al's* semi-quantitative theory reveals that ME induces breakdown of three dimensional (3D) tetrahedral structures of water at water-rich compositions. This is being followed by an ordered region due to possible H-bonded cosolvent−water complexation and then the usual disordered region due to packing imbalance. Comparison of ΔY(HI)−composition profiles for aqueous mixtures of t-butanol (Bu^{t}OH), ethylene glycol (EG), and 1,2-dimethoxy ethane (DME) also demonstrates that the remarkable enhancement of 3D water structures by the well known structure promoter Bu^{t}OH gets succintly diminished when cosolvent Bu^{t}OH is replaced by EG, ME, and DME, as is expected from structural and electronic considerations of the cosolvents.

PRABIR K. GUHA et KIRON K. KUNDU. Can. J. Chem. **63**, 798 (1985).

Opérant à sept températures équidistantes échelonnées de 15 à 45°C et faisant appel à des mesures de f.é.m. obtenues respectivement à l'aide des cellules Pt, H_2 (g, 1 atm)/HBr (m), solvant/AgBr−Ag et Pt, H_2 (g, 1 atm)/KOH (m_1), KI (m_2), solvant/AgI−Ag, on a déterminé les énergies (ΔG_t^0) et les entropies (ΔS_t^0) libres standards pour les transferts de HBr et de HI de l'eau vers des solutions aqueuses de méthoxy-2-éthanol (ME). Les valeurs de ΔG_t^0 déterminées pour HBr et HI ainsi que les valeurs équivalentes obtenues dans la littérature pour HCl et, en particulier, les valeurs obtenues pour les ions individuels en faisant l'hypothèse du tétraphénylarsonium tétraphénylbore (TATB), suggèrent que, alors que les ions H^+ sont de plus en plus stabilisés par des "basicités" de plus en plus élevées induites par le cosolvant, les ions halogénures (X^-) sont de plus en plus déstabilisés par des diminutions d'"acidité" induites par le cosolvant et par la constante diélectrique des solvants mixtes comparée à celle de l'eau. Si l'on effectue, à la lumière de la théorie semi-quantitative de Kundu et de ses collaborateurs, une analyse de la variation, en fonction de la composition, des valeurs observés pour $T\Delta S_t^0$(HX) et en particulier pour ΔY (= $T\Delta S_t^0(H^+) + T\Delta S_{t,ch}^0(X^-)$), on en conclut que le ME induit des ruptures dans les structures tétraédriques tridimensionnelles (3D) des compositions d'eau ou riches en eau. Ceci est suivi par une région ordonnée qui est peut être due à une complexation eau-cosolvant provenant d'une liaison hydrogène possible et finalement par la région désordonnée habituelle qui est due à une mauvaise balance dans l'entassement. Une comparaison des profils reliant le ΔY (HI) et la composition, pour des mélanges aqueux de t-butanol (t-BuOH), d'éthylène glycol (EG) et de diméthoxy-1,2 éthane (DME), permet aussi de démontrer que les structures tridimensionnelles de l'eau sont rehaussées d'une façon remarquable par le t-BuOH, qui est bien connu pour promouvoir des structures, alors qu'elles sont fortement diminuées lorsque le t-BuOH est remplacé par l'EG, le ME ou le DME; ces constatations correspondent à ce que l'on peut prévoir sur la base de considérations structurales et électroniques des cosolvants.

[Traduit par le journal]

Introduction

2-Methoxy ethanol (ME), variously known as methyl cellosolve, is a widely used organic solvent for various industrial processes because of its unique solvating properties associated with its quasi-aprotic character. In fact, being a hydroxyether it has partly protic and partly aprotic characters. Besides, by virtue of its unique structural characteristics it is also likely to have enhanced aprotic character, as is expected from the possible formation of intramolecular hydrogen-bonded aprotic form **B**

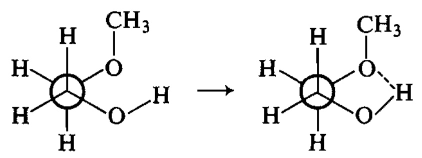

A **B**

Moreover, being a mono-methyl ether of ethylene glycol (EG), it is also likely to show some physico-chemical characteristics which would lie intermediate to protic EG and its dimethyl ether, i.e., aprotic 1,2-dimethoxy ethane (DME). Because of these reasons it should be very useful and interesting to evolve the knowledge of solvating and structural characteristics of the aqueous mixtures of these closely related cosolvents.

With that end in view we have recently undertaken comprehensive studies (1−4) on ion−solvent interactions of a series of ions like alkali metal ions (M^+), halide ions (X^-), H^+, OH^- etc. in the aqueous mixtures of these closely related cosolvents, as determined from emf measurements of suitable galvanic cells and by the use of widely used tetraphenylarsonium tetraphenylboron (TATB) reference electrolyte assumption (5):

$$\Delta G_t^0(Ph_4B^-) = \Delta G_t^0(Ph_4As^+) = \frac{1}{2}\,\Delta G_t^0(Ph_4AsPH_4B)$$

where Ph = phenyl and ΔG_t^0(i) denotes transfer free energies of the ion from the reference solvent water to the mixed solvents. These studies helped derive important reflections about

[1]Holder of a Junior Research Fellowship under University Grants Commission, New Delhi.

[2]To whom all correspondence should be addressed.

the solvating characteristics of these cosolvents, which conform fairly well with the structural and electronic considerations of these cosolvent molecules. Moreover, as part of gleaning three dimensional (3D) ice-like tetrahedral structures of water in aqueous mixtures of these cosolvents we have recently reported the standard electrode potentials (E^0) of Ag−AgX electrodes and the related transfer free energies ΔG_t^0(HX) and entropies ΔS_t^0(HX) of hydrogen halides (HX) for aqueous solutions of EG (1) and DME (4*a*) as the latter quantities have recently been shown (6) to be a useful probe for the relative 3D tetrahedral structures of water in various aquo-organic solvents. But although E^0 values of the Ag−AgCl electrode at different temperatures — the basis of ΔS_t^0(HCl) in aqueous ME solutions are already reported by Sadek *et al.* (7) those for the Ag−AgBr and Ag−AgI electrodes are yet to be determined. It should therefore be of particular interest to extend such studies for other two hydrogen halides namely HBr and HI.

In this paper we report E^0 values of the Ag−AgBr and Ag−AgI electrodes at different temperatures and the related transfer energetics of HBr and HI in this solvent system. E^0 values of the Ag−AgBr electrode have been determined by emf measurements of cell [C]

[C] Pt, H_2 (g, 1 atm)/HBr (*m*), solvent/AgBr−Ag

But owing to the gradual oxidation of I^- at low pH even when freshly distilled HI and freshly purified and also deoxygenated solvent ME were used, it was not possible to use the cell of the type [C] for the Ag−AgI electrode. Instead, as in aqueous like DME, THF, and dioxane (D), cell [D]

[D] Pt, H_2 (g, 1 atm)/KOH (m_1), KI (m_2), solvent/AgI−Ag

was found suitable for this solvent system as well. The required ionization constant (K_s) values of the solvents were known from a parallel study using a cell of the type [D] with KBr and AgBr−Ag electrode in place of KI and AgI−Ag electrode, respectively, which are reported in the following paper (8). In all the above cases the compositions of the solvent mixtures are 10, 30, 50, and 70 wt% ME and the temperatures are in the range of 15−45°C at 5° interval.

Experimental

2-Methoxy ethanol (Merck) was purified by refluxing and distilling successively over pieces of sodium for about 5 h and over $LiAlH_4$ for about 5 h. The distillate was stored in a desiccator and redistilled every time before use after refluxing with $LiAlH_4$ for about 5 h. The bp and density compared fairly well with literature values (3*a*, 7). Water used was triply distilled. HBr (Riedel) was purified just before use by digesting the acid with red phosphorous and then distilling in an all glass apparatus under oxygen free N_2 atmosphere (9*a*). Before collecting the distilled HBr the solvent was freed from dissolved air by passing purified H_2 gas through it, so as to avoid the possible oxidation of HBr in the solvent. KI (E. Merck, G.R.) was used after drying at about 150°C and then over a vacuum desiccator for about 2−3 days. The Ag−AgBr and Ag−AgI electrodes were of thermal type and prepared by the methods described by Ives and Janz (10). Other experimental details including the preparation of solvents, solutions, platinization of Pt-foil H_2 electrodes and also the procedure of measurements, were discussed earlier (6). The behaviour of the electrodes, the time for the attainment of equilibrium, and the criteria of equilibrium of the cells were essentially similar to that described earlier (6).

Results

The observed emf (corrected to pH_2 = 1 atm) for both the cells [C] and [D] at different temperatures for the corresponding molalities of HBr (cell [C]) and of KOH and KI (cell [D]) have been tabulated elsewhere.[3] The standard potential E_m^0 (molal scale) of the Ag−AgBr electrode at any temperature for any solvent was determined by extrapolating the observed linear plot of the usual extrapolation function $E^{0\prime}$ defined by relation [1] (11),

$$[1] \quad E^{0\prime} = E + 2k' \ln m - 2k'A_0B_0m^{1/2}(1 + a_0B_0m^{1/2})^{-1} - 2k' \ln(1 + 0.002\, M_s m) = E_m^0 - 2k'\beta m$$

against the molality m of HBr to $m = 0$. In eq. [1] E is the observed equilibrium emf value (corrected to pH_2 = 1) for the particular molality m of HBr, M_s the mean molar mass of the mixed solvents, $k' = RT/F$, A_0B_0 and B_0 are Debye−Hückel constants as given by

$$A_0B_0 = 1.8246 \times 10^6 (\ln 10)\, d_s^{1/2} (\epsilon_s T)^{-3/2} \text{ mol}^{-1/2} \text{ kg}^{1/2}$$

$$B_0 = 50.29 \times 10^{10}\, d_s^{1/2} (\epsilon_s T)^{-1/2}\, m^{-1} \text{ mol}^{-1/2} \text{ kg}^{1/2}$$

and β is an empirical constant for a given pair of solute and solvent but depending upon the adjustable ion-size parameter a_0. The required densities (d_s), the vapour pressure, and the dielectric constant (ϵ_s) of the solvents are taken from Sadek *et al*'s paper (7) and by interpolation where necessary. The dielectric constant data at 15 and 20°C were obtained by extrapolation of the observed linear plots of log ϵ_s vs. T^{-1} for each of the solvent mixtures. As earlier (6, 11), the value of a_0 was taken as zero, since this gave a good linear plot in each case and reasonable variation of a_0 had no significant influence of E_m^0 values.

The standard potential (E_m^0) of the Ag−AgI electrode at any temperature for any solvent mixture was obtained by extrapolating the observed linear plot of the usual extrapolation function $E^{0\prime}$ defined by [2] (4*b*)

$$[2] \quad E^{0\prime} = E + k \log m_{I^-}/m_{S^-} + k \log K_s = E^0 - k \log a_{SH}\gamma_{I^-}/\gamma_{S^-} = E_m^0 + f(\mu)$$

against the ionic strength μ to $\mu = 0$. In eq. [2] E is the observed equilibrium value (corrected to pH_2 = 1 atm) of cell [B],[3] K_s the autoinization constant of the mixed solvent (SH), as defined by $K_s = a_{H^+}\, a_{S^-}/a_{SH}$ (4*b*), where S^- stands for all the lyate ions (including OH^- and 2-methoxy ethylate ion) and H^+ counts all the H^+ (solvated) (including H_3O^+ and 2-methoxy ethoxonium ion ($Me - H^+$) and the other terms have usual significance.

As in the previous cases (4, 12) standard states are so chosen that at infinite dilution in each solvent mixture the activity coefficients (γ_i) of the ions concerned as well as the activity of the mixed solvent SH are unity. Also, as the term by $a_{SH}\, \gamma_{I^-}/\gamma_{S^-}$ in dilute solution in each solvent is as before (4*b*, 12) likely to be proportionate to μ, extrapolation of the function $E^{0\prime}$ [2] to $\mu = 0$ yielded E_m^0. Assuming that the electrolytes KOH and KI are completely dissociated in these mixed solvents m_{S^-} and m_{I^-} are taken as equal to m_1 and m_2, respectively, and $\mu = (m_1 + m_2)d_s$. The required values of K_s for computing $E^{0\prime}$ are obtained from the following paper (8). The values of E_m^0 for both Ag−AgBr and Ag−AgI electrodes are given in Table 1. The uncertainties in the values of E_m^0 for the Ag−AgBr elec-

[3]A complete set of the data referred to above is available, at a nominal charge, from the depository of Unpublished Data (CISTI), National Research Council of Canada, Ottawa, Ont., K1A 0S2.

TABLE 1. The values of E^0_m (V) of Ag–AgBr and Ag–AgI electrodes at different temperatures for ME + water mixtures

	E^0_m (V)						
wt. % ME	15°C	20°C	25°C	30°C	35°C	40°C	45°C
			Ag–AgBr electrode				
10	0.07295	0.07105	0.0688	0.0661	0.0633	0.0605	0.0573
30	0.0662	0.0638	0.0611	0.0566	0.0542	0.0505	0.0458
50	0.05295	0.04905	0.0444	0.0402	0.0357	0.0305	0.02455
70	0.0232	0.01655	0.0094	0.0015	−0.00605	−0.01375	−0.0213
			Ag–AgI electrode				
10	−0.1458	−0.1474	−0.1491	−0.1514	−0.1527	−0.1545	−0.1569
30	−0.1405	−0.1422	−0.1436	−0.1474	−0.1493	−0.1520	−0.1559
50	−0.1328	−0.1357	−0.1401	−0.1432	−0.1473	−0.1512	−0.1567
70	−0.1473	−0.1537	−0.1612	−0.1687	−0.1758	−0.1832	−0.1910

TABLE 2. The values of constants a, b, and c of eq. [3] for Ag–AgBr and Ag–AgI electrodes in ME + water mixtures

	Ag–AgBr electrode			Ag-AgI electrode		
wt.% ME	a/V	$10^4\ b$/V °C^{-1}	$10^6\ c$/V °C^{-2}	a/V	$10^4\ b$/V °C^{-1}	$10^6\ c$/V °C^{-2}
0[a]	0.06855	−5.1992	−2.7476	−0.1541	−3.520	−2.7523
10	0.06619	−5.2607	−4.6428	−0.1510	−3.650	−1.1904
30	0.05747	−6.7642	−5.8571	−0.1466	−5.107	−6.5238
50	0.04027	−9.3571	−6.4761	−0.1430	−7.850	−5.9523
70	0.00168	−14.9670	−3.1190	−0.1684	−14.621	−2.7142

[a]Computed from the data reported in ref. 9*a* for Ag–AgBr electrode and in ref. 9*b* for Ag–AgI electrode.

TABLE 3. Standard transfer free energies (ΔG^0_t), $T \times$ transfer entropies ($T\Delta S^0_t$), and the related quantities of transfer: ΔY (= $T\Delta S^0_t(H^+)$ + $T\Delta S^0_{t.ch}(X^-)$) of HX (X = Cl, Br, and I) from water to ME + water mixtures (mole fraction scale) at 35°C

		ΔG^0_t (kJ mol^{-1})			ΔG^0_t(i) (kJ mol^{-1})				$T\Delta S^0_t$ (kJ mol^{-1})			ΔY (= $T\Delta S^0_t(H^+)$ + $T\Delta S^0_{t.ch}(X^-)$ (kJ mol^{-1}))		
Wt.% ME	Mol.% ME	HCl[a]	HBr	HI	H^+ [b]	Cl^-	Br^-	I^-	HCl[a]	HBr	HI	HCl[a]	HBr	HI
10	2.56	0.29	−0.18	−0.71	−0.3	0.6	0.1	−0.4	1.49	0.76	−0.43	−0.16	−0.51	−1.62
30	9.21	0.84	−0.33	−2.14	−2.7	3.5	2.4	0.6	−1.01	−2.20	−2.30	1.23	−0.15	−0.18
50	19.14	1.70	0.19	−3.57	−5.6	7.3	5.8	2.0	−6.66	−8.50	−12.58	2.62	0.36	−4.24
70	35.58	(4.71)	2.16	−2.94	−8.2	(12.5)	10.4	5.3	−(19.00)	−24.21	−28.16	(0.00)	−2.53	−7.76

[a]Computed from the data in ref. 7.
[b]Modified data from ref. 3*a* as the original data were wrong due to computational error. Values in parentheses at 70 wt.% ME are extrapolated data as computed from the data in ref. 7, see text.

trode lie within ±0.3 mV, while those for the Ag–AgI electrode are within ±0.5 mV.

The E^0_m values for both the electrodes at different temperatures for each solvent mixture were then fitted by the method of least squares to eq [3]

$$[3] \quad E^0_m = a + b(t - 30) + c(t - 30)^2$$

where t is the temperature in °C. The coefficients a, b, and c for the two electrodes for each of the solvent mixtures are listed in Table 2. The coefficients of eq. [3] for water have been obtained by use of the data of Bates and co-workers (9) for the two electrodes, and are also included in Table 2.

The free energy changes, ΔG^0_t, accompanying the transfer of 1 mol HX (X = Br, I) from the standard state in water (w) so that in each of the mixed solvents (s), i.e., of the process HX (w) → HX (s), have been computed on the mole fraction scale at 25°C, using the relation

$$[4] \quad \Delta G^0_t(\mathrm{HX}) = -F\,[(E^0_m)_s - (E^0_m)_w] - 2\,RT \ln M_s/M_w$$

and the corresponding entropy changes, ΔS^0_t, at 25°C have been obtained by use of eq. [5]

$$[5] \quad \Delta S^0_t(\mathrm{HX}) = F\,[(b_s - b_w) - 10\,(c_s - c_w)] + 2\,R \ln M_s/M_w$$

where M_s and M_w are the average and pure molar mass of the mixed solvent and water, respectively, and T = 298.15 K. The values for ΔG^0_t and $T\Delta S^0_t$ so obtained for HBr and HI for all these solvents are presented in Table 3. The average estimated uncertainties in ΔG^0_t and ΔS^0_t are as before (16) ± 0.03 kJ mol^{-1} and ±1. J K^{-1} mol^{-1}, respectively.

For the sake of comparison, the corresponding values for HCl have also been computed in a similar manner, i.e., the reported E^0_m values in water (13) and in 10, 30, and 50 wt % ME (7) were first fitted into eq. [6]

$$[6] \quad E^0_m = a + b(t - 35) + c(t - 35)^2$$

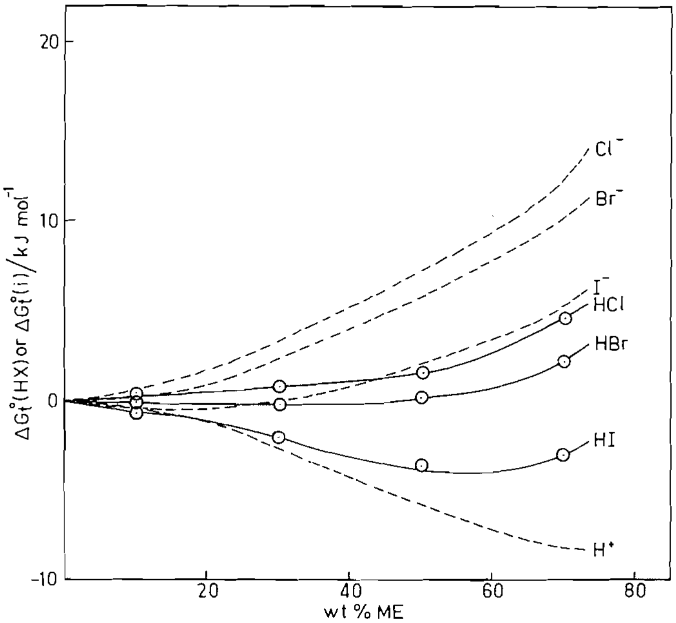

FIG. 1. Variation of ΔG_t^0(HX) (solid lines) and ΔG_t^0(i) for some ions (H^+, Cl^-, Br^-, I^-) (broken lines) with wt.% ME at 25°C.

and the coefficients so obtained were used to compute ΔG_t^0(HCl) and ΔS_t^0(HCl) values at 25°C by relations [7] and [8], respectively

$$[7]\quad \Delta G_t^0(\mathrm{HCl}) = -F\,[(a_s - a_w) - 10(b_s - b_w)] + 100\,(c_s - c_w) - 2RT \ln M_s/M_w$$

$$[8]\quad \Delta S_t^0(\mathrm{HCl}) = F\,[(b_s - b_w) - 20(c_s - c_w)] + 2R \ln M_s/M_w$$

ΔG_t^0 and $T\,\Delta S_t^0$ values of HCl so obtained at 25°C are also listed in Table 3. Since the E_m^0 values for 70 wt% ME are not available in Sadek *et al*'s paper the thermodynamic parameters for HCl in the corresponding solvent composition were not compared with our values.

Discussion

Free energies of transfer

ΔG_t^0(HX)−composition profiles (Fig. 1) for the hydrogen halides in this solvent system are found to be more or less typical of what have been observed in similar other aquo-organic solvents including aliphatic alcohols (14), EG (15), glycerol (GL) (16), or ethers like D (4*a*), THF (4*a*), and DME (4*a*). Thus, as in other aquo-organic solvents the observed gradual increase in ΔG_t^0(HCl) and ΔG_t^0(HBr) and the initial downward trends of ΔG_t^0(HI) followed by the upward trend at higher compositions and for a given composition the observed order: ΔG_t^0(HCl) > ΔG_t^0(HBr) > ΔG_t^0(HI) are the result of opposing behaviour of the individual ions like H^+ and X^- ions, which are likely to be guided by the acidity, basicity, and dielectric constant of the solvents. This is also evident from the corresponding profiles of the ions in the system as have been obtained by use of the widely used tetraphenylarsonium tetraphenylboron (TATB) reference electrolyte assumption (5) studied previously for this solvent system (3*a*). As can be seen from these profiles, while $\Delta G_t^0(H^+)$ values become increasingly negative, $\Delta G_t^0(X^-)$ values become increasingly positive. The increased solvation of H^+, as indicated earlier

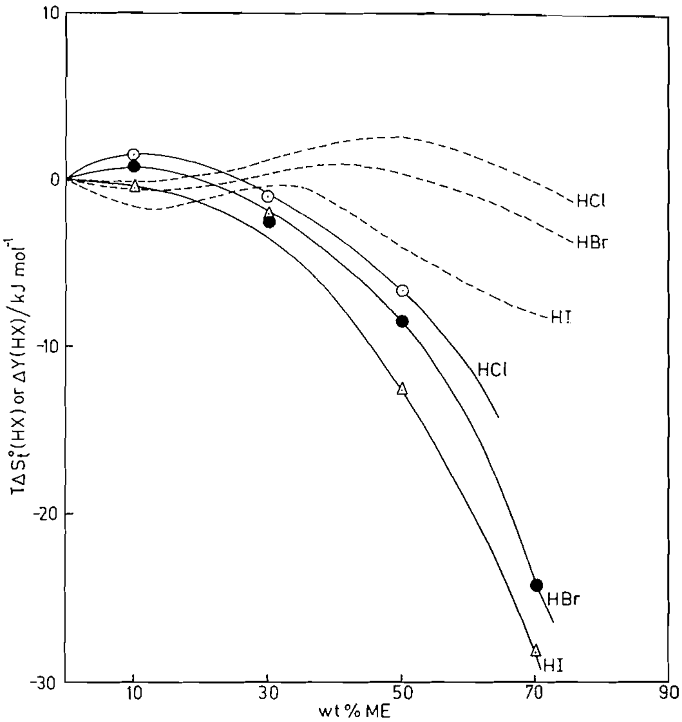

FIG. 2. Variation of $T\Delta S_t^0$(HX) (solid lines) and ΔY(HX) (broken lines) with wt.% ME at 25°C.

(3*a*), can be attributed to the cosolvent-induced larger basicity (17, 18) of the mixed solvents and their "cation—O—centre" type "acid−base" interactions (17, 18) with H^+. Similarly, the decreased solvation of X^- is attributable to the combined effects of cosolvent-induced decreased "acidity" or "anion−H−centre" type "acid−base" interactions (17, 18) with X^- ions, and the decreased dielectric constant causing increased Born-type electrostatic contribution in the mixed solvents compared to that in water. Moreover, the relative order of destabilization of the halide ions is the combined effect of the decreasing strength of "anion−H−centre" type interactions and the possible increasing strength of "soft−soft" interactions (19) between the increasingly polarizable anions and the softer cosolvent molecules or H-bonded aquo-cosolvent bases compared to that in water. Notably, the observed trend of relatively less destabilization of I^- compared to Cl^- and Br^- at higher cosolvent compositions in particular, is indicative of the possible enhanced "soft−soft" interactions due to enhanced softness of the possible aprotic form **B** of the cosolvent molecules or of the H-bonded aquo-cosolvent complexes of the type **E**:

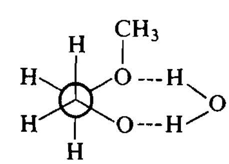

E

Entropies of transfer

The observed $T\Delta S_t^0$(HX)−composition profiles (Fig. 2) unlike in aqueous alcohols (6), glycol (6), glycerol (16), and THF (4*a*) but like in aqueous DME (4) pass through a slight hump around 10 wt. % ME and then move sharply downward at higher compositions and at any composition their relative order is HCl > HBr > HI. The observed slight hump is possibly the superimposed effect of dielectric constant on $\Delta S_t^0(HX)$, as have been observed in the case of aqueous DME (4*a*). That this is particularly true becomes all the more evident when we consider the partly rationalized quantities ΔY ($= T\Delta S_t^0(H^+) + T\Delta S_{t,ch}^0(X^-)$) as illustrated in Fig. 2. These ΔY values have been obtained by subtracting $T\Delta S_{t,ch}^0(X^-)$ values from the observed $T\Delta S_t^0(HX)$ values, the former values being tentatively computed as before (6) by use of Born equation (14, 20). The required $\theta_s(= -d \ln \epsilon_s/dT)$ values were taken from ref. 7 and obtained where necessary from the observed linear plots of ln ϵ_s vs T. As could be seen from Fig. 2, ΔY–composition profiles instead of retaining the characteristic maximum as in aqueous EG (6), or exhibiting a sharply downward trend as in DME (4*a*), exhibits a wavy or "roller-coaster" type behaviour (20, 21) at initial compositions, reflecting the effects of possible structural changes of aqueous ME.

The real implications of the observed $T\Delta S_t^0(HX)$– and especially ΔY–composition profiles, can be visualized in the light of our aforesaid semi-quantitative theory on $\Delta S_t^0(HX)$, which is essentially based on Frank and Wen's model (22) of ion-solvation and fairly well recognized (23) four-step transfer process (6, 24). According to this theory

(*a*) when 3D tetrahedral structuredness of aquo-organic solvent > 3D structuredness of pure water

$$\Delta Y > 0, \text{ and } \Delta Y(X = I) > \Delta Y(X = Br) > \Delta Y(X = Cl)$$

(*b*) when solvent structure < pure water structure

$$\Delta Y < 0, \text{ and } \Delta Y(X = I) < \Delta Y(X = Br) < \Delta Y(X = Cl)$$

The observed characteristic maxima of ΔY and their relative order: HI > HBr > HCl in water-rich compositions of aqueous mono-ols (6) and the sharply downward trends and the reverse order: HCl > HBr > HI at higher cosolvent compositions also substantiated the theory as the mono-ols are well known promoters of 3D structures at water-rich compositions and 3D structure breakers at higher compositions (25, 26). Moreover, the important conclusions regarding structural features of aqueous EG (6), GL (16), and of ethers like D, THF, and DME (4*a*) derived in the light of the above-noted tenets are also in fair agreement with those derived from various other studies in the respective solvents.

In the present ME–water system the observed roller-coaster type behaviour of $\Delta Y(HX)$ instead of the characteristic maxima as observed in aqueous mono-ols, followed by the usual downward trends at higher compositions and particularly the relative order: $\Delta Y(HCl) > \Delta Y(HBr) > \Delta Y(HI)$ observed all through suggest that unlike mono-ols but like D and DME, ME possibly causes break down of 3D structures of water right from the initial composition. The observed upward trend after the initial downward trend imparting roller-coaster type behaviour is seemingly the result of possible hydrogen bonded intercomponent complexation of the type **E**, making the solvents at these compositions somewhat more ordered. Such type of intercomponent complexes were attributed to similar upward trends observed in $\Delta Y(HX)$–composition profiles (6) or ΔS_t^0-composition profiles for *p*-nitroaniline (27) or benzoic acid (28) especially in aqueous mono-ols at higher compositions.

Referring to Fig. 3 where we have illustrated the ΔY–composition profiles for HI in aqueous mixtures of the closely related cosolvents like EG, ME, and DME, as well as for Bu^{t}OH, we find that the effect of remarkable enhancement of 3D water structures by the well known structure promoter — Bu^{t}OH (29) gets succintly diminished when cosolvent Bu^{t}OH is replaced by EG, ME, and DME. This diminution is so much that ME and DME are effectively weak and strong structure breakers respectively. Seemingly, the inductive effect of two (—CH_3) groups attached to the two flexible etherial O-atoms of the DME molecule makes it more hydrophilic than ME molecule containing one (—CH_3) group attached to one flexible etherial O-atom, which is again relatively more hydrophilic than EG. As structuring or destructuring ability of a cosolvent depends upon the ratio of hydrophobic to hydrophilic effects of the cosolvents (30) the observed slight structure making propensity of EG skeletal exceeds the hydrophilicity of two —OH groups attached to it. But on passing from EG to DME via ME by successive replacement of hydroxy H-atoms by electron donating —CH_3 groups enhances hydrophilic character of the cosolvents, which in turn imparts increasingly 3D structure breaking propensities of these cosolvents.

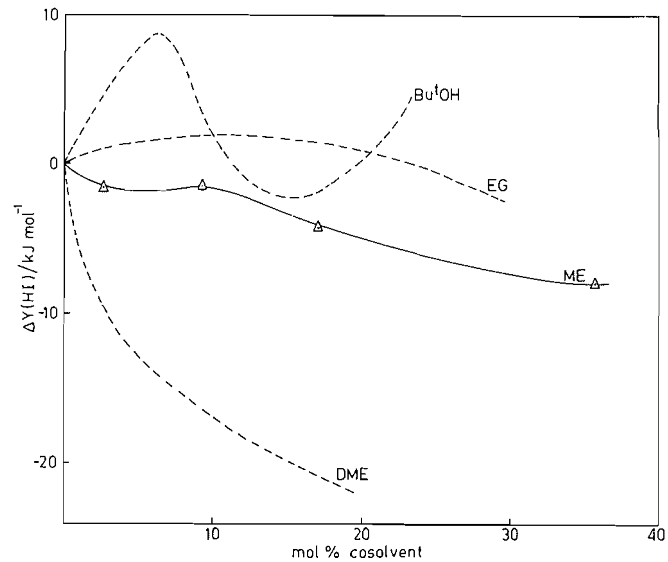

FIG. 3. Variation of ΔY(HI) in aqueous Bu^{t}OH, ME, DME, and EG.

Acknowledgement

Thanks are due to the University Grants Commission, Government of India for awarding a Junior Research Fellowship to P.K.G.

1. M. N. DAS and K. K. KUNDU. J. Ind. Chem. Soc. **51**, 266 (1974) and references therein.
2. A. K. DAS and K. K. KUNDU. Ind. J. Chem. **16**A, 47 (1978).
3. A. BHATTACHARYA, A. K. DAS and K. K. KUNDU. (*a*) Ind. J. Chem. **20**A, 347 (1981); (*b*) Ind. J. Chem. **20**A, 353 (1981); (*c*) Can. J. Chem. **59**, 1153 (1981).
4. J. DATTA and K. K. KUNDU. Can. J. Chem. (*a*) **59**, 3149 (1981); (*b*) **59**, 3141 (1981).
5. (*a*) E. GRUNWALD, G. BAUGHMANN, and G. KOHNSTAM. J. Am. Chem. Soc. **82**, 5801 (1960); (*b*) B. G. COX, G. R. HEDWIG, A. J. PARKER, and D. D. WATTS. Aust. J. Chem. **27**, 477 (1974) and references therein.
6. K. BOSE, K. DAS, A. K. DAS, and K. K. KUNDU. J. Chem. Soc. Faraday Trans. I, **74**, 1051 (1978), and references therein.
7. H. SADEK, TH. F. TADROS, and A. A. EL-HARAKANY. Electrochim. Acta. **16**, 339 (1971).
8. P. K. GUHA and K. K. KUNDU. Can. J. Chem. **63**, 804 (1985).
9. H. B. HETZER, R. A. ROBINSON, and R. G. BATES. J. Phys. Chem. (*a*) **66**, 1423 (1962); (*b*) **68**, 1929 (1964).

10. D. G. J. IVES and G. J. JANZ. Reference electrodes — theory and practice. Academic Press, New York. 1969. p. 208.
11. K. BOSE and K. K. KUNDU. J. Chem. Soc. Faraday Trans. I, **73**, 284 (1977).
12. H. S. HARNED and L. D. FALLON. J. Am. Chem. Soc. **61**, 2374 (1939).
13. H. S. HARNED and R. W. EHLERS. J. Am. Chem. Soc. **54**, 1350 (1932); 55, 2179 (1933).
14. R. G. BATES. *In* Hydrogen-bonded solvent systems. *Edited by* A. K. Covington and P. Jones. Taylor and Francis, London. 1968.
15. K. K. KUNDU, D. JANA, and M. N. DAS. Electrochim. Acta, **18**, 95 (1973).
16. I. N. BASUMULLICK and K. K. KUNDU. Can. J. Chem. **57**, 961 (1979).
17. D. FEAKINS. *In* Hydrogen-bonded solvent systems. *Edited by* A. K. Covington and P. Jones. Taylor and Francis, London. 1968.
18. A. DAS and K. K. KUNDU. J. Soln. Chem. **5**, 431 (1976).
19. R. G. PEARSON. J. Am. Chem. Soc. **85**, 3353 (1963).
20. K. K. KUNDU and K. MAZUMDAR. J. Chem. Soc. Faraday Trans. I, **69**, 806 (1973); **71**, 1422 (1975).
21. J. B. HYNE. Hydrogen-bonded solvent system. *Edited by* A. K. Covington and P. Jones. Taylor and Francis, London. 1968. p. 99.
22. H. S. FRANK and W. Y. WEN. Discuss. Faraday Soc. **24**, 133 (1957).
23. Y. POINTUD and J. JUILLARD. J. Chem. Soc. Faraday Trans. I, **73**, 1907 (1977).
24. K. K. KUNDU. Ind. J. Chem. **10**, 303 (1972).
25. (*a*) F. FRANKS and D. J. G. IVES. Q. Rev. **20**, 1 (1966); (*b*) F. FRANKS. *In* Physico-chemical processes in mixed aqueous solvents. *Edited by* F. Franks. Heineman, London. 1967. p. 105.
26. F. FRANKS and D. S. REID. *In* Water, a comprehensive treatise. Vol. 2. *Edited by* F. Franks. Plenum Press, London. 1973. Chapt. 5.
27. K. BOSE and K. K. KUNDU. Can. J. Chem. **35**, 3961 (1977).
28. K. DAS, A. K. DAS, K. BOSE and K. K. KUNDU. J. Phys. Chem. **82**, 1242 (1978).
29. J. JUILLARD. J. Chem. Soc. Faraday Trans. I, **78**, 43 (1982).
30. R. K. MOHANTY, T. S. SARMA, S. SUBRAMANIAN, and J. C. AHLUWALIA. Trans. Faraday Soc. **67**, 305 (1971).

Thermodynamics of autoionization of 2-methoxy ethanol + water mixtures and structuredness of the solvents

PRABIR K. GUHA[1] AND KIRON K. KUNDU[2]
Physical Chemistry Laboratories, Jadavpur University, Calcutta – 700 032, India

Received April 6, 1984

PRABIR K. GUHA and KIRON K. KUNDU. Can. J. Chem. **63**, 804 (1985).

Standard free energies (ΔG^0) and entropies (ΔS^0) of autoionization of aqueous mixtures of 10, 30, 50, and 70 wt.% of 2-methoxy ethanol (ME) have been evaluated from the autoionization constants (K_s) of the solvents as determined from emf measurements of the cell Pt, H_2 (g, 1 atm)/KOH (m_1), KBr (m_2), solvent/AgBr–Ag at seven equidistant temperatures ranging from 15 to 45°C. The observed increase in pK_s and the related $\delta(\Delta G^0)$ (= ${}_s\Delta G^0 - {}_w\Delta G^0$) has been ascribed to be the effect of decreased dielectric constant, increased basicity and decreased acidity of the mixed solvents compared to that of water. Analysis of relative entropic contributions of autoionization, $T\delta(\Delta S^0)$ (= $T({}_s\Delta S^0 - {}_w\Delta S^0)$) and their chemical part, $T\delta(\Delta S^0)_{ch}$ in the aqueous mixtures of ME as well as the closely related cosolvents like ethylene glycol (EG) and 1,2-dimethoxy ethane (DME), appears to suggest that unlike EG but like DME, ME has an overall structure breaking propensity of three dimensional (3D) tetrahedral structures of water. But the transfer entropies of water $\Delta S_t^0(H_2O)$ derived thereof, for these cosolvents suggest that while the structural changes induced by protic EG are seemingly obscured due to the involved multiple acid-base equilibria with water, and that by aprotic DME are disturbed by the formation of strong hydrogen-bonded DME–H_2O complexes around 4–14 mol% DME, quasi-aprotic ME appears to induce some order due to the possible formation of H-bonded ME–water complexes around 10–15 mol% ME.

PRABIR K. GUHA et KIRON K. KUNDU. Can. J. Chem. **63**, 804 (1985).

Opérant à sept températures équidistantes entre 15 et 45°C et utilisant des f.é.m. mesurées à l'aide de la cellule Pt, H_2 (g, 1 atm)/KOH (m_1), KBr (m_2), solvant/AgBr–Ag, on a évalué les constantes d'autoionisation (K_s) des solvants et puis les énergies libres (ΔG^0) ainsi que les entropies standards (ΔS^0) d'autoionisation de mélanges aqueux à 10, 20, 30, 50 et 70% en poids de méthoxy-2 éthanol (ME). On a observé une augmentation du pK_s ainsi que de la valeur apparentée $\delta(\Delta G^0)$ (= ${}_s\Delta G^0 - {}_w\Delta G^0$) et on attribue ces observations aux effets combinés d'une diminution de la constante diélectrique, d'une augmentation de la basicité et d'une diminution de l'acidité des solvants mixtes par rapport à celles de l'eau. L'analyse des contributions relatives de l'entropie d'autoionisation, $T\delta(\Delta S^0)$ (= $T({}_s\Delta S^0 - {}_w\Delta S^0)$) ainsi que de leur partie chimique $T\delta(\Delta S^0)_{ch}$ dans les mélanges aqueux de ME ainsi que dans des cosolvants très voisins comme l'éthylèneglycol (EG) et le diméthoxy-1,2 éthane (DME) semble suggérer que contrairement à ce que l'on observe avec l'EG mais d'une façon similaire à ce que l'on observe avec le DME, le ME possède une propension globale à briser les structures tridimentionnelles (3D) tétraédriques de l'eau. Toutefois, un examen des entropies de transfert de l'eau $\Delta S_t^0(H_2O)$ qui en dérivent pour ces cosolvants suggère qu'alors que les changements structuraux induits par l'EG protique semblent être masqués par des équilibres acide–base multiples et complexes avec l'eau et que les changements induits par le DME aprotique sont perturbés par la formation de complexes DME–H_2O qui, autour de compositions contenant de 4 à 14% de DME, sont liés par de fortes liaisons hydrogènes, le ME qui est quasi aprotique semble induire un certain ordre à cause de la formation possible de complexes ME–eau, qui à des concentrations de 10–15 mol% de ME, sont liés par des liaisons hydrogènes.

[Traduit par le journal]

Introduction

As part of our comprehensive studies (1–5) on acid–base properties, ion–solvent interactions, and solvent structures in the aqueous binaries of the closely related cosolvents like protic ethylene glycol (EG), quasi-aprotic 2-methoxy ethanol (ME) and aprotic 1,2-dimethoxy ethane (DME), we have reported in the previous paper (1) the transfer energies of hydrogen halides (HX) and derived important reflections on acid–base as well as the structural aspects of the aqueous mixtures of ME. But as previous studies by Kundu and co-workers (4*b*, 5) have shown, the autoionization constant (K_s) of different aquo-organic solvents at different temperatures and the related thermodynamic parameters are likely to reflect not only the acidity and basicity of the solvents, but also their structural features. So, it should be of particular interest to extend such studies to this solvent system as well. Previously, autoionization constants of this solvent system have been reported by Woolley *et al.* (6) but by use of glass–Ag–AgCl electrodes, while that by Bhattacharya *et al.* (3*c*) though by use of H_2– and Ag–AgCl electrodes, but at 25°C only.

In the aqueous mixtures of ME autoionization of the solvents can be represented by general eq. [1]

$$[1] \quad SH(s) + SH(s) = SH_2^+(s) + S^-(s)$$

where SH represents a solvent molecule in the mixed solvents, being either water or ME and SH_2^+ and S^- are lyonium and lyate ions and (s) essentially denotes that the species are in their standard state in the respective mixed solvents. But when ME acts as an intramolecularly H-bonded aprotic solvent (1), SH molecule essentially represents H_2O and SH_2^+ and S^- are respectively H_3O^+ and OH^- and the autoionization [1] will in effect stand for the ionization of water in the mixed solvents, as in the case of DME (4*b*). As in previous studies (4*b*, 5*c*), the thermodynamics of autoionization of these mixed solvents have been determined from the autoionization constant (K_s) of these solvents as obtained from emf measurements of cell [A]

$$[A] \quad \text{Pt, } H_2 \text{ (g, 1 atm)/KOH } (m_1), \text{ KBr } (m_2), \text{ solvent/AgBr–Ag}$$

at seven equidistant temperatures ranging from 15 to 45°C. The compositions studied are 10, 30, 50, and 70 wt.% ME.

---

[1] Holder of a Junior Research Fellowship under University Grants Commission, New Delhi.

[2] To whom all correspondence should be addressed.

TABLE 1. pK_s values (molal scale) for the autoionization of ME + water mixtures at different temperatures

	pK_s values at different temperatures (°C)						
Wt.% ME	15	20	25	30	35	40	45
0[a]	14.346	14.167	13.997	13.883	13.680	13.535	13.396
10	14.403	14.245	14.080 (14.06)[a] (14.13)[b]	13.935	13.785	13.645	13.522
30	14.630	14.485	14.330 (14.29)[a] (14.43)[b]	14.220	14.080	13.957	13.845
50	15.092	14.950	14.820 (14.69)[a] (14.82)[b]	14.690	14.567	14.457	14.352
70	15.795	15.685	15.580 (15.42)[a] (15.53)[b]	15.485	15.395	15.307	15.225

[a]Reference 3c.
[b]Reference 6.

TABLE 2. Coefficients of eq. [3] and the values of ΔG^0, ΔH^0, and ΔS^0 (molal scale), $T\delta(\Delta S^0_N)$ and $\Delta S^0_t(H_2O)$ for the autoionization of the ME + water mixtures

Wt.% ME	A/K	B	$C \times 10^2$/K^{-1}	ΔG^0(kJ mol^{-1})	ΔH^0(kJ mol^{-1})	ΔS^0(J K^{-1} mol^{-1})	$T\delta(\Delta S^0_N)$ (kJ mol^{-1})	$\Delta S^0_t(H_2O)$ (J K^{-1} mol^{-1})
0[a]	4627.68	−7.13007	1.8800	79.90	56.61	−78.1	0	0
10	3663.65	−1.32220	1.0450	80.38	52.35	−94.0	−4.34	24
30	3499.82	−0.97597	1.2006	81.81	46.51	−118.4	−10.71	40
50	3775.03	−2.73714	1.6413	84.60	44.35	−135.0	−14.57	73
70	3102.51	0.73714	1.4890	88.94	34.05	−184.1	−27.81	—

[a]Computed from the data reported in refs. 10 and 18.

Experimental

The quality and the method of purification of ME have been described earlier (1). Water used was triply distilled. KBr (E. Merck, G.R.) was used after drying at about 250°C and cooling in a vacuum desiccator for 3–5 days. Other experimental details including the preparation of solvents, solutions, Ag–AgBr and platinized Pt electrodes and also the methods of emf measurements were exactly similar as described in the preceding papers (1, 4*b*, 5*c*).

Results

The pK_s values (molal scale) in these mixed solvents were obtained by extrapolating the observed linear plots of function [2]

$$[2] \quad pK_s' = \frac{F[E - (E^0_m)_{Ag-AgBr}]}{2.303\,RT} + \log \frac{m_{Br}}{m_{S^-}}$$

$$= pK_s - \log a_{SH}\, \gamma_{Br^-}/\gamma_{S^-} = pK_a + f(\mu)$$

against the ionic strength μ to $\mu = 0$. Here the terms have exactly the same significance as described in the preceding paper. The required $(E^0_m)_{Ag-AgBr}$ values in the solvents were obtained from the said paper.

The emf data of cell [A] at different temperatures and the corresponding molalities of KOH and KBr for each of the solvent mixtures are given elsewhere.[3] The pK_s values at different temperatures for all the compositions of the mixed solvents are listed in Table 1. The estimated uncertainties in pK_s values is of the order of ±0.005 unit. Notably, pK_s values at 25°C compare fairly well with Bhattacharya *et al.*'s data (3*c*) at lower compositions but differ by 0.13 and 0.16 unit at 50 and 70 wt.% cosolvent, respectively. The present values, however, compare tolerably well with those of Woolley *et al.*'s data (6) except at 30 wt.% ME where deviation is about 0.10 unit. Evidently, our earlier doubts about the untoward behaviour of glass electrode at higher compositions in this solvent system seem unfounded. The discrepancies between our present and earlier data may result from the possible uncertainty in the involved $E^0_{Ag-AgCl}$ values of Sadek *et al.* (7), as these values yielded ΔG^0_t(HCl) values in these solvents, which are somewhat different from those by Smits *et al.* (8).

The pK_s values at different temperatures for each of the cosolvent compositions were fitted as before (1, 4*b*) into the Harned–Robinson expression [3] (9)

$$[3] \quad pK_s = A/T + B + CT$$

by the method of least squares. The values of the coefficients A, B, and C for each of the compositions of these mixed solvents are given in Table 2. These coefficients reproduce pK_s values to within ±0.005 unit of the experimental data.

The thermodynamic quantities, namely ΔG^0, ΔS^0, and ΔH^0 accompany the autoionization of 1 mol of the mixed solvents were evaluated at 25°C by using the standard relations (10) comprising the coefficients of eq. [3]. These values (molal scale) are presented in Table 2.

[3]A complete set of data referred to above is available at a nominal charge from the Depository of Unpublished Data, CISTI, National Research Council of Canada, Ottawa, Ont., Canada K1A 0S2.

TABLE 3. Values of $(pK_s)_N$, (ΔG^0_N), $\Delta G^0_t(H^+)$, $\Delta G^0_{t,ch}(H^+)$, $\Delta G^0_t(OH^-)_{app}$, $-\Delta G^0_{cell\text{-}A}$, $\Delta G^0_t(OH^-)_{app}$, $\Delta G^0_t(OH^-)$ and $\Delta G^0_{t,ch}(OH^-)$ for ME + water mixtures at 25°C (ΔG^0 values are in kJ mol^{-1})

Wt.%	Mol%	$(pK_s)_N$	$\delta(\Delta G^0_N)$	$\Delta G^0_t(H^+)^a$	$\Delta G^0_{t,ch}(H^+)$	$\Delta G^0_t(OH^-)_{app}$	$-\Delta G^0_{cell\text{-}A}$	$\Delta G^0_t(OH^-)'^a_{app}$	$\Delta G^0_t(OH^-)^a$	$\Delta G^0_{t,ch}(OH^-)$
0	0	17.49	0	0	0	0	0	0	0	0
10	2.56	17.50	0.08	−0.3	−0.5	0.4	2.54	1.3	0.9	0.6
30	9.21	17.59	0.61	−2.7	−3.4	3.3	7.62	8.2	4.9	3.6
50	19.14	17.89	2.35	−5.6	−7.4	8.0	13.60	16.2	8.2	5.0
70	35.58	18.41	5.15	−8.2	−12.2	13.5	20.76	26.3	12.8	5.7

[a] The values of $\Delta G^0_t(H^+)$ and $\Delta G^0_{cell\text{-}A}$ were obtained after due correction of this data reported in ref. 3*c*, which were wrong due to the involved computational error. Also, the values of $\Delta G^0_t(OH^-)'_{app}$ ($= \Delta G^0_{cell\text{-}A} - 2\,\Delta G^0_t(K^+)$, see ref. 3*c*) and of $\Delta G^0_t(OH^-)$ ($= \Delta G^0_t(OH^-)'_{app} - \Delta G^0_t(OH^-)_{app}$, vide ref. 3*c*) after due correction.

The standard free energy changes accompanying the autoprotolytic reaction [1] in the mixed solvent ${}_s\Delta G^0_N$, relative to that in pure water, ${}_w\Delta G^0_N$, have been computed on the mole function scale at 25°C using [4]

$$[4]\quad \delta(\Delta G^0_N) = {}_s\Delta G^0_N - {}_w\Delta G^0_N = 2.303RT[p({}_sK_s)_N - p({}_wK_s)_N]$$
$$= 2.303RT[p_sK_s + 2\log 1000/M_s] - [p_wK_s + 2\log 1000/M_w]$$

Similarly, those for entropy changes $\delta(\Delta S^0_N)$ were computed by use of eq. [5]

$$[5]\quad \delta(\Delta S^0_N) = {}_s\Delta S^0_N - {}_w\Delta S^0_N = 2.303R(B_w - B_s) + 4.606RT(C_w - C_s) + 2R\ln M_s/M_w$$

The subscripts s, w, N, M_w, and M_s have their usual significance as described in ref. 1. The values of (ΔG^0_N) and (ΔS^0_N) are listed in Table 3.

From the results in Table 1 it appears that the pK_s values of ME–water mixtures are increasingly greater than that of pure water. As is well known, autoprotolysis constant of an amphiprotic solvent is a composite function of the intrinsic acidity and basicity as well as dielectric constant of the solvent medium. In our preceding paper (1) it has been shown that ME is more basic and less acidic than water and also with increasing ME, dielectric constant decreases (7). Obviously, the observed pK_s values conform to the combined result of these three effects (2, 3*c*, 4*b*).

Moreover, as shown in our earlier paper on this aspect at 25°C (3*c*), the standard free energy change $\delta(\Delta G^0_N)$ accompanying the autoprotolysis of the mixed solvents relative to that of water is given by

$$[6]\quad \delta(\Delta G^0_N) = \Delta G^0_t(H^+) + \Delta G^0_t(OH^-)_{app}$$

where $\Delta G^0_t(H^+)$ and $\Delta G^0_t(OH^-)_{app}$ stand for the free energy changes for the processes [7] and [8], respectively

$$[7]\quad H_3O^+(w) + SH(s) = H_2O(w) + SH_2^+(s)$$

$$[8]\quad SH(s) + OH^-(w) = S^-(s) + H_2O(w)$$

Using the values of H^+ based on TATB method studied earlier for this solvent system (3*a*) $\Delta G^0_t(OH^-)_{app}$ could be computed by use of eq. [6]. Notably however, $\Delta G^0_t(H^+)$ values reported earlier (3*c*) involved some computational error. So also are the values $-\Delta G^0_{cell\text{-}A}$, $\Delta G^0_t(OH^-)'_{app}$, $\Delta G^0_t(OH^-)_{app}$, and $\Delta G^0_t(OH^-)$ reported in that paper (3*c*). Moreover, the present $\delta(\Delta G^0)$ values are also slightly different from the data reported in ref. 3*c*. So, the correct values for all the quantities including $\Delta G^0_t(OH^-)'_{app}$ as well as $\Delta G^0_t(OH^-)$, are given in Table 2. Notably of course, the new values hardly affect our earlier contention.

Besides, if Born-type electrostatic contributions $\Delta G^0_{t,el}(i)$ (12) for H^+ and OH^- be computed tentatively by using $r_{H_3O^+} = 0.276$ nm (13) and $r_{OH^-} = 0.156$ nm (14) and be subtracted from the values of $\Delta G^0_t(H^+)$ and $\Delta G^0_t(OH^-)$, respectively, the resulting $\Delta G^0_{t,ch}(H^+)$ and $\Delta G^0_{t,ch}(OH^-)$ values (see Table 3) suggest that the "chemical" basicity of the mixed solvents exceeds the "chemical" acidity of the corresponding compositions of the mixed solvents relative to that of water. The acidity constant of ME, ($pK_H = 15.2 \pm 0.5$) determined by Woolley and George (6) also partly substantiates this observation. This is possibly indicative of the partial quasi-aprotic character of ME as indicated in the previous paper (1).

Entropy of autoprotolysis

As is well recognized, entropy changes rather than enthalpy changes, are more informative about structural implications of the solvents (4, 5*b*, 5*c*, 15) accompanying a process in any aquo-organic solvents. So, as before (4*b*), analysis of the entropy changes of the autoprotolysis should be rewarding. The variation of $T\delta(\Delta S^0_N)$ ($= T({}_s\Delta S^0_N - {}_w\Delta S^0_N)$) with mol% of the cosolvent is shown in Fig. 1. For the sake of comparison those for the aqueous mixtures of the closely related cosolvents like EG and DME, taken from literature (4*b*, 16), are also illustrated in Fig. 1. Since the depolymerization of water molecules prior to self-protolysis contributes positive entropy changes to the overall entropy of autoionization, the larger is the extent of 3D tetrahedral water structures in the aquo-organic solvents, the larger is this contribution (5*c*). Consequently, the appearance of a maximum in $T\delta(\Delta S^0_N)$–composition profile would imply that the mixed solvents are more structured than pure water and a downward trend would imply less structured (4*b*, 5*b*). Apparently, the observed $T\delta(\Delta S^0_N)$–composition profiles (Fig. 1) suggest that all the cosolvents break down 3D structures of water. But at any composition the observed relative order of $T\delta(\Delta S^0_N)$: DME > EG > ME is indeed highly intriguing. In view of the fact that autoionization is a charge separation process, the relative variations of ϵ_s and θ_s ($= -d\ln \epsilon_s/dT$) dictating the Born-type electrostatic contribution $\delta(\Delta S^0)_{el}$ (11), are likely to contribute significantly to the observed order. To see the structural contributions free of this electrostatic effect, $\delta(\Delta S^0)_{el}$ values have been computed, tentatively though, by use of simple Born equation (11):

$$[10]\quad \delta(\Delta S^0)_{el} = \frac{Ne^2}{2}[(\epsilon_s\theta_s)^{-1} - (\epsilon_w\theta_w)^{-1}]$$

assuming that $r_{SH_2^+} \approx r_{H_3O^+} = 0.276$ nm (12) and $r_{S^-} \approx r_{OH^-} = 0.156$ nm (13) and obtaining the values of ϵ_s and θ_s from ref. 7 and ϵ_w and θ_w from ref. 10. On subtracting these from $\delta(\Delta S^0_N)$

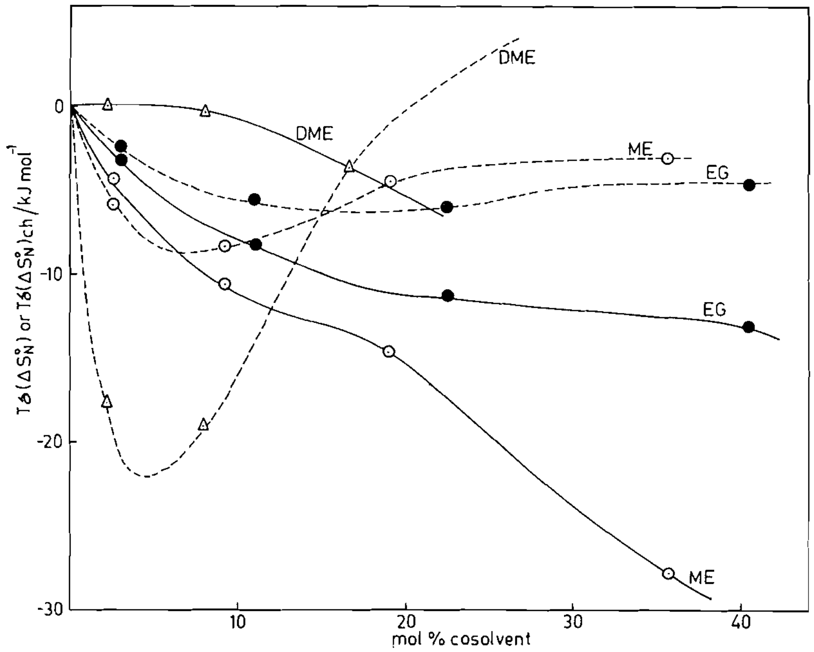

FIG. 1. Variation of $T\delta(\Delta S^0_N)$ (solid lines) and $T\delta(\Delta S^0_N)_{ch}$ (broken lines) accompanying the autoionization of aqueous mixtures of ME, DME, and EG.

values are obtained the "non-Born" or "chemical" contribution $\delta(\Delta S^0_N)_{ch}$ which are plotted against cosolvent compositions by dotted curves in Fig. 1. Interestingly enough, the observed plots apparently indicate that at water-rich compositions $|-T\delta(\Delta S^0)_{ch}|$ are in the order DME > ME > EG implying that the structure breaking propensities of the cosolvents are also in the same order conforming to what has been observed in the previous paper (1). But the observed upward trend and the reverse order of $\delta(\Delta S^0_N)_{ch}$–composition profiles at higher compositions are again apparently intriguing. This is because the effects of $\Delta S^0_t(H_2O)$ involved in $\delta(\Delta S^0_N)$ (loc. cit. eq. [11]) and the structural changes due to the packing imbalance with increased addition of cosolvents are likely to confuse the issue. So, consideration of the structural implications of $\delta(\Delta S^0_N)$ from another angle is in order.

If we assume that ME acts predominantly as quasi-aprotic (1) and that the autoionization of the ME–water mixed solvents is mainly dictated by autoionization of water, $T\delta(\Delta S^0_N)$ is likely to be involved by having a contribution of $\Delta S^0_t(H_2O)$ as has been indicated in DME–water mixtures (*4b*). Thus, since

$$[11] \quad \delta(\Delta S^0_N) = {}_s\Delta S^0_N - {}_w\Delta S^0_N = \Delta S^0_t(H^+) + \Delta S^0_t(OH^-) - \Delta S^0_t(H_2O)$$

and the contributions of $\Delta S^0_t(H^+) + \Delta S^0_t(OH^-)$ could be tentatively obtained from another source which is free from a_{H_2O}, it would be possible to estimate $\Delta S^0_t(H_2O)$ by subtracting the contributions of the sum: $(\Delta S^0_t(H^+) + \Delta S^0_t(OH^-))$ from $\delta(\Delta S^0_N)$. The tentative values of $(\Delta S^0_t(H^+) + \Delta S^0_t(OH^-))$ for different compositions of this solvent system have been obtained by plotting $(\Delta S^0_t(H^+) + \Delta S^0_t(X^-))$ where X = Cl^-, Br^-, and I^- against $(r_{X^-})^{-1}$ using $r_{Cl^-} = 0.181$ nm, $r_{Br^-} = 0.195$ nm and $r_{I^-} = 0.217$ nm (10) and reading out the values corresponding to $r_{OH^-} = 0.156$ nm (13). The required values of $\Delta S^0_t(H^+) + \Delta S^0_t(X^-)$ in ME–water mixtures for $X^- = Cl^-$ have been taken from ref. 7 and those for X = Br^- and I^- from our preceding paper (1). The $\Delta S^0_t(H_2O)$ values so obtained in ME–water mixtures are listed in Table 2 and the variation of

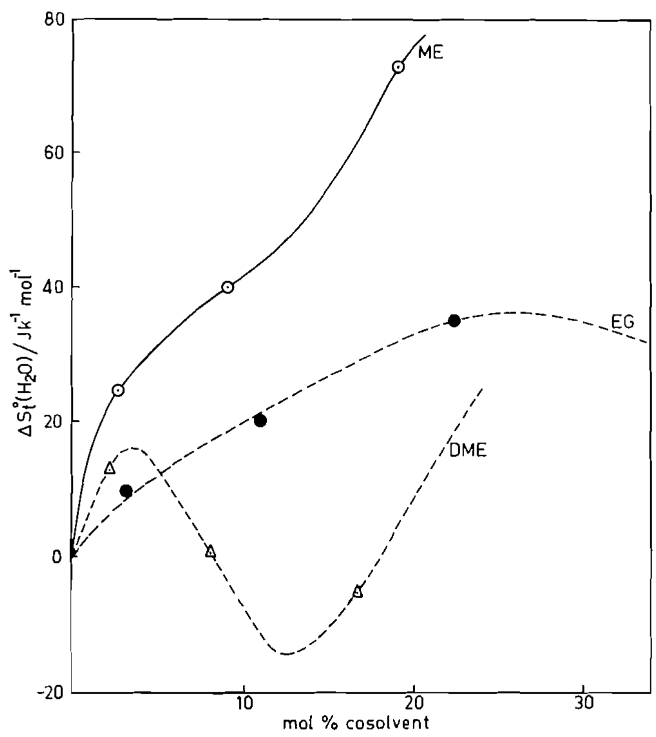

FIG. 2. Variation of $\Delta S^0_t(H_2O)$ in aqueous ME, DME, and EG.

$\Delta S^0_t(H_2O)$ at 25°C with mol% ME is shown in Fig. 2. For the sake of comparison, $\Delta S^0_t(H_2O)$ values in DME–water mixtures have been taken from the ref. *4b*. Also, assuming tentatively that in EG–water mixtures as well autoionization might be chiefly guided by ionization of water at least in water-rich compositions, $\Delta S^0_t(H_2O)$ values have been similarly computed from the reported values of $\delta(\Delta S^0_N)$ (15) and $\Delta S^0_t(HX)$ (*2a*) for that solvent system. The $\Delta S^0_t(H_2O)$–composition profiles for both DME–water mixtures and EG–water mixtures are illustrated in Fig. 2.

Now simple consideration of order–disorder phenomena indicates that the negative trend of the $\Delta S_t^0(H_2O)$–composition profile would imply more order and hence more "structure or cluster" in the mixed solvents than in water. But when the $\Delta S_t^0(H_2O)$–composition profile has a positive trend the reverse is true. The nature of the curves in Fig. 2 therefore suggests that addition of EG apparently induces breaking down of 3D water structures right from the beginning, contrary to the contentions expressed in our preceding paper (1, 16). But in the case of DME–water system as discussed earlier (4*b*) the observed sharp increases of $\Delta S_t^0(H_2O)$ at the initial compositions are indicative of the effect of the predominant structure breaking and the downward trend thereafter around 4–14 mol% DME is the result of increased order accompanying the possible formation of stable H-bonded bidentate DME–water complex (3*b*, 17). Similarly, in the case of ME–water system the observed sharp increases of $\Delta S_t^0(H_2O)$ with the addition of ME are indicative of the effect of structure breaking propensity of ME and then the observed downward trend resulting in a hump onward 10–15 mol% ME is possibly the result of the formation of H-bonded ME–water complexes referred to earlier (1). Lastly, the observed upward trends at still higher compositions in the cases of both ME and DME are the reflection of increased disorder due to the packing imbalance common to all other cosolvents.

Notably of course the observed anomalous order and features of $\Delta S_t^0(H_2O)$–composition profile for EG–water system is possibly indicative of the fact that the cosolvent EG being exclusively protic in nature, is possibly undergoing acid–base equilibria among themselves as well as with water molecules and thus obscuring the effect of ionization of water on which $\Delta S_t^0(H_2O)$ values are based.

Thus, the contentions of the present study are in fair agreement with those drawn from behaviour of $T\Delta S_t^0(HX)$ or $\Delta Y(HX)$ discussed in the preceding paper (1). Notably, however, that the structural information obtained from the observed hump of $\Delta S_t^0(H_2O)$ referred to in this paper is not exactly reflected in the behaviour of $T\Delta S_t^0(HX)$, $\Delta Y(HX)$, or $T\delta(\Delta S_N^0)$ values. Evidently, the behaviour of $\Delta S_t^0(H_2O)$ values, if free from uncertainties, is likely to be more informative than any of the other quantities, which after all, contain the Born-type electrostatic contributions.

Acknowledgement

Thanks are due to the University Grants Commission, New Delhi, for awarding a Junior Research Fellowship to P.K.G.

1. P. K. GUHA and K. K. KUNDU. Can. J. Chem. **63**, 000 (1985).
2. M. N. DAS and K. K. KUNDU. (*a*) J. Ind. Chem. Soc. **51**, 266 (1974) and references therein; (*b*) Ind. J. Chem. **16**A, 467 (1978).
3. A. BHATTACHARYA, A. K. DAS, and K. K. KUNDU. (*a*) Ind. J. Chem. **20**A, 347 (1981); (*b*) Ind. J. Chem. **20**A, 353 (1981); (*c*) Can. J. Chem. **59**, 1153 (1981).
4. J. DATTA and K. K. KUNDU. Can. J. Chem. (*a*) **59**, 3149 (1981); (*b*) **59**, 3141 (1981).
5. (*a*) K. K. KUNDU, P. K. CHATTOPADHYAY, D. JANA, and M. N. DAS. J. Phys. Chem. **74**, 2635 (1970); (*b*) A. K. DAS and K. K. KUNDU. J. Phys. Chem. **79**, 2604 (1975); (*c*) I. N. BASU MULLICK and K. K. KUNDU. Ind. J. Chem. **18**A, 1 (1979).
6. E. M. WOOLLEY and R. E. GEORGE. J. Soln. Chem. **3**, 119 (1974).
7. H. SADEK, TH. F. TADROS, and A. A. EL-HARAKANY. Electrochim. Acta, **16**, 334 (1971).
8. R. SMITS, D. L. MASSART, J. JUILLARD, and J. P. MOREL. Electrochim. Acta, **21**, 425 (1978).
9. H. S. HARNED and R. A. ROBINSON. Trans. Faraday Soc. **36**, 973 (1941).
10. H. S. HARNED and B. B. OWEN. Physical Chemistry of electrolyte solutions. Reinhold, New York. 1958.
11. U. SEN, K. K. KUNDU, and M. N. DAS. J. Phys. Chem. **71**, 3665 (1967).
12. M. PAABO, R. G. BATES, and R. A. ROBINSON. J. Phys. Chem. **70**, 247 (1966).
13. (*a*) D. FEAKINS. *In* Physico-chemical processes in mixed aqueous solvents. *Edited by* F. Franks. Heinemann, London. 1967; (*b*) D. Feakins. *In* Hydrogen-bonded solvent system. *Edited by* A. K. Covington and P. Jones. Taylor and Francis, London. 1966.
14. E. M. ARNETT, W. G. BENTRUDE, J. J. BURKE, and P. MAC DUGGLEBY. J. Am. Chem. Soc. **87**, 1541 (1965).
15. S. K. BANERJEE, K. K. KUNDU, and M. N. DAS. J. Chem. Soc. B, 166 (1967).
16. K. BOSE, K. DAS, A. K. DAS, and K. K. KUNDU. J. Chem. Soc. Faraday Trans. I, **74**, 1051 (1978).
17. A. JEANES and R. ADAMS. J. Am. Chem. Soc. **59**, 2608 (1937).
18. H. S. HARNED and L. D. FALLON. J. Am. Chem. Soc. **61**, 2374 (1939).

Ab initio studies on hydrogen bonded chains. V. The structure of infinite chains of methanol and water molecules

ALFRED KARPFEN AND PETER SCHUSTER

Institut für Theoretische Chemie und Strahlenchemie der Universität Wien, A-1090 Wien, Währingerstr. 17 Austria

Received July 17, 1984

This paper is dedicated to Professor C. Sandorfy on the occasion of his 65th birthday

ALFRED KARPFEN and PETER SCHUSTER. Can. J. Chem. **63**, 809 (1985).

Infinitely extended, periodic, bent chains of methanol and water molecules have been investigated with the aid of the *ab initio* crystal orbital method. Results on equilibrium geometries, stabilization energies, and other ground state properties are compared with the corresponding data obtained on monomers and homodimers. We also confront our computed results with experimental vapor phase and solid state data. Deviations from additivity of intermolecular interactions and the change of molecular properties from vapor phase monomer to molecules embedded in a periodic lattice are pointed out and compared to analogous effects as observed in other hydrogen bonded polymers. A few remarks on the evaluation of effective molecular dipole moments in molecular crystals are included as well.

ALFRED KARPFEN et PETER SCHUSTER. Can. J. Chem. **63**, 809 (1985).

Utilisant la méthode *ab initio* des orbitales cristallines, on a étudié des chaînes recourbées, périodiques et infiniment étendues de molécules de méthanol et d'eau. On compare les résultats obtenus relativement aux géométries d'équilibre, aux énergies de stabilisation et à d'autres propriétés de l'état fondamental avec des données correspondantes obtenues à l'aide de monomères et d'homodimères. On a aussi confronté nos résultats de calculs avec les données expérimentales obtenues tant en phase gazeuse qu'à l'état solide. On identifie les déviations par rapport à l'additivité des interactions intermoléculaires et le changement des propriétés moléculaires qui accompagne un changement du monomère en phase gazeuse en molécules imbriquées dans un réseau périodique et on les compare aux effets analogues observés dans d'autres polymères liés par des pont hydrogènes. On inclut aussi quelques remarques sur l'évaluation des moments dipolaires moléculaires effectifs dans des cristaux moléculaires.

[Traduit par le journal]

1. Introduction

Formation of hydrogen bonded chains is an often encountered structural feature in molecular crystals. Molecules which simultaneously can play the role of proton donors and acceptors such as hydrogen halides, simple alcohols and carboxylic acids, hydrogen cyanide, imidazole and many others preferentially crystallize in highly anisotropic structures containing sequentially aligned hydrogen bonds. Because of the large anisotropy in these systems many characteristic solid state properties may be reasonably well described by a treatment of the isolated hydrogen bonded chains.

In this series of papers the ground state properties of periodic, hydrogen bonded chains formed by hydrogen fluoride (1, 2), hydrogen cyanide (3), and formic acid molecules (4) have been investigated within the framework of the Hartree–Fock approximation. Here we wish to report results of similar *ab initio* studies on infinite chains of methanol and water molecules, respectively. To our best knowledge these are the first *ab initio* studies on these systems. Whereas the infinite chain of methanol molecules closely resembles the actual crystal structure of solid methanol, we regard the corresponding calculations on H_2O polymers mainly as a model study and as a first step towards a fully quantum chemical description of the various ice modifications.

Methanol adopts a polymeric, chain-like structure in the solid state (5). Various phase transitions have been detected in solid methanol (6–8). Structural differences between these phases consist mainly of varying degrees of puckering in the O—H---O chain. Moreover, the relative orientation and order of methyl groups changes as well. An elucidation of the relative stability of different periodic patterns in $(CH_3OH)_\infty$ goes far beyond the scope of this work, we note, however, that the chain structure persists in all solid phases of methanol. Detailed analysis of vibrational spectra of solid methanol substantiated the structural results (9–14).

The structure of the isolated methanol molecule in the vapor phase is well known (15–17). Corresponding detailed information on the preferred geometries of methanol dimers in the vapor phase is not available yet although the existence of vapor phase dimers and higher oligomers is well established (18–22). Experimental data on methanol dimer have been obtained by infrared spectroscopy in inert matrices (23–25) and by infrared photodissociation (26). Several *ab initio* studies on methanol dimers (21, 27–32) and trimers (27–29) have been reported. Higher oligomers are only dealt with in a single *ab initio* study (29) performed at a minimal basis set level.

Because of their overwhelming importance in nature vapor phase and particularly condensed phases of H_2O have been studied in great detail (33–35). The ability of H_2O to form four hydrogen bonds with surrounding water molecules leads to crystallization in essentially three-dimensional structures. Nevertheless, for various purposes, an isolated chain of water molecules has often been used as a model system in the past. Either it may be viewed as part of the ice lattice and constitutes therefore a simple model to study the influence of cooperative effects in a hydrogen bonded lattice, or, alternatively, a chain of water molecules has often served as the most primitive model for proton pumps (36–40).

As with the experimental work the number of quantum chemical studies on H_2O dimers and clusters is too numerous to be discussed here. For a recent review of experimental data and quantum chemical studies on $(H_2O)_n$ we refer to ref. 41 and also to newer *ab initio* calculations on H_2O clusters (42–44).

In this work, we aim towards a detailed and systematic description of a number of ground state properties of infinitely extended, periodic chains of methanol and water molecules, respectively. Nearly complete geometry optimization has been performed for both periodic structures. In case of the methanol polymer double ζ quality calculations have been performed only, whereas the H_2O chain has been treated by applying the same double ζ basis and additionally a more extended basis set containing a set of polarization functions on all atoms. In order to furnish an appropriate comparison monomers and homodimers of CH_3OH and H_2O have been treated at the same level. We report equilibrium geometries, stabilization energies, O—H stretching force constants and dipole moments. We also discuss some problems in the evaluation of effective dipole moments in molecular crystals or polymers. Finally we compare some aspects of the cooperative nature of hydrogen bonding in $(CH_3OH)_\infty$ and $(H_2O)_\infty$ with the behavior observed in related hydrogen bonded polymers.

2. Method of calculation

Ab initio Hartree–Fock calculations on one-dimensional, infinitely extended, periodic systems may nowadays be performed quite routinely. Explicit use of translational symmetry via the crystal orbital technique (45–47) offers considerable advantages over conventional cluster type approaches combined with subsequent attempts to extrapolate certain properties of interest to infinite chain length. Proper convergence is easily guaranteed and uncertainties in the extrapolation of quantities like total energies and geometrical parameters or conceptual difficulties connected with the evaluation of effective electrostatic moments in particular dipole moments per molecule are easily avoided. Moreover, full geometry optimization is easier since under the constraint of translational symmetry the number of internal degrees of freedom is much less than in open chain clusters. Recent methodical advances in *ab initio* crystal orbital calculations and several reviews dealing with applications in different fields of polymer physics may be found in ref. 48.

Computational techniques of our crystal orbital calculations have already been described in the previous papers of this series (1–4). We mention therefore only that all calculations on H_2O- and CH_3OH-polymers were performed in third neighbors' approximation. Remaining interaction terms could be treated with the aid of electrostatic approximations (49) without causing a significant loss in accuracy. Total energies per molecule obtained in this way are sufficiently converged (better than five digits) to ensure a reliable computation of potential energy surfaces and a meaningful comparison to monomer and dimer energies.

In a first step the equilibrium geometries of zig-zag H_2O- and CH_3OH-polymers were determined (see Fig. 1). In the case of $(CH_3OH)_\infty$ two geometric restrictions have been applied. Carbon atoms and the O—H---O backbone were confined to the same plane and methyl groups were oriented in a way to preserve a plane of symmetry. All remaining internal coordinates have been optimized. The dimer $(CH_3OH)_2$ has been treated under identical geometrical constraints. In case of $(H_2O)_\infty$ only planarity of the O—H---O backbone was required whereas hydrogen atoms not involved in hydrogen bonding point alternately above and below the O—H---O plane. Explicit use of an S_2 screw axis reduced the problem to a single molecule per primitive unit cell in $(H_2O)_\infty$ as well as in $(CH_3OH)_\infty$.

Both for $(H_2O)_\infty$ and $(CH_3OH)_\infty$ a double ζ type $7s3p/3s$ basis (50, 51) contracted to $4s2p/2s$ was applied. The choice of this comparatively small basis set was largely dictated by a compromise between desired flexibility and limitations in computing resources. Because of the presence of methyl groups large basis sets could not be applied for methanol chains. The only cluster calculations on larger methanol oligomers reported up to now in the literature have been performed with the minimal STO-3G basis applying additionally a frozen molecule approximation (29). STO-3G calculations usually grossly underestimate intermolecular distances. This tendency together with the well established correlation between X---Y bond lengths and X—H bond lengths often leads to an artificial stabilization of symmetric hydrogen bonds in polymers. An artefact of this type is e.g. obtained for hydrogen fluoride polymers in case the STO-3G basis is applied (52). We therefore decided to use at least a double ζ quality description for our calculations. The main drawback at this level of approximation is a large basis set superposition error resulting in a substantial overestimation of stabilization energies. Intermolecular distances are already quite reasonably described at this level although they turn out to be somewhat underestimated.

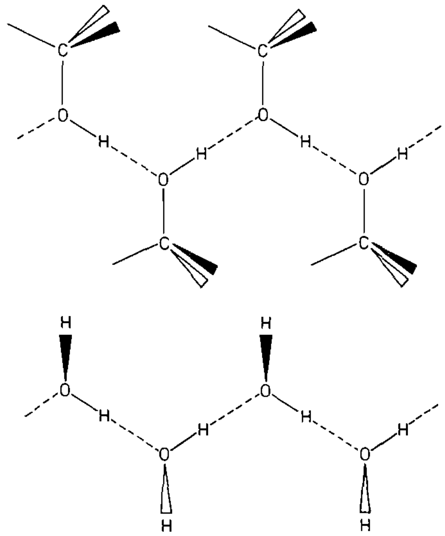

FIG. 1. Structure of $(CH_3OH)_\infty$ and $(H_2O)_\infty$.

In order to investigate the influence of basis set extension a $9s5p1d/5s1p \rightarrow [5,3,1/3,1]$ basis was additionally applied in case of $(H_2O)_\infty$. s and p basis sets were again taken from refs. 50, and 51. Exponents of polarization functions were 1.3 for d-functions on oxygen and 0.75 for p-functions on hydrogen atoms. Geometry optimizations have been performed under identical constraints as described for the smaller basis set.

3. Results and discussion

3.1. $(CH_3OH)_\infty$

Computed equilibrium structures of methanol monomer, dimer, and polymer are shown in Fig. 2. Although equilibrium geometries of monomer and dimer have been obtained via gradient optimization techniques and the polymer geometry has been found by a pointwise search on the energy surface we find satisfactory agreement in those geometrical parameters (methyl group geometry) not involved in hydrogen bonding. For future calculations it seems therefore a legitimate approximation to freeze the geometrical parameters of the methyl-group at the monomer value. Total energies, stabilization energies and other quantities which change substantially upon polymer formation, namely $r_{O\cdots O}$, r_{O-H}, f_{OH} and the dipole moment are displayed in Table 1.

As already mentioned before the main weakness of the current calculations is the strong overestimation of hydrogen bond — or stabilization energies. Dimer stabilization energies as obtained with STO-3G, 4-31G and 6-31G* basis sets are −5.57, −8.06, and −5.66 kcal/mol, respectively (32). We obtain −9.0 kcal/mol indicating that within the $7s3p/3s$ basis

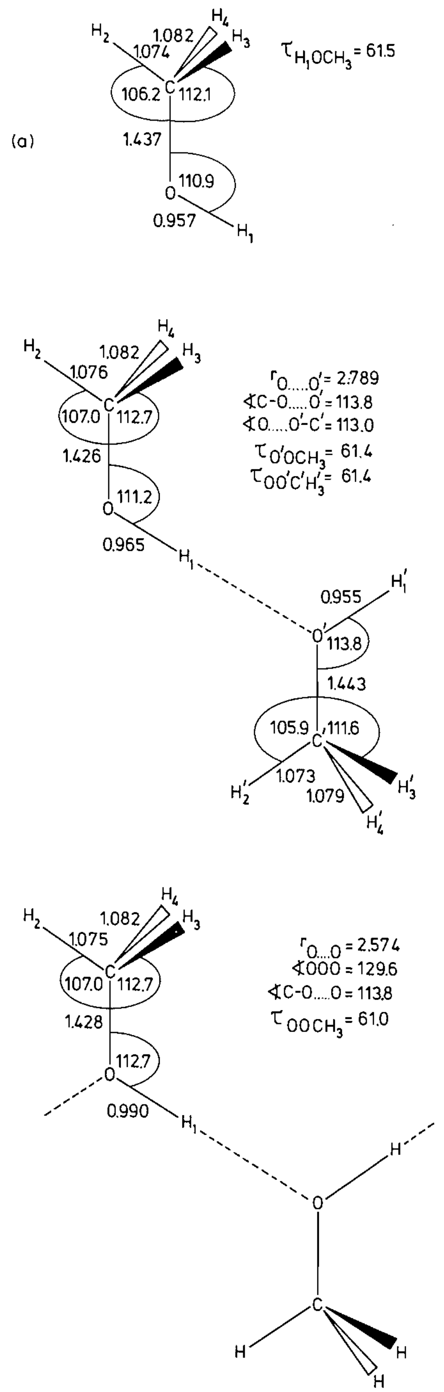

FIG. 2. Equilibrium geometries of monomer (*a*), dimer (*b*), and polymer (*c*) of methanol as obtained with the $7s3p/3s$ basis. Distances in Å, angles in deg.

the superposition error is even slightly larger than the one obtained with 4-31G. From previous experience (1–4), however, we are confident that relative changes occurring upon polymer formation are reasonably described. We observe an increase of the stabilization energy from −9.0 kcal/mol in the dimer to −13.4 kcal/mol in the polymer. Equally the intermolecular distance is substantially smaller in the polymer than in the dimer. In the solid state of methanol an O - - - O distance of 2.66 Å is observed, slightly larger than our computed value of 2.57 Å and consistent with the known tendency to underestimate intermolecular distances at the double ζ level.

TABLE 1. Selected ground state properties of methanol monomer, dimer, and polymer as obtained with the $7s3p/3s$

	Value		
Parameter	CH_3OH	$(CH_3OH)_2$	$(CH_3OH)_\infty$
Total energies (hartree)	−114.86109	−229.73653	−114.88251
ΔE (kcal/mol)	—	−9.0	−13.4
$r_{O\cdots O}$ (Å)	—	2.79	2.57
$r_{O—H}$ (Å)	0.957	0.965	0.990
$f_{O—H}$ (mdyn/Å)	8.19	7.55	5.29
μ (Debye)	2.151	4.163	2.331

Significant changes are also observed in O—H bond lengths and particularly in the corresponding force constant f_{OH}. We have not performed a full vibrational analysis and therefore the computation of the O—H frequency on the basis of f_{OH} alone would be premature. We note, however, that the vapor phase frequency of ν_{OH} is 3682 cm^{-1} (53). Matrix isolation of $(CH_3OH)_2$ yielded values of 3490–3528 cm^{-1} dependent on the type of matrix used (24) whereas the lowest OH-frequency in the solid is 3187 cm^{-1} (9). Vibrational frequencies in liquid methanol lie between the matrix and solid state data (54) indicating substantial self-association and polymer formation in the liquid. Our results therefore reproduce quite nicely the experimental trends.

3.2. $(H_2O)_\infty$

Equilibrium geometries of H_2O, $(H_2O)_2$, and $(H_2O)_\infty$ as obtained with the $7s3p/3s$ and the $9s5p1d/5s1p$ basis are shown in Fig. 3. Contrary to the case of $(CH_3OH)_2$ the water dimer has been treated in a configuration corresponding to the most stable dimer. This geometry differs from the $(H_2O)_\infty$ chain by a change in the torsional angle around O—O bonds. Whereas periodicity dictates that a screw axis remains as symmetry element in the polymer the corresponding symmetry is lacking in the case of the open chain dimer. The most important data obtained on H_2O, $(H_2O)_2$, and $(H_2O)_\infty$ are collected in Table 2. All of the changes observed to occur in the course of polymer formation of methanol are found to occur in H_2O polymers as well. Comparison to experimental data on ice is, however, less straightforward. The inherently three-dimensional structure of ice and the lack of anisotropy certainly causes substantial deviations from an idealized one-dimensional aggregate. From detailed studies of the amount of non-additive interactions in different types of H_2O-trimers (55) one may conclude that most of the attractive part of the non-additive interactions are already contained in our model polymer because it consists exclusively of a superposition of DA (donor–acceptor) trimers. DA-trimers are significantly more stable than either DD or AA trimers. Moreover, two thirds of the possible trimers in either ice I_h or ice I_c correspond to sequential trimers of the DA type.

With the above reservations in mind we observe experimentally a reduction of $r_{O\cdots O}$ from 2.98 Å in the vapor phase dimer (56) to 2.74 Å in ice I_c (33). The larger basis set calculations yield a corresponding reduction from 2.98 to 2.84 Å. From a comparison with our earlier calculation on $(HF)_\infty$ we estimate that a small fraction (about 10%) of the observed discrepancy is still due to basis set deficiencies in our calculations on one-dimensional H_2O chains. At the double ζ level we obtain a reduction of the intermolecular distance from 2.85 to 2.60 Å on going from the dimer to the polymer. 4-31G calculations, comparable in quality to our double zeta calcu-

TABLE 2. Selected ground state properties of H_2O monomer, dimer, and polymer as obtained with the $7s3p/3s$ and $9s5p1d/5s1p$ basis

Parameter	Value					
	H_2O		$(H_2O)_2$		$(H_2O)_\infty$	
Basis set	7,3/3	9,5,1/5,1	7,3/3	9,5,1/5,1	7,3/3	9,5,1/5,1
Total energy (hartree)	−75.88506	−76.04816	−151.78573	−152.10464	−75.907545	−76.05927
ΔE (kcal/mol)	—	—	−9.6	−5.2	−14.1	−7.0
$r_{O\cdots O}$ (Å)	—	—	2.85	2.98	2.60	2.84
r_{O-H} (Å)	0.958	0.942	0.965	0.946	0.991	0.954
f_{O-H} (mdyn/Å)	8.22	9.72	7.68	9.41	5.17	8.56
μ (Debye)	2.42	2.16	3.66	3.46	2.50	2.37

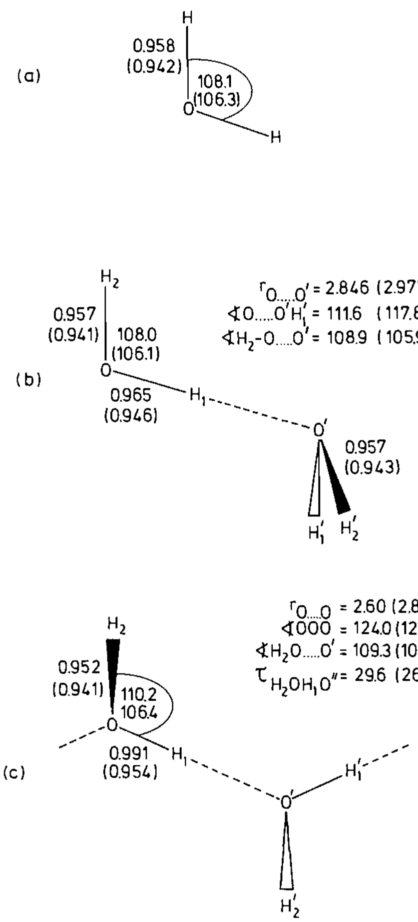

FIG. 3. Equilibrium geometries of monomer (*a*), dimer (*b*), and polymer (*c*) of H_2O as obtained with the $7s3p/3s$ and the $9s5p1d/5s1p$ basis. The latter values are given in parentheses. Distances in Å, angles in deg.

lations, by Tse *et al.* (32) on $(H_2O)_2$ and by Newton (44) on $(H_2O)_3$, $(H_2O)_5$, and $(H_2O)_6$ gave O---O distances of 2.85, 2.77, and 2.71 Å for dimer, DA-trimer and cyclic hexamer, respectively, whereas the dimer distance was recovered for a pentamer in which the molecule was tetrahedrally surrounded by four others.

3.3. *A note on dipole moments of molecules embedded in a periodic medium*

Recently Scheiner and Nagle (42) reported *ab initio* calculations on the charge partitioning between Bjerrum and ionic defects in ice. To this end they performed calculations on linear clusters of water molecules. For a more detailed discussion of this problem we refer to their work (42). For the following it is only important that they had to evaluate the *z*-component of the dipole moment of an H_2O molecule embedded in a linear H_2O polymer, where *z* is the direction in which the polymer extends. Their procedure was to evaluate μ_z for clusters of increasing chain length and then to divide by the number of molecules in the cluster. We shall demonstrate here that the above procedure, although valid, e.g., for the extrapolation of total energies per molecule, leads to effective dipole moments which always contain significant contributions from edge effects. For this purpose we performed model calculations on strictly linear hydrogen fluoride clusters containing 1, 3, 5, 7, and 9 HF molecules, respectively, and compared these to corresponding crystal orbital calculations. Results are given in Table 3.

In case a cluster is uncharged the total dipole moment is independent of the choice of the origin. This total dipole moment may now be partitioned into dipole moments of individual molecules in an infinite number of ways. For a short discussion of sources of arbitrariness see ref. 3 and references therein. Here we chose to partition the electron density in the same way as it is done in a Mulliken population analysis in close analogy to the evaluation of dipole moments via the crystal orbital approach (41, 49). Since molecules in the periodic, infinite chain are all identical and *neutral*, their dipole moment is independent of the choice of the origin. The same is asymptotically true for the innermost molecules of large clusters. Because of charge transfer molecules at the edge of the cluster are *charged*. Their dipole moments are consequently a function of the position of the origin. Because the amount of charge accumulated at the edge molecules converges as well with increasing cluster size, μ_{total}/n, converges too. However, invariably much too large values of the dipole moment are obtained in this way. This behavior is nicely reflected in our model calculations (see Table 3) and needs no further discussion.

In Table 4 we show dipole moment components of isolated H_2O molecules and those resulting from H_2O molecules embedded in the infinite chain as obtained with the $9s5p1d/5s1p$ basis. In order to obtain a comparison with the results of Scheiner and Nagle a single calculation on $(H_2O)_\infty$ in the ice geometry ($r_{O\cdots O}$ = 2.76 Å, r_{O-H} = 0.97 Å, all bond angles tetrahedral) has been performed as well. We obtain an increase of μ_z by 14 and 16% at the equilibrium geometry and at the ice configuration, respectively. As a consequence of the one-dimensional model, total dipole moments are increased by 9.8 and 8.7%. Scheiner and Nagle report increases of μ_z by 44 and 59%, respectively, dependent on the type of basis set used. In view of the above discussion we attribute their findings to an

TABLE 3. Dipole moments of HF molecules in linear clusters, all values in Debye

Number of HF molecules in the cluster	1	3	5	7	9	∞
4					5.386	
3				4.643	2.679	
2			3.893	2.572	2.431	
1		3.107	2.457	2.400	2.379	
0[a]	2.155	2.303	2.352	2.364	2.369	2.375
−1		2.937	2.387	2.372	2.371	
−2			3.734	2.482	2.398	
−3				4.507	2.573	
−4					5.276	
Total	2.155	8.349	14.823	21.336	27.861	∞
Total/n	2.155	2.783	2.965	3.048	3.096	3.279[b]
$\frac{\mu_{n+2}-\mu_n}{2}$	—	3.097	3.237	3.257	3.263	3.279[b]

[a] Central molecule in the cluster.
[b] Obtained by graphical extrapolation as in ref. 42.

TABLE 4. Dipole moments of isolated H_2O monomers and of H_2O molecules embedded in periodic chains as obtained with the $9s5p1d/5s1p$ basis

	Energy minimum[a]		Ice structure	
	H_2O	$(H_2O)_\infty$	H_2O	$(H_2O)_\infty$
μ_x	0.764	0.770	1.504	1.499
μ_y	0.714	0.634	0.0	−0.145
μ_z	1.888	2.150	1.504	1.752
			(1.186)[b]	(1.882)[b]
			(1.786)[c]	(2.565)[c]
μ_{total}	2.159	2.370	2.127	2.311

[a] Geometries as in Fig. 1c.
[b] STO-3G from ref. 42.
[c] 4-31G from ref. 42.

inadequate extrapolation procedure which yields results that depend on the detailed surface structure of the cluster. For other attempts in the literature to compute the induced moments of an H_2O molecule in the ice lattice we refer the reader to (57, 58).

Clearly within our one-dimensional model chain we cannot hope to obtain the dipole moment of H_2O in the ice modifications. The additional induced dipole moments strongly depend on the lattice type as, e.g., discussed recently by Johari (57).

4. Comparison to other hydrogen bonded polymers

In Table 5 we confront our results on H_2O and CH_3OH polymers with recent *ab initio* studies on similar hydrogen bonded polymers emphasizing the differences between properties of vapor phase dimers and infinite chains. We consider the extra stabilization energy per molecule ΔE over the dimer value gained by polymer formation, the reduction of intermolecular distances $\Delta r_{X\cdots Y}$, the elongations of X—H bond lengths and the corresponding reductions of X—H force constants, and finally the change of molecular dipole moments.

Turning first to a discussion of stabilization energies we observe in all cases a substantial enhancement of "hydrogen bond" energies in the polymers. A simple analysis of a strictly linear chain of dipoles (41) yielded an increase of 28% of the dimer stabilization solely on the basis of pairwise additive forces. From the species considered in Table 5 $(HCN)_\infty$ and $(HF)_\infty$ most closely approach this model system. Comparison of infinite chain and dimer properties is also easier in these systems because the equilibrium geometry of the vapor phase dimers closely resemble the polymer structure with respect to the relative orientation of neighboring molecules.

Non-additive contributions to intermolecular interactions are small in the case of $(HCN)_\infty$ which essentially behaves like a simple dipole system. Much larger cooperative contributions are found in $(HF)_\infty$. In case of the other polymers $(H_2O)_\infty$, $(CH_3OH)_\infty$, and $(HCOOH)_\infty$ a quantitative assessment of the degree of nonadditivity cannot be given by comparison to a simple linear chain of dipoles. Additional calculations on more detailed models would be necessary in order to define the appropriate reference system.

Of particular importance is the substantial reduction of intermolecular distances and the elongation of X—H bond lengths taking place upon polymer information. The size of these effects provides an estimate of the inherent failures of Monte-Carlo or molecular dynamics studies of condensed phases, liquid or solid, of hydrogen bonded molecules working with pair potentials derived from the vapor phase and relying consequently also on a frozen molecule approximation.

This deviation from the frozen molecule assumption is essential for a proper consideration of the lattice dynamical aspects of hydrogen bonded solids (2). The strong decrease of X—H force constants in the polymers causes large shifts in the corresponding vibrational frequencies, the most characteristic feature of hydrogen bonds from the experimental point of view. As already discussed before the detailed changes of effective dipole moments in the polymers is not easy to systematize unless the consequences of the specific structure of a given polymer are analysed on their own. Monomer dipole moments are, however, always modified considerably. The same clearly applies to higher moments as well.

Conclusions

Crystal orbital calculations on hydrogen bonded polymers offer a convenient way to study the influence of periodic environments on various molecular properties. Because of the explicit use of translational symmetry and the possibility to perform lattice summations in a numerically satisfactory way, truncation errors and uncertainties in extrapolation procedures from small clusters to periodic systems arising in conventional cluster calculations are completely avoided. Advantages of this kind of approach will be even more pronounced in three-

TABLE 5. Survey of the modifications of selected monomer and dimer properties occurring upon polymer formation in hydrogen bonded systems, all values in %

				Δr_{X-H}[c]		$-\Delta f_{X-H}$[c]			
Species	Basis set	$-\Delta E$[a]	$-\Delta r_{X\cdots Y}$[b]	Dimer	Polymer	Dimer	Polymer	$\Delta\mu$[c]	*Reference*
HF	(8,4/4)	67.0	8.9	—	3.0	4.0	25.6	15.2	
	(9,5,1/5,1)	54.4	7.6	0.4	2.0	—	18.2	15.4	2
	(10,6,2/6,1)	61.7	8.1	0.4	2.1	3.7	20.5	19.9	
H_2O	(7,3/3)	46.9	8.8	0.7	3.4	6.6	37.1	3.3	This work
	(9,5,1/5,1)	34.6	4.7	0.4	1.3	3.2	12.7	9.8	
CH_3OH	(7,3/3)	48.9	7.9	0.8	3.4	7.8	35.5	9.8	This work
HCOOH	STO-3G	24.5	2.2	1.9	3.0	—	—	68.7	4
	(7,3/3)	31.5	1.5	2.8	3.4	25.7	33.7	53.8	
HCN	STO-3G	43.8	4.7	—	1.0	—	8.4	18.4	
	(8,4/4)	39.3	4.9	—	0.7	—	7.5	9.7	3
	(10,6,1/6,1)	39.8	4.1	—	0.4	—	6.9	14.8	

[a] Increase over the dimer stabilization.
[b] Reduction of the dimer distance.
[c] Relative to monomer.

dimensional systems. With the advent of faster computers fully quantum chemical studies of hydrogen bonded solids will soon come into reach and will allow a more reliable discussion of condensed phase properties than models based on pairwise additive potentials.

Acknowledgements

Financial assistance by the Austrian "Fonds zur Förderung der wissenschaftlichen Forschung", Project No. 3669 and generous supply of computer time by the "Interfakultäres EDV-Zentrum", Wien are gratefully acknowledged.

1. A. KARPFEN. Chem. Phys. **47**, 401 (1980).
2. A. BEYER and A. KARPFEN. Chem. Phys. **64**, 343 (1982).
3. A. KARPFEN. Chem. Phys. **79**, 211 (1983).
4. A. KARPFEN. Chem. Phys. **88**, 415 (1984).
5. K. J. TAUER and W. N. LIPSCOMB. Acta Crystallogr. **5**, 606 (1952).
6. H. G. CARLSON and E. F. WESTRUM, JR. J. Chem. Phys. **54**, 1464 (1971).
7. A. WÜRFLINGER and R. LANDAU. J. Phys. Chem. Solids, **38**, 811 (1977).
8. F. FISCHER and R. FUHRICH. Z. Naturforsch. **38a**, 31 (1982).
9. M. FALK and E. WHALLEY. J. Chem. Phys. **34**, 1554 (1961); **34**, 1569 (1961).
10. R. J. JACOBSEN, J. W. BRASCH, and Y. MIKAWA. J. Mol. Struct. **1**, 309 (1967).
11. A. B. DEMPSTER and G. ZERBI. J. Chem. Phys. **54**, 3600 (1971).
12. P. T. T. WONG and E. WHALLEY. J. Chem. Phys. **55**, 1830 (1971).
13. A. PELLEGRINI, D. R. FERRO, and G. ZERBI. Mol. Phys. **26**, 577 (1973).
14. P. PIAGGIO, R. TUBINO, and G. DELLEPIANI. J. Mol. Struct. **96**, 277 (1983).
15. P. VENKATESWARLU and W. GORDY. J. Chem. Phys. **23**, 1200 (1955).
16. K. KIMURA and M. KUBO. J. Chem. Phys. **30**, 151 (1959).
17. R. M. LEES and J. G. BAKER. J. Chem. Phys. **48**, 5299 (1968).
18. E. TUCKER, S. B. FARNHAM, and S. D. CHRISTIAN. J. Phys. Chem. **73**, 3820 (1969).
19. V. CHEAM, S. B. FARNHAM, and S. D. CHRISTIAN. J. Phys. Chem. **74**, 4157 (1970).
20. J. A. ODUTOLA, P. VISWANATHAN, and T. R. DYKE. J. Am. Chem. Soc. **101**, 4787 (1979).
21. L. A. CURTISS, D. J. FRURIP, and M. BLANDER. J. Chem. Phys. **75**, 5900 (1981).
22. D. J. FRURIP, L. A. CURTISS, and M. BLANDER. Intern. J. Thermophys. **2**, 115 (1981).
23. M. VAN THIEL, E. D. BECKER, and G. C. PIMENTEL. J. Chem. Phys. **27**, 95 (1957).
24. A. J. BARNES and H. E. HALLAM. Trans. Faraday Soc. **66**, 1920 (1970).
25. W. A. P. LUCK and O. SCHREMS. J. Mol. Struct. **60**, 333 (1980).
26. M. A. HOFBAUER, C. F. GIESE, and W. R. GENTRY. J. Phys. Chem. **88**, 181 (1984).
27. J. E. DEL BENE. J. Chem. Phys. **55**, 4633 (1971).
28. Y. C. TSE and M. D. NEWTON. J. Am. Chem. Soc. **99**, 611 (1977).
29. L. A. CURTISS. J. Chem. Phys. **67**, 1144 (1977).
30. L. A. CURTISS. Intern. J. Quantum Chem. Symp. **11**, 459 (1977).
31. L. A. CURTISS and D. J. FRURIP. Intern. J. Quantum Chem. Symp. **15**, 189 (1981).
32. Y.-C. TSE, M. D. NEWTON, and L. C. ALLEN. Chem. Phys. Lett. **75**, 350 (1980).
33. D. EISENBERG and W. KAUZMAN. The structure and properties of water. Oxford University Press, Oxford. 1969.
34. E. WHALLEY, S. J. JONES, and L. W. GOLD (*Editors*). Physics and chemistry of ice. Royal Society of Canada, Canada. 1973.
35. F. FRANKS (*Editor*). Water, a comprehensive treatise. Vol. 1. Plenum, New York. 1972.
36. J. F. NAGLE and H. J. MOROWITZ. Proc. Natl. Acad. Sci. USA, **75**, 298 (1978).
37. J. F. NAGLE, M. MILLE, and H. J. MOROWITZ. J. Chem. Phys. **72**, 3959 (1980).
38. E. W. KNAPP, K. SCHULTEN, and Z. SCHULTEN. Chem. Phys. **46**, 215 (1980).
39. J. F. NAGLE and M. MILLE. J. Chem. Phys. **74**, 1367 (1981).
40. F. FREUND. Bioelectrochem. Bioenerg. **9**, 61 (1982).
41. A. BEYER, A. KARPFEN, and P. SCHUSTER. Top. Curr. Chem. **120**, 1 (1984).
42. S. SCHEINER and J. F. NAGLE. J. Phys. Chem. **87**, 4267 (1983).
43. M. D. NEWTON. J. Phys. Chem. **87**, 4288 (1983).
44. M. D. NEWTON. Acta Crystallogr. B**39**, 104 (1983).
45. T. E. PEACOCK and R. MCWEENY. Proc. R. Soc. London, **74**, 385 (1959).
46. G. DEL RE, J. LADIK, and G. BICZO. Phys. Rev. **155**, 997 (1967).
47. J. M. ANDRE, L. GOUVERNEUR, and G. LEROI. Intern. J. Quantum Chem. **1**, 451 (1967).
48. J. LADIK, J. M. ANDRE, and M. SEEL (*Editors*). Quantum chem-

istry of polymers – solid state aspects. NATO-ASI Series C 123, Reidel, Dordrecht. 1984.
49. L. PIELA and J. DELHALLE. Intern. J. Quantum Chem. **13**, 605 (1978).
50. S. HUZINAGA. Approximate atomic functions I. University of Alberta, Alta., Canada. 1981.
51. S. HUZINAGA. J. Chem. Phys. **42**, 1293 (1965).
52. A. KARPFEN. Unpublished results.
53. R. G. INSKEEP, J. M. KELLIKER, P. E. MCMAHON, and B. G. SOMERS. J. Chem. Phys. **28**, 1033 (1958).
54. C. BOURDÉRON, J. J. PÉRON, and C. SANDORFY. J. Phys. Chem. **76**, 869 (1972).
55. D. HANKINS, J. W. MOSKOWITZ, and F. H. STILLINGER. J. Chem. Phys. **53**, 4544 (1970).
56. T. R. DYKE, K. M. MACK, and J. S. MUENTER. J. Chem. Phys. **66**, 498 (1977).
57. P. JOHARI. J. Chem. Phys. **80**, 4413 (1984).
58. C. A. COULSON and D. EISENBERG. Proc. R. Soc. London Ser. A**291**, 445 (1966).

Synthèse et hydrolyse d'orthoesters trioxa-2,7,8 bicyclo[3.2.1] octanes et trioxa-2,8,9 bicyclo[3.3.1] nonanes

OTMANE BOUAB ET GÉRARD LAMATY
Laboratoire de Chimie Organique Physique, Université des Sciences et Techniques du Languedoc, Place Eugène Bataillon, 34060 Montpellier Cedex, France

ET

CLAUDE MOREAU
Laboratoire de Chimie Organique Physique et Cinétique Chimique Appliquées (U.A.CNRS 418), Ecole Nationale Supérieure de Chimie de Montpellier, 8, rue Ecole Normale, 34075 Montpellier Cedex, France

Reçu le 30 mars 1984

OTMANE BOUAB, GÉRARD LAMATY et CLAUDE MOREAU. Can. J. Chem. **63**, 816 (1985).

Les vitesse d'hydrolyse des orthoesters trioxa-2,7,8 bicyclo[3.2.1] octanes et trioxa-2,8,9 bicyclo[3.3.1] nonanes substitués en position 1 (R = H, CH_3, C_6H_5) ont été déterminées à deux températures dans un mélange eau/dioxanne 40:60 en volume. Ces nouveaux résultats confirment le comportement généralement observé dans l'hydrolyse des orthoesters ayant une conformation favorable pour s'hydrolyser avec contrôle stéréoélectronique.

OTMANE BOUAB, GÉRARD LAMATY, and CLAUDE MOREAU. Can. J. Chem. **63**, 816 (1985).

The rates of hydrolysis of 1-substituted 2,7,8-trioxabicyclo[3.2.1]octanes and 2,8,9-trioxabicyclo[3.3.1]nonanes (R = H, CH_3, C_6H_5) have been determined at two temperatures in dioxan/water (60:40 by volume). These new results confirm the behaviour generally observed in the hydrolysis of orthoesters which have a favourable conformation to hydrolyze under stereoelectronic control.

Introduction

Dans un précédent travail concernant l'hydrolyse des trioxa-2,4,10 adamantanes (1, 2) nous avons émis l'hypothèse que l'étape déterminant la vitesse de réaction était l'addition de l'eau sur l'ion carboxonium intermédiaire et non la formation de cet ion; en effet, l'encombrement stérique dû à la présence d'un cycle cyclohexanique est tel que le réaction favorisée est le retour vers l'acide conjugué du substrat (étape k_{-2}, schéma 1), hypothèse confirmée depuis par des travaux récents de McClelland (3).[1]

Afin de vérifier que le changement d'étape lente observé dans l'hydrolyse des trioxaadamantanes était dû à un encombrement stérique à l'approche de l'eau dans l'ion carboxonium intermédiaire, nous avons procédé à l'étude de modèles simples (4) et nous présentons maintenant l'étude réalisée sur deux séries de composés dont la structure est très voisine de celle des trioxaadamantanes – les trioxa-2,7,8 bicyclo[3.2.1] octanes substitués en position 1 : **1** (R = H), **2** (R = CH_3), **3** (R = C_6H_5) et les trioxa-2,8,9 bicyclo[3.3.1] nonanes substitués en position 1 : **4** (R = H), **5** (R = CH_3) et **6** (R = C_6H_5) – mais dans lesquels le retour interne vers l'acide conjugué du substrat à partir de l'ion carboxonium intermédiaire est fortement improbable (schéma 2), l'encombrement stérique d'une chaîne hydroxylée étant moindre que celui d'un cycle cyclohexanique.

Dans un premier temps, nous avons procédé à la synthèse des produits qui n'était pas connue pour quatre d'entre eux, **2**, **3**, **5** et **6**; dans un deuxième temps, nous avons procédé à l'analyse des produits de la réaction d'hydrolyse et à la détermination des constantes de vitesse d'hydrolyse et des grandeurs d'activation.

Résultats expérimentaux

Synthèse

Les orthoesters **1**, **2** et **3** ont été préparés par réaction de transestérification à partir du butanetriol-1,2,4 et des orthocarboxylates de triméthyle ou triéthyle correspondants; les orthoesters **4**, **5** et **6** ont été synthétisés, par réaction de transestérification également, à partir du pentanetriol-1,3,5 et des orthocarboxylates de triméthyle ou triéthyle correspondants. Les propriétés physico-chimiques des quatre nouveaux produits – **2**, **3**, **5** et **6** – sont données dans la partie expérimentale.

Analyse des produits de la réaction

L'analyse des produits d'hydrolyse peut apporter des renseignements utiles sur le sens d'ouverture des orthoesters. L'hydrolyse des orthoesters **1**, **2** et **3** peut conduire, tout en respectant les règles stéréoélectroniques, à trois produits (**10**, **11** et **12**, schéma 3); un seul produit d'hydrolyse (**10**) est observé. De même, l'hydrolyse des orthoesters **4**, **5** et **6** peut conduire, tout en respectant les mêmes règles stéréoélectroniques, à deux produits (**13** et **14**, schéma 4); là aussi, un seul produit d'hydrolyse est observé (**13**).

Ces aspects seront développés plus en détail dans la partie discussion.

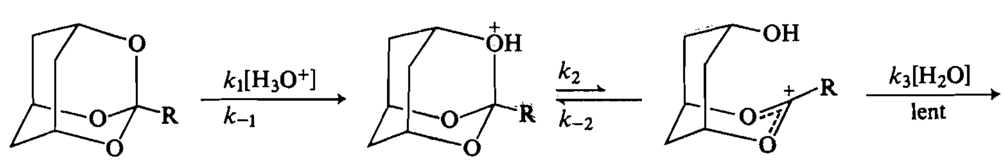

SCHÉMA 1

[1] Aussi R. A. McClelland. Communication personnelle.

TABLEAU 1. Hydrolyse des trioxa-2,7,8 bicyclo[3.2.1] octanes substitués en position 1

Trioxa-2,7,8 bicyclo[3.2.1] octane (**1**)				
HCl 10^{-3} *M*				
$k_{obs} = 0{,}134 \times 10^{-1}$ s^{-1} à 29,0°C				
$k_{obs} = 0{,}360 \times 10^{-1}$ s^{-1} à 41,5°C				
HCOOH/HCOONa [HCOOH]/[HCOONa] = 1; $pH_{réel}$ = 5,56[a]				
HCOOH (*M*)	0,0805	0,0402	0,0103	0 (intercept)[b]
$k_{obs} \times 10^3$ s^{-1} à 29,0°C	0,172	0,160	0,156	0,153 (r = 0,981)
Méthyl-1 trioxa-2,7,8 bicyclo[3.2.1] octane (**2**)				
HCOOH/HCOONa [HCOOH]/[HCOONa] = 1; $pH_{réel}$ = 5,57[a]				
HCOOH (*M*)	0,0402	0,0205	0,0103	0 (intercept)[b]
$k_{obs} \times 10^2$ s^{-1} à 28,7°C	0,871	0,800	0,768	0,731 (r = 0,999)
$k_{obs} \times 10$ s^{-1} à 41,8°C	0,205	0,186	0,176	0,166 (r = 0,999)
CH_3COOH/CH_3COONa $[CH_3COOH]/[CH_3COONa]$ = 1; $pH_{réel}$ = 6,89[a]				
CH_3COOH (*M*)	0.082	0.042	0,011	0 (intercept)[b]
$k_{obs} \times 10^4$ s^{-1} à 29,0°C	5,89	4,81	3,96	3,66 (r = 0,999)
Phényl-1 trioxa-2,7,8 bicyclo[3.2.1] octane (**3**)				
HCOOH/HCOONa [HCOOH]/[HCOONa] = 1; $pH_{réel}$ = 5,57[a]				
HCOOH (*M*)	0,0803	0,0405	0,0104	0 (intercept)[b]
$k_{obs} \times 10^2$ s^{-1} à 28,7°C	0,485	0,421	0,348	0,333 (r = 0,993)
$k_{obs} \times 10^2$ s^{-1} à 41,4°C	1,147	0,971	0,789	0,747 (r = 0,996)
CH_3COOH/CH_3COONa $[CH_3COOH]/[CH_3COONa]$ = 1; $pH_{réel}$ = 6,89[a]				
CH_3COOH (*M*)	0,082	0,042	0,011	0 (intercept)[b]
$k_{obs} \times 10^4$ s^{-1} à 29,0°C	4,46	3,35	2,67	2,35 (r = 0,998)

[a] $pH_{réel}$ = pH lu + 0,4 (5).
[b] Extrapolation à concentration nulle (régression linéaire).

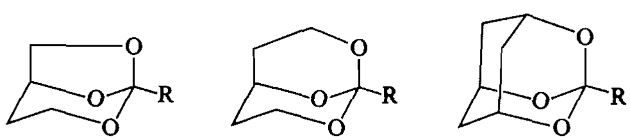

1 R = H   **4** R = H   **7** R = H
2 R = CH_3 **5** R = CH_3 **8** R = CH_3
3 R = C_6H_5 **6** R = C_6H_5 **9** R = C_6H_5

SCHÉMA 2

Résultats cinétiques

L'hydrolyse acido-catalysée des trioxa-2,7,8 bicyclo[3.2.1] octanes substitués en position 1 et des trioxa-2,8,9 bicyclo-[3.3.1] nonanes substitués en position 1 a été effectuée dans le solvant eau/dioxanne 40:60 en volume et à deux températures. Les couples acide/base utilisés pour tamponner le milieu sont acide formique/formiate de sodium et acide acétique/acétate de sodium. La force ionique a été maintenue constante à 0,1 *M* par addition de chlorure de potassium. Les résultats cinétiques sont rassemblés dans les tableaux 1 et 2 (la reproductibilité moyenne est de 3%). Les constantes catalytiques $k_{H_3O^+}$, k_{HCOOH} et k_{CH_3COOH} ont été obtenues en exploitant les résultats des tableaux 1 et 2 et en tenant compte des effets dus à la présence du dioxanne (5, 6); ces constantes ainsi que les grandeurs d'activation sont reportées dans le tableau 3.

Interprétation des résultats expérimentaux

L'examen des tableaux 1 et 2 montre que l'hydrolyse des trioxa-2,7,8 bicyclo[3.2.1] octanes substitués en position 1 et des trioxa-2,8,9 bicyclo[3.3.1] nonanes substitués en position 1 est soumise à une catalyse acide générale, type de catalyse compatible avec le concept de contrôle stéréoélectronique qui implique que la rupture d'une liaison C—O—alkyle est favorisée si les deux autres hétéroatomes ont chacun une paire d'électrons libres antipériplanaire par rapport à cette liaison (7).

Par ailleurs, les résultats expérimentaux sont en accord avec un mécanisme dans lequel l'étape déterminant la vitesse de réaction est la formation d'un ion carboxonium intermédiaire (8, 9): les entropies d'activation sont du même ordre de grandeur que celles reportées dans l'hydrolyse d'autres systèmes cycliques (4), faiblement négatives dans la réaction catalysée par H_3O^+ (mécanisme unimoléculaire A1) et fortement négatives dans la réaction catalysée par les acides faibles (mécanisme bimoléculaire A S_E2); le remplacement d'un hydrogène par un méthyle où un phényle entraîne une augmentation de la vitesse de l'hydrolyse en accord avec une meilleure stabilisation de l'état de transition pour les produits substitués et en accord également avec l'absence d'empêchement stérique à la conjugaison dans les dérivés cycliques, empêchement stérique observé en série aliphatique (tableau 4) par Kresge et coll. (10).

Ces résultats font donc apparaître un comportement totalement différent de celui observé avec les trioxa-2,4,10 adamantanes substitués en position 3 (tableau 5) et confirment la particularité du système adamantyle.

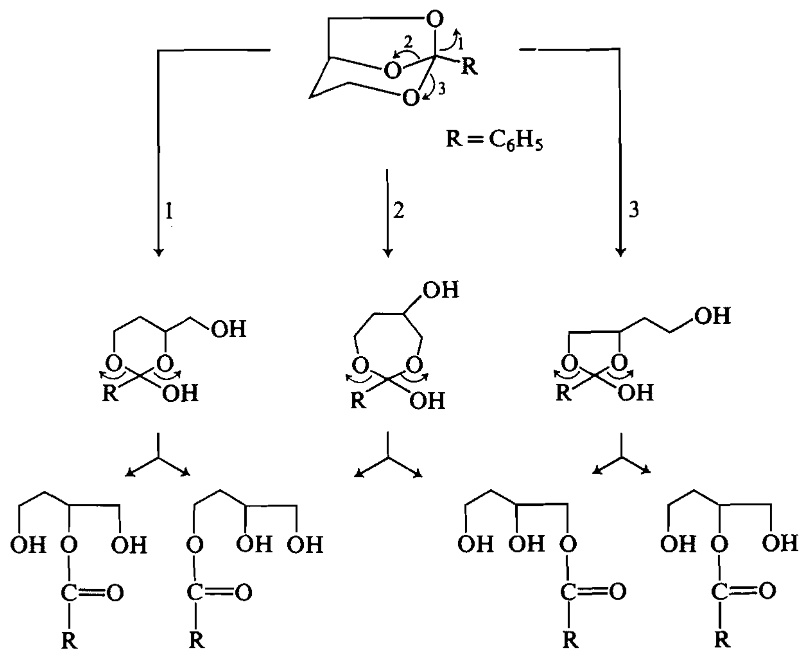

10 11 12 10

SCHÉMA 3

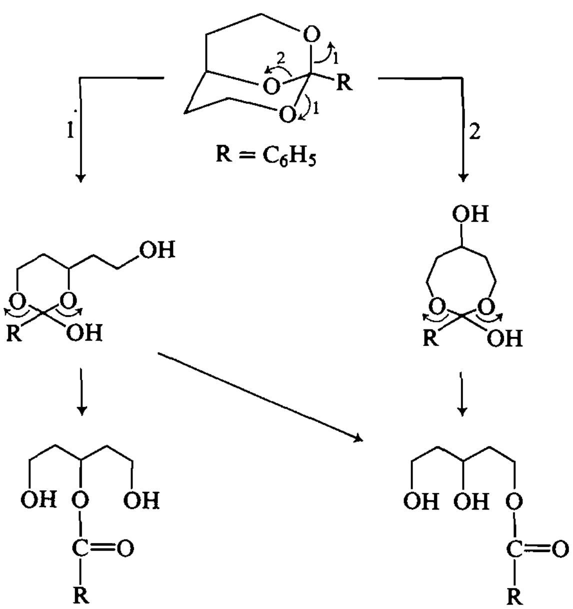

13 14

SCHÉMA 4

Discussion

Sens d'ouverture dans l'hydrolyse des trioxa-2,7,8 bicyclo-[3.2.1] octanes substitués en position 1

En appliquant les règles stéréoélectroniques (11), l'hydrolyse des orthoesters **1**, **2** et **3** peut s'effectuer par rupture de l'une quelconque des liaisons C—O, C(1)—O(7), C(1)—O(8) ou C(1)—O(2) (schéma 5) pour donner les ions carboxoniums cycliques à 5, 6 ou 7 éléments et conduire aux produits d'hydrolyse **10**, **11** ou **12**. Expérimentalement, l'hydrolyse de l'orthoester **3** (R = C_6H_5) conduit à un seul produit (**10**) ce qui exclurait la formation de l'ion carboxonium cyclique à 7 éléments et donc la rupture, en particulier au cours de l'étape cinétique, de la liaison C(1)—O(8). Par ailleurs, si on élimine le facteur tension de cycle dans l'état initial, facteur qui favoriserait la rupture de la liaison C(1)—O(7) (10), il ne reste que les stabilités relatives des ions carboxonium pour trancher et les avis sont partagés; selon Paulsen (11), les ions dioxolénium-1,3 seraient plus stables que les ions dioxénium-1,3 alors que pour McClelland ce serait l'inverse (12).[2]

Sens d'ouverture dans l'hydrolyse des trioxa-2,8,9 bicyclo-[3.3.1] nonanes substitués en position 1

En ce qui concerne le sens d'ouverture des orthoesters **4**, **5** et **6**, la situation est moins complexe; deux ions cycliques peuvent se former tout en respectant les mêmes règles stéréoélectroniques (schéma 6); il ne peut y avoir que deux produits d'hydrolyse, **13** ou **14**. Expérimentalement, l'hydrolyse de l'orthoester **6** conduit au produit **13** ce qui exclurait la formation d'un ion carboxonium à 8 éléments et par conséquent la rupture cinétique de la liaison C(1)—O(9).

Position de l'état de transition

Nous avons montré dans un précédent travail (4) que les effets de substituant étaient un des critères qui permettaient d'élucider le mécanisme de l'hydrolyse des acétals et des orthoesters; le rapport $k_{C_6H_5}/k_{CH_3}$ permet, en particulier, de mieux apprécier la position de l'état de transition le long du chemin réactionnel: dans l'hydrolyse des orthoesters, ce rapport est voisin de l'unité, tantôt inférieur, tantôt supérieur, mais loin du rapport $k_{C_6H_5}/k_{CH_3}$ que l'on trouve dans l'hydrolyse des acétals ($k_{C_6H_5}/k_{CH_3} \simeq 30$).

Les rapports $k_{C_6H_5}/k_{CH_3}$ déterminés dans ce travail, ($k_{C_6H_5}/k_{CH_3}$ = 0,4 à 0,9 pour la série bicyclo[3.2.1] octane et $k_{C_6H_5}/k_{CH_3}$ = 0,7 à 1,1 pour la série bicyclo[3.3.1] nonane), confirment l'analyse que nous avions faite, à savoir que seul un état de transition ayant peu de caractère ion carboxonium peut conduire à un rapport $k_{C_6H_5}/k_{CH_3}$ inférieur à l'unité, les effets inductifs (+*I* pour CH_3 et −*I* pour C_6H_5) pouvant entrer en

[2] Aussi H. K. Hall, Jr. Communication personnelle.

TABLEAU 2. Hydrolyse des trioxa-2,8,9 bicyclo[3.3.1] nonanes substitués en position 1

Trioxa-2,8,9 bicyclo[3.3.1] nonane (**4**)				
HCl 9,5 × 10^{-4} *M*				
k_{obs} = 0,235 × 10^{-1} s^{-1} à 14,2°C				
k_{obs} = 0,676 × 10^{-1} s^{-1} à 28,6°C				
HCOOH/HCOONa [HCOOH]/[HCOONa] = 1; $pH_{réel}$ = 5,56[a]				
HCOOH (*M*)	0,0803	0,0405	0,0104	0 (intercept)[b]
k_{obs} × 10^3 s^{-1} à 28,8°C	0,894	0,810	0,723	0,703 (r = 0,996)
k_{obs} × 10^2 s^{-1} à 42,2°C	0,236	0,215	0,194	0,189 (r = 0,997)
Méthyl-1 trioxa-2,8,9 bicyclo[3.3.1] nonane (**5**)				
HCOOH/HCOONa [HCOOH]/[HCOONa] = 1; $pH_{réel}$ = 5,56[a]				
HCOOH (*M*)	0,0803	0,0405	0,0104	0 (intercept)[b]
k_{obs} × 10^2 s^{-1} à 13,7°C	0,715	0,609	0,469	0,446 (r = 0,987)
k_{obs} × 10^2 s^{-1} à 29,2°C	0,201	0,160	0,132	0,120 (r = 0,999)
CH_3COOH/CH_3COONa [CH_3COOH]/[CH_3COONa] = 1; $pH_{réel}$ = 6,89[a]				
CH_3COOH (*M*)	0,083	0,042	0,011	0 (intercept)[b]
k_{obs} × 10^2 s^{-1} à 29,0°C	0,164	0,137	0,111	0,104 (r = 0,998)
k_{obs} × 10^2 s^{-1} à 42,0°C	0,372	0,289	0,242	0,218 (r = 0,997)
Phényl-1 trioxa-2,8,9 bicyclo[3.3.1] nonane (**6**)				
HCOOH/HCOONa [HCOOH]/[HCOONa] = 1; $pH_{réel}$ = 5,56[a]				
HCOOH (*M*)	0,0405	0,0210	0,0104	0 (intercept)[b]
k_{obs} × 10 s^{-1} à 29,0°C	0,132	0,107	0,0985	0,0853 (r = 0,994)
k_{obs} × 10 s^{-1} à 42,0°C	0,301	0,241	0,216	0,184 (r = 0,998)
CH_3COOH/CH_3COONa [CH_3COOH]/[CH_3COONa] = 1; $pH_{réel}$ = 6,89[a]				
CH_3COOH (*M*)	0,082	0,042	0,011	0 (intercept)[b]
k_{obs} × 10^3 s^{-1} à 29,0°C	1,19	0,874	0,664	0,575 (r = 0,999)
k_{obs} × 10^2 s^{-1} à 42,0°C	0,304	0,230	0,166	0,146 (r = 0,999)

[a] $pH_{réel}$ = pH lu + 0,4 (5).
[b] Extrapolation à concentration nulle (régression linéaire).

TABLEAU 3. Hydrolyse des orthoesters **1**, **2**, **3**, **4**, **5** et **6**. Constantes catalytiques et grandeurs d'activation à 25,0°C

Produits	Catalyseur	k_{cat} (M^{-1} s^{-1})[b]	$\Delta H^{\neq}$ (kcal/mole)[c]	$\Delta S^{\neq}$ (ue)[d]
1	H_3O^+	11	14,0	−7
	HCOOH	2,32 × 10^{-4}[a]		
2	H_3O^+	2,16 × 10^3	11,2	−6
	HCOOH	2,55 × 10^{-2}	14,2	−18
	CH_3COOH	2,72 × 10^{-3}[a]		
3	H_3O^+	9,18 × 10^2	11,3	−7
	HCOOH	1,44 × 10^{-2}	13,7	−21
	CH_3COOH	2,53 × 10^{-3}[a]		
4	H_3O^+	53,9	11,8	−11
	HCOOH	1,86 × 10^{-3}	12,1	−31
5	H_3O^+	3,3 × 10^3	10,5	−7
	HCOOH	7,53 × 10^{-2}	11,0	−27
	CH_3COOH	5,44 × 10^{-3}	12,7	−26
6	H_3O^+	2,3 × 10^3	10,4	−8
	HCOOH	8,35 × 10^{-2}	12,9	−20
	CH_3COOH	5,44 × 10^{-3}	13,4	−24

[a] t = 29,0°C.
[b] Erreur sur k_{obs} < 3%.
[c] Erreur sur $\Delta H^{\neq}$ < 0,8 kcal/mol.
[d] Erreur sur $\Delta S^{\neq}$ < 3 cal/mol/K.

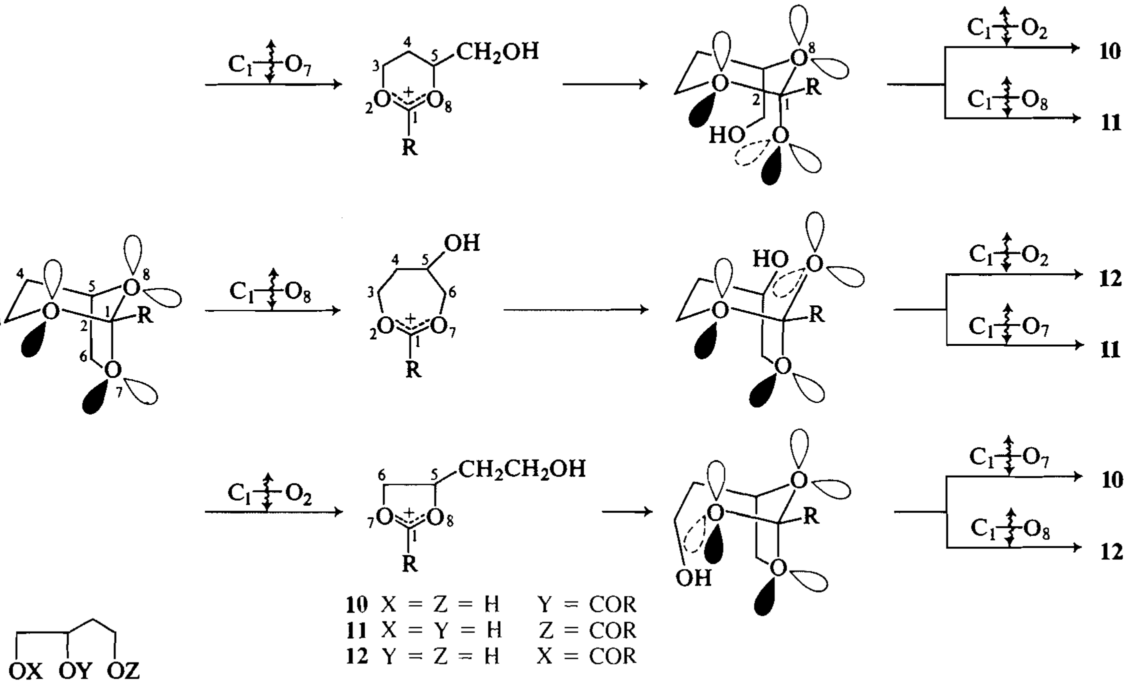

SCHÉMA 5

TABLEAU 4. Constantes de vitesse relatives k_{H^+} dans l'hydrolyse d'orthoesters cycliques et non cycliques

R	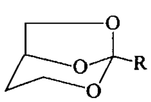	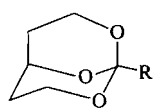	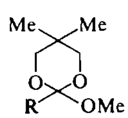	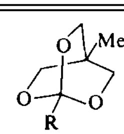	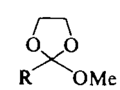	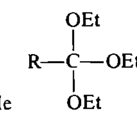
H	1	1	1	1	1	1
Me	196	61	221	63	77	38
Ph	83	43	99	88	30	0,6

TABLEAU 5. Comparaison avec l'hydrolyse des trioxa-2,4,10 adamantanes

Substrats	$k_{H_3O^+}$	$\Delta S^{\neq}$	Substrats	$k_{H_3O^+}$	$\Delta S^{\neq}$	Substrats	$k_{H_3O^+}$	$\Delta S^{\neq}$
1	11	−7	**4**	53,9	−11	**7**	$3{,}3 \times 10^{-2}$	−27
2	$2{,}2 \times 10^{3}$	−6	**5**	$3{,}3 \times 10^{3}$	−7	**8**	$6{,}2 \times 10^{-4}$	−19
3	$9{,}2 \times 10^{3}$	−7	**6**	$2{,}3 \times 10^{3}$	−8	**9**	$9{,}5 \times 10^{-5}$	−12

compétition avec les effets mésomères (stabilisation de l'ion carboxonium à la fois par CH_3 et C_6H_5).

Réactivité

L'examen du tableau 3 montre qu'il n'existe pratiquement pas de différence de réactivité entre les séries bicyclo[3.2.1] octane et bicyclo[3.3.1] nonane pour un substituant donné, confirmant ainsi de façon plus précise les résultats obtenus par Hall *et al.* (12) pour les dérivés non substitués **1** et **4**.

L'introduction d'un cycle à cinq chaînons en série bicyclo[3.2.1] octane n'a donc pas de conséquence notable sur la réactivité des orthoesters. Des observations similaires ont déjà été faites antérieurement: il n'existe pas de différence de réactivité entre le diéthoxy-2,2 tétrahydrofuranne et le diéthoxy-2,2 tétrahydropyranne (7) pas plus qu'il n'en existe entre les méthoxy-2 dioxolannes-1,3 et les méthoxy-2 dioxannes-1,3 (4). De même un travail récent de Kresge en série bicyclo[2.2.1] heptane confirme l'absence de tension de cycle ou tension angulaire dues à la présence de cycles à cinq éléments dans l'hydrolyse des orthoesters (13).

Le fait que l'état de transition de la réaction soit peu avancé le long du chemin réactionnel n'est probablement pas étranger au "tassement" de la réactivité des orthoesters; cependant, une caractéristique commune à tous les orthoesters étudiés jusqu'à maintenant est une orientation favorable des paires d'électrons libres sur les atomes d'oxygène permettant l'hydrolyse avec contrôle stéréoélectronique.

Partie expérimentale

Les spectres de rmn ^{1}H ont été enregistrés sur un appareil Varian EM 390 (référence interne: TMS).

Synthèse

Les orthoesters **1**, **2**, **3**, **4**, **5** et **6** ont été préparés par réaction de transestérification à partir du butanetriol-1,2,4 (**1**, **2** et **3**) ou du pentanetriol-1,3,5 (**4**, **5** et **6**) et des orthocarboxylates de triméthyle ou

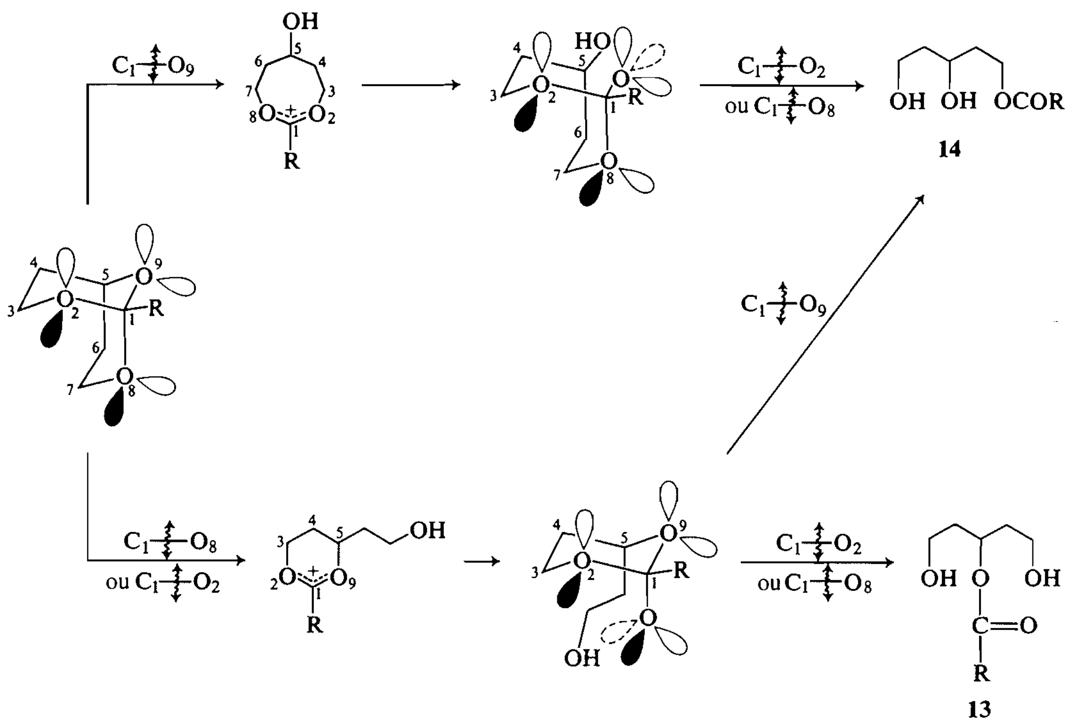

SCHÉMA 6

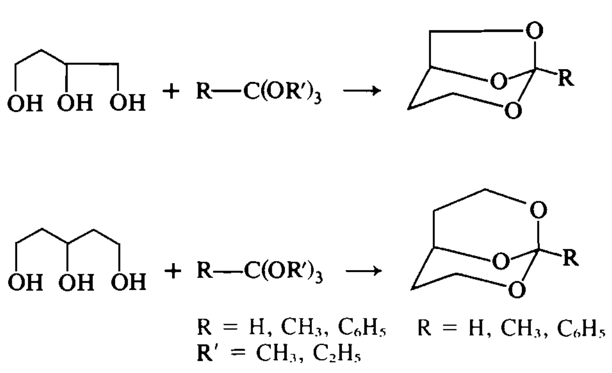

SCHÉMA 7

triéthyle correspondants (schéma 7).

1: La méthode reportée par Crank et Eastwood (14) conduit à des rendements médiocres. Ce produit a été obtenu en modifiant la procédure reportée par Hall *et al.* (12): un mélange de 14,8 g (0,1 mol) d'orthoformiate d'éthyle et 10,6 g de butanetriol-1,2,4 (Aldrich) est chauffé à 100°C pendant 3 h sous pression normale. On récupère ainsi les deux premières molécules d'alcool. La température est abaissée à 50°C et on fait barboter de l'acide chlorhydrique gazeux sec pendant 2 min. Le mélange est agité pendant 15 min et la pression abaissée à 20 Torr (1 Torr = 133.3 Pa). En chauffant progressivement, la troisième molécule d'éthanol est libérée et l'orthoester distillé. Une deuxième distillation soignée permet d'obtenir 6 g d'orthoester **1** pur; Eb. = 66–67°C/20 Torr; rendement: 52% (litt. (12) Eb. = 82°C/30 Torr; rendement: 70%); rmn ^{1}H ($CDCl_3$) δ: 1,2–1,4 (1H, deux multiplets, H4a), 2,1–2,5 (1H, multiplet symétrique, H4e), 3,6–4,1 (4H, multiplet, H méthyléniques sur C3 et C6), 4,5 (1H, multiplet, H5), 5,8 (1H, singulet, H1).

2: 16,2 g (0,1 mol) d'orthoacétate d'éthyle et 10,6 g de butane triol-1,2,4 (0,1 mol) sont dissous dans 50 mL d'alcool isobutylique anhydre. Ce mélange est chauffé progressivement jusqu'à 100°C. Une première fraction distille à 78°C; une deuxième fraction distille à 100°C; en abaissant la pression à 20 Torr on recueille l'orthoester entre 67°C et 72°C. Après redistillation, on obtient 5 g d'orthoester **2** pur; Eb. = 70°C/20 Torr; rendement: 38%; rmn ^{1}H ($CDCl_3$) δ: 1,2–1,5 (1H, deux multiplets, H4a), 1,58 (3H, singulet, méthyle sur C1), 2,2–2,5 (1H, multiplet symétrique, H4e), 3,7–4,2 (4H, multiplet, H méthyléniques sur C3 et C6), 4,6–4,8 (1H, multiplet, H5).

3: 3,7 g (0,02 mol) d'orthobenzoate de méthyle et 2,2 g (0,02 mol) de butanetriol-1,2,4 sont chauffés progressivement jusqu'à 140°C, période pendant laquelle on recueille du méthanol. Le résidu visqueux qui reste dans le ballon est distillé pour donner 2 g d'orthoester **3**; Eb. = 120°C/0,5 Torr; rendement: 60%; rmn ^{1}H ($CDCl_3$) δ: 1,3–1,6 (1H, deux multiplets, H4a), 2,2–2,6 (1H, multiplet symétrique, H4e), 3,9–4,5 (4H, multiplet, H méthyléniques sur C3 et C6), 4,80 (1H, multiplet, H5), 7,3–7,8 (3H, massif, H aromatiques).

4: Cet orthoester a été synthétisé suivant la procédure décrite par Hall *et al.* (12); Eb. = 78°C/10 Torr; rendement: 83% (litt. (12) Eb. = 78°C/ 10 Torr; rendement: 75%; rmn ^{1}H ($CDCl_3$) δ: 1,4–2,6 (4H, massif, H méthyléniques sur C4 et C6); 3,5–4,4 (5H, massif, H méthyléniques sur C3, C5 et C7), 5,78 (1H, singulet, H1).

5: Ce nouveau produit est préparé selon la procédure utilisée pour le composé **4**; Eb. = 125°C/0,03 Torr; rendement: 81%; rmn ^{1}H ($CDCl_3$) δ: 1,4–2,6 (3H, singulet à 1,45, méthyle sur C1; 4H, massif, H méthyléniques sur C4 et C6), 3,5–4,5 (5H, massif, H méthyléniques sur C3, C5 et C7).

6: 2,4 g (0,02 mol) de pentanetriol-1,3,5 et 3,7 g (0,02 mol) d'orthobenzoate de méthyle sont dissous dans 80 mL de xylène anhydre et portés à reflux pendant 48 h en présence de 100 mg d'acide paratoluènesulfonique. Au mélange refroidi on ajoute une solution saturée de carbonate de sodium. Après extraction du solvant, le produit brut est distillé. On obtient ainsi 1,5 g d'orthoester **6** pur; Eb. 111–113°C/0,08 Torr; rendement; 37%; rmn ^{1}H ($CDCl_3$) δ: 1,4–2,6 (4H, massif, H méthyléniques sur C4 et C6), 3,4–4,6 (5H, massif, H méthyléniques sur C3, C5 et C7), 7,2–7,7 (5H, massif, H aromatiques).

Analyse des produits d'hydrolyse

Après hydrolyse des orthoesters aromatiques **3** et **6** dans les conditions cinétiques, les produits d'hydrolyse sont analysés par rmn ^{1}H ($CDCl_3$). Dans les deux cas, la rmn ne révèle, aux erreurs d'intégration près, qu'un seul proton en α de la fonction benzoate. L'hydrolyse de **3** conduit donc essentiellement à l'ester **10** (cf. schéma 3) et l'hydrolyse de **6** conduit, quant à elle, uniquement à l'ester **13** (cf. schéma 4).

Caractéristiques rmn ^1H des produits d'hydrolyse ($CDCl_3$)

10: δ 1,8–2,4 (2H, massif, CH_2—CH_2OH), 2,85 (2H, massif, O—*H*), 3,8–4,2 (4H, massif, CH_2—O), 5,4–5,7 (1H, multiplet, *CH*—$OCOC_6H_5$), 7,3–7,6 et 7,9–8,1 (3H + 2H, deux multiplets, H aromatiques).

13: δ: 1,6–2,4 (4H, massif, CH_2—CH_2OH), 3,2–4,6 (6H, massif, CH_2OH), 5,1–5,4 (1H, multiplet, *CH*—$OCOC_6H_5$), 7,3–7,6 et 7,9–8,1 (3H + 2H, deux multiplets, H aromatiques).

Méthodes cinétiques

Les méthodes cinétiques sont analogues à celles décrites par ailleurs (2, 5).

1. O. Bouab, G. Lamaty et C. Moreau. J. Chem. Soc. Chem. Commun. 678 (1978).
2. O. Bouab, G. Lamaty, C. Moreau, O. Pomares, P. Deslongchamps et L. Ruest. Can. J. Chem. **58**, 567 (1980).
3. R. A. McClelland et P. K. W. Lam. Can. J. Chem. **62**, 1068 (1984); **62**, 1074 (1984).
4. O. Bouab, G. Lamaty, C. Moreau et O. Pomares. Nouv. J. Chim. **5**, 175 (1981).
5. G. Lamaty, C. Moreau et Z. Mouloungui. Can. J. Chem. **61**, 2643 (1983).
6. G. Douheret. Bull. Soc. Chim. Fr. 1412 (1967).
7. O. Bouab, C. Moreau et M. Zeh Ako. Tetrahedron Lett. 61 (1978).
8. E. H. Cordes et H. G. Bull. Chem. Rev. **74**, 581 (1974).
9. T. H. Fife. Acc. Chem. Res. **5**, 264 (1972).
10. Y. Chiang, A. J. Kresge, P. Salomaa et C. I. Young. J. Am. Chem. Soc. **96**, 4494 (1974).
11. P. Deslongchamps. Stereoelectronic effects in organic chemistry. Pergamon Press, London. 1983.
12. H. K. Hall, Jr., F. de Blauwe et T. Pyriadi. J. Am. Chem. Soc. **97**, 3854 (1975).
13. R. A. Burt, Y. Chiang, H. K. Hall, Jr. et A. J. Kresge. J. Am. Chem. Soc. **104**, 3687 (1982).
14. G. Crank et F. W. Eastwood. Aust. J. Chem. **17**, 1385 (1964).

γ-Phosphono-γ-lactones. The use of allyl esters as easily removable phosphonate protecting groups

MATTHIAS KAMBER AND GEORGE JUST[1]
Department of Chemistry, McGill University, Montreal, P.Q., Canada H3A 2K6

Received February 17, 1984

MATTHIAS KAMBER and GEORGE JUST. Can. J. Chem. **63**, 823 (1985).

During the synthesis of γ-lactones bearing a phosphonic acid group at the γ-position, difficulties were encountered generating the free phosphonic acids from corresponding esters. A protecting group used for carboxylic acids was adapted to phosphonic acids, making this transformation easy.

MATTHIAS KAMBER et GEORGE JUST. Can. J. Chem. **63**, 823 (1985).

Lors d'une synthèse de γ-lactones ayant un acide phosphonique en position γ, nous avons éprouvé des difficultés à transformer des esters phosphoniques en acides libres. Cette transformation a été rendue facile par adaptation aux acides phosphoniques d'un groupe utilisé pour protéger les acides carboxyliques.

Introduction

Some years ago (1), we pointed out that the steric strain responsible for the chemical reactivity and hence biological activity of the classical β-lactam antibiotics could be replaced by a strain generated by electron-withdrawing groups attached to the nitrogen atom of the β-lactam moiety. This concept was borne out by the discovery of monobactams (2) **1**, which are monocyclic β-lactams substituted by a sulfonic acid at the amidic nitrogen, and the synthesis of analogous monophosphams (3) of type **2**, of which the monomethyl ester **2** seemed to be the most active (3).

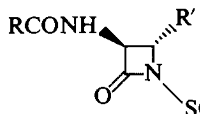

1 $R' = H, CH_3$

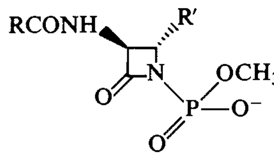

2

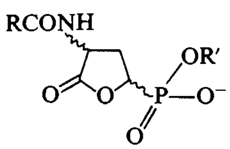

3*a* $R' = H, K^+$
b $R' = CH_3$

It occurred to us that the activated β-lactam function, $\nu \geq 1765\ cm^{-1}$, which most probably acts as an acylating agent (4), could be replaced by a γ-lactone, $\nu \simeq 1780\ cm^{-1}$, which should have similar acylating properties. We therefore decided to prepare γ-lactones **3***a and* **3***b*, the latter because of its similarity with monophospham **2**.

Synthesis of phosphonolactone 12

Glycine was transformed in 80% yield to its allyl ester hydrochloride, mp 68–71°C, using the recently described method of Brooks and Chan (5), and acylated in 80% yield with di-*tert*-butydicarbonate to **4**. Rearrangement of the bis-silylated dianion of **4** according to the procedure developed by Bartlett and Barstow (6) gave **6***a*, which was transformed to methyl ester **6***b*, using ethereal diazomethane.

Because of relatively low yields in the rearrangement step, and the necessity to esterify the carboxyl function with diazomethane on a large scale, carbobenzyloxyglycine was subjected to a similar sequence. Ester formation with allyl alcohol – trimethylsilyl chloride (Me_3SiCl) gave **5**, mp 36–37°C, and rearrangement of the bis-trimethylsilyl ether of the dianion of **5** gave crude acid **7***a*. Methylation with methanol–Me_3SiCl (5) gave **7***b*, mp 40–41°C, in 85% overall yield, based on carbobenzyloxyglycine.

Whereas the ozonolysis of analogous rearranged compounds derived from crotyl esters of type **7** to the corresponding aldehyde was apparently not possible (6), **7***b* could be easily ozonized at −78°C, using methylene chloride as solvent. Reductive work-up using dimethyl sulfide gave **8**, contaminated with a side-product which was difficult to remove.

Treatment of the crude aldehyde **8** with dimethyl phosphite in methylene chloride containing some triethylamine at 20°C overnight gave a mixture of the aldehyde-phosphonate adduct **13** and the cyclic phosphono-lactone **12** as a mixture of diastereoisomers. Stirring of the mixture in methylene chloride – trifluoroacetic acid (5:1) resulted in the complete conversion of the adduct **13** to the highly strained lactone **12**, $\nu = 1800\ cm^{-1}$.

Alternatively, phosphonolactone **12** was obtained, albeit in very low yield, in the following manner. Olefinic acid **7***a* was ozonolyzed to **9**, mp 139–142°C. Mesylation of **9** gave a mixture of mesylate **10** and chloride **11**. The latter was also obtained by treating **9** with thionyl chloride. Arbusov reaction of **11** with trimethyl phosphite gave **12** in very low yield.

Attempts to hydrolyse, partially or completely, dimethyl phosphonate **12** to monomethyl ester or diacid **3** ($R = OCH_2Ph$) failed. These attempts included (a) reaction with Me_3SiCl/KI or NaBr in acetonitrile (7, 8), which resulted either in opening of the lactone ring, or very slow reaction giving ill-defined products; (b) reaction with HBr/acetic acid (9), which gave polar products that did not provide starting material upon remethylation; (c) treatment with LiI/2,4,6-collidine in DMF (10) (similar to b); (d) reaction with thiourea (11): this gave what appeared to be the desired acid or acids, since remethylation provided starting material. However, the purification proved to be extremely difficult, and no clean acid could be isolated; (e) sodium bromide/benzyl triethylammonium chloride (12): the reaction was very slow, and no desired acid could be isolated.

It was clear that no good method was at hand, and that we required a phosphonic acid protecting group which could be removed under mild conditions, and where the requisite dialkyl or alkyl methyl phosphonate could be prepared and handled with relative ease. Furthermore, the resulting phosphonic acid

[1] Author to whom correspondence may be addressed.

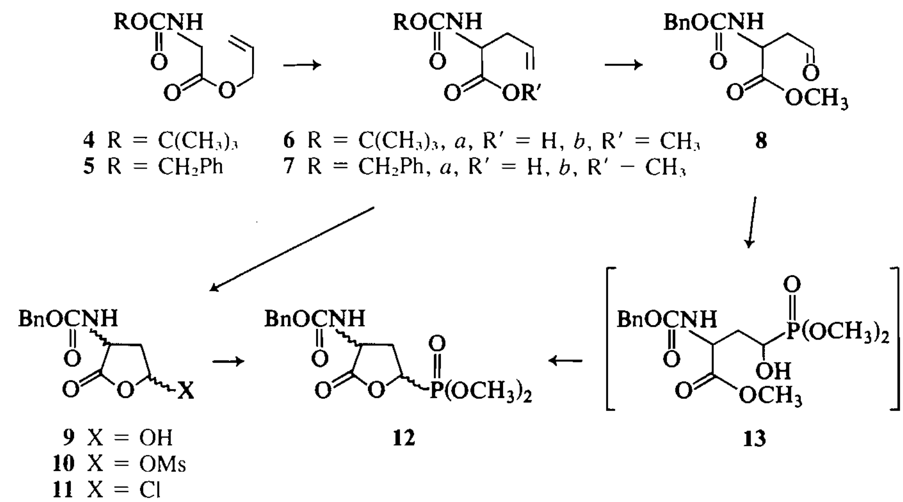

SCHEME 1

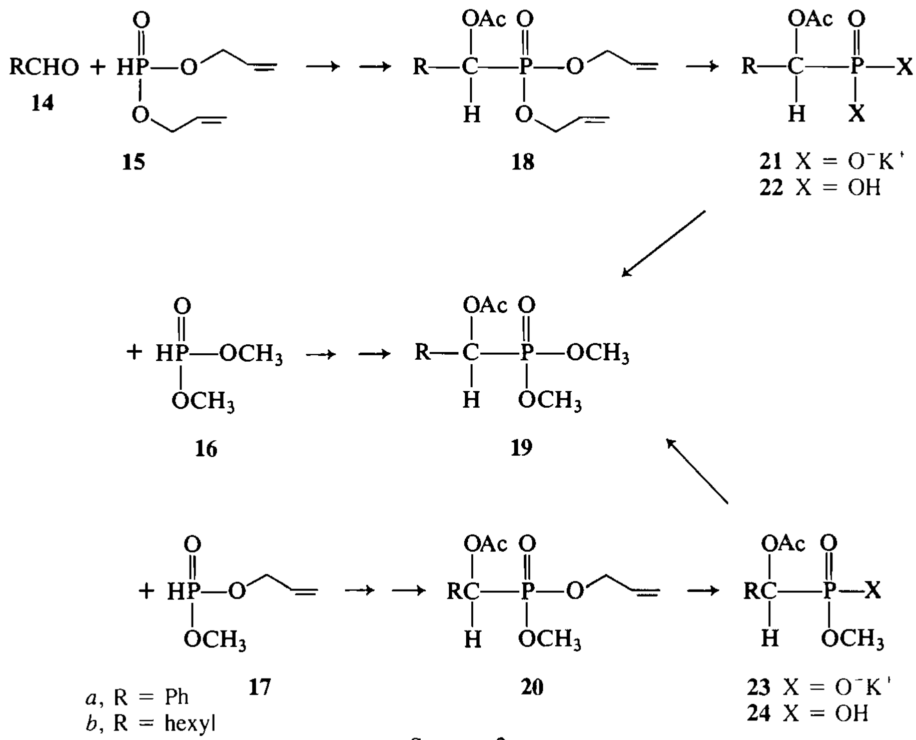

SCHEME 2

or salt should not require further purification beyond simple extraction or crystallization.

A variety of dialkyl phosphonates were investigated, and abandoned for the following reasons.

(a) Dibenzyl or benzyl methyl phosphonates are unstable compounds.

(b) Methyl trichloroethyl phosphonate is difficult to prepare, and trouble was anticipated in separating the free phosphonic acid from the zinc ions produced during Zn-mediated removal of the trichloroethyl group.

(c) Bis-trimethylsilylethyl phosphonate rearranges to trimethylsilyl phosphonate with extrusion of ethylene.

We then investigated the suitability of using diallyl and allyl methyl phosphonate as phosphonating agent. Diallyl phosphonate was prepared according to the general procedure described (13). After numerous trials (14, 15; also ref. 13, p. 28), allyl methyl phosphonate was prepared by reaction of allyl alcohol with phosphorus trichloride, and treating the resulting allyl phosphorodichloridite, bp 45–52°C (15 Torr; 1 Torr = 133.3 Pa), first with methanol–pyridine and then with water–pyridine.

For model studies, we prepared six α-acetoxyphosphonates **18**a, b, **19**a, b, and **20**a, b by treating benzaldehyde or heptanal with the appropriate diallyl, dimethyl, and allyl methyl phosphonates **15**, **16**, and **17**, and acetylating the resulting dialkyl hydroxyphosphonates. Three systems were used to try to remove the allyl group.

(1) Catalytic transfer hydrogenation using ammonium formate in methanol and 10% Pd/C (16). The results were not very reproducible, and methanolysis of the acetate group was observed.

(2) 3% $Pd(PPh_3)_4$/4–5%PPh_3/potassium 2-ethylhexanoate

in ethyl acetate (17). This system removed the allyl group smoothly to give potassium salts **21***a*, *b* and **23***a*, *b*. Their structures were proven by remethylation to give the dimethyl α-acetoxyphosphonates **19***a*, *b*. In each case, no starting materials **18***a*, *b* or **20***a*, *b* could be detected, and **19***a*, *b* was obtained as the major product (>90%), as established by tlc, and 200-MHz ^{1}H nmr in the case of **21***a*.

The isolation of the potasium salt was achieved by crystallization (**21***a*, 83%), or required evaporation to dryness, and washing with ether (**21***b*, **23***a*, **23***b*, 5–10% potassium 2-ethylhexanoate contamination). Other, more polar, diallyl phosphonates (see following paper) gave less soluble potassium salts which precipitated and were obtained in high yield and purity.

(3) Wilkinson's catalyst ($(Ph_3P)_3RhCl$). Heating to reflux of phosphonates **18***a*, **18***b*, **20***a*, and **20***b* in 15% aqueous acetonitrile containing 2–3% Wilkinson's catalyst for 1–2 hours (18) resulted in the disappearance of the starting material (tlc) and formation of **22***a*, **22***b*, **24***a*, and **24***b* in 71, 69, 86, and 78%, respectively. The work-up required evaporation of the solvent, dissolving the phosphonic acids in water, and separation from the precipitated Wilkinson's catalyst by filtration. Freeze-drying then gave the products. Their structures were proven by remethylation with ethereal diazomethane (tlc and, in the case of **24***a*, 200-MHz ^{1}H nmr).

None of the yields were optimized. Dimethyl phosphonates **19***a*, *b* were stable to the reaction conditions outlined under (2) and (3).

The application of this methodology to phosphono lactones **3** will be reported in due course.

Experimental

Thin-layer chromatography (tlc) was performed on Merck Silica Gel 60 F_{254} aluminum-backed plates. Flash chromatography was done on Woelm Silica (32–63 μm). Melting points (mp) were measured on a Gallenkamp block and are uncorrected, unless specified otherwise. The nmr spectra were recorded on Varian T-60, T-60A, and, where noted, XL-200 and Bruker WH-90 spectrometers. Infrared (ir) spectra were recorded on a Perkin Elmer 257 spectrophotometer. Abbreviations: br = broad, s = strong, m = medium, w = weak.

Mass spectra (ms) were obtained on HP 5984A or LKB 9000 spectrometers, in the direct inlet mode unless indicated otherwise.

Carbobenzyloxy (Cbz) glycine allyl ester 5

Cbz-glycine (6.3 g, 30 mmol) was dissolved in 35 mL allyl alcohol. Then Me_3SiCl (9.5 mL, 73 mmol) was added over a period of 5 min and the mixture left under a N_2 atmosphere at room temperature overnight (5). The solvent was evaporated and the product filtered through silica gel (short 3 × 5 cm column, methylene chloride). After crystallization from ether/petroleum ether, 7.20 g (28.9 mmol, 96%) of ester **5** was obtained, mp 36–37°C; ir ($CHCl_3$, cm^{-1}): 3860 m, 3620 m, 3450 m, 3020 s, 2990 m, 1745 s, 1725 s, 1515 m, 1420 m, 1210 s, 1050 m, 930 m, 750 s; ^{1}H nmr (60 MHz, $CDCl_3$) δ: 7.4 (s, 5H, C_6H_5), 6.2–5.6 (m, 2H, NH and =CH), 5.5–5.3 (m, 2H, H_2C=), 5.2 (s, 2H, Ar—CH_2—O), 4.7 (d, *J* = 6 Hz, 2H, O—CH_2—CH=CH_2), 4.1 (d, *J* = 6 Hz, 2H, CO—CH_2—N); ms (*m/z*, %): 249 (M^+, 6), 108 (41), 107 (31), 91 (100, 65 (11), 41 (17).

*Rearranged acid 7*a *(ref. 6)*

Hexamethyldisilazane (7 mL, 33 mmol) was dissolved in 100 mL dry tetrahydrofuran (THF) and cooled under N_2 to 0°C. Then n-butyllithium (20 mL, 1.55 *n* in hexane, 31 mmol) was added dropwise and after 10 min the solution was cooled to −78°C. The allyl ester **5** (3.75 g, 15.05 mmol, dissolved in 10 mL THF) was added over 5 min. After another 30 min, Me_3SiCl (4.2 mL, 33 mmol) was added, the mixture stirred for 15 min at −78°C, and then warmed up over 1 h to 20°C. The yellow solution was then warmed for 1–1.5 h to 55–60°C, cooled to 20°C, and diluted with 20 mL methanol. The solvents were evaporated to about 20% of their original volume, diluted with ether, and extracted 4 times with a 5% NaOH solution. Acidification of the combined water layers with cold 6 *N* HCl and extraction with methylene chloride (CH_2Cl_2) gave, after drying ($MgSO_4$) and evaporation, a quantitative yield of the crude acid **7***a* (7.5 g) as a yellowish oil. It was used without further purification; ir ($CHCl_3$, cm^{-1}): 3550–2500 br, m, 3440 m, 2950 m, 1720 s, 1500 m, 1340 m, 1050 m, 900 m; ^{1}H nmr (60 MHz, $CDCl_3$) δ: 10.5 (s, 1H, COOH), 7.3 (s, 5H, C_6H_5), 6.0–5.4 (m, 1H, =CH), 5.3–5.0 (m, approx. 3H, NH and H_2C=), 5.1 (s, 2H, Ar—CH_2—O), 4.4 (m, 1H, N—*CH*—COO), 2.6 (t, *J* = 6 Hz, 2H, CH_2—CH=CH_2); ms (*m/z*, %): 249 (M^+, 11), 208 (M^+ − 41, 2), 204 (M^+ − 45, 2), 108 (22), 107 (10), 91 (100), 79 (16), 65 (12), 41 (29).

*Methyl ester 7*b

Crude acid **7***a* (7.5 g) was dissolved in 30 mL methanol and Me_3SiCl (4.5 mL, 35.5 mmol) was added. Stirring overnight under N_2, evaporation to dryness, and recrystallization from ether/hexane gave the ester **7***b* as colourless crystals (3.47 g, 13.2 mmol, 88% from allylester **5**), mp 40–41°C; ir ($CHCl_3$, cm^{-1}): 3450 m, 2990 m, 1740 s, 1720 s, 1515 m, 1210 s, 1050 m, 920 m; ^{1}H nmr (60 MHz, $CDCl_3$) δ: 7.2 (s, 5H, C_6H_5), 5.9–5.3 (m, 2H, NH and =CH), 5.2–4.9 (m, 2H, H_2C=), 5.1 (s, 2H, Ar—CH_2—O), 4.4 (m, 1H, N—*CH*—COO), 3.7 (s, 3H, $COOCH_3$), 2.5 (t, *J* = 6 Hz, 2H, CH_2—CH=CH_2); ms (*m/z*, %): 263 (M^+, 17), 222 (M^+ − 41, 6) 204 (M^+ − 59, 4), 178 (4), 160 (4), 108 (8), 107 (3), 91 (100), 79 (4), 65 (8), 59 (2), 41 (5).

Aldehyde 8

The ester **7***b* (1.78 g, 6.75 mmol) was dissolved in CH_2Cl_2 and cooled to −78°C. Then ozone was bubbled through the solution until it turned blue. Excess ozone was removed with a steam of dry N_2. Dimethylsulfide (5 mL) was added and the reaction left at ~20°C overnight. The solvent was evaporated and the crude yellow oil partitioned between ether and saturated $NaHCO_3$ solution, and the ether layer dried over $MgSO_4$ and evaporated to give crude aldehyde **8** (1.73 g, 6.53 mmol, 96%) as a yellowish oil. The aldehyde **8** could be used without further purification; ir ($CHCl_3$, cm^{-1}): 3430 m, 2950 m, 2940 m, 1720 br s, 1500 s, 1430 m, 1330 m, 1050 m; ^{1}H nmr (60 MHz, $CDCl_3$) δ: 9.7 (s, 1H, CHO), 7.3 (s, approx. 5H, C_6H_5), 5.6 (m, 1H, NH), 5.2 (s, approx. 2H, Ar—CH_2—O), 4.7 (m, 1H, N—*CH*—COO), 3.7 (s, 3H, $COOCH_3$), 3.1 (d, *J* = 6 Hz, 2H, —CH_2—CHO); ms (*m/z*, %): 265 (M^+, 6), 206 (M^+ − 59, 3), 162 (M^+ − 59–44, 3), 115 (3), 108 (22), 107 (9), 91 (100), 79 (6), 77 (5), 69 (9), 65 (12), 59 (2), 55 (6), 44 (4), 43 (8), 41 (5).

Lactone 12

Crude aldehyde **8** (580 mg, 2.2 mmol) was dissolved in 1 mL CH_2Cl_2, dimethylphosphite (0.5 mL, 3.8 mmol) and triethylamine (0.1 mL) were added, and the mixture left overnight at ~20°C. The solvent was pumped off, 2.5 mL CH_2Cl_2 and 0.5 mL trifluoroacetic acid were added, and the mixture left for ~20 h. Flash chromatography (silica gel, ethyl acetate – hexane 5:1) gave 490 mg (1.43 mmol, 65%) of the lactone **12** as a mixture of 2 diastereoisomers; ir ($CHCl_3$, cm^{-1}): 3420 m, 2950 m, 2850 m, 1800 s, 1720 s, 1495 m, 1450 m, 1250 m, 1150 s, 1030 s; ^{1}H nmr (60 MHz, $CDCl_3$) δ: 7.3 (s, 5H, C_6H_5), 6.0–5.7 (m, 1H, NH), 5.1 (s, 2H, Ar—CH_2—O), 4.8–4.2 (m, 2H, P—CH and N—CH—COO), 3.8 (m, 6H, 2 P—O—CH_3), 2.9–2.1 (m, 2H, —CH_2—); ms (*m/z*, %): 343 (M^+, 19), 282 (3), 252 (17), 237 (7), 236 (76), 234 (2), 174 (4), 137 (13), 108 (10), 91 (100), 79 (11), 65 (11), 59 (4), 44 (6).

Allyl phosphorodichloridite

To 320 mmol PCl_3 at −75°C was added 320 mmol of freshly distilled allyl alcohol over a period of 5 h. The HCl formed was removed with a stream of dry N_2. The reaction mixture was warmed slowly to room temperature and kept stirring overnight (N_2 stream). Distillation was interrupted after 55 mmol (17%) allyl phosphorodichloridite, bp 35–40°C/10 Torr, was obtained because of reported spontaneous polymerization resulting in explosion of the mixture distilled to less than half of its volume.

Allyl methyl phosphonate 17

Allyl phosphorodichloridite (23.6 mmol) was dissolved in 80 mL dry THF and cooled under N_2 to −78°C. Then 23.6 mmol methanol and 23.6 mmol pyridine in 10 mL THF were added dropwise over a period of 30 min. Stirring was continued for another 1.5 h at −78°C, and for 2 h at 20–25°C. The reaction mixture was cooled to 0°C and 10 mL THF containing 25 mmol water and 26 mmol pyridine were added dropwise. The mixture was stirred 0.5 h at 0°C and then 2 h at 20–25°C. After filtration and evaporation, the crude yellow oil was dissolved in 2 mL of CH_2Cl_2 and filtered over 5 g silica gel using CH_2Cl_2 as eluant. After evaporation to dryness, the methyl allyl phosphonate **17** could be obtained as a clear oil (2.51 g, 18.5 mmol, 78.5%); ir ($CHCl_3$, cm^{-1}): 2440 (P—H), 1270–1180 (P=O, C—O); ^1H nmr (60 MHz, $CDCl_3$) δ: 6.85 (d, J = 700 Hz, 1H, PH), 6.2–5.7 (m, 1H, =CH), 5.6–5.1 (m, 2H, H_2C=), 4.7–4.4 (m, 2H, H_2COP), 3.8 (d, J = 12 Hz, 3H, H_3COP); ms (m/z, %): 137 (M^+ + 1, 0.5), 97 (29), 95 (M^+ − 41, 7), 80 (29), 79 (M^+ − 57, 100), 58 (66), 47 (25), 41 (27).

Diallyl phosphonate 15

Diallyl phosphonate was prepared in 86% yield from 1 equiv. phosphorus trichloride, 3 equiv. allyl alcohol, and 2 equiv. pyridine using the general procedure described (13); ir ($CHCl_3$, cm^{-1}): 2430 (P—H), 1270–1200 (P=O, C—O); ^1H nmr (60 MHz, $CDCl_3$) δ: 6.8 (d, J = 700 Hz, 1H, PH), 6.2–5.6 (m, 2H, =CH), 5.5–5.1 (m, 4H, H_2C=), 4.7–4.3 (m, 4H, H_2COP); ms (m/z, %): 121 (M^+ − 41 (C_3H_5), 51), 105 (M^+ − 57, 4), 83 (12), 80 (10), 79 (17), 65 (14), 58 (11), 57 (CH_2=$CHCH_2O$, 100), 41 (80).

Diallyl, methyl allyl, and dimethyl acetoxyphosphonates 18, 19, and 20

All six compounds were prepared in an identical manner, and their spectra were very similar. A representative example is described. To a methylene chloride (5 mL) solution of benzaldehyde **14***a* (2 mmol) was added diallyl phosphonate **15** (2.16 mmol) and 3 drops of triethylamine. After tlc indicated completion of the reaction (16 h), acetic anhydride (2 mL) and triethylamine (1 mL) were added at 0°C. After 2 h, diethyl ether and ice-water were added. Stirring for 0.5 h and washing to neutrality gave after drying ($MgSO_4$), evaporation, and flash chromatography (silica gel, petroleum ether – acetone 10:1) diallyl phosphonate **18***a* (1.36 mmol, 68%) as a clear oil.

18*a*: ir (film, cm^{-1}): 1755 (C=O), 1260 (P=O), 1220 (O—C), 1020 (P—O); ^1H nmr (60 MHz, $CDCl_3$) δ: 7.3 (m, 5H, C_6H_5), 6.1 (d, J = 13 Hz, approx. 1H, HCP), 6.1–5.5 (m, 2H, =CH), 5.4–5.0 (m, 4H, H_2C=), 4.6–4.3 (m, 4H, H_2COP), 2.1 (s, 3H, H_3CCO); ms (m/z, %): 310 (M^+, 0.2), 267 (M^+ − 43, 4), 162 ($HPO(OCH_2CH{=}CH_2)_2$, 10), 121 ($HPO_2OCH_2CH{=}CH_2$, 20), 107 (C_6H_5CHOH, 17), 77 (C_6H_5, 10), 57 ($H_2C{=}CHCH_2O$, 9), 43 ($COCH_3$, 100), 41 ($CH_2CH{=}CH_2$, 66).

Spectral characteristics of 18, 19, and 20

Dimethyl phosphonate **19***a*: 3.6 and 3.7 ppm (two d, J = 10 Hz, 6H, 2 CH_3OP); **19***b*: 3.78 and 3.80 ppm (two d, J = 10.6 Hz, 6H, 2 CH_3OP); allyl methyl phosphonate **20***a*: 3.6 and 3.7 ppm (two d, J 10 Hz, 3H, CH_3OP); **20***b*: 3.7 ppm (d, J = 10 Hz, 3H, CH_3OP); **18***a*, **19***a*, **20***a*: Ph—*CH*—*P*: J = 13 Hz, d; **18***b*, **19***b*, **20***b*: $C_5H_{11}CH_2$—*CH*—*P*: $J_{AX} + J_{BX}$ = 15 Hz, J(d) = 9 Hz. All mass spectra showed m/z for $HPO(OR)_2$; $HOP(OMe)_2$: **19***a* 110 (100%), **19***b* (97%); HOP(OM) ($OCH_2CH{=}CH_2$): **20***a* 136 (20%); **20***b* (80%); $HOP(OCH_2CH{=}CH_2)_2$: **18***a* 162 (10%); **18***b* (7%).

All phosphonate esters showed negligible (<0.4%) M^+ or $(M + 1)^+$ peaks except for **19***a*: M^+ 258.0664 (27.5%; calcd. 258.0657).

*Dipotassium salt 21*a

To 86 mg (0.28 mmol) of **18***a*, 1.33 mL 0.5 *M* (2.4 equiv.) potassium 2-ethylhexanoate in ethyl acetate, 20 mg (6.3 mol%) tetrakis-(triphenylphosphine)palladium(0), and 6 mg (8 mol%) triphenylphosphine were added. The reaction mixture was stirred at 20–25°C until all starting material had reacted (1.5 to 2 h). After addition of 2 mL acetone, the salt precipitated out as white crystals. Filtration gave 79 mg (83%) dipotassium salt **21***a*; ir (4% in KBr, cm^{-1}): 1705 (C=O), 1250 (P=O); ^1H nmr (60 MHz, CD_3OD) δ: 7.1 (m, 5H, C_6H_5), 5.5 (d, J = 13 Hz, 1H, HCP), 1.8 (s, 3H, H_3CCO), Dipotassium salt **21***a* was converted to its dimethyl ester **19***a* by dissolving it in methanol, and adding acidic ion-exchange resin (Amberlyte IR-120) and then ethereal diazomethane.

*Potassium salt 23*b

To 51 mg (0.17 mmol) **20***b*, 0.38 mL 0.5 *M* (1.12 equiv.) potassium 2-ethylhexanoate in ethyl acetate, 6 mg (3 mol%) tetrakis(triphenylphosphine)palladium(0), and 2 mg (4.5 mol%) triphenylphosphine were added and the mixture stirred at 20–25°C until all starting material had reacted (1.5 to 2 h). No crystals precipitated out, so the solvent was evaporated, and after the remaining yellowish oil was washed several times with ether, it solidified in the cold. Yield approximately 85–90%; ir ($CHCl_3$, cm^{-1}): 1725 (C=O), 1230 (P=O); ^1H nmr (60 MHz, $CDCl_3$) δ: 5.2 (m, 1H, HCP), 3.6 (d, J = 10 Hz, 3H, H_3COP), 2.2 (s, 3H, H_3CCO), 2.0–1.0 (br m, approx. 13H, alkyl) (^1H nmr spectrum shows approximately 5–8% impurities due to the remaining triphenylphosphine and 2-ethylhexanoate). The monopotassium salt **23***b* was converted to its dimethyl ester **19***b* as described earlier.

*Phosphonic acid 24*a

To a solution of 74 mg (0.26 mmol) **20***a* in 3 mL acetonitrile/ water (85:15), 5 mg (2 mol%) of Wilkinson's catalyst was added. After refluxing for 2 h all the starting material had reacted. The solvent was evaporated, and the residue stirred for 5 min in 5 mL of water. After filtration, the water layer was freeze-dried to give 65 mg (0.22 mmol, 86%) of the acid **24***a* as a yellow oil; ir ($CHCl_3$, cm^{-1}): 1740 (C=O), 1180 (P=O); ^1H nmr (60 MHz, $CDCl_3$) δ: 7.3 (br s, approx. 5H, C_6H_5), 6.1 (br s, 1H, HCP), 3.6 (br s, 3H, H_3COP), 2.2 (s, 3H, H_3CCO). The acid **24***a* was treated with ethereal diazomethane to give dimethyl ester **19***a*.

Acknowledgements

We wish to thank the Natural Sciences and Engineering Research Council of Canada and American Cyanamid Co. for generous financial support, and Dr. Orval Mamer and associates of the Biomedical Mass Spectrometry Unit, McGill University for the mass spectral data.

1. G. JUST and R. ZAMBONI. Can. J. Chem. **56**, 2720 (1978).
2. A. IMADA, K. KITANO, K. KINTAKA, M. MUROI, and M. ASAI. Nature, **289**, 590 (1981); R. B. SYKES, C. M. CIMARUSTI, D. P. BONNER, K. BUSH, D. M. FLOYD, N. H. GEORGOPAPADAKOU, W. H. KOSTER, W. C. LIU, W. L. PARKER, P. A. PRINCIPE, M. L. RATHNUM, W. A. SLUSARCHYK, W. H. TREJO, and J. S. WELLS. Nature, **291**, 489 (1981).
3. W. H. KOSTER, R. ZAHLER, D. P. BONNER, H. W. CHANG, C. M. CIMARUSTI, G. A. JACOBS, and M. PERRI. Monophosphams: monocyclic β-lactam antibiotics activated by N-1 phosphonic (-inic) acids. A comparative study of monobactams (2-oxoazetidine-1-sulfonic acids). Abstract 674, XXII Interscience Conference on Antimicrobial Agents and Chemotherapy Poster Session – New Monobactams. October 5, 1982.
4. D. D. KEITH, J. TENGI, P. ROSSMAN, L. TODARO, and M. WEIGELE. Tetrahedron, **39**, 2445 (1983).
5. M. BROOKS and T. H. CHAN. Synthesis, 201 (1983).
6. P. A. BARTLETT and J. F. BARSTOW. J. Org. Chem. **47**, 3933 (1982).
7. A. J. RUDINSKAS and T. L. HULLAR. J. Med. Chem. **19**, 1367 (1976).
8. (*a*) C. E. MCKENNA, M. T. HIGA, N. H. CHEUNG, and M. C. MCKENNA. Tetrahedron Lett. 155 (1977); (*b*) C. E. MCKENNA and J. SCHMIDHAUSER. J. Chem. Soc. Chem. Commun. 739 (1979).

9. A. VASELLA and R. VOEFFRAY. Helv. Chim. Acta, **65**, 1953 (1982).
10. E. J. COREY, D. H. HUA, B. C. PAN, and S. SEITZ. J. Am. Chem. Soc. **104**, 6818 (1982).
11. W. H. KOSTER, R. ZAHLER, H. W. CHANG, C. M. CIMARUSTI, G. A. JACOBS, and M. PERRI. J. Am. Chem. Soc. **105**, 3743 (1983).
12. I. PETNEHÁZY, G. Y. SZAKÁL, and L. TÖKE. Synthesis, 453 (1983).
13. HOUBEN-WEYL. Methoden der organischen Chemie. Band XII/2. Georg Thieme Verlay, Stuttgart. 1964. p. 21.
14. K. GRZÉSKOWIAK. Synthesis, 831 (1980).
15. M. KLUBA and A. ZWIERZAH. Synthesis, 134 (1978).
16. M. K. ANWER and A. F. SPATOLA. Synthesis, 929 (1980).
17. P. D. JEFFREY and S. W. MCCOMBIE. J. Org. Chem. **47**, 587 (1982).
18. B. LAGUZZA and B. GANEM. Tetrahedron Lett. 1483 (1981).

Synthesis of 3-chloro-4-(dichloromethyl)-5-hydroxy-2(5*H*)-furanone, a potent mutagen

ABEYSINGHE A. PADMAPRIYA AND GEORGE JUST[1]
Department of Chemistry, McGill University, Montreal, P.Q., Canada H3A 2A7

AND

NORMAN G. LEWIS[1]
Pulp and Paper Research Institute of Canada, 3420 University Street, Montreal, P.Q., Canada H3A 2A7

Received June 15, 1984

ABEYSINGHE A. PADMAPRIYA, GEORGE JUST, and NORMAN G. LEWIS. Can. J. Chem. **63**, 828 (1985).

Starting from tetrachloroacetone **1** and (carbomethoxymethylene)triphenylphosphorane **4**, the title compound **16** was prepared in five steps in 44% yield. Spectroscopic and chromatographic data indicated that this material was identical to a potent mutagen isolated from kraft pulp chlorination effluent. Various mutant *Salmonella typhimurium* strains (TA 98, 100, and 1537) behaved similarly when incubated with either **16** or the isolated mutagen.

ABEYSINGHE A. PADMAPRIYA, GEORGE JUST et NORMAN G. LEWIS. Can. J. Chem. **63**, 828 (1985).

A partir du tétrachloroacétone **1** et du triphénylphosphorane carboxyméthoxyméthylène **4**, le composé titre **16** a été préparé en cinq étapes dans un rendement de 44%. Cette substance était identique à un mutagène puissant isolé d'un effluent de chloration kraft. Différentes souches mutantes de *Salmonella typhimurium* (TA 98, 100 et 1537) ont réagi de façon semblable lorsque mises en incubation avec soit **16** ou le mutagène isolé.

Introduction

It is now firmly established that the effluent produced during the first chlorination stage of kraft and sulphite wood pulp bleaching is highly mutagenic (1−11). These findings generated considerable interest in the chemical structures of the mutagenic substances and various mutagens have now been identified, e.g. 2-chloropropenal and chlorinated acetones (4, 6, 7, 10, 11). In a related study it was reported that at least 30−50% of the total mutagenicity of kraft chlorination effluent was attributed to a single constituent (12, 13). This compound, tentatively proposed (12) to be the hydroxyfuranone **16** was highly mutagenic (~10^4 revertants/nmol) and, therefore, possibly carcinogenic (14).

In pulp manufacture, various effluent streams are required to remove unwanted materials formed at different stages of pulp production. These streams are subsequently combined prior to discharge into the receiving waters, and, *even* if biologically untreated, are only very weakly mutagenic (2, 5).

Nevertheless, the fate of the tentatively identified mutagen **16** deserves serious attention since its chemical stability, biodegradability, and bioaccumulation in aquatic organisms and plants is unknown.

As a first objective, therefore, a total synthesis of the hydroxyfuranone **16**, and a comparison of its mutagenicity to that of isolated effluent material was required.

Results and discussion

We considered that entry into the mutagen system could be achieved by the Wittig condensation of tetrachloroacetone **1** and (carbomethoxychloromethylene)triphenylphosphorane **7** or -phosphonate **5** (Scheme 1). Therefore, in a series of model studies, tetrachloroacetone **1** was condensed with phosphonates **2** and **3**, and phosphorane **4**. The reaction with the phosphonates proceeded slowly, and chromatography was required to obtain olefins **9** and **10** in 70−75% yield. However, phosphorane **4** reacted rapidly, with no subsequent chromatography needed, and **9** (80% yield) was crystallized directly from hexane.

[1]Authors to whom correspondence may be addressed.

Attempted hydrolysis of the ethyl ester **10**, with methanolic sodium hydroxide, afforded only the deconjugation product **11** based on nmr evidence; i.e., this compound had a one-proton singlet at δ 6.82 ($C\underline{H}Cl_2$) and a two-proton singlet at δ 3.66 ($\underline{CH_2}CO_2CH_2CH_3$). Further treatment of **11** gave a mixture of compounds that were not further investigated. In contrast, methyl ester **9** was converted to the desired acid **8**, as evidenced by nmr and ir, with no products of deconjugation being observed.

Having established that the condensation and hydrolysis of the methyl ester **9** proceeded without difficulty, we next turned our attention to the direct synthesis of the chloro-olefinic ester **13**.

Chlorophosphonate anion **5**, obtained by treatment of triethyl dichlorophosphonoacetate with n-butyllithium (15), reacted with tetrachloroacetone **1** but did not produce the expected pentachloro condensation product **13**. Instead, only aldolization products resulting from the condensation of the anion of tetrachloroacetone **1** with **1** were obtained (mass spectrometric evidence only).

Reaction of the corresponding chlorophosphorane **7** (16) with **1** did not afford **13** either, but, surprisingly, gave the *tetra*chloro olefin **9** in approximately 50% yield. Further investigation of this interesting reaction revealed that pentachloroacetone **19** was being formed. It therefore seems (Scheme 2) that the sterically hindered Wittig reagent **7** abstracted a proton from tetrachloroacetone **1**, which in turn removed chlorine from the chlorophosphonium salt **18** to give pentachloroacetone **19** and (carbomethoxymethylene)triphenylphosphorane **4**.

An alternate approach to generate **13** by reaction of tetrachloroacetone **1** with the anion of *tert*-butyl chlorotrimethylsilyl acetate **6** (17) also failed.

We therefore treated the olefinic ester **9** with chlorine in CH_2Cl_2, in the presence of ferric chloride, for 18−24 h to produce the hexachloro compound **12**. An ethereal solution of **12**, when treated with triethylamine, gave the desired pentachloro-olefin **13** (80% yield based on **9**).

The nmr spectra for the tetrachloro- and pentachloro-olefins **9** and **13** were very informative: apart from the methoxy resonances, **9** had a vinylic proton at δ 8.03 and another singlet at δ 6.73, corresponding to the two protons adjacent to the chlo-

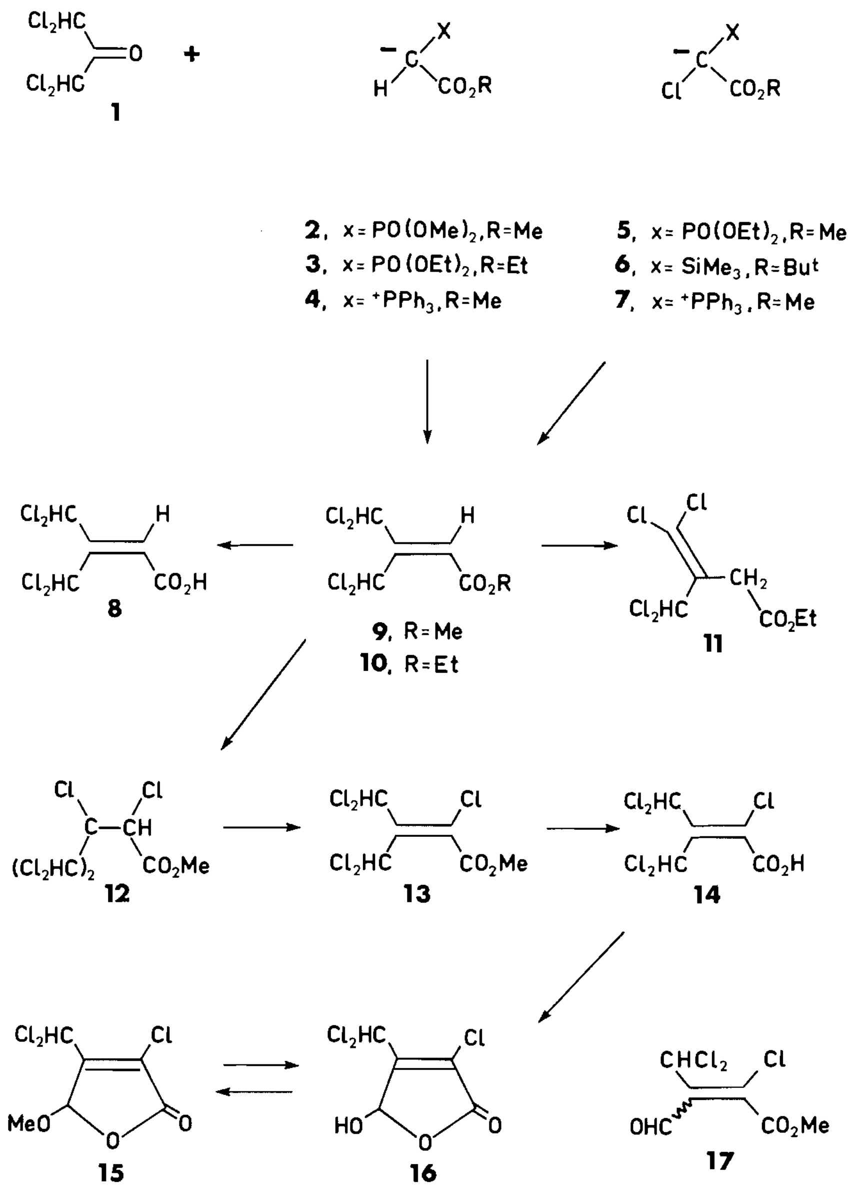

SCHEME 1

rine atoms. With **13**, only two one-proton singlets at δ 7.32 ($CHCl_2$ *cis* to $—CO_2CH_3$) and δ 6.72 ($CHCl_2$ *cis* to Cl) were observed. Mass spectra of both **9** and **13** were consistent with the structures assigned, but, under the conditions employed, no M^+ signal was evident. Only fragmentations due to the loss of at least one chlorine atom or the loss of a methoxy group were noted.

Unfortunately, conditions were not found for the direct conversion of ester **13** to the hydroxyfuranone **16**, e.g. treatment with two equivalents of lithium hydroxide gave a mixture of products that was not investigated further, and hydrolysis with potassium bicarbonate did not proceed at an acceptable rate.

However, hydroxyfuranone **16** was obtained as follows: reaction of **13** with one equivalent of lithium hydroxide (18) in tetrahydrofuran–water gave the carboxylic acid **14** in quantitative yield. Subsequent treatment of **14** with aqueous potassium carbonate afforded the hydroxyfuranone **16**, contaminated with very minor amounts of unidentified products.

The position of attachment of the dichloromethyl group was realized by simple inspection of the long range $^{13}C—^{1}H$ cou-

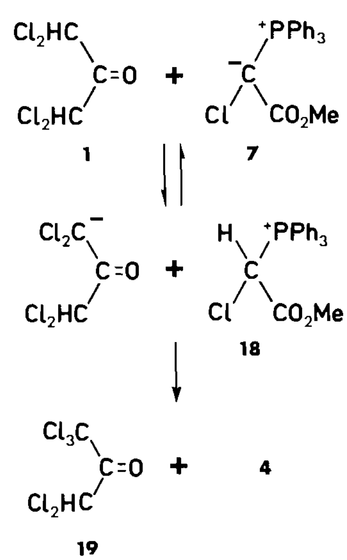

SCHEME 2

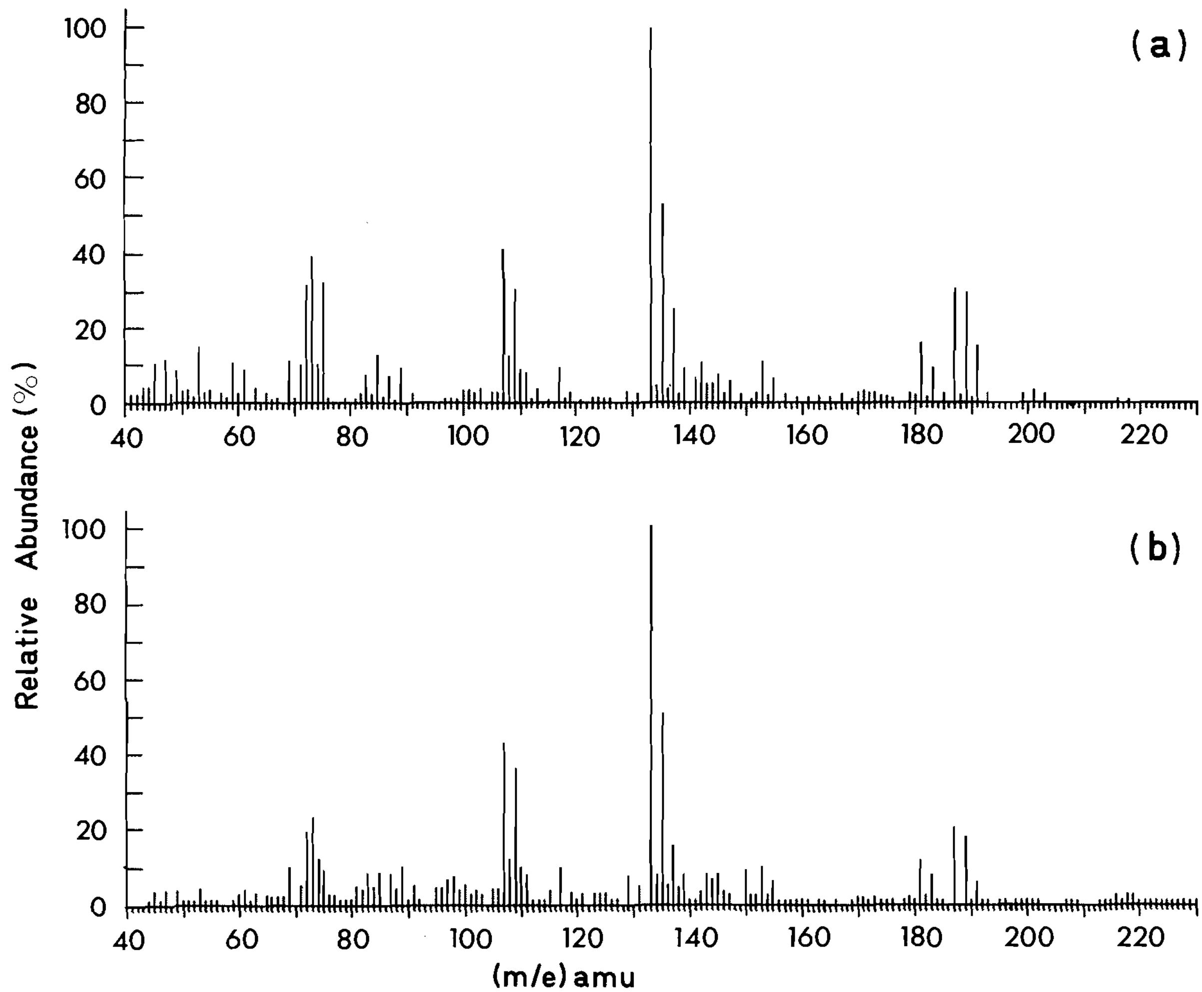

FIG. 1. Mass spectral fragmentation pattern of (a) synthetic hydroxyfuranone **16**, and (b) isolated mutagen. *Note*: The mass spectra of synthetic hydroxyfuranone **16** and the isolated mutagen were obtained on Hewlett–Packard quadrupole mass spectrometers 5980A and 5985A respectively. Both spectra were recorded in the electron impact mode.

pling in the nmr spectrum, e.g., the doublet at δ 164.51 (d, ^3J = 2.7 Hz, C═O) can only be rationalized by structure **16** since, if the other isomer were present, additional long range (^3J) coupling (CO—C—$CHCl_2$) would be observed.

Compound **16** had a retention time (gc, TMS derivative), uv spectrum, and a mass spectral fragmentation pattern (see Fig. 1) identical to that for the mutagen isolated from bleach plant effluent.

When acid **14** was submitted to the prolonged action of sodium hydroxide in methanol, a product was formed which appeared homogeneous by gc. However, gc/ms proved that it consisted of two products, the desired methyl ether **15** and what appeared to be **17**, of unknown geometry.

The methyl ether **15**, though, was smoothly obtained by the reaction of lactol **16** with methanolic hydrogen chloride. An identical gc retention time and mass spectral fragmentation pattern were recorded for this derivative, and the methyl ether previously produced from the isolated mutagen. Note also that lactol **16** could be regenerated from **15** by reaction with trifluoroacetic acid – THF–water.

Final confirmation of the mutagen's identity now required short-term bioassays with various mutant strains of *Salmonella typhimurium*. The mutagenic properties of synthetic trichlorolactol **16** are shown in Fig. 2. The corresponding test data for the isolated mutagen can be found in Fig. 6 of ref. 13.

When incubated with tester strain TA 100 (no metabolic activation), a strong mutagenic response occurred (~6000 revertants/nmol) in good agreement with previous observations for isolated material (13) (2,800–10,000 revertants/nmol). Further, when tester strain TA 100 was metabolically activated, neither the synthetic nor isolated mutagen produced a statistically significant number of revertants.

With tester strains TA 98 and TA 1537, synthetic **16** again behaved in a manner comparable to the effluent mutagen. In fact, the only difference observed was with strain TA 1535. Previously the effluent material had given a mild mutagenic effect but this was not observed for synthetic **16**. The reasons for this are not yet clear and require further investigation.

In conclusion, we have confirmed that the mutagen isolated from the chlorination effluent has the trichlorolactol structure **16**.

Experimental

General methods

Melting points were determined on a Gallenkamp MF-370 melting point apparatus and are uncorrected. Ultraviolet (uv) spectra were recorded on a Pye Unicam SP800 spectrophotometer in methanol solution. The wavelengths of absorption maxima are reported in nanometers (nm) with ε values in parentheses. Infrared (ir) spectra, measured on a Perkin–Elmer model 297 spectrophotometer, were

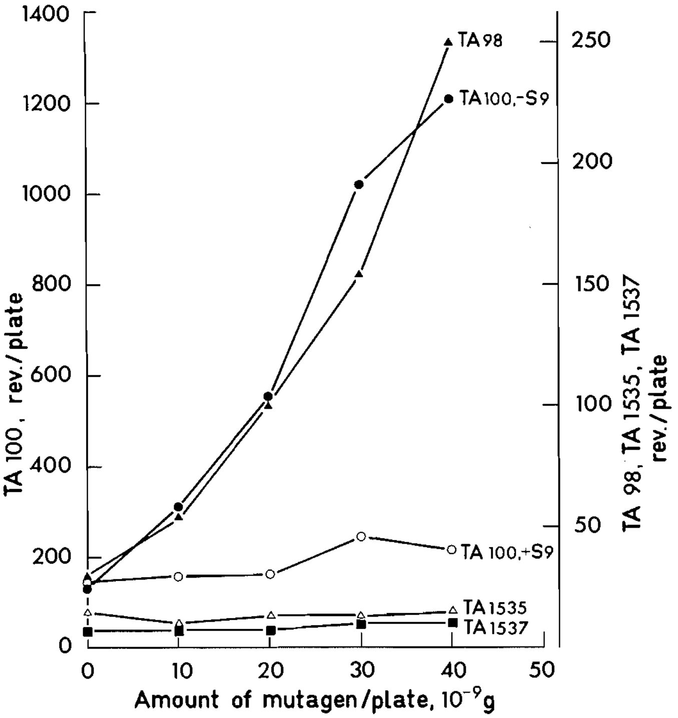

FIG. 2. Mutagenicity of synthetic hydroxyfuranone **16** on different test strains without metabolic activation. Testing against strain TA 100 was also made with metabolic activation (TA 100, +S9).

taken in chloroform solution, unless otherwise stated. The absorption maxima of each compound are reported in wavenumbers (cm^{-1}), and calibrated with respect to the absorption band of polystyrene at 1601 cm^{-1}. Proton magnetic resonance (^1H nmr) spectra were recorded on a Varian T-60 spectrometer, with TMS added as an internal standard. The integrated peak areas and proton assignments are given in parentheses. Carbon-13 magnetic resonance (^{13}C nmr) spectra were recorded in $CDCl_3$ solution on a Varian XL-300 spectrometer. Low resolution mass spectra (ms) were determined on a Hewlett–Packard model 5980A instrument and are reported in amu with relative abundances in parentheses. For simplicity, only the $^{35}Cl_n$ ion of the Cl_n cluster is reported. Microanalyses were carried out by Guelph Chemical Laboratories, Guelph, Ontario. Column chromatography utilized Merck (Kieselgel 60) silica gel (40–60 μm particle size). Thin layer chromatography utilized Merck art. 5554 alumina-backed silica gel 60 GF_{254} plates. As a matter of routine, all reagents and solvents were recrystallized or redistilled prior to use.

Ames mutagenicity testing was performed under contract by B.C. Research, Vancouver, B.C.

Methyl 3-(dichloromethyl)-4,4-dichlorocrotonate (9)

Methyl (triphenylphosphoranylidene)acetate (3.344 g, 10 mmol) and 1,1,3,3-tetrachloroacetone (1.96 g, 10 mmol) were dissolved in dry THF (10 mL), and the mixture stirred at room temperature for 14 h under nitrogen. The THF was then evaporated under reduced pressure and the residue dissolved in a minimum amount of CH_2Cl_2 (~ 3 mL). To this solution was added hexane (100 mL), with the resulting precipitate removed by filtration. The filtrate was evaporated and the residue recrystallized from hexane to give **9** (2.11 g, 84%), mp 50–51°C; ir ν_{max}: 3040, 3010, 1720, 1660; uv λ_{max}: 224(8464); ^1H nmr ($CDCl_3$) δ 3.90 (3H, s, CH_3), 6.73 (2H, s, 2 × $CHCl_2$), 8.03 (1H, s, CH); ms *m/e*: 219 (M^+ − OCH_3, 10%), 191 (M^+ − CO_2CH_3, 14%), 179 (M^+ − HCl, Cl, 100%). *Anal.* calcd. for $C_6H_6Cl_4O_2$: C 28.60, H 2.40, Cl 56.29; found: C 29.17, H 2.48, Cl 56.60.

Ethyl 3-(dichloromethyl)-4,4-dichlorocrotonate (10)

n-BuLi (1.5 *M*, 3.3 mL, 5 mmol) in hexane was added dropwise to a magnetically stirred solution of triethyl phosphonoacetate (0.92 mL, 5 mmol) in dry THF (4 mL) at −75°C under N_2. The reaction mixture was allowed to rise to room temperature, tetrachloroacetone (0.60 mL, 5 mmol) was added, and stirring was continued for 2 h. The mixture was then heated to reflux. After 14 h the reaction mixture was cooled, poured into cold water (20 mL), and extracted with hexane (3 × 25 mL). The organic extracts were dried (Na_2SO_4), and evaporated to give a brown oil. This was applied onto a silica gel column, and eluted carefully with Et_2O–hexane (5:95) by flash chromatography.

Selected eluent fractions were combined, and evaporated to give ester **10** (970 mg, 73%), mp 46–48°C; ir(KBr) ν_{max}: 3025, 2980, 1720, 1660, 780; uv λ_{max}: 223 (7528); ^1H nmr ($CDCl_3$) δ: 1.34 (3H, t, *J* = 6.5 Hz, CH_3), 4.28 (2H, q, *J* = 6.5 Hz, CH_2), 6.60 (2H, s, 2 × $CHCl_2$), 7.9 (1H, s, CH); ms *m/e*: 264 (M^+, 0.28%), 85 (100%).

Methyl 2,4,4-trichloro-2(dichloromethyl)crotonate (13)

A suspension of **9** (2.99 g, 11.9 mmol) and ferric chloride (5 mg) in CH_2Cl_2 (250 mL) was saturated with chlorine and allowed to stand at room temperature for 14 h. The solvent was then evaporated to give **12** (3.82 g, 100%) as a colorless oil; ir ν_{max}: 1752, 1340; ^1H nmr ($CDCl_3$) δ: 3.85 (3H, s, CH_3), 5.27 (1H, s, CHCl), 6.54 (1H, s, $CHCl_2$), and 6.64 (1H, s, $CHCl_2$).

To a magnetically stirred solution of **12** (3.82 g, 11.8 mmol) in dry Et_2O (30 mL) at room temperature was added triethylamine (2 mL, 14.3 mmol). Stirring was maintained for 30 min, and the organic mixture then removed and washed with water (3 × 10 mL). The organic solubles were dried (Na_2SO_4) and evaporated to give a light brown solid. Recrystallization from hexane gave **13** (2.72 g, 80%), mp 60–62°C; ir(KBr) ν_{max}: 3030, 3095, 2975, 1725, 1610, 1320, 805, 775, 725; uv λ_{max}: 232.5 (8244): ^1H nmr ($CDCl_3$) δ: 3.90 (3H, s, OCH_3), 6.72 (1H, s, $CHCl_2$, *trans* to CO_2CH_3), 7.32 (1H, s, $CHCl_2$, *trans* to Cl); ms *m/e*: 253 (M^+ − OCH_3, 5%), 250 (MH^+ − Cl, 22%), 248 (M^+ − HCl, 5%), 213 (M^+ − HCl, Cl, 100%). *Anal.* calcd. for $C_5H_5Cl_5O_2$: C 25.16, H 1.76, C 61.90; found: C 25.27, H 1.75, Cl 52.74. (No explanation has been found to account for the chlorine analyses.)

2,4,4-Trichloro-3-(dichloromethyl)-crotonic acid (14)

A solution of **13** (1 g, 3.49 mmol) and LiOH·H_2O (150 mg, 3.57 mmol) in THF–H_2O (7 mL, 6:1) was magnetically stirred at room temperature for 1 h. The solution was then concentrated (to ca. 2 mL), adjusted to pH 2 with 1 *M* hydrochloric acid, and extracted with ethyl acetate (3 × 10 mL). The organic solubles were dried (Na_2SO_4) and evaporated to give **14** (0.949 g, 99.8%), mp 118–120°C; ir (KBr) ν_{max}: 1690, 1610, 1600, 800, 770, 715; uv λ_{max}: 231 (7694); ^1H nmr ($CDCl_3$) δ: 6.80 (1H, s, $CHCl_2$, *cis* to CO_2H), 7.43 (1H, s, $CHCl_2$, *cis* to Cl), 11.05 (1H, s, CO_2H); ms *m/e*: 235 (M^+ − Cl, 17%), 199 (M^+ − HCl, − Cl, 37%), 44 (CO_2, 100%). *Anal.* calcd. for $C_5H_3Cl_5O_2$: C 22.05, H 1.11, Cl 65.09; found: C 22.21, H 1.16, Cl 65.24.

*3-Chloro-4-(dichloromethyl)-5-hydroxy-2(5*H*)-furanone (16)*

The acid **14** (0.79 g, 2.9 mmol) and $KHCO_3$ (0.581 g, 5.8 mmol) were dissolved in H_2O (25 mL) and heated for 3 h at 50°C under N_2. The reaction mixture was then cooled (to 20°C) and extracted with ethyl acetate (3 × 20 mL). The organic solubles were combined, dried (Na_2SO_4), and evaporated.

The crude product was applied to a silica gel column, and then carefully eluted with Et_2O–hexane (1:1) by flash chromatography. Trichlorolactol **16** (0.407 g, 65%) was obtained as a pale-yellow liquid by evaporation of selected chromatographic fractions; ir (neat) ν_{max}: 3400, 3000, 1780, 1660, 750, 690; uv λ_{max}: 224.5 (8129); ^1H nmr ($CDCl_3$) δ: 5.27 (1H, bs, OH), 6.40 (1H, s), 6.60 (1H, s); ^{13}C nmr ($CDCl_3$): 60.51 (d, $^1J_{C6-H6}$ = 181 Hz, $CHCl_2$), 96.55 (dt, $^1J_{C5-H5}$ = 178.8 Hz, $^2J_{C5-OH}$ = 3.85 Hz, CHOH), 125.19 (d, d, ^2J = 0.83 Hz, ^2J = 3.02 Hz, C=*C*—$CHCl_2$), 150.45 (bs, C3, =C—Cl), 164.51 (d, $^3J_{C2-H5}$, = 2.72 Hz, CO).

*3-Chloro-4-(dichloromethyl)-5-methoxy-2(5*H*)-furanone (15)*

To a solution of **16** (36 mg, 0.17 mmol) in methanol (0.2 mL) was added HCl-saturated methanol (3 drops), and the mixture was then stirred for 24 h at room temperature, under N_2. The solution was evaporated to give a residue which was redissolved in EtOAc (4 mL) and washed with water (1 × 2 mL). The organic solubles were dried (Na_2SO_4) and evaporated to give **15** (35 mg, 91%) as a colorless liquid; ir ν_{max}: 2930, 2840, 1795, 1725, 1655, 1600; uv λ_{max}: 226 (7781); ^{1}H nmr ($CDCl_3$) δ: 3.70 (3H, s, OCH_3), 6.05 (1H, s, C*H*OMe), 6.60 (1H, s, $CHCl_2$); ms *m/e*: 199 ($M^+ - OCH_3$, 32%).

*Conversion of **15** to **16***

A solution of **15** (40 mg, 1.73 mmol) in THF (0.6 mL) and trifluoroacetic acid (3 *N*, 0.4 mL) was stirred at room temperature for 96 h under N_2. The reaction mixture was then diluted with H_2O (3 mL) and extracted with ethyl acetate (3 × 10 mL). The organic extract was dried (Na_2SO_4) and evaporated. The crude product was applied to a silica gel column and carefully eluted with Et_2O−hexane (1:1) by flash column chromatography. Fractions containing the trichlorolactol were combined to give **16** (26 mg, 69%).

Acknowledgements

We wish to thank the Pulp and Paper Research Institute of Canada (PPRIC) and NSERC for financial support. We are indebted to Dr. R. H. Voss (PPRIC) for his continued interest and support of this project, to Dr. B. R. Holmbom (Abö Akademi, Turku, Finland) for the gc comparison of the synthetic trichlorolactol with the isolated mutagen, and to Dr. O. Mamer, Biomedical Mass Spectrometry Unit, for an excellent mass spectrometric service.

1. P. ANDER, K. E. ERIKSSON, M. C. KOLAR, K. KRINGSTAD, U. RANNUG, and C. RAMEL. Sven. Papperstidn. **80**, 454 (1977).
2. C. HÖGLUND, A. S. ALLARD, A. H. NEILSON, and L. LANDNER. Sven. Papperstidn. **82**, 447 (1979).
3. A. BJORSETH, G. E. CARLBERG, and M. MOLLER. Sci. Total Environ. **11**, 197 (1979).
4. (*a*) L. STOCKMAN, L. STRÖMBERG, and F. DE SOUSA. Cellul. Chem. Technol. **14**, 517 (1980); (*b*) M. A. NAZAR and W. H. RAPSON. Pulp Pap. Can. **81**(8), 75 (1980).
5. E. G. H. LEE, J. C. MUELLER, C. C. WALDEN, and H. STICH. Pulp. Pap. Can. **82**(5), 69 (1981).
6. A. B. MCKAGUE, E. G. H. LEE, and G. R. DOUGLAS. Mutat. Res. **91**, 301 (1981).
7. K. P. KRINGSTAD, P. O. LJUNGQUIST, F. DE SOUSA, and L. M. STRÖMBERG. Environ. Sci. Technol. **15**, 562 (1981).
8. G. P. DONNINI. Pulp Pap. Can. **82**(11), 106 (1981).
9. J. A. ELLENTON, G. R. DOUGLAS, and E. R. NESTMANN. Can. J. Genet. Cytol. **23**, 17 (1981).
10. G. R. DOUGLAS, E. R. NESTMANN, A. B. MCKAGUE, O. P. KAMRA, E. G. H. LEE, J. A. ELLENTON, R. BELL, D. KOWBEL, V. LIU, and J. POOLEY. *In* Application of short-term bioassays in the analysis of complex environmental mixtures. Vol. 3. *Edited by* M. Waters *et al.* Plenum Press, New York. 1983.
11. K. P. KRINGSTAD, P. O. LJUNGQUIST, F. DE SOUSA, and L. M. STRÖMBERG. *In* Water chlorination: environmental impact and health effects. Vol. 4. *Edited by* R. L. Jolley *et al.* Ann Arbor Science, Ann Arbor, MI. 1983.
12. B. R. HOLMBOM, R. H. VOSS, R. D. MORTIMER, and A. WONG. TAPPI, **64**(3), 172 (1981).
13. B. R. HOLMBOM, R. H. VOSS, R. D. MORTIMER, and A. WONG. Environ. Sci. Technol. **18**, 333 (1984).
14. J. MCCANN and B. N. AMES. Proc. Natl. Acad. Sci. U.S.A. **73**, 950 (1976).
15. J. VILLIERAS, P. PERRIOT, and J. F. NORMANT. Synthesis, **31**, (1978).
16. A. J. SPEZIALE and K. W. RATTS. J. Org. Chem. **28**, 465 (1963).
17. T. H. CHAN and M. MORELAND. Tetrahedron Lett. **6**, 515 (1978).
18. E. J. COREY, I. SZEKELY, and C. S. SHINER. Tetrahedron Lett **40**, 3529 (1977).

Formation threshold structures of some $[C_5H_7O]^+$ ions: use of general schemes for estimation of heats of formation of gas-phase organic ions

MEHRSHID ALAI, GIORGIO G. ATTARDO, AND ROBIN T. B. RYE[1]
Department of Chemistry, Concordia University, 1455 de Maisonneuve Blvd. W., Montreal, P.Q., Canada H3G 1M8

Received August 10, 1984

MEHRSHID ALAI, GIORGIO G. ATTARDO, and ROBIN T. B. RYE. Can. J. Chem. **63**, 833 (1985).

Recently published correlations between heat of formation and structure of gas-phase ions have been used to assign formation threshold structures to $[C_5H_7O]^+$ ions produced by methyl radical loss from molecular ions of mesityl oxide, 5-hexene-2-one, 3-methylcyclopentanone, and 2-cyclohexenol. An unambiguous structure assignment has been made for the $[C_5H_7O]^+$ daughter ion from mesityl oxide. For the three other precursors two common formation-threshold structures consistent with the thermochemical data are proposed.

MEHRSHID ALAI, GIORGIO G. ATTARDO et ROBIN T. B. RYE. Can. J. Chem. **63**, 833 (1985).

Des travaux publiés récemment ont établi des corrélations entre la chaleur de formation et la structure des ions en phase gazeuse; on a utilisé ces corrélations pour attribuer les structures, au niveau du seuil de formation, des ions $[C_5H_7O]^+$ qui se forment lorsque les ions de l'oxyde de mésityle, de l'hexène-5 one-2, de la méthyl-3 cyclopentanone ou du cyclohexène-2 ol perdent un radical méthyle. On a pu faire une attribution non ambigue de la structure de l'ion fille $[C_5H_7O]^+$ provenant de l'oxyde de mésityle. Pour les trois autres précursors, on propose deux structures communes, au niveau du seuil de formation, qui sont en accord avec les données thermodynamiques obtenues.

[Traduit par le journal]

Introduction

Collisional activation (CA) mass spectrometry has achieved prominence as a method for the determination of the structure of gas-phase ionic species (1). In spite of the widespread use of this technique, thermochemical characterization of ions at their formation threshold remains an essential component of any complete structure determination. This is so because the CA technique samples ions with a range of internal energies; the structures determined may therefore be different than those at threshold if isomerization reaction channels with low energy requirements are available.

Two recent publications (2, 3) have outlined general methods for correlating ionic heats of formation with the threshold structures of gaseous odd and even electron ions. We have now utilized these techniques to assign configurations to $[C_5H_7O]^+$ ions generated by methyl radical loss from 4-methyl-3-penten-2-one (mesityl oxide) (**1**), 5-hexene-2-one (**2**), 3-methylcyclopentanone (**3**), and 2-cyclohexenol (**4**).

Experimental

The $[C_5H_7O]^+$ ions of interest were generated by dissociative ionization using a monoenergetic electron beam. Appearance energies (AE) were measured as described elsewhere (4). The heats of formation of the neutral precursors were taken from the literature or calculated by additivity.

Results and discussion

(a) *Mesityl oxide, 1*

Zwinselman *et al.* (5) proposed the molecular ion of **1** as an intermediate structure preceding the loss of methyl radical from 2-methyl-3,4-dien-2-ol, with the acylium ion **c** as the daughter ion generated. Ion **a**, readily produced by methyl radical loss from ionized methyl vinyl ketone (6), can be represented by the two canonical structures shown; thus **c** corresponds to double methyl substitution at a charge-bearing site of **a**. The other member of the series, **b**, can be generated by H loss from crotonaldehyde (7). If the structural assignments are correct,

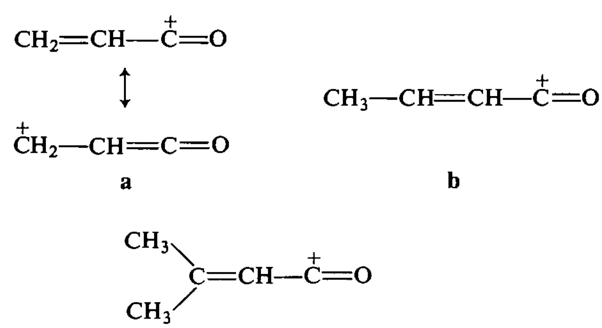

a **b** **c**

then, following the conclusions of Holmes and Lossing (3), the heats of formation of **a**, **b**, and **c** given in Table 1 should lie on a straight line when plotted against log (no. of atoms), and this straight line should roughly parallel similar plots for other methyl substitutions at C-atoms bearing a formal charge. Inspection of Fig. 1 and the data in Table 1 shows that such is the case, with the least-squares line for **a**, **b**, and **c** approximately parallel to line A (methyl substitution on CH_2O) and line B (methyl substitution on CH_2OH). We propose, therefore, that **c** is the configuration of the $[C_5H_7O]^+$ ion formed from **1** by $\dot{C}H_3$ loss.

Additional information can be extracted from Fig. 1. It will be noted that the datum for **b** lies significantly above the line (dotted line, Fig. 1) joining the data points for **a** and **c**. The structure of **b** was clearly established by CA and analysis of metastable peak charcteristics (7); we conclude that the reported ΔH_f for **b** is too high. This is not surprising; a conventional electron impact source (such as used for **b**) is known to give AE measurements which are higher than those obtained with the monoenergetic electron beam used in the case of **a** and **c** (4*c*). We may thus revise the ΔH_f for **b** downwards by approximately 40 kJ mol^{-1} to a value of 645 kJ mol^{-1}.

(b) *5-Hexene-2-one, 2*

Loss of methyl from the molecular ion of **2** can occur via simple cleavage to give a $[C_5H_7O]^+$ ion of structure **d**. While **d** may be a plausible structure, it is by no means certain that it is the correct one. The heat of formation of **d** can be estimated

[1]Author to whom all correspondence should be addressed.

TABLE 1. Thermochemical data

(*i*) $[C_5H_7O]^+$ Ions

Precursor	ΔH_f (neutral) kJ mol^{-1}	Reference	AE eV	ΔH_f (ion) kJ mol^{-1}
1	−189	8	9.48	577
2	−153	8	9.58	628
3	−219	8	10.38	636
4	−167	8	9.74	628

(*ii*) Other ions

Ion	ΔH_f kJ mol^{-1}	Reference	Figure/line
CH_2O	942	2	1/A
CH_3CHO	818	2	1/A
$(CH_3)_2CO$	720	2	1/A
CH_2OH	703	1	1/B
CH_3CHOH	582	1	1/B, 2/A
$(CH_3)_2COH$	502	1	1/B
CH_2CHCO	749	5	1/C
$CH_3CHCHCO$	690	6	1/C
$CH_3C(OH)_2$	314	2	2/A
CH_3CH_2	904	2	2/A
CH_2CH_2	1067	8*b*	2/B
CH_2CHOH	757	2	2/B
$CH_2C(OH)_2$	502	2	2/B
C_6H_6	975	8*b*	2/C
C_6H_5OH	724	2	2/C
$C_6H_4(OH)_2$	502	2	2/C
c-C_5H_7	833	3*b*	—

in the following manner. Ion **d** can be constructed by replacing the terminal CH_3 in $CH_3CH_2\overset{+}{C}{=}O$ with a $CH_2{=}CH{-}CH_2{-}$ group. It has been shown (2) that substitution on a site remote from the charge-bearing site has approximately the same effect on ΔH_f (ion) as on ΔH_f (neutral). The heats of formation of 2-propanone an **2** are −238.5 kJ mol^{-1} (8) and −153 kJ mol^{-1} (by additivity (9)), respectively. These data, when taken with a ΔH_f of 623 kJ mol^{-1} for $CH_3CH_2\overset{+}{C}{=}O$ (10), lead to a calculated heat of formation for **d** of 709 kJ mol^{-1}. The measured value (Table 1) of ΔH_f for $[C_5H_7O]^+$ from **2** is 628 kJ mol^{-1}, and it may therefore be concluded with some assurance that structure **d** is incorrect.

$H_2C{=}CH{-}CH_2{-}CH_2{-}\overset{+}{C}{=}O$

d

$H_3C{-}CH_2{-}CH{=}CH{-}\overset{+}{C}{=}O$

e

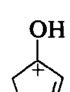

f

It is considerably more difficult to assign the correct structure, given the large number of possible configurations for $[C_5H_7O]^+$, but the estimation method can be used to determine whether proposed structures are consistent with the thermochemical data. The stabilizing effect of conjugation is well documented; we therefore wished to evaluate the conjugated ion **e** as a possible structure. The heat of formation of **e** can be estimated from the corrected ΔH_f for **b** (see Fig. 1 and text). Construction of **e** by replacement of the terminal CH_3 group in **b** wth CH_3CH_2 corresponds to substitution remote from the charge-bearing site and, as was done in the previous case, the effect of this substitution on ΔH_f (ion) was equated to the

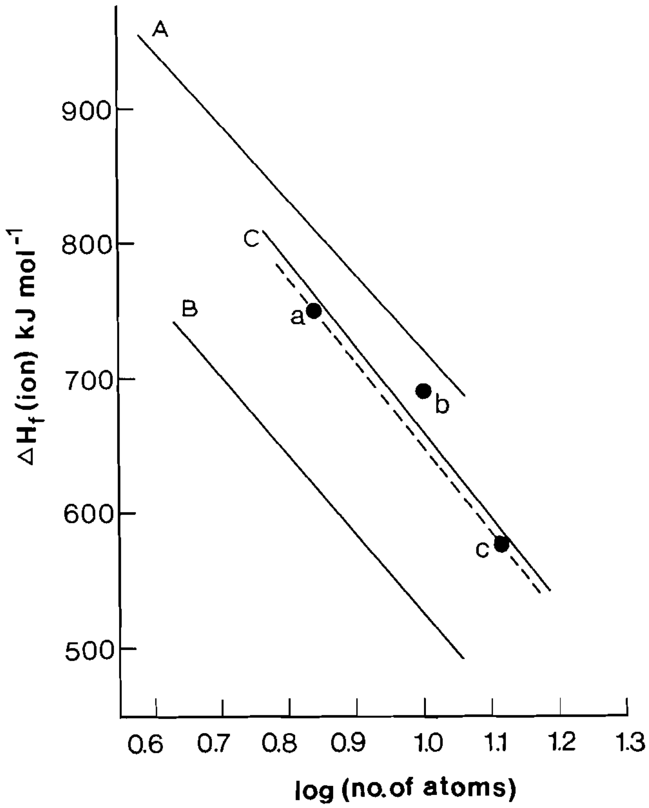

FIG. 1. Heats of formation vs. log (no. of atoms) for successive methyl substitution at charge-bearing site: **a**, [vinyl ketenium]$^+$; **b**, methyl-substituted vinyl ketenium cation; **c**, $[C_5H_7O]^+$ from mesityl oxide. Lines A, B, and C: see text.

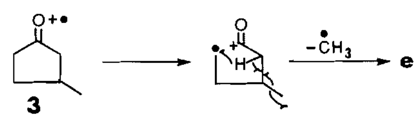

SCHEME. 1. Possible fragmentation pathways for production of ion **e** from the molecular ion of 3-methylcyclopentanone.

change in ΔH_f (neutral). This procedure leads to a calculated ΔH_f for **e** of 624 kJ mol^{-1}, in excellent agreement with the measured value. It would be unwise to conclude from this result that the ion structure has been unambiguously determined; this point is underlined by the results for **3** and **4** given below. It should also be noted that, at internal energies only slightly above threshold, other reaction channels and fragment ion structures may be involved. We have recently reported evidence (11) that this is the case for methyl radical loss from **2**.

(c) *3-Methylcyclopentanone,* **3**, *and 2-cyclohexene-1-ol,* **4**

The measured heat of formation of the $[C_5H_7O]^+$ ion from **3** and from **4** is the same, within experimental error, as that obtained with **2** as the precursor (Table 1). Formation of **e** from **3** can be easily rationalized in terms of CH_3 loss from α-cleaved molecular ion, as shown in Scheme 1. Methyl loss from **4** has been the subject of several reports (12–15). Buch and coworkers (14) studied the 70-eV spectra of **4** and a wide range of labelled analogues. Loss of CH_3 was observed to involve C(2) together with the hydrogen atoms from C(1), C(2), and C(3); a [1-hydroxy-cyclopentene-1]$^+$ ion with the charge located on C(2) was proposed as a plausible structure for the $[C_5H_7O]^+$ daughter ion. An alternative mechanism, based on

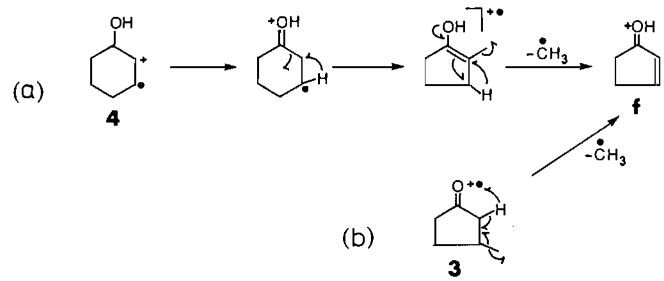

SCHEME. 2. Possible fragmentation pathways leading to ion **f** from the molecular ion of (a) 2-cyclohexenol (15) and (b) 3-methylcyclopentanone.

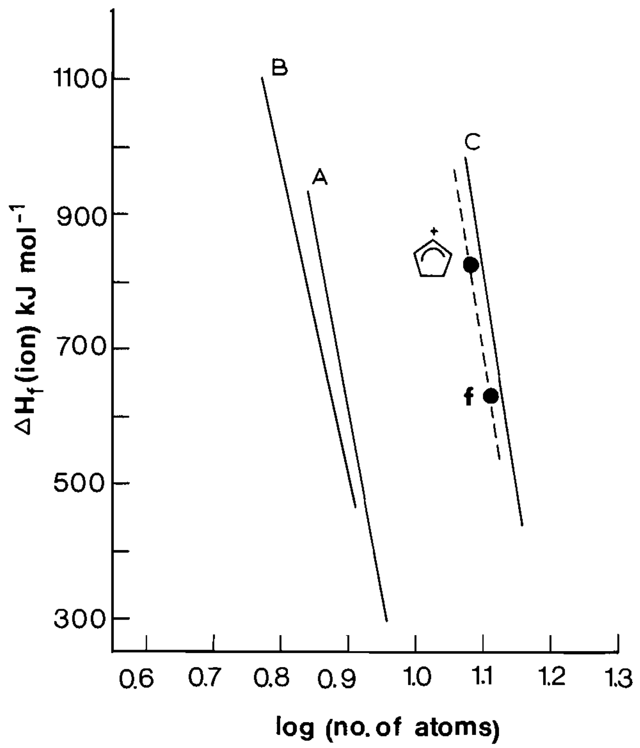

FIG. 2. Heats of formation vs. log (no. of atoms) for successive hydroxyl substitution at charge-bearing site: **f**, hydroxyl substitution on [cyclopentenium]$^+$ cation. Lines A, B, and C: see text.

the results of metastable ion studies, has been suggested by Lignac and Tabet (15). These authors propose that isomerization of the molecular ion of **4** to the enol form of methyl-2-cyclopentenol precedes methyl loss, with the latter process involving a shift of the hydrogen atom at C(4) (Scheme 2(a)). The $(M - CH_3)^+$ ion generated, **f**, is of interest because it could also be produced by methyl radical loss from **3**. A possible mechanism is shown in Scheme 2(b), although the 1,3-hydrogen shift indicated would imply an activation energy of at least 160 kJ mol^{-1} for this pathway (16). We wished to determine whether or not structure **f** was consistent with the measured ΔH_f for $[C_5H_7O]^+$ from **3** and **4**.

The procedure followed was analogous to that employed for **c**. Ion **f** can be viewed as resulting from —OH substitution on the charge-bearing site of the [cyclopentenium]$^+$ cation. It has been shown that plots of ΔH_f against log (no. of atoms) give roughy parallel lines for various series of successive —OH substitutions (3). The average value of the slopes of three such plots (lines A, B, and C, Fig. 2) was determined using the data in Table 1, the ΔH_f datum for [cyclopentenium]$^+$ (4*b*) used to calculate the intercept, and the estimated line for the effect of hydroxyl substitution on the charge-bearing a site of [cyclopentenium]$^+$ was plotted (dotted line, Fig. 2). The ΔH_f of **f** is estimated by this method to be 635 kJ/mol. Given the uncertainties associated with the above procedure, we conclude that threshold heat of formation measurements do not allow us to distinguish between ion structures **e** and **f**.

Summary

The methods developed by Holmes and Lossing have been used to assign the acylium structure **c** to the $[C_5H_7O]^+$ ion generated from **1** at the formation threshold.

For various series of both —OH and CH_3— substitutions at charge-bearing sites, roughly parallel plots of ΔH (ion) vs. log (no. of atoms) have been reported (3). This feature enables useful structural predictions to be made even in cases where only limited amounts of data are available. We have used this approach to show that at least two possible threshold configurations consistent with the thermochemical data, viz. **e** and **f**, are possible for the $[C_5H_7O]^+$ ion generated from **2**, **3**, and **4**.

Acknowledgements

We are indebted to Dr. F. P. Lossing for AE measurements and helpful discussion, and to Prof. J. L. Holmes for much valuable advice and comment. The financial support of the Natural Sciences and Engineering Research Council of Canada is gratefully acknowledged.

1. F. W. McLafferty. Acc. Chem. Res. **13**, 35 (1980).
2. J. L. Holmes, M. Fingas, and F. P. Lossing. Can. J. Chem. **59**, 80 (1981).
3. J. L. Holmes and F. P. Lossing. Can. J. Chem. **60**, 2365 (1982).
4. (*a*) K. Maeda, G. P. Semeluk, and F. P. Lossing. Int. J. Mass Spectrom. Ion Phys. **1**, 395 (1968); (*b*) F. P. Lossing and J. C. Traeger. Int. J. Mass Spectrom. Ion Phys. **19**, 9 (1976); (*c*) H. M. Rosenstock, K. Draxl, B. W. Steiner, and J. T. Herron. J. Phys. Chem. Ref. Suppl. 1, 6 (1977).
5. J. J. Zwinselman, N. N. Nibbering, B. Ciommer, and H. Schwarz. *In* Current topics in mass spectrometry and chemical kinetics. *Edited by* J. H. Beynon and M. L. McGlashan. Heyden and Son, London. 1982.
6. J. L. Holmes, J. K. Terlouw, and P. C. Burgers. Org. Mass Spectrom. **15**, 140 (1980).
7. H. Hommes and J. K. Terlouw. Org. Mass Spectrom. **14**, 51 (1979).
8. J. B. Pedley and J. Rylance. Sussex–N.P.L. computer analysed thermochemical data: organic and organometallic compounds. University of Sussex, England. 1977.
9. (*a*) S. W. Benson. Thermochemical Kinetics. 2nd ed. John Wiley and Sons, New York. 1976; (*b*) H. M. Rosenstock, D. Sims, S. S. Schroyer, and W. J. Webb. Ion energetics measurements. Part I. National Bureau of Standards, Washington, D.C. 1980.
10. R. H. Staley, R. D. Wieting, and J. L. Beauchamp. J. Am. Chem. Soc. **99**, 5964 (1977).
11. G. A. Attardo and R. T. B. Rye. Org. Mass Spectrom. **19**, 241 (1984).
12. R. T. Aplin, H. E. Browning, and P. Chamberlin. Chem. Commun. 1071 (1967).
13. T. J. Adley, G. Matteo, and R. T. B. Rye. Org. Mass Spectrom. **14**, 562 (1979).
14. D. Braem, F. O. Gulacar, U. Burger, and A. Buchs. Org. Mass Spectrom. **14**, 609 (1979).
15. C. Lignac and J. C. Tabet. Int. J. Mass Spectrom. Ion Phys. **47**, 375 (1983).
16. J. H. Vajda, A. G. Harrison, A. Hirota, and F. W. McLafferty. J. Am. Chem. Soc. **103**, 36 (1981).

Equilibrium structures, proton affinities, and ionization potentials of the fluoroacetones

SAI CHENG CHOI AND RUSSELL J. BOYD[1]

Department of Chemistry, Dalhousie University, Halifax, N.S., Canada B3H 4J3

Received July 9, 1984

SAI CHENG CHOI and RUSSELL J. BOYD. Can. J. Chem. **63**, 836 (1985).

Theoretical calculations on the fluoroacetones and their conjugate acids exhibit an inverse dependence of the proton affinity on the number of fluorine substituents. The good correlation between increasing proton affinity and decreasing ionization potential is attributed to the observation that the ionization of a nonbonding electron is essentially localized at a single atom which is also the site of protonation. The best quantitative agreement between the theoretical and experimental proton affinities is obtained at the 6-31G* level, while the STO-3G basis set leads to a satisfactory account of the additivity of fluorine substituents. The calculations corroborate the experimental interpretation of the preferred conformations of *p*-fluoroacetone molecules in terms of the presence of an intramolecular hydrogen bond between the carbonyl proton and the F on the adjacent carbon. Only one type of equilibrium conformation is predicted for the fluorinated acetones, whereas two types of equilibrium conformations are predicted for the conjugate bases.

SAI CHENG CHOI et RUSSELL J. BOYD. Can. J. Chem. **63**, 836 (1985).

D'après des calculs théoriques sur les fluoroacétones et sur leurs acides conjugués, l'affinité pour les protons varie d'une façon inverse avec le nombre de substituants fluor. C'est à l'observation que l'ionisation d'un électron non liant est essentiellement localisée sur un atome unique qui est aussi le site de la protonation que l'on attribue la bonne corrélation qui existe entre une augmentation de l'affinité pour les protons et la diminution du potentiel d'ionisation. C-est au niveau 6-31G* que l'on obtient les meilleurs accords quantitatifs entre les résultats expérimentaux et les valeurs calculées pour les affinités pour les protons; par ailleurs, l'utilisation de l'ensemble STO-3G conduit à une explication satisfaisante de l'additivité des substitutants fluor. Les calculs corroborent l'interprétation expérimentale des conformations privilégiées des molécules de *p*-fluoroacétones en fonction d'une liaison hydrogène intramoléculaire entre le proton du carbonyle et le F attaché au carbone voisin. Dans le cas des fluoroacétones, on ne prédit qu'un seul type d'équilibre conformationnel; toutefois, on prédit deux types d'équilibres conformationnels pour les bases conjuguées.

[Traduit par le journal]

Introduction

One of the major challenges of chemistry is to predict the effect of substituents on the properties of molecules and to develop models and theories which facilitate a better understanding of substituent effects. Most systematic studies of substituent effects have been carried out in solution, where the observed properties are often more a reflection of the effects of solvation than of the intrinsic properties of the species of interest. Recent advances in physical chemistry have provided several powerful methods for studying the reactions and structures of ions in the gas phase. Complementary information on the intrinsic properties of molecules and ions is provided, however, by *ab initio* molecular orbital theory.

Ion cyclotron resonance studies (1) of the gas-phase basicities of six fluorinated acetones have revealed a very regular decrease in proton affinity of 6.1 ± 0.4 kcal/mol for each successive fluorine substituent. This result has been interpreted in terms of a substituent effect which is almost purely inductive and correlates well with the group electronegativity of the methyl substituents. Furthermore, the linear dependence of the observed proton affinities on the number of fluorine substituents reveals a small stabilizing interaction of 2−3 kcal/mol in the protonated fluoroacetones, which is attributed to the formation of an intramolecular hydrogen bond. The additivity of fluorine substituent effects in the gas-phase basicities of fluorinated acetones stands in contrast to the less regular changes in acidities and basicities which are often associated, both in solution and in the gas phase, with multiple substitution in organic molecules (2, 3).

The Drummond and McMahon study of the fluorinated acetones is a remarkable application of one of the three techniques, namely high-pressure mass spectrometry (4, 5), flowing afterglow (6−8), and ion cyclotron resonance spectrometry (9−12), which yield reliable gas-phase data on the intrinsic acidities and basicities of molecules. Not only are the substituent effects additive, but up to six hydrogens in acetone can be replaced by fluorines. Furthermore, two isomers are possible for each of the di-, tri-, and tetrafluoro derivatives, and, therefore, a total of ten molecules are available for the study of multiple substituent effects. Given accurate proton affinities (1) for seven of these compounds, we have studied the ability of *ab initio* molecular orbital (MO) theory to account for the additivity of fluorine substituent effects in the acetone series. In this paper we focus our attention on equilibrium structures, proton affinities, and multiple substituent effects. We will present an analysis of intramolecular hydrogen bonding in the protonated fluoroacetones in a later paper (13).

Method

All computations were performed on a CDC CYBER 170-730 computer using the GAUSSIAN 76 program (14). In some cases an expanded version of the GAUSSIAN 76 program (15) was used. $CH_mF_{3-m}COCH_nF_{3-n}$ and their corresponding conjugate acids $CH_mF_{3-m}COHCH_nF^+_{3-n}$, where m and n are equal to 0, 1, 2, or 3 were optimized at the STO-3G level. For some species, in which the C—C bonds were found to be longer (1.56 to 1.63 Å) at the STO-3G level than normal ones (1.54 Å), partial 4-31G optimizations were carried out. The partial 4-31G optimizations are denoted by '4-31G' and consist of a 4-31G optimization on the C—C bonds followed by a minimal STO-3G optimization on the rest of the molecule. The '4-31G' optimization was employed on CH_2FCOCH_3, CHF_2COCH_3, CF_3COCH_3, CF_3COCF_3, and their corresponding conjugate acids. Partial optimizations with split-valence

[1]Author to whom correspondence should be addressed.

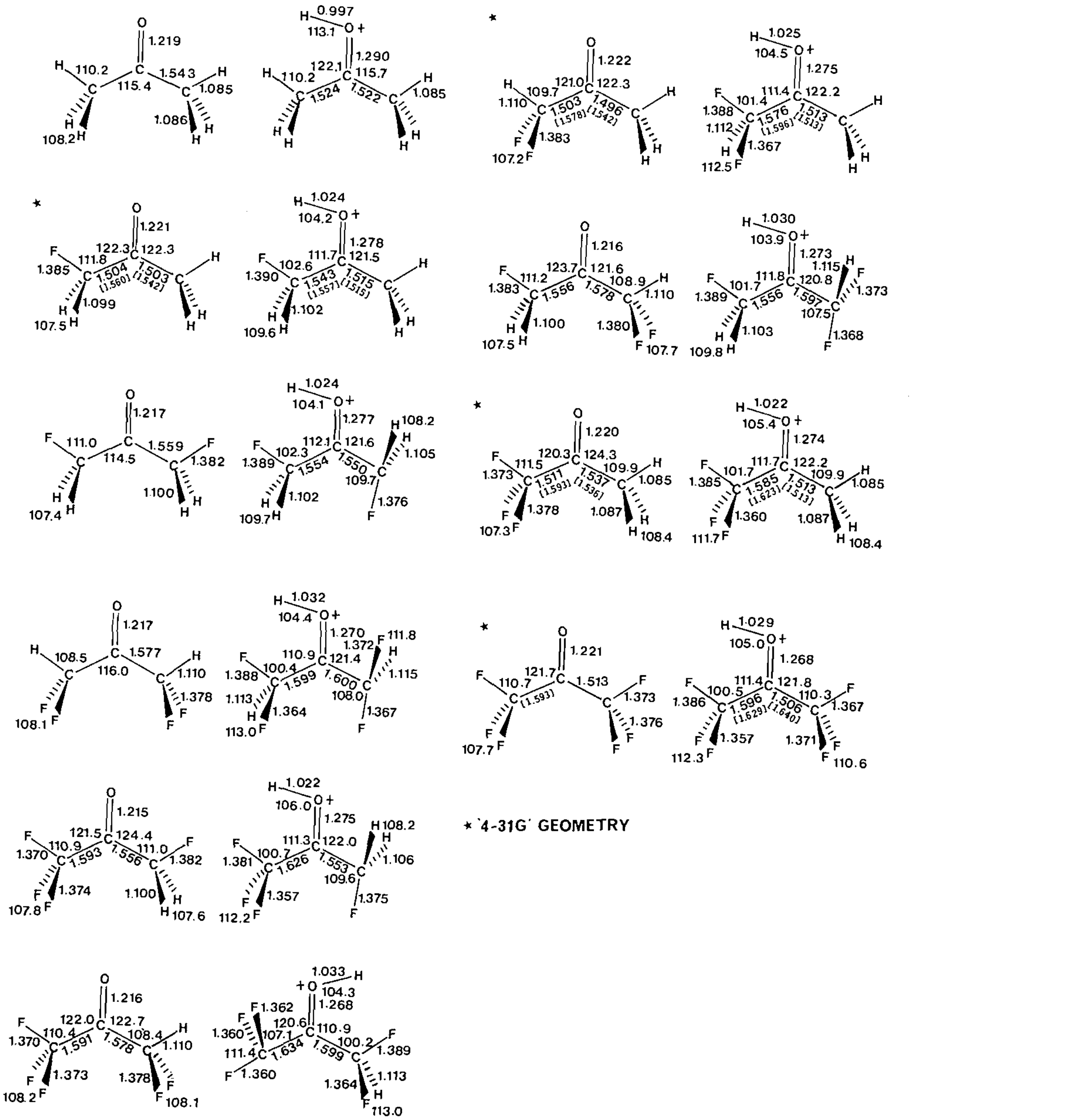

FIG. 1. Equilibrium geometries of the fluorinated acetones and their conjugate acids. For molecules optimized at the '4-31G' level, denoted by a star, the STO-3G values of the C—C bond lengths are given in square brackets.

basis sets have been shown (16) to yield good approximations to the full K-LMG optimizations in the case of *cis*-acetic acid and acetamide. A model geometry (r (C—H) = 1.085 Å and angle HCH = 108.2°) was used for all unsubstituted methyl groups. The STO-3G or '4-31G' equilibrium geometries of the fluorinated acetones and their conjugate acids are shown in Fig. 1.

Tables 1 and 2 list the STO-3G//STO-3G, 4-31G//STO-3G, 4-31G//'4-31G', and 6-31G*//STO-3G total energies and the point group symmetries of the equilibrium conformations in the neutral and protonated series, respectively. The theoretical proton affinities (PA), defined as the difference in total energies of the base and its conjugate acid, are listed in Table 5 together with the available experimental values. The zero-point energy and thermodynamic corrections have not been included. The latter are simply a function of the temperature, while the former should be essentially constant within a series of related molecules (16). Hence these omissions will not affect the chemical trends as significantly as the more serious basis set and correlation errors. Large basis sets and post Hartree–Fock calculations are impractical for the larger members of the series. Calculations at the 4-31G level are included for all members of the series, while the 6-31G* basis set has been used up to and including 1,1,1-trifluoroacetone and its conjugate acid.

Results and discussion

Equilibrium structures

The types of equilibrium conformations of the neutral and protonated series are shown in Fig. 2 where X and Y may be either hydrogen or fluorine. All neutral molecules show one type of conformation, namely that of type I, in which the unique atom occupies the X position. For CF_3COCH_3 and CF_3COCF_3, the question of the position of a unique atom does

TABLE 1. Total energies[a] of neutral fluoroacetones[b]

Molecule	STO-3G//STO-3G	4-31G//STO-3G	4-31G//'4-31G'	6-31G*//STO-3G
CH_3COCH_3 (C_{2v})	−189.53603	−191.67579		−191.95965
CH_2FCOCH_3 (C_s)	−286.97902	−290.39060	−290.39302	−290.79649
CH_2FCOCH_2F (C_{2v})	−384.42112	−389.10149		−389.63031
CHF_2COCH_3 (C_s)	−384.43944	−389.12641	−389.13013	−389.65628
$CH_2FCOCHF_2$ (C_s)	−481.88156	−487.83855		−488.49118
CF_3COCH_3 (C_s)	−481.91178	−487.86320	−487.86568	−488.51972
CHF_2COCHF_2 (C_{2v})	−579.33917	−586.56265		
CF_3COCH_2F (C_s)	−579.35291	−586.57197		
CF_3COCHF_2 (C_s)	−676.81038	−685.29659		
CF_3COCF_3 (C_{2v})	−774.28088	−784.02789	−784.02789	

[a]All energies are in atomic units: 1 au = 27.2116 eV.
[b]The notation A//B implies the energy has been calculated with basis set A at the equilibrium geometry of basis set B.

TABLE 2. Total energies[a] of protonated fluoroacetones[b]

Molecule	STO-3G//STO-3G	4-31G//STO-3G	4-31G//'4-31G'	6-31G*//STO-3G
$CH_3COHCH_3^+$ (C_s)	−189.93244	−191.99658		−192.28188
$CH_2FCOHCH_3^+$ (C_s)	−287.37654	−290.69485	−290.69497	−291.10776
$CH_2FCOHCH_2F^+$ (C_s)	−384.81055	−389.39619		−389.93378
$CHF_2COHCH_3^+$ (C_1)	−384.82202	−389.40022	−389.40026	−389.94299
$CH_2FCOHCHF_2^+$ (C_1)	−482.25649	−488.09947		−488.76755
$CF_3COHCH_3^+$ (C_s)	−482.28211	−488.11817	−488.11914	−488.79290
$CHF_2COHCHF_2^+$ (C_1)	−579.70118	−586.79899		
$CF_3COHCH_2F^+$ (C_s)	−579.71465	−586.81154		
$CF_3COHCHF_2^+$ (C_1)	−677.16258	−685.51291		
$CF_3COHCF_3^+$ (C_s)	−774.62180	−784.22648	−784.22989	

[a]All energies are in atomic units: 1 au = 27.2116 eV.
[b]See footnote *b* in Table 1.

not arise. As expected, those molecules with equal numbers of F atoms on each carbon have two equal C—C bonds. The reverse holds true, with the more highly substituted methyl group being associated with a longer C—C bond at both the STO-3G and '4-31G' levels.

In this work the site of protonation is assumed to be the carbonyl oxygen, in agreement with an earlier MNDO study (17) which showed that protonation at fluorine in CH_2FCOCH_3 is less stable by about 25 kcal/mol. In the two types of equilibrium conformation of the protonated series, position X on C_1 is always occupied by a F atom, thus forming a pseudo-five-membered ring. From Fig. 1, it is readily seen that five of the protonated molecules, $CH_3COHCH_3^+$, $CH_2FCOHCH_3^+$, $CHF_2COHCH_3^+$, $CF_3COHCH_3^+$, and $CF_3COHCF_3^+$, have type II equilibrium conformations while $CH_2FCOHCH_2F^+$, $CH_2FCOHCHF_2^+$, $CHF_2COHCHF_2^+$, $CF_3COHCH_2F^+$, and $CF_3COHCHF_2^+$, have type III equilibrium conformations. The apparent feature of the pseudo-five-membered ring in both types II and III equilibrium conformations indicates the presence of an intramolecular hydrogen bond between the carbonyl hydrogen and the F atom at C_1. This is in agreement with the experimental interpretation (1) of the dependence of the proton affinity on the number of fluorine substituents.[2] Note that in the protonated series, position X at C_3 is always occupied by a F atom, if possible, regardless of whether it is the unique atom or not. This is in contrast to that found in the neutral series. Figure 1 shows that, of the unsymmetrically substituted protonated

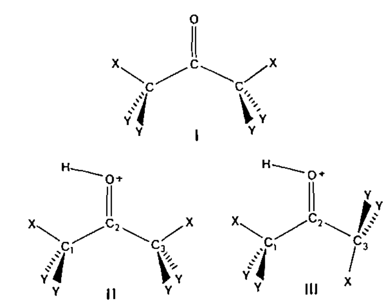

FIG. 2. Types of equilibrium conformations of the fluorinated acetones (I) and their conjugate acids (II and III).

acetones, the carbonyl proton is directed toward the carbon with the larger number of F substituents in the case of $CF_3COHCH_2F^+$, and toward the carbon atom with the smaller number of F substituents in the case of $CH_2FCOHCHF_2^+$ and $CF_3COHCHF_2^+$. With the exception of the latter two, the equilibrium conformations of the protonated species are characterized by an intramolecular hydrogen bond involving a F atom of the more highly substituted methyl group. Here it is interesting to note that Drummond and McMahon (1) have suggested that intramolecular hydrogen bond formation in pentafluoroacetone should occur to a fluorine in the CF_3 group rather than the CF_2H group, on the basis that the higher symmetry of the CF_3 group leads to a lower overall entropy associated with internal rotation, and thus the decrease in entropy due to restriction of the rotation should be less.

The equilibrium conformations of CH_3COCH_3, CH_2FCOCH_3, CF_3COCH_3, and CF_3COCF_3 remain unchanged upon

[2]Infrared studies (18, 19) of the protonated fluoroacetone and hexafluoroantimoniate salt (20) showed the absence of intramolecular hydrogen bonding when the halogen is fluorine.

protonation. In the case of CHF_2COCH_3 and CHF_2COCHF_2, protonation leads to a change in the conformation of the methyl group that is involved in the internal hydrogen bond. The conformation of the methyl group which is not involved in the internal hydrogen bond in CHF_2COCHF_2, $CH_2FCOCHF_2$, CHF_2COCHF_2, CF_3COCH_2F, and CF_3COCHF_2 remains unchanged upon protonation. Note that both methyl groups show changes in conformation upon protonation in the case of CHF_2COCHF_2.

The C—F bond length varies little from one molecule to another within the fluoroacetones, the range being from 1.370 Å (in CF_3COCH_2F) to 1.384 Å (in CH_2FCOCH_3) at the STO-3G level, whereas the C—H bond length shows a larger range of 0.025 Å. Previous studies (21, 22) have shown that the STO-3G basis set underestimates the effect of multiple substitution on the C—F bond lengths of the fluoromethanes. The bond angles in the neutral series are very close to the values typical of trigonally and tetrahedrally hybridized carbon. The only significant bond length variation is that of the C—C bond in both the neutral and protonated series. In general, at the minimal STO-3G level of optimization, the replacement of H by F results in the extension of the C—C bond (s). This is especially true in the protonated series. The degree of elongation in the protonated series is governed by the number of F atoms bonded to the adjacent carbon atom. In the case of the acetate anion, the C—C bond stretches by about 0.02 Å for each successive F substituent at the STO-3G level (16). This study shows similar elongation of the C—C bond(s) in both the neutral and protonated series. Relative to $CH_3COHCH_3^+$, the effect of a F substituent is to increase the adjacent C—C bond and to contract the opposite C—C bond of $CH_2FCOHCH_3^+$. In both the neutral and protonated series, the methyl carbon with a larger number of F atoms will have a longer C—C bond. With the increasing number of F substituents at both C_1 and C_3, the question arises as to whether such molecules are in fact on the verge of breaking up into two separate fragments. This is especially true in the case of $CF_3COHCF_3^+$. In short, the effect of fluorination in the protonated series can be summarized as shown in Table 3 with the $CH_3COHCH_3^+$ STO-3G structure as the reference. Use of a model methyl group is justified by the small changes of the optimized CH_3 group in CF_3COCH_3 as compared with that of CH_3COCH_3 at the STO-3G level.

As shown in Fig. 1, '4-31G' equilibrium structures were obtained for CH_2FCOCH_3, CHF_2COCH_3, CF_3COCH_3, CF_3COCF_3, and their corresponding acids. Analysis of the proton affinities and the total atomic charges at the 4-31G//'4-31G' level indicates only slight differences from the 4-31G//STO-3G values. Consequently, a significant improvement upon the STO-3G results for the two series is not expected as a result of reoptimization at the '4-31G' level. This is further justified by the poor agreement between the theoretical '4-31G' geometries of CF_3COCH_3 and CF_3COCF_3 with the experimental results of Adreassen and Bauer (23) and Bauer and co-workers (24), respectively.

This paper reports the first extensive theoretical study on the structures of the fluoroacetones and their conjugate acids. An *ab initio* study by Jost *et al.* (25) assumed model geometries for CH_3COCH_3, CH_2FCOCH_3, CH_2FCOCH_2F, and their corresponding conjugate acids based on the following parameters: C=O = 1.212 Å, C—H = 1.095 Å, C—C = 1.50 Å, C—F = 1.398 Å, and CCO = 121°. All other angles were assumed to be tetrahedral. On the basis of Del Bene and Vaccaro's work (26), Jost *et al.* argued that the C=O and $^+$O—H bond lengths and the COH^+ angle do not depend on the substituents and consequently do not require any optimization. Nevertheless, the present study clearly indicates that the number and positions of the F substituents do affect the geometry of the protonated species. This is especially noticeable in the pseudo-five-membered ring associated with the intramolecular hydrogen bond.

TABLE 3. Comparison of STO-3G equilibrium geometries in the protonated series

Parameter	*p*-fluoroacetone	*p*-acetone
r (O—H)	1.026	0.997
r (C=O)	1.273	1.290
r (C_1—C_2)	1.593	1.524
∠COH	104.9	113.1
$\angle OC_2C_1$	112.4	122.4
$\angle C_2C_1F$	101.2	110.2

TABLE 4. Comparison of neutral and protonated average equilibrium geometries at the STO-3G level

Parameter	Neutral	Protonated
r (C=O)	1.217	1.273
r (C_1—F) or C_3—F)	1.378	1.386
r (C_1—C_2)	1.578	1.593
r (C_2—C_3)	1.554	1.564
$\angle OC_2C_1$	122.1	112.4
$\angle OC_2C_3$	122.8	120.4
$\angle C_2C_1F$ or $\angle C_2C_3F$	111.3	101.2

A semi-empirical MNDO study (17) predicted a COH angle in the protonated species of about 120−125° and a slight increase in the O—H bond with the number of F substituents. However, this study shows an average COH angle of 104.9° at the STO-3G level. In addition, a large discrepancy is also observed for the O—H bond lengths: 1.026 Å on average at the STO-3G level versus 0.964 Å by MNDO. Nevertheless, the C=O bond in the protonated species is in close agreement, 1.277 and 1.273 Å according to the MNDO and STO-3G calculations, respectively. Table 4 summarizes the changes in structural parameters associated with protonation.

Proton affinities

Seven of the ten PA's are available from an ion cyclotron resonance (ICR) study (1). The extra three theoretical PA's are obtained from the three isomers of the di,- tri-, and tetrafluoroacetones. As shown in Table 5, the theoretical PA's decrease as the number of F substituents increases, in good agreement with the experimental observation. It is apparent that the minimal STO-3G basis set grossly overestimates the PA's by about 57 ± 3 kcal/mol. Since the amount of overestimation is fairly constant, the observed trends are well reproduced. The lack of experimental PA's for the three isomeric pairs precludes an assessment of the STO-3G prediction that maximizing the number of F's on one carbon decreases the basicity and hence increases the acidity of the protonated acetones.

PA's at the 4-31G//STO-3G level differ considerably from those at the STO-3G//STO-3G level, which does not in general provide reliable estimates of relative PA's of related bases (27, 28). The 4-31G//STO-3G calculations overestimate the PA of actone by about 7.4 kcal/mol and underestimate the

TABLE 5. Proton affinities[a]

Molecule	STO-3G//STO-3G	4-31G//STO-3G	4-31G//'4-31G'	6-31G*//STO-3G	Experiment[b]	MNDO[c]
CH_3COCH_3	248.8	201.3		202.2	193.9	189.0
CH_2FCOCH_3	249.4	190.9	189.5	195.3	190.0	182.2
CH_2FCOCH_2F	244.4	184.9		190.4	183.5	174.8
CHF_2COCH_3	240.1	171.8	169.5	179.9		
$CH_2FCOCHF_2$	235.3	163.7		173.4		
CF_3COCH_3	232.4	160.0	159.0	171.4	177.1	161.3
CHF_2COCHF_2	227.2	148.3			171.1	156.5
CF_3COCH_2F	227.0	150.3				
CF_3COCHF_2	221.0	135.7			165±2	146.9
CF_3COCF_3	213.9	124.6	123.4		159.3	136.5

[a]All protons affinities are in kcal/mol.
[b]See ref. 1.
[c]See ref. 17.

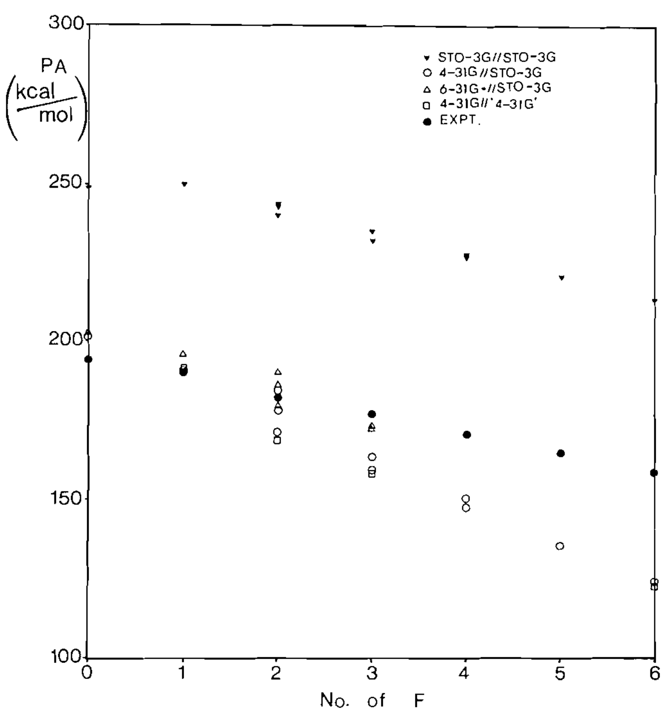

FIG. 3. Experimental and theoretical proton affinities (PA) versus the number of fluorine substituents in the fluoroacetones.

remaining PA's by up to 34.7 kcal/mol, with the error increasing as the number of F's increases. Note that, in the case of the tetrafluoroacetone pair of isomers, the prediction that maximizing the number of F's on one carbon atom increases the acidity of the protonated species does not hold at the 4-31G//STO-3G level. The slight difference between the 4-31G//'4-31G' and 4-31G//STO-3G results demonstrates that the application of partial split-valence optimizations does not significantly improve the PA's, in agreement with a study (16) of the carboxylate anions. However, at the 6-31G*//STO-3G level, a considerable improvement is observed, with the difference between the theoretical and experimental values not exceeding 10 kcal/mol. Even though the 6-31G*//STO-3G data are incomplete, it is obvious that the 6-31G* basis set gives the best estimate of the experimental PA's.

Figure 3 shows plots of the theoretical and experimental PA's versus the number of F substituents. The correlation coefficients (R^2) are 0.959, 0.979, 0.987, 0.904, and 0.991 for the STO-3G//STO-3G, 4-31G//STO-3G, 4-31G//'4-31G', 6-31G*//STO-3G, and experimental values, respectively. The correlation improves as the level of theory increases, with one exception, i.e. the 6-31G*//STO-3G data. Since only a few members of the series are included and they cover only a narrow range of n, the R^2 value for the 6-31G*//STO-3G data is insignificant. By comparison, the 4-31G//'4-31G' level gives the best R^2 value because the few PA values cover a larger range of n. Nevertheless, the R^2 value at the 4-31G//'4-31G' level is also insignificant due to the lack of a complete set of data. In fact the inability of the 4-31G basis set to account for the F substituent effect can be seen by making a comparison between the 4-31G and 6-31G* PA's at the STO-3G geometry. In acetone, the difference in PA between 4-31G//STO-3G and 6-31G*//STO-3G levels is only a small amount, 1 kcal/mol. With an increase in the number of F substituents, the difference in PA's between these two levels becomes excessive, indicating the inadequacy of the 4-31G basis set for the description of the effect of multiple F substituents.

Experimentally (1), a regular decrease of 6.1 kcal/mol in PA was observed with the addition of each F substituent. Least-squares fits to the data plotted in Fig. 3 yield 7.2, 13.7, 12.7, and 11.7 kcal/mol at the STO-3G//STO-3G, 4-31G//STO-3G, 4-31G//'4-31G', and 6-31G*//STO-3G levels, repectively. Hence the STO-3G//STO-3G calculations show an F substituent effect that is closest to the experimental result, while the larger basis sets show effects that are about twice as large. Even though the STO-3G//STO-3G calculations provide a more satisfactory account of multiple substituents, better quantitative agreement with experiment is obtained at the 6-31G*//STO-3G level.

A semi-empirical MNDO study by DeKock *et al.* (17) gave PA's that deviate considerably from the experimental results (see Table 5), with the deviations tending to increase as the number of F substituents increases. From a least-squares fit to the MNDO values (excluding acetone) in Table 5, we obtain a slope of 9.1 kcal/mol compared to the STO-3G and experimental values of 7.2 and 6.1 kcal/mol, respectively. A significant difference between the MNDO and *ab initio* results is evident from the equilibrium conformations. For the protonated species, all *ab initio* calculations yield equilibrium structures in which the carbonyl proton is directed toward a F on an adjacent methyl group. Thus the equilibrium structures are characterized by a pseudo-five-membered ring which is attributed to the formation of an intramolecular hydrogen bond. The MNDO results for protonated 1,1,1-trifluoroacetone place the energy

TABLE 6. Vertical ionization potentials[a]

Molecule	STO-3G//STO-3G	4-31G//STO-3G	6-31G*//STO-G	4-31G//'4-31G'	Experiment[b]	MNDO[c]
CH_3COCH_3	8.76	11.08	11.08		9.71	10.8
CH_2FCOCH_3	8.80	11.55	11.46	11.73	10.20	11.0
CH_2FCOCH_2F	8.85	12.02	11.83		10.46	11.3
CHF_2COCH_3	8.99	12.16	11.94	12.47	10.47	
$CH_2FCOCHF_2$	9.02	12.60	12.29			
CF_3COCH_3	9.20	12.83	12.51	13.05	11.00	12.0
CHF_2COCHF_2	9.17	13.08			11.33	11.9
CF_3COCH_2F	9.23	13.25				
CF_3COCHF_2	9.38	13.77				12.4
CF_3COCF_3	9.58	14.47		14.97	12.09	13.0

[a]All ionization potentials are in eV.
[b]See ref. 34.
[c]See ref. 17.

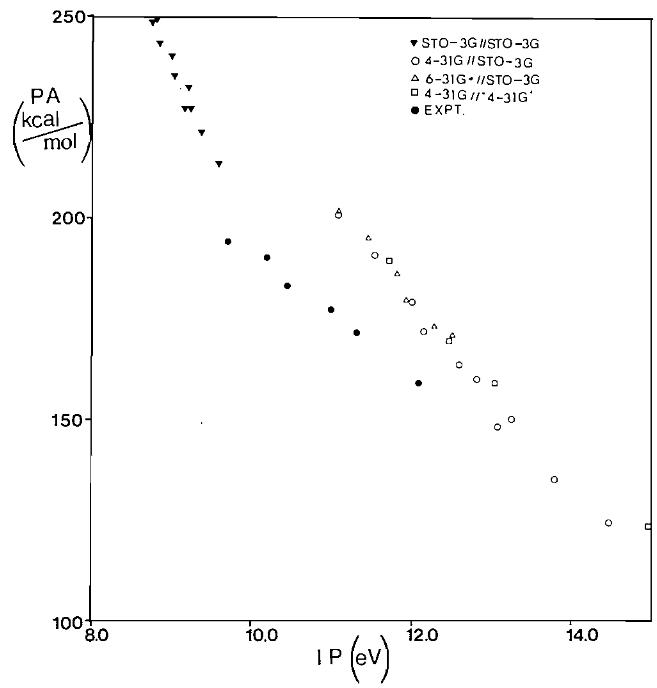

FIG. 4. Experimental and theoretical proton affinities (PA) versus the corresponding ionization potentials (IP) in the fluoroacetones.

of the hydrogen bonded conformation 1 kcal/mol above the conformation in which the carbonyl proton is directed toward the CH_3 group rather than the CF_3 group. At the 4-31G//4-31G level we find a difference of 1.7 kcal/mol in favour of the conformation which is interpreted in terms of a F---H—O intramolecular hydrogen bond. Thus our *ab initio* results are consistent with the original suggestion of Drummond and McMahon (1) and not with the MNDO results (17).

The overall free energy of stabilization of a protonated species due to the formation of an intramolecular hydrogen bond can be estimated from the difference between the acetone PA and the intercept obtained from a least-squares fit to the PA's of the fluoroacetones. This method leads to 7.7, 3.4, 6.0, 1.9, and 2.4 kcal/mol with the STO-3G//STO-3G, 4-31G//STO-3G, 6-31G*//STO-3G, experimental, and MNDO data, respectively. Thus the highly parameterized MNDO method leads to a better agreement with the experimental estimate of the stabilization due to the formation of an intramolecular hydrogen bond than do the *ab initio* calculations. Here it is interesting to note that the only previous *ab initio* study (25) of the proton affinities of acetone, monofluoroacetone, and 1,1-difluoroacetone attempted to assess the magnitude of the intramolecular hydrogen bond energy by comparing the energies of *syn* and *anti* conformations of the protonated forms. At the STO-3G and 4-31G levels with model geometries, Jost *et al.* (25) obtained 5.1 and 7.9 kcal/mol, respectively, for protonated monofluoroacetone. This is considerably higher than the 4-31G//4-31G value for protonated 1,1,1-trifluoroacetone (see the preceding paragraph). Such a procedure can not be applied, however, to the highly fluorinated acetones because a suitable *anti* conformation does not exist. We shall postpone a thorough discussion of the intramolecular hydrogen bond until a later paper (13) in which we will present a detailed analysis based on the topological properties of the charge density.

Ionization potentials

We wish to conclude our discussion by noting that there is a good correlation (see Fig. 4) between the theoretical values for the proton affinities and ionization potentials (IP) of the fluoroacetone bases. Similar correlations have been observed (29, 30) between experimental sets of data for a variety of systems, including the fluoroacetones (1), and in theoretical studies (27, 31, 32). The theoretical IP's for the fluoroacetones, as given by Koopmans' theorem (33), are tabulated in Table 6, together with the experimental (34) and MNDO (17) values. As expected, the STO-3G IP's are too low by about 1 to 2 eV, while the larger basis sets overestimate the IP's by similar amounts. Both theory and experiment indicate a correlation between increasing proton affinity and decreasing ionization potential for the fluoroacetones. The correlation is similar to that observed in other R_2CO molecules (32), and is expected in a related series of molecules in which ionization of a nonbonding electron is essentially localized at a single atom which is also the site of protonation. Del Bene has suggested (31) that the correlation between decreasing IP and increasing PA may arise from the common mechanism of stabilizing the resulting ions, which involves a polarization of electron density toward the basic site. The latter mechanism is a central feature of a model for the protonation of carbonyl bases (32).

Conclusion

The theoretical equilibrium structures are consistent with the interpretation of the gas-phase basicities in terms of the formation of an intramolecular hydrogen bond. The stereochemistry of the methyl group involved in the intramolecular hydrogen bond is always *cis* periplanar with the carbonyl group, whereas the other methyl group shows a preference for both *cis* and *trans* periplanar conformations. The fluoroacetones, like the parent molecule, are predicted to have equilibrium structures in which both methyl groups are *cis* periplanar with the carbonyl group, with the unique atom of the mono- and difluoromethyl groups lying in the carbonyl plane.

The theoretical PA's of the fluoroacetones have been shown to decrease as the number of F substituents increases, in agreement with the ICR study of Drummond and McMahon. The best quantitative agreement is obtained at the 6-31G*//STO-3G level, with the deviations being less than 10 kcal/mol. Although the minimal STO-3G basis overestimates the PA's by about 57 ± 3 kcal/mol, the minimal basis set provides a good estimate of the effect of each successive F substituent on the proton affinity: 7.2 kcal/mol versus the observed 6.1 kcal/mol. Larger basis sets lead to substituent effects which are about twice as great. Theoretical estimates of the intramolecular hydrogen bond energy have been obtained from the difference between the calculated PA of acetone and the intercept of a plot of the calculated PA's as a function of the number of F substituents. The STO-3G estimate is too high by nearly 6 kcal/mol whereas the 4-31G//STO-3G estimate is only 1.5 kcal/mol too high. In general, the *ab initio* calculations overestimate the effects of successive fluorine substituents. A good correlation between the theoretical proton affinities and ionization potentials of the fluoroacetones is consistent with the observation that the ionization of a nonbonding electron is essentially localized at a single atom which is also the site of protonation.

Acknowledgements

We thank Dr. T. B. McMahon for several helpful discussions and his interest in this work. The financial support of the Natural Sciences and Engineering Research Council of Canada and a generous allocation of computing time from the Dalhousie University Computer Centre are gratefully acknowledged.

1. D. F. DRUMMOND and T. B. MCMAHON. J. Phys. Chem. **85**, 3746 (1981).
2. M. J. S. DEWAR and R. C. DOUGHERTY. The PMO theory of organic chemistry. Plenum, New York. 1975.
3. R. W. TAFT. In Proton transfer reactions. *Edited by* E. F. Caldin and V. Gold. Chapman and Hall, London. 1975.
4. P. KEBARLE. Annu. Rev. Phys. Chem. **28**, 445 (1977).
5. J. B. CUMMING and P. KEBARLE. Can. J. Chem. **56**, 1 (1978).
6. J. H. STEWART, R. H. SHAPIRO, C. H. DEPUY, and N. M. BIERBAUM. J. Am. Chem. Soc. **99**, 7650 (1977).
7. G. I. MACKAY, R. S. HEMSWORTH, and D. K. BOHME. Can. J. Chem. **54**, 1624 (1976).
8. F. C. FEHSENFELD. Int. J. Mol. Spectrosc. Ion Phys. **16**, 151 (1975).
9. T. A. LEHMAN and M. M. BURSEY. Ion cyclotron resonance spectroscopy. Wiley. New York. 1976.
10. J. E. BARTMESS, J. A. SCOTT and R. T. MCIVER, JR. J. Am. Chem. Soc. **101**, 6046 (1979).
11. R. GYGAS, H. L. MCPETERS, and J. I. BRAUMAN. J. Am. Chem. Soc. **101**, 2657 (1979).
12. R. FARID, and T. B. MCMAHON. Can. J. Chem. **58**, 2307 (1980).
13. S. C. CHOI and R. J. BOYD. In preparation.
14. J. S. BINKLEY, R. A. WHITESIDE, P. C. HARIHARAN, R. SEEGER, J. A. POPLE, W. J. HEHRE, and M. D. NEWTON. QCPE, **11**, 368 (1978).
15. R. J. BOYD and K. E. EDGECOMBE. QCPE Bull. **2**, 10 (1982).
16. K. E. EDGECOMBE and R. J. BOYD. Can. J. Chem. **62**, 2881 (1984).
17. R. L. DEKOCK, C. P. JASPERSE, and M. S. KONINGS. J. Mol. Struct. (THEOCHEM), **94**, 343 (1983).
18. F. C. MARLER and H. HOPKINS. J. Phys. Chem. **74**, 4164 (1970).
19. L. J. BELLAMY and R. J. PACE. Spectrochim. Acta Part A, **25**, 319 (1969).
20. G. NOEL. These 3ᵉ Cycle, Université de Bordeaux I, France. 1973.
21. K. E. EDGECOMBE and R. J. BOYD. Can. J. Chem. **61**, 45 (1983).
22. R. A. WHITESIDE, M. J. FRISCH, J. S. BINKLEY, D. J. DEFREES, H. B. SCHLEGEL, K. RAGHAVACHARI and J. A. POPLE. Carnegie-Mellon, Quantum Chemistry Archive, 2nd ed. July 1981.
23. A. L. ANDREASSEN and S. H. BAUER. J. Mol. Struct. **12**, 381 (1972).
24. R. L. HILDERBRANDT, A. L. ANDREASSEN, and S. H. BAUER. J. Phys. Chem. **74**, 1586 (970).
25. R. JOST, J. SOMMER, and G. WIPFF. Nouv. J. Chim. **2**, 63 (1977).
26. J. E. DEL BENE and A. VACCARO. J. Am. Chem. Soc. **98**, 7526 (1976).
27. J. E. DEL BENE. J. Am. Chem. Soc. **99**, 3617 (1977).
28. J. E. DEL BENE. Chem. Phys. Lett. **55**, 235 (1978).
29. J. L. BEAUCHAMP. Annu. Rev. Phys. Chem. **22**, 527 (1971).
30. R. H. STALEY, J. E. KLECKNER and J. L. BEAUCHAMP. J. Am. Chem. Soc. **98**, 2081 (1976).
31. J. E. DEL BENE. J. Am. Chem. Soc. **100**, 1673 (1978).
32. J. E. DEL BENE and S. RADOVICK. J. Am. Chem. Soc. **100**, 6936 (1978).
33. T. KOOPMANS. Physica, **1**, 104 (1934).
34. V. Y. YOUNG and K. L. CHENG. J. Chem. Phys. **65**, 3187 (1976).

Intramolecular Michael-type additions. IV.[1] Synthesis of 2-azabicyclo[3.2.1]oct-3-enes from 4-chloroalkyl-1,4-dihydropyridines

BRIAN GREGORY,[2] ERIC BULLOCK, AND TENG-SONG CHEN

Department of Chemistry, Memorial University of Newfoundland, St. John's, Nfld., Canada A1B 3X7

Received June 20, 1984

BRIAN GREGORY, ERIC BULLOCK, and TENG-SONG CHEN. Can. J. Chem. **63**, 843 (1985).

2-Azabicyclo[3.2.1]oct-3-enes, including examples having a spiro centre at C(8), may be obtained by the reaction of anions derived from 1,3-diketones or cyclopentadiene with 4-chloroalkyl-1,4-dihydropyridines or with azepines. Intermediate 4,5-dihydro-1*H*-azepines have been isolated under milder conditions. The structures of the bicyclic compounds were established using infrared, ultraviolet, nuclear magnetic resonance, and mass spectrometry. Pharmacological examination of selected compounds revealed low antimicrobial and hypotensive activity.

BRIAN GREGORY, ERIC BULLOCK et TENG-SONG CHEN. Can. J. Chem. **63**, 843 (1985).

On peut obtenir des aza-2 bicyclo[3.2.1] octenes-3, y compris des exemples possédant un centre spiro en C(8), en faisant réagir des anions dérivant de dicétones-1,3 ou du cyclopentadiène avec des chloroalkyl-4 dihydro-1,4 pyridines ou avec des azépines. Utilisant des conditions expérimentales douces, on a pu isoler les dihydro-4,5 1*H*-azépines. On a déterminé les structures des composés bicycliques en faisant appel aux spectroscopies infrarouge et ultraviolette, à la rmn et à la spectrométrie de masse. Une étude pharmacologique de certains composés a permis d'établir qu'ils possèdent des activités hypotensive et antimicrobienne qui sont faibles.

[Traduit par le journal]

Saturated derivatives of 2-azabicyclo[3.2.1]octane are readily available through condensation reactions (2), from bicyclic ketones or their derived oximes using Schmidt or Beckmann reactions respectively (3−9), or by irradiation of bicycloheptane nitronate anions (10). Alkoxy derivatives have been obtained by the silver-(I) assisted solvolytic cyclization of a chloramine (11) and by photolytic decomposition of 1-azidonorbornane (12). The synthesis of 2-azabicyclo-[3.2.1]octenes and dienes has been achieved mainly through the reaction of norbornadiene with reagents such as benzenesulfonyl azide (13−17), cyanogen azide (18, 19), or nitrile oxides (20). Irradiation of 5-methylenenorbornene in the presence of nitrosamines gave 2-hydroxy-2-azabicyclo-[3.2.1]octa-3,6-dienes (21, 22), while 2-hydroxy-6-enes may be obtained by irradiation of cycloalkane nitronate anions (23). A 6-ene, in equilibrium with an isomeric cyclopentene, has been obtained by treatment of an equilibrium mixture of 2-oxabicyclo[3.2.1]octa-3,6-diene and *endo*-6-formylbicyclo-[3.1.0]hex-2-ene with methylamine (24). Spectroscopic evidence has recently been obtained using matrix isolation techniques for the photolytic preparation of the very reactive, anti-Bredt, bridgehead imine 2-azabicyclo[3.2.1]oct-1-ene (25). Only saturated derivatives appear to have been evaluated for pharmacological activity, prompted by structural relationships to pempidine (26) or the benzomorphan system (27). Reports describe assessment of hypotensive (28, 29), analgesic (30−32), narcotic antagonist (27), and ganglion-blocking activity (26).

Earlier, we have shown that 4-chloromethyl-1,4-dihydropyridines react with basic nucleophiles to give ring-expanded products (33) which may react further to give a variety of heterocyclic systems (34). Ashby and Eisner *et al.* have shown that the hydrosulfide anion reacts with the chloromethyldihydropyridine to give an 8-thia-2-azabicyclo[3.2.1]oct-3-ene, presumably through the intermediacy of a 4,5-dihydroazepine-4-thiol (35, 36). Other heteroatom bridged compounds prepared in this way include the 8-seleno-, 8-benzylamino-, and 8-oxa-2-azabicyclo[3.2.1]oct-3-enes (37, 38); use of thiourea followed by base affords 7-thia-2-azabicyclo[3.2.1]oct-3-enes (39), a reaction which does not involve nucleophile-induced ring expansion. It occurred to us that derivatives of 2-azabicyclo[3.2.1]oct-3-ene might be obtained by the action of a carbanion on a chloromethyl-1,4-dihydropyridine to give a 4-substituted-4,5-dihydro-1*H*-azepine, followed by intramolecular Michael addition as outlined in Scheme 1. The successful realization of this hypothesis is the subject of the present communication[3] and represents a departure from previous synthetic methodology, which mostly has involved ring expansion of preformed bicyclic skeleta. Further, the compounds available by this new route appeared interesting to screen for pharmacological activity.

Reaction of the 4-chloromethyl-1,4-dihydropyridine with sodium acetylacetonate in dimethylformamide at low temperatures afforded a crystalline product, $C_{17}H_{23}NO_6$, whose spectroscopic properties confirmed structure **3**. In particular, the ultraviolet absorption maxima at 231 nm (ϵ 12 100) and 329 nm (ϵ 12 300) were consistent with the presence of a 4,5-dihydroazepine-3,6-diester chromophore (33, 38), while the lack of a strong band at 250 nm[4] excluded the alternative structure **16**. In basic media, an additional strong absorption band at 297 nm (ϵ 26 300) was observed, due to the conversion of the β-diketone side chain to enolate. The failure to isolate the O-alkylation[5] product **16** may be due to the known propensity of dihydroazepines to lose 4-oxygen substituents to give the azepine **17** (37, 43), which is known to add nucleophiles (44), resulting in conversion to the more stable C-alkylation product **3**.

Reaction of **1**, **3**, or **17** with sodium acetylacetonate under

[1]Reference 1 is regarded as Part III of this series.

[2]Author to whom all correspondence should be addressed.

[3]For a preliminary account of this work in relation to Baldwin's Rules see ref. 1.

[4]Dimedone enol ethyl ether, a suitable model for the $\mathrm{{-}OCH{=}CH{-}\overset{\overset{\displaystyle O}{\|}}{C}{-}R}$ chromophore, has an ultraviolet maximum at 250 nm (ϵ 19 200) (40).

[5]For discussions of factors influencing C- and O-alkylation see refs. 41 and 42.

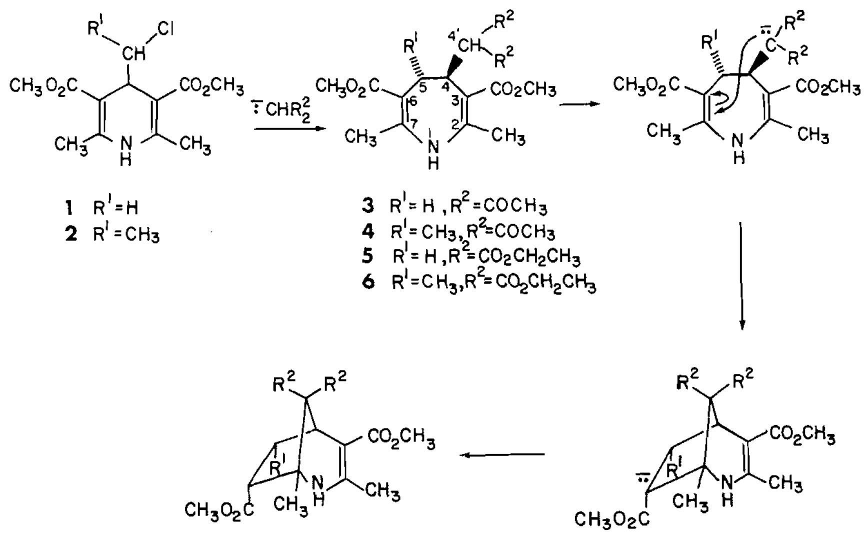

1 $R^1=H$
2 $R^1=CH_3$

3 $R^1=H, R^2=COCH_3$
4 $R^1=CH_3, R^2=COCH_3$
5 $R^1=H, R^2=CO_2CH_2CH_3$
6 $R^1=CH_3, R^2=CO_2CH_2CH_3$

7 $R^1=H, R^2=COCH_3$
8 $R^1=CH_3, R^2=COCH_3$
9 $R^1=H, R^2, R^2=-CH_2(-CH_2)_2-CH_2-$

SCHEME 1

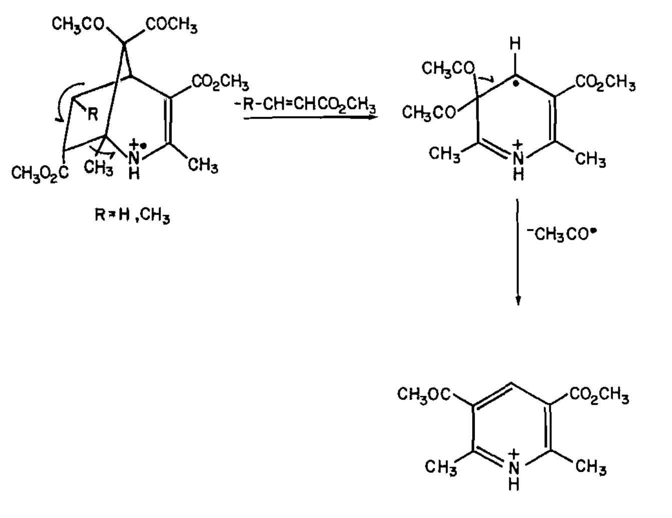

$R=H, CH_3$

$\frac{m}{z}$ 208

SCHEME 2

more vigorous conditions gave the 2-azabicyclo[3.2.1]oct-3-ene **7** whose structure follows from the presence of infrared bands due to NH (str), saturated ketone and ester, and unsaturated ester, and an ultraviolet spectrum showing an intense absorption at 289 nm similar to the 1,4,5,6-tetrahydronicotinic ester chromophore (45) in bridged systems (35–39).[6] The mass spectrum of **7** was dominated by a fragmentation pathway which involved loss of methyl acrylate and acetyl radical (Scheme 2) to give the substituted pyridinium ion at m/z 208. The [1]Hmr spectrum showed four methyl singlets at δ 1.79, 2.03, 2.14, and 2.27; the assignment of the signals at δ 1.79 and 2.27 to methyls at C(1) and C(3) respectively is based on a comparison with the [1]Hmr spectra of compounds **9–15** (see below) which lack signals due to acetyl methyl groups. The remaining signals in the spectrum were in good agreement with the assigned structure, although the signal due to the hydrogen at C(7) was obscured and an unequivocal assignment of the configuration of the methoxycarbonyl group was not possible. Since, based on [1]Hmr, the 7-methoxycarbonyl group of the 8,8-spirocyclopentadiene compounds **14** and **15** (see below) has an *endo*-configuration and we have shown earlier that, in an 8-thia analogue, the *exo*-7-methoxycarbonyl may be converted to *endo*-7-methoxycarbonyl by base-catalyzed equilibration (38), we believe the methoxycarbonyl group in **7** (and also in **8–13** below), which has a bridging group that is bulkier than sulfur, has an *endo*-configuration as shown. It is unlikely that under these conditions (6 h under basic conditions at 100°C in DMF) equilibration to the more stable epimer at C(7) had not taken place.

At room temperature, the action of sodium acetylacetonate on the chloroethyldihydropyridine **2** afforded a mixture of the dihydroazepine **4** (60%), whose methyl at C(5) is assigned a *trans*-configuration to the 4-diacetylmethyl group by analogy with earlier work (38), and the 2-azabicyclooctene **8** (13%). AT 100°C the bicyclic compound **8** was the major product, in 74% yield. These results indicate that the 4,5-dihydroazepine **4** is an intermediate in the formation of the 2-azabicyclooctene **8**, and this is supported by the observation that **8** is formed in 70% yield when sodium acetylacetonate or sodium methoxide is reacted with **4**. Further, it has been shown that the same azabicyclooctene **8** is formed in 80% yield when sodium acetylacetonate is reacted with the azepine **18** in DMF at 90°C. This reaction presumably involves Michael addition to C(4) in **18**, followed by intramolecular Michael addition. Thus, formation of **8** may involve the sequence **2** → **18** → **4** → **8**.[7] The *endo*-configuration of the methyl at C(6) in **8** is a necessary consequence of the *trans* stereochemistry at C(4,5) in the

[6]An alternative 9-oxa-2-azabicyclo[4.3.1]deca-3,7-diene structure **19**, formed by addition of the side chain enolate oxygen of **3** to C(2), would be expected to show an additional strong absorption band in the range 240–270 nm due to the additional 3-acetyl-5,6-dihydropyran chromophore (46, 47).

[7]Similar results also suggest the sequence **1** → **17** → **3** → **7**.

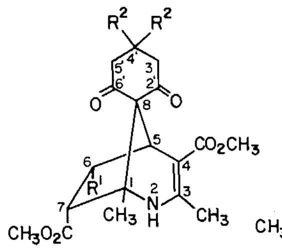

10 R' = H, R^2 = H
11 R' = CH$_3$, R^2 = H
12 R' = H, R^2 = CH$_3$
13 R' = CH$_3$, R^2 = CH$_3$

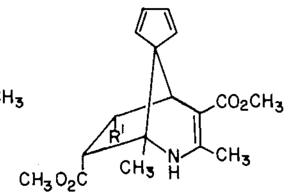

14 R' = H
15 R' = CH$_3$

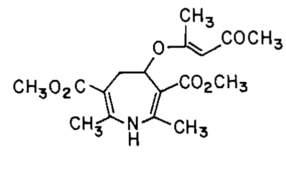

16

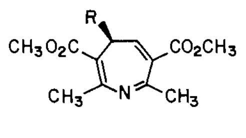

17 R = H
18 R = CH$_3$

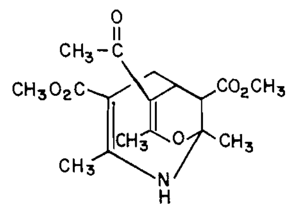

19

dihydroazepine **4** and is supported by ^{1}Hmr spectra of the spirocyclopentadiene compounds **14** and **15** (see below), while reasons for assigning *endo*-configuration for the 7-methoxycarbonyl group are given above. As with compound **7**, the mass spectrum was again dominated by the pyridinium ion at m/z 208, in this case arising by loss of methyl crotonate and acetyl radical. Although the mass spectra of **7** and **8** showed low abundance peaks at m/z 294 and 308 due to loss of acetyl radical, there is no evidence that loss of acetyl precedes loss of unsaturated ester in the formation of the pyridinium ion fragment. Indeed, since the mass spectra of the 8-thia analogues show loss of acrylate (35) or crotonate (38), we believe that loss of the unsaturated ester occurs prior to acetyl radical loss as shown in Scheme 2. The mass spectra of these compounds are being investigated further.

The use of sodium derivatives of cyclic 1,3-diketones, e.g. 1,3-cyclohexanedione or dimedone, afforded the novel spiro compounds **10**–**13** in yields of 60–90% at 65–90°C. In each case, the hydrogens at C(6,7) are obscured in the ^{1}Hmr spectrum and the configurations of the methyl and methoxycarbonyl groups are assigned by analogy (see above). Other spectroscopic features were consistent with the assigned structures.

The reaction has also been extended to the anion of cyclopentadiene in an attempt to provide compounds in which ^{1}Hmr signals due to protons at C(5) to C(7) may be seen clearly. Thus **1** or **2** afforded the spirocyclopentadienes **14** and **15** respectively. Although the expected ultraviolet absorption of the 5,5-dialkylcyclopentadiene chromophore at about 250 nm (48, 49) was hidden by the aminocrotonate absorption at 295 nm in **14**, it was apparent in **15**. In the infrared spectra, **14** and **15** showed saturated and unsaturated ester carbonyl and NH stretching absorptions. The ^{1}Hmr spectrum of **14** showed singlets at δ 1.21, 2.18, 3.62, and 3.71, due to methyls at C(1), C(3), and two methyl esters, respectively, a broad singlet at δ 4.28 (NH), and a four-proton multiplet at δ 6.31 due to the protons of the cyclopentadiene moiety.[8] In addition, the spectrum showed four multiplets consisting of a double doublet at δ 3.19 (J 4.9 and 11.8 Hz; this signal resembled the X part of an ABX system, and thus gave two coupling constants by direct measurement), a broadened doublet at δ 2.97 (J 5.8 and 1.0 Hz), and partly overlapping multiplets at δ 2.62 (J 4.9, 13.9, and 1.0 Hz) and δ 2.38 (J 11.8, 13.9, and 5.8 Hz). Examination of Dreiding models suggests that the dihedral angles subtended by C(5)—H with *exo* and *endo* C(6)—H are close to 30° and 90° respectively. Thus, the H at C(5) should be strongly coupled only to one proton, namely, *exo* H at C(6), and would be expected to be a doublet, J approx 6–7 Hz. Accordingly, the broadened doublet at δ 2.97 is assigned to the hydrogen at C(5); the broadening ($J \sim 1$ Hz) is due to coupling to the *endo*-hydrogen at C(6). The low field part (δ 2.62) of the higher field overlapping multiplets resembles the low field half of an AB system which is split by an additional proton, and consisted of 2 doublets with relative line intensities of approximately 1 : 1 : 3 : 3. The signals at δ 2.62 and 2.38 were therefore assigned to the two protons attached to C(6), and since only the latter signal shows a strong coupling (J 5.8 Hz) to C(5)—H, it must be due to the *exo*-hydrogen at C(6), while the δ 2.62 signal is due to the *endo*-hydrogen at C(6). The remaining signal, at δ 3.19, is consequently assigned to the hydrogen at C(7) and is *exo* (and the methoxycarbonyl is then *endo*) because it has a large coupling (J 11.8 Hz) to the *exo*-hydrogen at C(6) as required by the near zero dihedral angle. The assignments were confirmed by comparison with the ^{1}Hmr spectrum of **15** which, in particular, showed doublets at δ 1.07 (3H, J 6.5 Hz), 2.73 (1H, J 8.2 Hz), 2.97 (1H, J 5.2 Hz), and a multiplet at δ 3.08 (1H, J 5.2, 6.5, and 8.2 Hz) for the system —CH—CH(CH$_3$)—CH—. The doublet at δ 2.97 was assigned to the proton at C(5) and the size of the coupling indicated that it was coupled to *exo*-hydrogen at C(6), causing the methyl at C(6) to be assigned an *endo*-configuration. The doublet at δ 2.73 must then be due to *exo*-hydrogen at C(7) and this is confirmed by partial exchange using sodium methoxide in CH$_3$OD, when the NH signal disappeared and there was considerable diminution of intensity of the doublet at δ 2.73, while other signal intensities remained unchanged.

An interesting feature of the ^{1}Hmr spectrum of the bicyclooctenes is that in the compounds **7**, **8**, **10**–**13** derived from 1,3-diketones the signal due to the methyl at C(1) appears at

[8]The presence of 4 olefinic protons confirms that **14** and **15** are spiro-5,5-cyclopentadienes. Alkylation of cyclopentadienes with bis-alkylating agents such as dibromoethane is well known to produce 5,5-spirocyclopentadienes (48).

δ 1.61−1.79, while in spirodienes **14** and **15** it is found at δ 1.21 and 0.98 respectively. Since in the spirocyclopentane **9**, obtained by hydrogenation of **14**, the C(1) methyl signal is observed at δ 1.29, the above chemical shift variation must be due to deshielding by the carbonyl groups rather than shielding by the diene system.

Appropriate ring-opening of the tetrahydropyridine ring of spiro compounds **10**−**15** should furnish derivatives of the spiro[4,5]decane and spiro[4,5]nonane system and this is presently under investigation.

When the anion derived from diethyl malonate was reacted in tetrahydrofuran at 40°C with either chloromethyl compound **1** or chloroethyl compound **2**, substitution and ring expansion again took place to give the 4,5-dihydroazepines **5** and **6** respectively. In each case, the ^{1}Hmr signals due to ethyl esters (as with acetyl methyl groups in **3** and **4**) were non-equivalent and coupling constants between protons attached to C(4) and C(4′) were unusually high for substituted malonates (11 and 12 Hz in compounds **5** and **6** respectively), showing the lack of free rotation about C(4)—C(4′). Attempts to prepare the corresponding azabicyclo[3.2.1]octenes using more vigorous conditions, e.g. **1** or **2** with diethyl sodiomalonate in dimethylformamide at 120°C, were unsuccessful, yielding only **5** or **6**. The reasons for the failure to form the bicyclic compounds are not clear, but may involve prevention of the intramolecular Michael addition by the steric requirements of the two ethoxycarbonyl groups.

Three compounds were selected for evaluation in a broad pharmacological screen (see Acknowledgements). Compound **7** showed weak activity (MIC 100 μg/mL) against *Serratia marcescens* and *Klebsiella pneumoniae*. Compound **5** was active at a similar level against *S. marescens*, *K. pneumoniae*, and *Streptococcus fecalis*. It also exhibited activity at 100 mg/kg po (and slight activity at 25 mg/kg) in an antihypertensive assay using spontaneously hypertense rats. Low activity (MIC 50 μg/mL) against *Trichomonas vaginalis* was observed for compound **12**.

Experimental

Details concerning spectral measurements, analyses, etc., are provided in an earlier publication (34).

General method for preparation of 4,5-dihydroazepines or 2-azabicyclo[3.2.1]oct-3-enes

The 4-chloroalkyl compound **1** or **2** (0.01 mol) and the sodium enolate (or cyclopentadienylsodium) (0.022 mol) in dry dimethylformamide (10−30 mL per g of **1** or **2**) were stirred at the appropriate temperature for the specified time. The reaction mixture was then cooled, poured into 3.3 volumes of 10% aqueous ammonium chloride, and extracted three times with ether or chloroform. Evaporation of the organic solvent gave a crude product which was purified by column chromatography or recrystallization (see Table 1).

Dimethyl 4-(diacetylmethyl)-4,5-dihydro-2,7-dimethylazepine-3,6-dicarboxylate, **3**

Infrared ν_{max}: 3414 (NH), 1703 (ketone carbonyl), 1700 (unsaturated ester), and 1632 (C═C) cm^{-1}; uv (95% ethanol) λ_{max}: 231 nm (ε 12 100), 329 nm (ε 12 300); (0.01 *M* sodium hydroxide in 95% ethanol) λ_{max}: 234 nm (ε 11 900), 297 nm (ε 26 300), 326 nm (ε 12 100); ^{1}Hmr δ: 2.08 and 2.10 (s, s, acetyl methyls), 2.20 approx. (m, obscured by four methyl singlets), 2.25 and 2.33 (s, s, methyls at C(2), C(7)), 3.15 (dd, *J* 5.6 and 14.0 Hz, H at C(5)), 3.65 and 3.68 (s, s, methyl esters), 3.71 (d, *J* 11.0 Hz, —C*H*(COCH$_3$)$_2$), 4.29 (m, H at C(4) or C(5)), 5.68 (s, NH); ms *m/z*: 337(1.4, M$^+$), 237(50), 206(42), 205(40), 179(24), 178(91), 146(100), 118(39), 100(54), 85(60), 43(44), and 42(52).

TABLE 1. Preparation of 4,5-dihydroazepines and 2-azabicyclo[3.2.1]oct-3-enes

Compound	Reactants*	Solvent†	Temperature (°C)	Reaction time (h)	Yield (%)	Recrystallization solvent†	Melting point (°C)	Molecular formula	Analysis (%) Calculated C	Calculated H	Calculated N	Found C	Found H	Found N
3	**1**, Na^+A^-	DMF	0–5	6	58	E/P	147–148.5	$C_{17}H_{23}NO_6$	60.52	6.87	4.15	60.36	6.93	4.09
4	**2**, Na^+A^-	DMF	20	24	60‡	E/P	104–106	$C_{18}H_{25}NO_6$	61.52	7.17	3.98	61.55	7.25	3.97
5	**1**, Na^+B^-	THF	40	15	75.5	E/P	99–100.5	$C_{19}H_{27}NO_8$	57.43	6.85	3.53	57.29	6.93	3.43
6	**2**, Na^+B^-	THF	40	20	66	E/P	125.5–127	$C_{20}H_{29}NO_8$	58.37	7.10	3.40	58.42	7.13	3.36
7	**1**, Na^+A^-	DMF	60	10	85	E/P	192.5–193.5	$C_{17}H_{23}NO_6$	60.52	6.87	4.15	60.52	6.91	4.27
8	**2**, Na^+A^-	DMF	100	6	74	C/E/P	180–181	$C_{18}H_{25}NO_6$	61.52	7.17	3.98	61.39	7.33	3.89
10	**1**, Na^+C^-	DMF	70	10	90	E/P	219.5–220.5	$C_{18}H_{23}NO_6$	61.88	6.64	4.19	61.82	6.40	4.19
11	**2**, Na^+C^-	DMF	90	10	60‡	E/P	137–138.5	$C_{19}H_{25}NO_6$	62.80	6.93	3.85	62.65	6.93	3.79
12	**1**, Na^+D^-	DMF	65	8	82	C/P	221.5–222.5	$C_{20}H_{27}NO_6$	63.64	7.21	3.71	63.70	7.23	3.85
13	**2**, Na^+D^-	DMF	90	10	68	E/P	218.5–219.5	$C_{21}H_{29}NO_6$	64.43	7.47	3.58	64.38	7.49	3.39
14	**1**, Na^+E^-	DMF	60	6	68	E/P	195–196.5	$C_{17}H_{21}NO_4$	67.31	6.98	4.62	67.57	7.03	4.75
15	**2**, Na^+E^-	DMF	60	10	38	E/P	158–159.5	$C_{18}H_{23}NO_4$	68.12	7.30	4.41	67.87	7.42	4.34

*A−E represent 2,4-pentanedione, diethyl malonate, 1,3-cyclohexanedione, 5,5-dimethyl-1,3-cyclohexanedione, and cyclopentadiene, respectively.
†Solvents: DMF = dimethylformamide, E = diethyl ether, P = petroleum ether (boiling range 40−60°C), C = chloroform, THF = tetrahydrofuran.
‡Purification required column chromatography on silica gel H using benzene/ethyl acetate for elution.

Dimethyl 8,8-diacetyl-1,3-dimethyl-2-azabicyclo[3.2.1]oct-3-ene-4,7-dicarboxylate, 7

Infrared ν_{max} 3418 (NH), 1736 (saturated ester), 1721 (saturated ketone), and 1694 (unsaturated ester) cm^{-1}; uv λ_{max}: 289 nm (ϵ 13 600); ^{1}Hmr δ: 1.79 (s, methyl at C(1)), 2.03 and 2.14 (s, s, acetyl methyls), 2.27 (s, methyl at C(3)), 3.68 (s, ester methyl), 4.17 (s, NH), and, in addition, signals due to four protons between δ 1.4−3.9 which were partially obscured by signals due to methyl esters and C-methyl groups; ms m/z: 337(23, M^+), 306(10), 294(12), 208(100), and 43(21).

Alternate method

A solution of the 4,5-dihydroazepine **3** (6 mg) and sodium acetylacetonate (3 mg) in dry dimethylformamide (0.3 mL) was stirred at 60−65°C for 2 h and then worked up as above. The bicyclic product (4 mg, 66%) was obtained as white prisms, mp 192.5−193.5°C, and was shown to be identical with the product of the general method by mixed mp, uv, ir, and mass spectra.

Dimethyl 4-(diacetylmethyl)-4,5-dihydro-2,5,7-trimethylazepine-3,6-dicarboxylate, 4

Infrared ν_{max}: 3414 (NH), 1699 (saturated ketone and unsaturated ester), and 1631 (C=C) cm^{-1}; uv λ_{max}: 231 nm (ϵ 11 100), 328 nm (ϵ 12 700); ^{1}Hmr δ: 0.89 (d, J 6.8 Hz, methyl at C(5)), 2.08 and 2.10 (s, s, acetyl methyls), 2.29 and 2.30 (s, s, methyls at C(2) and C(7)), 3.25 (m, H at C(5)), 3.66 (d, J 11.0 Hz, CH($COCH_3)_2$), 3.67 and 3.70 (s, s, methyl esters), 4.07 (dd, J 5.5 and 11.0 Hz, H at C(4)), 5.76 (s, NH); ms m/z: 351 (9, M^+), 320(18), 319(9), 276(30), 252(54), 251(100), 220(81), 219(17), 211(19), 192(70), 179(80), 167(25), 160(35), 153(46), and 43(29).

Dimethyl 8,8-diacetyl-1,3,6-trimethyl-2-azabicyclo[3.2.1]oct-3-ene-4,7-dicarboxylate, 8

Infrared ν_{max}: 3436 (NH), 1733 (saturated ester), 1695 (unsaturated ester, saturated ketone), and 1668 (C=C) cm^{-1}; uv λ_{max}: 292 nm (ϵ 13 100); ^{1}Hmr (DMSO-d_6) δ: 0.84 (d, J 6.0 Hz, methyl at C(6)), 1.61 (s, methyl at C(1)), 2.03 and 2.08 (s, s, acetyl methyls), 2.27 (s, methyl at C(3)), 3.58 and 3.61 (s, s, methyl esters), 6.93 (s, NH); one ring proton at δ 3.6−3.8 was partially obscured by the methyl ester signals and the signals due to two other protons overlapped at δ 3.0−3.6; ms m/z: 351 (17, M^+), 320(8), 308(14), 276(6), 209(16), 208(100), 176(6), 148(6), and 43 (24).

Alternate method (a)

The 4,5-dihydroazepine **4** (10 mg) and sodium acetylacetonate (5 mg) in dry dimethylformamide (0.3 mL) were stirred at 60−65°C for 2 h. After being worked up as above, the bicyclic compound **8** (7 mg, 70%) was obtained as white prisms, mp 181−182°C.

Alternate method (b)

The 4H-azepine **18** (38) (160 mg) and sodium acetylacetonate (100 mg) in dry dimethylformamide (10 mL) were stirred at 90°C for 6 h and then worked up as above. The bicyclic compound **8** was obtained from ether − petroleum ether as white needles (180 mg, 80%), mp 180−181°C.

Dimethyl 1,3-dimethyl-2-azabicyclo[3.2.1]oct-3-ene-4,7-dicarboxylate-8-spiro-(2′,6′-dioxocyclohexane), 10

Infrared ν_{max}: 3416 (NH), 1725 (saturated ester), 1692 (unsaturated ester, saturated ketone), and 1659 (C=C) cm^{-1}; uv λ_{max}: 289 nm (ϵ 14 900); ^{1}Hmr δ: 1.75 (s, methyl at C(1)), 2.04 (s, methyl at C(3)), 3.68 and 3.69 (s, s, methyl esters), 4.20 (s, NH), and, in addition, one-proton signals at δ 3.5 and 3.8 were partially obscured by the ester methyl signal, while the other two ring protons and the six protons of the cyclohexanedione moiety appeared as overlapping multiplets at δ 1.2−3.3; ms m/z: 349(45, M^+), 318(24), 265(36), 231(20), 220(20), 207(55), 192(27), 179(100), and 165(22).

Dimethyl 1,3,6-trimethyl-2-azabicyclo[3.2.1]oct-3-ene-4,7-dicarboxylate-8-spiro(2′,6′-dioxocyclohexane), 11

Infrared ν_{max}: 3436 (NH), 1728 (saturated ester), 1695 (unsaturated ester, saturated ketone), and 1667 (C=C) cm^{-1}; uv λ_{max}: 292 nm (ϵ 15 250); ^{1}Hmr δ: 0.96 (d, J 7.0 Hz, methyl at C(6)), 1.65 (s, methyl at C(1)), 2.14 (s, methyl at C(3)), 3.69 and 3.71 (s, s, methyl esters), 3.85 (d, J 5.8 Hz, probably H at C(5)), 4.73 (s, NH), and a complex signal at δ 1.2−3.7 consisting of signals due to the remaining two ring protons and the six protons of the cyclohexanedione moiety; ms m/z: 363 (44, M^+), 332(21), 279(28), 220(23), 207(50), 192(32), 179(100), and 165(18).

Dimethyl 1,3-dimethyl-2-azabicyclo[3.2.1]oct-3-ene-4,7-dicarboxylate-8-spiro(4′,4′-dimethyl-2′,6′-dioxocyclohexane), 12

Infrared ν_{max}: 3416 (NH), 1727 (saturated ester), 1697 (unsaturated ester, saturated ketone), and 1662 (C=C) cm^{-1}; uv λ_{max}: 289 nm (ϵ 14 550); ^{1}Hmr δ: 0.84 and 1.19 (s, s, methyls of dimedone moiety), 1.73 (s, methyl at C(1)), 2.02 (s, methyl at C(3)), 3.68 (s, two ester methyls), 4.16 (s, NH), and complex signals between δ 1.6−3.9 due to eight additional protons; ms m/z: 377 (74, M^+), 346(28), 291(16), 259(34), 248(17), 220(26), 207(50), 179(100), 165(20), and 83(22).

Dimethyl 1,3,6-trimethyl-2-azabicyclo[3.2.1]oct-3-ene-4,7-dicarboxylate-8-spiro-(4′,4′-dimethyl-2′,6′-dioxocyclohexane), 13

Infrared ν_{max}: 3436 (NH), 1728 (saturated ester), 1696 (unsaturated ester, saturated ketone), and 1668 (C=C) cm^{-1}; uv λ_{max}: 292 nm (ϵ 15 050); ^{1}Hmr δ: 0.84 and 1.20 (s, s, methyls of dimedone moiety), 0.94 (d, J 7.0 Hz, methyl at C(6)), 1.63 (s, methyl at C(1)), 2.12 (s, methyl at C(3)), 3.64 and 3.67 (s, s, methyl esters), 3.80 (d, J 5.8 Hz, probably H at C(5)), 4.51 (s, NH), and a complex signal δ 1.8−3.7 consisting of the remaining two ring protons and four ring protons of the dimedone moiety; ms m/z: 391(77, M^+), 360(26), 279(14), 259(20), 248(17), 220(32), 207(50), 180(21), 179(100), 165(19), and 83(24).

Dimethyl 1,3-dimethyl-2-azabicyclo[3.2.1]oct-3-ene-4,7-dicarboxylate-8-spirocyclopentadiene, 14

Infrared ν_{max}: 3427 (NH), 1739 (saturated ester), and 1681 (unsaturated ester) cm^{-1}; uv λ_{max}: 295 nm (ϵ 16 200); ^{1}Hmr (HA 100) δ: 1.21 (s, methyl at C(1)), 2.18 (s, methyl at C(3)), 2.38 (m, J 5.8, 11.8, and 13.9 Hz, *exo*-H at C(6)), 2.62 (bdd, J 4.9, 13.9, and 1.0 Hz, *endo*-H at C(6)), 2.97 (bd, J 5.8 and approx 1.0 Hz, H at C(5)), 3.19 (dd, J 4.9 and 11.8 Hz, H at C(7)), 3.62 and 3.71 (s, s, methyl esters), 4.28 (s, NH), and 6.31 (m, cyclopentadiene ring protons); ms m/z: 303 (67, M^+), 288(13), 272(30), 244(100), 216(59), 212(27), 202(82), 184(34), 169(13), 158(63), 157(14), 156(16), 129(18), 128(19), 115(29), and 42(26).

Dimethyl 1,3-dimethyl-2-azabicyclo[3.2.1]oct-3-ene-4,7-dicarboxylate-8-spirocyclopentane, 9

The spirocyclopentadiene (250 mg) and platinum oxide (50 mg) in methanol (20 mL) were stirred under hydrogen at 1 atmosphere and room temperature. The hydrogen absorption required 0.5 h and stirring was continued for a further 0.5 h. The catalyst was removed by filtration and the solvent removed on the rotary evaporator. The spirocyclopentane was obtained after two recrystallizations from aqueous methanol as white prisms (242 mg, 96%), mp 212−213.5°C; ir ν_{max}: 3427 (NH), 1730 (saturated ester), and 1664 (unsaturated ester) cm^{-1}; uv λ_{max}: 296 nm (ϵ 16 950); ^{1}Hmr (HA 100) δ: 1.29 (s, methyl at C(1)), 1.62 (bs, eight cyclopentane ring protons), 2.10 (s, methyl at C(3)), 2.14 (m, J 5.5, 11.0, and 12.5 Hz, *exo*-hydrogen at C(6)), 2.35 (bdd, J 5.0, 12.5, and −0.5 Hz, *endo* hydrogen at C(6)), 2.70 (bd, J 5.5 and −0.5 Hz, H at C(5)), 2.94 (dd, J 11.0 and 5.0 Hz, H at C(7)), 3.64 and 3.68 (s, s, methyl esters), 4.04 (s, NH); ms m/z: 307 (48, M^+), 276(27), 248(14), 207(20), 206(100), 193(13), 192(37), and 179(32). *Anal.* calcd. for $C_{17}H_{25}NO_4$: *Mol. Wt.* 307, C 66.43, H 8.20, N 4.59; found: *Mol. Wt.* 307 (ms), C 66.27, H 8.22, N 4.69.

Dimethyl 1,3,6-trimethyl-2-azabicyclo[3.2.1]oct-3-ene-4,7-dicarboxylate-8-spirocyclopentadiene, 15

Infrared ν_{max}: 3422 (NH), 1728 (saturated ester), 1679 (unsaturated ester), and 1666 (C=C) cm^{-1}; uv λ_{max}: 241 nm (ϵ 3 100), 297 nm (ϵ 15 400); ^{1}Hmr (HA 100) δ: 0.98 (s, methyl at C(1)), 1.07 (d, J 6.5 Hz, methyl at C(6)), 2.26 (s, methyl at C(3)), 2.73 (d, J 8.2 Hz, H at C(7)), 2.97 (d, J 5.2 Hz, H at C(5)), 3.08 (m, J 5.2, 6.5, and 8.2 Hz, H at C(6)), 3.62 and 3.68 (s, s, methyl esters), 4.62 (s, NH), 6.10, 6.27, and 6.78 (each m, 1H, 2H, and 1H respectively, cyclopentadiene ring hydrogens); the 6-methyl doublet appeared as a singlet on irradiation at 308 Hz; ms m/z: 317 (46, M^+) 302(20), 286(16), 270(18), 258(56), 242(21), 226(22), 218(14), 217(80), 216(75), 203(19), 202(100), 198(18), 192(13), 184(17), 170(18), 158(25), 143(20), 142(15), 44(50), and 42(22).

Dimethyl 4-(diethoxycarbonylmethyl)-4,5-dihydro-2,7-dimethylazepine-3,6-dicarboxylate, ***5***

Infrared ν_{max}: 3417 (NH), 1750 (saturated ester), 1728 (saturated ester), 1705 (unsaturated ester), and 1633 (C=C) cm^{-1}; uv λ_{max}: 230 nm (ϵ 11 850) and 329 nm (ϵ 13 200); ^{1}Hmr δ: 1.19 and 1.24 (overlapping t, J 7.2 Hz, methyls of ethyl esters), 2.27 and 2.34 (s, s, methyls at C(2), C(7)), 3.30 (d, J 11.0 Hz, CH of malonate), 3.31 (dd partially obscured by signal at δ 3.30, J 16.0 and 6.0 Hz, H at C(5)), 3.65 and 3.69 (s, s, methyl esters), 4.06 and 4.15 (overlapping q, J 7.2 Hz, CH_2 of ethyl esters), 5.73 (s, NH); in addition, complex signals due to one proton at δ 2.0–2.4 and one proton at δ 4.15 were obscured by ring methyl and CH_2 of ethyl ester respectively; ms m/z: 397(4, M^+), 238(40), 237(82), 206(51), 205(42), 179(54), 178(97), 146(93), 133(72), 118(34), 115(100), and 43(80).

Dimethyl 4-(diethoxycarbonylmethyl)-4,5-dihydro-2,5,7-trimethylazepine-3,6-dicarboxylate, ***6***

Infrared ν_{max}: 3420 (NH), 1749 (saturated ester), 1727 (saturated ester), 1701 (unsaturated ester), and 1631 (C=C) cm^{-1}; uv λ_{max}: 230 nm (ϵ 11 800), 326 nm (ϵ 14 900); ^{1}Hmr δ: 0.93 (d, J 6.8 Hz, methyl at C(5)), 1.18 and 1.22 (overlapping t, J 7.3 and 7.2 Hz, methyls of ethyl esters), 2.32 (s, methyls at C(2) and C(7)), 3.21 (d, J 12.0 Hz, CH of malonate), 3.42 (m partially obscured by ester methyls and signal at δ 3.21, J 6.8, H at C(5)), 3.66 and 3.70 (s, s, methyl esters), 3.97 (dd, overlapping signals at δ 4.06, 4.14, J 6.0 and 12.0 Hz, H at C(4)), 4.06 and 4.14 (overlapping q, J 7.3 and 7.2 Hz, CH_2 of ethyl esters), 5.72 (s, NH); ms m/z: 411(3, M^+), 252(45), 251(87), 220(44), 192(39), 179(100), and 153(29).

Acknowledgements

The authors wish to thank Memorial University of Newfoundland and the Natural Sciences and Engineering Research Council of Canada for financial support and Memorial University for the award of a Fellowship to one of us (T.S.C.) In addition, the authors gratefully acknowledge the help of the late Dr. M. A. Davis and Ayerst Research Laboratories, Montreal, for arranging the pharmacological evaluation of compounds **5**, **7**, and **12**.

1. B. GREGORY, E. BULLOCK, and T-S. CHEN. J. Chem. Soc. Chem. Commun. 1070 (1979).
2. C. MANNICH and H. BUDDE. Arch. Pharm. **270**, 283 (1932).
3. R. W. COTTINGHAM. J. Org. Chem. **25**, 1473 (1960).
4. R. C. ELDERFIELD and E. T. LOSIN. J. Org. Chem. **26**, 1703 (1961).
5. B. L. FOX and J. E. REBOULET. J. Org. Chem. **36**, 3639 (1968).
6. H. ERDTMAN and S. THOREN. Acta Chem. Scand. **24**, 87 (1970).
7. A. ZABZA, C. WAWRZENCZYK, and H. KUZYNSKI. Bull. Acad. Pol. Sci. Ser. Sci. Chem. **20**, 623 (1972).
8. A. ZABZA. Pr. Nauk. Inst. Chem. Org. Fiz. Politech. Wroclaw, 1 (1971).
9. N. G. KOZLOV and T. PEHK. Zh. Org. Khim. **18**, 1118 (1982).
10. K. YAMADA, T. KANEKIYO, S. TANAKA, K. NARUCHI, and M. YAMAMOTO. J. Am. Chem. Soc. **103**, 7003 (1981).
11. P. G. GASSMAN, F. HOYDA, and J. DYGOS. J. Am. Chem. Soc. **90**, 2716 (1968).
12. J. O. REED and W. LWOWSKI. J. Org. Chem. **36**, 2864 (1971).
13. J. E. FRANZ and C. OSUCH. Chem. Ind. (London), 2058 (1964).
14. A. C. OEHLSCHLAGER and L. H. ZALKOW. J. Org. Chem. **30**, 4205 (1965).
15. K. UMANO, H. TANIGUCHI, H. INOUE, and E. IMOTO. Tetrahedron Lett. 247 (1979).
16. P. BARRACLOUGH, S. BILGIC, and D. W. YOUNG. Tetrahedron, **35**, 91 (1979).
17. K. UMANO and H. INOUE. Bull. Univ. Osaka Prefect. Ser. A, **29**, 95 (1980).
18. A. G. ANASTASSIOU. J. Org. Chem. **31**, 1131 (1966).
19. A. G. ANASTASSIOU and H. KASMAI. J. Chem. Soc. Chem. Commun. 201 (1975).
20. K. UMANO, S. MIZONE, K. TOKISATO, and H. INOUE. Tetrahedron Lett. **22**, 73 (1981).
21. Y. L. CHOW and S. K. PILLAY. Heterocycles, **5**, 171 (1976).
22. Y. L. CHOW, S. K. PILLAY, and H. H. QUON. J. Chem. Soc. Perkin Trans. 2, 1255 (1977).
23. K. YAMADA, S. TANAKA, K. NARUCHI, and M. YAMAMOTO. J. Org. Chem. **47**, 5283 (1982).
24. P. BARRACLOUGH and D. W. YOUNG. J. Chem. Soc. Perkin 1, 2354 (1975).
25. R. S. SHERIDAN and G. A. GANZER. J. Am. Chem. Soc. **105**, 6158 (1983).
26. N. D. EDGE, S. J. CORNE, G. E. LEE, and W. R. WRAGG. Brit. J. Pharmacol. **15**, 207 (1960).
27. K. NOGUCHI, M. TAKEDA, and S. NURIMOTO. Chem. Pharm. Bull. **25**, 890 (1977).
28. G. E. LEE, W. R. WRAGG, S. J. CORNE, N. D. EDGE, and H. W. READING. Nature, **181**, 1717 (1958).
29. P. GAILLIOT, J. BAGET, and P. SARET. U. S. PATENT 2,927,115; Chem. Abstr. **55**, P5542i (1961).
30. H. H. ONG and V. B. ANDERSON. Ger. Offen. 2,610,712; Chem Abstr. **86**, P29671f (1977).
31. H. H. ONG, V. B. ANDERSON, and J. C. WILKER. J. Med. Chem. **21**, 758 (1978).
32. H. H. ONG, V. B. ANDERSON, J. C. WILKER, T. C. SPAULDING, and L. R. MEYERSON. J. Med. Chem. **23**, 726 (1980).
33. P. J. BRIGNELL, E. BULLOCK, U. EISNER, B. GREGORY, A. W. JOHNSON, and H. WILLIAMS. J. Chem. Soc. 4819 (1963).
34. E. BULLOCK, B. GREGORY, and M. T. THOMAS. Can. J. Chem. **55**, 693 (1977), and references cited therein.
35. J. ASHBY and U. EISNER. J. Chem. Soc. (C), 1706 (1967).
36. U. EISNER, M. Z. HAQ, J. FLIPPEN, and I. KARLE. J. Chem. Soc. Perkin Trans. 1, 357 (1972), and references cited therein.
37. J. ASHBY, L. A. CORT, J. A. ELVIDGE, and U. EISNER. J. Chem. Soc. (C), 2311 (1968).
38. B. GREGORY, E. BULLOCK, and T. S. CHEN. Can. J. Chem. **57**, 44 (1979).
39. M. E. M. BAGGS and B. GREGORY. Can. J. Chem. **58**, 794 (1980).
40. E. G. MEEK, J. H. TURNBULL, and W. WILSON. J. Chem. Soc. 2891 (1953).
41. H. O. HOUSE. Modern synthetic reactions. 2nd ed. W. A. Benjamin, Inc., Menlo Park, California. 1972. p. 520.
42. L. M. JACKMAN and B. C. LANGE. Tetrahedron, **33**, 2737 (1977).
43. M. ANDERSON and A. W. JOHNSON. J. Chem. Soc. 2411 (1965).
44. P. J. BRIGNELL, U. EISNER, and H. WILLIAMS. J. Chem. Soc. 4226 (1965).
45. K. TSUDA, Y. SATCH, N. IKEKAWA, and H. MISHIMA. J. Org. Chem. **21**, 800 (1956).
46. F. E. BADER. Helv. Chim. Acta, **36**, 215 (1953).
47. A. I. SCOTT. Interpretation of the ultraviolet spectra of natural products. Pergamon Press, Oxford. 1964. p. 58.
48. S. MCLEAN and P. HAYNES. Tetrahedron **21**, 2313 (1965); **21**, 2329 (1965).
49. C. F. WILCOX and M. MESIROV. J. Org. Chem. **25**, 1841 (1960).

Total assignment of the ¹H and ¹³C spectra of mikanokryptin and comparison of its solution and solid state conformations

WILLIAM F. REYNOLDS
Chemistry Department, University of Toronto, Toronto, Ont., Canada M5S 1A1

RAUL G. ENRÍQUEZ, MARCO A. CHAVEZ, AND ANA L. SILBA
Unidad de Investigacion Biomedica en Medicina Tradicional, Y Herbolaria, IMSS, Luz Saviñón 214, México, D.F. 03100 México

AND

MIGUEL A. MARTINEZ
Instituto de Biologia, U.N.A.M., Ciudad Universitaria, México, D.F. 20 México

Received July 30, 1984

WILLIAM F. REYNOLDS, RAUL G. ENRÍQUEZ, MARCO A. CHAVEZ, ANA L. SILBA, and MIGUEL A. MARTINEZ. Can. J. Chem. **63**, 849 (1985).

The ¹H and ¹³C spectra of mikanokryptin are unambiguously assigned using a variety of one-dimensional nmr experiments (selective homonuclear decoupling, use of inversion–recovery pulse sequences to reveal hidden peaks, and DEPT spectral editing) in conjunction with normal and "long range" two-dimensional heteronuclear correlated experiments. Detailed comparison of vicinal, allylic, and homoallylic ¹H—¹H coupling constants with dihedral angles determined from an earlier crystal structure determination indicates that solution and solid state configurations are similar.

WILLIAM F. REYNOLDS, RAUL G. ENRÍQUEZ, MARCO A. CHAVEZ, ANA L. SILBA, et MIGUEL A. MARTINEZ. Can. J. Chem. **63**, 849 (1985).

Faisant appel à une variété d'expériences de rmn unidimensionnelle (découplage homonucléaire sélectif, séquences de pulsation avec inversion et récupération dans le but de révéler la présence de pics cachés et édition spectrale DEPT) ainsi qu'à des expériences hétéronucléaires en deux dimensions (normales ou à longue distance), on a pu faire une attribution non équivoque des signaux des spectres rmn du ¹H et du ¹³C de la mikanokryptine. Sur la base d'une comparaison détaillée des constantes de couplage ¹H—¹H viciniales, allyliques et homoallyliques avec les angles dièdres attribués antérieurement à l'aide de la structure cristalline, on a pu établir que les conformations à l'état solide et en solution sont semblables.

[Traduit par le journal]

Introduction

Mikania mikrantha H.B.K. and a number of different plants of the genus *Aristolochia* share the popular name "guaco" in Mexican traditional medicine and are all purported to be effective for treatment of dermatological affections (1). As part of a continuing phytochemical investigation of plants which are used for this purpose in traditional medicine (2), we have undertaken an investigation of *Mikania mikrantha* H.B.K. The first compound isolated was mikanokryptin, **1**, a lactone derivative first reported by Herz *et al.* (3). The structure and stereochemistry of **1** has been established by X-ray diffraction techniques (4) and its ¹H spectrum has been partially assigned (3)

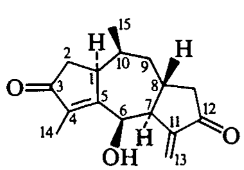

1

(more extensive assignments were reported for derivatives of **1** (3)).

In this manuscript, we report the complete and unambiguous assignment of ¹H and ¹³C spectra for **1**, using a variety of one- and two-dimensional nmr techniques. The solution and solid state conformations of **1** are also compared.

Results and discussion

(a) *¹H chemical shift assignments*

In the original report, five of the proton signals for **1** were obscured and two others overlapped (90 MHz $(CD_3)_2SO$ (3)). However, we found that in $CDCl_3$ (with ca. 5% $(CD_3)_2SO$ to promote solubility) at 200 MHz, $H(9)_\alpha$[1] was partially obscured by $C(14)H_3$, but all other peaks were clearly resolved (see Fig. 1(a) illustrating region 1.75–3.25). The multiplet structure for $H(9)_\alpha$ was resolved using a procedure first suggested by Hall and Preston (5). By utilizing a standard inversion–recovery pulse sequence and by choosing a delay time (0.88 s) for which the methyl signal is nulled, one can clearly observe the multiplet structure for $H(9)_\alpha$. (See Fig. 1(b); since the spin-lattice relaxation time, T_1, is significantly shorter for $H(9)_\alpha$ than for $C(14)H_3$, the former signal has almost completely recovered when the latter signal is nulled.) This approach has been surprisingly little used. However, it has some advantages even when compared to more sophisticated techniques such as homonuclear "*J* resolved" two-dimensional nmr spectra (6). Not only can the experiment be performed on routine spectrometers lacking the pulse programmer and large data storage capabilities necessary for 2D experiments but it will also succeed even when two signals have identical chemical shifts (provided they have different T_1 values). By contrast, homonuclear "*J* resolved" spectra cannot resolve peaks with identical shifts. Finally, the inversion–recovery spectra used to find the null provide useful qualitative relaxation information which

[1]Methylene protons are assigned as α or β on the basis of the known stereochemistry of **1** (4) plus the magnitudes of observed couplings to adjacent methine hydrogens. The two exocyclic methylene protons are labelled $H(13)_c$ and $H(13)_t$ depending on whether they are *cis* or *trans* to the lactone functionality.

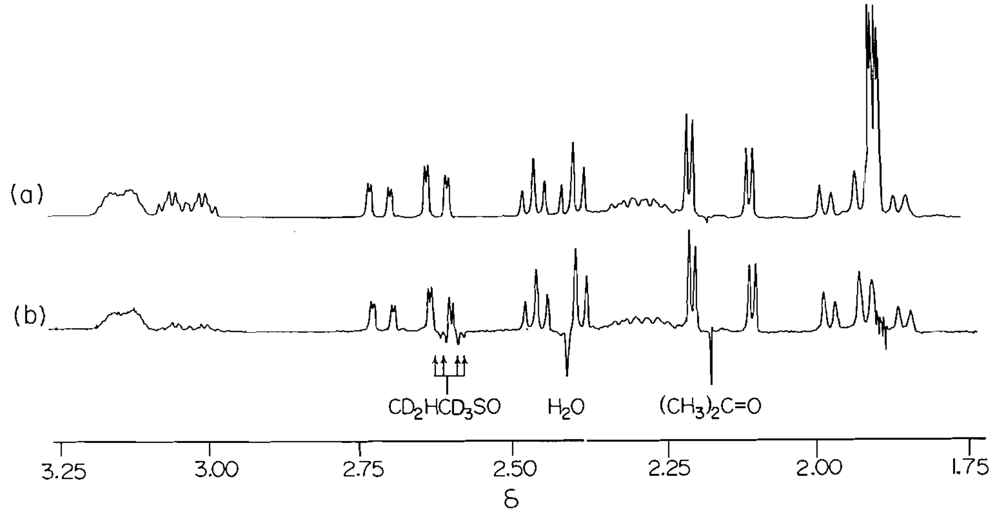

FIG. 1. Inversion–recovery ^{1}H spectra of **1** using the following delays betwen 180° (inverting) and 90° (sampling) pulses: (a) 2.25 s; (b) 0.88 s. The signal for $C(14)H_3$ is almost nulled with the shorter delay but nearly recovered with the longer delay. Also note that three small molecule impurity peaks (residual HCD_2CD_3SO, H_2O, and $(CH_3)_2C{=}O$ (solvent of crystallization)) which are inverted with the shorter delay are almost nulled with the longer delay, allowing clearer observation of $H(2)_\alpha$ and $H(9)_\beta$.

can aid in assigning peaks. For example, the low-field methylene proton (δ 6.40) was assigned as $H(13)_c$ on the basis of its longer relaxation time than $H(13)_t$ (δ 5.72). The latter proton is intramolecularly relaxed by dipole–dipole interactions with H(7), while there is no comparable proximate proton to relax $H(13)_c$.[2]

Remaining ^{1}H signals were assigned with the aid of a series of selective homonuclear decoupling experiments which established ^{1}H—^{1}H connectivities and also aided in determining the magnitudes of individual coupling constants. Final assignments of ^{1}H chemical shifts and coupling constants are given in Table 1. Allowing for differences due to solvent effects, the chemical shifts are consistent with the earlier partial assignment for **1** (3).

TABLE 1. ^{1}H chemical shifts (δ) and coupling constants (J, Hz) for **1** in 95% $CDCl_3$ – 5% $(CD_3)_2SO$

Proton[a]	δ[b]	J[c]
H(1)	3.12	6.8(2α), 2.2(10), 2.0(2$_\beta$), 2.0(14), 1.0(6)
H(2)$_\alpha$	2.65	19.1(2$_\beta$), 6.8(1), 1.1(6)
H(2)$_\beta$	2.17	19.1(2$_\alpha$), 2.0(1)
H(6)	5.13	5.6(OH), 3.5(7), 1.1(2$_\alpha$), 1.0(1), 0.8(14)
H(7)	3.01	9.6(8), 3.5(6), 3.4(13c), 3.0(13t)
H(8)	4.84	12.1(9$_\alpha$), 9.6(7), 3.5(9$_\beta$)
H(9)$_\alpha$	1.92	12.6(9)$_\beta$), 12.1(8), 3.9(10)
H(9)$_\beta$	2.42	12.6(9$_\alpha$), 3.5(8), 3.5(10)
H(10)	2.29	7.3(15), 3.9(9$_\alpha$), 3.5(9$_\beta$), 2.2(1)
H(13)$_c$	6.40[d]	3.4(7)
H(13)$_t$	5.72[d]	3.0(7)
H(14)$_3$	1.90	2.0(1), 0.8(6)
H(15)$_3$	0.86	7.3(10)
OH	4.54	5.6(6)

[a]Proton numbering as in **1**. This corresponds to labelling used in ref. 4. (Labelling of the two methyl groups was reversed in 3.)
[b]Chemical shift (in ppm) relative to internal $Si(CH_3)_4$.
[c]Magnitudes of couplings in Hertz and (in brackets) the proton to which the indicated proton is coupled.
[d]$H(13)_c$ is *cis* to the lactone function while $H(13)_t$ is *trans* to the lactone function.

(b) *^{13}C chemical shift assignments for 1*

Initial ^{13}C assignments were based on normal ^{1}H-decoupled ^{13}C spectra plus CH, CH_2, and CH_3 subspectra obtained using DEPT spectral editing (7) (see Fig. 2). This allowed assignment of individual carbons in terms of numbers of attached carbons. In order to complete the assignment of individual peaks with a minimum of ambiguity, a pair of heteronuclear (^{13}C–^{1}H) correlated two-dimensional experiments were performed. The first was a standard heteronuclear correlated experiment using delay times optimized for direct ^{13}C–^{1}H coupling (8). This provided the ^{13}C spectra of protonated carbons along one frequency axis with the ^{1}H spectra of the corresponding directly bonded hydrogens along the second axis at right angles (see Fig. 3). This allowed unambiguous assignment of all protonated carbons on the basis of the previously assigned ^{1}H spectral peaks (see Table 2).

This left five non-protonated carbons to be assigned. Since these covered a wide chemical shift range (δ 136–208), partial assignment could be made on the basis of chemical shifts of related model compounds and (or) additive chemical shift parameters (9). In particular, the signal at δ 208.0 could be unambiguously assigned to the α,β-unsaturated carbonyl, C(3), while the signals at δ 143.5 and δ136.3 could be tentatively assigned as C(4) and C(11) respectively. However, while the peaks at δ 170.9 and δ 169.9 obviously were due to C(5) and C(12), it was unclear which signal was which. In order to resolve these ambiguities, a "long range" heteronuclear correlated experiment (10) was carried out. This used the same pulse sequence as the previous experiment but with delay times optimized for geminal ($^2J_{CH}$) and vicinal ($^3J_{CH}$) couplings, allowing assignment of non-protonated carbons from couplings to known ^{1}H signals on adjacent carbons. For example, the peak at δ 170.9 is coupled to $H(14)_3$ while the δ 169.9 peak shows coupling to $H(13)_c$ and $H(13)_t$ (all $^3J_{CH}$), allowing unambiguous assignment of the former as C(5) and the latter as C(12) (see Fig. 4). Similarly, the peak at δ 143.5 is coupled to $H(14)_3$ while the peak at δ 136.3 is coupled to $H(13)_c$ and H(7) (all $^2J_{CH}$), confirming the tentative assignment of the former as C(4) and the latter as C(11). Finally, the δ 208.0 peak shows coupling to $H(14)_3$, $H(2)_\alpha$, and $H(2)_\beta$, consistent with its as-

[2]This was confirmed by an nOe measurement.

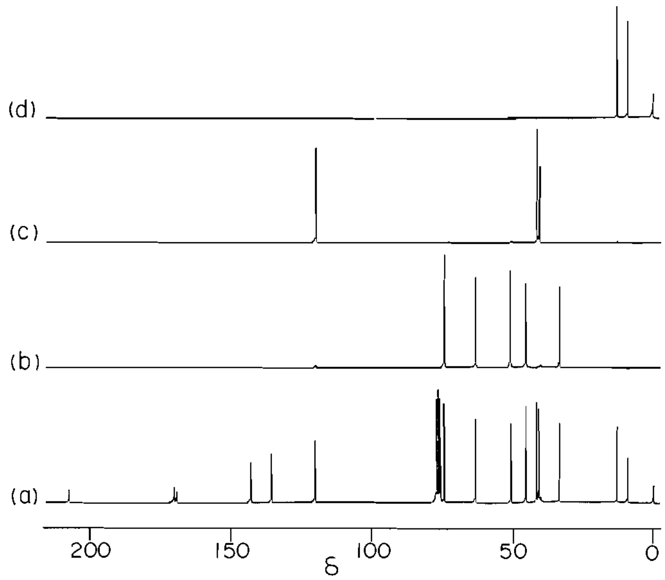

FIG. 2. (a) Normal ^{13}C spectrum of **1**; (b) edited (DEPT) spectrum for CH carbons only; (c) CH_2 only; (d) CH_3 only.

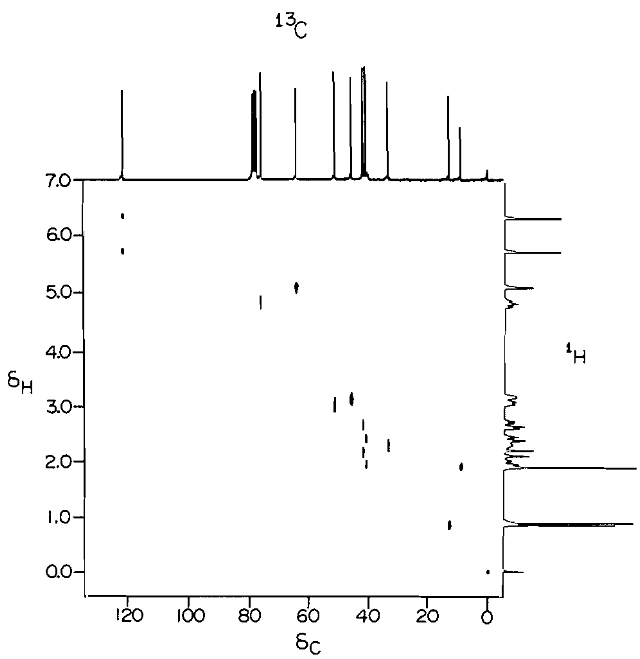

FIG. 3. Normal heteronuclear correlated spectrum of **1**, illustrating the protonated ^{13}C spectrum along the horizontal and the ^1H spectrum along the vertical.

signment of C(3). Note that the "long range" heteronuclear correlated experiment effectively divided the five non-protonated carbons into two subsets, the first (C(3), C(4), C(5)) coupled to $H(14)_3$ but not $H(13)_c$, and the second (C(11), C(12)) coupled to $H(13)_c$ but not $H(14)_3$ (see Fig. 4). Within each subset, chemical shift differences are sufficiently large ($\Delta\delta > 25$) to allow completely unambiguous assignment of individual peaks (see Table 2). This supports earlier evidence that "long range" heteronuclear correlated experiments provide an approach of considerable generality for assigning non-protonated ^{13}C peaks (10). This is important since the most obvious alternative, $^{13}C—^{13}C$ connectivity ("INADEQUATE") experiments (11), often cannot be carried out due to sensitivity limitations.

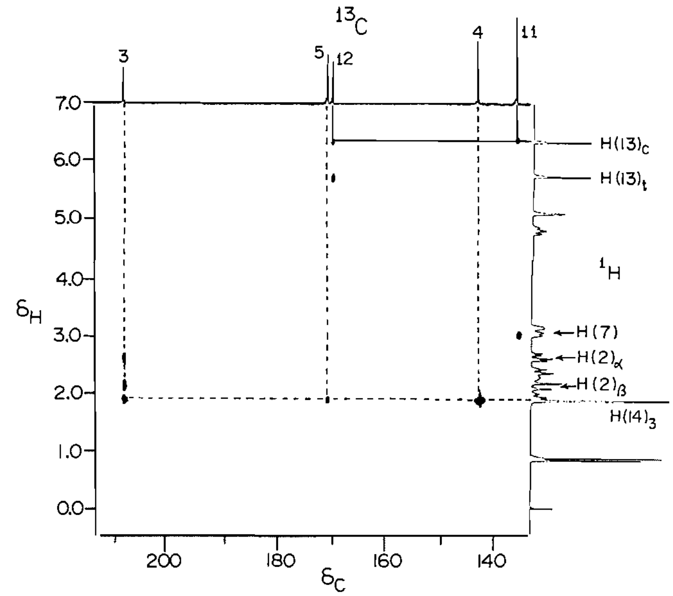

FIG. 4. "Long range" heteronuclear correlated spectrum of **1** with non-protonated ^{13}C spectrum along the horizontal and ^1H spectrum along the vertical; ------: connectivities of ^{13}C with $H(14)_3$; ——: connectivities of ^{13}C peaks with $H(13)_c$.

TABLE 2. ^{13}C chemical shifts (δ) for **1** in 95% $CDCl_3$ – 5% $(CD_3)_2SO$

Carbon[a]	δ[b]	Carbon	δ
C(1)[c]	45.17	C(9)[c]	40.46
C(2)[c]	41.34	C(10)[c]	33.05
C(3)[d]	208.03	C(11)[d]	136.28
C(4)[d]	143.52	C(12)[d]	169.91
C(5)[d]	170.90	C(13)[c]	120.94
C(6)[c]	63.52	C(14)[c]	8.96
C(7)[c]	50.68	C(15)[c]	12.76
C(8)[c]	75.18		

[a]Labelling as in **1**.
[b]^{13}C chemical shifts (in ppm) relative to internal $^{13}CH_3Si(CH_3)_3$.
[c]Chemical shifts assigned with aid of normal heteronuclear correlated two-dimensional spectra.
[d]Chemical shifts assigned with aid of "long range" heteronuclear correlated two-dimensional spectra.

(c) *Comparison of the solution and solid state conformations of 1*

The publication reporting the crystal structure of **1** does not list any dihedral angles involving hydrogens (4).[3] However, these are easily calculated from the reported atomic coordinates (4) and are listed in Table 3, along with the corresponding $^1H—^1H$ coupling constants. Vicinal ($^3J_{H-H}$) coupling constants are also plotted against the corresponding solid state H—C—C—H dihedral angles in Fig. 5. These show a good Karplus relationship, indicating that are are no major changes in conformation on going from the solid state to solution. Even the H—O—C(6)—H(6) coupling constant is consistent with the observed dihedral angle in the solid state. However, this may be fortuitous since the orientation of the OH group in the solid state is influenced by intermolecular hydrogen bonding (4) and since the observed coupling constant is also consistent with that expected for a freely rotating OH group.

[3]However, ref. 4 provides a three-dimensional representation of the conformation of **1**, along with all C—C—C—C dihedral angles.

TABLE 3. Comparison of observed vicinal, allylic, or homoallylic $^{1}H-^{1}H$ coupling constants for **1** in solution with the corresponding dihedral angles in the crystalline state

Angle	<[a]	Coupling	J (Hz)[b]
H(1)—C(1)—C(2)—H(2)$_\alpha$	1	$^{3}J_{H(1)H(2)_\alpha}$	6.8
H(1)—C(1)—C(2)—H(2)$_\beta$	117	$^{3}J_{J(1)H(2)_\beta}$	2.0
C(1)—C(10)—C(10)—H(10)	71	$^{3}J_{H(1)H(10)}$	2.2
H(6)—C(6)—C(7)—H(7)	65	$^{3}J_{H(6)H(7)}$	3.5
H(7)—C(7)—C(8)—H(8)	156	$^{3}J_{H(7)H(8)}$	9.6
H(8)—C(8)—C(9)—H(9)$_\alpha$	177	$^{3}J_{H(8)H(9)_\alpha}$	12.1
H(8)—C(8)—C(9)—H(9)$_\beta$	61	$^{3}J_{H(8)H(9)_\beta}$	3.5
H(9)$_\alpha$—C(9)—C(10)—H(10)	50	$^{3}J_{H(9)_\alpha H(10)}$	3.9
H(9)$_\beta$—C(9)—C(10)—H(10)	65	$^{3}J_{H(9)_\beta H(10)}$	3.5
H(6)—C(6)—O—H	43	$^{3}J_{H(6)OH}$	5.6
H(7)—C(7)—C(11)—C(13)	81	$^{4}J_{H(7)H(13)_c}$ (*transoid*)	3.4
		$^{4}J_{H(7)H(13)_t}$ (*cisoid*)	3.0
H(1)—C(1)—C(5)—C(4)	121	$^{5}J_{H(1)H(14)}$	2.0
H(6)—C(6)—C(5)—C(4)	54	$^{5}J_{H(6)H(14)}$	0.8

[a]Dihedral angle in degrees.
[b]Coupling constant (in hertz).

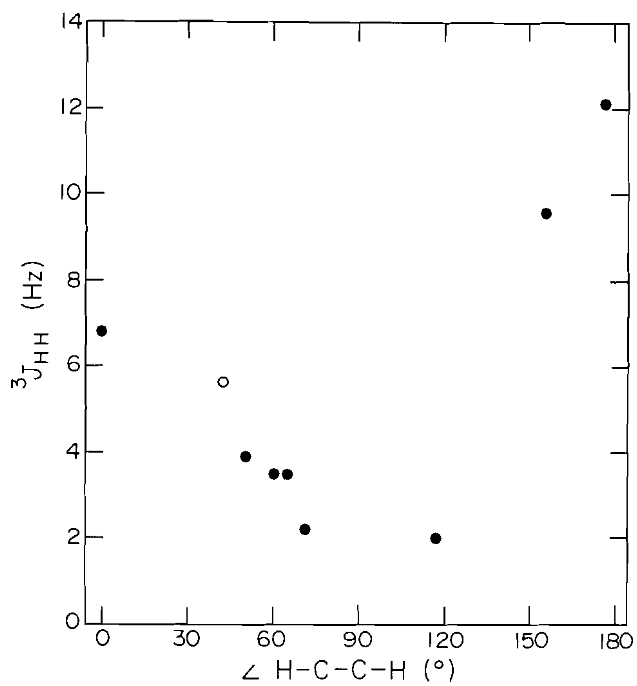

FIG. 5. Plot of vicinal $^{1}H—^{1}H$ coupling versus H—C—C—H dihedral angle. The open circle is the coupling to the OH proton.

Several of the observed long-range coupling constants are also consistent with the crystalline conformation. For example, the two allylic couplings involved H(7) and the exocyclic methylene protons are both $\geq$ 3 Hz. This is close to the maximum value for this type of coupling (12), as expected for the near-orthogonal orientations of H(7)—C(7) and C(11)—C(13) (allylic couplings show a maximum for <H—C—C=C $\simeq$ 90° (12)). The couplings of H(1) and H(6) to C(14)H_3 are respectively examples of *transoid* and *cisoid* homoallylic (H—C—C=C—C—H) couplings. Two factors probably account for the larger magnitude of the former coupling. First, *transoid* homoallylic couplings are generally larger than *cisoid* homoallylic couplings, e.g. the rotationally averaged homoallylic couplings in *cis* and *trans*-2-butene are respectively 1.20 Hz and 1.59 Hz (13). Second, homoallylic couplings are increased by having either C—H bond at right angles to the plane of the double bond (13). <H(1)—C(1)—C(5)—C(4) is closer to 90° than <H(6)—C(6)—C(5)—C(4), consistent with the larger magnitude of the former homoallylic coupling.

There is a small four-bond coupling between H(1) and H(6) and a five-bond coupling of similar magnitude between H(2)$_\alpha$ and H(6). However, no corresponding coupling is observed between H(2)$_\beta$ and H(6) (decoupling of H(6) gives no noticeable line narrowing for H(2)$_\beta$, suggesting $^{5}J_{H(2)_\beta H(6)} < 0.1$ Hz). The different couplings of H(2)$_\alpha$ and H(2)$_\beta$ to H(6) are surprising since the fragment C(2)—C(1)—C(5)—C(6) is almost planar (<C(2)—C(1)—C(5)—C(6) = 174°) and H(2)$_\alpha$—C(2) and H(2)$_\beta$—C(2) show fairly similar dihedral angles with respect to C(1)—C(5) (respectively 116° and 126°). Unfortunately, too little is known about the conformational dependence of this type of 5-bond coupling (14) to draw any conclusions concerning the reasons for these differences.

Finally, the large magnitude of the geminal coupling between H(2)$_\alpha$ and H(2)$_\beta$ (19.1 Hz) is consistent with a conformation in which the H—H axis is parallel to the π orbital of the adjacent carbonyl group (15), as indicated by the crystal structure (4).

In summary, we have used a variety of one-dimensional nmr techniques (selective decoupling, inversion–recovery sequences to reveal hidden resonances, and DEPT spectral editing) in conjunction with two-dimensional heteronuclear ($^{13}C—^{1}H$) correlated spectra to unambiguously assign the ^{1}H and ^{13}C spectra of mikanokryptin, **1**. Comparison of vicinal, allylic, and homoallylic $^{1}H—^{1}H$ coupling constants in solution with corresponding dihedral angles determined from the crystalline structure demonstrate that the solution and solid state conformations of **1** are similar.

Experimental

Specimens of *Mikania mikrantha* H.B.K. were harvested at Xanciutlalpan, Puebla, Mexico. Vouchers are on deposit at the IMSSM Herbarium (voucher numbers 3290, 3320, and 3452). Four hundred and fifty grams of dried, ground aerial parts (stems and leaves) were defatted with hexane by exhaustive maceration at room temperature, followed by extraction with methylene chloride (4 × 3 l) in a similar fashion. After *in vacuo* removal of solvent, 16 g of a residue were obtained. A solid separated spontaneously from this residue and was removed by filtration. Recrystallization from acetone–ethanol afforded crystals (mp 246–248°C) which were identified as mikanokryptin by comparison with previously reported ^{1}H nmr, uv, ir, and mass spectra data (3).

All nmr spectra were obtained on a Varian XL-200 nmr spectrometer, operating in pulsed Fourier transform mode at a probe temperature of 20°C. For ^1H spectra, ca. 5 mg of **1** were dissolved in 0.6 mL of 95% $CDCl_3$ − 5% $(CD_3)SO$ (with ca. 0.1% $(CH_3)_4Si$ as internal reference) and placed in a 5-mm tube. Spectra were obtained using 1600-Hz spectral widths and 16K data points (5-s acquisition time), zero filled to 32K (0.1-Hz data point resolution). Ninety degree pulses (7.5 μs) and 5-s recycle times were used and 32 transients were accumulated. For ^{13}C spectra, ca. 80 mg of **1** were dissolved in 2 mL of the same solvent mixture as for the ^1H spectra. Spectral widths of 12 000 and 1.33-s acquisition times (32K data points) were used for normal and DEPT spectra. For normal spectra, 45° (7.5 μs) pulses were used with a recycle time of 2 s and 10 000 transients were accumulated. Four DEPT spectra were obtained using θ pulses of 45°, 90°, 90°, and 135° (7) with 2500 transients for each spectrum. Edited subspectra were obtained using the editing program ADEPT incorporated in the standard Varian software (H release).

Normal and "long range" heteronuclear correlated spectra were obtained using a spectrum width of 11 000 Hz in the ^{13}C domain and 1500 Hz in the ^1H domain with 2048 data points for the former and 512 for the latter, 320 transients were collected per time increment with 128 time increments; 2-Hz line broadening was applied along each axis. For the normal spectrum, the delay times Δ_1 = 0.0036 s and Δ_2 = 0.0024 s were chosen, corresponding to optimum values for an average $^{13}C—^1H$ coupling of 140 Hz (6). For the long-range experiments, repeated preliminary measurements indicated best values of Δ_1 = 0.075 s and Δ_2 = 0.033 s. These are compromise values which are approximately optimized for both geminal and vicinal $^{13}C—^1H$ coupling involving methyl hydrogens (ca. 5 Hz (15)) and *anti*-vicinal $^{13}C—^1H$ coupling involving methylene and methine hydrogens (ca. 10 Hz (16)) (6).

Acknowledgements

Financial support from NSERCC is gratefully acknowledged (WFR).

1. J. L. DIAZ. Usos de las plantas medicinales de Mexico. IMEPLAN, Mexico. 1976.
2. R. G. ENRIQUEZ, M. A. CHAVEZ, and W. F. REYNOLDS. J. Nat. Prod. **47**, 896 (1984).
3. W. HERZ, A. SRINIVASAN, and D. S. KALYANAMARAN. Phytochemistry, **14**, 233 (1975).
4. M. J. BOVELL, M. H. P. GUY, G. A. SIM, D. N. J. WHITE, and W. HERZ. J. Chem. Soc. Perkin Trans. **2**, 53 (1979).
5. (*a*) L. D. HALL and C. M. PRESTON. Carbohydr. Res. **27**, 286 (1973); (*b*) L. D. HALL. Adv. Carbohydr. Chem. Biochem. **29**, 11 (1974).
6. A. BAX. Two-dimensional nuclear magnetic resonance in liquids. D. Reidel, Holland. 1982.
7. D. M. DODDRELL, D. T. PEGG, and M. R. BENDALL. J. Magn. Reson. **48**, 323 (1982).
8. (*a*) A. A. MAUDSLEY, L. MULLER, and R. R. ERNST. J. Magn. Reson. **28**, 463 (1977); (*b*) A BAX and G. A. MORRIS. J. Magn. Reson. **42**, 501 (1981).
9. (*a*) J. B. STOTHERS. Carbon-13 NMR spectroscopy. Academic Press, New York. 1972; (*b*) E. BREITMAIER and W. VOELTER. ^{13}C NMR spectroscopy. Verlag Chemie, Weinheim. 1974.
10. (*a*) C. WYNANTS, K. HALLENGA, G. VAN BINST, A. MICHEL, and J. ZANEN. J. Magn. Reson. **57**, 93 (1984); (*b*) J. C. BELOEIL, M. A. DELSUC, J. Y. LALLEMAND, G. DAUPHIN, and G. JEMINET. J. Org. Chem. **49**, 1797 (1984); (*c*) W. F. REYNOLDS, R. G. ENRIQUEZ, L. I. ESCOBAR, and X. LOZOYA. Can. J. Chem. **62**, 2421 (1984).
11. (*a*) A. BAX, R. FREEMAN, and G. A. MORRIS. J. Am. Chem. Soc. **102**, 4849 (1980). (*b*) T. H. MARECI and R. FREEMAN. J. Magn. Reson. **48**, 158 (1982).
12. M. BARFIELD, A. M. DEAN, C. J. FALLICK, R. J. SPEAR, S. STERNHELL, and P. W. WESTERMAN. J. Am. Chem. Soc. **97**, 1482 (1975).
13. M. BARFIELD and S. STERNHELL. J. Am. Chem. Soc. **94**, 1905 (1972).
14. M. BARFIELD and B. CHAKRABARTI. Chem. Rev. **69**, 757 (1969).
15. R. R. FRASER and B. F. RABY. J. Am. Chem. Soc. **94**, 3458 (1972).
16. P. E. HANSEN. Prog. Nucl. Magn. Reson. Spectrosc. **14**, 175 (1981).

Flow-tube studies of reactions of selected ions with cyanoacetylene

A. B. RAKSIT AND D. K. BOHME

Department of Chemistry and Centre for Research in Experimental Space Science, York University, Downsview, Ont., Canada M3J 1P3

Received August 10, 1984

A. B. RAKSIT and D. K. BOHME. Can. J. Chem. **63**, 854 (1985).

Rate constants and product distributions have been determined for ion/molecule reactions of cyanoacetylene (HC_3N) with He^+, $C^+(^2P)$, CH_3^+, C_2^+, C_2H^+, $C_2H_2^+$, CN^+, C_2N^+, $C_2N_2^+$, N_2^+, CO^+, H_3^+, N_2H^+, HCO^+, $C_2H_3^+$, H_3O^+, $CH_3NO_2H^+$, CH_3CNH^+, $(CH_3)_2COH^+$, i-$C_3H_7OH_2^+$, C_3H^+, and C_4N^+. The measurements were performed with the selected-ion flow-tube (SIFT) technique at 296 ± 2 K. The observed reactions exhibit a variety of pathways including charge transfer, proton transfer, condensation, and association. The condensation and association reactions are suited for molecular growth by ion/molecule reactions. Special consideration is given to the active role of cyanoacetylene in the possible molecular synthesis which occurs in dense interstellar gas clouds by ion/molecule reactions.

A. B. RAKSIT et D. K. BOHME. Can. J. Chem. **63**, 854 (1985).

On a déterminé les constantes de vitesse et les distributions des produits des réactions ions/molécules entre le cyanoacétylène (HC_3N) et les ions He^+, $C^+(^2P)$, CH_3^+, C_2^+, C_2H^+, $C_2H_2^+$, CN^+, C_2N^+, $C_2N_2^+$, N_2^+, CO^+, N_3^+, N_2H^+, HCO^+, $C_2H_3^+$, H_3O^+, $CH_3NO_2H^+$, CH_3CNH^+, $(CH_3)_2COH^+$, i-$C_3H_7OH_2^+$, C_3H^+ et C_4N^+. On a effectué les mesures à 296 ± 2 K en faisant appel à la technique des tubes à écoulement avec ions sélectifs (TEIS). Les réactions observées présentent une variété de voies réactionnelles, y compris des transferts de charges, des transferts de protons, des condensations et des associations. Les réactions de condensations et d'associations se prêtent bien à une croissance moléculaire par des réactions ions/molécules. On a accordé une considération spéciale au rôle actif que pourrait jouer le cyanoacétylène dans les synthèses moléculaires qui peuvent se produire, par des réactions ions/molécules, dans les nuages gazeux interstellaires denses.

[Traduit par le journal]

Introduction

Cyanoacetylene has attracted attention recently in astrochemistry as a consequence of its identification in the radiospectrum of several interstellar sources including cold dark molecular clouds and the circumstellar shells of late type stars (1). The molecular cloud TMC-1 is an example of such a source. This cloud also has been found to contain many related molecules such as the cyanopolyynes, $HC_{2n}CN$, with values of n up to 4, methylcyanoacetylene, CH_3C_2CN, and the radicals C_4H and C_3N (2). The concomitance of these molecules suggests that they have a common chemical lineage and that perhaps cyanoacetylene itself is a key progenitor. Here we report laboratory measurements of gas-phase reactions of various carbonaceous and organonitrogen ions with cyanoacetylene which begin to explore the latter possibility.

Gas-phase ion/molecule reactions have been invoked successfully in astrochemistry to account for the molecular synthesis of many simple molecules in interstellar clouds (3–5). Ion/molecule reactions are also expected to play an important role in the formation and destruction of larger and more complex molecules. The chemical paths to larger molecules become increasingly more difficult to track as the molecules become more complex and so they are not understood nearly as well. The studies reported here represent an attempt to identify such paths which are specific to cyanoacetylene.

A previous laboratory study of ion/molecule reactions with cyanoacetylene has led to the conclusion that the positive ion chemistry of cyanoacetylene is dominated by charge-transfer or proton-transfer reactions and is thus, by implication, of minor importance to the chemical synthesis of larger molecules (6). The observations reported here establish serious discrepancies with the earlier results for a number of key reactions and point towards an active rather than a passive role for cyanoacetylene in molecular growth by ion/molecule reactions.

Experimental

The measurements were performed with the selected-ion flow tube/flowing afterglow apparatus in the Ion Chemistry Laboratory at York University (7, 8). The reagent ions were derived from suitable parent gases by electron impact at low pressures. An axial electron impact ionizer (Extranuclear, Model 041-3) was used as the ion source. Typical ion injection energies were in the range 10 to 15 V. The carrier gas was either helium or hydrogen. To remove traces of water vapour the buffer gases were passed through zeolite traps (a 50:50 mixture of Union Carbide molecule sieves 4A and 13X) cooled to liquid nitrogen temperature. The cyanoacetylene was prepared in the laboratory from methyl propiolate (Aldrich) (9). Experiments with H_3^+ as the "chemical ionization" reagent indicated a purity of greater than 99%. All measurements were made at an ambient temperature of 296 ± 2 K.

Results

The reaction rate constants and product distributions obtained in this study for reactions of ions with cyanoacetylene are summarized in Table 1. Rate constants and product distributions were determined in the manner described previously (7, 10). Table 1 includes all the primary product ions which were observed to contribute more than 5% to the total product spectrum. The branching ratios have been rounded off to the nearest 5% and are accurate to ±30%. The experimental rate constants are compared with collision rate constants, k_c, derived according to a recent combined variational transition state theory/classical trajectory study of thermal energy ion polar molecule capture collisions (11) with an estimated polarizability for HC_3N of 5.29 Å^3 (12) and a dipole moment of 3.6 D (13).

He⁺

He^+ was derived from helium by electron impact at 26 eV and injected into helium buffer gas. Approximately 30% conversion to He_2^+ was observed at pressures of about 0.3 Torr. The conversion occurs by termolecular association along the length of the flow tube. The added cyanoacetylene was observed to react rapidly with both He^+ and He_2^+ although some of the observed decrease in the He_2^+ signal was due to depletion of the precursor He^+. Figure 1 shows the plethora of product

TABLE 1. Summary of rate constants (in units of 10^{-9} cm^3 molecule^{-1} s^{-1}) and product distributions measured for ion–molecule reactions with cyanoacetylene using the SIFT technique at 296 ± 2 K

Reactant ion	Products	Branching ratio	k_{exp}[a]	k_c[b]
He^+	C_2^+, C_3^+, C_2H^+, CN^+, C_2N^+, C_3N^+		6.9 (8.2)	9.0
C^+ (^2P)	$C_3H^+ + CN$	0.8	6.1 (8.7)	5.6
	$C_4N^+ + H$	0.2		
CH_3^+	$C_3H_3^+ + HCN$	0.6	4.2[c] (2.7)	5.1
	$CH_3^+ \cdot HC_3N$	0.4		
C_2^+	$C_3N^+ + C_2H$	0.5	4.8	4.3
	$C_5N^+ + H$	0.2		
	$C_3H^+ + C_2N$	0.2		
	$C_2N^+ + C_3H$	0.1		
C_2H^+	$HC_3NH^+ + C_2$	0.5	3.2	4.2
	$C_4H_2^+ + CN$	0.2		
	$HC_5N^+ + H$	0.2		
	$HC_3N^+ + C_2H$	0.1		
$C_2H_2^+$	$C_4H_2^+ + HCN$	0.5	3.2[c] (1.9)	4.2
	$C_2H_2^+ \cdot HC_3N$	0.5		
CN^+	$HC_3N^+ + CN$	0.8	3.9 (5.3)	4.2
	$C_3N^+ + HCN$	0.2		
C_2N^+	$C_3H^+ + C_2N_2$	1.0	3.1	3.7
$C_2N_2^+$	$HC_3N^+ + C_2N_2$	1.0	1.6	3.4
N_2^+	$HC_3N^+ + N_2$	1.0	4.1	4.1
CO^+	$HC_3N^+ + CO$	1.0	3.1 (2.3)	4.1
H_3^+	$HC_3NH^+ + H_2$	1.0	10.5 (9.1)	10.3
N_2H^+	$HC_3NH^+ + N_2$	1.0	4.2 (4.2)	4.0
HCO^+	$HC_3NH^+ + CO$	1.0	4.0 (3.7)	4.0
$C_2H_3^+$	$HC_3NH^+ + C_2H_2$	1.0	3.9 (1.8)	4.1
H_3O^+	$HC_3NH^+ + H_2O$	1.0	3.8 (4.0)	4.7
$CH_3NO_2H^+$	$HC_3NH^+ + CH_3NO_2$	0.5	1.8	3.3
	$(H_4C_4N^+ + HNO_2)$	0.5		
CH_3CNH^+	$CH_3CNH^+ \cdot HC_3N$	1.0	0.5[d]	3.6
$(CH_3)_2COH^+$	$(CH_3)_2COH^+ \cdot HC_3N$	1.0	0.05[e]	3.3
i-$C_3H_7OH_2^+$	i-$C_3H_7OH_2^+ \cdot HC_3N$	1.0	0.6[d]	3.3
C_3H^+	$C_3H^+ \cdot HC_3N$	1.0	1.3[f]	3.7
C_4N^+	$C_4N^+ \cdot HC_3N$	1.0	1[e]	3.3

[a]The accuracy of the rate constants is estimated to be better than ±30%. Values in parentheses are the flowing afterglow results reported by Freeman *et al.* in ref. 6.

[b]Collision rate constants derived from the combined variational transition state theory/classical trajectory study of Su and Chesnavich (11).

[c]In helium buffer gas at a total pressure of 0.31 Torr and concentration of 1.0×10^{16} atoms cm^{-3}.

[d]In hydrogen buffer gas at a total pressure of 0.21 Torr and concentration of 6.8×10^{15} molecules cm^{-3}.

[e]In hydrogen buffer gas at a total pressure of 0.185 Torr and concentration of 6.0×10^{15} molecules cm^{-3}.

[f]In helium buffer gas at a total pressure of 0.347 Torr and concentration of 1.1×10^{16} atoms cm^{-3}.

ions which appeared in response to these reactions. All of them can be derived by dissociative charge transfer. C^+, CH^+, and HCN^+ were also observed as primary product ions but they were produced in relatively small amounts and are not shown in Fig. 1. Also it should be noted that formation of HC_3N^+ itself was observed but the data analysis indicated that it could be accounted for entirely by secondary reactions. The secondary product spectrum was complex as would be expected from the high reactivity of all the primary product ions which is evident from the decays shown in Fig. 1. Several of these secondary reactions are elucidated in the following sections.

C^+

The C^+ ions were produced from C_2N_2 at an electron energy

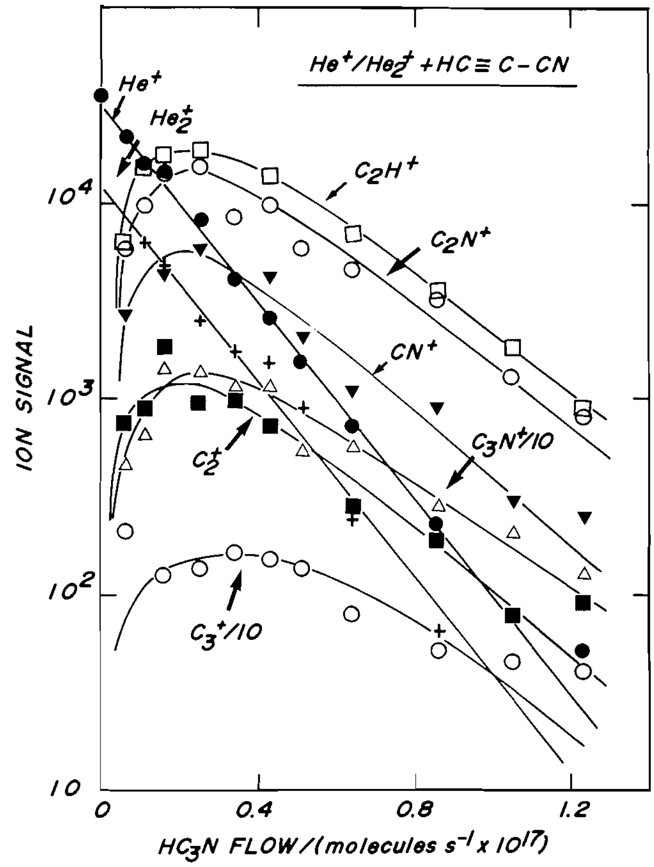

FIG. 1. The observed variations in ion signals recorded for the addition of HC_3N into the reaction region of the SIFT apparatus in which He^+ is initially established in helium buffer gas. P = 0.332 Torr, $\bar{v} = 7.4 \times 10^3$ cm s^{-1}, L = 46 cm, and T = 297 K. He^+ is derived from He at an electron energy of 25.7 eV.

of 32 eV and selected with an injection energy of 12.4 V. HCO^+ and C_2N^+ were two other ions observed in the C^+ spectrum downstream but with intensities less than 10% and 1% of the C^+ signal, respectively. Their origin can be attributed to reactions of C^+ with H_2O impurity in the buffer gas and with C_2N_2 which leaks through the selection quadrupole region. Separate experiments in which CO was added into the reaction region indicated that more than 95% of the C^+ generated in this fashion was in the ^2P ground state (14). Charge transfer to form CO^+ which is exothermic only with the excited ^4P state of C^+ was observed to proceed with less than 5% of the initial C^+ population.

Figure 2 shows data observed for the reaction of C^+ with HC_3N proceeding in our SIFT apparatus. The predominant primary product ion was identified as C_3H^+ and it was accompanied by some production of C_4N^+. The C_3H^+ and C_4N^+ ions may be formed by C—H insertion with elimination of CN and H, respectively. Formation of C_3^+ + HCN was not observed. Available heats of formation for C_3H^+ and C_3^+ (15, 16) indicate that formation of C_3^+ is approximately 30 kcal mol^{-1} less exothermic. The C_3H^+ product is likely to be the carbene cation $:\overset{+}{C}$—C≡CH whose chemistry we have investigated in detail in a separate study (8). The structure of the C_4N^+ product is uncertain as either $CCCCN^+$ or $CCCNC^+$ may be formed depending on which end of the molecule is attacked. Carbene character is also likely to be associated with this ion, as for example in $:\overset{+}{C}$—C≡C—CN. Figure 2 also shows rapid reac-

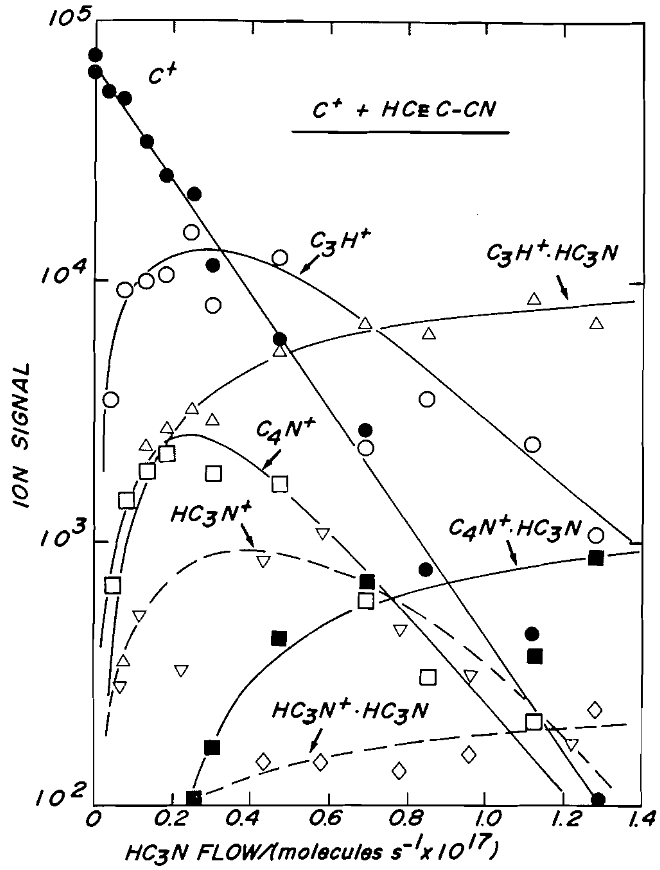

FIG. 2. The observed variations in ion signals recorded for the addition of HC_3N into the reaction region of the SIFT apparatus in which C^+ is initially established in helium carrier gas. P = 0.314 Torr, $\bar{v} = 7.2 \times 10^3$ cm s^{-1}, L = 46 cm, and T = 296 K. C^+ is derived from C_2N_2 at an electron energy of 32 eV.

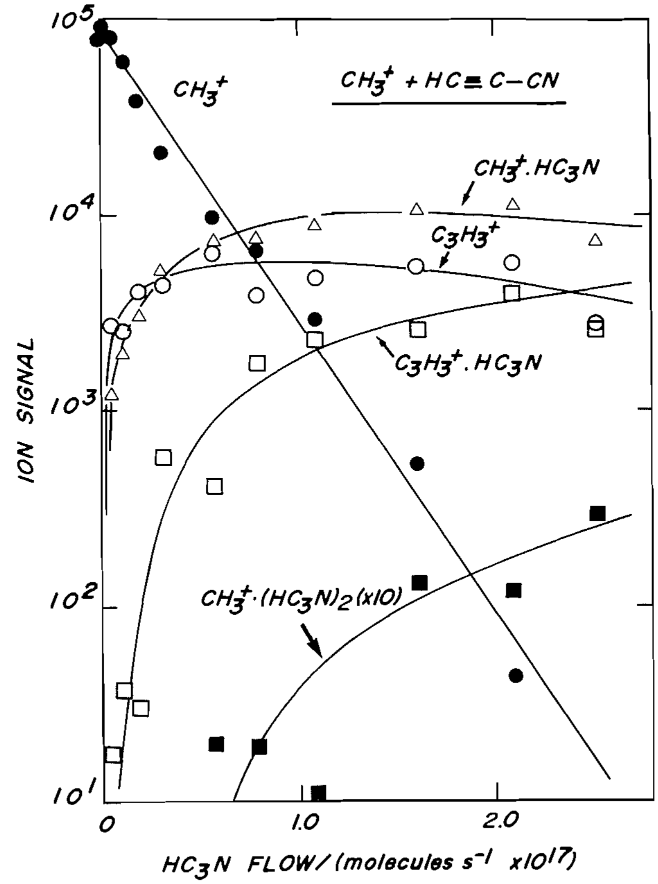

FIG. 3. The observed variations in ion signals recorded for the addition of HC_3N into the reaction region of the SIFT apparatus in which CH_3^+ is initially established in helium carrier gas. P = 0.311 Torr, $\bar{v} = 7.4 \times 10^3$ cm s^{-1}, L = 46 cm, and T = 295 K. CH_3^+ is derived from CH_4 at an electron energy of 24.1 eV.

tions of C_3H^+ and C_4N^+ with HC_3N to form the adducts $C_3H^+ \cdot HC_3N$ and $C_4N^+ \cdot HC_3N$. Also HC_3N^+ was produced as a primary ion and it reacted further to form the adduct $HC_3N^+ \cdot HC_3N$. The production of HC_3N^+, which accounts for about 5% of the initial C^+, may be attributed entirely to the excited ^4P component of C^+ which can react with HC_3N in an exothermic fashion by charge transfer. Not shown in Fig. 2 are the impurity ions at m/z 29 (HCO^+) and 38 (C_2N^+) which were present initially at levels of less than 10% and 1% of the initial C^+ signal, respectively. Separate experiments indicated that HCO^+ reacts by proton transfer to yield $H_2C_3N^+$ and that C_2N^+ produces C_3H^+. Also the observations allowed for some production (5%) of C_2N^+ directly from the reaction of C^+ with HC_3N.

CH_3^+

This ion was derived from CH_4 at 24 eV. Background ions were present at m/z = 19, 29, and 33. These were ascribed to H_3O^+, N_2H^+, and $CH_3^+ \cdot H_2O$. Figure 3 shows the appearance of the product ions which were assigned to the reaction of CH_3^+ with cyanoacetylene. Major primary products were observed at m/z = 39 and 66. Since formation of HC_2N^+ (m/z 39) + C_2H_3 is endothermic, the m/z 39 product must be $C_3H_3^+$. The ion with m/z 66 must be the adduct $CH_3^+ \cdot HC_3N$. Both product ions reacted further to form the adducts $C_3H_3^+ \cdot HC_3N$ and $CH_3^+ \cdot (HC_3N)_2$. An ion with m/z 52 was also observed in the product spectrum with an intensity up to 5% of the total product ions but its origin could be attributed entirely to proton-transfer reactions with the impurity ions.

The two primary product channels appear to reflect the position of attack on the cyanoacetylene molecule. Attack at the carbon α to the cyanogen group can lead to elimination of HCN and formation of the propargyl cation while attack at the β carbon would make HCN elimination less favourable and lead preferentially to an adduct which could be the cyanopropenylium ion, $CH_3\text{—}CH\text{=}\overset{+}{C}\text{—}CN$. However, neither of these structures can be considered to be established by these measurements. Alternatives include formation of the cyclopropenium isomer of $C_3H_3^+$ which is also exothermic and formation of an adduct which is electrostatically bound.

C_2^+

This ion was derived from C_2N_2 by electron impact at 50 eV. Background ions of known identity and origin were present at levels of less than 5% of the initial C_2^+ signal. Primary product ions with a contribution of more than 5% of the total observed included m/z 50 (C_3N^+), 74 (C_5N^+), 37 (C_3H^+), and 38 (C_2N^+). The corresponding reactions dictated by thermochemistry and their product distributions are indicated in Table 1. The predominant channel to produce C_3N^+ corresponds to hydride transfer. H atom elimination to form C_5N^+ leads to carbon chain lengthening. The mechanisms of the two remaining channels is less certain but they may arise from side-on attack by C_2^+. The adducts $C_3N^+ \cdot HC_3N$, $C_5N^+ \cdot HC_3N$, and $C_3H^+ \cdot HC_3N$ appeared to be formed rapidly by secondary reac-

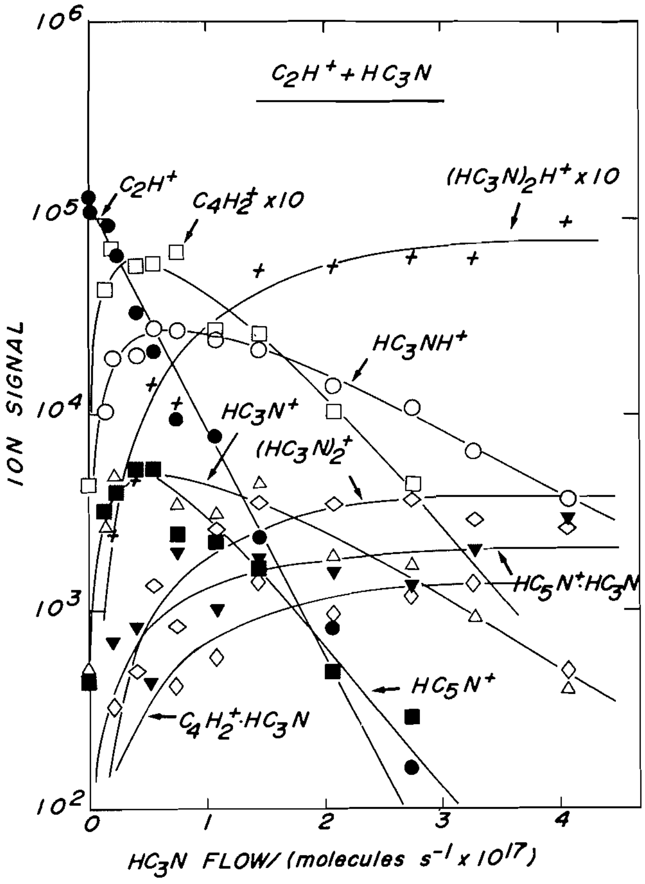

FIG. 4. The observed variations in ion signals recorded for the addition of HC_3N into the reaction region of the SIFT apparatus in which C_2H^+ is initially established in helium carrier gas. P = 0.339 Torr, v = 7.1 × 10^3 cm s^{-1}, L = 46 cm, and T = 297 K. C_2H^+ is derived from cyanoacetylene by electron impact at 31 eV.

tions with cyanoacetylene. Only the adduct of C_2N^+ was not observed. It is shown in a later section that this ion reacts with HC_3N to produce C_3H^+.

C_2H^+

This ion was generated from HC_3N by electron impact at 31 eV. The main impurity ions present initially were m/z 19 (H_3O^+), 26 ($C_2H_2^+$), and 42 ($H_2C_2O^+$) at 5%, 2%, and 2%, respectively, of the initial C_2H^+ signal. All three of these impurity ions have been shown in separate experiments to be derivatives of the reaction of C_2H^+ with H_2O impurity. Their presence was taken into account in the product analysis. The evolution of the product ions observed with addition of HC_3N is shown in Fig. 4. The predominant product channel corresponds to proton transfer and the minor channel apparently to charge transfer although CN transfer cannot be excluded. The two other intermediate channels both appear to result in C—C bond formation. The $C_4H_2^+$ product is likely to be ionized diacetylene which may arise by attack at the carbon α to CN while HC_5N^+, presumably ionized cyanodiacetylene, may be the result of attack at the β carbon with elimination of H. All four of the product ions reacted further with HC_3N to rapidly establish the adducts $(HC_3N)_2H^+$, $(HC_3N)_2^+$, $C_4H_2^+ \cdot HC_3N$, and $HC_5N^+ \cdot HC_3N$.

$C_2H_2^+$, $C_4H_2^+$

The $C_2H_2^+$ was derived from acetylene by electron impact at 31 to 51 eV. Major primary products were observed at m/z 50 and 77 which were assigned to $C_4H_2^+$ and $C_2H_2^+ \cdot HC_3N$, respectively. Production of m/z 50 = C_3N^+ is endothermic according to available heats of formation (16). The m/z 77 ion is produced exclusively from $C_2H_2^+$ and not from a secondary reaction of $C_4H_2^+$ with HC_3N which was shown in the C_2H^+ experiments to produce only the adduct $C_4H_2^+ \cdot HC_3N$. There was no indication for the formation of an ion at m/z 52 which would be indicative of proton transfer. Evidently carbon chain lengthening and association are the only two primary product channels. Proton transfer was identified as the only channel by earlier flowing afterglow measurements (6). It is possible that proton transfer is in fact endothermic although the energetics for proton transfer are not well known due to the uncertainty in the heat of formation of C_2H (17). Within the uncertainties of PA(C_2H) and PA(HC_3N) the change in enthalpy for the proton transfer is −4 ± 9 kcal mol^{-1}.

CN^+

CN^+ was derived from C_2N_2 by electron impact at ca. 55 eV. CN^+ reacts rapidly with H_2O and a number of ions derived from this reaction were present as impurity ions. The major reaction channel between CN^+ and HC_3N corresponds to charge transfer although C_2H transfer is also a possibility. Some production of an ion with m/z 50 was observed and it was ascribed to formation of C_3N^+ + HCN which may result from hydride transfer. Also an ion with m/z 52 (HC_3NH^+ or $C_2N_2^+$) was observed to be produced but its origin could be attributed entirely to a proton transfer between H_3O^+ and cyanoacetylene. The C_3N^+, HC_3N^+, and m/z 52 ions were all observed to undergo secondary reactions to form adducts with HC_3N.

C_2N^+

This ion was derived from cyanoacetylene at an electron energy of 35 eV. C_3H^+ was the only primary product observed and it reacted further to form the adduct $C_3H^+ \cdot HC_3N$. Separate experiments performed in our laboratory have shown that the C_2N^+ derived from HC_3N (and also from C_2N_2) is a mixture of at least two states. One component has been found to react rapidly with O_2 to form C_2NO^+ and O_2^+ and comprises about 5% of the total mixture. The remaining 95% was observed to be unreactive towards O_2. It is not clear whether the observed difference in reactivity is due to the two structural isomers C—N—C^+ and C—C—N^+ or whether singlet and triplet forms of this carbene cation are involved. Calculations have shown the C—N—C^+ isomer to be more stable than the C—C—N^+ isomer by ca. 30 kcal mol^{-1} (18).

H_3^+, N_2H^+, HCO^+, $C_2H_3^+$, H_3O^+

We have investigated proton transfer reactions with cyanoacetylene in a separate study directed towards a determination of the proton affinity of HC_3N by the bracketing technique (19). All five of the protonated species listed above were observed to react rapidly with HC_3N by proton transfer with rate constants in close agreement with predicted collision rate constants. The observations recorded for the fastest of these reactions, viz. the reaction with H_3^+, are shown in Fig. 5 which also includes the reactive behaviour of the impurity ions H_3O^+ and N_2H^+. The protonated cyanoacetylene reacts further to establish the protonated dimer.

$CH_3NO_2H^+$, NO^+

These two ions were generated by injecting $CH_3NO_2^+$ into H_2 buffer gas (19). At the injection energies employed (12.4 V) some NO^+ was present (≈ 10%) which is presumed to arise

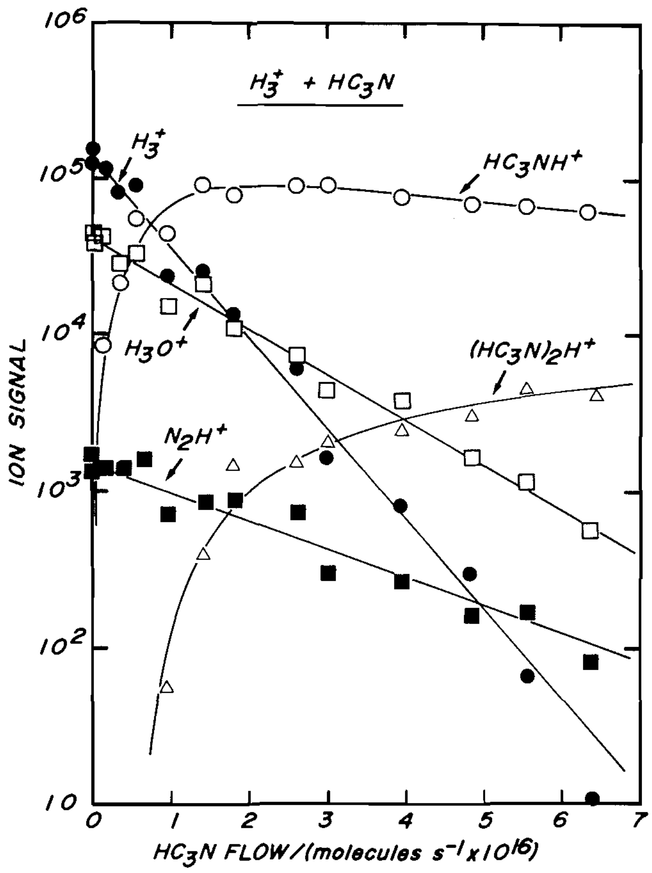

FIG. 5. The observed variations in ion signals recorded for the addition of HC_3N into the reaction region of the SIFT apparatus in which H_3^+ is initially established in hydrogen carrier gas. $P = 0.188$ Torr, $v = 6.5 \times 10^3$ cm s^{-1}, $L = 45$ cm, and $T = 296$ K. The selected ion is H_2^+ derived from H_2 by electron impact at 30 eV. H_3O^+ and N_2H^+ arise from reactions of H_3^+ with impurities in the carrier gas.

from collisional dissociation of $CH_3NO_2^+$. The NO^+ was observed to react only slowly to form the adduct $NO^+ \cdot HC_3N$. The rate constant for this association is estimated to be $< 1 \times 10^{-10}$ cm^3 $molecule^{-1}$ s^{-1} at a total pressure of 0.18 Torr and a hydrogen density of 5.9×10^{15} molecules cm^{-3}. The $CH_3NO_2H^+$ was observed to react rapidly to form two products in about equal proportions: an ion at m/z 52 which corresponds to protonated HC_3N and an ion at m/z 66 which may be $H_4C_4N^+$, $H_2C_4O^+$, or C_3NO^+. The possible m/z 66 product ions would involve concomitant production of the neutrals HNO_2, H_3N_2O, and H_5CNO, respectively. The first option appears most likely and could produce the cyanopropenylium ion as shown in reaction [1]

$$[1] \quad CH_3NO_2H^+ + HC{\equiv}C{-}CN \rightarrow CH_3{-}CH{=}\overset{+}{C}{-}CN + HNO_2$$

N_2^+, CO^+, $C_2N_2^+$

N_2^+ was derived from N_2 at an electron energy of 45 eV, $C_2N_2^+$ from C_2N_2 at 51 eV, and CO^+ from OCS at 34 eV. All these ions have recombination energies higher than the ionization energy of cyanoacetylene so that charge transfer was observed to be the dominant channel (>95%) for all three ions. Impurity ions were present at m/z 18 (H_2O^+), 19 (H_3O^+), and 29 (N_2H^+ or HCO^+) and these reacted predictably by proton transfer to establish HC_3NH^+. Both the HC_3N^+ produced by charge transfer and the HC_3NH^+ produced by proton transfer reacted further by addition of HC_3N to form $(HC_3N)_2^+$ and $(HC_3N)_2H^+$, respectively.

$(CH_3)_2COH^+$, CH_3CNH^+, i-$C_3H_7OH_2^+$

These three protonated species were observed to form adduct ions with cyanoacetylene. Each was generated in H_2 buffer gas by reaction [2]

$$[2] \quad X^+ + H_2 \rightarrow XH^+ + H$$

where X^+ was derived by electron impact of X = $(CH_3)_2CO$, CH_3CN, and i-C_3H_7OH, respectively (19). Table 1 shows that the association reactions with CH_3CNH^+ and i-$C_3H_7OH_2^+$ are quite rapid and about 10 times faster than the association reaction with $(CH_3)_2COH^+$. The adduct of CH_3CNH^+ was observed to react further with HC_3N in a manner which may be described by the solvated proton transfer reaction [3].

$$[3] \quad CH_3CNH^+ \cdot HC_3N + HC_3N \rightarrow HC_3NH^+ \cdot HC_3N + CH_3CN$$

The reverse of reaction [3] is actually the preferred direction. This was shown in a separate study in which $HC_3NH^+ \cdot HC_3N$ was generated in H_2 buffer gas by the reaction sequence [4] and [5]

$$[4] \quad H_2^+(H_3^+) + HC_3N \rightarrow HC_3NH^+ + H(H_2)$$

$$[5] \quad HC_3NH^+ + HC_3N \rightarrow HC_3NH^+ \cdot HC_3N$$

The $HC_3NH^+ \cdot HC_3N$ adduct was observed to react rapidly with CH_3CN by the reverse of reaction [3] with a rate constant of 1.9×10^{-9} cm^3 $molecule^{-1}$ s^{-1}. The analogue of reaction [3] was not observed for the adduct ions $(CH_3)_2COH^+ \cdot HC_3N$ and i-$C_3H_7OH_2^+ \cdot HC_3N$. The smaller rate constants for these two reactions are consistent with the larger intrinsic basicities of $(CH_3)_2CO$ (PA = 194 kcal mol^{-1}) and i-C_3H_7OH (PA = 190 kcal mol^{-1}). Finally, the observations indicated no measurable tendency of any of the adduct ions to add a second HC_3N molecule. The rate of addition of the second molecule of HC_3N is estimated to be at least 10 times slower than the rate of addition of the first. This difference in rate is likely to reflect a difference in the nature of the bonding in these adduct ions.

C_3H^+, C_4N^+

These two ions are likely to be the carbene cations with the linear structures $:\overset{+}{C}{-}C{\equiv}C{-}H$ and $:\overset{+}{C}{-}C{\equiv}C{-}CN$. When generated from the reaction of C^+ with HC_3N both ions were observed to add one molecule of HC_3N rapidly (see Fig. 2 and Table 1). Representative data for a separate study of the reaction of C_3H^+ with HC_3N where C_3H^+ is derived from electron impact of propylene is shown in Fig. 6. The two reactions were not investigated as a function of pressure. Stabilization of the adduct ions may proceed by collision with the buffer gas atoms but radiative association cannot be ruled out. The further addition of a second molecule of HC_3N was observed to proceed much more slowly.

Discussion and conclusions

The measurements reported here show that cyanoacetylene is very reactive towards ions at room temperature. The reactivity is manifested in a number of different ways. The moderate ionization potential of HC_3N and its moderately high proton affinity ensure that charge transfer and proton transfer can be effective. Cyanoacetylene also exhibits a range of interesting and rapid condensation and association reactions which are suited for molecular growth by ion/molecule reactions.

The ions selected in this study for reaction with cyano-

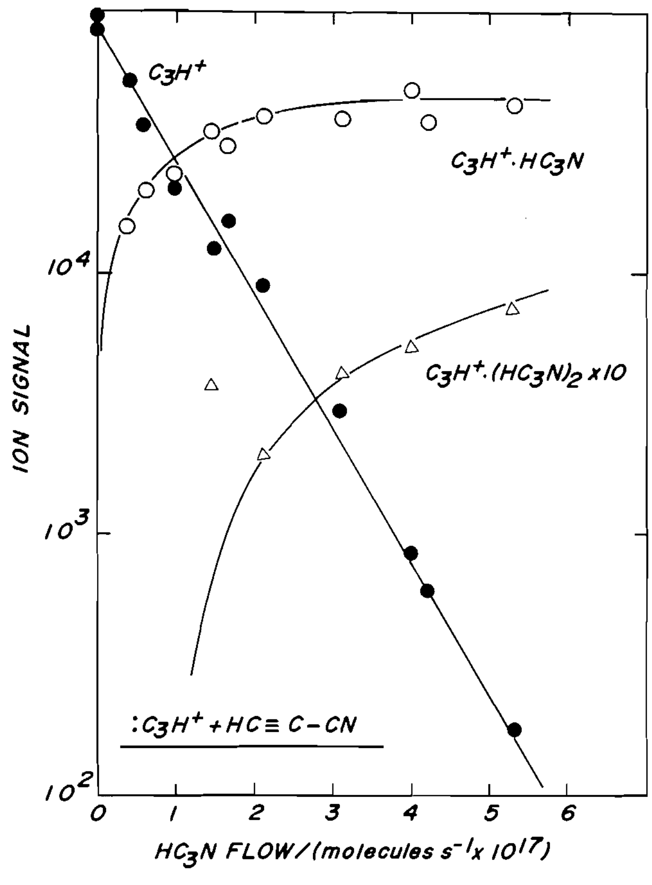

FIG. 6. The observed variations in ion signals recorded for the addition of HC_3N into the reaction region of the SIFT apparatus in which C_3H^+ is initially established in helium carrier gas. P = 0.347 Torr, $\bar{v} = 7.3 \times 10^3$ cm s^{-1}, L = 46 cm, and T = 296 K. C_3H^+ is derived from propylene by electron impact at 55 eV.

acetylene span a large range in recombination energy up to 24.6 eV for He^+. Charge transfer is exothermic for ions with a recombination energy greater than 11.60 ± 0.01 eV which is the ionization energy of HC_3N (20). Indeed charge transfer was an observed product channel with all of the ions which met this criterion, viz. He^+ (24.6), C^+ (^4P) (16.6), N_2^+ (15.6), CN^+ (15.1), CO^+ (14.0), $C_2N_2^+$ (13.4), and C_2H^+ (11.6), where the recombination energy is given in parentheses in eV (21). The charge transfer with He^+ was completely dissociative. For dissociative charge transfer to be exothermic to form any of the product ions indicated for He^+ in Table 1 the recombination energy of the ion must be greater than 17.7 eV and this is the case only for He^+. For the reactions of the other ions dissociative charge transfer is endothermic and was not observed. Charge transfer was observed to be only a minor channel with C_2H^+. The recombination energy of this ion is quite uncertain but appears to be very close to the ionization energy of cyanoacetylene. Values of 11.96 ± 0.05 eV (22), 11.6 ± 0.5 eV (17), 11.51 eV,[1] and 11.31 ± 0.13 eV (24) have been reported in the literature. Given this large uncertainty it is conceivable that charge transfer between C_2H^+ and HC_3N is in fact slightly endothermic at room temperature but this would still be consistent with our observation.

Freeman *et al.* (6) have reported flowing afterglow measurements of the charge transfer reactions of He^+, CN^+, and CO^+. The rate constants agree with those obtained in the SIFT study reported here within the combined error estimates of both experiments. However, Freeman *et al.* (6) did not report any dissociative charge transfer with He^+ and apparently also did not observe the small production of C_3N^+ from CN^+ which proceeds by hydride transfer. Furthermore these authors reported exclusive charge transfer for the reaction of C^+ with HC_3N which is not in agreement with our observations. Charge transfer between HC_3N and the $C^+(^2P)$ ground state is endothermic since the ionization energy of HC_3N (11.60 ± 0.01 eV) is higher than the recombination energy (11.260 eV) of $C^+(^2P)$. Charge transfer with C^+ should therefore not proceed rapidly at room temperature unless it is mostly in the (^4P) excited state. About 5% of the C^+ appeared to be in the (^4P) state in the SIFT experiments reported here and a charge transfer product was observed consistent with this population but the remaining 95% of the C^+ ions was seen to react to build up the carbon chain in the formation of C_3H^+ and C_4N^+.

Proton-transfer reactions with cyanoacetylene have been discussed in detail in a separate study directed towards a determination of the proton affinity of HC_3N (24). A value of 184 ± 4 kcal mol^{-1} was derived from bracketing measurements. Proton transfer was observed to proceed with H_3^+ (101), N_2H^+ (117), HCO^+ (141), $C_2H_3^+$ (153), H_3O^+ (166), and $CH_3NO_2H^+$ (180) but not with the CH_3CNH^+ (187) or $(CH_3)_2COH^+$ (194) where proton affinities are given in parentheses in kcal mol^{-1}. Proton transfer was observed by Freeman *et al.* (6) for H_3^+, N_2H^+, HCO^+, $C_2H_3^+$, and H_3O^+ and the rate constants obtained for these reactions with the two techniques again are in good accord. However, there are serious discrepancies for the reactions of CH_3^+ and $C_2H_2^+$ for which Freeman *et al.* (6) have also reported exclusive proton transfer. For these two ions the SIFT measurements indicate only condensation and association. The proton affinity of CH_2 can be calculated to be 197 kcal mol^{-1} from available thermochemical information (21) and this makes the proton transfer with HC_3N endothermic. The energetics of the proton-transfer reaction between $C_2H_2^+$ and HC_3N is less certain due to the uncertainty in the heat of formation of C_2H (17). Within the uncertainties of PA(C_2H) and PA(HC_3H) the change in enthalpy is −4 ± 9 kcal mol^{-1}. The SIFT measurements did not indicate occurrence of proton transfer which suggests that this channel is in fact endothermic also.

The remaining reactions which were investigated result predominantly in condensation and association and are of interest in chemical synthesis by ion/molecule reactions. Several condensation reactions lead to the buildup of purely carbonaceous ions as in the generation of C_3H^+ from C^+, $C_3H_3^+$ from CH_3^+, and $C_4H_2^+$ from C_2H^+ and $C_2H_2^+$. Others lead to the lengthening of the carbon backbone of the cyanoacetylene as in the formation of C_4N^+ from C^+, C_5N^+ from C_2^+, HC_5N^+ from C_2H^+ and possibly $H_4C_4N^+$ from $CH_3NO_2H^+$. The association reactions which were observed with HC_3N exhibited an interesting range in specific rate. The apparent bimolecular rate constants were generally $\geq 5 \times 10^{-11}$ cm^3 molecule^{-1} s^{-1} which is close to the collision limit. These are large values and as such are indicative of the formation "tight" adducts in which the bonding is quite strong (25, 26). Strong bonding is not entirely unexpected for the adducts observed. CH_3CNH^+, *i*-$C_3H_7OH_2^+$, and $(CH_3)_2COH^+$ should form proton bound adducts with HC_3N. The proton affinities of CH_3CN, *i*-C_3H_7OH, and $(CH_3)_2CO$ are within 10 kcal mol^{-1} of that for HC_3N. Charge delocalization is possible with $(CH_3)_2COH^+$ as is expressed in the resonance structures [6].

[1] S. I. Miller and J. Berkowitz. Referred to in ref. 22.

[6] 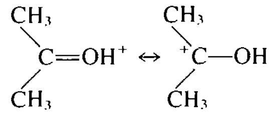

This may result in a weaker proton bond in this case and thus account for the smaller rate constant observed for the formation of $(CH_3)_2COH^+ \cdot HC_3N$.

With C_3H^+ and C_4N^+ and possibly also $C_2H_2^+$ and $C_4H_2^+$ the bonding in the observed adducts is likely to be covalent. The carbene cations C_3H^+ and C_4N^+ should react with HC_3N by C—H σ bond insertion in a manner analogous to the bimolecular insertion reactions already reported for C_3H^+ (8, 27). Sigma bond insertion would lead to the product ions [7] and [8].

[7] $HC{\equiv}C{-}\overset{+}{C}H{-}C{\equiv}C{-}C{\equiv}N$

[8] $N{\equiv}C{-}C{\equiv}C{-}\overset{+}{C}H{-}C{\equiv}C{-}C{\equiv}N$

Charge delocalization is possible in these two ions and this may account for the observed decrease in the rate of addition of a second molecule of HC_3N. The nature of the bonding in the adducts $C_2H_2^+ \cdot HC_3N$ and $C_4H_2^+ \cdot HC_3N$ is less certain.

In ionized environments such as, for example, dense molecular interstellar clouds, ion/molecule reactions proceed in competition with neutralization reactions. Neutralization may proceed by electron-ion recombination (EIR), charge transfer (CT), or proton transfer (PT) and, when coupled to an ion/molecule reaction leading to bond formation in the ion, may result in the synthesis of a neutral molecule in which the new bond is preserved (23). For example, electron–ion recombination or proton-transfer reactions with the carbonaceous ions C_3H^+, $C_3H_3^+$, and $C_4H_2^+$ may establish the neutral molecules C_3, C_3H_2, and C_4H, and with $H_4C_4N^+$ may establish methylcyanoacetylene. $C_4H_2^+$ may neutralize by charge transfer to form diacetylene while HC_5N^+ may charge transfer to form cyanodiacetylene. The new bond may also be preserved directly in the neutral product of an ion/molecule reaction as in the reaction of C_2N^+ with HC_3N to form C_3H^+ where the neutral product must be C_2N_2.

For the specific case of the molecular cloud TMC-1 the results obtained in this study provide an indication of the possible role of cyanoacetylene in the synthesis of derivative molecules. Efficient routes are available for the synthesis of C_4H and C_4N according to reactions [9] and [10], respectively.

[9] $C_2H_2^+ \xrightarrow{HC_3N} C_4H_2^+ \xrightarrow[EIR]{PT} C_4H$

[10] $C^+ \xrightarrow{HC_3N} C_4N^+ \xrightarrow{CT} C_4N$

C^+ and $C_2H_2^+$ are attractive ionic precursors in models of interstellar ion chemistry as they react with H_2 only slowly by association (23). CH_3^+ is attractive for the same reason. With cyanoacetylene it yields the propargyl cation which may neutralize to form the carbene $H_2C{=}C{=}C{:}$ as shown in reaction [11].

[11] $CH_3^+ \xrightarrow{HC_3N} C_3H_3^+ \xrightarrow{PT} C_3H_2$

The $CH_3^+ \cdot HC_3N$ adduct observed in the laboratory may form in the molecular cloud by radiative association and then neutralize to form methylcyanoacetylene according to reaction [12].

[12] $CH_3^+ \xrightarrow{HC_3N} CH_3{-}CH{=}\overset{+}{C}{-}CN \xrightarrow[EIR]{PT} CH_3C_2CN$

Another possible route towards methylcyanoacetylene is reaction [13]

[13] $CH_3NO_2H^+ \xrightarrow{HC_3N} CH_3{-}CH{=}\overset{+}{C}{-}CN \xrightarrow[EIR]{PT} CH_3C_2CN$

but this route is less attractive for TMC-1 as CH_3NO_2 has not been identified. Plausible routes are also available for the synthesis of cyanopolyynes. Cyanodiacetylene may be produced directly from C_2H^+ according to reaction [14].

[14] $C_2H^+ \xrightarrow{HC_3N} HC_5N^+ \xrightarrow{CT} HC_5N$

Several of the primary product ions allow build up of the cyanopolyynes in secondary reactions. For example, recent measurements of the reaction of C_4N^+ with CH_4 in our laboratory indicate a channel leading the $H_2C_5N^+$ which may neutralize to form cyanodiacethylene. Other intriguing possibilities include the neutralization of the adducts $C_2H_2^+ \cdot HC_3N$ and $C_4H_2^+ \cdot HC_3N$ to form HC_5N and HC_7N, respectively, by elimination of H_2. Also the radiative recombination counterparts of the adduct formation observed in the flow tube for the carbene cations C_3H^+ and C_4N^+ expressed in reactions [15] and [16]

[15] $C_3H^+ + HC_3N \rightarrow HC{\equiv}C{-}\overset{+}{C}H{-}C{\equiv}C{-}CN + h\nu$

[16] $C_4N^+ + HC_3N \rightarrow NC{-}C{\equiv}C{-}\overset{+}{C}H{-}C{\equiv}C{-}CN + h\nu$

may provide direct routes for the synthesis in the interstellar medium of the large neutral carbenes $:C(C_2H)C_2CN$ and $:C(C_2CN)_2$. These may form on neutralization by proton transfer or electron–ion recombination. They constitute a new class of complex organonitrogen molecules whose presence may provide still further opportunities for molecular growth in the interstellar medium.

Acknowledgements

We thank the Natural Sciences and Engineering Research Council of Canada for financial support. Also we thank N. Haese for valuable discussions and A. Fox for preparing samples of HC_3N.

1. G. WINNEWISER and C. M. WAMSLEY. Astrophys. Space Sci. **65**, 83 (1979).
2. N. W. BROTEN, J. M. MACLEOD, L. W. AVERY, W. M. IRVINE, B. HOGLUND, P. FRIBERG, and A. HJALMARSON. Astrophys. J. **276**, L25 (1984).
3. E. HERBST. *In* Protostars and planets. *Edited by* T. Gehrels. Tucson, U. of Arizona Press. 1978. pp. 88–99.
4. S. S. PRASAD and W. T. HUNTRESS. Astrophys. J. Suppl. **43**, 1 (1980).
5. S. S. PRASAD and W. T. HUNTRESS. Astrophys. J. **239**, 151 (1980).
6. C. G. FREEMAN, P. W. HARLAND, and M. J. MCEWAN. Mon. Not. R. Astr. Soc. **187**, 441 (1979).
7. G. I. MACKAY, G. D. VLACHOS, D. K. BOHME, and H. I. SCHIFF. Int. J. Mass Spectrom. Ion Phys. **36**, 259 (1980).
8. A. B. RAKSIT and D. K. BOHME. Int. J. Mass Spectrom. Ion Phys. **55**, 69 (1983).
9. C. MOUREU and J. C. BONGRAND. Ann. Chim. Rome, **14**, 47 (1920).
10. N. G. ADAMS and D. SMITH. J. Phys. B, **9**, 1439 (1976).
11. T. SU and W. J. CHESNAVICH. J. Chem. Phys. **76**, 5183 (1982).

12. E. R. LIPPINCOTT and J. M. STUTMAN. J. Phys. Chem. **68**, 3976 (1964).
13. A. A. WESTENBERG and E. B. WILSON. J. Ann. Chem. Soc. **72**, 199 (1950).
14. M. TICHY, A. B. RAKSHIT, D. G. LISTER, N. D. TWIDDY, N. G. ADAMS, and D. SMITH. Int. J. Mass Spectrom. Ion Phys. **23**, 123 (1977).
15. A. B. RAKSIT and D. K. BOHME. Int. J. Mass Spectrom. Ion Phys. **49**, 275 (1983).
16. J. L. FRANKLIN, J. G. DILLARD, H. M. ROSENSTOCK, J. T. HERRON, K. DRAXL, and F. H. FIELD. Natl. Stand. Ref. Data Ser. **26**, 41 (1969).
17. J. R. WYATT and F. E. STAFFORD. J. Phys. Chem. **76**, 1913 (1972).
18. M. YOSHIMINE and W. P. KRAEMER. Chem. Phys. Lett. **90**, 145 (1982).
19. A. B. RAKSIT and D. K. BOHME. Int. J. Mass Spectrom. Ion Processes, **57**, 211 (1984).
20. C. BAKER and D. W. TURNER. Proc. R. Soc. London, A**308**, 19 (1968).
21. H. M. ROSENSTOCK, K. DRAXL, B. W. STENER, and J. T. HERRON. J. Phys. Chem. Ref. Data Ser. 6, Suppl. 1 (1977).
22. H. OKABE and V. H. DIBELER. J. Chem. Phys. **59**, 2430 (1973).
23. H. I. SCHIFF and D. K. BOHME. Astrophys. J. **232**, 740 (1979).
24. Y. ONO and C. Y. NG. J. Chem. Phys. **74**, 6985 (1981).
25. E. HERBST. J. Chem. Phys. **70**, 2201 (1979).
26. A. GOOD. Trans. Faraday Soc. **67**, 3495 (1971).
27. D. K. BOHME, A. B. RAKSIT, and A. FOX. J. Am. Chem. Soc. **105**, 5481 (1983).

The crystal and molecular structure of *syn*-[4.4.3]propella-2,4,12-trien-11-ol 3,5-dinitrobenzoate

JUDITH C. GALLUCCI, KATSUO OHKATA, AND LEO A. PAQUETTE
Evans Chemical Laboratories, The Ohio State University, Columbus, OH 43210, U.S.A.

Received June 19, 1984

JUDITH C. GALLUCCI, KATSUO OHKATA, and LEO. A. PAQUETTE. Can. J. Chem. **63**, 862 (1985).

The crystal structure of *syn*-[4.4.3]propella-2,4,12-trien-11-ol 3,5-dinitrobenzoate, **2**, has been determined by single crystal X-ray diffraction and refined to an R value of 0.051. The crystal structure is triclinic with $a = 10.208(2)$, $b = 13.355(2)$, $c = 7.068(1)$ Å, $\alpha = 99.35(1)°$, $\beta = 100.63(1)°$, $\gamma = 100.79(1)°$, and the space group is $P\bar{1}$ with two molecules per cell, $D_{(calcd)} = 1.39$ g cm^{-3}. The unsaturated five-membered ring resides in an envelope conformation with C6—C11—C12—C13 lying essentially in a plane. The fifth atom, C1, is positioned 0.47 Å out of this plane on the side opposite O1. The latter is situated 1.38 Å away and projects the 3,5-dinitrobenzoate group above the central portion of the cyclohexadiene unit. Four contiguous carbon atoms in the latter ring are mutually coplanar and the fused cyclohexane ring adopts a chair conformation. The overall molecular geometry is reconcilable with its solvolytic behavior in aqueous acetone.

JUDITH C. GALLUCCI, KATSUO OHKATA, et LEO. A. PAQUETTE. Can. J. Chem. **63**, 862 (1985).

On a déterminé la structure cristalline du dinitro-3,5 benzoate du [4.4.3] propellatriène-2,4,12 ol-11-*syn*, **2**, par diffraction de rayons-X sur un cristal unique et on l'a affinée jusqu'à une valeur de $R = 0{,}051$. Le cristal est triclinique avec $a = 10{,}208(2)$, $b = 13{,}355(2)$, $c = 7{,}068(1)$ Å, $\alpha = 99{,}35(1)°$, $\beta = 100{,}63(1)°$, $\gamma = 100.79(1)°$. Le groupe d'espace est $P\bar{1}$ avec deux molécules par maille, $D_{(calc)} = 1{,}39$ g cm^{-3}. Le cycle insaturé à cinq chaînons existe dans une conformation enveloppe avec les 4 carbones C-6, C-11, C-12 et C-13 reposant essentiellement dans un plan. Le cinquième atome, C1, est situé à 0,47 Å hors de ce plan du côté opposé au O1. Ce dernier est à 1,38 Å plus loin et projette ainsi le groupe dinitro-3,5 benzoate au-dessus de la partie centrale de l'unité cyclohexadiénique. Quatre atomes de carbone contigus de ce dernier cycle sont mutuellement coplanaires et le noyau cyclohexanique qui lui est condensé adopte une conformation chaise. La géométrie moléculaire globale est en accord avec le comportement solvolytique dans l'acétone aqueuse.

[Traduit par le journal]

Introduction

The solvolytic behavior of the epimeric 3,5-dinitrobenzoates **1** and **2** in aqueous acetone has proven to be particularly informative with regard to the question of long-range charge delocalization (1). Despite the fact that the two molecules give rise to identical product distributions within experimental error, *anti* isomer **1** ionizes 100 times more rapidly than **2**. This widely divergent kinetic response was interpreted to be an indication of substantial π participation during rate-determining C—O bond heterolysis in **1** which fosters direct conversion to delocalized carbocation **3**. Because the *syn* isomer does not enjoy a comparably favorable stereochemical alignment, the initial ionization event leads to a simpler allyl cation. Only subsequently does the allyl → bishomotropylium electronic reorganization occur. The development of heightened charge delocalization as in **3** is almost certain to require disrotatory folding of the three- and unsaturated four-carbon bridges for the purpose of achieving through-space interaction and maximizing orbital overlap.

When the *anti/syn* rate ratio of 100 is compared to that previously determined for **4** and **5** (*exo/endo* = 12) (2), it becomes apparent that the presence of an additional fused cyclohexane ring is either more conducive to the development of bishomoaromatic character (see **3**) within **1** or less favorable to the ionization of **2**. For these reasons, we became interested in establishing the conformational preference of **2** and report here the results of its X-ray determined crystal structure.

X-ray structure results

Experimental

Preliminary precession photographs with MoKα radiation failed to find any Laue symmetry higher than $\bar{1}$; hence the space group possibilities are restricted to $P1$ and $P\bar{1}$. The pale yellow crystal used for data collection was a many-sided lump cut from a larger crystal and measured approximately 0.36 mm × 0.40 mm × 0.44 mm in size. The unit cell con-

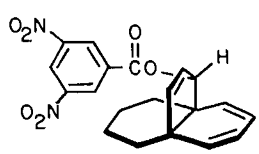

1

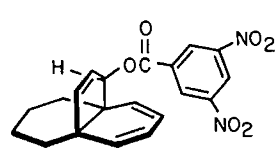

2

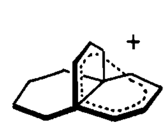

3

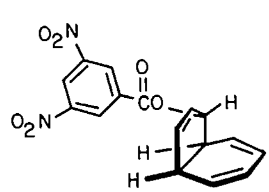

4

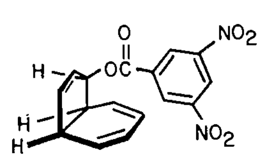

5

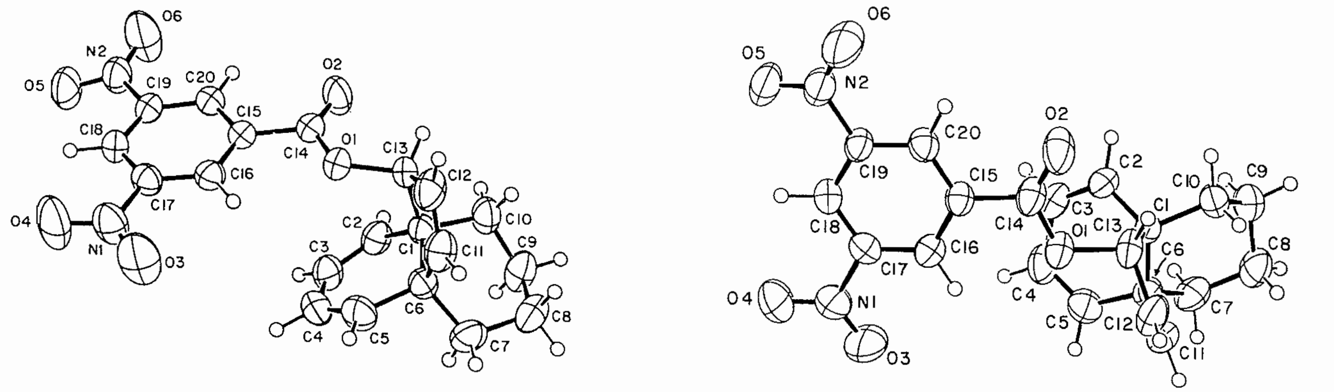

FIG. 1. ORTEP drawings of the molecular structure of **2** (left: side view; right: top view). The hydrogen atoms are drawn with an artificial radius for clarity; the nonhydrogen atoms are presented as 50% probability thermal ellipsoids.

stants a = 10.208(2), b = 13.355(2), c = 7.068(1) Å, α = 99.35(1)°, β = 100.63(1)°, and γ = 100.79(1)° were determined by the least-squares fit of the diffractometer setting angles for 26 reflections in the 2θ range 16 to 30° with MoKα radiation (λ(K$\bar{\alpha}$) = 0.71069 Å).

Data were collected at 21(1)°C by the $\theta-2\theta$ scan technique on a Syntex P$\bar{1}$ diffractometer equipped with graphite-monochromated MoKα radiation. The data were corrected for Lorentz and polarization effects and put on an absolute scale by means of a Wilson plot (3);[1] no absorption correction was applied. Five reflections saturated the detector during the data collection, the (0$\bar{1}$1), (101), (200), (3$\bar{1}\bar{1}$), and (30$\bar{1}$), and were not included in the data set. Six standard reflections were measured after every 100 reflections and gave no evidence of decay.

The additional pertinent crystallographic details are: $C_{20}H_{18}N_2O_6$ fw = 382.38 Triclinic, space group $P\bar{1}$, cell volume = 911 Å^3, Z = 2, $D_{(calcd)}$ = 1.39 g cm^{-3}, linear absorption coefficient = 0.98 cm^{-1}, 2θ limits = 4° ≤ 2θ ≤ 50°, scan speed = 2.0 to 24.0 deg min^{-1} in 2θ, background time/scan time = 0.5, scan range = 1.0° below Kα_1 to 1.2° above Kα_2, data collected = $+h$, $\pm k$, $\pm l$, unique data = 3219, unique data with $F_o^2 > 2\sigma(F_o^2)$ = 2083, final number of variables = 253, $R(F)$ = 0.051, $R_w(F)$ = 0.044, error in observation of unit weight = 1.80 e. ($R(F) = \Sigma||F_o| - |F_c||/\Sigma|F_o|$ and $R_w(F) = (\Sigma w(|F_o| - |F_c|)^2/\Sigma w|F_o|^2)^{1/2}$ with $w = 1/\sigma^2(F_o)$.)

Structure determination

Initial attempts to solve the structure with MULTAN 80 (4) in space group $P\bar{1}$ failed in that a pattern of planar hexagons was generated consistently in the E-maps. The structure was ultimately solved with MULTAN 80 with the following modifications: the two largest E-values were removed from the NORMAL file (these values are 4.6 and 4.5 for the (8$\bar{8}$3) and (833) reflections, respectively, and are significantly larger than the third largest value of 3.8) and the statistically weighted tangent refinement option was used. The resulting E-map clearly contained all the nonhydrogen atoms.

The SHELX-76 package (5) was used for full-matrix least-squares refinements; the function $\Sigma w(|F_o| - |F_c|)^2$ was minimized where $w = 1/\sigma^2(F_o)$. Isotropic refinement of the nonhydrogen atoms converged to an R index of 0.173. After one cycle of anisotropic refinement, a difference electron density map revealed the positions of all the hydrogen atoms. The hydrogens were then included in the model as fixed contributions at their calculated positions with C—H = 1.00 Å and $B_H = B_{C(iso)} + 1.0$ Å.^{2} The final refinement cycle on the anisotropic nonhydrogen atoms yielded agreement indices of $R(F)$ = 0.051 and $R_w(F)$ = 0.044 for the 2083 intensities with $F_o^2 > 2\sigma(F_o^2)$ and the 253 variables. The final cycle had a maximum shift/esd of 0.03. The final difference electron density map contains maximum and minimum peak heights of 0.15 and −0.18 e Å^{-3}. Scattering factors for the carbon, nitrogen, and oxygen atoms (6a) and for the hydrogen atoms (6b) are from the usual sources. The anisotropic thermal parameters,

TABLE 1. Final positional parameters and equivalent isotropic thermal parameters for **2**

Atom	x/a	y/b	z/c	B_{eq}(Å^2)[b]
C1	0.7681(3)[a]	0.2942(2)	0.3347(3)	3.43
C2	0.6740(3)	0.1948(2)	0.3421(4)	4.15
C3	0.5836(3)	0.1376(2)	0.1840(4)	4.69
C4	0.5644(3)	0.1716(2)	0.0001(4)	5.21
C5	0.6231(3)	0.2665(2)	−0.0112(4)	5.26
C6	0.7103(3)	0.3466(2)	0.1656(4)	3.78
C7	0.6193(3)	0.4223(2)	0.2209(4)	5.06
C8	0.6777(3)	0.4954(2)	0.4210(4)	5.47
C9	0.7005(3)	0.4306(2)	0.5744(4)	5.60
C10	0.8084(3)	0.3705(2)	0.5364(4)	4.77
C11	0.8393(3)	0.3985(2)	0.1154(4)	4.81
C12	0.9447(3)	0.3605(2)	0.1789(5)	5.26
C13	0.9066(3)	0.2769(2)	0.2871(4)	4.12
C14	0.9024(3)	0.0946(2)	0.2338(4)	4.31
C15	0.8500(3)	−0.0060(2)	0.0862(4)	3.53
C16	0.7911(3)	−0.0098(2)	−0.1093(4)	3.78
C17	0.7430(3)	−0.1057(2)	−0.2340(4)	3.89
C18	0.7484(3)	−0.1976(2)	−0.1736(4)	3.91
C19	0.8061(3)	−0.1906(2)	0.0212(4)	3.73
C20	0.8587(3)	−0.0973(2)	0.1522(4)	3.86
O1	0.8875(2)	0.1763(1)	0.1520(3)	4.20
O2	0.9508(3)	0.0993(1)	0.4025(3)	7.06
N1	0.6798(3)	−0.1113(3)	−0.4427(4)	5.55
N2	0.8107(3)	−0.2882(2)	0.0916(4)	5.13
O3	0.6626(3)	−0.0322(2)	−0.4925(3)	8.55
O4	0.6488(3)	−0.1961(2)	−0.5529(3)	8.32
O5	0.7471(2)	−0.3690(2)	−0.0159(3)	6.36
O6	0.8792(3)	−0.2832(2)	0.2518(3)	9.95

[a]Estimated standard deviations in the least significant figures are given in parentheses in all tables.
[b]$B_{eq} = 8\pi^2/3\ \Sigma_i\Sigma_j U_{ij}a_i^*a_j^*\mathbf{a}_i\cdot\mathbf{a}_j$.

[1]The programs used for data reduction are from the CRYM crystallographic computing package as modified by G. G. Christoph at The Ohio State University, Columbus, Ohio.

TABLE 2. Final bond lengths for **2**

Atoms	Length (Å)	Atoms	Length (Å)
C1—C2	1.501(3)	C14—O1	1.335(3)
C1—C6	1.559(3)	C14—O2	1.190(3)
C1—C10	1.547(3)	C14—C15	1.499(3)
C1—C13	1.561(4)	C15—C16	1.390(3)
C2—C3	1.327(3)	C16—C17	1.378(3)
C3—C4	1.438(4)	C17—C18	1.371(3)
C4—C5	1.318(4)	C18—C19	1.374(3)
C5—C6	1.516(3)	C19—C20	1.374(3)
C6—C7	1.548(4)	C15—C20	1.387(3)
C7—C8	1.527(4)	C17—N1	1.481(3)
C8—C9	1.505(4)	C19—N2	1.474(3)
C9—C10	1.517(4)	N1—O3	1.199(3)
C6—C11	1.501(4)	N1—O4	1.215(3)
C11—C12	1.311(4)	N2—O5	1.206(3)
C12—C13	1.485(4)	N2—O6	1.201(3)
C13—O1	1.474(3)		

TABLE 3. Final bond angles for **2**

Atoms	Angle (deg)	Atoms	Angle (deg)
C2—C1—C6	113.0(2)	C1—C13—O1	111.2(2)
C2—C1—C10	111.2(3)	C13—O1—C14	116.8(2)
C2—C1—C13	112.6(2)	O1—C14—O2	125.1(3)
C6—C1—C10	111.8(2)	O1—C14—C15	111.6(2)
C6—C1—C13	102.7(2)	O2—C14—C15	123.3(3)
C10—C1—C13	104.9(2)	C14—C15—C16	122.3(2)
C1—C2—C3	121.9(2)	C14—C15—C20	117.5(2)
C2—C3—C4	121.5(3)	C16—C15—C20	120.1(2)
C3—C4—C5	120.9(3)	C15—C16—C17	118.4(2)
C4—C5—C6	123.1(3)	C16—C17—C18	123.1(2)
C5—C6—C1	111.6(2)	C16—C17—N1	119.2(2)
C5—C6—C7	105.8(2)	C18—C17—N1	117.8(2)
C5—C6—C11	109.7(2)	C17—C18—C19	116.7(2)
C7—C6—C1	114.8(2)	C18—C19—C20	123.1(2)
C7—C6—C11	113.7(2)	C18—C19—N2	118.0(2)
C1—C6—C11	101.4(2)	C20—C19—N2	119.0(2)
C6—C7—C8	113.6(2)	C19—C20—C15	118.6(2)
C7—C8—C9	108.5(2)	C17—N1—O3	118.2(3)
C8—C9—C10	109.7(2)	C17—N1—O4	117.7(3)
C9—C10—C1	113.5(2)	O3—N1—O4	124.1(3)
C6—C11—C12	113.1(3)	C19—N2—O5	118.3(2)
C11—C12—C13	111.2(3)	C19—N2—O6	118.3(2)
C12—C13—C1	103.2(2)	O5—N2—O6	123.4(3)
C12—C13—O1	107.6(2)		

the hydrogen atom parameters, and the structure factors have been placed in the Depository of Unpublished Data.[2]

Discussion

The final positional parameters of the nonhydrogen atoms of **2** are presented in Table 1. ORTEP drawings of the molecule (7) giving the numbering system we have used are shown in Fig. 1. No unusual bond lengths (Table 2) or bond angles (Table 3) have been noted. Only one intermolecular contact significantly less than the sum of van der Waals radii (C 1.7, N 1.5, O 1.4, H 1.2 Å) was observed: O2···H20 = 2.41 Å where H20 is a phenyl ring hydrogen. Consequently, the geometry reported in Fig. 1 can be assumed, to a first approximation, to be that of the isolated molecule. A stereoscopic view of the unit cell is shown in Fig. 2.

The torsion angles of the five-membered ring (Table 4) disclose that the four atoms C6—C11—C12—C13 are closest to being coplanar (Table 5). The fifth atom of this ring, C1, lies 0.47 Å out of this plane and comprises the flap of the envelope.

[2]Copies of these tables may be obtained, at a nominal charge, from the Depository of Unpublished Data, CISTI, National Research Council of Canada, Ottawa, Ont., Canada K1A 0S2.

TABLE 4. Selected torsion angles for **2**[a]

Atoms	Angle (deg)
O1—C13—C1—C2	34.0(3)
O1—C13—C1—C10	155.1(2)
O1—C13—C1—C6	−87.9(2)
C13—C12—C11—C6	−1.0(4)
C11—C12—C13—C1	−17.2(4)
C12—C13—C1—C6	27.1(3)
C13—C1—C6—C11	−27.0(3)
C1—C6—C11—C12	18.6(4)
C1—C2—C3—C4	−4.4(5)
C2—C3—C4—C5	−8.8(5)
C3—C4—C5—C6	−1.8(5)
C4—C5—C6—C1	22.4(4)
C5—C6—C1—C2	−32.0(3)
C6—C1—C2—C3	25.2(4)

[a]The sign of the torsion angle is defined according to the convention in ref. 8.

TABLE 5. Least-squares planes for **2**

Coefficients of the plane equation $Ax + By + Cz = D$[a]

Plane	A	B	C	D
1	−0.070	0.519	0.732	2.755
2	0.942	−0.453	−0.292	4.399
3	0.970	−0.096	−0.415	8.172
4	0.554	0.714	−0.259	7.072

Deviations (Å) from planes

	Plane 1	Plane 2	Plane 3	Plane 4
C1	0.468†	0.521†		−0.533†
C2		0.201†		
C3		0.003(3)		
C4		−0.007(3)		
C5		0.007(4)		
C6	−0.003(2)	−0.003(3)		−0.051(2)
C7				0.054(3)
C8				0.715†
C9				−0.055(3)
C10				0.052(3)
C11	0.005(3)			
C12	−0.005(3)			
C13	0.003(2)			
O1	−1.380†			
C15			−0.001(3)	
C16			−0.006(3)	
C17			0.007(3)	
C18			0.001(3)	
C19			−0.008(3)	
C20			0.008(3)	

†Indicates an atom not included in the calculation of the plane.

[a]The plane is described in the crystal coordinate system according to the method given in ref. 9.

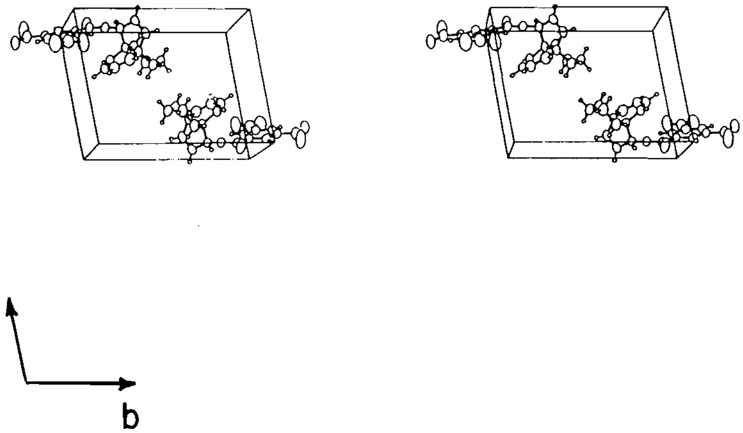

FIG. 2. Stereoscopic view of the unit cell for **2**.

Atom O1 lies on the opposite side of this four-atom plane and at a distance of 1.38 Å from it. The resulting cant projects the C13—O1 bond of the 3,5-dinitrobenzoate moiety directly over the central portion of the cyclohexadiene ring.

As concerns the latter, the data reveal that the four atoms C3—C4—C5—C6 most nearly define a plane. The remaining two atoms, C1 and C2, lie 0.52 Å and 0.20 Å, respectively, from this plane, and on the same side. The remaining cyclohexane ring is in a chair conformation. When a least-squares plane is fitted to the C6—C7—C9—C10 atoms, the C1 atom is 0.53 Å away from this plane, while the C8 atom is positioned 0.72 Å away and on the opposite side of this plane.

In view of the geometry characteristics of **2**, it is possible to conclude that its ionization is not sterically or torsionally impeded. Most notably, the three carbon atoms of the incipient allyl cation are not misaligned for eventual favorable interaction with the cyclohexadiene fragment. We presume therefore that the *exo/endo* rate differential which distinguishes **1/2** from **4/5** is most reasonably attributed to the facilitation of the direct conversion of **1** to **3** by the fused cyclohexane ring. The X-ray structure of molecule **1** might shed some light on this last point.

1. L. A. PAQUETTE, K. JELICH, and K. OHKATA. Tetrahedron Lett. **23**, 2749 (1982); L. A. PAQUETTE, K. OHKATA, K. JELICH, and W. KITCHING. J. Am. Chem. Soc. **105**, 2800 (1983).
2. J. C. BARBORAK and P. VON R. SCHLEYER. J. Am. Chem. Soc. **92**, 3184 (1970).
3. D. J. DUCHAMP. Program and abstracts. American Crystallographic Association Meeting, Bozeman, MT. 1964.
4. P. MAIN, S. J. FISKE, S. E. HULL, L. LESSINGER, G. GERMAIN, J.-P. DECLERCQ, and M. M. WOOLFSON. MULTAN 80. A system of computer programs for the automatic solution of crystal structures from X-ray diffraction data. Univs. of York, England and Louvain, Belgium. 1980.
5. G. M. SHELDRICK. SHELX-76. Program for crystal structure determination. University Chemical Laboratory, Cambridge, England. 1976.
6. (*a*) International tables for X-ray crystallography. Vol. IV. The Kynoch Press. Birmingham, England. 1974; (*b*) R. F. STEWART, E. R. DAVIDSON, and W. T. SIMPSON. J. Chem. Phys. **42**, 3175 (1965).
7. C. K. JOHNSON. ORTEP. Report ORNL-3794. Oak Ridge National Laboratory, Tennessee. 1965.
8. W. KLYNE and V. PRELOG. Experientia, **16**, 521 (1960).
9. V. SCHOMAKER, J. WASER, R. MARSH, and G. BERGMAN. Acta Crystallogr. **12**, 600 (1959).

Ambident nucleophiles. III. N-bonded vs. C-bonded adduct formation on reaction of imidazolide anions with 1,3,5-trinitrobenzene

M. P. SIMONNIN, J. C. HALLE, F. TERRIER, AND M. J. POUET

Laboratoire de Spectroscopie et de Physicochimie des Solutions, U.A. 403 du CNRS, E.N.S.C.P., 11 Rue Pierre et Marie Curie, 75231 Paris, Cedex 05, France

Received July 6, 1984

M. P. SIMONNIN, J. C. HALLE, F. TERRIER, and M. J. POUET. Can. J. Chem. **63**, 866 (1985).

Imidazolide anions of imidazole, 2- and 4-methylimidazoles, 4,5-dimethyl and 4,5-diphenylimidazoles react with 1,3,5-trinitrobenzene (TNB) in dimethylsulfoxide (DMSO) to yield, initially, N-bonded σ-adducts under kinetic control. These undergo a subsequent conversion to C-adducts, which are the thermodynamically stable products. The formation of N,C-diadducts from the reversible attack of a second TNB molecule on the imidazolide moiety of the C-adducts is also observed. Provided that the corresponding position of the parent imidazolide anion is free, the formation of C-adducts occurs preferentially at the C-4 or C-5 carbon atom. However, C-2 substitution is observed in 4,5-disubstituted derivatives. Structures and preferred conformations of some adducts and diadducts are deduced from nOe experiments. The mechanisms of the various reactions are discussed. Evidence is presented that adduct formation results in a low-field shift of methyl groups located in a position adjacent to the substitution site, while all the other protons move upfield. This unusual deshielding presumably reflects a proximity effect between a methyl group and the hydrogen atom attached to the sp^3 carbon of the adducts.

M. P. SIMONNIN, J. C. HALLE, F. TERRIER et M. J. POUET. Can. J. Chem. **63**, 866 (1985).

Dans le diméthylsulfoxyde (DMSO), le trinitro-1,3,5 benzène (TNB) réagit avec les anions imidazolate, méthyl-2 et méthyl-4 imidazolate, diméthyl-4,5 et diphényl-4,5 imidazolate pour donner initialement des complexes-σ azotés. Ces derniers disparaissent peu à peu au profit de complexes-σ carbonés qui sont les produits thermodynamiquement stables de la réaction. La formation de N,C-diadduits par attaque d'une seconde molécule de TNB sur la forme anionique des C-adduits est aussi observée. Le mécanisme des réactions est discuté. Il apparaît que les complexes carbonés résultent préférentiellement d'une attaque du TNB sur les carbones-4 ou -5 du noyau imidazole mais, dans les dérivés disubstitués-4,5 où ces positions sont occupées, la substitution électrophile se produit sur le carbone-2. Les structures et les conformations les plus favorisées des complexes ont été établies sur la base d'expériences nOe. Les études rmn montrent également, que, contrairement à ce qui se passe pour tous les autres protons, la formation des complexes entraîne un déplacement à champ faible d'un groupe méthyle adjacent au site de substitution. Ce résultat inattendu est probablement dû à un effet de proximité entre le groupe méthyle et l'hydrogène porté par le carbone sp^3 du complexe.

Imidazolide anions are known to be potential ambident nucleophiles, being able to undergo electrophilic attack by conventional electrophiles at a nitrogen or at a carbon atom (1, 2). Depending on the structures of the parent imidazoles and the experimental conditions, carbon attack may occur at C-2, C-4, or C-5.

In a recent communication (3), we have shown that unsubstituted imidazole anion $\mathbf{1}^-$ also acts as an ambifunctional nucleophile towards electron-deficient aromatics like 1,3,5-trinitrobenzene (TNB). In this case, the N-adduct **2** appears to form under kinetic control but the C-adduct **3**, which exists in the two tautomeric forms **3***a* and **3***b*, is the thermodynamically stable product. More significantly, the N,C-diadduct **4** was also observed. Inasmuch as this reaction provided the first example of the ambident reactivity of an imidazolide anion

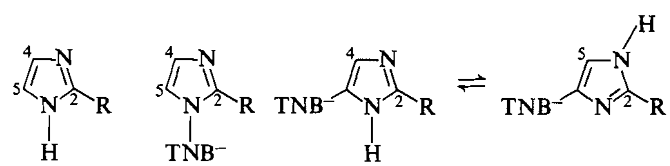

R = H, **1** 2 **3***a* **3***b*
R = Me, **6** **7** **8***a* **8***b*

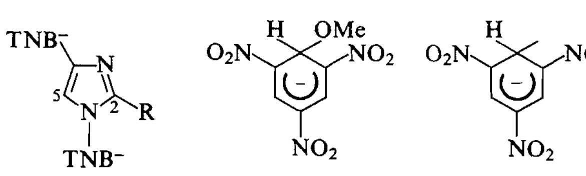

R = H, **4** **5** TNB⁻
R = Me, **9**

towards electrophilic aromatics, we thought it of interest to extend our study to differently substituted imidazolide anions. The results that we now report show that both N-1 and N-3 positions may be involved in the N-attack process when the anions are unsymmetrical. Moreover, TNB addition may take place at the three carbon positions of the imidazole ring.

Results

The reaction of TNB with imidazolide anions from 2-methyl, 4-methyl, 4,5-dimethyl, and 4,5-diphenyl imidazoles was studied in dimethylsulphoxide (DMSO) solution. The anions were generated first by adding an equimolar amount of methanolic potassium methoxide (5.54 *M*) to a solution of the parent imidazoles (0.3 *M*) in DMSO. Then, the resulting solution was added to a DMSO solution of TNB (0.3 *M*). Strong colors typical of TNB σ-adducts develop immediately. The course of the reactions was followed by ^{1}H nmr. An unambiguous distinction between N-bonded and C-bonded adducts could be made on the following grounds: (1) provided it could be observed, the presence of a broad NH signal at low field (~11 ppm) is typical of the C-adducts; (2) the observation that the AX_2 systems due to the cyclohexadienyl protons appear at higher field in the C-adducts than in the N-adducts, in agreement with electronegativity arguments and with previously reported results[1] (5–8). The cyclohexadienyl protons are noted $H_{1'}$, $H_{3'}$, $H_{5'}$ in the N-adducts and $H_{1''}$, $H_{3''}$, $H_{5''}$ in the C-adducts. In those instances where two N-bonded adducts were initially observed, nOe (nuclear Overhauser effect) experiments were carried out to determine structures. Also to be noted is the

[1] For recent reviews on Meisenheimer adducts, see ref. 4.

TABLE 1. ^{1}H nuclear magnetic resonance data of imidazole, 2-methylimidazole, and their TNB σ-adducts[a]

Compounds	δ_R	δ_{H_4}	δ_{H_5}	$\delta_{H_{1'}}$	$\delta_{H_{3'/5'}}$	$\delta_{H_{1''}}$	$\delta_{H_{3''/5''}}$	$^4J_{2-4}$	$^4J_{2-5}$	$^3J_{4-5}$	$^4J_{1'-3'/5'}$	$^4J_{1''-3''/5''}$	J
1	7.67	7.03						1.0					
2	7.61	6.78	6.89	7.07	8.53			0.9	1.3	1.2	0.8		
3*a* ⇄ **3***b*	7.38	6.82				5.77	8.31	1.2				0.5	$^5J_{1''-2} \sim 0.3$[b]
4	7.31		6.61	6.96	8.51	5.64	8.27		1.4		0.8	0.5	$^4J_{1'-2} \sim 0.4$[b]
6	2.28	6.85											$^5J_{1''-2} \sim 0.3$[b]
7	2.58	6.56	6.64	6.97	8.53_4					1.5	0.6_5		$^4J_{1'-5} = 0.4$
8*a* ⇄ **8***b*	2.15	6.65				5.69	8.31					0.4_5	
9	2.43		6.25	6.87	8.53	5.55	8.28				0.6	0.5	

[a]Chemical shifts in ppm relative to TMS as internal standard, J in Hertz, solvent DMSO-d_6.
[b]Unresolved coupling constants determined by double resonance experiments, see ref. 19.

TABLE 2. ^{1}H nuclear magnetic resonance data of 4(5)-methylimidazole and its TNB σ-adducts[a]

Compounds	δ_{NH}	δ_{H_2}	$\delta_{H_{5(4)}}$	δ_{Me}	$\delta_{H_{1'}}$	$\delta_{H_{3'/5'}}$	$\delta_{H_{1''}}$	$\delta_{H_{3''/5''}}$	$^4J_{1'-3'/5'}$	$^4J_{1''-3''/5''}$	$J_{2-5(4)}$	$J_{Me-5(4)}$	J
10	9.08	7.50	6.70	2.13							1.1	0.9	
11		7.51	6.56	2.00	6.97	8.53_4			0.7_5		1.4	0.9	
12		7.23	6.51	2.35	6.90	8.55			0.7		1.2	0.9	
13*a* ⇄ **13***b*	11.6	7.28		2.25			5.64	8.33		0.3_5			$J_{1''-2} = 0.3$
14		6.95		2.48	6.83	8.50	5.56	8.28	0.6	0.4			

[a]Chemical shifts in ppm relative to TMS as internal standard, J in Hertz, solvent DMSO-d_6.

initial presence of some amounts of unreacted imidazoles and of the TNB-methoxide adduct **5** in all experiments; the reasons for this formation will be discussed in the forthcoming section.

2-Methylimidazole 6

In a general way, the reactivity of 2-methylimidazolide anion $\mathbf{6}^-$ towards TNB resembles that of unsubstituted imidazolide anion $\mathbf{1}^-$ (3). Nuclear magnetic resonance (nmr) spectra showed the initial formation of the N-adduct **7**. With time, **7** disappeared while two new species, which may be identified as the C-adduct **8** and the N,C-diadduct **9**, appeared. After a few weeks, **8** was the only species which existed in the solution. Table 1 allows the comparison of nmr data for the adducts from **1** and **6**. Peculiar features of interest are the following. While the three imidazolic protons of the N-adduct **2** give an AMX system which provides an unambiguous assignment of these protons, the two imidazolic protons of **7** give an AB system. In this case, the existence of a long-range coupling $J_{H_AH_{1'}} = 0.4$ Hz allows us to assign the low-field signal (H_A) to H_5. Accordingly, H_5 is deshielded relative to H_4 in both N-adducts **2** and **7**.

The observation of a broad signal at δ = 6.65 ppm for the imidazolic proton $H_{4(5)}$ of the C-adduct **8** indicates the existence of a tautomeric exchange **8***a* ⇄ **8***b* which prevents the detection of the NH signal. A similar tautomery was observed between **3***a* and **3***b* (3).

The structure of the diadduct **9** was assigned by analogy with the results for **4** (3). In this latter case, the observed coupling constant of 1.4 Hz was only consistent with a $^4J_{25}$ coupling, and therefore with structure **4**. Note that steric reasons are also expected to favor **4** or **9** rather than diadduct structures with two vicinal TNB^- moieties.

The nOe experiments were performed on the N-adduct **7**, the C-adduct **8**, and the N,C-diadduct **9**. Irradiation of the methyl signal of **7** resulted in a 15% enhancement of the integrated intensity of $H_{1'}$. In contrast, no nOe enhancement was detected between $H_{1'}$ and H_5. On the other hand, irradiation of the $H_{1''}$ signal of the C-adduct **8** resulted in a 17% enhancement of the integrated intensity of the imidazolic proton of **8**. Similarly, a 20% enhancement of H_5 of the N,C-diadduct **9** was observed when irradiating the $H_{1''}$ signal of **9**. The implications of these results in terms of preferred conformations of these adducts are discussed in the subsequent section (see Scheme 2).

4(5)-Methylimidazole 10

Due to its dissymmetrical structure, 4-methylimidazolide anion $\mathbf{10}^-$ may attack TNB via either of the nitrogen atoms N-1 or N-3. Indeed, the two N-adducts **11** and **12** were initially observed, though in quite different proportions, i.e. ~80:20. The spectra showed the presence of two very close AX_2 systems and two sets of two imidazolic protons and of methyl signals, with distinct chemical shifts (Table 2). These were assigned by nOe experiments, which indicated that the major species is **11** and the minor one **12**. In the case of **11**, irradiation of the $H_{1'}$ signal enhanced the integrated intensity of the H_2 signal by 20%. On the other hand, irradiation of the methyl signal of **12** enhanced the integrated intensity of the $H_{1'}$ signal by 17% (see Scheme 2).

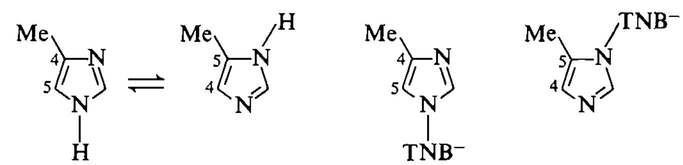

10*a* **10***b* **11** **12**

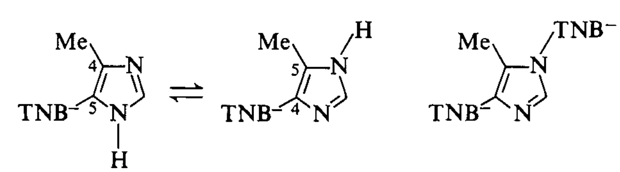

13*a* **13***b* **14**

Conversion of **11** and **12** into the C-adducts **13** was nearly complete in several days. The spectrum of **13** showed the presence of only one imidazolic proton at δ = 7.28 ppm and a broad NH signal at 11.6 ppm. A broad signal was also observed

TABLE 3. ^1H nuclear magnetic resonance data of 4,5-dimethyl and 4,5-diphenylimidazoles and their TNB σ-adducts[a]

Compounds	δ_{NH}	δ_{H_2}	$\delta_{Me(4)}$	$\delta_{Me(5)}$	$\delta_{H_{1'}}$	$\delta_{H_{3'/5'}}$	$\delta_{H_{1''}}$	$\delta_{H_{3''/5''}}$	$^4J_{1'-3'/5'}$	$^4J_{1''-3''/5''}$	$^5J_{Me-Me}$	J
15		7.37	2.05									
16		7.12	1.98	2.26	6.83	8.52			0.6		0.6	$^4J_{1'-2} \sim 0.3$[b] $J_{Me(4)-2} \sim 0.1_5$[b]
17*a* ⇄ **17*b***	11.0		1.95				5.64	8.32		0.3_5		
18		7.77										
20	12.48						5.88	8.44		0.2		

[a] Chemical shifts in ppm relative to TMS as internal standard, J in Hertz, solvent DMSO-d_6.
[b] Unresolved coupling constants determined by double resonance experiments; see ref. 19.

for the methyl group, suggesting the existence of a tautomeric equilibrium **13*a*** ⇄ **13*b***. An amount of the N,C-diadduct **14** was also evidenced by nmr, and its concentration was strongly increased by addition of a second equivalent of methoxide ion and of TNB. In addition to the two expected AX_2 systems, the spectrum of **14** showed only one imidazolic proton, the resonance of which gave a singlet. The structure **14** was attributed to this diadduct on steric grounds and confirmed by nOe experiments. Irradiation of the methyl signal of **14** enhanced the integrated intensities of $H_{1'}$ and $H_{1''}$ signals by 17% and 20% respectively. These effects unambiguously show that the two TNB^- moieties are not in a vicinal position, i.e. the diadduct corresponds to the tautomer **13*b*** of the C-adduct (see Scheme 2).

*4,5-Dimethyl and 4,5-diphenylimidazoles **15** and **18***

4,5-Dimethylimidazolide anion **15**$^-$ reacted with TNB to give the kinetically favored N-adduct **16**. The absence of a NH

R = Me, **15** R = Ph, **18**   **16** **19*** *Not observed

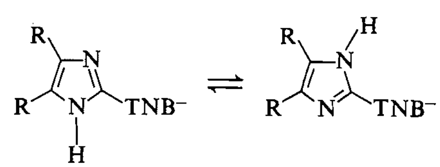

17*a* **20*a***   **17*b*** **20*b***

signal, the observation of a low-field imidazolic proton H-2, and the presence of two distinct methyl resonances with equal intensities are features typical of the dissymmetrical structure **16** (Table 3). With time, **16** disappeared and the C-adduct **17**, which has no imidazolic proton but a low-field NH signal, was formed. The observation of a single signal for the two methyl groups implies the existence of a rapid tautomeric exchange **17*a*** ⇄ **17*b***.

In contrast with its 4,5-dimethyl analog, 4,5-diphenylimidazolide anion **18**$^-$ does not form a N-adduct, i.e. **19**, on reaction with TNB. Only the formation of **5** with the concomitant recovery of the parent imidazole **18** was initially observed. Then, the nmr spectra showed the progressive formation of the C-adduct **20**, which was characterized by its cyclohexadienylic AX_2 system, a low-field NH signal at 11.5 ppm, and the absence of the H-2 imidazolic proton.

To be noted is that no N,C-diadduct formation could be detected, even under forcing conditions, i.e. with excess of methoxide ion and TNB, in these two 4,5-disubstituted imidazolic systems. Such adducts, which would necessarily have two vicinal cyclohexadienyl moieties, are expected to be disfavored on steric grounds. This conclusion is supported by the structure **14**, unambiguously established for the N,C-diadduct of 4(5)-methylimidazole (*vide supra*).

Discussion

Mechanism of adduct formation

pK_a measurements of various imidazoles have shown that these derivatives are relatively acidic in H_2O–DMSO mixtures rich in DMSO and may be completely ionized by hydroxide ion in these media (9).[2] For instance, imidazole, 2-methylimidazole, and 4,5-diphenylimidazole have pK_a values of 17.15, 18.08, and 15.55, respectively, at 20°C in 5% H_2O – 95% DMSO (v/v), which are much lower than the ionic product of this mixture (pK_s = 24) (ref. 10). A similar situation prevails in H_2O–DMSO mixtures with >95% DMSO, as well as in methoxide solutions in DMSO–MeOH mixtures. On this ground, the most reasonable mechanism describing the interaction between TNB and the various imidazole anions is depicted in Scheme 1, which refers to the 4(5)-methylimidazole – TNB system.

Since the π-electron system of the imidazole ring is not interrupted by bond making at a nitrogen atom while it is at a carbon atom, the reaction of TNB with all imidazolide anions except **18**$^-$ results in the initial and reversible formation of the N-adducts, e.g. **11** and **12**, under kinetic control. Although the equilibrium concentration of MeO^- ions is small, the reversible formation of the methoxide complex **5** competes with that of the N-adducts, as a result of the well-known highly favored kinetic and thermodynamic factors associated with the formation of **5** from TNB and MeO^- (4*c*, 11). This latter adduct is the only one initially formed in the 4,5-diphenylimidazolide anion – TNB system. In this case, the nonobservation of the N-adduct **19** may be accounted for in terms of severe steric compression.

The formation of the C-adduct occurs in an essentially irreversible two-step sequence. The first step is the reversible formation of an imidazolenine intermediate, e.g. **13**, H, which subsequently rearranges to give the thermodynamically stable C-adduct, e.g. **13**. The non-observation of the imidazolenine intermediates suggest that they are not stable and that their rearomatization into the C-adducts is very fast. Indeed, this behavior is similar to that encountered in the case of the formation of the C-adducts of TNB and pyrroles or indoles (6). As previously discussed, on the basis of the absence of reaction between TNB and N-methylimidazole under the same basic

[2] Also, J. C. Halle and F. Terrier, unpublished results.

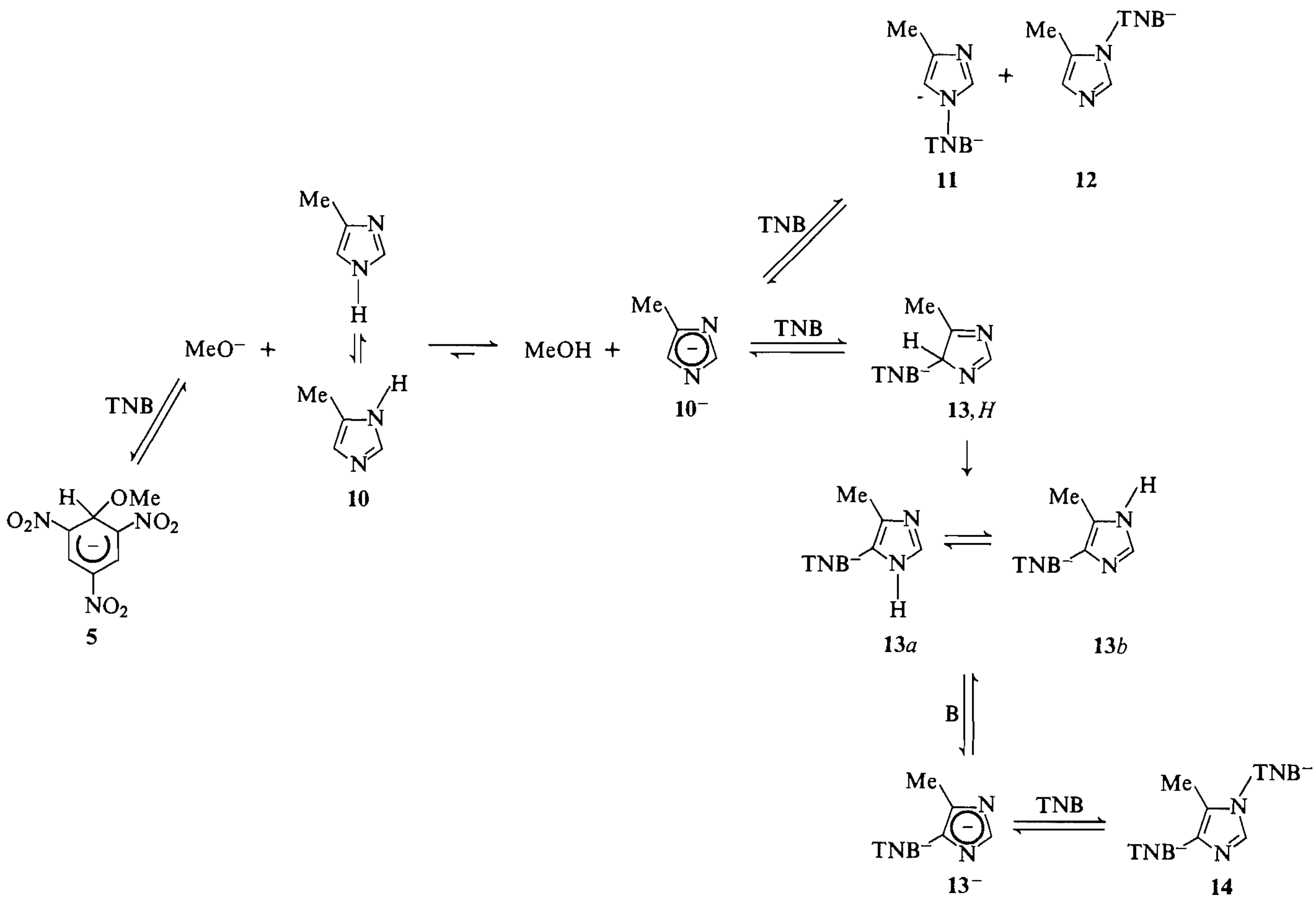

SCHEME 1

conditions as those used in this work (3), C-adduct formation from direct attack of carbanionic species of imidazoles may be safely excluded (12).

The negatively charged trinitrocyclohexadienate moiety is known to exhibit an appreciable acidifying effect (13–16). As a result, the NH group of the C-adducts is more acidic than that of the parent imidazoles and is deprotonated to some extent either by the equilibrium concentration of methoxide ions or by the imidazolide ions. Then, the resulting anions, e.g. **13⁻**, can attack free TNB, accounting for the reversible formation, under kinetic control, of the observed N,C-diadducts, e.g. **14**. As long as the experiments were performed in a 1 : 1 stoichiometry (1 equiv. Im^-/1 equiv. TNB), we observed that these N,C-diadducts ultimately disappear to give only the C-adducts. Clearly, the latter are thermodynamically more stable than the former. However, the N,C-diadducts could be regenerated by adding an equimolar mixture of MeO^- and TNB to the solutions of the C-adducts.

Although they are not thermodynamically stable products, the N-adducts may be isolated as crystalline potassium salts, provided that the experiments be done in acetonitrile instead of DMSO. Addition of ether precipitates red crystals, which rapidly turn to a gummy dark material if no care is taken to avoid contact with ambient moisture. Dissolution of these crystals in DMSO gives spectra similar to those observed from the *in situ* generation of the N-adducts. Similarly, we succeeded in precipitating the C-adducts by ether from the DMSO solution, when the isomerization of the N-adducts was essentially complete (see experimental section).

Preferred conformation of the adducts

Scheme 2 summarizes the results of the nOe experiments performed on various adducts. These suggest that the N- and C-adducts assume peculiar preferred conformations around their N—$C_{1'}$ or C—$C_{1''}$ bonds. In the case of the N-adduct **7** of 2-methylimidazole, the important effect between the 2-methyl group and $H_{1'}$ indicates a preferred conformation where $H_{1'}$ is spatially close to the methyl group, ie. where the TNB^- moiety is far removed from this group. In the corresponding C-adduct **8** and N,C-diadduct **9**, the nOe enhancements observed between $H_{1''}$ and H_5 suggest that, in their favored conformation, the C-TNB^- moiety lies in the vicinity of N-3. On the other hand, the N-TNB^- moiety of **9** presumably keeps the same orientation as in **7**.

However, the most interesting conformational results relate to the adducts of 4(5)-methylimidazole. Thus the nOe results show that the preferred conformation of the major N-adduct **11** is similar to that of **7**, despite the absence of a vicinal methyl group. In contrast, the $H_{1'}$ proton of the TNB^- moiety of the minor N-adduct **12** lies in the vicinity of the methyl group. Consequently, the H_2 proton of **12** is located in the proximity of the cyclohexadienate ring. A similar situation prevails in the favored conformation of the N,C-diadduct **14** where there is a proximal relationship between the 5-methyl group and each of the $H_{1'}$ and $H_{1''}$ protons.

The above results point out that the presence of a methyl substituent tends to favor a conformation where it is far away from the TNB^- moiety(ies). Such a situation was probably to be expected on the basis of steric grounds.

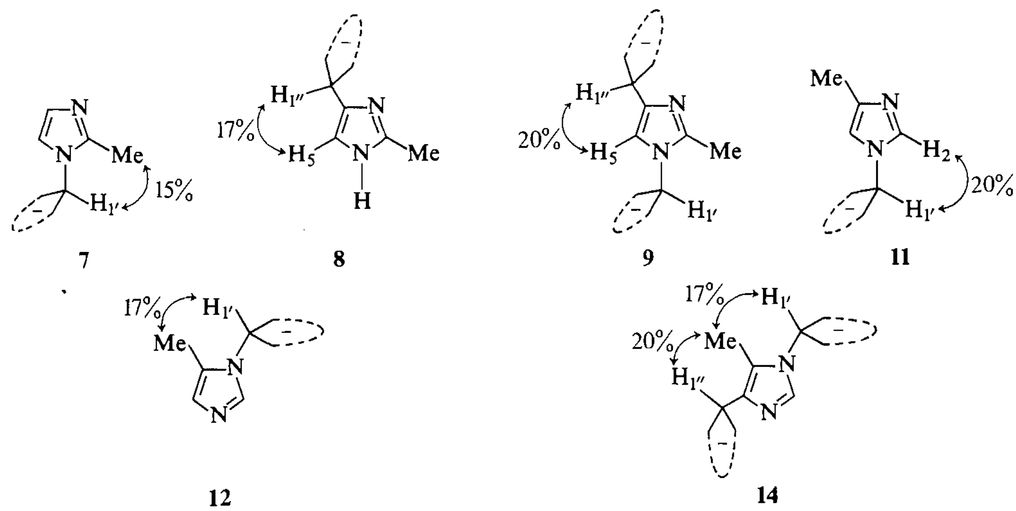

SCHEME 2

Proton chemical shifts

The imidazolic protons are more shielded in the N- and C-monoadducts than in the parent imidazoles. A further shielding occurs on formation of the N,C-diadducts. Similar trends are observed for the methyl groups when they are not attached at a carbon adjacent to the site of nucleophilic attack. In contrast, the methyl groups which are vicinal to a C-TNB^- or N-TNB^- moiety are deshielded relative to the parent imidazole. Moreover, in the N,C-diadduct **14**, where the methyl group is adjacent to both a N-TNB^- and a C-TNB^- moiety, an additional deshielding is observed relative to the N-adduct **12** or to the C-adduct **13**, suggesting that the effect is somewhat cumulative. Significantly, the deshielded methyl groups are those which are involved in a nOe enhancement, and consequently are spatially located close to the $H_{1'}$ or $H_{1''}$ protons bonded to the sp^3 carbons of the TNB^- moieties. This observation tends to indicate that the low-field shifts observed are related to a proximity effect (17, 18).[3] It is on this ground that we have attributed the two methyl resonances of the N-adduct **16** of 4,5-dimethylimidazole.

Experimental

Nuclear magnetic resonance spectra

The ^1H nmr spectra were recorded at 100 MHz (Varian XL 100) in the CW mode, using TMS as an internal standard. The nOe experiments were performed immediately after degassing the DMSO solutions by bubbling argon for 5 min.

Isolable adducts

Potassium salts of the C-adducts **3** and **13** of imidazole and 4-methylimidazole were precipitated from the DMSO solutions by addition of anhydrous diethyl ether (Et_2O). The purple crystals which formed were filtered, ground to a fine powder under an argon atmosphere, washed with copious amounts of anhydrous ether, and dried *in vacuo* to eliminate any associated solvent. The two adducts do not melt but decompose between 180 and 200°C. The ^1H nmr spectra of the isolated salts in DMSO-d_6 are similar to those observed in the *in situ* generation of **3** and **13**.

Anal. calcd. for the potassium salt of **3**, $C_9H_6N_5O_5K$: C 33.85, H 1.89, N 21.94; found: C 34.29, H 2.16, N 21.71.

Anal. calcd. for the potassium salt of **13**, $C_{10}H_8N_5O_6K$: C 36.03, H 2.42, N 21.01; found: C 36.39, H 2.81, N 20.73.

1. (*a*) M. R. GRIMMETT. Adv. Heterocycl. Chem. **27**, 288 (1980); (*b*) *In* Comprehensive organic chemistry. Vol. 4, *Edited by* Sir D. Barton, W. D. Ollis, and P. G. Sammes. Pergamon Press, Oxford. 1979. p. 370.
2. A. F. POZHARSKII, A. D. GARNOVSKII, and A. M. SIMONOV. Russ. Chem. Rev. **35**, 122 (1966).
3. F. TERRIER, F. DEBLEDS, J. C. HALLE, and M. P. SIMONNIN. Tetrahedron Lett. **23**, 4079 (1982).
4. (*a*) M. J. STRAUSS. Chem. Rev. **70**, 667 (1970); (*b*) S. SEKIGUCHI. Yuki Gosei Kagaku Kyokai Shi, **36**, 633 (1978); (*c*) F. TERRIER. Chem. Rev. **82**, 77 (1982); (*d*) E. BUNCEL. *In* The chemistry of amino, nitro- and nitroso compounds. Supplement F. *Edited by* S. Patai. Wiley, London. 1982. p. 1925; (*e*) G. A. ARTAMKINA, M. P. EGOROV, and I. P. BELETSKAYA. Chem. Rev. **82**, 427 (1982).
5. E. BUNCEL, M. R. CRAMPTON, M. J. STRAUSS, and F. TERRIER. *In* Electron-deficient aromatic- and heteroaromatic-base interactions. Elsevier, Amsterdam, Holland. 1984. Chapt. 2.
6. (*a*) J. C. HALLE, F. TERRIER, M. J. POUET, and M. P. SIMONNIN. J. Chem. Res. (S), 360 (1980); (*b*) J. C. HALLE, M. J. POUET, M. P. SIMONNIN, F. DEBLEDS, and F. TERRIER. Can. J. Chem. **60**, 1988 (1982).
7. M. J. STRAUSS, R. A. RENFROW, and E. BUNCEL. J. Am. Chem. Soc. **105**, 2473 (1983).
8. (*a*) R. J. SPEAR, W. P. NORRIS, and R. W. READ. Tetrahedron Lett. **24**, 1555 (1983); (*b*) W. P. NORRIS, R. J. SPEAR, and R. W. READ. Aust. J. Chem. **36**, 297 (1983).
9. C. F. BERNASCONI and F. TERRIER. J. Am. Chem. Soc. **97**, 7458 (1975).
10. J. C. HALLE, R. GABORIAUD, and R. SCHAAL. Bull. Soc. Chim. Fr. 1851 (1969).
11. C. F. BERNASCONI. J. Am. Chem. Soc. **92**, 4682 (1970).
12. (*a*) Y. TAKEUCHI, H. J. C. YEH, K. L. KIRK, and L. A. COHEN. J. Org. Chem. **43**, 3565 (1978); (*b*) Y. TAKEUCHI, K. L. KIRK, and L. A. COHEN. J. Org. Chem. **43**, 3570 (1978).
13. P. CAVENG, P. B. FISHER, E. HEILBRONNER, A. L. MILLER, and H. ZOLLINGER. Helv. Chim. Acta, **50**, 848 (1967).
14. M. R. CRAMPTON. J. Chem. Soc. B, 2112 (1971).
15. E. BUNCEL and J. G. K. WEBB. Can. J. Chem. **52**, 630 (1974).
16. C. F. BERNASCONI, M. C. MULLER, and P. SCHMID. J. Org. Chem. **44**, 3189 (1979).
17. T. W. MARSHALL and J. A. POPLE. Mol. Phys. **3**, 339 (1960).
18. C. G. CARDINAS. Tetrahedron Lett. 4013 (1969).
19. D. J. SARDELLA. J. Magn. Reson. **10**, 188 (1973)..

[3] A referee has suggested that another possible interpretation of this deshielding might be in terms of polarization of the methyl group (C-Me^+) by the adjacent and oppositively oriented dipole.

1,*n*-Radical ions. Photosensitized (electron transfer) and electrochemical oxidation of 1,1,2,2-tetraphenylcyclopropane[1]

DANIAL D. M. WAYNER AND DONALD R. ARNOLD[2]
Department of Chemistry, Dalhousie University, Halifax, N.S., Canada B3H 4J3

Received June 28, 1984

DANIAL D. M. WAYNER, and DONALD R. ARNOLD. Can. J. Chem. **63**, 871 (1985).

The photosensitized (electron transfer) and the electrochemical oxidation of 1,1,2,2-tetraphenylcyclopropane (**1**) have been studied. The products obtained from the photosensitized (electron transfer) study are 1,1,3,3-tetraphenylpropene (**2**), 1,3,3-triphenylindene (**3**), tetraphenylallene (**4**), and 3-methoxy-1,1,3,3-tetraphenylpropene (**8**). The product ratios are dramatically dependent upon the reaction conditions, particularly sensitizer (aromatic nitriles, tetracyanoethylene, chloranil, and 2,3-dichloro-5,6-dicyanobenzoquinone were used), and solvent. The variations in product ratios are attributed to variations in the redox behaviour of the sensitizer radical anion and upon the basicity and nucleophilicity of the medium. The products in the electrochemical study are **3**, **4**, and **8**. Common intermediates have been identified and a mechanism for the formation of products is proposed.

DANIAL D. M. WAYNER et DONALD R. ARNOLD. Can. J. Chem. **63**, 871 (1985).

On a étudié les oxydations photosensibilisées (transferts d'électrons) et électrochimiques du tétraphényl-1,1,2,2 cyclopropane (**1**). Les produits formés lors de l'étude photosensibilisée (transferts d'électrons) sont: le tétraphényl-1,1,3,3 propène (**2**), le triphényl-1,3,3 indène (**3**), le tétraphénylallène (**4**) et le méthoxy-3 tétraphényl-1,1,3,3 propène (**8**). Les rapports des produits formés varient d'une façon dramatique avec les conditions de la réaction et, en particulier, avec la nature du sensibilisateur (on a utilisé des nitriles aromatiques, le tétracyanoéthylène, le chloranil et la dichloro-2,3 dicyano-5,6 benzoquinone) ainsi qu'avec la nature du solvant. On attribue les variations observées dans les rapports des produits aux variations dans le comportement rédox de l'anion radicalaire du sensibilisateur et à la basicité ainsi qu'au caractère plus ou moins nucléophile du milieu. Lors des études électrochimiques, il y a formation de **3**, de **4** et de **8**. On a identifié la nature des intermédiaires communs et on propose un mécanisme pour la formation des produits.

[Traduit par le journal]

Introduction

The generation of radical ions in solution by photosensitization (electron transfer) is now recognized as a general reaction (3). There is intense research activity in this area, especially for the study of the formation and subsequent reactions of the radical cations (3). It is already apparent, however, that the observed reactions may not reflect the intrinsic reactivity of the radical cation: the nature of the acceptor radical anion often plays an important role, even in highly polar solvents where radical ion pair separation should be a fast process. Two recently reported examples, which involve initial formation of 1,3-radical cations, will illustrate this point.

The ultimate reaction of the 1,2-diphenylcyclopropane radical cation – sensitizer radical anion pair depends upon the sensitizer. When 1,4-dicyanonaphthalene is used as the electron accepting sensitizer, *cis–trans* isomerization of the 1,2-diphenylcyclopropane is observed (4). The proposed mechanism for this reaction, based upon a study involving photochemically induced dynamic nuclear polarization (CIDNP), indicates that back electron transfer from the sensitizer radical anion to the radical cation gives the 1,2-diphenylcyclopropane triplet (the trimethylene) which subsequently isomerizes. The energy of the donor–acceptor radical ion pair is greater than that of the triplet energy of 1,2-diphenylcyclopropane. On the other hand, when chloranil is used as the electron acceptor, no *cis–trans* isomerization occurs; CIDNP studies indicate the 1,2-diphenylcyclopropane radical cation is formed as before, but in this case back electron transfer yields only the sensitizer triplet, which is of lower energy than that of the 1,2-diphenylcyclopropane (4*b*). Apparently, *cis–trans* isomerization of the 1,2-diphenylcyclopropane radical cation is slow enough that it cannot compete with the back electron transfer process (5). In this case the critical factors which influence the reaction are the triplet energy of the radical ion pair and the triplet energy of the sensitizer relative to the triplet energy of the trimethylene.

In a closely related reaction, photosensitization (electron transfer) of phenylcyclopropane in methanol, using 1,4-dicyanobenzene as the acceptor, gives an almost equal mixture of the anti-Markownikoff addition product, methyl-3-phenylpropylether, and the photosubstitution product, 3-methoxy-1-(4-cyanophenyl)-1-phenyl propane (6). When 1,1-diphenylcyclopropane is subjected to these conditions, none of the analogous photosubstitution product is obtained; methyl-3,3-diphenylpropylether is formed in almost quantitative yield.

In both cases, the initial reaction of the radical cation is to add methanol to form the benzylic- or diphenylmethyl-type radical intermediate. In the case of phenylcyclopropane, coupling between the benzylic-type radical and the dicyanobenzene radical anion competes with the back electron transfer; i.e., reduction of the radical. With 1,1-diphenylcyclopropane, coupling between the diphenylmethyl-type radical and the dicyanobenzene radical anion cannot compete with reduction of the radical. The difference in reactivity is attributed to the differences in reduction potential of the intermediate radicals. The diphenylmethyl-type radical is considerably easier to reduce than the benzyl-type radical. While the reduction potential of this benzylic radical is not known, it will certainly be greater than that of the benzyl radical (−1.43 V vs. saturated calomel electrode (SCE), HMPA–THF, ref. 7) and may, in fact, be comparable to that of 1,4-dicyanobenzene (−1.6 V vs. SCE, acetonitrile, ref. 3). It therefore seems likely that the benzylic-type radical and anion will be in equilibrium with the dicyanobenzene radical anion and dicyanobenzene, while in the diphenylmethyl analogue ($E_{1/2}$ = −1.16 V vs. SCE, HMPA–THF, ref. 7) the equilibrium will be largely in favor of the anion. So, in this case, it is the reduction potential of the

[1]Portions of this work have been reported in preliminary communications (1, 2).
[2]Author to whom correspondence should be addressed.

sensitizer that ultimately determines the reactivity of the radical cation – radical anion pair.[3] A similar competition between addition of methanol and photosubstitution has been observed for olefin radical cations (8).

Another important characteristic of the sensitizer radical anion that can influence the fate of the radical cation is basicity; the radical cation may deprotonate, with the radical anion serving as base. The observed reaction will then depend upon the reactivity of the radical pair. The electron transfer process greatly increases the acidity of the donor (9) and the basicity of the acceptor, so proton transfer should frequently be favourable. Apparently, proton transfer is not always rapid enough to compete with other reactions or this process would be much more common.

Our awareness of the importance of these considerations originally developed from observations of the reactivity of 1,1,2,2-tetraphenylcyclopropane (**1**) radical cation that were apparently inconsistent. We have reported that the photosensitized (electron transfer) reaction of **1** in acetonitrile solution, using 1,4-dicyanonaphthalene as the electron accepting sensitizer, gave 1,1,3,3-tetraphenylpropene (**2**) in good yield (reaction [1] and ref. 1). In contrast, when tetracyanoethylene was used as the acceptor, 1,3,3-triphenylindene (**3**) was the only product (reaction [2]) (ref. 1). The mechanistic scheme we proposed for these reactions involved the 1,3-radical cation as a common intermediate which partitioned between two reaction pathways. Indene formation was thought to involve the 1,1,3,3-tetraphenylpropenyl cation. Yet it was known that this cation, generated by treatment of the alcohol precursor with acid, gave good yields of tetraphenylallene (**4**) (Reaction [3]) (ref. 10), and, the allene was not detected in either of these photosensitized reactions.

[1] 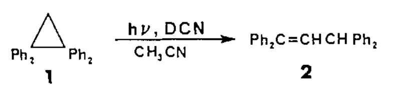

[2] 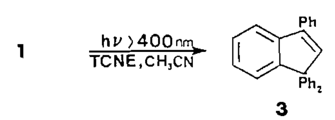

[3] 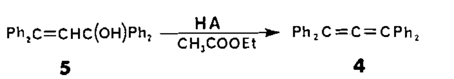

[4] 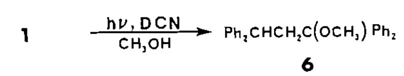

[5] 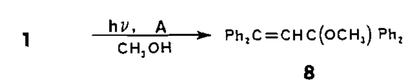

A further complication was obvious from the work of Rao and Hixson which was reported about the same time as our results (6). As mentioned previously, 1,1-diphenylcyclopropane gives the methanol addition product upon irradiation in methanol with 1,4-dicyanobenzene as the electron acceptor. Similar irradiation of 1,1,2,2-tetraphenylcyclopropane gave good yields of the 1,1,3,3-tetraphenylpropene (**2**); no 1-methoxy-1,1,3,3-tetraphenylpropane (**6**) was detected (reaction [4]) (ref. 6). If the 1,1,3,3-tetraphenylpropenyl cation were involved in this reaction, 3-methoxy-1,1,3,3-tetraphenylpropene (**8**) should have been formed (reaction [5]).

These results were particularly surprising, not only because the 1-methoxy-1,1,3,3-tetraphenylpropane was not formed, but also because the 1,1,3,3-tetraphenylpropene was apparently stable under these conditions. We have shown that 1,1-diphenylethylene and other phenyl alkenes yield the product from the anti-Markownikoff addition of alcohol under these conditions (11), and, by analogy, 1,1,3,3-tetraphenylpropene should give 2-methoxy-1,1,3,3-tetraphenylpropane (**7**). However, this product also was not observed.

This plethora of possible products, six in all (**2–4**, **6–8**), from one relatively simple starting material, in fact, may not be unusual for reactions of this type. We were intrigued by the possibility that we could understand this complex behavior to the point where we could direct the reaction toward a specific product through seemingly minor variation in reaction conditions. Such an understanding is essential to the development of synthetically useful reactions in this area in general.

TABLE 1. Calculated free-energy change for electron transfer from **1**[a]

Acceptor	E_{00} (kcal mol^{-1})	E_{red} (V vs. SCE)	ΔG_{ET}[b] (kcal mol^{-1})
1,4-Dicyanobenzene (DCB)	98.6[c]	−1.60	−31.7
1,4-Dicyanonaphthalene (DCN)	79.6[c]	−1.28	−17.6
9,10-Dicyanoanthracene (DCA)	66.6[c]	−0.89	−14.6
Methyl-4-cyanobenzoate (MCB)	74.5[c]	−1.77	−23.7
Tetracyanoethylene (TCNE)	[d]	−0.24	−15.5
Chloranil (TCQ)	[d]	0.02	−20.5
2,3-Dichloro-5,6-dicyanobenzoquinone (DDQ)	[d]	0.51	−31.8

[a]The oxidation potential of **1** is 1.36 V (E_p) in acetonitrile (1, 2).
[b]Calculated using the Weller equation (12) using $e^2/\epsilon\alpha$ = 0.06 eV.
[c]Reference 3.
[d]In these cases formation of a charge-transfer complex was indicated by a new adsorption band at long wavelength. The energy at the onset of the long wavelength charge-transfer absorption band is approximately 50 kcal mol^{-1}.

Results

*Photosensitized (electron transfer) irradiation of **1***

The pertinent characteristics of the electron accepting sensitizers used in this study are listed in Table 1. The reduction potentials were determined by cyclic voltammetry and, since analysis of the waves indicates the electrode processes are reversible, these values are thermodynamically significant. The anodic oxidation of **1**, however, is not reversible, so there is some uncertainty in the oxidation potential (2). The free energies for the electron transfer were calculated using the Weller equation (eq. [6]) (ref. 12).

$$[6] \quad \Delta G^0_{ET} = 23.06\,(E_{ox}(\text{donor}) - E_{red}\,(\text{acceptor}) - e^2/\epsilon\alpha) - E_{00}$$

The results of the irradiations are summarized in Table 2. Sensitizers 1,4-dicyanobenzene (DCB), 1,4-dicyanonaphthalene (DCN), 9,10-dicyanoanthracene (DCA), and methyl-4-

[3]Steric factors may also influence this reaction; it would be more difficult for the more hindered diphenylmethyl-type radical to couple with the dicyanobenzene radical anion.

TABLE 2. Photosensitized (electron transfer) irradiation of **1**

Acceptor	Product(s)	Yield (%)
DCB[a,b]	**2**	
DCN[a,b]	**2**	65–75
DCA[a]	**2**	
MCB[a]	**2**	
TCNE[a]	**3**(19):**4**(1)	71[c]
TCQ[a]	**3**(1):**4**(9)	75[c]
DDQ[a]	**3**(1):**4**(3.5)	47[c]
TCQ[b]	**8**	87[d]

[a]In acetonitrile.
[b]In acetonitrile–methanol (3:1, v/v).
[c]Combined yield of **3** and **4**.
[d]Combined yield of **4** and **5**, the decomposition products of **8** on a silica gel column.

TABLE 3. Controlled potential electrolysis of **1**

Solvent[a]	Conversion (%)	Current yield (%)[b]	Product(s)[c]	Yield (%)
CH_3CN	50	95	**3**	90
CH_3CN/0.1 *M* 2,6-lutidine	25	70	**3**	2
			4	55
CH_3CN/CH_3OH (3:1 v/v)	75	70	**8**	82

[a]0.1 *M* TEAP.
[b]Based on recovered starting material.
[c]These are the only products detected by hplc at 5% conversion.

cyanobenzoate (MCB) all lead to formation of 1,1,3,3-tetraphenylpropene (**2**) in acetonitrile solution (reaction [1]).

Rao and Hixson (6) have reported that **2** also was formed from **1** upon irradiation in methanol solution. We have confirmed this observation; when the irradiation is carried out in acetonitrile–methanol (3:1, v/v) only **2** is produced. No product resulting from the addition of methanol (neither **7** nor **8**) was detected. When this irradiation is carried out in acetonitrile – methanol – O-*d*, the product (**2**) has deuterium (>95%) incorporated at the allylic position. Extended irradiation of **2** under these conditions does *not* cause incorporation of deuterium nor methanol addition (7).

Using tetracyanoethylene (TCNE) as the acceptor, irradiation, in acetonitrile, of the charge-transfer band leads to the formation of 1,3,3-triphenylindene (**3**) (1). Careful analysis of this reaction mixture by high pressure liquid chromatography (hplc) indicates the presence of a trace of tetraphenylallene (**4**) (the ratio of indene (**3**) to allene (**4**) is 19:1) which was not detected in the previous work. Similar irradiation of this mixture, but with tetraethylammonium perchlorate (TEAP, 0.1 *M*) added, gives the same products in the same ratio.

On the other hand, with chloranil (TCQ) as the electron acceptor, irradiation of the charge-transfer complex in acetonitrile leads to the formation of tetraphenylallene (**4**) as the major product. Analysis of the reaction mixture by hplc indicates the ratio of **3** to **4** is 1:9 with this sensitizer. This ratio also does not change when the irradiation is carried out in acetonitrile containing 0.1 *M* TEAP. When this irradiation was carried out in acetonitrile–methanol (3:1, v/v) the product is 3-methoxy-1,1,3,3-tetraphenylpropene (**8**, reaction [5]).

When 2,3-dichloro-5,6-dicyanobenzoquinone (DDQ) is used as the electron accepting sensitizer, irradiation of the charge-transfer band, in acetonitrile solution, leads to the formation of substantial amounts of both **3** and **4** (1:3.5).

TABLE 4. Cyclic voltammetric data for **1**[a]

Sweep rate (V s^{-1})	E_{P1} (V)[b]	i_{P1} (μA)	E_{P2} (V)[b]	i_{P2} (μA)
0.050	1.285	30	1.504	9
0.100	1.294	40	1.540	5
0.200	1.320	53	1.564	3
0.400	1.360	72	1.575	2

[a]In acetonitrile (0.1 *M* TEAP).
[b]Versus sce.

Controlled potential electrolysis of 1

The results from the controlled potential oxidation of **1** under various conditions are summarized in Table 3. The anodic oxidation of **1** in acetonitrile (0.1 *M*, TEAP) at 1.3 V (vs. SCE) leads to the formation of 1,3,3-triphenylindene (**3**) (2); tetraphenylallene (**4**) was not detected. When the electrolysis is carried out under similar conditions, but with 2,6-lutidine (0.1 *M*) added to the anolyte, the product is predominantly **4**; only a trace (<3%) of **3** is present under these conditions. Electrolysis of **1** in acetonitrile–methanol (3:1, v/v) results in the formation of 3-methoxy-1,1,3,3-tetraphenylpropene (**8**, reaction [6]).

Electrochemical measurements of 1

Cyclic voltammetric studies were carried out in both acetonitrile (0.1 *M* TEAP), and dichloromethane (0.1 *M* tetrabutylammonium perchlorate, TBAP) (2). In acetonitrile, two irreversible anodic waves are observed at E_p = 1.36 V and E_p = 1.58 V, at a sweep rate of 400 mV s^{-1}. As the sweep rate increases from 50 mV s^{-1}, the relative height of the second wave decreases and it is not detected at sweep rates faster than 1.0 V s^{-1} (Table 4).

The cyclic voltammogram of 1,3,3-triphenylindene (**3**) reveals a sharp anodic wave ($E_p - E_p/2$ = 40 mV) at 1.58 V at a sweep rate of 400 mV s^{-1}. The cyclic voltammogram of this solution after an equimolar amount of **1** has been added does not exhibit the wave at 1.36 V. The peak current for the wave at 1.58 V, on the other hand, doubles in value for this mixture (Fig. 1).

The cathodic sweep reveals the presence of a reversible wave at $E_{1/2}$ = 0.34 V and an irreversible wave at E_p = 0.17 V. The intensity of the reversible wave decreases if the cathodic sweep is delayed.

At the onset of oxidation of **1**, the acetonitrile solution around the anode turns visibly purple. A solution of 1,1,3,3-tetraphenylpropenol (**5**) in acetonitrile (0.1 *M* TEAP) containing trifluoroacetic acid (5×10^{-3} *M*) turns the same colour. The cyclic voltammogram of this solution also reveals a reversible wave at $E_{1/2}$ = 0.34 V.

Cyclic voltammetric studies in dichloromethane (0.1 *M* TBAP) were similar to those in acetonitrile, the main difference being that while there is an anodic wave at 1.36 V, the second anodic wave at 1.58 V is not observed. There is a quasi-reversible wave at $E_{1/2}$ = 0.37 V. The onset of oxidation again is accompanied by the development of a purple colour near the surface of the electrode, as was the case in acetonitrile.

Spectroelectrochemical measurements

The anolyte turns purple as soon as the potential is applied. The visible absorption spectrum of this solution shows three broad absorption maxima (λ_{max} = 568 nm, 459 nm, 382 nm) of

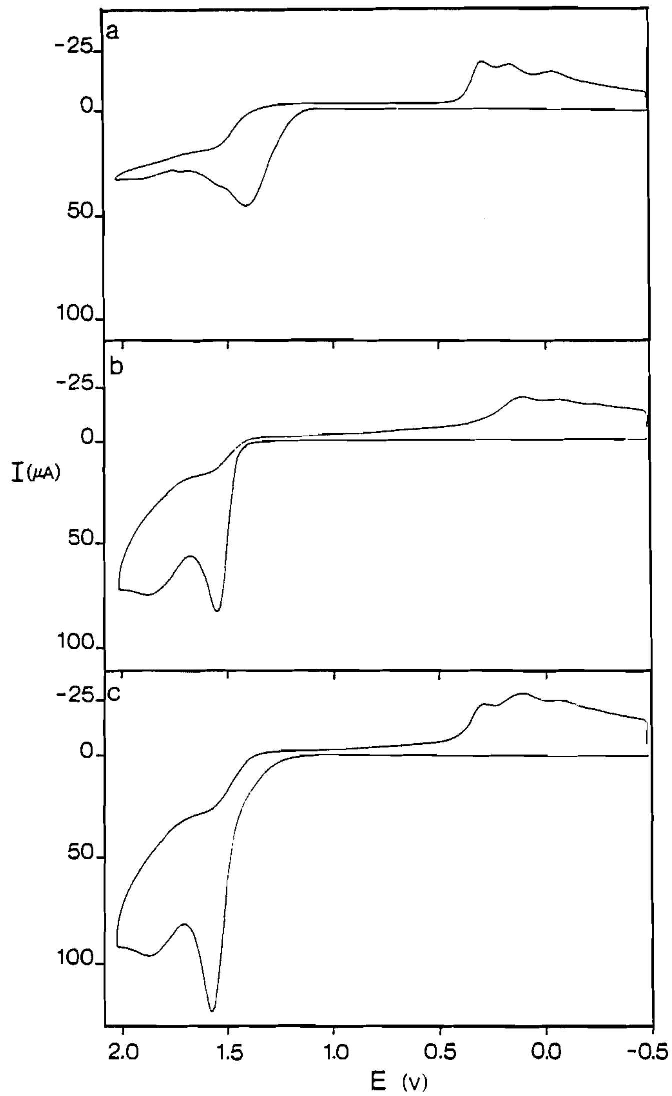

FIG. 1. Cyclic voltammograms in acetonitrile, 0.1 M TEAP at 400 mV s^{-1} of (a) **1** (1.5×10^{-3} M), (b) **3** (1.5×10^{-3} M), and (c) **1** (1.5×10^{-3} M) and **3** (1.5×10^{-3} M) illustrating that the adsorbed **3** insulates the electrode from the solution until the discharge potential of 1.58 V is reached.

approximately equal intensity. This spectrum is essentially identical to the spectrum obtained from the 1,1,3,3-tetraphenylpropenol in acetonitrile (0.1 M TEAP) to which trifluoroacetic acid has been added. The irradiation of the charge-transfer band between **1** and TCNE, TCQ, or DDQ results in the development of a coloured intermediate with a similar visible absorption spectrum, within a few seconds of irradiation. This colour slowly disappears if the vessel is removed from the irradiation source.

The rate of disappearance of the coloured intermediate can be measured using an electrolysis cell fitted with Pyrex windows (see Experimental). The rate of disappearance of the colour follows first-order kinetics with a rate constant of 2.87×10^{-2} s^{-1} at 23°C. The same rate constant is obtained whether monitoring the absorption at 460 nm or 570 nm (at 380 nm background absorption interferes with the measurement). Furthermore, the rate is independent of electrolyte concentration over the range 0.1 to 0.001 M TEAP (cell resistance precluded measurements at lower concentrations).

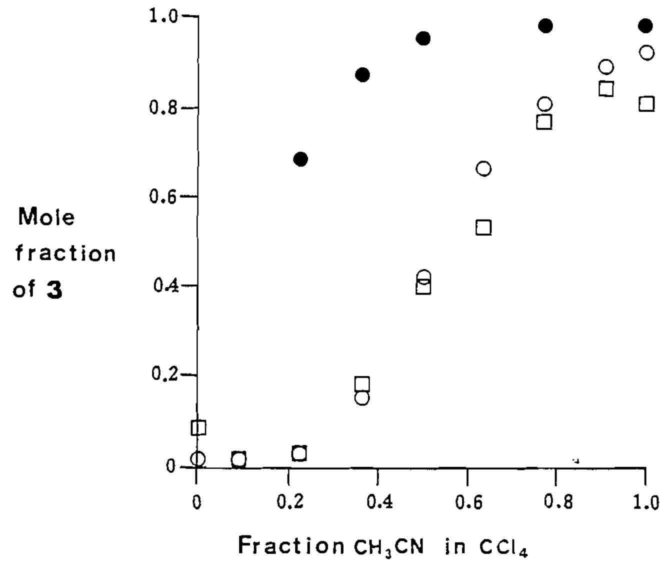

FIG. 2. Mole fraction of **3** (the remainder is **4**) versus the fraction (by volume) of acetonitrile in carbon tetrachloride from the reaction of **5** with (a) ● toluenesulphonic acid, (b) □ trifluoroacetic acid, and (c) ○ trichloroacetic acid.

TABLE 5. Effect of temperature on the rate of the unimolecular reaction of 1,1,3,3-tetraphenylpropenyl cation in acetonitrile (0.1 M TEAP)

T (°C)[a]	k_{obs} (s^{-1})
37.6	0.15±0.01
33.2	0.092±0.001
28.3	0.053±0.001
23.2	0.029±0.002
19.6	0.017±0.002
11.9	0.0063±0.0001

[a]±0.1°C.

The temperature dependence of the rate constant (Table 5) leads to an estimate of the activation energy for loss of the intermediate of 21.8±0.6 kcal mol^{-1} and a preexponential factor (log A) of 14.5 ± 0.4.

Solvent and acid effects on the ratio 3/4

The products obtained by treatment of **5** in mixtures of acetonitrile and carbon tetrachloride with an acid are **3** and **4**. These products are obtained in chemical yields greater than 90%. The ratio (**3**/**4**) decreases as the percentage of acetonitrile decreases (Fig. 2). While there appear to be no significant differences between trifluoroacetic acid and trichloroacetic acid, p-toluenesulphonic acid gives a significantly higher ratio (**3**/**4**) in all solvent mixtures.

Discussion

The products obtained upon photosensitized (electron transfer) oxidation of **1** are remarkably dependent upon reaction conditions, particularly solvent and sensitizer. Although some of these observations were reported several years ago (1, 6), the mechanism has never been discussed in detail. The sequence outlined in Scheme 1 can account for all the results.

The first two steps, initial excitation of the electron accepting sensitizer and electron transfer to give $1^{\cdot+}$ and $A^{\cdot-}$, are well established. All of the irradiations were carried out through

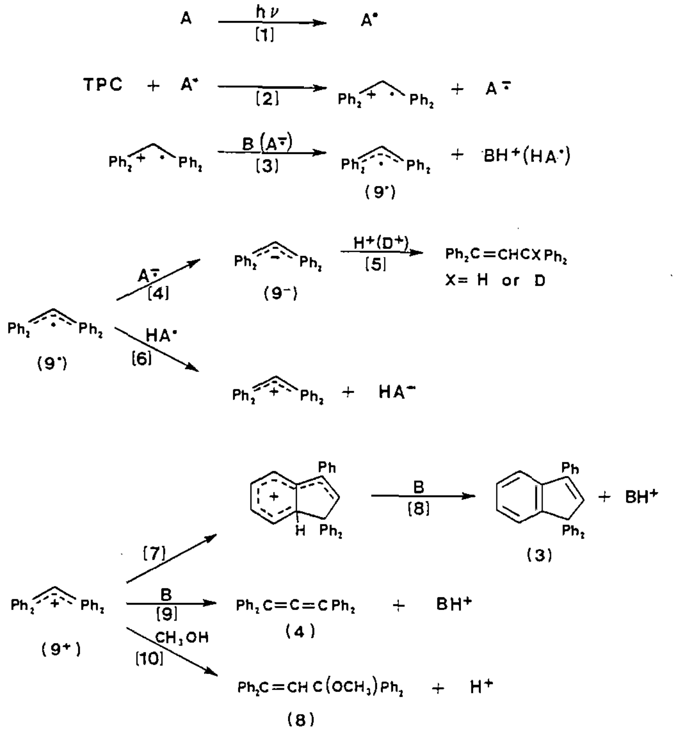

SCHEME 1

Pyrex, so wavelengths shorter than 290 nm are absorbed by the vessel. The sensitizers have appreciable absorption at longer wavelengths, while **1** is essentially transparent beyond 300 nm. The electron transfer step is thermodynamically favourable in every case (Table 2). Table 1 lists the free-energy change for this process as estimated by the Weller equation (12). With the quinone sensitizers (DDQ and TCQ) the triplet state is undoubtedly involved because of the rapid intersystem crossing in these cases. When the sensitizer forms a charge-transfer complex with **1** (TCNE, TCQ, DDQ) irradiation in the wavelength region of the charge-transfer transition can lead directly to the radical ion pair.

The deprotonation of $\mathbf{1}^{\cdot +}$ (Scheme 1, Step 3) dominates the chemistry after the electron transfer has occurred. In many instances in the literature, when a mechanism involving the deprotonation of a radical cation is proposed, the fate of the proton is essentially ignored until it is needed again to protonate another intermediate. In some cases the deprotonation does not seem to occur when it is predicted that it should, while in other cases the anion radical is thought to serve as the base. It is of fundamental importance to understand what is occurring and why. The first requirement is to estimate the pK_a of $\mathbf{1}^{\cdot +}$.

We have developed several thermochemical cycles which can be used to estimate the pK_a of a radical cation from available thermochemical data (9). An estimate can be made if the oxidation potential of RH (E^0_{RH}) and the bond dissociation energy of R—H (ΔG_{BDE}) are known. In this case, eq. [7] can be used,

$$[7] \quad pK_a = 0.73\,(-FE^0_{RH} + \Delta G^0_{BDE} + \Delta G^0_{tr(H^+)} + \Delta G^0_{f(H)} + \Delta G^0_{isom})$$

where $\Delta G_{tr(H^+)sol}$ is the free-energy associated with the transfer of a proton from water to the solvent of interest, $\Delta G_{f(H)g}$ is the free-energy of formation of a hydrogen atom and, ΔG_{isom} is the free-energy associated with the isomerization of the cyclopropyl radical to the allyl radical, Fig. 3.

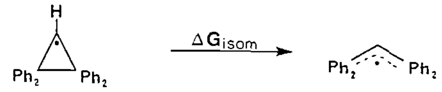

FIG. 3. The isomerization of 2,2,3,3-tetraphenylcyclopropyl radical to 1,1,3,3-tetraphenylpropenyl radical.

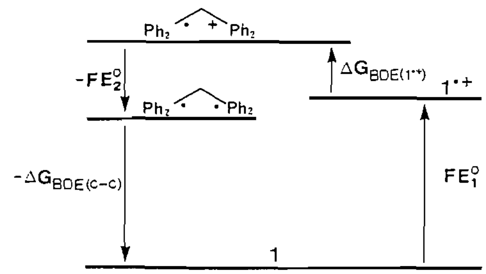

FIG. 4. Thermochemical cycle to estimate the strength of the one-electron, two-centre bond in $\mathbf{1}^{\cdot +}$.

To determine the pK_a of $\mathbf{1}^{\cdot +}$, the value of E^0_{RH} is estimated from the E_{ox} (1.48 V vs. NHE); $\Delta G_{tr(H^+)sol}$ is 11 kcal mol^{-1} for acetonitrile (13); $\Delta G_{f(H)g}$ is 48.6 kcal mol^{-1}, and $\Delta G_{BDE(RH)}$ is approximately 96±3 kcal mol^{-1} (14). The free-energy change associated with the isomerization from the cyclopropyl to the allylic structure must also be estimated. In the unsubstituted $C_3H_5^{\cdot}$ radical this value is approximately −25 kcal mol^{-1} (14). The extra stabilization associated with the four phenyl groups[4] should not account for more than −14±3 kcal mol^{-1}, so ΔG_{isom} should then be approximately −39±3 kcal mol^{-1}. Substitution of these values into eq. [7] gives an estimate of −11±4 for the pK_a of $\mathbf{1}^{\cdot +}$.

Another approach can be used to obtain an estimate of this number. The pK_a of the 1,1-diphenylethyl cation (in water) is approximately −6 (16). The pK_a value in acetonitrile, based on the free-energy of transfer of the proton (11 kcal mol^{-1}) and the hydrocarbon fragments (−2±2 kcal mol^{-1}), should be about 0.6±1. This number must be corrected for the allylic stabilization gained upon deprotonation (14±3 kcal mol^{-1}) and the strength of the one-electron two-centre bond being broken. An estimate of the strength of this bond may be obtained from the cycle shown in Fig. 4. The value of ΔG_{BDE} (C—C) is estimated from the activation barrier to thermal isomerization, which is about 30 kcal mol^{-1} (17). The oxidation potential E^0_2 should be approximately the same as the oxidation potential of the 1,1-diphenylethyl radical (approx. 0.42 V vs. NHE) (18) and the oxidation potential of **1** is given above. This gives an estimate of 6 kcal mol^{-1} for the strength of the one-electron two-centre bond of $\mathbf{1}^{\cdot +}$. Therefore, the pK_a of $\mathbf{1}^{\cdot +}$ should be:

$$pK_a = 0.6\pm1 - 0.728\,(14\pm3 - 6) = -5\pm3$$

It is, therefore, not surprising that $\mathbf{1}^{\cdot +}$ deprotonates. Furthermore, this process should be rapid because the C—H bond being broken can be parallel to the vacant *p*-orbital.

It is reasonable to assume that the sensitizer radical anion could serve as the base for the deprotonation of $\mathbf{1}^{\cdot +}$. In those cases where the sensitizer is reduced (TCNE, TCQ, and DDQ) this occurs. In fact, even in those cases where the sensitizer is not reduced (DCN, DCB, DCA, and MCB), and **2** is the

[4]This is based on ΔG^0_{BDE} (C—H) in diphenylmethane relative to the ΔG^0_{BDE} (C—H) in ethane (15).

product, protonation of the sensitizer radical anion still may be favourable.[5] However, in these cases, Scheme 1, Step 4 requires the radical anion to reduce $\mathbf{9}^{\cdot}$. If proton transfer to these radical anions is slow, the radical cation, $\mathbf{1}^{\cdot+}$, is acidic enough to protonate the solvent. There are other possible mechanisms for the formation of **2** which involve $HA^{\cdot}$, disproportionation of the radical $\mathbf{9}^{\cdot}$, for example. However, the observed deuterium incorporation in **2**, from methanol-O-*d*, argues against this alternative.

The next step in the reaction scheme, Step 4, involves a reduction of $\mathbf{9}^{\cdot}$ by the sensitizer radical anion. The reduction potential of $\mathbf{9}^{\cdot}$ is known (−0.94 V vs. SCE, ref. 21). Table 1, which lists the reduction potentials of the sensitizers, clearly indicates that the radical anions of all of the aromatic nitriles are capable of reducing $\mathbf{9}^{\cdot}$ to $\mathbf{9}^{-}$; even DCA, where the electron transfer is almost isoenergetic. Furthermore, the radical anions of the other sensitizers (TCNE, TCQ, and DDQ), which do not give **2** as a product, are *not* capable of reducing $\mathbf{9}^{\cdot}$. Following the reduction of $\mathbf{9}^{\cdot}$, protonation of $\mathbf{9}^{-}$ (Scheme 1, Step 5) completes the mechanism for the formation of **2**.

The reduction of $\mathbf{9}^{\cdot}$ and subsequent protonation of $\mathbf{9}^{-}$ explains the high degree of incorporation of deuterium at the allylic position with no scrambling. The absence of observable isotopic scrambling in **2** also rules out reversibility for the deprotonation of $\mathbf{1}^{\cdot+}$ (9).

An alternative mechanism for the incorporation of deuterium in **2** might be deprotonation of $\mathbf{2}^{\cdot+}$ to form $\mathbf{9}^{\cdot}$ followed by reduction and subsequent deuteration. However, when a solution of **2** and 1,4-dicyanonaphthalene (DCN) are irradiated in acetonitrile − methanol-O-*d*, no deuterium exchange is observed.

This result raises several new questions. Since the formation of the highly stabilized radical, $\mathbf{9}^{\cdot}$, should be a driving force for deprotonation of $\mathbf{2}^{\cdot+}$, it is not immediately obvious why $\mathbf{1}^{\cdot+}$ deprotonates while $\mathbf{2}^{\cdot+}$ does not[6]. Furthermore, the inability of both $\mathbf{1}^{\cdot+}$ and $\mathbf{2}^{\cdot+}$ to react with methanol is unexpected (3, 8), especially in the case of $\mathbf{2}^{\cdot+}$ since 1,1-diphenylethylene under similar conditions reacts to form the anti-Markownikoff

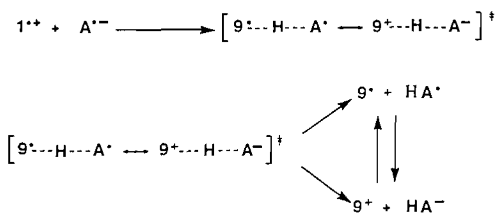

SCHEME 2

addition product in high yield (11). Also, 1,1-diphenylcyclopropane and phenylcyclopropane react to add methanol. Products resulting from the deprotonation of the radical cation of 1,1-diphenylcyclopropane or phenylcyclopropane were not reported in these cases either (6).

The radical cation $\mathbf{1}^{\cdot+}$ must preferentially deprotonate. The bulky phenyl groups will inhibit the addition of methanol, allowing the deprotonation to compete effectively. The addition of methanol to $\mathbf{2}^{\cdot+}$ must also be hindered. It is known that the rate of addition of methanol to olefin radical cations decreases markedly as the olefin becomes more heavily substituted (3, 18). The preferred conformation of the diphenylmethyl group in **2** (and presumably $\mathbf{2}^{\cdot+}$) has the C—H bond perpendicular to the olefinic π-bond.[7] The phenyl groups, therefore, effectively hinder the addition of methanol. This conformational preference, which has been observed in other systems (23), also accounts for the apparent lack of acidity of $\mathbf{2}^{\cdot+}$.

Consider next, Scheme 1, Step 6, the oxidation of $\mathbf{9}^{\cdot}$. It is clear that the deprotonation of $\mathbf{1}^{\cdot+}$ to $A^{\cdot-}$ (Step 3) and electron transfer (Step 6) can occur simultaneously, and that this process is equivalent to hydrogen atom transfer from $\mathbf{1}^{\cdot+}$ by $A^{\cdot-}$ (Scheme 2). In effect, the transition state can be more or less polar. Nevertheless, it is useful to consider these various steps independently in order to assess the energetics of the overall process.

If proton transfer were to occur between $\mathbf{1}^{\cdot+}$ and $\mathbf{A}^{\cdot-}$, then, if the reduction potential of $HA^{\cdot}$ is greater than the oxidation potential of $\mathbf{9}^{\cdot}$ (i.e., $E_{ox}(\mathbf{9}^{\cdot}) - E_{red}(HA^{\cdot}) < 0$), the subsequent electron transfer to form $\mathbf{9}^{+}$ would be fast. On the other hand, if $E_{ox}(\mathbf{9}^{\cdot}) - E_{red}(HA^{\cdot}) > 0$, then, even if hydrogen atom transfer were to occur, the ion pair would undergo an electron transfer to generate the radical pair.

There is independent evidence, at least in the case of TCQ, where $\mathbf{9}^{+}$ is observed, that $E_{ox}(\mathbf{9}^{\cdot}) - E_{red}(HA^{\cdot}) < 0$. The electrochemistry of several quinones and hydroquinones (not DDQ or TCQ) has been studied previously (24). The oxidation of hydroquinones in the presence of bases such as pyrrolidine, 2,6-lutidine, and pyridine results in a new wave at about 0.7 V below the oxidation potential of the hydroquinone (25). In the case of 1,4-hydroquinone (QH_2), the anodic wave for the oxidation of the hydroquinone disappears upon addition of two equivalents of 2,6-lutidine to the anolyte (25*b*). Under these conditions, a new wave at $E_p = 0.67$ V was attributed to the

[5]Consider, for example, the protonation of $DCN^{\cdot-}$ by $\mathbf{1}^{\cdot+}$. The required values of ΔG^0_{BDE}, ΔG^0_{isom}, and E^0_{ox} have been discussed above. The value of E_{red} for DCN is in Table 1. Therefore, only an estimate of ΔG_{BDE} of the C—H bond to be made in $DCNH^{\cdot}$ is required. The enthalpy of reaction for 1,4-dihydronaphthalene to give naphthalene and two hydrogen atoms can be calculated (109.9 kcal mol^{-1}) from information in standard tables (19). The BDE of the C—H bond in 1,4-dihydronaphthalene is approximately 75±2 kcal mol^{-1} (15). This would give a BDE of 35±2 for the second C—H bond. It is known that a cyano group decreases the C—H BDE by approximately 6 kcal mol^{-1} (20). On the other hand, the other cyano group will stabilize the radical ($DCNH^{\cdot}$) to some degree, and both cyano groups will be conjugated in the product. The overall effect on the BDE may be as much as −4±2 kcal mol^{-1}. This would give a value of 22±3 kcal mol^{-1} for ΔG^0_{BDE} ($DCNH^{\cdot}$). The ΔG^0 for protonation of $DCN^{\cdot-}$ by $\mathbf{1}^{\cdot+}$ would then be −27±6 kcal mol^{-1}. Similar reasoning suggests that protonation of the radical anion of DCB, DCA, and MCB is also favourable.

[6]Using a thermochemical cycle similar to that above, the pK_a of $\mathbf{2}^{\cdot+}$ also may be calculated. The oxidation potential (E_{ox} of **2** is 1.80 V (vs. NHE) and the free energy associated with the bond dissociation is about 72 kcal mol^{-1}. The estimated pK_a of $\mathbf{2}^{\cdot+}$ is −5±2. Therefore, $\mathbf{2}^{\cdot+}$ should deprotonate in methanol. Since deprotonation of $\mathbf{2}^{\cdot+}$ is favourable from thermochemical considerations, the reason for the lack of apparent acidity must be kinetic in nature.

[7]Evidence for this conformational preference is based on observed vicinal $^1H-^1H$ coupling constants (16). The $^1H-^1H$ coupling in **2** is 10 Hz while in an analogous compound, 1,3-diphenylindene, where the dihedral angle is approximately 60 degrees, the $^1H-^1H$ coupling constant is only 2 Hz (17). The proton chemical shifts for the allylic and vinyl proton in **2** are δ 4.75 and δ 6.45 respectively. Those for 1,3-diphenylindene are δ 4.55 and δ 6.49 respectively.

oxidation of $QH^- \rightarrow Q + H^+ + 2e^-$.[8] Similarly, the oxidation of $TCQH_2$ in acetonitrile occurs at E_p = 1.56 V. Addition of 2,6-lutidine (1.5 equivalents) to the anolyte produces a new wave at E_p = 0.60 V attributable to the oxidation of $TCQH^-$.[9] Since E_{ox} ($9^\cdot$) − E_{red} ($TCQH^\cdot$) = −0.26 V, the observation of 9^+ is expected.

Irradiation of the charge-transfer complex between **1** and TCNE, DDQ, or TCQ results in the formation of mixtures of **3** and **4** as well as the reduced acceptors. The mechanism for the formation of **3** and **4** via 9^+ is shown in Scheme 1, Steps 7–9.

The proposed cyclization of the cation 9^+ is in apparent contradiction of reported behavior. Treatment of 1,1,3,3-tetraphenylpropenol (**5**) with *p*-toluenesulphonic acid in ethyl acetate gave an almost quantitative yield of **4** (10). We find, however, *that with acetonitrile as solvent*, treatment of **5** with *p*-toluenesulphonic acid leads to an almost quantitative yield of **3** (2). As the percentage of carbon tetrachloride in acetonitrile increases, the proportion of **4** progressively increases (Fig. 2). A weaker acid (trifluoroacetic acid or trichloroacetic acid) produces a much more dramatic effect than the strong acid (*p*-toluenesulphonic acid).

These results are rationalized by considering the effect of the solvent polarity on the strength of the acid (or it's conjugate base) (28). The dielectric constant of binary solvent mixtures of carbon tetrachloride and acetonitrile as a function of mole fraction of carbon tetrachloride is almost linear. As the solvent polarity decreases, the strength of the conjugate base increases, so the deprotonation of 9^+ becomes more favourable. The strong acid (*p*-toluenesulphonic acid) leads to a higher ratio of **3**/**4**. The pK_a of trichloroacetic acid is similar to that of trifluoroacetic acid, so it is not surprising that the plots obtained in Fig. 2 are similar.

This explanation may be oversimplified. Acid–base equilibria in aprotic solvents are complex. Besides the equilibrium for salt formation, equilibria for acid dimerization, $(HA)_2$, homoconjugate ion formation, $(A—H——A)^-$, and, in the case of **5**, the pK_{R^+}, are also important. In general, weaker acids dimerize more readily in aprotic media. On the other hand, homoconjugate ion formation is more favourable with stronger acids. The ability of the conjugate base to accept a proton, however, depends on its charge, size, polarizability, and, to some extent, steric factors (i.e. the same factors that are important in aqueous media). However, it is clear that relative pK_a's in aprotic solvents are very much attenuated, relative to those values measured in water (28). Most of this difference is a result of the heat of transfer of the proton from water to acetonitrile. (In the reaction of 9^+ in ethyl acetate, the solvent apparently acts as the base.)

The formation of indenes from the allylic cations has been reported. Pittman and Miller (29) have found that allylic cations such as the 1,1,3-triphenylpropenyl cation are stable at low temperature in strong acid. Warming these solutions induced cyclization to form stable solutions of the indanyl cation. Quenching with base led to an almost quantitative yield of the corresponding indene. In these solutions, the intermediate cyclohexatrienyl cations were not observed, which implies that Scheme 1, Step 8 is rapid, probably a result of the driving force for aromatization upon proton loss.

It is clear, therefore, that the ratio of **3** to **4** is sensitive to the basicity of the medium. The observed dependence of the ratio of **3** to **4** on the sensitizer (Table 2) may be explained on this basis. The ratio of **3** to **4** decreases in the order TCNE > TCQ > DDQ. This follows expected base strength of the anions HA^-. The difference in base strength of the anions (HA^-) can also account for the qualitative observation that the steady-state concentration of 9^+ is greater with TCNE as the sensitizer than with TCQ (see below).

The possibility that $9^\cdot$ may cyclize to lead, ultimately, to **3**, or, that $9^\cdot$ may disproportionate to give **4** should be considered. Dietz *et al.* (21) found that a stable solution of 9^- could be oxidized to form a stable solution of $9^\cdot$ (which gave a well-resolved esr spectrum). The solution of $9^\cdot$ could be reduced back to 9^- with no apparent reaction.

The irradiation of the charge-transfer complex between **1** and TCQ in acetonitrile–methanol (3:1, v/v) leads to the formation of **8** in good yield (based upon hplc analysis of the crude reaction mixture). The isolation of **8** is not straightforward; only half of this ether was eluted from a silica gel flash chromatographic column even though the compound was on the column for less than 30 min. The remainder of the material was recovered as **5** on elution with methanol. The formation of **8** is consistent with the existence of 9^+ along the reaction pathway. Treatment of **5** in acetonitrile–methanol (3:1, v/v) with trifluoroacetic acid (10^{-2} *M*) produces **8** in good yield, based upon proton magnetic resonance (^{1}Hmr) spectroscopy and hplc.

Strong support for many of the mechanistic considerations proposed in Scheme 1 can be derived from the electrochemical study of the oxidation of **1** (2). The oxidation of **1** at a spherical platinum electrode occurs at E_p = 1.36 V in acetonitrile (0.1 *M* TEAP) using a sweep rate of 400 mV s^{-1}. At sweep rates less than 1.0 V s^{-1} a second anodic wave (E_p = 1.58 V at 400 mV s^{-1}) is observed. The relative height of the second wave increases as the sweep rate decreases (Table 4). The second wave is attributable to the oxidation of **3**, adsorbed on the working electrode. The sweep rate dependence is a result of a slow chemical step. The strong adsorption of **3** to the working electrode is evident from Fig. 2. The sharp anodic wave at E_p = 1.58 V is obtained for the cyclic voltammogram of **3**. Addition of an equivalent amount of **1** to this solution only results in an increase in the peak current for the second anodic wave. The first wave at E_p = 1.36 V is not observed, indicating that the working electrode is insulated from the solution until the discharge potential of **3** is reached.

The appearance of an anodic wave attributable to the oxidation of **3** clearly indicates that the anodic wave at E_p = 1.36 V represents a two-electron process. Radical cations generally are more stable in dichloromethane than in acetonitrile (30), so this solvent was used in an attempt to detect the individual one-electron transfer steps upon oxidation of **1**. The first wave at E_p = 1.36 V in dichloromethane appears to be identical to the wave in acetonitrile. Even at sweep rates as fast as 20 V s^{-1}, no evidence for two one-electron transfers is obtained.

At the onset of oxidation (in acetonitrile), the solution near the surface of the electrode becomes visibly purple. The cathodic sweep reveals two waves. The first cathodic wave is reversible with $E_{1/2}$ = 0.34 V. The second wave is at E_p = 0.17 V and is irreversible. The irreversible wave may be the reduc-

[8]Recently, Laviron has measured the E^0 value for this oxidation ($QH^- \rightleftarrows QH^\cdot$, + 0.22 V vs. SCE, aqueous) (26).

[9]Addition of 2,6-di-*tert*-butylpyridine has a similar effect, except forty equivalents must be added before the wave at E_p = 1.56 V is not observed, and the new wave occurs at E_p = 0.87 V. These differences can be attributed to a steric effect with this hindered base (27).

tion of a proton which occurs at $E_{1/2}$ = 0.24 V (31) in water, i.e., the normal hydrogen electrode (NHE). A likely candidate for the coloured intermediate is **9**$^+$. When the cation **9**$^+$ is generated in the electrolysis cell from the alcohol **5** by the addition of trifluoroacetic acid, the voltammogram of the resulting purple solution has the same reversible reduction wave at $E_{1/2}$ = 0.34 V. Furthermore, the irreversible wave at E_p = 0.17 V, associated with the proton reduction, is also observed.

Some uncertainty still remains regarding the mechanistic sequence of the anodic oxidation of **1** to **9**$^+$. Two possible pathways are the ECE and the EEC process. For the ECE mechanism the deprotonation of **1**$^{\cdot +}$ is thermodynamically feasible even considering acetonitrile as the base (9), and the oxidation of **9**$^\cdot$ would be rapid at 1.1 V. The alternative pathway (EEC) requires that the oxidation of **1**$^{\cdot +}$ to **1**$^{++}$ occurs at 1.1 V (the onset of oxidation), followed by deprotonation to give **9**$^+$. An estimate of the oxidation potential of **1**$^{\cdot +}$ can be made; it should be between the oxidation potential of tetraphenylethylene radical cation (1.45 V) (32) and the oxidation potential of the 1,1-diphenylethyl radical (−0.2 V (18)). The strength of the one-electron two-centre bond in **1**$^{\cdot +}$ is small (5), so the oxidation potential of **1**$^{\cdot +}$ should be closer to the value for the 1,1-diphenylethyl radical. Obviously, both pathways are thermodynamically feasible.

Controlled potential electrolysis of **1** gives further support to the suggestion that **9**$^+$ lies on the reaction pathway (Table 3). Electrolysis in acetonitrile (0.1 *M* TEAP) gives **3** in good yield. Addition of a base (2,6-lutidine) diverts the reaction from the original pathway and **4** is now the major product (only a trace of **3** is detected). In acetonitrile–methanol (3:1, v/v) (0.1 *M* TEAP) the product obtained is **8**. This, of course, parallels the expected behavior of **9**$^+$.

It is interesting to compare the controlled potential electrolysis (in methanol) of **1** to that reported for 1,2-diphenylcyclopropane (*cis* and *trans*) (33). In the case of 1,2-diphenylcyclopropane the product from the electrolysis was 1,3-dimethoxy-1,3-diphenylpropane. It was proposed that the radical cation of the cyclopropane reacted with methanol to form the benzylic radical which oxidized to the cation and reacted once again with methanol (ECEC). The radical cation of 1,2-diphenylcyclopropane showed no propensity for deprotonation under these conditions (the allylic ether analogous to **8** was not detected). This, of course, is consistent with the photosensitized (electron transfer) results (1, 6).

The isolation of **8** from the electrolysis of **1** does not confirm unambiguously the intermediacy of **9**$^+$. If methanol were to react with **1**$^{\cdot +}$ (or **1**$^{++}$), the resulting diphenylethyl-type cation could simply deprotonate to give **8**. Furthermore, since an excess of protons is produced in this reaction, 1,3-dimethoxy-1,1,3,3-tetraphenylpropane may be produced, and subsequently react via an acid-catalyzed elimination of methanol. Analysis of the reaction by hplc indicates that **8** is the only product formed, even at low conversion (<5%). The photosensitized (electron transfer) reaction of **1** in acetonitrile–methanol (3:1, v/v) indicates that **1**$^{\cdot +}$ deprotonates much faster than it reacts with methanol. Certainly the dication **1**$^{++}$ will be as, or more, acidic under similar conditions. The formation of **8**, via **9**$^+$, under the electrolysis conditions is, therefore, reasonable.

Treatment of **5**, in acetonitrile (0.1 *M* TEAP), with trifluoroacetic acid, produces a coloured solution which exhibits three broad absorption maxima at 568 nm, 459 nm, and 382 nm attributed to **9**$^+$. This spectrum can be compared to the spectrum of **9**$^-$ which exhibits visible absorption maxima at 564 nm and 463 nm (14). Similarity is expected; the energy difference between the HOMO and the NBMO (non-bonding molecular orbital) in the cation is the same as the difference between the NBMO and the antibonding MO in the anion (34).

Electrolysis of a solution of **1** gives a coloured solution which exhibits absorption maxima at 570 nm, 461 nm, and 381 nm. Similarly, irradiation of the charge-transfer band between **1** and TCNE, DDQ, or TCQ in acetonitrile produces a coloured solution with absorption maxima at 566 nm and 458 nm. We suggest that all three spectra represent the same intermediate, **9**$^+$.

The stability of **9**$^+$, the ease with which it is generated electrochemically from **1**, and the ease with which it is detected spectrophotometrically make it possible to measure the rate of disappearance as a function of temperature (Table 5). The rate of disappearance of **9**$^+$ (measured at either 570 nm or 460 nm) follows first-order kinetics. The temperature dependence gives an apparent activation energy of 21.8±0.6 kcal mol^{-1} and a preexponential factor, log *A*, of 14.5 ± 0.4. It is clear from the simple mechanism in Scheme 1, Steps 7 and 8, that this rate constant represents the rate of formation of **3**. The rate at 23°C is independent of the concentration of electrolyte between 0.1 and 0.001 *M* TEAP. The ratio of **3**/**4** with TCNE as acceptor does not change significantly when 0.1 *M* TEAP is added to the solution. Similarly the product ratio is the same with or without 0.1 *M* TEAP when TCQ is the acceptor. It is reasonable to conclude, therefore, that the rate constant for the formation of **3** will be the same in the photochemical experiments.

Conclusions

1$^{\cdot +}$ can undergo several different reactions which depend on the acceptor used and on the reaction conditions. The reduction potential of **9**$^\cdot$ is −0.94 V (14). The reduction potentials of all of the acceptors which lead to the formation of **2** are greater than, or within 0.05 eV of, this value. Conversely, for the sensitizer radical anions which lead to the formation of **3** and **4**, all the radical anions are incapable of reducing **9**$^\cdot$. Only one, DDQ, is capable of oxidizing **9**$^\cdot$. It is possible, however, for the protonated radical anions (HA$^\cdot$) of TCQ, DDQ, and TCNE to oxidize **9**$^\cdot$ since **9**$^+$ is observed spectroscopically in these cases.

The partitioning between **9**$^-$ and **9**$^+$ is easily interpreted in terms of the reduction potential of the acceptor. The partitioning between **3** and **4** depends on the basicity of the medium. The implication is that HA$^-$ is the base, since in the absence of base (i.e. in the electrolysis of **1**) **4** is not formed. This indicates that **4** results from deprotonation to a base other than solvent.

The complex behaviour observed with this seemingly simple system must pertain in general for photosensitized (electron transfer) reactions. This complexity, in fact, offers an opportunity of dramatically increasing the synthetic utility of this type of reaction if the factors which influence the preference of one reaction pathway over another can be understood and controlled.

Experimental

Acetonitrile (Fisher ACS grade) for preparative photolysis and electrolysis, as well as for electrochemical measurements, was distilled successively from sodium hydride (1 g/L) and phosphorus pentoxide (2 g/L), followed by passing through a column of basic alumina (100 g/L), refluxing over calcium hydride for 24 h in an inert atmosphere, and, finally, fractional distillation. Acetonitrile for the electrochemical measurements was used immediately after distillation while that for preparative work was stored over 3A molecular sieves. Tetraethylammonium perchlorate (Aldrich) was recrystallized three times from 90% ethanol and dried in a vacuum desiccator. Tetracyanoethylene (Aldrich) was sublimed and recrystallized three times from chlorobenzene. Chloranil (Eastman) was purified by recrystallization four times from benzene. 2,3-Dichloro-2,6-dicyanobenzoquinone (Aldrich) was purified by recrystallization four times from chloroform–benzene (4:1). 1,4-Dicyanobenzene (Aldrich) was purified by sublimation followed by recrystallization three times from ethanol. 1,4-Dicyanonaphthalene was prepared by the method of Heiss, *et al.* (35) from the reaction of *o*-phenylenediacetonitrile and *N*,*N*'-di-*tert*-butylglyoxaldiimine. The 1,4-dicyanonaphthalene was purified by column chromatography followed by recrystallization from methanol (three times). Methyl-4-cyanobenzoate was prepared by the acid-catalysed esterification of 4-cyanobenzoic acid (Aldrich) and purified by recrystallization (ethanol). 9,10-Dicyanoanthracene was prepared by the reaction of cuprous cyanide with 9,10-dibromoanthracene (36) and was purified by column chromatography followed by recrystallization (twice from benzene). The preparations of 1,1,2,2-tetraphenylcyclopropane (17), 1,3,3-triphenylindene (37), and tetraphenylallene (10) have been described.

The ^{1}Hmr spectra were recorded on a Varian T60 spectrometer and are reported in parts per million downfield from TMS. Melting points were obtained on a Sybron Corporation Thermodyne hot stage and are uncorrected. The hplc analysis was performed using a Waters Associates M-45 solvent delivery system in conjunction with a Tracor 970 variable wavelength absorbance detector. The column (Merck, Lichrosorb RP-18) was prepared by suspending the packing (1.1 g) in a mixture of carbon tetrachloride (10 mL) and tetrabromoethane (8 mL) by sonication for 3 min. The slurry was poured into a pre-column (18 cm × 1.5 cm diameter) and immediately packed into the analytical column (10 cm × 0.6 cm diameter) with n-heptane at a pressure of 3450 psi (using a Haskel air-driven fluid pump). The eluant was progressively changed to chloroform, then methanol. The analysis was done at a flow rate of 1.2 mL/min with 83% methanol–water. The absorbance was monitored at 247 nm (the isobestic point of **3** and **4**).

To calibrate the hplc, the apparent mole fraction of **3** (based on relative peak heights) was converted to a true mole fraction with a working curve. The working curve was a plot of apparent versus true mole fraction, constructed with ten accurately weighed samples of mixtures of **3** and **4**.

Electrochemical cell and apparatus

Cyclic voltammetric measurements were performed in a three-electrode cell (10 mL volume) fitted with a cooling jacket and a scintered glass frit through which nitrogen was passed in order to deoxygenate and stir the solution prior to measurement. The working electrode was a spherical platinum electrode (1mm diameter) embedded in soft glass and contacted with a Nichrome wire through a mercury pool. The counter electrode was a platinum coil embedded in soft glass and inserted through a sidearm of the cell. The reference electrode was a saturated calomel electrode (SCE) which was isolated from the solution by a glass tube (inserted in another sidearm) which ended in a Luggin capillary placed 0.5 mm from the surface of the working electrode. The working electrode was immersed in concentrated nitric acid for 30 min prior to use, washed with 5% bicarbonate, water, and methanol, then dried in an oven at 60°C. The electrochemical cell was cleaned by immersion in concentrated nitric acid (2 h) followed by rinsing with water, 5% sodium bicarbonate, water, and acetone, and dried at 100°C.

Solutions were degassed with dry nitrogen (presaturated with solvent) for 5 min prior to each measurement, and, during the measurement, the nitrogen atmosphere was maintained above the solution. Substrate concentrations were typically 0.001 *M* in a total volume of 7 mL.

The spectroelectrochemical cell consisted of a 4-cm cylinder (1 cm diameter) with optically flat Pyrex windows sealed at each end. The cell was surrounded by a water jacket. The temperature of the solution in the cell was maintained using a Polyscience Corporation, Model 90 temperature controlled circulating bath. The solution in the cell was continuously stirred with a magnetic stirring bar, placed in a shallow well below the light path. The working electrode (platinum mesh, 4 cm × 0.5 cm), inserted via an opening in the top of the cell, was held against the inside wall of the cell in order to keep it out of the light path. A thermistor probe (Cary 219 spectrophotometer accessory) was placed in a second opening in the top of the cell and protruded only slightly, by approximately 2 mm, into the light path. The reference electrode and counter electrode were isolated from the solution in a separate compartment which contacted the working compartment through a scintered glass frit. This compartment was inserted through an opening in the side of the cell, ending with a ground glass joint. The entire assembly was placed in the sample compartment of a Varian–Cary 219 spectrophotometer.

The substrate concentrations were 2.9×10^{-3} *M*. During each run, approximately 0.5 C were passed at constant current (0.05 equivalents). The cell was then open-circuited and the absorbance of the solution monitored as a function of time. The solution was replaced with fresh solution after every third measurement. The temperature did not vary by more than ±0.1 degree during any given measurement.

Controlled potential electrolysis was performed with a standard H-cell (total volume 100 mL). Both the working electrode and counter electrode were platinum mesh (9 cm^2). The reference electrode was introduced via a Luggin capillary.

Cyclic voltammetric measurements were obtained with a PAR (Princeton Applied Research) 173 potentiostat in combination with a PAR 175 universal programmer and a PAR 179 digital coulometer. Controlled potential electrolyses and spectroelectrochemical measurements were performed with the use of the PAR 173 potentiostat.

Irradiations were carried out in acetonitrile or acetonitrile–methanol (3:1) at a substrate concentration of 0.1 *M*. Solutions were degassed by bubbling dry nitrogen for 10 min prior to irradiation. Irradiations were carried out in 2 cm id Pyrex tubes (large scale) or 5-mm Pyrex nmr tubes. Two irradiation systems were employed, a 1-kW medium pressure mercury lamp (General Electric Co.) with a quartz cooling jacket which was immersed in a constant temperature bath at 10°C, and a Hanovia 450-W lamp with a quartz cooling jacket. When the Hanovia lamp was used, the irradiation tubes were contained in a Pyrex cooling jacket connected to a Polyscience Model 90 temperature controlled circulating bath. This jacket also served as a short-wavelength (<280 nm) filter. Reaction mixtures were chromatographed on a flash chromatographic column or with a medium pressure (15 psi, helium) lc system (8).

*Photosensitized (electron transfer) irradiation of **1** using 1,4-dicyanonaphthalene in acetonitrile*

1 (100 mg, 2.9×10^{-4} mol) and 1,4-dicyanonaphthalene (10 mg, 5.8×10^{-5} mol) were dissolved in acetonitrile (3.0 mL), degassed by bubbling nitrogen for 10 min, and irradiated at 10°C (through a Pyrex filter) with a 1-kW lamp for 4 h. Analysis (hplc) indicated only one major product. The solvent was evaporated under reduced pressure and the reaction mixture separated by medium pressure chromatography (silica gel, hexanes–dichloromethane gradient). **2** (66 mg, 73%) was isolated and recrystallized from absolute ethanol to give colourless crystals which melted at 126–128°C (lit (38) mp 127–128°C). The ^{1}Hmr spectrum was identical to an authentic sample (δ, $CDCl_3$; 7.20 (m, 20 H), 6.52 (d, J = 10 Hz, 1H), 4.75 (d, J = 10 Hz, 1H)).

Other compounds isolated from the column were unreacted starting material (**1**, 10 mg) and unreacted sensitizer (DCN, 8 mg, 80% recovery).

*Photosensitized (electron transfer) irradiation of **1** using 1,4-dicyanonaphthalene in acetonitrile-methanol-O-*d

1 (30 mg, 8.7×10^{-5} mol) and DCN (3 mg, 1.7×10^{-5} mol) were dissolved in a mixture of acetonitrile and methanol-O-*d* (3:1, v/v, 1.0 mL), degassed by bubbling nitrogen for 5 min, and irradiated (through Pyrex) with a 1-kW lamp for 1.5 h (at 10°C). The solvent was removed under reduced pressure and **2** was isolated by medium pressure chromatography (silica gel, hexanes–dichloromethane gradient); ^{1}Hmr (Nicolet 360-MHz nmr spectrometer) showed only the resonances at δ 7.20 (m, 20H) and 6.52 (s, 1H). The ^{2}Dmr spectrum showed only a singlet at δ 4.78.

*Photosensitized (electron transfer) irradiation of **1** using tetracyanoethylene*

1 (100 mg, 2.98×10^{-4} mol) and tetracyanoethylene (38 mg, 3.0×10^{-4} mol) in acetonitrile (3.0 mL) were degassed by bubbling nitrogen for 10 min and then irradiated through a sodium nitrite filter (> 400 nm) at 10°C for 72 h. Within a few seconds of irradiation, the solution became dark purple. This colour slowly faded when the tube was removed from the irradiation bath. After the irradiation was complete (monitored by hplc) a colourless solid, which had precipitated, was filtered and the solvent was evaporated under reduced pressure.

The residue, after evaporation, exhibited an ^{1}Hmr spectrum (δ, $CDCl_3$: 4.90 (s)) and an ir spectrum (KBr (cm^{-1}): 2819, 2606, 2484, 2274, 1620, 1302, 1201, 996, 908, 561) identical to an authentic sample of dihydrotetracyanoethylene (39). The crude yield was 28 mg (74%).

The precipitate was combined with the residue from the evaporation of solvent and separated by medium pressure chromatography (silica gel, hexanes–dichloromethane gradient) to give **3** (58 mg, 67%), **4** (3 mg, 4%), and **1** (14 mg). The identity of **3** and **4** was confirmed by comparison to authentic samples of each (refs. 10, 37).

*Photosensitized (electron transfer) irradiation of **1** using chloranil in acetonitrile*

1 (100 mg, 2.9×10^{-4} mol) and chloranil (63 mg, 3.0×10^{-4} mol) in acetonitrile (2.0 mL) were degassed by bubbling nitrogen for 10 min, then irradiated through a sodium nitrite filter solution (> 400 m) at 10°C for 4 h. The solution became only slightly purple within a few seconds of irradiation. Analysis (hplc) indicated that **3** (minor) and **4** (major) were formed. The solvent was evaporated under reduced pressure, the residue was dissolved in dichloromethane, and the tetrachlorohydroquinone (insoluble in dichloromethane) was filtered (42 mg, 67%) and identified by mass spectrometry (M^+ (246) and characteristic M+2, M+4, M+6) and ir (KBr (cm^{-1}): 3410(s), 1415(s), 1312(s), 1205(s), 888(s), 720(m), 708(m)).

The dichloromethane was evaporated under reduced pressure and the residue was separated by medium pressure chromatography (silica gel, hexanes–dichloromethane gradient). Isolated from the column were **4** (47 mg, 67%), **3** (5 mg, 7%), and **1** (30 mg).

*Photosensitized (electron transfer) irradiation of **1** using 2,3-dichloro-5,6-dicyanobenzoquinone in acetonitrile*

1 (100 mg, 2.9×10^{-4} mol) and 2,3-dichloro-5,6-dicyanobenzoquinone (68 mg, 3.0×10^{-4} mol) in acetonitrile (2.0 mL) were degassed by bubbling nitrogen for 10 min, then irradiated through a sodium nitrite filter solution (> 400 nm) at 10°C for 4 h. The solution became dark purple within a few seconds of irradiation. The solvent was evaporated and the residue extracted into dichloromethane. The hydroquinone precipitate (reduction product) was filtered to give a crude yield of 32 mg, 47%, and identified by mass spectrometry (M^+ (228) and characteristic M+2, M+4) and ir (KBr (cm^{-1}): 3260(s), 2260(m), 1578(m), 1455(s), 1360(m), 1280(s), 1200(s), 1078(m), 892(s), 778(m), 748(m), 703(w), 690(w)).

The dichloromethane was evaporated under reduced pressure and the residue was separated by medium pressure chromatography (silica gel, hexanes–dichloromethane gradient) to give **3** (7 mg, 10%), **4** (25 mg, 35%), and **1** (29 mg).

*Photosensitized (electron transfer) irradiation of **1** using chloranil in acetonitrile–methanol (3:1, v/v)*

1 (100 mg, 2.9×10^{-4} mol) and chloranil (63 mg, 3.0×10^{-4} mol) in acetonitrile–methanol (3:1, v/v, 2.0 mL) were degassed by bubbling nitrogen for 10 min, then irradiated through a sodium nitrite filter solution (>400 nm) at 10°C for 5 h. The solvent was evaporated under reduced pressure and the residue was extracted with dichloromethane (to separate the hydroquinone from the reaction mixture). The hydroquinone precipitate was filtered (43 mg, 68%), and characterized as above.

The dichloromethane was removed under reduced pressure and separated by medium pressure chromatography (silica gel, hexanes–dichloromethane gradient) to give **4** (7 mg, 10%), **5** (54 mg, 77%), and **1** (33 mg). Analysis (hplc) of the original reaction mixture indicated that only **8** was present; neither **4** nor **5** were detected, indicating that these products were a result of decomposition of **8** on the silica gel column.

*Controlled potential electrolysis of **1** in acetonitrile*

Into the anodic compartment of the electrolysis cell, containing acetonitrile (0.1 *M* TEAP, 100 mL), **1** (250 mg, 7.2×10^{-4} mol) was dissolved. The solution was stirred and a constant potential of 1.3 V (vs. SCE) was applied. When 90.8 C had been consumed, the reaction was stopped. The solvent was removed under reduced pressure and the residue taken up into benzene to remove the electrolyte. After gravity filtration and removal of the benzene the mixture was separated by medium pressure lc (silica gel, hexane–dichloromethane gradient). The compounds isolated were **1** (84 mg) and **3** (142 mg, 85%). The identity of **3** was confirmed by comparison to an authentic sample (37).

*Controlled potential electrolysis of **1** in the presence of base*

1 (100 mg, 2.9×10^{-4} mol) was added to the anodic compartment of the electrolysis cell containing acetonitrile, 100 mL 0.1 *M* TEAP, and 0.1 *M* 2,6-lutidine. The solution was stirred and a controlled potential of 1.4 V was applied until 19.9 C were consumed. The solvent was removed under reduced pressure and the residue was dissolved in benzene. This solution was filtered (to remove TEAP) and the benzene was removed under reduced pressure. The mixture was separated by medium pressure chromatography (silica gel, hexane–dichloromethane gradient). The compounds isolated were **1** (77 mg) and **4** (13 mg, 57%). Analysis (hplc) of the fractions containing **4** indicated the presence of a trace (<3%) of **3**. The identity of **4** was confirmed by comparison to an authentic sample (10).

*Controlled potential electrolysis of **1** in acetonitrile–methanol*

1 (100 mg, 2.9×10^{-4} mol) was added to the anodic compartment of the electrolysis cell containing a mixture of acetonitrile and methanol (3:1, v/v, 0.1 *M* TEAP). The solution was stirred and a controlled potential of 1.4 V was applied until 60.1 C had been consumed. The solvent was evaporated and the residue dissolved in benzene. The benzene solution was filtered and the solvent was removed under reduced pressure. The mixture was separated by flash chromatography (silica gel, hexane–dichloromethane gradient). The products isolated were **1** (27 mg) and **8** (43 mg, 55%). Elution of the flash chromatographic column with methanol gave **5** (20 mg, 27%). **5** was not detected by hplc analysis of ^{1}Hmr of the reaction mixture.

Acknowledgements

This work was supported by a grant from the Natural Sciences and Engineering Research Council of Canada (including a scholarship to D.D.M.W.). D.R.A. is grateful for a fellowship from the John Simon Guggenheim Foundation.

1. R. W. R. HUMPHREYS and D. R. ARNOLD. J. Am. Chem. Soc. **101**, 2743 (1979).
2. D. D. M. WAYNER and D. R. ARNOLD. J. Chem. Soc. Chem. Commun. 1087 (1982).
3. S. L. MATTES and S. FARID. Organic photochemistry. 6. *Edited by* A. Padwa. Marcel Dekker, New York. 1983. pp. 233–326.
4. (*a*) P. C. WONG AND D. R. ARNOLD. Tetrahedron Lett. 2101 (1979); (*b*) H. D. ROTH and M. L. M. SCHILLING. J. Am. Chem. Soc. **102**, 7956 (1980).
5. D. D. M. WAYNER, R. J. BOYD, and D. R. ARNOLD. Can. J. Chem. **61**, 2310 (1983).
6. V. R. RAO and S. S. HIXSON. J. Am. Chem. Soc. **101**, 6458 (1979).

7. B. JUAN, J. SCHWARTZ, and R. BRESLOW. J. Am. Chem. Soc. **107**, 5741 (1980).
8. R. M. BORG and D. R. ARNOLD. Can. J. Chem. **62**, 1785 (1984).
9. A. M. DEP. NICHOLAS and D. R. ARNOLD. Can. J. Chem. **60**, 2165 (1982).
10. A. R. UBBELOHDE and J. A. BURGESS. J. Chem. Soc. B, 1106 (1970).
11. (*a*) R. A. NEUNTEUFEL and D. R. ARNOLD. J. Am. Chem. Soc. **95**, 4080 (1973); (*b*) Y. SHIGEMITSU and D. R. ARNOLD. J. Chem. Soc. Chem. Commun. 407 (1975); (*c*) D. R. ARNOLD and A. J. MAROULIS. J. Am. Chem. Soc. **98**, 5931 (1976); (*d*) **99**, 7355 (1977); (*e*) A. J. MAROULIS, Y. SHIGEMITSU, and D. R. ARNOLD. J. Am. Chem. Soc. **100**, 535 (1978).
12. D. REHM and A. WELLER. Isr. J. Chem. **8**, 259 (1970).
13. B. G. COX, G. R. HEDWIG, A. J. PARKER, and D. W. WATTS. Aust. J. Chem. **27**, 477 (1974).
14. A. M. NICHOLAS and D. R. ARNOLD. Can. J. Chem. **60**, 3011 (1982).
15. D. F. MCMILLEN and D. M. GOLDEN. Ann. Rev. Phys. Chem. **33**, 493 (1982).
16. S. P. MCMANUS and C. V. PITTMAN, JR. Organic reactive intermediates. *Edited by* S. P. McManus. Academic Press, New York. 1973. pp. 193–335.
17. D. R. ARNOLD, D. D. M. WAYNER, and M. YOSHIDA. Can. J. Chem. **60**, 2313 (1982).
18. D. R. ARNOLD and A. OKAMOTO. Can. J. Chem. Submitted.
19. Codata Bulletin No. 28, ICSV Codata, Paris 1978. J. Chem. Thermodyn. **10**, 903 (1978).
20. G. LEROY. Int. J. Quantum Chem. **23**, 271 (1983).
21. R. DIETZ, M .E. PEOVER, and R. WILSON. J. Chem. Soc. B, 75 (1968).
22. W. G. MILLER and C. V. PITTMAN, JR. J. Org. Chem. **39**, 1955 (1974).
23. (*a*) F. D. LEWIS, T. I. HO, and J. T. SIMPSON. J. Am. Chem. Soc. **104**, 1924 (1982); (*b*) F. D. LEWIS and T. I. HO. J. Am. Chem. Soc. **102**, 1751 (1980); (*c*) P. J. WAGNER and A. E. PUCHALSKI. J. Am. Chem. Soc. **102**, 6177 (1980); (*d*) **100**, 5948 (1978).
24. J. Q. CHAMBERS. The chemistry of the quinonoid compounds. *Edited by* S. Patai. John Wiley and Sons, New York. 1974. Chapt. 14.
25. (*a*) V. D. PARKER. J. Chem. Soc. Chem. Commun. 716 (1969); (*b*) B. R. EGGINS and J. Q. CHAMBERS. J. Electrochem. Soc. **117**, 186 (1970).
26. E. LAVIRON. J. Electroanal. Chem. **164**, 213 (1984).
27. C. J. SCHLESENER, C. AMATORE, and J. K. KOCHI. J. Am. Chem. Soc. In press.
28. M. M. DAVIS. Acid–base behavior in aprotic organic solvents. NBS Monograph 105, 1968.
29. C. V. PITTMAN and W. G. MILLER. J. Am. Chem. Soc. **95**, 2947 (1973).
30. A. J. BARD and J. PHELPS. J. Electroanal. Chem. **25**, App 2 (1970).
31. R. C. WEAST (Editor). C.R.C. handbook of chemistry and physics. C.R.C. Publishing Co., Cleveland, Ohio. 1971.
32. J. D. STUART and W. E. OHNESORGE. J. Am. Chem. Soc. **93**, 4531 (1971).
33. T. SHONO and Y. MATSUMURA. J. Org. Chem. **35**, 4157 (1970).
34. A. STREITWIESER, JR. Molecular orbital theory for organic chemists. John Wiley and Sons Inc., New York. 1961.
35. L. HEISS, E. F. PAULUS, and H. REHLING. Justus Liebigs Ann. Chem. 1583 (1980).
36. C. S. MARVEL and W. S. SPERRY. Org. Synth. Coll. Vol. **1**, 95 (1964).
37. L. L. MILLER and R. F. BOYER. J. Am. Chem. Soc. **93**, 650 (1971).
38. J. E. HODGKINS and M. P. HUGHES. J. Org. Chem. **27**, 4187 (1962).
39. W. J. MIDDLETON, R. E. HECKERT, E. L. LITTLE, and C. G. KRESPAN. J. Am. Chem. Soc. **80**, 2783 (1958).

The preparation of some fused isothiazole derivatives

David M. McKinnon,[1] K. Ann Duncan, Aileen M. McKinnon, and Perry A. Spevack
Department of Chemistry, University of Manitoba, Winnipeg, Man., Canada R3T 2N2

Received June 26, 1984

David M. McKinnon, K. Ann Duncan, Aileen M. McKinnon, and Perry A. Spevack. Can. J. Chem. **63**, 882 (1985).

The treatment of di(2-amino-5-methylphenyl)methane with *N*-sulfinylmethanesulfonamide gives two materials, 3-(2-amino-5-methylphenyl)-5-methyl-2,1-benzisothiazole and what appears to be its tautomer, a 2,1-benzisothiazolo[2,3-*b*]-2,1-benzisothiazole derivative. Reaction of the former with methyl iodide gives mono-, di-, and trimethyl derivatives. The second of these also possesses the symmetrical 2,1-benzisothiazolo[2,3-*b*]-2,1-benzisothiazole structure. The structure of the other methylation product and of the acetylation products are discussed. Some 1,2-dithiol-3-ylidene-2-pyridylmethanes were made by condensation of 3-alkylthio-1,2-dithiolium salts with methyl 2-pyridylacetate. These demonstrate little sulfur–nitrogen interaction. 3-Methylthio-4-phenyl-1,2-dithiolium iodide reacts anomalously with methyl 2-pyridylacetate to form a quinolizinethione. 1,2-Benzisothiazolo[2,3-*a*]pyridinium triiodide was made by iodine oxidation of 2-(2-mercaptophenylpyridine).

David M. McKinnon, K. Ann Duncan, Aileen M. McKinnon et Perry A. Spevack. Can. J. Chem. **63**, 882 (1985).

La réaction du di(amino-2 méthyl-5 phényl) méthane avec le *N*-sulfinylméthanesulfonamide conduit à deux produits, le (amino-2 méthyl-5 phényl)-3 méthyl-5 benzisothiazole-2,1 et ce qui semble être son tautomère, un dérivé benzisothiazolo-2,1[2,3-*b*] benzisothiazole-2,1. La réaction du premier produit avec l'iodure de méthyle fournit des dérivés mono-, di- et triméthylés. Le deuxième de ces dérivés possède aussi la structure benzisothiazolo-2,1 [2,3-*b*] benzisothiazole. On discute de la structure des autres produits de méthylation et d'acétylation. On a préparé quelques dithiol-1,2 ylidène-3 pyridyl-2 méthanes par condensation de sels d'alkylthio-3 dithiolium-1,2 avec le pyridyl-2 acétate de méthyle. Ceci démontre qu'il n'y a que peu d'interaction entre le soufre et l'azote. L'iodure du méthylthio-3 phényl-4 dithiolium-1,2 réagit d'une façon anormale avec le pyridyl-2 acétate de méthyle; il en résulte la formation d'une quinolizinethione. On a préparé le triiodure du benzisothiazolo-1,2 [2,3-*a*] pyridinium par une oxydation à l'iode de la (mercaptophényl-2 pyridine)-2.

[Traduit par le journal]

Introduction

This paper will describe the preparation and properties of a number of fused systems containing actual or potential fused isothiazole rings which have been made as part of continuing studies on isothiazoles.

The 1,2-dithiolo[1,5-*b*]-1,2-dithioles[2] (**1**) are compounds in which the central sulfur atom possesses interesting valency properties, and many examples of compounds of this type have been described (1, 2). In fact many structural variations are possible to give compounds of analogous structure and properties, provided that the central atom is capable of valency shell expansion (1–3). Nevertheless, attempts to synthesize a dibenzo derivative of the system **1** have failed (4), although monobenzo derivatives are known. The most reasonable suggestion for this is that there is a steric repulsion of the interior *ortho* hydrogen atom on the benzo rings (2), since some dibenzo derivatives *linked* in the *ortho* positions do exist (5–7). Also, the 1,2-oxathiolo[1,5-*e*]-1,2-oxathiole system is known as the parent heterocycle, simple derivatives, a benzo, and as a dibenzo derivative (**2***b*) (8–11). In the dibenzo system the shortened S—O bond distances so change the geometry of the system that the *ortho* hydrogen atoms are no longer in a position for steric interference.

It was therefore of interest to construct isothiazole analogs of the dibenzo derivatives, i.e. the 2,1-benzisothiazolo[2,3-*b*]-2,1-benzisothiazole system (**2***c*), to further test this suggestion. Although some isothiazole analogs are known (12), these are of the parent heterocycle and simpler derivatives. No benzo derivatives appear to have been described.

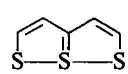

1

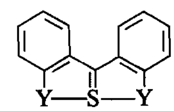

2

a Y = S
b Y = O
c Y = NR

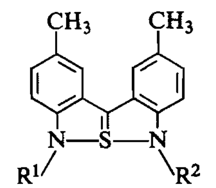

3

a $R^1 = R^2 = H$
b $R^1 = R^2 = CH_3$
c $R^1 = H, R^2 = CH_3$
d $R^1 = H, R^2 = COCH_3$

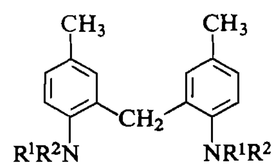

4

a $R^1 = R^2 = H$
b $R^1 = H, R^2 = CH_3$
c $R^1 = H, R^2 = COCF_3$
d $R^1 = Me, R^2 = COCF_3$

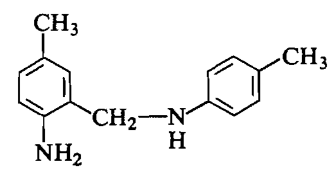

5

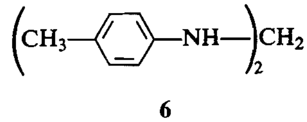

6

We directed our attention to the compounds of type **3** as being some of the simplest with respect to nitrogen substitution because the ring substituents would provide both a suitable nmr probe and facilitate the *ortho–ortho* linking of an aromatic amine starting material. The diamine **4***a* was a suitable starting material since 2,1-benzisothiazoles have been prepared from *o*-toluidine derivatives by reaction with either thionyl chloride

[1] Author to whom correspondence may be addressed.

[2] These compounds have been named variously as thiathiophthenes or 1,6,6aλ^4-trithiapentalenes. Similarly the compound **2***c* could be named as a thiadiazaindenoindene. However, in this paper we will use the nomenclature systems of Chemical Abstracts. The naming of these compounds has been discussed by N. Losac'h (1).

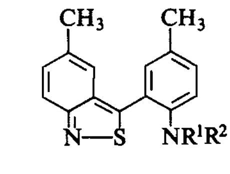

7

a R[1] = R[2] = H
b R[1] = H, R[2] = CH_3
c R[1] = H, R[2] = $COCH_3$
d R[1] = R[2] = $COCH_3$

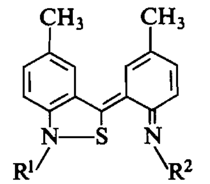

8

a R[1] = H, R[2] = CH_3
b R[1] = CH_3, R[2] = H

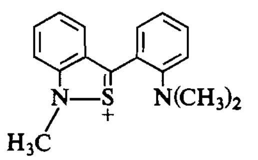

9

(13, 14) or *N*-sulfinylmethanesulfonamide (15, 16), which is reported to give better yields. This diamine **4***a* had been prepared (17) by the rearrangement of the amine **5**, itself prepared from the amine **6**, but we found it simpler to prepare the diamine **4***a* directly by a modified procedure. Treatment of **4***a* with *N*-sulfinylmethanesulfonamide gave a reddish oil whose mass spectrum was consistent with a compound of formula $C_{15}H_{14}N_2S$, i.e. that of the compound **3***a*. The nmr spectrum indicated two equivalent methyl groups (at δ = 2.33 ppm). A broad peak at δ = 6.55 ppm may be due to NH protons. However, over several days this oil crystallized to a yellow solid, which was also the product obtained when attempts were made to purify the oil by chromatography. This material had an analysis and mass spectrum corresponding to $C_{15}H_{14}N_2S$, but since the nmr spectrum showed non-equivalency of the two methyl groups (at δ = 2.30 and 2.40 ppm), it appears that this compound is the isomeric 3-(2-amino-5-methylphenyl)-5-methyl-2,1-benzisothiazole (**7***a*). Since the methyl protons of 5-methyl-2,1-benzisothiazoles absorb at δ = 2.30–2.33 ppm (16, 17), it is likely that the protons at δ = 2.42 are those of the methyl group on the phenyl substituent. It therefore appears likely that **3***a* and **7***a* are tautomers. This compound exhibited a broad absorption at δ = 3.8 ppm which disappeared on shaking with deuterium oxide and is assigned to the amino group protons. Also, when the reddish oil was shaken with deuterium oxide, its spectrum changed to that of the yellow solid.

Since the tautomerism should be blocked by *N*-alkylation, the solid material was treated with methyl iodide, giving three products, corresponding to mono-, di-, and trimethyl derivatives. The second of these was a deep crimson crystalline solid whose nmr showed only two types of methyl peaks, at δ = 3.71 and 2.67 ppm, corresponding in chemical shift to *N*- and *C*-methyl groups respectively. In addition, the spectrum of the aromatic protons demonstrated a typical ABX pattern. The ^{13}C nmr spectrum of **3***b* demonstrated the presence of only nine types of carbon atom, four of which were quaternary. These properties are consistent with the symmetrical structure of 1,4,8,11-tetramethyl-2,1-benzisothiazolo[2,3-*b*]-2,1-benzisothiazoles (**3***b*). It thus appears that the shorter S—N bond lengths in **3***b*, like those in compounds of type **2***b*, so favorably affect the geometry compared to dithiole analogs that the interior *ortho* hydrogen atoms do not interfere with each other.

It should also be noted that the spectrum of the aromatic protons in the putative **3***a* resembled those of **3***b*.

The monomethylated material was a yellow solid whose nmr spectrum indicated three different methyl groups, one of which was in the range expected for an *N*-methyl group. Since the two others, at δ = 2.33 and 2.42 ppm, are in the range observed for the yellow compound **7***a*, we consider on this basis that it is 5-methyl-3-(2-methylamino-5-methylphenyl)-2,1-benzisothiazole (**7***b*). Three other structures, the imines **8***a* and *b* and the fused structure **3***c* are eliminated for the following reasons: the imines **8***a*,*b* are *o*-quinonoid structures, and expected to be unstable, and in the fused structure **3***c* the aromatic methyl groups would be expected to be much more equivalent than found, by comparison with the compounds **2***a* and *b*. It is recognized that **8***a* and *b* and **3***c* may be resonance contributors to a single structure. The third material, obtained only in small amounts, appears on the basis of its solubility, and that it contains iodine, to be a salt, probably 1-methyl-3-(2-dimethylaminophenyl)-2,1-benzisothiazolium iodide (**9**).

We also attempted to make the compound **3***b* from di(2-methylamino-5-methylphenyl)methane (**4***b*). The synthesis of this compound from *N*-methyl *p*-toluidine is reported (17) although no experimental details were given. We therefore made it from the amine **4***a* by conversion to its *bis*-trifluoroacetamide **4***c* (18). Although such amides are reported (19, 20) to give secondary amines directly on treatment with methyl iodide and potassium hydroxide, with this compound we isolated the *N*,*N'*-dimethyl *bis*-trifluoroacetamide (**4***d*) which afforded **4***b* on prolonged alkaline hydrolysis. When this was treated with *N*-sulfinylmethanesulfonamide we were unable to isolate any isothiazole products. In contrast to **4***a*, the compound **4***b* cannot form an *N*-sulfinylamine. It has been suggested (14) that *N*-sulfinylamines are necessary intermediates in the conversion of *o*-toluidines to 2,1-benzisothiazoles. It also seems likely that if the bicyclic structure **3***a* is indeed produced in the above reaction, it is formed by tautomerism of an initially formed 3-(2-amino-5-methylphenyl-5-methyl-2,1-benzisothiazole (**7***a*).

Treatment of the compound **3***a* with acetic anhydride gave two products, corresponding to mono- and diacetyl derivatives. Since the former showed only two methyl singlets in the ratio of 1:2, it therefore appears that the two aromatic methyl peaks are fortuitously equivalent. Two structures, **3***d* and **7***c*, are possible. Because of the close similarity of the methyl groups in the bicyclic structure **3***d* we are inclined to favor this structure. This material also exhibited a broad peak at δ = 6.75 ppm which, as noted above, may be indicative of an N—H group in the bicyclic structure. The diacetyl derivative possessed two non-equivalent aromatic methyl groups, ruling out a symmetrical structure, and the most likely possibility is therefore the imide **7***d*. Although satisfactory nmr and mass spectra were obtained for these materials, they appear to be too unstable for proper analysis. 2,1-Benzisothiazoles and 2,1-benzisoxazoles rearrange to oxazines on treatment with acetic anhydride (21, 22) but these types of reactions require structural features not present here.

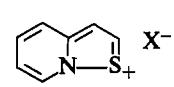

10

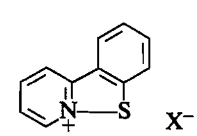

11

a X = I_3
b X = ClO_4

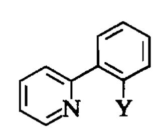

12

a Y = NH_2
b Y = SCSOEt
c Y = SH

Other types of compounds containing interesting fused isothiazole type nuclei are the isothiazolo[2,3-*a*]pyridinium salts **10** and 1,2-benzisothiazolo[2,3-*a*]pyridinium salts **11**, some of which have been made by oxidation of suitable thiones (23) or acid treatment of certain thiocyanates (24). In this work 2-(2-aminophenyl)pyridine (**12***a*) was diazotized and converted via the xanthate **12***b* to 2-(2-mercaptophenyl)pyridine (**12***c*), which on iodine oxidation gave the salt **10***a*. Treatment of this with perchloric acid gave the known (24) perchlorate **10***b*.

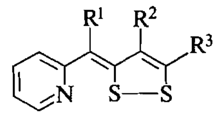

13

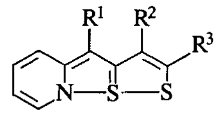

14

a $R^1 = CO_2Me$, $R^2 = H$, $R^3 = Ph$
b $R^1 = CO_2Me$, $R^2 = R^3 = Ph$
c $R^1 = CO_2Me$, $R^2 = R^3 = (CH{=}CH)_2$
d $R^1 = CO_2Me$, $R^2 = Ph$, $R^3 = H$
e $R^1 = R^2 = H$, $R^3 = Ph$
f $R^1 = H$, $R^2 = R^3 = Ph$
g $R^1 = CO_2Me$, $R^2 = Ph$, $R^3 = H$

Other compounds which may possess to some extent a fused isothiazole structure are 1,2-dithiole-3-ylidine-2-pyridylmethanes (**13**), if possible resonance structures **14** are considered. These compounds are therefore analogous to compounds in which similar interaction between the nitrogen atom of a pyrimidine or pyridine ring and the sulfur atom of a thiadiazole ring has been demonstrated (25, 26), although crystal studies (27) on a more related compound, 3-methyl-6-(5-phenyl-1,2-dithiol-3-ylideneamino)pyridine have in fact demonstrated only slight sulfur–nitrogen interaction. These compounds **13***a*–*c* were made by condensation of methyl 2-pyridylacetate with the appropriate 3-alkylthio-1,2-dithiolium salts and, of these, **13***a*, *b* gave the compounds **13***e*, *f* on acidic hydrolysis. With **13***c* the hydrolysis proceeded more extensively, giving benzo-1,2-dithiole-3-one. An examination of the ^{13}C spectra of **13***e*, *f* showed no absorption in the region δ = 170–180 ppm, which appears to be fairly characteristic of a number of compounds possessing hypervalent sulfur (2), e.g. 1,2-dithiolo[1,5-*b*]-1,2-dithioles and related compounds, and it thus appears that these compounds too are best represented by structures **13**.

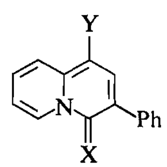

15

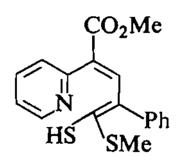

16

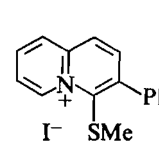

17

a X = S, Y = CO_2Me
b X = O, Y = CO_2Me
c X = S, Y = H

The reaction of 3-methylthio-4-phenyl-1,2-dithiolium iodide with methyl 2-pyridylacetate gave two compounds. One of these, obtained in low yield, corresponds to the condensation product **13***d*. The major product, a yellow crystalline solid, had properties consistent with a molecular formula of $C_{17}H_{13}NO_2S$ and appears to be a carboxylic ester. This is tentatively assigned the quinolizinethione structure **15***a* on the following basis: consideration of reaction mechanisms involving nucleophilic attack on the unhindered 5-position of the dithiolium salt would lead to the dithioester **16** or enethiol, which could form **15** by electrocyclization and loss of methanethiol. The ^{13}C nmr of the material exhibited an absorption at δ = 175.6 ppm, which is in the range exhibited by 2-pyridinethiones (29). Treatment of **15***a* with potassium permanganate in acetone afforded the quinolizinone **15***b*, and acid hydrolysis produced the quinolizinethione **15***b* which on methylation gave the salt **17**.

Experimental

The ^1H and ^{13}C nmr spectra were obtained in deuteriochloroform solution using tetramethylsilane as an internal standard, on a Varian model E.M. 360 spectrometer and on a Bruker model AM-300 spectrometer, respectively. Mass spectra were obtained on a Finnigan model 1015 spectrometer, and thick layer chromatography (tlc) was performed on Merck "Kieselgel 60 PF" silica gel. Where necessary, solutions were dried over anhydrous magnesium sulfate.

Di-p-toluidinylmethane (6)

This was prepared by the method of Eberhardt and Welter (28) and the product recrystallized from ethanol as pale yellow shiny leaflets, mp 85–87°C (lit. (28) mp 86°C).

Di-(2-amino-5-methylphenyl)methane (4a)

The method of Chakrabarti et al. (17) was modified as follows. Di-*p*-toluidinylmethane (**6**) (0.18 mol), *p*-toluidine hydrochloride (0.18 mol), and *p*-toluidine (1.8 mol) were mixed as solids, heated under nitrogen to 130°C, and stirred at this temperature for 14 h. On cooling, the mixture was neutralized with a slight excess of sodium hydroxide solution and *p*-toluidine was removed by steam distillation. The tarry residue was dissolved in warm 6 *M* hydrochloric acid, resinous material filtered off, and the filtrate slowly neutralized to pH 7 with sodium hydroxide solution. The brown amorphous mass which precipitated was kept at 5°C for 3 days and filtered. Recrystallization from hexane gave colorless needles, mp 93–94°C (lit. (17) mp 96°C).

Bis(2-trifluoroacetamido-5-methylphenyl)methane (4c)

The product was prepared from the diamine **3***a* by the method of Bruice et al. (19). Recrystallization from ethanol/water (1:3) gave colorless plates, mp 250–251°C.

*Bis(2-(*N*-methyltrifluoroacetamido)-5-methylphenyl)methane (4d)*

The method of Johnstone et al. (20) was modified as follows. The bis-trifluoroacetamide **4***c* (1.7 mmol), methyl iodide (9.4 mmol), and powdered potassium hydroxide (6.4 mmol) were added to dry acetone (20 mL) and the mixture refluxed for 30 min. Acetone and methyl iodide were removed *in vacuo*, and the resulting material dissolved in chloroform and filtered to remove potassium hydroxide. Evaporation of the filtrate gave a colorless viscous oil which crystallized on standing. Addition of petroleum ether gave colorless needles (83%), mp 100–101°C. This material was not analysed.

Di-(2-methylamino-5-methylphenyl)methane (4b)

The bis-*N*-methyltrifluoroacetamide **4***d* (1.5 mmol) was added to powdered potassium hydroxide (6.0 mmol) in water (10 mL) and methanol (5 mL), and the mixture refluxed for 17 h, cooled, acidified with 2 *N* hydrochloric acid, and extracted with chloroform. Drying followed by evaporation gave a colorless oil which crystallized on standing or upon addition of petroleum ether. Recrystallization from hexanes gave **4***b* as colorless prisms (77%), mp 88–89°C (lit. (17) mp 86°C).

*Reaction of di(2-amino-5-methylphenyl)methane (4a) with *N*-sulfinylmethane-sulfonamide to form 7a*

The procedure of Singerman (15) was used. Extraction of the final product with chloroform, followed by drying and evaporation, gave a viscous reddish oil which appears (tlc) to be substantially pure. This oil crystallized on standing several days and was further purified by chromatography. Isolation of a yellow band gave on work-up a deep yellow oil which crystallized on scratching. Recrystallization from hexane with rapid cooling gave deep yellow plates, mp 113–115°C (55%).

In some cases no reddish oil was obtained and the product gave yellow crystalline material directly on work-up. For the yellow material *7a*, The nmr spectrum, δ: 2.30 and 2.42 (two 3H singlets, the methyl groups), 3.75 (2H, broad, the NH_2 protons), 6.60–7.75 (6H bands, the aromatic protons) ppm. The mass spectrum M^+ 254, *M* calcd. 2.54. *Anal.* calcd. for $C_{15}H_{14}NS_2$: C 70.87, H 5.51, N 11.02, S 12.60; found: C 70.84, H 5.69, N 10.87, S. 12.41%.

For the reddish oil, tentatively **2***a*, the mass spectrum M^+ 254, *M* calcd. 254. The nmr spectrum, δ 2.35 ppm (two 3H singlets, the methyl groups), 6.55 (2H, broad, the two NH protons), 6.87–7.75 (6H bands, the aromatic protons) ppm. Treatment with D_2O gave a spectrum like that of **7***a*.

Reaction of 4b *with* N-*sulfinylmethanesulfonamide*

The procedure used was identical to that used for **3***a* (15). The final extraction showed no presence of the expected isothiazole **3***b* or of any other major product.

Reaction of 3a *with methyl iodide*

The 2,1-benzisothiazole **3***a* (0.4 mmol) and methyl iodide (5 mL) were heated under reflux for 20 h, methyl iodide removed *in vacuo*, and the resultant dark red solid chromatographed several times on silica in various chloroform/acetone blends. The monomethylation product **7** was a relatively non-polar yellow band which was isolated to give a yellow crystalline material (30%). Recrystallization from hexane gave deep yellow needles, mp 140–141°C. The nmr spectrum, δ: 2.33, 2.42 (two 3H singlets, the aromatic methyl groups), 2.82 (3H singlet, the *N*-methyl group), 3.75 (3H singlet, the *N*-methyl group), 3.75 ppm (1H, broad, the NH proton), 6.67–7.88 (6H bands, the aromatic protons) ppm. The mass spectrum M^+ 268, *M* calcd. 268. *Anal.* calcd. for $C_{16}H_{16}N_2S$: C 71.61, H 6.01, N 10.44, S 11.95; found: C 71.24, H 5.75, N 10.35, S 12.24%.

The dimethylation product **2***b* was a deep-red crystalline material and recrystallization from ethanol gave ruby colored prisms, mp 167–168°C. The nmr spectrum δ: 2.67 and 3.71 (two 6H's, the aromatic and *N*-methyl protons), 7.13–7.51 and 8.55–8.66 (4H, m and 2H, m respectively, the aromatic protons) ppm. When the peak at δ = 2.67 ppm was irradiated, the aromatic protons exhibited an ABX type pattern, J_{AB} = 8.5 Hz. The mass spectrum M^+ found: 282, *M* calcd.: 282. *Anal.* calcd. for $C_{17}H_{18}N_2S$: C 72.30, H 6.42, N 9.92, S 11.35; found: C 72.08, H 6.40, N 9.80, S 11.53%.

The third component, obtained in only a small amount (10 mg), was a highly polar deep yellow band which gave a dark yellow semi-crystalline oil on isolation. It was purified by crystallization from cyclopentanone followed by washing with small amounts of dry acetone. Deep amber prisms, mp 243–244°C, were obtained. This was not analyzed but appears to be salt-like and containes iodine. It is tentatively given the structure **9**.

Reaction of 2a *with acetic anhydride*

The isothiazole **2***a* (0.4 mmol) and acetic anhydride (5 mL) were refluxed for 20 min, cooled, extracted with chloroform, the chloroform extract washed with water, and dried. Evaporation gave an orange oil which was chromatographed on silica in a chloroform/acetone (6:1) mixture yielding 2 components.

The monoacetylation product **2***d* was a colorless fluorescent band (R_f 0.6) and gave a pale yellow oil (51%) which crystallized on standing. Recrystallization from methanol gave pale yellow needles, mp 164–165.5°C. The nmr spectrum, δ: 1.93 (3H, s, the acetyl methyl), 2.43 (two 3H, s, the aromatic methyl), 6.75 (1H broad, the NH), 7.10–8.25 (6H bands, the aromatic protons) ppm. The mass spectrum M^+ 292, *M* calcd. 292.

The diacetylation product **6***d* was a colorless band (R_f 1) with a bright blue fluorescence and gave a bright yellow oil (46%) upon isolation. The nmr spectrum, δ: 2.21 (6H, s, the acetyl methyls), 2.45, 2.57 (two CH_3, s, the aromatic methyls), 7.18–7.95 (6H bands, the aromatic protons) ppm. The mass spectrum M^+ 338, *M* calcd. 338. When the reaction time was increased to 1 h, the yield of **2***d* decreased to 11% while that of **6***d* increased to 87%.

These compounds begin to decompose after a few days and no satisfactory analyses were obtained.

*2-(2-Aminophenyl)pyridine (12*a*)*

2-(2-Nitrophenylpyridine) (ref. 30) (20 g, 0.1 mol) in 50% aqueous ethanol (50 mL) was warmed gently and sodium dithionite added slowly until the yellow color of the solution had disappeared. The solution was concentrated to remove ethanol and extracted with chloroform, which on evaporation gave the amine **10***a* as a colorless oil (80%).

*2-(2-Mercaptophenyl)pyridine (12*b*)*

2-(2-Aminophenylpyridine) (8.5 g, 0.05 mol) in dilute hydrochloric acid was diazotized and the mixture added to a warm (50°C) solution of potassium ethylxanthate (20 g) in water (100 mL). The mixture was allowed to cool and the oil extracted with chloroform. The dried chloroform extract was evaporated and the residual oil hydrolyzed in 20% aqueous sodium hydroxide solution at 100°C for 3 h. The mixture was treated with sodium dithionite (1 g) and refluxed 1 h more. The solution was separated from any unhydrolyzed material by decantation or filtration, adjusted to pH 7 with concentrated hydrochloric acid, and treated with ether. The dried ether extract gave the crude mercaptan as a yellow oil which was used directly in the next stage. Yield 2.5 g; 29%.

*2,1-Benzisothiazolo[2,3-*a*]pyridinium triodide (11*a*)*

The crude 2-(2-mercaptophenyl)pyridine (1.81 g, 0.01 mol) in ethanol (15 mL) was treated with a saturated solution of iodine in ethanol until precipitation of the crystalline product was complete. The product was filtered and recrystallized from nitromethane as brown needles, mp 166°C (60% based on crude starting material). *Anal.* calcd. for $C_{11}H_8NSI_3$: C 23.28, H 1.41, N 2.47, S 5.64, I 67.20; found: C 23.03, H 1.34, N 2.48, S 5.52, I. 67.07%. This material was treated in boiling acetic acid with perchloric acid and boiled to expel iodine, giving the perchlorate (**11***b*), mp 168°C (lit. (24) mp 168–169°C).

*Reaction of 1,2-dithiolium salts with methyl 2-pyridylacetate to form methyl 1,2-dithiol-3-ylidene-2-pyridylacetates (13*a–c*)*

The 3-methylthio-1,2-dithiolium salts (0.01 mol) and methyl 2-pyridylacetate (1.5 g) in acetonitrile (20 mL) were warmed gently for 5 min. The evolution of methanethiol was evident and the mixture became homogeneous. The solutions were diluted with water and extracted with chloroform, which was dried. Evaporation yielded red oils which crystallized on trituration with ethanol. Compounds were recrystallized from hexane–benzene, 1:1 mixtures. Results are summarized in Table 1.

*Hydrolysis of methyl 1,2-dithiol-3-ylidene-2-pyridylacetates to form 1,2-dithiol-3-ylidene-2-pyridylmethanes (13*c, f*)*

The esters (0.5 g) **12***a–c* were treated with amixture of acetic acid (5 mL) and concentrated hydrochloric acid (5 mL) under reflux for 24 h. Solutions were diluted with water and neutralized with sodium bicarbonate. The dried chloroform extracts were evaporated, giving the products as red or orange crystals which were recrystallized from toluene. Results are summarized in Table 1. Compound **12***c* gave only benzo-1,2-dithiole-3-one on hydrolysis.

*Reaction of 3-methylthio-4-phenyl-1,2-dithiolium iodide with methyl 2-pyridylacetate to form the quinolizenethione (15*a*)*

This reaction was performed as for the other 1,2-dithiolium salts. Work-up gave a viscous red oil which slowly crystallized under ethanol. The product (**15***a*) was collected and recrystallized from ethanol as fibrous yellow needles, mp, 166–168°C (61%). Work-up of the mother liquor gave more of this material and a small amount of the ester **13***g*.

For **15***a*, the ^{1}H nmr spectrum δ: 3.91 (3H, s, the methyl protons), 7.46–9.60 (10H bands, the aromatic and heterocyclic protons) ppm. The ^{13}C nmr spectrum, δ: 175.61 (C=S), 165.42 (C=O) ppm. The mass spectrum $M^+ - 1$ found: 294, $M - 1$ calcd.: 294. *Anal.* calcd. for $C_{17}H_{13}NSO_2$: C 69.15, H 4.41, N 4.75, S, 10.85; found: C 69.05, H 4.47, N 4.72, S 10.83%.

TABLE 1. Preparation of methyl 1,2-dithiol-3-ylidene-2-pyridylacetates (**12***a*–*c*) and 1,2-dithiol-3-ylidene-2-pyridylmethanes (**12***e*, *f*)

				Analysis							
				Calculated				Found			
Compound	Yield (%)	Melting point (°C)	Formula	C	H	N	S	C	H	N	S
12*a*	67	120–121	$C_{17}H_{13}NO_2S_2$	62.39	3.98	4.28	19.57	62.41	4.22	4.18	19.46
12*b*	95	214–215	$C_{23}H_{17}NO_2S_2$	68.49	4.22	3.47	15.88	68.66	4.03	3.61	15.92
12*c*	63	116–128*	$C_{15}H_{11}NO_2S_2$	59.80	3.65	4.65	21.26	59.61	3.39	4.43	21.51
12*d*	3	150–152	$C_{17}H_{13}NO_2S_2$	62.39	3.98	4.28	19.57	62.44	4.11	4.40	19.62
12*e*	79	153–154	$C_{15}H_{11}NS_2$	66.91	4.09	5.20	23.79	67.05	4.18	5.11	23.86
12*f*	82	175–176	$C_{12}H_{15}NS_2$	73.04	4.35	4.06	18.55	73.11	4.18	4.17	18.67

*This material appears (by nmr spectrum) to be a 3:1 mixture of two components, probably the two geometrical isomers. We have been unable to separate these by chromatography or crystallization.

*Preparation of methyl 3-phenyl-4-oxo-4*H*-quinolizine-1-carboxylate (15*b*)*

Methyl 3-phenyl-4-thio-4*H*-quinolizine-1-carboxylate (295 mg, 1 mmol) in acetone (10 mL) was titrated with a saturated solution of potassium permanganate in acetone until th solution just retained a purple color on standing. The mixture was filtered to remove manganese dioxide and purified by tlc using ether as an eluent. The product ran as a yellow band with a blue halo under uv light. Work-up and crystallization from an ethanol–benzene 1:1 mixture gave the product as bright yellow needles, mp 139.5–140.5°C (91%). The nmr spectrum, δ: 3.86 (3H, s, the methyl protons), 7.27–9.45 (10H bands, the aromatic and heterocyclic protons). The mass spectrum M^+ found: 279, *M* calcd.: 279. *Anal.* calcd. for $C_{17}H_{13}NO_3$: C 73.12, H 4.66, N 5.02; found: C 73.22, H 4.61, N 5.18%.

*Preparation of 3-phenyl-4*H*-quinolizine-4-thione (15*e*)*

The ester **15***a* (294 mg, 1 mmol) in acetic acid (10 mL), concentrated hydrochloric acid (10 mL), and water (10 mL) was refluxed 24 h. The yellow solution was neutralized with solid sodium bicarbonate and extracted with chloroform (3 × 50 mL). These extracts were dried and evaporated to give a yellow oil which was purified by chromatography. The material crystallized from ethanol as yellow needles, mp 135–136°C (91%). The mass spectrum, $M^+ - 1$ calcd.: 236, $M - 1$ found: 236. *Anal.* calcd. for $C_{15}H_{11}NS$: C 75.95, H 4.64, N 5.91, S 13.50; found: C 75.81, H 4.72, N 5.88, S 13.60%.

Preparation of 4-methylthio-3-phenylquinolizinium iodide (17)

3-Phenyl-4*H*-quinolizine-4-thione (118 mg, 0.5 mmol) was treated with methyl iodide (2 mL). The thione dissolved rapidly but soon precipitated a yellow oil which eventually crystallized. The material was collected and recrystallized from nitromethane with precipitation by ether as yellow needles, mp 146–148°C (97%). *Anal.* calcd. for $C_{16}H_{14}INS$: C 50.56, H 3.69, I 33.51, N 3.69, S, 8.44; found: C 50.47, H 3.81, I 33.45, N 3.69, S 8.81%.

Acknowledgements

We wish to thank the Natural Sciences and Engineering Research Council of Canada for financial support of this work. We also wish to thank Mr. W. Buchannon for preparation of the mass spectra, and Mr. K. Marat for preparation of the nmr spectra.

1. N. LOSAC'H. 1,6,6aS^{IV}-Trithiapentalenes and related structures. *In* Advances in heterocyclic chemistry. Vol. 13. *Edited by* A. R. Katritzky and A. J. Boulton. Academic Press, New York. 1971.
2. C. T. PEDERSEN. Sulfur Reports, **1**, 1 (1980).
3. A. G. BRIGGS, J. CZYZEWSKI, and D. H. REID. J. Chem. Soc. Perkin Trans. 1, 2340 (1979).
4. E. KLINGSBERG. J. Org. Chem. **37**, 3226 (1972).
5. E. P. GOODINGS, D. A. MITCHARD, and G. OWEN. J. Chem. Soc. Perkin Trans. 1, 1310 (1972).
6. N. R. AYYANGAR, S. R. PURAO, and B. D. TILAK. Indian. J. Chem. **16**B, 673 (1978).
7. (*a*) S. DAVIDSON, D. LEAVER, and J. H. STEVEN. *In* Organic sulfur chemistry, structure, mechanism and synthesis. *Edited by* C. J. M. Stirling. Butterworth, London. (1975). p. 443; (*b*) S. DAVIDSON, T. J. GRINTER, D. LEAVER, and J. H. STEVENS. J. Chem. Res (S), 221 (1980).
8. D. H. REID and R. G. WEBSTER. J. Chem. Soc. Perkin Trans. 1, 775 (1975).
9. I. H. POMERANTZ, L. J. MILLER, E. LUSTIG, D. MASTBROOKE, E. NANSEN, R. BARRON, N. OATES, and J.-Y. CHEN. Tetrahedron Lett. 5307 (1969).
10. I. H. POMERANTZ, L. J. MILLER, R. BARRON, D. MASTBROOK, and I. EGRY. Tetrahedron, **28**, 2183 (1972).
11. B. KRISCHE, W. WALTER, and G. ADIWIDJAJA. Chem. Ber. **115**, 3842 (1982).
12. A. S. INGRAM, D. H. REID, and J. D. SYMON. J. Chem. Soc. Perkin Trans. 1, 242 (1974).
13. M. DAVIS and A. W. WHITE. J. Chem. Soc. Chem. Commun. 1547 (1968).
14. M. DAVIS and A. W. WHITE. J. Org. Chem. **34**, 2985 (1969).
15. G. M. SINGERMAN. J. Heterocycl. Chem. **12**, 877 (1975).
16. B. DANYLEC and M. DAVIS. J. Heterocycl. Chem. **17**, 533 (1980).
17. P. CHAKRABARTI, K. VENKATESAN, T. S. CAMERON, T. DEMIR, and R. A. SHAW. J. Chem. Soc. Perkin Trans. 1, 206 (1981).
18. V. KLINGEBEIL and D. BESTMANN. Z. Naturforsch. Teil B, **34**, 123 (1979).
19. T. C. BRUICE, T. W. CHAN, J. P. TAULANE, I. YOKOE, D. L. ELLIOT, R. F. WILLAMS, and M. NOVAK. J. Am. Chem. Soc. **99**, 6713 (1977).
20. R. A. W. JOHNSTONE, D. W. PAYLING, and C. THOMAS. J. Chem. Soc. C, 2223 (1969).
21. M. DAVIS and S. P. POGANY. J. Heterocycl. Chem. **14**, 267 (1977).
22. K.-H. WUNSCH and A. J. BOULTON. Indoxazines and anthranils. *In* Advances in heterocyclic chemistry. Vol. 8. *Edited by* A. R. Katritzky and A. J. Boulton. Academic Press, New York. 1967.
23. G. G. ABBOTT and D. LEAVER. J. Chem. Soc. Chem. Commun. 150 (1973).
24. R. C. DAVIS, T. J. GRINTER, D. LEAVER, and R. M. O'NEIL. Tetrahedron Lett. 3339 (1979).
25. R. L. N. HARRIS. Aust. J. Chem. **25**, 993 (1972).
26. K. T. POTTS and J. KANE. J. Org. Chem. **39**, 3783 (1974).
27. C. GLIDEWELL and D. C. LILES. Acta Crystallogr. Sect. B, **37**, 1451 (1981).
28. C. EBERHARDT and A. WELTER. Chem. Ber. **27**, 1804 (1984).
29. I. W. J. STILL, N. PLAVAC, D. M. MCKINNON, and M. S. CHAUHAN. Can. J. Chem. **54**, 280 (1976).
30. J. W. HAWORTH, I. M. HEILBRON, and D. H. HEY. J. Chem. Soc. 349 (1940).

Azides. Part V. A kinetic study of the formation of *N*-(*p*-toluenesulphonyl)-1*H*-azepine by thermolysis of *p*-toluenesulphonylazide in benzene under nitrogen pressure[1]

NAGARAJ R. AYYANGAR, RAMESH B. BAMBAL, DATTATRAYA D. NIKALJE, AND KUMAR V. SRINIVASAN
National Chemical Laboratory, Pune 411 008, India

Received July 6, 1984

NAGARAJ R. AYYANGAR, RAMESH B. BAMBAL, DATTATRAYA D. NIKALJE, and KUMAR V. SRINIVASAN. Can. J. Chem. **63**, 887 (1985).

The course of thermolysis of *p*-toluenesulphonylazide (**A**) in benzene at 160°C and 40.1 atm of nitrogen pressure was followed by analysis of the reactants and products in the reaction mixture by hplc. The rate measurements indicate that the reaction follows first-order kinetics with respect to the formation of *N*-(*p*-toluenesulphonyl)-1*H*-azepine (**B**) and *p*-toluenesulphonamide (**D**). The concentration–time profile is consistent with the formation of *p*-toluenesulphonylanilide (**C**) from the azepine (**B**). The rate constants indicate that the azepine (**B**) decomposes to the anilide (**C**) at the same rate at which it is formed.

NAGARAJ R. AYYANGAR, RAMESH B. BAMBAL, DATTATRAYA D. NIKALJE et KUMAR V. SRINIVASAN. Can. J. Chem. **63**, 887 (1985).

Faisant appel à la clhp pour analyser les réactifs et les produits présents dans les mélanges réactionnels, on a déterminé le cours de la thermolyse de l'azoture de *p*-toluènesulfonyle (**A**) en solution dans le benzène, à 160°C et sous 40,1 atmosphères d'azote. Les vitesses mesurées indiquent que la réaction est du premier ordre par rapport à la formation de la *N*-(*p*-toluènesulfonyl) 1*H*-azépine (**B**) et du *p*-toluènesulfonamide (**D**). Le profil concentration–temps est en accord avec une formation du *p*-toluènesulfonylanilide (**C**) à partir de l'azépine (**B**). Les constantes de vitesse indiquent que la vitesse de formation de l'azépine (**B**) est égale à sa vitesse de décomposition en anilide (**C**).

[Traduit par le journal]

Introduction

Thermal decomposition of *p*-toluenesulphonylazide in dimethyl terephthalate at atmospheric pressure has been shown to result in the formation of 2-*p*-toluenesulphonamidoterephthalate and *N*-*p*-toluenesulphonyl-2,5-dicarbomethoxy-1*H*-azepine in 5% and 15% yields, respectively (1). Electron-withdrawing functional groups such as carbomethoxy, acetyl, and nitro lead preferentially to the formation of *N*-sulphonylazepines, whereas electron-donating groups such as methyl predominantly yield the sulphonanilides. This has been attributed to the influence of the substituents on the stability of the benzaziridine intermediate complex formed initially (2). It has been reported that, in the thermolysis mixture of methyl sulphonylazide in benzene, mainly the sulphonanilide (C—H insertion product) and the sulphonamide (hydrogen abstraction product) could be detected. Methyl sulphonylazepine, the ring expansion product (C═C insertion product) was not isolated, although its formation was evident and it was trapped as its tetracyanoethylene adduct (3).

Recently, the facile synthesis of *N*-sulphonyl-1*H*-azepines in good yields by the nitrene insertion reaction under nitrogen pressure has been reported by us, in which it was also shown that pressure has a remarkable effect on such insertion product formation involving ring expansion (4). This communication deals with the course of this reaction, which was followed kinetically by estimating the unreacted azide (**A**), the azepine (**B**), the sulphonanilide (**C**), and the sulphonamide (**D**) in the reaction mixture at various intervals of time by high performance liquid chromatography (hplc). The kinetic data indicated the reaction pathway as shown in Scheme 1.

The sulphonanilide (**C**) is exclusively formed from the azepine (**B**), by a consecutive reaction in series, viz. **A** → **B** → **C**. The sulphonamide derivative (**D**) is formed by abstraction of two hydrogens by the sulphonylnitrene (**I**), in a parallel reaction.

In contrast, when the thermolysis was carried out at atmo-

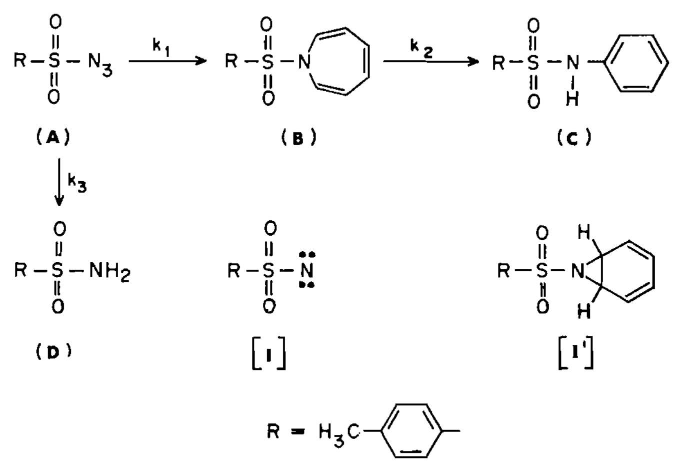

SCHEME I

spheric pressure and reflux temperature of benzene, the sulphonylazepine (**B**) was isolated only in poor yield (less than 1.5%). It was also shown that azepine formation increases with an increase in pressure. Furthermore, the reaction temperature of 155–160°C appeared to be critical. In one experiment, when the reaction was carried out at 140–145°C under otherwise similar reaction conditions, no sulphonylazepine (**B**) could be isolated. The use of nitrogen positive pressure serves the dual purpose of attaining the necessary critical temperature for the spontaneous irreversible thermolytic decomposition of the tosylazide (**A**) to the singlet nitrene (**I**), and of keeping the benzene in the liquid phase for a homogeneous reaction.

The interest in the azepine ring systems has been generated because of their presence in a number of drugs (5). The rhoeadine alkaloids have benzazepine as the basic structure (6). The sulphonyl azepines described here and elsewhere may exhibit promising biological activity.

Results and discussion

para-Toluenesulphonylazide was thermolysed in an excess

[1] NCL Communication No. 3403.

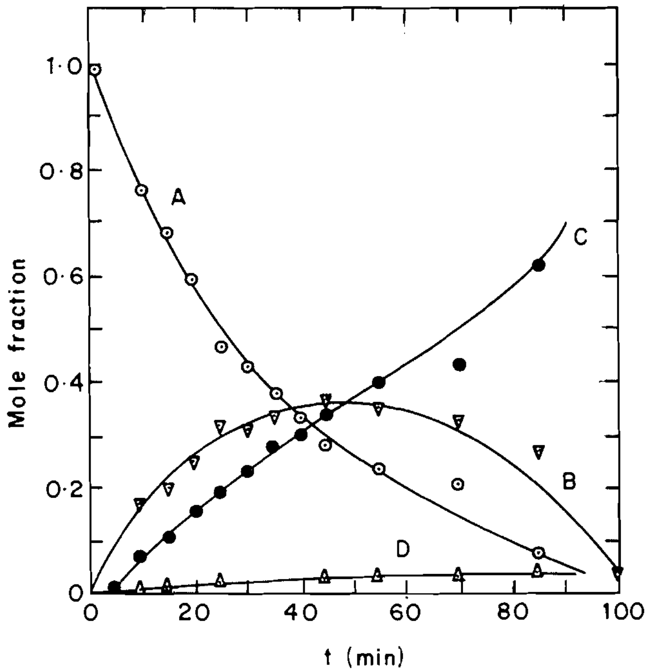

FIG. 1. Concentration–time curves.

of benzene at 160°C and 40.1 atm (1 atm = 101.3 kPa) of nitrogen pressure in a Parr autoclave. Aliquots of the reaction mixture were withdrawn at various intervals of time. They were subjected to hplc analysis for the estimations of the unconverted azide (**A**), and relative amounts of azepine (**B**), anilide (**C**), and amide (**D**), formed in the reaction (Table 1). Since benzene, one of the reactants, was in large excess, the reaction is zero order with respect to it. As such, it was removed from the samples before analysis. Preliminary investigations revealed that the reaction was initiated for a measurable conversion of the azide (**A**) to the nitrene (**I**) only at 160°C. Under the reaction conditions, this temperature was attained 50 min from the time the heating was started. This was taken to be the zero time of the reaction. The concentration vs. time curves for the azide (**A**), azepine (**B**), anilide (**C**), and amide (**D**) respectively are shown in Fig. 1. These are typical of those reported for consecutive first-order reactions (7). Since at the end of the reaction no azide (**A**) was present and the reaction could be carried out to complete conversion of the azepine (**B**) to the anilide (**C**), the thermolysis of *p*-toluenesulphonylazide (**A**) in benzene is a first-order consecutive irreversible reaction in series as shown in Scheme 1. The overall specific reaction rate ($k_1 + k_3$) for the thermal decomposition of the azide in benzene is the sum of the specific reaction rate for the formation of the azepine (**B**) (k_1) and that for the formation of the sulphonamide (**D**) (k_3) by a parallel reaction. Both reactions involve the nitrene (**I**) as intermediate.

The linear plot of $-\ln X_A$ vs. time t (Table 2, Fig. 2) indicated that the thermal decomposition of the azide **A** is a first-order reaction with an overall specific reaction rate

$$[1] \quad k_1 + k_3 = 0.028 \text{ min}^{-1}$$

The slope of the linear plot of X_B vs. X_D (Fig. 3) gives the value

$$[2] \quad k_1/k_3 = 5.349$$

TABLE 1. Analysis of compounds **A**, **B**, **C**, and **D**, in the reaction at different intervals of time by hplc

Reaction time t (min)	Composition X (mole fraction)			
	X_A	X_B	X_C	X_D
10	0.756	0.170	0.070	0.005
15	0.683	0.202	0.102	0.012
20	0.592	0.250	0.160	0.016
25	0.465	0.318	0.196	0.020
30	0.430	0.310	0.232	0.022
35	0.375	0.311	0.275	0.020
40	0.330	0.351	0.288	0.027
45	0.278	0.356	0.337	0.029
55	0.219	0.349	0.398	0.034
70	0.210	0.325	0.433	0.032
85	0.081	0.266	0.612	0.033
100	—	0.034	0.933	0.032

TABLE 2. Thermolysis of *p*-toluenesulphonyl azide in benzene at 160°C and at 40.1 atm

t (min)	X_A	$-\ln X_A$
5	0.996	0.004
10	0.756	0.28
15	0.683	0.38
20	0.592	0.52
25	0.465	0.77
30	0.430	0.84
35	0.375	0.98
40	0.330	1.11
45	0.278	1.28
55	0.219	1.52
70	0.210	1.56
85	0.082	2.50

Solving eq. [2] simultaneously with eq. [1], the values of k_1 and k_3 were evaluated as 0.0235 ± 0.0007 min^{-1} and 0.0044 ± 0.0001 min^{-1} respectively. To evaluate the value of k_2, the differential equation

$$[3] \quad \frac{dX_B}{dt} + k_2X_B = k_1e^{-k_1t}$$

for first-order consecutive irreversible reaction was simplified to

$$[4] \quad -\ln X_{B_{max}} = k_2t_{max}$$

Substituting the values for $X_{B_{max}}$ and t_{max} as 0.356 and 45 respectively from Fig. 1 and Table 1 in eq. [4], the value of k_2 was evaluated as 0.0228 ± 0.0006 min^{-1}. The second step of the series reaction was also confirmed to be first order by carrying out the reaction starting from different initial concentrations of the azide (**A**), under identical conditions. The mole fraction of the azepine (**B**) at t_{max}, i.e. $X_{B_{max}}$ remains constant and was independent of the initial azide concentration. Thus the results indicate that k_1 is nearly equal to k_2, in which case $X_{B_{max}} = 1/e = 0.368, \ldots$ from eq. [3]. The calculated value of $X_{B_{max}}$ as derived above matches well with the experimental value of 0.356 for $X_{B_{max}}$ (Fig. 1).

The kinetic data generated by us clearly indicate that the nitrene insertion in benzene at 160°C under pressure preferentially forms the sulphonyl azepine (**B**), possibly via the ben-

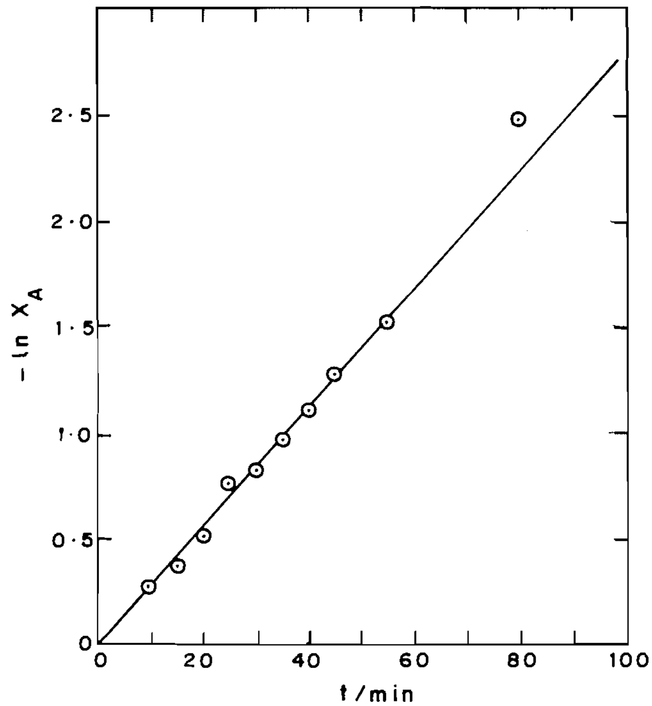

FIG. 2. First-order plot for the decomposition of azide **A** in benzene.

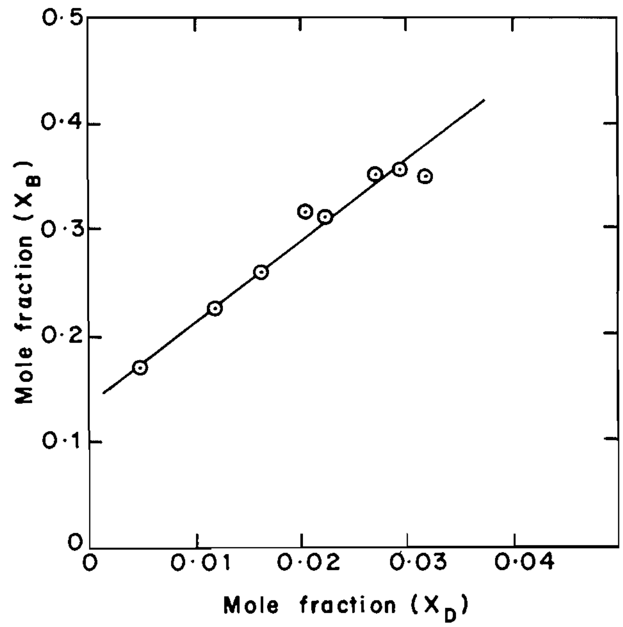

FIG. 3. Linear plot for the determination of k_1/k_3.

zaziridine intermediate (**I′**). The sulphonylazepine (**B**) then rearranges to the sulphonanilide (**C**) in a concerted manner, possibly involving a carbon–carbon σ-bond formation followed by aromatization. The rate constant evaluations show that the azepine (**B**) rearranges to the anilide (**C**) at the same rate at which it is formed. This indicates that, under the conditions of the reaction, both steps, viz. the formation of the azepine (**B**) and subsequent conversion to the sulphonanilide (**C**), are kinetically controlled.

Experimental

Melting points were recorded in capillary tubes. Benzene used for the reaction was distilled on phosphorous pentoxide. Petroleum ether used was of the boiling range 60–80°C unless otherwise specified. Reactions were carried out in a Parr bench-top mini reactor of 300-mL capacity provided with a heater, stirrer, pressure gauge, thermocouple, and temperature controller. A sample removal system in the form of a loop with inlet and outlet valves, fabricated out of a copper tube of 22 in. × 0.1 in. id, was fixed to the sampling point of the reactor. Reaction samples were analysed by reverse phase liquid chromatography on a Spectra-Physics SP 8000 high performance liquid chromatograph connected to a uv detector at 254 nm using an ODS (Spectra-Physics) column (250 mm × 4.6 mm id). The ir spectra were recorded as Nujol mulls using a Perkin–Elmer 221 spectrometer, the nmr spectra on a Varian T-60 spectrometer using tetramethyl silane as internal standard, and mass spectra on a CEC-21-110B mass spectrometer.

General procedure for the thermolysis of p-*toluenesulphonylazide in benzene*

In a typical run, the azide **A** (4.0 g, 0.005 mol) and benzene (200 g, 2.56 mol) were charged into the autoclave already purged with nitrogen. The reactor was pressurized to 27.2 atm with nitrogen and heated slowly to raise the temperature to 160°C in 1 h. The final pressure recorded on the gauge at 160°C was 40.1 atm, the generated nitrogen and the vapour pressure of benzene at reaction temperature contributing towards the increase in pressure. The first sample was removed at 145°C at 55 min and the rest at 160°C at various intervals of time (Table 1).

Procedure for sample removal

During each sample removal, the outlet valve of the sample tube was closed and the inlet valve opened to let the reaction mixture enter inside the loop. The inlet valve was then closed immediately. The loop was cooled externally by dipping in cold water and then the outlet valve opened to remove the reaction mixture inside the loop. Before removal of the next sample, the same operation was repeated to flush the inside of the loop free of the previous sampling. Each time nearly 10 mL of the sample was removed. The pressure drop noticed during each sample removal was compensated for by pressuring the system back to 40.1 atm with nitrogen every time.

High performance liquid chromatographic (hplc) analysis

Excess benzene was distilled off and the crude solid dissolved in methanol. The methanolic solution was filtered prior to analysis by hplc with the following operating parameters: detector at 254 nm at a sensitivity of 0.18 amp; mobile phase of methanol–water (6:4); flow rate of 2 mL/min; column inlet pressure of 1619 psi (1 psi = 6.89 kPa); and a chart speed of 1 cm/min; 10 μL of the sample were injected each time. The composition of the reactant and the products in the reaction mixture was then determined using the external standard quantitation method with the aid of the data processor unit present in the instrument. The order of elution of the components with their retention time(s) in parentheses are as follows: (1) *p*-toluenesulphonamide (**D**) (208); (2) *p*-toluenesulphonylanilide (**C**) (444); (3) *p*-toluenesulphonylazide (**A**) (534); and (4) *p*-toluenesulphonylazepine (**B**) (592). The analysis of the samples withdrawn at various intervals of time has been given in Table 1.

Preparation of standard compounds

The standard compounds were prepared according to methods reported in literature: (**A**) *p*-toluenesulphonylazide (8); (**B**) *p*-toluenesulphonyl-1*H*-azepine, mp 167°C (dec.) (lit. (4) mp 167°C); (**C**) *p*-toluenesulphonanilide, mp 103°C (lit. (9) mp 103°C); (**D**) *p*-toluenesulphonamide, mp 136°C (lit. (10) mp 136°C). All the products were characterized further by spectral and elemental analyses.

1. N. R. AYYANGAR, M. V. PHATAK, and B. D. TILAK. Indian J. Chem. **16B**, 547 (1978).
2. N. R. AYYANGAR, M. V. PHATAK, A. K. PUROHIT, and B. D. TILAK. Chem. Ind. (London), 853 (1979).
3. R. A. ABRAMOVITCH, T. D. BAILEY, T. TAKAYA, and V. UMA. J. Org. Chem. **39**, 340 (1974).
4. N. R. AYYANGAR, R. B. BAMBAL, and A. G. LUGADE. J. Chem.

Soc. Chem. Commun. 790 (1981).
5. J. F. M. GAGAN. Rodd's chemistry of carbon compounds. Elsevier, Amsterdam. 1979. p. 195.
6. T. KAMETANI and K. FUKUMOTO. Heterocycles, **3**, 931 (1975).
7. O. LEVENSPIEL. Chemical reaction engineering. Wiley Eastern Limited, New Delhi. 1975. p. 60.
8. R. FUSCO, G. BIANCHETTI, and D. POCAR. Gazz. Chim. Ital. **91**, 849 (1961).
9. D. ELAMANN and E. FABIENKE. Chem. Ber. **92**, 712 (1959).
10. A. L. CORDOVA. An. Fac. Farm. Bioquim., Univ. Nac. Mayor San Marcos, **1**, 515 (1950); Chem. Abstr. **47**, 5310 g (1953).

Reduction of dicarbonyl compounds on a mercury electrode. II. Reduction mechanism of acetylbenzoyl

J. M. RODRÍGUEZ-MELLADO, J. L. AVILA, AND J. J. RUIZ[1]
Departamento de Química Física, Facultad de Ciencias, Universidad de Córdoba, Spain

Received January 17, 1984[2]

J. M. RODRÍGUEZ-MELLADO, J. L. AVILA, and J. J. RUIZ. Can. J. Chem. **63**, 891 (1985).

A study on the electrochemical reduction of acetylbenzoyl on a mercury electrode has been carried out in the pH range 0–9 in buffered aqueous solutions. The effect of pH, drop time, temperature, and acetylbenzoyl concentration on polarographic and kinetic parameters has been studied. The occurrence of adsorption phenomena is inferred from the recordings of $C-E$ curves. Tafel slopes and reaction orders have been obtained at potentials corresponding to the foot of the wave. On the basis of these experimental data, a reaction mechanism is proposed for the zone of potentials where Tafel's law is satisfied.

J. M. RODRÍGUEZ-MELLADO, J. L. AVILA et J. J. RUIZ. Can. J. Chem. **63**, 891 (1985).

Utilisant des solutions aqueuses tamponées et opérant à des pH allant de 0 à 9, on a étudié la réduction électrochimique de l'acétylbenzoyle sur une électrode à mercure. On a étudié l'effet du pH, du temps de chute, de la température et de la concentration de l'acétylbenzoyle sur les paramètres polarographiques et cinétiques. Sur la base des enregistrements de courbes $C-E$, on croit qu'il existe des phénomènes d'adsorption. On a obtenu les pentes de Tafel et les ordres de la réaction à des potentiels correspondants au pied de la vague. Sur la base de ces données expérimentales, on propose un mécanisme réactionnel pour la zone de potentiels qui satisfait à la loi de Tafel.

[Traduit par le journal]

Introduction

There are only two papers in the chemical literature dealing with the electrochemical reduction of acetylbenzoyl, showing great discrepancies with respect to one another.

Thus, a paper by Arai (1) reports the occurrence of one or two reduction waves (depending on the pH of the medium) over the pH range 0–10, finding no waves above pH 10. According to this author, a dimerization process corresponds to the first wave found.

On the other hand, Fedoronko and Hudekova (2) state that acetylbenzoyl shows one, two, or three polarographic waves (also depending on the pH of the medium) over the pH range 0–12 and attribute them to the reduction of the unhydrated species, the monohydrate protonated form, and the monohydrate itself, respectively. These authors carried out a potential-controlled electrolysis at potentials corresponding to the limiting current (i_L) of the first wave, subsequently isolating the reaction product and identifying it as phenylacetylcarbinol by ir spectroscopy.

In any case, the reduction mechanism of acetylbenzoyl has not yet been discussed. Therefore, the aim of this paper has been to carry out a polarographic study of this compound, as well as to determine some kinetic parameters at potentials corresponding to the foot of the polarographic wave ($i/i_L < 0.05$), on the basis of which the reaction mechanism can be discussed.

Experimental

All reagents used were Merck p.a. grade. A buffered solution with the following components and concentrations was used as supporting electrolyte: 0.05 M CH_3COOH and 0.05 M H_3PO_4 for pH < 8, and 0.05 M H_3PO_4 and 0.05 M $NaHCO_3$ for pH > 8. The ionic strength was adjusted to 0.2 M with $NaNO_3$.

An electronic system made up of an Amel 551 potentiostat, a Hewlett–Packard 7045-A recorder, and a Hewlett–Packard 3310-A wave generator was used. All measurements were made in a thermostatted Amel 494 cell.

The working electrode was a Radiometer B 400 capillary with flux, $m = 2$ mg s^{-1} and drop time, $t = 4.19$ s, both parameters being measured in 0.05 M phosphate buffer at pH 2 and open circuit, the height of the mercury reservoir being 40 cm. A saturated Ingold 303-NS calomel electrode was used as reference and a platinum Ingold Pt-4805 acted as auxiliary.

Differential capacity–potential curves were recorded automatically by fitting our electronic system to a circuit devised by Roldán *et al.* (3). A Telequipment D-1011 oscilloscope was also used. The capillary was an Amel EA 1019/2 with $m = 1.02$ mg s^{-1}, its drop time being set at 4.8 s.

Both the voltammetric measurements and the determination of the number of electrons were performed by means of a Metrohm EA 290 hanging-drop mercury electrode. Differential pulse polarograms were recorded by using a Metrohm-Herisau 626 polarograph.

All measurements were made in a nitrogen medium at 25 ± 0.1°C, with the exception of those corresponding to the study of the effect brought about by a temperature change. All other experimental conditions were identical to those described in ref. 4.

Results and discussion

Polarographic behaviour

Acetylbenzoyl shows one or two reduction waves (depending on the pH) by DC polarography. The first one occurs over the whole pH range under study (0–9), whereas the second one can only be observed within the pH range 2–9. The sum of the heights of the two waves remains practically constant throughout the pH range studied (Fig. 1).

The limiting current of the first reduction wave is dependent on the pH of the solution. Figure 1 shows the variation of the former as a function of the latter. Above pH 10, the limiting current decreases with time (the higher the pH, the sharper the decrease) due to the instability of acetylbenzoyl in alkaline solutions.

An increase in pH shifts the $E_{1/2}$ of this first wave towards more negative potentials. The plot of $E_{1/2}$ vs. pH is linear with a slope of −58 mV per pH unit.

Below pH 1 and at potentials corresponding to the limiting current the process is controlled by diffusion, as is evident from the value of the temperature coefficient (1.4%/°C) and the slopes of the plots of log i_L vs. log t (0.19) and log i_L vs. log h (0.5) (h is the height of the mercury reservoir). Between pH

[1]All correspondence concerning this paper should be addressed to: J. J. Ruiz, Dpto. Química Física, Facultad de Ciencias, Av. Medina Azahara 9, Cordoba-5, Spain.

[2]Revision received September 27, 1984.

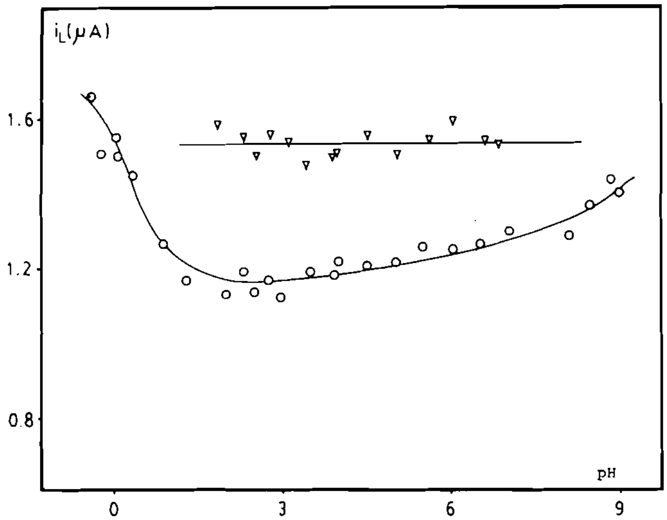

FIG. 1. Variation of i_L with pH. ○ First wave. △ Total limiting current.

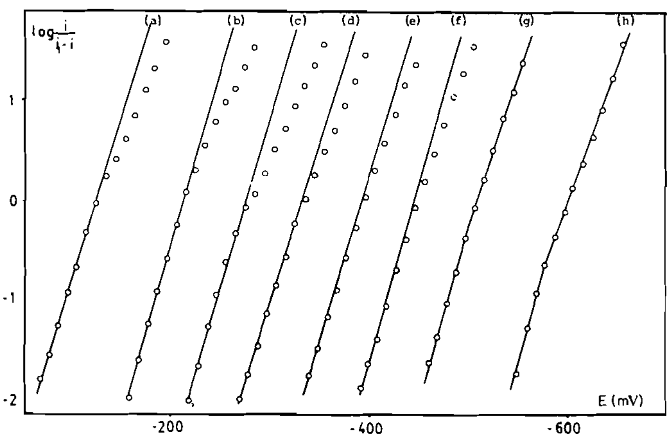

FIG. 2. Logarithmic analysis. pH: (a) 1.19; (b) 1.97; (c) 2.95; (d) 3.97; (e) 5.00; (f) 6.01; (g) 7.00; (h) 8.62.

1 and 9 the wave exhibits a certain kinetic character (at pH 4 the temperature coefficient is 2.8%/°C, $\partial\log i_L/\partial\log t = 0.25$, and $\partial\log i_L/\partial\log h = 0.42$). The variation of these parameters with pH, resembling that found for other α-dicarbonyl compounds (5), indicates that in the potential region corresponding to the plateau of the wave the process is partly controlled by the dehydration of the carbonyl group, a chemical reaction prior to the transfer process and subject to general acid–base catalysis. In order to show this kinetic character, we have plotted log $[i_L/(i_D - i_L)]$ vs. log t. The results so obtained satisfied the Koutecky equation (6), which, as modified for maximum current, reads:

$$[1] \quad i_L/(i_D - i_L) = 1.386\,(k_1K^2t)^{0.546}$$

The straight line obtained has a slope of 0.56 at pH 4, the value of k_1K^2 being 8.3 s^{-1}.

A logarithmic study of the first wave has been carried out over the whole pH range under study, its results being displayed in Fig. 2. The logarithmic study shows a linear segment corresponding to the lower part of the wave, whereas a deviation from linearity is observed for higher i values. The wave fulfils the Sluyters equation (7), derived for a weak adsorption of depolarizer, negligible for both products and intermediates.

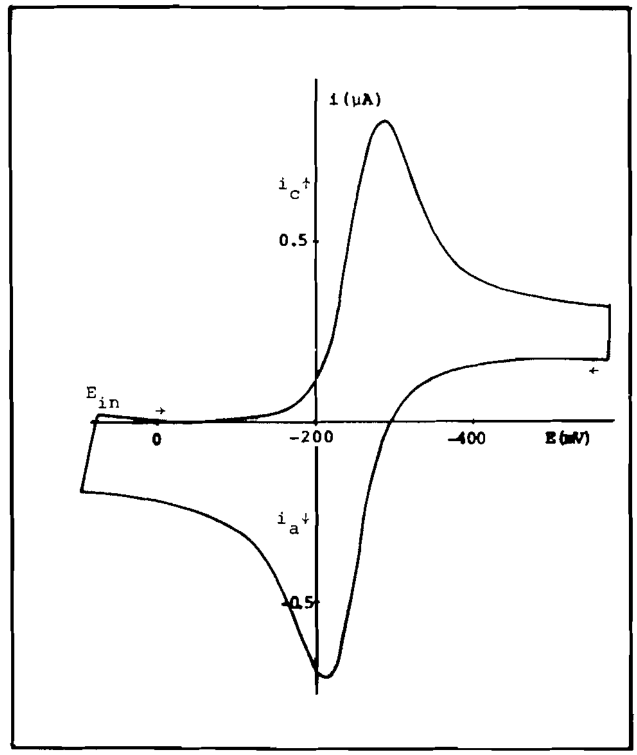

FIG. 3. Voltammograms. Sweep-rate = 400 mV s^{-1}. pH 2.12 ($E_p^{anodic} - E_p^{cathodic}$ = 82 mV). E_{in} indicates the potential initial.

The slope of the linear segment, −29 mV, indicates that the electron transfer is a reversible process, at least at potentials corresponding to the foot of the polarographic wave. In order to determine whether the overall reaction was reversible or postkinetic at these potentials, the influence of drop time on potential was studied at a constant i value corresponding to the foot of the wave, finding a slope of 15 mV for the linear plot of E vs. log t, which shows the overall process to be postkinetic. This conclusion is corroborated by the fact that the intensity is independent of the height of the mercury reservoir at potentials corresponding to the foot of the wave.

A voltammetric study has been carried out over the sweep range of 100–1000 mV s^{-1}. Figure 3 shows a typical voltammogram. The corresponding anodic peak is observed in addition to the cathodic one. The former can be attributed to the oxidation of the enol form of phenylacetylcarbinol. The difference between both peak potentials is greater than 2.303 $RT/2F$, which indicates that the overall process is not reversible. Above pH 7, the height of the anodic peak decreases with increase in pH, disappearing above pH 9.

With regard to the second reduction wave, its $E_{1/2}$ shifts towards more negative potentials (−110 mV/pH) with increase in pH. The value of the temperature coefficient (1.5%/°C) and the variation of the limiting current with the drop time ($\partial\log i_L/\partial\log t = 0.19$) and the height of the mercury reservoir ($\partial\log i_L/\partial\log h = 0.5$) show that the wave is governed by diffusion at potentials corresponding to the limiting current and is observable within the whole pH range.

A study of acetylbenzoyl reduction has been performed by differential pulse polarography, indicating that the peak corresponding to the second wave observed by DC polarography decreases in intensity between pH 4 and 6 and that a new peak appears at slightly more negative potentials. The variation of the area of both peaks with pH is the same shape as a titration

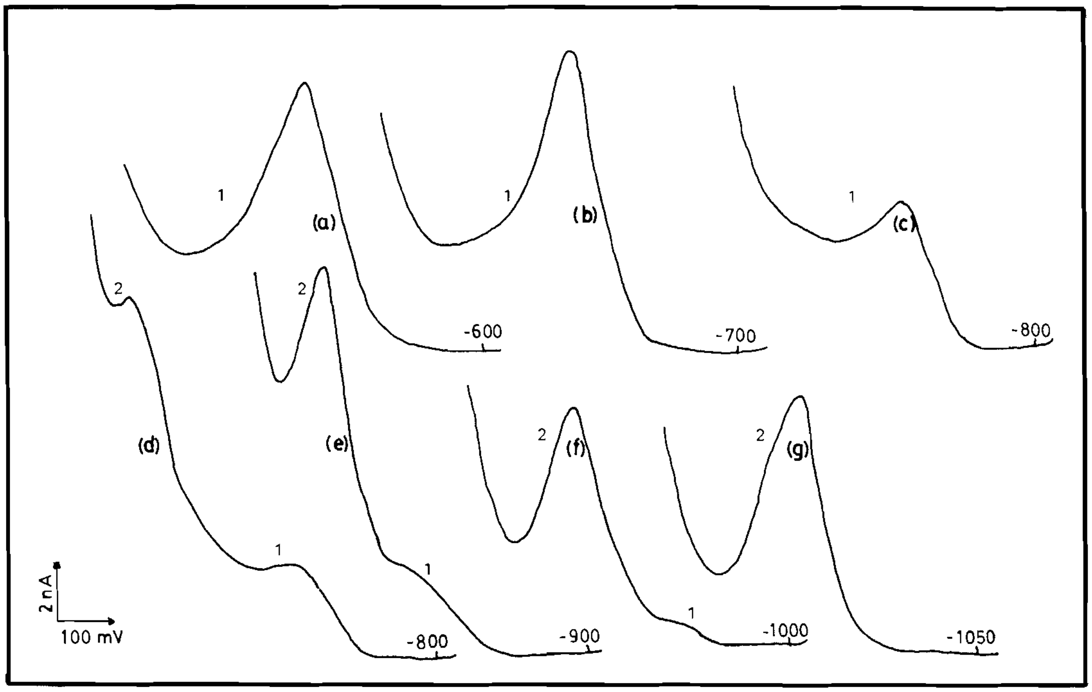

FIG. 4. Differential pulse polarograms. Second wave. Variation with pH. pH: (a) 3.01; (b) 3.51; (c) 4.02; (d) 4.49; (e) 5.09; (f) 5.49; (g) 6.00.

curve. Some of the recordings obtained are shown in Fig. 4.

The potentials of these peaks are the same as those corresponding to the second and third waves obtained by Fedoronko and Hudekova (2) by DC polarography. Moreover, we should indicate that the variation with pH of both the height and the potential of the aforementioned waves coincide exactly with the behaviour observed by us as regards the pH effect on the peaks obtained by DP polarography, and which should be, in our opinion, attributed to the processes suggested by Fedoronko and Hudekova for the second and third waves:

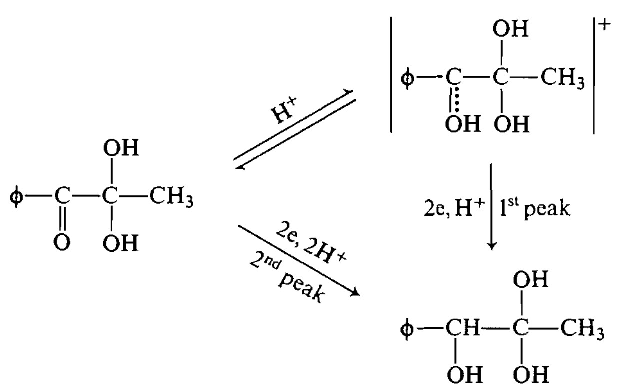

Determination of the number of electrons

The determination of the number of electrons taking part in the overall reduction reaction per mol of acetylbenzoyl was carried out by constant-potential chronoamperometry, using a hanging-drop electrode. One set of measurements was made at pH 0 and the potential corresponding to the limiting current of the first wave, and another set of measurements was performed at pH 4 and the potential corresponding to the limiting current of the second wave. A value of about 2 was found in every case.

$C-E$ *curves*

Capacity–potential curves were recorded for acetylbenzoyl

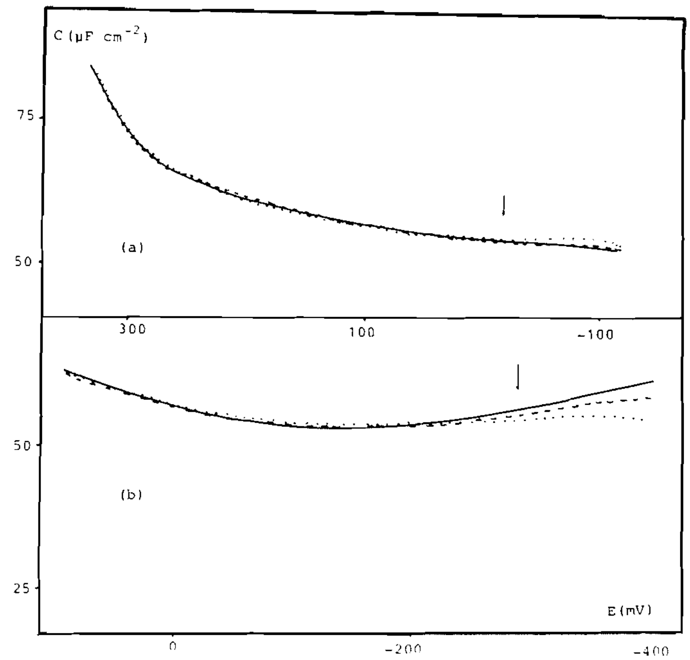

FIG. 5. Capacity–potential curves. (a) pH = 0; (b) pH = 4. ——— Supporting electrolyte. ----- Acetylbenzoyl 5×10^{-5} M. ······· Acetylbenzoyl 2×10^{-4} M. (Arrow indicates the potential of initiation of the reduction.)

at both the working concentration (2×10^{-4} M) and at 5×10^{-5} M. These recordings, performed at pH 0 and 4, together with those corresponding to the supporting electrolyte, are shown in Fig. 5. At pH 0 and 4 no practical difference can be observed between the three curves. Consequently, acetylbenzoyl adsorption must be very weak (and therefore unappreciable in the $C-E$ recordings) or nonexistent.

Nevertheless, the $C-E$ curves recorded at pH 10.3 do show the occurrence of adsorption, even at potentials corresponding to the beginning of the reduction process (around −650 mV).

Since the $C-E$ curves recorded below pH 9 do not show any extent of adsorption, we may consider that the reduction occurs in an homogeneous phase.

Tafel curves and reaction orders

Regarding $i-E$ polarization curves traced at potentials corresponding to the foot of the first polarographic wave, a study has been carried out on their variation with the concentration of reactants.

From the variation of $\log i$ with the concentration of reactants at a constant potential, the corresponding reaction orders were obtained. Figures 6 and 7 show some of the results. The average value of the Tafel slopes was −30 mV, while the reaction orders with respect to acetylbenzoyl and H^+ ion were 1.0 and 2.0 respectively.

With the aim of studying the influence of other proton donors of the solution on the reaction mechanism, the reaction orders corresponding to the buffer components were determined at varying pH and a constant ionic strength, indicating that this influence is only appreciable for high concentrations of the proton donors.

The following reaction mechanism, in agreement with the Tafel slopes and reaction orders found, is proposed for potentials corresponding to the foot of the wave:

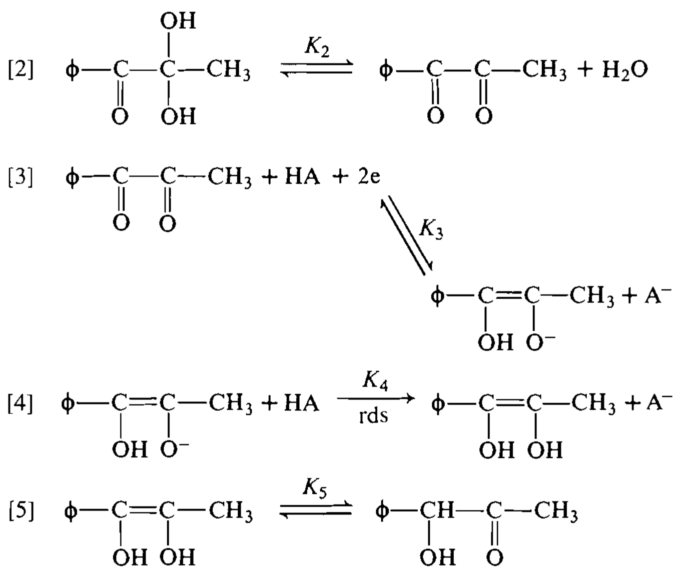

SCHEME 1

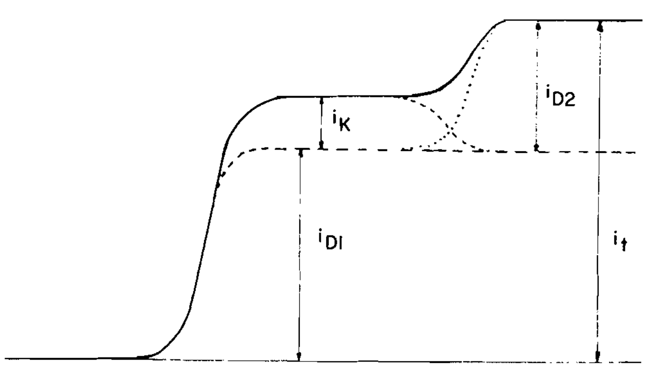

SCHEME 2

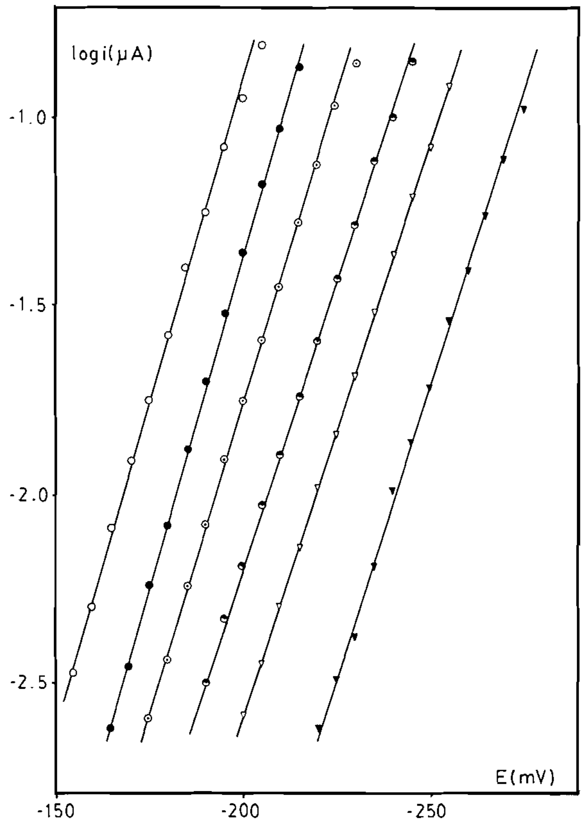

FIG. 6. Tafel plots at varying pH values. pH: ○ 1.69; ● 1.97; ⊙ 2.29; ◒ 2.48; △ 2.71; ▲ 3.04.

where HA represents any acidic species present in the interphase.[3]

Assuming reaction [4] to be the rate-determining step, the value of the cathodic current at the foot of the wave can be expressed as:

$$[6] \quad i = 2FKK'C\,C_H\,(k_H C_H + \sum_i k_{HA_i} C_{HA_i})\, e^{-2FE/RT}$$

where C and C_H stand for the concentration of acetylbenzoyl and H^+ ion, respectively; C_{HA_i} for the concentration of each acidic species (except H^+) present in the interphase; E for

[3]During the revision of this paper, it was suggested to us that reaction [3] should be written as 3 discrete steps:

[3*a*] $PhCOCOCH_3 + e^- = (PhCOCOCH_3)^{\cdot -}$

[3*b*] $(PhCOCOCH_3)^{\cdot -} + HA = (PhCOCOHCH_3)^{\cdot} + A^-$

[3*c*] $(PhCOCOHCH_3)^{\cdot} + AB^{\cdot -} = (PhCOCOHCH_3)^- + AB$

However, our experimental data prevent us from establishing the sequence of the elementary steps, in quasi-equilibrium, which precede the rate-determining step. Hence, we have opted for writing the sum of all these steps in reaction [3].

On the other hand, it could be considered that reactions such as [4] are generally very fast and often diffusion controlled and thus it is difficult to accept this as the rate-controlling step in the reaction. As a matter of fact, these reactions are generally fast, but our results clearly indicate the occurrence of a non-zero reaction order with respect to the proton donors of the supporting electrolyte, which indicates that these proton donors are involved in the rate-determining step. The occurrence of a protonation reaction as rate-determining step is, therefore, plausible.

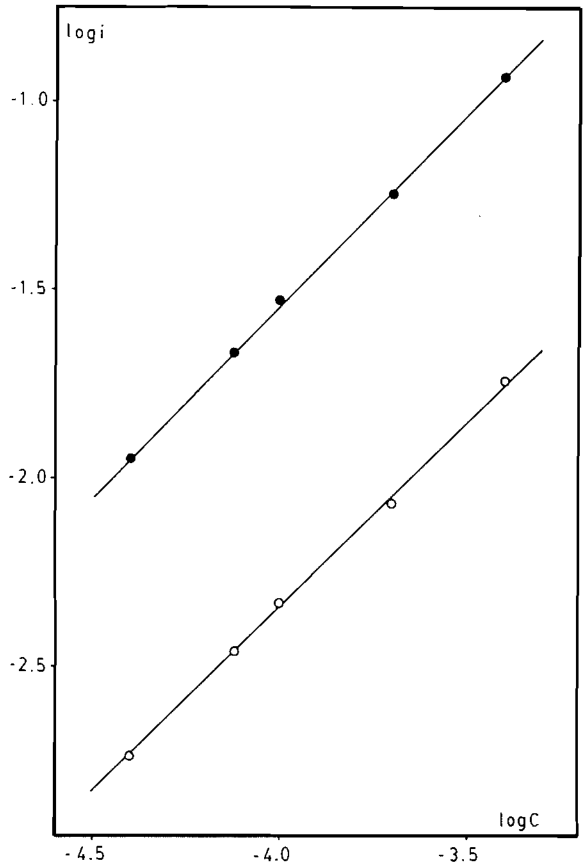

FIG. 7. Electrochemical order with respect to acetylbenzoyl. pH 4.00; ○ E = −275 mV; ● E = −300 mV.

potential applied; K for the product of the equilibrium constants of the stages prior to the rds; k_H and k_{HA_i} for the rate constants corresponding to the reaction of protonation by H^+ ion and HA_i species, respectively; and K' for $\exp(2F\Delta\Phi_{ref}/RT)$, $\Delta\Phi_{ref}$ being the potential of the reference electrode. The term $\sum_i k_{HA_i}C_{HA_i}$ takes into account the contribution of all acidic species present in the interphase, except the H^+ ion.

In the case of protonation by phosphoric acid, and according to eq. [6], the log i vs. log [HA] plot (where [HA] = $[H_2PO_4^-]$ + $[HPO_4^{2-}]$) should give rise (as is experimentally confirmed) to a curve with a slope approaching 1 or 0, depending on whether $k_{H_2PO_4^-}[H_2PO_4^-] + k_{HPO_4^{2-}}[HPO_4^{2-}]$ is much larger or smaller than k_HC_H, respectively. Furthermore, the plot of i vs. [HA] is linear (Fig. 8). The ratio between the slope and the intercept for this plot is independent of the potential, as may be expected from eq. [6], and clearly indicates that both H^+ ion and phosphoric acid are involved in the anion protonation (step [4]).

Since the $\sum_i k_{HA_i}C_{HA_i}$ term contribution is negligible at the values of the working buffer concentration, the reaction order with respect to H^+ ion can be expected to be close to 2, as it indeed happens to be.

Since the wave satisfies closely the Sluyters equation, the process must be complicated with adsorption phenomena. However, these deviations are not significant at potentials

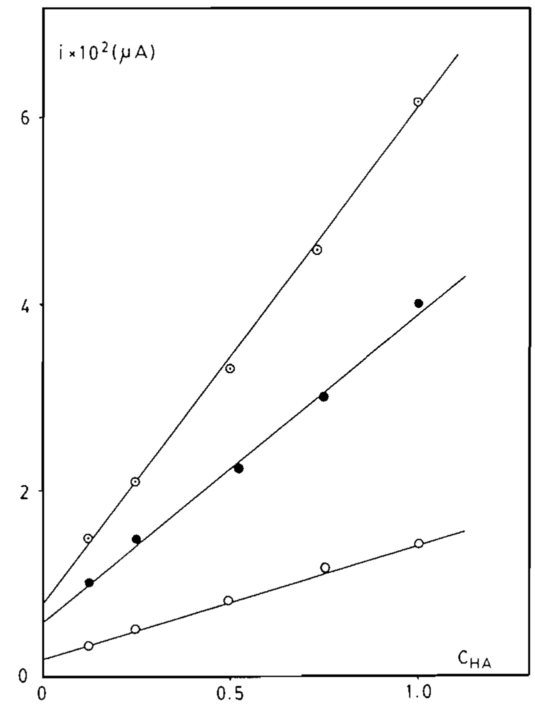

FIG. 8. Plot of i vs. $\{[H_2PO_4^-] + [HPO_4^{2-}]\}$ at pH 7.12. ○ E = −400 mV; ● E = −465 mV; ⊙ E = −480 mV.

corresponding to the foot of the wave.

The calculation of the polarographic and kinetic parameters corresponding to the second wave cannot be accomplished since, at potentials corresponding to the limiting current of the first wave, the reduction of both the unhydrated molecules already existing in the solution and those arising from the dehydration of the monohydrated form in the interphase takes place.

On the other hand, at potentials corresponding to any part of the second wave, the process involves the reduction of the monohydrate (a reaction allowed by the values of the potential) and the unhydrated species arising by diffusion from the bulk of the solution. This fact has prevented us from determining the limiting current for the first wave in the zone of potentials where the second one appears and, consequently, the value of the current for the latter. Therefore it is impossible to obtain electrochemical data for this process. Scheme 2 shows what has been stated above.

1. T. ARAI. Denki Kagaku, **30**, 175 (1962).
2. M. FEDORONKO and M. HUDEKOVA. Rev. Chim. Miner. **5**, 411 (1968).
3. E. ROLDÁN, D. GONZÁLEZ-ARJONA, and M. DOMÍNGUEZ. An. Quim. **78**, 158 (1982).
4. J. J. RUIZ, A. ALDAZ, and M. DOMÍNGUEZ. Can. J. Chem. **55**, 2799 (1977).
5. J. KRUPICKA and J. J. K. NOVÁK. Collect. Czech. Chem. Commun. **25**, 1275 (1960).
6. J. WEBER and J. KOUTECKY. Collect. Czech. Chem. Commun. **20**, 980 (1955).
7. M. SLUYTERS-REHBACH, S. GONZÁLEZ, and J. H. SLUYTERS. J. Electroanal. Chem. **51**, 405 (1974).

Pyrrole chemistry. XXVIII. Substitution reactions of 1-(phenylsulfonyl)pyrrole and some derivatives

HUGH J. ANDERSON, CHARLES E. LOADER,[1] RU XUN XU, NGHIA LÊ, NIALL J. GOGAN, ROBERT MCDONALD, AND LOUISE G. EDWARDS

Chemistry Department, Memorial University of Newfoundland, St. John's, Newfoundland, Canada A1B 3X7

Received August 13, 1984

HUGH J. ANDERSON, CHARLES E. LOADER, RU XUN XU, NGHIA LÊ, NIALL J. GOGAN, ROBERT MCDONALD, and LOUISE G. EDWARDS. Can. J. Chem. **63**, 896 (1985).

The preparative value of the 1-(phenylsulfonyl) *N*-blocking and directing group for the synthesis of 3-acylpyrroles has been further evaluated. Acetylation and benzoylation are strongly regiospecific and give good yields. However, the regiospecificity is not general and other substitution reactions give mixtures of 2- and 3-substitution or even mostly 2-substitution. Friedel and Crafts *tert*-butylation gives 3-*tert*-butyl-1-(phenylsulfonyl)pyrrole and provides a useful route to *tert*-butylpyrrole, but ethylation and isopropylation give mixtures. Acylations of 2- and 3-alkyl-1-(phenylsulfonyl)pyrroles show little evidence of useful regiospecificity.

HUGH J. ANDERSON, CHARLES E. LOADER, RU XUN XU, NGHIA LÊ, NIALL J. GOGAN, ROBERT MCDONALD et LOUISE G. EDWARDS. Can. J. Chem. **63**, 896 (1985).

On a évalué à nouveau l'utilité préparative du groupement phénysulfonyl-1 comme agent *N*-bloqueur et comme groupe directeur pour la synthèse d'acyl-3 pyrroles. L'acylation et la benzoylation sont très régiospécifiques et se produisent avec de bons rendements. Toutefois, la régiospécificité n'est pas générale et d'autres réactions de substitutions conduisent à des mélanges de produits substitués en 2 ou en 3 ou même à des produits qui sont principalement substitués en position 2. La réaction de *tert*-butylation selon Friedel et Crafts fournit le *tert*-butyl-3 (phénylsulfonyl)-1 pyrrole et cette réaction s'avère une route utile pour préparer du *tert*-butylpyrrole; toutefois les réactions d'éthylation ou d'isopropylation conduisent à des mélanges. Les réactions d'acylation des alkyl-2 (ou -3) (phénylsulfonyl)-1 pyrroles ne semblent pas présenter de régiospécificité utile.

[Traduit par le journal]

Recently, Kakushima *et al.* (1) provided a detailed account of their exploration of the Friedel–Crafts acylation of 1-(phenylsulfonyl)pyrrole.[2] Earlier, we (4) and they (5) had reported that this reaction gave mostly, and in some cases only, 3-substitution on the pyrrole ring, consequently affording a useful three-step synthesis of 3-acylpyrroles from pyrrole. Nevertheless, changes in the amount (4) and the nature (1) of the Lewis acid catalyst have been found to lead to more, or even exclusive, 2-substitution.

In contrast, the acylation of pyrroles having other electron-withdrawing groups on the nitrogen, such as the 1-alkoxycarbonyl, leads to almost exclusive 2-substitution (6). A closer model, 1-benzoylpyrrole, was also found to be acetylated at the 2-position. These acyl groups do have a trigonal carbon attached to the ring nitrogen and can occupy less space than the groups about the tetrahedrally substituted sulfur atom, particularly if complexation of the Friedel–Crafts catalyst with the *N*-substituent is important.

While the acetylation reaction was used to explore the potential of this acylation, most of our preparative efforts using the method have been directed toward the synthesis of some 3-aroylpyrroles that were of interest in other studies. These syntheses were generally carried through the acylation and hydrolysis steps without interruption to give the desired 3-aroylpyrrole in good yield where all steps were optimized (Table 1).

In the earlier communication (4) we reported that both formylation using dichloromethyl butyl ether/$AlCl_3$ or dimethylformamide/phosphorus oxychloride, and cyanation using cyanogen bromide/$AlCl_3$ or chlorosulfonyl isocyanate, resulted in 2-substitution of 1-(phenylsulfonyl)pyrrole. The Vilsmeier reaction gave a poor yield of product even under vigorous conditions. This contrasted strongly with the excellent 2-formylation of methyl 1-pyrrolecarboxylate (8). The cyanation reaction using chlorosulfonyl isocyanate was also relatively slow, but gave an almost quantitative yield of the 2-cyano derivative that was easily hydrolyzed to afford pyrrole-2-carbonitrile (69%) in three steps from pyrrole. However, a 73% yield may be obtained from the reaction of chlorosulfonyl isocyanate with pyrrole itself (9).

Kakushima *et al.* (1) found that oxalyl chloride/$AlCl_3$ gave 2-substitution (as the —COCl group) and they drew attention to the fact that a variety of one-carbon acylations all attacked the 2-position, in contrast to the 3-acylation of 1-(phenylsulfonyl)pyrrole obtained with acetyl and larger groups. However, the reaction of *S*-ethyl chlorothioformate/$AlCl_3$ gave a 65% yield of *S*-ethyl 1-(phenylsulfonyl)pyrrole-3-thiocarboxylate. It was hoped that this product would then afford easy access to pyrrole-3-carboxaldehyde, but stirring with Raney nickel under a variety of conditions (10, 11) produced no reaction or caused the loss of the entire thiol ester group. Removal of the 1-phenylsulfonyl group with KOH/methanol gave a good yield of methyl pyrrole-3-carboxylate contaminated with a small amount of *S*-ethyl pyrrole-3-thiocarboxylate. Similarly, aqueous base rapidly removed the phenylsulfonyl group but hydrolyzed the thiol ester more slowly.

Nitration of 1-(phenylsulfonyl)pyrrole with nitric acid/acetic anhydride under a variety of conditions gave a low yield of a crude oil that was a mixture of mostly 3- and some 2-nitrated product (nmr). The reaction caused considerable destruction of pyrrolic material. Crystallization from methanol

[1]Author to whom correspondence should be addressed.

[2]The phase transfer method of Illi (2) using powdered sodium hydroxide gave a 71% yield of 1-(phenylsulfonyl)pyrrole from pyrrole, while 50% aqueous sodium hydroxide afforded 84% of a very pure product (see Experimental). Either method is more convenient to use on a large scale than the original synthesis using pyrrolylpotassium (3).

TABLE 1. 3-Aroylpyrroles from 1-(phenylsulfonyl)pyrrole

3-Substituent	Yield (mp (°C))	Infrared (cm^{-1} ($CHCl_3$))	^1H nmr (ppm)
4-Methylbenzoyl-	45% (128–129.2)	1634	2.37 (3H, s), 6.68 (2H, m), 7.13 (2H, d), 7.23 (1H, m), 7.64 (2H, d), 9.53 (1H, b)
2-Methylbenzoyl-	57% (94.2–96.6)	1635	2.39 (3H, s), 6.60 (2H, m), 6.93 (1H, m), 7.16 (4H, m), 9.43 (1H, b)
4-Chlorobenzoyl-	42% (119–120)*	3200, 1615†	6.70 (1H, m), 6.83 (1H, m), 7.44 (2H, d), 7.78 (2H, b)
4-Methoxybenzoyl-	22% (105–106.5)	3170, 1605†	3.80 (3H, s), 6.70 (2H, m), 6.84 (1H, m), 7.77 (4H, m), 9.43 (1H, b)

*Literature mp (7) 121–122°C.
†Nujol mull.

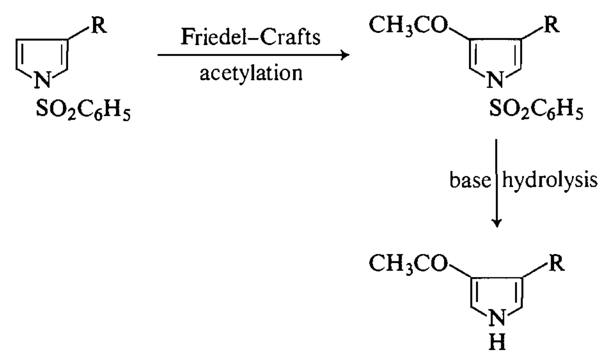

SCHEME 1

easily gave pure 3-nitro-1-(phenylsulfonyl)pyrrole. Although the yield was modest (20%), the purification and hydrolysis to 3-nitropyrrole seemed to make it a possible synthesis of the compound. An earlier preparation required chromatography to obtain a similar yield of 3-nitropyrrole (12). However, the recent method of Muchowski and Solas (13) affords close to 80% of 3-nitropyrrole in three steps from pyrrole.

Trichloroacetylation of 1-(phenylsulfonyl)pyrrole could not be obtained under any of the conditions tried. although it was possible to detect in both nmr and mass spectra trace amounts of the desired product following vigorous reactions. As trichloroacetylation does succeed with pyrrole-2-carbonitrile, the ring must be considerably deactivated. Further examples of the deactivated nature of 1-(phenylsulfonyl)pyrrole were: the failure of the HIO_3/I_2 iodination, a reaction that gives a modest yield with pyrrole-2-carboxaldehyde (14, 15), and of formylation with *N,N*-dimethylformamide/triphenylphosphinyl bromide perbromide (16) and with ethyl orthoformate/trifluoracetic anhydride (17).

The Friedel–Crafts alkylation of 1-(phenylsulfonyl)pyrrole with *tert*-butyl chloride and aluminum chloride catalyst afforded 3-*tert*-butyl-1-(phenylsulfonyl)pyrrole in excellent yield with only a trace of the 2-*tert*-butylated isomer (not isolated). Isopropylation with isopropyl chloride gave a mixture of the 2- (~55%) and 3- (~45%) isopropyl-1-(phenylsulfonyl)pyrrole. Separation of these isomers was fairly difficult using column chromatography, but was achieved with good recovery using medium pressure liquid chromatography (18) on silica gel. Ethylation of 1-(phenylsulfonyl)pyrrole with ethyl bromide in dichloromethane was very slow, giving a low yield contaminated with the product of the reaction with the solvent. This problem was overcome by using an excess of ethyl bromide as the solvent. The reaction was then fairly rapid but gave mostly 2-ethylation accompanied by the formation of considerable amounts of polymeric material. Under the conditions used, there was an almost complete lack of disubstitution during alkylations, even in the presence of a large excess of alkyl halide, again reflecting the low reactivity of 1-(phenylsulfonyl)pyrrole towards electrophilic attack.

The 2- or 3-alkyl-1-(phenylsulfonyl)pyrroles can be hydrolysed to the corresponding alkylpyrrole with base. The use of this path for the preparation of 3-*tert*-butylpyrrole has an advantage over the literature method (19) in that purification of the intermediate 1-phenylsulfonylated product is simple owing to the virtual absence of the other isomer. The separation of isomeric mixtures of 2- and 3-alkyl-1-(phenylsulfonyl)pyrroles is difficult, so the preparation of 3-ethylpyrrole by reduction/hydrolysis of 3-acetyl-(1-phenylsulfonyl)pyrrole as described below or by the reduction of the α-substituted succinonitriles with diisobutylaluminum hydride recently reported (20) (also suitable for 3-isopropylpyrrole) is preferable.

We were also interested in the effect of a 3-alkyl group on further Friedel–Crafts acetylation of the 1-phenylsulfonyl compounds. In general terms, would it be possible to extend the synthesis and obtain the 3,4-disubstituted pattern shown in Scheme 1.

To prepare 3-ethyl-1-(phenylsulfonyl)pyrrole for this investigation, attempts were made to reduce the carbonyl group on 3-acetyl-1-(phenylsulfonyl)pyrrole catalytically using Raney nickel, H_2/Pd, and $PdCl_2$/C. As well, hydrazine/tosyl hydrazide followed by reduction with $NaBH_4$ was tried, but these methods failed to give the desired product. As an alternative, the Huang–Minlon modification of the Wolff–Kishner reduction of 3-acetyl-1-(phenylsulfonyl)pyrrole gave 3-ethylpyrrole in one step and constitutes an efficient preparation of this compound (51% from pyrrole). The 1-phenylsulfonyl group was then replaced using its potassium salt (3). Later it was found possible to reduce 3-acetyl-1-(phenylsulfonyl)pyrrole directly to 3-ethyl-1-(phenylsulfonyl)pyrrole using the Clemmensen reduction.

These 3-alkyl-1-(phenylsulfonyl)pyrroles possessing groups of increasing size were subjected to Friedel–Crafts acetylation. However, instead of the 4-substitution hoped for, the products were all mixtures (as shown in Scheme 2) in which the predominant isomer arose from 5-substitution. As the alkyl group increased in size, the proportion of 2-substitution decreased. Some 4-substitution was observed (see Table 2).

Similarly, the cyanation of 3-*tert*-butyl-1-(phenylsulfonyl)-pyrrole gave mostly 5-cyanation, together with some 2-substitution, under the essentially neutral conditions of chlorosulfonyl isocyanate/*N,N*-dimethylformamide.

On the other hand, the Friedel–Crafts acetylation of

TABLE 2. The Friedel–Crafts acetylation of 3-alkyl-1-(phenylsulfonyl)pyrroles

	Product yield % (% of total isolated product)		
Alkyl-1-(phenylsulfonyl)pyrrole	2-Acetyl-	4-Acetyl-	5-Acetyl-
3-Ethyl-	5(9)	16(30)*	32(60)*
3-Isopropyl-	10(13)	Trace	66(87)
3-*tert*-butyl-	—	Trace	40(~100)(79)(~100)†

*Estimated from ^1H nmr of mixture of 4-acetyl and 5-acetyl isomers.
†$AlCl_3$ catalyst ($SnCl_4$ catalyst).

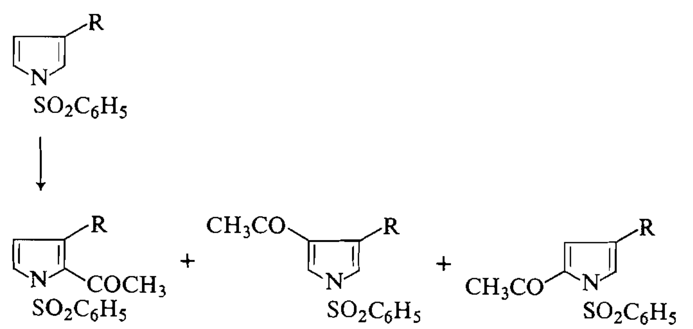

SCHEME 2

2-isopropyl-1-(phenylsulfonyl)pyrrole gave a mixture in which 4-substitution predominated, in contrast to the usual 5-attack on a 2-alkylpyrrole (21).

The product mixture obtained from the Friedel and Crafts reaction on the 3-alkyl-1-(phenylsulfonyl)pyrroles was very sensitive to reaction conditions and to the catalyst chosen for the reaction. Where a particular isomer is desired, careful choice of the reaction conditions can significantly improve its yield. The hoped-for high yields of the 4-substituted products were not obtained, but the procedure does offer a route to small amounts of some disubstituted pyrroles not easily obtainable by other methods.

Although the 1-(phenylsulfonyl) directing group does not provide a general pathway for the synthesis of 3-substituted pyrroles, it does afford a simple, efficient, and useful method for the synthesis of 3-acetylpyrrole and some other simple 3-acylpyrroles. In addition, useful yields of some 3-alkylpyrroles can be obtained. Other methods are available that are more selective and give better yields, but are often less convenient. The reason for the observed regiospecificity is unclear and we are continuing to investigate this aspect of the reaction. The fact that the presence of a 1-phenylsulfonyl group leads to "normal" (i.e. predominantly α-) substitution in the Friedel and Crafts acylation of 3-alkylpyrroles, while producing "abnormal" (i.e. mainly β-) substitution with 2-isopropylpyrrole, also needs explanation.

Experimental

Melting points are uncorrected. Elemental analyses were by Atlantic Microlabs, GA, U.S.A. The ir spectra were recorded on a Perkin–Elmer 237B or 1320 grating spectrophotometer as Nujol mulls unless otherwise stated. The ^1H nmr spectra (nmr) were determined using a Varian EM 360 or a Bruker WP-80 instrument and are expressed in ppm (δ values) relative to tetramethylsilane as internal reference in $CDCl_3$ unless otherwise stated. Low and high resolution mass spectra were recorded on a VG Micromass 7070HS spectrometer. Throughout, the term "petroleum" refers to the fraction of bp 60–80°C unless otherwise specified. The term "hexanes" refers to a mixture of isomers bp 65.8–69.0°C. For flash chromatography (22) "Baker Analyzed" silica gel, and for preparative thin-layer chromatography Whatman PLK5F plates, were used.

1-(Phenylsulfonyl)pyrrole

A mixture of pyrrole (52.8 g, 0.787 mol), dichloromethane (500 mL), tetrabutylammonium hydrogen sulfate (27.1 g), and sodium hydroxide solution (640 mL, 50% aqueous) was made in a 3-L 3-necked flask. The stirred mixture was cooled in cold water and phenylsulfonyl chloride (212 g) in dichloromethane (80 mL) was added fairly rapidly so that the mixture refluxed gently. When the addition was complete the mixture was stirred at room temperature for a further 20 h.

The inorganic precipitate was collected on a Celite pad by suction filtration and the filtrate was filtered through phase separation filter paper (Whatman IPS) to remove the aqueous layer. The organic filtrate was washed five times with water then dried ($MgSO_4$). The aqueous material that collected in the filter paper was diluted with an equal volume of water and then extracted with dichloromethane. The dichloromethane extracts were washed with water, combined with the organic material, and then dried ($MgSO_4$). The solvent was then removed to leave a thick oil that was crystallized from a dichloromethane/petroleum mixture affording off-white crystals. The product was recrystallized from methanol to give 1-(phenylsulfonyl)pyrrole (137 g, 84%), mp 88–89°C (lit. (3) mp 89–89.5°C).

Preparation of 3-benzoylpyrrole

Aluminum chloride (17.37 g, 130 mmol) was dissolved in the minimum amount of nitromethane and 1-(phenylsulfonyl)pyrrole (22.5 g, 109 mmol) in dichloromethane (600 mL) was added to the stirred mixture. Benzoyl chloride (18.3 g, 130 mmol) was then added over a period of 5 min and after a further 5 min stirring the mixture was poured slowly onto 600 mL of ice and water. The organic layer was separated and the aqueous layer was extracted with ether (3 × 75 mL). The combined organic extract was washed with sodium bicarbonate solution (2 × 75 mL, 5% aqueous), dried ($MgSO_4$), and the solvent removed. The medium-brown residue was added to a solution of potassium hydroxide (12.21 g) in aqueous methanol (120 mL water/120 mL methanol) and stirred overnight at 60°C. After cooling the methanol was flash-evaporated from the mixture, leaving a light-brown cloudy solution, which was extracted with dichloromethane (3 × 75 mL). The organic extract was dried ($MgSO_4$), and the solvent removed. Flash chromatography on silica gel of the light-brown gummy residue, using an ethyl acetate/hexanes mixture (15) as the eluting solvent, gave 3-benzoylpyrrole (9.44 g, 51% from 1-(phenylsulfonyl)pyrrole) as off-white crystals, mp. 98.5–99°C (lit. (23) mp 99.5–100°C), other properties identical with authentic material.

Other 3-aroylpyrroles prepared by this method are listed in Table 1.

2-Acetylpyrrole from 1-benzoylpyrrole

1-Benzoylpyrrole (0.71 g, 4.1 mmol) was dissolved in 1,2-dichloroethane (10 mL). To the stirred solution was added, at room temperature, aluminum chloride (1.22 g, 10 mmol) and acetic anhydride (0.45 mL, 4.3 mmol). After 2 h at room temperature the reaction mixture was poured into ice water (40 mL) and stirred vigorously. The layers were separated, the aqueous layers extracted three times with dichloroethane, and the combined layers washed with 5%

aqueous $NaHCO_3$, with saturated aqueous NaCl, dried ($MgSO_4$), and the solvent removed to give a dark oil. The ^1H nmr spectrum of the oil indicated almost entirely 2-acetyl-1-(phenylsulfonyl)pyrrole with less than 10% of 3-substitution.

The crude product was dissolved in a solution of methanol (30 mL) containing KOH (0.58 g, 10 mmol) and stirred at room temperature for 4 h. The solvent was flashed down and the product partitioned between water and ether. The aqueous layer was extracted 3 times with ether and the combined layers were washed with saturated aqueous NaCl and dried ($MgSO_4$). Removal of solvent gave 2-acetylpyrrole, (0.34, 75%). The sublimed product was identical to an authentic sample.

Vilsmeier formylation of 1-(phenylsulfonyl)pyrrole

1-(Phenylsulfonyl)pyrrole (500 mg, 2.4 mmol) was treated with a mixture of *N*,*N*-dimethylformamide (3 mL, 39 mmol) and $POCl_3$ (0.4 mL, 4.4 mmol) at 60°C for 48 h. The brown oil that formed was then cooled and dissolved in water. The aqueous solution was extracted with ether. The ether extracts were washed with water, dried ($CaCl_2$), and the solvent was removed. The residue was unchanged 1-(phenylsulfonyl)pyrrole. The aqueous layer was made strongly basic with 3 mol L^{-1} NaOH and stirred for 3 h. The yellow solution was then extracted with ether. The ether extracts were washed with water, dried (K_2CO_3), and the solvent was removed to leave a residue of pyrrole-2-carboxaldehyde (79 mg, 34%), identical with authentic material.

S-Ethyl 1-(phenylsulfonyl)pyrrole-3-thiocarboxylate

1-(Phenylsulfonyl)pyrrole (0.70 g, 3.4 mmol) was dissolved in 1,2-dichloroethane (10 mL). To the stirred solution at room temperature was added aluminum chloride (1.00 g, 7.5 mmol), followed by *S*-ethyl thiochloroformate (0.35 mL, 3.4 mmol). The solution was brought to the boiling point and stirred 1.5 h. The reaction mixture was poured into cold water (50 mL) and stirred vigorously. After the usual work-up, the dark solution was passed through a short column of Al_2O_3, eluting with dichloroethane. Removal of the solvent gave an oil that slowly crystallized. Recrystallization from dichloromethane/hexanes gave a colorless solid (0.65 g, 65%), mp. 67–68.5°C. Sublimation (which was very slow) gave mp 68–69°C; ir ν: 1650 cm^{-1}; nmr δ: 1.29 (3H, t, —CH_3), 3.00 (2H, q, —SCH_2-), 6.71 (1H, m, C-4), 7.16 (1H, m, C-5), 7.5–8.1 (6H, m, phenyl and C-2). *Exact Mass* calcd. for $C_{13}H_{13}NO_3S_2$: 295.03367; found: 295.0289, deviation 4.7 mmu.

3-Nitro-1-(phenylsulfonyl)pyrrole

Fuming nitric acid (0.35 mL) was added to ice-cold acetic anhydride (2 mL) and allowed to warm to room temperature. 1-(Phenylsulfonyl)pyrrole (1.081 g, 5.2 mmol) was dissolved in acetic anhydride (3 mL) and then cooled to −10°C. The solution of fuming nitric acid was then added dropwise to the stirred solution of 1-(phenylsulfonyl)pyrrole over about 5 min. The mixture was stirred for a further 1 h at −10°C and then poured onto about 150 g of ice. The aqueous mixture was extracted with ether, the organic extracts were combined, washed with water, dried ($CaCl_2$), and the solvent was removed. The ^1H nmr spectrum of the yellow residue showed that it contained about 30% of 3-nitro-1-(phenylsulfonyl)pyrrole and only a trace of the 2-nitro isomer. The residue in a little methanol was refrigerated overnight. The pale yellow crystals were collected, and washed with a small amount of cold methanol to give the product as a very pale yellow solid (321 mg, 24%), mp 102–103°C; nmr δ: 6.82 (1H, dd, C-4H), 7.13 (1H, dd, C-3H), 7.37–8.17 (6H, m); $J_{4,5}$ = 3.5, $J_{2,4}$ = 1.5, $J_{2,5}$ = 2.5 Hz; m/z = 252. *Anal.* calcd. for $C_{10}H_8N_2O_4S$: C 47.61, H 3.19, N 11.10; found: C 47.71, H 3.26, N 11.08.

3-Nitropyrrole

A solution of potassium hydroxide (1.2 g, 21 mmol) in methanol (25 mL) was added to the crude product of the nitration of 1-(phenylsulfonyl)pyrrole (1.081 g, 75 mmol) as above and the mixture was stirred at room temperature overnight. The solvent was then removed and water (100 mL) was added. The aqueous solution was extracted thoroughly with ether. The ether extracts were combined, washed with water, dried ($CaCl_2$), and the solvent was removed to leave a very pale yellow residue that was recrystallized from chloroform/petroleum to give 3-nitropyrrole (112 mg, 19% from 1-(phenylsulfonyl)pyrrole), mp 99.5–100.5°C (lit. (12) 99–101°C); nmr δ: 6.76 (2H, m), 7.68 (1H, dd). The aqueous layer from the extraction was made acid with 6 mol L^{-1} sulfuric acid and then again extracted with ether, which gave 302 mg of a yellow oil that contained only traces of 2- and 3-nitropyrrole. The bulk of this residue appeared to consist of products from the destruction of the 1-(phenylsulfonyl)pyrrole.

Similar hydrolysis of pure 3-nitro-1-(phenylsulfonyl)pyrrole (552 mg) gave pure 3-nitropyrrole (230 mg, 96%), mp. 99.5–100.5°C, as an almost colourless solid.

2-Cyano-1-(phenylsulfonyl)pyrrole

(a) 1-(Phenylsulfonyl)pyrrole (500 mg, 2.4 mmol) was dissolved in acetonitrile (5 mL) and cooled to 0°C in an ice bath. Chlorosulfonyl isocyanate (0.3 mL) was added dropwise to the stirred solution and then it was allowed to warm to room temperature and stirred for 5 h. *N*,*N*-Dimethylformamide (0.5 mL) was added to the mixture, stirring was continued for a further hour at room temperature, and the mixture was then poured onto ice. Solid 2-cyano-1-(phenylsulfonyl)pyrrole precipitated from the aqueous mixture as a light brown solid which was collected, washed with cold water, and air dried (556 mg, 99%). A sample of the almost pure crude product was sublimed for analysis (90°C, 0.1 Torr; 1 Torr = 133.3 Pa) to give the analytical sample, mp 94.5–95°C; ir ν: 2226 (CN) cm^{-1}; nmr δ: 6.27 (1H, q, C-4H), 6.90 (1H, q, C-3H), 7.46 (1H, q, C-5H), 7.41–8.16 (5H, m); m/z = 232. *Anal.* calcd. for $C_{11}H_8N_2O_2S$: C 56.88, H 3.47; found: C 56.91, H 3.50.

A sample of the product (329 mg) was hydrolysed as described above for 3-nitro-1-(phenylsulfonyl)pyrrole to give pyrrole-2-carbonitrile (90 mg, 69%), identical with an authentic sample.

(b) 1-(Phenylsulfonyl)pyrrole (1.035 g, 5 mmol) was dissolved in 1,2-dichloroethane (10 mL). To the stirred solution was added aluminum chloride (1.50 g, 22 mmol) and a solution of cyanogen bromide (0.53 g, 7 mmol) in 1,2-dichloroethane (5 mL) at room temperature; the solution was then stirred for 3 h. The reaction mixture was poured onto ice and stirred. The layers were separated and the aqueous layer was extracted three times with chloroform. The combined organic layers were washed with saturated aqueous NaCl and dried ($MgSO_4$). Removal of the solvent gave 1.15 g (99%) of light brown solid. A small sample was sublimed to give mp 94–95°C. A mixture mp with a sample from (a) was not depressed.

3-Ethylpyrrole

A mixture of 3-acetyl-1-(phenylsulfonyl)pyrrole (16.90 g, 67.8 mmol), KOH (16.90 g, 301 mmol), and $N_2H_4.H_2O$ (16.90 g, 338 mmol) in triethyleneglycol (170 mL) was stirred and refluxed for 1.5 h. Water was distilled from the mixture and it was refluxed for a further 4 h. Ether was added to the cooled mixture (ice and water) with stirring for 15 min. The organic layer was separated from the aqueous layer, which was extracted with ether (4 × 100 mL). The combined organic layer and extracts were washed once with water, dried ($MgSO_4$, 1 h), evaporated, and the residue vacuum distilled 86°C/20 Torr (lit. (24) bp 86–88°C/20 Torr), to give 3-ethylpyrrole (3.30 g, 51%). The ^1H nmr chemical shifts were identical to those of an authentic sample.

3-Ethyl-1-(phenylsulfonyl)pyrrole

(a) *From 3-ethylpyrrole*

3-Ethylpyrrole (3.30 g, 34.7 mmol) was dissolved in dry tetrahydrofuran (75 mL, freshly distilled) and then potassium metal was added slowly (excluding moisture) until an excess was present and the hydrogen evolution ceased. A solution of phenylsulfonyl chloride (6.75 g, 38.2 mmol) in tetrahydrofuran (10 mL) was then added dropwise at room temperature. The mixture was stirred overnight, filtered, and the solvent was evaporated. The residue was dissolved in water and extracted with ether (4 × 150 mL). The combined ethereal layer and extracts were washed once with water and dried ($MgSO_4$). The ether was removed and the residue was vacuum distilled (125–135°C/0.1 Torr) to give 3-ethyl-1-(phenylsulfonyl)pyrrole (2.38 g, 29%), an oil which solidified just below room temperature; nmr δ: 1.10 (3H, t, —CH_3), 2.40 (2H, q, —CH_2), 6.10 (1H, dd), 6.80 (1H, m), 7.00 (1H, dd), 7.3–7.8 (5H, m). *Exact Mass* calcd. for $C_{12}H_{13}NO_2S$: 235.06669; found: 235.0682, deviation 1.5 mmu.

(b) *From 3-acetyl-1-(phenylsulfonyl)pyrrole*

Amalgamated zinc (prepared from zinc (3.66 g, 56 mmol granular) and a solution of mercuric chloride (0.37 g, 1.4 mmol) in water (5 mL) and concentrated hydrochloric acid (0.5 mL)) was placed in a flask, together with water (2.5 mL), concentrated HCl (6 mL), and a solution of 3-acetyl-1-(phenylsulfonyl)pyrrole (1.09 g, 4.4 mmol) in toluene (25 mL). The solution was refluxed for 7 h, when more concentrated HCl (3 mL) was added and reflux continued to a total of 24 h. After cooling, the layers were separated, the aqueous layer extracted twice more with toluene, and the combined organic layers washed with saturated aqueous NaCl and dried ($MgSO_4$). Evaporation of solvent gave a thick brown oil. Short-path distillation gave 3-ethyl-1-(phenylsulfonyl)pyrrole (0.63 g, 61%), with spectral properties identical to the product above.

2- and 3-ethyl-1-(phenylsulfonyl)pyrrole

1-(Phenylsulfonyl)pyrrole (3.2 g, 15 mmol) was dissolved in bromoethane (5.0 mL) and cooled in an ice bath. Aluminum chloride (6.4 g, 48 mmol) was added rapidly with stirring and the mixture was heated under gentle reflux for 4.5 h, when the mixture was cooled and poured into ice/water. Following the usual work-up, removal of the solvent gave a brown oil (2.93 g) that was a mixture of products and polymeric by-products (^{1}H nmr). Flash chromatography of the oil on silica gel with elution by a 2% ethyl ether/petroleum (60–80°C bp) mixture gave (poor separation) the following.

2,5-Diethyl-1-(phenylsulfonyl)pyrrole (135 mg, 3%), mp 40.5–41.5°C (from ethyl ether/petroleum); nmr δ: 1.21 (6H, t, —CH_3), 2.78 (4H, q, —CH_2), 5.92 (2H, dd, C3,4-H), 7.32–7.87 (5H, m). *Exact Mass* calcd. for $C_{14}H_{17}NO_2S$: 263.09799; found: 263.0973, deviation 0.7 mmu.

2-Ethyl-1-(phenylsulfonyl)pyrrole (974 mg, 26%), mp 57–58°C (from methanol); nmr δ: 1.13 (3H, t, —CH_3), 2.76 (2H, q, —CH_2), 5.93 (1H, dd, C3-H), 6.16 (1H, dd, C5-H), 7.25 (1H, dd, C4-H), 7.35–8.18 (5H, m); m/z = 235. *Anal.* calcd. for $C_{12}H_{13}NO_2S$: C 61.25, H 5.56, N 5.95; found: C 61.34, H 5.61, N 5.90.

A mixture of 2- and 3-isomers (204 mg, 5%).

3-Ethyl-1-(phenylsulfonyl)pyrrole (483 mg, 13%), identical with the material obtained above from the reduction of 3-acetyl-1-(phenylsulfonyl)pyrrole.

2- and 3-isopropyl-1-(phenylsulfonyl)pyrrole

Aluminum chloride (9.65 g, 72.4 mmol) was mixed with dichloromethane (25 mL) and cooled in an ice bath. 1-(Phenylsulfonyl)pyrrole (5.0 g, 24.1 mmol) in dichloromethane (25 mL) was then added, followed by isopropyl chloride (2.58 g, 328 mmol) in dichloromethane (25 mL) dropwise. The pale yellow mixture was stirred in the ice bath for a further 5 h. It was then poured onto ice (100 g). Following the usual work-up, the solvent was removed to leave an oily residue (5.8 g, 96% as mixture). The ^{1}H nmr spectrum of the product indicated that it contained almost equal proportions of the 2- and 3-isopropylated products. Medium pressure chromatography (18) of the product (1-g sample) on silica gel (Merck Kieselgel 60) gave on elution with 3% ether/cyclohexane, in order of elution, the following.

2-Isopropyl-1-(phenylsulfonyl)pyrrole[3] (0.46 g, 23%). The product crystallized on cooling but melted below room temperature; nmr δ: 1.17 (6H, d), 1.36 (1H, septet), 6.03 (1H, m), 6.2 (1H, dd), 7.24 (1H, dd), 7.37–7.87 (5H, m), $J_{4,5}$ = 3.4, $J_{3,5}$ = 1.8, $J_{3,4}$ = 3.2, $J_{3,\text{isopropyl H}}$ = 0.7, $J_{\text{isopropyl}}$ = 6.8 Hz. *Exact Mass* calcd. for $C_{13}H_{15}NO_2S$: 249.08234; found: 249.0830, deviation 0.7 mmu.

3-Isopropyl-1-(phenylsulfonyl)pyrrole (0.31 g, 15%). The product was obtained as a colourless oil that slowly crystallized below 0°C; nmr δ: (6H, d), 2.64 (1H, septet), 6.17 (1H, dd), 6.87 (1H, m), 7.21 (1H, dd), 7.31–7.97 (5H, m), $J_{4,5}$ = 3.3, $J_{2,5}$ = 1.7 Hz. *Exact Mass* calcd. for $C_{13}H_{15}NO_2S$: 249.0823; found: 235.0831, deviation 0.8 mmu.

*3-*tert*-Butyl-1-(phenylsulfonyl)pyrrole*

1-(Phenylsulfonyl)pyrrole (5.0 g, 24 mmol) was added to a stirred mixture of aluminum chloride (9.65 g, 72 mmol) and dichloromethane (25 mL) cooled in an ice bath. A solution of *tert*-butyl chloride (2.8 g, 30 mmol) in dichloromethane (25 mL) was then added dropwise and the mixture allowed to warm to room temperature, stirred for 4.5 h, and poured onto ice. Following the usual work-up, the solvent was removed to leave the product as a pale yellow oil (5.9 g) that slowly crystallized. Recrystallization from methanol gave 3-*tert*-butyl-1-(phenylsulfonyl)pyrrole (5.12 g, 80%); mp 42°C; nmr δ: 1.17 (9H, s), 6.21 (1H, dd), 6.86 (1H, dd), 7.03 (1H, dd), 7.26–7.93 (5H, m), $J_{2,4}$ = 1.8, $J_{4,5}$ = 3.4, $J_{2,5}$ = 2.4 Hz; m/z = 263. *Anal.* calcd. for $C_{14}H_{17}NO_2S$: C 63.85, H 6.50; found: C 63.88, H 6.52. Base hydrolysis (4) of 3-*tert*-butyl-1-(phenylsulfonyl)pyrrole gave 3-*tert*-butylpyrrole (54% yield) with spectra identical to those of authentic material (24).

Cyanation of tert*-butyl-1-(phenylsulfonyl)pyrrole*

Cyanation of 3-*tert*-butyl-1-(phenylsulfonyl)pyrrole with chlorosulfonyl isocyanate using the procedure described above for 2-cyano-1-(phenylsulfonyl)pyrrole gave a 93% mixture of the two possible α-substituted products that proved to be very difficult to separate. The ^{1}H nmr spectrum showed that 2- and 5-cyano-4-*tert*-butyl-1-(phenylsulfonyl)pyrrole were present in a ratio of about 3:2. Medium pressure liquid chromatography (18) of 0.40 g of the crude product on silica gel (eluent 10:1 hexane/ethyl acetate) gave, in order of elution, the following.

*2-Cyano-4-*tert*-butyl-1-(phenylsulfonyl)pyrrole* (191 mg), mp 90.5–91.5°C; ir ν: 2201 cm^{-1}; nmr δ: 1.16 (9H, s, —$C(CH_3)_3$), 6.89 (1H, d, C-4H), 7.21 (1H, d, C-4H), 7.5–8.3 (5H, m), $J_{2,4}$ = 1.8 Hz. *Anal.* calcd. for $C_{15}H_{16}N_2SO_2$: C 62.47, H 5.59, N 9.71; found: C 62.57, H 5.63, N 9.66.

*2-Cyano-3-*tert*-butyl-1-(phenylsulfonyl)pyrrole* (25 mg), mp 81.5–83°C; ir ν: 2218 cm^{-1}; nmr δ: 1.35 (9H, s, —$C(CH_3)_3$), 6.29 (1H, d, C-5H), 7.42 (1H, d, C-4H), 7.5–8.2 (5H, m), $J_{4,5}$ = 3.4 Hz. *Exact Mass* calcd. for $C_{15}H_{16}N_2O_2S$: 288.09324; found: 288.0926, deviation 0.6 mmu.

In addition, between the two pure fractions a mixture (84 mg) of the two products was obtained.

Acetylation of 3-alkyl-1-(phenylsulfonyl)pyrroles

One molar equivalent of the 3-alkyl-1-(phenylsulfonyl)pyrrole was dissolved in an appropriate amount of dichloromethane, the mixture was cooled in ice and water, and 3 times the molar equivalent of catalyst ($AlCl_3$ or $SnCl_4$) was added followed by vigorous stirring at 0°C for 30 min. Acetyl chloride (2 molar equivalents) in dichloromethane was then added dropwise at 0°C. The reaction mixture was allowed to warm to room temperature and then stirred for 42 h. The reaction was quenched by pouring the mixture into a beaker containing ice and water, followed by stirring for 1 h. The layers were then separated and the aqueous layer was extracted with dichloromethane. The organic layer and the extracts were combined and washed three times with water, twice with 5% aqueous $NaHCO_3$, dried ($MgSO_4$), and the solvent was then removed to leave the crude products.

Acetylation of 3-ethyl-1-(phenylsulfonyl)pyrrole

Acetylation of 3-ethyl-1-(phenylsulfonyl)pyrrole (560 mg, 1.5 mmol) as described, and the residue subjected to preparative thin-layer chromatography on silica gel, developed with 10% ethyl ether in petroleum, gave the following.

[3]2-Isopropyl-1-(phenylsulfonyl)pyrrole rapidly turned yellow when stored at room temperature in air and was less stable than the 3-isopropyl isomer. Both compounds can be stored without decomposition below 0°C in air.

Unchanged starting material, 3-ethyl-1-(phenylsulfonyl)pyrrole (64 mg).

2-Acetyl-3-ethyl-1-(phenylsulfonyl)pyrrole (36 mg, 5%), mp 98–99°C; ir ν: 1667 cm^{-1}; nmr δ: 1.22 (3H, t, CH_2CH_3), 2.50 (3H, s, —$COCH_3$), 2.70 (1H, q, CH_2CH_3), 6.20 (1H, dd, $J_{4,5}$ = 3.2 Hz), 7.40–7.90 (6H, m, aromatic H). *Exact Mass* calcd. for $C_{14}H_{15}NO_3S$: 277.07726; found: 277.0770, deviation 0.3 mmu. Hydrolysis of this isomer in KOH and methanol gave 2-acetyl-3-ethylpyrrole; nmr δ: 1.30 (3H, t, CH_2CH_3), 2.46 (3H, s, —$COCH_3$), 2.80 (1H, q, CH_2CH_3), 6.10 (1H, dd), 6.85 (1H, dd).

A mixture (321 mg, 48%) of 4-acetyl-3-ethyl-1-(phenylsulfonyl)-pyrrole (16% yield based on ^{1}H nmr) and 5-acetyl-3-ethyl-1-(phenylsulfonyl)pyrrole (32% based on ^{1}H nmr). Recrystallization from ethyl ether/petroleum (60–80°C bp) gave pure *5-acetyl-3-ethyl-1-(phenylsulfonyl)pyrrole* as colourless needles, mp 94–95°C; ir ν: 1669 cm^{-1}; nmr δ: 1.25 (3H, t, CH_2CH_3), 2.35 (3H, s, —$COCH_3$), 2.52 (1H, q, CH_2CH_3), 6.90 (1H, d, $J_{2,4}$ = 2.0 Hz), 7.35–8.10 (6H, m, aromatic H). *Exact Mass* calcd. for $C_{14}H_{15}NO_3S$: 277.07726; found: 277.0762, deviation 1.1 mmu. Hydrolysis of this isomer in KOH and methanol gave 2-acetyl-4-ethylpyrrole; nmr δ: 1.30 (3H, t, CH_2CH_3), 2.40 (3H, s, —$COCH_3$), 2.55 (1H, q, CH_2CH_3), 6.60–6.85 (2H, m).

Preparative thin-layer chromatography (developing the plate with 30% ethyl ether/petroleum) of the mother liquors from the recrystallization gave some additional 5-acetyl-3-ethyl-1-(phenylsulfonyl)pyrrole and *4-acetyl-3-ethyl-1-(phenylsulfonyl)pyrrole*, mp 98–99°C; ir ν: 1663 cm^{-1}; nmr δ: 1.24 (3H, t, CH_2CH_3), 2.33 (3H, s, —$COCH_3$), 2.52 (1H, q, CH_2CH_3), 6.93 (1H, d, $J_{2,5}$ = 1.8 Hz), 7.35–8.10 (6H, m, aromatic H). *Exact Mass* calcd. for $C_{14}H_{15}NO_3S$: 277.07726; found: 277.0758, deviation 1.4 mmu.

Acetylation of 3-isopropyl-1-(phenylsulfonyl)pyrrole

As described above, the usual procedure with 3-isopropyl-1-(phenylsulfonyl)pyrrole (300 mg) gave a mixture which was separated by preparative thin-layer chromatography on silica gel developed with 10% ethyl ether in petroleum. Obtained were the following.

Unchanged 3-isopropyl-1-(phenylsulfonyl)pyrrole (16 mg).

2-Acetyl-3-isopropyl-1-(phenylsulfonyl)pyrrole (36 mg, 10%), mp 74–74.5°C; ir ν: 1676 cm^{-1}; nmr δ: 1.14 (6H, d, —$CH(CH_3)_2$), 2.52 (3H, s, —$COCH_3$), 3.06 (1H, m, —$CH(CH_3)_2$), 6.24, 7.37 (each 1H, d, $J_{4,5}$ = 3.23 Hz), 7.45–8.05 (5H, m, aromatic H). *Exact Mass* calcd. for $C_{15}H_{17}NO_3S$: 291.0929; found: 291.0912, deviation 1.7 mmu.

5-Acetyl-3-isopropyl-1-(phenylsulfonyl)pyrrole (232 mg, 66%), mp 132–133°C; ir ν: 1667 cm^{-1}; nmr δ: 1.21 (6H, d, —$CH(CH_3)$, 2.28 (3H, s, —$COCH_3$), 2.79 (1H, m, —$CH(CH_3)_2$), 6.90 (1H, d, $J_{2,4}$ = 2.15 Hz), 7.25–8.00 (6H, m, aromatic H). *Anal.* calcd. for $C_{15}H_{17}O_3S$: C 61.83, H 5.88, N 4.80; found: C 61.74, H 5.92, N 4.76.

The mother liquors showed the presence (^{1}H nmr) of a further compound which was difficult to purify. Slow sublimation of the gummy material along a glass tube gave a sublimate containing the product which was recrystallized from ethyl ether/petroleum to give *4-acetyl-3-isopropyl-1-(phenylsulfonyl)pyrrole*, mp 75–77°C; ir ν: 1673 cm^{-1}; nmr δ: 1.10 (6H, d, —$CH(CH_3)_2$), 2.35 (3H, s, —$COCH_3$), 3.33 (1H, m, —$CH(CH_3)_2$), 6.88 (1H, d, $J_{2,5}$ = 2.42 Hz), 7.25–8.00 (6H, m. aromatic H). *Exact Mass* calcd. for $C_{15}H_{17}NO_3S$: 291.0929; found: 291.0923, deviation 0.6 mmu.

*Acetylation of 3-*tert*-butyl-1-(phenylsulfonyl)pyrrole*

As described above, the usual procedure with 3-*tert*-butyl-1-(phenylsulfonyl)pyrrole (500 mg) afforded a highly crystalline mixture which on recrystallization from an ethyl acetate/petroleum mixture gave 5-acetyl-3-*tert*-butyl-1-(phenylsulfonyl)pyrrole (144 mg). Preparative thin-layer chromatography (10% ethyl ether in petroleum) of the residue from the mother liquor allowed further separation of the products as follows.

Unchanged 3-*tert*-butyl-1-(phenylsulfonyl)pyrrole (75 mg).

*5-Acetyl-3-*tert*-butyl-1-(phenylsulfonyl)pyrrole* (192 mg, total 236 mg 40%), mp 184–185°C; ir ν: 1672 cm^{-1}; nmr δ: 1.28 (9H, s), 2.31 (3H, s, —$COCH_3$), 6.93 (1H, d, $J_{2,4}$ = 2.06 Hz), 7.40–8.05 (6H, m, aromatic H); m/z = 305. *Anal.* calcd. for $C_{16}H_{19}NO_3S$: C 62.95, H 6.33; found: C 63.08, H 6.33. Hydrolysis (KOH/methanol) gave the known 2-acetyl-4-*tert*-butylpyrrole, mp 133–134°C (lit. (25) mp 133–134°C), ^{1}H nmr spectra identical.

The mother liquors from the recrystallization of the 5-acetyl-3-*tert*-butyl-1-(phenylsulfonyl)pyrrole contained some *4-acetyl-3-*tert*-butyl-1-(phenylsulfonyl)pyrrole*, mp 183–183.5°C; ir ν: 1673 cm^{-1}; nmr δ: 1.29 (9H, s), 2.40 (3H, s, —$COCH_3$), 6.85 (1H, d, $J_{2,5}$ = 2.35 Hz), 7.5–8.0 (6H, m, aromatic H). *Exact Mass* calcd. for $C_{16}H_{19}NO_3S$: 305.10856; found: 305.1064, deviation 2.2 mmu.

Acetylation of 2-isopropyl-1-(phenylsulfonyl)pyrrole

A solution of 2-isopropyl-1-(phenylsulfonyl)pyrrole (100 mg, 0.40 mmol) was acetylated with acetyl chloride and aluminum chloride in dichloromethane. After about 5 min the mixture was poured onto ice and stirred for 1 h, then allowed to warm to room temperature. After a total of 3 h, the yellowish mixture was worked up in the usual manner. Following filtration through phase separation paper to remove suspended water and drying (Molecular Sieves, Davison grade 512), removal of the solvent gave a mixture of acetylated products as an oil (90.5 mg, 77%). The ^{1}H nmr of the oil showed that the mixture contained three compounds. Flash chromatography of the product on silica gel gave on elution with 30% ether/petroleum (60–80°C bp), in order of elution; the following.

3-Acetyl-2-isopropyl-1-(phenylsulfonyl)pyrrole (trace).

5-Acetyl-2-isopropyl-1-(phenylsulfonyl)pyrrole (trace). The product crystallized on cooling but melted below room temperature; nmr δ: 1.23 (6H, d, —$CH(CH_3)_2$, 2.50 (3H, s, —$COCH_3$), 3.59 (1H, septet, —$CH(CH_3)_2$), 6.13 and 6.88 (each 1H, d, pyrrole H, $J_{3,4}$ = 3.7 Hz), 7.47–8.27 (5H, m, aromatic H).

4-Acetyl-2-isopropyl-1-(phenylsulfonyl)pyrrole (82.4 mg, 70%), as an oil that slowly crystallized, mp 73–74°C; ir ν: 1666 cm^{-1}; nmr δ: 1.11 (6H, d, —$CH(CH_3)_2$, 2.39 (3H, s, —$COCH_3$), 3.14 (1H, septet, —$CH(CH_3)$, 6.42 (1H, dd, $J_{3,5}$ = 1.8 Hz), 7.40–7.94 (6H, m, aromatic H). *Anal.* calcd. for $C_{15}H_{17}O_3S$: C 61.83, H 5.88, N 4.80; found: C 61.91, H 5.88, N 4.77.

A sample of this last compound (82.2 mg, 0.30 mmol) was hydrolysed (4) to give 4-acetyl-2-isopropylpyrrole (27.7 mg, 64%), mp 72–73°C (lit. (25) mp 68.5–69.5°C. An authentic sample (25) had mp 71–71.5°C and the mixture melting point was undepressed); ir ν: 3220, 1635 cm^{-1}; nmr δ: 1.27 (6H, d, —$CH(CH_3)$, 2.42 (3H, s, —$COCH_3$), 2.93 (1H, septet, —$CH(CH_3)_2$), 6.38 (1H, dd, 3-H, $J_{3,5}$ = 1.8, $J_{3,\text{isopropyl H}}$ = 0.9 Hz), 7.37 (1H, dd, 5-H, $J_{1,5}$ = 3.2 Hz).

Acknowledgements

We gratefully acknowledge the financial help of the Memorial University of Newfoundland and the Natural Sciences and Engineering Research Council of Canada. We also thank Dr. Brian Gregory for high resolution mass spectra and Mr. Avery Earle for Fourier transform nmr.

1. M. KAKUSHIMA, P. HAMEL, R. FRENETTE, and J. ROKACH. J. Org. Chem. **48**, 3214 (1983).
2. V. O. ILLI. Synthesis, 387 (1979).
3. E. P. PAPADOPOULOS and N. F. HAIDAR. Tetrahedron Lett. 1721 (1962).
4. R. X. XU, H. J. ANDERSON, N. J. GOGAN, C. E. LOADER, and R. MCDONALD. Tetrahedron Lett. **22**, 4899 (1981).
5. J. ROKACH, P. HAMEL, M. KAKUSHIMA, and G. M. SMITH. Tetrahedron Lett. **22**, 4901 (1981).
6. A. TREIBS and A. DIETL. Justus Liebigs Ann. Chem. **619**, 80 (1958).
7. J. R. CARSON and N. M. DAVIS. J. Org. Chem. **46**, 839 (1981).
8. C. F. CANDY, R. A. JONES, and P. H. WRIGHT. J. Chem. Soc. (C), 2563 (1970).
9. C. E. LOADER and H. J. ANDERSON. Can. J. Chem. **59**, 2673 (1981).

10. C. E. LOADER and H. J. ANDERSON. Tetrahedron, **25**, 3879 (1969).
11. H. J. ANDERSON and H. NAGY. Can. J. Chem. **50**, 1961 (1972).
12. K. J. MORGAN and D. P. MORREY. Tetrahedron, **27**, 245 (1971).
13. J. MUCHOWSKI and D. R. SOLAS. Tetrahedron Lett. **24**, 3455 (1983).
14. M. FARNIER and P. FOURNARI. C. R. Acad. Sci. Ser. C, **273**, 919 (1971).
15. M. FARNIER and P. FOURNARI. Bull. Soc. Chim. Fr. 351 (1973).
16. D. J. CHADWICK and S. T. HODGSON. J. Chem. Soc. Perkin Trans. 1, 93 (1983).
17. P. S. CLEZY, C. J. R. FOOKES, and A. J. LIEPA. Aust. J. Chem. **25**, 1979 (1972).
18. A. I. MEYERS, J. SLADE, R. K. SMITH, and E. D. MIKELICH. J. Org. Chem. **44**, 2247 (1979).
19. R. A. JONES and G. P. BEAN. The chemistry of pyrroles. Academic Press, London, New York, San Francisco. 1977. p. 144.
20. J. H. BABLER and K. P. SPINA. Tetrahedron Lett. **25**, 1659 (1984).
21. R. A. JONES and G. P. BEAN. The chemistry of pyrroles. Academic Press, London, New York, San Francisco. 1977. Chapt. 4.
22. W. C. STILL, M. KAHN, and A. MITRA. J. Org. Chem. **43**, 2923 (1978).
23. H. J. ANDERSON, C. E. LOADER, and A. FOSTER. Can. J. Chem. **58**, 2527 (1980).
24. J. K. GROVES, H. J. ANDERSON, and H. NAGY. Can. J. Chem. **49**, 2427 (1971).
25. H. J. ANDERSON and C. W. HUANG. Can. J. Chem. **48**, 1550 (1970).

n–π Electron donor–acceptor complexes. II. Aliphatic amines with dinitrobenzenes

JOAQUÍN O. SINGH, JORGE D. ANUNZIATA, AND JUANA J. SILBER[1]

Departamento de Química y Física, Universidad Nacional de Río Cuarto, Estafeta 9, Río Cuarto, 5800 Córdoba, Argentina

Received June 14, 1984

JOAQUÍN O. SINGH, JORGE D. ANUNZIATA, and JUANA J. SILBER. Can. J. Chem. **63**, 903 (1985).

The interaction of several aliphatic amines as *n*-donors and dinitrobenzenes (DNB) as π-acceptors has been studied in n-hexane. The formation of electron donor – acceptor (EDA) complexes is proposed to explain the spectroscopic behaviour of the mixtures. The stability constants (K_s) for these complexes have been calculated by an iterative procedure. For a given acceptor, the donor strength of $RNH_2 > R_2NH > R_3N$ was found. This order is explained by considering the role that steric effect may play in the EDA complex formation. On the other hand, the fact that for a given donor K_s follows the order 1,2-DNB > 1,3-DNB > 1,4-DNB, and that 1,2-DNB reacts with primary amines, led to the proposal of orientational complexes. These EDA complexes may be considered intermediates in aromatic nucleophilic substitution reactions.

JOAQUÍN O. SINGH, JORGE D. ANUNZIATA et JUANA J. SILBER. Can. J. Chem. **63**, 903 (1985).

On a étudié l'interaction de pluseurs amines aliphatiques, comme donneurs *n* et dinitrobenzens (DNB), comme accepteurs π, dans n-hexane. On propose la formation de complexes electron-donneur – accepteur (EDA) pour expliquer le comportement spectroscopique des mélanges. La constante de stabilité (K_s) pour ces complexes a été calculée au moyen d'une procédure itérature. Pour un accepteur donné, on a observé que la force du donneur était $RNH_2 > R_2NH > R_3N$. Cela s'explique en considérant le role que jouent les effects stériques dans la formation de complexes EDA. D'ailleurs le fait que K_s, pour un donneur donné, ait l'ordre 1,2-DNB > 1,3-DNB > 1,4-DNB et que 1,2-DNB réagisse avec amines primaires, conduit a proposer des complexes orientationnels. Ces complexes EDA peuvent etre considérés des intermediaires dans les réactions de substitution nucléophilique aromátique.

Introduction

The importance of the study of *n*-π Electron-Donor–Acceptor (EDA) complexes, as well as the need of a systematic study of their thermodynamic properties and their correlation with the structure of the component molecules, has been previously discussed (1).

To follow this line, the interaction of several aliphatic amines with 1,2-, 1,3-, and 1,4-dinitrobenzenes (DNB) in n-hexane has been studied in this work.

Several types of interactions between nitro-substituted aromatic compounds and aliphatic amines have been identified (2–5). They depend on the structure of the amine molecule and, to a great extent, on the nature of the solvent. In this sense the most studied nitro aromatic compound is 1,3,5-trinitrobenzene (s-TNB), for which evidence has been adduced (6, 7) for the formation of EDA complexes with primary, secondary, and tertiary amines dissolved in alkane solvents. In polar aprotic solvents, tertiary amines form solely EDA complexes with s-TNB (8, 9). However, in these solvents, for primary and secondary amines the addition to the aromatic ring resulting in a σ complex has been fully recognized (4, 5, 9). In addition, for *ortho*-dinitro aromatics, such as 1,2,4-TNB and also for 1,2-DNB, even in a nonpolar solvent as benzene, aromatic nucleophilic substitutions (S_NAr) of the nitro group by piperidine has been reported (10). The role that EDA complexes may play in the formation of the σ adducts and in S_NAr is yet unknown. The occurrence of such reactions via EDA complexes was proposed several years ago (3, 11). Also, a possible EDA complex between the nucleophile, either an aliphatic or aromatic amine, and the aromatic substrate, has recently been suggested to form previous to the σ complex intermediate, in order to explain the second-order kinetics in the amine, for fluorine substitution of 2,4-dinitro-1-fluorobenzene (12). However, no kinetic evidence has been obtained for the participation of the EDA complexes in this reaction. This is probably due to the high rate coefficient expected for the formation of this type of EDA complex (13). In the course of this investigation, the stability constants (K_s) for the formation of EDA complexes between aliphatic amines and dinitrobenzene have been determined. In order to correlate the values of K_s with the structure of the amines and the acceptors, orientational complexes are proposed. These types of complexes may be considered intermediates in S_NAr reactions.

Experimental

n-Hexane (Carlo Erba, R.P.), diethyl (DEA), triethyl (TEA), n-butyl (n-BA), di-n-butyl (DBA), and tri-n-butyl (TBA) amines (Aldrich Chemical Co.) were purified as previously described (1). To obtain reproducible results special care should be taken to assure the purity of the amine. The latter was controlled by glc (Porapak Q.-Apiezon L.), and by the ultraviolet cut-off point. The solvent and the amines were degassed and distilled in a high vacuum line just before use to ensure anhydrous conditions. 1,2-DNB (Fluka), 1,3-DNB (Merck), and 1,4-DNB (Fluka) were twice recrystallized from ethanol and then sublimed under vacuum.

Spectra were obtained in thermostatted cells in a Cary 17 spectrophotometer. The working temperatures were 16°, 27°, and 40°C ± 0.1°C.

Solutions were prepared by weighing. The ranges of concentration used were 1×10^{-4} to 3×10^{-4} *M* for DNB and 0.2 to 3 *M* for the amines. All solutions were freshly prepared prior to use.

Data processing was performed on a Digital PDP11/34 computer.

Results

The spectral characteristics of the systems amine–DNB studied show the same general features as observed for amine–benzonitrile (1). Although no new band is observed, there is an appreciable deviation from additivity of the optical density with respect to those of the components alone in the region of λ = 290 nm to 320 nm.[2] Typical spectral results are shown in Fig. 1. The spectral characteristics were maintained during the time measurement, except for the system n-BA – 1,2-DNB. For the latter system, a new band was observed at

[1]Author to whom correspondence should be addressed.

[2]The high absorption of both the amine and the DNB prevented observations at λ shorter than 290 nm.

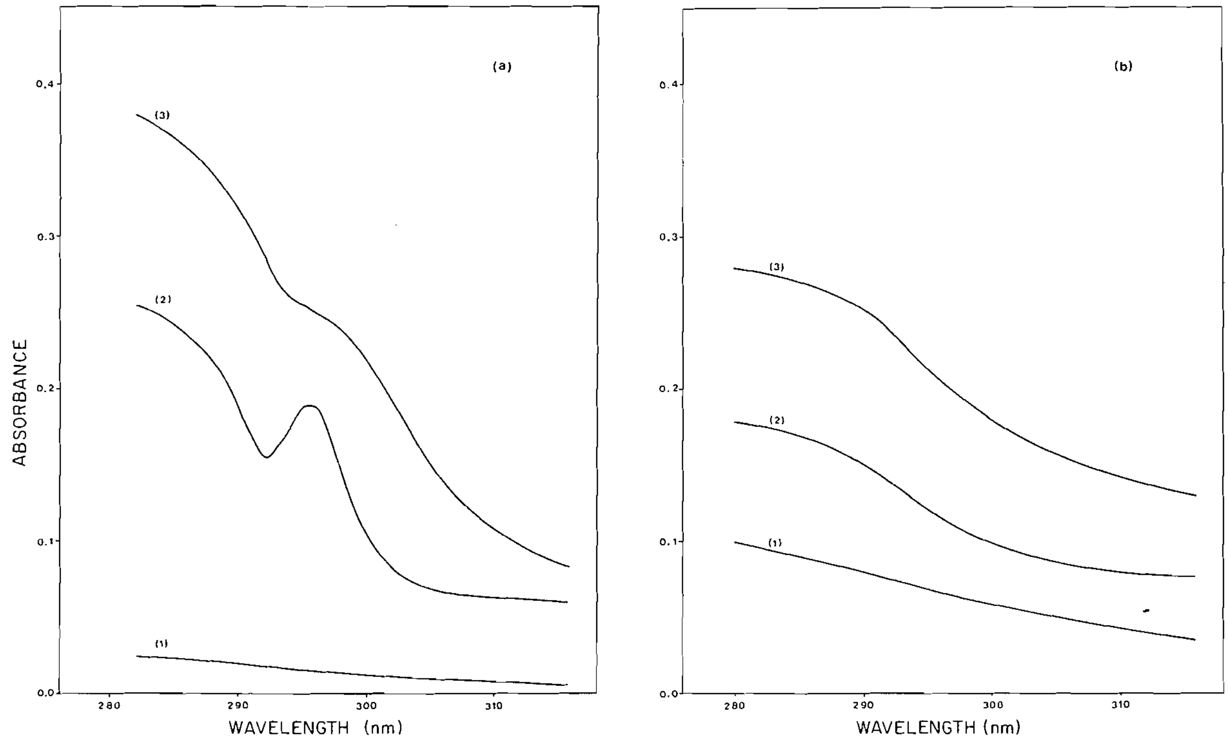

FIG. 1. Typical spectral results. (a) (1) n-BA 1.01 M; (2) 1,3-DNB 2.27×10^{-4} M; (3) mixture of n-BA 1.01 M and 1,3-DNB 2.27×10^{-4} M. (b) (1) DBA 1.19 M, (2), 1,2-DNB 1.21×10^{-4} M; (3) mixture of DBA 1.19 M and 1,2-DNB 1.21×10^{-4} M. Solvent: n-hexane. Temperature: 27 ± 0.1°C.

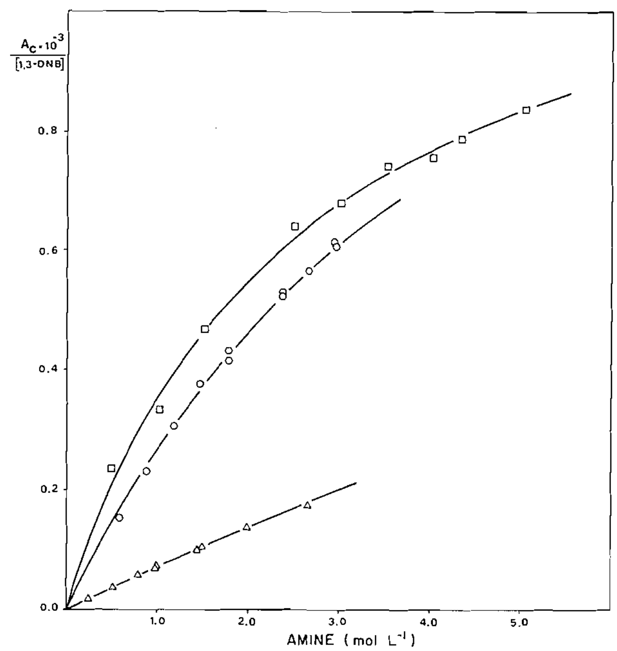

FIG. 2. Plots of $A_c/[A_0]$ vs. amine concentration for the systems. (□) 1,3-DNB − n-BA; (○) 1,3-DNB − DBA; (△) 1,3-DNB − TBA. The simulated curves are represented (see text) as a solid line.

$\lambda_{max} = 410$ nm immediately after mixing. This new band increased with time to a limited value depending on the 1,2-DNB concentration and it was assigned to the formation of N-n-butyl-2-nitroaniline, by S_NAr of the nitro group of 1,2-DNB by n-BA (14).

Actually, if the mixtures of the secondary amines with 1,2-DNB are allowed to stand for several hours, a new band also develops at around 400 nm, showing that these amines are also prone to produce S_NAr in 1,2-DNB. However, with the exception of the system n-BA − 1,2-DNB, these reactions are slow enough to allow the studies which are the purpose of this work. The enhanced absorbance for the systems amine−DNB was interpreted as due to a specific interaction, probably the formation of an EDA complex (1). Then, if a 1:1 complex is assumed, the observed absorbance, A_T, can be interpreted as the sum of three components (eq. [1])

$$[1] \quad A_T = A_A + A_D + A_{AD}$$

where A_A, A_D, and A_{AD} stand for the absorbance of the acceptor (DNB), the donor (amine), and the complex at equilibrium concentration.

An absorbance value, A_c, can now be defined as a function of the experimental values, A_T, and the corresponding values for the initial concentration of the acceptor, A_{A_0}, and the donor, A_{D_0}, (eq. [2])

$$[2] \quad A_c = A_T - (A_{A_0} + A_{D_0})$$

Then, A_c is a measure of the deviation from additivity of the mixtures. These values were determined for each system at 300 nm, which was the λ where they could be most accurately calculated. For every system, A_c was determined for different ratios of amine−DNB, in which the amine concentration $[D_0]$ was always at least 500-fold in excess with respect to the DNB concentration, $[A_0]$.

Typical plots of $A_c/[A_0]$ vs. amine concentration are shown in Fig. 2. For a given acceptor, the curvature of these plots is characteristic of a particular amine, giving a qualitative picture of the equilibrium conditions. The larger the deviation from a straight line, the greater the stability constant, K_s.

Approximate values of K_s and ϵ_c were determined graph-

TABLE 1. Results for K_s and ϵ_{AD} for amine–DNB complexes in n-hexane at 27°C and λ = 300 nm

Systems		Ratio	K_s	ϵ_{AD}	Correlation
Acceptor	Donor	$[D_0] \times 10^{-3}/[A_0]$	(L mol^{-1})[a]	(L mol^{-1} cm^{-1})[b]	coefficient
1,2-DNB	DBA	2.30–24.50	0.249±0.012	1661	0.9994
	TBA	1.73–13.75	0.098±0.010	1796	0.9996
1,3-DNB	n-BA	2.23–48.57	0.394±0.020	1764	0.9995
	DEA	2.05–25.10	0.243±0.012	2132	0.9993
	DBA	2.27–28.67	0.201±0.010	2133	0.9991
	TEA	3.05–16.13	0.089±0.009	2228	0.9983
	TBA	0.92–8.82	0.043±0.006	2267	0.9999
1,4-DNB	n-BA	2.96–29.56	0.356±0.008	3213	0.9992
	DBA	4.81–24.06	0.165±0.008	3295	0.9967
	TBA	0.52–4.60	0.032±0.005	6285	0.9938

[a]The error in K_s was calculated as in ref. 1.
[b]$\epsilon_{AD} = \epsilon_C + \epsilon_A + \epsilon_D$.

ically following eq. [3], derived (15) for the case where the absorption of the complex overlaps with that of the donor and the acceptor

$$[3] \quad \frac{[A_0][D_0]}{A_c([A_0] + [D_0])} = \frac{1}{K\epsilon_c}\frac{1}{([A_0] + [D_0])} + \frac{1}{\epsilon_c}$$

Then, the iterative procedure previously described (1) is used to calculate the final values of K_s and ϵ_c. In this procedure, K_s is varied to obtain the best fit to eq. [4].

$$[4] \quad A_c = \epsilon_c[AD]$$

[AD] being the equilibrium molar concentration of the complex. The fit to eq. [4] is measured by the correlation coefficient.

A further check to ensure the best values for K_s was developed. A computer simulation of the curves $A_c/[A_0]$ vs. $[D_0]$ was performed with the values of A_c calculated from the K_s obtained by the iterative procedure. A very good agreement between the experimental and the simulated curve was obtained, as is shown in Fig. 2. The results in K_s and ϵ_{AD} obtained for the systems studied are depicted in Table 1.

The behaviour of K_s with temperature was also studied for every system. Typical results are shown in Fig. 3. In general, as expected, small negative values of $-\Delta H$, around 8 kJ/mol, were found.

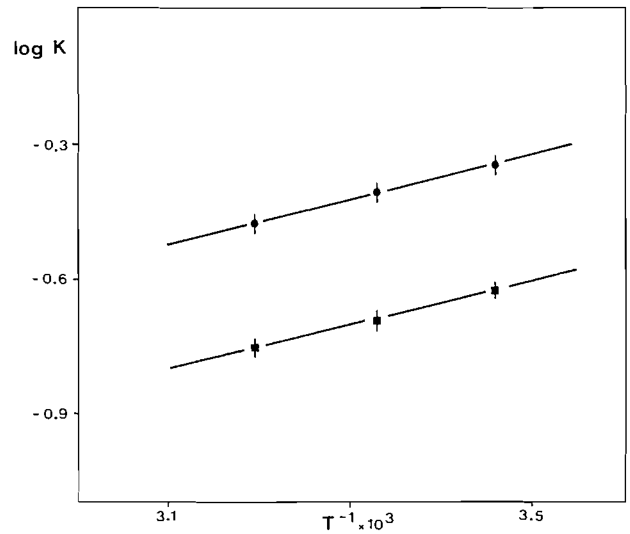

FIG. 3. Typical behavior of log K vs. T^{-1}: (●) n-BA – 1,3-DNB; (■) DBA – 1,3-DNB. Solvent: n-hexane.

Discussion

The fact that a value of K_s and a finite constant value of ϵ_{AD} could be determined from the enhanced absorbance of every mixture of amine–DNB in n-hexane can be taken as good evidence of formation of EDA complexes as was postulated for the same donors with benzonitrile, also in n-hexane (1).

Then, the difference in absorption of the mixture with respect to any single component may correspond (*i*) to broadening of a component band due to admixture of a component excited state with a charge transfer state (16); (*ii*) to an overlap with a new band of the EDA complexes. Although from the present experimental evidence it is not possible to distinguish between these two possibilities, the following considerations may favor (*ii*) as the more probable. It is expected that the maxima for the charge transfer band in these systems would lie in the ultraviolet region of the spectra (17), which is unreachable experimentally. These maxima are known to vary for similar sytems (1,3,5-TNB – aliphatic amines (6)) with the ionization potential (I_p) of the amine, in agreement with Mulliken's theory (18). In these systems it is observed that the lower the I_p of the electron donor, the smaller the transition energy ($h\nu_{AD}$) of the charge transfer band. Then, assuming that for the system DNB–amine the ϵ_{AD}(max) is not drastically different for the different amines, as was proposed for the systems benzonitrile–amines (1), it can be considered that the calculated ϵ_{AD} at 300 nm (see Table 1) represents the extinction coefficient of the tail of the charge transfer band. Consequently the difference in ϵ_{AD} would reflect the shift in ϵ_{AD} for any given acceptor, with the order $RNH_2 > R_2NH > R_3N$ as expected. On the other hand, and following the same reasoning, for a given donor the greatest value of ϵ_{AD} would be obtained for the acceptor with greatest electron affinities E_A (15). As can be seen in the table, for a given amine, ϵ_{AD} increases in the order 1,2-DNB < 1,3-DNB < 1,4-DNB which is also the order in which the E_A of the DNB increases (19). When the stability constant (K_s) values for a given acceptor are analyzed, it is clearly seen in the table that these follow the order $RNH_2 > R_2NH > R_3N$. This order is the inverse of the one that can be predicted from the inductive effects of the alkyl groups on the donor ability of the amines. There is a tendency, although it is only qualitative, for K_s to decrease with the dipole moment of the amine (20), which could suggest a contribution from dipolar association (21).

Actually the role of electrostatic force cannot be ruled out. It has been recently suggested that electrostatic interactions may make substantial contributions to the ground-state properties of EDA complexes (22). For the systems studied it is not possible, from the data, to establish the magnitude of this contribution, but it is not believed that it is the unique cause of the interactions. Previous studies in this laboratory, on solvatochromism in the ultraviolet spectra of π-acceptors such as benzonitrile (23) and nitrobenzene (24) as model compounds, have shown that the solvent effects on aliphatic amines cannot be accounted for only by dipolar interactions and that EDA complexation should be postulated. Similar considerations have been made to explain the mechanism of conductivity of triethylamine–nitrobenzene (25). Then, considering that the interaction is mostly through the EDA complex, the order of K_s with the amine structure could be explained through steric effects. Thus, for a given acceptor, the bulkier the substituents in the amine, the smaller the K_s. This consideration seems reasonable since the steric effects have been proposed to play an important role in EDA complexes having nitro aromatics as acceptors (26, 27). Moreover, in several types of EDA complexes having amines as donor, the effect of steric control on K_s (28–30) has been emphasized several times.

The values of K_s for the three DNBs studied are significantly greater than the values for the benzonitrile complexes with the same donor (1). These are expected results, since the presence of two nitro groups makes the aromatic ring more electron deficient and subsequently a better electron acceptor than benzonitrile.

The acceptor strength order generally observed for π–π complexes of these compounds (31) is 1,2-DNB $\sim$ 1,3-DNB $<$ 1,4-DNB. The explanation that has been given for these facts (32) does not seem to be satisfactory for the n–π complexes studied, since, for a given amine, the K_s follows the order of 1,2-DNB $>$ 1,3-DNB $>$ 1,4-DNB. The fact that both the donor and acceptor are unsymmetrical compounds suggests that there could be a preferred orientation of one molecule with respect to the other in the complex (33). Orientational complexes have been proposed for nitro aromatic complexes with indoles (33), methyl benzenes (34), and anilines (35).

Recently, energy changes calculated by CNDO/2 for complexing of ammonia, used as a model of an aliphatic amine donor, with quinones as acceptors (30) show that there are preferential sites of complexation at the midpoint of C(1)—C(2) on the quinone molecule. Nevertheless a stable complex is also predicted for any approach of the lone pair perpendicular to the quinone molecule.

In the present study, the fact that 1,2-DNB seems to be a better acceptor and at the same time gives S_NAr with the least sterically hindered amines suggests the possibility of formation of orientation complexes. In these complexes the amine nitrogen atom with its lone pair of electrons approachs the site of least electron density in the acceptor, which could be the carbon on the ring bonded to the nitro group (**I**). Such a type of complex has also been proposed as an intermediate in the reaction of amine with 1,3,5-TNB (36).

If such orientation is accepted, 1,2-DNB will probably be the better acceptor, due to the large inductive effect exerted by the *ortho* nitro group. This effect will be smaller for 1,3- and

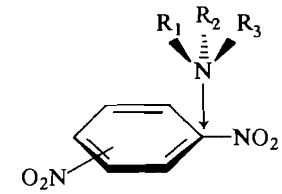

I

1,4-DNB. It should be mentioned that similar arguments are proposed to explain the usually more powerfully activating effect of the *o*-nitro with respect to the *p*-nitro in S_NAr (37).

Acknowledgements

Financial support from the Consejo Nacional de Investigaciones Científicas y Técnicas (CONICET) and Consejo de Investigaciones Científicas y Tecnológicas de la Provincia de Córdoba (CONICOR) is gratefully acknowledged.

1. J. Anunziata, J. Singh, and J. J. Silber. Can. J. Chem. **59**, 1291 (1981).
2. E. Buncel, A. R. Norris, and K. E. Russel. Q. Rev. Chem. Soc. **22**, 123 (1968).
3. M. J. Strauss, S. P. B. Taylor, and A. Reznick. J. Org. Chem. **37**, 3076 (1972).
4. F. Terrier. Chem. Rev. **82**, 77 (1982).
5. G. A. Artamkina, M. P. Egorov, and I. P. Beletskaya. Chem. Rev. **82**, 427 (1982).
6. R. Foster and R. K. Mackie. J. Chem. Soc. 3843 (1962).
7. W. Liptay and N. Tamberg. Z. Elektrochem. **66**, 59 (1962).
8. M. R. Crampton and V. Gold. J. Chem. Soc. B, 23 (1967).
9. M. J. Strauss. Chem. Rev. **70**, 667 (1970).
10. J. R. Beck. Tetrahedron, **34**, 2057 (1978).
11. G. Briegleb, W. Liptay, and M. Cantner. Z. Phys. Chem. (Frankfurt) **26**, 55 (1960).
12. L. Forlani and V. Tortelli. (*a*) J. Chem. Res. (S) 63 (1982); (*b*) 258 (1982).
13. C. F. Bernasconi. J. Am. Chem. Soc. **92**, 129 (1970).
14. J. O. Singh, J. D. Anunziata, and J. J. Silber. Acta Sudam. Quím. (Chile). Submitted.
15. S. D. Ross and M. M. Labes. J. Am. Chem. Soc. **79**, 76 (1957).
16. K. M. C. Davis and M. F. Farmer. J. Chem. Soc. B, 859 (1968).
17. (*a*) R. Foster and R. Mackie. Tetrahedron, **16**, 119 (1961); (*b*) R. Foster and C. A. Fyfe. Rev. Pure Appl. Chem. **16**, 61 (1966).
18. R. S. Mulliken and W. B. Person. Molecular complexes. Wiley, New York. 1962.
19. G. Briegleb. Angew. Chem. Int. Ed. Engl. **3**, 617 (1964).
20. J. A. Riddick and W. B. Bunger. Organic solvents. Techniques of Chemistry. Vol. II. 3rd ed. Wiley–Interscience, New York. 1970.
21. H. Fujiwara, T. Takaba, Y. Yamazaki, and Y. Sasaki. (*a*) J. Chem. Soc. Faraday Trans. 1, **75**, 79 (1979); (*b*) **78**, 347 (1982).
22. B. D. Ghosh and R. Basu. J. Phys. Chem. **84**, 1887 (1980).
23. J. Anunziata, J. O. Singh, and J. Chessa de Silber. An. Asoc. Quim. Argentina, **71**, 401 (1983).
24. L. Zingaretti, J. Anunziata, J. Singh, N. Toselli, and J. Chessa de Silber. Proceedings of the Third Physical Chemistry Congress, Argentina. 1983.
25. M. F. Mayahi and H. A. Husain. J. Indian Chem. Soc. L, 34 (1973).
26. R. Foster. J. Chem. Soc. 1075 (1960).
27. O. D. Bonner and G. B. Woolsey. Tetrahedron, **24**, 3625 (1968).
28. H. C. Brown and G. G. Pai. J. Org. Chem. **46**, 4713 (1981).

29. A. S. N. MURTHY and A. P. BHARDWAJ. J. Chem. Soc. Faraday Trans. 2, **78**, 1811 (1982).
30. M. J. M. CAMPBELL, B. DEMETRIOU, and R. JONES. J. Chem. Soc. Perkin Trans. 2, 917 (1983).
31. R. FOSTER. Organic charge transfer complexes. Academic Press, New York. 1969. Chapt. 7.
32. R. FOSTER and T. J. THOMSON. Trans. Faraday Soc. **59**, 2287 (1963).
33. R. FOSTER and C. A. FYFE. J. Chem. Soc. (B) 926 (1966).
34. N. B. JURINSKI and P. A. D. DE MAINE. J. Am. Chem. Soc. **86**, 3217 (1964).
35. J. LANDAWER and H. MCCONNELL. J. Am. Chem. Soc. **74**, 1221 (1952).
36. R. E. MILLER and W. F. K. WYNNE-JONES. J. Chem. Soc. 2378 (1959).
37. R. E. PARKER and T. O. READ. J. Chem. Soc. 3149 (1962).

Étude physico-chimique des solutions concentrées en acide phosphorique par voie électrochimique. Propriétés acido-basiques et oxydo-réductrices

C. LOUIS ET J. BESSIÈRE

Laboratoire de Chimie et d'Électrochimie Analytique, Faculté des Sciences, Université de Nancy I, B.P. 239, 54506 Vandoeuvre Les Nancy, France

Reçu le 25 juin 1984

C. LOUIS et J. BESSIÈRE. Can. J. Chem. **63**, 908 (1985).

Les propriétés acido-basiques des milieux $H_2O-H_3PO_4$ (1 à 14 *M*) sont caractérisées par la fonction d'acidité R_0(H) et les fonctions basiques $R_0(H_2PO_4^-)$, $R_0(HPO_4^{2-})$, $R_0(PO_4^{3-})$ qui représentent respectivement l'activité du proton et le pouvoir donneur des particules $H_2PO_4^-$, HPO_4^{2-}, PO_4^{3-}. Les limites thermodynamiques du domaine de potentiel accessible ainsi que la nature de l'équilibre d'ionisation de l'acide sont précisées. Les niveaux d'acidité *H* et *R* des milieux phosphoriques sont comparés à ceux des milieux sulfurique, chlorhydrique et fluorhydrique. L'identité du niveau d'acidité R_0(H) de ces milieux pour une même valeur de l'acitvité en eau des solutions est montrée.

C. LOUIS and J. BESSIÈRE. Can. J. Chem. **63**, 908 (1985).

Acid–base properties in 1 to 14 *M* H_3PO_4 solutions are characterized with a R_0(H) acidity function and $R_0(H_2PO_4^-)$, $R_0(HPO_4^{2-})$, $R_0(PO_4^{3-})$ functions which respectively represent the H^+ activity in these media and their ability to give $H_2PO_4^-$, HPO_4^{2-}, PO_4^{3-} species. The thermodynamic limits of potential and the nature of the ionization equilibrium are studied. *H* and *R* acidity levels in phosphoric media are compared to those of sulfuric, hydrochloric, and hydrofluoric acid media. The identity of their R_0(H) acidity level for the same value of water activity is shown.

Introduction

L'acide phosphorique est un intermédiaire important dans la synthèse des engrais et dans l'élaboration de produits purs destinés à l'industrie alimentaire et au traitement de surface. La séparation des éléments valorisables (uranium, vanadium, terres rares) ou toxiques (cadmium, arsenic, molybdène, métaux lourds) qu'il contient est généralement réalisée par des opérations d'extraction liquide–liquide ou de précipitation. Les résines échangeuses d'ions et la flottation ionique ont également été envisagées à l'echelle du laboratoire et de l'installation pilote.

Le niveau d'acidité des milieux phosphoriques conditionne le pouvoir extractant des agents chélatants utilisés en milieu non miscible, la protonation des collecteurs de flottation ionique ainsi que le pouvoir oxydo-réducteur des solutés. Au cours de cet article, la variation du niveau d'acidité R_0(H) des milieux phosphoriques avec la concentration de l'acide (de 1 *M* à 14 *M*) et le diagramme potentiel–pH généralisé de ces milieux sont établis. Leur pouvoir donneur des espèces $H_2PO_4^-$, HPO_4^{2-}, PO_4^{3-} est caractérisé par les fonctions $R_0(H_2PO_4^-)$, $R_0(HPO_4^{2-})$, $R_0(PO_4^{3-})$, ce qui permet de préciser en particulier la nature de l'équilibre d'ionisation dans les milieux phosphoriques. L'importance du terme activité de l'eau dans la fixation du niveau d'acidité des milieux eau–acide est ensuite étudiée.

Experimental

Réactifs

Acide phosphorique: Prolabo; ferrocène: Sigma; indicateurs de Hammett: Aldrich; 1,4-benzoquinone et hydroquinone: Fluka.

Procédures et matériel

Les mesures potentiométriques à intensité nulle ont été faites au moyen du millivoltmètre Aries 10000 Tacussel. Les tracés polarographiques ont été obtenus sur le polarographe PRG 3 Tacussel.

Pour les tracés voltampérométriques sur électrode solide, réalisés avec l'ensemble Tipol EPL 2 Tacussel, un montage classique à trois électrodes a été utilisé. Le dégazage des milieux réactionnels est obtenu par passage d'azote.

L'électrode au calomel saturé aqueuse placée dans un compartiment séparé contenant H_3PO_4 0,1 *M* est en général utilisée comme électrode de référence (1).

REMARQUE: Elle a été comparée aux électrodes suivantes (2): électrode au calomel saturé aqueuse, électrode au calomel saturé préparée *in situ*, electrode AgCl/Ag, électrode Hg_2HPO_4/Hg, électrode $BiPO_4$/Bi.

L'électrode auxiliaire est constituée par un fil de platine. Les différentes électrodes de travail utilisées sont: électrode de platine EDI Controvit Tacussel (diamètre 1 mm) ou fil de platine (diamètre 0,8 mm) serti dans du verre ou du Teflon; électrode de carbone vitreux EDI Controvit Tacussel (diamètre 3 mm) ou barreau de carbone vitreux serti dans du verre (diamètre 2 mm). La vitesse de rotation est habituellement de 600 tours/min.

L'électrode à hydrogène est préparée selon la méthode préconisée par G. Charlot *et al.* (3).

Résultats et discussion

1. *Fonction d'acidité* $R_0(H)$ *des milieux* $H_2O-H_3PO_4$

La fonction d'acidité R_0(H) introduite par Strehlow et coll. pour caractériser le niveau d'acidité des solutions (4, 5) est déterminée expérimentalement à partir de la mesure du potentiel pris par une électrode indicatrice de pH en utilisant le système ferricinium/ferrocène comme référence de potentiel.

Dans le cas où l'électrode à hydrogène sert d'électrode indicatrice, la fonction d'acidité R_0(H) est donnée par la relation:

$$[1] \quad R_0(\mathrm{H}) = (E_0^{\mathrm{H_2O}} - E^{\mathrm{H_2O-H_3PO_4}})/0{,}058$$

où $E_0^{\mathrm{H_2O}} = -0{,}400$ V est le potentiel standard de l'électrode à hydrogène dans l'eau à 25°C et $E^{\mathrm{H_2O-H_3PO_4}}$ son potentiel dans une solution acide de composition donnée exprimé par rapport à Fc^+/Fc. Lorsque l'on utilise l'électrode 1,4-benzoquinone/hydroquinone saturée comme électrode indicatrice, la fonction R_0(H) est donnée par la relation:

$$[2] \quad R_0(\mathrm{H}) = (E_{\mathrm{Q_s/QH_{2s}}}^{\mathrm{H_2O}} - E_{\mathrm{Q_s/QH_{2s}}}^{\mathrm{H_2O-H_3PO_4}})/0{,}058$$

où $E_{\mathrm{Q_s/QH_{2s}}}^{\mathrm{H_2O}} = +0{,}316$ V est le potentiel standard du couple 1,4-benzoquinone saturée/hydroquinone saturée dans l'eau et $E_{\mathrm{Q_s/QH_{2s}}}^{\mathrm{H_2O-H_3PO_4}}$ son potentiel dans la solution acide exprimé par rapport à Fc^+/Fc.

La fonction R_0(H) s'identifie au pH si l'on admet que le potentiel standard du système ferricinium/ferrocène est indépendant de la nature du solvant. Dans la relation:

TABLEAU 1. Potentiels des systèmes Fc^+/Fc et H^+/H_2 dans les milieux $H_2O-H_3PO_4$ (mV vs. ECS dans H_3PO_4 0,1 *M*)

	H_3PO_4 *M*							
	0,1	1,02	2,04	5,10	7,15	10,0	12,0	14,0
$E_{1/2Fc^+/Fc} = E_0$ sur Hg (mV vs. ECS H_3PO_4 0,1 *M*)	+130	+80	+50	−30	−85	−190	−290	−380
E_{H^+/H_2} (mV vs. ECS H_3PO_4 0,1 *M*)	−347	−335	−337	−330	−327	−315	−300	−260

[3] $\mathrm{pH} = R_0(\mathrm{H}) + \log f_{Fc}/f_{Fc^+}$

les coefficients d'activité f_{Fc} et f_{Fc^+} sont alors égaux.

1.1. *Système de comparaison: ferricinium/ferrocène*

Le ferrocène (Fc) est peu soluble dans les milieux $H_2O-H_3PO_4$. Il s'oxyde en ferricinium (Fc^+) de coloration bleue sous l'action de l'oxygène ou des protons seuls lorsque le milieu est suffisamment concentré en acide.

Des réactions susceptibles de modifier le comportement redox du système Fc^+/Fc ont été mentionnées dans le cas d'autres milieux. Ainsi la protonation du ferrocène sur l'atome de métal a été mise en évidence par rmn dans les milieux H_2SO_4 concentrés (6). La complexation de l'ion ferricinium par les anions, qui a été montrée pour les chlorure, les perchlorate, les thiocyanate ainsi que pour les anions des acides carboxyliques, n'a pas lieu dans le cas des ions phosphate (7, 8). L'hydrolyse de l'ion ferricinium, qui peut se produire à température élevée (8), se fait lentement à température ambiante dans les milieux phosphoriques de concentration supérieure à 11,5 *M* où nous avons constaté l'apparition d'espèces Fe(II).

Etant donné les caractéristiques de rapidité et de réversibilité du système Fc^+/Fc dans les milieux $H_2O-H_3PO_4$, son potentiel normal est pris égal au potentiel de demi-vague de réduction de Fc^+ déterminé en polaragraphie. Les valeurs expérimentales des potentiels normaux du système Fc^+/Fc exprimées par rapport à l'électrode de référence ECS aqueuse dans un compartiment séparé contenant H_3PO_4 à la concentration 0,1 *M*, sont données dans le tableau 1.

1.2. *Système indicateur de H^+: H^+/H_2. Electrode à hydrogène*

Le bon fonctionnement de l'électrode à hydrogène dans les milieux phosphoriques peut en principe être vérifié en suivant la variation de son potentiel en fonction de la pression d'hydrogène. Mais l'analyse précise des voltampérogrammes est délicate car ils sont peu reproductibles. Leur allure générale est néanmoins en faveur d'un système rapide. La convergence de la fonction d'acidité calculée à partir de ces résultats et des fonctions d'acidité dont la détermination est fondée sur d'autres systèmes indicateurs de H^+ a confirmé a posteriori le fonctionnement correct de l'électrode à hydrogène dans les milieux phosphoriques. Les valeurs expérimentales de potentiel de l'électrode à hydrogène mesurées par rapport à l'électrode de référence ECS aqueuse dans H_3PO_4 0,1 *M* sont données dans le tableau 1.

1.3. *Système indicateur de H^+: 1,4-benzoquinone/hydroquinone*

Les deux composés 1,4-benzoquinone et hydroquinone sont solubles dans les milieux $H_2O-H_3PO_4$. Dans tout le domaine de concentration en H_3PO_4, les tracés voltampérométriques sur électrode de platine poli montrent que le système 1,4-benzoquinone/hydroquinone est lent. L'oxydation de l'hydroquinone est caractérisée par une vague de diffusion pure d'après le critère de Levich. Le signal correspondant à la réduction de la quinone n'a pas cette propriété et indique que l'espèce se transforme lentement.

TABLEAU 2. Potentiels des systèmes Q/QH_2 et Q_s/QH_{2s} dans les milieux $H_2O-H_3PO_4$ (mV vs. Fc^+/Fc)

	H_2O	H_3PO_4 *M*				
		2,0	5,5	8,0	11,5	14,0
$E_{0(Q/QH_2)}$ (mV vs. Fc^+/Fc)	+299	+328	+400	+460	+600	+720
$E_{Q_s/QH_{2s}}$ (mV vs. Fc^+/Fc)	+315	+320	+420	+505	+655	+780

Les études faites par potentiométrie à intensité nulle sur électrode de platine montrent que la loi de Nernst est vérifiée dans les différents milieux phosphoriques et que la pente des droites $E = f(\log[Q]/[QH_2])$ reste égale à 30 mV. Le système Q/QH_2 est donc reversible dans les milieux $H_2O-H_3PO_4$ selon le processus:

[4] $Q + 2H^+ + 2\,e^- \rightleftharpoons QH_2$

Les potentiels normaux du système Q/QH_2 ainsi que les potentiels mesurés à saturation des espèces Q et QH_2, exprimés par rapport au système Fc^+/Fc sont donnés dans le tableau 2.

1.4. *Fonction $R_0(H)$*

Les variations avec la concentration d'acide de la fonction $R_0(\mathrm{H})$ calculée à partir du système H^+/H_2 (relation [1]) et du système Q_s/QH_{2s} (relation [2]) sont présentées en fig. 1.

Les valeurs calculées à partir des deux systèmes indicateurs coïncident jusqu'à la concentration H_3PO_4 11,5 *M* (écart inférieur à 0,3 unité). Pour des concentrations d'acide comprises entre 11,5 et 14 *M*, nous utiliserons de préférence les valeurs déterminées à partir du système de l'hydrogène en raison de la modification de la quinone dans les milieux concentrés en acide.

La fonction d'acidité $R_0(\mathrm{H})$ qui caractérise l'acidité des milieux $H_2O-H_3PO_4$ présente une variation de 9 unités environ lorsque la concentration d'acide passe de 1,0 *M* à 14 *M*. L'écart entre les niveaux d'acidité des milieux phosphoriques correspondant aux concentrations industrielles 5,5 et 11,5 *M* est de 4 unités.

1.5. *Domaine de potentiel accessible dans les milieux $H_2O-H_3PO_4$. Diagramme potentiel–$R_0(H)$ du solvant*

D'un point de vue thermodynamique, le domaine des poten-

TABLEAU 3. Limites thermodynamiques du domaine des potentiels accessibles dans les milieux $H_2O-H_3PO_4$

	H_2O	H_3PO_4 *M*					
		1,0	2,0	5,5	8,0	11,5	14,0
R_0(H)		+0,2	−0,2	−1,9	−3,2	−6,1	−8,9
$-\log a_{H_2O}$[a]		0,009	0,021	0,100	0,217	0,52	0,92
E_{H^+/H_2}[b]	−400	−411	−387	−290	−205	−46	+120
E_{O_2/H_2O}[c]	+829	+817	+841	+942	+1020	+1197	+1371
ΔE[d]		1228	1228	1232	1225	1237	1251

[a] D'après la réf. 9.
[b] mV vs. Fc^+/Fc, d'après le tableau 1.
[c] mV vs. Fc^+/Fc, d'après la relation [7].
[d] mV d'après la relation [8].

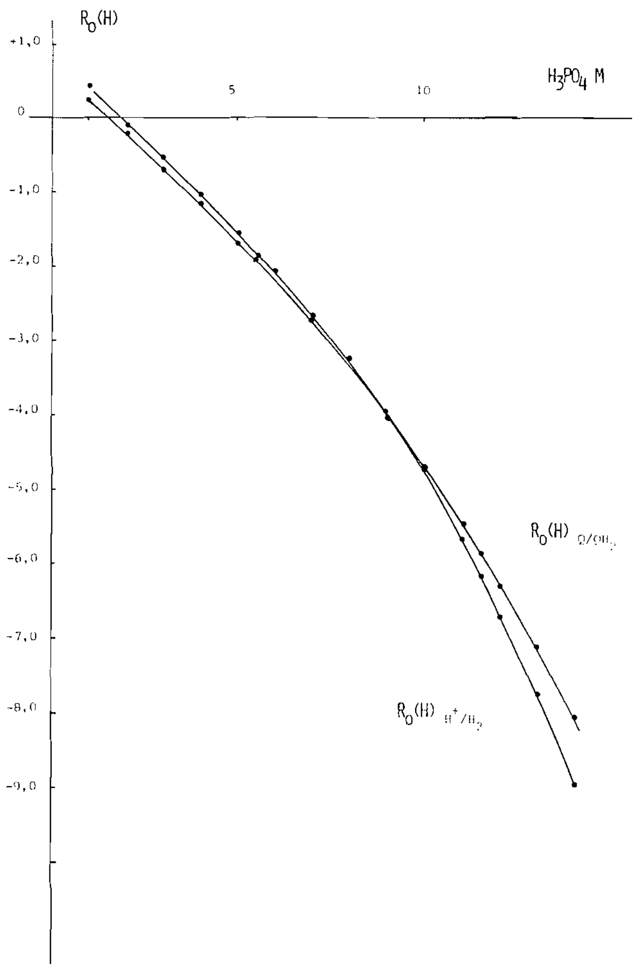

FIG. 1. Fonction R_0(H) en fonction de la concentration de H_3PO_4; (a) déterminée à partir du système H^+/H_2; (b) déterminée à partir du système Q_s/QH_{2s}.

tiels accessibles dans les milieux $H_2O-H_3PO_4$ est limité par les propriétés oxydantes du proton et les propriétés réductrices de l'eau. Les limites sont données par la variation des systèmes H^+/H_{2g} et O_{2g}/H_2O avec la concentration de l'acide.

Si l'on considère la réaction:

$$[5] \quad 2H^+ + 2e^- \rightleftharpoons H_{2g}$$

la variation du potentiel du système H^+/H_2 ne dépend que de la fonction d'acidité selon la relation [1].

Si l'on considère la réaction:

$$[6] \quad O_{2g} + 4H^+ + 4e^- \rightleftharpoons 2H_2O$$

la limite thermodynamique des potentiels accessibles en oxydation est donnée par la relation:

$$[7] \quad E = E^{H_2O}_{0_{O_2/H_2O}} - 0{,}058\ R_0(H) - 0{,}029 \log a_{H_2O}$$

avec $E^{H_2O}_{0_{O_2/H_2O}} = +0{,}829$ V. Elle dépend de l'acidité du milieu et de son activité en eau (9). L'étendue du domaine accessible en potentiel est donc donnée par la relation:

$$[8] \quad \Delta E = E^{H_2O}_{0_{O_2/H_2O}} - E^{H_2O}_{0_{H^+/H_2}} - 0{,}029 \log a_{H_2O}$$

Elle est pratiquement constante et égale à 1,23 V. En effet, le terme 0,029 log a_{H_2O} est négligeable jusqu'à une concentration d'acide de 8 *M* et sa valeur est de 28 mV dans les milieux les plus concentrés (tableau 3).

Le diagramme $E-R_0$(H) des milieux $H_2O-H_3PO_4$ est présenté en fig. 2.

REMARQUE: L'electrolyse sur électrode de platine de mélanges $H_2O-H_3PO_4$ donne O_2 et H_2 par décomposition de H_2O. Cependant, la formation d'ozone est sensible, même pour de faibles concentrations d'acide (10–12). Cette méthode a été préconisée pour la préparation de milieux concentrés d'acide phosphorique (12).

1.6. *Comparaison des fonctions d'acidité dans les milieux $H_2O-H_3PO_4$*

L'acidité des milieux $H_2O-H_3PO_4$ a été caractérisée par des fonctions *H*: H_0, H_0', H_0''', H_R, H_R' (13–16), ainsi que par des fonctions *R*: H_{GF} (8). Le tableau 4 présente les variations de ces différentes fonctions et permet de les comparer à la fonction R_0(H) que nous avons déterminée.

1.6.1. *Comparaison des fonctions* R_0*(H) et* H_0

Comme dans les autres milieux eau–acide, les fonctions d'acidité R_0(H) et H_0 présentent un écart sensible qui augmente avec la teneur en acide. Si l'on admet que la fonction R_0(H) traduit le mieux le niveau d'acidité du milieu du fait de la structure du système de comparaison Fc^+/Fc, d'après la relation:

$$[9] \quad pH = H_0 + \log f_I/f_{IH^+}$$

l'écart entre les deux fonctions mesure la quantité $\log f_I/f_{IH^+}$. Afin de préciser la part due à chacun des constituants du couple IH^+/I, nous avons étudié la variation de solvatation d'un indicateur de Hammett, l'anthraquinone I′, dont la protonation ne peut être réalisée dans les milieux phosphoriques, même concentrés.

En milieu 5,5 *M*, c'est la 4-chloro-2-nitroaniline I qui permet d'évaluer H_0 ($pK_{H_2O} = -0{,}9$). Les deux indicateurs de

TABLEAU 4. Fonctions d'acidité H et R dans les milieux $H_2O-H_3PO_4$

H_3PO_4 M	H_0	H'_0	H'''_0	H_R	H'_R	H_{GF}	$R_0(H)$
1,0	+1,8	+0,70	+0,55	+0,63	+0,63	+0,6	+0,2
2,0	+0,42	+0,27	+0,5	−0,1	−0,1	−0,1	−0,2
3,0	+0,06	−0,1	−0,45	−0,8	−0,8	−0,77	−0,7
4,0	−0,025	−0,4	−0,9	−1,32	−1,32	−1,35	−1,1
5,0	−0,55	−0,7	−1,40	−2,05	−1,95	−1,85	−1,7
5,5	−0,70	−0,83	−1,60	−2,4	−2,27	−2,1	−1,9
6,0	−0,83	−0,97	−1,85	−2,75	−2,60	−2,35	−2,1
7,0	−1,07	−1,25	−2,33	−3,45	−3,25	−2,85	−2,7
8,0	−1,35	−1,5	−2,75	−4,15	−3,95	−3,4	−3,2
9,0	−1,65	−1,75	−3,20	−4,92	−4,60	−4,0	−3,9
10,0	−1,95	−2,03	−3,60	−5,70	−5,32	−4,65	−4,7
11,0	−2,40	−2,35	−4,0	−6,45	−6,0	−5,35	−5,6
11,5	−2,60	−2,5	−4,2	−6,83	−6,3	−5,75	−6,1
12,0	−2,77	−2,7	−4,45	−7,22	−6,65	−6,08	−6,7
13,0	−3,17	−2,95	−4,9	−8,0	−7,30	−7,0	−7,7
14,0	−3,55	−3,30	−5,5	−8,8	−7,9	−8,0	−8,9

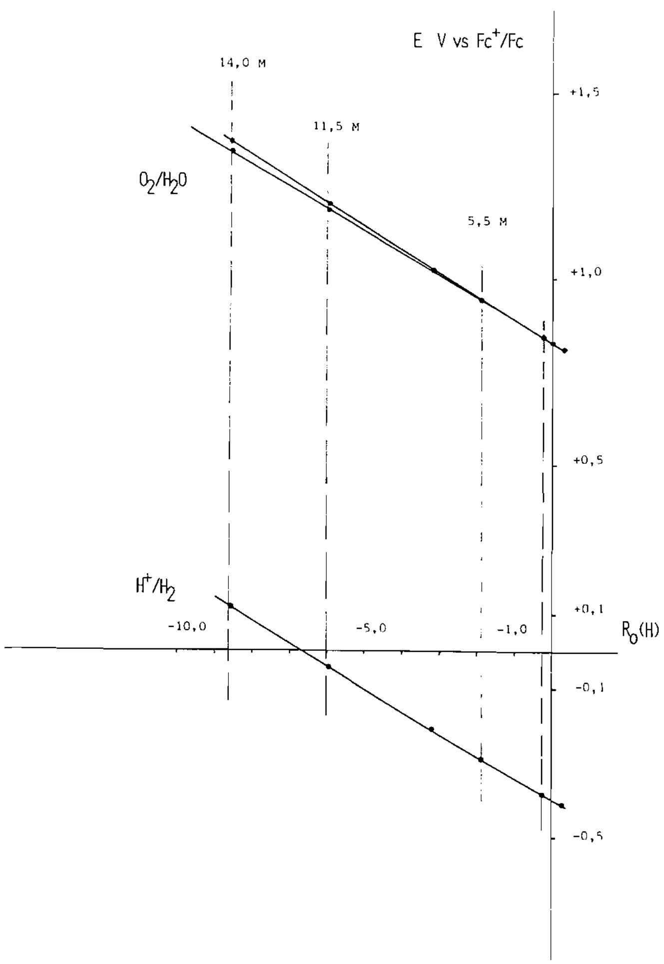

FIG. 2. Diagramme $E-R_0(H)$ des milieux $H_2O-H_3PO_4$.

Hammett obéissent à la relation:

[10] $f_I/f_{IH^+} = f_{I'}/f_{I'H^+}$

Or, la solubilité de l'anthraquinone ne varie pratiquement pas lorsque l'on passe de l'eau au milieu phosphorique 5,5 M. Donc, $f_{I'}$ est peu différent de 1 et la différence $R_0(H) - H_0$ mesure la quantité $-\log f_{I'H^+}$ (relation [9]). En milieu phosphorique 5,5 M, $-\log f_{I'H^+}$ est donc égal à $-1,2$. Cette valeur est voisine de celles trouvées pour les coefficients d'activité de cations monovalents qui ne subissent pas d'interaction spécifique avec les ions du solvant.[1]

Globalement, l'écart entre les fonctions $R_0(H)$ et H_0 est dû à une desolvatation rapide de IH^+ quand la teneur en acide augmente alors que la solvatation de la molécule neutre varie peu. Il semble que, du fait de leur structure, les indicateurs de Hammett soient plus sensibles aux effets de la solvatation par l'eau que les indicateurs conduisant aux fonctions $R_0(H)$ et H'_R.

1.6.2. *Comparaison des fonctions* $R_0(H)$, H_{GF} *et* H'_R

Les variations des fonctions d'acidité H_{GF} et $R_0(H)$ en fonction de la concentration de H_3PO_4 sont très voisines. Ceci valide indirectement l'utilisation de l'électrode de verre comme indicateur de niveau d'acidité. Contrairement aux électrodes à hydrogène et à quinhydrone dont le bon fonctionnement peut être vérifié, l'électrode de verre ne donne, pour chaque milieu, qu'une valeur de potentiel de membrane qui est fixé par la composition de la solution.

La concordance existant entre les fonctions H'_R et $R_0(H)$ est analogue à celle observée dans le cas des milieux $H_2O-H_2SO_4$ (17). Elle peut s'expliquer par le fait que les lois de variation des cofficients d'activité relatifs au ferrocène et au ferricinium sont très proches de celles observées pour les édifices hydrocarbonés insaturés, protonés ou non, conduisant à la fonction H'_R. Dans cette famille d'indicateurs, la présence de groupements substitués n'a pour effet que de modifier le pK_{H_2O} des couples indicateurs et n'a pratiquement pas d'influence sur la valeur du rapport des coefficients d'activité relatifs aux deux constituants du couple acide–base (18).

REMARQUE: À notre connaissance, l'exploitation des résultats existant concernant l'acidité des milieux phosphoriques pour le calcul d'une fonction d'acidité d'excès (19) n'a pas été faite.

2. *Fonctions* $R_0(H_2PO_4^-)$, $R_0(HPO_4^{2-})$ *et* $R_0(PO_4^{3-})$ *dans les milieux* $H_2O-H_3PO_4$

La fonction $R_0(H)$ traduit l'aptitude du milieu eau–acide à céder la particule H^+. Par analogie, les fonctions $R_0(H_2PO_4^-)$, $R_0(HPO_4^{2-})$ et $R_0(PO_4^{3-})$ sont définies pour caractériser l'ap-

[1] Le calcul et l'analyse des coefficients d'activité des anions et des cations dans les milieux phosphoriques seront présentés dans un article intitulé: Solvatation des espèces ioniques dans les milieux $H_2O-H_3PO_4$. À paraître. C. Louis et J. Bessière.

titude des milieux $H_2O-H_3PO_4$ à céder les particules $H_2PO_4^-$, HPO_4^{2-} et PO_4^{3-}.

Elles peuvent être déterminées expérimentalement à partir de la mesure du potentiel pris par une électrode M dont le fonctionnement fait intervenir un équilibre électrochimique engageant l'une des espèces phosphate et le composé insoluble correspondant. Ainsi, si l'on considère l'équilibre redox:

[11] $MHPO_{4s} + 2e^- \rightleftharpoons M_s + HPO_4^{2-}$

le potentiel du système $MHPO_{4s}/M_s$ dans les différents milieux est donné par la relation:

[12] $$E^{H_2O-H_3PO_4} = E_0^{H_2O} - \frac{0,058}{2} \log a_{HPO_4^{2-}}$$

Il ne dépend que de l'activité de l'espèce HPO_4^{2-} et la fonction

[13] $$R_0(HPO_4^{2-}) = \frac{E^{H_2O-H_3PO_4} - E_0^{H_2O}}{0,029}$$

est directement liée à l'écart des potentiels du système $MHPO_{4s}/M_s$ dans le milieu eau–acide et dans l'eau, ceux-ci étant exprimés par rapport au système de comparaison Fc^+/Fc.

Les fonctions $R_0(H_2PO_4^-)$ et $R_0(PO_4^{3-})$ peuvent être déterminées de la même manière. Néanmoins, elles ne sont pas indépendantes. En effet, en solution diluée, les activités des espèces participant aux équilibres:

[14] $H_2PO_4^- \rightleftharpoons H^+ + HPO_4^{2-}$ $\quad pK_2 = 7,2$

[15] $HPO_4^{2-} \rightleftharpoons H^+ + PO_4^{3-}$ $\quad pK_1 = 12,4$

sont liées au pH, à pK_1 et pK_2 par les relations:

[16] $pK_2 = pH + p(HPO_4^{2-}) - p(H_2PO_4^-)$

[17] $pK_1 = pH + p(PO_4^{3-}) - p(HPO_4^{2-})$

Dans les milieux concentrés, l'expression des constantes des équilibres de protonation reste la même et les trois fonctions sont liées par des relations formellement analogues à celles établies dans les milieux dilués:

[18] $pK_2 = R_0(H) + R_0(HPO_4^{2-}) - R_0(H_2PO_4^-)$

[19] $pK_1 = R_0(H) + R_0(PO_4^{3-}) - R_0(HPO_4^{2-})$

Ces fonctions permettent de préciser la nature de l'équilibre d'ionisation des mélanges $H_2O-H_3PO_4$ et de prévoir l'évolution de la solubilité d'un phosphate minéral avec la teneur en acide.

2.1. *Système Hg_2HPO_{4s}/Hg_s. Fonction* $R_0(HPO_4^{2-})$

L'oxydation électrochimique du mercure dans les milieux $H_2O-H_3PO_4$ se traduit par la formation d'un précipité qui a été identifié par diffraction X comme Hg_2HPO_4, quelle que soit la composition du milieu acide. La réaction d'oxydo-réduction est:

[20] $Hg_2HPO_{4s} + 2e^- \rightleftharpoons 2Hg_s + HPO_4^{2-}$

Le potentiel pris par une électrode au phosphate mercureux préparée *in situ* ne dépend donc que de l'activité des espèces HPO_4^{2-} (relation [12]). La fonction $R_0(HPO_4^{2-})$ est calculée d'après le relation [13] où $E^{H_2O} = -0,024$ V.

Les résultats sont présentés dans le tableau 5. Ils montrent que les propriétés réductrices du mercure en milieu $H_2O-H_3PO_4$ diminuent quand la concentration d'acide augmente.

2.2. *Système $BiPO_{4s}/Bi_s$. Fonction* $R_0(PO_4^{3-})$

Le phosphate de bismuth est peu soluble dans les milieux $H_2O-H_3PO_4$ et précipite uniquement sous la forme $BiPO_4$, quelle que soit la concentration de l'acide (20). $BiPO_4$ est réductible en bismuth métal selon le processus redox:

[21] $BiPO_{4s} + 3e^- \rightleftharpoons Bi_s + PO_4^{3-}$

Le potentiel E_{BiPO_{4s}/Bi_s} ne dépend que de l'acitvité des espèces PO_4^{3-}. Expérimentalement, il est donné par l'électrode de bismuth utilisée *in situ* (20). En effet, dans les différents milieux $H_2O-H_3PO_4$, l'électrode de bismuth se couvre instantanément d'une couche de phosphate de bismuth. La fonction $R_0(PO_4^{3-})$ est calculée d'après la relation:

[22] $$-\log a_{PO_4^{3-}} = R_0(PO_4^{3-}) = \frac{E^{H_2O-H_3PO_4} - E'^{H_2O}}{0,058/3}$$

où $E'^{H_2O} = -0,593$ V est le potentiel du système $BiPO_{4s}/Bi_s$ dans l'eau. Les résultats sont présentés dans le tableau 5.

REMARQUE: Les deux fonctions $R_0(HPO_4^{2-})$ et $R_0(PO_4^{3-})$ ont été déterminées indépendamment. Nous avons vérifié que la quantité:

$$R_0(H) + R_0(PO_4^{3-}) - R_0(HPO_4^{2-})$$

théoriquement égale à 12,4 (relation [19]), restait pratiquement constante et comprise entre 12,3 et 12,8, ce qui est satisfaisant puisque les fonctions R_0 sont déterminées chacune à 0,2 unité près.

2.3. *Fonction* $R_0(H_2PO_4^-)$

La fonction $R_0(H_2PO_4^-)$, calculée d'après la relation [18], figure également dans le tableau 5.

L'ensemble des propriétés acide–base des milieux $H_2O-H_3PO_4$ (1 *M* à 14 *M*) est présenté sous la forme d'un diagramme: $R_0(H_2PO_4^-)$, $R_0(HPO_4^{2-})$, $R_0(PO_4^{3-})$, $R_0(H)$, log a_{H_2O}, log $a_{H_3PO_4}$ en fonction de la concentration de H_3PO_4 (fig. 3).

2.4. *Application: équilibre d'ionisation dans les milieux $H_2O-H_3PO_4$*

Si l'équilibre:

[23] $H_3PO_4 + 4H_2O \rightleftharpoons H_9O_4^+ + H_2PO_4^-$

rend compte des phénomènes dans les milieux concentrés en acide, les fonctions $R_0(H)$ et $R_0(H_2PO_4^-)$, l'activité de l'eau a_{H_2O} et l'activité de l'acide $a_{H_3PO_4}$ sont liées par la relation:

[24] $R_0(H) + R_0(H_2PO_4^-) + \log a_{H_3PO_4} + 4 \log a_{H_2O} = 2,1$

A partir de nos résultats et des données de la littérature (9) nous avons calculé l'expression:

[25] $A_n = R_0(H) + R_0(H_2PO_4^-) + \log a_{H_3PO_4} + n \log a_{H_2O}$

en fonction de la concentration de l'acide pour $n = 4,2,1$. Les résultats sont donnés dans le tableau 6.

Il existe donc une concordance satisfaisante entre les données expérimentales et l'expression A_4 ($n = 4$) jusqu'à des concentrations d'acide voisines de 8 *M*. Pour des concentrations comprises entre 8 *M* et 12 *M*, la corrélation est bonne pour $n = 2$ puis $n = 1$. Ceci implique que le nombre des molécules d'eau solvatant le proton diminue à ces concentrations de H_3PO_4. L'équilibre de dissociation de H_3PO_4 est alors représenté par:

[26] $H_3PO_4 + H_2O \rightleftharpoons H_3O^+ + H_2PO_4^-$

Pour les milieux les plus concentrés (concentration supérieure à 12 *M*), l'expression [25] cesse d'être valable. Ceci peut être attribué à des phénomènes de dimérisation (21) ou de poly-

TABLEAU 5. Potentiels des systèmes Hg_2HPO_{4s}/Hg_s et $BiPO_{4s}/Bi_s$ dans les milieux $H_2O-H_3PO_4$. Fonctions $R_0(H_2PO_4^-)$, $R_0(HPO_4^{2-})$ et $R_0(PO_4^{3-})$

H_3PO_4 *M*	$E_{Hg_2HPO_{4s}/Hg_s}$ [a]	E_{BiPO_{4s}/Bi_s} [a]	$R_0(H_2PO_4^-)$ [b]	$R_0(HPO_4^{2-})$	$R_0(PO_4^{3-})$
1,0	+220	−190	+1,4	8,4	20,8
2,0	+250	−160	+2,0	9,4	22,4
3,0	+270	−135	+2,2	10,1	23,7
4,0	+295	−110	+2,6	11,0	25,0
5,0	+320	−90	+2,9	11,8	26,0
5,5	+330	−75	+3,1	12,2	26,8
6,0	+345	−65	+3,4	12,7	27,3
7,0	+375	−35	+3,8	13,7	28,8
8,0	+405	−5	+4,3	14,8	30,4
9,0	+437	+30	+4,3	15,9	32,2
10,0	+470	+70	+4,7	17,0	34,3
11,0	+505	+110	+5,0	18,2	36,3
11,5	+525	+135	+5,3	18,9	37,6
12,0	+540	+150	+5,5	19,4	38,4
13,0	+580	+185	+5,8	20,8	40,2
14,0	+620	+220	+6,0	22,2	42,0

[a] mV vs. Fc^+/Fc.
[b] D'après la relation [10].

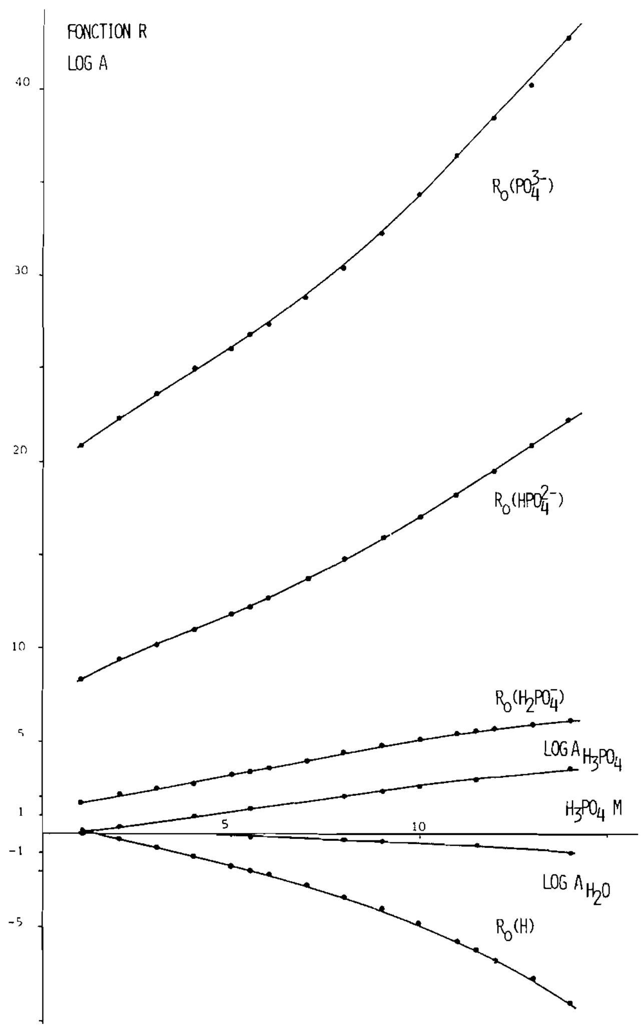

FIG. 3. Caractéristiques acide–base des milieux $H_2O-H_3PO_4$.

mérisation de l'acide phosphorique. L'équilibre [26] ne traduit plus à lui seul l'ionisation dans les milieux $H_2O-H_3PO_4$.

REMARQUE: Des phénomènes analogues ont été observés pour les milieux $H_2O-H_2SO_4$ et H_2O-HF. Des discontinuités au niveau des propriétés physiques (densité, conductivité) se manifestent à partir des concentrations $1H_2SO_4-2H_2O$ et $2HF-1H_2O$ (70% HF) (17, 22). Au delà de ces concentrations, il faut considérer les milieux comme des solvants différents dont les propriétés ne peuvent être déduites des lois concernant les mélanges.

3. *Comparaison de l'acidité de différents milieux eau–acide*

Les fonctions d'acidité d'excès apporteront probablement de nouveaux éléments dans la comparaison des milieux eau–acide (23). Nous avons, pour notre part, comparé les niveaux d'acidité $R_0(H)$ de différents milieux eau–acide pour des valeurs égales de leur activité en eau comme cela a été fait pour les fonctions d'acidité *H*.

3.1. *Comparaison de l'acidité à partir des fonctions* H_o

De nombreuses études ont porté sur l'analyse des relations susceptibles d'exister entre les valeurs des fonctions H_0 et l'activité de l'eau d'un mélange eau–acide de composition donnée. Ce sont principalement les travaux de Bascombe et Bell (24) et Wyatt (25) qui ont permis de préciser le rôle de l'activité de l'eau dans la fixation du niveau d'acidité H_0 des solutions acides.

3.1.1. *Cas des milieux eau–acides forts*

Dans le cas des acides forts, ces auteurs montrent que la fonction H_0 est la même pour des solutions ayant la même activité en eau. La relation entre la fonction d'acidité et l'activité de l'eau est:

$$[27] \quad H_0 = -5{,}02 + \log \frac{(1 + 20a_c + 150a_c^2 + 500a_c^3 + 625a_c^4)(1 - a_c)}{2a_c}$$

Elle s'applique avec une bonne précision aux mélanges $H_2O-HClO_4$, H_2O-HNO_3, $H_2O-H_2SO_4$, H_2O-HCl pour des teneurs inférieures à 60% en poids d'acide. Le modèle de Wyatt fait intervenir des équilibres successifs d'hydratation des différentes espèces participant à la réaction de protonation de l'indicateur. Ce résultat implique que, une fois l'activité de l'eau fixée, le terme $\log f_I/f_{IH^+}$ est indépendant de la nature des anions de l'acide et conduit à admettre que, dans les milieux eau–acide fort, les degrés d'aquation du proton, de I et de IH^+

TABLEAU 6. Calcul de l'expression [25] $A_n = R_0(\mathrm{H}) + R_0(\mathrm{H_2PO_4^-}) + \log a_{\mathrm{H_3PO_4}} + n \log a_{\mathrm{H_2O}}$ pour n = 4, 2, 1

H_3PO_4 *M*	R_0(H)	$R_0(H_2PO_4^-)$[a]	$\log a_{H_3PO_4}$	$\log a_{H_2O}$	A_4	A_2	A_1
1,0	+0,2	+1,7	+0,0	−0,009	1,91	1,93	1,94
2,0	−0,2	+2,2	+0,43	−0,021	2,34	2,38	2,41
4,0	−1,1	+2,8	+1,0	−0,057	2,47	2,58	2,64
5,5	−1,9	+3,3	+1,38	−0,10	2,38	2,58	2,68
8,0	−3,2	+4,3	+2,05	−0,217	2,28	2,71	2,93
9,0	−3,9	+4,7	+2,3	−0,285	1,96	2,53	2,81
10,0	−4,7	+5,0	+2,57	−0,371	1,38	2,13	2,50
11,5	−6,1	+5,6	+2,93	−0,52	0,35	1,39	1,91
14,0	−8,9	+6,0	+3,47	−0,92	−3,11	−1,27	−0,35

[a] Valeur moyenne résultant du calcul de $R_0(H_2PO_4^-)$ d'une part à partir de la relation [18] (système Hg_2HPO_{4s}/Hg_s) et d'autre part de la combinaison des relations [18] et [19] (système $BiPO_{4s}/Bi_s$).

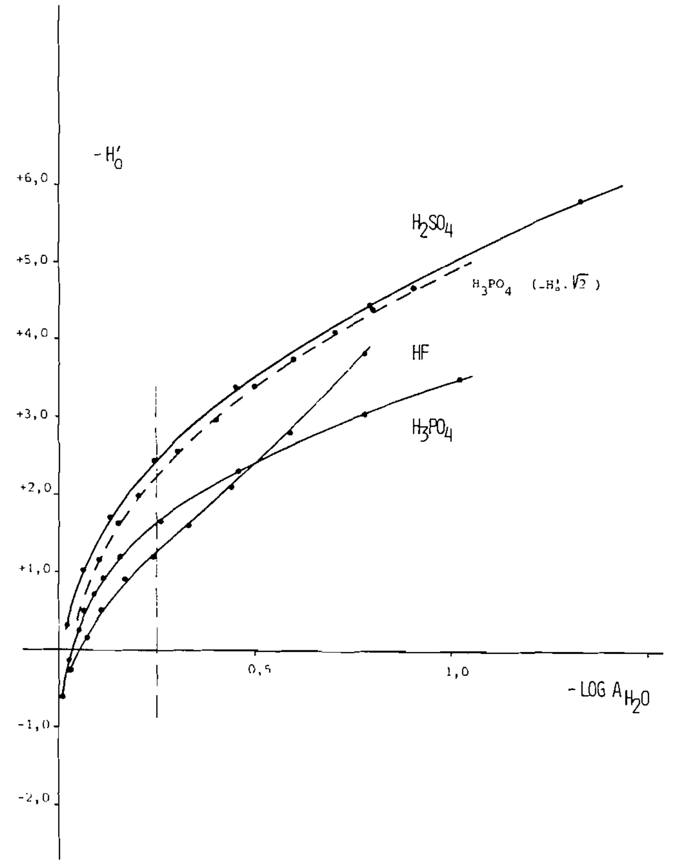

FIG. 4. Relation entre les fonctions H_0' et l'activité de l'eau dans les milieux $H_2O-H_2SO_4$, $H_2O-H_3PO_4$, H_2O-HF.

sont les mêmes et que les anions de l'acide ne participent pas à la solvatation de ces espèces.

3.1.2. *Cas des milieux eau–acides faibles*

Si l'on envisage le comportement d'acides faibles comme H_3PO_4 ou HF, on constate (fig. 4) que, pour une même activité de l'eau, le terme $-H_0$ est plus élevé dans le cas des acides forts que dans le cas d'un acide faible. Wyatt (25) a attribué cette différence au degré d'ionisation de l'acide d'après la relation:

$$[28] \quad H_0(\text{acide faible}) - H_0(\text{acide fort}) = \log \frac{1 + \alpha}{2\alpha}$$

Dans le cas de l'acide phosphorique, le coefficient α reste relativement faible. Il est de 0,126 pour H_3PO_4 42,5% (5,5 *M*)

TABLEAU 7. Calcul du coefficient d'ionisation [28] en fonction de la teneur (%) en acide pour H_3PO_4 et HF

$\log a_{H_2O}$	$C_{H_3PO_4}$ %	$C_{H_3PO_4}$ *M*	$\alpha_{H_3PO_4}$	C_{HF}	α_{HF}
−0,05	31	3,8	0,11	12	0,059
−0,1	42,5	5,5	0,126	19	0,046
−0,2	55	7,7	0,086	27,5	0,036
−0,3	62	9,2	0,059	34	0,028
−0,4	68	10,3	0,046	38,5	0,031
−0,5	72	11,3	0,036	42	0,036
−0,6	75	12,1	0,029	45	0,052
−0,7	79	12,7	0,025	48	0,086
−0,8	80	13,3	0,020		
−0,9	83	13,9	0,017		

et de 0,036 pour H_3PO_4 72,5% (11,5 *M*) (tableau 7). Contrairement aux solutions d'acides forts, les milieux $H_2O-H_3PO_4$ comportent à la fois des molécules d'eau et des molécules d'acide non dissociées susceptibles de participer à la solvatation des espèces H^+, I, IH^+. Ceci est confirmé par la conductibilité relativement faible de ces milieux par rapport à celle des milieux sulfuriques par exemple.

Le phénomène est probablement plus complexe dans le cas des milieux H_2O-HF où les molécules HF solvatent les ions F^- pour donner les espèces HF_2^- (22, 26–30). Ces équilibres secondaires perturbent les conditions d'application du modèle de Wyatt.

REMARQUE: Une analyse plus attentive des relations possibles entre l'activité de l'eau et la fonction H_0' dans les milieux $H_2O-H_3PO_4$ nous a conduit à constater que, dans tout le domaine de concentration envisagé, une solution phosphorique d'activité en eau donnée est caractérisée par un niveau d'acidité équivalent à celui d'une solution d'acide fort dont l'activité en eau est égale à la racine carrée de l'activité en eau de la solution phosphorique (fig. 4). Dans l'hypothèse où cette relation serait une propriété caractéristique des mélanges eau–acides faibles, elle devrait être vérifiée en particulier pour les milieux H_2O-HF. Or, d'après la fig. 4, nous voyons qu'il n'en est rien. Cependant, le comportement particulier des milieux H_2O-HF pourrait expliquer cette divergence et l'existence d'une relation entre les fonctions d'acidité H_0 des acides forts et des acides faibles n'est pas à exclure a priori. Elle devrait faire intervenir, en principe, les mêmes modèles que ceux utilisés dans les milieux $H_2O-H_2SO_4$ très concentrés (25, 31–34) où il existe des molécules d'acide non dissociées.

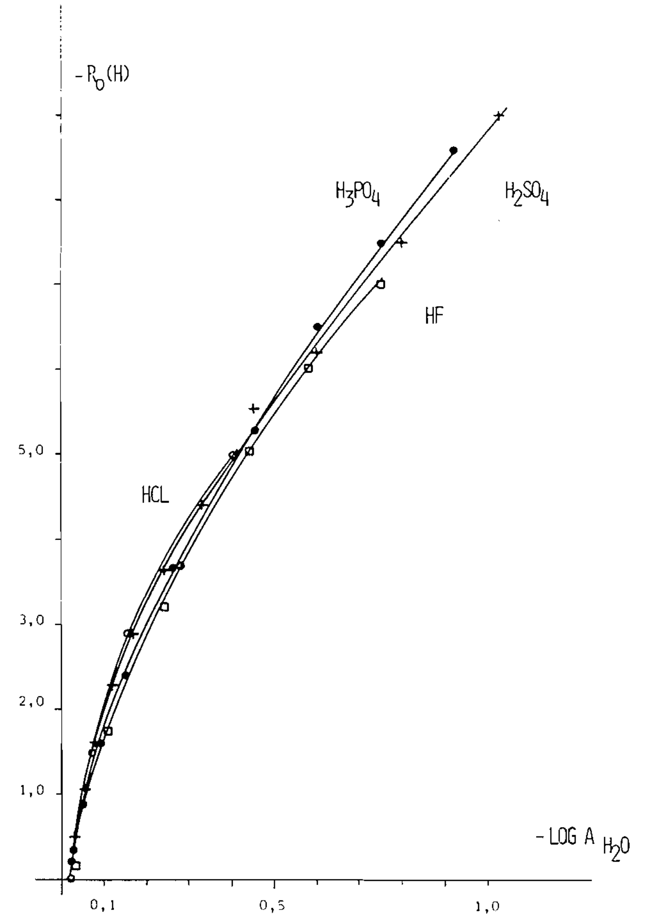

FIG. 5. Relation entre les fonctions R_0(H) et l'activité de l'eau dans les milieux $H_2O-H_2SO_4$, H_2O-HCl, $H_2O-H_3PO_4$, H_2O-HF.

3.2. *Comparaison de l'acidité à partir de la fonction* H'_R

Contrairement à ce qui a été observé avec les indicateurs de Hammett, il n'existe pas de relation univoque entre les fonctions H'_R et l'activité de l'eau dans les milieux eau–acides forts (35–41). Pour une même activité de l'eau, l'ordre de variation du terme $-H'_R$ est:

$$-H'_R(HCl) < -H'_R(H_2SO_4) < -H'_R(HNO_3) < -H'_R(HClO_4)$$

Les acides $HClO_4$ et HNO_3 ont un comportement voisin ($\Delta H'_R$ = 0,1 à 0,2 unités). Mais il existe un écart sensible dans tout le domaine de concentration entre le comportement des acides $HClO_4$ et HCl ($\Delta H'_R$ = 2 unités pour $-\log a_{H_2O}$ = 0,7).

D'autre part, les acides faibles comme H_3PO_4 (9, 16) ne se différencient pas nettement des acides forts. L'écart des fonctions H'_R pour les milieux H_2O-HCl, $H_2O-H_2SO_4$, $H_2O-H_3PO_4$ reste inférieur à 0,3 unités pour $-\log a_{H_2O}$ = 0,7.

3.3. *Comparaison de l'acidité à partir de la fonction* $R_o(H)$

La figure 5 présente les variations de la fonction R_0(H) avec l'activité en eau dans les milieux $H_2O-H_2SO_4$ (17), H_2O-HCl (42), H_2O-HF (26, 43), $H_2O-H_3PO_4$. Il apparaît que, dans le cas des acides forts H_2SO_4 et HCl, le niveau d'acidité est le même pour une même valeur de l'activité en eau. Ce résultat est analogue à celui obtenu avec les fonctions H_0 (25).

L'identité de la fonction R_0(H) à activité en eau donnée reste vraie dans le cas des acides faibles H_3PO_4 et HF. Il semble donc que les molécules non dissociées de H_3PO_4 ou de HF ne modifient pas le comportement du système de comparaison Fc^+/Fc comme elles le font dans le cas des indicateurs de Hammett. De plus, à activité en eau donnée, le niveau d'acidité R_0(H) est le même, que l'on soit en présence d'un acide fort ou d'un acide faible.

Ce résultat est important car il permet de comparer les solutions acides entre elles et d'apprécier, dans la modification de solvatation d'une espèce ionique ou moléculaire, la part due à l'activité en eau et celle qui peut être attribuée aux ions du milieu. Il sera appliqué en particulier à la comparaison des propriétés de solubilité des espèces et des caractéristiques d'oxydo-réduction de systèmes.[2]

Conclusion

Nous avons caractérisé le niveau d'acidité des milieux phosphoriques par la fonction d'acidité R_0(H). Sa variation est de 9 unités lorsque la concentration de l'acide passe de 1 à 14 *M* et de 4 unités entre les milieux industriels 5,5 et 11,5 *M*. Ces résultats permettront de préciser l'influence du niveau d'acidité sur le pouvoir oxydo-réducteur de nombreux systèmes, notamment de l'uranium.[3] Le diagramme potentiel – niveau d'acidité de ces milieux a été établi. L'étendue thermodynamique du domaine des potentiels accessibles reste proche de 1,23 V. Nous disposons ainsi des limites thermodynamiques de stabilité des oxydants et des réducteurs dans les milieux phosphoriques.

L'utilisation des systèmes électrochimiques du mercure et du bismuth nous a permis de déterminer les fonctions basiques $R_0(H_2PO_4^-)$, $R_0(HPO_4^{2-})$ et $R_0(PO_4^{3-})$. Elles seront utiles pour évaluer les variations thermodynamiques de solubilité des phosphates minéraux avec la teneur en acide.[4] L'analyse de la relation existant entre R_0(H), $R_0(H_2PO_4^-)$, les activités de l'eau et de l'acide phosphorique montre que l'équilibre d'ionisation de H_3PO_4 défini en solution aqueuse diluée reste valable pour les solutions concentrées en acide. Nous avons montré que le niveau d'acidité R_0(H) des milieux H_2O-HCl, $H_2O-H_2SO_4$, H_2O-HF et $H_2O-H_3PO_4$ était le même pour une même valeur du terme activité de l'eau. Ce résultat conduit à envisager la comparaison des propriétés d'oxydo-réduction et de complexation de systèmes, notamment ceux pour lesquels la solvatation spécifique des espèces mises en jeu par les anions du milieu n'est pas un facteur déterminant.

1. C. LOUIS et J. BESSIÈRE. Anal. Lett. **13**(A11), 937 (1980).
2. C. LOUIS. Thèse de Doctorat d'Etat, Université de Nancy 1, France. 1983. p. 145.
3. G. CHARLOT, J. BADOZ-LAMBLING et B. TREMILLON. Les réactions électrochimiques. Méthodes électrochimiques d'analyse. Masson, Paris. 1959. p. 147.
4. H. M. KOEPP, H. WENDT et H. STREHLOW. Z. Electrochem. **64**, 483 (1960).
5. H. STREHLOW. Electrode potentials in non-aqueous solvents. *Dans* The chemistry of non-aqueous solvents. Vol. 1. *Édité par* J. J. Lagowski. Academic Press, New York. 1966. Chap. 4. p. 129.
6. T. J. CURPHEY, J. O. SAUTER, M. ROSENBLUM et J. H.

[2] Cf. note 1.

[3] Les variations avec la concentration de l'acide des caractéristiques d'oxydo-réduction des systèmes sont étudiées dans un article intitulé: Diagrammes potentiel – niveau d'acidité dans les milieux $H_2O-H_3PO_4$. I. Systèmes redox ne faisant pas intervenir le proton. II. Systèmes redox faisant intervenir le proton. À paraître. C. Louis, N. Benlakhdim et J. Bessière.

[4] Cf. note 1.

RICHARDS. J. Am. Chem. Soc. **82**, 5249 (1960).
7. J. JANATA et G. JANSEN. J. Chem. Soc. Faraday Trans I, 1656 (1972).
8. T. A. MODRO, K. YATES et J. JANATA. J. Am. Chem. Soc. **97**, 1492 (1975).
9. K. L. ELMORE, C. M. MASSON et J. H. CHRISTENSEN. J. Am. Chem. Soc. **68**, 2528 (1946).
10. M. L. JOSIEN et G. SOURISSEAU. Ozone. *Dans* Nouveau traité de chimie minérale. Tome 13. *Edité par* P. Pascal. Masson, Paris. 1960. p. 243.
11. M. KUWA, T. SAJI et M. MUKAI. Denki Kagaku, **34**, 275 (1966).
12. M. KUWA, T. SAJI et M. MUKAI. Denki Kagaku, **34**, 420 (1966).
13. A. I. GEL'BSHTEIN, G. G. SCHCHEGLOVA et M. I. TEMKIN. J. Inorg. Chem. USSR, **1**, 282 (1956).
14. E. HEILBRONNER et S. WEBER. Helv. Chim. Acta, **32**, 1513 (1949).
15. E. M. ARNETT et G. W. MACH. J. Am. Chem. Soc. **86**, 2671 (1964).
16. E. M. ARNETT et G. W. MACH. J. Am. Chem. Soc. **88**, 1177 (1966).
17. M. BOUCHET. Thèse de Doctorat d'Etat, Paris. 1973.
18. R. W. TAFT. J. Am. Chem. Soc. **86**, 116 (1964).
19. R. A. COX et K. YATES. Can. J. Chem. **61**, 2225 (1983).
20. J. DE GYVES et J. BESSIÈRE. 14° Congrès latino-américain de Chimie. San José, Costa Rica, 1981.
21. K. L. ELMORE, J. D. HATFIELD, R. L. DUNN et A. D. JONES. J. Phys. Chem. **69**, 3520 (1965).
22. A. VAILLANT, J. DEVINCK et B. TREMILLON. Electroanal. Chem. Interfac. Electrochem. **57**, 219 (1974).
23. P. G. TRAVERSO. Can. J. Chem. **62**, 153 (1984).
24. K. N. BASCOMBE et R. P. BELL. Faraday Discuss. Chem. Soc. **24**, 158 (1957).
25. P. A. H. WYATT. Faraday Discuss. Chem. Soc. **24**, 162 (1957).
26. A. VAILLANT. Thèse de Doctorat de 3° cycle, Paris, 1974.
27. R. P. BELL, K. N. BASCOMBE et J. C. MACCOUBREY. J. Chem. Soc. 1286 (1956).
28. H. H. HYMAN, M. KILPATRICK et J. J. KATZ. J. Am. Chem. Soc. **79**, 3668 (1957).
29. L. DOMANGE. Fluor, acide fluorhydrique: solution aqueuse. *Dans* Nouveau traité de chimie minérale. Tome 16. *Edité par* P. Pascal. Masson, Paris. 1960. p. 117.
30. M. KILPATRICK. J. Chem. Educ. **37**, 403 (1960).
31. M. J. JORGENSON et D. R. HARTTER. J. Am. Chem. Soc. **85**, 878 (1963).
32. J. C. D. BRAND. J. Chem. Soc. 997 (1950).
33. J. C. D. BRAND, W. C. HORNING et M. B. THORNLEY. J. Chem. Soc. 1374 (1962).
34. N. C. DENO et R. W. TAFT. J. Am. Chem. Soc. **76**, 244 (1954).
35. N. C. DENO, H. E. BERKHEIMER, WM. L. EVANS et H. J. PETERSON. J. Am. Chem. Soc. **81**, 2344 (1959).
36. N. C. DENO, J. J. JARUZELSKI et A. J. SCHRIESHEIM. J. Am. Chem. Soc. **77**, 3044 (1955).
37. J. N. PEARCE et A. F. NELSON. J. Am. Chem. Soc. **55**, 3075 (1933).
38. R. A. ROBINSON et O. J. BAKER. Trans. R. Soc. N. Z. **76**, 250 (1946).
39. U. HALDNA, I. KOPPEL et H. I. KUURA. Russ. J. Phys. Chem. **40**, 899 (1966).
40. M. RANDALL et L. E. YOUNG. J. Am. Chem. Soc. **50**, 989 (1928).
41. International Critical tables. **3**, 304.
42 D. D. BABALE. Thèse de Doctorat de 3° cycle, Yaounde, 1981.
43. A. VAILLANT, J. DEVINCK et B. TREMILLON. Anal. Lett. **6**, 1095 (1973).

Photochemical reactions of quinonoid compounds with phosphorus derivatives

ANGELO ALBERTI[1]
Istituto dei Composti del Carbonio Contenenti Eteroatomi e loro Applicazioni, CNR, 89 Via Tolara di Sotto, 40064 Ozzano Emilia, Italy

ANDREW HUDSON
School of Chemistry and Molecular Sciences, University of Sussex, Falmer, Brighton BN1 9QJ, United Kingdom

GIAN FRANCO PEDULLI
Istituto Chimico dell'Universita', 09100 Cagliari, Italy

AND

W. GRANT MCGIMPSEY AND JEFFREY K. S. WAN
Department of Chemistry, Queen's University, Kingston, Ont., Canada K7L 3N6

Received May 29, 1984

ANGELO ALBERTI, ANDREW HUDSON, GIAN FRANCO PEDULLI, W. GRANT MCGIMPSEY, and JEFFREY K. S. WAN. Can. J. Chem. **63**, 917 (1985).

The photoreactions of tetraethylpyrophosphite, tetraphenylbiphosphine, diphenylphosphine oxide, and tetraethylbiphosphine disulphide with five quinones or quinonoid compounds have been studied by esr spectroscopy; $\dot{P}(O)Ph_2$ and $\dot{P}(O)(OEt)_2$ radicals add to both carbon–carbon and carbon–oxygen double bonds, whilst with $Ph_2\dot{P}$ and $\dot{P}(S)Et_2$ radicals only the species resulting from addition to a carbonyl group are observed. It is also reported that the photogenerated quinone triplets react with tetraethylpyrophosphite leading to the formation of diethoxyphosphonyl radicals, which in turn add to other ground state quinone molecules, the diethoxyphosphinyl adduct to a carbonyl group being also formed in the process.

ANGELO ALBERTI, ANDREW HUDSON, GIAN FRANCO PEDULLI, W. GRANT MCGIMPSEY et JEFFREY K. S. WAN. Can. J. Chem. **63**, 917 (1985).

Faisant appel à la spectroscopie rpe, on a étudié les photoréactions du tétraéthylpyrophosphite, de la tétraphénylbiphosphine, de l'oxyde de diphénylphosphine et du disulfure de la tétraéthylbiphosphine avec cinq quinones ou composés quinonoïdes; les radicaux $\dot{P}(O)Ph_2$ et $\dot{P}(O)(OEt)_2$ s'additionnent tant aux doubles liaisons carbone–carbone que carbone–oxygène alors que, avec les radicaux $Ph_2\dot{P}$ et $\dot{P}(S)Et_2$, on n'observe que la formation des produits résultant d'une addition sur le groupement carbonyle. On rapporte aussi que les triplets de quinones qui sont photogénérés réagissent avec le tétraéthylpyrophosphite en conduisant à la formation de radicaux diéthoxyphosphonyle qui s'additionnent à leur tour à l'état fondamental des molécules de quinones; l'adduit diéthoxyphosphinyle sur le groupement carbonyle se forme aussi dans ce processus.

[Traduit par le journal]

Introduction

The reactions of phosphorus-centered radicals with carbonyl compounds have received little attention to date. It has been reported that dialkylphosphinyl radicals $\dot{P}R_2$ (R = Me, Et) add to di-*tert*-butyl ketone to give $t\text{-}Bu_2\dot{C}OPR_2$ (1); similarly, the radical resulting from the addition of the photolytically generated $\dot{P}Ph_2$ to the less hindered oxygen atom of 2,6-di-*tert*-butyl-*p*-benzoquinone has been observed by one of us (2).

In order to achieve a deeper insight into the nature of the radical intermediates formed during the reactions of phosphorus-centred radicals with unsaturated derivatives containing the carbonyl function, we have undertaken an electron spin resonance (esr) investigation of the reactions between phosphinyl, phosphonyl, and thiophosphonyl radicals and a number of quinones.

There has been continuing controversy about radical addition to quinones and their analogs. This is mainly because of the two distinct reactive sites in these species. These substrates can in fact lead to different radical adducts depending on the pathway followed by the addition reaction, i.e. attack either at a carbon–carbon or a carbon–oxygen double bond by the incoming $R_n\dot{P}$ radicals. Analogous isomeric adducts have been actually observed in the addition of silyl and germyl radicals to unsaturated carbonyl derivatives such as maleic anhydride and other related compounds (3).

In the course of the present study both kinds of adducts were detected in the addition of phosphonyl radicals to most of the investigated quinones, while only the oxygen adducts could be observed with phosphinyl and thiophosphonyl radicals. We know of no previous reports of the addition of phosphonyl and thiophosphonyl radicals to the carbonyl function. It is hoped that these results will be useful to phosphorus chemists in their understanding of the reactions and reaction mechanisms involving phosphines, phosphites, and pyrophosphites.

Experimental

All phosphorus compounds were commercially available, as were quinones **1–3**; dithiolactone **4** (4) and dione **5** (5) were obtained as described in the literature.

The esr spectra were recorded on either a Varian E104 or a Bruker ER200 esr spectrometer equipped with an nmr gaussmeter (field calibration), a frequency counter (*g* factor determination), and standard variable temperature devices.

Benzene or *tert*-butylbenzene solutions of the appropriate quinone and tetraphenylbiphosphine (TPBP) or tetraethylbiphosphine disulphide (TPBPS) were irradiated within the cavity of the esr spectrometer by means of 1-kW or 200-W high pressure mercury lamps; di-*tert*-butyl peroxide (BOOB) solutions were used in the photoreactions of tetraethylpyrophosphite (TEP) and diphenylphosphine oxide (DPPO). A Bausch & Lomb grating monochromator was also used in some of the experiments.

Results and discussion

We have studied the reactions of diphenylphosphinyl, $\dot{P}Ph_2$;

[1] Author to whom correspondence may be addressed.

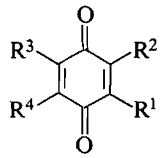

1; R^1 = R^2 = R^3 = R^4 = H
2; R^1 = R^2 = R^3 = R^4 = Me
3; R^1 = R^4 = H, R^2 = R^3 = t-Bu

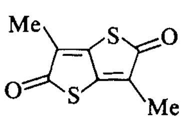

4

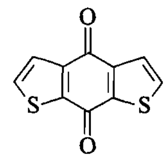

5

diphenylphosphonyl, $O\dot{P}Ph_2$; diethoxyphosphonyl, $O\dot{P}(OEt)_2$; and diethylthiophosphonyl, $S\dot{P}Et_2$; radicals with *p*-benzoquinone (**1**, BQ), duroquinone (**2**, DQ), 2,6-di-*tert*-butyl-*p*-benzoquinone (**3**, DTBQ), 3,6-dimethylthieno[3,2-*b*]thiophen-2,5-dione (**4**, DMTTD), and benzo[1,2-*b*;5,4-*b*′]dithiophen-4,8-dione (**5**, BDTD).

Tetraphenylbiphosphine, P_2Ph_4, is known to be a good source of $\dot{P}Ph_2$ radicals when irradiated with uv light (2). Homolytic cleavage of the phosphorus–phosphorus bond presumably also occurs upon irradiation of TEBPS with formation of diethylthiophosphonyl radicals $S\dot{P}Et_2$. The diethoxyphosphonyl radical $O\dot{P}(OEt)_2$ has been generated by the displacement reaction [1] of photolytically produced *tert*-butoxyl radicals with TEP (6), and the diphenylphosphonyl radical $O\dot{P}Ph_2$ via hydrogen abstraction from DPPO by t-Bu$\dot{O}$ [2]:

[1] $[(EtO)_2P]_2O + t\text{-Bu}\dot{O} \rightarrow t\text{-BuOP(OEt)}_2 + O\dot{P}(OEt)_2$

[2] $Ph_2P(O)H + t\text{-Bu}\dot{O} \rightarrow t\text{-BuOH} + O\dot{P}Ph_2$

As mentioned in the introduction, phosphorus-centered radicals may react with carbonyl compounds by attacking the oxygen atom; in such quinones as DTBQ or BDTD, where the two carbonyl functions are inequivalent, isomeric adducts can be formed depending on which of the two oxygens undergoes addition. Moreover, quinones contain carbon–carbon double bonds which also are potential sites of addition for the incoming radicals. The formation of several kinds of spin adducts is therefore to be expected when reacting quinones with phosphorus-centered radicals.

p-Benzoquinones (1–3)

In principle, the addition reaction of $\dot{P}R_n$ radicals to BQ, DQ, and DTBQ can be schematized as outlined in eq. [3];

[3] 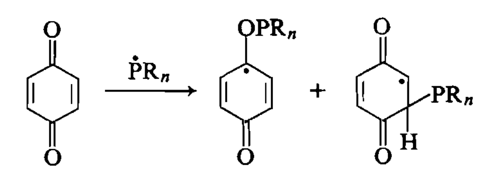

(a) (b)

When using the unsubstituted derivative **1**, no adducts of either kind could be observed with $\dot{P}Ph_2$, $O\dot{P}Ph_2$, and $S\dot{P}Et_2$, while with $O\dot{P}(OEt)_2$ the species resulting from addition of the phosphonyl radical to a carbonyl group was detected. The low persistence of the possible adducts of BQ (**1***a*) and (**1***b*) likely makes these species difficult to detect. Since increasing the steric hindrance in the proximity of a radical centre usually leads to longer-lived paramagnetic species, the reaction was repeated using substituted quinones.

With DTBQ both the adducts **3***a* and **3***b* are obtained by reaction with $O\dot{P}Ph_2$ and $O\dot{P}(OEt)_2$, while $S\dot{P}Et_2$ and $\dot{P}Ph_2$ only give the oxygen adducts **3***a*. However, in the $\dot{P}Ph_2$ case the esr spectra also indicate the presence of a ring adduct **3***b* whose spectral parameters are identical with those exhibited by the corresponding species resulting through addition of $O\dot{P}Ph_2$ radicals to DTBQ. Because of the unsymmetrical nature of this quinone, two pairs of oxygen and ring adducts might be formed. The small triplet splitting (1.2–1.6 G) detected for radicals **3***a* clearly indicates that addition of $\dot{P}R_n$ radicals takes place at the less hindered carbonyl group. This assignment is confirmed in the case of $O\dot{P}Ph_2$ and $O\dot{P}(OEt)_2$ adducts by a comparison between the appropriate values collected in Table 1 and the hfs constants previously reported by Rieker for the authentic radicals **3***a* obtained by oxidation of the corresponding phenols (7). The detection of radical **3***a* (where PR_n is a $P(O)Ph_2$ group) in the thermal reaction of DTBQ with DPPO followed by oxidation has also been reported recently. (8).

The ring adducts of DTBQ originate from attack of $O\dot{P}R_2$ at an unsubstituted carbon of the quinone; addition to positions 2 or 6 would in fact result in the formation of a radical species which should show a ca. 20-G splitting from the single proton linked to the radical centre (3). We therefore assign the structure **3***b* to the ring adducts, although the actual values of the

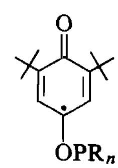

3*a*

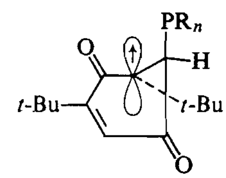

3*b*

β-proton and ^{31}P splittings (see Table 1) are, respectively, smaller and larger than expected. It seems that the presence of the bulky *tert*-butyl group α to the radical centre induces a significant distortion of the quinone ring, forcing the hydrogen atom into a quasi-equatorial position, i.e. into the nodal plane of the $2p_z$ orbital containing the unpaired electron, and the $P(O)R_2$ substituent closer to the axial position where the C—P bond can strongly overlap the singly occupied orbital. Similar trends have been previously reported for highly hindered cyclohexadienyl radicals (9, 10).

With duroquinone, only two adducts could be positively identified, i.e. the species **2***b* resulting from addition of $O\dot{P}Ph_2$ and $O\dot{P}(OEt)_2$ radicals to the ring of DQ. The identification of these radicals is straightforward, as their spectra consist of doublets, $a(^{31}P)$ = 33–38 G, of quartets, a(3H) = 23–24 G, further split into smaller quartets, a(3H) = 0.36 G, the magnitude of the couplings being consistent wth the presence of a methyl group α to a carbon radical centre and of another methyl group and a phosphorus nucleus β to it.

While the observed radicals are unambiguously identified, some questions concerning the nature of the initiating species may arise. We have therefore examined the photoreactions of 2,6-di-*tert*-butyl-*p*-benzoquinone, which was chosen because of the relatively high persistence of its radical adducts, upon irradiation in the regions of its uv absorption maxima, viz. 254 nm, 318 nm, and 446 nm (11). With BOOB-free solutions of

TABLE 1. Electron spin resonance parameters* for the radical adducts of BQ, DQ, and DTBQ

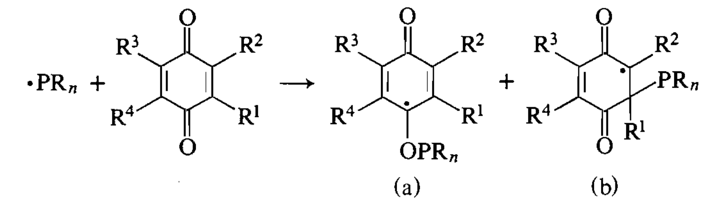

Compound	PR_n	Radical	a_{R^1}	a_{R^2}	a_{R^3}	a_{R^4}	$a_{^{31}P}$	g	T (K)
1	$P(O)(OEt)_2$	(a)	0.70	5.56	5.56	0.70	1.63	2.0050_6	298
2	$P(O)Ph_2$	(b)	0.36(3H)	23.60(3H)	—	—	33.05	2.0047_0	193
2	$P(O)(OEt)_2$	(b)	0.36(3H)	24.70(3H)	—	—	37.90	2.0047_0	193
3	PPh_2	(a)	1.16	—	—	1.16	2.09	2.0047_4	213
3	PPh_2	(a)	1.22	—	—	1.22	3.62	2.0047_4	313
3	$P(O)Ph_2$	(a)	1.59	—	—	1.59	6.44	2.0048_0	273
3	$P(O)Ph_2$	(b)	9.94	0.40(9H)	—	—	57.42	2.0047_5	223
3	$P(O)(OEt)_2$	(a)	1.57	—	—	1.57	7.72	2.0048_5	296
3	$P(O)(OEt)_2$	(a)	1.62	—	—	1.62	8.16	2.0048_5	323
3	$P(O)(OEt)_2$	(b)	9.30	0.35(9H)	—	—	77.60	2.0040_0	323
3	$P(S)Et_2$	(a)	1.54	—	—	1.54	10.76	2.0047_0	303

*Couplings in gauss.

3 containing TEP a weak esr signal developed after awhile, its intensity, although increasing with time, never matching that of the spectra obtained by irradiation in the presence of peroxide. The signal clearly indicated the presence of three radical species: the ring- and oxygen-diethoxyphosphonyl adducts **3***a* and **3***b*, and a third species with a g factor 2.0047_5 and exhibiting coupling of the unpaired electron with two protons (a = 1.26 G) and a ^{31}P nucleus (a = 3.52 G). A probable mechanism accounting for the formation of $O\dot{P}(OEt)_2$ radicals involves

[4] 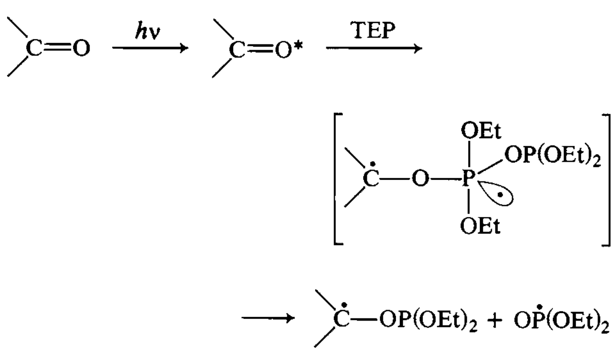

attack of the photogenerated quinone triplet on the pyrophosphite, followed by α-fragmentation of the intermediate biradical. This mechanism also nicely accounts for the detection of a third radical species, whose esr couplings are consistent with the diethoxyphosphinyl adduct of DTBQ.

No esr signals were, however, detected when irradiating in the aforementioned regions solutions of **3** containing either TPBP or TEBPS, thus indicating that the reactions leading to the phosphinyl and thiophosphonyl adducts are not initiated by an excited state of the quinone. Although one would expect that irradiation at shorter wavelengths, where both TPBP and TEBPS absorb, would lead to the formation of $\dot{P}Ph_2$ and $S\dot{P}Et_2$ radicals, it is likely that the intensity of the radiation emerging from the monochromator is not sufficient for the cleavage of the P—P bond. Also in the case of DPPO, no signal from adducts **3***a* and **3***b* could be observed, unless BOOB was added to the solutions.

*3,6-Dimethylthieno[3,2-*b*]thiophen-2,5-dione (**4**)*

The reaction of both $O\dot{P}Ph_2$ and $O\dot{P}(OEt)_2$ radicals with the dione **4** leads to the simultaneous formation of the oxygen (**4***a*) and ring (**4***b*) adducts, the proton hyperfine splitting constants of the former species being similar to those of the analogous oxygen adducts with group IVB organometallic radicals (12). Attack at the ring might in principle occur at the carbons either in positions 3,6 or 4,5; in the former case the structure of the resulting adducts will be closely related to a substituted allylic system and a methyl splitting of ca. 10 G would be expected; in the other case addition would result in α-ketoalkyl radicals characterized by much larger methyl couplings (ca. 20 G), as for the DQ adducts. The ca. 8–9 G quartet splitting (see Table 2) clearly indicates that $O\dot{P}R_2$ radicals attack positions 3 or 6 of DMTTD.

Similarly to what was found with BQ, DQ, and DTBQ, the reaction of dione **4** with $S\dot{P}Et_2$ and $\dot{P}Ph_2$ radicals only led to the detection of the oxygen adducts **4***a*, although in the latter case esr evidence for the simultaneous formation of the $O\dot{P}Ph_2$ ring adduct **4***b* was also obtained.

*Benzo[1,2-*b*;5,4-*b*′]dithiophen-4,8-dione (**5**)*

On reaction of phosphorus-centered radicals with BDTD, addition seems to occur only at the oxygen atoms. Due to their inequivalence, two isomers **5***a* and **5***a*′ are expected to form, and indeed they have been observed with $\dot{P}Ph_2$, $O\dot{P}Ph_2$, and $O\dot{P}(OEt)_2$; surprisingly enough, with $S\dot{P}Et_2$ only isomer **5***a* could be detected. The identification of the isomers, accomplished by analogy with the related hydrogen and group IVB adducts (12), was based on the assumption that larger splittings at the protons 2,5 (see Table 3) should be observed for isomer (a), due to the possibility of delocalizing the unpaired electron on these positions. The relative concentration of isomer (a) increases along the sequence $PPh_2 < P(O)Ph_2 < P(O)(OEt)_2 < P(S)Et_2$; no traces of **5***a*′ could actually be observed for the last adduct.

General remarks

The $\dot{P}Ph_2$, $S\dot{P}Et_2$, and $O\dot{P}Ph_2$ radicals which lead to the observed spin adducts with quinones **1–5** are formed via ho-

TABLE 2. Electron spin resonance parameters* for the radicals adducts of DMTTD

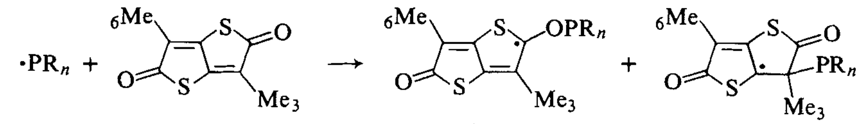

(a) (b)

PR_n	Radical	a^H_{Me6}	a^H_{Me3}	$a_{^{31}P}$	g	T (K)
PPh_2	(a)	8.12	1.12	5.46	2.0034_5	296
$P(O)Ph_2$	(a)	8.56	1.44	9.68	2.0034_2	353
$P(O)Ph_2$	(b)	8.67	—	30.43	2.0035_2	296
$P(O)(OEt)_2$	(a)	8.22	1.23	6.21	2.0034_0	393
$P(O)(OEt)_2$	(b)	8.70	—	41.01	2.0034_9	393
$P(S)Et_2$	(a)	8.58	1.45	13.11	2.0035_2	373

*Couplings in gauss.

TABLE 3. Electron spin resonance parameters* for the radical adducts of BDTD

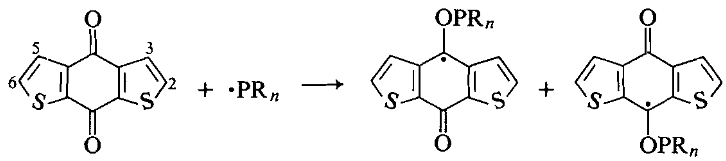

(a′) (a)

PR_n	Radical	$a_{2,6}$	$a_{3,5}$	$a_{^{31}P}$	g	T (K)	Relative amount (%)
PPh_2	(a)	2.77	0.22	6.48	2.0049_0	295	57
PPh_2	(a′)	1.27	0.57	11.39	2.0052_9	295	43
$P(O)Ph_2$	(a)	3.06	0.25	15.12	2.0048_9	323	~60
$P(O)Ph_2$	(a′)	1.36	0.64	16.36	2.0052_6	323	~40
$P(O)(OEt)_2$	(a)	2.82	0.29	5.92	2.0048_4	343	70
$P(O)(OEt)_2$	(a′)	1.29	0.60	8.67	2.0052_9	343	30
$P(S)Et_2$	(a)	3.03	0.19	20.94	2.0049_1	295	>90

*Couplings in gauss.

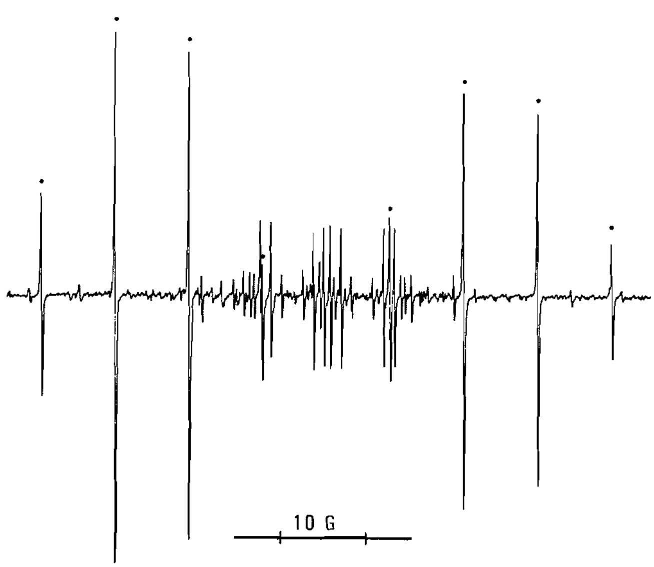

FIG. 1. The esr spectrum observed at 393 K upon uv irradiation of a solution of the dithiolactone **4** containing TEP and di-*tert*-butyl peroxide. The marked lines are due to the radical adduct **4***b*.

molysis of tetraphenylbiphosphine and tetraethylbiphosphine disulphide or by hydrogen abstraction from diphenylphosphine oxide by *tert*-butyl radicals. Diethoxyphosphonyls $\dot{O}P(OEt)_2$ may instead be formed through two alternative pathways, viz. reactions [1] and [4]. On the other hand, as it has been recently shown (13) that *t*-Bu$\dot{O}$ radicals react with pyrophosphite at a diffusion-controlled rate ($k_{[1]} = 2.85 \times 10^9\ M^{-1}\ s^{-1}$), we believe that in peroxide solutions the mechanism outlined in reaction [4] only plays a minor role. This seems to be further substantiated by the fact that the diethoxyphosphinyl oxygen adduct **3***a* was only detected when using peroxide-free solutions of DTBQ and TEP.

Reaction [4] is nevertheless an interesting and quite general process. Thus diethoxyphosphonyl adducts were detected in the absence of peroxide also with quinones **1**, **4**, and **5**, while intense esr signals from both $Ph_2\dot{C}OP(OEt)_2$ and $Ph_2\dot{C}OP(O)(OEt)_2$ were observed by irradiation of solutions of benzophenone and TEP (14).

Phosphinyl, phosphonyl, and thiophosphonyl radicals do not exhibit uniform behaviour in their reactions with compounds **1**–**4**; $\dot{O}P(OEt)_2$ and $\dot{O}PPh_2$ are in fact the only species for which adducts resulting from addition to the quinone ring could be observed along with those originating from addition to the carbonyl function. A knowledge of rates of addition of phosphorus-centered radicals to unsaturated and carbonyl compounds would of course be very useful in establishing whether the failure to observe a particular paramagnetic species is due to a slow rate of formation or to a fast rate of radical loss. Unfortunately, although the use of kinetic esr (15) and of laser flash photolysis techniques (16) has now made available a considerable amount of kinetic data for many radical reactions, only very few refer to processes involving phosphorus-centered radicals, and it would appear that attention has been mainly focussed on $\dot{O}P(OEt)_2$ (9, 17, 18). A substantial body of information is instead available on the reactivity of silyl radicals, whose reaction rates with various substrates have been determined (19). Although silicon- and phosphorus-centered radicals often react with the same substrates to give structurally related adducts, extrapolation of kinetic data is often dangerous. For example $\dot{O}P(OEt)_2$ and $\dot{S}iEt_3$ add to furan and thiophene with similar rates, while the reaction of silyl radicals with benzene is two orders of magnitude faster than that of diethoxyphosphonyls (13). Also, the silyl adduct to the double bond of maleic anhydride is detected at or below room temperature, but the oxygen adduct is the only observable species at higher temperature (3); the phosphonyl adducts **3**a, **3**b, **4**a, and **4**b are instead observed over a wide temperature range (−80 to +80°C), although in varying relative amounts.

All the observed $\dot{P}Ph_2$, $\dot{S}PEt_2$, $\dot{O}PPh_2$, and $\dot{O}P(OEt)_2$ radical adducts detected in this study are to be considered persistent (20), and, with the exceptions only of **1**a, **5**a, and **5**a', they could be observed over significant time intervals (several minutes to hours) when photolysis was interrupted. It is worth noting that in the case of the two phosphonyl derivatives **4**b the radical concentration can be increased or decreased reversibly in the absence of uv irradiation by simply raising or lowering the temperature, which clearly indicates that a monomer–dimer equilibrium is being observed.

Dione **5** represents a particular case; one might expect that the rates of addition to a ring and of decay of the resulting radicals did not differ drastically from the values determined in a laser flash photolysis experiment of the addition of $\dot{O}P(OEt)_2$ radicals to thiophene (13), i.e. $k_a = 1.7 \times 10^6\,M^{-1}\,s^{-1}$ and $2k_t = 10^9\,M^{-1}\,s^{-1}$ at −80°C, although a slight reduction of the rate of radical loss may be expected due to partial delocalization of the unpaired electron onto a carbonyl group. Although rates of addition of $\dot{P}R_n$ radicals to the carbonyl function are not available for comparison, it seems unlikely, at least in thermodynamic terms, that the incoming radicals add to one of the rings with consequent destruction of an aromatic system, when addition to one of the carbonyl groups would result in a stabilized phenoxyl radical.

A peculiar feature of the reactions of TPBP with quinones is that, besides the species resulting from addition of $\dot{P}Ph_2$ radicals to a carbonyl group, the $\dot{P}(O)Ph_2$ spin adducts to the ring of the quinone are detected; similar adducts were also formed when using diphenylphosphine to produce $\dot{P}Ph_2$ radicals. This is likely to be the result of contamination of TPBP or DPP by the corresponding oxides. It is in fact known that both secondary phosphines (21) and polyphosphines (22) are highly sensitive to oxidizing agents and, according to reactions [5] and [6], may lead to precursors of diphenylphosphonyl radicals.

$$[5]\quad 2Ph_2PH \xrightarrow{O_2} 2Ph_2P(O)H$$

$$[6]\quad Ph_2P\text{—}PPh_2 \xrightarrow{O_2} Ph_2(O)P\text{—}P(O)Ph_2$$

Acknowledgements

The authors are grateful to NSERC for financial assistance; financial support from CNR (Rome) is also acknowledged by G.F.P.

1. I. G. NEIL and B. P. ROBERTS. J. Organomet. Chem. **102**, C17 (1982).
2. K. S. CHEN, T. FOSTER, and J. K. S. WAN. J. Chem. Soc. Perkin Trans. 2, 1238 (1979).
3. A. ALBERTI, A. HUDSON, and G. F. PEDULLI. Tetrahedron, **38**, 3749 (1982).
4. G. MARTELLI, L. TESTAFERRI, M. TIECCO, and P. ZANIRATO. J. Org. Chem. **40**, 3384 (1975).
5. D. W. H. MCDOWELL and J. C. WISOWATY. J. Org. Chem. **37**, 1712 (1972).
6. A. G. DAVIES, D. GRILLER, and B. P. ROBERTS. J. Am. Chem. Soc. **94**, 1782 (1972).
7. A. RIEKER. Z. Naturforsch. Teil B, **21**, 647 (1966).
8. A. I. PROKOF'EV, N. P. PROVOTOROVA, N. A. KARDANOV, N. N. BUBNOV, S. P. SOLODOVNIKOV, N. N. GODOVIKOV, and M. I. KABACHNIK. Izv. Akad. Nauk SSSR, Ser. Khim. 1865 (1981); Chem. Abstr. **95**, 169311z (1981).
9. D. GRILLER, K. DIMROTH, T. M. FYLES, and K. U. INGOLD. J. Am. Chem. Soc. **97**, 5526 (1975).
10. P. G. COOKSON, A. G. DAVIES, and B. P. ROBERTS. J. Chem. Soc. Chem. Commun. 289 (1976).
11. A. RIEKER, W. RUNDEL, and H. KESSLER. Z. Naturforsch. Teil B, **24**, 547 (1969).
12. A. ALBERTI, A. HUDSON, G. F. PEDULLI, and P. ZANIRATO. J. Organomet. Chem. **198**, 145 (1980).
13. T. J. BURKEY, D. GRILLER, L. LUNAZZI, and A. S. NAZRAN. J. Org. Chem. **48**, 3704 (1983).
14. A. ALBERTI, D. GRILLER, and G. F. PEDULLI. To be published.
15. D. GRILLER and K. U. INGOLD. Acc. Chem. Res. **13**, 193 (1980); **13**, 317 (1980).
16. H. PAUL, R. D. SMALL, JR., and J. C. SCAIANO. J. Am. Chem. Soc. **100**, 4520 (1978); J. C. SCAIANO. J. Am. Chem. Soc. **102**, 7747 (1980), and references therein.
17. D. GRILLER, P. R. MARIOTT, D. C. NONHEBEL, M. J. PERKINS, and P. C. WONG. J. Am. Chem. Soc. **103**, 7761 (1981).
18. D. GRILLER, J. W. COOPER, and K. U. INGOLD. J. Am. Chem. Soc. **97**, 4269 (1975).
19. J. A. BABAN, M. D. COOK, and B. P. ROBERTS. J. Chem. Soc. Perkin Trans 2, 1247 (1982); C. CHATGILIALOGLU, K. U. INGOLD, and J. C. SCAIANO. J. Am. Chem. Soc. **104**, 5119 (1982), and references therein.
20. D. GRILLER and K. U. INGOLD. Acc. Chem. Res. **9**, 13 (1976).
21. M. M. RAUHUT and H. A. CURRIER. J. Org. Chem. **26**, 4626 (1961).
22. D. J. H. SMITH. *In* Comprehensive organic chemistry. Vol. 2. *Edited by* D. Barton, W. D. Ollis, and I. O. Sutherland. Pergamon Press, New York. 1979. p. 1159.

An electrochemical investigation on mononuclear and dinuclear copper(I) aminocarbonyl complexes

PIERO ZANELLO[1]
Dipartimento di Chimica dell'Università di Siena, Piano dei Mantellini, 44, 53100 Siena, Italy

AND

PIERO LEONI
Istituto di Chimica Generale dell'Università di Pisa, Via Risorgimento, 35, 56100 Pisa, Italy

Received July 5, 1984

PIERO ZANELLO and PIERO LEONI. Can. J. Chem. **63**, 922 (1985).

The electrochemical behaviour of some copper(I) aminocarbonyl derivatives, namely, $[Cu(dien)(CO)]^+$ (dien = diethylenetriamine), $[Cu(Medpt)(CO)]^+$ (Medpt = *N,N*-bis(3-aminopropyl)methylamine), $[Cu_2(tmen)_2(\mu\text{-}PhCO_2)(\mu\text{-}CO)]^+$ (tmen = *N,N,N',N'*-tetramethylethylenediamine), has been studied in dimethyl sulfoxide solution at platinum electrodes by cyclic and dc voltammetry, and controlled potential coulometry. In all studied complexes each copper(I) centre undergoes one-electron charge transfers in both anodic and cathodic processes. The electrogenerated copper(II) complexes, fully characterized, can be reversibly reduced to the starting copper(I) carbonyl derivatives in the presence of carbon monoxide. The electron-transfer sequences in which these copper(I) complexes may be involved have been elucidated.

PIERO ZANELLO et PIERO LEONI. Can. J. Chem. **63**, 922 (1985).

Faisant appel à la voltamétrie cyclique et à cd ainsi qu'à la coulométrie à potentiel contrôlé et opérant en solution dans le diméthylsulfoxyde, on a étudié le comportement électrochimique de quelques dérivés aminocarbonyles du cuivre (I) au niveau d'électrodes de platine; on a examiné en particulier le $[Cu(dien)(CO)]^+$ (dien = diéthylènetriamine), $[Cu(Medpt)(CO)]^+$ (Medpt = *N,N*-bis(amino-3 propyl)méthylamine), $[Cu_2(tmen)_2(\mu\text{-}PhCO_2)(\mu\text{-}CO)]^+$ (tmen = *N,N,N',N'*-tétraméthyl-éthylènediamine). Dans tous les complexes étudiés, chaque centre de cuivre(I) subit un transfert de charge d'un électron, tant dans le processus anodique que cathodique. Les complexes de cuivre(II), générés d'une manière électrochimique, ont été complètement caractérisés et, en présence de monoxyde de carbone, ils peuvent facilement être reconvertis en dérivés aminocarbonyles de cuivre(I) de départ. On a élucidé les suites de transferts électroniques dans lesquels ces complexes de cuivre(I) peuvent être impliqués.

[Traduit par le journal]

Introduction

The redox chemistry of copper(I) derivatives may serve to understand the function of a number of naturally occurring cuproproteins (1).

Increasing attention is paid to the electrochemistry of copper(I)/copper(II) redox couples of biological relevance (2–15). However, the electrochemical behaviour of copper(I) derivatives is seldom directly dealt (9, 11, 13). For the most part the redox properties of copper(II) derivatives are investigated, with a particular attention to the responses in the presence of carbon monoxide.

We present here the electrochemical behaviour in nonaqueous solvent of a number of copper(I) aminocarbonyl derivatives, $[Cu(Medpt)(CO)]^+$, $[Cu(dien)(CO)]^+$, and $[Cu_2(tmen)_2(\mu\text{-}PhCO_2)(\mu\text{-}CO)]^+$ (**I**, **II**, **III**), whose anodic oxidation leads to decarbonylated copper(II) species, $[Cu(Medpt)(S)]^{2+}$, $[Cu(dien)(S)]^{2+}$, and $[Cu_2(tmen)_2(\mu\text{-}PhCO_2)(S)]^{3+}$ (S = solvent) (**IV**, **V**, **VI**), able to be cathodically reduced to **I**, **II**, and **III**, respectively, in the presence of carbon monoxide.

Because of the coordination geometry around copper, the nature of the donor atoms in **I**–**III**, the presence of a dicopper(I) unit in **III** which binds 1 CO/2 Cu, and the relatively

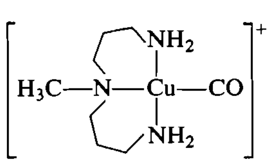

I

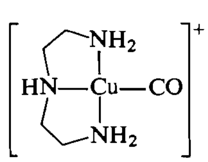

II

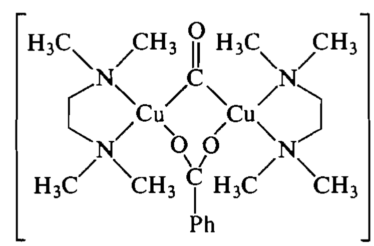

III

high electrode potentials for copper(I)/copper(II) charge transfers, this study can contribute to the elucidation of reversible oxidation and carbon monoxide binding processes in mononuclear and dinuclear copper proteins.

Results and discussion

In Fig. 1 the response at a platinum microelectrode, both in dc voltammetry at an electrode with periodical renewal of the diffusion layer (DLRPE) and in cyclic voltammetry, of **I** in dimethyl sulfoxide (DMSO) solution is reported.

As it can be seen the copper(I) complex gives rise to both an anodic and a cathodic process. Controlled potential coulometric tests at potentials corresponding to the limiting current of either oxidation or reduction process show that each process involves one electron per molecule of starting copper(I) compound. Quantitative deposition of copper metal occurs in the cathodic electrolysis.

As regards the anodic process, the analysis of CV responses with scan rate (16), from 0.02 to 5 V s^{-1} (at higher scan rates the response becomes ill-shaped), indicates the occurrence of an uncomplicated one-electron charge transfer quasi-reversible

[1]To whom all correspondence should be addressed.

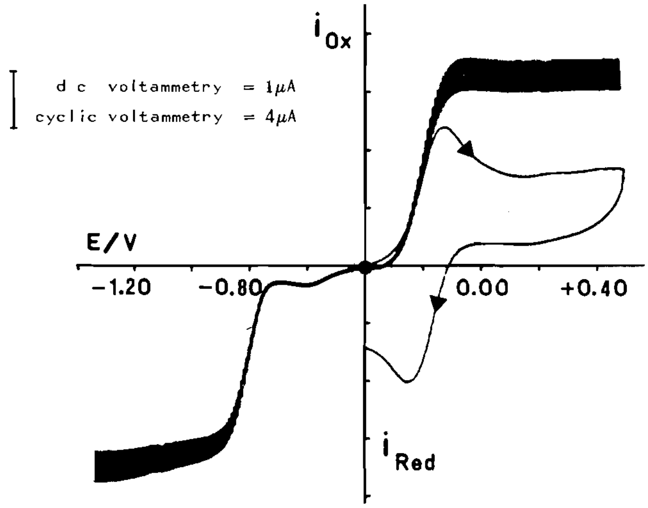

FIG. 1. Electrochemical behaviour of a DMSO solution containing $[NEt_4][ClO_4]$ (0.1 mol dm^{-3}) and $[Cu^I(Medpt)(CO)]BPh_4$ (8.2×10^{-4} mol dm^{-3}) in dc voltammetry and in cyclic voltammetry. Platinum working microelectrode. Cyclic voltammetric responses at 0.2 V s^{-1}. (●) Starting potential.

in character at a formal electrode potential $E^{0\prime} = -0.20$ V ($\Delta E_p = 160$ mV at $v = 0.2$ V s^{-1}). The dc voltammogram ($E_{1/2} = -0.20$ V) confirms the quasi-reversibility of the process in that it shows an ($E_{3/4} - E_{1/4}$) value of 75 mV and its logarithmic analysis gives a ratio $\Delta E/\Delta \log [i/(i_d - i)]$ of 72 mV. These data seemed to support the electrode formation of a previously unknown copper(II) carbonyl species. However, macroelectrolysis experiments performed at +0.2 V did not reveal any presence of copper(II) carbonyls; in fact, while the colourless copper(I) solution displays an ir spectrum with a CO band at 2045 cm^{-1}, the electrogenerated blue copper(II) solution shows no CO stretching frequencies. Notwithstanding coulometric experiments helped us in the elucidation of the electrode mechanisms involved in both anodic and cathodic processes. Figure 2 reports the CV responses after a series of exhaustive electrode oxidations and reductions of the starting copper(I) derivative.

The anodic oxidation of the copper(I) carbonyl species, $[Cu^I(CO)L]^+$ leads to a decarbonylated copper(II) derivative, $[Cu^{II}L]^{2+}$ (*vide infra*), able to display a voltammetric response at $E^{0\prime} = -0.20$ V, i.e. at the same potentials of the initial peak system A–B ($E^{0\prime} = -0.20$ V) (Fig. 2*b*). The $[Cu^{II}L]^{2+}$ compound can be reversibly reduced to the $[Cu^IL]^+$ analogue ($E_p^c = -0.27$ V) (Fig. 2*c*), which, in turn, can be reoxidized to the $[Cu^{II}L]^{2+}$ form ($E_p^a = -0.13$ V) (Fig. 2*d*). By saturation with CO, the $[Cu^{II}L]^{2+}$ species can be reduced to a copper(I) carbonyl derivative ($E_p^c = -0.20$ V) (Fig. 2*e*). As it can be seen this last step occurs at potentials more positive than the reduction to $[Cu^IL]^+$, in agreement with the well known behaviour of other copper(II) derivatives (4, 6, 7, 13). Infrared spectra on solutions from bulk electrolysis under CO atmosphere ($p = 1$ atm) of previously electrogenerated $[Cu^{II}L]^{2+}$ species show the starting copper(I) carbonyl compound to be restored.

In view of the tested quasi-reversibility of the $[Cu^{II}L]^{2+}/[Cu^IL]^+$ redox couple, and assuming the same degree of reversibility for the reduction of $[Cu^{II}L]^{2+}$ to $[Cu^I(CO)L]^+$, it is possible, following Gagné's suggestions (6), to compute the equilibrium constant for the reaction:

$$[Cu^IL]^+ + CO \overset{K^I}{\rightleftarrows} [Cu^I(CO)L]^+$$

on the basis of the anodic shift of the peak potentials (ΔE) of the reduction process copper(II)/copper(I) complex in the presence and in the absence of CO, through the simplified relation:

$$e^{\Delta E(nF/RT)} - 1 = K^I[CO]$$

A value of about 1.3×10^4 M^{-1} has been estimated.

Under nitrogen the decarbonylated copper(II) derivative can be further reduced to the corresponding copper(0) derivative $[Cu^0L]$ at the potentials of the peak system G–H ($E^{0\prime} = -0.55$ V) (Fig. 2*b–d*); decomposition to copper metal follows the charge transfer, as shown by the appearance of peaks E and F in the reverse scan, due to the charge transfers of electrodeposited copper metal to free copper(I) ion and of the copper(I) ion to free copper(II) ion, respectively. The reduction to $[Cu^0(CO)L]$ species of the starting $[Cu^I(CO)L]^+$ occurs at potentials of the peak system C–D ($E^{0\prime} = -0.64$ V), as shown in Fig. 2 *a* and *e*.

Ultimately the following scheme depicts the whole electrode activity of $[Cu^I(Medpt)(CO)]^+$:

$E_p^a = -0.13$ V

$[Cu^I(CO)L]^+ \xrightarrow{-e^-} [Cu^{II}(CO)L]^{2+} \xrightarrow[-CO]{\text{fast}} [Cu^{II}L]^{2+}$

$E^{0\prime} = -0.64$ V $+e^- \rightleftarrows -e^-$ +CO, $+e^-$ $E_p^c = -0.20$ V $+e^- \rightleftarrows -e^-$ $E^{0\prime} = -0.20$ V

$[Cu^0(CO)L]$ $[Cu^IL]^+$

$\downarrow t_{1/2} \cong 3$ s $+e^- \rightleftarrows -e^-$ $E^{0\prime} = -0.55$V

$Cu^0 + CO + L$ $[Cu^0L]$

$\downarrow t_{1/2} \cong 3$ s

$Cu^0 + L$

The decarbonylation step of $[Cu^{II}(CO)L]^{2+}$ could have been described as an equilibrium step; however, even in CO atmosphere ($p = 1$ atm) the anodic electrolysis of $[Cu^I(CO)L]^+$ did not lead to copper(II) carbonylated species.

Lifetimes reported have been obtained according to the Nicholson's method for a charge transfer followed by an irreversible first-order chemical reaction (17).

The fact that the anodic oxidation of starting $[Cu^I(CO)L]^+$

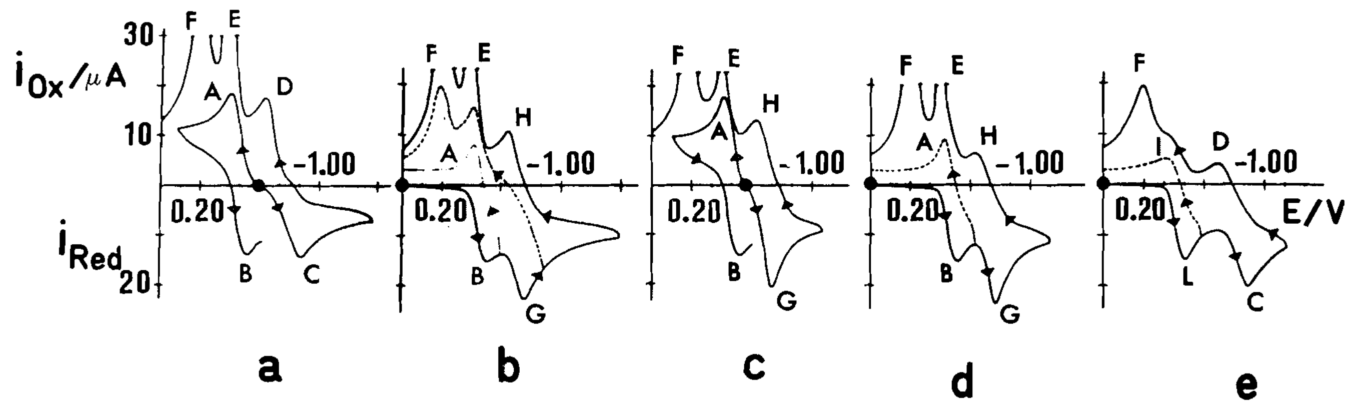

FIG. 2. Cyclic voltammetric responses of a deaerated DMSO solution containing $[Cu^I(Medpt)(CO)]BPh_4$ (2.1×10^{-3} mol dm^{-3}) and $[NEt_4][ClO_4]$ (0.1 mol dm^{-3}) in the following experimental conditions: initial (*a*); after complete oxidation to copper(II) derivative at E_W = +0.2 V (*b*); after complete re-reduction to copper(I) derivative at E_W = −0.3 V (*c*); after complete re-oxidation to copper(II) derivative at E_W = +0.2 V (*d*); saturated with CO (*e*). Platinum working microelectrode. Scan rate: 0.2 V s^{-1} (E_W = working potential).

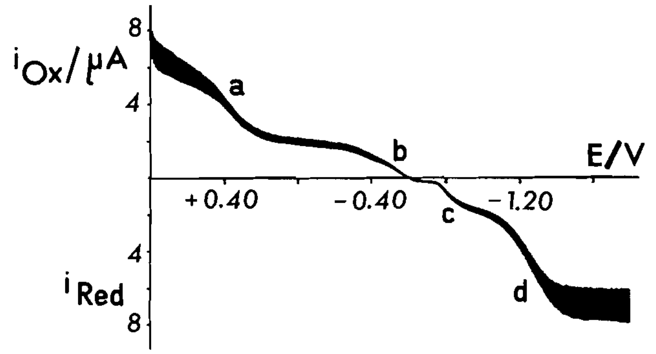

FIG. 3. Dc voltammogram recorded on a DMSO solution containing $[Cu^I(dien)(CO)]BPh_4$ (1.38×10^{-3} mol dm^{-3}) and $[NEt_4]$-$[ClO_4]$ (0.1 mol dm^{-3}). Platinum working microelectrode.

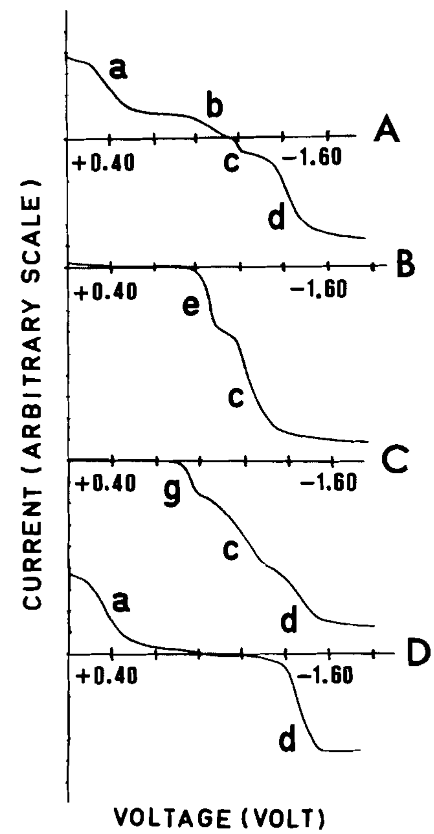

FIG. 4. Schematic dc voltammetric responses of a deaerated DMSO solution containing $[Cu^I(dien)(CO)]BPh_4$ (1.03×10^{-2} mol dm^{-3}) and $[NEt_4][ClO_4]$ (0.1 mol dm^{-3}) in the following experimental conditions: initial (*A*); after complete oxidation to copper(II) derivative at E_W = +0.6 V (*B*); in the same conditions of (*B*) but under CO atmosphere (p = 1 atm) (*C*); after re-reduction under CO atmosphere at E_W = −0.75 V of electrogenerated copper(II) species.

appears in cyclic voltammetry as an uncomplicated charge transfer must be attributed to the quickness of the decarbonylation reaction in comparison with the testable potential scan rates.

It must be said that **I** gives rise to a further anodic process at potentials higher than +1.0 V, but the closeness to the solvent discharge prevents any reliable investigation. Nevertheless its peak height in cyclic voltammetry about three times greater than that of the above reported one-electron oxidation, allowing us to disregard the formation of a copper(III)−amine compound, contrary to some tetraamine complexes (18), very likely suggests this process to be ligand based.

The electrochemical behaviour of **II** can be investigated less deeply than that of **I**, because cyclic voltammetric responses are hardly reproducible. However, dc voltammetry at a platinum DLPRE gives an exhaustive picture of the electron transfer processes in which this species can be involved. Figure 3 reports the dc voltammogram at a platinum electrode obtained from **II** in a deaerated DMSO solution. Two oxidation, *a* ($E_{1/2}$ = +0.38 V) and *b* ($E_{1/2}$ = −0.52 V), and two reduction processes, *c* ($E_{1/2}$ = −0.85 V) and *d* ($E_{1/2}$ = −1.27 V) are present. Controlled potential coulometric tests performed in correspondence to the limiting current of process *b* indicates the consumption of one electron per molecule of starting copper(I) compound; by performing the electrolysis at potentials corresponding to the limiting current of process *a* an overall consumption of one electron per molecule of starting copper(I) compound occurs too. This datum suggests that in DMSO solution an equilibrium exists between two copper(I) species, only one of which contains the Cu—CO unit (single CO stretching band at 2050 cm^{-1}). Coulometry at potentials corresponding to the limiting current of process *d* shows the overall consumption of one electron per molecule of starting copper(I) compound; electrodeposition of copper metal occurs.

Figure 4 schematizes the dc voltammetric responses from a series of exhaustive electrolyses on **II**.

Bulk electrolysis on a deaerated solution of starting copper(I) carbonyl compound $[Cu^I(CO)L]^+$ at potentials varying from −0.3 to 0.7V always leads to a blue copper(II) compound $[Cu^{II}L]^{2+}$, the ir spectrum of which shows no CO adsorption bands; this species can be electroreduced in two steps e ($E_{1/2}$ = −0.52 V), just located at the potentials of process b, and c ($E_{1/2}$ = −0.85 V) (Fig. 4B). As visible in Fig. 4C, under CO atmosphere (p = 1 atm) the voltammetric picture relevant to $[Cu^{II}L]^{2+}$ shows the process e to shift to more anodic potentials giving rise to the process g ($E_{1/2}$ = −0.33 V), attributable to the electrogeneration of a copper(I) carbonyl compound, followed by two processes at the same potentials of processes c and d. Under CO atmosphere the electrolysis of $[Cu^{II}L]^{2+}$ performed at potentials ranging between those corresponding to the limiting current of process g and those corresponding to the foot of process d (from −0.45 V to −0.8 V) gives rise to a copper(I) compound which substantially displays a response with one anodic and one cathodic process corresponding to processes a and d of the starting copper(I) compound, processes b and c being strongly lowered (Fig. 4D). In addition the ir spectrum of the so-electrogenerated copper(I) species is coincident with the one of starting **II**. This last step markedly throws light on the aforementioned equilibrium existing in DMSO solutions of **II**, which can be hence formulated as:

$$[Cu^I(dien)(CO)]^+ \xrightleftharpoons{+S\ (S\ =\ DMSO)} [Cu^I(dien)(S)]^+ + CO$$

In confirmation of this, the dc voltammogram of **II** under CO atmosphere appears as that of Fig. 4D.

An analogous equilibrium could not be detected in the case of **I** under the adopted experimental conditions. The more basic Medpt, which would strengthen the Cu—CO bond, as suggested by ir data, might be responsible for this different behaviour.

The voltammogram of **II** at p_{CO} = 1 atm allows us a reliable determination of the instability constant for copper(I) carbonyl compound in DMSO solvent simply from the limiting current values of the two copper(I) species; it results of the order of 1.6 × 10^{-4} M. Indeed this datum implies that the shift of the reduction potential of $[Cu^{II}(dien)]^{2+}$ towards more anodic potentials in the presence of CO had to be 52 mV instead of the measured value of 190 mV. We think the discrepancy must be attributed to the high degree of irreversibility of the electrode processes which makes unapplicable the previously cited Gagné's computation.

The irreversibility of the one-electron process a ($E_{1/2}$ = +0.38 V) is witnessed by an ($E_{3/4} - E_{1/4}$) value of 240 mV.

In conclusion, if one neglects the decarbonylation equilibrium due to DMSO solvent, the following scheme holds for the electrode activity of $[Cu^I(dien)(CO)]^+$:

$$E_{1/2} = +0.38\ V$$

$$[Cu^I(CO)L]^+ \xrightarrow[-e^-]{} [Cu^{II}(CO)L]^{2+} \rightarrow [Cu^{II}L]^{2+}$$

$$E_{1/2} = -1.27\ V \quad \downarrow +e^- \qquad +CO,\ +e^- \qquad +e^- \downarrow\uparrow -e^- \quad E^{0\prime} = -0.52\ V$$

$$[Cu^0(CO)L] \qquad E_{1/2} = -0.33\ V \qquad [Cu^IL]^+$$

$$\downarrow \qquad\qquad +e^- \downarrow \quad E_{1/2} = -0.85\ V$$

$$Cu^0 + CO + L \qquad\qquad [Cu^0L]$$

$$\downarrow$$

$$Cu^0 + L$$

It must be noted that no carbonyl copper(II) compound has been obtained even in macroelectrolysis tests at +0.7 V under CO atmosphere.

Also in this case ligand-centred anodic oxidation processes are present at potentials higher than +1.0 V.

At this stage the nature of the electrogenerated compound $[Cu^{II}L]^{2+}$ in the case of both **I** and **II** has to be discussed. In order to identify the oxidation product we synthesized several copper(II) complexes with different Cu/triamine ratios in DMSO. Their electrochemical behaviour was compared with that of the electrogenerated $[Cu^{II}L]^{2+}$ species. The voltammetric picture of the electrode oxidation product $[Cu^I(dien)(CO)]^+$ was paralleled by that of $[Cu(dien)(DMSO)_3]^{2+}$. This result was not unexpected, since for instance the possible rearrangement of $[Cu(dien)(CO)]^+$ to the common species $[Cu(dien)_2]^{2+}$ (19) should have involved the release of free copper ions easily detectable in voltammetry. The same pathway holds when dien is replaced by Medpt. This accounts for the formalism adopted in the description of the electrode activity of both **I** and **II**. It must be also pointed out that the cathodic reduction under CO atmosphere at the potentials of the first reduction step of both $[Cu(Medpt)(DMSO)_3]^{2+}$ and $[Cu(dien)(DMSO)_3]^{2+}$, chemically synthesized, leads to **I** and **II**, respectively, as shown by ir spectra.

As pointed out elsewhere (20), the existence of the complex **III** is limited to the solid state (bridging CO frequency at 1926 cm^{-1}), or in solution of nonpolar solvents (bridging CO frequency in toluene at 1945 cm^{-1}). In THF solution the following equilibrium holds:

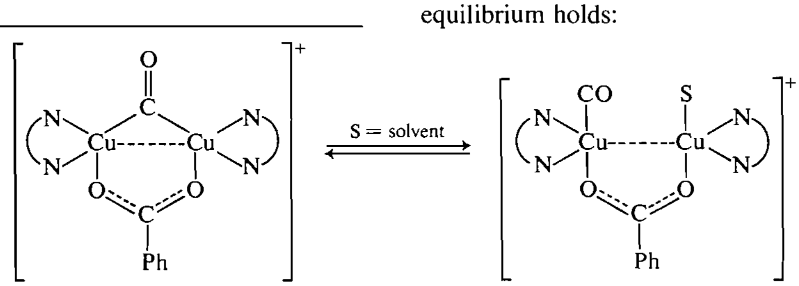

III **III′**

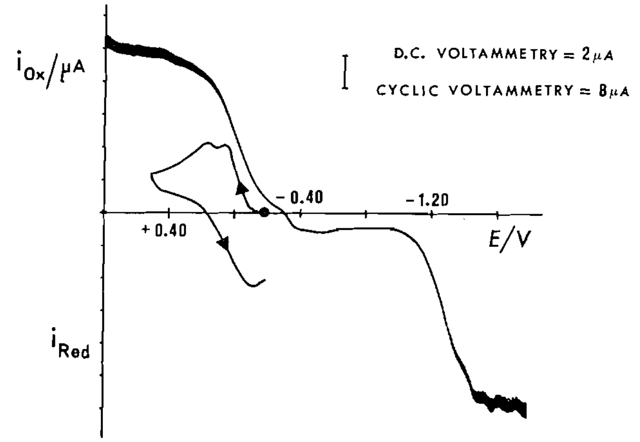

FIG. 5. Voltammetric responses of a DMSO solution containing $[NEt_4][ClO_4]$ (0.1 mol dm^{-3}) and $[Cu_2(tmen)_2(Ph—CO_2)(CO)(S)]$-$BPh_4$ (2.46 × 10^{-3} mol dm^{-3}). Platinum working microelectrode. (●) Starting potential for cyclic voltammetric response; scan rate 0.2 V s^{-1}.

In fact, the ir spectrum shows both bridging (1930 cm^{-1}) and terminal (2060 cm^{-1}) CO bands. In DMSO the equilibrium is completely shifted to the right, as shown by the presence in the ir spectrum of only one CO stretching band at 2055 cm^{-1}. Therefore, the electrochemistry below discussed refers to this CO-unbridged form, **III′**. Figure 5 reports the voltammetric responses obtained from a **III′** solution at a platinum microelectrode.

As it can be seen the CV response shows the presence of two oxidation processes very close to each other (E_p^a = +0.04 V, +0.15 V), whereas dc voltammetry indicates the presence of only one oxidation process ($E_{1/2}$ = −0.02 V). Unfortunately the CV responses have a low degree of reproducibility, preventing any accurate study of the underlying electrode mechanisms. The cathodic reduction of the starting dicopper(I) complex occurs at $E_{1/2}$ = −1.28 V; cyclic voltammetry shows that the charge transfer is followed by decomposition of the electrogenerated zero-valent copper complex. Some amounts of air-oxidized product are also present, which undergoes a preceding reduction at $E_{1/2} \cong -0.3$ V. Also in this case the oxidation of the ligand occurs at potentials higher than +1.0 V, close to the solvent discharge. Controlled potential coulometric tests at +0.5 V indicate the consumption of 2 mol of electrons per mole of starting complex. Two mole of electrons per mole of starting complex are also consumed in the cathodic electrolysis at −1.7 V, which is followed by electrodeposition of copper metal. An ($E_{3/4} - E_{1/4}$) value of 200 mV for the anodic response indicates the irreversibility of the involved charge transfer. The presence of some inflexions on the rising part of the cathodic response prevents any graphical analysis of the relevant process. The clear detection of two subsequent oxidation processes in cyclic voltammetry suggests the mixed-valence $Cu^{II}Cu^{I}$ species (7) to exist only on the short-time scale. The available CV data do not allow us to distinguish the oxidation process of copper(I) carbonylated centre from that of copper(I) solvated centre. However, by analogy with the voltammetric behaviour of a series of dinuclear copper(I) complexes able to form monocarbonylated species (13), we are tempted by way of speculation to assign the less anodic peak of Fig. 4 to the oxidation of copper(I) carbonylated moiety and the more anodic peak to the oxidation of copper(I) solvated moiety.

Further information on electrode processes have been gained once again by dc voltammetry on solutions of **III′** exhaustively oxidized at the potential of +0.5 V. As expected the resulting blue dicopper(II) solution, which shows no carbonyl absorption band in its ir spectrum, is electroreduced in two successive steps schematically corresponding to the reduction of the dicopper centre from $Cu^{II}Cu^{II}$ to $Cu^{I}Cu^{I}$ ($E_{1/2} \cong -0.4$ V) and from $Cu^{I}Cu^{I}$ to $Cu^{0}Cu^{0}$ ($E_{1/2} \cong -1.0$ V), respectively. The less cathodic response is difficult to analyze because of the presence of a maximum of the first kind. Under CO atmosphere (p = 1 atm) this first step shifts anodically about 30 mV. The electrolytic reduction of the electrogenerated blue dicopper(II) species to dicopper(I) species at potentials varying from −0.35 V to −0.55 V, when performed under CO atmosphere, restores a pale green solution which displays a dc voltammogram identical to that reported in Fig. 5. In addition, the ir spectrum of this electrogenerated dicopper(I) species is coincident with that of the starting **III′**. In conclusion the electrode behaviour of the dinuclear copper(I) carbonyl complex $[Cu_2(tmen)_2(\mu\text{-}PhCO_2)(CO)(S)]^+$ can be best schematized:

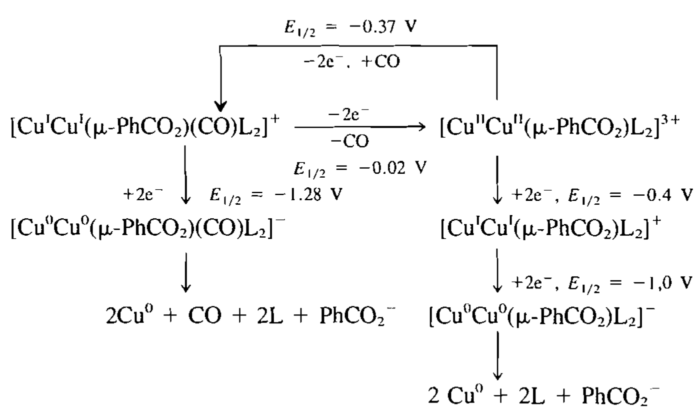

Conclusions

The electron-transfer sequences in which **I**, **II**, and **III** may be involved have been studied in non-aqueous solvent. The anodic oxidation of **I**, **II**, **III** gives rise to the corresponding decarbonylated copper(II) derivatives, which in the presence of carbon monoxide can be quantitatively electroreduced to the starting copper(I) aminocarbonyl complexes, indicating that no irreversible change upon oxidation occurs in the skeleton of molecules **I**, **II**, and **III**.

A comparison between the electrode processes of **I** and **II** reveals that **I** is more easily oxidized to copper(II) species and more easily reduced to copper(0) species than **II**. It seems likely that the presence of the electron-donating methyl group in **I** favours the oxidation step, as well as the presence of a more flexible cavity, increased in size, favours the reduction step.

Finally it has to be underlined that the redox potentials of the copper(I)/copper(II) couples measured for **I**, **II**, and **III** are high enough to approach those of the copper sites in common cuproproteins (3, 7).

Experimental

Materials

[Cu(dien)(CO)]BPh_4, [Cu(Medpt)(CO)]BPh_4, and $[Cu_2(tmen)_2(\mu\text{-}PhCO_2)(\mu\text{-}CO)]BPh_4$ were prepared as previously described (20, 21). $[Cu(dien)(DMSO)_3]^{2+}$ and $[Cu(Medpt)(DMSO)_3]^{2+}$ were obtained as perchlorate salts by mixing in methanol equimolar amounts of $Cu(ClO_4)_2.6H_2O$ and the appropriate triamine in the presence of an excess of DMSO. The salts precipitated as blue microcrystalline solids and afforded satisfactory elemental analyses.

Reagent grade DMSO (Carlo Erba) was dried with 0.3-nm molecular sieves (Union Carbide). The supporting electrolyte tetraethylammonium perchlorate $[NEt_4][ClO_4]$ (Carlo Erba) was dried in a vacuum oven and used without further purification. Extra pure nitrogen was employed to remove oxygen from tested solutions. Carbon monoxide was passed through Oxy-Trap (Alltech Associates) to remove residual oxygen.

Apparatus

A PAR model 170 Electrochemistry System was used as polarizing unit; the recording devices were either a Houston Instruments model 2000 XY recorder or, for potential scan rates higher than 0.5 V s^{-1}, a Hewlett-Packard model 1123A storage oscilloscope.

Cyclic voltammetric tests were performed in a three electrode cell having a platinum sphere working microelectrode surrounded by a platinum-spiral counter electrode. The potential of the working microelectrode was probed by a Luggin capillary reference electrode compartment.

An electrode with periodical renewal of the diffusion layer (DLPRE) was obtained by moving the platinum electrode with a time-controlled knocker.

Controlled potential coulometric tests were performed in an H-shaped cell with anodic and cathodic compartments separated by a sintered glass disk. The working macroelectrode was a platinum gauze. In these tests an Amel potentiostat model 551, with an associated Amel model 558 coulometer integrator, were used.

Potential values refer to an aqueous saturated calomel reference electrode (sce). All experiments were carried out at 20 ± 0.1°C.

Infrared solution spectra were recorded on a Perkin-Elmer Model 597 spectrophotometer in the wavenumber range 4000–400 cm^{-1}.

Methods

Cyclic voltammetric current–potential curves have been analysed as a function of the scan rate, v, on the basis of the anodic, or cathodic peak potential (E_p^a, or E_p^c), the difference between the peak potential value of a response and that of the reverse one (($E_p^a - E_p^c$) for an anodic process, or ($E_p^c - E_p^a$) for a cathodic process), the quotient of the peaks current of the reverse and the direct response ((i_p^c/i_p^a) for an anodic process, or (i_p^a/i_p^c) for a cathodic process), the quotient of the peak current of the response and the square root of the scan rate ($i_p/v^{1/2}$). Unless otherwise specified, peak potential values refer at a scan rate of 0.2 V s^{-1}. Formal electrode potentials, $E^{0\prime}$, for quasi-reversible charge transfer have been computed as the average of the anodic (or cathodic) peak potential and the directly associated cathodic (or anodic) peak potential, under the usual assumption that the transfer coefficient α ranges between 0.3 and 0.7.

In dc voltammetry the location of irreversible charge transfer processes is expressed by $E_{1/2}$; for quasi-reversible process the $E^{0\prime}$ symbol has been used.

The solubility of CO in dimethylsulphoxide at P_{CO} = 1 atm has been taken as 1.1×10^{-3} mol dm^{-3} (20 ± 1°C) (22).

Acknowledgments

The authors wish to thank Professor M. Pasquali for helpful discussions. Financial support by Consiglio Nazionale delle Ricerche of Italy is gratefully acknowledged.

1. E. I. SOLOMON. *In* Copper proteins. *Edited by* G. T. Spiro. Wiley, New York. 1982. Chapt. 2. p. 41.
2. N. MAKINO, P. MCMAHILL, H. S. MASON, and T. H. MOSS. J. Biol. Chem. **249**, 6062 (1974).
3. G. S. PATTERSON and R. H. HOLM. Bioinorg. Chem. **4**, 257 (1975).
4. R. R. GAGNÉ, J. L. ALLISON, R. S. GALL, and C. A. KOVAL. J. Am. Chem. Soc. **99**, 7170 (1977).
5. A. W. ADDISON, M. CARPENTER, L. K-M. LAU, and M. WICHOLAS. Inorg. Chem. **17**, 1545 (1978).
6. R. R. GAGNÉ, J. L. ALLISON, and D. M. INGLE. Inorg. Chem. **18**, 2767 (1979).
7. R. R. GAGNÉ, C. A. KOVAL, T. J. SMITH, and M. CIMOLINO. J. Am. Chem. Soc. **101**, 4571 (1979).
8. R. R. GAGNÉ, R. P. KREH, and J. A. DODGE. J. Am. Chem. Soc. **101**, 6917 (1979).
9. T. N. SORRELL, M. R. MALACHOWSKI, and D. L. JAMESON. Inorg. Chem. **21**, 3250 (1982).
10. K. D. KARLIN, J. C. HAYES, S. JUEN, J. P. HUTCHINSON, and J. ZUBIETA. Inorg. Chem. **21**, 4106 (1982).
11. T. N. SORRELL and D. L. JAMESON. J. Am. Chem. Soc. **104**, 2053 (1982).
12. S. K. MANDAL and K. NAG. J. Chem. Soc., Dalton Trans. 2429 (1983).
13. S. KITAGAWA, M. MUNAKATA, and N. MIYAJI. Bull. Soc. Jpn. **56**, 2258 (1983).
14. P. ZANELLO, P. A. VIGATO, U. CASELLATO, S. TAMBURINI, and G. A. MAZZOCCHIN. Transition Met. Chem. **8**, 294 (1983).
15. R. C. LONG and D. N. HENDRICKSON. J. Am. Chem. Soc. **105**, 1513 (1983).
16. E. R. BROWN and R. F. LARGE. *In* Physical methods of chemistry. Part IIA. Electrochemical methods. *Edited by* A. Weissberger and B. W. Rossiter. Wiley Interscience, New York. 1971.
17. R. S. NICHOLSON and I. SHAIN. Anal. Chem. **36**, 706 (1964).
18. L. FABBRIZZI, A. POGGI, and P. ZANELLO. J. Chem. Soc. Dalton Trans. 1495 (1984).
19. F. S. STEPHENS. J. Chem. Soc. A, 883 (1969).
20. M. PASQUALI, C. FLORIANI, G. VENTURI, A. GAETANI-MANFREDOTTI, and A. CHIESI-VILLA. J. Am. Chem. Soc. **104**, 4092 (1982).
21. M. PASQUALI, F. MARCHETTI, and C. FLORIANI. Inorg. Chem. **17**, 1684 (1978).
22. C. ERCOLANI, F. MONACELLI, G. PENNESI, G. ROSSI, E. ANTONINI, P. ASCENZI, and M. BRUNORI. J. Chem. Soc. Dalton Trans. 1120 (1981).

Complex formation between cuprous iodide and phenyl phosphine: a nuclear magnetic resonance and X-ray crystallographic study

RAYMOND J. BATCHELOR, THOMAS BIRCHALL,[1] AND ROMOLO FAGGIANI

Department of Chemistry and Institute for Materials Research, McMaster University, 1280 Main Street West, Hamilton, Ont., Canada L8S 4M1

Received July 27, 1984

RAYMOND J. BATCHELOR, THOMAS BIRCHALL, and ROMOLO FAGGIANI. Can. J. Chem. **63**, 928 (1985).

The X-ray crystal structure of di-μ-iodobis[bis(phenylphosphine)copper(I)] has been determined: $R_1 = 0.0460$. The crystals were monoclinic, space group *Cc*, $a = 10.625(2)$ Å, $b = 25.115(8)$ Å, $c = 11.361(2)$ Å, $\beta = 105.929(15)°$, fw = 821.28, and Z = 4. The molecular structure consists of two $CuI(C_6H_5PH_2)_2$ units bridged via the iodines so that each copper achieves tetrahedral coordination. Nuclear magnetic resonance data provides evidence that the phenylphosphines remain coordinated in solution but undergo rapid exchange at room temperature.

RAYMOND J. BATCHELOR, THOMAS BIRCHALL et ROMOLO FAGGIANI. Can. J. Chem. **63**, 928 (1985).

Faisant appel à la diffraction des rayons-X, on a déterminé la structure cristalline du di-μ-iodobis[bis(phénylphosphine)-cuivre(I)] jusqu'à une valeur de $R_1 = 0{,}0460$. Les cristaux sont monocliniques, groupe d'espace *Cc*, $a = 10{,}625(2)$, $b = 25{,}115(8)$ et $c = 11{,}361(2)$ Å, $\beta = 105{,}929(15)°$, mm = 821,28 et Z = 4. La structure moléculaire comporte deux unités $CuI(C_6H_5PH_2)_2$ qui sont reliées par les iodes d'une façon telle que chaque atome de cuivre atteint une coordination tétraédrique. Sur la base des données de la rmn, on peut affirmer que, en solution, les phénylphosphines restent coordinnées mais qu'elles subissent un échange rapide à la température ambiante.

[Traduit par le journal]

Introduction

Although basicity and donor ability are well known properties of trivalent compounds of the group 5 elements there has been relatively little investigation of the coordination chemistry of hydrides and organohydrides of these elements other than nitrogen. Presumably this is because the tertiary derivatives, especially the triphenyl compounds, are much easier to work with and much less susceptible to oxidation. While it is reasonable to expect that the coordination chemistry of primary and secondary phosphines will be very similar to that of tertiary derivatives potential differences do exist. For example, there is evidence for the dissociation of P—H bonds with resultant formation of phosphido complexes (1). Also it has been noted that the order of basicity for phosphines is tertiary > secondary > primary > PH_3 (2).

The coordinating ability of a phosphine, however, depends on features other than simple basicity. For example, the extent to which π-acidity of the ligand can contribute to the stability of the coordinative interaction has been the centre of much controversy (3). It is unlikely that π-back donation into *d*-orbitals of the ligand is significant for tertiary organophosphines, but for PF_3 and for phosphites it is apparently important (4). Vibrational studies on the C—O stretching frequency of a carbonyl group *trans* to a given phosphine ligand indicate that PH_3 is intermediate in "π-accepting" ability between tertiary phosphines and phosphites (4).

It has also been shown that, for tertiary phosphines, the steric bulk of the ligand appears to be the deciding factor in the stability of the coordinative interactions between these ligands and transition metals (5–7) although there appear to be exceptions to this general rule (8). With much smaller phosphine ligands such as PH_3 or the primary phosphines, steric interactions should be greatly reduced (cf. the cone angles: PH_3 87°, $C_6H_6PH_2$ 101°, $P(C_6H_5)_3$ 145° (5)). For complexes containing small ligands, electronic factors should assume increased relative importance.

The systems $(CuX)_m(L)_n$ (X = halide, L = amine, phosphine, arsine) appeared to be potentially useful for investigations concerning the relative importance of steric and electronic factors because a large number of X-ray crystallographic studies have shown that the steric bulk of both the neutral ligands and the halides have a tremendous influence on the degree of association and resulting structure of such complexes (9, 10). Spectroscopic characterization of these complexes has proven to be somewhat problematic, however, and as a consequence of this they have been largely studied by X-ray crystallography (3, 10).

In early vapour pressure studies (11, 12) it was concluded that cuprous halides could form complexes with PH_3 in ratios of $CuX \cdot 2PH_3$ and $CuX \cdot PH_3$ but that these were unstable to loss of PH_3. Much later, Abel *et al.* (13) studied the complexes formed between $(C_6H_5)_2PH$ and cuprous halides in the hope that vibrational and ^1H nmr spectroscopy, with specific focus on the hydrogen bonded to phosphorus, would yield further information on the characterization of these kinds of complexes. These authors found complexes possessing most of the known stoichiometries for $(CuX)_m(PR_3)_n$, where $m/n = 1/3, 1/2, 2/3, 1/1$. However, while nmr and infrared spectroscopies could differentiate between free and complexed $(C_6H_5)_2PH$, these techniques could not discriminate between the different stoichiometries and structures of the complexes. These studies appear to be the only previous investigations of cuprous halide complexes of non-tertiary phosphines.

Here we report our results on the interaction of cuprous iodide with phenylphosphine and with phosphine. Nuclear magnetic resonance evidence is presented which indicates that complex formation takes place with both phenylphosphine and phosphine but only in the former case could solid complexes be isolated. One of these, $CuI \cdot 2C_6H_5PH_2$, has been subjected to analysis by single crystal X-ray diffraction and is shown to be dimeric, with bridging iodine atoms so that each copper achieves four coordination.

Experimental

Phosphorus-31 nmr spectra were recorded on a Bruker WH-90 spectrometer.

[1]To whom all correspondence should be addressed.

TABLE 1. Crystal and diffraction data acquisition parameters for $[CuI(C_6H_5PH_2)_2]_2$

Crystal parameters (at −65°C)[a]	
a = 10.625(2) Å	Monoclinic
b = 25.115(8) Å	Space group Cc
c = 11.361(2) Å	Z = 4
β = 105.929(15)°	fw = 821.28
V = 2914.6(12) Å^3	ρ_c = 1.8716(9) g cm^{-3}
$\mu(MoK_\alpha)$ = 38.5 cm^{-1}	ρ_o = 1.8(1) g cm^{-3}[b]
Conditions : hkl : $h+k = 2n$, $h0l$: $l = 2n$	
Crystal dimensions : 0.3 × 0.3 × 0.2 mm[c]	
Intensity measurements	
Radiation	MoK_α (λ = 0.71069 Å; graphite monochromator)
Scan mode	θ:2θ
Scan range	(K_{α_1} −1.0°) to (K_{α_2} +1.0°)
Scan rates[d]	5.86 to 29.30° min^{-1}
Reflections measured	$\pm h,k,\pm l$
Maximum 2θ	45°
Standard reflections[e]	5 −5 0 (esd 2.93%)
	4 −8 1 (esd 1.53%)
Details of refinement[f]	
Unique reflections	3820 (Friedel opposites not averaged)
"Unobserved reflections"	less than 3σ:381, zero intensity:36[g]
R factors[h]	R_1 = 0.0460, R_2 = 0.0593
Weighting scheme	$w = [\sigma_F^2 + 0.001741\ F^2]^{-1}$
"Secondary extinction"	$F^* = F(1-2.9 \times 10^{-8}F^2/\sin\theta)$
Final |shift/error|	Maximum 0.090, average 0.006
Highest peak[i] in final difference map	1.010 e Å^{-3}
Lowest trough in final difference map	−0.655 e Å^{-3}
$F(000)$ = 1583.9	

[a]15 reflections 20° ≤ 2θ ≤ 30° were used to determine the cell constants using MoK_{α_1} radiation (λ = 0.70926 Å).
[b]Neutral buoyancy in aqueous $ZnBr_2$.
[c]The crystal was a rectangular prism; the dimensions given are approximate; measurement of more precise crystal dimensions was unfortunately forestalled by decomposition and liquefaction of the crystal upon rewarming to room temperature after the acquisition of intensity data.
[d]Dependent on the intensity of a preliminary count.
[e]Measured after every 48 reflections; displayed no systematic deviations in intensity.
[f]Data reduction, including Lorentz and polarization corrections, was performed using programs from the XRAY-76 package of crystallographic programs (14). Absorption corrections were not applied (estimated maximum conceivable error in F is ~35%).
[g]Reflections of zero intensity were given a weight of zero in the refinement.
[h]$R_1 = \Sigma(|F_o| - |F_c|)/\Sigma(F_o)$; $R_2 = [\Sigma(w(|F_o| - |F_c|)^2)/\Sigma(wF_o^2)]^{1/2}$
[i]This peak occurs at (0.4035, 0.4229, 0.7104) which is 1.00 Å from I_1. The second most intense peak occurs at 1.09 Å from I_2.

X-ray crystallography

Crystals of $CuI \cdot 2C_6H_5PH_2$, suitable for single crystal X-ray analysis, were obtained by recrystallization from ethanol containing 5% tetrahydrofuran. The structure was initially solved using a partial set of intensity data collected at ambient temperature using a Syntex-Nicolet P2$_1$ diffractometer. The atomic temperature factors determined in this initial refinement were somewhat large, therefore a full data set was acquired at reduced temperature using an LT-1 low temperature attachment. Details of the crystal and diffraction data parameters are summarised in Table 1.

The symmetry and systematic absences of the weighted reciprocal lattice indicated that $C2/c$ and Cc were possible space groups for the crystal. The structure was solved by Patterson techniques and refined using the program SHELX 76 (14). The XRAY 76 package of programs (15) was used to perform data reduction and to create the ORTEP drawings of the structure. No solution to the Patterson map could be found in the centrosymmetric space group $C2/c$. Analysis of the normalized squared structure factors (E^2) gives an average value of $|E^2 - 1|$ of 0.82. A centrosymmetric structure would be expected to give a value of 0.97 and a non-centrosymmetric structure a value of 0.74 (14).

TABLE 2. Final atomic positional fractional coordinates × 10^3 and equivalent isotropic thermal parameters for the non-hydrogen atoms of $[CuI(C_6H_5PH_2)_2]_2$

Atom	x	y	z	U_{eq} (Å^2 × 10^{-3})[a]
I(1)	500[b]	423.29(2)	750[b]	36.3(5)
I(2)	591.9(1)	318.56(2)	503.3(1)	39.9(5)
Cu(1)	530.1(1)	420.58(5)	525.9(1)	39.7(9)
Cu(2)	575.8(1)	322.41(5)	731.7(1)	40.9(9)
P(1)	771.9(3)	316.9(1)	871.8(3)	40(2)
P(2)	336.2(3)	431.0(1)	386.8(3)	39(2)
P(3)	687.9(3)	477.2(1)	509.7(3)	43(2)
P(4)	411.9(3)	270.4(1)	754.8(2)	43(2)
C(1)	786.9(9)	348.9(4)	1018.8(9)	34(2)
C(2)	900(1)	377.0(4)	1080.5(9)	41(2)
C(3)	906(1)	399.0(5)	1189(1)	56(3)
C(4)	808(1)	395.1(5)	1246(1)	56(3)
C(5)	695(1)	366.7(5)	1188(1)	60(3)
C(6)	686(1)	344.9(4)	1073.6(9)	43(3)
C(7)	314.9(9)	402.0(4)	235.1(9)	33(2)
C(8)	259(1)	352.3(5)	205(1)	57(3)
C(9)	253(2)	332.7(7)	85(2)	81(4)
C(10)	294(2)	362.0(6)	6(2)	80(4)
C(11)	350(1)	408.5(6)	37(1)	68(4)
C(12)	361(1)	428.8(4)	150(1)	42(3)
C(13)	859(1)	464.1(4)	590.2(9)	38(2)
C(14)	961(1)	478.2(4)	542(1)	51(3)
C(15)	1089(1)	466.8(5)	609(1)	60(3)
C(16)	1114(1)	442.4(5)	716(1)	63(3)
C(17)	1015(1)	428.8(5)	770(1)	57(3)
C(18)	887(1)	439.3(5)	703(1)	48(3)
C(19)	243(1)	286.6(4)	677.2(9)	39(2)
C(20)	140(1)	270.1(5)	723(1)	58(3)
C(21)	11(1)	284.5(5)	659(1)	61(3)
C(22)	−14(1)	311.9(5)	552(1)	60(3)
C(23)	87(2)	326.5(5)	511(1)	61(3)
C(24)	215(1)	315.3(4)	573(1)	47(3)

[a]Equivalent positions: x,y,z; $x + 1/2, y + 1/2, z$; $x, \bar{y}, z + 1/2$; $x + 1/2, 1/2 - y, z + 1/2$; $U_{eq} = (1/3)\sum_i\sum_j U_{ij}a_i^*a_j^*\mathbf{a}_i \cdot \mathbf{a}_j$; U_{iso} for carbon atoms.
[b]Coordinates fixed arbitrarily to define the origin of the unit cell.

The structural solution in the non-centrosymmetric space group Cc was fully refined for all non-hydrogen atoms and included anisotropic temperature factors for Cu, I, and P. The hydrogen atoms associated with the carbon atoms of the phenyl rings were not well defined in the difference map: these atoms were fixed at positions 0.95 Å (16) from each carbon atom along a vector bisecting each C—C—C angle and in the plane defined by those atoms. Each hydrogen atom was assigned an isotropic temperature factor fixed at 1.5 times that of the carbon atom to which it was bonded. Because of these somewhat arbitrary constraints on the C—H groups, and as there is only passing interest in the phenyl groups themselves, no attempt was made to refine the carbon atoms anisotropically. The positions and temperature factors of the hydrogen atoms were recalculated after each cycle of refinement and were fixed at these new values for the subsequent cycle. The hydrogen atoms bonded to phosphorus could not be found in the electron difference map and were not included in the refinement.

The final positional parameters and equivalent isotropic temperature factors are given in Table 2. Anisotropic temperature factors for the heavy atoms are listed in Table 3. The calculated and observed structure factors and σ-values, selected least-squares planes and di-

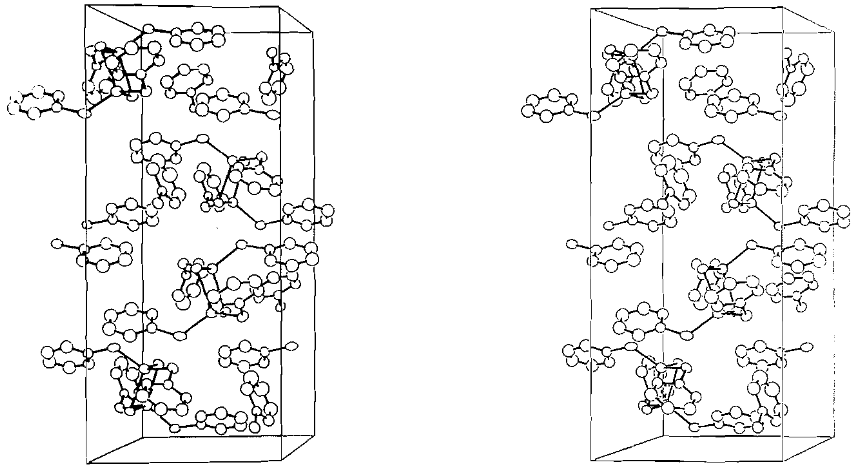

FIG. 1. Packing of $[CuI(C_6H_5PH_2)_2]_2$ molecules in the unit cell. Stereoscopic ORTEP diagram showing the contents of one unit cell plus atoms to complete all four molecules and all phenylphosphine groups which protrude into the cell.

TABLE 3. Anisotropic temperature factors for the heavy atoms in $[CuI(C_6H_5PH_2)_2]_2$ ($Å^2 \times 10^{-3}$)

Atom	U_{11}	U_{22}	U_{33}	U_{12}	U_{13}	U_{23}
I(1)	40.3(4)	30.5(4)	32.0(4)	4.0(3)	7.9(3)	−4.6(3)
I(2)	46.3(4)	34.4(4)	33.4(4)	7.3(3)	12.9(3)	−3.8(3)
Cu(1)	36.9(8)	39.2(8)	34.7(8)	0.4(5)	2.2(6)	−1.1(5)
Cu(2)	44.1(8)	37.8(7)	32.6(8)	3.5(5)	3.6(6)	−0.5(5)
P(1)	40(2)	39(2)	32(2)	9(1)	5(1)	3(1)
P(2)	37(2)	41(2)	32(2)	6(1)	5(1)	3(1)
P(3)	43(2)	30(1)	48(2)	1(1)	5(1)	6(1)
P(4)	58(2)	29(1)	35(2)	−4(1)	7(1)	3(1)

hedral angles as well as positional coordinates and thermal parameters for the hydrogen atoms have been deposited on Supplementary Information and are available on request (Tables 5, 6, and 7 respectively).[2]

Results and discussion

Description of the structure

The crystal consists of discrete molecular dimers, $[\{CuI(C_6H_5PH_2)_2\}_2]$, separated by normal van der Waals distances. Each molecule comprises one asymmetric unit of the structure.

The packing of the molecules in the unit cell, shown in Fig. 1, is particularly interesting because it demonstrates how the packing of structurally symmetric molecules can cause those molecules to assume asymmetric conformations. The molecules of $[\{CuI(C_6H_5PH_2)_2\}_2]$ pack so that three of the phenyl-groups, namely those bonded to P(1), P(3), and P(4), from each molecular unit are incorporated into infinite sliding stacks in which each ring is related to the ring three levels further along the stack by the *c*-centering operation. Therefore the axes of these "pseudo-graphitic" stacks are oriented parallel to the $[1,\bar{1},0]$ and $[1,1,0]$ directions. Stacks possessing these two different orientations are related to each other by the *c*-glide plane. Two of the crystallographically unique rings in a given stack are very nearly parallel to one another. The dihedral angle between them is 4.8°. The third ring is tilted somewhat with respect to the other two, giving dihedral angles of 20.6° and 21.4°. This tilting of the ring bonded to P(1) arises because the fourth crystallographically unique phenyl-ring, bonded to P(2) is situated between adjacent pseudo-graphitic stacks separated by unit translations along *a* and is in close contact with the former ring. This last phenyl ring is oriented approximately parallel to the axes of the neighbouring stacks and packs edge to edge with Cu_2I_2 rhombuses of adjacent molecules so that it is nearly coplanar with these latter fragments (Fig. 1). The dihedral angle between the plane of this ring and that of an adjacent Cu_2I_2 rhombus is 11.0°. The structure, therefore, contains sets of infinite "ribbons" parallel to $(1,\bar{1},0)$ and $(1,1,0)$ consisting of alternating phenyl-rings and Cu_2I_2 rhombuses. These "ribbons" are sandwiched between the "sliding stacks" of phenyl-rings and thus represent another facet of the same packing condition which gives rise to the orientations of the stacks. The absence of significant voids in this structure suggests that it represents an optimum packing geometry.

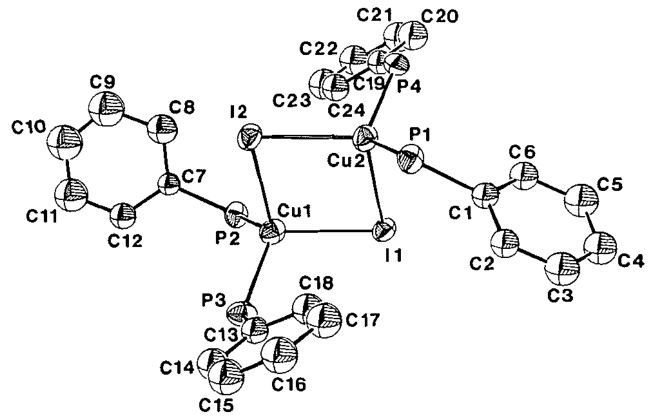

FIG. 2. The $[CuI(C_6H_5PH_2)_2]_2$ molecule viewed towards the *b,c* face.

Molecular structure

A diagram of an individual molecule is given in Fig. 2 and shows clearly the relative orientations of the phenyl-groups discussed above. There is a slight puckering of the Cu_2I_2 rhombus indicated by a dihedral angle of 5° between planes I1,Cu1,I2 and I1,Cu2,I2. Such puckering is commonly observed in structures of this type (17) and is no doubt attributable to packing forces. The interatomic distances and bond angles are listed in Table 4.

[2]Complete set of data is available, at a nominal charge, from the Depository of Unpublished Data, CISTI, National Research Council of Canada, Ottawa, Ont., Canada K1A 0S2.

TABLE 4. Interatomic distances (Å) and bond angles (deg) for $[CuI(C_6H_5PH_2)_2]_2$

(*a*) Bond distances

Bond	Distance	Bond	Distance
I(1) —Cu(1)	2.652(1)	I(2) —Cu(1)	2.675(1)
I(1) —Cu(2)	2.684(1)	I(2) —Cu(2)	2.648(2)
I(1) —I(2)	4.151(1)	Cu(1)—Cu(2)	3.340(2)
Cu(1)—P(2)	2.241(3)	Cu(2)—P(1)	2.252(3)
Cu(1)—P(3)	2.244(3)	Cu(2)—P(4)	2.249(3)
P(2) —C(7)	1.83(1)	P(1) —C(1)	1.82(1)
P(3) —C(13)	1.83(1)	P(4) —C(19)	1.82(1)
C(1) —C(2)	1.40(1)	C(7) —C(8)	1.39(2)
C(1) —C(6)	1.38(2)	C(7) —C(12)	1.37(2)
C(2) —C(3)	1.34(2)	C(8) —C(9)	1.44(2)
C(3) —C(4)	1.37(2)	C(9) —C(10)	1.33(3)
C(4) —C(5)	1.40(2)	C(10)—C(11)	1.32(2)
C(5) —C(6)	1.39(2)	C(11)—C(12)	1.36(2)
C(13)—C(14)	1.39(2)	C(19)—C(20)	1.40(2)
C(13)—C(18)	1.38(2)	C(19)—C(24)	1.35(2)
C(14)—C(15)	1.39(2)	C(20)—C(21)	1.41(2)
C(15)—C(16)	1.33(2)	C(21)—C(22)	1.36(2)
C(16)—C(17)	1.40(2)	C(22)—C(23)	1.33(2)
C(17)—C(18)	1.40(2)	C(23)—C(24)	1.38(2)

(*b*) Bond angles

Bonds	Angle	Bonds	Angle
Cu(1)—I(1) —Cu(2)	77.50(4)	Cu(1)—I(2) —Cu(1)	77.73(5)
I(1) —Cu(1)—I(2)	102.36(5)	I(1) —Cu(2)—I(2)	102.24(5)
I(1) —Cu(1)—P(2)	110.2(1)	I(1) —Cu(2)—P(1)	104.03(8)
I(1) —Cu(1)—P(3)	110.60(9)	I(1) —Cu(2)—P(4)	106.3(1)
I(2) —Cu(1)—P(2)	104.26(9)	I(2) —Cu(2)—P(1)	113.2(1)
I(2) —Cu(1)—P(3)	113.00(9)	I(2) —Cu(2)—P(4)	110.72(9)
P(2) —Cu(1)—P(3)	115.5(1)	P(1) —Cu(2)—P(4)	118.5(1)
Cu(1)—P(2) —C(7)	118.1(3)	Cu(2)—P(1) —C(1)	116.9(3)
Cu(1)—P(3) —C(13)	120.5(4)	Cu(2)—P(4) —C(19)	120.5(4)
P(2) —C(7) —C(8)	121.5(9)	P(1) —C(1) —C(2)	121.8(9)
P(2) —C(7) —C(12)	119.6(7)	P(1) —C(1) —C(6)	119.9(7)
P(3) —C(13)—C(14)	122.4(8)	P(4) —C(19)—C(20)	121.7(8)
P(3) —C(13)—C(18)	118.5(9)	P(4) —C(19)—C(24)	119.6(9)
C(8) —C(7) —C(12)	119(1)	C(2) —C(1) —C(6)	118(1)
C(7) —C(8) —C(9)	116(1)	C(1) —C(2) —C(3)	119(1)
C(8) —C(9) —C(10)	121(2)	C(2) —C(3) —C(4)	123(1)
C(9) —C(10)—C(11)	122(2)	C(3) —C(4) —C(5)	119(1)
C(10)—C(11)—C(12)	120(2)	C(4) —C(5) —C(6)	118(1)
C(7) —C(12)—C(11)	122(1)	C(1) —C(6) —C(5)	122(1)
C(14)—C(13)—C(18)	119.2(9)	C(20)—C(19)—C(24)	119(1)
C(13)—C(14)—C(15)	119(1)	C(19)—C(20)—C(21)	119(1)
C(14)—C(15)—C(16)	122(1)	C(20)—C(21)—C(22)	121(1)
C(15)—C(16)—C(17)	122(1)	C(21)—C(22)—C(23)	118(1)
C(16)—C(17)—C(18)	117(1)	C(22)—C(23)—C(24)	123(1)
C(13)—C(18)—C(17)	122(1)	C(19)—C(24)—C(23)	120(1)

The dimeric molecule contains two pseudotetrahedrally coordinated copper atoms bridged by two iodine atoms. The other coordination sites are occupied by the phosphorus atoms of the phenylphosphine ligands. This molecule may therefore be described as a "normal" dimer in that it has the most commonly occurring geometries about halogen and copper found in copper(I) halide – phosphine complexes. Although a number of compounds have been prepared which possess the same stoichiometric ratio of ligand to metal halide and which probably possess the same structure, no crystal structure has previously been reported for a simple "binary" dimeric complex of this stoichiometric ratio of CuI to monodentate phosphine ligand, nor has any similar structure been reported in which the phosphine ligands were not tertiary phosphines.

Recently the structures of a series of dimeric molecules based on the Cu_2I_2 unit have been reported (10). The neutral ligands in all of these cases were nitrogen bases. Two related structures of mixed-ligand dimeric $Cu_2I_2L_4$ complexes have been reported in which two neutral ligands are nitrogen bases and the other two coordinate via arsenic (18, 19). Two structures have been published (17) which consist of molecules possessing the Cu_2I_2 core and phosphorus-coordinating neutral ligands. Neither of these, however, is a simple $Cu_2I_2L_4$ complex. The one whose geometry most closely approaches that of the present structure is $[\{CuI[P(C_6H_5)_2CH_3]_2\}_2 \cdot SO_2]$ which has the same structural geometry as $[\{CuI(C_6H_5PH_2)_2\}_2]$ except that it contains a molecule of SO_2 which is weakly coordinated, via sulphur, to one of the bridging iodine atoms. The other complex is $[(CuI)_2\{P(C_6H_5)_3\}_3]$ in which one of the copper atoms is only pseudo-trigonally coordinated. Coordination of a fourth triphenylphosphine ligand in this molecule is thought to be prohibited as a consequence of the steric bulk of the triphenylphosphine ligands. The former compound containing $P(C_6H_5)_2CH_3$ ligands as well as the compound $[\{CuI(C_6H_5PH_2)_2\}_2]$, presented here, both demonstrate that the use of smaller phosphine ligands permits full tetrahedral coordination of the copper atoms.

Various authors have concluded that the molecular structures of cuprous halide – tertiary phosphine complexes are the net results of electronic, steric and packing factors (6, 9, 10, 17, 20). When the phosphine ligands and halide ions are large (e.g. $P(C_6H_5)_3$ and I^-) non-bonded intramolecular interactions are dominant in deciding the structural geometry and stoichiometry in concert with the metal–ligand and metal–halide bond distances which appear to be a function of the coordination number about the metal (9). The bond angles about copper and halogen appear to be quite variable and adopt values which presumably minimize steric interactions. In $[\{CuI(C_6H_5PH_2)_2\}_2]$, as well as in other compounds possessing Cu_2I_2 units, the geometry of this unit is apparently governed, to a large extent, by the minimum distance of mutual approach of the two iodine atoms (4.151(1) Å for $[\{CuI(C_6H_5PH_2)_2\}_2]$; 4.109(1) Å for $[\{CuI[(C_6H_5)_2CH_3]_2\}_2 \cdot SO_2]$; 4.302(1) Å for $[(CuI)_2\{P(C_6H_5)_3\}_3]$. Twice the accepted van der Waals radius of iodine is 4.30 Å (21).

Comparison with the nitrogen–donor adducts (10) shows that the change from phosphorus to nitrogen ligands is accompanied by expansion of the intramolecular I. . . I separation and the I—Cu—I angles along with corresponding contraction of the Cu---Cu separation and Cu—I—Cu angles. This may be related to the fact that the N—Cu—N angles are smaller than the corresponding P—Cu—P angles.

The Cu—Cu distance in $[\{CuI(C_6H_5PH_2)_2\}_2]$ is non-bonding (3.340(2) Å). The distance in Cu metal is 2.56 Å. However, separations of Cu atoms in similar compounds show a considerable range of values and can approach bonding distances. It has been postulated (22) that there may be a net "soft attractive" interaction between Cu atoms in such complexes rendering the structures relatively indifferent to the magnitude of the metal–metal separation. The result is that this distance is merely a consequence of the minimum halogen–halogen distance and normal Cu—X bond lengths.

The CuI bond lengths, average = 2.665(18) Å, are in the range normally found for tetrahedrally coordinated copper (I) (2.62–2.81 Å) (10, 17, 20). There do not appear to be any identifiable trends in these bond lengths with the nature of the neutral ligand. The Cu—P distances, average = 2.247(5) Å, are the same as those found with tertiary phosphines in similar structures, namely, 2.24 to 2.27 Å (17, 20). The phenylphosphine ligands display no unusual features in bond lengths or angles. The P—C bond lengths, average = 1.823(4) Å, are normal for a phosphorus–carbon single bond. The phosphorus atoms deviate very little from the planes of their associated phenyl rings. Apparent deviations in the C—C bond distances from the expected 1.395 Å, especially for those between *meta* and *para* carbon atoms, may result from systematic errors caused by rigid-body thermal motions. Specifically, wagging motions of the phenylphosphine groups may cause the C—C bond lengths furthest from the point of attachment of the ligand to the Cu atom to be systematically low (20).

Nuclear magnetic resonance of cuprous iodide – phosphine solutions

It has been demonstrated (6) that the steric bulk of a tertiary phosphine ligand is the dominant contributing factor to the dissociation of their complexes with cuprous halides in solution. Complexes between cuprous halides and the much smaller primary phosphines or PH_3 itself might reasonably be expected to be more stable since, in addition to their smaller cone angles (5), they have also been postulated to have greater π-acidity than tertiary phosphines (23). In fact a possible order of "complexing power" of P(III) ligands has been suggested to be as follows:

$$P(OR)_3 > PF_3 > PH_3 > PR_3 > P(OPh)_3 > PPh_3 \simeq PBu'_3$$

(4), though such a listing is of course somewhat arbitrary.

Earlier workers (11, 12) found that adducts between PH_3 and cuprous halides are unstable to loss of PH_3 under standard conditions. This suggests that ligand basicity is the dominant factor contributing to the energetics of the metal–phosphine interaction in the absence of steric effects.The relative basicities of PH_3 and the phenylphosphines, as given by the pK_a values of the conjugate phosphonium ions, are $P(C_6H_5)_3$, $pK_a = 2.73$; $P(C_6H_5)_2H$, $pK_a = 0.03$; $P(C_6H_5)H_2$, pK_a est. (−1.7); PH_3, $pK_a = -14$ (2). For compounds with Cu(I) it seems that π-back-donation into phosphorus d-orbitals is not sufficient to compensate for the weaker σ-donor ability of PH_3 relative to the phenyl-substituted phosphines. This may be due, in part, to the d^{10} filled-shell configuration of Cu(I).

To confirm the earlier conclusions regarding the interaction between PH_3 and CuI, solutions of PH_3 and CuI in THF were prepared and examined by ^{31}P nmr. It was found that indeed a considerable excess of PH_3 was required in the sealed nmr tubes in order to dissolve all of the cuprous iodide. ^{31}P nmr spectra of these solutions confirmed complex formation by revealing a complexation shift of approximately 20 ppm to low field and an increase in J_{PH} from 187 Hz for free PH_3 to approximately 233 Hz in the solution. The existence of only one ^{31}P signal, an ^1H-coupled quartet, regardless of the exact composition of the solution indicated that as with other phosphines the complexes undergo rapid ligand exchange in solution at room temperature. Raman spectra of the solutions confirmed this. A sharp band at 2307 cm^{-1}, attributed to the P—H stretching vibration of free PH_3, as well as a broader, possibly multiple, band centred at 2344 cm^{-1}, attributed to bound PH_3, were observed. Such an increase in P—H stretching frequency is in agreement with the observation that the P—H stretching frequency of $(C_6H_5)_2PH$ increases by about 33 to 41 cm^{-1} upon coordination to copper (I) (13). The nmr and vibrational results are consistent with a strengthening of the P—H bond upon complexation.

When low-temperature ^{31}P nmr spectra of the solutions were recorded, in an attempt to "freeze out" the ligand exchange process, a white solid precipitated and the time averaged ^{31}P nmr parameters shifted back towards those of free PH_3. This process was observed to be reversible and possibly indicates that $CuI-PH_3$ complex formation is endothermic. Crystals of the precipitated solid were shown by X-ray diffraction to be cuprous iodide (24).

The reaction of excess cuprous iodide with phenylphosphine in THF yielded a highly soluble product. The weight of unreacted CuI suggested that the stoichiometry of the soluble product was approximately $(CuI)_{0.8} \cdot C_6H_5PH_2$. The ^{31}P nmr spectrum of this solution consisted of a triplet at $\delta = -106.62(3)$ ppm having the spin–spin coupling $^{1}J_{PH} = 303(3)$ Hz. Below −70°C the ^{31}P resonance of the above solution broadens considerably; however, no new features were observed before the freezing point of the solution was reached. Since the observed room temperature chemical shift is to low field of that of free phenylphosphine by approximately 20 ppm and the P—H coupling constant is ~100 Hz greater than that of free phenylphosphine, it must be concluded that these nmr parameters represent a coordinated ligand. Perhaps these ligands undergo rapid exchange, at room temperature, between species of different geometry and degree of association as has been observed for tertiary phosphine adducts (7, 25). Attempts were made to isolate crystals suitable for X-ray crystallographic analysis from this solution, but although crystalline material was obtained we have not yet been able to characterise this product because of its tendency to decompose and release $C_6H_5PH_2$.

When two equivalents of phenylphosphine were allowed to react with cuprous iodide a crystalline product was obtained after recrystallization from ethanol containing 5% THF. A THF solution of the product yielded room temperature ^{31}P and ^{13}C nmr spectra which were essentially identical with those found for the previous solutions prepared using excess CuI. Upon cooling, however, the ^{31}P nmr spectrum initially displayed some broadening of the observed triplet until below −90°C further fine structure was resolved (Fig. 3). The low temperature spectrum can be accounted for by postulating a ^{31}P—^{31}P spin–spin coupling between two phenylphosphine ligands bound to the same coppper atom.

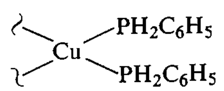

Although these two phosphorus atoms are chemically equivalent and thus have the same chemical shift, they are magnetically inequivalent by virtue of the strong coupling to the protons directly bound to them. Figure 3 includes a simulated spectrum which represents the best fit to the observed peak positions assuming only coupling between directly bound phosphorus and hydrogen ($^{1}J_{PH}$ = 299 Hz) and the two bond ^{31}P—^{31}P coupling ($^{2}J_{PP}$ = 107 Hz). The three bond ^{31}P—^{1}H coupling was fixed at zero for this simulation. The changes in ^{31}P chemical shift and one-bond ^{31}P—^{1}H coupling upon reducing the temperature were insignificant and no new resonances appeared. Therefore, it is apparent that at room temperature the bound phosphine ligands are being exchanged rapidly between different copper atoms. It is not possible to deduce whether this exchange is inter- or intramolecular. However, since it is known that these kinds of complexes may undergo ligand dissociation in solution (26), it is quite possible that the exchange is intermolecular in nature. The species in solution at low temperature could have the dimeric structure found in the solid state. Dimeric species are known to exist in benzene solutions of CuCl and $P(C_6H_5)_3$ or $PCH_3(C_6H_5)_2$ when the ligand to CuCl ratio is less than 3:1 (26). However, for the THF solutions of $[CuI(C_6H_5PH_2)_2]$ the possibility that a THF solvent molecule assumes one coordination position, and thus breaks-up the dimers, cannot be ruled out.

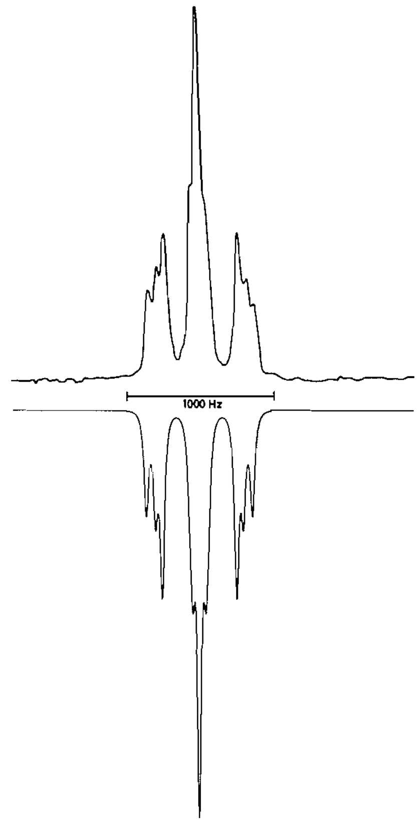

FIG. 3. ^{31}P nmr spectrum of $[CuI(C_6H_5PH_2)_2]_2$ in the THF solution at −99°C; upper, actual spectrum; lower, simulated spectrum.

Acknowledgements

We thank the Natural Sciences and Engineering Research Council of Canada for financial support and for a scholarship to R. J. Batchelor. The authors wish to acknowledge the helpful advice of Dr. C. J. L. Lock and Dr. J. F. Britten.

1. C. S. KRAIHANZEL. J. Organomet. Chem. **73**, 137 (1974).
2. W. A. HENDERSON and G. A. STREULI. J. Am. Chem. Soc. **82**, 5791 (1960).
3. C. A. MCAULIFFE and W. L. LEVASON. Phosphine, arsine, stibine complexes of the transition elements. Elsevier, New York. 1979.
4. J. EMSLEY and D. HALL. The chemistry of phosphorus. J. Wiley and Sons, New York. 1976.
5. C. A. TOLMAN. Chem. Rev. **77**, 313 (1977).
6. S. J. LIPPARD and G. J. PALENIK. Inorg. Chem. **10**, 1322 (1971).
7. S. J. LIPPARD and J. J. MAYERLE. Inorg. Chem. **11**, 753 (1972).
8. R. G. GOEL and A. L. BEAUCHAMP. Inorg. Chem. **22**, 395 (1983).
9. J. T. GILL, J. J. MAYERLE, P. S. WELKER, D. F. LEWIS, D. A. UCKO, D. J. BARTON, D. STOWENS, and S. J. LIPPARD. Inorg. Chem. **15**, 1155 (1976).

10. P. C. HEALY, C. PAKAWATCHAI, and A. H. WHITE. J. Chem. Soc. Dalton Trans. 1917 (1983).
11. R. HÖLTJE and H. SCHLEGEL. Z. Anorg. Allg. Chem. **243**, 246 (1940).
12. R. SCHOLDER and K. PATTOCK. Z. Anorg. Allg. Chem. **220**, 250 (1934).
13. E. W. ABEL, R. A. N. MCLEAN, and I. H. SABHERWAL. J. Chem. Soc. A, 133 (1969).
14. G. M. SHELDRICK. Shelx 76. Program for crystal structure determination. University of Cambridge, England. 1976.
15. J. M. STEWART. X-RAY 76 package of crystallographic programs, Tech. Rep. TR-446. Univ. of Maryland, College Park, MD.
16. M. R. CHURCHILL. Inorg. Chem. **12**, 1213 (1973).
17. P. G. ELLER, G. J. KUBAS, and R. R. RYAN. Inorg. Chem. **16**, 2454 (1977).
18. R. GRAZIANI, G. BOMBIERI, and E. FORSELLINI. J. Chem. Soc. A, 2331 (1971).
19. M. R. CHURCHILL and J. R. MISSERT. Inorg. Chem. **20**, 619 (1981).
20. M. R. CHURCHILL, B. G. DEBOER, and D. J. DONOVAN. Inorg. Chem. **14**, 617 (1975).
21. L. PAULING. The nature of the chemical bond and the structure of molecules and crystals. 3rd ed. Cornell University Press, Ithica, NY. 1960.
22. P. K. MEHROTRA and R. HOFFMANN. Inorg. Chem. **17**, 2187 (1978).
23. E. O. FISCHER, E. LOUIS, and C. G. KREITER. Angew. Chem. Int. Edn. Eng. **8**, 377 (1969).
24. R. BATCHELOR and T. BIRCHALL. Acta Crystallogr. B**38**, 1260 (1982).
25. E. L. MUETTERTIES and C. W. ALEGRANTI. J. Am. Chem. Soc. **92**, 4114 (1970).
26. D. J. FIFE, W. M. MOORE, and K. W. MORSE. Inorg. Chem. **23**, 1684 (1984).

High temperature potential/pH diagrams for the chlorine–water system

BARBARA KOLODZIEJ[1] AND FATHI HABASHI
Department of Mining and Metallurgy, Laval University, Quebec City, P.Q., Canada G1K 7P4

Received March 26, 1984[2]

BARBARA KOLODZIEJ and FATHI HABASHI. Can. J. Chem. **63**, 935 (1985).

Thermodynamic evidence supports the view that the reaction $2\,Cl^- + 2H^+ + \frac{1}{2}O_2 \rightarrow Cl_2(aq) + H_2O$ takes place above 127°C at pH = 0. An increase in HCl concentration and/or oxygen partial pressure allow the reaction to proceed at lower temperature.

BARBARA KOLODZIEJ et FATHI HABASHI. Can. J. Chem. **63**, 935 (1985).

Des données thermodynamiques suggérent que la réaction $2Cl^- + 2H^+ + \frac{1}{2}O_2 \rightarrow Cl_2(aq) + H_2O$ peut se produire à une température supérieure à 127°C et à un pH de 0. Si la concentration de HCl et/ou la pression partielle d'oxygène est augmentée, la réaction peut se produire à des températures plus basses.

[Traduit par le journal]

During the aqueous oxidation of some sulfide minerals at high temperature and pressure, it was observed that the rate of reaction in HCl solution is higher than that in H_2SO_4 solution of the same normality, all other factors being the same (1–4). This was explained to be due to the formation of chlorine according to the reaction

$$2Cl^- + 2H^+ + \tfrac{1}{2}O_2 \rightarrow Cl_2(aq) + H_2O$$

Aqueous chlorine is known to be a strong oxidant for sulfides; that is why its formation would enhance the dissolution. The present report is a thermodynamic analysis of the above reaction using E–pH diagrams prepared especially for elevated temperatures.

Method of calculation

Potential/pH diagrams for the chlorine–water system can be derived for temperatures up to 150°C by a method based largely on the Criss and Cobble Entropy Correspondence Principle (5). For representing equilibrium conditions in aqueous solutions we utilized the work by Pourbaix (6) which contains diagrams at 25°C. For easy comparison of the diagrams presented in the paper with those provided by Pourbaix we use his system of numbering of reactions.

The diagrams presented in this paper were constructed using the Correspondence Principle together with various other data from sources shown in Table 1. The reactions considered in the chlorine–water systems are shown in Table 2. All reactions were considered in the general form

$$[1] \quad aA + xH^+ + ze^- = bB + cH_2O$$

so that the reduction potential at temperature T becomes

$$[2] \quad E_T = E_T^0 + \frac{RT}{zF} \ln \frac{a_A^a a_{H^+}^x}{a_B^b a_{H_2O}^c}$$

If the activity of water is assumed to be equal to unity, the term $-\log a_{H^+}$ defined as pH, and with

$$[3] \quad \Delta G_T^0 = -zFE_T^0$$

it follows that

$$[4] \quad \frac{zFE_T}{2.303RT} = -\frac{\Delta G_T^0}{2.303RT} + \log \frac{a_A^a}{a_B^b} - x\ \mathrm{pH}$$

A change in free energy for each reaction at temperatures 90 and 150°C was calculated from the equation with T_1 = 298 K,

$$[5] \quad \Delta G_{T_2}^0 = \Delta G_{T_1}^0 - (T_2 - T_1)\Delta S_{T_1}^0 + (T_2 - T_1)\Delta \bar{C}_p^0]_{T_1}^{T_2} - T_2 \Delta \bar{C}_p^0]_{T_1}^{T_2} \ln (T_2/T_1)$$

using the G_{298}^0 and S_{298}^0 values shown in Table 1 and heat capacity data shown in Tables 3, 4. The ion heat-capacity functions have been presented by Criss and Cobble in the following form

$$[6] \quad \bar{C}_p^0]_{298}^{T_2} = a_{T_2} + b_{T_2} \cdot S_{298}^0 \text{ (absolute)}$$

where a_{T_2} and b_{T_2} are temperature dependent and S_{298}^0 (absolute) is the entropy based on $S_{H^+}^0 = -5.0$.

TABLE 1. Thermodynamic data at 25°C

Formula	$G_{298\,K}^{0}$ [b] (kcal/mol)	$S_{298\,K}^{0}$ [c] (cal/mol deg)
$O_2(g)$	0	49.0
$H_2(g)$	0	31.2
$H_2O(l)$	−56.688	16.71
Cl_2[a](aq)	1.650	29.0
$Cl_2(g)$	0	53.29
$HCl(g)$	−22.769	44.646
H^+	0	
Cl^-	−31.350	13.5
ClO_4^-	−2.470	43.5

[a] Dissolved chlorine.
[b] From Pourbaix (6).
[c] From Latimer (7).

TABLE 2. Chlorine–water system

	Reaction involving the stability of water
[b]	$O_2(g) + 4H^+ + 4e^- = 2H_2O(l)$
	Two dissolved substances
[3]	$2Cl^- = Cl_2(aq) + 2e^-$
[9]	$Cl^- + 4H_2O = ClO_4^- + 8H^+ + 8e^-$
[15]	$Cl_2(aq) + 8H_2O = 2ClO_4^- + 16H^+ + 14e^-$
	Two gaseous substances
[25]	$2HCl(g) = Cl_2(g) + 2H^+ + 2e^-$
	One gaseous substance and one dissolved substance
[31]	$HCl(g) = Cl^- + H^+$
[35]	$2Cl^- = Cl_2(g) + 2e^-$
[41]	$Cl_2(g) + 8H_2O = 2ClO_4^- + 16H^+ + 14e^-$

[1] Present address: Institute of Inorganic Chemistry, Polytechnic University, Wrocław, Poland.
[2] Revision received October 16, 1984.

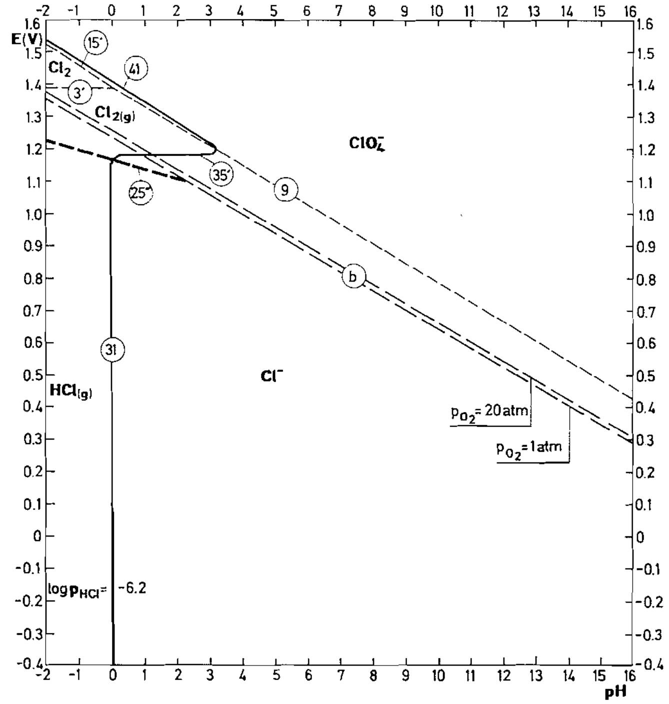

FIG. 1. Potential–pH equilibrium diagram for the system chlorine–water at 298 K, for solution containing 1 g-atom Cl/L.

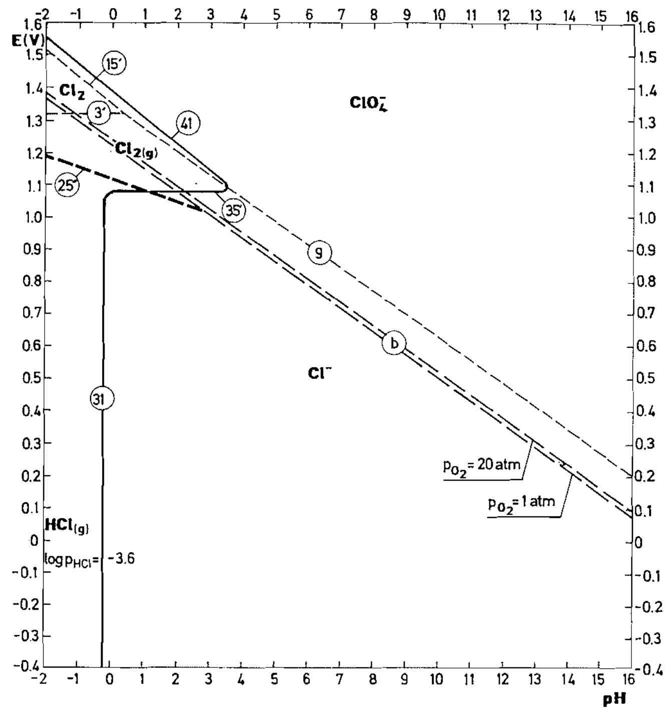

FIG. 2. Potential–pH equilibrium diagram for the system chlorine–water at 363 K, for solutions containing 1 g-atom Cl/L.

TABLE 3. Values of partial molar heat capacities for some ions and non-ionic species

Formula	$\bar{C}^0_{p\,298}$	$\bar{C}_p^0]^{363}_{298}$	$\bar{C}_p^0]^{423}_{298}$
H^+	28[a]	31[a]	33[a]
Cl^-	−32.6[a]	−58[a]	−62[a]
ClO_4^-		−56.9[a]	−57[a]
Cl(aq)		65.0[b]	109.0[b]
Cl_2(g)	8.11[c]	8.35[c]	8.46[c]
O_2(g)	7.00[c]	7.22[c]	7.36[c]
H_2(g)	6.42[c]	6.71[c]	6.78[c]
HCl(g)	6.96[c]	6.97[c]	6.98[c]
H_2O(l)	18.1[c]	18.1[c]	18.1[c]

[a] From Criss and Cobble (5).
[b] From Helgeson (8).
[c] From Kelley (9).

Results and conclusions

The equations for various reactions in the Cl–H_2O system presented in Table 2 were used in the construction of the potential/pH diagrams shown in Figs. 1, 2, 3, 4. The potential/pH equilibrium diagram for 25°C presented according to Pourbaix was supplemented with an expression related to equilibrium [31].

The equation presenting equilibrium [31] (Table 2) allows for the partial pressure of HCl over the aqueous 1 *M*, 3 *M* hydrochloric acid solution at 298, 363, and 423 K. Partial pressures of HCl in aqueous hydrochloric acid solutions at various concentrations and temperatures (10) are provided in Table 5. The diagrams presented in Figs. 1, 2, 3, 4 provide a suitable value of log p_{HCl} apart from the equilibrium line for reaction [31]. In order to determine the effect of hydrochloric acid concentration on the equilibria in question at 150°C also the potential/pH diagram for HCl was plotted (Fig. 4).

Analysis of the equilibria presented in the potential/pH diagrams at various temperatures shows that an increase in temperature results in a considerable decrease in the reaction potentials denoted in Table 2 by [3], [25], [35]. Thus, with the increasing temperature the area of thermodynamical stability of gaseous chlorine in equilibrium with gaseous HCl and Cl^- ions becomes enlarged and also the region of relative predominance of free chlorine Cl_2(aq) contained in hydrochloric acid solution becomes enlarged.

On the other hand, an increase in temperature results in an increase of the oxygen reduction potential

$$[7] \quad O_2 + 4H^+ + 4e^- = 2H_2O$$

which depends also on its partial pressure. By analyzing a possibility for reaction $2Cl^- = Cl_2(aq) + 2e^-$ (Table 4, reaction [3]) to occur, it was found on the grounds of the above mentioned relationships that at 25°C the potential of this reaction over the entire pH range lies above the reduction potential of O_2 to H_2O. Only a slight potential difference for reaction $2Cl^- = 2Cl(g) + 2e^-$ (Table 4, reaction [35]), and for reduction of oxygen of maximum 0.06 V for HCl solutions at pH $<$ 1.2 might indicate the oxidation reaction of Cl^- to Cl_2(g) to occur. An increase in temperature up to 90°C favours the oxidation reaction of Cl^- to Cl_2(g). At this temperature the difference in potentials between oxidation reaction of Cl^- ions to Cl_2(g) and reduction reaction of oxygen to H_2O in HCl solution at pH $<$ 2.2 is max. 0.17 V. On the other hand, for the course of reaction

$$[8] \quad 2Cl^- + \tfrac{1}{2}O_2 + 2H^+ = Cl_2(aq) + H_2O$$

the temperature of 90°C is still too low. Though for pH $<$ 1.4 the potential of oxidation reaction of Cl^- ions to Cl_2(aq) is slightly higher than that for reduction of oxygen but in this pH region, as shown by the diagram, one does not deal with the HCl solution. Analysis of equilibria for the same reactions at 150°C (Fig. 3) indicates that the course of oxidation reaction of

TABLE 4. Standard free energy ΔG^0 and equations relating E_T, pH, and activity

Equation	T (K)	ΔG_T^0 (cal/mol)	E_T/pH relationships Volts/pH/activity
[b]	298	−113 380	$E_T = 1.229 - 0.059\text{pH} + 0.015 \log P_{O_2}$
	363	−112 950	$= 1.224 - 0.072\text{pH} + 0.018 \log P_{O_2}$
	423	−115 540	$= 1.209 - 0.084\text{pH} + 0.021 \log P_{O_2}$
[3]	298	−64 398	$E_T = 1.395 + 0.0295 \log \frac{[Cl_2]_{aq}}{[Cl^-]^2}$
	363	−61 036	$= 1.320 + 0.0360 \log \frac{[Cl_2]_{aq}}{[Cl^-]^2}$
	423	−53 256	$= 1.15 + 0.042 \log \frac{[Cl_2]_{aq}}{[Cl^-]^2}$
[9]	298	−255 554	$E_T = -1.380 - 0.0591\text{pH} + 0.0074 \log \frac{[ClO_4^-]}{[Cl^-]}$
	363	−248 746	$= 1.35 - 0.072\text{pH} + 0.009 \log \frac{[ClO_4^-]}{[Cl^-]}$
	423	−239 989	$= 1.30 - 0.084\text{pH} + 0.0105 \log \frac{[ClO_4^-]}{[Cl^-]}$
[15]	298	−446 714	$E_T = 1.385 - 0.0675\text{pH} + 0.0042 \log \frac{[ClO_4^-]^2}{[Cl_2]_{aq}}$
	363	−436 239	$= 1.350 - 0.082\text{pH} + 0.0051 \log \frac{[ClO_4^-]^2}{[Cl_2]_{aq}}$
	423	−425 033	$= 1.316 - 0.096\text{pH} + 0.006 \log \frac{[ClO_4^-]^2}{[Cl_2]_{aq}}$
[25]	298	−54 098	$E_T = 0.987 - 0.0591\text{pH} + 0.0295 \log \frac{p_{Cl_2}[H^+]^2}{p^2_{HCl}}$
	363	−51 829	$= 0.986 - 0.072\text{pH} + 0.036 \log \frac{p_{Cl_2}[H^+]^2}{p^2_{HCl}}$
	423	−48 624	$= 0.970 - 0.084\text{pH} + 0.042 \log \frac{p_{Cl_2}[H^+]^2}{p^2_{HCl}}$
[31]	298	−8 595	$\log [Cl^-] = 6.30 + \text{pH} + \log p_{HCl}$
	363	−6 351	$\log [Cl^-] = 3.84 + \text{pH} + \log p_{HCl}$
	423	−3 883	$\log [Cl^-] = 2.0 + \text{pH} + \log p_{HCl}$
[35]	298	−62 744	$E_T = 1.359 + 0.0295 \log \frac{p_{Cl_2}}{[Cl^-]^2}$
	363	−60 231	$= 1.30 + 0.036 \log \frac{p_{Cl_2}}{[Cl^-]^2}$
	423	−52 516	$= 1.14 + 0.042 \log \frac{p_{Cl_2}}{[Cl^-]^2}$
[41]	298	−44 864	$E_T = 1.389 - 0.0675\text{pH} + 0.042 \log \frac{[ClO_4^-]^2}{p_{Cl_2}}$
	363	−439 102	$= 1.36 - 0.082\text{pH} + 0.0051 \log \frac{[ClO_4^-]^2}{p_{Cl_2}}$
	423	−427 411	$= 1.32 - 0.096\text{pH} + 0.006 \log \frac{[ClO_4^-]^2}{p_{Cl_2}}$
Limits of the domains of relative predominance of the dissolved substances			
[3′]	298		$E_T = 1.395 - 0.0295 \log C^*$
$Cl^-/Cl_2(aq)$	363		$= 1.320 - 0.0360 \log C$
	423		$= 1.15 - 0.042 \log C$

TABLE 4. (*Concluded*)

Equation	T (K)	ΔG_T^0 (cal/mol)	E_T/pH relationships Volts/pH/activity
[15′]	298		$E_T = 1.385 - 0.0675\text{pH} + 0.0042 \log C$
$Cl_2(aq)/ClO_4^-$	363		$= 1.350 - 0.082\text{pH} + 0.0051 \log C$
	423		$= 1.316 - 0.096\text{pH} + 0.006 \log C$
Limits of the domains of relative predominance of the gaseous substances			
[25″]†	298		$E_T = 1.173 - 0.0295\text{pH} - 0.0295 \log [Cl^-]$
$HCl(g)/$	363		$= 1.124 - 0.036\text{pH} - 0.036 \log [Cl^-]$
$Cl_2(g), Cl^-$	423		$= 1.054 - 0.042\text{pH} - 0.042 \log [Cl^-]$
Solubility in g-atoms of chlorine per litre			
[35′]	298		$E_T = 1.359 - 0.0591 \log C + 0.0295 \log p_{Cl_2}$
$Cl^-/Cl_2(g)$	363		$= 1.30 - 0.072 \log C + 0.036 \log p_{Cl_2}$
	423		$= 1.14 - 0.084 \log C + 0.042 \log p_{Cl_2}$

*Concentration C calculated in moles of dissolved substance per litre.
†The relation E_T is explained in the Appendix.

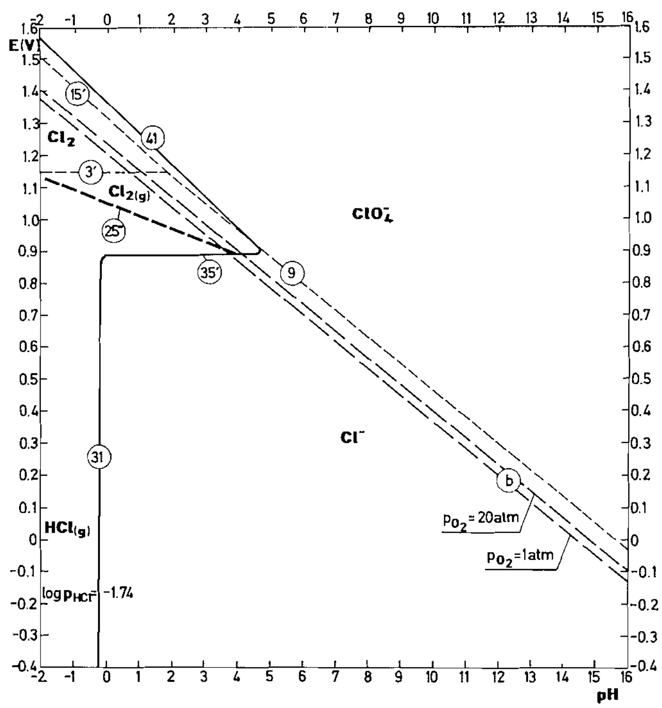

FIG. 3. Potential–pH equilibrium diagram for the system chlorine–water at 423 K, for solutions containing 1 g-atom Cl/L.

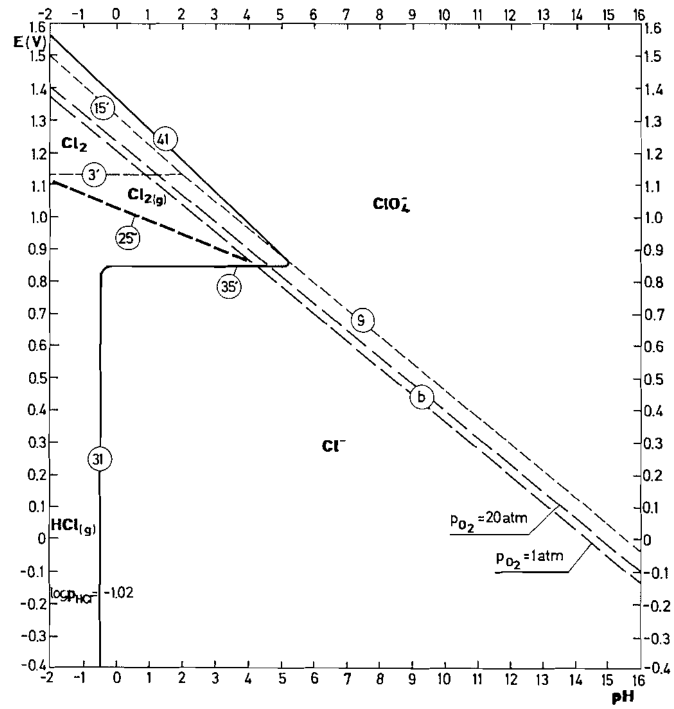

FIG. 4. Potential–pH equilibrium diagram for the system chlorine–water at 423 K, for solutions containing 3 g-atom Cl/L.

Cl^- ions to $Cl_2(aq)$ is thermodynamically justified. If the partial pressure of oxygen is 20 atm, the maximum difference of potentials for oxidation of Cl^- and reduction of oxygen in HCl solution at pH < 1 is 0.1 V for the reaction whose product is $Cl_2(g)$ and 0.37 V for the reaction which yields $Cl_2(aq)$, respectively. An increase in the hydrochloric acid concentration up to 3 M causes that under the same conditions the maximum potential difference increases up to 0.14 V and 0.43 V, respectively (Fig. 4). In order to estimate the temperature at which the course of oxidation reaction of Cl^- ions to $Cl_2(aq)$ becomes thermodynamically justified the following procedure was applied. The E_T potential of oxygen reduction was determined at 25, 90, and 150°C, assuming $P_{O_2} = 20$ atm and pH of solution equals 0. It amounts to 1.25, 1.24, 1.24 V, respectively. Because of such insignificant changes it was assumed that its value does not depend on temperature and is 1.24 V. Then the relation of E_T versus temperature for oxidation reaction of Cl^- ions to $Cl_2(aq)$ was determined. On this basis it was found that the E_T potential of this reaction assumes the

TABLE 5. Partial pressures (in atm) of HCl in aqueous hydrochloric acid solutions at various concentrations and temperatures

HCl	Temperature (K) 298	363	423
1 M	6.31×10^{-7}	2.48×10^{-4}	1.79×10^{-2}
3 M	7.0×10^{-6}	1.92×10^{-3}	9.42×10^{-2}

* Extrapolated values (on the grounds of $\log p_{HCl} = f(T)$).

value of 1.24 V at about 127°C. Thus one should infer that above this temperature the course of oxidation of the Cl^- ions to $Cl_2(aq)$ under oxygen pressure in HCl solution at pH = 0 is thermodynamically justified only at temperatures exceeding 127°C. Similar considerations carried out for solutions with varying pH and, hence, at various HCl concentrations indicate that an increase in HCl concentration allows this reaction to proceed at correspondingly lower temperatures. An increase in partial pressure of oxygen has a similar effect on the course of oxidation reaction of Cl^- ions to $Cl_2(aq)$: the higher the partial pressure of oxygen, the lower the temperature at which this reaction can take place.

Recent experimental work by Kiwi and Grätzel (11) has shown that chloride ion in acid medium can be oxidized in presence of solid catalysts. Thus, at pH ≈ 1, and 10^{-3} M Ce^{4+}, a solution of 10^{-3} M NaCl generates Cl_2 at the rate of 60 μM/L h in presence of ruthenium oxide, $RuO_2 \cdot xH_2O$. In view of the thermodynamic calculations presented here, the formation of Cl_2 during the aqueous oxidation of sulfide minerals in HCl medium seems plausible.

Acknowledgements

The authors acknowledge with thanks the financial aid of the Institute of Inorganic Chemistry, Polytechnic University in Wrocław, Poland, and the Canadian Natural Sciences and Engineering Research Council.

1. F. Habashi and T. Toor. Met. Trans. **10**B, 49 (1979).
2. T. Mizoguchi and F. Habashi. Trans. Inst. Min. Met. **92**C, 14 (1983).
3. T. Mizoguchi and F. Habashi. Intern. J. Min. Process. **8**, 177 (1981).
4. K. Naito and F. Habashi. Trans. Inst. Min. Met. C**93**, 69 (1984).
5. C. M. Criss and J. W. Cobble. J. Am. Chem. Soc. **86**, 5385 (1964).
6. M. Pourbaix. Atlas of electrochemical equilibria in aqueous solution. Pergamon, Oxford. 1966.
7. W. M. Latimer. The oxidation states of the elements and their potentials in aqueous solution. Prentice-Hall, New York. 1952.
8. C. J. Helgeson. J. Phys. Chem. **71**, 3121 (1967).
9. K. K. Kelley. Contributions to the data on theoretical metallurgy. Bulletin 584, US Bureau of Mines, Washington, D.C., 1960.
10. Perry's Chemical Engineer Handbook. 4th ed. McGraw-Hill, New York. 1974. pp. 3–60 and 3–61.
11. J. Kiwi and M. Grätzel. Chem. Phys. Lett. **78** (2), 241 (1981).

Appendix

The equilibrium between the two gaseous substances HCl(g) and $Cl_2(g)$ should be referred to in the chlorine–water system under consideration which contains also the Cl^- ions derived from dissociation of aqueous hydrochloric acid solution. Hence, in order to determine the limits of the domain of relative predominance of HCl(g) and $Cl_2(g)$ in the presence of the Cl^- ions one should consider two reactions denoted by [25] and [31] in the Table 4. The equilibrium of reaction [25] is described by the Nernst equation:

$$E_{(T)} = E_{0(T)} + \frac{2.303RT}{2F} \log \frac{p_{Cl_2}[H^+]^2}{p_{HCl}^2}$$

while that of reaction [31] by the equation

$$\log [Cl^-] = \log K_T + pH + \log p_{HCl}$$

where $K_T = [Cl^-][H^+]/p_{HCl}$

The following combination of the above two relationships:

$$E_{(T)} = E_{0(T)} + \frac{2.303RT}{2F} \log \frac{p_{Cl_2}}{p_{HCl}} + \frac{2.303RT}{2F} \log \frac{[H^+]^2}{p_{HCl}}$$

$$= E_{0(T)} + \frac{2.303RT}{2F} \log K_T - \frac{2.303RT}{2F} pH - \frac{2.303RT}{2F} \log [Cl^-]$$

yields an equation used for determination of the limits of the domains of relative predominance of the HCl(g) and $Cl_2(g)$ in the presence of the Cl^- ions. This equation is denoted by [25″] in Table 4 (according to the Pourbaix nomenclature) and is given for the respective temperatures 298, 363, and 423 K.

Synthesis of novel, highly reactive 1-oxyl-2,2,6,6-tetramethyl-1,2,5,6-tetrahydropyridine derivatives

JÓZSEF CSEKÖ, H. OLGA HANKOVSZKY, AND KÁLMÁN HIDEG[1]

Central Laboratory, Chemistry, University of Pécs, P.O. Box 99, H-7643 Pécs, Hungary

Received July 19, 1984

JOZSEF CSEKÖ, H. OLGA HANKOVSZKY, and KÁLMÁN HIDEG. Can. J. Chem. **63**, 940 (1985).

New multipurpose spin labels and synthons can be synthesized from 1-oxyl-2,2,6,6-tetramethyl-1,2,5,6-tetrahydropyridine-4-carboxylic acid (**1**). Either **1**, its pentafluorophenylester (**2**), or acylcarbonate (**3**) (prepared from **1** with ethyl chloroformate) can be reduced to 1-oxyl-2,2,6,6-tetramethyl-4-hydroxymethyl-1,2,5,6-tetrahydropyridine (**4**). The methanesulfonate (**6**) and the bromo compound (**7**) are highly reactive alkylating reagents due, in large part, to the allylic linkage in the nitroxide ring. The latter can be reacted with $KSSO_2CH_3$ to give methanethiolsulfonate (**9**). A novel side chain spin-labelled α-amino acid ester (**11**) is made by a phase-transfer alkylation of a Schiff base with **7**. Compound **11** can be coupled with the protected L-phenylalanine in the presence of dicyclohexylcarbodiimide (DCC) to produce the nitroxide dipeptide (**12**).

JOZSEF CSEKÖ, H. OLGA HANKOVSZKY et KÁLMÁN HIDEG. Can. J. Chem. **63**, 940 (1985).

On peut synthétiser de nouveaux synthons et de nouveaux marqueurs de spin à usage multiple à partir de l'acide oxyl-1 tétraméthyl-2,2,6,6 tétrahydro-1,2,5,6 pyridinecarboxylique-4 (**1**). On peut réduire soit le composé **1**, soit son ester pentafluorophényle (**2**) ou son acylcarbonate (**3**) (que l'on peut préparer à partir de **1** par réaction avec le chloroformate d'éthyle) en oxyl-1 tétraméthyl-2,2,6,6 hydroxyméthyl-4 tétrahydro-1,2,5,6 pyridine (**4**). Le méthanesulfonate (**6**) ainsi que le dérivé bromé (**7**) sont des réactifs alkylants très réactifs à cause, en grande partie, de la liaison allylique dans le cycle nitroxyde. On peut faire réagir le dérivé bromé avec le $KSSO_2CH_3$ pour obtenir le méthanethiosulfonate **9**. On a préparé le nouvel ester **11** d'un acide α-aminé portant un marqueur de spin sur la chaîne latérale en effectuant une alkylation par transfert de phase d'une base de Schiff par le composé **7**. Dans le but d'obtenir le nitroxyde dipeptide (**12**), on peut coupler le composé **11** avec une L-phénylalanine en présence de dicyclohexylcarbodiimide (DCC).

[Traduit par le journal]

Introduction

Reactive functional groups attached to stable nitroxide free radicals have been used as spin labels for studying biomolecules in recent decades (1). The most frequently used types of nitroxides are the pyrroline- the pyrrolidine-, and the piperidine-*N*-oxyls:

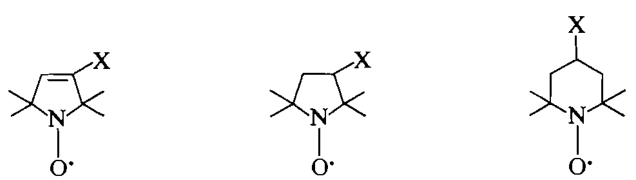

Hsia and co-workers reported the synthesis of 1-oxyl-2,2,6,6-tetramethyl-1,2,5,6-tetrahydropyridine-4-carboxylic acid (**1**) (2). We wish to report the reduction of the acid **1** to the alcohol **4** and the oxidation of **4** to the aldehyde **5**. The corresponding pyrroline derivatives have proved to be highly reactive and versatile synthons (3). The tetrahydropyridine derivative has opened further opportunities for spin-labelling molecules of biological interest.

Results and discussion

The synthesis of the acid **1** was achieved by the method of Hsia and co-workers (2). The alcohol **4** can be obtained either directly from **1** with sodium bis(2-methoxyethoxy)aluminium hydride (SMEAH) in toluene, from the reduction of the active ester **2**, or from the mixed anhydride ester **3** with sodium borohydride. The **4** can be oxidized to the unsaturated aldehyde **5** with activated manganese dioxide. The conversion of **4** to the mesylate (**6**) can be carried out with methanesulfonyl choride in the presence of triethylamine (TEA). Compound **6** with lithium bromide in acetone gives the bromo compound (**7**) in high yield. The bromo compound **7** shows high reactivity as observed in the corresponding pyrroline analogue (4), due to its allylic structure. The bromo compound **7** can be converted into the benzoate without allylic rearrangement because the same benzoate (**8**) can be obtained when the alcohol (**4**) is directly benzoylated with benzoyl chloride in pyridine. The methanethiolsulfonate derivative (**9**) can be prepared from **7** with potassium methanethiolsulfonate, utilizing the method described earlier for the synthesis of the pyrroline analogue (5). The importance of this method lies in the fact that α-amino acid derivatives can be prepared which bear the nitroxide moiety in the side-chain having no other chiral centre in the molecule.

The synthesis of a pyrroline α-amino acid (**10**) in our laboratory has been described earlier (6). Two reviews deal with synthesis and spin-labelling of α-amino acids and peptides (7, 8). We show here a synthesis of the new paramagnetic α-amino acid ester, **11**, utilizing O'Donnell's method (9) applied in our earlier work which described the synthesis of **10**. Amino ester **11** can be acylated with L-*N*-trifluoroacetyl phenylalanine (TFA-Phe) in the presence of dicyclohexylcarbodiimide (DCC) in dry tetrahydrofuran to give **12** (Scheme 1).

The presence of an allylic system in the nitroxide ring confers a substantial increase in reactivity upon halide derivatives of those nitroxides relative to the saturated ring nitroxides. This is of great importance for synthetic applications where these niroxides are coupled to biologically important, but often heat-labile molecules such as drugs, hormones, and macromolecules.

A second important aspect of our paper concerns the orientation of the nitroxide in a derivatized molecule. We emphasize that the five- and six-membered rings result in quite different alignments of the N—O$^\bullet$ bond of the nitroxide relative to a derivatized molecule. This can have a significant impact upon spectral analysis when a bound species is undergoing aniso-

[1] Author to whom correspondence may be addressed.

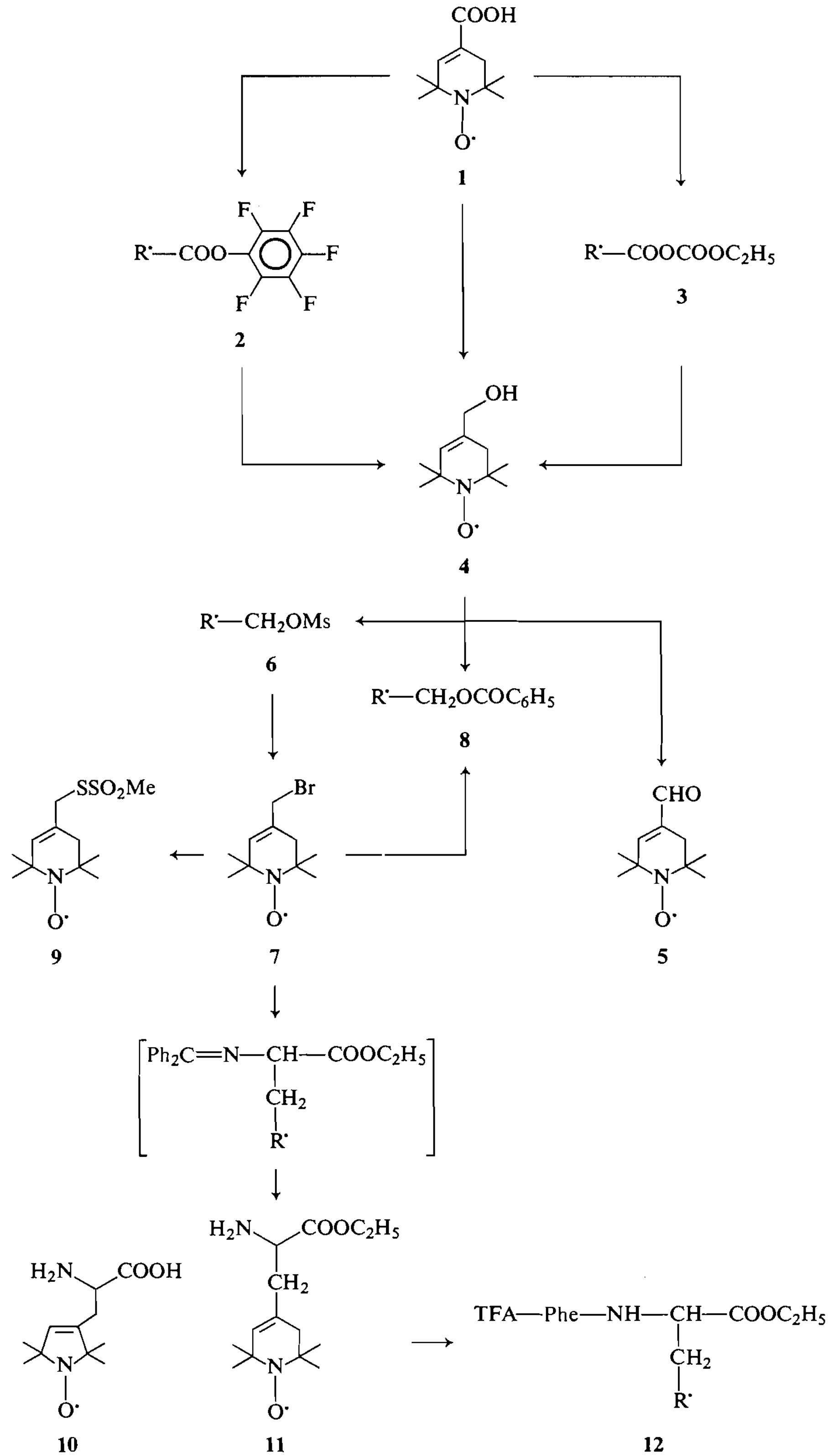

SCHEME 1

tropic motion, e.g. in a biological membrane. Thus, the availability of allylic nitroxides for alkylation in addition to the α,β-unsaturated aldehydes for various reactions provides a needed versatility when synthesizing spin-labelled analogues which retain biological activity, and yields the best opportunities for interpretation of esr spectra.

Experimental

Melting points were measured using a Boetius micro instrument and are not corrected. The ir spectra were measured with a Zeiss Specord 75 type instrument. The esr spectra were obtained from a 10^{-3} M solution on a Zeiss ER9 spectrometer. All the monoradicals exhibited three equidistant lines with a_N = 14.8–15.0 G. The mass spectra were taken in a Varian-MAT-SM-1 instrument.

1-Oxyl-2,2,6,6-tetramethyl-1,2,5,6-tetrahydropyridine-4-carboxylic acid pentafluorophenyl ester (2)

To a stirred solution of carboxylic acid (**1**) (594 mg, 3 mmol) and pentafluorophenol (552 mg, 3 mmol) in dry ethyl acetate (10 mL), a solution of DCC (619 mg, 3 mmol) in dry ethyl acetate (3 mL) was added at 0°C. The mixture was stirred 3 h at room temperature. The dicyclohexylurea (DCU) was filtered off, the filtrate was extracted with 5% sodium hydrogen carbonate solution and with water, dried over anhydrous sodium sulfate, and evaporated to dryness. The pure yellow ester (**2**) was crystallized from chloroform/ether, yield: 820 mg (75%); mp 113–114°C; ir (Nujol): 1745 (CO) cm^{-1}. *Anal.* calcd. for $C_{16}H_{15}F_5NO_3$ (mol. wt. 364.3): C 52.75, H 4.15, N 3.85; found: C 52.40, H 4.22, N 3.80.

(Carbonic acid-1-oxyl-2,2,6,6-tetramethyl-1,2,5,6-tetrahydro-pyridine-4-carboxylic acid)anhydride ethyl ester (3)

To a stirred solution of **1** (1.98 g, 10 mmol) in ether (20 mL) triethylamine (TEA) (1.21 g, 12 mmol) was added, then the mixture was cooled to 0°C, and under stirring a solution of ethyl chloroformate (1.30 g, 12 mmol) in ether (10 mL) was added dropwise. After the addition had been completed, stirring was continued for 3 h at room temperature. TEA hydrochloride was filtered off, the filtrate was evaporated, then the residue was taken up in hexane and kept in a refrigerator. The crystals separated gave **3**, yield: 2.43 g (90%); mp 43–44°C; ir (Nujol): 1805, 1730 (COOCOO) cm^{-1}; ms, *m/e*: M^+ 270 (41), 196 (18), 182 (15), 168 (100). *Anal.* calcd. for $C_{13}H_{20}NO_5$ (mol. wt. 270.3): C 57.76, H 7.46, N 5.18; found: C 57.79, H 7.32, N 5.26.

1-Oxyl-4-hydroxymethyl-2,2,6,6-tetramethyl-1,2,5,6-tetrahydro-pyridine (4)

Method A

The active acid derivative (**2** or **3**) (10.0 mmol) was added to a stirred suspension of sodium borohydride (0.5 g) in ethanol (30 mL) at 0°C, stirred for 1 h, then the mixture evaporated to dryness. Water (10 mL) was added to the residue, extracted with chloroform (3 × 10 mL), the organic phase was dried, and evaporated to dryness. The solid residue was crystallized from ether/hexane; yield of **4** from **2**: 1.6 g (87%); from **3**: 1.63 (89%); mp 37–38°C; ir (Nujol): 3500–3100 (OH) cm^{-1}. *Anal.* calcd. for $C_{10}H_{18}NO_2$ (mol. wt. 184.3): C 65.19, H 9.84, N 7.60; found: C 65.39, H 9.70, N 7.89.

Method B

A toluene solution of sodium bis(2-methoxyethoxy)aluminium hydride (13.75 mL, 70%) was added dropwise to a stirred suspension of acid (**1**) (4.950 g, 25 mmol) in dry toluene (300 mL). The solution was refluxed for 2 h. The mixture was then added dropwise to a cooled and stirred 5% aqueous solution of sodium hydroxide (125 mL). The toluene phase was separated, dried, and evaporated to dryness, and the orange solid residue was crystallized from ether/hexane to give **4**, yield: 2.73 g (59%); mp 36–37°C. The product is identical with compound **4** obtained by Method A.

1-Oxyl-4-formyl-2,2,6,6-tetramethyl-1,2,5,6-tetrahydropyridine (5)

To a stirred solution of unsaturated alcohol (**4**) (1.84 g, 10 mmol) in tetrachloromethane (30 mL) was added active manganese dioxide (18 g); the solution was refluxed for 30 min, then filtered, and the filtrate was evaporated to dryness. The yellow residue was recrystallized from hexane to give pure aldehyde (**5**), yield: 1.21 g (66%); mp 69–70°C; ir (Nujol): 1670 (CO) cm^{-1}; ms, *m/e*: M^+ 182 (37), 168 (30), 152 (100). *Anal.* calcd. for $C_{10}H_{16}NO_2$ (mol. wt. 182.3): C 65.90, H 8.85, N 7.69; found: C 66.01, H 8.88, N 7.61.

1-Oxyl-2,2,6,6-tetramethyl-1,2,5,6-tetrahydropyridine-4-yl methyl sulfonate (6)

To a stirred solution of **4** (2.764 g, 15 mmol) and TEA (1.670 g, 16.5 mmol) in dichloromethane (25 mL) at −10°C, methanesulfonyl chloride (1.890 g, 16.5 mmol) was added dropwise, and stirred for 3 h at room temperature. The mixture was extracted with water (15 mL) and washed with a solution of 5% sodium hydrogen carbonate (20 mL). The organic phase was dried and evaporated to dryness. The product was a dark red oil (**6**), yield: 3.55 g (90%); ir (film): 1160 (OSO_2) cm^{-1}. *Anal.* calcd. for $C_{11}H_{20}NO_4S$ (mol. wt. 262.4): C 50.36, H 7.68, N 5.34, S 12.23; found: C 50.04, H 7.70, N 5.01, S 12.37.

1-Oxyl-4-bromomethyl-2,2,6,6-tetramethyl-1,2,5,6-tetrahydro-pyridine (7)

A solution of mesylate (**6**) (3.411 g, 13 mmol) and lithium bromide (3.387 g, 39 mmol) in dry acetone (20 mL) was refluxed for 30 min, diluted with water (10 mL), and extracted with ether (2 × 20 mL). The ether phase was dried and evaporated to dryness. The residual bromo compound (**7**) is a dark red oil, yield: 2.67 g (83%); ir (film): 1620 (C=C) cm^{-1}. *Anal.* calcd. for $C_{10}H_{17}BrNO$ (mol. wt. 247.2): C 48.59, H 6.93, N 5.67, Br 32.33; found: C 48.47, H 6.80, N 5.51, Br 32.77.

1-Oxyl-2,2,6,6-tetramethyl-1,2,5,6-tetrahydropyridine-4-yl methyl benzoate (8)

Method A

To the solution of **7** (247 mg, 1 mmol) in dry dimethylformamide (3 mL) sodium benzoate (173 mg, 1.2 mmol) was added. The mixture was heated (60°C) for 3 h, diluted with water (5 mL), and extracted with ether (3 × 10 mL). The organic phase was washed with water, dried, and evaporated. The residual **8** is a red oil, yield: 200 mg (69%); ir (film): 1720 (CO) cm^{-1}. *Anal.* calcd. for $C_{17}H_{22}NO_3$ (mol. wt. 288.4): C 70.81, H 7.69, N 4.86; found: C 70.75, H 7.58, N 4.49.

Method B

To a stirred solution of **4** (184 mg, 1.0 mmol) in dry pyridine, benzoylchloride (154 mg, 1.1 mmol) was added dropwise at 5°C. The mixture was allowed to stand for 3 h, then poured into crushed ice, and extracted with ether (3 × 10 mL). The organic phase was washed with 1 *N* hydrochloric acid, water, dried, and evaporated to dryness to give the **8** as an orange oil, yield: 220 mg (76%). The **8** was essentially the same as obtained by Method A.

(1-Oxyl-2,2,6,6-tetramethyl-1,2,5,6-tetrahydropyridine-4-methyl)-methanethiolsulfonate (9)

A solution of bromomethyl compound (**7**) (247 mg, 1.0 mmol) and potassium methanethiolsulfonate (150 mg, 1.0 mmol) in dry ethanol (10 mL) was refluxed for 3 h, then diluted with brine (10 mL), and extracted with ether (3 × 10 mL). The ether phase was dried and evaporated to dryness. The pure **9** was crystallized from ether/hexane, yield: 160 mg (57%); mp 38–40°C; ir (Nujol): 1325 (SO_2) cm^{-1}. *Anal.* calcd. for $C_{11}H_{20}NO_3S_2$ (mol. wt. 278.4): C 47.45, H 7.24, N 5.04, S 23.03; found: C 47.35, H 7.14, N 5.08, S 23.29.

Ethyl[2-amino-3-(1-oxyl-2,2,6,6-tetramethyl-1,2,5,6-tetrahydro-pyrid-4-yl)]propionate (11)

A solution of sodium hydroxide (2 *N*, 1.2 mL, 2.4 mmol) was added to a methylene chloride solution (3 mL) of the ethyl *N*-(diphenylmethylene)glycinate (10) (267 mg, 1.0 mmol), tetrabutylammonium hydrogen sulfate (TBAH) (407 mg, 1.2 mmol), and **7** (297 mg, 1.2 mmol) and stirred at room temperature for 3 h. The organic phase was evaporated, washed with water, dried, and evaporated to dryness. The residue was taken up in ether (30 mL) and filtered to remove quaternary bromide. The filtrate was evaporated to dryness. Aqueous citric acid (10%, 2 mL) was added to the tetrahydrofuran solution (2 mL) of the alkylated Schiff's base and stirred for 1 h. The reaction mixture was diluted with water (5 mL) and extracted with chloroform (2 × 10 mL) to remove the benzophenone. The aqueous phase was basified wth a solution of 2 *N* sodium hydroxide to pH 8, extracted with chloroform (3 × 10 mL), dried, and evaporated to dryness to give **11** as a red oil. The crude compound was subjected to preparative thin-layer chromatography (tlc) (Merck, Kieselgel 60; chloroform/MeOH, 9:1), the major band was eluted with ethyl acetate. Yield: 130 mg (48%); ir (film): 3400–3200 (NH_2), 1730 (CO) cm^{-1}; ms, *m/e*: M^+ 269 (9), 255 (14), 239 (23), 102 (100). *Anal.* calcd. for $C_{14}H_{25}N_2O_3$ (mol. wt. 269.4): C 62.43, H 9.36, N 10.40; found: C 62.09, H 9.25, N 10.47.

N-Trifluoroacetyl-L-phenylalanyl-2-amino-3-(1-oxyl-2,2,6,6-tetramethyl-1,2,5,6-tetrahydropyrid-4-yl) ethyl propionate (**12**)

To a stirred solution of L-*N*-trifluoroacetylphenylalanine (262 mg, 1.0 mmol) and **11** (269 mg, 1.0 mmol) in tetrahydrofuran (5 mL) was added a solution of DCC (206 mg, 1.0 mmol) in dry tetrahydrofuran (5 mL) at 0°C and stirred for 3 h at room temperature. The dicyclohexylurea (DCU) was filtered off, and the filtrate evaporated to dryness. The residue was taken up in ethylacetate (20 mL), washed with 1 *N* HCl at 0°C, then with 5% sodium hydrogen carbonate and water, dried, and evaporated to dryness. The pure product (**12**) was obtained with preparative tlc (Merck, Kieselgel 60; chloroform/ether, 9:1). Yield: 160 mg (31%); mp 57–59°C; ir (Nujol): 3400 (NH), 1730 (CO) cm^{-1}; ms, *m/e*: M^+ 512 (100), 482 (70), 346 (28). *Anal.* calcd. for $C_{25}H_{33}F_3N_3O_5$ (mol. wt. 512.6): C 58.58, H 6.49, N 8.20; found: C 58.32, H 6.52, N 8.25.

Acknowledgements

This work was supported in part by the Hungarian Academy of Sciences, Grant No. 301/A/82. The authors are indebted to Dr. J. Belágyi for the esr spectra and for the mass spectra to Dr. J. Jerkovich, Institute for Drug Research, Budapest, and to Mrs. M. Ott for the microanalyses.

1. L. J. BERLINER (*Editor*). Spin labeling, theory and applications. Academic Press, New York. Vol. I (1976) and Vol. II (1979).
2. L. T. L. WONG, R. SCHWENK, and J. C. HSIA. Can. J. Chem. **52**, 3381 (1974).
3. K. HIDEG, H. O. HANKOVSZKY, L. LEX, and GY. KULCSÁR. Synthesis, 911 (1980).
4. K. HIDEG, H. O. HANKOVSZKY, L. LEX, and GY. KULCSÁR. Synthesis, 914 (1980).
5. L. J. BERLINER, S. GRÜNWALD, H. O. HANKOVSZKY, and K. HIDEG. Anal. Biochem. **119**, 450 (1982).
6. L. LEX, K. HIDEG, and H. O. HANKOVSZKY. Can. J. Chem. **60**, 1448 (1982).
7. H. R. WENZEL, H. TSCHESCHE, and E. GOLDAMMER. Spin-labelled amino acids, peptides and proteins – synthesis and applications. *In* Modern methods in protein chemistry. *Edited by* H. Tschesche. Walter de Gruyter, Berlin, New York. 1983. p. 385.
8. K. HIDEG and H. O. HANKOVSZKY. The chemistry of spin-labelled amino acids, peptides. Some newer mono- and bifunctionalized nitroxide free radicals. *In* Paramagnetic models of drugs and biochemicals. *Edited by* R. I. Zhdanov, CRC Press, Cleveland, Ohio, USA. (In press).
9. M. J. O'DONNELL, J. M. BONIECE, and S. E. EARP. Tetrahedron Lett. 2641 (1978).
10. P. L. PICKARD, and T. L. TOLBERT. Organic Syntheses, Collect. Vol. V. Wiley, New York. 1973. p. 520.

L'isomérisation de radicaux insaturés. II. Les radicaux α-éthallyles et α,γ-diméthallyles formés dans la photolyse de l'hexène-3 et du méthyl-4-pentène-2 à 147,0 et 184,9 nm

GUY J. COLLIN[1] ET HÉLÈNE DESLAURIERS

Département des Sciences Fondamentales, Université du Québec à Chicoutimi, Chicoutimi, Qué., Canada G7H 2B1

Reçu le 20 juin 1984

GUY J. COLLIN et HÉLÈNE DESLAURIERS. Can. J. Chem. **63**, 944 (1985).

Nous avons étudié la photodécomposition du *cis*-hexène-3 et du méthyl-4-*cis*-pentène-2 à 147,0 et 184,9 nm. La fragmentation de la molécule photoexcitée suit le mécanisme habituel. La rupture primaire a essentiellement lieu (≃80%) sur le lien C—C situé en position β par rapport à la double liaison. Des ruptures α(C—C), β(C—H) et α(C—H) viennent compléter ce panorama. La formation des radicaux α-éthallyles et α,γ-diméthallyles est donc importante dans chacun des deux cas, et nous avons pu montrer que ces deux radicaux doivent s'isomériser l'un dans l'autre pour pouvoir expliquer la formation d'une partie du pentadiène-1,3 dans le cas de l'hexène-3 et de la totalité du butadiène-1,3 dans le cas du méthyl-4-pentène-2. Cette isomérisation demande un transfert interne d'un atome d'hydrogène en 1,4.

GUY J. COLLIN and HÉLÈNE DESLAURIERS. Can. J. Chem. **63**, 944 (1985).

The photolysis of *cis*-3-hexene and 4-methyl-*cis*-2-pentene has been studied at 147.0 and 184.9 nm. The fragmentation pattern of the photoexcited molecule is normal: it requires, mainly, the split of a C—C bond located in the β position relative to the double bond (≃80%). Some α(C—C), β(C—H), and α(C—H) primary splits complete this mechanism. The formation of α-ethallyl and α,γ-dimethallyl radicals is important in 3-hexene and 4-methyl-2-pentene, respectively. An isomerization process, involving these two radicals, is necessary to explain the formation of part of the 1,3-pentadiene in the 3-hexene system and of all the 1,3-butadiene in the 4-methyl-2-pentene system. This process involves a 1,4-hydrogen atom transfer.

Introduction

Nous avons établi récemment que les radicaux excités α,α-diméthallyles s'isomérisent vers la structure α,β-diméthallyles et réciproquement par transfert interne 1,4 d'un atome d'hydrogène (1). La présente étude vise à observer le même processus avec les radicaux α-éthallyles et α,γ-diméthallyles. Pour ce faire, nous proposons d'étudier la photolyse du *cis*-hexène-3 et du méthyl-4-*cis*-pentène-2. En effet, il est connu que, dans la région de l'uv sous vide, ou de l'uv très lointain, la fragmentation la plus importante implique la rupture du lien β(C—C) (2, 3). Dans ces conditions, on peut s'attendre à obtenir les radicaux mentionnés plus haut avec des rendements importants.

Partie expérimentale

Les techniques utilisées dans ce travail sont classiques (1–3). La lampe émettant à 147,0 nm est une lampe de résonance à xénon (4) de fabrication domestique, l'autre est une lampe "basse pression" à mercure achetée chez Philipps. Les échantillons sont préparés dans un système en Pyrex dans lequel le vide est maintenu par deux pompes: une pompe à diffusion à huile (deux étages) est située en amont d'une pompe mécanique. Les analyses sont faites par chromatographie en phase gazeuse par deux appareils équipés de système de détection à double flamme ionisante et comprenant l'un une colonne de squalane (5) l'autre une colonne de UCON LB 550 × 20% (6). Les rendements quantiques sont obtenus par comparaison photochimique en éclairant dans les mêmes conditions le *cis*-butène-2.

Les échantillons de monomère sont des produits API. Les taux d'impuretés affichés sur ces échantillons sont: le *cis*-hexène-3, 0,086 ± 0,013% et le méthyl-4-*cis*-pentène-2, 0,08 ± 0,07%. Les analyses chromatographiques montrent que le *cis*-hexène-3 contient de l'hexène-1 (12 ± 0,5 ppm); on n'a pas mesuré le contenu d'hexène-2, ni celui en *trans*-hexène-3. Quant au méthyl-4-*cis*-pentène-2 il contient du méthyl-2-pentadiène-1,4 (10 ± 1 ppm), du méthyl-2-hexane (≃6 ppm), un composé inconnu en C_6 (10 ± 1 ppm). Ici, également, on n'a pu mesurer le contenu en isomère *trans*.

[1]Auteur à qui adresser toute correspondance.

Résultats

Ceux-ci apparaissent sous forme de rendements quantiques dans les tableaux qui accompagnent le texte.

La photolyse du cis-*hexène-3 à 147 nm*

Les figures 1 et 2 montrent l'inverse du rendement des produits majeurs formés en présence d'oxygène: ce sont le butadiène-1,3, le pentadiène-1,3 (*cis* + *trans*) et l'éthylène. En présence d'oxygène moléculaire (+10%) les rendements en acétylène et en butyne-1 sont plutôt constants: $\Phi(C_2H_2)$ = $0{,}03_5 \pm 0{,}00_5$ et Φ(butyne-1) = 0,045 ± 0,005. En l'absence d'oxygène, les rendements en hydrocarbures saturés légers sont les suivants: $\Phi(CH_4)$ = 0,035 ± 0,01, $\Phi(C_2H_6)$ = 0,43 ± 0,05 et $\Phi(C_3H_8)$ = 0,10 ± 0,02 pourvu que la pression du monomère soit comprise entre 2 et 40 Torr (1 Torr = 133,3 Pa). On n'a pas observé de formation de méthyl-3-pentène-1 en l'absence d'oxygène.

La photolyse du cis-*hexène-3 à 184,9 nm*

Le tableau 1 donne un panorama complet des produits formés. Le butadiène-1,3 est encore le produit majeur formé en présence d'oxygène; son rendement est cependant plus faible que celui mesuré à 147 nm à pression égale. Il en est de même du pentadiène-1,3 et de l'éthylène. En l'absence d'oxygène, l'éthane est le produit majeur à toute pression. On observe aussi la formation de méthyl-3-pentène-1.

*La photolyse du méthyl-4-*cis-*pentène-2 à 147 nm*

Le tableau 2 donne une vue complète des produits formés auxquels il faut ajouter les diènes apparaissant dans les figures 3 et 4. Ces butadiène-1,3, pentadiènes-1,3 et isoprène ont des rendements qui décroissent avec l'augmentation de la pression. En présence d'oxygène, le propène et le pentadiène-2,3 ont des rendements qui décroissent aussi avec l'augmentation de la pression. Ainsi la valeur Φ(propène) passe de 0,11 à 1 Torr à 0,045 à 60 Torr et celle du pentadiène-2,3 de $0{,}02_3$ à $0{,}01_6$ sur le même intervalle de pression. Par contre, toujours en présence d'oxygène, les rendements en méthane, acétylène, propyne et méthyl-3-butyne-1 sont plutôt constants entre 5 et

TABLEAU 1. Photolyse du *cis*-hexène-3 pur à 184,9 nm

P (Torr)	ΦCH_4[b]	C_2H_4	C_2H_6[a]	C_3H_8[a]	Butadiène-1,3	M3P1[a]	Pentadiène-1,3	CH_3'[c]
5,2	0,02	0,02$_4$	0,44	0,05$_3$	0,40	0,06$_2$	0,01$_5$	0,76$_5$
9,9	0,03	0,02$_0$	0,38$_5$	0,04$_9$	0,31$_2$	0,06$_2$	nm[d]	0,77$_5$
19,8	0,03	0,01$_4$	0,25$_5$	0,05$_2$	0,16$_6$	0,06$_6$	0,00$_7$	0,62$_2$
40,0	0,03	0,00$_4$	0,11$_7$	0,01$_6$	0,07$_3$	0,03$_6$	nm	0,28$_5$
60,2	0,03	0,00$_3$	0,08$_4$	0,01$_2$	0,03$_6$	0,02$_8$	nm	0,22$_7$
80,0	0,01	0,00$_2$	0,09$_3$	0,01$_3$	0,02$_6$	0,031$_0$	0,00$_4$	0,26$_6$
99,8	0,01	0,00$_4$	0,07$_1$	0,01$_0$	0,01$_9$	0,025$_8$	0,00$_3$	0,21$_2$

[a]Le rendement quantique de ces produits se réduit à zéro en présence de 10% d'oxygène.
[b]Le rendement $\Phi(CH_4)$ est inférieur à 0,005 en présence de 10% d'oxygène.
[c]Voir texte: relation [B].
[d]Non mesuré.

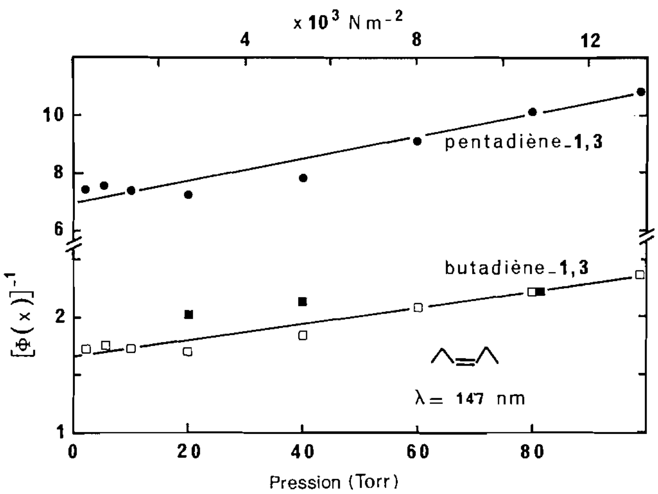

FIG. 1. Photolyse du *cis*-hexène-3 à 147,0 nm pure [□] ou en présence de 10% d'oxygène (●, ■). Inverse des rendements quantiques en fonction de la pression du monomère.

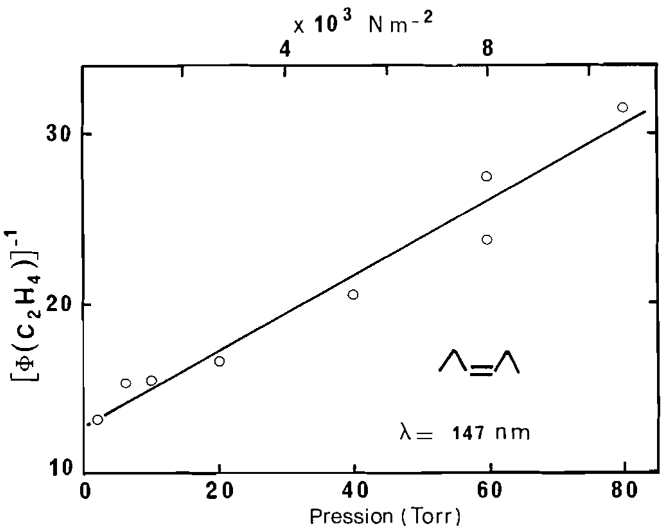

FIG. 2. Photolyse du *cis*-hexène-3 à 147,0 nm en présence de 10% d'oxygène. Inverse du rendement quantique de l'éthylène en fonction de la pression du monomère.

60 Torr: $\Phi(CH_4) = 0{,}03 \pm 0{,}01$, $\Phi(C_2H_2) = 0{,}04_0 \pm 0{,}00_4$, Φ(propyne) $= 0{,}015 \pm 0{,}005$ et $\Phi(C_5H_8) = 0{,}01_4 \pm 0{,}00_2$.

*La photolyse du méthyl-4-*cis*-pentène-2 à 184,9 nm*

Le tableau 3 indique qu'à cette longueur d'onde l'éthane est le produit majeur en l'absence d'oxygène et son rendement décroît avec la pression. En présence d'oxygène, le butadiène-1,3 et le pentadiène-1,3, dont les rendements sont similaires, sont les produits majeurs.

Enfin il faut signaler la formation de petites quantités de butène-1 (cas de l'hexène-3) et de propène, méthyl-3-butène-1 et pentène-2 (cas du méthyl-4-pentène-2) en présence de 10% d'oxygène. Le rendement quantique du butène-1 diminue de 0,02 sous une pression de 2 Torr à 0,01 sous une pression de 100 Torr. Celui du propène est similaire et ceux du méthylbutène et du pentène sont toujours inférieurs à 0,01 dans la même zone de pression. Ces produits sont probablement formés par décomposition des radicaux C_6H_{13} vibrationnellement excités. Ces derniers sont le résultat de l'addition des atomes d'hydrogène présents dans chacun des systèmes sur la double liaison du monomère (7, 8). Ce mécanisme ne sera pas discuté plus loin.

Discussion

La photolyse du cis-*hexène-3 (H3)*

(a) *À 147,0 nm*

La photofragmentation du *cis*-hexène-3 suit le mécanisme habituel déjà observé dans d'autres systèmes (2, 3). Ainsi la rupture prépondérante a lieu sur la liaison C—C située en position β par rapport à la double liaison. La molécule étant symétrique, deux liaisons C—C sont ainsi placées.

[1] $CH_3CH_2CH{=}CHCH_2CH_3 + h\nu \rightarrow CH_3CH_2CH{=}CHCH_2CH_3^{**}$

[2] $H3^{**} \rightarrow CH_3 + \dot{C}H_2\dot{C}H\dot{C}HCH_2CH_3^{*}$ $\quad \Delta H \simeq 295$ kJ mol^{-1} (réf. 9)

[3*a*] $\dot{C}H_2\dot{C}H\dot{C}HCH_2CH_3^{*} \xrightarrow{k_d} CH_3 + CH_2{=}CHCH{=}CH_2$ $\quad \Delta H \simeq 155$ kJ mol^{-1}

[3*b*] $\dot{C}H_2\dot{C}H\dot{C}HCH_2CH_3^{*} + M \xrightarrow{k_M} M + \dot{C}H_2\dot{C}H\dot{C}HCH_2CH_3$

L'énergie du photon incident est de 811 kJ Einstein^{-1}. A la température ordinaire, l'énergie vibrationnelle de la molécule est voisine de 14 kJ mol^{-1}, de telle sorte que la molécule photoexcitée, M**, contient environ 825 kJ mol^{-1}. Ainsi, après rupture du lien β(C—C) il reste encore 530 kJ mol^{-1} à distribuer entre les deux fragments. Le radical α-éthallyle, pourvu que la distribution de cet excédent soit convenable, a suffisamment d'énergie interne pour se fragmenter, à moins qu'une collision ne vienne lui en soustraire suffisamment auquel cas il est stabilisé. Ce simple mécanisme est du type

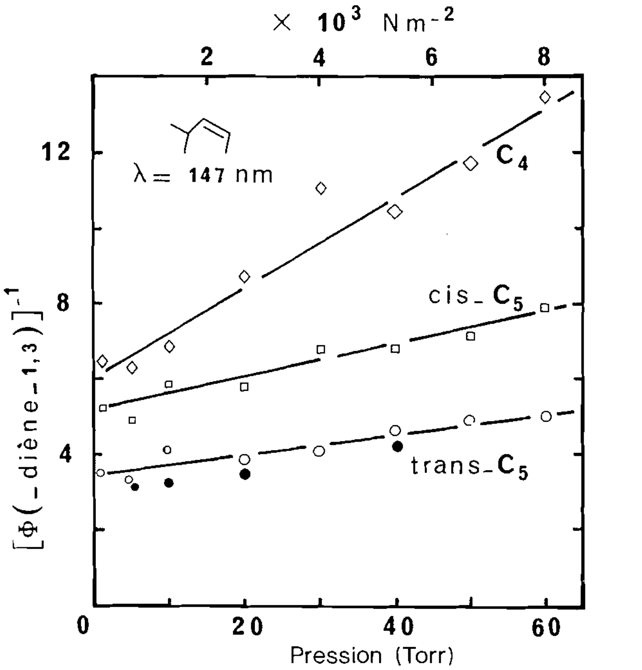

FIG. 3. Photolyse du méthyl-4-*cis*-pentène-2 à 147,0 nm pur (●) ou en présence de 10% d'oxygène (○, □, ◇). Inverse des rendements quantiques en fonction de la pression du monomère.

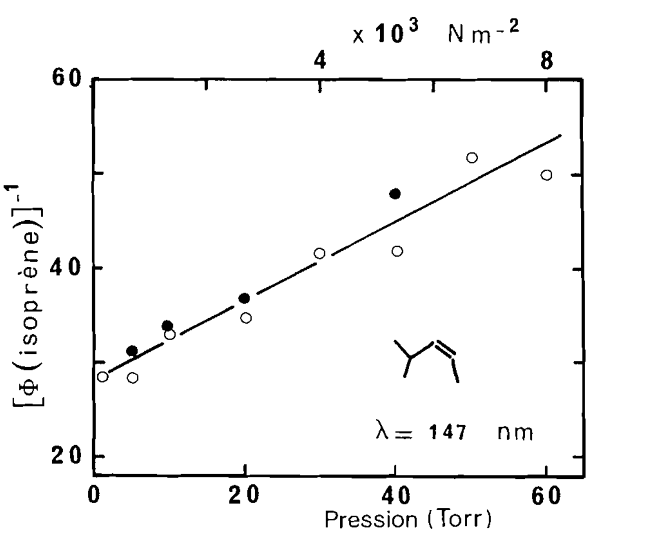

FIG. 4. Photolyse du méthyl-4-*cis*-pentène-2 à 147,0 nm pur (●) ou en présence de 10% d'oxygène (○). Inverse du rendement quantique de l'isoprène en fonction de la pression du monomère.

Stern–Volmer (10) et l'inverse du rendement quantique en butadiène-1,3 (B13) varie linéairement en fonction de la pression dans la chambre réactionnelle:

[A] $[\Phi(\mathrm{B13})]^{-1} = [\Phi_0(\mathrm{B13})]^{-1}(1 + k_s[\mathrm{M}]/k_d)$

La figure 1 montre la validité de la relation [A], et l'interception de la droite de Stern–Volmer à pression nulle donne la valeur maximum du rendement quantique en butadiène-1,3: Φ_0(butadiène-1,3) $\simeq 0{,}60_4$.

Le pentadiène-1,3 (*cis* + *trans*) a un comportement de type Stern–Volmer (fig. 1). Ce rendement est appréciable: Φ_0(pentadiène-1,3) = 0,145. Au moins deux routes peuvent être proposées pour leur formation. La première, et peut-être la plus importante, sera mieux circonscrite plus loin: elle réclame l'isomérisation du radical α-éthallyle vers la structure symétrique α,γ-diméthallyle par transfert interne 1,4 d'un atome d'hydrogène (11):

TABLEAU 2. Photolyse du méthyl-4-*cis*-pentène-2 pur à 147,0 nm. Rendements quantiques

Produits	Pression (Torr) 5	10	20	41
Méthane	$0{,}04_8$	0,07	0,04	0,02
Acétylène[b]	$0{,}04_2$	$0{,}04_7$	$0{,}04_6$	$0{,}04_1$
Éthylène[b]	$0{,}03_5$	$0{,}02_7$	$0{,}02_6$	$0{,}02_0$
Éthane[a]	0,30	0,31	$0{,}26_7$	$0{,}26_7$
Propène[b]	0,10	0,09	0,08	$0{,}07_5$
Propane[b]	0,03	0,02	0,02	0,02
Propyne[b]	0,03	0,03	0,02	$0{,}02_4$
Butène-1[b]	$0{,}02_5$	$0{,}02_5$	$0{,}02_5$	$0{,}02_7$
Isobutane[a]	$0{,}03_6$	$0{,}03_4$	$0{,}02_7$	$0{,}03_1$
Méthyl-3-butyne-1[b] (?)	$0{,}01_8$	$0{,}01_6$	$0{,}01_6$	$0{,}01_5$
Isoprène[b]	$0{,}03_1$	$0{,}02_9$	$0{,}02_6$	$0{,}02_1$
Méthyl-2-pentane[a]	$0{,}04_7$	$0{,}03_0$	0,00	0,00
Diméthyl-2,4-pentène-2[a]	0,04	$0{,}01_6$	$0{,}02_4$	$0{,}01_1$
Diméthyl-2,4-pentane[a]	0,07	0,07	0,04	0,06
Diméthyl-2,3-pentane[a]	0,15	0,16	0,12	$0{,}12_6$

[a]Le rendement quantique de ces produits est essentiellement zéro en présence de 10% d'oxygène.
[b]Le rendement quantique de ces produits est essentiellement inchangé en présence de 10% d'oxygène.

[4] $CH_3CH_2\dot{C}H\dot{C}H\dot{C}H_2^* \rightarrow CH_3\dot{C}H\dot{C}H\dot{C}HCH_3^*$

$\Delta H = -14\ \mathrm{kJ\ mol^{-1}}$ (réf. 12)

[5*a*] $CH_3\dot{C}H\dot{C}H\dot{C}HCH_3^* \rightarrow CH_3CH{=}CHCH{=}CH_2 + H$

$\Delta H = 204\ \mathrm{kJ\ mol^{-1}}$

[5*b*] $CH_3\dot{C}H\dot{C}H\dot{C}HCH_3^* + M \rightarrow M + CH_3\dot{C}H\dot{C}H\dot{C}HCH_3$

L'autre mécanisme fait appel à la rupture primaire d'un lien C—H situé en position α par rapport à la double liaison:

[6] $H3^{**} \rightarrow CH_3CH_2\dot{C}H\dot{C}H\dot{C}HCH_3^* + H$

[7*a*] $CH_3CH_2\dot{C}H\dot{C}H\dot{C}HCH_3^* \rightarrow CH_3 + CH_2{=}CHCH{=}CHCH_3$

[7*b*] $CH_3CH_2\dot{C}H\dot{C}H\dot{C}HCH_3^* + M \rightarrow CH_3CH_2\dot{C}H\dot{C}H\dot{C}HCH_3$

De la même manière la rupture en α d'un lien C—C peut conduire à la formation d'éthylène (fig. 2) et aussi d'acétylène et de butyne-1:

[8] $H3^{**} \rightarrow CH_3CH_2^* + \dot{C}H{=}CHCH_2CH_3^*$

[9*a*] $CH_3CH_2^* \rightarrow C_2H_4 + H$

[9*b*] $CH_3CH_2^* + M \rightarrow M + C_2H_5$

[10*a*] $\dot{C}H{=}CHCH_2CH_3^* \rightarrow CH{\equiv}CH + C_2H_5$

[10*b*] $\dot{C}H{=}CHCH_2CH_3^* \rightarrow CH{\equiv}CCH_2CH_3 + H$

Le rendement minimum du processus [8] peut-être obtenu soit par la valeur du rendement en éthylène à pression nulle: $\Phi_0(C_2H_4) = 0{,}08$ (fig. 2), soit par la somme des rendements en acétylène et butyne-1: $\Phi(C_2H_2) + \Phi$(butyne-1) = 0,08 (voir résultats)!

La rupture d'un lien α(C—C) est très probablement plus facile que la rupture d'un lien α(C—H). En fait, à des énergies similaires, la fragmentation d'un lien α(C—C) semble à peu

TABLEAU 3. Photolyse du méthyl-4-*cis*-pentène-2 pur à 184,9 nm. Rendements quantiques

P (Torr)	ΦCH_4	C_2H_6[a]	Propène	Propyne	Butadiène-1,3[c]	Pentadiène-1,3[c]	Isobutane[a]	$\Phi(CH_3')$[b]
1,95	0,03	0,37	$0{,}04_3$	$0{,}01_5$	$0{,}10_3$	$0{,}08_8$	$0{,}01_6$	0,60
5,1	nm[d]	nm	$0{,}03_4$	$0{,}01_0$	$0{,}06_2$	$0{,}06_4$	$0{,}01_9$	nm
10,2	0,02	0,32	$0{,}04_3$	$0{,}01_4$	$0{,}05_4$	$0{,}04_8$	$0{,}01_6$	0,60
20,2	$0{,}01_5$	0,23	$0{,}03_3$	$0{,}01_2$	$0{,}02_8$	$0{,}02_9$	$0{,}00_9$	$0{,}43_5$
30,1	$0{,}01_6$	0,20	$0{,}03_1$	$0{,}01_4$	$0{,}02_7$	$0{,}02_2$	$0{,}01_1$	0,38
40,6	$0{,}01_1$	0,14	$0{,}02_6$	$0{,}01_8$	$0{,}01_9$	$0{,}02_0$	$0{,}00_7$	0,27
50,1	$0{,}01_0$	0,09	$0{,}02_2$	$0{,}01_6$	$0{,}01_3$	$0{,}01_5$	$0{,}00_5$	0,24

[a]Le rendement quantique de ces produits s'annule en présence de 10% d'oxygène.
[b]Voir texte: relation [C].
[c]En présence de 10% d'oxygène, les rendements de ces produits sont ≈30% plus élevés.
[d]Non mesuré.

près aussi facile que celle d'un lien β(C—H) (13, 14). Cette remarque tend à montrer que la valeur $\phi([6])$ est inférieure à celle de $\phi([8])$, et la fragmentation en pentadiène-1,3 serait surtout le fait du mécanisme impliquant l'isomérisation du radical excité α-éthallyle.

Le bilan de la formation de tous les produits radicalaires est loin d'être complet. En particulier tous les produits de combinaison des radicaux en C_5 n'ont pas été mesurés. On peut cependant, sans démonstration élaborée, indiquer que le mécanisme ci-haut proposé est suffisant pour expliquer la formation de méthane, éthane et de propane en l'absence d'oxygène (voir résultats).

(*b*) *À 184,9 nm*

Le mécanisme discuté plus haut doit encore être valide. Cependant, l'énergie du photon est maintenant de 644 kJ Einstein^{-1}, on peut donc prévoir des fragmentations secondaires moins importantes et même, éventuellement, une stabilisation par collision de la molécule photoexcitée. Le tableau 1 montre la formation prépondérante du butadiène-1,3, avec encore un peu de pentadiène-1,3, mais de façon relativement beaucoup moins importante. Tout se passe comme si la diminution de l'énergie interne du radical α-éthallyle entraîne une diminution de l'importance de l'isomérisation et donc favorise sa stabilisation par collision.

Il faut ici relever la formation de méthyl-3-pentène-1. Celui-ci est tout probablement le résultat de la combinaison des radicaux méthyles et α-éthallyles:

[11*a*] $CH_3 + CH_3CH_2\dot{C}H\dot{C}H\dot{C}H_2 \rightarrow$ H3

[11*b*] $CH_3 + CH_3CH_2\dot{C}H\dot{C}H\dot{C}H_2 \rightarrow CH_3CH_2CH(CH_3)CH{=}CH_2$ (M3P1)

Le rapport des constantes de vitesse des réactions [11*a*] et [11*b*] n'est pas connu des auteurs. On peut cependant faire l'hypothèse que le rapport k_{11a}/k_{11b} est le même que celui observé lorsque le radical éthyle substitue le radical méthyle: soit k_{11a}/k_{11b} = 2,05 (15). On peut dès lors non seulement estimer le rendement des radicaux méthyles, mais encore celui des radicaux méthyles formés dans le processus primaire [2], $\Phi(CH_3')$, et ce à toute pression (tableau 1):

$$[B] \quad \Phi(CH_3') = 2\Phi(C_2H_6) + \Phi(C_3H_8) + 3{,}05\ \Phi(\mathrm{M3P1}) - \Phi(\mathrm{B13})$$

En effet, l'éthane est formé par la combinaison de deux radicaux méthyles, le propane et le méthyl-3-pentène-1 par celle d'un radical méthyle et d'un autre radical éthyle ou

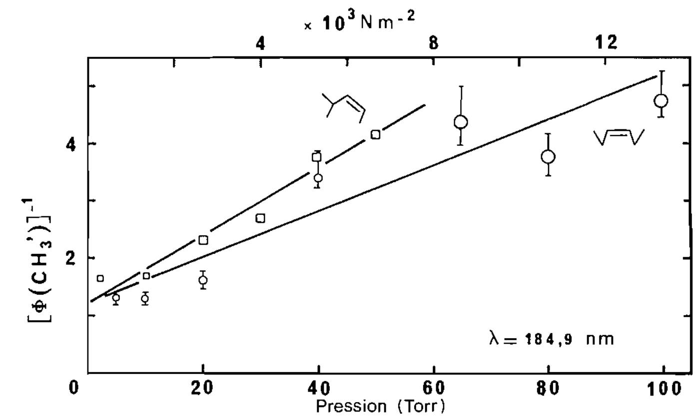

FIG. 5. Photolyse du *cis*-hexène-3 (○) et du méthyl-4-*cis*-pentène-2 (□) purs à 184,9 nm. Inverse du rendement quantique de la formation du radical méthyle primaire: formules [B] et [C]. L'incertitude expérimentale est représentée par une barre verticale.

α-éthallyle. Cependant, la formation de butadiène-1,3 libérant un second radical méthyle, il y a lieu de soustraire cette formation pour ne mesurer que le rendement de radicaux méthyles liés au processus primaire [2]. Les résultats de la relation [B] apparaissent dans le tableau 1. Traduits sous forme du mécanisme de Stern–Volmer, et ce malgré une incertitude expérimentale importante, ils permettent de mesurer ce rendement à pression nulle: $\Phi_0(CH_3') = 0{,}81_4\ (\pm 10\%)$ (fig. 5). Ainsi près de 80% de la molécule photoexcitée se fragmentent par rupture du lien β(C—C) à cette longueur d'onde.

Les autres produits apparaissant dans le tableau 1 ne demandent pas d'autres explications que celles déjà avancées à 147,0 nm. Tous ces résultats sont rassemblés dans le tableau 4. Ce dernier synthétise la photofragmentation de la molécule *cis*-hexène-3 photoexcitée.

*La photolyse du méthyl-4-*cis*-pentène-2 (M4cP2)*

(*a*) *À 147,0 nm*

A nouveau le mécanisme général de photofragmentation s'applique. On s'attend donc à obtenir principalement du pentadiène-1,3 (fig. 3): Φ_0 (pentadiène-1,3) = 0,47.

[12] $CH_3CH(CH_3)CH{=}CHCH_3 + h\nu \rightarrow CH_3CH(CH_3)\dot{C}H{=}CHCH_3^{**}$ (M4*c*P2**)

[13] M4*c*P2** $\rightarrow CH_3 + CH_3\dot{C}H\dot{C}H\dot{C}HCH_3^{*}$

TABLEAU 4. Photolyse du *cis*-hexène-3. Fragmentation[a]

	147,0	184,9 nm
$C_6H_{12}^{**} \rightarrow CH_3CH_2\dot{C}H\dot{C}H\dot{C}H_2^{*} + CH_3$		$0,81_4$[b]
↳ $CH_2{=}CHCH{=}CH_3 + CH_3$	$0,60_4$	(≃0,48)
↓ $CH_3\dot{C}H\dot{C}H\dot{C}HCH_3^{*}$		
↳ $CH_3CH{=}CHCH{=}CH_2 \rightarrow \{H, CH_3\}$	$0,14_5$	$0,01_5$
$\rightarrow CH_3CH_2\dot{C}H\dot{C}H\dot{C}HCH_3^{*} + H$		
$\rightarrow CH_3CH_2CH{=}\dot{C}H^{*} + C_2H_5^{*}$	≥0,08	$\geq 0,05_5$[d]
↳ $C_2H_4 + H$	(0,08)	$0,02_5$
↳ C_2H_2[c] $+ C_2H_5$	$(0,03_5)$[c]	$0,00_1$
↳ $CH_3CH_2C{\equiv}CH$[c] $+ H$	$(0,04_5)$[c]	0,00
Total[e]	$\geq 0,83_2$	>0,91

[a]Les rendements quantiques des produits moléculaires sont obtenus par extrapolation à pression nulle, sauf cas indiqués.
[b]$\Phi_0(CH_3')$: voir texte, relation [B].
[c]Rendements quantiques indépendants de la pression: $2 < P < 100$ Torr.
[d]Φ(propane) $\simeq \Phi(C_2H_5)$: combinaison des radicaux méthyles et éthyles.
[e]Le rendement total des réactions primaires de fragmentation est au moins égal, sinon supérieur, aux valeurs indiquées puisque celles-ci sont, en partie, déterminées par rapport aux rendements des réactions secondaires de fragmentation.

réactions suivies des réactions [5*a*] et [5*b*].

Il faut tout de suite ajouter que le butadiène-1,3 présente lui aussi un comportement de type Stern–Volmer avec un rendement à pression nulle fort appréciable: Φ_0(butadiène-1,3) = 0,16! Ici, la seule voie simple pour sa formation réside dans l'isomérisation du radical α,γ-diméthallyle vers la structure α-éthallyle.

La fragmentation primaire d'une liaison C—C située en position α par rapport à la double liaison conduit aux réactions suivantes:

[14] $M4cP2^{**} \rightarrow CH_3CH(CH_3)CH{=}\dot{C}H^{*} + CH_3$

[15*a*] $CH_3CH(CH_3)CH{=}\dot{C}H^{*} \rightarrow i\text{-}C_3H_7 + CH{\equiv}CH$

[15*b*] $CH_3CH(CH_3)CH{=}\dot{C}H^{*} \rightarrow CH_3\dot{C}(CH_3)\dot{C}H\dot{C}H_2^{*}$

[16] $CH_3\dot{C}(CH_3)\dot{C}H\dot{C}H^{*} \rightarrow H + CH_2{=}C(CH_3)CH{=}CH_2$

[17] $M4cP2^{**} \rightarrow i\text{-}C_3H_7^{*} + \dot{C}H{=}CHCH_3^{*}$

[18] $i\text{-}C_3H_7^{*} \rightarrow C_3H_6 + H$

[19] $\dot{C}H{=}CHCH_3^{*} \rightarrow CH_3 + CH{\equiv}CH$

réactions suivies ou en parallèles avec les réactions de stabilisation habituelles. Les formations d'acétylène et de propène sont aisément expliquées. Il faut ajouter que les produits moléculaires issus de la fragmentation de radicaux excités vinyliques ont des rendements quantiques peu sensibles à l'effet de pression. La formation d'isoprène est un peu plus complexe (fig. 4). L'isomérisation (transfert interne 1,3 d'une atome d'hydrogène) du radical méthyl-3-butènyl-1 vers la structure α,α-diméthallyle (16) est probablement assez facile étant donné la position tertiaire et allylique de l'atome d'hydrogène déplacé.[2] Finalement, les ruptures primaires de liens α(C—H) permettent d'expliquer les formations de

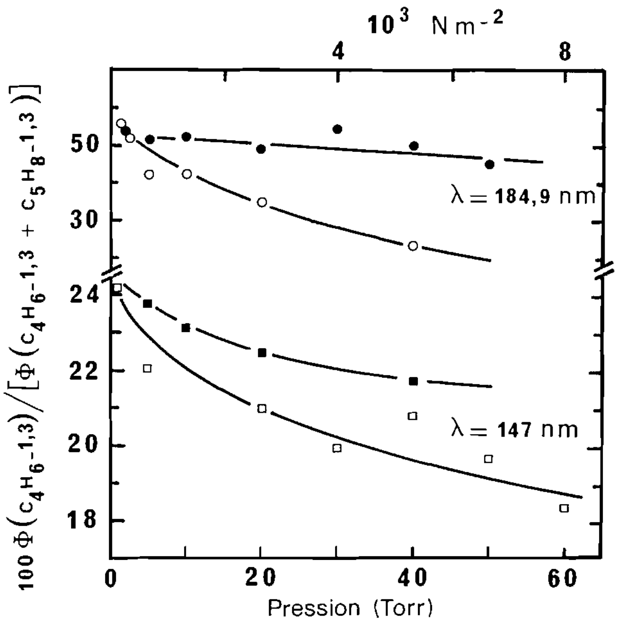

FIG. 6. Photolyse du méthyl-4-*cis*-pentène-2. Variation du rapport $\Phi(C_4H_6\text{-}1,3)/[\Phi(C_4H_6\text{-}1,3) + \Phi(C_5H_8\text{-}1,3)]$ en fonction de la pression du monomère en l'absence (■, ●) ou en présence de 10% d'oxygène (□, ○).

propyne, pentadiène-2,3 et méthyl-3-butyne-1 (tableau 2).

[20] $M4cP2^{**} \rightarrow H + CH_3CH(CH_3)CH{=}\dot{C}CH_3^{*}$

[21] $CH_3CH(CH_3)CH{=}\dot{C}CH_3^{*} \rightarrow i\text{-}C_3H_7 + CH_3C{\equiv}CH$

[22] $M4cP2^{**} \rightarrow H + CH_3CH(CH_3)\dot{C}{=}CHCH_3^{*}$

[23*a*] $CH_3CH(CH_3)\dot{C}{=}CHCH_3^{*} \rightarrow CH_3 + CH_3CH{=}C{=}CHCH_3$

[23*b*] $CH_3CH(CH_3)\dot{C}{=}CHCH_3^{*} \rightarrow CH_3CH(CH_3)C{\equiv}CH + CH_3$

Pour compléter ce mécanisme, il faudrait aussi proposer les réactions de ruptures primaires impliquant les liaisons β(C—H). Sans entrer dans le détail, ces réactions pourraient

[2]Ici, il faut mentionner que l'isomérisation du radical méthyl-3-butène-1-yl-1 vers la forme méthyl-2-butène-3-yl-1 a été observée (17*a*) et que cette dernière forme semble en équilibre avec le radical pentène-4-yl-1 (17*b*).

TABLEAU 5. Photofragmentation du méthyl-4-*cis*-pentène-2[a]

	147,0	184,9 nm
M4cP2** → $CH_3\dot{C}H\dot{C}H\dot{C}HCH_3$* + CH_3		≥0,79[b]
↳ $CH_3CH{=}CHCH{=}CH_3$ + H	0,47	(0,26)
↓ $CH_3CH_2\dot{C}H\dot{C}H\dot{C}H_2$*		
↳ $CH_2{=}CHCH{=}CH_2$ + CH_3	0,16	(0,15$_4$)
↱ $CH_3CH{=}CH_2$ + H	0,11	0,05
→ i-C_3H_7* + $CH_3CH{=}\dot{C}H$*		
↳ CH_3 + ; ↱ i-C_3H_7 + } CH≡CH	0,04[c]	0,00
→ $CH_3CH(CH_3)CH{=}\dot{C}H$* + CH_3		
↓ $CH_3\dot{C}(CH_3)\dot{C}H\dot{C}H$*		
↳ iso-C_5H_8 + H	0,03$_5$	0,00
→ $CH_3CH(CH_3)CH{=}\dot{C}CH_3$* + H		
↳ $CH_3C{\equiv}CH$ + i-C_3H_7	0,03[c]	0,01$_5$
→ $CH_3CH(CH_3)\dot{C}{=}CHCH_3$* + H		
↳ $CH_3CH{=}C{=}CHCH_3$ + CH_3	0,02$_5$[c]	0,00
↳ $CH_3CH(CH_3)C{\equiv}CH$ + CH_3	0,02[c]	0,00
Total[d]	≃0,89	≥0,855

[a]Les rendements quantiques des produits moléculaires sont obtenus par extrapolation à pression nulle, sauf cas indiqués.
[b]$\Phi_0(CH_3^{\cdot})$: voir texte, relation [C].
[c]Rendements quantiques indépendants de la pression: $2 < P < 100$ Torr.
[d]Voir note *e*; tableau 2.

ajouter un peu de pentadiène-1,3 et de méthyl-3-pentadiène-1,3 (ce dernier produit n'ayant pas été mesuré).

(b) *À 184,9 nm*

Les résultats apparaissant dans le tableau 3 montrent encore la prépondérance du rendement en pentadiène: Φ_0(pentadiène-1,3) = 0,26. Cependant, par rapport aux rendements observés à 147,0 nm, le rendement en butadiène-1,3 a gagné de l'importance: Φ_0(butadiène-1,3) = 0,15$_4$. Quant aux autres réactions de fragmentation primaires, elles ne sont guère observables si ce n'est à travers la formation de quantités mineures de propène et de propyne.

De la même manière, les produits radicalaires (ceux dont la formation est inhibée par la présence d'oxygène) permettent d'évaluer qualitativement la présence de radicaux méthyles (formation de l'éthane) et isopropyles (formation d'isobutane). Malheureusement, la combinaison des radicaux méthyles et α,γ-diméthallyles reforme le monomère et celle impliquant les radicaux méthyles et α-éthallyles n'ont pu être mesurés. Il est dès lors hasardeux de vouloir établir le rendement quantique de formation des radicaux méthyles issus de la réaction de fragmentation primaire, réaction [13], puisque la relation suivante est incomplète:

$$[C] \quad \Phi(CH_3^{\cdot}) \geq 2\Phi(C_2H_6) + \Phi(\text{iso-}C_4H_{10}) - \Phi(\text{butadiène-1,3})$$

Cette relation donne une valeur minimum au rendement $\phi([13])$: $\phi([13]) \geq 0,60$ et son extrapolation à pression nulle attribue une valeur $\Phi_0(CH_3^{\cdot}) \simeq 0,79$ (tableau 3 et fig. 5).

L'isomérisation des radicaux α-éthallyles et α,γ-diméthallyles

Le tableau 4 montre, à partir des rendements de produits à pression nulle, que l'isomérisation (réaction [4]) est importante à 147,0 nm puisque le rapport Φ_0(pentadiène-1,3)/-Φ_0(butadiène-1,3) ≃ 0,24 et négligeable à 184,9 nm. Par contre, tableau 5, le rapport similaire est nettement plus important à 184,9 nm dans le cas du méthyl-pentène: Φ_0(butadiène-1,3)/Φ_0(pentadiène-1,3) = 0,59 à cette longueur d'onde comparativement à 0,34 à 147,0 nm (fig. 6). Cette dernière observation est, au prime abord, en désaccord avec la diminution d'énergie disponible lorsque la longueur d'onde croît entre 147,0 et 184,9 nm. On peut cependant proposer une explication simple pour cet apparent désaccord. On peut en effet admettre que, quelle que soit la longueur d'onde, le processus limitant n'est pas le processus primaire. En effet en tenant compte de l'énergie interne disponible à la température ordinaire, environ 658 kJ mol^{-1} sont disponibles, c'est-à-dire beaucoup plus que les 295 kJ mol^{-1} requis pour la rupture primaire. A 184,9 nm il ne reste donc qu'un maximum de 360 kJ mol^{-1} pour la fragmentation secondaire ou pour l'isomérisation.

La fragmentation du radical α-éthallyle (réaction [3*a*]) implique la rupture d'un lien β(C—C) tandis que celle du radical α,γ-diméthallyle (réaction [5*a*]) demande celle d'un lien β(C—H). Par conséquent, on peut admettre que l'énergie d'activation du processus [5*a*] est supérieure à celle du processus [3*a*]. Il s'ensuit que l'apparent équilibre observé ici en faveur de la formation du butadiène-1,3 est gouverné non pas par l'équilibre entre les deux formes radicalaires, mais plutôt par la facilité relative de chacun des deux radicaux à se fragmenter. La réaction [5a] est plus endothermique que la réaction [3a] de quelque 59 kJ mol^{-1}. La réaction [$-3a$] a une énergie d'activation d'environ 9 à 15 kJ mol^{-1} tandis que celle de la réaction [$-5a$] est de l'ordre de 5 kJ mol^{-1} (18). En tenant compte des facteurs de fréquence, encore à l'avantage de la réaction [3a], cette différence est insuffisante pour faire en sorte que la constante de vitesse de la réaction [5a] soit aussi rapide que celle de la réaction [3a].

Remerciements

Nous voulons exprimer nos remerciements et notre gratitude au Conseil de recherches en sciences naturelles et en génie du Canada et au Fonds pour la Formation de chercheurs et d'actions concertées du Québec pour l'aide accordée tout au long de ce travail.

1. H. DESLAURIERS et G. J. COLLIN. Can. J. Chem. **63**, 62 (1985).
2. D. HOUDE, H. DESLAURIERS et G. J. COLLIN. Can. J. Chem. **61**, 962 (1983).
3. H. DESLAURIERS, G. J. COLLIN et B. SIMARD. J. Photochem. **21**, 19 (1983).
4. R. GORDEN, JR., R. E. REBBERT et P. AUSLOOS. NBS Technical Note 496 (1969).
5. R. A. HIVELY et R. E. HINTON. J. Gas Chromatogr. **6**, 903 (1968).
6. J. GAWŁOWSKI, J. NIEDZIELSKI et A. BIERZYNSKI. Chem. Anal. Warsaw, **15**, 721 (1970).
7. A. B. TRENWITH et B. S. RABINOVITCH. J. Phys. Chem. **86**, 3447 (1982).
8. C. W. LARSON, B. S. RABINOVITCH et D. C. TARDY. J. Chem. Phys. **47**, 4570 (1967).
9. A. B. TRENWITH. Int. J. Chem. Kinet. **5**, 67 (1973).
10. W. FORST. *Dans* Theory of unimolecular reactions. *Edité par* E. M. Loebl. Academic Press, New York, NY. 1973.
11. W. P. L. CARTER et D. C. TARDY. J. Phys. Chem. **78**, 2201 (1974).
12. F. P. LOSSING et J. C. TRAEGER. Int. J. Mass Spectrom. Ion Phys. **19**, 9 (1976).
13. P. BORRELL et P. CASHMORE. Trans. Faraday Soc. **65**, 1595 (1969).
14. F. BAYRAKCEKEN, J. H. BROPHY, R. D. FINK et J. E. NICHOLAS. J. Chem. Soc. Faraday Trans. 1, **69**, 228 (1973).
15. D. L. BAULCH, P. K. CHOWN et D. C. MONTAGUE. Int. J. Chem. Kinet. **11**, 1055 (1979).
16. G. J. COLLIN, H. DESLAURIERS et J. DESCHÊNES. Can. J. Chem. **57**, 870 (1979).
17. (*a*) K. W. WATKINS et L. A. O'DEEN. J. Phys. Chem. **75**, 2665 (1971); (*b*) W. P. L. CARTER et D. C. TARDY. J. Phys. Chem. **78**, 1245 (1974).
18. P. I. ABELL. *Dans* Comprehensive Chem. Kinet. Vol. 18. *Edité par* C. H. Bamford et C. F. H. Tipper. Elsevier Sci. Publ. Co., New York, NY. 1976.

Utilization of thiocarbonyl transfer reagents. Preparation of thioamides, mercapto esters, and thiapyran derivatives[1]

David N. Harpp,[2] J. Gavin MacDonald, and Charles Larsen[3]
Department of Chemistry, McGill University, Montreal, P.Q., Canada H3A 2K6

Received July 9, 1984

David N. Harpp, J. Gavin MacDonald, and Charles Larsen. Can. J. Chem. **63**, 951 (1985).

The reaction of 1,1′-thiocarbonyldiimidazole and 1,1′-thiocarbonylbis(1,2,4-triazole) with several aldonitrones has been found to afford thioamides in good yield. Several 1,1′-thiocarbonylbisazoles, which have been shown to undergo Diels–Alder additions with dienes to give cyclic and bicyclic adducts, can be further converted to mercapto esters, thiapyrans, and thiapyranones in good yield.

David N. Harpp, J. Gavin MacDonald et Charles Larsen. Can. J. Chem. **63**, 951 (1985).

On a trouvé que la réaction du thiocarbonyl-1,1′ diimidazole ou du thiocarbonyl-1,1′ bis(triazole-1,2,4) avec plusieurs aldonitrones conduit aux thioacétamides, avec de bons rendements. Il est bien connu que plusieurs thiocarbonyl-1,1′ bisazoles peuvent subir des réactions de Diels–Alder, par additions de diènes, pour conduire à des adduits cycliques et bicycliques; on démontre que l'on peut transformer ces hétérocycles en mercapto esters, thiapyrannes et thiapyrones, avec de bons rendements.

[Traduit par le journal]

In recent years, heterocyclic thiocarbonyl transfer reagents (1) have found several important applications in the synthesis of new compounds (2). For instance, both 1,1′-thiocarbonyldiimidazole (**1**) and -1,2,4-triazole (**2**) react with various nucleophiles in a selective fashion, permitting the facile synthesis of unsymmetrically substituted thioureas and related compounds (3). They have also been used in a stereospecific olefin synthesis from 1,2-diols (4), and in the configurational assignment of olefins, diols, and epoxides (5).

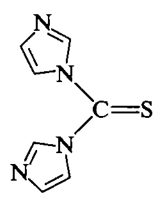

1

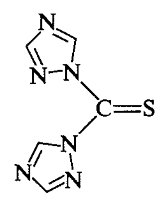

2

Our interest in utilizing thiocarbonyl transfer reagents in organic synthesis (5) is focused on the cycloaddition reactions of these systems with various nitrones and dienes. In this paper we wish to describe the preparation of thioamides (for a preliminary report, see ref. 6) from the reaction of aldonitrones with thiocarbonyl transfer reagents and to extend earlier work on the Diels–Alder adducts of these thiocarbonylazoles to the synthesis of thiapyrans, thiapyranones, and mercapto esters (7).

Results and discussion

Although there are several methods in the literature for the preparation of thiocarbonyl transfer reagents, we have found that the trimethylsilylazoles offered the greatest potential for the one-pot synthesis of 1,1′-thiocarbonylbisazoles in excellent yields (3).

Treatment of a variety of nitrones (**3**) with 1,1′-thiocarbonyldiimidazole (**1**) or triazole derivative (**2**) in refluxing benzene provides thioamides (**4**) in good overall isolated yield (Table

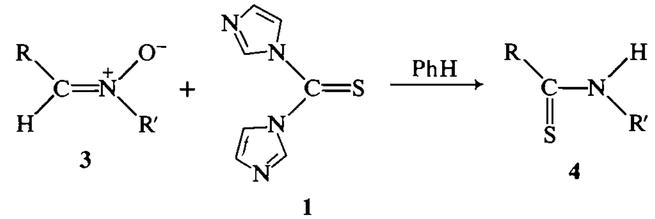

1). The formation of **4** can be postulated[4] to arise by an initial 1,3-dipolar cycloaddition of the nitrone followed by elimination of 1,1′-carbonyldiimidazole.

It was found that treatment of 4,5,5-trimethyl-Δ′-pyrroline-1-oxide (**5**) with 1,1′-thiocarbonyldiimidazole (**1**) in benzene at room temperature gave 4,5,5-trimethylpyrroline-2-thione (**6**) in high yield.

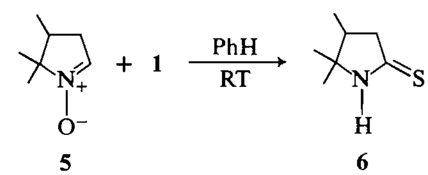

The solvent polarity did not have an appreciable effect as reaction with benzene, chlorobenzene, or ethyl acetate all gave the product in similar yield. The presence of a trace amount of pyridine in the reaction mixture cut the reaction time in half (8 to 4 h) with no significant change in yield. It is likely that the base (B) assists in the elimination step (eq. [1]).

[1]

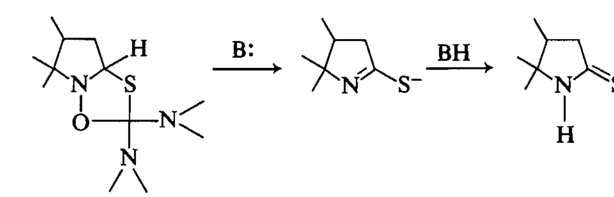

[1] Organic Sulfur Chemistry. Part 48. For Part 47, see ref. 26.

[2] Author to whom correspondence may be addressed.

[3] Kemisk Laboratorium II, H.C. Orsted Institutet, Copenhagen, Denmark.

[4] To substantiate this, we found that benzonitrile oxide reacted with **2** to give the cycloadduct as a stable, white, crystalline product (see Experimental).

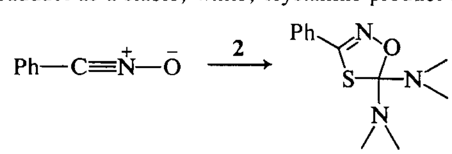

TABLE 1. Reaction of nitrones ($\mathrm{RHC{=}\overset{+}{N}(\overset{-}{O})R'}$) with **1** to give thioamides

Product	R	R′	Isolated yield (%) of thioamide
4*a*	Ph	Me	75
4*b*	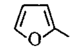	Me	68
4*c*	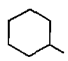	Me	67
4*d*	Ph	—CH_2Ph	70

Reaction of thiocarbonylazole (**1**) with ketonitrones **7***a* and **7***b* in refluxing benzene gave no thioamide, with only starting material being recovered even after 3 days. Possibly some cycloadduct **8** is formed but there is no hydrogen on the ketonitrone carbon so the elimination step cannot take place as suggested for the aldonitrones in eq. [1]. The possibility that thioamide formation is light induced (8) was eliminated when **6** was formed in a dark reaction.

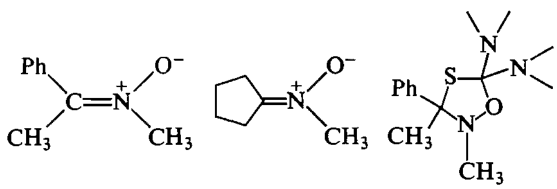

7*a* **7***b* **8**

Examples of cycloaddition reactions between nitrones and thiocarbonyl compounds are not common (8, 9). Cyclic aldonitrones are reported to be converted to the related thiolactams by refluxing in carbon disulfide (10); however, noncyclic nitrones are instead isomerized by this method[5] (11). Reaction of *C*-phenyl-*N*-methylnitrone (**3***a*) with thiophosgene at room temperature in benzene gave only *N*-methylbenzamide, providing an interesting contrast with the related thiocarbonylazoles.

In addition to nitrone cycloadditions, the Diels–Alder reactions of thiocarbonyl transfer reagents with reactive dienes can be of broad utility in the construction of functionalized ring systems (7). Accordingly, we examined the [4 + 2] cycloaddition reaction of several thiocarbonylbisazoles with 2,3-dimethyl-1,3-butadiene (**9***a*) and 1,4-diphenyl-1,3-butadiene (**9***b*).

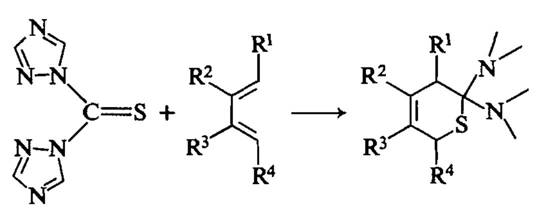

9*a*; R^1, R^4 = H; R^2, R^3 = CH_3 **10***a*
9*b*; R^1, R^4 = Ph; R^2, R^3 = H **10***b*

Treatment of 1,1′-thiocarbonylbis(1,2,4-triazole) (**2**) with 2,3-dimethyl-1,3-butadiene (**9***a*) in methylene chloride at room temperature for 10 h gave a nearly quantitative yield (98%) of 3,4-dimethyl-6,6-bis(1,2,4-triazol-1-yl)-5,6-dihydro-2*H*-thiopyran (**10***a*). Similarly, reaction of 1,4-diphenyl-1,3-butadiene (**9***b*) with the thiocarbonylbisazole (**2**) in refluxing benzene gave the corresponding dihydrothiapyran (**10***b*) in good yield. The cycloadducts of these thiocarbonylazoles are crystalline and moisture stable. This contrasts with the adducts formed by the parent thiophosgene (12), which tend to be unstable and must be stored in the cold. Interestingly, treatment of 2,3-dimethyl-1,3-butadiene (**9***a*) with 1,1′-thiocarbonyldibenzotriazole (**11**) in refluxing benzene for 8 h gave 3,4-dimethyl-6-(benzotriazol-1-yl)-2*H*-thiapyran (**12**). It is proposed that the cycloadduct is formed, which then eliminates one of the benzotriazole groups under the reaction conditions. In contrast to this, we found that similar reaction of butadiene (**9***a*) with 1,1′-thiocarbonyldibenzimidazole did not yield any product; only starting materials were isolated even after prolonged reflux.

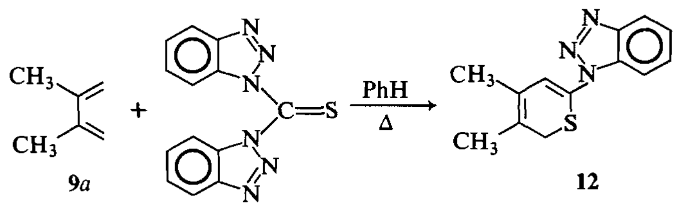

9*a* **11** **12**

Several reviews of the Diels–Alder reaction involving thiocarbonyl dienophiles have been published (13) and illustrate that thiocarbonyl groups of all kinds are highly reactive as dienophiles, much more so than the corresponding carbonyl compound. Thioketones are effective dienophiles and add to most dienes in high yield at exceptionally low temperatures to afford stable adducts (14). The few reports on the regiochemical selectivity of thioketone additions to unsymmetrical dienes indicate that mixtures are obtained (15). *In situ* thioaldehydes also undergo Diels–Alder additions to dienes to yield stable thiapyran ring systems (7*b*, 16).

The chemistry of cycloadducts **10***a* and **10***b* has been investigated. The behavior of **10***a* and **10***b* under solvolytic conditions was found to be quite interesting. Refluxing dihydrothiapyran **10***a* in dilute hydrochloric acid for 1 h provided 3,4-dimethyl-3-hydro-2*H*-thiapyran-6-one (**13**) in high yield (80%). The structure of **13** was assigned on the basis of its physical and spectral data.

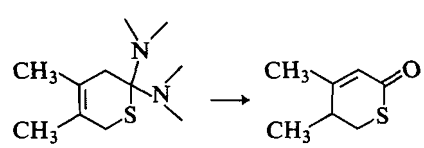

10*a* **13**

The formation of the thiapyranone presumably proceeds by way of acid-catalyzed elimination of the triazole groups with subsequent formation of the more stable conjugated enone system.

We have also observed that these dihydrothiapyran systems **10***a* and **10***b*, on treatment with cupric sulfate (0.5 equivalent) in a refluxing methanol–water mixture (4:1) for 1 h, gave the corresponding thiapyrans (**14**) in high yield.

Other cupric and cuprous salts (e.g. Cu^I I and Cu^{II} Cl_2) were also found to promote the elimination of one of the triazole groups under similar conditions. The copper cation was dem-

[5] Aldonitrones are known to rearrange to the isomeric amides by treatment with a variety of reagents such as phosgene, SO_2, PCl_3, and acetyl chloride.

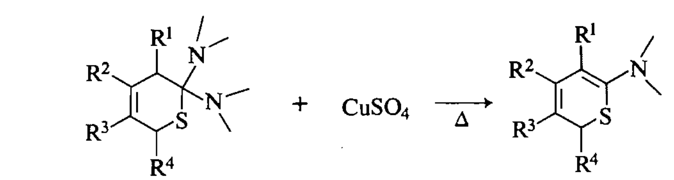

10*a*; R^1, R^4 = H; R^2, R^3 = CH_3 **14***a*
10*b*; R^1, R^4 = Ph; R^2, R^3 = H **14***b*

onstrated to be the active agent, as only starting material was recovered when ammonium sulfate was used, even after prolonged reflux. The copper ion is thought to complex with the triazole groups, thus assisting the elimination. While copper salts are well known to accelerate Diels–Alder additions (17), reports of copper-assisted eliminations do not appear to be common.

Treatment of 3,4-dimethyl-6,6-bis(1,2,4-triazol-1-yl)-5,6-dihydro-2*H*-thiapyran (**10***a*) or 2,5-diphenyl-6,6-bis(1,2,4-triazol-1-yl)-5,6-dihydro-2*H*-thiapyran (**10***b*) with methyl iodide in refluxing acetonitrile was also found to give the corresponding thiapyran (**14***a* or **14***b*) in high yield. The structure of the products was unambiguously confirmed by their physical and spectral data. Methyl iodide is thought to alkylate one of the triazole groups and thus activating it towards elimination under the solvolysis conditions.

Thiapyran (**14***a*) was also formed in high yield (95%) when 3,4-dimethyl-6,6-bis(1,2,4-triazol-1-yl)-5,6-dihydro-2*H*-thiapyran (**10***a*) was heated at reflux in a methanol solution containing one equivalent of phenol; presumably, phenol promotes the elimination of a triazole group by acid catalysis.

The solvolysis of these dihydrothiapyran systems in alcoholic solvents was found to depend on the acid concentration as well as the ratio of alcohol to water. Thus treatment of dihydrothiapyran **10***a* in refluxing methanol with dry HCl for 1 h gave the mercapto ester **15** in good yield[6] (18). In contrast, similar reaction of the dihydrothiapyran **10***a* in a 10:1 methanol–

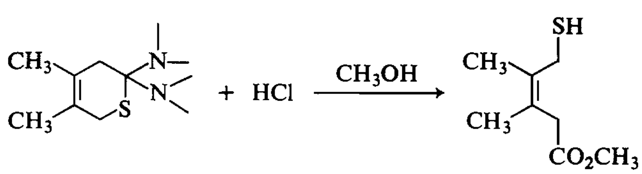

10*a* **15**

water mixture at reflux containing a small amount of acid gave a mixture of 3,4-dimethyl-6-(1,2,4-triazol-1-yl)-2*H*-thiapyran (**14***a*, 80%) and 3,4-dimethyl-5-hydro-2*H*-thiapyran-6-one

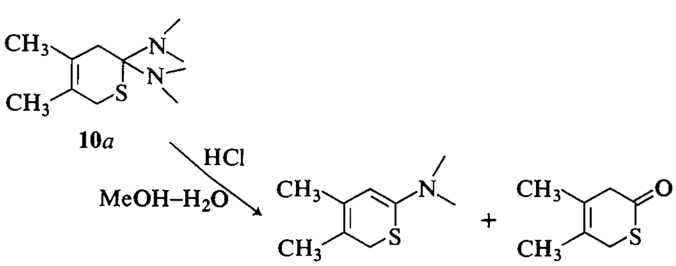

	14*a*	**16***a*
Ratio, 10:1	80%	10%
4:1	60%	33%

[6] Acyclic mercapto carboxylic acids have also been prepared by lithium/ammonia reduction of 2-thiophenecarboxylic acid.

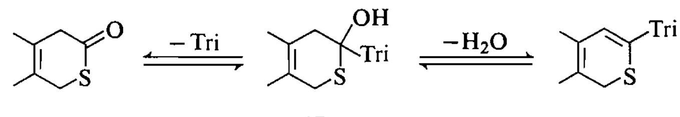

17

Tri = $C_2H_2N_3$

(**16***a*, 10%); this was easily separated by silica gel chromatography. Increasing the water concentration to a 4:1 mixture of methanol–water was found to increase the yield of the thiapyranone (**16***a*, 33%) at the expense of the thiapyran (**14***a*, 60%). As a working hypothesis, we propose that the mechanism involves competition between elimination of the second triazole group and dehydration of the intermediate[7] (17). Earlier studies also showed that product distribution was a function of alcohol used (7).

We also investigated the chemistry of the bicycloadduct (**18**) obtained from reaction of 1,3-cyclohexadiene with 1,1′-thiocarbonyl-bis(1,2,4-triazole) **2**. Treatment of **18** with an acidic methanol–water mixture (4:1) under reflux for 1 h gave a mixture of 2-thiabicyclo[2,2,2]oct-5-ene-3-one (**19**, 56%) and methyl 4-mercapto-2-cyclohexenecarboxylate (7) (**20**, 38%); these compounds were easily separated and characterized. In contrast, only the mercapto ester **20** was isolated in good yield when **18** was treated with cupric sulfate (0.25 equivalent) in a refluxing methanol–water mixture for 1 h. The observed difference in solvolysis between the bicyclic and cyclic systems is probably due to release of strain in the bicyclic case.

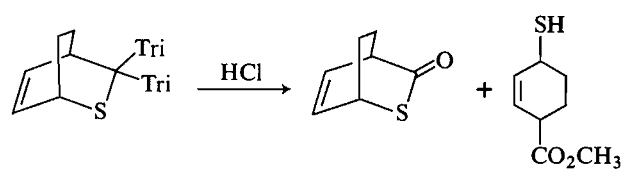

18 **19** **20**

We decided to further explore this copper-ion assisted solvolysis for the preparation of pure thiapyrans. A sample of myrcene (**21**) was reacted with 1,1′-thiocarbonylbis(1,2,4-triazole) (**2**) in refluxing benzene for 1 h to provide a mixture of the two isomeric cycloadducts **22***a*, *b* in high yield. Treatment of these dihydropyrans **22** with copper sulfate in a 4:1 methanol–water mixture at reflux for 1 h gave only the corresponding thiapyrans **23**[8] in good yield. It is interesting to note that similar treatment of **22** with an acidic methanol–water mixture (4:1) gave both thiapyrans **23** and thiapyranones **24**, as products. Thus, copper sulfate does appear to be a selective and general reagent for the preparation of thiapyrans from bis-triazole dihydrothiapyrans.

In summary, we have found that thiocarbonyl transfer reagents undergo ready cycloaddition with a variety of systems in synthetically useful yield. The cycloadducts of these reagents with dienes have been shown to undergo further reaction to

[7] Thiapyran **14***a* was shown not to be a precursor of thiapyranone **16***a* when a sample of **14***a* was refluxed in an acidic methanol–water mixture (4:1) for 4 h to yield only recovered starting material.

[8] We questioned whether thiapyran **23** might undergo internal Diels–Alder cycloaddition. Heating a benzene solution of **23** in a sealed tube at 180°C failed to yield any internal cycloadducts even after prolonged thermolysis; only slow decomposition was observed. Cycloaddition with maleic anhydride under similar conditions was also unsuccessful. This is likely due to the non-planarity of the thiapyran ring system.

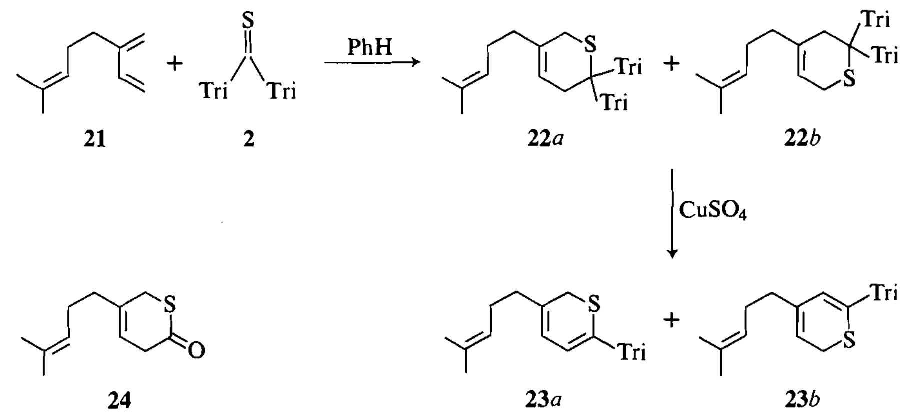

give thiapyrans, thiapyranones, and mercapto esters under appropriate conditions. Further applications of the cycloaddition reactions of these compounds in organic sysnthesis are currently under investigation.

Experimental

All melting points and boiling points are uncorrected. Elemental analyses were performed by Guelph Chemical Laboratories Ltd., Guelph, Ontario. The infrared spectra were determined on a Perkin–Elmer 580 infrared spectrophotometer. The proton magnetic resonance spectra were determined at 60 MHz with a Varian Associates T-60A spectrometer. Mass spectra were obtained on a Du Pont 21-492B mass spectrometer, using a direct insertion probe. Apart from nitrones **3***d*(19), **5**(20), and **7***b*(21) all the others were easily prepared in high yield (ca. 98%) from the corresponding aldehyde or ketone with *N*-methylhydroxylamine hydrochloride in the presence of sodium acetate in ethanol at room temperature. All gave satisfactory physical and spectral data.

Reaction of C-*phenyl*-N-*methylnitrone (***3***a) with 1,1′-thiocarbonyldiimidazole (***1***)*

A mixture of 0.90 g (6.6 mmol) of *C*-phenyl-*N*-methylnitrone and 1.18 g (6.6 mmol) of 1,1′-thiocarbonyldiimidazole in 40 mL of dry benzene was heated at reflux under a nitrogen atmosphere for 8 h. The solvent was then removed under reduced pressure and the crude residue subjected to silica gel chromatography with a 50% ethyl acetate – hexane mixture as eluent. The major fraction isolated was a pale yellow crystalline solid (0.75 g, 75%) whose structure was assigned as *N*-methylthiobenzamide (**4***a*) on the basis of the following data: mp 79–80°C (lit. (22) mp 79–80°C); ir (Nujol): 3300, 1590, 1350, 1230, 1035, 1020, 992, 934, 914, and 765 cm^{-1}; nmr ($CDCl_3$) δ: 3.22 (d, 3H) and 7.7–7.2 (m, 6H); ms, *m/e*: 151 (M^+), 136, 121, and 77. *Anal.* calcd. for C_8H_9NS: C 63.54, H 6.00, N 9.26; found: C 63.62, H 5.99, N 9.12.

Reaction of C-*(2-furyl)*-N-*methylnitrone (***3***b) with 1,1′-thiocarbonyldiimidazole (***1***)*

A mixture of 0.50 g (3.9 mmol) of *C*-(2-furyl)-*N*-methylnitrone and 0.69 g (3.9 mmol) of 1,1′-thiocarbonyldiimidazole in 40 mL of dry benzene was heated at reflux under a nitrogen atmosphere for 8 h. The solvent was then removed under reduced pressure and the crude residue subjected to silica gel chromatography with a 50% ethyl acetate – hexane mixture as eluent. The major fraction isolated was a pale yellow crystalline solid (0.38 g, 68%) whose structure was assigned as *N*-methyl-2-thiofuramide (**4***b*) on the basis of the following data: mp 70–71°C (lit. (23) mp 71°C); ir (Nujol): 3220, 1580, 1510, 1330, 1275, 1157, 1031, 1010, 955, 865, 825, 745, and 700 cm^{-1}; nmr ($CDCl_3$) δ: 3.30 (d, 3H), 6.42 (m, 1H), and 7.33 (m, 2H); ms, *m/e*: 141 (M^+), 124, 111, 100. *Anal.* calcd. for C_6H_7NOS: C 51.04, H 4.99, N 9.92; found: C 51.00, H 4.93, N 9.84.

Reaction of C-*cyclohexyl*-N-*methylnitrone (***3***c) with 1,1′-thiocarbonyldiimidazole (***1***)*

A mixture of 2.55 g (18 mmol) of *C*-cyclohexyl-*N*-methylnitrone and 3.19 g (18 mmol) of 1,1′-thiocarbonyldiimidazole in 40 mL of dry benzene was heated at reflux under a nitrogen atmosphere for 8 h. The solvent was then removed under reduced pressure and the crude residue subjected to silica gel chromatography with a 50% ethyl acetate – hexane mixture as eluent. The major fraction isolated was a pale yellow crystalline solid (1.89 g, 67%) whose structure was assigned as *N*-methylthiocyclohexylamide (**4***c*) on the basis of the following data: mp 66–67°C; ir (Nujol): 3300, 1535, 1335, 1290, 1205, 1105, 1020, 975, 884, 843, 804, and 714 cm^{-1}; nmr ($CDCl_3$) δ: 1.3–2.0 (m, 11H) and 3.20 (d, 3H); ms, *m/e*: 157 (M^+), 142, 124, and 102. *Anal.* calcd. for $C_8H_{15}NS$: C 61.09, H 9.61, N 8.90; found: C 60.93, H 9.65, N 8.75.

Reaction of C-*phenyl*-N-*benzylnitrone (***3***d) with 1,1′-thiocarbonyldiimidazole (***1***)*

A mixture of 2.38 g (17 mmol) of *C*-phenyl-*N*-benzylnitrone and 3.0 g (17 mmol) 1,1′-thiocarbonyldiimidazole in 40 mL of dry benzene was heated at reflux under a nitrogen atmosphere for 8 h. The solvent was then removed under reduced pressure and the crude residue subjected to silica gel chromatography with a 60% ethyl acetate – hexane mixture as eluent. The major fraction isolated was a pale yellow crystalline solid (2.7 g, 70%) whose structure was assigned as *N*-(phenylmethylene)-benzenecarbothioamide (**4***d*) on the basis of the following data: mp 82–83°C; ir (Nujol): 3300, 3075, 3060, 3025, 1617, 1510, 1320, 1280, 1200, 1058, 1025, 916, 900, 760, and 740 cm^{-1}; nmr ($CDCl_3$) δ: 4.95 (d, 2H) and 7.0–7.8 (m, 10H); ms, *m/e*: 227 (M^+), 195, 165, 103, and 91; *Anal.* calcd. for $C_{14}H_{13}NS$: C 73.97, H 5.76, N 6.16; found: C 74.02, H 5.70, N 6.11.

*Reaction of 4,5,5-trimethyl-Δ′-pyrroline-1-oxide (***5***) with 1,1′-thiocarbonyldiimidazole (***1***)*

A mixture of 0.300 g (2.4 mmol) of 4,5,5-trimethyl-Δ′-pyrroline-1-oxide and 0.420 g (2.4 mmol) of 1,1′-thiocarbonyldiimidazole in 20 mL of dry benzene was stirred at room temperature under a nitrogen atmosphere for 8 h. The solvent was then removed under reduced pressure and the crude residue subjected to silica gel chromatography with a 10% ethyl acetate – hexane mixture as eluent. The major fraction isolated was a pale yellow crystalline solid (0.285 g, 84%) whose structure was assigned as 4,5,5-trimethyl-pyrroline-2-thione (**6**) on the basis of the following data: mp 144–145°C; nmr ($CDCl_3$) δ: 1.00 (d, 3H), 1.15 (s, 3H), 1.30 (s, 3H), and 2.2–3.2 (m, 3H); ms, *m/e*: 143 (M^+), 128, 95, and 58. *Anal.* calcd. for $C_7H_{13}NS$: C 9.15, H 9.15, N 9.78; found: C 58.98, H 9.55, N 9.30.

*Reaction of 1,1′thiocarbonylbis(1,2,4-triazole) (***2***) with* C-*phenyl*-N-*methylnitrone (***3***a),* C-*(2-furyl)*-N-*methylnitrone (***3***b), and* C-*phenyl*-N-*benzylnitrone (***3***d)*

In a similar fashion to the above reactions, a mixture of 1.4 mmol of 1,1′-thiocarbonylbis(1,2,4-triazole) and 1.4 mmol of the corresponding nitrone in 30 mL of dry benzene was stirred at room temperature under a nitrogen atmosphere for 8 h. Work-up was similar to that described with the imidazole experiments. The thioamides produced were found to be identical in every respect to those obtained by the thiocarbonyldiimidazole route. The isolated yields were *N*-

methylthiobenzamide (**4***a*), 62%; *N*-methyl-2-thiofuramide (**4***b*), 58%; and *N*-(phenylmethylene)-benzenecarbothioamide (**4***d*), 60%.

Reaction of N-*methyl*-C-*phenylnitrone (3*a*) with thiophosgene*

To a stirred solution of 0.30 g (2.2 mmol) *N*-methyl-*C*-phenylnitrone in 10 mL of dry benzene at room temperature was slowly added 0.25 g of thiophosgene in 5 mL of dry benzene. The thiophosgene solution was observed to decolorize immediately on contact with the nitrone solution. The resultant mixture was stirred for 2 h, after which the solvent was removed under reduced pressure. The crude residue was subjected to silica gel chromatography with a 50% ethyl acetate – hexane mixture was eluent. The major fraction isolated was a colorless crystalline solid (0.22 g, 73%) whose structure was assigned as *N*-methylbenzamide on the basis of the following data and by comparison with an authentic sample: mp 77–78°C (lit (24) mp 80–81°C); nmr ($CDCl_3$) δ: 3.00 (d, 3H), 6.8 (br s, 1H), and 7.2–7.8 (m, 5H); ms, *m/e*: 135 (M^+), 105, and 77.

Reaction of 1,1′-thiocarbonylbis(1,2,4-triazole) (2) with benzonitrile oxide

To a stirred solution of 0.22 g (1.4 mmol) benzohydroximoyl chloride (25) and 0.20 g (1.1 mmol) of 1,1′-thiocarbonylbis(1,2,4-triazole) in 20 mL of dry methylene chloride at 0°C was slowly added 0.4 g of trimethylamine. After the mixture was stirred for 2 h it was filtered and the solvent was removed under reduced pressure. The resulting residue was purified by silica gel chromatography with a 50% ethyl acetate – hexane mixture to give 0.284 g (87%) of 5,5-bis(1,2,4-triazol-1-yl)-5-phenyl-1,4,2-oxathiazole: mp 120–121°C; ir (Nujol): 3090, 1280, 1190, 1130, 995, 840, 755, and 670 cm^{-1}; nmr ($CDCl_3$) δ: 7.3–7.6 (m, 5H), 8.12 (s, 2H), and 8.53 (s, 2H); ms, *m/e*: 299 (M^+), 231, and 77.

Reaction of 2,3-dimethyl-1,3-butadiene with 1,1′-thiocarbonylbis-(1,2,4-triazole) (2)

A mixture of **2** (1.8 g, 0.01 mol) and 0.8 g (0.01 mol) of 2,3-dimethyl-1,3-butadiene in dry methylene chloride (35 mL) was stirred at room temperature for 10 h. Removal of the solvent under reduced pressure gave faint pink crystals. The product was recrystallized from benzene (or a mixture of benzene and cyclohexane) to give a nearly colorless product (2.6 g, 98%) with a melting point of 121–122°C. The product was assigned the structure 3,4-dimethyl-6,6-bis(1,2,4-triazol-1-yl)-5,6-dihydro-2*H*-thiapyran **10***a* on the basis of the following data: ir (Nujol): 3100, 1340, 1260, 1175, 1124, 990, 932, 843, 760, and 635 cm^{-1}; nmr ($CDCl_3$) δ: 1.76 (s, 6H), 3.25 (s, 2H), 3.72 (s, 2H), 8.02 (s, 2H), and 8.58 (s, 2H); ms, *m/e*: 194, 193, 178, 124, and 69. *Anal.* calcd. for $C_{11}H_{14}N_6S$: C 50.35, H 5.38, N 32.04; found: C 50.30, H 5.35, N 32.00.

*Reaction of 1,4-diphenyl-1,3-butadiene (9*b*) with 1,1′-thiocarbonylbis(1,2,4-triazole) (2)*

A mixture of 1.80 g (0.01 mol) of **2** and 2.06 g (0.01 mol) of 1,4-diphenyl-1,3-butadiene (**9***b*) in 40 mL of benzene was refluxed for 12 h. Removal of the solvent under reduced pressure gave a pale brown crystalline solid. The product was recrystallized from benzene to yield 2.6 g (67%) of colorless product with a melting point of 196–197°C. The structure of the product was assigned as 2,5-diphenyl-6,6-bis(1,2,4-triazol-1-yl)-5,6-dihydro-2*H*-thiapyran (**10***b*) on the basis of the following data: ir (Nujol): 3100, 1340, 1270, 1176, 1125, 980, 815, 734, and 665 cm^{-1}; nmr ($CDCl_3$) δ: 4.55 (d, 1H), 5.40 (m, 1H), 6.10 (m, 2H), 7.27 (s, 5H), 7.47 (s, 5H), 7.68 (s, 2H), 8.13 (s, 1H), and 8.87 (s, 1H). *Anal.* calcd. for $C_{21}H_{18}N_6S$: C 65.26, H 4.69, N 21.75; found: C 65.10, H 4.28, N 21.45.

Reaction of 1,3-cyclohexadiene with 1,1′-thiocarbonylbis(1,2,4-triazole) (2)

A mixture of 1.8 g (0.01 mol) of **2** and 0.8 g (0.01 mol) of 1,3-cyclohexadiene was heated at reflux for 10 h. Removal of the solvent under reduced pressure gave an almost colorless product. The crude product was recrystallized from cyclohexane to give a colorless crystalline product (2.44 g, 94%) with a melting point of 113–114°C. The structure of the product was assigned as 3,3-bis(1,2,4-triazol-1-yl)-2-thiabicyclo[2.2.2]oct-5-ene (**18**) on the basis of the following data: ir (Nujol): 3095, 1270, 1175, 1130, 1000, 940, 882, 830, 722, and 658 cm^{-1}; nmr ($CDCl_3$) δ: 1.57 (m, 4H), 3.88 (m, 1H), 4.53 (m, 1H), 6.10 (m, 1H), 6.65 (m, 1H), 7.85 (s, 1H), 7.93 (s, 1H), 8.45 (s, 1H), and 8.70 (s, 1H); ms, *m/e*: 260 (M^+), 191, 122, and 69. *Anal.* calcd. for $C_{11}H_{12}N_6S$: C 50.75, H 4.65, N 32.29; found: C 50.65, H 4.66, N 32.33.

Reaction of 1,1′-thiocarbonyldibenzotriazole (11) with 2,3-dimethyl-1,3-butadiene

A mixture of 2.0 g (7.2 mmol) of **11** and 0.59 g (7.2 mmol) of 2,3-dimethyl-1,3-butadiene in 30 mL of dry benzene was heated at reflux for 8 h. The solvent was then removed under reduced pressure and the crude residue subjected to silica gel chromatography with a 50% ethyl acetate – hexane mixture as eluent. The major fraction isolated was a pale yellow crystalline solid (1.0 g, 60%) whose structure was assigned as 3,4-dimethyl-6-(benzotriazol-1-yl)-2*H*-thiapyran (**12**) on the basis of the following data: mp 88–89°C; ir (Nujol): 1610, 1590, 1530, 1285, 1214, 1170, 1050, 1000, 970, and 860 cm^{-1}; nmr ($CDCl_3$) δ: 1.94 (s, 6H), 3.52 (s, 2H), 6.50 (s, 1H), and 7.2–8.0 (m, 4H); ms, *m/e*: 243 (M^+), 214, and 125.

*Reaction of 3,4-dimethyl-6,6-bis(1,2,4-triazol-1-yl)-5,6-dihydro-2*H*-thiapyran (10*a*) in dilute hydrochloric acid*

A suspension of 0.2 g (0.76 mmol) of **10***a* in 15 mL of water containing 8 drops of concentrated HCl was heated at reflux for 1 h. The resultant clear yellow solution was poured into 60 mL of cold water and the mixture extracted with methylene chloride (2 × 50 mL). The combined organic extracts were washed with water (100 mL), dried ($MgSO_4$), and the solvent removed under reduced pressure to yield a yellow oil. The crude residue was subjected to silica gel chromatography with a 10% ethyl acetate – hexane mixture as eluent. The major fraction isolated was a light yellow oil (87 mg, 80%) whose structure was assigned as 3,4-dimethyl-3-hydro-2*H*-thiopyran-6-one (**13**) on the basis of the following data: bp 60°C at 0.01 Torr (Kugelrohr) (1 Torr = 133.3 Pa); ir (neat): 2970, 2930, 2880, 1644, 1624, 1450, 1432, 1372, 1307, 1200, 1176, 1125, 1100, 1024, 846, and 700 cm^{-1}; nmr ($CDCl_3$) δ: 1.41 (d, 3H), 2.02 (s, 3H), 2.90 (m, 2H), 3.62 (dd, 1H, J = 12, 4 Hz), and 5.92 (br s, 1H); ms, *m/e*: 142 (M^+), 114, 99, and 67.

*Reaction of 3,4-dimethyl-6,6-bis(1,2,4-triazol-1-yl)-5,6-dihydro-2*H*-thiapyran (10*a*) with cupric sulfate*

A suspension of 0.2 g (0.76 mmol) 3,4-dimethyl-6,6-bis(1,2,4-triazol-1-yl)-5,6-dihydro-2*H*-thiapyran and 0.1 g (0.40 mmol) cupric sulfate in 20 mL of a 4:1 mixture of methanol–water was heated at reflux for 1 h. The mixture was then poured into 100 mL of water and the solution extracted with CH_2Cl_2 (2 × 20 mL). The combined organic extracts were washed with water, dried ($MgSO_4$), and the solvent removed under reduced pressure to yield pale yellow crystals. The crude product was subjected to silica gel chromatography with a 50% ethyl acetate – hexane mixture as eluent. The major fraction isolated was a white crystalline solid (0.12 g, 82%) whose structure was assigned as 3,4-dimethyl-6-(1,2,4-triazol-1-yl)-2*H*-thiapyran (**14***a*) on the basis of the following data: mp 96–97°C; ir (Nujol): 3100, 1620, 1580, 1415, 1292, 1270, 1210, 1145, 1100, 1000, 952, 900, 875, and 830 cm^{-1}; nmr ($CDCl_3$) δ: 1.94 (br s, 6H), 3.46 (s, 2H), 6.67 (s, 1H), 8.01 (s, 1H), and 8.42 (s, 1H); ms, *m/e*: 193 (M^+), 178, 124, and 91.

*Reaction of 2,5-diphenyl-6,6-bis(1,2,4-triazol-1-yl)-5,6-dihydro-2*H*-thiapyran (10*b*) with cupric sulfate*

A suspension of 0.6 g (1.55 mmol) of **10***b* and 0.5 g (2.00 mmol) cupric sulfate in 20 mL of a 4:1 mixture of methanol–water was heated at reflux for 1 h. The reaction mixture was then poured into 100 mL of water and the solution extracted with methylene chloride (2 × 20 mL). The combined organic extracts were washed with water (100 mL), dried ($MgSO_4$), and the solvent removed under reduced pressure to yield a light yellow solid. The crude product was easily purified by silica gel chromatography with a 20% ethyl acetate – hexane mixture as eluent to give 0.42 g (85%) of a white crystalline solid. The structure of the product was assigned as 2,5-diphenyl-6-(1,2,4-triazol-1-yl)-2*H*-thiapyran (**14***b*) on the basis of the following data: mp 121–122°C; ir (Nujol): 3108, 3058, 1620, 1594, 1486, 1400, 1352, 1274, 1200, 1124, 990, 942, 876, and 865 cm^{-1}; nmr ($CDCl_3$) δ: 5.08 (d, 1H, J = 5 Hz), 6.00 (dd, 2H, J = 10, 5 Hz), 6.66 (d, 1H, J = 10 Hz), 7.1–7.4 (m, 10H), 7.67 (s, 1H), and 7.90 (s, 1H); ms, *m/e*: 317 (M^+), 249, 172, and 149.

*Reaction of 3,4-dimethyl-6,6-bis(1,2,4-triazol-1-yl)-5,6-dihydro-2*H*-thiapyran (10*a*) with methyl iodide*

A mixture of 0.10 g (0.4 mmol) of **10***a* and 0.20 g (1.5 mmol) of methyl iodide in 10 mL of dry acetonitrile was heated at reflux for 1 h. The solvent was then removed under reduced pressure and the crude residue subjected to silica gel chromatography with a 50% ethyl acetate – hexane mixture as eluent. The major fraction isolated was a white crystalline solid (0.06 g, 82%) whose structure was assigned as 3,4-dimethyl-6-(1,2,4-triazol-1-yl)-2*H*-thiapyran (**14***a*) as its physical and spectral data were identical to a sample of **14***a* obtained in the $CuSO_4$ reaction.

*Reaction of 2,5-diphenyl-6,6-bis(1,2,4-triazol-1-yl)-5,6-dihydro-2*H*-thiapyran (10b) with methyl iodide*

A mixture of 0.5 g (1.3 mmol) of **10***b* and 0.5 g (3.5 mmol) of methyl iodide in 20 mL of dry acetonitrile was heated at reflux for 1 h. The solvent was then removed under reduced pressure and the crude residue subjected to silica gel chromatography with a 50% ethyl acetate – hexane mixture as eluent. The major fraction isolated was a white crystalline solid (0.3 g, 73%) whose structure was assigned as 2,5-diphenyl-6-(1,2,4-triazol-1-yl)-2*H*-thiapyran (**14***b*) on the basis of the following data: mp 121–122°C; ir (Nujol): 3080, 3057, 3022, 1625, 1594, 1558, 1487, 1400, 1352, 1274, 1200, 1124, 980, 875, and 867 cm^{-1}; nmr ($CDCl_3$) δ: 5.08 (d, 1H, J = 5 Hz), 6.02 (dd, 1H, J = 10, 5 Hz), 6.67 (d, 1H, J = 10 Hz), 7.0–7.6 (m, 10H), 7.70 (s, 1H), and 7.94 (s, 1H); ms, *m/e*: 317 (M^+), 249, 172, and 149.

*Reaction of 3,4-dimethyl-6,6-bis(1,2,4-triazol-1-yl)-5,6-dihydro-2*H*-thiapyran (10a) with phenol*

A mixture of 0.2 g (0.7 mmol) of **10***a* and 0.07 g (0.7 mmol) of phenol in 20 mL of acetone was heated at reflux for 3 h. The solvent was then removed under reduced pressure and the crude residue subjected to silica gel chromatography with a 50% ethyl acetate – hexane mixture as eluent. The major fraction isolated was assigned as 3,4-dimethyl-6-(1,2,4-triazol-1-yl)-2*H*-thiapyran (**14***a*) as its physical (including undepressed mixture mp) and spectral data were identical to a sample of **14***a* obtained with the $CuSO_4$ reaction.

*Acidic hydrolysis of 3,4-dimethyl-6,6-bis(1,2,4-triazol-1-yl)-5,6-dihydro-2*H*-thiapyran (10a)*

(a) *HCl in dry methanol*

Dry HCl was bubbled through a solution of 0.2 g (0.76 mmol) **10***a* in methanol (15 mL) at reflux for 40 min. Reflux was continued for an additional 60 min. The solvent was then removed under reduced pressure to yield a yellow oil. The crude product was easily purified by silica gel chromatography with a 10% ethyl acetate – hexane mixture as eluent. The colorless oil (0.10 g, 76%) was assigned as methyl 3,4-dimethyl-5-mercapto-3-pentenecarboxylate (**15**) on the basis of the following data: ir (neat): 2950, 2861, 2540, 1720, 1460, 1270, 1200, 1165, 1014, and 780 cm^{-1}; nmr ($CDCl_3$) δ: 1.60 (br s, 1H), 1.95 (s, 6H), 3.00 (s, 2H), 3.50 (m, 2H), and 3.9 (s, 3H); ms, *m/e*: 174 (M^+), 173, 159, 141, and 114.

(b) *HCl in a 10:1 methanol–water mixture*

A solution of 0.200 g (0.76 mmol) of **10***a* in 15 mL of a 10:1 methanol–water mixture containing 6 drops of concentrated hydrochloric acid was heated at reflux for 1 h. The cooled solution was poured into 50 mL of water and the mixture extracted with methylene chloride (2 × 20 mL). The combined organic extracts were washed with water (50 mL), dried ($MgSO_4$), and the solvent removed under reduced pressure. The crude residue was shown by tlc to contain two products which were easily separated and purified by silica gel chromatography with a 10% ethyl acetate – hexane mixture as eluent. The first fraction isolated was a colorless crystalline solid (120 mg, 80%) whose structure was assigned as 3,4-dimethyl-6-(1,2,4-triazol-1-yl)-2*H*-thiapyran (**14***a*) on the basis of the following data: mp 96–97°C; ir (Nujol): 3100, 1620, 1580, 1415, 1292, 1270, 1210, 1145, 1100, 1000, 952, 900, 875, and 830 cm^{-1}; nmr ($CDCl_3$) δ: 1.94 (br s, 6H), 3.46 (s, 2H), 6.67 (s, 1H), 8.01 (s, 1H), and 8.42 (s, 1H); ms, *m/e*: 193 (M^+), 178, 124, and 91.

The second fraction isolated was a colorless oil (10 mg, 10%) whose structure was assigned as 3,4-dimethyl-5-hydro-2*H*-thiopyran-6-one (**16***a*) on the basis of the following data: bp 68–70°C at 0.01 Torr (Kugelrohr); ir (neat): 2910, 2855, 1672, 1430, 1213, 1141, 1104, 1040, 903, and 742 cm^{-1}; nmr ($CDCl_3$) δ: 1.93 (s, 6H), 3.19 (s, 2H), and 3.63 (s, 2H); ms, *m/e*: 142 (M^+), 99, 82, and 67.

(c) *HCl in a 4:1 methanol–water mixture*

The above experiment was repeated; however, this time a 4:1 methanol–water mixture was used as solvent. Work-up as described gave 90 mg (60%) 3,4-dimethyl-6-(1,2,4-triazol-1-yl)-2*H*-thiapyran (**14***a*) and 35 mg (33%) 3,4-dimethyl-5-hydro-2*H*-thiapyran-6-one (**16***a*). The physical and spectral properties were identical to those described earlier.

Acidic hydrolysis of 3,3-bis(1,2,4-triazol-1-yl)-2-thiabicyclo[2.2.2]-oct-5-ene (18)

To a solution of 0.2 g (0.76 mmol) of **18** in 10 mL of a 4:1 mixture of methanol–water was added 3 drops concentrated HCl and the mixture heated at reflux for 3 h. The resultant solution was poured into 60 mL of water and the mixture extracted with CH_2Cl_2 (2 × 30 mL). The combined organic extracts were washed with water (50 mL), dried ($MgSO_4$), and the solvent removed under reduced pressure. The crude residue was subjected to silica gel chromatography using a 10% ethyl acetate – hexane mixture as eluent. The first fraction isolated was a colorless oil (50 mg, 38%) whose structure was assigned as methyl 4-mercapto-2-cyclohexenecarboxylate (**20**). The second fraction was a white crystalline solid (60 mg, 56%) whose structure was assigned as 2-thiabicyclo[2.2.2]oct-5-ene-3-one (**19**). Both these compounds were identified on the basis of their physical and spectral data: (**20**) ir (neat): 3030, 2900, 2725, 2560, 1728, 1430, 1290, 1265, 1195, 1165, 1030, 1014, 905, and 735 cm^{-1}; nmr ($CDCl_3$) δ: 1.78 (d, 1H), 2.02 (m, 4H), 3.13 (m, 1H), 3.75 (s, 3H), and 5.87 (m, 2H); ms, *m/e*: 172 (M^+), 139, 112, 108, and 79. (**19**) mp 73–74°C; ir (Nujol): 1680, 1618, 1350, 1330, 1180, 1070, 1010, 905, 880, 835, and 805 cm^{-1}; nmr ($CDCl_3$) δ: 2.0–2.6 (m, 4H), 3.98 (m, 1H), 4.50 (m, 1H), and 6.4–7.2 (m, 2H); ms, *m/e*: 140, 80, and 79.

Treatment of 3,3-bis(1,2,4-triazol-1-yl)-2-thiabicyclo[2.2.2]oct-5-ene (18) with cupric sulfate

A mixture of 100 mg (0.38 mmol) of **18** and 30 mg (0.12 mmol) of cupric sulfate in 20 mL of a 4:1 mixture of methanol–water was heated at reflux for 1 h. The cooled solution was poured into 50 mL of water and the mixture extracted with CH_2Cl_2 (2 × 20 mL). The combined organic extracts were washed with water (100 mL), dried ($MgSO_4$), and the solvent removed under reduced pressure. The crude residue was subjected to silica gel chromatography using a 10% ethyl acetate – hexane mixture as eluent. The major fraction isolated was a colorless liquid (62 mg, 93%) whose structure was assigned as methyl 4-mercapto-2-cyclohexenecarboxylate (**20**) as its physical and spectral data were identical to those described earlier.

Reaction of myrcene (21) with 1,1′-thiocarbonylbis(1,2,4-triazole) (2)

A mixture of 0.75 g (5.5 mmol) of myrcene and 1.0 g (5.5 mmol) of 1,1′-thiocarbonylbis(1,2,4-triazole) in 30 mL of dry benzene was heated at reflux under a nitrogen atmosphere for 1 h. On cooling, the solvent was removed under reduced pressure and the crude residue was subjected to silica gel chromatography with a 50% ethyl acetate – hexane mixture as eluent. The major fraction isolated was a colorless oil (7.5 g, 83%) which contained a 1:1 mixture of the two isomers 6,6-bis(1,2,4-triazol-1-yl)-5,6-dihydro-3-(4-methyl-pent-3-enyl)-2*H*-thiapyran (**22***a*) and its 4-(4-methyl-pent-3-enyl) isomer (**22***b*) identified on the basis of the following data: ir (neat): 3120, 2964, 2920, 2850, 1500, 1380, 1355, 1280, 1200, 1180, 1135, 1005, 950, 880, 820, and 750 cm^{-1}; nmr ($CDCl_3$) δ: 1.76 (br s, 6H), 2.20 (m, 4H), 3.34 (m, 2H), 3.87 (m, 2H), 5.07 (m, 1H), 5.66 (m, 1H), 7.98 (s, 2H), and 8.62 (s, 2H); ms, *m/e*: 316 (M^+), 248, and 136.

*Reaction of 6,6-bis(1,2,4-triazol-1-yl)-5,6-dihydro-3(and the 4 isomer)-(4-methyl-pent-3-enyl)-2*H*-thiapyran (22) with cupric sulfate*

A mixture of 0.60 g (1.9 mmol) of **22***a*, *b* and 0.16 g (0.66 mmol) of cupric sulfate in 10 mL of a 4:1 methanol–water mixture was heated at reflux for 1 h. The cooled reaction mixture was poured into 100 mL of water and the solution extracted with methylene chloride (2 × 50 mL). The combined organic extracts were washed with water (100 mL), dried ($MgSO_4$), and the solvent removed under reduced pressure. The crude residue was then subjected to silica gel chromatography with a 50% ethyl acetate – hexane mixture as eluent. The major fraction isolated was a pale yellow crystalline solid (0.42 g, 90%) which contained a 1:1 mixture of the two isomers, 4-(4-methyl-pent-3-enyl)-6-(1,2,4-triazol-1-yl)-2*H*-thiapyran (**23***b*) and its 3-(4-methyl-pent-3-enyl)- isomer (**23***a*). The structures were assigned on the basis of the following data: ir (Nujol) (**22***a* + **22***b*): 3120, 1645, 1570, 1500, 1270, 1200, 1134, and 100 cm^{-1}; nmr ($CDCl_3$) δ: 1.80 (s, 6H), 2.32 (s, 4H), 3.58 (m, 2H), 5.17 (m, 1H), 5.47 (m, 1H), 6.68 (s, 1H), 8.02 (s, 1H), and 8.46 (s, 1H); (**23***a*) δ: 1.70 (s, 6H), 2.38 (s, 4H), 3.54 (m, 2H), 5.17 (m, 1H), 5.98 (m, 2H), 8.02 (s, 1H), and 8.46 (s, 1H); ms, *m/e* (mixture): 247 (M^+), 232, 204, 178, and 79.

*Acidic hydrolysis of 6,6-bis(1,2,4-triazol-1-yl)-5,6-dihydro-3(and the 4 isomer)-4methyl-pent-3-enyl)-2*H*-thiapyran (22a, b)*

A solution of 0.86 g (2.7 mmol) of **22** in 30 mL of a 4:1 mixture of methanol–water was heated at reflux for 1 h. The cooled solution was poured into 100 mL of water and the mixture extracted with CH_2Cl_2 (2 × 30 mL). The combined organic extracts were washed with water (100 mL), dried ($MgSO_4$), and the solvent removed under reduced pressure. The crude residue was subjected to silica gel chromatography using a 50% ethyl acetate – hexane mixture as eluent. The first fraction isolated was a colorless oil (0.22 g, 41%) whose structure was assigned as 5-hydro-3(and the 4-isomer)-(4-methyl-pent-3-enyl)-2*H*-thiapyran-6-one (**24**) on the basis of the following spectral data: ir (neat): 2950, 2900, 1725, 1655, 1425, 1365, 1247, 1150, 1095, 1062, 1028, 880, 820, and 745 cm^{-1}; nmr ($CDCl_3$) δ: 1.73 (m, 12H), 2.25 (m, 8H), 3.17 (br s, 4H), 3.63 (br s, 2H), 3.78 (br s, 2H), 5.17 (br s, 2H), 5.72 (m, 1H), and 5.95 (m, 1H); ms, *m/e*: 196 (M^+), 168, 136, 128, and 79.

The second fraction isolated was a pale yellow crystalline solid (0.29 g, 43%) whose structure was assigned as 5-hydro-3(and the 4-isomer)-(4-methyl-pent-3-enyl)-6-(1,2,4-triazol-1-yl)-2*H*-thiapyran (**23**) on the basis of its spectral data and comparison with a sample reported earlier in the experimental section.

Acknowledgements

We thank the Natural Sciences and Engineering Research Council of Canada and the Department of Education of Quebec for financial support of this work.

1. H. A. STAAB. Angew. Chem. **73**, 148 (1961); H. A. STAAB and G. WALTHER. Justus Liebigs Ann. Chem. **657**, 98 (1962).
2. U. G. ANHTHONI, C. LARSEN, and P. H. NIELSON. Acta. Chem. Scand. **20**, 1714 (1966); C. R. JOHNSON, J. E. KEISER, and J. C. SHARP. J. Org. Chem. **34**, 860 (1969); B. ZWANENBURG, L. THIJS, J. B. BROENS, and J. STRATING. Recl. Trav. Chim. Pays-Bas, **91**, 443 (1972); E. BLOCK. Org. React. **30**, 457 (1984).
3. C. LARSEN, K. STELIOU, and D. N. HARPP. J. Org. Chem. **43**, 337 (1978); C. LARSEN and D. N. HARPP. J. Org. Chem. **46**, 2465 (1981); Phosphorus Sulfur, **19**, 91 (1984).
4. E. J. COREY and R. A. E. WINTER. J. Am. Chem. Soc. **85**, 2677 (1963).
5. A. KRIEF, L. HEVESI, J. B. NAGY, and E. G. DEROUANE. Angew. Chem. **89**, 103 (1977).
6. D. N. HARPP and J. G. MACDONALD. Tetrahedron Lett. 4927 (1983).
7. (*a*) C. LARSEN and D. N. HARPP. J. Org. Chem. **45**, 3713 (1980); (*b*) E. VEDEJS, D. A. PERRY, K. N. HOUK, and N. G. RONDAN. J. Am. Chem. Soc. **105**, 6999 (1983).
8. D. ST. C. BLACK and K. G. WATSON. Aust. J. Chem. **26**, 2491 (1973).
9. G. MAZZANTI, G. MACCAGNANI, B. F. BONINI, and P. PEDRINI. Gazz. Chim. Ital. **110**, 163 (1980).
10. D. ST. C. BLACK and K. G. WATSON. Angew. Chem. Int. Ed. Engl. **11**, 47 (1972).
11. J. HAMER and A. MACALUSO. Chem. Rev. **64**, 473 (1964).
12. W. J. MIDDLETON. J. Org. Chem. **30**, 1390 (1965); G. LABAN and R. MAYER. Z. Chem. **7**, 227 (1967); C. R. JOHNSON, J. E. KEISER, and J. C. SHARP. J. Org. Chem. **34**, 860 (1969); H. J. REICH and J. E. TREND. J. Org. Chem. **38**, 2637 (1973).
13. J. HAMER (*Editor*). 1,4-Cycloaddition reactions. Academic Press, New York. 1967; H. WOLLWEBER. Diels–Alder reaktion. Thieme Verlag, Stuttgart. 1972; S. M. WEINREB and R. R. STAIB. Tetrahedron, 3087 (1982).
14. W. J. MIDDLETON. J. Org. Chem. **30**, 1395 (1965); M. S. RAASCH. J. Org. Chem. **40**, 161 (1975); A. SHONBERG and B. KONIG. Tetrahedron Lett. 3361 (1965); K. YAMADA, M. YOSHIOKA, and N. SUGIYAMA. J. Org. Chem. **33**, 1240 (1968); Y. OKMOTE, M. YOSHIOKA, K. YAMADA, and N. SUGIYAMA. J. Org. Chem. **32**, 3676 (1967); K. HARTKLE, T. KISSEL, J. QUANTE, and G. HENSSEN. Angew. Chem. Int. Ed. Engl. **17**, 953 (1978); K. FRIEDRICH and H. J. GALLMEIER. Tetrahedron Lett. 2971 (1981).
15. A. OHNA, Y. OHNISHI, and G. TSUCHIHASHI. Tetrahedron, 871 (1969).
16. J. E. BALDWIN and R. C. G. LOPEZ. J. Chem. Soc. Chem. Commun. 1029 (1982); C. M. BLADON, I. E. G. FERGUSON, G. W. KIRBY, A. W. LOCKHEAD, and D. C. MCDOUGALL. J. Chem. Soc. Chem. Commun. 423 (1983); E. VEDEJS, T. H. EBERLEIN, and D. L. VARIE. J. Am. Chem. Soc. **104**, 1445 (1982); E. VEDEJS and D. A. PERRY. J. Org. Chem. **49**, 573 (1984).
17. E. J. COREY, N. M. WEINSHENKER, T. K. SCHAAF, and W. HUBER. J. Am. Chem. Soc. **91**, 5675 (1969).
18. W. G. BLENDERMAN, M. M. JOULLIE, and G. PRETI. J. Org. Chem. **48**, 3206 (1983), and references cited therein.
19. H. E. DE LA MARE and G. M. COPPINGER. J. Org. Chem. **28**, 1068 (1963).
20. R. BONNETT, R. F. C. BROWN, V. M. CLARK, I. O. SUTHERLAND, and A. J. TODD. J. Chem. Soc. 2094 (1959).
21. O. EXNER. Collect. Czech. Chem. Commun. **16**, 258 (1951).
22. P. WOLKOFF and S. HAMMERUM. Acta Chem. Scand. Ser. B, **30**, 837 (1976).
23. R. I. MELTZER, A. D. LEWIS, and J. A. KING. J. Am. Chem. Soc. **77**, 4062 (1955).
24. BEILSTEIN'S. Handbuch der organischen Chemie. Vol. 9. p. 201.
25. K. C. LUI, B. R. SHELTON, and R. K. HOWE. J. Org. Chem. **45**, 3916 (1980).
26. D. N. HARPP, T. AIDA, J. DE CESARE, P. TISNES, and T. H. CHAN. Synthesis. In press.

Stéréochimie des complexes du chlorure d'iode avec les bases carbonylées

MICHEL BERTHELOT, MARYVONNE HELBERT ET CHRISTIAN LAURENCE[1]

Laboratoire de Spectrochimie Moléculaire – U.E.R. de Chimie, Université de Nantes, 2, rue de la Houssinière, 44072 Nantes, France

Reçu le 13 juillet 1984

MICHEL BERTHELOT, MARYVONNE HELBERT et CHRISTIAN LAURENCE. Can. J. Chem. **63**, 958 (1985).

Le dédoublement des bandes ν(I—Cl) et ν(C═O) des complexes du chlorure d'iode avec des bases carbonylées en solution très diluée dans l'heptane a été attribué à l'existence de deux complexes 1 : 1 stéréoisomères: un complexe linéaire (ICl dans l'axe de la liaison carbonyle) et un complexe angulaire (ICl dans la direction d'une paire libre de l'oxygène). Dans les séries RCOOEt, RCOPh, RCO*t*-Bu, R_2CO, $RCONPh_2$ et $RCONMe_2$ où R = Me, Et, i-Pr ou *t*-Bu, on passe progressivement du complexe angulaire pour R = Me au complexe linéaire pour R = *t*-Bu car la présence de substituants encombrants sur le groupe carbonyle déstabilise le complexe angulaire. Dans les séries RCOH et RCOMe le complexe est angulaire quel que soit l'effet stérique de R car ICl se fixe sur la paire libre proche de H ou Me, substituants non encombrants. En présence d'un excès de ICl un complexe 1:2 apparaît.

MICHEL BERTHELOT, MARYVONNE HELBERT, and CHRISTIAN LAURENCE. Can. J. Chem. **63**, 958 (1985).

The splitting of the ν(I—Cl) and ν(C═O) bands of ICl complexes with carbonyl bases in highly diluted heptane solutions is explained by the existence of two 1 : 1 stereoisomeric complexes: a linear complex (ICl along the axis of the carbonyl bond) and an angular complex (ICl in the direction of a lone pair). In the series RCOOEt, RCOPh, RCO*t*-Bu, R_2CO, $RCONPh_2$, and $RCONMe_2$, where R = Me, Et, i-Pr, or *t*-Bu, the angular complex for R = Me transforms into the linear complex for R = *t*-Bu, since bulky substituents on the carbonyl group destabilize the angular arrangement. In the series RCOH and RCOMe the complex is angular whatever the steric effect of R, since ICl is located on the lone pair near the small H or Me substituents. When ICl is added in excess, a 1:2 complex appears.

Introduction

Dans un article précédent (1) nous avons mis en évidence deux complexes stéréoisomères (a) et (b) lors de la formation d'une liaison hydrogène sur le groupe carbonyle à partir du dédoublement de la vibration de valence ν(XH...). Dans le complexe (a) la géométrie est déterminée par une optimisation

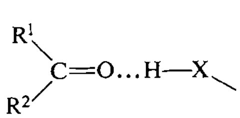

(a)

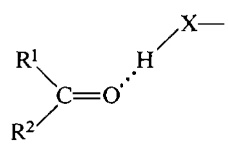

(b)

de l'interaction électrostatique et dans le complexe (b) par une optimisation de l'interaction covalente. L'énergie de répulsion dépend de l'encombrement stérique du donneur de proton et des substituants R^1 et R^2 et est minimum dans la configuration (a).

Il est intéressant de savoir si d'autres acides de Lewis que les donneurs de proton présentent cette stéréoisomérie de complexation en solution. Parmi les acides de Lewis d'encombrement et de caractère électrostatique/covalent différents de ceux des donneurs de proton, le chlorure d'iode a été choisi dans ce travail car sa vibration de valence ν(I—Cl) (à 375,6 cm^{-1} dans l'heptane) s'abaisse fortement par complexation avec des bases de Lewis (2–6) et il donne des complexes suffisamment forts avec les bases carbonylées[2] pour provoquer également un abaissement important de la vibration ν(C═O) (7).

En confrontant les résultats obtenus par l'étude simultanée des vibrateurs ν(C═O) et ν(I—Cl) il est alors possible de mettre en évidence trois types de complexes (a), (b) et (c) dans les solutions d'ICl et de base carbonylée dans l'heptane.

[1]Auteur à qui toute correspondance doit être adressée.

[2]Les enthalpies de formation varient de −25,5 kJ mol^{-1} pour MeCOOEt (8) à −39,7 kJ mol^{-1} pour $MeCONEt_2$ (9).

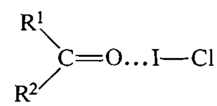

(a)

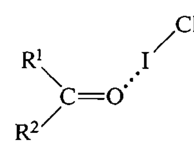

(b)

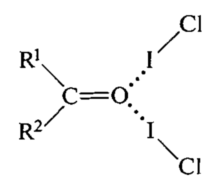

(c)

Partie expérimentale

Produits

La purification et la dessiccation de l'heptane et des bases carbonylées ont été précédemment décrites (1). Le chlorure d'iode Aldrich, garanti à 98%, est conservé et manipulé à l'abri de l'humidité.

Spectres

Ils sont enregistrés immédiatement après préparation de la solution sur un spectrophotomètre Perkin–Elmer 580B balayé par de l'air sec, travaillant à une résolution de 2 cm^{-1} dans les régions ν(CO) et ν(I—Cl). Les opérations de stockage, soustraction (des spectres du solvant et de ICl libre ou de la base libre), expansion et lissage des spectres sont effectuées sur une station de données PE 3500 grâce au logiciel PE 580.

Cellules et solutions

Les solutions sont effectuées dans l'heptane, solvant apolaire qui doit minimiser l'ionisation des complexes (5,6). Dans la région ν(I—Cl) une cellule en polyéthylène avec une cale d'épaisseur en Teflon permet d'éviter l'attaque des faces et de la cale par ICl. Une épaisseur de 6 mm permet de travailler avec des concentrations en ICl environ 10^{-2} *M* suffisamment faibles pour retarder d'éventuelles réactions d'halogénation de la base ou pour éviter la précipitation des complexes. La concentration de la base varie de 0,5 *M* à 10^{-2} *M* selon la stabilité du complexe. Dans la région ν(CO) une cellule CaF_2 de 1 mm permet de travailler avec des concentrations de l'ordre de celles de la région ν(I—Cl). Les solutions sont préparées et les cellules sont remplies en boîte sèche. Dans le spectrophotomètre les cellules sont thermorégulées à 20°C.

Décomposition des spectres

La soustraction de la bande ν(CO) libre ou de la bande ν(ICl) libre est effectuée directement sur la station de données, ce qui évite une décomposition mathématique du massif constitué par la superposition

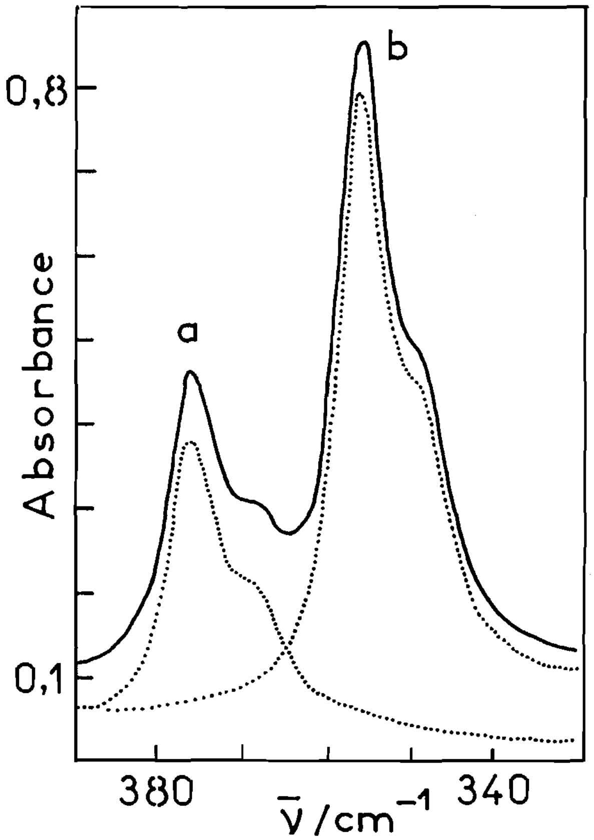

FIG. 1. Bandes ν(I—Cl) libre (a) et complexée (b) montrant la formation équilibrée d'un complexe cyclobutanone−ICl dans l'heptane. Concentrations: ICl ~0,01 *M* et cyclobutanone ~0,03 *M*.

des bandes du complexe et des molécules libres. Dans les cas où les bandes de plusieurs complexes se recouvrent la décomposition est effectuée mathématiquement comme précédemment (1).

Résultats

Région ν(I—Cl)

La bande d'absorption infrarouge ν(I—Cl) à 375,6 cm^{-1} dans l'heptane présente un épaulement aux basses fréquences attribué à l'isotope I^{37}Cl. Les rapports expérimentaux des fréquences et des absorbances au maximum des deux composantes du massif obtenues après décomposition sont en bon accord avec le rapport ν(I—^{37}Cl)/ν(I—^{35}Cl) = 0,9786 calculé dans l'approximation de l'oscillateur harmonique et avec l'abondance 24,5% de l'isotope ^{37}Cl.

Comme l'illustre la fig. 1, l'addition d'une base carbonylée à une solution de ICl dans l'heptane provoque, par formation équilibrée d'un complexe, l'apparition d'une nouvelle bande aux basses fréquences, déplacée de 3,5 cm^{-1} pour CF_3COOEt à 42,6 cm^{-1} pour la diméthyl-2,6-γ-pyrone.

Pour un certain nombre de cétones et d'esters, deux nouvelles bandes dénotées b (basse fréquence) et h (haute fréquence) apparaissent (fig. 2F, 2G). L'examen de l'évolution des fréquences et des intensités des deux nouvelles bandes dans les séries RCOOEt, RCOPh, RCO*t*-Bu et R_2CO, où R=Me puis Et puis i-Pr puis *t*-Bu, montre que c'est principalement la bande b qui est présente quand R=Me et la bande h quand R=*t*-Bu, alors que pour R=i-Pr ou Et, généralement les deux bandes b et h coexistent en proportions variables (fig. 2E à 2H).

Pour quelques complexes la bande ν(I—Cl) du complexe est plus fine que la bande ν(I—Cl) libre. Ceci provoque une meilleure résolution des deux isotopes et il apparaît, comme dans le cas précédent, deux bandes mais leurs fréquences et leurs intensités sont dans les rapports isotopiques 0,9786 et 24,5% ce qui permet de les attribuer aux deux isotopes et non aux bandes b et h précédentes (fig. 2H).

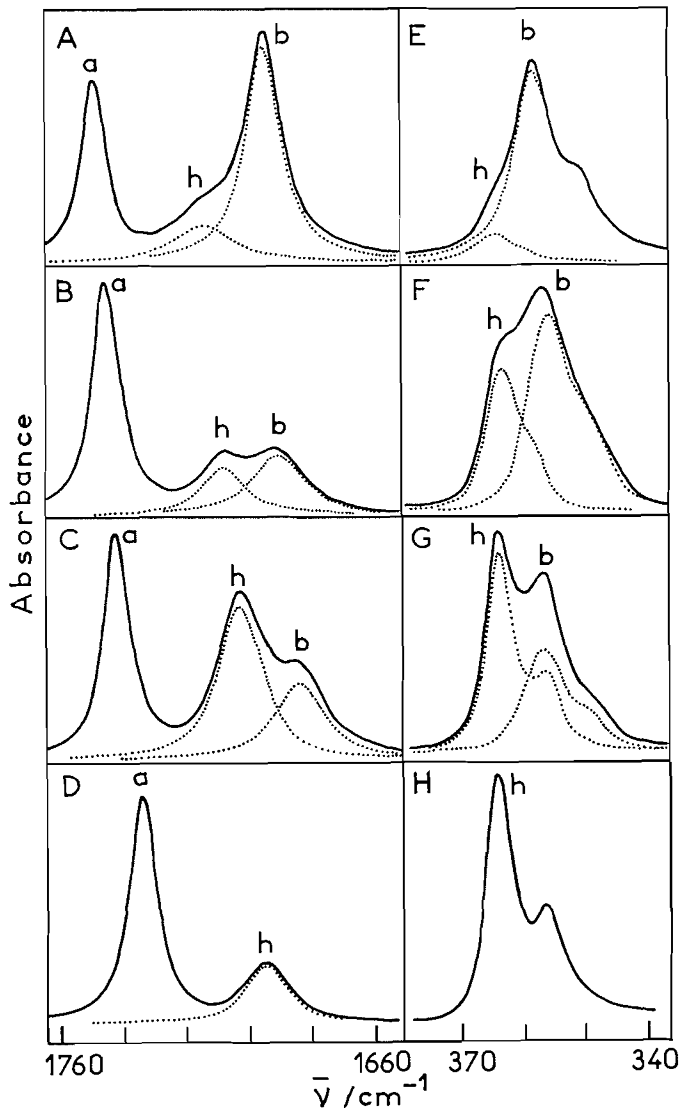

FIG. 2. Bandes ν(I—Cl) et ν(C=O) des complexes de ICl avec MeCOOEt (A et E), EtCOOEt (B et F), i-PrCOOEt (C et G) et *t*-BuCOOEt (D et H). Les bandes libres ont été soustraites dans la région ν(I—Cl). (a) Bande ν(C=O) libre, (h) complexe linéaire, (b) complexe angulaire.

Région ν(C=O)

L'addition de ICl à une solution de base carbonylée dans l'heptane provoque l'apparition d'une nouvelle bande aux basses fréquences, déplacée de 22 cm^{-1} pour MeCOH à 72 cm^{-1} pour $EtCONMe_2$.

Quand deux bandes b et h étaient apparues dans la région ν(I—Cl), on observe également deux nouvelles bandes dans la région ν(C=O) dans un rapport d'intensité voisin de celui observé pour ν(I—Cl) (fig. 2B et 2C).

Dans de rares cas deux nouvelles bandes apparaissent dans la région ν(C=O) par addition de ICl, alors qu'une seule nouvelle bande avait été observée dans la région ν(I—Cl) par addition de base carbonylée. La propension de la fondamentale

TABLEAU 1. Déplacements $\Delta\nu$(I—Cl) (cm^{-1}) pour les complexes linéaire (bande h) et angulaire (bande b) de ICl avec les bases carbonylées dans l'heptane

Base	$\Delta\nu$(I—Cl) h	$\Delta\nu$(I—Cl) b	Base	$\Delta\nu$(I—Cl) h	$\Delta\nu$(I—Cl) b	Base	$\Delta\nu$(I—Cl) h	$\Delta\nu$(I—Cl) b
Esters, carbonates			*Amides*			*Cétones*		
CCl_3COOEt	~4,6		$ClCONPh_2$		13,2	Cyclobutanone		19,8
CF_3COOEt	~3,5		$ClCONMe_2$		15	Cyclopentanone		22,8
ClCOOEt		9,6	CF_3CONMe_2	12,1		Cyclohexanone		23,2
HCOOPh		11	CCl_3CONMe_2	12,4		MeCOMe		20,3
Ethylène carbonate		~12,8	$PhCONPh_2$		26,7	MeCOEt		21,5
HCOOMe		11,4	$HCONPh_2$		27,5	MeCOi-Pr		21,8
HCOOEt		13	HCONMePh		29,2	MeCO*t*-Bu		23,4
Propylène carbonate		13,8	$PhCONMe_2$		32,4	MeCO Adamantyl		23,3
MeOCOOMe	8,1		*N*-méthylpipéridone-2		34,0	EtCOEt	[a]	21,4
MeOCOOEt	9		$i\text{-}PrCONMe_2$	25,3		i-PrCOi-Pr	13,6	21,2
EtOCOOEt	9,5		*t*-$BuCONMe_2$	25,3		*t*-BuCO*t*-Bu	10,9	
PhCOOMe	10,6		$MeCONMe_2$		34,5	*t*-BuCOEt	12,5	21
MeCOOMe		16,5	$EtCONMe_2$		35,1	*t*-BuCOi-Pr	13,5	
Cyclohexyl COOMe	11,5		$MeCONEt_2$		36,0	Cyclopropyl COMe		23
PhCOOEt	11,3		$HCONMe_2$		36,1	$(Cyclopropyl)_2CO$	15,5	24,4
EtCOOEt	12,7	18,5	*p*-$MeOC_6H_4CONEt_2$		36,3	$MeCOCCl_3$		~6,8
i-PrCOOEt	11,8	18,3	$HCONEt_2$		37,1	$MeCOCF_3$		~4,7
MeCOOEt		16,9	*N*-formylpipéridine		38,1	$PhCOCF_3$		~4,8
t-BuCOOEt	11,2		$MeCONPh_2$		30,0	PhCOMe		21,8
γButyrolactone		18,7	$i\text{-}PrCONPh_2$	22,5		*p*-$NO_2C_6H_4COMe$		15,7
Cyclopropyl COOMe	11,4	19,3				*m*-$NO_2C_6H_4COMe$		16,1
Cyclopropyl COOEt	12,0	19,7	*Aldéhydes*			*p*-$OMeC_6H_4COMe$		25,6
						PhCOEt	13,1	21,8
Urées			MeCOH		15,2	PhCOi-Pr	13,1	
			EtCOH		16,6	PhCO*t*-Bu	12	
$Me_2NCONMe_2$	34,4		i-PrCOH		17,1	PhCOPh		19,1
$Et_2NCONEt_2$	36,4		Cyclohexyl COH		18,8	1-Naphtyl COMe		22,2
			t-BuCOH		19,8	2-Naphtyl COMe		23,4
Carbamates			PhCOH		19,3	α-Tetralone		25,4
			p-$MeOC_6H_4COH$		23,8	Indanone-1		26,8
$EtOCONMe_2$	21,4		*p*-MeC_6H_4COH		24,7	Xanthone	17,9	
$MeOCONMe_2$	20,2					Chromone		30,9
$EtOCONPh_2$	18,2		*Chlorures d'acide*			γ-Pyrone		32,6
$MeOCONPh_2$	16,7					Dimethyl-2,6-γ-pyrone		42,6
$PhOCONPh_2$	15,9		MeCOCl		~5,4	Flavone		36,4
			PhCOCl		~7	Diméthyl-5,5-cyclohexénone		25,8
						Isophorone		29,7
						Diméthyl-5,5-Cl-3-cyclohexénone		23,3

[a]Présence d'une bande h difficilement pointable.

ν(C=O) à entrer en résonance de Fermi avec des bandes harmoniques ou de combinaison dans ces molécules complexes généralement sans élément de symétrie peut expliquer cette discordance.

L'addition d'un excès de ICl, correspondant à la quasi-disparition de la bande ν(C=O) libre, permet d'observer dans de nombreux cas l'apparition d'une bande supplémentaire au massif ν(C=O) obtenu en solution diluée de ICl (fig. 3).

Les tableaux 1 et 2 rassemblent les déplacements de fréquence $\Delta\nu$(I—Cl) = ν(I—Cl)libre − ν(I—Cl)complexe et $\Delta\nu$(C=O) = ν(C=O)libre − ν(C=O)complexe, mesurés pour un certain nombre d'esters, carbonates, urées, carbamates, amides, aldéhydes et cétones. Ces $\Delta\nu$ se rapportent aux complexes b et/ou h, en fonction de la discussion ci-dessous.

Discussion

Complexe angulaire et complexe linéaire

Bien qu'aucun calcul théorique n'ait été effectué, à notre connaissance, sur les complexes de ICl avec les composés carbonylés, il est évident que trois principaux termes contribuent à l'énergie d'interaction entre ICl et une base carbonylée: un terme électrostatique (le moment dipolaire de ICl vaut 1,48 D dans le cyclohexane (10)), un terme covalent et un terme de répulsion. Il est clair que l'interaction électrostatique est optimisée dans la configuration linéaire $\overrightarrow{C{=}O}\ldots\overrightarrow{ICl}$. Il est probable que, comme pour les donneurs de proton, l'interaction covalente est optimisée lorsque ICl se place dans l'axe d'une paire libre. Une telle configuration angulaire a été trouvée, à l'état solide, pour le complexe acétone–dibrome (11). Il est enfin évident que la présence de groupes volumineux R^1 et R^2 sur le carbonyle augmente plus l'énergie de répulsion dans le complexe angulaire que dans le complexe linéaire.

La concordance entre les régions ν(C=O) et ν(I—Cl) et la dilution des solutions étudiées indiquent qu'il peut se former deux complexes 1:1 en solution. Par analogie avec les complexes des bases carbonylées avec des donneurs de proton (1),

TABLEAU 2. Déplacements $\Delta\nu(C{=}O)$ (cm^{-1}) pour les complexes linéaire (bande h) et angulaire (bande b) de ICl avec les bases carbonylées dans l'heptane

Base	$\Delta\nu(C{=}O)$ h	$\Delta\nu(C{=}O)$ b	Base	$\Delta\nu(C{=}O)$ h	$\Delta\nu(C{=}O)$ b	Base	$\Delta\nu(C{=}O)$ h	$\Delta\nu(C{=}O)$ b
Esters			$MeCONPh_2$		67,5	MeCOi-Pr		37,9
			i-$PrCONPh_2$	55,9		MeCO*t*-Bu		34,5
MeCOOEt	~35	54,5	*N*-méthylpipéridone-2		66,5	EtCOEt	22,1	38,6
EtCOOEt	38,7	54,9	CF_3CONMe_2	31,6		i-PrCOi-Pr	26,4	43,9
i-PrCOOEt	40	57				*t*-BuCO*t*-Bu	25,6	
t-BuCOOEt	37,9		*Aldéhydes*[a]			*t*-BuCOEt	26,2	~39
Cyclopropyl COOMe	38,8	51,4				*t*-BuCOi-Pr	26,4	
			MeCOH		22,8	PhCOMe		38
Amides			*t*-BuCOH		26,8	PhCOEt	25,3	46,4
						PhCOi-Pr	27,9	
$MeCONMe_2$		65,2	*Cétones*			PhCO*t*-Bu	23,1	
$EtCONMe_2$		71,6				$(Cyclopropyl)_2CO$	32,9	51,4
i-$PrCONMe_2$	52,2		MeCOMe		26,8[b]			
t-$BuCONMe_2$	50		MeCOEt		34,6			

[a]Des multiplets de Fermi perturbent l'étude de EtCHO et i-PrCHO.
[b]Valeur faible comparativement à MeCOEt du fait d'une résonance de Fermi sur la fondamentale libre.

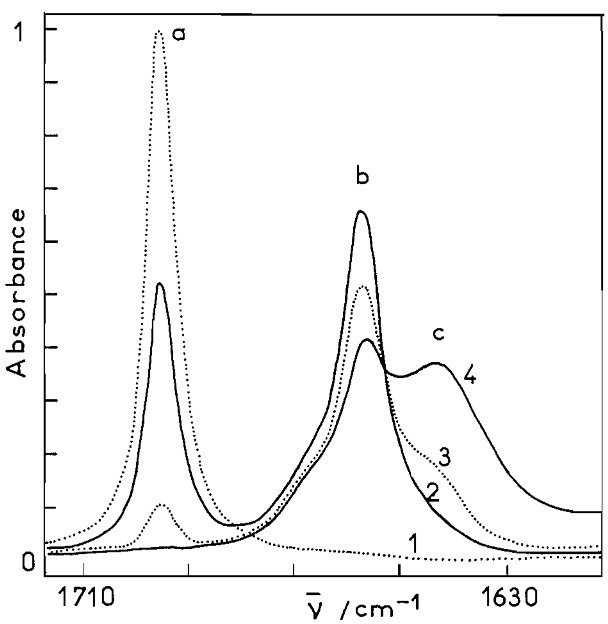

FIG. 3. Modification de la région $\nu(C{=}O)$ de l'acétophénone 0,015 *M* dans l'heptane par addition de quantités croissantes de ICl: (1) 0 (2) 0,03 *M* (3) 0,15 *M* (4) 0,5 *M*. (a) Bande libre, (b) complexe angulaire 1:1, (c) complexe 1:2.

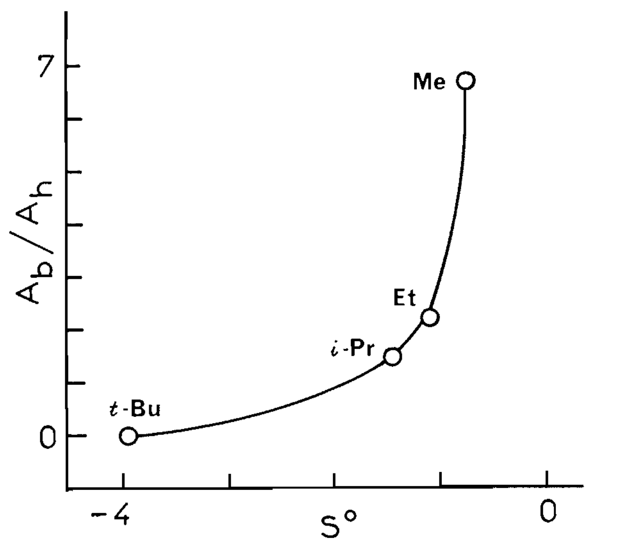

FIG. 4. Rapports d'intensité des bandes h et b (région $\nu(C{=}O)$) pour les complexes RCOOEt—ICl en fonction du paramètre stérique S^0 de R.

nous pensons que ces deux complexes sont l'un le complexe angulaire, l'autre le complexe linéaire.

*Attribution de la bande b au complexe angulaire et de la bande h au complexe linéaire par variation stérique dans les séries RCOOEt, RCOPh, RCO*t*-Bu et R_2CO*

La bande b disparaît au profit de la bande h dans les séries RCOOEt, RCOPh, RCO*t*-Bu et R_2CO quand l'encombrement du substituant variable R, mesuré par le paramètre stérique S^0(12), augmente en passant de Me à *t*-Bu (fig. 4). Les substituants constants OEt, Ph et *t*-Bu étant suffisamment volumineux ($S^0 = -1{,}36$, $-1{,}82$ et $-3{,}94$ respectivement) pour restreindre l'approche de ICl de leur côté, nous expliquons ce phénomène par un empêchement progressif de l'attaque angulaire de ICl sur la paire libre voisine de R, lorsqu'on passe de R = Me à R = *t*-Bu. Nous attribuons donc la bande b au complexe angulaire et, par voie de conséquence, la bande h au complexe linéaire, beaucoup moins sensible aux effets stériques.

Attribution angulaire ou linéaire dans le cas d'un complexe unique. Séries RCOMe, RCOH, $RCONMe_2$ et $RCONPh_2$

Dans les séries RCOMe et RCOH, on observe toujours un seul complexe quel que soit le volume stérique de R. De plus ce complexe ne change pas de structure pour R=Me, Et, i-Pr ou *t*-Bu puisque les déplacements $\Delta\nu(I{-}Cl)$ et $\Delta\nu(C{=}O)$ varient peu, ou régulièrement, dans ces séries (ce qui était attendu du fait des effets électriques voisins de ces quatre alkyles sur la basicité de l'oxygène). L'étude de la série RCO*t*-Bu ayant montré que pour MeCO*t*-Bu ce complexe est angulaire, il s'ensuit que pour MeCOEt, MeCOi-Pr et Me_2CO ce complexe est également angulaire car S^0(Me,Et ou i-Pr) < S^0(*t*-Bu). A fortiori HCOMe, HCOEt, HCOi-Pr et HCO*t*-Bu donnent aussi un complexe angulaire puisque S^0(H) < S^0(Me).

L'invariance de structure du complexe en dépit de l'évolution dramatique de l'encombrement stérique de R dans les séries RCOMe et RCOH provient à l'évidence de la fixation de ICl sur la paire libre restée dégagée du côté des petits substituants constants $H(S^0 = 0)$ et $Me(S^0 = -0{,}73)$.

Dans la série $RCONMe_2$ on observe également toujours un seul type de complexe. Mais les valeurs de $\Delta\nu$(I—Cl) montrent que l'on passe d'un complexe angulaire pour R=Me et Et ($\Delta\nu$ = 34,5 et 35,1 cm^{-1}) à un complexe linéaire pour R=i-Pr et *t*-Bu ($\Delta\nu$ = 25,3 cm^{-1}). Par analogie il est probable que la valeur $\Delta\nu$(I—Cl) = 30 cm^{-1} de $MeCONPh_2$ correspond au complexe angulaire et la valeur 22,5 cm^{-1} de i-Pr $CONPh_2$ au complexe linéaire.

Pour les autres bases carbonylées R^1COR^2 montrant des bandes ν(I—Cl) et ν(C=O) de complexe uniques, une tentative d'attribution "angulaire" ou "linéaire" est effectuée dans les tableaux sur la base (*i*) de l'encombrement des paires libres: les faibles valeurs de S^0 pour un substituant (séries $HCOR^2$, $ClCOR^2$ et $MeCOR^2$) et la cyclisation qui dégage les paires (carbonates cycliques, lactones, cycloalcanones, lactames) favorisent le complexe angulaire tandis que les fortes valeurs de S^0 pour les deux substituants R^1 et R^2 (urées, carbamates) et la conformation s-*cis*,s-*cis* des carbonates favorisent le complexe linéaire; (*ii*) des séquences de basicité obtenues précèdemment avec les donneurs de proton (1): ainsi $\Delta\nu$(I—Cl) = 11,5 et 16,5 cm^{-1} respectivement pour $C_6H_{11}COOMe$ et MeCOOMe alors que $C_6H_{11}COOMe$ apparaît plus basique vis-à-vis du méthanol; l'inversion est attribuée au passage d'un complexe angulaire pour MeCOOMe à un complexe linéaire pour $C_6H_{11}COOMe$.

Complexe 1:2.

Puisqu'une bande supplémentaire apparaît lorsque ICl est en excès par rapport à la base carbonylée, nous l'attribuons à un complexe d'ordre supérieur à 1:1. La possibilité pour une molécule de base oxygénée de fixer deux molécules d'acide de Lewis grâce aux deux paires libres de l'oxygène déjà été mise en évidence (*i*) pour les donneurs de proton avec les bases carbonylées (13), (*ii*) pour le cyanure d'iode avec l'oxyde de triphénylarsine (14) et (*iii*) pour l'iodophénylacétylène et l'iodocyanoacétylène avec l'oxyde de triphénylarsine (15). Nous attribuons donc cette bande supplémentaire au complexe 1:2 du type (c) représenté ci-dessus.

1. C. LAURENCE, M. BERTHELOT et M. HELBERT. Spectrochim. Acta Part A. Sous presse.
2. W. B. PERSON, R. E. HUMPHREY, W. A. DESKIN et A. I. POPOV. J. Am. Chem. Soc. **80**, 2049 (1958).
3. W. B. PERSON, R. E. ERICKSON et R. E. BUCKLES. J. Am. Chem. Soc. **82**, 29 (1960).
4. J. YARWOOD et W. B. PERSON. J. Am. Chem. Soc. **90**, 3930 (1968).
5. S. G. W. GINN et J. L. WOOD. Trans. Faraday Soc. **62**, 777 (1968).
6. G. A. BOWMAKER, K. H. TAN et M. J. TAYLOR. Aust. J. Chem. **33**, 1743 (1980).
7. E. AUGDAHL et P. KLABOE. Acta Chem. Scand. **16**, 1647 (1962).
8. D. G. BROWN, R. S. DRAGO et T. F. BOLLES. J. Am. Chem. Soc. **90**, 5706 (1968).
9. M. QUEIGNEC et C. LAURENCE. J. Chim. Phys. **79**, 603 (1982).
10. A. L. MCCLELLAN. Tables of experimental dipole moments. Freeman, San Francisco. 1963.
11. O. HASSEL et K. O. STROMME. Acta Chem. Scand. **13**, 275 (1959).
12. U. BERG, R. GALLO, G. KLATTE et J. METZGER. J. Chem. Soc. Perkin Trans. 2, 1350 (1980).
13. P. COMBELAS, C. GARRIGOU-LAGRANGE et J. LASCOMBE. Ann. Chim. (France), **5**, 315 (1970).
14. J. GRUNDNES et R. DAHL. Spectrochim. Acta Part A, **26**, 541 (1970).
15. C. LAURENCE, M. QUEIGNEC-CABANETOS et B. WOJTKOWIAK. J. Chem. Soc. Perkin Trans. 2, 1605 (1982).

Cyclopentadienyl ruthenium complexes. Part III.[1] Reactivity of some η^5-cyclopentadienylbis(triphenylphosphine)ruthenium(II) complexes with nitrosyl tribromide[2] and dinitrogen trioxide

R. F. N. ASHOK, M. GUPTA, K. S. ARULSAMY, AND U. C. AGARWALA
Department of Chemistry, Indian Institute of Technology, Kanpur 208 016, India

Received May 25, 1984

R. F. N. ASHOK, M. GUPTA, K. S. ARULSAMY, and U. C. AGARWALA. Can. J. Chem. **63**, 963 (1985).

Mixed ruthenium(II) nitrosyls have been synthesized in yields larger than 60% by a general reaction of $[Ru(\eta^5\text{-}C_5H_5)(PPh_3)L]^+X^-$ (L = 2,2′-bipyridine or 1,10-phenanthroline, X^- = Cl^- or Br^-) or $[Ru(\eta^5\text{-}C_5H_5)(PPh_3)(L)X]$ (L = PPh_3, pyridine, 3-picoline, 4-picoline, $\frac{1}{2}$(2,2′-bipyridine), or $\frac{1}{2}$(1,10-phenanthroline); X^- = Cl^-, Br^-, I^-, CN^-, NCS^-, H^-, or $SnCl_3^-$) with $NOBr_3$ and N_2O_3. In these complexes NO seems to bind with the metal ion as NO^+. The reactions of N_2O_3 gave either nitrito or nitrosyl dinitrito complexes. The reactions of $NOBr_3$ with trichlorostannate complexes did not yield nitrosyl complexes, instead nitrito complexes were isolated in which spectroscopic evidence (ir, ^{1}H nmr) suggest π-interaction of one of the phenyl rings of the triphenylphosphine ligand to the ruthenium center. All products are characterised by elementary microanalyses, conductivity, magnetic moment measurements, electronic, ir, and ^{1}H nmr spectral data.

R. F. N. ASHOK, M. GUPTA, K. S. ARULSAMY et U. C. AGARWALA. Can. J. Chem. **63**, 963 (1985).

Faisant appel à une réaction générale du $[Ru(\eta^5\text{-}C_6H_5)(PPh_3)L]^+X^-$ (L = bipyridine-2,2′ ou phénanthroline-1,10, X^- = Cl^- ou Br^-) ou du $[Ru(\eta\text{-}C_5H_5)(PPh_3)(L)X]$ (L = PPh_3, pyridine, picoline-3, picoline-4, (1/2)(bipyridine-2,2′) ou (1/2)(phénanthroline); X^- = Cl^-, Br^-, I^-, CN^-, NCS^-, H^- ou $SnCl_3^-$) avec le $NOBr_3$ ou le N_2O_3, on a réussi à synthétiser des nitrosyles mixtes de ruthénium avec des rendements supérieurs à 60%. Dans ces complexes, il semble que le NO soit lié au métal sous la forme d'un ion NO^+. Les réactions impliquant le N_2O_3 conduisent à des complexes des types nitrito ou nitrosyl dinitrito. Les réactions du $NOBr_3$ avec les complexes trichlorostannates ne fournissent pas de complexes de type nitrosyle; on a plutôt isolé des complexes de type nitrito pour lesquels les données spectroscopiques (ir et rmn du ^{1}H) suggèrent l'existence d'une interaction-π de l'un des cycles phényles du ligand triphénylphosphine avec le centre ruthénium. On a caractérisé tous les produits grâce à leurs analyses élémentaires, à des mesures de conductivité et de moments dipolaires et à leurs spectres électroniques, ir et de rmn du ^{1}H.

[Traduit par le journal]

Introduction

During the course of our studies of the reactions of NOX′ (X′ = Cl^-, Br^-, Br_3^-, or NO_2^-) with various transition metal complexes (1−4), it has been found that these can be used as a good nitrosylating agent. In continuation with our investigations on the reactivities of some π-cyclopentadienyl ruthenium(II) complexes (5, 6), we report here a number of mixed ligand complexes $[Ru(NO)(PPh_3)LX_nY_{3-n}]$ ((X = Cl^-, Br^-, I^-, CN^-, NCS^-), (Y = Cl^-, Br^-, NO_2^-), n = 1−3), $[Ru(PPh_3)(NO_2)(SNCl_3)L]$ synthesized by the reactions of $[Ru(\eta^5\text{-}C_5H_5)(PPh_3)L]^+X^-$ (where L = 2,2′-bipyridine or 1,10-phenanthroline; X = Cl^- or Br^-) or $[Ru(\eta^5\text{-}C_5H_5)(PPh_3)(L)X]$ (where L = PPh_3, Py, 3-picoline, 4-picoline, $\frac{1}{2}$(2,2′-bipyridine) or $\frac{1}{2}$(1,10-phenanthroline); X = Cl^-, Br^-, I^-, H^-, CN^-, NCS^-, or $SnCl_3^-$) with $NOBr_3$ and N_2O_3 under homogeneous reaction conditions. It has also been shown that one of the phenyl rings of PPh_3 is π-bonded to ruthenium in $[Ru(NO_2)(PPh_3)(SnCl_3)L]\cdot xN_2O_3$ (x = 0−2). The yield of the complexes was found to be more than 60% in every reaction.

Experimental

All chemicals used were of Analar grade. The solvents were dried and distilled before use. The reactions were carried out under pure and dry nitrogen.

$NOBr_3$ and N_2O_3 were prepared by literature methods (7, 8) and used as saturated solution in dry dichloromethane.

The $[Ru(\eta\text{-}C_5H_5)(PPh_3)_2Cl]$ (9), $[Ru(\eta\text{-}C_5H_5)(PPh_3)_2Br]$, $[Ru(\eta\text{-}C_5H_5)(PPh_3)_2I]$, $[Ru(\eta\text{-}C_5H_5)(PPh_3)_2H]$, $[Ru(\eta\text{-}C_5H_5)(PPh_3)_2(CN)]$, $[Ru(\eta\text{-}C_5H_5)(PPh_3)(NCS)]$, $[Ru(\eta\text{-}C_5H_5)(PPh_3)_2(SnCl_3)]$ (10), and complexes $[Ru(\eta\text{-}C_5H_5)(PPh_3)(Py)Cl]$, $[Ru(\eta\text{-}C_5H_5)(PPh_3)(3\text{-}Pic)Cl]$, $[Ru(\eta\text{-}C_5H_5)(PPh_3)(4\text{-}Pic)Cl]$, $[Ru(\eta\text{-}C_5H_5)(PPh_3)(Bipy)]^+Cl^-$, $[Ru(\eta\text{-}C_5H_5)(PPh_3)(o\text{-phen})]^+Cl^-$, $[Ru(\eta\text{-}C_5H_5)(PPh_3)(Py)Br]$, $[Ru(\eta\text{-}C_5H_5)(PPh_3)(3\text{-}Pic)Br]$, $[Ru(\eta\text{-}C_5H_5)(PPh_3)(4\text{-}Pic)Br]$, $[Ru(\eta\text{-}C_5H_5)(PPh_3)(Bipy)]^+Br^-$, $[Ru(\eta\text{-}C_5H_5)(PPh_3)(o\text{-Phen})]^+Br^-$, $[Ru(\eta\text{-}C_5H_5)(PPh_3)(Py)I]$, $[Ru(\eta\text{-}C_5H_5)(PPh_3)(3\text{-}Pic)I]$, $[Ru(\eta\text{-}C_5H_5)(PPh_3)(4\text{-}Pic)I]$, $[Ru(\eta\text{-}C_5H_5)(PPh_3)(Bipy)_{1/2}I]$, $[Ru(\eta\text{-}C_5H_5)(PPh_3)(o\text{-Phen})_{1/2}I]$, $[Ru(\eta\text{-}C_5H_5)(PPh_3)(Py)(CN)]$, $[Ru(\eta\text{-}C_5H_5)(PPh_3)(3\text{-}Pic)(CN)]$, $[Ru(\eta\text{-}C_5H_5)(PPh_3)(4\text{-}Pic)(CN)]$, $[Ru(\eta\text{-}C_5H_5)(PPh_3)(Bipy)_{1/2}CN]$, $[Ru(\eta\text{-}C_5H_5)(PPh_3)(o\text{-Phen})_{1/2}(CN)]$, $[Ru(\eta\text{-}C_5H_5)(PPh_3)(Py)(NCS)]$, $[Ru(\eta\text{-}C_5H_5)(PPh_3)(3\text{-}Pic)(NCS)]$, $[Ru(\eta\text{-}C_5H_5)(PPh_3)(4\text{-}Pic)(NCS)]$, $[Ru(\eta\text{-}C_5H_5)(PPh_3)(Bipy)_{1/2}(NCS)]$, $[Ru(\eta\text{-}C_5H_5)(PPh_3)(o\text{-Phen})_{1/2}(NCS)]$, $[Ru(\eta\text{-}C_5H_5)(PPh_3)(Py)(SnCl_3)]$, $[Ru(\eta\text{-}C_5H_5)(PPh_3)(3\text{-}Pic)(SnCl_3)]$, $[Ru(\eta\text{-}C_5H_5)(PPh_3)(4\text{-}Pic)(SnCl_3)]$, $[Ru(\eta\text{-}C_5H_5)(PPh_3)(Bipy)_{1/2}(SnCl_3)]$, $[Ru(\eta\text{-}C_5H_5)(PPh_3)(o\text{-Phen})_{1/2}(SnCl_3)]$ were prepared as reported elsewhere (5).

[A] Reactions of NOX′ (X′ = Br_3^- or NO_2^-) with $[Ru(\eta^5\text{-}C_5H_5)(PPh_3)(L)^+X^-]$ (L = Bipy or 1,10-phen; X = Cl or Br), $[Ru(\eta^5\text{-}C_5H_5)(PPh_3)(L)X]$ (L = PPh_3, Py, 3-Pic or 4-Pic), or $[Ru(\eta^5\text{-}C_5H_5)(PPh_3)(L)X]$ (L = PPh_3, Py, 3-Pic or 4-Pic, $\frac{1}{2}$Bipy or $\frac{1}{2}$(1,10-Phen); X = I or NCS, $SnCl_3$)

A saturated solution of NOX′ in dichloromethane (*ca.* 5 mL) was very slowly added to a well stirred solution of the appropriate complex (*ca.* 0.6 mmol) in a mixed solvent containing 20 mL of dichloromethane and 40 mL of methanol at 30°C. The resulting mixture was heated under reflux for 10−15 min, whereupon microcrystals of the corresponding complex were separated. The product was filtered, washed with methanol, water, methanol, ether, and petroleum ether (40−60°C) and dried *in vacuo*. The samples were recrystallized from CH_2Cl_2/methanol mixture or CH_2Cl_2/petroleum ether, though the initial crop itself contained analytically pure complexes (yield, 70% approximately). These complexes were analyzed for the complexes whose compositions are shown in Table 1. In the case of the bromo

[1]For Part II, see ref. 6.

[2]The compound was synthesized in 1923. Though it has been formulated as $NOBr_3$, there is a possibility that it might be a mixture. For our reactions we have assumed it to be $NOBr_3$.

TABLE 1. Reactions of $[Ru(\eta^5\text{-}C_5H_5)(PPh_3)(L)X]$ with NOX′ — characterisation data of complexes‡

	$[Ru(\eta^5\text{-}C_5H_5)(PPh_3)(L)X]$		NOX′		Analyses, found (calcd.)%§					Infrared bands	λ_{max} (nm)
No.	L =	X =	X′ =	Product †colour, mp (°C)	C	H	X	N	P	(cm^{-1}) KBr discs	($CHCl_3$ solvent)
1	PPh_3	Cl	Br_3	$[Ru(NO)(PPh_3)_2Br_3]$ [A]	48.5	3.5	26.5	1.6	6.8	1864	465, 350, 300, 230
				B, 280	(48.3)	(3.4)	(26.8)	(1.6)	(6.9)		
2	Py	Cl	Br_3	$[Ru(NO)(PPh_3)(Py)Br_3)$ [A]	38.9	2.7	33.6	3.7	4.2	1865	460, 350, 300, 230
				B, 250	(38.8)	(2.8)	(33.7)	(3.9)	(4.4)		
3	3-Pic	Cl	Br_3	$[Ru(NO)(PPh_3)(3\text{-Pic})Br_3]$ [A]	39.8	3.1	33.0	3.7	4.4	1868	460, 315, 235
				YB, 245	(39.7)	(3.0)	(33.1)	(3.9)	(4.3)		
4	4-Pic	Cl	Br_3	$[Ru(NO)(PPh_3)(4\text{-Pic})Br_3]$ [A]	39.8	3.1	33.1	3.8	4.2	1865	460, 310, 230
				YB, 245	(39.7)	(3.0)	(33.1)	(3.9)	(4.3)		
***5**	2,2′-Bipy	Cl	Br_3	$[Ru(NO)(PPh_3)(Bipy)_{1/2}Br_3]$ [A]	38.7	2.6	33.7	3.7	4.3	1870	460, 310, 225
				B, 250	(38.8)	(2.7)	(33.8)	(3.9)	(4.4)		
***6**	1,10-Phen	Cl	Br_3	$[Ru(NO)(PPh_3)(o\text{-Phen})_{1/2}Br_3]$ [A]	39.9	2.5	33.1	3.8	4.2	1868	680, 460, 310
				B, 230	(39.8)	(2.6)	(33.2)	(3.9)	(4.3)		
7	PPh_3	Cl	NO_2	$[Ru(NO)(NO_2)_2Cl(PPh_3)\cdot\frac{1}{2}CH_2Cl_2$ [A]	53.0	3.7	8.7	5.0	7.4	1868, 1340, 1320, 840, 310	430, 335, 290, 253, 225
				B, 240	(53.1)	(3.8)	(8.6)	(5.1)	(7.5)		
8	Py	Cl	NO_2	$[Ru(NO)(NO_2)_2Cl(PPh_3)Py]CH_2Cl_2$ [A]	42.0	3.3	15.7	8.4	4.6	1870, 1340, 1320, 840, 310	450, 340, 290, 250, 225
				B, 280	(42.1)	(3.2)	(15.6)	(8.2)	(4.5)		
9	3-Pic	Cl	NO_2	$[Ru(NO)(NO_2)_2Cl(PPh_3)(3\text{-Pic})]$ [A]	46.7	3.5	5.9	9.2	5.0	1868, 1340, 1320, 840, 310	460, 345, 290, 250, 225
				B, 280	(46.9)	(3.6)	(5.8)	(9.1)	(5.1)		
10	4-Pic	Cl	NO_2	$[Ru(NO)(NO_2)_2Cl(PPh_3)(4\text{-Pic})CH_2Cl_2$ [A]	42.8	3.1	15.1	7.9	4.5	1874, 1340, 1320, 840, 310	463, 345, 290, 250, 225
				B, 280	(42.9)	(3.0)	(15.2)	(8.0)	(4.4)		
***11**	2,2′-Bipy	Cl	NO_2	$[Ru(NO)(NO_2)_2Cl(PPh_3)(Bipy)_{1/2}]\frac{1}{2}CH_2Cl_2$ [A]	43.9	3.2	11.0	8.6	4.9	1868, 1340, 1320, 840, 810, 310	475, 350, 280, 250, 225
				B, 240	(44.0)	(3.1)	(11.1)	(8.7)	(4.8)		
***12**	1,10-Phen	Cl	NO_2	$[Ru(NO)(NO_2)_2Cl(PPh_3)(o\text{-Phen})_{1/2}]\frac{1}{4}CH_2Cl_2$ [A]	45.9	3.0	8.3	8.8	4.7	1872, 1340, 1320, 950, 840, 810, 310	480, 355, 275, 240, 225
				B, 280	(46.0)	(3.1)	(8.4)	(8.9)	(4.9)		
13	PPh_3	Br	Br_3	$[Ru(NO)(PPh_3)_2Br_3]$ [A]	48.2	3.3	26.9	1.7	6.8	1864	465, 350, 300, 230
				B, 240	(48.3)	(3.4)	(26.8)	(1.6)	(6.9)		
14	Py	Br	Br_3	$[Ru(NO)(PPh_3)(Py)Br_3]$ [A]	38.9	2.9	33.8	3.8	4.5	1865	460, 350, 300, 230
				OB, 250	(38.8)	(2.8)	(33.7)	(3.9)	(4.4)		
15	3-Pic	Br	Br_3	$[Ru(NO)(PPh_3)(3\text{-Pic})Br_3]$ [A]	39.9	3.1	33.2	3.8	4.5	1865	460, 310, 230
				YB, 245	(39.7)	(3.0)	(33.1)	(3.9)	(4.3)		
16	4-Pic	Br	Br_3	$[Ru(NO)(PPh_3)(4\text{-Pic})Br_3]$ [A]	39.9	3.1	33.0	3.8	4.4	1865	460, 310, 230
				YB, 245	(39.7)	(3.0)	(33.1)	(3.9)	(4.3)		
***17**	2,2′-Bipy	Br	Br_3	$[Ru(NO)(PPh_3)(Bipy)_{1/2}Br_3]$ [A]	38.7	2.9	33.7	3.8	4.3	1870	460, 310, 225
				B, 250	(38.8)	(2.7)	(33.8)	(3.9)	(4.4)		
***18**	1,10-Phen	Br	Br_3	$[Ru(NO)(PPh_3)(o\text{-Phen})_{1/2}Br_3]$ [A]	39.9	2.7	33.1	3.8	4.2	1868	680, 460, 310, 225
				B, 230	(39.8)	(2.6)	(33.2)	(3.9)	(4.3)		
19	PPh_3	Br	NO_2	$[Ru(NO)(NO_2)_2(PPh_3)_2Br]\cdot\frac{3}{4}CH_2Cl_2$ [A]	49.6	3.6	14.9	4.6	6.9	1870, 1340, 1320, 830, 310	575, 430, 345, 250, 225
				YB, 202	(49.5)	(3.5)	(15.0)	(4.7)	(7.0)		
20	Py	Br	NO_2	$[Ru(NO)(NO_2)_2(PPh_3)(Py)Br]\frac{1}{2}CH_2Cl_2$ [A]	41.0	3.0	16.7	8.1	4.6	1870, 1340, 1320, 830, 310	560, 435, 330, 230
				OB, 255	(41.1)	(3.1)	(16.8)	(8.2)	(4.5)		
21	3-Pic	Br	NO_2	$[Ru(NO)(NO_2)_2(PPh_3)(3\text{-Pic})Br]\frac{1}{2}CH_2Cl_2$ [A]	41.9	3.2	16.6	7.9	4.3	1868, 1340, 1320, 840, 310	565, 435, 325, 230
				OB, 280	(42.0)	(3.3)	(16.5)	(8.0)	(4.4)		
22	4-Pic	Br	NO_2	$[Ru(NO)(NO_2)_2(PPh_3)(4\text{-Pic})Br]\frac{1}{2}CH_2Cl_2$ [A]	41.9	3.2	16.4	8.1	4.5	1872, 1340, 1320, 840, 310	568, 432, 325, 230
				OB, 280	(42.0)	(3.3)	(16.5)	(8.0)	(4.4)		

TABLE 1 (*Continued*)

No.	$[Ru(\eta^5\text{-}C_5H_5)(PPh_3)(L)X]$ L =	X =	NOX′ X′ =	Product †colour, mp (°C)	Analyses, found (calcd.)%§ C	H	X	N	P	Infrared bands (cm^{-1}) KBr discs	λ_{max} (nm) ($CHCl_3$ solvent)
*23	2,2′Bipy	Br	NO_2	$[Ru(NO)(NO_2)_2(PPh_3)(Bipy)_{1/2}Br)$ [A] G, 260	42.8 (42.9)	3.2 (3.1)	12.6 (12.4)	8.6 (8.7)	4.7 (4.8)	1874, 1340, 1320, 840, 810, 310	530, 430, 320, 230
*24	1,10-Phen	Br	NO_2	$[Ru(NO)(NO_2)_2(PPh_3)(o\text{-Phen})_{1/2}Br]\frac{1}{4}CH_2Cl_2$ [A] B, 220	43.1 (43.0)	2.8 (2.9)	14.4 (14.5)	8.2 (8.3)	4.5 (4.6)	1870, 1340, 1320, 930, 840, 810, 310	535, 435, 315, 225
25	PPh_3	I	Br_3	$[Ru(NO)(PPh_3)_2Br_3]$ [A] B, 240	48.4 (48.3)	3.3 (3.4)	26.7 (26.8)	1.8 (1.6)	6.7 (6.9)	1864	465, 350, 300, 230
26	Py	I	Br_3	$[Ru(NO)(PPh_3)(Py)Br_3]CH_2Cl_2$ [A] O, 238	36.0 (36.1)	2.7 (2.8)	39.2 (39.0)	3.4 (3.5)	3.8 (3.9)	1865	460, 350, 300, 230
27	3-Pic	I	Br_3	$[Ru(NO)(PPh_3)(3\text{-Pic})Br_3]$ [A] YB, 248	39.8 (39.7)	3.1 (3.0)	33.0 (33.1)	3.8 (3.9)	4.4 (4.3)	1868	460, 315, 235
28	4-Pic	I	Br_3	$[Ru(NO)(PPh_3)(4\text{-Pic})Br_3]$ [A] YB, 246	39.6 (39.7)	3.0 (3.0)	33.0 (33.1)	3.7 (3.9)	4.2 (4.3)	1865	460, 310, 230
29	½(2,2′-Bipy)	I	Br_3	$[Ru(NO)(PPh_3)(Bipy)_{1/2}IBr_2]$ [A] O, 246	36.5 (36.4)	2.4 (2.5)	37.7 (37.9)	3.6 (3.7)	4.0 (4.1)	1870	460, 310, 225
30	½(1,10-Phen)	I	Br_3	$[Ru(NO)(PPh_3)(o\text{-Phen})_{1/2}Br_3]$ [A] O, 243	39.7 (39.8)	2.5 (2.6)	33.1 (33.2)	3.7 (3.9)	4.4 (4.3)	1868	680, 460, 310, 225
31	PPh_3	I	NO_2	$[Ru(NO)(NO_2)_2(PPh_3)_2I]\cdot\frac{1}{2}CH_2Cl_2$ [A] RB, 165	47.6 (47.8)	3.3 (3.4)	17.5 (17.7)	4.5 (4.6)	6.7 (6.8)	1870, 1340, 1320, 835, 310	580, 435, 330, 295, 225
32	Py	I	NO_2	$[Ru(NO)(NO_2)_2(Py)I]$ [A] O, 160	13.9 (14.0)	1.1 (1.2)	29.7 (29.6)	13.0 (13.1)	—	1872, 1340, 1320, 838, 310	425, 330, 290, 230
33	3-Pic	I	NO_2	$[Ru(NO)(NO_2)_2(3\text{-Pic})I]$ [A] YB, 275	16.4 (16.3)	1.5 (1.6)	28.6 (28.7)	12.4 (12.6)	—	1870, 1340, 1320, 838, 310	430, 335, 290, 270, 230
34	4-Pic	I	NO_2	$[Ru(NO)(NO_2)_2(4\text{-Pic})I]$ [A] YB, 268	16.5 (16.3)	1.5 (1.6)	28.9 (28.7)	12.5 (12.6)	—	1868, 1340, 1320, 838, 310	440, 330, 300, 225
35	½(2,2′-Bipy)	I	NO_2	$[Ru(NO)(NO_2)_2(Bipy)I]$ [A] O, 160	14.1 (14.0)	1.0 (0.9)	29.6 (29.7)	13.0 (13.1)	—	1870, 1338, 1320, 838, 310	445, 330, 300, 225
36	½(1,10-Phen)	I	NO_2	$[Ru(NO)(NO_2)_2(o\text{-Phen})I]$ [A] O, 167	16.3 (16.4)	1.0 (0.9)	28.8 (28.9)	12.6 (12.7)	—	1870, 1340, 1320, 935, 840, 810, 310	455, 330, 300, 225
37	PPh_3	CN	Br_3	$[Ru(NO)(PPh_3)_2Br_3]$ [B] B, 242	48.5 (48.3)	3.5 (3.4)	26.5 (26.8)	1.6 (1.6)	6.8 (6.9)	1864	465, 350, 300, 230
38	Py	CN	Br_3	$[Ru(NO)(PPh_3)(Py)Br_3]$ [B] O, 240	38.7 (38.8)	2.9 (2.8)	33.5 (33.7)	3.7 (3.9)	4.6 (4.4)	1865	460, 350, 300, 230
39	3-Pic	CN	Br_3	$[Ru(NO)(PPh_3)(3\text{-Pic})Br_3]$ [B] YB, 249	39.8 (39.7)	3.1 (3.0)	33.2 (33.1)	3.8 (3.9)	4.4 (4.3)	1868	460, 315, 235
40	4-Pic	CN	Br_3	$[Ru(NO)(PPh_3)(4\text{-Pic})Br_3]$ [B] YB, 248	39.8 (39.7)	3.1 (3.0)	33.0 (33.1)	3.8 (3.9)	4.4 (4.3)	1865	460, 310, 230
41	½(2,2′-Bipy)	CN	Br_3	$[Ru(NO)(PPh_3)(Bipy)_{1/2}(CN)Br_2]CH_2Cl_2$ [B] G, 280	40.6 (40.4)	2.7 (2.8)	31.4 (31.1)	5.5 (5.1)	4.1 (4.2)	1858, 2048	500, 350, 350, 315, 230
42	½(1,10-Phen)	CN	Br_3	$[Ru(NO)(PPh_3)(o\text{-Phen})_{1/2}Br_3]$ [B] O, 243	39.7 (39.8)	2.8 (2.6)	33.4 (33.2)	3.8 (3.9)	4.4 (4.3)	1868	680, 460, 310, 225
43	PPh_3	CN	NO_2	$[Ru(NO)(NO_2)_2(CN)(PPh_3)_2]$ [B] B, 280	57.3 (57.4)	3.7 (3.9)	—	7.2 (7.3)	8.2 (8.0)	2050, 1875, 1340, 1320, 835, 310	535, 450, 310, 230
44	Py	CN	NO_2	$[Ru(NO)(NO_2)_2(CN)(PPh_3)Py]$ [B] B, 280	48.6 (48.8)	3.1 (3.2)	—	9.4 (9.5)	5.5 (5.3)	2050, 1872, 1340, 1320, 830, 310	540, 460, 300, 235

TABLE 1 (*Continued*)

No.	$[Ru(\eta^5\text{-}C_5H_5)(PPh_3)(L)X]$ L =	X =	NOX′ X′ =	Product †colour, mp (°C)	Analyses, found (calcd.)%§ C	H	X	N	P	Infrared bands (cm^{-1}) KBr discs	λ_{max} (nm) ($CHCl_3$ solvent)
45	3-Pic	CN	NO_2	$[Ru(NO)(NO_2)_2(CN)(PPh_3)(3\text{-Pic})]$ [B]	49.6	3.5	—	9.4	5.2	2050, 1874, 1340,	545, 460, 300,
				B, 280	(49.7)	(3.6)		(9.3)	(5.1)	1320, 830, 310	235
46	4-Pic	CN	NO_2	$[Ru(NO)(NO_2)_2(CN)(PPh_3)(4\text{-Pic})]$ [B]	49.6	3.5	—	9.5	5.3	2050, 1880, 1340,	535, 460, 310,
				B, 280	(49.7)	(3.6)		(9.3)	(5.1)	1320, 830, 310	230
47	$\frac{1}{2}$(2,2′-Bipy)	CN	NO_2	$[Ru(NO)(NO_2)_2(CN)(PPh_3)Bipy)_{1/2}]$ [B]	48.7	3.3	—	9.7	5.4	2055, 1875, 1340,	585, 465, 300,
				YB, 244	(48.9)	(3.2)		(9.5)	(5.3)	1320, 830, 310	230
48	$\frac{1}{2}$(1,10-Phen)	CN	NO_2	$[Ru(NO)(NO_2)_2(CN)(PPh_3)(o\text{-Phen})_{1/2}]$ [B]	49.7	3.1	—	9.2	5.3	2055, 1865, 1340,	530, 460, 310,
				B, 280	(49.9)	(3.2)		(9.3)	(5.2)	1320, 940, 830, 310	225
49	PPh_3	NCS	Br_3	$[Ru(NO)(PPh_3)_2Br_3]$ [B]	48.2	3.5	26.7	1.7	6.7	1864	465, 350, 300
				B, 241	(48.3)	(3.4)	(26.8)	(1.6)	(6.9)		
50	Py	NCS	Br_3	$[Ru(NO)(PPh_3)(Py)Br_3]$ [B]	38.6	2.6	33.9	3.8	4.3	1865	460, 350, 300,
				O, 240	(38.8)	(2.8)	(33.7)	(3.9)	(4.4)		230
51	3-Pic	NCS	Br_3	$[Ru(NO)(PPh_3)(3\text{-Pic})Br_3]$ [B]	39.6	3.1	33.3	3.8	4.2	1868	460, 315, 235
				YB, 248	(39.7)	(3.0)	(33.1)	(3.9)	(4.3)		
52	4-Pic	NCS	Br_3	$[Ru(NO)(PPh_3)(4\text{-Pic})Br_3]$ [B]	39.6	3.1	33.2	3.8	4.4	1865	460, 310, 230
				YB, 249	(39.7)	(3.0)	(33.1)	(3.9)	(4.3)		
53	$\frac{1}{2}$(2,2′-Bipy)	NCS	Br_3	$[Ru(NO)(PPh_3)(Bipy)_{1/2}Br_3]$ [B]	38.7	2.9	33.6	3.7	4.5	1870	460, 310, 225
				B, 250	(38.8)	(2.7)	(33.8)	(3.9)	(4.4)		
54	$\frac{1}{2}$(1,10-Phen)	NCS	Br_3	$[Ru(NO)(NCS)Br_2(PPh_3)]_2$ [B]	37.1	2.4	26.0	4.5	5.0	2140, 1855	465, 350, 230
				G, 220	(37.3)	(2.5)	(26.2)	(4.6)	(5.1)		
55	PPh_3	NCS	NO_2	$[Ru(NO)(NCS)(NO_2)_2(PPh_3)_2]$ [B]	55.4	3.6	—	6.9	7.8	2144, 1865, 1340,	445, 350, 290,
				YB, 175	(55.2)	(3.7)		(7.0)	(7.7)	1320, 830, 310	225
56	Py	NCS	NO_2	$[Ru(NO)(NCS)(NO_2)_2(PPh_3)(Py)]$ [B]	46.2	3.0	—	8.9	4.9	2144, 1865, 1340,	440, 340, 290,
				Y, 280	(46.3)	(3.1)		(9.0)	(5.0)	1320, 830, 310	225
57	3-Pic	NCS	NO_2	$[Ru(NO)(NCS)(NO_2)_2(PPh_3)(3\text{-Pic})]$ [B]	47.1	3.6	—	8.6	4.8	2144, 1865, 1340,	460, 350, 290,
				YG, 184	(47.2)	(3.5)		(8.8)	(4.9)	1320, 830, 310	230
58	4-Pic	NCS	NO_2	$[Ru(NO)(NCS)(NO_2)_2(PPh_3)(4\text{-Pic})]$ [B]	47.4	3.6	—	8.9	5.0	2144, 1865, 1340,	465, 350, 290,
				YG, 185	(47.2)	(3.5)		(8.8)	(4.9)	1320, 830, 310	230
59	$\frac{1}{2}$(2,2′-Bipy)	NCS	NO_2	$[Ru(NO)(NCS)(NO_2)_2(PPh_3)(Bipy)_{1/2}]$ [B]	46.3	3.0	—	8.9	4.9	2144, 1865, 1340,	455, 290, 230
				YB, 275	(46.4)	(3.2)		(9.0)	(5.0)	1320, 830, 310	
60	$\frac{1}{2}$(1,10-Phen)	NCS	NO_2	$[Ru(NO)(NCS)(NO_2)_2(PPh_3)(o\text{-Phen})_{1/2}]$ [B]	47.3	3.1	—	8.7	4.8	2144, 1865, 1340,	450, 290, 230
				YB, 280	(47.4)	(3.0)		(8.8)	(4.9)	1320, 945, 830, 310	
61	PPh_3	$SnCl_3$	Br_3	$[Ru(NO_2)(SnCl_3)(PPh_3)_2]\cdot\frac{1}{2}CH_2Cl_2$ [A]	46.5	3.4	15.0	1.7	6.8	1500, 1480, 1430,	560, 450, 325,
				OP, 290	(46.6)	(3.8)	(15.1)	(1.5)	(6.6)	1370, 1350, 1340, 1310, 850, 800	280, 260, 230
62	Py	$SnCl_3$	Br_3	$[Ru(NO_2)(SnCl_3)(PPh_3)Py]\cdot\frac{3}{4}CH_2Cl_2$ [A]	37.8	2.6	21.0	3.6	4.0	1500, 1480, 1430,	555, 425, 310,
				O, 210	(37.7)	(2.7)	(21.1)	(3.7)	(4.1)	1370, 1350, 1340, 1310, 850, 840	225
63	3-Pic	$SnCl_3$	Br_3	$[Ru(NO_2)(SnCl_3)(PPh_3)(3\text{-Pic})]\frac{1}{2}CH_2Cl_2$ [A]	39.1	3.0	18.7	3.5	4.1	1500, 1482, 1430,	550, 525, 315,
				O, 218	(39.3)	(3.1)	(18.9)	(3.7)	(4.1)	1370, 1350, 1340, 1310, 850, 800	230
64	4-Pic	$SnCl_3$	Br_3	$[Ru(NO_2)(SnCl_3)(PPh_3)(4\text{-Pic})]\frac{3}{4}CH_2Cl_2$ [A]	38.4	3.0	20.6	3.7	4.1	1500, 1482, 1430,	560, 420, 315,
				OY, 188	(38.6)	(3.1)	(20.7)	(3.6)	(4.0)	1370, 1350, 1340, 1310, 850, 800	230

TABLE 1 (*Concluded*)

No.	$[Ru(\eta^5\text{-}C_5H_5)(PPh_3)(L)X]$ L =	X =	NOX′ X′ =	Product †colour, mp (°C)	Analyses, found (calcd.)%§ C	H	X	N	P	Infrared bands (cm^{-1}) KBr discs	λ_{max} (nm) ($CHCl_3$ solvent)
65	½(2,2′-Bipy)	$SnCl_3$	Br_3	$[Ru(NO_2)(SnCl_3)(PPh_3)(Bipy)_{1/2}]2CH_2Cl_2$ [A] Y, 185	34.6 (34.8)	2.6 (2.7)	28.4 (28.8)	3.1 (3.2)	3.5 (3.6)	1500, 1482, 1430, 1370, 1350, 1340, 1310, 850, 800	590, 435, 310 225
66	½(1,10-Phen)	$SnCl_3$	Br_3	$[Ru(NO_2)(SnCl_3)(PPh_3)(o\text{-Phen})_{1/2}$ [A] O, 190	39.6 (39.7)	2.5 (2.6)	14.9 (14.7)	3.8 (3.9)	4.1 (4.3)	1500, 1482, 1430, 1370, 1350, 1340, 1310, 850, 800	570, 450, 300, 260,
67	PPh_3	$SnCl_3$	NO_2	$[Ru(NO_2)(SnCl_3)(PPh_3)_2].N_2O_3$ [A] O, 190	44.2 (44.4)	3.0 (3.1)	10.8 (11.0)	4.4 (4.3)	6.3 (6.4)	1850, 1340, 1320, 810	580, 450, 315, 280, 225
68	Py	$SnCl_3$	NO_2	$[Ru(NO_2)(SnCl_3)(PPh_3)Py].3N_2O_3$ [A] B, 202	29.1 (29.3)	1.9 (2.0)	11.4 (11.3)	11.7 (11.9)	3.5 (3.3)	1850, 1345, 1320, 805	560, 445, 300, 270, 225
69	3-Pic	$SnCl_3$	NO_2	$[Ru(NO_2)(Cl)(PPh_3)(3\text{-Pic})].3N_2O_3$ [A] O, 195	36.3 (36.1)	2.8 (2.9)	4.8 (4.6)	14.4 (14.6)	4.1 (4.0)	1850, 1345, 1325, 810	585, 455, 310, 290, 230
70	4-Pic	$SnCl_3$	NO_2	$[Ru(NO_2)(Cl)(PPh_3)(4\text{-Pic}).3N_2O_3$ [A] O, 199	36.2 (36.1)	2.7 (2.9)	4.5 (4.6)	14.7 (14.6)	4.2 (4.0)	1852, 1345, 1325, 810	580, 455, 310, 290, 230
71	½(2,2′-Bipy)	$SnCl_3$	NO_2	$[Ru(NO_2)(SnCl_3)(PPh_3)(Bipy)_{1/2}]N_2O_3$ [A] O, 196	35.2 (35.0)	2.5 (2.4)	13.6 (13.5)	7.3 (7.1)	3.8 (3.9)	1854, 1340, 1320, 805	545, 450, 280, 225
72	½(1,10-Phen)	$SnCl_3$	NO_2	$[Ru(NO_2)(SnCl_3)(PPh_3)(o\text{-Phen})_{1/2}]2N_2O_3$ [A] O, 183	32.7 (32.9)	2.3 (2.2)	12.3 (12.2)	12.6 (12.8)	3.6 (3.5)	1852, 1340, 1320, 930, 805	550, 445, 270, 230

*These complexes are ionic having composition $[Ru(\eta^5\text{-}C_5H_5)(PPh_3)L]^+X^-$.

†B = Brown, OB = Orange Brown, YB = Yellowish Brown, G = Green, O = Orange, RB = Reddish Brown, YG = Yellowish Green, OR = Orange Red, OY = Orange Yellow, Y = Yellow. [A][B] = methods used for preparation.

‡^{1}H-nmr spectra showed broad multiplet resonance at around δ7.2 ppm due to phosphine and *N*-heterocyclic base protons. In addition, complexes **61–72** showed multiplet absorption at δ 6.2 due to π-bonded phenyl protons of the PPh_3 ligand. The complexes having picolines as coligands exhibited an additional signal in the region δ 1.8–2.0 for the methyl protons.

§Error limit ±1%. The complexes having NCS as one of the anionic ligands, analysed satisfactorily for sulphur.

complexes, the reaction mixture was stirred at room temperature for about half an hour, followed by the concentration of the resulting solution under reduced pressure to about 5 mL. The concentrate was centrifuged and the complex was precipitated by the addition of about 25 mL of *n*-hexane.

[B] Reactions of NOX′ (X′ = Br_3^- or NO_2^-) with [Ru(η^5-C_5H_5)(PPh_3)(L)X] (where L = PPh_3, Py, 3-Pic, ½(Bipy), or ½(1,10-Phen); X = CN^- or SCN^-)

The complex (150 mg, 0.2 mmol) was dissolved in a mixture of 10 mL of dichloromethane and 25 mL of methanol, followed by the addition of 2–3 mL of a saturated dichloromethane solution of NOX′. The reaction mixture was heated under reflux for about 30 min. The colour of the solution changed to blackish green. After the usual work-up (Method I, Bromocomplexes), an oily product was obtained from which a pure crystalline solid was difficult to separate. However, in a few cases the repeated process of dissolution of the oil in CH_2Cl_2 or $CHCl_3$, and precipitation with light petroleum (40–60°C) gave a dark green solid in rather low yield (*ca.* 15%) which was filtered, washed with *n*-hexane, and dried *in vacuo*.

If the foregoing procedure was slightly modified by adding about 25 mL of triphenylphosphine into the reaction mixture while under reflux, an instantaneous formation of an orange brown to orange yellow shining crystals in high yield (*ca.* 90%) was observed. These were separated, washed with methanol and ether, and finally dried *in vacuo*. The complexes contained bromide in place of CN^- or SCN^-).

[C] Reactions of NOX′ (X′ = Br_3^- or NO_2^-) with [Ru(η^5-C_5H_5)(PPh_3)$_2$H]

The bright yellow complex [Ru(η^5-C_5H_5)(PPh_3)$_2$H] when dissolved in CH_2Cl_2 or $CHCl_3$ gave the chloro complex, [Ru(η^5-C_5H_5)(PPh_3)$_2$Cl]; in $CHBr_3$ the bromo complex, [Ru(η^5-C_5H_5)(PPh_3)$_2$Br]. As a result, when NOX′ was reacted with the hydrido complex by method [A], the isolated products were found to be identical to those obtained from the chloro, or bromo complex, depending on the solvent chosen for dissolving the hydrido complex prior to its reaction with $NOBr_3$.

The melting points of the complexes were found on a Fisher-Johns melting point apparatus.

The electronic spectra (210–700 nm) of the complexes in chloroform solution were recorded on the Cary 17-D model spectrophotometer.

The ir spectra were recorded as KBr discs on a Perkin-Elmer 580 spectrophotometer in the range 200–400 cm^{-1}.

Magnetic moments were measured, by the Gouy method using $Hg[Co(NCS)_4]$ as the calibrant.

Nuclear magnetic resonance spectra of the complex were taken on the Perkin Elmer, HA-100 spectrometer.

All complexes exhibited bands due to protons of PPh_3 and heterocyclic bases around δ 7.0; of C_5H_5, around δ 4.0; and those of methyl protons of picolines, around δ 5.0.

Carbon, hydrogen, and nitrogen were estimated in the microanalytical laboratory of the I.I.T., Kanpur. The sulphur and halogen were estimated by the standard methods (11). The phosphorus in the complexes were estimated as mentioned elsewhere (12).

Results and discussion

The reactions of $NOBr_3$ or N_2O_3 with [Ru(η^5-C_5H_5)(PPh_3)(L)X] gave bright coloured air-stable mixed ligand complexes (yield 60%) having a general formula [Ru(NO)(PPh_3)X_nY_{3-n}L] (X^- = Cl^- or Br^-; Y^- = Br^-, NO_2^-; n = 1–3) except those with $SnCl_3$. In the latter case, the reaction products obtained have a general formula [Ru(NO_2)($SnCl_3$)(PPh_3)L]. The analytical data of these complexes are given in Table 1. They were found to be diamagnetic and non-conducting.

They were readily soluble in haloform solvents but were practically insoluble in alcohols and non-polar solvents. The products derived from the trichlorostannate complexes have poor solubility in haloform solvents too. In order to confirm the proposed formulation of the complexes, the spectral studies (uv, visible, ir, nmr) have been carried out on these complexes whose results are discussed under the following heads.

Infrared spectra

(1) Reactions with $NOBr_3$

The ir spectra of complexes having $SnCl_3^-$ as an anion differed from those of the remaining ones in three respects. (*i*) They failed to exhibit any band around 1850 cm^{-1}, indicating that $NOBr_3$ could not nitrosylate them. (*ii*) They showed four new bands characteristic of the coordinated NO_2^- (21) around 1340(s) cm^{-1}, 1320(m-w) cm^{-1}, 840(m-w) cm^{-1} and around 300(w) cm^{-1}. Since NO_2^- may co-ordinate both as nitro or nitrito group, the absence of the diagnostic band of the coordinated nitro group around 650 cm^{-1}, unless masked by the intense PPh_3 bands around 600 cm^{-1}, was tentatively taken as evidence for its being bonded to the metal ion through oxygen. (*iii*) They exhibited a characteristic pattern of five bands in the region 1500–1350 cm^{-1} which has previously been used as diagnostic of PPh_3 complexes where one of the phenyl groups of PPh_3 is π-bonded to the metal ion (5, 13–27). (*iv*) They also showed the presence of three bands in 690–820 cm^{-1} region, while PPh_3 coordinated through phosphorus exhibits only two bands around 690 and 740 cm^{-1}. In case the phenyl group of PPh_3 is π-bonded, it is also expected that the absorption bands due to out-of-plane C—H bending modes should show a shift in their positions. It has, therefore, been assumed that the third band around 790–800 cm^{-1} could arise because of the out-of-plane bending mode of C—H of the π-bonded phenyl ring.

The ir spectra of the remaining complexes (other than trichlorostannate ones) showed an intense absorption band in the region 1840–1880 cm^{-1} besides the bands due to other coligands (29–32). Since the position of ir frequency due to ν_{NO} corrected by Ibers rule (28) in the complexes has been found to be greater than 1620 cm^{-1}, these can be regarded as complexes between Ru(II) and NO^+.

During the course of reactions of cyanato and thiocyanato complexes, it has been noted that the reaction products invariably appeared as oils, from which all attempts to separate the crystalline product were not successful in most cases. In a few cases, however, a solid product could be isolated and its spectra showed bands due to CN or NCS groups around 2000 or 2100 cm^{-1}, respectively. As stated in the Experimental section the addition of a few milligrams of PPh_3 in the refluxing reaction mixture led to the separation of very pure product in relatively good yield in which CN^- or NCS^- had been substituted by Br^-. It is, however, difficult to assess the role which PPh_3 plays in the crystallization process.

Generation of sulfate ion during the course of the reaction with the thiocyanato complexes has also been detected by the analytical data of the product separated by evaporating the refluxed-solution to dryness, followed by washing the residue with ether or petroleum ether. In the spectra of these complexes, the exhibited typical absorption bands of bridged sulfato group (33) appeared at the appropriate positions (1200 cm^{-1}, 1050 cm^{-1}, 850 cm^{-1}, and 600 cm^{-1}) besides the bands of the other attached groups.

(2) Reaction with N_2O_3

Although N_2O_3 reacts with [Ru(η^5-C_5H_5)(PPh_3)(L)X] (where X = Cl, Br, I, CN, or NCS) to yield nitrosyls, the reaction products of complexes having $SnCl_3^-$ as anion were different in two respects: (*i*) NO group is not coordinated with the metal ion. (*ii*) The reaction products crystallised out with N_2O_3 as adducts. These differences have been indicated by their ir spectra which exhibited all the characteristic bands due to NO_2^- except that at 650 cm^{-1} (1340 cm^{-1}, 1320 cm^{-1}, 840 cm^{-1}, and 300 cm^{-1}) and those, due to N_2O_3 (1870, 1340, 1320, 840 cm^{-1}) with a slight unsystematic shifts in their positions. The absence of 650 cm^{-1} band suggested NO_2^- to be bonded as nitrito group. Although all the spectra have shown a band around 1850 cm^{-1}, but compared to the position of NO^+ band, its position in $SnCl_3$ complexes was shifted slightly towards higher wave numbers and it was relatively a broader band. Though 1850 cm^{-1} band may also indicate the presence of NO^+, but the presence of other characteristic bands of N_2O_3 around 1340, 1320, and 840 cm^{-1} suggested the absence of NO and further, the presence of bonded NO^+ group in the complexes will require an extra negative ion for balancing the charge on the complex. It was therefore envisaged that 1850 cm^{-1} band suggested the presence of N_2O_3 rather than NO^+. Besides their ir spectra also exhibited the characteristic pattern of five bands in the 1500–1350 cm^{-1} region, and three bands in 820–690 cm^{-1} region, suggesting the presence of π-interaction between ruthenium ion and one of the phenyl rings of PPh_3.

Interestingly, N_2O_3 adducts were formed only with the complexes in which ruthenium is coordinated with PPh_3 through π-interaction of one of its phenyl ring. Although the assignment of a reason for the interesting behaviour of these complexes will be speculative, literature indicates that a number of aromatic compounds like toluene, *m*-xylene, etc., form adducts with N_2O_3 by donating electron density from the aromatic ring to N_2O_3 (34). The formulation of these adducts as $[NOR]^+[NO_2]^-$ has also been discarded on the grounds of electrolytic conductivity (35). In the complexes, a weak acid–base interaction between uncoordinated phosphorus atom (base) and N_2O_3 (acid) could possibly explain the N_2O_3-adduct formation.

Though this simple explanation is highly speculative, it could be suggested that the triphenylphosphine molecule coordinated to the metal ion through π-interaction of the phenyl group is playing some role in the adduct formation.

¹H nmr spectra

All the complexes ¹H nmr spectra were studied to confirm the presence of the co-ligand molecules. These exhibited a poorly resolved broad multiplet due to the protons of the phenyl groups of PPh_3 and those of *N*-heteronuclear group in the region around δ 7.0 and an additional band due to methyl protons around δ 2.0 in the case of picolines. The absence of a sharp signal in δ 4.5 region, further confirmed the loss of η-C_5H_5 moiety during nitrosylation.

Owing to the low solubility of the $SnCl_3$ complexes, only low intensity, poorly-resolved spectra were obtained. However, a broad resonance around δ 7.2 and a weak multiplet around δ 5.2 were observed in every case. The latter signal has been assigned to the π-bonded phenyl ring of PPh_3 (17). The upfield shift of the band compared to that obtained in triphenylphosphine or P-bonded triphenylphosphine complexes is supportive of the π-interaction of the phenyl ring of PPh_3 with ruthenium. Though a single crystal X-ray study will ultimately give a conclusive proof for the π-arene interaction with the Ru atom, the present spectroscopic evidences (ir and ¹H nmr) nevertheless strongly suggest that the only structure of the nitrito chlorostannate complexes which is consistent with all the data is the one in which phenyl ring of triphenylphosphine is bound to metal with a π-arene type linkage (Fig. 1).

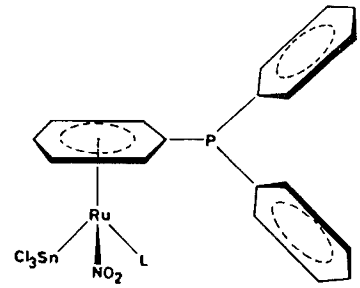

FIG. 1. Structure of cyclopentadienyl ruthenium complexes (L = PPh_3, pyridine, 3-picoline, 4-picoline, $\frac{1}{2}$(2,2′-bipyridine), or $\frac{1}{2}$(1,10-phenanthroline)).

Magnetic and uv, visible spectral data

All the complexes were diamagnetic in the solid state. This points towards an octahedral geometry of ligand atoms around the d^6 ruthenium ion in a strong ligand field causing a low spin configuration.

Table 1 lists the λ_{max} of the electronic spectra of the complexes obtained at room temperature in chloroform solution.

In order to seek some information about the π-interaction of one of the phenyl rings of phosphine molecules with the metal center, uv spectra of the $SnCl_3$ complexes were studied. But because of the presence of a number of π-bonded molecules like phosphine, pyridines, picolines, 2,2′-bipyridyl, 1,10-phenanthroline, NO_2^-, NO^+, SCN^-, or CN^- in the complexes, practically a continuous and strong absorption was observed beyond 350 nm. Hence no information could be gathered from their uv spectra, though in a few cases the positions of one or two shoulder bands around 270 nm did shift towards the higher energy side.

In the visible region a rather broad band of medium intensity, centering around 450 nm, was exhibited by all the complexes. As it is generally believed that d–d or the (MLCT) transition in ruthenium(II) octahedral complexes occur under a broad envelope at around 450 nm (36), the presence of a similar band in the present complexes suggested an octahedral geometry of ligands around Ru(II) ion. While comparing the spectral positions of this band with those of parent ones $[Ru(\eta^5\text{-}C_5H_5)(PPh_3)(L)X]$ (*ca.* 550 nm) a considerable band shift towards higher energy has been found in the nitrosyl or nitrito complexes. By taking into account the large number of donor groups which are capable of creating a stronger field around the metal ion an observed blue shift is quite understandable. Further, the position of the 450 nm band showed variation in its position for the series of Cl, Br, I, CN, $SnCl_3$, NCS complexes, in accordance with the ligand position in the spectrochemical series. The substitution of a phosphine ligand by a pyridine or picolines caused a red shift in consonance with their lower positions compared to phosphine in the spectrochemical series. The shift in 2,2′-bipyridine or 1,10-phenanthroline complexes was found to be erratic. Since 450 nm band seems to be ligand field dependent, it may be assigned to be arising due to MLCT. The probability of this band being due purely to a d–d transition is rather low, because of the availability of low lying empty π^* orbitals of the ligand.

Further the compositions of all the reaction products suggest an octahedral geometry. The complexes, being mixed ligand ones, may exist in a number of isomeric forms. However, no attempt has been made to assign any particular geometry to these complexes except that PPh_3 and L molecules may be *cis* to each other, if one assumes that no molecular rearrangement has taken place during the reaction.

A few of the complexes contain dichloromethane as a CH_2Cl_2 of crystallization. Since the number of protons in CH_2Cl_2 is two per molecule of CH_2Cl_2, it is difficult to observe these protons because of the solubility limitation of the complexes. However it has been observed that in a couple of cases (compounds **26** and **41**) where the solubility of the complexes was found to be rather large, a very weak band corresponding to one or two protons, around δ 4.2 was observed which has been assigned to CH_2Cl_2 bands.

Finally, it may be emphasized that although it is difficult to postulate any mechanistic path-way for these reactions, one may speculate the following tentative scheme of these reactions.

It is well known that the following equilibrium in the methanolic solution of $[Ru(\eta^5\text{-}C_5H_5)(PPh_3)_2X]$ exists:

$$[Ru(\eta^5\text{-}C_5H_5)(PPh_3)_2X] \rightleftharpoons [Ru(\eta^5\text{-}C_5H_5)(PPh_3)_2]^+ + X^-$$

It is, therefore, conceivable that the reacting species in these reactions could possibly be $[Ru(\eta^5\text{-}C_5H_5)(PPh_3)_2L]^+$ which interacts with $NOBr_3$ or N_2O_3 or NO^+ in a concerted or stepwise process to give an intermediate

$$[Ru(\eta^5\text{-}C_5H_5)(PPh_3)L(NO)]^{2+}$$

The latter subsequently undergoes substitution reaction with $X^- = Cl^-$, Br^-, NO_2^-, etc., to yield the final product $[Ru(NO)X_{3-n}Y_n(PPh_3)L]$.

Acknowledgement

R.F.N.A. wishes to thank the University Grants Commission, New Delhi, for the financial assistance in the form of a Teacher Fellowship. We also thank one of the referees for his valuable suggestions.

1. K. K. PANDEY, S. DATTA, and U. C. AGARWALA. Transition Metal Chem. **4**, 337 (1979).
2. K. K. PANDEY and U. C. AGARWALA. Z. Anorg. Allg. Chem. **457**, 235 (1979).
3. K. K. PANDEY and U. C. AGARWALA. J. Inorg. Nucl. Chem. **42**, 293 (1980).
4. K. C. JAIN, K. K. PANDEY, R. PARASHAD, T. SINGH, and U. C. AGARWALA. Ind. J. Chem. **19**A, 1089 (1980).
5. R. F. N. ASHOK, K. S. ARULSAMY, M. GUPTA and U. C. AGARWALA. Inorg. Chim. Acta. To be published.
6. R. F. N. ASHOK, M. GUPTA, and U. C. AGARWALA. Inorg. Chim. Acta. To be published.
7. R. L. DATTA and N. R. CHATTERJEE. J. Am. Chem. Soc. **45**, 481 (1923).
8. G. BRAUER. Handbook of preparative inorganic chemistry. Vol. I. Academic Press, New York. 1963. p. 488.
9. M. I. BRUCE and N. J. WINDSOR. Aust. J. Chem. **30**, 1601 (1977).
10. T. WILCZEWSKI, M. BOCHENSKA, and J. F. BIERNAT. J. Organomet. Chem. **215**, 87 (1981).
11. A. I. VOGEL. A textbook of quantitative inorganic analysis. Longmans Green, London. 1961. p. 491.
12. K. K. PANDEY and U. C. AGARWALA. Indian J. Chem. **20**A, 240 (1981).
13. J. T. PRICE and T. S. SORESEN. Can. J. Chem. **46**, 515 (1968).
14. M. J. NOBLE, G. CRAFER, and L. M. HAINES. J. Chem. Soc. Chem. Commun. 1406 (1969).
15. J. A. OSBORN. Inorg. Chem. **9**, 2339 (1970).
16. R. J. HAINES and A. L. DU PREEZ. J. Am. Chem. Soc. **93**, 2820 (1971).
17. R. COTTON and C. J. RIX. Aust. J. Chem. **24**, 2461 (1971).
18. J. A. BOWDEN and R. COTTON. Aust. J. Chem. **24**, 2471 (1971).
19. M. D. RAUSCH, G. A. MOSER, E. J. ZAIKO, and A. L. LIPMAN, JR. J. Organomet. Chem. **23**, 185 (1970).
20. J. J. HOUGH and E. SINGLETON. J. Chem. Soc. Chem. Commun. 371 (1972).
21. J. R. SANDERS. J. Chem. Soc. Dalton Trans. 743 (1973).
22. G. J. KRUGER, A. L. DU PREEZ, and R. J. HAINES. J. Chem. Soc. Dalton Trans. 1302 (1974).
23. J. C. MCCONWAY, A. C. SKAPSKI, L. PHILIPS, R. J. YOUNG, and G. WILKINSON. J. Chem. Soc. Chem. Commun. 327 (1974).
24. R. J. HAINES and A. L. DU PREEZ. J. Organomet. Chem. **84**, 357 (1975).
25. R. J. YOUNG and G. WILKINSON. J. Chem. Soc. Dalton Trans. 719 (1976).
26. T. V. ASHWORTH, M. J. NOLTE, R. H. REIMANN, and E. SINGLETON. J. Chem. Soc. Chem. Commun. 937 (1977).
27. R. USON *et al.* J. Organomet. Chem. **256**, 331 (1983).
28. B. L. HAYMORE and J. I. IBERS. Inorg. Chem. **14**, 3060 (1975).
29. L. MAIER. Prog. Inorg. Chem. **5**, 27 (1963).
30. R. L. BOHON, R. ISAAC, H. HOFTEIZER, and R. J. ZELLNER. Anal. Chem. **30**, 245 (1958).
31. D. P. BIDDISCOMBE, E. A. COULSON, R. HANDLEY, and E. F. G. HERRINGTON. J. Chem. Soc. 1957 (1954).
32. A. A. SCHILT and R. C. TAYLOR. J. Inorg. Nucl. Chem. **9**, 211 (1959).
33. K. NAKAMOTO. Infrared and Raman spectra of inorganic and coordination compounds. 3rd ed. Wiley-Interscience, New York. 1977. pp. 142, 239–241.
34. A. J. VOSPER and E. NICIECKI. J. Chem. Soc. Dalton Trans. 1721 (1978).
35. A. W. SHAW, A. J. VOSPER, and M. PRITCHARD. J. Chem. Soc. Dalton Trans. 2172 (1974).
36. C. R. JOHNSON and R. E. SHEPERD. Inorg. Chem. **22**, 2439 (1983) and references therein.

The biosynthesis of cyclopropane fatty acids. III. pH Dependence of methyl hydrogen exchange: gas chromatographic – mass spectral studies

PETER H. BUIST AND JUDY M. FINDLAY
The Ottawa–Carleton Institute for Research and Graduate Studies in Chemistry, Carleton University, Ottawa, Ont., Canada K1S 5B6

Received August 28, 1984

PETER H. BUIST and JUDY M. FINDLAY. Can. J. Chem. **63**, 971 (1985).

L-Methionine-methyl-d_3 was administered to *Lactobacillus plantarum* and the deuterium content of the biosynthetic lactobacillic acid examined by gc–ms. By conducting the biosynthetic experiments in media of varying pH, it was shown that the production of d_1-cyclopropane fatty acid increases with decreasing pH. Factors such as culture age and total activity of cyclopropane synthetase do not directly influence the extent of exchange.

PETER H. BUIST et JUDY M. FINDLAY. Can. J. Chem. **63**, 971 (1985).

On a administré de la L-méthionine-méthyl-d_3 au *Lactobacillus plantarum* et, faisant appel à la cpg/sm, on a examiné le contenu en deutérium de l'acide lactobacillique biosynthétique. En effectuant les expériences de biosynthèse dans des milieux de pH variés, on a pu démontrer que la production d'acide gras comportant un cyclopropane-d_1 augmente avec une diminution du pH. Des facteurs comme l'age de la culture et l'activité totale de la synthésase de cyclopropane n'influencent pas directement le degré d'échange.

[Traduit par le journal]

Enzymic processes which take place in hydrophobic environments form an important subset of all biological reactions. The detailed mechanisms of these reactions are of interest since the chemical reactivity of species subjected to solvent-free environments is often startlingly different from their behaviour in solution. One important example of this type of chemistry is the biomethylenation of olefinic fatty acyl phospholipids as it takes place in many bacterial cell membranes (1). The methylene bridge is derived from *S*-adenosyl-L-methionine (S.A.M.) and the reaction is presumed to involve methyl transfer, formation of a carbocationic intermediate, and 1,3 proton elimination to give the cyclopropyl product. An active site model for this reaction has been presented previously (2) and the essential features are displayed in Scheme 1. The precise structure of the carbocationic intermediate is unknown. Feeding experiments using specifically deuterated substrates and the microorganism, *Lactobacillus plantarum*, have established that if a protonated cyclopropane (3) is involved, then it is sufficiently short-lived to preclude any significant scrambling of deuterium label, as determined by nmr experiments (2, 4). Fluorine substituent effect studies are currently underway in order to gain more insight into this intriguing biological reaction. (For a preliminary account, see ref. 5.)

Feeding experiments using methionine, bearing a trideutero methyl group, have also provided mechanistic information. Interestingly, up to 17% of a monodeuterated species is observed in the mass spectrum of biosynthetic cyclopropane fatty acid (lactobacillic acid) obtained in these feedings. After a complete analysis of the various possible pathways for hydrogen exchange, it was concluded that exchange at the methyl group was probably occurring as a consequence of the fact that the deprotonation step leading to cyclopropane formation is reversible (2).

Recently, the existence of the exchange process has been confirmed in every detail by running the simultaneously proton and deuterium decoupled ^{13}C nmr spectrum of biosynthetic lactobacillic acid derived from methionine-methyl-d_3, which was enriched with carbon-13 in the methyl group.[1] Again,

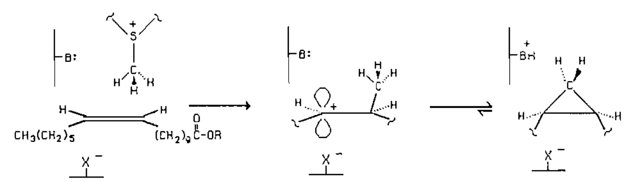

SCHEME 1

approximately 20% of a 1 : 1 mixture of the two possible diastereomeric d_1-species was observed in this experiment.

With the exchange phenomenon firmly documented by two independent analytical techniques, we decided to investigate this very unusual process more closely. Previously (2) it had been noted that the production of exchanged material seemed to increase with increasing culture age in feeding experiments with *Lactobacillus plantarum*. Since the pH of the culture medium also decreases with the extent of growth, due to lactic acid production, it was thought that the exchange process might be dependent on pH. We wish to report the results of experiments which show quite conclusively that this is, in fact, the case.

The simplest way to begin testing our hypothesis was to run the feeding experiments using methionine-methyl-d_3 in media of varying pH, and to analyze the biosynthetic cyclopropane for d_1-content by gc–ms. Two sets of feeding experiments were carried out, the results of which are shown in Table 1. In the first incubation, the pH of the culture was constantly adjusted during growth to the initial pH of 7, by the addition of sterile base to neutralize lactic acid produced by the organism (Expt. #1). In the second experiment, the incubation was started at a pH of 5 and allowed to drop to a final pH of 4.2 (Expt. #2). In this way, we were able to examine the exchange process in two complementary pH domains. We could not perform incubations where the initial pH of the culture was significantly greater than 7.0, since the microorganism cannot tolerate these conditions. In each case, a control experiment was performed (Controls #1 and #2), in which the pH of the medium was allowed to drop from an initial value of 7.0 to a value of approximately 4.0 at the end of the incubation. Experiment #3 refers to previously published work (2), in which the incubation

[1] Unpublished results, obtained in collaboration with A. G. McInnes, J. A. Walter and J. L. C. Wright.

TABLE 1. pH-Dependence of methyl group exchange during cyclopropane fatty acid biosynthesis

pH range (Ave. pH)	Cell yield[a] (mg/100 mL)	% Biomethylenation[b]	$\%d_2$[c]	$\%d_1$	$\%d_0$	$\%d_1/(\%d_1 + \%d_2)$
Expt. #1						
7.0–6.5 (6.75)	245	39	86.5	7.8	5.7	8.3 ± 1.2
Control #1						
7.0–4.4 (5.7)	155	39	83.6	11.3	5.1	11.9 ± 1.3
Expt. #2						
5.0–4.2 (4.6)	74	69	75.2	14.6	10.2	16.3 ± 1.5
Control #2						
7.0–4.1 (5.55)	216	41	80.4	11.5	8.1	12.5 ± 1.4
Expt. #3 (ref. 2)						
7.0–5.9 (6.45)	69	29	83.0	7.3	8.0	8.1 ± 1.3
Control #3 (ref. 2)						
7.0–4.4 (5.7)	124	54	84.3	11.3	4.4	11.8 ± 1.3

[a] The cell yields are given in terms of dry cell weight per 100 mL of culture.
[b] The fatty acids were extracted and analyzed by capillary gc to determine the % biomethylenation: [amt. cyclopropane/(amt. cyclopropane and amt. olefin)] × 100.
[c] For a discussion of errors in the determination of deuterium content, see the experimental section.

was carried out at uncontrolled pH, but part of the same culture was harvested during exponential phase (final pH 5.9) and the remaining portion in lag phase (final pH 4.4).

The following parameters were measured.

(1) Average pH at which biomethylenation was taking place. Our data shows that a substantial amount of cyclopropane formation occurs at all pH values.

(2) Cell yield, as an indication of extent of growth.

(3) % Biomethylenation, the % conversion of olefin to cyclopropane as a measure of the total activity of the cyclopropane synthetase.

(4) The extent of exchange, indicated by the amount of d_1-cyclopropane as a percentage of the total deuterated material. The contribution by d_0 species was neglected, as endogenous cyclopropane from the inoculum was always a major source of this material. Also, an inherent $M - 2$ peak in the mass spectrum of these compounds made it difficult to quantitate the d_0 species accurately. In any case, further loss of deuterium from a monodeuterated cyclopropane is expected to be small, due to a substantial intramolecular isotope effect (2).

When the extent of exchange given by the parameter $\%d_1/(\%d_1 + \%d_2)$ is plotted versus average pH of the medium, it is readily apparent that the extent of exchange increases with decreasing pH (see Fig. 1. At this stage we do not know the mathematical form of the pH dependence). The excellent reproducibility of the data is indicated by the results of Control #1 and Control #3. In contrast, the extent of exchange does not correlate in any obvious way with cell yield, as is readily seen by comparing the results of Expts. #2 and #3. It appears that the extent of exchange also increases with % biomethylenation (graph not shown). We believe that this latter correlation is an indirect one and is due to the fact that, in general, the total activity of cyclopropane synthetase is increased by a drop in pH due to a complex induction phenomenon, as discussed in further detail below.

Consideration of our active site model for this reaction may provide an explanation for the pH dependence of exchange (see

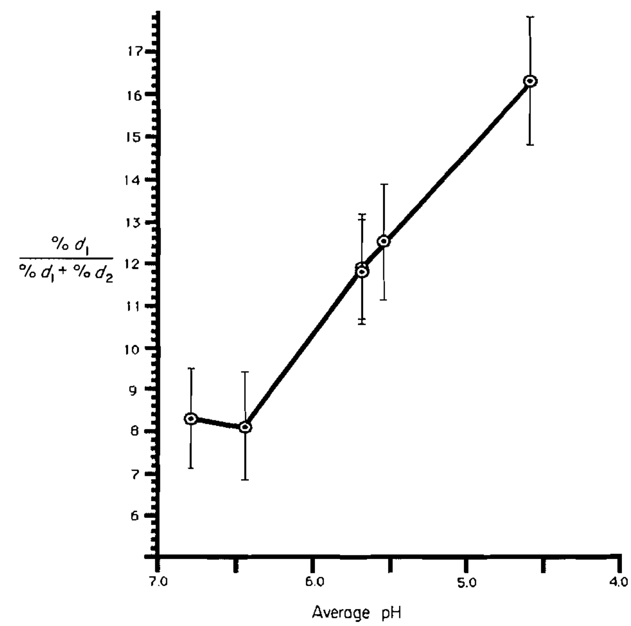

FIG. 1. Dependence of extent of methyl hydrogen exchange on pH.

Scheme 1). Using arguments first developed by Akhtar and Jones (6), we suggest that just as the sulfonium salt is activated by desolvation to allow delivery of a methyl group to an isolated double bond, so the equally unsolvated, conjugate acid (e.g. an ammonium group) is able to protonate the cyclopropane ring.

Assuming for the moment that this is the case, then one might intuitively expect that a lowering of external pH would cause an increase in d_1-cyclopropane production. At lower pH, the equilibrium between the base and its conjugate acid will be shifted to favour the conjugate acid form and hence favour reprotonation of the cyclopropane ring. This equilibrium may be established via one or more amino acid residues acting as a proton shuttle between the active site and the external environment. Thus the extent to which a dideutero-cyclopropane fatty acid is reopened will be greater under these "more acidic" conditions and thus lead to an enhanced production of exchanged material.

Another, perhaps less likely, explanation for the pH dependence of exchange might be that the tertiary structure of the cyclopropane synthetase is altered at lower pH so that the rate of product release is decreased relative to the rate of reprotonation of the cyclopropane.

Either of these effects may also lead to a decrease in specific acitivity of the enzyme. It is interesting to note in this connection that previous work with a cyclopropane synthetase from *Clostridium butyricum* has shown that the pH optimum for the enzyme is, in fact, 7.0 with a rather broad range of 3 pH units on either side of neutrality (7). Unfortunately, a pH profile for the enzyme from *Lactobacillus plantarum* has not been carried out; however, assays of this enzyme are routinely carried out at a pH of 7. The most recent enzymological work with a cyclopropane synthetase from *E. coli* also did not include a pH profile of enzyme activity (8). In vivo studies with *Lactobacillus plantarum* have shown that lowering of pH of the medium enhances lactobacillic acid production but that this effect involves protein synthesis (9), which indicates a more complex inductive effect than at first realized (10).

In summary, we have shown that the exchange at the methyl group in biomethylenation is pH dependent, and thus have provided a basis for further work using purified enzyme preparations buffered over a wider range of pH values. In this way, one should be able to determine the exact form of the pH dependence and gain some clues as to the nature of the base present in the active site. Also, it may be possible to monitor the in vitro exchange process directly by ^{13}C nmr, if S.A.M. enriched with carbon-13 in the methyl group is employed.

Methyl hydrogen exchange seems to be a general phenomenon in "difficult" biomethylations, i.e. methyl transfer to unactivated double bonds, particularly where elimination at the methyl group is the mode of collapse of the carbocationic intermediate (see ref. 2 for a complete discussion). We believe that the observance of exchange in these systems is a consequence of the high reactivity of separated ion pairs in the hydrophobic microenvironment required for these methyl transfers to proceed (6). A search for a similar pH dependence of methyl group exchange as found in this work is warranted in other systems.

Experimental

Apparatus, methods, and materials

L-Methionine-methyl-d_3 was purchased from Merck, Sharpe and Dohme, Pointe Claire, Quebec. Examination of the *bis*-TMS derivative of this material showed that it was essentially 100% trideuterated, with only traces of exchanged species present.

Mass spectrometric determination of deuterated species was performed on a VG 7070-E mass spectrometer, coupled to a DANI 3800 gas chromatograph which was equipped with a 6% OV 101 column and operated isothermally at 250°C. The mass spectrometer was operated at 70 eV, with an accelerating voltage of 6 kV. The ion source was heated at 210°C. Deuterium determinations were performed by injecting a 1% hexane solution of the biosynthetic fatty acids as their methyl esters, scanning the molecular ion cluster repetitively over the entire gc peak due to methyl lactobacillate, and summing the intensities of each individual peak. In this manner each deuterated species could be determined as a percentage with an absolute maximum error of ±1%. The resultant error in $\%d_1/(\%d_1 + \%d_2)$ was calculated in the usual way. In plotting this data, vertical error bars are used, since the error in the parameter plotted along the ordinate is considered to be much larger than the error in the parameter plotted along the abscissa.

The microorganism used in this study was *Lactobacillus plantarum* ATCC 8014 and was obtained from the American Type Culture Collection, Rockville, MD, U.S.A. The basal medium used for each feeding experiment was that of Henderson and Snell (11). The microorganism was grown without shaking at 37°C and harvested by centrifugation at 4°C at 5000 rpm. The cells were then freeze-dried and weighed. Fatty acids were isolated from the bacterial cells by saponification as described below and quantitated as their methyl esters by capillary gc analysis using a Varian Vista 6000 gas chromatograph equipped with a J. and W. DB-5, 0.25-μm capillary column and an FID detector.

Methionine-methyl-d_3 feedings: experiment #1 and control #1

L-Methionine-methyl-d_3 (25 mg) in 3 mL of 50% ethanol and a sterilized solution of biotin (2.5 μg) in 0.25 mL of water were added to 250 mL of filter sterilized basal medium (pH 7.0). Ninety milliliters of this medium were added to a Florence flask, which was then inoculated with a saline suspension (0.5 mL) of freshly grown cells and the culture grown for 26 h to give a final pH of 4.4. The cells were harvested and fatty acids extracted as usual.

One hundred and fifty milliliters of the same medium were transferred to a 250-mL beaker fitted with a 3-holed rubber stopper. A pH electrode was wiped with ethanol and inserted into the medium. An inlet tube connected via tubing to a burette filled with sterile 2 *N* KOH was also inserted. The third port was used to inoculate the medium. The beaker was placed in a constant temperature bath set to 37°C. As growth proceeded the pH of the medium was kept between 6.5 and 7.0 by adding base. After 26 h the cells were harvested and fatty acids extracted by the procedure described below.

Isolation of microbial fatty acids

The dried cells were hydrolyzed with 20 mL of 1 *M* KOH in 1:1 ethanol/water at reflux, under nitrogen, with stirring, for 2 h. The ethanol was then removed *in vacuo* at 40°C. The aqueous residue was transferred to a separatory funnel and washed once with 30 mL of ether. The aqueous layer was acidified with 50% H_2SO_4 and the pH was monitored with Congo Red paper. The fatty acids were extracted with 3 × 10 mL of ether and the combined ether layers were washed with 10 mL of water. After drying with 4 g of sodium sulphate, the ether layer was filtered and the solvent removed *in vacuo*. Residual water was removed as an azeotrope with acetone. The fatty acid residue was dissolved in 2 mL of ether contained in a 25-mL round-bottomed flask and a freshly prepared ethereal solution of diazomethane was distilled into the flask until the yellow colour of diazomethane persisted. The solvent was removed *in vacuo*.

The fatty acid methyl esters were stored in hexane solution in Teflon-capped vials.

Methionine-methyl-d_3 feedings: experiment #2 and control #2

L-Methionine-methyl-d_3 (40 mg) in 50% ethanol (4 mL) and biotin (4.0 μg) in 0.4 mL of sterile water were added to 400 mL of filter sterilized basal medium which was then divided into 200-mL portions between two Florence flasks. The pH of one portion was adjusted to 7.0 (Control #2) and the pH of the other portion was lowered to 5.0 (Expt. #2). Both flasks were inoculated with a 1.0-mL saline suspension of freshly grown cells. Growth was allowed to proceed for 48 h, after which the cells were harvested and fatty acids extracted as usual.

Acknowledgements

We thank the Natural Sciences and Enigneering Research Council of Canada for financial support. The technical assistance of Dr. C. Kazakoff with the gc–ms work is gratefully acknowledged. One of us (J.M.F.) thanks NSERC for an Undergraduate Summer Research Award.

1. J. H. LAW. Acc. Chem. Res. **4**, 199 (1971).
2. P. H. BUIST and D. B. MACLEAN. Can. J. Chem. **60**, 371 (1982).
3. M. SAUNDERS, P. VOGEL, E. L. HAGEN, and J. ROSENFELD. Acc. Chem. Res. **6**, 53 (1973).
4. P. H. BUIST and D. B. MACLEAN. Can. J. Chem. **59**, 828 (1981).
5. P. H. BUIST and J. M. FINDLAY. Tetrahedron Lett. **25**, 1433 (1984).
6. M. AKHTAR and C. JONES. Tetrahedron, **34**, 813 (1978).
7. H. ZALKIN, J. H. LAW, and H. GOLDFINE. J. Biol. Chem. **238**, 1242 (1963).
8. F. R. TAYLOR and J. E. CRONAN. Biochemistry, **18**, 3292 (1979).
9. D. D. SMITH. Ph.D. Thesis, North Texas State University, Denton, Texas (1981).
10. L. A. HALPER. Ph.D. Thesis, North Texas State University, Denton, Texas (1976).
11. L. M. HENDERSON and E. E. SNELL. J. Biol. Chem. **172**, 15 (1948).

Mécanisme des réactions du chlorite et du dioxyde de chlore. 3. La dismutation du chlorite

GUY SCHMITZ ET HENRI ROOZE

Faculté des Sciences Appliquées, Université Libre de Bruxelles, 50, Avenue F. Roosevelt, 1050 – Bruxelles, Belgique

Reçu le 20 juin 1984

GUY SCHMITZ et HENRI ROOZE. Can. J. Chem. **63**, 975 (1985).

La dismutation du chlorite a été étudiée en solutions d'acide perchlorique 0,01 *M* à 1 *M*, à 25°C et pour une force ionique de 1 *M*. Les résultats impliquent au moins trois processus réactionnels. Le premier est catalysé par les ions Cl^-, le second donne une loi d'ordre deux et le troisième est catalysé par le fer. Sa loi cinétique est

$$\frac{d[ClO_2]}{dt} = \frac{[Fe^{3+}][ClO_2^-][HClO_2]}{[ClO_2]}\left(1{,}39 + \frac{0{,}11}{[H^+]}\right)$$

Elle peut être interprétée par la réaction réversible $ClO_2^- + Fe^{3+} \rightleftharpoons ClO_2 + Fe^{2+}$ suivie de deux étapes déterminantes $Fe^{2+} + HClO_2 \rightarrow$ produits et $Fe^{2+} + ClO_2^- \rightarrow$ produits. Nous déduisons de cette étude et de la précédente faite en présence d'*ortho*-tolidine, que la réaction d'ordre deux correspond à un mécanisme radicalaire en chaîne.

GUY SCHMITZ and HENRI ROOZE. Can. J. Chem. **63**, 975 (1985).

The disproportionation of chlorite was studied in 0.01 to 1 *M* perchloric acid solutions at 25°C and an ionic strength of 1 *M*. The results suggest at least three reaction paths. The first is catalysed by Cl^- ions, the second gives a second-order rate law, and the third is catalysed by iron. Its rate law is

$$\frac{d[ClO_2]}{dt} = \frac{[Fe^{3+}][ClO_2^-][HClO_2]}{[ClO_2]}\left(1.39 + \frac{0.11}{[H^+]}\right)$$

This can be interpreted by the reversible reaction $ClO_2^- + Fe^{3+} \rightleftharpoons ClO_2 + Fe^{2+}$ followed by two rate-determining reactions $Fe^{2+} + HClO_2 \rightarrow$ products, $Fe^{2+} + ClO_2^- \rightarrow$ products. From this study and the former, made with added *ortho*-tolidine, we conclude that the second-order reaction proceeds by a radical chain mechanism.

Introduction

La thermodynamique, la stoechiométrie et certains aspects de la cinétique de la dismutation du chlorite ont été discutés dans nos articles précédents (1, 2). Cette dismutation peut résulter d'au moins trois réactions.

(a) La réaction catalysée par les ions Cl^- (1). Elle peut intervenir même s'il n'y a pas d'ions Cl^- initialement, car la dismutation du chlorite en produit. Sa contribution n'est alors significative qu'aux acidités et conversions élevées. Elle peut être négligée lors de toutes les expériences discutées ci-après.

(b) La réaction classique d'ordre 2.

$$[1] \quad -d[HClO_2]/dt = k_1[HClO_2]^2$$

La loi [1], bien établie en milieux très acides, n'est plus vérifiée si $[H^+] \leq 0{,}2\ M$ (3).

(c) La réaction catalysée par des traces de fer dont nous avons étudié la cinétique en présence d'*ortho*-tolidine (2). Nous l'étudions ici en son absence. La technique expérimentale a été décrite antérieurement (1, 2). La concentration totale du chlorite, $[HClO_2] + [ClO_2^-]$, sera désignée par $[NaClO_2]$ et la concentration totale du fer ajouté par [Fe].

Résultats préliminaires

Nous avons confirmé l'observation de Kieffer et Gordon (3), la loi [1] n'est plus satisfaite si $[H^+] \leq 0{,}2\ M$, et en avons découvert la raison: la catalyse de la dismutation du chlorite par les traces de fer inévitablement présentes dans les réactifs. Rappelons (fig. 1 de la réf. 2) qu'en absence d'*ortho*-tolidine, si $[HClO_4] = 0{,}1\ M$, 5×10^{-6} mol/L de fer font plus que doubler la vitesse de formation du dioxyde de chlore. Cet effet du fer est très spécifique (4).

Lors de nos mesures préliminaires nous avons également observé un effet inhibiteur du dioxyde de chlore. Cet effet semblant contredire d'autres travaux, nous en donnons une preuve directe. La figure 1 montre l'évolution de la concentration du ClO_2 dans une solution de chlorite à pH = 2. On observe une diminution rapide de la vitesse qui ne peut résulter ni d'une perte de ClO_2 ni de la variation de la concentration du chlorite. Après 9 min la vitesse a diminué d'un facteur 3 environ, alors que la conversion est inférieure à 10%. La courbe (b) prouve que ceci résulte d'un effet inhibiteur du ClO_2 sur sa vitesse de formation. On a fait passer un courant d'azote pour chasser le ClO_2 dans une fraction de la solution donnant la courbe (a). Toutes autres choses étant égales, les vitesses sont plus grandes si $[ClO_2]$ est plus petit. D'autre part nous n'avons trouvé aucun effet du chlorate.

Résultats en présence de fer ajouté

Dans le domaine d'acidité étudié et sans chlorure ni fer ajouté, la stoechiométrie correspond assez bien à [2] avec une tendance à la formation d'un peu plus de chlorate (1, 3).

$$[2] \quad 4HClO_2 = 2ClO_2 + ClO_3^- + Cl^- + 2H^+ + H_2O$$

Nous avons vérifié qu'en présence de fer ajouté cette équation reste valable, les écarts semblant même moins importants qu'en son absence. Avec 3×10^{-4} mol/L de fer nous avons obtenu

$$[ClO_2]/\Delta[NaClO_2] = 0{,}49 \pm 0{,}02$$

rapport indépendant du chlorite initial, $[NaClO_2]_0 = 10^{-3}$ à $10^{-2}\ M$, et de l'acidité, $[HClO_4] = 10^{-2}$ à $2\ M$.

Pour une acidité fixée et une quantité de fer ajoutée suffisante (elle dépend de l'acidité et sera précisée plus loin) nous avons obtenu la loi cinétique [3]

$$[3] \quad \frac{d[ClO_2]}{dt} = k_3\frac{[NaClO_2]^2}{[ClO_2]}$$

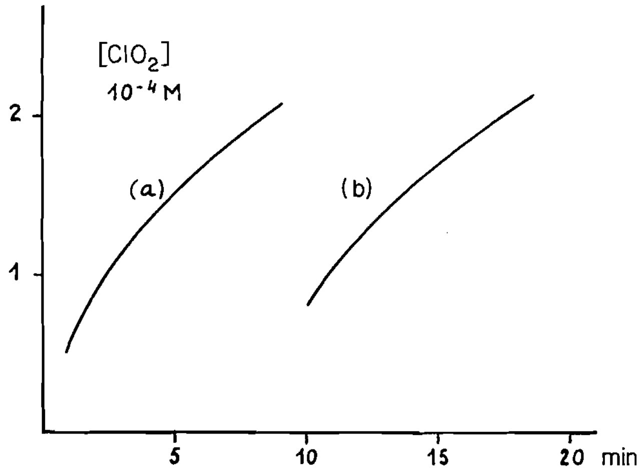

FIG. 1. Evolution de la concentration du ClO_2 dans deux fractions de la même solution; (a) sans barbotage d'azote; (b) après barbotage d'azote pendant 9 min. $[NaClO_2] = 5{,}4 \times 10^{-3}\ M$; $[HClO_4] = 9{,}0 \times 10^{-3}\ M$.

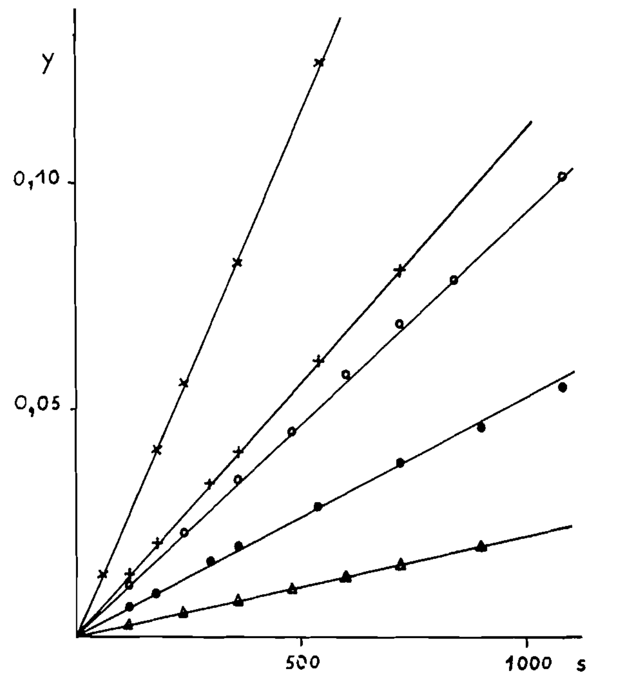

FIG. 2. Transformée Y de la conversion en fonction du temps; $[NaClO_2]_0 = 5{,}7 \times 10^{-3}\ M$. $4Y = [NaClO_2]_0/[NaClO_2] - 1 - \ln [NaClO_2]_0/[NaClO_2]$. $[H^+] = 0{,}0520\ M$, $[Fe] = 3{,}0 \times 10^{-4}\ M$ (X); $[H^+] = 0{,}0520\ M$, $[Fe] = 1{,}2 \times 10^{-4}\ M$ (+); $[H^+] = 0{,}0520\ M$, $[Fe] = 6{,}0 \times 10^{-5}\ M$ (●); $[H^+] = 0{,}208\ M$, $[Fe] = 6{,}0 \times 10^{-4}\ M$ (○); $[H^+] = 0{,}208\ M$, $[Fe] = 1{,}2 \times 10^{-4}\ M$ (△).

Par intégration, avec $[NaClO_2] = [NaClO_2]_0 - 2[ClO_2]$, on obtient [4].

$$[4] \quad \frac{[NaClO_2]_0}{[NaClO_2]} - 1 - \ln \frac{[NaClO_2]_0}{[NaClO_2]} = 4k_3t$$

La figure 2 donne quelques exemples de nos mesures et la figure 3 montre que la constante cinétique apparente k_3 est proportionnelle à la concentration du fer et indépendante de la valeur initiale du chlorite. L'effet de l'acidité sur k_3 apparaît dans le tableau 1 et conduit à expliciter [3] sous la forme [5].

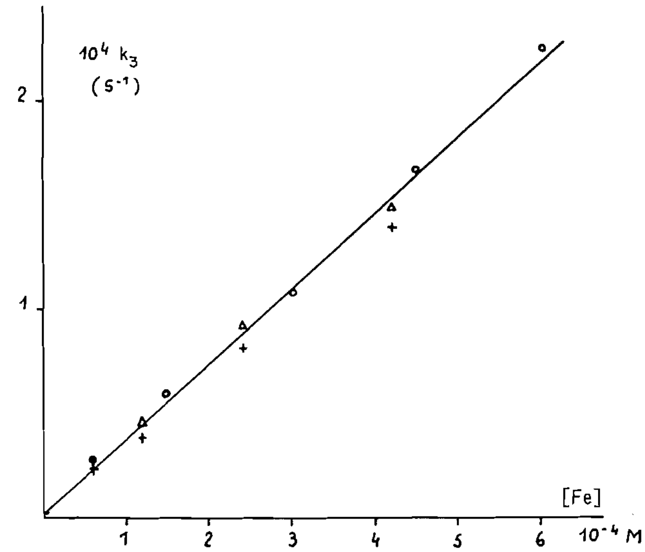

FIG. 3. Variation de k_3 en fonction du fer ajouté. $[H^+] = 0{,}104\ M$; $[NaClO_2]_0 = 3{,}2 \times 10^{-3}\ M$ (+), $5{,}7 \times 10^{-3}\ M$ (○), $8{,}0 \times 10^{-3}\ M$ (△), $1{,}6 \times 10^{-2}\ M$ (●).

TABLEAU 1. Effet de l'acidité sur k_3, 25°C, $I = 1\ M$

$[H^+]$ (M)[a]	$k_3/[Fe]$ $(M^{-1}\ s^{-1})$ Exp.	Calc.[b]
0,052	0,765	0,757
0,104	0,368	0,373
0,208	0,165	0,178
0,416	0,0866	0,0853
1,039	0,0334	0,0330

[a]Les valeurs de $[H^+]$ sont légèrement inférieures à celles de $[HClO_4]$ à cause de la formation de $[HClO_2]$.
[b]Valeurs calculées par [6].

$$[5] \quad \frac{d[ClO_2]}{dt} = \frac{[Fe][ClO_2^-]}{[ClO_2]}(k_5'[HClO_2] + k_5''[ClO_2^-])$$

On déduit de

$$[HClO_2] = \frac{[H^+]}{[H^+] + K_a}[NaClO_2];$$

$$[ClO_2^-] = \frac{K_a}{[H^+] + K_a}[NaClO_2]$$

la relation [6] entre k_3 et l'acidité.

$$[6] \quad \frac{k_3}{[Fe]}\frac{([H^+] + K_a)^2}{K_a} = k_5'[H^+] + k_5''K_a$$

En portant les valeurs du premier membre de [6], calculées avec $K_a = 2{,}4 \times 10^{-2}$ pour $T = 25$°C et une force ionique $I = 1\ M$ (2, 5), en fonction de $[H^+]$ on obtient une droite dont la pente et l'ordonnée à l'origine donnent:

$$k_5' = 1{,}39\ M^{-1}\ s^{-1}; \qquad k_5''K_a = 0{,}11\ s^{-1}$$

Résultats en absence de fer ajouté

En absence de fer ajouté la production de ClO_2 résulte à la fois de la réaction d'ordre deux et de celle catalysée par les traces de fer inévitablement présentes dans les réactifs (2, 4). Tant que la réaction catalysée par les ions Cl^- est négligeable, on obtient [7].

$$[7] \quad \frac{d[ClO_2]}{dt} = k_2[HClO_2]^2 + \frac{[Fe][ClO_2^-]}{[ClO_2]} \times (k_5'[HClO_2] + k_5''[ClO_2^-])$$

Pour une valeur donnée de la concentration du fer, la contribution du deuxième terme est d'autant plus petite que $[ClO_2]$ est grand. Elle diminue donc lorsque la conversion augmente. Cette contribution diminue également si l'acidité augmente, ce qui explique que Kieffer et Gordon (3) aient vérifié la loi d'ordre deux en milieux perchloriques 1,2 M mais pas en milieux moins acides.

Soit α un coefficient stoechiométrique valant 2 si [2] est exactement suivi, un peu supérieur si l'on forme un peu plus de chlorate.

$$[NaClO_2] = [NaClO_2]_0 - \alpha[ClO_2]$$

Si le deuxième terme de [7] était négligeable, on devrait vérifier la forme intégrée [8].

$$[8] \quad \frac{1}{[NaClO_2]} - \frac{1}{[NaClO_2]_0} = \alpha k_2' t$$

$$k_2' = k_2\left[\frac{[H^+]}{[H^+]+K_a}\right]^2$$

La figure 4(a) donne quelques exemples de nos résultats. La loi d'ordre deux n'est pas vérifiée aux faibles conversions parce que, conformément à [7], la réaction catalysée par le fer n'est pas négligeable. Elle ne le devient qu'à partir de conversions d'autant plus grandes que $[H^+]$ et $[NaClO_2]_0$ sont petits. Dans le domaine où $1/[NaClO_2]$ varie linéairement en fonction du temps, nous obtenons à 25°C

$$k_2 = 5{,}1 \pm 0{,}2 \times 10^{-3}\ M^{-1}\ s^{-1}$$

valeur indépendante du chlorite, $[NaClO_2]_0 = 10^{-3}$ à 10^{-2} M, et de l'acidité, $[HClO_4] = 0{,}2$ à 1,2 M. Nous avons utilisé $\alpha = 2$. Avec α un peu plus grand on calculerait $[NaClO_2]$ un peu plus petit, $\alpha k_2'$ un peu plus grand et par un effet de compensation pratiquement la même valeur de k_2. Hong et Rapson (5) ont obtenu $k_2 = 5{,}5 \times 10^{-3}$ et Kieffer et Gordon (3) $\alpha k_2 = 1{,}17 \times 10^{-2}$.

Les importances relatives des deux termes de [7] correspondent bien aux teneurs en fer des réactifs déterminées par spectroscopie d'émission de plasma (4). Par exemple pour l'expérience de la figure 4(a) faite avec $[HClO_4] = 1{,}2$ M et $[NaClO_2]_0 = 2{,}18 \times 10^{-3}$ M on peut estimer que l'on avait $[Fe] \sim 2 \times 10^{-6}$ M. On en déduit avec les constantes cinétiques ci-dessus $r(\text{fer})/r(\text{ordre 2}) = 1{,}2 \times 10^{-5}/[ClO_2]$ ou encore $r(\text{fer}) = r(\text{ordre 2})$ si $[NaClO_2]^{-1} - [NaClO_2]_0^{-1} = 5$ en bon accord avec l'expérience.

L'équation [7], basée sur nos mesures de la production de ClO_2, est en accord avec les mesures de Kieffer et Gordon (3) de la consommation du $NaClO_2$. La figure 4(b) en donne un exemple. En milieu acide perchlorique 1,2 M, pour lequel ils ont admis la loi d'ordre 2, on obtient bien une droite mais elle ne passe pas par l'origine. La présentation adoptée fait apparaître la contribution, petite mais significative, de la catalyse par le fer au début de cette expérience. Nous avons également vérifié que leurs résultats en milieux moins acides (par

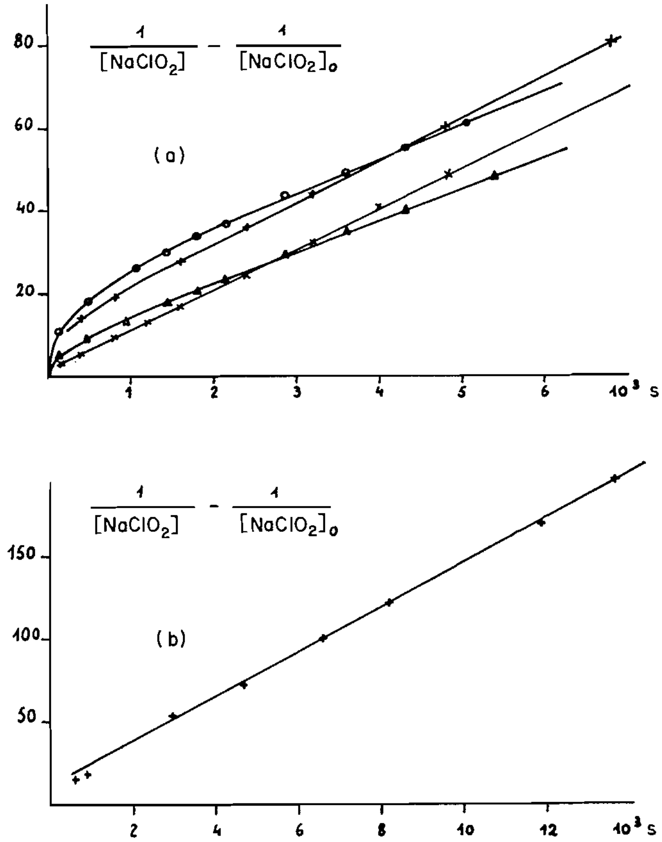

FIG. 4. (a) Résultats en absence de fer ajouté: $[H^+] = 1{,}2$ M, $[NaClO_2]_0 = 1{,}09 \times 10^{-2}$ M (X); $[H^+] = 1{,}2$ M, $[NaClO_2]_0 = 2{,}18 \times 10^{-3}$ M (+); $[H^+] = 0{,}2$ M, $[NaClO_2]_0 = 1{,}04 \times 10^{-2}$ M ($\triangle$); $[H^+] = 0{,}2$ M, $[NaClO_2]_0 = 4{,}15 \times 10^{-3}$ M ($\bigcirc$). (b) Résultats de Kieffer et Gordon (réf. 3, p. 243): $[H^+] = 1{,}2$ M, $[NaClO_2]_0 = 3{,}64 \times 10^{-3}$ M.

exemple p. 238 de la réf. 3; $[HClO_4] = 3{,}33 \times 10^{-3}$ M) satisfont la relation [4]. Dans ces milieux, la réaction catalysée par le fer présent dans les réactifs est prépondérante.

Interprétation des résultats

Catalyse par le fer

Pour interpréter nos résultats en présence d'*ortho*-tolidine nous avions admis (2) les réactions [9] et [10].

$$[9] \quad ClO_2^- + Fe^{3+} \rightleftharpoons ClO_2 + Fe^{2+}$$

$$[10'] \quad HClO_2 + Fe^{2+} \rightarrow ClO + Fe(OH)^{2+}$$

$$[10''] \quad ClO_2^- + Fe^{2+} + H_2O \rightarrow ClO + Fe(OH)_2^+$$

Ces mêmes réactions permettent d'interpréter la catalyse par le fer observée ici, la seule différence étant la réversibilité de [9]. L'*ortho*-tolidine réduisant très rapidement le ClO_2, en sa présence la réaction [9] est déterminante. Ici par contre, le ClO_2 est un produit de la réaction globale et [9] est un quasi-équilibre. On retrouve la loi [5] en admettant que les étapes déterminantes sont [10'] et [10''].

$$[Fe^{2+}] = K_9 \frac{[ClO_2^-][Fe^{3+}]}{[ClO_2]}$$

$$r_{10} = K_9 \frac{[ClO_2^-][Fe^{3+}]}{[ClO_2]} (k_{10}'[HClO_2] + k_{10}''[ClO_2^-])$$

Les constantes des équilibres d'hydrolyse

$$Fe^{3+} + H_2O \rightleftharpoons Fe(OH)^{2+} + H^+$$

$$Fe^{3+} + 2H_2O \rightleftharpoons Fe(OH)_2^+ + 2H^+$$

étant petites, respectivement 9×10^{-4} et $4,9 \times 10^{-7}$ (6, 7), les concentrations des formes hydroxylées sont négligeables dans le domaine d'acidité étudié. Celles des complexes avec les ions Cl^- le sont également (8). La valeur de la constante d'équilibre $K_9 = 2,7 \times 10^{-4}$ estimée en annexe implique que dès les plus faibles conversions observées, on a $[Fe^{2+}] \ll [Fe^{3+}]$ et par conséquent

$$[Fe^{3+}] = [Fe]$$

L'expression de r_{10} correspond bien à la loi expérimentale [5].

Réaction d'ordre deux

La réaction d'ordre deux étant supprimée par l'*ortho*-tolidine, nous avons souligné (2) que $2HClO_2 \rightarrow HClO + ClO_3^- + H^+$ n'est pas une réaction simple. Elle fait intervenir au moins un intermédiaire éliminé par l'*ortho*-tolidine. Ceci suggère un mécanisme radicalaire en chaîne de la forme générale suivante.

Initiation

[i] $HClO_2 + X \rightarrow R^1 + \ldots$

Chaîne

[c1] $HClO_2 + R^1 \rightarrow ClO_3^- + H^+ + R^2$

[c2] $HClO_2 + R^2 \rightarrow HClO + R^1$

Rupture

[r] $R^1 + X \rightarrow \ldots$

ou $R^2 + X \rightarrow \ldots$

La quasi-stationnarité des concentrations des radicaux R^1 et R^2 donne

$$k_i[HClO_2] = k_r[R^1] \text{ ou } k_r[R^2]$$

et une vitesse de la chaîne proportionnelle à $[HClO_2]^2$.

Admettons que la réaction d'initiation soit [10], c'est-à-dire $X \equiv Fe^{2+}$ et $R^1 \equiv ClO$. On obtient la chaîne [11], [12].

[11] $HClO_2 + ClO \rightarrow ClO_3^- + H^+ + Cl$

[12] $HClO_2 + Cl \rightarrow HClO + ClO$

La rupture peut être [13] ou [14].

[13] $Cl + Fe^{2+} \rightarrow Cl^- + Fe^{3+}$

[14] $ClO + Fe^{2+} \rightarrow ClO^- + Fe^{3+}$

D'autre part nous savons (1) que le HClO formé réagit très rapidement avec le chlorite suivant [15] et [16].

[15] $HClO + 2HClO_2 \rightarrow 2ClO_2 + Cl^- + H^+ + H_2O$

[16] $HClO + HClO_2 \rightarrow ClO_3^- + Cl^- + 2H^+$

Dans les milieux acides et riches en chlorite la réaction [15] est prépondérante.

La stoechiométrie de la chaîne résulte de [11] + [12] soit

$$2HClO_2 \rightarrow HClO + ClO_3^- + H^+$$

Si le HClO réagissait uniquement suivant [15] on obtiendrait exactement [2]. La petite contribution de [16] conduit à un excès de chlorate. On retrouve ainsi la stoechiométrie expérimentale.

Effet du choix de la réaction de rupture

A. Si on admet que la rupture de la chaîne se fait suivant [13] on obtient:

Initiation–rupture

Sa stoechiométrie résulte de 2 × [9] + [10] + [11] + [13] soit

$$4HClO_2 \rightarrow 2ClO_2 + ClO_3^- + Cl^- + 2H^+ + H_2O$$

Sa vitesse est donnée par l'expression de r_{10} ci-dessus. On retrouve bien la stoechiométrie et la cinétique de la réaction catalysée par le fer.

Chaîne

Nous venons de montrer que sa stoechiométrie est en accord avec l'expérience. Sa vitesse est obtenue en écrivant la relation de quasi-stationnarité:

$$k'_{10}[HClO_2][Fe^{2+}] + k''_{10}[ClO_2^-][Fe^{2+}] = k_{13}[Cl][Fe^{2+}]$$

d'où

$$r_{12} = \frac{k_{12}}{k_{13}}[HClO_2]^2\left(k'_{10} + k''_{10}\frac{K_a}{[H^+]}\right)$$

La comparaison de r_{10} avec la loi expérimentale [5] donne

$$\frac{k''_{10}K_a}{k'_{10}} = \frac{k''_5K_a}{k'_5} = 0,08$$

Dans les milieux acides où la réaction d'ordre deux est étudiée la contribution du terme en k''_{10} est petite et la cinétique correspond parfaitement à l'expression de r_{12}.

B. Si on admet que la rupture de la chaîne se fait suivant [14] on obtient:

Initiation–rupture

Sa stoechiométrie résulte de 2 × [9] + [10] + [14] soit

$$3HClO_2 \rightarrow 2ClO_2 + HClO + H_2O$$

suivi de [15] et [16]. Sa vitesse est donnée par l'expression de r_{10}.

Chaîne

Sa stoechiométrie est la même que ci-dessus. Sa vitesse est obtenue en écrivant la relation de quasi-stationnarité

$$k'_{10}[HClO_2][Fe^{2+}] + k''_{10}[ClO_2^-][Fe^{2+}] = k_{14}[ClO][Fe^{2+}]$$

d'où

$$r_{11} = \frac{k_{11}}{k_{14}}[HClO_2]^2\left[k'_{10} + k''_{10}\frac{K_a}{[H^+]}\right]$$

On retrouve également la loi cinétique de la réaction d'ordre deux.

La seule différence notable entre les deux hypothèses concerne la stoechiométrie de l'initiation–rupture. Avec [14], du fait de la prépondérance de [15] par rapport à [16], on prévoit une formation relative de ClO_2 beaucoup plus importante que celle obtenue expérimentalement pour la réaction catalysée par le fer. Nous admettons donc que, dans nos conditions, la rupture est [13]. Ce n'est pas nécessairement vrai en milieux moins acides. En effet lorsque la majorité du chlorite se trouve sous la forme ClO_2^-, le ClO produit par [10] pourrait réagir suivant [14] plutôt que suivant [11]. On expliquerait ainsi la forte proportion de ClO_2 obtenue par Kieffer et Gordon (3) si $[HClO_4] = 3,3 \times 10^{-3}$ *M*.

Comparaison avec les résultats de Ondrus et Gordon

Ondrus et Gordon (9) ont étudié la réduction du chlorite par un excès de Fe(II). L'étape déterminante correspond à l'échange d'un seul électron et leurs résultats sont interprétés par [10′] et [10″]. Nous avons recalculé leurs valeurs en prenant $K_a = 2,4 \times 10^{-2}$ et obtenu (2)

$$k'_{10} = 930\ M^{-1}\ s^{-1}$$

$$k''_{10}K_a = 64\ s^{-1}\ (25°C, I = 2\ M)$$

D'autre part la comparaison de [5] avec $d[ClO_2]/dt = 2r_{10}$ donne

$$2K_9k'_{10} = 1,39\ M^{-1}\ s^{-1}$$

$$2K_9k''_{10}K_a = 0,11\ s^{-1}\ (25°C, I = 1\ M)$$

L'accord entre les deux séries de valeurs serait parfait avec $K_9 = 8 \times 10^{-4}$ au lieu de $K_9 = 2,7 \times 10^{-4}$ estimé en annexe. Comparant des constantes cinétiques déduites d'études très différentes et tenant compte de l'imprécision de l'estimation de K_9, due surtout aux effets de force ionique, il faut considérer que ceci confirme que [10] est l'étape déterminante de la dismutation du chlorite catalysée par le fer.

Conclusion et discussion

Ce qui apparaissait déjà dans le travail de Kieffer et Gordon a été confirmé et complété par nos mesures. La stoechiométrie et la cinétique de la dismutation du chlorite sont compliquées par des compétitions entre diverses réactions. Le mécanisme que nous proposons repose sur un très grand nombre de faits expérimentaux et peut être représenté par le schéma suivant.

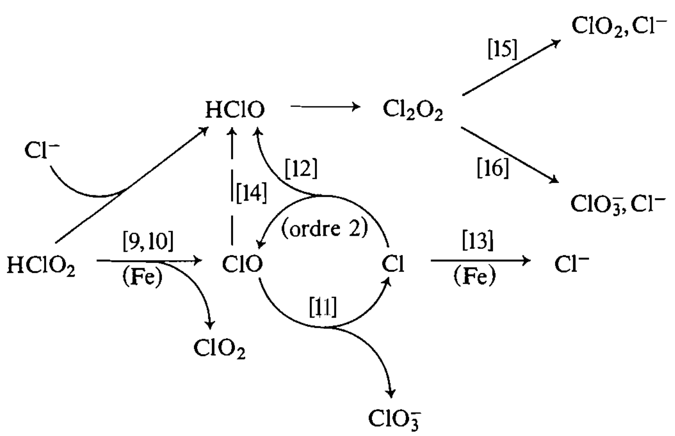

On retrouve dans ce schéma les trois processus réactionnels cités dans l'introduction.

(a) La réaction catalysée par les ions Cl^- que nous avons étudiée antérieurement (1) correspond à la partie supérieure.

(b) Au centre on voit la chaîne donnant la loi d'ordre deux. Elle existe dans tout le domaine de pH étudié mais n'est prépondérante qu'en milieux assez acides et pour des conversions ni trop faibles (effet du fer) ni trop élevées (effet du chlorure).

(c) L'initiation–rupture de cette chaîne correspond à la réaction catalysée par le fer et inhibée par le dioxyde de chlore. Les traces de fer présentes dans l'acide perchlorique "pour analyses" ou dans le chlorite recristallisé plusieurs fois suffisent pour la faire apparaître. A pH = 0 elle devient négligeable par rapport à la réaction d'ordre 2 dès les faibles conversions; à pH = 2 elle reste importante jusqu'aux conversions très élevées.

Dans le premier article de cette série (1) nous avions laissé un fait expérimental étonnant inexpliqué. Lors de la réaction $HClO + HClO_2$ on peut obtenir plus de ClO_2 que le maximum prévu par [15]. Ceci avait également été observé par Emmenegger et Gordon (10) qui avaient suggéré que l'acide hypochloreux catalyse la dismutation du chlorite. Une telle catalyse peut se comprendre dans le cadre de notre mécanisme. Lorsque le HClO est présent dans le système en concentration macroscopique il faut tenir compte d'une réaction supplémentaire, $HClO + Fe^{2+} \rightarrow Cl + Fe(OH)^{2+}$, initiant la décomposition en chaîne de $HClO_2$ suivant [11] et [12].

Hong et Rapson (5) ont observé vers pH = 1 que lorsqu'on augmente la concentration des ions Cl^-, la vitesse de formation du ClO_2 passe par un minimum. Nous avons confirmé cette observation. L'augmentation de la vitesse après le minimum est évidemment due à la réaction catalysée par les ions Cl^-. L'interprétation de sa diminution avant le minimum donnée par ces auteurs ne peut être retenue car elle fait intervenir la réaction $HClO + Cl^- + H^+ \rightarrow Cl_2 + H_2O$ en exigeant qu'elle soit irréversible dans ces conditions, ce qui est exclu (11). Dans le cadre de notre mécanisme cette diminution peut s'expliquer simplement par la réaction $Cl + Cl^- \rightleftharpoons Cl_2^-$ (12). Si Cl_2^- disparait plutôt par une réaction de rupture que par une réaction analogue à [12], les ions Cl^- diminuent la vitesse de la décomposition en chaîne de $HClO_2$. Ces réactions n'ont pas été considérées ci-dessus car les données actuelles ne permettent pas un traitement quantitatif de cet effet.

Lorsqu'on augmente le pH, la vitesse de dismutation du chlorite passe par un maximum vers pH = 2 (3, 13). Ce fait ne peut être interprété simplement en remarquant que, pour une valeur donnée de $[NaClO_2]$, le produit $[ClO_2^-][HClO_2]$ passe par un maximum à ce pH. Il faut également tenir compte de la formation des formes hydroxylées $Fe(OH)^{2+}$ et $Fe(OH)_2^+$. Celles-ci semblent avoir également un effet catalytique en tampon acétate à pH = 4 (14).

Les travaux antérieurs avaient fait apparaître la complexité de la stoechiométrie et de la cinétique de la dismutation du chlorite. L'utilisation de l'*ortho*-tolidine nous a donné les clefs de leur interprétation: l'effet catalytique du fer et le fait que $2HClO_2 \rightarrow HClO + ClO_3^- + H^+$ ne soit pas une réaction élémentaire. Le mécanisme que nous proposons ici est en accord avec tous les faits expérimentaux connus entre pH = 0 et pH = 2. Son extension aux milieux moins acides nécessiterait de nouvelles expériences.

1. G. Schmitz et H. Rooze. Can. J. Chem. **59**, 1177 (1981).
2. G. Schmitz et H. Rooze. Can. J. Chem. **62**, 2231 (1984).
3. R. G. Kieffer et G. Gordon. Inorg. Chem. **7**, 235 (1968); **7**, 239 (1968).
4. H. Rooze. Anal. Chem. **56**, 601 (1984).
5. C. C. Hong et W. H. Rapson. Can. J. Chem. **46**, 2053 (1968).
6. B. O. Hedström. Ark. Kemi. **6**, 1 (1953).
7. L. N. Mulay et P. W. Selwood. J. Am. Chem. Soc. **76**, 6207 (1954).
8. U. Strahm, R. C. Patel et E. Matijevic. J. Phys. Chem. **83**, 1689 (1979).
9. M. G. Ondrus et G. Gordon. Inorg. Chem. **11**, 985 (1972).
10. F. Emmenegger et G. Gordon. Inorg. Chem. **6**, 633 (1967).
11. M. Eigen et K. Kustin. J. Am. Chem. Soc. **84**, 1335 (1962).
12. C. G. Jayson, B. J. Parsons et A. J. Swallow. J. Chem. Soc. Faraday Trans. 1, **69**(9), 1597 (1973).
13. W. Buser et H. Hanisch. Helv. Chim. Acta, **35**, 2547 (1952).
14. H. F. Launer, W. K. Wilson et J. H. Flynn. J. Res. Natl. Bur. Stand. **51**(5), 237 (1953).
15. W. H. Latimer. Oxidation potentials. Prentice Hall, New York. 1952.
16. W. C. Schumb, M. S. Sherrill et S. B. Sweetser. J. Am.

Chem. Soc. **59**, 2360 (1937).
17. L. B. MAGNUSSON et J. R. HUIZENGA. J. Am. Chem. Soc. **75**, 2242 (1953).
18. A. J. ZIELEN et J. C. SULLIVAN. J. Phys. Chem. **66**, 1065 (1962).
19. G. SCHMITZ. J. Chim. Phys. **76**, 209 (1979).

Annexe

Constante d'équilibre de [9]

Le potentiel standard E^0 du couple Fe^{3+}/Fe^{2+} vaut 0,771 V (15). Sa valeur apparente E' dépend du milieu et de la force ionique (16–18). En solutions perchloriques 1 M elle vaut 0,739 ± 0,002 V. Pour le couple ClO_2/ClO_2^- l'incertitude est plus grande. L'examen des sources nous ayant conduit à adopter 0,950 V (1) indique que cette valeur est une bonne estimation de E' en milieu perchlorique 1 M. Elle est supérieure au potentiel standard admis antérieurement $E^0 = 0{,}935$ V (19). L'effet de la force ionique sur ce potentiel est en accord avec celui observé par Hong et Rapson (5) sur la constante d'acidité K_a. En effet:

$$E' = E^0 - \frac{RT}{F} \ln \gamma^2_{HClO_2}$$

En prenant comme estimation du coefficient d'activité

$$\gamma^2_{HClO_2} = K_a^0/K_a'(1\ M) = 1{,}1/2{,}4$$

on obtient

$$E'(1\ M) - E^0 = 0{,}020$$

De $E'(Fe^{3+}/Fe^{2+}) = 0{,}739$ V et $E'(ClO_2/ClO_2^-) = 0{,}950$ V, on déduit

$$K_9 = \frac{[ClO_2][Fe^{2+}]}{[ClO_2^-][Fe^{3+}]} = 2{,}7 \times 10^{-4}$$

(25°C, milieu perchlorique 1 M)

Au cours de nos expériences on avait

$$\frac{[Fe^{2+}]}{[Fe^{3+}]} = 2{,}7 \times 10^{-4} \frac{[ClO_2^-]}{[ClO_2]} = \frac{6{,}5 \times 10^{-6}}{[H^+] + 2{,}4 \times 10^{-2}} \frac{[NaClO_2]}{[ClO_2]}$$

et $[Fe^{3+}] \gg [Fe^{2+}]$ dès les plus faibles conversions observées.

The mechanism of enzymic hydroxyl group removal from C-21 of tetrahydrodeoxycorticosterone

HERBERT L. HOLLAND AND ELLY RIEMLAND
Department of Chemistry, Brock University, St. Catharines, Ont., Canada L2S 3A1

Received August 2, 1984

HERBERT L. HOLLAND and ELLY RIEMLAND. Can. J. Chem. **63**, 981 (1985).

The C-21 hydroxyl group of C-17- and C-21-deuterium labelled tetrahydrodeoxycorticosterone is removed by the anaerobic intestinal bacterium *Eubacterium lentum* ATCC 25559 with retention of deuterium label at C-17α and loss of one of the two deuterium atoms originally present at C-21. Dehydroxylation at C-21 proceeds with an apparent primary kinetic isotope effect, K_H/K_D, at C-21 of 2.6. These data suggest a route for C-21 dehydroxylation involving a C-20(21)-enediol intermediate.

HERBERT L. HOLLAND et ELLY RIEMLAND. Can. J. Chem. **63**, 981 (1985).

Sous l'influence de la bactérie anaérobique intestinale *Eubacterium lentum* ATCC 25559, le groupement hydroxyle C-21 de la tétrahydrodéoxycorticostérone, marquée au deutérium dans les positions C-17 et C-21, est éliminé avec rétention du marqueur en C-17α et avec perte de l'un des deux atomes de deutérium originalement présents en position C-21. La déhydroxylation en C-21 se produit avec un effet isotopique cinétique primaire apparent, K_H/K_D, en C-21 qui est égal à 2,6. Ces données suggèrent que la déhydroxylation en C-21 implique un intermédiaire ènediol-C-20(21).

[Traduit par le journal]

Introduction

Those 21-hydroxycorticosteroids which undergo enterohepatic circulation in the body (passage through the intestines and reabsorption into the liver) are eventually excreted in a modified form lacking the C-21 hydroxyl group (1). In contrast, those which are directly excreted retain this functionality (2). The 21-dehydroxylation reaction is performed by the anaerobic intestinal microflora (3), the species responsible having been identified as *Eubacterium lentum* (4). This reaction can provide one of the major routes for the metabolism (and hence deactivation) of administered corticosteroids such as tetrahydrodeoxycorticosterone (**1***a*) (5) and aldosterone (6), and in view of its widespread relevance (in addition to any intrinsic chemical interest), we have undertaken a study of its mechanism.

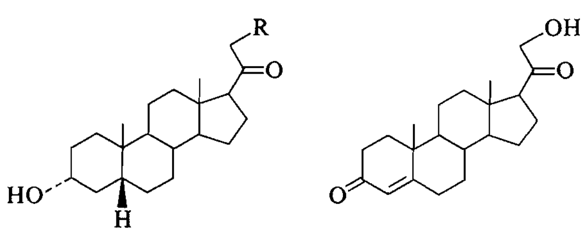

1*a* R = OH
b R = H

2

Enzymological studies from Bokkenheuser's laboratory have established that the C-21 dehydroxylating enzyme from *E. lentum* requires a reduced flavin cofactor ($FMNH_2$) (4, 7), is inhibited by metal chelating agents (8), functions at pH 6.5–7.3 (1), and dehydroxylates only those substrates with a C-20 carbonyl function (1). Preliminary mechanistic work has also been carried out (9), which determined that C-21 dehydroxylation of ^{3}H labelled deoxycorticosterone (21-hydroxypregn-4-ene-3,20-dione, **2**) by human fecal flora proceeded with substantial but unreproducible loss of label from a site assumed to be C-21. However, this reference includes no details of the method of preparation of labelled substrate, or of the criteria used to establish the homogeneity or position of label, so the data must be interpreted with caution. Our data, discussed below, remove this ambiguity and expand upon the mechanistic details of the dehydroxylation.

Results and discussion

We have used the intestinal bacterium *E. lentum* ATCC 25559, in anaerobic mixed culture with *Esherichia coli*, to perform the conversion of **1***a* to **1***b*. The latter microorganism serves to generate the highly reducing environment necessary for *E. lentum* to carry out this biotransformation (1, 4). In our hands, this mixed but defined bacterial culture was not able to dehydroxylate **2** as previously reported in the case of undefined fecal bacteria (9) and the related bacterium *E. lentum* VPI 0255 (1), but **1***a* was quantitatively dehydroxylated at C-21 within seven days.

Labelled substrate **1***a* was prepared from unlabelled material by base catalysed exchange, using the method developed by Johnson for the preparation of side-chain labelled corticosteroids (10), and analysed by ^{1}H and ^{2}H nmr analysis. Product **1***b*, both of enzymic origin and as prepared by exchange, was additionally analysed by electron impact mass spectrometry. The latter technique could not be applied to labelled **1***a* because of the lack of an observable molecular ion: other mass spectral techniques (e.g. FAB) could not be used for quantitative deuterium estimation.

The deuterium content of **1***a* at C-21 was estimated by ^{1}H nmr using the C-3 hydrogen signal as internal reference, and thence at C-17 by the relative areas of the signals assigned to deuterium at C-21 and C-17 in the ^{2}H nmr spectrum. Reported values represent the average of ten integrations. The content and location of label in **1***b* were determined by mass spectral, ^{1}H and ^{2}H nmr data (see Experimental). The values obtained for starting material, biotransformation product, and control incubation samples are listed in Table 1.

Control experiments confirm that the integrity of label in **1***a* is maintained under the incubation conditions; thus **1***a* recovered from a pH 6.3 phosphate buffer after 7 days, and from a short (4 day) incubation at pH 6.2–6.5 with *E. lentum*, showed no appreciable loss or scrambling of label. Similarly, product **1***b* did not lose any label from C-17 or -21 during a seven-day exposure to an active culture of *E. lentum*/*E. coli*. Analysis of **1***b* produced from labelled **1***a*, however, clearly shows that the C-21 dehydroxylation reaction takes place without appreciable loss of label from C-17α, but with loss of one of the two labelled hydrogen atoms originally present at C-21.

Incubation of substrate consisting of an equimolar mixture of

TABLE 1. Metabolism of labelled **1***a* by *E. Lentum*

Substrate	Conditions	Product	Yield, %	^{2}H Content % C-17	^{2}H Content % C-21
1*a*	Synthetic sample			44*	95†
1*b*	Synthetic sample			>95	80‡
1*a*	Phosphate buffer pH 6.3 7 days	**1***a* recovered	92	44	95†
1*a*	*E. lentum* 4 days	**1***a* recovered	50	45	95†
1*b*	*E. lentum* 7 days	**1***b*	94	>95	80‡
1*a*	*E. lentum* 4 days	**1***b*	30	38	52†
1*a*	*E. lentum* 7 days	**1***b*	80	41	47†

*Values are accurate to ±2%.
†Percentage of two deuterons.
‡Percentage of three deuterons.

labelled and unlabelled **1***a* gave a sample of **1***b* whose deuterium content, following the assumption of the loss of one deuterium atom from C-21 during dehydroxylation, enabled the apparent primary kinetic isotope effect, K_H/K_D, for the reaction to be calculated using the equation (11):

$$K_H/K_D = \frac{\ln 1 - f\dfrac{1 + AD_0/AH_0}{1 + XD/XH}}{\ln 1 - rf\dfrac{1 + AD_0/AH_0}{1 + XD/XH}}$$

where AD_0/AH_0 = ratio of labelled to unlabelled substrate at time zero; XD/XH = ratio of products arising from labelled (XD) and unlabelled (XH) substrates; $r = (XD/XH)/(AD_0/AH_0)$; and $f = (XH + XD)/(AH_0 + AD_0)$ = fraction of conversion. Using the values $AD_0/AH_0 = 1$, $XD/XH = 0.54$, and $f = 0.52$ (see Experimental) the value of K_H/K_D is 2.6 ± 0.1. This value is similar to those observed for some other enzyme catalysed enolizations (12–14) and, together with the substrate and cofactor requirements discussed above, and a possible role for metal ions in the reaction, suggests the route for C-21 dehydroxylation proposed in Scheme 1.

During dehydroxylation, the substrate may bind irreversibly in the C-20(21)-enediol form **3** to an as yet unidentified metal ion of the enzyme. Metal ions are common binding sites in the enzymic coordination of α-ketols (e.g. glyoxalase (15)), and can provide Lewis acid activation for substrate enolization (16). Reduction of **3** by $FMNH_2$ may then be followed by metal catalysed dehydration (17) to release the product **1***b* in its enol form.

The route presented in Scheme 1 is somewhat similar to the routes established for the enzymic dehydroxylation of bile acids at C-7 (18, 19) and of 16α-hydroxyprogesterone at C-16 (20) by *Eubacteria*. In these cases, the reactions proceed by dehydration followed by reduction of the resultant carbon–carbon olefinic bond. Scheme 1 is consistent with all the available data on the C-21 dehydroxylation reaction. The nature of the metal ion and the stereochemical details of the deprotonation at C-21 remain to be investigated.

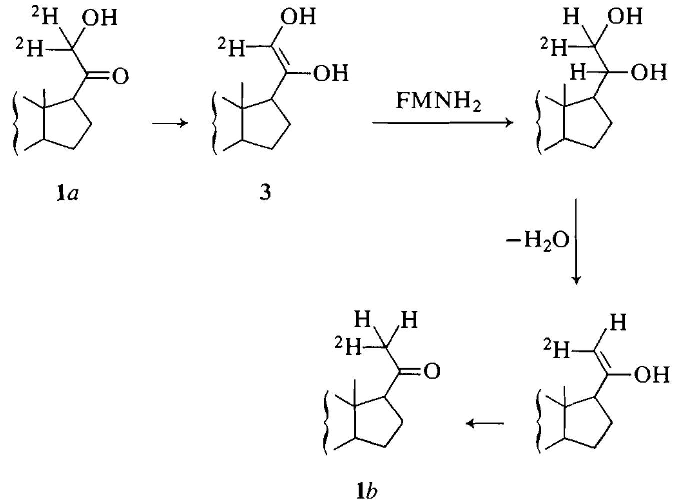

SCHEME 1. Proposed route for C-21 dehydroxylation by *E. lentum*.

Experimental

Apparatus, materials, and methods

Melting points were determined with a Gallenkamp apparatus and are uncorrected. The ^{1}H nmr spectra were obtained at 80 MHz on a Bruker WP-80CW using $CHCl_3$ as solvent and TMS as internal standard, and the ^{2}H nmr spectra at McMaster University, Hamilton, on a Bruker WM 250, using $CHCl_3$ as solvent and internal standard. Mass spectra were obtained with an AEI MS30 interfaced to a Kratos DS 55 data system. Deuterium content was determined by repeated scanning of the appropriate molecular ion and $M - H_2O$ regions and correction for natural isotopic abundances. Column chromatography was performed on silica gel (Merck 230–400 mesh) and thin layer chromatography on Merck silica gel 60F-254 (0.2 mm). *Eubacterium lentum* ATCC 25559 was maintained in continuous culture as described below.

Maintenance of E. lentum

Growth medium consisting of dehydrated brain heart infusion broth (Difco, 37 g/L) and cysteine hydrochloride (0.5 g/L) was autoclaved and cooled to room temperature under a continuous degassing stream of argon. The pH of the medium was 6.2–6.5. This medium was inoculated under anaerobic conditions with the stock *E. lentum* culture (12 mL per L of new medium) and allowed to grow out at 37°C. The culture was maintained by transfers at intervals not exceeding 14 days.

Synthesis of substrates

*5β-Pregnan-3α, 21-diol-20-one, 17,21,21-*d$_3$ *(***1***a)*

Unlabelled **1***a* (Sigma, 61.6 mg) was dissolved in methanol-OD (3 mL) and this solution added to a solution of tris(hydroxymethyl)-methylamine (1.05 g) in D_2O (25 mL) and methanol-OD (25 mL). The resulting mixture was maintained at 60°C for 24 h, then cooled and acidified with 35% DCl in D_2O to pH 5. The methanol was removed under reduced pressure and the aqueous residue extracted with dry ethyl acetate (3 × 25 mL). The extract was dried (Na_2SO_4) and evaporated to yield 61.7 mg of labelled **1***a*, identical in physical properties (mp, tlc) to unlabelled material. The ^{1}H nmr included signals at δ 0.63 (3H, s, C-18 H), 0.93 (3H, s, C-19 H), and 3.65 (1H, m, C-3 H) ppm. The area of the signal at δ 4.15 ppm was used to estimate the residual ^{1}H content at C-21 (5%, see Table 1). FAB mass spectral analysis gave a cluster of ions at m/e 334–337. The ^{2}H nmr included signals at δ 2.43 (C-17 H) and 4.12 (C-21 H) ppm.

*5β-Pregnan-3α-ol-20-one, 17,21,21,22,-*d$_4$ *(***1***b)*

To a solution of 5β-pregnan-3α-ol-20-one (0.1 g) and tetra-n-butyl ammonium bromide (0.1 g) in dry benzene (5 mL) was added a solution of NaOD in D_2O (5%, 10 mL). The resulting two-phase system was stirred and refluxed under protection from atmospheric moisture for 48 h. The reaction mixture was then cooled, and the organic layer separated, washed with pH 6.86 phosphate buffer (3 × 10 mL), dried, and evaporated to yield labelled **1***b* (81.5 mg), which had identical physical (mp and tlc) properties to an unlabelled sample. The ^1H nmr included signals at δ 0.58 (3H, s, C-18 H), 0.93 (3H, s, C-19 H), and 3.63 (1H, m, C-3 H) ppm. The ^2H nmr included signals at δ 2.07 (C-21 H) and 2.51 (C-17 H) ppm. Other spectral data (ir, ^{13}C nmr) were consistent with the proposed structure.

Exposure of labelled **1**a *to pH 6.3 buffer*

Labelled **1***a* (40 mg) was dissolved in ethanol (95%, 1 mL) and the resulting solution added to phosphate buffer (pH 6.3, 50 mL). The mixture was kept at 37°C for 7 days, then cooled, and extracted with chloroform (3 × 50 mL). The extract was dried and evaporated to give recovered **1***a* (37 mg). Deuterium content is listed in Table 1.

Incubations with E. lentum *(Table 1)*

The substrate (50 mg) was dissolved in ethanol (95%, 4 mL), and 1 mL portions of this solution added to each of four 250-mL aliquots of growth medium, prepared as described above. The medium was then autoclaved, cooled and degassed under argon, and each portion then inoculated with 3 mL of *E. lentum* stock culture (7 days old) and 3 mL of *E. coli* stock culture (Boreal). The cultures were then maintained at 37°C for 4–7 days (see Table 1). Products and recovered substrates were isolated as described (21), and purified by crystallization following column chromatography. Compounds were identified by physical (mp, tlc) and spectral (nmr) comparison with authentic samples. Details of recovery and yields are listed in Table 1.

For the mixed labelling isotope effect study, labelled and unlabelled **1***a* (37.5 mg each) were mixed and incubated as described above for 4 days. The product **1***b* (39 mg) was found by mass spectral analysis to have the following isotopic content: d_0, 70%; d_1, 18%; d_2, 12%. Based on the overall isotopic composition of the starting material (d_1 = 15%, d_2 = 47%, d_3 = 35%), the fraction XD/XH is calculated as below. Percent product arising from unlabelled substrate (XH) is $p.d_0$: % product arising from labelled substrate (XD) is $0.15\, q.d_0 + 0.47\, q.d_1 + 0.35\, q.d_2$ (assuming the loss of one deuterium on conversion). Total d_0 product is therefore $(p + 0.15q)$%, total d_1 product is $0.47q$%, and total d_2 product is $0.35\,q$%. Since $p + 0.15\,q = 70$, $0.47\,q = 18$, $0.35\,q = 12$, and $p + q = 100$, therefore $p = 65$, $q = 35$, and $XD/XH = q/p = 0.54$. The degree of conversion, f, was 0.52 based on the isolation of 38.9 mg of product. The remainder of the starting material was isolated unchanged, giving a quantitative recovery of steroid.

Acknowledgements

We thank the Natural Sciences and Engineering Research Council of Canada for financial support, Mr. T. Jones for mass spectral analyses, and Mr. B. Sayer, McMaster University, Hamilton for ^2H nmr spectra.

1. J. WINTER and V. D. BOKKENHEUSER. J. Steroid Biochem. **9**, 379 (1978).
2. I. A. MACDONALD, V. D. BOKKENHEUSER, J. WINTER, A. M. MCLERNON, and E. H. MOSBACH. J. Lipid Res. **24**, 675 (1983).
3. E. ERIKSSON, J. A. GUSTAFSSON, and J. SJOVALL. Eur. J. Biochem. **9**, 550 (1969).
4. V. D. BOKKENHEUSER, J. WINTER, P. DEHAZYA, and W. J. KELLY. Appl. Environ. Microbiol. **34**, 571 (1977).
5. J. WINTER, V. D. BOKKENHEUSER, and L. PONTICORVO. J. Biol. Chem. **254**, 2626 (1979).
6. V. D. BOKKENHEUSER, J. WINTER, J. W. HONOUR, and C. H. L. SHACKLETON. J. Steroid Biochem. **11**, 1145 (1979).
7. S. D. FEIGNER, V. D. BOKKENHEUSER, J. WINTER, and P. B. HYLEMAN. Biochem. Biophys. Acta, **574**, 154 (1979).
8. S. D. FEIGNER and P. B. HYLEMAN. J. Lipid Res. **21**, 585 (1980).
9. W. G. KELLY, O. DELEON, J. WINTER, and V. D. BOKKENHEUSER. J. Steroid Biochem. **8**, 73 (1977).
10. D. M. JOHNSON. J. Org. Chem. **47**, 198 (1982).
11. C. C. MCMULLEN and H. G. THODE. *In* Mass spectrometry. *Edited by* C. A. McDowell. McGraw-Hill, Toronto. 1980.
12. W. W. MILLER and J. H. RICHARDS. J. Am. Chem. Soc. **91**, 1498 (1969).
13. J. RETEY and J. A. ROBINSON. Stereospecificity in organic chemistry and enzymology. Verlag Chemie, Weinheim. 1982. p. 105.
14. R. V. J. CHARI and J. W. KOZARICH. J. Biol. Chem. **256**, 9785 (1981).
15. K. A. DAVIS and G. R. WILLIAMS. Biochim. Biophys. Acta, **113**, 393 (1966).
16. S. S. HALL, A. M. DOWEYKO, and F. JORDAN. J. Am. Chem. Soc. **100**, 5934 (1978).
17. H. DUGAS and C. PENNEY. Bio-organic chemistry. Springer Verlag, New York. 1981. pp. 329, 339.
18. B. SAMUELSSON. J. Biol. Chem. **235**, 361 (1960).
19. B. A. WHITE, D. A. M. PAONE, A. F. CACCIAPUOTI, R. J. FRICKE, E. H. MOSBACH, and P. B. HYLEMON. J. Lipid Res. **23**, 145 (1982).
20. J. WINTER, S. O'ROURKE, V. D. BOKKENHEUSER, P. B. HYLEMON, and T. L. GLASS. J. Steroid Biochem. **16**, 231 (1982).
21. V. D. BOKKENHEUSER, J. B. SUZUKI, S. B. POLOVSKY, J. WINTER, and W. G. KELLY. Appl. Microbiol. **30**, 82 (1975).

Extended basis *ab initio* calculations on conformers of propanal

V. P. GUPTA
Department of Physics, University of Jammu, Jammu Tawi – 180001, India

Received May 28, 1984

V. P. GUPTA. Can. J. Chem. **63**, 984 (1985).

Extended basis *ab initio* calculations on four conformations of propanal at the 4-31G and 6-31G** levels followed by many-body perturbative interaction calculations MP2 and MP3 have been conducted. Optimized geometries, heights of rotational barriers, dipole moments, ionisation potentials, and diagonal harmonic force constants have been reported. The *s-cis* conformer (dihedral angle CCCO = 0°) is found to be more stable than the *gauche* conformer (dihedral angle CCCO = 129.84°) by 5.07 kJ mol^{-1}. Torisonal potential barriers *s-cis/gauche*, *gauche/s-cis*, and *gauche/gauche* have values 8.81, 3.74, and 1.84 kJ mol^{-1}, respectively. It appears that meaningful values of rotational barriers can be obtained only after a careful optimization of the geometries of the conformations involved.

V. P. GUPTA. Can. J. Chem. **63**, 984 (1985).

Opérant aux niveaux 4-31G et 6-31G**, on a effectué des calculs *ab initio* sur quatre conformations du propanal; on a ensuite effectué des calculs MP2 et MP3 impliquant une interaction perturbative de plusieurs corps. On rapporte les géométries optimisées, les hauteurs des barrières à la rotation, les moments dipôlaires, les potentiels d'ionisation et les constantes de force harmonique diagonale. On a trouvé que le conformère *s-cis* (angle dièdre CCCO = O°) est plus stable que le conformère *gauche* (angle dièdre CCCO = 129,84°) par 5,07 kJ/mol. Les valeurs des barrières au potentiel de torsion sont respectivement 8,81, 3,74 et 1,84 kJ/mol pour *s-cis/gauche*, *gauche/s-cis* et *gauche/gauche*. Il semble que l'on ne peut obtenir de valeurs significatives pour les barrières à la rotation qu'après avoir effectué une optimisation adéquate des géométries des conformations impliquées.

[Traduit par le journal]

Introduction

Several studies using different experimental techniques such as microwave (1–3), vibrational (4–8) and nmr (9) spectroscopy, and the theoretical techniques such as molecular dynamics (10) and molecular orbital calculations (11–14) have been reported in the literature for the determination of the conformation of propanal in gaseous and liquid phases. Some statistical mechanical calculations (15, 16) of the chemical and thermodynamic properties of propanal in the gaseous state have also been reported. All these studies indicate that propanal exists as a mixture of *s-cis* and *gauche* conformers with the methyl group eclipsing the carbonyl bond in the *s-cis* (**I**) conformation and skewed out of plane to a dihedral angle of ca. 130° in the *gauche* (**III**) conformer. In a separate communication (17), we have reported photorotamerisation studies on this molecule in low temperature argon and nitrogen matrices and have found that at 10 K the concentrations of the two conformers are 95% *s-cis* and 5% *gauche* which changes to 47% and 53% respectively, on irradiation with a broad band ir radiation. A considerable uncertainty exists in the literature about the conformations of the lowest energy conformer and also about the enthalpy difference between the two stable conformers (2, 4, 14, 17, 18). Similarly, different values have been reported in the literature for the potential energy barriers between conformers *s-cis/gauche* and *gauche/s-cis* and the dihedral angle φ_0 (C_1—C_2—C_3=O_4) in the *gauche* conformer (2, 4, 10).

Ab initio calculations on propanal were first reported by Radom *et al.* (11) who studied the variation of the RHF energy for the molecule with the change in the dihedral angle φ_0 (C_1—C_2—C_3=O_4). The calculations were performed using the 4-31G basis set and a model geometry as proposed by Pople *et al.* (19). However, no attempt was made to optimize the geometry of the molecule and as such the results were in large error from the experimental values. Allinger *et al.* (10) reported *ab initio* calculations using a $5s2p$ basis set of Gaussian orbitals (20) without a geometry optimization. They optimized geometries of the lowest energy conformations **I** and **III** by the method of molecular mechanics. In two recent studies (3, 33) that appeared after the present work was completed *ab initio* 4-21G results have been reported. In an earlier communication (17) we reported, in part, results of our *ab initio* calculations on propanal using the 4-31G extended basis set and the optimized geometries of the *s-cis* and *gauche* conformers.

In order to have a more complete understanding about the structure of propanal and for obtaining the diagonal force constants we carried out extended basis set 4-31G and 6-31G** *ab initio* calculations followed by many body Møller-Plesset perturbative interaction calculations MP2 and MP3.

Configurational notations and computational methods

The notations used in this paper for conformers of propanal are similar to those in alcohols (29, 30) as well as that published in our earlier communication (17). Propanal is a single rotor system in which different configurations can be obtained by rotation around the C_2—C_3 axis. The conformations with respect to the dihedral angle φ_0 (C_1—C_2—C_3=O_4) are denoted as **I** (or C; φ_0 = 0°), *II* (φ_0 = 72.9°), **III** (or G; φ_0 = 130°), and **IV** (φ_0 = 180°). Computer drawings of these conformations are given in Fig. 1. Rotation of the CH_3 group about the C_1—C_2 axis does not give any new conformer.

The calculations were carried out on computers Univac 1108, Burrough B7800, and Vax-11 using programmes Gaussian-76 (31) and Gaussian-80 (32). Geometries of all the four conformers were optimized in the 4-31G basis set by the usual iterative process using Gaussian-76. First, the coordinates of the *s-cis* (**I**) species (Fig. 1) were optimized, since this conformer was expected to be the lowest energy species. Then, using the *s-cis* geometry, the influence of the rotation of the CHO group in intervals of 10° was studied (i.e., varied from 0° to 180°); this calculation gave approximate φ_0 values for the maxima and minima. The geometries of the other three conformations (**III** corresponding to a minimum and **II** and **IV** corresponding to energy maxima) were then optimized. The

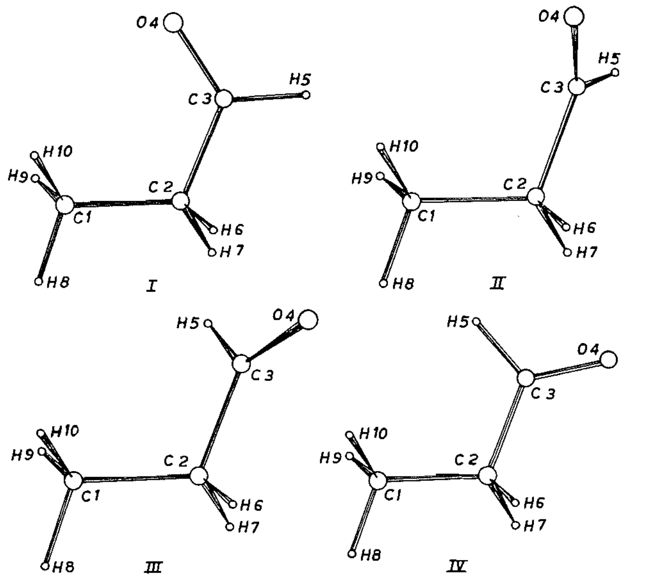

FIG. 1. Computer-drawn drawing of the conformations of propanal.

energy maxima do not seem to be first order saddle point. A semi-rigid 4-31G potential energy surface was constructed (cf. ref. (17)). For each calculated point on the curve, the geometry of the nearest optimized conformation was used. To obtain reliable results for the diagonal force constants, the geometries were carefully optimized till the bond lengths changed by no more than 0.2 pm (0.002 Å), angles no more than 0.2° and dihedral angles no more than 0.5°. Optimization of the angles required at least five iteration cycles. The optimizations of the minimum energy conformations **I** and **III** were verified by the gradient optimisation method of the program Gaussian 80 (31), in which case the residual forces on the cartesian coordinates were less than or equal to 1×10^{-3} mdyn. These optimized geometries were then used for the 6-31G** level calculations involving polarization functions at every atom. MP2 and MP3 level calculations also used the same geometries.

Results and discussion

The results of calculations are summarized in Tables 1 to 3. Table 1 contains the optimized geometries of all the four conformations in the 4-31G basis set. The energies of these conformations, rotational barriers; and the ionization potentials (based on Koopman's theorem), as obtained from the different levels calculations, are given in Table 2. The atomic and bond populations and the dipole moments obtained from 6-31G** calculations and the harmonic force constants obtained at the optimized geometries and at small displacements from these geometries for the *s-cis* and gauche conformations are included in Table 3.

From Tables 1 and 2 it follows that conformations **I** and **III** correspond to the energy minima and **II** and **IV** to the energy maxima. 6-31G** calculations elevate the energies of these conformations over their 4-31G values whereas the MP2 and MP3 calculations stabilize these values. The enthalpy difference between **I** and **III** from MP3 calculations is 5.07 kJ mol^{-1}. This value is higher than the experimental values 2.88 − 4.16 kJ mol^{-1} (2, 4, 9, 18, 21). The dihedral angle φ_0 (C_1—C_2—C_3=O_4) for conformation **III** obtained from 4-31G geometry optimization is 129.84° which lies within the experimental range 131 ± 6° suggested by Butcher and Wilson (2) from

TABLE 1. 4-31G results for the optimized conformations of propanal; bond lengths are in pm and angles in degrees

Internal coordinates etc.	Conformations			
	I	II	III	IV
C_1—C_2	152.44	153.51	153.41	152.62
C_2—C_3	149.85	150.27	149.78	150.46
C_3—O_4	120.97	121.04	120.96	120.93
C_3—H_5	108.59	108.52	108.69	109.00
C_2—H_6	108.74	108.36	108.11	108.50
C_2—H_7	108.74	108.33	108.71	108.50
C_1—H_8	108.22	108.20	108.15	108.30
C_1—H_9	108.12	108.38	108.39	108.30
C_1—H_{10}	108.12	108.18	108.27	108.30
C_1—C_2—C_3	113.67	112.47	111.88	113.52
C_2—C_3—O_4	124.59	122.72	124.47	123.37
C_2—C_3—H_5	115.67	117.40	115.72	116.80
C_3—C_2—H_6	107.67	107.91	108.52	107.81
C_3—C_2—H_7	107.67	108.40	108.01	107.81
C_2—C_1—H_8	110.52	110.73	110.48	110.94
C_2—C_1—H_9	110.95	111.31	111.30	111.08
C_2—C_1—H_{10}	110.95	110.53	111.12	111.08
C_1—C_2—H_6	110.91	109.60	111.31	110.65
C_1—C_2—H_7	110.91	110.43	109.34	110.65
H_8—C_1—H_9	108.41	107.88	107.76	107.74
H_8—C_1—H_{10}	108.41	108.23	107.93	107.74
φ_0(C_1—C_2—C_3=O_4)	0.0	72.90	129.84	180.00

microwave measurements and is quite close to the value 128.2° calculated by Allinger *et al.* (9) from molecular dynamics. The dihedral angle φ_0 (C_1—C_2—C_3=O_4) for conformation **II** is found to be 72.9° which is in agreement with a value of ca. 70° obtained by Pickett and Scroggin (1).

MP3 calculations predict **I** → **III** rotational barrier of 8.81 kJ mol^{-1} which is in agreement with the experimental value 8.80 kJ mol^{-1} estimated by Pickett *et al.* (1) from microwave studies. It may, however, be noted that a value of 15 kJ mol^{-1} calculated by Radom *et al.* (11) using a model geometry for the molecule in 4-31G basis set is very much higher than the experimental value as well as our calculated value. It thus appears that meaningful values for the torsional potential barriers through *ab initio* calculations can be obtained only after a careful geometry optimization. The calculated values of *gauche/s-cis* and *gauche/gauche* barriers are 3.74 and 1.84 kJ mol^{-1}, respectively.

It has been pointed out by earlier workers (22−24) that the calculated dipole moment at the 4-31G level overestimates the experimental value by about 25%. A similar situation is found in the case of the *s-cis* conformer of propanal where the calculated value of the dipole moment in the 4-31G level is 3.27 D as against the experimental value of 2.58 D (25). Extension of the basis set and introduction of polarisation functions at each atom, as in the 6-31G** level calculations, improves upon the value of the dipole moment. The 6-31G** value of dipole moment of *s-cis* propanal is thus found to be 3.01 D. The corresponding dipole moment for the *gauche* conformer is 3.23 D.

Experimental observations indicate that conformations involving a methyl group in *cis*-position to carbonyl have lower energy. Radom *et al.* (11) explain this observation by suggesting that a methyl group provides a polarizable group close to the highly intrinsic dipole of carbonyl. Our results seem to support this hypotheses. It is found that the population density

TABLE 2. Relative RHF energy, rotational barriers, and ionisation potential of different conformations of propanal at 4-31G, 6-31G**, MP2 and MP3 levels

Conformation	Level of calculation 4-31G	6-31G**	MP2	MP3	Literature[e]
Energy (kJ mol⁻¹)					
I (C)	0.0[a]	0.0[b]	0.0[c]	0.0[d]	—
II	8.97	9.30	8.79	8.81	8.80(c)[1], 9.5±0.5 (c)[2], 12.3(c)[4], 10.0(t)[3], 8.75(t)[10,13]
III (G)	4.75	4.92	5.07	5.07	4.1(c)[12], 6.0(t)[3], 2.9(c)[4], 3.33(t)[10], 3.91(t)[11]
IV	6.71	7.46	6.85	6.91	6.7(c)[1], 8.64(t)[3], 4.1(t)[10]
Ionisation potential (eV)					
I	11.41	11.38			
II	11.28	11.30			
III	11.35	11.32			
IV	11.30	11.32			
Rotational barrier (kJ mol⁻¹)					
I(C)/**III**(G)	8.97	9.30	8.79	8.81	8.80(c)[1], 9.5±0.5(c)[2], 12.3(c)[4], 8.75(t)[10,13], 10.0(t)[3]
III(G)/**I**(C)	4.22	4.38	3.72	3.74	4.7(c)[1], 5.8(c)[2], 9.6(c)[4], 1.0(t)[11], 5.41(t)[13]
III(G)/**III**(G)	1.96	2.54	1.78	1.84	2.4(c)[1], 4.1±0.4(c)[2], 5.05(c)[4]

[a]Absolute value −191.666003 au.
[b]Absolute value −191.960968 au.
[c]Absolute value −192.064364 au.
[d]Absolute value −192.079369 au.
[e]Letters c and t in parenthese refer to experimental and theoretical data respectively.

TABLE 3. Atom and bond populations[a] (q-values), dipole moments[a] and diagonal quadratic force constants[b] for the optimised *cis* (**I**) and *gauche* (**III**) conformations of propanal

Atom or bond population	Conformations I	III	Diagonal force constants	Conformations I	III
qC_1	6.3254	6.3582	kC_1C_2	4.5236[d]	4.4077
qC_2	6.3286	6.3188	kC_2C_3	5.2525	5.4555
qC_3	5.6169	5.6081	kC_3O_4	15.4968	15.3873
qO_4	8.4978	8.4979	kC_3H_5	5.6672	5.4868
qH_5	0.8958	0.9030	kC_2H_6	5.5520	5.5740
qH_6	0.8595	0.8416	kC_2H_7	5.5520	5.4963
qH_7	0.8595	0.8585	kC_1H_8	5.5240	5.6538
qH_8	0.8858	0.8660	kC_1H_9	5.5572	5.5235
qH_9	0.8654	0.8802	kC_1H_{10}	5.5572	5.5678
qH_{10}	0.8654	0.8675	$kC_1C_2C_3$	2.4659[e]	1.9375
qC_3—O_4	0.5603	0.5600	$kC_2C_3O_4$	2.6020	2.1718
qO_4—H_8	0.0003	0.0	$kC_2C_3H_5$	1.5613	1.5320
qO_4—H_9	0.0020	0.0	$kC_3C_2H_6$	2.6629	1.7595
qO_4—H_{10}	0.0020	0.0003	$kC_3C_2H_7$	2.6629	1.6473
Dist. O_4—H_9[c]	278.84	391.20	$kC_2C_1H_8$	1.9232	1.7829
μ	3.01	3.23	$kC_2C_1H_9$	2.3693	1.5986
			$kC_2C_1H_{10}$	2.3693	1.6561
			$kC_1C_2H_6$	2.5836	1.7633
			$kC_1C_2H_7$	2.5836	1.5873
			$kH_8C_1H_9$	2.2467	1.5991
			$kH_8C_1H_{10}$	2.2467	1.6557
			$kCCCO$	—	0.0317

[a]Values based on 6-31G** level calculations.
[b]Values based on 4-31G level calculations. Other values in the force constant matrix can be obtained by writing to the author.
[c]Distances are in pm.
[d]Bond stretch force constants are in mdyn $Å^{-1} = 10^2$ N m^{-1}.
[e]Angle bending and torsional force constants are in mdyn $Å^{-1}$ $rad^{-2} = 10^{-18}$ Nm rad^{-2}.

of electron overlap between the atoms O_4 and H_9 or O_4 and H_{10} in conformation **I** is 0.0020 as against values between 0 and 0.0003 for the other three conformations.

It has been indicated by Pulay (26) that the *ab initio* calculations have a tendency to overestimate the diagonal force constants. However, trends in the values of the calculated force constants for molecules having similar structure are quite reliable and informative. Murto *et al.* (27) adopted scaling down procedure for using the STO-3G calculated force constants in the calculation of the frequencies of vibrations of fluoro- and chloroethanols. In the present case we have listed the unscaled diagonal force constants for the *cis* (**I**) and *gauche* (**III**) conformers of propanal in Table 3. It may be seen that the C═O stretching force constants for conformers **I** and **III** are 15.4968 and 15.3873 mdyn Å^{-1}, respectively, predicting a higher carbonyl stretching frequency in conformer **I**. This fact is confirmed from experiment where the C═O stretching absorption bands appear at 1743 cm^{-1} and 1727 cm^{-1} in conformers **I** and **III**, respectively, in argon matrix at 10 K (17). It is found that while diagonal force constants need to be scaled down by 15−20% to provide a good agreement with the experimental frequencies, the non-diagonal force constants (not reported here) do not need any scaling (28).

In quite recent study, Van Nuffel *et al.* (3) calculated the vibrational frequencies of *cis* (**I**) and *gauche* (**III**) conformers on the basis of a force field obtained through *ab initio* calculations using the 4-21G basis and predicted a higher frequency for C═O stretching vibration for conformer **III** (1756.2 cm^{-1}) than for conformer **I** (1754.7 cm^{-1}). This contradicts the experimental findings (17) and raises doubts about the unscaled values of their C═O stretching force constants (14.23 mdyn Å^{-1} for **I** and 14.24 mdyn Å^{-1} for **III**). Similarly, their predictions for several other frequencies of *cis* and *gauche* conformers do not agree with the experimental data (5, 17). However, they corroborate our conclusion regarding the magnitude of scaling down the *ab initio* diagonal force constants.

Acknowledgements

The author is grateful to Professor J. Murto, Department of Physical Chemistry, Helsinki University, Helsinki, Finland, for making the computer time available for the present calculations and for many helpful discussions.

1. H. M. PICKETT and D. G. SCROGGIN. J. Chem. Phys. **61**, 3954 (1974).
2. S. S. BUTCHER and E. B. WILSON JR. J. Chem. Phys. **40**, 1671 (1964).
3. P. VAN NUFFEL, L. VAN DEN ENDEN, C. VAN ALSENOY, and W. J. GEISE. J. Mol. Struct. **116**, 99 (1984).
4. J. R. DURIG, D. A. C. COMPTON, and A. Q. MCARVER. J. Chem. Phys. **73**, 719 (1980).
5. S. G. FRANKISS and W. KYNASTON. Spectrochim. Acta, **28**A, 2149 (1972).
6. E. F. WORDEN JR. Spectrochim. Acta, **18**A, 1121 (1962).
7. S. G. FRANKISS. J. Chem. Soc. Faraday Trans. **70**, 1516 (1974).
8. A. CHAPPUT, B. ROUSSEL, and G. FLEURRY. J. Raman. Spectrosc. **2**, 117 (1974).
9. R. J. ABRAHAM and J. A. POPLE. Mol. Phys. **3**, 609 (1960).
10. N. L. ALLINGER and S. M. J. HICKEY. J. Mol. Struct. **17**, 233 (1973).
11. L. RADOM, W. A. LATHAN, W. J. HEHRE, and J. A. POPLE. Aust. J. Chem. **25**, 1601 (1972).
12. M. R. PETERSON, B. R. DE MARE, I. G. CSIZMADIA, and O. P. STRAUSZ. J. Mol. Struct. **86**, 131 (1981).
13. H. J. KOHLER. Z. Chem. **11**, 467 (1971).
14. M. J. ARONEY, R. J. W. LE FEVRE, and A. N. SINGH. J. Chem. Soc. 564 (1965).
15. H. A. G. CHERMIN. Petroleum Refiners, **40**, 181 (1961).
16. I. A. VASIL'EV and A. A. VVEDENSKII. Zhur. Fiz. Khim. **40**, 842 (1966).
17. V. P. GUPTA, T. LOTTA, J. MURTO, M. RÄSÄNEN, and A. ASPIALA. Chem. Phys. **90**, 291 (1984).
18. G. SBRAMA and V. SCHETTINO. J. Mol. Spectrosc. **83**, 110 (1970).
19. J. A. POPLE, and M. S. GORDON. J. Am. Chem. Soc. **89**, 4253 (1967).
20. N. L. ALLINGER and S. M. J. HICKEY. Tetrahedron, **28**, 2157 (1972).
21. G. J. KARBASTOS and N. HSI. J. Am. Chem. Soc. **87**, 2864 (1965).
22. P. GEORGE, C. W. BOCK, and A. SCHMIEDEKAMP. J. Mol. Struct. Theochem. **76**, 363 (1981).
23. P. KOLLMANN, J. MCKELVEY, A. JOHANSSON, and S. ROTHENBERG. J. Am. Chem. Soc. **97**, 955 (1975).
24. M. D. NEWTON and G. A. JEFFREY. J. Am. Chem. Soc. **99**, 2413 (1977).
25. E. C. HURDIS and C. P. SMYTH. J. Am. Chem. Soc. **65**, 89 (1943).
26. P. PULAY. Direct use of gradient for investigating molecular energy surfaces. *In* Applications of electronic structure theory. *Edited by* H. F. Schaefer. Plenum Press, New York, p. 153, 1977.
27. J. MURTO, M. RÄSÄNEN, A. ASPIALA, and L. HOMANEN. J. Mol. Struct. Theochem. **92**, 45 (1983).
28. V. P. GUPTA. Unpublished results.
29. M. RÄSÄNEN, A. ASPIALA, and J. MURTO. J. Chem. Phys. **79**, 107 (1983).
30. A. ASPIALA, T. LOTTA, J. MURTO, M. RÄSÄNEN, and V. P. GUPTA. Chem. Phys. Lett. **9**, 179 (1984).
31. QCPE Program No. 391, Quantum Chemistry Program Exchange, Indiana University, Department of Chemistry. 1980.
32. J. S. BINKLEY, R. A. WHITESIDE, R. KRISHNAN, R. SEEGER, D. J. DE FREES, H. B. SCHLEGEL, S. TOPIOL, L. R. KAHN, and J. A. POPLE. Gaussian 80, Department of Chemistry, Carnegie Mellon University, Pittsburgh, PA.
33. V. J. KLIMKOWSKI, P. VAN NUFFEL, L. VAN DEN ENDEN, C. VAN ALSENOY, H. J. GEISE, J. N. SCARSDALE, and L. SCHÄFER. J. Comput. Chem. **5**, 122 (1984).

Identification of the product from the reduction of permanganate ion by trimethylamine in aqueous phosphate buffers

FERNANDO MATA-PEREZ AND JOAQUIN F. PEREZ-BENITO[1]

Departamento de Química Física, Facultad de Ciencias, Universidad de Valladolid, 47002 Vallodolid, Spain

Received July 24, 1984

FERNANDO MATA-PEREZ and JOAQUIN F. PEREZ-BENITO. Can. J. Chem. **63**, 988 (1985).

The product obtained from the reduction of potassium permanganate by trimethylamine in aqueous phosphate buffers has been identified as a soluble form of colloidal manganese dioxide which is stabilized in solution by adsorption of phosphate ions on its surface. The dependence of the rate of flocculation on several experimental variables has been studied. Phosphate ions have been found to increase the solubility of the colloid by increasing the apparent energy of activation of the flocculation process. This could explain the well-known capacity of those ions for retarding the precipitation of manganese dioxide.

FERNANDO MATA-PEREZ et JOAQUIN F. PEREZ-BENITO. Can. J. Chem. **63**, 988 (1985).

On a identifié le produit obtenu lors de la réduction du permanganate de potassium par de la triméthylamine dans des tampons aqueux de phosphates; il s'agit d'une forme colloïdale de dioxyde de manganèse qui est stabilisée en solution par une adsorption des ions phosphates sur sa surface. On a étudié la relation entre le taux de floculation et diverses variables expérimentales. On a trouvé que les ions phosphates augmentent la solubilité du colloïde par le biais d'une augmentation de l'énergie d'activation apparente du processus de floculation. Ceci pourrait expliquer la capacité bien connue de ces ions à retarder la précipitation du dioxyde de manganèse.

[Traduit par le journal]

Introduction

Manganese dioxide is a brown substance whose insolubility in water is well-known. However, its precipitation has been found to be substantially delayed in the presence of phosphate ions (1, 2). This property has made phosphate buffers useful for the study of a great variety of permanganate ion oxidations in aqueous medium. When they are present a soluble brown–yellow product, instead of a precipitate, is obtained. However, despite its extensive occurrence in permanganate ion oxidations performed in phosphate buffered solutions, the nature of that species has never been established.

Although it has been sometimes suggested that this soluble species could be $H_2MnO_4^{2-}$ (3*a*), H_2MnO_3 (4) or a phosphate complex (4, 5), we wish to report some spectrophotometric findings which strongly support that it is actually a soluble form of colloidal manganese dioxide stabilized in solution by the existence of phosphate ions on the surface of the colloidal particles.

The reducing agent used in this study was trimethylamine. The spectra recorded at the end of the reaction showed that the product is the same than those obtained using different reducing agents such as uracils (4), unsaturated acids (4), or dimethylamine (6), in phosphate buffers.

Although the organic products obtained from the permanganate ion oxidation of amines have been carefully determined (7–9), and some kinetic studies of the permanganate ion oxidation of trimethylamine in phosphate buffers have been published (10, 11), no identification of the soluble brown–yellow product has been reported. The present paper aims to resolve this missing point.

Experimental

The reactants were potassium permangante and trimethylammonium chloride (in excess). A buffer mixture $KH_2PO_4-K_2HPO_4$ was also used. Potassium chloride was added to the solutions to keep the ionic strength of the medium constant when necessary. The solvent was water twice distilled from potassium permanganate.

All the spectrophotometric operations (periodic scanning during reaction, recording of the spectra at the end of the reaction and monitoring of the flocculation process) were performed by means of a Hewlett-Packard UV-VIS Spectrophotometer, equipped with a temperature controlled cuvette holder.

The pH measurements were made by using a Corning Model 7 pH Meter, provided with a combined electrode.

To determine the oxidation state of manganese in the product, five solutions of $KMnO_4$ ($2 \times 10^{-4} - 1 \times 10^{-3}$ *M*) and $Me_3N \cdot HCl$ (3×10^{-2} *M*) were allowed to react in an aqueous buffered system. When the spectrophotometer showed that all the permanganate had been consumed, concentrated perchloric acid and an excess of potassium iodide were added to the solutions; the iodine released was titrated against standard thiosulfate solution, using starch as indicator.

Results

The iodometric technique previously used by other authors (4, 12, 13) allowed us to determine the oxidation state of manganese in the soluble brown–yellow product. An average value of 3.93 ± 0.13, which is quite consistent with a Mn(IV) species, was obtained.

On the other hand, when the reaction was scanned under the experimental conditions given in Fig. 1 no isosbestic point was found; instead the intersection of the successive spectra showed a shift to higher wavelengths as the reaction advanced. However, a 2.5-fold increase in the concentration of the buffer substances (all the other experimental conditions remaining constant) led to the observation of a sharp isosbestic point at 470 nm (see Fig. 2).

The spectrum of the soluble Mn(IV) species at the end of the reaction was also found to be dependent on the phosphate concentration; for the same Mn(IV) concentration the absorbance at every wavelength increases as the phosphate concentration decreases (see Fig. 3).

In order to establish the nature of the product more definitely, the influence of several experimental variables on the rate of conversion of the soluble Mn(IV) species into MnO_2 precipitate was studied. When sequential scans showed that all the permanganate had been reduced by trimethylamine, the evolution of the product was followed by monitoring the in-

[1]To whom all correspondence should be addressed. Present address: Department of Chemistry, University of Regina, Regina, Sask., Canada S4S 0A2.

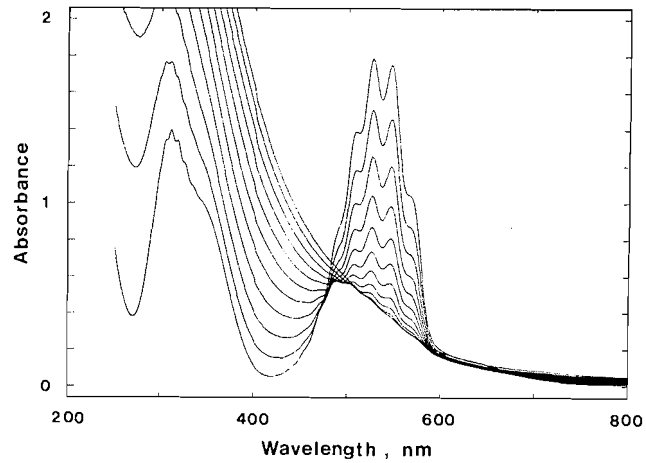

FIG. 1. Successive scans at 6 min intervals during the reaction between permanganate ion (8×10^{-4} M) and trimethylamine (3×10^{-2} M). [KH_2PO_4] = 2×10^{-2} M, [K_2HPO_4] = 2×10^{-2} M, ionic strength 0.23 M (KCl), pH 6.74, 45.0°C.

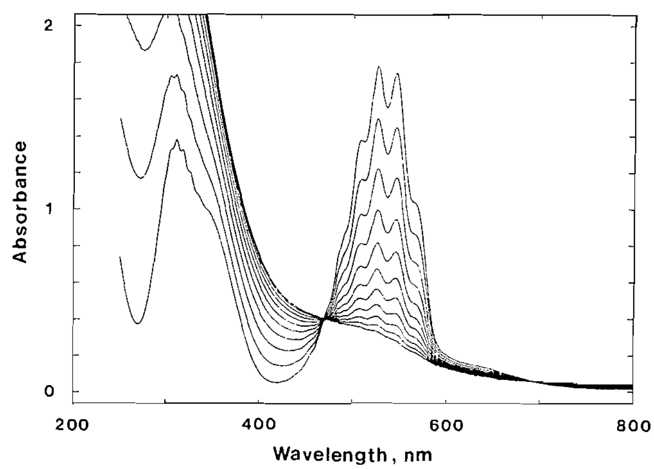

FIG. 2. Successive scans at 6 min intervals during the reaction between permanganate ion (8×10^{-4} M) and trimethylamine (3×10^{-2} M). [KH_2PO_4] = 5×10^{-2} M, [K_2HPO_4] = 5×10^{-2} M, ionic strength 0.23 M, pH 6.74, 45.0°C.

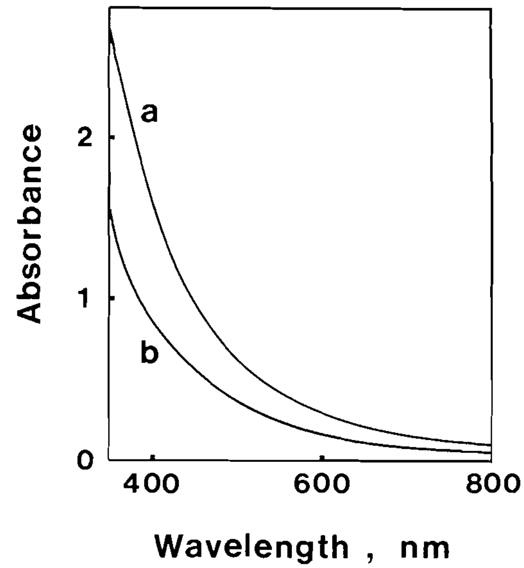

FIG. 3. Spectra at the end of the reaction between permanganate ion (8×10^{-4} M) and trimethylamine (3×10^{-2} M). Ionic strength 0.23 M (KCl), pH 6.74, 45.0°C. [KH_2PO_4] = [K_2HPO_4] = 2×10^{-2} M (a) and 5×10^{-2} M (b).

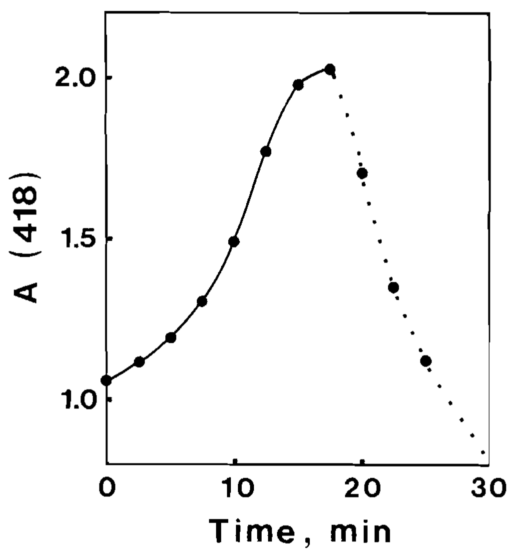

FIG. 4. Variation of the absorbance at 418 nm with time after the end of the reaction between permanganate ion (8×10^{-4} M) and trimethylamine (3×10^{-2} M). [KH_2PO_4] = 3×10^{-2} M, [K_2HPO_4] = 3×10^{-2} M, ionic strength 0.23 M (KCl), pH 6.74, 60.0°C. The dotted line shows when precipitation has already begun.

crease in absorbance at a chosen wavelength (for instance, at 418 nm) until a maximum was obtained. A typical example has been represented in Fig. 4. The highest value of the absorbance corresponded to the start of precipitation, and the subsequent decrease in that magnitude is due to the removal of MnO_2 from the solution by precipitation.

The time necessary for precipitation (t_p) was taken to be the period of time which elapsed between the end of the permanganate–trimethylamine reaction and the observation of a maximum in the absorbance at 418 nm. The inverse of t_p was selected as a way to estimate the rate of conversion of the soluble Mn(IV) species into MnO_2 precipitate.

By measuring t_p under different experimental conditions, it was found that the rate of conversion of the soluble Mn(IV) species into MnO_2 precipitate increases with the initial permanganate concentration in the system (Fig. 5) and also with the potassium chloride concentration (Fig. 6). On the contrary, phosphate ions inhibit the precipitation process, as Fig. 7 clearly shows.

Finally, t_p was found to decrease with temperature; these data are presented in Fig. 8 in an Arrhenius-type fashion. From the slopes of the ln $(1/t_p)$ vs. $1/T$ linear relationships apparent values of the energies of activation for the conversion of the soluble Mn(IV) species into MnO_2 precipitate at four different phosphate concentrations were determined, and the results have been listed in Table 1. We can see that an increase in the phosphate concentration results in an increase in the apparent energy of activation; i.e., precipitation is retarded.

Discussion

All the results obtained in this study can be adequately explained by accepting that the soluble Mn(IV) species is present in the system in the form of colloidal particles of manganese dioxide stabilized temporarily in solution by adsorption of

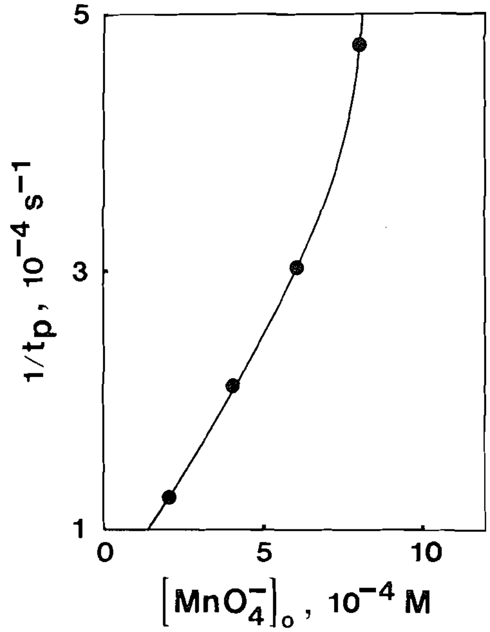

FIG. 5. Dependence of the rate of conversion of the soluble Mn(IV) species into MnO_2 precipitate on the initial permanganate concentration. [Me_3N] = 3 × 10^{-2} M, [KH_2PO_4] = 2 × 10^{-2} M, [K_2HPO_4] = 2 × 10^{-2} M, ionic strength 0.23 M (KCl), pH 6.74, 45.0°C.

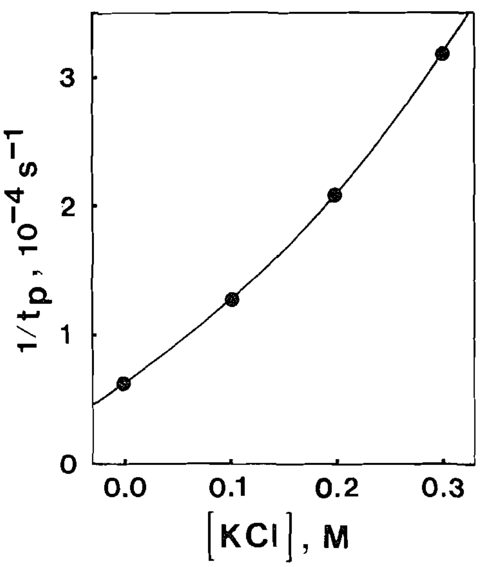

FIG. 6. Dependence of the rate of conversion of the soluble Mn(IV) species into MnO_2 precipitate on the potassium chloride concentration. [MnO_4^-]$_0$ = 8 × 10^{-4} M, [Me_3N] = 3 × 10^{-2} M, [KH_2PO_4] = 5 × 10^{-2} M, [K_2HPO_4] = 5 × 10^{-2} M, pH 6.74, 45.0°C.

phosphate ions on their surface. This hypothesis appears to be the only one which is consistent with the totality of experimental findings.

It has been found that for the soluble Mn(IV) species there is a good linear relationship between the logarithm of the absorbance and the logarithm of the wavelength, with the slope being slightly dependent on the experimental conditions and the amount of time elapsed after the end of the permanganate-trimethylamine reaction. The average slope for 54 different spectra recorded was 4.3 ± 0.6. This appears to be a reflection of Rayleigh's Law, according to which the absorbance due to

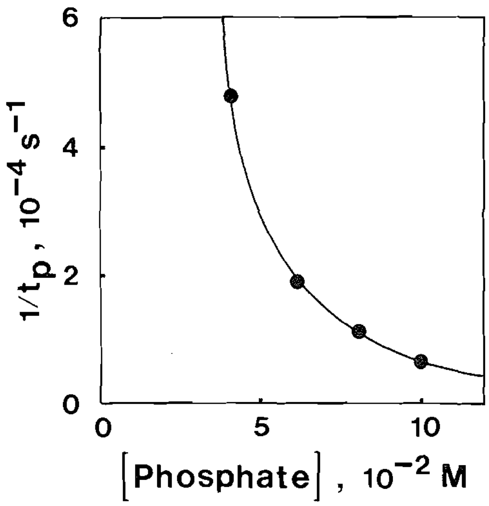

FIG. 7. Dependence of the rate of conversion of the soluble Mn(IV) species into MnO_2 precipitate on the total concentration of phosphate ions (equimolar amounts of KH_2PO_4 and K_2HPO_4). [MnO_4^-]$_0$ = 8 × 10^{-4} M, [Me_3N] = 3 × 10^{-2} M, ionic strength 0.23 M (KCl), pH 6.74, 45.0°C.

TABLE 1. Apparent energies of activation for the conversion of the soluble Mn(IV) species into MnO_2 precipitate for different phosphate concentrations

[Phosphate] (10^{-2} M)[a]	E_a (kJ mol^{-1})[b]
4	82±5
6	98±3
8	105±3
10	128±1

[a]Total concentration of phosphate ions (equimolar amounts of KH_2PO_4 and K_2HPO_4).
[b][MnO_4^-]$_0$ = 8 × 10^{-4} M, [Me_3N] = 3 × 10^{-2} M, ionic strength 0.23 M (KCl) pH 6.74.

scattering of light by a solution of colloidal particles is inversely proportional to the fourth power of the wavelength (14). One of these linear relationships, in excellent agreement with Rayleigh's Law, is shown in Fig. 9.

The absence of an isosbestic point in Fig. 1 could be explained in principle as a consequence of the existence of some manganese intermediate between Mn(VII) and Mn(IV) in appreciable concentration; however, both Mn(VI) and Mn(V) are known to be instable in solutions buffered near neutrality (3b). Moreover, none of the characteristic bands of Mn(VI) or Mn(V) can be observed in Fig. 1. The lack of a good isosbestic point must then be due to an unfulfillment of Beer's Law by the soluble Mn(IV) species. However, this anomalous behavior cannot be due to an aggregative process of the soluble Mn(IV) species at the molecular level (such as dimerization), for a dimer could not produce a strong light-scattering phenomenon as is experimentally observed (see Fig. 9). The existence of a sharp isosbestic point at higher phosphate concentration (see Fig. 2) indicates that for these conditions Beer's Law is fulfilled.

To clarify this point, the absorbance at 526 nm for the experiments shown in Figs. 1 and 2 has been represented in Fig. 10 vs. the absorbance at 418 nm.

Since both permanganate ion and the soluble Mn(IV) species

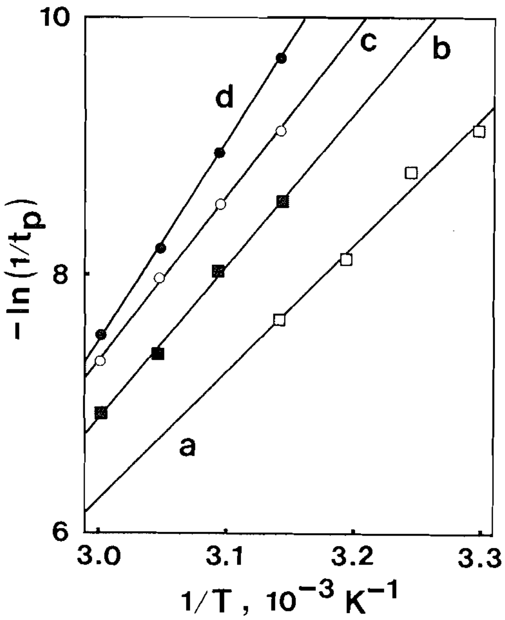

FIG. 8. Arrhenius-type plots for the conversion of the soluble Mn(IV) species into MnO_2 precipitate. $[MnO_4^-]_0 = 8 \times 10^{-4}$ *M*, $[Me_3N] = 3 \times 10^{-2}$ *M*, ionic strength 0.23 *M* (KCl), pH 6.74. $[KH_2PO_4] = [K_2HPO_4] = 2(a), 3(b), 4(c), 5(d) \times 10^{-2}$ *M*.

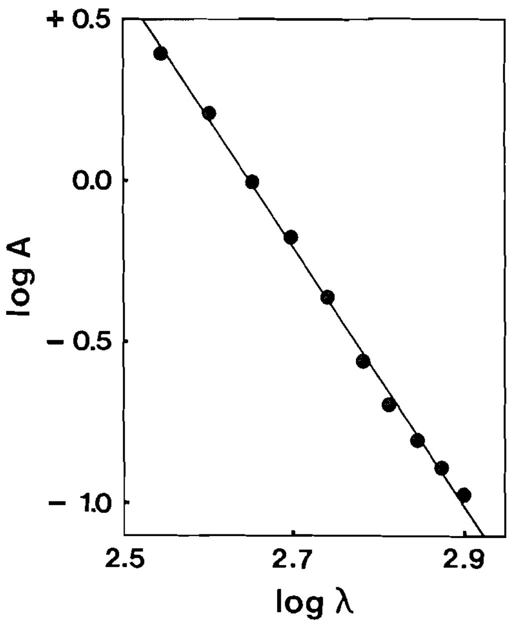

FIG. 9. Rayleigh's Law for the spectrum recorded an hour after the end of the reaction between permanganate ion (8×10^{-4} *M*) and trimethylamine (3×10^{-2} *M*). $[KH_2PO_4] = 2 \times 10^{-2}$ *M*, $[K_2HPO_4] = 2 \times 10^{-2}$ *M*, ionic strength 0.23 *M* (KCl), pH 6.74, 35.0°C. Slope = −3.99, r = 0.998.

absorb light at 526 nm, the absorbance at this wavelength can be written as follows:

[1] $A(526) = \epsilon_R^{526} c + \epsilon_P^{526}(c_0 - c)$

where ϵ_R^{526} and ϵ_P^{526} are respectively the extinction coefficients of reactant and product at 526 nm, and c is the permanganate concentration, its initial value being c_0. In eq. [1] it has been taken into consideration that the concentration of possible manganese intermediates between Mn(VII) and Mn(IV), if present

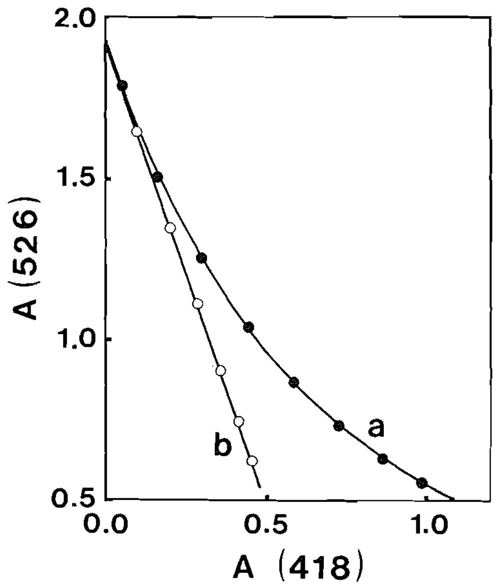

FIG. 10. Absorbance at 526 nm vs. absorbance at 418 nm during the reaction between permanganate ion (8×10^{-4} *M*) and trimethylamine (3×10^{-2} *M*). Ionic strength 0.23 *M* (KCl), pH 6.74, 45.0°C. $[KH_2PO_4] = [K_2HPO_4] = 2 \times 10^{-2}$ *M* (*a*) and 5×10^{-2} *M* (*b*).

at all, is negligible, as pointed out above.

Given that permanganate ion is transparent at 418 nm, the absorbance at this wavelength will be:

[2] $A(418) = \epsilon_P^{418}(c_0 - c)$

where ϵ_P^{418} is the extinction coefficient of the product at 418 nm.

From eqs. [1] and [2] we can deduce:

[3] $A(526) = \epsilon_R^{526} c_0 - [(\epsilon_R^{526} - \epsilon_P^{526})/\epsilon_P^{418}]A(418)$

Hence, a linear relationship would be expected for a plot of $A(526)$ vs. $A(418)$ during the course of reaction. However, as can be seen in Fig. 10 a linear plot is obtained only for the experiments completed at higher phosphate concentrations. Albeit we knew already from Fig. 1 that for the case of lower phosphate concentrations, the soluble Mn(IV) species does not fulfill Beer's Law, Fig. 10 provides an important information. We can observe for this case that the $A(526)$ vs. $A(418)$ relationship is actually a concave curve and that the linear relationship corresponding to higher phosphate concentration coincides with the tangent to the curve at the beginning of the reaction.

This concave curve is a consequence of the flocculation process. It is known that the intensity of radiation scattered by colloidal particles increases with the size of those particles (14). Hence, an increase in the size of the colloidal particles as the reaction is advancing will provoke an increase in the extinction coefficients of the product at 418 and 526 nm, and so a decrease in the absolute value of the slope of the $A(526)$ vs. $A(418)$ relationship (see eq. [3]). As a result, a concave curve, instead of a linear relationship, is found.

On the contrary, when the reaction is followed in the presence of a more concentrated buffer, phosphate ions will adsorb on the colloidal manganese dioxide in a greater proportion and the rate of flocculation will decrease because of the negative electrostatic charges accumulated on the colloid surface. Since the flocculation process is now much slower, the extinction coefficients of the product will be approximately constant and eq. [3] becomes a linear relationship.

The fact that this linear relationship is a tangent to the concave curve at the beginning of the reaction indicates that the size of the colloidal particles is initially the same in both cases. However, while the particles grow by flocculation throughout the reaction in the presence of a diluted phosphate buffer, the initial size of the colloidal particles is "frozen" in the presence of a more concentrated phosphate buffer.

The difference in the rate of flocculation explains the absence or presence of an isosbestic point in Figs. 1 and 2 respectively, and also the different intensity of the spectra recorded at the end of the reaction in both experiments (see Fig. 3). In the case of lower phosphate concentration the size of the colloidal particles is bigger as is the intensity of the radiation scattered by them.

The stabilization of colloids in solution by adsorption of anions on their surface is certainly a well-known phenomenon (15). Given that the experiments were made in systems near neutrality, the concentration of PO_4^{3-} ions was too small to be regarded as the stabilizing agent. Thus, either HPO_4^{2-} or $H_2PO_4^-$ must be responsible for that effect. Although both of them are probably stabilizing the colloidal particles, HPO_4^{2-} will likely account for a greater contribution, because of its greater charge.

Although the adsorption of phosphate ions greatly decreases the number of effective collisions between charged colloidal particles per unit of time, they will not be totally suppressed. Consequently, when all the permanganate has been reduced, flocculation will be made evident spectrophotometrically by a gradual increase in absorbance. Then, the start of the precipitation of manganese dioxide provokes a sudden decrease in that magnitude (see Fig. 4).

An explanation of the results shown in Fig. 5 is evident. An increase in the initial permanganate concentration will result in an increase in the concentration of the soluble Mn(IV) species at the end of the reaction and, accordingly, an increase in the number of colloidal particles of manganese dioxide. Since the collisions of colloidal particles per unit of time will increase parallelly, so will do the rate of flocculation.

The results summarized in Fig. 6 are a consequence of the well-known capacity of electrolytes for increasing the rate of flocculation of colloids (15).

Figure 7 confirms the fact already known from the analysis of Fig. 10, that phosphate ions inhibit the flocculation of colloidal particles and, so, delay the appearance of a precipitate of manganese dioxide.

The acceleration of the flocculation process with temperature shown in Fig. 8 is a consequence of an increase in the number of effective collisions between colloidal particles per unit of time. The fact that this is an activated process fulfilling an Arrhenius-type equation allows us to check the ideas so far developed. Since the stability of the colloidal particles in solution is due to the electrostatic charge that increases the energy necessary to surmount their mutual repulsion, and since this charge is originated by the selective adsorption of phosphate ions on the surface of colloidal manganese dioxide, an increase in the phosphate concentration will result in an increase in the amount of phosphate ions adsorbed and, so, in an increase in the apparent energy of activation of the flocculation process. This is in total agreement with the results compiled in Table 1.

On the other hand, the information presented in this paper might be useful to resolve a current controversy concerning a long-lived species detected in the permanganate oxidation of alkenes. The fact that the spectra recorded for this species are quite similar to the ones shown in Fig. 3 could support a Mn(IV) species, as suggested by some authors (4, 12, 13), rather than the widely accepted cyclic manganate(V) diester (16–24).

Acknowledgments

Discussions with Dr. D. G. Lee during the preparation of this manuscript, as well as the concession to J.F.P.B. by the Spanish Ministry of Education and Science of a grant to study at the University of Regina, Canada, where a part of the experimentation was made, are gratefully acknowledged.

1. R. STEWART. Oxidation mechanisms. Benjamin, New York. 1964. p. 60.
2. F. FREEMAN. React. Species Chem. React. **1**, 179 (1976).
3. R. STEWART. *In* Oxidation in organic chemistry. Part A. *Edited by* K. B. Wiberg. Academic Press, New York. 1965. (*a*) p. 6. (*b*) p. 2.
4. F. FREEMAN, C. O. FUSELIER, C. R. ARMSTEAD, C. E. DALTON, P. A. DAVIDSON, E. M. KARCHEFSKI, D. E. KROCHMAN, M. N. JOHNSON, and N. K. JONES. J. Am. Chem. Soc. **103**, 1154 (1981).
5. K. B. WIBERG and R. STEWART. J. Am. Chem. Soc. **77**, 1786 (1955).
6. F. MATA, J. PEREZ-BENITO, and A. ARRANZ. Z. Phys. Chem. Neue Folge. **135**, 141 (1983).
7. H. SHECHTER, S. S. RAWALAY, and M. TUBIS. J. Am. Chem. Soc. **86**, 1701 (1964).
8. H. SHECHTER and S. S. RAWALAY. J. Am. Chem. Soc. **86**, 1706 (1964).
9. S. S. RAWALAY and H. SHECHTER. J. Org. Chem. **32**, 3129 (1967).
10. D. H. ROSENBLATT, G. T. DAVIS, L. A. HULL, and G. D. FORBERG. J. Org. Chem. **33**, 1649 (1968).
11. S. SENENT, F. MATA, and M. A. DE LA PEÑA. Rev. Roum. Chim. **23**, 841 (1978).
12. L. I. SIMANDI and M. JAKY. J. Am. Chem. Soc. **98**, 1995 (1976).
13. L. I. SIMANDI, M. JAKY, F. FREEMAN, C. O. FUSELIER, and E. M. KARCHEFSKI. Inorg. Chim. Acta, **31**, L457 (1978).
14. G. M. BARROW. Physical chemistry. 2nd ed. McGraw-Hill, New York. 1966. pp. 803–804.
15. W. J. MOORE. Physical chemistry. 2nd ed. Prentice-Hall, Englewood Cliffs, NJ. 1955. p. 523.
16. D. G. LEE and J. R. BROWNRIDGE. J. Am. Chem. Soc. **95**, 3033 (1973).
17. K. B. WIBERG, C. J. DEUTSCH, and J. ROCEK. J. Am. Chem. Soc. **95**, 3034 (1973).
18. D. G. LEE and J. R. BROWNRIDGE. J. Am. Chem. Soc. **96**, 5517 (1974).
19. F. FREEMAN, C. O. FUSELIER, and E. M. KARCHEFSKI. Tetrahedron Lett. 2133 (1975).
20. F. FREEMAN and E. M. KARCHEFSKI. Biochim. Biophys. Acta, **447**, 238 (1976).
21. T. OGINO and K. MOCHIZUKI. Chem. Lett. 443 (1979).
22. K. TOYOSHIMA, T. OKUYAMA, and T. FUENO. J. Org. Chem. **45**, 1600 (1980).
23. T. OGINO. Tetrahedron Lett. **21**, 177 (1980).
24. D. G. LEE and K. C. BROWN. J. Am. Chem. Soc. **104**, 5076 (1982).

COMMUNICATIONS

Stereoselective total syntheses of (±)-sinularene and (±)-5-epi-sinularene: a general intramolecular Diels–Alder approach to tricyclic sesquiterpenes

KAZIMIERZ ANTCZAK, JOHN F. KINGSTON, AND ALEX G. FALLIS
Department of Chemistry, Memorial University of Newfoundland, St. John's, Nfld., Canada A1B 3X7

Received November 30, 1984

KAZIMIERZ ANTCZAK, JOHN F. KINGSTON, and ALEX G. FALLIS. Can. J. Chem. **63**, 993 (1985).

Stereoselective total synthesis of (±)-sinularene and (±)-5-epi-sinularene are described. The sequence employs a "blocked" cyclopentadiene in which the cyclopropane unit also serves as a latent methyl group. Thus intramolecular [4+2] cycloaddition of the substituted methyl spiro[2.4]hepta-4,6-dien-1-yl)-2-pentenoate **11** affords 5-benzyloxy-6-isopropyl-8-carbomethoxy-tetracyclo[$5.4.0^{1,7}.0^{2,4}.0^{2,9}$]undec-10-ene (**12**) which after selective hydrogenolysis generates the tricyclo[$4.4.0^{1,6}.0^{2,8}$]decane (sinularene) ring system. Removal of the secondary hydroxyl function ($Ph_3P/CCl_4/CH_3CN$; $H_2/Pd/C$), reduction of the methyl ester ($LiAlH_4$), and introduction of the exocyclic double bond (acetate pyrolysis, 550°C) completes the synthesis of (±)-sinularene in 14 steps from cyclopentadiene. A parallel series of reactions employing the isopropyl epimer of **12** affords (±)-5-epi-sinularene.

KAZIMIERZ ANTCZAK, JOHN F. KINGSTON et ALEX G. FALLIS. Can. J. Chem. **63**, 993 (1985).

On décrit des synthèses stéréosélectives totales du (±)-sinularène et du (±)-épi-5 sinularène. La synthèse implique l'utilisation d'un cyclopentadiène "bloqué" dans lequel l'unité cyclopropanique sert aussi de groupement méthyle latent. La cycloaddition intramoléculaire [4+2] du spiro[2.4]heptadiène-4,6 yl-1 pentène-2 oate de méthyle (**11**) conduit donc au benzyloxy-5 isopropyl-6 carbométhoxy-8 tétracyclo[$5.4.0^{1,7}.0^{2,4}.0^{2,9}$]undécène-10 (**12**) qui, après une hydrogènolyse sélective, conduit au système cyclique tricyclo[$4.4.0^{1,6}.0^{2,8}$]décane (sinularène). L'élimination de la fonction hydroxyle secondaire ($Ph_3P/CCl_4/CH_3CN$; $H_2/Pd/C$), la réduction de l'ester méthylique ($LiAlH_4$) et l'introduction de la double liaison exocyclique (pyrolyse de l'acétate à 550°C) complètent la synthèse du (±)-sinularène, en 14 étapes à partir du cyclopentadiène. Une série parallèle de réactions faisant appel à l'épimère isopropyle de **12** conduit au (±)-épi-5 sinularène.

[Traduit par le journal]

There is considerable current interest in the intramolecular Diels–Alder reaction and it has been applied to a number of natural product syntheses with notable success (1–4). Among the diverse structures produced in nature, the bridged sesquiterpenes sinularene (5, 6), longifolene (7, 8), and sativene (9, 10) occupy a prominent position. All have been the object of a variety of synthetic approaches and served as a challenge for new synthetic methodology (sinularene syntheses (11, 12),[1] longifolene syntheses (13–18), sativene syntheses (17–25)). In principle these structures could be synthesized via an intramolecular Diels–Alder reaction of an appropriate 5-alkylcyclopentadiene. In practice, however, as an early approach to longifolene showed (26), the propensity of substituted cyclopentadienes to undergo facile 1,5-sigmatropic rearrangement prior to cyclization takes precedence. Thus for this strategy to succeed, rearrangement must be blocked or conditions developed where cyclization can compete efficiently (27, 28). Unfortunately, blocking the sigmatropic reaction is not necessarily straightforward, since even chlorine migrates prior to cyclization in a related case (29).[2]

We report herein a successful solution to this problem, in which the sigmatropic rearrangement is blocked by the cyclopropane moiety present in the spiro[2.4]heptadiene system **1** (Scheme 1). Intramolecular cycloaddition affords a tetracyclic compound of type **2** and selective cyclopropane ring opening provides the requisite tricyclo[$4.4.0^{1,6}.0^{2,8}$]decane skeleton for the interesting marine natural product sinularene.

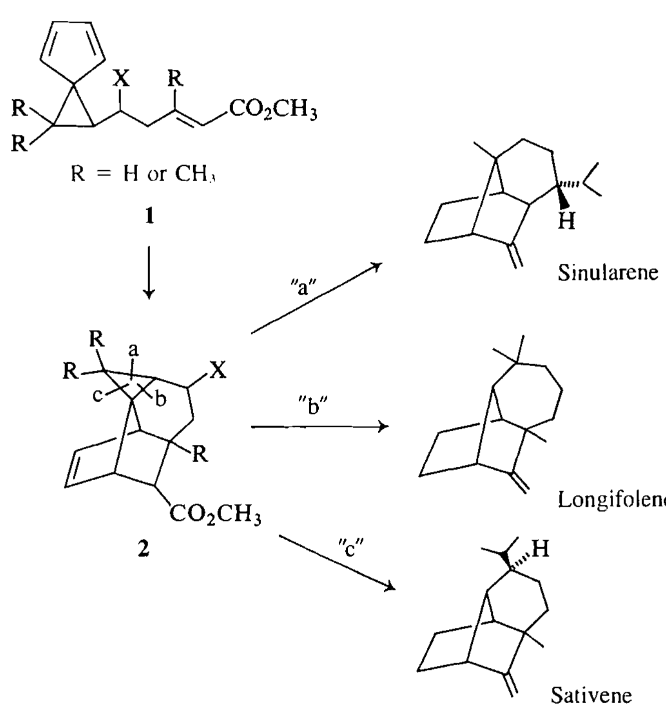

SCHEME 1

[1]After submission of this manuscript we learned of an additional sinularene synthesis by E. Piers and G. L. Jung (see following Communication). We are grateful to Professor Piers for a preprint of their paper.

[2]As we have pointed out elsewhere (38), an alternative solution employs a brexane intermediate followed by a ring expansion. This approach has been used by Snowden for the total synthesis of sativene (24).

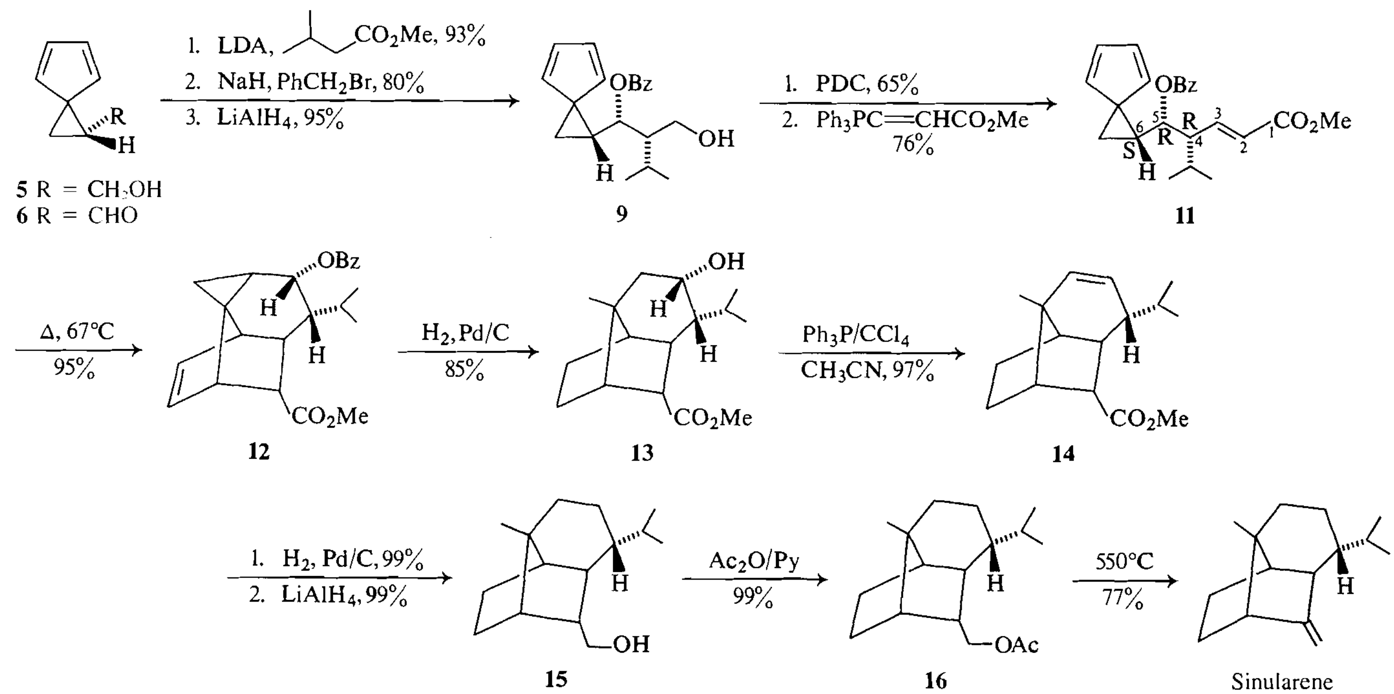

SCHEME 2

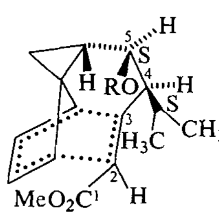

3

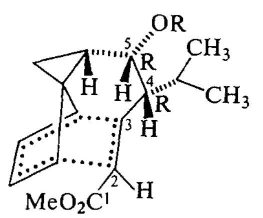

4

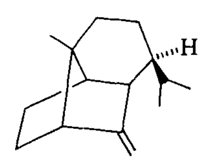

5-Epi-sinularene

With suitably substituted precursors, controlled cleavage of the other cyclopropane bonds should permit entry to the longifolene and sativene series as illustrated (30).

Our initial studies revealed (31) that a C5 oxygen substituent was essential to ensure that the desired intramolecular cycloaddition proceeded. In addition, by carrying the isopropyl function in the sidechain, it seemed likely that its stereochemistry could be controlled as a consequence of steric constraints in the Diels–Alder transition state. Thus the substituted triene **11** (Scheme 2) was selected as a suitable intermediate target. It is apparent that the nonbonded interactions between the developing *exo*-hydrogen and the isopropyl substituent are reduced in **4** compared to **3** and were expected to favour preferential cyclization to the natural stereoisomer.[3] Experimentally, the ether function (R = benzyl) was of greater significance and inhibited cyclization of the C5 (S) diastereomers.[4]

As outlined in Scheme 2, the substituted triene **11** was elaborated from a series of condensations commencing with the aldehyde **6**, obtained by oxidation of the known alcohol **5** (32, 33) (MnO_2, 83%). The initial coupling (LDA/THF, −78°C) with methyl 3-methylbutyrate generated the hydroxyl centre selectively (≃5:1) due to preferential attack on the aldehyde carbonyl from the less hindered direction. This led to a 93% yield of hydroxy-ester comprised of a 47:30:14:2 ratio of stereoisomers. The major diastereomer **8** (47%, illustrated)

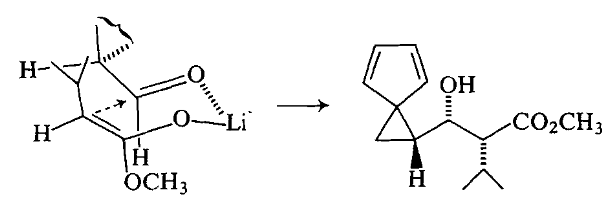

7 8

arose from condensation with the Z(O) enolate as illustrated in **7** and was the isomer necessary for conversion to (±)-sinularene. The 30% component, produced from the *E*(O) enolate, differed in the orientation of the isopropyl group as required for (±)-5-epi-sinularene. The major diastereomer **8** was converted to the C4(R)C5(R) triene **11** as follows. The secondary alcohol was protected as a benzyl ether (80%, NaH, $PhCH_2Br$, DME) and the ester function reduced to the primary alcohol **9** (95%, $LiAlH_4$). Oxidation of **9** (PDC, 65%) gave the aldehyde **10** which was subjected to Wittig condensation with methyl (triphenylphosphoranylidene)acetate in refluxing THF. These conditions resulted in simultaneous cyclization of triene **11** to the tetracyclic ester **12** in 72% overall yield. A parallel series of

[3]All the compounds discussed are racemic but only the enantiomers leading to the natural configuration of sinularene and 5-epi-sinularene are illustrated, commencing with the *S* enantiomer of aldehyde **6**.

[4]For consistency and clarity the chiral centres are numbered according to the triene **11**.

reactions on the 30% diastereomer (isopropyl epimer of **8**) afforded the C4(S)C5(R) triene (not illustrated), which also cyclized at 67°C. In contrast, the related C5(S) triene isomers, failed to cyclize even in refluxing dichlorobenzene (180°C).

Thus the cycloaddition was specific, as confirmed by the success of the synthesis and X-ray analysis of the minor, crystalline isopropyl(S)-benzyl(R) adduct corresponding to **12** from which (±)-5-epi-sinularene was prepared. The nonbonded interactions in the transition state were clearly significant and find a partial parallel in the total synthesis of patchouli alcohol (34), in which only one diastereomer cyclized.

Consistent with our preliminary studies of related cyclopropyl ketones (30), hydrogenolysis of **12** cleaved the least substituted cyclopropane bond exclusively, to release the latent methyl group with concomitant removal of the benzyl function and hydrogenation of the double bond (H_2, 10% Pd/C, 85%). Attempted conversion of **13** to a secondary bromide with triphenylphosphinedibromide afforded a significant amount of the olefin **14** accompanied by unreacted alcohol. Elimination is known to compete with substitution in these cases (35) and, by conducting the reaction in acetonitrile with triphenylphosphine/carbon tetrachloride, the single olefin **14** was obtained in 97% yield (^{13}C nmr, 135.3, 128.9). Hydrogenation of **14** (H_2, 10% Pd/C, CH_3OH, 1 atm. (101.3 kPa), 99%) followed by lithium aluminum hydride reduction of the resulting ester provided the primary alcohol **15** quantitatively. Introduction of the exocyclic methylene using either selenoxide elimination or dehydrobromination proved impractical. Thus authentic (±)-sinularene was prepared from **15** *via* pyrolysis (550°C, 77%) of the acetate **16**, and possessed spectral features (^1H nmr, ir, ms) identical to those published for the natural product (5).

This completes a direct stereoselective synthesis of (±)-sinularene in 22% overall yield from the major aldol diastereomer **8** (9% from **5**) and 14 steps from cyclopentadiene, the same ultimate starting material as employed in the Australian (11) and Swiss (12) syntheses. A parallel series of reactions from the minor isopropyl(S) adduct corresponding to **12** afforded (±)-5-epi-sinularene.

These concepts and procedures are also applicable to the preparation of 12-acetoxysinularene (36, 37) and are currently being extended to an asymmetric synthesis of (+)-longifolene, utilizing this intramolecular Diels–Alder:cyclopropane ring opening strategy.

Acknowledgements

We are grateful to Memorial University of Newfoundland and the Natural Sciences and Engineering Research Council of Canada for financial support of this research, G. Gallacher and S. K. Attah-Poku for preliminary experiments, B. Gregory for high resolution mass spectra, A. Hanson (NRC, Halifax, Canada) for X-ray analysis, and H. J. Liu (University of Alberta) for 400 MHz ^1H nmr spectra.

1. A. G. FALLIS. Can. J. Chem. **62**, 183 (1984).
2. E. CIGANEK. Org. React. **32**, 1 (1984).
3. G. BRIEGER and J. N. BENNETT. Chem. Rev. **80**, 63 (1980).
4. W. OPPOLZER. Angew. Chem. Int. Ed. Engl. **16**, 10 (1977).
5. C. M. BEECHAM, C. DJERASSI, and H. EGGERT. Tetrahedron, **34**, 2503 (1978).
6. C. M. BEECHAN, C. DJERASSI, J. S. FINER, and J. CLARDY. Tetrahedron Lett. 2395 (1977).
7. G. OURISSON. Bull. Soc. Chim. Fr. 895 (1955).
8. J-C. THIERRY and R. WEISS. Tetrahedron Lett. 2663 (1969).
9. P. DE MAYO and R. E. WILLIAMS. J. Am. Chem. Soc. **87**, 3275 (1965).
10. L. A. SMEDMAN, E. ZAVARIN, and R. TERANISHI. Phytochemistry, 1457 (1969).
11. P. A. COLLINS and D. WEGE. Aust. J. Chem. **32**, 1819 (1979).
12. W. OPPOLZER, H. F. STRAUSS, and D. P. SIMMONS. Tetrahedron Lett. **23**, 4673 (1982).
13. E. J. COREY, M. OHNO, R. B. MITRA, and P. VATAKENCHERRY. J. Am. Chem. Soc. **86**, 478 (1964).
14. J. E. MCMURRY and S. J. ISSER. J. Am. Chem. Soc. **94**, 7132 (1972).
15. R. A. VOLKMANN, G. C. ANDREWS, and W. S. JOHNSON. J. Am. Chem. Soc. **97**, 4777 (1975).
16. W. OPPOLZER and T. GODEL. J. Am. Chem. Soc. **100**, 2583 (1978).
17. W. OPPOLZER. Pure Appl. Chem. **53**, 1181 (1981).
18. W. OPPOLZER and T. GODEL. Helv. Chim. Acta, **67**, 1154 (1984).
19. J. E. MCMURRY. J. Am. Chem. Soc. **90**, 6821 (1968).
20. G. L. HODGSON, D. F. MACSWEENEY, and T. MONEY. J. Chem. Soc. Perkin Trans. 1, 2113 (1973).
21. E. PIERS, M. B. GERAGHTY, R. D. SMILLIE, and M. SAUCY. Can. J. Chem. **53**, 2849 (1975).
22. H. HAGIWARA, M. MIYASHITA, H. UDA, and A. YOSHIKOSHI. Bull. Chem. Soc. Jpn. **48**, 3723 (1975).
23. P. BAKUZIS, O. O. S. CAMPOS, and M. L. F. BAKUZIS. J. Org. Chem. **41**, 3261 (1976).
24. M. YANAGIYA, K. KANEKO, T. KAJI, and T. MATSUMOTO. Tetrahedron Lett. 1761 (1979).
25. R. L. SNOWDEN. Tetrahedron Lett. **22**, 101 (1981).
26. G. BRIEGER. J. Am. Chem. Soc. **85**, 3783 (1963).
27. E. J. COREY, N. M. WEINSHENKER, T. K. SCHAFF, and W. HUBER. J. Am. Chem. Soc. **91**, 5675 (1969).
28. E. J. COREY, U. KOELLIKER, and J. NEUFFER. J. Am. Chem. Soc. **93**, 1489 (1971).
29. R. S. GLASS, J. D. HERZOG, and R. L. SOBCZAK. J. Org. Chem. **43**, 3209 (1978).
30. S. K. ATTAH-POKU, K. ANTCZAK, S. J. ALWARD, and A. G. FALLIS. Can. J. Chem. **62**, 1717 (1984).
31. G. GALLACHER, A. S. NG, S. K. ATTAH-POKU, K. ANTCZAK, S. J. ALWARD, J. F. KINGSTON, and A. G. FALLIS. Can. J. Chem. **62**, 1709 (1984).
32. K. BANGERT and V. BOEKELHEIDE. Tetrahedron Lett. 1119 (1963).
33. M. NEUENSCHWANDER, D. MEUCHE, and H. SCHALTEGGER. Helv. Chim. Acta, **46**, 1760 (1963).
34. F. NAF, R. DECORZANT, W. GIERSCH, and G. OHLOFF. Helv. Chim. Acta, **64**, 1387 (1981).
35. R. APPEL and H-D. WIHLER. Chem. Ber. **109**, 3446 (1976).
36. J. C. BRAEKMAN, D. DALOZE, A. DUPONT, B. TURSCH, J. P. DE CLERCQ, G. GERMAIN, and M. VAN MEERSSCHE. Tetrahedron, **37**, 179 (1981).
37. W. OPPOLZER, T. BEGLEY, and A. ASHCROFT. Tetrahedron Lett. **25**, 825 (1984).
38. A. G. FALLIS and E. G. BREITHOLLE. International Symposium on Stereochemistry, Kingston, Ont., Canada. June 27 – July 2, 1976. Abstract M1.

Thermal rearrangement of functionalized 6-*exo*-(1-alkenyl)bicyclo[3.1.0]hex-2-enes. A total synthesis of (±)-sinularene

EDWARD PIERS AND GRACE L. JUNG

Department of Chemistry, University of British Columbia, 2036 Main Mall, University Campus, Vancouver, B.C., Canada V6T 1Y6

Received November 30, 1984

EDWARD PIERS and GRACE L. JUNG. Can. J. Chem. **63**, 996 (1985).

A total synthesis of the racemic form of the marine sesquiterpenoid (−)-sinularene (**1**) is described. The key step of the synthesis involved the stereoselective thermal rearrangement of the highly functionalized bicyclo[3.1.0]hexene **12** to provide, in 86% yield, the substituted bicyclo[3.2.1]octadiene **13**. Conversion of the latter substance into (±)-sinularene (**1**) was accomplished via an efficient 4-step sequence.

EDWARD PIERS et GRACE L. JUNG. Can. J. Chem. **63**, 996 (1985).

On décrit une synthèse totale de la forme racémique du sesquiterpénoïde marin, (−)-sinularène (**1**). L'étape clé de la synthèse implique la transposition thermique stéréosélective du bicyclo[3.1.0]hexène **12** hautement fonctionnalisé qui conduit au bicyclo[3.2.1]octadiène **13** substitué avec un rendement de 86%. On a opéré la transformation de **13** en (±)-sinularène (**1**) en faisant appel à une séquence très efficace de quatre réactions.

[Traduit par le journal]

In 1977, the constitution and absolute stereochemistry of the structurally unusual sesquiterpenoid (−)-sinularene, isolated from the soft coral *Sinularia mayi*, were determined to be as shown in **1** (1). Subsequently, two related natural products, 12-acetoxysinularene (**2**) and 12-acetoxycyclosinularene (**3**),

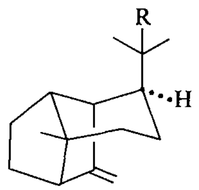

1 R = H
2 R = OAc

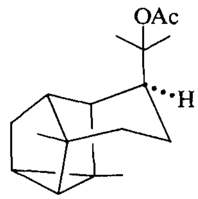

3

were obtained from a dichloromethane extract of *Clavularia inflata* (2). Up to the present time, two total syntheses of (±)-sinularene (**1**) have been reported (3, 4) and another has been completed.[1] In addition, the preparation of (±)-12-acetoxysinularene (**2**) has been described (5). We record herein our total synthesis of (±)-**1** via a route (summarized in Scheme 1) which is very different from those employed previously.

Reaction of 1-lithio-3-methyl-1-butyne with methacrolein (tetrahydrofuran, −30°C → room temperature, 1 h) provided the alcohol **4**[2] which, when treated with hot (130°C) triethyl orthoacetate in the presence of propionic acid (6), was converted stereoselectively into the ester **5** (58%). Transformation of the latter material into the diazoketone **6** (59% overall), followed by sequential carbenoid ring closure of **6** and hydrogenation (Lindlar's catalyst) of the resultant bicyclic alkyne **7**, provided cleanly the keto alkene **8** (62% from **6**).

Treatment of the trimethylsilyl enol ether of ketone **8** with $Pd(OAc)_2$ in acetonitrile (7) gave the enone **9** in 65% yield. When **9** was allowed to react with lithium divinylcuprate, the two epimeric conjugate addition products **10** and **11** were produced in a ratio of 9.4:1, respectively[3] (65% yield). These substances were separated by column chromatography. Evidence that the major (expected) product was the desired compound **10** was obtained by ^1H nmr spectroscopy. Thus, in a difference nOe experiment, irradiation at δ 2.15 (H_A, see **10**) caused enhancement of the signal (δ 2.91) due to the proton adjacent to the vinyl group (R in **10**).

In our overall synthetic plan, the key step was envisaged to be the thermal rearrangement of the enol silyl ether **12**, (hopefully) to produce the bicyclic triene **13**.[4] Presumably this process would involve isomerization of **12** to the epimer **17**, which would then undergo a Cope rearrangement (9). However, it should be pointed out that the thermally induced bond reorganization of **12** could proceed via an alternative pathway involving a homo-[1,5]-sigmatropic hydrogen migration (10) to provide (at least initially) the highly substituted cyclopentene **18**. In the anticipated transition state for the desired Cope process (see **A**), there is a significant destabilization due to steric repulsion between the isopropyl group and H_X. On the other hand, the presumed transition state for the sigmatropic

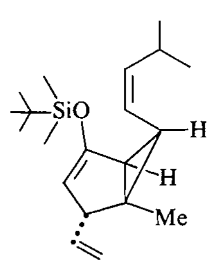

17

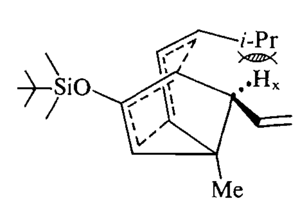

A

[1]Work by K. Antczak, J. F. Kingston, and A. G. Fallis. We are grateful to Professor Fallis for a preprint which describes their work (see preceding Communication).

[2]All compounds reported herein exhibited spectra (ir, ^1H nmr) in full accord with structural assignments. New substances gave satisfactory elemental analyses and (or) high resolution mass spectrometric molecular mass determinations.

[3]Interestingly, the reaction of **9** with vinylmagnesium bromide in the presence of $CuBr \cdot Me_2S$ (catalyst) was significantly less stereoselective, producing **10** and **11** in a ratio of 2.25:1 (63%).

[4]For previous reports concerning the synthesis of functionalized bicyclo[3.2.1]octane systems by thermolysis of 6-(1-alkenyl)bicyclo-[3.1.0]hex-2-enes, see ref. 8.

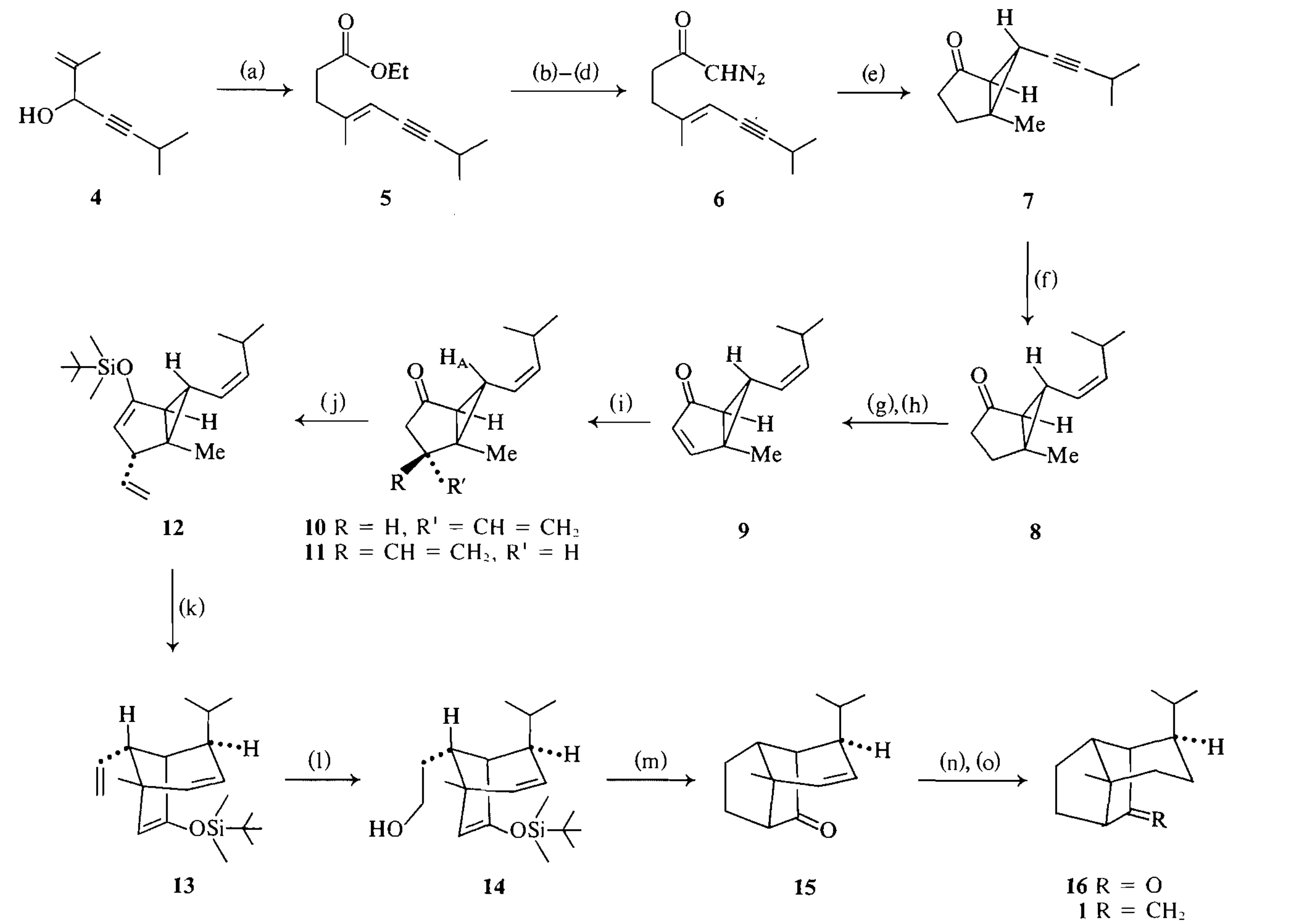

SCHEME 1. (a) $MeC(OEt)_3$, $EtCO_2H$, 130°C, 40.5 h; (b) KOH, H_2O, MeOH, reflux; H^+; (c) $(COCl)_2$, C_6H_6, reflux, 1 h; (d) CH_2N_2, Et_2O, 0°C; (e) $Cu(acac)_2$, C_6H_6, reflux, 2 h; (f) H_2, Pd–$CaCO_3$, $Pb(OAc)_2$, quinoline, pentane, room temperature, 5 h; (g) Me_3SiI, Et_3N, CH_2Cl_2, −78°C; (h) $Pd(OAc)_2$, MeCN, room temperature, 1 h; (i) $(CH_2{=}CH)_2CuLi$, Et_2O, −63°C to −30°C; NH_4Cl–H_2O; (j) LiN(*i*-Pr)$_2$, THF, −78°C; *t*-$BuMe_2SiCl$, THF–HMPA, −78°C to room temperature, 4 h; (k) 220°C, C_6H_6, sealed tube; (l) Sia_2BH, THF; H_2O_2, NaOH; (m) *p*-$MeC_6H_4SO_2Cl$, 4-dimethylaminopyridine, CH_2Cl_2, room temperature; (n) H_2, Pd–C, MeOH, room temperature; (o) $Ph_3P{=}CH_2$, THF, reflux, 69 h.

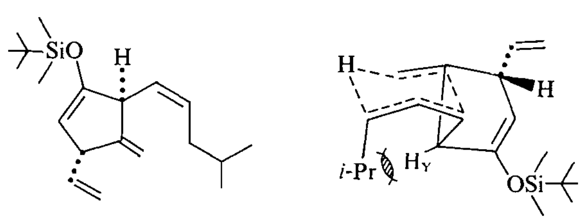

18 **B**

hydrogen shift suffers from a similar interaction involving the isopropyl group and H_Y (see **B**). Thus, it is difficult to make a clear-cut prediction as to which mode of rearrangement would be preferred.

Fortunately (and happily), thermolysis of **12** produced, in 86% yield, a single product, the spectra of which showed clearly that it was the desired triene **13**. Chemoselective hydroboration–oxidation of the latter compound, followed by treatment of the resultant alcohol **14** with *p*-toluenesulfonyl chloride in the presence of 4-dimethylaminopyridine, afforded directly the tricyclic ketone **15** (68% from **13**). Hydrogenation of **15** provided the ketone **16**, which was spectrally and chromatographically identical with the same compound prepared by Collins and Wege (3).[5]

Conversion of **16** into (±)-sinularene (**1**) has been accomplished previously via a three-step sequence (3). However, we have shown that this transformation can be carried out conveniently by treatment of **16** with methylenetriphenylphosphorane in refluxing tetrahydrofuran. Although the reaction was slow, it provided (±)-**1** cleanly (66% yield from **15**). Racemic sinularene (**1**) thus obtained was identical with an authentic sample.[5]

Acknowledgements

We are grateful to the Natural Sciences and Engineering Research Council of Canada for financial support and for a Postgraduate Scholarship (to G.L.J.).

1. C. M. BEECHAN, C. DJERASSI, J. S. FINER, and J. CLARDY. Tetrahedron Lett. 2395 (1977).
2. J. C. BRAEKMAN, D. DALOZE, A. DUPONT, B. TURSCH, J. P.

[5]We thank Professor Wege for copies of the ^{1}H nmr and ir spectra of (±)-**16** and Professor Oppolzer for copies of the ^{1}H nmr, ir, and mass spectra of (±)-sinularene (**1**).

DECLERCQ, G. GERMAIN, and M. VAN MEERSSCHE. Tetrahedron, **37**, 179 (1981).
3. P. A. COLLINS and D. WEGE. Aust. J. Chem. **32**, 1819 (1979).
4. W. OPPOLZER, H. F. STRAUSS, and D. P. SIMMONS. Tetrahedron Lett. **23**, 4673 (1982).
5. W. OPPOLZER, T. BEGLEY, and A. ASHCROFT. Tetrahedron Lett. **25**, 825 (1984).
6. K. A. PARKER and R. W. KOSLEY, JR. Tetrahedron Lett. 691 (1975).
7. Y. ITO, T. HIRAO, and T. SAEGUSA. J. Org. Chem. **43**, 1011 (1978).
8. E. PIERS and E. H. RUEDIGER. J. Org. Chem. **45**, 1725 (1980); E. PIERS, G. L. JUNG, and N. MOSS. Tetrahedron Lett. **25**, 3959 (1984).
9. S. J. RHOADS and N. R. RAULINS. Org. React. **22**, 1 (1975); J. E. BALDWIN and K. E. GILBERT. J. Am. Chem. Soc. **98**, 8283 (1976).
10. C. W. SPANGLER. Chem. Rev. **76**, 187 (1976); E. M. MIL'VITSKAYA, A. V. TARAKANOVA, and A. F. PLATE. Russ. Chem. Rev. **45**, 469 (1976).

Formation de l'état triplet du benzaldéhyde dans sa réaction en phase gazeuse avec l'azote activé

ODILE DESSAUX, CHRISTIAN DUPRET ET PIERRE GOUDMAND[1]

Laboratoire de Spectroscopie de la réactivité chimique, Chimie Physique, Université des Sciences et Techniques de Lille, Domaine Universitaire Scientifique, 59655 Villeneuve d'Ascq Cedex, France

Reçu le 10 octobre 1984

ODILE DESSAUX, CHRISTIAN DUPRET et PIERRE GOUDMAND. Can. J. Chem. **63**, 998 (1985).

La réaction en phase gazeuse de l'azote activé avec le benzaldéhyde donne une réaction chimiluminescente attribuée essentiellement à la transition $T_1(n\pi^*) \rightarrow S_0$ du benzaldéhyde. Deux étapes dans le mécanisme de la réaction sont proposées.

ODILE DESSAUX, CHRISTIAN DUPRET, and PIERRE GOUDMAND. Can. J. Chem. **63**, 998 (1985).

The reaction of active nitrogen with benzaldehyde gives a chemiluminescent reaction mainly attributed to the $T_1(n\pi^*) \rightarrow S_0$ transition of benzaldehyde. Two steps of the mechanism are proposed.

Introduction

L'azote activé par décharge électrique microonde est un vecteur d'énergie de réactivité physicochimique très importante (1). Il constitue un milieu en évolution dynamique du fait du mécanisme complexe de recombinaison des atomes d'azote (2, 3) mettant en jeu des états moléculaires triplets ou singulet vibrationnellement excités (4). Le comportement de l'azote activé apparaît différent suivant l'état physique du réactif sur lequel il réagit: en phase gazeuse il entraîne, en général, une fragmentation de la cible moléculaire pour former des radicaux ou molécules mono, di ou triatomiques, pouvant être accompagnée d'une fixation d'azote atomique (1), tandis que ses réactions avec des matrices solides contenant un dérivé aromatique à faible température (77 K ou 4,2 K) ont pour effet essentiel une excitation à l'état triplet par transfert radiatif (5).

La possibilité de l'intervention de l'état triplet de la molécule cible comme intermédiaire primaire dans la réaction de l'azote activé est souvent postulée (1) sans aucune preuve directe: l'une des raisons essentielles de la difficulté de la mise en évidence d'une telle étape est le caractère fortement inhibiteur des atomes $N(^4S)$ pour des états triplets; c'est ainsi que s'interprète la faible concentration stationnaire de $N_2(^3\Sigma_u^+)$ dans le gaz activé où cette molécule à l'état triplet le plus bas est détruite par la réaction très rapide [1]:

$$[1] \quad N_2(^3\Sigma_u^+) + N(^4S) \rightarrow N_2(^1\Sigma_g^+) + N(^4S).$$

Nous rendons compte de la mise en évidence expérimentale de l'état triplet de la cible moléculaire dans la réaction chimiluminescente, en phase gazeuse, de l'azote activé sur le benzaldéhyde.

Partie expérimentale

L'azote activé est produit et réagit sur le benzaldéhyde C_6H_5CHO à l'aide d'un dispositif déjà décrit antérieurement (3). Les réactifs sont des produits chimiquement purs utilisés sans purification complémentaire. Le dispositif d'observation spectroscopique est constitué par la chaîne de détection et d'enregistrement: monochromateur "Coderg MSV" – photomultiplicateur "EMI 9558 QB" couplé à un enregistreur.

La réaction se présente comme une chimiluminescence bleue très localisée, dans la zone de mélange des deux flux gazeux. Ce phénomène ne peut être mis en évidence que dans des conditions très strictes de débit des deux réactifs qui impliquent la consommation complète des atomes d'azote qui se traduit par une disparition totale de la chimiluminescence jaune.

Le spectre d'émission de la chimiluminescence (fig. 1) présente essentiellement la transition triplet–singulet $T_1(n\pi^*) - S_0$ du benzaldéhyde. Les longueurs d'onde sont mesurées, avec une précision de 1 nm, à 460 nm, 426 nm et 397 nm, ce qui correspond avec une bonne précision à la vibration d'élongation de C=O dont la fréquence moyenne apparaît être de 1725 cm^{-1} dans notre travail. L'émission du système $^2\Sigma^+ - {}^2\Sigma^+$ du radical CN est également présente mais sous une intensité faible; la comparaison des spectres 1a et 1b montre qu'elle est présente sur le spectre d'un témoin enregistré après l'arrêt de l'arrivée du benzaldéhyde et semble indiquer que l'origine de cet émetteur très sensible est une impureté.

Discussion

Deux étapes mécanistiques de la réaction peuvent être dégagées dans ce travail préliminaire.

[1]Auteur à qui adresser la correspondance.

DECLERCQ, G. GERMAIN, and M. VAN MEERSSCHE. Tetrahedron, **37**, 179 (1981).
3. P. A. COLLINS and D. WEGE. Aust. J. Chem. **32**, 1819 (1979).
4. W. OPPOLZER, H. F. STRAUSS, and D. P. SIMMONS. Tetrahedron Lett. **23**, 4673 (1982).
5. W. OPPOLZER, T. BEGLEY, and A. ASHCROFT. Tetrahedron Lett. **25**, 825 (1984).
6. K. A. PARKER and R. W. KOSLEY, JR. Tetrahedron Lett. 691 (1975).
7. Y. ITO, T. HIRAO, and T. SAEGUSA. J. Org. Chem. **43**, 1011 (1978).
8. E. PIERS and E. H. RUEDIGER. J. Org. Chem. **45**, 1725 (1980); E. PIERS, G. L. JUNG, and N. MOSS. Tetrahedron Lett. **25**, 3959 (1984).
9. S. J. RHOADS and N. R. RAULINS. Org. React. **22**, 1 (1975); J. E. BALDWIN and K. E. GILBERT. J. Am. Chem. Soc. **98**, 8283 (1976).
10. C. W. SPANGLER. Chem. Rev. **76**, 187 (1976); E. M. MIL'VITSKAYA, A. V. TARAKANOVA, and A. F. PLATE. Russ. Chem. Rev. **45**, 469 (1976).

Formation de l'état triplet du benzaldéhyde dans sa réaction en phase gazeuse avec l'azote activé

ODILE DESSAUX, CHRISTIAN DUPRET ET PIERRE GOUDMAND[1]

Laboratoire de Spectroscopie de la réactivité chimique, Chimie Physique, Université des Sciences et Techniques de Lille, Domaine Universitaire Scientifique, 59655 Villeneuve d'Ascq Cedex, France

Reçu le 10 octobre 1984

ODILE DESSAUX, CHRISTIAN DUPRET et PIERRE GOUDMAND. Can. J. Chem. **63**, 998 (1985).

La réaction en phase gazeuse de l'azote activé avec le benzaldéhyde donne une réaction chimiluminescente attribuée essentiellement à la transition $T_1(n\pi^*) \rightarrow S_0$ du benzaldéhyde. Deux étapes dans le mécanisme de la réaction sont proposées.

ODILE DESSAUX, CHRISTIAN DUPRET, and PIERRE GOUDMAND. Can. J. Chem. **63**, 998 (1985).

The reaction of active nitrogen with benzaldehyde gives a chemiluminescent reaction mainly attributed to the $T_1(n\pi^*) \rightarrow S_0$ transition of benzaldehyde. Two steps of the mechanism are proposed.

Introduction

L'azote activé par décharge électrique microonde est un vecteur d'énergie de réactivité physicochimique très importante (1). Il constitue un milieu en évolution dynamique du fait du mécanisme complexe de recombinaison des atomes d'azote (2, 3) mettant en jeu des états moléculaires triplets ou singulet vibrationnellement excités (4). Le comportement de l'azote activé apparaît différent suivant l'état physique du réactif sur lequel il réagit: en phase gazeuse il entraîne, en général, une fragmentation de la cible moléculaire pour former des radicaux ou molécules mono, di ou triatomiques, pouvant être accompagnée d'une fixation d'azote atomique (1), tandis que ses réactions avec des matrices solides contenant un dérivé aromatique à faible température (77 K ou 4,2 K) ont pour effet essentiel une excitation à l'état triplet par transfert radiatif (5).

La possibilité de l'intervention de l'état triplet de la molécule cible comme intermédiaire primaire dans la réaction de l'azote activé est souvent postulée (1) sans aucune preuve directe: l'une des raisons essentielles de la difficulté de la mise en évidence d'une telle étape est le caractère fortement inhibiteur des atomes $N(^4S)$ pour des états triplets; c'est ainsi que s'interprète la faible concentration stationnaire de $N_2(^3\Sigma_u^+)$ dans le gaz activé où cette molécule à l'état triplet le plus bas est détruite par la réaction très rapide [1]:

$$[1] \quad N_2(^3\Sigma_u^+) + N(^4S) \rightarrow N_2(^1\Sigma_g^+) + N(^4S).$$

Nous rendons compte de la mise en évidence expérimentale de l'état triplet de la cible moléculaire dans la réaction chimiluminescente, en phase gazeuse, de l'azote activé sur le benzaldéhyde.

Partie expérimentale

L'azote activé est produit et réagit sur le benzaldéhyde C_6H_5CHO à l'aide d'un dispositif déjà décrit antérieurement (3). Les réactifs sont des produits chimiquement purs utilisés sans purification complémentaire. Le dispositif d'observation spectroscopique est constitué par la chaîne de détection et d'enregistrement: monochromateur "Coderg MSV" – photomultiplicateur "EMI 9558 QB" couplé à un enregistreur.

La réaction se présente comme une chimiluminescence bleue très localisée, dans la zone de mélange des deux flux gazeux. Ce phénomène ne peut être mis en évidence que dans des conditions très strictes de débit des deux réactifs qui impliquent la consommation complète des atomes d'azote qui se traduit par une disparition totale de la chimiluminescence jaune.

Le spectre d'émission de la chimiluminescence (fig. 1) présente essentiellement la transition triplet–singulet $T_1(n\pi^*) - S_0$ du benzaldéhyde. Les longueurs d'onde sont mesurées, avec une précision de 1 nm, à 460 nm, 426 nm et 397 nm, ce qui correspond avec une bonne précision à la vibration d'élongation de C=O dont la fréquence moyenne apparaît être de 1725 cm^{-1} dans notre travail. L'émission du système $^2\Sigma^+ - {}^2\Sigma^+$ du radical CN est également présente mais sous une intensité faible; la comparaison des spectres 1a et 1b montre qu'elle est présente sur le spectre d'un témoin enregistré après l'arrêt de l'arrivée du benzaldéhyde et semble indiquer que l'origine de cet émetteur très sensible est une impureté.

Discussion

Deux étapes mécanistiques de la réaction peuvent être dégagées dans ce travail préliminaire.

[1]Auteur à qui adresser la correspondance.

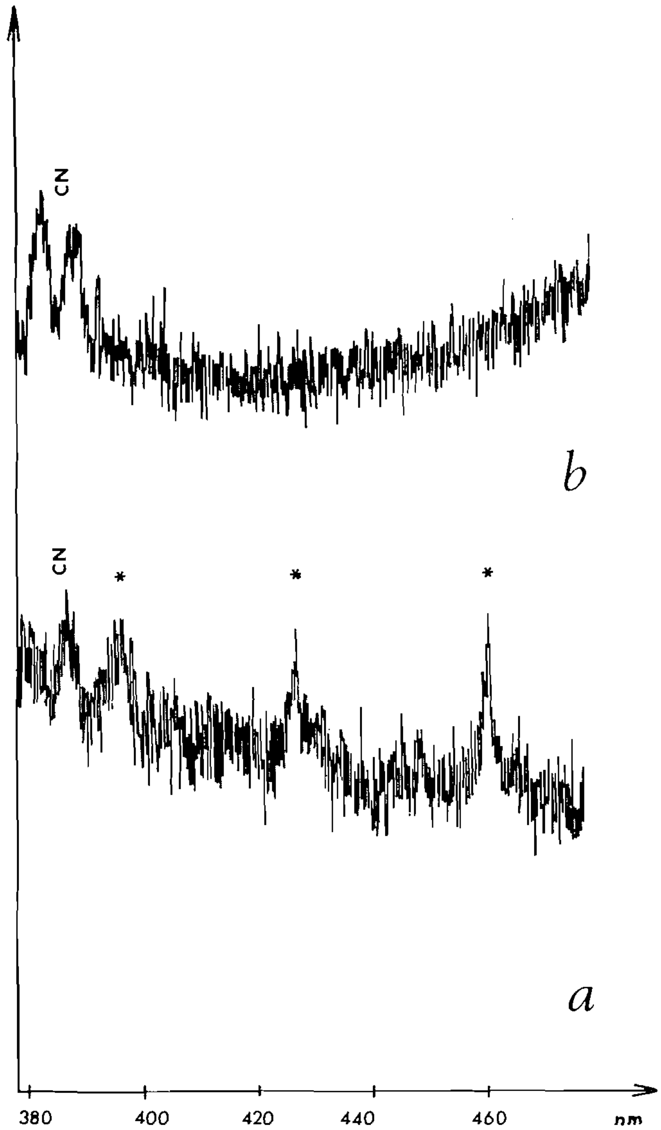

FIG. 1. (a) Enregistrement du spectre de la chimiluminescence du benzaldéhyde avec l'azote activé. (b) Enregistrement témoin en l'absence de benzaldéhyde.

(a) L'excitation de l'état $T_1(n\pi^*)$ du benzaldéhyde peut être interprétée, a priori; soit par un transfert d'énergie à partir de molécules d'azote présentes dans le milieu $N_2(^3\Pi_g)$: T_2 ou $N_2(^3\Sigma_u^+)$: T_1

[2] $N_2(T) + \phi CHO(S_0) \rightarrow N_2(S_0) + \phi CHO(T_1 n\pi^*)$

soit par une triple collision

[3] $N(^4S) + N(^4S) + \phi CHO(S_0) \rightarrow N_2(S_0) + \phi CHO(T_1 n\pi^*)$

Les réactions du modèle [2] ne sont efficaces que si elles sont très rapides, étant donné la court durée de vie des espèces $N_2(T)$ dans l'azote activé: $N_2(T_2)$, du fait de sa transition radiative permise vers $N_2(T_1)$, cette dernière à cause de la réaction [1]. La réaction [3] apparaît ainsi la plus probable comme responsable du peuplement de l'état triplet de ϕ-CHO. En tout état de cause les réactions [2] ou [3] de formation de $\phi CHO(T_1 n\pi^*)$ ne sont pas des réactions élémentaires et en particulier la réaction [3] peut mettre en jeu des états électroniquement excités de l'azote. Le diagramme énergétique (fig.

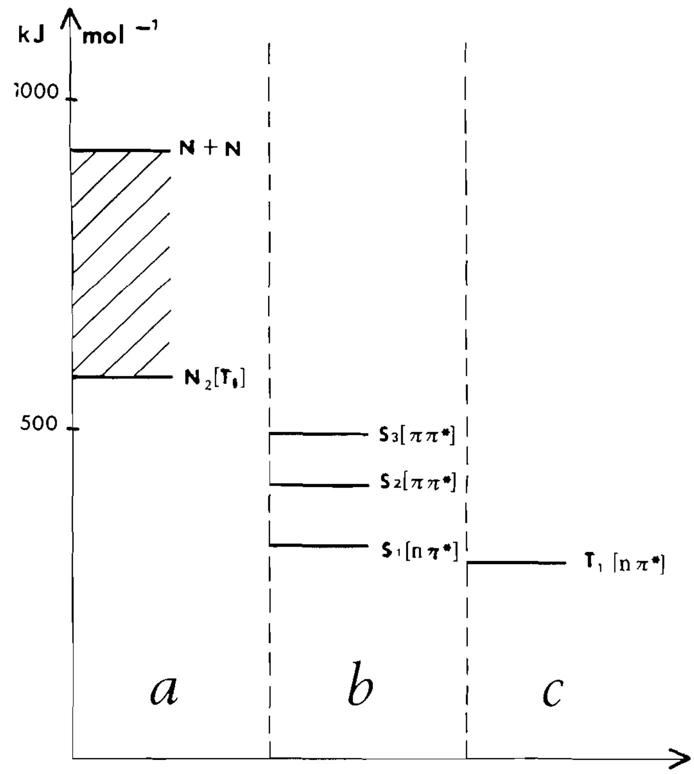

FIG. 2. Diagramme énergétique. (a) Niveaux d'énergie susceptibles d'être mis en jeu dans les réactions de l'azote activé. (b) Niveaux d'énergie des premiers singulets de ϕCHO. (c) Niveau d'énergie de l'état triplet de ϕCHO.

2) permet de comparer les énergies susceptibles d'être mises en jeu dans le transfert — qui doit se faire d'une manière isoénergétique: l'énergie de l'état triplet $T_1(n\pi^*)$ du benzaldéhyde, et celles de ses états excités singulets — qui constituent une limite supérieure pour l'énergie de l'état triplet correspondant. Ce schéma montre que l'état $T_1(n\pi^*)$ ne peut être produit qu'après un processus de relaxation énergétique important mettant en jeu des mécanismes de conversion interne (par cascade d'états triplets successifs), mais éventuellement aussi des conversions intersystèmes vers des états singulets.

(b) La nécessité d'opérer dans des conditions de disparition totale des atomes $N(^4S)$ étaye l'hypothèse d'une désactivation cinétique très rapide:

[4] $\phi CHO(T_1 n\pi^*) + N(^4S) \rightarrow \phi CHO(S_0) + N(^4S)$.

1. A. N. WRIGHT et C. A. WINKLER. Active nitrogen. Academic Press, New York. 1968.
2. (*a*) I. M. CAMPBELL et B. A. THRUSH. Proc. R. Soc. A, **296**, 201 (1967); (*b*) R. A. YOUNG. J. Chem. Phys. **60**, 5050 (1974).
3. (*a*) O. DESSAUX, P. GOUDMAND et B. MUTEL. J. Quant. Spectrosc. Radiat. Transfer, **30**, 137 (1983); (*b*) O. DESSAUX, P. GOUDMAND et B. MUTEL. J. Quant. Spectrosc. Radiat. Transfer, **30**, 311 (1983).
4. B. MUTEL, M. BRIDOUX, M. CRUNELLE-CRAS, O. DESSAUX, F. GRASE, P. GOUDMAND et G. MOREAU. Chem. Phys. Lett. **104**, 290 (1984).
5. (*a*) O. DESSAUX. J. Chim. Phys. **67**, 1137 (1970); (*b*) P. DEVOLDER, O. DESSAUX et P. GOUDMAND. J. Photochem. **15**, 265 (1981).
6. (*a*) Y. HIRATA et E. C. LIM. J. Chem. Phys. **72**, 5505 (1980); (*b*) L. GOODMAN, M. LAMOTTE et M. KOYANAGI. Chem. Phys. **47**, 329 (1980).

^{1}H and ^{13}C nuclear magnetic resonance studies on the Diels–Alder adducts of isoquinolin-3(2*H*)-ones[1]

GÁBOR TÓTH[2] AND ATTILA ALMÁSY
NMR Laboratory of the Institute for General and Analytical Chemistry, Technical University, Budapest, H-1521, Hungary

AND

LÁSZLÓ HAZAI, ANTAL SCHNITTA, AND GYULA DEÁK
Institute of Experimental Medicine, Hungarian Academy of Sciences, Budapest, H-1450, P.O.B. 67, Hungary

Received July 6, 1984

GÁBOR TÓTH, ATTILA ALMÁSY, LÁSZLÓ HAZAI, ANTAL SCHNITTA, and GYULA DEÁK. Can. J. Chem. **63**, 1001 (1985).

The stereochemistry of the adducts of isoquinolin-3(2*H*)-ones and maleimides was studied and ^{1}H and ^{13}C spectral parameters of the *endo* and *exo* stereoisomers were determined. The predominant rotamers generated by rotation about the C(7)—C(7a) and (C1)—C(1′) bonds were identified.

GÁBOR TÓTH, ATILLA ALMÁSY, LÁSZLÓ HAZAI, ANTAL SCHNITTA et GYULA DEÁK. Can. J. Chem. **63**, 1001 (1985).

On a étudié la stéréochimie des adduits obtenus par condensation des 2*H*-isoquinoléinones-3 sur les maléimides et on a déterminé les paramètres, en rmn du ^{1}H et du ^{13}C, des stéréoisomères *endo* et *exo*. On a identifié les rotamères prédominants qui sont générés par des rotations autour des liaisons C(7)—C(7a) et C(1)—C(1′).

[Traduit par le journal]

Introduction

Earlier, we reported that some isoquinolin-3(2*H*)-ones, prepared in our laboratory, which are partly present as their *ortho*-quinoidal lactam tautomer, are amenable to Diels–Alder reaction with active dienophiles (1–3). Thus, a number of adducts with maleic acid derivatives have been prepared employing *N*-phenyl- and *N*-carbamoyl-maleimide, as well as maleic anhydride, as dienophiles. The products contain various substituents, such as alkyl, aryl, aralkyl, and heteroaryl groups, and may be condensed with a benzene ring in positions (*f*), (*g*), or (*h*). The unsubstituted maleimide adduct **1** was prepared by an indirect route (1).

Results and discussion

The products may be of either *exo* or *endo* configuration. Usually only one adduct could be isolated, except in the case of **5** where both isomers could be separated (2). The numbering used in the assignment of nmr data is shown in the formula for *exo* **5*b*** (Scheme 2).

The earlier misconception that, in the *endo* isomers, the *ortho*-hydrogens of the condensed benzene ring (H-9a and H-9d) are highly shielded by the nearby imide carbonyl led to incorrect conclusions concerning the stereostructure of the above adducts and their congeners (4–6). It has been shown later that the two proton signals in question should rather be assigned to the *ortho*-hydrogens of the *N*-phenyl group (7–9). This assumption is supported by our present ^{1}H and selective ^{13}C{^{1}H} decoupling studies on compounds **1**–**6**. However, the assumption that increased shielding of the methyne protons is diagnostic for the *exo* stereoisomer (7) could not be confirmed.

Characteristic ^{1}H nmr data for compounds **1**–**7**, along with further Lis (Lanthanide induced shift) values for **5*a*** on addition of Eu(fod)$_3$ graphically interpolated to a 1:1 substrate/reagent ratio are compiled in Table 1.

We have found that the spectra of *exo* and *endo* isomers characteristically differ in the chemical shifts of the *ortho*-protons of the *N*-phenyl group, which in the latter are shifted upfield to 6.40 ppm owing to the diamagnetic anisotropic effect of the condensed benzene ring. The proton H-9a is in turn more

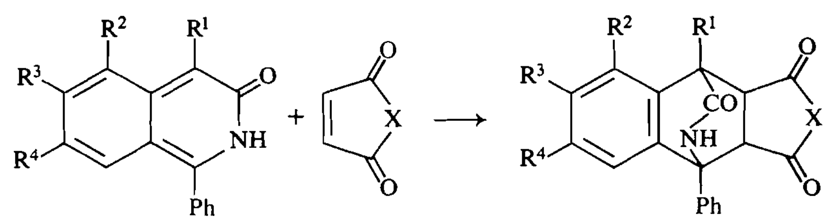

X = NH, NPh, NCONH$_2$, O

	R^1	R^2	R^3	R^4	X
1	Me	H	H	H	NH
2	Me	H	H	H	NPh
3	H	Me	H	H	NPh
4	Me	Me	H	H	NPh
5*a*	CH$_2$Ph	H	H	H	NPh
5*b*	CH$_2$Ph	H	H	H	NPh
6	CH$_2$Ph	H	MeO	MeO	NPh

[1]Diels–Alder reaction of 3(2*H*)-isoquinolinones, Part 4. For Part 3, see ref. 1.

[2]To whom all correspondence should be addressed. Present address: Department of Chemistry, University of Alberta, Edmonton, Alta., Canada, T6G 2G2.

TABLE 1. ^{1}H nuclear magnetic resonance data δ(ppm); *J*(Hz) of compounds **1**–**6** and LIS values of **5***a*

Compound	2-H	6-H	9d-H	4b-H_2	NH	R^1	Aromatic H's	Others
1[a,c]	3.28d	4.47d	6.38d		8.70	1.78 (3 H, s)	7.1–7.8 (8 H, m)	
2[a,d]	3.42d	4.65d	6.77d	6.40m	8.59	1.84 (3 H, s)	7.0–7.85 (11 H, m)	
3[a,d]	3.91dd	4.58d	6.57d	6.40m	8.51	4.34 (1 H, d, 2 Hz)	7.0–7.85 (10 H, m)	2.32 (3 H, s, Me)
4[a,d]	3.42d	4.52d	6.58d	6.42m	8.53	2.11 (3 H, s)	7.0–7.85 (10 H, m)	2.47 (3 H, s, Me)
5*a*[b,c]	3.48d	4.22d	6.59d	6.40m		3.89 (2 H, br s)[e]	7.0–7.85 (16 H, m)	
Δδ	6.3	2.4		1.3		8.6, 10.9	9a-H 5.0, 1b-H_2 9.1 7b-H_2 3.6	
5[b,c]	3.64d	3.99d	6.38d	7.00	7.04	4.00 (1 H, d, 17 Hz) 4.24 (1 H, d)[e]	7.0–7.6 (18 H, m)	
6[b,c]	3.53d	4.25d	6.46s	6.40m	6.95	3.89 (2 H, br s)	7.1–7.85 (13 H, m)	3.63 (3 H, s, Me)

[a]Solvent: [$^2H_6$]DMSO.
[b]Solvent: $CDCl_3$.
[c]Temperature: 25°C.
[d]Temperature: 70°C.
[e]Other signals in overlapping with aromatic H's.

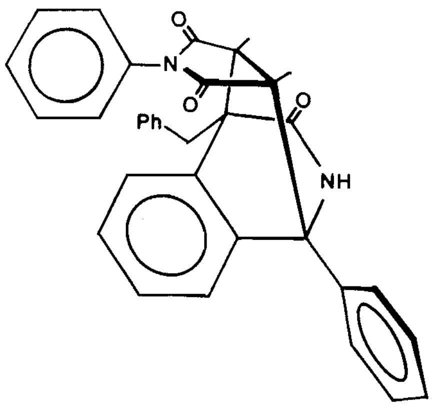

5*a*

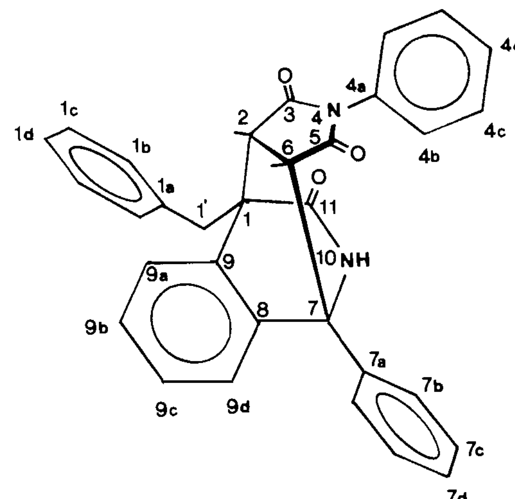

5*b*

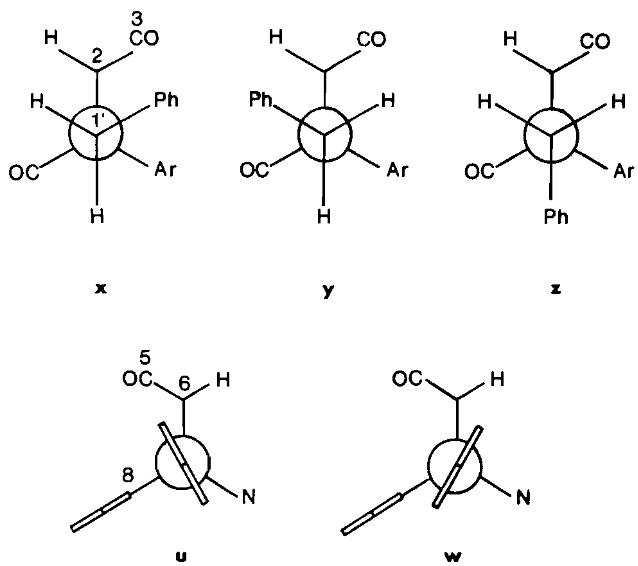

SCHEME 1

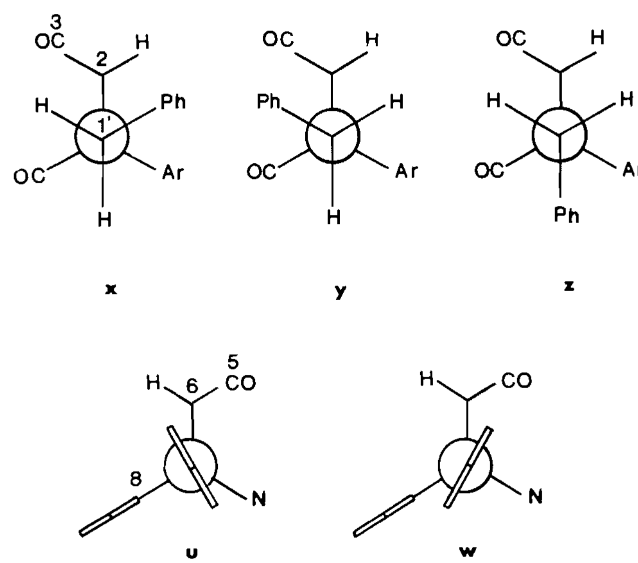

SCHEME 2

shielded in the *exo* isomers. When R^1 = CH_2Ph (**5***a* and **6**) diastereotopic methylene protons produce a broad singlet in the *endo* isomers, while an AB-type doublet in *exo* **5***b*. Lis measurements have revealed that, similar to 4-benzyl-1-phenyl-dihydro-3(2*H*)-isoquinolines (10), Eu(fod)$_3$ was associated with the amide carbonyl. Accordingly, highest induced shifts were observed at the methylene and *ortho*-hydrogens of the benzyl group. The accidental anisochrony of the methylene protons was lifted by the shift reagent, proving that the coincidence of chemical shifts was not due to averaging by fast

TABLE 2. ^{13}C chemical shifts of compounds **1**–**7** in [$^2H_6$]DMSO

Carbon	1	2	3	4	5*a*[a]	5*b*[a]	6[a]	7[a]
1	48.3	48.3	43.9	51.2	52.9	52.8	52.9	48.5
2	48.8	47.9	45.7	49.5[b]	44.2	47.1	44.8	
3	175.5	172.9	175.1	174.8	173.3	172.7	173.6	
5	175.2	172.9	173.8	173.5	172.9	172.9	172.8	
6	51.3	50.1	49.2	49.8[b]	49.4	50.5	49.9	
7	63.5	63.8	65.6	63.8	64.4	64.8	64.5	59.4
8	135.3	135.0	135.1	135.3	134.7	134.1	129.3	135.2
9	137.4	137.4	134.2	135.8	137.1	137.4	130.3	136.3
9a	123.0	122.9	133.1	134.5	123.6	123.5	107.7	127.8
9b	126.7	126.7	129.7	132.4	126.3	126.1	148.0	126.6
9c	127.7	127.8	127.1	126.7	127.4	127.3	149.1	127.0
9d	123.3	123.4	121.8	122.6	124.5	125.7	108.7	127.0
11	173.4	173.3	171.9	173.5	173.7	173.7	173.8	173.1
1′	12.9	12.8		18.0	31.8	32.5	32.1	41.4
9a′			18.0	21.8				
1a					138.1	137.7	135.0	137.6
1b					132.6	130.6	132.2	130.8
1c					128.9	128.9	129.0	128.8
1d					128.9	128.9	129.0	128.8
4a		131.5	131.8	131.8	131.0	131.4	131.0	
4b		126.3	126.8	126.7	126.3	126.6	126.2	
4c		128.4	128.9	129.0	128.5	128.3	128.6	
4d		128.4	128.9	129.0	128.5	128.3	128.6	
7a	140.3	140.0	140.4	141.3	139.7	144.1	137.2	141.3
7b	129.9	129.8	130.3	130.4	129.8	128.9	129.6	129.3
7c	127.7	127.6	128.2	127.9	127.7	127.3	127.8	127.7
7d	128.3	128.3	129.2	128.6	128.5	128.9	128.9	128.3
MeO							56.4	

[a]In $CDCl_3$

[b]Tentative assignment.

rotation around the C(1)—C(1′) bond. The Lis value (1.3 ppm) for the *ortho*-protons of the *N*-phenyl group at the same time supported the *endo* configuration in which *N*—Ph is remote from C(11)═O. Unequal Lis values for the angular H-2 and H-6 proton signals also confirm their assignment. ^{13}C chemical shifts for compounds **1**–**6** as well as of *cis*-4-benzyl-1-phenyl-1,4-dihydro-3(2*H*)-isoquinolinone **7**, used as a model, are shown in Table 2. Assignments were based on those for **7** (10). It has to be noted that, in view of recent data reviewed by Ewing (11), assignments for the *ortho*- and *meta*-carbons of the benzyl group had to be interchanged.

For *N*-phenyl-succinimides, some unassigned ^{13}C chemical shifts have been reported (12). *N*—Ph shifts can, however, be assigned by comparing the spectra of **1** and **2**. Selective $^{13}C\{^1H\}$ decoupling of the two-proton signal at 6.40 indicated that the signal at 126.3 belongs to C(4*b*). On N—H → N—Ph substitution the imide carbonyl signals were shifted upfield by 2.3–2.6 ppm. Identification of the close C(2) and C(6) methyne signals was possible by the appearance of a ^3J(C, H) = 3.6 Hz coupling in the former, arising by interaction with the 1-methyl group. ^1J(C, H) couplings were 142.8 and 141.0 Hz, respectively.

Assignment of the lower field signal to C(6) could also be substantiated by comparing data for **2** and **3**. By removing the methyl group in the γ-position, this signal was essentially unaffected, while that for C(2) shifted, as expected, upfield. Accordingly, the signal for the β-positioned C(11) moved upfield while that for the γ-positioned C(3) moved downfield. Changes caused in the signals of the condensed aromatic ring effected by $R^2 = CH_3$ substitution also corroborated their assignment.

In **4** ($R^1 = R^2 = CH_3$) interaction of the *peri* methyl groups resulted in a slight deformation of the molecular skeleton, which may explain small deviations of chemical shifts from those calculated by additivity rules for carbons in the vicinity of C(1) and C(9). Downfield shifts of the two methyl group signals due to a δ-effect are quite characteristic (13).

Replacement of $R^1 = CH_3$ (**2**) for CH_2Ph (**5***a*, **5***b*, and **6**) involves a characteristic downfield shift of the C(1) signals. For the C(2) signal, a marked upfield shift was observed in **5***a* and **6**, and a small downfield shift in **5***b*. This can be interpreted by considering the rotamers **x**, **y**, and **z**, generated by rotation around the C(1)—C(1′) bond. With **5***a* and **6** rotamer **x**, and with **5***b* rotamer **y** involve severe steric interaction and can thus be discounted as being predominant conformers. In both **x** and **y**, γ-gauche interaction between C(2) and Ph—C(1′) is expected, while the same groups are γ-anti disposed in **z**. In the light of the observed shifts (see above), the predominant conformer for **5***a* and **6** is **y**, while for **5***b* it is **z**. Differences in the C(1b) chemical shifts also reflect changes of conformation.

There is a notable difference of the C(7a) shifts in the *exo* and *endo* isomers which can also be traced back to conformational changes. In the *endo* series, steric interaction between C(5)═O and H_2-7b is avoided in rotamer **w**, in which the planes of C(7)-phenyl and of the condensed benzene ring are at about 30°, while in rotamer **u**, characteristic for *exo*-(**5***b*), this angle is about 90°.

This assumption is supported by an upfield shift of 0.5 ppm of the H-9d signal in **5***b* under the well-known anisotropic effect of the phenyl group, as compared with the values recorded for **5***a*.

The characteristic chemical shifts observed for the signals of the condensed aromatic ring of the dimethoxy compound **6** provided further evidence for our assignments. The close C(9a) and C(9d) signals were assigned with the aid of selective $^{13}C\{^{1}H\}$ decoupling.

Experimental

The ^{1}H and ^{13}C nmr spectra were recorded on a JEOL FX-100 nmr spectrometer in PFT mode (16 K data points for FID) at ambient temperature at 99.6 and 25.0 MHz, respectively, using tetramethylsilane as internal standard.

Acknowledgments

The authors are grateful to Professor O. P. Strausz and Dr. M. Torres for helpful discussions. One of us (G.T.) thanks the Natural Sciences and Engineering Research Council of Canada for a visiting fellowship.

1. L. Hazai, A. Schnitta, Gy. Deák, G. Tóth, and Á. Szöllősy. Acta Chim. Acad. Sci. Hung. **117**, 99 (1984).
2. L. Hazai, Gy. Deák, G. Tóth, A. Schnitta, Á. Szöllősy, and J. Tamás. Acta Chim. Acad. Sci. Hung. **113**, 237 (1983).
3. L. Hazai, Gy. Déak, A. Schnitta, J. Hasko-Breuer, and E. Horváth. Acta Chim. Acad. Sci. Hung. **116**, 303 (1984).
4. M. P. Cava and N. M. Pollack. J. Am. Chem. Soc. **88**, 4112 (1966).
5. D. W. Jones. J. Chem. Soc. C, 1729 (1969).
6. N. J. Mruk and H. Tieckelmann. Tetrahedron Lett. **14**, 1209 (1970).
7. D. W. Jones and G. Kneen. Chem. Commun. 1356 (1971).
8. J. M. Holland and D. W. Jones. J. Chem. Soc. C, 536 (1970).
9. D. W. Jones and R. L. Wife. J. Chem. Soc. Perkin Trans. 1, 2722 (1972).
10. G. Tóth, L. Hazai, Gy. Deák, and H. Duddeck. Justus Liebigs Ann. Chem. 1103 (1978).
11. D. F. Ewing. Org. Magn. Reson. **12**, 499 (1979).
12. U. H. Brinker, G. Wilk, and K. Gomann. Angew. Chem. Suppl. 1228 (1983).
13. (*a*) F. W. Wehrli and T. Wirthlin. Interpretation of carbon-13 NMR spectra. Heyden, London. 1980. p. 39; (*b*) W. A. Ayer, L. M. Browne, S. Fung, and J. B. Stothers. Org. Magn. Reson. **11**, 73 (1978).

Free radical mechanisms for the oxidation of 2,3-dihydroxy-2-propenal (triose reductone) by hexacyanoferrate(III)

YASUO ABE, TAKAAKI DOHMARU, HIDEO HORII, AND SETSUO TANIGUCHI
Radiation Center of Osaka Prefecture, Shinke-cho, Sakai, Osaka 593, Japan

Received August 27, 1984

YASUO ABE, TAKAAKI DOHMARU, HIDEO HORII, and SETSUO TANIGUCHI. Can. J. Chem. **63**, 1005 (1985).

Kinetic studies of the oxidation of 2,3-dihydroxy-2-propenal (triose reductone, RH_2) by hexacyanoferrate(III), $[Fe(CN)_6]^{3-}$, were carried out in acidic media ($[H^+] = 0.02-0.1$ *M* (1 *M* = 1mol dm^{-3})) at various temperatures (10–30°C). The ionic strength of the media ($I = 0.04-0.4$ *M*) was adjusted using sodium perchlorate. The second-order rate constants in M^{-1} s^{-1} are (0.86 ± 0.06) – (2.83 ± 0.14) for the reactions of hexacyanoferrate(III) with RH_2 and [(4.16 ± 0.03) – (12.4 ± 0.2)] × 10^3 for those with RH^- ion. Activation parameters for the oxidation have been reported and compared with those of the oxidation of triose reductone with peroxodisulfate ion. A probable mechanism is proposed for the reaction.

YASUO ABE, TAKAAKI DOHMARU, HIDEO HORII et SETSUO TANIGUCHI. Can. J. Chem. **63**, 1005 (1985).

Opérant en milieu acide ($[H^+]$ = 0,02 à 0,1 *M* (1 *M* = 1 mol dm^{-3})) et à diverses températures allant de 10 à 30°C, on a effectué des études cinétiques sur l'oxydation du dihydroxy-2,3 propène-2 al (triose de la réductone, RH_2) par l'hexacyanoferrate(III), $[Fe(CN)_6]^{3-}$. On a ajusté la force ionique du milieu (*I* = 0,04 à 0,4 *M*) en utilisant du perchlorate de sodium. Les constantes de vitesse du second ordre (en M^{-1} s^{-1}) se situent entre 0,86 ± 0,06 et 2,83 ± 0,14 pour les réactions de l'hexacyanoferrate(III) avec RH_2 et entre (4,14 ± 0,03) × 10^3 et (12,4 ± 0,2) × 10^3 pour celles avec l'ion RH^-. On rapporte les paramètres d'activation pour l'oxydation et on les compare avec ceux obtenus pour l'oxydation du triose de la réductone par l'ion peroxodisulfate. On propose un mécanisme probable pour la réaction.

[Traduit par le journal]

Triose reductone (RH_2) has been well known for its reducing properties in aqueous solutions. The reductone is the simplest in structure of the compounds having an enediol group; the physiologically important L-ascorbic acid is a typical compound of this structure. Thus kinetic studies on the reaction of triose reductone would help to clarify the mechanisms of the physiological activities of enediol compounds. It has been reported that the rates of oxidation of RH_2 by molecular oxygen (1) and peroxodisulfate ($S_2O_8^{2-}$) (2) are dependent on the hydrogen ion concentrations. In the latter case, the mechanism was interpreted in terms of the successive one-electron transfers, while the rate constant for the triose reductone radicals was not determined. The existence of the triose reductone free radicals has been confirmed by pulse radiolysis of the reductone (3). Thus it is of current interest to get any kinetic information on the electron transfer reaction involving $RH^{\cdot}$. Hexacyanoferrate(III) is a typical one-electron oxidizing agent (4) and is often used in a model reaction of biologically important cytochrome c. In the present paper, we make kinetic studies of the oxidation reactions of RH_2 with hexacyanoferrate(III) in aqueous acidic solution, present the most probable reaction mechanism, and give the rate constants of some of the elementary reactions involved.

Experimental

Materials

Triose reductone was prepared and purified by the method described in the literature (5). Sodium perchlorate, potassium hexacyanoferrate(III), and potassium hexacyanoferrate(II) of analytical grade (E. Merck) were used without further purification. All the other chemicals were guaranteed reagents of the Wako Pure Chemicals Co. Ltd.

Reaction solution

The hexacyanoferrate(III) solution was prepared by dissolving 65.9 mg of the solid in 250 cm^3 of a dilute sulfuric acid solution containing 0.5 mmol of disodium dihydrogen ethylenediaminetetraacetate (EDTA) and a given weight of sodium perchlorate. EDTA was added to complex heavy metal ions which catalyse the oxidation of triose reductone (1) and which react with hexacyanoferrate(III) ion to produce complex precipitates. The triose reductone solution was prepared by dissolving 31.0 mg of the compound in 30 cm^3 of the same acid solution as described above. It was then saturated with argon (high-purity argon gas was bubbled through the solution to remove the dissolved oxygen).

Kinetic method

The hexacyanoferrate(III) solution (2.9 cm^3) was transferred into a gas-tight optical cell and argon gas was bubbled through the solution by means of injection needles and a septum cap for 0.5–1 h. The reaction was started by adding the triose reductone solution (0.1 cm^3). The temperature of the reaction solution was kept constant during the reaction. Kinetic data were obtained by following the decreasing absorption of hexacyanoferrate(III) at 420 nm (neither triose reductone nor hexacyanoferrate(II) absorbed light at this wavelength under the reaction conditions). The acidity was kept constant at a value in the range of 0.01–0.05 *M* in sulfuric acid. The temperature was controlled by circulating thermostated water around the cell housing. The pH values of the triose reductone solution in the course of the measurement of the pK_a values were corrected for various ionic strengths. The activity coefficients f_i for protons at varying ionic strengths (I) were obtained by using $\log f_i = -0.358 z_i^2 I^{1/2}/(1 + 10^8 a_i \times 0.2325 I^{1/2})$ with $10^8 a_i = 9$ and $z_i = 1$ (6). The activity coefficients used in this paper were 0.89 (0.04), 0.85 (0.1), 0.83 (0.2), and 0.80 (0.4): the ionic strength is given in parentheses.

Results and discussion

Stoichiometry

By maintaining a slight excess of oxidizing agent and by performing spectrophotometric measurements at 420 nm, the following stoichiometric equation was found:

[1] $2Fe(III) + RH_2 \rightarrow 2Fe(II) + DR + 2H^+$

where RH_2 and DR represent triose reductone and dehydroreductone, 1,2,3-propane-trione, respectively.

Dissociation constant of triose reductone

The pK_a values of the first dissociation of triose reductone (RH_2) for the equilibrium, $RH_2 \rightleftharpoons RH^- + H^+$, were determined by the spectrophotometric method reported previously (1) at an ionic strength of 0.4 *M* (with the temperature (°C) in paren-

TABLE 1. Second-order rate constants, $k_0(M^{-1}\ s^{-1})$, for the reaction between triose reductone and hexacyanoferrate(III)[a]

Temperature (°C)	$I(M)$	$[H^+]$ (M) 0.1	0.04	0.025	0.02
10	0.4	1.56±0.10	2.72±0.03	3.79±0.15	4.44±0.14 (4.48±0.02)[b]
15	0.4	2.16±0.11	3.61±0.16	5.09±0.20	5.83±0.09 (5.92±0.02)[b]
20	0.4	2.73±0.12	4.63±0.22	6.93±0.18	7.64±0.11 (7.77±0.03)[b]
25	0.4	3.59±0.06 (3.52±0.02)[b]	5.89±0.13	8.52±0.26	9.88±0.11 (9.82±0.05)[b]
30	0.4	4.80±0.17	8.09±0.25	11.2±0.2	13.0±0.2 (12.8±0.1)[b]
25	0.04	2.39±0.04	3.11±0.11	3.75±0.19	4.34±0.10
25	0.1	2.68±0.05 (2.63±0.03)[b]	3.76±0.14	5.11±0.15	5.50±0.02
25	0.2	3.14±0.06	4.74±0.11	6.49±0.12	7.70±0.20

[a]Initial concentrations: $K_3[Fe(CN)_6]$, 7.743×10^{-5} M; triose reductone, 3.872×10^{-5} M.
[b]Additional 7.743×10^{-5} M of $K_4[Fe(CN)_6]$ was dissolved.

theses): 4.95 (10), 4.91 (15), 4.86 (20), 4.82 (25), and 4.78 (30), and at 25°C (with the I in parentheses): 4.95 (0.04), 4.88 (0.1), 4.84 (0.2), and 4.82 (0.4).

Kinetics of the reaction

When pseudo-first-order conditions, $[TR]_0/[Fe(III)]_0 = 10$, were adopted, plots of log A_t vs. t were linear to at least 80% completion, where $[TR] = [RH_2] + [RH^-]$ and A_t indicates the absorbance of $K_3[Fe(CN)_6]$ at 420 nm at a certain time (t) of reaction. When second-order conditions, $[Fe(III)]_0/[TR]_0 = 2$, were adopted, second-order plots, $[Fe(III)]^{-1}$ vs. t, were also linear for 75% completion; some examples of the plots are given in Fig. 1. Thus, the following empirical rate law and the relationship between $[Fe(III)]^{-1}$ and t can be suggested, respectively:

$$[2]\quad -1/2\mathrm{d}[Fe(III)]/\mathrm{d}t = k_0[Fe(III)][TR]$$

$$[3]\quad [Fe(III)]^{-1} = k_0 t + [Fe(III)]_0^{-1}$$

Values of k_0 obtained at various temperatures, ionic strengths, and acidities are collected in Table 1.

The second-order rate constants k_0 increase with decreasing acidity. The conventional treatment of the reactions involving the acid dissociation equilibrium gives k_0 as in eq. [4],

$$[4]\quad k_0 = k_1 + (k_2 - k_1)K_a/([H^+] + K_a)$$

where k_1 and k_2 are the rate constants of the reactions of RH_2 and RH^- with Fe(III), respectively. In the present experiment, $[H^+]$ were much larger than K_a ($K_a = 10^{-5}$). Therefore, eq. [4] can be simplified to eq. [5],

$$[5]\quad k_0 = k_1 + (k_2 - k_1)K_a/[H^+]$$

The plots of k_0 vs. $[H^+]^{-1}$ showed a linear relationship; the plots are given in Figs. 2 and 3. The k_1 and k_2 values are listed in Table 2.

Effect of the reduced form

Some kinetic runs were performed in the presence of reduced species of metal complex, namely, hexacyanoferrate(II), in the same concentration as the corresponding oxidized form. No significant effect was observed on the calculated rate constants (see the values in parentheses in Table 1).

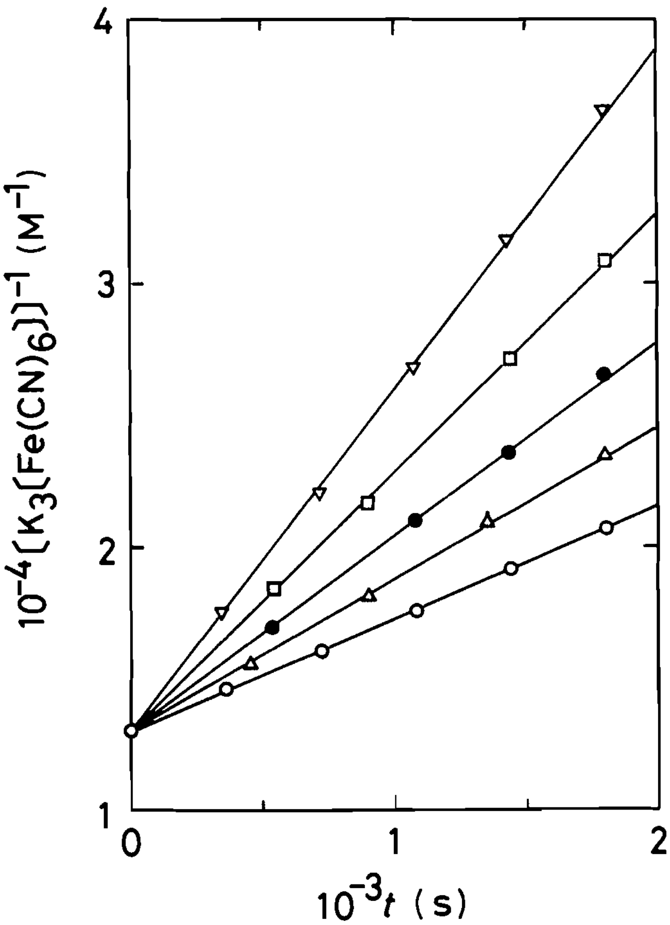

FIG. 1. Relation between 10^{-4} $[Fe(III)]^{-1}$ and time for the reduction of Fe(III) with triose reductone at I = 0.4 and various temperatures. ○: 10°C, △: 15°C, ●: 20°C, □: 25°C, ▽: 30°C.

Effect of ionic strength

In order to investigate the ionic-strength effect, kinetic runs were performed at 25°C with increasing addition of $NaClO_4$ up to 0.40 M. Values of second-order rate constants obtained for this portion of the investigation are listed in Table 2 and are

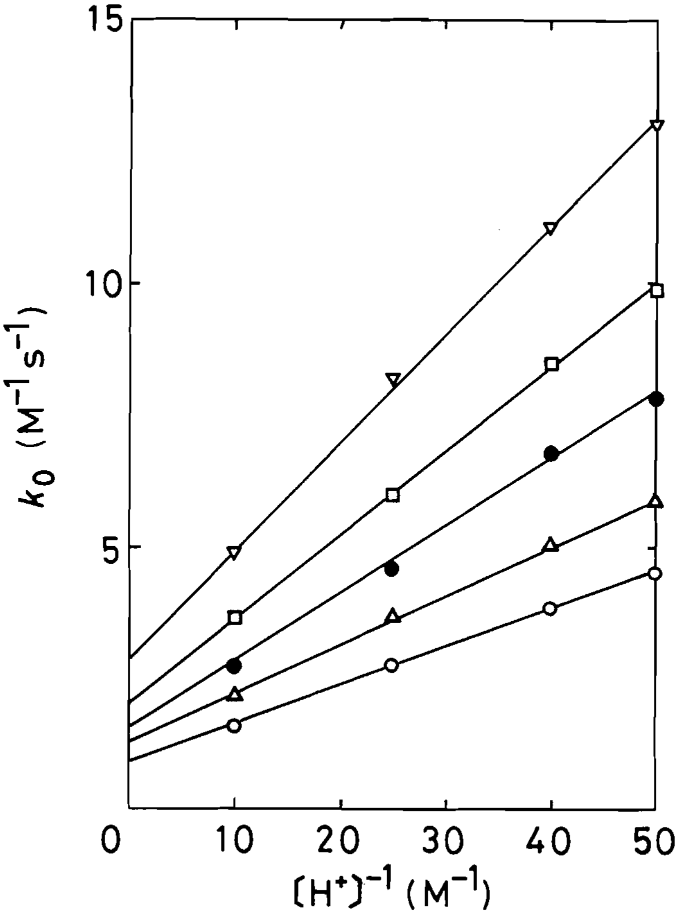

FIG. 2. Relation between k_1 and $[H^+]^{-1}$ for the oxidation of triose reductone with $K_3[Fe(CN)_6]$ at $I = 0.4$ and various temperatures. Each plot denotes the mean value of three experimental data. ○: 10°C, △: 15°C, ●: 20°C, □: 25°C, ▽: 30°C.

observed to increase with increasing ionic strength, as would be expected for reaction of the triose reductone monoanion with negatively charged oxidizing species.

Davies has normalized a great deal of kinetic data relating to specific cation effects by considering the effect of ion-pair formation between the specific cation and the reactants on the ionic strength or some function of the ionic strength by using the following equation (7),

$$[6] \quad \log k = \log k_0 + 2Az_az_bF(I)$$

$$F(I) = I^{1/2}/(1 + I^{1/2}) - 0.2I$$

where A is the Debye–Hückel coefficient, z_a and z_b are the charges on the reactant, and k_0 is the bimolecular rate constant at zero ionic strength. Swinehart applied Davies' equation to the reaction of hexacyanoferrate(III) with sulfite in the presence of sodium chloride and obtained a good relationship between rate constant and ionic strength (8).

The plots of log k_2 vs. $F(I)$ showed a straight line, with the relationship $\log k_2 = 3.17 \pm 0.05 + (2.75 \pm 0.21)F(I)$. This dependence is expected for the reaction between two ions of the same sign: the positive value of 2.75 is in good agreement with that of $z_az_b = 3.0$.

The fact that the ionic-strength dependence of rate constant in the reaction of triose reductone with peroxodisulfate in the presence of sodium perchlorate agreed with the Debye–Hückel equation (ref. 2) suggests that neither triose reductone anion

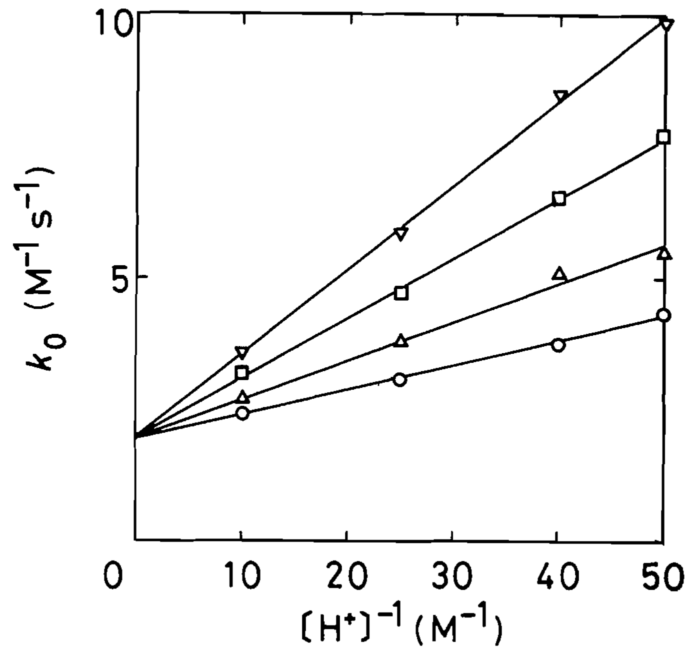

FIG. 3. Relation between k_1 and $[H^+]^{-1}$ for the oxidation of triose reductone with $K_3[Fe(CN)_6]$ at 25°C and various ionic strengths. Each plot denotes the mean value of three experimental data. ○: 0.04 M, △: 0.1 M, □: 0.2 M, ▽: 0.4 M.

TABLE 2. Temperature and ionic-strength dependence of rate constants and kinetic parameters

Temperature (°C)	$I(M)$	k_1 (M^{-1} s^{-1})	$10^{-3}k_2$ (M^{-1} s^{-1})
10	0.4	0.86±0.06	6.45±0.17
15	0.4	1.26±0.08	7.55±0.21
20	0.4	1.46±0.12	9.36±0.27
25	0.4	1.95±0.10	10.6±0.0
30	0.4	2.83±0.14	12.4±0.2
25	0.04	1.95±0.10	4.16±0.03
25	0.1	1.95±0.10	5.60±0.04
25	0.2	1.95±0.10	7.90±0.03
$\Delta H^{\ddagger}$ (kJ mol^{-1})		38±3	21±1
$\Delta S^{\ddagger}$ (J deg^{-1} mol^{-1})		−112±11	−97±3

nor peroxodisulfate anion form an ion pair. Therefore, it is suggested that hexacyanoferrate(III) forms an ion pair with sodium cation as indicated in eq. [7], although no empirical data has been reported in the literature.

$$[7] \quad [Fe(CN)_6]^{3-} + Na^+ \rightleftharpoons Na[Fe(CN)_6]^{2-}$$

The association constant of hexacyanoferrate(III) and potassium cation was estimated to be about 20 at 25°C (9). Assuming that a maximum value of the equilibrium constant for eq. [7] is 10^1 and that the activity coefficient of the ion pair is the same as for $[Fe(CN)_5NO]^{2-}$ (6), the fraction of the ion pair is expected to be less than 20% at the present reaction conditions.

Temperature dependence

The activation parameters corresponding to the specific rate

[1]Equilibrium constants for sodium ion-pair formation are usually less than half of those for potassium ion.

constants at $I = 0.4$ were calculated from the slope of the Eyring plot ($\ln k/T$ vs. $1/T$) and listed in Table 2. The absolute values of both enthalpy and entropy of activation for RH^- are less than those for the oxidation with peroxodisulfate ($\Delta H^\ddagger = 37 \pm 1$ kJ mol^{-1} and $\Delta S^\ddagger = -123 \pm 5$ J deg^{-1} mol^{-1}) (2) and also less than those for the oxidation of L-ascorbic acid with hexacyanoferrate(III) ($\Delta H^\ddagger = 45.2$ kJ mol^{-1} and $\Delta S^\ddagger = -166.5$ J deg^{-1} mol^{-1}) (10).

Mechanism of the reaction

From the results of ionic strength, it is suggested that the resulting ion pair has less oxidizing ability than hexacyanoferrate(III). Therefore, a mechanism consistent with the present experimental observation can now be written (eqs. [8]–[13]). The role of Na^+ has been ignored in the discussion that follows.

$$[8] \quad RH_2 \overset{K_a}{\rightleftharpoons} RH^- + H^+$$

$$[9] \quad [Fe(CN)_6]^{3-} + RH_2 \xrightarrow{k_1} RH^\cdot + [Fe(CN)_6]^{4-} + H^+$$

$$[10] \quad [Fe(CN)_6]^{3-} + RH^- \xrightarrow{k_2} RH^\cdot + [Fe(CN)_6]^{4-}$$

$$[11] \quad RH^\cdot \overset{K_2}{\rightleftharpoons} R^{-\cdot} + H^+$$

$$[12] \quad [Fe(CN)_6]^{3-} + RH^\cdot \xrightarrow{k_3} DR + H^+ + [Fe(CN)_6]^{4-} + H^+$$

$$[13] \quad [Fe(CN)_6]^{3-} + R^{-\cdot} \xrightarrow{k_4} DR + [Fe(CN)_6]^{4-}$$

The presence of free radicals in the oxidation of triose reductone was confirmed by esr measurement (11) and kinetic considerations (2). The linearity of pseudo-first-order plots and the absence of an effect of the presence of reduced species indicate that no reverse reactions are kinetically relevant.

Considering the K_2 value, which is estimated to be about 1.5 by us (unpublished result) at the equilibrium eq. [11], triose reductone free radicals exist in both forms $RH^\cdot$ and $R^{-\cdot}$ under the present conditions. Although absolute values of the rate constants k_3 and k_4 are unknown, the following experimental rate law [14] suggests that $k_3, k_4 \gg k_1, k_2$.

$$[14] \quad -1/2\, d[Fe(III)]/dt = (k_1 + k_2K_a/[H^+])[Fe(III)][TR]$$

Another mechanism for the consumption of triose reductone free radicals by disproportionation is also possible (3).

$$[15] \quad 2RH^\cdot \xrightarrow{k_5} RH_2 + DR$$

$$[16] \quad 2R^{-\cdot} + 2H^+ \xrightarrow{k_6} RH_2 + DR$$

If the radicals were eliminated only by the disproportionation, the rate law of the decrease of hexacyanoferrate(III) must be according to eq. [17].

$$[17] \quad -d[Fe(III)]/dt = (k_1 + k_2K_a/[H^+])[Fe(III)][TR]$$

The rate constant of the disproportionation was reported as $2 \times 10^8\ M^{-1}\ s^{-1}$ at pH 9.6 (3). Although the rate constant is much larger than the values of k_1 and k_2 even when the reaction conditions are different, the concentration of radicals at steady state is very small. Therefore, eqs. [15] and [16] can be neglected for the reaction mechanism of the oxidation of triose reductone, even though they might become important after 85% completion.

Acknowledgements

The authors wish to express their thanks to Professor S. Yamabe and Dr. T. Minato of Nara University of Education for their helpful discussions.

1. Y. Abe, H. Horii, S. Taniguchi, K. Kamai, and M. Takagi. Bull. Chem. Soc. Jpn. **56**, 467 (1983).
2. Y. Abe, H. Horii, and S. Taniguchi. Bull. Chem. Soc. Jpn. **57**, 222 (1984).
3. H. Horii, Y. Abe, S. Taniguchi, S. Maeda, and T. Watanabe. Chem. Lett. 1313 (1983).
4. B. S. Thyagarajan. Chem. Rev. **58**, 439 (1958).
5. H. v. Euler and C. Martius. Justus Liebigs Ann. Chem. **505**, 73 (1933).
6. J. Kielland. J. Am. Chem. Soc. **59**, 1675 (1937).
7. C. W. Davies. *In* Progress in reaction kinetics. Vol. 1. *Edited by* G. Porter. Pergamon Press, Oxford. 1961. pp. 163–186.
8. J. H. Swinehart. J. Inorg. Nucl. Chem. **27**, 2313 (1967).
9. J. C. James and C. B. Monk. Trans. Faraday Soc. **46**, 1041 (1950).
10. U. S. Mehrotra, M. C. Agrawal, and S. P. Mushran. J. Phys. Chem. **73**, 1996 (1969).
11. I. Yamazaki and L. H. Piette. Biochim. Biophys. Acta, **77**, 47 (1963).

Relaxation and related ¹H nmr studies on "asperlin." Configuration and conformation of the epoxypropyl side-chain

PHOTIS DAIS AND ARTHUR S. PERLIN
Department of Chemistry, McGill University, Montreal, P.Q., Canada H3A 2A7
Received August 7, 1984

PHOTIS DAIS and ARTHUR S. PERLIN. Can. J. Chem. **63**, 1009 (1985).

Monoselective and biselective spin-lattice relaxation rates, together with nOe experiments, have been used to examine the configuration and conformation of the epoxypropyl side-chain of "asperlin" (**1**) in benzene solution. The data confirm earlier evidence that the oxirane ring is *trans*, and indicate that **1** is the 6*R*,7*S* diastereomer. Moreover, it is shown that in the most probable conformation of the side-chain about the C-5,C-6 bond, H-5 and H-6 are *anti*.

PHOTIS DAIS et ARTHUR S. PERLIN. Can. J. Chem. **63**, 1009 (1985).

Dans le but d'examiner la configuration et la conformation de la chaîne latérale époxypropyle de l' "asperline" (**1**) en solution dans le benzène, on a utilisé des vitesses de relaxation spin-réseau mono et bi-sélectives ainsi que des expériences d'effet nucléaire Overhauser. Les données confirment les indications antérieures à l'effet que le cycle oxiranne est *trans* et elles indiquent que le composé **1** est le diastéréomère 6*R*,7*S*. De plus, on démontre que dans la conformation la plus probable de la chaîne latérale autour de la liaison C-5,C-6, les hydrogènes H-5 et H-6 sont *anti*.

[Traduit par le journal]

Introduction

The structure of 5-acetoxy-5,6-dihydro-6-(1,2-epoxypropyl)-2-pyrone (**1**) ("asperlin"), a metabolite of *Aspergillus nidulans* (1), has been studied (2, 3) by ¹H and ¹³C nmr spectroscopy, using reference compounds derived mainly from carbohydrates of known stereochemistry, as well as by chemical synthesis (3). It was concluded that the pyrone ring of **1**

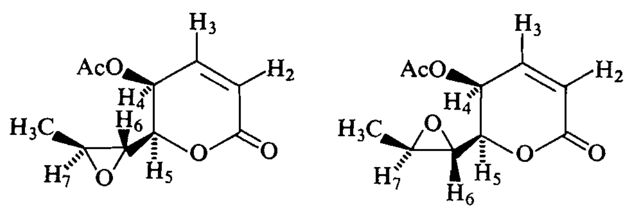

a *b*

1

assumes a semi-planar conformation, that the 4,5-substituents of the ring[1] have the L-*threo* configuration, and also that the exocyclic epoxypropyl moiety is *trans*. The present paper describes spin-lattice relaxation and nuclear Overhauser enhancement (nOe) measurements, carried out primarily to examine the configuration of the oxirane ring (i.e., as in diastereoisomer **1***a* or **1***b*),[2] as well as the conformation of the epoxypropyl side-chain.

Proton monoselective spin-lattice relaxation and nOe data, and (or) mono- and biselective experiments (4), provide a rigorous approach to the structure of molecules in solution, without the need of reference compounds. Obviously, this offers practical advantages when model compounds are not readily available or easily synthesized. The principle inherent in applying measurements of proton relaxation rates and nOe is the dependence of pairwise dipolar interactions on interatomic distances, viz., these interactions decrease approximately as a simple sixth power of the interatomic distance (5). Hence, by calculation of the pertinent interproton dimensions for a given molecule, structural and conformational features may be determined. Applied to asperlin, this general approach has afforded information about the most probable orientation of the epoxypropyl side-chain around the C-5,C-6 bond, and also about which of the two possible diastereoisomers (**1***a* or **1***b*) corresponds to the natural product.

[1]In keeping with the numbering used earlier (3) in correlating the stereochemistry of asperlin with that of carbohydrate models, the carbonyl carbon of **1** is herein designated C-1, and the α-proton, H-2.

[2]It has not proven feasible to determine the structure of asperlin by X-ray crystallography, because the only form of the compound available consists of twinned crystals (G. Donnay, private communication).

Experimental

¹H and ¹³C nuclear magnetic resonance spin-lattice relaxation and nOe measurements

All of the nmr experiments were conducted at 400 MHz (¹H) and 100 MHz (¹³C) with a Bruker-400 spectrometer, at 20°C. A 0.15 *M* solution of asperlin in benzene-d_6 was used for the ¹H experiments, and a 0.5 *M* solution in benzene-d_6 for the ¹³C experiments. Each sample was carefully degassed by using 5 to 6 "freeze–pump–thaw" cycles, following which the nmr tube was sealed. ¹³C spin-lattice relaxation times and ¹H nonselective relaxation rates were measured by the two-pulse inversion recovery technique. Details of the procedure used in the nonselective relaxation and nOe experiments are given elsewhere (6, 7). Statistical errors in the fit of semilogarithmic plots were within ±2% and ±5% for ¹H and ¹³C nmr relaxation rates.

Monoselective relaxation rates for H-4 to H-7 protons were measured by using a long (15–20 ms), weak pre-irradiation pulse which selectively inverted the required resonance frequency. The selective 180° pulse was provided by the decoupler channel. In performing bi-(double) selective experiments the computer of the spectrometer was used to control a train of two selective 180° pulses provided consecutively by the decoupler at the resonance frequencies of protons H-5 and H-7 and (or) H-4 and H-7. The time interval between the two pulses (~200 ns) and the total duration of the two pulses (~30 ms) were negligibly small compared to the long relaxation times of these protons, ensuring thereby the effectiveness of the experiment, i.e., no significant relaxation during excitation. Typical mono- and biselective inversions are shown in Fig. 1. Mono- and biselective partially relaxed spectra were obtained by the inversion recovery method. Typically 20 to 30 τ values covering the range ~0–2T_1 were used for the initial rate approximation. The total magnetization intensity for each resonance was processed by a two-parameter linear regression analysis to obtain selective relaxation rates. Each relaxation rate value presented is an average of 2 or 3 separate measurements. The statistical error and reproduciblity of the various relaxation rates were better than ±3% and ±5%, respectively.

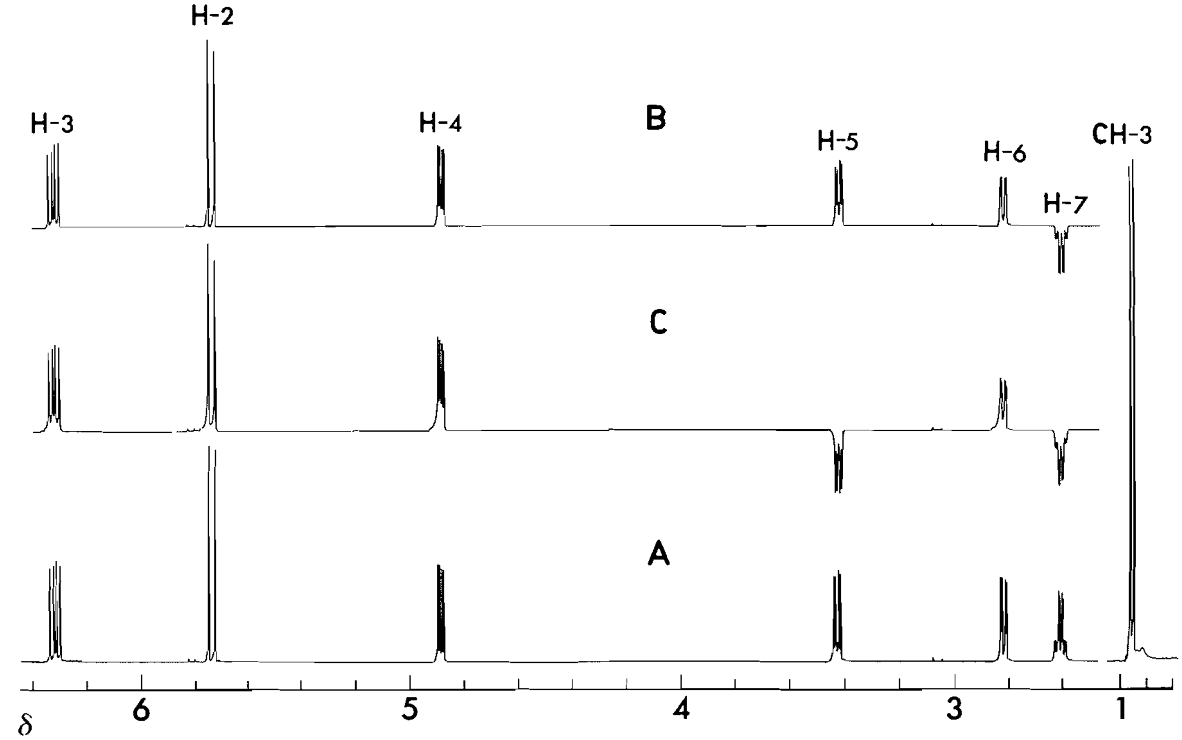

FIG. 1. (A) Normal ^{1}H nmr spectrum of **1** benzene-d_6 at 400 MHz; (B) representative ^{1}H monoselective spin-lattice relaxation experiment with **1**; the H-7 signal was inverted by a selective 180° pulse (~15 ms), τ = 0.01 s; (C) representative ^{1}H biselective spin-lattice relaxation experiment in which two signals, H-5 and H-7, were inverted simultaneously by two consecutive selective 180° pulses (~15 ms each) provided by the decoupler channel, τ = 0.1 s.

TABLE 1. Proton and carbon-13 nuclear magnetic resonance data for "asperlin"[a]

Proton	δ^1H[b]	$^3J_{\text{H–H}}$[c]	R_1^{ns}[d]	R_1^{s}[e]	$R_1^{\text{ns}}/R_1^{\text{s}}$	R_1^{bs}[f]	Carbon	δ^{13}C[b]	R_1[g]
H-2	5.71	$J_{\text{H-2,H-3}}$ = 9.72	187	—	—	—	C-1	161.05	—
							C-2	124.78	0.57
H-3	6.30	$J_{\text{H-3,H-4}}$ = 5.69	255	—	—	—	C-3	140.35	0.51
H-4	4.87	$J_{\text{H-4,H-5}}$ = 2.81	288	189	1.52	204	C-4	62.23	0.51
H-5	3.40	$J_{\text{H-5,H-6}}$ = 6.85	285	196	1.45	213	C-5	78.38	0.49
H-6	2.79	$J_{\text{H-6,H-7}}$ = 1.95	215	142	1.51	—	C-6	55.14	0.38
H-7	2.58	$J_{\text{H-7,CH}_3}$ = 5.20	263	178	1.48	194	C-7	53.85	0.39
CH_3	0.93	—	—	—	—	—	CH_3	16.90	0.38

[a]0.15 M and 0.5 M solutions in benzene-d_6 for ^{1}H and ^{13}C experiments, respectively. The chemical shifts for the acetyl group are not shown.
[b]In ppm relative to TMS.
[c]Coupling constants in Hz.
[d]Nonselective ^{1}H spin-lattice relaxation rates in ms^{-1}.
[e]Monoselective ^{1}H spin-lattice relaxation rates in ms^{-1}.
[f]Double-selective ^{1}H spin-lattice relaxation rates in ms^{-1}.
[g]Carbon-13 spin-lattice relaxation times in s. The measured ^{13}C nOe values for all protonated carbons were 3.00 ± 0.15.

Results and discussion

At 400 MHz, with benzene-d_6 as the solvent, the ^{1}H nmr spectrum of **1** (Fig. 1A) is completely resolved. Whereas at lower field (3) the H-6 and H-7 signals overlapped, these signals now appear in slightly distorted form as a doublet of doublets and a quartet of doublets, respectively. Analysis of these signals, together with those of the methyl protons as an ABX_3 spectrum, gave the following parameters: J_{AB} = 1.95 Hz, J_{AX} = 0 Hz, J_{BX} = 5.20 Hz, ν_A = 559.17 Hz, ν_B = 516.84 Hz, and ν_X = 185.83 Hz, where A = H-6, B = H-7, and X_3 = CH_3. Proton chemical shifts and coupling constants are shown in Table 1. These nmr parameters, along with the ^{13}C chemical shifts, are in accord with previous (2, 3) interpretations of the stereochemistry of **1**.

The nonselective spin-lattice relaxation rates (R_1^{ns}) also shown in Table 1, give complementary information about the stereochemstry of **1**. For the ring protons, it can be seen that the R_1^{ns} values for H-4 and H-5 are the same, whereas the relaxation rates of H-2 and H-3 are lower by ~35% and 11%, respectively, and H-2 relaxes ~27% more slowly than H-3. Inspection of possible inter-ring relaxation pathways cannot satisfactorily explain these relaxation rates. For instance, H-3 and H-4 would be expected to have the fastest relaxation rates, due to the *gauche* and eclipsed disposition of their neighbouring protons. Moreover, the primary relaxation pathways for H-2 and H-5 are provided by H-3 and H-4, respectively, and al-

TABLE 2. ^1H nuclear Overhauser enhancement measurements on "asperlin" (**1**)

Proton irradiated	Proton observed				
	H-4	H-5	H-6	H-7	CH_3[a]
H-4	—	0.122 (±0.006)	0.025 (±0.013)	0.063 (±0.008)	—
H-5	0.118 (±0.011)[b]	—	—	0.086 (±0.010)	—
H-6	—	—	—	−0.080 (±0.008)	—
H-7	0.075 (±0.012)	0.063 (±0.007)	−0.051 (±0.010)	—	—
CH_3[a]	—	—	0.092 (±0.006)	0.108 (±0.004)	—

[a]Methyl of epoxypropyl group. Irradiation of the acetoxymethyl protons did not significantly affect the other protons (including H-2 and H-3).
[b]Values in parentheses are standard deviations based on the measured intensities.

though the relative proximity of each pair of protons is nearly the same, the relaxation rate of H-5 is ~35% faster than that of H-2. In part, these variations reflect the sensitivity of proton relaxation rates to changes in the rates of anisotropic modes of reorientation of **1**. That is, ^{13}C spin-lattice relaxation measurements demonstrate that **1** tumbles anisotropically in benzene, inasmuch as the ^{13}C R_1 value for C-2 (Table 1) is smaller than those of the other ring carbons, which are nearly the same within experimental error. This difference, ~14%, indicates that **1** tumbles anisotropically about a preferential axis of rotation, which forms a small angle with the C-2, H-2 relaxation vector. The theory of dipole−dipole relaxation in anisotropically tumbling molecules shows (8) that relaxation vectors which lie on, or parallel to, the major axis of rotation are more efficient than vectors at an angle to this axis. It follows that the H-3,H-4 pathway is expected to be more efficient that those of H-2,H-3 and H-4,H-5. In addition, however, the fact that the relaxation rates of H-4 and H-5 are faster than for H-3 suggests that the two former protons interact with protons of the epoxypropyl moiety. Similarly, the methyl protons, which provide a primary relaxation pathway for vicinal H-7, should have an influence on H-6 commensurate with a *trans* configuration (2, 3) for the epoxide, as compared to a *cis* configuration in which the methyl protons and H-6 would be further apart. These considerations have a bearing on such questions as the configuration and conformation of this side chain, because of their relationship to molecular dimensions, as will now be discussed.

Interproton distances may be measured effectively from combinations of mono- (R_1^s) and biselective (R_1^{bs}) spin-lattice relaxation rates and nOe values. The experimentally determined interproton distances may then be compared with molecular models in order to assess stereochemical possibilities. Theory shows (4, 5, 9) that internuclear distances between spins i and j can be measured by combining monoselective relaxation rates and nOe values and (or) mono- and biselective relaxation rates, i.e.,

$$[1]\quad (r_{ij})^6 = \frac{0.5\,\gamma_i^2\gamma_j^2\hbar^2}{R_{1,i}^{s}\cdot f_i(j)}$$

and

$$[2]\quad R_{1,i}^{bs} = R_{1,i}^{s} + \sigma_{ij} \text{ and (or) } R_{1,j}^{bs} = R_{1,j}^{s} + \sigma_{ji}$$

where $\sigma_{ij} = \sigma_{ji}$ the cross-relaxation term given by

$$[3]\quad \sigma_{ij} = \frac{0.5\,\gamma_i^2\gamma_j^2\hbar^2}{(r_{ij})^6}\,\tau(ij)$$

$\tau(ij)$ is the rotational correlation time of the internuclear vector r_{ij}, $f_i(j)$ is the nOe value of spin i upon irradiation of spin j, and $R_{1,i}^2$, $R_{1,i}^{bs}$ are the mono- and biselective spin-latice relaxation rates of spin i, respectively. In the present study, intermolecular dipolar contributions were kept to a minimum by restricting the relaxation measurements to a degassed, dilute solution. Other competing relaxation mechanisms (e.g., spin-rotation, etc.) were found to be absent. This is demonstrated by the ratios of the nonselective rates to monoselective rates for the pertinent protons (Table 1), which are very close to the theoretical value 1.5 (5, 9) confirming the preponderance of dipole−dipole interactions in the relaxation of these protons. Problems associated with nonexponential decay of the magnetization vectors in the relaxation experiments (4, 9) were avoided by confining measurements to "initial" relaxation rates (4, 5, 9). Hence, three factors affecting relaxation rates, and thereby calculated interproton distances, were kept to a minimum.

Another factor to be assessed is motional anisotropy. Equations [1]−[3] hold under isotropic reorientation of the r_{ij} vector. In this case $\tau(ij)$ can be measured from ^{13}C spin-lattice relaxation experiments, assuming that the proton−proton correlation time is the same as the correlation time of the $^{13}C-^1H$ vector. For asperlin, the overall reorientation is anisotropic as evidenced by the ^{13}C T_1 values of the pyrone ring carbons (Table 1). The $\tau(ij)$ correlation time is, in fact, an effective correlation time containing contributions from the correlation times of molecular reorientation about the principle axes of the diffusion tensor. A study (10) of the motional behavior of **1** indicates that its rotational dynamics can be represented adequately by the diffusion of a prolate ellipsoid with the major axis passing through the C-2,H-2 bond. The correlation times for rotations about, and perpendicular to, the major axis were found to be $\tau_\parallel = 30.3 \pm 1.7$ ps and $\tau_\perp = 23.5 \pm 1.2$ ps. This ~22% difference in the correlation times for parallel and perpendicular rotations about the major axis leads to a reduction in the error in the calculated distances by a factor of six (see eqs. [1] and [3]). Therefore the estimated error in the calculations introduced by molecular anisotropy is ~4%, which is too small to invalidate the quantitative determination of internuclear distances.

By using the relaxation parameters in Table 1, the nOe values in Table 2, and eqs. [1]−[3], interatomic distances were calculated for the proton pairs H-4,H-6 and H-5,H-7 (Table 3). The other data in Table 3 are values of interatomic distances derived from stereochemical models[3] of the two diastereoisomeric forms of the *trans* epoxide (**1**a and **1**b), as well as those of the *cis* isomer, in which O-4 and H-5 are *anti* (3), and the dihedral angle between H-5 and H-6 is 180 ± 30°. This latter range is commensurate with the dihedral angle indicated by $^3J_{5,6}$ (6.85 Hz, Table 1), by reference to the Karplus relationship (11), whereas the alternate value of 0 ± 30° can be rejected because, as shown by the lack of a mutual nOe response between H-5 and H-6 (Table 2), these protons cannot have a *syn* relationship.

[3]HGS Molecular Models (Benjamin/Maruzen), using the "bent bonds" furnished to construct the oxirane ring of **1**.

TABLE 3. Interproton distances (Å) for "asperlin" from molecular models and nuclear magnetic resonance data

	Models					
	trans epoxide		*cis* epoxide			
Protons	**1***a*	**1***b*	**2***a*[b]	**2***b*[b]	R_1^s and nOe[a]	R_1^s and R_1^{bs} [a]
H-4,H-7	3.04−1.75	4.20−3.67	3.36−3.00	4.90−4.37	2.92±0.13 2.81±0.09	2.79±0.10
H-5,H-7	2.07−2.70	2.66−1.89	3.29−3.68	3.68−3.32	2.88±0.11 2.78±0.08	2.73±0.09
H-4,H-5	2.38[c]				2.60±0.07	2.58±0.08

[a]The limits of error cited are the propagated errors in the various experimental quantities, including the error introduced by motional anisotropy.
[b]Corresponding to **1***a* and **1***b*, respectively.
[c]See footnote 3.

The interatomic distances taken from molecular models are regarded as approximations only. Although the structure of oxirane has been determined (12), we are uncertain as to dimensions of the angles and distances in the disubstituted oxirane structure comprising carbons 5 to 8 of **1**. With this reservation, a comparison of the experimentally determined values for the distance between H-4 and H-7 (~2.8 Å, Table 3), with those expected for the various diastereoisomeric forms, shows that the experimental value falls within the range for the two extreme orientations in **1***a*, whereas it lies well outside the range of values for the other *trans* isomer (**1***b*) and for both *cis* forms. Hence, the nmr measurements provide an independent proof that, as proposed earlier (2, 3), the epoxide ring of **1** is *trans*. An analogous comparison of distances between H-5 and H-7 finds no difference between **1***a* and **1***b* although in both instances the dimensions from models nearly overlap[4] the experimental value of ~2.8 Å.

Structures **1***a* and **1***b* may be compared in a different manner. According to the nmr measurements on **1**, H-4 and H-5 are equidistant from H-7 (~2.8 Å). By rotating the epoxypropyl side chain in a molecular model of **1***a* around the C-5,C-6 bond, so as to locate H-4, H-5, and H-7 in that fashion, H-6 becomes oriented *anti* with respect to H-5. This is in accord with the preceding comments on the significance of $^3J_{5,6}$. In marked contrast, however, when the analogous operation is applied to a model of **1***b*, the H-5,H-6 dihedral angle is found to be around 90°, i.e., requiring $^3J_{5,6} \simeq 0$ Hz.

Overall, then, the present findings are more fully compatible with structure **1***a* – the 6*R*,7*S* isomer – than with its diastereoisomeric structural alternatives. It is noteworthy that a tentative choice of **1***a* was made (13), on the basis of the minimal hindrance to epoxide formation expected, in the synthesis of (the D-enantiomer of) asperlin (3).

[4]Moreover, it may be noted that the molecular model afforded a value for the distance between H-4 and H-5 of the pyrone ring (having a more rigid geometry) that is ~9% smaller than the experimentally determined value (Table 3). With this "correction", isomer **1***a* also accommodates the H-5,H-7 interproton distance predicted by the nmr measurements.

1. A. D. ARGOUDELIS, J. H. COATES, and R. R. HERR. Antimicrob. Agents Chemother. 801 (1965); S. P. OWEN and B. K. BHUYNAN. Antimicrob. Agents Chemother. 804 (1965).
2. S. LESAGE and A. S. PERLIN. Can. J. Chem. **56**, 2889 (1978).
3. S. LESAGE and A. S. PERLIN. Can. J. Chem. **56**, 3117 (1978).
4. P. DAIS, T. K. M. SHING, and A. S. PERLIN. J. Am. Chem. Soc. **106**, 3082 (1984).
5. J. H. NOGGLE and R. E. SHIRMER. The nuclear Overhauser effect. Academic Press, New York. 1971 p. 4.
6. P. DAIS and A. S. PERLIN. Can. J. Chem. **60**, 1648 (1982).
7. P. DAIS, T. K. M. SHING, and A. S. PERLIN. Carbohydr. Res. **122**, 305 (1983).
8. D. E. WOESSNER. J. Chem. Phys. **37**, 647 (1982); Mol. Phys. **34**, 899 (1977).
9. R. FREEMAN, J. D. W. HILL, B. L. TOMLINSON, and L. D. HALL. J. Chem. Phys. **61**, 4466 (1974).
10. P. DAIS and A. S. PERLIN. Abstract OR 2-3, 67th Annual CIC Conference, Montreal. June 3–6, 1984.
11. M. KARPLUS. J. Am. Chem. Soc. **85**, 2870 (1963).
12. C. HIROSE. Bull. Chem. Soc. Jpn. **47**, 1311 (1974).
13. S. LESAGE. Ph.D. thesis, Aug. 1977. McGill University, Montreal, P.Q. p. 94.

Synthesis of D-norisomorphinans ((±)-[14α]-D-normorphinans)

JOHN P. YARDLEY[1] AND RICHARD W. REES
Wyeth Laboratories, Inc., P.O. Box 8299, Philadelphia, PA 19101, U.S.A.

Received March 28, 1984[2]

JOHN P. YARDLEY and RICHARD W. REES. Can. J. Chem. **63**, 1013 (1985).

A synthesis of the D-norisomorphinan ring system is described. Conversion of the initial synthetic target, *trans*-1,3,4,9,10,10a-hexahydro-6-methoxy-9-oxo-4a(2*H*)-phenanthrenecarboxamide (**10***c*) into the D-norisomorphinan (**6***b*) proved possible only after removal of the carboxamide ambident functionality. The successful route proceeds via hypobromous acid addition to *trans*-1,3,4,10a-tetrahydro-6-methoxy-4a(2*H*)-phenanthrenemethanamine (**21**) followed by a facile intramolecular cyclization to the D-norisomorphinan (**23**).

JOHN P. YARDLEY et RICHARD W. REES. Can. J. Chem. **63**, 1013 (1985).

On décrit une synthèse du système cyclique du D-norisomorphinane. On a d'abord obtenu l'hexahydro-1,3,4,9,10,10a méthoxy-6 oxo-9 2*H*-phénanthrène carboxamide-4a *trans* (**10***c*) comme première cible de la synthèse; ce n'est qu'après avoir éliminé la fonction carboxamide ambidente que l'on a pu transformer **10***c* et obtenir le D-norisomorphane (**6***b*). La voie permettant d'effectuer cette réalisation implique une addition d'acide hypobromeux sur la tétrahydro-1,3,4,10a méthoxy-6 2*H*-phénanthrène méthanamine-4a *trans* (**21**) suivie d'une cyclisation intramoléculaire facile en D-norisomorphinane (**23**).

[Traduit par le journal]

Introduction

(−)3-Hydroxy-*N*-methyl-morphinan (**1**) has clinical utility as an analgesic, while potent analgesic activity has been uncovered in the corresponding B/C-*trans* fused or isomorphinan structure (**2**) (ref. 1). As part of a program to extend the

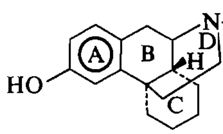

1

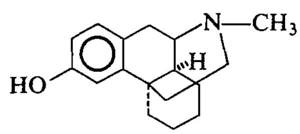

2

structure–activity relationships to the ring D-nor compounds, synthesis of the D-norisomorphinan ring system was required. Belleau, Conway, and co-workers have already described (2) a synthesis of the ring B/C *cis*-fused, D-normorphinan (**5***a*), which proceeds via 4a-aminomethyl-4a,10a-*cis*-1,2,3,4,10,-10a-hexahydrophenanthrene (**4***a*). Compound **4***a* was obtained by a base catalysed rearrangement of **3***a*; B/C-*trans* fused products were not observed. The synthesis described below passes through a 4a,10a-*trans* counterpart of **4***c* and leads to 3-hydroxy-*N*-methyl-D-norisomorphinan (**6***b*).

Results and discussion

At the outset it appeared that a viable synthesis of the D-normorphinan or D-norisomorphinan ring system could be modeled on Schenker's approach (3) to 2,3,4,5-tetrahydro-1,4-methano-1*H*-3-benzazepine (**9**), the key step of which was the cyclization of **7** to **8**. Thus a synthesis of **6** would require construction of the intermediate **10**. The synthesis of **10** is outlined in Scheme 2.

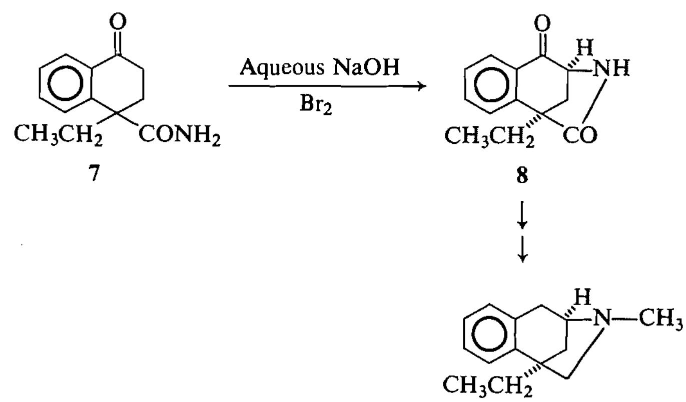

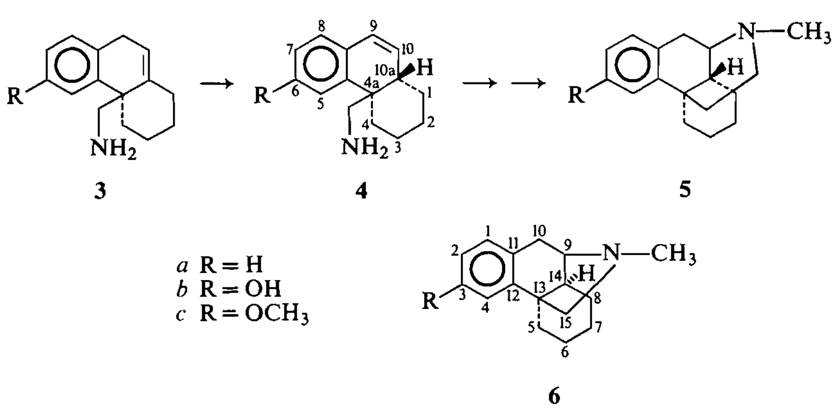

SCHEME 1

[1] Author to whom correspondence may be addressed.
[2] Revision received October 19, 1984.

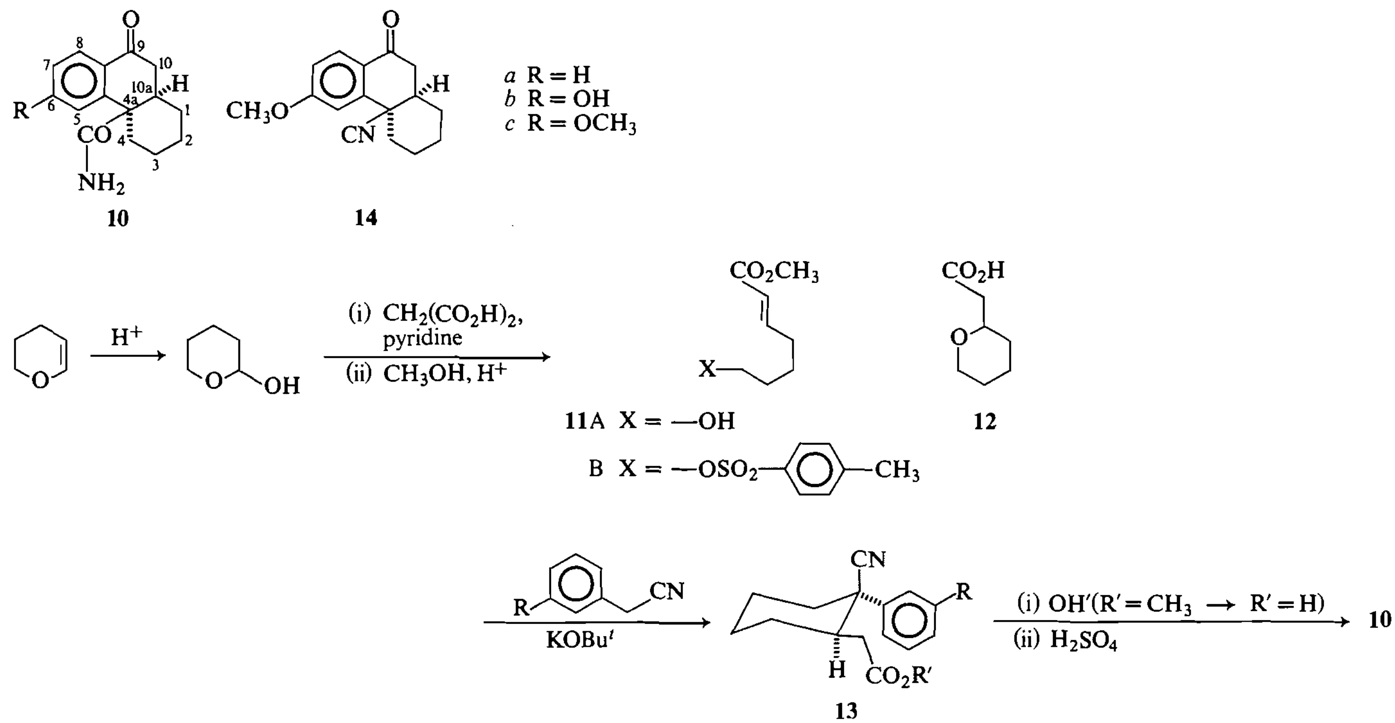

SCHEME 2

Methyl 7-hydroxy-*trans*-2-heptenoate (**11**A) is readily available by Raphael's procedure (4) starting from dihydropyran; in a minor modification, the intermediate 7-hydroxy-*trans*-2-heptenoic acid was not distilled but converted directly to the methyl ester using methanolic hydrogen chloride. In our hands, attempted distillation of the crude acid gave **12** as the predominant product. Cycloaddition was not a major problem in the distillation of **11**A, presumably due to the lower distillation pot temperatures involved. The oily tosylate (**11**B), together with *m*-methoxyphenylacetonitrile, added to a refluxing solution of potassium *tert*-butoxide in *tert*-butanol led, in a combined alkylation – Michael addition step, to **13***c* ($R^1 = CH_3$). **13***c* was not purified but hydrolysed to the acid **13***c* ($R^1 = H$) which in turn was cyclized directly to **10***c*. If the cyclization in sulfuric acid is conducted at 0°C rather than at room temperature, a small yield of the nitrile (**14**) may be isolated in addition to **10***c*, and this argues against participation of glutaric intermediates in the cyclization step. *para*-Activation is not required for cyclization, a virtually identical yield of **10***a* being obtained by a similar sequence from phenylacetonitrile.

Compound **10***c* showed the appropriate mass ions at 273 (M^+) and 229 ($M^+ - CONH_2$), a 1,2,4-trisubstituted benzene ^{1}Hmr pattern, and primary amide and aryl ketone ir absorptions at 1690, 1660, 1595, and 1555 cm^{-1}. No trace of a second diasteriomer with B/C rings *cis* fused was detected and this deserves comment. Regardless of whether the Michael-addition step, a perpendicular attack on the conjugated system by a *m*-methoxyphenylacetonitrile anion, or nucleophilic displacement of the tosylate occurs first, the final step involves formation of a cyclohexane ring. The preferred transition state will presumably have the bulky *m*-methoxyphenyl and carboxymethyl groups in a low energy *trans* diequatorial relationship leading to **13***c* ($R^1 = CH_3$). Proof of the *trans* stereochemistry follows from the ^{1}Hmr of rigid transformation products, *vide infra*, all of which lack visible coupling between the H(9) and H(14) protons for which the Karplus equation predicts (5) a dihedral angle of 100°, in agreement with measurements from Dreiding models. The value for the corresponding B/C *cis*-fused, D-normorphinans J_{H9H14} is 5 Hz, in agreement with the observed dihedral angle $\phi_{H9H14} = 37°$ (2).

Bromination experiments

Schenker reports (3) the synthesis of **8** by a heterogeneous reaction of **7** in aqueous sodium hydroxide with bromine. Using the substrate **10***c* no reaction was observed, presumably a consequence of the extreme insolubility of **10***c*. Repetition of the reaction with the addition of tetrahydrofuran, initially added as a cosolvent, rather surprisingly afforded a two-phase system;[3] thin-layer chromatography indicated rapid loss of starting material. The product isolated in essentially quantitative yield was the Hofmann rearrangement product, the isocyanate (**15**), rather than the expected bromoketone (Scheme 3). If the isocyanate is not isolated, but the two-phase reaction mixture stirred overnight at room temperature, the products are the bridged structure (**17**) and a minor component – the amine (**16**). Compound **17** presumably arises via intramolecular attack of the enol form of **15** on the isocyanate moiety, formation of an α-enolate anion from this ketone with sodium hydroxide being unlikely. It is worth noting that **17** had the mass, mass spectral fragmentation pattern, and an ir expected for **18**. The ^{1}Hmr of **17** has a sharp one-proton singlet at 3.00 ppm, assigned to the H(10) proton. Lack of coupling with the H(10a) proton was the first evidence that rings B and C were *trans* fused.

Bromination of **10***c* in anhydrous tetrahydrofuran with no added base afforded **19**. The appropriate mass ion at 271 (M^+) was observed and the ir showed typical ammonium bands. Again a peak at 5.39 ppm, assigned to the H(10) proton in the ^{1}Hmr was a sharp singlet. The isolation of **17** and **19** rather than

[3] The lowered solubility of tetrahydrofuran in strong alkali proved useful in the synthesis of both **15** and **23**.

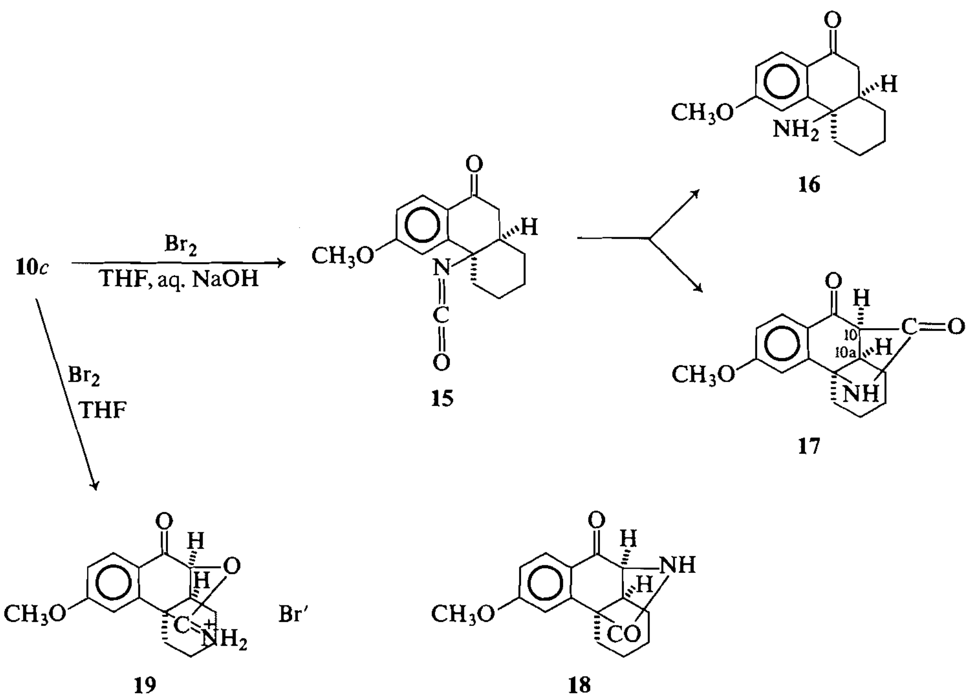

SCHEME 3

18, while disappointing, suggested that the D-norisomorphinan would be obtainable once the ambident functionality of the amide was removed, e.g., by intramolecular cyclization of the aminomethyl compound **21**.

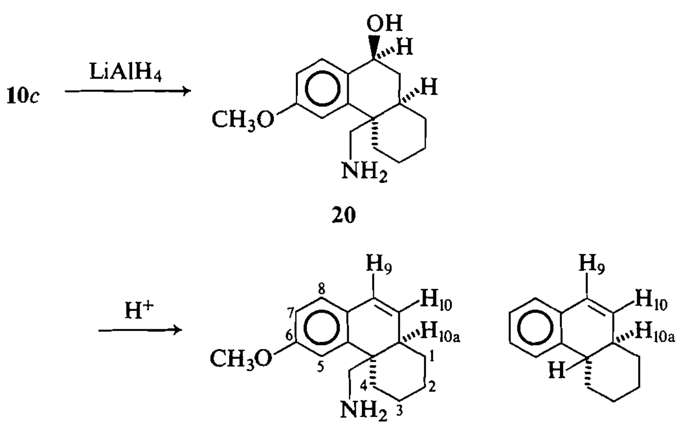

Conversion of **10***c* into **21** was achieved in two steps – a prolonged reduction with $LiAlH_4$ to the hydroxyamine (**20**), followed by formation of **21** by an acid-catalysed elimination of the benzylic hydroxyl. Compound **20** was isolated as a sharp-melting crystalline solid. Its isolation as a single isomer upon reduction reflects the lack of steric hindrance to α-face approach by the reducing agent. The quasi-equatorial stereochemical assignment for the ring hydroxyl was inferred from the broad width of the benzylic ^{1}Hmr proton signal at 4.8 ppm, reflecting the large diaxial interaction with the 10β proton. In practice, it proved convenient to convert the total crude reaction mixture directly to **21** using *p*-toluenesulfonic acid in benzene. Overall yields of 60% from **10***c* were obtained.

The ^{1}Hmr spectrum of **21** deserves comment; the C(10) olefinic proton is observed as the B portion of an ABX system. The Karplus equation (5) predicts a value $J_{H10H10a} \cong 0.1$ Hz for the 4a,10a-*trans* system where the dihedral angle, $\phi_{H10H10a} = 100°$ is found and, indeed, $J_{H10H10a} = 0–1$ Hz is observed in the model system (**22**) reported by Nelson *et al.* (6). In **21** the C(10) proton is observed as a doublet of doublets split by both H(9), $J_{H9H10} = 9$ Hz, and by H(10a), $J_{H10H10a} = 2.2$ Hz, suggesting a small increase in the $\phi_{H10H10a}$ dihedral angle.

A possible explanation may be made using Bucort's principles of conformational transmission, considering rings B and C as a *trans*-fused octalin system (see, for example, references to Bucorts' papers in ref. 7). The *syn* 1,3-diaxial interactions between the large aminomethyl group and the axial hydrogens at C(1) and C(3) are intensified by the ring B unsaturation. In opposition a decrease in steric pressure is obtained by a decrease in the dihedral angle formed by C(4)—C(4a)—C(10a)—C(1) and is not reflected in Dreiding models. The net result of the compromise is an increase in the $\phi_{H10H10a}$ angle.

Formation of the D*-norisomorphinan*

Two concurrent efforts to form the D-norisomorphinan ring system were made. One approach, an attempted synthesis of the azetidium structure[4] (**i**) by assisted solvolysis of an *N*-chloroamine derivative was unsuccessful. Lithium aluminum hydride reduction of **i** might be expected to afford a D-norisomorphinan. The other, a successful method, involved an attempt to prepare a 10α-bromo, 9ϵ-hydroxybromohydrin from **20** by treatment with *N*-bromoacetamide in aqueous tetrahydrofuran. α-Face attack by the bromonium ion is to be expected on both steric and electronic grounds, since the β-face is swept by the positively charged aminomethyl group. α-Face attack would presumably occur via perpendicular attack on the 9,10-olefin in a pre-boat form and lead to a 10α-bromo-

[4]
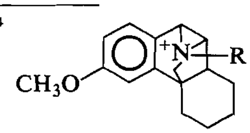

i

derivative, since solvent attack is to be expected at the benzylic position. After addition of excess sodium hydroxide the reaction mixture because two-phase and the product isolated after a 45-minute wait proved to be the D-norisomorphinan **23**. Bromohydrin formation is obviously followed by a facile intramolecular alkylation of the amine upon neutralization of the perchloric acid. Conversion of **23** to **24** by vigorous hydrogenolysis confirmed the benzylic location of the hydroxyl function. The benzylic proton of **23** appears in the nmr as a doublet, $J_{9/10}$ = 4.5 Hz, a value that is ambiguous with regard to configurational assignment.

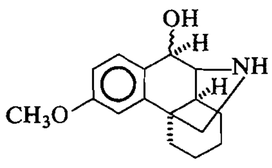

23

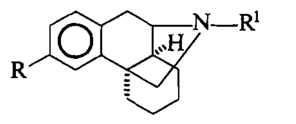

24 R = OCH_3, R' = H
25 R = OCH_3, R' = $CO_2CH_2CH_3$
6*b* R = OH, R' = CH_3
6*c* R = OCH_3, R' = CH_3

Completion of the synthesis proved straightforward; **24** was converted to the *N*-methyl compound (**6*c***) via the intermediate urethane **25**. Demethylation of the aromatic methoxyl in **6*c*** proceeded smoothly, by brief treatment with hydrogen bromide at 140°C, affording 3-hydroxy-*N*-methyl-D-norisomorphinan **6*b***. Overall the synthetic route is represented by the sequence **10*c*** → **20** → **21** → **23** → **24** → **25** → **6*c*** → **6*b***.

Experimental

Melting points (uncorrected) were obtained on a Thomas–Hoover apparatus. The nmr and mass spectra were determined on Jeolco Model C-60HL and Associated Electrical Industries MS-9 spectrometers.

Methyl 7-hydroxy-trans-*2-heptenoate,* p-*toluenesulfonate (11B)*

Methyl 7-hydroxy-*trans*-2-heptenoate (85 g; 5.4 × 10^{-1} mol) in pyridine (450 mL) at 0°C was treated over 2 min with *p*-toluenesulfonyl chloride (123 g; 6.5 × 10^{-1} mol) and the mixture allowed to reach room temperature over 6 h. Ice was added and the mixture stirred for a further 45 min. After dilution with water the mixture was extracted with ether (2×) and the extracts washed successively with water, dilute sulfuric acid, water, $NaHCO_3$ solution, and brine and dried over Na_2SO_4. After evaporation of the solvent the oily tosylate was used directly; ir: 1730, 1660, 1600, 1360, 1180 cm^{-1}.

trans-*1,3,4,9,10,10a-Hexahydro-6-methoxy-9-oxo-4a(2*H*)-phenanthrenecarboxamide (10*c*)*

A mixture of *m*-methoxyphenylacetonitrile (20 g; 1.35 × 10^{-1} mol) and **11B** (39.6 g; 1.27 × 10^{-1} mol) in *tert*-butanol (550 mL) was added dropwise, during 3 h, to a refluxing solution of potassium *tert*-butoxide (16.4 g; 1.46 × 10^{-1} mol) in *tert*-butanol (300 mL). The reaction mixture was refluxed for a further 3 h under nitrogen and then stirred at room temperature overnight. Acetic acid (20 mL) was added and the reaction mixture stripped to a small volume, diluted with water, and extracted with diethyl ether (2×). The ether extracts were washed with water, brine, and evaporated; the residue in methanol (350 mL) was heated under reflux with 20% NaOH solution (100 mL; 5 × 10^{-1} mol) during 2.5 h. The reaction mixture was stripped to a small volume, diluted with water, and extracted with ether (rejected). The aqueous solution was acidified strongly with hydrochloric acid and extracted (2×) with ether. The ether extracts were washed with brine, dried (Na_2SO_4), and evaporated to a partially crystalline residue (35 g). The total residue was stirred with cold concentrated H_2SO_4 (1 L) overnight and poured onto ice. A highly crystalline product (14 g) precipitated and was recrystallized from acetone to yield **10*c*** (10 g, 29%), mp 225–228°C; ir: 3350 (s), 3140 (s), 1690 (s), 1660 (s), 1595 (s), 1555 infl. cm^{-1}; ^{1}H nmr (DMSO) δ: 3.71 (3H, s, —OCH_3), 6.75 (C(7)-H centre of a pair of d, $J_{5/7}$ 2.5 cps, $J_{7/8}$ 8.5 Hz), 6.99 (C(5)-H d, $J_{5/7}$ 2.5 Hz, $J_{5/8}$ 0 Hz), 7.62 (C(8)-H d, $J_{7/8}$ 8.5 Hz), 6.66 (2H, br m, $CONH_2$) ppm; ms *m/e*: 273 (M^+), 229 (M^+ – $CONH_2$), 187, 167. *Anal.* calcd. for $C_{16}H_{19}NO_3$: C 70.31, H 7.01, N 5.13; found: C 70.03, 70.54; H 7.04, 7.17; N 5.53, 5.15%.

If the concentrated sulfuric acid cyclization step in the above example is allowed to proceed at 0°C rather than at room temperature, small amounts of a more soluble (methanol), less polar, intermediate carbonitrile may be isolated: *trans*-1,3,4,9,10,10a-hexahydro-6-methoxy-9-oxo-4a(2*H*)-phenanthrenecarbonitrile (**14**), mp 174–177°C; ir: 2220 (very weak), 1685 (s), 1605 (s) cm^{-1}. *Anal.* calcd. for $C_{16}H_{17}NO_2$: C 75.21, H 6.71, N 5.49; found: C 75.06, H 6.71, N 5.49%.

Bromination experiments

trans-*2,3,4,4a,10,10a-Hexahydro-4a-isocyanato-6-methoxy-9(1*H*)-phenanthrenone (15)*

Bromine (144 μL, 0.45 g; 2.8 × 10^{-3} mol) was added to a stirred, two-phase solution prepared from **10*c*** (600 mg; 2.2 × 10^{-3} mol), sodium hydroxide (1 g), water (10 mL), and tetrahydrofuran (10 mL). Thin-layer chromatography indicated complete loss of starting material within 5 min. The reaction mixture was diluted with water and methylene chloride. The methylene chloride extract was washed with water (2×), brine, dried (Na_2SO_4), and concentrated to a residue. Crystallization from methylene chloride – hexane afforded **15** (500 mg, 84%), mp 112–113.5°C; ir: 2250 (s) cm^{-1}. *Anal.* calcd. for $C_{16}H_{17}NO_3$: C 70.83, H 6.32, N 5.16; found: C 70.60, H 6.45, N 5.04%.

trans-*4a-Amino-2,3,4,4a,10,10a-hexahydro-6-methoxy-9(1*H*)-phenanthrenone (16) and (4aα,10α,10aβ)-1,2,3,4,10,10a-hexahydro-6-methoxy-9*H*-4a,10(iminomethano)phenanthrene-9,11-dione (17)*

Bromine (720 μL, 2.23 g; 1.4 × 10^{-2} mol) was added over 10 min to a stirred two-phase solution prepared from **10*c*** (3 g; 1.1 × 10^{-2} mol), sodium hydroxide (3 g), water (40 mL), and tetrahydrofuran (45 mL). The reaction mixture was stirred at room temperature overnight, diluted with water, and extracted with methylene chloride. The methylene chloride extract was washed with water (2×), brine, dried (Na_2SO_4), and concentrated to a residue. Trituration of the residue with ether afforded a crystalline residue of **17** (1.24 g, 42%) that, after two recrystallizations from methylene chloride – methanol, had mp 239–243°C (dec.).

The ether triturate was evaporated and the residue recrystallized from ether–hexane (charcoal) and then methylene chloride – hexane to afford **16** (360 mg, 13%, mp 101–103°C. Compound **16**: ms *m/e*: 245 (M^+), 228, 202, 188. *Anal.* calcd. for $C_{15}H_{19}NO_2$: N 5.71; found: N 5.48, 5.49%. Compound **17**: ms *m/e*: 271 (M^+), 243, 228, 214. *Anal.* calcd. for $C_{16}H_{17}NO_3$: C 70.83, H 6.32, N 5.16; found: C 70.50, H 6.32, N 5.33%.

*(4aα,10α,10aβ)-1,2,3,4,10,10a-Hexahydro-12-imino-6-methoxy-9*H*-10,4a-(epoxymethano)phenanthren-9-one (19)*

Bromine (0.85 μL, 2.64 g; 1.7 × 10^{-2} mol) in tetrahydrofuran (40 mL) was added dropwise to a suspension of **10*c*** (4 g; 1.46 × 10^{-2} mol) in tetrahydrofuran (40 mL). Complete solution was followed by a voluminous precipitate of **19** (4.3 g, 83%). The analytical sample, mp 216–218°C (dec.), was obtained by rapid recrystallization from methanol–ether; ms *m/e*: 271 (M^+). *Anal.* calcd. for $C_{16}H_{17}NO_3 \cdot HBr$: C 54.56, H 5.15, N 3.98, Br 22.69; found: C 54.67, H 5.39, N 3.96, Br 22.06%.

(4aα,10aβ)-4a-Aminomethyl-1,2,3,4,4a,9,10,10a-octahydro-6-methoxy-9-phenanthrenol (20)

Compound **10*c*** (30 g) and lithium aluminum hydride (20 g) in tetrahydrofuran (3 L) were refluxed under nitrogen during 2 days. The cooled reaction mixture was treated dropwise with 100 mL, 3% NaOH solution, filtered, and evaporated to a crystalline residue of **20** (28 g) suitable for further transformation. An analytical sample, mp 149–151°C, was obtained by recrystallization from ethyl ether – hexane; ^{1}H nmr ($CDCl_3$–D_2O) δ: AB q of aminomethyl protons with *J* 13.5 Hz at 2.81 and 2.99, 3.84 (3H, s, OCH_3), 4.83 (1H center approximate t, C(9)-H) ppm; ms *m/e*: 243 ($M^+ - H_2O$). *Anal.* calcd. for $C_{16}H_{23}NO_2$: C 73.53, H 8.87, N 5.36; found: C 73.24, H 8.82, N 5.33%.

trans-*1,3,4,10a-Tetrahydro-6-methoxy-4a(2*H*)-phenanthrenemethanamine (21)*

Compound **20** (25 g; 8.5 × 10^{-2} mol) and *p*-toluenesulfonic acid monohydrate (18 g; 9.5 × 10^{-2} mol) in benzene (1 L) were heated under reflux using a Dean–Stark head; after 1 h the reaction mixture was stripped to a small volume, diluted with ether, and extracted with water. The aqueous phase together with a crystalline precipitate were washed with ether (rejected), basified strongly with NaOH solution, and extracted with ether (2×). The ether extracts were washed with brine, dried (Na_2SO_4), evaporated to a small volume, and filtered through a Woelm alumina column (Grade I, basic 120 g); the product (16 g) eluted with ether and was obtained as a colorless oil; ir: 1610, 1570 cm^{-1}; ^{1}H nmr ($CDCl_3$) δ: 2.87 (2H, multiplet, $W_{1/2}$ H 5 Hz), 3.79 (3H, s, —OCH_3), AB q $J_{9/10}$ 9 Hz, protons centered at 5.48 (C(10)-H) and 6.36 (C(9)-H) further split by C(10a)-H, $J_{10a/10}$ 2.2 Hz, $J_{9/10a}$ 3 Hz ppm.

*(±)-(14α)-3-Methoxy-*D*-normorphinan-10-ol (23)*

Compound **21** (4.86 g; 2 × 10^{-2} mol) in tetrahydrofuran (150 mL) containing 0.5 *N* $HClO_4$ (80 mL; 4 × 10^{-2} mol) was cooled to 0°C and treated, under nitrogen, with *N*-bromoacetamide (3 g; 2.2 × 10^{-2} mol) added over 1–2 min. Thin-layer chromatography indicated that there was a rapid loss of starting material; after 20 min, excess NaOH solution (20 mL; 50%) and ice were added. The two-phase solution was stirred for 45 min. After dilution with benzene the organic layer was washed with water (2×), brine, dried (Na_2SO_4), and evaporated to a residue which readily crystallized on trituration with boiling ether to give the product (4 g; free base form), mp 140–143.5°C. Recrystallization from methanol–ether gave a higher mp form, mp 174–177°C; ^{1}H nmr ($CDCl_3$) δ: 2H, AB q, *J* 10 Hz, aminomethyl protons centered at 2.53 and 3.57; 2H, AB q, $J_{9/10}$ 4.5 Hz, $J_{9/14}$ 0 Hz centered at 3.24 (C(9)-H) and 4.66 (C(10)-H); 3.79 (3 Hs, —OCH_3) ppm. *Anal.* calcd. for $C_{16}H_{21}NO_2$: C 74.10, H 8.16, N 5.4; found: C 73.69, H 8.16, N 5.34%.

Salt (**23**·HCl), mp 244–245°C, crystallized from methanol–ether. *Anal.* calcd. for $C_{16}H_{22}NO_2Cl$: C 64.96, H 7.50, N 4.74, Cl 11.95; found: C 64.60, H 7.47, N 4.69, Cl 11.72%. In a repeat experiment, **21** (14.4 g) was converted into **23**·HCl (8.1 g, 46%), mp 243–245°C, without isolation or purification of the free base.

*(±)-(14α)-3-Methoxy-*D*-normorphinan (24)*

Compound **23** (5.0 g), acetic acid (80 mL), 70% perchloric acid (2 mL), and 5% Pd on $BaSO_4$ (2.0 g) were stirred at 80°C in an atmosphere of hydrogen overnight (1 mol uptake). After cooling, 30 mL of 10% K_2CO_3 solution were added and following filtration the reaction mixture was evaporated, basified with NaOH solution, taken into CH_2Cl_2, and washed with brine. After evaporation of the solvent, the residue in ether was dried (Na_2SO_4) and treated with isopropanolic hydrogen chloride to give a crystalline precipitate which after trituration with boiling acetone afforded **24**·HCl (4.14 g, 86%), mp 228–231°C (some previous decomposition). The analytical sample, mp 238°C (dec.), was obtained by recrystallization from acetone; ms *m/e*: 243 (M^+). *Anal.* calcd. for $C_{16}H_{22}NOCl \cdot \frac{1}{4} H_2O$: C 67.59, H 7.98, N 4.93, Cl 12.47; found: C 67.45, 67.35; H 7.75, 7.84; N 4.82, 4.67; Cl 12.97%.

*(±)-(14α)-3-Methoxy-17-methyl-*D*-normorphinan (6c)*

Compound **24** (4 g; 1.43 × 10^{-2} mol) in a stirred mixture of methylene chloride (300 mL) and saturated $NaHCO_3$ solution (300 mL) was treated with ethyl chloroformate (1.8 mL; 1.88 × 10^{-2} mol) at room temperature during 30 min. After standing overnight, the organic layer was separated and evaporated. The residue in ether was washed with dilute HCl, brine, dried (Na_2SO_4), and evaporated to give the urethane (**25**, 4.2 g). The urethane in ether–tetrahydrofuran (1 : 1, 400 mL) was heated under reflux with $LiAlH_4$ (2.5 g) during 4 h. After standing overnight the reaction mixture was treated with 12.5 mL 3% NaOH solution, filtered, and evaporated. The residue in ether was filtered through a Woelm alumina column (40 g, Grade I, basic) and eluted with ether. The total eluate was treated with isopropanolic hydrogen chloride and the precipitate, after crystallization from acetone, afforded **6***c*·HCl (2.9 g, 70%), mp 238–240°C; ^{1}H nmr ($CDCl_3$–D_2O) δ: 2.9 (3H, s, N-CH_3), 3.88 (3H, s, —OCH_3), 3.38 (ca. 2H, d, *J* = 3 Hz – actually center peaks of AB quartet (CH_2—N—CH_3)) ppm; ms *m/e*: 257 (M^+). *Anal.* calcd. for $C_{17}H_{24}NOCl$: C 69.49, H 8.23, N 4.77, Cl 12.07; found: C 69.30, H 8.29, N 4.64, Cl 12.35%.

*(±)-(14α)-17-Methyl-*D*-normorphinan-3-ol (6b)*

Compound **6***c*·HCl (1.8 g) and 47–49% aqueous hydrogen bromide (30 mL) were heated under reflux during 45 min. The cooled reaction was treated with ice and an excess of concentrated ammonium hydroxide to give a crystalline precipitate of the product (free base form). After aging (1 h) the precipitate (1.6 g) was filtered off. A small portion recrystallized from acetone had mp 223–225°C (dec.). *Anal.* calcd. for $C_{16}H_{21}NO$: C 78.97, H 8.70, N 5.76; found: C 78.93, H 8.91, N 5.73%.

The remainder in acetone was treated with a slight excess of isopropanolic hydrogen chloride and concentrated. The crystalline precipitate was recrystallized from methanol–ether; the product, **6***b*·HCl (1.15 g, 66%), had mp 255–258°C (with effervescence); ms *m/e*: 243 (M^+). *Anal.* calcd. for $C_{16}H_{22}NOCl$: C 68.68, H 7.93, N 5.01, Cl 12.67; found: C 68.17, H 7.86, N 4.85, Cl 11.97%.

Acknowledgements

We wish to thank Mr. C. Kuhlman and Dr. C. Hetzel for mass spectra, Dr. C. Hetzel for nmr determinations, Dr. Herchel Smith for his interest, and Miss P. Stevens for secretarial assistance.

1. (*a*) S. J. HELLERBACH, O. SCHNIDER, H. BESENDORF, and B. PELLMONT. Morphinans. *In* Synthetic analgesics, International Series of Monographs in Organic Chemistry, 8, part IIA. Pergamon Press, New York. 1966. pp. 33–73; (*b*) M. R. JOHNSON and G. M. MILNE. *In* Burger's medicinal chemistry. 4th ed. Part III. *Edited by* M. E. Wolff. Wiley–Interscience, New York. 1981. p. 699; (*c*) M. GATES and W. B. WEBB. J. Am. Chem. Soc. **80**, 1186 (1958).
2. T. T. CONWAY, T. W. DOYLE, Y. G. PERRON, J. CHAPUIS, and B. BELLEAU. Can. J. Chem. **53**, 245 (1975).
3. K. SCHENKER. U. S. Patent 3,474,463. Oct. 21, 1969. Equivalent Neth. Appl. 6,057,339 Dec. 13, 1965; Chem. Abstr. **65**, 696F (1966).
4. J. KENNEDY, N. J. MCCORKINDALE, and R. A. RAPHAEL. J. Chem. Soc. 3813 (1961).
5. (*a*) M. KARPLUS. J. Am. Chem. Soc. **85**, 2870 (1963); (*b*) S. STERNWELL. Q. Rev. **23**, 236 (1969).
6. W. L. NELSON, D. D. MILLER, and E. SHEFTER. J. Org. Chem. **35**, 3433 (1970).
7. L. VELLUZ, J. VALLS, and G. NOMME. Angew. Chem. Int. Ed. Engl. **4**, 181 (1965).

Oxidation of hydrocarbons. 13. The oxidation of cinnamate ion by alkaline permanganate

DONALD G. LEE[1] AND KASINATHAN NAGARAJAN
Department of Chemistry, University of Regina, Regina, Sask., Canada S4S 0A2

Received April 17, 1984

DONALD G. LEE and KASINATHAN NAGARAJAN. Can. J. Chem. **63**, 1018 (1985).

The rates of oxidation of cinnamate ion by permanganate have been compared under conditions where distinctly different products (MnO_4^{2-} and MnO_2) are obtained. Since the rates of both reactions respond in similar ways to substituent effects, deuterium substitution on the double bond, and to temperature changes, it may be concluded that the different products are due to post transition state reactions. Reaction sequences that are consistent with this conclusion and with the observed stoichiometries have been suggested.

DONALD G. LEE et KASINATHAN NAGARAJAN. Can. J. Chem. **63**, 1018 (1985).

On a comparé les vitesses d'oxydation de l'ion cinnamate par le permanganate dans des conditions où l'on obtient d'une façon distincte deux produits différents (MnO_4^{2-} et MnO_2). Les vitesses des deux réactions répondent de la même manière aux effets de substituants, à l'introduction de deutérium sur la double liaison et à des changements de température; on en conclut que les différents produits proviennent de réactions se produisant après l'état de transition. On suggère des séries de réactions qui sont en accord avec cette conclusion et avec les stoïchiométries observées.

[Traduit par le journal]

Introduction

It has been assumed for almost one century that all permanganate–alkene reactions proceed by way of the same intermediate, a cyclic manganate(V) diester (1). This is a large assumption for a reaction in which the nature of the products is very sensitive to experimental conditions. Depending on the conditions employed, the organic products can be diols, ketols, or cleavage products, while the inorganic products are MnO_4^{2-}, MnO_2, or Mn^{3+} (2–4). Consequently, it is apparent that the assumption of a common intermediate should be carefully tested. In attempting to apply such a test, we have chosen to study the reaction under two sets of conditions that give distinctly different products, and to compare the effect of substituents, the effect of isotopic substitution and the effect of temperature changes on the rates of reaction.

Experimental

Materials

The oxidant was Fisher analyzed reagent grade potassium permanganate. The substituted *trans*-cinnamic acids were obtained from the Aldrich Chemical Co. and repeatedly recrystallized until they gave sharp melting points which agreed with those reported in the literature. The deuterated cinnamic acids were prepared using methods previously described (5). Water, collected from an all-glass still, was redistilled from alkaline permanganate (6).

Silicate solutions were prepared by dilution of commercial sodium silicate solutions (Harrisons and Crosfield) in the following way. A concentrated silicate solution (2 mL) was added to 1 L of distilled water and heated gently for 1 h with stirring. After cooling, the solution was centrifuged in portions, filtered, diluted to 2 L, and stored in polyethylene bottles. The density of this solution was 1.044 g/mL; its pH was 11.3. At this pH the product of the reaction is manganese(IV) oxide, which first flocculates and then precipitates (as MnO_2) if the reaction is carried out in an aqueous solution. However, the presence of silicate stabilizes manganese dioxide (7), prevents flocculation, and vastly improves the linearity of the kinetic rate plots.

When the reaction of permanganate with cinnamic acid is carried out in 0.50 *M* NaOH the product can be identified as MnO_4^{2-} from its spectrum (2). Under these conditions it is stable for a long period relative to the half-life of the reaction, thus making it possible to obtain reliable kinetic plots and to assign the observed spectral changes with high confidence.

TABLE 1. Rate constants for the oxidation of cinnamate ion by permanganate in 0.5 *M* NaOH[a]

[Cinnamate ion] ($M \times 10^3$)	k_1 (s^{-1})[b]	k_2 (M^{-1} s^{-1})[c]
8.11	7.01 ± 0.07	864 ± 9
14.9	12.1 ± 0.6	812 ± 40
20.3	16.4 ± 0.5	808 ± 24

[a]Temperature = 25.0 ± 0.1°C, $[MnO_4^-] = 3.8 \times 10^{-4}$ *M*.
[b]Pseudo-first-order rate constants (see Fig. 1).
[c]$k_2 = k_1$/[cinnamate ion].

Kinetic methods

The reactions were followed by monitoring spectral changes using a rapid-scan stopped-flow spectrophotometer (System 777-RS, supplied by Update Instruments Inc.). Reaction rates were determined under pseudo-first-order conditions by measuring the decrease in absorbance at 526 nm.

Results

Oxidations in 0.50 M NaOH

When the rate of oxidation was studied in 0.50 *M* NaOH using a large excess of the reductant, cinnamate ion, linear plots of $-\ln (A - A_f)$ vs. time were obtained (Fig. 1). This indicates that the rate of reaction is first order with respect to permanganate ion (8). The pseudo-first-order rate constants so obtained were found to be directly proportional to the cinnamate ion concentration, thus indicating that the reaction is also first order in reductant (Table 1).

Inverse secondary isotope effects were observed when the rates for *trans*-cinnamate ion-α-*d* and *trans*-cinnamate ion-β-*d* were compared with unlabelled *trans*-cinnamate ion (Table 2).

The rates of oxidation in 0.5 *M* NaOH were found to be quite insensitive to the presence of ring substituents (Table 3). A ρ value of 0.13 is obtained from a Hammett plot for the reaction, with a significantly better fit being obtained when σ^- substituent constants are used (Fig. 2).

Activation parameters for the reaction (Table 4) were deter-

[1] Author to whom correspondence should be addressed.

TABLE 2. Deuterium isotope effects[a]

Substrates	[Substrate] ($M \times 10^3$)	Conditions	$k_2(M^{-1}\ s^{-1})$[b]	k^H/k^D
Cinnamate ion	8.11	0.5 M NaOH	864 ± 9	
Cinnamate ion-α-d	8.05	0.5 M NaOH	982 ± 14	0.87
Cinnamate ion-β-d	8.10	0.5 M NaOH	970 ± 14	0.89
Cinnamate ion	4.39	pH 11.3	742 ± 5	
Cinnamate ion-α-d	4.30	pH 11.3	799 ± 3	0.93
Cinnamate ion-β-d	4.43	pH 11.3	797 ± 3	0.93

[a]Temperature = 25.0 ± 0.1°C. $[MnO_4^-] = 3.8 \times 10^{-4}\ M$.
[b]k_2 defined in Table 1.

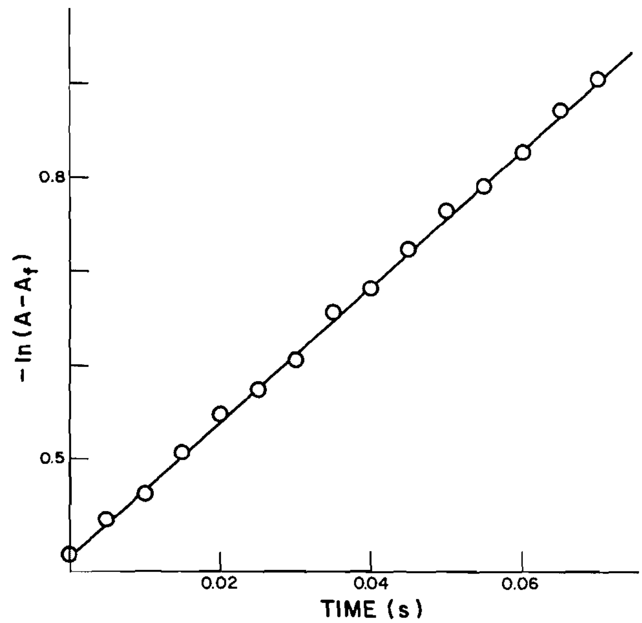

FIG. 1. Typical pseudo-first-order plot for the oxidation of cinnamate ion by permanganate in 0.5 M NaOH. [Cinnamate ion] = $8.11 \times 10^{-3}\ M$. $[KMnO_4^-] = 3.80 \times 10^{-4}\ M$. Temperature = 25°C. Slope = 7.03 s^{-1}. Correlation coefficient = 0.999.

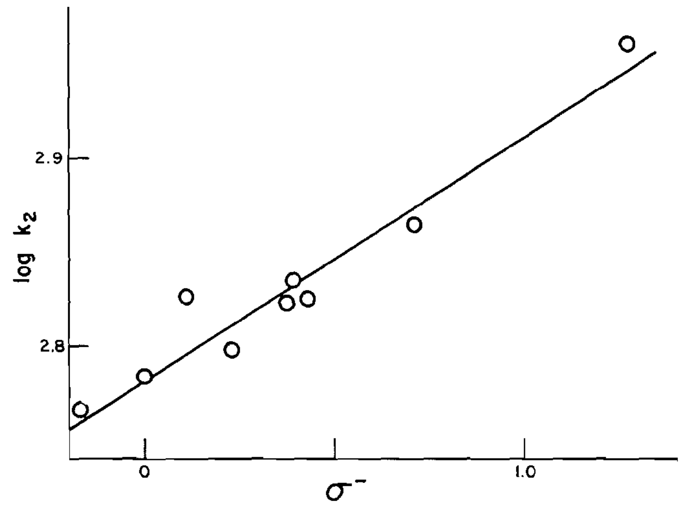

FIG. 2. Hammett plot for the oxidation of substituted cinnamate ions by permanganate in 0.5 M NaOH. Slope = 0.13, correlation coefficient = 0.97. When σ substituent values are used the slope increases to 0.16 and the correlation coefficient drops to 0.87.

mined from a plot of ln k_2/T vs. $1/T$. See Fig. 3.

With less than a ten-fold excess of cinnamate ion, good isosbestic points were observed at 469 and 577 nm when the solutions were successively scanned as the reaction progressed (Fig. 4), and one mole of manganate(VI) was formed for each mole of permanganate consumed. When larger excesses of cinnamate ion were used the isosbestic points were less sharply defined, and less than the calculated amount of manganate(VI) was formed. This suggests that manganate(VI) slowly reacts with cinnamate ion when it is present in large concentrations. Under all conditions manganate(VI) was slowly reduced to manganese dioxide on standing at room temperature.

Stoichiometric studies indicated that one mole of olefin consumed two moles of permanganate.[2]

Oxidations at pH 11.3

When the reaction was carried out in silicate solutions at pH 11.3 a stable pale brown solution (or suspension) was produced. Iodometric titrations showed that the manganese present was in the +4 oxidation state. A similar stabilization of manganese dioxide in silicate or phosphate solutions has previously been observed in other laboratories (7, 9).

An isosbestic point at 460 nm was observed when spectra were taken at intervals as the reaction progressed (Fig. 5). Stoichiometric studies indicated that 0.9 mole of permanganate was consumed for each mole of reductant present.[2]

TABLE 3. Rate constants for the oxidation of substituted cinnamate ions by potassium permanganate

Substituent	$k_2(M^{-1}\ s^{-1})$[a]	$k_2(M^{-1}\ s^{-1})$[b]
p-Methyl	587 ± 3	699 ± 11[c]
H	608 ± 12	736 ± 18
m-Methoxy	672 ± 10	880 ± 16
p-Chloro	628 ± 11	678 ± 16
m-Chloro	665 ± 20	855 ± 4
m-Bromo	684 ± 2	
m-Trifluoromethyl	668 ± 4	834 ± 39
m-Nitro	733 ± 15	965 ± 6
p-Nitro	914 ± 43	1190 ± 20

[a][NaOH] = 0.5 M, temperature = 15.0 ± 0.1°C, $[MnO_4^-] = 3.8 \times 10^{-4}\ M$, [substrate]/$[MnO_4^-]$ = 20.
[b]pH = 11.3, temperature = 25.0 ± 0.1°C, $[MnO_4^-] = 3.8 \times 10^{-4}\ M$, [substrate]/$[MnO_4^-]$ = 20.
[c][Substrate]/$[MnO_4^-]$ = 10.

[2]The initial product formed when cinnamate is oxidized proved to be somewhat reactive toward permanganate, thus making stoichiometric studies difficult. However, when other unsaturated carboxylates (such as 4-cyclohexene-1,2-dicarboxylate) were used, stable products were obtained and the stoichiometry could be established accurately and without difficulty.

TABLE 4. Activation parameters under different conditions

Reductant	Conditions	$\Delta H^{\ddagger}$ (kcal/mol)	$\Delta S^{\ddagger}$ (eu)	$\Delta G^{\ddagger}$ (kcal/mol)[e]
Cinnamate ion[a]	0.5 M NaOH	4.7 ± 0.5	−29 ± 1	13.3 ± 0.8
Cinnamate ion[b]	pH 11.3	4.5 ± 0.4	−31 ± 1	13.7 ± 0.7
Cinnamic acid[c]	1 M $HClO_4$	4.2 ± 0.5	−30 ± 2	13.1 ± 1.1
Methyl cinnamate[d]	Nonaqueous	5.6 ± 0.8	−38 ± 3	16.9 ± 1.7
Cinnamate ion[f]	pH 6.5–13	3.3 ± 0.7	−36 ± 2	14.0 ± 1.3

[a]Temperature range, 17–40°C.
[b]Temperature range, 0–40°C.
[c]From ref. 12.
[d]From ref. 13.
[e]At 25°C.
[f]From ref. 14.

The rate of reaction was found to be first order in both permanganate (Fig. 6) and cinnamate ion (Table 5). Inverse secondary deuterium isotope effects, similar in magnitude to those found when the reaction was studied in 0.5 M NaOH, were observed when the rates of cinnamate ion-α-d and cinnamate ion-β-d were compared with unlabelled substrate (Table 2).

A Hammett plot almost identical to that observed in 0.5 M NaOH was obtained (Fig. 7). Activation parameters obtained from a plot of ln k/T vs. $1/T$ (Fig. 3) have been summarized in Table 4.

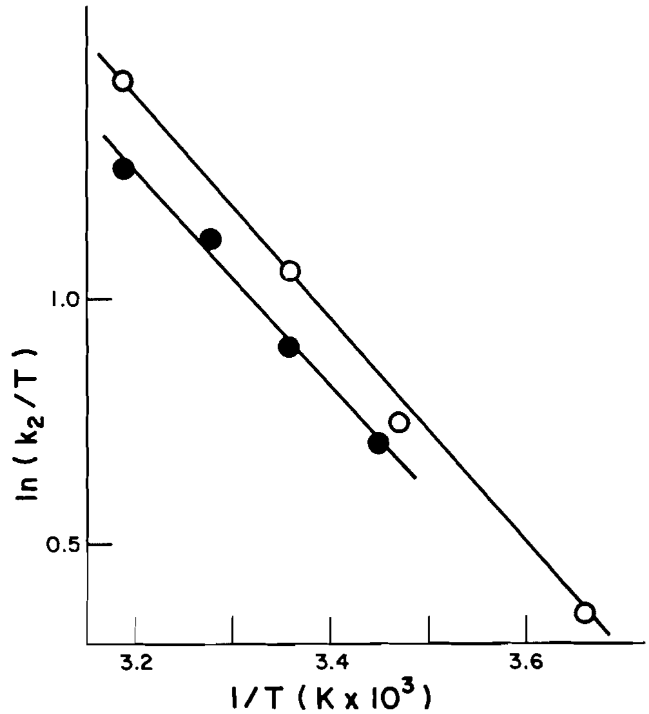

FIG. 3. Activation energy plots. ● 0.50 M NaOH. ○ silicate solutions (pH = 11.3).

Discussion

The results obtained under both sets of conditions described above are consistent with a reaction that is initiated by formation of a cyclic manganate(V) diester in the rate-limiting step, as has previously been suggested by several authors (2, 3, 10):

[1] 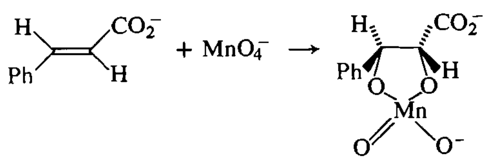

1

The small, positive ρ value may be associated with a stabilization of the ground state by electron-donating groups rather than an effect on the transition state. Stabilization by resonance of the type depicted in structures **2***a* and **2***b* would lead to reduced rates of reaction for those compounds bearing electron-donating substituents.

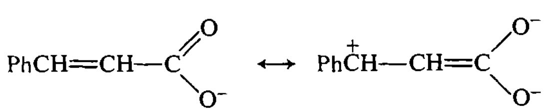

2*a* **2***b*

The inverse secondary deuterium isotope effects, which indicate a change in hybridization from sp^2 in the ground state to sp^3 in the transition state (11), are reminiscent of those obtained when the oxidation of cinnamic acid was studied in 1 M perchloric acid solutions (12). Consequently, it appears as if the transition state may be quite similar under acidic conditions as well. This suggestion is reinforced by noting that similar activation parameters are also obtained under basic, acidic, and nonaqueous conditions (Table 4). However, it is quite possible that a somewhat different transition state is obtained during the oxidation of methyl cinnamates by quaternary ammonium permanganate in nonaqueous solvents, where the observed rate constants are smaller, the substituent effects larger, and the isotope effects different (13).

If the rate-determining steps are the same under both sets of experimental conditions it follows that the different products obtained (MnO_4^{2-} and MnO_2) must be a consequence of post transition state reactions. In 0.5 M NaOH, where the product is MnO_4^{2-}, the stoichiometry indicates that two moles of permanganate are reduced. Consequently, it appears as if the cyclic manganate(V) diester formed in the rate-determining step must be oxidized by permanganate, giving two moles of manganate(VI). The exact point at which this oxidation takes place is, however, open to speculation and at least three possibilities can be considered. In one, the cyclic manganate(V) diester could be oxidized and then hydrolyzed as in eqs. [2] and [3] (2, 14).

[2] 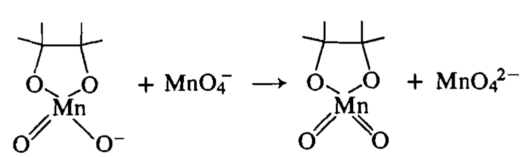

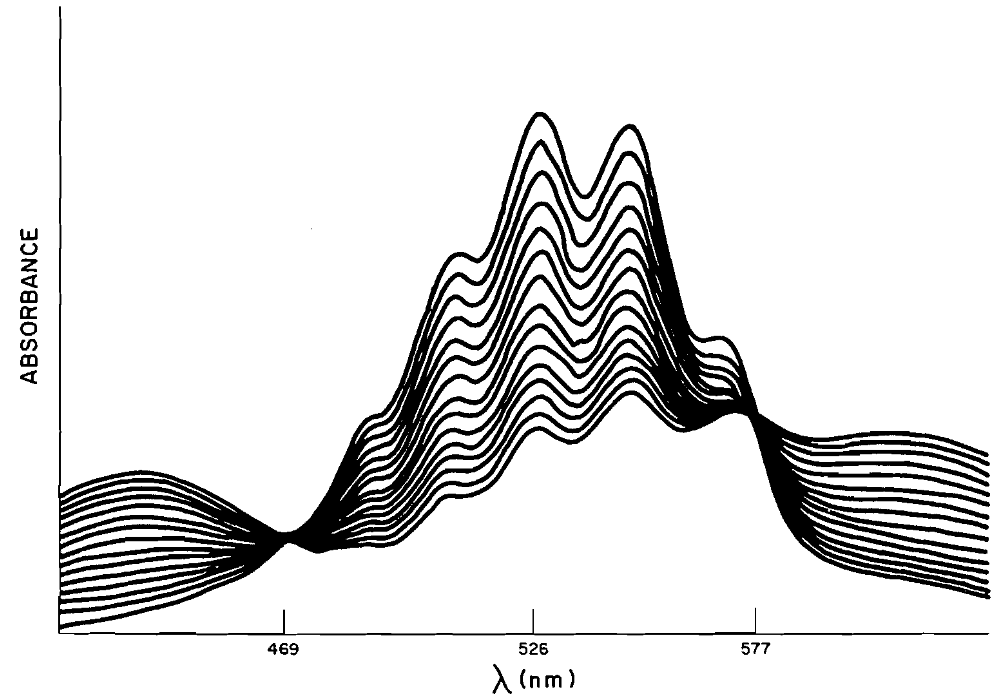

FIG. 4. Sequential scans obtained at 40-ms intervals during the oxidation of cinnamate ion (1.49×10^{-3} *M*) by permanganate (3.80×10^{-4} *M*) in 0.5 *M* NaOH at 25°C.

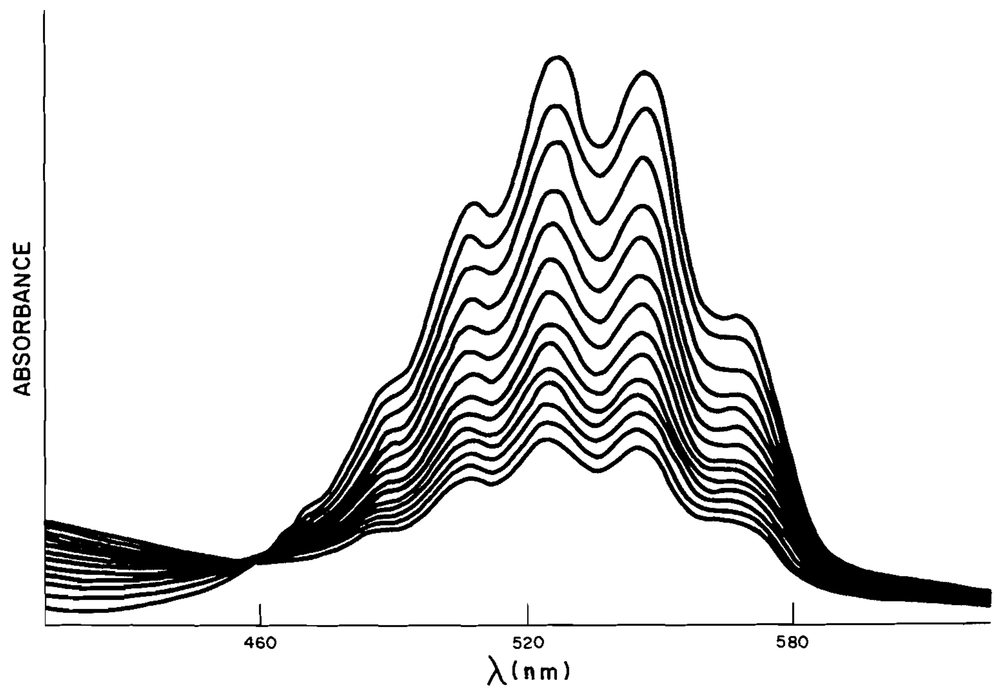

FIG. 5. Sequential scans obtained at 20-ms intervals during the oxidation of cinnamate ion (8.07×10^{-3} *M*) by permanganate (3.88×10^{-4} *M*) in a silicate solution (pH 11.3) at 17°C.

[3] 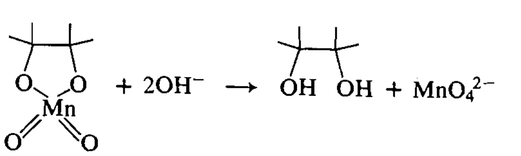

An alternative possibility is suggested by reports that manganate(V) rapidly dimerizes in aqueous solutions (15, 16). Dimerization of **1** followed by oxidation and hydrolysis would also result in the formation of MnO_4^{2-} as the product:

[4] 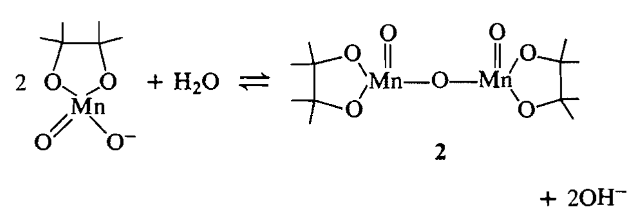

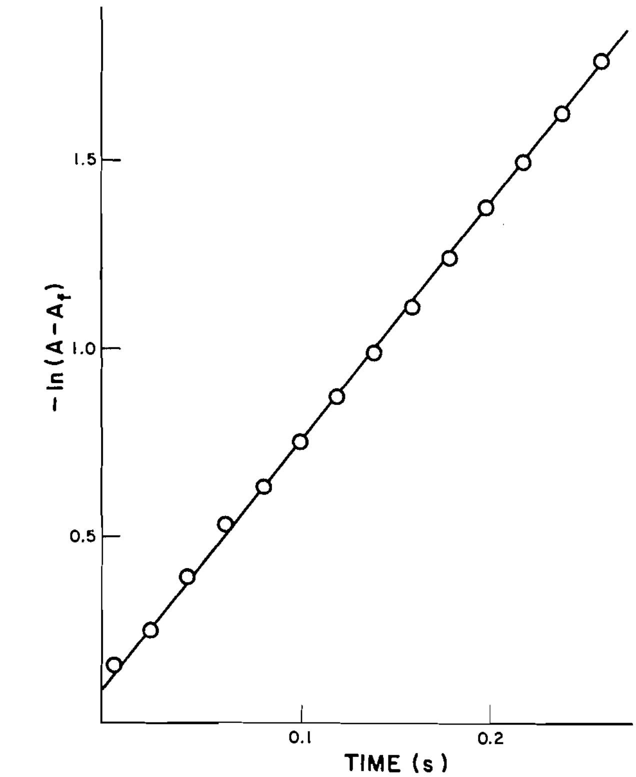

FIG. 6. Typical pseudo-first-order plot for the oxidation of cinnamate ion in silicate solutions. pH = 11.3. [Cinnamate ion] = 8.09 × 10^{-3} *M*. [$KMnO_4^-$] = 3.80 × 10^{-4} *M*. Temperature = 25°C. Slope = 6.10 s^{-1}. Correlation coefficient = 0.999.

[5] $2 + 2MnO_4^- + 2OH^-$

$\longrightarrow$ 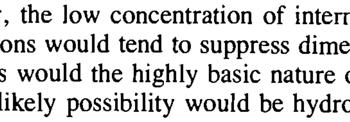 $+ 2MnO_4^{2-} + H_2O$

3

[6] $3 + 4OH^- \longrightarrow 2$ 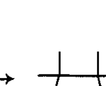 $+ 2MnO_4^{2-}$

However, the low concentration of intermediate present in these solutions would tend to suppress dimer formation (reaction [4]), as would the highly basic nature of the solutions.

A more likely possibility would be hydrolysis of the intermediate followed by oxidation of $HMnO_4^{2-}$ to MnO_4^{2-} as in eqs. [7] and [8].

[7] $1 + H_2O + OH^- \longrightarrow$ 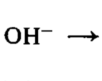 $+ HMnO_4^{2-}$

[8] $MnO_4^- + HMnO_4^{2-} + OH^- \longrightarrow 2MnO_4^{2-} + H_2O$

Whether the first or the third possibility would predominate depends on the relative magnitudes of the bimolecular rate constants for reactions [2] and [7], both of which would be expected to be large. However, the hydrolysis reaction would probably be faster because of the much larger concentration of hydroxide ions as compared to oxidant (0.5 *M* vs. 3 × 10^{-4} *M*). Consequently, although it is impossible to exactly specify the nature of fast reactions which follow the rate-limiting step, it seems most reasonable to propose a sequence consisting of reactions [1], [7], and [8].

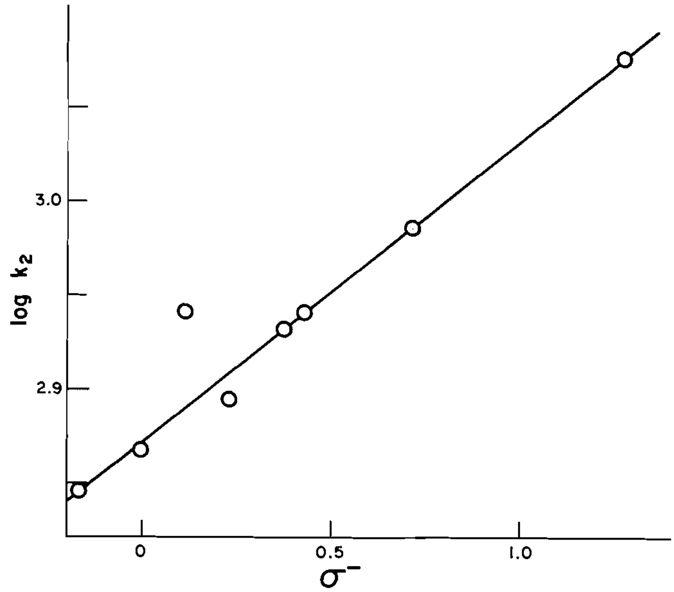

FIG. 7. Hammett plot for the oxidation of substituted cinnamate ions by permanganate in sodium silicate solutions (pH 11.3). Slope = 0.15, correlation coefficient = 0.96. When σ substituent values are used the slope increases to 0.20 and the correlation coefficient drops to 0.91.

TABLE 5. Rate constants for the oxidation of cinnamate ion by permanganate in silicate solutions at pH 11.3[a]

[Cinnamate ion] ($M \times 10^3$)	$k_1(s^{-1})$[b]	$k_2(M^{-1}\ s^{-1})$[c]
4.39	3.26 ± 0.02	742 ± 5
8.09	5.95 ± 0.15	736 ± 18
11.82	8.96 ± 0.26	758 ± 22

[a] Temperature = 25.0 ± 0.1°C, [MnO_4^-] = 3.8 × 10^{-4} *M*.
[b] Pseudo-first-order rate constants (see Fig. 6).
[c] $k_2 = k_1$/[cinnamate ion].

At pH 11.3, where the stoichiometry of the reaction is 0.9 : 1 and the product is manganese dioxide, a different sequence of reactions must follow the rate-determining step. The most likely possibility is that manganate(V), formed in reaction [7], is not stable under these less basic conditions and is immediately reduced to MnO_2 by reaction with the solvent as in eq. [9] (15, 17). This suggestion is consistent with the observation made by Carrington and Symons (17) that manganate(V) is stable only under very basic conditions; in more acidic solutions reduction to manganese dioxide is rapid and autocatalytic (15).

[9] $2HMnO_4^{2-} + H_2O \rightarrow 2MnO_2 + 1/2O_2 + 4OH^-$

This sequence of reactions requires a stoichiometry of $KMnO_4$/alkene = 1 : 1, which is slightly larger than the experimental value of 0.9 : 1. Consequently, there may be a competing reaction sequence that uses oxidant more efficiently. For example, the reaction at pH 11.3 could parallel that in 0.5 *M* NaOH, resulting in the formation of manganate(VI) which would also be unstable under these conditions (2, 17–19). Disproportionation of MnO_4^{2-} according to eq. [10] would lead to a stoichiometry of 0.66:1. A combination of these two sequences could then give the observed stoichiometry.

In order to test this possibility K_2MnO_4 was dissolved in 0.1 *M* NaOH and then diluted with either silicate solution or water to give two solutions of equal basicity. The solution containing silicate disproportionated rapidly according to eq. [10], while the solution not containing silicate reacted much

$$[10] \quad 3MnO_4^{2-} + 2H_2O \rightarrow 2MnO_4^- + MnO_2 + 4OH^-$$

more slowly. Consequently, the possibility exists that the reaction in silicate solutions at pH 11.3 could also consist of eqs. [1] and [7] followed by [8] and [10], or [9]. In any event, it must be assumed that the reactions following the rate-determining step are rapid because no long-lived intermediates were apparent under these conditions (Fig. 5).

In summary, it can be concluded that the formation of different products (MnO_4^{2-} and MnO_2) is not associated with any fundamental change in the mechanism of the reaction between permanganate and carbon–carbon double bonds. Instead, the change in products appears to be due to the greater reactivity of manganese(V) oxides in the less basic solution.

Acknowledgment

The authors are grateful to the Natural Sciences and Engineering Research Council of Canada for financial support, and to Vivekananda College, Madras, for a sabbatical leave to K.N.

1. G. WAGNER. J. Russ. Phys. Chem. Soc. **27**, 219 (1895).
2. R. STEWART. *In* Oxidation in organic chemistry. Part A. *Edited by* K. B. Wiberg. Academic Press, New York. 1965. pp. 1–68.
3. D. G. LEE. *In* Oxidation in organic chemistry. Part D. *Edited by* W. S. Trahanovsky. Academic Press, New York. 1982. pp. 147–206.
4. D. ARNDT. Manganese compounds as oxidizing agents in organic chemistry. Open Court, La Salle. 1981.
5. D. G. LEE and J. R. BROWNRIDGE. Can. J. Chem. **51**, 2102 (1973).
6. I. M. KOLTHOFF and E. B. SANDELL. Textbook of quantitative inorganic analysis. 3rd ed. MacMillan, New York. 1955. p. 181.
7. M. G. HICKS. U.S. Patent No. 4,268,487 (1981).
8. S. W. BENSON. The foundations of chemical kinetics. McGraw–Hill, New York. 1960.
9. E. NARITA and T. OKABE. Ind. Eng. Chem. Prod. Res. Dev. **21**, 662 (1982).
10. F. FREEMAN, C. O. FUSELIER, C. R. ARMSTEAD, C. E. DALTON, P. A. DAVIDSON, E. M. KARCHESFSKI, D. E. KROCHMAN, M. N. JOHNSON, and N. K. JONES. J. Am. Chem. Soc. **103**, 1154 (1981); M. JAKY and L. I. SIMANDI. J. Chem. Soc. 939 (1976); S. WOLFE and C. F. INGOLD. J. Am. Chem. Soc. **103**, 940 (1981); K. B. WIBERG, C. J. DEUTSCH, and J. ROCEK. J. Am. Chem. Soc. **95**, 3034 (1973); A. K. RAPPE and W. A. GODDARD. J. Am. Chem. Soc. **104**, 3287 (1982).
11. E. A. HALEVI. Prog. Phys. Org. Chem. **1**, 109 (1963).
12. D. G. LEE and J. R. BROWNRIDGE. J. Am. Chem. Soc. **96**, 5517 (1974).
13. D. G. LEE and K. C. BROWN. J. Am. Chem. Soc. **104**, 5076 (1982).
14. K. B. WIBERG and R. D. GEER. J. Am. Chem. Soc. **88**, 5827 (1966).
15. S. WOLFE, C. F. INGOLD, and R. U. LEMIEUX. J. Am. Chem. Soc. **103**, 938 (1981).
16. B. JEZOWSKA-TRAEBIATOWSKA and J. NAWOJSKA. Bull. Acad. Pol. Sci. Ser. Sci. Chim. **10**, 361 (1962).
17. A. CARRINGTON and M. C. R. SYMONS. J. Chem. Soc. 3373 (1956).
18. F. R. DUKE. J. Phys. Chem. **56**, 882 (1952).
19. H. I. SCHLESINGER and H. B. SIEMS. J. Am. Chem. Soc. **46**, 1965 (1924).

Viscosities and densities of binary liquid mixtures of *m*-cresol with substituted anilines. Part 3

RAMAMURTHY PALEPU,[1] JOAN OLIVER, AND BRIAN MACKINNON
Department of Chemistry, University College of Cape Breton, Sydney, N.S., Canada B1P 6L2

Received August 15, 1984

RAMAMURTHY PALEPU, JOAN OLIVER, and BRIAN MACKINNON. Can. J. Chem. **63**, 1024 (1985).

Densities and viscosities were determined for the binary systems of *m*-cresol with aniline, *N*-methylaniline, *N,N*-dimethylaniline, *N*-ethylaniline, and *N,N*-diethylaniline at five different temperatures. From the experimental results, the excess volume, excess viscosity, excess molar free energy of activation of flow, excess partial molar volume, and partial molar volumes were calculated. Also various thermodynamic parameters of activation of flow were calculated from the dependence of viscosity on temperature. The deviations from ideality of thermodynamic and transport functions are explained on the basis of molecular interactions between the components of the mixture.

RAMAMURTHY PALEPU, JOAN OLIVER et BRIAN MACKINNON. Can. J. Chem. **63**, 1024 (1985).

Opérant à cinq températures différentes, on a déterminé les densités et les viscosités des systèmes binaires formés d'une part de *m*-crésol et d'autre part d'aniline, de *N*-méthylaniline, de *N,N*-diméthylaniline, de *N*-éthylaniline et de *N,N*-diéthylaniline. A partir de ces résultats expérimentaux, on a calculé les volumes en excès, les viscosités en excès, les énergies libres molaires en excès pour l'activation de l'écoulement, les volumes molaires partiels en excès et les volumes molaires partiels. En se basant sur la variation de la viscosité avec la température, on aussi calculé divers paramètres thermodynamiques pour l'activation de l'écoulement. Il existe des déviations par rapport à l'idéalité des fonctions thermodynamiques et de transport que l'on explique en fonction d'interactions moléculaires entre les composantes des mélanges.

[Traduit par le journal]

Introduction

This paper deals with investigations of the thermodynamic and transport properties of binary liquid mixtures and is a continuation of our previous studies (1–4). The excess viscosity (η^E), excess volume (V^E), excess free energy of activation of flow (G^{*E}), and partial molar volumes ($\bar{V}_i$) have been computed from the experimental results on densities and viscosities for the systems *m*-cresol (MC) + aniline (A), *m*-cresol + *N*-methylaniline (MA), *m*-cresol + *N,N*-dimethylaniline (DMA), *m*-cresol + *N*-ethylaniline (EA), and *m*-cresol + *N,N*-diethylaniline (DEA) at five different temperatures.

Experimental

The methods used in the present investigation have been described previously (3, 4).

Materials and solutions

Chemicals used in the present study are either B.D.H. or Aldrich and purified by standard procedures (5). Only colourless middle fractions were collected and the mixtures were prepared by mixing weighed amounts of pure liquids. Caution was taken to prevent evaporation.

Results

The experimental results for pure liquids agree well with the values from literature (6, 7). Excess volumes for the systems MC + A and MC + DMA were reported by Solimo and Katz at 25°C (8), and the results of the present investigation are in excellent agreement with the published data. The experimental values for all systems at different temperatures[2] were used to calculate the excess thermodynamic functions with the following equations:

$$[1] \quad V = (X_1M_1 + X_2M_2)/\rho$$

$$[2] \quad V^E = V - (X_1V_1^* + X_2V_2^*)$$

$$[3] \quad \eta^E = \eta - (X_1\eta_1^* + X_2\eta_2^*)$$

$$[4] \quad G^{*E} = RT \ln \eta V - (X_1 \ln \eta_1^*V_1^* + X_2 \ln \eta_2^*V_2^*)$$

Here ρ, η, and V are the density, viscosity, and molar volume of the mixture, M_1, M_2, V_1^*, V_2^*, η_1^*, η_2^* are molecular masses, molar volumes, and viscosities of pure components 1 and 2, respectively, and X_i represents the mole fraction of the component i in the solution. The excess quantities Y^E were fitted to the Redlich–Kister (9) equation:

$$[5] \quad Y^E = X_1(1 - X_1)\sum_{j=1}^{n} a_j(1 - 2X_1)^{j-1}$$

Values of coefficients (a_j) of this equation, together with the standard error of estimate (σ) are summarized in Tables 1–3. Figures 1, 2, and 3 show the values of η^E, V^E, and G^{*E} as a function of the mole fraction of *m*-cresol.

The continuous curves were generated using a plotter (Watanabe Miplot), CBM 8032 microcomputer and the values of a_j from eq. [5]. Excess partial molar volumes (V_1^E) and the partial molar volume ($\bar{V}_1$) were computed using the equations:

$$[6] \quad (V_1^E) = (V^E)_{1,2} + (1 - X_1)\left[\frac{\partial(V^E)_{1,2}}{\partial X_1}\right]_{P,T}$$

$$[7] \quad (\bar{V}_1) = V_1^* + (V_1^E)$$

Figures 4 and 5 show the values of $(V_1)^E$, and $(\bar{V}_1)$ as a function of mole fraction of *m*-cresol. Continuous curves were generated with the aid of the plotter.

Various thermodynamic parameters of activation of viscous flow were determined using Eyring's equation (10). According to Eyring

$$[8] \quad \eta = \frac{hN}{V}\exp(\Delta H^{\ddagger}/RT - \Delta S^{\ddagger}/R)$$

where η is the viscosity of the solution, h, N, and V are Planck's constant, Avogadros number, and molar volume,

[1]To whom all correspondence should be addressed.

[2]Five tables containing viscosity and density data are available, at a nominal charge, from the Depository of Unpublished Data, CISTI, National Research Council of Canada, Ottawa, Ont., Canada K1A 0S2.

TABLE 1. Coefficients for least-square fit of results by eq. [5] for excess viscosity (cP)

System	T (K)	a_1	a_2	a_3	a_4	a_5	a_6	σ
Aniline +	298	7.92	−12.01	−2.47	−7.03	2.42	15.78	0.001
m-cresol	303	6.08	−7.54	−4.50	−5.36	7.24	10.74	0.003
	308	4.78	−5.36	−3.65	−1.78	5.06	2.73	0.002
	313	3.74	−3.16	−3.08	−7.84	5.96	9.63	0.004
	318	2.78	−2.88	−0.70	−4.14	1.29	4.95	0.004
N-Methylaniline	298	−4.78	−5.65	5.49	−0.10	−0.99		0.002
+ *m*-cresol	303	−3.00	−4.50	1.72	3.70	3.27		0.001
	308	−1.70	−3.30	2.35	1.31	−2.89		0.003
	313	−1.07	−2.55	0.60	3.63	−1.38	−3.20	0.004
	318	−0.70	−2.55	−3.49	3.32	4.55		0.001
N,*N*-Dimethylaniline	298	−13.03	4.88	0.20	−8.32	7.86		0.006
+ *m*-cresol	303	−8.88	2.81	0.50	−4.34	3.22		0.005
	308	−6.07	1.97	−0.52	−3.50	3.52		0.004
	313	−4.43	1.52	−0.60	−2.66	2.46		0.004
	318	−5.13	−0.45	−4.58	−1.89	−1.58	−8.73	0.019
N-Ethylaniline	298	−3.75	−11.87	10.94	3.70	−5.97		0.015
+ *m*-cresol	303	−2.13	−8.99	4.50	4.91	−0.76		0.007
	308	−1.10	−7.21	2.19	5.76			0.001
	313	−0.64	−5.55	7.30	5.74			0.004
	318	−0.38	−4.55	−0.41	6.22			0.001
N,*N*-Diethylaniline	298	−9.78	−0.97	10.17	−17.63	−1.16	15.56	0.006
+ *m*-cresol	303	−6.59	−1.67	7.91	−10.49	−2.86	10.62	0.006
	308	−4.25	−2.14	4.50	−1.63	−1.37		0.056
	313	−3.31	−2.09	4.57	0.06	−3.64		0.003
	318	−2.58	−1.69	4.54	0.62	−5.02		0.001

TABLE 2. Coefficients for least-square fit of results by eq. [5] for excess molar free energy of activation flow (J mol^{-1})

System	T (K)	a_1	a_2	a_3	a_4	a_5	a_6	σ
Aniline +	298	3922.00	−1212.00	−1945.00	−3582.00	1427.00	5057.00	9.0
m-cresol	303	3694.00	−918.90	−2557.00	−3638.00	3392.00	5542.00	9.8
	308	3445.00	−1080.00	−1943.00	−701.60	1785.00		13.0
	313	3217.00	−496.40	−2433.00	−5620.00	3695.00	6790.00	9.0
	318	2863.00	−906.40	−1097.00	−3491.00	911.20	3550.00	7.2
N-Methylaniline	298	1996.00	−1698.00	102.50	95.09			2.2
+ *m*-cresol	303	1815.00	−1820.00	−1240.00	1666.00	4670.00	2627.00	2.0
	308	1777.00	−1408.00	15.28	312.80	−1179.00		4.4
	313	1620.00	−1412.00	−380.40	247.30	−987.10	−2999.00	3.3
	318	1509.00	−1948.00	−5285.00	−50.12	6974.00	4245.00	5.3
N,*N*-Dimethylaniline	298	−816.10	−837.90	1017.00	−2217.00			16.0
+ *m*-cresol	303	−668.90	−773.00	548.10	−1584.00			11.0
	308	−495.80	−389.20	−35.62	−2076.00	446.30		6.6
	313	−482.90	−96.47	−40.75	−2308.00			12.0
	318	−4047.00	−2697.00	−5843.00	−8672.00	−7739.00	−7295.00	15.0
N-Ethylaniline	298	2448.00	−3545.00	142.70	1837.00			10.0
+ *m*-cresol	303	2248.00	−3714.00	−1447.00	2904.00	2486.00		10.0
	308	2155.00	−3777.00	−1934.00	3917.00	3281.00		12.0
	313	1994.00	−3611.00	−2284.00	4388.00	3338.00		12.0
	318	1814.00	−3708.00	−2994.00	5502.00	3803.00		14.0
N,*N*-Diethylaniline	298	29.79	−2247.00	1954.00	−3551.00	−611.30	4697.00	17.0
+ *m*-cresol	303	41.30	−2542.00	2485.00	13.97	−2123.00		23.0
	308	310.9	−1532.00	303.7	−6276.00	868.50	9038.00	17.0
	313	−23.25	−2689.00	2117.00	2623.00	−2586.00	−2648.00	2.8
	318	−181.6	−2565.00	3137.00	3577.00	−4490.00	−3758.00	2.1

respectively.

When ln ($\eta V/hN$) is plotted against $1/T$, the slope is equal to $\Delta H^{\ddagger}/R$ and the intercept is equal to $-\Delta S^{\ddagger}/R$. Using both graphical and least-squares method, the activation parameters $\Delta H^{\ddagger}$ and $\Delta S^{\ddagger}$ were obtained and $\Delta G^{\ddagger}$ was obtained using the equation:

$$[9] \quad \Delta G^{\ddagger} = \Delta H^{\ddagger} - T\Delta S^{\ddagger}$$

Values obtained are presented in Table 4.

Discussion

Association of phenol and substituted phenols through inter-

TABLE 3. Coefficients for least-square fit of results by eq. [5] for excess volume ($cm^3\ mol^{-1}$)

System	T (K)	a_1	a_2	a_3	a_4	a_5	a_6	σ
Aniline +	298	−1.41	0.12	0.55	0.13	−0.47		0.005
m-cresol	303	−1.37	0.12	0.31	0.05	−0.09		0.006
	308	−1.40	0.06	0.24	0.11			0.002
	313	−1.42	−0.022	0.26	0.15	0.003		0.007
	318	−1.36	0.079	−0.08	0.05	0.63		0.002
N-Methylaniline	298	−1.38	0.13	0.16	0.43	−0.09		0.009
+ *m*-cresol	303	−1.35	0.36	−0.23	−0.33	0.57		0.007
	308	−1.33	0.32	0.06	−0.37			0.009
	313	−1.32	0.48	0.14	−0.60	0.37		0.012
	318	−1.26	0.50	−0.07	−0.51	0.64		0.013
N,*N*-Dimethylaniline	298	−1.48	−0.14	1.87	1.10	−3.41		0.009
+ *m*-cresol	303	−1.41	0.56	0.17				0.004
	308	−1.42	0.65	0.06	−0.27			0.005
	313	−1.41	0.59	0.04	−0.29			0.008
	318	−1.35	0.58	−0.15	−0.38	0.51		0.005
N-Ethylaniline	298	−2.29	0.55	0.66				0.009
+ *m*-cresol	303	−2.19	0.05	−0.13	0.52	0.11		0.006
	308	−2.07	0.24	0.18	0.35	0.58		0.007
	313	−2.04	0.08	0.70	0.55	2.20	−1.80	0.011
	318	−2.17	0.14	−2.70	−2.97	8.13	7.14	0.017
N,*N*-Diethylaniline	298	−2.77	1.03	−0.19	0.24	−0.24		0.015
+ *m*-cresol	303	−0.82	4.76	−10.42	−7.59	12.31		0.010
	308	−0.81	4.26	−12.02	−7.08	14.51		0.014
	313	−0.72	4.33	−8.82	−7.05	9.81		0.014
	318	−0.67	4.55	−11.30	−6.90	14.04	−1.07	0.008

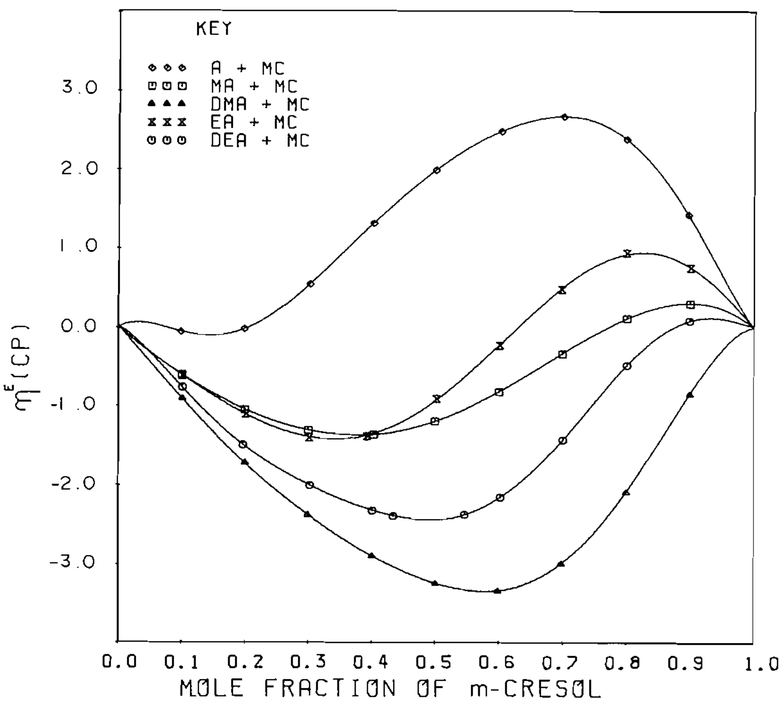

FIG. 1. Plot of excess viscosity vs. mole fraction of *m*-cresol.

molecular hydrogen bonding has been inferred on the basis of studies relating to physical properties (11). The hydrogen bond in the association of phenols is of O—H---O type, the strength of which is determined by the geometry of the molecules and the nature of the substituents in the phenol molecules. The choice of *m*-cresol was based on its ability to form intermolecular hydrogen bonds, compared to the limited ability of *o*-chlorophenol to form intermolecular hydrogen bonding. This is useful when comparing the present result to the results of *o*-chlorophenol with anilines (4). The above systems can be classified as both polar and associated systems (12). In nonelectrolyte systems, positive deviations from ideal behaviour are attributed to dispersion forces (13) and negative deviations to the geometric considerations (14). Attempts have been made to explain the behaviour of liquid mixtures on the basis of sign and magnitude of the excess viscosity and excess volume.

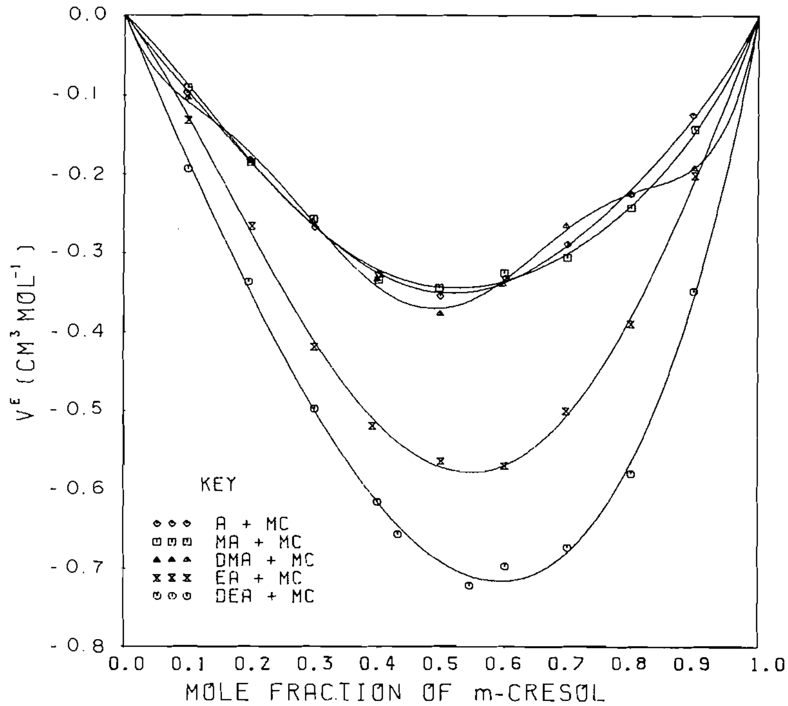

FIG. 2. Plot of excess volume vs. mole fraction of *m*-cresol.

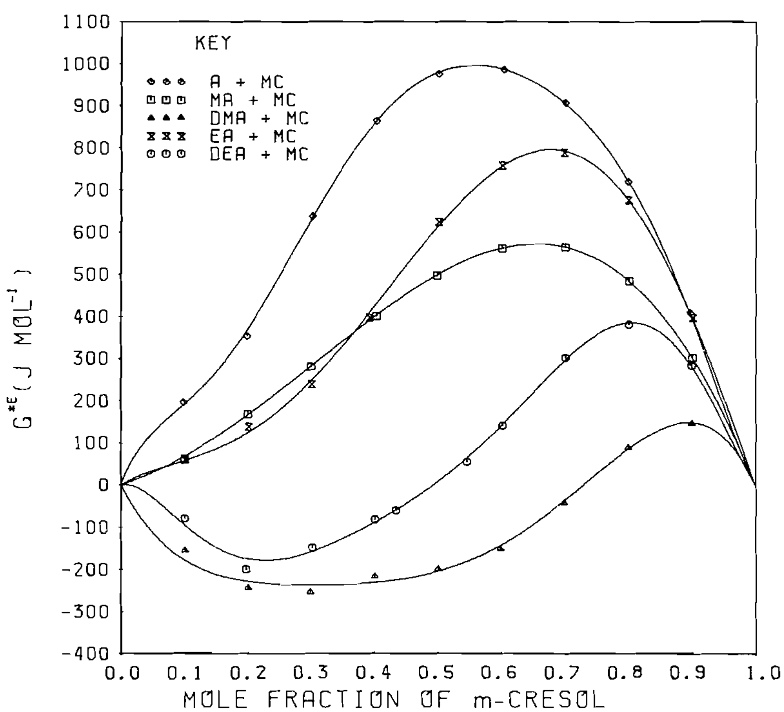

FIG. 3. Plot of excess free energy of activation vs. mole fraction of *m*-cresol.

Examination of Fig. 1 shows that the values of η^E become negative initially when MC is added and positive at higher mole fraction of MC. However, in the case of the system (DMA + MC) the η^E values remain negative in the entire range of composition. According to Fort and Moore (15) the values of η^E are negative for systems of different molecular size in which dispersion forces are dominant. The η^E values become less negative and then increasingly positive as the strength of the interaction increases. In the present study, all the chemical species are cyclic, so that small differences of size in the molecules are not important in the excess viscosity. The positive η^E values for the systems (A + MC), (MA + MC), and (EA + MC) indicate the strength of interaction increases at higher concentration of *m*-cresol probably due to association between *m*-cresol and anilines through hydrogen bonding. The values of η^E are equal to zero for all systems except (DEA + MC) at a definite mole fraction of MC. The composition at which η^E is equal to zero depends on the type of system and

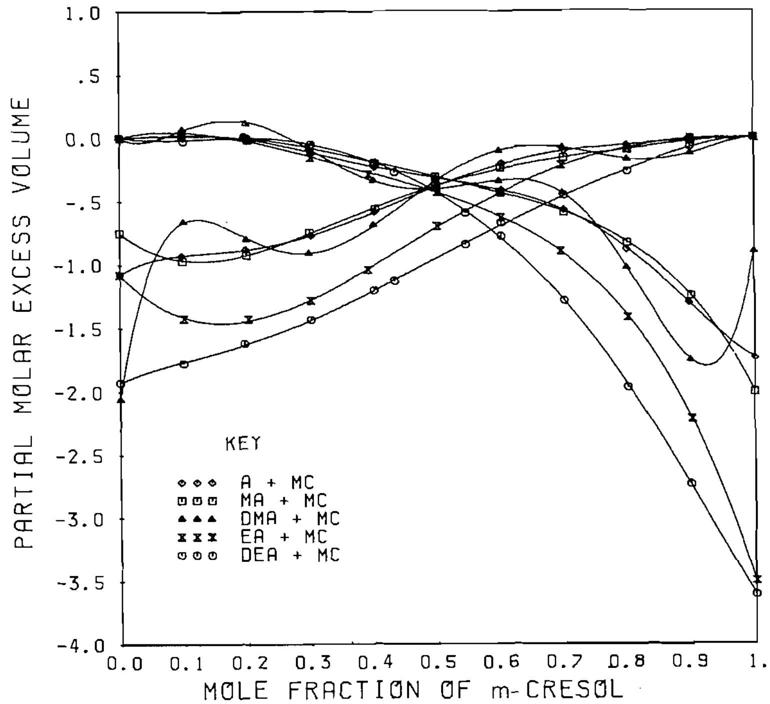

FIG. 4. Plot of partial molar excess volumes vs. mole fraction of *m*-cresol.

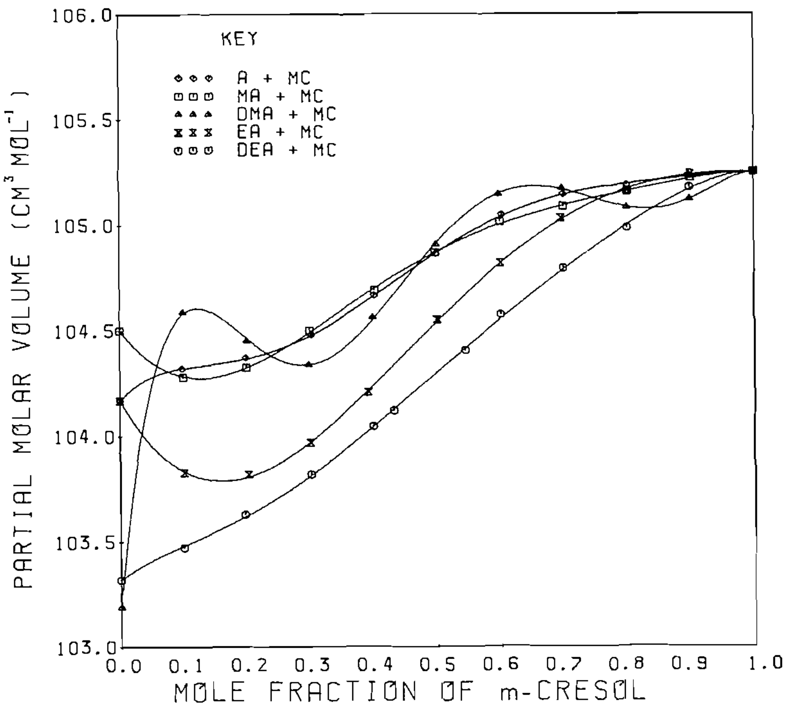

FIG. 5. Plot of partial molar volume vs. mole fraction of *m*-cresol.

whether or not the system behaves like an ideal one at this composition.

The negative values of V^E in Fig. 2 for the five systems are explained by Prigogine (16) in terms of different sizes of the molecules or the dipole–dipole interaction between them. The intermolecular association complex also contributes to these negative values. Since all the species are cyclic, the small differences of size in the molecules are not important in the excess molar volume. The minimum values of V^E for these systems can be explained in terms of acid–base interaction between *m*-cresol and anilines. The strength of the base follows the order DEA > EA > DMA > MA > A. The value at the minima for the system (A + MC) is slightly more negative than that of (MA + MC), and this may be due to the ability of aniline to form stronger hydrogen bonds with *m*-cresol than MA with MC. If H is defined as η/η_i where η is the experimental viscosity of the mixture and $\ln \eta_i = X_1 \ln \eta_1 + X_2 \ln \eta_2$ then according to Stairs (17), H is related to the ideal free

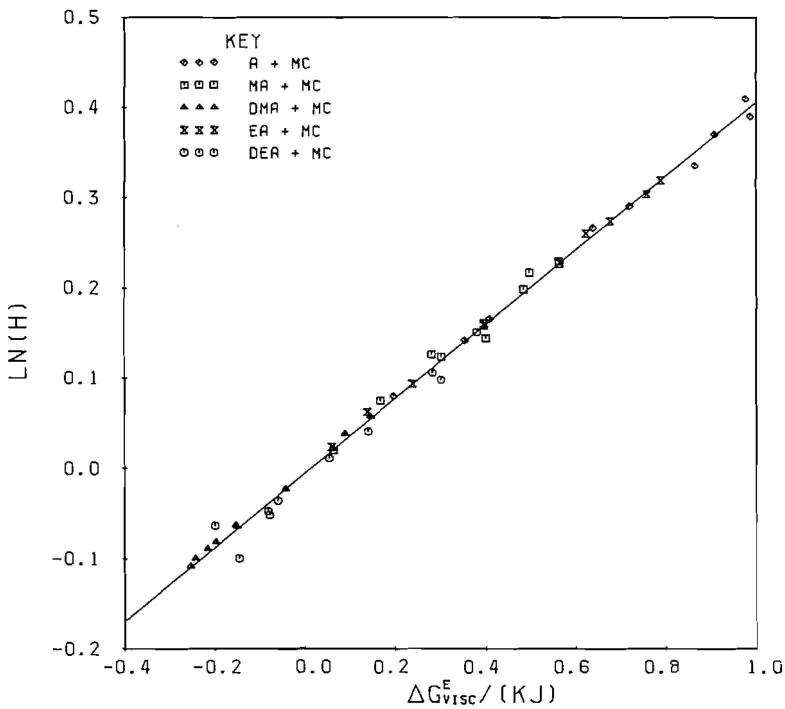

FIG. 6. Plot of ln H vs. G^{*E}.

TABLE 4. Activation parameter for viscous flow

System	x_1^*	$\Delta H^{\ddagger}$	$\Delta S^{\ddagger}$	$\Delta G^{\ddagger}$
Aniline + *m*-cresol	0.0000	22.30	19.17	16.59
	0.0989	25.36	27.56	17.15
	0.1989	27.56	33.29	17.64
	0.3022	30.20	40.10	18.26
	0.4024	32.82	46.98	18.82
	0.4997	34.88	52.42	19.26
	0.6028	36.57	56.91	19.61
	0.6996	37.36	58.79	19.34
	0.7998	37.51	58.79	20.00
	0.8970	37.28	57.88	20.03
	1.0000	37.87	60.09	19.97
N-Methylaniline + *m*-cresol	0.0000	16.47	3.32	15.48
	0.1000	20.26	14.07	16.07
	0.2003	24.21	25.52	16.61
	0.2996	26.26	30.64	17.13
	0.4033	27.66	33.46	17.69
	0.4984	29.38	37.50	18.21
	0.6003	32.10	44.85	18.73
	0.6996	35.18	53.67	19.18
	0.8006	37.86	61.41	19.56
	0.9002	38.84	63.84	19.82
	1.0000	37.87	60.09	20.00
N,*N*-Dimethylaniline + *m*-cresol	0.0000	10.53	−14.36	14.81
	0.1006	12.84	−7.82	15.17
	0.1999	15.59	−0.07	15.62
	0.2985	16.94	2.79	16.11
	0.4002	19.01	7.90	16.65
	0.4997	22.01	16.19	17.19
	0.5979	26.46	29.22	17.76
	0.6977	31.28	43.24	18.39
	0.7997	35.16	54.11	19.04
	0.8992	37.09	58.72	19.59
	1.0000	37.87	60.09	19.97
N-Ethylaniline + *m*-cresol	0.0000	16.49	2.16	15.84
	0.1010	17.61	4.29	16.33
	0.2022	22.50	19.15	16.79
	0.3013	25.62	27.91	17.31
	0.3924	27.58	32.65	17.85
	0.5013	30.12	38.89	18.53
	0.6010	32.80	46.06	19.07
	0.6981	35.85	54.85	19.51
	0.8003	38.70	63.38	19.82
	0.9008	39.92	66.97	19.96
	1.0000	37.88	60.10	19.97
N,*N*-Diethylaniline + *m*-cresol	0.0000	15.24	−3.80	16.38
	0.1005	18.22	4.51	16.68
	0.1971	18.36	5.66	16.38
	0.3018	21.78	14.95	17.32
	0.4008	25.03	24.41	17.76
	0.4336	25.78	26.43	17.90
	0.5455	28.12	32.58	18.41
	0.6016	29.50	36.28	18.69
	0.7004	32.65	45.13	19.20
	0.8005	36.10	55.21	19.64
	0.8988	38.12	61.18	19.89
	1.0000	37.87	60.09	19.97

*Mole fraction of *m*-cresol, units: $\Delta H^{\ddagger}$, $\Delta G^{\ddagger}$ (kJ mol^{-1}), $\Delta S^{\ddagger}$ (J mol^{-1}).

volume (V_i) of the solution by the equation:

$$[10] \quad H^{-1} = (V_i + V^{E})/V_i$$

According to eq. [10], a plot of H^{-1} vs. V^{E} should be linear. However, when H^{-1} is plotted against V^{E}, a nonlinear plot was obtained in the present study. In our previous studies (3, 4) when ln H is plotted against G^{*E}, a single straight line with a zero intercept was obtained. This type of result is not unexpected, because the expression for G^{*E} takes into account both viscosity and volume.

All the systems involved in our previous studies exhibited positive η^E and negative V^E; however, in the present study when ln H is plotted against G^{*E}, a single straight line with nonzero intercept is obtained (Fig. 6). This behaviour is not unusual since in the present study the η^E values are both positive and negative and V^E values are negative. In the temperature range investigated, the values of $\Delta H^{\ddagger}$ are positive and vary in the order MC > A > EA > MA > DEA > DMA, indicating that association and dipole–dipole interactions increase the value of $\Delta H^{\ddagger}$. Except for DEA and DMA, the $\Delta S^{\ddagger}$ values are positive. The values of $\Delta H^{\ddagger}$ and $\Delta G^{\ddagger}$ for the mixtures are positive for each binary system studied and increase with increase in *m*-cresol concentration. Entropy of activation is positive for all systems except for DMA and DEA with MC in amine-rich regions.

According to Reed and Taylor (18) and Meyers *et al.* (19), the G^{*E} parameter may be considered a reliable measure to detect the presence of interaction between molecules. Positive values of G^{*E} can be seen in binary systems where specific interactions between molecules take place. G^{*E} values are positive at all compositions for the mixtures of MC with A, MA, and EA. For the other systems it is negative at low concentrations of MC and becomes positive at higher concentrations. From the values of G^{*E}, one can conclude that the strength of specific interactions varies in the order A + MC > EA + MC > MA + MC > DEA + MC > DMA + MC.

Examination of Fig. 5 reveals that the addition of 1 mol of *m*-cresol in a large volume of the different bases produces a volume contraction in the order MA < EA ≅ A < DEA < DMA. According to Somsen and co-workers (20) better information on interactions in binary mixtures can be deduced from the shape of the curve obtained when partial molar volume is plotted against composition. A pronounced minimum in the curve indicates the strength of the interactions.

From the analysis of the results one can conclude that the strength of specific interactions between *m*-cresol with substituted anilines varies in the order A + MC > EA + MC > MA + MC > DEA + MC > DMA + MC. The type of interactions are mainly acid–base interactions and hydrogen bonding. Also the strength of interactions is less pronounced in *m*-cresol compared to *o*-chlorophenol. This could be attributed to these facts: (*a*) *o*-chlorophenol is a stronger acid than *m*-cresol and (*b*) absence of polymerization through intermolecular hydrogen bonding in *o*-chlorophenol compared to *m*-cresol.

Acknowledgements

The financial support of the Natural Science and Engineering Council of Canada and C.E.R.P. (UCCB) is appreciated. The authors (J.O. and B.M.) wish to acknowledge the summer research stipends provided by the Cape Breton Development Corporation.

1. R. PALEPU and L. MOORE. Thermochem. Acta, **30**, 384 (1979).
2. R. PALEPU and L. MOORE. Thermochem. Acta, **37**, 109 (1980).
3. D. J. G. IRWIN, R. JOHNSON, and R. PALEPU. Thermochem. Acta. In press.
4. R. PALEPU, J. OLIVER, and D. CAMPBELL. J. Chem. Eng. Data, To be published.
5. A. WEISSBERGER, E. S. PROSKAUER, J. A. RIDDICK, and E. E. ROOPS. Organic solvents. Vol. VII. 2nd ed. Interscience Publ., New York. 1955.
6. J. TIMMERMANS. Physico-chemical constants of pure organic compounds. Elsevier Publishing Co. Inc., New York. 1950.
7. R. R. DREISBACH. Adv. Chem. Ser. 15 (1955).
8. H. N. SOLIMO and M. KATZ. An. R. Soc. Esp. Fis. Quim. **72**, 297 (1976).
9. O. REDLICH and A. T. KISTER. Ind. Eng. Chem. **40**, 345 (1948).
10. H. EYRING, R. E. POWELL, and W. E. ROSEWEARE. Ind. Eng. Chem. **33**, 837 (1941).
11. C. G. PIMENTEL and L. A. MCCLELLAN. The hydrogen bond. W. H. Freeman, London. 1960.
12. J. A. BARKER and F. SMITH. J. Chem. Phys. **22**, 375 (1954).
13. J. O. HIRSCHFELDER, C. F. CURTIS, and R. B. BIRD. Molecular theory of gases and liquids. John Wiley and Sons, Inc., NY. 1954.
14. E. A. GUGGENHEIM. Mixtures. Oxford University Press, Oxford. 1952. p. 29.
15. R. J. FORT and W. R. MOORE. Trans. Faraday Soc. **62**, 1112 (1966).
16. I. PRIGOGINE. The molecular theory of solutions. North Holland Publishing Co., Amsterdam. 1957.
17. R. A. STAIRS. Can. J. Chem. 58, 296 (1980).
18. T. M. REED and T. E. TAYLOR. J. Phys. Chem. **63**, 58 (1959).
19. R. MEYER, M. MEYER, J. METZER, and A. PENELOUX. J. Chem. Phys. **62**, 405 (1971).
20. C. DEVISSER, W. J. M. HEUVELSLAND, L. A. DUNN, and G. SOMSEN. J. Chem. Soc. Faraday Trans. 1, **74**, 1159 (1978).

Dipole moments of some aromatic and aliphatic aldehydes. Their dependence on the solvent and the atomic polarization

CONSTANTINO GROSSE,[1] MAGDALENA MECHETTI, AND PEDRO BRITO

Instituto de Física, Facultad de Ciencias Exactas y Tecnología, Universidad Nacional de Tucumán, 4000 Tucumán, R. Argentina

Received May 2, 1984

CONSTANTINO GROSSE, MAGDALENA MECHETTI, and PEDRO BRITO. Can. J. Chem. **63**, 1031 (1985).

The dipole moments of 21 aromatic and aliphatic aldehydes were determined. Permittivity measurements were performed on highly diluted cyclohexane solutions at 20°C. The limiting forms of Debye's, Onsager's, and Bordewijk's expressions were used. The influence of the solvent on the dipole moment values was studied using decalin and heptane mixtures. Only the Debye's values presented an apparent solvent effect while the Onsager's and Bordewijk's values remained independent of the solvent. Dipole moment values obtained using the refractive indexes of the components were also compared with those derived using the refractive indexes of the mixtures. This permitted one to estimate in 0.07 the relation between atomic and electronic polarization.

CONSTANTINO GROSSE, MAGDALENA MECHETTI et PEDRO BRITO. Can. J. Chem. **63**, 1031 (1985).

On a mesuré les moments dipolaires de vingt et un aldéhydes aliphatiques et aromatiques. On a effectué les mesures de permitivité à 20°C, sur des solutions très diluées dans le cyclohexane. On a utilisé les formes limites des expressions de Debye, Onsager et Bordewijk. De plus, utilisant des mélanges de décaline et d'heptane, on a étudié l'influence des solvants sur les valeurs des moments dipolaires. Les valeurs obtenues à l'aide de l'expression de Debye sont les seules à présenter un effet apparent de solvant; les valeurs obtenues à l'aide des expressions de Onsager ou de Bordewijk sont indépendantes du solvant. On a aussi comparé les valeurs des moments dipolaires obtenues à l'aide des indices de réfraction des composantes avec les valeurs que l'on peut dériver des indices de réfraction des mélanges. Sur cette base, on peut évaluer à 0,07 la relation entre les polarisations atomique et électronique.

[Traduit par le journal]

1. Introduction

The main purpose of this work is to determine the dipole moments of a series of aromatic and aliphatic aldehydes. This was accomplished as usual (1, 2) by measuring the static dielectric permittivity of dilute polar − non-polar solutions.

A definite theoretical expression relating the solution permittivity with microscopic properties has not yet been obtained. Existing treatments generally assume an ideal behaviour neglecting correlations, complex formation, volume variations, and molecular anisotropies. In the high dilution limit, a linear variation of the static dielectric permittivity with concentration is expected. Different theories lead to different slopes and consequently, to different values for the dipole moment of the solute molecule. Despite its being an old problem this subject maintains a permanent interest as can be seen from the literature (3−7).

In this paper the high dilution limiting forms of the expressions due to Debye (1), Onsager (2), and Bordewijk (5), were used. In order to determine the importance of the solvent effect, some aldehydes were studied in three different solvents. Using measurements of the refractive indexes of these same mixtures, the values of the atomic polarization were also estimated.

2. Theoretical expressions for the static dielectric permittivity of solutions

The theoretical expressions most currently used to determine the molecular dipole moments in solution are those deduced by Debye and Onsager. In the limit of very low concentrations, they can be written, respectively, as

$$[1]\quad \epsilon_{1,2} = \epsilon_2 + K_1\left(\frac{N_1\mu^2_{\mathrm{Deb}}}{9\epsilon_0 kT}\right)\frac{(\epsilon_2+2)^2}{3} + K_1\frac{(\epsilon_{\infty 1}-\epsilon_2)(\epsilon_2+2)}{(\epsilon_{\infty 1}+2)}$$

$$[2]\quad \epsilon_{1,2} = \epsilon_2 + K_1\left(\frac{N_1\mu^2_{\mathrm{Ons}}}{9\epsilon_0 kT}\right)\frac{3\epsilon_2^2(\epsilon_{\infty 1}+2)^2}{(2\epsilon_2+\epsilon_{\infty 1})^2} + K_1\frac{(\epsilon_{\infty 1}-\epsilon_2)3\epsilon_2}{(2\epsilon_2+\epsilon_{\infty 1})}$$

where $\epsilon_{1,2}$ and ϵ_2 are the mixture and solvent permittivities, $\epsilon_{\infty 1}$ is the part of the solute permittivity associated with its total induced polarization, N_1 is the number of solute molecules per unit volume in pure state, and K_1 is the volume concentration. Equations [1] and [2] have been deduced in the framework of a continuum approach. A more rigorous expression for the permittivity has been obtained by Bordewijk (5). For polar−non-polar solutions of isotropic non-correlated molecules it writes as

$$[3]\quad \frac{(\epsilon_{1,2}-\epsilon_{\infty 1,2})(2\epsilon_{1,2}+\epsilon_{\infty 1,2})}{\epsilon_{1,2}(\epsilon_{\infty 1,2}+2)^2} = K_1\left(\frac{N_1\mu^2_{\mathrm{Bord}}}{9\epsilon_0 kT}\right)\left(\frac{3\epsilon_{\infty 1,2}(\epsilon_{\infty 1}+2)}{(2\epsilon_{\infty 1,2}+\epsilon_{\infty 1})(\epsilon_{\infty 1,2}+2)}\right)$$

where $\epsilon_{\infty 1,2}$ is the solution permittivity associated with the total induced polarization.

Before comparing the limiting form of eq. [3] with expressions [1] and [2], a functional relation between $\epsilon_{\infty 1,2}$ and $\epsilon_{\infty 1}$, ϵ_2, and K_1 is needed. Assuming that this relation is given by the Clausius−Mossotti equation (8, 9),

$$[4]\quad \frac{(\epsilon_{\infty 1,2}-\epsilon_2)}{(\epsilon_{\infty 1,2}+2)} = K_1\frac{(\epsilon_{\infty 1}-\epsilon_2)}{(\epsilon_{\infty 1}+2)}$$

the following result is obtained:

[1] Member of the Consejo Nacional de Investigaciones Científicas y Técnicas de la República Argentina, to whom all correspondence should be addressed.

TABLE 1. Molecular weights, densities, static dielectric permittivities, and refractive indexes of the solvents used

Substance	M_2	d_2 (g/cm^3)	ϵ_2	n_{D2}
Cyclohexane	84.16	0.779	2.021	1.426
Heptane	100.21	0.683	1.920	1.387
Decalin	138.26	0.886	2.165	1.480

TABLE 2. Molecular weights and densities of pure solutes, measured variations with the concentration of the static dielectric permittivity of cyclohexane solutions

Substance	M_1	d_1 (g/cm^3)	$\frac{\epsilon_{1,2} - \epsilon_2}{x}$
Benzaldehyde	106.12	1.05	9.35
o-Toluyaldehyde	120.15	1.04	8.72
m-Toluyaldehyde	120.15	1.02	10.36
p-Toluyaldehyde	120.15	1.02	12.36
2-Fluorbenzaldehyde	124.12	1.19	9.92
3-Fluorbenzaldehyde	124.12	1.18	8.33
4-Fluorbenzaldehyde	124.12	1.179	4.52
Mesitylen-2-carbaldehyde	148.21	1.020	10.27
1-Naphtaldehyde (α)	156.19	1.140	10.03
Piridine 3-aldehyde	107.11	1.140	6.11
Piridine 4-aldehyde	107.11	1.139	3.52
Furfural	96.09	1.16	11.64
Thiophen 2-aldehyde	112.15	1.226	12.76
n-Formylpiperidine	113.16	1.019	16.52
Cyclohexancarbaldehyde	112.17	0.903	6.53
Bromal	280.76	2.67	3.08
Pivaldehyde	86.14	0.778	3.75
Butyraldehyde	72.11	0.803	5.25
Crotonaldehyde	70.09	0.855	12.36
Hidrozimtaldehyde	134.18	1.01	6.10
n-Valeraldehyde	86.14	0.808	6.32

$$[5] \quad \epsilon_{1,2} = \epsilon_2 + K_1\left(\frac{N_1\mu^2_{\mathrm{Bord}}}{9\epsilon_0 kT}\right)\frac{3\epsilon_2^2(\epsilon_{\infty 1} + 2)^2}{(2\epsilon_2 + \epsilon_{\infty 1})^2} + K_1\frac{(\epsilon_{\infty 1} - \epsilon_2)(\epsilon_2 + 2)}{(\epsilon_{\infty 1} + 2)}$$

This expression combines the best features of eq. [1] and [2]: the non-dipolar part of Debye and the dipolar part of Onsager.

3. Experimental details

Static dielectric measurements were performed at the Microwave Laboratory of the Johannes Gutenberg University of Mainz, Germany, by one of us (C.G.). The apparatus and the experimental techniques used have been previously described (10, 11). For most measurements the solvent was cyclohexane which is, probably, the solvent best suited for dielectric studies (12). Heptane and decalin were also used to estimate the solvent effect.

The solvents, Table 1, were obtained from Merck and dried with 3 Å molecular seeds. The solutes, Table 2, in the highest purity available, usually purissimus grade, were obtained from Fluka. The solutions were also dried with molecular seeds. The data included in these tables, and later used in the calculation, were taken from the supplier's catalogs except for those in the last column in Table 2.

The parameters deduced from the measurements performed on highly diluted solutions are all linear functions of concentration. Therefore, the significant values are the corresponding slopes rather than the absolute values. In our case, the important quantity is the difference between the static dielectric permittivities of the solutions and of the pure solvent divided by the molar concentration: $(\epsilon_{1,2} - \epsilon_2)/x$.

In order to improve the precision of the results, measurements were performed at the following concentrations: x = 0.001, 0.002, 0.003, and 0.004, and the slopes were obtained by least-squares fits. The results obtained appear on Table 2, their accuracy being of the order of 1%.

4. Determination of the dipole moments

Before using eqs. [1], [2], and [5], in order to obtain the values of the dipole moments of the different solute molecules, the values of the permittivities $\epsilon_{\infty 1}$ must be assessed. They can not be directly measured since at high frequencies other absorption processes are present (13). Therefore, the induced polarization, $P_i = P_e + P_a$, where P_e is the electronic and P_a the atomic polarization, is often taken as being equal to P_e or proportional to it. The proportionality constant depends on the molecule considered and usually ranges between 1 and 1.15 (14). In this paper, both these extreme cases were considered. The dipole moments thus obtained are given in Table 3, where the first values in each column correspond to the case $\epsilon_{\infty 1} = n^2_{D1}$, while the second ones corresponds to

$$(\epsilon_{\infty 1} - 1)/(\epsilon_{\infty 1} + 2) = 1.15(n^2_{D1} - 1)/(n^2_{D1} + 2)$$

They are also compared to existing values (14) measured in solution at 20−25°C. When more than one dipole moment is reported the extreme values are indicated.

It is apparent from this table that the values of μ_{Ons} are very different from μ_{Deb}. These differences are, in general, greater than the experimental uncertainties in the determination of the dipole moments which are less than 1%. This shows the importance of choosing the best theoretical expression for μ. Table 3 also shows that the values of μ_{Ons} are almost equal to those of μ_{Bord}. The differences between the three dipole moment values can be estimated by writing $\epsilon_{\infty 1} = \epsilon_2 + \Delta$ and expanding eqs. [1], [2], and [5] in powers of Δ. This leads to

$$[6] \quad \mu_{\mathrm{Deb}} = \mu_{\mathrm{Ons}}\left[1 + \frac{2}{3}\Delta\frac{(\epsilon_2 - 1)}{\epsilon_2(\epsilon_2 + 2)}\right]$$

$$[7] \quad \mu_{\mathrm{Bord}} = \mu_{\mathrm{Ons}}\left[1 + \Delta^2\frac{(\epsilon_2 - 1)\epsilon_{1,2}(\epsilon_{\infty 1,2} + 2)^2}{(\epsilon_{1,2} - \epsilon_{\infty 1,2})(2\epsilon_{1,2} + \epsilon_{\infty 1,2})(\epsilon_2 + 2)^3}\right]$$

Equation [6] shows, in agreement with Table 3, that μ_{Deb} can be less or greater than μ_{Ons}, depending on the sign of Δ (6). On the contrary, the difference between μ_{Bord} and μ_{Ons} is independent of this sign, eq. [7], being one order smaller.

As for the variation of the moments obtained using extreme values of the atomic polarization, it is also comparable with the experimental error. The corresponding differences are smaller when Debye's expression is used increasing strongly with the use of Onsager's or Bordewijk's formulas.

5. Influence of the solvent

In order to estimate the influence of the solvent on the dipole moment values, additional measurements in heptane and decalin were performed on *ortho*, *meta*, and *para*-toluylaldehydes, Table 4. The results obtained with the three solvents appear on Table 5 and lead to the following conclusions. In view of the experimental uncertainties, no solvent effect could be detected for the substances considered when Onsager's or Bordewijk's formulas were used. On the contrary, Debye's formula leads to an apparent solvent effect since the corresponding variations with the solvent of the dipole moment values are roughly two

TABLE 3. Dipole moment values (D) in cyclohexane at 20°C

Substance	μ_{Deb}	μ_{Ons}	μ_{Bord}	$\mu_{literature}$
Benzaldehyde	2.91–2.95	2.76–2.86	2.77–2.87	3.02–3.03
o-Toluyaldehyde	2.79–2.84	2.64–2.75	2.65–2.75	
m-Toluyaldehyde	3.06–3.11	2.91–3.02	2.91–3.02	
p-Toluyaldehyde	3.36–3.40	3.19–3.30	3.19–3.31	2.78
2-Fluorbenzaldehyde	3.01–3.05	2.88–2.98	2.89–2.98	
3-Fluorbenzaldehyde	2.75–2.79	2.62–2.72	2.63–2.72	
4-Fluorbenzaldehyde	1.97–2.03	1.88–1.98	1.88–1.98	
Mesitylen 2-carbaldehyde	3.02–3.07	2.85–2.98	2.86–2.98	2.95–2.96
1-Naphtaldehyde (α)	2.93–2.99	2.70–2.83	2.71–2.84	2.87
Piridine 3-aldehyde	2.32–2.36	2.20–2.29	2.20–2.30	2.34–2.37
Piridine 4-aldehyde	1.71–1.77	1.63–1.72	1.63–1.73	1.74–1.79
Furfural	3.29–3.32	3.14–3.24	3.14–3.24	3.23–3.54
Thiophen 2-aldehyde	3.42–3.45	3.21–3.32	3.21–3.32	3.48
n-Formylpiperidine	3.95–3.97	3.83–3.93	3.83–3.93	
Cyclohexancarbaldehyde	2.44–2.49	2.38–2.48	2.38–2.47	
Bromal	1.51–1.59	1.41–1.53	1.42–1.53	
Pivaldehyde	1.89–1.93	1.88–1.95	1.88–1.95	
Butyraldehyde	2.24–2.27	2.22–2.29	2.22–2.29	
Crotonaldehyde	3.43–3.45	3.35–3.44	3.35–3.44	2.77–3.44
Hidrozimtaldehyde	2.30–2.36	2.19–2.31	2.20–2.31	
n-Valeraldehyde	2.45–2.49	2.43–2.51	2.43–2.51	

TABLE 4. Measured variations with the concentration of the static dielectric permittivity and of the square of the refractive index

Substances	$(\epsilon_{1,2} - \epsilon_2)/x$	$(n^2_{D1,2} - n^2_{D2})/x$
o-Toluyaldehyde in		
Decalin	5.99	0.11
Cyclohexane	8.72	0.40
Heptane	6.20	0.53
m-Toluyaldehyde in		
Decalin	7.21	0.11
Cyclohexane	10.36	0.34
Heptane	7.37	0.38
p-Toluyaldehyde in		
Decalin	8.60	0.11
Cyclohexane	12.36	0.41
Heptane	8.78	0.39

TABLE 5. Dipole moment values in decalin, cyclohexane, and heptane at 20°C

Substances	μ_{Deb}	μ_{Ons}	μ_{Bord}
o-Toluyaldehyde in			
Decalin	2.70–2.77	2.58–2.72	2.59–2.72
Cyclohexane	2.79–2.84	2.64–2.75	2.65–2.75
Heptane	2.80–2.87	2.64–2.75	2.64–2.76
m-Toluyaldehyde in			
Decaline	2.98–3.03	2.86–2.98	2.86–2.98
Cyclohexane	3.06–3.11	2.91–3.02	2.91–3.02
Heptane	3.07–3.12	2.90–3.01	2.91–3.01
p-Toluyaldehyde in			
Decalin	3.27–3.31	3.13–3.25	3.14–3.25
Cyclohexane	3.36–3.40	3.19–3.30	3.19–3.31
Heptane	3.37–3.41	3.19–3.29	3.19–3.30

times greater than those for the other two expressions. All this is in agreement with the conclusions of ref. 6.

6. Estimation of the atomic polarization P_a

Equations [1] and [2] were obtained as low dilution limiting forms of the general formulae for the static dielectric permittivity, written as functions of the molecular parameters μ_i and α_i. The polarizabilities were then eliminated in terms of the high frequency permittivities of the pure compounds with the help of Clausius–Mossotti's expression.

On the contrary, Bordewijk's permittivity expression [3] is a function of the mixture high frequency permittivity $\epsilon_{\infty 1,2}$. This made it necessary to use the high frequency formula [4] in order to obtain the limiting result [5] comparable with eqs. [1] and [2]. This leads to the conclusion that, at least in the case of Bordewijk's formula, a better way to determine dipole moment values is to measure the permittivity variations with the concentration both at low, $(\epsilon_{1,2} - \epsilon_2)/x$, and high, $(\epsilon_{\infty 1,2} - \epsilon_2)/x$, frequencies.

In order to compare this procedure with the usual one, measurements of $(n^2_{D1,2} - n^2_{D2})/x$ for *o*-, *m*-, and *p*-toluylaldehyde in heptane, cyclohexane, and decalin were performed, Table 4. Dipole moment values were calculated by using the expressions:

$$[8] \quad \epsilon_{1,2} = \epsilon_{\infty 1,2} + K_1\left(\frac{N_1\mu^2_{Deb}}{9\epsilon_0 kT}\right)\frac{(\epsilon_2 + 2)^2}{3}$$

for the Debye model, and

$$[9] \quad \epsilon_{1,2} = \epsilon_{\infty 1,2} + K_1\left(\frac{N_1\mu^2_{Ons}}{9\epsilon_0 kT}\right)\frac{3\epsilon_2^2(\epsilon_{\infty 1} + 2)^2}{(2\epsilon_2 + \epsilon_{\infty 1})^2}$$

for both Onsager and Bordewijk's models.

As previously, the relation between $(\epsilon_{\infty 1,2} - \epsilon_2)/x$ and $(n^2_{D1,2} - n^2_{D2})/x$, was evaluated in the extreme cases:

$$[10] \quad \frac{\epsilon_{\infty 1,2} - \epsilon_2}{x} = \frac{n^2_{D1,2} - n^2_{D2}}{x}$$

and

$$[11] \quad \frac{\epsilon_{\infty 1,2} - \epsilon_2}{x} = 1.15\frac{n^2_{D1,2} - n^2_{D2}}{x} + 0.05\,(\epsilon_2 - 1)(\epsilon_2 + 2)$$

TABLE 6. Dipole moment values obtained using the mixture's refractive indexes

Substances	μ_{Deb}	μ_{Ons}, μ_{Bord}
o-Toluyaldehyde in		
Decalin	2.76−2.70	2.71−2.59
Cyclohexane	2.83−2.79	2.75−2.65
Heptane	2.79−2.73	2.70−2.58
m-Toluyaldehyde in		
Decalin	3.04−2.98	2.98−2.86
Cyclohexane	3.11−3.07	3.03−2.93
Heptane	3.10−3.05	3.00−2.89
p-Toluyaldehyde in		
Decalin	3.32−3.27	3.26−3.13
Cyclohexane	3.40−3.36	3.30−3.20
Heptane	3.40−3.35	3.28−3.17

The results obtained appear in Table 6, where the first values correspond to assumption [10] and the second ones to [11].

This table, when compared with Table 5, shows very similar values but appearing in each column in the inverse order. This means that the results obtained using expressions [1], [2], and [5], together with the assumption $P_a = 0$ ($P_a = 0.15P_e$) give approximately the same results as when using formulas [8] and [9] with condition [11] ([10]).

Therefore, the results of Tables 5 and 6 become compatible for intermediate $P_a = 0.07P_e$ values.

7. Acknowledgments

We thank Professor F. Hufnagel for providing experimental facilities, help, and hospitality at Mainz as well as to the Alexander von Humboldt Foundation for a fellowship given to one of us.

1. P. DEBYE. Polar molecules. Dover Publication, New York. 1929.
2. L. ONSAGER. J. Am. Chem. Soc. **58**, 1486 (1936).
3. C. GROSSE and J. L. GREFFE. J. Chim. Phys. **72**, 1297 (1975).
4. C. F. BÖTTCHER and P. BORDEWIJK. Theory of electric polarization. Vol. 2. Elsevier. 1978.
5. P. BORDEWIJK. Chem. Phys. **33**, 451 (1978).
6. R. FINSY and R. VAN LOON. J. Phys. Chem. **80**, 2783 (1976).
7. M. BARÓN and H. MECHETTI. J. Phys. Chem. **86**, 3464 (1982).
8. C. F. BÖTTCHER. Theory of electric polarization. Vol. 1, Elsevier. 1973.
9. W. F. BROWN. J. Chem. Phys. **18**, 1193 (1950).
10. K. KREUTER. Z. Naturforsch. **23**a, 1728 (1968).
11. H. KILP. Z. Argew. Phys. **30**, 288 (1970).
12. F. HUFNAGEL and H. KILP. Z. Naturforsch. **18**a, 6 (1963).
13. G. KLAGES and G. KRAUSS. Z. Naturforsch. **26**a, 1272 (1971).
14. A. L. MCCLELLAN. Tables of experimental dipole moments. Vol. 2. Rahara Enterprises, El Cerrito, CA. 1974.

The synthesis and characterization of 3,3-disubstituted pent-4-enals and their 2,2-(trimethylenedithio)pent-4-enal precursors, including the X-ray crystal structure of (*R*)-3-ethyl-3-phenyl-2,2-(trimethylenedithio)pent-4-enal

CHARLES G. YOUNG, BRIAN R. JAMES,[1] AND STEVEN J. RETTIG[2]

Department of Chemistry, University of British Columbia, 2036 Main Mall, Vancouver, B.C., Canada V6T 1Y6

Received July 30, 1984

CHARLES G. YOUNG, BRIAN R. JAMES, and STEVEN J. RETTIG. Can. J. Chem. **63**, 1035 (1985).

A variety of 3,3-disubstituted pent-4-enals (**5***a*, R = Me, R′ = Et; **5***b*, R = Me, R′ = Ph; **5***c*, R = Et, R′ = Ph) has been prepared by the Raney nickel desulfurization of the corresponding 3,3-disubstituted 2,2-(trimethylenedithio)pent-4-enal precursors **4***a*–**4***c*. The precursor compounds were prepared by the alkylation of 2-formyl-1,3-dithiane with the appropriate 3,3-disubstituted allylic bromide. The new compounds have been characterized by elemental analysis, infrared and nmr spectroscopy, and mass spectrometry. The crystal and molecular structure of (*R*)-**4***c* has also been determined by X-ray crystallography. At temperatures of ca. 130°C, compounds **4***a*–**4***c* undergo intramolecular rearrangement to form the trisubstituted alkenes **6***a*–**6***c*, which have also been characterized by the present study.

CHARLES G. YOUNG, BRIAN R. JAMES et STEVEN J. RETTIG. Can. J. Chem. **63**, 1035 (1985).

On a préparé divers pentène-4 als disubstitués en position 3 (**5***a*, R = Me, R′ = Et; **5***b*, R = Me, R′ = Ph; **5***c*, R = Et, R′ = Ph) en désulfurant les précurseurs correspondants (**4***a*–**4***c*), triméthylènedithio-2,2 pentène-4 als disubstitués en position 3, à l'aide de nickel de Raney. On a préparé ces précurseurs en alkylant le formyl-2 dithiane-1,3 avec le bromure allylique approprié disubstitué en position 3. On a caractérisé les nouveaux composés par analyse élémentaire, par spectroscopies ir et rmn et par spectrométrie de masse. On a également déterminé la structure cristalline et la structure moléculaire du composé (*R*)-**4***c* par diffraction des rayons X. A des températures d'environ 130°C, les composés **4***a*–**4***c* subissent des transpositions intramoléculaires conduisant aux alcènes trisubstitués **6***a*–**6***c* que l'on a également caractérisés au cours de la présente étude.

[Traduit par le journal]

Introduction

Our ongoing investigation of catalytic asymmetric cyclization and decarbonylation reactions of pent-4-enals (1) has necessited the preparation of a series of racemic 3,3-disubstituted pent-4-enal substrates. Two methods have been reported (2) for the preparation of such compounds and the 2,3-disubstituted analogues. One method, of somewhat limited scope for synthesis of the 3,3-compounds, involves the conjugate addition of vinylcuprate(I) reagents to α,β-unsaturated aldehydes. The second, more versatile, reaction involves the addition of ethylene oxide to allylic Grignard reagents, followed by oxidation of the resulting alcohol. The methods are dependent on the availability and nature of the ultimate alkenic reagents and, for the latter method, the ease of oxidation of the alcohol precursor. We have developed an alternative approach to the desired substrates, one which involves the Raney nickel desulfurization of 2,2-(trimethylenedithio)pent-4-enal precursors. This paper reports the preparation and characterization of the new pent-4-enals **5***a*–**5***c*, their precursors **4***a*–**4***c*, and the compounds produced by the thermal rearrangement of these precursors (compounds **6***a*–**6***c*).

Results and discussion

The synthesis of the title compounds follows the reactions of eqs. [1]–[3] within Scheme 1. The preparation of the allylic bromides **3***a*–**3***c* is straightforward, and these compounds may

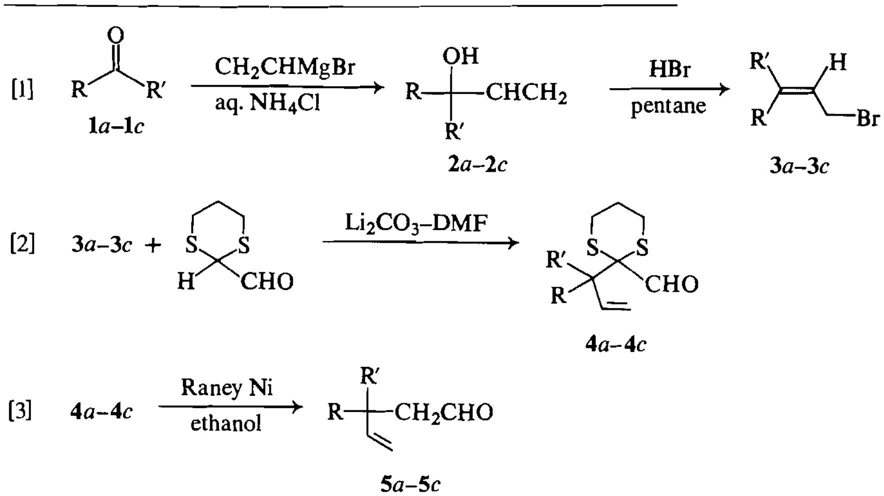

SCHEME 1. The preparation of **5***a*–**5***c* via **4***a*–**4***c*. (The substituents are as follows: (*a*) R = Me, R′ = Et; (*b*) R = Me, R′ = Ph; (*c*) R = Et, R′ = Ph).

[1] Author to whom correspondence should be addressed.
[2] Experimental Officer, U.B.C. Crystal Structure Service.

be stored at 0°C for several days before use. Both *E* and *Z* isomers are present in **3***a*–**3***c*, the isomer ratio being dictated by the usual steric interactions (see experimental section). Reaction [2] also proceeds smoothly at room temperatures and good yields of **4***a*–**4***c* are obtained after ca. 5 days. These compounds are air-stable, white, crystalline solids which are readily isolated and purified by recrystallization. This feature makes 2-formyl-1,3-dithiane the thioacetal of choice in these reactions, as considerable difficulty was experienced in the purification of the liquid products derived from bis(ethylthio)acetal (these reactions were not pursued). From unsuccessful attempts to obtain other compounds of series **4**, we have discerned two features associated with reactions [1] and [2] which limit their synthetic generality and that of Scheme 1 as a whole. Firstly, the use of ketones with bulky substitutents (e.g. R = Me, R′ = 2,4,6-$Me_3C_6H_2$) can prevent initial reaction with vinylmagnesium bromide, presumably because the Grignard reagent is unable to approach the carbonyl carbon atom. Secondly, the use of ketones with two aryl substituents (e.g. R = Ph, R′ = *p*-$MeOC_6H_4$) enhances, following reaction [2], the rapid rearrangement of the series **4** product according to eq. [4]. Thus, when R = R′ = aryl, only products of series **6** are isolated by room temperature manipulations. Series **4** products of this type, however, may be accessible by suitable low temperature syntheses. Various analogs of **4***a*–**4***c* have been previously prepared by the *in situ* alkylation of 2-formyl-1,3-dithiane (3).

Compounds **4***a*–**4***c* are characterized by the following spectroscopic properties (see experimental section for details). In their infrared spectra, the compounds display characteristic absorptions at ca. 1700 ($\nu_{C=O}$), 1600 ($\nu_{C=C}$), and 600 (ν_{CSC}) cm^{-1}, while the mass spectra display peaks assignable to the molecular ion, a fragment formed by loss of CHO, the 2-formyl-1,3-dithianyl ion (m/e = 148), and cyclic disulfide ions (m/e = 107/106/105). The cyclic disulfide fragments have been observed also in the mass spectra of related 1-aryl-1,3-dithianes (4, 5). The 400-MHz ^1H nmr spectra of the compounds exhibit several features of interest; that of **4***c* (Fig. 1a) exemplifies the salient features for the series.[3] In all cases the resonances due to the aldehyde, vinyl, methyl, and aromatic protons are readily identified. As well, the spectra of **4***a* and **4***c* clearly display the diastereotopic nature of the methylene protons of the R′ and R groups, respectively. In **4***c*, two unique six-line resonances (δ_A 2.22, δ_B 2.53) are produced by the diastereotopic H_A and H_B protons (J_{AB} = 14.5 Hz, $^3J_{CH_3,A}$ = $^3J_{CH_3,B}$ = 7.5 Hz). The presence of the chiral centre in these molecules also dictates the inequivalence of the six heterocyclic ring protons and this is reflected in the observation of six unique resonances attributable to these protons (see Fig. 1a).

TABLE 1. Bond lengths in (*R*)-**4***c* with estimated standard deviations in parentheses

Bond	Length (Å)	Bond	Length (Å)
S(1)—C(2)	1.811(6)	C(4)—C(5)	1.319(9)
S(1)—C(6)	1.812(7)	C(6)—C(7)	1.531(9)
S(2)—C(2)	1.848(5)	C(7)—C(8)	1.489(10)
S(2)—C(8)	1.812(7)	C(9)—C(10)	1.490(9)
O —C(1)	1.128(11)	C(11)—C(12)	1.388(8)
C(1)—C(2)	1.508(9)	C(11)—C(16)	1.391(8)
C(2)—C(3)	1.583(7)	C(12)—C(13)	1.393(8)
C(3)—C(4)	1.539(8)	C(13)—C(14)	1.354(11)
C(3)—C(9)	1.540(8)	C(14)—C(15)	1.377(12)
C(3)—C(11)	1.537(7)	C(15)—C(16)	1.392(8)

The couplings observed for these ring protons[3] are consistent with the rings having a chair conformation in solution, a feature persistent in the solid state structure of (*R*)-**4***c* (see below). The ^{13}C-{^1H} nmr spectra of all compounds display the expected resonances, as detailed in the experimental section.

As confirmation of the spectroscopically derived formulations of **4***a*–**4***c*, the single crystal X-ray structure of (*R*)-**4***c* was determined. A stereoview of the molecule is given in Fig. 2. Pertinent bond lengths and angles are given in Tables 1 and 2, respectively. In this molecule the substituents of the adjacent quaternary carbon atoms C(2) and C(3) are in the least sterically encumbered staggered positions. Indeed, steric interactions appear to dictate the general conformations of all groups relative to their neighbours. On the (*R*)-C(3) atom the vinyl and ethyl substituents were unambiguously differentiated in the crystallographic study, the groups possessing bond lengths of 1.319(9) Å and 1.490(9) Å, respectively. The carbonyl group has a C—O bond length of 1.128(11) Å and the oxygen atom has close interatomic contacts with H(6a) (2.56 Å, C—H··O 121°) and H(8a) (2.70 Å, C—H··O 124°), and an intermolecular contact with H(8e) (−*x*, 1/2*y*, −*z*; 2.49 Å, C—H··O 140°). The trimethylenedithio ring possesses a chair conformation as found in solution by nmr. In the two structurally inequivalent C—S bonds, significantly different bond lengths of 1.811(6) and 1.848(5) Å are observed. Close intramolecular contacts are noted also between S(1)··H(92) (2.68 Å, C—H··S 110°), S(2)··H(91) (2.70 Å, C—H··S 110°), and S(2)··H(4) (2.62 Å, C—H··S 111°). The chair structure of the trimethylenedithio ring has been structurally characterized previously, for example in 2-phenyl-1,3-dithiane (6).

Intramolecular thermal rearrangement of **4***a*–**4***c* occurs readily at ca. 130°C, eq. [4]; the products that result from formal [1,3] sigmatropic shifts have been isolated and characterized as the trisubstituted alkenes **6***a*–**6***c*. Although we have not made a detailed study of the rates of rearrangement of

[4]

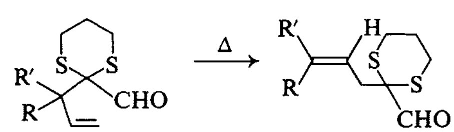

4*a*–**4***c* **6***a*–**6***c*

4*a*–**4***c*, it is clear from the observed reaction times (see experimental section) that **4***b* and **4***c* rearrange more readily than does **4***a*. Besides offering greater steric relief to the strained adjacent quaternary centers, rearrangement of **4***b* and **4***c* produces stabilized, more highly substituted (indeed, conjugated) alkenes. The lower steric strain of **4***a* and the absence of conjugate

[3] With the exception of the R groups, the numbering scheme used in Fig. 1 is applicable to all series **4**, **5**, and **6** compounds, i.e. C(1)—C(5) and C(6)—C(8) pertain to pent-4-enal and trimethylenedithio carbon atoms, respectively. In the nmr assignments of these compounds, protons are numbered according to the carbon atom to which they are bonded. The subscripts a = axial, e = equatorial, *g* = geminal, *t* = *trans*-, and *c* = *cis*- further specify the ring and olefinic protons and their couplings. The unique R group protons are identified separately. Typical proton coupling constants in the heterocyclic rings were $J_{6a6e} = J_{7a7e} = J_{8a8e}$ = 13.5 Hz, $J_{7a6e} = J_{7a8e}$ = 3.5 Hz, $J_{7e6e} = J_{7e8e}$ = 4.3 Hz, J_{6e8e} = 1.6 Hz, $J_{7e6a} = J_{7e8a}$ = 2.8 Hz, $J_{7a6a} = J_{7a8a}$ = 11.8 Hz. Other abbreviations used in the spectral data are: s = singlet, d = doublet, t = triplet, q = quartet, m = multiplet; ir, s = strong, m = medium, w = weak.

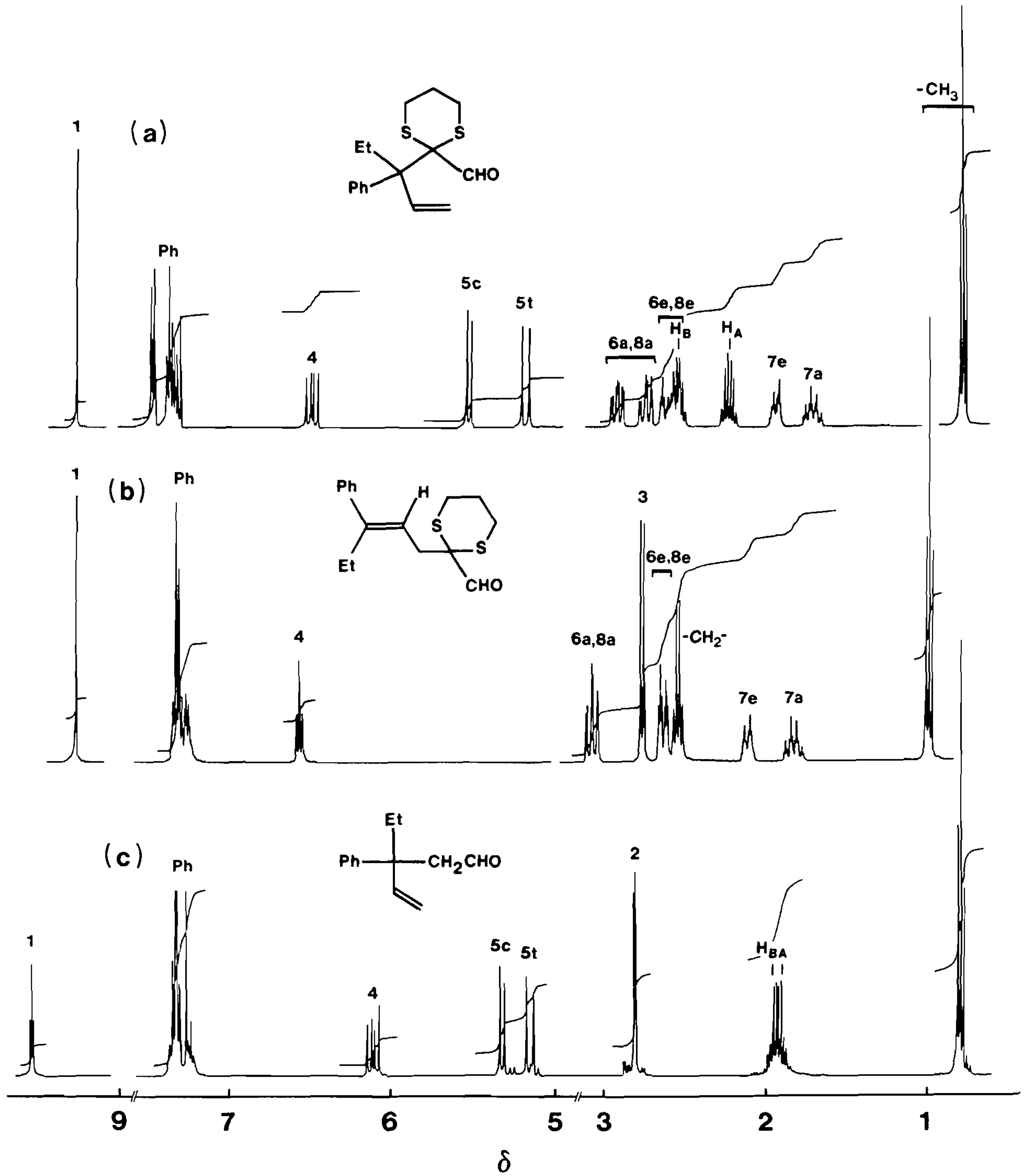

FIG. 1. The 400-MHz [1]H nmr spectra of (a) **4**c, (b) **6**c, and (c) **5**c, the archetypal members of the three classes of compounds described herein (see also footnote 3).

stabilization in **6**a lead to a slower rearrangement in this case. These rate-determining factors are consistent with the earlier mentioned room temperature rearrangement of 3,3-bis(aryl) compounds of series **4**. With the exception of the **4**a → **6**a rearrangement where both E- and Z-**6**a form, only the E isomer is formed during the rearrangement of **4**b and **4**c. A directly analogous rearrangement of 2,2-bis(ethylthio)-3,3-dimethylpent-4-enal has been studied recently by Bates and Ramaswamy (7), and their kinetic data were interpreted in terms of a biradical mechanism.

The loss of the chiral centre and its associated asymmetry upon the rearrangement of **4**a–**4**c lead to relatively simple nmr spectra for **6**a–**6**c. For example, in the [1]H nmr spectrum of **6**c (Fig. 1b), the diastereotopic methylene proton resonances and the six trimethylenedithio proton resonances of **4**c are replaced by a simple quartet resonance and a set of four ring proton resonances (due to H(7a),H(7e), and equivalent H(6a),H(8a) and H(6e),H(8e) pairs), respectively. Again, a chair conformation in the heterocyclic ring is indicated by the nmr data. The vinyl resonances of **4**c are replaced by triplet and doublet resonances due to the new alkene and β-methylene protons, respectively. Other spectral data are consistent with the pro-

TABLE 2. Bond angles in (*R*)-**4***c* with estimated standard deviations in parentheses

Bond	Angle (deg)	Bond	Angle (deg)
C(2)—S(1)—C(6)	103.8(3)	C(9)—C(3)—C(11)	112.7(4)
C(2)—S(2)—C(8)	101.7(3)	C(3)—C(4)—C(5)	127.7(6)
O —C(1)—C(2)	130.3(9)	S(1)—C(6)—C(7)	114.8(5)
S(1)—C(2)—S(2)	111.2(3)	C(6)—C(7)—C(8)	112.8(5)
S(1)—C(2)—C(1)	114.7(5)	S(2)—C(8)—C(7)	113.9(4)
S(1)—C(2)—C(3)	109.0(3)	C(3)—C(9)—C(10)	118.0(5)
S(2)—C(2)—C(1)	102.5(4)	C(3)—C(11)—C(12)	121.9(5)
S(2)—C(2)—C(3)	109.5(3)	C(3)—C(11)—C(16)	121.4(5)
C(1)—C(2)—C(3)	109.8(4)	C(12)—C(11)—C(16)	116.6(5)
C(2)—C(3)—C(4)	109.7(4)	C(11)—C(12)—C(13)	121.4(6)
C(2)—C(3)—C(9)	110.5(4)	C(12)—C(13)—C(14)	120.3(6)
C(2)—C(3)—C(11)	106.9(4)	C(13)—C(14)—C(15)	120.4(6)
C(4)—C(3)—C(9)	104.6(5)	C(14)—C(15)—C(16)	119.0(6)
C(4)—C(3)—C(11)	112.4(4)	C(11)—C(16)—C(15)	122.1(6)

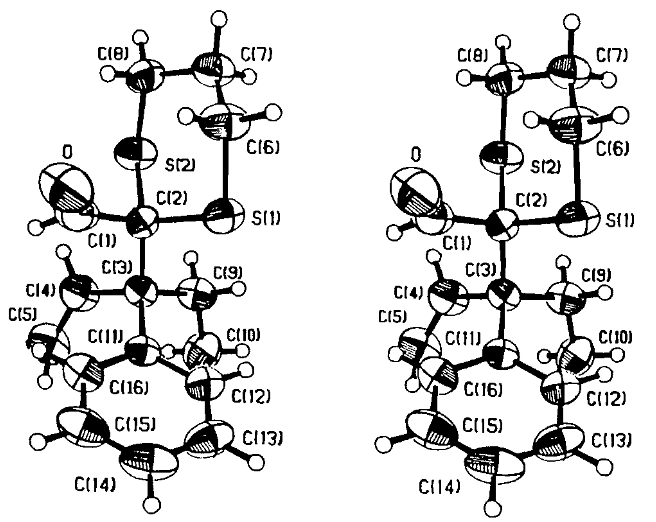

FIG. 2. ORTEP stereoview of (*R*)-**4***c* with the atom numbering scheme. Non-hydrogen atoms are shown as ellipsoids of 50% probability. Hydrogen atoms are spheres of convenient arbitrary size.

posed formulations.

The desulfurization of **4***a*–**4***c* leads to the formation of the desired pent-4-enal. This reaction is, however, critically dependent upon the nature of the Raney nickel used. In previous desulfurization studies (8–10), the possible concomitant reduction of functional groups such as aldehydes and alkenes by the Raney nickel has been noted. Only highly deactivated forms of Raney nickel (effected by a 2-h reflux in acetone (11)) have been found useful for the deuslfurization of **4***a*–**4***c*. The somewhat variable nature of the nickel makes monitoring by tlc the most reliable method of assessing the course of the reaction. Extensive reaction times or the use of highly activated nickel leads to sequential aldehyde, and then alkene, reduction. The pent-4-enals **5***a*–**5***c* are colourless liquids which are best stored under nitrogen at <0°C. Possible isomerization to the Prins product was not observed over a period of weeks (at room temperature, $CDCl_3$), although decomposition via autooxidation processes occurs over a period of several months.

The pent-4-enals exhibit infrared absorptions assignable to ν(C=O), ν(C=C), ν(=CH_2) as well as characteristic bands at ca. 768 and 705 cm^{-1}. The mass spectra exhibit peaks due to the molecular ion, and fragments resulting from the loss of CHO, CH_2CHO, and other substituent fragments. The 400-MHz ^{1}H nmr data of the compounds are summarized in the experimental section, and the spectrum of **5***c* is shown in Fig. 1c. With the exception of the R and R′ resonances, the nmr spectra of **5***a*–**5***c* display similar features due to the common pent-4-enal backbone. A characteristic vinyl group resonance is observed in the 5- to 6.5-ppm region (Fig. 1c), and a triplet resonance at ca. 9.5 ppm may be readily assigned to the CHO proton, which appears to be equally coupled ($^3J \sim 2.8$ Hz) to the two diastereotopic protons of the adjacent methylene group. The AB pattern associated with these CH_2 protons is displayed upon selective decoupling of the aldehyde proton. In **5***b* the significiantly different chemical shifts of these diastereotopic protons ($\Delta = 0.07$ ppm) produces a typical AB pattern in the CH_2 region, each peak being split by the small CHO coupling. However, the near equivalent chemical shifts of the diastereotopic protons in **5***c* ($\Delta = 0.02$ ppm) produce the triplet pattern and associated satellite peaks observed in Fig. 1c. The R and R′ resonances may be readily assigned and, where present, diastereotopic protons within these groups produce characteristic nmr resonances: e.g. the —CH_2CH_3 resonance of **5***c* results from the overlapping patterns of AB protons (J_{AB} = 15.6 Hz) equally coupled to the adjacent CH_3 protons. The small "duplicate" peaks in spectrum **1***c* indicate a small amount of a second rotamer in solutions of **5***c*.

In conclusion, we feel that the methodology described in this paper provides a general route to compounds of series **4**, **5**, and **6**. While our interest has been directed only at compounds where R ≠ R′, the synthesis of many other derivatives with R = R′ would be straightforward. We note again, however, the two conditions which limit the complete generality of this methodology: viz., the presence of bulky R and (or) R′ substituents, or R = R′ = aryl substituents. Substituents which contain functional groups that are reactive towards the reagents used in Scheme 1 may also prove to be problematic.

Experimental

Reagent grade solvents and chemicals were used without further purification unless otherwise stated. Liquid ketone starting materials were distilled prior to use. Tetrahydrofuran was distilled from sodium/benzophenone, and *N*,*N*-dimethylformamide was dried and stored over 4 Å molecular sieve. The acetone used was of spectroscopic grade. The method of Meyers and Strickland (11) was employed in the preparation of 2-formyl-1,3-dithiane. Thin layer chromatography was carried out on commercial silica gel plates (Bakerflex IB2-F, J.T. Baker Co.), while column chromatography employed 230–400 mesh silica gel (E. Merck). Plates were developed by 5% dodecamolybdophosphoric acid in ethanol.

Melting points were measured in air and are uncorrected. Infrared spectra were recorded on a Perkin Elmer Model 598 instrument as Nujol mulls or neat liquid samples. Nuclear magnetic resonance spectra were obtained on Brüker WH 400 (400 MHz, for ^{1}H) and Varian CFT-20 (19.9 MHz, for ^{13}C) spectrometers using tetramethylsilane as internal standard. Spectral assignments[3] were aided by routine decoupling experiments, computer simulation of the resonances and, for $^{13}C-\{^{1}H\}$ nmr, SFORD experiments. Mass spectra were recorded on a Varian MAT CH4-B spectrometer. Microanalyses were performed by Mr. P. Borda of this department.

Preparation of compounds

*4*a–*4*c

Bromoethene (6.41 g, 0.06 mol) in tetrahydrofuran (5 mL) was slowly added, at a rate which effected smooth boiling, to a mixture of magnesium turnings (2.5 g, 0.103 mol) in tetrahydrofuran (15 mL containing 4 drops of 1,2-dibromoethane activator) under an atmosphere of dinitrogen. A further 15 mL of tetrahydrofuran were added and the mixture allowed to stir for 45 min. The brown vinylmagnesium bromide mixture was cooled to 0°C and treated dropwise with the ketone (**1***a*–**1***c*, 0.06 mol). The mixture was sitrred at 0°C for 20 min, and then at room temperature for 40 min. It was then poured into a stirred saturated aqueous solution of NH_4Cl (150 mL) and upon dissolution of the magnesium was extracted with diethyl ether (3 × 50 mL). The combined ether extracts were washed with water, dried ($MgSO_4$), and the solvent removed *in vacuo*. The allylic alcohols **2***a*–**2***c* were obtained (identified by nmr).

The above product was dissolved in pentane (30 mL) and treated with 48% hydrobromic acid (7.5 mL). After stirring for 2 h, the pentane phase was washed with water (2 × 80 mL), dried ($MgSO_4$), and the solvent removed *in vacuo*. The allylic bromides **3***a*–**3***c* were obtained (identified by nmr). Isomeric ratios were, for **3***a*, 66% *E*, 34% *Z*; **3***b*, 77% *E*, 23% *Z*; **3***c*, 66% *E*, 34% *Z*.

A mixture of the above allylic bromide (0.05 mol), 2-formyl-1,3-dithiane (7.42 g, 0.05 mol), and lithium carbonate (5.55 g, 0.076 mol) in *N,N*-dimethylformamide (35 mL) was stirred under a slow flow of dinitrogen for 4–6 days (tlc monitor, 18% ethylacetate in petroleum ether 35–60°C bp). Diethyl ether (100 mL) was then added and the mixture washed with water (3 × 70 mL), 10% aqueous sodium hydroxide solution (3 × 60 mL), and then brine (2 × 60 mL). The ether solution was dried ($MgSO_4$) and the solvent removed under vacuum. For the high melting point solids (**4***b*, **4***c*), dissolution of the residue in ethanol/ether (~1:3) mixtures, followed by evaporation of the ether component, led to white crystals of product. These were collected, washed with ethanol, and vacuum dried. Low melting point **4***a* was purified by rapid distillation under vacuum (bp 100°C, 0.8 Torr (1 Torr = 133.3 Pa)). The purified liquid **4***a* solidified upon cooling. The products may also be purified by column chromatography (18% ethylacetate in petroleum ether 35–60°C bp).

*Compound 4*a

White crystalline solid, yield 8.0 g (70%), mp 38–40°C; ir (film, cm^{-1}): ν(C—H, CHO), 2840s, 2720s; ν(C=O), 1708s; ν(C=C) 1635w; ν(CSC), 620s; ^{1}H nmr ($CDCl_3$) δ: 0.77 (t, 3H, J = 7.5 Hz, CH_2CH_3), 1.24 (s, 3H, CH_3), 1.76 (m, 1H, H-7a), 1.85 (ABX_3, J_{AB} = 14.0 Hz, $J_{AX} = J_{BX}$ = 7.5 Hz, diast. CH_2 of Et), 1.99 (m, 1H, H-7e), 2.62, 2.66 (m's, 2H, H-6e,8e), 2.85, 2.95 (m's, 2H, H-6a,8a), 5.09 (dd, 1H, J_t = 17.6 Hz, J_g = 0.8 Hz, H-5*t*), 5.29 (dd, 1H, J_c = 11.2 Hz, J_g = 0.8 Hz, H-5*c*), 5.96 (dd, 1H, H-4), 9.35 (s, 1H, H-1); $^{13}C-\{^{1}H\}$ nmr ($CDCl_3$) δ: 8.13, 28.29 (CH_3CH_2), 17.39 (CH_3), 24.44, 26.97, 26.97 (C-7, C-6, and C-8), 47.16 (C-3), 68.19 (C-2), 116.73 (C-5), 139.57 (C-4), 190.69 (C-1); *m/e* (25°C): 232/231/230 (M^+), 203/202/201 (M − CHO), 150/149/148, 147, 107/106/105. *Anal.* calcd. for $C_{11}H_{18}OS_2$: C 57.35, H 7.88; found: C 57.2, H 8.0%.

*Compound 4*b

White crystalline solid, yield 11.8 g (85%), mp 53°C; ir (Nujol, cm^{-1}): ν(C—H, CHO) 2840s, 2720s; ν(C=O), 1695s; ν(CSC), 612s; ^{1}H nmr ($CDCl_3$) δ: 1.80 (s, 3H, CH_3), 1.70 (m, 1H, H-7a), 1.96 (m, 1H, H-7e), 2.59 (m, 2H, H-6e,8e) 2.78, 2.90 (m's, 2H, H-6a,8a), 5.16 (dd, 1H, J_t = 17.2 Hz, J_g = 0.8 Hz, H-5*t*), 5.35 (dd, 1H, J_c = 11.0 Hz, J_g = 0.8 Hz, H-5*c*), 5.75 (dd, 1H, H-4), 7.4 (m, 5H, Ph), 9.26 (s, 1H, H-1); $^{13}C-\{^{1}H\}$ nmr ($CDCl_3$) δ: 22.11 (CH_3), 23.89, 27.21, 27.21 (C-7, C-6, and C-8), 50.44 (C-3), 67.13 (C-2), 116.25 (C-5), 140.97 (C-4), 141.4–126.9 (Ph), 189.12 (C-1); *m/e* (65°C); 280/279/278 (M^+), 251/250/249 (M − CHO), 150/149/148, 147, 131, 107/106/105, 91. *Anal.* calcd. for $C_{15}H_{18}OS_2$: C 64.71, H 6.52; found: C 64.8, H 6.4%.

*Compound 4*c

White crystalline solid, yield 11.7 g (80%), mp 77°C; ir (Nujol, cm^{-1}): ν(C—H, CHO) 2840s, 2720s; ν(C=O), 1712s; ν(CSC), 620s; ^{1}H nmr ($CDCl_3$) δ: 0.78 (t, 3H, J = 7.5 Hz, CH_3), 2.22(A) and 2.53(B) (ABX_3, 2H, J_{AB} = 14.5 Hz, $J_{AX} = J_{BX}$ = 7.5 Hz, diast. CH_2 of Et) 1.71 (m, 1H, H-7a), 1.94 (m, 1H, H-7e), 2.54, 2.61 (m's, 2H, H-6e,8e), 2.75, 2.91 (m's, 2H, H-6a,8a), 5.15 (dd, 1H, J_t = 17.4 Hz, J_g = 1.3 Hz, H-5*t*), 5.49 (dd, 1H, J_c = 11.3 Hz, J_g = 1.3 Hz, H-5*c*), 6.46 (dd, 1H, H-4), 7.35 (m, 5H, Ph), 9.26 (s, 1H, H-1); $^{13}C-\{^{1}H\}$ nmr ($CDCl_3$) δ: 8.92, 24.62 (CH_3CH_2), 24.10, 27.46, 27.46 (C-7, C-6, and C-8), 55.95 (C-3), 68.41 (C-2), 118.76 (C-5), 127.55–137.00 (Ph), 136.62 (C-4), 189.07 (C-1); *m/e* (70°C): 294/293/292 (M^+), 265/264/263 (M − CHO), 150/149/148, 147, 145, 107/106/105, 91. *Anal.* calcd. for $C_{16}H_{20}OS_2$: C 65.71, H 6.89, O 5.50; found: C 65.5, H 7.0, O 5.5%.

*5*a–*5*c

Raney nickel (Aldrich Chemicals, 50-μ particle size, 30 g) was washed with water until the washings were neutral. The water was replaced by acetone (100 mL) and the mixture stirred under reflux for 2 h. The acetone was then replaced by an ethanol (anhydrous for **4***a*) solution of **4***a*–**4***c* (0.002 mol in 70 mL) and the mixture stirred for ca. 8 h (24 h for **4***a*. Monitor by tlc, 18% ethyl acetate/petroleum ether 35–60°C bp). Upon removal of the ethanol solvent (*in vacuo*), the residue was extracted with diethyl ether (3 × 100 mL). The combined extracts were filtered through Florisil, dried ($MgSO_4$), and reduced in volume to yield an oil. Column chromatography (18% ethyl acetate/petroleum ether 35–60°C bp) yields **5***a*–**5***c*.

*Compound 5*a

Volatile colourless liquid, difficult to free from solvent. Yield and analysis therefore precluded; ir (film, cm^{-1}): ν(C—H, CHO) 2810s, 2710s; ν(C=O) 1720s; ν(C=C) 1638m; ν(=CH_2) 920s, 768s; 705s; ^{1}H nmr ($CDCl_3$) δ: 0.84 (t, 3H, J = 7.4 Hz, CH_2CH_3), 1.12 (s, 3H, CH_3), 1.44(A) and 1.46(B) (ABX_3, 2H, J_{AB} = 14.0 Hz, $J_{AX} = J_{BX}$ = 7.4 Hz, diast. CH_2 of Et), 2.33 (d of AB quartets, 2H, δ_A = 2.29, δ_B = 2.37, J_{AB} = 15.0 Hz, J_{12} = 2.8 Hz, diast. H-2), 4.97 (dd, 1H, J_t = 17.0 Hz, J_g = 0.8 Hz, H-5*t*), 5.10 (dd, 1H, J_c = 10.6 Hz, J_g = 0.8 Hz, H-5*c*), 5.85 (dd, 2H, H-4), 9.73 (t, 1H, J_{12} = 2.8 Hz, H-1); $^{13}C-\{^{1}H\}$ nmr ($CDCl_3$) δ: 8.17, 33.84 (CH_3CH_2), 23.08 (CH_3), 39.19 (C-3), 52.77 (C-2), 113.16 (C-5), 145.01 (C-4), 203.28 (C-1); *m/e*: 128/127/126 (M^+), 97 (M − CHO), 83.

*Compound 5*b

Colourless oil, yield 0.23 g (66%); ir (film, cm^{-1}): ν(C—H, CHO) 2810s, 2710s; ν(C=O) 1720s; ν(C=C) 1638m; ν(=CH_2) 920s; 768s; 705s; ^{1}H nmr ($CDCl_3$) δ: 1.53 (s, 3H, CH_3), 2.795 (d of AB quartets, 2H, δ_A = 2.76, δ_B = 2.83, J_{AB} = 15.2 Hz, J_{12} = 2.8 Hz, diast. H-2), 5.13 (dd, 1H, J_t = 17.2 Hz, J_g = 0.8 Hz, H-5*t*), 5.23 (dd, 1H, J_c = 10.2 Hz, J_g = 0.8 Hz, H-5*c*), 6.12 (dd, 1H, H-4), 7.3 (m, 5H, Ph), 9.59 (t, 1H, J_{12} = 2.8 Hz, H-1); $^{13}C-\{^{1}H\}$ nmr ($CDCl_3$) δ: 26.15 (CH_3), 42.91 (C-3), 53.34 (C-2), 113.14 (C-5), 126.3–145.6 (Ph), 145.12 (C-4), 202.16 (C-1); *m/e*: 176/175/174 (M^+), 145 (M − CHO), 131. *Anal.* calcd. for $C_{12}H_{14}O$: C 82.72, H 8.10; found: C 82.8, H 8.2%.

*Compound 5*c

Colourless oil, yield 0.3 g (80%); ir (film, cm^{-1}): ν(C—H, CHO) 2820s, 2720s; ν(C=O) 1718s; ν(C=C) 1635w; ν(=CH_2) 920s; 768s; 705s; ^{1}H nmr ($CDCl_3$) δ: 0.79 (t, 3H, J = 7.4 Hz, CH_3), 1.90(A) and 1.95(B) (ABX_3, 2H, J_{AB} = 13.9 Hz, $J_{AX} = J_{BX}$ = 7.4 Hz, diast. CH_2 of Et), 2.80 (d of AB quartets, 2H, δ_A = 2.79, δ_B = 2.81, J_{AB} = 15.6 Hz, J_{12} = 2.9 Hz, diast. H-2), 5.15 (dd, 1H, J_t = 17.7 Hz, J_g = 0.6 Hz, H-5*t*), 5.32 (dd, 1H, J_c = 11.1 Hz, J_g = 0.6 Hz, H-5*c*), 6.02 (dd, 1H, H-4), 7.3 (m, 5H, Ph), 9.54 (t, 1H, J_{12} =

2.9 Hz, H-1); ^{13}C-{^1H} nmr ($CDCl_3$) δ: 8.35, 31.77 (CH_3CH_2), 46.50 (C-3), 49.94 (C-2), 114.31 (C-5), 125.9–144.0 (Ph), 143.60 (C-4), 202.93 (C-1); *m/e*: 190/189/188 (M^+), 159 (M − CHO), 145. *Anal.* calcd. for $C_{13}H_{16}O$: C 82.94, H 8.57; found: C 82.9, H 8.5.

*6*a–*6*c

Glass ampoules containing *4a*–*4c* (50 mg) were sealed under vacuum and heated at 130°C. Reaction times of 2 h were employed for *4b* and *4c*, but *4a* required extended (24 h) reaction periods. The products were purified by column chromatography (18% ethyl acetate/petroleum ether 35–60°C bp).

*Compound (*Z,E*)-6*a

Colourless oil, yield 0.045 g (90%); ir (film, cm^{-1}): ν(C=O), 1709s; ν(CSC) 630m; ^1H nmr ($CDCl_3$) δ: 0.98 (t, 3H, J = 7.5 Hz, CH_2CH_3), 1.64 (dt, $J_{Me,4}$ = 1.3 Hz, $J_{Me,3}$ = 0.7 Hz, CH_3 *E* isomer, 64%), 1.70 (dt, *J*'s as above, CH_3 *Z* isomer, 36%), 1.80 (qt, 1H, H-7a), 2.01 (q, 2H, J = 7.5 Hz, CH_2CH_3), 2.09 (m, 1H, H-7e), 2.55 (d(br), 2H, J_{34} = 7.5 Hz, H-3), 2.59 (dq, 2H, H-6e,8e), 3.01 (ddd, 2H, H-6a,8a), 5.10 (t(br), J_{34} = 7.5 Hz, H-4, *Z*), 5.14 (tq, J_{34} = 7.5 Hz, $J_{Me,4}$ = 1.3 Hz, H-4, *E*), 7.3 (m, 5H, Ph), 9.15 (s, 1H, H-1); *m/e*: 232/231/230 (M^+), 203/202/201 (M − CHO), 150/149/148, 147, 107/106/105.

*Compound (*E*)-6*b

Colourless oil, yield 0.046 g (92%); ir (film, cm^{-1}): ν(C=O) 1709s; ν(CSC) 630s; ^1H nmr ($CDCl_3$) δ: 1.83 (qt, 1H, H-7a), 2.07 (dt, 3H, $J_{Me,4}$ = 1.3 Hz, $J_{Me,3}$ = 0.7 Hz, CH_3), 2.10 (m, 1H, H-7e), 2.62 (dq, 2H, H-6e,8e) 2.75 (d, 2H, J_{34} = 7.5 Hz, H-3), 3.05 (ddd, 2H, H-6a,8a), 5.75 (tq, 1H, J_{34} = 7.5 Hz, J_{45} = 1.3 Hz, H-4), 7.3 (m, 5H, Ph), 9.15 (s, 1H, H-1); *m/e*: 280/279/278 (M^+), 251/250/249 (M − CHO), 150/149/148, 147, 131, 107/106/105, 91.

*Compound (*E*)-6*c

Colourless oil, yield 0.046 g (92%); ir (film, cm^{-1}): ν(C=O) 1710s; ν(CSC) 630s; ^1H nmr ($CDCl_3$) δ: 0.99 (t, 3H, J = 7.4 Hz, CH_3), 1.82 (qt, 1H, H-7a), 2.10 (m, 1H, H-7e), 2.53 (q, 2H, J = 7.4 Hz, CH_2CH_3), 2.62 (dq, 2H, H-6e,8e), 2.74 (d, 2H, J_{34} = 7.5 Hz, H-3), 3.05 (ddd, 2H, H-6a,8a), 5.59 (t, 1H, J_{34} = 7.5 Hz, H-4), 7.3 (m, 5H, Ph), 9.25 (s, 1H, H-1); *m/e*: 294/293/292 (M^+), 265/264/263 (M − CHO), 150/149/148, 147, 107/106/105, 91.

*X-ray crystallographic study of (*R*)-4*c

A single crystal of what proved to be (*R*)-*4c* ($C_{16}H_{20}OS_2$, mol. wt. = 292.45), grown by the slow evaporation of a diethyl ether solution of **4c**, was selected for the crystallographic study. The crystal was monoclinic, space group $P2_1$, with a = 6.7224(9), b = 7.0172(3), and c = 16.269(2) Å, β = 98.443(6)°, and with d_{calcd} = 1.280 g cm^{-3} for Z = 2 and V = 759.1 $Å^3$. The intensity data were measured at 22°C on an Enraf–Nonius CAD4-F diffractometer (graphite monochromated Cu-K_α radiation, ω–2θ scans at a scan rate of 0.91–10.06° min^{-1} and scan range (deg in ω) of 0.90 + 0.14 tan θ). The size of the crystal used for data collection was approximately 0.16 × 0.30 × 0.31 mm. A total of 1698 unique reflections was measured for θ < 75° of which 1536 had $I \geq 3\sigma(I)$ (data collected for $+h$, $+k$, $\pm l$). The intensities of three check reflections, measured every hour throughout the data collection, showed only small random fluctuations. The data were processed[4] and corrected for absorption (12, 13) (μ = 30.3 cm^{-1}). The structure[5] was solved by conventional heavy-atom methods, the coordinates of the sulfur atoms being determined from the Patterson function and those of the oxygen and carbon atoms from subsequent difference maps. Hydrogen coordinates and thermal parameters were calculated (C(sp^3)—H = 0.98 Å, C(sp^2)—H = 0.97 Å) and included as fixed atoms. The non-hydrogen atoms were refined anisotropically to R = 0.071 and R_w = 0.091 (function minimized $\Sigma w(|F_o| - |F_c|)^2$ where $w = 1/\sigma^2(F)$; $\sigma^2(I) = S + 2B + [0.025(S - B)]^2$ where S = scan count and B = normalized background count). In the final cycle, the maximum parameter shift was 0.09 σ (mean Δ/σ = 0.01) and the residual electron density ranged from −1.0 to 0.58 e $Å^{-3}$. Refinement of the opposite enantiomorph resulted in higher values of R and R_w. The R value ratios (rejected enantiomorph/accepted enantiomorph) were 1.009 on R, and 1.011 on R_w, both significant at >99.5% probability level (14). The atomic scattering factors used were taken from Cromer and Mann (15) and (for hydrogens) Stewart *et al.* (16), and anomalous scattering factors (for S and O atoms) were taken from Cromer and Liberman (17).

[4] The computer programs used include locally written programs for data processing and locally modified versions of the following: ORFLS, full-matrix least-squares, and ORFFE, function and errors, by W. R. Busing, K. O. Martin and H. A. Levy; FORDAP, Patterson and Fourier syntheses, by A. Zalkin; ORTEP II, illustrations, by C. K. Johnson.

[5] A detailed account of the structure determination (Table 3), final atomic parameters (Tables 4 and, for hydrogen, 6), thermal parameters (Tables 5 and, for hydrogen, 6), torsion angles (Table 7), and a table of measured and calculated structure factor amplitudes (12 pages), are available, at a nominal charge, from the Depository of Unpublished Data, CISTI, National Research Council of Canada, Ottawa, Ont., Canada K1A 0S2.

Acknowledgements

We thank Dr. G. S. Bates for directing our attention to this method of pent-4-enal preparation and for helpful discussions, and also Dr. J. Trotter for use of the departmental X-ray facilities.

1. B. R. JAMES and C. G. YOUNG. J. Chem. Soc. Chem. Commun. 1215 (1983); J. Organomet. Chem. In press.
2. R. C. LAROCK, K. OERTLE, and G. F. POTTER. J. Am. Chem. Soc. **102**, 190 (1980), and references therein.
3. S. R. WILSON and J. MATHEW. Synthesis, 625 (1980).
4. J. H. BOWIE and P. Y. WHITE. Org. Mass Spectrom. **2**, 611 (1969).
5. C. J. SHAW and V. V. KANE. Org. Mass Spectrom. **15**, 502 (1980).
6. H. T. KALFF and C. ROMERS. Acta Crystallogr. **20**, 490 (1966).
7. G. S. BATES and S. RAMASWAMY. Can. J. Chem. **59**, 3120 (1981).
8. G. B. SPERO, A. V. MCINTOSH, and R. H. LEVIN. J. Am. Chem. Soc. **70**, 1907 (1948).
9. L. B. BARKLEY, M. W. FARRAR, W. S. KNOWLES, and H. RAFFELSON. J. Am. Chem. Soc. **76**, 5017 (1954).
10. R. MOZINGO, D. E. WOLF, S. A. HARRIS, and K. FOLKERS. J. Am. Chem. Soc. **65**, 1013 (1943).
11. A. I. MEYERS and R. C. STRICKLAND. J. Org. Chem. **37**, 2579 (1972).
12. P. COPPENS, L. LEISEROWITZ, and D. RABINOVICH. Acta Crystallogr. **18**, 1035 (1965).
13. W. R. BUSING and H. A. LEVY. Acta Crystallogr. **22**, 457 (1967).
14. W. C. HAMILTON. Statistics in physical sciences. Ronald Press, New York. 1964. p. 157.
15. D. T. CROMER and J. B. MANN. Acta Crystallogr. Sect. A, **24**, 321 (1968).
16. R. F. STEWART, E. R. DAVIDSON, and W. T. SIMPSON. J. Chem. Phys. **42**, 3175 (1965).
17. D. T. CROMER and D. LIBERMAN. J. Chem. Phys. **53**, 1891 (1970).

Compounds of W(VI) with *l*(−)malic acid: a polarimetric and ^{1}H nuclear magnetic resonance study of the formation and interconversion equilibria in excess of W(VI)

ANTONIO CERVILLA, JOSÉ A. RAMÍREZ, AND ELISA LLOPIS

Departamento de Química Inorgánica, Facultad de Ciencias Químicas, Universidad de Valencia, Spain

Received October 20, 1983[1]

ANTONIO CERVILLA, JOSÉ A. RAMÍREZ, and ELISA LLOPIS. Can. J. Chem. **63**, 1041 (1985).

Complex formation occurring between *l*(−)malic acid and W(VI) has been investigated by polarimetric and cryoscopic measurements, and also by proton nmr spectroscopy. The complexing ability of malic acid depends on the metal–ligand ratio. With excess W(VI), four different complexes are formed. The pH of the medium is the principal variable controlling complex formation and the various interconversion equilibria. At high pH (>7.0), the stable complex is a monomer, while at lower pH values dimers predominate. Conditional dissociation constants of some species have been evaluated and they show that the complexes formed with excess W(VI) have a higher stability than those found when malic acid is in excess. Comparison of the proton coupling constants shows that the conformation of malic acid in its metal complexes depends on which reagent is in excess, and leads to a number of conclusions about the structure of the dimeric species.

ANTONIO CERVILLA, JOSÉ A. RAMÍREZ et ELISA LLOPIS. Can. J. Chem. **63**, 1041 (1985).

La formation de complexes entre l'acide malique et le W(VI) a été étudiée par polarimétrie, cryoscopie et spectroscopie ^{1}H nmr. Le pouvoir de coordination de l'acide malique dépend du rapport metal–ligande. Sous un excés de W(VI), quatre différents complexes sont formés; nous avons étudié leurs équilibres de formation et interconversion qui sont function du pH du milieu. Le complexe stable au plus haut valeur de pH est un monomére, tandis que les trois autres sont des diméres. Les constants conditionnelles de dissociation de quelques espéces ont été mesurées et leurs valeurs montrent que les complexes formés sous un excés de W(VI) sont plus stables que ceux qui sont formés en excés d'acide malique. La comparaison des constants de couplement du proton montre que la conformation de l'acide malique dépend du réactif qui est en excés et nous en tirons des conclusions sur la structure des espéces dimériques.

Introduction

The formation of complexes between W(VI) and *l*(−)malic acid (H_2L) has been investigated earlier by conductimetric, potentiometric, and polarimetric methods (ref. 1, and references therein).

In excess of H_2L, previous papers showed that malic acid can form, with W(VI) (1) or Mo(VI) (2), three different complexes which are similar to those formed by tartaric (3), oxalic (4), and lactic (5) acids: one monomeric 1:2 (metal/ligand) species and two dimeric species of stoichiometry 2:2, which are stable in a more acidic medium.

However, it is worth emphasizing that in contrast to what was observed for the above ligands and for the malonic acid (6) and sorbitol (7), the complexation behaviour of the malic acid depends on which reagent (W(VI) or H_2L) is in excess. As we shall see, with excess W(VI), the malic acid gives rise to other different complex species, pointing out that there must be some essential structural difference between the malic acid and the above ligands.

On the other hand, in a more recent paper, V. Gil *et al.* (8) have reported that the ^{1}H nmr spectra of a solution of Na_2WO_4 and H_2L show several X-type signals, arising from H—C—OD protons, that reveal the formation of three different complexes: two 1:2 metal/ligand monomeric species and one dimeric, of 2:2 stoichiometry. (A fourth 2:1 complex having an ABX spectrum whose X part was very broad and of low intensity could also be considered.) These authors also found that the conformation of the complex species depended on the pH and on which reagent was in excess; however, in spite of what would be expected, they found that the monomeric species were more stable at lower pH than the dimeric ones.

This paper tries to complete the study of the W(VI) – malic acid system and is directed, together with the data already published, toward elucidating the relationship between ligand structure and complex-formation ability for oxotungsten– and oxomolybdenum–ligand species.

Results and discussion

Evidence for the different complexes

In curve A of Fig. 1 we have plotted the changes in the rotatory power, $\hat{D}$, produced by the neutralization with NaOH of a solution 10^{-2} *M* in malic acid (H_2L). This curve was modified when the neutralization was carried out in the presence of Na_2WO_4, which forms stable complex species in solution. Curve C shows the effect produced by the addition of a constant Na_2WO_4 excess to the malic acid solution ($W(VI)/H_2L = 25$). In this curve, given that in the presence of a large excess of W(VI) we can assume that all the malic acid will be complexed, the only contributions to the rotatory power of the solution are those due to the complex species themselves. Five discontinuities can be distinguished: at pH = 10.00, 7.25, 5.50, 4.00, and 1.50. These discontinuities or breaks define five pH zones: (a) 10.00 > pH, the $\hat{D}$ values correspond to the free *l*(−)malate ions, meaning that there is no interaction between the WO_4^{2-} and L^{2-} ions; (b) 10.00 > pH > 7.25, the noticeable rotatory power increase by acidification must be due to the formation of a complex species, and at its maximum (pH = 7.25) we can consider that all the ligand will be forming this complex; (c) 7.25 > pH > 5.50, in this pH region the rotatory power fall can be related to the presence of a second complex in equilibrium with the first one; (d) 5.50 > pH > 4.00, in this pH interval there is a rotatory power increase, implying the existence of a third complex which produces a maximum of $\hat{D}$ at pH = 4.00; (e) 4.00 > pH > 1.50, finally, further acidification gives a drop of $\hat{D}$, which becomes stabilized at pH = 1.50. At this pH the $\hat{D}$ value is different from the one due to the free malic acid, showing the existence of a fourth complex in this pH medium.

On the other hand, curve B shows that the behaviour of this

[1] Revision received October 22, 1984.

TABLE 1. Rotatory power as a function of tungstate concentration[a]

v(mL)	$C_w(10^2)$ (M)	$\hat{D}$(degrees)	v(mL)	$C_w(10^2)$ (M)	$\hat{D}$(degrees)
0.50	2	0.116	3.00	12	0.298
0.75	3	0.152	3.50	14	0.309
1.00	4	0.179	4.00	16	0.322
1.50	6	0.227	4.50	18	0.328
2.00	8	0.258	5.00	20	0.335
2.50	10	0.282	6.00	24	0.347

[a] $\hat{D}_{\text{lim}} = 0.430$; pH = 7.40; λ = 436 nm; v_0 = 1 mL of H_2L ($a_0 = 0.25\ M$) v, mL of Na_2WO_4 ($b_0 = 1\ M$); V_T = 25 mL.

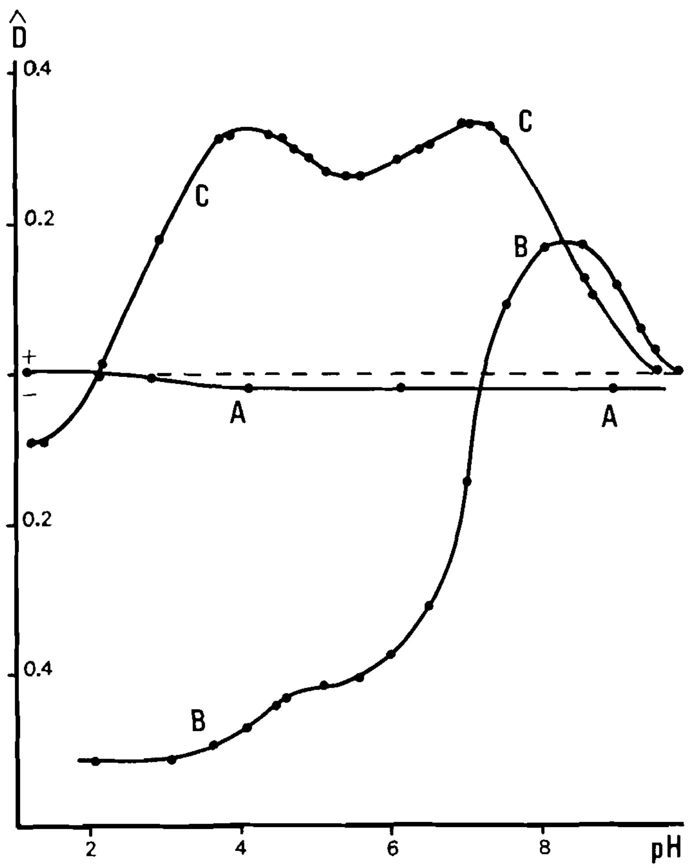

FIG. 1. Optical activity variations as a function of pH. Curve A: $10^{-2}\ M$ in malic acid; curve B: complexes formed with excess of H_2L, $10^{-2}\ M$ in Na_2WO_4 (L/W = 25); curve C: complexes formed with excess of W(VI), $10^{-2}\ M$ in H_2L (W/L = 25).

system when there is an excess of ligand in the solution is totally different from that observed when it is in deficit. When excess of ligand is present (H_2L/W(VI) = 25), the changes in the rotatory power with pH reveal the formation of three different complexes (one 1:2 and two 2:2) whose formation from tungstate and malate ions requires 2, 2, and 2.5 H^+ moles per mole of W(VI), respectively (1).

From the rotatory power data plotted in curves B and C it is seen that below pH 7.25 the complex species present when the ligand is in excess have a strong levorotatory character, while in excess of metal the complex species stable at lower pH (<2.0) has a slightly levorotatory character and the other three are dextrorotatory.

Stoichiometry and stability constants of the complexes

The above observations imply that the composition of these complexes cannot be determined by Job's method since its application requires that a single species is present in solution independent of which reagent is in excess (10).

In order to determine the stoichiometry and stability constants of the complexes formed in excess of W(VI), the generalized molar-ratio procedure (11) and Asmus "straight-line" method (12) were applied. For both methods, the presentation here will follow in detail these earlier papers, where any symbols or notations not defined in the present report will be found and explained.

A series of samples containing a constant amount of $l(-)$malic acid ($C_L = a_0 v_0/V_T$) and varying concentrations of W(VI) ($C_W = b_0 v/V_T$) was prepared by dilution of the appropriate amounts of the standard solutions (a_0, b_0) until V_T = 25 mL. All the solutions were made 1 M in $NaClO_4$ and their pH adjusted to the required value by adding appropriate amounts of concentrated NaOH and (or) $HClO_4$ (70%). The measured values of the rotatory power, $\hat{D}$ (degrees), of the solutions are given in Table 1 at pH = 7.40, first break.

For the application of the generalized Asmus' method, we may assume a general equilibrium of the type:

$$\delta L + n\delta\, W \rightleftarrows L_\delta W_{n\delta}$$

The mass action law can be written as:

$$K' = K_d^{1/\delta} = [L] \cdot [W]^n/[L_\delta W_{n\delta}]$$

and the following relation holds:

$$[1] \quad \frac{\hat{D}^{1/\delta}}{v^n} = \frac{a_0 b_0^n v_0}{V_T^{\,n+1}}\, \epsilon^{1/\delta} \frac{1}{K'} - \frac{(b_0)^n}{(V_T)^n}\, \delta\epsilon^{1/\delta - 1} \frac{1}{K'}\, \hat{D}$$

where ϵ denotes the specific molar rotation of the complex.

According to this relation the graphical plot of $\hat{D}^{1/\delta}/v^n$ vs. $\hat{D}$ is linear only when values δ and n are chosen correctly.

In Fig. 2 we show the plots obtained at pH = 5.60. The dimeric character of this complex (δ = 2) and its stoichiometric ratio 1:1 (n = 1) are clearly inferred from it. For this straight line the abscissa at the origin leads to the value (ϵ = 42.6)[2] which allows us to calculate from the slope the conditional stability constant K_d of the complex as $K_d = 3.41 \times 10^{-7}$.

From the data at pH = 7.40, the stoichiometric coefficients found for this complex are δ = 1 (monomeric species) and n = 1, with a conditional stability constant of $K_d = 5.51 \times 10^{-2}$.

On the other hand, the generalized molar-ratio method can also be applied using the data in Table 1. In this method, the formation of a single complex is described by an equilibrium of the type:

$$mL + nW \rightleftarrows L_m W_n$$

[2] In, deg mol^{-1} L dm.

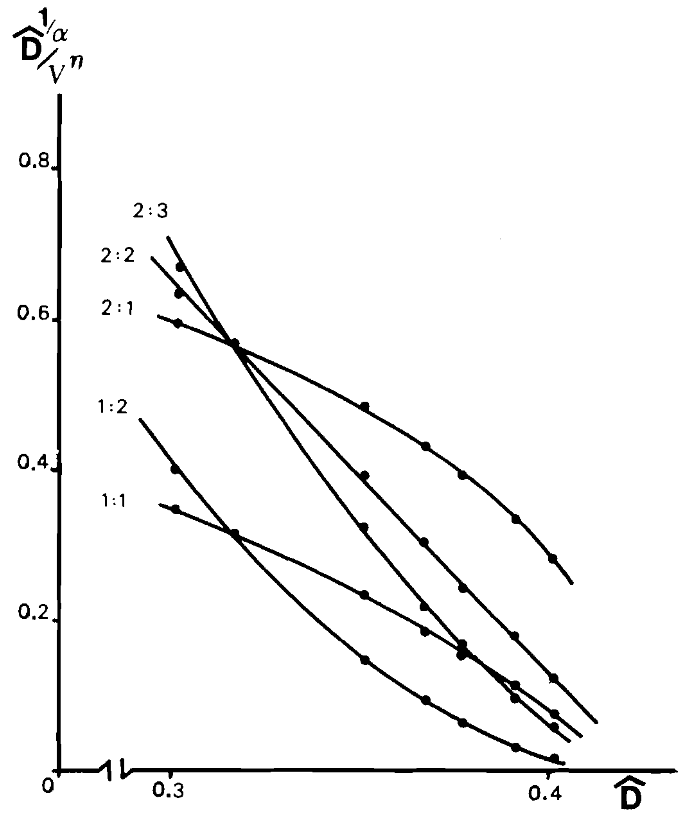

FIG. 2. Asmus modified method, pH = 5.60. ($\hat{D}^{1/\delta}/v^n$) vs. $\hat{D}$ for selected δ (degree of condensation) and n (stoichiometric ratio) values. Only when δ = 2 and n = 1 (stoichiometry 2:2) is a straight line obtained. $C_L^0 = 2 \times 10^{-2}$ M; v, mL of Na_2WO_4 0.25 M ($2.0 < v < 10.0$); V_T = 25 mL.

and now, the mass action law can be written as:

$$[2] \quad K^* = (1/K_{eq}C_L^{m-1})^{1/n} = \frac{C_W(x) - nC_Lx/m}{[x/m(1-x)^m]^{1/n}}$$

with $K_{eq} = 1/K_d$; C_L the concentration of ligand ($C_L = a_0v_0/V_T$), and C_W the metal concentration given by $[L_mW_n] = xC_L/m$ ($0 < x < 1$), where $x = \hat{D}/\hat{D}_{limit}$, and $\hat{D}_{limit}$ is equal to $\hat{D}$ of a solution having a large enough C_W/C_L ratio to assume that $[L_mW_n] = C_L/m$.

Plotting K^* against x, eq. [2] only leads to a horizontal line for the correct m and n values. As illustrated in Fig. 3, we have plotted the results obtained using the data given in Table 1 at pH = 7.40: $m = n = 1$, and the conditional stability constant is $K_d = 5.01 \times 10^{-2}$. At pH = 5.60 the m and n values found are $m = n = 2$, with the constant $K_d = 3.97 \times 10^{-7}$. These results are in excellent agreement with our Asmus' method results.

For the stoichiometries of the species present at lower pH, the above methods are unreliable because the high stability of the complexes makes the variation of the concentration of complex formed with the metal/ligand ratio negligible.

For these two species we have obtained indirect evidence of their stoichiometry from the ^1H nmr spectra. The low-pH ^1H nmr spectra recorded for a solution of 1:1 composition show a complete conversion of unbound to bound ligand resonances, and these complexes are so stable that a slight excess of ligand immediately gives rise to additional nmr signal corresponding to the free ligand. This fact points out that both species have a stoichiometric ratio W/L = 1. Furthermore, we shall present below additional polarimetric and cryoscopic results which provide a similar conclusion on the stoichiometry of these complexes.

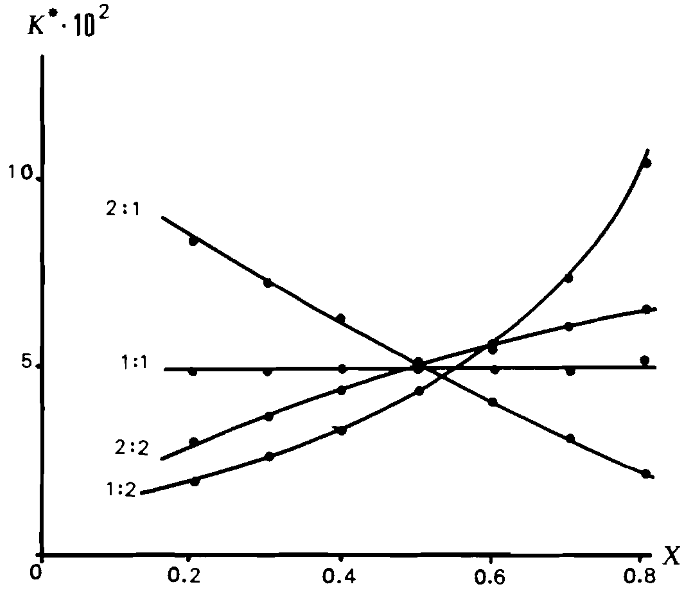

FIG. 3. Molar-ratio generalized method, pH = 7.40. K^* vs. x function only leads to a horizontal line for a stoichiometry 1:1.

Formation and interconversion equilibria

Given that all the complexes present when W(VI) is in excess have a 1:1 composition, the interconversion equilibria between different species can be written according to equilibria of the type:

$$[3] \quad \text{Complex A} + n\text{H}^+ \rightleftarrows 1/a \text{ Complex B}$$

in which the value of a is related to the degree of condensation of the complexes. For these equilibria we can write (9):

$$\text{constant} = \log(\beta^{1/a}/1 - \beta) + n\,\text{pH}$$

where constant = $\log K + 1/a \log a - \log C(1/a - 1)$, C being the initial concentration of the complex A and β the molar fraction of complex B formed.

Data in Fig. 1 (curve C) have been used to perform calculations which permit the determination of the coefficients n and a. As we have noted above, there are four pH zones, defined by the breaks, in which we can assume that an equilibrium of the type [3] takes place. For each of these intervals, the values of β can be calculated, for each pH, according to the relation:

$$[4] \quad \hat{D} = \hat{D}_B\beta + (1 - \beta)\hat{D}_A$$

where $\hat{D}$ is the value of the rotatory power at the pH mentioned and $\hat{D}_A$ and $\hat{D}_B$ the rotatory power corresponding to those pH values for which the curve C has the breaks, assuming that practically all the ligand is present in a single complex species.

Equation [4] implies that if we plot $\log(\beta^{1/a}/1 - \beta)$ as a function of pH for different values of $1/a$ we will obtain a linear relationship only for the correct value of a, and the slope of this straight line gives us the value of n. A summary of the results obtained is given in Table 2.

According to these data, and given that the stoichiometries of the complexes are known, we can write the following complexation equilibria, valid when W/L > 1:

TABLE 2. Calculated values of the a and n coefficients in the formation and interconversion reactions

pH zone	Proposed equilibrium	$\hat{D}$ limits values	a	n
9.50 > pH > 7.00	$W + L + nH^+ = 1/a$ I	$\hat{D}_{I} = 0.336$	1	1.07
7.00 > pH > 5.50	$I + zW + nH^+ = 1/a$ II	$\hat{D}_{II} = 0.267$	2	1.02
5.50 > pH > 4.00	$II + zW + nH^+ = 1/a$ III	$\hat{D}_{III} = 0.325$	1	2.05
4.00 > pH > 1.00	$III + zW + nH^+ = 1/a$ IV	$\hat{D}_{IV} = -0.090$	1	1.05

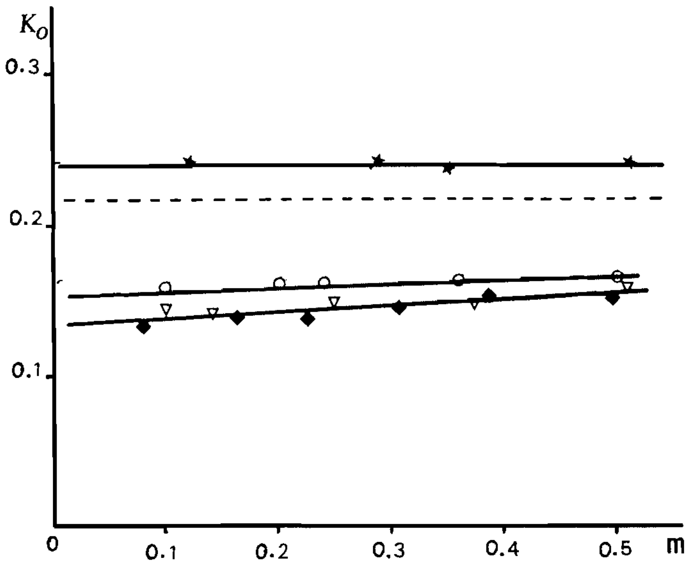

FIG. 4. Cryoscopic molal decreases K (°C) vs. molality (moles of W(VI)/kg of solvent). Malate/tungstate = 1, and (+) H^+/WO_4^{2-} = 1, (▽) H^+/WO_4^{2-} = 2, (◆) H^+/WO_4^{2-} = 3, (○) H^+/WO_4^{2-} = 3.5.

9.50 > pH > 7.00

$$WO_4^{2-} + C_4H_4O_5^{2-} + H^+ \rightleftarrows \{WO_2(C_4H_3O_5)(OH)_2\}^{3-}$$

7.00 > pH > 5.50

$$\{WO_2(C_4H_3O_5)(OH)_2\}^{3-} + H^+ \rightleftarrows 1/2\{[WO(OH)_2(C_4H_3O_5)]_2O\}^{4-} + 1/2H_2O$$

5.50 > pH > 4.00

$$\{[WO(OH)_2(C_4H_3O_5)]_2O\}^{4-} + 2H^+ \rightleftarrows \{[WO(OH)_2(C_4H_4O_5)]_2O\}^{2-}$$

4.00 > pH > 1.00

$$\{[WO(OH)_2(C_4H_4O_5)]_2O\}^{2-} + H^+ \rightleftarrows \{[WO(OH)(C_4H_4O_5)]_2O(OH)\}^{-} + H_2O$$

In summary, the formation of these complexes from WO_4^{2-} and $C_4H_4O_5^{2-}$ ions requires 1.0, 2.0, 3.0, and 3.5 equivalents of H^+ ions per each mole of W(VI) complexed, respectively, and the degree of condensation calculated agrees with those found by the stoichiometric methods.

Saline cryoscopy

In order to check the above polarimetric results we have applied an independent technique, saline cryoscopy in Glauber salt (13). The particular method used was the stationary state procedure (14).

It should be mentioned that the rotatory power of an equimolar solution of W(VI) and ligand has a dextrorotatory character, and the values of the rotatory power measured indicate that in this solution the ligand is predominantly involved in the formation of the complexes described when W(VI) is in excess (data not reported). This fact agrees with the higher stability constants found for these complex species.

In Fig. 4 we have plotted the molal decrease (K) in the transition temperature of $Na_2SO_4 \cdot 10H_2O$ as a function of the molality of solutions (moles of W(VI)/kg of Glauber salt) for a series of samples containing malate/tungstate and H^+/tungstate ratios corresponding to the above deduced stoichiometries. H^+ ions were added to the solutions as $NaHSO_4$, according to Haase's observation (15). Urea was employed as a non-electrolyte to determine the cryoscopic constant of the apparatus, resulting in a value equal to 0.22°C/mol urea.

Extrapolation of the straight lines in Fig. 4 to infinite dilution leads to K_0, the molal decrease at the origin. These values can be used to calculate n, the number of cryoscopically active particles per W(VI) in the solutions since $n = K_0/0.22$. The results obtained agree with the polarimetric data.

Structural considerations

Since the vicinal H—H coupling constant J_{H-H} depends among other factors on the H—C—C—H bond angle, ^{1}H nmr spectroscopy has proved particularly suitable for the study of the conformation of malic acid in the complexes where the binding is inert.

For the free malic acid, the J_{H-H} values have been found to vary with pH, essentially as a result of conformational changes caused by electrostatic and steric effects. Those changes may be discussed in terms of the populations of the three staggered rotational isomers (16):

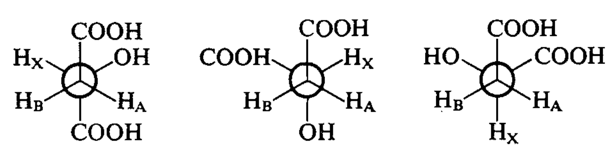

a **b** **c**

By assuming reasonable values for vicinal coupling constants in the three rotamers (J_{trans} = 16.0 Hz and J_{gauche} = 4.0 Hz) it has been possible to deduce, from the observed coupling constants, the relative populations of the isomers **a**, **b**, and **c** as a function of the pH (17, 18). The assignment of protons A and B has been based on the reasonable assumption that the malate ions exist mainly in form **a**, thus justifying $J_{AX} > J_{BX}$. Complexation with W(VI) leads to a negligible low shift of the AB pattern and a larger low field shift of the X multiplet.

In the presence of excess ligand, all spectra obtained for the complexes exhibit three broad peaks in the X-region that are nearly pH independent. This fact suggests that the conformation of the malic acid is fundamentally the same in all of them, but a complete analysis was not possible (see Table 3). Only $J_{AX} + J_{BX}$ = 12.5 Hz could be calculated for the complex present at pD = 5.00.

This agrees with the result obtained by Gil *et al.* (8), who found that, at pD = 5.50 using a 100 MHz spectrometer, the spectrum showed more lines, and separate values $J_{AX} = 10.5$ Hz and $J_{BX} = 2.4$ Hz could be calculated. According to these authors, the increase of J_{AX} and decrease of J_{BX} observed on going from the free ligand (malate ions at pD = 5.50; J_{AX} = 9.7 and J_{BX} = 3.3 Hz) to the complex with W(VI) shows that the formation of these complexes stabilizes conformation **a**. It was concluded that, in the presence of an excess ligand, the malic acid acts as bidentate ligand through a carboxylic acid centre and a β-positioned alcoholic group.

However, as mentioned in the Introduction, if we consider that these complexes are dimers with a $H_2L/W(VI) = 1$ ratio (1), and not monomers of 1:2 composition as indicated by Gil, the following structures can be proposed. In both structures, the ligand has the same **a** conformation:

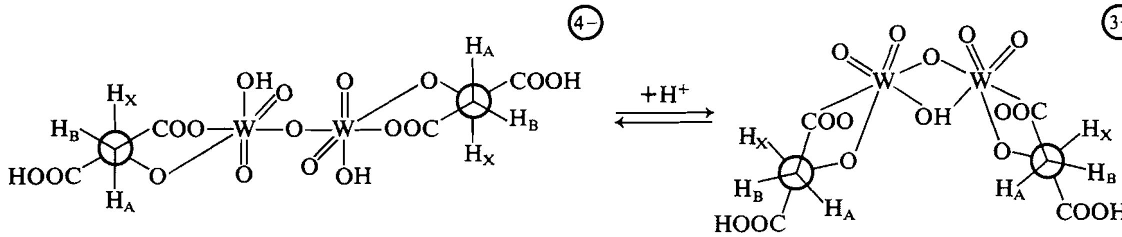

Evidence for similar structures has been obtained for oxalate (4), malonate (6), lactate (5), tartrate (3), and sorbitol (7) derivatives, and the presence of a double bridge in protonated species has also been previously suggested.

In Fig. 5, ^{1}H nmr spectra when W(VI) is in excess are given at pD values where only one complex species is predominant. In this set of ABX spectra, the spectrum which does not appear is that recorded for the monomeric 1:1 complex (pH = 7.50), owing to the proximity of the X part to water which prevented a reliable measurement of the coupling constant.

Two aspects of these spectra are of interest. First, in agreement with our polarimetric findings, the ^{1}H nmr spectra show that for excess metal three 2:2 tungstate–malate complexes can be formed depending on pD. Second, these complexes give rise to room-temperature spectra with narrower lines than those obtained with excess ligand. This might indicate that, in agreement with the above calculated values of K_d, the complexes formed are more dissociated under these conditions. In fact, as has been already reported (8), on lowering the temperature the spectra in the presence of excess ligand become appreciably narrower and, accordingly, the broadening at room temperature may be assigned to ligand exchange.

In Table 3 are summarized the values of J_{AX} and J_{BX} obtained from ABX analysis of the spectrum of each of the three 2:2 complexes (19, 20). However, for the complex stable at pD = 2.60, due to the coincidence of peaks in its ABX spectrum, only ($J_{AX} + J_{BX}$) could be calculated.

The value of J_{BX} = 4.4 Hz obtained for the dimeric complex at higher pD is essentially a *gauche* coupling constant, whereas the value of J_{AX} = 8.6 Hz implies a mixture of *trans* and *gauche* arrangements for A and X. The conclusion is that, in this complex, forms **a** and **c** could have the most important contributions. However, since the complex is quite strong, ligand exchange is slow, and internal rotation of the ligand would be difficult in the complex. The observed coupling constant might better be interpreted in terms of a single conformation. Among the three staggered rotamers, conformation **a** is the one that is more in agreement with the observed J-values. However, J_{BX} is high and J_{AX} low enough to postulate a twisting of structure **a**, in the sense that the H_B—C—C—H_X dihedral angle increases with a concomitant decrease in H_A—C—C—H_X.

At pD = 4.50, according to Gil *et al.* (8), the observed values of J_{AX} = 1.2 Hz and J_{BX} = 6.3 Hz are close to the expected values for a conformation of the ligand in which the A and B protons are in a *gauche* arrangement with respect to the X proton. Thus **c**, or a conformation close to it, appears to be the preferred geometry in this case.

From these nmr results we can propose the following structures for the three 2:2 complexes formed in excess of W(VI):

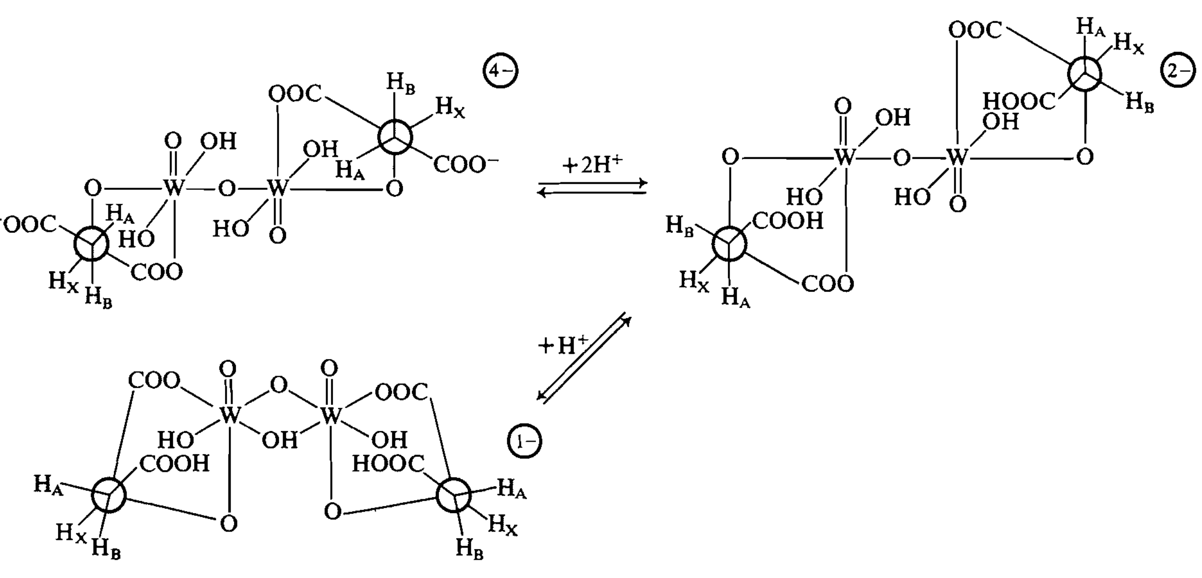

TABLE 3. Proton coupling constants and chemical shifts (in Hz) referred to *tert*-butanol, at 90 MHz[a]

Complex ion	pD	J_{AB}	$(J_{AX} + J_{BX})$	J_{AX}	J_{BX}	$(\nu_x - \nu_B)$	$(\nu_B - \nu_A)$
$\{[WO(C_4H_3O_5)(OH)_2]_2O^{4-}\}$	6.50	14.5	13.0	8.6	4.4	234.43	7.64
$\{[WO(C_4H_4O_5)(OH)_2]_2O^{2-}\}$	4.40	18.0	7.5	1.2	6.3	229.24	16.50
$\{[WO(C_4H_4O_5)(OH)]_2O(OH)^{1-}\}$	2.60	—	11.6	—	—		

[a] Spectra are shown in Fig. 5.

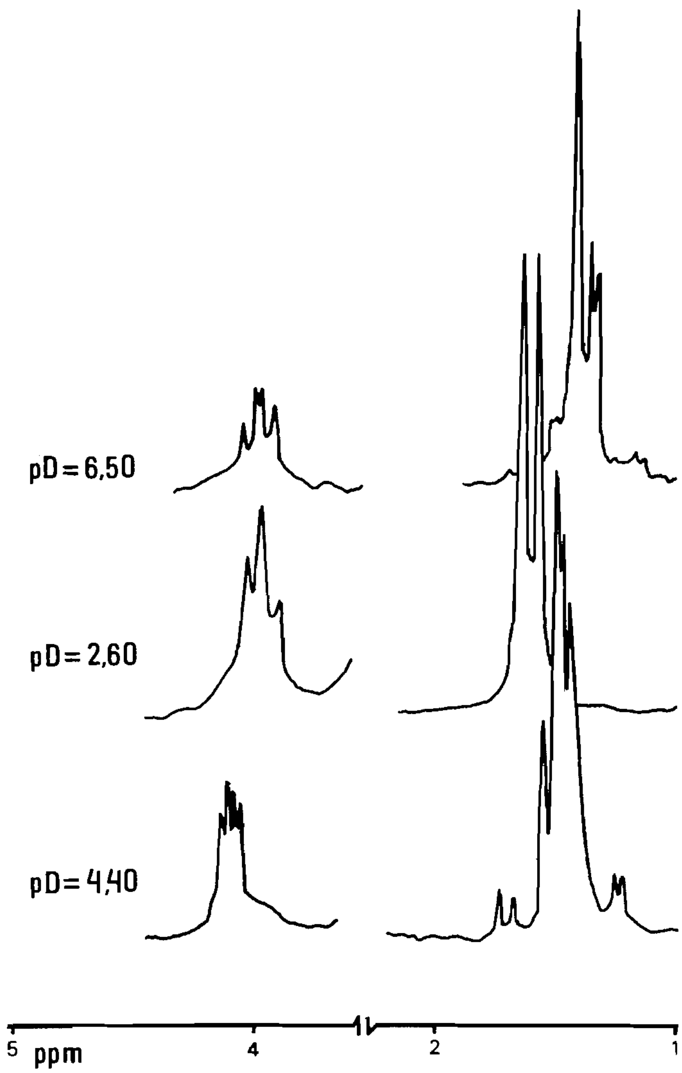

FIG. 5. 90-MHz Proton nmr spectra of a 4:1 solution of tungstate/malic acid in D_2O, for a range of pD values.

In all these structures we have assumed a bidentate complexing ability for the malic acid, which implies a chelation to each W atom through a carboxylic and an α-positioned alcoholic group. However, for the two last species which are stable at a lower pD, a facial tridentate coordination might also be expected. The five-membered rings in these complexes should be more stable than the six-membered rings formed in the complexes when ligand is in large excess. The higher stability of the former can thus be rationalized on the basis of the formation of five-membered, instead of six-membered, chelate rings. This feature would also account for previous reports of varying stabilities of the 2:2 Mo(VI)–ligand complexes with oxalic acid (4), malonic acid (6), and succinic acid (21). A dependence on the length of the carbon chain in the organic acid molecule, and thus chelate ring size, appears to exist. The oxalate complex is the most stable, the value of the dissociation constant for the malonate complex being two orders lower than for oxalate. No complex formation could be detected for the succinate complex (22).

Experimental

Solutions were prepared using analytical grade sodium tungstate and *l*(−)malic acid.

Rotatory power and pH were measured in a manner similar to that described previously (1). All samples were prepared to be 1 *M* in $NaClO_4$ to maintain the ionic strength of the medium and the pH was adjusted to the required value by adding the appropriate amounts of concentrated NaOH and (or) $HClO_4$ (70%).

The optical rotations of the solutions measured immediately and again after 24 h showed that immediate formation of stable complexes occurred.

For the cryoscopic measurements, a Knauer electronic measuring instrument was employed, using only a thermistor temperature probe. The standard sample volume was 0.15 mL and the reproducibility in the freezing point of the Glauber's salt was ±0.002°C. For concentrated solutions, the measuring error was smaller than 1%.

Samples for nmr spectroscopy were prepared by dissolving the appropriate amounts of Na_2WO_4 and *l*(−)malic acid in D_2O. In order to reduce the OH signal, the sample mixture was lyophilized from a D_2O solution and adjustment of the pD was done by dropwise addition of dilute DCl and NaOD solutions.

Proton nmr spectra were obtained at 90 MHz on a Perkin–Elmer R-32 spectrometer at a probe temperature of 35 ± 1°C.

1. A CERVILLA, A. BELTRÁN, and J. BELTRÁN. Can. J. Chem. **57**, 773 (1979).
2. A. BELTRÁN, A. CERVILLA, and J. BELTRÁN. J. Inorg. Nucl. Chem. **43**, 1337 (1981).
3. A CERVILLA, A. BELTRÁN, and J. BELTRÁN. Proc. Indian Acad. Sci. **90**, 297 (1981).
4. A. BELTRÁN, F. CATURLA, A. CERVILLA, and J. BELTRÁN. J. Inorg. Nucl. Chem. **43**, 3277 (1981).
5. A. BELTRÁN-PORTER, F. CATURLA, M. JOSÉ VILA, and A. CERVILLA. Trans. Metal Chem. **8**, 324 (1983).
6. A. BELTRÁN-PORTER, A. CERVILLA, F. CATURLA, and B. SEGURA. Trans. Metal Chem. **8**, 222 (1983).
7. A. CERVILLA, J. A. RAMIREZ, and A. BELTRÁN-PORTER. Trans. Metal Chem. **8**, 21 (1983).
8. V. M. S. GIL, M. E. T. L. SARAIVA, M. M. CALDEIRA, and A. M. D. PEREIRA. J. Inorg. Nucl. Chem. **42**, 389 (1980).
9. B. VIOSSAT. Rev. Chim. Miner. **9**, 737 (1972).
10. M. JONES and K. KEITH. J. Am. Chem. Soc. **62**, 1005 (1958).
11. A. BELTRÁN-PORTER, D. BELTRÁN-PORTER, A. CERVILLA, and J. A. RAMIREZ. Talanta, **30**, 124 (1983).
12. A. BELTRÁN-PORTER and J. A. RAMIREZ. Can. J. Chem. **61**, 1100 (1983).
13. P. SOUCHAY. Bull. Soc. Chem. Fr. **14**, 914 (1947); **15**, 143 (1948).
14. R. U. BONER *et al.* Number average molecular weights. Interscience, New York. 1958.

15. R. HAASE. Z. Naturforsch. **81**, 380 (1953).
16. L. E. ERICKSON. J. Am. Chem. Soc. **87**, 1867 (1965).
17. J. S. MARIANO and V. M. S. GIL. Mol. Phys. **17**, 313 (1969).
18. R. A. ALBERTY and P. BENDER. J. Am. Chem. Soc. **81**, 542 (1959).
19. E. D. BECKER. High resolution NMR. Academic Press, London. 1972.
20. J. A. POPLE, W. G. SCHNEIDER, and H. J. BERNSTEIN. High-resolution nuclear magnetic resonance. McGraw–Hill, New York. 1959.
21. A. BELTRÁN, F. CATURLA, A. CERVILLA, and J. BELTRÁN. An. Quim. **77**, B, 405 (1981).
22. K. B. YATSIMIRSKII and K. E. PRIK. Russ. J. Inorg. Chem. **7**, 821 (1962).

Total assignment of the ^{13}C spectrum of taraxasteryl acetate by $^{13}C-^{13}C$ connectivity experiments and determination of the stereochemistry of taraxasterol by X-ray diffraction

WILLIAM F. REYNOLDS AND JEFFERY F. SAWYER
Department of Chemistry, University of Toronto, Toronto, Ont., Canada M5S 1A1

RAÚL G. ENRÍQUEZ, LAURA I. ESCOBAR, AND MARCO A. CHAVEZ
Unidad de Investigación Biomédica en Medicina Tradicional y Herbolaria, I.M.S.S., Luz Saviñón 214, México, D.F. 03100, México

AND

JAMES N. SHOOLERY
Varian Instrument Group, 611 Hansen Way, Palo Alto, CA 94303, U.S.A.

Received July 30, 1984

WILLIAM F. REYNOLDS, JEFFERY F. SAWYER, RAÚL G. ENRÍQUEZ, LAURA I. ESCOBAR, MARCO A. CHAVEZ, and JAMES N. SHOOLERY. Can. J. Chem. **63**, 1048 (1985).

$^{13}C-^{13}C$ connectivity (INADEQUATE) experiments have been used to reassign the ^{13}C spectrum of taraxasteryl acetate. This shows that there were ten errors in an earlier ^{13}C spectral assignment for this compound. An X-ray diffraction investigation of taraxasterol shows that ring E adopts a slightly distorted boat conformation. It is suggested that severe steric interactions in the chair form force it to adopt this unusual conformation. On the basis of the $^{1}H-^{1}H$ coupling constants, it is concluded that taraxasteryl acetate adopts a very similar conformation in solution. Crystals of taraxasterol–ethanol solvate are orthorhombic, space group $P2_12_12_1$ wih a = 7.447(1) Å, b = 17.637(2) Å, c = 22.269(4) Å, U = 2925 Å^3, and D_{calc} = 1.07 g cm^{-3} for Z = 4.

WILLIAM F. REYNOLDS, JEFFERY F. SAWYER, RAÚL G. ENRÍQUEZ, LAURA I. ESCOBAR, MARCO A. CHAVEZ et JAMES N. SHOOLERY. Can. J. Chem. **63**, 1048 (1985).

On a fait appel à des expériences de conjonction (INADEQUATE) du $^{13}C-^{13}C$ pour faire de nouvelles attributions du spectre du ^{13}C de l'acétate de taraxastéryle. Ces expériences ont permis de démontrer que la première interprétation du spectre du ^{13}C de ce composé comporte dix erreurs. Une étude par diffraction de rayons X du taraxastérol montre que le cycle E adopte une conformation bateau légèrement déformée. On suggère que c'est la présence de fortes interactions stériques dans la forme chaise qui oblige cette dernière à adopter cette conformation inhabituelle. En se basant sur les constantes de couplage $^{1}H-^{1}H$, on conclut que l'acétate de taraxastéryle adopte à peu près la même conformation en solution. Les cristaux du taraxastérol solvaté avec de l'éthanol appartiennent au groupe d'espace orthorhombique $P2_12_12_1$ avec a = 7.447(1) Å, b = 17.637(2) Å, c = 22.269(4) Å, U = 2925 Å^3, D_{calc} = 1.07 g cm^{-3} et Z = 4.

[Traduit par le journal]

Introduction

As part of an investigation of medicinal properties of natural products extracted from *Montanoa tomentosa* Cerv. (1), we isolated a white crystalline compound (mp 245–246°C) which, according to high resolution mass spectrometry, had the empirical formula $C_{32}H_{52}O_2$. Comparison with previously reported infrared (2), ^{1}H nmr (2), and ^{13}C nmr (3) spectral data and melting point data (2, 4) indicated that the compound was the pentacyclic triterpenoid taraxasteryl acetate, **1** (5). While this compound is known to occur in a wide variety of plants (2, 4), this represented the first report of its isolation from *Montanoa tomentosa*.

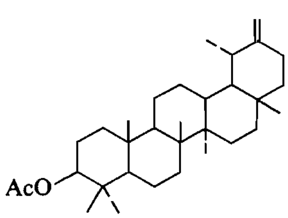

1

During the course of its characterization, we noted that there were at least six errors in the recently reported ^{13}C spectral assignments for **1** (3). Furthermore, certain of the coupling constants observed in the ^{1}H spectrum appeared to be inconsistent with the accepted stereochemistry (5) of **1**. Consequently, we undertook a more detailed nmr and X-ray diffraction investigation of **1** in order to obtain unambiguous spectral and stereochemical assignments. These investigations are reported below.

Results and discussion

(a) *Reassignment of the ^{13}C spectrum of 1*

As part of the characterizations of **1**, we applied spectral editing techniques to its ^{13}C spectrum. In Fig. 1, the ^{1}H-decoupled ^{13}C spectrum of the aliphatic region is reproduced, along with three edited subspectra (CH, CH_2, and CH_3), obtained using the pulse sequence DEPT (6). The latter spectra allow unambiguous assignment of ^{13}C peaks in terms of numbers of attached hydrogens. This revealed that there were at least six errors in the previously reported ^{13}C peak assignments (3) for **1** (see Table 1).

One possibility was simply that three pairs of carbons were interchanged (Table 1). However, it was uncertain whether these were the only incorrect assignments since spectral editing can only detect errors based on incorrect numbers of attached protons and not, for example, a pair of misassigned CH_3 groups. Consequently, we undertook a two-dimensional $^{13}C-^{13}C$ connectivity (INADEQUATE) experiment (7) in order to obtain an unambiguous total ^{13}C assignment of **1** based on carbon–carbon bond networks. The resultant spectrum is illus-

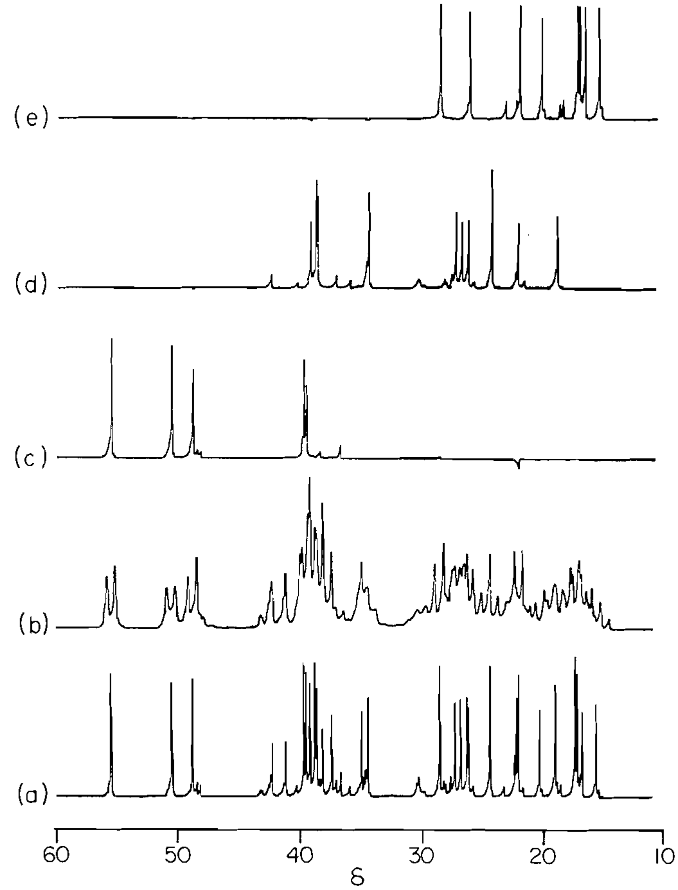

FIG. 1. (*a*) Normal ^{13}C spectrum of **1** for region δ 10–60; (*b*) SFORD spectrum; (*c*) subspectrum showing CH carbons only, obtained by DEPT spectral editing; (*d*) subspectrum showing CH_2 carbons only; (*e*) subspectrum showing CH_3 carbons only.

TABLE 1. ^{13}C peaks for **1** with incorrect numbers of attached protons in the previous assignment

δ^a	$n_H{}^b$
25.49 (25.4)	3 (2)
26.15 (26.1)	2 (3)
38.29 (38.3)	2 (1)
38.85 (38.8)	2 (1)
39.15 (39.1)	1 (2)
39.38 (39.3)	1 (2)

[a] ^{13}C chemical shifts in $CDCl_3$ (relative to $^{13}CH_3Si(CH_3)_3$). The first values are from this work while the values in brackets are from ref. 3.

[b] Number of attached protons for each ^{13}C peak as determined in this work by DEPT spectral editing. Incorrect values in brackets are from ref. 3 and were estimated from SFORD spectra.

trated in Fig. 2. Each directly bonded $^{13}C-^{13}C$ pair appears as a pair of AX or AB doublets having the same double quantum frequency, i.e. falling on the same horizontal line. Each doublet is centered about the corresponding chemical shift in the standard ^{1}H-decoupled ^{13}C spectrum with the doublet splitting, $^{1}J_{CC}$, typically being 35–70 Hz. Furthermore, each AX or AB spectrum must be symmetric about a line of slope 2 passing through the origin defined by the r.f. carrier (7). Due to these severe constraints, it is easy to distinguish data from artifacts and consequently establish the carbon–carbon connectivity pattern. The only unusual features in Fig. 2 concern the connectivities between C(20) and C(19) and C(21). The former peak is not observed since it lies outside the spectral window and digital filtering prevents folding in. However, C(20) still participates in double quantum coherence with C(19) and C(21). Based on the chemical shifts of these nuclei, the expected double quantum frequencies are, respectively, ca. 7300 Hz and 6150 Hz for C(19) and C(21). Since these lie outside the double quantum spectral window, these peaks appear folded in at respective double quantum frequencies of ca. −4700 Hz (doublet a in Fig. 2) and −5850 Hz (doublet b in Fig. 2). Note that there is no digital filtering in the double quantum dimension.

Final assignments are straightforward, based on the data in Fig. 2, and are given in Table 2. Individual carbons are also labelled on the stick diagram at the top of Fig. 2. These results reveal that there were ten misassigned ^{13}C peaks, all corresponding to protonated aliphatic carbons, in the earlier assignment (3). This represents over 40% of the 24 carbons of this type in **1**. There are at least two possible reasons for this disturbingly large number of misassignments. The first is that single frequency off-resonance decoupled (SFORD) spectra (obtained at 20 MHz) were used to assign ^{13}C peaks (3). However, even a 50.1-MHz SFORD ^{13}C spectrum for the aliphatic region of **1** (see Fig. 1) is far too complex to allow reliable assignments of all carbon multiplicities. Figure 1 provides a striking illustration of why this obsolete technique should be abandoned in favor of spectral editing techniques such as DEPT (6), INEPT (8), or APT (9). It should be noted that while DEPT and INEPT require a spectrometer with a sophisticated pulse programmer and phase shifters, APT can be implemented even on routine pulsed FT nmr spectrometers (9).

The second possible source of errors is in the use of model compounds as aids in assignment. This assumes (a) that the spectra of the model compounds are correctly assigned and (b) that they are sufficiently similar in structure and stereochemistry to the compound in question to be reliable models. In the case of **1**, germanicol acetate, **2**, (10) and lupeol, **3**, (11) were used as models. However, both **2** and **3** differ significantly from **1** in the structure of ring E. Interestingly, seven of the ten misassigned carbons are either ring D or E carbons or CH_3 groups bonded to ring D and (or) E (see Table 2). In addition, C(12) is spatially proximate to $C(29)H_3$. The significance of these observations will become apparent in part (b).

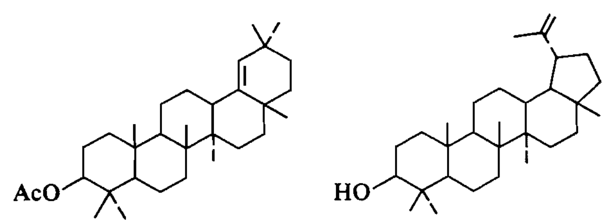

2 **3**

(b) *Determination of the relative configuration and conformation of taraxasteryl by X-ray diffraction methods*

The accepted structure for taraxasterol is 3β,18α,19α-

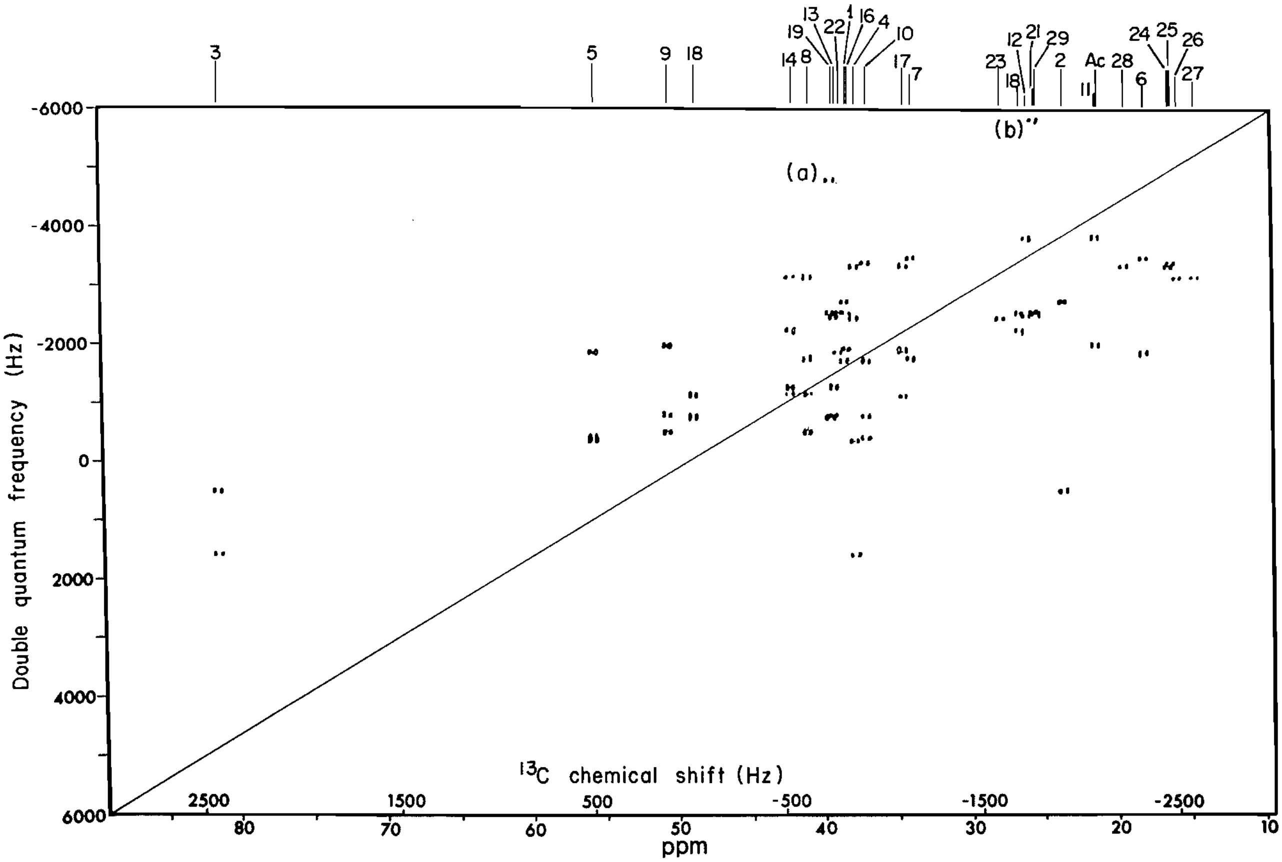

FIG. 2. Two-dimensional $^{13}C-^{13}C$ connectivity spectrum for **1**. Normal frequency axis is along the horizontal while the double quantum frequency is along the vertical. Peaks between coupled ^{13}C nuclei appear along the horizontal, distributed symmetrically with respect to the diagonal line. The final assignments are shown in the stick spectrum at the top. Doublets a (due to C(19)) and b (due to C(21)) are discussed in the text.

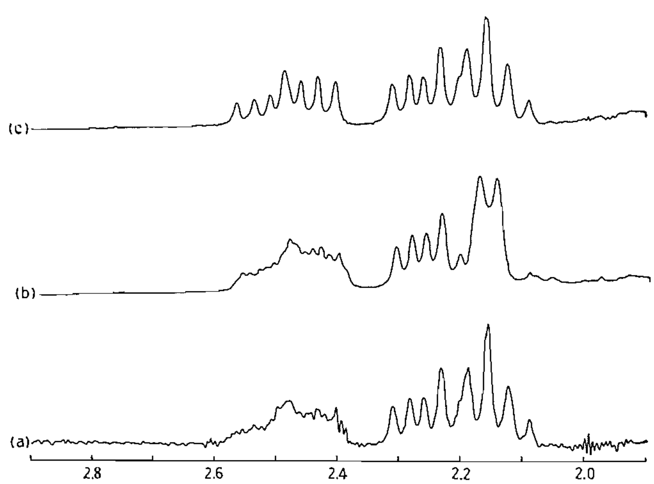

FIG. 3. ^1H spectrum of **1** in C_6D_6 showing allylic hydrogens. (*a*) Normal ^1H spectrum; (*b*) corresponding spectrum with decoupling of C(29) methyl doublet (δ 1.10); (*c*) corresponding spectrum with decoupling of exocyclic methylene protons (δ 4.92).

urs-20(30)-en-3-ol with the C(29) methyl group in an equatorial orientation in the assumed chair form of ring E (5, 12). However, the 200-MHz ^1H spectrum of **1** showed features which seemed inconsistent with this stereochemistry. In C_6D_6, the multiplets for protons allylic to the double bond are cleanly separated from other ^1H signals (see Fig. 3). Selective decoupling of the C(29) methyl doublet collapsed one of these multiplets to a doublet with $J_{HH} = 6.5$ Hz. This must be H(19) with the doublet reflecting vicinal coupling to H(18). This should be an *anti* (diaxial or a,a) coupling, according to the accepted structure. However, the magnitude of $J_{H(18)H(19)}$ seems more consistent with a *gauche* (axial–equatorial, a,e) coupling, e.g. $J_{H(a)H(a)} = 13.5$ Hz, $J_{H(a)H(e)} = 4–5$ Hz in methylenecyclohexane (13). Furthermore, selective decoupling of the methylene hydrogens reveals near-zero coupling of these protons to H(19). If H(19) is axially oriented, one would expect strong allylic coupling (ca. 2–3 Hz) to each of the methylene hydrogens, while this coupling should be near zero if H(19) is equatorial (14) (note that only one of the two C(21) protons (at δ 2.46 in Fig. 3) shows significant allylic coupling).

Both of these observations suggest that $C(29)H_3$ is in an axial or pseudo-axial orientation. One possible explanation is that the accepted structure for taraxasterol is incorrect and that it is actually 3β,18α,19β-urs-20(30)-en-3-ol. This would have $C(29)H_3$ axial and H(19) equatorial, assuming a chair form for ring E. In fact, the structure of taraxasterol has never been determined by an unambiguous technique such as X-ray diffraction. Rather, it was deduced from a complex series of isomerization and interconversion reactions (5). Consequently, we undertook an X-ray diffraction investigation of taraxasterol[1] in order to resolve these structural ambiguities.

The actual crystal structure of taraxasterol is shown in Fig.

[1] Taraxasterol was chosen for this investigation in preference to its acetate, **1**, since the former gave better crystals.

TABLE 2. Final assigned ^{13}C peaks for **1** from $^{13}C-^{13}C$ connectivity experiment

Carbon[a]	δ^b	Carbon	δ^b
C(1)	38.44 (38.4)	C(17)	34.53 (34.4)
C(2)	23.70 (23.6)	C(18)	48.63 (48.6)
C(3)	80.96 (80.8)	C(19)	39.28 (39.3, C(22))
C(4)	37.79 (37.7)	C(20)	154.64 (154.4)
C(5)	55.40 (55.4)	C(21)	25.61 (25.5, C(12))
C(6)	18.18 (18.1)	C(22)	38.85 (38.8, C(13))
C(7)	33.99 (33.9)	C(23)	27.94 (27.8)
C(8)	40.91 (40.8)	C(24)	16.51 (16.4)
C(9)	50.39 (50.3)	C(25)	16.34 (16.2, C(26))
C(10)	37.04 (37.0)	C(26)	15.89 (15.8, C(25))
C(11)	21.46 (21.4)	C(27)	14.72 (14.6)
C(12)	26.15 (26.1, C(28))	C(28)	19.49 (19.4, C(29))
C(13)	39.15 (39.1, C(16))	C(29)	25.49 (25.4, C(21))
C(14)	42.03 (41.9)	C(30)	107.12 (107.1)
C(15)	26.64 (26.6)	CH_3—CO_2—	21.33 (21.1)
C(16)	38.29 (38.3, C(19))	CH_3—CO_2—	171.01 (170.8)

[a]Labelling as shown below.
[b]^{13}C chemical shifts in $CDCl_3$ (relative to internal $^{13}CH_3Si(CH_3)_3$). The first values are from this work while the values in brackets are from ref. 3. In cases where peaks were misassigned in ref. 3, the previous assignment is given after the δ value, e.g. (26.1, C(28)) illustrates that C(12) had previously been assigned as C(28).

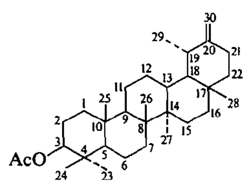

Numbering of taraxasteryl acetate

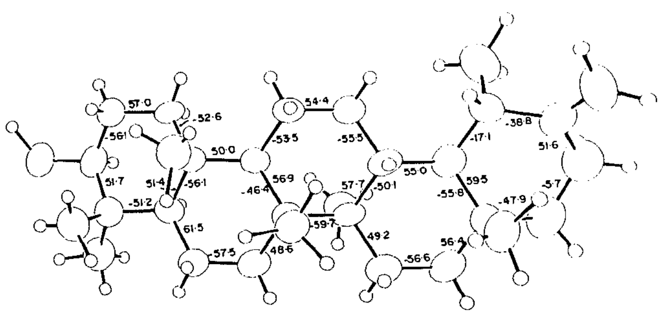

FIG. 4. ORTEP view of the molecular structure of taraxasterol. Thermal ellipsoids are drawn at the 50% probability level. The crystallographic numbering scheme corresponds to the chemical notation. The correct absolute configuration (using the inverted coordinates of Table 3) is indicated. Intraring C—C—C—C dihedral angles (°) are indicated for each ring. Note the close contact for $C(12)H_2$ and $C(29)H_3$.

4, while atomic coordinates are summarized in Table 3. In fact, the configuration of taraxasterol is identical to that previously proposed. However, while intraring dihedral angles for rings A–D (see Fig. 4) show that they exist in slightly flattened chair forms (an idealized chair would show alternating dihedral angles of +60° and −60°), ring E is in a distorted boat conformation (i.e. note the near zero values for ∠C(17)—C(18)—C(19)—C(20) and ∠C(17)—C(22)—C(21)—C(20)) with $C(29)H_3$ in a pseudo-axial orientation.

It is interesting to consider why ring E adopts the normally disfavored boat conformation. This cannot be primarily due to the presence of the exocyclic methylene group or to any steric interactions of $C(29)H_3$ with this group, since methylenecyclohexane prefers a slightly distorted chair form (15) while the methyl group in 1-methyl-2-methylenecyclohexane favors an equatorial orientation over an axial orientation by 1.0 kcal/mol (16). Rather, it appears that a steric interaction between $C(12)H_2$ and $C(29)H_3$ forces ring E into the boat conformation. Even in this conformation, the closest hydrogen–hydrogen separation between $C(12)H_2$ and $C(29)H_3$ is 2.46 Å, roughly the sum of hydrogen van der Waals radii. This distance would be significantly decreased if the molecules attempted to adopt a chair conformation for ring E.

The alternative possibility, that the ring E conformation results from crystal packing forces, can be conclusively ruled out on the basis of the X-ray and nmr data. The crystal packing diagram (see Fig. 5) shows a hydrogen bond O(1)—H(1) . . . . O(2) (O(1)—H(1) = 1.18 Å; O(2)—H(1) = 1.60 Å, ∠O(1)—H(1) - - - O(2) = 147.7°) involving the solvent. However, all other intermolecular contacts are weak. Furthermore, the ^1H nmr data indicate that **1** has a solution conformation which is very similar to the crystal structure conformation of taraxasterol. For example, the H(18)—C(18)—C(19)—H(19) dihedral angle of 142° in the crystal structure is consistent with $^3J_{H(18)H(19)}$ = 6.5 Hz in **1** while the H(19)—C(19)—C(20)—C(30) dihedral angle of 30° is also consistent with the near-zero allylic coupling of H(19) to the methylene protons. Thus the apparently inconsistent features in the ^1H spectrum of **1** can be rationalized in terms of a boat conformation for ring E. This also likely accounts for many of the misassigned ^{13}C peaks. For example, among the incorrectly assigned carbons are four of the five carbons in the sequence C(12)—C(13)—C(18)—C(19)—C(29) which is perturbed by the $C(12)H_2$—$C(29)H_3$ steric interaction. This clearly points out the risks in using

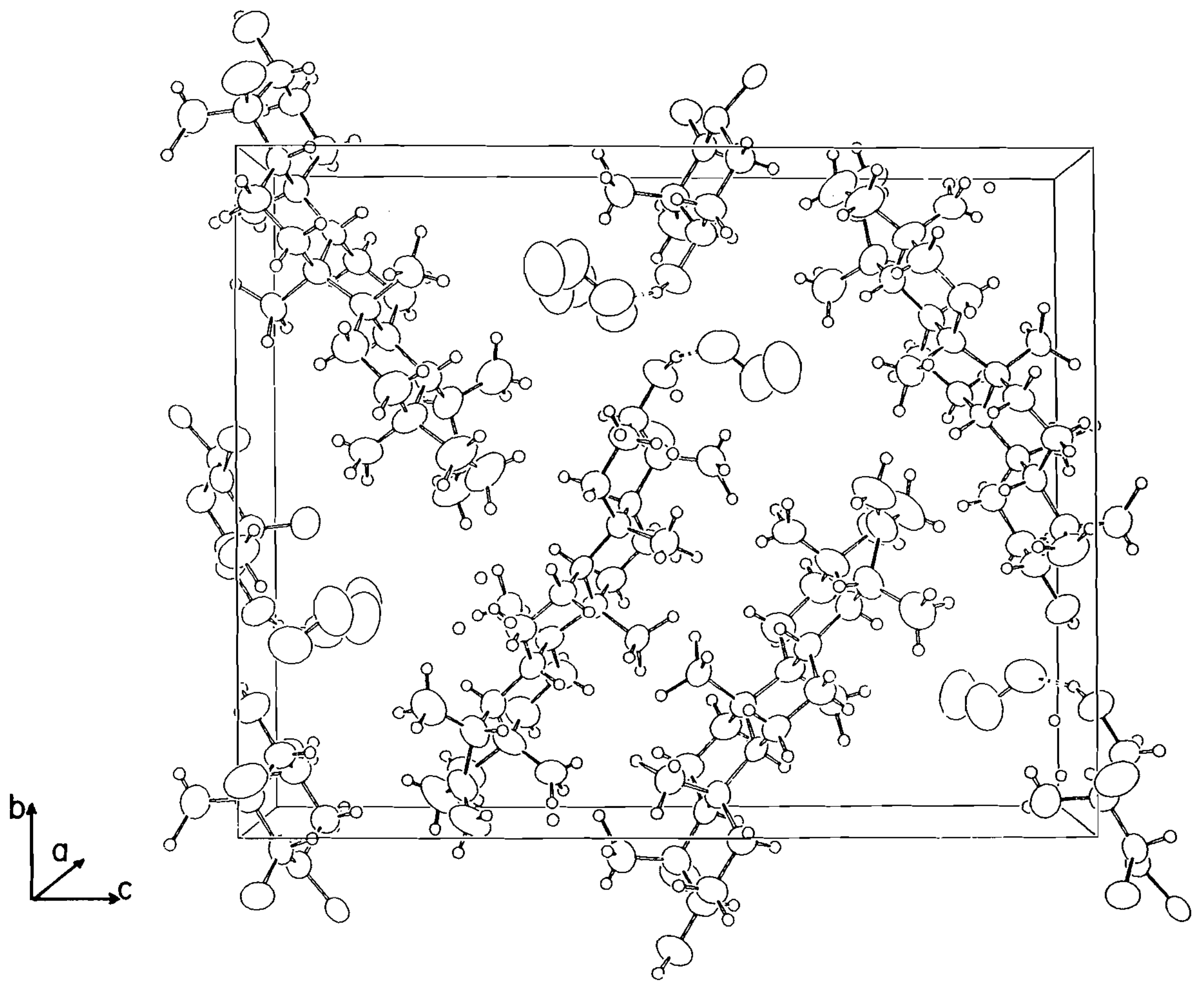

FIG. 5. Crystal packing diagram for taraxasterol–ethanol solvate.

model compounds to assign ^{13}C peaks in a compound of uncertain stereochemistry.

Conclusions

$^{13}C-^{13}C$ connectivity ("INADEQUATE") experiments have been used to unambiguously assign the ^{13}C signals in **1**. Comparison with a previous ^{13}C spectral assignment shows that 10 of 24 protonated aliphatic carbons had been incorrectly assigned (3). This is attributed to the use of an unreliable experimental method (SFORD) plus the use of inappropriate model compounds. It is concluded that SFORD spectra should be abandoned in favor of spectral editing (APT, INEPT, or DEPT) techniques while, at the very least, model compounds should only be used for assignment purposes when one is totally confident of the stereochemistries of both the model and target compounds. Wherever possible, one should use an unambiguous technique such as $^{13}C-^{13}C$ connectivity experiments for assignment of ^{13}C spectra (7). If this is impossible due to sensitivity limitations, it may often be possible to use heteronuclear correlated 2D spectra which are optimized for long-range $^{13}C-^{1}H$ couplings to unambiguously assign ^{13}C peaks (17).

Ring E of taraxasterol prefers a distorted boat conformation in the solid state, probably due to nonbonded interactions between $C(12)H_2$ and $C(29)H_3$. Taraxasteryl acetate, **1**, apparently has a very similar conformation in solution, accounting for the unexpected features in the ^{1}H spectrum of this compound.

Experimental

Dried ground leaves (1.2 kg) of *Montanoa tomentosa* Cerv. were macerated at room temperature with petroleum ether (bp 30–60°C) for periods of 48 h, three times. The extracts evaporated *in vacuo* were collected, yielding 87 g of syrupy residue. Twenty-five grams of this extract were chromatographed on a column of silica gel deactivated with 5% H_2O. Elution was carried out using 250-mL fractions of solution varying in concentration from pure hexane to 94% hexane/6% ethyl acetate (v/v%). Twenty-five fractions were collected in this way with **1** appearing in fractions 8–15. The collected fractions were rechromatographed under similar conditions, yielding 1.3 g of crude compound. Recrystallization from ethanol yielded 0.7 g of **1** (mp 245–246°C).

Most ^{1}H and ^{13}C spectra of **1** were obtained on a Varian XL-200 spectrometer operating in pulsed Fourier transform mode at a probe temperature of 20°C. ^{1}H spectra were recorded for C_6D_6 solutions containing ca. 5 mg of sample in 0.5 mL of solvent in a 5-mm tube with 0.1% tetramethylsilane as internal reference. Spectral width was 2000 Hz with 32K data points. 90° (7 μs) pulse widths were used with a repetition time of 8 s; 32 transients were collected. ^{13}C spectra were recorded for $CDCl_3$ solutions containing 150 mg of sample in 2.5 mL of solvent in a 10-mm tube. Spectral width was 10,000 Hz with 32K data points. 45° (7.5 μs) pulse widths were used with a repetition time of 1.6 s, and 4000 transients. Four DEPT spectra were collected using θ pulses of 45°, 90°, 90°, and 135° with 1200 transients for each

TABLE 3. Table of positional parameters and their estimated standard deviations

Atom	x	y	z	B(Å²)	Atom	x	y	z	B(Å²)
O(1)	0.3103(6)	−0.1831(2)	0.5080(2)	6.3(1)	C(21)	0.282(1)	0.4710(4)	0.7850(3)	8.7(2)
C(1)	0.1335(8)	−0.0104(3)	0.5878(3)	4.5(1)	C(22)	0.456(1)	0.4443(4)	0.7555(4)	7.3(2)
C(2)	0.1308(9)	−0.0830(3)	0.5522(3)	4.9(1)	C(23)	0.636(1)	−0.0887(4)	0.5155(4)	7.0(2)
C(3)	0.3179(9)	−0.1135(3)	0.5417(3)	5.2(1)	C(24)	0.400(1)	−0.0477(4)	0.4440(3)	6.0(2)
C(4)	0.4422(8)	−0.0560(3)	0.5105(3)	4.6(1)	C(25)	0.1431(9)	0.0784(3)	0.5029(3)	5.0(1)
C(5)	0.4332(8)	0.0200(3)	0.5467(2)	4.0(1)	C(26)	0.3480(9)	0.2291(3)	0.5377(2)	4.6(1)
C(6)	0.5608(8)	0.0804(3)	0.5249(3)	4.7(1)	C(27)	0.5124(8)	0.1831(3)	0.7022(3)	4.9(1)
C(7)	0.5853(8)	0.1408(3)	0.5720(3)	4.6(1)	C(28)	0.366(1)	0.4398(3)	0.6469(3)	6.2(2)
C(8)	0.4100(7)	0.1796(3)	0.5919(2)	3.7(1)	C(29)	0.024(1)	0.3266(4)	0.7915(3)	8.2(2)
C(9)	0.2661(7)	0.1177(3)	0.6065(2)	3.4(1)	C(30)	−0.010(1)	0.4980(4)	0.7406(4)	8.2(2)
C(10)	0.2436(7)	0.0518(3)	0.5600(2)	3.7(1)	O2	0.9702(8)	0.2804(3)	0.0634(3)	9.4(2)
C(11)	0.0952(8)	0.1546(3)	0.6280(2)	4.0(1)	C1	1.188(2)	0.3150(6)	0.1389(4)	12.0(3)
C(12)	0.1222(8)	0.2087(3)	0.6798(3)	4.6(1)	C2	1.008(1)	0.3283(6)	0.1128(4)	10.3(3)
C(13)	0.2606(7)	0.2702(3)	0.6680(2)	4.0(1)					
C(14)	0.4444(7)	0.2311(3)	0.6495(3)	3.9(1)					
C(15)	0.5832(8)	0.2920(4)	0.6370(3)	5.3(2)					
C(16)	0.5972(9)	0.3524(4)	0.6862(3)	6.3(2)					
C(17)	0.4238(8)	0.3930(3)	0.7001(3)	5.4(1)					
C(18)	0.2808(8)	0.3300(3)	0.7174(2)	4.8(1)					
C(19)	0.1044(8)	0.3665(4)	0.7368(3)	5.2(1)					
C(20)	0.1198(9)	0.4496(4)	0.7528(3)	5.7(2)					

Anisotropically refined atoms are given in the form of the isotropic equivalent thermal parameter defined as: $(4/3)[a^2B(1,1) + b^2B(2,2) + c^2B(3,3) + ab(\cos\gamma)B(1,2) + ac(\cos\beta)B(1,3) + bc(\cos\alpha)B(2,3)]$.

spectrum (16 K data points, repetition rate = 1.6 s, [^{1}H] pulse width = 37 s). Edited subspectra were obtained using the subroutine ADEPT incorporated in the Varian software (H2 release).

The two-dimensional $^{13}C-^{13}C$ connectivity experiment was carried out with a Varian XL-300 nmr spectrometer using 300 mg of taraxasteryl acetate in 2.0 mL $CDCl_3$ and a 10-mm broadband probe tuned for ^{13}C at 75 MHz. The INADEQUATE pulse sequence (7) was set up to apply a final detection pulse of 135°. Broadband decoupling was applied continuously. The spectral width was 6000 Hz (80 ppm), the acquisition time was 0.170 s, and the resulting number of data points in the chemical shift dimension was 2048. The number of increments in the evolution time (delay between creation of double quantum coherence and observation of the signal) was 128, but zero-filling allowed second dimension Fourier Transformation using 256 data points in the double quantum frequency dimension. The first dimension FIDs were weighted by an exponential line-broadening function of 5 Hz; the second dimension interferograms were weighted by an exponential broadening function of 20 Hz.

Each increment was acquired for 320 pulse sequences, with a 3.0-s delay between sequences to allow substantial recovery of magnetization even for the quaternary carbons. This gave a total acquisition time of 36 h. The timing of the INADEQUATE sequence was calculated and set by the CCC2D program of the XL-300, based on the value of 37 Hz estimated for the average $^{13}C-^{13}C$ coupling constant.

Taraxasterol was prepared by hydrolyzing **1** in 0.1 *N* NaOH in 50% ethanol–water followed by neutralization, recovery of precipitated taraxasterol, and recrystallization from ethanol. The crystals were colorless blocks and needles. Precession photographs were used to obtain preliminary cell and space group information. Initially data were collected on an Enraf–Nonius CAD-4 diffractometer by the use of graphite monochromatized Mo K$\bar{\alpha}$ radiation (λ = 0.71069 Å). Subsequently a more extensive data set was obtained using Cu radiation (λ = 1.54184 Å) and a block-shaped crystal of overall dimensions 0.35 × 0.1875 × 0.1125 mm in the directions [1,0,0], [0,1,$\bar{1}$], and [0,1,1] respectively.

Crystal data

$C_{30}H_{50}O \cdot C_2H_6O$ fw = 472.8

Orthorhombic, space group $P2_12_12_1$ with a = 7.447(1) Å, b = 17.637(2) Å, c = 22.269(4) Å, U = 2925 Å^3, and D_c = 1.07 g cm^{-3} for Z = 4. Cu K$\bar{\alpha}$ radiation (λ = 1.54184 Å), μ(Cu K$\bar{\alpha}$) = 4.5 cm^{-1}.

Cell constants were obtained by least-squares refinement of the setting angles of 25 reflections within the range $9.6 < \theta < 20.4°$. Intensity data were collected at room temperature in coupled ω:2θ modes using scan ranges of 0.85 + 0.147 tan θ° within a maximum scan time of 95 s. For each reflection, backgrounds were obtained by extending the scan by 25% on either side of the peak and were measured for half the time taken to collect the peak. A total of 2986 reflections in the quadrant h,k,l with $2\theta \leq 130°$ was obtained. No significant variations in the intensities of 3 standard reflections monitored after every 8500 s of exposure time were observed.

Lorentz and polarization corrections were applied to all reflections. The rejection of systematically absent and zero F_{obs} data then gave a final data set of 2528 reflections. The structure was initially solved using direct methods (MULTAN 11) (18) on the data set collected with Mo radiation. Missing atoms and the presence of a molecule of ethanol solvent in the lattice were indicated in subsequent Fourier maps. Hydrogen atoms were placed in calculated positions or were located in difference Fourier maps (CH_3 groups) with fixed thermal parameters (B = 7.5 or 10.0 Å^2) but were not refined.

Least-squares refinement of the structure using the Cu data set and including an extinction correction g to the data converged (max. shift/error = 0.07) to the final residuals R_1 = 0.0773 (R_w = 0.0902) for 1941 reflections (308 variables) with $I > 1.5\sigma(I)$. The final value of g was 1.4(2) × 10^{-6} and weights were given by $1/\sigma(F)^2$ where $\sigma(F) = 4F^2/(\sigma(I)^2 + (0.07F^2)^2)^{1/2}$. A final difference Fourier contained no peak greater than 0.22 e Å^{-3}.

All calculations were performed on a PDP 11/23 computer using programs in the Enraf–Nonius structure determination package (19). Tables of positional parameters of the hydrogen atoms, anisotropic, thermal parameters, bond lengths, bond angles, and final structure factor amplitudes have been deposited as Supplementary Material.[2]

1. X. LOZOYA, R. G. ENRIQUEZ, and E. BEHAR. Contraception, **27**, 267 (1983).
2. S. K. TALAPATRA, M. BHATACHARYA, and M. P. TALPATRA. Indian J. Chem. **11**, 166 (1981).

[2]These tables are available, at a nominal charge, from the Depository of Unpublished Data, CISTI, National Research Council of Canada, Ottawa, Ont., Canada K1A 0S2.

3. A. PATRA, A. K. MUKHOPADHYAY, and A. K. MITRA. Org. Magn. Reson. **17**, 166 (1981).
4. (*a*) N. AHMAD and G. HAHN. Pak. J. Sci. Med. Res. **2**, 55 (1959); (*b*) J.-H. CHU and P.-C. YAN. Hua Hsueh Hsueh Pao, **25**, 179 (1959); (*c*) C. P. NAMBOORIDYSAD, G. H. KULKARNI, and G. R. KELKAR. Curr. Sci. **37**, 350 (1968); (*d*) W. H. HUI and W. K. LEE. Phytochemistry, **10**, 889 (1971); (*e*) C. P. DUTTA, L. P. K. RAY, and D. N. ROY. Phytochemistry, **11**, 2267 (1972); (*f*) X. A. DOMINGUEZ, P. ROJAS, M. DEL C. DUENOS WIARCO, and S. ESCAVARIA. Phytochemistry, **13**, 224 (1973); (*g*) X. A. DOMINGUEZ, D. BUTRUILLA, and P. PEREYA. Rev. Latinoam. Quim. **7**, 98 (1976); (*h*) H. KOHDA, O. TANAKA, and K. NISHI. Chem. Pharm. Bull. **24**, 1040 (1976); (*i*) L. QUIJANO, J. S. CALDERON, F. COMGEZ, J. T. GARDUNS, and T. RISS. Phytochemistry, **19**, 175 (1980).
5. T. G. HALSALL, E. R. H. JONES, and R. E. H. SWAYNE. J. Chem. Soc. 1905 (1954).
6. D. M. DODDRELL, D. T. PEGG, and M. R. BENDALL. J. Magn. Reson. **48**, 323 (1982).
7. T. H. MARECI and R. FREEMAN. J. Magn. Reson. **48**, 158 (1982).
8. G. A. MORRIS. J. Am. Chem. Soc. **102**, 428 (1980).
9. S. L. PATT and J. N. SHOOLERY. J. Magn. Reson. **46**, 535 (1982).
10. A. K. PATRA, A. K. MITRA, T. K. CHATTERJIE, and A. K. BARUA. Org. Magn. Reson. **17**, 148 (1981).
11. E. WENKERT, G. V. BORDDELAY, I. R. BURFELT, and L. N. MORENO. Org. Magn. Reson. **11**, 337 (1978).
12. P. DE MAYO. The higher terpenoids. Interscience, New York. 1959. p. 180.
13. J. T. GERIG and R. A. RIMERMAN. J. Am. Chem. Soc. **92**, 1219 (1970).
14. M. BARFIELD and B. CHAKRABARTI. Chem. Rev. **69**, 757 (1969).
15. (*a*) F. A. L. ANET and I. YOVARI. Tetrahedron, **34**, 2879 (1978); (*b*) R. J. ABRAHAM, M. J. BOVILL, D. J. CHADWICK, L. GRIFFITHS, and F. SANCASSAN. Tetrahedron, **36**, 279 (1980).
16. J. LESSARD, P. V. M. TAN, R. MARTINO, and J. K. SAUNDERS. Can. J. Chem. **55**, 1015 (1977).
17. (*a*) C. WYNANTS, K. HALLINGA, G. VAN BINST, A. MICHEL, and J. ZANEN. J. Magn. Reson. **57**, 93 (1984); (*b*) H. KESSLER, C. GRIESINGER, J. ZARBOCK, and H. R. LOOSLI. J. Magn. Reson. **57**, 331 (1984); (*c*) W. F. REYNOLDS, R. G. ENRIQUEZ, L. I. ESCOBAR, and X. LOZOYA. Can. J. Chem. **62**, 2421 (1984).
18. P. MAIN *et al.* MULTAN 11/82 system of programs for the automatic solution of crystal structures from X-ray diffraction data. University of York, England. 1982.
19. B. A. FRENZ *et al.* Enraf–Nonius structure determination package. College Station, Texas. 1981.

Magnetic properties of anhydrous and hydrated dimethylphosphinates of manganese(II). The crystal and molecular structure of poly-bis(μ-dimethylphosphinato)diaquomanganese(II)

WALTER V. CICHA, JOHN S. HAYNES, KATHERINE W. OLIVER, STEVEN J. RETTIG, ROBERT C. THOMPSON,[1] AND JAMES TROTTER

Department of Chemistry, University of British Columbia, 2035 Main Mall, Vancouver, B.C., Canada V6T 1Y6

Received August 7, 1984

WALTER V. CICHA, JOHN S. HAYNES, KATHERINE W. OLIVER, STEVEN J. RETTIG, ROBERT C. THOMPSON, and JAMES TROTTER. Can. J. Chem. **63**, 1055 (1985).

The dimethylphosphinate of manganese(II), $Mn[(CH_3)_2PO_2]_2$, and its dihydrate have been prepared and studied using magnetic susceptibility, differential scanning calorimetry, and electronic and vibrational spectroscopic methods. The dihydrate was obtained in crystalline form and a single crystal X-ray diffraction study revealed a polymeric structure.

Crystals of poly-bis(μ-dimethylphosphinato)diaquomanganese(II) are monoclinic, a = 20.722(3), b = 4.8652(2), c = 11.0689(14) Å, β = 102.209(7)°, Z = 4, space group $C2/c$. The structure was solved by conventional heavy-atom methods and was refined by full-matrix least-squares procedures to R = 0.030 and R_w = 0.033 for 983 reflections with $I \geq 3\sigma(I)$. The structure consists of infinite centrosymmetric chains of Mn(II) atoms linked by double phosphinate bridges and extending along the crystallographic b axis. The water molecules are involved in both interchain and bifurcated intrachain hydrogen bonding (O···O = 2.734(2), 2.899(3) and 3.120(3) Å). The coordination about Mn is slightly distorted octahedral with libration-corrected bond lengths Mn—O(phosphinato) = 2.156(2) and 2.212(2), Mn—OH_2 = 2.247(2) Å.

Magnetic susceptibility studies on the dihydrate from 300 to 4.2 K reveal a magnetic moment of ~5.9 BM over most of the range and give no evidence for significant magnetic exchange. The anhydrous compound, which is considered on the basis of indirect evidence to retain the double phosphinate bridged structure exhibited by the dihydrate, shows relatively strong antiferromagnetic behaviour. The data have been analyzed according to two theoretical models both of which employ the isotropic Heinsenberg Hamiltonian. The scaling model of Wagner and Friedberg gives $J = -2.94$ cm^{-1} and g = 2.02 and the interpolation scheme of Weng gives $J = -2.69$ cm^{-1} and g = 2.01. The magnitude of the exchange coupling is considered in relation to that observed in related manganese compounds and possible reasons for the observed damping of the exchange on hydration are discussed.

WALTER V. CICHA, JOHN S. HAYNES, KATHERINE W. OLIVER, STEVEN J. RETTIG, ROBERT C. THOMPSON et JAMES TROTTER. Can. J. Chem. **63**, 1055 (1985).

On a préparé le diméthylphosphinate de manganèse(II), $Mn[(CH_3)_2PO_2]_2$ ainsi que son hydrate double et on les a étudiés en faisant appel à la susceptibilité magnétique, à la calorimétrie à balayage différentiel et à la spectroscopie électronique et vibrationnelle. On a obtenu l'hydrate double sous forme cristalline et une étude par diffraction de rayons X sur un cristal unique révèle qu'il existe sous une forme polymérisée.

Les cristaux de poly-bis(μ-diméthylphosphinato)diaquomanganèse(II) appartiennent au groupe d'espace monoclinique $C2/c$, avec a = 20,722(3), b = 4,8652(2), c = 11,0689(14) Å, β = 102,209(7)°, Z = 4. On a résolu la structure par la méthode conventionnelle aux atomes lourds et on l'a affinée par la méthode des moindres carrés (matrice entière) jusqu'à des valeurs de R = 0,030 et de R_w = 0,033 pour 983 réflexions avec $I \geq 3\sigma(I)$. La structure comprend des chaînes centrosymétriques infinies d'atomes de Mn(II) liés par un double pont phosphinato et s'étendent le long de l'axe cristallographique b. Les molécules d'eau sont impliquées dans des liaisons hydrogènes interchaînes et intrachaînes bifurquées (O···O) = 2,734(2), 2,899(3) et 3,120(3) Å. La coordination autour du Mn est un octaédrique, légèrement déformée avec des longueurs de liaison, corrigées pour la libration, de Mn—O(phosphinato) = 2,156(2) et 2,212(2) et Mn—OH_2 = 2,247(2) Å.

Les études de susceptibilité magnétique, réalisées avec l'hydrate double à des températures allant de 300 à 4,2 K, révèlent la présence d'un moment magnétique de 5,9 BM environ sur presque tout l'intervalle considéré. Le composé anhydre, qui, d'après des preuves indirectes, conserverait la structure pontée double phosphinate qui existe dans le dihydrate, exhibe un comportement antiferromagnétique relativement fort. On a analysé les données selon deux modèles théoriques qui utilisent l'Hamiltonien isotrope de Heinsenberg. Le modèle proportionné de Wagner et Friedberg permet de prédire des valeurs de $J = -2{,}94$ cm^{-1} et g = 2,02 alors que le schéma d'interpolation de Weng conduit à des valeurs de $J = -2{,}69$ cm^{-1} et g = 2,01. On considère l'amplitude du couplage d'échange en rapport avec celui observé avec des composés apparentés du manganèse et on discute des raisons qui pourraient expliquer le fait que l'échange accompagnant l'hydratation est amoindri.

[Traduit par le journal]

Introduction

The poly(metal phosphinates) are a class of inorganic coordination polymers in which metal centres are bridged by —OPR_2O— groups to form, typically, one-dimensional extended chains (1–6). These materials have generated interest from chemists and physicists alike over the past twenty years. Their polymeric nature leads generally to thermal and chemical stability as well as to some plastic and other properties of interest to industry (7) while the presence of paramagnetic transition metal sites throughout the polymeric lattice holds potential for the propagation of magnetic exchange and other interesting solid state properties (5, 6, 8). Earlier work on the dialkylphosphinates of copper(II) has shown that these compounds provide examples of both antiferromagnetic and ferromagnetic one-dimensional chains, the sign and magnitude of the exchange coupling in these compounds being related to relatively minor structural differences (6). To fully explore magneto-structural correlations in these systems we have been studying the effects of varying both the nature of the phosphinate bridge and the metal. In addition, in the present work we have discovered that hydration of the metal ion, in this instance at least, has a significant effect on the magnetic properties. We report here the synthesis and magnetic properties of the dimethylphosphinate of manganese(II), $Mn[(CH_3)_2PO_2]_2$,

[1] To whom all correspondence should be addressed.

and its dihydrate. The structure of the dihydrate was determined by single crystal X-ray diffraction methods. The existence of a monohydrate, reported earlier (9), was not confirmed in the present work.

Experimental

Preparations

Dimethylphosphinic acid, $(CH_3)_2PO_2H$

The synthetic route chosen involved the synthesis first of tetramethyldiphosphine disulfide, $(CH_3)_2P(S)P(S)(CH_3)_2$ according to a scaled-down version of Parshall's method (10) followed by oxidation and subsequent hydrolysis to the acid. Oxidation of the disulfide using hydrogen peroxide (11), chlorine (which gave dimethyltrichlorophosphorane, $(CH_3)_2PCl_3$, and which could be subsequently hydrolyzed to the acid) (12, 13) and mercuric oxide (14) all gave the desired product; however, the best yields were obtained by the method described in detail below involving oxidation with an excess of sulfuryl chloride to give dimethylphosphinic chloride, $(CH_3)_2POCl$, followed by hydrolysis to the acid.

The Grignard reaction between 1.65 mol of magnesium in 200 mL of dry ether and 1.50 mol of methyl iodide in 100 mL of dry ether was initiated by the addition of a few grains of iodine. The methyl iodide was added over 3 h at such a rate as to maintain a gentle reflux and when addition was complete, the mixture was refluxed for a further 1/2 h. The resulting solution was cooled in an ice bath and freshly distilled thiophosphoryl chloride (0.51 mol) in 50 mL dry ether was added slowly. A vigorous reaction resulted in the formation of a white precipitate. After addition was completed, the reaction mixture was cooled and poured over 350 g of ice after which 600 mL of 10% sulfuric acid was added and the mixture was stirred overnight. The resulting white precipitate was filtered from the solution and recrystallized from 5:1 (by volume) benzene–ethanol yielding 30.8 g of tetramethyldiphosphine disulfide (mp 226–227.5°C; lit. 227°C (10)).

Following the observation by Maier (14) that oxidation of tetraalkyldiphosphine disulfides with an excess of sulfuryl chloride results in the formation of dialkylphosphinic chloride, we added 0.49 mol of sulfuryl chloride dropwise, with stirring, to a cooled (0°C) benzene solution of $(CH_3)_4P_2S_2$ (0.10 mol). The solution immediately became cloudy yellow. After addition was complete the mixture was refluxed for 45 min, cooled, and the solvent, any remaining sulfuryl chloride and volatile reaction by-products were removed by pumping under vacuum. Crude $(CH_3)_2POCl$ was isolated from the dried reaction mixture by vacuum sublimation and was dissolved in water. The solution was filtered and the hydrochloric acid produced in the hydrolysis reaction was neutralized with aqueous sodium hydroxide. The residue from the evaporation of the aqueous solution was taken up in dry acetonitrile and filtered to remove sodium chloride. The desired acid was obtained in 89% yield by evaporation of the acetonitrile solution. Melting point 86–89°C (lit. 87.5–88.5 (15)). *Anal.* calcd. $C_2H_7PO_2$: C 25.54, H 7.50; found: C 25.50, H 7.63.

Poly-bis(μ-dimethylphosphinato)diaquomanganese(II), $Mn(H_2O)_2[(CH_3)_2PO_2]_2$

Manganese(II) acetate tetrahydrate (5.0 mmol) was dissolved in 400 mL of ethanol and the solution was then added dropwise with stirring to a solution of dimethylphosphinic acid (10.0 mmol) dissolved in 600 mL of ethanol. The resulting solution was stirred for about 2 days then the volume was reduced to about 300 mL by flash evaporation. Over the next 5 days small, pale pink crystals of the dihydrate, suitable for X-ray diffraction studies, were obtained. These were collected by filtration, washed with cold ethanol, and allowed to air dry. A further crop of crystals were obtained by reducing the volume of the filtrate by about a half and allowing the solution to stand for about a week (total yield, 26%). *Anal.* calcd. for $MnC_4H_{16}P_2O_6$: C 17.33, H 5.83, O 34.64; found: C 17.22, H 5.99, O 34.35.

In order to obtain pure crystals of the diaquo species it is necessary to crystallize slowly from dilute solutions as described above. More rapid crystallization yields non-crystalline materials of intermediate degrees of hydration. For example, when a solution of 7.5 mmol of manganese(II) acetate tetrahydrate in 250 mL ethanol was mixed with a solution of 15.1 mmol of dimethylphosphinic acid in 125 mL ethanol an immediate precipitate formed, the composition of which corresponded to a hemi-hydrate. *Anal.* calcd. for $MnC_4H_{13}P_2O_{4.5}$: C 19.21, H 5.24; found: C 19.14, H 5.25.

Poly-bis(μ-dimethylphosphinato)manganese(II), $Mn[(CH_3)_2PO_2]_2$

The anhydrous compound may be obtained by heating the diaquo compound or the hemi-hydrate to 60–70°C under vacuum for several hours. *Anal.* calcd. for $MnC_4H_{12}P_2O_4$: C 19.93, H 5.02, O 26.55; found: C 19.78, H 5.02, O 26.30.

Carbon, hydrogen, and oxygen were determined by P. Borda of the Department of Chemistry, The University of British Columbia.

Differential scanning calorimetry (DSC)

DSC studies were made using a Mettler DSC 20 cell and a Mettler TC10 TA processor.

$Mn(H_2O)_2[(CH_3)_2PO_2]_2$ exhibits an endothermic peak (ΔH = 343 J g^{-1}) at 107°C due to loss of water followed by a second endothermic event (ΔH = 40 J g^{-1}) at 208°C. $Mn[(CH_3)_2PO_2]_2$ exhibits an endothermic peak (ΔH = 41 J g^{-1}) at 200°C. Both materials undergo oxidative decomposition above 310°C.

Infrared spectra

Spectra in the range 4000 to 250 cm^{-1} were recorded on a Perkin-Elmer Model 598 spectrometer using samples mulled in Nujol as well as hexachlorobutadiene and pressed between KRS-5 plates (Harshaw Chemical Co.).

$Mn(H_2O)_2[(CH_3)_2PO_2]_2$: 3410 m br, 3160 m br, 2980 w, 2919 w, 1650 w br, 1425 w br, 1294 m, 1282 m, 1137 s, 1121 s, 1065 m, 1032 w sh, 903 w, 868 m, 735 m, 455 m.

$Mn[(CH_3)_2PO_2]_2$: 2985 w, 2920 w, 1424 w, 1302 m, 1288 m, 1123 s, 1031 s, 919 vw, 875 m sh, 867 m, 741 w, 726 vw sh, 497 w, 485 w, 455 w sh, 440 m (w = weak, m = medium, s = strong, v = very, br = broad, sh = shoulder).

Magnetic susceptibilities

Variable temperature magnetic susceptibilities were measured over the temperature range 4.2 to 300 K using equipment and methods described previously (6). The diamagnetic corrections used were −14, −42, and -13×10^{-6} cm^3 mol^{-1} for Mn^{2+}, $(CH_3)_2PO_2^-$, and H_2O, respectively.

X-ray crystallographic analysis of $Mn(H_2O)_2[(CH_3)_2PO_2]_2$

A crystal bounded by the eight faces (followed by their distances in mm from a common origin): ±(100), 0.031, ±(010), 0.244, ±(101), 0.063, ±(10 − 2), 0.075, was mounted in a general orientation. Unit-cell parameters were refined by least-squares on 2 sin θ/λ values for 25 reflections (2θ = 35–45°) measured on a diffractometer with Mo-K_α radiation ($\lambda(K_{\alpha_1})$ = 0.70930, $\lambda(K_{\alpha_2})$ = 0.71359 Å). Crystal data at 22°C are:

$C_4H_{16}MnO_6P_2$ fw = 277.05

Monoclinic, a = 20.722(3), b = 4.8652(2), c = 11.0689(14) Å, β = 102.209(7)°, V = 1090.7(2) Å^3, Z = 4, ρ_c = 1.687 g cm^{-3}, $F(000)$ = 572, μ(Mo-K_α) = 14.49 cm^{-1}. Absent reflections: hkl, $h + k$ odd, and $h0l$, l odd, space group $C2/c$ (C^6_{2h}, No. 15) from structure analysis.

Intensities were measured with graphite-monochromated MoK_α radiation on an Enraf-Nonius CAD4-F diffractometer. An ω–2θ scan at 0.87–6.71° min^{-1} over a range of (0.80 + 0.35 tan θ)° in ω (extended by 25% on both sides for background measurement) was employed. Data were measured to 2θ = 65°. The intensities of three check reflections, measured every hour throughout the data collection, showed only small random fluctuations. After data reduction,[2] an

[2]The computer programs used include locally written programs from data processing and locally modified versions of the following: ORFLS, full-matrix least-squares, and ORFFE, functions and errors, by W. R. Busing, K. O. Martin, and H. A. Levy; FORDAP, Patterson and Fourier syntheses, by A. Zalkin; ORTEP II, illustrations, by C. K. Johnson.

TABLE 1. Final positional (fractional × 10^5, C × 10^4, H × 10^3) and isotropic thermal parameters ($U \times 10^3$ Å^2) with estimated standard deviations in parentheses

Atom	x	y	z	U^*_{eq}/U_{iso}
Mn	25000	25000	0	18
P	13868(3)	74982(15)	588(5)	19
O(1)	17339(9)	54730(36)	−6189(15)	23
O(2)	18166(9)	97911(36)	7279(14)	22
O(3)	27455(10)	49045(42)	17629(17)	28
C(1)	724(2)	8994(8)	−1056(3)	38
C(2)	1006(2)	5756(7)	1158(3)	35
H(0a)	288(2)	474(7)	255(3)	46(10)
H(0b)	279(3)	658(11)	155(5)	95(16)
H(1a)	45(2)	994(8)	−61(3)	48(9)
H(1b)	46(2)	779(8)	−146(4)	58(13)
H(1c)	89(2)	1000(8)	−160(4)	75(14)
H(2a)	73(2)	704(8)	143(4)	58(12)
H(2b)	71(2)	448(9)	79(4)	78(14)
H(2c)	133(2)	509(9)	187(4)	94(16)

* (1/3) trace U_{diag}.

absorption correction was applied using the Gaussian integration method (16, 17). Transmission factors ranged from 0.809 to 0.920 for 112 sampling points. Of the 1989 independent reflections measured, 983 (49.4%) had intensities greater than $3\sigma(I)$ above background where $\sigma^2(I) = S + 2B + (0.04(S - B))^2$ with S and B the normalized scan and background counts.

The centrosymmetric space group $C2/c$ was indicated by both the E-statistics and the Patterson function, from which the Mn and P coordinates were determined. The Mn atom is constrained to lie either on a twofold axis or at a centre of symmetry, the latter being the case. The coordinates of all remaining atoms were determined from subsequent difference maps. In the final stages of refinement the hydrogen atoms were refined with isotropic, and the non-hydrogen atoms with anisotropic thermal parameters. The scattering factors and anomalous scattering terms for Mn and P were taken from ref. 18. Convergence was reached at $R = 0.030$ and $R_w = 0.033$ for 983 reflections with $I \geq 3\sigma(I)$. The function minimized was $\Sigma w(|F_o| - |F_c|)^2$ (where $w = 1/\sigma^2(F)$), $R = \Sigma||F_o| - |F_c||/\Sigma|F_o|$, $R_w = (\Sigma w(|F_o| - |F_c|)^2/\Sigma w|F_o|^2)^{1/2}$.

On the final cycle of refinement the mean and maximum parameter shifts corresponded to 0.002 and 0.02σ, respectively, and the mean error in an observation of unit weight was 1.286. The largest residuals on the final difference map (−0.69, +0.39 e Å^{-3}) were in the vicinity of P and Mn, respectively. The final positional and isotropic thermal parameters are given in Table 1. Anisotropic thermal parameters (Table 7) and measured and calculated structure factors have been placed in the Depository of Unpublished Data.[3]

Bond distances have been corrected for libration using the TLS model (19). The rms standard error in the temperature factors σU_{ij} (derived from the least-squares analyses) is 0.0010 Å^2. Two structural sub-units were analysed: the centrosymmetric MnO_6 unit and the O_2PC_2 fragment (rms σU_{ij} = 0.0024 and 0.0011 Å^2, respectively). Bond lengths corrected for libration (19, 20) appear in Table 2 along with the uncorrected distances. Bond angles, details of hydrogen bonding, and intraannular torsion angles are given in Tables 3–5, respectively.

Results and discussion

Although organophosphinates of manganese(II) have been reported in the literature (8, 9, 21–27), no detailed X-ray crystallographic or cryomagnetic studies on these compounds have been previously undertaken. We found that slow crystallization of the dimethylphosphinate derivative from dilute solution gave well-formed pale pink crystals which, according to elemental analysis and infrared studies, incorporate two molecules of water per manganese. The DSC thermogram for this material shows an endothermic event beginning around 60–70°C and peaking at about 107°C corresponding to the loss of the water molecules. Consistent with this, bulk samples of the hydrated derivative may be completely dehydrated by heating for several hours at 60 to 70°C under vacuum. There is no evidence in the thermogram for a stable monohydrate (9) or any other distinct hydrated phase. Whereas the variable temperature magnetic properties of the anhydrous material indicate a relatively strongly magnetically coupled system, the hydrated material gives little evidence for magnetic concentration (see below). In order to establish the manner in which the water molecules are incorporated and to determine whether we were dealing with a polymeric or molecular system, a single crystal X-ray diffraction study was undertaken on a crystal of the hydrate.

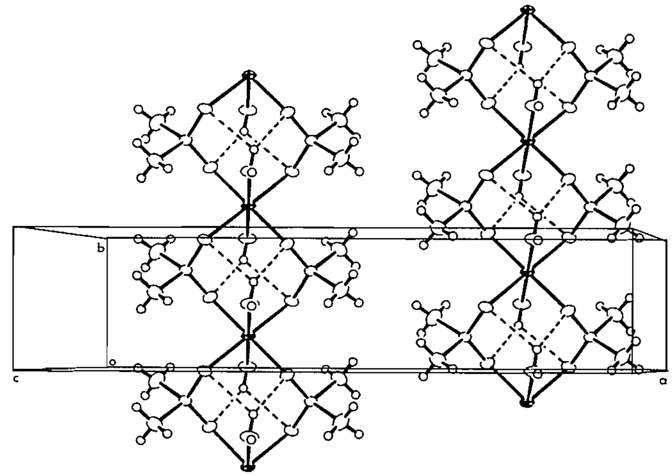

FIG. 1. View of $Mn(H_2O)_2[(CH_3)_2PO_2]_2$ showing two chains extending along the b axis. 50% probability thermal ellipsoids are shown for the non-hydrogen atoms; hydrogen atoms have been assigned arbitrarily small thermal parameters for the sake of clarity. Mn atoms are represented by shaded ellipses. Broken lines indicate hydrogen bonds.

The crystal structure of $Mn(H_2O)_2[(CH_3)_2PO_2]_2$ consists of closely packed infinite chains of identical cages (each having twelve vertices and six non-planar faces) propagating along the crystallographic b-axis (Fig. 1). The manganese atoms are connected in the chains by double phosphinate bridges with four oxygens from four different phosphinates forming a roughly square planar array around each manganese. Water molecules coordinated above and below this plane complete an MnO_6 chromophore. Atom labelling and the coordination geometry about Mn is shown in Fig. 2. Hydrogen atoms from the two water molecules coordinated to the same metal are involved in intrachain bifurcated hydrogen bonds with phosphinate oxygen atoms bonded to adjacent manganese atoms. These hydrogens together with the six chromophore oxygens make up eight of the cage vertices. The remaining four vertices are supplied by two phosphorus and two manganese atoms, the latter of which form shared corners between cages and hence serve as links in the infinite chains. The second hydrogen atom on each water molecule is involved in a strong hydrogen bond with a phos-

[3] Complete set of data is available, at a nominal charge, from the Depository of Unpublished Data, CISTI, National Research Council of Canada, Ottawa, Ont., Canada K1A 0S2.

TABLE 2. Bond lengths (Å) with estimated standard deviations in parentheses

Bond	Length Uncorr.	Length Corr.	Bond	Length Uncorr.	Length Corr.
Mn —O(1)	2.150(2)	2.156	P —O(2)	1.519(2)	1.526
Mn —O(2)[1]	2.208(2)	2.212	P —C(1)	1.795(3)	1.803
Mn —O(3)	2.239(2)	2.247	P —C(2)	1.796(3)	1.804
P —O(1)	1.510(2)	1.516			
O(3)—H(0a)	0.86(3)		C(1)—H(1c)	0.89(5)	
O(3)—H(0b)	0.86(5)		C(2)—H(2a)	0.94(4)	
C(1)—H(1a)	0.94(4)		C(2)—H(2b)	0.90(5)	
C(1)—H(1b)	0.86(4)		C(2)—H(2c)	0.97(5)	

[1] Symmetry operation $1/2 - x$, $1/2 - y$, $-z$.

TABLE 3. Bond angles (deg) with estimated standard deviations in parentheses*

Bonds	Angle (deg)	Bonds	Angle (deg)
O(1)—Mn —O(2)[2]	91.75(7)	O(1)—P —C(1)	107.37(14)
O(1)—Mn —O(2)[3]	88.25(7)	O(1)—P —C(2)	110.61(13)
O(1)—Mn —O(3)	86.71(7)	O(2)—P —C(1)	108.78(14)
O(1)—Mn —O(3)[1]	93.29(7)	O(2)—P —C(2)	108.22(13)
O(2)[2]—Mn—O(3)	92.23(7)	C(1)—P —C(2)	106.0(2)
O(2)[2]—Mn—O(3)[1]	87.77(7)	Mn —O(1)—P	132.69(10)
O(1)—P —O(2)	115.45(10)		
Mn —O(3)—H(0a)	143(2)	H(1b)—C(1)—H(1c)	109(3)
Mn —O(3)—H(0b)	106(3)	P —C(2)—H(2a)	107(2)
H(0a)—O(3)—H(0b)	109(4)	P —C(2)—H(2b)	112(3)
P —C(1)—H(1a)	107(2)	P —C(2)—H(2c)	112(3)
P —C(1)—H(1b)	113(2)	H(2a)—C(2)—H(2b)	102(3)
P —C(1)—H(1c)	110(3)	H(2a)—C(2)—H(2c)	109(3)
H(1a)—C(1)—H(1b)	102(3)	H(2b)—C(2)—H(2c)	114(4)
H(1a)—C(1)—H(1c)	116(3)		

*Here and elsewhere in this report superscripts refer to the following symmetry operations: [1] $1/2 - x, 1/2 - y, -z$; [2] $x, y - 1, z$; [3] $1/2 - x, 3/2 - y, -z$; [4] $x, y + 1, z$; [5] $1/2 - x, y - 1/2, 1/2 - z$.

phinate oxygen on a neighbouring chain with the result that the chains are connected together in the *c* direction by two interchain hydrogen bonds per cage (Fig. 3). The overall structure can then be thought of as consisting of well-separated layers of cages stacked up approximately along the *a* axis. The strength of the hydrogen bonding interactions between adjacent chains is apparent from the differences between the intra and interchain hydrogen bonding parameters (Table 4). The shorter interchain distances suggest that hydrogen bonding is stronger between chains than within chains; this strong interchain interaction accounts, in part at least, for the relatively high crystal density of this material compared to, for example, that of copper(II) diethylphosphinate (5).

The intrachain distance between manganese atoms is 4.8652(2) Å and the minimum interchain distance is 6.046(1) Å. The intrachain distance is less than 0.1 Å shorter than the Cu—Cu distances in polymeric copper(II) phosphinates. The Mn—O bond distances of 2.156(2) and 2.212(2) Å are typical for this type of bond (28) and, as expected, are slightly longer than the Cu—O distances observed in the copper(II) phosphinates (4–6). Bond distances and angles involving the R_2PO_2 moieties are comparable to those found in other polymeric phosphinates (3–6) and exhibit no unusual features.

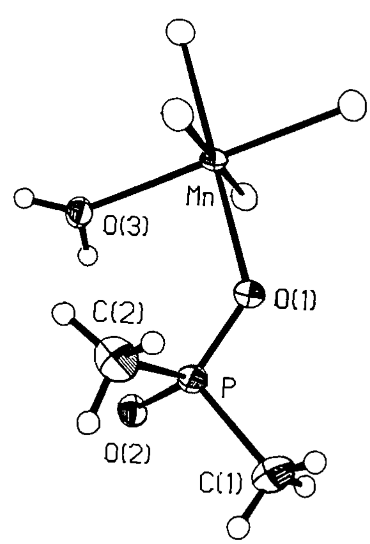

FIG. 2. View of $Mn(H_2O)_2[(CH_3)_2PO_2]_2$ showing the atom numbering scheme and the coordination about Mn.

Attempts to obtain crystals of anhydrous $Mn[(CH_3)_2PO_2]_2$ suitable for X-ray studies have not been successful. Certain conclusions regarding its structure may, however, be drawn from other evidence. It seems likely that the removal of the two water molecules on dehydration of the hydrate does not significantly alter the double phosphinate bridged backbone structure of the material. This is supported by the DSC thermogram which shows a single endothermic peak due to loss of water and no other thermal events which might accompany a major

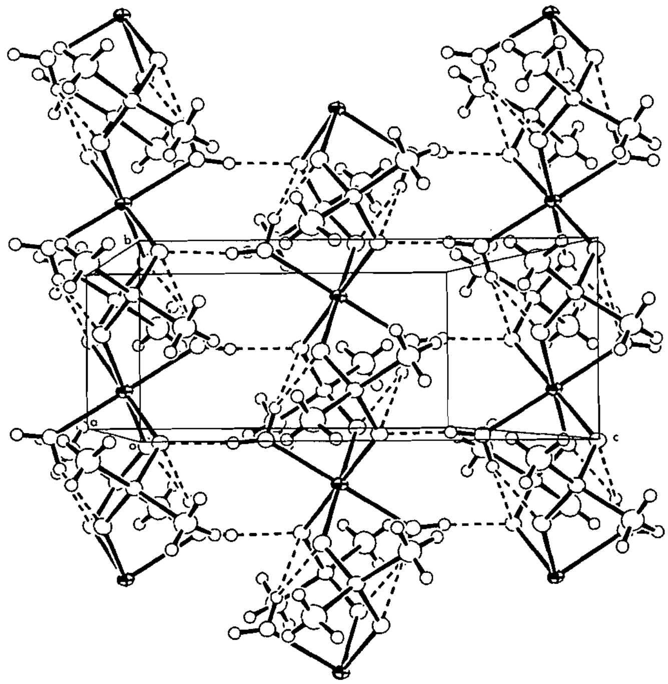

FIG. 3. View of $Mn(H_2O)_2[(CH_3)_2PO_2]_2$ showing hydrogen bonding interactions connecting the chains in the c direction. Mn atoms represented by shaded ellipses. Broken lines indicate H-bonds.

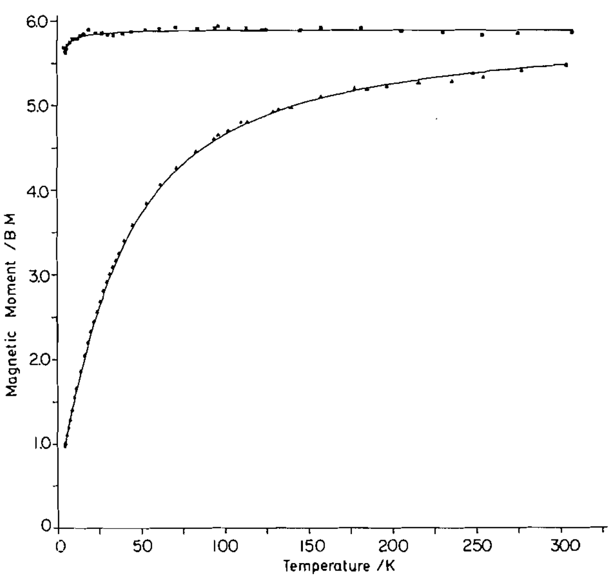

FIG. 4. Magnetic moment versus temperature plots for $Mn(H_2O)_2[(CH_3)_2PO_2]_2$ (■) and $Mn[(CH_3)_2PO_2]_2$ (▲). Solid lines are the best fit to the Wagner–Friedberg model.

change in structure up to ~195°C. The endothermic peak which appears near this temperature is not due to melting (visual observation on heating a sample in a melting point tube) and is probably due to a high temperature structural phase change. Further support for the contention that a polymeric lattice is maintained comes from solubility tests. The anhydrous compound was found to be only very sparingly soluble in methanol, ethanol, and acetone and insoluble in carbon tetrachloride, chloroform, and petroleum ether. Moreover the relatively strong magnetic exchange observed for this material is consistent with the presence of a polymeric lattice (see below) and not with a molecular species. It has been suggested that information regarding the mode of phosphinate coordination may be obtained from infrared studies particularly in the PO_2 stretching region (29). The antisymmetric and symmetric PO_2 stretching frequencies which occur at 1137 and 1065 cm^{-1} in the hydrated compound shift to 1123 and 1031 cm^{-1} on dehydration. A shift in frequencies would be expected as the hydrogen bonding interactions with the coordinated water molecules are removed. The increase in the separation between the two frequencies (from 72 cm^{-1} in the hydrate to 92 cm^{-1}) suggests that the phosphinate bridging may be more unsymmetrical in the anhydrous material (29). This might arise if, on dehydration, the phosphinate oxygens formerly involved in interchain hydrogen bonding now occupy axial positions vacated by the water molecules in a tetragonally distorted MnO_6 chromophore. The pale pink colour of the anhydrous material is consistent with such a chromophore or, in the limit of negligible interchain interactions, with a square planar environment about manganese (30).

TABLE 4. Hydrogen bond data (distances in Å and angles in deg)*

Atoms	H···A	D···A	D—H···A
	Intrachain		
O(3)—H(0b)···O(1)^3	2.56(5)	3.120(3)	124(4)
O(3)—H(0b)···O(2)	2.13(5)	2.899(3)	149(5)
	Interchain		
O(3)—H(0a)···O(2)^5	1.88(3)	2.734(2)	174(3)

*See footnote to Table 3.

TABLE 5. Intra-annular torsion angles (deg) standard deviations in parentheses*

Atoms	Value (deg)
O(2)^3—Mn—O(1)—P	−107.61(15)
O(2)—P —O(1)—Mn	66.0(2)
O(1)—P —O(2)—Mn^4	49.1(2)
P —O(2)—Mn^4—O(1)^3	−89.81(13)

*Symmetry-related torsion angles have the opposite sign.

Magnetic susceptibility data are recorded in Table 6 and the magnetic moments are plotted in Fig. 4. The moment for $Mn[(CH_3)_2PO_2]_2$ varies from just above 5.4 BM at room temperature to about 1.0 BM at 4.2 K and the susceptibility versus temperature plot (Fig. 5) shows a broad maximum at 34 K. These properties suggest one-dimensional antiferromagnetic exchange as found, for example, in the triple chlorine bridged tetramethylammonium manganese(II) chloride (31).

Two models are available for the theoretical analysis of antiferromagnetic exchange in linear chain manganese(II) compounds, the scaling model of Wagner and Friedberg (32) and the interpolation scheme developed by Weng (33). Both models use the isotropic Heisenberg Hamiltonian, which is appropriate in the case of Mn^{2+} (^6S ground state). According to the Wagner and Friedberg model,

$$\chi_M = \frac{Ng^2\beta^2S(S+1)}{3kT}\cdot\frac{1+U}{1-U}$$

where $U = \coth K - 1/K$ and $K = 2JS(S+1)/kT$.

Hiller *et al.* have generated a series of coefficients for mag-

TABLE 6. Magnetic susceptibilities

T (K)	$10^6\chi_m$ ($cm^3\ mol^{-1}$)	T (K)	$10^6\chi_m$ ($cm^3\ mol^{-1}$)	T (K)	$10^6\chi_m$ ($cm^3\ mol^{-1}$)
		$Mn(H_2O)_2[(CH_3)_2PO_2]_2$			
307.3	14 000	94.2	46 500	14.0	304 000
275.2	15 590	83.4	52 400	11.9	353 000
253.6	16 810	71.0	61 600	10.4	405 000
230.1	18 690	61.0	71 500	9.39	448 000
205.3	21 040	52.7	82 500	7.82	528 000
181.7	24 080	44.4	97 400	6.78	603 000
157.7	27 810	39.4	109 000	5.76	697 000
145.4	29 830	34.2	125 000	5.32	746 000
124.6	34 900	30.7	139 000	4.99	828 000
122.6	35 460	27.1	158 000	4.96	803 000
112.8	38 700	23.4	184 000	4.35	914 000
102.5	42 700	19.3	225 000	4.22	963 000
96.1	45 870	16.2	264 000		
		$Mn[(CH_3)_2PO_2]_2$			
303.4	12 410	102.0	27 300	25.2	36 300
276.6	13 340	95.5	28 600	23.2	35 900
253.9	14 090	92.9	28 700	21.5	35 500
247.7	14 730	82.4	30 300	19.7	35 000
234.8	14 990	70.8	32 300	17.9	34 400
214.9	16 210	61.3	34 000	15.9	33 700
196.0	17 490	52.9	35 300	13.4	32 800
184.6	18 350	44.5	36 300	11.0	31 900
177.0	19 210	39.7	36 800	9.82	31 400
156.7	20 890	36.3	36 900	8.16	30 700
139.6	22 340	34.5	37 000	7.02	30 300
131.9	23 420	32.8	37 000	6.16	29 900
128.5	23 700	31.0	36 900	5.32	29 700
113.3	25 600	29.1	36 800	4.48	29 500
109.4	26 530	27.4	36 600	4.22	29 400

netic susceptibility to reproduce Weng's numerical results (34). Accordingly

$$\chi_M = \frac{Ng^2\beta^2}{kT}\,\frac{[A + BX^2]}{[1 + CX + DX^3]}$$

and for $S = 5/2$, $A = 2.9167$, $B = 208.04$, $C = 15.543$, $D = 2707.2$, and $X = |J|/kT$.

The experimental results were analyzed using both models with fits made to the susceptibility data with J and g as fitting parameters. Best fits were obtained by minimizing the function

$$F = \left[\frac{1}{n}\sum_i^n \left(\frac{\chi_i^{calc} - \chi_i^{obs}}{\chi_i^{obs}}\right)^2\right]^{1/2}$$

where n is the number of data points. The best fit values are $-2.69\ cm^{-1}$ for J, the exchange coupling constant, and 2.01 for g ($F = 0.0151$) using the Weng model and $-2.94\ cm^{-1}$ for J and 2.02 for g ($F = 0.0222$) using the Wagner–Friedberg model. As expected g is ~2.00 in both cases. For comparison, $[(CH_3)_4N]MnCl_3$ has $J = -4.38\ cm^{-1}$ (31) and $CsMnCl_3\cdot 2H_2O$, a single chloro-bridged chain, has $J = -2.16\ cm^{-1}$ (35). The magnetic interaction in the phosphinate compound is particularly interesting when one considers that although the exchange pathway involves a three-atom bridge, the magnitude of the exchange is at least comparable to that found in the chloro-bridged compounds.

A series of complexes with a similar bridging network to that found in the phosphinates are those of type $M(N_2H_5)_2(SO_4)_2$. The zinc compound has been shown to contain bidentate sulfate anions forming a double bridge between adjacent zinc ions to link them in a linear chain (36). The manganese compound (assumed to have the same structure) is antiferromagnetic with $J = -0.42\ cm^{-1}$ (37), seven times smaller than the J obtained for the phosphinate-bridged species. It is not obvious whether this difference in J's is due to the nature of the bridging anion (sulfate versus phosphinate) or due to the presence of extensive hydrogen bonding which is present in the sulfate-bridged com-

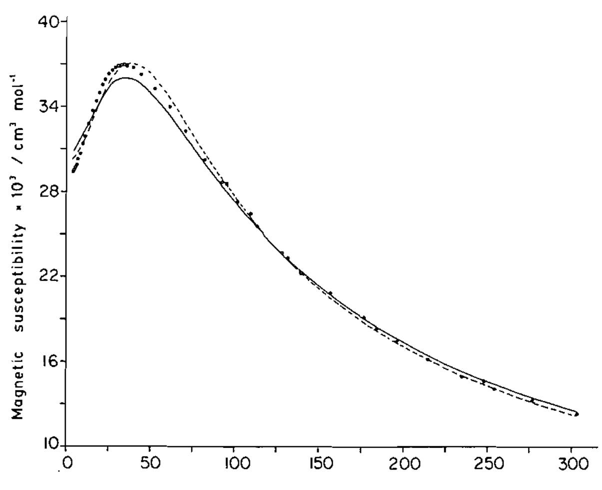

FIG. 5. Magnetic susceptibility versus temperature plots for $Mn[(CH_3)_2PO_2]_2$. Circles are experimental data. Solid line is the best fit to the Wagner–Friedberg model and the broken line is the best fit to the Weng model.

plex but absent in the phosphinate. Of relevance to this consideration is the fact that the hydrated manganese phosphinate derivative studied in the present work also has an extensive hydrogen bonded network and shows little, if any, magnetic exchange (see below).

Both theoretical models represent the experimental magnetic data reasonably well especially at temperatures above ~80 K. Discrepancies with both models are, however, seen at lower temperatures and, moreover, the Weng model does not reproduce the temperature of the rounded maximum in the χ_M plot as well as the other model (Fig. 5). Any or all of the following factors could account for the discrepancies. A small amount of paramagnetic impurity will affect the shape of the susceptibility versus temperature curve especially for antiferromagnets at lower temperatures. Both models ignore zero-field splitting effects (38) and although these should be small in the case of Mn(II) they may have a significant effect at low temperatures. Also, interchain interactions are ignored in both models. The possibility of some weak association between chains to raise the coordination number of manganese to six was discussed above. Unfortunately, without single crystal X-ray diffraction studies on this compound it is difficult to conclude whether such interactions are likely to be significant.

In contrast to the magnetic behaviour seen in the anhydrous compound, $Mn(H_2O)_2[(CH_3)_2PO_2]_2$ has a moment of ~5.9 BM over the range 300 to 10 K as expected for magnetically dilute, spin-free, manganese(II). There is a small decrease in moment from 10 to 4.2 K and while this can be fit to theory (Wagner and Friedberg model, $g = 2.00$ and $J = -0.02$ cm^{-1} (Fig. 4)), the fit should not be interpreted as definite evidence for exchange in this material; such small decreases in moment at low temperatures could be accounted for by zero-field splitting effects (38). Nonetheless, the fit does place an upper limit of -0.02 cm^{-1} on J and shows that any net exchange in the hydrate must be very weak indeed compared to that present in the anhydrous compound. Two possible explanations are suggested for this difference in magnetic properties. In the anhydrous compound relatively strong antiferromagnetic intrachain exchange takes place. On hydration the water molecules, through their coordination to manganese, will effectively decrease the metal's acidity towards the bridging phosphinate groups and, through hydrogen bonding to the phosphinate oxygens, they will effectively decrease the phosphinate basicity towards manganese. The net effect is weaker phosphinate–manganese bonds, poorer orbital overlap and weaker intrachain exchange. Another possible source of the effective damping of significant net magnetic exchange in the hydrate is suggested by the work on $MnCl_2 \cdot 2H_2O$ (39). This compound exhibits some structural similarities to the hydrate studied here. The compound has a chain structure with manganese atoms joined by double chloride bridges. Water molecules coordinated in axial positions form hydrogen bonds with chlorides in neighbouring chains. In this compound there is both intrachain antiferromagnetic exchange via the chlorides and interchain ferromagnetic exchange via the hydrogen-bonded water molecules with the magnitudes of the two almost equal. This raises the possibility that in $Mn(H_2O)_2[(CH_3)_2PO_2]_2$ antiferromagnetic intrachain exchange effects are also present but are roughly cancelled by interchain ferromagnetic exchange via the water molecules.

Acknowledgements

We thank the Natural Sciences and Engineering Research Council of Canada for financial support and the University of British Columbia Computing Centre for assistance. K.W.O. and J.S.H. thank the U.B.C. Graduate Scholarship Committee and K.W.O. also thanks NSERC for scholarship awards.

1. F. Giordano, L. Randaccio, and A. Ripamonti. J. Chem. Soc. Chem. Commun. 19 (1967).
2. F. Giordano, L. Randaccio, and A. Ripamonti. Acta Crystallogr. Sect. B, **25**, 1057 (1969).
3. P. Colamarino, P. L. Orioli, W. D. Benzinger, and H. D. Gillman. Inorg. Chem. **15**, 800 (1976).
4. R. Cini, P. Colamarino, P. L. Orioli, L. S. Smith, P. R. Newman, H. D. Gillman, and P. Nannelli. Inorg. Chem. **16**, 3223 (1977).
5. K. W. Oliver, S. J. Rettig, R. C. Thompson, and J. Trotter. Can. J. Chem. **60**, 2017 (1982).
6. J. S. Haynes, K. W. Oliver, S. J. Rettig, R. C. Thompson, and J. Trotter. Can. J. Chem. **62**, 891 (1984).
7. B. P. Block. Inorg. Macromol. Rev. **1**, 115 (1970).
8. J. C. Scott, A. F. Garito, A. J. Heeger, P. Nannelli, and H. D. Gillman. Phys. Rev. B, **12**, 356 (1975).
9. E. I. Matrosov and B. Fisher. Izv. Akad. Nank SSSR, Neorg. Mater. **3**, 545 (1967).
10. G. W. Parshall. Org. Synth. **45**, 102 (1965).
11. H. Reinhardt, D. Bianchi, and D. Mölle. Chem. Ber. **90**, 1656 (1957).
12. K. D. Gallicano. Ph.D. dissertation, University of British Columbia, 1980.
13. W. Kuchen, H. Buchwald, K. Strokenberg, and J. Metten. Lieb. Annal. Chem. **652**, 28 (1962).
14. L. Maier. Chem. Ber. **94**, 3051 (1961).
15. P. C. Crofts. Organic phosphorus compounds. Vol. 6. *Edited by* G. M. Kosolapoff and L. Maier. Wiley-Interscience, New York. 1973. Chapt. 14.
16. P. Coppens, L. Leiserowitz, and D. Rabinovich. Acta Crystallogr. **18**, 1035 (1965).
17. J. De Meulenaer and H. Tompa. Acta Crystallogr. **19**, 1014 (1965).
18. International tables for X-ray crystallography. Vol. 4. Kynoch Press, Birmingham. 1974.
19. V. Schomaker and K. N. Trueblood. Acta Crystallogr. Sect. B, **24**, 63 (1968).
20. D. W. J. Cruickshank. Acta Crystallogr. **9**, 747 (1956); **9**, 754 (1956); **14**, 896 (1961).
21. V. V. Korshak, A. M. Polyakova, O. V. Vinogradova, K. N. Anisimov, N. E. Kolobova, and M. V. Kotova. Izv. Akad. Nank SSSR, Ser. Khimi. **3**, 642 (1968).
22. S. V. Vinogradova, V. V. Korshak, O. V. Vinogradova, A. M. Polyakov, K. N. Anisimov, and N. Ye. Kolobova. Vysokomol. soyed. A**15**, 516 (1973).
23. H. D. Gillman and J. L. Eichelberger. Inorg. Chem. **15**, 840 (1976).
24. H. D. Gillman and J. L. Eichelberger. Inorg. Chim. Acta, **24**, 31 (1977).
25. C. M. Mikulski, J. Unruh, R. Rabin, F. J. Iaconianni, L. L. Pytlewski, and N. M. Karayannis. Inorg. Chim. Acta, **44**, L77 (1980).
26. C. M. Mikulski, J. Unruh, D. F. Delacato, F. J. Iaconianni, L. Pytlewski, and N. M. Karayannis. J. Inorg. Nucl. Chem. **43**, 1751 (1981).
27. J. Emsley, A. P. Dunning, R. J. Parker, J. K. Williams, S. Brown, S. Earnshaw, and D. S. Moore. Polyhedron, **3**, 125 (1984).
28. J. L. Hoard, B. Pedersen, S. Richards, and J. V. Silverton. J. Am. Chem. Soc. **83**, 3533 (1961).
29. H. D. Gillman. Inorg. Chem. **13**, 1921 (1974).
30. F. A. Cotton and G. Wilkinson. Advanced inorganic chemistry. 4th ed. Interscience Publishers, New York. 1980.

31. R. DINGLE, M. E. LINES, and S. L. HOLT. Phys. Rev. **187**, 643 (1969).
32. G. R. WAGNER and S. A. FRIEDBERG. Phys. Lett. **9**, 11 (1964).
33. C. H. WENG. Ph.D. Dissertation, Carnegie-Mellon University, Pittsburgh, P.A. 1968.
34. W. HILLER, J. STRÄHLE, A. DATZ, M. HANACK, W. E. HATFIELD, L. W. TER HAAR, and P. GÜTLICH. J. Am. Chem. Soc. **106**, 329 (1984).
35. T. SMITH and S. A. FRIEDBERG. Phys. Rev. **176**, 660 (1968).
36. C. K. PROUT and H. M. POWELL. J. Chem. Soc. 4177 (1961).
37. H. T. WITTEVEEN and J. REEDIJK. J. Solid State Chem. **10**, 151 (1974).
38. W. E. HATFIELD, W. E. ESTES, W. E. MARSH, M. W. PICKENS, L. W. TER HAAR, and R. W. WELLER. *In* Extended linear chain compounds. Vol. 3. *Edited by* J. S. Miller. Plenum Press, New York. 1983. Chapt. 2.
39. J. N. MCELEARNEY, S. MERCHANT, and R. L. CARLIN. Inorg. Chem. **12**, 906 (1973).

Preparation, crystal and molecular structures of $Ph_2CNSNSO$ and a comparison of the —SNSO and —SNSS chromophores

TRISTRAM CHIVERS,[1] RICHARD T. OAKLEY,[2] ROGER PIETERS, AND JOHN F. RICHARDSON
Department of Chemistry, University of Calgary, Calgary, Alta., Canada T2N 1N4

Received August 7, 1984

TRISTRAM CHIVERS, RICHARD T. OAKLEY, ROGER PIETERS, and JOHN F. RICHARDSON. Can. J. Chem. **63**, 1063 (1985).

The sulphenyl chloride, Ph_2CNSCl, prepared *in situ* from $Ph_2CNSiMe_3$ and sulphur dichloride, has been employed in the synthesis of $Ph_2CNSNSO$ and $Ph_2CNSNSNSNCPh_2$ by reaction with Me_3SiNSO and $Me_3SiNSNSiMe_3$, respectively. An X-ray structural determination of $Ph_2CNSNSO$ shows it to consist of a planar *cis–trans* chain. The crystals are triclinic and belong to the space group $P\bar{1}$, a = 9.9078(8), b = 10.0967(9), c = 15.1682(14) Å, α = 78.646(7), β = 71.065(7), γ = 63.449(7)°, V = 1281.5(5) Å^3, Z = 4. The final R and R_w values were 0.033 and 0.027, respectively. The $\pi^* \rightarrow \pi^*$ excitation energies for the RSNSO and RSNSS chromophores are compared for different R groups and discussed in the light of MNDO calculations on the model compounds HSNSX (X = S, O). The thermal decomposition of both $Ph_2CNSNSO$ and $Ph_2CNSNSNSNCPh_2$ produced S_4N_4 and Ph_2CO or $(Ph_2CN)_2S$, respectively.

TRISTRAM CHIVERS, RICHARD T. OAKLEY, ROGER PIETERS et JOHN F. RICHARDSON. Can. J. Chem. **63**, 1063 (1985).

On a utilisé le chlorure de sulfényle, Ph_2CNSCl, préparé *in situ* à partir du $Ph_2CNSiMe_3$ et du dichlorure de soufre, pour effectuer la synthèse du $Ph_2CNSNSO$ et du $Ph_2CNSNSNSNCPh_2$ par réaction avec soit du Me_3SiNSO ou du $Me_3SiNSNSiMe_3$. Une détermination de la structure du $Ph_2CNSNSO$ par diffraction des rayons-X a permis de montrer qu'il existe sous la forme d'une chaîne planaire *cis–trans*. Les cristaux sont tricliniques, groupe d'espace $P\bar{1}$, avec a = 9,9078(8), b = 10,0967(9), c = 15,1682(14) Å, α = 78,646(7), β = 71,065(7), γ = 63,449(7)°, V = 1281,5(5) Å^3 et Z = 4. Les valeurs finales de R et R_w sont respectivement 0,033 et 0,027. On a comparé les énergies d'excitation $\pi^* \rightarrow \pi^*$ pour les chromophores RSNSO et RSNSS portant différents groupements R et on en discute à la lumière de calculs MNDO sur les composés modéles HSNSX (X = S, O). Les décompositions thermiques de $Ph_2CNSNSO$ et $Ph_2CNSNSNSNCPh_2$ conduisent respectivement au S_4N_4 et Ph_2CO ou au $(Ph_2CN)_2S$.

[Traduit par le journal]

Introduction

Recently we have characterized a number of species containing the —SNSS chromophore (e.g. $SNSS^-$ (1), $SSNSS^-$ (2, 3), and $Ph_3PNSNSS$ (4)). We have also noted that π-donor ligands, R, induce a large bathochromic shift on the $\pi^* \rightarrow \pi^*$ transition of RSNSS derivatives and explained this effect in terms of qualitative MO considerations (5). Several compounds of the type RSNSO are known, e.g. CF_3SNSO (6) and Me_2NSNSO (7, 8), but quantitative data concerning their molecular structures or electronic spectra are lacking with the exception of $S(NSO)_2$ (9). In order to assess the effect of replacing a terminal sulphur atom by oxygen in these derivatives we have synthesized and determined the crystal and molecular structures of $Ph_2CNSNSO$. We have also carried out MNDO calculations on the model compound HSNSO and compared the results with those found for HSNSS. A secondary interest in RNSNSO compounds was that they might provide a convenient source of S_2N_2, and hence $(SN)_x$, via thermally induced elimination of RO in derivatives where R is a strong oxophile.

Experimental

Reagents and general procedures

Solvents were dried (methylene dichloride (P_2O_5) and acetonitrile (CaH_2 and P_2O_5)) and freshly distilled before use. All reactions were conducted under an atmosphere of nitrogen (99.98% purity passed through Ridox and silica gel). The progress of reactions involving trimethylsilyl reagents was monitored by ^1H nmr spectroscopy, and the non-volatile reaction products were analyzed initially by tlc on silica gel. Chemical analyses were performed by MHW Laboratories, Phoenix, AZ.

Sulphur dichloride (Thiokol/Ventron Division) was distilled before use and the following reagents were prepared by literature procedures: Ph_2CN_2 (10), S_4N_4 (11), $(Ph_2CN)_2S$ (12), $Ph_2CNSiMe_3$ (13), Me_3SiNSO (14), $Me_3SiNSNSiMe_3$ (15).

Instrumentation

Infrared spectra (4000–250 cm^{-1}) were recorded as Nujol mulls (CsI windows) on a Perkin-Elmer 467 grating spectrophotometer. Ultraviolet–visible spectra were obtained by use of a Cary 219 spectrophotometer. Routine ^1H nmr spectra were recorded on a Hitachi Perkin-Elmer R-24B instrument, and mass spectra were run on a Varian CH5 spectrometer (EI/70 eV) or a VG Micromass 7070F instrument (C.I./Ar).

Preparation of diphenylmethyleneamino(thionylimino)sulphide, $Ph_2CNSNSO$

$Ph_2CNSiMe_3$ (2.4 g, 9.3 mmol) in methylene dichloride (5 mL) was added dropwise to a solution of SCl_2 (0.96 g, 9.3 mmol) in methylene dichloride (20 mL) at −78°C. The reaction mixture was allowed to warm up slowly to −60°C during 3 h and then Me_3SiNSO (1.3 g, 9.3 mmol) in methylene dichloride (5 mL) was added at −78°C to the solution which was allowed to reach 23°C slowly. After 3 days solvent was removed from the orange solution *in vacuo* to give a very viscous residue which was redissolved in CH_2Cl_2–CH_3CN. Removal of solvent *in vacuo* produced a yellow solid which was dissolved in the minimum amount of toluene. A small amount of white precipitate, $Ph_2CNH_2^+Cl^-$ (ir spectrum), was removed by filtration. A tlc of the toluene solution indicated two major components which were separated by chromatography on a BioBeads SX-8 column. The first fraction yielded $(Ph_2CN)_2S$ (0.065 g, ir spectrum (12)). The residue obtained after removal of toluene from the second fraction was dissolved in the minimum amount of CH_2Cl_2 (ca. 10 mL) and then an excess of CH_3CN (ca. 40 mL) was added. After several days at −20°C this solution produced orange–red crystals of $Ph_2CNSNSO$ (0.94 g, 3.4 mmol) mp 95–96°C. *Anal.* calcd. for $C_{13}H_{10}N_2OS_2$: C 56.91, H 3.67, N 10.21, S. 23.37, O 5.83; found: C 56.21, H 3.71, N 10.12,

---

[1] To whom all correspondence should be addressed.
[2] Present address: Department of Chemistry and Biochemistry, University of Guelph, Guelph, Ont., Canada N1G 2W1.

S 22.98, O 6.98 (by diff.). Infrared (major bands): 1550(m), 1463(s), 1320(m), 1298(m), 1191(vs), 1181(vs), 1175(vs), 1010(m), 991(m), 952(m), 787(m), 705(m), 695(s), 377(m) cm^{-1}. Ultraviolet and visible spectrum (CH_3CN), $\lambda_{max}(\epsilon)$: 370 (2×10^4) nm (M^{-1} cm^{-1}). Ms: (E.I. source temperature 100°C) 274(100), 212(62), 180(76), 109(41), 77(87), 51(36), (C.I. source temperature 90°C) 274(19), 212(39), 180(53), 109(39), 104(28), 77(100).

Preparation of bis(diphenylmethylene)trisulphur tetranitride, $Ph_2CNSNSNSNCPh_2$

$Ph_2CNSiMe_3$ (8.3 g, 33 mmol) in CH_2Cl_2 (50 mL) was added dropwise to a solution of SCl_2 (3.4 g, 33 mmol) in CH_2Cl_2 (50 mL) at −78°C. After ca. 3 h a solution of $Me_3SiNSNSiMe_3$ in CH_2Cl_2 (50 mL) was added dropwise to the reaction mixture. The resulting red solution was allowed to reach 23°C slowly. Solvent was removed *in vacuo* and the dark red residue was recrystallized from acetonitrile to give pure (tlc) $Ph_2CNSNSNSNCPh_2$ (2.2 g, 4.5 mmol) λ_{max} 505 nm, $\epsilon = 2 \times 10^{-4}$ M^{-1} cm^{-1} (cf. lit: λ_{max} 508 nm (16)). The infrared spectrum was identical to that of an authentic sample prepared from Ph_2CN_2 and S_4N_4 (16, 17).

Thermolysis of $Ph_2CNSNSNSNCPh_2$

A solution of $Ph_2CNSNSNSNCPh_2$ (0.50 g, 1.0 mmol) in CH_3CN (50 mL) changed colour from deep red to pale orange during 48 h at reflux. After removal of solvent *in vacuo* the residue was dissolved in toluene and chromatographed on a Biobeads SX-8 column. Four fractions were collected and the following products were isolated: (*i*) an inseparable mixture of $Ph_2CNSNSNSNCPh_2$ and $(Ph_2CN)_2S$, (*ii*) and (*iii*) $(Ph_2CN)_2S$ (0.060 g, 0.22 mmol), and (*iv*) S_4N_4 (0.066 g, 0.36 mmol).

X-ray analysis of $Ph_2CNSNSO$

Crystal data

$C_{13}H_{10}N_2OS_2$ fw = 274.37
Space group $P\bar{1}$, $a = 9.9078(8)$, $b = 10.0967(9)$, $c = 15.1682(14)$ Å, $\alpha = 78.646(7)$, $\beta = 71.065(7)$, $\gamma = 63.449(7)°$, $V = 1281.5(5)$ Å^3, $Z = 4$, $\rho_c = 1.422$ g cm^{-3} (21(1)°C; MoKα, $\lambda = 0.71069$ Å, graphite monochromator) and μ(MoKα) = 3.95 cm^{-1}.

A red–orange sample of approximate dimensions 0.40 × 0.40 × 0.30 mm was cut from a large crystal and mounted on an Enraf-Nonius CAD4F diffractometer. Intensity data were collected at room temperature using the $\omega-2\theta$ scan technique with a scan range of 1.5(0.60 + 0.347 tan θ) and scan speeds varying from 0.6 to 5.0° min^{-1}. The intensity was calculated as $I = (P - 2(B1 + B2))Q$, where P is the central 64 steps of a 96 step scan, $B1$ and $B2$ are the background counts, and Q is the scan rate. The standard deviation of the intensity $\sigma(I) = [P + 4(B1 + B2)]^{1/2}Q$. Three standard reflections measured every 2000 s of X-ray exposure time showed no decomposition of the crystal had occurred during the data acquisition period. A total of 5866 unique reflections were measured for the octants $\pm h$, $+k$, $\pm l$ to a maximum $\theta = 27.5°$, of which 2932 were considered observed ($F_o > 3\sigma(F_o)$). The data were corrected for background, Lorentz and polarization effects but an absorption correction was not considered necessary. Extensive photographic studies of a number of crystals supported the choice of space group.

The coordinates of the CNSNSO fragment of one of the two molecules in the asymmetric unit were determined by direct methods (MULTAN 78) (18). Structure factor and difference Fourier calculations revealed the positions of the remaining non-hydrogen atoms. The structure was refined by full-matrix least-squares techniques based on F, minimizing the function $\Sigma w(|F_o| - |F_c|)^2$, where $w = [\sigma(F_o)^2]^{-1}$. All computations were performed using the XRAY 76 system of programs (19) implemented on a Honeywell computer with a Multics operating system. Scattering factors for non-hydrogen atoms were those of Cromer and Mann (20) and those for H were taken from ref. 21. Anomalous dispersion corrections were included for non-hydrogen atoms (22). H atoms were readily located from a difference Fourier map and included in the model in idealized positions (sp^2 at C, C—H = 0.95 Å) with isotropic thermal parameters set to 1.1 times B_{eq} of the atom to which they are bonded. H parameters were not refined. The model converged for 4332 reflections (observed reflections plus those for which $I_c > 3\sigma(I_o)$) and 325 variables with the agreement factors $R = \Sigma(||F_o| - |F_c||)/\Sigma|F_o| = 0.033$ and $R_w = [\Sigma w(|F_o| - |F_c|)^2/\Sigma w|F_o|^2]^{1/2} = 0.027$. In the final cycle the goodness of fit value was 0.82 and the largest peak of residual electron density was 0.28 e Å^{-3} and was of no chemical significance.

Tables giving the thermal parameters for non-hydrogen atoms (S I), positional and thermal parameters for hydrogen atoms (S II), and the structure factors for $Ph_2CNSNSO$ (S III) have been placed in the Depository of Unpublished Data.[3]

Computational method

The use of the MNDO (modified neglect of diatomic overlap) method (23) for the study of binary sulphur–nitride molecules has been reported by several groups (24–26).

Results and discussion

Preparation of $Ph_2CNSNSO$ and $Ph_2CNSNSNSNCPh_2$

Previous synthetic routes to RSNSO derivatives include the reactions of CF_3SNH_2 with SOF_2 (6), $Me_3SiNR'_2$ (R = Me, Et) with $S(NSO)_2$ (8), or Me_3SiNSO with R''_2NSCl (R″ = Me, Et, *n*-Pr, *i*-Pr) (7). In view of the ready availability of sulphenyl chlorides, the latter could constitute a general method and it has now been applied to the synthesis of $Ph_2CNSNSO$ via Ph_2CNSCl prepared *in situ* (reaction [1]).[4] Attempts to prepare related derivatives (R = Ph_3P, Ph_2S) were unsuccessful. However, this synthetic approach has been extended to provide an alternative preparation of $Ph_2CNSNSNSNCPh_2$ (reaction [2]), a member of a class of compounds which have been used as electrophotographic pigments (27).

$$Ph_2CNSiMe_3 + SCl_2 \xrightarrow{-Me_3SiCl} Ph_2CNSCl$$

[1] $$Ph_2CNSCl \xrightarrow[-Me_3SiCl]{Me_3SiNSO} Ph_2CNSNSO$$

[2] $$Ph_2CNSCl \xrightarrow[-2Me_3SiCl]{Me_3SiNSNSiMe_3} (Ph_2CNSN)_2S$$

Crystal and molecular structure of $Ph_2CNSNSO$

An ORTEP drawing of the molecule is shown in Fig. 1. Table 1 gives the positional parameters and Table 2 gives the bond lengths and bond angles for non-hydrogen atoms in the two different molecules of $Ph_2CNSNSO$ (**A** and **B**). The

[3] Tables S I – S III are available at a nominal charge, from the Depository of Unpublished Data, CISTI, National Research Council of Canada, Ottawa, Ont., Canada K1A 0S2.

[4] The reaction of Ph_2CNLi with SCl_2 to produce $(Ph_2CN)_2S$ has been reported (ref. 12).

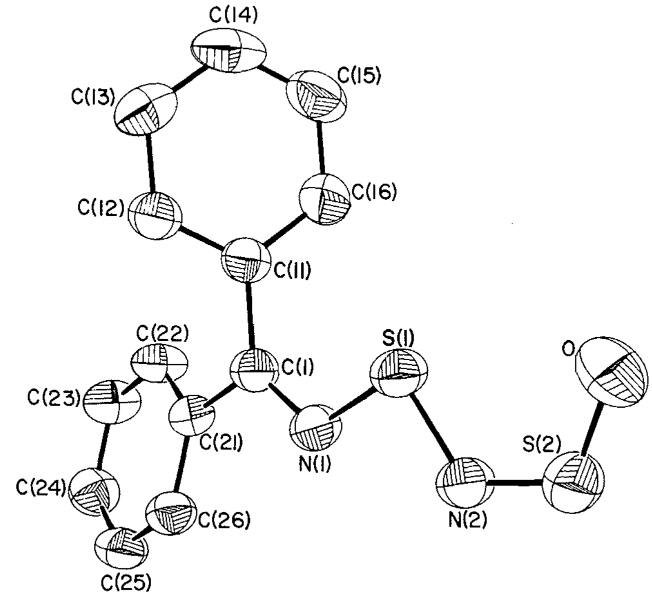

FIG. 1. An ORTEP drawing of $Ph_2CNSNSO$ showing the atomic numbering scheme for molecule **A**.

CNSNSO unit is an essentially planar, *cis–trans* chain,[5] the largest deviations from the best plane being 0.067 Å for S(1) in molecule **A** and −0.087 Å for S(1) in molecule **B** (Table 3). The detailed geometric arrangement bears a marked similarity to that found for the planar chain in OSNSNSO, which has a *cis, trans* geometry for both SNSO units (ref. 9, Table 4). The short C═N bond length (1.286(3) Å) and the alternation in the S—N bond lengths involving N(2) (1.644(2) and 1.529(3) Å) suggest that the valence bond structure **1** is a reasonable approximate representation for $Ph_2CNSNSO$. Furthermore the S(1)—N bond lengths (1.644(2) and 1.680(3)) Å and bond

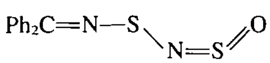

1

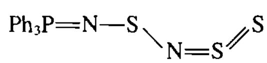

2

angle at S(1) (96.9(1)°) are comparable to the corresponding values for $Ph_2CNSNCPh_2$ (d(S—N) = 1.675(2) Å and ∠NSN 94.7(1)°) (28), which are typical for two coordinate sulphur(II) (29). These data and a comparison of the structural parameters found for the thiosulphinyl derivative, **2** (4), suggest that delocalization of π electrons across S(1) is not well developed in **1**. In **2** the S—N bond lengths involving N(2) are equal (1.592(4) and 1.587(4) Å) and the bond angle at S(1) is 107.7(2)°.

The dihedral angles between the planes of the two phenyl groups attached to C(1) differ for the two molecules **A** and **B** (77.4 vs. 66.7°). Small differences are also observed in the dihedral angles between the individual phenyl groups and the CNSNSO plane (59.6 and 22.9° for **A** vs. 56.0 and 26.3° for **B**).

Electronic structure and uv–visible spectra of RSNSO derivatives

Ab initio HFS MO calculations on a model *cis*-$SNSS^-$ ion indicate that the ground state corresponds to a six π-electron system and that the strong absorption band at 470 nm represents a π* (HOMO) → π* (LUMO) excitation (1). Neutral molecules RSNSS also exhibit intense visible absorption bands attributed to π* → π* transitions and π donor ligands, R, induce a bathochromic shift on this absorption which is larger for soft ligands (e.g. S in $SSNSS^-$, λ_{max} 582 nm) (2) than for hard

[5] *Cis, trans* refers to the geometrical arrangement of the substituents attached to the S(1)—N(2) and S(1)—N(1) bonds, respectively.

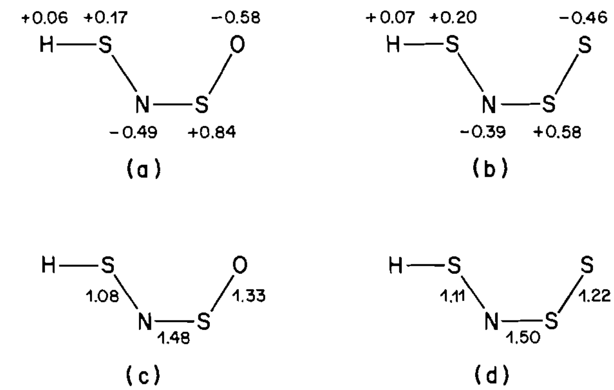

FIG. 2. Atomic charges, (*a*) and (*b*), and bond orders, (*c*) and (*d*), for planar HSNSO and HSNSS.

TABLE 1. Positional parameters ($\times 10^4$) and B_{eq} ($\times 10$) for the non-hydrogen atoms of $Ph_2CNSNSO$[a]

Atom	x/a	y/b	z/c	B_{eq}
S(1) **A**	4689.7(8)	8911.0(8)	4184.9(5)	39
S(2) **A**	1607.3(9)	10611.8(8)	5091.8(5)	45
N(1) **A**	5961(2)	9575(2)	3455(1)	35
N(2) **A**	3215(2)	10513(2)	4474(1)	39
O(1) **A**	1462(2)	9217(2)	5434(1)	63
C(1) **A**	7320(3)	8636(3)	3049(2)	34
C(11) **A**	7853(3)	6994(3)	3188(2)	33
C(12) **A**	9103(3)	6149(3)	3566(2)	38
C(13) **A**	9579(3)	4635(3)	3729(2)	41
C(14) **A**	8817(4)	3946(3)	3505(2)	48
C(15) **A**	7599(3)	4761(3)	3120(2)	55
C(16) **A**	7108(3)	6279(3)	2963(2)	48
C(21) **A**	8435(3)	9217(3)	2395(2)	32
C(22) **A**	9631(3)	8374(3)	1693(2)	39
C(23) **A**	10631(3)	8920(3)	1047(2)	42
C(24) **A**	10441(3)	10340(3)	1093(2)	44
C(25) **A**	9262(3)	11195(3)	1794(2)	46
C(26) **A**	8259(3)	10651(3)	2444(2)	38
S(1) **B**	6501.7(8)	5037.2(8)	736.6(5)	44
S(2) **B**	8787.3(9)	5505.9(8)	−789.7(5)	49
N(1) **B**	5939(2)	3665(2)	817(1)	38
N(2) **B**	7742(2)	4687(2)	−306(1)	39
O(1) **B**	8682(2)	6648(2)	−288(1)	67
C(1) **B**	4971(3)	3420(3)	1567(2)	33
C(11) **B**	4695(3)	2081(3)	1587(2)	34
C(12) **B**	3334(3)	1962(3)	2141(2)	40
C(13) **B**	3075(3)	735(3)	2128(2)	51
C(14) **B**	4183(4)	−389(3)	1570(2)	55
C(15) **B**	5548(3)	−303(3)	1029(2)	50
C(16) **B**	5798(3)	928(3)	1034(2)	42
C(21) **B**	4178(3)	4349(3)	2384(2)	33
C(22) **B**	3417(3)	5881(3)	2264(2)	39
C(23) **B**	2756(3)	6750(3)	3018(2)	48
C(24) **B**	2854(3)	6105(3)	3902(2)	53
C(25) **B**	3575(3)	4583(3)	4039(2)	48
C(26) **B**	4211(3)	3706(3)	3284(2)	38

[a] For molecule **B**, C(1) in Fig. 1 is C(21) and C(12) is C(22) etc.

TABLE 2. Bond lengths (Å) and angles (deg) for $Ph_2CNSNSO$

Bond	Distance A	Distance B[a]
S(1)—N(1)	1.679(2)	1.681(3)
S(1)—N(2)	1.641(2)	1.646(2)
S(2)—N(2)	1.533(2)	1.525(2)
S(2)—O	1.455(2)	1.451(3)
C(1)—N(1)	1.281(2)	1.292(3)
C(1)—C(11)	1.491(3)	1.487(4)
C(1)—C(21)	1.479(4)	1.483(3)
C(11)—C(12)	1.383(4)	1.381(4)
C(12)—C(13)	1.380(4)	1.378(5)
C(13)—C(14)	1.378(6)	1.369(4)
C(14)—C(15)	1.361(5)	1.367(5)
C(15)—C(16)	1.381(4)	1.374(5)
C(16)—C(11)	1.386(5)	1.381(3)
C(21)—C(22)	1.378(3)	1.389(3)
C(22)—C(23)	1.376(4)	1.379(4)
C(23)—C(24)	1.373(4)	1.384(4)
C(24)—C(25)	1.376(3)	1.381(4)
C(25)—C(26)	1.379(4)	1.388(4)
C(26)—C(21)	1.392(4)	1.396(4)

Atoms	Angles A	Angles B[a]
C(1)—N(1)—S(1)	117.8(2)	120.8(2)
N(1)—S(1)—N(2)	97.5(1)	96.3(1)
S(1)—N(2)—S(2)	121.6(1)	123.9(2)
N(2)—S(2)—O	116.9(1)	117.5(1)
N(1)—C(1)—C(11)	124.4(2)	115.5(2)
N(1)—C(1)—C(21)	117.9(2)	124.7(3)
C(11)—C(1)—C(21)	117.7(2)	119.8(2)
C(1)—C(11)—C(12)	120.0(3)	121.5(2)
C(1)—C(11)—C(16)	121.7(2)	120.2(2)
C(12)—C(11)—C(16)	118.4(2)	118.3(3)
C(11)—C(12)—C(13)	120.8(3)	120.8(2)
C(12)—C(13)—C(14)	119.9(3)	119.9(3)
C(13)—C(14)—C(15)	119.9(3)	120.2(3)
C(14)—C(15)—C(16)	120.4(4)	119.9(2)
C(15)—C(16)—C(11)	120.6(3)	121.0(3)
C(1)—C(21)—C(22)	120.6(3)	120.5(2)
C(1)—C(21)—C(26)	121.0(2)	120.7(2)
C(22)—C(21)—C(26)	118.4(2)	118.8(2)
C(21)—C(22)—C(23)	121.6(3)	120.4(2)
C(22)—C(23)—C(24)	119.7(2)	120.3(2)
C(23)—C(24)—C(25)	119.5(3)	120.2(3)
C(24)—C(25)—C(26)	120.9(3)	119.5(3)
C(25)—C(26)—C(21)	119.9(2)	120.7(2)

[a] For molecule **B**, C(11) in Fig. 1 is C(21) and C(12) is C(22), etc.

TABLE 3. Deviations from best plane in $Ph_2CNSNSO$[a]

Atom	Deviation Molecule **A**	Deviation Molecule **B**
C(1)	−0.035	0.054
N(1)	−0.015	0.003
S(1)	0.067	−0.087
N(2)	0.036	−0.031
S(2)	−0.030	0.023
O	−0.023	0.038

[a] The equations of the planes are $6.094x + 2.836y + 14.324z = 11.312$ for molecule **A**, and $6.534x - 2.858y + 8.183z = 3.498$ for molecule **B**.

TABLE 4. Comparison of bond lengths (Å) and angles (deg) in $Ph_2CNSNSO$ and $S(NSO)_2$

Parameter	$Ph_2CNSNSO$[a]	$S(NSO)_2$ (*9a*)[b]	$S(NSO)_2$ (*9b*)[c]
N(1)—S(1)	1.680(3)	1.657(2)	1.647(3)
S(1)—N(2)	1.644(2)	1.657(2)	1.647(3)
N(2)—S(2)	1.529(2)	1.534(2)	1.535(3)
S(2)—O	1.453(3)	1.465(2)	1.446(4)
N(1)—S(1)—N(2)	96.9(1)	97.2(1)	97.3(2)
S(1)—N(2)—S(2)	122.7(2)	123.6(2)	124.3(2)
N(2)—S(2)—O	117.2(1)	117.5(1)	118.0(2)

[a] Average of values for molecules **A** and **B**.
[b] Determined at −105°C.
[c] Determined at 31°C.

TABLE 5. Molecular orbital energies (eV) and eigenvector coefficients for planar HSNSO and HSNSS

	ϵ_i	S	N	S	O(S)
			HSNSO		
π_4	−1.825	0.260	−0.624	0.618	−0.401
π_3	−9.707	−0.619	0.424	0.319	−0.584
π_2	−12.547	−0.684	−0.406	0.239	0.557
π_1	−15.706	0.285	0.515	0.682	0.433
			HSNSS		
π_4	−2.557	0.298	−0.643	0.582	−0.398
π_3	−9.512	−0.437	0.417	0.150	−0.782
π_2	−12.155	−0.749	−0.171	0.482	0.420
π_1	−15.588	0.398	0.618	0.638	0.229

ligands (e.g. Ph_3PN in $Ph_3PNSNSS$, λ_{max} 491) (4). This trend has been explained in terms of the change in the energies of the frontier orbitals of RSNSS caused by the substituent R (5), and it is expected to be qualitatively similar for the SNSO chromophore. In order to assess the effect of the replacement of a terminal sulphur atom by oxygen on the electronic structure of RSNSS we have carried out MNDO calculations for the model compounds HSNSO and HSNSS. As indicated in Fig. 2, the bonds are more polar in HSNSO than in HSNSS, but the bond orders are similar. The S—N bond orders of 1.08 and 1.48 for HSNSO are consistent with the observed bond lengths of 1.644(2) and 1.529(3) Å, respectively, for $Ph_2CNSNSO$ (*vide supra*). The corresponding bond orders of 1.11 and 1.50 for HSNSS do not corroborate the equal S—N bond lengths found for $Ph_3PNSNSS$ (4). It should be noted, however, that both "long–short" and "short–long" S—N bond sequences have been observed for $SSNSS^-$ (3), as predicted by *ab initio* MO calculations (2).

The energies and eigenvector coefficients of the π orbitals for planar HSNSO and HSNSS are compared in Table 5. The major difference is the higher energy of the LUMO (π_4) in HSNSO. Since the HOMO energies are similar, the π^* (HOMO) $\rightarrow$ π^* (LUMO) transition is expected to occur at higher energy for RSNSO compared to RSNSS. The experimental data given in Table 6 are consistent with this prediction, and a

TABLE 6. λ_{max} values (nm) for RSNSO and RSNSS derivatives

Compound	λ_{max}	Reference
CF_3SNSO	Colourless	6
OSNSNSO	365	4
$Ph_2CNSNSO$	370	This work
Me_2NSNSO	Intense yellow	7, 8
$C_7H_8(SNSS)_2$[a]	408, 433	5
$SNSS^-$	470	1
$Ph_3PNSNSS$	491	4
$SSNSS^-$	582	2

[a]The appearance of two bands is the result of an excitonic coupling of the two chromophores.

similar trend has been observed for the $\pi \rightarrow \pi^*$ transition energies of carbonyls (30) and thiocarbonyls (31).

Thermal decomposition of $Ph_2CNSNSO$ and $Ph_2CNSNSNSNCPh_2$

Although $Ph_2CNSNSO$ exhibits moderate thermal stability, it does decompose at ca. 200°C in the solid state to give S_4N_4 and Ph_2CO (tlc). The formation of S_4N_4 is good evidence for the elimination of S_2N_2 (cf. thermolysis of $Ph_3As{=}N{-}S_3N_3$ (4)), but attempts to trap S_2N_2 using an apparatus described in ref. 4 were thwarted by co-sublimation of $Ph_2CNSNSO$. For comparison, the pyrolysis of $S(NSO)_2$ of 200–400°C under ultrahigh vacuum did not produce S_2N_2 (32).

The thermal decomposition of $Ph_2CNSNSNSNCPh_2$ in acetonitrile at reflux produced S_4N_4 in 72% yield (reaction [3]).

[3] $2Ph_2CNSNSNSNCPh_2 \rightarrow S_4N_4 + 2(Ph_2CN)_2S$

Conclusions

A comparison of RSNSO and RSNSS derivatives shows that they both adopt *cis, trans* chain structures, but the bonds are more polar and the $\pi^* \rightarrow \pi^*$ transition energy is higher in the former. The synthesis of RSNSO compounds (from RSCl) is more straightforward due to the availability of the reagent Me_3SiNSO.

Acknowledgements

The financial support of the Natural Sciences and Engineering Research Council of Canada through operating grants, a strategic grant (No. G0262) and a summer research assistantship (R.P.) is gratefully acknowledged.

1. J. BOJES and T. CHIVERS. J. Chem. Soc. Chem. Commun. 1023 (1980); J. BOJES, T. CHIVERS, W. G. LAIDLAW, and M. TRSIC. J. Am. Chem. Soc. **104**, 4837 (1982).
2. T. CHIVERS and R. T. OAKLEY. J. Chem. Soc. Chem. Commun. 752 (1979); T. CHIVERS, W. G. LAIDLAW, R. T. OAKLEY, and M. TRSIC. J. Am. Chem. Soc. **102**, 5773 (1980).
3. N. BURFORD, A. W. CORDES, R. T. OAKLEY, W. PENNINGTON, and P. N. SWEPSTON. Inorg. Chem. **20**, 4430 (1981).
4. T. CHIVERS, A. W. CORDES, R. T. OAKLEY, and P. N. SWEPSTON. J. Chem. Soc. Chem. Commun. 35 (1980); T. CHIVERS, A. W. CORDES, R. T. OAKLEY, and P. N. SWEPSTON. Inorg. Chem. **20**, 2376 (1981).
5. A. W. CORDES, H. KOENIG, M. C. NOBLE, and R. T. OAKLEY. Inorg. Chem. **22**, 3375 (1983).
6. A. HAAS and P. SCHOTT. Chem. Ber. **101**, 3407 (1968).
7. D. A. ARMITAGE and C. C. TSO. J. Chem. Soc. Chem. Commun. 1413 (1971); D. A. ARMITAGE and A. W. SINDEN. J. Inorg. Nucl. Chem. **36**, 993 (1974).
8. H. W. ROESKY and W. SCHAPER. Chem. Ber. **107**, 3451 (1974).
9. (*a*) R. STEUDEL, J. STEIDEL, and N. RAUTENBERG. Z. Naturforsch. **35**b, 792 (1980); (*b*) G. MACLEAN, J. PASSMORE, P. S. WHITE, A. BANISTER, and J. A. DURRANT. Can. J. Chem. **59**, 187 (1981).
10. H. STAUDINGER, E. ANTHES, and F. PFENNINGER. Chem. Ber. **49**, 1932 (1916).
11. M. VILLENA-BLANCO and W. L. JOLLY. Inorg. Synth. **9**, 98 (1967).
12. A. J. BANISTER, J. A. DURRANT, J. S. PADLEY, and K. WADE. J. Inorg. Nucl. Chem. **41**, 1415 (1979).
13. C. SUMMERFORD and K. WADE. J. Chem. Soc. A, 1487 (1969).
14. O. J. SCHERER and P. HORNIG. Angew. Chem. Int. Ed. Engl. **5**, 729 (1966).
15. O. J. SCHERER and R. WIES. Z. Naturforsch. **25**b, 1486 (1970).
16. E. FLUCK. Z. Anorg. Allg. Chem. **312**, 195 (1961).
17. E. M. HOLT, S. L. HOLT, and K. J. WATSON. J. Chem. Soc. Dalton Trans. 1357 (1974).
18. P. MAIN, S. E. HULL, L. LESSINGER, G. GERMAIN, J.-P. DECLERCQ, and M. M. WOOLFSON. MULTAN 78, A system of computer programs for the automatic solution of crystal structures from X-ray diffraction data. University of York, York, England. 1978.
19. J. M. STEWART (*Editor*). Technical Report TR-446. Computer Science Centre, University of Maryland.
20. D. T. CROMER and J. B. MANN. Acta Crystallogr. A**24**, 321 (1968).
21. R. F. STEWART, E. DAVIDSON, and W. SIMPSON. J. Chem. Phys. **42**, 3175 (1965).
22. International tables for X-ray crystallography. Kynoch Press, Birmingham, England. 1974.
23. M. J. S. DEWAR and W. THIEL. J. Am. Chem. Soc. **99**, 4899 (1977); **99**, 4907 (1977); QPCE (1977), No. 353 (MNDO).
24. T. CHIVERS, P. W. CODDING, W. G. LAIDLAW, S. W. LIBLONG, R. T. OAKLEY, and M. TRSIC. J. Am. Chem. Soc. **105**, 1186 (1983).
25. R. GLEITER and R. BARTETZKO. Z. Naturforsch. **36**b, 492 (1981).
26. (*a*) S. SENSARMA and A. G. TURNER. Inorg. Chim. Acta, **64**, L161 (1982); (*b*) A. G. TURNER. Inorg. Chim. Acta, **65**, L201 (1982).
27. B. GRUSHKIN. U.S. Patents Nos. 3,615,409 and 3,616,393, October 26, 1971; Chem. Abstr. **76**, 40262 (1972); **76**, 40283 (1972).
28. M-T. AVERBUCH-POUCHOT, A. DURIF, A. J. BANISTER, J. A. DURRANT, and J. HALFPENNY. J. Chem. Soc. Dalton Trans. 221 (1982).
29. A. J. BANISTER and J. A. DURRANT. J. Chem. Res. (M), 1928 (1978).
30. G. PORTER and P. SUPPAN. Trans. Faraday Soc. **61**, 1664 (1965).
31. J. FABIAN, H. VIOLA, and R. MAYER. Tetrahedron, **23**, 4323 (1967).
32. H. W. ROESKY, J. ANHAUS, and W. S. SHELDRICK. Inorg. Chem. **23**, 75 (1984).

Electrostatic effects on ionization equilibria: MNDO study of proton and hydrogen transfer reactions of 5-fluoropentanoic acid

ZDENEK FRIEDL[1]
Department of Chemistry, University of Alberta, Edmonton, Alta., Canada T6G 2G2

Received July 6, 1984

ZDENEK FRIEDL. Can. J. Chem. **63**, 1068 (1985).

Relative proton transfer enthalpies $\delta\Delta H^0$ and homolytic bond strengths $\delta\Delta H^0$ (A—H) of *sp* and *ap* conformers of 5-fluoropentanoic acid, as well as some related aliphatic and 4-X-bicyclo[2.2.2]octane-1-carboxylic halogenoacids, have been calculated by the MNDO method. The results, together with literature data concerning the gas phase acidities, were compared with the prediction of the electrostatic theory. It is shown that the substituent effects on acidities of carboxylic acids are largely due to substituent interactions in the anions and only to a smaller extent to interactions in the neutral acids. A small contribution (about one-eighth to one-fourth as large in magnitude but of opposite sign) is possibly also made by substituent effects on homolytic bond strengths DH^0 (A—H).

ZDENEK FRIEDL. Can. J. Chem. **63**, 1068 (1985).

Utilisant la méthode MNDO, on a calculé les enthalpies relatives de transferts de protons ($\delta\Delta H^0$) et les forces relatives des liaisons homolytiques ($\delta\Delta H^0$ (A—H)) des conformères *sp* et *ap* de l'acide fluoro-5 pentanoïque, de quelques halogénoacides aliphatiques apparentés et de quelques acides X-4 bicyclo[2.2.2] octanecarboxyliques-1. On a comparé les résultats obtenus ainsi que des données tirées de la littérature relatives aux acidités en phase gazeuse avec des prédictions obtenues à l'aide de la théorie électrostatique. On démontre que les effets des substituants sur les acidités des acides carboxyliques sont dus en grande partie à des interactions des substituants dans les anions alors que les interactions des substituants des acides neutres n'ont qu'une faible influence. Il est possible que les effets des substituants puissent faire une légère contribution (de l'ordre du huitième au quart de l'amplitude mais de signe inverse) sur les forces des liaisons homolytiques DH^0 (A—H).

[Traduit par le journal]

Introduction

Substituent effects on proton transfer reactions may be theoretically predicted within the framework of classical electrostatics. Considering ionization equilibria in the gas phase (1, 2), the electrostatic theory developed by Smallwood (3) seems to be more appropriate than the generally used theory of Kirkwood and Westheimer (4, 5). The second theory was created especially for the description of solvent effects on ionization equilibria in aqueous solutions. These effects are expressed by means of the effective relative permittivity ϵ_{ef}, which must be calculated from the solvent bulk permittivity ϵ_{ext} and the internal relative permittivity ϵ_{int} attributed to the solute molecule (4, 5). On the other hand, Smallwood (3) had cancelled all the solvation terms and considered the effect of the dipolar substituent X on the isodesmic reaction [1]

$$[1] \quad \text{X—A—H} + \text{A}^- = \text{X—A}^- + \text{A—H}$$

as the change of reaction enthalpy $\delta\Delta H^0$ in the gas phase.

Provided that effective relative permittivity ϵ_{ef} equals one for the gas phase, the electrostatic field effect F_D on the equilibrium [1] is expressed in both theories by the same equation, eq. [2]

$$[2] \quad \delta\Delta H^0 \cong \delta\Delta E^0 = Ze\mu \cos\theta / r^2 \epsilon_{ef}(4\pi\epsilon_0)$$

where Z is the charge valence (± 1), e the electronic charge, μ is the dipole moment of substituent X, r the distance between charge Ze and μ, and θ is the angle between r and μ.

Equation [2] generally assumes that the remaining substituent effects have been eliminated by the proper choice of system (i.e., especially resonance R_π and steric S_D effects between the substituent X and the anion in X—A$^-$). Until now, great attention was paid to the testing of electrostatic theory from this point of view (2, 6) or simply changing of the geometrical variables r and θ in eq. [2] (refs. 2, 6–8). However, as we mentioned in our previous papers (9–12), two basic assumption of the theory still remain that have not been adequately tested: the equality of the homolytic bond strengths in the substituted and unsubstituted acids, and the consideration of the substituent effect as a direct field effect F_D acting exclusively on the ionizable proton in the neutral acid X—A—H.

At present there are only very limited experimental data about the changes of DH^0 (A—H) due to substitution from gas phase experiments (13–15), and none of them deal with carboxylic acids. In a similar way there are only a few papers (16–18) which consider the F_D effect in both the neutral acid and the anion.

For the reasons mentioned above, we decided to test the common assumption of the equality of homolytic bond strengths at a semiempirical quantum chemical level using the MNDO method. The *sp* and *ap* conformers of 5-fluoropentanoic acid (structure **1**) were chosen as model compounds, which allow us to test the F_D effects of the carbon–fluorine dipole even for the different geometrical parameters r and θ in eq. [2]. The applicability of the MNDO method (19, 20) for the

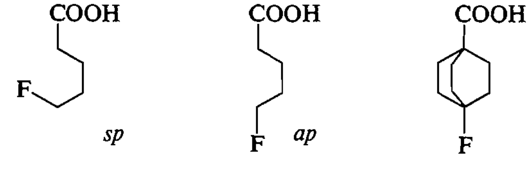

1 **2**

proton transfer reactions was checked on some related aliphatic and bicyclo[2.2.2]octane-1-carboxylic acids (structure **2**) whose gas phase acidities are known (13).[2]

[1] Permanent address: Department of Organic Chemistry, Slovak Technical University, CS-81237 Bratislava, Czechoslovakia.

[2] Also, R. W. Taft and I. Koppel, unpublished results.

TABLE 1. MNDO calculated heats of formation and net atomic charges of the compounds R—$CH_2CH_2CH_2CH_2$—X shown in eq. [3] (in kJ mol^{-1})

X	Twist angle[a] (°)	$-\Delta H_f^0$ R = COOH	COO^-	$COO^{\bullet}$	q_H[b] (electron)	q_O[c] (electron)
sp H	0	442.567	484.397	126.279	0.21557	−1.21189
H	45	450.872	492.396	—	0.21549	−1.21183
H	90	445.825	487.572	—	0.21555	−1.21182
H	135	441.858	483.730	—	0.21551	−1.21139
ap H	180	451.354	493.082	135.087	0.21556	−1.21188
sp F	0	606.189	644.489	290.927	0.21511	−1.21246
F	45	623.355	664.544	—	0.21564	−1.21057
F	90	629.942	679.862	—	0.21690	−1.20646
F	135	626.204	682.199	—	0.21747	−1.20372
ap F	180	635.974	693.934	317.515	0.21773	−1.20352
sp H	0	R = H	86.106			
sp H	180		94.687			
sp F	0		250.327			
ap F	180		281.619			

[a]Twist angle between the C—X and C—C bonds of the carbon skeleton.
[b]Net atomic charge on the carboxyl proton.
[c]Sum of net atomic charges of the carboxylate oxygen atoms.

Computational section

The quantum chemical calculations were made at the semi-empirical MNDO level (21) by using the MNDO (22) and MNDOC (23) programs. The standard geometry parameters (24) were used as a starting value for the geometry optimization, but the C—H bond lengths (109 pm) and the C—C—H bond angles (109.47°) were held constant. During the optimization the carboxyl group was kept coplanar with the carbon chain of the *sp* and *ap* conformers of **1**, and the most stable orientations were taken into account.

The geometrical constraints mentioned above were tested for the case of neutral and anionic forms of the *sp* and *ap* conformers of **1**. Despite this restriction, only a negligible influence upon $\delta\Delta H^0$ was found (less than 0.1 kJ mol^{-1}), in comparison with the fully optimized geometry.

The calculated heats of formation ΔH_f^0, the net atomic charges on the carboxyl proton q_H, and the sum of charges on the carboxylate oxygens q_O are given in Table 1 for all structures mentioned above. The same MNDO parameters for some aliphatic and bicyclo[2.2.2]octane-1-carboxylic acids are given in Table 2.

TABLE 2. MNDO calculated heats of formation and net atomic charges of some related aliphatic and bicyclic halogenoacids (in kJ mol^{-1})

Acid		$-\Delta H_f^0$ COOH	COO^-	q_H[a] (electron)	q_O[b] (electron)
Acetic		423.411	460.718	0.21610	−1.22573
Fluoroacetic[c]		603.945	680.355	0.22121	−1.17335
Chloroacetic[d]		440.888	524.526	0.22297	−1.15817
Propionic	*sp*	429.162	468.957	0.21572	−1.21463
	ap	436.569	476.907	0.21572	−1.21470
2-Cl-Propionic	*sp*	437.741	492.757	0.21816	−1.17413
	ap	468.432	546.329	0.22024	−1.18631
BCO[e]		434.994	489.564	0.21744	−1.18598
4-F-BCO		601.222	672.494	0.21838	−1.17723
4-Cl-BCO		456.176	531.975	0.21859	−1.17345

[a,b]Net atomic charges as described in Table 1.
[c]The most stable O═C—C—F (*ap*) conformation.
[d]The most stable O═C—C—Cl (*sp*) conformation.
[e]BCO means bicyclo[2.2.2]octane-1-carboxylic.

Electrostatic calculations

The relative electrostatic energies $\delta\Delta E^0$ were calculated from eq. [2] using $\epsilon_{cf} = 1$ and introducing the difference $\mu_X - \mu_H$ for μ. Standard bond moments (25) were used (in 10^{-30} C m): C—H, −1.0; C—F, 4.67; and C—Cl, 5.67. The geometrical parameters r and θ were both calculated from the MNDO optimized atomic coordinates and from the standard geometry parameters (24). In the second case, the ionizable proton of the carboxyl group was localized (4) at a distance of 145 pm from the carbonyl carbon in the direction of the prolonged bond C—C(O). The negative charge on the carboxylate anions was localized in both cases in the middle of the linkage of the carboxylate oxygens.

The electrostatic energies $\delta\Delta E^0$ for reaction [1] were calculated by means of eq. [2], taking charge valence $Z = +1$, while in the case of the relative electron affinities $\delta\Delta E^0$ (EA) the charge valence was taken as $Z = -1$. This means that $\delta\Delta E^0$ values express the energy change accompanying the removal of a proton from the neutral X—A—H molecule, while $\delta\Delta E^0$ (EA) predict the energy of removal of an electron from the electrostatic field due to a substituent dipole in the anion $X—A^-$.

The relative electrostatic energies $\delta\Delta E^0$ and electron affinities $\delta\Delta E^0$ (EA) calculated on the basis of optimized MNDO and standard geometry parameters are given in Table 3.

Discussion

Reynolds *et al.* have shown that *ab initio* molecular orbital calculations at the minimal basis set STO-3G level can be successfully used to predict substituent polar effects (6). This was illustrated, for example, on 4-substituted styrenes (26), 4-substituted benzoic acids (27), and substituted methylamines and pyridines (28). Since the investigated structures contained eight to twelve heavy atoms, the choice of fixed geometries (24) was necessitated by cost considerations. In this respect the semiempirical MNDO method (21) with the geometry opti-

TABLE 3. Relative electrostatic energies $\delta\Delta E^0$ and electron affinities $\delta\Delta E^0$ (EA) of investigated halogenoacids (in kJ mol^{-1})

Acid	Twist angle (°)		$\delta\Delta E^0$ MNDO[a]	$\delta\Delta E^0$ Std.[b]	$\delta\Delta E^0$ (EA) MNDO[a]	$\delta\Delta E^0$ (EA) Std.[b]
5-F-Pentanoic	*sp*	0	7.1	14.0	−6.0	−19.7
		45	4.5	—	−3.2	—
		90	−2.8	—	5.3	—
		135	−8.4	—	11.9	—
	ap	180	−10.4	−12.7	14.3	16.9
Fluoroacetic[c]		180	−10.2	−23.7	49.1	46.1
Chloroacetic[d]		0	−30.4	−28.3	56.7	53.9
2-Cl-Propionic	*sp*	0	−7.1	12.9	13.0	−7.1
	ap	180	−17.7	−25.9	34.3	36.5
4-F-BCO		180	−11.3	−12.7	16.1	16.9
4-Cl-BCO		180	−12.6	−14.0	17.6	18.4

[a] The geometry parameters cos θ and *r* calculated from the MNDO optimized atomic coordinates.
[b] The geometry parameters cos θ and *r* calculated from the standard geometry parameters (ref. 24).
[c,d] The most stable O=C—C—X conformers.

TABLE 4. Proton transfer enthalpies $\delta\Delta H^0$ and relative net atomic charges δq_H and δq_O of investigated halogenoacids (in kJ mol^{-1})

Acid	Twist angle (°)		$\delta\Delta H^0$ MNDO	$\delta\Delta H^0$ Expt.	δq_H[a] (10^3 electron)	δq_O[b] (10^3 electron)
5-F-Pentanoic	*sp*	0	3.5	—	−0.46	−0.57
		45	0.3	—	0.15	1.26
		90	−8.2	—	1.35	5.36
		135	−14.1	—	1.96	7.67
	ap	180	−16.2	—	2.17	8.36
Fluoroacetic[c]		180	−39.1	−45.6[e]	5.11	52.38
Chloroacetic[d]		0	−46.3	−49.8[e]	6.87	67.56
2-Cl-Propionic	*sp*	0	−15.2	−27.2[e]	2.44	40.50
	ap	180	−37.6		4.52	28.39
4-F-BCO		180	−16.7	−23.0[f]	0.94	8.75
4-Cl-BCO		180	−21.2	−25.5[f]	1.15	12.53

[a] Difference $q_H(X) - q_H(H)$.
[b] Difference $q_O(X) - q_O(H)$.
[c,d] The most stable O=C—C—X conformers.
[e] Reference 13.
[f] See footnote 2.

mization can be considered as a promising approach (19, 20), especially as regards still important (2, 8) bicyclo[2.2.2]octane and 1-azabicyclo[2.2.2]octane systems in the future.

As mentioned in the introduction, there is a quite fundamental question as to whether the MNDO method is adequate for the description of the substituent effects on proton transfer reactions. For this reason we calculated MNDO $\delta\Delta H^0$ enthalpies for fluoroacetic, chloroacetic, 2-chloropropionic, 4-fluorobicyclo[2.2.2]octane-1-carboxylic (4-F-BCO), and 4-chlorobicyclo[2.2.2]octane-1-carboxylic (4-Cl-BCO) acids, as their experimental gas phase acidities $\delta\Delta H^0_{\mathrm{exptl}}$ are known (13).[2]

The consistency of the calculated and experimental data of Table 4 is reasonably good considering not only the electronegativity and polarizability effects (the chloro derivatives are stronger acids), but also the absolute $\delta\Delta H^0$ values. In particular, the satisfactory agreement of $\delta\Delta H^0$ values of the *ap* conformer of **1** and 4-F-BCO acid (structure **2**) with the experimental $\delta\Delta H^0_{\mathrm{exptl}}$ of 4-F-BCO acid (−16.2 and −16.7 kJ mol^{-1} versus −23.0 kJ mol^{-1}, Table 4) suggests that MNDO provides a proper description of the F_D effect on proton transfer reactions, because both acids have practically the same geometry parameters cos θ and *r* (see structure **1**), and thus the same theoretical magnitude of the F_D effect.

Comparison of the electrostatic theory with the MNDO calculations is presented in Tables 3 and 4. The problem is whether the gas phase acidities $\delta\Delta H^0$ are better predicted by the $\delta\Delta E^0$ or the $\delta\Delta E^0$ (EA) values.[3] In order to test this problem the following three types of isodesmic reactions [3] were formed,

[3] 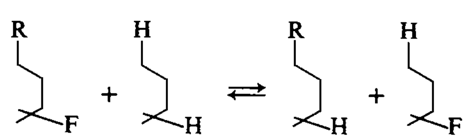

where R is either the carboxyl group COOH, carboxylate anion COO^-, or carboxyl radical $COO^\bullet$ in both *sp* and *ap* conformers of 5-fluoropentanoic acid. The effect of the substituent on acidity $\delta\Delta H^0$ (Table 4) is then given by the energy change for reaction [1], which is just the difference in the $\delta\Delta H_3^0$ energies for the COOH and COO^- groups. In a similar way, the substituent effects on the homolytic bond strengths δDH^0 (A—H) are given by the energy change for reaction [4]:

[4] $\mathrm{X{-}A{-}H + A^\bullet = X{-}A^\bullet + A{-}H}$

and eq. [5] expresses the substituent effects on electron affinity of the radical $\delta EA(A^\bullet)$:

[5] $\mathrm{X{-}A^- + A^\bullet = X{-}A^\bullet + A^-}$

The substituent effects on the gas phase acidity are then given with regard to eqs. [1], [4], and [5] by eq. [6]:

[6] $\delta\Delta H^0 = \delta DH^0\,(\mathrm{A{-}H}) - \delta EA\,(\mathrm{A^\bullet})$

TABLE 5. MNDO calculated $\delta\Delta H_3^0$ energies of reaction [3], homolytic bond strengths δDH^0 (A—H), and electron affinities δEA ($A^\bullet$) of eq. [6] (in kJ mol^{-1})

R	$\delta\Delta H_3^0$ *sp*	$\delta\Delta H_3^0$ *ap*	δDH^0 (A—H) *sp*	δDH^0 (A—H) *ap*	δEA ($A^\bullet$) *sp*	δEA ($A^\bullet$) *ap*
COOH	−0.6	−2.3	−1.0	2.2	−4.5	18.4
COO^-	−4.1	13.9	—	—	—	—
$COO^\bullet$	0.4	−4.5	—	—	—	—

The MNDO calculated $\delta\Delta H_3^0$ energies, the homolytic bond strengths δDH^0 (A—H), and electron affinities δEA ($A^\bullet$) are given in Table 5. When comparing these data, it is obvious that the predominant substituent effect on $\delta\Delta H^0$ is largely due to substituent interactions in the anions (16–18) and only to a smaller extent to interactions in the neutral acids and the carboxyl radicals.

In order to test the electrostatic theory we plotted the $\delta\Delta E^0$ and $\delta\Delta E^0$ (EA) values against the $\delta\Delta H^0$ energies. Figure 1 reveals that evidently the best agreement is with the MNDO geometry based $\delta\Delta E^0$ (EA) electron affinities. The electrostatic energies $\delta\Delta E^0$ generally underestimate $\delta\Delta H^0$, especially with respect to short-chain aliphatic halogenoacids (points 6–8, Fig. 1). The same pattern can be seen from the relative net atomic

[3] This approach differs slightly from Yoder's treatment (18) and, as regards the geometry used, is discussed below.

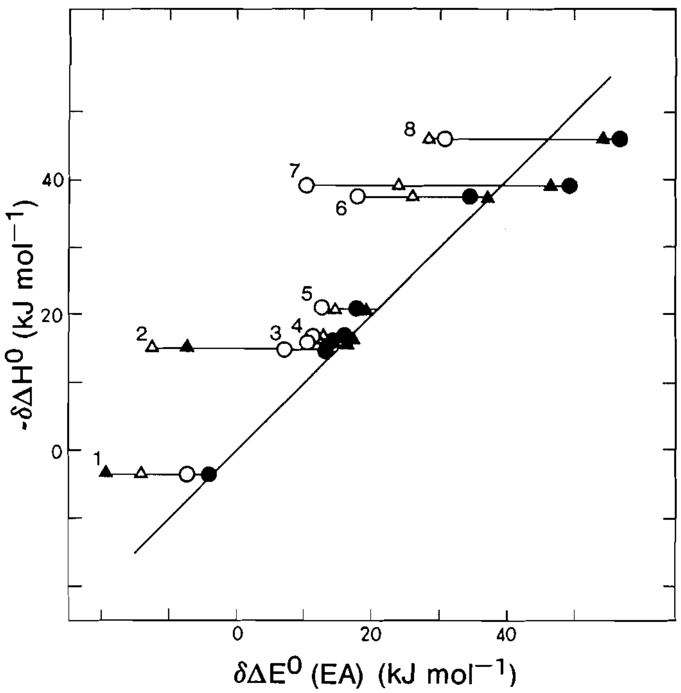

FIG. 1. Test of the electrostatic theory for variable halogenoacids. The MNDO $\delta\Delta H^0$ energies of various halogenoacids are plotted against $\delta\Delta E^0$ (○ MNDO, △ standard geometry) and (or) $\delta\Delta E^0$ (EA) (● MNDO, ▲ standard geometry). Parent acids: 1, *sp* 5-F-pentanoic; 2, *sp* 2-Cl-propionic; 3, *ap* 5-F-pentanoic; 4,4-F-BCO; 5,4-Cl-BCO; 6, *ap* 2-Cl-propionic; 7, fluoroacetic; 8, chloroacetic. The straight line has the theoretical slope.

charges δq_H and δq_O which are listed in Table 4. The ratio of $\rho(\delta q_O)/\rho(\delta q_H) = 3.3$ for the conformers of 5-fluoropentanoic acid, and for the related aliphatic halogenoacids it is even higher – approximately 10. In other words, these facts mean that the substituent effects on $\delta\Delta H^0$ are predominantly due to effects in the carboxylate anions so that the relative electron affinities $\delta\Delta E^0$ (EA) give a more appropriate description of the proton transfer reaction [1] at the empirical level of the electrostatic theory.

Note the failure of the standard geometry based $\delta\Delta E^0$ (EA) values (18) as regards a description of the reversed substituent effect in acids 1 and 2 (Fig. 1). In order to reach reasonable agreement with the $\delta\Delta H^0$ energies, the use of a corresponding fully optimized geometry is necessary.

The remaining problem is the possible substituent effects on homolytic bond strength DH^0 (A—H) during the proton transfer reaction [1]. If there was a set of experimental $\delta\Delta H^0$ and δEA (A$^\cdot$) values it would probably be possible to obtain δDH^0 (A—H) energies, even given their large uncertainty (29). Due to the lack of experimental data we tried to obtain δDH^0 (A—H) energies for reaction [4], at least at a MNDO method level.

The relevant data are assembled in Tables 4 and 5. When we compare $\delta\Delta H_3^0$ and $\delta\Delta H^0$ energies (Table 4) it is obvious that substituent effects on acidity are largely determined by effects in carboxylate anions, but their magnitudes in the corresponding neutral acids and carboxyl radicals are practically the same. Regardless of the small absolute values of δDH^0 (A—H), which are given in Table 5 (about one-eight (*ap*) to one-fourth (*sp*) as large in magnitude but of opposite sign), the general pattern of F_D effects on reaction [4] is quite reasonable: the lower the polarity of the O—H bond, the lower the δDH^0 (A—H) energy. Table 4 shows this relationship more explicitly in terms of the relative atomic charges δq_H, which predict an increase of electron density on the reaction centre of the *sp* conformer of 5-fluoropentanoic acid.

A somewhat less accurate approach based on the MNDO calculated IP (i.e., the negative HOMO energies of the anions X—A$^-$) gives δEA (A$^\cdot$) −2.9 kJ mol^{-1} for the *sp* and 18.4 kJ mol^{-1} for the *ap* conformer. Even so, the corresponding homolytic bond strengths (0.6 and 2.2 kJ mol^{-1}, respectively) agree fairly well with the δDH^0 (A—H) in Table 5.

The relative homolytic bond strength δDH^0 (A—H) is usually neglected within the framework of electrostatic theory (3–6). However, if the respective proton transfer reaction were transferred from the gas phase into solution, the magnitude of δDH^0 (A—H) would become more important for a predominant solvent effect on δEA (A$^\cdot$). For example, in the following reaction [7] we calculated that the $\delta\Delta H^0$ energies would

[7] $X—A—H + A^- \ldots H_2O = X—A^- \ldots H_2O + A—H$

decrease by 0.2 kJ mol^{-1} for the *sp* and 0.4 kJ mol^{-1} for the *ap* conformer of 5-fluoropentanoic acid. This trend agrees in general with the solvent attenuation factor (2) for the substituted acetic acids (SAF(aq) = $\rho_I(gas)/\rho_I(aq)$ = 4.1). Summarizing the present evidence, we can state that the homolytic bond strengths DH^0 (A—H) do not necessarily cancel, and that a competent experimental examination will be desirable in future studies.

Acknowledgements

I am very grateful to Professor Paul Kebarle for helpful comments and for support of this research. I thank Professor Robert W. Taft for providing results of gas phase acidities of bicyclo[2.2.2]octanecarboxylic acids. The financial support of the National Research Council of Canada is gratefully acknowledged.

1. P. KEBARLE. Ann. Rev. Phys. Chem. **28**, 445 (1977).
2. R. W. TAFT. Prog. Phys. Org. Chem. **14**, 247 (1983).
3. H. M. SMALLWOOD. J. Am. Chem. Soc. **54**, 3048 (1932).
4. J. G. KIRKWOOD and F. H. WESTHEIMER. J. Chem. Phys. **6**, 506 (1938).
5. F. H. WESTHEIMER and J. G. KIRKWOOD. J. Chem. Phys. **6**, 513 (1938).
6. W. F. REYNOLDS. Prog. Phys. Org. Chem. **14**, 165 (1983).
7. R. D. TOPSOM. J. Am. Chem. Soc. **103**, 39 (1981).
8. R. D. TOPSOM. Acc. Chem. Res. **16**, 292 (1983).
9. O. EXNER and Z. FRIEDL. Collect. Czech. Chem. Commun. **43**, 3227 (1978).
10. Z. FRIEDL, J. HAPALA, and O. EXNER. Collect. Czech. Chem. Commun. **44**, 2928 (1979).
11. K. KALFUS, Z. FRIEDL, and O. EXNER. Collect. Czech. Chem. Commun. **49**, 179 (1984).
12. Z. FRIEDL. Can. J. Chem. **62**, 2337 (1984).
13. J. B. CUMMING and P. KEBARLE. Can. J. Chem. **56**, 1 (1978).
14. R. H. STALEY, M. TAAGEPERA, W. G. HENDERSON, I. KOPPEL, J. L. BEAUCHAMP, and R. W. TAFT. J. Am. Chem. Soc. **99**, 326 (1977).
15. J. E. BARTMESS and R. T. MCIVER, JR. *In* Gas phase ion chemistry. Vol. 2. *Edited by* M. T. Bowers. Academic Press, New York. 1979. p. 87.
16. (*a*) A. PROSS, L. RADOM, and R. W. TAFT. J. Org. Chem. **45**, 818 (1980); (*b*) G. KEMISTER, A. PROSS, L. RADOM, and R. W. TAFT. J. Org. Chem. **45**, 1056 (1980).
17. J. T. EDWARD, P. G. FARRELL, J. L. JOB, and B.-L. POH. Can.

J. Chem. **56**, 1122 (1978).
18. C. S. YODER and C. H. YODER. J. Am. Chem. Soc. **102**, 1245 (1980).
19. M. J. S. DEWAR. J. Mol. Struct. **100**, 41 (1983).
20. S. DEBRUIJN. Int. J. Quant. Chem. **25**, 367 (1984).
21. M. J. S. DEWAR and W. THIEL. J. Am. Chem. Soc. **99**, 4899 (1977); **99**, 4907 (1977).
22. W. THIEL. QCPE, **11**, 353 (1978).
23. W. THIEL. QCPE, **15**, 438 (1983).
24. J. A. POPLE and M. GORDON. J. Am. Chem. Soc. **89**, 4253 (1967).
25. O. EXNER. Dipole moments in organic chemistry. Thieme, Stuttgart. 1975. p. 33.
26. W. F. REYNOLDS, P. G. MEZEY, and G. K. HAMER. Can. J. Chem. **55**, 522 (1977).
27. P. G. MEZEY and W. F. REYNOLDS. Can. J. Chem. **55**, 1567 (1977).
28. W. F. REYNOLDS, P. G. MEZEY, W. J. HEHRE, R. D. TOPSOM, and R. W. TAFT. J. Am. Chem. Soc. **99**, 5821 (1977).
29. B. K. JANOUSEK and J. I. BRAUMAN. *In* Gas phase ion chemistry. Vol. 2. *Edited by* M. T. Bowers. Academic Press, New York. 1979. p. 53.

Syntheses of model oligosaccharides of biological significance. 4. Synthesis of a fucosylated *N*,*N*′-diacetylchitobioside and related oligosaccharides[1]

DAVID A. SCHWARTZ AND HO-HUAT LEE

Ludwig Institute for Cancer Research, Toronto Branch, 9 Earl Street, Toronto, Ont., Canada M4Y 1M4

JEREMY P. CARVER

Departments of Medical Genetics and Medical Biophysics, University of Toronto, Toronto, Ont., Canada M5S 1A8

AND

JIRI J. KREPINSKY[2]

Ludwig Institute for Cancer Research, Toronto Branch, 9 Earl Street, Toronto, Ont., Canada M4Y 1M4 and Departments of Medical Genetics and Medical Biophysics, University of Toronto, Toronto, Ont., Canada M5S 1A8

Received June 18, 1984

This paper is dedicated to Professor Peter Yates on the occasion of his 60th birthday

DAVID A. SCHWARTZ, HO-HUAT LEE, JEREMY P. CARVER, and JIRI J. KREPINSKY. Can. J. Chem. **63**, 1073 (1985).

The synthesis of two trisaccharides and one disaccharide containing L-fucose and 2-acetamido-2-deoxy-D-glucose is reported. Methyl 3,6-di-*O*-benzyl-2-deoxy-2-phthalimido-β-D-glucopyranoside was glycosylated with a 3,4,6-tri-*O*-acetyl-2-deoxy-2-phthalimido-β-D-glucopyranosyl bromide. Removal of the phthalimido protecting groups by hydrazinolysis followed by *N*-acetylation and debenzylation yielded methyl *N*,*N*′-diacetylchitobioside 3′,4′,6′-triacetate. The latter was selectively fucosylated at the 6-position with 2,3,4-tri-*O*-benzyl-α-L-fucopyranosyl bromide to yield, after debenzylation and de-*O*-acetylation, methyl 2-acetamido-4-*O*-(2-acetamido-2-deoxy-β-D-glucopyranosyl)-2-deoxy-6-*O*-(α-L-fucopyranosyl)-β-D-glucopyranoside. When methyl 3-*O*-benzyl-2-deoxy-2-phthalimido-β-D-glucopyranoside was fucosylated, its 6-*O*- and 4,6-di-*O*-(α-L-fucopyranosyl) derivatives were obtained by use of 1 and 2 equivalents, respectively, of the protected fucosyl bromide.

DAVID A. SCHWARTZ, HO-HUAT LEE, JEREMY P. CARVER et JIRI J. KREPINSKY. Can. J. Chem. **63**, 1073 (1985).

On rapporte la synthèse de deux trisaccharides et d'un disaccharide contenant du L-fucose et de l'acétamido-2 déoxy-2 D-glucose. On a glycosylé le di-*O*-benzyl-3,6 déoxy-2 phtalimido-2 β-D-glucopyrannoside de méthyle avec le bromure de tri-*O*-acétyl-3,4,6 déoxy-2 phtalimido-2 β-D-glucopyrannosyle. L'hydrazinolyse du groupe protecteur phtalimido, suivie d'une *N*-acétylation et d'une débenzylation, conduit au N triacétate-3′,4′,6′ du *N*,*N*′-diacétylchitobioside de méthyle. La fucolisation sélective de ce dernier en position 6 à l'aide du bromure de tri-*O*-benzyl-2,3,4 α-L-fucopyrannosyle, conduit, après débenzylation et dé-*O*-acétylation, à l'acétamido-2 *O*-(acétamido-2 déoxy-2 β-D-glucopyrannosyl)-4 déoxy-2 *O*-(α-L-glucopyrannosyl)-6 β-D-glucopyrannoside de méthyle. La fucosylation du *O*-benzyl-3 déoxy-2 phtalimido-2 β-D-glucopyrannoside par 1 ou 2 équivalents de bromure de fucosyle protégé de méthyle permet d'obtenir les dérivés *O*-6 ou di-*O* (α-L-fucopyranosyle)-4,6.

[Traduit par le journal]

Glycoproteins containing N-linked oligosaccharides are ubiquitous on cell surfaces. All such oligosaccharides contain a core structure which is invariably attached through an *N*,*N*′-diacetylchitobiosyl linkage to L-asparagine (1), and in some cases this disaccharide moiety is glycosylated with L-fucose (2). We are studying the role of the three-dimensional structure of oligosaccharides such as **1** and **2** in biosynthetic pathways as well as in cell–cell recognition. In addition to this, the complete structures or their fragments can be used as determinants of artificial antigens which may be useful for the prep-

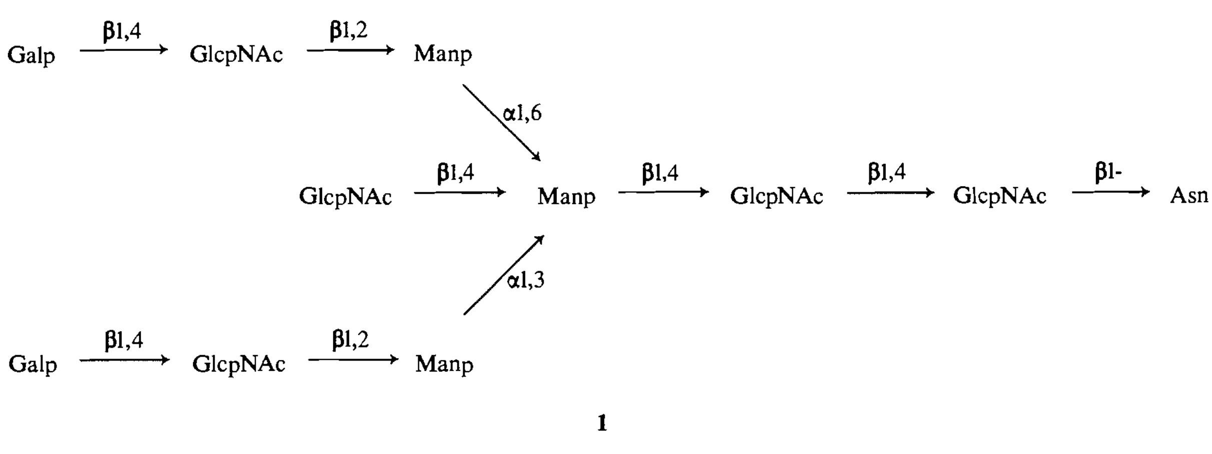

1

[1] For part 3, see ref. 23.

[2] Author to whom correspondence may be addressed.

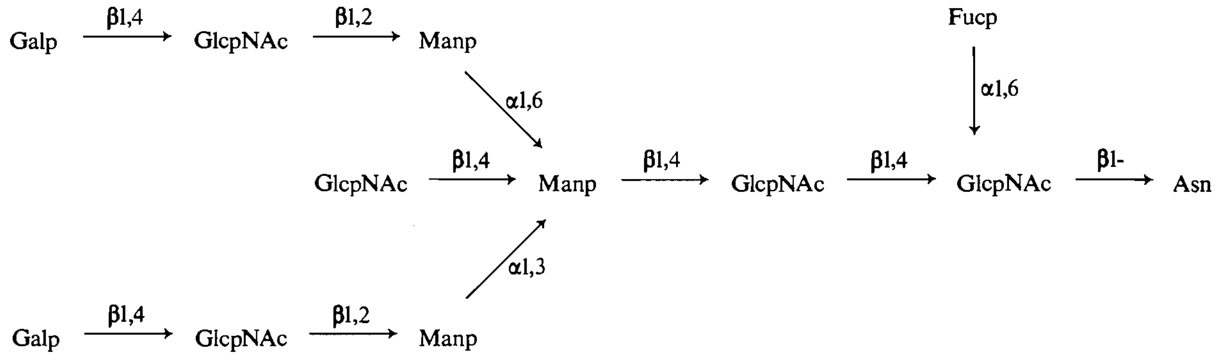

2

aration of diagnostic reagents (2, 3). In our overall synthetic strategy we sought to develop a methodology for the efficient syntheses of smaller oligosaccharides which can be linked together to form **1** or **2**. Thus we have previously reported the syntheses of the mannose-containing portion of the core (4, 5), and herein we describe an efficient and simple synthesis of the chitobiose-fucose part of **2**, i.e. the model trisaccharide **3***a*. We also wanted to prepare the disaccharide **4**, and in the course of this synthesis we observed that the reactivities of OH-6 and OH-4 differ sufficiently to allow a simple preparation of either **4** or **5**.

Trisaccharide **3***b* has already been synthesized (6) in a fairly complicated procedure employing 1,6-anhydro derivatives (20 steps in 1% overall yield). Since OH-4 is much more reactive in the latter than in the conventional $^4C_1$ conformation it seems advantageous to utilize this property for the formation of the 1,4-linkage of chitobiose. However, the use of 1,6-anhydro sugars is also extremely time-consuming, so we set out to design a shorter route which would allow the preparation of substantial quantities of **3***a* and related oligosaccharides relatively rapidly. The efficiency of the synthetic sequence is of particular importance because, eventually, isotopically labelled

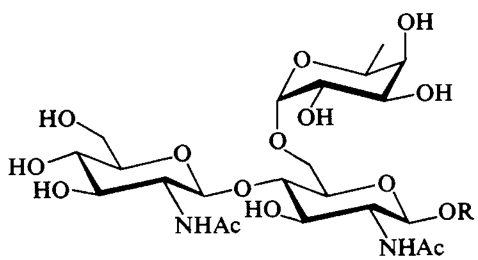

3*a* R = Me
b R = H

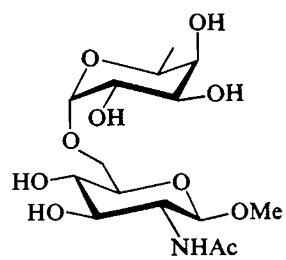

4

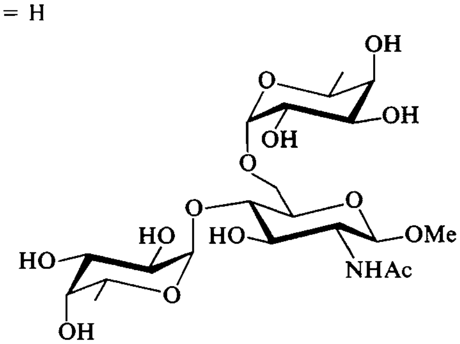

5

fucose is to be incorporated.

Lemieux *et al.* (7) have shown that the OH-4 in 2-amino-2-deoxyglucose is not so unreactive in the $^4C_1$ conformation as to warrant the use of 1,6-anhydro derivatives (8, 9). It was also shown previously (7, 11) that the protection of the amino function as its *N*-phthalimido derivative in glycosylating agents leads to exclusive formation of the desired β-anomer in similar situations. Moreover, in an aglycon moiety, the *N*-phthalimido group cannot participate in an imidate formation as the acetamido group does (10). We have therefore adopted the *N*-phthalimido approach to form a chitobiosyl derivative as, for instance, in the condensation of the aglycon **6***a* with the bromide **7** using silver triflate/collidine as a promoter, which resulted in a 60% yield of the disaccharide **8***a* (11).

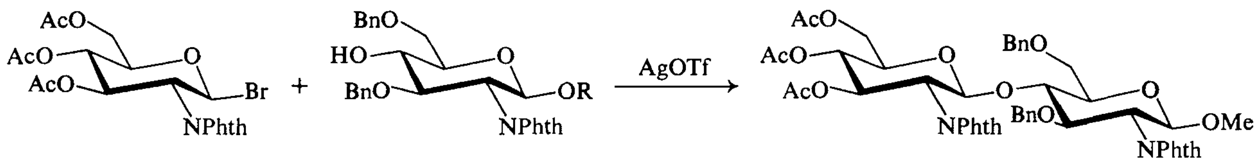

7

6*a* R = CH_2CCl_3
b R = Me

8*a* R = CH_2CCl_3
b R = Me

The aglycon required for the synthesis of trisaccharide **3***a* should be a derivative of **8** in which the OH-6 is free. Therefore, any protection of this OH group should be removable in the presence of other blocking groups. First we considered the combinations **9** (R = Bn, R' = Ac) and **10** (R = *tert*-butyldimethylsilyl, R' = Ac).

Glycosylation of bromide **7** with methanol using silver triflate/collidine as promoter yielded **11** in 79% yield, with complete β-anomeric specificity (as determined by 360-MHz ^{1}H nmr spectroscopy). This glycosylation was subsequently accomplished more readily and in higher yield (95%) using silver zeolite (13) as the promoter with no loss of anomeric specificity.

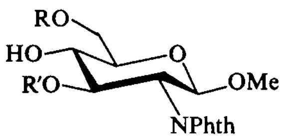

9 R = Bn; R' = Ac
10 R = Me_2tBuSi—; R = Ac

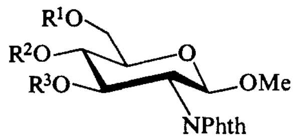

11 R' = R² = R³ = Ac
12 R' = R² = R³ = H
15 R' = R² = H; R³ = Ac
16 R' = Ac; R² = R³ = H
17 R' = Bn; R² = R³ = H
18 R' = R³ = Bn; R² = H
23 R' = R² = H; R³ = Bn

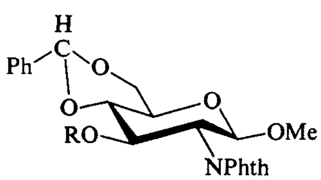

13 R = H
14 R = Ac
19 R = Bn

Zemplén deacetylation gave in 85% yield the triol **12** which after benzylidenation with α,α-dimethoxytoluene/*p*-toluenesulphonic acid gave **13** in 85% yield. Acetylation followed by hydrolysis of the benzylidene moiety gave the 3-acetyl derivative **15** in 80% yield. The structure of **15** was confirmed by its ^{1}H nmr spectrum which exhibited a signal at δ 5.63 characteristic of an acetylated H-3 (dd, J = 10.6 and 9.1 Hz).

An attempt to synthesize **9** from diol **15** using phase transfer catalysis (14) resulted in isolation of **16** formed by migration of the secondary acetate group to the primary hydroxyl group. The stannylation technique of benzylation (11) yielded only the 6-benzyl derivative **17**, as the acetate was labile under the reaction conditions. We could not obtain the 3,6-dibenzyl derivative by this procedure as has been reported previously (15) for methyl α-D-mannopyranoside.

Unable to synthesize alcohol **9** we turned our attention to alcohol **10**. Direct silylation of diol **15** with *tert*-butyldimethylsilyl chloride and imidazole in DMF gave the desired alcohol **10** in 66% yield. Attempted glycosylation of alcohol **10** with bromide **7** using silver triflate/3,4-dihydro-2*H*-pyrido[1,2-*a*]-pyridinone-2-one (11, 16) in dichloroethane was unsuccessful, presumably because of the steric encumbrance of the bulky silyl protecting group.

Stymied by our previous approaches to make monosaccharides **9** and **10** with differential protection at the 3- and 6-positions of the glycon, we felt that the synthesis of disaccharide **20** (cf. ref. 11) or **8***b*, followed by their debenzylation, would lead to diols which could be selectively fucosylated at the desired, and more accessible, primary 6-position. Acetamido groups in **20** could be a potential problem as they can form an imidate in glycosidation reactions using strong promoters (10). However, it has been shown previously that in glycosidations in which mild promoters were used, certain bases present in the reaction mixture could be responsible for the imidate formation (e.g. Hünig's base, ref. 7*c*). The avoidance of such bases, particularly when the hydroxyl group to be glycosylated is the more reactive primary one (as would be the case in the standard, bromide ion-catalyzed fucosylation (12) of an *N*,*N'*-diacetylchitobiose derivative by tri-*O*-benzyl-α-L-fucopyranosyl bromide) should therefore suppress the imidate formation.

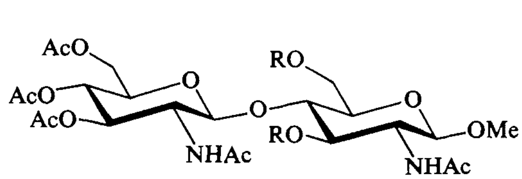

20 R = Bn
21 R = H

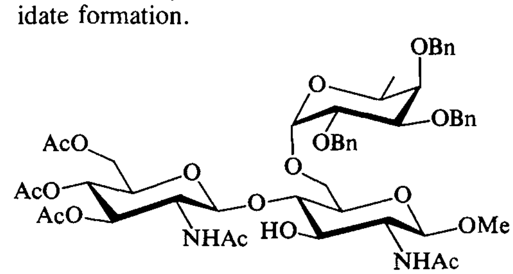

22

The synthesis of the starting alcohol **18** began from the benzylidene derivative **13** which was alkylated in 86% yield with sodium hydride and benzyl bromide in diethoxyethane to give **19** (11). Selective reduction of the benzylidene acetal in **19** using sodium cyanoborohydride (17) gave the desired alcohol **18** in 95% yield. The overall yield of **18** from **7** was 50%.

Glycosylation of alcohol **18** with bromide **7** to give the desired disaccharide **8***b* was accomplished in 46% yield using silver triflate/collidine in nitromethane. The ^{1}H nmr spectrum of **8***b* exhibited a doublet at δ 5.53, (J = 8.4 Hz, H-1) and a doublet at 4.87, (J = 8.3 Hz, H-1′). These assignments were confirmed by decoupling experiments (cf. also ref. 11).[3]

In order to synthesize the trisaccharide **3***a* starting from **8***b* we considered two approaches differing in whether the fucosylation would be performed on *N*-phthalimido or *N*-acetyl derivatives. As it as desirable to keep the number of synthetic steps after fucosylation to a minimum because, eventually, isotopically labelled fucose is to be incorporated, the latter was preferred.

Hydrazinolysis of **8***b* and subsequent acetylation gave the desired *N,N′*-diacetylchitobiose derivative **20** in 75% yield. This disaccharide was debenzylated by hydrogenolysis over palladium-on-charcoal in methanol to give diol **21**. Diol **21** was selectively fucosylated in 65% yield with 1.2 equivalents of 2,3,4-tri-*O*-benzyl-α-L-fucopyranosyl bromide (18) using the halide ion-catalyzed procedure (12), i.e., tetraethylammonium bromide and 4A molecular sieves in dichloromethane/DMF. Trisaccharide **22** was deprotected by hydrogenolysis followed by Zemplén deacetylation to give trisaccharide **3***a* in 55% yield.

The structure of **3***a* was confirmed by its ^{1}H nmr spectrum, which exhibited three anomeric doublets: δ 4.91, (J = 3.8 Hz, H-1, α-fucopyranosyl moiety), 4.64, (J = 7.6 Hz, H′) and 4.43 (J = 8.0 Hz, H-1). The broadened quartet at δ 4.13, J = 6.3 Hz and <0.5 Hz is assigned to H-5 on the fucose moiety and is characteristic for a fucose substituted at the 6-position of *N,N′*-diacetylchitobiose (19).

Synthesis of saccharides **4** and **5** began with the hydrolysis of **19** in 60% aqueous acetic acid to give diol **23** in 88% yield. The protected disaccharide **24** was prepared from **23** by taking advantage of the higher reactivity of the primary hydroxyl group in **23** towards 2,3,4-tri-*O*-benzyl-α-L-fucopyranosyl bromide **28** (18) in comparison with the secondary hydroxyl. Consequently, the use of 1.2 equivalents of **28** for shorter periods of time leads to almost exclusive formation of **24**, while 2.4 equivalents or more of **28** and prolonged reaction times yield mostly the trisaccharide derivative **25**. It is, however, easy to separate **24** from **25** by chromatography.

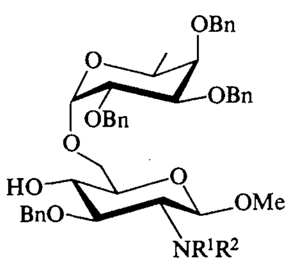

24 R¹, R² = Phth
26 R¹ = Ac, R² = H

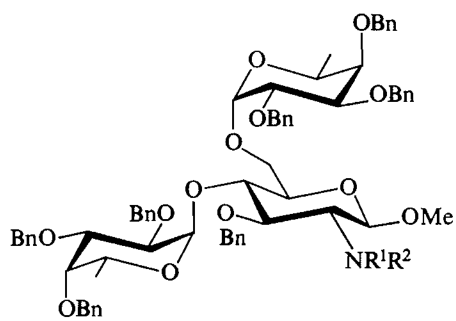

25 R¹, R² = Phth
27 R¹ = Ac, R² = H

Deprotection of both **24** and **25** by hydrazinolysis followed by *N*-acetylation and hydrogenolysis gave disaccharide **4** and trisaccharide **5**, respectively. The ^{1}H nmr spectra of **4** and **5** were in complete agreement with their structures. Thus, for example, **4** showed two anomeric proton resonances at δ 4.49 (d, J = 3.9 Hz, H-1′) and δ 4.45 (d, J = 8.5 Hz, H-1), a one-proton quartet at δ 4.14 (J = 6.5 Hz, J_2 < 0.5 Hz, H-5′), and a three-proton doublet at δ 1.23 (J = 6.6 Hz, H-6′). Similarly, **5** showed three anomeric proton resonances at δ 5.00 (J = 3.6 Hz, H-1′), 4.91 (J = 3.9 Hz, H-1″), and at 4.44 (J = 8.3, H-1), as well as two three-proton doublets at δ 1.22 and δ 1.14 (J = 6.6 Hz, H-6′ and H-6″).

Complete analysis of the nmr spectra of **3***a*, **4**, and **5** will be published elsewhere in connection with our conformational studies of these oligosaccharides.

Experimental

General methods

Melting points were determined on a Reichert Thermovar melting point apparatus and are uncorrected. Optical rotations were measured with a Perkin–Elmer polarimeter (Model 140) at 26 ± 1°C. Microanalyses were performed by the Microanalytical Laboratory Ltd., Markham, Ontario. The ^{1}H nmr spectra were recorded at 360 MHz with a Nicolet spectrometer at the Toronto Biomedical NMR Centre, University of Toronto. They were obtained at 23 ± 2°C either in $CDCl_3$ containing 1% TMS as the internal standard or in D_2O (99.996%, Merck, Sharp, and Dohme) with acetone (0.1%, 2.225 ppm relative to internal DSS) as the internal standard. FAB mass spectrometry was performed with a VG Analytical ZAB HF reverse geometry instrument (for general conditions cf. ref. 22 and references therein) at the Institute of Physiological Chemistry, University of Bonn.

Thin layer chromatography (tlc) was performed on silica gel $60F_{254}$ (Merck) plastic plates using the following solvent systems: A, hexane/ethyl acetate (1:1); B, ethyl acetate (100%); and visualized by quenching of ultraviolet fluorescence and (or) spraying with 50% aqueous sulfuric acid and heating at 100°C. Silica gel 60 (230–400 mesh; Merck was used for flash chromatography. All glycosylation reactions were performed under an argon atmosphere. All starting materials were dried overnight under vacuum (10^{-3} Torr; 1 Torr = 133.3 Pa) prior to use and all solvents were distilled from appropriate drying agents. Solutions were concentrated at water aspirator pressure unless indicated *in vacuo* (10^{-3} Torr).

The symbols ′ and ″ are used as follows:

$$\text{G}' \text{ (or F}') \xrightarrow[1,6]{1,4 \text{ or}} \text{G} \rightarrow \text{aglycon}$$

$$\begin{array}{ccccc} & & \text{F}'' & & \\ & & \downarrow{\scriptstyle 1,6} & & \\ \text{G}' & \xrightarrow{1,4} & \text{G} & \xrightarrow{1,6} & \text{aglycon} \end{array}$$

[3]Symbols used to distinguish monosaccharide units in oligosaccharides are defined in the experimental part.

$$
\begin{array}{ccccc}
 & & F' & & \\
 & & \downarrow & & \\
F'' & \xrightarrow[1,4]{} & G & \xrightarrow{1,6} & \text{aglycon}
\end{array}
$$

where G represents an *N*-acetylglucosamine unit and F represents a fucose unit.

*Methyl 3,4,5-tri-*O*-acetyl-2-deoxy-2-phthalimido-β-D-glucopyranoside (11)*

Method A

To a cooled solution (−30°C) of methanol (0.9 mL), collidine (3.0 mL; 22.9 mmol), and silver triflate (5.80 g; 22.6 mmol) in nitromethane (25 mL) was added a solution of bromide **7**[4] (9.96 g; 20.0 mmol) in nitromethane (15 mL). The reaction mixture was stirred at −30°C for 1 h (tlc monitored), warmed to room temperature, and filtered through Celite. The filtrate was washed successively with 0.5 *N* aqueous HCl, saturated aqueous $NaHCO_3$, and brine. The organic extract was dried ($MgSO_4$) and concentrated to give a yellow oil from which **11** was crystallized after dilution with hexane/ethyl acetate (1:1) as a white solid (6.15 g in two crops; 79% yield).

Method B

To a stirred mixture of silver zeolite (20 g) (ref. 13), methanol (6 mL), and dichloromethane (75 mL) was added a solution of bromide (α or β) **7** (20.4 g; 40.9 mmol) in dichloromethane (50 mL). The reaction mixture was protected from light and was stirred at room temperature for 1 h, filtered through Celite, and the filtrate was concentrated to give a syrup (18.0 g) which after recrystallization from hexane/ethyl acetate (1:1) gave microcrystalline **11** (17.0 g; 95% yield from three crops); mp 155–157°C; $[\alpha]_D$ +42.2° (*c* 1.0, chloroform) (lit. (20) mp 160.5–162.0°C; $[\alpha]_D$ +44.7° (*c* 1.1, chloroform); (lit. (21) mp 156–157°C; $[\alpha]_D$ +45.5° (*c* 3.23, chloroform)); R_f(A) 0.3; ^{1}H nmr δ: 7.75–7.90 (m, 4H, $N(CO)_2C_6H_4$), 5.78 (dd, 1H, *J* = 10.6, 9.2 Hz, H-3), 5.30 (d, 1H, *J* = 8.5 Hz, H-1), 3.45 (s, 3H, OCH_3), 2.15, 2.05, and 1.88 (s, 9H, $COCH_3$).

Methyl 2-deoxy-2-phthalimido-β-D-glucopyranoside (12)

This compound was prepared in 85% yield from triacetate **11** and sodium methoxide in methanol according to ref. 20; mp 200–202°C; $[\alpha]_D$ −9.1° (*c* 1.0, methanol) (lit. (20) mp 202.5–204.5°C; $[\alpha]_{589}$ −8.62° (*c* 1.0, methanol)); R_f(A) 0.0, (B) 0.3; ^{1}H nmr δ: 7.85–7.95 (m, 4H, $N(CO)_2C_6H_4$), 5.17 (d, 1H, *J* = 8.3 Hz, H-1), 3.43 (s, 3H, OCH_3).

*Methyl 4,6-*O*-benzylidene-2-deoxy-2-phthalimido-β-D-glucopyranoside (13)*

Compound **13** was prepared in 85% yield from triol **12**, α,α-dimethoxytoluene, and *p*-toluenesulphonic acid in acetonitrile (7). After recrystallization from hexane/ethyl acetate (1:1) a colourless microcrystalline solid was isolated; mp 192–194°C; $[\alpha]_D$ +63.2° (*c* 1.0, chloroform); R_f(A) 0.43; ^{1}H nmr δ: 7.72–7.88 (m, 4H, $N(CO)_2C_6H_4$), 7.36–7.51 (m, 5H, C_6H_5CH), 5.60 (s, 1H, CHC_6H_5CH), 5.21 (d, 1H, *J* = 8.4 Hz, H-1), 3.45 (s, 3H, OCH_3), 2.38 (s, 1H, D_2O exch., *OH*). *Anal.* calcd. for $C_{22}H_{21}NO_7$: C 64.23, H 5.14, N 3.40; found: C 64.44, H 5.20, N 3.46.

*Methyl 3-*O*-acetyl-4,6-benzylidene-2-deoxy-2-phthalimido-β-D-glucopyranoside (14)*

Acetic anhydride (12.5 mL) was mixed with a cooled solution (0°C) of **13** (5.95 g; 14.4 mol) in pyridine (25 mL) and the reaction mixture was stirred overnight at room temperature. The colourless solution was poured onto crushed ice; the separated solid was collected by filtration, and dried *in vacuo*, to give **14** as an amorphous solid (5.90 g; 90% yield); $[\alpha]_D$ +4.0° (*c* 1.0, chloroform); R_f(A) 0.46; ^{1}H nmr δ: 7.7–7.9 (m, 4H, $N(CO)_2C_6H_4$)), 7.3–7.5 (m, 5H, C_6H_5CH), 5.88 (dd, 1H, *J* = 10.2 and 9 Hz, H-3), 5.55 (s, 1H, C_6H_5CH), 5.37 (d, 1H, *J* = 8.4 Hz, H-1), 3.45 (s, 3H, OCH_3). *Anal.* calcd. for $C_{24}H_{23}NO_8$: C 63.57, H 5.11, N 3.09; found: C 63.44, H 5.26, N 3.14.

[4]This compound and some other intermediates were purchased from Toronto Research Chemicals, 100 College St., Toronto, Ont., Canada M5G 1L5.

*Methyl 3-*O*-acetyl-2-deoxy-2-phthalimido-β-D-glucopyranoside (15)*

A solution of **14** (1.05 g; 2.31 mmol) in 60% acetic acid (50 mL) was heated at 100°C for 30 min (tlc monitored). The solvent was removed *in vacuo* to give diol **15** as a colourless solid (748 mg; 88% yield). Recrystallization from hexane/ethyl acetate gave **15** as a microcrystalline solid; mp 84–86°C; $[\alpha]_D$ +74.4° (*c* 1.0, chloroform); R_f(B) 0.45; ^{1}H nmr δ: 7.85–7.95 (m, 4H, $N(CO)_2C_6H_4$), 5.63 (dd, 1H, *J* = 10.6 and 9.1 Hz, H-3), 5.30 (d, 2H, *J* = 8.4 Hz, H-1), 3.45 (s, 3H, OCH_3), 2.8 (br s, 2H, *OH*), 1.95 (s, 3H, $COCH_3$).

*Methyl 6-*O*-acetyl-2-deoxy-2-phthalimido-β-D-glucopyranoside (16)*

A solution of diol **15** (200 mg; 0.54 mmol), tetra-*n*-butylammonium hydrogen sulfate (40 mg; 0.11 mmol), and benzyl bromide (0.1 mL; 0.82 mmol) in dichloromethane was added to a solution of aqueous NaOH (1 *M*; 0.65 mL; 0.65 mmol) in water (5 mL), and heated under reflux for 16 h. The organic phase was separated, dried ($MgSO_4$), filtered, and concentrated to a colourless oil. Flash chromatography on silica gel (hexane/ethyl acetate (35:65)) gave **16** as an amorphous solid; R_f(B) 0.44; ^{1}H nmr δ: 7.85–7.95 (m, 4H, $N(CO)_2C_6H_4$), 5.15 (d, 1H, *J* = 8.4 Hz, H-1), 4.67 (dd, 1H, *J* = 12.4 and 3.5 Hz, H-6), 4.29 (dd, *J* = 12.4 and 2.2 Hz, H-6′), 3.44 (s, 3H, OCH_3), 2.05 (s, 3H, $COCH_3$).

*Methyl 6-*O*-benzyl-2-deoxy-2-phthalimido-β-D-glucopyranoside (17)*

A solution of diol **15** (200 mg; 0.55 mmol) and bis(tri-*n*-butyl tin) oxide (0.30 mL; 0.58 mmol) in toluene (8 mL) was heated under reflux with continuous removal of water for 3 h. The solution was cooled to room temperature, the solvent was removed *in vacuo*, and the residue was dissolved in benzyl bromide (5 mL) and heated at 85°C for 18 h. After processing as described (11), the colourless residual oil was purified by flash chromatography on silica gel (ethyl acetate) to give **17** as an oil; R_f(B) 0.55; ^{1}H nmr δ: 7.85–7.95 (m, 4H, $N(CO)_2C_6H_4$), 6.82–7.03 (m, 5H, $C_6H_5CH_2$), 5.15 (d, 1H, *J* = 8.4 Hz, H-1), 3.85 (m, 2H, H-6), 3.43 (s, 3H, OCH_3).

*Methyl 3-*O*-acetyl-6-*O*-(*tert*-butyl)dimethylsilyl-2-deoxy-2-phthalimido-β-D-glucopyranoside (10)*

A solution of diol **14** (560 mg; 3.83 mmol) in DMF (5 mL) containing *tert*-butyldimethylsilyl chloride (277 mg; 1.84 mmol) and imidazole (260 mg; 3.83 mmol) was stirred overnight at room temperature. The colourless solution was diluted with ether, washed successively with water and brine, dried ($MgSO_4$), filtered, and concentrated. The residual oil was purified by flash chromatography on silica gel using hexane/ethyl acetate (1:1) as eluant; a colourless solid was isolated which was crystallized from hexane/ethyl acetate (490 mg; 66% yield); mp 138.5–140°C; $[\alpha]_D$ +0.6 (*c* 1.0, chloroform); R_f(A) 0.45; ^{1}H nmr δ: 7.85–7.95 (m, 4H, $N(CO)_2C_6H_4$), 5.65 (dd, 1H, *J* = 10.7, 8.3 Hz, H-3), 5.28 (d, 1H, *J* = 8.5 Hz, H-1); 3.45 (s, 3H, OCH_3), 1.95 (s, 3H, $COCH_3$), 1.6 (s, 1H, D_2O exch., *OH*), 0.95 (s, 9H, $(CH_3)_3C$), 0.10 (s, 6H, $SiCH_3$). *Anal.* calcd. for $C_{23}H_{33}NO_8Si$: C 57.60, H 6.93, N 2.92; found: C 57.71, H 7.04, N 2.90.

*Methyl 3-*O*-benzyl-4,6-benzylidene-2-deoxy-2-phthalimido-β-D-glucopyranoside (19)*

Compound **19** was prepared in 86% yield from alcohol **13**, sodium hydride, and benzyl bromide in dimethoxyethane as described (11). Following work-up, the residual oil was crystallized from hexane/ethyl acetate (1:1); mp 124–125°C; $[\alpha]_D$ +58.0° (*c* 1.0, chloroform); R_f(A) 0.55; ^{1}H nmr δ: 7.72 (br s, 4H, $N(CO)_2C_6H_4$), 7.42–7.6 (m, 5H, C_6H_5CH), 6.85–7.05 (m, 5H, $C_6H_5CH_2$), 5.63 (s, 1H, C_6H_5CH), 5.15 (d, 1H, *J* = 8.5 Hz, H-1), 4.20 (dd, 1H, *J* = 10.4 and 8.5 Hz, H-2), 3.40 (s, 3H, OCH_3). *Anal.* calcd. for $C_{29}H_{27}NO_7$: C 69.45, H 5.43, N 2.79; found: C 69.28, H 5.23, N 2.82.

*Methyl 3,6-di-*O*-benzyl-2-deoxy-2-phthalimido-β-D-glucopyranoside (18)*

To a mixture of compound **19** (1.0 g; 2.0 mmol), powdered molecular sieves (3A Linde; 25 g), and sodium cyanoborohydride (385 mg;

6.0 mmol) in THF (50 mL) was added dropwise a saturated solution of HCl in dry diethyl ether until the gas evolution ceased (17). The reaction mixture was stirred at room temperature until the starting material completely disappeared (1 h; tlc monitored). When compound **19** was present after 1 h, a small amount of ethereal HCl was added and stirring was continued. After the work-up as described (17), a colourless oil was isolated; $[\alpha]_D$ 39.4° (*c* 1.9, chloroform); R_f(A) 0.40; ^{1}H nmr δ: 7.6–7.75 (m, 4H, $N(CO)_2C_6H_4$), 7.2–7.4 (m, 5H, $C_6H_5CH_2$), 6.9–7.1 (m, 5H, $C_6H_5CH_2$), 5.06 (d, 1H, J = 8.3 Hz, H-1) 4.23 (dd, 1H, J = 10.7 and 8.3 Hz, H-3), 4.13 (dd, 1H, J = 10.7 and 8.3 Hz, H-2), 3.38 (s, 3H, OCH_3), 2.95 (s, 1H, D_2O exch., OH). *Anal.* calcd. for $C_{29}H_{29}NO_7$: C 69.17, H 5.80, N 2.78; found: C 68.92, H 5.63, N 2.69.

Methyl 3,6-di-O-benzyl-2-deoxy-2-phthalimido-4-O-(3,4,6-tri-O-acetyl-2-deoxy-2-phthalimido-β-D-glucopyranosyl)-β-D-glucopyranoside (8b)

To a solution of silver triflate (479 mg; 1.86 mmol), collidine (0.250 mL; 1.90 mmol), and alcohol **18** (875 mL; 1.74 mmol) in dry nitromethane (5 mL) cooled to −25°C was added a solution of bromide **7** (942 mg; 1.89 mmol) in dry nitromethane (3 mL). The reaction mixture was stirred at −25°C for 4 h, allowed to warm to room temperature, and a second equivalent of silver triflate (480 mg; 1.86 mmol) and collidine (0.250 mL; 1.90 mmol) was added followed by the addition of a solution of bromide **7** (950 mg; 1.97 mmol) in nitromethane (5 mL). The reaction mixture was protected from light, stirred overnight, and then filtered through Celite. The filtrate was diluted with dichloromethane (25 mL) and washed successively with 1 *N* aqueous HCl, saturated aqueous $NaHCO_3$, and brine, dried ($MgSO_4$), filtered, and concentrated to a brown syrup (2.8 g). Further purification by flash chromatography on silica gel using hexane/ethyl acetate (1:1) gave starting alcohol **18** (470 mg) and disaccharide **8*b*** as an oil (742 mg; 46% yield); $[\alpha]_D$ −8.6, (*c* 2.1, chloroform); R_f(A) 0.26; ^{1}H nmr δ: 7.75–7.95 (m, 4H, $N(CO)_2C_6H_4$), 7.65 (br s, 4H, $N(CO)_2C_6H_4$), 7.30–7.35 (m, 5H, $C_6H_5CH_2$), 6.80–7.05 (m, 5H, $C_6H_5CH_2$), 5.79 (dd 1H, J = 11.0 and 9.0 Hz, H-3'), 5.53 (d, 1H, J = 8.4 Hz, H-1), 4.87 (d, 1H, $J_{1,2}$ = 8.3 Hz, H-1'), 3.28 (s, 3H, OCH_3), 2.00, 1.97, and 1.84 (3s, 9H, $COCH_3$). *Anal.* calcd. for $C_{49}H_{48}N_2O_{16}$: C 63.91, H 5.25, N 3.04; found: C 63.70, H 5.41, N 2.90.

Methyl 2-acetamido-4-O-(2-acetamido-3,4,6-tri-O-acetyl-2-deoxy-β-D-glucopyranosyl)-3,6-di-O-benzyl-2-deoxy-β-D-glucopyranoside (20)

A solution of disaccharide **8*b*** (248 mg; 0.27 mmol), hydrazine hydrate (85%; 2 mL), and 95% aqueous ethanol (10 mL) was gently heated under reflux for 30 min. After cooling to 0°C the reaction mixture was filtered and the filtrate was evaporated to dryness (pale yellow solid, 230 mg). The residue was dissolved in pyridine (5 mL) and acetic anhydride (2 mL) and stirred overnight at room temperature. After the usual work-up the residue was triturated with hexane/ethyl acetate (1:1), the solid **20** was isolated by filtration (75 mg), and another portion of **20** (75 mg) was isolated by concentration of the filtrate followed by crystallization from hexane/ethyl acetate (1:1). The total yield of **20** was 75%; mp 246–248°C; $[\alpha]_D$ −10.6° (*c* 1.0, methanol); R_f(B) 0.64; ^{1}H nmr δ: 7.3–7.5 (m, 10H, $C_6H_5CH_2$), 6.15 (d, 1H, J = 9 Hz, $NHCOCH_3$), 5.19 (d, 1H, J =9 Hz, $NHCOCH_3$), 4.49 (d, 1H, J = 6.0 Hz, H-1), 4.36 (d, 1H, J = 8.4 Hz, H-1'), 3.43 (s, 3H, OCH_3), and 2.09, 2.04, 2.03, 2.01, and 1.96 (5s, 15H, $COCH_3$). *Anal.* calcd. for $C_{37}H_{48}N_2O_{14}$: C 59.67, H 6.50, N 3.76; found: C 59.50, H 6.39, N 3.69.

Methyl 2-acetamido-4-O-(2-acetamido-3,4,6-tri-O-acetyl-2-deoxy-β-D-glucopyranosyl)-2-deoxy-β-D-glucopyranoside (21)

Compound **20** (300 mg; 0.40 mmol) was hydrogenolyzed over palladium-on-carbon in methanol (10 mL) at atmospheric pressure for 16 h. After the usual work-up **21** was obtained as a colourless solid (235 mg; 87% yield). This product was used without further purification; $[\alpha]_D$ −21.7° (*c* 1.0, methanol); ^{1}H nmr δ: 5.10 (t, 1H, J = 8.6 Hz, H-3'), 5.04 (t, 1H, J = 8.6 Hz, H-4'), 4.62 (d, 1H, J = 8.6 Hz, H-1'), 4.42 (d, 1H, J = 8.3 Hz, H-1), 3.48 (s, 3H, OCH_3), 2.09, 2.04, 2.03, 2.01, and 1.96 (5s, 15H, $COCH_3$). *Anal.* calcd. for $C_{23}H_{36}N_2O_{14}$: C 48.93, H 6.43, N 4.96; found: C 49.03, H 6.55, N 5.03.

Methyl 2-acetamido-4-O-(2-acetamido-3,4,6-tri-O-acetyl-2-deoxy-β-D-glucopyranosyl)-6-O-(2,3,4-tri-O-benzyl-α-L-fucopyranosyl)-2-deoxy-β-D-glucopyranoside (22)

To a mixture of diol **21** (290 mg; 0.51 mmol), tetraethylammonium bromide (323 mg; 1.53 mmol), and powdered molecular sieves (4A Linde; 1.5 g) in dry dichloromethane (5 mL) and DMF (5 mL) was added a solution of tribenzylfucopyranosyl bromide (ref. 18) (310 mg; 0.624 mmol) in dichloromethane (5 mL). After stirring at room temperature for 16 h, the solids were removed by filtration and the filtrate was washed with water, dried ($MgSO_4$), filtered, and evaporated to dryness to give an amorphous white solid (600 mg) which after trituration with hexane/ethyl acetate (1:1) gave crystalline **22** (325 mg; 65% yield); mp 258–260°C; $[\alpha]_D$ −60.3° (*c* 1.0, methanol); R_f(B) 0.14; ^{1}H nmr δ: 7.2–7.6 (m, 15H, $C_6H_5CH_2$), 6.6 (d, 1H, J = 10.5 Hz, $NHCOCH_3$), 5.42 (d, 1H, J = 10.5 Hz, $NHCOCH_3$), 4.69 (d, 1H, J = 3.5 Hz, H-1''), 4.41 (d, 1H, J = 8.6 Hz, H-1'), 4.30 (d, 1H, J = 8.3 Hz, H-1), 3.41 (s, 3H, OCH_3), 2.09 (s, 3H, $COCH_3$), 2.0 (s, 6H, $COCH_3$), 2.02 (s, 3H, $COCH_3$), 1.77 (s, 3H, $COCH_3$), 1.12 (d, 3H, J = 6.4 Hz, H-6''). *Anal.* calcd. for $C_{50}H_{64}N_2O_{18}$: C 61.21, H 6.58, N 2.85; found: C 61.09, H 6.73, N 2.92.

Methyl 2-acetamido-4-O-(2-acetamido-2-deoxy-β-D-glucopyranosyl)-2-deoxy-6-O-(α-L-fucopyranosyl)-β-D-glucopyranoside (3a)

Compound **21** (280 mg; 0.48 mmol) was debenzylated by hydrogenolysis as described for **22**. The product was de-*O*-acetylated with sodium methoxide in methanol and neutralized with 10% aqueous acetic acid. Following evaporation of the solvent, the residue was dissolved in distilled water and passed through a column (150 mm × 15 mm) of mixed bed resin (BioRad AG501-X8). Trisaccharide **3*a*** was isolated as a white crystalline solid (85 mg, 55% yield). Recrystallization from ethanol/water gave an analytical sample; mp 298–300°C (dec.); $[\alpha]_D$ −4.3° (*c* 0.57, H_2O); ^{1}H nmr δ: 4.91 (d, 1H, J = 8.0 Hz, H-1''), 4.64 (d, 1H, J = 7.6 Hz, H-1'), 4.43 (d, 1H, J = 8.0 Hz, H-1), 4.13 (br q, 1H, J = 6.5, J_2 < 0.5 Hz, H-5''), 2.08 (s, 3H, $COCH_3$), 2.03 (s, 3H, $NHCOCH_3$), 1.23 (d, 3H, J = 6.6 Hz, H-6''); *m/e*: 583, $(M - 1)^-$. *Anal.* calcd. for $C_{23}H_{40}N_2O_{15}$: C 47.25, H 6.90, N 4.79; found: C 47.19, H 6.82, N 4.83.

Methyl 3-O-benzyl-2-deoxy-2-phthalimido-β-D-glucopyranoside (23)

A solution of **19** (4.10 g; 8.15 mmol) in 60% aqueous acetic acid (50 mL) was heated at 100°C for 30 min (tlc monitored). The solvents were removed *in vacuo* to give diol **23** accompanied by a small amount of the 6-acetate derivative. Pure **23** was obtained by flash chromatography on silica gel using ethyl acetate as a microcrystalline solid (2.90 g; 88% yield); mp 120.5–122°C; $[\alpha]_D$ +57.2° (*c* 1.0, chloroform); R_f(A) 0.12; ^{1}H nmr δ: 7.75 (br s, 4H, $N(CO)_2C_6H_4$), 7.0–7.15 (m, 5H, $C_6H_5CH_2$), 5.10 (d, 1H, J = 8.4 Hz, H-1), 3.40 (s, 3H, OCH_3). *Anal.* calcd. for $C_{22}H_{23}NO_7$: C 63.92, H 5.61, N 3.39; found: C 63.78, H 5.80, N 3.34.

Methyl 3-O-benzyl-2-deoxy-2-phthalimido-6-O-(2,3,4-tri-O-benzyl-α-L-fucopyranosyl)-β-D-glucopyranoside (24)

To a mixture of diol **23** (450 mg; 1.09 mmol), tetraethylammonium bromide (1.14 g; 5.4 mmol), and powdered molecular sieves (4A Linde; 2.5 g) in dichloromethane (10 mL) was added a solution of tribenzylfucosyl bromide (ref. 18) (650 mg; 1.3 mmol) in dichloromethane (5 mL). The reaction mixture was stirred at room temperature for 6 h and filtered through Celite. The filtrate was washed with water, dried ($MgSO_4$), filtered, and concentrated to give a colourless oil (1.2 g). Flash chromatography on silica gel (hexane/ethyl acetate (2:1)) gave **24** as a colourless oil (380 mg; 42% yield); $[\alpha]_D$ −7.0° (*c* 0.86, chloroform); R_f(A) 0.42; ^{1}H nmr δ: 7.6–7.8 (m, 4H, $N(CO)_2C_6H_4$), 7.2–7.6 (m, 15H, $C_6H_5CH_2$), 6.9–7.1 (m, 5H, $C_6H_5CH_2$), 5.01 (d, 1H, J = 8.4 Hz, H-1) 4.82 (d, 1H, J = 4.4 Hz, H-1'), 3.33 (s, 3H, OCH_3), 1.16 (d, 1H, J = 6.5 Hz, H-5'). *Anal.* calcd. for $C_{49}H_{51}NO_{11}$: C 70.91, H 6.19, N 1.69; found: C 70.80, H 6.22, N 1.73.

Methyl 3-O-benzyl-2-deoxy-2-phthalimido-4,6-di-O-(2,3,4-tri-O-benzyl-α-L-fucopyranosyl)-β-D-glucopyranoside (25)

To a mixture of diol **23** (625 mg; 1.51 mmol), tetraethylammonium bromide (1.59 g; 7.57 mmol), and powdered freshly activated molecular sieves (4A Linde; 1.50 g) in dichloromethane (10 mL) was added a solution of tribenzylfucosyl bromide (ref. 18) (1.45 g; 2.91 mmol) in dichloromethane (5 mL). The reaction mixture was stirred overnight at room temperature and filtered through Celite. The filtrate was washed with water, dried ($MgSO_4$), filtered, and concentrated to 2.2 g of a brown oil. Flash chromatography on silica gel using hexane/ethyl acetate (2:1) as eluant gave two major fractions. The more polar fraction, R_f(A) 0.42, was disaccharide **24** (365 mg; 30% yield).

The less polar fraction, R_f(A) 0.61, was trisaccharide **25** (425 mg) as a colourless oil; $[\alpha]_D$ −38.2° (*c* 0.6, chloroform); ^{1}H nmr δ: 7.6–7.8 (m, 4H, $N(CO)_2C_6H_4$), 7.2–7.5 (m, 30H, $C_6H_5CH_2$), 7.0 (m, 5H, $C_6H_5CH_2$), 5.35 (d, 1H, *J* = 3.2 Hz, H-1), 3.26 (s, 3H, OCH_3), 1.04 (d, 3H, *J* = 6.5 Hz, H-6′ or H-6″), 0.82 (d, 3H, *J* = 6.5 Hz, H-6′ or H-6″). *Anal.* calcd. for $C_{76}H_{79}NO_{15}$: C 73.23, H 6.39, N 1.12; found: C 73.11, H 6.45, N 1.01.

Methyl 2-acetamido-3-O-*benzyl-2-deoxy-6-*O-*(2,3,4-tri-*O-*benzyl-α-L-fucopyranosyl)-β-D-glucopyranoside (26)*

A solution of **24** (250 mg; 0.31 mmol) and hydrazine hydrate (85%; 2 mL) in 95% aqueous ethanol (10 mL) was gently heated under reflux for 20 min. The reaction mixture was concentrated to dryness to give a non-crystalline yellowish residue which was dissolved in a mixture of 50% aqueous methanol (10 mL) and acetic anhydride (3 mL) and sitrred at room temperature overnight. The precipitate which formed was isolated by filtration and dried *in vacuo* to give crystalline **26** (133 mg; 60% yield); mp 197–200°C; $[\alpha]_D$ −44.5° (*c* 0.7, chloroform); R_f(B) 0.48; ^{1}H nmr δ: 7.2–7.5 (m, 20H, $C_6H_5CH_2$), 5.37 (d, 1H, *J* = 9 Hz, N*H*COCH$_3$, 3.42 (s, 3H, OCH_3), 1.90 (s, 3H, $NHCOCH_3$), 1.17 (d, 3H, *J* = 6.5 Hz, H-6′). *Anal.* calcd. for $C_{43}H_{51}NO_{10}$: C 69.61, H 6.94, N 1.89; found: C 69.82, H 7.11, N 1.94.

*Methyl 2-acetamido-2-deoxy-6-*O-*(α-L-fucopyranosyl)-β-D-glucopyranoside (4)*

Compound **26** (210 mg; 0.28 mmol) was stirred with 10% palladium-on-charcoal (50 mg) in 75% aqueous methanol (10 mL) under hydrogen (1 atm (= 101.3 kPa)) for 18 h. Following filtration through Celite the filtrate was concentrated *in vacuo* and the resulting colourless solid was dissolved in water and passed through a column (150 mm × 15 mm) of mixed bed resin (BioRad AG501-X8) to give a desalted solution of disaccharide **4**. Pure **4** was obtained following lyophilization as an amorphous solid (89 mg; 83% yield); $[\alpha]_D$ −20.6° (*c* 0.38; H_2O); ^{1}H nmr δ: 4.94 (d, 1H, *J* = 3.9 Hz, H-1′), 4.45 (d, 1H, *J* = 8.5 Hz, H-1), 4.14 (br q, 1H, *J* = 6.5, J_2 < 0.5 Hz, H-5′), 3.50 (s, 3H, OCH_3), 2.04 (s, 3H, $NHCOCH_3$), 1.23 (d, 3H, *J* = 6.5 Hz, H-6′); *m*/*e*: 380 $(M-1)^-$. *Anal.* calcd. for $C_{15}H_{27}NO_{10}$: C 47.24, H 7.14, N 3.69; found: C 7.01, H 7.02, N 3.58.

*Methyl 2-acetamido-3-*O-*benzyl-2-deoxy-4,6-di-*O-*(2,3,4-tri-*O-*benzyl-α-D-fucopyranosyl)-β-D-glucopyranoside (27)*

A solution of compound **25** (248 mg; 0.21 mmol) and hydrazine hydrate (85%; 1 mL) in 95% aqueous ethanol (5 mL) was gently heated under reflux for 20 min. The reaction mixture was evaporated to dryness *in vacuo* and the resulting yellow amorphous residue was treated at room temperature with pyridine (5 mL) and acetic anhydride (1 mL). After the usual work-up a colourless oil (220 mg) was isolated. Flash chromatography on silica gel using hexane/ethyl acetate (2:3) gave **27** as a colourless oil (110 mg; 48% yield); $[\alpha]_D$ −41.5° (*c* 1.0, chloroform); R_f(A) 0.25; ^{1}H nmr δ: 7.1–7.5 (m, 35H, $C_6H_5CH_2$), 6.29 (d, 1H, *J* = 9.2 Hz, N*H*COCH$_3$, 5.29 (d, 1H, *J* = 3.1 Hz, H-1), 3.38 (s, 3H, OCH_3), 1.63 (s, 3H, $NHCOCH_3$), 1.03 (d, 3H, *J* = 6.4 Hz, H-6′ or H-6″), 0.96 (d, 3H, *J* = 6.4 Hz, H-6′ or H-6″).

*Methyl 2-acetamido-2-deoxy-4,6-di-*O-*(α-L-fucopyranosyl-β-D-glucopyranoside (5)*

Compound **27** (200 mg; 0.17 mmol) was deprotected to give **5** in a similar manner as it was used to prepare **4**. Trisaccharide **5** was a colourless amorphous solid (77 mg; 85% yield); $[\alpha]_D$ −3.8° (*c* 0.63, H_2O); ^{1}H nmr δ: 5.00 (d, 1H, *J* = 3.6 Hz, H-1′ or H-1″), 4.91 (d, 1H, *J* = 3.9 Hz, H-1′ or H-1″), 4.44 (d, 1H, *J* = 8.3 Hz, H-1), 4.34 (br q, 1H, *J* = 6.6 Hz, H-5′ or H-5″), 4.13 (br q, 1H, *J* = 6.6 Hz, H-5′ or H-5″), 3.49 (s, 3H, OCH_3), 1.22 (d, 3H, *J* = 6.6 Hz, H-6′ or H-6″), 1.14 (d, 3H, *J* = 6.6 Hz, H-6′ or H-6″).

Acknowledgements

This work was in part supported by grants from the Medical Research Council of Canada (to J.P.C.). We thank Dr. R. U. Lemieux for discussions of some aspects of this work. Our thanks are due also to Dr. A. A. Grey for help in interpretation of some nmr spectra, Mr. A. Lee for recording the nmr spectra, and Dr. H. Egge for the mass spectra. We also thank Dr. G. O. Aspinall for use of the polarimeter and Mr. Jose Baptista for measuring the optical rotations.

1. J. MONTREUIL. Adv. Carbohydr. Chem. Biochem. **37**, 157 (1980).
2. R. U. LEMIEUX, K. BOCK, L. T. J. DELBAERE, S. KOTO, and V. S. RAO. Can. J. Chem. **58**, 631 (1980).
3. R. U. LEMIEUX, D. A. BAKER, W. M. WEINSTEIN, and C. M. SWITZER. Biochemistry, **20**, 199 (1981).
4. F. M. WINNIK, J.-R. BRISSON, J. P. CARVER, and J. J. KREPINSKY. Carbohydr. Res. **103**, 15 (1982).
5. F. M. WINNIK, J. P. CARVER, and J. J. KREPINSKY. J. Org. Chem. **47**, 2701 (1982).
6. S. OGURI and S. TEJIMA. Chem. Pharm. Bull. **29**, 1629 (1981).
7. (*a*) R. U. LEMIEUX, T. TAKEDA, and B. Y. CHUNG. Am. Chem. Soc. Symp. Ser. **39**, 90 (1976); (*b*) R. U. LEMIEUX, S. Z. ABBAS, and B. Y. CHUNG. Can. J. Chem. **60**, 58 (1982); (*c*) O. HINDSGAUL, T. NORBERG, J. LEPENDU, and R. U. LEMIEUX. Carbohydr. Res. **109**, 109 (1982).
8. H. PAULSEN. Angew. Chem. Int. Ed. Engl. **21**, 155 (1982).
9. S. KOTO, N. MORISHIMA, and S. ZEN. J. Synth. Org. Chem. Jpn. **41**, 691 (1983).
10. (*a*) J.-R. POUGNY, U. KRASKA, and P. SINAY. Carbohydr. Res. **60**, 383 (1978); (*b*) U. KRASKA, J.-R. POUGNY, and P. SINAY. Carbohydr. Res. **50**, 181 (1976).
11. T. OGAWA, S. NAKABAYSHI, and K. SASAJIMA. Carbohydr. Res. **96**, 29 (1981).
12. R. U. LEMIEUX, K. B. HENDRIKS, R. V. STICK, and R. JAMES. J. Am. Chem. Soc. **97**, 4056 (1975).
13. P. J. GAREGG and P. OSSOWSKI. Acta Chem. Scand. Ser. B, **37**, 249 (1983).
14. P. J. GAREGG, T. IVERSEN, and S. OSCARSON. Carbohydr. Res. **50**, C12 (1976).
15. J. ARNARP and J. LONNGREN. J. Chem. Soc. Perkin Trans. 1, 2070 (1981).
16. T. MUKAIYAMA, Y. AIKAWA, and S. KOBAYASHI. Chem. Lett. 57 (1976).
17. (*a*) P. J. GAREGG, H. HULTBERG, and S. WALLIN. Carbohydr. Res. **108**, 97 (1982); (*b*) P. J. GAREGG, H. HULTBERG, and S. OSCARSON. J. Chem. Soc. Perkin Trans. 1, 2395 (1982).
18. M. DEJTER-JUSZYNSKI and H. M. FLOWERS. Carbohydr. Res. **18**, 219 (1971).
19. (*a*) J. F. G. VLIEGENTHART, L. DORLAND, and H. VAN HALBEEK. Adv. Carbohydr. Chem. Biochem. **41**, 209 (1983); (*b*) A. A. GREY, S. NARASIMHAN, J.-R. BRISSON, H. SCHACHTER, and J. P. CARVER. Can. J. Biochem. **60**, 1123 (1982).
20. D. R. BUNDLE and S. JOSEPHSON. Can. J. Chem. **58**, 2679 (1980).
21. S. AKLYA and T. OSAWA. Chem. Pharm. Bull. (Tokyo) **8**, 583 (1960).
22. H. EGGE, J. PETTER-KATALINIC, J. PAZ-PARENTE, G. STRECKER, J. MONTREUIL, and B. FOURNET. FEBS Lett. **156**, 357 (1983).
23. F. M. WINNIK, J. P. CARVER, and J. J. KREPINSKY. J. Labelled Compd. Radiopharm. **20**, 983 (1983).

Thermodynamic properties of the dilute solutions of silver chloride and aluminum trichloride in alkali chlorides by electromotive force measurements

P. J. TUMIDAJSKI AND S. N. FLENGAS

Department of Metallurgy and Materials Science, University of Toronto, Toronto, Ont., Canada M5S 1A4

Received March 5, 1984

P. J. TUMIDAJSKI and S. N. FLENGAS. Can. J. Chem. **63**, 1080 (1985).

Thermodynamic data for dilute solutions of AgCl and $AlCl_3$ in molten alkali chlorides were derived from the emf's of formation and of galvanic cells, respectively, given as, Ag/AgCl – ACl/C,Cl_2 and Ag/AgCl – ACl//$AlCl_3$ – ACl/Al. ACl represents NaCl, KCl, CsCl, or the equimolar mixtures of NaCl–CsCl and KCl–CsCl. It was found that the thermodynamic properties of the ternary melts could be predicted from the results of the binary melts using the relationship (17, 20, 21), $(\overline{\Delta Z})_{123} = (1 - t)\,(\overline{\Delta Z})_{12} + t(\overline{\Delta Z})_{13}$, where Z represents any partial molar property. The ternary solution is denoted by the subscript 1, 2, 3 while the two binaries are denoted by 1, 2 and 1, 3; t is a concentration variable given as $t = X_3/(X_2 + X_3)$. These expressions are valid when the binary and the ternary solutions have the same content of either AgCl or $AlCl_3$, respectively.

P. J. TUMIDAJSKI et S. N. FLENGAS. Can. J. Chem. **63**, 1080 (1985).

En se basant sur les fem de formation et des cellules galvaniques Ag/AgCl – ACl/C, Cl_2 et Ag/AgCl – ACl//$AlCl_3$ – ACl/Al dans lesquelles ACl représente NaCl, KCl, CsCl ou des mélanges équimolaires de NaCl–CsCl ou de KCl–CsCl, on a évalué les données thermodynamiques de solutions diluées de AgCl et de $AlCl_3$ dans des chlorures alcalins fondus. On a trouvé que l'on peut prédire les propriétés thermodynamiques des sels ternaires fondus en se basant sur les résultats obtenus avec des sels binaires fondus et en utilisant la relation (17, 20, 21) $(\overline{\Delta Z})_{123} = (1 - t)\,(\overline{\Delta Z})_{12} + t(\overline{\Delta Z})_{13}$, où Z représente n'importe quelle propriété molaire partielle. On utilise les indices 1, 2, 3 pour désigner la solution ternaire et les indices 1, 2 et 1, 3 pour désigner les deux solutions binaires; t est une variable de concentration que l'on représente par $t = X_3/(X_2 + X_3)$. Ces expressions sont valables quand les solutions ternaires contiennent chacune des quantités semblables de AgCl ou de $AlCl_3$.

[Traduit par le journal]

Introduction

The thermodynamic properties of the solutions of AgCl or $AlCl_3$ in alkali chloride melts have been the subject of several studies. For the former, the systems investigated include the binary solutions of AgCl–NaCl (1–3), AgCl–KCl (1, 3, 4), AgCl–CsCl (1, 3) and AgCl–RbCl (3), and the ternary solutions of AgCl–LiCl–KCl (5, 6), AgCl–NaCl–KCl (3), and AgCl–NaCl–CsCl (3). For the case of $AlCl_3$, the following systems have been studied: $AlCl_3$–NaCl (7–12), $AlCl_3$–KCl (7), $AlCl_3$–RbCl (7), $AlCl_3$–CsCl (7), and $AlCl_3$–NaCl–KCl (13). These measurements were taken with concentrated solutions of AgCl or $AlCl_3$. The behaviour of dilute solutions of AgCl or $AlCl_3$ where Henry's law is expected to be valid have not yet been investigated. The thermodynamic properties of the dilute solutions of AgCl in the binary systems AgCl–NaCl, AgCl–KCl, AgCl–CsCl, and in the ternary systems AgCl–NaCl–CsCl and AgCl–KCl–CsCl have been obtained from emf measurements on formation cells of the type, Ag/AgCl – ACl/C,Cl_2. The thermodynamic properties of the dilute solutions of $AlCl_3$ in the binary systems $AlCl_3$–NaCl, $AlCl_3$–KCl, $AlCl_3$–CsCl, and in the ternary systems $AlCl_3$–NaCl–CsCl and $AlCl_3$–KCl–CsCl have been obtained from emf measurements on galvanic cells of the type Al/$AlCl_3$ – ACl//AgCl – ACl/Ag. For both cells, ACl represents the salt components NaCl, KCl, CsCl, or the equimolar mixtures of NaCl–CsCl and KCl–CsCl.

Experimental

The AgCl and alkali chlorides used were reagent grade and were purified and dehydrated by treatment in an anhydrous HCl atmosphere at 673 K. The $AlCl_3$ was anhydrous of reagent grade. Iron contaminants were removed by vacuum sublimation. Aluminum trichloride was introduced into the alkali chloride salt by reacting an excess of the $AlCl_3$ vapor with a known quantity of alkali chloride in a two compartment non-isothermal cell described in detail elsewhere (14). The reaction is $AlCl_{3(g)} + ACl = A(AlCl_4)_{(l)}$. The weight gain of ACl following the reaction yields the exact stoichiometry of the product. Furthermore, A($AlCl_4$) type compounds have a lower decomposition vapor pressure compared to pure $AlCl_3$ (8, 15). Weighing, handling, and transfer of all chemicals were conducted in a drybox filled with anhydrous argon gas. All graphite used in the experiments was high density, research grade graphite (Aremco), and it was purified by chlorine treatment at 1273 K, as described previously (16, 17).

The design of the electrochemical cells employed in the present investigation are given in Figs. 1 and 2 for the AgCl and $AlCl_3$ systems, respectively. For the AgCl experiments, the cell consisted of the Ag indicator electrode and the Cl_2 gas reference electrode. The half cell compartments were separated by a diaphragm consisting of an asbestos fibre fused in quartz (16). The $AlCl_3$ cell contained the Al indicator electrode and the Ag/AgCl secondary reference electrode. The half cell compartments were separated by the asbestos diaphragm described previously.

At the beginning of a run, the appropriate weights of salts were transferred to the respective electrode compartments. Then the cell was heated in a furnace for 24 h while anhydrous argon gas passed over the salts to remove any remaining traces of moisture. Afterwards, the temperature was gradually raised above the melting point of the salts and emf measurements begun. After 2 h the emf's became stable and the potentials recorded. Reversibility was confirmed by temperature cycling and by polarization tests. For the latter, 1 mA was passed through the cell in each direction using an external dc source. After disconnecting the dc source, in each case the cell emf returned to the original value in less than 1 min. Cell emf's were stable and reproducible to within ±1 mV within the 24 h required for each run. The adjustment to the cell emf for the Ag—C thermoelectric potential was established by connecting the Ag and C electrode tips in the absence of the electrolyte and measuring the resulting emf.

The spontaneous reaction for the silver chloride formation cell is

$$Ag_{(s)} + \tfrac{1}{2}Cl_{2(g,\,1\,atm)} = \underline{AgCl}$$

The line under a salt species denotes a species in solution. The corresponding Nernst equation is:

$$[1] \qquad E_{cell} = E^0_{AgCl} - \frac{RT}{F}\ln\,(X_{AgCl}) - \frac{RT}{F}\ln\,(\gamma_{AgCl})$$

where E^0_{AgCl} is the standard formation cell potential of pure liquid AgCl. The values of E^0_{AgCl} used in this investigation were determined

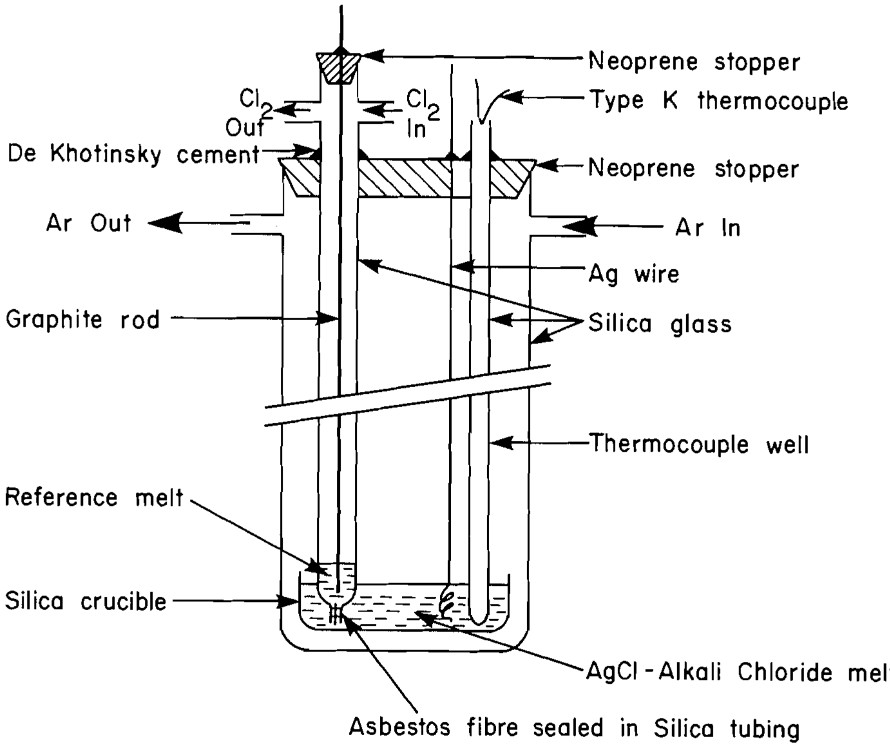

FIG. 1. Experimental cell for the AgCl experiments.

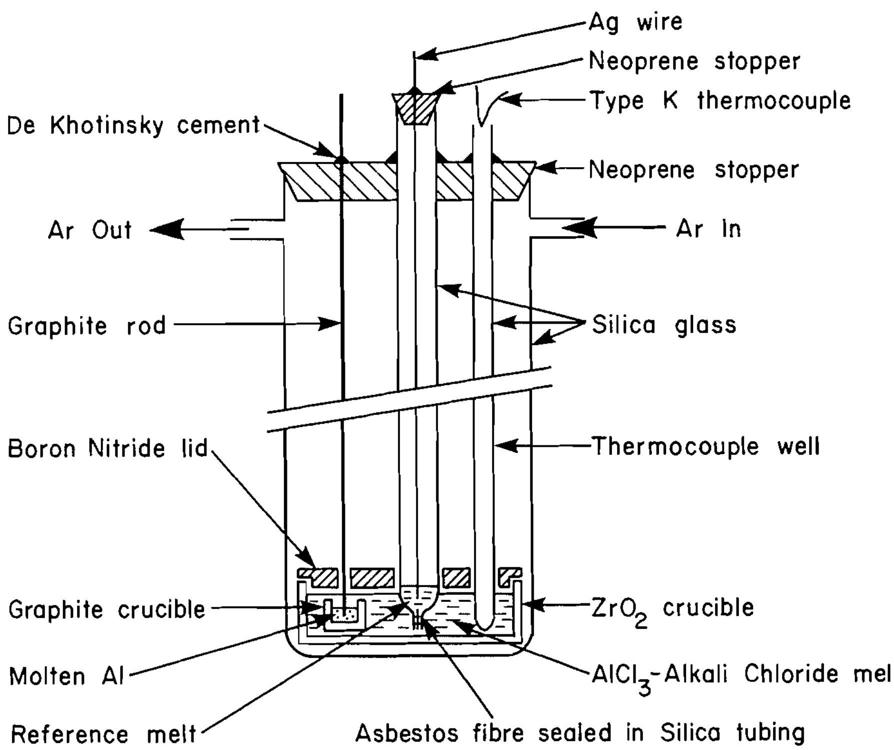

FIG. 2. Experimental cell for the $AlCl_3$ experiments.

previously in this laboratory (1). F is the Faraday's constant given as 96 487 J/V mol and R is the gas constant given as 8.3144 J/mol K. The standard state was chosen to be the pure liquid AgCl at the temperature of the experiments. For dilute compositions of AgCl, where Henry's law is expected to be valid, γ^{h}_{AgCl} should be constant. Accordingly, the formal potential of AgCl is defined as:

$$[2] \qquad E^{0}_{f(AgCl)} = E^{0}_{AgCl} - \frac{RT}{F} \ln (\gamma^{h}_{AgCl})$$

The final form of eq. [1] is

$$[3] \qquad E_{cell} = E^{0}_{f(AgCl)} - \frac{RT}{F} \ln (X_{AgCl})$$

and the plot of E_{cell} against log (X_{AgCl}) should be linear, having a slope of $2.303RT/F$, and an intercept equal to $E^{0}_{f(AgCl)}$.

The spontaneous cell reaction for the Al–Ag galvanic cell is

$$Al_{(l)} + 3\underline{AgCl} = \underline{AlCl_3} + 3Ag_{(s)}$$

TABLE 1. E_{cell} versus temperature for the AgCl systems

Solvent	X_{AgCl}	$E = AT + B$ (V)		C coeff.	Range (K)
		$A \times 10^4$	B		
NaCl	1.31×10^{-3}	3.781	0.987	0.994	1089–1178
(t = 0)	1.00×10^{-2}	0.671	1.126	0.965	1078–1183
	5.00×10^{-2}	−1.590	1.229	−0.991	1095–1176
	1.00×10^{-1}	−1.066	1.107	−0.996	1065–1180
KCl	1.14×10^{-3}	2.782	1.177	0.973	1079–1175
(t = 0)	9.89×10^{-3}	0.966	1.190	0.991	1058–1182
	5.00×10^{-2}	−0.878	1.230	−0.987	1020–1177
	1.00×10^{-1}	−4.056	1.557	−0.942	1040–1169
CsCl	5.15×10^{-3}	−1.853	1.709	−0.999	969–1172
(t = 1)	1.02×10^{-2}	−3.979	1.799	−0.997	965–1169
	4.98×10^{-2}	−0.788	1.295	−0.993	952–1178
	1.00×10^{-1}	0.953	1.065	0.974	1010–1171
NaCl–CsCl*	1.35×10^{-3}	2.035	1.234	0.998	981–1170
(t = 1/2)	1.05×10^{-2}	0.917	1.199	0.969	981–1173
	5.00×10^{-2}	−1.784	1.328	−9.968	984–1183
	1.00×10^{-1}	−1.403	1.221	−0.981	983–1176
KCl–CsCl*	5.22×10^{-3}	0.851	1.331	0.996	999–1173
(t = 1/2)	1.05×10^{-2}	−1.532	1.498	−0.999	975–1160
	5.06×10^{-2}	−0.734	1.254	−0.986	974–1159
	1.06×10^{-1}	−1.826	1.316	−0.997	982–1171

* Equimolar.

TABLE 2. E_{cell} versus temperature for the $AlCl_3$ systems

Solvent	X_{AlCl_3}	X_{AgCl}	$E = AT + B$ (V)		C coeff.	Range (K)
			$A \times 10^4$	B		
NaCl	1.00×10^{-1}	1.01×10^{-1}	−8.095	1.801	−0.998	1076–1193
(t = 0)	4.97×10^{-2}	5.03×10^{-2}	−8.373	1.790	−0.999	1088–1197
	1.03×10^{-2}	1.19×10^{-2}	−8.643	1.734	−0.999	1100–1203
	1.04×10^{-3}	1.63×10^{-3}	−9.062	1.667	−0.998	1077–1188
KCl	1.01×10^{-1}	1.00×10^{-1}	−7.542	1.677	−0.999	1051–1191
(t = 0)	5.00×10^{-2}	4.97×10^{-2}	−7.991	1.686	−0.999	1061–1186
	1.00×10^{-2}	1.23×10^{-2}	−8.715	1.689	−0.998	1058–1190
	1.00×10^{-3}	5.17×10^{-3}	−8.870	1.697	−0.999	1055–1196
CsCl	1.02×10^{-1}	9.45×10^{-2}	−7.153	1.573	−0.994	998–1189
(t = 1)	4.97×10^{-2}	4.78×10^{-2}	−7.866	1.611	−0.999	986–1203
	9.99×10^{-3}	2.28×10^{-2}	−7.739	1.579	−0.997	1001–1179
	5.39×10^{-3}	4.65×10^{-3}	−9.202	1.606	−0.999	993–1169
NaCl–CsCl*	9.50×10^{-2}	1.00×10^{-1}	−7.744	1.710	−0.999	997–1188
(t = 1/2)	4.93×10^{-2}	4.89×10^{-2}	−8.180	1.710	−0.999	1003–1193
	1.02×10^{-2}	1.50×10^{-2}	−8.859	1.719	−0.999	993–1205
	5.15×10^{-3}	5.00×10^{-3}	−9.620	1.718	−0.999	982–1205
KCl–CsCl*	1.01×10^{-1}	1.06×10^{-1}	−7.517	1.658	−0.999	1005–1200
(t = 1/2)	4.98×10^{-2}	5.15×10^{-2}	−7.869	1.647	−0.999	1004–1179
	1.01×10^{-2}	1.25×10^{-2}	−8.427	1.621	−0.999	988–1193
	5.17×10^{-3}	5.00×10^{-3}	−8.938	1.607	−0.999	990–1198

* Equimolar.

The Nernst equation is

[4] $$E_{cell} = (E^0_{AlCl_3} - E^0_{AgCl}) - \frac{RT}{3F}\ln(X_{AlCl_3}/X^3_{AgCl}) - \frac{RT}{3F}\ln(\gamma_{AlCl_3}/\gamma^3_{AgCl})$$

where $E^0_{AlCl_3}$ is the standard formation cell potential of pure liquid $AlCl_3$. The values of $E^0_{AlCl_3}$ were available at 500 K from the thermochemical tables (18), and were calculated at higher temperatures assuming a temperature independent specific heat capacity. The uncertainty in $E^0_{AlCl_3}$ values is estimated to be ±5%. The standard state was chosen to be the pure molten chloride at the temperature of the experiments. For dilute solutions obeying Henry's law, $\gamma^h_{AlCl_3}$ and γ^h_{AgCl} are expected to be constant, and the formal potential should be:

[5a] $$E^0_{f(cell)} = E^0_{AlCl_3} - E^0_{AgCl} - \frac{RT}{3F}\ln(\gamma^h_{AlCl_3}/(\gamma^h_{AgCl})^3)$$

or

TABLE 3. Formal potentials for the AgCl systems*

System	$E^0_{f(AgCl)}$ (±0.002 V) 1073 K Expt.	1073 K Theor.	1123 K Expt.	1123 K Theor.	1173 K Expt.	1173 K Theor.
NaCl	−0.780		−0.758		−0.735	
KCl	−0.895		−0.870		−0.851	
CsCl	−0.950		−0.931		−0.910	
NaCl–CsCl†	−0.868	−0.865	−0.853	−0.845	−0.825	−0.823
KCl–CsCl†	−0.911	−0.923	−0.890	−0.901	−0.869	−0.880
NaCl–KCl‡	−0.820	−0.838	−0.807	−0.814	−0.795	−0.793

*These potentials represent the overall cell reaction, $(AgCl)_{X=1,\text{ but at an infinitely diluted thermodynamic state}} = Ag_{(s)} + (1/2)Cl_{2(g,\ 1\ atm)}$.
† Equimolar.
‡ Reference 16.

TABLE 4. Formal potentials for the $AlCl_3$ systems*

System	$E^0_{f(AlCl_3)}$ (±0.003 V) 1073 K Expt.	1073 K Theor.	1123 K Expt.	1123 K Theor.	1173 K Expt.	1173 K Theor.
NaCl	−1.853		−1.805		−1.758	
KCl	−1.874		−1.827		−1.780	
CsCl	−1.912		−1.860		−1.807	
NaCl–CsCl*	−1.873	−1.883	−1.822	−1.833	−1.771	−1.783
KCl–CsCl*	−1.896	−1.894	−1.845	−1.844	−1.794	−1.794

*These potentials represent the overall cell reaction, $(AlCl_3)_{X=1,\text{ but at an infinitely diluted thermodynamic state}} = Al_{(l)} + (3/2)Cl_{2(g,\ 1\ atm)}$.
† Equimolar.

$$[5b]\quad E^0_{f(cell)} = E^0_{f(AlCl_3)} - E^0_{f(AgCl)}$$

where $E^0_{f(AgCl_3)}$ and $E^0_{f(AgCl)}$ are the formal potentials of $AlCl_3$ and AgCl respectively. Thus, eq. [4] can be written as

$$[6]\quad E_{cell} = E^0_{f(cell)} - \frac{RT}{3F}\ln\left(X_{AlCl_3}/X^3_{AgCl}\right)$$

Plotting E_{cell} against log (X_{AlCl_3}/X^3_{AgCl}), a straight line should be obtained with a slope of $-2.303RT/3F$ and an intercept equal to $E^0_{f(cell)}$. It should be mentioned that the formal potentials of eqs. [2] and [5] represent the free energy of a hypothetical state of unit mole fraction of solute, having in all respects the properties of the solute at its state in an infinitely diluted solution.

Results and discussion

Tables 1 and 2 summarize the measured cell emf's which have been expressed as least-squares lines of the form $E = AT + B$, where E is cell potential in V, and T is the temperature in K. Cell emf's have been corrected for the thermo-electric effects of Ag and C. Melt compositions are expressed in mole fractions of AgCl and $AlCl_3$, respectively. For ternary solutions, the composition variable t has been defined as

$$[7a]\quad t = X_{CsCl}/(X_{CsCl} + X_{NaCl})$$

or

$$[7b]\quad t = X_{CsCl}/(X_{CsCl} + X_{KCl})$$

The correlation coefficients in Tables 1 and 2 indicate that the plots of cell potential versus temperature should be linear. The estimate for the standard deviation of cell potential for the regression of cell potential on temperature is approximately 4 mV for all cases.

Nernst plots for the five AgCl – alkali chloride systems as expressed by eq. [2] are given in Fig. 3. The experimental data for AgCl indicate a one-electron electrode reaction, as expected. For the Ag–Al galvanic cell, plots of E_{cell} versus log (X_{AlCl_3}/X^3_{AgCl}) are given in Fig. 4. The curves are linear and correspond to a three-electron electrode reaction, as expected. Linear regression analysis for the Nernst plots gave correlation coefficients of almost unity for all cases. The linearity of the plots in Figs. 3 and 4 indicates that the dilute solutions of AgCl and $AlCl_3$ in molten alkali chlorides obey Henry's law. Values of $E^0_{f(AgCl)}$ and $E^0_{f(AlCl_3)}$ determined graphically as indicated in Figs. 3 and 4, are recorded in Tables 3 and 4 in accordance with the IUPAC convention (19). For both AgCl and $AlCl_3$, the magnitude of the values of the formal potentials increase as CsCl is added and decrease as the temperature is increased. Included in Tables 3 and 4 are the theoretical values for the formal potentials in the ternary solutions calculated from the equation which has been derived previously (17, 20, 21),

$$[8]\quad E^0_{f(123)} = (1-t)E^0_{f(12)} + tE^0_{f(13)}$$

where $E^0_{f(123)}$ is the formal potential of AgCl or $AlCl_3$ in a ternary solution and $E^0_{f(12)}$ and $E^0_{f(13)}$ are the formal potentials in the component binary systems. The t parameter was defined in eq. [7]. Figures 5 and 6 are the plots of $E^0_{f(AgCl)}$ and $E^0_{f(AlCl_3)}$ versus the t parameter at 1123 K for the AgCl – alkali chloride and $AlCl_3$ – alkali chloride systems, respectively. It is readily seen that the experimental results for $t = 1/2$ are in agreement

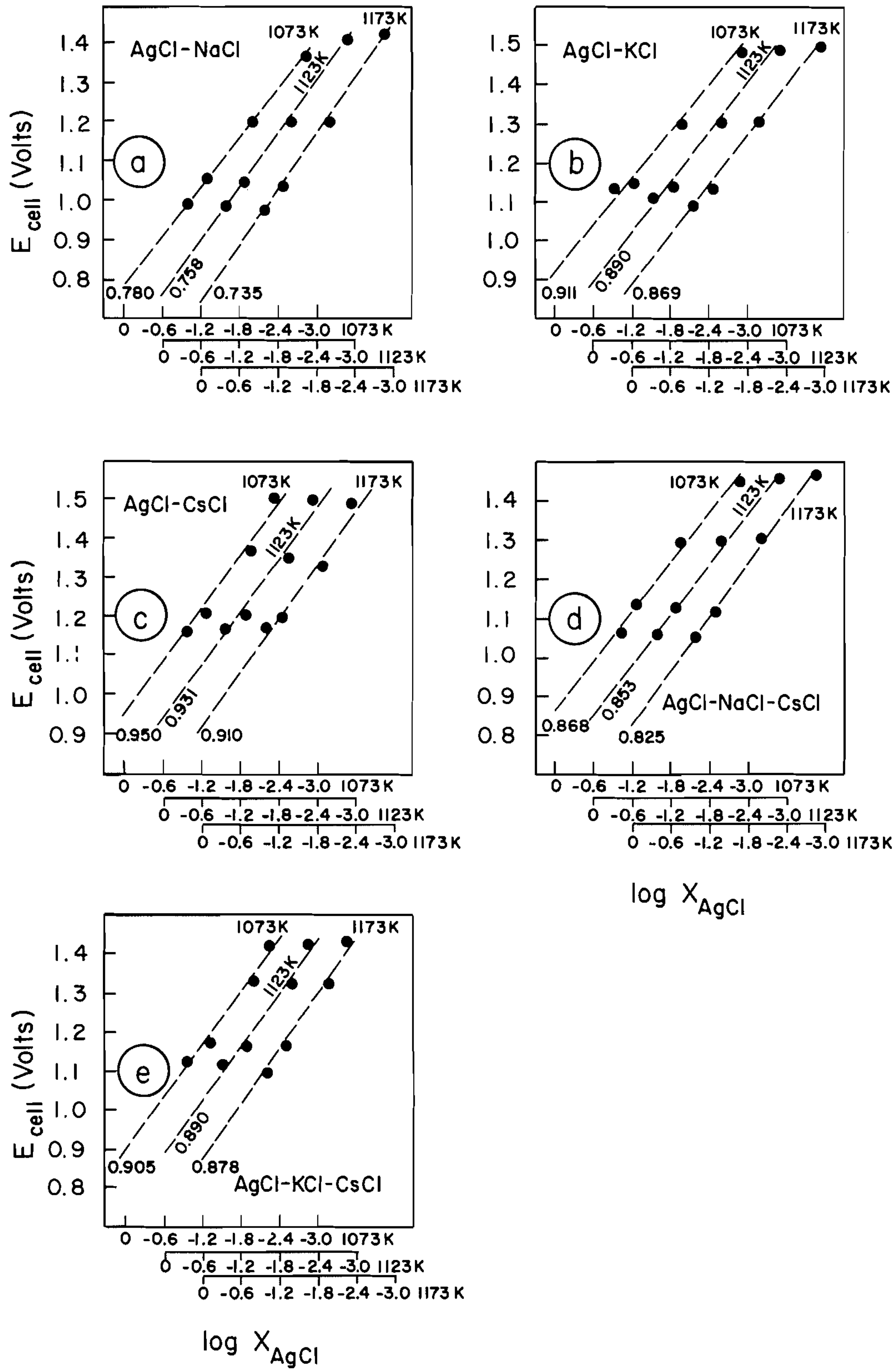

FIG. 3. Concentration dependence of E_{cell} in the AgCl – alkali chloride systems at 1073 K, 1123 K, and 1173 K.

to within 2% or better with the predicted values from eq. [8].

Activity coefficients for AgCl and $AlCl_3$, respectively, are summarized in Tables 5 and 6. The uncertainty in these values is estimated as ±5%. A comparison of the activity coefficients indicates the pronounced effect of CsCl in creating thermodynamically stable solutions. The large negative deviations from ideality shown by the magnitude of the activity coefficients of $AlCl_3$, indicates the strong tendency of the $AlCl_3$ to form complex species in these melts. Negative deviations from ideality have also been observed for the concentrated solutions of $AlCl_3$ in alkali chloride melts, and have been interpreted as indicating the presence of the complex species in solution (11,

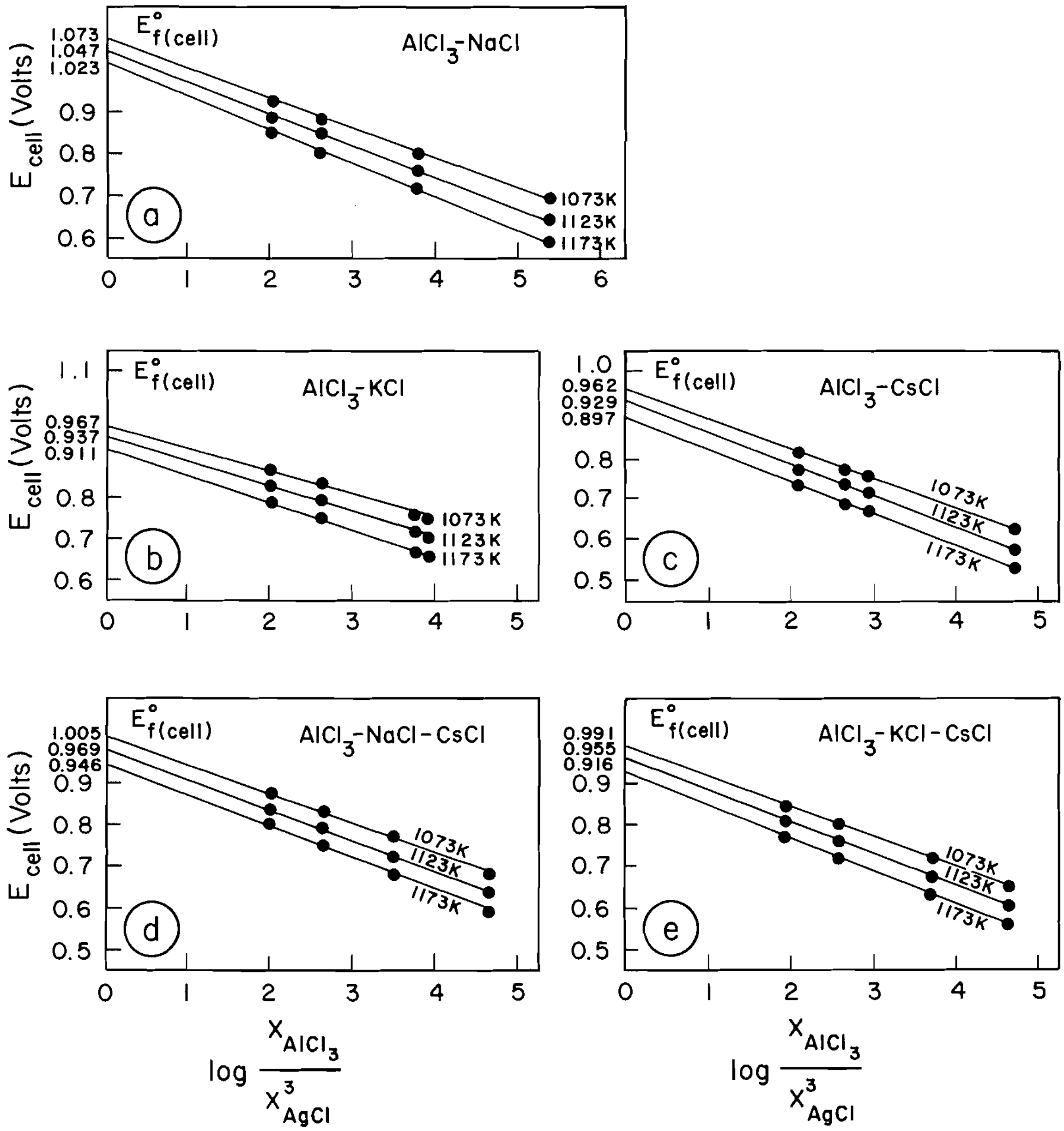

FIG. 4. Concentration dependence of E_{cell} in the $AlCl_3$ – alkali chloride systems at 1073 K, 1123 K, and 1173 K.

TABLE 5. Thermodynamic properties for the AgCl systems*

System	$(\overline{\Delta H})_{AgCl}$	$(\overline{\Delta S})^{ex}_{AgCl}$	γ^h_{AgCl} 1073 K	1123 K	1173 K
NaCl	−17.6	−20.3	1.592	1.747	1.884
KCl	−27.7	−19.5	0.459	0.549	0.598
CsCl	−28.9	−15.5	0.253	0.292	0.333
NaCl–CsCl†	−23.7	−17.9	0.615	0.655	0.773
KCl–CsCl†	−27.9	−18.0	0.384	0.447	0.491

*Units: $(\overline{\Delta H})_{AgCl}$ kJ/mol, $(\overline{\Delta S})^{ex}_{AgCl}$ J/mol K.
†Equimolar.

TABLE 6. Thermodynamic properties for the $AlCl_3$ systems*

System	$(\overline{\Delta H})_{AlCl_3}$	$(\overline{\Delta S})^{ex}_{AlCl_3}$	$\gamma^h_{AlCl_3} \times 10^2$ 1073 K	1123 K	1173 K
NaCl	−179	−130	1.17	2.92	6.52
KCl	−182	−127	0.594	1.48	3.39
CsCl	−227	−159	0.173	0.530	1.52
NaCl–CsCl†	−207	−151	0.613	1.72	4.43
KCl–CsCl†	−214	−150	0.291	0.844	2.24

*Units: $(\overline{\Delta H})_{AlCl_3}$ kJ/mol, $(\overline{\Delta S})^{ex}_{AlCl_3}$ J/mol K.
†Equimolar.

12). For both the AgCl and $AlCl_3$ systems, the activity coefficients increase with temperature increase, indicating the dissociation of complexes at higher temperatures. The $AlCl_3$ – alkali chloride solutions could be suitable as electrolytes for the production of aluminum metal by fused salt electrolysis. The most thermodynamically stable systems appear to be the $AlCl_3$–CsCl binary and the $AlCl_3$–KCl–CsCl ternary solutions. Figures 7 and 8 are the plots of $\log \gamma^h_{AgCl}$ and $\log \gamma^h_{AlCl}$ versus the t parameter at 1123 K for the AgCl – alkali chloride and $AlCl_3$ – alkali chloride systems, respectively. The

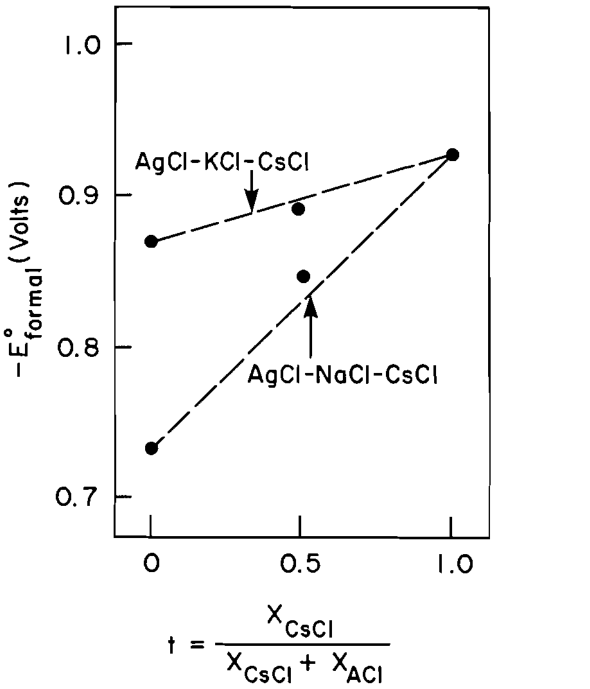

FIG. 5. $E^{0}_{f(AgCl)}$ versus t at 1123 K for the AgCl–NaCl–CsCl and AgCl–KCl–CsCl systems.

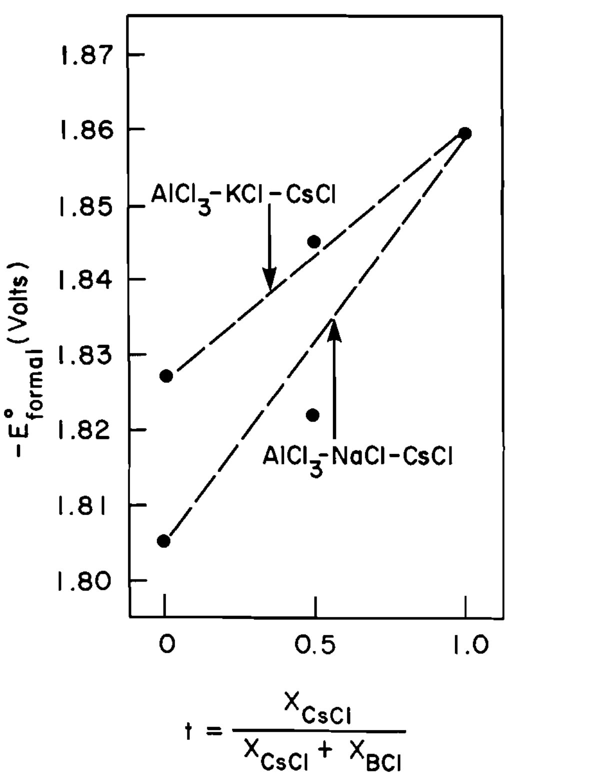

FIG. 6. $E^{0}_{f(AlCl_3)}$ versus t at 1123 K for the $AlCl_3$–NaCl–CsCl and $AlCl_3$–KCl–CsCl systems.

predicted values at $t = 1/2$ are in good agreement with those obtained experimentally.

The partial molar enthalpies and excess entropies of mixing for AgCl and $AlCl_3$ are given in Tables 5 and 6, respectively.

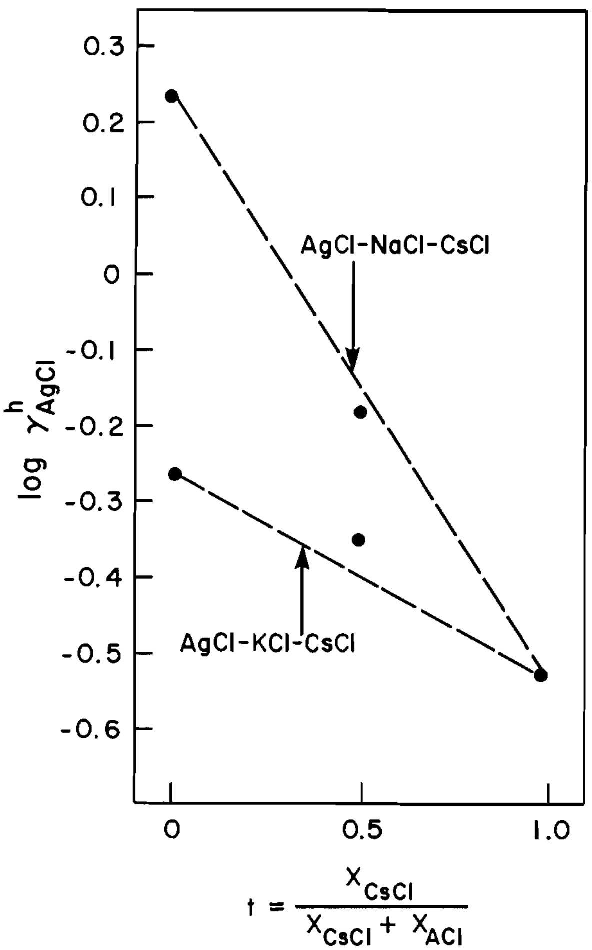

FIG. 7. $\log \gamma^{h}_{AgCl}$ versus t at 1123 K for the AgCl–NaCl–CsCl and AgCl–KCl–CsCl systems.

The error in the values of the enthalpies and entropies is approximately ±2.1 kJ/mol and ±2.1 J/mol K, respectively. The magnitude of the values of the enthalpies and entropies for $AlCl_3$ are much larger than the corresponding values for AgCl. This is consistent with the magnitude of the activity coefficients for $AlCl_3$, and with the pronounced reactivity of $AlCl_3$ with alkali chloride, and the subsequent formation of complex species in solution. For both AgCl and $AlCl_3$, the exothermicity increases as the size of the alkali metal cation in the alkali chloride solvent changes from Na^+ to Cs^+, indicating that in the presence of larger solvent cations there is an increase in the interaction between the silver or aluminum cation and the surrounding anions (22). The values of $(\overline{\Delta H})_{AgCl}$ or $(\overline{\Delta H})_{AlCl_3}$ in the ternary melts are in agreement to within 5% or better with those calculated from the previously derived expression (17, 20, 21) given as

$$[9] \quad (\overline{\Delta H})_{123} = (1 - t)(\overline{\Delta H})_{12} + t(\overline{\Delta H})_{13}$$

which is valid when the component binaries 1,2 and 1,3, respectively, and the ternary 1,2,3, contain the same amount of a reactive metal chloride like AgCl or $AlCl_3$, which are thought of as behaving like ligand acceptors.

The relationship is depicted schematically in Figs. 9 and 10 for the AgCl – alkali chloride and $AlCl_3$ – alkali chloride systems, respectively.

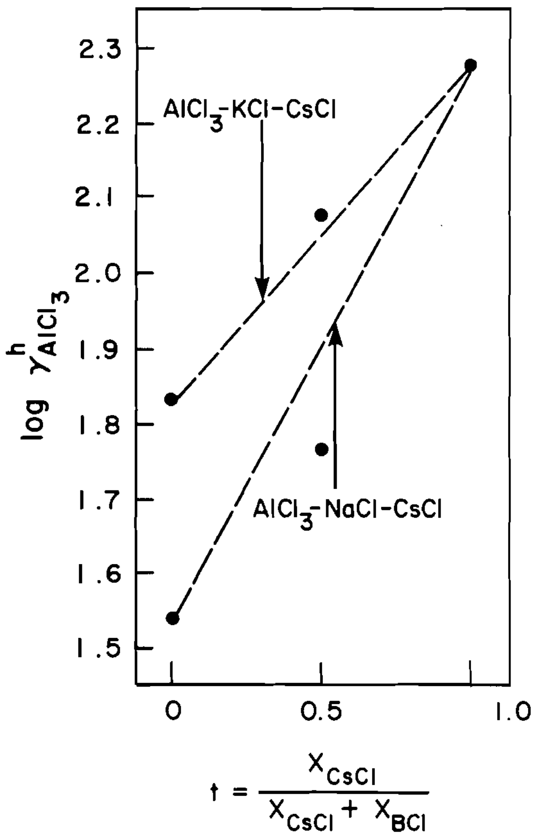

FIG. 8. log $\gamma^{h}_{AlCl_3}$ versus t at 1123 K for the $AlCl_3$–NaCl–CsCl and $AlCl_3$–KCl–CsCl systems.

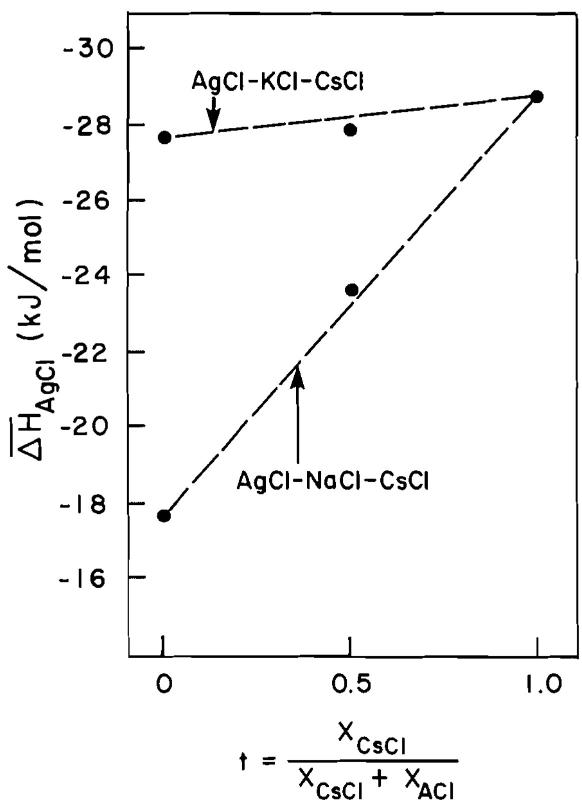

FIG. 9. $(\overline{\Delta H})_{AgCl}$ versus t for the AgCl–NaCl–CsCl and AgCl–KCl–CsCl systems.

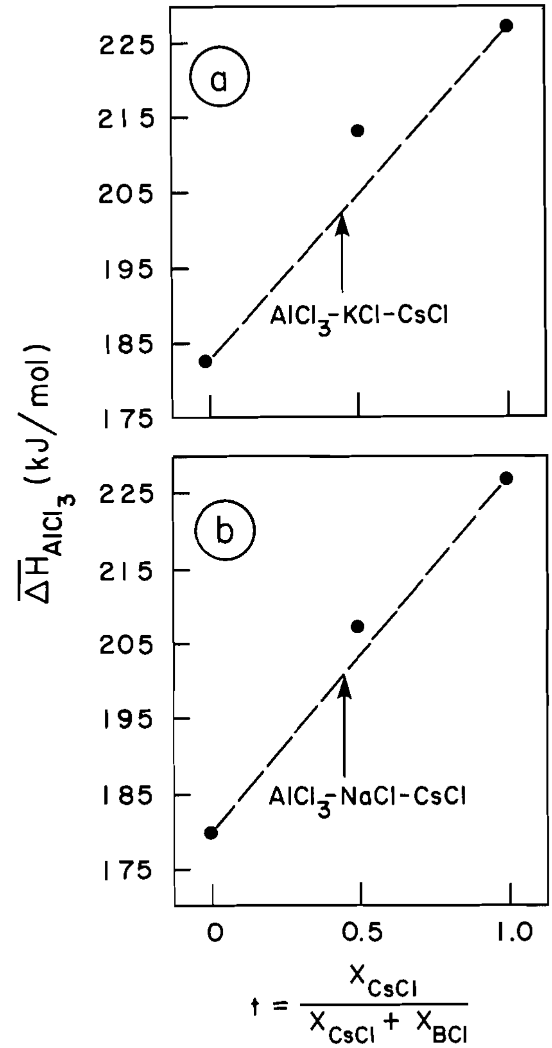

FIG. 10. $(\overline{\Delta H})_{AlCl_3}$ versus t for the $AlCl_3$–NaCl–CsCl and $AlCl_3$–KCl–CsCl systems.

Acknowledgements

Financial assistance by the Natural Sciences and Engineering Research Council of Canada to one of the authors (P.J.T.) in the form of a Postgraduate Scholarship is gratefully acknowledged.

1. A. D. PELTON and S. N. FLENGAS. J. Electrochem. Soc. **117**, 1130 (1970).
2. Z. MOSER, W. GASIOR, and K. RZYMAN. J. Electrochem. Soc. **126**, 1467 (1979).
3. J. GUION, M. BLANDER, D. HENGSTENBERG, and K. HAGEMARK. J. Phys. Chem. **72**, 2086 (1968).
4. Z. MOSER, M. KUCHARSKI, and K. RZYMAN. J. Electrochem. Soc. **125**, 692 (1978).
5. A. C. GRUNER and W. T. THOMPSON. Can. J. Chem. **53**, 1084 (1975).
6. Z. MOSER and K. RZYMAN. Electrochim. Acta, **25**, 183 (1980).
7. K. SCHULZE, D. STEINLY, and H. HOFF. Z. Naturforsch. **289**, 1847 (1973).
8. E. DEWING. Met. Trans. B, **12**B, 705 (1981).
9. V. STOROZHENKO. Zh. Fiz. Khim. **48**, 1709 (1974).
10. A. BJORGUM, A. STERTEN, V. B. SORENSON, J. THONSTAD, and R. TUNOLD. Electrochim. Acta, **26**, 487 (1981).
11. A. BJORGUM, A. STERTEN, J. THONSTAD, and R. TUNOLD. Elec-

trochim. Acta, **26**, 491 (1981).
12. H. LINGA, K. MOTZFELDT, and H. OYE. Ber. Bunsen. Phys. Chem. **82**, 586 (1978).
13. Y. BORISGLEBSKII, M. VETYUKOV, and Z. SHATOVA. Zh. Prikl. Khim. **51**, 1188 (1978).
14. R. LISTER and S. N. FLENGAS. Can. J. Chem. **43**, 2947 (1965).
15. E. DEWING. J. Am. Chem. Soc. **77**, 2639 (1955).
16. S. N. FLENGAS and T. R. INGRAHAM. J. Electrochem. Soc. **106**, 714 (1959).
17. D. R. SADOWAY and S. N. FLENGAS. J. Electrochem. Soc. **122**, 515 (1975).
18. D. STULL and H. PROPHET. JANAF Thermochemical Tables, 2nd ed. NSRDS-NBS 37, Washington. 1971.
19. T. LICHT and A. DE BETHUNE. J. Chem. Educ. **34**, 443 (1957).
20. D. R. SADOWAY and S. N. FLENGAS. *In* Extractive metallurgy of refractory metals. *Edited by* H. Sohn, N. Carlson, and J. Smith. AIME, Warrendale, PA. 1981. pp. 315–339.
21. S. N. FLENGAS and D. R. SADOWAY. *In* Proceedings of the Third International Symposium on Molten Salts. *Edited by* G. Mamantov, M. Blander, and G. P. Smith. The Electrochemical Society, NJ. 1981. pp. 68–94.
22. O. J. KLEPPA. Ann. Rev. Phys. Chem. **16**, 187 (1965).

Chemical deoxygenation of the epoxide moiety in deoxynivalenol (vomitoxin)

RUSSELL R. KING

Research Station, Research Branch, Agriculture Canada, Fredericton, N.B., Canada E3B 4Z7

AND

ROY GREENHALGH

Chemistry and Biology Research Institute, Agriculture Canada, Ottawa, Ont., Canada K1A 0C6

Received September 27, 1984

RUSSELL R. KING and ROY GREENHALGH. Can. J. Chem. **63**, 1089 (1985).

Reaction of triacetoxydeoxynivalenol (**3**) with hydrobromic acid – acetic acid at reflux temperatures yielded 3α,7α,13,15-tetraacetoxy-2-bromo apotrichothec-9-en-8-one (**5**) and 3α,7α,15-triacetoxy-13-bromo-12-hydroxytrichothec-9-en-8-one (**4**). Dehalohydrination of the 13,12-bromohydrin derivative with Zn – acetic acid followed by deacetylation with sodium ethoxide gave 3α,7α,15-trihydroxytrichothec-9,12-dien-8-one (**2**). This compound proved identical to the transformation product isolated from incubation of deoxynivalenol (vomitoxin) in vitro with rumen microorganisms.

RUSSEL R. KING et ROY GREENHALGH. Can. J. Chem. **63**, 1089 (1985).

La réaction du triacétoxydéoxynivalenol (**3**) lors d'un reflux avec un mélange d'acide hydrobromique et d'acide acétique fournit les produits: tétraacétoxy-3α,7α,13,15 bromo-2 ène-9, one-8 apotrichothec (**5**) et triacétoxy-3α,7α,15 bromo-13 ène-9, one-8 hydroxy-12 trichothec (**4**). D'autre part, la déhalohydrination du dérivé bromo-13 hydrin-12 à l'aide de zinc et d'acide acétique suivie de déacétylation avec l'éthoxide de sodium produit le trihydroxy-3α,7α,15 diène-9,12 one-8 trichothec (**2**). Le dérivé s'avère identique au produit de transformation récemment isolé lors de l'incubation in vitro du déoxynivalenol (vomitoxine) avec des microorganismes du rumen.

Deoxynivalenol (**1**) (3α,7α,15-trihydroxy-12,13-epoxy trichothec-9-en-8-one or vomitoxin) is one of the predominant trichothecene mycotoxins associated with infection of cereal grains by certain fusarium species (1). As a result of the consumption of such contaminated products, animals may suffer sublethal toxicoses (2). As yet, the exact metabolic fate of the toxin when ingested is unknown. Our recent investigations (3) involving incubation of deoxynivalenol in vitro with rumen microorganisms demonstrated that the predominant biotransformation consisted of deoxygenation of the 12,13-epoxide moiety to a 12,13-double bond. Yoshizawa *et al.* (4) have also observed a similar transformation when deoxynivalenol was administered to rats. Since there is good evidence to suggest that the toxicity of trichothecenes is conferred by the 12,13-epoxide group and that the elimination of it substantially detoxifies the substances (5), our primary interest was to prepare a sufficient quantity of the deoxygenated metabolite (i.e., 3α,7α,15-trihydroxytrichothec-9,12-dien-8-one (**2**)) in order to determine its relative toxicity.

Two standard approaches for transforming the 12,13-epoxide moiety to a double bond were investigated. One route was direct epoxide deoxygenation; the other, halohydrin formation (via epoxide cleavage) prior to dehalohydrination. Of the two approaches, only the latter eventually provided an acceptable measure of success.

Although Gutzwiller *et al.* (7) obtained low yields of the C-12,13 vinyl analogue of verrucarol (4β,15-diacetoxytrichothec-9,12-diene) on reaction with $LiAlH_4$, only complex mixtures (devoid of the vinyl derivative) were obtained on subjecting deoxynivalenol to similar reaction conditions. This result was not entirely unexpected and is presumably attributable to the presence of the reactive 9-en-8-one system. Attempted direct deoxygenation utilizing a Cu–Zn catalyst (8) (under a variety of reaction conditions) again did not elicit the required result.

Preliminary investigations involving a variety of reagents previously utilized for the deoxygenation of epoxides (9) (via halohydrin intermediates) also failed to bring about the desired reaction with deoxynivalenol. This behaviour may be ascribed to an inaccessibility towards the catalyst or to the possibility that conformational changes on cleavage of the epoxide group are energetically unfavourable and a thermodynamic driving force is required.

Eventually, it was determined that refluxing a solution of deoxynivalenol (**1**) and sodium iodide in acetic acid, prior to the addition of powdered zinc, furnished a quantity of the required diene (**2**). The yield was extremely small (<1%), however, and tlc analysis showed the reaction mixture contained many more substances than would be expected from a simple epoxide opening, followed by dehalohydrination. In an attempt to reduce unwanted side reactions, the triacetyl derivative (**3**) of deoxynivalenol was formed and hydrobromic acid was substituted for sodium iodide. Under these conditions, and although relatively longer reaction times were involved, tlc analysis confirmed that triacetoxydeoxynivalenol (**3**) was transformed into just two major compounds.

The new compounds were readily separated by preparative tlc and further purified by crystallization. The less polar of the two compounds (R_f 0.77, 19.4%) was found, by spectroscopic and chemical means, to exhibit properties consistent with those of the 13,12-bromohydrin derivative (**4**). For example (*i*) the tertiary nature of the hydroxyl group (indicated by ir) was confirmed by its lack of reactivity towards both chromic acid and trifluoroacetic anhydride; (*ii*) the parent ion from mass spectral determinations was increased by 81 *m/e*; and (*iii*) in the ^1H nmr spectrum (Table 1) no resonances ascribable to a spiro epoxide group were found. Compound **4** with the stereochemistry assigned is the product anticipated from a normal S_N2 epoxide opening (i.e., nucleophilic *trans* attack at the less highly substituted carbon atom) (10).

Identification of the other major product (R_f 0.68, 30.8%) from the reaction of triacetoxydeoxynivalenol (**3**) with hydrobromic acid – acetic acid proved more complex. First, the ir spectrum was devoid of hydroxyl absorptions. Secondly, both the mass spectrum and ^1H nmr spectrum indicated the presence of another acetoxyl group. Since its mass spectrum also dem-

TABLE 1. ^{1}H nuclear magnetic resonance spectra of compounds (chemical shifts, δ)

Hydrogen no.	Compound 3	4	5	6	7	8
2	3.96 (d, 1H) J = 4.4 Hz	4.28 (d, 1H) J = 4.8 Hz	4.26 (d, 1H) J = 8.5 Hz	5.49 (d, 1H) J = 5.9 Hz	4.50 (d, 1H) J = 4.4 Hz	3.92 (d, 1H) J = 4.4 Hz
3	5.26 (m, 1H)	5.41 (m, 1H)	5.13 (m, 1H)	6.00 (m, 1H)	4.96 (m, 1H)	5.38 (m, 1H)
4	2.18 (ABX, 2H)	2.13, 2.44 (ABX, 2H)	1.98, 2.08 (ABX, 2H)	2.05, 2.79 (ABX, 2H)	2.04, 2.38 (ABX, 2H)	2.14 (ABX, 2H)
7	6.08 (s, 1H)	5.83 (s, 1H)	6.01 (s, 1H)	5.99 (s, 1H)	5.90 (s, 1H)	—
10	6.58 (d, d, 1H) J = 5.0 Hz	6.51 (d, d, 1H) J = 5.0 Hz	6.64 (d, d, 1H) J = 5.4 Hz	6.63 (d, d, 1H) J = 5.4 Hz	6.54 (d, d, 1H) J = 5.8 Hz	2.55, 2.98 (q, 2H) J_{ab} = 18.8, $J_{10,11}$ = 2.2 Hz
11	4.78 (d, 1H) J = 4.8 Hz	4.82 (d, d, 1H) J = 4.8 Hz	4.62 (d, d, 1H) J = 5.2 Hz	4.16 (d, d, 1H) J = 5.2 Hz	4.71 (d, 1H) J = 5.8 Hz	4.48 (d, d, 1H) $J_{10,11}$ = 4.8 Hz
13	2.94, 3.16 (AB, 2H) J = 3.4 Hz	3.73, 4.46 (AB, 2H) J = 9.6 Hz	4.14, 4.54 (AB, 2H) J = 12.5 Hz	4.09, 4.37 (AB, 2H) J = 12.5 Hz	5.27 (s, 1H), 4.88 (s, 1H) J = 1.0 Hz	1.50 (s, 3H)
14	0.98 (s, 3H)	1.17 (s, 3H)	1.28 (s, 3H)	1.16 (s, 3H)	1.23 (s, 3H)	1.28 (s, 3H)
15	4.30, 4.44 (AB, 2H) J = 11.8 Hz	4.24, 4.61 (AB, 2H) J = 11.5 Hz	4.28, 4.42 (AB, 2H) J = 11.4 Hz	4.12, 4.48 (AB, 2H) J = 11.5 Hz	4.26, 4.38 (AB, 2H) J = 12.2 Hz	4.11, 4.60 (AB, 2H) J = 11.4 Hz
16	1.86 (s, 3H)	1.88 (s, 3H)	1.88 (s, 3H)	1.86 (s, 3H)	1.82 (s, 3H)	1.88 (s, 3H)
Ac	1.94 (s, 3H) 2.16 (s, 3H) 2.24 (s, 3H)	1.85 (s, 3H) 2.15 (s, 3H) 2.20 (s, 3H)	1.86 (s, 3H) 2.13 (s, 3H) 2.15 (s, 3H) 2.20 (s, 3H)	1.85 (s, 3H) 2.14 (s, 3H) 2.17 (s, 3H)	1.91 (s, 3H) 2.14 (s, 3H) 2.20 (s, 3H)	2.06 (s, 3H) 2.12 (s, 3H) 2.26 (s, 3H)

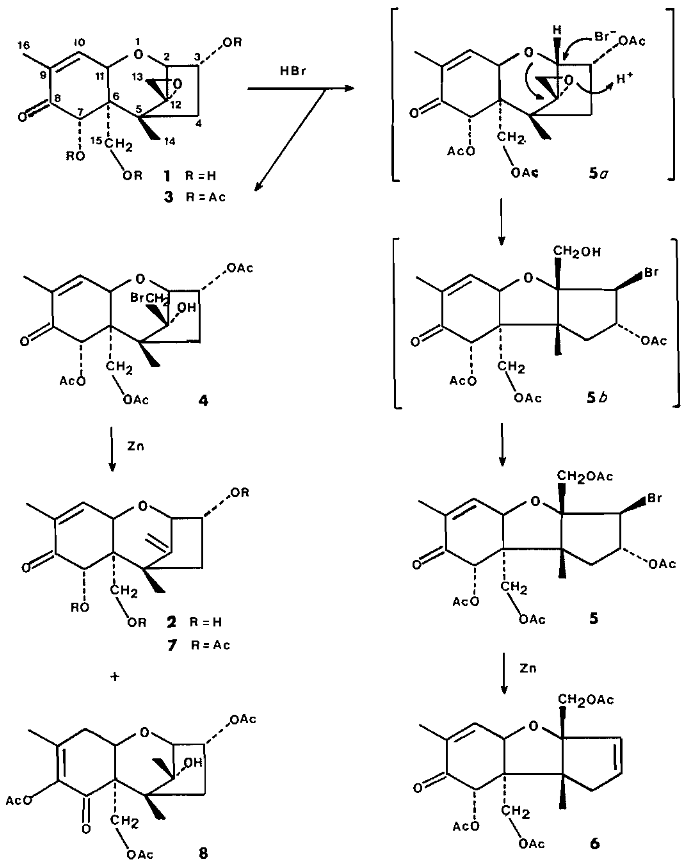

FIG. 1.

onstrated introduction of a bromine atom, and its ^{1}H nmr profile confirmed loss of epoxide-associated absorptions, the compound was initially formulated as a 13-acetoxy-12-bromo derivative. This compound was assumed to originate from acid-catalyzed acetylation of a 12-bromo-13-hydroxy precursor arising from an alternate mode of bromide attack on the 12,13-epoxide. In the light of a subsequent chemical transformation, however, it was established that skeletal rearrangement to an apotrichothecene ring system (11) (Fig. 1) had occurred, and the bromohydrin acetate was assigned the structure **5**. Again, it was assumed that acid-catalyzed acetylation takes place after the initial rearrangement.

Although acid-catalyzed rearrangements of the trichothecene to the apotrichothecene ring system are well documented (12), we believe this is the first such observation reported for the nivalenol series. This particular intramolecular process is thought to proceed by nucleophilic attack of the position one oxygen atom on the protonated epoxide moiety (i.e., **5***a*). Such a pathway obviously represents a comparable energy barrier to external nucleophilic attack by Br^- and, if our structural assignments are correct, is a severe limiting factor in our synthetic design.

Although neither of the bromo derivatives **4** and **5** were affected when treated with Zn in acetic acid at room temperature, they both reacted rapidly at reflux temperatures. The bromoapotrichothecene derivative (**5**) yielded just one major product (73.9%). As anticipated, mass spectral and ^{1}H nmr data confirmed elimination of bromine and an acetoxyl group (13). The ^{1}H nmr spectrum also indicated that resonances previously ascribed to the C-2, C-3 protons were replaced by signals representative of alkene protons in a 5-membered ring system (14). These data were considered supportive of the apotrichothec-2,9-diene structure (**6**) and are consistent with the rationale utilized to formulate the structure of its 2-bromo-apotrichothecene precursor (**5**).

In contrast to the bromoapotrichothecene compound (**5**), treatment of the 13-bromo-12α-hydroxy analogue (**4**) with Zn and acetic acid yielded one major and several minor compounds. The mass spectrum of the major compound (43.4%, isolated by preparative tlc) exhibited a molecular ion at m/e 406, suggesting the elimination of a bromine atom and a hydroxyl group. Its ^{1}H nmr had doublet resonances at δ 4.88 and 5.27 (each 1H, J = 1.0 Hz) which were assigned to terminal methylene protons at the C-13 position. Treatment of the compound with m-chloroperbenzoic acid in chloroform quantitatively converted it into triacetoxydeoxynivalenol (**3**). Based upon this data, the compound was assigned the 9,12-dien-8-one structure **7**. Accordingly, deacetylation with sodium ethoxide furnished the required 3α,7α,15-trihydroxy-trichothec-9,12-dien-8-one (**2**).

Of the minor products produced by treatment of the bromohydrin (**4**) with Zn − acetic acid, only one was isolated in quantities amenable to ready identification. Mass spectral data for this compound indicated loss of bromine and acquisition of a hydrogen atom. Its ^{1}H nmr spectrum exhibited a new 3-proton singlet at 1.50 and other changes (i.e., no resonances at δ 6.6 (H-10) or δ 6.05 (H-7), those for H-11 had moved upfield to δ 4.43, and a new two-proton quartet at δ 2.96, 2.55) were consistent with isomerization of the A-ring to an 8-acetoxy-8-en-7-one system (15). Based upon this data, the structure **8** was proposed for the compound. The formation of **8** from the bromohydrin **4** is possibly facilitated by proximity of the Zn−bromide−hydroxyl complex (16) to the 7β-hydrogen atom.

Experimental

Melting points are uncorrected and were determined on a Kofler hot stage microscope. Infrared (ir) spectra were determined on a Beckman IR-20A spectrophotometer in Nujol mulls. Nuclear magnetic resonance (nmr) spectra were obtained in $CDCl_3$ solutions with Me_4Si as an internal standard on a Bruker W.M. 250 nmr spectrophotometer at 250 MHz. The mass spectra were obtained on either of two systems, one a VG 7070H and the other a VG 12000 quadrupole instrument. Thin layer chromatograms were run on glass plates coated with silica gel GF (layer thickness 0.25 mm). Separated components were detected by ultraviolet fluorescence and (or) by charring after a spray of 5% sulfuric acid in ethanol.

3α,7α,15-Triacetoxy-12,13-epoxytrichothec-9-en-8-one (2)

A solution of *deoxynivalenol* (**1**, 400 mg) in acetic anhydride (3 mL) and pyridine (4 mL) was stirred overnight at room temperature and then neutralized by decantation into a cold saturated solution of sodium bicarbonate (80 mL). After extraction of the neutral solution with chloroform (2 × 80 mL) the chloroform extracts were concentrated under vacuum, and the residue crystallized from diethyl ether furnished *3α,7α,15-triacetoxy-12,13-epoxytrichothec-9-en-8-one* (**3**, 514 mg, R_f 0.70) (silica gel, hexane − ethyl acetate 1:1), mp 154−156°C (lit. (1) mp 155−157°C); ir (Nujol) ν_{max}: 1735 (acetates), 1680 (αβ-unsaturated ketone) cm^{-1}; ^{1}H nmr (see Table 1).

Reaction of 3α,7α,15-triacetoxy-12,13-epoxytrichothec-9-en-8-one (3) with hydrobromic acid/acetic acid

A solution of *3α,7α,15-triacetoxy-12,13-epoxytrichothec-9-en-8-one* (**3**, 380 mg) in glacial acetic acid (30 mL) was treated with an excess of 48% hydrobromic acid (0.25 mL) and refluxed with stirring until tlc studies (hexane − ethyl acetate 1:1) indicated that reaction was complete (4 h). The reaction solution was then cooled and the acetic acid removed *in vacuo*. The residue was subsequently purified by preparative thin layer chromatography (ethyl acetate − hexane 2:3). Crystallization of the major component (152 mg, R_f 0.68) from diethyl ether gave *3α,7α,13,15-tetraacetoxy-2-bromo apotrichothec-7-en-8-one* (**5**), mp 164−165°C; ir (Nujol) ν_{max}: 1740, 1725, and 1690 cm^{-1}; ^{1}H nmr (see Table 1). Mass spectrum m/e: 544.0933 (M^+); calculated for $C_{23}H_{29}Br^{79}O_{10}$: (m.wt.) 544.2628. Crystallization of the minor component (88 mg, R_f 0.77) from diethyl ether gave *3α,7α,15-triacetoxy-13-bromo-12-hydroxytrichothec-7-en-8-one* (**4**), mp 85−86°C; ir (Nujol) ν_{max}: 3460, 1748, 1735, 1716, and 1690 cm^{-1}; ^{1}H nmr (see Table 1). Mass spectrum m/e: 502.1387 (M^+); calculated for $C_{21}H_{27}Br^{79}O_9$: (m.wt.) 502.2392.

7α,13,15-Triacetoxyapotrichothec-2,9-dien-8-one (6)

3α,7α,13,15-Tetraacetoxy-2-bromo-apotrichothec-7-en-8-one (**5**, 60 mg) in glacial acetic acid (5 mL) was refluxed, with stirring, in the presence of powdered zinc (200 mg) for 5 min. The reaction solution was cooled, decanted into a rotary evaporator flask, and the acetic acid removed *in vacuo*.

The residue was taken up in chloroform (60 mL), washed with bicarbonate solution, and the chloroform removed *in vacuo*. Crystallization of the residue from ethanol furnished *7α,13,15-triacetoxy-apotrichothec-2,9-dien-8-one* (**6**, 33 mg, R_f 0.66), mp 120−121°C; ir (Nujol) ν_{max}: 1746, 1735, and 1692 cm^{-1}; ^{1}H nmr (see Table 1). Mass spectrum m/e: 406.1625 (M^+); calculated for $C_{21}H_{26}O_8$: (m.wt.) 406.1574.

Reaction of 3α,7α,15-triacetoxy-13-bromo-12-hydroxytrichothec-7-en-8-one (4) with zinc − acetic acid

3α,7α,15-Triacetoxy-13-bromo-12-hydroxytrichothec-7-en-8-one (**4**, 60 mg) in glacial acetic acid (10 mL) was refluxed, with stirring, in the presence of powdered zinc (200 mg) for 5 min. The reaction solution was cooled, decanted into a 100-mL rotary evaporator flask, and the acetic acid removed *in vacuo*. The residue was taken up in chloroform (60 mL), washed with bicarbonate solution, and the chloroform removed *in vacuo*. The residue was then purified by preparative thin layer chromatography (ethyl acetate − hexane 2:3). The minor component (5.2 mg, R_f 0.46) was crystallized from ether − hexane to yield *3α,8,15-triacetoxy-12-hydroxy-13-methyltrichothec-8-en-7-one* (**8**), mp 171−72°C; ir (Nujol) ν_{max}: 3410, 1758, 1735, 1718, 1655, and 1635 cm^{-1}; ^{1}H nmr (see Table 1). Mass spectrum m/e: 424.1752 (M^+); calculated for $C_{21}H_{28}O_9$: (m.wt.) 424.1734). The major component (21 mg, R_f 0.65), *3α7α,15-triacetoxytrichothec-9,12-dien-8-one* (**7**), had ir (Nujol) ν_{max}: 1735 and 1690 cm^{-1}; ^{1}H nmr (see Table 1). Compound **7** (20 mg) in absolute ethanol (5 mL) was treated for 15 min at room temperature with 0.1 M sodium ethoxide (5 mL). The reaction mixture was deionized with Amberlite IR-120 (H^+) ion-exchange resin and the ethanol removed *in vacuo*.

The residue was purified by preparative thin layer chromatography (ethyl acetate) and gave a compound (9.8 mg, R_f 0.51) as an amorphous solid; ir (Nujol) ν_{max}: 3360−3410, and 1672 cm^{-1}; ^{1}H nmr δ 1.46 (s, 3H, H-14), 1.88 (q, 3H, H-16), 2.18 (ABX, 2H, H-4), 3.85 (AB, 2H, H-15, J = 11.8), 4.25 (d, 1H, H-2, J = 4.5), 4.30 (m, 1H, H-3), 4.75 (d, 1H, H-11, J = 6.0), 4.76 (d, 1H, H-7, J = 1.5), 5.11, 5.24 (2s, 2H, H-13), and 6.63 (d, d, 1H, H-10, J = 6.0). Mass spectrum m/e: 280.1455; calculated for $C_{15}H_{20}O_5$: (m.wt.) 280.1312. These data are compatible with the structure 3α,7α,15-trihydroxytrichothec-9,12-dien-8-one (**2**), which is identical to the transformation product isolated from incubation of deoxynivalenol (**1**) with rumen microorganisms.

Acknowledgements

We thank Greg Lonergan, Chemistry Department, University of New Brunswick, Fredericton, New Brunswick, for the nmr determinations.

1. T. Yoshizawa and N. Morooka. Agric. Biol. Chem. **37**, 2933 (1973); R. F. Vesonder, A. Ciegler, and A. H. Jensen. Appl. Microbiol. **26**, 1008 (1973); M. M. Blight and J. F. Grove.

J. Chem. Soc. Perkin Trans. I, 1691 (1974); Y. UENO. *In* Advances in nutritional research. Vol. 3. *Edited by* H. H. Draper. Plenum Press, New York. 1980. pp. 301–353.
2. T. YOSHIZAWA and N. MOROOKA. J. Food Hyg. Soc. Japan, **15**, 261 (1974); R. F. VESONDER, A. CIEGLER, A. H. JENSEN, W. K. ROHWEDDER and D. WEISLEDER. Appl. Environ. Microbiol. **31**, 280 (1976); O. M. FORSYTH, T. YOSHIZAWA, N. MOROOKA and J. TUITE. *ibid.*, **34**, 547 (1977); T. YOSHIZAWA, T. SHIROTA and N. MOROOKA. J. Food Hyg. Soc. Jpn. **19**, 178 (1978).
3. R. R. KING, R. E. MCQUEEN, D. LEVESQUE, and R. GREENHALGH. J. Agric. Food Chem. **32**, 1181 (1984).
4. T. YOSHIZAWA, H. TAKEDA, and T. OHI. Agric. Biol. Chem. **47**, 2133 (1983).
5. J. F. GROVE and P. H. MORTIMER. Biochem. Pharmacol. **18**, 1473 (1969); M. D. GROVE, H. R. BURMEISTER, S. L. TAYLOR, D. WEISLEDER, and R. D. PLATTNER. J. Agric. Food Chem. **32**, 541 (1984).
6. H. SUZUKI, T. FUCHITA, A. IWASA, and T. MISHINA. Synthesis, 905 (1978), and references therein.
7. J. GUTZWILLER, R. MAULI, H. P. SIGG, and CH. TAMM. Helv. Chim. Acta, **47**, 2234 (1964).
8. S. M. KUPCHAN and M. MARUYAMA. J. Org. Chem. **36**, 1187 (1971).
9. R. N. BARUAH, R. P. SHARMA, and J. N. BARUAH. Chem. Ind. **13**, 524 (1983), and references therein.
10. R. E. PARKER and N. S. ISAAC. Chem. Rev. **59**, 737 (1959); S. WINSTEIN and R. B. HENDERSON. *In* Heterocyclic compounds. Vol. 1. *Edited by* R. C. Elderfield. Wiley, New York. 1950. pp. 1–60.
11. G. G. FREEMAN, J. E. GILL, and W. S. WARING. J. Chem. Soc. 1105 (1959).
12. J. R. BAMBURG and F. M. STRONG. *In* Microbial toxins. Vol. VII. *Edited by* S. Kadis, A. Ciegler, and S. J. Ajl. Academic Press, New York. 1971. pp. 224–227.
13. S. G. LEVINE and M. E. WALL. J. Am. Chem. Soc. **81**, 2826 (1959).
14. R. M. SILVERSTEIN, G. C. BASSLER, and T. G. MORRILL (*Editors*). Spectrometric identification of organic compounds. 3rd ed. Wiley, New York. 1974. pp. 223–227.
15. R. GREENHALGH, J. GILBERT, R. R. KING, B. A. BLACKWELL, J. R. STARTIN, and M. J. SHEPARD. J. Agric. Food Chem. **32**, 1416 (1984).
16. J. W. CORNFORTH, R. H. CORNFORTH, and K. K. MATHEW. J. Chem. Soc. 112 (1959).

Competitive photochlorination and kinetic isotope effects for hydrogen/deuterium abstraction from the methyl group in C_2H_6, C_2D_6, CH_3CHCl_2, CD_3CHCl_2, CH_3CCl_3, and CD_3CCl_3

E. TSCHUIKOW-ROUX,[1] JAN NIEDZIELSKI,[2] AND F. FARAJI
Department of Chemistry, University of Calgary, Calgary, Alta., Canada T2N 1N4

Received March 23, 1984[3]

E. TSCHUIKOW-ROUX, JAN NIEDZIELSKI, and F. FARAJI. Can. J. Chem. **63**, 1093 (1985).

The abstraction of hydrogen and deuterium from ethane, 1,1-dichloroethane, 1,1,1-trichloroethane, and some of their deuterated analogs by photochemically generated ground state chlorine atoms has been investigated in the temperature range 7–95°C using methane as competitor. Rate constants and their temperature coefficients are reported for the following reactions:

$$C_2H_6 + Cl \rightarrow CH_3CH_2 + HCl \quad k_1$$
$$C_2D_6 + Cl \rightarrow CD_3CD_2 + DCl \quad k_2$$
$$CH_3C\mathit{H}Cl_2 + Cl \rightarrow CH_3CCl_2 + HCl \quad k_3$$
$$C\mathit{H}_3CHCl_2 + Cl \rightarrow CH_2CHCl_2 + HCl \quad k_4$$
$$CD_3C\mathit{H}Cl_2 + Cl \rightarrow CD_3CCl_2 + HCl \quad k_5$$
$$C\mathit{D}_3CHCl_2 + Cl \rightarrow CD_2CHCl_2 + DCl \quad k_6$$
$$C\mathit{H}_3CCl_3 + Cl \rightarrow CH_2CCl_3 + HCl \quad k_7$$
$$C\mathit{D}_3CCl_3 + Cl \rightarrow CD_2CCl_3 + DCl \quad k_8$$

An Arrhenius law temperature dependence was observed in all cases. Mixed primary and α-secondary kinetic isotope effects are $k_1/k_2 = 2.79 \pm 0.27$, $k_4/k_6 = 4.13 \pm 0.32$, $k_7/k_8 = 1.46 \pm 0.12$ at 298 K and decrease to $k_1/k_2 = 2.53 \pm 0.22$, $k_4/k_6 = 4.06 \pm 0.28$, $k_7/k_8 = 1.45 \pm 0.09$ at 370 K, showing a "normal" temperature dependence. The kinetic isotope effect for H/D abstraction from the methyl group decreases with increasing number of chlorine substituents in the adjacent chloromethyl group. The β-secondary isotope effect, k_3/k_5, is close to unity and shows a slight inverse temperature dependence.

E. TSCHUIKOW-ROUX, JAN NIEDZIELSKI et F. FARAJI. Can. J. Chem. **63**, 1093 (1985).

Opérant à des températures allant de 7 à 95°C et utilisant le méthane comme produit de compétition, on a étudié la réaction d'enlèvement d'hydrogène ou de deutérium de l'éthane, du dichloro-1,1 éthane, du trichloro-1,1,1 éthane et de quelques-uns de leurs analogues deutérés par des atomes de chlore générés d'une façon photochimique et existants dans leur état fondamental. On rapporte les constantes de vitesse et les coefficients de température appropriés pour les réactions suivantes:

$$C_2H_6 + Cl \rightarrow CH_3CH_2 + HCl \quad k_1$$
$$C_2D_6 + Cl \rightarrow CD_3CD_2 + DCl \quad k_2$$
$$CH_3C\mathit{H}Cl_2 + Cl \rightarrow CH_3CCl_2 + HCl \quad k_3$$
$$C\mathit{H}_3CHCl_2 + Cl \rightarrow CH_2CHCl_2 + HCl \quad k_4$$
$$CD_3C\mathit{H}Cl_2 + Cl \rightarrow CD_3CCl_2 + HCl \quad k_5$$
$$C\mathit{D}_3CHCl_2 + Cl \rightarrow CD_2CHCl_2 + DCl \quad k_6$$
$$C\mathit{H}_3CCl_3 + Cl \rightarrow CH_2CCl_3 + HCl \quad k_7$$
$$C\mathit{D}_3CCl_3 + Cl \rightarrow CD_2CCl_3 + DCl \quad k_8$$

Dans tous ces cas, on a observé une relation du type d'Arrhénius entre les vitesses et la température. A 298 K, on a déterminé les effets isotopiques cinétiques mixtes, primaires et secondaires en α, $k_1/k_2 = 2{,}79 \pm 0{,}27$, $k_4/k_6 = 4{,}13 \pm 0{,}32$ et $k_7/k_8 = 1{,}46 \pm 0{,}12$ et, à 370 K, ces valeurs diminuent vers $k_1/k_2 = 2{,}53 \pm 0{,}22$, $k_4/k_6 = 4{,}06 \pm 0{,}28$, $k_7/k_8 = 1{,}45 \pm 0{,}09$; ces résultats sont en accord avec une relation "normale" avec la température. L'effet isotopique cinétique pour l'enlèvement des H/D de groupements méthyles diminue avec une augmentation du nombre de chlores qui sont présents dans le groupe chlorométhyle voisin. L'effet isotopique secondaire-β se rapproche de l'unité et il présente une légère dépendence inverse avec la température.

[Traduit par le journal]

Introduction

The abstraction of hydrogen by ground state chlorine atoms from partially chlorinated methanes and ethanes has been the subject of a number of investigations. Earlier competitive results have been reviewed by Fettis and Knox (1) and, lately, the data have been updated and revised (2, 3). Recent environmental concern regarding the indirect effect of chlorofluoromethane release on the stratospheric ozone balance (4) has resulted in an upsurge of interest in the reactivity of atomic chlorine with hydrogen-containing atmospheric constituents which may provide a sink for Cl atoms, thereby removing them from the Cl/ClO cycle which catalytically destroys odd oxygen in the stratosphere. Although the concentrations of chloroalkanes in the stratosphere are relatively low, they are not negligible, and this has prompted several studies using modern "direct" techniques. Clyne and Walker (5) investigated the reactions of Cl atoms with CH_3Cl, CH_2Cl_2, and $CHCl_3$ using a discharge flow – mass spectrometric technique, and Manning and Kurylo (6) reported on the reaction Cl + CH_3Cl employing the flash photolysis – resonance fluorescence method. Two direct studies have been reported on mono-, di-, and trichloroethanes by Wine *et al.* (7, 8), in which chlorine atoms were produced by 355-nm pulsed laser photolysis of Cl_2 and mon-

[1]Author to whom correspondence should be adressed.
[2]Permanent address: Department of Chemistry, Warsaw University, Warsaw, Poland.
[3]Revision received October 30, 1984.

itored by time-resolved resonance fluorescence spectroscopy. Though, in principle, the direct studies are to be preferred, the technique employed of following the rate of decay of the chlorine atom concentration suffers from its inability to distinguish between the different types of hydrogen in the chloroethane molecule, and, moreover, it cannot match the internal accuracy of modern competitive measurements.

In a recent paper from this laboratory (9) the photochlorination of C_2H_5Cl and C_2D_5Cl was examined using the competitive method. Accurate rate parameters were obtained and, surprisingly, a marked difference was observed in the magnitude of the intermolecular isotope effect involving the α and β hydrogens. To better understand these results, the measurements are presently extended to include the photochlorination of 1,1-dichloro- and 1,1,1-trichloroethane and their deuterated analogs. The experiments on ethane and perdeuterated ethane were also included to check the reliability of the earlier data (10), and for the sake of consistency in searching for the trends in a set of related compounds.

Experimental

The apparatus, light source, and experimental procedures have been described previously (9). Photolyses were carried out in a static system over the temperature range 7−95°C using filtered visible light centered at 424 nm. Only chlorine absorbs at this wavelength, and the ensuing decomposition of an excited Cl_2 molecule yields Cl atoms which are in their ground electronic state for all practical purposes ($Cl(^2P_{3/2}) > 99.2\%$ $Cl(^2P_{1/2}) < 0.8\%$ at 298 K). The temperature of the reactor was kept uniform to within 0.2°C, and dark reactions were never observed.

Three systems were examined: C_2H_6/C_2D_6, CH_3CHCl_2/CD_3CHCl_2, and CH_3CCl_3/CD_3CCl_3. The complementary data for the system CH_3CH_2Cl/CD_3CH_2Cl were taken from our recent publications (11, 12). The only carbon-containing products observed were the primary chlorination products: C_2H_5Cl, C_2D_5Cl, CH_3CCl_3, $CH_2ClCHCl_2$, CD_3CCl_3, $CD_2ClCHCl_2$, CH_2ClCCl_3, CD_2ClCCl_3, and CH_3Cl, the latter originating from the competitor, CH_4. Analyses were performed by isothermal gas chromatography using a 2-m Durapak column and flame ionization detection, at temperature settings in the range 110−150°C depending on compound. Quantitative analysis involved corrections for the relative sensitivities of the F.I. detector response, which were accurately determined (see discussion).

All chemicals used in this study were obtained commercially: research grade chlorine and methane from Matheson; 1,1-dichloroethane from Eastman Organic Chemicals; 1,1,1-trichloroethane (with no stabilizers added) from Matheson, Coleman, and Bell, Manufacturing Chemists; and deuterated compounds from Merck, Sharp and Dohme (Canada). The overall purity of the samples was on the average about 99%. All reactants were purified by repeated distillations *in vacuo* at either methanol or toluene slush temperatures (∼−94°C) until the level of the most deleterious impurities (viz. CH_3Cl and those corresponding to the C_2-photochlorination products) was below the limit of detection. The residual impurities, not exceeding 0.2%, were innocuous and were tolerated. The isotopic purity of the deuterated samples stated by the manufacturer was above 98% in all cases, and was confirmed by mass-spectral analysis.

Results and discussion

The reagents (ethane or one of the chloroethanes, CH_4 as competitor, and Cl_2) were photolyzed at λ ∼424 nm over the temperature range 7−95°C at total pressures of about 21 Torr (1 Torr = 133.3 Pa). Competing reactants were used in at least twenty-fold excess over chlorine to satisfy the requirement of long chains and insure that chain termination is predominantly by radical combination. In several experiments the excess of competing reactants over Cl_2 was varied up to seventy-fold and was found to have no effect on the product ratios. As expected, neither had a factor of ∼10 variation in light intensity. The pertinent rate laws, as well as the verification of the long-chain assumption, have been presented elsewhere (9).

Under these conditions the relevant processes are the eight abstraction reactions

$$[1] \quad C_2H_6 + Cl \rightarrow CH_3CH_2 + HCl$$

$$[2] \quad C_2D_6 + Cl \rightarrow CD_3CD_2 + DCl$$

$$[3] \quad CH_3C\mathit{H}Cl_2 + Cl \rightarrow CH_3CCl_2 + HCl$$

$$[4] \quad C\mathit{H}_3CHCl_2 + Cl \rightarrow CH_2CHCl_2 + HCl$$

$$[5] \quad CD_3C\mathit{H}Cl_2 + Cl \rightarrow CD_3CCl_2 + HCl$$

$$[6] \quad C\mathit{D}_3CHCl_2 + Cl \rightarrow CD_2CHCl_2 + DCl$$

$$[7] \quad CH_3CCl_3 + Cl \rightarrow CH_2CCl_3 + HCl$$

$$[8] \quad CD_3CCl_3 + Cl \rightarrow CD_2CCl_3 + DCl$$

followed by:

$$[9] \quad R + Cl_2 \rightarrow RCl + Cl$$

where R denotes any of the ethyl or chloroethyl radicals formed in reactions [1]−[8]. Since the radicals R are thermal, they can neither decompose nor undergo any internal rearrangements prior to reaction with Cl_2. As has been shown previously in analogous cases (11), under the experimental conditions used, other side reactions involving free radicals such as metathetical hydrogen/deuterium and (or) chlorine exchange, or the abstraction of H or D from the product hydrogen chlorides, are unimportant. These conclusions are also valid for the present system.

In the absence of these complicating features, the rate constant ratio for the competitive photochlorination of RH with a reference compound R′H is given by

$$[10] \quad \frac{k}{k_r} = \frac{\ln\,[RH]_0 - \ln\,[RH]_f}{\ln\,[R'H]_0 - \ln\,[R'H]_f}$$

where the subscripts 0 and f denote initial and final concentrations. Equation [10] is exact, subject only to the long-chain assumption. Since the consumption method is experimentally inconvenient and, moreover, cannot distinguish between different types of H-atoms in the reactant, eq. [10] can be expressed in terms of the product yields.

$$[11] \quad \frac{k}{k_r} = \frac{\ln\,\{1 - [RCl]/[RH]_0\}}{\ln\,\{1 - [R'Cl]/[R'H]_0\}}$$

At very low conversions with respect to both RH and R′H, eq. [11] may be simplified without noticeable error to

$$[12] \quad \frac{k}{k_r} = \frac{[RCl]\,[R'H]_0}{[R'Cl]\,[RH]_0}$$

The approximations involved in the derivation of this expression have been discussed elsewhere and shown to be justified (9, 11).

Equation [12] was used to reduce the data in experiments on di- and trichloroethanes. In experiments on C_2H_6 and C_2D_6 the difference in reactivity between the ethanes and methane is very large. Consequently, CH_4 was necessarily used in large (80- to 150-fold) excess. Still, the conversion of ethane in these experiments was as high as 7−8% for C_2H_6 and about 3 times smaller for C_2D_6. In these cases the simplified eq. [12] was modified by applying a correction factor (13) which, in the

TABLE 1. Relative Arrhenius parameters for H/D abstraction by chlorine atoms[a]

Competitors R_iH/R_jH	A_i/A_j [b,c]	$(A_i/A_j)_{corr}$ [b,d]	$-(E_i-E_j)/R$ (K)
C_2H_6/CH_4	7.41±0.37	7.33±0.38	1298±15
C_2D_6/CH_4	4.16±0.17	4.25±0.18	1147±13
CH_3CH_2Cl/CH_4[e]	1.224±0.013	1.294±0.029	684.2±3.4
CD_3CH_2Cl/CH_4[f]	0.616±0.009	0.661±0.016	343.4±4.4
CH_3CHCl_2/CH_4	0.451±0.011	0.709±0.018	129±8
CD_3CHCl_2/CH_4	0.118±0.005	0.18_8±0.01	102±14
CH_3CCl_3/CH_4	0.432±0.015	1.015±0.038	−541±11
CD_3CCl_3/CH_4	0.301±0.012	0.716±0.03	−550±12
CH_3CHCl_2/CH_4	0.488±0.016	0.619±0.021	894±10
CD_3CHCl_2/CH_4	0.435±0.016	0.575±0.022	920±12

[a]Stated uncertainty limits are ±1σ. Both precision of analyses and errors involved in the determination of the respective correction factors for the F.I. detector sensitivites are accounted for.
[b]Statistical A-factor ratio (*not* reduced on a per atom basis).
[c]A-factor ratios based on initially assumed relative F.I. detector sensitivities of $S = 1$ for all chlorinated C_2-products, but measured $S = 0.51$ for the reference product, CH_3Cl (C.F. (CH_3Cl) = 1.96 relative to CH_3CHCl_2, Table 2).
[d]Corrected A-factor ratios using correction factors (C.F.) from Table 2.
[e]Data taken from ref. 11.
[f]Data taken from ref. 12.

limit, reduces to eq. [11], but which does not require a direct determination of the ratio, $[RCl]/[RH]_0$, the latter being inconvenient and subject to experimental error. These corrections were small, on the level of 2–4%.

In all cases studied, the rate constant ratios conformed to the Arrhenius rate law over the temperature range of this investigation. The results are listed in Table 1, and are based on the usual least-squares treatment, where the quoted error limits are one standard deviation. For each compound examined two different reagent mixtures using two different batches of this compound were prepared. The agreement between these two sets of results was always satisfactory. The uncertainties stated in Table 1 for the pre-exponential factor ratios, A_i/A_j, and activation energy differences $(E_i - E_j)/R$, account for random errors only. These incorporate uncertainties in pressure measurements in the preparation of mixtures, errors in gas-chromatographic peak area determinations, and varying levels of trace impurities from one mixture to another, and from one sample to another.

The differences in flame ionization detector sensitivity towards the compounds of interest are the major contributing factors to systematic errors. These differences were established using authentic samples, and relative correction factors are tabulated in Table 2, with CH_3CHCl_2 arbitrarily chosen as a reference. These correction factors are very significant for the different chloroethanes: the sensitivity decreases markedly with chlorine substitution, and also depends on the position of the halogen(s) for geometric isomers. Further, a discernible isotope effect is observed: the sensitivity decreases with increasing deuterium substitution in the molecule. In two cases authentic samples of the deuterated compounds were not available ($CD_2ClCHCl_2$ and CD_2ClCCl_3). In this instance the correction factors were evaluated by interpolation (Table 2).

The sensitivity corrections which affect the pre-exponential factor ratios but not the activation energy differences have been allowed for in Table 1 under the heading $(A_i/A_j)_{corr}$. Other systematic errors, e.g. those due to the isotopic impurities, deviations from the true Gaussian distribution, and to the as-

TABLE 2. Correction factors (C.F.) for the relative sensitivity of the flame ionization detector towards chlorohydrocarbons of interest

RCl	C.F.[a]
CH_3CHCl_2	1.00[b]
CH_3Cl	1.96±0.003
C_2H_5Cl	0.989±0.011
C_2D_5Cl	1.022±0.013
CH_2ClCH_2Cl	1.057±0.013
CH_2ClCD_2Cl	1.072±0.013
CH_3CCl_3	1.268±0.014
CD_3CCl_3	1.321±0.021
$CH_2ClCHCl_2$	1.571±0.009
$CD_2ClCHCl_2$[c]	1.59±0.02
CH_2ClCCl_3	2.349±0.035
CD_2ClCCl_3[d]	2.38±0.05

[a]The correction factor is defined as: C.F. (RCl) = $S(CH_3CHCl_2)/S(RCl)$.
[b]1,1-Dichloroethane was arbitrarily chosen as a reference.
[c]Estimate: C.F.($CD_2ClCHCl_2$) = C.F.($CH_2ClCHCl_2$) × C.F. (CD_2ClCH_2Cl)/C.F.(CH_2ClCH_2Cl).
[d]Estimate: C.F.(CD_2ClCCl_3) = C.F.(CH_2ClCCl_3) × C.F.(CD_2ClCH_2Cl)/C.F.(CH_2ClCH_2Cl).

sumptions inherent in the simplified reaction mechanism are estimated to be of little importance.

Rate constants and absolute Arrhenius parameters

Based on the relative rate parameters reported in Table 1, the absolute Arrhenius parameters were calculated and assembled in Table 3 using the absolute rate constant value ($cm^3\ s^{-1}$) for the chlorination of methane determined by Keyser (14) for the temperature range 291 to 423 K,

$$[13]\quad k_{CH_4} = (1.65 \pm 0.32) \times 10^{-11} \exp[-(1530 \pm 68)/T]$$

We consider this value to be more appropriate for our range of temperatures than that recommended by the NASA panel (3) in the range 200–300 K applicable to stratospheric temperatures. Our rate parameters for the photochlorination of C_2H_6 differ significantly from those recommended by the NASA panel. However, if their preferred value for the methane reference reaction were to be adopted, reasonable agreement is achieved. This may be taken as an indication that Keyser's values for the rate parameters are too large. Nevertheless, for the sake of consistency with our former data on chloroethane, Keyser's value for k_{CH_4} is retained, particularly since it overlaps our temperature range.

In the case of the other compounds reported here, data from other laboratories that could be compared with our results are sparse. Chiltz *et al.* (10) reported the rate constant ratios, k_1/k_2, at several temperatures in the range 302–433 K for the direct competition in C_2H_6/C_2D_6 mixtures using a mass spectrometric technique. Although these data show a high degree of scatter when plotted according to the Arrhenius rate law, an approximate temperature dependence is given by $\ln(k_1/k_2) = 0.53 + 137/T$, in satisfactory agreement with our value of $\ln(k_1/k_2) = 0.545 + 151/T$ based on the data in Table 1.

Cillien *et al.* (15) have reported the relative and absolute parameters for the chlorination of 1,1-dichloroethane, in the absence and presence of CH_3Cl as competitor. The values of the Arrhenius parameters for this reference reaction used in the

TABLE 3. Absolute rate parameters for H/D atom abstraction by chlorine atoms[a,b]

Reactant	A	E/R	k_{298}	k_{298}/n	Reference
$\mathrm{C_2H_6}$	121±24(6)	232±70(15)	56±15	9.3	This work
	77	90±90	57	9.5	3
$\mathrm{C_2D_6}$	70±14(3)	383±69(13)	19±5	3.2	This work
	45	226±(>100)[c]	21	3.5	10[d]
	68	368±(>100)[c]	20	3.3	10[e]
$\mathit{CH_3}\mathrm{CH_2Cl}$	21.3±4(0.5)	846±68(3)	1.25±0.3	0.4	11
$\mathrm{CH_3}\mathit{CH_2}\mathrm{Cl}$	23.5±4(0.4)	417±68(3)	5.8±2.7	2.9	11
$\mathit{CD_3}\mathrm{CH_2Cl}$	10.8±2(0.3)	1189±68(4)	0.20±0.05	0.067	12
$\mathit{CH_3}\mathrm{CHCl_2}$	11.7±2(0.3)	1401±68(8)	0.11±0.03	0.035	This work
	9.6	1460±360	0.071_5	0.024	15[f]
	8.5±1.8	1420±298	0.072±0.05	0.024	15[g]
$\mathrm{CH_3}\mathit{CH}\mathrm{Cl_2}$	10.2±2(0.3)	636±68(10)	1.2±0.3	1.2	This work
	7.6±2	665±300	0.8±0.5	0.8	15[g]
	8.2±1	554±36	1.3±0.2		8[h]
$\mathit{CD_3}\mathrm{CHCl_2}$	3.1±0.6(0.1)	1428±69(14)	0.026±0.007	0.0086	This work
$\mathrm{CD_3}\mathit{CH}\mathrm{Cl_2}$	9.5±2(0.4)	610±68(12)	1.2±0.3	1.2	This work
$\mathit{CH_3}\mathrm{CCl_3}$	16.7±3(0.6)	2071±68(11)	0.016±0.004	0.0053	This work
	2.4	1856±535	0.0047	0.0016	15[f]
	2.1±0.7	1817±500	0.0047±0.03	0.0016	15[g]
		>1200	<0.037		7[i]
$\mathit{CD_3}\mathrm{CCl_3}$	11.8±2(0.5)	2080±68(12)	0.011±0.003	0.0037	This work

[a]Units for A and k_{298} are 10^{-12} cm^3 s^{-1}. k_{298}/n = rate constant per available hydrogen. Units for E/R are Kelvin.
[b]Stated uncertainties in Arrhenius factors allow for error limits of the reference reaction: $\mathrm{Cl + CH_4 \rightarrow CH_3 + HCl}$. Unless otherwise indicated, values in brackets denote uncertainties in competitive experiments only.
[c]Estimated lower error limits.
[d]Data based on competitive experiments against $\mathrm{C_2H_6}$; recalculated using rate parameters for reference reaction recommended in ref. 3.
[e]Data based on competitive experiments against $\mathrm{C_2H_6}$; recalculated using rate parameters for $\mathrm{C_2H_6}$ reported in this work.
[f]Data based on competitive experiments against $\mathrm{CH_3Cl}$; recalculated using rate parameters for $\mathrm{CH_3Cl}$ from ref. 3.
[g]Data based on competitive experiments against $\mathrm{CH_3Cl}$; recalculated using rate parameters for $\mathrm{CH_3Cl}$ from ref. 13.
[h]Direct laser FP–RF measurements; primary and tertiary hydrogens were not distinguishable.
[i]Direct laser FP–RF measurement; only lower limit for E/R determined.

original work are no longer tenable. The reevaluated rate constant (cm^3 s^{-1}) for methyl chloride

$$[14] \quad k_{\mathrm{CH_3Cl}} = 3.4 \times 10^{-11} \exp\,[-(1260 \pm 200)/T]$$

recommended by the NASA panel (3) based on the preferred absolute measurements of Manning and Kurylo (6) agrees well with our competitive measurements against ethyl chloride (13)

$$[15] \quad k_{\mathrm{CH_3Cl}} = (3.02 \pm 0.61) \times 10^{-11} \exp\,[-(1221 \pm 68)/T]$$

Using these new values to recalculate the absolute rate parameters of Cillien *et al.* we obtain good agreement with respect to the activation energy (Table 3). It should be noted that $\mathrm{CH_3CHCl_2}$ represents an internally competitive system, and the product ratio determines the relative rate constants directly: $k_3/k_4 = [\mathrm{CH_3CCl_3}]/\mathrm{CH_2ClCHCl_2}]$. In the case of simultaneous internal competition against an external standard, eq. [12] is also valid for each identifiable product. The results are shown in Table 4 and compared with $\mathrm{CH_3CH_2Cl}$ and with the internal competition data for $\mathrm{CH_3CHCl_2}$ of Cillien *et al.* (15) over the temperature range 303–353 K. It should be noted that since no external competitor is involved, the uncertainties associated with the latter do not enter into this direct comparison. The agreement in the activation energy difference between tertiary and primary hydrogens in $\mathrm{CH_3CHCl_2}$ is excellent, while the ratio of pre-exponential factors differs by about 30%. This discrepancy could result if the differences in sensitivities of the detector response toward tri-substituted photolysis products were not accounted for in the earlier work. The only other report on the rate parameters for the chlorination of $\mathrm{CH_3CHCl_2}$ is by Wine and Semmes (8) based on laser flash photolysis – resonance fluorescence measurements. Unfortunately, as noted earlier, in this direct investigation no distinction can be made between the abstraction of tertiary and primary hydrogens in the molecule, since the reaction was followed by measuring only the rate of decay of Cl atoms. Their rate constant for the abstraction reaction is therefore a composite of two contributions. In the light of the Arrhenius parameters for the primary and tertiary hydrogen abstraction presented in Table 3, the activation energy for the "mixed" processes reported by Wine and Semmes seems to be too low.

The reaction of chlorine atoms with 1,1,1-trichloroethane has also been investigated competitively by Cillien *et al.* (15) and directly by Wine, Semmes, and Ravishankara (7). In this case only one type of hydrogen is available and the results of

TABLE 4. Relative rate parameters for internal competition: Cl + CH_3CH_2Cl and Cl + CH_3CHCl_2[a]

Compound	$A_{s,t}/A_p$[b]	$(A_{s,t}/n_{s,t})/(A_p/n_p)$[c]	$-(E_{s,t}-E_p)$ (cal mol^{-1})	$(k_{s,t}/n_{s,t})/(k_p/n_p)$[c] at 298 K	Reference
CH_2CH_2Cl	1.099±0.015	1.649±0.023	853±4	6.96±0.11	11
CH_3CHCl_2	0.89±0.21	2.67±0.60	1500±150	34±12	15
	1.145±0.05	3.435±0.145	1520±23	45±2.5	This work

[a]Stated uncertainties represent $\pm 1\sigma$.
[b]Subscripts s and t refer to secondary hydrogens in CH_3CH_2Cl or to tertiary hydrogen in CH_3CHCl_2, respectively; subscript p refers to primary hydrogens in the methyl groups of both compounds.
[c]Ratios given per available C—H bond.

both methods should be comparable directly. Regrettably, due to the slow nature of the reaction and the onset of complicating features attributed to secondary processes at the higher temperatures, Wine *et al.* could only establish a lower limit for the activation energy (Table 3). Comparison among the competitive studies shows that the activation energy determined in this work agrees with the recalculated values of Cillien *et al.*, given the large uncertainty in the latter work. However, the pre-exponential factors are in marked disagreement and, in this case, can not be reconciled on the basis of detector sensitivity corrections.

Inspection of Table 3 shows that both the *A*-factors and the activation energies are affected by chlorine substitution. The dominant feature with respect to reactivity is, firstly, the progressive increase in activation energies, in both the α and β positions, with increasing Cl substitution on the same carbon atom. Secondly, hydrogen abstraction is faster from the *substituted* carbon atom in a molecule with the *same* number of chlorine atoms, viz., $k(CH_3C\mathit{H}_2Cl) > k(C\mathit{H}_3CH_2Cl)$; $k(CH_3C\mathit{H}Cl_2) > k(C\mathit{H}_3CHCl_2)$. The highest activation energy and the slowest rate are observed for CH_3CCl_3 where there are only primary hydrogens. Similar trends have also been found in the case of fluoroethanes (13, 16, 17). A plausible qualitative explanation of these observations may be sought in terms of repulsive and electron withdrawal effects by the bound chlorine atom(s). The general trend of increasing activation energy and hence lower reactivity with increasing number of chorine substituents may then be attributed to the repulsion of the approaching chlorine atom by the bonded chlorine(s). It would appear that such repulsion should be more pronounced at the chlorinated site, yet the attack on the secondary hydrogen in CH_3CH_2Cl and tertiary hydrogen in CH_3CHCl_2 is faster than on the vicinal methyl group. This may be attributed to the electron-withdrawing power of the electronegative chlorine: the electrons are drawn towards the bound Cl atom(s), thus weakening the C—H bonds in the methylene and methine groups, respectively. Thus there is evidently a concerted effect of repulsion and electron withdrawal by the bound chlorines. The fact that hydrogen abstraction from the chlorinated group in CH_3CHCl_2 is slower than in CH_3Cl_2Cl further suggests that the repulsive effect increases with the number of chlorine substituents.

Although the argument based on repulsion and electronegativity considerations is simple and adequate, an opposite point of view has been presented by Johnston and Goldfinger (18) to rationalize the strong disagreement between the observed trend of activation energy with bond energy for hydrogen abstraction by Cl atoms from chlorinated methanes and ethanes (based on the then available data) and that calculated from LEPS and BEBO potential energy surfaces. Seeking an explanation in terms of nonbonding interactions between the incident and bound chlorine atoms (considered as symmetrical groups), these authors evaluated the Lennard–Jones 6–12 potential function and showed that for the dimensions of their activated complexes the interactions were on the attractive part of the potential. Therefore, the observed activation energies were ascribed not to van der Waals repulsions, but to dynamic effects of attractive dispersion forces between bound and free chlorine atoms. According to Johnston and Goldfinger, the preferential attraction of the chlorine atom by the bound chlorine results in collision complexes of the form >CH—Cl---Cl predominating over those of the form >CCl—H---Cl; thus unless the approaching atom has a relatively high kinetic energy, the hydrogen atom transfer complex never forms. This rather curious conclusion must be questioned in the light of more recent data on the activation energies for H by Cl abstraction and C—H bond dissociation energies, at least in the case of the chloromethane series. A comparison of the activation energies (values in kcal mol^{-1}) in CH_3Cl (3.6), CH_2Cl_2 (2.9), $CHCl_3$ (2.8) reported by Clyne and Walker (5) shows a distinct trend, if not a one-to-one correspondence, with the C—H bond dissociation energies: 102.9; 100.6; 95.2 kcal mol^{-1}, respectively, reported most recently by Weissman and Benson (19). The activation energy for Cl + CH_3Cl determined by Clyne and Walker is higher than that reported by Manning and Kurylo (6) and may be subject to a systematic error (3); however, we have used it here for the sake of internal consistency in this comparison. It is tempting to provide a similar comparison for the chloroethane series. Unfortunately, to date, "measured" C—H bond dissociation energies are not available for most of the chloroethanes, except for $CHCl_2CHCl_2$ and C_2HCl_5 (20). It was based on these data and the known value of $D(C_2H_5$—H) that Franklin and Huybrechts (21) assumed that $D(R_{Cl}$—H) = 98.0, 96.7, and 95.4 kcal mol^{-1} for primary, secondary, and tertiary C—H bonds, respectively, in those chloroethanes for which experimental values are not available. This is inadequate for the present purpose, especially in view of the kinetic data for the chlorination of CH_3CCl_3. Wine and Semmes (8) have argued convincingly that the substitution of Cl on one carbon atom substantially increases the C—H bond strength on the adjacent carbon atom, citing in support of CH_3CCl_3 its fluorinated analog, CH_3CF_3, in which the C—H bond is known to be extremely strong, $D(CF_3CH_2-H) = 106.7$ kcal mol^{-1} (20). A similar view with respect to fluoroethanes has been expressed by McMillen and Golden (20). In fact, Wine and Semmes carried the analogy of the reactivity trends observed in the chloromethane series to the chloroethanes, and suggested that the substitution of Cl in the α-position not only strengthens the C—H bond on the β carbon but also weakens the remaining C—H bonds on the α-carbon. Our results on the chlorination of both chloroethanes and fluoroethanes (13) support this contention.

TABLE 5. Kinetic isotope effects[a] for hydrogen/deuterium abstraction by chlorine atoms

	k_i/k_j			
	T=280 K	310 K	340 K	370 K
CH_3CH_3/CD_3CD_3[b]	2.88 ± 0.28	2.74 ± 0.26	2.62 ± 0.23	2.53 ± 0.22
CH_3CH_2Cl/CD_3CH_2Cl	6.62 ± 0.21	5.88 ± 0.18	5.34 ± 0.16	4.92 ± 0.15
CH_3CHCl_2/CD_3CHCl_2	4.15 ± 0.33	4.11 ± 0.31	4.08 ± 0.29	4.06 ± 0.28
CH_3CCl_3/CD_3CCl_3	1.46 ± 0.12	1.46 ± 0.12	1.45 ± 0.10	1.45 ± 0.09
CH_3CHCl_2/CD_3CHCl_2[c]	$0.97_8\pm0.08$	$0.98_7\pm0.08$	$0.99_5\pm0.07$	1.00 ± 0.07

[a]Primary and α-secondary kinetic isotope effects are not separated.
[b]Unless otherwise noted, any contributions from the β-secondary kinetic isotope effect (KIE) are not taken into account.
[c]Pure β-secondary KIE.

TABLE 6. Comparison of kinetic isotope effects for H/D abstraction by Cl atoms at 298 K

RH/R'D	k_H/k_D	ΔH^0_{298} (kcal mol^{-1})[a]	Reference
C_2H_6/C_2D_6	2.69[b]	−5.1	10
	5.88		[c]
	3.4		24
	2.79		This work
CH_3CH_2Cl/CD_3CH_2Cl	6.20	−5.2[d]	11, 12
CH_3CH_2Cl/CH_3CD_2Cl	2.23	−6.5[d]	11
$CHCl_3/CDCl_3$	4.0[b]	−7.8	10
	2.5		24
CH_3CHCl_2/CD_3CHCl_2	4.13	−5.2[d]	This work
CH_3CCl_3/CD_3CCl_3	1.46	−5.6[d]	This work

[a]Enthalpy change for the reaction RH + Cl → R + HCl.
[b]From a plot of the data in ref. 10 according to the Arrhenius rate law.
[c]Calculated from reevaluated absolute Arrhenius parameters in ref. 2.
[d]Based on thermochemical data and interpolated heats of formation for haloethyl radicals from ref. 21 (but see text).

Isotope effects

Rate constant ratios for H/D atom abstraction from compounds of interest at four selected temperatures are listed in Table 5. A few literature values that are available are included for comparison in Table 6. It should be emphasized that the measured intermolecular hydrogen−deuterium kinetic isotope effects consist of contributions from the primary and secondary isotope effects. Secondary contributions arise since the isotopic composition of the residual ethyl or chloroethyl groups is different. Although the contributions from the α-secondary isotope effect are, as recently shown (22), small, but not negligible, the present results do not permit us to extricate these contributions.

Our data on the C_2H_6/C_2D_6 system are in close agreement with those of Chiltz *et al.* (10). The isotope effect is rather weak compared to the so-called "theoretical maximum", which is based on a one-dimensional three-particle model but which ignores any tunneling correction. According to this simplified treatment applicable to hydrogen atom transfer reactions, the maximum kinetic isotope effect is related to the zero-point energy difference of the atoms being transferred in the reactants (23):

$$[16] \quad (k_H/k_D)_{max} = \exp\,[(E_{Z,RH} - E_{Z,RD})/RT]$$

For the C_2H_6/C_2D_6 system, $(k_H/k_D)_{max} \approx 8$ at 298 K. The temperature dependence of the primary (plus α-secondary) kinetic isotope effects (KIE) for this and the three chlorine substituted systems is normal: the KIE decreases with temperature (Table 5). A comparison of the chlorinated pairs with C_2H_6/C_2D_6 shows a significant change: the KIE for H/D abstractions from the methyl group is ~2.2 times larger in the case of the monochlorinated species. With increasing chlorine substitution the KIE decreases markedly, such that for the CH_3CCl_3/CD_3CCl_3 system it is about 1/2 the value for C_2H_6/C_2D_6. A comparison of H/D abstraction associated with the methyl and methylene groups in the chloroethane pairs (Table 6) reveals that the KIE for the primary hydrogens is about 3 times larger. In this instance the qualitative generalization postulated by Lewis (23): "With two hydrogen atom transfers of equal exothermicity, the one of higher activation energy will have the more nearly symmetrical transition state and hence the higher isotope effect" is roughly obeyed, given the uncertainties in the heats of reaction. However, this conclusion cannot be extended to the KIE associated with the pairs CH_3CH_2Cl/CD_3CH_2Cl, CH_3CHCl_2/CD_3CHCl_2, and CH_3CCl_3/CD_3CCl_3 based on the thermochemical data and interpolations of Franklin and Huybrechts (21) which predict almost equal exothermicities for hydrogen abstraction by Cl atoms for the three chloroethanes (Table 6). Since the activation energy increases significantly in going from CH_3CH_2Cl to CH_3CHCl_2 to CH_3CCl_3 (Table 3) while the KIE shows a strong opposite trend (Table 6), either the generalization of Lewis breaks down in this case, or the thermochemical data are inadequate. Our results, taken in conjunction with those of Cillien *et al.* (15) and Wine *et al.* (7, 8) strongly suggest that the C—H bond energies in chloroethanes and the estimated heats of formation of chlorinated ethyl radicals are in need of revision.

Finally, it is worth noting that our results yield the magnitude of the β-secondary kinetic isotope effect in the system CH_3CHCl_2/CD_3CHCl_2, k_3/k_5. This weak effect is unity within the limits of experimental error. However, the pre-exponential factors and activation energies for reactions [3] and [5] are different. The difference is barely outside the quoted error limits but the trends confirm our former observations concerning β-secondary kinetic isotope effects in the photochlorination of ethyl chlorides (11, 12): both the A-factor and the activation energy decrease as a result of deuterium substitution in the adjacent group, i.e., in going from CH_3CHCl_2 to CD_3CHCl_2, the activation energy difference accounting for the inverse temperature dependence.

Acknowledgement

The financial support of the Natural Sciences and Engineering Research Council of Canada is gratefully acknowledged.

1. G. C. FETTIS and J. H. KNOX. *In* Progress in reaction kinetics. Vol. 2. *Edited by* G. Porter. Pergamon Press and Macmillan, New York. 1964.
2. J. A. KERR and S. J. MOSS (*Editors*). CRC Handbook of bimolecular and termolecular gas reactions. Vol. 1. CRC Press Inc., Boca Raton, Florida. 1981.
3. Chemical kinetics and photochemical data for use in stratospheric modeling. Evaluation No. 6, JPL Publication 83-62, Jet Propulsion Laboratory, Pasadena, California, 1983, and references cited therein.
4. F. S. ROWLAND and M. J. MOLINA. Rev. Geophys. Space Phys. **13**, 1 (1975).
5. M. A. A. CLYNE and R. F. WALKER. J. Chem. Soc. Faraday Trans. I. **69**, 1547 (1973).
6. R. G. MANNING and M. J. KURYLO. J. Phys. Chem. **81**, 291 (1977).
7. P. H. WINE, D. H. SEMMES, and A. R. RAVISHANKARA. Chem. Phys. Lett. **90**, 128 (1982).
8. P. H. WINE and D. H. SEMMES. J. Phys. Chem. **87**, 3572 (1983).
9. E. TSCHUIKOW-ROUX, T. YANO, and J. NIEDZIELSKI. J. Phys. Chem. **88**, 1408 (1984).
10. G. CHILTZ, R. ECKLING, P. GOLDFINGER, G. HUYBRECHTS, H. S. JOHNSTON, L. MEYERS, and G. VERBEKE. J. Chem. Phys. **38**, 1053 (1963).
11. J. NIEDZIELSKI, E. TSCHUIKOW-ROUX, and T. YANO. Int. J. Chem. Kinet. **16**, 621 (1984).
12. J. NIEDZIELSKI and E. TSCHUIKOW-ROUX. Chem. Phys. Lett. **105**, 527 (1984).
13. E. TSCHUIKOW-ROUX, T. YANO, and J. NIEDZIELSKI. J. Chem. Phys. **82**, 65 (1985).
14. L. F. KEYSER. J. Chem. Phys. **69**, 214 (1978).
15. C. CILLIEN, P. GOLDFINGER, G. HUYBRECHTS, and G. MARTENS. Trans. Faraday Soc. **63**, 1631 (1967).
16. P. CADMAN, A. W. KIRK, and A. F. TROTMAN-DICKENSON. J. Chem. Soc. Faraday Trans. 1, **72**, 1027 (1976).
17. G. J. MARTENS, M. GODFROID, J. DELVAUX, and J. VERBEYST. Int. J. Chem. Kinet. **8**, 153 (1976).
18. H. S. JOHNSTON and P. GOLDFINGER. J. Chem. Phys. **37**, 700 (1962).
19. H. WEISSMAN and S. W. BENSON. J. Phys. Chem. **87**, 243 (1983).
20. D. F. MCMILLEN and D. M. GOLDEN. Ann. Rev. Phys. Chem. **33**, 493 (1982).
21. J. A. FRANKLIN and G. H. HUYBRECHTS. Int. J. Chem. Kinet. **1**, 3 (1969).
22. E. TSCHUIKOW-ROUX and J. NIEDZIELSKI. J. Photochem. **27**, 141 (1984).
23. E. S. LEWIS. *In* Isotopes in organic chemistry. Vol. 2. *Edited by* E. Buncel and C. C. Lee. Elsevier Scientific Publishing Co., Amsterdam. 1976. p. 127.
24. E. S. LEWIS. Top. Curr. Chem. **74**, 31 (1978).

The sorption of uranyl species on a hematite sol[1]

C. H. HO AND D. C. DOERN

Research Chemistry Branch, Whiteshell Nuclear Research Establishment, Atomic Energy of Canada Limited, Pinawa, Man., Canada R0E 1L0

Received December 20, 1983[2]

C. H. HO and D. C. DOERN. Can. J. Chem. **63**, 1100 (1985).

The sorption of uranyl species on a hematite sol of narrow size distribution has been studied as a function of uranium concentration and solution pH. The adsorption increases with increasing uranium content in the solution. Raising the pH from 5 to about 6.2 markedly enhances the uptake of uranium. The enhanced uptake coincides with a proportional increase of $(UO_2)_3(OH)_5^+$. The sudden increase in adsorption around this pH region does not appear to be due to changes in surface charge of the hematite particles. It may be due to specific interactions between $(UO_2)_3(OH)_5^+$ and the hematite particles. Results of desorption experiments show that different binding sites may exist on the hematite surface.

C. H. HO et D. C. DOERN. Can. J. Chem. **63**, 1100 (1985).

On a étudié la variation de la sorption d'espèces d'uranyles, sur un sol d'hématite avec une distribution étroite de la taille des particules, en fonction de la concentration de l'uranium et du pH de la solution. L'adsorption augmente avec une augmentation de la concentration de l'uranium dans la solution. Une augmentation du pH de 5 à 6,2 fait augmenter l'adsorption d'uranium d'une façon importante. L'augmentation de l'adsorption coïncide avec une augmentation proportionnelle de la concentration du $(UO_2)_3(OH)_5^+$. L'augmentation subite de l'adsorption autour de cette région de pH ne semble pas due à des changements dans la charge de la surface des particules d'hématite. Elle pourrait être due à des interactions spécifiques entre le $(UO_2)_3(OH)_5^+$ et les particules d'hématite. Les résultats des expériences de désorption montrent qu'il pourrait exister différents sites de fixation sur la surface de l'hématite.

[Traduit par le journal]

Introduction

The sorption of metal ions on oxide surfaces is important in many technical areas such as ore processing and environmental pollution studies. It is also important when considering the transport of radionuclides in a geological waste-disposal vault. Waste forms could be subjected to groundwater attack, and actinides such as uranium could be released into the groundwater and adsorbed onto mineral surfaces or particulates (such as iron oxyhydroxides) already in the groundwater (1).

We have chosen to study uranium as the first step in a more general study of actinide adsorption onto colloidal particles. A number of studies on adsorption of uranium from aqueous solution have been reported (2–4). Most have emphasized adsorption on natural geological materials such as clay and basalt. Because not enough is known about either the state of the adsorbed uranium or the sorption mechanism onto any specific adsorbent, it is difficult to predict accurately the effect of sorption on the mobility of uranium.

The present study was directed towards achieving a better understanding of the mechanism of uranium adsorption on hematite. Hematite is an important component of geological formations found in close association with uranium under natural conditions (5). Therefore, information about the adsorption of actinides onto hematite will help in assessing actinide mobility. To this end, a hematite sol of narrow size distribution was synthesized and characterized. The adsorption and desorption of uranium on this sol were investigated over a range of pH values ($3 \leq pH \leq 6.2$), with particular emphasis on the correlation of uranium adsorption with the uranyl species present over this pH range.

Experimental

Materials

Distilled water was passed through two ion-exchange columns and then redistilled in a grease-free Pyrex still. The ferric chloride was Baker Analyzed Reagent. All other chemicals were reagent grade and were used without further purification.

The hematite sol was prepared by hydrolysis at 100°C of ferric chloride for about 24 h, and the particles were examined in an International Scientific Instrument DS Model 130 scanning electron microscope equipped with a Tracor Northern Particle Recognition and Characterization device for particle size and size distribution analysis. Specific surface area measurements were obtained by the BET method, using nitrogen gas as the adsorbate. The composition of the particles was determined by X-ray diffraction. The isoelectric point was obtained using a Rank Brothers Microelectrophoresis Apparatus. Infrared spectra were obtained in KBr medium using a Nicolet Model MX-1 Fourier Transform Infrared Spectrometer.

Methods

Uranium adsorption was determined by measuring the depletion of uranyl ions in a supernatant solution with a Cary 210 Ultraviolet spectrophotometer, using 2-(5-bromo-2-pyridylazo)-5-diethylaminophenol as a chromogenic reagent (6). A constant particle concentration of 0.2 g dm^{-3} was used with a contact time of 16 h. Trial experiments showed that adsorption did not change significantly for a longer contact time of 40 h. The experimental procedure was as follows: A series of uranyl solutions and the hematite sol were prepared at the required concentration, pH, and ionic strength (using 5×10^{-4} mol dm^{-3} NaCl, NaOH, or HCl). Then 10 cm^3 of the hematite sol was transferred to a polycarbonate centrifuge bottle containing 10 cm^3 of uranyl nitrate solution. The mixture was shaken for 16 h in a water bath at 25 ± 0.1°C. The solid was separated from the liquid in a Beckman L8-55 Ultracentrifuge and the supernatant solution was analyzed for uranium content. The pH of the supernatant was also noted. A control without hematite was prepared, and duplicate runs were performed for each series of experiments. The electrophoretic mobility of the particles was determined after diluting a portion of uranium-loaded hematite particles with centrifuged supernatant to give a suitable concentration for observation. Only the pH of the supernatant solution was used in the results.

Desorption of uranium from loaded hematite was studied in two separate experiments. In the first, a portion of the supernatant solution was replaced by the same volume of fresh solution with the same pH and salt concentration as the adsorption solution. In the second, the pH

[1]AECL No. 8038.
[2]Revision received May 18, 1984.

TABLE 1. Characteristics of the hematite particles

Characteristic	Value
Particle size (μm)	0.12
Specific surface area ($m^2\ g^{-1}$)	34
Chemical composition (% α-Fe_2O_3)	>98
Isoelectric point	7.6

of the mixture was lowered fom 6.19 to about 4 using concentrated HCl immediately after the adsorption process. After equilibrating the mixture for an appropriate time, aliquots of the supernatant were removed, and the uranium concentration was determined. The pH of the supernatant was also measured.

Results and discussion

Characterization

Table 1 shows the characteristics of the synthesized hematite particles. The particle shape is uniform and the size distribution is very narrow. X-ray diffraction data were consistent with the particles being α-Fe_2O_3 containing less than 2% β-FeO(OH).

Adsorption

Figure 1 shows the dependence of the amount of uranium adsorbed on the equilibrium solution concentration of uranium at various pH values of the media. Significant adsorption does occur, even though the hematite particles possess net positive charge in the pH range from 3 to 6.5. This suggests that there must be a non-electrostatic contribution to the overall free energy of adsorption that outweighs the repulsive coulombic and solvation forces. The adsorption was greatest at a pH of about 6.2 and decreased markedly at lower pH values.

In an earlier study, Borovec (3) used the Freundlich isothermal relation to interpret his experimental data for the adsorption of uranyl ions by fine clay. Borovec's data conformed well with the Freundlich equation for uranyl concentrations below 1×10^{-4} mol dm^{-3}. Recently, Langmuir (7) used the Langmuir equation to analyze his data for the adsorption of uranium on iron oxyhydroxide. He suggested that the non-linearity of the plot might be due to different adsorption mechanisms. However, in the present study, the experimental data were not analyzed by the conventional adsorption isotherms because (*i*) a number of uranyl species exist in the solution; (*ii*) one or more uranyl species may be involved in the adsorption process; and (*iii*) the proportions of uranyl species change with the total uranium content in the solution.

Several attempts have been made to explain the variation in adsorption of hydrolyzable cations with respect to pH. In general, hydrolysis of cations to form other soluble and/or insoluble species is assumed to be an important factor in this variation; however, quantitative data on the hydrolysis of uranium(VI) are scarce. Calculations based on Sillen and Martell's thermochemical data (8) have shown that the hydrolysis of uranium (VI) could form a variety of aquo complexes such as $UO_2(OH)^+$, $(UO_2)_2(OH)_2^{2+}$, and $(UO_2)_3(OH)_5^+$. The proportion of each species depends on the total uranyl ion concentration and solution pH. Recently, Toth and Begun (9) used Raman spectroscopy to detect different hydrolyzed uranium species in an aqueous medium, and found that the predominant species in the pH region 1.30 to 4.02 were UO_2^{2+}, $(UO_2)_2(OH)_2^{2+}$, and $(UO_2)_3(OH)_5^+$. Although their uranyl ion concentrations were higher than those of other workers, the results agree with the data from Sillen and Martell (8) and Baes and Mesmer (10).

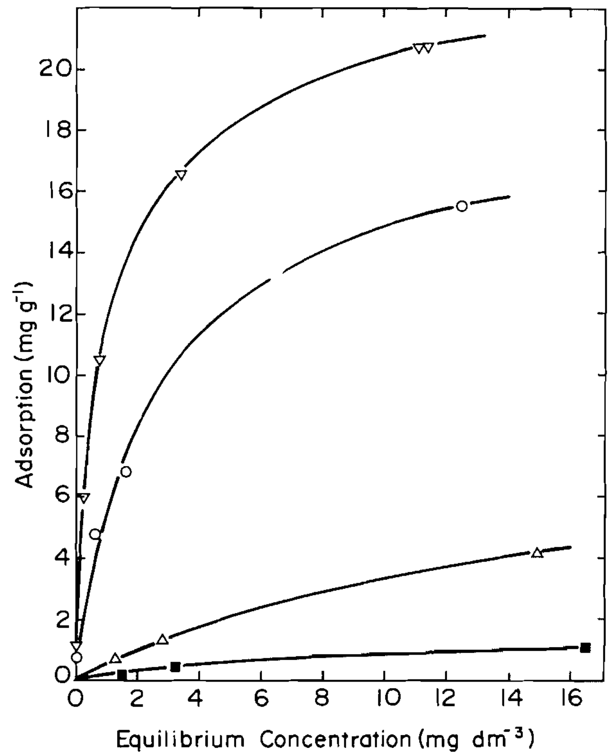

FIG. 1. Effect of pH on the adsorption of uranyl species on hematite at 25°C in 5×10^{-4} mol dm^{-3} NaCl: ∇, pH 5.95–6.19; $\bigcirc$, pH 5.26–5.45; $\triangle$, pH 4.51–4.58; $\blacksquare$, pH 3.04–3.06.

Figure 2 shows the fraction of uranium adsorbed as a function of pH, together with the hydrolysis data from Baes and Mesmer (10), at a uranyl ion concentration of 1×10^{-5} mol kg^{-1}. At pH < 4, where UO_2^{2+} is the predominant species, the adsorption is very small. This suggests that UO_2^{2+} is not the active species involved in adsorption. As the pH is increased, the adsorption of uranium increases abruptly. The sudden increase in adsorption around pH 5 could not be related to the surface charge of the hematite particles. As shown in Fig. 4, a change of solution pH from 4 to 6.2 results in only a slight decrease in the electrophoretic mobility of the hematite particles (dotted line). The reduction in the ζ potential of the hematite particles is considered to be too small to produce such a dramatic effect on the adsorption of uranium ions. However, this sudden increase in adsorption coincides with a marked increase in the amount of $(UO_2)_3(OH)_5^+$ and, therefore, $(UO_2)_3(OH)_5^+$ may be responsible for the increased uptake of uranium. The coulombic repulsion between $(UO_2)_3(OH)_5^+$ and the positively charged oxide surface is presumably less than for UO_2^{2+}, thereby permitting increased uptake of uranium. Moreover, the lowering of the ionic charge of hydrolyzed uranium (VI) ion would cause a decrease in secondary solvation energy, thereby enhancing the adsorption. Similar adsorption behaviour has been observed with other hydrolyzable cations. For instance, the adsorption of thorium(IV) (11) on silver iodide was observed to increase sharply as soon as hydrolysis became significant. Although other uranyl species such as UO_2OH^+ and $(UO_2)_2(OH)_2^{2+}$ are present in the pH region from 4 to 6, they are of minor importance when compared with $(UO_2)_3(OH)_5^+$ (see Fig. 2), and cannot account for the sudden increase in uptake of uranium.

In a recent paper, Maya and Begun (12) have demonstrated the existence of $(UO_2)_2CO_3(OH)_3^-$ in addition to $UO_2(CO_3)_2^{2-}$

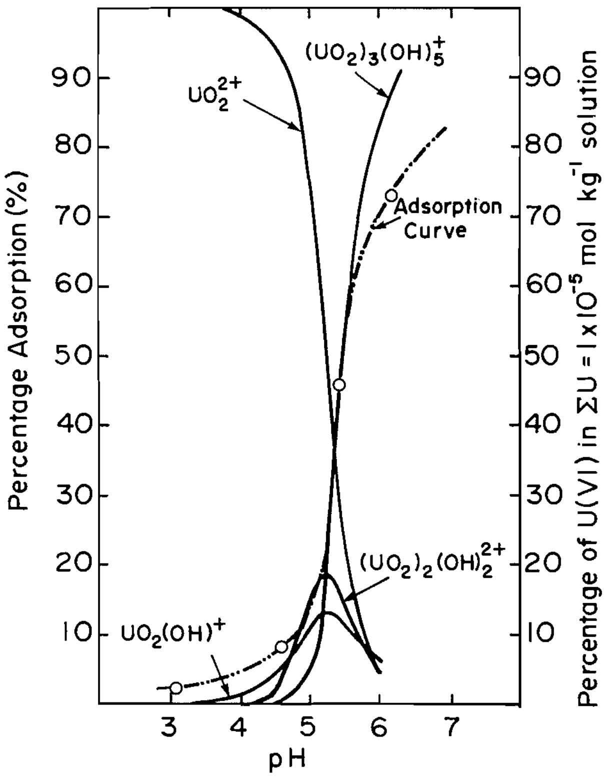

FIG. 2. Comparison of the pH dependence of the adsorption of uranyl species on hematite at 25°C with the percentage of the major hydrolysis products of U(VI) (ΣU = 1 × 10^{-5} mol kg^{-1}) (from ref. 10).

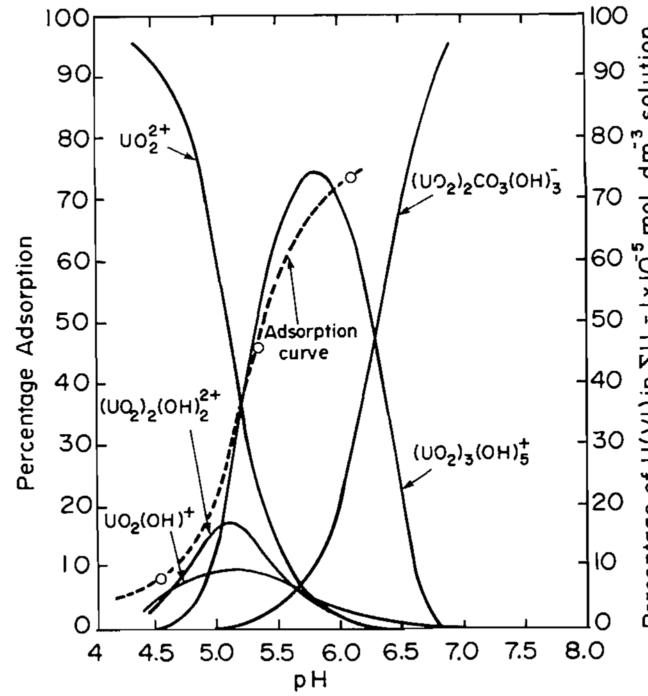

FIG. 3. Comparison of the pH dependence of the adsorption of uranyl species on hematite at 25°C with the percentage of the major hydrolysis products of U(VI) (ΣU = 1 × 10^{-5} mol dm^{-3}) from Lemire.

and $UO_2(CO_3)_3^{4-}$. Computer calculations that included these carbonate complexes (formed from dissolved atmospheric carbon dioxide) were performed by Lemire at Whiteshell Nuclear Research Establishment and the results are shown in Fig. 3. When the adsorption data are compared with the proportions of major hydrolysis products of U(VI) from Lemire's calculation (see Fig. 3), the agreement is very good, though the proportion of $(UO_2)_2CO_3(OH)_3^-$ begins to increase at a pH value of around 6.

The electrophoretic mobility results (see Fig. 4) show that the mobility of hematite depends on the amount of uranium adsorbed. For pH < 4, only a small amount of non-hydrolyzed UO_2^{2+} is adsorbed, and the electrophoretic mobility does not change significantly. As the pH is increased, a pronounced effect is observed, especially for solutions with higher uranium content. In each case, the isoelectric point tends to shift towards lower pH values. This behaviour is often observed for "specifically adsorbed" ions. As shown in the previous section, the proportion of $(UO_2)_3(OH)_5^+$ increases with pH. Such species contain more than one hydroxyl group per ion, and these hydroxyl groups can become attached to the positively charged hematite surface, lowering the overall surface charge of the particle. In fact, Matijevic and Janauer (13) have advanced the same idea to explain the reversal of charge of silver bromide sol by ferric ions.

One may question whether or not the above phenomenon can be explained by the interfacial precipitation model (14). This model would regard the adsorption as an interfacial precipitation of uranium(VI) oxide, which occurs at a pH lower than the bulk value. A comparison of the electrophoretic mobility data of the oxide with that of uranium-loaded hematite particles

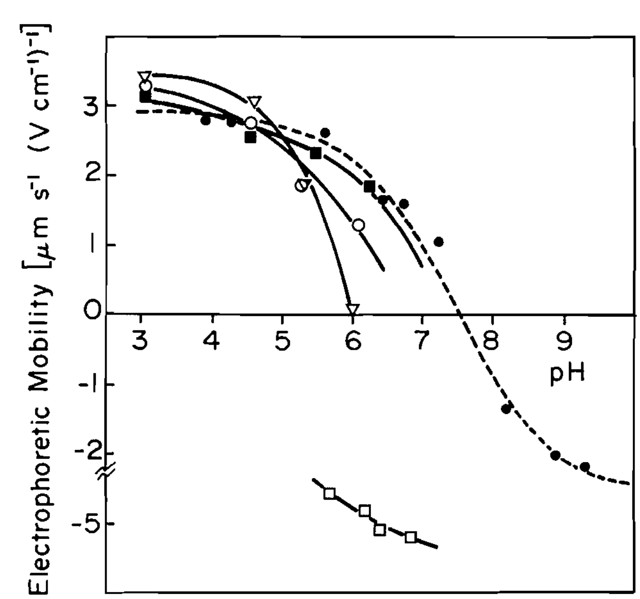

FIG. 4. Electrophoretic mobility of hematite sol in the absence and presence of uranyl species together with the electrophoretic mobility of U(VI) oxide as a function of pH at 25°C in 5 × 10^{-4} mol dm^{-3} NaCl: ∇, ΣU = 5 × 10^{-5} mol dm^{-3}; □, U(VI) oxide; ○, ΣU = 1 × 10^{-5} mol dm^{-3}; ●, hematite; ■, ΣU = 1 × 10^{-6} mol dm^{-3}.

should give some elucidation of the above question. A series of hydrolysis experiments were performed on aqueous UO_2^{2+} ions at slightly higher solution pH. The precipitates obtained were identified by electron diffraction to be U(VI) oxides. The variation of the electrophoretic mobility of the oxide with solution pH, as shown in Fig. 4, does not resemble that of the uranium-loaded hematite, indicating that the oxide is not the species involved in the adsorption.

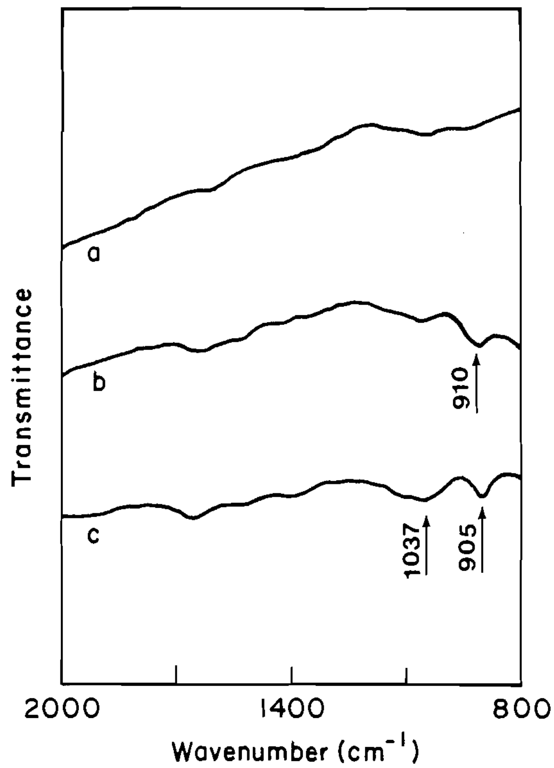

FIG. 5. Infrared spectra of (*a*) hematite,(*b*) hematite loaded with uranium at pH 4.30, and (*c*) hematite loaded with uranium at pH 6.08.

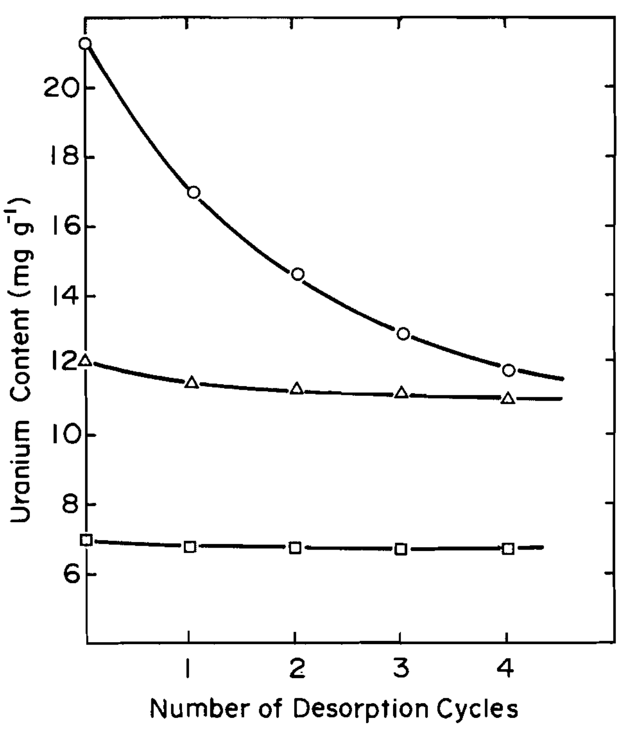

FIG. 6. Desorption of uranyl species from hematite sol as a function of desorption cycle at pH 6.2 in 5 × 10^{-4} mol dm^{-3} NaCl. The amounts of uranium adsorbed onto the hematite before desorption are ○, 21.17 mg g^{-1}; △, 12.10 mg g^{-1}; □, 6.97 mg g^{-1}.

Figure 5 shows the ir spectra (2000 cm^{-1} to 800 cm^{-1} range) of hematite and uranium-loaded hematites for two pH values. No defined bands were detected for hematite (Fig. 5*a*). For uranium-loaded hematites: at pH 4.30, UO_2^{2+} ions are adsorbed

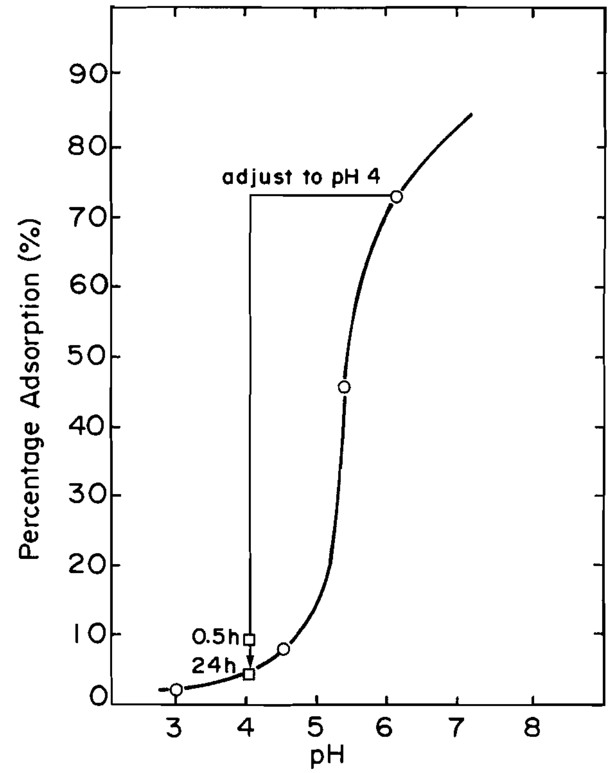

FIG. 7. The desorption of uranyl species from hematite sol.

and the characteristic uranium band appears at 910 cm^{-1} (Fig. 5*b*). The position of this band shifts to 905 cm^{-1} at pH 6.08 (Fig. 5*c*), indicating that the sorption product is different from UO_2^{2+}. From known hydrolysis data, this band can only be accounted for if $(UO_2)_3(OH)_5^+$ is adsorbed. The presence of an absorption band at 1037 cm^{-1} may be due to the hydroxyl groups in $(UO_2)_3(OH)_5^+$. The above results further substantiate our conclusion that $(UO_2)_3(OH)_5^+$ may be the major species involved in the adsorption.

Desorption

Desorption studies were carried out in two ways, using the uranium-loaded hematite particles immediately after the adsorption experiment. The results from successive desorption into water with the same pH and salt concentration as the adsorption solution are shown in Fig. 6. In most cases the adsorbed uranium is retained, even after several desorption cycles. At a pH of about 6.20, the predominant solution species is $(UO_2)_3(OH)_5^+$. It follows that this species may be adsorbed irreversibly. This is consistent with the behaviour of specifically adsorbed cations.

In addition, the amount of uranium desorbed depends on the initial amount of uranium adsorbed (Fig. 6), possibly because of different binding sites on the surface of the hematite. In a recent paper, Benjamin and Leckie (15) have shown that the surface of iron oxyhydroxide has different binding sites (Multiple-site Adsorption Model). The binding strength for cations may vary between sites by more than an order of magnitude. At high adsorption density, some cations are bound to weaker binding sites and these would come off first during desorption, however, at low adsorption density, most cations are bound to stronger binding sites and only a few would come off during desorption.

The effect of pH on the desorption process is shown in Fig. 7. The percentage of uranium adsorbed was plotted as a function of solution pH. After equilibrating the reaction system for 16 h at pH 6.2, the mixture was adjusted to pH 4. The results indicate a fast release of adsorbed uranium over a period of 30 min. Similar results were obtained when the solution pH was lowered to 3. Thus, it seems that the adsorption process is reversible with respect to solution pH. This can be explained if we assume that the added acid could alter the chemical form of the adsorbed species and/or destroy the bonding between the adsorbent and the adsorbate. As has already been mentioned, UO_2^{2+} is the predominant species at pH 4. A change in solution pH (to 4) could reverse the hydrolysis reaction:

$$3UO_2^{2+} + 5\ OH^- \rightarrow (UO_2)_3(OH)_5^+$$

Since the affinity of hematite for UO_2^{2+} is not high, most of the UO_2^{2+} is released from the surface of the oxide.

Acknowledgements

The authors wish to thank Dr. G. J. Howard, Dr. N. H. Sagert, and Dr. R. J. Lemire for their helpful comments. We also wish to thank our colleagues in the Materials Science and Analytical Science Branches for X-ray diffraction and electron diffraction analyses, BET measurements, and scanning electron micrograph work.

1. W. STUMM and J. J. MORGAN. Aquatic chemistry: an introduction emphasizing chemical equilibria in natural waters. John Wiley and Sons, New York, NY. 1981.
2. L. L. AMES, J. E. MCGARRAH, B. A. WALKER, and P. F. SALTER. Chem. Geol. **35**, 205 (1982).
3. Z. BOROVEC. Chem. Geol. **32**, 45 (1981).
4. VAN DER WEIJDEN and D. LANGMUIR. The Geological Society of America Annual Meetings, Denver, Abstract with program, Vol. 8. No. 6. 1976.
5. R. A. RICH, H. D. HOLLAND, and U. PETERSON. Developments in economic geology 6, American Elsevier Publishing Co., NY. 1977.
6. D. A. JOHNSON and T. M. FLORENCE. Anal. Chim. Acta, **53**, 73 (1971).
7. D. LANGMUIR. *In* Adsorption from aqueous solutions. *Edited by* P. H. Tewari. Plenum Press, NY. 1981.
8. L. G. SILLEN and A. E. MARTELL. Stability constants of metal-ion complexes. Chem. Soc., Burlington House, London, Spec. Publ. No. 17 and No. 25. 1964 and 1971.
9. L. M. TOTH and G. M. BEGUN. J. Phys. Chem. **85**, 547 (1981).
10. C. F. BAES and R. E. MESMER. The hydrolysis of cations. John Wiley and Sons, New York, NY. 1976.
11. K. F. SCHULZ and M. J. HERAK. Croat. Chem. Acta, **30**, 127 (1958).
12. L. MAYA and G. M. BEGUN. J. Inorg. Nucl. Chem. **43**, 2827 (1981).
13. E. MATIJEVIC and G. E. JANAUER. J. Colloid Interface Sci. **21**, 197 (1966).
14. E. S. HALL. Discuss. Faraday Soc. **42**, 197 (1966).
15. M. M. BENJAMIN and J. O. LECKIE. J. Colloid Interface Sci. **79**, 209 (1981).

Cation transport in isomeric pentanes: effects of temperature, density, and molecular shape[1]

ISTVAN GYÖRGY, NORMAN GEE, AND GORDON R. FREEMAN
Chemistry Department, University of Alberta, Edmonton, Alta., Canada T6G 2G2

Received May 15, 1984

ISTVAN GYÖRGY, NORMAN GEE, and GORDON R. FREEMAN. Can. J. Chem. **63**, 1105 (1985).

The cation mobility μ_+ is measured in *n*-pentane, *iso*-pentane, *neo*-pentane, and mixtures of *n*- and *neo*-pentane over conditions from the normal liquid, through the critical fluid, to the low density gas. Most of the liquid data correlate with the reduced temperature T/T_c. The T/T_c reflects free volume and viscosity changes. Comparison is made to neutral molecule diffusion. The transition from viscosity control of mobility in the liquid to density control in the dilute gas occurs over the reduced viscosity region $3 > \eta/\eta_c > 0.6$, which corresponds to the reduced density region $1.9 > n/n_c > 0.5$. In the saturated gas $n\mu_+$ is similar in all pentanes, but *iso*- $\geqslant$ *n*- > *neo*-pentane. At constant density $d\mu_+/dT \geq 0$ for gases. The average momentum transfer cross sections in the *n*-/*neo*-pentane mixtures are similar to those in *neo*-pentane at low T but similar to those in *n*-pentane at high T. The present findings are combined with previous electron mobility data in addressing the effect of hydrocarbon molecular (external) shape on the electric breakdown strength of gases.

ISTVAN GYÖRGY, NORMAN GEE et GORDON R. FREEMAN. Can. J. Chem. **63**, 1105 (1985).

On a mesuré la mobilité μ_+ du cation dans le *n*-pentane, l'*iso*-pentane, le *néo*-pentane et dans les mélanges de *n*- et de *néo*-pentane dans des conditions allant du liquide normal, au fluide critique et finalement jusqu'au gaz de faible densité. Pour la plupart des données relatives au liquide, il existe une corrélation avec la température réduite T/T_c. Le rapport T/T_c reflète les variations du volume libre et de la viscosité. On a établi une comparaison avec la diffusion de molécules neutres. La transition, à partir du contrôle viscosimétrique de la mobilité du liquide jusqu'au contrôle de la densité du gaz dilué, se produit dans la région de viscosité réduite $3 > \eta/\eta_c > 0{,}6$ qui correspond à la région de densité réduite $1{,}9 > n/n_c > 0{,}5$. Dans les gas saturés, la valeur de $n\mu_+$ est identique dans tous les pentanes et elle varie suivant: *iso*- $\gtrsim$ *n*- > *néo*-pentane. Pour une densité constante, $d\mu_+/dT \geq 0$ pour les gaz. A basse température, les sections droites moyennes des transferts de moment dans les mélanges de *n*-/*néo*-pentane sont identiques à celles du *néo*-pentane; par ailleurs, à hautes températures, elles sont identiques à celles du *n*-pentane. On combine ces renseignements avec les données obtenues antérieurement sur la mobilité de l'électron pour étudier l'effet de la forme externe de l'hydrocarbure à l'état moléculaire sur la force de rupture électrique des gaz.

[Traduit par le journal]

Introduction

Ion mobilities in low density gases are limited by the gas density n, the molecular polarizability α, and the molecule–ion reduced mass M_r (1, 2). Gas density remains a dominating parameter up to the critical region (3–5). In the liquid phase, ion mobilities are limited by the viscosity η and the ion radius r (6). Stokes' law applies quite well at $\eta/\eta_c \gtrsim 2.5$, where η_c is the viscosity of the critical fluid (4, 5, 7). The transition from density to viscosity control of ion diffusion has previously been investigated in two ways. In argon gas at atmospheric pressure, ions have been clustered with increasing numbers m of water molecules until, with $m \gtrsim 1000$, the ionic radius was large enough, $\gtrsim 1.4$ nm, that Stokes' law applied in the gas phase (8). The other way was to increase the fluid density continuously from that of the low density gas to that of the dense liquid, and measure the change in mobility behavior (4, 5).

The possibility of an additional factor, that of molecular shape, emerges from a comparison of cation mobilities in *n*-hexane and cyclohexane (3*a*), or in benzene and toluene (3*b*), or in propane, propene, and cyclopropane (4). However, changes in polarizability might have complicated an apparent shape effect. In the present article, cation mobilities are reported for the isomeric series *n*-, *iso*-, and *neo*-pentane, and in mixtures of *n*- and *neo*-pentane, for which α is constant (9). The density was varied from the dilute gas through the critical region to the dense liquid.

Experimental

A. Materials

The pentanes were Phillips Research Grade. Further purification of the samples was effected in a grease-free vacuum line. After degassing, each pentane was stirred on sulfuric acid (>72 h), distilled onto potassium hydroxide pellets and stirred (>24 h), distilled onto a nearly equal volume of Davison Molecular Sieves 5A (>24 h), and finally distilled onto sodium–potassium alloy and stirred (>72 h). The acid removed traces of olefin, the hydroxide removed carbon dioxide and residual traces of sulfuric acid, the molecular sieves removed water, and the alloy removed residual traces of oxygen. The pentane was degassed by several freeze–pump–thaw cycles between each distillation. Prior to filling a cell, the liquid was subjected to a final distillation, transferred to a measuring burette, and the amount required to attain the critical fluid density at $T > T_c$ was distilled into the cell reservoir at 77 K. The cell was sealed with a flame after the cell pressure had been reduced to $<10^{-5}$ Pa.

B. Cells

The conductance cells had ~11 mm thick glass walls (10). Liquid phase measurements were performed in a cell in which the parallel plates were immersed in the liquid (10*a*) and gas phase in a cell in which the plates were above the liquid (10*b*). The cells were cut open at the end of the series of experiments, and the plate separations were measured with Do All models M-1 Minus measuring rods. The cell for the liquid phase had a drift distance of 3.10 mm; in the gas cell it was 3.20 mm.

C. Techniques

The samples were irradiated by 1 μs pulses of 1.7 MeV X-rays from a Van de Graaff generator. The electron drift times were <1% of those of the ions. The transient current was amplified with a Princeton Applied Research 113 preamplifier, integrated and stored in a Fabritek 1062 signal averager (4). The average of 16 or 32 signals was used to measure the ion drift time t_d (typically 10 to 1000 ms). The mobility is given by $\mu = l^2/t_d V$, where l is the drift distance and V the applied voltage. Voltages up to 6 kV were obtained from a Fluke 408B High Voltage Power Supply, and >6 kV from a Spellman High Voltage DC Supply.

The temperature was varied by heating the cell in a thermostated hot

[1] Assisted financially by the Natural Sciences and Engineering Research Council of Canada.

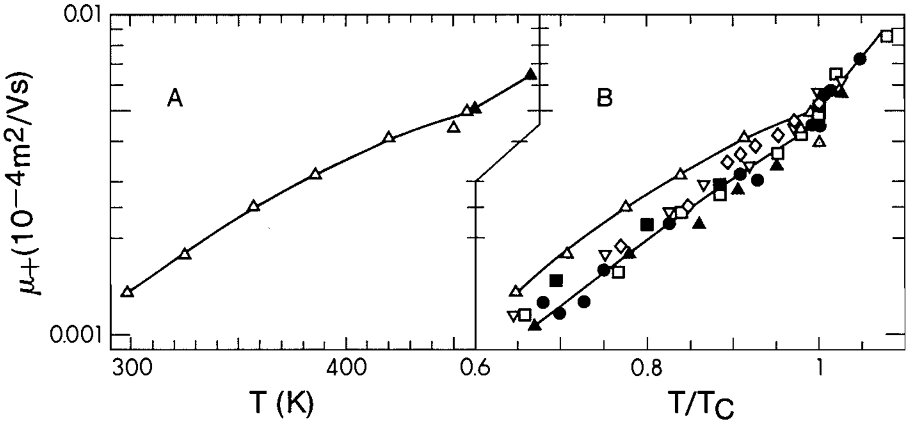

FIG. 1. Cation mobilities as functions of temperature (A) and reduced temperature (B) in the liquid and supercritical gas phases. A: *iso*-pentane, liquid under its vapor pressure (△), and gas at n_c (▲); B; *n*-pentane (■), *iso*-pentane (△), *neo*-pentane (●); *n*-pentane/*neo*-pentane mixtures containing 10 (◇), 25 (▲), 50 (□), and 75 (▽) mol% *n*-pentane.

air bath (10*a*). The cell temperature was monitored near the electrodes and at the end of the cell farthest from the electrode, by copper–constantan thermocouples (Thermo-electric Canada Ltd.). A third thermocouple in the bath was connected to the LFE Corp. Model 226-A21 temperature controller, which varied the current supplied to the heating coil of the Master Appliance Model AH-751 heat gun.

D. Physical properties

The critical constants and physical properties were obtained from refs. 11 and 12. No data were available for the mixtures; they were assumed to be ideal (13). The evaporation points and critical temperatures were visually monitored and no deviation from ideality was observed (13).

Viscosity data are available for *n*-pentane over a large range including the critical region (12, 14); the value of η_c is 26.7 μPa s. Data for *neo*-pentane are more sparse (15, 16); no critical region data were found. Data for liquid *iso*-pentane exist only for $T \leq 293$ K (17).

Results

A. Liquid phase

Data for the co-existence liquid and the supercritical gas of *iso*-pentane are plotted in Fig. 1*A*. The mobility μ_+ increases approximately as the exponential of the temperature. Such is also the case for *n*-pentane, *neo*-pentane, and mixtures of *n*-pentane/*neo*-pentane. Further, most of the differences between μ_+ in *n*-pentane, *neo*-pentane, and their mixtures disappear in a corresponding states plot (Fig. 1*B*).

B. Gas phase

Mobilities in *n*-pentane and *neo*-pentane gases are shown in Fig. 2, and those in *iso*-pentane and *n*-pentane/*neo*-pentane mixtures in Fig. 3. In each case μ_+ decreases along the co-existence curve as T increases, due to the concomitant increase of density n. However, at constant n the mobility is constant or increases with T. The relative increase is greater for a greater n.

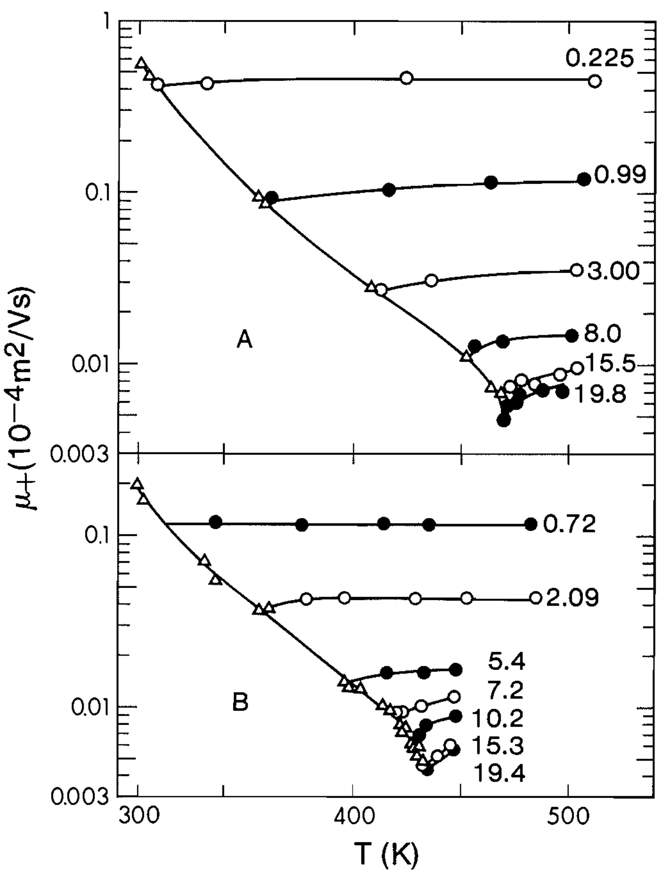

FIG. 2. Cation mobilities in the gas phase. △, coexistence vapor; circles, constant density n (10^{26} molecule/m^3). A: *n*-pentane; B: *neo*-pentane.

Discussion

A. Gas phase

1. Low density nonsaturated gas

At low gas densities, $d\mu/dT$ is near zero in all the pentane isomers and in the *n*-pentane/*neo*-pentane mixtures (Figs. 2 and 3). This is like the cation behavior in *n*-hexane (3*a*), benzene and toluene (3*b*) at $n \leq 3 \times 10^{25}$ molecules/m^3. In contrast, $d\mu/dT$ in cyclopentane and cyclohexane (3*a*) at $n \lesssim 5 \times 10^{25}$ molecules/m^3, or in the C_1–C_4 alkanes and alkenes at $\gtrsim 7 \times 10^{25}$ molecules/m^3 (4), is appreciably greater than zero, especially near the liquid–vapor co-existence curve. The value $d\mu/dT = 0$ implies that scattering is dominated by the long range attractive polarization potential (2). Combination of the Nernst–Einstein relation with the Chapman–Enskog diffusion expression gives (2)

$$[1] \quad n\mu_+ = \frac{3e\sqrt{\pi}}{8M_r}\left(\frac{2kT}{M_r}\right)^{5/2} \bigg/ \int_0^\infty v^5\sigma_m \exp\left(-M_r v^2/2kT\right) dv$$

where M_r is the ion–molecule reduced mass, v the relative velocity, k Boltzmann's constant, e the electronic charge, and σ_m the momentum transfer cross section. In terms of an average

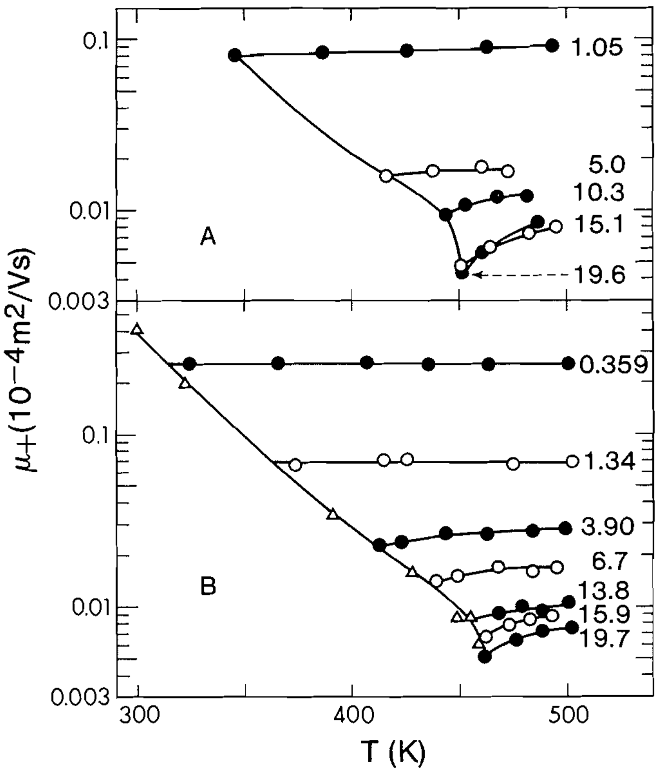

FIG. 3. Cation mobilities in the gas phase. Symbols as in Fig. 2. *A*: 50/50, *n*-pentane/*neo*-pentane; *B*: *iso*-pentane.

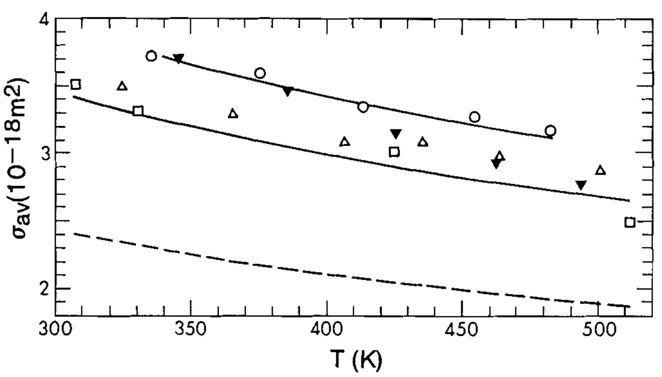

FIG. 4. Average scattering cross sections σ_{av} for cations in *neo*-pentane (○), *iso*-pentane (△), *n*-pentane (□), and 50 mol% *n*-pentane/*neo*-pentane mixture (▼), as functions of T. The values were calculated from eq. [4], using μ in the lowest constant density gases of Figs. 2 and 3, and assuming $M_r = M$. The solid lines serve as visual guides to the *neo*-pentane and *n*-pentane data. The dashed line indicates the polarization limit.

cross section σ_{av} (4*a*),

$$[2] \quad \sigma_{av} = \langle v^3\sigma_m\rangle/\langle v^3\rangle$$

$$[3] \quad = \left(\frac{3}{4}\right)\left(\frac{e}{M_r}\right)\frac{1}{\langle v\rangle n\mu_+}$$

with $\langle v\rangle = (8kT/\pi M_r)^{1/2}$, so that

$$[4] \quad \sigma_{av} = \frac{3}{8}\, e\left(\frac{\pi}{2M_rkT}\right)^{1/2}\frac{1}{n\mu_+}$$

For unclustered ions and molecules, M_r equals $M/2$, where M is the molecular mass. The radiolyses of *neo*-pentane (18) and *n*-pentane (19) initially generate C_1–C_5 cations. However, the smaller cations react rapidly with parent gas molecules, mainly by hydride transfer, so that the ions drifting in the cell would be C_5-cations (18, 19), probably clustered by molecules (4). For heavily clustered ions, M_r equals M. The latter was assumed in calculating the average cross sections in Fig. 4. The cross sections are largest for cations in *neo*-pentane and smallest for cations in *n*-pentane; the *iso*-pentane results are intermediate. The solid lines indicate the results for *neo*-pentane and for *n*-pentane if $d\mu/dT$ were zero. The cation cross sections in the *n*-pentane/*neo*-pentane mixture are similar to *neo*-pentane values at low temperatures, but decrease towards *n*-pentane values as T increases. The dashed line represents the polarization limit (2) for scattering by a molecule of average polarizability $\alpha = 10 \times 10^{-30}$ m^3, which is the value for each pentane (9). The line was obtained by calculating the Langevin small ion mobility (2) and combination of that with eq. [4]. All the pentane cross sections are larger than the polarization limit.

2. *Saturated gas*

As the gas density is increased along the vapor–liquid coexistence curve, the behavior is dominated by the fluid density (3–5). The product $n\mu_+$ varies by only ~25% on going from the low density gas to the critical fluid (Fig. 5). It passes through a shallow minimum at $n \approx 4 \times 10^{26}$ molecules/m^3, or $n/n_c \approx 0.2$. Data for ions in *iso*-pentane are shown in Fig. 5*A* to illustrate the behavior. Data for the three pentane isomers are given in Fig. 5*B* to permit comparison. The general behavior is similar for the three isomers, but the values of $n\mu_+$ are in the order *iso* $\gtrsim$ *n* $>$ *neo*. The slightly lower values in *neo*-pentane, which lacks flexibility in the molecular structure, suggests that molecular rigidity tends to increase the extent of clustering of molecules about the ion.

The increase of $n\mu_+$ at $n > 0.5n_c$ is attributed to the destructive interference of the multimolecular scattering interactions (5). At $n \gtrsim 1.9n_c$ the value of $n\mu_+$ decreases due to the restriction of motion by the reduction of free volume.

Similar behavior has been observed for ions in other liquids (3–5). The transition from normal gas phase behavior (density control) to normal liquid phase behavior (viscosity control) occurs in the region $0.5 \lesssim n/n_c \lesssim 1.9$.

B. *Liquid phase*

1. *Arguments against Arrhenius plots*

Traditionally, discussions of liquid phase diffusion coefficients (20–24) or ion mobilities (3) center around Arrhenius plots and the associated activation energies. Such procedures are unnecessary (25). Transport properties are describable in terms of temperature and density without emphasizing energy barriers or activation (26). Diffusion involves repeated small displacements, each much smaller than the diameter of a fluid molecule. The temperature has a small role but the dominant factor is the free volume ($V - V_0$), where V_0 is the lower limit of the volume V where the molecules are too crowded to permit diffusion or bulk flow (25–31).

The dispensibility of Arrhenius plots can be illustrated using the self diffusion coefficient D in liquid *n*-pentane. The data are presented in Fig. 6*A*, as in the original work (20). While the linear approximation (dashed line) is fair, plotting log D versus T (Fig. 6*B*) results in nearly as straight a line. The closest fit in either case is attained by a curve (solid line).

Values of log D in liquid *iso*-pentane and *neo*-pentane plotted against T likewise result in nearly straight lines (Fig. 6*B*). *Neo*-pentane data at $T > 299$ K of ref. 22 were abnormally high due to possible bubbling effects (23) and were not used. In a

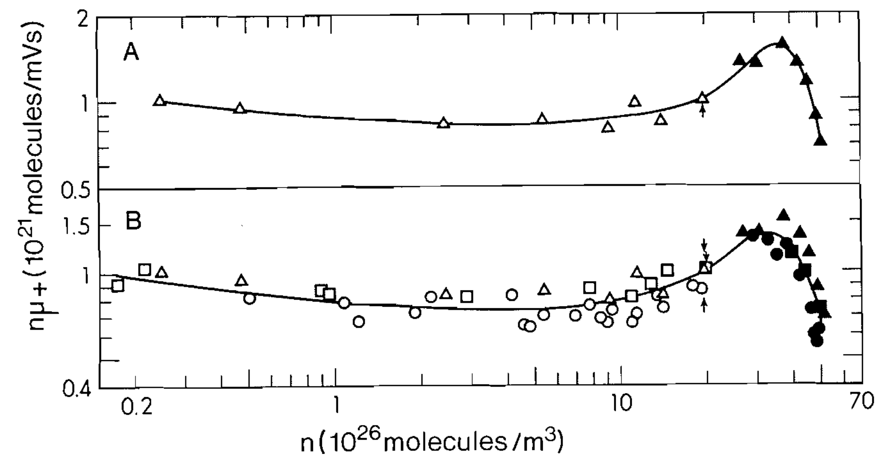

FIG. 5. Density dependence of $n\mu_+$ in the coexistence vapor and liquid of *iso*-pentane (△, ▲), *n*-pentane (□, ■), and *neo*-pentane (○, ●). Open symbols, vapor; closed symbols, liquid. The arrows indicate n_c.

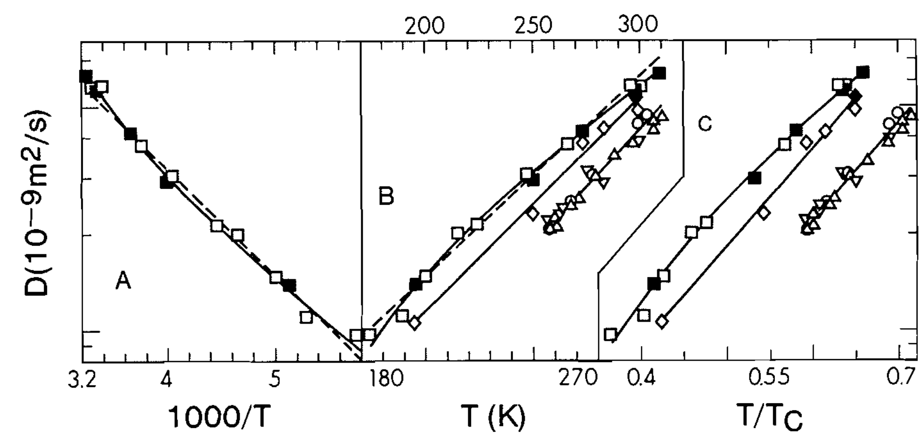

FIG. 6. Plot of log D versus: A, $1000/T$; B, T; C, T/T_c, where T_c is 433.8 K for *neo*-pentane, 460.4 K for *iso*-pentane, and 469.7 K for *n*-pentane. The liquids are (symbols, reference): *n*-pentane (□, 20), (■, 21); *iso*-pentane (◇, 21), (◆, 20*b*); *neo*-pentane (▽, 22), (△, 23), (○, 24).

corresponding states plot (Fig. 6*C*) the order remains *n*-pentane > *iso*-pentane > *neo*-pentane, unlike ion mobility where *iso*- > *n*- ≳ *neo*-pentane.

The log D versus T behavior largely reflects changes in $(V - V_0)$. The self-diffusion constant can be related to $(V - V_0)/V_0$, $T^{1/2}$, $M^{1/2}$, and the collision diameter (25, 28). If V_0 and the collision diameter are approximately constant, $D \propto T^{1/2}\,(V - V_0)/V_0$. For *n*-pentane a plot of D against $T^{1/2}\,(V - V_0)/V_0$ is slightly curved (Fig. 7). The curvature may be due to temperature dependence of V_0 or of the collision diameter (28).

In summary, a log D or log μ_+ versus T plot is preferred to an Arrhenius plot. The presentation of experimental data is more direct, and the attribution of the free volume effect to a hypothetical activation barrier is avoided. Therefore in this work log μ_+ versus T plots are used.

2. Possible molecular shape effect

Earlier studies (20–22), noted that at a given T/T_c, D is larger for the flexible molecules *n*-pentane than for the more rigid *neo*-pentane. The *iso*-pentane results are intermediate. These and related viscosity data (12, 14–17) lead to conjectures about the role of molecular shape (15, 21). The value of V/V_c is expected to be similar for the isomers at a given T/T_c. The values of V_c of the pentane isomers differ by only 2%, so each V should be similar at a given T/T_c. The diffusion data (Fig. 6*C*) then indicate that translation of a more rigid, sphere-like molecule at a given V is hindered with respect to the motion of a more flexible, chainlike molecule in accordance with theoretical expectation (32).

The ion mobility values in like manner are lower in the more rigid, sphere-like *neo*-pentane than in the more flexible *iso*-pentane at a given $T/T_c < 0.9$ (Fig. 1*B*). However, the values in *n*-pentane and in the *n*-pentane/*neo*-pentane mixtures are similar to those in *neo*-pentane, and they are lower than those in *iso*-pentane. At $T/T_c > 0.9$, the data for all liquids merge together. In contrast to neutral molecule diffusion, there is no clear shape effect for the motion of ions. The difference may lie in the effect of the charge on the local environment of the ion (32), and in the structures of the ions themselves.

3. Effect of viscosity

To connect the ion mobility to a physical property of the fluid, the mobility of ions in liquids has long been correlated with the viscosity η (6, 33–35). Values of $\eta\mu_+$ are presented in Fig. 8. The behavior is similar for each of the isomers wherever they can be compared. At $\eta > 100$ μPa s, $\eta\mu_+$ is constant. Using Stokes' law, the radius of the diffusing particle is

$$[5] \quad r = e/C\eta\mu_+$$
$$= 1.6 \times 10^{-19}/C\eta\mu_+, \text{ m}$$

where $\eta\mu_+$ is in kg m/V s^2 and the constant C is 6π for ions

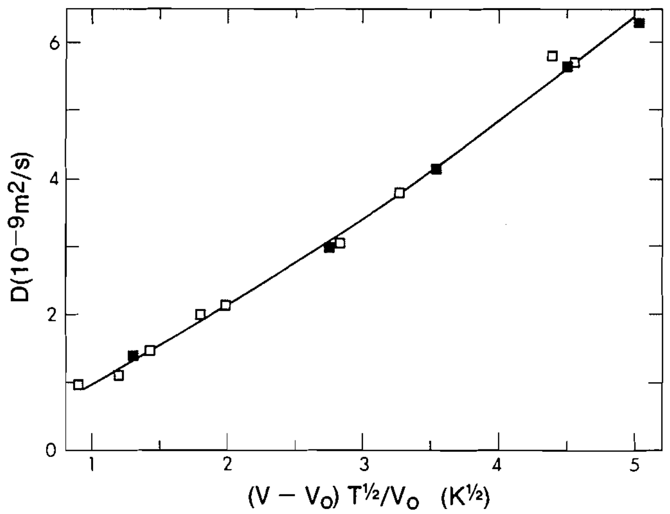

FIG. 7. Plot of D versus $(V - V_0)T^{1/2}/V_0$, where V_0 is 153×10^{-30} m^3/molecule (25*a*). Liquid symbols as Fig. 6.

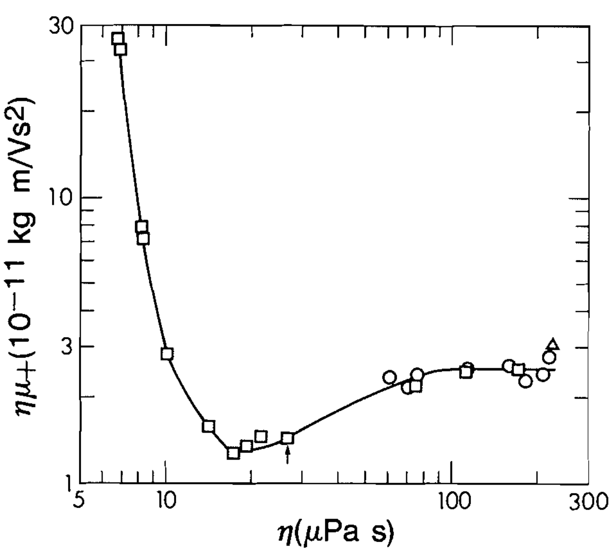

FIG. 8. Viscosity dependence of $\eta\mu_+$ in coexistence vapor and liquid *n*-pentane (□), *iso*-pentane (△) and *neo*-pentane (○). The arrow indicates η_c for *n*-pentane.

(stick condition). A radius of 3.3×10^{-10} m is inferred at $\eta >$ 100 μPa s in *n*- and *neo*-pentane, and of 2.8×10^{-10} m in *iso*-pentane. For a range of neutral molecules, C is near 4π (36). Assumption of 4π (slip condition) in eq. [5] in combination with the Nernst–Einstein relation gives radii in 10^{-10} m of 2.5 (*n*-pentane), 2.8 (*iso*-pentane), and 3.8 (*neo*-pentane) from D and η at 298 K. The ion and molecule radii are similar in size.

The decrease at $\eta < 80$ μPa s indicates breakdown of viscosity control and gives a limit $\eta/\eta_c \sim 3$ for normal liquid ion behavior. The $\eta\mu_+$ decreases through the critical region (arrow) to a minimum at $\eta \sim 18$ μPa s ($\eta/\eta_c \sim 0.7$) and increases at yet lower viscosity. The decrease as the critical region is approached has been ascribed to electrostriction exerting a greater effect as the compressibility of the fluid increases (4, 5, 7). The increase at $\eta < 16$ μPa s, $\eta/\eta_c < 0.6$, indicates the transition towards density control ($n\mu_+ \sim$ constant) and corresponds to $n/n_c < 0.5$ (Fig. 5). The transition region between density and viscosity control of ion transport in the pentanes is thus $0.5 \lesssim n/n_c \lesssim 1.9$, or equivalently $0.6 \lesssim \eta/\eta_c \lesssim 3$.

C. Application to dielectric breakdown strength

The present ion mobilities are reflected in the relative breakdown strength of pentane isomers. In an investigation of the breakdown strength of hydrocarbon gases, a structure dependence was observed but discounted (37). Chain branching increases the strength (*iso*- relative to *n*-butane; *neo*-relative to *iso*- and *n*-pentane). Hemispherical electrodes were used. In breakdown from a positive tip the electron mobility does not seem to be important; the initiation current depends on the cations (38–41). On the other hand, breakdown from a negative point is dependent upon the electron mobility. The present work indicates that at a given density the cation mobility is similar in all pentanes (Fig. 5). However, the slight differences are in the order indicated by the breakdown strength (37). In *n*-butane and *iso*-butane the cation mobilities are also similar (4). Further, the electron mobility depends on the physical shape of the molecules (12, 42) and is lower for a gas of more branched, more sphere-like molecules. Although the electrons are "hot" at the fields required for breakdown, a brief comparison of thermal electron mobilities indicates the tendencies. At a given low gas density, μ_e in *n*-butane is twice of that in *iso*-butane (42). For the pentanes, μ_e in *n*-pentane is 1.3 times that in *iso*-pentane and 3 times that in *neo*-pentane. The trends in the observed cation mobilities and the effect of increased sphericity on the electron mobility combine to confirm that dielectric breakdown strength is greater in gases of more branched, more sphere-like hydrocarbon molecules (37).

Acknowledgement

We thank the staff of the Radiation Research Center for assistance with the design and construction of equipment.

1. J. C. MAXWELL. Philos. Trans. R. Soc. London **157**, (1866).
2. E. W. MCDANIEL. Collision phenomena in ionized gases. John Wiley and Sons, New York. 1964. Chapt. 9.
3. S. S.-S. HUANG and G. R. FREEMAN. J. Chem. Phys. (*a*) **70**, 1538 (1979); (*b*) **72**, 1989 (1980).
4. N. GEE and G. R. FREEMAN. Can. J. Chem. (*a*) **59**, 2988 (1981); (*b*) **60**, 1034 (1982).
5. N. GEE, S. S.-S. HUANG, T. WADA, and G. R. FREEMAN. J. Chem. Phys. **77**, 1411 (1982).
6. G. G. STOKES. Trans. Cambridge Philos. Soc. **9**, 8 (1850).
7. N. GEE and G. R. FREEMAN. Can. J. Chem. **58**, 1490 (1980).
8. D. E. HAGEN, P. C. YUE, and J. L. KASSNER, JR. J. Coll. Interf. Sci. **52**, 526 (1975).
9. J. APPLEQUIST, J. R. CARL, and K.-K. FUNG. J. Am. Chem. Soc. **94**, 2952 (1972).
10. (*a*) J.-P. DODELET and G. R. FREEMAN. Can. J. Chem. **55**, 2264 (1977); (*b*) T. WADA and G. R. FREEMAN. Phys. Rev. Lett. **42**, 715 (1979).
11. T. R. DAS, C. O. REED, JR., and P. T. EUBANK. J. Chem. Eng. Data, **22**, 3 (1977); **22**, 9 (1977); **22**, 16 (1977).
12. N. B. VARGAFTIK. Tables on the thermophysical properties of liquids and gases. 2nd ed. J. Wiley and Sons, Halsted Press, New York. 1975.
13. I. GYÖRGY, N. GEE, and G. R. FREEMAN. J. Chem. Phys. **79**, 2009 (1983).
14. A. L. LEE. Viscosity of light hydrocarbons. Monograph on API Res. Project 65, API, New York. 1965.
15. M. K. PHIBBS. J. Chem. Phys. **19**, 1420 (1951).
16. M. H. GONZALEZ and A. L. LEE. J. Chem. Eng. Data, **13**, 55 (1968).
17. J. M. GEIST and M. R. CANNON. Ind. Eng. Chem. Anal. Ed. **18**,

611 (1946).
18. R. E. REBBERT and P. AUSLOOS. J. Res. NBS, **76A**, 329 (1972).
19. S. LUKAC. Rad. Phys. Chem. **15**, 713 (1980).
20. (*a*) D. C. DOUGLASS and D. W. MCCALL. J. Phys. Chem. **62**, 1102 (1958); (*b*) D. W. MCCALL, D. C. DOUGLASS, and E. W. ANDERSON. J. Chem. Phys. **31**, 1555 (1959).
21. E. FISHMAN and T. VASSILIADES. J. Phys. Chem. **63**, 1217 (1959).
22. D. C. DOUGLASS, D. W. MCCALL, and E. W. ANDERSON. J. Chem. Phys. **34**, 152 (1961).
23. D. KESSLER, A. WEISS, and H. WITTE. Ber. Bunseg. Phys. Chem. **71**, 3 (1967).
24. J. J. VAN LOEF. Physica, **95B**, 34 (1978).
25. (*a*) J. H. HILDEBRAND. Science, **174**, 490 (1971); (*b*) B. J. ALDER and J. H. HILDEBRAND. Ind. Eng. Chem. Fundam. **12**, 387 (1973).
26. J. H. DYMOND and B. J. ALDER. J. Chem. Phys. **45**, 2061 (1966).
27. J. J. VAN LOEF. Physica, **62**, 345 (1972); **94B**, 105 (1978).
28. J. H. DYMOND. J. Chem. Phys. **60**, 969 (1974); Chem. Phys. **17**, 101 (1976).
29. H. J. M. HANLEY and R. O. WATTS. Mol. Phys. **29**, 1907 (1975).
30. J. H. DYMOND and L. A. WOOLF. J. Chem. Soc. Faraday Trans. 1, **78**, 991 (1982).
31. F. P. RICCI and D. ROCCA. J. Phys. Chem. **86**, 3047 (1982).
32. C. MUCKENFUSS and C. F. CURTIS. J. Chem. Phys. **29**, 1257 (1958).
33. M. BORN. Z. Phys. **1**, 221 (1920).
34. P. WALDEN and H. ULICH. Z. Phys. Chem. **107**, 219 (1923).
35. I. ADAMECZEWSKI. Ann. Phys. **8**, 309 (1937).
36. J. JONAS, D. HASHA, and S. G. HUANG. J. Chem. Phys. **71**, 3996 (1979); J. Phys. Chem. **84**, 109 (1980).
37. J. C. DEVINS and R. W. CROWE. J. Chem. Phys. **25**, 1053 (1956).
38. W. F. SCHMIDT and D. R. PUGH. J. Phys. D**10**, 1139 (1977).
39. J. GERHOLD. Cryogenics, **19**, 571 (1979).
40. J. C. DEVINS, S. J. RZAD, and R. J. SCHWABE. J. Appl. Phys. **52**, 4531 (1981).
41. E. O. FORSTER. Proc. 7th Int. Conference on Conduction and Breakdown in Dielectric Liquids. Berlin. 1981. p. 199.
42. N. GEE and G. R. FREEMAN. J. Chem. Phys. **78**, 1951 (1983).

Magnetic concentration and polymorphism in di-n-octyl-, di-n-decyl-, and di-n-dodecylphosphinates of copper(II)

JOHN S. HAYNES, KATHERINE W. OLIVER, AND ROBERT C. THOMPSON
Department of Chemistry, University of British Columbia, 2036 Main Mall, Vancouver, B.C., Canada V6T 1Y6

Received September 27, 1984

JOHN S. HAYNES, KATHERINE W. OLIVER, and ROBERT C. THOMPSON. Can. J. Chem. **63**, 1111 (1985).

Phosphinates of copper(II) of the type $Cu(R_2PO_2)_2$ where R is n-octyl, n-decyl, and n-dodecyl have been synthesized and characterized by differential scanning calorimetry, vibrational and electronic spectroscopy, and variable temperature (300 to 4.2 K) magnetic susceptibility studies. Each of these compounds was obtained in distinct α and β structural forms. All materials appear to have the double phosphinate bridged extended chain structure and the magnetic data have been successfully analyzed according to the isotropic Heisenberg model for linear chains. The α forms exhibit antiferromagnetic behaviour with J values of -25, -29, and -29 cm^{-1} for the octyl, decyl, and dodecyl derivatives respectively. The β forms are ferromagnetic and have corresponding J values of 1.8, 2.1, and 2.3 cm^{-1} respectively. Magneto-structural correlations in these extended chain coordination polymers are discussed.

JOHN S. HAYNES, KATHERINE W. OLIVER et ROBERT C. THOMPSON. Can. J. Chem. **63**, 1111 (1985).

On a synthétisé des phosphinates de cuivre(II) du type $Cu(R_2PO_2)_2$ où R = n-octyle, n-décyle, et n-dodécyle et on les a caractérisés en faisant appel à la calorimétrie à balayage différentiel, aux spectroscopies vibrationnelle et électronique et à des études de susceptibilité magnétique à température variable (de 300 à 4,2 K). On a obtenu chacun de ces composés sous les deux formes structurales α et β. Tous les composés semblent avoir une structure en chaîne allongée avec deux ponts phosphinates. On a analysé avec succès les données magnétiques selon le modèle isotrope de Heisenberg pour les chaînes linéaires. Les formes α ont un comportement antiferromagnétique avec des valeurs de J de -25, -29 et -29 cm^{-1} respectivement pour les dérivés octyle, décyle et dodécyle. Les formes β sont ferromagnétiques et les valeurs correspondantes de J sont respectivement de 1,8, 2,1 et 2,3 cm^{-1}. On discute des corrélations magnéto-structurales dans ces chaînes allongées de polymères de coordination.

[Traduit par le journal]

Introduction

The diethyl-, di-n-butyl-, and di-n-hexylphosphinates of copper(II), $Cu(R_2PO_2)_2$, have been shown to be chain polymers with structures consisting of copper atoms with flattened tetrahedral coordination geometry (D_{2d} local symmetry) linked by double phosphinate bridges (1–3). Such structures provide the possibility of pathways for magnetic exchange; weak antiferromagnetic exchange was observed in the ethyl derivative while both the butyl and hexyl compounds showed ferromagnetic exchange (3). This dependence of the sign of the magnetic exchange on the type of alkyl group attached to phosphorus prompted the present extension of our studies to include phosphinates with longer chain alkyl groups. We were also encouraged in this particular direction by earlier observations of polymorphism in metal phosphinates (4–6) with the possibility that different forms of the same material might exhibit different magnetic properties.

We report here the synthesis and study of n-alkyl phosphinates $Cu(R_2PO_2)_2$, where R = n-C_8H_{17}, n-$C_{10}H_{21}$, and n-$C_{12}H_{25}$. Each of these may be obtained in a high melting (mp 120–130°C) α form from solution and a low melting (mp 90–100°C) β form from the melt. Each form shows distinct magnetic properties. Infrared, near-infrared, and visible spectra have been used to investigate structural similarities and differences in these materials, none of which can be obtained in crystalline form suitable for single crystal X-ray diffraction studies. The polymorphism exhibited by these compounds has been examined using differential scanning calorimetry (DSC).

Experimental

Synthesis of the phosphinic acids, di-n-octylphosphinic acid, (n-C_8H_{17})$_2PO_2H$

The phosphinic acids were synthesized by the peroxide catalyzed reaction between the appropriate 1-alkene and hypophosphorus acid (7). Di-n-octylphosphinic acid was prepared following the procedure of Peppard *et al.* (8), except that the quantities of the reactants used were reduced by one half, and recrystallization from acetone was required to remove a coating of light yellow oil from the crude product; mp 82–83.5°C (lit. (9) mp 85°C). *Anal.* calcd. for $C_{16}H_{35}PO_2$: C 66.17, H 12.15; found: C 66.34, H 12.09.

The n-decyl and n-dodecyl derivatives were prepared in a manner similar to the n-octyl compound; however, it was found that the procedure outlined (8) for the removal of the monosubstituted acid ((C_8H_{17})(H)(PO_2H) in the n-octyl case (by conversion to the sodium salt and subsequent extraction into aqueous sodium hydroxide) was not applicable to the ten- and twelve-carbon chain compounds. In the synthesis of these compounds the monosubstituted acids appeared to be the major products, despite attempts to promote the formation of the disubstituted derivatives by increasing the mole ratio of benzoyl peroxide to hypophosphorus acid (from 0.05:1.0 to 0.13:1.0) and by adding the peroxide in 4 portions over 9 h. However, the monosubstituted acids occurred as one component of an oil, which was easily removed from the solid disubstituted compounds by washing with cold ethanol or acetone, as described below.

Di-n-decylphosphinic acid, (n-$C_{10}H_{21}$)$_2PO_2H$

A mixture of 1-decene (0.50 mol), aqueous hypophosphorus acid (0.24 mol), water (24 mL), ethanol (170 mL), and benzoyl peroxide (a total of 28 mmol, one third being added in 3 portions, at 3-h intervals), contained in a round-bottomed flask, was refluxed for 26 h. When cooled, the mixture separated into two layers with a white solid in the top (organic) layer. The solution was extracted with 300 mL of benzene, after acidification with hydrochloric acid (500 mL of 1.0 *M* HCl). The benzene layer was scrubbed with two 125-mL portions of 1.0 *M* HCl, isolated, and evaporated, yielding a mixture of a white solid and an oil, which was removed by washing with cold ethanol. Recrystallization of the solid from benzene gave the desired di-n-decylphosphinic acid in 14% yield; mp 85.6°C (lit.(10) mp 87–88°C, (7) mp 87.7–88.3°C). *Anal.* calcd. for $C_{20}H_{43}PO_2$: C 69.32, H 12.51; found: C 69.07, H 12.70.

Di-n-dodecylphosphinic acid, (n-$C_{12}H_{25}$)$_2PO_2H$

After refluxing a mixture of 1-dodecene (0.29 mol), aqueous hypophosphorus acid (0.14 mol), water (10 mL), ethanol (45 mL), and benzoyl peroxide (16 mmol, added as described above for the n-decyl compound) for 24 h, the two-phase mixture was poured into 1.0 *M* HCl (250 mL) and thoroughly stirred. A total of 300 mL of benzene was needed to dissolve all the white solid that was present in the organic phase. This benzene was separated and the aqueous phase was extracted with a further 150 mL of benzene. The combined benzene layers were evaporated to a mixture of a solid and an oil, which was removed by washing with cold acetone. The crude acid was dissolved in chloroform and reprecipitated by the addition of acetone to yield di-n-dodecylphosphinic acid in 25% yield; mp 93.5°C (lit. (7) mp 93.8–94.8°C). *Anal.* calcd. for $C_{24}H_{51}PO_2$: C 71.59, H 12.77; found: C 71.54, H 12.75.

Synthesis of the copper(II) phosphinate α *forms*

A problem routinely encountered in the synthesis of the copper(II) phosphinate compounds under discussion was the formation of copolymers containing both the phosphinate ligand and the anion of the copper-containing starting material (usually the sulfate anion). It was found generally that dilution of the partially neutralized acid solution and (or) the reaction mixture with water prevented the copolymerization from occurring.

α-Poly-bis(μ-di-n-octylphosphinato)copper(II),
α-Cu[(n-C$_8$H$_{17}$)$_2$PO$_2$]$_2$

This compound was prepared in a manner analogous to that used by Gillman (4); however, dilution with water was needed to prevent the formation of the copolymer.

A solution of di-n-octylphosphinic acid (22 mmol) in methanol (500 mL) was partially neutralized (pH 6) with aqueous sodium hydroxide, then added dropwise with stirring to a solution of copper(II) sulfate pentahydrate (11 mmol) in 60% aqueous methanol (185 mL). Precipitation of a bright blue solid began immediately, and when the addition was complete, water (400 mL) was added and the mixture was stirred for 2 h. The solid was removed by filtration, washed with methanol, water, and, finally, methanol, and air dried. Yield: 98%. *Anal.* calcd. for $CuC_{32}H_{68}P_2O_4$: Cu 9.89, C 59.83, H 10.67; found: Cu 9.87, C 60.04, H 10.73.

α-Poly-bis(μ-di-n-decylphosphinato)copper(II),
α-Cu[(n-C$_{10}$H$_{21}$)$_2$PO$_2$]$_2$

This compound was prepared by essentially the same method as that previously reported for the n-hexyl derivative (3), although addition of water to the ethanolic acid solution, prior to the addition of the copper(II) solution, was required to prevent the formation of the copolymer in this case.

Di-n-decylphosphinic acid (9 mmol), dissolved in ethanol (500 mL), was partially neutralized with aqueous sodium hydroxide (8 mmol in 90 mL water). After filtration, water was added until the solution became cloudy (this cloudiness was, presumably, the water insoluble phosphinic acid, and was dispelled by the addition of a small volume of ethanol), giving a total volume of ca. 1 L. Copper(II) sulfate pentahydrate (4 mmol in 60 mL water) was added dropwise, with stirring, resulting in the precipitation of a bright blue solid. When the addition of the copper was complete, the reaction mixture was stirred for 1.5 h, after which the solid was removed by filtration, washed with ethanol, water, and, finally, ethanol, and air dried. Yield: 93%. *Anal.* calcd. for $CuC_{40}H_{84}P_2O_4$: Cu 8.42, C 63.87, H 11.22; found: Cu 8.33, C 63.84, H 11.12.

α-Poly-bis(μ-di-n-dodecylphosphinato)copper(II),
α-Cu[(n-C$_{12}$H$_{25}$)$_2$PO$_2$]$_2$

The preparation of two samples of the dodecyl compound, one the pure α form, and the other a mixture of the α and β forms (labelled α′), is described here. Whether some β isomer is formed in the synthesis of the α form appears to depend on the rate of formation of the product, which, in turn, depends on the concentrations of the reacting solutions, specifically, that of the phosphinic acid. Hence the α′ sample was obtained with rapid polymer formation from concentrated solutions. It is of note that Drinkard and Kosolapoff (10) appear to have formed the purely β-form of the copper n-decyl compound (on the basis of the melting point, 94°C (10) versus 92°C reported here), from a very concentrated aqueous solution of the phosphinic acid. The pure α-Cu[(n-C$_{12}$H$_{25}$)$_2$PO$_2$]$_2$ was synthesized in a manner analogous to that used to obtain the n-decyl derivative, with the exception that the solutions were more dilute.

Di-n-dodecylphosphinic acid (2.5 mmol), dissolved in ethanol (900 mL), was partially neutralized with sodium hydroxide (2.4 mmol in 75 mL water), and, after filtration, an additional 400 mL of water was added. Dropwise addition of aqueous copper(II) sulfate pentahydrate (1.2 mmol in 100 mL water) resulted in the precipitation of a very fine, blue solid. When the addition of Cu(II) was complete, a further 300 mL of water was added and the reaction mixture was stirred for 1.5 h. The solid was separated by filtration, washed with ethanol, and air dried. Yield 80%. *Anal.* calcd. for $CuC_{48}H_{100}P_2O_4$: Cu 7.33, C 66.51, H 11.63; found: Cu 7.28, C 66.40, H 11.43.

The α′-Cu[(n-C$_{12}$H$_{25}$)$_2$PO$_2$]$_2$ sample was prepared by the same method as described above for the pure α form; however, the partially neutralized phosphinic acid solution was much more concentrated (8 mmol in 1200 mL versus 2.5 mmol in ca. 1500 mL), and no water was added to the reaction mixture after the addition of the Cu(II) was complete. Yield 98%. *Anal.* found: Cu 7.37, C 66.51, H 11.70.

Synthesis of the copper(II) phosphinate β *forms*

The β isomers were obtained from the melt of samples of the analytically pure α forms. (Dissolution in, and subsequent evaporation of, an organic solvent such as chloroform also produces the β isomers.) In a typical conversion, the compound (ca. 1 g) was placed in a 100-mL Kjeldahl flask and melted in an oil bath at a temperature just above the appropriate melting point (given below). When judged, visually, to be completely melted, the sample was removed from the oil bath and allowed to freeze completely. It was then remelted and recooled, the process being repeated at least three times to ensure complete conversion of the α form to the β.

β-Poly-bis(μ-di-n-octylphosphinato)copper(II),
β-Cu[(n-C$_8$H$_{17}$)$_2$PO$_2$]$_2$

Oil bath temperature: 135°C. *Anal.* calcd. for $CuC_{32}H_{68}P_2O_4$: Cu 9.89, C 59.83, H 10.67; found: Cu 9.87, C 59.98, H 10.70.

β-Poly-bis(μ-di-n-decylphosphinato)copper(II),
β-Cu[(n-C$_{10}$H$_{21}$)$_2$PO$_2$]$_2$

Oil bath temperature: 130°C. *Anal.* calcd. for $CuC_{40}H_{84}P_2O_4$: Cu 8.42, C 63.87, H 11.22; found: Cu 8.36, C 63.63, H 11.10.

β-Poly-bis(μ-di-n-dodecylphosphinato)copper(II),
β-Cu[(n-C$_{12}$H$_{25}$)$_2$PO$_2$]$_2$

Oil bath temperature: 130°C. *Anal.* calcd. for $CuC_{48}H_{100}P_2O_4$: Cu 7.33, C 66.51, H 11.63; found: Cu 7.31, C 66.30, H 11.55.

Experimental techniques

Infrared spectra were obtained on a Perkin–Elmer model 598 spectrophotometer. Samples were mulled in Nujol and pressed between KRS-5 plates (Harshaw Chemical Co.). Electronic spectra (from 3,800 to 30 000 cm^{-1}) were obtained on Nujol mulls using a Cary 14 spectrophotometer.

Magnetic susceptibilities over the range 125–4.2 K were measured using a P.A.R. Model 155 vibrating sample magnetometer and over the range 80–300 K using a Gouy balance. This equipment was described in detail earlier (3). Magnetic susceptibilities were corrected for the diamagnetism of all atoms. These corrections were (in 10^{-6} cm^3 mol^{-1}): copper, −11; $(n\text{-}C_8H_{17})_2PO_2^-$, −210; $(n\text{-}C_{10}H_{21})_2PO_2^-$, −257; $(n\text{-}C_{12}H_{25})_2PO_2^-$, −300. A value of 60×10^{-6} cm^3 mol^{-1} was used to correct for the temperature independent paramagnetism of copper(II).

Differential scanning calorimetry measurements were obtained with a Mettler DSC 20 Standard Cell, a Mettler TC10 TA Processor, and a Print Swiss Matrix RO-80 printer/plotter. Powered samples (2–4 mg) were sealed in standard aluminum pans (40 μL). Two small holes punched in the lid allowed for free access to the measuring cell atmosphere, in this case, air. The heating rate was 4°C/min. The temperature was calibrated from 25–600°C with standard indium, zinc, and lead samples. Heat flow calibration was achieved using carefully weighed samples of indium.

Carbon and hydrogen microanalyses were obtained by P. Borda of

TABLE 1. DSC data for $Cu(R_2PO_2)_2$

R	Form	T_{fus} (°C)[a]	ΔH_{fus}[a] (kJ mol^{-1})	T_d (°C)[b]	Comments[c]
n-C_8H_{17}	α	123.8	63	265	Broad irreversible melting
n-C_8H_{17}	β	89.4	53	265	Sharp, low temp. sh., reversible melting
n-$C_{10}H_{21}$	α	122.7	93	250	Broad, irreversible melting
n-$C_{10}H_{21}$	β	92.0	71	250	Sharp, low temp. sh., reversible melting
n-$C_{12}H_{25}$	α	129.1	96	235	Broad, irreversible melting
n-$C_{12}H_{25}$	β	94.5, 96.8	94	235	Sharp doublet, reversible melting
n-$C_{12}H_{25}$	α′	97.1	19	—	Sharp
		125.3	86	235	Broad, irreversible melting

[a] T_{fus} and ΔH_{fus} are temperature and enthalpy of fusion.
[b] T_d represents the temperature at which oxidative decomposition begins.
[c] Sharp, broad, and doublet refer to the shape of the DSC curve; sh., shoulder, temp., temperature.

the Department of Chemistry, The University of British Columbia. Copper was determined by EDTA titration.

Solubilities

Qualitative solubility tests show β-$Cu[(n\text{-}C_8H_{17})_2PO_2]_2$ to be soluble (in excess of 0.1 g in 100 mL) in chloroform and slightly soluble in dichloromethane, carbon tetrachloride, and benzene. β-$Cu[(n\text{-}C_{10}H_{21})_2PO_2]_2$ is soluble in chloroform, slightly soluble in carbon tetrachloride, and insoluble in dichloromethane and benzene. The α forms of the above are slightly soluble in the chlorinated solvents and insoluble in benzene. Both α and β forms of $Cu[(n\text{-}C_{12}H_{25})_2PO_2]_2$ are slightly soluble in chloroform and dichloromethane and insoluble in carbon tetrachloride and benzene. All six of these compounds were found to be insoluble in petroleum ether, water, methanol, ethanol, and acetone.

Results and discussion

Syntheses, thermal properties, and solubilities

Reaction of a partially neutralized solution of di-n-octylphosphinic acid in methanol with an aqueous methanol solution of copper(II) sulfate pentahydrate gave a quantitative yield of α-$Cu[(n\text{-}C_8H_{17})_2PO_2]_2$. This material was first prepared, by a very similar method, by Gillman, who labelled it form I (4). Our observed melting point of 123.8°C and ΔH of 63 kJ mol^{-1} (Table 1) are in good agreement with the values obtained by Gillman. We found that remelting of the sample occurred at 89.4°C compared to Gillman's 81°C. The heat of fusion in this case also differs somewhat from that reported earlier. This second form, which we have labelled β-$Cu[(n\text{-}C_8H_{17})_2PO_2]_2$, is easily prepared in bulk by the repeated heating and cooling (135°C to room temperature) of a sample of the α form. We believe that this thermal cycling ensures complete conversion to the β form. This was not done in the earlier work and probably accounts for the differences observed in our β form and Gillman's form II.

Reaction of sodium di-n-decylphosphinate with copper(II) sulfate in aqueous ethanol yields α-$Cu[(n\text{-}C_{10}H_{21})_2PO_2]_2$. As for the octyl derivative, repeated heating to above the melting point of bulk samples of this material, followed by cooling to room temperature, results in complete conversion to the β form. In 1952 Drinkard and Kosolapoff (10) reported the preparation of what appears to have been the β form of this material (from the reported mp of 94°C); no mention of polymorphism was made in this early work.

No previous studies on copper(II) n-dodecylphosphinate have been reported. We obtained α and β forms by procedures identical to those used to obtain the corresponding decyl derivatives. In this instance we observed, however, that it is possible to have significant β contamination of the α form (the so-called α′ sample) if precipitation occurs too rapidly from concentrated solutions. The β contaminant was easily discernible in the DSC thermogram; whereas the pure α material shows a single endothermic peak at 125°C due to melting, the contaminated sample gave, in addition, an endothermic peak at 97.1°C due to melting of the β impurity.

The DSC data are given in Table 1. The heats of fusion, ΔH_{fus}, range from ~50 to 100 kJ mol^{-1}, for these long alkyl chain compounds. The values tend to decrease as the alkyl group gets shorter; this trend continues with the hexyl, butyl, and ethyl derivatives, where ΔH_{fus} values of 40, 28, and 13 kJ mol^{-1} respectively have been reported (3). This result suggests that the melting process involves the breakup of the interchain associative interactions and that these arise primarily from the intermeshing of alkyl groups on neighbouring chains (3). The extent of intermeshing would be expected to decrease as R gets smaller.

While the enthalpies of fusion tend to decrease as R gets smaller, the opposite trend is observed in the melting temperatures (compare the values in Table I to the values 109, 155, and 280°C reported for the hexyl, butyl, and ethyl derivatives (3)). This implies that while less energy is required to disrupt interchain interactions in the shorter R compounds, this effect is outweighed by the smaller increase in entropy on melting; therefore, a higher temperature of melting results.

Another effect of decreasing alkyl chain length in these polymeric phosphinates is to increase the oxidative stability. While the compounds studied here (and the hexyl derivative (3)) oxidatively decompose around 230–260°C, the ethyl and butyl derivatives decompose at 280°C (3). This effect has been observed before and has been attributed to the decreasing ease of oxidation of the alkyl group as R gets smaller (11, 12).

The accessibility of the polar inorganic backbone to polar solvents, as determined by the size of the alkyl groups attached to phosphorus, appears to be an important factor in determining the solubilities of these polymers. Hence, while the ethyl derivative is relatively soluble in polar solvents (3), the long alkyl chain compounds studied here are insoluble in water, methanol, ethanol, and acetone. Solubilities in chlorinated solvents, where presumably dipole-induced dipole interactions between the polymer backbone and the solvent are important, also tend to be slightly greater when R is small.

Electronic spectra

The α forms of the octyl, decyl, and dodecyl compounds exhibit broad absorption maxima at 12.3 × 10^3 cm^{-1} (±200

TABLE 2. Infrared spectra[a] in the regions 1000–1200 cm^{-1} and 700–810 cm^{-1} for $Cu(R_2PO_2)_2$

	$Cu[(n\text{-}C_8H_{17})_2PO_2]_2$		$Cu[(n\text{-}C_{10}H_{21})_2PO_2]_2$		$Cu[(n\text{-}C_{12}H_{25})_2PO_2]_2$	
Assignment	α form	β form	α form	β form	α form	β form
	1192 w sh					1189 w
	1180 w sh	1196 w	1189 m sh	1190 w	1186 w sh	1162 vw sh
	1170 m sh	1119 s sh	1171 m sh	1160 vw sh	1171 m sh	1115 vs sh
ν_{asy} (PO_2)	1107 vs	1112 vs	1109 vs	1111 vs	1111 vs	1111 vs
	1097 s sh		1100 s sh	1090 m sh	1100 s sh	1099 s sh
				1064 m sh	1082 m sh	
			1072 m sh	1057 m sh		1068 m sh
		1065 m sh	1058 s sh	1048 m sh		1054 m sh
ν_{sym} (PO_2)	1043 vs	1046 s	1043 vs	1042 s	1046 vs	1044 s
	1029 s sh					1025 m sh
ν_{asy} (PC_2)	772 m br	804 m–s	773 m br	805 m–s	775 m br	806 m
		779 w		780 w		783 w
		756 vw sh		763 vw		765 vw
	742 vw sh	740 w sh		741 w sh	740 w sh	
ν_{sym} (PC_2)	721 m–s	722 m	723 m–s	723 m	724 m–s	723 m
	707 vw sh	711 m sh	707 w sh	714 w sh	710 w sh	

[a] s = strong, m = medium, w = weak, m–s = medium to strong, sh = shoulder, v = very, br = broad.

cm^{-1}) with shoulders at 14.3, 14.3, and 14.4 × 10^3 cm^{-1} (±400 cm^{-1}) respectively. Within the experimental uncertainty these spectra are identical to that reported previously for $Cu[(C_2H_5)_2PO_2]_2$ (2). The absorption maxima for the β forms are at 11.4, 11.4, and 11.6 × 10^3 cm^{-1} (±200 cm^{-1}) for the octyl, decyl, and dodecyl derivatives respectively; shoulders are observed at 13.2 × 10^3 cm^{-1} (±400 cm^{-1}) for all three. These spectra are indistinguishable from those of $Cu[(n\text{-}C_4H_9)_2PO_2]_2$ and $Cu[(n\text{-}C_6H_{13})_2PO_2]_2$ (3). As discussed previously (2), the principal absorption may be assigned to the $^2B_2 \rightarrow {}^2A_1$, ^2E transition and the shoulder to $^2B_2 \rightarrow {}^2B_1$ in D_{2d} symmetry.

It was shown (3) that the difference in the electronic spectra between the ethyl derivative, on the one hand, and the butyl and hexyl compounds, on the other, could be accounted for by slight differences in the geometries of the CuO_4 chromophores involved, the more compressed (towards square planar) geometry of the ethyl derivative shifting its absorptions to higher energies. It seems reasonable to conclude that the α forms studied here have CuO_4 chromophores which are similar in geometry to that found in $Cu[(C_2H_5)_2PO_2]_2$ and are more compressed towards square planar geometry than those of the β forms.

Infrared spectra

In view of the lack of precise structural data from X-ray diffraction studies, the infrared spectra were examined in some detail for indications of structural differences between the α and β forms. The most informative regions of the spectra were found to be those in which the P—O and P—C stretching vibrations occur and a listing of observed frequencies in these regions is given in Table 2. Absorptions in the 1000–1200 cm^{-1} region are readily assigned to PO_2 stretching vibrations of coordinated phosphinate groups (2). Although there is more structure associated with these absorptions for the octyl, decyl, and dodecyl compounds compared with the shorter alkyl chain derivatives, the principal bands in this region occur near 1110 cm^{-1} for the antisymmetric PO_2 vibration and 1045 cm^{-1} for the symmetric vibration in all compounds. Moreover, the separation between the bands of about 65 cm^{-1} falls into the range expected for equivalent P—O bonds (4, 6, 13). This supports the conclusion that all of these polymeric copper(II) phosphinates have the same basic inorganic backbone involving chains of copper ions joined by double bridging phosphinate groups. Other structures involving alternating single–triple phosphinate bridges, terminal phosphinate groups, or unsymmetrical bridging (non-equivalent P—O bonds) would be expected to give distinctly altered spectra in the PO_2 stretching region (4, 6, 13). Numerous shoulders of varying intensity are observed on the principal PO_2 absorptions of the compounds where R is large. This has been seen in other transition metal phosphinates and has been ascribed to overtones, combination bands, or PO_2 stretching frequencies caused by phosphinate structures not predominant in the bulk polymer (14, 15). Another possible cause is the presence of phosphinate groups in slightly different environments along the polymer chain. In the hexyl compound, for example, there are two crystallographically distinct rings; one ring has Cu—O—P—O—Cu moieties that involve one long (1.932 Å) and one short (1.896 Å) Cu—O bond while the other two Cu—O bonds are both relatively short (1.902 Å and 1.907 Å) (3). This difference in bonding results in two distinct types of phosphinate group and may be the cause of the structure seen in the PO_2 stretching region of this compound. By comparison, the Cu—O bonds are all nearly equivalent in the ethyl (1.916–1.922 Å) and butyl (1.916–1.926 Å) derivatives (2, 3) and for both of these, simple, unstructured two-band spectra are observed in the PO_2 stretching region.

Examination of the PC_2 stretching region (Table 2) reveals significant differences between the α and β forms. The former show a broad, medium intensity antisymmetric PC_2 stretch in the 770–775 cm^{-1} region, close to the frequency observed in the ethyl derivative. In contrast, in the β forms this band has shifted to about 805 cm^{-1} and become a relatively sharp, medium to strong absorption, comparable to the antisymmetric stretches observed in the butyl and hexyl derivatives. This particular band was seen in the spectrum of the preparation of the α-dodecyl derivative, which we concluded from DSC studies contained significant β impurity (so-called α′ material). The symmetric PC_2 stretch is virtually the same (~725 cm^{-1})

in all compounds, although in the ethyl and α derivatives this band is somewhat more intense than the antisymmetric stretch, while for the butyl, hexyl, and β forms it is generally less intense.

Other regions of the infrared spectra were generally less informative; however, there are features in the 450–600 cm^{-1} region, where angle bending modes of the C_2PO_2 groups normally occur (13, 16–21), which also group the β forms with the butyl and hexyl derivatives. These compounds all exhibit two relatively strong bands around 555 and 520 cm^{-1} with differing numbers of weaker bands depending on R. The α forms also exhibit two relatively strong bands but at higher frequencies (~585 and 550 cm^{-1}), as well as a number of weaker bands depending on R. In this instance the ethyl derivative is somewhat unique, exhibiting two medium intensity absorptions at lower energy than observed in the β forms (2). The region below 400 cm^{-1} contains bands due to Cu—O stretching and lattice vibrations. Most compounds studied here show a single medium intensity band around 360–380 cm^{-1} accompanied usually by several weaker bands. There are no clear features in this region that classify the compounds into distinct groups.

This analysis of the vibrational data has revealed spectral similarities among the ethyl and α derivatives on the one hand and the butyl, hexyl, and β derivatives on the other, and strongly suggests that there are important structural similarities within each group and differences between groups. Moreover, the greatest spectral differences between groups involve vibrations of the PC_2 moiety, suggesting that the differences primarily involve the orientations and inter- and intrachain packing of the alkyl groups while the inorganic Cu—O—P—O—Cu backbone remains relatively constant in all compounds (except for small differences in the CuO_4 geometry, as discussed above). This is consistent with the reported X-ray results on the shorter alkyl chain compounds (3). One of the structural features noted in this earlier work was that in the ethyl compound one of the $Cu(OPR_2O)_2Cu$ rings has two alkyl groups axial and two equatorial to the ring, whereas in the butyl and hexyl derivatives all alkyl groups are axial. Such differences likely occur in the α and β forms of the long alkyl chain compounds.

Magnetic properties

Magnetic susceptibilities from 4.2 to 300 K are given in Table 3[1] and magnetic moments are plotted as a function of temperature in Fig. 1. The strong spectral (and therefore, presumably, structural) correlation between $Cu[(C_2H_5)_2PO_2]_2$ and the α forms of the long alkyl chain compounds occurs also with the magnetic properties. In common with the ethyl compound, all α derivatives exhibit magnetic moments which decrease with temperature, behaviour indicative of antiferromagnetic coupling. As the temperature is lowered the magnetic susceptibility of α-$Cu[(n\text{-}C_{10}H_{21})_2PO_2]_2$ passes through a broad maximum at ~48 K and a minimum at ~16 K and then rises sharply with further decrease in temperature (Fig. 2). For both the α-octyl and α-dodecyl derivatives the low temperature rise in susceptibility occurs just below the temperature of the maximum and hence the maximum is not as well defined. This increase in susceptibility at the lowest temperatures is indicative of the presence of paramagnetic monomer impurity.

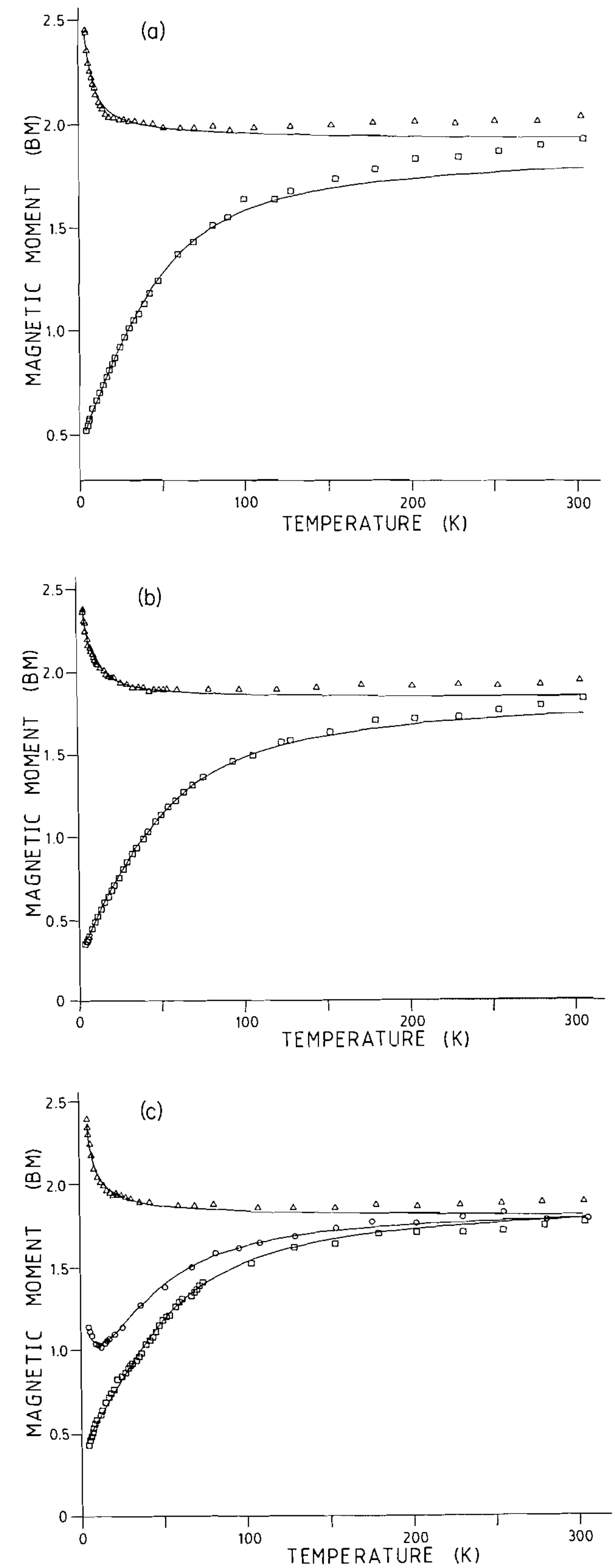

FIG. 1. Magnetic moment vs. temperature plots. Solid lines are calculated from theory using best fit values of magnetic parameters (see text). (a) □ α-$Cu[(n\text{-}C_8H_{17})_2PO_2]_2$, △ β-$Cu[(n\text{-}C_8H_{17})_2PO_2]_2$; (b) □ α-$Cu[(n\text{-}C_{10}H_{21})_2PO_2]_2$, △ β-$Cu[(n\text{-}C_{10}H_{21})_2PO_2]_2$; (c) □ α-$Cu[(n\text{-}C_{12}H_{25})_2PO_2]_2$, ○ α′-$Cu[(n\text{-}C_{12}H_{25})_2PO_2]_2$, △ β-$Cu[(n\text{-}C_{12}H_{25})_2PO_2]_2$.

[1] Available at a nominal charge from the Depository of Unpublished Data, CISTI, National Research Council of Canada, Ottawa, Ont., Canada, K1A 0S2.

TABLE 4. Magnetic parameters

Compound	J (cm^{-1})	g	F^a	% Monomer
α-$Cu[(n\text{-}C_8H_{17})_2PO_2]_2$	−25	2.23	0.022	5.2
α-$Cu[(n\text{-}C_{10}H_{21})_2PO_2]_2$	−29	2.19	0.017	1.4
α-$Cu[(n\text{-}C_{12}H_{25})_2PO_2]_2$	−29	2.25	0.023	3.8
α'-$Cu[(n\text{-}C_{12}H_{25})_2PO_2]_2$	{ −24	2.24	0.027	2.3 (monomer)
	{ +2.3			18.0 (ferromagnet)
β-$Cu[(n\text{-}C_8H_{17})_2PO_2]_2$	+1.8	2.24	0.017	—
β-$Cu[(n\text{-}C_{10}H_{21})_2PO_2]_2$	+2.1	2.13	0.012	—
β-$Cu[(n\text{-}C_{12}H_{25})_2PO_2]_2$	+2.3	2.11	0.018	—

$^a F$ = fitting function (see text). Fit to $T < 100$ K data only.

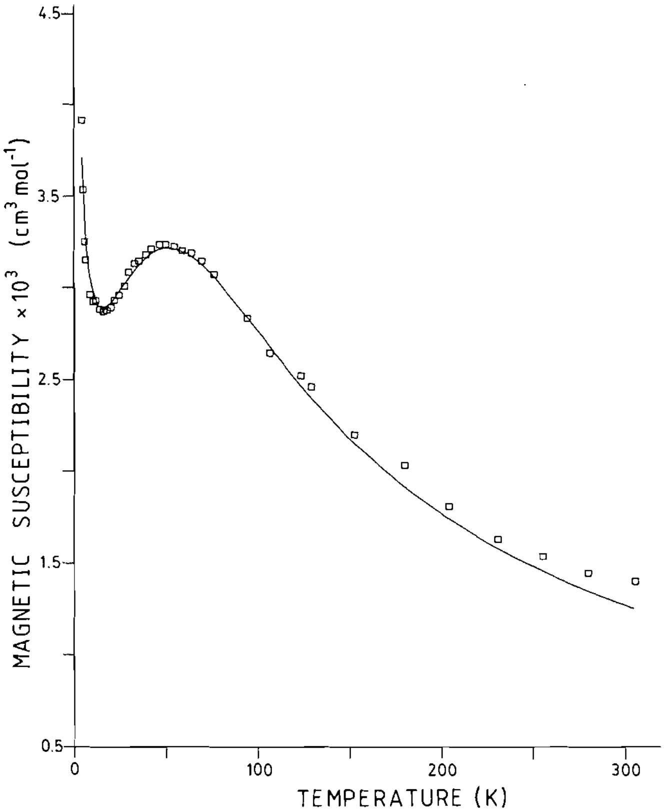

FIG. 2. Magnetic susceptibility vs. temperature plot for α-$Cu[(n\text{-}C_{10}H_{21})_2PO_2]_2$. Solid line is theory (see text).

As before (3), the magnetic data were analyzed according to the isotropic Heisenberg model for exchange coupled linear chains employing the polynomial expression for the magnetic susceptibility developed by Hall (22, 23). Computer fits were made to the susceptibility data with J, g, and percent paramagnetic impurity as variables. For the purpose of these fits the paramagnetic contribution was assumed to follow Curie law and to have the same g value as that of the bulk antiferromagnetically coupled polymer. The criterion used for the best fit was that set of parameters which gave the minimum value of the function:[2]

$$F = \left[\frac{1}{n}\sum_i^n \left(\frac{\chi_i^{calc} - \chi_i^{obs}}{\chi_i^{obs}}\right)^2\right]^{1/2}$$

[2]This was the fitting function used in ref. 3 where it was termed the rms deviation. The values quoted in ref. 3 are in error; they should read 12×10^{-3}, 18×10^{-3}, and 13×10^{-3} for the ethyl, butyl, and hexyl derivatives respectively. The quantities are dimensionless.

where n is the number of data points and χ_i^{obs} and χ_i^{calc} are the experimental and calculated susceptibilities. We were not always able to obtain satisfactory agreement between experiment and theory over the entire temperature range from 4.2 to 300 K for the compounds studied in this work. In view of the inherent uncertainty, due to packing errors, in the absolute susceptibility determined by the Gouy method ($\sim\pm5\%$), we chose to fit the low temperature (<100 K) magnetometer data (estimated uncertainty in χ_M of $\pm2\%$) only. The best fit values of the magnetic parameters as well as the corresponding values of F for the various compounds are given in Table 4. The solid lines in Figs. 1 and 2 are calculated using these parameters and, as can be seen, the agreement with experiment is good, particularly over the low temperature region.

These long alkyl chain α derivatives differ from $Cu[(n\text{-}C_2H_5)_2PO_2]_2$ in two important ways. First, the magnetic data indicate the presence of paramagnetic impurities. This may reflect a small concentration of monomeric phosphinate in which the R_2PO_2 groups chelate or may reflect the effect of a smaller degree of polymerization and consequently a higher concentration of terminal copper atoms. In any event the microanalytical data suggest the impurity is "structural" rather than "chemical", reflecting the presence of a small amount of a paramagnetic form of copper(II) phosphinate different from that present in the bulk phosphinate bridged chain. The second way in which the α forms differ from the diethylphosphinate derivative is that the former have significantly larger absolute values of the exchange coupling constant J.

The β forms of the copper(II) dioctyl-, didecyl-, and didodecylphosphinates all exhibit ferromagnetic behaviour. The low temperature magnetic susceptibility data (4.2–100 K) were fit to theory employing the polynomial expression of Baker *et al.* for ferromagnetically coupled $S = 1/2$ chains (23, 24). Attempts to include paramagnetic impurity produced no improvement in agreement between experiment and theory in these cases. This may reflect the lack of such impurity; however, it must be appreciated that because of the large susceptibilities observed at low temperatures for ferromagnetic samples the detection of a small amount of paramagnetic impurity would be very difficult. Magnetic moments are shown compared to theory in Fig. 1 and best fit values of the magnetic parameters, as well as the corresponding values of the fitting parameter F, are listed in Table 4. An interesting feature of these results is that, in contrast to the results for the antiferromagnetic materials, the J values are all small ($\approx +2$ cm^{-1}) and very close to those observed for the ferromagnetic butyl and hexyl derivatives (3).

The sample of the α-dodecyl compound that DSC and infrared studies indicate contains significant β impurity (α' material) exhibits magnetic properties completely consistent with this conclusion. The magnetic moment, which decreases on lowering the temperature, shows a minimum at ~11 K, then increases again to 4.2 K (Fig. 1). This behaviour cannot be accounted for by paramagnetic impurity alone in an antiferromagnetic sample but is indicative of the presence of ferromagnetic impurity. In fact, the best fit was found assuming both paramagnetic and ferromagnetic impurity (Table 4). In fitting the data for this sample the value of J for the ferromagnetic impurity was fixed at the value observed for the pure β form. The values of g and J for the antiferromagnetic component that constitutes the major part of the sample (Table 4) obtained in the fit are in good agreement with the values obtained for the pure α form.

This work completes detailed magnetic studies on a series of straight chain dialkylphosphinates of copper(II). It has shown that, whereas the compounds containing short alkyl chains (C_2,C_4,C_6) exist in either antiferromagnetic or ferromagnetic forms, the longer alkyl chain compounds (C_8,C_{10},C_{12}) exhibit polymorphism and are readily obtainable in both forms. Spectroscopic evidence suggests all compounds have the same extended chain, double phosphinate bridged structure with differences involving the orientations of the alkyl groups with respect to the plane of the inorganic backbone. This in turn affects the packing of the chains and may result in the small differences observed in the detailed geometry of the CuO_4 chromophores. We suggested earlier (3) that both ferromagnetic and antiferromagnetic pathways for superexchange may be available in these compounds, with a feature such as the flattening of the CuO_4 chromophore favouring the latter pathway. These ideas may be taken further as a result of the current study. The exchange coupling constant is virtually the same in all of the ferromagnetic samples but $-J$ varies from ~1 cm^{-1} in the ethyl compound to ~30 cm^{-1} in the other antiferromagnetic materials. This suggests that the ferromagnetic pathway involves primarily σ-type orbital overlap, which is relatively insensitive to small changes in geometry, while the antiferromagnetic pathway involves the π-type orbital overlap, which is more sensitive to changes in geometry. Hence when the latter dominates, as it seems to do in the ethyl and α octyl, decyl, and dodecyl forms, greater differences in the magnitude of exchange coupling between compounds are observed.

Acknowledgements

We thank the Natural Sciences and Engineering Research Council of Canada for financial support and the University of British Columbia Computing Centre for assistance. K.W.O. and J.S.H. thank the U.B.C. Graduate Scholarship Committee and K.W.O. also thanks NSERC for scholarship awards.

1. R. Cini, P. Colamarino, P. L. Orioli, L. S. Smith, P. R. Newman, H. D. Gillman, and P. Nannelli. Inorg. Chem. **16**, 3223 (1977).
2. K. W. Oliver, S. J. Rettig, R. C. Thompson, and J. Trotter. Can. J. Chem. **60**, 2017 (1982).
3. J. S. Haynes, K. W. Oliver, S. J. Rettig, R. C. Thompson, and J. Trotter. Can. J. Chem. **62**, 891 (1984).
4. H. D. Gillman. Inorg. Chem. **13**, 1921 (1974).
5. V. Giancotti and A. Ripamonti. J. Chem. Soc. (A), 706 (1969).
6. H. D. Gillman. Inorg. Chem. **11**, 3124 (1972).
7. R. H. Williams and L. A. Hamilton. J. Am. Chem. Soc. **77**, 3411 (1955).
8. D. F. Peppard, G. W. Mason, and S. Lewey. J. Inorg. Nucl. Chem. **27**, 2065 (1965).
9. R. H. Williams and L. A. Hamilton. J. Am. Chem. Soc. **74**, 5418 (1952).
10. W. C. Drinkard and G. M. Kosolapoff. J. Am. Chem. Soc. **74**, 5520 (1952).
11. P. Nannelli, B. P. Block, J. P. King, A. J. Saraceno, O. S. Sprout, Jr., N. D. Peschko, and G. H. Dahl. J. Polym. Sci. Polym. Chem. Ed. **11**, 2691 (1973).
12. B. P. Block, S. H. Rose, C. W. Schaumann, E. S. Roth, and J. Simkin. J. Am. Chem. Soc. **84**, 3200 (1962).
13. E. I. Matrosov, K. A. Andrianov, I. Ya. Manevich, and Yu. A. Buslaev. Izv. Akad. Nauk SSSR, Neorg. Mater. **1**, 464 (1965); Engl. translation: Inorg. Mater. (USSR), **1**, 428 (1965).
14. H. D. Gillman and J. L. Eichelberger. Inorg. Chem. **15**, 840 (1976).
15. H. D. Gillman and J. L. Eichelberger. Inorg. Chim. Acta, **24**, 31 (1977).
16. A. D. Delman, J. Kelly, J. Mironov, and B. B. Simms. J. Polym. Sci. Part A-1, **4**, 1277 (1966).
17. E. J. Matrosov and B. Fisher. Izv. Akad. Nauk SSSR, Neorg. Mater. **3**, 545 (1967); Engl. Translation: Inorg. Mater. (USSR), **3**, 485 (1967).
18. T. S. Wei, J. C. Scott, A. F. Garito, A. J. Heeger, H. D. Gillman, and P. Nannelli. Phys. Rev. B, **12**, 5297 (1975).
19. M. Tsuboi. J. Am. Chem. Soc. **79**, 1351 (1957).
20. K. Nakamoto, P. J. McCarthy, A. Ruby, and A. E. Martell. J. Am. Chem. Soc. **83**, 1066 (1961).
21. D. E. C. Corbridge. Top. Phosphorus Chem. **6**, 235 (1969).
22. J. W. Hall. Ph.D. thesis, University of North Carolina, 1977.
23. W. E. Estes, W. E. Hatfield, J. A. C. van Ooijen, and J. Reedijk. J. Chem. Soc. Dalton Trans. 2121 (1980).
24. G. A. Baker, Jr., G. S. Rushbrook, and H. E. Gilbert. Phys. Rev. A, **135**, 1272 (1964).

The oxidation of organic sulphides by *Mortierella isabellina*. 2. Effects of substituents on the stereochemistry of sulphoxide formation

Herbert L. Holland, Heike Pöpperl, Ronald W. Ninniss, and P. Chinna Chenchaiah
Department of Chemistry, Brock University, St. Catharines, Ont., Canada L2S 3A1

Received September 19, 1984

Herbert L. Holland, Heike Pöpperl, Ronald W. Ninniss, and P. Chinna Chenchaiah. Can. J. Chem. **63**, 1118 (1985).

A series of *para*-substituted alkyl aryl sulphides has been transformed stereoselectively to the sulphoxide by incubation with the fungus *Mortierella isabellina*. The enantiomeric purity of the products was dependent on the nature of substitution in the aromatic ring and at sulphur. Comparisons of the enantiomeric purities obtained from sulphides with *para* substituents of the same steric size but different electronic properties indicate that the stereoselectivity of *S* oxidation is susceptible to electron withdrawing or donating factors. This conclusion lends credence to a stepwise oxidation mechanism involving an electron deficient sulphur intermediate.

Herbert L. Holland, Heike Pöpperl, Ronald W. Ninniss et P. Chinna Chenchaiah. Can. J. Chem. **63**, 1118 (1985).

Par incubation avec des champignons *Mortierella isabellina*, on a transformé stéréosélectivement en sulfoxydes une série de sulfures d'alkyles et d'aryles substitués en *para*. La pureté énantiomérique des produits dépend de la nature des substituants sur le noyau aromatique et au niveau du soufre. En se basant sur une comparaison des puretés énantiomériques obtenues avec des sulfures portant des substituants en *para* qui ont des encombrements stériques semblables mais des propriétés électroniques différentes, on peut déduire que la stéréosélectivité de l'oxydation du soufre est susceptible aux factuers électro-affinitaires ou électro-donneurs des substituants. Cette conclusion supporte le concept d'un mécanisme par étape impliquant un intermédiaire sulfuré déficient en électrons.

[Traduit par le journal]

In spite of the continued interest in chiral sulphoxides, both in the study of sulphur stereochemistry (1) and as intermediates in asymmetric synthesis (2), the best direct chemical methods for their generation from sulphides (3) have not yet achieved the high degree of enantiomeric purity desirable in modern asymmetric synthesis. High enantiomeric excesses (>35%) are routinely available for *p*-tolyl alkyl sulphoxides (only) by a modification (4) of the Anderson synthesis (5) using sulfinate esters, or by the use of biological oxidizing agents employing sulphides as substrates.

In the latter area, the use of actively growing or resting cultures of fungi has been the most widely used technique for the production of sulphoxides of good optical purity (6–8). Other methods of biotransformation, using enzymes of mammalian origin (9,10) or peroxide oxidation in the presence of enzyme templates (11), are not generally applicable to preparative scale work.

In an extension of our earlier work on the mechanism of alkyl aryl sulphide oxidation by the fungus *Mortierella isabellina* (12), in which we proposed that cytochrome P-450 dependent mono-oxygenase enzymes of the fungus were responsible for oxidation at sulphur, we have now studied the effects of substitution at the *para* position of the aromatic ring, and at sulphur, on the degree of enantiomeric enrichment of the resultant sulphoxide. The sulphides used in this study, **1** and **4**, gave the corresponding sulphoxides, **2** and **5**, respectively, as major products on incubation with *M. isabellina*; this is summarized in Table 1. In the case of methyl *p*-nitrophenyl sulphide (1*g*) and *p*-bromophenyl methyl sulphide (1*j*), the sulphones (3*a* and 3*b*, respectively) were also obtained. Fungal oxidation of sulphoxides to sulphones is well documented (13).

The enantiomeric enrichments reported in Table 1 were determined by the ^{1}H nmr chiral shift reagent method. In the presence of 0.25 molar equivalents of Eu(hfc)$_3$ the methyl singlets for the two enantiomers of **1**, the *S*-alkyl α hydrogen signals of 4*a*, 4*b*, and 4*d*, and the *S*-alkyl β hydrogen signals of 4*c* were well resolved (ΔΔδ ca. 0.2–0.4 ppm). In addition, the C-2 and C-6 aromatic hydrogen signals of **1** were also separated into a pair of half AB quartets whose relative areas

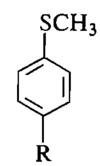

1

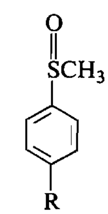

2

a R = H
b R = CH_3
c R = C_2H_5
d R = $CH(CH_3)_2$
e R = $C(CH_3)_3$
f R = OCH_3
g R = NO_2
h R = F
i R = Cl
j R = Br
k R = CN

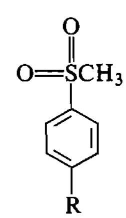

3 *a* R = Br
b R = NO_2

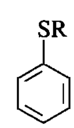

4

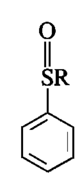

5

a R = C_2H_5
b R = $CH(CH_3)_2$
c R = $C(CH_3)_3$
d R = *n*.C_3H_7

TABLE 1. Transformation of sulphides **1** and **4** by *M. isabellina*

	Sulphoxide formation				
		Enantiomeric excess (%)			
Substrate	Isolated yield (%)	Nmr	Rotation (ref.)	$[\alpha]_D^{21}$ (°)	Configuration
1*a*	65	58	55(14)	+98	*R*
1*b*	52	46	43(6)	+77	*R*
1*c*	20	90		+95	*R*
1*d*	30	84	80(16)	+135	*R*
1*e*	27	76		+82	*R*
1*f*	50	72		+121	*R*
1*g*	6[a]	20		+41	*R*
1*h*	45	70		+97	*R*
1*i*	69	90		+135	*R*
1*j*	66[b]	100		+110	*R*
1*k*	35	80	80(17)	+105	*R*
4*a*	70	86	83(18)	+154	*R*
4*b*	55	83		+145	*R*
4*c*	15	58	62(14)	+110	*R*
4*d*	52	100		+192	*R*
(±)**2***g*	100	0		—	—
(±)**2***j*	100	0		—	—

[a]Accompanied by sulphone (30%).
[b]Accompanied by sulphone (5%).

could be used as an internal check on the values obtained from the methyl singlets. The values for enantiomeric enrichments so obtained were checked where possible by optical rotation measurements. Our estimate of optical purity for the sulphoxide 1*b* differs from that previously reported by Sih and co-workers (8) for 1*b* obtained from the same fungus. The latter group, however, estimated their optical purity solely from rotation measurements; at least three different values for the specific rotation of (*R*)-1*b* appear in the literature (6,15).

The values reported in Table 1 for the enantiomeric enrichment of sulphoxides 2*g* and 2*j* may not be directly attributable to stereospecific sulphide oxidation. In these cases the formation of sulphone **3** was also obtained, raising the possibility that the values listed for the enrichments of 2*g* and 2*j* may be attributable at least in part to stereoselectivity in the oxidation of sulphoxide to sulphone (13). In an attempt to investigate this, racemic sulphoxides 2*g* and 2*j* were administered as substrates to *M. isabellina*, but under these conditions the formation of sulphone did not occur. It therefore seems likely that, in the case of sulphone formation from 2*g* and 2*j*, both oxidations occur without the substrate leaving the enzyme's active site; it may therefore not be possible to directly determine the stereoselectivity of the second oxidation. The assignment of absolute stereochemistry to the predominant sulphoxide enantiomers in Table 1 follows from the results reported for the absolute stereochemistry of alkyl aryl sulphoxides of known optical rotation (14,15,19,20).

Walsh and co-workers noted an intrinsic lack of stereospecificity in the cytochrome P-450 catalysed enzymic oxidation of *p*-tolyl ethyl sulphide to sulphoxide (21,22). A similar result has been recorded by others (23) and rationalized in terms of the diagram of Fig. 1. The alternatives are either specific binding with non-specific oxidation occurring at either A or B, or a non-specific binding mode in which oxidation occurs from only one of the directions shown. The latter interpretation has been proposed by Oae and co-workers (23) for the liver microsomal oxidation of sulphides on the basis of a change in absolute stereochemistry of the oxidation of PhSR where R = *tert*-butyl, compared with the stereochemistry observed for R = methyl, and the assumption that *tert*-butyl is sterically larger than phenyl.

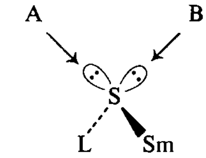

L = large substituent
Sm = small substituent

FIG. 1. Stereoselectivity in enzymic sulphide oxidation

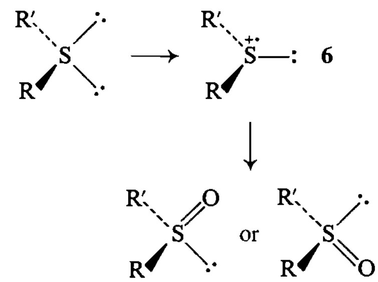

FIG. 2. Mechanism of enzymic sulphide oxidation (12,24)

This interpretation cannot hold in the present case, as all the sulphides listed in Table 1 gave sulphoxide of positive rotation (*R* stereochemistry; see above). We therefore prefer the earlier interpretation of Henbest and co-workers (6) of a specific binding mode and non-stereospecific oxidation. This proposal is also consistent with the conclusions of Walsh (21,22).

A non-stereospecific oxidation may be the result of a "loose" active site in which oxidation can occur from either direction (Fig. 1). In this event an additional possibility is raised by a consideration of the mechanism of oxidation at sulphur, and is presented in Fig. 2. Previous work (12,24) has indicated that this reaction is a stepwise process; the intermediate has been formulated as the radical cation (**6**) (Fig. 2) (24) or a similar species coordinated to the active site of the enzyme (12). In either case, the intermediate will not possess the regular tetrahedral geometry characteristic of sulphides or sulphoxides. Spectroscopic and theoretical studies of the related molecules H_2S and $H_2S^{+\cdot}$ indicate that the barrier to linearity is substantially reduced by ionization at sulphur (25,26) and that the ionized species can invert at room temperature (25).

Intermediate **6** will therefore not necessarily possess the stereochemical integrity of the substrate. The oxidation of **6** to sulphoxide is fast compared with the initial ionization step (12,27,28). The rates for similar reactions (e.g. C—H oxidation) catalysed by cytochrome P-450 dependent enzymes suggests that this rate can approach that of radical inversion (29), raising the possibility that the absolute stereochemistry of product may be determined, in part, by the stability of the radical cation **6**.

A comparison of the enantiomeric excesses (ee) of sulphoxides obtained from isosteric sulphides (Table 1) suggests that the ee is dependant at least in part on the electron density at sulphur. Thus with substrates 1*a*/1*h* (*para* H vs. *para* F), ee increases from 58 to 70%. A similar effect is found for 1*f* vs. 1*c* (72% to 90%), and 1*b* vs. 1*k* (46% to 80%), suggesting that, for these compounds, an increase in electron withdrawal by the aromatic ring and the resultant destabilization of the intermediate **6** has a positive effect on enantiomeric purity.

In the absence of more detailed information on reaction rates and intermediate structures this effect cannot be unambiguously attributed to a variation in radical lifetimes, but this hypothesis is an attractive one which is consistent with the data. It is, of course, not the only factor which affects enantiomeric excess. There clearly exist both *para* steric factors (cf. **1**, R = CH_3 vs. C_2H_5), and *S*-alkyl steric factors (cf. 1*a* vs. 4*a* and 4*d*), but in the results from the isosteric substrates described above these steric factors are minimized.

The data presented herein can therefore be rationalized in the following terms. The stereoselectivity of sulphoxide formation is determined largely by binding parameters, which are susceptible to steric factors (Fig. 1); in addition, there is an electronic effect of the substituent at the *para* position of the aromatic ring of **1** whose influence can be understood in terms of the stepwise mechanism of sulphoxidation presented in Fig. 2.

Experimental

Apparatus, materials, and methods

Melting points were determined on a Gallenkamp apparatus and are uncorrected. Infrared spectra were recorded on an Analect FX6260 FTIR spectrometer. Proton nmr spectra were obtained at 80 MHz with a Varian WP80CW instrument, using $CDCl_3$ as solvent and TMS as internal standard. Enantiomeric ratios were determined in a mixture of $CDCl_3$ and CCl_4 (1:4) in the presence of tris[3-(heptafluoropropylhydroxymethylene)-*d*-camphorato] europium(III). Mass spectra were obtained with an AEI MS30 interfaced to a Krato DS-55 data system. Column chromatography was performed on silica gel and thin layer chromatography on Merck silica gel 60F-254 (0.2 mm). Optical rotations were determined with a Perkin–Elmer 241MC polarimeter using chloroform as solvent. *Mortierella isabellina* NRRL 1757 was maintained as described previously (12).

Preparation of substrates

Thioanisole (1*a*) was a commercial sample. The methyl sulphides 1*b*–1*k* were prepared from the corresponding thiols as previously described (12). The alkyl sulphides 4*a*, 4*b*, and 4*d* were prepared by alkylation of the corresponding thiol with alkyl bromide (12), and 4*c* by addition of thiophenol to isobutene as described (30). Racemic sulphoxides 2*g* and 2*j* were prepared from the sulphide by oxidation with sodium metaperiodate (31). All compounds exhibited spectral and physical properties consistent with their structures.

Incubations with M. Isabellina

Mortierella isabellina NRRL 1757 was grown as described, and the incubations performed as previously detailed (12). Yields and enantiomeric purities of products are listed in Table 1.

Acknowledgements

Financial support was provided by the Natural Sciences and Engineering Research Council of Canada. We are grateful to Mr. T. Jones for help in obtaining spectral data.

1. J. G. Tillett. Chem. Rev. **76**, 747 (1976).
2. G. Solladie. Synthesis, 185 (1981).
3. F. A. Davis, R. H. Jenkins, S. B. Awad, O. D. Stringer, W. H. Watson, and J. Galloy. J. Am. Chem. Soc. **104**, 5412 (1982).
4. J. Drabowicz, B. Bujnicki, and M. Mikolajczyk. J. Org. Chem. **47**, 3325 (1982).
5. K. K. Anderson. Tetrahedron Lett. 93 (1962).
6. B. J. Auret, D. R. Boyd, H. B. Henbest, and S. Ross. J. Chem. Soc. C, 2371 (1968).
7. B. J. Auret, D. R. Boyd, H. B. Henbest, C. G. Watson, K. Balenovic, V. Polak, V. Johanides, and S. Divjak. Phytochemistry, **13**: 64 (1974).
8. E. Abushanab, D. Reed, F. Suzuki, and C. J. Sih. Tetrahedron Lett. 3415 (1978).
9. D. J. Waxman, D. R. Light, and C. Walsh. Biochemistry, **21**, 2499 (1982).
10. T. Takata, M. Yamazaki, K. Fujimori, Y. H. Kim, T. Iyanagi, and S. Oae. Bull. Chem. Soc. Jpn. **56**, 2300 (1983).
11. T. Sugimoto, T. Kokubo, J. Miyazaki, S. Tanimoto, and M. Okano. Bioorg. Chem. **10**, 311 (1981).
12. H. L. Holland and I. M. Carter. Can. J. Chem. **60**, 2420 (1982).
13. B. J. Auret, D. R. Boyd, and H. B. Henbest. J. Chem. Soc. C, 2374 (1968).
14. U. Felli, D. Tarossi, F. Montanari, and G. Torre. J. Chem. Soc. C, 1317 (1968).
15. K. Mislow, M. M. Green, P. Laur, J. T. Melillo, T. Simmons, and A. L. Ternay. J. Am. Chem. Soc. **87**, 1958 (1965).
16. G. Modena, U. Quintilly, and G. Scorrano. J. Am. Chem. Soc. **94**, 202 (1972).
17. W. H. Pirkle, M. S. Hoekstra, and W. H. Miller. Tetrahedron Lett. 2109 (1976).
18. K. Kamiyama, H. Minato, and M. Kobayashi. Bull. Chem. Soc. Jpn. **46**, 3895 (1973).
19. R. S. Cooke and G. S. Hammond. J. Am. Chem. Soc. **92**, 2739 (1970).
20. U. DeLaCamp and H. Hope. Acta Crystallogr. Sect. B, **26**, 846 (1970).
21. D. R. Light, D. J. Waxman, and C. Walsh. Biochemistry, **21**: 2490 (1982).
22. D. J. Waxman, D. R. Light, and C. Walsh. Biochemistry, **21**, 2499 (1982).
23. T. Takata, M. Yamazaki, K. Fujimori, Y. H. Kim, S. Oae, and T. Iyanagi. Chem. Lett. 1441 (1980).
24. Y. Watanabe, T. Iyanagi, and S. Oae. Tetrahedron Lett. **21**, 3685 (1980).
25. R. N. Dixon, G. Duxbury, M. Horani, and J. Rostas. Mol. Phys. **22**, 977 (1971).
26. F. B. Brown. J. Chem. Phys. **58**, 827 (1973).
27. C. Srinivasan, P. Kuthalingham, and N. Arumugan. Can. J. Chem. **56**, 3043 (1978).
28. Y. Watanabe, S. Oae, and T. Iyanagi. Bull. Chem. Soc. Jpn. **55**, 188 (1982).
29. H. L. Holland. Chem. Soc. Rev. **11**, 371, 394 (1982).
30. W. Hahn. Ger. Patent 1,110,631 (July 13th, 1961); Chem. Abstr. **56**, 3416 (1962).
31. N. J. Leonard and C. R. Johnson. J. Org. Chem. **27**, 282 (1962).

Microbial hydroxylation of steroids. 10. Rearrangement during epoxidation and hydroxylation, and the stepwise nature of these enzymic reactions

HERBERT L. HOLLAND AND ELLY RIEMLAND
Department of Chemistry, Brock University, St. Catharines, Ont., Canada L2S 3A1

Received September 27, 1984

HERBERT L. HOLLAND and ELLY RIEMLAND. Can. J. Chem. **63**, 1121 (1985).

A series of unsaturated steroids has been incubated with fungi which are known to hydroxylate at a site corresponding to the allylic position in the analogous saturated steroids. In some cases, the anticipated hydroxylation occurred without rearrangement of the double bond. In a number of instances, however, products were obtained whose structures implied that allylic rearrangement had occurred during the reaction. The formation of these products is consistent with a stepwise mechanism of enzymatic oxidation. Possible routes for product formation are presented which incorporate this proposal.

HERBERT L. HOLLAND et ELLY RIEMLAND. Can. J. Chem. **63**, 1121 (1985).

On a fait incuber une série de stéroïdes non saturés avec des champignons connus pour hydroxyler à une site correspondant à la position allylique des stéroïdes saturés analogues. Dans quelques cas, l'hydroxylation prévue se produit sans transposition de la double liaison. Toutefois, dans un bon nombre de cas, on a obtenu des produits dont les structures impliquent que des transpositions allyliques se sont produites au cours de la réaction. La formation de ces produits est en accord avec un mécanisme de l'oxydation enzymatique qui impliquerait plusieurs étapes. On propose des voies réactionnelles possibles qui incorporent cette proposition.

[Traduit par le journal]

Introduction

The enzymatic conversion of a saturated carbon–hydrogen bond to hydroxyl, and the related enzymatic epoxidation of olefins, are most often catalyzed by cytochrome P-450 dependent mono-oxygenase enzymes (1). The mechanism of these oxidations is still in doubt, currently favoured possibilities being presented in Scheme 1 (for hydroxylation) and Scheme 2 (for epoxidation) (2).

Evidence has recently been accumulating which supports a stepwise route for both of these reactions (routes B, Schemes 1 and 2) (3–8). This has taken the form of epimerization during hydroxylation (4), the trapping of carbon radical intermediates (5, 6), the observation of inversion of olefin geometry during epoxidation (3), and the detection of rearrangements during olefin oxidation (7, 8).

The hydroxylation of steroids by fungi has been shown in many cases to be a cytochrome P-450 dependent mono-oxygenase reaction (9–12). In order to further study the mechanism of the enzymatic oxidation of steroid substrates, we have now investigated the metabolism of a series of unsaturated steroids by fungi which are known to hydroxylate analogous saturated steroids at a position corresponding to an allylic carbon (13). The putative existence of a radical intermediate such as those shown in routes B of Schemes 1 and 2 now allows for the possibility of allylic rearrangements in these cases, and it was this aspect of the problem which we set out to study.

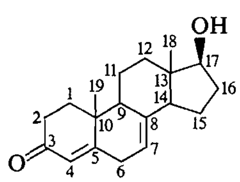

1

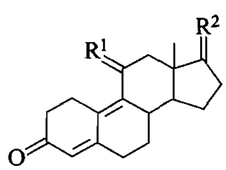

2 *a* $R^1 = H_2$, $R^2 = \alpha H, \beta OH$
b $R^1 = H_2$, $R^2 = 0$
c $R^1 = R^2 = \alpha H, \beta OH$

The substrates used in the main body of this work, **1**, **2*a***, **3**, and **4** were prepared by published procedures. The synthesis of **3** has been described only in outline, and is therefore presented

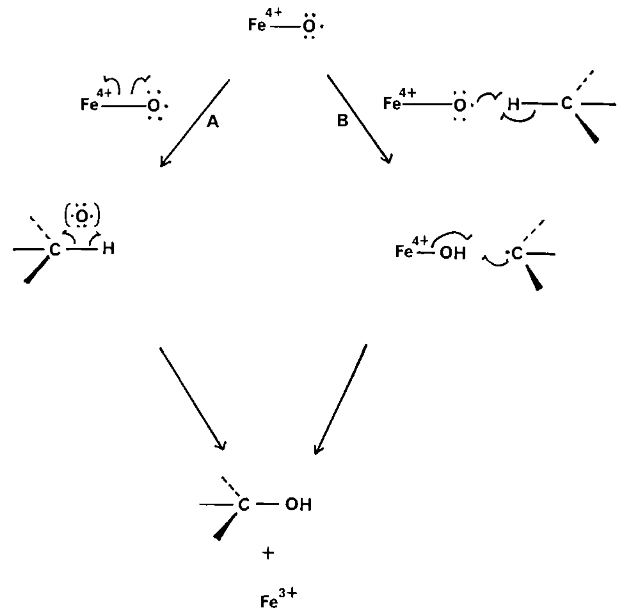

SCHEME 1. Possible routes for hydroxylation at saturated carbon by cytochrome P-450 dependent mono-oxygenases.

in detail herein. The ^{13}C nmr chemical shifts of these compounds, together with the ketone **2*b*** (which was prepared from **2*a*** by Jones oxidation to aid in chemical shift assignments) are presented in Table 1. The assignments were straightforward and were based on chemical shifts, multiplicity in off-resonance decoupled spectra, and published values for analogous steroids (14).

Results

The results of the incubations are summarized in Table 2. The $\Delta^{7,8}$ steroid **1** was recovered unchanged from incubation with *R. arrhizus*, a fungus known to hydroxylate Δ^4-3-keto-steroids at C-6β following the abstraction of the C-6β hydrogen (15). We attribute the absence of metabolism in this case to the failure of **1** to be bound by the enzyme's active site. The conjugated estradiene **2*a***, incubated with the C-11β hydroxy-

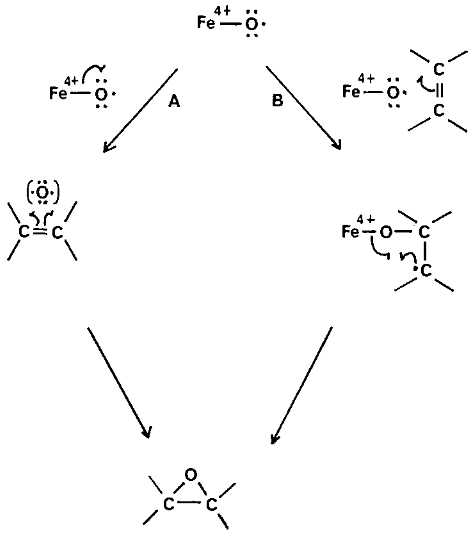

SCHEME 2. Possible routes for epoxidation of olefins by cytochrome P-450 dependent mono-oxygenases.

lating fungus *C. lunata*, gave only the product of 11β hydroxylation, **2***c*. No rearranged species were detected. The structure of **2***c* follows from its ^{13}C nmr spectrum (Table 3), which clearly shows the shifts anticipated for 11β hydroxlation (14) when applied to the spectrum of the unsubstituted substrate **2***a* (Table 1). Incubation of **2***a* with the C-11α hydroxylator *R. stolonifer* did not result in detectable metabolism.

The use of $\Delta^{8(9)}$-progesterone (**3**) as a substrate for fungi which hydroxylate progesterone (**14***a*) at C-7 or C-11 yielded some products whose structures indicate that the double bond is involved in their formation. Incubation of **3** with the 11α/7β hydroxylator *R. stolonifer* gave, in addition to normal 7β hydroxylation yielding **6**, a compound (**5**) which was assigned the structure shown. The ^{13}C and ^{1}H nmr spectra of **5** clearly show the presence of the $\Delta^{1,4}$-dien-3-one grouping and the lack of 17β acetyl side chain. The presence of the 9,11α epoxide can be deduced from ^{1}H nmr (the 11β hydrogen resonating at δ 3.38 ppm), and the presence of the shifts in the ^{13}C nmr spectrum (particularly at C-1 and C-7, and C-14) predicted for **5** on the basis of the application of shift parameters for a 9,11α epoxide (obtained from **4** and **12**) to **9**.

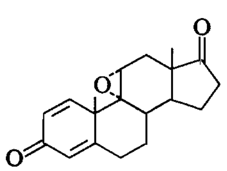

5

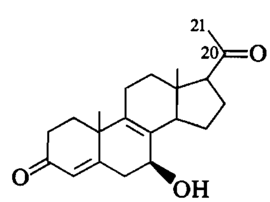

6

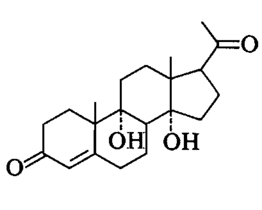

7

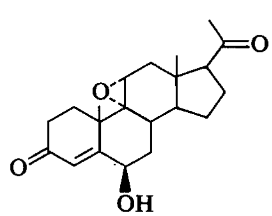

8

The same substrate when incubated with the C-11β hydroxylator *C. lunata* gave a single metabolic product, **7**. Again, ^{13}C

TABLE 1. ^{13}C nuclear magnetic resonance chemical shifts of substrates **1**–**4**

	δ ppm				
Carbon	**1**	**2***a*	**2***b*	**3**	**4**
1	35.8	25.7	25.6	34.3	34.3
2	33.7	36.6	36.7	34.3	33.8
3	199.2	200.0	199.5	198.9	199.1
4	122.3	122.0	122.3	123.3	124.1
5	168.9	157.6	156.5	170.5	169.6
6	32.4	30.8	31.2	28.5	32.9
7	115.3	25.7	24.9*	34.3	32.1
8	138.5	39.4	38.5	129.2	37.3
9	45.5	146.8	144.6	132.2	145.2
10	37.7	125.4	126.0	38.9	41.0
11	21.3	27.1	26.2*	23.2	118.4
12	32.7	37.1	30.4	35.7	40.7
13	43.5	42.8	47.2	43.4	42.4
14	49.2	51.1	50.9	51.7	52.9
15	21.5	23.4	21.6	24.1	25.4
16	29.8	30.5	35.5	23.0	23.0
17	81.1	81.1	219.5	62.1	63.4
18	10.8	10.5	12.9	12.9	13.0
19	20.9			21.9	26.0
20				209.1	209.0
21				31.3	31.2

* Chemical shifts marked with asterisks may be interchanged.

nmr was instrumental in structure assignment. The key shifts were those caused by γ *gauche* interactions (C-1, -7, -12, and -17), and the *trans*-antiperiplanar shift of C-18 caused by the presence of hydroxyl at C-14α (16, 17). The 7α hydroxylating fungus *M. griseocyanus*, when incubated with **3**, gave the product of 6β-hydroxylation and $\Delta^{9(11)}$ epoxide formation, **8**. The structure of **8** was deduced by nmr spectral analysis. The ^{13}C nmr spectrum showed shifts entirely in agreement with those calculated by applying the shift parameters for C-6β hydroxylation (14) and C-9,11 epoxidation (above) to the spectrum of **4**.

In order to allow for the possibility that $\Delta^{8(9)}$-progesterone, **3**, may contain the $\Delta^{9(11)}$ isomer **4** as a trace impurity produced during its preparation, a separate series of control incubations was performed using **4** as substrate. *R. stolonifer* gave only the product of ring A oxidation and side chain cleavage (**9**), together with a mixture of the 12-alcohols **10**. The structures of the

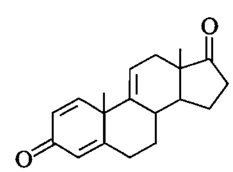

9

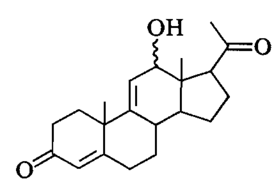

10

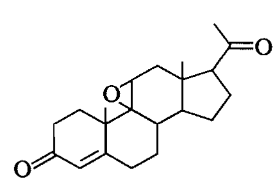

11

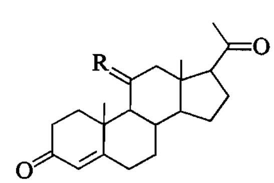

14 *a* R = H_2
b R = αH, βF
c R = O
d R = αOH, βH

TABLE 2. Incubations with fungi

Substrate	Fungus	Normal site of hydroxylation (ref. 13)	Time (h)	Products (% isolated)
1	*R. arrhizus*	6β	96	**1** (80)
2*a*	*R. stolonifer*	11α, 7β	96	**2***a* (58)
	C. lunata	11β	72	**2***a* (35), **2***c* (42)
3	*R. stolonifer*	11α, 7β	96	**3** (65), **5** (8), **6** (21)
	C. lunata	11β	72	**3** (12), **7** (12)
	M. griseocyanus	7α	48	**3** (10), **8** (17)
4	*R. Stolonifer*	11α, 7β	72	**4** (56), **9** (14), **10** (14)
	C. lunata	11β	72	**4** (10), **11** (13)
	M. griseocyanus	7α	72	**4** (21), **12** (?), (?)
14*a* + **14***b*	*R. stolonifer*	11α, 7β	55	**14***d* (18.5), **14***c* (1.5)

TABLE 3. ^{13}C nuclear magnetic resonance chemical shifts of products **2** and **5**–**12**

	δ ppm						
Carbon	**2***c*	**5**	**7**	**8**	**9**	**12**	**13**
1	27.1	149.6	31.8	29.3	154.4	27.6	28.3
2	37.1	130.2	34.0	34.7	127.4	34.9	33.8
3	194.1	186.0	199.4	199.6	186.2	198.0	199.2
4	124.4	126.3	126.7	128.5	124.0	125.7	126.5
5	156.2	163.6	169.0	164.8	166.3	166.5	169.3
6	30.6	34.7	32.9	73.0	33.6	32.4	33.8
7	25.3	28.7	21.7	33.4	32.0	26.4	25.0
8	36.0	31.6	38.3	28.4	36.1	32.9	37.2
9	145.5	70.7	77.9	67.6	143.6	67.0	76.1
10	129.5	48.4	44.7	41.9	46.0	41.2	43.6
11	66.2	54.4	27.1*	53.7	120.0	52.8	26.7
12	43.9	32.4	27.6*	38.6	33.8	38.0	31.6
13	42.2	43.5	48.2	39.7	46.0	39.7	43.6
14	50.2	41.0	86.6	45.6	48.4	45.3	49.2
15	23.5	21.9	27.8	24.3	22.9	24.0	24.0
16	29.8	36.2	21.4	23.3	36.1	22.9	22.7
17	82.1		59.0	63.3	220.5	62.7	63.1
18	12.7	16.4	17.5	15.1	13.9	14.7	12.3
19		23.2	20.1	23.3	26.7	20.7	19.7
20			210.6	209.1		208.3	209.3
21			31.5	31.2		30.7	31.3

*Chemical shifts marked with asterisks may be interchanged.

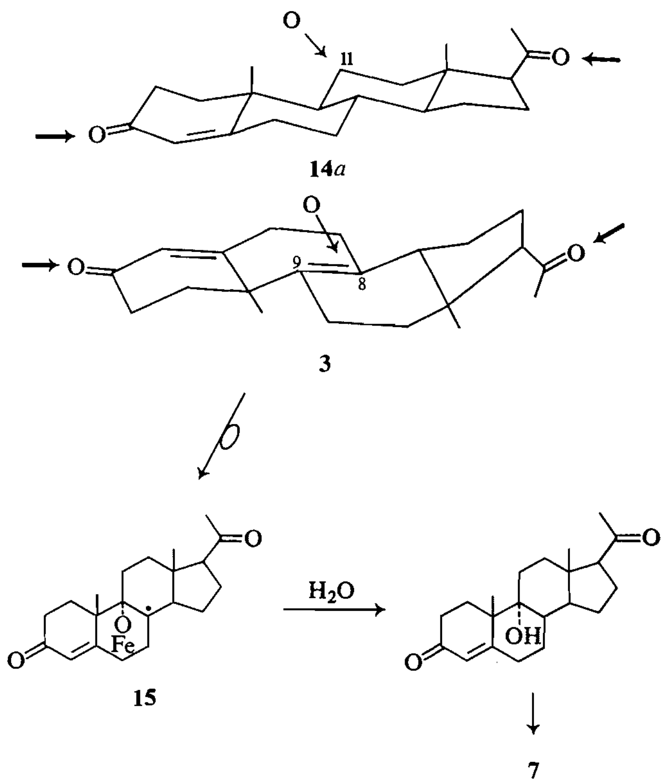

SCHEME 3. Possible route for hydroxylation of **3** at C-9α by *C. lunata*.

latter were confirmed by ^1H nmr decoupling experiments between the C-11 and C-12 hydrogens (see Experimental). This mixture could not be separated by any of the chromatographic techniques at our disposal. *C. lunata* gave only the reported (18) 9,11β epoxide on incubation with **4**, but *M. griseocyanus* gave a low yield of a complex mixture which, although chromatographically homogeneous (tlc), was shown by ^1H nmr analysis to contain at least three different steroids. The appearance of the characteristic C-11β hydrogen resonance as a doublet (J = 8 Hz) at δ 3.23 ppm indicated, however, that 9,11α epoxidation, probably producing **12**, had occurred.

Discussion

The oxidative removal of the C-17β acetyl side chain, and the introduction of Δ^1 unsaturation, has been reported to occur with several fungal species (19, 20), but not previously with *Rhizopus*. The introductions of hydroxyl at C-11β (in **2***c*) and C-14α (in **7**) by *C. lunata* represent normal modes of hydroxylation (13), as do the C-7β hydroxylation of **3** by *R. Stolonifer*, giving **6**, and the C-6β hydroxylation of **3** to give **8** (13). The hydroxylation of **4** at C-12 by *R. stolonifer* is not exceptional: the allylic C-12 position of the substrate is both activated (2) and adjacent to the normal site of hydroxylation (13).

The formation of the epoxides **5** and **8**, and the 9α hydroxylation giving **7**, cannot, however, be rationalized on the basis of simple oxidative metabolism. In the case of **7**, 9α-hydroxylation may occur via the route outlined in Scheme 3. The three-dimensional arrangement of binding (at C-3 and C-20) and hydroxylation (at C-11β) sites of progesterone, (**14***a*) (2), is also shown. Inspection of models shows that the $\Delta^{8(9)}$ substrate **3** best fits into this binding arrangement in an inverted manner. The "back-to-front" binding of steroid substrates for hydroxylation has been well documented by the Oxford group (2); "upside-down" binding has been proposed previously (21) to explain the results of some non-stereospecific hydroxylations at C-11.

Binding of **3** in the manner shown to the hydroxylase of *C. lunata* would expose the α face of the $\Delta^{8(9)}$ bond to the oxidizing site. Previous work has demonstrated that steroid hydroxylation and epoxidation can both be performed by the same enzyme (22, 23) and, in this event, the application of the stepwise mechanisms of Scheme 2 can result in 9α hydroxylation. The intermediate radical **15** does not collapse internally to epoxide in this case. The conformation of **15**, now that the restraining influence of the olefinic bond is removed, is such that the C-9α oxygen and the radical density of C-8 are rigidly *trans*-diaxial and therefore unable to recombine. Hydrogen transfer from solvent completes the process.

That the C-8β hydrogen of **7** is provided by the aqueous medium has been demonstrated by the incubation of **3** with *C. lunata* in the presence of 10% deuterium enriched water. The product thus isolated was examined by ^{2}H nmr and showed signals centered at 1.25 and 2.57 ppm. The latter were exchangeable and assigned to deuterium at enolic sites, but the former was not, and is close to the reported resonance position for the C-8β hydrogen of normal steroids (24).

The epoxide grouping present in **5** and **8** must also be the result of a stepwise oxidation process. In the case of the metabolism of **3** by *M. griseocyanus*, a C-7α hydroxylator of normal steroids, inverse binding of **3** to the active site now exposes the C-11 position to the oxidizing species. Abstraction of a hydrogen from this position (cf. route B, Scheme 1) can produce the allylic radical **16**, which can rearrange to **17**, pick up hydrogen from the medium as above, and be epoxidized in the normal way (Scheme 4). The direct incubation of the $\Delta^{9(11)}$ steroid, **4**, with *M. griseocyanus* indicates that this epoxidation does indeed occur.

The formation of **5** from incubation of **3** with *R. stolonifer* can proceed in a similar manner, except that it is not necessary in this case to propose an inverted binding of substrate, as this fungus is a known C-11α hydroxylator. In this case, however, the $\Delta^{9(11)}$ olefin **4** is not itself directly epoxidized by *R. stolonifer*, suggesting that a preferred mode of reaction in this latter case is the removal of the side chain (giving **9**), after which the enzyme will not accept the androstene derivative as a substrate.

In an attempt to further confirm the radical nature of hydroxylation at C-11, we have also studied the competitive hydroxylations of progesterone (**14*a***) and its 11β-fluoro derivative (**14*b***) by *R. stolonifer*. The former yields only 11α-hydroxy progesterone (**14*d***), and we have previously demonstrated that the latter gives rise only to 11-keto progesterone (**14*c***), probably via a halohydrin intermediate (25). One might expect a rate retardation in the metabolism of **14*b*** compared with that of **14*a*** in the event that the reaction proceeded via a radical abstraction process (Scheme 1, route B). For a direct, concerted oxidation (Scheme 1, route A), with a transition state resembling substrate (2), the effect of the fluorine substituent should be minimal. In the event, the ratio of **14*c*** (from **14*b***) to **14*d*** (from **14*a***) observed from incubation of an equimolar mixture of these isosteric substrates with *R. arrhizus* was 1:12, indicating that **14*a*** is metabolized preferentially.

In the absence of information about the transport and binding of these substrates, these latter data are not conclusive. However, the results of this and the other incubations discussed herein generally support the stepwise, radical abstraction mechanisms of routes B, Schemes 1 and 2, for the hydroxylation and epoxidation of steroid substrates.

Other possible routes such as olefin hydration/dehydration have been considered for the formation of rearranged products and, in view of the fact that the products obtained result from

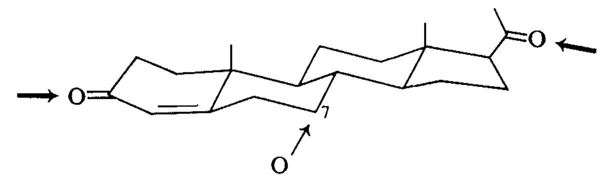

14*a*

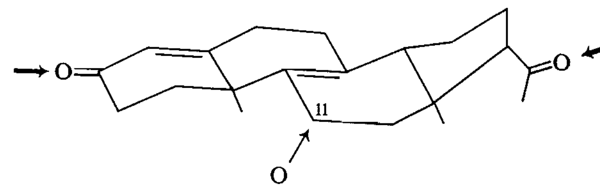

3

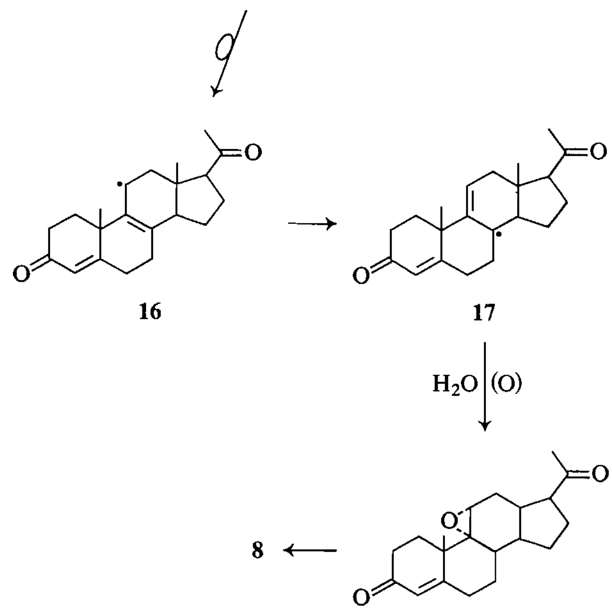

SCHEME 4. Possible route for 9,11α epoxidation of **3** by *M. griseocyanus*.

whole organism metabolism, these possibilities cannot be entirely discounted. However, the available data on steroid hydroxylating fungi suggest that these rearrangements are not generally observed (13, 20) and we found no evidence for such rearrangement when not in concert with hydroxylation or epoxidation reactions.

Experimental

Apparatus, materials, and methods

Melting points were determined on a Kofler heating stage and are uncorrected. Infrared spectra were recorded with a Perkin–Elmer 237B spectrometer. The nmr spectra were obtained with a Bruker WP60, WP80CW, or WH400 (at the Southwestern Ontario nmr Centre, Guelph) using $CDCl_3$ as solvent and TMS as internal standard. Mass spectra were obtained with an AEI MS 30 spectrometer fitted with a Kratos DS-55 data system. Thin layer chromatography was performed on Merck silica gel 60F-254 and column chromatography on Merck silica gel (230–400 mesh). Elemental analyses were performed by Guelph Chemical Laboratories, Guelph, Ontario.

Incubations with fungi

Curvularia lunata NRRL 2380 (26), *Mucor griseocyanus* ATCC 1207 (27), *Rhizopus arrhizus* ATCC 11145 (28), and *Rhizopus stolonifer* ATCC 6227b (28) were grown and the incubations performed as

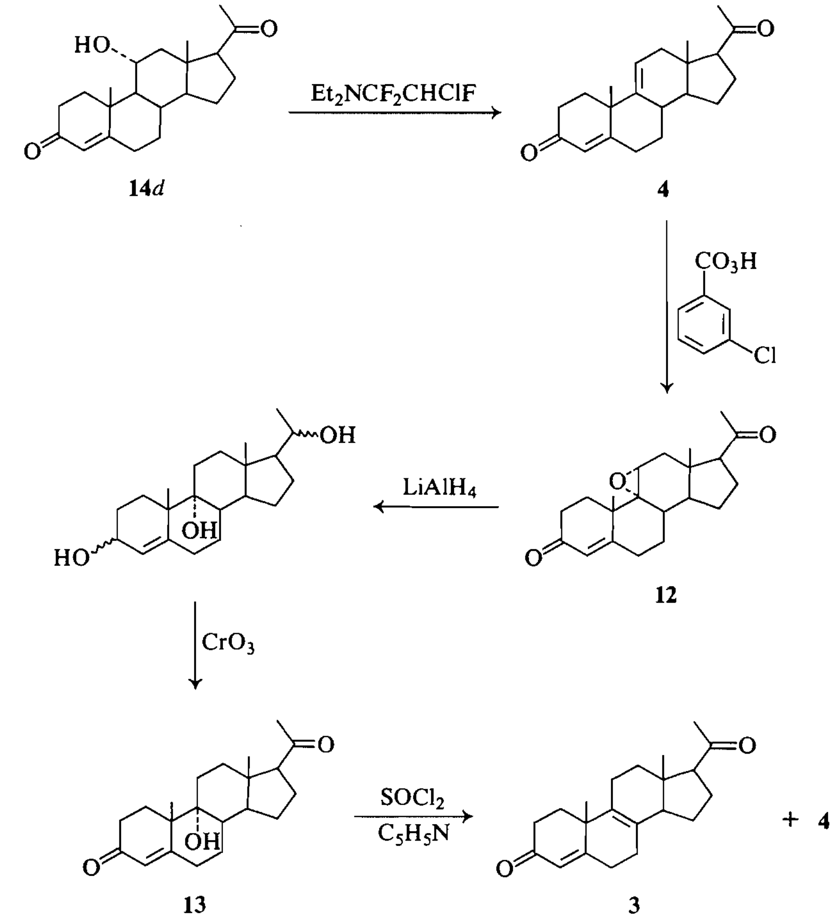

SCHEME 5. Synthesis of pregna-4,8(9)-diene-3,20-dione (**3**) (ref. 32).

described. Details of times, products, and yields are summarized in Table 2.

Synthesis of substrates

The following compounds were prepared by the literature procedures, and gave satisfactory spectral and analytical data: androsta-4,7-dien-17β-ol-3-one (**1**) (29), estra-4,9(10)-dien-17β-ol-3-one (**2***a*) (30), and pregna-4,9(11)-diene-3,20-dione **4** (31). The ^{13}C nmr data are listed in Table 1.

Pregna-4,8(9)-diene-3,20-dione (3)

This compound was prepared by the route outlined by Schneider and Jackson (32) and presented in Scheme 5.

9,11α-Epoxypregn-4-ene-3,20-dione (12)

A solution of pregna-4,9(11)-diene-3,20-dione (**4**) (7.82 g) in chloroform (50 mL) was cooled to 5°C, and then a solution of *m*-chloroperoxybenzoic acid (5.1 g) in chloroform (50 mL) added. The resulting mixture was kept at 5°C for 6 h, then washed with aqueous sodium sulfite (3 × 100 mL), water, and dried over sodium sulfate. Evaporation gave a sample of **12** (7.01 g), mp 180–185°C (lit. (32) mp 180–192°C), which was used directly in the next step. The ^{13}C nmr data are listed in Table 3.

Pregn-4-ene-3β,9α,20β-triol

Lithium aluminum hydride (8.0 g) was added to dry ether (275 mL), and then a solution of **12** (7.0 g) in dry benzene (80 mL) added slowly with stirring. When the addition was complete, the resulting mixture was refluxed for 5 h, then cooled and the residual reducing agent decomposed (33). Work-up in the usual way gave a crude sample of the title compound (7.46 g) which was oxidized directly to **13** by the usual method (34, 35).

Pregna-4,8(9)-diene-3,20-dione (3)

A solution of **13** (4.5 g) in dry pyridine (100 mL) was cooled to 0°C. Thionyl chloride (5 mL), previously treated to remove traces of HCl and Cl_2, was then added at such a rate that the temperature was maintained below 5°C. The solution was then poured into ice water (500 mL), and extracted with ether (4 × 200 mL). The extract was washed with aqueous HCl (5%), then water, dried over sodium sulfate, and then evaporated. The residue was chromatographed (silica gel, benzene-to-ether stepwise gradient) to yield a sample (2.1 g) consisting of a mixture of the compound **3** and the $\Delta^{9(11)}$ isomer **4**. Crystallization from ethyl acetate/hexane gave pure **3** (1.05 g, 25%), mp 158–160°C (lit. (32) mp 162–167°C). The ^{1}H nmr included signals at δ 0.65 (3H, s, C-18H), 1.33 (3H, s, C-19H), 2.15 (3H, s, C-21H), and 5.72 (1H, s, C-4H) ppm. The ^{13}C nmr data are listed in Table 1. Also recovered was **4** (0.8 g) which was recycled in the synthesis.

Fungal metabolic products

Hitherto unreported data for the products of incubation of **2–4** with the fungi listed above are summarized below. The ^{13}C nmr data are listed in Table 3.

Estra-4,9(10)-diene-11β,17β-diol-3-one (2c)

Infrared ν_{max}: 1640, 2900, 3350 cm^{-1}; ^{1}H nmr included signals at δ 1.08 (3H, s, C-18H), 3.60 (1H, br m, C-11α, 17 H's), and 5.73 (1H, s, C-4H) ppm; ms *m/z* (%): 288 (36) 270 (100), 260 (30). M^+ 288.1701; $C_{18}H_{24}O_3$ requires M^+ 288.1725.

9,11α-Epoxyandrosta-1,4-diene-3,17-dione (5)

Melting point 196–198°C; ^{1}H nmr included signals at δ 0.98 (3H, s, C-18H), 1.53 (3H, s, C-19H), 3.38 (1H, m, C-11βH), 5.73 (1H, s, C-4H), 6.20 (1H, d, J = 10 Hz, C-2H), and 6.63 (1H, d, J = 10 Hz, C-1H) ppm; ms *m/z* (%): 298 (35), 282 (35), 256 (100), 241 (37). M^+ 298.1551; $C_{19}H_{22}O_3$ requires M^+ 298.1569.

Pregna-4,8-diene-3,20-dion-7β-ol (6)

Melting point 128–130°C. ir ν_{max}: 1620, 1665, 1720, 2929, 3430 cm^{-1}; ^{1}H nmr included signals at δ 0.55 (3H, s, C-18H), 1.33 (3H, s, C-19H), 2.13 (3H, s, C-21H), 4.53 (1H, t, J = 5 Hz, C-7αH), and 5.75 (1H, s, C-4H) ppm; ms m/z (%): 328 (60), 310 (25), 295 (31), 267 (28), 253 (16), 225 (100). M^+ 328.1989; $C_{21}H_{28}O_3$ requires M^+ 328.2039.

Pregn-4-ene-9α,14α-diol-3,20-dione (7)

Melting point 100–106°C; ^1H nmr included signals at δ 0.78 (3H, s, C-18H), 1.30 (3H, s, C-19H), 2.10 (3H, s, C-21H), and 5.83 (1H, s, C-4H) ppm; ms m/z (%): 346 (100%), 324 (55), 308 (52), 267 (93). M^+ 346.2162; $C_{21}H_{30}O_4$ requires M^+ 346.2144.

9,11α-Epoxypregn-4-ene-3,20-dion-6β-ol (8)

Melting point 177–179°C; ir ν_{max}: 1670, 1700, 2930, 3350 cm^{-1}; ^1H nmr included signals at δ 0.70 (3H, s, C-18H), 1.63 (3H, s, C-19H), 2.10 (3H, s, C-21H), 3.18 (1H, d, J = 5 Hz, C-11βH), 4.40 (1H, t, J = 4 Hz, C-6αH), and 5.90 (1H, s, C-4H) ppm; ms m/z (%): 344 (100), 326 (41), 311 (20), 301 (14), 283 (45), 267 (18). *Anal.* calcd. for $C_{21}H_{28}O_4$: C 73.23, H 8.19%; found: C 73.10, H 8.47%.

Androsta-1,4,9(11)-triene-3,17-dione (9)

Melting point 148–150°C; ir ν_{max}: 1625, 1665, 1740, 2940 cm^{-1}; ^1H nmr included signals at δ 0.93 (3H, s, C-18H), 1.43 (3H, s, C-19H), 5.55 (1H, br s, C-11H), 6.05 (1H, s, C-4H), 6.24 (1H, d, J = 10 Hz, C-2H), and 7.16 (1H, d, J = 10 Hz, C-1H) ppm; ms m/z (%): 282 (100), 267 (43), 239 (26). M^+ 282.1684; $C_{19}H_{22}O_2$ requires M^+ 282.1621.

Pregna-4,9(11)-diene-3,20-dione-12-α/β-ols (10)

Infrared ν_{max}: 1650, 1685, 1710, 2950, 3350 cm^{-1}; ^1H nmr included signals at δ 0.60 and 0.65 (each 3H, s, C-18H), 1.38 and 1.40 (each 3H, s, C-19H), 2.15 (3H, s, C-21H), 4.00 (1H, d, J = 6 Hz, C-12ξH), 4.43 (1H, d, J = 8 Hz, C-12ξH), 5.75 (1H, s, C-4H), 5.85 (1H, dd, J = 6, 8 Hz, C-11H) ppm. Irradiation at δ 5.85 caused collapse of the signals at δ 4.0 and 4.43 ppm to singlets. Mass spectra m/z (%): 328 (31), 313 (10), 311 (17), 295 (11), 284 (100).

9,11β-Epoxypregn-4-ene-3,20-dione (11)

Melting point 185–190°C; ^1H nmr included signals at δ 0.83 (3H, s, C-18H), 1.43 (3H, s, C-19H), 2.15 (3H, s, C-21H), 3.40 (1H, m, C-11αH), and 5.78 (1H, s, C-4H) ppm; ms m/z (%): 328 (100), 313 (66), 312 (51), 295 (68), 267 (98), 252 (45).

*Incubation of **3** with* C. lunata *in D_2O*

The fungus was grown in the normal way (26), collected by filtration, and resuspended in 10% (v/v) deuterium oxide in distilled water. The cells were allowed to equilibrate for 30 min in this environment, and then substrate (**3**) (0.45 g) was added in the normal manner (3). Subsequent incubation and work-up followed the procedure used for preparative incubations (see Table 2 and ref. 28). The product **7**, isolated by chromatography, was examined by ^2H nmr and showed signals centered at δ 1.25 and 2.57 ppm. Recovered substrate showed only natural abundance levels of deuterium.

Acknowledgements

This work was supported by the Natural Sciences and Engineering Research Council of Canada through an operating grant (to H.L.H.) and a postgraduate scholarship (to E.R.). We acknowledge the assistance of T. Jones (Brock), the Southwestern Ontario nmr Centre (Guelph), and Mr. B. Sayer (McMaster) in obtaining spectral data.

1. F. P. GUENGERICH and T. L. MACDONALD. Acc. Chem. Res. **17**, 9 (1984).
2. H. L. HOLLAND. Chem. Soc. Rev. **11**, 371 (1982).
3. S. W. MAY, S. L. GORDON, and M. STELTENKAMP. J. Am. Chem. Soc. **99**, 2017 (1977).
4. J. T. GROVES, G. A. MCCLUSKY, R. E. WHITE, and M. J. COON. Biochem. Biophys. Res. Commun. **81**, 154 (1978).
5. O. AUGUSTO, H. S. BEILAN, and P. R. ORTIZ DE MONTELLANO. J. Biol. Chem. **257**, 11288 (1982).
6. P. R. ORTIZ DE MONTELLANO, O. AUGUSTO, F. VIOLA, and K. L. KUNZE. J. Biol. Chem. **258**, 8623 (1983).
7. D. C. LIEBLER and F. P. GUENGERICH. Biochemistry, **22**, 5482 (1983).
8. D. MANSUY, J. LECLAIRE, M. FONTECAVE, and M. MOMENTEAU. Biochem. Biophys. Res. Commun. **119**, 319 (1984).
9. K. BRESKVAR and T. HUDNIK-PLEVNIK. Biochem. Biophys. Res. Commun. **74**, 1192 (1977).
10. K. BRESKVAR and T. HUDNIK-PLEVNIK. J. Steroid Biochem. **14**, 395 (1981).
11. D. GHOSH and T. B. SAMANTA. J. Steroid Biochem. **14**, 1063 (1981).
12. M. HAYANO, A. SAITO, D. STONE, and R. I. DORFMANN. Biochim. Biophys. Acta, **21**, 380 (1956).
13. W. CHARNEY and H. L. HERZOG. Microbial transformations of steroids. Academic Press, New York. 1967.
14. J. W. BLUNT and J. B. STOTHERS. Org. Magn. Reson. **9**, 439 (1977).
15. H. L. HOLLAND, P. CH. CHENCHAIAH, E. M. THOMAS, B. MADER, and M. J. DENNIS. Can. J. Chem. **62**, 2740 (1984).
16. W. A. AYER, L. M. BROWNE, S. FUNG, and J. B. STOTHERS. Can. J. Chem. **54**, 3272 (1976).
17. H. L. HOLLAND and E. M. THOMAS. Can. J. Chem. **57**, 3069 (1979).
18. Y. KUROSAWA, M. HAYANO, and B. M. BLOOM. Agr. Biol. Chem. (Tokyo), **25**, 838 (1961).
19. F. VIOLA, O. CAPUTO, G. BALLIANO, L. DELPRINO, and L. CATTEL. J. Steroid Biochem. **19**, 1451 (1983).
20. L. L. SMITH. *In* Terpenes and steroids. Vol. 4. The Chemical Society, London. 1974. p. 515.
21. D. R. BRANNON, F. W. PARRISH, B. J. WILEY, and L. LONG. J. Org. Chem. **32**, 1521 (1967).
22. M. H. GELB, P. MÄLKÖNEN, and S. G. SLIGAR. Biochem. Biophys. Res. Commun. **104**, 853 (1982).
23. F. N. CHANG and C. J. SIH. Biochemistry, **3**, 1551 (1964).
24. L. D. HALL, J. K. M. SANDERS, and S. SUKUMAR. J. Chem. Soc. Chem. Commun. 366 (1980).
25. H. L. HOLLAND and E. M. THOMAS. Can. J. Chem. **60**, 160 (1982).
26. Y. Y. LIN, M. SHIBAHARA, and L. L. SMITH. J. Org. Chem. **34**, 3530 (1969).
27. K. SINGH, S. N. SEGAL, and C. VEZINA. Can. J. Microbiol. **13**, 1271 (1967).
28. H. L. HOLLAND and B. J. AURET. Can. J. Chem. **53**, 2041 (1975).
29. D. S. IRVINE and G. KRUGER. J. Org. Chem. **35**, 2418 (1970).
30. L. VELLUZ, G. NOMINÉ, and J. MATHIEU. Angew. Chem. **72**, 725 (1960).
31. D. E. AYER. Tetrahedron Lett. 1065 (1962).
32. W. SCHNEIDER and R. W. JACKSON. U.S. Patent 3,040,065 (June 19th, 1962); Chem. Abstr. **57**, 13849f (1962).
33. V. M. MICOVIC and M. L. MIHAILOVIC. J. Org. Chem. **18**, 1190 (1953).
34. R. M. DODSON and R. D. MUIR. J. Am. Chem. Soc. **83**, 4631 (1961).
35. J. FRIED. U.S. Patent 3,141,877 (July 21st, 1964); Chem. Abstr. **61**, 9563d (1964).

Microbial hydroxylation of steroids. 11. Hydroxylation of *A*-nor-, *B*-homo-Δ^1-, and Δ^1-testosterone acetates by *Rhizopus arrhizus*

HERBERT L. HOLLAND AND P. CHINNA CHENCHAIAH

Department of Chemistry, Brock University, St. Catharines, Ont., Canada L2S 3A1

Received September 19, 1984

HERBERT L. HOLLAND and P. CHINNA CHENCHAIAH. Can. J. Chem. **63**, 1127 (1985).

The testosterone derivatives *A*-nortestosterone acetate and *B*-homo-Δ^1-testosterone acetate have been incubated with *Rhizopus arrhizus*, a fungus which hydroxylates testosterone at the C-6β and C-11α positions. These modes of hydroxylation were also observed for the *A*-nor steroid. The *B*-homo steroid, however, was oxidized at C-2β and concurrently hydroxylated at C-6β and C-7aβ (but not at C-11) by *R. arrhizus*. Δ^1 steroids of conventional skeleton were hydroxylated at C-11α by *R. arrhizus*; in addition, Δ^1-androstenedione was epoxidized at the 1,2β position. No C-6 hydroxylation of conventional $\Delta^{1,4}$-3-ketosteroids was observed.

HERBERT L. HOLLAND et P. CHINNA CHENCHAIAH. Can. J. Chem. **63**, 1127 (1985).

On a fait incuber les dérivés de la testostérone, acétates de *A*-nortestostérone et *B*-homo Δ^1-testostérone, avec le *Rhizopus arrhizus*, un champignon qui provoque des hydroxylations en positions C-6β et C-11α. On a aussi observé ces modes d'hydroxylation avec le *A*-nor stéroïde. Toutefois, le *R. arrhizus* provoque une oxydation du *B*-homostéroïde en C-2β ainsi qu'une hydroxylation concurente en C-6β et en C-7aβ (mais pas en C-11). Sous l'influence du *R. arrhizus*, les Δ^1-stéroïdes avec un squelette conventionnel sont hydroxylés en C-11α; de plus, la Δ^1-androstènedione subit une époxydation en position 1,2β. On n'a observé aucune hydroxylation en C-6 avec les $\Delta^{1,4}$ céto-3 stéroïdes conventionnels.

[Traduit par le journal]

A-norandrostanes have recently been found to be capable of interacting with estrogen and androgen receptor proteins in a specific way (1), while the naturally occurring plant hormone brassinolide is a steroid with a 7-membered B ring (2). In view of these developments, and as part of our continuing programme of investigation of steroid hydroxylations by *Rhizopus arrhizus* and other fungi (3), we have now studied *A*-nor and *B*-homo steroids as substrates. The microbial hydroxylations of *A*-nor steroids at C-1β, -6β, -7α, -9α, -11α, -11β, -12β, -14α, -16α, and -21 have been reported, representing in most cases normal modes of hydroxylation by the microorganisms concerned (4, 5); however, the incubations of *A*-nor or *B*-homo steroids with *R. arrhizus* have not been reported.

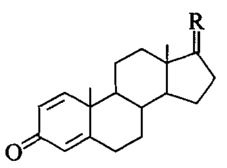

1 *a* R = αH, βOH
b R = αH, βOAc
c R = 0

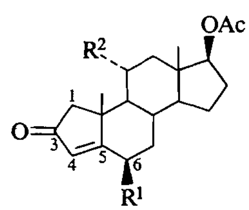

2 *a* R' = R² = H
b R' = H, R² = OH
c R' = OH, R² = H

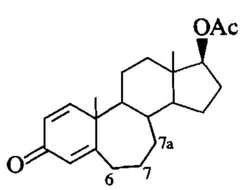

3

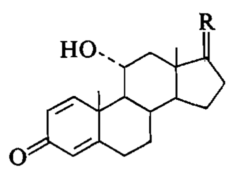

4 *a* R = αH, βOH
b R = αH, βOAc
c R = 0

It was our intention to study the *A*-nor compound **2***a* and *B*-homotestosterone acetate as substrates; the former was readily synthesized, and the corresponding saturated *B*-homo steroid **7***a* was synthesized by Ringold's route (6). The analogous compound in the pregnane series has been converted to *B*-homoprogesterone by monobromination at C-4 followed by dehydrobromination (7) (an exceptional result, since the monobromination of 5α-3-ketosteroids normally occurs at C-2 (8)). When we applied the same procedures to **7***a*, however, we were unable to isolate any C-4 monobrominated product. Even in the presence of limiting bromine concentrations, the major product was the 2,4-dibromide **7***b*, which could be converted to the $\Delta^{1,4}$-dien-3-one **3** in moderate yield.

Faced with the dienone **3** as the only available *B*-homo steroid, we decided to study the $\Delta^{1,4}$-dien-3-ones of normal skeleton **1**, as substrates for the hydroxylating enzymes of *R. arrhizus*. Steroids of this structure have not previously been extensively examined for their ability to act as substrates in these reactions (4, 5).

The ^{13}C nmr spectra of substrates **1**–**3** are reported in Table 1. Product structures were deduced largely from ^{13}C and ^{1}H nmr data. The ^{13}C nmr spectrum of **1***c* has been previously reported; our assignments of resonances to C-7 and C-12 represent a reversal of the original literature values (9), and are based on the shifts predicted (10) from the wider range of substituents at C-17 now available to us. The assignment of resonances in **2***a* and **3** was straightforward and in agreement with those predicted from the values reported for analogous steroids of normal skeleton (10).

Hydroxylation of *A*-nortestosterone acetate **2***a* by *R. arrhizus* gave the C-11α and -6β hydroxysteroids **2***b* and **2***c* respectively. The structures of **2***b* and **2***c* follow from their ^{13}C nmr (Table 3) and ^{1}H nmr (Experimental) spectra, the former being particularly diagnostic in showing clearly the shifts for hydroxyl substitution at C-11α and C-6β anticipated from the published parameters (10).

In contrast, the $\Delta^{1,4}$-dien-3-ones **1** were not hydroxylated at C-6β by *R. arrhizus*, but gave the corresponding 11α-hydroxy derivatives, **4**, as major products (Table 2). Hydroxylations at C-6β and C-11α by *R. arrhizus* represent normal modes of oxidation of Δ^4-3-ketosteroids (4, 11). In the case of the dione **1***c*, however, a second product was also obtained in low yield, to which structure **5** has been assigned. The presence of an epoxy grouping at C-1,2 was indicated by the appearance in the ^{1}H nmr spectrum of an AB quartet at δ 3.37 and 3.62 ppm, one

TABLE 1. ^{13}C nuclear magnetic resonance chemical shifts of substrates **1**, **2**a, and **3**

Carbon	δ ppm				
	1*a*	**1***b*	**1***c*	**2***a*	**3**
1	156.1	155.5	155.2	50.7	158.5
2	127.4	127.6	127.6	—	127.5
3	186.5	186.1	186.0	208.3	186.5
4	123.7	124.0	124.0	125.6	126.4
5	169.5	168.7	168.2	188.9	169.3
6	32.7*	32.6*	32.3*	27.5	32.6
7	33.1*	33.0*	32.5*	32.2	29.8
7a	—	—	—	—	27.0*
8	35.5	35.3	35.0	35.5	36.7
9	52.6	52.3	52.3	53.7	57.0
10	43.6	43.5	43.4	46.1	46.3
11	22.5	22.3	22.0	23.1	24.6
12	36.3	36.5	31.2	36.6	38.8
13	43.1	42.7	47.6	43.0	42.2
14	50.2	49.9	50.4	50.1	50.2
15	23.5	23.6	21.8	23.6	24.6
16	30.2	27.4	35.5	27.5	27.5*
17	81.2	82.2	219.6	82.5	82.5
18	11.1	12.0	13.8	12.2	11.9
19	18.6	18.7	18.7	20.0	18.7
OAc	—	21.1	—	21.1	21.1
		171.0		171.2	171.1

*Chemical shifts marked with asterisks may be interchanged.

TABLE 2. Incubations with *Rhizopus arrhizus*

Substrate	Product (% isolated)
1*a*	**1***a* (51), **4***a* (13)
1*b*	**1***b* (42), **4***b* (15)
1*c*	**1***c* (62), **4***c* (15), **5** (1.5)
2*a*	**2***a* (65), **2***b* (20), **2***c* (6)
3	**3** (64), **6***a* (8), **6***b* (12)

half of which (3.37) was also coupled to the C-4 proton at δ 5.70 ppm. Both ^{13}C and ^{1}H nmr confirmed the absence of the Δ^1 olefinic bond, and the appearance of new ^{13}C resonances at 55.3 and 61.1 ppm is diagnostic of an epoxide (12).

The β stereochemistry of the 1,2 epoxide of **5** was deduced from ^{1}H nmr, where the downfield shift of the C-19 hydrogen signal indicates the presence of oxygen in a position 1,3-diaxial to the methyl group (13), and ord (optical rotatory dispersion) data (see Experimental), which show the presence of a weak negative $n \rightarrow \pi^*$ Cotton effect between 350 and 450 nm. Application of the octant rules for epoxy ketones (14, 15) predict that **5** should show a weak negative $n \rightarrow \pi^*$ Cotton effect, whereas the α isomer should show an effect of similar magnitude but opposite sign. This finding is in accord with the observed weak positive effect for 2β-hydroxy testosterone (16), and the fact that the epoxide grouping is known to be an "anti-octant" substituent (17).

The *B*-homo steroid **3** gave two products on incubation with *R. arrhizus*, assigned structures **6***a* and **6***b*. The ^{1}H and ^{13}C nmr spectra of **6***a* clearly showed the absence of the Δ^1 bond and the presence of two secondary alcohol groups in a *B*-homo-Δ^4-3-ketosteroid skeleton. One of the hydroxy groups was assigned to the C-2β position on the following rounds. The ^{13}C chemical shift (85.1 ppm) and ^{1}H shift of the associated methine hydro-

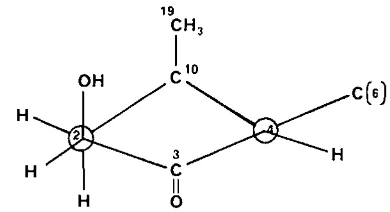

FIG. 1. Conformation of ring A of **6***a* and **6***b*.

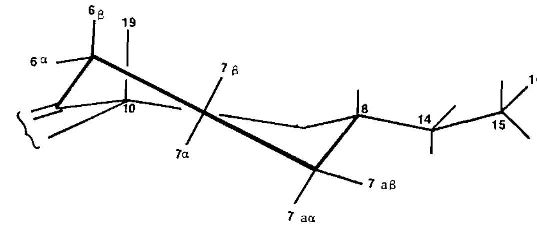

FIG. 2. Conformation of ring B of **6***a*.

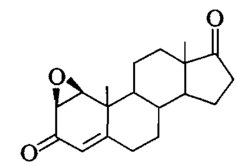

5

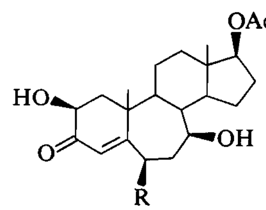

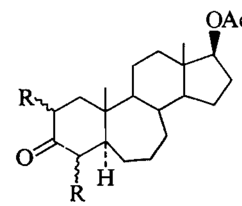

6 *a* R = H
b R = OH

7 *a* R = H
b R = Br

gen (4.12 ppm) locate the hydroxyl either adjacent to carbonyl or in an allylic position. The observation of the C-4 hydrogen as a doublet, coupled to the C-6β hydrogen (18), rules out the latter site of substitution. The β stereochemistry of substitution at C-2 follows from the downfield shift of the C-19 methyl group in both the ^{1}H and ^{13}C nmr spectra. Inspection of models of **6***a* and **6***b* (Fig. 1) shows that the C-2α hydrogen exactly bisects the C-1αH—C-1βH angle; the observed multiplicity of the C-2α hydrogen (triplet, J = 7.3 Hz) is in accord with this expectation. The conformation shown in Fig. 1 is different from that found for 2β-hydroxy-Δ^4-3-ketosteroids of normal skeleton (16), but the presence of the seven-membered B-ring in **6***a* and **6***b* introduces conformational restraints on ring A which are absent in normal steroids.

The location of the second hydroxyl group of **6***a* is not obvious, but the multiplicity and chemical shift of the associated methine hydrogen, and the ^{13}C nmr differences between **6***a* and **6***b* (see below), led to the location of this group at C-7aβ. The hydrogen now assigned as C-7aα has the multiplicity anticipated from the dihedral angles (ϕ C-7aαH—C-8H = 180°, ϕ C-7aαH—C-7αH = 90°, ϕ C-7aαH—C-7βH ≃ 145°) present in the predominant C-7 twist chair conformation of ring B shown in Fig. 2 (19). The ^{13}C nmr chemical shift assignments for **6***a* (Table 3) are also consistent with this structure. No other position of hydroxylation in ring B was consistent with these

TABLE 3. ^{13}C nuclear magnetic resonance chemical shifts of products **2** and **4–6**

	δ ppm							
Carbon	**2***b*	**2***c*	**4***a*	**4***b*	**4***c*	**5**	**6***a*	**6***b*
1	53.7	52.0	160.4	158.7	159.0	61.1	42.7*	43.3*
2	—	—	124.2	125.3	125.1	55.3	85.1	85.7
3	209.8	208.5	187.3	186.5	186.9	194.3	194.1	198.2
4	126.3	127.4	123.9	124.8	124.8	119.8	125.0	128.3
5	188.7	184.9	169.8	167.7	167.9	168.4	167.4	166.0
6	27.6	67.4	33.1	33.2	32.3*	33.3*	29.8	76.3
7	31.4	39.6	33.1	33.2	32.9*	32.9*	36.1	45.6
7a	—	—	—	—	—	—	77.1	77.3
8	34.4	30.3	34.6	34.1	34.1	35.5	35.3	36.2
9	59.1	54.2	60.5	60.7	60.2	51.5	60.5	61.5
10	45.2	46.1	44.3	44.1	44.1	41.3	45.1	45.1
11	68.1	23.0	67.4	68.0	67.7	20.9	22.9	22.8
12	46.9	36.6	43.2	48.2	42.3	31.1	42.0*	42.2*
13	43.3	43.0	47.3	43.3	47.9	47.5	42.7	42.5
14	49.6	50.0	49.3	50.0	49.7	50.4	51.2	51.4
15	23.1	23.6	23.3	23.6	21.9	21.8	24.2	26.2
16	27.5	27.5	29.9	27.8	35.9	35.5	28.3	28.4
17	81.7	82.5	80.3	81.7	218.4	219.6	81.5	81.4
18	13.3	12.2	12.2	13.2	14.6	13.9	14.1	14.2
19	20.8	22.1	18.5	18.9	18.7	17.0	20.8	21.6
OAc	21.0	21.1		20.9			21.1	21.2
	171.1	171.3		170.9			171.0	171.1

*Chemical shifts marked with asterisks may be interchanged.

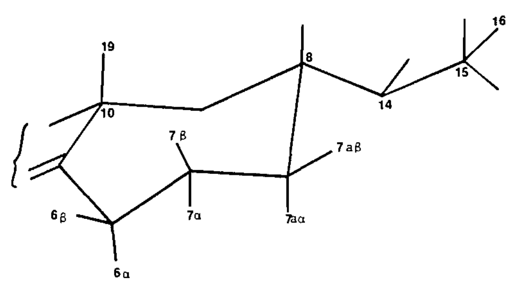

FIG. 3. Conformation of ring B of **6***b*.

values: rings C and D were clearly ruled out as sites of hydroxylation by the unambiguous observation of unperturbed ^{13}C nmr resonances at δ 22.9 (C-11), 24.2 (C-15), and 28.3 (C-16) ppm. *R. arrhizus* has been previously reported to hydroxylate normal steroids at C-7β (4).

The ^1H nmr spectrum of **6***b* clearly shows the presence of an additional hydroxyl group relative to **6***a*, and suggests its location at C-6β. This follows from the chemical shift of the associated methine hydrogen (δ 4.48 ppm) and the observation of the C-4 hydrogen signal as a sharp singlet (cf. **6***a* above), shifted downfield to δ 5.92 ppm. Closer examination of the ^{13}C nmr of **6***b* reveals the following: the C-19 signal, although downfield with respect to that of **6***a*, has not shifted to the extent normally associated with C-6β hydroxylation in normal steroids (10); there has been a 2-ppm downfield shift of the C-15 resonance, and the resonances at C-8 and C-9 show small downfield shifts. These facts are explicable by the assumption that ring B of **6***b* now adopts the alternative C-8 chair conformation shown in Fig. 3 (19). This conformation relieves the C-6β hydroxy – C-19 methyl interaction present in the alternative conformation of Fig. 2, and also has the effect of bringing the C-7aβ alcohol into close proximity with the C-15 hydrogens. In the conformation of Fig. 3, the steric relationship between C-15 and C-7aβ is identical to that of normal steroids, in which hydroxylation at C-7β causes an average downfield shift at C-15 of +2.8 ppm (10). This is not true of either C-7α hydroxylation, nor the presence of hydroxyl at C-7aβ in the conformation of **6***a* shown in Fig. 2. The observed multiplicity of the C-6α hydrogen signal of **6***b* is entirely consistent with that predicted from the C-6—C-7 dihedral angles estimated from the structure of Fig. 3 (C-6αH—C-7βH ≃ 160°, C-6αH—C-7αH ≃ 40°).

The remaining spectral data for **6***a* and **6***b* also accord with the structures discussed above. The absence of a molecular ion in the spectrum of **6***b*, and its low intensity in the spectrum of **6***a*, are probably attributable to a facile loss of water involving the C-2 alcohol, producing the cross conjugated keto group as a stable ion (and indeed as the base peak in the case of **6***b*).

We therefore conclude that, although hydroxylation of A-nortestosterone acetate by *R. arrhizus* shows no effects attributable to the lack of a carbon in the A-ring, the presence of an additional carbon in ring B (as in **3**), coupled with a Δ^1 bond, leads to a new site of oxidation, C-2β, in addition to the more usual hydroxylations at C-6 and C-7. The oxidation of **3** at C-2β is clearly not a conventional mono-oxygenase dependent hydroxylation of the type normally occurring at saturated carbon. However, direct conversion of steroid olefins to saturated alcohols has been observed during fungal hydroxylation,[1] and attributed to a variant of the normal enzymic epoxidation mechanism. It is therefore relevant that $\Delta^{1,4}$ steroids of normal skeleton can be epoxidized at the 1,2β position by *R. arrhizus*. The relationship, if any, between the epoxidation of **1***c* and the hydroxylation at C-2β of **3** will be the subject of future investigation.

[1] See the preceding paper of the series in this journal, ref. 3.

Experimental

Apparatus, materials, and methods

Melting points were determined on a Kofler heating stage and are uncorrected. Infrared spectra were recorded with an Analect 6260FX FTIR. The nmr spectra were obtained with a Bruker WP60 (^{13}C) or WP80CW (^{1}H) at Brock, or with a WM250 at McMaster University, using $CDCl_3$ as solvent and TMS as internal standard. Mass spectra were obtained with an AEI MS30 spectrometer fitted to a Kratos DS-55 data system. Thin layer chromatography was performed on Merck silica gel 60F-254, and column chromatography on silica gel (200–430 mesh). Optical rotation measurements were made at McMaster University using a Perkin–Elmer 241MC polarimeter. The solvent used was chloroform and the path length 1 dm. Elemental analyses were performed by Guelph Chemical Laboratories, Guelph, Ontario, or by the Pascher microanalytical Laboratory, Bonn, W. Germany.

Substrates

The following were commercial samples (Sigma): androsta-1,4-dien-17β-ol-3-one (**1***a*), androsta-1,4-dien-17β-ol-3-one acetate (**1***b*), and androsta-1,4-diene-3,17-dione (**1***c*). *A*-nortestosterone acetate (**2***a*) was prepared from testosterone by the published procedure (20, 21). *B*-homoandrosta-1,4-dien-17β-ol-3-one acetate (**3**) was prepared as outlined below.

*2ξ,4ξ-Dibromo-*B*-homo-5α-androstan-17β-ol-3-one acetate (***7*b*)

B-Homo-5α-androstan-17β-ol-3-one acetate (**7***a*) (100 mg) obtained by Ringold's synthesis (6) was treated with bromine in acetic acid by the procedure used by Himizu and Shichita in the synthesis of *B*-homoprogesterone (7). A single product, **7***b*, was obtained in 48% yield. No monobromo derivative was identified in the reaction mixture. Variation of stoichiometric ratio of reactants and time gave **7***b* and unreacted **7***a* as the only isolable steroids. The title compound had mp 171–172°C. *Anal.* calcd. for $C_{22}H_{32}Br_2O_3$: C 52.38, H 6.35, Br 31.75%; found: C 52.40, H 6.27, Br 32.10%.

B*-Homoandrosta-1,4-dien-17β-ol-3-one acetate (***3***)*

The dibromide **7***b* (0.135 g) was dissolved in DMF (7 mL) to which lithium chloride (0.135 g) had been added, and the mixture kept at 120°C under a nitrogen atmosphere for 16 h. Work-up in the usual way afforded a mixture which contained a single uv absorbing component (tlc). Column chromatography afforded **3** (0.035 g, 40%) as an oil which could not be induced to crystallize. The ^{1}H nmr included signals at δ 0.85 (3H, s, C-18H), 1.30 (3H, s, C-19H), 2.07 (3H, s, OAc), 4.57 (1H, t, J = 7 Hz, C-17αH), 6.07 (1H, s, C-4H), 6.15 and 7.05 (2H, ABq, J = 9 Hz, C-2 and -1 H's respectively); ^{13}C nmr, see Table 1; ms m/z (%): 342 (44), 320 (5), 300 (5), 286 (8), 282 (13), relative to 83 (100). M^+ 342.2322; $C_{22}H_{30}O_3$ requires M^+ 342.2195. *Anal.* calcd. for $C_{22}H_{30}O_3$: C 77.19, H 8.77%; found: C 77.51, H 8.62%.

Incubations with R. arrhizus *ATCC 11145*

Rhizopus arrhizus ATCC 11145 was maintained and incubations were performed as previously described (22), except that an incubation period of 72 h was used. Hitherto unreported spectral and physical data for products **2** and **4**–**6** are listed below. The ^{13}C nmr data are presented in Table 3.

A*-Norandrost-4-ene-11α,17β-diol-3-one, 17-acetate (***2**b*)

Oil; ir ν_{max}: 1682, 1731, 3443 cm^{-1}; ^{1}H nmr included signals at δ 0.88 (3H, s, C-18H), 1.26 (3H, s, C-19H), 2.05 (3H, s, OAc), 3.70–4.15 (1H, m, C-11βH), 4.65 (1H, t, J = 7 Hz, C-17αH), 5.77 (1H, s, C-4H) ppm; ms m/z (%): 332 (26), 314 (33), 304 (9), 286 (7), 279 (29) relative to 149 (100). M^+ 332.1938; $C_{20}H_{28}O_4$ requires M^+ 332.1988. *Anal.* calcd. for $C_{20}H_{28}O_4$: C 72.29, H 8.43%; found: C 72.10, H 8.12%.

A*-Norandrost-4-ene-6β,17β-diol-3-one, 17-acetate (***2**c*)

Melting point 189–191°C; ir ν_{max}: 1685, 1730, 2930, 3369 cm^{-1}; ^{1}H nmr included signals at δ 0.87 (3H, s, C-18H), 1.35 (3H, s, C-19H), 2.03 (3H, s, OAc), 2.25 (2H, br s, C-1H?), 4.65 (1H, t, J = 7 Hz, C-17αH), 4.85 (1H, t, J = 3 Hz, C-6αH), 5.78 (1H, s, C-4H) ppm; ms m/z (%): 332 (2), 316 (12), 288 (56), 274 (10), 256 (38) relative to 147 (100). M^+ 332.1929; $C_{20}H_{28}O_4$ requires M^+ 332.1988. *Anal.* calcd. for $C_{20}H_{28}O_4$: C 72.29, H 8.43%; found: C 72.64, H 8.18%.

*Androsta-1,4-diene-11α,17β-diol-3-one (***4**a*) and androsta-1,4-diene-3,17-dion-11α-ol (***4**c*)*

Spectral data for these compounds are in agreement with those previously published (23).

*Androsta-1,4-diene-11α,17β-diol-3-one, 17-acetate (***4**b*)

Oil; ^{1}H nmr included signals at δ 0.80 (3H, s, C-18H), 1.20 (3H, s, C-19H), 1.92 (3H, s, OAc), 4.0 (1H, d of t, J = 10, 6 Hz, C-11βH), 4.60 (1H, t, J = 8 Hz, C-17αH), 5.95 (1H, s, C-4H), 6.03 and 7.65 (2H, ABq, J = 10 Hz, C-2 and -1H's) ppm; ms m/z (%): 344 (12), 326 (2), 284 (2), 266 (4), 251 (3) based on 122 (100). M^+ 344.2031; $C_{21}H_{28}O_4$ requires M^+ 344.1987.

*1,2β-Epoxyandrost-4-ene-3,17-dione (***5***)*

Melting point 200–202°C; ir ν_{max}: 1663, 1738, 2956 cm^{-1} (no O—H stretch); $[\alpha]^{21}_{589}$ −79° (c = 0.31), $[\alpha]^{21}_{576}$ −85°, $[\alpha]^{21}_{546}$ −107°, $[\alpha]^{21}_{434}$ −331°, $[\alpha]^{21}_{404}$ −433°, $[\alpha]^{21}_{366}$ −201°; ^{1}H nmr included signals at δ 0.92 (3H, s, C-18H), 1.40 (3H, s, C-19H), 3.37 (dd, J = 2, 4 Hz) and 3.62 (d, J = 4 Hz) (each 1H, AB, C-2 and C-1 H's respectively), and 5.70 (1H, d, J = 2 Hz, C-4H) ppm; ms m/z (%): 300 (4), 284 (3), 272 (2), 226 (50), based on 57 (100). M^+ 300.1817; $C_{19}H_{24}O_3$ requires M^+ 300.1725. *Anal.* calcd. for $C_{19}H_{24}O_3$: C 76.0, H 8.0%; found: C 75.72, H 8.0%.

B*-Homoandrost-4-ene-2β,7aβ,17β-triol-3-one, 17-acetate (***6**a*)

Oil; ir ν_{max}: 1665, 1729, 2930, 3460 cm^{-1}; ^{1}H nmr included signals at δ 0.89 (3H, s, C-18H), 1.33 (3H, s, C-19H), 2.03 (3H, s, OAc), 3.90 (1H, d of t, J = 4, 11.5 Hz, C-7aαH), 4.12 (1H, t, J = 7.3 Hz, C-2αH), 4.64 (1H, t, J = 8 Hz, C-17αH), and 5.77 (1H, d, J = 1.4 Hz, C-4H) ppm; ms m/z (%): 374 (1.3), 358 (49), 343 (7), relative to 55 (100). $M^+ - H_2O$ 358.2124. $C_{22}H_{30}O_4$ ($M - H_2O$) requires 358.2144.

B*-Homoandrost-4-ene-2β,6β,7aβ,17β-tetrol-3-one, 17-acetate (***6**b*)

Oil; ir ν_{max}: 1663, 1729, 2931, 3430 cm^{-1}; ^{1}H nmr included signals at δ 0.89 (3H, s, C-18H), 1.46 (3H, s, C-19H), 2.02 (3H, s, OAc), 4.0 (1H, d of t, J = 3.5 and 11.5 Hz, C-7aαH), 4.15 (1H, t, J = 7.3 Hz, C-2αH), 4.48 (1H, d of d, J = 7.6, 9.6 Hz, C-6αH), 4.63 (1H, t, J = 8 Hz, C-17αH), and 5.92 (1H, s, C-4H) ppm; ms m/z (%): 374 (100), 359 (7), 332 (10), 314 (6). $M^+ - H_2O$ 374.2087. $C_{22}H_{30}O_5$ ($M^+ - H_2O$) requires 374.2093.

Acknowledgements

Financial support was provided by the Natural Sciences and Engineering Research Council of Canada. We are grateful to Mr. T. Jones (Brock) and Mr. B. Sayer (McMaster) for their help in obtaining spectral data.

1. J. Canceill, J. Jacques, M. M. Bouton, M. Fortin, and C. Tournemine. J. Steroid Biochem. **18**, 643 (1983).
2. M. D. Gove, G. F. Spencer, W. K. Rohweddler, N. Mandava, J. F. Worley, J. D. Warthen, G. L. Steffens, J. L. Flippen-Anderson, and J. C. Cook. Nature, **281**, 216 (1979).
3. H. L. Holland and E. Riemland. Can. J. Chem. **63**, 1121 (1985).
4. W. Charney and H. L. Herzog. Microbial hydroxylation of steroids. Academic Press, New York. 1967.
5. L. L. Smith. *In* Terpenes and steroids. Vol. 4. The Chemical Society, London. 1974. p. 394.
6. H. J. Ringold. J. Am. Chem. Soc. **82**, 961 (1960).
7. J. Himizu and T. Shichita. Chem. Pharm. Bull (Toyko), **13**, 1145 (1965).
8. D. N. Kirk and M. P. Hartshorn. Steroid reaction mechanisms. Elsevier, London. 1968. p. 163.
9. J. R. Hanson and M. Siverns. J. Chem. Soc. Perkin Trans. 1, 1956 (1975).
10. J. W. Blunt and J. B. Stothers. Org. Magn. Reson. **9**, 439 (1977).

11. H. L. HOLLAND. Acc. Chem. Res. **17**, 398 (1984).
12. H. L. HOLLAND, P. R. P. DIAKOW, and G. J. TAYLOR. Can. J. Chem. **56**, 3121 (1978).
13. J. E. BRIDGEMAN, P. C. CHERRY, A. S. CLEGG, J. M. EVANS, SIR EWART R. H. JONES, A. KASAL, V. KUMAR, G. D. MEAKINS, Y. MORISAWA, E. E. RICHARDS, and P. O. WOODGATE. J. Chem. Soc. (C), 250 (1970).
14. G. SNATZKE. Tetrahedron, **21**, 413 (1965).
15. C. DJERASSI, W. KLYNE, T. NORIN, G. OHLOFF, and E. KLEIN. Tetrahedron, **21**, 163 (1965).
16. R. D. BURNETT and D. N. KIRK. J. Chem. Soc. Perkin Trans. 1, 1830 (1973).
17. H. WYNBERG and B. MARSMAN. J. Org. Chem. **45**, 158 (1961).
18. T. A. WITTSTRUCK, S. K. MALHOTRA, and H. J. RINGOLD. J. Am. Chem. Soc. **85**, 1699 (1963).
19. L. KOHOUT, J. FAJKOS, and F. SORM. Collect. Czech. Chem. Commun. **34**, 601 (1969).
20. F. L. WEISENBORN. U.S. Patent 3,210,406 (Oct. 5th 1965). Chem. Abstr. **63**, 18219 d (1965).
21. F. L. WEISENBORN, D. C. REMY, and T. L. JACOBS. J. Am. Chem. Soc. **76**, 552 (1954).
22. H. L. HOLLAND and B. J. AURET. Can. J. Chem. **53**, 2041 (1975).
23. SIR EWART R. H. JONES, G. D. MEAKINS, J. O. MINORS, J. H. PRAGNELL, and A. L. WILKINS. J. Chem. Soc. Perkin Trans. 1, 1552 (1975).

Surface tension and density of the molten $PbCl_2$–KCl–NaCl ternary system

T. FUJISAWA,[1] T. UTIGARD, AND J. M. TOGURI

Department of Metallurgy and Materials Science, University of Toronto, Toronto, Ont., Canada M5S 1A4

Received August 15, 1984

T. FUJISAWA, T. UTIGARD, and J. M. TOGURI. Can. J. Chem. **63**, 1132 (1985).

The maximum bubble pressure method was used to determine the surface tension and density of melts within the $PbCl_2$–KCl–NaCl system. The temperature range of this study was from 450 to 800°C. In all cases, the surface tension was found to decrease with increasing temperature. At constant molar ratios of KCl to NaCl, a minimum in the surface tension was observed at approximately 40 mol% $PbCl_2$. The ternary surface tension values were found to obey the simple additivity expression of the binary surface tensions of $PbCl_2$–KCl and $PbCl_2$–NaCl. Based on these findings, constant surface tension contours have been drawn.

The density obtained in the present study agree well with the previously determined densities using a bottom-balance Archimedean technique reported by this laboratory.

T. FUJISAWA, T. UTIGARD et J. M. TOGURI. Can. J. Chem. **63**, 1132 (1985).

On a utilisé la méthode de la pression maximale de la bulle pour déterminer la tension de surface et la densité de produits fondus dans le système $PbCl_2$–KCl–NaCl. On a effectué cette étude de 450 à 800°C. Dans tous les cas, la tension superficielle diminue avec une augmentation de la température. A des rapports constants de KCl/NaCl, on a trouvé qu'il existe un minimum dans la tension superficielle qui se situe à environ 40 mole pourcent de $PbCl_2$. On a trouvé que les valeurs des tensions superficielles tertiaires obéissent à une expression simple d'additivité des tensions superficielles binaires du $PbCl_2$–KCl et $PbCl_2$–NaCl. Sur la base de ces observations, on a pu établir des contours de tensions superficielles constantes.

La densité obtenue au cours du présent travail est en bon accord avec les densités déterminées antérieurement en utilisant une technique mise au point dans notre laboratoire et faisant appel à une balance d'Archimède.

[Traduit par le journal]

Introduction

The present process for the extraction of lead from lead sulphide concentrates involves sintering followed by high temperature carbon reduction in a blast furnace. Although this process is effective for lead production from high grade lead sulphide concentrates, it does give rise to problems with respect to environmental concerns and to the treatment of complex lead ores. The public concern of the environmental effects of lead will no doubt introduce strict legislation controlling the emissions of heavy metals as well as sulphur dioxide.

In anticipation of such regulations, new processes have been proposed. One such process is the conversion of lead sulphide to a chloride followed by fused-salt electrolysis to produce metallic lead and chlorine (1–3). The chlorine produced is recycled directly or indirectly for the production of lead chloride. Various steps in this process are being actively investigated in Canada by CANMET.

Fused-salt electrolysis for the recovery of lead poses a number of problems. Lead chloride alone is not a good electrolyte. It has a high vapour pressure and exhibits poor current efficiency with respect to lead production. However, the addition of alkali chlorides decreases the fuming of lead chloride and improves the electrical conductivities. The favoured electrolyte composition appears to be the $PbCl_2$–KCl–LiCl ternary system. One problem with this system is the hygroscopic nature of LiCl. For this reason, the $PbCl_2$–KCl–NaCl ternary system has been suggested and serves as an alternative electrolyte in spite of its slightly lower molar conductivity.

Unfortunately, the physical properties of these ternary systems are scarce. Recently, the densities and molar volumes of melts in both the $PbCl_2$–KCl–NaCl and $PbCl_2$–KCl–LiCl ternary systems were determined in this laboratory (4). During this study, it was noted that alkali chloride melts containing $PbCl_2$ tended to creep up the crucible wall. Such observation suggests that the surface tension of these melts is quite low and could give rise to creeping of the electrolyte during cell operation. This phenomenon could lead to poor current efficiency. However, surface tension data on these systems are not available in the literature.

Consequently, the present study was undertaken to determine the surface tension of the molten salt system $PbCl_2$–KCl–NaCl as a function of composition and temperature in the range of interest for the electrolytic process of lead recovery.

Experimental

The maximum bubble pressure technique was selected as the method for the determination of the surface tension of the molten salts. With this method, the density of the liquid salt can be measured simultaneously with the surface tension. The maximum bubble pressure method at high temperatures has been used in many investigations (5–7) of the surface tension of molten salts and is known to give accurate and reproducible values. The principles of this method are well established. It involves the slow formation of a gas bubble at the tip of a capillary immersed in the liquid. Simultaneously, the pressure of the gas used to form the bubble is measured in order to determine the maximum pressure developed inside the bubble at the very instant it bursts. Schrödinger (8) developed the following relationship between the surface tension and the maximum bubble pressure.

$$[1] \quad \gamma = \frac{rP_\gamma}{2}\left[1 - (2/3)\left(\frac{r\rho g}{P_\gamma}\right) - (1/6)\left(\frac{r\rho g}{P_\gamma}\right)^2\right]$$

γ is the surface tension, r is the radius of the capillary, P_γ is the maximum pressure difference inside and outside the bubble at the level of the end of the tip, ρ is the density difference between the liquid salt and the gas, and g is the acceleration of gravity.

Apparatus

The overall apparatus used in this investigation is shown in Fig. 1. The furnace had a uniform temperature (2.5°C) region of 5 cm. The salt mixtures were contained in graphite crucibles with an inner diameter of 26 mm and a height of 47 mm under a purified argon

[1]Present address: Department of Metallurgy, Nagoya University, Nagoya, Japan.

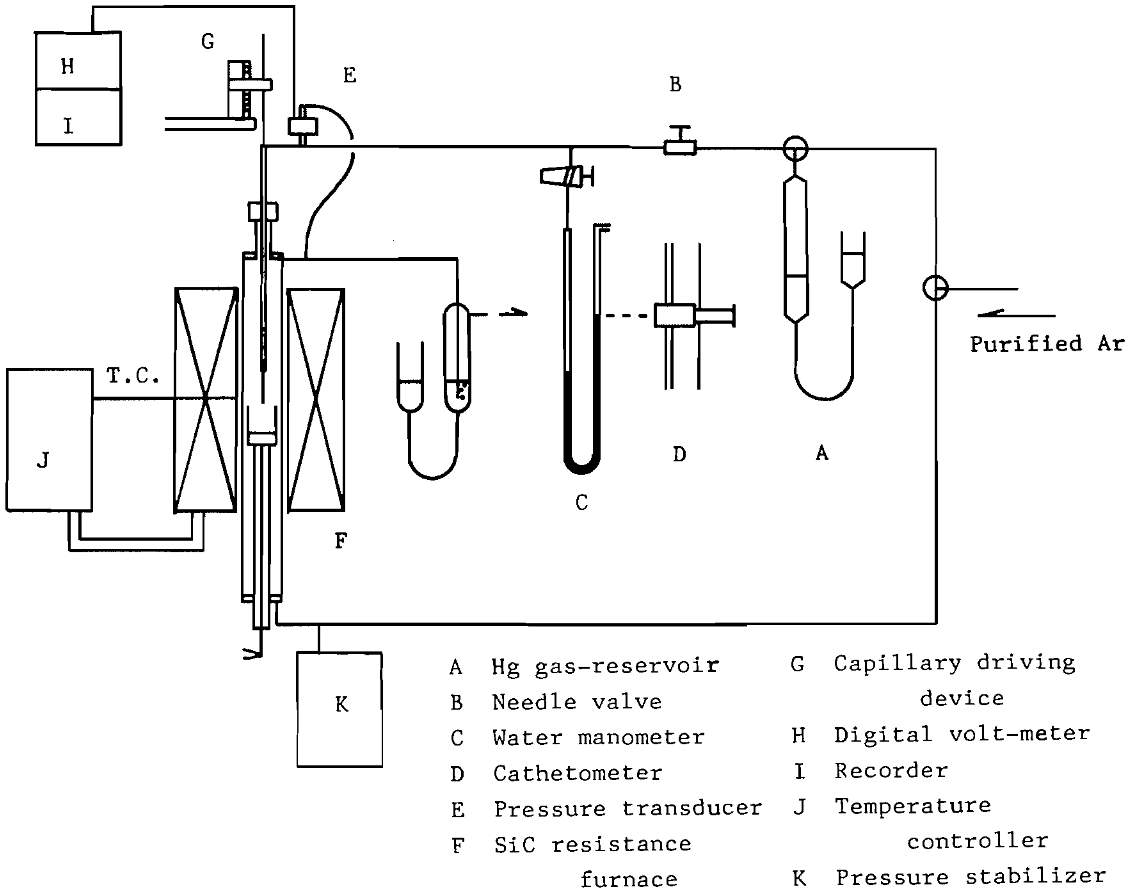

FIG. 1. Surface tension apparatus.

atmosphere. The capillary quartz tubes were 5 cm long, with an outer diameter of about 2.1 mm and with an inner diameter of about 1.03 mm. In order to obtain precise results, it was necessary to pay careful attention to the capillary tip. The bore must be as round as possible, the end flat and perpendicular to the axis of the capillary, and the edge of the orifice very sharp. A microscope was used to check the condition and the diameter of the orifice. All measurements were corrected for thermal expansion of the capillary orifice.

The quartz capillary tube was connected to an alumina tube with alumina cement (Ceramabond #503). This assembly was connected to a stainless steel tube which could be moved slowly (0.417 mm/min) up or down with a motor. The immersion depth of the capillary into the liquid was measured with a cathetometer and also calculated from the rotating speed of the motor. The pressure inside the capillary tube was measured with a pressure transducer (Model PL283TC-2.5-350, Stathan Instruments Inc., Los Angeles) with a sensitivity of 0.001 mV corresponding to 1 Pa. The high purity argon (99.999% min.) used to form the bubbles was passed through a copper getter furnace and through two drying columns packed with drierite and P_2O_5 to remove any possible traces of oxygen and water.

Materials

The potassium chloride (Fisher A.C.S. grade), the sodium chloride (Fisher U.S.P. grade), and the lead chloride (Baker Analysed reagent grade) were pre-dried in a vacuum oven at 150°C. As required, certain amounts of each salt were mixed together to form the desired salt mixture. This mixture was placed into a graphite crucible located in the purification furnace and kept at about 180°C under vacuum (1 Pa) for about 10 h. Argon was then introduced and the salt mixture heated to just above the melting point. Chlorine gas was bubbled through the melt for about 1 h. to remove any oxides. This was followed by bubbling of purified argon gas through the melt for about 1 h to remove any dissolved chlorine. The melt was then quenched and stored in a desiccator until required. The vaporization loss of lead chloride during the purification treatment was found to be negligibly small.

Procedure

A graphite crucible with the premixed, purified salt mixture was positioned inside the furnace. The capillary tip was cleaned with alcohol and dried with an argon gas jet before it was placed about 5 cm above the surface of the salt mixture. Each capillary tip was used for only one experiment. The furnace was then flushed with argon and slowly heated up to the desired temperature. Excess pressure was applied to the capillary while it was lowered towards the melt surface. The capillary was then lowered very slowly until a sudden pressure jump was registered by the pressure transducer as shown in Fig. 2, indicating that the capillary had touched the melt surface. The capillary was then stopped and the surface position was recorded. The bubbling rate was adjusted to about 1 bubble/min which was in the region where the transducer output was independent of the gas flow-rate. The pressure was increased linearly with the immersion depth until a bubble was released at the capillary tip followed by a sudden decrease in pressure. The capillary immersion depth was changed several times while the maximum bubble pressure was recorded. The pressure drop caused by the formation of a bubble at the capillary tip is the difference in the pressure just before the bubble bursts and after it has burst as shown by the sawtoothed curve in Fig. 2. By measuring the maximum bubble pressure at different immersion depths, the density of the salt can be calculated from the slope of the curve formed when the maximum pressure is plotted as a function of immersion depth as shown in Fig. 3. From the same plot, the pressure drop caused by the formation of the bubble can be found as the maximum pressure for zero immersion depth. Using this pressure value the surface tension of the salt mixture can be calculated using Schrodinger's equation. The temperature effect on the surface tension and the density

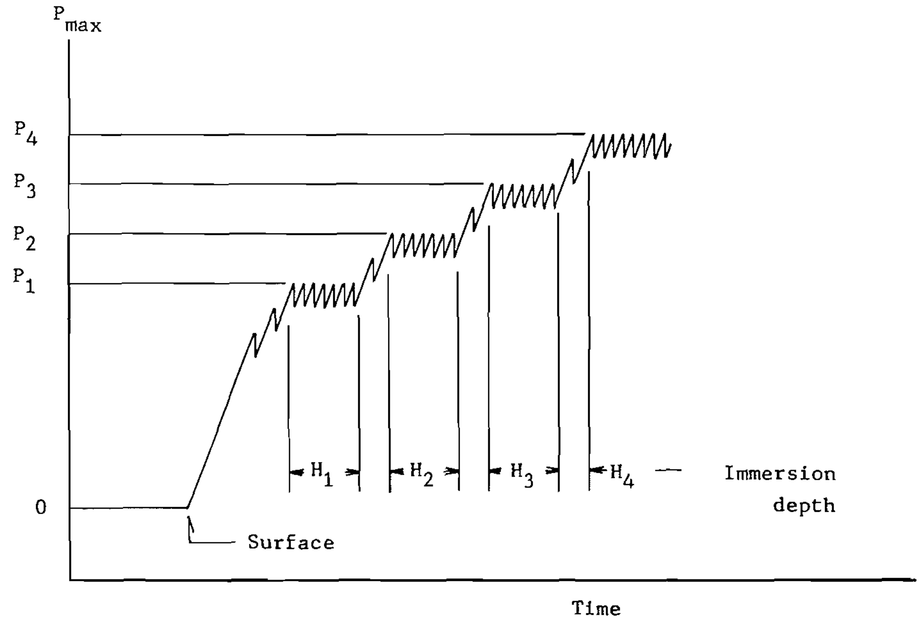

FIG. 2. Typical pressure transducer output.

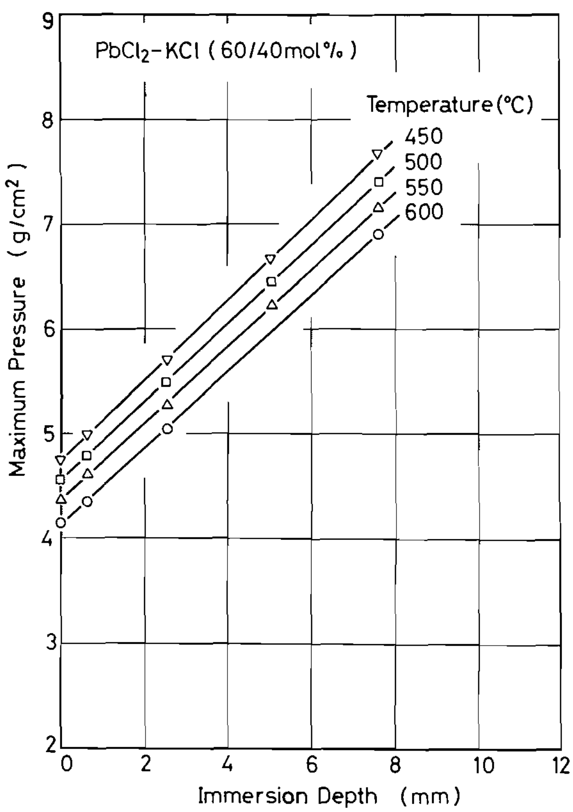

FIG. 3. Effect of immersion depth on the maximum pressure: $PbCl_2$–KCl system.

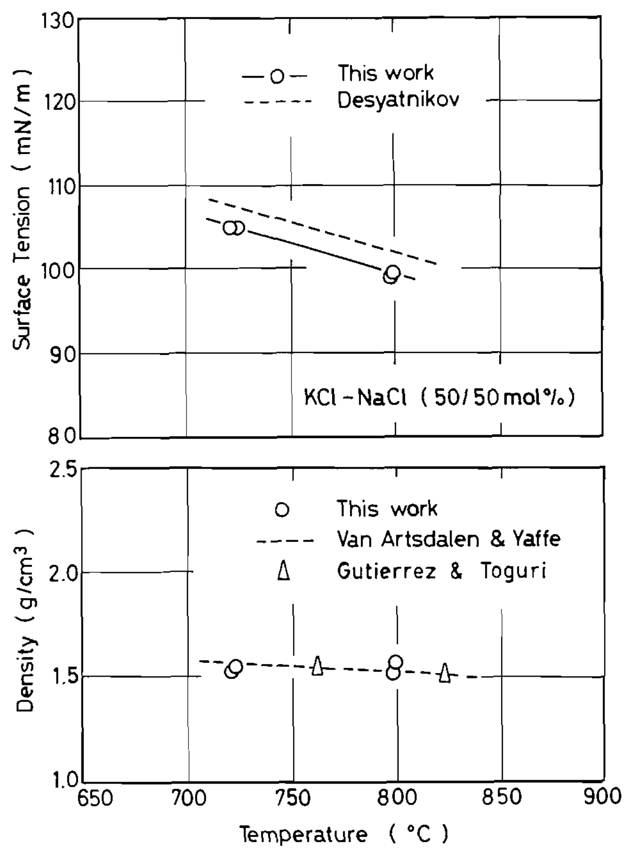

FIG. 4. Surface tension and density of KCl–NaCl (50/50 mole ratio) as a function of temperature.

were determined during both heating and cooling cycles.

A typical linear relationship between the maximum pressure and immersion depth is shown in Fig. 3 for a melt containing 60 mol% $PbCl_2$ and 40 mol% KCl. The effect of increasing the temperature is to decrease the maximum bubble pressure for a constant depth of immersion.

Results and discussion

The maximum bubble pressure apparatus was tested by measuring the surface tension and density of a 50 mol% mixture of NaCl–KCl. The results of this study are shown in Fig. 4. The surface tension obtained with the present apparatus is within 2.5% of the data of Desyatnikov (7) which are recommended by Janz *et al.* (9). Desyatnikov also used the maximum bubble pressure method. On the other hand, the density data obtained are in excellent agreement with both the recent data of

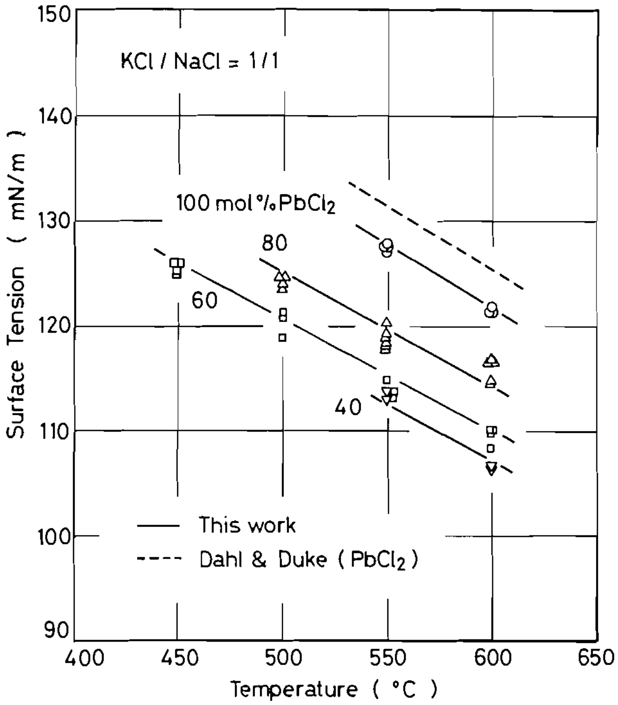

FIG. 5. Temperature dependency of surface tension at constant KCl/NaCl molar ratio in the $PbCl_2$–KCl–NaCl system.

Gutierrez and Toguri (4) and the older data of Van Artsdalen and Yaffe (10).

Based on these results, the surface tension and the density of pure $PbCl_2$ and the binary and ternary mixtures of $PbCl_2$, KCl, and NaCl have been measured within the temperature range of 450 to 600°C.

In the case of pure $PbCl_2$, the experiments were performed at two temperatures, 550 and 600°C. The upper limit was dictated by the vaporization loss of $PbCl_2$ and the lower limit by its melting point. Within the experimental temperature range the surface tension can be represented by the following equation:

$$[2] \quad \gamma = 227.9 - 0.122T \text{ (mN/m)}$$

As shown in Fig. 5, the present results are approximately 3.7% below those reported by Dahl and Duke (11) which are shown by the dotted line and which were obtained using the maximum bubble pressure method.

Our results both for the pure $PbCl_2$ and for the NaCl–KCl binary melts are approximately 2.5 to 3.7% below the reported values (7, 11). One likely systematic error is that as the quartz tube comes in contact with the liquid surface, the tube gets wetted and the liquid advances up the side of the tube. It has been estimated that due to this phenomenon, the true liquid surface falls approximately 0.1 mm in comparison with the surface detected when the capillary tube enters the liquid. The uncertainty in the measurements of the capillary immersion depth using a cathetometer is estimated to 0.15 mm giving a total of 0.25 mm with a corresponding uncertainty in the surface tension values of approximately 2%. With an additional error of approximately 1% caused by the measurements of the capillary radius and the maximum bubble pressure, the total uncertainty is estimated to be 3%.

The effect of temperature on the surface tension of melts containing equimolar mixtures of KCl and NaCl with varying amounts of $PbCl_2$ is also shown in Fig. 5. The results indicate

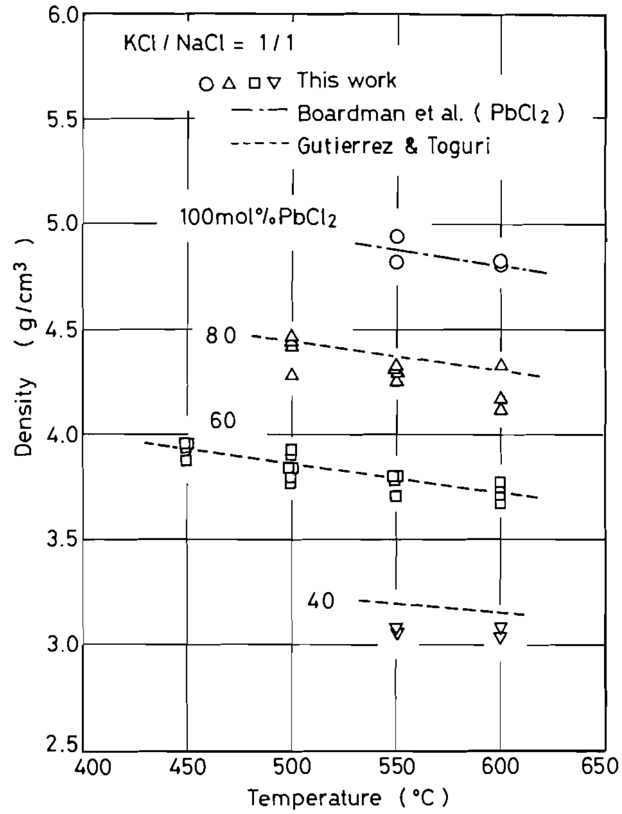

FIG. 6. Temperature dependency of density at constant KCl/NaCl molar ratio in the $PbCl_2$–KCl–NaCl system.

that the surface tension decreases linearly with increasing temperature and decreases with decreasing amount of $PbCl_2$ for melts containing more than 40 mol% $PbCl_2$. The corresponding density values are given in Fig. 6. The density for pure $PbCl_2$ obtained in the present study is in good agreement with that of Boardman *et al.* (12). The effect of temperature on the density of ternary melts is also illustrated and shows a linear decrease with increasing temperatures. Good agreement is found with the reported values of Gutierrez and Toguri (4) as shown by the dotted lines. Decreasing the concentration of $PbCl_2$ leads to a decrease in melt density.

The surface tension and the density were also measured for mixtures with a constant amount of $PbCl_2$ (60 mol%) and with varying amounts of KCl and NaCl. Figure 7 shows typical results for the effect of NaCl addition on the surface tension at various temperatures. Within the experimental accuracy, the surface tension increases linearly with increase in NaCl at constant $PbCl_2$ concentration. Increasing the temperature decreases the surface tension. The corresponding densities are illustrated in Fig. 8.

The surface tension of the binary mixture of $PbCl_2$–NaCl is higher than that of a mixture containing $PbCl_2$ and KCl. From the obtained data, an almost linear relation can be observed between the surface tension of the ternary mixtures and the ratio of KCl to NaCl at constant $PbCl_2$ contents. Similar relations are observed also for the density values with the highest density values in the $PbCl_2$–NaCl binary.

The compositions of the ternary system can be expressed by the parameters y and t, where

$$[3] \quad y = x_{PbCl_2}$$

$$[4] \quad t = x_{KCl}/(x_{KCl} + x_{NaCl})$$

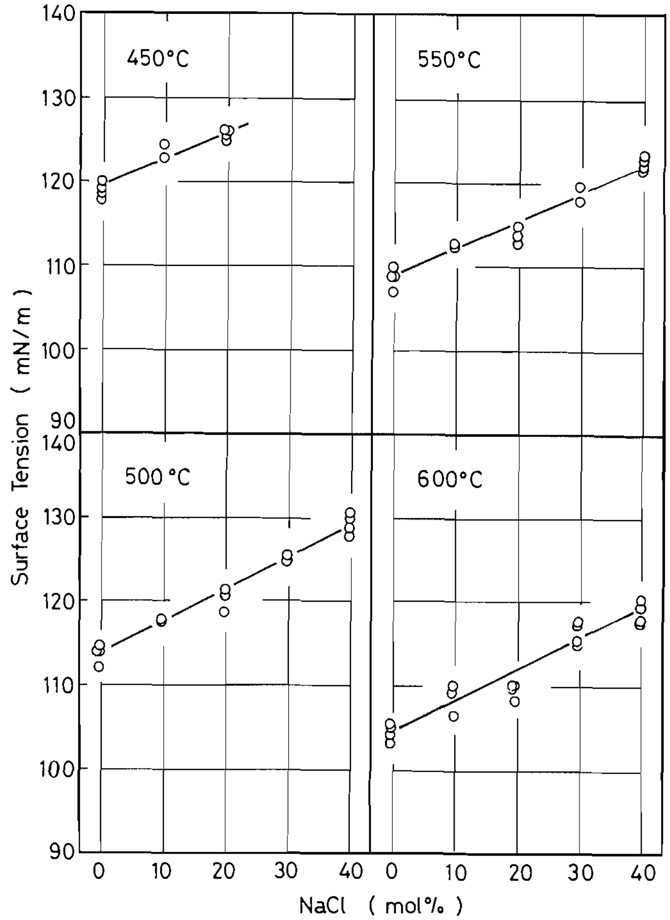

FIG. 7. Composition dependency of surface tension at constant $PbCl_2$ content (60 mol%) in the $PbCl_2$–KCl–NaCl ternary system.

The average surface tension values at each temperature and composition are given in Table 1 together with the fitted coefficients of the linear equation

$$[5] \quad \gamma = A + B^{*}T(\mathrm{K})\,(\mathrm{mN/m})$$

The corresponding average density values are given in Table 2 together with the fitted coefficients of the linear equation

$$[6] \quad \rho = C + D^{*}T(\mathrm{K})\,(\mathrm{g/cm^3})$$

Dahl and Duke (11) showed that the surface tension of the lead chloride-alkali chloride binary mixtures have a minimum value at approximately 40 mole percent $PbCl_2$. The extent of this minimum increases as the size of the alkali ion increases (from Na to Cs). A similar minimum in the surface tension was observed in this work. By extrapolating the values of the equimolar binary mixture of KCl and NaCl to 823 and 873 K, a pronounced minimum can be observed at a $PbCl_2$ content of approximately 40 mol%, as shown in Fig. 9. The plotted points are based on the average experimental values and the lines are the least-squares fitted second order polynomials. This behaviour corresponds well with that observed by Dahl and Duke (11) and by Sternberg *et al.* (13). This behaviour may be explained by the formation of surface active $PbCl_{2+n}^{n-}$ complexes, where the value of *n* may be 1, 2, or 4. Support for this suggestion comes from studies of Raman spectra (14), surface tension measurements (11), and density measurements (15). Similar complex formation has also been suggested in mixtures

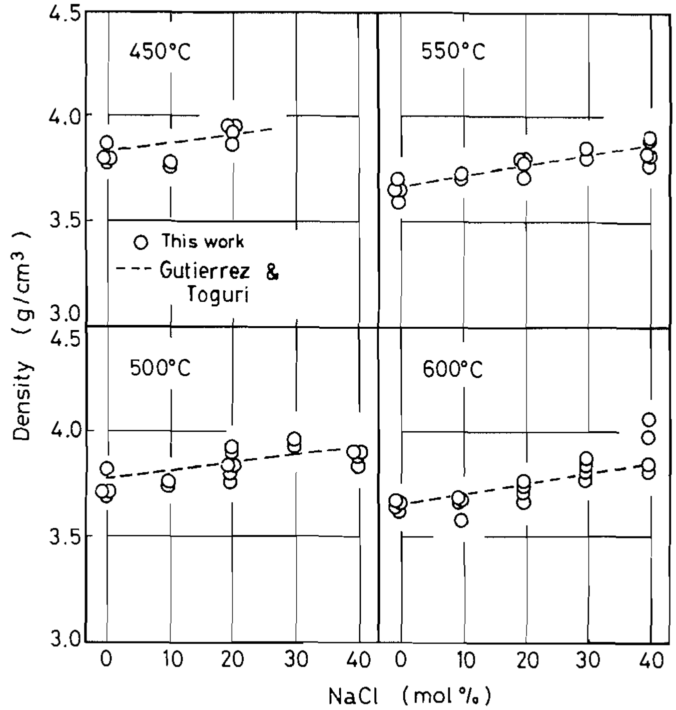

FIG. 8. Composition dependency of density at constant $PbCl_2$ content (60 mol%) in the $PbCl_2$–KCl–NaCl ternary system.

TABLE 1. Surface tension for the $PbCl_2$–KCl–NaCl system

Composition*		Temperature				$\gamma = A + BT(\mathrm{K})$†	
y	*t*	723 K	773 K	823 K	873 K	*A*	*B*
1.0		—	—	127.5	121.4	227.9	−0.122
0.8	0.5	—	124.1	118.8	115.8	187.9	−0.083
0.6	1.0	119.4	114.4	109.4	103.7	194.9	−0.104
0.6	1.0	118.5	113.0	107.9	105.2	183.0	−0.090
0.6	0.75	123.7	117.7	112.5	108.6	196.2	−0.101
0.6	0.5	125.2	—	—	109.2	202.3	−0.107
0.6	0.5	126.1	120.3	113.4	109.9	206.0	−0.111
0.6	0.25	—	125.2	118.8	116.4	192.6	−0.088
0.6	0.0	—	130.3	123.4	—	237.0	−0.138
0.6	0.0	—	128.4	122.2	118.9	201.4	−0.095
0.4	0.5	—	—	113.5	106.5	228.7	−0.140
0.0	0.5	105.1 (996 K)		99.3 (1073 K)	179.8	−0.075	

*y, mole fraction of $PbCl_2$; t, mole fraction of KCl over sum of mole fractions of KCl and NaCl.
†Surface tension (γ) is given in mN/m.

of $CdCl_2$ with alkali chlorides based on surface tension measurements (16).

The surface tension of ternary mixtures with a given $PbCl_2$ mole fraction can be calculated, within experimental errors from the two binary systems $PbCl_2$–KCl and $PbCl_2$–NaCl by the following expression:

$$[7] \quad \gamma(\text{ternary}) = t^{*}\gamma_{12} + (1 - t)^{*}\gamma_{13}$$

where γ_{12} and γ_{13} are the surface tension of the binaries $PbCl_2$–KCl and $PbCl_2$–NaCl with the required $PbCl_2$ content. By assuming that this additive relation is valid throughout the ternary system, it is possible to calculate the surface tension of any mixture from the data of the two binaries $PbCl_2$–KCl and $PbCl_2$–NaCl. This additive behaviour has previously been

TABLE 2. Density for the $PbCl_2$–KCl–NaCl ternary system

Composition*		Temperature				$\rho = C + DT$(K)†	
y	t	723 K	773 K	823 K	873 K	C	$10^4 D$
1.0		—	—	4.89	4.82	6.04	−14.0
0.8	0.5	—	4.40	4.29	4.21	5.86	−14.0
0.6	1.0	3.80	3.71	3.65	3.63	4.58	−11.0
0.6	1.0	3.82	3.75	3.65	3.67	4.60	−11.0
0.6	0.75	3.77	3.75	3.65	3.67	4.28	−7.0
0.6	0.5	3.94	—	—	3.71	5.02	−15.0
0.6	0.5	3.92	3.80	3.75	3.74	4.76	−12.0
0.6	0.25	—	3.95	3.83	3.83	4.86	−12.0
0.6	0.0	—	3.91	3.89	—	4.22	−4.0
0.6	0.0	—	3.86	3.85	3.83	4.09	−3.0
0.4	0.5	—	—	3.07	3.06	3.15	−1.0
0.0	0.5	1.54(996 K)		1.55(1073 K)		1.44	+1.0

*y, mole fraction of $PbCl_2$; t, mole fraction of KCl over sum of mole fractions of KCl and NaCl.
†Density is given in g/cm³.

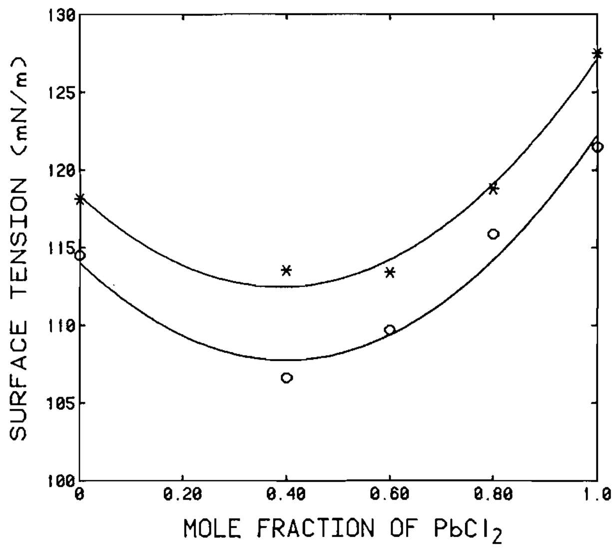

FIG. 9. Composition dependency of surface tension at constant KCl/NaCl molar ratio (50/50).

found (4) to be valid for the molar volumes of ternary mixtures of $PbCl_2$, KCl, and NaCl. By using reported (9) binary surface tension values, the following equations were found by a least squares curve fitting:

$PbCl_2$–KCl:

$$[8] \quad \gamma_{12} = 177.35 - 17.82*y + 73.49*y^2 - (6.44 + 5.94*y)*T$$

$PbCl_2$–NaCl:

$$[9] \quad \gamma_{13} = 218.45 - 39.2*y + 42.02*y^2 - (9.52 + 1.44*y)*T$$

$PbCl_2$–KCl–NaCl

$$[10] \quad \gamma = t*\gamma_{12} + (1 - t)*\gamma_{13}$$

By using these equations, constant surface tension lines can be calculated. Figure 10 shows the liquidus lines and the constant surface tension lines for the $PbCl_2$–KCl–NaCl ternary system at 873 K. For a constant $PbCl_2$ content the surface tension

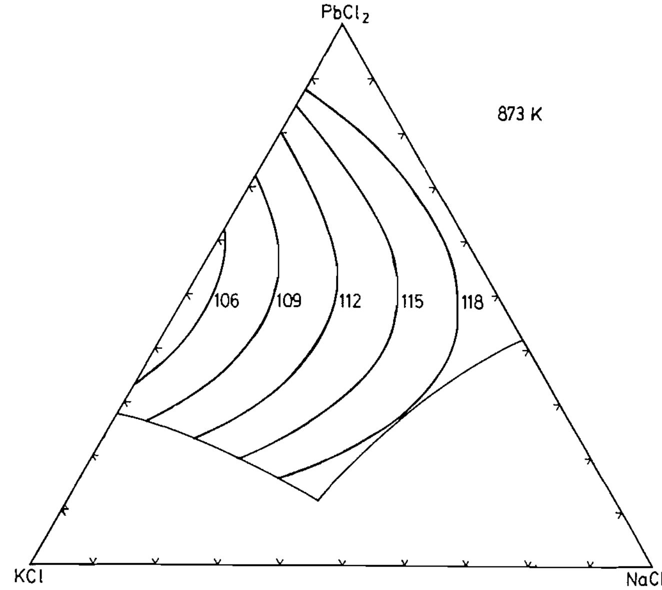

FIG. 10. Constant surface tension lines for the $PbCl_2$–KCl–NaCl ternary system at 873 K.

increases on going from the KCl- to the NaCl-rich side. For a given KCl-to-NaCl ratio a minimum in the surface tension is observed at approximately 45 mol% $PbCl_2$, which is slightly higher than that found in this study. The values measured in this work are all within 3% from those calculated by the above equations with the exception of the mixture of equimolar amounts of KCl and NaCl with 40 mol% $PbCl_2$ where the deviation is 4%. This is consistent with the present study in which the minimum in the surface tension was obtained for mixtures containing 40 mol% $PbCl_2$.

The density values obtained in this work using the maximum bubble pressure method are not expected to be of the same accuracy as those obtained by direct Archimedean methods. Nevertheless, the data obtained in the present study were in excellent agreement with those of Gutierrez and Toguri (4) who used a bottom-balance Archimedean technique.

Conclusions

(*1*) The surface tension and densities of the $PbCl_2$–KCl–NaCl ternary system have been determined over the temperature range 450 to 650°C by a maximum bubble pressure method.

(*2*) The surface tension of these melts were found to be additive at constant values of y and this behaviour could be described by the additivity rule with respect to t:

$$\gamma = t*\gamma_{12} + (1 - t)*\gamma_{13}$$

where the two binary systems, each containing $PbCl_2$, are denoted by the subscripts 12 and 13.

Acknowledgements

This research was carried out under contract and with the financial support of Canada Centre for Mineral and Energy Technology; Energy, Mines and Resources, Canada; Contract No. 05SU 23440-1-9064. We are grateful to Dr. J. E. Dutrizac of CANMET for many helpful discussions.

1. F. P. HAVER, C. E. ELGES, and M. M. WONG. Rep. Invest.-U.S., Bur. Mines 1976. R18166.

2. J. E. MURPHY, F. P. HAVER, and M. M. WONG. Rep. Invest.-U.S., Bur. Mines 1974. R17913.
3. M. M. WONG and F. P. HAVER. Symposium on molten salt electrolysis in metal production. Institute of Mining and Metallurgy: London. 1977.
4. A. GUTIERREZ and J. M. TOGURI. J. Chem. Eng. Data, **27**, 109 (1982).
5. D. A. NISSEN and R. W. CARLSTEN. J. Electrochem. Soc. **121**, 500 (1974).
6. Z. MOSER, W. GASIOR, and K. RZYMAN. J. Electrochem. Soc. 129, (1982).
7. O. G. DESYATNIKOV. Zhur. Priklad. Khim. **29**, 870 (1956).
8. E. SCHRÖDINGER. Ann. Physik. **46**, 488 (1917).
9. G. J. JANZ, R. P. T. TOMKINS, C. B. ALLEN, J. R. DOWNEY, G. L. GARDNER, U. KREBS, and S. K. SINGER. J. Phys. Chem. Ref. Data, **4**, 871 (1975).
10. E. R. VAN ARTSDALEN and I. S. YAFFE. J. Phys. Chem. **59**, 118 (1955).
11. I. L. DAHL and F. R. DUKE. USAEC Report ISC-923, 1958.
12. N. F. BOARDMAN, F. H. DORMAN, and E. HEYMANN. J. Phys. Chem. **53**, 375 (1949).
13. S. STERNBERG, M. TERZI, and M. KUCHARSKI. Archiwum Hutnictwa, **22**, 169 (1977).
14. M. TANAKA, K. BALASUBRAMANYAM, and J. O. M. BOCKRIS. Electrochim. Acta, **8**, 621 (1963).
15. H. BLOOM (*Editor*). The chemistry of molten salts. W. A. Benjamin, Inc. 1967.
16. G. BERTOZZI and G. SOLDANI. J. Phys. Chem. **72**, 353 (1968).

Photoreduction of water by visible light in the presence of montmorillonite

GILLES VILLEMURE
Ottawa–Carleton Institute for Research and Graduate Studies in Chemistry, Ottawa University Campus, Ottawa, Ont., Canada K1N 9B4

HIDEOMI KODAMA
Chemistry and Biology Research Institute, Research Branch, Agriculture Canada, Ottawa, Ont., Canada K1A 0C6

AND

CHRISTIAN DETELLIER[1]
Ottawa–Carleton Institute for Research and Graduate Studies in Chemistry, Ottawa University Campus, Ottawa, Ont., Canada K1N 9B4

Received July 20, 1984

GILLES VILLEMURE, HIDEOMI KODAMA, and CHRISTIAN DETELLIER. Can. J. Chem. **63**, 1139 (1985).

A pH 7.0 solution of methyl viologen, tris(2,2′-bipyridyl)ruthenium(II) chloride and triethanolamine acting as a sacrificial donor, produces hydrogen when irradiated by visible light (>395 nm) in the presence of a montmorillonite. We have observed a maximum production of hydrogen corresponding to an optimum ratio methyl viologen/clay. Preferential adsorption studies have allowed us to relate this optimum ratio to a particular distribution of the dicationic organic species on the clay surface: methyl viologen is intercalated into the layers and shares the occupancy of the external surface area in a ratio three-to-one with tris(2,2′-bipyridyl)ruthenium(II). Nine different homoionic clays were prepared and, compared to the natural one, showed no drastic difference in the hydrogen production.

GILLES VILLEMURE, HIDEOMI KODAMA et CHRISTIAN DETELLIER. Can. J. Chem. **63**, 1139 (1985).

En présence d'une montmorillonite, soumise à l'irradiation par la lumière du visible (>395 nm), une solution de viologène de méthyle, de chlorure de tris(2,2′)-bipyridyle de ruthénium(II) et d'un donneur sacrificiel (la triéthanolamine), produit de l'hydrogène. Nous avons observé une production maximum d'hydrogène correspondant à un rapport optimum de viologène de méthyle/argile. Des études d'adsorption préférentielle ont permis de relier ce rapport optimum à une distribution particulière des espèces chargées dicationiques sur la surface de l'argile: le viologène de méthyle est intercalé entre les couches et partage l'occupation de la surface externe avec le bipyridyle de Ruthénium dans un rapport trois/un. Neuf argiles homoioniques différentes ont été préparées et ne montrent pas de différence notable pour ce qui est de la production d'hydrogène, lorsque comparées à l'argile naturelle.

Introduction

Montmorillonite is a naturally occurring aluminosilicate (1) with a layer structure. Each layer is built up of two tetrahedral Si—O_4 sheets with their vertices pointing inwards, between which cations, mainly Al(III), are octahedrally coordinated. Isomorphous replacement of aluminum(III) by magnesium(II) or iron(II) in the octahedral sheet and/or of silicon(IV) by aluminum(III) in the tetrahedral sheets results in a global negative charge which is balanced by aquated cations (Na^+ and/or Ca^{2+}) occupying the interlamellar space. Those cations are exchangeable and can be replaced by any positively charged organic or inorganic species. Interlamellar water molecules can also be exchanged with organic neutral molecules. Therefore, this fascinating material has known many applications. "Maya Blue", an acid, base, or temperature-resistant pigment was obtained by Mayas in the eighth century by incorporating an organic pigment (indigo) into a clay (attapulgite) (2, 3). Clays may have played an important role in the prebiotic formation of oligopeptides (4, 5). Recently, organic reactions effected by clay supported, or intercalated, reagents have been developed (6), and a rhodium catalyst intercalated into hectorite layers displays selectivity for olefin reduction (7). Clays play an important role in protecting ground water sources from contamination by capturing heavy metals (8) or organic herbicides such as paraquat (9, 10).

Paraquat (1,1′-dimethyl-4,4′-dipyridinium dichloride), also called methyl viologen, is used as an effective electron relay in the process of water photoreduction (11). Hydrogen production from water photosplitting by visible light is an important goal in solar energy conversion and storage. A system consisting of an electron relay, such as methyl viologen (MV^{2+}), a photosensitizer, such as tris(2,2′-bipyridine)ruthenium(II) ($Ru(bpy)_3^{2+}$), a sacrificial donor, such as triethanolamine (TEOA), and a catalyst, such as colloidal platinum, can effect water photoreduction (12). We have shown that this system in the absence of platinum, but in the presence of a natural clay, called Wyoming Bentonite, produces hydrogen, if irradiated by visible light, at pH 7.0 (13). Clay minerals (sepiolite or hectorite) have been used as a supporting material for a water photooxidation catalyst, RuO_2 (14), or as a simultaneous support for two catalysts, RuO_2 — in view of water photooxidation — and Pt — in view of water photoreduction (15). We show in this article how hydrogen is photoproduced in the presence of a natural clay, and we propose an interpretation for the role of the clay.

Experimental

Tris(2,2′-bipyridyl)ruthenium(II) chloride was purchased from Alfa, methyl viologen, triethanolamine, and sodium ethylene diamine tetraacetate (EDTA) from Aldrich, and were used without further purification. Buffers were Fisher solutions (monobasic potassium phosphate and sodium hydroxide for pH 7.0 and potassium biphthalate for pH 4.0). The clay was a Wyoming Bentonite from Clay Spur, Wyoming, USA. The <0.2 μm fraction of Wyoming Bentonite was separated using conventional techniques (gravitation).

Homoionic clays were prepared by saturating the original bentonite (mainly Na-form) with one of the following chloride solutions: Ni(II), Cu(II), Zn(II), Co(II), Mg(II), Ca(II), Sr(II), Li(I), or NH_4(I). Excess salts were removed by dialysis. The reaction mixtures used for the

[1]To whom all correspondence should be addressed.

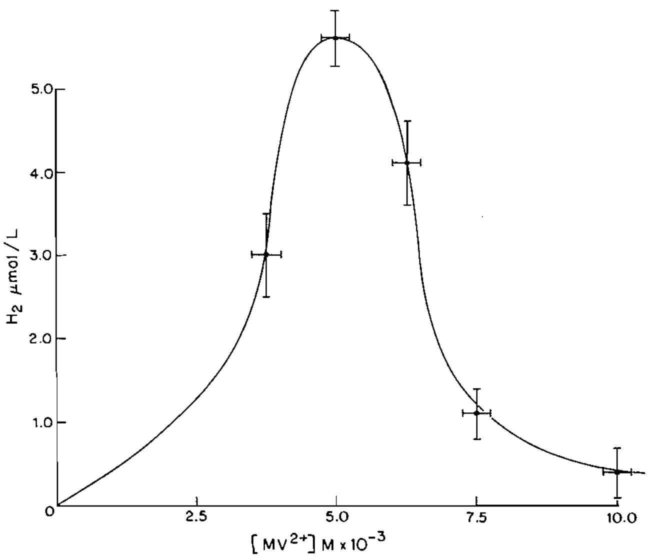

FIG. 1. Production of hydrogen as a function of MV^{2+} concentration (see Experimental part for description of the conditions).

experiment given in Fig. 1 were prepared in the following way, keeping the same order of addition of the various reagents under argon: 10 mL of the pH 7.0 buffered solution was added to 0.8 mL of TEOA, followed by the addition of 0.2 g of clay, a variable amount of MV^{2+}, 0.0192 g of $Ru(bpy)_3^{2+}$, and deoxygenated and deionized water in order to keep a constant total volume of 60 mL. Other experiments were based on the same typical procedure. The reaction mixture in a round bottom flask (cross-sectional area 75 cm^2) was then illuminated under argon with a 300 W tungsten–halogen lamp (at 25 cm from the center of the solution) through a 395 nm glass filter (Ealing, GG-395). Quantitative determinations of the hydrogen produced was effected by gas chromatographic analysis on a 5 Å molecular sieves column. Oriented thin films of clay which had been exchanged by MV^{2+} and $Ru(bpy)_3^{2+}$ were examined by an X-ray diffraction method to measure the change in d_{001}-spacing of the clay. The clay films were prepared by drying clay suspension (containing 20 mg sample) on glass slides. Diffraction patterns were recorded on a Scintag computer-automated X-ray diffractometer using Co radiation. Adsorption of methyl viologen or $Ru(bpy)_3^{2+}$ by montmorillonite was quantitatively measured by uv–visible spectra of the supernatant after 15 h stirring of the Na^+-exchanged clay in the methyl viologen (257.5 nm band) or $Ru(bpy)_3^{2+}$ (452 nm band) solutions.

Results and discussion

We have previously shown (13) that a solution of MV^{2+}, $Ru(bpy)_3^{2+}$, and TEOA at pH 7.0, in the presence of clay, produces a maximum amount of hydrogen at a given clay concentration. We have now checked that this maximum corresponds to an optimum value of the ratio MV^{2+}/clay and not to an opacity effect due to a too large clay concentration. Figure 1 shows the production of hydrogen as a function of methyl viologen concentration for a given amount of clay (3.3 g/L).[2] In the previously reported (13) experiment, and in this experiment, the maximum amount of hydrogen evolved corresponds to the same ratio [MV^{2+}]/[clay], equal to 1.5 mmol of MV^{2+}/g clay. This is three times higher than the typical cation exchange capacity of montmorillonite (100 mequiv./100 g) (10).

The production of hydrogen was also followed as a function of the concentration of clay and MV^{2+}, when their ratio was kept at a value close to the optimum observed value (Table 1). Since the concentration of $Ru(bpy)_3^{2+}$ was kept constant, the hydrogen production should increase with an increase in the MV^{2+} concentration. However, the observed hydrogen production increase depended only slightly upon the quantity of MV^{2+} in the experiment (Table 1). The opacity of the reaction mixture becomes important at high clay concentrations and can counterbalance a higher concentration of electron relay species. We checked that the system was independent of the nature of the cation with which the clay was saturated. That is for the nine different homoionic montmorillonites used (Table 2), we did not observe any synergistic effect between methyl viologen and the interlayer cation for the hydrogen production. The order of magnitude of the hydrogen production is the same as the one observed in the case of the original clay.

We determined the adsorption capacity of a homoionic clay (<0.2 μ) for MV^{2+} and $Ru(bpy)_3^{2+}$ (see Experimental). The maximum quantity of MV^{2+} and $Ru(bpy)_3^{2+}$ adsorbed by the clay were 89 ± 8 mequiv./100 g and 83 ± 5 mequiv./100 g, respectively. These values are in good agreement with literature data (10) for MV^{2+} (100 mequiv./100 g) and close to the exchange capacity of a typical montmorillonite (102 mequiv./100 g) (10). Figures 2 and 3 show the competitive adsorptions of MV^{2+} and $Ru(bpy)_3^{2+}$ by the montmorillonite.

When the two cations were added simultaneously to the clay suspension (Fig. 2), we observed a quasi-equal distribution of the cationic species between the two phases. At low $Ru(bpy)_3^{2+}/MV^{2+}$ ratios, no preferential adsorption is observed. The clay and the water phases contain the same molar ratio in $Ru(bpy)_3^{2+}$ vs. total concentration of charged organic species. At high $Ru(bpy)_3^{2+}$ concentrations a slight preferential adsorption of MV^{2+} is observed. In our experimental procedure Ru-

TABLE 1. Hydrogen production as a function of MV^{2+} and clay concentrations, at constant ratio (1.67 mmol MV^{2+}/g clay)

[MV^{2+}] (10^{-3} M)	[clay] (g/L)	H_2[a] (μmol/L)
2.50	1.50	3.9±0.5
5.00	3.00	5.4±0.6
7.50	4.50	4.3±0.7
10.00	6.00	6.3±0.7

[a]H_2 produced after 20 h of illumination of a system containing $Ru(bpy)_3^{2+}$ (5×10^{-4} M), TEOA (1.0×10^{-1} M), MV^{2+} and montmorillonite at pH = 7.0, under argon.

TABLE 2. Effect of the clay associated metal cation on hydrogen production in the presence of homoionic montmorillonites

Clay-associated metal cation	H_2[a] (μmol/L)
Cu^{2+}	5.6±0.8
Ni^{2+}	4.8±0.7
Sr^{2+}	4.6±0.7
Zn^{2+}	4.3±0.7
Ca^{2+}	3.8±0.7
Cd^{2+}	2.9±0.7
Mg^{2+}	2.9±0.7
NH_4^+	2.4±0.7
Natural	3.9±0.5

[a]H_2 produced after 20 h of illumination of a system containing MV^{2+} (2.5×10^{-3} M), $Ru(bpy)_3^{2+}$ (5.0×10^{-4} M), TEOA (1.0×10^{-1} M), clay (1.5 g/L) at pH 7.0 under argon.

[2]Under the same conditions, but at pH 4.0, using EDTA as the sacrificial donor, the hydrogen production is ten times higher.

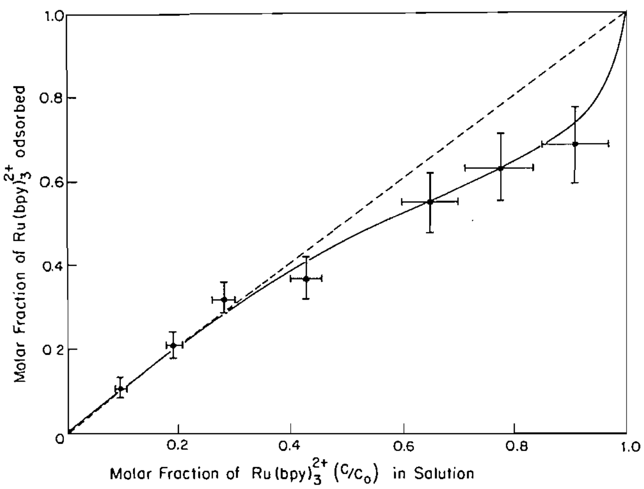

FIG. 2. Molar fraction of $Ru(bpy)_3^{2+}$ adsorbed on clay $[Ru(bpy)_3^{2+}]_{ads}/([Ru(bpy)_3^{2+}]_{ads} + [MV^{2+}]_{ads})$ as a function of molar fraction of $Ru(bpy)_3^{2+}$ in solution (see text).

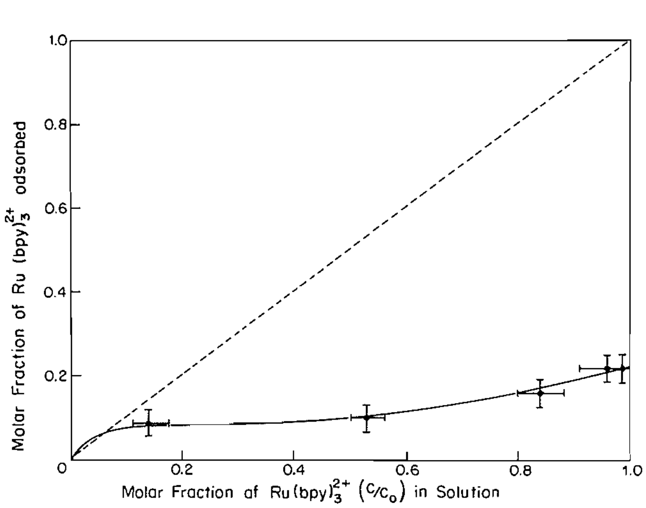

FIG. 3. Molar fraction of $Ru(bpy)_3^{2+}$ adsorbed on a clay on which MV^{2+} has been previously adsorbed, as a function of molar fraction of $Ru(bpy)_3^{2+}$ in solution (see text).

$(bpy)_3^{2+}$ was added to the system after MV^{2+}, when the clay interlamellar sodium has already been exchanged with MV^{2+}. The ability of $Ru(bpy)_3^{2+}$ to displace preadsorbed MV^{2+} was therefore studied (Fig. 3). $Ru(bpy)_3^{2+}$ can displace only a limited fraction of the MV^{2+}. Even with $Ru(bpy)_3^{2+}/MV^{2+}$ ratio equal to 10, only 22 ± 3% of the MV^{2+} is displaced (see Fig. 3). X-ray results showed that the d_{001} spacing was much smaller for MV^{2+} (12.55 Å) than for $Ru(bpy)_3^{2+}$ (17.4 Å) (Table 3). The thickness of the silicate layer being 9.6 Å, an interlamellar space of 2.95 Å accommodates methyl viologen. This space is too narrow by far to permit the incorporation of $Ru(bpy)_3^{2+}$. One can estimate the ratio between external areas and total areas of a montmorillonite to be about 30% (16). Therefore, small amounts of $Ru(bpy)_3^{2+}$ can be adsorbed on the external area of the clay, entering in competition with MV^{2+} for occupation of these sites, the internal sites not being available for $Ru(bpy)_3^{2+}$. This is in agreement with the optimum MV^{2+}/clay concentrations ratio observed for hydrogen production. When the MV^{2+} concentration is too high, the clay surface is saturated with MV^{2+} (Table 3).

All these observations lead us to a model for the active site

TABLE 3. Adsorption of MV^{2+} and $Ru(bpy)_3^{2+}$ by montmorillonite and X-ray determined basal spacings (see Experimental section)

Cation	Amount adsorbed (mequiv./g)	Basal spacings	
		Measured (Å)	Literature (Å)
Na^+	—	10.7	10.6(9)
MV^{2+}	0.89±0.08	12.6	12.4(10)
$Ru(bpy)_3^{2+}$	0.83±0.05	17.4	18.0(21)

responsible of the electron transfer to H^+: (*a*) MV^{2+} displaces Na^+, and/or any other interlamellar metal cations completely in such a way that the maximum exchange capacity of the clay has been attained. (*b*) The aggregate clay/MV^{2+} is particularly stable, with the dication probably adopting a flat conformation squeezed in a 2.95 Å intersheet distance. (*c*) $Ru(bpy)_3^{2+}$ can enter in competition with MV^{2+} adsorbed on external sites on the clay. The distribution of $Ru(bpy)_3^{2+}$ and MV^{2+} between external sites and the solution is not preferential. One dication out of three on the external sites is $Ru(bpy)_3^{2+}$, reflecting the organic cations solution ratio under our optimum experimental conditions. (*d*) MV^{2+} is reduced to $MV^{\dot{+}}$ on the external surface and/or on contact sites between external $Ru(bpy)_3^{2+}$ and intercalated MV^{2+}. Efficient charge separation can be achieved in aqueous suspensions of colloidal silica (17). Similarly the clay colloidal suspension suppress at least partially the reverse electron transfer between $Ru(bpy)_3^{2+}$ and $MV^{\dot{+}}$. The coexistence of electron acceptor sites, such as aluminum at the crystal edges (18) and electron donating sites, such as transition metals in the reduced states (18) can effect the electronic transfer to the protons, generated at the highly acidic montmorillonite surface (19). Titanium(III) exchanged zeolite A in water yields hydrogen under visible illumination (20). Local clay area containing titanium could be involved in the electronic transfer process.

Acknowledgements

We acknowledge the Natural Sciences and Engineering Research Council of Canada (NSERCC) for financial support. One of us (G. V.) is grateful to NSERCC for a postgraduate scholarship.

1. W. A. DEER, R. A. HOWIE, and J. ZUSSMAN. Rock forming minerals. Vol. 3. Sheet silicates. Longmans, Green and Co., London. 1962. pp. 226–245.
2. H. VAN OLPHEM. Science, **154**, 645 (1966).
3. R. KLEBER, L. MASSCHELEIN-KLEINER, and J. THISSEN. Stud. Conserv. **12**, 41 (1967).
4. N. LAHAV and S. CHANG. J. Mol. Evol. **8**, 357 (1976).
5. J. G. LAWLESS and N. LEVI. J. Mol. Evol. **13**, 281 (1979).
6. A. CORNELIS, P. LASZLO, and P. PENNETREAU. Clay Minerals, **18**, 437 (1983).
7. T. J. PINNAVAIA, R. RAYTHATHA, J. G.-S. LEE, L. J. HALLORAN, and J. R. HOFFMAN. J. Am. Chem. Soc. **101**, 6891 (1979).
8. P. MONSEF-MIRZAI and W. R. MCWHINNIE. Inorg. Chim. Acta, **73**, 41 (1983).
9. S. B. WEED and J. B. WEBER. Am. Mineral. **53**, 478 (1968).
10. M. RAUPACH, W. W. EMERSON, and P. G. SLADE. J. Coll. Interf. Sci. **69**, 398 (1979).
11. A. HARRIMAN and M. A. WEST (*Editors*). Photogeneration of hydrogen. Academic Press. 1982.
12. J. KIWI, K. KALYANASUNDARAM, and M. GRÄTZEL. Struct. Bonding, **49**, 37 (1982).

13. C. DETELLIER and G. VILLEMURE. Inorg. Chim. Acta, **86**, L19 (1984).
14. H. NIJS, H. VAN DAMME, F. BERGAYA, A. HABTI, and J. J. FRIPIAT. J. Mol. Catal. **21**, 223 (1983).
15. H. NIJS, J. J. FRIPIAT, and H. VAN DAMME. J. Phys. Chem. **87**, 1279 (1983).
16. D. T. B. TENNAKOON, J. M. THOMAS, M. J. TRICHER, and J. O. WILLIAMS. J. Chem. Soc. Dalton Trans. 2207 (1974).
17. I. WILLNER, J. M. YAND, C. LAANE, J. W. OTVOS, and M. CALVIN. J. Phys. Chem. **85**, 3277 (1982).
18. R. A. DELLA GUARDIA and J. K. THOMAS. J. Phys. Chem. **87**, 990 (1983).
19. J. HELSEN. J. Chem. Educ. **59**, 1063 (1982).
20. S. M. KUZNICKI and E. M. EYRING. J. Am. Chem. Soc. **100**, 6790 (1978).
21. D. KRENSKE, S. ABDO, H. VAN DAMME, M. CRUZ, and J. J. FRIPIAT. J. Phys. Chem. **84**, 2447 (1980).

The conformations of prostacyclin and related prostaglandins[1]

HELMUT BEIERBECK AND GEORGE KOTOVYCH[2]
Department of Chemistry, University of Alberta, Edmonton, Alta., Canada T6G 2G2

AND

MAKIKO SUGIURA
Kobe Women's College of Pharmacy, Kobe, Japan

Received August 28, 1984

HELMUT BEIERBECK, GEORGE KOTOVYCH, and MAKIKO SUGIURA. Can. J. Chem. **63**, 1143 (1985).

The conformations of prostacyclin, PGI_2, and three of its analogues, 6*R*- and 6*S*-PGI_1 and carbacyclin, were studied by high field ^1H nmr spectroscopy. The *cis*-bicyclo- and *cis*-oxabicyclo[3.3.0]octane ring conformations were completely assigned. The minima for the pseudorotational conformations are observed at $^7E/_{12}E$ for PGI_2, $^{6}_{6a}T/^{11}_{12}T$ for 6*R*-PGI_1, and $_6E/^{11}E$ for 6*S*-PGI_1 and carbacyclin. The data indicate that each molecule adopts a narrow pseudolibrational range, if not a single conformation. The α- and ω-side chain conformations were characterized, but not unambiguously. Vicinal coupling constants and nuclear Overhauser enhancements proved to be the most useful spectroscopic parameters in this study.

HELMUT BEIERBECK, GEORGE KOTOVYCH et MAKIKO SUGIURA. Can. J. Chem. **63**, 1143 (1985).

Faisant appel à la rmn du ^1H à haut champ, on a étudié les conformations de la prostacycline, PGI_2, et de trois de ses analogues, les 6*R*- et 6*S*-PGI_1 et la carbacycline. On a réussi à faire des attributions complètes pour les conformations des cycles *cis*-bicyclo et *cis*-oxabicyclo[3.3.0] octanes. On a observé les positions des minima des conformations pseudorotationnelles du PGI_2, 6*R*-PGI_1 ainsi que 6*S*-PGI_1 et carbacycline qui se situent respectivement à $^7E/_{12}E$, $^{6}_{6a}T/^{11}_{12}T$, et $_6E/^{11}E$. Ces données indiquent que les variations conformationnelles de chaque molécule sont limitées, mais qu'elles ne sont pas limitées à une seule conformation. On a caractérisé les conformations des chaînes latérales α et ω; toutefois ces caractérisations ne sont pas sans ambiguités. Les constantes de couplage vicinales et les effets Overhauser nucléaires se sont avérés les paramètres spectroscopiques les plus utiles de cette étude.

[Traduit par le journal]

In a recent series of articles (1–4) we reported ^1H nmr chemical shifts and coupling constants for prostacyclin and three of its derivatives, compounds of considerable pharmacological interest. Prostacyclin or PGI_2, first isolated in 1976, is a potent vasodilator and inhibitor of platelet aggregation (5, 6). It is rather unstable, however, and a number of biologically active analogues were developed (5), among them the isomeric 5,6-dihydroprostacyclins, 6*R*-PGI_1 and 6*S*-PGI_1, and carbacyclin, in which the ether oxygen is replaced by a methylene group. In the present study we have undertaken a detailed conformational analysis, based on ^1H nmr coupling constants and nuclear Overhauser effects, of this important group of prostaglandins.

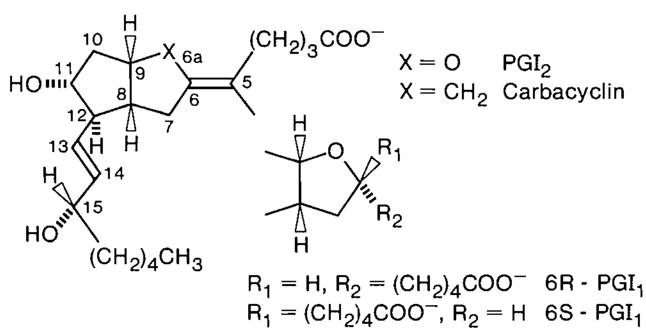

Experimental

The samples of PGI_2, 6*S*-PGI_1, 6*R*-PGI_1, and carbacyclin used in this study were gifts from Drs. R. A. Johnson, J. E. Pike, and D. R. Morton of Upjohn, Kalamazoo. For the measurements of coupling constants in chloroform solution, CD_3OD was distilled into nmr tubes containing PGI_2 methyl ester or 6*S*-PGI_1, respectively, to exchange labile protons; the methanol was then evaporated and $CDCl_3$ added. The prostaglandin concentrations were ~0.005 *M*. The samples were sealed after four freeze–pump–thaw cycles. PGI_2 samples were prepared in glycine/D_2O buffer solutions at pH ≥ 10. Solutions were 0.005 *M* PGI_2 in a 0.20 *M* and 0.015 *M* buffer and 0.017 *M* in 0.02 *M* buffer to check for the effect of concentration on the T_1 data. The high pH was necessary to prevent PGI_2 hydrolysis. For 6*S*- and 6*R*-PGI_1, a 0.10 *M* phosphate/D_2O buffer of pH = 7.0 was used. The samples were weighed into nmr tubes, buffer solution added, the solvent evaporated, fresh 100% D_2O added, and oxygen removed in four freeze–pump–thaw cycles. 6*S*-PGI_1 concentrations were 0.005 *M*, 0.008 *M*, and 0.013 *M* while the 6*R*-PGI_1 solutions were 0.005 *M*. All glassware was cleaned extensively, including a nitric acid wash, to eliminate paramagnetic impurities.

All nmr measurements were carried out on a Bruker WH-400 FT nmr spectrometer equipped with an Aspect 2000 data system, using 16K, 32K, or 64K of memory, as required. The solvent deuterium resonances served as lock signal. All ^1H nmr spectra were run at ambient temperature, but the ^{13}C measurements were carried out at 277 K to minimize decomposition. The nonselective longitudinal ^1H relaxation times were determined using the $180°-t-90°$ pulse sequence as discussed previously (1).

Quantitative nOe's were determined as follows. The decoupler was set to the first of three or four multiplets and eight transients recorded in quadrature detection mode, the decoupler moved to the next multiplet, and finally far off resonance. The control free induction decay (FID) was subtracted from each nOe FID, and the decoupler reset to the first multiplet for the next cycle. Each multiplet was irradiated for a time $t \gtrsim 5T_1$ with sufficient power to just saturate that signal. The nOe's were derived from the integration curves of the signals of interest and the saturated signal in the difference spectrum. Each quoted nOe value is the average of at least three determinations.

The ^{13}C chemical shift assignments for PGI_2 are based on the spin-echo technique with gated decoupling and on selective $^{13}C-\{^1H\}$ decoupling experiments. With the exception of C_1 to C_3, our values are in good agreement with literature data for the PGI_2 methyl ester in

[1]Paper No. 10 in a series of high-field nmr studies on the prostaglandins and leukotrienes.

[2]Author to whom correspondence should be addressed.

$CDCl_3$ (7). The 180°$-t-$90° pulse sequence was used in the ^{13}C T_1 experiments.

Calculations

Coupling constants

Vicinal coupling constants in $HR_1R_2C—CHR_3R_4$ segments were calculated with Altona's equation (ref. 8)

$$[1]\quad {}^3J_{HH} = 13.86 \cos^2 \phi - 0.81 \cos \phi + \sum_i^4 \Delta\chi_i\{0.56 - 2.32 \cos^2 (\xi_i\phi + 17{\cdot}9|\Delta\chi_i|)\}$$

where

ϕ = proton–proton torsion angle
$\Delta\chi_i$ = difference in Huggins electronegativities (9) between R_i and H ($\chi_C - \chi_H = 0{\cdot}4$, $\chi_O - \chi_H = 1.3$)
ξ_i = +1 and −1 for substituent R_i clockwise and counterclockwise from the coupled geminal proton.

Three- and four-bond vinyl–allylic coupling constants were estimated with Garbisch' equations (ref. 10)

$$[2]\quad {}^3J_{HH} = 6.6 \cos^2 \phi + 2.6 \sin^2\phi \qquad 0° \le \phi \le 90°$$
$$= 11.6 \cos^2\phi + 2.6 \sin^2\phi \qquad 90° \le \phi \le 180°$$

$$[3]\quad {}^4J_{HH} = 1.3 \cos^2\phi - 2.6 \sin^2\phi \qquad 0° \le \phi \le 90°$$
$$= -2.6 \sin^2\phi \qquad 90° \le \phi \le 180°$$

Nuclear Overhauser effects

For the case of isotropic motion and dipole–dipole relaxation the fractional enhancement $f_d(s)$ at nucleus d on saturating signal s is given (11) by

$$[4]\quad f_d(s) = A\left[\sum_s g_d(s) - \sum_{i\neq d,s} f_i(s)g_d(i)\right]$$
$$= -A \sum_{i\neq d} f_i(s)g_d(i), \qquad f_s(s) = -1$$

where

$g_d(i)$ = the geometric term
$= N_i\langle r_{di}^{-6}\rangle \Big/ \sum_j N_j\langle r_{dj}^{-6}\rangle$
N_j = number of magnetically equivalent nuclei j
r_{dj} = distance between protons d and j
A = the correlation term
$= [6\tau_C/(1 + 4\omega^2\tau_C^2) - \tau_C]/[\tau_c + 3\tau_c/(1 + \omega^2\tau_c^2) + 6\tau_c/(1 + 4\omega^2\tau_c^2)]$

The brackets in $\langle r_{dj}^{-6}\rangle$ indicate conformational averages (12), where appropriate. The nOe's for a given molecular conformation were obtained as follows. Coordinates for that conformation were generated as outlined below, proton–proton distances were derived from these coordinates, and the $g_d(i)$ in eq. [4] were evaluated. The nOe's were then obtained by an iterative fit of expression [4] to the observed values, calculating the constant A from an assumed correlation time or treating it as an adjustable variable in a least-squares fit.

Relaxation times

Nonselective ^1H relaxation times were calculated by a least-squares fit of eq. [5] (11) to the observed values, treating B as variable.

$$[5]\quad T_{1i} = B\Big/\left[\sum_{j\neq i} N_j\langle r_{ij}^{-6}\rangle + (N_i - 1)r_{ii}^{-6}\right]$$

where

$$B = 10/\{\hbar^2\gamma_H^4 \times [3\tau_C/(1 + \omega^2\tau_c^2) + 12\tau_c/(1 + 4\omega^2\tau_c^2)]\}$$

Ring conformations

In order to simplify the pseudorotational analysis of the ring systems, PGI_2 and the PGI_1 isomers were assumed to be *cis*-bicyclo[3.3.0]octane derivatives like carbacyclin. The conformations of cyclopentane may be described by Altona's pseudorotation equation (ref. 13)

$$[6]\quad \phi_j = \phi_{max}\cos (p_k + 144j);\ j = 0, 1\ldots4$$

where

ϕ_j = C—C torsion angle about C_{j-1}—C_j
ϕ_{max} = maximum torsion angle
p_k = phase angle of pseudorotation
$= 18k$; $k = 0, 1\ldots19$

With ϕ_{max} = 48° the torsion angles in the twist and envelope conformations have the following values.

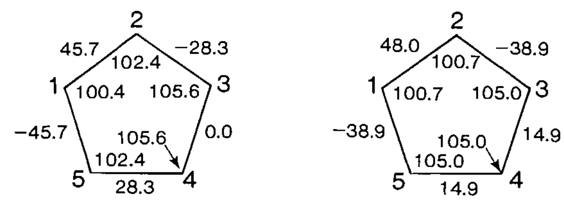

^1E $\qquad$ ^1_2T

The valency angles shown are Hendrickson's (14) values for Pitzer's (15) cyclopentane conformations, and were used in the derivation of ring coordinates.

In order to form *cis*-bicyclo[3.3.0]octane, two cyclopentane rings have to be joined at bonds with identical torsion angles. Since the rings may be combined up–up or up–down, 2×20 conformations are generated (the two combinations give identical results, when the torsion angle about the common bond is $\pm\phi_{max}$). Protons and carbon substituents were attached to the rings as shown.

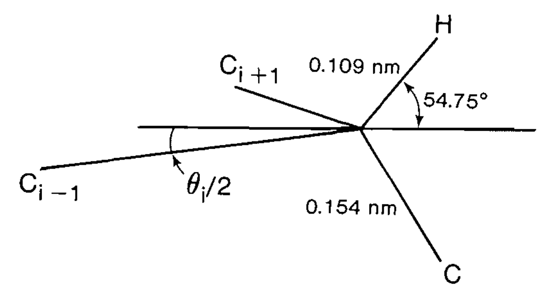

Side chain conformations

Only coordinates and conformer populations for segment H_3-H_{17} were needed, since T_1's and nOe's were only available within the range H_5-H_{15}. The conformations of the abbreviated α- and ω-chains were built with C—C and C=C bond lengths of 0.154 and 0.134 nm, tetrahedral and trigonal bond angles, and eclipsed $C(sp^2)-C(sp^3)$ and staggered $C(sp^3)-C(sp^3)$ rotamers. Side chain conformations with *syn*-axial δ-interactions were excluded. The population χ_1 of a given chain conformation is the product of the populations p_{ik} of the rotational states of the constituent bonds (16)

$$[7]\quad \chi_1 = \prod_j^n p_{jk} \Big/ \sum_j^n \sum_k^3 \prod_j^n p_{jk}, \qquad 1 = 1, 2\ldots3^n$$

TABLE 1. Experimental and calculated coupling constants (in Hz) for the ring protons in PGI_2, 6*R*-PGI_1, 6*S*-PGI_2, and carbacyclin

	PGI_2			6*R*-PGI_1		6*S*-PGI_1			Carbacyclin	
	Observed		Calcd.	Observed	Calcd.	Observed		Calcd.	Observed	Calcd.
	$CDCl_3$[a]	D_2O(1)	$^{7}E/_{12}E$	D_2O(2)	$^{6}_{6a}T/^{11}_{12}T$	$CDCl_3$[b]	D_2O(3)	$_{6}E/^{11}E$	$CDCl_3$(4)	$_{6}E/^{11}E$
6aα,9									2.0	0.7
6aβ,9									8.9	8.5
6α,7α						4.8	4.6	4.1		
6α,7β						9.8	10.4	11.4		
6β,7α				9.1	10.9					
6β,7β				6.3	5.3					
7α,7β	15.4	15.5		12.0		12.5	12.4		14.8	
7α,8	0	0	1.2	5.0	6.8	0	0.5	0.7	0	0.7
7β,8	8.0	7.6	5.4	9.1	10.3	8.3	8.1	8.5	8.7	8.5
8,9	6.3	6.5	6.4	7.2	8.1	7.2	7.6	9.2	8.7	10.3
8,12	8.8	10.7	11.3	9.7	10.5	9.0	10.0	9.0	9.7	9.0
9,10α	2.8	3.0	2.8	4.4	5.3	5.5	6.0	7.8	7.7	9.5
9,10β	6.4	7.2	9.8	7.2	9.8	7.0	7.6	8.6	8.2	8.7
10α,10β	14.4	14.3		13.6		13.6	12.9		12.2	
10α,11	8.1	8.7	7.8	9.3	9.5	9.6	10.5	10.4	10.0	10.4
10β,11	7.8	8.7	8.6	7.2	7.2	6.9	6.8	6.1	7.0	6.1
11,12	8.1	8.7	9.7	9.3	10.0	9.5	10.0	9.7	9.8	9.7

[a]Experiments carried out on the methyl ester. Side chain coupling constants (Hz): $J_{5,7\alpha} \simeq 0$, $J_{5,7\beta} = 1.7$, $J_{12,13} = 8.1$, $J_{13,14} = 15.3$, $J_{14,15} = 6.6$, $J_{15,16} \simeq J_{15,16^*} = 6.4$.

[b]ω-chain coupling constants are similar to $PGI_2/CDCl_3$ values.

where n = number of bonds with three rotational states. Rotamer populations were derived from coupling constants or treated as variables. The χ_i are the weighing factors for the r_{dj}^{-6}.

Results and discussion

The conformational analysis of PGI_2, the PGI_1's, and carbacyclin is based on two complimentary ^1H nmr parameters, namely coupling constants (Table 1), which define the orientation of vicinal protons, and nOe's (Table 2), which are sensitive probes of steric interactions. Relaxation times (Table 3) proved less informative, since conformational variations of internuclear distances tend to average in the sum of the relaxation contributions. For this reason, however, T_1's are useful motional probes, i.e. they define the molecular region in which the isotropic correlation time approximation for nOe's is justified. The nonselective relaxation times for PGI_2 and the PGI_1's are well reproduced for $H_5{-}H_{15}$ and $H_6{-}H_{15}$, respectively (Table 3), and the ^{13}C NT_1's for PGI_2 are approximately equal from C_5 to C_{15} (Table 4), as in $PGF_{2\alpha}$ (17, 18). The nOe expression [4] should therefore be applicable in this range, and indeed agreement is satisfactory (Table 2). Correlation times derived from the nOe's (τ_c = 0.24 ns) and T_1's (τ_c = 0.1 ns) are somewhat different, however. Relaxation times derived with τ_c = 0.24 ns are about 70% of the values obtained with τ_c = 0.1 ns. This discrepancy should not affect the conformational arguments.

The ring conformations for all four substrates are readily derived from the vicinal coupling constants. Plots of standard deviations between calculated and observed coupling constants vs. pseudorotational conformations (Figs. 1a and 1b) show well-defined minima at $^{7}E/_{12}E$ (PGI_2), $^{6}_{6a}T/^{11}_{12}T$ (6*R*-PGI_1), and $_{6}E/^{11}E$ (6*S*-PGI_1 and carbacyclin), indicating that each molecule adopts a narrow pseudolibrational range, if not a single conformation. In all cases the C_{11}—C_{12} torsion angle is at or near its maximum and the 11- and 12-substituents are pseudo-equatorial. The 6*R*-PGI_1 and carbacyclin conformation $_{6}E/^{11}E$ is the conformational minimum of *cis*-bicyclo[3.3.0]octane (19, 20).

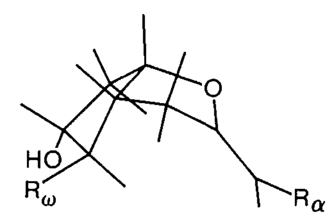

PGI_2 Conformation $^{7}E/_{12}E$

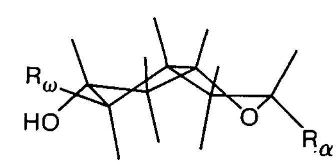

6R – PGI_1 Conformation $^{6}_{6a}T/^{11}_{12}T$

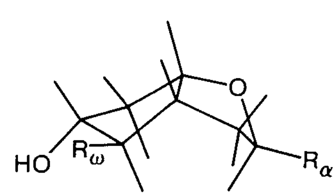

6S – PGI_1 Conformation $_{6}E/^{11}E$

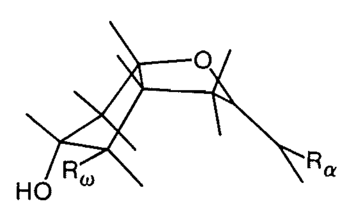

Carbacyclin Conformation $_{6}E/^{11}E$

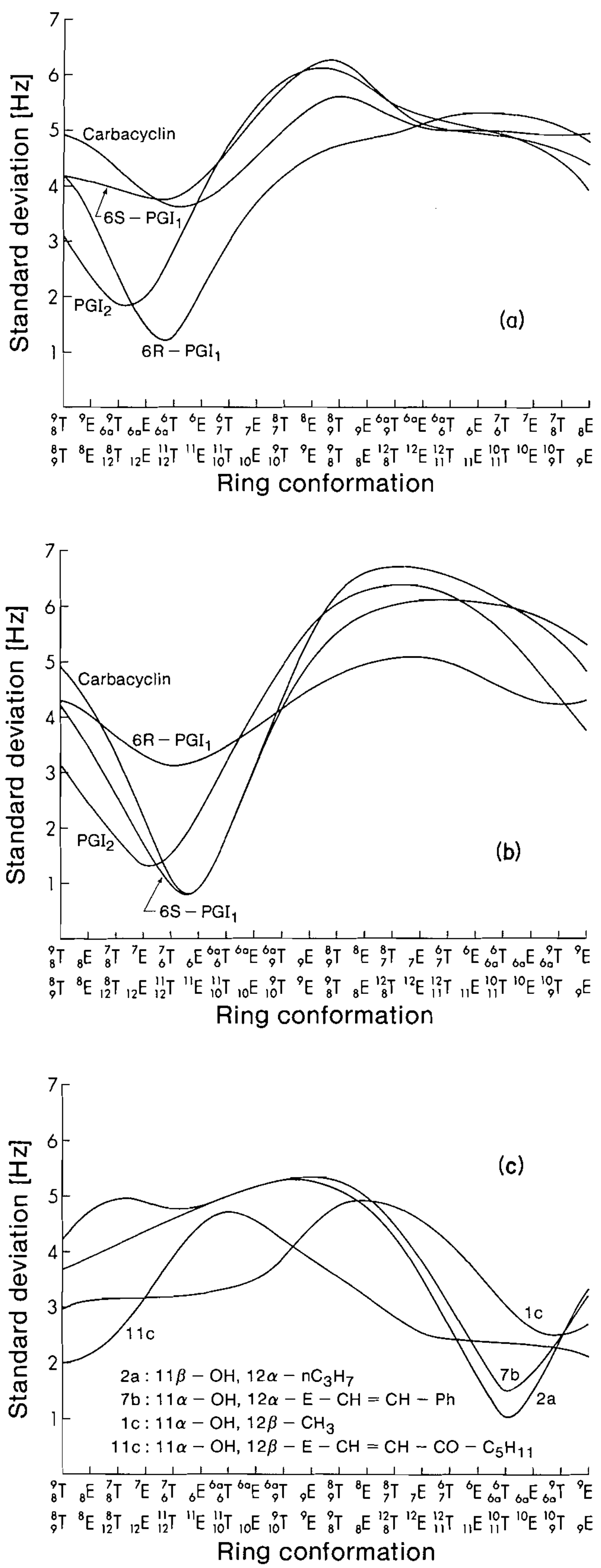

FIG. 1. Plots of standard deviations between calculated and observed vicinal proton coupling constants vs. pseudorotational conformations for PGI$_2$, 6R-PGI$_1$, 6S-PGI, and carbacyclin (1a and 1b), and for 11-hydroxy, 12-alkyloxabicyclo[3.3.0]octan-6-one data taken from ref. 21 (1c).

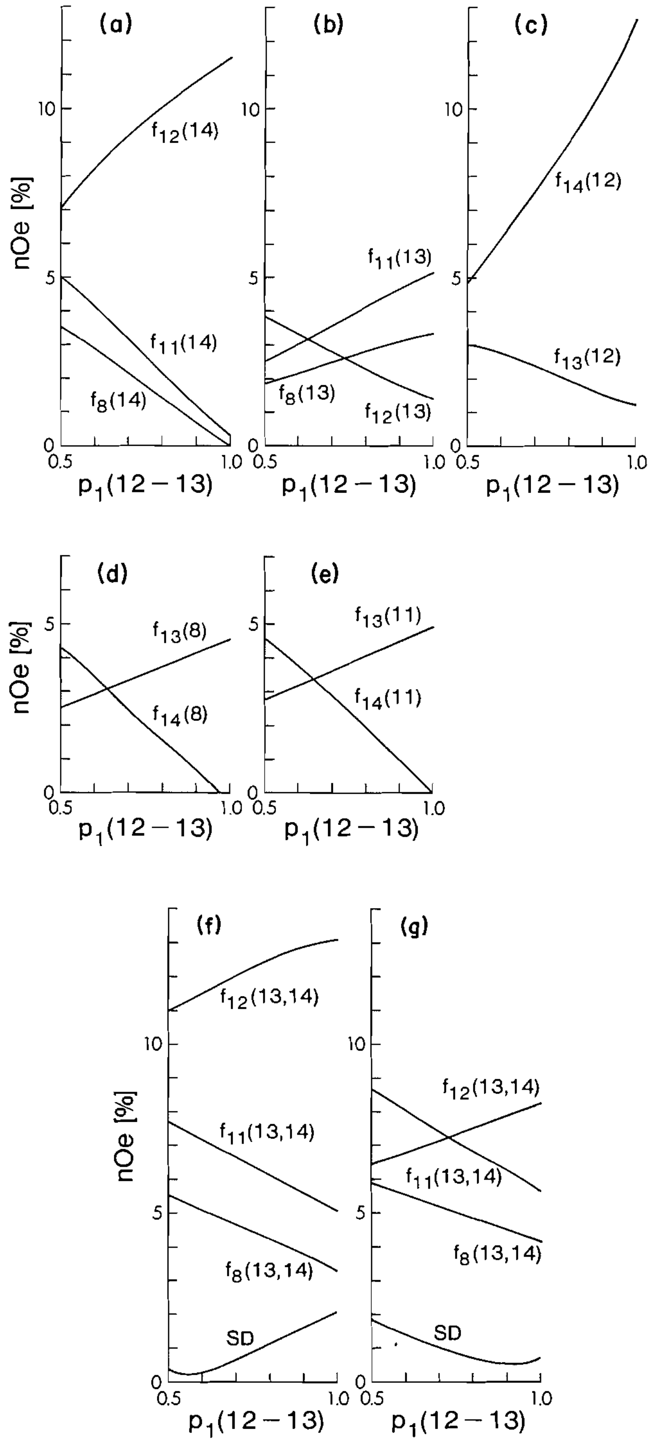

FIG. 2. Plots of calculated nuclear Overhauser effects and standard deviations (SD) between calculated and measured nOe's vs. the population of the principal C_{12}—C_{13} rotamer. Figs. 2a–2f: PGI$_2$; Fig. 2g: 6S-PGI$_1$.

The PGI$_2$ minimum in Fig. 1a is not much shallower than the minimum in Fig. 1b. Only two of the nine coupling constants of PGI$_2$, $J_{7\alpha,8}$ and $J_{7\beta,8}$, depend specifically on the ether ring conformation, and the minima in Figs. 1a and 1b are essentially determined by the cyclopentane ring conformation $_{12}E$. That the ether ring conformation is indeed ^{7}E (minimum in Fig. 1b), and not $_{6a}E$, is readily apparent from the vicinal coupling constants $J_{7\alpha,8}$ and $J_{7\beta,8}$,

	$J_{7\alpha,8}$	$J_{7\beta,8}$
${}_{6a}E/{}_{12}E$	3.9 Hz	11.0 Hz
${}^{7}E/{}_{12}E$	1.2 Hz	5.4 Hz
Exp.	~0	7.6 Hz

from the long range coupling constants $J_{5,7\alpha}$ and $J_{5,7\beta}$,

	$\phi_{5,7\alpha}$	$\phi_{5,7\beta}$	$\lvert J_{5,7\alpha}\rvert$	$\lvert J_{5,7\beta}\rvert$
${}_{6a}E/{}_{12}E$	−88.3°	31.7°	2.6 Hz	0.2 Hz
${}^{7}E/{}_{12}E$	−14.3°	105.7°	1.4 Hz	2.4 Hz
Exp.			0	1.6 Hz

and from the nOe's between H_5, $H_{7\alpha}$, and $H_{7\beta}$.

	$f_5(7\alpha)$	$f_5(7\beta)$	$f_{7\alpha}(5)$	$f_{7\beta}(5)$
${}_{6a}E/{}_{12}E$	0.5%	4.2%	0.2%	1.0%
${}^{7}E/{}_{12}E$	4.9%	0	1.4%	0
Exp.	5.0%	1.8%	3.0%	0

Nuclear Overhauser effects also provide convincing support for the 6S-PGI$_1$ conformation ${}_6E/{}^{11}E$ established on the basis of vicinal coupling constants (Fig. 1b).

	r_{6-12}	$g_6(12)$	$f_6(12)$	$g_{12}(6)$	$f_{12}(6)$	$r_{7\alpha-12}$	$g_{12}(7\alpha)$	$f_{12}(7\alpha)$
${}^{7}_{6}T/{}^{11}_{12}T$	0.202 nm	0.455	11.6%	0.497	12.6%	0.268 nm	0.091	1.9%
${}_6E/{}^{11}E$	0.239 nm	0.199	4.9%	0.241	5.7%	0.243 nm	0.218	5.1%
${}^{6a}_{6}T/{}^{11}_{10}T$	0.293 nm	0.048	0.9%	0.068	1.3%	0.219 nm	0.392	9.9%
Obs.			3.2%		4.0%			4.2%

The H_6—H_{12} and, to a lesser extent, $H_{7\alpha}$—H_{12} distances are undoubtedly overestimated by using *cis*-bicyclo[3.3.0]octane as model. Nevertheless, the assignment seems unambiguous, since r_{6-12} and $r_{7\alpha-12}$ vary significantly and in opposite directions from one conformation to the next on the pseudorotation path.

De Clercq and Samson (21) published coupling constants for a series of synthetic lactone analogues of PGI$_2$, and it seemed worthwhile to look at the effect of replacing C_6=C_5 by C_6=O on the ring conformations. Surprisingly, no clear minimum could be found for the 11α-hydroxy, 12β-alkyl derivatives of oxabicyclo[3.3.0]octan-6-one (Fig. 1c), for which the authors (21) proposed the ${}^{10}_{11}T$ conformation (prostaglandin system). Averages over several contiguous conformations gave similar negative results. Interestingly, reasonably sharp minima at ${}^{6}_{6a}T/{}^{10}_{11}T$ were obtained for the 11α-hydroxy, 12α-alkyl and 11β-hydroxy, 12α-alkyl derivatives (Fig. 1c).

Acyclic C(sp^2)—C(sp^3) bonds like C_4—C_5 in PGI$_2$ or carbacyclin, C_{12}—C_{13} and C_{14}—C_{15} in the ω-chain, are known (see, for instance, ref. 22) to prefer rotational states in which the double bond eclipses a single bond. This is borne out in the crystal structures of prostaglandins (23−27), where the C_{12}—H and C_{15}—H bonds are more or less coplanar with C_{13}=C_{14}. However, the vicinal coupling constants in solution (e.g. $J_{12,13}$ = 8.1 Hz for PGI$_2$) certainly do not agree with an exclusive *trans* orientation, for which eq. [2] estimates a value of 11.6 Hz. Either C_{12}—C_{13} is in a rotational state with an H_{12}—H_{13} angle close to 150°, as suggested by Conover and Fried (17), or other eclipsed rotamers are significantly populated. If $J_{60°}$ = 3.6 Hz, C_{12}—C_{13} rotamers 2 and 3 would have to be occupied about half the time,

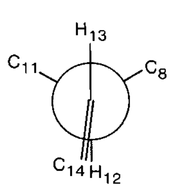

1

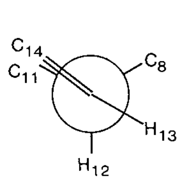

2

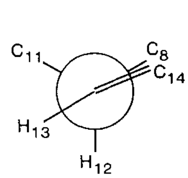

3

$$p_1 \times 11.6 + (1 - p_1) \times 3.6 = 8.1, \qquad p_1 = 0.56$$

although it is difficult to place confidence limits on that value. The nOe technique seemed well suited for estimating C_{12}—C_{13} rotamer populations, since H_8, H_{11}, and H_{12} provide close contacts for H_{13} and especially H_{14} at each stop on the C_{12}—C_{13} rotation path. Consequently the average distances, and therefore the nOe's, change significantly and in opposite directions on varying $p_1(12-13)$ (Figs. 2a−2e). Unfortunately H_{13} and H_{14} form an AB system and only the $f_i(13,14)$ are available, with contradictory results. The nOe's for PGI$_2$ confirm the coupling constant evidence, $p_1(12-13)$ = 0.6 (Fig. 2f), whereas, according to the $f_i(13,14)$ for 6R-PGI$_1$, there is essentially only one conformation, $p_1(12-13)$ = 0.9 (Fig. 2g). The nOe's and T_1's in Tables 2 and 3 were calculated with $p_1(12-13)$ = 0.5, but only a substrate with well-separated H_{13} and H_{14} signals is likely to provide an unambiguous answer.

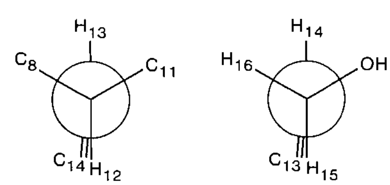

The substitution pattern around C_{14}—C_{15} is similar to C_{12}—C_{13}, except for a replacement of carbon by oxygen. Equation [2] for vinyl−allylic coupling constants does not have a substituent term, but the electronegativity correction term of eq. [1]

$$(1.3 - 0.4)\{0.56 - 2.32\cos^2(-\phi + 17.9 \times (1.3 - 0.4)\}$$
$$= [-1.4(\phi = 180°) - 0.6(\phi = 60°)]/2 = 1.0 \text{ Hz}$$

accounts well for the observed difference $J_{14,15} - J_{12,13}$ = (6.6 − 7.8)Hz in 6S-PGI$_1$; i.e. the rotational behaviour about C_{14}—C_{15} is similar to C_{12}—C_{13}.

C_4 in PGI$_2$ or carbacyclin would be expected to occupy the skew positions, since eclipsing C_4—C_5 with the double bond

TABLE 2. Experimental[a] and calculated ^1H nuclear Overhauser effects (in %) and molecular correlation times τ_C for PGI_2 and 6S-PGI_1

		PGI$_2$[b]					τ_C = 0.24 ns				
s		*d*=5	7α	8	7β	10β	9	11	12	13	14
5	Exp.		3.0		0						
	Calcd.		1.4	0	0						
7α,8	Exp.	5.0					8.5			11.3	
	Calcd.	4.9					8.3			2.5	4.3
7β,10β	Exp.	1.8					9.3	10.3			
	Calcd.	0					11.7	7.7			
9	Exp.		6.7								
	Calcd.		0	6.2							
11	Exp.		2.6		4.3				3.7	6.3	
	Calcd.		0	2.9	0	3.2			1.7	2.7	4.5
13,14	Exp.		5.0					7.5	11.2		
	Calcd.		0	5.5				7.7	11.0		
15	Exp.									10.5	
	Calcd.									4.9	1.7

			6S-PGI$_1$[c]				τ_C = 0.24 ns					
s		*d*=6α	7α	7β	8	10β	9	10α	11	12	13	14
6,15	Exp.		2.8							4.0		
	Calcd.		2.4							5.7		
7α	Exp.	5.3		19.0						4.2		
	Calcd.	3.7		20.4						5.1		
8,10β	Exp.						18.0	21.0	10.8		5.7	
	Calcd.						18.3	18.8	8.8		3.3	4.2
9	Exp.				10.0							
	Calcd.				6.9	3.3						
11	Exp.				5.8						6.0	
	Calcd.				1.5	2.5					2.6	4.5
12	Exp.	3.2	1.5		2.3			3.3			10.3	
	Calcd.	4.9	2.8		1.0	0		1.9			2.9	5.0
13,14	Exp.				4.2				6.0	7.0		
	Calcd.				5.9				8.5	6.4		

[a]Estimated error limits ±1 (%).
[b]Calculations based on the following molecular conformation: rings = $^7E/_{12}E$; $p_1(3-4) = 0.7$; $p_1(4-5) = 0.0$; $p_1(12-13) = p_1(14-15) = 0.5$; $p_1(15-16) = 0.0$.
[c]Calculations based on the following molecular conformation: rings $_6E/^{11}E$; $p_1(3-4) = p_1(4-5) = 0.7$; $p_1(5-6) = 0.0$; $p_1(12-13) = p_1(14-15) = 0.5$; $p_1(15-16) = 0.0$.

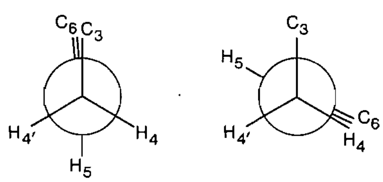

1 2 3

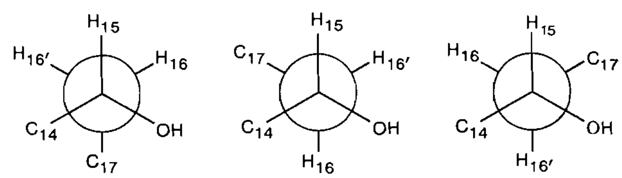

1 2 3

would introduce *syn*-axial δ-interactions with the ester oxygen or 6a-methylene bridge. Indeed, the observed H_4—H_5 coupling constants of 7.2 Hz for PGI_2/D_2O (1) and 6.7 Hz for carbacyclin/$CDCl_3$ (4) agree satisfactorily with 7.6 Hz, the value calculated with $p_2 = p_3 = 0.5$.

The coupling constants between H_{15} and the diastereotopic protons H_{16} and $H_{16'}$ are essentially equal, if not identical. With $J_{15,16}$ = 6.6 Hz (3) (6S-PGI_1/D_2O) the following rotamer populations are obtained.

$$p_1 = 0.13, p_2 = 0.47, p_3 = 0.40$$

The simpler model $p_1 = 0.0$, $p_2 = p_3 = 0.5$ was used in the nOe and T_1 calculations, which reproduces the coupling constants equally well, $J_{15,16}$ = 6.8 Hz, $J_{15,16'}$ = 7.6 Hz. A more detailed analysis on the basis of coupling constants seems unwarranted, and segmental motion as well as signal overlap eliminate nOe's. The situation is similar around C_5—C_6 in the PGI_1 series, where $J_{65} \simeq J_{65'}$ = 6.3 Hz (3). Again $p_2 = p_3$ = 0.5 was used in the calculations.

Finally, *trans* rotamer populations of 70% were assumed for all n-butane segments. For example, $J_{2,3}$ = 7.5 Hz (6S-PGI_1/D_2O) (3) gives $p_1(2-3) = 0.73$, in excellent agreement with the value of 0.72 obtained from the *gauche/trans* butane energy difference of 0.966 kcal/mol (28).

Proton relaxation times and nuclear Overhauser effects de-

TABLE 3. Experimental[a] and calculated nonselective ^{1}H relaxation times (in s) and molecular correlation times τ_c for PGI_2, 6R-PGI_1, and 6S-PGI_1

	PGI_2[b]		6R-PGI_1[c]		6S-PGI_1[b]	
	Obs.	Calcd.	Obs.	Calcd.	Obs.	Calcd.
5	1.28	1.47				
6α					0.70[d]	0.56
6β			0.88[d]	0.81		
7α	0.44[d]	0.39	0.31	0.38	0.31	0.35
7β	0.39[e]	0.39	0.42[e]	0.37		0.38
8	0.63[d]	0.64	0.49	0.63	0.49[e]	0.62
9	1.04	0.87	0.94	0.85	0.94	0.90
10α		0.41		0.43		0.35
10β	0.39[e]	0.34	0.36	0.37	0.36[e]	0.36
11	0.99	0.88	0.88[d]	0.98	0.88	1.06
12		1.14	0.67[e]	0.79	0.67	0.68
13		0.92	1.00[f]	0.97	1.01[f]	0.88
14		0.78	1.00[f]	0.84	1.01[f]	0.93
15	0.96	0.96		1.03	0.94[f]	0.97
τ (ns)		0.09		0.08		0.09

[a]Estimated error limits ±0.05 (s).
[b]Calculations based on the molecular conformation described in Table 2.
[c]Calculations based on the following molecular conformation: rings ${}^{6}_{6}T/{}^{11}_{12}T$; side chains as in 6S-$PGI_1$ (see Table 2).
[d–f]Identically labelled signals partially overlap, reducing the precision of the measured T_1 values.

TABLE 4. ^{13}C nuclear magnetic resonance chemical shifts[a] and relaxation times[b] for PGI_2[c]

	δ	NT_1(s)		δ	NT_1(s)		δ	NT_1(s)
1	184.29	[d]	8	44.98	0.36	15	72.84	0.44
2	37.30	0.94	9	83.98	0.38	16	36.02	0.72
3	26.55	0.72	10	39.93	0.56	17	24.57	0.82
4	24.79	0.64	11	76.41	0.31	18	30.97	1.20
5	97.55	0.32	12	53.61	0.36	19	22.11	1.78
6	154.28	[d]	13	131.64	0.36	20	13.47	[d]
7	32.31	0.44	14	135.31	0.39			

[a]Chemical shifts quoted relative to "internal" TMS. The reference spectrometer frequency was determined by adding the $^{1}HOD - {}^{1}HCCl_3$ frequency difference at 277 K to the $(^{13}CH_3)_4Si/CDCl_3$ spectrometer frequency.
[b]Estimated error limits ±10%.
[c]Experiments carried out on a 0.017 *M* PGI_2 solution in 0.02 *M* glycine buffer of pH 10.3 at 277 K.
[d]T_1 too long for recycle time employed.

rived from this conformational model agree reasonably well with experiment, although some of the conformational details in the side chains remain to be worked out. The C_{12}—C_{13} rotamer problem in particular requires derivatives with well-resolved H_{13} and H_{14} signals. The conformations of the ring systems, on the other hand, are well defined. Not only is there good agreement between calculation and experiment, but alternative conformations could unambiguously be eliminated on the basis of nOe comparisons. Thus, as in the leukotriene series (29, 30), quantitative nuclear Overhauser effects and, to a lesser extent, relaxation time measurements proved useful complements to vicinal coupling constants in the conformational analysis of complex molecules of biological interest.

Acknowledgments

The authors wish to thank Drs. R. A. Johnson, J. E. Pike, and D. R. Morton of Upjohn for providing the samples used in this study, Mr. W. Moffat for expert technical assistance, and the Natural Sciences and Engineering Research Council of Canada, the Alberta Heart Foundation, and the University of Alberta for generous financial support.

1. G. KOTOVYCH, G. H. M. AARTS, T. T. NAKASHIMA, and G. BIGAM. Can. J. Chem. **58**, 974 (1980).
2. G. KOTOVYCH and G. H. M. AARTS. Can. J. Chem. **58**, 2649 (1980).
3. G. KOTOVYCH, G. H. M. AARTS, and T. T. NAKASHIMA. Can. J. Chem. **59**, 1449 (1981).
4. G. KOTOVYCH and G. H. M. AARTS. Org. Magn. Reson. **18**, 77 (1982).
5. J. R. VANE and S. BERGSTRÖM (*Editors*). Prostacyclin. Raven Press, New York. 1979.
6. C. PACE-ASCIAK and R. GRYGLEWSKI. *In* Prostaglandins and related substances. *Edited by* C. Pace-Asciak and E. Granström. Elsevier Science Publ., New York. 1983.
7. R. A. JOHNSON, F. H. LINCOLN, E. G. NIDY, W. P. SCHNEIDER, J. L. THOMPSON, and U. J. AXEN. J. Am. Chem. Soc. **100**, 7690 (1978).
8. C. A. G. HAASNOOT, F. A. A. M. DE LEEUW, and C. ALTONA. Tetrahedron, **36**, 2783 (1980).
9. M. L. HUGGINS. J. Am. Chem. Soc. **75**, 4123 (1953).
10. E. W. GARBISCH. J. Am. Chem. Soc. **86**, 5561 (1964).
11. J. H. NOGGLE and R. E. SCHIRMER. The nuclear Overhauser effect. Academic Press, New York. 1971.
12. R. E. SCHIRMER, J. P. DAVIS, J. H. NOGGLE, and P. A. HART. J. Am. Chem. Soc. **94**, 2561 (1972).
13. C. ALTONA, H. J. GEISE, and C. ROMERS. Tetrahedron, **24**, 13 (1968).
14. J. B. HENDRICKSON. J. Am. Chem. Soc. **83**, 4537 (1961).
15. K. S. PITZER and W. E. DONATH. J. Am. Chem. Soc. **81**, 3213 (1959).
16. H. BEIERBECK and J. K. SAUNDERS. Can. J. Chem. **58**, 1258 (1980).
17. W. W. CONOVER and J. FRIED. Proc. Natl. Acad. Sci. U.S.A. **71**, 2157 (1974).
18. C. CHACHATY, Z. WOLKOWSKI, F. PIRIOU, and G. LUKACS. J. Chem. Soc. Chem. Commun. 951, (1973).
19. R. GRANGER, L. BARDET, C. SABLAYROLLES, and J. P. GIRARD. C.R. Acad. Sci. Ser. C, **270**, 1326 (1970).
20. N. L. ALLINGER, M. T. TRIBBLE, M. A. MILLER, and D. H. WERTZ. J. Am. Chem. Soc. **93**, 1637 (1971).
21. P. DE. CLERCQ and M. G. SAMSON. Org. Magn. Reson. **11**, 262 (1978).
22. D. A. C. COMPTON, S. C. HSI, H. H. MANTSCH, and W. F. MURPHY. J. Raman. Spectrosc. **13**, 30 (1982), and references therein.
23. S. ABRAHAMSSON. Acta Crystallogr. **16**, 409 (1963).
24. J. W. EDMONDS and W. L. DUAX. Prostaglandins, **5**, 275 (1974).
25. J. W. EDMONDS and W. L. DUAX. J. Am. Chem. Soc. **97**, 413 (1975).
26. D. A. LANGS, M. G. ERMAN, and G. T. DETITTA. Science, **197**, 1003 (1977).
27. S. FORTIER, M. G. ERMAN, D. A. LANGS, and G. T. DETITTA. Acta Crystallogr. Sec. B, **36**, 1099 (1980).
28. A. L. VERMA, W. F. MURPHY, and H. BERNSTEIN. J. Chem. Phys. **60**, 1540 (1974).
29. M. SUGIURA, H. BEIERBECK, P. C. BÉLANGER, and G. KOTOVYCH. J. Am. Chem. Soc. **106**, 4021 (1984).
30. M. SUGIURA, H. BEIERBECK, P. C. BÉLANGER, and G. KOTOVYCH. Can. J. Chem. **62**, 1640 (1984).

Substituent effects on benzyl radical hyperfine coupling (hfc) constants. Part 3. Comparison of the α-hfc for substituted benzyl radicals with the β-hfc for substituted cumyl radicals

DONALD R. ARNOLD,[1] A. MARTIN DE P. NICHOLAS, AND MILES S. SNOW
Department of Chemistry, Dalhousie University, Halifax, N.S., Canada B3H 4J3

Received August 16, 1984

DONALD R. ARNOLD, A. MARTIN DE P. NICHOLAS, and MILES S. SNOW. Can. J. Chem. **63**, 1150 (1985).

The electron spin resonance (esr) spectra of eighteen *para*-substituted cumyl radicals were analyzed. The relationship between the β-hyperfine coupling (β-hfc) constants of these cumyl radicals and the corresponding α-hfc constants of benzyl radicals was studied. Although there is a general trend for the α- and β-hfc values to vary in a similar manner, specific deviations from a linear correlation between these parameters were observed. These deviations were rationalized by considering charge effects on spin delocalization. The correlation coefficient for the linear regression analysis of these α- and β-hfc values was found to significantly improve when parameters reflecting charge effects on spin delocalization were included in an extended Hammett treatment of the spectral data.

DONALD R. ARNOLD, A. MARTIN DE P. NICHOLAS et MILES S. SNOW. Can. J. Chem. **63**, 1150 (1985).

On a analysé les spectres de résonance paramagnétique électronique (rpe) de dix-huit radicaux cumyles substitués en position *para*. On a étudié la relation existant entre la constante de couplage hyperfin-β (chf-β) de ces radicaux cumyles et les constantes chf-α correspondantes des radicaux benzyles. Les valeurs des chf-α et chf-β tendent généralement à varier de la même façon: cependant on observe des déviations spécifiques par rapport à la corrélation linéaire entre ces paramètres. On rationalise ces écarts en considérant les effets de la charge sur la délocalisation du spin. On a trouvé, que pour ces valeurs de chf-α et chf-β, le coefficient de corrélation de l'analyse de répression linéaire est amélioré d'une façon significative lorsque les paramètres qui reflètent les effets de la charge sur la délocalisation de spin sout inclus dans un traitement de Hammett élargi des données spectrales.

[Traduit par le journal]

Introduction

The study of substituent effects on radical reactivity and stability is a topic of great interest. Several linear free-energy ($\sigma^{\cdot}$) scales based upon relative reactivity have been proposed (1, 2). Most of these scales have failed to unambiguously separate radical and polar effects. We have suggested that the $\sigma^{\cdot}_{\alpha}$ scale, based upon electron spin resonance (esr) α-hyperfine coupling constants (α-hfc), is a true reflection of the nature of the radical and is therefore free from complications caused by steric and polar effects inherent at a transition state (1). The validity and utility of the $\sigma^{\cdot}_{\alpha}$ scale was demonstrated by the satisfactory correlation obtained between $\sigma^{\cdot}_{\alpha}$ and the logarithm of the rate constant for the thermal isomerization of a series of 2-aryl-3,3-dimethylmethylenecyclopropanes studied by Creary (1, 3).

In Part 1 of this series (1), we defined $\sigma^{\cdot}_{\alpha}$, for a substituent x, from the benzylic α-hydrogen hyperfine coupling constant (α-hfc$_x$):

$$[1] \quad (\sigma^{\cdot}_{\alpha})_x = 1 - [(\alpha\text{-hfc}_x)/(\alpha\text{-hfc}_H)]$$

We believe that these $\sigma^{\cdot}_{\alpha}$ values represent the substituent effect on the component of energy that may be attributed to spin delocalization in these benzyl radicals. The $\sigma^{\cdot}_{\alpha}$ scale offers major advantages over other $\sigma^{\cdot}$ scales, because the substituent effects are attributable only to effects on the radical and not on any closed shell species. We have shown that the effects of charge on the stability of even relatively non-polar species, like hydrocarbons and hydrocarbon radicals, are not negligible (4). Consequently, the other $\sigma^{\cdot}$ scales, which have ignored effects on neutral closed shell species, cannot be used as an indication of radical stability.

In Part 2 of this series we extended the $\sigma^{\cdot}_{\alpha}$ scale to over thirty substituents. We also described in detail the mode of action of sulphur-containing substituents on benzyl radical delocalization. Several *para*-substituted benzyl radicals of the general form $R(O_n)SC_6H_4CH_2$. (n = 0, 1, 2; R = Me, Ph, Tol, COMe, OMe) were studied (2).

In this work[2] we extend our study of substituent effects on benzyl radical hfc values to the α,α-dimethylbenzyl (cumyl) system. This study is significant, because it enables the comparison of the substituent effects on the α-and β-hfc values of two closely related series of radicals. Since both α- and β-hfc values depend primarily on spin density they will correlate, if the major effect of substituents is on spin delocalization. Moreover, if such a correlation exists between these two parameters it will add considerable strength to the argument that the $\sigma^{\cdot}_{\alpha}$ scale is primarily a measure of spin density. It will give confidence to the $\sigma^{\cdot}_{\alpha}$ values that have already been established. In addition, if the substituent effect on both α- and β-hfc is in general the same, specific deviations from a linear correlation between these two parameters may provide valuable information about the factors which influence spin density and hence stabilization of a radical by spin delocalization. This understanding is required for the general application of $\sigma^{\cdot}_{\alpha}$ to benzylic radicals other then benzyl itself.

While the overall change in α-hfc values is large (>10%), the small effects (<0.03 G) caused by some substituents cannot be readily distinguished. It would therefore be useful to have a scale with a larger variation in hfc constants as a function of substitution. Studies of carbon based radicals containing hydrogens both α and β to the radical centre show that β-hfc values are frequently greater than the corresponding α-hfc values (5, 6). Consequently, we may find that the cumyl series, where

[1]Author to whom correspondence should be addressed.

[2]Presented in part at the 67th Annual Chemical Institute of Canada Conference, Montreal, Quebec, June 3–6, 1984; Abstract no: OR-2-7.

TABLE 1. Hyperfine coupling constants for *para*-substituted cumyl radicals[a]

Substituent	a_β [b]	a_o [b]	a_m [b]	a_x [b]
1. COMe	15.07	4.55	1.55	<0.50[c]
2. COPh	15.07	4.52	1.53	—
3. CN	15.37	4.60[d]	1.60[d]	0.80[d,e]
4. COOMe	15.40	4.57	1.55	<0.35[c]
5. SPh	15.60	4.72	1.65	—
6. $S(O)_2Ph$	15.76	4.61	1.55	—
7. Cl	16.03	4.85	1.65	0.36,[f] 0.30[g]
8. OCH_3	16.10	4.75[d]	1.50[d]	0.60[c,d]
9. OPh	16.10	4.82	1.62	—
10. CH_3	16.10	4.70[d]	1.60[d]	5.8[c,d]
11. Et	16.13	4.60[d]	1.60[d]	2.90[d,h]
12. CF_3	16.15	4.70	1.58	8.40[i]
13. i-Pr	16.17	4.75	1.55	2.35[j]
14. *t*-Bu	16.17	4.75	1.55	—
15. OCOPh	16.24	4.83	1.65	—
16. H	16.28	4.70	1.65	5.55
17. OCOMe	16.30	4.85	1.65	—
18. F	16.35	4.75	1.55	12.65[k]

[a]All values are in G. Unless indicated otherwise the uncertainty is ±0.03 G.
[b]Subscript indicates position.
[c]Hydrogens of methyl.
[d]Uncertainty is ±0.06 G.
[e]Nitrogen of CN.
[f]^{35}Cl.
[g]^{37}Cl.
[h]α-Hydrogens of ethyl.
[i]Fluorine of CF_3.
[j]α-Hydrogen of isopropyl.
[k]^{19}F.

TABLE 2. The effect of *para*-substituents (X) on α- and β-hyperfine coupling constants of benzylic radicals[a]

X	a_β [b]	a_α [c]	a_β/a_α
COMe	15.07	15.28	0.986
COPh	15.07	15.35	0.982
CN	15.37	15.60	0.985
COOMe	15.40	15.55	0.990
SPh	15.60	15.30[d]	1.020
$S(O)_2Ph$	15.76	15.95[d]	0.988
Cl	16.03	16.07	0.998
OCH_3	16.10	15.95	1.009
OPh	16.10	15.95[d]	1.009
CH_3	16.10	16.00	1.006
Et	16.13	16.05[d]	1.005
CF_3	16.15	16.39	0.985
i-Pr	16.17	16.10[d]	1.004
t-Bu	16.17	16.12	1.003
OCOPh	16.24	16.25[d]	0.999
H	16.28	16.25	1.002
OCOMe	16.30	16.33	0.998
F	16.35	16.42	0.996

[a]All values are in G. The uncertainty is ±0.03 G.
[b]β-hfc values of cumyl radicals from Table 1.
[c]α-hfc values of benzyl radicals, unless stated otherwise, from ref. 1.
[d]Reference 2.

β-hfc values are being measured, will be more sensitive to changes in spin density. On the other hand, the significant decrease in the delocalization of spin into the ring, caused by the two α-methyl groups, will attenuate the substituent effect. The relative importance of these two opposing factors cannot be predicted a priori.

Results

The cumyl radicals were generated photochemically in the microwave cavity of the esr spectrometer, either by hydrogen atom abstraction from the corresponding cumene or by bromine atom abstraction from the appropriate cumyl bromide. The esr spectra were recorded with the aid of a signal averager and the hfc values were determined by computer simulation of the spectra.

The data (Table 1) represent a consistent series, produced under similar conditions. Typically, the best signal-to-noise ratio was obtained at the lowest temperature possible, above the freezing point of the solution. But most of the spectra were recorded at 253 K to maintain a consistency in the conditions. The esr spectra of two of these radicals have been reported previously (5); the agreement between our values and those reported is good. In several cases, the effect of variation of the spectra as a function of temperature was studied; the β-hfc was found to be independent of temperature over the range 213 to 333 K. Details are reported in the experimental section.

Discussion

In general, α-hfc is believed to arise primarily from a spin-polarization mechanism, while β-hfc results mostly from a hyperconjugative type of interaction (6–9). Thus, α- and β-hfc interactions need not show the same sensitivity to substituent effects. In fact, it has been shown that α- and β-hfc in hydrocarbon radicals are affected differently by such factors as deviation from planarity (i.e., the state of hybridization of the radical centre (6*b*)). β-Hfc values are also known to be very dependent on torsional angle, so conformation of the singly occupied orbital relative to the β-carbon–hydrogen bond is important (7).

Within a closely related series of substituted benzyl or cumyl radicals, factors other than spin density that could influence hfc should remain constant. In addition, the esr spectra of all the cumyl radicals studied showed a single hfc value for all the hydrogens of the α-methyl groups. This indicates that all of the methyl hydrogens are equilibrated, throughout the temperature range (213 to 333 K) used in this work. Thus, the methyl groups must be rapidly rotating so that torsional effects are averaged. Consequently, substituent effects on β-hfc values of the cumyl radical series can also be expected to be related primarily to spin delocalization.

In Table 2 the benzylic α-hfc constants of *para*-substituted benzyl radicals are compared with the β-hfc constants of the corresponding cumyl radicals. If both of these hfc values correlate, a constant ratio, α-hfc/β-hfc, is expected. Table 2 shows that for most substituents this ratio is close to the value for the unsubstituted radicals (α-hfc/β-hfc = 1.002). Thus there is a general trend for the β-hfc values in cumyl radicals to vary in a similar manner to that of the α-hfc values in benzyl radicals. However, Table 3 and Fig. 1 clearly show that significant deviations from a linear correlation between the α- and β-hfc values, much larger than the experimental error of ±0.03 G, are observed for some substituents. Because of these specific deviations, the correlation between the two types of hfc values is far from satisfactory (r = 0.92, 18 data points, see Fig. 1 and Table 3). In the plot shown in Fig. 1 the substituents that lie below (above) the least-squares regression line have a relatively lower (higher) ratio of α-hfc/β-hfc and hence show an unexpectedly large (small) effect in the cumyl series with

TABLE 3. A linear regression analysis of charge effects on the relationship between the benzylic β-hfc values of cumyl radicals (a_β) and the benzylic α-hfc values of the benzyl radicals (a_α)[a,b]

Regression equation[c]	r[d]
$a_\beta = (1.06\pm0.23)a_\alpha-(0.9\pm3.7)$	0.92
$a_\beta = (0.92\pm0.13)a_\alpha-(0.45\pm0.15)\sigma_p+(1.3\pm2.1)$	0.98
$a_\beta = (0.88\pm0.24)a_\alpha-(0.41\pm0.33)(\lvert a_o\rvert+\lvert a_m\rvert)-(3.3\pm3.7)$	0.94

[a]Hyperfine coupling values (hfc) from Tables 1 and 2. σ_p values from refs. 12 and 13.
[b]Number of data points is eighteen.
[c]The uncertainty indicated in the coefficients is the standard error at the 95% confidence level.
[d]Correlation coefficient. Corrected for degrees of freedom.

respect to the benzyl series. Figure 1 also shows that all electron-withdrawing (donating) groups cause a larger (smaller) spin delocalizing effect on the β-hfc in the cumyl than the α-hfc of the benzyl radical system.

Charge effects on spin delocalization have been discussed in terms of merostabilization (10) or capto-dative stabilization (11). Figure 2 shows how the electron-withdrawing nature of a *para*-substituent can affect spin delocalization.[3] These charge separated valence-bond structures show that α-substituents that can stabilize an incipient positive charge on the benzylic carbon will enhance spin delocalization by electron-withdrawing groups at the *para*-position. Therefore, the cumyl system, with two α-methyl substituents that stabilize a positive charge better than the α-hydrogens in the benzyl radicals, should be more sensitive than the corresponding benzyl system to charge effects. Hence, the deviations observed in Fig. 1 can be a result of a greater contribution of charge separated valence-bond structures, such as Figs. 2 (b) and (c), in the cumyl than in the benzyl radicals.

The specific deviation of each point from the correlation line shown in Fig. 1 is plotted against the Hammett substituent constant σ in Fig. 3. This parameter was chosen because a consistent set of values was available (12, 13).[4]

The sign of the slope of the line in Fig. 3 reflects the fact that electron-withdrawing groups generally have a greater influence increasing spin delocalization in the cumyl series relative to the benzyl series. This is consistent with a greater contribution of the charge separated valence-bond structures (Figs. 2 (b) and (c)) in the cumyl series.

We have defined the substituent effect on spin delocalization ($\sigma^{\bullet}_\alpha$) based upon the α-hfc of the benzyl radical. Of course, there must be *some* inherent charge effect on this system as well. A quantitative indication of the increased importance of charge effects on the cumyl radical series, relative to the benzyl series, can be obtained by plotting the β-hfc values against the two parameters α-hfc and σ (Fig. 4).[4]

The ρ_α value reflects the balance between the inherently larger β-hfc and the diminished delocalization into the ring, since considerable spin is distributed among the α-methyl groups.

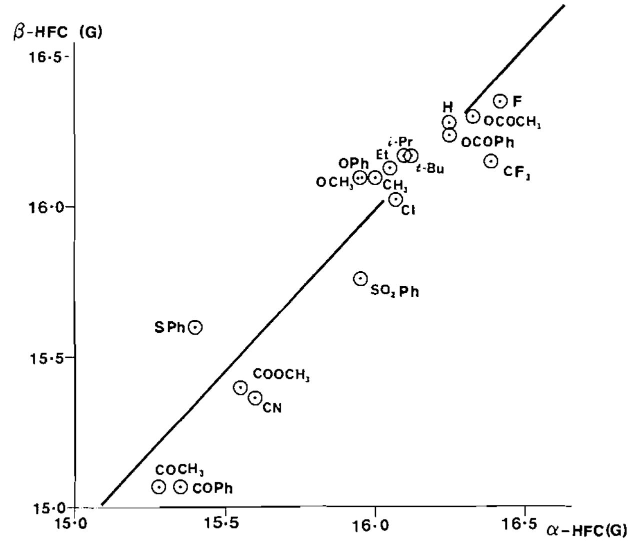

FIG. 1. A linear regression analysis of the relationship between β-hfc of cumyl radicals (a_β) and the benzylic α-hfc of benzyl radicals (a_α). $(a_\beta) = 1.06(a_\alpha) - 0.93$ ($r = 0.92$, 18 data points)

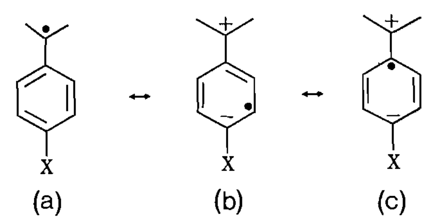

FIG. 2. Charge effects on spin delocalization in benzylic radicals.

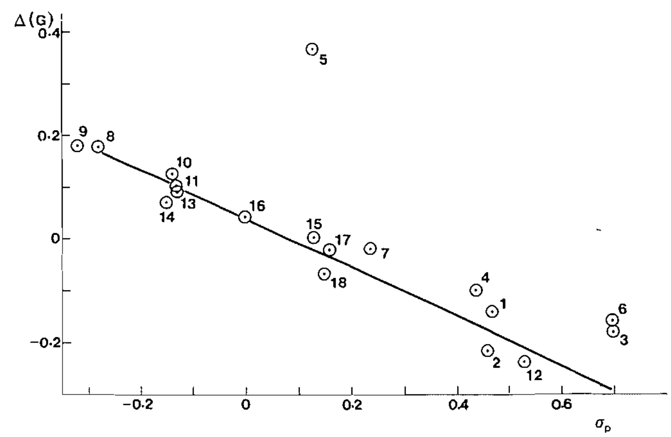

FIG. 3. A plot of Δ ($\Delta = a_\beta - 1.06(a_\alpha) + 0.93$), versus the Hammett substituent constant σ_p. Points are numbered according to Table 1.

The magnitude of ρ_σ indicates the increased importance of spin delocalization away from the benzylic position through a greater contribution of the valence-bond structures Figs 2(b) and (c), in the cumyl series relative to the benzyl series. The importance of charge effects on the relationship between the benzylic hfc values is now clear. Therefore it will be useful to determine if there are any other manifestations of charge effects on spin delocalization in the esr spectra of the cumyl radicals.

The valence-bond structures (b) and (c) in Fig. 2 clearly show that spin delocalization induced by charge effects will

[3]Effects resulting from the development of a negative charge on the benzylic carbon have been ignored in the absence of electron-withdrawing α-substituents. However, such effects, if present, will be opposite to the charge effects described in Figs. 2 (b) and (c).

[4]The correlation coefficient for the least-squares line in Fig. 3 is $r = 0.79$. σ^- Values are not available for all the substituents. For the data plotted in Fig. 4, the correlation coefficient is $r = 0.98$.

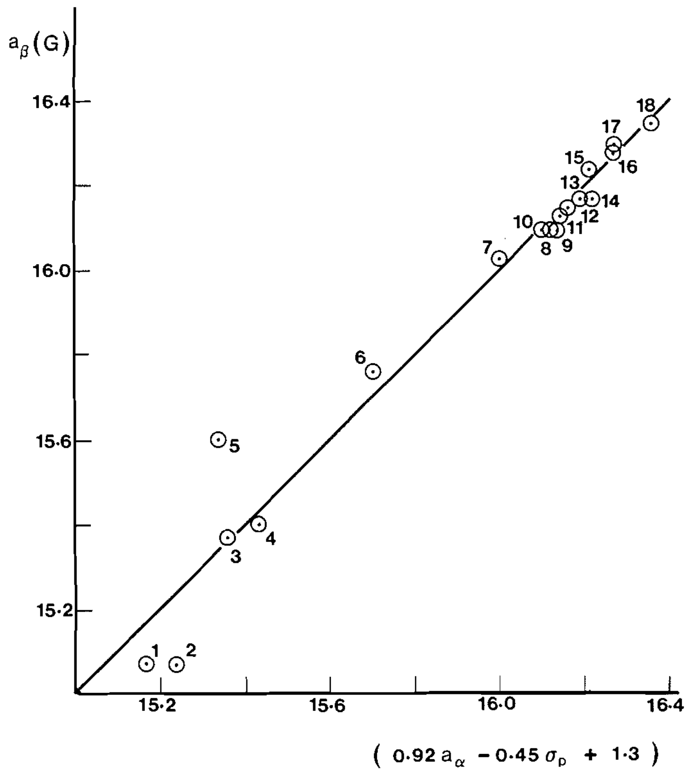

FIG. 4. Two-parameter Hammett correlation. A plot of β-hfc values of cumyl radicals (a_β) vs. (0.92 a_α(benzyl) − 0.45 σ_p + 1.3). Points are numbered according to Table 1.

cause an increase in α-spin[5] at the *meta*- and *ipso*-positions (14). This will result in a concomitant decrease in α-spin at the benzylic position. Moreover, such changes in spin distribution will decrease the absolute value of the hfc at the *ortho* and *meta* ring positions. In fact, all substituents displaying enhanced delocalizing effects in the cumyl system do have relatively lower $|a_o|$ and $|a_m|$ values. Moreover, the hypothesis that the variation in the $|a_o|$ and $|a_m|$ values are a manifestation of charge effects can be tested by the multiple linear regression analysis of α- and β-hfc values (denoted a_α and a_β respectively in Table 2), with the inclusion of an additional parameter, namely, the sum of the absolute values of the *ortho*- and *meta*-hyperfine coupling constants (i.e. $2(|a_o| + |a_m|)$).

This is admittedly a semi-quantitative approach to correct for charge effects on spin delocalization. However, the improvement in the correlation coefficient (r), corrected for the degrees of freedom (r = 0.92 becomes r = 0.94), suggests that this is a valid analysis (Table 3). Consequently, $2(|a_o| + |a_m|)$ may prove to be a useful parameter for describing the charge-related effects on spin delocalization.

The hypothesis that the α- and β-hfc values of benzylic radicals have the same functional dependence on spin density can be tested directly (free from charge effects) only if the relevant α- and β-hydrogens are on the same radical, such as the phenethyl radical system. Preliminary studies of this system indicate that the α- and β-hfc values do show the same functional dependence on spin density.[6] The complete study of this series is now underway.

[5]By convention, a radical is assumed to have excess α-spin.

[6]D. R. Arnold, A. M. de P. Nicholas, and K. M. Young. Unpublished results.

Conclusion

The present study shows that there is a general trend: β-hfc values of cumyl radicals vary in a similar manner to the α-hfc values of benzyl radicals. However, specific deviations are observed from a linear correlation between these α- and β-hfc values. These deviations are rationalized by considering charge effects on spin delocalization. Electron-withdrawing (donating) substituents show a greater (smaller) delocalizing effect in the cumyl radicals relative to the benzyl radicals.

Charge effects on spin delocalization should be general, and should depend upon the electron-withdrawing and donating ability of the groups attached to the radical centre (11).

We have shown that the variations in the hfc values at the *ortho* and *meta* positions reflect the changes in the spin delocalizing efficiency of a substituent in the cumyl radicals relative to the corresponding benzyl system.

Since the extent of spin delocalization of a radical is inherently dependent upon charge effects, it will be difficult to assess the relative importance of radical stabilizing effects and polar factors from studies of relative reactivity.

Experimental

General information

The esr spectra were recorded on a Varian Associates E-109 B electron paramagnetic resonance spectrometer, equipped with a liquid nitrogen variable temperature accessory, at 0.5-mW microwave power and 0.5−0.8 G modulation amplitude. All spectra were recorded with the aid of a Nicolet 1170 signal averager. Typically, twelve, 100-G wide, scans were accumulated (0.5 min/scan). Coupling constants were measured directly from the oscilloscope and refined by computer simulation (15) using an IBM-PC.

The ^{1}Hmr spectra were recorded on a Varian CFT-20 spectrometer or a Nicolet Model 360 NB spectrometer, coupled to an Oxford Instruments superconducting magnet and a Nicolet 192 Kword data acquisition system, and are reported in parts per million downfield from TMS. Infrared spectra were recorded on either an air-purged Perkin−Elmer 180 grating infrared spectrometer, a Pye Unicam SP1000, or a Perkin−Elmer 283B or 237B infrared spectrometer and are reported in wavenumbers (relative to the 1601.8 cm^{-1} absorption of polystyrene). Mass spectra were obtained on a modified Du Pont CEC Model 21-104 mass spectrometer. Melting points, recorded on a Sybron Corporation Thermodyne hotstage apparatus, are corrected.

Substituted cumenes (liquids) were purified by gas chromatography using a 5 ft × 3/8 in. column packed with 5% SE-30 on Chromosorb-W (60/80) and helium as the carrier gas.

Materials

Di-*tert*-butyl peroxide (DTBP) and triethylsilane were obtained from Pfaltz and Bauer Inc. and were used without further purification. Hexamethylditin and hexabutylditin were obtained from Alpha Products and used without further purification. Chlorobenzene (J. T. Baker Chemicals Inc.) was stirred over concentrated sulphuric acid, washed successively with water, saturated sodium bicarbonate, and water, dried over anhydrous magnesium sulphate, and distilled through a Vigreux column. All solvents were distilled prior to use.

Synthesis

4-Isopropyldiphenyl ether

4-Isopropyldiphenyl ether was prepared by refluxing a mixture of 4-isopropylphenol, bromobenzene, cuprous oxide, and γ-collidine (2, 16). The yield of 4-isopropyldiphenyl ether was 87% as a colourless oil; ir PE 180 (neat) cm^{-1}: 1600, 1500, 1250, 875, 760; ^{1}Hmr (80 MHz, $CDCl_3$) δ: 7.34−6.87(m, 9H), 2.90(m, 1H), 1.24(d, 6H).

4-Isopropylacetophenone

4-Isopropylacetophenone was prepared by the reaction of cumene and acetyl chloride in the presence of aluminum chloride, using carbon disulphide as the solvent. The reaction mixture was purified by vacuum distillation. 4-Isopropylacetophenone was obtained as a colourless oil (17); ir SP1000 (neat) cm^{-1}: 1680, 1610, 830; ^{1}Hmr (361.1 MHz, $CDCl_3$) δ: 7.90(m,2H), 7.31(m,2H), 2.97(m,1H), 2.59(s,3H), 1.27(d,6H).

4-Isopropylbenzophenone

4-Isopropylbenzophenone was prepared by a procedure similar to that used for the acetophenone except using benzoyl chloride. Vacuum distillation afforded 4-isopropylbenzophenone as a colourless oil (18); ir SP1000 (neat) cm^{-1}: 1660, 1610, 850, 700; ^{1}Hmr (361.1 MHz, $CDCl_3$) δ: 7.32–7.81(m,9H), 2.99(m,1H), 1.29(d,6H).

4-Isopropyldiphenyl sulphone

4-Isopropyldiphenyl sulphone was prepared in essentially quantitative yield by the addition of 4-isopropylsulphonyl chloride to a solution of benzene and aluminum chloride (2). The sulphonyl chloride was prepared in 94% yield by the addition of chlorosulphonic acid to cumene at 0°C (19). Recrystallization of the crude product from alcohol, with added Norite, produced colourless needles, mp 101–101.5°C (lit. (30) mp. 98.5–99.5°C); ir PE 180 (KBr) cm^{-1}: 1610, 1325, 1170, 840, 760, 690, 650; ^{1}Hmr (80 MHz, $CDCl_3$) δ: 7.81–8.00(m,4H), 7.28–7.53(m,5H), 2.94(m,1H), 1.22(d,6H).

4-Isopropyldiphenyl sulphide

4-Isopropyldiphenyl sulphone, 2.0 g (7.7 mmol), was placed in a 50-mL round bottom flask equipped with a reflux condenser and septum inlet. The flask was purged with dry nitrogen and 5.5 g of diisobutylaluminum hydride (DIBAL-H) (38.7 mmol) in toluene (20 mL) was added through the septum via a syringe. The solution was refluxed under a nitrogen atmosphere until the reaction was complete (3–4 days). The reaction mixture was poured into aqueous ammonium chloride and extracted with ether. The combined organic layers were washed with a saturated salt solution, dried with magnesium sulphate, and evaporated (20). The residue was chromatographed on a silica gel column using methylene chloride as the eluent. The yield of the purified product was 1.57 g (90%); ir PE 180 (neat) cm^{-1}: 2980, 1595, 1490, 1450, 1395, 1375, 830, 745, 695; ^{1}Hmr (361.1 MHz, $CDCl_3$) δ: 7.16–7.32(m,9H), 2.88(m,1H), 1.24(d,6H).

Methyl 4-isopropylbenzoate

In a 250-mL 3-necked flask equipped with a magnetic stirrer, reflux condenser, and a constant pressure dropping funnel was placed 12.2 g (91 mmol) of aluminum chloride. To the aluminum chloride was added 10.0 g (83 mmol) of cumene dissolved in 175 mL of carbon disulphide. The flask was cooled in an ice bath; to the cooled mixture was added a solution of 11.6 g (91 mmol) of oxalyl chloride in 25 mL of carbon disulphide. After the evolution of gases (**caution: carbon monoxide!**) had ceased, the mixture was allowed to warm to room temperature. The mixture was then refluxed for 1.5 h and the cooled mixture was poured into 200 mL of methanol. The carbon disulphide was removed by distillation and the residue was poured into water and extracted with ether. The combined organic layers were washed with 5% sodium hydroxide, saturated salt solution, dried with magnesium sulphate, and evaporated. The yield of a pale yellow oil was 11.3 g (76%). The product was distilled under vacuum to yield a colourless oil (21); ir PE 283B (neat) cm^{-1}: 1735, 1620, 1285, 1120; ^{1}Hmr (80 MHz, $CDCl_3$) δ: 7.91–8.01(m,2H), 7.22–7.32(m,2H), 3.89(s,3H), 2.95(m,1H), 1.25(d,6H).

4-Fluorocumyl alcohol

4-Fluorocumyl alcohol was prepared by the reaction of ethyl 4-fluorobenzoate with methyl magnesium iodide, mp 36–37°C uncorrected (lit. (22) mp 37.8°C); ir 283B (neat) cm^{-1}: 3400, 1605, 1510, 1235, 1160, 835; ^{1}Hmr (80 MHz, $CDCl_3$) δ: 6.99–7.53(m,4H), 1.89(s,1H), 1.56(s,6H).

4-Trifluoromethylcumene

Method a: 4-trifluoromethylcumene was prepared by catalytic hydrogenation of 4-trifluoromethyl-α-methylstyrene using palladium-on-carbon (49% overall yield from the cumyl alcohol). The styrene was prepared by the acid catalyzed dehydration of 4-trifluoromethylcumyl alcohol (23, 24) using 4-tolunenesulphonic acid in refluxing benzene.

Method b: 4-trifluoromethylcumene was prepared by the reduction of 4-trifluoromethylcumyl alcohol using hydriodic acid and red phosphorus (refluxing overnight) (24). The yield was 58%; ir 283B (neat) cm^{-1}: 1625, 1335, 1175, 1135, 1080, 1020, 845; ^{1}Hmr (80 MHz, $CDCl_3$) δ: 7.18–7.59(m,4H), 2.96(m,1H), 1.25(d,6H).

4-Methylcumyl alcohol

4-Methylcumyl alcohol (22, 25) was prepared by the reaction of methyl 4-toluate with methyl magnesium iodide; ir 283B (neat) cm^{-1}: 3420, 1520, 1370, 960, 820; ^{1}Hmr (361.1 MHz, $CDCl_3$) δ: 7.37(m,2H), 7.15(m,2H), 2.34(s,3H), 1.79(s,1H), 1.57(s,6H).

4-Chlorocumene

4-Chlorocumene was prepared by a Sandmeyer reaction using the diazonium salt from 4-isopropylaniline and cuprous chloride (26); ir 283B (neat) cm^{-1}: 1500, 1100, 1020, 830; ^{1}Hmr (80 MHz, $CDCl_3$) δ: 7.06–7.32(m,4H), 2.87(m,1H), 1.21(d,6H); ms *m/e* (rel. intensity): 154(M^+,30), 139(100).

4-Isopropylphenyl benzoate

4-Isopropylphenyl benzoate was prepared by the reaction between 4-isopropylphenol and benzoyl chloride in 3 *M* aqueous sodium hydroxide (27); mp 75°C (lit. (28) mp 72–74°C); ir 283B cm^{-1}: 1735, 1200, 1055, 880, 720; ^{1}Hmr (361.1 MHz, $CDCl_3$) δ: 8.20(m,2H), 7.11–7.62(m,7H), 2.94(m,1H), 1.27(d,6H).

4-Isopropylphenyl acetate

4-Isopropylphenyl acetate (29) was prepared by a procedure similar to that used for the benzoate; ir 283B (neat) cm^{-1}: 1780, 1510, 1375, 1225, 1205, 1020, 915, 850; ^{1}Hmr (80 MHz, $CDCl_3$) δ: 6.92–7.28(m,4H), 2.90(m,1H), 2.27(s,3H), 1.23(d,6H).

4-Ethylcumyl alcohol

4-Ethylcumyl alcohol was prepared by the addition of 4-ethylacetophenone to methyl magnesium iodide (22); ir 283B (neat) cm^{-1}: 3400, 1510, 1460, 1365, 1170, 955, 830; ^{1}Hmr (80 MHz, $CDCl_3$) δ: 7.10–7.45(m,4H), 2.62(q,2H), 1.88(s,1H), 1.55(s,6H), 1.23(t,3H).

*4-*tert*-Butylcumyl alcohol*

4-*tert*-Butylcumyl alcohol was prepared by the addition of methyl 4-*tert*-butylbenzoate to a solution of methyl magnesium iodide; mp 78°C (lit. (22) mp 79°C); ir 283B (neat) cm^{-1}: 3350, 1370, 960, 830; ^{1}Hmr (80 MHz, $CDCl_3$) δ: 7.38(s,4H), 1.73(s,1H), 1.57(s,6H), 1.31(s,9H).

4-Cyanocumene

4-Cyanocumene (30) was prepared by a Sandmeyer reaction using the diazonium salt formed from 4-isopropylaniline and cuprous cyanide (27); ir 237B cm^{-1}: 2240; ^{1}Hmr (361.1 MHz, $CDCl_3$) δ: 7.59(m,2H), 7.33(m,2H), 2.97(m,1H), 1.27(d,6H).

4-Methoxycumene

4-Methoxycumene was prepared by the reaction of 4-isopropylphenol with dimethyl sulphate in 5% aqueous potassium hydroxide. The product was purified by column chromatography using silica gel; ir 283B (neat) cm^{-1}: 1620, 1520, 1250, 1040, 830; ^{1}Hmr (361.1 MHz, $CDCl_3$) δ: 7.15(m,2H), 6.85(m,2H), 3.79(s,3H), 2.86(m,1H), 1.23(d,6H).

Preparation of cumyl bromides

The method of Grice and Owen (31) was used for the conversion of substituted cumyl alcohols to the bromides. Typically, the cumyl alcohol (0.02 mol) was dissolved in pentane or benzene (100 mL). Hydrogen bromide gas was passed through the solution for 0.5 h. The solution was then dried over anhydrous magnesium sulphate, filtered, and the solvent removed at reduced pressure.

Electron spin resonance experiments

Cumenes

A static solution of DTBP (0.3 mL)[7] and the cumene (30–60 mg) was irradiated in the esr spectrometer cavity using filtered (methanol in a quartz tube) light from a 1-kW Hanovia Xe–Hg high-pressure lamp. All samples were purged with nitrogen for 5 min prior to

[7]To increase the solubility of the *para*-SO_2Ph derivative, 0.2 mL of benzene was added to the DTBP solution.

irradiation and examined at 253 K.

The observed spectrum of the 4-methoxycumyl radical, generated by this procedure, was complicated by the competitive hydrogen abstraction from the methoxy methyl group. Simulation indicated a ratio of cumyl to α-aryloxymethyl radical of ca. 1 : 1. The α-aryloxy radical was simulated by $a(CH_2)$ = 17.40 G.

Cumylbromides

Three procedures were used to generate the cumyl radicals from the bromide. In procedure 1, a static solution of DTBP (0.2 mL), triethylsilane (0.2 mL), and the bromide (50–100 mg), diluted if necessary with chlorobenzene, was purged with nitrogen and irradiated as described above in the esr spectrometer cavity. The 4-*tert*-butylcumyl radical was generated by this procedure at 233 K. In procedure 2, a solution of the bromide (50–100 mg) in *tert*-butylbenzene or chlorobenzene was continuously purged with nitrogen while hexamethylditin (0.1 mL) was injected via the purge tube. It was necessary to have a glass wool plug in the purge tube to filter the hexamethylditin. This solution was irradiated as described above. The use of chlorobenzene allowed cooling of the sample to temperatures as low as 233 K without precipitation of the hexamethylditin. The 4-fluoro and 4-ethyl derivatives were generated by this method at 263 K and 233 K, respectively. In procedure 3, the bromide (100 mg) was purged with nitrogen and hexabutylditin (0.1 mL) added in a glove box under an inert atmosphere. This solution was irradiated as described above. The 4-methyl derivative was generated by this method at 253 K.

Control experiments

Linearity of field was checked against the lines of $[Cr(NH_3)_5Cl]Cl_2$ doped with 2% $[Co(NH_3)_5Cl]Cl_2$ (32). Accuracy of the field was checked against the couplings for Wurster's blue perchlorate in ethanol (33). The effects of moderate temperature changes on the spectra of six representative cumyl radicals, 4-chloro, 4-isopropyl, 4-acetyl, 4-carbomethoxy, 4-benzoyl, and 4-phenylsulfonyl, were studied by recording the spectrum at 20-deg intervals from 213 to 273 K, and also at 333 K for 4-chloro and 4-acetyl, and at 293 K for 4-isopropyl, 4-benzoyloxy, and 4-phenylsulfonyl. In all cases the benzylic β-hfc value was invariant. However, for the 4-isopropyl derivative, a change in the hfc value for the isopropyl group with a lowering of temperature was observed, indicating the hindered rotation of the isopropyl group.

Acknowledgements

This work was supported by a grant from the Natural Sciences and Engineering Research Council of Canada. We thank the Atlantic Regional Magnetic Resonance Centre at Dalhousie University for the 360-mHz nmr spectra. A.M.N. is grateful for the award of an Izaak Walton Killam Memorial scholarship. The authors also acknowledge the contribution of R. Subramanian.

1. J. M. DUST and D. R. ARNOLD. J. Am. Chem. Soc. **105**, 1211 (1983); **105**, 6531 (1983).
2. D. D. M. WAYNER and D. R. ARNOLD. Can. J. Chem. **62**, 1164 (1984).
3. X. CREARY. J. Org. Chem. **45**, 280 (1980).
4. (*a*) A. M. DE P. NICHOLAS and D. R. ARNOLD. Can. J. Chem. **62**, 1850 (1984); (*b*) A. M. DE P. NICHOLAS and D. R. ARNOLD. Can. J. Chem. **62**, 1860 (1984).
5. (*a*) R. LIVINGSTON, H. ZELDES, and M. S. CONDRADI. J. Am. Chem. Soc. **101**, 4312 (1979); (*b*) K. H-. HELLWEGE (*Editor*). Landolt–Bornstein Handbook. Vol. 9. Part b. Organic C-centred radicals. Springer Verlag, Berlin. 1977.
6. (*a*) J. E. WERTZ and J. R. BOLTON. Electron spin resonance. McGraw–Hill, New York. 1972; (*b*) P. B. AYSCOUGH. Electron spin resonance in chemistry. Methuen, London, 1967; (*c*) H. FISHER. Free radicals. Vol II. *Edited by* J. K. Kochi. Wiley, New York. 1973. Chapt. 19; (*d*) A. CARRINGTON and A. D. MCLACHLAN. Introduction to magnetic resonance. Harper and Row, New York, NY. 1967. Chapt. 6; (*e*) L. SALEM. The molecular orbital theory of conjugated systems. W. A. Benjamin, Inc., New York. 1966. p. 278.
7. (*a*) D. GRILLER and K. U. INGOLD. J. Am. Chem. Soc. **96**, 6715 (1974); (*b*) H. NAKATSUJI, H. KATO, and T. YONEZAWA. Bull. Chem. Soc. Jpn. **43**, 698 (1970); (*c*) R. BERSOHN. J. Chem. Phys. **24**, 1066 (1956); (*d*) D. B. CHESNUT. J. Chem. Phys. **29**, 43 (1958).
8. H. M. MCCONNELL. J. Chem. Phys. **24**, 764 (1956).
9. P. B. AYSCOUGH. Electron spin resonance in chemistry. Methuen, London. 1967. p. 77.
10. (*a*) W. J. LEIGH and D. R. ARNOLD. Can. J. Chem. **59**, 609 (1981); (*b*) W. J. LEIGH and D. R. ARNOLD. Can. J. Chem. **59**, 3061 (1981); (*c*) R. W. BALDOCK, P. HUDSON, A. R. KATRITZKY, and F. SOTI. J. Chem. Soc. Perkin Trans. 1, 1422 (1974); (*d*) W. J. VAN DEN HOEK, B. A. C. ROUSSEEUW, J. SMIDT, W. G. B. HUYSMANS, and W. J. MIJS. Chem. Phys. Lett. **13**, 429 (1972).
11. (*a*) H. G. VIEHE, R. MERE'NYI, L. STELLA, and Z. JANOUSEK. Angew. Chem. Int. Ed. Engl. **18**, 917 (1979); (*b*) H. G. VIEHE, Z. JANOUSEK, and R. MERE'NYI. Acc. Chem. Res. In press.
12. M. CHARTON. Prog. Phys. Org. Chem. **13**, 119 (1981).
13. O. EXNER. *In* Correlation analysis in chemistry. Recent advances. *Edited by* N. B. Chapman and J. Shorter. Plenum Press, New York. 1978. Chapt. 10.
14. (*a*) A. CARRINGTON and A. D. MCLACHLAN. Introduction to magnetic resonance. Harper and Row, New York, NY. 1967. p. 91; (*b*) P. B. AYSCOUGH. Electron spin resonance in chemistry. Methuen, London. 1967. p. 255.
15. U. M. OEHLER and E. G. JANZEN. Can. J. Chem. **60**, 1542 (1982).
16. R. G. R. BACON and O. J. STEWART. J. Chem. Soc. 4953 (1965).
17. R. MURPHY and R. H. PRAGER. J. Organomet. Chem. **156**, 133 (1978).
18. J. A. SMITH and R. A. TURLE. J. Org. Chem. **37**, 126 (1971).
19. E. H. HUNTRESS and F. H. CARTEN. J. Am. Chem. Soc. **62**, 511 (1940).
20. J. N. GARDNER, S. KAISER, A. KRUBINER, and H. LUCAS. Can. J. Chem. **51**, 1419 (1973).
21. F. VAN MEURS and H. VAN BEKKUM. J. Organomet. Chem. **133**, 321 (1977).
22. H. C. BROWN, Y. OKAMOTO, and G. HAM. J. Am. Chem. Soc. **79**, 1906 (1957).
23. G. A. OLAH, M. B. COMISAROW, and C. J. KIM. J. Am. Chem. Soc. **91**, 1458 (1969).
24. A. N. BLAKITNYI, E. V. KONOVALOV, A. P. SEVAST'YAN, YU. A. FIALKOV, and L. M. YAGUPOL'SKII. Zh. Org. Khim. **10**, 512 (1974).
25. A. FISCHER and R. RODERER. Can. J. Chem. **54**, 423 (1976).
26. A. K. MANGLIK, R. B. MOODIE, K. SCHOFIELD, G. D. TOBIN, R. G. COOMBES, and P. HADJIGEORGIOU. J. Chem. Soc. Perkin Trans. **2**, 1606 (1980).
27. A. I. VOGEL. Vogel's textbook of practical organic chemistry. 4th ed. Longman Inc., New York. 1978. pp. 607, 1102–1103.
28. J. R. NORELL. J. Org. Chem. **38**, 1924 (1973).
29. C. E. BARNES, K. S. FELDMAN, M. W. JOHNSON, H. W. H. LEE, and P. C. MYHRE. J. Org. Chem. **44**, 3925 (1979).
30. N. KORNBLUM, S. C. CARLSON, and R. G. SMITH. J. Am. Chem. Soc. **101**, 647 (1979).
31. R. GRICE and L. N. OWEN. J. Chem. Soc. 1947 (1963).
32. W. T. M. ANDRIESSEN. J. Magn. Reson. **23**, 339 (1976).
33. J. E. WERTZ and J. R. BOLTON. Electron spin resonance. McGraw–Hill, New York. 1972. Appendix.

Novel coincidence effects in a bimetallic phase transfer catalyzed reaction. Biphasic reduction reactions catalyzed by rhodium carbonylmetallate clusters

FERENC JOÓ AND HOWARD ALPER[1]

Ottawa-Carleton Chemistry Institute, Department of Chemistry, University of Ottawa, Ottawa, Ont., Canada K1N 9B4

Received July 24, 1984

FERENC JOÓ and HOWARD ALPER. Can. J. Chem. **63**, 1157 (1985).

Bimetallic and cluster rhodium carbonyl complexes catalyze the biphasic reduction of nitro compounds under mild conditions (using CO/5 *M* NaOH, C_6H_6 or $PhCH_3$). Rate studies indicate the sensitivity of the reaction to the nature of the organic substrate, base concentration, and the temperature. A previously observed bimetallic ($Co_2(CO)_8$ and $(1,5\text{-HDRhCl})_2$) and phase transfer catalyzed [$R_4N^+X^-$] reduction of nitro compounds was found to be a consequence of the inhibition and reactivation of the true catalyst by the quaternary ammonium salt and cobalt carbonyl, respectively.

FERENC JOÓ et HOWARD ALPER. Can. J. Chem. **63**, 1157 (1985).

Opérant en deux phases et sous des conditions douces (utilisant CO/NaOH 5 *M*, C_6H_6 ou $PhCH_3$), les complexes, bimétalliques et sous forme d'agrégats, du rhodium carbonyle peuvent catalyser la réduction des composés nitrés. Des données cinétiques indiquent que la réaction est sensible à la nature du substrat organique, à la concentration en base et à la température. Une réduction, bimétallique et catalysée par un transfert de phase [$R_4N^+X^-$], des composés nitrés a été observée antérieurement; on a trouvé que cette réduction est une conséquence d'inhibition et de réactivation du vrai catalyseur qui sont respectivement provoquées par le sel d'ammonium quaternaire et le cobalt carbonyle.

[Traduit par le journal]

Group 8 metal complexes play an important role in the homogeneously catalyzed reduction of nitro compounds (1–4). One of us has demonstrated that by application of phase transfer techniques, the reaction conditions could be made significantly milder in the ruthenium carbonyl (3) and the dichlorotris(triphenylphosphine)ruthenium (5) catalyzed processes. Recently, the use of bimetallic phase transfer catalysis for the reduction of nitro compounds has been described, whereby the synergistic effect of cobalt carbonyl and chloro(1,5-hexadiene)rhodium(I) dimer $[1,5\text{-HDRhCl}]_2$ facilitates amine formation when dodecyltrimethylammonium chloride (DTAC) is the phase transfer agent in a mixture of 5 *N* sodium hydroxide and benzene, (reaction [1]). No reaction occurred when only one of the two metal catalysts were used under the phase

$$[1]\quad \mathrm{ArNO_2} \xrightarrow[\mathrm{Co_2(CO)_8,\,[1,5\text{-}HDRhCl]_2,\ rt,\ 1\ atm}]{\mathrm{CO,\ 5}\,M\,\mathrm{NaOH,\ C_6H_6,\ C_{12}H_{25}N(CH_3)_3{}^+Cl^-}} \mathrm{ArNH_2}$$

transfer conditions (6).

While there has been considerable interest in the use of two different metal complexes for catalyzing various organic transformations, little is understood about such processes. An investigation was therefore undertaken in order to gain some insight into the mechanism of the intriguing phase transfer reduction reaction. Several noteworthy findings were made which are reported herein: (*i*) rhodium carbonyl clusters are able to catalyze the nitro reduction in two-phase media in the *absence* of phase transfer agents and cobalt carbonyl; and (*ii*) the bimetallic nature of the above reaction ([1]) is a consequence of the coincidence of inhibition and reactivation of the true catalyst by the quaternary ammonium salt and cobalt carbonyl, respectively.

Results and discussion

When a nitro compound and a catalytic quantity of $[1,5\text{-HDRhCl}]_2$ or chlorodicarbonylrhodium(I) dimer, dissolved in a mixture of 5 *M* NaOH and either toluene or benzene, were placed under 1 atm of carbon monoxide at room temperatre ($[1,5\text{-HDRhCl}]_2$ is converted to $Rh(CO)_2Cl$ under these conditions), a relatively fast gas uptake began which corresponded to the nitro-amine conversion. The latter was verified by gas volumetry as well as by product isolation and characterization. However, *no* reaction was observed when a phase transfer catalyst was present [dodecyltrimethylammonium chloride, tetrabutylammonium chloride, tetrabutylammonium hydroxide].

The reactivity pattern (Table 1) is basically the same as that found with the $[1,5\text{-HDRhCl}]_2/Co_2(CO)_8$/DTAC catalyst system, i.e., the reaction is selective for the reduction of the nitro group in the presence of olefin, halogen, and carbonyl functionalities (6). The reaction of sterically hindered or aliphatic nitro compounds is slow compared to the non-hindered aromatic ones; nevertheless, it does occur.

Both temperature and base concentration are important for a favorable process to occur. At even slightly elevated temperatures (40°C), the catalyst is destroyed in the first few minutes of the reaction which then stops completely. At low base concentrations (0.1 *M*) a green aqueous phase is formed instead of the dark brown one in 5 *M* NaOH, and reaction is slow, if it occurs at all. A plot of the effect of hydroxide ion concentration on the rate of nitrobenzene reduction is illustrated in Fig. 1. The fastest reaction occurs at 3 *M* NaOH, while the rate is less at higher base concentrations. Variation in the base concentration will not only affect the solubility of the reactant species (including carbon monoxide), but also the ease of attack by hydroxide ion on coordinated carbonyl, and the interconversion of carbonylrhodates (discussed below). It is also noteworthy that deactivation of the catalyst is accompanied by uptake of carbon monoxide, and therefore a long pretreatment of the rhodium solutions with CO/H_2O should be avoided even at room temperature.

It is interesting to note that Alessio *et al.* (7) have found $Rh_6(CO)_{16}$ and chloro(1,5-cyclooctadiene)rhodium(I) completely inactive for the reduction of nitrobenzene in the absence of a chelating phenanthroline-type ligand by CO/H_2O in 95% ethanol at elevated pressure (30 atm) and temperature (165°C — no base was added). In the present study, however, $Rh_6(CO)_{16}$ or even aqueous $RhCl_3$ can be used as catalyst pre-

[1] To whom all correspondence should be addressed.

TABLE 1. Specific rates of reduction of nitro compounds by CO/H_2O catalyzed by rhodium carbonyl clusters under biphasic conditions and in homogeneous solutions

Substrate	Rate*
4-Nitrochlorobenzene	13.9[a]
	12.8[b] (92%)†
Nitrobenzene	11.7[a]
4-Nitrobenzophenone	9.5[c] (91%)†
4-Nitrotoluene	6.9[a]
	6.5[c]
	4.8[d]
	0.8[e]
3-Nitrotoluene	8.3[a]
4-Nitro-*trans*-stilbene	3.0[a]
	2.8[c] (90%)†
Benzyl-4-nitrophenyl ether	1.8[a]
Nitromesitylene	0.7[a]
Nitrocyclohexane	0.3[a]
Nitrobenzene‡	17.3[f]
4-Nitrotoluene‡	11.2[f]
	0.4[g]

*Rates are expressed as mol RNO_2 reduced to RNH_2 per mol Rh per hour based on the conversion reached in the first 30 min. Biphasic systems: 15 mL 5 *M* NaOH, 20 mL toluene, 30°C, CO to 1 bar total pressure, and (*a*) 0.3 mmol substrate, 0.030 mmol Rh as [Rh(hexadiene)Cl]$_2$; (*b*) 1 mmol substrate, 0.033 mmol Rh as $[Rh(CO_2Cl]_2$; (*c*) 1 mmol substrate, 0.125 mmol Rh as $[Rh(CO)_2Cl]_2$; (*d*) 0.3 mmol substrate, 0.125 mmol Rh as $Rh_6(CO)_{16}$; (*e*) 1 mmol substrate, 0.100 mmol Rh as $RhCl_3 \cdot aq$; (*f*) 1 mmol substrate, 0.100 mmol Rh as $[Rh(CO)_2Cl]_2$; (*g*) as (*f*) but 500 mg NaOAc instead of 1 mL 5 *M* NaOH.

†Yield of isolated and chromatographically purified 4-aminochlorobenzene, 4-aminobenzophenone, and 4-amino-*trans*-stilbene (reaction time: 280, 65, and 260 min, respectively).

‡Homogeneous solutions: 9 mL MeOH, 1 mL H_2O, 1 mL 5 *M* NaOH, 30°C, CO to 1 bar total pressure.

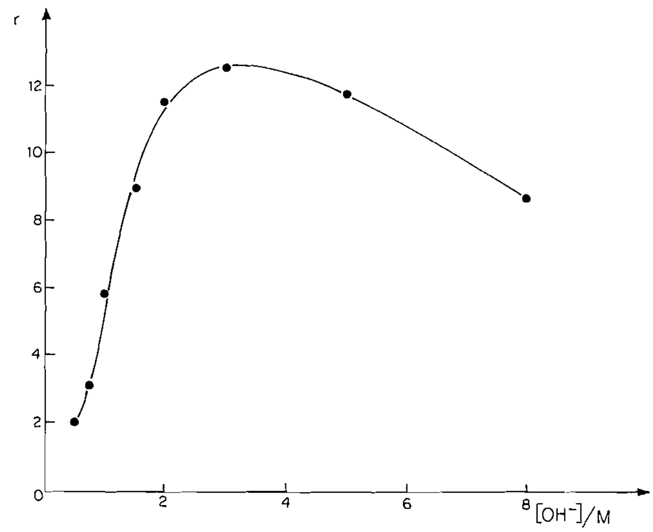

FIG. 1. Effect of base concentration on the rate of reduction of nitrobenzene. Conditions: 15 mL NaOH solution, 20 mL toluene, 0.03 mmol Rh as $[Rh(CO)_2Cl]_2$, 0.3 mmol $PhNO_2$, carbon monoxide up to 1 bar total pressure (30°C). Rates are calculated on the basis of gas uptake in the first 30 min of the reaction and are expressed as mol $PhNO_2$ reduced/mol Rh h.

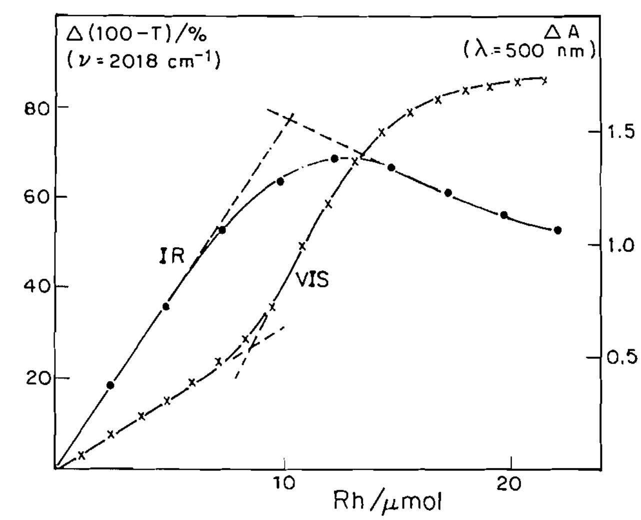

FIG. 2. Spectrophotometric titration of $Co(CO)_4^-$ with $[Rh(CO)_2Cl]_2$ under CO. Infrared: 9.50 μmol of $C_{12}H_{25}N(CH_3)_3^+Co(CO)_4^-$ in $PhCH_3$ titrated with 0.25 μmol Rh/μL solutions of $[Rh(CO)_2Cl]_2$ in $PhCH_3$. The break on the graph corresponds to 1.07 Rh/Co. VIS: 8.53 μmol $PPN^+Co(CO)_4^-$ in CH_2Cl_2 (3.0 mL) titrated with 0.12 μmol Rh/μL solutions of $[Rh(CO)_2Cl]_2$ in CH_2Cl_2. The break on the graph corresponds to 1.01 Rh/Co.

cursors (Table 1).

Pioneering work by Chini and co-workers[2] showed that various rhodium complexes can react with carbon monoxide and base to give a series of carbonylrhodates (via formation of $[Rh(CO)_2Cl]_2$ and $Rh_4(CO)_{12}$), including inter alia $[Rh_{12}(CO)_{30}]^{2-}$ (violet), $[Rh_5(CO)_{15}]^-$ (red–brown), $[Rh_7(CO)_{16}]^{3-}$ (green), and $[Rh_6(CO)_{14}]^{4-}$ (dark red). Furthermore, halo- and hydridocarbonylrhodates are also formed in the presence of halogen and hydrogen, respectively. Under the conditions employed by us, both $[1,5\text{-HDRhCl}]_2$ and $[Rh(CO)_2Cl]_2$ consume carbon monoxide up to the ratio of CO/Rh = 3.5, accompanied by the transfer of the rhodium containing species to the aqueous phase, forming a dark brown solution. The reaction is complex indeed, and the infrared spectra of the quaternary ammonium carbonylrhodate salts did not correlate well with the published spectral data of the noted carbonylrhodates. However, it was found that $Rh_{12}(CO)_{30}^{2-}$ (9) and $Rh_7(CO)_{16}^{3-}$ (10), prepared by the methods of Chini *et al.*, proved to be catalytically active for nitro reduction in homogeneous methanol/water solutions. As the reduction requires base, the slight activity of violet-red solutions of $Rh_{12}(CO)_{30}^{2-}$ (possibly also containing $Rh_5(CO)_{15}^-$) (11) may be due to the presence of some $Rh_7(CO)_{16}^{3-}$ as the real catalytic species. Use of the latter as catalyst results in the maintenance of a green color of the solution throughout the reaction; however, if one uses an excess of nitro compound compared to base, the color turns red when the OH^- ion is consumed, indicating that the nitro compound oxidized the green species (formal oxidation number −0.429) to the red one(s) (FON −0.166 and −0.2, respectively). The higher specific rates in aqueous alcohol than under biphasic conditions is probably a result of the homogeneous conditions. On the other hand, the low activity of the

[2] For an account of this subject, see ref. 8.

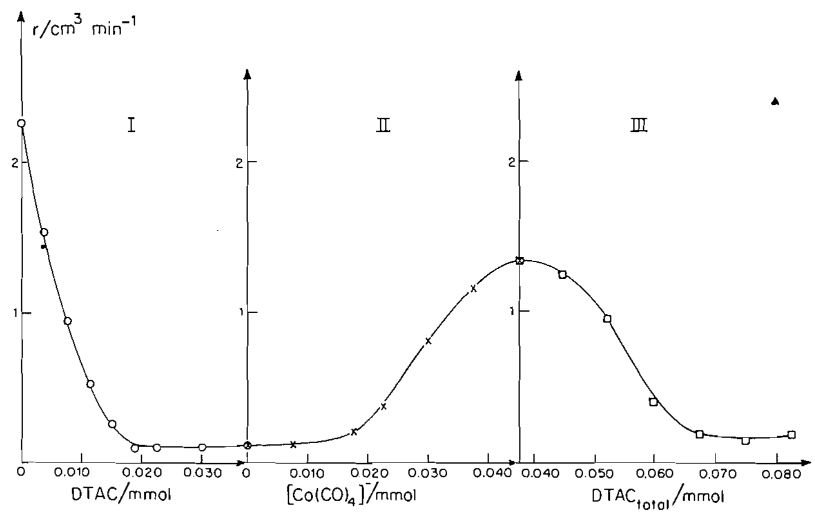

FIG. 3. Effect of (*I*) $C_{12}H_{25}N(CH_3)_3{}^+Cl^-$; (*II*) $Co(CO)_4{}^-$, formed from the added $Co_2(CO)_8$; and (*III*) $C_{12}H_{25}N(CH_3)_3{}^+Cl^-$ added subsequently, on the rate of reduction of $PhNO_2$ by CO/H_2O, catalyzed by $[Rh(CO)_2Cl]_2$. Conditions: 3 mmol $PhNO_2$, 0.10 mmol Rh, 15 mL 5 *M* NaOH, 20 mL $PhCH_3$, 30°C, 1 bar total pressure. The rate observed in the presence of 0.080 mmol of NaCl (and in the absence of $C_{12}H_{25}N(CH_3)_3{}^+Cl^-$) is also shown (▲).

green weakly basic aqueous solutions previously mentioned may be due to the low solubility of the aromatic nitro compounds in dilute aqueous base solutions, while 5 *M* NaOH is a reasonably good solvent for polar organic substrates.

Strongly basic aqueous solutions of rhodium carbonyls are known to catalyze the water gas shift reaction (1, 4, 12) and $Rh_{12}(CO)_{30}{}^{2-}$ was suggested as a catalytically active intermediate (13). We have also found that solutions of $[Rh(CO)_2Cl]_2$ in 5 *M* NaOH under carbon monoxide produce hydrogen at room temperature and 1 bar total pressure with a rate of about 0.1 mol H_2/mol Rh h.

In order to determine the cause of the synergistic effect of $[1,5\text{-HDRhCl}]_2$ and $Co_2(CO)_8$ in the phase transfer catalyzed reduction of nitro compounds by CO/H_2O (6) an investigation was made of the reaction of $[Rh(CO)_2Cl]_2$ and $R_4N^+Co(CO)_4{}^-$ in dry toluene. An intense red–brown color develops on the addition of $[Rh(CO)_2Cl]_2$ to $C_{12}H_{25}N(CH_3)_3{}^+Co(CO)_4{}^-$ in toluene or methylene chloride. The reaction can be followed by visible spectrophotometry at 500 nm and a plot of ΔA vs. [Rh] (Fig. 2) reveals the formation of a complex with a 1:1 Co/Rh ratio (not $Co_2Rh_2(CO)_{12}$).[3] Solutions of this composition show absorptions in the infrared region at 2062, 2018, 1986, 1948, and 1908 cm^{-1} (all strong — toluene solutions), and the formation of this complex is also established by ir spectrophotometric titration (Fig. 2). The structure of this complex may be $C_{12}H_{25}N(CH_3)_3{}^+Rh(CO)_2Cl(Co(CO)_4)^-$ in which $Co(CO)_4{}^-$ acts as a pseudohalide. The ir spectrum is in accord with this structure since there are only terminal carbonyl bands present, and the number of these bands is consistent with C_{2v} molecular symmetry with a staggered conformation. Attempts to obtain analytically pure materials have proved unsuccessful (15).

Addition of further amounts of $[Rh(CO)_2Cl]_2$ to the bimetallic anionic complex gives a new complex having a 2:1 Rh/Co ratio. This complex is much less stable in solution than the 1:1 complex. On addition of tetrabutylammonium chloride, the red–brown solution of the 1:1 Co/Rh complex turns light green, and the Co–Rh complex decomposes to give $Rh(CO)_2Cl_2{}^-$ (ir ν_{CO}: 2065 and 1988 cm^{-1}) and $Co(CO)_4{}^-$, in agreement with the anticipated higher nucleophilicity of Cl^- than that of $Co(CO)_4{}^-$.

The presumed bimetallic complex $R_4N^+Rh(CO)_2Cl\text{-}[Co(CO)_4]^-$ is destroyed by addition of either tetrabutylammonium hydroxide or 5 *M* NaOH to give $R_4N^+Co(CO)_4{}^-$, as can be readily observed by monitoring the characteristic absorption of cobalt tetracarbonyl anion at 1885 cm^{-1}. If there is an equivalent, or less, of R_4N^+ to $Co(CO)_4{}^-$ in the system, the rhodium-containing species formed by the action of base moves to the aqueous phase. However, when there is an excess of R_4N^+ compared to $Co(CO)_4{}^-$ the insoluble salts of the anionic carbonylrhodates are produced and are finely dispersed in the toluene phase, collecting at the interphase on standing. Addition of $Co_2(CO)_8$ gives $R_4N^+Co(CO)_4{}^-$ which migrates to the organic phase and forces the rhodium carbonyls back to the aqueous solution. This inhibition/reactivation sequence is illustrated in Fig. 3, which also indicates the formation of higher nuclearity rhodium clusters (inhibition by dodecyltrimethylammonium chloride occurs at much below the rhodium concentration). Separate experiments show that inhibition is not due to chloride ion.

In conclusion, the rhodium(I) biphasic reaction is a simple and selective homogeneously catalyzed nitro reduction process. The above results account for the "bimetallic" phase transfer reaction, and in particular establish the fascinating effects of a quaternary ammonium salt and a second metal complex catalyst on the rhodium catalyzed biphasic reaction.

Experimental section

The nitro compounds, rhodium and cobalt compounds, as well as phase transfer agents were commercial materials. Solutions of the violet $Rh_{12}(CO)_{30}{}^{2-}$ were prepared by reacting 19.5 mg (0.1 mmol Rh) of $[Rh(CO)_2Cl]_2$ with carbon monoxide in a 9:1 methanol–water solution (10 mL) containing 0.5 g of sodium acetate. When 1% water/tetrahydrofuran was used as the solvent, the initial violet color turned deep red in approximately 30 min, and an ir showed bands at 2070 w, 2042 vs, 2010 vs, 1870 m, 1840 m, and 1779 vs cm^{-1}, characteristic of $Rh_5(CO)_{15}{}^-$. Addition of 5 *M* NaOH (1.0 mL) to the above solutions gave rise to an intense green solution, and the

[3] The related, neutral complex $(PEt_3)_2(CO)RhCo(CO)_4$ has been successfully isolated from the reaction of *trans*-$RhCl(CO)(PEt_3)_2$ with $KCo(CO)_4$ (14).

$Rh_7(CO)_{16}^{3-}$ anion could be precipitated after dilution with water, as the Bu_4N^+ salt. This compound, owing to its extreme air-sensitivity, was characterized in acetonitrile solution: ir-ν_{CO} 1990 m, 1955 vs, 1905 m, 1815 w, and 1770 s cm^{-1}.

General procedure for the biphasic reduction of nitro compounds

A mixture of 5 *M* NaOH (15 mL), toluene or benzene (20 mL) and nitro compound (1.0 mmol) was degassed in a constant pressure, thermostatted manometric apparatus, which was finally filled with carbon monoxide. The rhodium catalyst (0.033 mmol) in toluene was added (by syringe). The mixture was stirred until the desired conversion had occurred (indicated by gas uptake) at which time stirring was stopped. The two phases were separated, the aqueous phase was extracted with toluene or ether (2 × 20 mL) and the combined organic solution was dried ($MgSO_4$) and concentrated. When there was less than 100% conversion, the product and starting material were separated by column chromatography on silica gel using toluene:ether (1:1) as eluant. Products were identified by comparison of R_f values (TLC) and spectral data with those of authentic materials.

Infrared and visible spectrophotometric studies

Visible spectrophotometric titrations were carried out under carbon monoxide using a screw-thread headed pyrex-glass cell closed with a silicone–rubber septum. For infrared measurements (Perkin-Elmer 783 spectrophotometer), stock solutions were prepared and mixed under carbon monoxide and samples were withdrawn by means of hypodermic syringes.

Illustrative preparation of $R_4N^+Co(CO)_4^-$ for ir spectrophotometric titrations: $Co_2(CO)_8$ (0.171 g, 1.0 mmol) and dodecyltrimethylammonium chloride (0.456 g of a 50% w/w $R_4N^+Cl^-$ in 1:1 H_2O-isopropanol) were dissolved in a degassed mixture of 5 *M* NaOH (25 mL) and toluene (40 mL) under carbon monoxide. The solution was stirred for 40 min, during which time it became almost colorless. The organic phase was removed (syringe) and dried ($MgSO_4$) under carbon monoxide. An infrared spectrum showed only one carbonyl band at 1885 cm^{-1}, characteristic of $Co(CO)_4^-$, the concentration of which was found, by the iodine oxidation method (16), to be 19 μmol Co/mL.

Bis(triphenylphosphine)iminium tetracarbonylcobaltate was prepared for visible studies. To 16 mL of a methylene chloride solution of $Bu_4N^+Co(CO)_4^-$ (containing 63 μmol Co/mL) was added 0.552 g of PPNCl followed by ether (40 mL). The desired compound was filtered, washed with hexane, and dried under nitrogen: ν_{CO} 1886 cm^{-1} (CH_2Cl_2). Yield: 0.465 g (68%).

Acknowledgments

We are grateful to the Natural Sciences and Engineering Research Council's Strategic Grant Program for support of this work. We are indebted to Johnson-Matthey Limited for a loan of hydrated rhodium chloride.

1. K. CANN, T. COLE, W. SLEGEIR, and R. PETTIT. J. Am. Chem. Soc. **100**, 3969 (1978).
2. A. F. M. IQBAL. Tetrahedron Lett. 3385 (1971).
3. H. ALPER and S. AMARATUNGA. Tetrahedron Lett. 2603 (1980).
4. K. KANEDA, M. HIRAKI, T. IMANAKA, and S. TERANISHI. J. Mol. Catal. **12**, 385 (1981).
5. K. JANUSZKIEWICZ and H. ALPER. J. Mol. Catal. **19**, 139 (1983).
6. K. E. HASHEM, J. F. PETRIGNANI, and H. ALPER. J. Mol. Catal. In press.
7. E. ALESSIO, F. VINZI, and G. MESTRONI. J. Mol. Catal. **22**, 327 (1984).
8. R. S. DICKSON. Organometallic chemistry of rhodium and iridium. Academic Press, New York. 1983.
9. P. CHINI and M. MARTINENGO. Inorg. Chim. Acta, **3**, 299 (1969).
10. P. CHINI and S. MARTINENGO. Chem. Commun. 1091 (1969).
11. A. FUMAGALLI, T. F. KOETZLE, F. TAKUSAGAWA, P. CHINI, and S. MARTINENGO. J. Am. Chem. Soc. **102**, 1970 (1980).
12. C. UNGERMANN, V. LANDIS, S. A. MOYA, H. COHEN, H. WALKER, R. G. PEARSON, R. G. PINKER, and P. C. FORD. J. Am. Chem. Soc. **101**, 5922 (1979).
13. R. M. LAINE. J. Am. Chem. Soc. **100**, 6451 (1978).
14. D. A. ROBERTS, W. C. MERCER, S. M. ZAHURAK, G. L. GEOFFROY, C. W. DEBROSSE, M. E. CASS, and C. G. PIERPOINT. J. Am. Chem. Soc. **104**, 910 (1982).
15. S. MARTINENGO, P. CHINI, V. G. ALBANO, F. CARIATI, and T. SALVATORI. J. Organomet. Chem. **59**, 379 (1973).
16. H. W. STERNBERG, I. WENDER, and M. ORCHIN. Anal. Chem. **9**, 174 (1952).

Metabolites of *Lachnellula fuscosanguinea* (Rehm). Part 1. The isolation, structure determination, and synthesis of lachnelluloic acid[1]

WILLIAM A. AYER AND J. DANIEL FIGUEROA VILLAR

Department of Chemistry, University of Alberta, Edmonton, Alta., Canada T6G 2G2

Received September 27, 1985

WILLIAM A. AYER and J. DANIEL FIGUEROA VILLAR. Can. J. Chem. **63**, 1161 (1985).

The metabolites produced in liquid culture by the fungus *Lachnellula fuscosanguinea* (Rehm) Dennis have been examined and two antifungal agents, lachnelluloic acid and lachnellulone, have been isolated. The structure of lachnelluloic acid has been established as (−)-4-hydroxy-3-octanoyl-6-pentyl-5,6-dihydro-2-pyrone (**1**) by chemical and spectroscopic methods. The total synthesis of racemic lachnelluloic acid, starting from 6,8-tridecanedione (**6**) is reported. Lachnelluloic acid (**1**) shows strong antifungal activity against *Ceratocystis ulmi*, the causative agent of Dutch elm disease.

WILLIAM A. AYER et J. DANIEL FIGUEROA VILLAR. Can. J. Chem. **63**, 1161 (1985).

On a étudié les métabolites produits, au cours d'une culture liquide, par le champignon *Lachnellula fuscosanguinea* (Rehm) Dennis et on a isolé deux agents fongicides, l'acide lachnelluloïque et la lachnellulone. Faisant appel à des méthodes chimiques et spectroscopiques, on a démontré que la structure de l'acide lachnelluloïque correspond à celle de la (−)-hydroxy-4 octanoyl-3 pentyl-6 dihydro-5,6 pyrone-2 (**1**). On rapporte une synthèse totale de l'acide lachnelluloïque racémique faisant appel à la tridécanedione-6,8 (**6**) comme produit de départ. L'acide lachnelluloïque (**1**) présente une forte activité fongicide contre le *Ceratocystis ulmi*, l'agent provoquant la maladie de la tordeuse de bourgeons.

[Traduit par le journal]

The fungus *Lachnellula fuscosanguinea* (Rehm) Dennis (1, 2) has been shown to be antagonistic to the Dutch elm disease fungus *Ceratosystis ulmi* and to the wood rotting fungus *Fomes pini*.[2] Initial studies in our laboratories showed that a methylene chloride extract of liquid cultures of *L. fuscosanguinea* displayed antifungal activity against *C. ulmi*. We report here the isolation of two active antifungal agents and the structure (**1**) of one of these compounds, which we have named lachnelluloic acid.

Lachnelluloic acid (**1**) was isolated from the mycelium extract (CH_2Cl_2) of *L. fuscosanguinea* by flash chromatography followed by column chromatography on silica gel. The colorless, crystalline, low melting (39–40°C) substance possesses the molecular formula $C_{18}H_{30}O_4$ and gives a positive ferric chloride test. The infrared (ir) spectrum does not show OH absorption, but does show absorption at 1708, 1695, and 1555 cm^{-1}. The latter absorption band, and the lack of apparent OH absorption, is attributed to the strongly chelated enolized β-diketone functionality in **1**.

The ultraviolet spectrum of lachnelluloic acid shows strong absorption bands at 218 and 274 nm, shifted to 250 nm in the presence of base, very reminiscent of that of alternaric acid (**2**)

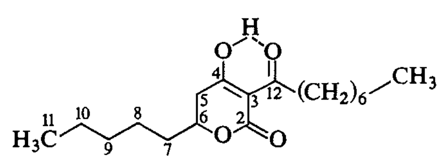

1

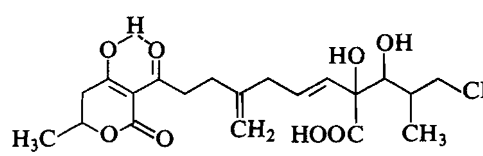

2

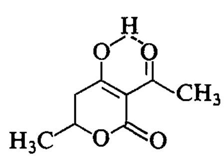

3

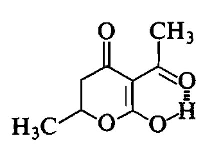

4

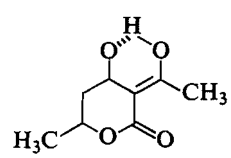

5

(**3**) and similar to that of dihydrodehydroacetic acid (**3**) (see below).

The ^1H nmr spectrum of **1** confirms the presence of the strongly H-bonded enolic proton, showing a signal at δ 17.9, similar to that observed in dihydrodehydroacetic acid (**3**). Homonuclear decoupling experiments suggested the partial structures A and B (Scheme 1) for lachnelluloic acid. Thus, simultaneous irradiation of the signal at δ 4.38 (proton *geminal* to the ethereal oxygen) induces decoupling of the *geminal* methylene protons at δ 2.68 and δ 2.58 (C-5 H's) as well as protons at δ 1.80 and δ 1.66, methylene protons of an alkyl side chain,

[1] The isolation and structure determination of lachnelluloic acid was first reported at the 9th Simposium Internacional de Química de Productos Naturales, Monterrey, Mexico, April 1982, Abstract no. 6. The synthesis of lachnelluloic acid was first presented at the Chemical Institute of Canada 66th Chemical Conference, Calgary, June 1982, Abstract OR 15-3.

[2] A. Tsuneda and Y. Hiratsuka, Northern Forest Research Centre, Canadian Forestry Service, Edmonton, personal communication. We thank Drs. Tsuneda and Hiratsuka for cultures of *L. fuscosanguinea*. The fungus was discovered growing on *Pinus contorta* in Jasper National Park and was identified by Dr. D.W. Minter, Commonwealth Mycological Institute (accession number CMI 250255).

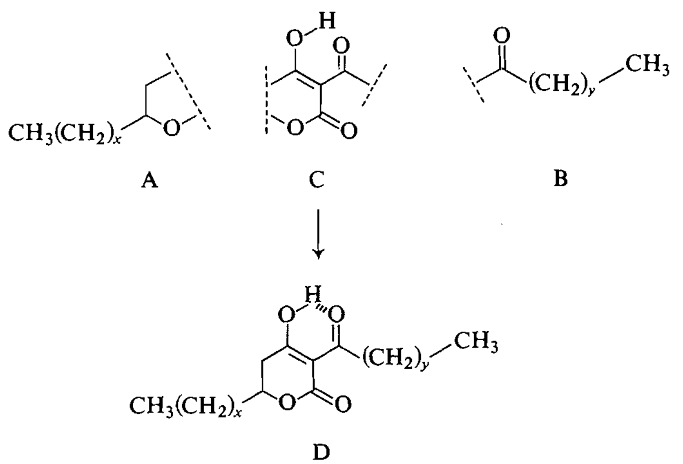

SCHEME 1

suggestive of partial structure A. The *geminal* pair of protons at δ 3.06 and δ 2.96, α to a carbonyl, are coupled to protons at δ 1.66, also part of an alkyl side chain, in keeping with partial structure B (see Experimental for complete assignments).

The ^{13}C nmr spectrum of **1** accounts for the 18 carbon atoms, two as methyl groups, eleven methylenes, one methine bearing oxygen, and four sp^2 hybridized carbons. The latter include a ketonic carbonyl at δ 204, a lactone or ester at δ 164, and the highly polarized double bond carbons of an enol at δ 195 and δ 103 (4, 5). In dihydrodehydroacetic acid (**3**) these signals appear at δ 201.2, 164.4, 195.0, and 103.4 (5).[3] This established the presence of part structure C in lachnelluloic acid.

Since lachnelluloic acid contains only four oxygen atoms, the part structures A, B, and C lead to structure D (Scheme 1) for lachnelluloic acid. The lengths of the side chains were deduced from the fragmentations observed in the electron impact mass spectrum of lachnelluloic acid. The base peak at m/z 239 corresponds to the loss of C_5H_{11} and represents the loss of the side chain *geminal* to the ethereal oxygen. A strong peak at m/z 226 ($M^+ - C_6H_{12}$) corresponds to McLafferty fragmentation of the acyl side chain. Thus in structure D, $x = 4$, and $y = 6$.

As a model for lachnelluloic acid, dihydrodehydroacetic acid (**3**) (6) was prepared by hydrogenation of dehydroacetic acid in benzene containing traces of pyridine. Compound **3** displays similar spectral characteristics (ir, uv, ^1H nmr, and ^{13}C nmr) to those of lachnelluloic acid (**1**). The direction of enolization in **3**, which must be the same as that in lachnelluloic acid, was determined to be as in **3** and not **4**, since the coupled ^{13}C nmr spectrum shows the lactone carbonyl as a broad singlet which is unaffected by deuterium exchange of the enolic hydrogen. Enolization as in **5**, although considered less likely, is not excluded by this datum (see also ref. 5).

In order to complete the assignment of the structure of lachnelluloic acid, racemic compound **1** was prepared by total synthesis as outlined in Scheme 2. Condensation of 6,8-tridecanedione (**6**), prepared by condensation of 2-heptanone and methyl hexanoate, with malonyl dichloride (**7**) afforded the pyrone **7** in 58% yield. Deacylation of **7** (90% H_2SO_4, 120–130°C) gave 4-hydroxy-6-pentyl-2-pyrone (**8**) in 87% yield. Hydrogenation of **8** over palladium–charcoal gives a quantitative yield of β-ketolactone **9** (spectral characteristics (see Experimental) and a negative ferric chloride test indicate that this compound exists in the unenolized form). Direct *C*-acylation of **9** with octanoyl chloride in refluxing trifluoroacetic acid (8) gave racemic lachnelluloic acid (**1**) in low (~10%) yield. Better results are obtained using Tanabe's method (9), which involves first *O*-acylation to provide **10** (~90% yield), followed by base-catalyzed thermal isomerization to provide racemic lachnelluloic acid (**1**) in 75% yield (34% overall yield from **6**), identical (ir, uv, nmr, ms) with the natural product. The absolute configuration of natural, levorotatory lachnelluloic acid has not been determined.

Direct acylation of the pyrone **8** with octanoyl chloride gave dehydrolachnelluloic acid **11** in high yield. All attempts to transform **11** into lachnelluloic acid by catalytic hydrogenation

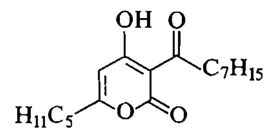

11

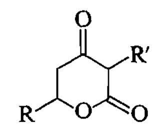

12 R = C_5H_{11}, R′ = C_8H_{17}
13 R = CH_3, R′ = C_2H_5

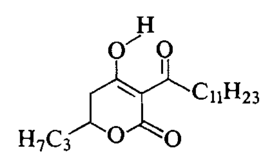

14

(as was successful with dehydroacetic acid above) were unsuccessful. Hydrogenation over palladium–charcoal in ethyl acetate gave the deoxygenated β-ketone lactone **12** in virtually quantitative yield. Hydrogenation–hydrogenolysis of lachnelluloic acid under identical conditions also provided **12**, and similar hydrogenation of dehydroacetic acid gave **13**.

Lachnelluloic acid, which shows antifungal activity against *C. ulmi*, bears a structural similarity to the recently reported (10) podoblastins (e.g., podoblastin A (**14**)), compounds which also show antifungal activity. The structure of the second antifungal metabolite isolated from *L. fuscosanguinea*, lachnellulone, will be the subject of the next paper in this series.

Experimental

General

High resolution electron impact mass spectra (hreims) were recorded on an AEI MS-50 mass spectrometer. Chemical ionization mass spectra (cims) and low resolution electron impact mass spectra (lreims) were obtained using an AEI MS-4 mass spectrometer. Fast atom bombardment (FAB) spectra were obtained using an AEI MS-50 spectrometer. The data were processed in DS-50 and DS-9 computers. Fourier transform infrared (ftir) spectra were recorded as $CHCl_3$ casts on a Nicolet 7199 FT interferometer. Single scan infrared (ir) were recorded on a Perkin Elmer 297 spectrometer. Routine nmr spectra were obtained on a Varian A-56/60A spectrometer, a Bruker WP-80 spectrometer, and a Varian 4A-100 spectrometer with a Digilab FTS/NMR-3 data system. Tetramethylsilane was used as the internal standard. High field ^1H nmr and ^{13}C nmr spectra were recorded on Bruker WH-200 or WH-400 spectrometers with an Aspect 2000 computer system. Ultraviolet (uv) spectra were obtained on a Unicam SP 1700 spectrophotometer and optical rotations on a Perkin Elmer 141 polarimeter. Melting points are uncorrected and were determined on a Fisher–Johns melting point apparatus. E. Merck silica gel 60 (less than 230 mesh) was used for column chromatography, and E. Merck

[3] We wish to thank Prof. J.B. Stothers for valuable discussion and for performing a 2D INADEQUATE experiment on **3** (see ref. 5).

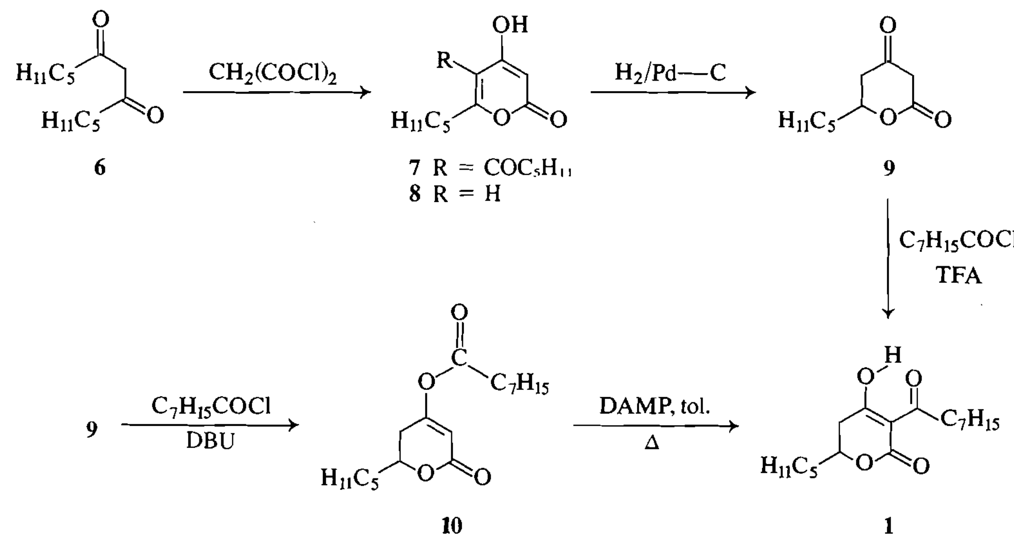

SCHEME 2

silica gel 60 (230–400 mesh) was used for flash chromatography. Preparative thin layer chromatography (ptlc) was carried out on Terochem silica gel G containing 1% Retma P-1 electronic phosphor (General Electric), 20 × 20 cm plates, 0.35–0.50 mm thickness. Analytical thin layer chromatography (tlc) was done on BDH precoated plates of silica gel 60 F-254. Visualization was carried out using uv light or iodine vapor (ptlc), and using 10% H_2SO_4 or 5% phosphomolybdic acid containing a trace of ceric sulfate in 5% sulfuric acid (tlc), followed by careful charring on a hot plate. All solvents were distilled prior to use. Skellysolve B refers to Skelly Oil Company light petroleum, bp 62–70°C.

Fermentations were carried out in a New Brunswick Scientific MF-214 microferm fermentor or a New Brunswick Scientific magnaferm fermentor.

Culturing of Lachnellula fuscoanguinea

Strain C-693 (Canadian Forestry Service, accession number of the Commonwealth Mycological Institute CMI 250255 and 250256) of *Lachnellula fuscosanguinea* was found growing on *Pinus contorta* on Maligne Lake Road, Jasper National Park, in 1979. A slant tube culture of this fungus was obtained from the Northern Forest Research Center, Edmonton. The original slant tube culture was transferred to potato dextrose agar (PDA) slant tubes which were kept as stock cultures at 4°C.

Shake cultures of the fungus were obtained by transferring small pieces of mycelium from the slant tubes to 300-mL Erlenmeyer flasks containing 150 mL of sterile potato dextrose broth (PDB). After two weeks at 17°C the shake cultures were ready to use as inoculum.

When a fermentor was used, 450 mL of inoculum was transferred to 10 L of sterile PDB in the fermentation tank. The conditions in the fermentor were kept as follows: temperature 20°C, air flow 1 L/min, pressure 4 psi (1 psi = 6.9 kPa), drive speed 170 rpm, and foam breaker speed 600 rpm. The fermentation was worked up after 3 weeks.

In the case of still culture, 25-mL aliquots of inoculum were transferred to 2.8-L Fernbach flasks, each containing 1 L of sterile PDB. The flasks were then kept at 17–20°C for at least 70 days.

Extraction of the metabolites

The culture mixture was separated into broth and mycelium by filtration through cheese cloth. The broth was extracted, without previous concentration, by CH_2Cl_2 liquid–liquid extraction (3 × 500 mL of CH_2Cl_2 for every 3 L of broth). The CH_2Cl_2 extract was then dried over anhydrous Na_2SO_4, filtered, and concentrated to dryness under reduced pressure at 35°C. Higher yields of extract were obtained when the broth was first concentrated (5 L to 500 mL, reduced pressure, 35°C) and then extracted with ethyl acetate in a continuous liquid–liquid extractor.

The mycelium was air dried for two days, then extracted with CH_2Cl_2 in a Soxhlet extractor. The CH_2Cl_2 extract was dried (anhydrous H_2SO_4) and concentrated.

Isolation of lachnelluloic acid (1)

A 50-mm diameter column was filled with 8 in. of silica gel for flash chromatography and packed using $CHCl_3$. The sample (1.5 g of crude extract) was applied as a concentrated solution in chloroform and the column was eluted with solvent at the rate of 2 in./min while collecting 50-mL fractions.

Fractions 20–30, eluted with $CHCl_3$, provided a waxy crystalline substance (305 mg). Column chromatography of this fraction (40 g of silica gel G mesh 270, 2-cm diameter column, Skellysolve B/$CHCl_3$, 1:1) gave a pure crystalline substance (204.2 mg), mp 39–40°C; $[\alpha]_D^{25}$ −26.6° (*c* 10, MeOH); tlc, R_f 0.5 (Skellysolve B/$CHCl_3$/HOAc, 50:50:1); ftir ($CHCl_3$, cast or solution): 2955, 2925, 2860, 1708, 1695, 1555, 1465, and 1065 cm^{-1}; uv (MeOH) λ_{max}: 218 (ϵ 700), 274 nm (ϵ 1090); uv (MeOH + NaOH) λ_{max}: 250 nm (ϵ 1375); uv (MeOH + HCl) λ_{max}: 275 nm (ϵ 1095); ^1H nmr (400 MHz, $CDCl_3$) δ: 17.9 (enolic H), 4.38 (H-6, dddd, J = 4.0, 5.0, 7.0 and 11.0 Hz, coupled to 2.58, 2.68, 1.80 and 1.66), 3.06 (H-13a, ddd, J = 6.5, 8.5, and 15.0 Hz, coupled to 1.66), 2.96 (H-13b, ddd, J = 6.5, 8.5, 15.0 Hz, coupled to 1.66), 2.68 (H-5a, dd, J = 11.0, 17.0 Hz, coupled to 4.38 and 2.58), 2.58 (H-5b, dd, J = 4.0, 17.0 Hz, coupled to 4.38 and 2.68), 1.80 (1H, dddd, J = 5.0, 7.0, 10.0, 13.0 Hz, coupled to 4.38, 1.66, and 1.53), 1.66 (3H, m, coupled to 4.38, 3.06, 2.96, and 1.80), 1.53 (1H, quintet, J = 5.0), 1.34–1.30 (14H, m, coupled to 0.90 and 0.92), 0.92 (3H, vt, J = 6.0, coupled to 1.34 and 1.30), 0.90 (3H, vt, J = 7.0, coupled to 1.34 and 1.30); ^{13}C nmr (100 MHz, $CDCl_3$) δ: 204.22 (s), 194.88 (s), 163.92 (s), 102.93 (s), 73.57 (d), 38.25 (t), 37.65 (t), 34.40 (t), 31.43 (t), 31.22 (t), 29.05 (t), 28.75 (t), 24.82 (t), 24.14 (t), 22.33 (t), 22.21 (t), 13.76 (q), and 13.66 (q); hreims *m/z* (formula, intensity, fragment): 310.2136 (calculated for $C_{18}H_{30}O_4$, 310.2144, 33, M^+), 292 ($C_{18}H_{28}O_3$, 6, M − H_2O), 240 ($C_{13}H_{20}O_4$, 15), 239 ($C_{13}H_{19}O_4$, 100.0, M − C_5H_{11}), 226 ($C_{12}H_{18}O_4$, 41, M − C_6H_{12}), 222 ($C_{13}H_{18}O_3$, 12) 221 ($C_{13}H_{17}O_3$, 62, M − $C_5H_{13}O$), 155 ($C_7H_7O_4$, 17), 129 ($C_5H_5O_4$, 10). The compound showed a positive ferric chloride test.

Isolation of lachnellulone[4]

Fractions 35–40 of the above mentioned flash chromatography of 1.5 g of crude extract of *L. fuscosanguinea*, eluant now 1% MeOH in $CHCl_3$, afforded a white crystalline material which was recrystallized from acetone/Skellysolve B to yield 20 mg of pure lachnellulone, mp

[4]The structure of lachnellulone will be discussed in part 2 of this series.

126–127°C; tlc, R_f 0.44 in $CHCl_3$; $[\alpha]_D^{25}$ +48.4 (*c* 10, CH_3OH). The spectral characteristics of lachnellulone will be described in the full paper.[4]

Hydrogenation of dehydroacetic acid

Dehydroacetic acid (1.0 g or 6 mmol) was mixed with 5% Pd–C (0.1 g) and benzene (20 mL) containing five drops of pyridine. The reaction mixture was then pressurized with hydrogen (60 psi) in a Parr hydrogenator for 40 h at room temperature. The reaction mixture was filtered to remove the catalyst and concentrated to dryness *in vacuo*. The solid residue was purified by crystallization from Skellysolve B/ethyl acetate to afford, in 95% yield, white crystals of dihydrodehydroacetic acid (**3**), mp 93–94°C; tlc, R_f 0.3 in $CHCl_3$/Skellysolve B/HOAc, 2:1:1; ftir (film): 2980, 2920, 1715, 1560, 1458, 1080, and 770 cm^{-1}; uv (MeOH) λ_{max}: (ϵ 20 700), 274 nm (ϵ 26 100); uv (MeOH + NaOH) λ_{max}: 208, 248 nm; ^1H nmr (200 MHz, $CDCl_3$) δ: 17.9 (1H, s), 4.52 (1H, m), 2.63 (2H, dd, *J* = 2.5, 6 Hz), 2.60 (3H, s), 1.44 (3H, d, *J* = 6 Hz); ^{13}C nmr (50 MHz, $CDCl_3$) δ: 201.18 (s), 195.04 (s), 164.35 (s), 103.43 (s), 70.25 (d), 39.45 (t), 26.47 (q), and 20.56 (q). The gated ^{13}C nmr spectra for deuterium-labelled (enolic H) dihydrodehydroacetic acid, δ: 201 (q, *J* = 6.5 Hz), 194 (m), 164 (bs), 103 (m), 70 (ddm, *J* = 147.5, 3.5 Hz), 39 (tbq, *J* = 130.0, 4.5 Hz), 26 (q, *J* = 230 Hz), and 20 (qq, *J* = 127.5, 2.0 Hz).

6,8-Tridecanedione (6)

Sodium amide (1 mol) was suspended in dry tetrahydrofuran (THF) (100 mL) in a 500-mL two-neck round bottom flask to which a dropping funnel and a reflux condenser ($CaCl_2$ drying tube) had been attached. 2-Heptanone (0.33 mol) in (THF) (50 mL) was added from the funnel over a period of 10 min. After 5 min stirring, methyl hexanoate (70 mL) in THF (50 mL) was added slowly to the reaction mixture. The viscous mixture was heated under reflux for 1 h and let cool to room temperature, then acidified with 10% HCl until all the precipitate had dissolved. The upper organic layer was separated, washed with distilled water, dried over anhydrous Na_2SO_4, filtered, and concentrated to yield a red liquid. Vacuum distillation (3 Torr; 1 Torr = 133.3 Pa) produced a fraction (130°C) containing the desired β-diketone, which was further purified by complexation with copper acetate (~100 mL of saturated solution). The copper complex was separated by filtration and washed with 95% EtOH. The green crystals of complex were then dissolved in $CHCl_3$ (100 mL) and decomposed with 10% H_2SO_4 (200 mL). The colorless $CHCl_3$ solution afforded, after drying and concentration, pure (by tlc) 6,8-tridecanedione (**6**), 35 g (54%), η_D^{20} 1.442; tlc, R_f 0.65 in Skellysolve B/ethyl acetate, 9:1; ir (cast): 2960, 2930, 2860, 1705 (w), 1610, 1460, 1150, 1110, 950, and 780 cm^{-1}; ^1H nmr (80 MHz, $CDCl_3$) δ: 15.40 (1H, bs), 5.50 (1H, s), 3.58 (fraction, s), 2.52 (fraction, t), 2.30 (4H, t), 1.62 (4H, bt), 1.30 (8H, m), 0.90 (6H, vt); hreims *m/z* (formula, intensity): 212.1775 (calculated for $C_{13}H_{24}O_2$, 212.1775, 11), 170 ($C_{10}H_{18}O_2$, 13), 156 ($C_9H_{16}O_2$, 34), 141 ($C_8H_{13}O_2$, 100), 100 ($C_5H_8O_2$, 50), and 99 ($C_6H_{11}O$, 77).

Condensation of 6,8-tridecanedione (6) with malonyl dichloride

6,8-Tridecanedione (24 mmol) was added to a round bottom flask connected to a dropping funnel and a gas outlet. Malonyl dichloride (24 mmol) was added slowly from the dropping funnel to the β-diketone and the reaction mixture was heated in a water bath at 80°C. A copious amount of hydrogen chloride, which was removed using a water aspirator, was produced in the darkening reaction mixture. When the evolution of HCl had stopped (30 min), the reaction mixture was dissolved in ether and washed with distilled water and then with brine. The ether extract was dried over anhydrous Na_2SO_4 and concentrated *in vacuo* to afford a red-brown solid residue which was recrystallized from hexane/ether (1:1) several times to give pale yellow flakes of 5-hexanoyl-4-hydroxy-6-pentyl-2-pyrone (**7**), 3.9 g (58% yield), mp 91–92°C; tlc, R_f 0.55 in 2% MeOH, 2% HOAc in $CHCl_3$; ftir (KBr): 3370, 2960, 2930, 2860, 2620, 2500, 1705, 1690, 1620, 1565, 1460, 1290, 985, and 830 cm^{-1}; uv (MeOH) λ_{max}: 225 (ϵ 6050); 261 (ϵ 5410), 288 nm (ϵ 5250); ^1H nmr (200 MHz, $CDCl_3$) δ: 16.71 (1H, bs), 5.56 (1H, s), 2.82 (2H, t, *J* = 7.5 Hz), 2.73 (2H, bt, *J* = 8.0 Hz), 1.70 (4H, m), 1.31 (8H, m), and 0.90 (6H, vt); ^{13}C nmr (50 MHz, $CDCl_3$) δ: 202.6 (s), 169.8 (s), 169.2 (s), 165.1 (s), 115.4 (s), 90.1 (d), 44.4 (t), 32.5 (t), 31.3 (t), 31.2 (t), 27.4 (t), 23.8 (t), 22.3 (t), 22.1 (t), 13.8 (q), and 13.7 (q); hreims *m/z* (formula, intensity, fragment): 280.1673 (calculated for $C_{16}H_{24}O_4$, 280.1675, 25, M^+), 252 ($C_{15}H_{24}O_3$, 22, M − CO), 237 ($C_{13}H_{17}O_4$, 15, M − C_3H_7), 224 ($C_{12}H_{16}O_4$, 18), 210 ($C_{11}H_{14}O_4$, 8), 209 ($C_{15}H_{13}O$, 100, M − C_5H_{11}), 206 ($C_{12}H_{14}O_3$, 27), 196 ($C_{11}H_{16}O_3$, 23), 181 ($C_9H_9O_4$, 14), 168 ($C_8H_8O_4$, 44), 153 ($C_7H_5O_4$, 26), and 99 ($C_6H_{11}O$, 67). *Anal.* calcd. for $C_{16}H_{24}O_4$: C 68.55, H 8.63; found: C 68.76, 68.92; H 8.70, 8.69.

Synthesis of 4-hydroxy-6-pentyl-2-pyrone (8)

5-Hexanoyl-4-hydroxy-6-pentyl-2-pyrone (**7**, 12.8 mmol) was dissolved in 90% H_2SO_4 (10 mL) and heated to 120–130°C for 60 min. The reaction mixture was cooled, diluted with 10% $NaHCO_3$, and extracted with ether. The ether extract was dried over anhydrous Na_2SO_4 and concentrated to yield an oil which crystallized under high vacuum. This compound was recrystallized from Skellysolve B/ether (1:1) to yield 1.8 g of the hydroxypyrone **8**. The mother liquors were purified by flash chromatography (30-mm diameter column, 2% MeOH, 2% HOAc in $CHCl_3$) to give, in fractions 9 to 13, 0.255 g of pyrone **8** (87% yield), mp 52–52.5°C; tlc, R_f 0.38 in 2% MeOH, 2% HOAc, 96% $CHCl_3$; ftir ($CHCl_3$ cast): 2960, 2930, 2845, 2520 (br), 1690 (w), 1640 (w), 1570, 1540, 1500, 1350, 1310, 1285, 1250, 1140, 920 (br), 885, 840, and 820 cm^{-1}; ^1H nmr (80 MHz, $CDCl_3$) δ: 10.9 (1H, bs), 6.1 (1H, s), 5.6 (1H, s), 2.5 (2H, t), 1.7 (2H, bt), 1.4 (4H, m), 0.9 (3H, vt); hreims *m/z* (formula, intensity, fragment): 182.0940 (calculated for $C_{10}H_{14}O_3$, 182.0942, 33, M^+), 164 ($C_{10}H_{12}O_2$, 2, M − H_2O), 154 ($C_9H_{14}O_2$, 7, M − CO), 141 ($C_8H_{13}O_2$, 10, M − C_2HO), 139 ($C_7H_7O_3$, 11, M − C_3H_7), 126 ($C_6H_6O_3$, 100, M − C_4H_8), 111 ($C_5H_3O_3$, 72), 98 ($C_5H_6O_2$, 44), and 84 ($C_4H_4O_2$, 64). *Anal.* calcd. for $C_{10}H_{14}O_3$: C 65.92, H 7.72; found: C 66.04, H 7.80.

Hydrogenation of 4-hydroxy-6-pentyl-2-pyrone (8)

4-Hydroxy-6-pentyl-2-pyrone (**8**, 1.37 mmol) was mixed with 5% Pd–C (30 mg) and ethyl acetate (20 mL) in a hydrogenation bottle. The reaction flask was connected to a Parr hydrogenator and pressurized to 70 psi with hydrogen. The reaction mixture was shaken for 24 h at room temperature. Filtration and concentration of the reaction mixture afforded 4-oxo-6-pentyl-3,4,5,6-tetrahydro-2-pyrone (**9**) in quantitative yield as a white solid (mp 64–65°C); tlc, R_f 0.33, 1% MeOH in $CHCl_3$; ftir ($CHCl_3$, cast): 3100, 2960, 2925, 2860, 2570, 1700 (w), 1595, 1390, 1290, 1040, 885, and 830 cm^{-1}; ^1H nmr (400 MHz, $CDCl_3$) δ: 4.62 (1H, dddd, *J* = 3, 5, 8, 12 Hz, coupled to δ 2.70, 2.47, 1.82, 1.71), 3.56 (1H, d, *J* = 19 Hz, coupled to δ 3.41), 3.41 (1H, d, *J* = 19 Hz, coupled to δ 3.56), 2.70 (1H, dd, *J* = 3, 18 Hz, coupled to δ 4.62, 2.47), 2.47 (1H, dd, *J* = 12, 18 Hz, coupled to δ 4.62, 2.70), 1.82 (1H, dddd, *J* = 5, 8, 9, 14 Hz, coupled to δ 4.62, 1.71, 1.56, 1.46), 1.71 (1H, dddd, *J* = 5, 5, 11, 18 Hz, coupled to δ 4.62, 1.82, 1.56, 1.46), 1.56 (1H, m), 1.46 (1H, m), 1.36 (4H, m) and 0.92 (3H, vt); hreims *m/z* (formula, intensity, fragment): 184.1098 (calculated for $C_{10}H_{16}O_3$, 184.1100, 5, M^+), 166 ($C_{10}H_{14}O_2$, 4, M − H_2O), 129 ($C_6H_9O_3$, 24, M − C_4H_7), 125 ($C_8H_{13}O$, 29, M − $C_2H_3O_2$), 115 ($C_5H_7O_3$, 17, M − C_5H_9), 113 ($C_5H_5O_3$, 100, M − C_5H_{11}), 111 ($C_6H_7O_2$, 19, M − C_4H_9O).

O-Acylation of 4-oxo-6-pentyl-3,4,5,6-tetrahydro-2-pyrone (9)

β-Ketolactone **9** (0.71 mmol) was dissolved in benzene (2 mL) containing 1,8-diazabicyclo[5.4.0]undec-7-ene (DBU) (0.73 mmol) and octanoyl chloride (0.73 mmol) at 0°C. This mixture was stirred in an ice-water bath for 3 h. The reaction mixture was treated with distilled water (20 mL) and extracted with benzene (2 × 10 mL). The combined benzene extracts were washed with 5% HCl (1 × 20 mL) and brine. The benzene solution was then dried over anhydrous Na_2SO_4 and concentrated to give an oil which was shown to be a single compound (tlc), the enol ester **10** (91% yield). This compound was unstable and was used immediately in the next step; ^1H nmr (200 MHz, $CDCl_3$) δ: 5.82 (1H, s), 4.40 (1H, m), 2.40 (2H, m).

Lachnelluloic acid (1)

6-Pentyl-4-oxyoctanoyl-5,6-dihydro-2-pyrone (**10**, 0.65 mmol) was dissolved in dry toluene (3 mL) and mixed with 4-*N*,*N*-dimethylaminopyridine (DMAP, catalytic amount). The resulting solution was heated under reflux for 5 h. The reaction mixture was worked up by adding water and extracting with toluene. The combined toluene extracts were washed with 5% HCl and brine. After drying over anhydrous Na_2SO_4 the solution was concentrated to give an oily residue. Flash chromatography of this residue (20-mm diameter column, Skellysolve B/EtOAc (95:5)) afforded, in fractions 7 to 11, pure racemic lachnelluloic acid (150 mg, 75% yield) as an oil, identical (tlc, ir, uv, ^{1}H nmr, hreims) with an authentic sample. *Anal.* calcd. for $C_{18}H_{30}O_4$: C 69.64, H 9.74, O 20.62; found: C 69.72, H 9.82.

Synthesis of dehydrolachnelluloic acid (11)

4-Hydroxy-6-pentyl-2-pyron (**8**, 1.38 mmol) was dissolved in trifluoroacetic acid (TFA) (10 mL) and mixed with octanoyl chloride (1.85 mmol). The reaction mixture was heated under reflux for 24 h. The resulting yellow solution was diluted to 100 mL with ether, extracted with 10% $NaHCO_3$ (2 × 200 mL), washed with water, dried over anhydrous Na_2SO_4, and concentrated to yield an oily residue. Flash chromatography of this residue (20-mm diameter column, Skellysolve B/chloroform (2:1)) afforded the pure crystalline dehydrolachnelluloic acid (0.4 g, 94%), mp 35–36°C; tlc, R_f 0.6 in chloroform/Skellysolve B (2:1); ftir ($CHCl_3$, cast): 3090 (w), 2960, 2930, 2830, 1725, 1635, 1605, 1560, 1445, 1225, 990, 850, and 700 cm^{-1}; ^{1}H nmr (200 MHz, $CDCl_3$) δ: 16.87 (1H, s), 5.92 (1H, s), 3.08 (2H, t, J = 7 Hz), 2.45 (2H, t, J = 8 Hz), 1.67 (4H, m), 1.35 (12H, m), 0.91 (3H, vt), and 0.89 (3H, vt); hreims m/z (formula, intensity, fragment): 308.1990 (calculated for $C_{18}H_{28}O_4$, 308.1988, 22, M$^+$), 290 ($C_{18}H_{26}O_3$, 8, M − H_2O), 252 ($C_{14}H_{20}O_4$, 3, M − C_4H_8), 237 ($C_{13}H_{17}O_4$, 64, M − C_5H_{11}), 224 ($C_{12}H_{16}O_4$, 100, M − C_6H_{12}), 210 ($C_{11}H_{14}O_4$, 41 M − C_7H_{14}), 204 ($C_{14}H_{20}O$, 31), 168 ($C_8H_8O_4$, 48), 153 ($C_7H_5O_4$, 10). *Anal.* calcd. for $C_{18}H_{28}O_4$: C 70.10, H 9.15; found: C 69.96, H 9.33.

Hydrogenation of dehydrolachnelluloic acid (11)

Dehydrolachnelluloic acid (0.78 mmol) was dissolved in ethyl acetate (20 mL) and transferred to a hydrogenation bottle containing 10% Pd–C catalyst (0.05 g). This mixture was pressurized to 60 psi of hydrogen in a Parr hydrogenator and shaken for 24 h. Thin layer chromatography of the reaction mixture showed the presence of a product different from lachnelluloic acid. After work-up the reaction product afforded the β-ketolactone **12**, in quantitative yield, as a viscous oil; tlc, R_f 0.2 in chloroform/Skellysolve B/HOAc (2:1:trace); ftir ($CHCl_3$, cast): 2960, 2930, 2865, 1610, 1384, 1250, 1120, 1040, and 740 cm^{-1}; ^{1}H nmr (200 MHz, $CDCl_3$) δ: 4.68 (1H, m, coupled to δ 2.73 and δ 2.42), 3.41 (1H, t, J = 7 Hz, coupled with δ 1.92, exchangeable with D_2O), 2.73 (1H, dd, J = 3, 18 Hz, coupled to δ 4.68 and δ 2.42), 2.42 (1H, dd, J = 12.0, 18.0 Hz, coupled to δ 4.68 and δ 2.73), 1.92 (2H, bt, coupled to δ 3.41 and δ 1.3), 1.3 (16H, m), and 0.90 (6H, vt); ^{13}C nmr (50 MHz, $CDCl_3$) δ: 201.05 (1.7), 169.07 (1.0), 73.81 (3.1), 56.49 (2.0), 43.42 (2.5), 34.23 (2.9), 31.60 (2.3), 31.18 (2.3), 29.44 (2.7), 29.08 (3.6), 29.00 (2.6), 27.02 (2.2), 24.17 (3.0), 22.90 (2.7), 22.40 (3.1), 22.20 (2.6), 13.82 (2.8), and 13.67 (3.4).

Hydrogenation of natural lachnelluloic acid (1)

Lachnelluloic acid (**1**, 3.1 mg) was mixed with 5% Pd–C (1 mg) and ethyl acetate (10 mL). The mixture was shaken at 60 psi of hydrogen for 24 h. The reaction mixture was filtered and concentrated to give a white solid which was purified by preparative tlc (20 × 20 cm, 0.35-mm thickness, $CHCl_3$) to afford β-ketolactone **12** (3 mg), identical (tlc, ftir, ^{1}H nmr, ms) with that prepared above.

Hydrogenation of dehydroacetic acid to give 13

Dehydroacetic acid (6 mmol) was mixed with 10% Pd–C catalyst (0.1 g) in a hydrogenation bottle, ethyl acetate (20 mL) was added to the mixture, and the flask was pressurized to 60 psi of hydrogen and shaken for 24 h at room temperature. Filtration and concentration of the reaction mixture afforded a yellow solid which was recrystallized from Skellysolve B/acetone to give white crystals of the β-ketolactone **13** in quantitative yield, mp 138–139°C. This compound gives a negative ferric chloride test; tlc, R_f 0.3 in Skellysolve B/$CHCl_3$/HOAc (30:70:1); ftir (film): 2960, 2930, 2860, 2540 (broad), 1603, 1385, 1270, 1120, 900 cm^{-1}; ir ($CHCl_3$): 1760 and 1720 cm^{-1}; hreims m/z (formula, intensity, fragment): 156.0788 (calculated for $C_8H_{12}O_3$, 156.0787, M$^+$), 128 ($C_6H_8O_3$, 53, M − C_2H_4), 87 ($C_4H_7O_2$, 9, M − C_4H_5O), 87 ($C_3H_3O_3$, 11, M − C_5H_9), and 55 (C_3H_3O, 100, M − $C_5H_9O_2$). *Anal.* calcd. for $C_8H_{12}O_3$: C 61.52, H 7.74; found: C 61.12, H 7.56.

Acknowledgements

We gratefully acknowledge the financial support provided by the Natural Sciences and Engineering Research Council of Canada. We also wish to thank the Alberta Heritage Foundation for Medical Research for a studentship (J.D.F.V.) and research allowance. We thank Drs. A. Tsuneda and Y. Hiratsuka, Northern Forest Research Centre, Edmonton, for bringing this problem to our attention and for providing cultures of *L. fuscosanguinea*, and Dr. A. Stoessl for providing a sample of alternaric acid.

1. A. Tsuneda. Fungal morphology and ecology. Tokyo Press, Tokyo. 1982. p. 99.
2. C. G. Dharne. Phytopath. Z. **53**, 101 (1965).
3. J. R. Bartels-Keith. J. Chem. Soc. 1662 (1960).
4. J. B. Stothers. Carbon-13 NMR spectroscopy. Academic Press, New York. 1972. p. 183.
5. A. Stoessl and J. B. Stothers. Can. J. Chem. **62**, 549 (1984).
6. S. Gelin and R. Gelin. Bull. Soc. Chim. Fr. 288 (1968).
7. M. A. Butt and J. A. Elvidge. J. Chem. Soc. 4483 (1963).
8. E. Marcus, J. F. Stephen, and J. K. Chan. J. Heterocycl. Chem. **6**, 13 (1969).
9. Y. Tanabe, M. Miyakado, N. Ohno, and Y. Yoshioka. Chem. Lett. 1543 (1982).
10. M. Miyakado, S. Inoue, Y. Tanabe, K. Watanabe, N. Ohno, H. Yoshioka, and T. Mabry. Chem. Lett. 1539 (1982).

Crystal structure determination of the conformation of two bicyclo[3.3.1]nonan-ones

JOHN F. RICHARDSON AND TED S. SORENSEN
The Department of Chemistry, University of Calgary, Calgary, Alta., Canada T2N 1N4

Received July 5, 1984

JOHN F. RICHARDSON and TED S. SORENSEN. Can. J. Chem. **63**, 1166 (1985).

The molecular structures of *exo*-7-methylbicyclo[3.3.1]nonan-3-one, **3**, and the *endo*-7-methyl isomer, **4**, have been determined using X-ray diffraction techniques. Compound **3** crystallizes in the space group $I\bar{4}$ with a = 15.115 (1), c = 7.677 (2) Å, and Z = 8 while **4** crystallizes in the space group $P2_1$, with a = 6.446 (1), b = 7.831 (1), c = 8.414 (2) Å, β = 94.42 (2)°, and Z = 2. The structures were solved by direct methods and refined to final agreement factors of R = 0.041 and R = 0.034 for **3** and **4** respectively. Compound **3** exists in a chair−chair conformation and there is no significant flattening of the chair rings. However, in **4**, the non-ketone ring is forced into a boat conformation.These results are significant in interpreting what conformations may be present in the related sp^2-hybridized carbocations.

JOHN F. RICHARDSON et TED S. SORENSEN. Can. J. Chem. **63**, 1166 (1985).

Utilisant des techniques de diffraction des rayons-X, on a déterminé les structures moléculaires de la méthyl-7 *exo* bicyclo[3.3.1] nonanone-3, **3**, et de son isomère méthyl-7 *endo*, **4**. Le composé **3** cristallise dans le groupe d'espace $I\bar{4}$, avec a = 15,115(1), c = 7,677(2) Å et Z = 8 alors que **4** cristallise dans le groupe d'espace $P2_1$, avec a = 6,446(1), b = 7,831(1), c = 8,414(2) Å, β = 94,42(2)° et Z = 2. On a résolu les structures par des méthodes directes et on les a affinées jusqu'à des valeurs respectives de R de 0,041 et 0,034 pour les composés **3** et **4**. Le composé **3** existe dans une conformation chaise−chaise et il n'y a pas d'aplatissement notable des cycles en formes chaises. Toutefois, dans le composé **4**, le cycle qui ne porte pas la cétone est forcé de prendre une conformation bateau. Ces résultats sont importants pour interpréter la nature des conformations qui peuvent être présentes dans les carbocations apparentés qui ont une hybridation sp^2.

[Traduit par le journal]

A number of organic reactions, where a carbocation intermediate is involved, undergo a rearrangement reaction characterized by a n,1-hydride shift, where position 1 is the carbocation centre and n is a C—H function located at a separation of 2, 3, 4, 5.... carbon atoms distant.

In some recent examples where n = 5 and 6, it has been possible to directly observe a symmetrical μ-hydrido-bridged carbocation **1**, where p and q define a medium ring, i.e. p + q = 6, 7, 8, or 9 (1−3). In the case of p = q = 3, R = H, it has also been possible to show the existance of **1** as an intermediate in solvolysis or acid-catalysis reactions (4, 5).

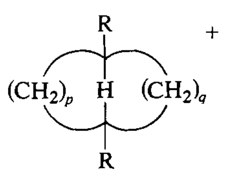

1

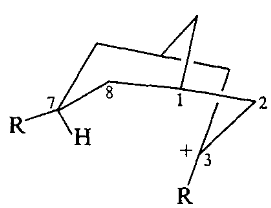

2

Like the simple ring compounds, the bicyclo[3.3.1]nonyl system **2** has been observed in many instances (6−8) to transfer a hydrogen between positions 3 and 7. However, the situation regarding a possible μ-hydrido-bridged carbocationic intermediate in solvolysis reactions has still not been definitively settled, although most of the evidence has been against such an intermediate. We have recently prepared the observable carbocation **2**, R = CH_3, and significantly, this is *not* a μ-hydrido-bridged structure,[1] involving instead a very rapid transfer of the hydrogen over a small barrier, i.e. a degenerate rearrangement involving a "normal" tertiary carbocation. The cation related to **2** but with an *endo*-methyl group was also prepared.[1]

The most likely cause of the difference between cations **1** and **2**, as discussed by Eakin *et al.* (6*a*), concerns the more rigid framework of the bicyclo[3.3.1]nonane ring system and the consequent difficulty in bringing C(3) and C(7) within "bonding" distance.

As an aid in the study of the observable carbocations, we were interested in getting structural data on the related ketones **3** and **4**. Ketone **3** was expected to be a di-chair structure and our principle interest was in looking at the expected "flattening" of the chairs because of transannular interactions. On the basis of nmr work, ketone **4** had been proposed to have a chair− boat structure (9). We were interested in confirming

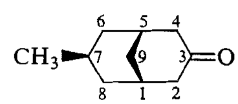

3

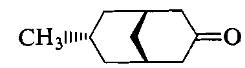

4

this and in using **4** as a model for a "non-flattening" chair structure. The structure of **4** is also of interest in light of very recent work by Renzoni and Borden (10), in which a 7-*endo*-carbomethoxybicyclo[3.3.1]nonan-3-one is postulated to have a dichair structure.

In looking at base-catalyzed hydride transfer, Murray-Rust *et al.* (11) have determined the structure of *exo*-7-hydroxybicyclo[3.3.1]nonan-3-one, **5**, and the corresponding methyl ether, **6**, and both have a di-chair structure (the former has a slight disorder problem).

Experimental

X-Ray analysis

The ketones **3** and **4** were prepared as outlined in refs. 6*a* and 12, respectively. Ketone **4** was further purified by vpc and crystals of both isomers were obtained by slow sublimation. Due to the facile sublimation of the ketones, suitable crystals of each were quickly affixed to a goniometer head at room temperature and immediately placed in the cold stream on an Enraf−Nonius CAD4F automated diffractometer fitted with a low-temperature device. The crystal systems were identified as tetragonal and monoclinic, respectively, using the indexing routines of the instrument. The distribution of intensity data

[1]T. S. Sorensen, unpublished results.

TABLE 1. Crystal data

Parameters	Isomer 3	Isomer 4
Formula	$C_{10}H_{16}O$	$C_{10}H_{16}O$
Formula wt., amu	152.24	152.24
Crystal description	Colorless plates	Colorless plates
Space group	$I\bar{4}$	$P2_1$
a, Å	15.115(1)	6.446(1)
b, Å	15.115(1)	7.831(1)
c, Å	7.677(2)	8.414(2)
β, deg	90	94.42(1)
U, Å^3	1753.8(5)	423.4(1)
Z	8	2
D_c, g cm^{-3}	1.15	1.19
F(000)	672.0	168.0
Radiation	Mokα, λ = 0.71069 Å (graphite monochromator)	
Temperature, °C	−83(1)	−172(2)
Max θ, deg	25	27.5
Scan range Δω, deg	1.5(0.70 + 0.347 tan θ)	1.5(0.70 + 0.34 tan θ)
Octants collected	$-h$, $+k$, $\pm l$	$\pm h$, $+k$, $-l$
Crystal dimensions, mm	0.20 × 0.30 × 0.30	0.10 × 0.25 × 0.30
μ(Mokα), cm^{-1}	0.78	0.81
Unique data collected	842	1033
Observed data ($I > 3\sigma(I)$)	594	886
No. data used in final cycle*	729	978
No. variables in final cycle	100	99
GOF	1.43	1.42
Max (shift/error)	0.03	0.03
R, R_w†	0.041, 0.032	0.034, 0.031

*Observed data plus those for which $I_c > 3\sigma(I_o)$.
†$R = \Sigma(\|F_o\| - \|F_c\|)/\Sigma\|F_o\|$; $R_w = [\Sigma w(\|F_o\| - \|F_c\|)^2/\Sigma w\|F_o\|^2]^{1/2}$.

TABLE 2. Positional parameters ($\times 10^4$) and B_{equiv} (**3** × 10, **4** × 100) for the non-hydrogen atoms of *exo*-, *endo*-7-methylbicyclo[3.3.1]-nonan-3-ones **3** and **4**. B_{eq} is calculated from 1/3 the trace of the B_{ij} matrix

Atom	x/a	y/b	z/c	B_{eq} (Å^2)
Compound 3				
C(1)	3413(2)	8702(2)	3608(5)	26(2)
C(2)	3864(2)	9401(2)	4717(5)	30(2)
C(3)	3264(2)	9861(2)	6007(5)	29(2)
C(4)	2556(2)	9303(2)	6852(4)	28(2)
C(5)	2142(2)	8607(2)	5661(5)	27(2)
C(6)	1533(2)	9014(2)	4282(5)	28(2)
C(7)	2029(2)	9606(2)	2984(5)	23(2)
C(8)	2813(2)	9111(2)	2217(5)	28(2)
C(9)	2879(2)	8083(2)	4774(5)	28(2)
C(10)	1414(2)	9954(2)	1566(5)	37(2)
O	3372(2)	10631(2)	6401(4)	47(2)
Compound 4				
C(1)	763(3)	−344(3)	7067(2)	132(8)
C(2)	926(3)	1238(4)	6003(2)	157(9)
C(3)	2924(3)	2222(3)	6363(2)	151(9)
C(4)	4885(3)	1166(4)	6589(2)	155(8)
C(5)	4603(3)	−384(3)	7677(2)	135(8)
C(6)	4311(3)	190(3)	9415(2)	141(8)
C(7)	2240(3)	−378(3)	10006(2)	122(8)
C(8)	455(3)	162(3)	8818(2)	137(8)
C(9)	2734(3)	−1420(3)	6990(2)	148(8)
C(10)	1939(3)	326(3)	11666(2)	166(8)
O	2947(2)	3770*	6448(2)	230(7)

*Coordinate fixed to define origin.

and the systematic extinctions observed during data collection are consistent with the space groups $I4$, $I\bar{4}$, and $I4/m$ (hkl, $h + k + l = 2n + 1$) for **3** and $P2_1$ and $P2_1/m$ ($0k0$, $k = 2n + 1$) for **4**. The acentric distribution of E values (K curve) for **4** indicated $P2_1$; however, the distribution was ambiguous for **3**. The final choices of the space groups as $I\bar{4}$ and $P2_1$ were substantiated by the successful solution and refinement of the structures. All attempts to solve the structures in the centric space groups or to transform the indices of the molecular mirror plane to the appropriate crystallographic mirror plane ($z = 0$ for $P2_1$, $y = 1/4, 3/4$ for $I4/m$) were unsuccessful. The crystal data and experimental conditions are summarized in Table 1. Three standard reflections measured every 1500 s of X-ray exposure time showed no decomposition of the crystals had occurred during the data acquisition period. The data were corrected for background, Lorentz, and polarization effects but an absorption correction was not performed as it was impossible to accurately measure faces on the data crystals before sublimation had occurred.

The structures were solved by direct methods (MULTAN 78) (13) and refined by full-matrix least-squares techniques based on F, minimizing the function $\Sigma w(|F_o| - |F_c|)^2$. The weighting schemes used were $w = [\sigma^2(F_o) + 0.0001(F_o)^2]^{-1}$ and $w = [\sigma^2(F_o) + 0.0002(F_o)^2]^{-1}$, where $\sigma(F_o)$ was derived from counting statistics, for **3** and **4** respectively. All computations were performed using the XRAY 76 system of programs (14) implemented on a Honeywell computer with a MULTICS operating system. Scattering factors for non-hydrogen atoms were those of Cromer and Mann (15) and those for H were taken from ref. 16. Anomalous dispersion corrections were included for non-hydrogen atoms (17). H atoms were readily located from difference Fourier syntheses and included in the models in ideal positions (d(C—H) = 1.00 Å) with isotropic thermal parameters set to 1.1 times B_{equiv} of the C atoms to which they are bonded. H atom parameters were recalculated after each of the final cycles, but not refined. For each structure, the final difference Fourier map showed that the largest peak of residual electron density was 0.17 e Å^{-3} and

TABLE 3. Bond lengths (Å) and angles (deg) for *exo*-, *endo*-7-methylbicyclo[3.3.1]nonan-3-ones **3** and **4**

	3	**4**
Bond	Distance	
C(1)—C(2)	1.520(5)	1.536(3)
C(2)—C(3)	1.512(5)	1.512(3)
C(3)—C(4)	1.508(5)	1.510(3)
C(3)—O	1.214(5)	1.215(2)
C(4)—C(5)	1.529(5)	1.540(3)
C(5)—C(6)	1.532(5)	1.555(3)
C(6)—C(7)	1.537(5)	1.526(3)
C(7)—C(8)	1.521(5)	1.525(3)
C(7)—C(10)	1.524(5)	1.528(3)
C(8)—C(1)	1.532(5)	1.554(3)
C(1)—C(9)	1.526(5)	1.530(3)
C(9)—C(5)	1.527(5)	1.529(3)
Atoms	Angle	
C(8)—C(1)—C(2)	112.1(3)	111.5(2)
C(9)—C(1)—C(2)	109.6(3)	109.0(2)
C(8)—C(1)—C(9)	110.1(3)	110.3(2)
C(1)—C(2)—C(3)	114.7(3)	112.9(2)
C(2)—C(3)—C(4)	116.7(3)	116.0(2)
C(2)—C(3)—O	121.6(3)	121.8(2)
C(4)—C(3)—O	121.6(3)	122.2(2)
C(3)—C(4)—C(5)	114.7(3)	111.8(2)
C(4)—C(5)—C(6)	112.5(3)	111.1(2)
C(4)—C(5)—C(9)	108.9(3)	108.6(2)
C(6)—C(5)—C(9)	109.8(3)	111.1(2)
C(5)—C(6)—C(7)	113.0(3)	113.2(2)
C(6)—C(7)—C(8)	110.1(3)	109.9(2)
C(6)—C(7—C(10)	111.6(3)	111.6(3)
C(8)—C(7)—C(10)	111.6(3)	110.9(2)
C(7)—C(8)—C(1)	113.0(3)	114.0(2)

was of no chemical significance. Atomic coordinates and $B_{\text{equivalent}}$ values for non-hydrogen atoms are given in Table 2 and bond lengths and angles are summarized in Table 3.[2]

Results and discussion

The bicyclo[3.3.1]nonane skeleton has been the subject of numerous conformational analyses, mainly involving nmr spectroscopy or X-ray crystallography. We will restrict our discussion to those cases involving one keto centre at C-3.

The finding of a dichair structure for **3** (Fig. 1) is entirely expected. The deformations in this conformer are discussed in the next section. The chair–boat structure found for **4** (Fig. 2), with the ketone ring as the chair, is not unexpected, and serves to confirm the earlier analysis made by nmr spectroscopy (9). However, it is probable that the chair–boat and chair–chair conformers of **4** have quite similar energies since the corresponding *endo*-carbomethoxy compound is apparently a dichair (10). The steric bulk of a methyl group is generally considered to be somewhat larger than that of carbomethoxy (18), consistent with the observations, but also indicative of a fine dividing line here between conformations.

[2]A complete set of structure factor listings, anisotropic thermal parameters, and hydrogen atom parameters is available at a nominal charge, upon request from the Depository of Unpublished Data, CISTI, National Research Council of Canada, Ottawa, Ontario, Canada K1A 0S2.

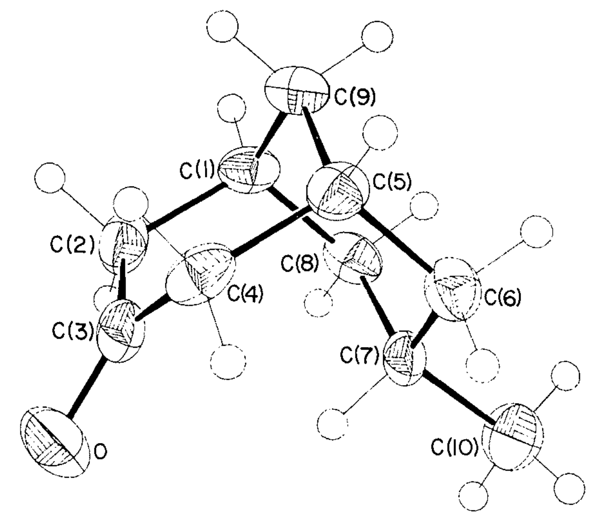

FIG. 1. A perspective view (Ortep) of the ketone **3** showing the atomic numbering scheme. Ellipsoids are drawn at the 50% probability level and hydrogens are included as spheres of radius 0.1 Å.

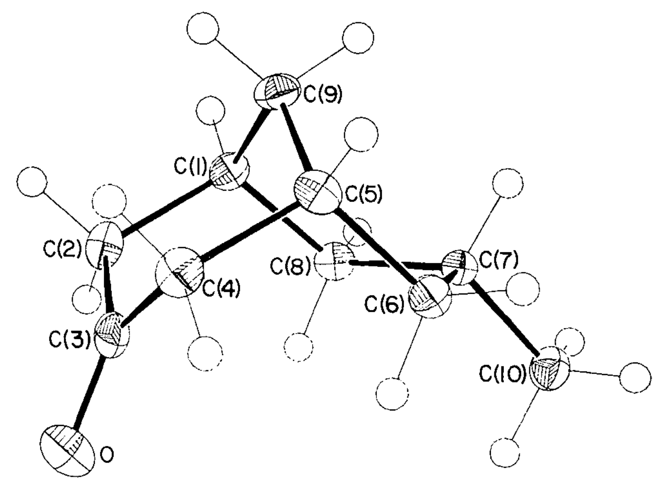

FIG. 2. A perspective view (Ortep) of the ketone **4** showing the atomic numbering scheme. Ellipsoids are drawn at the 50% probability level and hydrogens are included as spheres of radius 0.1 Å.

The crystal structures consist of discrete molecular units with the closest intermolecular contact being 2.54 Å for **3** (H10A(x, y, z) to H10C ($y - 1/2$, $1 - x$, $-z$)) and 2.38 Å for **4** (H10C (x, y, z) to H5 ($1 - x$, $1/2 + y$, $2 - z$)). Individual bond lengths and angles within the bicyclo[3.3.1]nonane skeletons of **3** and **4** show only minor deviations from the average values of 1.536(2) Å and 111.5° found in an electron diffraction study of the unsubstituted nonane (19). As one would expect, these deviations are greatest around atoms C(3) and C(7). A more detailed comparison between the present structures, **3** and **4**, and those determined by Murray-Rust *et al.* (11) **5** and **6**, is given in Table 4. The values are in general agreement within experimental error, with two minor exceptions: C_1—C_8(C_5—C_6) in **4** and the C=O distance for **5** are significantly longer than in the other structures. The latter has been ascribed to the disorder found in the crystal structure (11). The former could be a result of the chair–boat conformation which brings the *endo* H atoms on C(2), C(8) and C(4), C(6) closer than that found for **3** (avg. 2.43 Å for **3** vs. 2.34 Å for **4**). This is relieved in part by a slight lengthening of the C(1)—C(8)(C(5)—C(6)) and C(1)—C(2)(C(4)—C(5)) bonds.

TABLE 4. A comparison of bond lengths for **3**,* **4**,* *exo*-7-hydroxybicyclo[3.3.1]-nonane-3-one, **5**,† and *exo*-7-methoxybicyclo[3.3.1]nonane-3-one, **6**†

Bond (avg.)	Bond length (Å) 3	4	5	6
C(2)—C(3)(C(3)—C(4))	1.510(5)	1.511(3)	1.488(3)	1.500(7)
C(1)—C(2)(C(4)—C(5))	1.525(5)	1.538(3)	1.534(3)	1.510(7)
C(1)—C(9)(C(5)—C(9))	1.527(5)	1.530(3)	1.522(3)	1.520(7)
C(1)—C(8)(C(5)—C(6))	1.532(5)	1.555(3)	1.525(3)	1.527(7)
C(6)—C(7)(C(7)—C(8))	1.529(5)	1.526(3)	1.518(3)	1.508(7)
C(3)—O	1.214(5)	1.215(2)	1.245(3)	1.218(7)

*This work.
†Reference 11.

TABLE 5. Deformation of the chair rings in ketones **3** and **4** as measured by dihedral angles

Dihedral	Ketone	Angle (avg.*)
H(1)C(1)C(2)H(2) (*exo*)	**3**	46.4
	4	50.6
H(1)C(1)C(2)H(2) (*endo*)	**3**	71.5
	4	68.5
H(1)C(1)C(8)H(8) (*exo*)	**3**	54.3
	4	†
H(1)C(1)C(8)H(8) (*endo*)	**3**	64.5
	4	†

*Average of the 1, 2, 8 and 4, 5, 6 sides of the molecule.
†Boat conformation.

Ring deformations in 3

Repulsion between the C(3) and C(7) centres is expected to flatten both chairs in **3**. This deformation is most readily seen by looking at the $H_1C_1C_2H_2$ (*exo* or *endo*) and the H(1)C(1)-C(8)H(8) (*exo* or *endo*) dihedral angles. These are listed in Table 5. The best way to evaluate the flattening of the ketone chair in **3** is to compare the dihedral angles with those in **4**, where there is no C(3)—C(7) repulsion. This "extra" dihedral angle distortion is about 3–4° (Table 5). The other chair in **3** is also distorted from the theoretical 60° dihedrals by about 5°.

As a consequence of these distortions, the C(3)—C(7) distance in **3** is 3.004(5) Å and the *endo*-H(7)—C(3) distance is 2.43 Å. The details of the carbocation work on **2** and other 3-bicyclo[3.3.1]nonyl cations will be given in a separate paper. On the basis of the present structural work, it appears very probable that the undistorted C(3)—C(7) distance in a bicyclo[3.3.1]nonane is simply too long for the establishment of a μ-hydrido-bridged structure for **2**.

Acknowledgements

We thank Gerald Dimnik for his help in preparing ketones **3** and **4**, Dr. K. A. Kerr for the use of the diffractometer, and the Natural Sciences and Engineering Research Council of Canada for generous financial support.

1. R. P. KIRCHEN and T. S. SORENSEN. J. Am. Chem. Soc., **101**, 3240 (1979).
2. R. P. KIRCHEN, K. RANGANAYAKULU, A. RAUK, B. P. SINGH, and T. S. SORENSEN. J. Am. Chem. Soc., **103**, 588 (1981).
3. R. P. KIRCHEN, K. RANGANAYAKULU, B. P. SINGH, and T. S. SORENSEN. Can. J. Chem. **59**, 2173 (1981).
4. J. E. NORDLANDER, P. O. OWUOR, D. J. CABRAL, and J. E. HAKY. J. Am. Chem. Soc. **104**, 201 (1982).
5. J. E. NORDLANDER, K. D. KOTIAN, D. E. RAFF II, F. G. NJOROGE, and J. J. WINEMILLER. J. Am. Chem. Soc. **106**, 1427 (1984).
6. (*a*) M. A. EAKIN, J. MARTIN, W. PARKER, C. EGAN, and S. H. GRAHAM. Chem. Commun. 337 (1968); (*b*) W. T. MOODIE, W. PARKER, and I. WATT. J. Chem. Soc. Perkin Trans. 2, 664 (1979).
7. L. STÉHELIN, L. KANELLIAS, and G. OURISSON. J. Org. Chem., **38**, 847 (1973).
8. S. SAITO, T. YABUKI, T. MORIWAKE, and K. OKAMOTO. Bull. Chem. Soc. Jpn. **51**, 529 (1978).
9. A. G. YURCHENKO, S. D. ISAEV, T. N. UTOCHKA, and E. N. MARTYNOVA. Zh. Org. Khim. **10**, 1182 (1974).
10. G. E. RENZONI and W. T. BORDEN. J. Org. Chem., **48**, 5231 (1983).
11. J. MURRAY-RUST, P. MURRAY-RUST, W. C. PARKER, R. L. TRANTER, and C. I. F. WATT. J. Chem. Soc. Perkin Trans. 2, 1496 (1979).
12. K. KIMOTO, T. IMAGAWA, and M. KAWANISI. Bull. Chem. Soc. Jpn. **45**, 3698 (1972).
13. P. MAIN, S. E. HULL, L. LESSINGER, G. GERMAIN, J-P. DECLERCQ, and M. M. WOOLFSON. MULTAN 78, a system of programs for the automatic solution of crystal structures from X-ray diffraction data. University of York, York, England 1978.
14. J. M. STEWART. (*Editor*). Technical Report TR-446. Computer Science Centre, University of Maryland.
15. D. T. CROMER and J. B. MANN. Acta Crystallogr. Sect. A, **24**, 321 (1968).
16. R. F. STEWART, E. DAVIDSON, and W. SIMPSON. J. Chem. Phys., **42**, 3175 (1968).
17. International tables for X-ray crystallography. Kynoch Press, Birmingham, England. 1974.
18. E. L. ELIEL. Stereochemistry of carbon compounds. McGraw–Hill, New York. 1962.
19. E. L. OSINA, V. S. MASTRYUKOV, L. V. VILKOV, and N. A. BELIKOVA. J. Chem. Soc. Chem. Commun., 12 (1976).

Bicyclization of aza-compounds by positive halide ions. I. Cyclic amines[1]

R. M. ELOFSON, F. F. GADALLAH, AND J. K. LAIDLER
Alberta Research Council, Edmonton, Alta., Canada T6G 2G2

Received January 9, 1984[2]

R. M. ELOFSON, F. F. GADALLAH, and J. K. LAIDLER. Can. J. Chem. **63**, 1170 (1985).

Cyclic amines are oxidized to the bicyclic compounds by electrochemical oxidation. The presence of halide ions is found necessary for the reaction to proceed and to produce any bicyclic products. It is postulated that a positive halide species, $X^{(+)}$, is produced electrochemically and stabilized under the specific reaction conditions. The $X^{(+)}$ ion forms a complex with the parent cyclic amine which decomposes to the bicyclic product and HX. An analogy between the Hofer–Moest reaction to produce $C^{(+)}$ and this reaction to produce $X^{(+)}$ is postulated

R. M. ELOFSON, F. F. GADALLAH et J. K. LAIDLER. Can. J. Chem. **63**, 1170 (1985).

L'oxydation électrochimique des amines cycliques conduit à des composés bicycliques. On a trouvé que la présence d'ions halogénures est nécessaire pour que la réaction se produise et qu'elle conduise à des composés bicycliques. On fait le postulat qu'il y a production électrochimique d'un halogénure positif, X^+, qui est stabilisé dans les conditions spécifiques de la réaction. L'amine cyclique de base et l'ion X^+ formeraient un complexe qui se décomposerait en produit bicyclique et en HX. On fait le postulat qu'il existe une analogie entre la réaction de Hofer–Moest qui conduit à la formation de C^+ et cette réaction qui fournit des X^+.

[Traduit par le journal]

Introduction

Some time ago, Edwards and co-workers (1) succeeded in preparing indolizidine in 68% yield from *N*-chloroazacyclonane **1** in the presence of silver ions and aqueous dioxane. The reaction, as shown in [1], had every appearance of proceeding by way of a nitrenium ion **11**. After that discovery,

[1]

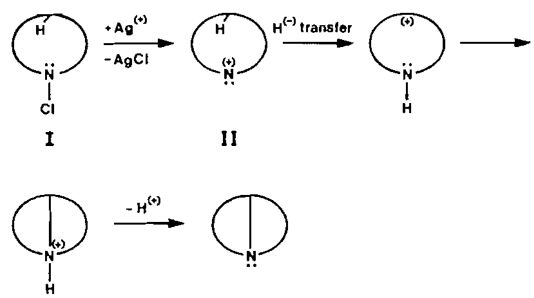

rapid development of nitrenium ion chemistry began, principally in Gassmann's laboratories (2).

Later, Edwards and Vocelle (3) found that silver (Ag^0) also leads to bicyclization. They presented evidence that the bicyclization involves a free radical mechanism with a transannular hydrogen abstraction (t.a.h.a.) via a homolytic pathway, as illustrated in [2].

[2]

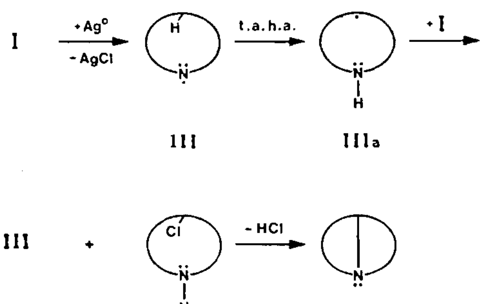

Earlier, Wawzonek and Culbertson (4) worked on a closely related problem. Those workers effected the cyclization of dibutylamine by irradiating chloramine **V**. As shown in [3],

[3]

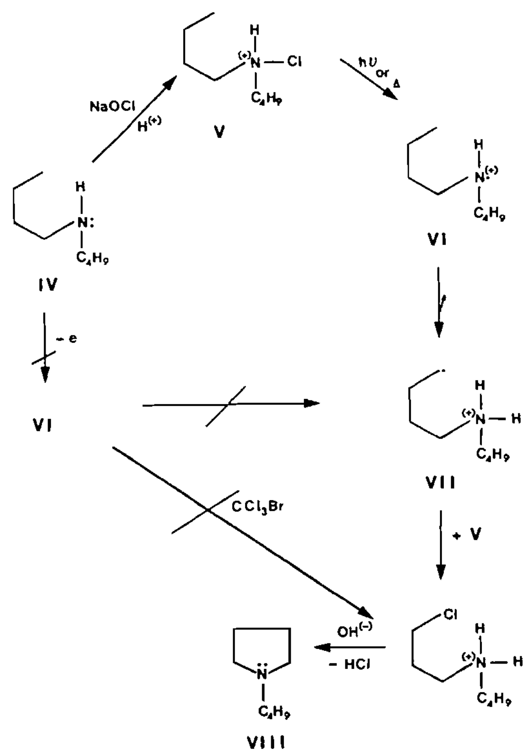

the cation–radical intermediate, **VI**, was proposed. However, Wawzonek's later attempts (5) to produce the cyclicized product, **VIII**, by anodic oxidation of the amine, **IV**, in a methanol–water mixture containing tetramethylammonium tetrafluroborate were unsuccessful.

Later, Waegell and co-workers (6) achieved the production of *N*-chloro, *N*-methyl, 5-methylaminobicyclo[2.2.1]hept-2-ene in neutral medium. The authors verified that, under conditions thought to induce formation of nitrinium ions, only the homolytic reactions occurred.

Edward's (3) and Wawzonek's (4) mechanisms for cycliza-

[1]Alberta Research Council Contribution No. 1311. Parts of this paper were discussed in talks at The North American Chemical Congress, Mexico City, 1975; Electrochemical Society, Washington, DC, 1976; and 6th North American Meeting of Catalysis Society, Chicago, 1979.

[2]Revision received August 28, 1984.

TABLE 1. E (V) vs. sce (V) of amines, amides, and halide ions

Species	E_1*	E_2*
Amines	+1.2 to 1.3	
$Cl^{(-)}$	+1.1	+1.7
$Br^{(-)}$	+1.03	+1.39
$I^{(-)}$	+0.25	+0.55

*E_1 and E_2 are half-wave potentials.

tion or bicyclization of haloamines are very similar in that they proceed via intramolecular hydrogen abstraction and the abstraction of Cl· from the starting material by a reactive intermediate, **III***a* or **VII**, respectively.

Starting with a cyclic amine, a prediction of the intermediate products is shown in [4]. The parent compounds **IX** would lose an electron on the anode to give a cation radical **X**. Route A or B would follow. Because the transannular hydrogen abstraction would have a faster rate than hydrogen abstraction from the solvent, route A was preferred over B. Since protonation is prevented in basic media, bicyclization would be encouraged. Reaction [4] shows the loss of two electrons and two protons in routes A and B.

[4]

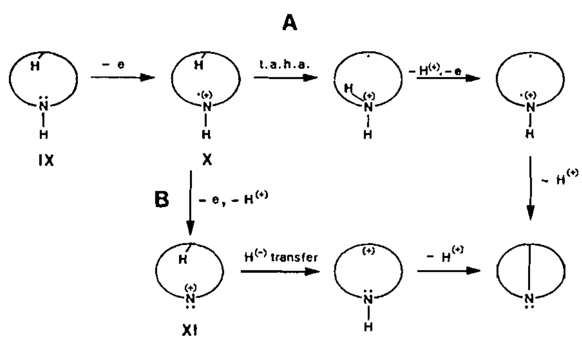

Results and discussion

Attemps to carry out the oxidation of azacyclononane in acetonitrile, tetrabutylammonium fluoroborate or perchlorate as the electrolytic support and Pt, C, Hg, or stainless steel anodes at controlled potentials of 1.3 V corresponding to one electron oxidation or at controlled currents corresponding to much higher voltages of either the amine or the halide ions, Table 1, produced no detectable bicyclic products. Loss of starting material occurred due to other reactions. It seems that the cation radical as it was produced, abstracted hydrogen from (*a*) the solvent to produce electrochemically inactive ammonium ion, or (*b*) from an adjacent carbon leading to Schiff's base (7, 8). To discourage hydrogen abstraction from the solvent and to encourage proton removal, water was added to the reaction mixture, but no bicyclization occurred. This implies that t.a.h.a., which should produce bicyclic products via route A, did not occur. However, when a graphite anode was used in 10% water in acetonitrile in the presence of lithium chloride and 100 mA current, 3% bicyclic product was obtained. More bicyclic product, 64%, was obtained with lithium bromide using 20% of water as in [5].

We found that specific conditions have to be attained to produce the respectable yields for medium sized rings (C_7-C_9 amines) shown in Table 2. These specific conditions are (*1*) water, halide ion, and hydroxide ion or basic medium; and (*2*) a carbon anode and a current of 100 to 150 mA corresponding to a potential of approximately 2.3 V.

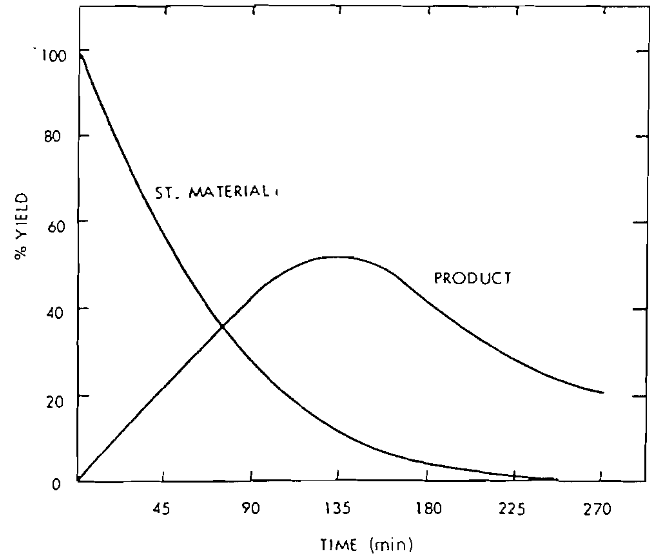

FIG. 1. Production and destruction of cyclic and bicyclic amines by further oxidation.

TABLE 2. Bicyclization of cyclic amines: 20% H_2O in CH_3CN, C anode, 0.1 *M* LiBr, 100 mA

Cyclic amine	Bicyclic product*		%	Time (h)
C_7NH_{15}	a	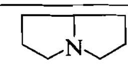	52	2.5
C_8NH_{17}	b	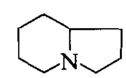	71	2.5
C_9NH_{19}	c	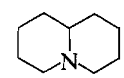	10	3.0
	d	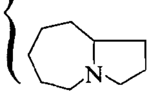	3.5	

*a = azabicyclo [3.3.0] octane, b = azabicyclo [4.3.0] nonane, c = azabicyclo [4.4.0] decane, d = azabicyclo [5.3.0] decane.

However, high current and high voltage at the anode also cause the destruction of the starting material as well as the products. Figure 1 shows the time course of anodic oxidation of C_7 cyclic amine. The reaction must be monitored to obtain maximum yields.

The experimental conditions necessary to obtain significant yields are similar to those of the Kolbe acid oxidation (9) and specifically to the Hofer–Moest reaction (10). This implies a similar reaction mechanism. Beyond this, caution must be exercised in postulating a mechanism. As stated in a review on the Kolbe and Hofer–Moest reactions, "The course of a particular oxidation, thus, depends on both the nature of the intermediate radical and the experimental conditions, and the proper choice of reaction parameters frequently permits the predominant formation of either radical derived or cation derived products. As we can see, all aspects of the mechanism of these reactions are subject to controversy" (11). At this stage it is only possible to point out some analogies for a possible mechanism for the bicyclization of cyclic amines described here.

An explanation for the way in which these reactions proceed was found in Anson's studies on the pattern of ionic and molecular adsorption at a smooth platinum electrode in aqueous media (12). However, his findings could be extended to accommodate our system. Anson found that at high positive charge densities, such as in our system, the halide ions are strongly adsorbed. But neutral molecules such as amines are weakly adsorbed, and "the interaction energy of the water dipole with the electric field at the surface becomes so large that the water molecules are preferentially adsorbed and the organic molecules, i.e. amine, thereby desorbed from the surface" (12).

In the case of the Hofer–Moest reaction, caboxylate anions are adsorbed and oxidized at the anode first to an alkyl radical plus carbon dioxide. The alkyl radical, still at the carbon anode, loses another electron to produce a carbonium ion which upon desorption from the positively polarized anode undergoes further reaction to produce the varied products of this well known reaction. In the case of the bicyclization described here, it is clear from Anson's review that halide ions would be adsorbed and the cyclic amines would be desorbed at the high positive potentials in the partly aqueous media used. In analogy with the Hofer–Moest reaction, it is here suggested that the halide atoms may lose another electron before desorption from the anode whereupon reaction occurs with the amine, Table 1. If indeed a positive halide species is produced it would first be produced as a ground state triplet $X^{\uparrow\uparrow}$ (Hund's rule). This triplet would rapidly change to the hydrated singlet due to energy of solvation, although it might be stabilized at the carbon electrode for a short time. In any event there would appear to be a close relationship between the electrochemical bicyclizations caused by positive halide ion as proposed and the formation of a carbonium ion which was suggested by Koehl (13) to produce methyl acetate as the major product instead of ethane when carbon was used instead of platinum as anodic material in the oxidation of potassium acetate. Further work on these mechanisms remains to be done. It should be noted, however, that *N*-chloroamines were stable in the presence of the carbon anode but when current was passed through the system a little bicyclization (0.6%) occurred. When lithium bromide was added and current applied, 3.5% bicyclization occurred in 4 h. Under the standard electrochemical conditions described in Table 2, very good yields were obtained.

Experimental

Reagents

All reagents and solvents were purified by published methods (14) except as specified. Solid reagents and reference compounds were recrystallized and melting points agreed with literature values.

Cyclic and bicyclic amines

C_7 and C_8 cyclic amines were obtained from Aldrich. C_8—N—Cl was prepared by a method in ref. 3. C_{12} amine was prepared by $LiAlH_4$ reduction of the parent lactam and purified by distillation. C_9 cyclic and C_7–C_9 bicyclic amines were otained from Dr. O. E. Edwards, N.R.C., Ottawa.

Electrodes

Natural graphite (George F. Pettisos, Canada). Porous carbon, 60 (Union Carbide S2408-60). Porous carbon, 45 (Union Carbide S2584-45). All the above cut to 5 cm high and 1.5 cm diameter. Stainless steel 304, 1/8 in rod. Platinum in fine mesh in a cylinder 5 cm high and 1.5 cm diameter.

Procedure

A three-neck round bottle flask served as the electrolytic cell. The flask could be fitted with a side arm and a fine fritted glass disc to provide two compartments for the cathode and anode. However, separation of the electrodes did not produce any significant differences in the results.

Since each reaction has to be monitored to ensure maximum yield, samples were withdrawn periodically for analysis. Each sample (2.3 mL) was made alkaline enough in the cold to separate the organic and aqueous layer. The organic layer was separated and the aqueous solution washed with ether. The ether solutions were added to thc organic layer, dried, concentrated, and used for glc analysis.

The final reaction mixture was acidified, concentrated to 1/10 of its original volume, made alkaline, extracted with ether, and dried. The ether was concentrated to a known volume and then used for analysis.

Instrumental analysis

Gas liquid chromatography: Hewlett-Packard 810 Res. Chromatograph, dual column, T.C. detector. Mass spectrometry: Perkin-Elmer 270. Column, 10% SE30 on Chemosorb W.AW. DMCS 60/80 mesh, 1/8 in × 12 in, temperature programming 20°C/mt to 280°C.

Acknowledgements

We are grateful to Drs. O. E. Edwards and M. H. Benn for their helpful discussions, generous supply of the cyclic and bicyclic compounds and general support.

1. O. E. EDWARDS, D. VOCELLE, J. W. APSIMON, and F. HAGUE. J. Am. Chem. Soc. **87**, 678 (1965).
2. P. G. GASSMANN. Acc. Chem. Res. **3**, 26 (1970), and references therein.
3. O. E. EDWARDS and D. VOCELLE. Can. J. Chem. **50**, 1167 (1972).
4. S. WAWZONEK and T. P. CULBERTSON. J. Am. Chem. Soc. **81**, 336 (1959).
5. S. WAWZONEK and S. M. HEILMANN. J. Electrochem. Soc. **121**, 378 (1974).
6. R. FURSTOSS, R. TADAYONI, and B. WAEGELL. Nouv. J. Chem. **1**, 167 (1977).
7. C. K. MANN and K. K. BARNES. Electrochemical reactions in non-aqueous systems. Debber, New York. 1970 Chapt. 9.
8. M. MASNI and H. SAYO. J. Chem. Soc. B. 1593 (1971).
9. H. KOLBE. Ann. Chem. Pharm. **69**, 257 (1849).
10. H. HOFER and M. MOEST. Justus Liebigs Ann. Chem. **323**, 285 (1902).
11. S. D. ROSS, M. FINKELSTEIN, and E. F. RUDD. *In* Anodic oxidation. Vol. 32. Organic chemistry, a series of monographs. *Edited by* Alfred T. Blomquist and Harry H. Wasserman. Academic Press, New York. 1975. p. 134.
12. F. C. ANSON. Acc. Chem. Res. **8**, 400 (1975).
13. W. J. KOEHL, JR. J. Am. Chem. Soc. **87**, 4686 (1964).
14. F. F. GADALLAH and R. M. ELOFSON. J. Org. Chem. **34**, 3335 (1969).

The electronic absorption spectra of some coumarins. A molecular orbital treatment

RAFIE H. ABU-EITTAH AND BAHGAT ALI H. EL-TAWIL
Department of Chemistry, Faculty of Science, King Abdulaziz University, Jeddah, Saudi Arabia

Received June 14, 1984[1]

RAFIE H. ABU-EITTAH and BAHGAT ALI H. EL-TAWIL. Can. J. Chem. 63, 1173 (1985).

The electronic absorption spectra of coumarin and its derivatives umbelliferone (6-hydroxycoumarin), esculetin (6, 7-dihydroxycoumarin), and scopoletin (6-methoxy-7-hydroxycoumarin) were investigated. The $n \rightarrow \pi^*$ transition was not observed in the spectrum of coumarin but was observed in the spectra of some of its derivatives. Molecular orbital calculations, using the INDO procedures, were carried out on coumarin and some of its derivatives. The activities of the different sites of the molecules are discussed in terms of the coefficients of the atomic orbitals constituting the HOMO and the LUMO. The correspondence between the calculated and experimental transition energy and band intensity is satisfactory.

RAFIE H. ABU-EITTAH et BAHGAT ALI H. EL-TAWIL. Can. J. Chem. 63, 1173 (1985).

On a étudié les spectres d'absorption électronique de la coumarine et de ses dérivés, à savoir l'umbelliférone (hydroxy-6-couramine), l'esculétine (dihydroxy-6,7, coumarine) et la scopolétine (méthoxy-6-hydroxy-7 coumarine). On n'a pas observé de transition $n \rightarrow \pi^*$ dans le spectre de la coumarine mais on l'observe dans le spectre de certains dérivés. On a effectué des calculs d'orbitales moléculaires, selon les méthodes INDO, sur la coumarine et sur certains de ses dérivés. On discute de l'activité des différents sites des molécules en fonction des coefficients des orbitales atomiques haute occupée et basse vacante. On trouve satisfaisant la concordance entre les valeurs calculées et expérimentales des énergies de transition des intensités des bandes.

[Traduit par le journal]

Introduction

Coumarin and many of its derivatives have such marked physiological effects as active hypotoxicity, carcinogenicity, anticoagulant action, and antibiotic activity. Perhaps of the greatest fundamental biochemical interest is the photosensitizing effect on cells of certain linear furanocoumarins, which is intimately associated with their cross-linking of the strands of DNA.

An attempt to correlate the biological activities and electronic structures of some coumarins was made by Heathcote and Hibbert (1); Hückel molecular orbital calculations were performed and were used to extend previous calculations (2) performed on aromatic hydrocarbons.

Link's group (3) early examined 106 samples of 4-hydroxycoumarins and found dicoumarol to have a higher anticoagulant activity than any of the synthetic coumarins tested. The minimal structural requirement for such an activity was an intact 4-hydroxycoumarin residue.

Coumarins showed a varying inhibiting effect on enzymes. The structure of coumarin is responsible for the specific inhibition of the enzyme. Umbelliferon (7-hydroxycoumarin) had no inhibition effect, contrary to 4-hydroxycoumarin (4, 5). Dihydroxy derivatives were more effective than monohydroxy ones, especially when occupying vicinal positions. Electron transport processes were also inhibited by dihydroxycoumarins (5).

Wald and Feuer (6) conducted a structure–activity relationship study on the ability of coumarin and nine of its natural and synthetic derivatives to induce drug-metabolism enzymes in rat liver. They calculated σ and π-electron density at the various positions of the coumarin nucleus and related the enzyme induction to the calculated values.

Recent studies have indicated some antitumour activity by simple coumarins. Coumarin itself has been reported to be a moderately potent inhibitor of chemical carcinogen-induced neoplasia (7), and other related coumarins have antitumour activity (8, 9).

Coumarins are known by their lasing effect. The coumarin class of laser dyes has either an hydroxyl or amino group at C-7 of the coumarin nucleus. The effects of substituents on the lasing characteristics of these compounds have been reported (10–13). The synthesis of several new laser dyes and the effects of substituents on their fluorescence maxima and fluorescence quantum yields have also been reported (14).

Fluorescence spectra excited by 2-photon absorption of the 6943-A° line of a ruby laser was investigated (15*a*). Results show large single values of non-linear second-order optical susceptibility. Kobayashi (15*b*) studied the picosecond kinetics of 7-hydroxy-4-methylcoumarin in the lowest singlet excited state and confirmed that the excited anion of this coumarin system is formed through the excited state of the neutral molecule.

In spite of the vast biological importance of coumarins, a detailed study of their spectra and electronic structure is lacking in the literature. The reported spectral behaviour has only been for diagnostic purposes and the observed bands were assigned to the benzene and pyrone rings (16, 17). The spectra of hydroxycoumarins and many of their derivatives, have been reported (18). Useful for diagnostic purposes was the finding that acetylated phenolic coumarins show uv spectra similar to those of the corresponding parent hydrocarbons (19, 20).

The shifts observed when running the spectra of coumarins in alkaline media have been widely used for differentiation (21–23) and diagnostic purposes (24). Spectral shifts produced when other inorganic reagents are added to ethanolic solutions of certain coumarins are also of diagnostic value (25, 26).

The only MO calculations performed on coumarins were on its π-system or using the EHT procedures (27). In this work the electronic absorption spectra of some coumarins, namely, coumarin, umbelliferone (7-hydroxycoumarin), escoletin (6,7-dihydroxycoumarin), and scopoletin (6-methoxy-7-hydroxycoumarin) were investigated. Molecular orbital calculations using all valence electrons by means of the INDO procedure were performed on the above compounds as well as on some aminocoumarins. The calculated parameters, namely, total energy, transition energy, charge density, dipole moment, σ and π population analysis, etc. are not available in the literature and

[1]Revision received November 16, 1984.

are essential in understanding the electronic structure of the compounds studied.

Experimental

Ethanol (Koch light spectroscopic reagent grade) and dioxan (Merck reagent grade) were used without further purification.

Coumarin, umbelliferone, esculetin, and scopoletin were obtained from Sarsyntex Laboratories, Sarget. The purity of the samples was confirmed by tlc procedures.

The spectra were recorded on a Cary-17 spectrophotometer using 1.0-cm^3 fused silica cells.

Results and discussion

A. *Electronic absorption spectra*

(i) Coumarin

The spectra of coumarin reported in the literature were not investigated further. The positions of band maxima, and their shift on varying the medium were used for identification purposes. The bands observed were sometimes assigned to transitions either on the benzene nucleus or on the pyrone nucleus. Such an interpretation is a rather crude one since the two chromophores, benzene and pyrone, are fused together and the

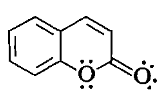

molecular orbitals will encompass the whole molecule and will not be localized on one of the chromophores. The π-electrons of the molecule are delocalized and the observed transitions should be assigned to the molecule as one unit. The method of "bisecting" the molecule to a number of non-interacting chromophores is an approximate one and has a meaning only if the chromophores are separated by more than one σ bond or if steric effects operate to distort the coplanarity of the different chromophores constituting the molecule. In the case of coumarin it is meaningless to bisect it into separate chromophores, and the observed spectral bands should be assigned to electronic transitions between molecular orbitals characteristic of the molecule.

The coumarin spectrum, in the accessible uv region, may show an $n \rightarrow \pi^*$ transition in addition to a number of $\pi \rightarrow \pi^*$ transitions. The $n \rightarrow \pi^*$ transition would be mainly localized on the C=O chromophore and may not be the lowest energy transition. The C—O—C bond angle in coumarin is 1.22°, indicating an sp^2 hybridization of the ring-oxygen atom (28). Hence, one of the lone pairs of electrons on that atom occupies a $2p_z$ atomic orbital and is a part of the π-system of the molecule.

Figure 1 shows the electronic absorption spectra of coumarin using ethanol and dioxan as solvents. Solvent polarity did not affect the position of band maxima, indicating that the polarity of the excited state is not significantly different from the polarity of the ground state. Electronic transitions which lead to polar states are stabilized in polar solvents, leading to a red shift of band maxima. The spectrum of coumarin shows three absorption bands none of which correspond to an $n \rightarrow \pi^*$ transition. This conclusion is supported by the high intensity (ϵ varied from 6,000 to 15,000) of the observed bands. Usually, $n \rightarrow \pi^*$ transitions are symmetry forbidden and ϵ is less than 100. Also, the absorption bands corresponding to $n \rightarrow \pi^*$ transitions are blue-shifted and blurred in polar solvent. The absorption band around 275 nm is asymmetric and the presence

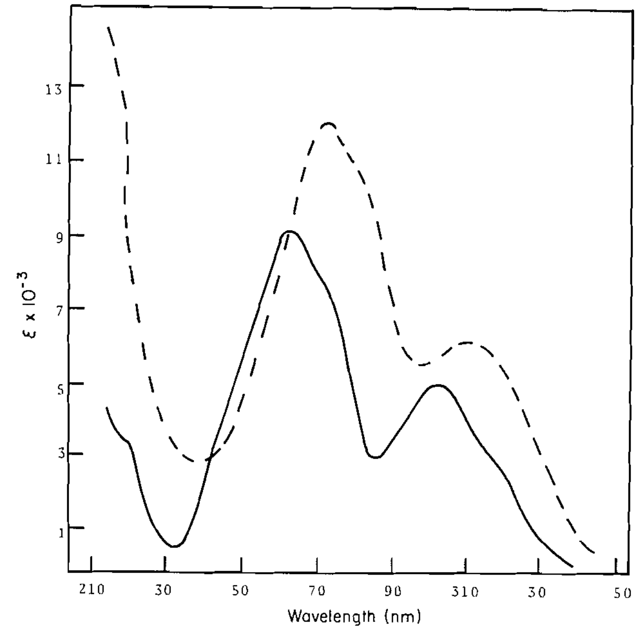

FIG. 1. The electronic absorption spectra of coumarin in dioxan (———); in ethanol (----).

TABLE 1. Numerical values of band maxima and intensities of the studied coumarins in ethanol

Compound	λ_{max} (nm)	ϵ (M^{-1} L^{-1})	f
Coumarin	310	6000	0.23
	285	10000	0.14
	274	12000	0.23
	220		
Umbeliferone	370	2200	0.04
	330	16830	0.43
	290	7300	0.15
	255, 240	4200, 5400	0.18
	220	14 290	—
Esculetin	400	3100	0.05
	350	11900	0.29
	300	5900	0.12
	260	5700	0.11
	230	16000	0.52
Scopoletin	400	3060	0.05
	345	12810	0.30
	300	5570	0.15
	253	6200	0.16
	230	15600	0.52

of a long wavelength shoulder is quite apparent. This observation may indicate that the band represents two overlapping electronic transitions; confirmation of such a conclusion will be by means of MO calculations.

The observed bands (Fig. 1) correspond to $\pi \rightarrow \pi^*$ transitions and the expected $n \rightarrow \pi^*$ transition is submerged under the strong $\pi \rightarrow \pi^*$ one. The position of the $n \rightarrow \pi^*$ transition will be predicted by MO calculations. As is evident, none of the observed $\pi \rightarrow \pi^*$ transitions can be assigned to the benzene or to the pyrone chromophores of the coumarin molecule. The observed bands correspond to transitions between MO's characteristic of the coumarin molecule.

Table 1 gives the values of band maxima, molar extinction coefficient, and oscillator strength of the observed bands.

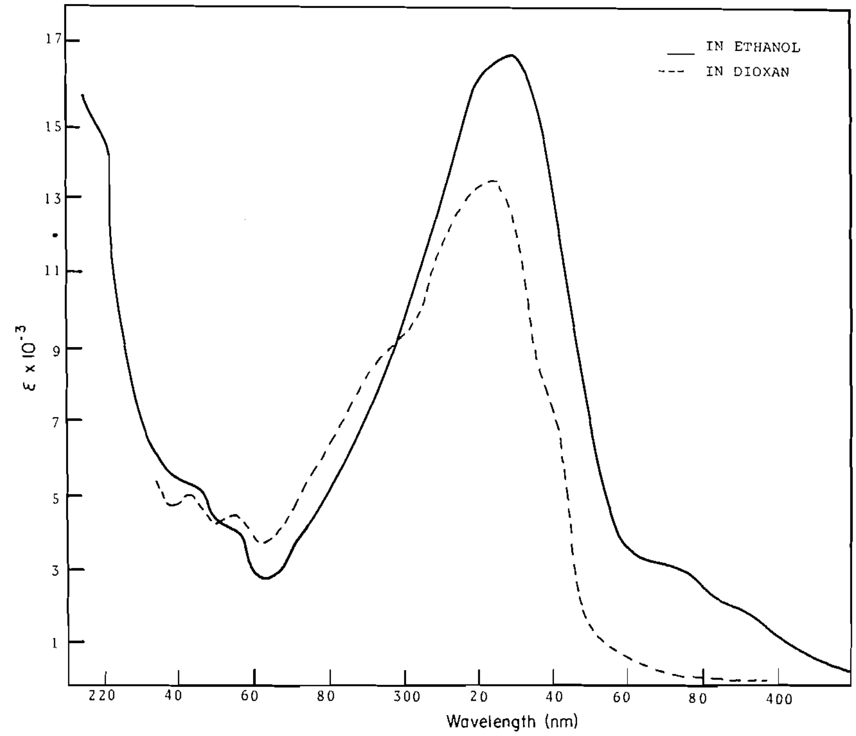

FIG. 2. The electronic absorption spectra of umbelliferone.

(ii) Substituted coumarins

Substitution in the coumarin nucleus by chromophores such as —OH, —OCH_3, —CH_3, and —NH_2 perturbs the electronic transitions of coumarin. The pertubation effect depends on

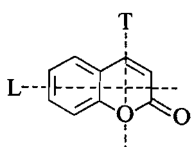

the extent of the interaction between the substituent and the π-system of the coumarin nucleus. The bands which will be perturbed depend on the position of the substituent, whether along the transverse, T, or the longitudinal, L, axis.

Figure 2 shows the electronic absorption spectra of umbelliferone (7-hydroxycoumarin). Substitution by an —OH group in the ring perturbed the spectrum significantly. Polar forms such as (b) are expected to contribute to the ground and mainly to the excited states. This contribution has resulted in a significant lowering of the energy levels as compared to those of coumarin. A pronounced red shift is encountered with all the

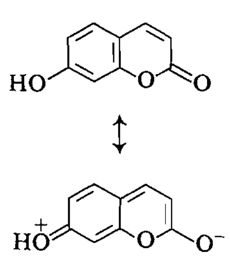

(a)

(b)

observed transitions; the lowest energy one appears in the region of 370 nm compared to 310 nm in coumarin, indicating that the contribution of tautomer (b) to the structure of umbelliferone is significant. The spectrum of umbelliferone shows at least five electronic transitions in the accessible uv region compared to the possibility of four electronic transitions for coumarin in the same region. The broad, intense and unsymmetric band in the region of 320 nm (Fig. 2) represents two overlapping transitions. The presence of a shoulder at the short wavelength end of the band is quite apparent. The observed bands represent $\pi \rightarrow \pi^*$ transitions, the weak $n \rightarrow \pi^*$ transition is submerged by the stronger $\pi - \pi^*$ one.

Substitution by another —OH group at C(6) facilitates the formation of the polar tautomer (c); hence one expects a further

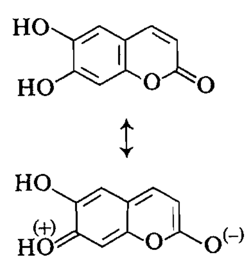

(c)

red shift in band maxima. The bands of esculetin (6, 7-dihydroxycoumarin) are red-shifted (Fig. 3) compared to those of umbelliferone but the same electronic transitions are observed in both compounds. An interesting observation is that the two overlapping transitions (in the region of 300 nm) in the case of umbelliferone are resolved in the case of esculetin. The predominant contribution of tautomer (c) to the structure of esculetin explains the significant variation of its spectrum from that of coumarin.

The replacement of one of the —OH groups in esculetin with a methoxy group (scopoletin) produces a minor effect on the spectrum (Fig. 4). The methoxy group is a stronger electron donor than the hydroxy group but the extent of their interaction with the π-electron system of the coumarin nucleus is the same.

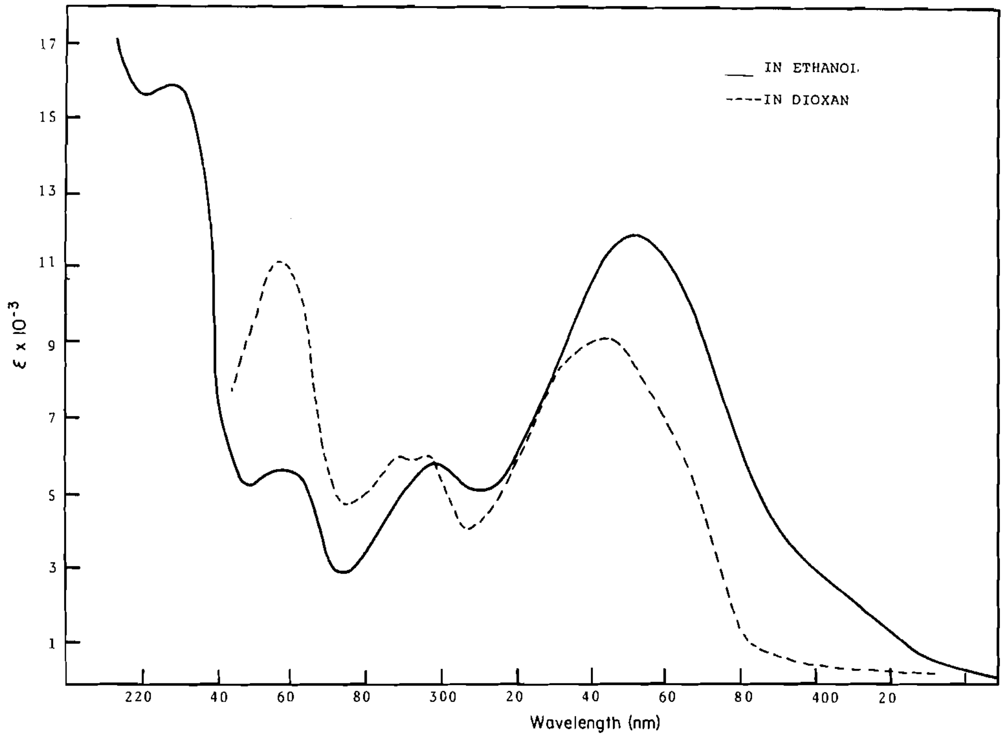

FIG. 3. The electronic absorption spectra of esculetin.

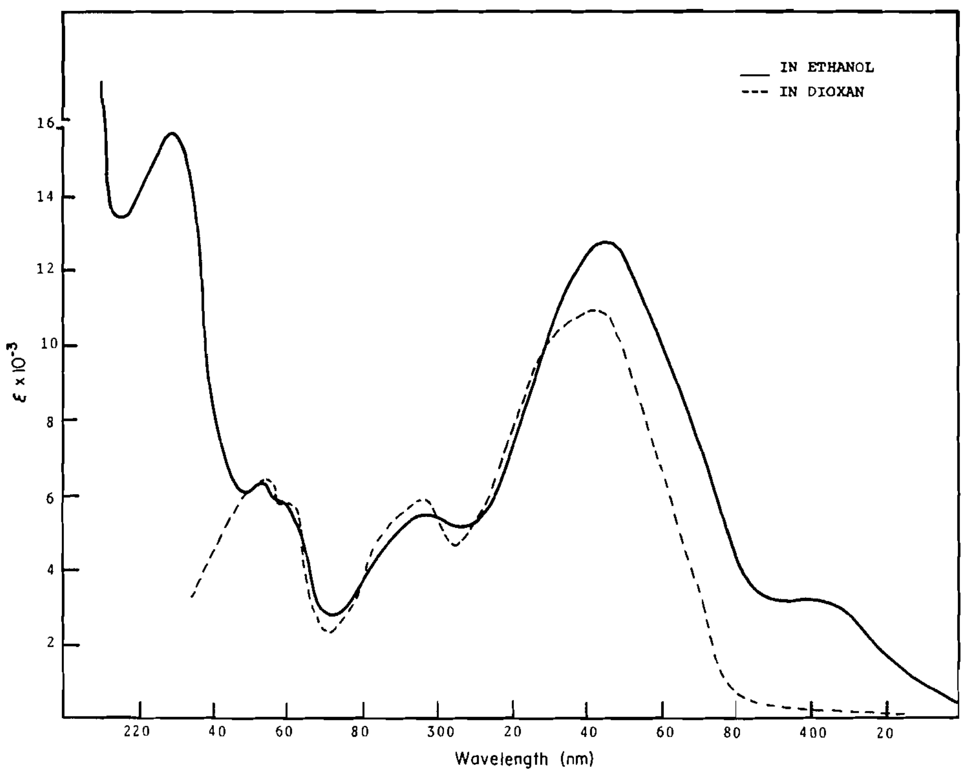

FIG. 4. The electronic absorption spectra of scopoletin.

This is seen when comparing the values of band maxima in the spectra of the two compounds; minor differences, if any, are detected. The values of band intensity confirm that all the observed transitions are $\pi \rightarrow \pi^*$ ones.

B. *Molecular orbital calculations*

It is established that a "structure–function" relationship exists for many biological compounds. The previously reported structural investigations considered only the "π" system of coumarins (1, 2, 27). In this work molecular orbital calculations were performed, using the INDO procedure, on coumarin and some of its derivatives, namely, 6-hydroxy-, 6,7-dihydroxy-, 6-amino-, 6,7-diamino-, 6-hydroxy-7-amino-, and 6-amino-7-hydroxycoumarins. Some of these coumarins and

TABLE 2. The numerical values of the charge density and the coefficients of AO's of selected atoms in the HOMO and LUMO of some coumarins

Compound	Atom C(2)	C(3)	C(4)	O(11)
6-Hydroxycoumarin	0.1099*	0.5865	0.2093	−0.3335
	0.1811†	0.4356	−0.4182	−0.1841
	0.4386‡	−0.1633	0.0971	−0.4698
7-Hydroxycoumarin	−0.1110	−0.6149	−0.1906	0.3274
	−0.1689	−0.4018	0.4199	0.1681
	0.4383	−0.2021	0.1139	−0.4759
6,7-Dihydroxycoumarin	−0.1109	−0.5929	−0.1881	0.3258
	0.1720	0.4166	−0.4143	−0.1741
	0.4404	−0.1902	0.1123	−0.4728
6-Aminocoumarin	0.1093	0.5863	0.2042	−0.3323
	0.1785	0.4319	−0.4197	−0.1815
	0.4399	−0.1719	0.1031	−0.4699
7-Aminocoumarin	0.1102	0.6073	0.1869	−0.3236
	−0.1702	−0.4063	0.4219	0.1699
	0.4393	−0.2014	0.1140	−0.4747
6,7-Diaminocoumarin	−0.1121	−0.5762	−0.1649	0.3156
	−0.1723	−0.4134	0.4192	0.1734
	0.4388	−0.1915	0.1091	−0.4741
6-Hydroxy-7-amino-coumarin	0.1118	0.5873	0.1769	−0.3200
	0.1726	0.4314	−0.4172	−0.1735
	0.4387	−0.1892	0.1083	−0.4737
6-Amino-7-hydroxycoumarin	−0.1113	−0.5809	−0.1758	0.3216
	−0.1722	−0.4166	0.4163	0.1742
	0.4405	−0.1924	0.1132	−0.4731
Coumarin	−0.1070	−0.6149	−0.2209	0.3369
	0.1747	0.4239	−0.4231	−0.1767
	0.4415	−0.1899	0.1140	0.4709

*Coefficients of the AO's in the HOMO (π).
†Coefficients of the AO's in the LUMO (π)*.
‡Net atomic charges density.

TABLE 3. A comparison of the calculated parameters of the studied isomeric coumarins

Compound	Total energy (eV)	Lowest transition energy (eV)	Dipole moment (D)
6-Hydroxycoumarin	−832	3.61	7.72
7-Hydroxycoumarin	−833	3.49	7.17
6-Aminocoumarin	−706	3.39	8.69
7-Aminocoumarin	−706	3.47	9.03
6-Hydroxy-7-amino-coumarin	−929	3.46	8.30
6-Amino-7-hydroxycoumarin	−930	3.46	7.23
Coumarin	−607	3.60	8.22

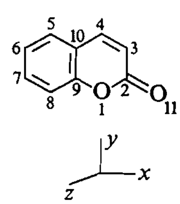

their heteroanalogues are used as laser sources and information about their electronic structure is essential.

The formalism and parameterizations of the INDO procedure may be found in the literature (29, 30). The values of bond lengths and bond angles required to define the geometry of the compounds studied have been reported previously (28, 31). The configuration we used in our calculations is shown.

The results of computations are given in Tables 2 and 3. The numerical values of the coefficients of the atomic orbitals of the active sites C(2), C(3), C(4), and O(11), participating in the highest occupied and lowest vacant molecular orbitals, as well as the net charge on these sites are given in Table 2.

A comparison of the calculated parameters for some isomeric coumarins is given in Table 3. Table 4 compares the experimentally found transition energies and oscillator strengths with theoretically calculated ones.

Discussion and conclusions

The coumarins studied are strong dipoles, hence excitation

TABLE 4. Comparison between experimentally found and theoretically calculated transition energy and oscillator strength

Compound	Transition energy		Oscillator strength	
	Exp.	Calcd.	Exp.	Calcd.
Coumarin	—	3.19	—	0.0
	3.9	3.6	0.23	0.79
	4.35	4.65	0.14	0.29
	4.51	4.71	0.23	0.34
	5.60	5.21	—	0.18
Umbelliferon (7-hydroxycoumarin)	3.35	3.35	0.04	0.00
	3.75	3.49	0.43	0.84
	4.27	4.48	0.21	0.32
	5.12	4.73	0.18	0.23
		5.06		0.17
Esculetin (6,7-dihydroxycoumarin)	3.2	3.27	0.05	0.00
	3.5	3.4	0.29	0.84
	4.13	4.5	0.12	0.37
	4.77	4.55	0.11	0.37
	5.39	5.10	0.52	0.27

of an electron is not expected to affect the polarity of the ground state. As a result, band maxima of the observed electronic transitions will not be apparently affected by solvent polarity. This result is evident when comparing the spectra of the coumarins studied in ethanol and dioxan.

The spectral behaviour of these coumarins indicates that substitution by an —OH group apparently affects the observed transitions. This result is evidence that tautomers such as (b) and (c) contribute significantly to the structures of hydroxycoumarins. The spectra of umbelliferon, esculetin, and scopoletin show a long wavelength shoulder which, most likely, corresponds to the forbidden $n \rightarrow \pi^*$ transition. The apparent high intensity of this transition results from its lying on the border of a relatively intense $\pi \rightarrow \pi^*$ transition. On the other hand, the coumarin spectrum does not show an isolated band (or shoulder) for the $n \rightarrow \pi^*$ transition. The solubility of the studied compounds is rather poor in non-polar solvents. Consequently, the weak $n \rightarrow \pi^*$ transitions were not clearly observed in dioxan. Molecular orbital calculations predicted the positions of the $n \rightarrow \pi^*$ transitions nicely (Table 4).

It is interesting to note that the electronic transitions which were overlapping in the spectrum of umbelliferone, in the region of 270–360 nm (Fig. 2), were nicely resolved in the spectrum of esculetin. This is evidence that tautomer (c) apparently contributes to the structure of that compound. Such a resolution appeared even better, when the —OH was replaced by an —OCH_3 group (scopoletin, Fig. 4).

Coumarins are α, β-unsaturated ketones. The active sites in the molecule are the C(2)═O(11) and C(3)═C(4). An important result of the performed calculations is the larger differences of the SCF-coefficients of these atoms in the HOMO than in the LUMO. In the former, the coefficient of the oxygen atom is significantly larger than that of C(2) and the coefficient of C(3) is larger than that of C(4). When considering the LUMO there is no significant difference in the values of the coefficients of C(2) and O(11) or between C(3) and C(4). Also, the charge on C(3) is always negative whereas that on C(4) is positive. The correspondence between the calculated and observed values of some parameters (transition energy and oscillator strength, Table 4) is satisfactory.

The spectra of amino- and hydroxyamino- coumarins are not available yet; our calculations indicate that their electronic spectra would not differ from their hydroxy analogues.

Molecular orbital calculations indicated that coumarin is a stronger dipole than hydroxycoumarins (Table 3). This result indicates that substitution by the —OH group creates a dipole in the opposite direction to that of the parent coumarin. The reverse behaviour is encountered on substitution by an —NH_2 group. It is found that amino-coumarins are stronger dipoles than coumarin, a result which means that substitution by the amino group creates a dipole in the same direction as that originally present in coumarin.

It may be interesting to compare some physical parameters for the isomers 6-hydroxy- and 7-hydroxy-coumarins; 6-amino- and 7-amino-coumarins; 6-hydroxy-7-amino- and 6-amino-7-hydroxy-coumarins (Table 3). No significant difference is detected in the total energy of any of the two isomers, and only slight differences are found in the lowest transition energy of any of the two isomers. However, significant differences in dipole moments are found between any of the two isomers.

1. J. G. HEATHCOTE and J. R. HIBBERT. Biochem. Soc. Trans. **2**, 301 (1974).
2. A. PULLMAN and B. PULLMAN. *In* Comprehensive biochemistry. Vol. 22. *Edited by* M. Florkin and E. H. Stotz. Elsevier, Amsterdam. 1967, p. 1.
3. R. S. OVERMAN, M. A. STAHMANN, C. F. HUEBNER, W. R. SULLIVAN, L. SPERO, D. G. DOHERTY, M. IKAWA, L. GRAF, S. ROSEMAN, and K. P. LINK. J. Biol. Chem. **153**, 5 (1974).
4. V. DADAK and P. ZBORIL. Collect. Czech Chem. Commun. **32**, 4118 (1967).
5. P. ZBORIL, J. HOLASOVA, and V. DADAK. Collect. Czech. Chem. Commun. **35**, 2983 (1970).
6. R. W. WALD and G. FUER. J. Med. Chem. **14**, 1081 (1971).
7. L. W. WATTENBURG, L. K. T. LAM, and A. V. FLADMORE. Cancer Res. **39**, 1651 (1979).
8. J. M. CASSADY, N. OJIMA, C.-J. CHANG, and J. L. MCLOUGHLIN. J. Nat. Prod. **42**, 274 (1979).
9. R. A. FINNEGAN, K. E. MERKEL and N. BACK. J. Pharm. Sci. **61**, 1599 (1972).
10. E. J. SCHMITSCHEK, J. A. TRIAS, R. HAMMOND, and R. L. ATKINS. Opt. Commun. **11**, 352 (1974).
11. P. R. HAMMOND, A. N. FLETCHER, R. A. HENRY, and R. L. ATKINS. Appl. Phys. **8311**, 315 (1975).
12. E. J. SCHMITISCHECK, J. A. TRIAS, P. R. HAMMOND, R. A.

HENRY, and R. L. ATKINS. Opt. Commun. **16**, 313 (1976).
13. S. G. SCHULMAN and L. S. ROSENBERG. J. Phys. Chem. **83**, 447 (1979).
14. R. L. ATKINS and D. E. BLISS. J. Org. Chem. **43**, 1975 (1978).
15. (*a*) K. K. SHARMA and M. L. GOYAL. Indian J. Pure. Appl. Phys. **19**, 731 (1981); (*b*) T. KOBAYASHI. J. Phys. Chem. **82**, 2277 (1978).
16. K. V. MASRANI, H. S. RAMA, and S. L. BAFNA. J. Appl. Chem. Biotechnol. **24**, 331 (1974).
17. (*a*) B. E. NIELSEN. Dan. Tidsskr. Farm. **44**, 111 (1970); Chem. Abstr. **74**, 20314 (1971); (*b*) V. P. BURYAK and N. K. STARCHEVSKAYA, Formatsiya, **30**(5), 26 (1981); Chem. Abstr. **95**, 219476e (1981).
18. R. H. GOODWIN and B. M. POLLOCK. Arch. Biochem. Biophys. **49**, 1 (1954).
19. K. DRLICA and M. SNYDER. J. Mol. Biol. **120**, 145 (1978).
20. (*a*) W. L. STANLEY and S. H. VANNIER. Phytochemistry, **6**, 585 (1967), (*b*) S. O. WOLFBEIS and K. SCHUFFNER. Photochem. Photobiol. **32**, 143 (1980).
21. F. M. DEAN and B. PARTON. J. Chem. Soc. C., 256 (1969).
22. R. M. HOROWITZ and B. GENTILI. J. Org. Chem. **25**, 2183 (1960).
23. N. R. KRISHNASWAMI, T. R. SESHADRI, and B. R. SHARM. Indian J. Chem. **4**, 120 (1966).
24. W. M. BANDARANAYAKE, S. S. SELLIAH, M. U. S. SULTANBAWA, and D. E. GAMES. Phytochemistry, **14**, 265 (1975).
25. J. MENDEZ and M. I. LOGO. Microchem. J. **14**, 567 (1969).
26. B. S. JOSHI and V. N. KAMAT. Tetrahedron Lett. 5767 (1966).
27. R. SAIRAM and N. K. RAY. Ind. J. Chem. **19**B, 989 (1980).
28. V. S. SHUKLA, and S. C. DUTTA, R. N. BARUAH, R. P. SHARMA, G. THYAGARAJAN, W. HERZ, N. KUMAR, K. WATANABE, and J. F. BLOUNT. Phytochemistry, **21**, 1725 (1982).
29. J. A. POPLE, D. L. BEVERIDGE, and P. A. DOBOSH. J. CHem. Phys. **47**, 2026 (1967).
30. J. A. POPLE and D. L. BEVERIDGE. Approximate molecular orbital theory. McGraw–Hill, New York. 1970.
31. J. BEGLEY, L. CROMBIE, D. A. SACK, and D. A. WHITING. J. Chem. Soc. Perkin Trans. 1 2402 (1977).

Thermodynamic behaviour of adenosine in water–DMSO mixtures in the presence of K^+ and Ca^{2+} ions at 25, 30, 35, and 40°C

ANIL K. PURI[1]

Department of Chemistry, University of Allahabad, Allahabad – 211002, India

Received April 6, 1984

ANIL K. PURI. Can. J. Chem. **63**, 1180 (1985).

Partial molar volume (ϕ_v^0), partial molar compressibility (ϕ_k^0), Jones–Dole viscosity *B* coefficient, and solute activation parameters of adenosine in water–DMSO mixtures in the presence of Ca^{2+} and K^+ ions have been calculated from ultrasonic, volumetric, and viscometric studies at 25, 30, 35, and 40°C (±0.01°C). The results are discussed in terms of the Jones–Dole viscosity *B* coefficients and the transition state parameters for viscous flow.

ANIL K. PURI. Can. J. Chem. **63**, 1180 (1985).

Utilisant les résultats d'études ultrasoniques, volumétriques et viscosimétriques effectuées à 25, 30, 35 et 40°C (±0.01°C), on a calculé les volumes molaires partiels (ϕ_v^0), les compressibilités molaires partielles (ϕ_k^0, les coefficients de viscosité *B* de Jones–Dole et les paramètres d'activation de solution de l'adénosine dans des mélanges eau/DMSO, en présence d'ions Ca^{2+} et K^+. On discute des résultats en fonction des coefficients de viscosté B de Jones–Dole et des paramètres de l'état de transition de l'écoulement visqueux.

[Traduit par le journal]

Introduction

Adenosine is one of the most important nucleosides in the study of molecular biology (1). Conformational properties of adenosine, the interaction of its different functional groups with solvent molecules in solution and temperature dependence of these interactions play an important role in the understanding of the thermodynamic behaviour of biochemical processes in living cells. The ultrasonic velocity in solution can be used to study the solute–solvent and solute–solute interactions, which are determined by the chemical structure of the solute and solvent molecules. Ultrasonic velocity measurements are mostly limited to obtaining the hydration numbers in aqueous (2–5) and non aqueous solution (6). Hemmes *et al.* (1) made a successful attempt to study the dependence of solute–solvent interactions on the chemical structure of nucleic acid derivatives in an aqueous solution. Interaction studies of bivalent metal ions with uracil, thymine, and cytosine have been investigated potentiometrically (7–10). Many attempts have been made to study the solution properties of DMSO–water mixtures (11–14), since DMSO is particularly suitable for biophysico chemical processes. Excess thermodynamic properties of DMSO–water mixtures at 20, 30, 40, and 60°C have been discussed in terms of molecular interactions by Pandey and Tiwari (15). The interaction of DMSO with *N*-benzoyl amino acids has been recently shown by Fong and Grant (16) using the ^1H nmr technique. Results show that the intermolecular H-bonding between DMSO and the amino-hydrogen atom increases the effective steric size of the amino hydrogen. Recently kinetic studies of ligand substitution have been carried out in the DMSO–water system by Coetzee and Karakatsanis (17). Relative viscosity of solution of sodium and potassium bromides and iodides in DMSO–water at 25, 35, and 45°C have been reported by Feakins and Lawrence (18–20). Results are discussed in terms of Jones–Dole viscosity *B* coefficients and transition state treatment.

The present article deals with the results of ultrasonic, volumetric, and viscosity studies of adenosine in DMSO–water mixtures in the presence of K^+ and Ca^{2+} ion at 25, 30, 35, and 40°C (±0.01°C). Results have been discussed in terms of partial molar volume (ϕ_v^0), partial molar compressibility (ϕ_k^0), Jones–Dole viscosity *B* coefficient, and transition state theory.

[1]Present address: 2125 McKesson Drive, Richmond, VA 23235, U.S.A.

Experimental

Adenosine (supplied by Sigma chemicals, U.S.A.) was of extra pure "Grade-Reagent" quality. Purity was checked by tlc and paper chromatography according to well known methods (32).

Dimethyl sulphoxide (DMSO) was distilled in a stream of dry nitrogen over sodium hydroxide at a pressure of 2.6 kPa using a 50 cm column packed with Finskihelices. A conductivity cell was attached to the still head and solvent collected when the electrolytic conductivity (k) of distillate had fallen to 4×10^{-6} S m^{-1}. The solvent was stored, and all manipulations on the solutions were made in a nitrogen filled dry box. KCl was of AR grade while hydrated $CaCl_2 \cdot 2H_2O$ was dried at 110°C and stored in dessicator. A solution of adenosine (0.01 *M*) was prepared in DMSO solvent. Stock solutions of 0.1 *M* KCl and 0.1 *M* $CaCl_2$ were prepared in double distilled water.

Two sets of ten solutions each of adenosine–(water–DMSO)–Ca^{2+} and adenosine–(water–DMSO)–K^+ designated as system A and system B were prepared in varying composition from 10–75% by weight of DMSO.

The densities of solutions were determined with the help of a calibrated bicapillary pyknometer at 25, 30, 35, and 40°C (±0.01°C), respectively. The estimated error in the density measurements was of the order of ±0.05%.

Ultrasonic velocity (u) in different solutions were measured using variable temperature, ultrasonic interferometry with a quartz crystal having a frequency of 2 MHz. The estimated error was ±0.01%.

Viscosity measurements were carried out using a calibrated Ostwold viscometer at 25, 30, 35, 40°C, respectively, with maintained temperature of ±0.01°C. The time of flow for water was selected in the range of 15–25 s, while for dilute solutions at least 30 s or more was used. The estimated errors in viscosity measurements were of the order of ±0.004%.

Results

Density data for adenosine in the mixed solutions of electrolytes have been used for the calculation of apparent molar volume (ϕ_v^0) as a function of total molality of co-solute and water–DMSO solvent composition. The corresponding equation in terms of densities is

$$\phi_v = \frac{1000\,(\bar{d}^0 - d)}{m_t \bar{d}^0\, d} + \frac{\bar{M}}{\bar{d}^0}$$

TABLE 1. (*a*) Apparent molar volume at infinite dilution (ϕ_v^0) for adenosine–water–DMSO in presence of Ca^{2+} (system A); adenosine = 0.01 *M*, $CaCl_2$ = 0.1 *M*

Temperature (°C)	$-\phi_v^0 \times 10^{-3}$ mL mol^{-1} when [DMSO] is									
	10 wt.%	20 wt.%	30 wt.%	40 wt.%	50 wt.%	55 wt.%	60 wt.%	65 wt.%	70 wt.%	75 wt.%
30	92.07	46.51	32.85	22.35	19.73	18.24	16.72	15.25	13.95	12.78
35	90.39	25.44	17.29	13.88	11.53	10.56	9.69	8.92	8.08	7.39
40	85.79	22.88	16.45	13.78	11.43	10.51	9.77	9.19	8.05	7.31

(*b*) Apparent molar volume at infinite dilution (ϕ_v^0) for adenosine–water–DMSO in presence of K^+ (system B); adenosine = 0.01 *M*, KCl = 0.1 *M*

Temperature (°C)	$-\phi_v^0 \times 10^{-3}$ mL mol^{-1} when [DMSO] is									
	10 wt.%	20 wt.%	30 wt.%	40 wt.%	50 wt.%	55 wt.%	60 wt.%	65 wt.%	70 wt.%	75 wt.%
25	88.98	46.43	30.90	24.02	19.71	17.87	16.53	15.17	13.89	12.68
30	89.58	46.54	31.32	24.10	19.74	18.22	16.58	15.25	14.00	12.69
35	90.25	46.57	31.65	24.30	19.76	18.56	16.97	15.54	14.11	12.14
40	91.15	46.69	31.80	24.38	19.89	18.65	17.19	15.65	14.19	12.94

TABLE 2. Experimental slope (S_v) for adenosine–water–DMSO in the presence of Ca^{2+} (system A) and K^+ (system B); adenosine = 0.01 *M*, $CaCl_2$ = 0.1 *M*, and KCl = 0.1 *M*

Temperature (°C)	S_v	
	System A	System B
25	—	0.200
30	0.200	0.180
35	0.140	0.167
40	0.090	0.133

TABLE 3. Apaprent molar compressibility at infinite dilution (ϕ_k^0) for adenosine–water–DMSO in the presence of K^+ and Ca^{2+} ion; adenosine = 0.01 *M*, $CaCl_2$ = 0.1 *M*, KCl = 0.1 *M*

Temperature (°C)	$-\phi_k^0$ (cm^3 mol^{-1} bar^{-1} $\times 10^{-3}$)	
	System A	System B
25	—	182
30	120	185
35	140	186
40	150	92

where $\bar{d}^0$ and d are the densities of the DMSO–water solvent and adenosine solution respectively. The value of $\bar{d}^0$ was determined from $\bar{d} = \Sigma d_i y_i$ where y_i represents weight fraction, m_t is the total molality of the co-solute in DMSO–water solvent and can be determined by $m_t = \Sigma m_i$ where m_i is the molarity of ith component. The mean molecular weight of the two solutes ($\bar{M}$) was obtained from $\bar{M} = \Sigma M_i y_i$, here M_i is the molecular weight of component i. Apparent molar volume at infinite dilution (ϕ_v^0) has been evaluated from the equation.

$$[2] \quad \phi_v = \phi_v^0 + S_v\sqrt{m_t}$$

where S_v is the experimental slope of ϕ_v vs. $\sqrt{m_t}$ plot. Values of partial molar volume (ϕ_v^0) at different DMSO compositions and different temperatures are recorded in Table 1.

S_v values are given in Table 2 for systems A and B. From density and ultrasonic velocity the isentropic compressibility (β_s) of solution has been calculated from the relationship

TABLE 4. Viscosity *B* coefficient for adenosine–DMSO–water in the presence of K^+ and Ca^{2+} ions

Temperature (°C)	*B* coefficient (mol^{-1} cm^{-3})	
	System A	System B
25	—	0.0150
30	0.0054	0.0078
35	0.0050	0.0070
40	0.0050	0.0056

$$[3] \quad \beta_s = \frac{1}{u^2 d}$$

where u is the ultrasonic velocity and d is the density of the medium. The isentropic aparent molar compressibility (ϕ_k) of solute was obtained from the relation

$$[4] \quad \phi_k = \frac{1000(\beta_s - \beta_0)}{m_t \bar{d}^0} + \beta_s\phi_v$$

where β_s and β_0 are the compressibilites of solution and solvent. Apparent molar compressibility at infinite dilution (ϕ_k^0) has been extrapolated from the linear plot of ϕ_k vs $\sqrt{m_t}$. Graphically estimated values of ϕ_k^0 are given in Table 3.

The experimental viscosity data were analysed in terms of the Jones–Dole equation (21) below which accounts for both solute–solvent and solute–solute interactions.

$$[5] \quad \frac{\eta^0}{\eta} = 1 + A\sqrt{m_t} + Bm_t$$

Here η^0/η is the relative viscosity of solution. The constants *A* and *B* are evaluated from the intercept and slope of the $(\eta^0/\eta - 1)/\sqrt{m_t}$ vs. $\sqrt{m_t}$ plot. The coefficient *A* represents the contribution from interionic electrolytic forces (22) and the coefficient *B* measures the order or disorder introduced by ions into the solvent structure. This constant is specific and approximates the additive property of electrolytes at a given temperature (23) although no satisfactory theoretical treatment has yet been given.

B coefficient values for systems A and B are given in Table 4. The viscosity and density data have been utilized for the calculation of activation parameter (24). The free energy of

TABLE 5. Activation parameters for adenosine in DMSO–water mixtures in the presence of K^+

Weight % of solvent	Temperature (°C)	$\Delta\mu^*$ (kcal/mol)	$-\Delta S^*$ eu	$-\Delta H^*$ (kcal/mol)
10	25	15.45	64.58	3.79
	30	15.71	64.77	3.91
	35	16.07	64.77	3.84
	40	16.09	64.41	4.07
20	25	15.66	72.61	5.97
	30	15.92	72.94	6.18
	35	16.03	72.78	6.38
	40	16.24	72.98	6.60
30	25	15.81	75.50	6.68
	30	16.02	75.68	6.91
	35	16.30	76.07	7.31
	40	16.44	76.09	7.37
40	25	16.03	78.57	7.38
	30	16.23	79.21	7.99
	35	16.59	79.48	7.88
	40	16.64	79.96	8.15
50	25	16.24	82.85	8.45
	30	16.45	83.32	8.79
	35	16.69	83.47	8.97
	40	16.85	84.41	9.57
55	25	16.35	83.46	8.50
	30	16.59	83.96	8.82
	35	16.75	83.96	9.11
	40	16.97	84.28	9.41
60	25	16.46	84.15	8.61
	30	16.71	84.56	8.91
	35	16.88	84.71	9.21
	40	17.11	85.03	9.50
65	25	16.59	85.76	8.96
	30	16.79	86.02	9.27
	35	17.00	86.30	9.58
	40	17.19	86.53	9.89
70	25	16.68	87.24	9.32
	30	16.91	87.61	9.63
	35	17.13	88.14	10.02
	40	17.34	88.24	10.27
75	25	16.79	88.82	9.43
	30	17.04	89.24	9.99
	35	17.41	90.07	10.33
	40	17.46	89.92	10.68

TABLE 6. Activation parameters for adenosine in DMSO–water mixtures in the presence of Ca^{2+}

Weight % solvent	Temperature (°C)	$\Delta\mu^*$ (kcal/mol)	$-\Delta S^*$ (eu)	$-\Delta H^*$ (kcal/mol)
10	30	15.66	91.87	12.17
	35	15.77	92.08	12.59
	40	16.08	92.65	12.91
20	30	15.81	82.17	9.08
	35	16.06	82.64	9.24
	40	16.29	83.04	9.70
30	30	16.00	79.82	7.88
	35	16.21	78.09	7.84
	40	16.47	78.53	8.11
40	30	16.21	72.09	5.63
	35	16.46	72.34	5.82
	40	17.70	72.57	6.01
50	30	16.43	114.22	18.17
	35	16.67	115.12	18.78
	40	16.96	116.14	19.39
55	30	16.55	94.82	12.18
	35	16.79	95.45	12.31
	40	17.08	96.11	13.29
60	30	16.67	85.05	9.09
	35	16.89	85.35	9.39
	40	17.15	85.79	9.67
65	30	16.82	85.49	9.08
	35	17.02	85.77	9.13
	40	17.28	86.21	9.58
70	30	16.86	103.63	14.54
	35	17.15	104.12	14.91
	40	17.40	105.18	15.52
75	30	17.17	79.48	6.90
	35	17.37	78.31	6.75
	40	17.58	79.72	7.37

activation for viscous flow (25, 33) is given by eq. [6],

$$[6]\quad \Delta\mu^* = RT \ln \frac{\eta^0 V}{hN}$$

where h is Planck constant and N is the Avogadro number, η^0 is the viscosity of solution, and V may be regarded as the volume of 1 mol of solution particles and is given by

$$V = \frac{1000}{n_1 + \nu n_2}\ \mathrm{cm}^3$$

where ν is the number of species into which a solute molecule dissociates and n_2 is the number of moles of solute per litre of solution. The number of moles n_1 of the solvent per litre of solution is given by

$$n_1 = \frac{1000\,\bar{d}^0 - n_2 \bar{M}_2}{\bar{M}_1}$$

where $\bar{M}_1$ and $\bar{M}_2$ are the molecular weights of co-solvent DMSO–water and co-solute adenosine and electrolytes, respectively. Furthermore, by measuring the B coefficient at different temperatures, enthalpies (ΔH^*), and entropies (ΔS^*) of activation can be obtained by using equations (24)

$$[7]\quad \Delta S^* = -\mathrm{d}(\Delta\mu^*)/\mathrm{d}T$$

$$[8]\quad \Delta H^* = \Delta\mu^* + \Delta S^*$$

Calculated values of $\Delta\mu^*$, ΔH^*, and ΔS^* are recorded in Tables 5 and 6 for sets A and B.

Discussion

The results in Table 1 reveal that the values of ϕ_v^0 (partial molar volume) gradually decrease with increase in temperature from 30 to 40°C for the system A and increase with temperature for system B for the whole range of solvent composition (10–75 wt.%). At the same time the positive S_v slopes for both the systems A and B gradually decrease with increasing temperature. It may therefore be concluded that ϕ_v^0 values correspond to a maximum for system B, thereby suggesting that solute–solvent interactions are stronger than solute–solute interactions in the temperature range 25–40°C. The increase in values of partial molal volume ϕ_v^0 for system B with increase in temperature are due to the dehydration of adenosine. S_v values are decreased with increase in temperature. It can be argued that solute–solute interactions can be affected by the influence of K^+ (system A) on the structure of DMSO as interionic attractions are stronger in DMSO (dipolar aprotic solvent) than in water because of the lower dielectric constant value of DMSO than water. The occurrence of maximum ϕ_v^0 values and lower S_v values in the case of system B is in agreement with the above inference.

According to Kaulgud and Patil (26), negative ϕ_v^0 values are associated with the "promotion" of solvent structure, i.e., addition of adenosine in the presence of an electrolyte in DMSO–water may lead to an incipient structure that enhances the water structure. This result might be due to the accommodation of adenosine in the cavity created by the displacement of water molecule into the interstices.

Apparent partial molar compressibilities (ϕ_k^0) (Table 3) increase with increasing temperature for system A for solvent compositions varying from 10–75 wt. %. The same trend in ϕ_k^0 values observed for system B except at 40°C, where the value of ϕ_k^0 is significantly lower. It is evident from Table 3 that both systems A and B the values of (ϕ_k^0) are negative at all temperatures. It can be interpreted as due to the loss of structural compressibility of water on account of population increase of four bonded water molecules in the vicinity of adenosine molecules. Critical evaluation for all the available physicochemical studies of DMSO–water mixtures by Frank and Ives (27) led to the conclusion that there must be reinforcement of the water structure in the neighborhood of DMSO molecules in dilute solution. There is also a greater loss of structural compressibility of water employing a greater ordering effect by ions on solvent structure as in the case of systems A and B except at 40°C in system B.

Viscosity B coefficients of the Jones–Dole equation are positive for both systems. The B values gradually decrease with increasing temperature. Positive B values indicate strong alignment of solvent molecules with ions, i.e., strong DMSO interaction with K^+ or Ca^{2+} ions and with amino site of adenosine, which reveals the "structure-making" behaviour of solvent structure. The B values decrease with increasing temperature indicating that ion–solvent interactions are being influenced in the temperature range from 20 to 40°C. A number of factors are believed to contribute to the B values in solutions of K^+ and Ca^{2+} ions in DMSO–water mixture. Dimethylsulfphoxide, a dipolar aprotic solvent (19), is pyramidal in shape with two C-atoms, the O-atom, and S-atom at the vertices (28). The bonding characteristics of the sulphur atom have been explained by Burg (29). Both the sulphur and the oxygen atoms possess a lone pair of electrons and for sulphur the lone pair is tetrahedrally disposed to the methyl groups and oxygen atom. A strong electrostatic interaction between the positive charge on the cation and the lone pair on the oxygen of each solvent molecule is envisaged when a cation solvent complex is formed as shown by the following mechanism.

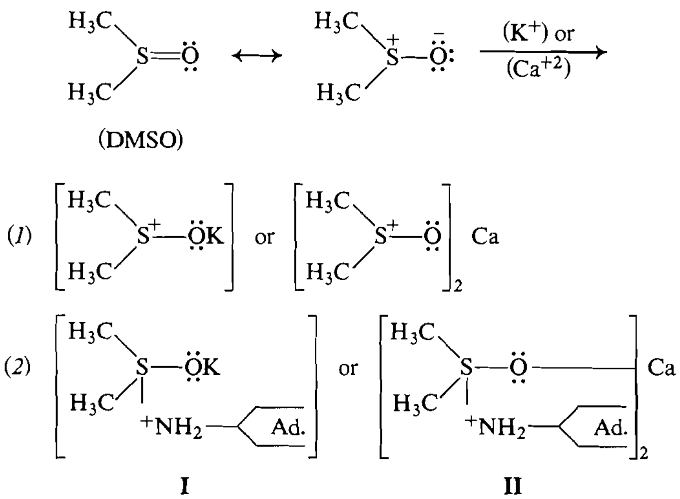

SCHEME 1. Possible mechanism: addition of metal ions with adenosine

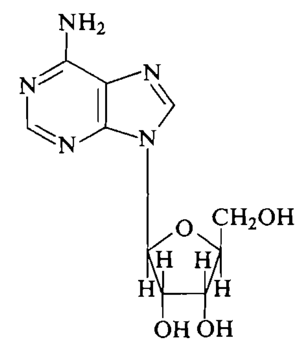

Adenosine

The cation–solvent complex of K^+ and Ca^{2+} with adenosine in the presence of DMSO–water co-solvent are represented by **I** and **II**, respectively (Scheme 1). It is evident that DMSO interacts strongly with the cations and this is reflected by the values of B coefficent shown in Table 4.

The analysis of solute–activation parameters reveals (Tables 5 and 6) that ΔS^* and ΔH^* are negative for systems A and B and increase gradually with increasing composition of DMSO–water from 10–75 wt.%.

This fact indicates that in the solvent mixture the average transition state is associated with bond making and an increase in the order. The system B on the other hand with an increase in the percentage of DMSO from 55 to 75 wt.% in the mixture, the values of ΔS^* and ΔH^* are comparatively lower. In the latter case it can be assumed that the transition state for viscous flow is accompanied by the breaking and distortion of intermolecular bonds. Moreover, the smooth progression of the values of ΔS^* and ΔH^* found in system A and B, Tables 5 and 6 confirm the absence of structural enhancement of water by DMSO. In fact, when the water structure is increased by the addition of co-solvent, maxima or minima in the values of activation parameters of viscous flow were obtained for electrolytes in water–ethanol (30) and water–acetone (31) systems. It is evident from Table 5 that free energy of activation ($\Delta\mu^*$) is positive for all proportions of solvent composition and at all temperatures studied in the present investigation. The results show that adenosine is higher in free energy state, i.e. formation of the transition state is less favourable in

DMSO−water mixtures from 10−75 wt.%, suggesting that water has more affinity for adenosine in DMSO−water cosolvent mixture in the presence of K^+ and Ca^{2+}. Similarly, other activation parameters for adenosine as ΔH^* and ΔS^* show negative contribution in DMSO−water mixtures, suggesting that entropies (ΔS^*) are less effective in the presence of cations K^+ or Ca^{2+} ions, and therefore, the net amount of order created by cations in DMSO−water mixture is substantial.

Acknowledgements

The author is deeply indebted to professors R. G. Bass, S. J. Silvers, and D. D. Shillady, Department of Chemistry, Virginia Commonwealth University, for reviewing this manuscript and for helpful discussion.

1. P. HEMMES and A. P. SARVAZYAN. J. Phys. Chem. **84**, 692 (1980).
2. H. SHIIO. J. Am. Chem. Soc. **80**, 70 (1958).
3. J. STUHER and E. YEAGER. Physical acoustics. Vol. II. Part A. *Edited by* Mason Academic press, New York Chapt. 6. 1965.
4. F. I. BRAGINSKAYA and S. KH. SADIKHOVA. Biofizika, **20**, 20 (1975).
5. A. JUSZKLEWL and D. SUGAR. J. Phys. Chem. **86**, 4831 (1982).
6. M. M. T. KHAN and C. R. KRISHNAMOORTHY. J. Inorg. Nucl. Chem. **36**, 711 (1974).
7. A. REINERT and A. DEUT. Berlin KI Med. **6**, 373 (1964).
8. R. C. SRIVASTAVA and M. N. SRIVASTAVA. J. Inorg. Nucl. Chem. **40**, 1439 (1978).
9. M. M. T. KHAN and M. S. JYOTI. J. Inorg. Nucl. Chem. **40**, 1731 (1978).
10. J. J. CHRISTENSEN, J. H. RYTTING, and R. M IZZAT. J. Chem. Soc. **B**, 1643 (1970).
11. M. D. ARCHEAR and R. P. H. GASSER. Trans. Faraday Soc. **62**, 3451 (1966).
12. N. P. YAO and D. M. BENNION. J. Phys. Chem. **75**, 1727 (1971).
13. R. L. BLOKHRA and M. L. PARMAR. Austral. J. Chem. **27**, 1407 (1974).
14. W. ADOLPH and W. SEIDEL. Z. Phys. Chem. Frankfurt, **93**, 173 (1974).
15. J. D. PANDEY and V. TIWARI. Acoust. Lett. **2**, 116 (1978).
16. C. W. FONG and G. G. GRANT. Aust. J. Chem. **34**, 1869 (1981).
17. J. F. COETZEE and C. G. KARAKATSANIS. J. Solution. Chem. **11**, 389 (1982).
18. K. G. LAWRENCE and R. T. M. BICKNELL. J. Chem. Soc. Faraday I, **72**, 307 (1976).
19. K. G. LAWRENCE and D. FEAKINS. J. Chem. Soc. Faraday I, **76**, 637 (1980).
20. K. G. LAWRENCE and D. FEAKINS. J. Chem. Soc. A, 212 (1966).
21. G. JONES and M. DOLE. J. Am. Chem. Soc. **51**, 2950 (1929).
22. H. FALKENHAGEN and E. L. VERNON. Physik, z. **33**, 140 (1932).
23. W. M. COX and J. H. WOLFENDEN. Proc. R. Soc. London, A**145**, 475 (1934).
24. A. SACCO. J. Chem. Soc. Faraday I, **78**, 1507 (1982).
25. M. KAMINSKY. Discuss. Faraday Soc. I, **24**, 171 (1957).
26. V. M. KAULGUD and K. J. PATIL. J. Phys. Chem. **78**, 714 (1974).
27. F. FRANK and D. J. G. IVES. Q. Rev. Chem. Soc. **20**, 1 (1966).
28. R. THOMAS and K. ERIKS. Acta Crystallogr. **21**, 12 (1966).
29. A. B. BURG. Organic sulphur compounds. *Edited by* N. Karash. Pergamon Press, London. **1**, 35 (1961).
30. D. D. MCDONALD, M. D. SMITH, and J. B. HYNE. Can. J. Chem. **49**, 2818 (1971).
31. M. CASTAGNOLO and A. SACCO. Thermochim Acta, **44**, 67 (1981).
32. I. B. MAFIN and D. M. DAFY. Anal. Chem. **21**, 965 (1961).
33. E. R. NIGHTINGALE and R. F. BENCK. J. Phys. Chem. **68**, 1777 (1959).

Propagation of error in fulvic acid titration data: a comparison of three analytical methods

WILLIAM FISH AND FRANÇOIS M. M. MOREL
R. M. Parsons Laboratory, 48-425, Massachusetts Institute of Technology, Cambridge, MA 02139, U.S.A.

Received July 24, 1984

WILLIAM FISH and FRANÇOIS M. M. MOREL. Can. J. Chem. **63**, 1185 (1985).

Many methods have been employed for measuring the interactions of trace metals and humic materials but little consideration has been given to the magnitude of error in the resulting titration data. Most common metal-titration methods can be placed into one of three categories based on the chemical species that is most directly measured: free ionic metal, total labile metal, or ligand-bound metal. The propagation of random instrument error into a titration data set is not uniform throughout a titration and the pattern of propagation is shown to be characteristic of the category of method used. Standard deviations are determined for measurements by ion-selective electrodes, fluorescence quenching, and fixed potential amperometry (each representative of a category of methods). Error propagation in resulting titration data is quantified. No single titration method yields uniformly precise data in all concentration ranges and a combination of complementary methods yields the best characterization of metal binding to a humic material.

WILLIAM FISH et FRANÇOIS M. M. MOREL. Can. J. Chem. **63**, 1185 (1985).

Plusieurs méthodes ont été utilisées pour mesurer les interactions entre des métaux à l'état de trace et les substances humiques; toutefois, peu de cas a été fait de l'amplitude de l'erreur qui entache les données de titration qui en résultent. En se basant sur la nature des espèces chimiques qui sont mesurées le plus directement, on peut classer la plupart des méthodes usuelles de titrages des métaux dans l'une des trois catégories suivantes: soit les métaux ioniques libres, les métaux totaux labiles ou les métaux liés à des ligands. La propagation de l'erreur instrumentale au hasard dans un ensemble de données de titrage n'est pas uniforme dans l'ensemble d'un titrage et on montre que le schéma de propagation est une caractéristique de la catégorie de méthode utilisée. On a déterminé les écarts standards pour des mesures faisant appel aux électrodes sélectives pour des ions, au piégage de la fluorescence et à l'ampérométrie à potentiel fixe (chacune représentant une catégorie de méthodes). On quantifie la propagation de l'erreur dans les données de titrage qui en résultent. Aucune méthode de titrage simple ne fournit des données uniformément précises dans tous les intervalles de concentration et une combinaison de méthodes complémentaires s'avère la meilleure façon de caractériser la liaison d'un métal à une substance humique.

[Traduit par le journal]

Introduction

In recent years researchers have amassed a substantial body of information about the interactions of humic materials with trace metals. In gathering these data, many analytical methods have been used, each of which measures a single chemical quantity such as free or ligand-bound metal. The additional quantities necessary for mathematically modeling the system have been indirectly obtained by data transformations.

Valid comparisons among results of different methods are possible if each method yields, either directly or indirectly, the same concentration of a metal species for a particular system. Tuschall and Brezonik (1) applied this test to four commonly used analytical methods: ion-selective electrodes, anodic stripping voltammetry, fluorescence quenching, and continuous flow ultrafiltration. Saar and Weber (2) compared and intercalibrated ion selective electrode and fluorescence quenching data and Waite and Morel (3) compared fulvic acid titrations using ion-selective electrodes and fixed-potential amperometry. The results of these comparisons suggest that, over certain concentration ranges and with certain exceptions, the measurements of each chemical quantity by several different methods are in approximate agreement.

With the variety of apparently comparable techniques available, criteria are needed to guide the choice of methodologies appropriate to a particular application. In a review of the titration methods currently available, Saar and Weber (4) emphasized the special merits and problems associated with each technique, such as sensitivity, interferences, and the metals that can be measured. In addition to matching the experimental capabilities of the method to the system under study, it is important to recognize the differences in the precision of data obtained from each method as a result of the different chemical species that are measured. The distinctions are a consequence of the arithmetic manipulations needed to calculate indirectly a species concentration. Errors propagate, resulting in different degrees of uncertainty for the directly and indirectly measured quantities.

Previous comparisons of techniques have not fully considered the implications of errors in transformed data. Parameters that characterize humic materials, such as stability constants and equivalent ligand concentrations, vary widely in accuracy depending on the titration method and the metal concentrations used. Frequently, limitations of time and materials preclude repetitive titrations and error intervals are not determined for model parameters. An alternative to numerous replicate titrations is to measure the precision of the analytical methods and then quantify the propagation of error for each transformation of the data. The latter approach is employed in this study.

We examined the most useful analytical methods and grouped them into three classes based on the quantities they measure. We selected a representative method from each class and showed that this method, in addition to its particular practical limitations, is subject to predictable errors characteristic of its class and that these errors propagate through the transformations needed to model the experimental results. As a consequence, no single technique can yield a complete and optimally precise set of metal-binding data. Results from different methods were overlapped to yield data that possess minimal error over a wide titration range. We applied these principles to series of Cu(II) titrations of fulvic acid obtained with each representative method. The predicted region of minimal error for each method was demonstrated by comparing the standard deviations of conditional stability constants obtained.

Theory

Classes of methods

Commonly used titration techniques fall into three general classes, each defined by the quantity that is measured as a function of total metal added during the titration: free ionic metal, labile metal species, or bound metal species.

Free-ionic metal activity may be measured with a solid-state, ion-selective electrode (ISE). These Nernstian devices generate a potential proportional to the logarithm of the free-metal activity in solution. Because stability constants are conventionally written in terms of the free metal species, the output of an ISE titration is especially convenient to use in speciation models. Furthermore, the logarithmic scaling allows data to be collected over many orders of magnitude. This feature is useful for characterizing humic materials which typically have a wide range of apparent metal-binding strengths.

Ion-selective electrodes have several well-known practical limitations. While very low free-metal activity can be measured, the lowest *total* metal concentrations possible are at or above the average concentrations typically found in unpolluted natural waters. Cupric ISEs, which are the most commonly used means of studying metal—humic interactions, are also subject to a large, uncorrectable interference from chloride ions (5). To overcome these problems, ion exchange methods have been proposed for determining ionic activities of metals in titrations (6). Such procedures fall into this class because the metal that partitions onto the exchanger surface is proportional to free-metal activity. Unfortunately, these methods still require relatively high ligand concentrations and are difficult to calibrate and interpret because of ligand adsorption on the exchanger (7). Consequently, the ion-selective electrode, which is very reliable within its optimal operating range (in the absence of interferences), was chosen for this study as the representative method of its class.

The second class comprises methods that yield arithmetically scaled labile-metal concentrations. The labile-metal fraction is operationally defined for each method but is ideally taken to be the sum of all metal species except the organo-metallic complexes of interest. Anodic stripping voltammetry and fixed-potential amperometry (3) fall into this category as well as all titration techniques involving separations, such as dialysis (8), gel-permeation chromatography (9), and ultrafiltration (1). The separation techniques offer great flexibility in the choice of reactant metals and background electrolytes, but uncertain molecular-size cutoffs make unclear the composition of the labile-metal fraction.

Because of its sensitivity and convenience, anodic stripping voltammetry (ASV) has been the most widely used technique in this class. Yet it is not clear which metal species are electrochemically stable and which are decomposed as "labile" at the negative potentials employed in the plating step (1, 10, 11). Much debate has centered on the accuracy of ASV techniques and there is substantial reason to believe that characterizations of metal binding agents by ASV methods are ambiguous or subject to artifact.

Waite and Morel (3) describe fixed-potential amperometry (FPA) as a method of labile-copper analysis that appears to have a sensitivity comparable to ASV methods yet is free of the major artifacts associated with mercury electrodes operating in the negative potential region. The FPA method has been intercalibrated with cupric ISE data and is used in this study as the representative method for this class.

The third class of methods are those that directly measure the formation of organo-metallic complexes during the titration. Spectrophotometry is the classical technique in this category (12) but has been little used for humic substances because of the weak absorptivity of metal—humate complexes. Methods that extract organo-metallic complexes onto a hydrophobic column such as the C-18 Sep-Pak column procedure described by Mills and Quinn (13) also fall into this class. Such methods are useful in estimating the extent of organic metal-binding in natural samples but are poorly suited to detailed titrimetric procedures because the kinetics of humic complex formation and dissociation in the column are not well defined. Quenching of natural humic fluorescence by certain paramagnetic metals (such as Cu^{2+}) has been recently applied to metal binding studies with considerable success (1, 14). Fluorescence quenching (FQ) is relatively sensitive and provides a direct, arithmetically scaled measure of metal-complex concentration. It is employed here as the third representative method.

Error propagation in data transforms

Developing a thermodynamic equilibrium model of metal interactions with humic materials requires knowledge of the free ionic activity of the metal, [M], the ligand-bound metal concentration, [ML], and the unbound-ligand concentration, L_f, over a range of values. In practice, all three quantities are not measured directly or independently. One quantity is measured as a function of the total metal added to the system and the two remaining quantities are determined indirectly from conservation of mass considerations. Several transformations of the original data are necessary to obtain the three quantities used in an equilibrium model.

For example, in ISE titrations the electrode potential is converted to the logarithm of the metal activity by multiplying by a calibration factor (A). The log of activity is exponentiated to obtain the arithmetic metal activity, which in turn is multiplied by a proportionality constant (K_0) to generate the concentration of inorganic metal complexes, M_i. This value is subtracted from the total concentration of metal in solution to determine, indirectly, the concentration of ligand-bound metal. The value of L_f must be obtained by subtracting [ML] from the total ligand concentration, L_T. In each of these transformations the uncertainty in the quantity obtained increases as errors propagate through the data set. We can quantify this propagation by simple statistical methods, summarized in Table 1.

Examination of the error propagation equations leads to the observation that the least error in each quantity results from methods that most directly measure that quantity. Note also that many of the error terms are based on relative errors and that the absolute error in a derived quantity may be dependent on the magnitude of the terms used in the derivation. Uncertainty in the indirectly measured quantities may increase dramatically through the course of a titration as concentrations of total metal and the directly measured species increase. This effect can be demonstrated graphically by drawing calculated error bars on plots of titration data.

The plots in Fig. 1 are the so-called formation functions which depict bound metal as a function of the negative log of the free metal activity (pM). The underlying formation function is identical for the three plots and represents a simulated metal

TABLE 1. Standard deviations and error propagation equations for chemical quantities measured by three exemplary methods. Subscript "r" denotes relative standard deviation. Chemical species are in units of mol/L. Propagation formulas after Skoog and West (23)

Quantity	Symbol	ISE	FQ	FPA
ISE potential (mV)	$V \pm S_v$	$S_v = 0.5$ mV	—	—
ISE calibration	$A \pm S_a$	$S_a = 0.4$ mV/unit pCu	—	—
FQ calibration	$B \pm S_b$	—	$S_{br} = 0.05$	—
FPA calibration	$C \pm S_c$	—	—	$S_{cr} = 0.01$
$-\log [Cu^{2+}]$	$pCu \pm S_p$	$S_{pr} = (S_{ar}^2 + S_{vr}^2)^{1/2}$	—	—
Percent quenching	$\%Q \pm S_q$	—	$S_q = 0.001(RFU_0)$	—
Charge transferred	$U \pm S_u$	—	—	$S_u = 0.4 + 0.01(U)$
$[Cu^{2+}]$	$Cu^{2+} \pm S_m$	$S_{mr} = S_p/0.434$	$S_{mr} = (S_{ir}^2 + S_{0r}^2)^{1/2}$	$S_{mr} = (S_{ir}^2 + S_{0r}^2)^{1/2}$
Inorganic constant	$K_0 \pm S_0$	[a]	[a]	[a]
Inorganic Cu(II)	$Cu_i \pm S_i$	$S_{ir} = (S_{0r}^2 + S_{mr}^2)^{1/2}$	$S_i = (S_l^2 + S_t^2)^{1/2}$	$S_{ir} = (S_{ur}^2 + S_{cr}^2)^{1/2}$
Total Cu(II) added	$Cu_T \pm S_t$	$S_{tr} = 0.02$	$S_{tr} = 0.02$	$S_{tr} = 0.02$
Humic-bound Cu(II)	$CuL \pm S_l$	$S_l = (S_t^2 + S_i^2)^{1/2}$	$S_{lr} = (S_{qr}^2 + S_{br}^2)^{1/2}$	$S_l = (S_t^2 + S_i^2)^{1/2}$
Free ligand	$L_f \pm S_f$	$S_f = S_l$	$S_f = S_l$	$S_f = S_l$

[a] $S_0 = 0.02$ (pH 6.0) or $S_0 = 19$ (pH 8.5) for all methods.

titration of a hypothetical three-ligand mixture calculated with the computer-based equilibrium program MINEQL (15). The three ligands yield titration curves essentially the same as those of humic acid but can be used to generate titration data to an arbitrarily high degree of accuracy (16).

The standard deviations in the quantities measured by ISE, FPA, and FQ were calculated from experimental data obtained in this laboratory (as discussed below) and were translated through the propagation equations for each method. Error intervals of one standard deviation from the computer-calculated mean values for both pM and [ML] (the 68% confidence intervals) were drawn about each point in the calculated formation functions.

As noted earlier, the error intervals for each metal species are smallest for the methods that most directly measure that species: free metal for Classes I and II, bound metal for Class III. The wide error bars on the low pM values for the Class II (FPA-type) measurements (Fig. 1*b*) reflect the detection limit of this method for a solution in which the labile metal approximately equals the free-metal activity; a similar error region would also be observed in the Class I measurements if the titration were conducted below the detection limit of the electrode.

Above the detection limits, indirectly measured species exhibit the greatest error and the magnitude of this error varies widely across the titration range. For example, bound-metal errors increase greatly near the end of the titrations that measure unbound metal. This reflects the propagation of relative errors as well as the fact that errors become most severe when we attempt to calculate a species concentration by subtracting two relatively large numbers.

A mathematical model of humic binding is of greatest predictive value if it is fitted to the most precise data in any concentration range. For each class of methods there is a titration region of minimal error in determinations of both free and bound metal. Figure 1 indicates that the best approach to modeling entails fitting Class I titration data in the high to moderate pM range and Class III titration data in the moderate to low pM range. Class II titrations might also be desirable, because of the high sensitivity of FPA, or for calibrating a model to data from a high-chloride medium.

Before combining the results of different techniques, the methods should be intercalibrated so there is reasonable congruence among the data. Intercalibration can be achieved in the central region of the titrations where all three titration classes yield data of nearly equal precision. From this central region, the data set can be extended for both free- and bound-metal species in either concentration direction with data from the appropriate methods. If only a single method is used, careful consideration should be given to the poor precision of data in certain regions of the titration and the resulting errors in the modeling parameters derived for that region.

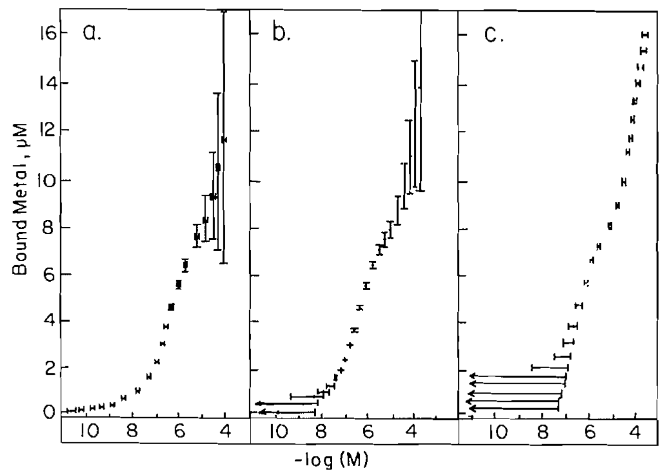

FIG. 1. A comparison of error propagation in hypothetical titration data: bound metal vs. −log free metal activity (formation functions). Error bars represent ± one standard deviation for: a. ion-selective electrode type data; b. fixed potential amperometry type data; c. fluorescence quenching type data.

Experimental

Fulvic acid was obtained from 20 L of Grassy Pond water (Bedford, MA) by adsorption onto XAD-8 resin according to the method of Thurman and Malcolm (17). The freeze-dried extract was 49% carbon by weight and this factor was used to prepare an aqueous stock solution of 50 mg-C/L of Grassy Pond fulvic acid (GP-FA). The stock solution was stored in a foil-covered flask (to exclude light) at 5°C and at pH 8. After preparation, stock solutions were allowed 48 h to dissolve and hydrolyze completely before any dilutions for titrations were made.

Solutions of fulvic acid for ion-selective electrode and fluorescence quenching titrations at 0.5, 1.0, and 5.0 mg-C/L were prepared with deionized water. Ionic strengths were adjusted using 1 *M* $NaClO_4$ to give an electrolyte concentration of 10^{-3} *M*. For fixed potential amperometry a background electrolyte of 0.5 *M* NaCl and 2 m*M* $NaHCO_3$ was used. The electrolyte was prepared from a 5 *M* NaCl, 20 m*M* $NaHCO_3$ stock solution that was passed through a Chelex resin column to remove contaminating trace metals according to the methods of Morel *et al.* (18).

Ion-selective electrode titrations were performed using a Radiometer F3000 Selectrode with a Cu(II) sensing membrane coupled with an Orion 90-02 double-junction reference electrode. The pH was monitored using a Fisher E5-A combination pH electrode and the pH was maintained by adjusting the alkalinity and bubbling with 1% CO_2/99% N_2 gas mixture. Electrode potentials were measured by a pair of Orion 801 Ionanalyzer meters. The ISE was calibrated with a series of copper solutions the day before each titration and was allowed to equilibrate overnight in a 1 m*M* Na_2EDTA/0.1 *M* TRIS buffer solution at pH 6.2. This procedure maximized electrode sensitivity in the low copper range. The fulvic acid solutions were titrated in 100-mL, water-jacketed beakers at 15°C with total copper concentrations ranging from 0.1 μ*M* to 100 μ*M*.

Fluorescence quenching titrations were performed using a Perkin–Elmer LS-5 Fluorescence spectrophotometer equipped with a 1-cm flow cell coupled by Teflon tubing and a peristaltic pump to a 50-mL, water-jacketed titration vessel maintained at 15°C. The pH was maintained with a CO_2/N_2 mixture as in the ISE titrations. Fulvic acid solutions were deoxygenated by several hours of bubbling with the CO_2/N_2 gas mixture in order to eliminate the minor quenching of the fulvic acid fluorescence by O_2. For GP-FA titrations the excitation and emission wavelengths were set for maximum fluorescence at 325 nm and 405 nm respectively. Slit widths were set at 10 nm. Kinetic studies indicated that quenching equilibrium was reached within 10 min at copper concentrations less than 1 μ*M* and in less than 5 min above 1 μ*M* copper. In subsequent titrations equilibration times were allowed, accordingly, before measurements were taken. Fulvic acid solutions were titrated over the same total copper range as in the ISE experiments: 0.1 μ*M* to 100 μ*M*.

Fixed potential amperometry was employed according to the methods of Waite and Morel (3). Measurements were made with an Environmental Science Associates (ESA) Model 3040 charge transfer analyzer equipped with a tubular pyrolytic graphite working electrode, a platinum wire counter electrode, and an Ag/AgCl, saturated NaCl reference electrode. The electrode potential was set at 90 mV and measurements were taken after a 10-min equilibration period following each copper addition. Titrations were performed with total copper ranging from 10 to 330 n*M*.

Results and discussion

Error analyses

The millivolt output of the ISE system was recorded to within 0.1 mV and analysis of five pairs of replicate titrations indicates that the standard deviation in electrode potential is ±0.5 mV. A slightly higher deviation is obtained at low Cu_T and pCu levels but, as an approximation, the standard deviation in potential was considered to be constant at ±0.5 mV.

The calibration factors for the electrode were determined by measurements of standard Cu(II) solutions. The deviation from Nernstian response allowed in the calibration slope was ±0.5 mV per decade pCu and the standard deviation was statistically derived from this spread to be ±0.4 mV per decade pCu.

The hydroxo and carbonato complexes of copper were calculated with stability constants selected from the literature. Stability constants and standard deviations for the carbonato complexes are given by Smith and Martell (19) as $\log \beta_1 = 6.75 \pm 0.02$ and $\log \beta_2 = 9.92 \pm 0.09$. There is greater variability in the constants for the hydroxo complex. For example, Smith and Martell (19) offer $\log \beta_1 = 6.3$ while Sunda and Hanson (20) reported $\log \beta_1 = 6.48$. The reported stability constants for the dihydroxo complex are particularly variable but, in two careful studies, values of $\log \beta_2 = 11.78$ (20) and 11.80 (21) were obtained. The mean of these is used in the present study. Standard deviations are not available for the hydroxo constants but it is reasonable to assume that both log β values are known to within ±0.10 log units. Because the concentrations of the hydroxide and the carbonate ions were held constant during the titrations, an aggregate proportionality factor, K_0, relating total inorganic and free ionic copper was calculated from the stability constants. The pH and $p(CO_3^{2-})$ were maintained within ±0.05 log units and incorporating all of these error terms in the calculation yielded $K_0 = 1.12 \pm 0.02$ for pH 6.0 and 170 ± 19 for pH 8.5.

The relative error associated with the calculation of inorganic copper becomes very significant when the inorganic copper concentration equals or exceeds the copper-fulvate concentration. This condition is dependent on both the metal/ligand ratio and the pH and is attained when either quantity is relatively high. Determinations of weak metal binding behavior by ion-selective electrode are therefore most accurate at low pH. Because apparent binding strength also decreases with pH, an appropriate compromise is to perform titrations near pH 6 where inorganic copper-complex concentrations and proton competition for the ligands are both acceptably small.

The standard deviation in the fluorescence measurements of a fulvic acid solution was uniform throughout the titration and equal to approximately 0.1% of the unquenched fluorescence. The relative fluorescence data are converted to bound-metal concentration by a calibration factor, *B*, linearly relating the percent-quenching (%*Q*) of fluorescence to the concentration of metal–fulvate complex. The simplest and most direct method for obtaining *B* is to plot percent quenching against the concentration of total metal added. If sufficiently small additions of Cu(II) (relative to the concentration of fulvic acid) are made, there is a region at the beginning of the titration in which there is a linear relationship between the metal added and the percent quenching. This region corresponds to the strong metal-binding portion of the titration in which essentially all of the metal added quantitatively binds to the fulvic acid. The slope of a least-squares fit of this region provides a quenching calibration factor for a given concentration of fulvic acid. This factor is assumed to be constant throughout the titration. The appropriateness of this assumption is discussed below.

The variation in the relative fluorescence translates into a standard deviation for the bound metal of ±0.1 × (calibration factor). For a typical titration of 5 mg-C/L GP-FA in which the calibration factor was 0.25 μ*M* bound Cu(II) per unit percent of quenching, the standard deviation on the bound copper measurements was ±0.025 μ*M*. The absolute error in bound metal is constant throughout so the relative error decreases as the titration advances. As a result, the relative error in the determination of free metal also decreases throughout the titration.

The labile copper measured by fixed potential amperometry includes all Cu(II) species that are reducible at the electrode potential, set in this system at +90 mV. At this potential only the hydrated cupric ion or the inorganic complexes are reduced and the current transferred over a fixed time interval, *U*, is proportional to the total inorganic copper in solution [Cu_i]. The proportionality factor, *C*, is obtained from a set of standard solutions. After systematic errors were corrected (3) we found the standard deviation in the current to be described by the equation:

$$[1] \quad S = \pm[S_x + S_{cr}(U)]$$

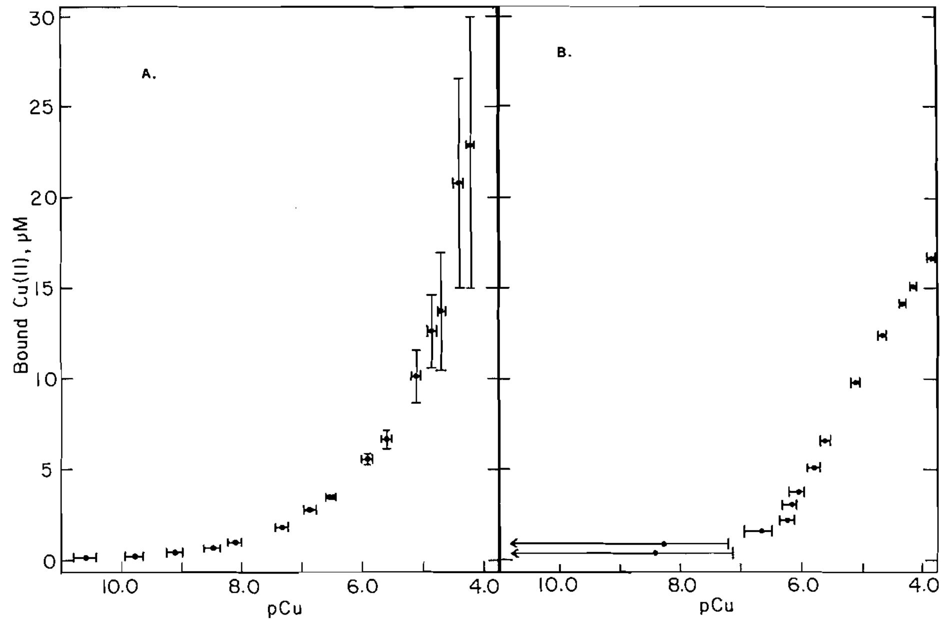

FIG. 2. Formation functions and standard deviations for Grassy Pond fulvic acid at 5.0 mg-C/L and pH 6.0. A. ISE titration; B. FQ titration.

in which S_x is a constant "background" error and $S_{cr}(U)$ represents the error that is proportional to the inorganic Cu(II) measured. For the experiments described here we found S_x = 0.4 nM and S_{cr} = 0.01; the latter value is the relative standard deviation in the proportionality factor. The minimum labile Cu(II) concentration accurately measurable was about 5 nM and the maximum copper concentration was about 350 nM.

The Davies equation was used to calculate the single-ion activity coefficients necessary for comparing the results of the FPA titrations to those of ISE titrations performed at lower ionic strength. Although there is significant uncertainty associated with these coefficients, the standard error could not be quantified and so is not incorporated in the error calculations.

Because total inorganic copper is directly measured by FPA, bound copper concentrations are more directly obtained with this method than by ISE. The inorganic copper concentration was converted to the cupric ion activity by the factor K_0 as defined earlier. For the solution conditions of the titration the minimum cupric ion activity measurable was about 0.01 nM or pCu = 11.0.

A summary of the standard deviations for the data from the three methods is presented in Table 1.

Comparison of titration results

Data from the ISE and FQ titrations of 1.0 and 5.0 mg-C/L solutions of Grassy Pond fulvic acid at pH 6.0 were converted by the arithmetic transformations described into both the directly and indirectly measured species concentrations. Plots of formation functions (bound metal vs. pCu) were prepared using the results of both techniques and are presented in Fig. 2 for comparison. The standard deviation for each data point was calculated with the error propagation equations, and error bars representing one standard deviation were placed around the symbols. The plots reveal systematic differences between the two methods as well as pronounced differences in the propagation of random error.

The formation functions demonstrate the limited sensitivity of fluorescence quenching for determining free-metal activity. Metal activity below 0.1 μM is measurable only by the ISE. The sensitivity of the ISE to low pCu allows the accurate calculation of stability constants or other model parameters for the strong binding region of the titration. Reliance on fluorescence quenching alone would preclude any quantification of this important property of humic materials.

The smallest amount of bound metal detectable in a fluorescence quenching titration is proportional to the smallest change in relative fluorescence distinguishable from noise. For the system described here that quantity is about 0.1 μM of bound copper and is independent of the total fulvic acid in solution. This amount is coincidentally the same as the smallest amount of strongly bound copper measurable with an ISE (equal to the minimum Cu_T).

Throughout the titration the ion-selective electrode provides relatively accurate measurements of pCu. Error propagation analysis reveals, however, that the accuracy of the ISE in measuring free metal does not translate into accurate bound-metal measurements over the entire titration range. The bound copper measured directly by fluorescence quenching exhibits higher accuracy than the indirect ISE data when [ML] > 2 μM. Accuracy in the high-metal region of the titration is critical for estimating the total ligand concentration, L_T.

In order to compare directly the species concentrations measured by these two methods, plots of the formation functions for both the ISE and the FQ titrations were overlaid (without error bars, for clarity) in Fig. 3.

In the low total-metal regions of the titrations, both ISE and FQ yield nearly identical bound metal values. The free-metal values in this region differ because of the poor precision with which fluorescence quenching measures unbound metal at low M_T. In the mid-range the formation functions overlap but, in the titration region corresponding to weak metal-binding, fluorescence quenching measures smaller bound-metal concentrations than does the ISE, a phenomenon observed in several other studies (1, 14). One explanation is that the weak binding sites have a different fluorescence efficiency than the stronger sites. Ryan and Weber (14) suggested that some of the weak binding occurs on molecules that have already been quenched by strongly bound Cu(II). Another explanation is simply that a greater proportion of the weaker binding is due to either sites not associated with fluorophores or a strictly electrostatic effect

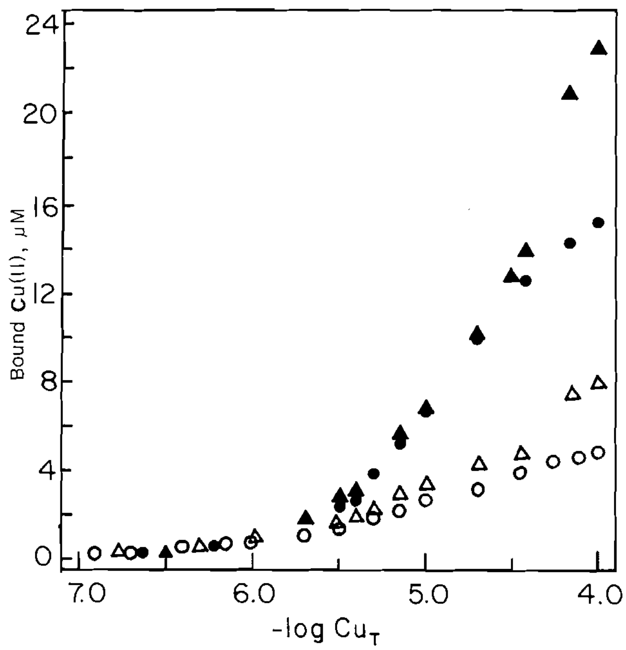

FIG. 3. Formation functions for Grassy Pond fulvic acid at pH 6.0. 5.0 mg-C/L: ISE (▲), FQ (●). 1.0 mg-C/L: ISE (△), FQ (○).

that does not involve the alteration of fluorescing electrons. No definitive explanation is currently possible and the discrepancy only adds greater uncertainty to the poorly defined end region of fulvic acid titrations.

The fulvic acid concentrations in these titrations are representative of many surface, freshwater systems but are perhaps an order of magnitude higher than in some deep groundwater or marine systems. The relatively high total copper concentrations required by the ISE seriously limit the usefulness of the method for characterizing humic matter at concentrations below 1 mg-C/L.

A fixed-potential amperometry titration of a 0.5 mg-C/L solution of Grassy Pond fulvic acid at pH 8.5 in 0.5 *M* NaCl demonstrates that FPA can quantify binding behavior for Cu(II)-fulvate present in concentrations below the sensitivity of other methods. The pH and background electrolyte furnish information about fulvic acid behavior under marine solution conditions.

The results of the FPA and ISE titrations were converted, as in the previous section, into both the directly and indirectly measured quantities and the data from both methods presented in comparative plots (Fig. 4). All activities were corrected to the lower ionic strength (I = 0.001) by coefficients calculated with the Davies equation. The formation functions demonstrate the relative merits of the two methods in the low-copper range. The ion-selective electrode is limited to measurements for which the total copper concentration is greater than about 0.1 μ*M* although the cupric-ion activity can be measured at less than 10^{-10} *M*. Total Cu(II) concentrations can be two orders of magnitude lower for the FPA titration than with the ISE, but FPA has the same sensitivity for both total and labile Cu(II). Therefore, the minimum cupric-ion activity measurable by FPA in the presence of strong binding agents is higher than for the ISE.

A comparison of the plots indicates good agreement in the cupric ion activities determined by both methods for pCu $\leq$ 9.2. At lower copper concentrations the activities measured by the ISE fall below the FPA data (Fig. 5). At these low total-

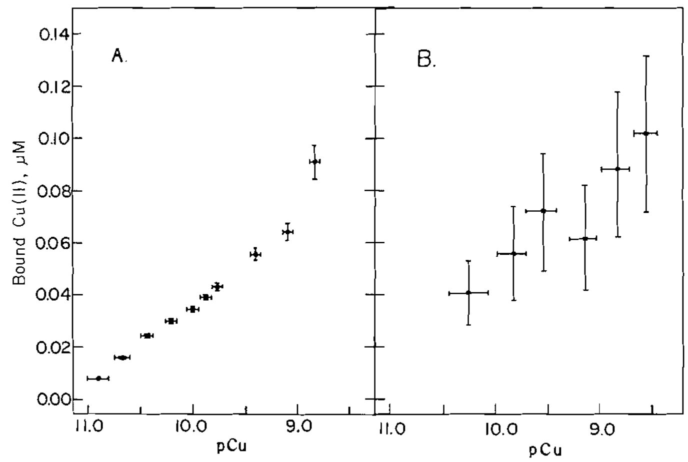

FIG. 4. Formation functions and standard deviations for Grassy Pond fulvic acid at 0.5 mg-C/L and pH 8.5. A. FPA titration; B. ISE titration.

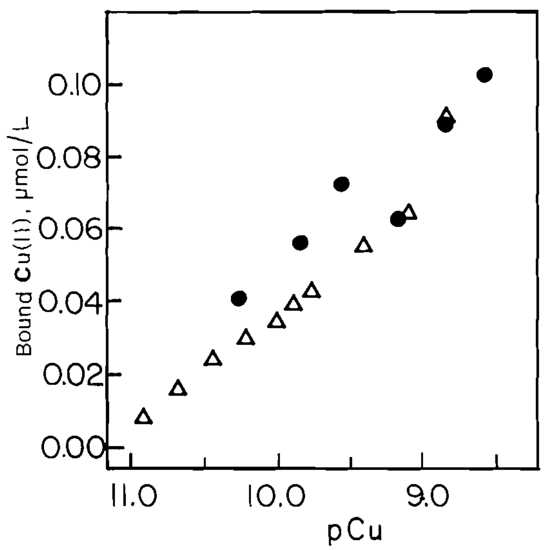

FIG. 5. Formation functions for Grassy Pond fulvic acid at 0.5 mg-C/L and pH 8.5. FPA titration (△); ISE titration (●).

copper concentrations the ISE is functioning below its optimal range and the equilibration time for the electrode is very slow, on the order of 2–10 h, depending on pH and pCu (low pCu and high pH have the slowest equilibration). Because the electrode potential drifts so slowly upward during this extended period it is likely the apparent equilibrium reached and recorded for these data points was short of true equilibration. Another likely problem was the loss of copper through surface adsorption at high pH, given the extended equilibration period. We estimated this quantity from atomic absorption spectrophotometry measurements of Cu_T in solution to be about 10% of total copper for Cu_T less than 1.0 μ*M*.

In the same Cu(II) concentration range, fixed-potential amperometry operates under optimal solution conditions and we expect the FPA data to be more accurate than those of the ISE operating outside its appropriate range. Measurements at the low metal/ligand ratios confirm the binding behavior observed in more concentrated fulvic acid solutions with other methods and are of great use in evaluating the metal complexing properties of marine waters.

Note also that the bound-metal data obtained by the ISE are particularly imprecise at the higher pH of this titration, compared to titrations at pH 6. The uncertainty in the inorganic complexation factor, K_0, is the primary cause. Recall that this constant is not needed in obtaining bound-copper values from FPA data because the total inorganic Cu(II) is measured directly by FPA.

The major limitations on FPA are the maximum permissible strong ligand concentration (about 0.1 μM), the maximum Cu(II) concentration (about 350 μM in the present system), and the need for relatively high chloride concentrations. These restrictions do not hinder the special usefulness of FPA for marine studies but indicate that the method cannot fully characterize humic material over a wide range of species concentrations, especially in the weak metal-binding region. While these problems are specific to FPA, all methods in Class II (linear, labile-metal) are hindered by the difficulty of collecting metal binding data over many orders of magnitude with a linearly responding method. As a class, these methods appear to be most useful for measuring a limited titration range under solution conditions that preclude the use of methods such as ISE and FQ.

The results of the fixed-potential amperometry titrations were not compared directly to the fluorescence quenching results because there is only a small region of overlap in the concentration ranges of the two methods. The overlap is in the region of least precision for free-metal measurements by fluorescence quenching. Hence, FPA and FQ, while complementary in the concentration ranges measured, cannot be directly intercalibrated.

Total ligand measurements

Determination of the total ligand concentration in solution is essential for defining conditional stability constants or parameters for other models of humic–metal interactions. If the bound-metal concentration in a plot of the complex-formation function levels off, the maximum concentration of bound metal is taken to equal L_T. Unfortunately, such unambiguous endpoints are rarely seen in Cu(II) titrations of humic materials. The large proportion of weak binding sites may not be fully saturated at the maximum metal activity in the titration. Formation of copper hydroxide solid at cupric ion activities greater than 10^{-4} M poses an upper limit for Cu(II) titrations, as does the flocculation of humic colloids (1).

The absence of a clear endpoint is exacerbated in ISE titrations by the scattered bound-metal data in the end region. Low ligand concentrations favor the likelihood of reaching the endpoint before pCu 4 and a low pH (less than 5) would permit continuing the titration to higher cupric-ion activities. However, L_T determinations are not improved by these conditions because the bound-metal concentration at the end of the titration in either case is smaller, while the error in the data remains about the same.

For Grassy Pond fulvic acid the best estimate of L_T, based on the ISE titration of 1.0 mg-C/L, is 6.0 ± 1.5 mequiv./mg-C (the standard deviation represents the variance in the bound-metal determination). For the fluorescence quenching titration of the same solution, L_T = 4.7 mequiv./mg-C. Although the uncertainty in the bound-metal measurements on which the latter figure is based is ±0.025 μM, the error in L_T is presumably greater than that because of uncertainty as to the degree of saturation of binding sites, coagulation effects, and uncertainty in the assumption that the FQ calibration factor is constant. Because the definition of endpoint remains rather arbitrary for all methods, the uncertainty cannot be quantified by replicate titrations. The error in L_T may be the single largest error in the calculation of metal–humic interactions. Many models of metal–humic interactions normalize bound-metal concentrations to L_T (i.e., $\bar{\nu} = [ML]/L_T$). Normalizing data to such a poorly defined quantity decreases the precision with which model parameters can be fitted.[1] Eliminating the L_T term from empirical binding models would obviate this analytically intractable problem.

In general, L_T is a difficult parameter to measure by any method, or, in fact, to properly define. The poor resolution of L_T has been little recognized in studies of metal–humic interactions and an examination of the literature indicates that most L_T values or "complexation capacities" are actually operationally defined endpoints that do not reflect the true concentrations of humic binding sites. The errors in titration end-regions also suggest that "total ligand concentration" or "binding capacity" should not be used as a descriptive parameter for comparing humic materials. The concentration of humic material, the method used, and the solution pH all have a dramatic effect on the maximum amount of metal binding observed.

Comparison of individual and combined data sets

Conditional stability constants for Cu(II)–fulvate complexes were derived from the results of the three exemplary methods by applying FITEQL, a computer-based, discrete-ligand optimization routine (22). The concentrations and stability constants obtained are, of course, only fitting parameters but they are useful for both reproducing the titration data and for comparing different data sets.

In order to compare the effects of error propagation, the standard deviations calculated for the titration data from each method were used to estimate confidence intervals for the derived stability constants and ligand concentrations. The solution scheme in FITEQL has provisions only for fixed relative standard deviations in the titration data. Since relative errors are not constant over the entire titration, the fitting optimizations were repeated for each ligand with the appropriate relative standard deviations substituted. The values used each time were the mean relative standard deviations for the titration region in which that ligand is predominant. The optimally fitted stability constants and equivalent ligand concentrations for all methods are presented in Table 2.

The results of applying a single analytical method to complicated mixtures such as fulvic acids are reflected in the diversity of standard deviations in the stability constants obtained. The regions of high error for each method translate predictably into poor accuracy for the conditional stability constants that predominate in those regions. This can be demonstrated by plotting the standard deviations associated with the ratios of bound metal to free metal for each titration (Fig. 6).

Prediction of bound-metal and free-metal concentrations is the goal of metal–humic speciation models and the error in the ratio of the two quantities is a convenient way of summarizing the errors expected in model calculations based on these data. The ratio is also proportional to the apparent stability constant that would be calculated at any point in the titration. In addition, the plot is a useful summary of the concentration ranges over which each method is operational.

The region in which the bound-metal/free-metal ratio is high

[1]W. Fish and F. M. M. Morel. In preparation (1985).

TABLE 2. Conditional stability constants, discrete ligand concentrations, and associated standard deviations for Grassy Pond fulvic acid (GP-FA). Values calculated with FITEQL using errors defined in Table 1

GP-FA (mg-C/L)	Method	Stability constants			Ligand concentrations, μequiv./L		
		log K_1	log K_2	log K_3	L_1	L_2	L_3
0.5[a]	ISE	—	9.02±0.90	—	—	0.40±0.25	—
	FPA	—	9.27±0.04	—	—	0.33±0.02	—
1.0[b]	ISE	—	8.25±0.29	6.27±0.18	—	0.25±0.10	1.98±0.35
	FQ	—	8.10±0.36	5.25±0.10	—	0.53±0.11	3.98±0.28
5.0[b]	ISE	10.52±0.34	8.28±0.20	5.63±0.14	0.18±0.06	1.34±0.26	9.15±1.20
	FQ	—	8.57±0.25	5.14±0.05	—	1.53±0.25	8.80±0.80

[a]pH 8.5, 0.5 *M* NaCl.
[b]pH 6.0 × 10^{-3} *M* $NaClO_4$.

(the left-hand side of the plot) corresponds to the low Cu_T, strong-binding region of the titration. The ISE data here have much lower relative standard deviations than do the FQ data. Conversely, in the region of low bound-metal/free-metal ratios at the right-hand side (weak metal-binding), the FQ data are more precise. The entire range of the FPA titration lies in the high-ratio region and the method yields lower relative standard deviations in the strong-binding region than does the ISE.

The results in Fig. 6 also indicate that each method is more accurate at higher fulvic acid concentrations. Examination of the error propagation equations shows that higher ligand concentrations result in smaller relative errors in the bound-metal data, hence less error in stability constants.

Only a combination of several methods yields the most precise set of ligand parameters. Within any broad region of a titration only two of the three methods operate within their concentration limits and the more precise data of the two sets available can be used to create a combined-methods data set.

Conclusions

Any comprehensive study of the interactions of a humic material with one or more metals is subject to unnecessary imprecision if only a single analytical method is employed or if inappropriate methods are selected. Precision at high bound-metal/free-metal ratios is important for quantifying the strongest metal binding behavior of a humic substance while accuracy at low bound-metal/free-metal ratios is critical for assessing the total number of sites available for binding. We have demonstrated that analytical methods can be grouped according to the quantity that they most directly measure and that the precision of metal binding data over a wide range of solution conditions can be enhanced if methods from at least two different classes are used. Examining the error propagation associated with the formation-function plots for each class is helpful in choosing complementary methods that yield the most precise data throughout a wide titration range. If only a single method can be utilized, the variance calculations and error propagation equations listed in Table 1 can be used to estimate confidence intervals for species concentrations or model parameters.

An overall improvement in the precision of titration data leads to better predictive calculations of trace-metal speciation in natural waters. Quantification of the variance in the parameters used to describe metal−humic interactions allows for more useful and realistic comparisons among the results of different studies. Error analysis can also indicate which

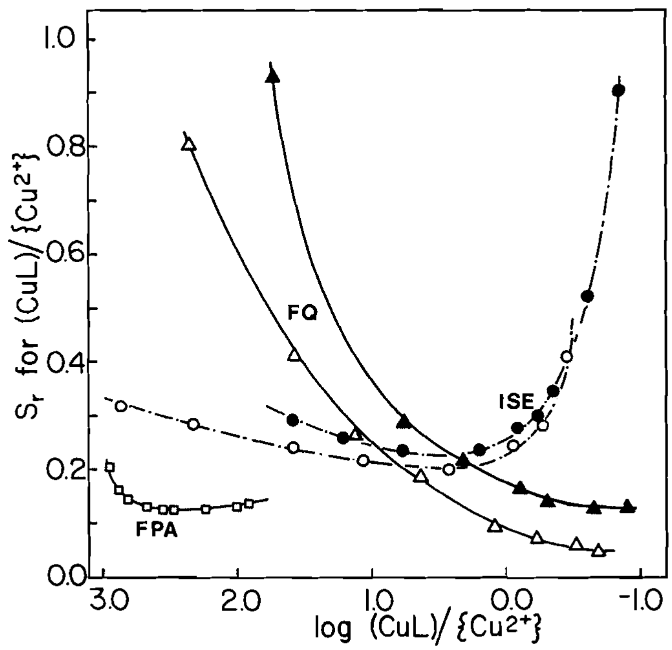

FIG. 6. Relative standard deviations for the ratio of bound Cu(II) to free Cu(II) for all titrations plotted against the log of the ratio. ISE: 1 mg-C/L (●), 5 mg-C/L (○). FQ: 1 mg-C/L (▲), 5 mg-C/L (△). FPA: 0.5 mg-C/L (□).

parameters (L_T for example) should not be incorporated in models or used for comparison.

Acknowledgments

The authors thank P. Gschwend and S. Chisholm for useful comments. This work was supported by International Copper Research Association (INCRA) Project No. 346 and by NSF grant OCE81-18103 and NOAA grant NA 79AA-D-00077. W. Fish is the recipient of an INCRA fellowship.

1. J. R. TUSCHALL and P. L. BREZONIK. *In* Aquatic and terrestrial humic materials. *Edited by* R. F. Christman and E. T. Gjessing. Ann Arbor Science, Ann Arbor, MI. 1983.
2. R. A. SAAR and J. H. WEBER. Anal. Chem. **52**, 2095 (1980).
3. T. D. WAITE and F. M. M. MOREL. Anal. Chem. **55**, 1268 (1983).
4. R. A. ŞAAR and J. H. WEBER. Environ. Sci. Technol. **16**, 510 (1982).
5. J. C. WESTALL, F. M. M. MOREL, and D. N. HUME. Anal. Chem. **51**, 1792 (1979).

6. C. M. G. VAN DEN BERG and J. R. KRAMER. *In* Chemical modeling in aqueous systems. *Edited by* E. Jenne. Proc. ACS Symposium. American Chemical Society, New York, NY. 1979.
7. C. M. G. VAN DEN BERG, P. T. S. WONG, and Y. K. CHAU. J. Fish. Res. Board Can. **36**, 901 (1979).
8. R. E. TRUITT and J. H. WEBER. Environ. Sci. Techol. **15**, 1204 (1981).
9. R. F. C. MANTOURA and J. P. RILEY. Anal. Chim. Acta, **78**, 193 (1975).
10. J. R. TUSCHALL and P. L. BREZONIK. Anal. Chem. **53**, 1986 (1981).
11. P. L. BREZONIK and J. R. TUSCHALL. Anal. Chem. **54**, 1000 (1982).
12. M. SCHNITZER and E. H. HANSEN. Soil Sci. **109**, 333 (1970).
13. G. MILLS and J. G. QUINN. Mar. Chem. **10**, 93 (1981).
14. D. K. RYAN and J. H. WEBER. Anal. Chem. **54**, 986 (1982).
15. J. C. WESTALL, J. L. ZACHARY, and F. M. M. MOREL. Technical Report No. 18, M.I.T., Cambridge, MA. 1976.
16. W. FISH, D. A. DZOMBAK, and F. M. M. MOREL. Environ. Sci. Technol. (1984) Submitted.
17. E. M. THURMAN and R. L. MALCOLM. Environ. Sci. Technol. **15**, 463 (1981).
18. F. M. M. MOREL, J. G. RUETER, D. M. ANDERSON, and R. R. L. GUILLARD. J. Phycol. **15**, 135 (1979).
19. R. M. SMITH and A. E. MARTELL. Critical stability constants. Vol. 4: inorganic complexes. Plenum, New York, NY. 1976.
20. W. G. SUNDA and P. J. HANSON. *In* Chemical modeling in aqueous systems. *Edited by* E. Jenne. Proc. ACS Special Symposium. American Chemical Society, New York, NY. 1979.
21. A. J. PAULSON. Potentiometric studies of cupric hydroxide complexation. MS Thesis, University of Rhode Island, Kingston, RI. 1978. 102 pp.
22. J. C. WESTALL. Technical Report. Department of Chemistry, Oregon State University, Corvallis, OR. 1982.
23. D. A. SKOOG and D. M. WEST. Fundamentals of analytical chemistry. 4th ed. Saunders College Publishing, Philadelphia, PA. 1982.

Kinetics and isotope effects of the β-elimination reactions of some 2,2-di(4-nitrophenyl)chloroethanes promoted by tetramethylguanidine in aprotic solvents

ARNOLD JARCZEWSKI AND MALGORZATA WALIGORSKA
Department of Chemistry, Adam Mickiewicz University, 60-780 Poznan, Poland

AND

KENNETH T. LEFFEK
Department of Chemistry, Dalhousie University, Halifax, N.S., Canada B3H 4H6

Received August 2, 1984

ARNOLD JARCZEWSKI, MALGORZATA WALIGORSKA, and KENNETH T. LEFFEK. Can. J. Chem. **63**, 1194 (1985).

Rate constants for the β-elimination of HCl from 2,2-di(4-nitrophenyl)-1,1-dichloroethane (I) and 2,2-di(4-nitrophenyl)-1,1,1-trichloroethane (II) promoted by tetramethylguanidine in the aprotic solvents acetonitrile, tetrahydrofuran, and n-hexane have been measured. The activation parameters are characterized by small enthalpies of activation (4.1 to 7.3 kcal mol^{-1}) and large negative entropies of activation (-35 to -50 cal mol^{-1} deg^{-1}). The primary deuterium isotope effects at 20°C range from k_H/k_D = 4.8 to 10.3. The results are interpreted to indicate an $(EcB)_I$ mechanism for both substrates I and II in acetonitrile solvent and an E2H or mixed $(ElcB)_I$–E2H mechanism in the less polar solvents, tetrahydrofuran and n-hexane.

ARNOLD JARCZEWSKI, MALGORZATA WALIGORSKA et KENNETH T. LEFFEK. Can. J. Chem. **63**, 1194 (1985).

On a mesuré les constantes de vitesse des éliminations β de HCl du di(nitro-4 phényl)-2,2 dichloro-1,1 éthane (I) et du di(nitro-4 phényl)-2,2 trichloroéthane (II) sous l'influence de la tétraméthylguanidine dans des solvants aprotiques comme l'acétonitrile, le tétrahydrofuranne et le n-hexane. Les paramètres d'activation sont caractérisés par des enthalpies d'activation faibles (4,1 à 7,3 kcal mol^{-1}) et par des entropies d'activation importantes et négatives (-35 à -50 cal mol^{-1} deg^{-1}). A 20°C, les effets isotopiques primaires du deutérium s'étalent de k_H/k_D = 4,8 à 10,3. Sur la base des résultats obtenus, on croit que, dans l'acétonitrile comme solvant, les deux substrats I et II réagissent par un mécanisme $(EcB)_I$ alors que dans des solvants moins polaires, comme le tétrahydrofuranne et le n-hexane, les produits réagiraient par un mécanisme E2H ou par un mécanisme mixte $(ElcB)_I$–E2H.

[Traduit par le journal]

Introduction

The kinetics and mechanism of the β-elimination reaction of HCl from diarylchloroethanes with different bases in a variety of solvents have been examined by McLennan and Wong (1–5) and by Cristol *et al.* (6, 7). Also, a study of proton transfer reactions to yield stable carbanions has been used to assess the importance of this step in determining the reaction parameters of β-eliminations (8) or the contribution of the E1cB mechanism to the overall mechanism of elimination (9). Primary deuterium isotope effects have been found to be useful in defining the character of the mechanism.

In this study, therefore, arylchloroethanes in which different numbers of chlorine atoms on the α-carbon atom modify the acidity of the hydrogen on the β-carbon atom, have been used to investigate the influence of this acidity on the rate and mechanism of the β-elimination reaction. The effect of electron-withdrawing substituents in the phenyl rings (10, 11) has been investigated, using *p*-nitrophenyl groups to compare with the *p*-chlorophenyl groups previously studied (1–5).

In this paper the changes are examined in the activation parameters, isotope effects, and mechanism of the β-elimination reaction of HCl from 2,2-di(4-nitrophenyl)-1,1-dichloroethane (I) and 2,2-di(4-nitrophenyl)-1,1,1-trichloroethane (II) promoted by the base 1,1′,3,3′-tetramethylguanidine (TMG) in several solvents of different polarity.

Results and discussion

The second-order rate constants for the elimination of HCl from the substrates I and II are shown in Tables 1 and 2, together with the primary deuterium isotope effects. These rate constants increase with increasing polarity of the solvent as expected, except that the elimination of DCl from the deuterated substrates is slightly faster in tetrahydrofuran than it is in acetonitrile. The second-order rate constants in acetonitrile for both I and II are about 1×10^3 greater than the corresponding rate constants for the elimination of HCl from DDT and DDD by the same TMG base (12). This indicates a Hammett ρ value for this reaction of more than 5 if the σ^0 scale is assumed to apply (13, 14) or about 3 if the σ^- scale is used. In either case this is a greater value than the largest ρ value (2.0) which has been found for proton transfer reactions (13, 14). Values of 4 and 5 were reported (15) for the base catalyzed cleavage of a series of *trans* and *cis* 1-phenyl-2-arylcyclopropanols but, although the transition state for this does involve a proton transfer, the authors concluded that it, in fact, contains relatively little proton transfer. Thus, this reaction is controlled mainly by the rate for carbon–carbon bond cleavage.

No doubt the replacement of the *p*-chloro substitutent by the *p*-nitro group increases the acidity of the hydrogen on the β-carbon atom of I and II, but the effect on the rate of elimination is greater than can be ascribed to the acidity change alone. Thus, a change of mechanism is indicated by this result.

The activation parameters for the reactions were calculated from the second-order rate constants by a linear least-squares method and are collated in Tables 3 and 4. The enthalpies of activation are quite low for both substrates and all solvents, although slightly larger values are obtained in the more polar solvent acetonitrile than in the non-polar hexane solvent. The low $\Delta H^{\ddagger}$ values, compared to other β-elimination reactions (4, 5, 7, 12, 16–18), suggest that the mechanism may be of the E1cB-type and that $\Delta H^{\ddagger}$ is largely controlled by the energy requirement to break the initial state solvation shell and allow the proton to transfer to the base.

The entropies of activation are all large and negative, with

TABLE 1. Second-order rate constants for the reaction of $(O_2NC_6H_4)_2$-$CHCHCl_2$ and its deuterated analogue with TMG base in acetonitrile, tetrahydrofuran, and hexane solvents

Temp. (°C)	k_{2H}(dm^3 mol^{-1} s^{-1}) ±std. dev.	k_{2D}(dm^3 mol^{-1} s^{-1}) ±std. dev.	k_H/k_D ±std. dev.
Acetonitrile			
10.0	0.291 ± 0.003	0.028 ± 0.001	10.6 ± 0.3
20.0	0.474 ± 0.004	0.049 ± 0.001	9.6 ± 0.1
30.0	0.707 ± 0.005	0.082 ± 0.001	8.6 ± 0.2
35.0	1.111 ± 0.003	0.141 ± 0.001	7.9 ± 0.1
40.0	1.67 ± 0.01	0.218 ± 0.001	7.6 ± 0.1
Tetrahydrofuran			
10.0	0.238 ± 0.002	0.034 ± 0.001	6.9 ± 0.1
20.0	0.371 ± 0.004	0.056 ± 0.001	6.6 ± 0.1
30.0	0.551 ± 0.004	0.088 ± 0.001	6.2 ± 0.1
40.0	0.775 ± 0.007	0.135 ± 0.001	5.7 ± 0.1
50.0	1.12 ± 0.01	0.198 ± 0.001	5.6 ± 0.1
Hexane			
10.0	0.058 ± 0.000_5	0.012 ± 0.000_1	4.9 ± 0.1
20.0	0.081 ± 0.002	0.017 ± 0.000_1	4.8 ± 0.1
30.0	0.109 ± 0.001	0.024 ± 0.000_2	4.5 ± 0.1
40.0	0.145 ± 0.001	0.033 ± 0.000_1	4.3 ± 0.0_3
50.0	0.189 ± 0.002	0.045 ± 0.000_3	4.2 ± 0.0_5

TABLE 2. Second-order rate constants for the reaction of $(O_2NC_6H_4)_2$-$CHCCl_3$ and its deuterated analogue with TMG base in acetonitrile, tetrahydrofuran, and hexane solvents

Temp. (°C)	k_{2H}(dm^3 mol^{-1} s^{-1}) ±std. dev.	k_{2D}(dm^3 mol^{-1} s^{-1}) ±std. dev.	k_{2H}/k_{2D} ±std. dev.
Acetonitrile			
10.0	0.339 ± 0.009	0.026 ± 0.001	12.8 ± 0.6
20.0	0.477 ± 0.004	0.046 ± 0.001	10.3 ± 0.2
30.0	0.674 ± 0.008	0.077 ± 0.001	8.7 ± 0.1
40.0	1.021 ± 0.01	0.124 ± 0.002	8.2 ± 0.2
50.0	1.53 ± 0.01	0.198 ± 0.001	7.7 ± 0.1
Tetrahydrofuran			
10.0	0.286 ± 0.003	0.039 ± 0.001	7.3 ± 0.1
20.0	0.415 ± 0.003	0.061 ± 0.001	6.8 ± 0.1
30.0	0.571 ± 0.002	0.088_5 ± 0.000_5	6.5 ± 0.0_4
40.0	0.767 ± 0.003	0.130 ± 0.001	5.9 ± 0.0_4
50.0	1.026 ± 0.001	0.183 ± 0.001	5.6 ± 0.0_5
Hexane			
10.0	0.045 ± 0.000_3	0.008 ± 0.000_1	5.7 ± 0.1
20.0	0.061 ± 0.000_2	0.011 ± 0.000_1	5.4 ± 0.0_5
30.0	0.079 ± 0.001	0.016 ± 0.000_1	5.1 ± 0.0_5
40.0	0.101 ± 0.001	0.022 ± 0.000_2	4.6 ± 0.1
50.0	0.125 ± 0.001	0.029 ± 0.000_3	4.3_5 ± 0.0_5

the values increasing as the polarity of the solvent is decreased, a trend previously observed by Cockerill (19). These results are consistent with an increase in the strength of the solvation shell during the activation process and that increase is greatest where the initial state solvation is weakest, in hexane solvent. The entropies of activation are generally consistent with a transition state of increased charge separation relative to the initial state.

The values of the primary deuterium isotope effect, given in Tables 1 and 2, are quite high for a β-elimination reaction, varying between k_H/k_D = 10.3 to 4.8 at 20°C. These show clearly that the rate-determining step involves the proton transfer. However, the isotope effect varies with the polarity of the solvent in the reverse manner to that observed for proton transfer reactions (20), in that the magnitude of the effect decreases with decreasing polarity of the solvent. This variation may not, therefore, be explained in terms of an increase in the active mass of the proton in polar solvents, as was suggested for the proton transfer reactions (19), but must be due to a variation in the mechanism. In the more polar acetonitrile solvent the $(E1cB)_I$ mechanism would be expected to be favoured, so that the full isotope effect would be observed. In the less polar solvents the mechanism should change to an E2H-type transition state, where the proton transfer is jointly rate controlling with the breaking of the bond to the leaving group, giving rise to the observation of a smaller deuterium isotope effect.

The isotope effects on the enthalpies of activation are about 1 kcal mol^{-1}, which would be expected for the loss of the carbon–hydrogen stretching frequency in the activation process, except for the reactions carried out in acetonitrile. In that solvent, where the mechanism is probably $(E1cB)_I$ (Scheme 1), the isotope effect on the enthalpies of activation of dichloro and trichloro substrates at 1.6 ± 0.2 and 2.3 ± 0.3 kcal mol^{-1} indicates that some proton tunnelling is probably taking place. The largest such isotope which can be accounted for by loss of the C—H stretching vibration and both C—H bending vibrations is about 2.1 kcal mol^{-1}. The absence of this evidence for tunnelling in the less polar solvents, where it is normally expected (20), is consistent with the operation of an E2H mechanism (Scheme 2), or a mixed E1cB–E2H mechanism.

The similarity of the second-order rate constants for the dichloro and trichloro substrates indicates that the effect of the chlorine atom on the acidity of the hydrogen on the β-carbon is very small. Therefore, the same mechanistic conclusions apply to both substrates.

In fact, in hexane solvent the trichloro substrate shows a slightly smaller second-order rate constant than the dichloro compound, showing no relationship with the acidity of the hydrogen on the β-carbon atom, in contrast to the findings for the analogous reactions of DDT and DDD (9).

Experimental

Materials

2,2-Diphenyl-1,1,1-trichloroethane was prepared by the method of McLennan and Wong (5) from acetophenone by chlorination with Cl_2 gas followed by reduction with $LiAlH_4$. The product 2,2-diphenyl-1,1,1-trichloroethane was recrystallized from methanol, mp 64.5–65°C (lit. (5) mp 64.5–65.5°C).

The ethane was nitrated by the method of Haskelberg and Lavie (21). The nitrated product had a mp 169°C (lit. (1, 21) mp 169°C); nmr, aliphatic proton, δ = 5.30 ppm (lit. (1) δ = 5.35 ppm).

2,2-Di(4-nitrophenyl)-1,1-dichloroethane was prepared according to McLennan and Wong (5) and Aston *et al.* (22). 1-Chloroacetophenone (20 g) in glacial acetic acid (150 g) was chlorinated by bubbling in Cl_2 gas for 7 h at 60°C under a 250-W lamp. The reaction mixture was poured onto crushed ice and the organic layer separated. The aqueous layer was extracted with diethyl ether and the ether extracts were added to the organic layer. After removal of the ether, the product 1,1-dichloroacetopheone was distilled at reduced pressure.

The 2,2-di(4-nitrophenyl)-1,1-dichloroethane was prepared from this ketone by the same procedure as for the trichloro compound, mp 179.5°C (lit. (1) mp 177–178°C); nmr, aliphatic proton, δ = 4.85 ppm (lit. (1) δ = 4.83 ppm).

The deuterated analogues of the two substrates were obtained using $LiAlD_4$ for the reduction of the ketones. The extent of deuteration was estimated to be at least 99% from the nmr spectra.

Reagent grade acetonitrile was purified by the method of O'Donnell *et al.* (23), with a final fractional distillation from P_2O_5. The fraction

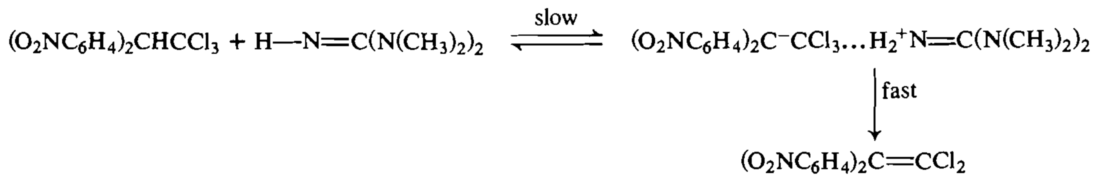

SCHEME 1

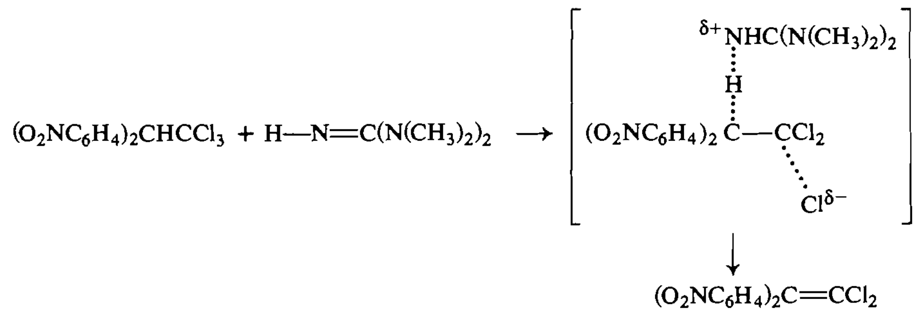

SCHEME 2

TABLE 3. Activation parameters for the reaction of $(O_2NC_6H_4)_2CHCHCl_2$ and its deuterated analogue with TMG base in acetonitrile, tetrahydrofuran, and hexane solvents

Parameter	Normal substrate		Deuterated substrate
Acetonitrile			
$\Delta H^{\ddagger}$ (kcal mol^{-1})	7.3 ± 0.1		8.9 ± 0.1
$\Delta S^{\ddagger}$ (cal mol^{-1} deg^{-1})	−35.1 ± 0.4		−34.3 ± 0.3
$\Delta G^{\ddagger}$ (kcal mol^{-1})	17.8 ± 0.2		19.1 ± 0.1
$(\Delta H_D^{\ddagger} - \Delta H_H^{\ddagger})$		1.6 ± 0.2	
$(\Delta S_D^{\ddagger} - \Delta S_H^{\ddagger})$		0.8 ± 0.5	
$(\Delta G_D^{\ddagger} - \Delta G_H^{\ddagger})$		1.3 ± 0.2	
Tetrahydrofuran			
$\Delta H^{\ddagger}$ (kcal mol^{-1})	6.4 ± 0.1		7.4 ± 0.1
$\Delta S^{\ddagger}$ (cal mol^{-1} deg^{-1})	−38.8 ± 0.3		−39.1 ± 0.1
$\Delta G^{\ddagger}$ (kcal mol^{-1})	17.9 ± 0.1		19.0 ± 0.1
$(\Delta H_D^{\ddagger} - \Delta H_H^{\ddagger})$		1.0 ± 0.1	
$(\Delta S_D^{\ddagger} - \Delta S_H^{\ddagger})$		−0.3 ± 0.3	
$(\Delta G_D^{\ddagger} - \Delta G_H^{\ddagger})$		1.1 ± 0.2	
Hexane			
$\Delta H^{\ddagger}$ (kcal mol^{-1})	4.8 ± 0.1		5.6 ± 0.1
$\Delta S^{\ddagger}$ (cal mol^{-1} deg^{-1})	−47.2 ± 0.1		−47.7 ± 0.1
$\Delta G^{\ddagger}$ (kcal mol^{-1})	18.9 ± 0.1		19.8 ± 0.1
$(\Delta H_D^{\ddagger} - \Delta H_H^{\ddagger})$		0.8 ± 0.1	
$(\Delta S_D^{\ddagger} - \Delta S_H^{\ddagger})$		−0.5 ± 0.2	
$(\Delta G_D^{\ddagger} - \Delta G_H^{\ddagger})$		0.9 ± 0.1	

which distilled at 82.0°C was collected.

Reagent grade tetrahydrofuran was purified by Paul's procedure (24). After work-up with NaOH and Al_2O_3, the solvent was fractionally distilled over sodium, with collection of the fraction distilling at 66.0°C.

Reagent grade hexane was purified by the method of Tonberg and Johnston (25). The hexane was shaken for 8 h with a mixture of H_2SO_4 (58%), HNO_3 (25%), and H_2O (17%) by weight. The solvent was then washed with concentrated H_2SO_4, then H_2O, and dried over a molecular sieve (4A). A final fractional distillation from sodium yielded a product, bp 68.7°C.

Tetramethylguanidine was dried over NaOH and fractionally distilled. The fraction distilling at 161°C was collected.

Product analyses

2,2-Di(4-nitrophenyl)-1,1,1-trichloroethane (0.5 g) was reacted in NaOEt in ethanol by refluxing the reaction mixture for 1 h. The mixture was cooled, poured into water, and the olefin product extracted with diethyl ether. The olefin was obtained by evaporation of the solvent and was recrystallized several times from ethanol, mp 172.5°C (lit. (1) mp 172–173°C).

The same method was used to prepare the olefin, 2,2-di(4-nitrophenyl)-1-chloroethene, from the dichloro substrate. After the solid products were recovered from the ether extract, they were separated by thin layer chromatography using benzene. The olefin was extracted from the tlc plate with isopropanol, mp 145°C (lit. (1) mp 145–146°C).

Kinetic measurements

The reactions were followed by monitoring the appearance of the olefin products at 324 nm using Specord uv–vis and VSU-2P spectrophotometers fitted with a constant temperature bath to control the temperature of the cell block within 0.1°C. In all three solvents the reaction went to 100% conversion to the olefin. The concentration of

TABLE 4. Activation parameters for the reaction of $(O_2NC_6H_4)_2CHCCl_3$ and its deuterated analogue with TMG base in acetonitrile, tetrahydrofuran, and hexane solvents

Parameter	Normal substrate		Deuterated substrate
Acetonitrile			
$\Delta H^{\ddagger}$ (kcal mol^{-1})	6.2 ± 0.3		8.5 ± 0.1
$\Delta S^{\ddagger}$ (cal mol^{-1} deg^{-1})	−38.6 ± 1.1		−35.5 ± 0.1
$\Delta G^{\ddagger}$ (kcal mol^{-1})	17.8 ± 0.5		19.1 ± 0.1
$(\Delta H_D^{\ddagger} - \Delta H_H^{\ddagger})$		2.3 ± 0.3	
$(\Delta S_D^{\ddagger} - \Delta S_H^{\ddagger})$		3.1 ± 1.1	
$(\Delta G_D^{\ddagger} - \Delta G_H^{\ddagger})$		1.3 ± 0.5	
Tetrahydrofuran			
$\Delta H^{\ddagger}$ (kcal mol^{-1})	5.2 ± 0.1		6.4 ± 0.1
$\Delta S^{\ddagger}$ (cal mol^{-1} deg^{-1})	−42.6 ± 0.2		−42.3 ± 0.2
$\Delta G^{\ddagger}$ (kcal mol^{-1})	17.9 ± 0.1		19.0 ± 0.1
$(\Delta H_D^{\ddagger} - \Delta H_H^{\ddagger})$		1.2 ± 0.1	
$(\Delta S_D^{\ddagger} - \Delta S_H^{\ddagger})$		0.3 ± 0.3	
$(\Delta G_D^{\ddagger} - \Delta G_H^{\ddagger})$		1.1 ± 0.1	
Hexane			
$\Delta H^{\ddagger}$ (kcal mol^{-1})	4.1 ± 0.1		5.3 ± 0.1
$\Delta S^{\ddagger}$ (cal mol^{-1} deg^{-1})	−50.2 ± 0.3		−49.2 ± 0.2
$\Delta G^{\ddagger}$ (kcal mol^{-1})	19.0 ± 0.1		20.0 ± 0.1
$(\Delta H_D^{\ddagger} - \Delta H_H^{\ddagger})$		1.2 ± 0.1	
$(\Delta S_D^{\ddagger} - \Delta S_H^{\ddagger})$		1.0 ± 0.3	
$(\Delta G_D^{\ddagger} - \Delta G_H^{\ddagger})$		1.0 ± 0.1	

TABLE 5. Reaction of 2,2-di(4-nitrophenyl)-1,1,1-trichloroethane with tetramethylguanidine in acetonitrile solvent at 20°C; initial concentration substrate = 0.5×10^{-4} M, initial concentration TMG = 1.1×10^{-2} M

	Absorbance	
Time (s)	A_1	A_2
0	0.065	0.400
24	0.125	0.415
48	0.175	0.425
72	0.215	0.430
96	0.250	0.435
120	0.280	0.440
144	0.310	0.445
168	0.330	0.450
192	0.350	0.455
216	0.370	0.460
240	0.385	0.465

Guggenheim analysis yields, $k_{obs} = 5.89 \times 10^{-3}$ s^{-1}

the base was always in large excess over that of the substrate, ensuring pseudo-first-order kinetics. Freshly prepared stock solutions were used to prepare the reaction mixtures in stoppered uv cells. Pseudo-first-order rate constants were calculated from the trace of absorbance vs. time using the Guggenheim method; an example run is given in Table 5. The second-order rate constants were calculated by a linear least-squares fit of the variation of k_{obs} with base.

The activation parameters were calculated using the transition state theory equation, again using a linear least-squares fit. The errors quoted in Tables 3 and 4 are the standard deviations.

1. D. J. McLennan and R. J. Wong. J. Chem. Soc. Perkin Trans. 2, 279 (1972).
2. D. J. McLennan and R. J. Wong. Tetrahedron Lett. 2887 (1972).
3. D. J. McLennan and R. J. Wong. Tetrahedron Lett. 2891 (1972).
4. D. J. McLennan and R. J. Wong. J. Chem. Soc. Perkin Trans. 2, 1373 (1974).
5. D. J. McLennan and R. J. Wong. J. Chem. Soc. Perkin Trans. 2, 526 (1974).
6. S. J. Cristol. J. Am. Chem. Soc. **67**, 1494 (1945).
7. S. J. Cristol, N. L. Hause, A. J. Quant, H. W. Miller, K. R. Eilar, and J. S. Meek. J. Am. Chem. Soc. **72**, 3333 (1952).
8. A. Jarczewski and K. T. Leffek. Can. J. Chem. **50**, 24 (1972).
9. G. Schroeder and A. Jarczewski. Polish J. Chem. **52**, 265 (1978).
10. J. F. Bunnett. J. Org. Chem. **44**, 1463 (1979).
11. E. Baciocchi, P. Perucci, and C. Rol. J. Chem. Soc. Perkin Trans. 2, 329 (1975).
12. A. Jarczewski and G. Schroeder. Rocz. Chem. **49**, 2025 (1975).
13. W. J. Boyle, Jr. Ph.D. Thesis, Northwestern University. 1971.
14. M. Hojatti and K. T. Leffek. Can. J. Chem. **62**, 2653 (1984).
15. A. Thibblin and W. P. Jencks. J. Am. Chem. Soc. **101**, 4963 (1979).
16. G. Schroeder, A. Jarczewski, and K. T. Leffek. Rocz. Chem. **51**, 279 (1977).
17. A. Jarczewski, G. Schroeder, and K. T. Leffek. J. Chem. Soc. 866 (1979).
18. K. T. Leffek and G. Schroeder. Can. J. Chem. **60**, 3077 (1982).
19. A. F. Cockerill. J. Chem. Soc. B, 964 (1967).
20. E. F. Caldin and S. Mateo. J. Chem. Soc. Faraday Trans. 1, **71**, 1876 (1974).
21. L. Haskelberg and D. Lavie. J. Am. Chem. Soc. **68**, 2267 (1947).
22. J. G. Aston, J. D. Newkirk, D. M. Jenkins, and J. Dorsky. Org. Synth. Coll Vol III, 538 (1955).
23. J. F. O'Donnell, J. T. Ayers, and C. K. Mann. Anal. Chem. **37**, 1161 (1965).
24. J. A. Riddick and W. B. Bunger. Techniques of organic chemistry. 2nd ed. Vol II. Wiley–Interscience, New York. 1979. p. 594.
25. J. A. Riddick and W. B. Bunger. Techniques of organic chemistry. 2nd ed. Vol. II. Wiley–Interscience, New York. 1979. p. 705.

Kinetics and mechanism of the oxidation of benzenediols and ascorbic acid by *bis*(1,4,7-triazacyclononane)nickel(III) in aqueous perchlorate media

A. McAuley, Lee Spencer, and P. R. West
Department of Chemistry, University of Victoria, Victoria, B.C., Canada V8W 2Y2

Received September 4, 1984

A. McAuley, Lee Spencer, and P. R. West. Can. J. Chem. **63**, 1198 (1985).

The reactions of the outer-sphere electron transfer reagent, $Ni(9\text{-aneN}_3)_2^{3+}$, (*bis*(1,4,7-triazacyclononane)nickel(III) ion) with ascorbic acid, hydroquinone, catechol, and resorcinol have been investigated. The absence of any proton related equilibria with the oxidant provides a means of ascribing the observed inverse hydrogen ion dependences to reactions of the dissociated ascorbate or quinolate ions, (HA^-). The data are consistent with the rate-determining one-electron transfer reactions:

$$Ni(9\text{-aneN}_3)_2^{3+} + H_2A \xrightarrow{k_1} Ni(9\text{-ane N}_3)_2^{2+} + H_2A^+$$

$$Ni(9\text{-aneN}_3)_2^{3+} + HA^- \xrightarrow{k_2} Ni(9\text{-ane N}_3)_2^{2+} + HA$$

followed by rapid oxidation of the radical ions formed. In the reaction with ascorbic acid, $k_1 \sim 0$ and k_2 (T = 25°C) = 5.2 × 10^6 M^{-1} s^{-1} ($\Delta H^{\ddagger}$ = 10.1 ± 2.5 kcal mol^{-1}, $\Delta S^{\ddagger}$ = 5.7 ± 5.1 cal mol^{-1} K^{-1}). For hydroquinone, catechol, and resorcinol, k_1 = 2.9 × 10^3, 2.8 × 10^2, and ~0 M^{-1} s^{-1} and k_2 = 6.9 × 10^9, 4.1 × 10^9, and 2.8 × 10^8 M^{-1} s^{-1}, respectively. These data have been combined with those from other similar reactions leading, by use of a Marcus correlation, to self-exchange rate constants for the $HAsc^-/HAsc^{\cdot}$ couple of 3.5 × 10^5 M^{-1} s^{-1} and for the $H_2Quin^{0/+}$ and $H_2cat^{0/+}$ systems of 5 × 10^7 and 2 × 10^7 M^{-1} s^{-1}, respectively. The importance of the effect of bond-reorganisation on electron transfer is discussed.

A. McAuley, Lee Spencer et P. R. West. Can. J. Chem. **63**, 1198 (1985).

On a étudié les réactions du réactif de transfert d'électron externe $Ni(Nonane\text{-}N_3)_2^{3+}$, (ion *bis*(triaza-1,4,7 cyclononane) nickel(III)) avec l'acide ascorbique, l'hydroquinone, le catéchol et le résorcinol. L'absence de tout proton relié à l'équilibre avec l'oxydant permet d'attribuer l'effet inverse observé pour l'ion hydrogène aux réactions des ions ascorbate et quinoléate dissociés (HA^-). Les données sont en accord avec des réactions impliquant un transfert à un électron comme étape déterminante

$$Ni(Nonane\text{-}N_3)_2^{3+} + H_2A \xrightarrow{k_1} Ni(Nonane\text{-}N_3)_2^{2+} + H_2A^+$$

$$Ni(Nonane\text{-}N_3)^{3+} + HA^- \xrightarrow{k_2} Ni(Nonane\text{-}N_3)_2^{2+} + HA$$

qui seraient suivies d'oxydations rapides des ions radicalaires formés. Pour la réaction avec l'acide ascorbique $k_1 \sim 0$ et k_2 (T = 25°C) = 5,2 × 10^6 M^{-1} s^{-1} ($\Delta H^{\ddagger}$ = 10,1 ± 2,5 kcal mol^{-1}, $\Delta S^{\ddagger}$ = 5,7 ± 5,1 cal mol^{-1} K^{-1}). Dans le cas de l'hydroquinone, du catéchol et du résorcinol, on a respectivement k_1 = 2,9 × 10^3, 2,8 × 10^2 et ~0 M^{-1} s^{-1} et k_2 = 6,9 × 10^9, 4,1 × 10^9 et 2,8 × 10^8 M^{-1} s^{-1}. On a combiné ces données à d'autres pour des réactions semblables afin d'obtenir, par l'emploi d'une corrélation de Marcus, une constante de vitesse d'autoéchange pour le couple $HAsc^-/HAsc^{\cdot}$ de 3,5 × 10^5 M^{-1} s^{-1} et pour les sytèmes $H_2Quin^{0/+}$ et $H_2cat^{0/+}$ de 5 × 10^7 et 2 × 10^7 M^{-1} s^{-1} respectivement. On discute de l'importance de la réorganisation de la liaison sur le transfert d'électron.

[Traduit par le journal]

Introduction

Although ascorbic acid (1–4) and other diols (5, 6) have been identified as reductants in biological processes, the recent interest (7–10) in electron transfer processes involving such species reflects the need for a precise understanding of the accompanying redox mechanisms. A feature of many of these reactions is the rate dependence on hydrogen ion concentration, normally associated with the varying degrees of protonation of the reductants. (In the case of ascorbic acid, for example, all three species H_2Asc, $HAsc^-$, and Asc^{2-} have been invoked as reactants in the oxidation by thioureapentacyanoferrate(III) ion (11)). Although early assessments (2) of the redox potentials for the H_2Asc^+/H_2Asc and $HAsc^{\cdot}/HAsc^-$ couples (~1.35 and 0.93 V, respectively) were based on large self exchange rates, more recent estimates (8, 12) are consistent with a value of 0.70–0.72 V for the ascorbate/ascorbate radical couple.

Investigations into the chemistry of nickel(III) species have led to the identification of species of considerable kinetic stability in aqueous media. In our laboratories, we have characterised recently (13) the *bis*(1,4,7-triazacyclononane)nickel(III) cation, ($Ni(9\text{-aneN}_3)_2^{3+}$) which, unlike other solvated tetraazanickel(III) macrocycles (14), shows only ~1% decomposition at pH ~ 3 over a 24 h period. Studies with several reducing systems have exhibited a lack of any pH dependence on electron transfer of this Ni(III)/(II) species and the reduction potential (0.945 V) renders it an appropriate outer-sphere reagent for examination of the kinetic parameters involved in redox reactions of organic substrates.

In this paper we wish to present data on the kinetics of oxidation of ascorbic acid and other benzene diols. From a knowledge of the self-exchange rate for the metal-ion couple, it is possible to derive information on the one-electron self-exchange processes for these organic reductants.

Experimental section

Materials

Bistriazacyclononanenickel(II) perchlorate (15), $[Ni(9\text{-aneN}_3)_2](ClO_4)_2$, was prepared using a modified preparation of the ligand as described (13). The corresponding nickel(III) salt was formed on addition of a slight stoichiometric excess of aquocobalt(III) (16) in ~1 M $HClO_4$. The resulting brown–green complex formed was recrystallised from ~10^{-3} M $HClO_4$. The solid was kept for months

TABLE 1. Rate data for the reaction of $[Ni(9\text{-}aneN_3)_2]^{3+}$ with ascorbic acid; $I = 1.00$ M (Li/H ClO_4), $\lambda = 350$ nm, $[H_2A] = (0.2-1.01) \times 10^{-3}$ M

$[H^+]/M$	$10^{-3}k_0/M^{-1}$ s^{-1}			
	10.5°C	15.0°C	25.0°C	30.0°C
1.00	0.205±0.013	0.264±0.005	—	0.720±0.004
0.70	0.269±0.006	0.352±0.003	0.96±0.05	—
0.40	0.555±0.008	0.68_0±0.005	1.53±0.08	1.89 ±0.01
0.20	—	—	3.06±0.05	—
0.10	2.01 ±0.04	2.90 ±0.02	5.55±0.04	7.22 ±0.19
0.05	3.91 ±0.07	5.35 ±0.43	11.4 ±0.21	14.0 ±0.3
0.02	—	—	29.4 ±0.15	36.3 ±0.7
0.01	—	—	—	—
0.005	30.6 ±0.15	37.4 ±0.16	111.0 ±1	—
$10^5K_a/M$	7.45	8.38	10.6	11.9
k_2K_a/s^{-1}	152	185	554	725
$10^{-6}k_2/M^{-1}$ s^{-1}	2.0_3	2.2	5.2	6.1

$\Delta H^{\ddagger} = 10.1 \pm 2.5$ kcal mol^{-1}
$\Delta S^{\ddagger} = 5.7 \pm 5.1$ cal mol^{-1} K^{-1}

in a dessicator without any apparent decomposition. Hydroquinone (Aldrich), catechol (Fisher), resorcinol (MCB) were purified either by vacuum distillation or recrystallised from ethanol, dried with ether, and stored at 0°C. Ascorbic acid (Sigma) was used without further purification. Lithium perchlorate was prepared by neutralisation of Li_2CO_3 with ~3 M $HClO_4$ and recrystallised three times from distilled water.

Kinetic studies

Solutions of the benzene diols and of ascorbic acid were freshly prepared using nitrogen-saturated water and maintained under an inert atmosphere. For the oxidant, the required amount of solid $[Ni(9\text{-}aneN_3)_2](ClO_4)_3$ was added to a N_2-saturated, thermostatted solution prior to use. Kinetic experiments were carried out using a stopped-flow apparatus described previously (17). The reduction of $[Ni(III)]^{3+}$ (ca. $1-3 \times 10^{-5}$ M) was followed at 340–350 nm under pseudo first order conditions of excess reductant $(0.2-1.4) \times 10^{-3}$ M. At all pH's studied, plots of ln ΔOD against time were linear for at least three half-lives. Ionic strength and hydrogen ion concentration were maintained using $H^+/Li^+-ClO_4^-$ mixtures. At higher pH's (>3) acetate buffers (10^{-2} M) were used, with no observed kinetic dependence on the buffer concentration.

Results

(I) Reaction of $[Ni(9\text{-}aneN_3)_2]^{3+}$ with ascorbic acid (H_2Asc)

The green-coloured nickel(III) complex ($\lambda_{max} = 312$ nm, $\epsilon = 1.01 \times 10^4$ M^{-1} cm^{-1}) is reduced rapidly by ascorbic acid to yield the corresponding nickel(II) ion (λ_{max} 322 nm, $\epsilon = 11$ M^{-1} cm^{-1}). A spectrophotometric titration ($\lambda = 350$ nm) revealed an oxidant:reductant ratio of 2.02(±0.05):1 consistent with the overall reaction:

[1] $2Ni(III) + H_2Asc \rightarrow 2Ni(II) + Asc + 2H^+$

The reaction rate was observed to exhibit a first-order dependence on ascorbic acid concentration under all conditions used in conformity with the rate equation

[2] $-d[Ni(III)]/dt = 2k_0[Ni(III)][H_2Asc]$

Kinetic measurements were made at several reductant concentrations at each $[H^+]$ used. A summary of the data is presented in Table 1. The full details are available as supplementary material (Table S1).[1] At all temperatures, plots of the second order rate constant, k_0, against $[H^+]^{-1}$ were linear (Fig. 1) over the range studied. Intercepts of such plots did not vary statistically from zero.

Since there are no proton-related equilibria associated with the oxidant, a mechanism consistent with the observed data may be written as

[3] $H_2Asc \rightleftharpoons H^+ + HAsc^-$ (K_a)

[4] $Ni(9\text{-}aneN_3)_2^{3+} + HAsc^- \xrightarrow{k_2} Ni(9\text{-}aneN_3)_2^{2+} + HAsc^{\cdot}$

[5] $HAsc^{\cdot} \rightleftharpoons H^+ + Asc^{\cdot-}$

[6] $Ni(9\text{-}aneN_3)_2^{3+} + Asc^{\cdot-} \xrightarrow{\text{fast}} Ni(9\text{-}aneN_3)_2^{2+} + Asc$

The ascorbate radical intermediate $HAsc^{\cdot}$ is known to be a strong acid (16) ($pK_r(HAsc) = -0.45$) so that the predominant form under the present experimental conditions is $Asc^{\cdot-}$. The radical ion may then react with a second mole of nickel(III) to yield the de-hydroascorbic acid product. The large driving forces for reactions of this type ($E^0(Asc/Asc^{\cdot-}) = 0.14$ V (12)) have led to the suggestion (7) that reaction [6] is close to diffusion controlled. An alternative secondary step [7]

[7] $Asc^{\cdot-} + Asc^{\cdot-} \xrightarrow{H^+} H_2Asc + Asc$

must also be considered since the disproportionation reaction ($k_7 \geq 10^8$ M^{-1} s^{-1}) (18, 19) would result in the observed overall stoicheiometry.

Using the above mechanism, k_0 may be expressed in the form

[8] $$k_0 = \frac{k_1[H^+] + k_2K_a}{[H^+] + K_a}$$

where k_1 is the rate constant for the reaction of the nickel(III) species with the undissociated form of the acid, H_2Asc. From Fig. 1 and the data in Table 1 it is seen that $k_1[H^+] \ll k_2K_a$ and

[1]Complete set of data is available upon request, at a nominal charge, from the Depository of Unpublished Data, CISTI, National Research Council of Canada, Ottawa, Ont., Canada K1A 0S2.

TABLE 2. Rate data for the reactions of $[Ni(9\text{-aneN}_3)_2]^{3+}$ with hydroquinone, catechol, and resorcinol; $I = 1.00\ M$, $T = 25°C$, $\lambda = 350$ nm, $[H_2Q] = (0.3-1.4) \times 10^{-3}\ M$

Hydroquinone			Catechol			Resorcinol	
$[H]/M$	pH	$10^{-3}k_0{}^a/M^{-1}\ s^{-1}$	$[H^+]/M$	pH	$10^{-2}k_0{}^a/M^{-1}\ s^{-1}$	pH	$k_0{}^a/M^{-1}\ s^{-1}$
1.00		2.34±0.02	1.00		1.90± 0.07	3.19	54.9± 2
0.70		2.44±0.10	0.70		2.03± 0.11	3.65	145 ± 4
0.40		2.64±0.02	0.50		2.29± 0.03	3.90	323 ± 4
0.10		2.83±0.02	0.20		2.49± 0.01	4.10	478 ± 9
	2.00	3.25±0.03		1.30	3.30± 0.02	4.30	841 ±10
	3.44	5.02±0.02		2.00	4.72± 0.06	4.40	1 493 ±16
	3.76	7.69±0.05		3.19	29.7 ± 0.5		
	4.09	14.3 ±0.3		3.65	74 ± 1		
	4.23	19.5 ±0.3		4.09	185 ± 4		
	4.70	50.5 ±0.4		4.42	431 ±17		

$^a k_0$ values are the average of rate constants obtained using at least two and more usually three or four different substrate concentrations.

in the range $[H^+] = 0.005-1.00\ M$, $[H^+] \gg K_a$ ($pK_a = 3.96$) (20)), so that eq. [8] may be written as

$$[9] \quad k_0 = k_2K_a/[H^+]$$

as is observed (Fig. 1). The rate constants, k_2, evaluated from data on the temperature dependence of K_a at $I = 1.0\ M$ (20, 21) are presented in Table 1.

(2) Reaction of $[Ni(9\text{-aneN}_3)_2]^{3+}$ with hydroquinone, catechol, and resorcinol

Spectrophotometric titration at 350 nm (1.0 M $HClO_4$) revealed in all cases an oxidant:reductant ratio of 2(±0.1):1 corresponding to the overall reaction

$$[10] \quad 2[Ni(9\text{-aneN}_3)_2]^{3+} + H_2Q \rightarrow 2[Ni(9\text{-aneN}_3)_2]^{2+} + 2H^+ + Q$$

where H_2Q is the benzene diol and Q the corresponding quinone. As in the case of the ascorbic acid reaction, the rates were first order in both [Ni(III)] and $[H_2Q]$. No simple overall hydrogen ion dependence was observed over the range studied $[H^+] = 1.00\ M$ – pH 4.8, but two regimes were discernible. Representative rate data are presented in Table 2. Full details of rate data are provided in supplementary Table S2.[1]

(a) 0.1 M < $[H^+]$ < 1.0 M

In this range, for the substrates (hydroquinone and catechol) studied, a small but consistent retardation in rate was observed with increasing $[H^+]$. There is no spectroscopic evidence for any change in oxidant species under these conditions and in other redox systems (13, 22) where no protonation equilibria are involved there is no observed rate dependence of $[Ni(9\text{-aneN}_3)_2]^{3+}$ with $[H^+]$. The retardation may therefore be attributed to protonation of the quinol as is shown

$$[11] \quad H_3Q^+ \overset{K_b}{\rightleftharpoons} H_2Q + H^+$$

$$[12] \quad [Ni(9\text{-aneN}_3)_2]^{3+} + H_2Q \xrightarrow{k_3} [Ni(9\text{-aneN}_3)]^{2+} + SQ^{\cdot}$$

$$[13] \quad Ni(III) + SQ^{\cdot} \xrightarrow{\text{fast}} Ni(II) + Q$$

where $SQ^{\cdot}$ is the semiquinone radical with no assumption made as to the state of protonation of the species. A rate expression consistent with the reaction scheme may be written in the form

$$[14] \quad -d[Ni(III)]/dt = 2k_3[H_2Q][Ni(III)]\cdot K_b/([H^+] + K_b)$$

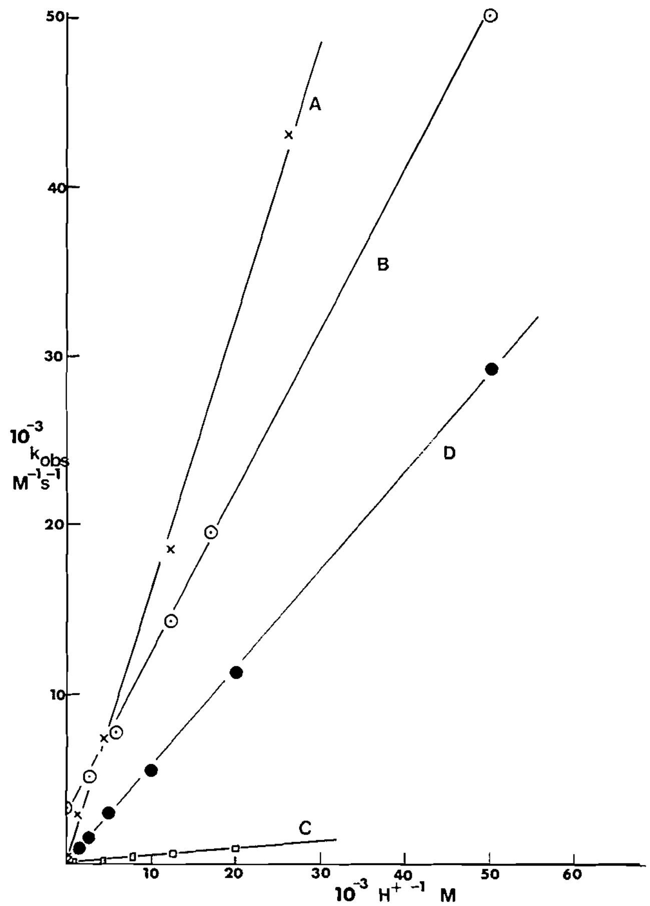

FIG. 1. Hydrogen ion dependences of the rates of oxidation of hydroquinone (*A*), catechol (*B*), and resorcinol (*C*), and ascorbic acid (*D*) ($T = 25°C$).

The observed second order rate constant, k_0, may be expressed as

$$[15] \quad k_0 = k_3K_b/([H^+] + K_b)$$

Equation [15] may be rearranged as

$$[16] \quad k_0 = k_3 - k_0[H^+]/K_b$$

such that a plot of k_0 against $k_0[H^+]$ should be linear with slope $-1/K_b$ and intercept k_3. Good linear plots were obtained for

TABLE 3. Rate constants for the reaction of $[Ni(9\text{-aneN}_3)_2]^{3+}$ with benzenediols and related anions

Reductant	K_b/M	$10^{10}K_a/M$	$10^{-3}k_3{}^a/M^{-1}\ s^{-1}$	$10^{-9}k_4/M^{-1}\ s^{-1}$
H_2Quin	4.2	1.40	2.9 (2.6)	6.9±0.3
H_2cat	1.8	3.55	0.28 (~0.2)	4.1±0.5[b]
H_2Res	—	1.55	~0	0.28±0.05[b]

[a]Values in parentheses are derived from higher pH conditions (see Fig. 2). More accurate values obtained at $[H^+] > 0.1\ M$.
[b]Corrections for diffusion related contributions lead to k_4 values of 3×10^{10} $M^{-1}\ s^{-1}$ ($Hcat^-$) and $3.1 \times 10^8\ M^{-1}\ s^{-1}$ ($HRes^-$), respectively. See text.

both reductants with (T = 25°C) $k_3 = 2.9 \times 10^3\ M^{-1}\ s^{-1}$ (hydroquinone) and $k_3 = 2.85 \times 10^2\ M^{-1}\ s^{-1}$ (catechol). Corresponding K_b values are $4.2 \pm 1.1\ M$ and $1.8 \pm 1.2\ M$, respectively. The rate data are consistent with the better reducing properties of hydroquinone. Similar behaviour to the above was observed in the oxidation by $Ni(cyclam)(H_2O)_2^{3+}$ (23) where the equilibrium data derived were $K_b = 4.5 \pm 1.2\ M$ (hydroquinone) and $3.3 \pm 0.9\ M$ (catechol) in good agreement with the present findings.

(b) $[H^+] < 0.1$ M

A marked increase in rate is observed with increasing pH which may be associated with the acid dissociation of the reductants, the almost identical pH profiles for each reaction reflecting the similarity of pK_a values for the substrates.

$$[17]\quad H_2Q \overset{K_a}{\rightleftharpoons} HQ^- + H^+$$

$$[18]\quad Ni(9\text{-aneN}_3)_2^{3+} + H_2Q \xrightarrow{k_3} Ni(9\text{-aneN}_3)_2^{2+} + SQ^{\bullet} + H^+$$

$$[19]\quad Ni(9\text{-aneN}_3)_2^{3+} + HQ^- \xrightarrow{k_4} Ni(9\text{-aneN}_3)_2^{2+} + SQ^{\bullet}$$

$$[20]\quad Ni(III) + SQ^{\bullet} \xrightarrow{\text{fast}} Ni(II) + Q$$

This mechanism is identical to that invoked in the ascorbic acid reduction and based on eq. [8] with the assumption that $[H^+] \gg K_a$ (pK_a = 9.5–11 for the reductants):

$$[21]\quad k_0 = k_3 + k_4K_a/[H^+]$$

Excellent linear plots of k_0 against $[H^+]$ were derived (Fig. 1). The individual rate constants are shown in Table 3. It may be noted that very good agreement is observed between k_3 values obtained at both high and low acid concentrations. In the case of resorcinol, however, there is no evidence within experimental error of any pathway attributable to k_3.

Discussion

The reactions of $[Ni(9\text{-aneN}_3)_2]^{3+}$ with the substrates under consideration may be assigned an outer-sphere mechanism since the oxidant is known to be substitution inert under the present experimental conditions. Two one-electron transfer steps may be expected in the oxidation of each substrate, the rate-determining process being the formation of the organic radical (or radical ion). Also, owing to the lack of any proton related equilibrium in the oxidant, the reactions of H_2A and HA^- may be attributed with a degree of certainty not often present in other oxidations. With aquo ions as reactants, the so-called "proton ambiguity" persists deriving from hydrolysis of the metal cations. The large difference in reactivity between the protonated ($k_3 \leq 10^3\ M^{-1}\ s^{-1}$) and dissociated forms ($k_4 \sim 10^7-10^9\ M^{-1}\ s^{-1}$) may be rationalised in terms of the redox potentials and self-exchange parameters. The rate constants for the reactions of $HQuin^-$ and $Hcat^-$ are very large and close to the limit of diffusion controlled systems. For the reaction of a 3+ ion of the type under consideration with a 1− anion, where an activated complex of radius ~10 Å is anticipated, a value of $k_{diff} \sim 4.7 \times 10^9\ M^{-1}\ s^{-1}$ may be estimated (24). It may be seen (Table 3) that the observed values for the reactions of $HQuin^-$ and $Hcat^-$ are of this order of magnitude and these systems must be considered as reacting predominantly via a diffusion controlled process. In the case of $HRes^-$, the rate constant is ~20-fold lower. The contribution to the observed value from diffusion may be eliminated (7) (eq. [22])

$$[22]\quad \frac{1}{k_{act}} = \frac{1}{k_4} - \frac{1}{k_{diff}}$$

where k_{act} and k_{diff} are the activation- and diffusion-controlled rate constants, respectively. Correction in this manner leads to k_4 values of $\sim 3 \times 10^{10}\ M^{-1}\ s^{-1}$ for the reaction with catecholate anion, $Hcat^-$, and $3.4 \times 10^8\ M^{-1}\ s^{-1}$ for the reaction involving $HRes^-$. The lower rate with the resorcinol anion may be interpreted in terms of the reduction of resonance stabilisation in the $HRes^{\bullet}$ radical formed on oxidation compared with that present in the $HQuin^{\bullet}$ or $Hcat^{\bullet}$ systems.

For the reactions under consideration, the cross-reaction rate constants are a function of the redox potentials of the reductants (25), consistent with the Marcus relationship. In terms of a recent modification of the theory (26), the rate constant for a cross reaction, k_{12}, is related to the rate constants for the component self-exchange reactions, k_{11} and k_{22}, and the equilibrium constant for the cross reaction, K_{12}, by

$$[23]\quad k_{12} = (k_{11}k_{22}K_{12}f_{12})^{1/2}W_{12}$$

where

$$[24]\quad \ln f_{12} = \frac{[\ln K_{12} + (W_{12} - W_{21})/RT]^2}{4\left[\ln\left(\frac{k_{11}k_{22}}{A_{11}A_{22}}\right) + \frac{W_{11} + W_{22}}{RT}\right]}$$

$$[25]\quad W_{12} = \exp\left[-(W_{12} + W_{21} - W_{11} - W_{22})/2RT\right]$$

$$[26]\quad W_{ij} = \frac{Z_iZ_je^2}{D_s\sigma_{ij}(1 + \beta\sigma_{ij}\sqrt{\mu})}$$

$$[27]\quad A_{ii} = \left[\frac{4\pi N\sigma^2\nu b\gamma r}{1000}\right]_{ii}$$

In these expressions W_{ij} is the work required to bring ions i and j (charges Z_i and Z_j) to the separation distance σ_{ij} (taken equal to the sum of a_i and a_j, the radii of ions i and j), $\beta = (8\pi Ne^2/1000D_skT)^{1/2}$, νb is the nuclear frequency that destroys the activated complex configuration ($\sim 9 \times 10^{12}\ s^{-1}$) (27), and γr is the thickness of the reaction layer (typically ~0.8 Å). Values of A/σ^2 are in the range $3-8 \times 10^{10}\ M^{-1}\ Å^{-2}\ s^{-1}$ and for the Ni(III) complex a value of $4.8 \times 10^{10}\ M^{-1}\ Å^{-2}\ s^{-1}$ has been derived (7). This value has been used in the present work.

The potentials of the H_2Q^+/H_2Q (E_1^0) and $HQ^{\bullet}/HQ^-$ (E_2^0) couples may be estimated using the expressions

$$[28]\quad E_1^0 = E_3^0 + 0.059\{pK_1 + pK_2 - pKr_1 - pKr_2\}$$

$$[29]\quad E_2^0 = E_3^0 + 0.059\{pK_2 - pKr_2\}$$

where E_3^0 represents the potential for the $Q^{\bullet-}/Q^{2-}$ couple (28) and pK_n and pKr_n are related to the dissociation of the diol or the corresponding radical.

Analysis of the data for $HRes^-$ (E_2^0 = 0.56 V), using k_{11}

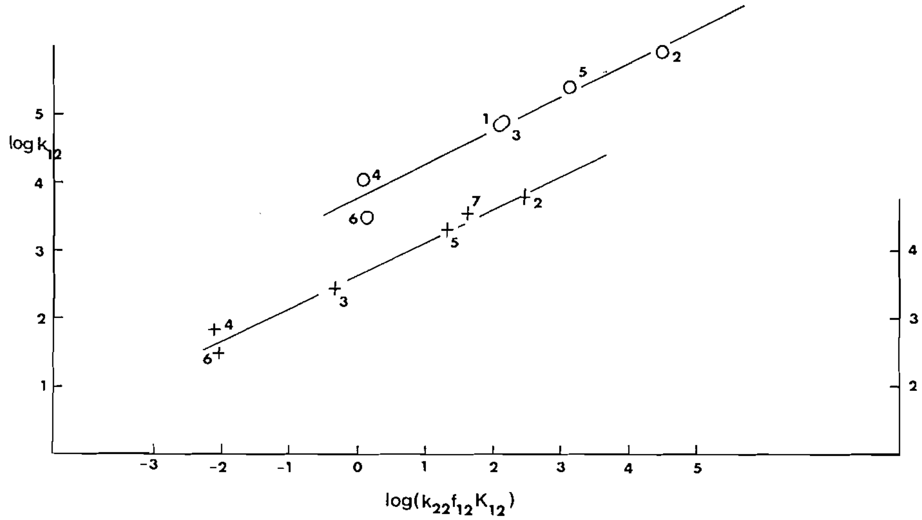

FIG. 2. Marcus correlations (plots of log k_{12} against log $f_{12}K_{12}k_{22}$) for the reactions of hydroquinone (○) and catechol (+) with various oxidants. *1*, $IrCl_6^{2+}$ (27); *2*, $[Ir(Cl_5)(OH_2)]^{3-}$ (26); *3*, $[IrBr_6]^{3-}$ (26); *4*, $[Ni(cyclam)(OH_2)_2]^{3+}$ (21); *5*, $[Ni(tet\text{-}c)(OH_2)_2]^{3+}$ (9); *6*, $[Ni(9\text{-aneN}_3)_2]^{3+}$; *7*, $Ni(tet\text{-}d)(OH_2)_2]^{3+}$ (9). Lines are drawn in accordance with a predicted slope of 0.50. Right hand ordinates refer to catechol data.

$(Ni(9\text{-aneN}_3)_2)^{3+/2+}$ = 6 × 10^3 M^{-1} s^{-1} (22) leads to a calculated value for the $HRes^-/HRes^{\cdot}$ self-exchange rate of 5.8 × 10^7 M^{-1} s^{-1} (ΔG^{*}_{22} ~ 4.4 kcal mol^{-1}).

In the case of the ascorbate ion, $HAsc^-$, a similar evaluation procedure leads to a self-exchange rate constant for the $HAsc^{\cdot}/HAsc^-$ couple of 3.5 × 10^5 M^{-1} s^{-1}. This is in excellent agreement with the value derived (1 × 10^5 M^{-1} s^{-1}) recently by Macartney and Sutin (7), confirming the outer-sphere character of the oxidant.

There are relatively few experimental data for the H_2Q^+/H_2Q couples. Using an analysis similar to that (eqs. [28], [29]) above, Pelizzetti *et al.* (29, 30) have evaluated redox potentials for the H_2Quin^+/H_2Quin and H_2cat^+/H_2cat couples (−1.14 and −1.25 V, respectively). The largest uncertainty in these values lies in the pKr_1 values ($H_2Q^+ \rightarrow HQ^{\cdot} + H^+$) where a value of 1− has been estimated. Using these data, we have plotted the results of several cross reactions using the form of the Marcus equation:

[30] $\log k_{12} = (1/2) \log k_{11} + (1/2) \log k_{22}K_{12}f_{12}$

where the work terms associated with the reaction of a neutral species approximate to zero. From eq. [30] it may be seen that a plot of log k_{12} against log $k_{22}f_{12}K_{12}$ should be linear with slope 0.50 and intercept (1/2) log k_{11}. The data for the oxidation of hydroquinone and catechol are shown in Fig. 2. Slopes are drawn as 0.5 leading to self-exchange rates of 5 × 10^7 M^{-1} s^{-1} (ΔG^* = 4.5 kcal mol^{-1}) and 2 × 10^7 M^{-1} s^{-1} (ΔG^* = 5.05 kcal mol^{-1}) for hydroquinone and catechol, respectively. These values are close to those derived previously (5). An uncertainty of a pK unit in the estimated value of pKr_1 would result in an uncertainty of about an order of magnitude in k_{11} (H_2Q/H_2Q^+).

The ratio of the rates of self-exchange of H_2Asc/H_2Asc (2 × 10^3 M^{-1} s^{-1}) (7) and $HAsc^-/HAsc^{\cdot}$ (3.5 × 10^5 M^{-1} s^{-1}) is ~6 × 10^{-3}. Using the rate of reaction of $Ni(9\text{-aneN}_3)_2^{3+}$ with $Hcat^-$, corrected for diffusion, (3 × 10^{10} M^{-1} s^{-1}) it is possible using (30) to derive a rough estimate of ~3.2 × 10^9 M^{-1} s^{-1} for the self-exchange rate involving the $Hcat/Hcat^{\cdot}$ couple. This is about two orders of magnitude greater than for the H_2cat/H_2cat^+ system. In the case of the ascorbate ion radical, however, the absolute rate is ~10^4 lower. This is probably the result of the extensive C—C and C═O bond re-organisation required on radical ion formation. A more facile electron redistribution with a minimum of bond length changes is possible for the $Hcat^-/Hcat^{\cdot}$ couple. The value for the corresponding resorcinol reaction is slower than that for catechol possibly owing to the lack of resonance stabilisation of the radical formed. However, it is clear that the benzenediol monoanions differ not only in the resonance delocalization which is uniquely available to *ortho*- and *para*-disubstituted aromatics (i.e. $Hcat^-/Hcat^{\cdot}$). The balance of the intermolecular and external hydrogen bonding forces in the two cases must be incor-

HCat⁻ 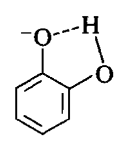

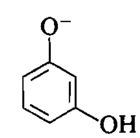 HRes⁻

porated. Such protic solvent effects play a substantial role in the position of keto−enol equilibrium, e.g., for acetylacetone (31). In general terms, differences in self exchange rates may well exhibit solvent trends reminiscent of Z values (or related solvatochromic scales) (32) where the energies of charge transfer bonds are related to solvation. It would be instructive to compare self exchange rates for the benzenediols in polar aprotic solvents (i.e., acetonitrile) and such studies are planned. Detailed analysis of these features must also await structural characterisation of the various radical species involved. It appears, however, that using coordination complexes employing outer sphere electron transfer pathways, it is possible to derive self-consistent data on organic redox couples where structural differences lead to significant variations in the electron-transfer parameters.

Acknowledgements

We are grateful to the Natural Sciences and Engineering Research Council of Canada and the University of Victoria for financial support. The authors thank Drs. P. R. Norman and O. Olubuyide for helpful discussions.

1. M. T. KHAN and A. E. MARTELL. J. Am. Chem. Soc. **89**, 4176 (1967).
2. E. PELIZZETTI, E. MENTASTI, and E. PRAMAURO. Inorg. Chem. **15**, 2898 (1976); **17**, 1181 (1978).
3. R. A. RICHMAN, R. L. SORENSEN, K. O. WATKINS, and G. DAVIES. Inorg. Chem. **16**, 1570 (1977).
4. R. C. PERKINS, A. H. BETH, L. S. WILKERSON, W. SERAFIN, L. R. DALTON, C. R. PARK, and J. H. PARK. Proc. Nat. Acad. Sci. U.S.A. **77**, 790 (1980).
5. E. PELIZZETTI, E. MENTASTI, and C. BAIOCCHI. J. Phys. Chem. **80**, 2979 (1976).
6. J. G. CLEMMER, G. K. HOGABOOM, and R. A. HOLWERDA. Inorg. Chem. **18**, 2567 (1979).
7. D. H. MACARTNEY and N. SUTIN. Inorg. Chim. Acta, 1983.
8. N. H. WILLIAMS and J. K. YANDELL. Austral. J. Chem. **35**, 1133 (1982).
9. A. McAULEY, T. OSWALD, and R. I. HAINES. Can. J. Chem. **61**, 1120 (1983).
10. D. H. MACARTNEY and A. McAULEY. J. Chem. Soc. Dalton Trans. 103 (1984).
11. D. H. MACARTNEY and A. McAULEY. Can. J. Chem. **59**, 132 (1981).
12. C. CREUTZ. Inorg. Chem. **20**, 4449 (1981).
13. A. McAULEY, P. R. NORMAN, and O. OLUBUYIDE. Inorg. Chem. **23**, 1938 (1984).
14. K. NAG and A. CHAKRAVORTY. Coord. Chem. Rev. **33**, 87 (1980).
15. R. YANG and L. J. ZOMPA. Inorg. Chem. **15**, 1499 (1976).
16. J. C. BRODOVITCH and A. McAULEY. Inorg. Chem. **20**, 1667 (1981); G. DAVIES and B. WARNQVIST. Coord. Chem. Rev. **5**, 349 (1970).
17. A. G. LAPPIN and A. McAULEY. J. Chem. Soc. Dalton Trans. 1564 (1975).
18. G. P. LAROFF, R. W. FESSENDEN, and R. H. SCHULER. J. Am. Chem. Soc. **94**, 9062 (1972).
19. B. H. J. BIELSKI, A. O. ALLEN, and H. A. SCHWARTZ. J. Am. Chem. Soc. **103**, 3516 (1981).
20. M. KIMURA, M. YAMAMOTO, and S. YAMABA. J. Chem. Soc. Dalton Trans. 423 (1982).
21. Z. AMJAD, J. C. BRODOVITCH, and A. McAULEY. Can. J. Chem. **55**, 3581 (1977).
22. A. McAULEY, P. R. NORMAN, and O. OLUBUYIDE. J. Chem. Soc. Dalton Trans. 1501 (1984).
23. J. C. BRODOVITCH, A. McAULEY, and T. OSWALD. Inorg. Chem. **21**, 3442 (1982).
24. W. RYBAK, A. HAIM, T. L. NETZEL, and N. SUTIN. J. Phys. Chem. **85**, 2856 (1981).
25. R. A. MARCUS. J. Phys. Chem. **72**, 891 (1968).
26. N. SUTIN. Acc. Chem. Res. **15**, 275 (1982); Prog. Inorg. Chem. **30**, 441 (1983).
27. B. S. BRUNSCHWIG, C. CREUTZ, D. H. MACARTNEY, T. K. SHAM, and N. SUTIN. Faraday Discuss. Chem. Soc. **74**, 113 (1982).
28. S. STEENKEN and P. NETA. J. Phys. Chem. **83**, 1134 (1979).
29. E. PELIZZETTI, E. MENTASTI, and E. PRAMAURO. J. Chem. Soc. Perkin II, 620 (1978).
30. E. MENTASTI, E. PELIZZETTI, and C. BAIOCCHI. J. Chem. Soc. Dalton Trans. 132 (1977).
31. K. D. GRANDE and S. M. ROSENFELD. J. Org. Chem. **45**, 1626 (1980).
32. E. M. KOSOWER. J. Am. Chem. Soc. **80**, 3253 (1958).

Isolation and structure of bryostatins 5−7[1]

GEORGE R. PETTIT,[2] YOSHIAKI KAMANO, CHERRY L. HERALD, AND MACHIKO TOZAWA[3]
Cancer Research Institute and Department of Chemistry, Arizona State University, Tempe, AZ 85287, U.S.A.

Received November 14, 1984

GEORGE R. PETTIT, YOSHIAKI KAMANO, CHERRY L. HERALD, and MACHIKO TOZAWA. Can. J. Chem. **63**, 1204 (1985).

American (Gulf of Mexico), Mexican (Gulf of California), and Japanese (Gulf of Sagami) specimens of the marine bryozoan *Bugula neritina* were found to contain in addition to bryostatin 4 (**3***a*) the new bryostatins 5−7 (**3***b*−*d*) as major antineoplastic components effective against the murine P388 lymphocytic leukemia. A total of 50 kg of wet *B. neritina* from the Northeastern Gulf of Mexico led to bryostatins 5−7 in 14.1, 61.9, and 31.2 mg yields respectively. The structural assignments for each of these potentially important substances were derived from detailed interpretation of the 400 MHz ^{1}H nmr and solution phase secondary ion mass spectral measurements, combined with the results of selective acid-catalyzed hydrolyses.

GEORGE R. PETTIT, YOSHIAKI KAMANO, CHERRY L. HERALD et MACHIKO TOZAWA. Can. J. Chem. **63**, 1204 (1985).

On a trouvé que les échantillons américains (Golfe du Mexique), mexicains (Golfe de la Californie) et japonais (Golfe de Sagami) du bryozoaire marin *Bugula neritina* contiennent, en plus de la bryostatine 4 (**3***a*), de nouvelles bryostatines 5−7 (**3***b*−*d*) qui sont des composants antinéoplastiques majeurs, efficaces contre la leucémie lymphocytique P388 murine. Un total de 50 kg de *B. neritina* humide, provenant du nord-est du Golfe du Mexique, a permis d'isoler 14,1, 61,9 et 31,2 mg respectivement des bryostatines 5−7. On a attribué les structures des chacune de ces substances potentiellement importantes en se basant sur une interprétation détaillée des spectres rmn du ^{1}H à 400 MHz et sur des mesures de spectrométrie de masse combinées aux résultats d'hydrolyses acido-catalysées sélectives.

[Traduit par le journal]

The bryozoan, *Bugula neritina* (Linnaeus) has proved to be a surprisingly productive reservoir of potentially useful anticancer constituents. A 15-year study (2) of this tiny marine animal in our laboratory has led to the discovery of bryostatins 1−3 (ref. 3, **1***a*, *b*, **2**) in Eastern Pacific Ocean specimens and bryostatin 4 (ref. 4, **3***a*) in Western Pacific Ocean, Gulf of California, and Gulf of Mexico samples. Each has exhibited activity against the U.S. National Cancer Institute's (NCI) murine P388 lymphocytic leukemia (PS system) at <46 μg/kg/inj. dose levels.

Further detailed investigations of *Bugula neritina* have now led to the isolation and structural elucidation of three new and potentially important bryostatins from Gulf of Mexico (Florida, USA), Gulf of California (Sonora, Mexico), and Gulf of Sagami (Japan) collections. Continuation of the bryostatin nomenclature (3*b*) has been employed to name these new PS cell growth inhibitory and antineoplastic substances bryostatin 5 (NSC-362616, PS cell line ED_{50}, 1.3×10^{-3} to 2.6×10^{-4} μg/mL, in vivo, 88% life extension at 185 μg/kg), bryostatin 6 (NSC-362617, PS cell line ED_{50}, 3.0×10^{-3} μg/mL, in vivo, 82% life extension at 185 μg/kg), and bryostatin 7 (NSC-362619, PS cell line ED_{50}, 2.6×10^{-5} μg/mL, in vivo 77% life extension at 92 μg/kg). Bryostatins 5−7 were discovered during a very careful examination of antineoplastic (PS) fractions leading to bryostatin 4 (4). In a typical approach, a Florida collection of *Bugula neritina* (50 kg wet wt) was extracted with methylene chloride − methanol−water and the methylene chloride phase was entered into an extensive separation procedure guided by bioassay using the PS leukemia. The biologically active methylene chloride fraction prepared (5) from the 9:1 → 4:1 methanol−water solvent partition sequence was subjected to detailed fractionation employing gel permeation (steric exclusion), silica gel and Sephadex (LH-20) partition, preparative layer, reverse phase, and high performance liquid (hplc) chromatography (4). Rigorous application of this improved separation sequence led to 44.5 mg of bryostatin 4 (**3***a*), bryostatin 5 (**3***b*, 14.1 mg), bryostatin 6 (**3***c*, 61.9 mg), and bryostatin 7 (**3***d*, 31.2 mg).

The reddish-purple color observed upon developing thin layer chromatograms of bryostatins 5−7 with anisaldehyde sulfuric acid reagent first suggested the relationship to bryostatin 4 and this superficial interpretation was further substantiated by careful interpretation of the high resolution (400 MHz) ^{1}H (Table 1) and ^{13}C nmr spectra (**3***b*) (Table 2). Except for the ester substituents at C-7 and C-20, all of the structural features characteristic of bryostatin 4 were apparent in the proton and carbon spectra of bryostatins 5−7. The solution phase secondary ion mass spectra of bryostatins 5−7 were quite revealing when the new techniques we developed (6) for detecting molecular ions of hitherto refractory substances were utilized. By this exceptionally useful method (employing an alkali metal iodide such as sodium iodide or silver tetrafluoroborate or thallium tetrafluoroborate in sulfolane) the molecular ions corresponding to bryostatins 5−7 were easily detected. Interpretation of the molecular ion with the few fragment ions produced proved to be very valuable; namely, for bryostatin 5, 889 $[M+Na]^+$, 871 $[M+Na-18]^+$, 829 $[M+Na-60]^+$, and 788 $[M+Na-102]^+$; bryostatin 6, 875 $[M+Na]^+$, 857 $(M+Na-18]^+$, 815 $[M+Na-60]^+$, and 787 $[M+Na-88]^+$; and bryostatin 7, 847 $[M+Na]^+$, 829 $[M+Na-18]^+$, and 787 $[M+Na-60]^+$. Loss of 60 and 102 mass units by mass spectral fragmentation of bryostatin 5 suggested acetate and valerate ester substituents. Similarly, loss of 60 and 88 from the bryostatin 6 molecular ion indicated acetate and butyrate esters. The cleavage of only 60 units from bryostatin 7 suggested a diacetate derivative.

Each of the preceding assumptions was further confirmed by completing the ^{1}H and ^{13}C nmr interpretations and these analyses were consistent with the mass spectral fragmentation results. Exact assignment for each of the ester substituents was achievable by the results of careful acid-hydrolysis experiments. As part of earlier structural studies involving bryostatins 1 (**1***a*) and 4 (**3***a*) it was found that the former substance

[1]Dedicated to Professor Carl Djerassi on the occasion of his 60th birthday. Manuscript 98 in the series Antineoplastic Agents; for part 97, see ref. 1.

[2]Author to whom correspondence may be addressed.

[3]Department of Chemistry, The Jikei University School of Medicine, Kokuryo, Chofu-shi, Tokyo 182, Japan.

TABLE 1. High resolution (400 MHz) ^{1}H nuclear magnetic resonance chemical shift assignments for bryostatins 5–7 in deuteriochloroform solution

Structure 3 assignment no.	Bryostatin 5 (3*b*)		Bryostatin 6 (3*c*)		Bryostatin 7 (3*d*)	
	δ (ppm)	Multiplicity (*J*, Hz)	δ (ppm)	Multiplicity (*J*, Hz)	δ (ppm)	Multiplicity (*J*, Hz)
2	2.46	(m)	2.42	(m)	2.41, 2.51	(m, m)
3	4.12	(m)	4.17	(m)	4.14	(m)
4	1.65, 2.03	(m, m)	1.53, 1.99	(m, m)	1.62, 2.00	(m, m)
5	4.21	(m)	4.21	(m)	4.21	(m)
6	1.20, 1.70	(m, m)	1.43, 1.71	(m, m)	1.45, 1.67	(m, m)
7	5.08	(m)	5.14	(m)	5.13	(m)
10	1.70, 2.08	(m, m)	1.79, 2.02	(m, m)	1.50, 1.99	(m, m)
11	3.88	(m)	3.95	(m)	3.95	(m)
12	2.15, ~2.18	(m)	2.17	(m)	2.17	(m)
14	1.85, 2.05	(m, m)	1.94, 2.05	(m, m)	1.83, 2.05	(m, m)
15	4.06	(m)	4.07	(m)	4.06	(m)
16	5.29	(dd; 8.4, 15.8)	5.29	(dd; 8.34, 15.72)	5.30	(dd; 8.44, 15.76)
17	5.75	(d; 15.8)	5.73	(d; 15.72)	5.74	(d; 15.76)
20	5.16	(s)	5.07	(s)	5.08	(s)
22	1.89, 2.03	(m, m)	1.85, 2.03	(m, m)	1.80, 2.05	(m, m)
23	3.98	(m)	3.96	(m)	3.62	(m)
24	1.83, 1.97	(m, m)	1.84, 1.94	(m, m)	1.90, 2.00	(m, m)
25	5.11	(m)	5.07	(m)	5.17	(m)
26	3.75	(m)	3.71	(m)	3.60	(m)
27	1.20	(d; 6.46)	1.20	(d; 7.21)	1.21	(d; 6.45)
28[a]	1.13	(s)	1.12	(s)	1.13	(s)
29[a]	0.99	(s)	0.97	(s)	0.97	(s)
30	5.65	(s)	5.64	(s)	5.65	(s)
32[a]	0.98	(s)	0.97	(s)	0.97	(s)
33[a]	0.91	(s)	0.90	(s)	0.91	(s)
34	5.95	(s)	5.94	(s)	5.95	(s)
36	3.68	(s)	3.67	(s)	3.68	(s)
37	3.65	(s)	3.65	(s)	3.65	(s)
2′	2.46	(m)	2.26	(m)	2.05	(s)
3′	1.8–1.9	(m)	1.60	(m)		
4′, 5′	1.16	(d; 14.5)	0.90	(7.2)[a]		
2″	2.05	(s)	2.05	(s)	2.04	(s)

[a]Assignments for these four positions may be interchanged.

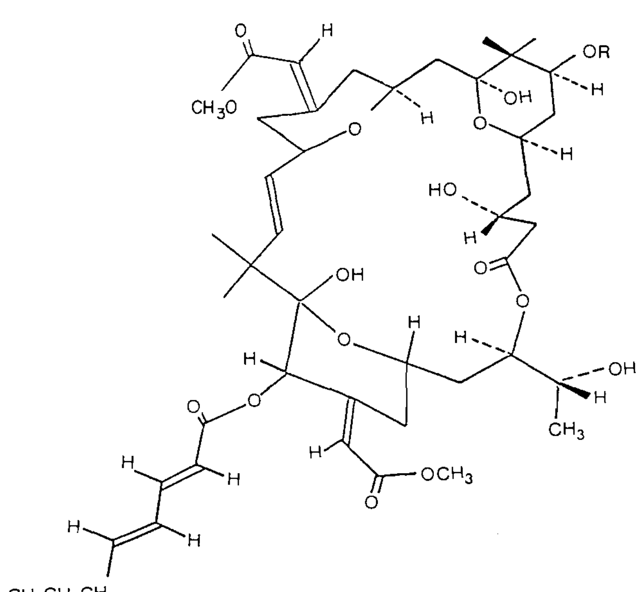

1*a*, R = CO—CH$_3$
Bryostatin 1
b, R = H
Bryostatin 2

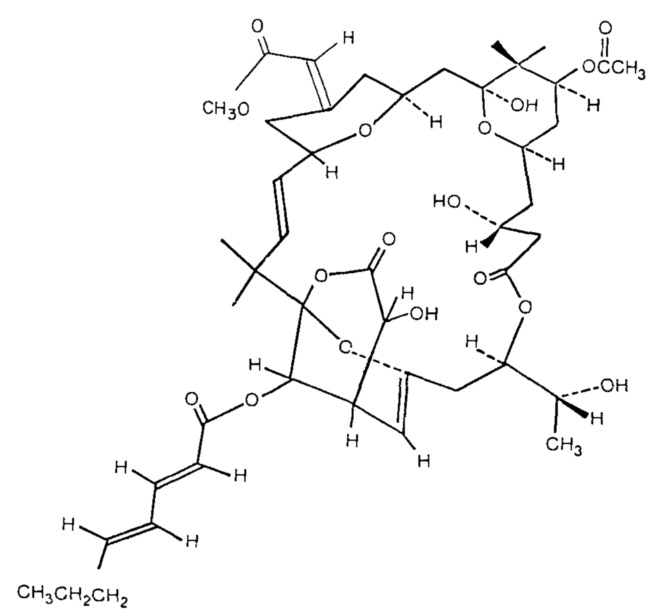

2
Bryostatin 3

TABLE 2. ^{13}C nuclear magnetic resonance chemical shift assignments (δ in ppm) for bryostatins 5–7 in deuteriochloroform solution

Structure **3** assignment no.	Bryostatin 5 (**3***b*)	Bryostatin 6 (**3***c*)	Bryostatin 7 (**3***d*)
1	178.04	173.52	172.22
2	44.19	44.26	44.23
3	64.76	64.80	64.76
4	31.26	31.26	31.20
5	73.73	73.76	73.70
6	33.27	33.47	33.40
7	72.37	72.66	72.95
8	41.27	41.11	41.04
9	101.87	101.90	101.87
10	42.41	42.34	42.34
11	65.84	65.74	65.71
12	42.05	42.05	42.02
13	156.46	156.85	156.82
14	36.40	39.59	36.43
15	70.22	70.22	70.25
16	139.24	139.11	139.11
17	129.62	129.72	129.66
18	44.88	44.88	44.84
19	98.95	98.91	98.88
20	79.16	79.13	79.13
21	151.88	151.75	151.72
22	35.87	35.94	36.00
23	74.48	74.48	74.45
24	40.00	40.00	39.94
25	71.55	71.59	71.59
26	68.56	68.56	68.50
27	19.85	19.82	19.85
28, 29	16.93	16.96	16.86
30	114.55	114.32	114.29
31	167.02	167.02	166.96
32	24.63 or 21.06	24.63 or 21.12	24.60 or 21.12
33	21.06 or 24.63	21.12 or 24.63	21.12 or 24.60
34	119.78	119.78	119.74
35	166.73	166.76	166.73
36, 37	51.05	51.08	51.05
1′	172.19	172.29	171.08
2′	39.06	39.50	21.48
3′	29.31	18.59	
4′	27.17	13.68	169.30
5′			21.12
1″	169.30	169.33	
2″	21.45	21.48	

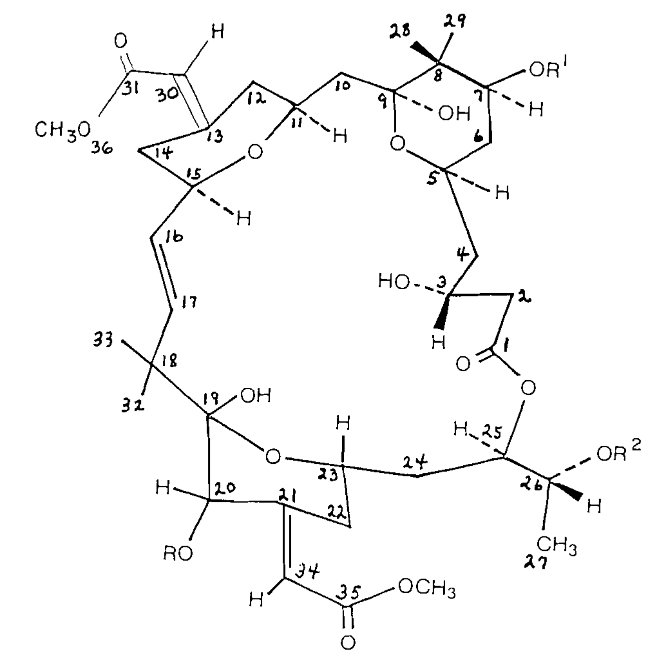

3*a*, R = $COCH_2CH_2CH_3$, R′ = $COCH_2CH(CH_3)_2$, R^2 = H. Bryostatin 4
b, R = $COCH_3$, R′ = $COCH_2CH(CH_3)_2$, R^2 = H. Bryostatin 5
c, R = $COCH_3$, R′ = $COCH_2CH_2CH_3$, R^2 = H. Bryostatin 6
d, R = R′ = $COCH_3$, R^2 = H. Bryostatin 7
e, R = $COCH_3$, R′ = R^2 = H
f, R = R^2 = H, R′ = $COCH_2CH(CH_3)_2$
g, R = R^2 = H, R′ = $COCH_2CH_2CH_3$
h, R = $COCH_2CH_2CH_3$, R′ = $COCH_2CH(CH_3)_2$, R^2 = $COCH_3$

could be selectively hydrolyzed to bryostatin 2 (**1***b*) as major product, presumably because of steric hindrance in the vicinity of the C-20 ester. Analogously, hydrochloric acid (1% in aqueous methanol)-catalyzed hydrolysis (24 h at room temperature) of bryostatin 5 (1 mg) afforded C-20 acetate **3***e* (300 μg) as major product accompanied by a lesser quantity (100 μg) of C-7 *iso*-valerate **3***f*. Comparable results were obtained employing bryostatin 6 (1 mg) which led to C-20 acetate **3***e* (350 μg, identical with the acetate from bryostatin 5) as major product accompanied by C-7 butyrate (**3***g*, 150 μg). Also, hydrochloric acid-catalyzed hydrolysis of bryostatin 7 (1 mg) afforded only C-20 acetate **3***e*, which was the same product from bryostatins 5 and 6. The data obtained from the selective hydrolyses allowed assignment of structures **3***b* and **3***c* respectively to bryostatins 5 and 6. The structure of bryostatin 7 (**3***d*) was based entirely upon conclusions reached from analyzing nmr and mass spectra.

Structural elucidation of bryostatins 4–7 allowed the course of some reactions explored as initial chemical probes of the molecular geometry to be better understood. For example, acetylation of bryostatin 4 (**3***a*) with acetic acid – pyridine (2 h at room temperature) was found to be very selective and afforded C-26 acetate **3***h*. Presumably due to intramolecular hydrogen bonding, the hydroxyl group at C-3 was essentially unaffected. Location of the 26-acetate (**3***h*) was based on interpretation of the high resolution (400 MHz) ^1H nmr spectrum. The 26-proton usually observed at δ 3.77 was shifted downfield to δ 4.99 (m). Conversely the C-3 proton signal in acetate **3***h* at δ 4.13 (m) was essentially the same as that in bryostatin 4 (**3***a*) at δ 4.16.

Some of the biological implications apparent from inspecting the structures of bryostatins 4–7 are particularly noteworthy. From evidence now in hand, *Bugula neritina* indigenous to the U.S. West Coast seems to have a special ability for synthesis of the C-20 (*E*,*E*)-octa-2,4-dienoate ester. Interestingly, this substituent may be in part responsible for the reduced cytotoxicity of this series. While no evidence for even trace amounts of bryostatins 1–3 could be detected in the various Gulf specimens of *Bugula neritina*, we were able to find barely detectable (by thin layer chromatography) amounts of bryostatins 4–7 in the Eastern Pacific *Bugula neritina*. The trace amounts (tlc only) of bryostatins 4–7 came from about 500 kg (wet weight) of California *Bugula neritina*. Presently bryostatins 4–7 are being readied for further evaluation against the NCI key experimental tumor systems. The results and other on-going studies should allow a better view of structure/activity relationships among this fascinating group of marine animal anticancer components.

Experimental

All solvents employed for chromatographic purposes were redistilled. Column chromatography was performed using either Sephadex LH-20, from Pharmacia Fine Chemicals, AB, Uppsala, Sweden, or silica gel (70–230 mesh) from E. Merck, Darmstadt. The hplc columns (9.4 × 500 mm) employed were the Partisil-10 M-9-ODS-2 (C-18 reversed phase) and Partisil-10 M-9 columns from Whatman, Inc., Clifton, New Jersey. An Altex hplc unit with System Controller Model 420 and Model 110A pumps was utilized for final separations. Preparative and reversed phase (KC-18) tlc plates were Whatman products. Silica gel GF Uniplates were supplied by Analtech, Inc., Newark, Delaware. All tlc plates were developed by uv light and (or) detected by anisaldehyde – acetic acid – sulfuric acid spray (plates heated to about 150°C for 5 to 10 min). Fractions were collected with either Gilson FC-80 (microfractionator) or FC-220 (racetrack fractionator) equipment in conjunction with a Gilson uv monitor Model HM.

All melting points are uncorrected and were observed with a Kofler-type melting point apparatus. Ultraviolet spectra (methanol solution) were recorded with a Hewlett–Packard 8450A uv/vis spectrometer. Optical rotations (methanol solution) were observed using a Perkin–Elmer Model 214 polarimeter. Mass spectra were determined with a MAT-312 mass spectrometer equipped for solution phase secondary ion mass spectrometry (SP-SIMS) employing sodium iodide in sulfolane (6). Infrared spectra (KBr) were obtained with a Nicolet FTIR Model MX-1 spectrometer. The nmr spectra were measured with Bruker WH-90 and WH-400 instruments, and deuteriochloroform was employed as solvent with tetramethylsilane as internal standard.

Collection and extraction

A July 1982 re-collection of *Bugula neritina* from the Eastern Gulf of Mexico (Alligator Harbor, Franklin County, Florida) provided 50 kg (wet weight) of marine animal which was preserved in 2-propanol, extracted, and subjected to preliminary separation as described before (see ref. 4 for details). By this means 37.6 g of bryostatin-enriched methylene chloride extract (PS ED_{50}, 0.058 μg/mL) was obtained and subjected to a series of column chromatographic separations to yield bryostatin 4 (44.5 mg) and, as summarized below, bryostatins 5–7.

Bryostatin 5 (3b)

From the succession of silica gel and gel permeation (Sephadex LH-20) column chromatographic steps previously used (4) to concentrate bryostatin 4 (**3***a*), an active fraction (0.38 g) was isolated as a white amorphous powder (PS cell line ED_{50}, 1.6×10^{-3} μg/mL) containing bryostatins 4–7 (evidenced by tlc using 7:3 n-hexane – acetone and 2:3 n-hexane – ethyl acetate). By extensive dry column (2 × 60 cm) silica gel chromatographic methods with solvent gradients of n-hexane – acetone (5:1 → 1:1) and n-hexane – ethyl acetate (2:1 → 1:2), six fractions were selected for further purification. The first fraction contained bryostatin 4. The second, third, and fifth fractions were subjected to hplc using a Partisil C-18 reversed phase column with a 1:1 → 9:1 methanol–water gradient (flow rate of 2 mL/min). The second fraction (15 mg) yielded pure bryostatin 5 (14.1 mg), melting at 169–172°C (needles from methylene chloride – methanol): $[\alpha]_D^{27}$ +106.92 (*c* 0.028); uv λ_{max}: 226 nm (ε 36 300); ir: 3465, 2980–2935, 1740, 1725, 1660–1640, 1440, 1385, 1370, 1290, 1230, 1165, 1100, 1080, 1060, and 1000 cm^{-1}; SP SIMS (6) ms *m/z* 889 $[M + Na]^+$ for $C_{44}H_{66}O_{17}$. See Tables 1 and 2 for the nmr data and the discussion section for additional mass spectral ions.

Bryostatin 6 (3c)

The third fraction (65 mg) was subjected to the same hplc final purification procedures as summarized for obtaining bryostatin 5, to afford bryostatin 6 (61.9 mg) as needles from methylene chloride – methanol: mp 172–175°C $[\alpha]_D^{27}$ +39.92 (*c* 0.05); uv λ_{max}: 228 nm (ε 36 350); ir: 3460, 2980–2950, 1740, 1720, 1660–1650, 1440, 1380, 1370, 1280, 1240, 1160, 1100, 1080, 1060, and 1000 cm^{-1}; SP-SIMS (6) ms *m/z* 875 [M + Na] for $C_{41}H_{60}O_{17}$. The nmr data have been recorded in Tables 1 and 2 and mass fragmentation ions in the discussion.

Bryostatin 7 (3d)

The fifth fraction (33 mg) was also purified by hplc as above to yield bryostatin 7, 31.2 mg, mp 176–179°C (needles from CH_2Cl_2–CH_3OH); $[\alpha]_D^{27}$ +39.92 (*c* 0.05); uv λ_{max}: 228 nm (ε 36 350); ir (KBr): 3460, 2980–2950, 1740, 1720, 1660–1650, 1440, 1380, 1370, 1280, 1240, 1160, 1100, 1080, 1060, and 1000 cm^{-1}; SP-SIMS ms *m/z* 824 for $C_{41}H_{60}O_{17}$.

Acid-catalyzed hydrolysis of bryostatin 5 (3b)

A specimen of bryostatin 5 (**3***b*, 1 mg) was subjected to hydrolysis in 1% hydrochloric acid (0.5 mL) for 24 h at room temperature. The product obtained by extraction with methylene chloride was washed with water, dried (*in vacuo*), and separated by hplc reversed phase (C-18) column chromatography. A methanol–water gradient from 1:1 to 9:1 was employed to give C-20 acetate **3***e* (300 μg) and C-7 isovalerate **3***f* (100 μg).

The C-20 acetate (**3***e*) was obtained as an amorphous powder from aqueous methanol: mp 153–156°C: ir: 3475, 2980–2950, 1740, 1720, 1660–1638, 1435, 1380–1370, 1290, 1240, 1160, 1100, 1090, 1075, 1048, 1005, and 870 cm^{-1}; SP-SIMS (6) ms, *m/z* 805 $[M + Na]^+$ for $C_{39}H_{58}O_{16}$, 787 $[M + Na - 18]^+$ and 745 $[M + Na - 60]^+$.

The C-7 *iso*-valerate (**3***f*) was obtained as an amorphous solid melting at 147–152°C from aqueous methanol; ir: 3470, 3435, 2975–2950, 1738, 1720, 1660–1635, 1440, 1390–1370, 1290, 1240, 1160, 1100, 1075, 1050, 1000, and 870 cm^{-1}; SP-SIMS, ms, *m/z* 847 $[M + Na]^+$ for $C_{42}H_{64}O_{16}$, 829 $[M + Na - 18]^+$ and 745 $[M + Na - 102]^+$. The C-7 *iso*-valerate was found to be identical[4] with the compound (**3***f*) derived from bryostatin 4 (**3***a*) by analogous acid hydrolysis.

Acid-catalyzed hydrolysis of bryostatin 6

A specimen of bryostatin 6 (**3***c*, 1 mg) was hydrolyzed and the products separated by reversed phase hplc as described for bryostatin 5 to provide C-20 acetate **3***e* (350 μg), identical[4] to that obtained from bryostatin 5, and C-7 butyrate **3***g* (150 μg).

The C-7 butyrate (**3***g*) was obtained as an amorphous solid melting at 166–170°C; ir (KBr): 3475, 3430, 2975–2945, 1736, 1720, 1640, 1620, 1440, 1390, 1095, 1080, 1040, and 870 cm^{-1}; SP-SIMS (6) ms, *m/z* 833 $[M + Na]^+$ for $C_{41}H_{62}O_{16}$, 815 $[M + Na - 18]^+$ and 745 $[M + Na - 88]^+$.

Acid-catalyzed hydrolysis of bryostatin 7

A sample of bryostatin 7 (**3***d*, 1 mg) was hydrolyzed and the crude material purified by reversed phase hplc as outlined for bryostatin 5. The major product was 20-acetate **3***e* (370 μg) and it was found[4] to be the same product analogously obtained from bryostatin 5 (**3***b*).

Acetylation of bryostatin 4

A sample of bryostatin 4 (9.0 mg) was treated with acetic anhydride (0.14 mL) and pyridine (0.2 mL) at room temperature for 4 h. The mixture was poured into ice-water and extracted with methylene chloride. The extract was washed with dilute hydrochloric acid and water, concentrated, and dried under reduced pressure. The crude product (9.5 mg) was purified by reversed phase hplc using the same procedure as described above for bryostatin 5. Pure bryostatin 4 acetate (**3***h*, 8.0 mg, 88.9% yield) was obtained as colorless needles from methylene chloride – methanol: mp 159–162°; $[\alpha]_D^{27}$ +58.71 (*c* 0.034); uv λ_{max}: 227 nm (ε 36 600); ir: 3460, 2985–2935, 1745, 1730, 1660–1640, 1440, 1380, 1370, 1290, 1240, 1165, 1100, 1080, 1050, and 1000 cm^{-1}; SP-SIMS ms, *m/z* 959 $[M + Na]^+$ (*M* = 936 for $C_{48}H_{72}O_{18}$), 941 $[M + Na - 18]^+$, 899 $[M + Na - 60]^+$, $[M + Na - 88]^+$– and 857 $[M + Na - 102]^+$.

[4]By tlc and mass spectral comparisons.

Acknowledgments

In addition to the financial aid provided by Eleanor W. Libby, the Waddell Foundation (Donald Ware), Mary Dell Pritzlaff, The Olin Foundation (Spencer T. and Ann W.), the Fannie E. Rippel Foundation, the Flinn Foundation, the Robert B. Dalton Endowment Fund, the Upjohn Co., Virginia L. Bayless, PHS Grant No. CA-16049-08 awarded by the National Cancer Institute, DHHS, and Contract NO1-CM-97262 with the Division of Cancer Treatment, NCI, DHHS, we are also pleased to thank for other necessary assistance Drs. H. Cohen, D. L. Doubek, P. D. Ellis, G. Hendler, L. W. Knapp, P. Lohavanijaya, M. I. Suffness, J. M. Schmidt, Mr. J. J. Rudloe, the Smithsonian Institution Oceanographic Sorting Center, and the National Science Foundation Regional Facility at the University of South Carolina (CHE 82-07445). Also, we are pleased to acknowledge assistance with the collection and initial extraction of the Japanese *Bugula neritina* by Drs. T. Kajiwara and T. Miura, University of Tokyo, and Dr. T. Takahashi and Mr. C. Hashimoto, the Jikei University School of Medicine.

1. G. R. PETTIT, G. M. CRAGG, C. W. HOLZAPFEL, and D. P. GIESCHEN. Biomed. Mass Spectrom. In press.
2. G. R. PETTIT, J. F. DAY, J. L. HARTWELL, and H. B. WOOD. Nature, **227**, 962 (1970).
3. (*a*) G. R. PETTIT, C. L. HERALD, D. L. DOUBEK, D. L. HERALD, E. ARNOLD, and J. CLARDY. J. Am. Chem. Soc. **104**, 6846 (1982); (*b*) G. R. PETTIT, C. L. HERALD, Y. KAMANO, D. GUST, and R. AOYAGI. J. Nat. Prod. **46**, 528 (1983); (*c*) G. R. PETTIT, C. L. HERALD, and Y. KAMANO. J. Org. Chem. **48**, 5354 (1983).
4. G. R. PETTIT, Y. KAMANO, C. L. HERALD, and M. TOZAWA. J. Am. Chem. Soc. **106**, 6768 (1984).
5. G. R. PETTIT, G. M. CRAGG, D. GUST, P. BROWN, and J. M. SCHMIDT. Can. J. Chem. **60**, 939 (1982); G. R. PETTIT and R. H. ODE. Biosynthetic products for cancer chemotherapy. Plenum Publishing Corp., New York, NY. 1979. p. 59.
6. G. R. PETTIT, C. W. HOLZAPFEL, G. M. CRAGG, C. L. HERALD, and P. WILLIAMS. J. Nat. Prod. **46**, 917 (1983).

The preparation of S_7BrMF_6 (M = As, Sb), and the preparation and crystal structure of $(S_7Br)_4S_4(AsF_6)_6$ containing the bromo-cycloheptasulphur (1+) cation

JACK PASSMORE, GEORGE SUTHERLAND, TOM K. WHIDDEN, PETER S. WHITE, AND CHI-MING WONG
Department of Chemistry, University of New Brunswick, Fredericton, N.B., Canada E3B 6E2

Received July 9, 1984

JACK PASSMORE, GEORGE SUTHERLAND, TOM K. WHIDDEN, PETER S. WHITE, and CHI-MING WONG. Can. J. Chem. **63**, 1209 (1985).

S_7BrMF_6 (M = As, Sb) were prepared essentially quantitatively by a variety of similar routes to those that led to S_7IMF_6; and in addition, by the reaction of bromine and S_7IAsF_6. $(S_7Br)_4S_4(AsF_6)_6$ was prepared essentially quantitatively directly from sulphur, bromine, and arsenic pentafluoride in the appropriate ratios. Crystals of $(S_7Br)_4S_4(AsF_6)_6$ are isostructural with $(S_7I)_4S_4(AsF_6)_6$, space group $P4/n$, a = 19.19(3), c = 8.01(1) Å. The structure was refined from a low temperature set of data to a final R = 0.12. The salt contains a discrete planar S_4^{2+} and bromo-cycloheptasulphur (1+) cations, the latter having a similar geometry, sulphur–sulphur bond distances and an intra-cationic halogen–sulphur contact to that observed in S_7I^+.

JACK PASSMORE, GEORGE SUTHERLAND, TOM K. WHIDDEN, PETER S. WHITE et CHI-MING WONG. Can. J. Chem. **63**, 1209 (1985).

Utilisant diverses méthodes semblables à celles qui ont permis de préparer le S_7IMF_6, on a préparé le S_7BrMF_6 (M = As, Sb) avec un rendement pratiquement quantitatif; on l'a aussi obtenu par la réaction du brome et du S_7IAsF_6. Par réaction du soufre, du brome et du pentafluorure d'arsenic dans des proportions appropriés, on a préparé le $(S_7Br)_4S_4(AsF_6)_6$ avec un rendement essentiellement quantitatif. Les cristaux de $(S_7Br)_4S_4(AsF_6)_6$ sont isostructuraux avec ceux du $(S_7I)_4S_4(AsF_6)_6$, groupe d'espace $P4/n$, a = 19,19(3), c = 8,01(1) Å. On a affiné la structure, jusqu'à une valeur finale de R = 0,12, à l'aide d'un ensemble de données obtenues à basse température. Le sel contient des ions individuels S_4^{2+} plan et bromo-cycloheptasoufre (1+); la géométrie, les distances soufre–soufre et le contact intracationique halogène–soufre de ce dernier sont semblables à ce qui a été observé avec le cation S_7I^+.

[Traduit par le journal]

Introduction

We have recently prepared and determined the crystal structures of the sulphur iodine cations S_7IMF_6 (M = As, Sb) (1–3), $[(S_7I)_2I][SbF_6]_3 \cdot 2AsF_3$ (4, 5), $(S_7I)_4S_4(AsF_6)_6$ (4, 6), and $S_2I_4(AsF_6)_2$ (7). It was of interest to determine whether iodine was unique in its ability to form cations of this sort, therefore, we explored the analogous sulphur–bromine system, and the results are reported in detail below. A preliminary communication briefly mentioned $(S_7Br)_4S_4(AsF_6)$ (6). Prior to this work the known binary sulphur–bromine species were S_xBr_2 (x = 2 to ca. 10) (of which only S_2Br_2 is stable) (8), SBr_3MF_6 (M = As, Sb) (9) salts, and the rather unstable NH_4SBr (8).

Experimental

Chemicals and techniques have been described (5, 10), in addition bromine (Anachemia, Reagent Grade) was dried and stored over P_2O_5 prior to use. Elemental analyses were obtained from A. Bernhardt, W. Germany and Butterworth, Teddington, England. Table 1 includes experimental weights for experiments described below.

(1) Preparation of S_7BrMF_6

(A) Reaction of sulphur with arsenic pentafluoride and bromine. In a typical reaction, AsF_5 (2.40 g, 14.1 mmol) was condensed onto excess S_8 (2.79 g, 10.9 mmol) in AsF_3 (14.26 g) in a two-bulbed Pyrex vessel separated by a coarse sintered glass frit and equipped with a Rotaflo or J. Young Teflon-stemmed Pyrex valve. After 12 h, Br_2 (0.77 g, 4.81 mmol) was added and the mixture stirred for 2 h, yielding a red–brown solution containing solids. The products were separated by filtration and the volatile material removed. A noncrystalline soluble red–brown solid and unreacted S_8 were obtained. *Anal.* calcd. for S_7BrAsF_6 (the soluble product): S 45.50, Br 16.20, As 15.19, F 23.11; found: S 45.16, Br 16.52, As 15.03, F 22.90.

Other similar reactions with approximately stoichiometric amounts of S_8 were performed leading to microcrystalline products (weights given in Table 1). Reactions carried out by adding Br_2 before the AsF_5 gave material of very poor quality (i.e. containing S_xBr_2).

(B) Reaction of excess sulphur with antimony pentafluoride and bromine. In a typical reaction, SbF_5 (3.04 g, 14.0 mmol) was condensed onto S_8 (3.03 g, 11.8 mmol) in SO_2 (8.67 g) and the mixture stirred for 1 h. Br_2 (0.73 g, 4.56 mmol) was then added and the red–brown mixture stirred for 2 h. The soluble and insoluble products were separated by filtration and SO_2ClF (3.01 g) added to the solution to facilitate crystal formation. Removal of the volatile material at 0°C over a 12 h period yielded what appeared to be a highly crystalline red–brown soluble solid and a mixture of sulphur and a reduced antimony pentafluoride product, $(SbF_3)_3SbF_5$. Several well formed crystals of soluble product were examined by X-ray precession photography but were found to diffract X-rays very poorly. *Anal.* calcd. for S_7BrSbF_6 (the soluble crystalline product): S 41.55, Br 14.80, Sb 22.54, F 21.11; found (*1*) S 41.92, 41.86, Br 14.69, Sb 22.32, F 20.78; (*2*) (a different reaction) S 41.13, Br 14.89, Sb 22.50, F 20.99.

(C) Reaction of $S_x(AsF_6)_2$ (average x ca. 17), with bromine. In one reaction, excess S_8 (4.88 g, 19.1 mmol) was reacted with stirring with AsF_5 (3.05 g, 17.9 mmol) in SO_2 (11.86 g) for 12 h. Separation of the deep red soluble product from unreacted S_8 was followed by addition of Br_2 (1.03 g, 6.44 mmol). The section of the vessel containing the excess sulphur was previously flame sealed at a constriction to prevent reaction of the sulphur with Br_2. The weight of unreacted sulphur (1.56 g, 6.09 mmol) indicated that the average stoichiometry of the red sulphur polyatomic cation was $S_{17.4}^{2+}$. The red–brown solution was separated from the precipitated sulphur after 4 days, and removal of the volatile material over a 24 h period resulted in a red–brown microcrystalline soluble solid, and insoluble S_8.

(D) Reactions of S_7IAsF_6 with Br_2. In one reaction, AsF_5 (2.43 g, 14.3 mmol) was reacted with a mixture of S_8 (2.48 g, 9.68 mmol) and I_2 (4.66 g, 18.3 mmol) in SO_2 (11.60 g) for 2 h with vigorous agitation. The soluble and insoluble (excess S_8/I_2) materials were separated as in (*C*). The weight of excess S_8 and I_2 remaining was found to be 3.64 g (3.79 g calculated for formation of S_7IAsF_6 based on AsF_5). After 4 days Br_2 (0.82 g, 5.13 mmol) was condensed onto the solution resulting in a red–brown solution containing no precipitate. Subsequently, the solution was pumped to dryness over a 24 h period yielding a red–brown microcrystalline solid. *Anal.* calcd. for S_7BrAsF_6: S 45.50, Br 16.20, As 15.19, F 23.11; found: S 45.16, Br 16.49, As 15.50, F 23.05, I 0.00.

(E) Reaction of $S_8(AsF_6)_2$ with KBr. In one reaction, SO_2 (6.63 g) was condensed onto $S_8(AsF_6)_2$ (1.17 g, 1.85 mmol) in a previously

TABLE 1. Weights of reactants and products

Experimental Section: Target reaction as per equation given in the discussion	Reactant Weights (g)	Product weight (g) Soluble Observed	Soluble Calculated[a]	Insoluble Observed	Insoluble Calculated[a]
1(*A*) Eq. [1]	S_8 + AsF_5[b] + Br_2				
	2.79 2.40 0.77[c]	4.64	4.64	0.56[f]	0.68
	1.48 1.69 0.57[d]	3.31	3.27	[e]	—
	2.55 2.95 0.92[d]	5.69	5.70	[e]	—
1(*B*) Eq. [2]	S_8 + SbF_5[b] + Br_2				
	3.03 3.04 0.73[c]	4.51	4.54	2.28[g]	2.20
	2.89 2.79 0.71[d]	4.50	4.17	1.89[g]	2.14
	4.79 3.24 1.08[d]	4.32	4.84	4.19[g]	3.90
1(*C*) Eq. [3]	$S_{17.4}(AsF_6)_2$[b] + Br_2				
	5.59 1.03[c]	5.95	5.89	0.54[f]	0.65
1(*E*) Eq. [5]	$S_8(AsF_6)_2$[b] + KBr				
	1.17 0.22[c]	0.78	0.91	0.54[h]	0.48
2 Eq. [6]	S_8[b] + AsF_5 + Br_2				
	1.30 1.97 0.40	3.15	3.14	[e]	—
	1.34 2.18 0.48[c]	3.44	3.25	[e]	—

[a] Calculated weights are for the target compound according to the appropriate equation based on (*b*).
[b] Limiting reagent.
[c] Data for the experiment described in the text.
[d] Data for experiment similar to that described in the text.
[e] No insolubles since approximately stoichiometric quantities of S_8, Br_2, and AsF_5 were used.
[f] Elemental S_8.
[g] Mixture of S_8 and $(SbF_3)_3SbF_5$ (14).
[h] Mixture of S_8 and $KAsF_6$.

isolated section of the apparatus and the blue solution quantitatively added to KBr (0.22 g, 1.85 mmol). After 6 h the red–brown solution containing solids was filtered into a third bulb and SO_2ClF (2.80 g) added to facilitate crystal formation. Removal of the volatile material over a 4 h period resulted in a noncrystalline red soluble solid. The insoluble solid was identified as a mixture of S_8 and $KAsF_6$ by Raman spectroscopy and X-ray powder diffraction photography.

Identification of S_7BrMF_6 bulk material

X-ray powder photographs (Cu Kα radiation) of material from preparations 1(*A*) and 1(*C*) to 1(*E*) were obtained and all were found to be similar, showing three strong lines at $2\theta \simeq 18.3$, 22.5, and 29.0° ($I/I_0 = 100$, 20, and 50, respectively). In addition, some photographs showed other much less intense lines. Attempts at obtaining reproducible Raman spectra, using a spinning cell at −196°C, were unsuccessful.

Stability of S_7BrMF_6

Solid S_7BrAsF_6 decomposed after several days at room temperature while S_7BrSbF_6 was stable for several weeks. In addition, samples of both salts in concentrated (SO_2) solution deposited a yellow solid (presumably S_8) with evolution of a dark red liquid (presumably S_xBr_2) on standing for several weeks. Both salts were found to be stable in the solid phase for at least several months at −20°C. Redissolving solid samples in fresh SO_2 or AsF_3 resulted in decomposition.

(2) Preparation of $(S_7Br)_4S_4(AsF_6)_6$

In one reaction AsF_5 (2.18 g, 12.8 mmol) was condensed onto S_8 (1.34 g, 5.22 mmol) over SO_2 (8.95 g). Br_2 (0.48 g, 2.92 mmol) and SO_2ClF (2.95 g) were added after 1 h. On warming to room temperature a dark green–brown solution over a dark precipitate was obtained. (We found that slight excess of Br_2 and AsF_5 with addition of SO_2ClF yielded better quality crystals). After 12 h the solution was dark red, tinted somewhat with green. Most of the volatile material was slowly (~4 days) condensed to the other side of the reaction vessel with a temperature gradient of 10°C between the two bulbs. Red needle-shaped crystals were obtained. The crystals were washed quickly with a small amount of solvent and then the volatile material was removed. This and other similar preparations yielded crystals suitable for single crystal X-ray analysis.

Stability of $(S_7Br)_4S_4(AsF_6)_6$

A crystalline sample of $(S_7Br)_4S_4(AsF_6)_6$ showed no apparent loss of crystallinity on storage for several weeks at room temperature. The crystals were found to partially decompose to a red liquid on irradiation with X-rays (Mo-Kα).

X-ray crystal structure of $(S_7Br)_4S_4(AsF_6)_6$

Suitable crystals, manipulated in a Vacuum Atmosphere Corp. dry box with the aid of an externally mounted Wild M3 microscope of long focal length, were sealed under dry nitrogen in rigorously dried glass capillary tubes. An initial photographic investigation showed the crystals to be tetragonal, space group $P4/n$ and apparently isostructural with $(S_7I)_4S_4(AsF_6)_6$ (4, 6). Initial attempts at collecting intensity data were abandoned because of excessive crystal movement and it was observed that a layer of red liquid formed on the surface of the crystals on exposure to X-rays. A number of attempts were made to secure the crystals inside the capillaries, but none were successful. At this point it was decided to try and collect data at low temperature, thereby using the liquid decomposition product to freeze the crystal in place.

The crystal was mounted on a Picker FACS-I diffractometer equipped with a modified Enraf-Nonius low temperature attachment, using graphite monochromated MoKα radiation. The cell dimensions and an orientation matrix were determined by a least-squares fit to the centered coordinates of 12 Friedel pairs of reflections in the range 30° ≤ 2θ ≤ 45°. Intensity data for two unique sets of reflections were collected using an ω–2θ scan of 2° (2θ) corrected for dispersion of the Kα doublet, at a scan speed of 2° (2θ) min^{-1}. Backgrounds were measured for 1/10 scan-time at each end of a scan and if the peak was considered significant ($I > 2\sigma(I)$) an analysis of the peak profile was performed. Three reference reflections, measured every 100 reflections, showed no indication of sample decomposition during the data

TABLE 2. Crystal data for $(S_7Br)_4S_4(AsF_6)_6$

Space Group	$P4/n$ (C^3_{4h}, #85)
a	19.19(3) Å
c	8.01(1) Å
V	2949 Å^3
Z	2
M.wt.	2479.0
$F(000)$	2348
D_{calcd}	2.71 Mg m^{-3}
Crystal size	0.4 × 0.4 × 0.2 mm
μ	7.20 mm^{-1}
$2\theta_{max}$	45°
λ(Mo Kα)	0.71073 Å
Number of unique reflections collected	1033
Number of observed reflections ($I \geq 3\sigma(I)$)	878
Final $R = \Sigma\|\Delta F\|/\Sigma\|F_o\|$	0.12
$= \Sigma\omega(\Delta\|F\|)^2/\Sigma\omega\|F\|^2$	0.14
Temperature	100 K

TABLE 3. Fractional atomic coordinates (esd's in parentheses)

Atom	x/a	y/b	z/c	U_{iso}
Br(1)	0.1601(3)	0.4347(3)	0.2568(7)	0.038
S(1)	0.1729(7)	0.5390(8)	0.336(2)	0.047
S(2)	0.2680(6)	0.5245(7)	0.516(2)	0.034
S(3)	0.2850(7)	0.4255(7)	0.519(2)	0.050
S(4)	0.2189(7)	0.3849(7)	0.718(2)	0.047
S(5)	0.1692(7)	0.4667(8)	0.802(2)	0.043
S(6)	0.0817(7)	0.4718(7)	0.644(2)	0.046
S(7)	0.0941(6)	0.5591(6)	0.512(2)	0.042
S(8)	0.2359(8)	0.6795(7)	0.005(3)	0.079
As(1)	0.5393(2)	0.1371(3)	0.0103(7)	0.032
F(11)	0.527(1)	0.224(1)	0.063(4)	0.041
F(12)	0.495(1)	0.113(2)	0.175(4)	0.045
F(13)	0.590(1)	0.165(1)	−0.168(4)	0.049
F(14)	0.468(2)	0.137(2)	−0.119(5)	0.087
F(15)	0.559(2)	0.051(2)	−0.029(4)	0.054
F(16)	0.616(1)	0.142(2)	0.126(4)	0.070
As(2)	0.25	0.25	0.168(2)	0.036
F(21)	0.25	0.25	−0.051(6)	0.070
F(22)	0.25	0.25	0.390(9)	0.066
F(23)	0.176(1)	0.293(1)	0.178(4)	0.063
As(3)	0.25	0.75	0.5	0.041
F(31)[a]	0.220(2)	0.688(3)	0.369(10)	0.15
F(32)[a]	0.176(3)	0.770(5)	0.390(12)	0.46

[a]To approximate the disorder F(31) and F(32) were included with occupancies of 3/4.

collection. However, it was found necessary to redetermine the orientation matrix each time the liquid N_2 dewar was refilled (about every 12 h). Crystal data are given in Table 2.

An initial attempt to use the atomic positions from $(S_7I)_4S_4(AsF_6)_6$ (4, 6) was not successful so the structure was solved by the direct methods program MULTAN (11), from which all the S, Br, and As atomic positions were obtained. The fluorines were located in subsequent difference syntheses, those about As(1) and As(2) behaved normally. The environment about As(3) showed eight peaks, indicating a disordered AsF_6^- similar to that in $(S_7I)_4S_4(AsF_6)_6$. Attempts to fit a set of octahedral fluorine atom arrangements failed and the fluorine positions were approximated by assigning F's with 3/4 occupancies to the positions found in the original difference synthesis. After correction of the data for absorption by Gaussian integration (transmission coefficients 0.06–0.25), the structure was refined by least-squares techniques. A weighting scheme based on counter statistics was used, the function minimised was $\Sigma\omega(\Delta|F|)^2$. The final agreement factors were R $(=\Sigma|\Delta F|/\Sigma|F|)$ = 0.12 and R_ω $(=\Sigma\omega(\Delta|F|)^2/\Sigma\omega|F|^2)$ = 0.14, with all the atoms refined anisotropically. Such mediocre agreement factors are not unusual in compounds similar to this one, and can be attributed not only to the disorder of one AsF_6^- but to the high thermal motion of all the anions. This may have been exacerbated by errors in the absorption correction due to the crystal shape being modified by surface decomposition. A final difference synthesis showed no abnormal features, the maximum was 1.9e$^-$ in the region of Br. Scattering factors were taken from the International tables for crystallography (12) and were corrected for anomalous dispersion. Computations were performed using SHELX-76 (13). Final positional parameters are given in Table 3.

Discussion

Preparation of S_7BrMF_6 (M = As, Sb)

We have found that S_7BrMF_6 may be prepared essentially quantitatively in liquid sulphur dioxide according to reactions [1] to [5] below:

$$[1]\quad nS_8 + 3AsF_5 + Br_2 \rightarrow 2S_7BrAsF_6 + AsF_3 + \left(n - \frac{7}{4}\right) S_8 \quad \left(n \geq \frac{7}{4}\right)$$

$$[2]\quad nS_8 + 10SbF_5 + 3Br_2 \rightarrow 6S_7BrSbF_6 + (SbF_3)_3\cdot SbF_5\ (14) + \left(n - \frac{21}{4}\right) S_8 \quad \left(n \geq \frac{21}{4}\right)$$

$$[3]\quad S_x(AsF_6)_2\ (x \approx 17) + Br_2 \rightarrow 2S_7BrAsF_6 + \left(\frac{x-14}{8}\right) S_8$$

$$[4]\quad S_7IAsF_6 + \frac{1}{2}Br_2 \rightarrow S_7BrAsF_6 + \frac{1}{2}I_2$$

$$[5]\quad S_8(AsF_6)_2 + KBr \rightarrow S_7BrAsF_6 + KAsF_6 + \frac{1}{8}S_8$$

Experimental weight changes taken as a whole (Table 1), and analytical data (five separate analyses from four different preparations) support formation of S_7BrMF_6. Although evidence of this type may be misleading (c.f. S_{19}^{2+} (15, 16) and Te_6^{4+} (17–19)), in view of the well established (1–3) existence of S_7I^+ and the X-ray crystal structure determination of $(S_7Br)_4S_4(AsF_6)_6$ (see below) it is reasonable to conclude that S_7BrMF_6 was formed in all of these reactions. Thus S_7BrMF_6 can be prepared by a variety of routes.

It is noteworthy that the final product of these reactions was never S_8BrMF_6. Reactions [1] and [2] were carried out with excess sulphur (see Table 1), allowing for the formation of S_8BrMF_6, and, reasonably S_8Br^+ was initially formed in reaction [4] from S_8^{2+} and Br^-, which presumably disproportionates to the observed S_7Br^+ and elemental sulphur. Reactions [1] and [2] likely proceed wih initial formation of sulphur polyatomic cations. In a separate experiment, a mixture of sulphur polyatomic cations of average composition $S_{17.4}^{2+}$ were reacted with bromine to give S_7Br^+ and elemental sulphur (reaction [3]). In addition, it is noted that sulphur and arsenic and antimony pentafluorides react very rapidly in the presence of bromine to form sulphur polyatomic cations (6). Bromine cations are not likely intermediates in reaction [1] or [2] since bromine cations react with the solvent, sulphur dioxide, to give SO_2BrF (20). S_7BrAsF_6 was also formed by the reaction of S_7IAsF_6 and bromine. The enthalpies of atomisation of I_2(s) and Br_2(l) are essentially the same (Br, 26.7; I, 25.5 kcal/g atom 25°C (21)), and in two coordinate sulphur compounds the S—Br bond (ca. 56 kcal/mmol (8)) is stronger than the S—I bond (49 kcal/mmol (22)). Therefore reaction [4] is likely exothermic and is observed to proceed as indicated.

TABLE 4.

(*a*) Bond distance (esd's in parentheses)

Bond	Distance (Å)	Bond	Distance (Å)
	S_7Br^+		
S(1)—Br(1)	2.114(16)	S(4)—S(3)	2.182(22)
S(2)—S(1)	2.344(19)	S(5)—S(4)	1.955(20)
S(7)—S(1)	2.106(20)	S(6)—S(5)	2.105(20)
S(3)—S(2)	1.928(19)	S(7)—S(6)	1.995(19)
	S_4^{2+}		
S(8)—S(8)′	1.951(19)		
	AsF_6^-'s		
F(11)—As(1)	1.74(3)	F(21)—As(2)	1.75(5)
F(12)—As(1)	1.63(3)	F(22)—As(2)	1.78(7)
F(13)—As(1)	1.81(3)	F(23)—As(2)	1.65(2)
F(14)—As(1)	1.71(4)		
F(15)—As(1)	1.72(3)		
F(16)—As(1)	1.74(3)		

(*b*) Bond angles (esd's in parentheses)

Bonds	Angle (deg)	Bonds	Angle (deg)
	S_7Br^+		
S(2)—S(1)—Br(1)	99.4(7)	S(4)—S(3)—S(2)	105.2(9)
S(7)—S(1)—Br(1)	106.9(7)	S(5)—S(4)—S(3)	104.4(8)
S(7)—S(1)—S(2)	99.7(8)	S(6)—S(5)—S(4)	102.7(9)
S(3)—S(2)—S(1)	104.7(8)	S(7)—S(6)—S(5)	105.2(8)
		S(6)—S(7)—S(1)	106.7(8)
	S_4^{2+}		
S(8)′—S(8)—S(8)″	89.9(8)		
	AsF_6^-'s		
F(12)—As(1)—F(11)	90.0(14)	F(15)—As(1)—F(14)	93.3(16)
F(13)—As(1)—F(11)	88.7(12)	F(16)—As(1)—F(11)	85.8(14)
F(13)—As(1)—F(12)	177.8(14)	F(16)—As(1)—F(12)	91.2(13)
F(14)—As(1)—F(11)	92.7(15)	F(16)—As(1)—F(13)	86.9(13)
F(14)—As(1)—F(12)	94.7(16)	F(16)—As(1)—F(14)	173.9(16)
F(14)—As(1)—F(13)	87.2(16)	F(16)—As(1)—F(15)	88.2(15)
F(15)—As(1)—F(11)	174.0(14)	F(22)—As(2)—F(21)	180.0(0)
F(15)—As(1)—F(12)	89.8(15)	F(23)—As(2)—F(21)	92.7(13)
F(15)—As(1)—F(13)	91.3(13)	F(23)—As(2)—F(22)	87.3(13)

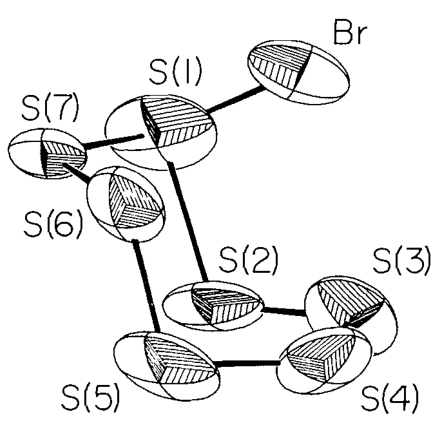

FIG. 1. The structure of the S_7Br^+ cation.

Preparation and characterization of $(S_7Br)_4S_4(AsF_6)_6$

This compound was prepared in ca. 90% yield (see Table 1) in sulphur dioxide solution according to reaction [6]:

$$[6] \quad 4S_8 + 2Br_2 + 9AsF_5 \rightarrow (S_7Br)_4S_4(AsF_6)_6 + 3AsF_3$$

X-ray powder diffraction photographs of this material were not inconsistent with the diffraction pattern calculated on the basis of single crystal diffractometer data. In addition, approximately 20 crystals from this preparation were identified as the title compound by single crystal X-ray precession photography. The experimental data are therefore consistent with the bulk of the material being $(S_7Br)_4S_4(AsF_6)_6$, and not a mixture of various species with this average stoichiometry.

It is noteworthy that $(S_7Br)_4S_4(AsF_6)_6$ is very soluble in the mixture of liquid SO_2 and AsF_3 present at the end of reaction [6], whereas $S_4(AsF_6)_2$ alone has low solubility. Thus, either the cations in solution are different from those in the solid state, or the solubility of $S_4(AsF_6)_2$ is greatly enhanced by the presence of S_7BrAsF_6.

The stabilities of the S_7Br^+*-containing salts*

The S_7Br^+-containing salts are less stable than the corresponding iodides. In addition, we were unable to prepare bro-

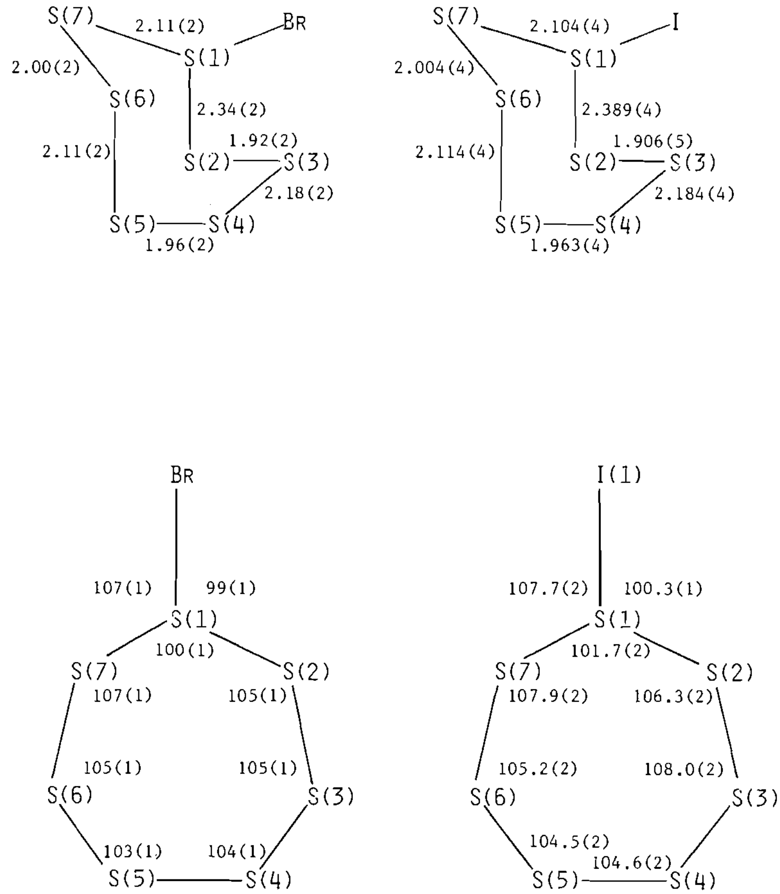

FIG. 2. A comparison of the bond distances (Å) and angles (deg) in S_7Br^+ with those in S_7I^+ in S_7ISbF_6 (3).

mine analogues of $(S_7I)_2I(SbF_6)_3 \cdot 2AsF_3$ (4, 5), and $S_2I_4(AsF_6)_2$ (7), or chlorine analogues of any of the sulphur–iodine cations. This is the opposite of what would be expected on the basis of the relative strengths of the sulphur–halogen bonds, and the relative stabilities of the hitherto known sulphur chlorides, bromides, and iodides, i.e. chlorides are more stable than bromides, which are more stable than iodides. This may, in part, be due to the greater stability of the products of disproportionation of the sulphur bromine (chlorine) cations, S_xBr_2 (S_xCl_2) and SBr_3^+ (9) (SCl_3^+). We note that SI_3^+ has not yet been identified, and S_xI_2 are not stable at room temperature. The relative stabilities of the sulphur bromine cations appears to decrease in the order $(S_7Br)_4S_4(AsF_6)_6 \geq S_7BrSbF_6 > S_7BrAsF_6$, a similar order to that of the corresponding iodides.

The crystal structure of $(S_7Br)_4S_4(AsF_6)_2$

The S_7Br^+ cation is illustrated in Fig. 1, and its geometry is compared to that of S_7I^+ (2, 3) in Fig. 2. Both S_7I^+ and S_7Br^+ have similar geometries to that of S_7O (23), with the sulphur ring having a distorted chair conformation. The neutral S_7 has a chair conformation of essentially C_s symmetry (24). Table 4 lists relevant bond distances and angles for S_7Br^+ and S_4^{2+}, and the ordered AsF_6^-'s. The sulphur–sulphur bond distances and angles within the cation are essentially identical to those of S_7I^+ (2, 3) (see Fig. 2), and the bond alternations within the ring are the same. As in S_7I^+, S(5)S(4)S(3)S(2) and BrS(1)S(2)S(3) are essentially planar, and the angle between the planes is 89.6°. The Br—S(3) contact (3.19(2) Å) is substantially less than the sum of the corresponding van der Waal's radii (3.80 Å) (25) indicating some Br—S(3) interaction. The S(1)—Br distance of 2.11(2) Å is somewhat shorter than the sum of the covalent radii of sulphur and bromine (2.18 Å) and other sulphur bromine bond distances (e.g. SO_2BrF, 2.155(6) (26); SBr_3^+, 2.16 (estimated in ref. 27); S_2Br_2, 2.164(5) (28); $SBrF_5$, 2.190(7) (29, 30); $(BrS)CS_2N_2^+Br_3^+$, 2.205(4) Å (31)). The shortest cation–anion contact is that to bromine, which is nearly linear (Br—F(23) = 2.81(3) Å, S(1)—Br—F(23) = 166(1)°). These features find a parallel in S_7I^+ (2, 3). The rather large standard deviations found for S_7Br^+ data do not allow a meaningful detailed comparison of the two structures. However, the average sulphur–sulphur bond distances and angles within the sulphur rings in S_7I^+ and S_7Br^+ are very similar (S_7I^+ in S_7ISbF_6, 2.095 Å, 105.5°; S_7Br^+, 2.09 Å, 104.1°; compare S_7, 2.066 Å, 104.95° (24)). It is noteworthy that the S_7X^+ unit has been identified in the crystal structures of $(S_7Br)_4S_4(AsF_6)_2$, S_7IMF_6 (M = As, Sb) (2, 3), $[(S_7I)_2I][SbF_6]_3 \cdot 2AsF_6$ (4, 5), and in $S_{19}(AsF_6)_2$ (16), whereas there is no evidence (3) for S_8X^+. Reasons why this might be the case have been suggested (3).

The S_4^{2+} cation is square and planar as is $S_4(AsF_6)_2 \cdot 0.6SO_2$ (6), and $(S_7I)_4S_4(AsF_6)_6$ (4, 6), with an S(8)—S(8') distance of 1.95(2) Å, not significantly different from those found in $S_4(AsF_6)_2 \cdot 0.6SO_2$ (2.015(3), 2.013(3) Å), and $(S_7I)_4S_4(AsF_6)_6$ (1.98(1) Å).[1]

[1] Complete set of data, which includes tables of anisotropic thermal parameters, torsional angles, and dihedral angles in S_7Br^+, and observed and calculated structure factors, may be obtained at a nominal charge, upon request, from the Depository of Unpublished Data, CISTI, National Research Council of Canada, Ottawa, Ont., Canada K1A 0S2.

Acknowledgement

We wish to thank the Natural Sciences and Engineering Research Council of Canada for financial support.

1. G. SUTHERLAND. Ph.D. Thesis. University of New Brunswick. 1981.
2. J. PASSMORE, P. TAYLOR, T. K. WHIDDEN, and P. S. WHITE. J. Chem. Soc. Chem. Commun. 689 (1976).
3. J. PASSMORE, G. SUTHERLAND, P. TAYLOR, T. K. WHIDDEN, and P. S. WHITE. Inorg. Chem. **20**, 3839 (1981) and references therein.
4. J. PASSMORE and G. SUTHERLAND. Inorg. Chem. **21**, 2717 (1982).
5. J. PASSMORE, G. SUTHERLAND, and P. S. WHITE. J. Chem. Soc. Chem. Commun. 901 (1979).
6. J. PASSMORE, G. SUTHERLAND, and P. S. WHITE. J. Chem. Soc. Chem. Commun. 330 (1980).
7. J. PASSMORE, G. SUTHERLAND, T. K. WHIDDEN, and P. S. WHITE. J. Chem. Soc. Chem. Commun. 289 (1980).
8. P. S. MAGEE. Sulphur in organic and inorganic chemistry. Vol. 1. *Edited by* A. Senning. Marcel Dekker Inc., New York. 1971. p. 261.
9. J. PASSMORE, E. K. RICHARDSON, and P. TAYLOR. Inorg. Chem. **17**, 1681 (1978).
10. J. PASSMORE and P. TAYLOR. J. Chem. Soc. Dalton Trans. 804 (1976).
11. P. MAIN, M. M. WOOLFSON, and G. GERMAIN. Acta Crystallogr. A**27**, 368 (1971).
12. C. H. DAUBEN and D. H. TEMPLETON. International tables for crystallography. Vol. IV. Kynoch Press, Birmingham. 1974.
13. G. M. SHELDRICK. SHELX-76 A Program for Crystal Structure Determination. Cambridge University. 1976.
14. W. A. S. NANDANA, J. PASSMORE, P. TAYLOR, D. C. N. SWINDELLS, and P. S. WHITE. J. Chem. Soc. Dalton Trans. 619 (1983).
15. R. J. GILLESPIE, J. PASSMORE, P. K. UMMAT, and O. C. VAIDYA. Inorg. Chem. **10**, 1327 (1971).
16. R. C. BURNS, R. J. GILLESPIE, and J. F. SAWYER. Inorg. Chem. **19**, 1423 (1980).
17. J. BARR, R. J. GILLESPIE, G. P. PEZ, P. K. UMMAT, and O. C. VAIDYA. J. Am. Chem. Soc. **92**, 1081 (1970).
18. R. J. GILLESPIE, W. C. LUK, and D. R. SLIM. J. Chem. Soc. Chem. Commun. 791 (1976).
19. R. C. BURNS, R. J. GILLESPIE, W. C. LUK, and D. R. SLIM. Inorg. Chem. **18**, 3086 (1979).
20. J. PASSMORE, W. A. S. NANDANA, E. K. RICHARDSON, and P. TAYLOR. J. Fluorine Chem. **15**, 435 (1980).
21. R. T. SANDERSON. Inorganic chemistry. Reinhold. 1976. p. 65.
22. R. J. HWANG and S. W. BENSON. J. Am. Chem. Soc. **101**, 2615 (1979).
23. R. STEUDEL, T. SANDOW, and R. REINHARDT. Angew. Chem. Int. Ed. **16**, 715 (1977).
24. R. STEUDEL, J. STEIDEL, J. PICKART, and F. SCHUSTER. Z. Naturforsch. **35**b, 1378 (1980).
25. F. A. COTTON and G. WILKINSON. Advanced inorganic chemistry. 3rd ed. Interscience, Toronto. 1972. p. 120.
26. J. M. RALEY, J. E. WOLLRAB, and R. W. LOVEJOY. J. Mol. Spectrosc. **48**, 100 (1973).
27. J. PASSMORE, E. K. RICHARDSON, T. K. WHIDDEN, and P. S. WHITE. Can. J. Chem. **58**, 851 (1980).
28. R. KNIEP, L. KORTE, and D. MOOTZ. Z. Naturforsch. **38**B, 1 (1983).
29. E. W. NEWAR and A. W. JACHE. J. Chem. Phys. **39**, 596 (1963).
30. C. VERRY, R. JUREK, P. GOULET, and B. LAMALLE. J. Phys. **42**, 223 (1981).
31. G. WOLMERSHAUSER, C. KRUGER, and Y.-H. TSAY. Chem. Ber. **115**, 1126 (1982).

Solid state and solution conformations of 1-(β-D-2′,3′-secoribofuranosyl)-5,6-dichlorobenzimidazole, an acyclonucleoside analogue[1]

GEORGE I. BIRNBAUM
Division of Biological Sciences, National Research Council of Canada, Ottawa, Ont., Canada K1A 0R6

RYSZARD STOLARSKI AND ZYGMUNT KAZIMIERCZUK
Department of Biophysics, Institute of Experimental Physics, University of Warsaw, 02-089 Warsaw, Poland

AND

DAVID SHUGAR
Institute of Biochemistry and Biophysics, Academy of Sciences, 02-532 Warsaw, Poland

Received September 17, 1984

GEORGE I. BIRNBAUM, RYSZARD STOLARSKI, ZYGMUNT KAZIMIERCZUK, and DAVID SHUGAR. Can. J. Chem. **63**, 1215 (1985).

The title compound crystallizes in the monoclinic space group $P2_1$ with two independent molecules in the asymmetric unit (Z = 4). The unit cell dimensions are a = 11.861(2), b = 7.897(1), c = 14.527(3) Å, β = 91.28(1)°. X-ray intensity data were measured on a diffractometer, and the crystal structure was determined by direct methods. Least-squares refinement converged at R = 0.036 for 2980 reflections. The glycosidic torsion angle [C(2)—N(1)—C(1′)—O(1′)] is 53.9° in molecule A and 129.8° in molecule B. In both molecules, the orientation of C(1′)—O(1′) to C(2′)—O(2′) is *trans*. The conformations about C(3′)—C(4′) and C(4′)—C(5′) are different in each of the two molecules. These features are compared with those of acyclonucleoside analogues with antiviral activity. The conformation in aqueous medium was examined with the aid of high-resolution ^{1}H nmr spectroscopy, and the results are compared with those obtained from the X-ray analysis.

GEORGE I. BIRNBAUM, RYSZARD STOLARSKI, ZYGMUNT KAZIMIERCZUK et DAVID SHUGAR. Can. J. Chem. **63**, 1215 (1985).

Le composé mentionné dans le titre cristallise dans le groupe d'espace $P2_1$, avec deux molécules indépendantes dans l'unité asymétrique (Z = 4). Les dimensions de la maille unitaire sont a = 11,861(2), b = 7,897(1), c = 14,527(3) Å, β = 91,28(1)°. On a mesuré les données d'intensité à l'aide d'un diffractomètre et on a déterminé la structure cristalline par des méthodes directes. Un affinement par le méthode des moindres carrés conduit à une valeur de R = 0,036 pour 2980 réflexions. L'angle de torsion glycosidique [C(2)—N(1)—C(1′)—O(1′)] est égal à 53,9° dans la molécule A et 129,8° dans la molécule B. Dans chacune des molécules, l'orientation de C(1′)—O(1′) à C(2′)—O(2′) est *trans*. Les conformations autour de C(3′)—C(4′) et C(4′)—C(5′) sont différentes dans chacune des deux molécules. On compare ces caractéristiques avec celles d'analogues acyclonucléosides possédant une activité antivirale. On a étudié la conformation en solution aqueuse en faisant appel à la rmn du ^{1}H à haute résolution et on a comparé les résultats avec ceux obtenus par diffraction des rayons X.

[Traduit par le journal]

Introduction

The 2′,3′-dialdehyde derivatives of ribonucleosides and ribonucleotides, obtained by periodate oxidation of the parent nucleosides and nucleotides, have been reasonably well characterized (1–3) and have been employed as affinity labels in a number of enzymatic systems (4, 5). Their subsequent reduction by borohydride leads to 2′,3′-seco analogues, which differ from the parent compounds only by the absence of the C(2′)—C(3′) bond. A number of such seconucleosides (and -nucleotides) have been prepared (6) and their biological activities examined (7, 8).

The foregoing take on added significance in relation to the known antiviral activities of other acyclonucleoside analogues in which the pentose ring is replaced by an acyclic chain. Interest in these originally stemmed from reports that acyclovir (ACV) is a potent antiherpes agent (9, 10), now licensed for treatment of herpes simplex type 2 virus infections. Subsequent members of this class include, amongst many others, 9-(1,3-dihydroxy-2-propoxymethyl)guanine (DHPG, 2′NDG), with in vitro antiviral activity superior to that of acyclovir (11–13), and others with lower activities, e.g. 9-(2,3-dihydroxypropyl)adenine (DHPA) (14), 9-(2,3-dihydroxy-1-propoxymethyl)guanine (DHPMG) (15, 16), and 9-(3,4-dihydroxybutyl)guanine (DHBG) (17).

Although the flexibility of the acyclic chains of these analogues would be expected to lead to equilibrium mixtures of conformers in solution, they are all capable of adopting conformations resembling a portion of the pentose rings, a factor

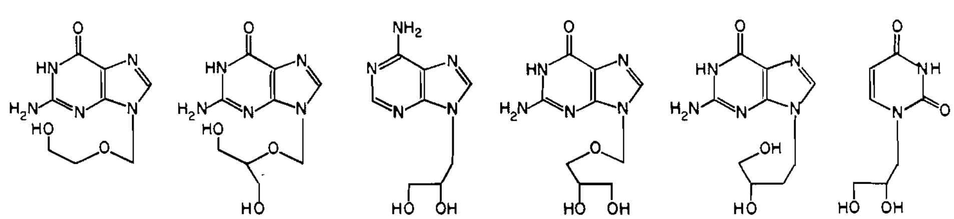

ACV DHPG DHPA DHPMG DHBG DHPU

[1] NRCC No. 24008.

which undoubtedly plays a role in their biological activities (18) and, in particular, in their reactions with enzyme systems involved in such activities. For example, yeast tRNA^{Phe}, in which the 3′-terminal AMP residue has been converted to the 2′,3′-seco form by oxidation–reduction, readily undergoes aminoacylation (19). Since it is the 3′-hydroxyl which is specifically aminoacylated in the unmodified tRNA (20), it may be inferred that the stereochemistry of this group in the seco-tRNA is retained, at least on interaction with the enzyme.

Although little is known about preferred solution conformations, the solid state structures and conformations of several of them have been determined (21–23; Hirschfield and Hoogsteen, unpublished). During the course of an investigation (24) on structure–activity relationships of 5,6-dichloro-1-β-D-ribofuranosylbenzimidazole (DRB), a known reversible inhibitor of nuclear RNA synthesis (25, 26) some analogues of which also possess antiviral activity (27), periodate oxidation and subsequent borohydride reduction gave the 2′,3′-seco derivative of DRB (seco-DRB) in the form of crystals suitable for X-ray diffraction. We report here on the solid-state and solution conformations of this analogue of acyclonucleosides. Such data should be of relevance to some of the reported activities in biological systems of oxidized–reduced nucleosides and nucleotides. In separate studies on the biological properties of such acyclonucleosides, now in progress, we have found that 2′,3′-secoguanosine is a more effective inhibitor of purine nucleoside phosphorylase than ACV or DHPG (unpublished observations).

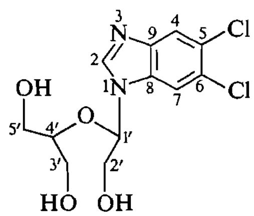

Experimental

Seco-DRB was prepared according to the general procedure described by Lerner (6) and Rosenthal *et al.* (1). To 1 g (3 mmol) of DRB, dissolved by heating in 20 mL dioxane and 40 mL water, and then cooled to room temperature, was added 0.9 g (4 mmol) KIO_4 with stirring over a period of 30 min. The mixture was stirred for an additional hour and the reaction terminated by addition of 0.6 mL of ethylene glycol. The product was then reduced by addition of 2.2 g $NaBH_4$ and stirring for 3 h. Excess borohydride was decomposed by acidification to pH 1 and the solution was then brought to neutrality and loaded on a column (6 × 30 cm) of 100/200 XAD-4. Elution was with a 0–90% aqueous methanol linear gradient. The fractions between 70 and 80% methanol were pooled and brought to dryness below 35°C under vacuum to yield 0.64 g (65%) of seco-DRB. A portion was taken up in water at 80°C (50 mg/mL) and allowed to cool slowly to give four- and five-sided plates, mp 148°C.

The ^{1}H nmr spectrum of a single crystal of seco-DRB dissolved in 0.4 mL of 99.8 at.% D_2O at 310 K was recorded at 500 MHz. A Bruker AM-500 spectrometer was used with 32 K points for the free induction decay. Chemical shifts are expressed relative to the signal for HOD, δ 4.60 ppm at 310 K, which also corresponds to 1% dioxane at δ 3.71 ppm as the external reference. Gated presaturation of the HOD resonance was employed for solvent suppression, and homonuclear decoupling was conducted in combination with suppression of the HOD signal.

X-ray precession photographs indicated space group $P2_1$. A crystal fragment measuring 0.40 × 0.40 × 0.15 mm was mounted on a CAD4 diffractometer; the crystal data are as follows:

TABLE 1. Final atomic coordinates and thermal parameters[a]

Atom	x/a	y/b	z/c	U_{eq}
N(1A)	1465(2)	5786(4)	7211(2)	330
C(2A)	539(3)	4977(5)	6846(2)	406
N(3A)	−152(2)	4395(4)	7461(2)	394
C(4A)	11(2)	4504(5)	9194(2)	379
C(5A)	688(3)	5084(4)	9907(2)	373
Cl(5A)	291(1)	4671(2)	11027(1)	608
C(6A)	1700(2)	5951(4)	9746(2)	344
Cl(6A)	2536(1)	6651	10657(1)	496
C(7A)	2055(2)	6261(4)	8872(2)	319
C(8A)	1366(2)	5686(4)	8153(2)	290
C(9A)	350(2)	4825(4)	8303(2)	327
C(1′A)	2381(2)	6615(5)	6724(2)	349
O(1′A)	1980(2)	7817(4)	6095(2)	434
C(2′A)	3057(3)	5368(5)	6165(2)	446
O(2′A)	3649(2)	4211(4)	6730(2)	504
C(3′A)	1801(3)	10274(5)	7155(3)	437
O(3′A)	2798(2)	11099(3)	6880(2)	532
C(4′A)	1286(2)	9167(4)	6408(3)	396
C(5′A)	1046(4)	10113(6)	5504(3)	553
O(5′A)	250(3)	11399(5)	5567(3)	652
N(1B)	6272(2)	8034(4)	7010(2)	332
C(2B)	5306(3)	8836(4)	6748(2)	396
N(3B)	4673(2)	9273(4)	7437(2)	427
C(4B)	4991(2)	8854(5)	9151(2)	396
C(5B)	5737(3)	8191(4)	9789(2)	382
Cl(5B)	5463(1)	8449(2)	10946(1)	553
C(6B)	6722(2)	7363(4)	9523(2)	350
Cl(6B)	7632(1)	6486(1)	10344(1)	447
C(7B)	7011(2)	7216(4)	8605(2)	335
C(8B)	6272(2)	7933(4)	7963(2)	309
C(9B)	5264(2)	8726(4)	8220(2)	352
C(1′B)	7094(2)	7313(4)	6385(2)	326
O(1′B)	7353(2)	5652(3)	6632(1)	321
C(2′B)	8221(3)	8255(4)	6415(2)	392
O(2′B)	8145(2)	9828(4)	5971(2)	475
C(3′B)	6231(3)	3811(5)	5639(2)	383
O(3′B)	5293(2)	2700(4)	5574(2)	484
C(4′B)	6443(2)	4442(4)	6619(2)	313
C(5′B)	6806(3)	3098(5)	7300(2)	402
O(5′B)	7862(2)	2375(3)	7083(2)	464

[a] All values were multiplied by 10^4.

$C_{12}H_{14}N_2O_4Cl_2$ fw = 321.2
Monoclinic, a = 11.861(2), b = 7.897(1), c = 14.527(3) Å, β = 91.28(1)°, V = 1360.35 Å^3, ρ_c = 1.57 g cm^{-3}, Z = 4 (20°C; MoKα_1, λ = 0.70930 Å); F(000) = 664, μ(MoKα) = 4.9 cm^{-1}.

Intensities were measured with monochromatized MoKα radiation, using ω/2θ scans with variable scan ranges and speeds. There were 3506 unique reflections with 2θ ≤ 56°; of those, 2985 had $I \geq 3\sigma(I)$ and were considered observed. The intensities were corrected for Lorentz and polarization factors; absorption corrections were considered unnecessary.

The structure was determined by direct methods with the aid of the computer program MULTAN78 (28). Of the 12 starting sets subjected to tangent refinement, the solution with the highest combined figure of merit yielded an E map on which 37 of the 40 nonhydrogen atoms in the asymmetric unit (two independent molecules, labelled A and B) could be located. The other three atoms were found on difference Fourier maps. The atomic parameters of these atoms were refined by block-diagonal least squares with anisotropic temperature parameters. All hydrogen atoms were located on difference Fourier maps and most were refined with isotropic temperature parameters. The atomic parameters of H(5″A) and the temperature parameters of seven other hydrogen atoms were not refined. The scattering factors were taken

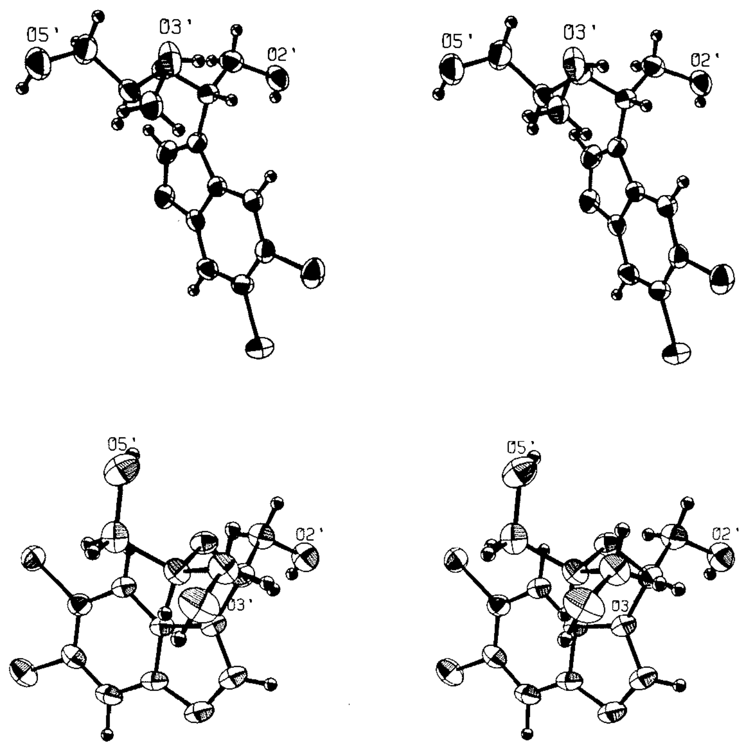

FIG. 1. Stereoscopic views of molecules A (top) and B (bottom) of seco-DRB; the thermal ellipsoids correspond to 50% probability.

from the International Tables for X-Ray Crystallography (29) and the chlorine curve was corrected for anomalous dispersion. Throughout the refinement the function $\Sigma w(|F_o| - |F_c|)^2$ was minimized and a factor of 0.8 applied to all shifts. The following weighting scheme was used during the final stages: $w = w_1 \cdot w_2$, where $w_1 = 1$ for $|F_o| \leq 20$, $w_1 = 20/|F_o|$ for $|F_o| > 20$; and $w_2 = \sin^2\theta/0.2$ for $\sin^2\theta < 0.2$, $w_2 = 1$ for $\sin^2\theta \geq 0.2$. This scheme made the average values of $w(\Delta F^2)$ independent of $|F_o|$ and $\sin^2\theta$. After the final cycle the average parameter shift equalled 0.1σ and the largest one 0.4σ. The conventional residual index R is 0.036 and the weighted index R' is 0.043 for 2980 reflections (five reflections suffered from extinction and were given zero weights). A final difference Fourier map showed no significant features. The coordinates of nonhydrogen atoms are listed in Table 1. Anisotropic temperature parameters, hydrogen atom parameters, deviations of atoms from mean planes, and a list of observed and calculated structure factors are available.[2] Stereoscopic views of the two molecules are shown in Fig. 1.

Results and discussion

Benzimidazole moieties

In molecule A all atoms of the benzimidazole ring system are coplanar, the largest deviation from planarity (for C(2)) being 0.010(4) Å. Cl(6) lies in the mean plane but Cl(5) and C(1′) are displaced from it by 0.039(1) and 0.029(4) Å, respectively. In molecule B the imidazole ring is perfectly planar but the benzene ring has the shape of a shallow boat with C(5) and C(8) deviating from the mean plane by 0.013(4) and 0.011(3) Å, respectively. The displacements of the substituents are larger than in molecule A.

Most bond lengths and bond angles (Fig. 2) in the two molecules are in excellent agreement. The differences between the exocyclic angles at N(1) are undoubtedly due to the different conformations of the acyclic sugar moiety (see below), but there does not appear to be a reasonable explanation for the difference in the C(6)—C(7) bond length. Details of the geometry may be compared with values observed in unsubstituted benzimidazoles (30–32) and in two riboside derivatives (33, 34). A striking feature is the absence of symmetry in both groups of compounds. In the solid state, only one tautomer of the imidazole ring is observed, leading to asymmetry about a

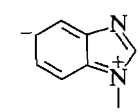

line passing through C(2) and bisecting C(5)—C(6). Furthermore, there is no symmetry in the benzene rings, even in unsubstituted benzimidazoles. After averaging the bond lengths, we see that the longest ones are C(5)—C(6), C(8)—C(9), and C(7)—C(8). The shortest bond is C(6)—C(7), followed by C(4)—C(9). These results appear to indicate that, of the various charged resonance forms of benzimidazole, the one shown below is the most significant. The distribution of bond angles is also asymmetric. Thus, C(6)—C(7)—C(8) is the smallest angle in the benzene ring, C(9)—C(4)—C(5) being the next smaller one. The same pattern is also observed in some substituted benzimidazoles (33, 34). Cl substitution of the benzene ring would be expected to deform the bond angles by up to 1.2° (35) but disubstitution of two *ortho* atoms almost cancels this effect.

Sugar moieties

The conformation of the acyclic sugar moiety (Fig. 3) is different in each of the two molecules. The glycosidic torsion angle [C(2)—N(1)—C(1′)—O(1′)] is in the *syn* range in molecule A and in the *anti* range in molecule B. In each case an N—C bond is *gauche* to the C(1′)—O(1′) and the C(1′)—C(2′) bonds, while another N—C bond almost eclipses

[2]These tables may be obtained, at a nominal charge, from the Depository of Unpublished Data, CISTI, National Research Council of Canada, Ottawa, Ont., Canada K1S 0S2.

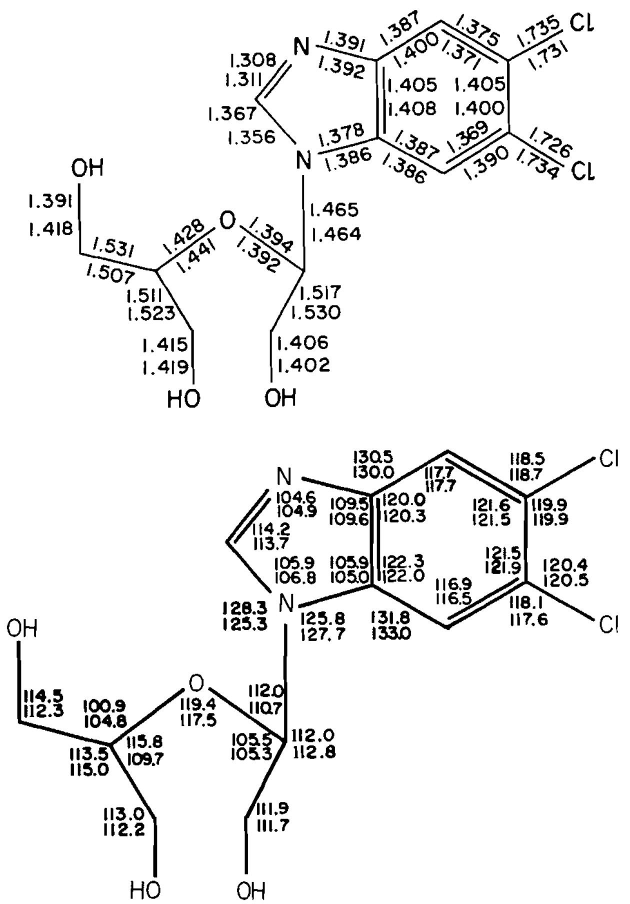

FIG. 2. (Top) Bond distances (in ångströms); their estimated standard deviations (esd's) are 0.003–0.005 Å, except for C(4′)—C(5′) and C(5′)—O(5′) in molecule A (0.006 Å). (Bottom) Bond angles (in degrees); their esd's are 0.2–0.3°. The upper and lower values refer to molecules A and B, respectively.

the C(1′)—H(1′) bond. It should be noted that in both molecules the O(1′)—C(1′)—N(1)—C torsion angle is smaller than C(2′)—C(1′)—N(1)—C. These are clearly the most stable conformations; their equivalence is illustrated by identical C(8)···H(1′) (mol. A) and C(2)···H(1′) (mol. B) distances (2.55–2.56 Å). We would predict that these conformations will be found in other acyclonucleoside analogues in which C(1′) is a tertiary carbon atom. On the other hand, in those analogues in which C(1′) is secondary, as in acyclovir (21), DHPG (Hirschfield and Hoogsteen, unpublished), *S*- and *RS*-DHPA (22), and in a derivative of 1-(2,3-dihydroxypropyl) uracil (DHPU) (23) the conformation about N—C(1′) is such that the C(1′)—X bond (where X is O(1′) or C(2′)) is approximately perpendicular (90 ± 20°) to the aglycon.

The orientation of the aglycon with respect to the sugar moiety appears unusual (Fig. 1), but a 120° rotation about the C(1′)—O(1′) bond brings about a conformation normal for β-nucleosides. In both molecules C(2′)—O(2′) is *trans* to C(1′)—O(1′). This is the conformation which is observed in ribofuranose rings with a C(2′)-*endo* pucker. C(3′)—O(3′) is *gauche*$^+$ with respect to C(4′)—O(1′) in molecule A and *trans* in molecule B. These conformations correspond to C(3′)-*endo* furanose rings with *xylo* and *ribo* configurations, respectively. Finally, C(5′)—O(5′) is *gauche*$^-$ to C(3′)—C(4′) in molecule A and *gauche*$^+$ in molecule B. Thus, of the six O—C—C—O interactions in the two molecules, four are found in *trans* and two in *gauche* conformations. As pointed out recently (18, 36), the *gauche* effect (37) is rather weak for C—O/C—O interactions and can be easily overcome by intermolecular hydrogen bonds or other packing forces. Nevertheless, its influence should become apparent when one surveys a large number of structures, because the effects of packing forces would be largely cancelled out. In the 1984 Cambridge Structural Database (38) we found 231 O—CH_2—CR_2—O fragments for which we calculated the O—C—C—O torsion angles. In the absence of the *gauche* effect, we would expect the *trans* rotamer, in which steric interactions are reduced, to be preferred over the two *gauche* conformers. In fact, we found only 53 *trans* rotamers, which confirms the existence, but also the weakness, of the *gauche* effect. These results are in general agreement with the observation of both *trans* and *gauche* conformations of C—OH bonds in acyclic polyols (39).

Most bond lengths in the two molecules are in very good agreement (Fig. 2), the only significant differences being at C(4′)—C(5′) and C(5′)—O(5′). The latter is most likely attributable to the different thermal parameters of O(5′). It is noteworthy that in this acyclic moiety C(1′)—O(1′) is significantly shorter than O(1′)—C(4′), a phenomenon generally observed in nucleosides. The bond angles at C(1′), C(2′), and C(3′) are not only the same in both molecules but also quite similar to those observed in ribofuranose rings. On the other hand, the angles at O(1′), C(4′), and C(5′) are different in both respects. C(1′)—O(1′)—C(4′) is unusually large, significantly larger than in acyclovir and in DHPG. It is possible that short intramolecular contacts between H(1′) and H(3′), 2.24–2.25 Å, are responsible for this (see Fig. 1). The differences between the angles at C(4′) are probably attributable to the different conformations about C(3′)—C(4′) and C(4′)—C(5′) (Fig. 3).

Hydrogen bonding and packing

Each molecule has three hydroxyl protons capable of participating in hydrogen bonds. The network formed by these bonds can be described as follows:

O(5′A)—H···O(2′B)—H···O(5′B)—H···N(3A)
O(3′B)—H···O(2′A)—H···O(3′A)—H···N(3B)

The geometry of the hydrogen bonds is given in Table 2. As commonly observed in X-ray analyses, the O—H bonds appear shorter than their real length. By extending the covalent bond lengths to their nominal value of 0.97 Å one obtains corrected H···*A* distances which reflect more accurately the strengths of these hydrogen bonds. The strongest bonds are seen to be those in which the proton donor also acts as an acceptor, a phenomenon known as the cooperativity effect (40). The O(2′B)—H···O(5′B) bond is unusually strong, particularly since it is part of a very short chain.

The molecules are packed so as to form pleated sheets, consisting of hydrophobic benzimidazole rings in molecules A and B and extending along *x* (Fig. 4). The dihedral angle between adjacent benzimidazoles is 121.4°. Located between the hydrophobic sheets are hydrophilic regions consisting of the carbohydrate moieties. The packing is stabilized by the hydrogen bond network described above.

Solution conformation

Solution conformations of 2′,3′-seconucleosides and -nucleotides have hitherto received relatively little attention. It was originally proposed by Cramer *et al.* (41), from an examination of CPK models, that a seconucleoside molecule should have a relatively rigid acyclic chain because of the steric effects of the

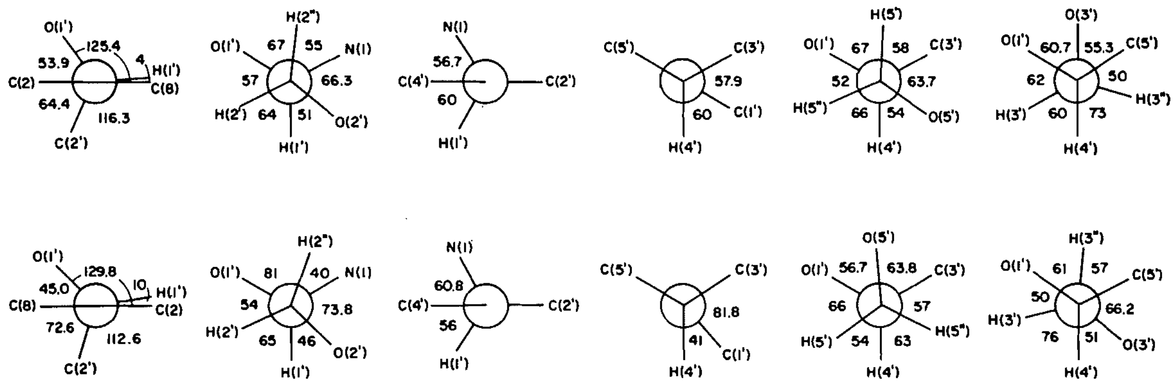

FIG. 3. Newman projections along N(1)—C(1′), C(1′)—C(2′), C(1′)—O(1′), O(1′)—C(4′), C(4′)—C(5′), and C(3′)—C(4′) in molecules A (top) and B (bottom).

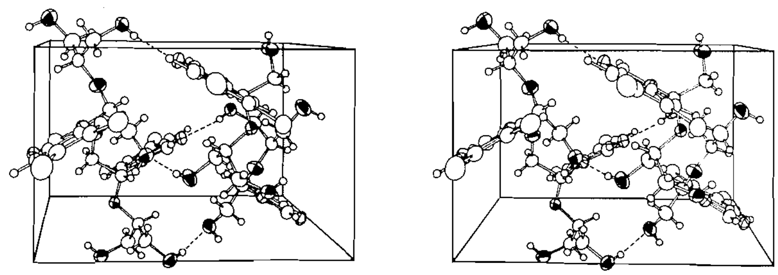

FIG. 4. Stereoscopic view of the molecular packing in the crystal.

TABLE 2. Distances and angles for hydrogen bonds

D A	A at	Distances, Å $D\cdots A$	$H\cdots A$	$H\cdots A_{corr}$	Angles, deg D—$H\cdots A$
O(5′A)—H···O(2′B)	$-1+x, y, z$	2.861	1.93	1.90	169
O(2′B)—H···O(5′B)	$x, 1+y, z$	2.607	1.74	1.65	168
O(5′B)—H···N(3A)	$1+x, y, z$	2.888	2.12	1.92	175
O(3′B)—H···O(2′A)	x, y, z	2.862	2.04	1.90	170
O(2′A)—H···O(3′A)	$x, -1+y, z$	2.668	1.90	1.75	157
O(3′A)—H···N(3B)	x, y, z	2.758	2.07	1.82	162

additional hydrogens at C(2′) and C(3′). However, a subsequent examination of the ^{1}H nmr spectra of the seco-nucleotides derived from AMP and ATP (19) led to the conclusion that free rotation about the C(1′)—C(2′) bond is possible. An analogous conclusion was arrived at by Lowe and Beechey (2) from an analysis of the 360-MHz ^{1}H spectrum of seco-ATP. These authors further proposed that similar free rotation is possible about the C(3′)—C(4′) bond. However, only the H(1′) and H(2′) signals were resolved in the foregoing investigations, and no attempts were made to determine relative rotamer populations.

The conformation of seco-DRB in solution was examined with the aid of ^{1}H nmr spectroscopy. A 500-MHz spectrum of an aqueous solution yielded chemical shifts and coupling constants listed in Table 3. The population values of the staggered rotamers about the three C—C bonds in the acyclic moiety (Fig. 5) were evaluated from the Karplus relation, assuming a dynamic equilibrium between conformers and using the relationship with six parameters (three substituents other than protons on each C—C fragment) proposed by Haasnoot *et al.* (42). The proton–proton torsion angles were assumed to be ±60° or 180°. For each bond one can calculate rotamer populations for both the possible assignments of the AB protons in an ABX system. The results of these calculations are given in Table 4. While we cannot determine which of the two sets is the correct one, we can compare these values with the results of the X-ray analysis (Fig. 3) which, fortuitously, established the conformation of two independent molecules. In the case of the C(1′)—C(2′) bond, the first set of values indicates a 2:1:1 distribution of the *trans*, *gauche*$^+$, and *gauche*$^-$ rotamers, respectively, while the second one points to a preference of *gauche*$^+$. The X-ray analysis revealed a *trans* conformation in both molecules. For the C(3′)—C(4′) bond, both sets indicate a slight preference for the *gauche*$^+$ rotamer with a secondary preference for either *trans* or *gauche*$^-$. In the solid state we found one *gauche*$^+$ and one *trans* rotamer. Finally, for the C(4′)—C(5′) bond, there is a choice between equal populations of either *trans* and *gauche*$^-$ or *gauche*$^+$ and *gauche*$^-$ rotamers. In the crystal structure we observe one *trans* and one *gauche*$^-$ conformation. Thus, the first set of values in Table 4 is in better agreement with the results of the X-ray analysis than the second one. It should be pointed out that there is no dom-

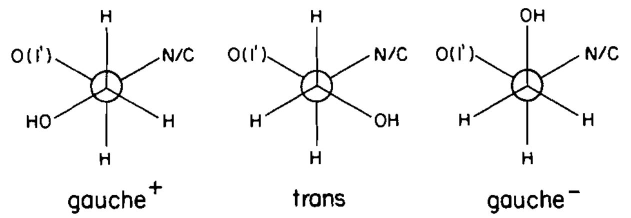

FIG. 5. *Gauche*$^+$, *trans*, and *gauche*$^-$ conformations about the C(1')—C(2'), C(3')—C(4'), or C(4')—C(5') bonds.

TABLE 3. Proton chemical shifts (in ppm) and proton–proton vicinal coupling constants (in Hz) in D_2O

H	δ(H)	H,H	J(H,H)
H(2)	8.343	1',2'	5.2, 6.3
H(4)	7.855	2',2'	−12.7
H(7)	7.927	3',3'	−12.3
H(1')	5.905	3',4'	3.8, 5.6
H(2')	4.049, 3.965	4',5'	6.0, 4.3
H(3')	3.772, 3.673	5',5'	−12.2
H(4')	3.56		
H(5')	3.39		

TABLE 4. Population of conformers (in %) in aqueous solution[a]

Bond	*gauche*$^+$	*trans*	*gauche*$^-$
C(1')—C(2')	26	47	27
	45	30	25
C(3')—C(4')	50	35	15
	46	11	43
C(4')—C(5')	18	40	42
	45	17	38

[a]For each bond, the values in the second row were obtained from reverse assignment of geminal AB protons.

inant conformation about any of these three bonds, indicating a relatively low energy barrier to rotation. We conclude, therefore, that the molecule can easily adopt whatever conformation is necessary for binding to an enzyme or other receptor.

We also obtained ^{1}H nmr spectra in DMSO-d_6 and in CD_3OD on a 100-MHz spectrometer. Owing to poor resolution, we were able to calculate relative populations only about the C(1')—C(2') bond. The results are in qualitative agreement with the values in Table 4.

Acknowledgements

We are very much indebted to Dr. David R. Bundle for recording the 500-MHz spectra and to Dr. Irena Ekiel for assistance with the nmr analysis. We are grateful to Dr. R. L. Tolman (Merck Sharp & Dohme Research Laboratories) for the results of the X-ray analysis of DHPG. Apart from the MULTAN system, all crystallographic calculations were carried out with programs written by Ahmed *et al.* (43). Figures 1 and 4 were drawn with the ORTEP program of Johnson (44).

1. L. P. ROSENTHAL, H. P. C. HOGENKAMP, and J. W. BODLEY. Carbohydr. Res. **111**, 85 (1982).
2. P. N. LOWE and R. B. BEECHEY. Bioorg. Chem. **11**, 55 (1982).
3. O. HOWARTH, A. S. JONES, R. T. WALKER, and P. G. WYATT. J. Chem. Soc. Perkin Trans. 2, 261 (1984).
4. S. B. EASTERBROOK-SMITH, J. C. WALLACE, and D. B. KEECH. Eur. J. Biochem. **62**, 125 (1976).
5. P. K. TSAI and H. P. C. HOGENKAMP. Arch. Biochem. Biophys. **226**, 276 (1983).
6. L. M. LERNER. Carbohydr. Res. **13**, 465 (1970).
7. J. NEMEC, J. M. RHOADES, P. W. TINSLEY, T. L. AVERY, and G. S. GERMAIN. Abstracts of Papers, 186th National Meeting of the American Chemical Society, Washington, DC. MEDI 78 (1983).
8. A. J. GRANT and L. M. LERNER. Biochemistry, **18**, 2838 (1979).
9. G. B. ELION, P. A. FURMAN, J. A. FYFE, P. DE MIRANDA, L. BEAUCHAMP, and H. J. SCHAEFFER. Proc. Natl. Acad. Sci. U.S.A. **74**, 5716 (1977).
10. H. J. SCHAEFFER, L. BEAUCHAMP, P. DE MIRANDA, G. B. ELION, D. J. BAUER, and P. COLLINS. Nature (London), **272**, 583 (1978).
11. K. O. SMITH, K. S. GALLOWAY, W. L. KENNELL, K. K. OGILVIE, and B. K. RADATUS. Antimicrob. Agents Chemother. **22**, 55 (1982).
12. W. T. ASHTON, J. D. KARKAS, A. K. FIELD, and R. L. TOLMAN. Biochem. Biophys. Res. Commun. **108**, 1716 (1982).
13. J. C. MARTIN, C. A. DVORAK, D. F. SMEE, T. R. MATTHEWS, and J. P. H. VERHEYDEN. J. Med. Chem. **26**, 759 (1983).
14. E. DE CLERCQ and A. HOLY. J. Med. Chem. **22**, 510 (1979).
15. W. T. ASHTON, L. F. CANNING, R. L. TOLMAN, J. D. KARKAS, R. LIOU, and A. K. FIELD. Abstracts of Papers, 23rd Interscience Conference on Antimicrobial Agents and Chemotherapy, Las Vegas, NV. Abstract No. 146 (1983).
16. T. S. LIN and M. C. LIU. Tetrahedron Lett. **25**, 905 (1984).
17. A. LARSSON, B. F. OEBERG, S. ALENIUS, C. E. HAGBERG, N. G. JOHANSSON, B. LINDBORG, and G. B. STENING. Antimicrob. Agents Chemother. **23**, 664 (1983).
18. G. I. BIRNBAUM and D. SHUGAR. *In* Topics in nucleic acid structure. Part 3. *Edited by* S. Neidle. Macmillan, London. 1985.
19. F. VON DER HAAR, E. SCHLIMME, M. GÓMEZ-GUILLEN, and F. CRAMER. Eur. J. Biochem. **24**, 296 (1971).
20. J. SONNENBICHLER, H. FELDMANN, and H. G. ZACHAU. Hoppe-Seyler's Z. Physiol. Chem. **341**, 249 (1965).
21. G. I. BIRNBAUM, M. CYGLER, and D. SHUGAR. Can. J. Chem. **62**, 2646 (1984).
22. G. S. D. KING and L. SENGIER. J. Chem. Res. Synop. 121 (1981).
23. P. M. KAISER and H. J. LINDNER. *In* Nucleosides, nucleotides and their biological applications. *Edited by* F. C. Alderweireldt and E. L. Esmans. University of Antwerp, Antwerpen. 1982. p. 293.
24. E. EGYHAZI, A. OSSOINAK, U. TAYIP, Z. KAZIMIERCZUK, and D. SHUGAR. Biochim. Biophys. Acta, **697**, 213 (1982).
25. P. B. SEHGAL and I. TAMM. Biochem. Pharmacol. **27**, 2475 (1978).
26. R. ZANDOMENI, B. MITTLEMAN, D. BUNICK, S. M. ACKERMAN, and R. WEINMANN. Proc. Natl. Acad. Sci. U.S.A. **79**, 3167 (1982).
27. A. DIWAN, C. N. GOWDY, R. K. ROBINS, and W. H. PRUSOFF. J. Gen. Virol. **3**, 393 (1968).
28. P. MAIN, S. E. HULL, L. LESSINGER, G. GERMAIN, J. P. DECLERCQ, and M. M. WOOLFSON. MULTAN78, University of York, England, and University of Louvain, Belgium. 1978.
29. International Tables for X-ray Crystallography. Vol. IV. Kynoch Press, Birmingham. 1974.
30. C. J. DIK-EDIXHOVEN, H. SCHENK, and H. VAN DER MEER. Cryst. Struct. Commun. **2**, 23 (1973).
31. A. ESCANDE and J. L. GALIGNÉ. Acta Crystallogr. Sect. B, **30**, 1647 (1974).
32. A. QUICK and D. J. WILLIAMS. Can. J. Chem. **54**, 2482 (1976).
33. S. SPRANG and M. SUNDARALINGAM. Acta Crystallogr. Sect. B, **29**, 1910 (1973).
34. Z. RUZIĆ-TOROS. Acta Crystallogr. Sect. B, **35**, 1277 (1979).

35. R. NORRESTAM and L. SCHEPPER. Acta Chem. Scand. Ser. A, **35**, 91 (1981).
36. G. I. BIRNBAUM, M. CYGLER, K. A. WATANABE, and J. J. FOX. J. Am. Chem. Soc. **104**, 7626 (1982).
37. S. WOLFE. Acc. Chem. Res. **5**, 102 (1972).
38. F. H. ALLEN, S. BELLARD, M. D. BRICE, B. A. CARTWRIGHT, A. DOUBLEDAY, H. HIGGS, T. HUMMELINK, B. G. HUMMELINK-PETERS, O. KENNARD, W. D. S. MOTHERWELL, J. R. RODGERS, and D. G. WATSON. Acta Crystallogr. Sect. B, **35**, 2331 (1979).
39. S. J. ANGYAL and R. LE FUR. Carbohydr. Res. **126**, 15 (1984).
40. G. A. JEFFREY and J. MITRA. Acta Crystallogr. Sect. B, **39**, 469 (1983).
41. F. CRAMER, F. VON DER HAAR, and E. SCHLIMME. FEBS Lett. **2**, 136 (1968).
42. C. A. G. HAASNOOT, F. A. A. M. DE LEEUW, and C. ALTONA. Tetrahedron, **36**, 2783 (1980).
43. F. R. AHMED, S. R. HALL, M. E. PIPPY, and C. P. HUBER. J. Appl. Crystallogr. **6**, 309 (1973).
44. C. K. JOHNSON. ORTEP II Report ORNL-5138, Oak Ridge National Laboratory, Oak Ridge, TN.

Structure–sweetness relationships for fructose analogs. Part II. Synthesis and properties of 1,6-dihydroxy-2-hexanone, a simple analog of the ketohexoses, and X-ray structure determination of the corresponding dianhydrides

WALTER A. SZAREK, OLIVIER R. MARTIN, AND ROBERT J. RAFKA
Carbohydrate Research Institute and Department of Chemistry, Queen's University, Kingston, Ont., Canada K7L 3N6

AND

T. STANLEY CAMERON
Department of Chemistry, Dalhousie University, Halifax, N.S., Canada B3H 4J3

Received March 9, 1984[1]

WALTER A. SZAREK, OLIVIER R. MARTIN, ROBERT J. RAFKA, and T. STANLEY CAMERON. Can. J. Chem. **63**, 1222 (1985).

Labile 1,6-dihydroxy-2-hexanone (**4**) was prepared from the corresponding triol by selective di-*O*-tritylation, Collins oxidation, and careful detritylation of the resulting keto compound **3** under mild, acidic conditions. As shown by its ^{1}Hmr and ^{13}Cmr spectra, **4** exists as a 3:2 mixture of open-chain and cyclic forms, respectively, at equilibrium in deuterium oxide (25°C). Upon standing, **4** is slowly converted into a hemiacetalic dimer. Under acidic conditions, dehydrative dimerization takes place to give the corresponding tricyclic dianhydride, one or both of the possible isomers (1:1 mixture) of which being formed according to the presence or absence of water in the medium. The structure (*trans*) of the thermodynamic isomer **5** was firmly established by an X-ray crystallographic analysis.

WALTER A. SZAREK, OLIVIER R. MARTIN, ROBERT J. RAFKA et T. STANLEY CAMERON. Can. J. Chem. **63**, 1222 (1985).

La dihydroxy-1,6-hexanone-2 (**4**), un analogue simple et relativement instable des cétohexoses, a été préparée à partir du triol correspondant par di-*O*-tritylation sélective, oxidation de Collins, et détritylation acido-catalysée du composé cétonique protégé **3** dans des conditions très douces. D'après les spectres de rmn (^{1}H, ^{13}C), les deux formes tautomères ouverte et cyclique de **4** sont présentes en proportion 3:2 à l'équilibre dans l'eau lourde (25°C). Au repos, le composé **4** se transforme peu à peu en un dimère hémiacétalique. En milieu acide, **4** subit une dimérisation déshydratante pour conduire au dianhydride tricyclique correspondant, ce dernier étant obtenu sous la forme d'un seul ou des deux isomères possibles selon que le milieu contient de l'eau ou non. La structure (*trans*) de l'isomère thermodynamique **5** est établie sans ambiguité par une analyse cristallographique aux rayons X.

Introduction

In continuation of our studies related to the origin of the high sweet taste of D-fructose (1), we turned our attention to a very simple analog of the ketohexoses, namely 1,6-dihydroxy-2-hexanone, or 2-hydroxy-2-(hydroxymethyl)tetrahydropyran in its cyclic, hemiacetalic form. This compound was of interest because of the fact that, according to Shallenberger (2) and Kier (3), it contains, in its cyclic form, only the AH, B, γ (OH, CH_2OH, 6-CH_2) unit considered as the major site of binding of

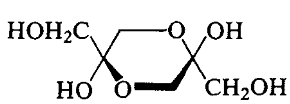

I

D-fructose with the sweet taste receptor, and because of the fact that, according to Birch (4), it should be able to "polarize" on the receptor, in contrast to the slightly sweet, "symmetrical" dimer of dihydroxyacetone (I). The presence of a large proportion of non-cyclic form in the constitutional equilibrium of this "trideoxyketose", however, might impose serious limitations to the validity of sweetness evaluation tests.

Previous ring-chain tautomerism studies of the simplest analogs of the ketoses (5) have established that 5-hydroxy-2-pentanone and 6-hydroxy-2-hexanone are less prone to exist in the cyclic form than the corresponding ω-hydroxyaldehydes (6), as expected from the lower reactivity of ketones as compared to aldehydes, and show a slight preference for the open-chain form in most organic solvents. If the presence of substituents on the ring stabilizes the cyclic form and increases the cyclic/open-chain ratio, the effect of a substituent (OH) at C(1) on this ratio was expected to be weak and a substantial proportion of open-chain form was anticipated for 1,6-dihydroxy-2-hexanone.

The only attempted preparation of 1,6-dihydroxy-2-hexanone has been reported by Owen and Peto (7). Ozonolysis of 2-methylene-1,6-hexanediol and treatment of the resulting ozonide with zinc and acetic acid gave a dianhydride which could not be cleaved to the expected dihydroxyketone. We describe in this article the first synthesis and the unusual properties of this "trideoxyketose" as well as an X-ray crystal structure determination of the corresponding *trans*-dianhydride **5**.

Results and discussion

The synthesis of 1,6-dihydroxy-2-hexanone (**4**) was realized in three steps from the corresponding triol **1** (Scheme 1). Commercially available **1** was selectively protected as its 1,6-di-*O*-trityl ether **2** and the secondary alcohol function of **2** oxidized, using $CrO_3 \cdot 2py - CH_2Cl_2$ (8), to the crystalline keto derivative **3** in excellent yield. The first attempts of detritylation of **3** rapidly revealed the unstable nature of **4**, and its formation from **3** constitutes the critical step of the synthesis. Catalytic hydrogenation of **3** did not give any satisfactory result, and the trityl groups of **3** had to be removed by acid-catalyzed hydrolysis. The best results were obtained by treating **3** in 7:2 (v/v) 1,4-dioxane – water (clear solution of **3**) with trifluoroacetic acid (final concentration ~6% (v/v)) at 55°C for 2 h, after which time the analysis of the mixture showed the presence of the expected product and triphenylcarbinol only. Upon processing under the mildest conditions (complete neutralization of the mixture with a basic ion-exchange resin before

[1] Revision received November 28, 1984.

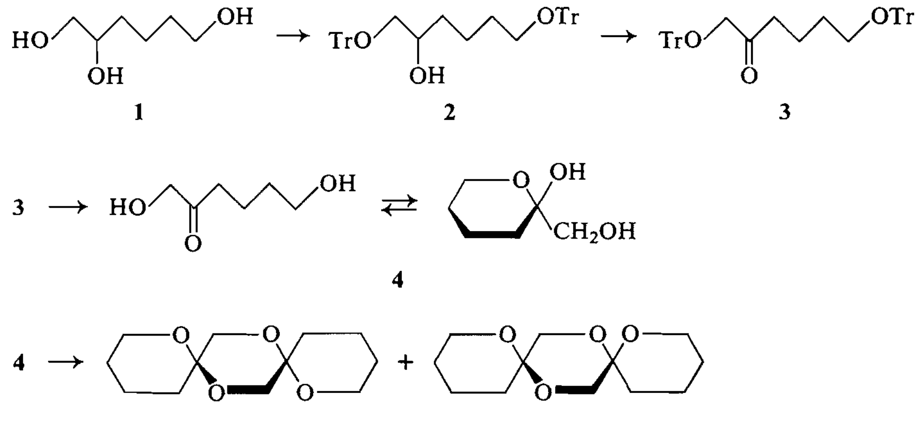

SCHEME 1

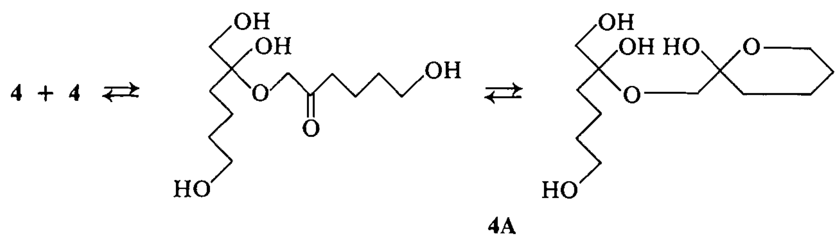

SCHEME 2

any other operation is essential), homogeneous **4** could be isolated in 62% yield. Rapid chromatography on silica gel gave a very pure sample of syrupy 1,6-dihydroxy-2-hexanone (**4**).

The difficulties in obtaining clean detritylation of **3** arise mainly from the high tendency of **4** to form a tricyclic dianhydride under acidic conditions. Thus, for example, treatment of **3** with 80% acetic acid at reflux temperature gave a mixture of **4**, the dianhydride **5**, and two other compounds of intermediate mobility (tlc) which disappeared after addition of an aqueous base (most probably the 2-acetate of **4** and another acylhemiacetal); **4** and **5** were isolated in yields of 45% and 11%, respectively.

The complete dehydrative dimerization of **4** could be achieved, for example, in anhydrous 1,4-dioxane in the presence of trifluoroacetic acid; under these conditions, the two possible isomers **5** and **6** were formed in a 1 : 1 ratio, the former *trans*-isomer being identical to the dianhydride reported by Owen and Peto (7).

Finally, upon standing, 1,6-dihydroxy-2-hexanone (**4**) was found to give slowly, among other minor products, a slightly faster-moving (tlc) compound which was separated from the original material by column chromatography. Upon treatment with an aqueous acid, this compound yielded immediately and quantitatively the starting **4**, a behavior consistent with the dimeric, hemiacetalic constitution **4A** (Scheme 2).

Structural analysis

The ^{1}Hmr spectral analysis of **4** showed that the open-chain, keto form is slightly preponderant (55%) in deuterated dimethylsulfoxide, as in the case of 6-hydroxy-2-hexanone (5). However, the behavior of **4** in water is very different; as shown by the ^{1}Hmr spectrum, the proportion of the cyclic form of **4** is appreciable (40%), whereas no hemiacetalic form was observed for 6-hydroxy-2-hexanone in aqueous medium. The ^{13}Cmr spectrum of **4** in deuterium oxide is given in Fig. 1. The higher polarity of 2-hydroxy-2-(hydroxymethyl)tetrahydropyran as compared to 2-hydroxy-2-methyltetrahydropyran does not seem to be a sufficient reason to account for this result, no difference being observed between the two hydroxyketones in polar solvents such as dimethylsulfoxide; favorable hydrogen bonding with the solvent, involving a proton-donor and a proton-acceptor group, might also be a factor stabilizing the cyclic form of 1,6-dihydroxy-2-hexanone in water.

The electron-impact mass spectrum of **4** exhibits two major fragmentations which are driven by the high stability of the (di)oxonium cations derived from its cyclic form (see Scheme 3).

The tricyclic dianhydrides of **4** are the simplest analogs of the long-known diheterolevulosans I and IV, two of the di-D-fructose dianhydrides obtained by the action of concentrated acid on D-fructose (9, 10). The 1,4-dioxane ring of the C_i-symmetrical *trans*-isomer (see **5**, *trans*) is expected to adopt a stable chair conformation with both OR substituents (C(6)—O(1) and C(9)—O(10) bonds) in an axial disposition (anomeric effect, see ref. 11 for the conformation of a related di-D-fructose dianhydride) whereas the C_2-symmetrical *cis*-isomer (see **6**, *cis*) undergoes rapid interconversion between two identical chair conformers.

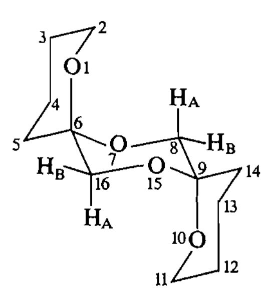

5, *trans*

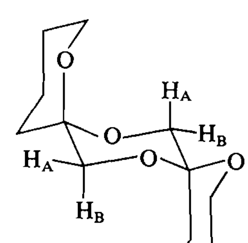

6, *cis*

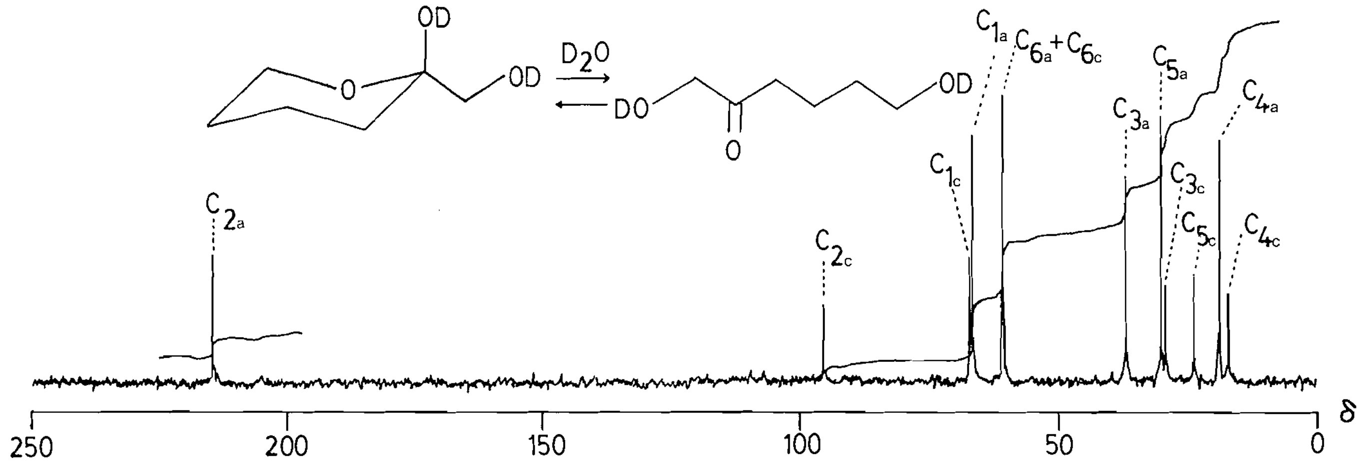

FIG. 1. ^{13}C nuclear magnetic resonance spectrum of **4** in deuterium oxide (25°C); a = acyclic, c = cyclic form.

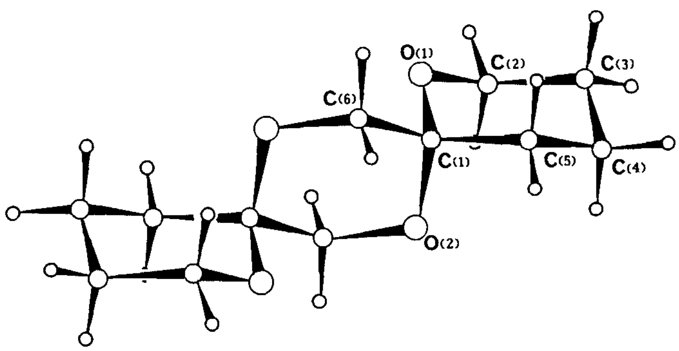

FIG. 2. Perspective view of **5** (crystallographic numbering).

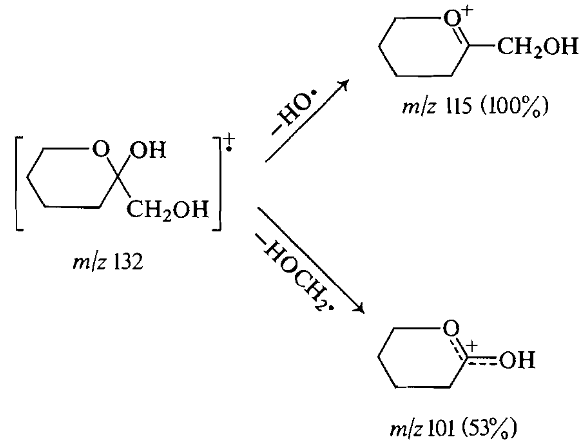

SCHEME 3

TABLE 1. Atomic coordinates (× 10^4) for compound **5**

Name	X/a	Y/b	Z/c
C(1)	464(4)	4348(3)	1305(2)
C(2)	3928(5)	3431(4)	2110(3)
C(3)	3663(5)	3346(4)	3508(3)
C(4)	2080(5)	4515(3)	3744(3)
C(5)	79(5)	4360(3)	2701(3)
C(6)	−1448(4)	3990(3)	263(3)
O(1)	1992(3)	3261(2)	1160(2)
O(2)	1185(3)	5824(2)	1065(2)

The ^{1}Hmr spectra of the two isomers are very similar and exhibit in each case a typical AB system for the two equivalent pairs of protons of the 1,4-dioxane ring. The well-resolved signals of the protons at C(2), C(11) and C(5), C(14) of the *cis*-isomer **6** indicate that the tetrahydropyran rings of the tetraoxadispirohexadecane system probably adopt the chair conformation in which the C(6)—O(7) and C(9)—O(15) bonds are axially oriented with respect to these rings, the same conformation existing in the solid state (see Fig. 2).

The relative configurations of **5** and **6** cannot be assessed on the basis of their ^{1}Hmr spectra at room temperature. Although their thermodynamic stabilities strongly suggested the *trans*-diaxial configuration of **5** (see below), their structures were firmly established by an X-ray crystallographic analysis of the highly crystalline isomer **5**. Figure 2 shows a perspective view of the molecule; the atomic parameters are documented in Tables 1–3.

X-ray crystallographic analysis of **5**

Crystallographic numbering (see Fig. 2) has been used in this Section and in Tables 1–3.

$C_{12}H_{20}O_4$ fw = 228.29

Monoclinic $P2_1/c$, $a = 6.532(1)$, $b = 8.856(3)$, $c = 10.268(4)$ Å, $\beta = 102.30(2)°$, $V = 580.33$ Å^3, $Z = 2$, $\rho_c = 1.306$ g cm^{-3} (22 ± 1°C; MoKα_1, $\lambda = 0.70926$ Å (graphite monochromator) $\mu = 0.58$ cm^{-1}), $F(000) = 248$.

A crystal of about 0.3 × 0.4 × 0.6 mm was mounted along the long axis. The cell dimensions were refined from 25 general reflections with the Bragg angle θ in the range 12–14° on a CAD4 diffractometer. 1131 reflections were measured in the range θ 2–25° of which 578 had $I > \sigma(I)$. The data were reduced to a standard scale by routine procedures (12) and were corrected for Lorentz and polarization factors but not for extinction or absorption. Reflections with E 1.2 were used to solve the structure by an application of the tangent formula that examined 4096 (2^{12}) sets of starting phases and eliminated progressively all but the most likely combinations. This procedure is part of an X-ray system written by Sheldrick (13). The positions of all but the hydrogen atoms were found on the resultant E map.

The structure was refined by full-matrix, least-squares procedures, minimizing $\Sigma w(\Delta F)^2$ with isotropic temperature factors on all the atoms. The hydrogen atoms were located from a difference Fourier synthesis when R was 0.07. Refinement continued with anisotropic temperature factors on all but the hydrogen atoms, and it converged with $R = 0.041$. The stan-

TABLE 2.[a] Interatomic distances and interbond angles for compound **5**

Atoms	Distance (Å)	Bonds	Angle (degrees)
		C(5)—C(1)—C(6)	113.5(2)
C(1)—C(5)	1.507(4)	C(5)—C(1)—O(1)	111.6(2)
C(1)—C(6)	1.496(4)	C(5)—C(1)—O(2)	106.6(2)
C(1)—O(1)	1.417(3)	C(6)—C(1)—O(1)	106.3(2)
C(1)—O(2)	1.428(3)	C(6)—C(1)—O(2)	109.1(2)
C(2)—C(3)	1.484(5)	O(1)—C(1)—O(2)	109.8(2)
C(2)—O(1)	1.431(4)	C(3)—C(2)—O(1)	112.7(3)
C(3)—C(4)	1.519(4)	C(2)—C(3)—C(4)	110.1(3)
C(4)—C(5)	1.509(4)	C(3)—C(4)—C(5)	109.9(3)
C(6)—O(2′)	1.420(3)	C(1)—C(5)—C(4)	112.4(2)
		C(1)—C(6)—O(2′)	114.2(2)
		C(1)—O(1)—C(2)	113.4(2)
		C(1)—O(2)—C(6′)	112.6(2)

[a]The transformation to generate the coordinates of the atoms of the other half of the molecule, from those given in Table 1, is $1 - x$, $-y$, $1 - z$.

TABLE 3. Selected torsional angles for compound **5**

Bonds	Angle (degrees)
C(6)—C(1)—C(5)—C(4)	172.3(2)
C(5)—C(1)—C(6)—O(2′)	171.8(2)
O(1)—C(1)—C(5)—C(4)	52.3(3)
C(5)—C(1)—O(1)—C(2)	−54.7(3)
C(5)—C(1)—O(1)—O(1)	69.1(4)
O(2)—C(1)—C(5)—C(4)	−67.6(3)
C(5)—C(1)—O(2)—C(6′)	−175.2(2)
O(1)—C(1)—C(6)—O(2′)	−65.2(3)
C(6)—C(1)—O(1)—C(2)	−179.0(2)
C(6)—C(1)—O(2)—C(6′)	−52.5(3)
O(2)—C(1)—C(6)—O(2′)	53.1(3)
O(2)—C(1)—O(1)—C(2)	63.2(3)
O(2)—C(1)—O(1)—O(1)	−172.9(2)
O(1)—C(1)—O(2)—C(6′)	63.6(3)
O(1)—C(2)—C(3)—C(4)	−56.0(4)
C(3)—C(2)—O(1)—C(1)	57.9(4)
C(2)—C(3)—C(4)—C(5)	52.6(4)
C(3)—C(4)—C(5)—C(1)	−51.4(3)
C(1)—O(2)—C(6′)—C(1′)	55.0(3)

dard deviation (σ) for each reflection was used for the weights during the refinement and the values of σ were determined from the diffractometer counting statistics.

Table 1 gives the final atomic coordinates.[2] The atomic scattering factors are taken from International Tables for X-ray Crystallography (1974). The interatomic distances, interbond angles, and torsional angles are given in Tables 2 and 3. Figure 2 shows a view of the molecule projected down *a*.

The crystal is constructed from isolated molecules of **5**, with the molecules themselves each containing a crystal symmetry center. There is no sign of disorder and thus **5** is confirmed to have the *trans* configuration. The C—C bond lengths are in the range 1.484(5)—1.519(4) Å, with C(2)—C(3) at 1.484(5) being possibly just significantly shorter than the others and with C(3)—C(4) at 1.519(4) just significantly longer. The C—O bond lengths are essentially equivalent with a range of 1.417(3)—1.431(4) Å. All three rings have the chair conformation; the torsional angles of the ring bonds in the central ring are 53.1(3), −52.5(3), and 55.0(3)° for the angles about C(6)—C(1), C(1)—O(2), and O(2)—C(6), respectively (the remaining three angles are related by the center of symmetry to the three already quoted, where they have the appropriate value with the opposite sign); the torsional angles in the external rings are −54.7(3), 57.9(4), −56.0(4), 52.6(4), −51.4(3), and 52.3(3)° for C(1)—O(1), O(1)—C(2) . . . . C(5)—C(1). In the central and external rings the mean torsional angles are ±53.5 and 54.1° which are somewhat less than ±55.9° that has been observed for cyclohexane (14).

Mechanistic aspects of dimer formation

The assignment of a labile, dimeric structure to compound **4A**, which is spontaneously formed from **4**, is supported by its chemical behaviour and by its mass spectrum, the latter being very similar to the spectrum of **4** as a consequence of a reversion of the equilibrium between the monomer and the dimer upon volatilization; however, its detailed structure is not definitely established. On the basis of the presence in its ^{1}Hmr spectrum of signals attributable to a tetrahydropyran ring (in particular, $\delta = 1.53$, td, in acetone-d_6), it would appear that the dimer **4A** is formed by the addition of the 1-OH function of one molecule of **4** to the keto group of a second molecule of **4** (see Scheme 2). This dimerization is important because it probably is the initial, reversible step for the formation of the dianhydrides of **4** in a protic medium. As shown by the behaviour of the two isomers under these conditions, **5** is the *thermodynamic* dianhydride, and the subsequent steps for its formation involve a series of reversible, internal acetalizations of a tautomer of **4A**. Thus, treatment of pure isomer **6** in 4:1 (v/v) 1,4-dioxane – water containing trifluoroacetic acid (10%) led rapidly to the disappearance of **6** and the formation of **4** and **5** (~1:1 ratio, equilibrium composition); the formation, although more slowly, of the monomer **4** from **5** was observed also under the same conditions. Furthermore, the dianhydride **6** was converted immediately into **4** and some **5** in 80% acetic acid at reflux temperature, a result which is in agreement with the exclusive formation of the thermodynamic isomer **5** during the detritylation of **3** under these conditions.

In contrast, the kinetically controlled formation of the two dianhydrides from **4** was achieved under anhydrous conditions

[2]A complete list of atomic parameters (Table 1) and a list of the structure factors (Table 3) are available from the Depository of Unpublished Data, CISTI, National Research Council of Canada, Ottawa, Ont., Canada K1A 0S2.

(trifluoroacetic acid in 1,4-dioxane); this interpretation was confirmed by the observation of the extremely slow conversion of **6** into **5** under a similar set of conditions (trifluoroacetic acid in tetrahydrofuran, less than 25% of **5** from **6** after 10 days at 20°C). A different dimerization mechanism might be involved in this case such as, for example, an initial "glycosylation" of 2-hydroxy-2-(hydroxymethyl)tetrahydropyran by a second molecule of **4** through its 1-OH group.

Because of the presence of a large proportion of the open-chain form at equilibrium in water, sweetness tests of **4**, to assess the taste of 2-hydroxy-2-(hydroxymethyl)tetrahydropyran, would be of doubtful value and have thus not been undertaken.

Experimental

Melting points were determined on a Fisher–Johns apparatus or on a Thomas Hoover capillary melting point apparatus and are uncorrected. Infrared spectra were recorded with a Perkin–Elmer 598 spectrophotometer. The nmr spectra were recorded with a Bruker CXP-200 spectrometer (^{1}H: 200 MHz, ^{13}C: 50.307 MHz) in chloroform-*d* with tetramethylsilane (TMS) as internal standard, unless otherwise stated; TMS was used as external standard for the spectra in deuterium oxide. Chemical shifts are given in parts per million downfield from TMS. Mass spectra were recorded on a Hewlett–Packard HP 5985 B gc–ms spectrometer. Thin-layer chromatography (tlc) was performed using silica gel G as the adsorbent in the following solvent systems (v/v): (A) toluene; (B) ethyl acetate; (C) toluene – ethyl acetate 2:1; (D) hexane – ethyl acetate 3:1; (E) hexane – ethyl acetate 4:1; (F) petroleum ether – acetone 2:1. The developed plates were dried and compounds located by spraying with 10% aqueous sulfuric acid containing 1% cerium sulfate and 1.5% molybdic acid, and heating at 150°C. Column chromatography was performed on silica gel 60 (70–230 mesh, Merck). 1,2,6-Hexanetriol was purchased from Aldrich and used without further purification. The term "petroleum ether" refers to the fraction of bp 30–60°C.

1,2,6-Hexanetriol 1,6-ditrityl ether (2)

To a solution of 1,2,6-hexanetriol (**1**, 0.8 g, 5.96 mmol) in dry pyridine (30 mL) was added triphenylmethyl chloride (3.65 g, 13.1 mmol, 2.2 equiv.). The mixture was stirred for 64 h at room temperature, and then poured into ice-water (100 g) and chloroform (60 mL). The organic phase was separated and the aqueous layer washed with chloroform (30 mL). The combined organic phases were washed at 0°C with 1 *N* hydrochloric acid to remove pyridine, then washed with a saturated aqueous sodium hydrogen carbonate solution (2 × 20 mL) and with water (2 × 20 mL), dried ($MgSO_4$), and concentrated. Column chromatography (solvent A; then A–B, 10:1 (v/v)) of the crude product afforded **2** (3.45 g, 94%) contaminated by a small amount of triphenylcarbinol. An analytical sample was obtained by column chromatography (solvent A–B, 50:1 (v/v)) and crystallization from ether; mp 129.5–130.5°C; R_f 0.26 (solvent A); ν_{max} (KBr): 3570, 3430 (OH), 1595, 1488, 1445, 1215, 1070, 760, 705 cm^{-1}; ^{1}Hmr δ: 1.2–1.47 (m, 4H) and 1.47–1.70 (m, 2H) (2H(3), 2H(4), 2H(5)), 2.34 (d, 1H, $J_{2,OH}$ = 3.3 Hz, exchanged in D_2O, 2-OH), 3.05 (dd, 1H, $J_{1A,1B}$ = 9.8 Hz, $J_{1A,2}$ = 7.5 Hz, H(1A)), 3.06 (t, 2H, $J_{5,6}$ = 6.1 Hz, 2H(6)), 3.21 (dd, 1H, $J_{1B,2}$ = 3.0 Hz, H(1B)), 3.73 (br m, 1H, H(2)), 7.22–7.55 (m, 30 H, $2(C_6H_5)_3C$). *Anal.* calcd. for $C_{44}H_{42}O_3$ (618.81): C 85.40, H 6.84; found: C 85.19, H 6.69.

1,6-Dihydroxy-2-hexanone ditrityl ether (3)

To a solution of dry pyridine (7.67 g, 97.0 mmol, 12 equiv.) in dry methylene chloride (125 mL) was added chromium trioxide (4.85 g, 48.5 mmol, 6 equiv.) and the mixture stirred for 30 min at room temperature. A solution of compound **2** (5.0 g, 8.08 mmol) in methylene chloride (45 mL) was then added in one portion. The reaction mixture was stirred for 17 min at room temperature, the solution decanted, and the black residue washed with ether (3 × 60 mL). The combined organic phases were washed successively with a 5% (v/v) aqueous sodium hydroxide solution (4 × 85 mL), cold 1 *N* hydrochloric acid (85 mL), a saturated aqueous sodium hydrogen carbonate solution (3 × 85 mL) and a saturated aqueous sodium chloride solution (3 × 85 mL), dried ($MgSO_4$), and concentrated. Crystallization of crude **3** from ether gave pure **3** (3.69 g, 73.9%); mp 145–147°C; R_f 0.44 (solvent A); ν_{max} (KBr): 1715 (C═O), 1595, 1490, 1450, 1220, 1070, 765, 748, 732, 713, 698 cm^{-1}; ^{1}Hmr δ: 1.64 (m, 4H, 2H(4), 2H(5)), 2.51 (br t, 2H, 2H(3)), 3.06 (br t, 2H, 2H(6)), 3.74 (s, 2H, 2H(1)), 7.16–7.50 (m, 30 H, $2(C_6H_5)_3C$). *Anal.* calcd. for $C_{44}H_{40}O_3$ (616.80): C 85.68, H 6.54; found: C 85.67, H 6.45.

1,6-Dihydroxy-2-hexanone, 2-hydroxy-2-(hydroxymethyl)tetrahydropyran (4)

Procedure A

Ketone **3** (10.5 g, 17.02 mmol) was gently heated at reflux temperature in 80% acetic acid (300 mL) for 1.5 h. The clear solution was cooled and concentrated under reduced pressure. The residue was triturated with water (150 mL) and the insoluble triphenylcarbinol derivatives removed by filtration. The aqueous solution of crude **4** was treated then with 20% sodium hydroxide (15 mL) for 0.5 h, neutralized with Dowex 50W-X8 (H^+) resin and concentrated. Column chromatography (solvent B) of the residue afforded compound **5** (205 mg, 10.5%) and pure, syrupy **4** (1.01 g, 45%).

Procedure B

To a solution of ketone **3** (1.1 g, 1.78 mmol) in 1,4-dioxane (70 mL) was added water (20 mL) and trifluoroacetic acid (5.4 mL). The mixture was stirred for 2 h at 55°C, cooled, and then neutralized with Amberlite IRA-400 (OH^-) resin; the resin and the precipitated triphenylcarbinol were removed by filtration and the filtrate concentrated. The residue was triturated with water, the resulting suspension filtered through Celite, and the filtrate concentrated to afford homogeneous and colorless **4** (146 mg, 62%); R_f 0.26 (solvent B); ν_{max} (film): 3380 (very broad, OH), 1720 (C═O), 1405, 1080, 1045 cm^{-1}; ^{1}Hmr (a = acyclic, c = cyclic form), (D_2O, 60% acyclic form) δ: 0.83–1.13 (br m, 4.8H, 2H(3c), 2H(4), 2H(5)), 1.88 (t, 1.2H, *J* = 6 Hz, 2H(3a)), 2.81 (s, 0.8H, 2H(1c)), 2.97 (t, 1.2H, *J* = 6 Hz, 2H(6a)), 3.0–3.38 (m, 0.8H, 2H(6c)), 3.74 (s, 1.2H, 2H(1a)); (DMSO-d_6, 55% acyclic form) δ: 1.31–1.61, 1.61–1.88 (m, 4.9H, 2H(3c), 2H(4), 2H(5)), 2.41 (t, 1.1H, *J* = 7 Hz, 2H(3a)), 3.19 (br t, 0.9H, 2H(1c)), 3.10–3.90 (s, DOH; several m, 2H(6)), 4.05 (d, 1.1H, $J_{1,OH}$ = 5.5 Hz, 2H(1a)), 4.41 (t, 0.55H, $J_{6,OH}$ = 5 Hz, 6a-OH), 4.59 (t, 0.45H, $J_{1,OH}$ = 6 Hz, 1c-OH), 5.06 (t, 0.55H, 1a-OH), 5.13 (s, 0.45H, 2c-OH); ^{13}Cmr (D_2O) acyclic form δ: 19.46 (C(4)), 30.77 (C(5)), 37.51 (C(3)), 61.29 (C(6)), 67.12 (C(1)), 214.45 (C(2)); cyclic form δ: 17.68 (C(4)), 24.41 (C(5)), 29.75 (C(3)), 61.44 (C(6)), 67.60 (C(1)), 95.85 (C(2)); *m/z* (%): 115 (100) ($M^{+\cdot} - HO^{\cdot}$), 101 (53) ($M^{+\cdot} - HOCH_2^{\cdot}$), 97 (51), 83 (30), 55 (29), 98 (25), 57 (13), 69 (11), 41 (10), 43 (10).

Dimer 4A

Upon standing, compound **4** was slowly converted into several new products including the dianhydride **5**. The main new compound, **4A**, was separated from **4** by column chromatography (solvent F, R_f of **4**: 0.17), syrup, R_f 0.22 (solvent F); ν_{max} (film): 3430 (OH), 1705 (C═O); *m/z* (%): 43 (100) (from residual Me_2CO), 115 (53), 101 (37), 55 (30), 58 (27) ($Me_2CO^{+\cdot}$), 97 (25), 83 (24), 41 (19), 98 (19), 100 (16), 114 (13), 57 (10).

(6R,9S and 6S,9R)-1,7,10,15-tetraoxadispiro[5,2,5,2]hexadecane (5) (trans-isomer)

The sample of compound **5** obtained during detritylation of ketone **3** (Procedure A above) was recrystallized from ether – petroleum ether; mp 163–164°C (lit. (7) mp 161°C); R_f 0.58 (solvent C), 0.29 (solvent E); ν_{max} (KBr): 1430, 1282, 1222, 1180, 1030, 935, 870 cm^{-1}; ^{1}Hmr δ: 1.34 (td, 2H) and 1.47–2.03 (several m, 10H) (2H(3), 2H(4), 2H(5), 2H(12), 2H(13), 2H(14)), 3.39 (d, 2H, J_{AB} = 11 Hz, H(8A), H(16A)), 3.70 (d and m, 6H, H(8B), H(16B), 2H(2), 2H(11)); *m/z* (%): 98 (100), 100 (18), 99 (7), 101 (7), 83 (7), 55 (7), 115 (5), 228 (4) ($M^{+\cdot}$), 70 (4), 129 (3.3). *Anal.* calcd. for $C_{12}H_{20}O_4$ (228.29): C 63.14, H 8.83; found: C 63.04, H 8.96.

(6R,9R and 6S,9S)-1,7,10,15-tetraoxadispiro[5,2,5,2]hexadecane (6) (cis-isomer)

To a solution of compound **4** (52 mg, 0.39 mmol) in 1,4-dioxane (1.1 mL) was added trifluoroacetic acid (0.11 mL) and, after 6 h at room temperature, 4 Å molecular sieves. The mixture was stirred further for 15 h, diluted with ether (10 mL), filtered, and the filtrate washed with a saturated aqueous sodium hydrogen carbonate solution (5 mL). The separated aqueous phase was washed with ether (5 mL), the combined organic phases washed with water (5 mL), dried ($MgSO_4$), and concentrated. Column chromtography (solvent D) of the residue containing **5** and **6** in an ~1:1 ratio afforded 12 mg (27%) of the faster-moving isomer **6** and 12 mg (27%) of **5**. A crystalline sample of **6** was obtained by crystallization from pentane at −15°C; mp 44.5−45°C; R_f 0.39 (solvent E); ν_{max} (KBr): 1440, 1360, 1290, 1220, 1185, 1110, 1080, 1055, 1040, 960, 895, 875 cm^{-1}; ^{1}Hmr (a = axial, e = equatorial) δ: 1.41 (td, 2H, $J_{5a,5e} = J_{14a,14e} = 13$ Hz, $J_{4a,5a} = J_{13a,14a} = 13$ Hz, $J_{4e,5a} = J_{13e,14a} = 4.3$ Hz, H(5a), H(14a)), 1.51−1.92 (m, 8H, 2H(3), 2H(4), 2H(12), 2H(13)), 2.00 (dm, 2H, H(5e), H(14e)), 3.44 (d, 2H, $J_{AB} = 12$ Hz, H(8A), H(16A)), 3.68 (d, 2H, H(8B), H(16B)), 3.70 (dm, 2H, $J_{2a,2e} = J_{11a,11e} \simeq 11$ Hz, H(2e), H(11e)), 3.92 (td, 2H, $J_{2a,3a} = J_{11a,12a} \simeq 11$ Hz, $J_{2a,3e} = J_{11a,12e} \simeq 3.5$ Hz, H(2a), H(11a)); *m/z* (%): 98 (100), 41 (18), 55 (16), 228 (15) ($M^{+\cdot}$), 114 (14), 83 (13), 43 (11), 101 (11), 115 (10), 198 (9). *Anal.* calcd. for $C_{12}H_{20}O_4$ (228.29): C 63.14, H 8.83; found: C 63.18, H 8.74.

Acknowledgements

The authors are grateful to the Natural Sciences and Engineering Research Council of Canada for its support of this work in the form of grants (to W.A.S. and T.S.C.) and to the Fonds National Suisse de la Recherche Scientifique for its award of a fellowship (to O.R.M.).

1. O. R. MARTIN, S.-L. KORPPI-TOMMOLA, and W. A. SZAREK. Can. J. Chem. **60**, 1857 (1982).
2. R. S. SHALLENBERGER. J. Food Sci. **28**, 584 (1963); New Sci. **407**, 569 (1964); Pure Appl. Chem. **50**, 1409 (1978); R. S. SHALLENBERGER and T. E. ACREE. Nature, **216**, 480 (1967); J. Agric. Food Chem. **17**, 701 (1969).
3. L. B. KIER. J. Pharm. Sci. **61**, 1394 (1972).
4. G. G. BIRCH. CRC Critical Rev. Food Sci. Nutr. **8**, 54 (1976).
5. J. E. WHITING and J. T. EDWARD. Can. J. Chem. **49**, 3799 (1971).
6. C. D. HURD and W. H. SAUNDERS. J. Am. Chem. Soc. **74**, 5324 (1952).
7. L. N. OWEN and A. G. PETO. J. Chem. Soc. 1146 (1956).
8. R. RATCLIFFE and R. RODEHORST. J. Org. Chem. **35**, 4000 (1970).
9. E. J. MCDONALD. Adv. Carbohydr. Chem. **2**, 253 (1946).
10. R. W. BINKLEY, W. W. BINKLEY, and A. A. GREY. Carbohydr. Res. **28**, 365 (1973).
11. R. U. LEMIEUX and R. NAGARAJAN. Can. J. Chem. **42**, 1270 (1963).
12. T. S. CAMERON and R. E. CORDES. Acta Crystallogr. Sect. B, **38**, 748 (1979).
13. G. M. SHELDRICK. X-ray system report. University Chemical Laboratories, Lensfield Road, Cambridge, England. 1976.
14. R. BUCOURT. *In* Topics in stereochemistry. Vol. 8. *Edited by* E. L. Eliel and N. L. Allinger. Wiley–Interscience, New York. 1974. p. 159.

Protonation of purines and related compounds in dimethylsulfoxide and water

ROBERT L. BENOIT, DANIELLE BOULET, LUC SÉGUIN, AND MONIQUE FRÉCHETTE
Département de Chimie, Université de Montréal, Montréal (Que.), Canada H3C 3V1

Received September 24, 1984

ROBERT L. BENOIT, DANIELLE BOULET, LUC SÉGUIN, and MONIQUE FRÉCHETTE. Can. J. Chem. **63**, 1228 (1985).

The ionization constants of the conjugated acids BH^+ of purine, adenine, 9-methyladenine, adenosine, guanine, and hypoxanthine, and of the related compounds imidazole, *N*-methylimidazole, benzimidazole, and 4-amino-2,6-dimethylpyrimidine have been determined potentiometrically in Me_2SO. The heats of solution and the heats of protonation of most of these bases have been obtained by calorimetry. Some additional determinations were carried out in water so that thermodynamic data in Me_2SO and in water could be compared. Our discussion of the solvent effect on these data is largely based on a consideration of the enthalpies of transfer of B and BH^+ and emphasizes the contrasting H-bonding properties of the solvents and of the functional groups on the solutes B and BH^+.

ROBERT L. BENOIT, DANIELLE BOULET, LUC SÉGUIN et MONIQUE FRÉCHETTE. Can. J. Chem. **63**, 1228 (1985).

On a déterminé par potentiométrie dans le Me_2SO les constantes d'ionisation des acides conjugués BH^+ de la purine, de l'adénine, de la méthyl-9 adénine, de l'adénosine, de la guanine et de l'hypoxanthine, et des composés voisins, imidazole, *N*-méthylimidazole, benzimidazole et amino-4 diméthyl-2,6 pyrimidine. Les chaleurs de solution et les chaleurs de protonation de la plupart de ces bases ont été obtenues par calorimétrie. Des déterminations supplémentaires ont été effectuées dans l'eau afin de pouvoir comparer les données thermodynamiques dans le Me_2SO et l'eau. Notre discussion de l'effet du solvant sur ces données est, en grande partie, basée sur une considération des enthalpies de transfert de B et BH^+ et met l'accent sur les différences au niveau des propriétés "donneur–accepteur" de liaisons-H tant avec les solvants qu'avec les groupements fonctionnels des solutés B et BH^+.

Purines are important constituents of nucleic acids, and their reactions with the proton and metal ions form the subject of many studies. While the thermodynamics of the first protonation steps of purines in aqueous media is well documented (1), there are few data on these reactions in dimethylsulfoxide even though this solvent, because of its high solubilizing power, is widely used as a reaction medium for related studies, particularly for nmr work. Since we have already compared the thermodynamics of protonation of some nitrogen bases in Me_2SO and in water (2), we have extended our study to include some important purine bases: purine, adenine, 9-methyladenine, adenosine, guanine, and hypoxanthine, as well as some parent and related compounds: imidazole, *N*-methylimidazole, benzimidazole, and 4-amino-2,6-dimethylpyrimidine. We present here the results of our research. The compounds used are listed below.

Experimental

Materials

Purine, pyrimidine (Sigma), adenine, adenosine, *N*-methylimidazole (Aldrich), and hypoxanthine and guanine (L. Light) were used without further purification. Imidazole (Aldrich) was doubly recrystallized in benzene and dried under vacuum at 50°C for 30 min. Benzimidazole (Sigma) was doubly recrystallized in distilled water and dried under vacuum at 60°C for 2 h. 4-Amino-2,6-dimethylpyrimidine (Aldrich) was recrystallized in a 2:1 mixture of ethyl acetate and absolute ethanol and dried under vacuum at room temperature for 2 h. 9-Methyladenine was synthesized as follows. An

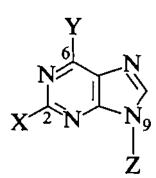

X-2	Y-6	Z-9	Purine
H	H	H	Purine (Pur)
H	NH_2	H	Adenine (Ade)
H	NH_2	D-Ribose	Adenosine (Ado)
H	NH_2	CH_3	9-Methyladenine (MeAde)
NH_2	OH*	H	Guanine (Gua)
H	OH*	H	Hypoxanthine (Hyp)

* Tautomerization

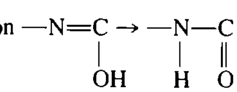

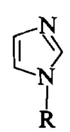

R = H, imidazole (Im)
R = CH_3, *N*-methylimidazole (MeIm)

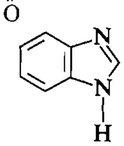

Benzimidazole
(BzIm)

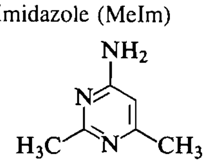

4-Amino-2,6-dimethylpyrimidine
(Dap)

TABLE 1. Ionization constants K of BH^+ ions at 25°C

	pK	
B	Me_2SO	H_2O
Pur	1.83 ± 0.06	(2.39)[a]
Ade	4.06 ± 0.09	(4.12)[b]
MeAde	3.69 ± 0.02	3.88 ± 0.01
Ado	3.18 ± 0.05	(3.55)[b]
Gua	3.74 ± 0.02	(3.3)[b]
Hyp	1.94 ± 0.02	(1.79),[b] (1.9)[c]
Im	6.26 ± 0.06	(7.14)[d]
MeIm	6.15 ± 0.01	(7.20)[d]
BzIm	4.36 ± 0.06	(5.77)[a]
Py	(3.45)[e]	(5.17)[e]
Dap	6.38 ± 0.03	6.85 ± 0.01, (6.98)[f]
ϕNH_2	(3.72)[e]	(4.60)[e]

[a]Reference 3.
[b]Reference 1.
[c]Reference 8.
[d]Reference 9.
[e]Reference 2*b*.
[f]Reference 10.

ethanolic solution of adenine and methyl iodide was heated under reflux at about 80°C for 1 h. The solid obtained was washed with a dilute sodium hydroxide solution, recrystallized in water, and dried under reduced pressure at 40°C for 2 h. The compound was identified by its ^1H and ^{13}C nmr spectra. All samples were checked for purity by means of acid–base titrations in acetic acid or in dimethylsulfoxide (Me_2SO), or by comparing their uv spectra with those published (3).

Trifluoromethanesulfonic acid (Aldrich) and HCl (McArthur) were used as supplied. Picric acid (BDH) (HPic) was dried under reduced pressure over P_2O_5 for 48 h. The HCF_3SO_3 and HPic solutions were prepared by weight or dilution and standardized with NaOH. Potassium chloride (McArthur) was used as received. Tetraethylammonium perchlorate (Eastman Kodak) was recrystallized in a 4:1 mixture of water and ethanol and dried under vacuum at room temperature for 1 h. Finally, Me_2SO (BDH, analytical reagent) was used without further purification.

Potentiometry

Potentiometric titrations of Me_2SO solutions of the bases (10^{-4} to 10^{-2} *M*) with standardized 0.1 *M* HCF_3SO_3 or HPic in Me_2SO were carried out at 25.0 ± 0.1°C in a thermostated cell. The electrodes used were a Radiometer G202B glass electrode and an I^-/I_3^- reference electrode consisting of a platinum wire in a Me_2SO solution 10^{-2} *M* in I_2 and 2×10^{-2} *M* in I^- (2). The junction connecting the reference electrode to the cell was a 10^{-1} *M* Et_4NClO_4 solution in Me_2SO. The solution was made initially 0.100 *M* in Et_4NClO_4 to keep the ionic strength constant. The potentials were measured either with a laboratory-constructed or with a Radiometer PHM 84 potentiometer. The glass electrode was calibrated before each series of experiments with standardized 0.1 *M* HCF_3SO_3 or HPic to give a 62 ± 2 mV slope (intercept 75 ± 5 mV, $r = 0.9996$) in a ΔE vs. pH plot. Potentiometric titrations of 0.1 *M* KCl aqueous solutions of the bases with standardized HCl were similarly obtained using a Radiometer K401 reference calomel electrode.

Calorimetry

The heat of solution and neutralization of solid and liquid bases were determined at 25.00 ± 0.01°C. The LKB Model 8721-1 Isoperibol Calorimeter and procedure have been described (4). The amount of base dissolved or reacted was known from the weights of the glass ampoules. An excess of 0.1 *M* HCF_3SO_3 or HPic in Me_2SO and 0.1 *M* HCl in water was used in the protonation experiments. For each base, 3–10 separate determinations were made at different concentrations.

Results

Ionization constants

The values of the ionization constants K of the protonated bases BH^+ in Me_2SO and water were obtained from the potentiometric neutralization data using the slightly modified program described previously (5). Our pK values, which are strictly valid for 0.10 ionic strength, are given in Table 1 with literature data. No corrections were made for the effect of ionic strength, which would be small for such a type of protonation reaction.

Solution enthalpies

The values of the heats of solution of the liquid (l) or solid (c) bases B in 100 mL Me_2SO or water were plotted against the number of moles of base dissolved (1 to 14×10^{-4} mol for Im, BzIm, Dap, Ade, Me Ade, Ado, and Pur, and 1 to 9×10^{-3} mol for MeIm). The slopes of the least-squares lines gave the enthalpy of solution of B, $\Delta H_s(B)$ (kJ mol^{-1}) which refers to eq. [1].

$$[1] \quad B(l \text{ or } c) = B(s)$$

No concentration dependence was observed in the range of base concentrations used, so that the $\Delta H_s(B)$ values were taken as being equal to $\Delta H_s^0(B)$. These ΔH_s^0 values are given in Table 2 together with published data. The corresponding enthalpies of transfer from water to Me_2SO, on the molar scale

$$[2] \quad \Delta H_t^0 = \Delta H_s^0 - \Delta H_w^0$$

are also given in Table 2.

Protonation enthalpies

The heats of solution of the bases in Me_2SO solutions of 0.1 *M* HCF_3SO_3 or HPic (both strong acids in Me_2SO (6)) and in aqueous 0.1 *M* HCl were plotted against the number of moles of bases dissolved (2 to 12×10^{-4} mol). The plots were linear and the least-squares slopes gave $\Delta H_n^0(B)$ (kJ mol^{-1}), the heat of neutralization of the base, according to

$$[3] \quad B(l \text{ or } c) + H^+(s) = BH^+(s)$$

For Pur, the weakest base in the series, a correction, based on the value of K, was made to account for its incomplete protonation. By combining the $\Delta H_n^0(B)$ values with those of $\Delta H_s^0(B)$, we calculated the heat of protonation of B, $\Delta H_p^0(B)$, in Me_2SO or water, for

$$[4] \quad B(s) + H^+(s) = BH^+(s)$$

with

$$[5] \quad \Delta H_p^0(B) = \Delta H_n^0(B) - \Delta H_s^0(B)$$

The existence of a second step in the protonation of the purines introduces a small error in our values for ΔH_n^0 and hence for ΔH_p^0. Using the values of the ionization constants K_{BH^+} and $K_{BH_2^{2+}}$ (4), the error calculated for ΔH_p^0 is estimated to be 3.0% or less for Ade, assuming that the heat of protonation for the second step is equal to or less than that for the first step. Similarly, the error calculated would be 1.2% or less for MeAde and negligible for Pur and Ado.

Some of the bases (marked with a double asterisk in Tables 2 and 3) were either too insoluble or dissolved too slowly to give meaningful heat changes. Therefore, for MeAde, ΔH_p^0 was determined directly in both solvents, by adding acid to a solution of B. Our value for ΔH_p^0 in water was combined with ΔH_n^0 to yield ΔH_s^0 according to eq. [5]. For BzIm, the value for

TABLE 2. Solution enthalpies (kJ mol^{-1}) of bases at 25°C and enthalpies of transfer from water to Me_2SO

	ΔH^0_s(B)*		
B	Me_2SO	H_2O	ΔH^0_t(B)
Pur	+13.7 ± 0.2(13.6)[a]	+18.3 ± 0.1(18.8)[a,b]	−4.6
Ade	+10.0 ± 0.1(10.8)[a]	(+29.9 to +33.5)[a,c,d]	−23.5
MeAde	+6.5 ± 0.7	+26.1 ± 0.4**(+28.7)[e]	−19.6
Ado	+1.3 ± 0.3	(+32.3)[f]	−31.0
Im	+11.0 ± 0.2	+12.8 ± 0.2(+12.9)[g]	−1.8
MeIm(1)	−0.1 ± 0.3	−9.6 ± 0.3(−9.41)[h]	+9.5
BzIm	+11.3 ± 0.1	+19.0 ± 0.2(+20.3)[b]	−7.7
Py(1)	(+1.2)[i]	(−9.7)[i]	+10.9
Pym(1)	+0.22 ± 0.04	(−9.8)[b]	+10.0
Dap	+14.6 ± 0.2	+9.7 ± 0.2	+4.9
ϕNH_2(1)	(−9.36)[i]	(+1.84)[i]	−11.2

[a]Reference 18.
[b]Reference 17.
[c]Reference 19.
[d]Reference 11.
[e]Reference 12.
[f]Reference 16.
[g]Reference 8.
[h]Reference 13.
[i]Reference 2*b*.
*Errors on the least-square slopes; ** see text.

TABLE 3. Enthalpies (kJ mol^{-1}) and entropies (J mol^{-1} K^{-1}) of protonation of bases at 25°C and enthalpies of transfer of BH^+ ions from water to Me_2SO

	ΔH^0_p(B)*		ΔS^0_p(B)[a]		
B	Me_2SO	H_2O	Me_2SO	H_2O	$\Delta H^0_t(BH^+)$
Pur	−19.5 ± 0.1	−8.8 ± 0.4	−30	16	−40.8
Ade	−25.8 ± 0.1	(−17.6)[b]	−9	20	−57.3
MeAde	−25.8 ± 0.1**	−19.4 ± 0.5**	−16	9	−51.5
Ado	−21.0 ± 0.1	(−15.9)[c]	−10	15	−61.6
Im	−42.4 ± 0.4	−36.8 ± 0.9(−36.4)[d]	−23	13	−32.9
MeIm	−38.8 ± 0.7	−32.9 ± 0.3(−31.6)[e]	−13	27	−21.9
BzIm	−30.7 ± 0.7	(−30.0)[f]	−20	10	−33.9
Py	(−27.7)[g]	(−20.3)[g]	−27	31	−22.0
Dap	−42.4 ± 0.4	−34.2 ± 0.5	−20	16	−28.8
ϕNH_2	(−30.8)[g]	(−30.1)[g]	−32	−13	−37.4

[a]Standard state defined as a one molar solution of base in 0.10 *M* acid media.
[b]Reference 14.
[c]Reference 1.
[d]Reference 8.
[e]Reference 9.
[f]Reference 15.
[g]Reference 2*b*.
*Errors on the least-square slopes; ** see text.

ΔH^0_p was taken from the literature and then combined with our ΔH^0_n to give ΔH^0_s. The ΔH^0_p values presented in Table 3 correspond to a 0.1 (usually 0.1 *M* acid) ionic strength. Judging from data of Hepler and co-workers (8) for Im in water, the values of ΔH^0_p at zero ionic strength are not likely to be very different: their ΔH^0_p values are −36.4 kJ mol^{-1} (μ = 0.02), −36.9 (μ = 0.2), while we found −36.8 (μ = 0.1) and 2 other values near −38.0 (μ = 0.5) have been reported (15, 20). However, as pointed out by a referee, for Ade μ may have a large effect on ΔH^0_p (14): ΔH^0_p passes from −21.4 kJ mol^{-1} (μ = 0.025) to −17.6 (μ = 0.10). This large effect is surprising and needs to be confirmed, particularly when one considers that for related Ado, ΔH^0_p varies only from −16.4 kJ mol^{-1} ($\mu \approx$ 0) to −15.9 (μ = 0.1). Our ΔH^0_p(B) values were combined with the ΔG^0_p(B) values calculated from the p*K* in Table 1 to give the protonation entropies ΔS^0_p listed in Table 3.

Discussion

First, if we look at the solvent effect on the ionization constants *K* of the conjugate acids BH^+ of the purines and related bases, the data in Table 1 show only minor changes of the p*K* when passing from water to Me_2SO, and this is particularly noticeable for the purines. Just as we observed with pyridine and anilines (2), the p*K* values are slightly lower in Me_2SO (except, interestingly enough, for the two hydroxypurines) but by less than 1.4 units. On the basis of eq. [1] it is clear that the lower pK's of BH^+ in Me_2SO, which means that they are stronger acids in Me_2SO, are qualitatively in line with the known higher basicity of this solvent compared with that of water. However, if we attempt to give figures for this, given that the free energy of solvation of H^+ is 18.8 kJ mol^{-1} more exothermic in Me_2SO than in water (2), the pK values should have been 3.3 units lower in Me_2SO than in water. Clearly, there are some compensating solvation effects on B and BH^+ which must be considered with those on H^+ to account fully for the small solvent effect on eq. [1] and the resulting pK changes.

Since the free energy data on B (and BH^+) are not easily attainable, we will pursue our discussion of the solvent effect on eq. [1] by comparing, in turn, the enthalpy data for B (Table 2), and then for BH^+ (Table 3), both in Me_2SO and in water. We first note in Table 3 that, contrary to what we would have expected, the protonation enthalpies $\Delta H^0_p(B)$ are more exothermic in Me_2SO than in water even though the enthalpy of solvation of H^+ is 25.5 kJ mol^{-1} more exothermic in Me_2SO than in water (2), which again emphasizes large solvation effects on B and BH^+. If we begin by examining the solution enthalpies and enthalpies of transfer of B, the data in Table 2 show some very interesting differences which we will attempt to relate to the contrasting H-bond properties of Me_2SO and water and to the nature of B functional groups. First, we see that for MeIm, ΔH^0_s is some 10 kJ mol^{-1} more exothermic in water than in Me_2SO ($\Delta H^0_t \approx +10$ kJ mol^{-1}), just as it is for Py and for Pym, while for benzene, which could approximate Py (and MeIm) for cavity and non-specific effects, $\Delta H^0_t = -0.3$ kJ mol^{-1} (7). Since MeIm and Py are both related H-bond acceptors but have no donor properties, we can advance that their more exothermic ΔH^0_s in water is due in part to the formation of H-bonds, H_2O acting as a donor. For Im, the smallness of ΔH^0_t (-1.8 kJ mol^{-1}) when compared with that of ΔH^0_t for Py or Pym and MeIm, can be viewed as resulting from a positive ΔH^0_t contribution due to the "pyridine" nitrogens counterbalanced by a negative contribution of the "pyrrole" —NH group, which gives stronger H-bonds with Me_2SO than with water. Then for Dap, ignoring the contribution of the Me groups on the basis of data for toluene (7), the negative contribution of the —NH_2 group, deduced from $\Delta H^0_t = -11$ kJ mol^{-1} for ϕNH_2, is more than offset by the positive contribution of the "pyridine" nitrogens. Now, it is not possible to relate the ΔH^0_t of the fused ring compounds to those of their imidazole and benzene or pyrimidine moieties. This is shown, for example, by comparing $\Delta H^0_t \sim -8$ kJ mol^{-1} for BzIm with the values for Bz, -0.3 kJ mol^{-1}, and for Im, -1.8 kJ mol^{-1}. A similar situation has recently been observed for such transfers from water to methanol (18). However, if we take BzIm as the reference base, we can also discuss the ΔH^0_t of the purines on the basis of group contributions. Thus, proceeding from BzIm to Pur, we note a positive ΔH^0_t increment, admittedly small, due to the "pyridine" nitrogens. Form Pur to Ade, there is the expected negative ΔH^0_t contribution from the —NH_2 group, although it is larger than that observed with ϕNH_2. From MeAde to Ade, we find the predictably negative increment due to the NH group, though smaller than when passing from MeIm to Im. Finally, for Ado, the replacement of the Me substituent of MeAde by the D-ribose group gives rise to a -8 kJ mol^{-1} contribution to ΔH^0_t, which we can attribute to stronger —OH interactions with Me_2SO.

Let us now consider the solvent effect on BH^+ ions. The paucity of data on proton affinities and heats of sublimation of the bases studied (unlike Py and ϕNH_2(2)) made it impossible to calculate and compare the solvation enthalpies of the gaseous ions BH^+. We have therefore based our discussion on the enthalpies of transfer ΔH^0_t of BH^+ ions from water to Me_2SO, calculated according to:

$$[6] \quad \Delta H^0_t(BH^+) = \Delta H^0_t(B) + \Delta H^0_t(H^+) + \Delta H^0_{p,s} - \Delta H^0_{p,w}$$

where $\Delta H^0_{p,s}$ and $\Delta H^0_{p,w}$ are the enthalpies of protonation of B in Me_2SO and water respectively, and $\Delta H^0_t(H^+)$ is taken as being equal to -25.5 kJ mol^{-1} (2). The values of $\Delta H^0_t(B)$ come from Table 2, those of ΔH^0_p from Table 3, and the results for $\Delta H^0_t(BH^+)$ are given in Table 3. The uniformly large negative values of ΔH^0_t, going from -20 to -60 kJ mol^{-1}, indicate a strong stabilization of BH^+ ions when passing from water to Me_2SO. This increased stabilization must come in part from stronger H-bonding of BH^+ with the more basic solvent Me_2SO. We have attempted to determine whether $\Delta H^0_t(BH^+)$ could not be decomposed into a non-electrostatic term approximated by $\Delta H^0_t(B)$ as well as an electrostatic term (2). This latter electrostatic contribution to the transfer of BH^+ is found to be near 32 kJ mol^{-1} for most of the bases considered. Such a constant contribution would mean, by considering eq. [6], that $\Delta H^0_{p,s} - \Delta H^0_{p,w}$ should be constant at about 7 kJ mol^{-1}. The values in Table 3 generally indicate differences of that magnitude. When we plot $\Delta H^0_t(BH^+)$ against $\Delta H^0_t(B)$, we also obtain $\Delta H^0_t(BH^+) = 0.92\,\Delta H^0_t(B) - 32.0$ ($r = 0.981$) excluding values for ϕNH_2, which is the only base that does not protonate on a pyridine nitrogen.

The entropy data for the protonation of the bases in Table 3 show wide differences for Me_2SO and water, i.e. negative entropy values in Me_2SO contrasting with the positive values in water. We have already observed similar results for the protonation of other nitrogen bases (2). This decrease in the protonation entropy when passing from water to Me_2SO reflects an increased amount of solvent immobilized in the protonation process, with likely contributions from all three particles involved, H^+, B, and BH^+. Finally, we have reported (2) a linear relation between the enthalpy of ionization ($\Delta H^0_{i,s} = -\Delta H^0_{p,s}$) and the p$K$ of the conjugate acids BH^+ of alkylamines, anilines, and pyridine in Me_2SO: $\Delta H^0_{i,s} = 6.855$ p$K + 4.907$ ($r = 0.997$). When we add our present data for the 8 nitrogen bases, we still obtain a fair correlation, $\Delta H^0_{i,s} = 7.02$ p$K + 1.86$ ($r = 0.990$) now for 18 bases with $1.8 <$ p$K < 11.0$, this is evidence of a clear enthalpy–entropy type relationship.

Acknowledgements

The financial assistance of the Natural Sciences and Engineering Research Council and of the Ministère de l'Education is gratefully acknowledged. We also thank Hélène Perreault, holder of a NSERC undergraduate scholarship, for her contribution to the work on MeAde.

1. R. M. IZATT, J. J. CHRISTENSEN, and J. H. RYTTING. Chem. Rev. **71**, 439 (1971).
2. (*a*) A. MUCCI, R. DOMAIN, and R. L. BENOIT. Can. J. Chem. **58**, 953 (1980); (*b*) R. L. BENOIT, M. J. MACKINNON, and L. BERGERON. Can. J. Chem. **59**, 1501 (1981).
3. S. F. MASON. J. Chem. Soc. 2071 (1954).
4. R. L. BENOIT and M. FRÉCHETTE. Can. J. Chem. **62**, 995 (1984).
5. R. L. BENOIT, A. L. BEAUCHAMP, and M. DENEUX. J. Phys. Chem. **73**, 3268 (1968).
6. R. L. BENOIT and C. BUISSON. Electrochim. Acta, **18**, 105 (1973).
7. E. M. ARNETT and D. R. MCKELVEY. J. Am. Chem. Soc. **88**, 2599 (1966).

8. E. L. WOOLLEY, R. W. WILTON, and L. G. HEPLER. Can. J. Chem. **48**, 3250 (1970).
9. A. C. M. PARVA, L. JULIANO, and P. BOSCHCOV. J. Am. Chem. Soc. **98**, 7645 (1976).
10. D. J. BROWN. The chemistry of heterocyclic compounds: the pyrimidines. Suppl. 1. Interscience Publishers, J. Wiley & Sons, New York, London. 1970. p. 371.
11. H. DEVOE and S. P. WASIK. J. Solution Chem. **13**, 51 (1984).
12. L. B. CLARK, G. P. PISCHEL, and I. TINACO. JR. J. Phys. Chem. **69**, 3615 (1965).
13. J. N. SPENCER, E. S. HOLMBOE, M. R. KIRSHENBAUM, S. W. BARTON, K. A. SMITH, W. S. WOLBACH, J. F. POWELL, and C. CHORAZY. Can. J. Chem. **60**, 1183 (1982).
14. S. ZIMMER and R. BILTONEN. J. Solution Chem. **1**, 291 (1972).
15. M. J. BLAIS, O. ENEA, and G. BERTHON. Thermochim. Acta, **20**, 335 (1977).
16. J. H. STERN and D. R. OLIVER. J. Chem. Eng. Data, **25**, 221 (1980).
17. J. N. SPENCER, S. W. BARTON, K. A. SMITH, W. S. WOLBACH, J. F. POWELL, M. R. KERSHENBAUM, D. W. FIRTH, E. M. HARRIS, and T. A. JUDGE. Can. J. Chem. **61**, 2695 (1983).
18. F. I. KANBOUR, J. K. AHMED, and G. A. W. DERWISH. J. Solution Chem. **12**, 763 (1983).
19. J. N. SPENCER and T. A. JUDGE. J. Solution Chem. **12**, 847 (1983).
20. F. MARSICANO and R. D. HANCOCK. J. Chem. Soc. Dalton Trans. 228 (1978).

A nuclear magnetic resonance study of the self-association of adriamycin and daunomycin in aqueous solution[1]

I. J. McLennan, R. E. Lenkinski, and Y. Yanuka

Guelph–Waterloo Centre for Graduate Work in Chemistry, Guelph Campus, Guelph, Ont., Canada N1G 2W1

and

Department of Pharmacy, Hebrew University of Jerusalem, Jerusalem, Israel

Received October 2, 1984

I. J. McLennan, R. E. Lenkinski, and Y. Yanuka. Can. J. Chem. **63**, 1233 (1985).

A study of the self-association of the anthracycline antibiotics adriamycin and daunomycin was undertaken in D_2O and methanol using nmr at 400 MHz. From the concentration dependence of the ^2H linewidths obtained on selectively deuterated daunomycin it was determined that daunomycin forms a dimer in aqueous solution. The concentration dependence of the chemical shift of the 4 methoxy group of adriamycin was fit to a dimer model in which only the non-protonated neutral species of adriamycin participated in the self-association process. The data were in agreement with the dimer model if a pK of 7.4 was used. The pH dependence of the self-association was fit to two ionizations, one with a pK of 8.2 and the other with a pK of 8.8. The latter pK was attributed to the ionization of the phenol based on the work of Eksborg. It was concluded that only the deprotonated amine of adriamycin took part in the dimerization process. The dimerization of adriamycin is characterized by a ΔS of approximately 3 cal deg^{-1} M^{-1} and a ΔH of -3.45 kcal M^{-1}. At room temperature the association constant for the dimerization process was found to be 4.0×10^5 M^{-1}. These results were discussed in terms of earlier studies by Barthelemy-Clavey *et al.*, Martin, and Chaires *et al.*

I. J. McLennan, R. E. Lenkinski et Y. Yanuka. Can. J. Chem. **63**, 1233 (1985).

Faisant appel à la rmn à 400 MHz, on a entrepris une étude sur l'auto-association des antibiotiques anthracyclines, adriamycine et daunomycine, en solutions dans le D_2O et le méthanol. En se basant sur la corrélation qui existe entre la concentration et les largeurs des bandes ^2H, obtenue à l'aide d'une daunomycine deutérée sélectivement, on a déterminé que la daunomycine forme un dimère en solution aqueuse. La corrélation qui existe entre la concentration et la déplacement chimique du groupement méthoxyle en position 4 suggère l'existence d'un modèle dans lequel seules les espèces neutres non-protonées de l'adriamycine participeraient dans le processus d'auto-association. Si on utilise un pK de 7,4, les données sont en accord avec le modèle dimère. La corrélation qui existe entre le pH et l'auto-association correspond à deux ionisations, une avec un pK de 8,2 et une autre avec un pK de 8,8. En se basant sur le travail de Eksborg, on attribue ce dernier pK à l'ionisation du phénol. On en conclut que seule l'amine déprotonée de l'adriamycine prend part au processus de dimérisation. La dimérisation de l'adriamycine est caractérisée par un ΔS d'environ 3 cal deg^{-1} M^{-1} et un ΔH de $-3{,}45$ kcal M^{-1}. À la température ambiante, on a trouvé que la constante d'association du processus de dimérisation est égale à $4{,}0 \times 10^5$ M^{-1}. On discute de ces résultats en fonction d'études antérieures de Barthelemy-Clavey et ses collaborateurs, Martin et Chaires et ses collaborateurs.

[Traduit par le journal]

Introduction

Adriamycin (doxorubicin, Adm) (**I**) and daunomycin (daunorubicin) are aminoglycoside anthracycline antibiotics that have been found to be effective antineoplastic agents in the treatment of promyelocytic leukemia and other lymphomas (1). Adm differs from daunomycin in that it has a hydroxyl group on the C14 of the keto-alkyl side chain on the A ring. Since the discovery of Adm in the early 1950's a large amount of information has been accumulated on its mechanism of action both at the molecular and cellular level (2, 3). These anthracyclines are known to bind strongly to DNA in vitro although different modes of binding have been observed (4, 5). In addition, alternate modes of activity have been proposed (6).

There have been several reports of metal ion complexes of Adm (7). We have recently shown that Adm can form complexes of relatively high stability with the trivalent lanthanide ions (8). These complexes were characterized by a variety of spectroscopic techniques including ^1H nmr. In the course of these latter studies we found that in aqueous solution the chemical shifts of several of the resonances of the antibiotic were dependent on the concentration of the drug present. This phenomenon is usually indicative of self-association (9, 10). Similar observations have been reported by Barthelemy-Clavey *et al.* (11), Martin (12), and Chaires *et al.* (13), all of whom have interpreted the concentration dependence of nmr chemical shifts in terms of the self-association of Adm. The self-association process has also been investigated by Eksborg (14) using partitioning experiments based on an extraction procedure. Eksborg (14) determined an effective association constant for the dimerization process of 3.09×10^4 M^{-1}, whereas the dimerization constant determined by Barthelemy-Clavey *et al.* was 570 M^{-1} and that of Martin ranged from 5000 to 9000 M^{-1}. Both of these latter studies utilized visible absorption and circular dichroism spectroscopy. This has been a more traditional approach in examining the aggregation of planar aromatic systems in solution. Recently, Chaires *et al.* (13) have examined the self-association process by visible absorption spectroscopy and ^1H nmr. Using a dimer model they obtained a dimerization constant for Adm of 3300 M^{-1}. These authors have also employed a second more complicated model called the indefinite association model, which takes into account higher aggregates. Using this model, Chaires *et al.* (13) obtained an intrinsic association constant of 1500 M^{-1} from an analysis of sedimentation equilibrium measurements. With the exception of the treatment by Eksborg (14) all of the above analyses neglected the various possible ionization equilibria for Adm in aqueous solution. This implies that all of the species

[1]Supported by the Natural Sciences and Engineering Research Council of Canada (R.E.L.).

(i.e. protonated, nonprotonated) of Adm present in solution can participate equally in the self-association process. Since we have found the self-association process to be pH dependent, *vide infra*, we believe that the neglect of the various ionization processes is a serious flaw in these analyses. In view of the apparent discrepancies in the reported self-association constants for Adm in solution, we undertook a systematic nmr investigation of the self-association process. Our main motivation for this study stems from our view that a knowledge of the solution properties of the antibiotic is important in understanding the metal binding properties and perhaps even the biological effects at the molecular level.

In this study we monitored the effects of variations in Adm concentration, pH, ionic strength, and temperature on the chemical shifts of Adm. The data were fit to an association process that took into account the ionization of the amino group on the glycosidic moiety of Adm. We have also employed ^2H relaxation time measurements as a means of monitoring the extent of self-association. We have analyzed the ^2H linewidths of daunomycin, specifically deuterated at position 14, in aqueous solutions to obtain estimates of the volume of the aggregate(s) formed. We report the results of these studies in the present communication.

Materials and methods

Materials

Adriamycin hydrochloride and daunomycin hydrochloride were kindly supplied by Dr. F. Arcamone of Adria Farmitalia Carlo Erba (Milan, Italy) and were used without further purification. D_2O (99.8%), deuterated methanol, and sodium dimethyl-2-silapentanesulfonate (DDS) were obtained from Merck, Sharp and Dohme. DCl (37% in D_2O) and NaOD (40% in D_2O) were obtained from Sigma. The KCl and EDTA (analytical grade) were from Baker.

Daunomycin specifically deuterated at position 14 was prepared by treating a solution of daunomycin (~6 mM) in methanol-d_4 with metallic sodium. After the reaction was complete (i.e. ca. 10 min) the solution was treated with D_2O and dilute DCl. The resulting solution was evaporated. The remaining solid was extracted with D_2O. A significant amount of nonwater-soluble red-coloured material was observed, suggesting that the aglycone may have formed. The 400-MHz ^1H nmr spectrum of the product was identical to that of daunomycin with the resonance at 2.48 (assigned to the C-14 methyl) missing in the product. The ^2H nmr spectrum obtained at 61.4 MHz showed only one resonance at 2.48, indicating that the methyl group at C-14 of daunomycin had been deuterated.

Nuclear magnetic resonance experiments

The ^1H nmr experiments were performed on a Bruker WH-400 spectrometer operating at 400.13 MHz in the Fourier transform mode using quadrature phase detection. Field/frequency lock was achieved by locking on D_2O in the samples. The temperature was controlled and was calibrated to ±1°C with neat ethylene glycol. For variable temperature experiments the samples were equilibrated for 10 min prior to acquisition of spectra. All spectra were referenced to the internal standard (DSS), whose chemical shift did not change significantly with the temperature and pH ranges used in this study. The shifts of DSS have been reported to change with varying concentrations of purine and uridine (32). However, the concentrations of Adm used in our studies were below 10 mM and hence any perturbations in the shift of DSS due to interactions between DSS and Adm were negligible. This was verified experimentally by examining the chemical shifts of a number of non-aromatic resonances of Adm. At all concentrations employed, all of the chemical shifts of these resonances were indentical. The chemical shift of DSS has been reported to be invariant with temperature over the range of 19° to 90°C (32). We have verified this observation with our own studies down to the temperature of 0°C where we found that the chemical shifts of certain nonaromatic protons

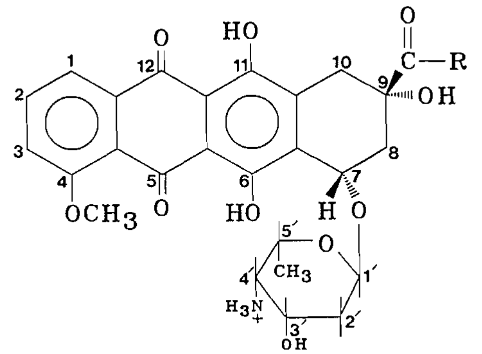

I

(H1′, H2′, H3′, 5′ Me) are invariant within experimental error (<5 Hz) (c.f. I). Typical acquisition parameters were: pulse width 4.5 μs (90°) at 400 MHz, relaxation delay 1 s, sweep width 7000 Hz, and 16 K data points. Approximately 60 to 200 FID's were accumulated depending on the concentration of the sample.

The adriamycin concentration was determined by monitoring the absorbance at 477 nm (ϵ = 11 500 M^{-1} cm^{-1}) (15). The solutions of Adm were made up in D_2O within 24 h prior to use and the pH was adjusted with 0.01 M NaOD or 0.01 M DCl using a Fisher model 620 pH meter with an Ingold model 6060-02 electrode directly in the nmr tube. The pH values reported are uncorrected for any isotope effects. For all of the experiments the ionic strength was adjusted with KCl. The calculation of K_D and curve fitting routines were performed on an OHIO 8000 16K Computer.

Results and discussion

The analysis of ^2H relaxation times of deuterated daunomycin

The applications of ^2H relaxation time measurements to monitor molecular dynamics have been reviewed by Mantsch *et al.* (16). In the extreme narrowing limit, the relaxation rates of a deuterium nucleus are given by (17)

$$[1] \quad \frac{1}{T_1} = \frac{1}{T_2} = \frac{3}{8}\left(\frac{e^2qQ}{\hbar}\right)^2\left(1 + \frac{n}{3}\right)\tau_c$$

where $(e^2qQ/\hbar)$ is the quadrupolar coupling constant along the deuteron–carbon bond, n is the asymmetry parameter (usually assumed to be close to zero), and τ_c is the correlation time for overall molecular reorientation. In the case of a freely-rotating CD_3 group with a correlation time of τ_i attached to a rigid molecule undergoing molecular reorientation with a correlation time of τ_c, eq. [1] can be modified as follows (18).

$$[2] \quad \frac{1}{T_1} = \frac{1}{T_2} = \frac{3}{8}\left(\frac{e^2qQ}{\hbar}\right)^2(0.11\tau_c)$$

if $\tau_c \geq \tau_i$.

For a spherical molecule the correlation time for molecular reorientation is given by

$$[3] \quad \tau_c = \frac{4\pi\eta a^3}{3kT}$$

where η is the viscosity of the solution, a is the radius of the molecule, k is Boltzmann's constant, and T is the temperature in degrees Kelvin. Glasel *et al.* (19) analyzed the ^2H spin lattice relaxation times of 7-methylguanine deuterated at the 7-methyl position to provide information concerning the rotational motion of 7-methylguanine and poly-7-methylguanylic acid. Ellis and co-workers (20) have shown that the linewidth of specifically deuterated molecules can be used as a measure of the real transverse relaxation rate of the deuterium nucleus in

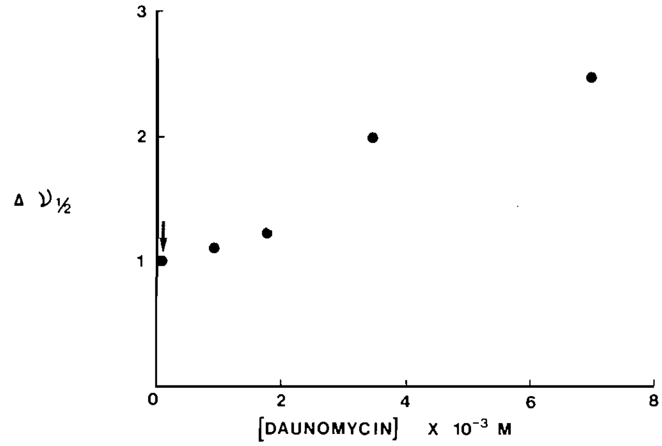

FIG. 1. The variation in the ^2H linewidth of daunomycin deuterated at position 14, with daunomycin concentration. The pH was 6.92, ionic strength 0.052, and the temperature was 22°C. These linewidths were corrected for inhomogeneity by monitoring the linewidth of ^2H from natural abundance deuterium in H_2O (0.5 Hz). The point indicated by an arrow is the linewidth obtained in methanol.

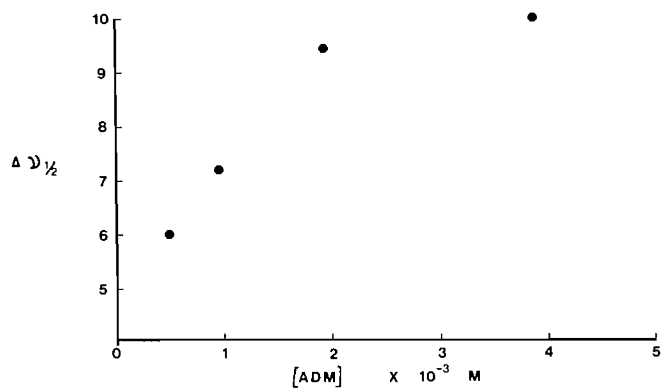

FIG. 2. The variation in the linewidth of the 4-O-methyl resonances of Adm with Adm concentration. The pH was 6.92, ionic strength 0.052, and temperature 21°C.

the molecule. In carrying out our analysis we employed an approach similar to the one described by Egan (21) in his analysis of the association of AMP in aqueous solution using ^2H nmr.

The variation in the linewidth of the deuterium resonance of 14-CD_3-daunomycin with the concentration of drug present is shown in Fig. 1. These linewidths have been corrected for any inhomogeneity of the magnetic field. Note that in Fig. 1 the linewidth at infinite dilution is around 1.0 Hz.

We can obtain an estimate for the correlation time of daunomycin as a monomer in H_2O at 22°C from [3]. From molecular models we find that daunomycin has molecular dimensions approximated by a sphere of ca. 3 Å radius. This corresponds to a correlation time of 8×10^{-11} s in eq. [3]. By using a value for the quadrupolar coupling constant of 170 kHz, a value for the linewidth of the ^2H resonance of 1.2 Hz can be obtained from eq. [2]. The good agreement between the linewidth observed at low daunomycin concentrations and estimated values for the ^2H linewidth indicates that daunomycin exists as a monomer at low concentrations in aqueous solution.

From Fig. 1 it is clear that the ^2H linewidth at higher daunomycin concentrations reaches a limit of around 2.5 Hz. This indicates that there is self-association occurring in solution. This is confirmed by the change in the chemical shifts observed

TABLE 1. ^1H Chemical shift data for adriamycin in methanol

Position	δ (ppm from DSS)	Position	δ (ppm from DSS)
H1	7.97	H4′	3.66
H2	7.85	H3′	3.56
H3	7.59	H10	3.05
H1′	5.45	H8	2.36
H7	5.11	H8	2.18
H14 OH	4.71	H2′	2.04
H5′	4.28	H2′	1.88
4 OMe	4.04	5′CH_3	1.29

in the molecule as well (*vide infra*). Moreover it is clear that the rotational correlation time of the associated species is twice that observed for the monomer. This strongly suggests that the associated species is a dimer in aqueous solution. This conclusion is also qualitatively supported by the variation observed in the linewidth of the ^1H resonance of the 4-O-methyl resonance of Adm with Adm concentration shown in Fig. 2.

Analysis of the chemical shift data

Figure 3 shows a ^1H 2D COSY spectrum (22) of Adm in methanol at 250 MHz. Analysis of the spectrum confirms some of the assignments based on homonuclear decoupling experiments performed at 400 MHz with Adm in methanol. In addition, selective nOe experiments performed at 400 MHz established the assignments of the three aromatic protons.[2] The assignments of the ^1H spectrum in methanol are summarized in Table 1. In methanol, the chemical shift positions of all of the peaks in the proton spectrum of Adm did not vary with the concentration of the drug present. On the other hand, in D_2O there were substantial changes in the chemical shifts of many of the resonances at higher concentrations. As outlined in the Introduction, several workers have analyzed the shifts of resonances of nuclei in Adm and other planar aromatic systems in examining the self-association process in aqueous solutions.

The analysis of chemical shifts in this study was based on a dimer model for Adm first proposed by Barthelemy-Clavey *et al.* (11) and is similar to the method of analysis used by Stein and Tomkiewicz (23). The equilibrium for the dimerization of Adm in aqueous solution can be written as

$$[4] \quad A + A \rightleftharpoons A_2$$

and, K_D, the dimerization constant can be defined as

$$[5] \quad K_D = \frac{[A_2]}{[A][A]}$$

where A is the free monomer, A_2 is the dimer, and the square brackets denote equilibrium concentrations. Similarly for the ionization of the glycosidic amine

$$[6] \quad K_a = \frac{[A][H^+]}{[AH]}$$

where K_a is the ionization constant for the 3′-amino group of Adm. Since we observed only one set of ^1H resonances throughout our study, and the self-association process of planar aromatic systems has been found to be fast on the ^1H nmr chemical shift time scale (24), we may write

$$[7] \quad \delta_{obs} = \frac{\delta_M([AH] + [A] + \delta_D[A_2]}{A_T}$$

[2]McLennan and Lenkinski, unpublished results.

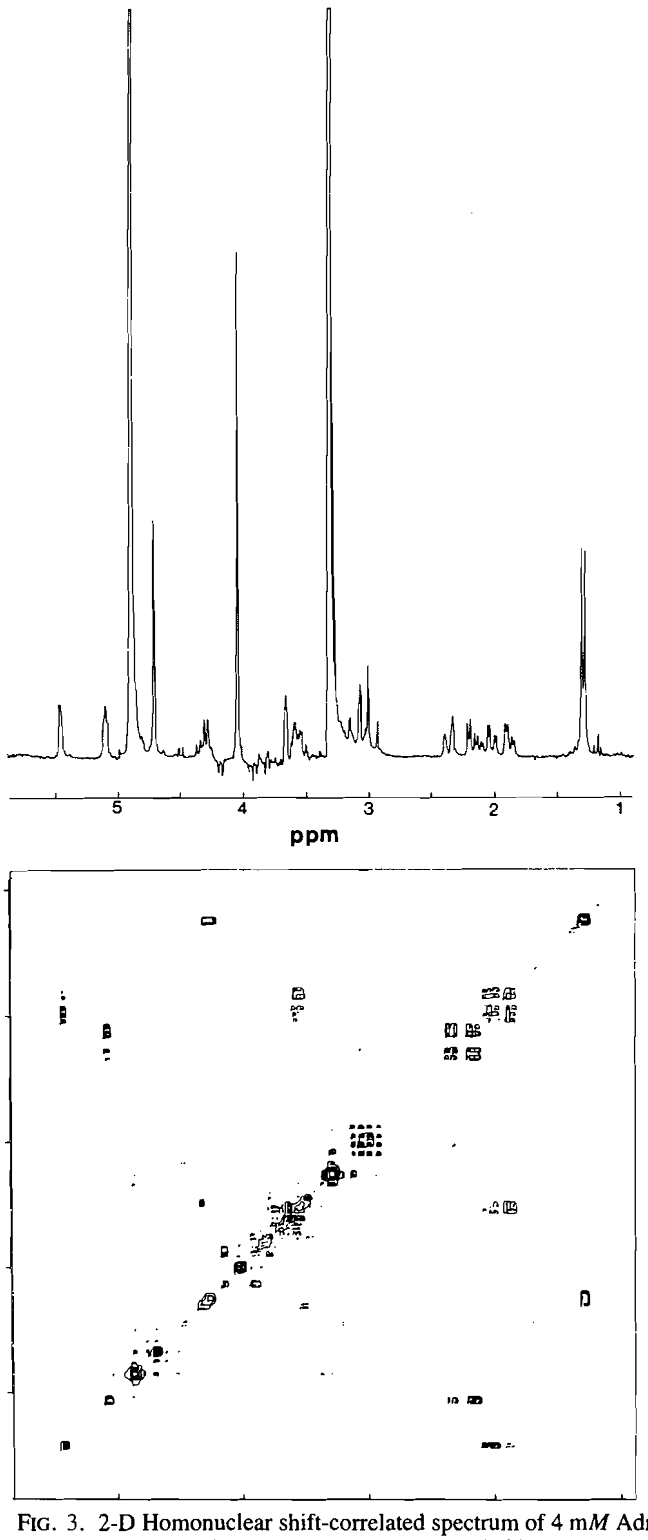

FIG. 3. 2-D Homonuclear shift-correlated spectrum of 4 mM Adm in deuterated methanol at 250 MHz. For chemical shift assignments see Table 1.

(assuming the phenolate anion does not participate in the association process) where AH refers to the protonated amine, A_T is the total Adm concentration, δ_{obs} is the observed chemical shift, δ_M is the chemical shift of the monomer, and δ_D is the chemical shift of the dimer. Substituting eqs. [5] and [6] into eq. [7] and rearranging gives eq. [8].

$$[8] \quad \delta_{obs} = \frac{[AH] + [A]}{A_T}(\delta_D - \delta_M) + \delta_M$$

A mass balance equation can be written in terms of A_T as

$$[9] \quad A_T = [A] + [AH] + 2[A_2]$$

and by substituting eqs. [5] and [6] into eq. [9] we can obtain a quadratic equation in [A],

$$[10] \quad [A]^2 K_A K_D + [A](K_A + [H^+]) - K_A A_T = 0$$

which can be solved by standard mathematical methods. The chemical shift data used to determine K_D was fit to eq. [10] using an interative method based on a sum of squares routine which utilized eq. [8]. A plot of δ_{obs} versus $([AH] + [A])/A_T$ yields both δ_M and δ_D. A similar procedure was used for determining the pK's from the pH titration data. The 4-methoxy peak was chosen as a monitor of the self-association since it is particularly sensitive ($\Delta\delta_{obs} \simeq 70$ Hz) to the Adm concentration. Also, this resonance occurs in a region of the ^{1}H nmr spectrum where there is minimal overlap with any other peaks and thus its chemical shift can be measured relatively precisely even at higher concentrations of Adm where linebroadening occurs (>2.1 mM). It should be noted that in eq. [7] we have made the assumption that δ_M is the same for all of the monomeric forms of Adm, i.e. both protonated and nonprotonated (AH and A respectively). This assumption was verified in experiments in methanol where the chemical shifts of both the protonated and nonprotonated forms of Adm have been measured. The chemical shift of the protonated form of Adm in methanol was found to be 3.98 ppm and the shift for the phenolate anion was found to be 3.96, which is well within the experimental error of the experiment. In addition, as was pointed out earlier, it is reasonable to assume that there is no self-association of Adm in methanol based on the chemical shift of the 4-methoxy resonance (Table 1).

The variation in the chemical shift of the 4-methoxy peak with the temperature and concentration of Adm is presented in Fig. 4. The solid lines represent the calculated shifts based on eq. [10]. Note the good agreement between the calculated and experimental data with a slight deviation seen at $T = 0$°C. This deviation may represent partial freezing of the sample, although this could not be observed visually.

The overall temperature dependence of the association process is shown in Fig. 5. The enthalpy for the process (derived from the slope of the plot in Fig. 5) was found to be -3.45 kcal M^{-1} with an estimate for ΔS (obtained from the intercept) of ca. 3 cal deg^{-1} M^{-1}. Due to the limitations of performing a variable temperature study in aqueous systems only an estimate of ΔS can be obtained, but this is a reasonable value, characteristic of stacking interactions in solutions of high dielectric constant (25).

The results obtained in this study are in agreement with a number of studies of other planar aromatic ring systems (11, 12, 26). In solutions of high dielectric constant the degree of self-association should be greater and this is seen in Fig. 6, which shows the effect of ionic strength on the self-association process. This has been attributed to non-specific interactions between the aromatic rings (27).

A value of K_D of $4.0 \times 10^5\ M^{-1}$ at 22°C contrasts with values of K_D of $5.0 \times 10^3\ M^{-1}$ determined by Martin (12) and $5.7 \times 10^2\ M^{-1}$ determined by Barthelemy-Clavey (11). Although in their studies they used daunomycin, the presence of the hydroxyl group at C14 is not expected to account for the large difference in K_D. Chaires *et al.* (13) have reported a value of 1500 M^{-1} for the association constant based on an analysis employing an indefinite association model. As was pointed out

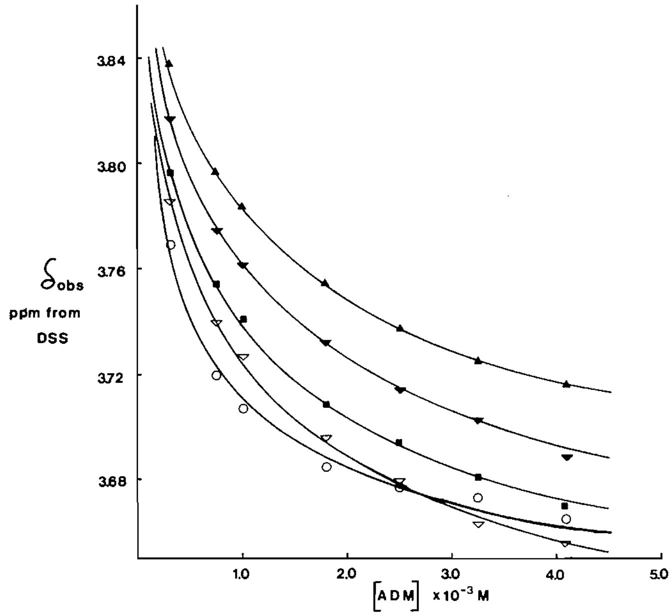

FIG. 4. Plots of δ_{obs}, the chemical shift of the 4-OMe resonance, versus Adm concentration referenced to internal DSS. $\mu = 0.052\ M$, pH 6.91 in D_2O. ○—○ 0°C, ▽—▽ 10°C, ■—■ 22°C, ▼—▼ 35°C, ▲—▲ 50°C. The solid line is calculated from the dimer model.

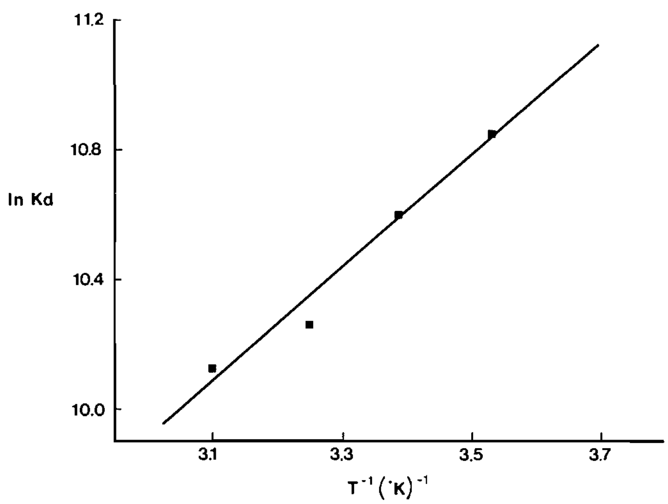

FIG. 5. A van't Hoff plot for the temperature dependence of the dimerization process from the data presented in Fig. 4.

earlier, the same authors also analyzed their data in terms of a dimerization model ($K = 3300\ M^{-1}$). A direct comparison between their results and the dimerization constant determined in the present study may not be relevant because none of the models proposed by Chaires *et al.* (13) take into account the pH dependence of the association process. A plausible reason for these differences is that by taking into account the ionization of the amino group (and assuming the phenolate anion does not participate in the dimerization process) the effective K_D is raised in our model. The pH dependence studies on the dimerization of Adm, shown in Fig. 7, appear to support this.

Eksborg (14) concluded that the free amine was the only species taking part in the dimerization process. In our studies the best fit was obtained using a dimer model in which only the free amine participates in dimerization. Using this model (based on eqs. [8] and [10]) we found a value for the pK of

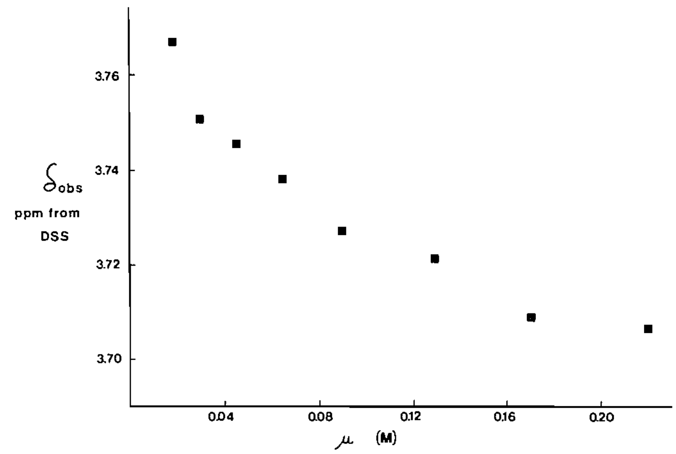

FIG. 6. The variation in δ_{obs} with the ionic strength of the solution. $1.71 \times 10^{-3}\ M$ Adm, pH 6.76, $T = 22°C$.

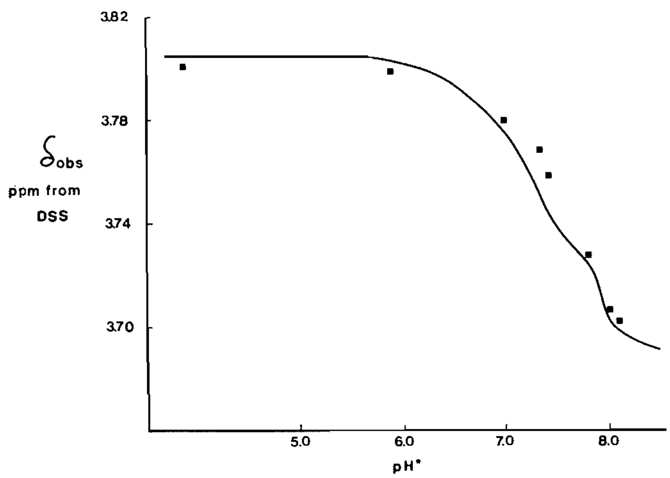

FIG. 7. The pH dependence on the self-association process of Adm in which the ionic strength was initially adjusted to $0.052\ M$. The solid line is calculated from the dimer model. 2 mM Adm, $T = 22°C$.

7.4 ± 0.2 for the protonation of the amine. Eksborg (14) has determined the pK_a of the glycosidic amine to be 8.2, whereas Righetti *et al.* (28) have determined it to be 7.8. The difference between our pK and the values reported by these authors (determined in H_2O) falls within the isotope effect of D_2O on the pK of primary amines, which is approximately -0.60 at this particular pH range (29). Taking into account our assumption about the phenolate anion, the isotope effect would make 7.4 a reasonable value. Figure 7 shows the results of a pH titration of 2 mM Adm in D_2O. Using the dimer model in the analysis of the chemical shift data, the data were fit to two ionizations characterized by pK's of 8.2 ± 0.2 and 8.8 ± 0.2, corresponding to the glycosidic amine and one of the phenols, respectively. Note that the value for the K_D obtained from this titration is $4.0 \times 10^4\ M^{-1}$, which is in good agreement with the value obtained from our previous analysis of the data for the concentration dependence of the chemical shift shown in Fig. 4. We believe that the discrepancy between the value obtained for the pK of the amino group (8.2 ± 0.2 in this case, 7.4 ± 0.2 for the data in Fig. 4) can be ascribed to differences in the ionic strength at which the two experiments were performed.

Lam and Neville (30) determined binding constants for acridine orange using visible absorption spectroscopy. Two models were proposed for its self-association, one involving anion participation and another involving only the neutral species of acridine orange. It was found that both models gave good agreement with the experimental data. Acridine orange has served as a prototype for many studies of stacking interactions of planar aromatic systems, although in the case of Adm direct anion participation in the self-association process has been ruled out based on the arguments stated earlier in the results and discussion.

A serious drawback to using visible absorption spectroscopy or nmr to monitor the extent of dimerization is that there are no clear criteria for ascertaining whether the absorbance peak or resonance signal arises from only monomer–dimer interactions or higher order association into *n*-mers. In the case of Adm, where the crystal structure of the dimer is not accurately known, Pople's treatment (9) cannot be used with confidence to determine whether the shifted resonance signal is strictly due to shielding interactions that arise from the dimerization between two monomers.

We have provided evidence (based on our ^2H relaxation measurements) that the two anthracyclines probably form only dimers in aqueous solution. There is no evidence that, at the higher concentrations employed in this study, the self-association process includes higher order association into tetramers or *n*-mers. This is contrary to the model proposed by Chaires *et al.* (13).

There has been some controversy regarding the validity of calculating binding constants by various graphical methods. To this end we have avoided the use of double reciprocal plots in evaluating K_D. The data were fit directly to the model equation (eq. [10]) as explained in the materials and methods. Deranleau (31) has pointed out (based on information theory) that meaningful conclusions regarding the validity of the equilibrium model and the value of the binding constant can be obtained when the observed data cover 75% of the binding curve. Using the value of $\Delta\delta_{obs}/(\delta_D - \delta_M)$ as a measure of the degree of observable data, relative to the complete binding curve, we have obtained data covering approximately 50% of the total binding curve for the various temperatures (Fig. 4). Unfortunately, due to solubility problems with Adm in water (>6 m*M*) and the sensitivity problems associated with the nmr experiment, it was difficult to obtain data covering a larger portion of the binding curve.

Conclusion

The self-association of Adm was studied using ^1H nmr. The results of the ^2H relaxation data provide strong evidence in support of a dimer model for Adm in aqueous solutions. The chemical shift data fit closely to a dimer model which took into account the ionization of the glycosidic amine. From the temperature dependence of the dimerization process it was determined that the process was characterized by an enthalpy of -3.45 kcal M^{-1} and an approximate value for ΔS of 3 cal $\deg^{-1} M^{-1}$. The relative value of K_D determined in our studies should aid in the understanding of metal ion binding and the interaction of Adm with DNA.

Acknowledgements

We thank Dr. Charles Rodger of Bruker Spectrospin (Canada) for help in obtaining the 2-D spectrum of Adm. The ^1H nmr and ^2H experiments, at 400 MHz in this study, were performed at the Southwestern Ontario High Field NMR Centre at the University of Guelph, which was established by a Major Installation grant from the Natural Sciences and Engineering Research Council of Canada. We would like to thank Dr. R. Wasylishen for helpful discussions.

1. F. ARCAMONE. Doxorubicin. *In* Anticancer antibiotics. Vol. 17. Academic Press, New York. 1981.
2. T. SKOVSGAARD. Biochem. Pharmacol. **26**, 215 (1977).
3. T. SKOVSGAARD. Biochem. Pharmacol. **27**, 1221 (1978).
4. T. R. TRITTON, S. A. MURPHEE, and A. C. SCARTORELLI. Biochem. Biophys. Res. Commun. **84**, 802 (1978).
5. D. R. PHILLIPS and G. A. CARLYLE. Biochem. Pharmacol. **30**, 2021 (1981).
6. L. GIANNI, B. J. CORDEN, and C. E. MEYERS. Rev. Biochem. Toxicol. **5**, 1 (1983).
7. (*a*) M. SPINELLI and J. C. DABROWIAK. Biochemistry, **21**, 5862 (1982); (*b*) F. T. GREENAWAY and J. C. DABROWIAK. J. Inorg. Biochem. **16**, 91 (1982).
8. R. E. LENKINSKI, S. SIERKE, and M. H. VIST. J. Less-Common Met. **94**, 359 (1983).
9. J. A. POPLE. J. Chem. Phys. **24**, 1111 (1956).
10. J. A. POPLE, W. G. SCHNEIDER, and H. J. BERNSTEIN. High-resolution nuclear magnetic resonance. McGraw Hill Co., New York. (1959). pp. 165–183.
11. V. BARTHELEMY-CLAVEY, J. MAURIGOT, J. DIMICOLI, and P. SICARD. FEBS Lett. **46**, 5 (1974).
12. S. R. MARTIN. Biopolymers, **19**, 713 (1980).
13. J. B. CHAIRES, N. DATTAGUPTA, and D. M. CROTHERS. Biochemistry, **21**, 3927 (1982).
14. S. EKSBORG. J. Pharm. Sci. **67**, 782 (1978).
15. E. J. GABBAY, D. GRIER, R. E. FINGERLE, R. REINER, R. LEVY, S. W. PEARCE, and W. D. WILSON. Biochemistry, **15**, 2062 (1976).
16. H. H. MANTSCH, H. SAITO, and I. C. P. SMITH. Prog. Nucl. Magn. Reson. Spectrosc. **11**, 211 (1977).
17. A. ABRAGAM. The principles of nuclear magnetism. Oxford University Press, Oxford. (1961). pp. 313–315.
18. M. D. ZEIDLER. Ber. Bunsenges. Physik. Chem. **69**, 659 (1963); D. E. WOESSNER, B. S. SNOWDEN, and G. H. MEYER. J. Chem. Phys. **50**, 719 (1969); D. E. WOESSNER and B. S. SNOWDEN. Adv. Mol. Relaxation Processes, **3**, 181 (1972).
19. J. A. GLASEL, S. HENDLER, and P. R. SRIMVASAN. Proc. Natl. Acad. Sci. U.S.A. **60**, 1038 (1968).
20. A. P. ZENS, P. T. FOGLE, T. A. BRYSON, R. B. DUNLAP, R. R. FISHER, and P. O. ELLIS. J. Am. Chem. Soc. **98**, 3760 (1976); A. P. ZENS, T. A. BRYSON, R. B. DUNLAP, R. R. FISHER, and P. D. ELLIS. J. Am. Chem. Soc. **60**, 7559 (1976).
21. W. EGAN. J. Am. Chem. Soc. **98**, 4091 (1976).
22. W. P. AUE, E. BARTHOLDI, and R. R. ERNST. J. Chem. Phys. **64**, 2229 (1976).
23. G. STEIN and M. TOMKIEWICZ. Trans. Faraday Soc. **66**, 517 (1970).
24. G. G. HAMMES and C. D. HUBBARD. J. Phys. Chem. **70**, 1615 (1966).
25. A. R. MONAHAN and D. F. BLOSSEY. J. Phys. Chem. **74**, 4014 (1970).
26. D. J. BLEARS and S. S. DANYLUK. J. Am. Chem. Soc. **89**, 21 (1967).
27. G. BAUR. J. Phys. Chem. **65**, 1457 (1961).
28. P. G. RIGHETTI, M. MENOZZI, E. GIANNAZZA, and L. VALENTINI. FEBS Lett. **101**, 51 (1979).
29. P. M. LAUGHTON and R. E. ROBERTSON. *In* Solute–solvent interactions. *Edited by* J. F. Coetzee and C. D. Ritchie. Marcel Dekker, New York. 1969. pp. 399–538.
30. M. E. LAMM and D. M. NEVILLE. Jr. J. Phys. Chem. **69**, 3872 (1965).
31. D. A. DERANLEAU. J. Am. Chem. Soc. **91**, 4044 (1969).
32. D. H. LIVE and S. I. CHAN. Org. Magn. Reson. **5**, 275 (1973).

Nuclear magnetic resonance studies of molecular motion in guanidinium chloride, bromide, and iodide [1]

CHRISTOPHER I. RATCLIFFE

Chemistry Department, University of British Columbia, Vancouver, B.C., Canada V6T 1W5

and

Division of Chemistry, National Research Council of Canada, Ottawa, Ont., Canada K1A 0R9

Received September 24, 1984

CHRISTOPHER I. RATCLIFFE. Can. J. Chem. **63**, 1239 (1985).

Guanidinium $[C(NH_2)_3^+]$ chloride, bromide, and iodide salts have been studied by ^1H and ^2H nmr as a function of temperature. The ^2H powder lineshapes show conclusively that reorientation of the guanidinium ion occurs about the principal three-fold axis in the chloride, bromide, and high temperature phase of the iodide. Activation energies for this process have been obtained from ^1H spin-lattice relaxation results. The question of whether or not there are concurrent two-fold flips of the —NH_2 units is discussed, but must presently remain unresolved. It was found that the high temperature phase of the iodide can be supercooled.

CHRISTOPHER I. RATCLIFFE. Can. J. Chem. **63**, 1239 (1985).

Faisant appel à la rmn du ^1H ou du ^2H à des températures variables, on a étudié les chlorure, bromure et iodure de guanidinium $[C(NH_2)_3^+]$. Sur la base de la forme des raies des spectres ^2H de poudres, on démontre sans ambiguité que la réorientation de l'ion guanidinium se produit autour d'un axe principal ternaire dans le chlorure et le bromure ainsi que dans la phase à haute température de l'iodure. On a déduit les énergies d'activation de ces processus en se basant sur les résultats obtenus pour la relaxation spin-réseau du ^1H. On discute de la possibilité de l'existence de deux inversions concurrentes des unités —NH_2; toutefois, cette question n'est pas résolue. On a trouvé que la phase à haute température de l'iodure peut donner lieu à de la surfusion.

[Traduit par le journal]

Introduction

The guanidinium ion $[C(NH_2)_3]^+$ is one of a number of molecules in which the —NH_2 groups, and in this case the whole molecule, are planar because of π overlap of the P_z orbitals of nitrogen and carbon. This has been substantiated by *ab initio* calculations (1–4). Further examples include urea and other amide groups. Barriers to rotation about the C—N bond are expected to be much higher than in materials such as amines where the π-bonding is not present. The barriers obtained in the *ab initio* calculations (1–4) differ among themselves, but from one nmr study of the guanidinium ion in liquid crystal solution a barrier of 13 kcal/mol was reported (1). This value seems rather low, however, when compared to the barriers reported from nmr studies of formamide and acetamide in solution, which are upwards of 16 kcal/mol (e.g. refs. 5–7) and solvent dependent. In solids the barriers would, if anything, be expected to increase due to external hindrances, but no values have as yet been reported.

The work done on simple salts of guanidinium has not been extensive. Infrared and Raman studies (8–13) and early ^1H nmr lineshape studies (14–16) helped to establish the planar structure of the ion. An NQR study has reported ^{14}N quadrupole coupling parameters for a number of salts (17).

Concerning motions of the ion, Kotera *et al.* (14) reported rigid lattice ^1H nmr second moments for the iodide at liquid nitrogen (20.94 G^2) and Dry Ice temperatures (20.02 G^2) and a value of 13.81 G^2 at room temperature. Lundin *et al.* (16) interpreted second moments for $[C(NH_2)_3]Al(SO_4)_2 \cdot 6H_20$ in terms of C_3 reorientation of the guanidinium above ~130 K with an estimated activation energy of 6 kcal/mol. Pająk *et al.* (18) recently reported ^1H second moment (M_2) and spin-lattice relaxation (T_1) results for $[C(NH_2)_3]ClO_4$ and suggested that C_3 reorientation of the whole ion occurs concurrently with two-fold flips of the —NH_2 groups.

This paper presents the results of ^1H T_1 studies of guanidinium chloride, bromide, and iodide performed at an earlier date (1977), together with some recent ^2H nmr lineshapes which have helped to clarify what motions occur. X-ray structural information is available on all three salts (19, 20). At room temperature the chloride and bromide are orthorhombic. The iodide is hexagonal, but a higher temperature modification previously thought to be orthorhombic has been reported (21). The hexagonal structure is interesting in that it has two inequivalent guanidinium ions; however, its space group is piezoelectric (22), a property which sometimes makes nmr measurements difficult if not impossible.

At the time of writing of this manuscript, Grottel and Pająk (23) published results which included ^1H M_2 and T_1 results of the Cl^-, Br^-, I^-, and BF_4^- salts. They also mention that X-ray powder results on the high temperature phase of the iodide suggest that it is cubic. While their T_1 results qualitatively resemble those presented here, a number of quantitative differences have been found which will be discussed in context. The results presented here also extend the T_1 measurements for the high temperature phase of the iodide into the metastable region below 350 K.

Experimental

The three halide salts were prepared by addition of the appropriate dilute acid to a solution of guanidinium carbonate until neutral. The resulting solutions were then evaporated until crystallization set in on cooling and the filtered products were then recrystallized from water.

Proton spin lattice relaxation times (T_1) were measured at 30.2 MHz over a range of temperatures using an inversion–recovery, $\pi - t - \pi/2$ pulse sequence on a Bruker B-KR322S spectrometer described before (24) (Chemistry Department, University of British Columbia). The free induction decay was apparently exponential within experimental error for the chloride, bromide, and higher temperature phase of the iodide. Further measurements on the bromide were obtained at 16 MHz.

The hexagonal phase of the iodide proved to be more unusual. In

[1]Issued as NRCC No. 24143.

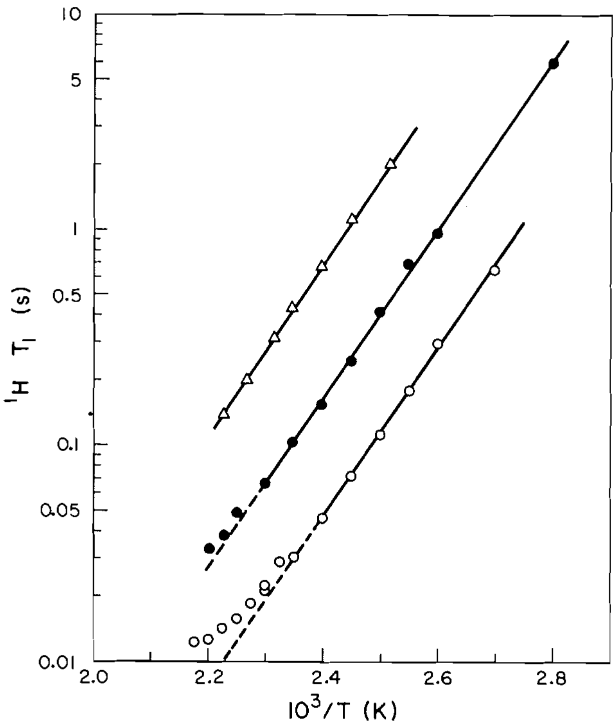

FIG. 1. The temperature dependence of the proton spin-lattice relaxation times observed for guanidinium chloride (△) at 30.2 MHz, bromide (●) at 30.2 MHz, and bromide (○) at 16.0 MHz. The solid lines indicate the linear least-squares fits.

the first place its piezoelectric nature was confirmed by the presence of a "noise" superimposed on the free induction decay. The noise was also present if the sample was removed from the magnetic field. Such signals often make measurement of T_1 impossible without special screening of the sample from the r.f. coil (25). However, in this case the piezoelectric signal was not excessive, appearing as a weaker signal superimposed on the free induction decay, and its pattern remained constant with each pulse. Consequently measurements of the magnetization recovery were still attempted. However, the relaxation proved to be quite non-exponential. An approximate relaxation parameter T_1' was therefore obtained from the time at which the magnetization recovery crossed zero assuming $T_1' \approx (t_0)/\ln 2$ (the so-called "null" method). The reasons for this non-exponential behaviour are obscure, but one is inclined to believe, in the absence of other obvious factors, that it may be due to an error introduced by the superimposed piezoelectric noise. Neither the piezoelectric behaviour nor the non-exponential decay were mentioned by Grottel and Pająk (23).

Deuterated samples of the salts were prepared from the fully protonated materials by repeated dissolution in and evaporation from D_2O (3 times). The ^2H nmr powder lineshapes were obtained at 27.63 MHz using a Bruker CXP 180 spectrometer, a Bruker/Oxford Instruments cryomagnet, and a variable temperature N_2 gas-flow probe with a Bruker B-VT-1000 temperature controller (Chemistry Division, NRCC). A quadrupole echo pulse sequence (26) was used with a delay time of 35 μs between X and Y pulses of 2.5 μs, and phase alternation. The cycle repetition rates varied from 0.4 to 20 s depending on T_1.

Results and analysis

Plots of log T_1 vs. $1000/T$ are shown in Figs. 1 and 2. The chloride and bromide have very long T_1's up to temperatures of about 370 K. Above this temperature the results show the linear low temperature slope of some relaxation mechanism, up to the highest temperatures before the samples melt. The results at

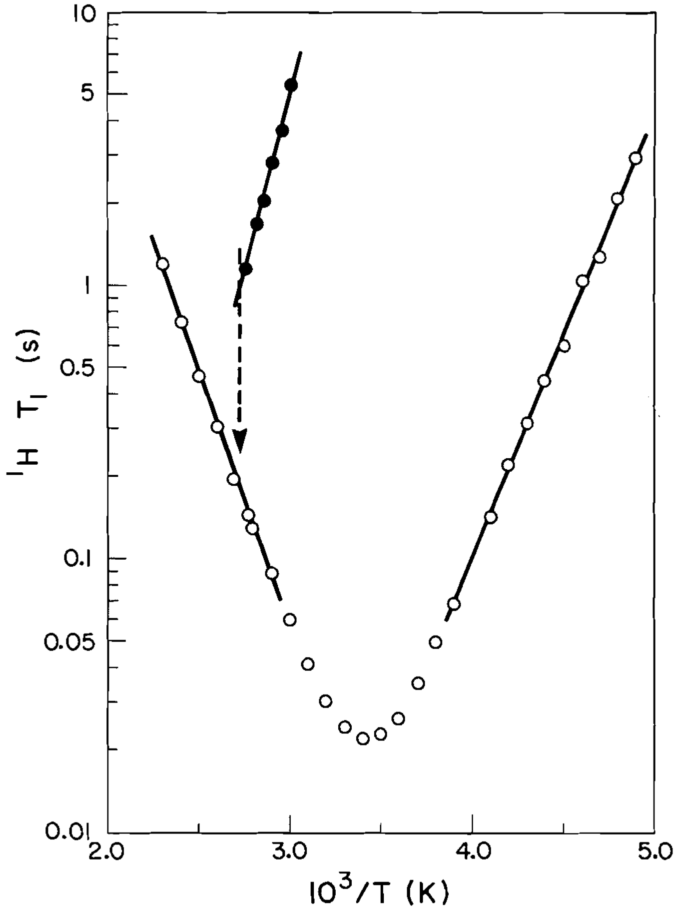

FIG. 2. The temperature dependence of the proton spin-lattice relaxation times observed for guanidinium iodide at 30.2 MHz; hexagonal phase (●), high temperature (and metastable) phase (○). The solid lines indicate the linear least-squares fits.

16 MHz for the bromide were obtained specifically to try to reach a T_1 minimum and, as can be seen, this was practically achieved. A value for $(T_1)_{min}$ = 12.0 ms at 460 K and 16 MHz is indicated. (An equivalent minimum at 30.2 MHz should therefore be 22.7 ms.) Also note that the T_1 results at the two frequencies fit the expected ω_0^2 dependence.

For the iodide the behaviour at the phase change varied somewhat, dependent upon the history of the sample. On warming, as the phase change was reached T_1 decreased dramatically and the piezoelectric effect disappeared over a period of several minutes. For a sample which had been previously melted to achieve greater packing in the sample tube this change took place at about 350 K, but for a powdered sample it occurred at about 365 K. This high temperature phase of both samples could then be supercooled. When left in this state at room temperature the powdered sample reverted to the hexagonal phase within an hour whereas the melted sample took much longer. Both gave similar values of T_1 in the supercooled state. (Note that Grottel and Pająk's (23) results do not extend into the supercooled region.) The complete T_1 curve in Fig. 2 thus represents the higher temperature phase. The higher temperature slope is greater than the lower temperature slope. The curve reaches a $(T_1)_{min}$ of 22 ms consistent with the bromide result (converted to 30.2 MHz), which suggests that the two minima are representative of similar relaxation mechanisms. Since the chloride appears to behave in a manner similar to the bromide it seems reasonable to assume that it too is relaxing by the same mechanism.

The few T_1−null results for the hexagonal phase of the iodide fall on a straight line, forming the low temperature slope of a T_1 curve. There is insufficient information in this to determine the relaxation mechanism, though one might again anticipate C_3' reorientation. It should be remembered, however, that for this phase (hexagonal) there are two inequivalent guanidinium ions in the cell, which might reorient at different rates.

Theoretical calculations of ^1H $(T_1)_{min}$ values for different motions

The T_1 results may be interpreted using the framework of the modified B.P.P. theory (27, 28). Modulation of the internuclear dipole−dipole interactions by molecular motions leads to spin-lattice relaxation. For an interproton vector:

$$\left(\frac{1}{T_1}\right)_{H-H} = \frac{3}{2}\gamma_H^4\hbar^2 I(I+1)[J^{(1)}(\omega_H) + J^{(2)}(2\omega_H)]$$

γ_H = magnetogyric ratio for ^{1}H, $\hbar = h/2\pi$, $I = 1/2$ for ^{1}H, ω_H = ^{1}H Larmor frequency. The $J^{(n)}(\omega)$ represent the spectral density functions for the particular motion concerned.

For a proton−nitrogen vector the situation is more complex (29), but it was shown in a previous paper concerning —NH_3^+ group ^{1}H relaxation (30) that the cross-relaxation terms had little effect on the observed ^{1}H T_1. Assuming a similar situation in the present case, the ^{14}N contribution to the proton relaxation is then well approximated by

$$\left(\frac{1}{T_1}\right)_{N-H} = \gamma_H^2\gamma_N^2\hbar^2 S(S+1) \times \left[\frac{1}{12}J^{(0)}(\omega_H - \omega_N) + \frac{3}{2}J^{(1)}(\omega_H) + \frac{3}{4}J^{(2)}(\omega_H + \omega_N)\right]$$

where $S = 1$ for ^{14}N. (Note this also neglects any ^{14}N quadrupolar interactions.)

The spectral density functions $J^{(n)}(\omega)$ must then be evaluated for each motion. The methods of Woessner (31) are probably the most frequently used to do this. However, in cases where the internuclear distance is changed by the motion, it is more convenient to use an apparently less well-known method (29, 32, 33). To obtain the overall relaxation rate for a particular motion one must (1) calculate, for each proton, the sum of the effects of motion on all the dipole−dipole vectors connecting that target proton to other nuclei, and (2) assuming rapid spin diffusion, average over all protons.

Calculated theoretical $(T_1)_{minimum}$ values for a number of possible motions are outlined below (values are given in Table 1). The molecular parameters used were N—H = 1.00 Å, C—N = 1.33 Å, and all bond angles 120° in the plane.

The final expressions for motions of the ion when *no internal rotation* occurs are relatively simple. For reorientation about the 3-fold axis (C_3' motion)

$$\left(\frac{1}{T_1}\right)_{C_3'} = \frac{9}{40}\frac{\gamma_H^4\hbar^2}{\omega_H}f(\omega_H\tau_c)\sum_i\frac{1}{r_{Hi}^6} + 2\frac{\gamma_H^2\gamma_N^2\hbar^2}{\omega_H}f'(\omega_H\tau_c)\sum_j\frac{1}{r_{Nj}^6}$$

where

$$f(\omega_H\tau_c) = \left[\frac{\omega_H\tau_c}{1+\omega_H^2\tau_c^2} + \frac{4\omega_H\tau_c}{1+4\omega_H^2\tau_c^2}\right]$$

and

TABLE 1. Calculated T_1 minimum values (ms) for motions of the guanidinium ion

Motion	T_1 (ms) 16 MHz	30.2 MHz
C_3' threefold axis	9.2	17.3
C_2' twofold axis	18.3	34.6
Isotropic	6.9	13.0
C_2 internal twofold reorientation of —NH_2	91.0	171.7
All 3 —NH_2 groups performing C_2	60.6	114.5

$$f'(\omega_H\tau_c) = \left[\frac{\omega_H\tau_c}{1+\omega_H^2\tau_c^2}\right]$$

and the r_{Hi}, r_{Nj} are the H---H and N---H distances. Implicit in the expression $f'(\omega_H\tau_c)$ for the N---H contribution is the approximation that $(\omega_H - \omega_N) \approx \omega_H \approx (\omega_H + \omega_N)$. τ_c is the correlation time for the motion and is assumed to have an Arrhenius dependence on temperature T and the activation energy E_a:

$$\tau_c = \tau_c^0 \exp(E_a/RT)$$

For isotropic motion one finds

$$\left(\frac{1}{T_1}\right)_{iso} = \frac{4}{3}\left(\frac{1}{T_1}\right)_{C_3'}$$

For reorientation about a two-fold axis (C_2' motion)

$$\left(\frac{1}{T_1}\right)_{C_2'} = \frac{9}{40}\frac{\gamma_H^4\hbar^2}{\omega_H}f(\omega_H\tau_c)\sum_i\left[\frac{\sin^2(2\Delta i)}{r_{Hi}^6}\right] + \frac{2\gamma_H^2\gamma_N^2\hbar^2}{\omega_H}f'(\omega_H\tau_c)\sum_j\left[\frac{\sin^2(2\Delta j)}{r_{Nj}^6}\right]$$

where Δi, Δj refer to the angle between an internuclear vector and the rotation axis. Coincidentally it is found that for this specific case where all bond angles in the plane are 120°

$$\left(\frac{1}{T_1}\right)_{C_2'} = \frac{1}{2}\left(\frac{1}{T_1}\right)_{C_3'}$$

For C_2 rotation of one NH_2 group with the rest of the molecule rigid (i.e. internal reorientation), the final expression is more complex:

$$\left(\frac{1}{T_1}\right)_{C_2} = \frac{1}{20}\frac{\gamma_H^4\hbar^2}{\omega_H}f(\omega_H\tau_c)\sum_i \times\left[\frac{1}{r_{Hi}^6} + \frac{1}{s_{Hi}^6} - (3\cos^2\Omega_i - 1)\cdot\frac{1}{r_{Hi}^3}\cdot\frac{1}{s_{Hi}^3}\right] + \frac{2}{9}\frac{\gamma_H^2\gamma_N^2\hbar^2}{\omega_H}f'(\omega_H\tau_c)\sum_j \times\left[\frac{1}{r_{Nj}^6} + \frac{1}{s_{Nj}^6} - (3\cos^2\Omega_j - 1)\cdot\frac{1}{r_{Nj}^3}\cdot\frac{1}{s_{Nj}^3}\right]$$

where the summations over i, j cover the interaction between *one of the mobile protons* and the other protons or nitrogens. r and s refer to the internuclear distances in the two sites and Ω refers to the angle between the two orientations. If all three —NH_2 groups are able to rotate with similar correlation times then the above expression for C_2 motion must be multiplied by

TABLE 2. Activation energies (kcal/mol)*

Salt	High temperature slope		Low temperature slope	
Cl^-			18.29±0.12 (0.9999)	[16.2]
Br^- 30.2 MHz			17.93±0.19 (0.9997)	
Br^- 16.0 MHz			17.85±0.33 (0.9994)	[14.8]
I^- (hexagonal)			12.04±0.32 (0.9986)	[10.0]
I^- (metastable)	8.62±0.11 (0.9995)	[8.1]	7.43±0.11 (0.9992)	
ClO_4^-		[7.9]		[10.0]
BF_4^-		[6.2]		

*Least-squares correlation coefficients are given in ( ). Grottel and Pająk's (23) results given in [ ].

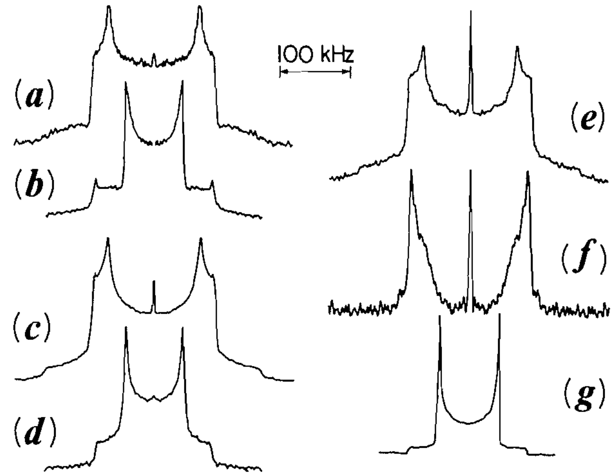

FIG. 3. The ^2H nmr powder lineshapes of guanidinium chloride (a) 307 K; (b) 425 K; bromide (c) 303 K, (d) 420 K; hexagonal iodide (e) 302 K, (f) 345 K; and metastable iodide (g) 311 K.

3/2. (Note these are independent flips, not a concerted reorientation of all three NH_2 groups at once.)

When the molecular parameters have been introduced, all the expressions above reduce to the form

$$\frac{1}{T_1} = (A + B)\left(\frac{\omega_H\tau_c}{1 + \omega_H^2\tau_c^2}\right) + 4A\left(\frac{\omega_H\tau_c}{1 + 4\omega_H^2\tau_c^2}\right)$$

which can then be solved for a minimum in T_1. Results are given in Table 1. It should be pointed out that the contribution to T_1 (at the minimum) of N—H interactions in the cases where the molecule is internally rigid is ~26%, whereas for internal rotation of $—NH_2$ groups this contribution jumps to ~67%. In the latter case it is then quite possible that cross-relaxation terms, which were neglected earlier, could affect the ^1H relaxation behaviour to some degree. However, further calculations to take this effect into account are not really warranted at this point, since it is quite clear that internal rotations of $—NH_2$ groups are far less efficient at producing ^1H relaxation than any of the rigid ion motions.

The observed T_1 minima for the bromide and iodide clearly correspond most closely to the calculated value for C_3' motion. (Calculated T_1 values are almost invariably found to be slightly less than those observed and in any case depend on the structural parameters chosen.) However, one more type of motion which should be considered is the composite motion of NH_2 flips concurrent with whole ion C_3' motion. Without going into a complex and very involved calculation for this particular case, one can assert that if the two processes have similar correlation times then the resultant T_1 minimum should not be less than that given by

$$\left(\frac{1}{T_1}\right)_{\text{composite min}} = \left(\frac{1}{T_1}\right)_{C_3' \text{ min}} + \left(\frac{1}{T_1}\right)_{C_2 \text{ min}}$$

For all three NH_2 groups flipping, this means that the T_1 minimum value should be no lower than 15 ms (30.2 MHz). This is not much different from the value for C_3' alone. Considering experimental errors and the usual discrepancies between observed and calculated T_1 minima, it does not seem realistic to distinguish between these two types of motion. In either case C_3' motion occurs and is the principal cause of relaxation, so that one can be reasonably certain from the T_1 results that such a motion is occurring. The question of whether or not there are concurrent NH_2 flips, however, should remain open. At this point the author diverges from the view of Grottel and Pająk (23) who interpreted their T_1 and M_2 results in terms of the $(C_3' + C_2)$ model. There is no reason to believe that their M_2 results provide any firmer grounds than the T_1 results for preferring $(C_3' + C_2)$ over C_3' alone.

Activation energies obtained from the linear slopes of the ln T_1 vs. $1000/T$ plots by least-squares fits are given in Table 2. It is in these activation energies that one first notices discrepancies between Grottel and Pająk's (23) and the present results. Also, when the difference in frequencies is taken into account it is found that the T_1 values for the chloride and bromide salts in the current work are lower than Grottel and Pająk's, but the situation is reversed for the high temperature phase of the iodide. The reasons for these differences are obscure at the present. Attempts were also made to fit the complete T_1 curve for the metastable iodide, using the model for C_3' motion including $^1H{-}{-}{-}^{14}N$ terms. However, the appreciable difference in slope on either side of the minimum would not permit a satisfactory fit, though the attempted fit gave an indication of the order of magnitude of the correlation time constant τ_c^0 as roughly 6×10^{-15} s.

^2H Lineshapes

Conclusive confirmation of motion around the C_3' axis comes from the ^2H lineshapes shown in Fig. 3. Close to room temperature the chloride, bromide, and hexagonal iodide have essentially rigid lattice lineshapes (Fig. 3 a, c, e, respectively) characteristic of planar $—ND_2$ groups involved in a π-bonding system. Note that this shows that both crystallographic types of guanidinium in the hexagonal iodide are rigid. The quadrupole coupling constants and asymmetry parameters are very similar to those observed in urea and thiourea (34, 35), Table 3.

The chloride and bromide at temperatures above 410 K and the high temperature phase of the iodide (even when supercooled to room temperature) show narrowed lineshapes (Fig. 3 b, d, g, respectively) corresponding to an axially symmetric coupling tensor, Table 3. At 345 K the hexagonal phase of the iodide is clearly undergoing a line narrowing transition but unfortunately does not reach the rapid motion limit before the phase change sets in (Fig. 3f). Figure 4 shows the calcu-

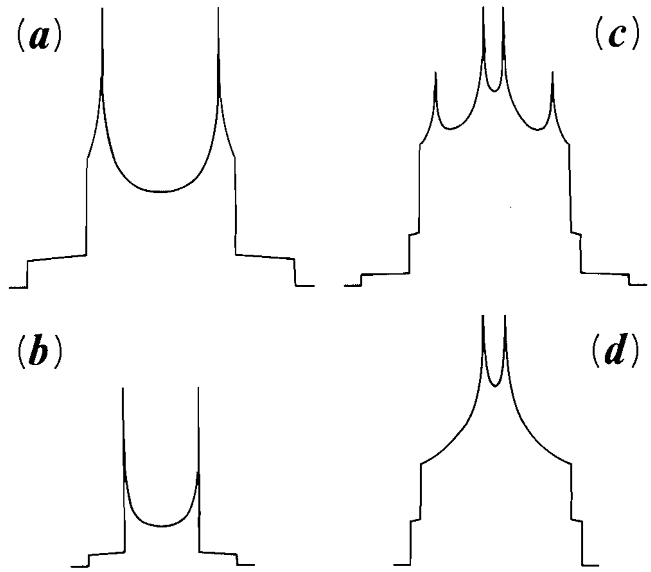

FIG. 4. Calculated ^{2}H powder nmr lineshapes for different motional processes (a) rigid, (b) C_3' reorientation, (c) C_2' reorientation, and (d) C_2 (NH_2) reorientation.

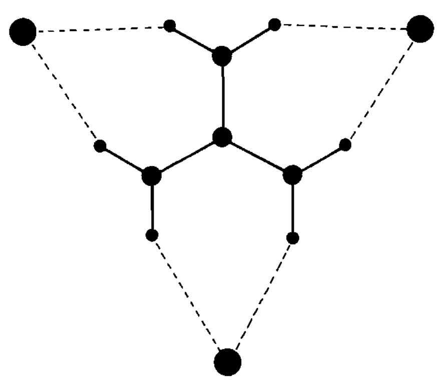

FIG. 5. A view down the C_3 axis of the chloride showing the arrangement of the three chloride ions with which there are hydrogen bonding contacts.

lated lineshapes for various cases of rapid motional averaging, assuming a rigid lattice value of $\eta = 0.12$ and bond angles all 120°. If the rigid q_{zz} is assumed to be along the ND bond axis then q_{yy} turns out to be perpendicular to the molecular plane (q_{xx} in the plane). (Lineshapes, other than rigid, are calculated by averaging the tensor components at all the equilibrium positions sampled by the motion, see ref. 36.) It is quite clear from a comparison of observed and calculated lineshapes that C_3' motion occurs; however, one again cannot distinguish between C_3' alone and C_3' concurrent with C_2 flips (the averaged lineshapes would be the same).

Structural considerations

It is informative to consider the immediate environment of the guanidinium ions, using the structural information available (19, 20). Since accurate H atom positions are not available, the lattices were regenerated in Cartesian space and the original (X-ray) CN_3 units were replaced by the symmetrical guanidinium ion, including the six H atoms, which was used earlier in the paper. Closest contacts of the protons in the rigid lattice case and their closest approaches to the surrounding atoms for C_2, C_2', and C_3' motions were then calculated. Contacts less than the sum of the van der Waals radii were taken as significant. The following important features emerged.

TABLE 3. ^{2}H Quadrupole coupling constants and asymmetry parameters

		Rigid lattice		Rapid C_3' motion	
Salt	T (K)	e^2qQ/h (Hz)	η	e^2qQ/h	η
Chloride	307	200 500	0.1445		
	425			107 400	0
Bromide	303	205 100	0.1416		
	420			109 900	0
Iodide Hexagonal	302	206 000	0.1331		
Iodide	311			112 800	0
Metastable	350			112 000	0
Thiourea*	250	207 800	0.1206		
Urea*	301	215 083	0.131		

*Obtained from powder samples in this laboratory, see refs. 34 and 35 for older single crystal results.

TABLE 4. Closest contacts with halide ions at equilibrium and during C_3' rotation (Å) (idealized guanidinium geometry as used in text)

	Cl	Br	I1*	I2*
C_3' rotation	1.73	1.86	2.14	2.38
Equilibrium	2.33	2.42	2.75	2.94

*The hexagonal iodide has two inequivalent guanidinium ions.

(1) In all cases, at the equilibrium position (rigid case) each H atom has only *one* significant overlap and that occurs with a halide ion. This is indicative of a hydrogen-bonding interaction.

(2) In all cases, three halide ions which are close to the plane of the guanidinium ion form a 3-fold or near 3-fold arrangement around the C_3 axis of the guanidinium. (In the cases of the bromide and iodide these three ions fall in a plane parallel to the plane of the guanidinium.) Figure 5 shows a view down the C_3 axis of the chloride, indicating these contacts. The view is essentially the same for the bromide and for the two types of guanidinium ion in the hexagonal iodide, except that the halide ions are further removed from the central axis.

(3) These three halide ions are also the only atoms which overlap the H atoms of the guanidinium during a C_3' reorientation.

(4) In all cases it was found that a C_2 flip of NH_2 would cause overlaps with halide ions to about the same extent as in the equilibrium position, and in most cases *slight* overlaps with one H atom (other than those within the guanidinium ion).

(5) In all cases C_2' rotation would cause a large number of overlaps with all types of atoms, suggesting that this motion should be sterically very unfavourable.

It is difficult to judge at what point a close approach to a halide ion becomes a repulsive rather than attractive (hydrogen-bonding) interaction, but these two forces presumably come into play in the C_3' motion (which has now been shown to occur in these materials). Table 4 lists the closest contacts with the three neighbouring halide ions. At the equilibrium position the geometry is most favourable for hydrogen bonding to all the protons and appreciable overlaps are already present. During the C_3' rotation the overlaps become much greater, first for one set of three protons and then the other three, but since these positions are not at the equilibrium position the interaction has presumably become more repulsive than attractive. The 3-fold arrangement of halide ions around the C_3' axis also means that the contributions to the total barrier from each individual halide ion add up constructively. The large barriers (particularly in the chloride and bromide) are then quite understandable.

In concluding, it is worth returning to the question of whether or not C_2 flips occur concurrently with the C_3' motion. One can advance some arguments against C_2 flips, based on observed and anticipated barriers. Note that the C_3' barrier depends *entirely* on interactions with atoms external to the guanidinium ion, and hence the large variations from one salt to another are easily rationalized. On the other hand, the barrier to C_2 flipping depends both on an internal and an external barrier. It was pointed out in the introduction that the internal barrier to C_2 flips should be at the very least 13 kcal/mol and probably significantly higher. This internal barrier should be similar in all salts and any difference from one salt to another would then be due to the additional external barrier. Clearly the activation energies observed in the I^-, ClO_4^-, and BF_4^- salts (this work and refs. 18, 23) are well below the minimum level anticipated for the internal barrier alone, for C_2 flips. This is perhaps the strongest argument against concurrent ($C_3' + C_2$) motions, at least for these salts. Further, one would not expect C_3' and C_2 motions to occur simultaneously in *all* the salts, especially when the observed range of barriers is so great and particularly when it would appear that the internal barrier dominates the C_2 flipping motion. A complete resolution of this question, however, must await further experimental evidence from a technique which is able to sufficiently distinguish the two motions.[2]

Acknowledgements

The author would like to express sincere thanks to Dr. B. A. Dunell of the University of British Columbia, in whose laboratory the ^1H T_1 measurements were performed, and to the National Research Council of Canada (now NSERC) for a Grant-in-Aid of that research, made to Dr. B. A. Dunell.

1. T. Bally, P. Diehl, E. Haselbach, and A. S. Tracey. Helv. Chim. Acta, **58**, 2398 (1975).
2. P. Kollman, J. McKelvey, and P. Gund. J. Am. Chem. Soc. **97**, 1640 (1975).
3. J. F. Capitani and L. Pederson. Chem. Phys. Lett. **54**, 547 (1978).

[2]Interested readers are referred to a paper by S. Gima *et al.* (37), which appeared after acceptance of the current paper.

4. A. M. Sapse and L. J. Massa. J. Org. Chem. **45**, 719 (1980).
5. H. Kamei. Bull. Chem. Soc. Jpn. **41**, 2269 (1968).
6. T. Drakenberg and S. Forsén. J. Phys. Chem. **74**, 1 (1970).
7. T. Drakenberg. Tetrahedron Lett. **18**, 1743 (1972).
8. C. L. Angell, N. Sheppard, A. Yamaguchi, T. Shimanouchi, T. Miyazawa, and S. Mizushima. Trans. Faraday Soc. **53**, 589 (1957).
9. J. Gupta. J. Ind. Chem. Soc. **13**, 575 (1936).
10. J. T. Edsall. J. Phys. Chem. **41**, 133 (1937).
11. O. D. Bonner and C. F. Jordan. Spectrochim. Acta, Part A, **32**, 1243 (1976).
12. R. Mecke and W. Kutzelnigg. Spectrochim. Acta, **16**, 1225 (1960).
13. O. D. Bonner. J. Phys. Chem. **81**, 2247 (1977).
14. A. Kotera, T. Morita, S. Aoyagi, Y. Kakiuchi, S. Nagakura, and K. Kume. Nippon Kagaku Zasshi, **82**, 302 (1961).
15. K. S. Aleksandrov, A. G. Lundin, and G. M. Mikhailov. Sov. Phys. Crystallogr. **5**, 77 (1960).
16. A. G. Lundin, G. M. Mikhailov, and S. P. Habuda. Sov. Phys. JETP, **13**, 903 (1961).
17. T. Oja. J. Chem. Phys. **59**, 2668 (1973).
18. Z. Pająk, M. Grottel, and A. E. Koziol. J. Chem. Soc. Faraday Trans. 2, **78**, 1529 (1982).
19. W. Theilacker. Z. Kristallogr. **90**, 51 (1935); **90**, 77 (1935); **90**, 256 (1935).
20. D. J. Haas, D. R. Harris, and H. H. Mills. Acta Crystallogr. **19**, 676 (1965).
21. R. Cadoret and J.-C. Monier. C.R. Acad. Sci. **256**, 5110 (1963).
22. J. C. Burfoot. Ferroelectrics. Van Nostrand, London. 1967.
23. M. Grottel and Z. Pająk. J. Chem. Soc. Faraday Trans. 2, **80**, 553 (1984).
24. C. I. Ratcliffe and B. A. Dunell. J. Chem. Soc. Faraday Trans. 2, **73**, 493 (1977).
25. L. Pandey and D. G. Hughes. J. Magn. Reson. **56**, 443 (1984).
26. J. H. Davis, K. R. Jeffrey, M. Bloom, M. I. Valic, and T. P. Higgs. Chem. Phys. Lett. **42**, 390 (1976).
27. N. Bloembergen, E. M. Purcell, and R. V. Pound. Phys. Rev. **73**, 679 (1948).
28. R. Kubo and K. Tomita. J. Phys. Soc. Jpn. **9**, 888 (1954).
29. A. Abragam. The principles of nuclear magnetism. Oxford. 1961.
30. C. I. Ratcliffe. J. Magn. Reson. **38**, 283 (1980).
31. D. E. Woessner. J. Chem. Phys. **36**, 1 (1962).
32. U. Haeberlen and G. Maier. Z. Naturforsch. Teil A, **22**, 1236 (1967).
33. A. Watton. J. Chem. Phys. **65**, 3653 (1976).
34. D. E. O'Reilly, E. M. Peterson, and Z. M. El Saffar. J. Chem. Phys. **54**, 1304 (1971).
35. T. Chiba. Bull. Chem. Soc. Jpn. **38**, 259 (1965).
36. R. G. Barnes. *In* Advances in nuclear quadrupole resonance. Vol. 1. *Edited by* J. A. S. Smith. Heyden, New York. 1974. p. 335.
37. S. Gima, Y. Furukawa, and D. Nakamura. Ber. Bunsenges. Phys. Chem. **88**, 939 (1984).

Kinetics of the reduction of nicotinonitrile cations by 1,4-dihydronicotinamides

JOHN W. BUNTING AND JOHN C. BREWER[1]
Department of Chemistry, University of Toronto, Toronto, Ont., Canada M5S 1A1

Received September 20, 1984

JOHN W. BUNTING and JOHN C. BREWER. Can. J. Chem. **63**, 1245 (1985).

The rates of reduction of a series of 1-(Z-benzyl)nicotinonitrile cations by a series of 1-(X-benzyl)-1,4-dihydronicotinamides have been studied at 25°C in 20% CH_3CN – 80% H_2O (pH 7.0 (5 m*M* phosphate), ionic strength 1.0 (KCl)). Spectral studies indicate the formation of 1,4-dihydronicotinonitrile products, without the formation of the isomeric 1,2-dihydro- or 1,6-dihydro-nicotinamide intermediates. Second-order rate constants (k_2) for these reductions are closely correlated with the Hammett σ constants for X and Z. Thus, for X = H, $\log k_2 = 0.63\sigma_z - 1.05$, while for Z = 4-CN, $\log k_2 = -0.64\sigma_x - 0.65$. The close correspondence between these ρ_x and ρ_z values indicates that charge neutralization on the nicotinonitrile cation exactly balances charge generation on the nicotinamide cation product in the rate-determining transition state. Thus the migrating hydrogen species is electrically neutral in the rate-determining transition state, which contrasts with the hydridic transition states previously reported in the reduction of isoquinolinium cations by 1,4-dihydronicotinamides. When 1-benzyl-4,4-dideuterio-1,4-dihydronicotinamide is used as the reductant, primary kinetic isotope effects of 3.0 and 2.7 are observed for the reduction of the 1-methylnicotinonitrile and 1-(4-cyanobenzyl)-nicotinonitrile cations, respectively. These data are evaluated in terms of the various mechanistic possibilities for hydride transfer.

JOHN W. BUNTING et JOHN C. BREWER. Can. J. Chem. **63**, 1245 (1985).

Opérant à 25°C, dans des solutions à 20% CH_3CN – 80% H_2O, à un pH de 7,0 (5 m*M* de phosphate) et à une force ionique de 1,0 (KCl), on a déterminé les vitesses de réduction d'une série de cations (Z-benzyl)-1 nicotinonitrile par une série de (X-benzyl)-1 dihydro-1,4 nicotinamides. Des études spectrales indiquent qu'il y a formation de produits dihydro-1,4 nicotinonitrile, sans formation des intermédiaires isomères dihydro-1,2 ou dihydro-1,6 nicotinamides. Il existe une corrélation entre les constantes de vitesse du deuxième ordre (k_2) de ces réductions et les constantes σ de Hammett des substituants X et Z. Ainsi, pour X = H, $\log k_2 = 0,63\sigma_z - 1,05$, alors que pour Z = CN-4, $\log k_2 = -0,64\sigma_x - 0,65$. La bonne correspondance entre ces valeurs de ρ_x et de ρ_z indique que, dans l'état de transition déterminant la vitesse de la réaction, la neutralisation de la charge du cation nicotinonitrile contrebalance exactement la génération de la charge sur le produit cationique nicotinamide. Dans l'état de transition qui détermine la vitesse de la réaction, l'hydrogène qui migre est électriquement neutre et ceci est en opposition avec les états de transition impliqués dans les réductions par les hydrures dont il était fait mention dans les rapports antérieurs sur la réduction de cations isoquinolinium par les dihydro-1,4 nicotinamides. Lorsqu'on utilise la benzyl-1 dideutéro-4,4 dihydro-1,4 nicotinamide comme réducteur, on observe des effets isotopiques primaires de 3,0 et 2,7 respectivement pour les réductions des cations méthyl-1 nicotinonitrile et (cyano-4 benzyl)-1 nicotinonitrile. On évalue ces données en fonction des diverses possibilités mécanistiques pour le transfert d'hydrure.

[Traduit par le journal]

We have recently reported kinetic studies of the reduction of a variety of quinolinium (1), isoquinolinium (2, 3), 3,4-dihydroisoquinolinium (4), and acridinium cations (5) by 1,4-dihydronicotinamides as part of our continuing investigation of the kinetics and mechanisms of hydride transfer in such reactions. For isoquinolinium and 3,4-dihydroisoquinolinium cations, the combination of substituent effects in the hydride donor and acceptor and deuterium primary kinetic isotope effects are only consistent with a direct one-step hydride transfer in which the migrating hydrogen bears a significant fractional negative charge and is thus clearly hydridic in character. Kinetic data for the reduction of quinolinium and acridinium cations (1, 5) are not easily rationalized in terms of one-step hydride transfer, and the possibility of one of the often considered one-electron reduction mechanisms ($e^- + H\cdot$ or $e^- + H^+ + e^-$) is thus indicated in these cases. This interpretation is supported by the enhanced rates of 1,4-dihydronicotinamide reduction that are found for quinolinium (at C-4) and acridinium cations relative to the analogous reaction for isoquinolinium cations. This rate enhancement is particularly dramatic in comparison with the rates of other nucleophilic attacks on these heteroaromatic cations (1, 5).

Van Eikeren *et al.* (6, 7) have studied the degenerate reaction between 1-benzyl-1,4-dihydronicotinamide and the 1-benzylnicotinamide cation and have concluded that this reaction is best rationalized in terms of an $e^- + H^+ + e^-$ mechanism for the formal hydride transfer. The reductions of quinolinium and acridinium cations by 1,4-dihydronicotinamides also differ from isoquinolinium cation reductions in generating 1,4-dihydropyridine derivatives rather than 1,2-dihydropyridines as reaction products. It therefore seems possible that one-electron mechanisms for hydride transfer predominate over direct hydride transfer for the formation of 1,4-dihydropyridines.

As a further test of this hypothesis we have now studied substituent effects in both the hydride donor and acceptor for the reduction of a series of 1-(Z-benzyl)nicotinonitrile cations by 1-(X-benzyl)-1,4-dihydronicotinamides (eq. [1]). This reaction is closely related to the degenerate hydride transfer

[1]

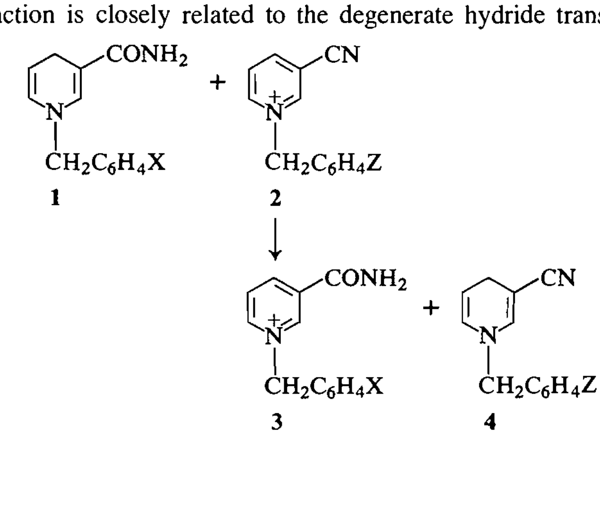

[1]Recipient of a 1983 NSERC Summer Bursary for undergraduate research.

studied by van Eikeren and Grier (6), but has the advantage of being somewhat faster because of the electronic effect of the cyano group, and also of easily allowing independent evaluation of substituent effects in the hydride donor and acceptor.

Experimental

1-(X-benzyl)-1,4-dihydronicotinamides and 1-benzyl-4,4-dideuterio-1,4-dihydronicotinamide were prepared and characterized as previously described (2).

1-(Z-benzyl)nicotinonitrile bromides

Nicotinonitrile (2 g) and the appropriately substituted benzyl bromide (in 20% stoichiometric excess) were refluxed in acetone (35 mL) for 10–16 h. The bromide salts precipitated from this solvent as fine white powders that were recrystallized from either ethanol or aqueous ethanol in the presence of a few drops of concentrated hydrobromic acid. These salts were characterized by ^{1}Hmr spectroscopy, and their purities determined to be 100 ± 2% by titration of the bromide ion by the Volhard method (8).

1-Methylnicotinonitrile bromide was prepared by stirring nicotinonitrile with methyl bromide in a pressure bottle at room temperature, and was similarly characterized.

Kinetic studies

All kinetic data were obtained spectrophotometrically on either Varian Cary 219 or Unicam SP-1800 instruments at 25°C. All reactions were studied in 20% acetonitrile – 80% water solutions buffered at pH 7.0 (5 m*M* phosphate) in the presence of 1 *M* potassium chloride. The decrease in absorbance due to the consumption of the dihydronicotinamide derivative (0.05–0.1 m*M*) was monitored at 380 nm in the presence of at least six different concentrations of each nicotinonitrile cation in the range 1.0–50 m*M*. Individual concentration ranges were determined by the solubility of the bromide salt and the reactivity of each cation. All reactions displayed absorbance changes that were strictly pseudo first order in the dihydronicotinamide over at least the first three reaction half-times. Rates of decomposition of the dihydronicotinamide derivatives were found to be insignificant under the current reaction conditions.

The equilibrium constant for the addition of cyanide ion to the 1-benzylnicotinonitrile cation was measured in aqueous solution at pH 11.0 (1 m*M* KOH) at 25°C in the presence of 1 *M* KCl, as previously described (9) for cyanide ion addition to nicotinamide cations. Potassium cyanide concentrations in the range 1.0–40 m*M* were employed.

Results

Reaction products

The time dependence of the electronic absorption spectrum of an equimolar mixture of 1-benzyl-1,4-dihydronicotinamide and the 1-benzylnicotinonitrile cation in 20% CH_3CN – 80% H_2O, ionic strength 1.0 at 25°C, is shown in Fig. 1. The shift to shorter wavelength of the long wavelength maximum during the course of this reaction is consistent with the formation of 1-benzyl-1,4-dihydronicotinonitrile, since 1,4-dihydronicotinonitriles are known to have absorption maxima at shorter wavelength than their 1,4-dihydronicotinamide analogs (10). The reaction product in Fig. 1 displays $\lambda_{max}(\epsilon)$ = 344 nm (6200 M^{-1} cm^{-1}) which is in agreement with 341 nm (5750 M^{-1} cm^{-1}) observed for a genuine sample of **4**:Z = H in neat acetonitrile solution (3).

The course of these reductions was also monitored by ^{1}Hmr spectroscopy. The overlapping of reactant and product signals is minimized in the reaction of 1-benzyl-1,4-dihydronicotinamide with the 1-methylnicotinonitrile cation. Changes in the ^{1}Hmr spectrum of an equimolar (0.1 *M*) solution of each of these species in 50% CD_3CN – 50% D_2O were monitored over a period of 4 h. All signals appearing in the spectra of this

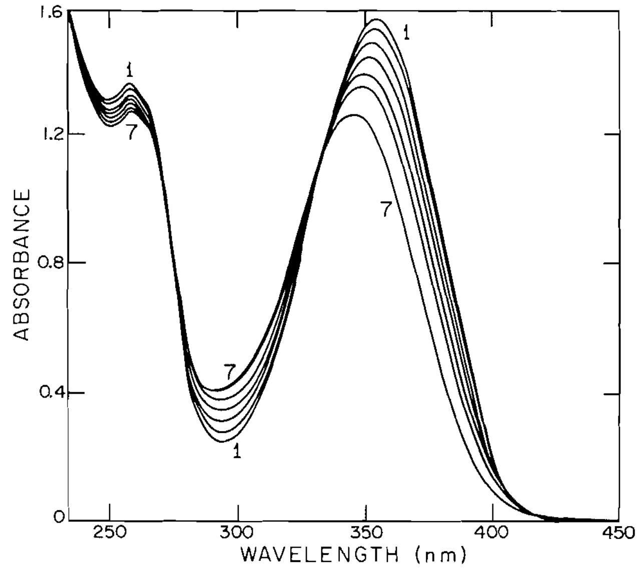

FIG. 1. Time dependence of the electronic absorption spectrum (1-mm path length) of a solution containing 1-benzyl-1,4-dihydronicotinamide (2.0 m*M*) and 1-benzylnicotinonitrile bromide (2.1 m*M*) in 20% CH_3CN – 80% H_2O at 25°C (pH 7.0, ionic strength 1.0). Curves 1–7 are recorded at reaction times of 0, 6, 16, 31, 56, 86, 240 min.

reaction in progress were readily attributable to signals from either these reactants or the products, 1-benzylnicotinamide cation and 1,4-dihydro-1-methylnicotinonitrile, by comparison with the spectra of genuine samples of each of these four species in this solvent system. There were no extraneous signals which might have been attributable to reaction intermediates. Signal integrations indicated no exchange with solvent deuterium during the course of this reaction. In particular, the multiplet centered at δ 3.00 ppm and attributable to the C-4 methylene group of the 1,4-dihydro-1-methylnicotinonitrile product integrates for two hydrogen atoms, and the signal for H-5 also has the appropriate multiplicity for coupling with two protons at C-4. It is thus clear that this formal hydride transfer reaction occurs without exchange of the migrating hydrogen atom with solvent deuterium.

Kinetic studies

Rates of all reactions were studied spectrophotometrically in the presence of limiting concentrations of the 1,4-dihydronicotinamide reductant and 10- to 400-fold excesses of the nicotinonitrile cations in 20% CH_3CN – 80% H_2O, ionic strength 1.0 at 25°C. Under these conditions, all reactions proved to be kinetically first order in reductant over greater than 90% reaction. Pseudo-first-order rate constants were evaluated, and found to be strictly proportional to nicotinonitrile cation concentration in each case. This allowed the evaluation of the second-order rate constants (k_2) reported in Table 1.

Rates of reduction of the 1-methylnicotinonitrile and 1-(4-cyanobenzyl)-nicotinonitrile cations by 1-benzyl-4,4-dideuterio-1,4-dihydronicotinamide were also measured (Table 1). These data allow the evaluation of the (predominantly) primary kinetic isotope effects of $k_2^H/k_2^D = 3.0 \pm 0.3$ and 2.7 ± 0.1 respectively.

The substituent effects on k_2 reported in Table 1 are closely correlated with the Hammett σ constants for the X and Z substituents. Thus, for the reaction of 1-benzyl-1,4-dihydronicotinamide with a series of 1-(Z-benzyl)nico-

TABLE 1. Second-order rate constants for the reduction of 1-(Z-benzyl)nicotinonitrile cations (**2**) by 1-(X-benzyl)-1,4-dihydronicotinamides (**1**)[a]

X	Z	k_2 (M^{-1} s^{-1})
H	4-CH_3	0.067 ±0.002
	H	0.092 ±0.004
	4-Br	0.127 ±0.008
	4-CF_3	0.183 ±0.002
	4-CN	0.246 ±0.004
	4-CN[b]	0.092 ±0.002
	4-NO_2	0.268 ±0.005
4-CH_3	4-CN	0.265 ±0.005
4-F		0.187 ±0.004
4-Br		0.171 ±0.004
3-F		0.143 ±0.003
3-CN		0.088 ±0.004
4-CN		0.084 ±0.002
H	N-methyl[c]	0.0184±0.0004
	N-methyl[b,c]	0.0062±0.0004

[a]Data in 20% CH_3CN – 80% H_2O, pH 7.0 (5 mM phosphate), ionic strength 1.0, 25°C.
[b]Data for 1-benzyl-4,4-dideuterio-1,4-dihydronicotinamide.
[c]Data for 3-cyano-1-methylpyridinium cation.

tinonitrile cations, eq. [2] is obtained.

[2] $\log k_2 = 0.63(\pm 0.03)\sigma_z - 1.05(\pm 0.01)$ (corr. coeff. = 0.996)

For the reduction of the 1-(4-cyanobenzyl)nicotinonitrile cation by a series of 1-(X-benzyl)-1,4-dihydronicotinamides the correlation eq. [3] is obtained.

[3] $\log k_2 = -0.64(\pm 0.05)\sigma_x - 0.65(\pm 0.02)$ (corr. coeff. = 0.982)

We have also investigated the equilibrium between the 1-benzylnicotinonitrile cation and 1-benzyl-4-cyano-1,4-dihydronicotinonitrile in the presence of cyanide ion. We find a dissociation constant of $9.2(\pm 0.5) \times 10^{-4}$ M for this equilibrium in aqueous solution under the same conditions as previously used for evaluation of the analogous equilibrium for 1-benzylnicotinamide cations (9). The dissociation constant for 1-benzyl-4-cyano-1,4-dihydronicotinamide under these conditions is 0.41 M (9).

Discussion

The electronic and ^{1}Hmr spectral data reported above are both consistent with the 1,4-dihydronicotinonitriles being the predominant products of the reaction of these nicotinonitrile cations with 1-benzyl-1,4-dihydronicotinamides. We cannot of course rule out the presence of minor amounts (<5%) of the corresponding 1,2-dihydro- and 1,6-dihydro-nicotinonitriles in the products. This observation is consistent with previous studies which have indicated that 1,4-dihydronicotinamides cleanly transfer hydride to C-4 of other nicotinamide cations and 3-acetylpyridinium cations (6, 11–17). There seems to be just one report of the formation of a 1,6-dihydropyridine in a 1,4-dihydronicotinamide reduction of a C-3 substituted pyridinium cation; Minato *et al.* (18) have reported the establishment of a 4:1 equilibrium mixture of 1,4-dihydro-1-methylnicotinamide and its 1,6-dihydro isomer when the former isomer is treated with the 1-methylnicotinamide cation in D_2O at 34°C.

The clean isosbestic points observed in Fig. 1, and the lack of any extraneous signals in the ^{1}Hmr spectra indicate the absence of any significant concentration of intermediate species in these reactions. While this observation does not unconditionally rule out 1,2- or 1,6-dihydronicotinonitriles as intermediates in these reactions, it does put very stringent requirements on rates of reactions leading to, and from, such potential intermediates. Thus both their formation and also their subsequent reaction with a further nicotinonitrile cation would have to be much faster than the rate of the overall reaction to prevent the accumulation of significant concentrations of these species. These conditions are inconsistent with the observations of Minato *et al.* (18) mentioned above; the second-order rate constant for the equilibration of the 1,4-dihydro- and 1,6-dihydro-1-methylnicotinamides via reaction with the 1-methylnicotinamide cation is several orders of magnitude smaller than observed for the current reactions in Table 1. Furthermore, van Eikeren and Grier (6) report that the transfer of deuterium from 1-benzyl-4,4-dideuterio-1,4-dihydronicotinamide to C-4 of the 1-benzylnicotinamide cation occurs without any exchange at C-2 or C-6. We therefore feel that we can safely rule out the 1,2-dihydro and 1,6-dihydro isomers as intermediates in the formation of the 1,4-dihydronicotinonitriles in the current reaction.

The second-order rate constant for reaction of 1-benzyl-1,4-dihydronicotinamide with the 1-benzylnicotinonitrile cation (0.092 M^{-1} s^{-1} at 25°C (Table 1)) is at least 50-fold greater than the rate constant reported by van Eikeren and Grier (6) for the degenerate hydride transfer between 1-benzyl-1,4-dihydronicotinamide and the 1-benzylnicotinamide cation (0.002 M^{-1} s^{-1} in 25% CH_3CN – 75% H_2O at 40°C). This is consistent with the greater electrophilicity of the former cation than that of the latter; for instance the equilibrium constant for cyanide ion addition at C-4 is 450-fold larger for the 1-benzylnicotinonitrile cation than for the 1-benzylnicotinamide cation. The 5-fold greater rate of attack on the 1-benzylnicotinonitrile cation than on the corresponding 1-methyl cation (Table 1) is also consistent with the relative susceptibilities of N-methyl and N-benzyl heteroaromatic cations to nucleophilic attack.

Reduction of the 1-methylnicotinonitrile cation (k_2 = 0.018 M^{-1} s^{-1} (Table 1)) by 1-benzyl-1,4-dihydronicotinamide occurs much more slowly than for the 1-methyl-3-cyanoquinolinium cation (121 M^{-1} s^{-1} (1) under the current experimental conditions). We have also shown (1) that the second-order rate constants for reduction of 1-methylquinolinium cations at C-4 are correlated with the pK_{R^+} values for these cations by eq. [4].

[4] $\log k_2 = -0.54\ pK_{R^+} + 7.3$

The direct estimation of pK_{R^+} for pseudobase formation by nicotinonitrile cations is difficult since these cations readily undergo a variety of decomposition reactions in aqueous base (19–21). However, we can estimate pK_{R^+} for pseudobase formation at C-4 of the 1-methylnicotinonitrile cation to be approximately 12.8 from the known pK_{R^+} of 13.3 for the 3-acetyl-1-methylpyridinium cation (22) and the relative affinities of these two cations for cyanide ion addition at C-4. Use of pK_{R^+} = 12.8 in eq. [4] then allows a prediction of k_2 = 2 M^{-1} s^{-1}, which is 100-fold larger than the value actually observed. Thus the linear free energy relationship established for quinolinium cations does not seem to be applicable to the

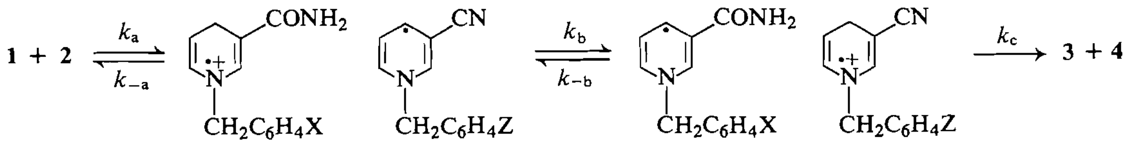

SCHEME 1

dihydronicotinamide reduction of pyridinium cations. It is not clear at present whether this result is due to inherent differences in the reactivities of pyridinium and quinolinium cations or, alternatively, to differences in the mechanisms of reduction for these two series of heterocyclic cations.

A further difference between the 1,4-dihydronicotinamide reductions of pyridinium and quinolinium cations can be found in the primary deuterium kinetic isotope effects for these reactions. The relationship in eq. [5] has been established (1) for the C-4 reduction of quinolinium cations by 1-benzyl-1,4-dihydronicotinamide and its 4,4-dideuterio derivative.

$$[5] \quad \ln (k_2^{H}/k_2^{D}) = 1.66\,(1 - ((pK_{R^+} - 14.6)/8.4)^2)$$

Application of this relationship to the reduction of the 1-methylnicotinonitrile cation ($pK_{R^+} = 12.8$ estimated above) and the 1-(4-cyanobenzyl)nicotinonitrile cation (estimated $pK_{R^+} = 11.2$) gives $k_2^{H}/k_2^{D} = 4.9$ and 4.0, respectively. These estimates are somewhat larger than the experimental values of 3.0 and 2.7. These experimental isotope effects are also much smaller than found for the 1-benzyl-1,4-dihydronicotinamide reduction of the 2-benzyl-5-nitroisoquinolinium cation ($k_2^{H}/k_2^{D} = 6.6$ (2)) which has $pK_{R^+} = 11.3$ (23) and is reduced at a similar rate ($k_2 = 0.4\ M^{-1}\ s^{-1}$ (2)) to the 1-(4-cyanobenzyl)nicotinonitrile cation ($k_2 = 0.246\ M^{-1}\ s^{-1}$ (Table 1)).

Comparison of the Hammett ρ values in eqs. [2] and [3] with the equilibrium ρ = 0.95 for unit positive charge neutralization in nicotinamide cations (9) indicates that positive charge development is about 65% complete on the nicotinamide moiety in the rate-determining transition state, and that charge neutralization is also about 65% complete on the nicotinonitrile moiety in this transition state.[2] This exact balance between charge creation and neutralization on the hydride donor and acceptor respectively is quite different from the situation found in analogous studies of the 1,4-dihydronicotinamide reductions of 5-nitroisoquinolinium (2) and 3,4-dihydroisoquinolinium cations (4). In these cases, positive charge development on the hydride donor "gets ahead" of charge neutralization on the hydride acceptor, and results in a fractional negative charge (0.3–0.4 unit charge) being borne by the migrating hydrogen atom in the transition state. The similarity of the two ρ values in eqs. [2] and [3] indicates that the migrating hydrogen atom must be essentially electrically neutral in the transition state for the reaction in the current study.

The mechanism of the degenerate transhydrogenation between 1-benzyl-1,4-dihydronicotinamide and the 1-benzylnicotinamide cation has been interpreted by van Eikeren *et al.* (6, 7) as involving successive electron, proton, and electron transfer steps, with the proton transfer being rate determining as indicated by the primary deuterium kinetic isotope effect of 6.2. The current data for the reduction of nicotinonitrile cations can be accommodated by such a mechanism provided that neither the initial electron transfer, nor the proton transfer, are clearly rate determining, and provided the migrating proton is not assigned any electron deficiency (i.e. no fractional positive charge). Such a mechanism is outlined in Scheme 1, and in simplified form in eq. [6], where A and B represent the appropriate radical – radical cation caged species and it is assumed that the k_c step is essentially irreversible.

$$[6] \quad \mathbf{1} + \mathbf{2} \underset{k_{-a}}{\overset{k_a}{\rightleftharpoons}} A \underset{k_{-b}}{\overset{k_b}{\rightleftharpoons}} B \xrightarrow{k_c} \mathbf{3} + \mathbf{4}$$

Assuming steady-state concentrations of A and B in eq. [6], one derives an overall second-order rate constant:

$$[7] \quad k_2 = \frac{k_a k_b k_c}{k_{-a}(k_{-b} + k_c) + k_b k_c}$$

Clearly, neither k_a nor k_c can be cleanly rate determining, since either of these conditions would require k_2^{H}/k_2^{D} close to unity. On the other hand, if k_b were cleanly rate determining the initial electron transfer would be a rapid pre-equilibrium, and the Hammett ρ values would be expected to reflect complete unit charge generation and neutralization in the hydride donor and acceptor respectively, and also k_2^{H}/k_2^{D} would be expected to be larger than is observed.

The small isotope effects upon k_a, k_{-a}, and k_c may be neglected, and the general expression for k_2^{H}/k_2^{D} then becomes

$$[8] \quad k_2^{H}/k_2^{D} = \frac{k_{-a}k_b^{H}(k_{-b}^{D} + k_c) + k_b^{H}k_b^{D}k_c}{k_{-a}k_b^{D}(k_{-b}^{H} + k_c) + k_b^{H}k_b^{D}k_c}$$

and for the condition $k_c \gg k_{-b}$, this further simplifies to

$$[9] \quad k_2^{H}/k_2^{D} = \frac{k_b^{H}(k_{-a} + k_b^{D})}{k_b^{D}(k_{-a} + k_b^{H})}$$

Equations [8] and [9] both predict experimentally observed isotope effects less than the true isotope effect (k_b^{H}/k_b^{D}) for the proton transfer step.

The alternative mechanism of electron followed by hydrogen atom transfer (eq. [10]) leads to eq. [11] for k_2, and also predicts eq. [9] for k_2^{H}/k_2^{D}.

$$[10] \quad \mathbf{1} + \mathbf{2} \underset{k_{-a}}{\overset{k_a}{\rightleftharpoons}} A \xrightarrow{k_b} \mathbf{3} + \mathbf{4}$$

$$[11] \quad k_2 = \frac{k_a k_b}{k_{-a} + k_b}$$

For this case, also, k_2^{H}/k_2^{D} is too large to allow k_a to be cleanly rate determining. Again, a cleanly rate-determining k_b would be inconsistent with the observed magnitude of the ρ values.

We have a situation then in which the mechanisms of eqs. [6] and [10] cannot be readily distinguished via substituent effects and isotope effects if more than one rate constant contributes significantly to the observed k_2. The $e^- + H^+ + e^-$ process of eq. [6] has the precedent of the related transhydrogenation between nicotinamide species studied by van Eikeren and Grier (6). On the other hand, the $e^- + H^{\bullet}$ process of eq. [10] is particularly attractive in the light of the requirement for an

[2]The assumptions inherent in the conversion of Hammett ρ values to fractional charges have been detailed previously (2).

electrically neutral migrating hydrogen species in the rate-determining transition state. This latter mechanism has also been proposed as a rationalization of the substituent effects and isotope effects found in the reduction of acridinium cations by 1,4-dihydronicotinamides in aqueous solutions (5).

Additionally, we cannot unambiguously rule out a direct one-step hydride transfer mechanism for these nicotinonitrile cation reductions at the present time, although the measured primary isotope effects in these reactions are somewhat less than the range found for analogous reactions which are believed to be genuine one-step hydride transfer processes (15, 24, 25). We note that k_2 for C-4 reduction of nicotinonitrile cations is of the order predicted from the linear free energy relationship (eq. [12]) established (3) for reduction of isoquinolinium cations by 1-benzyl-1,4-dihydronicotinamide. Such isoquinolinium cation reductions have been established to occur via direct one-step hydride transfers.

$$[12] \quad \log k_2 = -0.5\ \mathrm{p}K_{\mathrm{R}^+} + 4.9$$

However, the current linear free energy relationships (eqs. [2] and [3]) indicate that, unlike isoquinolinium cation reductions, the migrating hydrogen species in nicotinonitrile cation reductions does not bear any significant excess negative charge in the transition state.

Acknowledgements

We appreciate the continued support of this work by the Natural Sciences and Engineering Research Council of Canada. We also thank Ms. J. Bolton and Ms. Y. Goda for several experimental contributions to the data in the current study.

1. J. W. BUNTING and N. P. FITZGERALD. Can. J. Chem. **63**, 655 (1985).
2. J. W. BUNTING and S. SINDHUATMADJA. J. Org. Chem. **46**, 4211 (1981).
3. J. W. BUNTING, V. S. F. CHEW, and G. CHU. J. Org. Chem. **47**, 2303 (1982).
4. J. W. BUNTING, V. S. F. CHEW, and G. CHU. J. Org. Chem. **47**, 2308 (1982).
5. J. W. BUNTING, V. S. F. CHEW, G. CHU, N. P. FITZGERALD, A. GUNASEKARA, and H. T. P. OH. Bioorg. Chem. **12**, 141 (1984).
6. P. VAN EIKEREN and D. L. GRIER. J. Am. Chem. Soc. **99**, 8057 (1977).
7. P. VAN EIKEREN, P. KENNEY, and R. TOKMAKIAN. J. Am. Chem. Soc. **101**, 7406 (1979).
8. D. A. SKOOG and D. M. WEST. Fundamentals of analytical chemistry. 2nd ed. Holt, Rinehart and Winston, Inc., New York. 1969. p. 233.
9. J. W. BUNTING and S. SINDHUATMADJA. J. Org. Chem. **45**, 5411 (1980).
10. U. EISNER and J. KUTHAN. Chem. Rev. **72**, 1 (1972).
11. M. J. SPIEGEL and G. R. DRYSDALE. J. Biol. Chem. **235**, 2498 (1960).
12. G. CILENTO. Arch. Biochem. Biophys. **88**, 352 (1960).
13. J. LUDOWIEG and A. LEVY. Biochemistry, **3**, 373 (1964).
14. C. BERNOFSKY and W. J. GALLAGHER. Biochim. Biophys. Acta, **659**, 1 (1981).
15. R. M. G. ROBERTS, D. OSTOVIC, and M. M. KREEVOY. Faraday Discuss. Chem. Soc. **74**, 257 (1982).
16. J. B. JONES and K. E. TAYLOR. Can. J. Chem. **54**, 2974 (1976).
17. W. VAN GERRESHEIM, C. KRUK, and J. W. VERHOEVEN. Tetrahedron Lett. 565 (1982).
18. H. MINATO, T. ITO, and M. KOBAYASHI. Chem. Lett. 13 (1977).
19. E. M. KOSOWER and J. W. PATTON. Tetrahedron, **22**, 2081 (1966).
20. F. MICHELETTI MORACCI, A. CASINI, F. LIBERATORE, and V. CARELLI. Tetrahedron Lett. 3723 (1976).
21. J. H. BLANCH and K. FRETHEIM. J. Chem. Soc. (C), 1892 (1971).
22. R. B. MARTIN and J. G. HULL. J. Biol. Chem. **239**, 1237 (1964).
23. J. W. BUNTING and D. J. NORRIS. J. Am. Chem. Soc. **99**, 1189 (1977).
24. D. OSTOVIC, R. M. G. ROBERTS, and M. M. KREEVOY. J. Am. Chem. Soc. **105**, 7629 (1983).
25. M. F. POWELL and T. C. BRUICE. J. Am. Chem. Soc. **105**, 7139 (1983).

^{13}C nuclear magnetic resonance studies. 114.[1] An examination of the [3.3.1.0] → [4.3.0.0] rearrangement via β-enolization and H/D exchange in tricyclic ketones

ARTHUR J. RAGAUSKAS AND J. B. STOTHERS
Department of Chemistry, University of Western Ontario, London, Ont., Canada N6A 5B7

Received October 15, 1984

ARTHUR J. RAGAUSKAS and J. B. STOTHERS. Can. J. Chem. **63**, 1250 (1985).

The behavior of the *exo* and *endo* isomers of 7,7-dimethyltricyclo[3.3.1.0^{2,4}]nonan-6-one (**5**, **6**) under strongly basic conditions (t-BuO$^-$/t-BuOH/185°C) has been examined. In sharp contrast to their [3.2.1.0^{2,4}] analogs, the *endo* isomer is stable while the *exo* readily rearranges to 8,8-dimethyltricyclo-[4.3.0.0^{2,4}]nonan-7-one (**16**). Experiments were carried out in *tert*-butyl alcohol-O-d_1 to establish the sites of deuterium incorporation in the initial ketones as well as the relative rates and stereoselectivities of the exchange processes. Ketones **5** and **6** were prepared through ring expansion by ketonization of cyclopropoxides generated from the [3.2.1.0] homologs; the stereochemistry of these ketonizations was established by ^{2}H labelling.

ARTHUR J. RAGAUSKAS et J. B. STOTHERS. Can. J. Chem. **63**, 1250 (1985).

On a étudié le comportement des isomères *exo* et *endo* (**5** et **6**) de la diméthyl-7,7 tricyclo[3.3.1.0^{2,4}]nonanone-6 dans des conditions fortement basiques (t-BuO$^-$/t-BuOH/185°C). Par opposition au comportement de leurs analogues [3.2.1.0^{2,4}], l'isomère *endo* est stable alors que le produit *exo* se transpose facilement en diméthyl-8,8 tricyclo[4.3.0.0^{2,4}]nonanone-7 (**16**). On a réalisé des expériences dans le *tert*-butanol-O-d_1 afin de déterminer les sites d'incorporation du deutérium dans les cétones initiales ainsi que les vitesses relatives et les stéréosélectivités des processus d'échanges. On a préparé les cétones **5** et **6** grâce à une extension de cycle par le biais d'une cétonisation de cyclopropoxydes générés à partir des analogues [3.2.1.0]; on a déterminé la stéréochimie de ces cétonisations grâce à des marquages au ^{2}H.

[Traduit par le journal]

Introduction

Since the discovery of homoenolization (1), several examples for both acyclic and polycyclic monoketones have been found in which proton abstraction occurs from centres other than the α-carbons in ketones under strongly basic conditions (2). For most of these systems, proton abstraction from β-carbons, or β-enolization, has been observed, but there are a few examples of γ-enolization. The removal of a remote proton can lead to skeletal rearrangement and (or) deuterium exchange, if the reaction is carried out in a deuterated medium. The factors governing the regioselectivity and relative reactivity of such proton abstractions are of considerable interest since, in principle, the rearrangements (isomerizations) can provide a means of generating carbon skeletons which are not readily accessible through other routes. Some examples of the use of β-enolization in the syntheses of some naturally occurring carbon skeletons from more readily available systems have been described (3–5). With a better understanding of both the regioselectivity and stereoselectivity of β- and γ-enolization the scope of their synthetic applications could be enhanced.

Earlier, we reported the unidirectional conversion of 3,3-dimethylbicyclo[3.2.1]octan-2-one (**1**) to the isomeric [3.3.0] system **2** (6) and of 7,7-dimethyl-*endo*-tricyclo[3.2.1.0^{2,4}]-octan-6-one (**3**) to 4,4-dimethyltricyclo[3.3.0.0^{2,8}]octan-3-one (**4**) (7) as examples of β- and γ-enolization, respectively. To examine the question of relative reactivity in a closely related system, we elected to study the behavior of the 7,7-dimethyltricyclo[3.3.1.0^{2,4}]nonan-6-ones, under typical homoenolization conditions, t-BuO$^-$/t-BuOH at 185°C. By analogy with **1** and **3**, one could envisage proton abstraction to occur from C-3 and C-9 in the *endo* isomer **5**, constituting an intramolecular competition between γ- and β-enolization, respectively, while a comparison of the behavior of the *exo* isomer **6** with that of the *exo* counterpart of **3** was of interest because of the some-

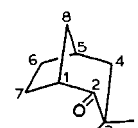

1

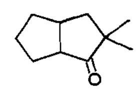

2

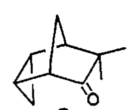

3

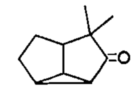

4

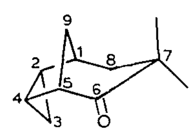

5

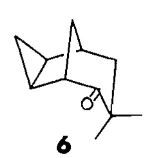

6

what surprising H/D exchange results found for the latter (7). For this reason, the sites and stereoselectivity of proton abstraction in **5** and **6** were established by the requisite H/D exchange experiments. The results of these experiments with **5** and **6** are described in this paper.

Results and discussion

Syntheses

The preparation of **5** and **6** was accomplished by ring expansion of the lower homologs in the [3.2.1.0^{2,4}] series through cyclopropanation of the enol ethers followed by base-catalyzed ketonization of the corresponding cyclopropoxides, as illustrated by **7a** → **10** for the *exo* series, and α,α-dimethylation of the resulting ketones. The ^{13}Cmr data for each of the intermediates in this sequence for the *exo* and *endo* series are listed in Table 1. Some stereochemical features of the conversion of **8** → **10** merit comment.

[1]For part 113 see ref. 5.

TABLE 1. ^{13}C shieldings[a] of the intermediates in the preparation of **5** and **6**

Compound	C-1	C-2	C-3	C-4	C-5	C-6	C-7	C-8	C-9	Other
exo-Series										
7[a]	34.4	16.6	5.4	9.4	48.0	214.4	44.5	25.1		
8[b]	40.7	24.7	18.8	20.8	45.6	169.0	109.3	36.3		0.0 (Me_3Si)
9[c]	36.2	17.4	6.3	15.5	41.8	67.0	15.4	25.5	18.1	1.0 (Me_3Si)
10	33.8	17.4	5.2	17.1	50.8	213.5	35.4	31.0	28.3	
6[d]	34.8	18.8	6.6	17.0	50.4	217.3	42.2	45.2	26.0	30.4 (*endo*-Me) 31.7 (*exo*-Me)
endo-Series										
endo-Tricyclo[3.2.1.0^{2,4}]-octan-6-one	34.1	21.5	18.6	18.7	50.7	215.6	42.4	52.5		
6-TMSO-tricyclo[3.2.1.0^{2,4}]-oct-6-ene[b]	40.7	17.3	17.9	12.8	47.0	157.3	100.9	61.7		0.0 (Me_3Si)
11[b,c]	36.2	20.1	10.1	19.8	43.2	59.0	19.0	22.9	45.5	1.0 (Me_3Si)
14	31.3	26.4	17.1	24.4	48.6	214.9	35.0	22.6	43.7	
5[d]	32.8	26.8	17.4	24.7	48.5	219.2	41.8	39.2	43.4	25.8 (*endo*-Me) 34.0 (*exo*-Me)

[a]In ppm from TMS for $CDCl_3$ solutions unless otherwise indicated.
[b]In C_6D_6 solution.
[c]For ease of comparison of the data, the unconventional numbering shown for **9** has been used.
[d]Assignments confirmed $^{13}C\{^1H\}$ correlation (see text).

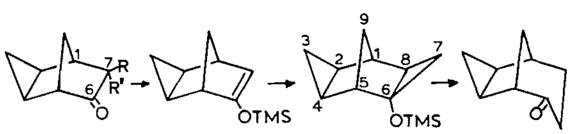

7*a* R = R' = H **8** **9** **10**
b R = Me, R' = H
c R = R' = Me

Since finding that this sequence provides an efficient means of ring expansion for a variety of polycyclic ketones (8), we have accumulated more than two dozen examples (3, 5, 9) and in each case a single cyclopropanation product was obtained. The stereochemical assignment for **9** followed from its ^{13}Cmr spectrum, which contained three methylene signals at δ_C 6.3, 15.4, and 18.1 which were assigned to C-3, -7, and -9, respectively.[2] The high field positions of these absorptions is only consistent with cyclopropanation at the *exo* face of **8** since an *endo* cyclopropyl ring in these systems tends to deshield C-9 substantially (10) such that its absorption would be expected to be near δ_C 40. For the corresponding cyclopropanation product **11** in the *endo* series leading to **5**, the three methylene carbons

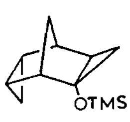

11

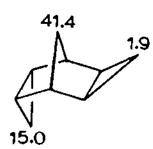

12

absorb at 10.0, 19.0, and 45.5 (C-3, -7, and -9, respectively[2]); these shieldings agree reasonably with the methylene data for **12** (10) after allowance for the presence of the *endo* oxygen in **11**. Hence we conclude that *exo* cyclopropanation also occurs in the *endo* series.

Upon cleavage of the trimethylsilyl ethers with base, the resulting cyclopropoxides can ketonize in two ways, either to produce the α-methyl derivative of the initial ketone or to undergo ring expansion to the homologous ketone. We could anticipate that the cleavage of **9** would favor ring expansion to **10** rather than generation of **7***b*, on the basis of earlier results in related systems (8). In the event, treatment of both **9** and **11** with NaOH–MeOH at 0°C furnished single ketones having no methyl absorption in their ^{1}H and ^{13}Cmr spectra. Although cleavage of the corresponding cyclopropyl TMS ether from norcamphor leads predominantly to ring expansion, the product contains 12% of 3-methylnorcamphor. Presumably the fact that **10** and its *endo* counterpart are less strained than **7***b* and its *endo* isomer governs the course of the ketonization of **9** and **11**, since it has been demonstrated that the process is subject to thermodynamic control (2, 11).

The opening of the cyclopropoxide anion **13**, generated by base-catalysed cleavage of TMS ether **9**, can proceed in either of two ways, i.e. with retention or inversion of configuration. These are shown as a and b in Scheme 1, to illustrate that the stereochemistry of the process can be determined by cleavage in a deuterated medium. While, in general, ketonizations of cyclopropoxides in polycyclic systems have been found to undergo inversion of configuration, there are some strained systems which exhibit retention (2). Thus it was of interest to establish the point in the present cases. To distinguish between paths a and b, **9** was cleaved in KOD/*t*-BuOD and the product treated with KOH/MeOH to back-exchange the α-deuterium picked up by exchange after the cleavage. The ^{13}Cmr spectrum of a 1:1 mixture of the **10**-d_1 obtained in this manner and **10** was recorded to determine the stereochemistry of the deuterium atom at C-8 in the latter material, since the magnitude of vicinal $^2H-^{13}C$ coupling interactions and the ^{2}H-induced isotope shifts depends on the relative orientation of the two nuclei (12). From this spectrum *exo*-deuterium incorporation was revealed; the observed isotope effects on the ^{13}C shieldings in ppb and the resolved couplings are shown in **10**-X. A key feature is the fact that vicinal $^{13}C-^2H$ coupling was readily apparent for the cyclopropyl methine carbon (C-2) with J = 1.5 Hz, while the C-9 signal was only slightly broadened; this is consistent with

[2]For ease of comparison of the shielding data listed in Table 1, the unconventional numbering scheme shown in **9** has been employed for **9** and **11**.

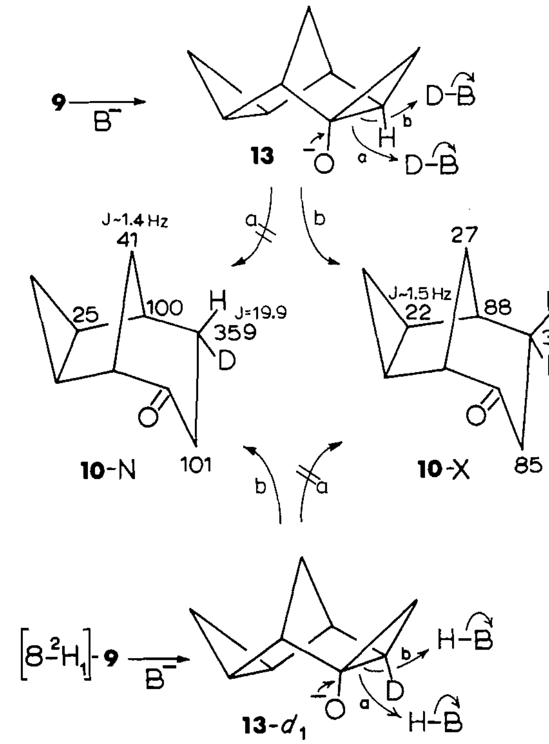

SCHEME 1

deuterium antiperiplanar to C-2 and, therefore, in the *exo*-orientation. To confirm this assignment, a sample of [7,7-$^2H_2$]-**7**a was converted to [8-$^2H_1$]-**9** which was subsequently opened with NaOH/MeOH to form **10**-d_1. The ^{13}Cmr spectrum of a 1:1 mixture of this material and **10** revealed the ^{2}H effects shown for **10**-N (Scheme 1). In this case, C-9 exhibited vicinal coupling of 1.4 Hz while the C-2 signal was only broadened by the deuterium, indicating that C-9 and the deuterium atom are antiperiplanar. These results establish that the cleavage of **13** proceeds with inversion. Treatment of **11** with KOD/t-BuOD followed by back-exchange with KOH/MeOH gave **14**-d_1 for which the ^{2}H effects in its ^{13}Cmr spectrum are shown. These constitute good evidence for the presence of *exo*-deuterium at C-8 and, hence, for inversion of configuration upon homoketonization of the cyclopropoxide generated from **11**.

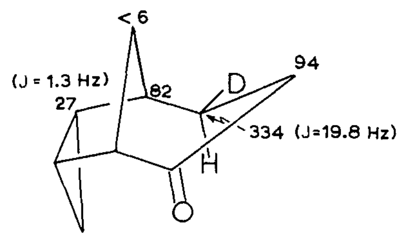

14-d_1

For **10**-X and **14**-d_1 it may be noted that the ^{2}H-induced shifts as well as the $^2H-^{13}C$ vicinal coupling with C-2 differ, presumably reflecting conformational differences in the two ring systems. In **14**, the *endo* disposition of C-3 will preclude a chair conformation for the six-membered ring which is probably the favored arrangement for **10** and in which the dihedral angle relating an *exo*-8-deuterium and C-2 is ~180°. In contrast, for a boat-like conformation of the six-membered ring, as is likely for **14**-d_1, this dihedral angle will be reduced to ~120°.

Homoenolization experiments

The behavior of **5** under homoenolization conditions was examined initially following our usual procedures (13); **5** was dissolved in anhydrous t-BuO$^-$/t-BuOH and aliquots were transferred to predried glass tubes under nitrogen, which were sealed and heated at ≥180°C for varying periods of time. The neutral product (~80% yields) was isolated and analyzed by gas–liquid chromatography (glc). In each case, the starting material was recovered unchanged and there was no indication of the formation of isomeric material in the neutral fraction even after >200 h at 185°C.

In contrast, under the same conditions and with the same batch of t-BuO$^-$/t-BuOH employed for some of the experiments with **5**, the *exo*-tricyclic ketone **6** was smoothly transformed to a new isomeric ketone which contained a cyclopentanone moiety on the basis of its carbonyl absorption data (1730 cm^{-1}, δ_C 223.9). The half-life for the disappearance of **6** and the appearance of the new ketone was found to be ca. 75 h at 180°C. The ^{13}C spectrum of the product contained ten

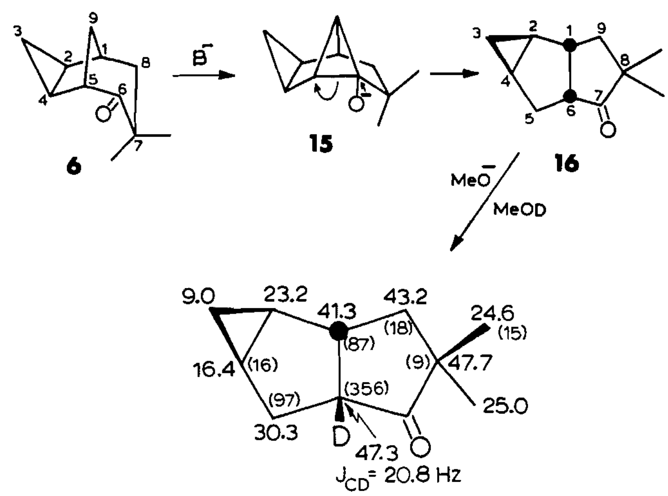

16-d_1

signals in addition to the carbonyl peak, δ_C ($CDCl_3$): 24.6, 25.0 (2 × CH_3), 9.0, 30.3, 43.2 (3 × CH_2), 16.4, 23.2, 41.3, 47.3 (4 × CH), and 47.7 (quat. C). From these data the ketone could be tentatively assigned structure **16** which could arise by proton abstraction from C-9 of **6** to generate β-enolate **15**, or its equivalent, subsequently opening with protonation at the original C-5 site. This rearrangement is constrained to give the *cis*, *anti*, *cis*-tricyclo[4.3.0.0^{2,4}]nonane skeleton.

To confirm this structure and the initial ^{13}Cmr signal assignments, a sample of the ketone was treated with MeONa/MeOD under mild conditions. Mass spectrometry indicated that exchange occurred at a single site (99.5% d_1) and in the ^{13}C spectrum of the recovered material the δ 47.3 α-methine signal was transformed to a 1:1:1 triplet, J_{CD} = 20.8 Hz, shifted upfield by 356 ppb. Precise isotope shifts for the signals of the neighboring carbons were obtained from the spectrum of a 1:1 mixture of **16** and **16**-d_1; these data are shown in the formula with the isotope shifts (in ppb) given in parentheses; these are entirely consistent with expectations for the assigned structure. As a final confirmation of structure **16**, the individual coupling constants for the sp^3 carbons in the skeleton were determined from its INADEQUATE spectrum (14); these results are sum-

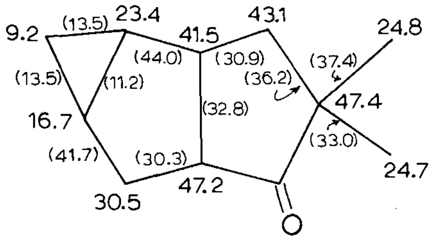

16A

marized in **16A** with the J values in parentheses. Since these spectra were run in C_6D_6 the shieldings differ slightly from those given with **16**-d_1 in $CDCl_3$.

The ^1H spectrum of **16** contained eight one-proton multiplets, one two-proton pattern, and two methyl singlets, δ 1.097 and 1.013. The cyclopropyl methylene protons appeared at highest field, δ 0.015 (*syn*-3-H, d(t), J = 5.1, 3.9 Hz) and 0.460 (*anti*-3-H, d(t), J = 5.1, 7.9 Hz), while the cyclopropyl methine protons gave rise to a complex multiplet, δ 1.24–1.38. The lowest field multiplet, δ 2.73 (d(t), J = 7.4, 11.2 Hz), was assigned to H-1 with a somewhat broadened pattern, δ 2.404 (ddd, J = 7.4, 9.2, 10.0 Hz), arising from H-6. A clear doublet of doublets, δ 2.156 (J = 10.0, 13.0 Hz), and an ill-defined 8-line pattern, δ 1.720, were assigned to the 5-protons while a clean multiplet, δ 1.995 (ddd, J = 1.6, 7.4, 12.8 Hz), and a somewhat broadened doublet of doublets, δ 1.492 (J = 11.2, 12.8 Hz), could be ascribed to the 9-protons. These ^1H assignments were confirmed by a $^{13}C(^1H)$ two-dimensional heteronuclear correlation experiment.

The stability of **5** under these strongly basic conditions stands in direct contrast to the behavior of **1** and **3**, which are smoothly transformed to **2** and **4**, respectively, upon treatment with t-BuO$^-$/t-BuOH at elevated temperatures (6, 7). Our original notion that **5** could conceivably provide an intramolecular competition for β- and γ-enolization was clearly incorrect and more subtle factors must play a role in governing isomerization via homoenolization. By analogy with **1**, in which proton abstraction from C-8 leads to rearrangement to form **2**, we anticipated that abstraction from C-9 in **5** would give the corresponding rearrangement product, while proton abstraction from C-3 could provide the [4.3.0.0] homolog of **4**, but there is no evidence of formation of isomeric material. On the other hand, **6** is smoothly converted to **16**, a rearrangement which is strictly analogous to the **1** → **2** conversion and which must involve proton abstraction from C-9 in **6**, as noted above, to form **15** with subsequent opening to **16**. The difference in behavior of **5** and **6** suggests that the relative orientation of the carbonyl group and C-9 must be highly important. While the six-membered ring in **6** can adopt a chair conformation, this arrangement is precluded for **5** because the *endo*-orientation of C-3 and its six-membered ring presumably assumes a boat-like conformation. An inspection of molecular models indicates that the dihedral angle between C-9 and the carbonyl oxygen increases from ca. 120° to ca. 170° with the chair-to-boat change for the six-membered ring in **6** and **5**, respectively. This change tips the π-system of the carbonyl group away from C-9, thereby rendering potential overlap with a developing carbanionic centre at C-9 less likely. It seems reasonable to suggest that this difference in the relative orientation of the carbonyl group and the methano bridge carbon in **5** and **6** may account for the marked change in reactivity. Some experiments to test this suggestion are in progress. The reluctance of **5** to rearrange via γ-enolization at C-3, in a manner analogous to that found for **3**, is more difficult to interpret. A comparison of the orientation of the carbonyl group with respect to C-3 in **3** and **5** indicates little difference except that the separation between the carbonyl carbon and C-3 is ca. 10% greater in **5**. It may be noted that, from Dreiding models, the distance between C-9 and the carbonyl carbon in **6** is comparable to that between C-3 and the carbonyl carbon in **3**, both of which isomerize under the reaction conditions. It may be relevant that there is a similar separation between the carbonyl carbon and the methylene carbon involved in the γ-enolate rearrangement of half-cage ketone **17** to **18**, which was the first example of this

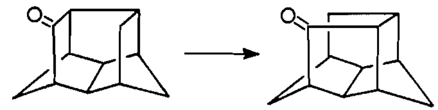

17 **18**

phenomenon (15). At the present time, we lack an alternative rationalization for the failure of **5** to undergo γ-enolate rearrangement and can only suggest that the separation between the carbonyl group and C-3 exceeds some critical value required for effective interaction of the carbonyl group with an incipient carbanionic centre. To gain further insight into the behavior of **5** and **6** under our reaction conditions, the results of H/D exchange experiments were also examined.

H/D exchange experiments

Although ketone **5** was found to be stable under strongly basic conditions, this does not preclude the occurrence of H/D exchange and, thus, it was of interest to examine samples after treatment with t-BuO$^-$/t-BuOD at 185°C for various times. After 88 h, recovered **5**-d_x was found to contain 3.96 atoms ^2H/molecule by mass spectrometry and ^{2}Hmr revealed five sites of incorporation; the relative amounts for each were determined by integration. The ^{2}Hmr signals and ^2H content were found to be δ 0.42 (0.64), 0.60 (0.16), 0.93 (1.66), 1.52 (0.75), 2.77 (0.75). The ^{1}Hmr spectrum of **5** contained methyl singlets at δ 0.930 and 1.060 which correlate with the ^{13}C methyl signals at δ_C 19.2 and 11.2, respectively, and can be assigned to the *exo*- and *endo*-methyl groups, respectively. Thus, **5** undergoes exchange at the *exo*-methyl site preferentially, as expected by analogy with several related systems. In addition, the bridgehead protons H-1 and -5 gave rise to multiplets at δ 2.405 and 2.765, respectively, while the methano bridge protons at C-9 appeared at δ 1.767 and 1.858, J_{AB} = 11.5 Hz. The 3-methylene protons absorb at δ 0.416 and 0.603, J_{AB} = 6.3 Hz, with the higher field component exhibiting additional couplings of 8.1 Hz to two protons and 1.8 Hz to one other proton; the lower field component contained a coupling of 3.6 Hz to two other protons. The higher field absorption, δ 0.416, therefore, was assigned to the *exo*-3-proton since it is well-established that $J_{cis} > J_{trans}$ for vicinal coupling in cyclopropyl rings (16); the small 1.8-Hz coupling was subsequently shown to involve the H-9 absorption at δ 1.858, by spin decoupling, thus identifying the latter as the *syn* proton. A somewhat broadened doublet, δ 1.102, J = 14.5 Hz, and a doublet of doublets, δ 1.418, J = 7.5 and 14.5 Hz, could be readily ascribed to the *endo*- and *exo*-protons on C-8, while the remaining absorptions, a pair of multiplets at δ 1.403 and 1.518, arise from H-2 and -4, respectively. From these data, it was concluded that deuterium exchange occurred at C-3, -4, -5, and the *exo*-methyl sites in **5**.

Confirmation for these sites of exchange was obtained by examination of the ^{13}C spectra of the **5**-d_x samples. Characteristic triplets, centred upfield from the normal **5** signals, arising by one-bond $^{13}C-^{2}H$ coupling were apparent for the bridgehead C-5 (J_{CD} = 19.6 Hz, isotope shift (Δ) = 398 ppb), the cyclopropyl methine C-4 (J_{CD} = 26.5 Hz, Δ = 404 ppb), the C-3 methylene (J_{CD} = 24.2 Hz, Δ = 292 ppb), and the *exo*-methyl carbon (J_{CD} = 19.5 Hz, Δ = 287 ppb), while the remaining absorptions exhibited the effects typical of deuterium substitution at neighboring carbons. Precise measurements of the ^{2}H-induced shifts for each of the patterns were accomplished by examination of the spectra of 1 : 1 mixtures of **5** and **5**-d_x. The *exo*-methyl absorption consisted of the original singlet at δ_C 34.0 and a pair of triplets, the signals of which were separated by 17 ppb. This small shift is attributable to the long range effect of deuterium at C-5. The *endo*-methyl absorption contained singlets for species containing deuterium at C-5 and at the *exo*-methyl carbon, with isotope shifts of 24 and 30 ppb, respectively. The quaternary C-7 pattern also consisted of three singlets because of isotope shifts in the corresponding deuterated species; these effects are 29 (C-5) and 64 (*exo*-Me) ppb. Similarly, the 8-methylene carbon pattern contained components exhibiting isotope shifts of 24 and 30 ppb while the C-1 pattern appeared to contain similar components but was too ill-resolved to permit precise measurements, presumably because of small isotope shifts and weak $^{13}C-^{2}H$ coupling in the various deuterated species. The absorption for C-2 contained three isotope-shifted components ascribable to species having deuterium at C-3 (114 ppb), at C-4 (84 ppb), and at both C-3 and -4. A similar pattern was found for C-9 because of deuterium at C-5 (68 ppb) and at C-4 (21 ppb). The isotope shifts in ppb for the remaining centres were found to be: C-3, 121 (C-4), 23 (C-5); C-4, 76 (C-3), 82 (C-5); C-5, 86 (C-4), 23 (C-3). These ^{13}C data establish the presence of deuterium at C-3, -4, -5, and the *exo*-methyl carbon, while the ^{2}Hmr spectrum showed that both methylene protons on C-3 undergo exchange, albeit at distinctly different rates. From results for a series of samples of **5**-d_x, recovered after treatment with *t*-BuO$^-$/*t*-BuOD at 195°C for 3, 6, 12, and 19 h, the relative proportions of deuterium at the various sites of exchange were determined; these data aided the determination of the specific isotope shifts noted above and permitted the extraction of approximate first-order rate constants for the exchange processes which are considered later.

To determine the regio- and stereoselectivity of proton abstraction in **6** under these homoenolization conditions, a series of experiments in deuterated base was carried out. Samples of **6**-d_x were isolated from the resulting mixtures with **16** by preparative glc after reaction times of 10, 20, and 40 h at 185°C in *t*-BuO$^-$/*t*-BuOD. The 40-h sample contained 1.84 atoms ^{2}H/molecule by mass spectrometry and its ^{2}Hmr spectrum revealed six sites of deuterium incorporation for which the relative amounts were measured by integration. These absorptions and the ^{2}H content were found at δ 0.13 (0.38), 0.28 (0.055), 0.87 (0.18), 0.93 (0.22), 1.14 (0.11), and 2.66 (0.89). The ^{1}Hmr spectrum of **6** exhibited methyl singlets at δ 1.142 and 1.111, which were found to correlate with the ^{13}C methyl signals at δ 31.7 and 30.4 and could be assigned to the *exo*- and *endo*-methyl groups, respectively, since deuterium exchange occurred exclusively at the former site. The bridgehead protons in **6** absorbed at δ 2.665 (d, J = 4.4 Hz, H-5) and 1.925 (m, H-1) while an AB pattern, each component of which contained

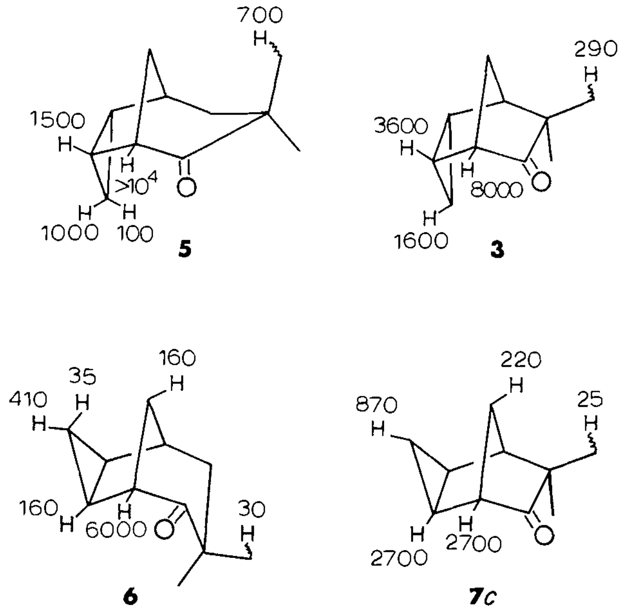

FIG. 1. Deuterium exchange rates ($k \times 10^8$ s^{-1}) at the various sites in **3**, **5**, **6** and **7***c* by β- and γ-enolization at 185°C in *t*-BuO$^-$/*t*-BuOD.

additional couplings, was readily ascribed to the 8-methylene protons: δ 1.341 (J = 4.1, 14.0 Hz) and 1.480 (J = 2.0, 2.8, 14.0 Hz); the latter pattern correlated with the methylene carbon signal at δ_C 45.2. A second AB pattern, each component of which appeared as a triplet, could be assigned to the 3-methylene protons: δ 0.133 (J = 5.4, 7.7 Hz) and 0.278 (J = 3.6, 5.4 Hz), and was found to correlate with the methylene carbon signal at δ_C 6.6. The larger vicinal couplings for the higher field pattern show it to be due to the proton *cis* to the cyclopropyl methine protons, H-2 and -4. A third AB pattern, which correlated with the methylene carbon at δ_C 26.0, was discernible for the 9-methylene protons; the higher field portion, δ 0.873, was a doublet, J = 12.5 Hz, broadened by small, unresolved couplings, while the lower field portion, δ 0.995, was partially masked by one of the two remaining multiplets, δ 0.79 and 0.93. The latter were assigned to H-2 and -4, and were found to correlate with the methine carbon signals at δ_C 18.8 and 17.0, respectively. An inspection of molecular models indicated that the dihedral angles between the *syn*-9-proton and the 1- and 5-bridgehead protons are ~90°. Hence the slightly broadened doublet at δ 0.873 could be assigned to *syn*-H-9. From these data we deduce that deuterium exchange occurred at C-3, -4, -5, -9, and the *exo*-methyl carbon. For further confirmation of deuterium incorporation at C-4, the C-3 absorption in the ^{13}Cmr spectrum of **6**-d_x recovered after 10 h was examined carefully. This pattern contained, in addition to a small singlet at δ_C 6.6 arising from non-deuterated material, a prominent singlet shifted upfield by 16 ppb owing to [5-$^{2}H_1$]-**6**, a 1 : 1 : 1 triplet, J_{CD} = 24.2 Hz, Δ = 298 ppb from [3,5-$^{2}H_2$]-**6**, and a weak singlet, Δ = 109 ppb, attributable to [4,5-$^{2}H_2$]-**6**. While both methylene hydrogens at C-3 undergo exchange, although at distinctly different rates, only the *syn*-hydrogen at C-9 was involved.

Approximate first-order rate constants for exchange at the various sites in **5** and **6** were extracted from the deuterium incorporation data and are given in Fig. 1, together with the earlier results (7) for their [3.2.1.0] analogs, **3** and **7***c*. In each case, exchange at the 3-methylene sites is highly stereoselective, indicative of steric hindrance, and the rates for the more reactive proton are comparable, although this centre is only involved in enolate rearrangement in the case of **3**. This seems to indicate that the carbonyl group has little influence on proton abstraction from C-3 and the reactivity of these protons can be attributed to the fact that cyclopropyl methylene hydrogens are more acidic than their alicyclic counterparts. On the other hand, their less acidic vicinal neighbors, the cyclopropyl methine hydrogens, are distinctly activated by the carbonyl group, since exchange occurred only at C-4 in each compound with no evidence of exchange at C-2. It is curious, however, that the rate of exchange at C-4 in **6** is slower than that at C-3 while the reverse was found for **3**, **5**, and **7***c*. The detection of exchange at the methano bridge in the related systems, fenchone and 3,3,6,6-tetramethylnorcamphor, is relatively recent (17). Hence it is interesting that the *syn*-proton at this position undergoes exchange selectively, but only in the *exo* series, **6** and **7***c*, and at comparable rates. In the bicyclic systems, *syn* exchange is strongly favored but proceeds at only ca. 1/100 of the rate found for **6** and **7***c*; this increased reactivity is difficult to explain.[3] The incorporation of a *syn*-deuterium at C-9 in **6** would suggest that the cleavage of β-enolate **15** to regenerate **6** proceeds with retention of configuration if this is indeed the mode of exchange. However, the absence of deuterium at the corresponding position in **1** (C-8) indicated that the conversion of **1** → **2** is unidirectional. For **6** it is conceivable that exchange at C-9 involves a different intermediate species than **15**. As already noted, methyl exchange occurred preferentially at the *exo*-groups, with the puzzling difference that this process is distinctly faster in the *endo* examples **3** and **5** than their *exo* counterparts, **6** and **7***c*.[3] Clearly, rather subtle factors govern the reactivity of exchange in these compounds and additional data are required before definitive interpretations can be devised.

Experimental

Boiling points are uncorrected. Gas–liquid chromatography was carried out on Varian 920 and 3700 instruments using columns of 10% Carbowax 20 M, 6% FFAP, or 10% SE-30 on Chromosorb W, as indicated. Tetrahydrofuran (THF) and ether were dried over sodium and freshly distilled before use. Diisopropyl amine, triethyl amine, and pyridine were distilled from CaH_2 and stored over 4A molecular sieves; methyl iodide was dried over 4A sieves. The ketones, *exo*-tricyclo[3.2.1.0^{2,4}]octan-6-one (**7**) and its *endo* isomer, were the starting materials for the preparation of **5** and **6** and had been described previously (10).

Infrared spectra were recorded with a Beckman 4250 instrument and mass spectra were obtained on a Varian MAT-311A system at 70 eV (direct inlet). Routine ^{1}Hmr spectra were obtained with either Varian T-60 or EM-360 instruments while data for pure samples were collected with a Varian XL-200 instrument. The latter spectrometer and a Varian XL-300 were employed to record the ^{2}H and ^{13}Cmr spectra, and comparison of the fully decoupled ^{13}C spectra with those obtained with either the APT (18) or DEPT (19) sequences identified the methyl, methylene, methine, and fully-substituted carbon signals. Correlation of the ^{1}H and ^{13}C spectra for **5** and **6** was accomplished using the HETCOR sequence of the XL software with a 2048 × 128 data matrix, 3600 (**5**) and 2600 Hz (**6**) spectral widths for ^{13}C and 1000 Hz for ^{1}H, transforming 2048 and 512 points, respectively. INADEQUATE (14) spectra of **16** were recorded with the C13SAT sequence of the XL software using a 3200-Hz sweep width (sp^3 carbons only), 12 and 16-s repetition rates, 60 000 points, and 64K transforms.

*6-Trimethylsilyloxy-*exo*-tricyclo[3.2.1.0^{2,4}]oct-6-ene (8)*

To a stirred solution of LDA (prepared from diisopropyl amine (3.31 mL, 23.6 mmol), THF (23 mL), *n*-BuLi (2.50 *M*, 8.26 mL) at −78°C, 30 min) under nitrogen was added **7** (1.80 g, 14.8 mmol) in THF (4.0 mL) and stirring was continued for 45 min at −78°C. A quenching solution (prepared by centrifugation of a mixture of trimethylsilyl chloride (3.37 mL, 26.6 mmol) and Et_3N (1.23 mL) in THF (3 mL) in a N_2-purged tube) was added and stirring was continued for 2 h after removal of the Dry Ice cooling bath. The reaction was then cooled to 0°C and cold saturated aqueous Na_2CO_3 solution (30 mL) was added by syringe with vigorous stirring. The organic layer was decanted, the aqueous layer extracted with pentane (3 × 25 mL), and the combined extracts washed with Na_2CO_3 solution (25 mL) and H_2O (2 × 25 mL) before drying over $MgSO_4$. Removal of the solvent under reduced pressure gave crude **8** which was purified by bulb-to-bulb distillation, bp 90–95°C/4 Torr (1 Torr = 133.3 Pa), 2.57 g, 90% yield; glc analysis (FFAP) indicated >90% purity. An analytical sample was collected by preparative glc, for characterization; ir ($CHCl_3$): 1598 cm^{-1} (C=C); ^{1}Hmr (C_6D_6) δ: 0.20 (s, 9H, Me_3Si), 0.5–1.5 (complex absorption, 6H), 2.53 (m, 2H, H-1, H-4), 5.05 (bd, 1H, H-7); ^{13}Cmr, see Table 1. *Exact Mass* calcd. for $C_{11}H_{18}OSi$: 194.1127; found: 194.1125.

2-Trimethylsilyloxytetracyclo[3.3.1.0^{2,4}0^{6,8}]nonane (9)

A zinc–silver couple (2.22 g, 34 mmol) was placed in a N_2-purged flask fitted with a reflux condenser and magnetic stirring bar and the apparatus was flame dried before cooling to room temperature. Methylene iodide (1.50 mL, 18.6 mmol) and Et_2O (4 mL) were added and the flask warmed to initiate reaction. On completion of the exothermic reaction, enol ether **8** (2.00 g, 10.3 mmol) in Et_2O (46 mL) was added with stirring and the resulting mixture was refluxed for 8 h. After cooling to 0°C, a 50:50 mixture of pyridine–ether (10 mL) was added. The precipitate was removed by filtration through Celite and the filtrate was concentrated under reduced pressure. The residue was taken up in pentane and the last traces of precipitate removed by filtration. Evaporation of the solvent gave oily liquid **9** (1.98 g, 92%); glc analysis (FFAP) indicated the product to be ca. 80% pure. An analytical sample (prep. glc) was collected for characterization; ^{1}Hmr ($CDCl_3$) δ: 0.18 (s, 9H, Me_3Si), 0.35 (m, 2H), 0.72 (m, 3H), 1.06 (m, 3H), 1.76 (m, 1H), 2.18 (m, 1H), 2.32 (m, 1H); ^{13}Cmr, see Table 1. *Exact Mass* calcd. for $C_{12}H_{20}OSi$: 208.1283; found: 208.1279.

exo-*Tricyclo[3.3.1.0^{2,4}]nonan-6-one (10)*

The tetracyclic TMS ether **9** (1.88 g) was added to methanolic NaOH solution (3 *M*, 90 mL) and allowed to stir for 24 h at 0°C before the addition of H_2O (70 mL). The product was extracted with pentane (4 × 50 mL) and the combined extracts washed with H_2O (3 × 40 mL); the combined aqueous washings were back-extracted with pentane (50 mL). The pentane extracts were dried over $MgSO_4$ before removal of the solvent by distillation to give **10** (1.09 g, 82%). Preparative glc was used to obtain pure samples for further work. The absence of **7***b* in the ketonization product was confirmed by glc since samples of the latter were available from earlier studies (10); ir ($CHCl_3$): 1710 cm^{-1} (C=O); ^{13}Cmr, see Table 1. *Exact Mass* calcd. for $C_9H_{12}O$: 136.0888; found: 136.0886.

Preparation of exo-*deuterio-**10**-d$_1$ (**10**-X)*

A solution of KOD in *t*-BuOD (2 *M*, 2 mL) was added to **9** (90 mg) and allowed to stand with stirring under a nitrogen atmosphere overnight. After the addition of D_2O (3 mL), the product was isolated as described for **10** to furnish **10**-d_3 (60 mg); ms: 0.9% d_0, 2.9% d_1, 19.7% d_2, 76.5% d_3 (total 2.715 D/molecule). This material was added to methanolic NaOH solution (3.6 *M*, 1.5 mL) and allowed to stand with stirring overnight before the addition of 10% NaCl solution (3 mL) and extraction with pentane (4 × 10 mL). The combined extracts were washed with 10% NaCl solution (3 × 10 mL) and the aqueous washings extracted once with pentane (30 mL). The pentane extracts were dried over $MgSO_4$ before removal of the solvent by

[3]A reviewer has suggested that a homoconjugative interaction between the *exo*-cyclopropyl ring and the carbonyl group may facilitate exchange at the methano bridges of **6** and **7***c*. This interaction could reduce the "electrophilicity" of the carbonyl group and thereby reduce its activation of the α-methyl carbons.

distillation to furnish *exo*-8-deuterio-**10**-d_1 (57 mg); ms: 7.7% d_0, 83.1% d_1, 5.1% d_2 (total 0.93 D/molecule); ^{13}Cmr, see text.

Preparation of endo-*8-deuterio-**10**-*d$_1$ *(**10-N**)*

The sequence **7** → **10** described above was repeated using 7,7-dideuterio-**7**-d_2 as the starting material prepared as follows. To a solution of NaOD/D_2O (0.5 *M*, 9.5 mL) was added **7** (1.40 g) under a nitrogen atmosphere and the solution was refluxed for 22 h. The product was extracted with pentane (3 × 10 mL) and the combined extracts washed with 10% NaCl solution (3 × 10 mL). The aqueous portion was reextracted with pentane (30 mL) and the pentane extracts dried over $MgSO_4$ before removal of the solvent by distillation to afford **7**-d_2 (1.34 g). The ^{13}Cmr spectrum of this product indicated almost complete exchange of the α-methylene hydrogens and this material was employed directly for the generation of **10**-d_1 via 7-deuterio-**8**-d_1 followed by cyclopropanation and ketonization as described above for **9** and **10**. The resulting product, *endo*-8-deuterio-**10**-d_1, was characterized by ^{13}Cmr (see text) and ms: 9.3% d_0, 70.7% d_1 (total 0.707 D/molecule).

*7,7-Dimethyl-*exo-*tricyclo[3.3.1.0^{2,4}]nonan-6-one (**6**)*

A solution of **10** (0.12 g, 0.9 mmol) in anhydrous Et_2O (6 mL) was added to $NaNH_2$ (0.19 g, 4.9 mmol) in Et_2O (5 mL) under a N_2 atmosphere and the mixture refluxed for 4 h. After cooling, methyl iodide (0.33 mL, 5.3 mmol) was added and the mixture refluxed overnight. Methyl iodide (0.11 mL, 1.8 mmol) was added and the mixture stirred for 3 h before cooling to 0°C. Water (5 mL) was slowly added and the organic phase decanted. The aqueous phase was extracted with pentane (3 × 8 mL) and the organic extracts washed with H_2O (3 × 6 mL). The combined washings were reextracted with pentane (10 mL). The combined extracts were dried over $MgSO_4$ before removal of the solvent which furnished crude **6**. Pure **6** (0.11 g, 76%) was obtained by column chromatography on alumina using pentane–ether, 90:10, as eluent; ir ($CHCl_3$): 1712 cm^{-1} (C=O); ^{1}Hmr, see text; ^{13}Cmr, see Table 1. *Exact Mass* calcd. for $C_{11}H_{16}O$: 164.1201; found: 164.1198.

*7,7-Dimethyl-*endo-*tricyclo[3.3.1.0^{2,4}]nonan-6-one (**5**)*

The analogous sequence described for **6** was employed for the preparation of **5**.

(*i*) 6-Trimethylsilyloxy-*endo*-tricyclo[3.2.1.0^{2,4}]oct-6-ene was obtained from the corresponding ketone (0.719 g, 5.8 mmol) using LDA (diisopropyl amine (1.30 mL, 9.3 mmol), THF (13 mL), *n*-BuLi (2.26 *M*, 3.60 mL) at −78°C) and trimethylsilyl chloride (1.20 mL, 9.5 mmol), Et_3N (0.45 mL, 3.2 mmol), and THF as described in detail above for **8**. The desired enol ether was purified by bulb-to-bulb distillation (bp 114–122°C/17 Torr) to yield 0.79 g (70% yield) for which glc (FFAP) indicated a purity of >98%; ir ($CHCl_3$); 1610 cm^{-1} (C=C); ^{1}Hmr ($CDCl_3$) δ: 0.30 (s, 9H, Me_3Si), 0.5–2.0 (complex absorption, 6H), 2.62, 2.72 (overlapping m, 1H each), 4.62 (bd, 1H, H-7); ^{13}Cmr, see Table 1. *Exact Mass* calcd. for $C_{11}H_{18}OSi$: 194.1127; found: 194.1123.

(*ii*) Cyclopropanation of this enol ether was accomplished using a Zn/Ag couple (0.87 g, 13 mmol), methylene iodide (0.59 mL, 7.3 mmol) in Et_2O (2 mL), and the work-up described for **9**. This procedure furnished **11** (0.70 g) which glc indicated to be >90% pure. Preparative glc (SE-30) furnished pure samples for characterization and for the following step in the sequence; ^{1}Hmr ($CDCl_3$) δ: 0.18 (s, 9H, Me_3Si) with one-proton multiplets at 0.36, 0.88, 2.11, 2.18, and 2.33 and two-proton multiplets at 0.71, 1.25, and 1.29; ^{13}Cmr, see Table 1. *Exact Mass* calcd. for $C_{12}H_{20}OSi$: 208.1283; found: 208.1277.

(*iii*) Tetracyclic ether **11** was ketonized in 90% yield with methanolic NaOH solution in a manner analogous to that described above for **9** and, as is the case for **9**, a single ketonic product was obtained; ir ($CHCl_3$): 1715 cm^{-1} (C=O); ^{13}Cmr, see Table 1. *Exact Mass* calcd. for $C_9H_{12}O$: 136.0888; found: 136.0889.

In a separate experiment **11** (95 mg) was treated with KOD in *t*-BuOD (2 *M*, 2 mL) using the procedure described above for the preparation of the trideuterated **10**-X. The trideuterated ketone produced contained (ms) 2.6% d_0, 7.9% d_1, 35.5% d_2, 54.0% d_3 (total 2.41 D/molecule). Subsequent treatment with methanolic NaOH solution (3.6 *M*, 2 mL) at room temperature overnight, followed by the usual work-up, furnished **14**-d_1, the ^{13}Cmr spectrum of which indicated the presence of ca. 0.8 atoms D/molecule at C-8 (see text).

(*iv*) The protio analog of **14** (0.20 g, 1.5 mmol) was dimethylated as described above for **10**, using $NaNH_2$ (0.33 g) in Et_2O (11 mL) and methyl iodide (0.58 mL for the first addition, and 0.19 mL for the second addition). The usual work-up furnished **5** (0.20 g, 83%); ir ($CHCl_3$): 1703 cm^{-1} (C=O); ^{1}Hmr, see text; ^{13}Cmr, see Table 1. *Exact Mass* calcd. for $C_{11}H_{16}O$: 164.1201; found: 164.1201.

Homoenolization experiments

The general procedures for the rearrangement and exchange experiments, reported previously (13), were followed as illustrated for **6**. To a solution of *t*-BuO$^-$/*t*-BuOH (1.27 *M*, H_2O content = 250 μg/mL) was added **6** to give a solution which was 0.26 *M* in ketone. To a series of 5-mL predried, thick-walled glass tubes were transferred 0.5-mL aliquots of the reaction solution; the tubes were degassed and sealed before immersion in an oil bath at 180°C. Tubes were removed at various times, cooled before opening, and the contents removed by washing with H_2O (10 mL). The organic product was isolated by pentane extraction (3 × 15 mL) and the combined extracts backwashed with H_2O (3 × 10 mL). The aqueous washings were reextracted with pentane (2 × 15 mL) and the pentane extracts dried over $MgSO_4$. Removal of the solvent by distillation afforded a neutral organic product, representing 75–80% yields from the various tubes, which was analyzed by glc to reveal the presence of two components, one of which was the starting ketone. The new component was ketonic (1730 cm^{-1}) and isomeric with the initial ketone; *Exact Mass* calcd. for $C_{11}H_{16}O$: 164.1201; found: 164.1198. This new ketone was identified as **16** by ^{13}Cmr as described in the text. Two other series of tubes were examined in a similar fashion using an oven at 185 ± 5°C. With reaction times >300 h, the starting material could not be detected in the product. A series of samples using *tert*-butyl alcohol-O-d_1 (99% deuterated, H_2O content = 264 μg/mL) was also run to examine the exchange processes occurring under these reaction conditions; the results are described in the text. An exactly analogous series of experiments was carried out using **5** as the starting material. In all cases, the neutral product, ~80% recovery, contained only the initial ketone; even after >300 h at 180°C there was no evidence (glc, ^{13}Cmr) of the presence of a new component.

*Preparation of **16**-*d$_1$

Ketone **16** (60 mg) was added to a stirred solution of MeONa/MeOD (1 *M*, 2.6 mL) under a N_2 atmosphere and stirring was continued for 12 h at room temperature. After the addition of D_2O (3 mL), the product was extracted with pentane (4 × 10 mL) and the combined extracts washed with 10% NaCl solution (2 × 15 mL) and H_2O (15 mL) before drying over $MgSO_4$. Removal of the solvent by distillation furnished **16**-d_1 (60 mg), the ^{13}Cmr spectrum of which indicated essentially complete deuteration at C-6; ms: 1.2% d_0, 98.8% d_1 (total 0.988 D/molecule).

Acknowledgements

We are grateful for the financial support provided by the Natural Sciences and Engineering Research Council of Canada.

1. A. NICKON and J. L. LAMBERT. J. Am. Chem. Soc. **84**, 4604 (1962); **88**, 1905 (1966).
2. N. H. WERSTIUK. Tetrahedron, **39**, 205 (1983).
3. J. L. JURLINA, H. A. PATEL, and J. B. STOTHERS. Can. J. Chem. **62**, 1159 (1984).
4. H. A. PATEL and J. B. STOTHERS. Can. J. Chem. **62**, 1926 (1984),
5. B. A. DAWSON, A. K. GHOSH, J. L. JURLINA, A. J. RAGAUSKAS, and J. B. STOTHERS. Can. J. Chem. **62**, 2521 (1984).
6. A. L. JOHNSON, N. O. PETERSEN, M. B. RAMPERSAD, and J. B.

STOTHERS. Can. J. Chem. **52**, 4143 (1974).
7. A. K. CHENG, A. K. GHOSH, and J. B. STOTHERS. Can. J. Chem. **62**, 1385 (1984).
8. Y. HOYANO, V. PATEL, and J. B. STOTHERS. Can. J. Chem. **58**, 2730 (1980).
9. V. PATEL and J. B. STOTHERS. Can. J. Chem. **58**, 2728 (1980); B. A. DAWSON and J. B. STOTHERS. Org. Magn. Reson. **21**, 217 (1983).
10. A. K. CHENG and J. B. STOTHERS. Org. Magn. Reson. **9**, 355 (1977).
11. A. NICKON, D. F. COVEY, D. G. PANDIT, and J. J. FRANK. Tetrahedron Lett. 368 (1975).
12. J. L. JURLINA and J. B. STOTHERS. J. Am. Chem. Soc. **104**, 4677 (1982); R. AYDIN, J. R. WESENER, H. GUNTHER, R. L. SANTILLAN, M. E. GARIBAY, and P. JOSEPH-NATHAN. J. Org. Chem. **49**, 3845 (1984).
13. A. L. JOHNSON, J. B. STOTHERS, and C. T. TAN. Can. J. Chem. **53**, 212 (1975).
14. A. BAX, R. FREEMAN, and S. P. KEMPSELL. J. Am. Chem. Soc. **102**, 4849 (1980).
15. HOWE and S. WINSTEIN. J. Am. Chem. Soc. **87**, 915 (1965); T. FUKUNAGA. J. Am. Chem. Soc. **87**, 916 (1965); T. FUKUNAGA and R. A. CLEMENT. J. Org. Chem. **42**, 270 (1977).
16. L. M. JACKMAN and S. STERNHELL. Applications of nuclear magnetic resonance spectroscopy in organic chemistry. Pergamon Press Ltd., Oxford. 1969. p. 286.
17. N. H. WERSTIUK, S. YEROUSHALAMI, and G. TIMMINS. Can. J. Chem. **61**, 1945 (1983).
18. S. L. PATT and J. N. SHOOLERY. J. Magn. Reson. **46**, 535 (1982).
19. D. M. DODDRELL, D. T. PEGG, and M. R. BENDALL. J. Magn. Reson. **48**, 323 (1982).

Minor anthraquinonoid metabolites of *Cercospora arachidicola*[1]

ALBERT STOESSL AND J. B. STOTHERS

London Research Centre, Agriculture Canada and the Department of Chemistry, University of Western Ontario, London, Ont., Canada N6A 5B7

Received October 22, 1984

ALBERT STOESSL and J. B. STOTHERS. Can. J. Chem. **63**, 1258 (1985).

Minor metabolites of the fungus *Cercospora arachidicola* have been identified as the known pigments versicolorin B (**3**), averantin (**4**), and nidurufin (**2*b***) and the new, but closely related compounds 4′-deoxydothistromin (**1*b***), 3′,4′-dehydro-4′-deoxydothistromin (**5*a***), and 4′,5-bisdeoxydothistromin (**1*d***). The ^{1}H and ^{13}Cmr spectra of **1*d***, **2*b***, and the tetracetates **1*c*** and **5*b*** are presented in detail. Biosynthetic and chemotaxonomic aspects are discussed.

ALBERT STOESSL et J. B. STOTHERS. Can. J. Chem. **63**, 1258 (1985).

On a identifié les métabolites mineurs du champignon *Cercospora arachidicola* comme étant les pigments connus versicolorine B (**3**), averantine (**4**) et nidurufine (**2*b***) ainsi que les nouveau composés déoxy-4′ dothistromine (**1*b***), déhydro-3′,4′ déoxy-4′ dothistromine (**5*a***) et bisdéoxy-4′,5 dothistromine (**1*d***) qui leurs sont très apparentés. On rapporte en détail les spectres rmn du ^{1}H et du ^{13}C des composés **1*d*** et **2*b*** ainsi que ceux des tétraacétates **1*c*** et **5*b***. On discute des aspects biosynthétiques et chémotaxonomiques.

[Traduit par le journal]

The peanut pathogen *Cercospora arachidicola* was found recently to produce dothistromin (**1*a***) and averufin (**2*a***) in a liquid medium (1). Subsequent work, employing a solid agar medium, resulted in greatly increased yields of **1*a*** and **2*a*** and in the isolation of brassicasterol and substantial amounts of long-chain fatty aldehydes as other metabolites of the fungus (2). Several other anthraquinones were also isolated, in small amounts, and their identities are reported here. Three of these compounds, versicolorin B (**3**), averantin (**4**), and nidurufin (**2*b***) are well-known fungal metabolites that are implicated in or close to the biosynthetic routes to sterigmatocystin and the aflatoxins (3–5). Three other compounds, **1*b***, **1*d***, and **5*a***, closely related to dothistromin (**1*a***), are reported here for the first time.

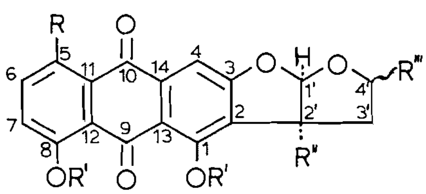

1

	R	R′	R″	R‴
a	OH	H	OH	OH
b	OH	H	OH	H
c	OAc	Ac	OAc	H
d	H	H	OH	H
e	H	H	H	H
f	OH	H	H	H

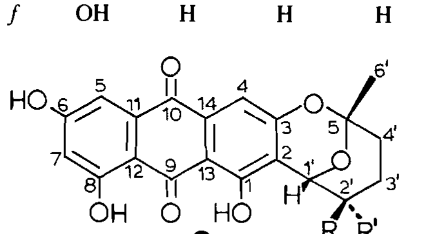

2

	R	R′
a	H	H
b	OH	H
c	H	OH

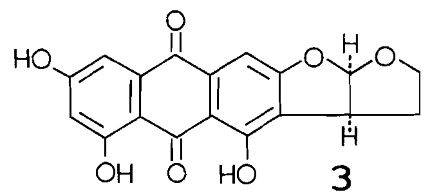

3

The identification of **3** followed unambiguously from its physical and spectroscopic data together with its negative optical rotation at 589 mμ. The identification of averantin (**4**) is tentative, based on its ^{1}Hmr and mass spectra and the melting point (227–235°C) compared to literature data but the sample decomposed before it could be fully characterized. Nidurufin

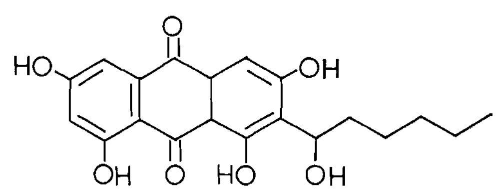

4

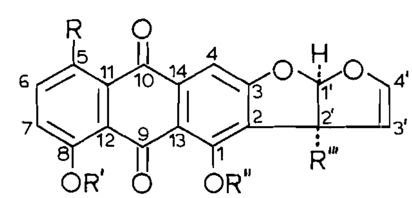

5

	R	R′	R″	R‴
a	OH	H	H	OH
b	OAc	Ac	Ac	OAc
c	OAc	Ac	H	H
d	OH	H	H	H
e	H	Me	H	H

[1]Part 116 of ^{13}Cmr studies; for Part 115 see ref. 22, Part 114 see ref. 23.

(**2***b*) melted at 267–268°C, with prior darkening, partial melting and resetting at ca. 200°C, in contrast to the mp (188°C) reported previously (6). A plausible explanation for this divergence may be dehydration of our samples on the Kofler stage to the anhydro compound. A comparison sample of authentic nidurufin, originally described as a metabolite of *Aspergillus nidulans* (6), could not be obtained. For this reason we present full ^{1}H and ^{13}Cmr data, which have not been specified in the other reports (4, 7) on the compound, but our ^{1}Hmr data (DMSO-d_6 solutions) are in reasonable accord with the few details given in the original publication (6) for acetone-d_6 solutions. The ^{1}Hmr spectrum contained three aryl proton absorptions at δ 6.89 (s), 7.00 (d, J = 2.5 Hz), and 6.50 (d, J = 2.5 Hz) assignable to H-4, -5, and -7, respectively, together with methine patterns at δ 5.00 (H-1′) and 5.38 (H-2′), methylene absorptions at δ 1.55, 1.78, 2.12, and 2.45 (H-3′, -4′) and a methyl singlet at δ 1.50. Phenolic hydroxyl signals were found at δ 12.00 (6-OH) and 12.40 (1- and 8-OH). The ^{13}Cmr spectrum bears a strong resemblance to that reported (8) for averufin (**2***a*), as expected, since the two compounds differ only by the additional hydroxyl group at C-2′ in **2***b*. The observed shieldings for **2***b* are shown in **6**. The dif-

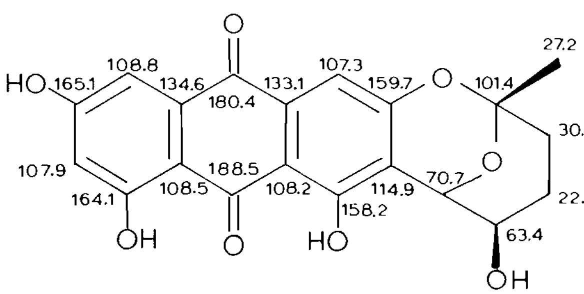

6

ferences, $\Delta\delta_C(\mathbf{2}b - \mathbf{2}a)$, found for C-1′ (+4.4 ppm), −2′ (+36.3 ppm), and −3′ (+7.1 ppm) are reasonable for hydroxyl substitution at C-2′, while the upfield −5.3 ppm shift for C-4′ indicates that the hydroxyl group is axial, i.e., *exo* with respect to the ring system, in complete agreement with the stereochemical assignment reported on the basis of synthesis (4) and contrasting with the original proposal of **2***c* (6). From our evidence we conclude that the metabolite isolated from *C. arachidicola* is identical with the synthetic *exo*-alcohol of Townsend and Christensen (4) and, hence, also with authentic nidurufin.

The two 2-deoxydothistromins **1***b* and **5***a*, separable only with considerable difficulty, were obtained as amorphous red solids. These were characterized as the tetraacetates **1***c* and **5***b*, which were easily purified by chromatography and crystallization. Their ^{1}Hmr, ^{13}Cmr, and mass spectra led to the structural assignments. Additional support was provided by the remarkable similarities of the ^{1}Hmr data (see Experimental) with those for the corresponding protons in **5***c*, which was used to characterize **5***d* reported as a cometabolite of **1***a* in *Dothistroma pini* (7). The ^{13}C spectrum of **1***c* contained methyl absorptions at δ_C 20.7, 20.9, 21.1, and 21.2, methylene signals at δ_C 37.5 (C-3′) and 67.2 (C-4′), methine peaks at 106.4 (C-4), 113.4 (C-1′), 130.3, and 131.2 (C-6, -7), and sixteen signals arising from nonprotonated carbons: δ 179.6, 180.5 (C-9, -10), 168.7, 169.2, 169.4, 169.7 (MeCO—), 165.6 (C-3), 147.3, 147.8, 147.9 (C-1, -5, -8), 138.8 (C-14), 125.5, 125.6, 126.8 (C-11, -12, -13), 119.5 (C-2), and 91.1 (C-2′). Apart from the replacement of the methylene signals with methine absorption at δ_C 101.7 and 151.1 (C-3′ and -4′), the ^{13}C spectrum of **5***b* was very similar, having methyl signals at δ_C 20.9, 21.0, 21.2, 21.3, methine peaks at 107.0 (C-4), 113.6 (C-1′), 130.3, 131.2 (C-6, -7), and sixteen nonprotonated carbon signals: 179.4 (C-9), 180.2 (C-10), 168.5, 169.1, 169.2, 169.4 (MeCO—), 164.6 (C-3), 146.3 147.7, 147.8 (C-1, -5, -8), 137.9 (C-14), 125.4, 126.6, 126.7 (C-11, -12, -13), 113.6 (C-1′), and 93.6 (C-2′). The signals arising from the anthraquinone moiety in each of the derivatives were readily assigned upon comparison with the data reported for an array of acetoxyanthraquinones (9).

Metabolite **1***d*, although obtained only in very small amount, crystallized readily. Its uv spectrum, differing markedly from those of its cometabolites, was typical of a 1,3,8-trioxyanthraquinone, as exemplified by 6-deoxy-8-*O*-methyl versicolorin A (**5***e*) from *Aspergillus ustus* (10). The mass spectrum indicated a composition of $C_{18}H_{12}O_7$ and that the sample was contaminated with an O-homolog $C_{18}H_{12}O_8$. This impurity, possibly **1***b* or other deoxydothistromin, must, however, be present in very small amounts since there was no evidence of its presence in the nmr spectra.

The ^{13}Cmr spectrum, 1.2 mg in DMSO-d_6, contained eighteen signals, seven of which were shown to arise from protonated carbons by a DEPT spectrum (11). Methylene signals appeared at δ 37.8 and 69.0 with CH absorptions at δ 102.3, 116.9, 119.4, 124.5, and 136.9. Signals for fully substituted carbons were found at δ 86.5, 111.3, 115.4, 120.4, 132.9, 136.6, 160.3, 161.1, 166.2, 180.8, and 190.7. From these data it was apparent that the two signals at lowest field must represent the carbonyl centres of the anthraquinone moiety with the more deshielded of the pair (C-9) flanked by two *peri*-hydroxyl groups. Comparison with the shieldings for 1,8-dihydroxy anthraquinone (9) led readily to assignments for C-5, -6, -7, -8, -11, and -12 which differ, on average, by 0.2 ppm from those of the model. Earlier detailed study of several anthraquinones has established that substitution on one of the aryl rings has relatively little effect on the ^{13}C shieldings of the other ring (9). Assignments for each of the remaining signals were made by comparison with the data observed for **3** and reported for versicolorin C (12), which require allowances for the additional hydroxyl substituent at C-2′. The differences of +4.0, +43.3, and +7.8 ppm for C-1′, -2′, and -3′, respectively, are quite consistent with this substitution. For C-1, -2, -3, -4, -13, and -14, the differences average 1.4 ppm, which also seem reasonable. The specific assignments are set out in **7**. The ^{1}Hmr

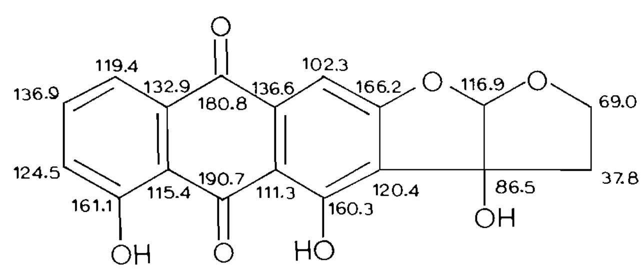

7

spectrum in $CDCl_3$ exhibited three signals readily ascribed to hydroxyl protons through their facile exchange with D_2O. Two of these, δ 12.05 and 12.56, must arise from strongly hydrogen-bonded phenolic groups while the third, appearing as a broad singlet at 2.88, could be attributed to an aliphatic hydroxyl. There were four aryl proton absorptions: a singlet, δ 7.343, and three doublets of doublets characteristic of three contiguous protonated centres, δ 7.826 (J = 1.3, 7.6 Hz), 7.676 (J = 7.6, 8.3 Hz), 7.308 (J = 1.3, 8.3 Hz). A one-proton singlet, δ 6.155, was clearly evident while the four remaining protons appeared as multiplets at 2.520, 2.786, 3.811, and 4.324, from which it was apparent that each was coupled to each of the others. The multiplet at δ 2.786 contained an "extra" coupling of 0.9 Hz which collapsed upon exchange of the hydroxyl protons, showing it to be coupled to the aliphatic hydroxyl proton. The coupling constants for the 2.786 absorption were 12.4, 4.7, and 0.9 Hz while the multiplet at δ 2.520 exhibited couplings of 12.4, 12.4, and 7.9 Hz; these data lead to the assignment of these as the methylene protons at C-3′. The pattern at δ 3.811 showed couplings of 12.4, 9.4, and 4.7 Hz while J values of 9.4, 7.9, and 0.9 Hz were apparent for the 4.324 pattern; thus these absorptions arise from the 4′-methylene protons. The observed J values are consistent with the relative orientations indicated in **8**.

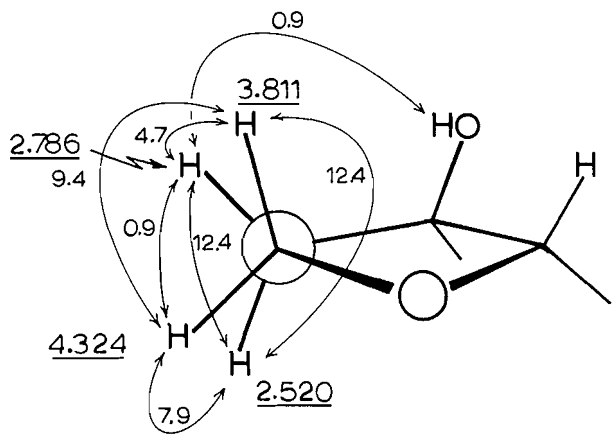

8

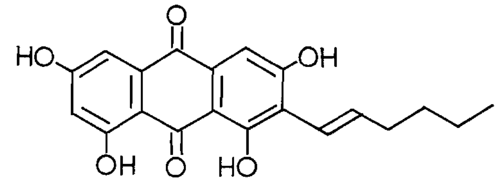

9

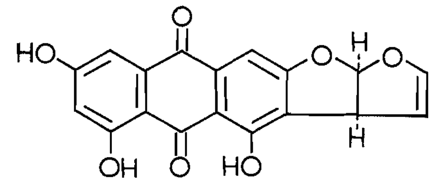

10

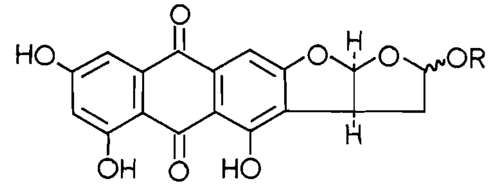

11

a R = H

b R = Ac

The isolation from *C. arachidicola* of small amounts of **1***b*,*d*, **2***a*,*b*, **3**, **4**, **5***a* as congeners of the major metabolite dothistromin (**1***a*) illustrates the remarkable similarity in the metabolism of certain *Cercospora* spp. and *Dothistroma pini*. The latter fungus has been found to produce **1***a* as a major metabolite, together with small amounts of **2***a*,*b*, averythrin (**9**), deoxyversicolorin C (**1***e*, identified tentatively), **1***f*, and **5***d* (7). The last three compounds are formally related to the *C. arachidicola* metabolites **1***d*,*b*, and **5***a*, respectively, merely by hydroxyl substitution at C-2′. Numerous *Cercospora* species, but exclusive of *C. arachidicola*, have been the subject of a chemotaxonomic study by Assante *et al.* (13, 14). Among other, not directly pertinent metabolites, they found **1***a* in *C. smilacis* and seven other spp., and **2***a* and **9** in *C. smilacis*. A deoxydothistromin, apparently not identical with **1***b* from *C. arachidicola*, was identified as a *D. pini* metabolite by mass spectral and preliminary unpublished evidence (15) but no evidence for this compound was obtained for *C. smilacis* (13).

While dothistromin and derivatives thus far appear to have been found only in *D. pini* and *Cercospora* spp., averufin (**2***a*) is known from *Aspergillus* spp. (16), *Bipolaris sorokiniana* (6, 17), and *Monocillium nordinii* (18). Versicolorin B similarly is known from *Aspergilli* (16*a*, *b*) while averantin occurs in *A. versicolor* (16*a*), *A. parasiticus*, and *Solorina crocea* (16*b*). Averantin (**4**), derived from polyacetate via norsolorinic acid, is well established as a precursor of averufin (**2***a*) which, in turn, is converted via versiconal acetate and subsequent steps to sterigmatocystin and hence, the aflatoxins (3–5, 16*b*, *c*). It has recently been suggested that the biotransformation of **2***a* into versiconal acetate may proceed with nidurufin (**2***b*) as a crucial intermediate (4, 19); the isolation of **2***b* as a congener of **2***a* in *A. nidulans* (6), *D. pini* (7), and now also *C. arachidicola* is therefore of some moment. Further, the mechanism of conversion of versiconal acetate into sterigmatocystin has been postulated to involve versicolorin A (**10**), which is indeed known to be incorporated into sterigmatocystin and the aflatoxins (3, 16*b*). Recently, however, it was found that versicolorin A hemiacetal (**11***a*) and its acetate **11***b*, but not **5***e*, were efficiently incorporated into aflatoxin B. It was suggested that **11***a* and **11***b* may be the true intermediates while versicolorin A (**10**) and versicolorin C (racemic-**3**) may be shunts which, however, can reenter the pathway (20). The compounds **11***a* and **11***b* were prepared from **10** by chemical methods and do not appear to be known as fungal products; it is therefore of considerable interest that the salient tetrahydro-2-hydroxybisfuran grouping occurs in dothistromin (**1***a*) (as well as in some aflatoxins).

Averufin and the versicolorins have long been regarded as mycotoxins (3, 12) while dothistromin (**1***a*) has considerable importance as a phytotoxin directly implicated in Dothistroma blight of pine (21); preliminary evidence from our laboratory (1) and elsewhere[2] suggests that it is also a mycotoxin. It is

[2]R. A. Franich, personal communication.

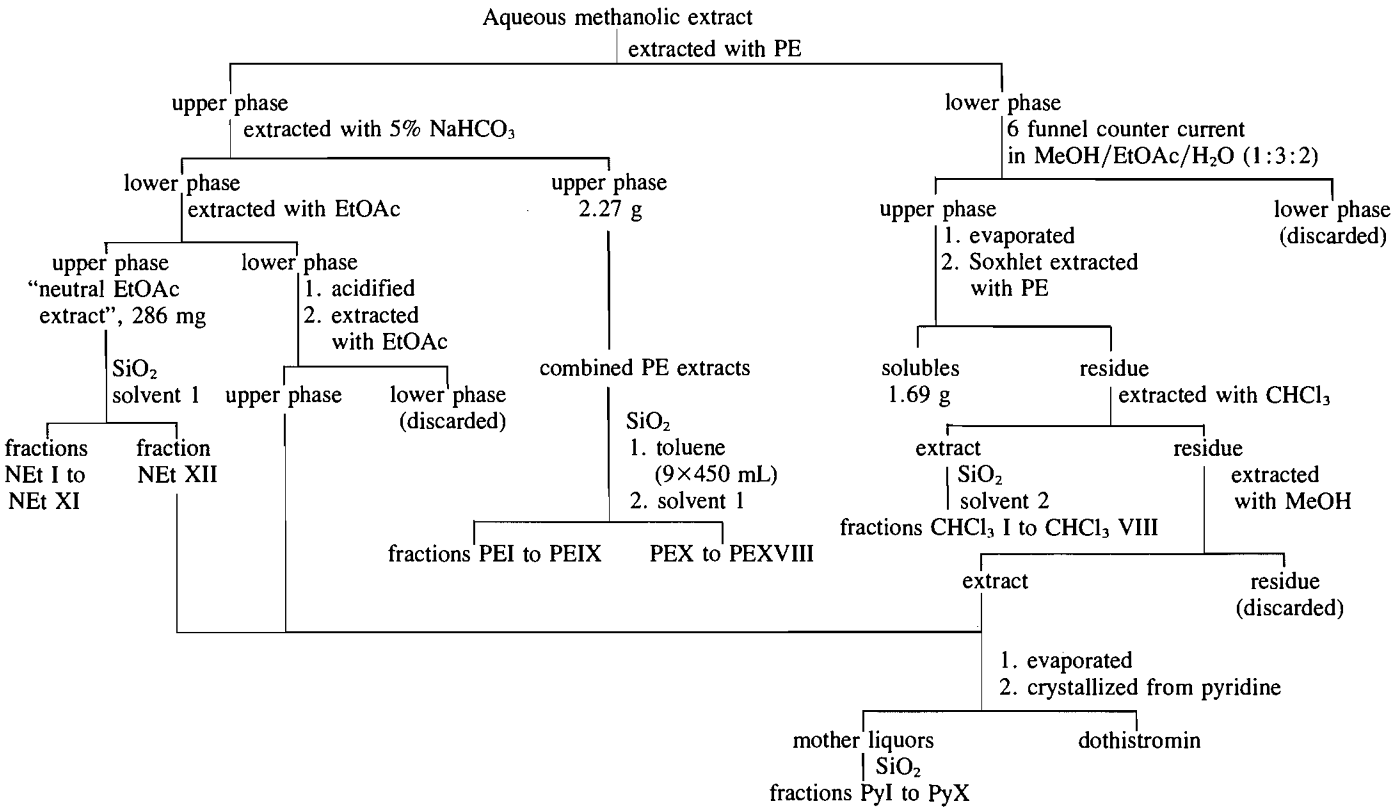

SCHEME 1. Fractionation of *C. arachidicola* extract

probable that similar biological activities are attached to some of the other anthraquinones from *C. arachidicola*; the compounds should therefore be handled with caution.

Experimental

The compounds described here were obtained in the same experiment as the aldehydes reported previously (2). In summary, *C. arachidicola* ATCC 18667 was cultured on potato-dextrose agar (320 Petri dishes, 20 mL each), the cultures being extracted with EtOAc/MeOH (1:1) after 3 weeks. After concentration till aqueous, the extracts were fractionated (Scheme 1) to provide light petrol extracts (PE I, PE II, . . .), neutral ethyl acetate extracts (NEt I, NEt II, . . .), chloroform extracts ($CHCl_3$ I, $CHCl_3$ II, . . .), dothistromin (from pyridine), and dothistromin mother liquors (Py I, Py II, . . .), where the Roman numerals denote consecutive fractions obtained by column chromatography over silica (Camag DF O), with EtOAc/toluene/HOAc (30:60:1; solvent 1) and $EtOAc/CH_2Cl_2/HOAc$ (20:80:1; solvent 2) as irrigants.

General procedures, materials, and instrumentation were as previously specified (2). The ^{13}Cmr spectra were obtained with Varian XL-200 and -300 instruments at 50.3 and 75.4 MHz, respectively (30° pulses, 4-s rep rates with 200-ppm sweep widths, and 32 K points/32 K transforms (XL-200) or 60 000 points/64 K transforms (XL-300) at ambient temperatures). Optical rotations were determined with a Perkin–Elmer 141 polarimeter; we thank Prof. W. A. Ayer for these measurements.

Dothistromin (**1***a*) was obtained substantially pure (824 mg) by one crystallization of the appropriate fraction (Scheme 1) from pyridine. Its identity (1) was further confirmed by acetylation (1, 15) of a recrystallized sample (24 mg) which on chromatography (solvent 1) gave as the only pure product the tetraacetate (14 mg), mp 125–128°C (from EtOH); ^{1}Hmr, $\delta(CDCl_3)$: 7.47 (s, H-6 and H-7), 7.28 (s, H-4), 6.56 (d, $J \sim$ 3Hz, H-4′), 6.54 (s, H-1′), 2.95 (m, H_2-3′), 2.51 and 2.49 (2s, 5-, 8-OAc), 2.14 (s, 2′-OAc), and 1.75 (s, 4′-OAc).

Averufin (**2***a*) was isolated by rechromatography and (or) recrystallization from fractions PE XIII, PE XIV, and NEt VI. It had the requisite uv and ^{1}Hmr spectra and was also identical with an authentic specimen (14) by tlc (several systems), mp, mp in admixture, and ms.

Versicolorin B (**3**) (10 mg) was obtained by repeated rechromatography and (or) crystallization (H_2O/isopropanol or MeOH/EtOAc) from fractions PE XV, NEt VII and VIII, and $CHCl_3$ III, and identified by comparison of its mp (303–306°C), uv, ^{1}Hmr, ^{13}Cmr, and ms parameters with literature data (12). The compound had $[\alpha]_D$ −155.2° (*c* 0.32, dioxane).

Averantin (**4**) (6 mg) was isolated by repeated rechromatography ($MeOH/CHCl_3/HOAc$ 5:95:0.1) of fractions NEt VII and VIII, and $CHCl_3$ IV; mp 213–219°C (from toluene/EtOAc), 227–235°C (from $CHCl_3$); λ_{max} (ϵ): 221 (42 800), 255 (sh) (20 900), 264 (23 400), 293 (38 600), 324 (19 500), 452 (11 300), and 462 (sh) (11 200); ^{1}Hmr, δ(DMSO-d_6): 7.16 (d, J = 2.5 Hz, H-5), 7.14 (s, H-4), 6.62 (d, J = 2.5 Hz, H-7), 5.17 (t, J = 6 Hz, H-1′), 1.80 (m, H_2-2′), 1.5–1.1 (m, H_2-3′, H_2-4′, H_2-5′), and 0.84 (t, J = 6 Hz, Me). The mass spectrum was indistinguishable from that published (5).

Nidurufin (**2***b*) (8 mg) was obtained from fractions NEt X and $CHCl_3$ XI, VII, and VIII, mostly by extensive refractionations (solvents 1, 2, $MeOH/CHCl_3/HOAc$ 10:90:1, and EtOAc/HOAc 99:1) and was recrystallized from MeOH/EtOAc; λ_{max} (ϵ): 221 (35 800), 256 (sh) (16 100), 264 (17 600), 293 (29 600), 315 (13 600), and 459 (8 000); *m/e*: 384, 366 (100%), 326, 323, 314, 299, 297, 286; $[\alpha]_D$ −12.6° (*c* 0.37, dioxane). *Exact mass* calcd. for $C_{20}H_{16}O_3$: 384.08452; found: 384.08464.

4′-Deoxydothistromin (**1***b*) and 3′,4′-dehydro-4′-deoxydothistromin (**5***a*) were separable from each other only by extensive rechromatography, substantial proportions of the compounds being invariably eluted as a mixture. Final yields were substantially pure **1***b*, 18 mg; **5***a*, 21 mg; unresolved mixture, 33 mg.

Acetylation (pyridine/Ac_2O 3:2, room temperature, overnight) of crude **1***b* (11 mg) gave the tetraacetate **1***c* (7.9 mg after chromatography in solvent 1); crystals from $MeOH/CHCl_3$, dec. >220°C without melting; λ_{max} (ϵ): 209 (15 600), 238 (10 200), 272 (23 900), 348 (3 500); ^{1}Hmr, $\delta(CDCl_3)$: 7.54 (s, 1H, H-4), 7.40 (s, 2H, H-6 and H-7), 6.47 (s, 1H, H-1′), 4.25 (m, 1H, H-4′ eq), 3.70 (m, 1H, H-4′ ax), ca. 2.6 (m, 2H, H-3′), 2.47 (s, 6H, 2 ArOAc), 2.42 (s, 3H, ArOAc), and 2.04 (s, 3H, 2′-OAc); *m/e*: 524, 482, 440 (100%), 398, 338 (100%), 310 (100%); $[\alpha]_D$ −72.4° (*c* 0.32, $CHCl_3$). *Exact Mass* calcd for $C_{26}H_{20}O_{12}$: 524.05941; found: 524.09587.

3′,4′-Dehydro-4′-deoxydothistromin (**5***a*) had [1]Hmr, δ(DMSO-d_6): 7.41 (br s, 2H, H-6, -7), 7.27 (br s, 1H, H-4), 6.48 (s, 1H, H-1′), and 5.66 (d, J = 3 Hz, 1H, H-3′). The tetraacetate **5***b*, prepared as **1***c*, was recrystallized from MeOH/$CHCl_3$; mp 211–213°C; λ_{max} (ε): 209 (29 700), 239 (16 400), 272 (30 500), 344 (6 200); [1]Hmr, δ($CDCl_3$): 7.58 (s, 1H, H-4), 7.37 (s, 2H, H-6 and H-7), 6.86 (s, 1H, H-1′), 6.69 (d, J = 2.8 Hz, 1H, H-4′), 5.43 (d, J = 2.8 Hz, 1H, H-3′), 2.46 (s, 6H, 2 ArOAc), 2.42 (s, 3H, ArOAc), and 2.06 (s, 3H, 2′-OAc); *m/e*: 522, 480, 462, 438, 420, 396, 378, 354, 336 (100%); $[\alpha]_D$ −49.5° (*c* 0.67, $CHCl_3$). *Exact Mass* calcd. for $C_{26}H_{18}O_{12}$: 522.07956; found: 522.07941.

4′-5-Bisdeoxydothistromin (**1***d*), 1.8 mg on repeated rechromatography of fractions NEt IX and X, and $CHCl_3$ IV, 1.0 mg after recrystallization ($CHCl_3$), had mp 254–258°C; λ_{max} (ε) 248 (16 300), 268 (22 200), 279 (21 400), 432 (4 500), and 455 (sh) (4 100). *m/e*: 356, 340 (M^+, 100%), 322, 312, 311, 294, 283, 281, 267, 256, 240, and 228. *Exact Mass* calcd. for $C_{18}H_{12}O_7$: 340.05827; found: 340.05935.

NOTE ADDED IN PROOF: The role of nidurufin as an aflatoxin precursor has become doubtful on the basis of a very recent study (ref. 24).

Acknowledgements

Thanks are due to G. L. Rock for general experimental assistance, D. Hairsine and S. Wilson for measuring mass and 200-MHz [1]Hmr spectra, and to the Natural Sciences and Engineering Research Council of Canada for financial support. We are very grateful to Dr. R. A. Franich for communicating results on the mutagenicity of dothistromin prior to their publication.

1. A. STOESSL. Mycopathologia, **86**, 165 (1984).
2. A. STOESSL. Can. J. Microbiol. **31**, 129 (1985).
3. P. S. STEYN, R. VLEGGAAR, and P. L. WESSELS. The biosynthesis of aflatoxin and its congeners. *In* The biosynthesis of mycotoxins. *Edited by* P. S. Steyn. Academic Press, New York. 1980. pp. 105–155.
4. C. A. TOWNSEND and S. B. CHRISTENSEN. Tetrahedron, **39**, 3575 (1983).
5. J. W. BENNETT, L. S. LEE, S. M. SHOSS, and G. H. BOUDREAUX. Appl. Environ. Microbiol. **39**, 835 (1980).
6. P. J. AUCAMP and C. W. HOLZAPFEL. J. S. Afr. Chem. Inst. **23**, 40 (1970).
7. A. V. DANKS and R. HODGES. Aust. J. Chem. **27**, 1603 (1974).
8. C. P. GORST-ALLMANN, K. G. R. PACHLER, P. S. STEYN, P. L. WESSELS, and DE B. SCOTT. J. Chem. Soc. Perkin Trans. 1, 2181 (1977).
9. G. HOFLE. Tetrahedron, **33**, 1963 (1977).
10. R. M. HORAK, P. S. STEYN, R. VLEGGAAR, and C. J. RABIE. S. Afr. J. Chem. **35**, 60 (1982).
11. D. M. DODDRELL, D. T. PEGG, and M. R. BENDALL. J. Magn. Reson. **48**, 323 (1982).
12. R. J. COLE and R. H. COX. Handbook of toxic fungal metabolites. Academic Press, New York. 1981. pp. 102–106.
13. G. ASSANTE, L. CAMARDA, L. MERLINI, and G. NASINI. Phytochemistry, **16**, 125 (1977).
14. G. ASSANTE, R. LOCCI, L. CAMARDÀ, L. MERLINI, and G. NASINI. Phytochemistry, **16**, 243 (1977).
15. R. T. GALLAGHER and R. HODGES. Aust. J. Chem. **25**, 2399 (1972).
16. (*a*) W. B. TURNER. Fungal metabolites. Academic Press, London and New York. 1971; (*b*) W. B. TURNER and D. G. ALDRIDGE. Fungal metabolites II. Academic Press, London. 1983; (*c*) T. J. SIMPSON, A. E. DE JESUS, P. S. STEYN, and R. VLEGGAAR. J. Chem. Soc. Chem. Commun. 631 (1982); 632 (1982).
17. C. M. MAES and P. S. STEYN. J. Chem. Soc. Perkin Trans. 1, 1137 (1984).
18. W. A. AYER, S. P. LEE, A. TSUNEDA, and Y. HIRATSUKA. Can. J. Microbiol. **26**, 766 (1980).
19. Z. AHMED and M. P. CAVA. J. Am. Chem. Soc. **105**, 682 (1983).
20. M. F. DUTTON and M. S. ANDERSON. Appl. Environ. Microbiol. **43**, 548 (1982).
21. L. SHAIN and R. A. FRANICH. Physiol. Plant Pathol. **19**, 49 (1981).
22. M. ESSENBERG, A. STOESSL, and J. B. STOTHERS. J. Chem. Soc. Chem. Commun. In press.
23. A. J. RAGAUSKAS and J. B. STOTHERS. Can. J. Chem. **63**, 1250 (1985).
24. C. A. TOWNSEND and S. B. CHRISTENSEN. J. Am. Chem. Soc. **107**, 270 (1985).

The reactions of some α-halo-β-ketosulfones with hard and soft nucleophiles. A preparation of sulfinate esters

J. STUART GROSSERT,[1] PRAMOD K. DUBEY, AND TOM ELWOOD
Department of Chemistry, Dalhousie University, Halifax, N.S., Canada B3H 4J3

Received November 25, 1983[2]

J. STUART GROSSERT, PRAMOD K. DUBEY, and TOM ELWOOD. Can. J. Chem. **63**, 1263 (1985).

The α-halo-β-ketosulfonyl functionality was attacked by ethanethiolate at the halogen which, in the presence of a proton source, usually resulted in reduction to the β-ketosulfone. A range of other soft nucleophiles did not react, whereas hard nucleophiles invariably attacked at the carbonyl, with subsequent cleavage to α-halosulfones. Ambident arylsulfinate anions usually attacked at halogen to form the sulfonyl halide, which reacted with excess sulfinate to give an intermediate that is readily attacked by alcohols. This reaction resulted in the formation of alkyl arylsulfinate esters in reasonable yields. The same reaction occurred when sulfonyl chlorides were reacted with sulfinate salts and it was rationalized by using HSAB principles. Spectral properties of some sulfinate esters are presented.

J. STUART GROSSERT, PRAMOD K. DUBEY et TOM ELWOOD. Can. J. Chem. **63**, 1263 (1985).

On a fait réagir l'éthanethiolate sur l'halogène de composés α-halo β-cétosulfonyle qui, en présence d'une source de protons, conduisent habituellement à une réduction en β-cétosulfone. Un certain nombre d'autres nucléophiles nous ne réagissent pas tandis que les nucléophiles durs attaquent invariablement le carbonyle avec un clivage subséquent conduisant aux α-halosulfones. Les anions arylsulfinates possèdent deux positions réactives et réagissent habituellement au niveau de l'halogène pour conduire à l'halogénure de sulfonyle qui réagit alors avec un excès de sulfinate pour donner un intermédiaire que les alcools attaquent facilement. Cette réaction conduit à la formation d'esters arylsulfinates alkyles avec des rendements raisonnables. La même réaction se produit lorsqu'on fait réagir des chlorures de sulfonyles avec des sels de sulfinates et on rationalise cette réaction en faisant appel aux principes ABDM. On présente les propriétés spectrales de quelques esters sulfinates.

[Traduit par le journal]

Introduction

The α-halo-β-ketosulfone functionality (**A**) has not been extensively studied (1–4), yet has considerable potential as a complex functionality in which interactions between proximate groups can be studied. For instance, it combines an α-halosulfone, a functionality that is known to undergo substitution reactions at carbon with difficulty, with an α-haloketone, a functionality that is usually susceptible to such substitutions (5). There are several ways in which **A** could react with a

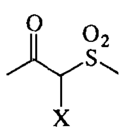

A

nucleophile, namely (*1*) attack at the α-carbon with displacement of the best leaving group, that is, the halogen X; (*2*) attack at the halogen X (6), with displacement of the enolate anion; (*3*) removal of the acidic α-proton (pK_a ~10)[3] if the attacking nucleophile is sufficiently basic; or, (*4*) attack at the β-carbonyl carbon, either to give a carbonyl addition product, or to displace an α-halosulfonyl carbanion as a leaving group (cleavage of C—C bond).

We have reported on reactions of the 4th type (4) in which cleavage could be induced by hydroxide or alkoxide anions, anions that are classified as hard in the HSAB terminology. Owing to our interest in the preparation of sulfenylated β-ketosulfones (7), we were attracted by the possible reaction of thiolate anions (soft nucleophiles) with **A**. This could, in principle, provide a route to α-sulfenylated-β-ketosulfones (and thus be of synthetic utility), and it could provide evidence as to whether a sulfonyl or a carbonyl group would control the course of a substitution reaction (and thus be of mechanistic interest). Our results (*vide infra*) have shown that the reaction is of little synthetic utility, but did provide some interesting evidence regarding mechanism. Also reported on are the reactions of **A** with a series of nucleophiles that can be classified as having varying degrees of hardness or softness.

Results and discussion

Reactions with thiolate anions

The α-halo-β-ketosulfones $PhCOCHBrSO_2Me$ (**1**) and $PhCOCHClSO_2Me$ (**2**) were used to study the reaction with thiolate since they were readily available (4). The results (Table 1) can be divided into three groups, namely entries 1, 2, entries 3–5, and entries 6–10. In the first group, the solvent was polar and protic, the product was that due to a reduction reaction, and attack by thiolate was therefore apparently exclusively at the halogen. Previous work on the reaction of α-halosulfones with nucleophiles has shown that reduction is significantly favoured over substitution as the degree of substitution at the halogen-bearing carbon is increased (6, 8, 9), especially in a protic solvent. In the case of **1** and **2**, attack at the halogen could be expected since the carbonyl group would stabilize the resulting anion. The other product of this reaction (eq. [1]) will be the sulfenyl halide, which is decomposed by the ethanol solvent. Reduction must be a rapid reaction since no cleavage products (4) from attack on **1** or **2** by ethoxide, formed by the reaction depicted in eq. [2], were detected.

$$[1]\quad RCO\cdot CHX\cdot SO_2Me + EtS^- \rightarrow [RCO\cdot CH\cdot SO_2Me]^- + EtSX$$

$$[2]\quad [RCO\cdot CH\cdot SO_2Me]^- + EtOH \rightarrow PhCOCH_2SO_2Me\ (\mathbf{3}) + EtO^-$$

The use of a polar, aprotic solvent (DMF, entries 3–5) permitted isolation of both the reduction product (**3**) and the

---

[1] Author to whom correspondence may be addressed.
[2] Revision received October 10, 1984.
[3] Work to be published, with J. Hoyle, J. N. M. Glover, and P. K. Dubey.

TABLE 1. The reactions of 2-bromo-2-methylsulfonyl-1-phenylethanone (**1**) and 2-chloro-2-methylsulfonyl-1-phenylethanone (**2**) with sodium ethanethiolate* at room temperature

Entry	Substrate*	Solvent	Time (h)	Products (yield)†
1	**1**	EtOH	8	$PhCOCH_2SO_2Me$ (**3**, 95%)‡
2	**2**	EtOH	5	**3**, 72%‡
3	**2**	DMF	24	**3**, 47% + EtSSEt (**4**, 59%)
4	**2**	DMF§	24	**3**, 55% + **4**, 55%§
5	**2**	DMF§	24	**3**, 36% + **4**, 59%§
6	**1**	THF	24	**3**, 46% + **4**, 62% + $PhCO\cdot CHSEt\cdot SO_2Me$ (**5**, 48%)
7	**2**	THF	24	**3**, 56% + **4**, 66% + **5**, 34%
8	**2**	THF§	24	**3**: **5** = ca. 2:1
9	**2**	THF§	24	**3**: **5** = ca. 1:1
10	**2**	PhMe	24	**3** + **4** + **5**‖

*All reactions were carried out on a 2-mmol scale with 4 mmol of thiolate, except for entries 1 and 2 when 10 mmol was used.
†Yields are estimated from integration of an ^1H nmr spectrum of weighed material that was also examined by tlc against reference compounds, unless otherwise stated.
‡Yield of pure, isolated material.
§The reaction was carried out in the dark in the presence of nitrobenzene (4 mmol, entries 4 and 8) or *m*-dinitrobenzene (2 mmol, entries 5 and 9), more than 80% of which was present in a product mixture.
‖The yields were not determined.

disulfide, **4**, formed by attack of excess thiolate on the intermediate sulfenyl chloride (eq. [3]).

$$[3]\quad EtSX + EtS^- \rightarrow EtSSEt\ (\mathbf{4}) + X^-$$

Repetition of the experiments in the presence of the radical-chain inhibitors nitrobenzene and *m*-dinitrobenzene (10) had no obvious effects, thus suggesting that the reaction most likely involves a two-electron attack of thiolate on halogen. No sign of any substitution product $PhCO\cdot CHSEt\cdot SO_2Me$ (**5**) was observed in the proton nmr spectra of crude reaction mixtures.

In aprotic solvents of lower polarity (THF, dimethoxyethane (DME), or toluene), both **1** and **2** yielded mixtures of the reduction product **3**, the substitution product **5**, plus the disulfide, **4**. The production of **5** must involve a process described in eq. [4] in competition with that in eq. [3], since it is unlikely

$$[4]\quad [RCO\cdot CH\cdot SO_2Me]^- + EtSX \rightarrow RCO\cdot CHSEt\cdot SO_2Me\ (\mathbf{5}) + X^-$$

that the mechanism of the reaction would change on switching solvents from DMF to THF. The results for DME as solvent were quite similar to entry 6 (Table 1) and are thus not reported. The complex product mixtures obtained from the experiments for checking whether a radical-chain reaction was involved (entries 8, 9) could not be analyzed with sufficient confidence to merit publication and thus bear further investigation.

It does seem reasonable to conclude from the above experiments that the reaction leading to the substitution product **5** does not involve a nucleophilic attack by thiolate at carbon (an S_N2 reaction), but rather an attack at the halogen, followed by subsequent reaction of the intermediate carbanion with the resulting sulfenyl halide. This type of reaction (eq. [1] followed by eq. [4]) has been suggested previously, but has not been definitively proven (8). We propose that the differences between the three classes of solvent reflect differences in solvation around the intermediate carbanion and the degree of reactivity of the solvent with the sulfenyl halide, and that attack both on carbon and on halogen, operating in competition during a given reaction (9), does not occur. The determination of the actual relative energy barriers for the various processes remains to be made.

TABLE 2. The reactions* of 2-chloro-2-methylsulfonyl-1-phenylethanone (**2**) with various nucleophiles in absolute ethanol solvent

Entry	Reagent	Conditions	Products
1	$Me\cdot CS\cdot NH_2$	14 h,	**2** + $Me\cdot CS\cdot NH_2$ cryst. residue
2	$H_2N\cdot CS\cdot NH_2$	16 h,	**2**, 87% recovered
3	KSCN	4 h, rt	**2**, 75% recovered
4	NaI†	12 h, rt	**2**, 95% recovered
5	KI	5 h, rt	**2**, $ClCH_2SO_2Me$ (**6**) and EtOBz‡ (**7**)§
6	KNO_3	24 h, rt	**2**, 88% recovered
7	KOCN	24 h, rt	**6**, 48% + **7**, 71%‖
8	KCN	4 h, rt	**6**, 75% + **7**, 65%‖
9	$KF\cdot 2H_2O$	4 h, rt	**6**, 68% + **7**, 59%‖

*All reactions were carried out on a 2-mmol scale.
†Reaction done in acetone solvent.
‡Bz = —CO·Ph.
§Products were a complex mixture; those given were identified by a comparison of chemical shifts in the ^1H nmr spectrum.
‖These yields were estimated from the ^1H nmr spectra. No other products were observed.

Reactions with various hard and soft nucleophiles

Since we have observed attack on **1** and **2** at the carbonyl by hard oxygen nucleophiles and at the halogen by soft sulfur nucleophiles, we extended the range of nucleophiles to encompass others of varying degrees of hardness. The results for reactions with **2** are reported in Table 2.

Thioamides and thioureas are known (11, 12) to be excellent nucleophiles for attack at electrophilic sp^3-hybridized carbons. Apparently they are not efficient nucleophiles for attack at chlorine, as they did not effect reduction of **2**. Likewise, thiocyanates can be good nucleophiles for attack at carbon (13), yet no reaction was observed. These experiments reinforce the belief, implied by the results in the previous section, that nucleophilic attack at carbon in α-halo-β-ketosulfones has a relatively high energy of activation.

The results with iodide (entries 4, 5) are not readily explicable; the reaction with potassium iodide in ethanol was re-

TABLE 3. The reactions of 2-bromo-2-methylsulfonyl-1-phenylethanone (**1**) and 2-chloro-2-methylsulfonyl-1-phenylethanone (**2**) with sodium benzenesulfinate dihydrate at room temperature

Entry	Substrate*	Solvent	Time (h)	Products (yield)[†]
1	**1**	MeCN	24 h	**3**, 95% + **1**[‡]
2[§]	**1**	DMF–EtOH	48 h	**3**, 38% + Ph·SO·OEt (**8**, 63%)
3	**1**	EtOH	24 h	**3**, **7**, **8** in mixture
4	**2**	MeCN	24 h	**3**, 95% + **2**[‖]
5	**2**	DMF	72 h	**3**, 69%, isolated
6[§]	**2**	DMF–EtOH	72 h	**3**, 50% + **8**, 82%
7[§]	**2**	DMF–MeOH	70 h	**3**, 60% + Ph·SO·OMe (**9**, 80%)
8[¶]	**2**	DCM**	24 h	**3**, 95% + **2**[††]
9[§,¶]	**2**	DCM–EtOH	48 h	**3**, 62% + **8**, 67% + **2**[‡‡]

*All reactions were done on a 2-mmol scale with 4 mmol of reagent.
[†]Yields are estimated from integration of a ^{1}H nmr spectrum of weighed product that was checked against reference compounds, except for entry 5 in which a single compound was isolated.
[‡]The yield of **3** ($PhCOCH_2SO_2Me$) is based on 59% of **1** being recovered.
[§]Entry 2, solvent was DMF–EtOH = 4:1 v/v; entries 6,7 = 2:1; entry 9 = 1:1 dichloromethane–ethanol.
[‖]The yield of **3** is based on 78% of **2** being recovered.
[¶]The reagent was triethylammonium benzene sulfinate, see Experimental.
**DCM = dichloromethane.
[††]The yield of **3** is based on 85% of **2** being recovered.
[‡‡]The yields of **3** and **8** are based on 29% of **2** being recovered.

producible, yet yielded a complex mixture of products that was not readily amenable to analysis. Further work in this area is required.

The reactions of **2** with hard nucleophiles paralleled those with alkoxides (4). In each case, only cleavage products were observed, corresponding to preferred attack at the carbonyl carbon.

Reactions with sulfinate salts

The sulfinate anion is especially interesting since it is an ambident nucleophile, with a soft center on sulfur and a hard center on oxygen (14–16). It has a significant affinity for electrophilic carbon (17), although it has been used to reduce α-halosulfones (18). Our results, obtained from carrying out the reaction under a wide range of conditions, are presented in Table 3. Two facts stand out: (*a*) the predominant reaction is reduction, as found previously for α-halosulfones (18); (*b*) in ethanol (entry 3), attack at the carbonyl is competitive since the cleavage product, ethyl benzoate (**7**), was present in the product mixture.

The reduction of bromo compound **1** (entry 1) was more facile than that of chloro compound **2** (entry 4), as would be expected if reaction is occurring by attack at the halogen. Reaction was only really effective in more polar solvents, even when a solubilizing counterion (entry 8) was used. Similar reductions of active halogen compounds by sulfinate anions have in fact been known for many years (19).

If a sulfinate anion attacked an active halogen atom at sulfur the product would be a sulfonyl halide (eq. [5]). It was thus rather surprising to find that the sulfur-containing products in

$$[5] \quad R{-}SO_2^- + Cl{-}Z \rightarrow R{-}SO_2{-}Cl + :Z^-$$

Table 3, entries 2, 6, 7, and 9, were sulfinate rather than sulfonate esters. The origin of these sulfinate esters was determined when we investigated the reaction of sodium arylsulfinates with arylsulfonyl chlorides in mixed DMF–alcohol solvents, the major product being the alkyl arylsulfinate esters. The relatively unstable oils were characterized by independent syntheses using the classical route through the sulfinyl chlo-

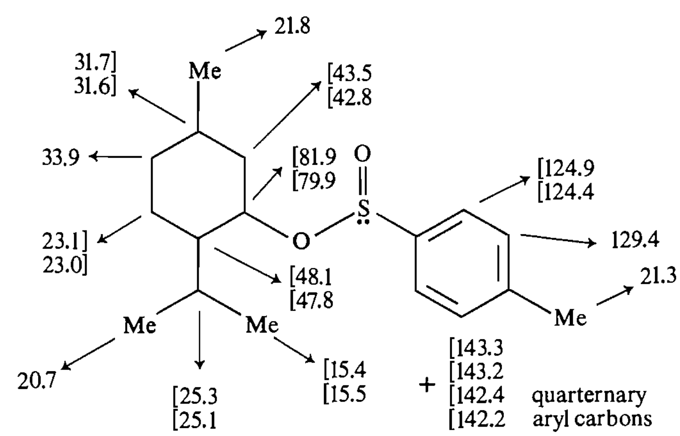

FIG. 1. (−)-Menthyl *p*-toluenesulfinate, **12**, with ^{13}C chemical shifts expressed as δ values.

rides. Spectral properties of the sulfinate esters synthesized by the two routes were identical; especially interesting were the ^{1}H nmr spectra of the ethyl sulfinate esters, which showed their methylene absorptions as classic 16-line patterns of an ABX_3 system (20). At 80 MHz these showed as two pairs of separated double quartets, but all the lines were not separated at 60 MHz. The ^{13}C nmr spectrum of the (−)-menthyl sulfinate (see Fig. 1) provided clear evidence that the sample was a diastereomeric mixture. The assignments of the resonances in this spectrum were made by comparison with the literature assignment for the spectrum of (−)-menthol (21), which agreed very closely with our own spectrum of (−)-menthol. The infrared spectrum of our sample of ethyl *p*-toluenesulfinate was identical to that previously published (22). The fragmentation pattern of the sulfinate esters under electron impact was straightforward, with the expected $ArSO_2]^+$, $ArSO]^+$, $ArS]^+$, and $Ar]^+$ ions predominating. In the case of the ethyl esters, the McLafferty rearrangement ions, $ArSO_2H]^{+\bullet}$, were important also.

We propose therefore that the sulfinate esters observed in entries 2, 6, 7, and 9 are formed by the reaction depicted in eq. [5], followed by two subsequent reactions (eqs. [6], [7]).

[6] $Ar \cdot SO_2 \cdot Cl + Ar \cdot SO \cdot O^- \rightarrow Ar \cdot SO_2 \cdot O \cdot SO \cdot Ar$ (**10**)

[7] **10** + $ROH \rightarrow ArSO_3H + RO \cdot SO \cdot Ar$

The attack by $ArSO_2^-$ at oxygen on the sulfur of the sulfonyl chloride would lead to an intermediate mixed anhydride **10**.[4] This species would be susceptible to nucleophilic attack at the sulfinyl sulfur (25), thus leading to sulfinate esters as depicted in eq. [7]. These reactions provide an elegant example of the ambidence of the sulfinate anion, with two nucleophilic centers having differing degrees of hardness. The reactions may, under certain circumstances, have some preparative merit and they appear to be of comparable convenience to a recently reported synthesis of sulfinate esters (26).

Two further points merit comment. Kohler and MacDonald (27) found that sodium *p*-toluenesulfinate and an arylsulfonyl chloride reacted in water–ether to give an α-disulfone, albeit in an unspecified yield.[5] We believe that this reaction also proceeds through **10**, which could undergo thermal rearrangement to an α-disulfone. Indeed, α-disulfones were a persistent minor contaminant in all our reactions leading to the sulfinate esters, but the formation of these disulfones was not efficient even if the sulfinate salt was warmed with the sulfonyl chloride in a solution of DMF.

The second point concerns the stability of aryl sulfinate esters. We have found these to be quite unstable at room temperature and were intrigued to find that the mass spectrum of a decomposed sample of ethyl *p*-toluenesulfinate, **11**, could readily be interpreted as resulting almost entirely from the disulfide **13** and the ethyl sulfonate ester **14**. The spectrum was very clean and the intensities of the isotope peaks for both molecular ions and for two fragment ions from **14** fitted their correct empirical formulae. There was apparently some *p*-toluenesulfonic acid present in the mixture also, although the evidence for this is less certain.

Thermal disproportionation reactions of sulfinate esters have been described by Müller and Schank (28), who found thiolsulfonates and disulfides as major products, these presumably being formed by the intermediacy of sulfenic acids. Apparently, the formation of sulfonate esters has not been described previously. The sulfonate likely derives from a nucleophilic attack of the sulfinate ester oxygen on the sulfur of a second ester molecule, leading to a sulfonate and sulfenate ester pair

[8] $2ArSO \cdot OR \rightarrow ArSO_2 \cdot OR + ArS \cdot OR$

(eq. [8]). Disproportionation reactions of sulfinate esters therefore merit further work.

Conclusions

The reactions of α-halo-β-ketosulfones described in this and in the previous (4) paper can be explained either by preferred attack of hard nucleophiles at the carbonyl group or by attack of soft nucleophiles at the halogen. With a suitable ambident nucleophile and solvent (cf. Table 3, entry 3) both processes can be observed, suggesting that the relative energy barriers are quite comparable. There does not seem to be any evidence for S_N2 attack at carbon. The results obtained, however, do not permit any assessment to be made whether the barrier for S_N2 attack has been raised vis-à-vis an alkyl halide, or whether the observed reactions occur because their activation energies are lowered as a result of structural features in α-halo-β-ketosulfones. Qualitative assessments of the reactions were assisted by the application of HSAB principles.

Experimental

General

Solvents were dried (usually 4 Å molecular sieves) or distilled as appropriate; THF was stored over P_2O_5, distilled from fresh P_2O_5, and then stored under nitrogen over $NaAlH_4$, from which it was freshly distilled before use. Sodium hydride (Alfa or Aldrich, 50% in oil dispersion) was washed several times with dry ligroin (bp 40–60°C) and dried *in vacuo*. The preparation of the halosulfones **1** and **2** has been described previously (4). For some experiments, sodium benzenesulfinate dihydrate was dried at 100°C/0.1 Torr (1 Torr = 133.3 Pa). Most reactions were carried out under a nitrogen atmosphere and volatile solvents were rotary evaporated before work-up; work-up was by pouring into water, appropriate adjustment of the pH, and extraction with dichloromethane; this extract was then washed with water, dried ($MgSO_4$), and evaporated. However, reactions performed in *N,N*-dimethylformamide (DMF) solvent were always extracted with diethyl ether, and then thoroughly washed with water to remove residual DMF. Since **3** is not very ether-soluble, recoveries by this procedure were not outstanding. Diethyl disulfide, **4** (Table 1, entries 6–9), was isolated by extracting the crude reaction products (after rotary evaporation) with ligroin (bp 40–60°C), which did not dissolve **1**–**3**.

Reduction of 2-chloro-2-methylsulfonyl-1-phenylethanone (**2**) *with sodium ethanethiolate in ethanol – typical procedure*

Freshly cut and washed sodium metal (263 mg) was dissolved in absolute EtOH (10 mL) to which was added EtSH (~1 mL, 12 mmol), followed by **2** (471 mg, 2 mmol). The resulting clear solution was stirred for 5 h (with protection from moisture) and rotary evaporated to an oil which was partitioned between dilute HCl and dichloromethane to give a colourless crystalline solid (290 mg, 72%), ^{1}H nmr identical to authentic **3**. Recrystallization (toluene) gave mp 105–107°C (lit. (4) mp 106–107°C).

Reaction of **2** *with sodium ethanethiolate in THF – typical procedure*

A solution of **2** (2 mmol) in dry THF (30 mL) was added under nitrogen to a solution of sodium ethanethiolate (4 mmol) in dry THF (20 mL), generated from NaH and EtSH. After stirring for 24 h, the solvent was rotary evaporated and the resulting oil triturated with ligroin (3 × 25 mL) to give diethyl disulfide (**4**) as a colourless oil (166 mg, 66% based on **2**). The residue was partitioned between dilute HCl and dichloromethane in the usual way to give an oil which solidified on standing (397 mg). Examination by tlc and ^{1}H nmr showed only $PhCOCH_2SO_2Me$ (**3**) and $PhCO \cdot CHSEt \cdot SO_2Me$ (**5**) to be present, in a molar ratio of 5:3. The identity of **5** was established by its preparation in an alternative manner (7).

The reaction of **2** *with sodium ethanethiolate in DMF – typical procedure*

The reaction was carried out as above, when THF was used as a solvent. After stirring for 24 h, the mixture was rotary evaporated at room temperature for 30 min before being partitioned between dilute HCl and ether in the usual way. The product was an oily solid (330 mg) that on careful examination by tlc and ^{1}H nmr was found to be a mixture of sulfone **3** and EtSSEt (**4**) in a molar ratio of 8:10. The identity of **4** was confirmed by comparison with an authentic sample using glc, and **3** could be washed free of **4** with ligroin for crystallization and comparison with an authentic sample; mp 105–106°C, (lit. (4) mp 106–107°C).

The reaction of **2** *with sodium phenylsulfinate – typical procedure*

A combination of **2** (465 mg, 2 mmol) and $PhSO_2Na \cdot 2H_2O$ (864

[4] Although sulfinic acid anhydrides $RSO \cdot O \cdot SOR$ (23) have been shown actually to be sulfinylsulfones $RSO \cdot SO_2R$ (22), the existence of species with structures very similar to **10** has to be invoked to explain the results of Kobayashi and Terao (24).

[5] A referee has pointed out that, for a number of years, this reported formation of α-disulfones has been known informally among some sulfur chemists to be incorrect; that these disulfones are formed in very poor yields was confirmed by the present work.

mg, 4.3 mmol) in a mixture of DMF (40 mL) and MeOH (20 mL) was stirred at room temperature under nitrogen for 72 h. Most of the methanol was removed by rotary evaporation; the solution was then poured into dilute HCl (200 mL, pH ~2) and extracted with diethyl ether (3 × 100 mL). Usual work-up gave a colourless oil (505 mg) that by tlc and ^{1}H nmr consisted of **3** (60%) and Ph·SO·OMe (**9**, 80% based on **2**). The sulfinate ester **9** was identified by its ^{1}H nmr (δ 3.50), coincident with the resonance of an authentic sample prepared by reacting PhSOCl (from $PhSO_2Na$ + $SOCl_2$) and MeOH in the presence of Et_3N. This was different from authentic Ph·SO_2·OMe (δ 3.77).

The preparation of triethylammonium phenylsulfinate

A solution of $PhSO_2Na\cdot 2H_2O$ (675 mg, 4 mmol) and triethylammonium chloride (585 mg, 4 mmol) in methanol was stirred at room temperature for 3 h. The solvent was removed by rotary evaporation and the syrupy residue was lixiviated with chloroform which was dried, filtered, and evaporated to a clear syrup; the ^{1}H nmr spectrum corresponded to a formulation of $PhSO_2\cdot HNEt_3$.

The reaction of sodium benzenesulfinate with benzenesulfonyl chloride in the presence of ethanol – the preparation of ethyl benzenesulfinate

Dried sodium benzenesulfinate (360 mg, 2.2 mmol) in dry DMF (10 mL) was added portionwise over a 20-min period to a stirred solution (N_2 atmosphere) of benzenesulfonyl chloride (0.29 mL, 2 mmol) in dry DMF (20 mL) and EtOH (5 mL). The reaction mixture was heated to 50°C for 15 min, poured into dilute NaCl solution, and worked up with ether in the usual way to give an oil that was lixiviated with ligroin (bp 40–60°C). The ligroin-soluble fraction gave ethyl benzenesulfinate (**8**) as a colourless oil (210 mg, 62%); ir (film) ν_{max}: 1135 cm^{-1}; ^{1}H nmr ($CDCl_3$) δ (TMS): 1.27 (3H, t, J = 7.1 Hz), 3.73, 4.11 (2H of ABX_3, J_{AX} = 7.1 Hz, J_{AB} = 10.1 Hz), 7.4–7.9 (5H, m); ^{13}C nmr ($CDCl_3$) δ (TMS): 15.3 (—CH_2CH_3), 60.8 (—CH_2CH_3), 124.9 (*ortho* C), 128.7 (*meta* C), 131.8 (*para* C), 144.6 (quart. Ph *C*); ms m/z: 172 (4.1), 171 (8.0), 170 (77.1), 142 (50), 141 (38), 126 (14), 125 (100), 110 (31), 109 (27), 97 (14), 94 (24), 78 (62), 77 (92).

This oil was identical (^{1}H nmr and tlc) to the oil obtained by reacting PhSOCl (from $PhSO_2Na$ + $SOCl_2$) and EtOH in the presence of Et_3N.

The preparation of ethyl p-*toluenesulfinate (11)*

This was prepared from sodium *p*-toluenesulfinate and TsCl on a 2-mmol scale to give a 63% yield of a colourless oil; ir (film) ν_{max}: 1130 cm^{-1}, identical to the published spectrum (23); ^{1}H nmr ($CDCl_3$) δ (TMS): 1.25 (3H, t, J = 7 Hz), 2.41 (3H, s), 3.69, 4.06 (2H of ABX_3, J_{AX} = 7, J_{AB} = 10 Hz), 7.20–7.62 (4H AA′BB′, J_{AB} = 8 Hz); ^{13}C nmr ($CDCl_3$) δ (TMS): 15.2 (—CH_2—CH_3), 21.1 (CH_3—Ar), 60.4 (—O—CH_2—), 124.8 (—SO—C—*C*(Ar)), 129.3 (Me—C—*C*(Ar)), 141.6 (—SO—*C*(Ar)), 142.2 (Me—*C*(Ar)).

The preparation of (−)-menthyl p-*toluenesulfinate (12)*

This was prepared in DMF solvent as above, on a 2-mmol scale, except that the reaction was stirred for 24 h at room temperature. The product (**12**), after chromatography over silica gel with dichloromethane as the eluant, crystallized in fine colourless needles as a mixture of diastereomers, 300 mg, 51%; mp 104–106°C (lit. (27) mp 102–106°C);[6] for ^{13}C nmr, see Fig. 1.

The decomposition of ethyl p-*toluenesulfinate (11)*

A sample of **11** was left on the laboratory bench for 1 week, at which point it was a colourless semisolid that was devoid of **11**. The material gave a mass spectrum that could readily be assigned as m/z: 248 (10.0), 247 (17.1), 246 (100), 214 (2), 123 (57), and 91 (205) with m^* = 186 ($214^2/246$ = 186.2) arising from *p*-tolyl disulfide (**13**), and m/z: 202 (2.4), 201 (4.8), 200 (43.2), 174 (4.4), 173 (7.3), 172 (83.1), 157 (3.5), 156 (6.8), 155 (63.1), 108 (26), 107 (36), and 91 (205) with m^* = 67.2 ($108^2/172$ = 67.8 or $91^2/123$ = 67.3, see above) arising from ethyl *p*-toluenesulfonate (**14**); ions at m/z 244 (6) and 211 (2) could not be assigned. The ion at m/z 172 varied in intensity over several scans and could probably be assigned to some free *p*-toluenesulfonic acid in the mixture. No other ions above m/z 155 were detected.

[6] We thank Dr. J. Hoyle for assistance with this experiment.

Acknowledgments

We thank the Natural Sciences and Engineering Research Council of Canada and Dalhousie University for financial support, and gratefully acknowledge the award by the Government of India of a scholarship for overseas study to P.K.D. We also thank Dr. J.-H. Kim for running the mass spectra.

1. R. Otto and W. Otto. J. Prakt. Chem. [2] **36**, 401 (1887).
2. D. Diller and F. Bergman. J. Org. Chem. **37**, 2147 (1972); J. Ficini and G. Stork. Bull. Soc. Chim. Fr. 723 (1964).
3. F. Bohlmann and G. Haffer. Chem. Ber. **102**, 4017 (1969).
4. J. S. Grossert, P. K. Dubey, G. H. Gill, T. S. Cameron, and P. A. Gardner. Can. J. Chem. **62**, 798 (1984).
5. F. G. Bordwell and W. T. Brannen, Jr. J. Am. Chem. Soc. **86**, 4645 (1964).
6. N. S. Zefirov and D. I. Makhon'kov. Chem. Rev. **82**, 615 (1982).
7. J. S. Grossert and P. K. Dubey. J. Chem. Soc. Chem. Commun. 1183 (1982).
8. F. G. Bordwell and B. B. Jarvis. J. Org. Chem. **33**, 1182 (1968).
9. R. F. Langler and J. A. Pincock. Can. J. Chem. **55**, 2316 (1977).
10. N. Kornblum, S. C. Carlson, and R. G. Smith. J. Am. Chem. Soc. **101**, 647 (1979).
11. F. Duus. *In* Barton and Ollis' comprehensive organic chemistry. Vol. 3. *Edited by* D. N. Jones. Pergamon, Oxford. 1979. pp. 449, 456–459.
12. H. Singh. J. Indian Chem. Soc. **56**, 545 (1979).
13. R. G. Guy. *In* The chemistry of cyanates and their thio derivatives. *Edited by* S. Patai. Wiley–Interscience, Chichester. 1977. pp. 819–886.
14. T.-L. Ho. Hard and soft acids and bases. Principles in organic chemistry. Academic Press. New York. 1977. p. 143.
15. M. Kobayashi. Bull. Chem. Soc. Jpn. **39**, 1296 (1966).
16. J. S. Meek and J. S. Fowler. J. Org. Chem. **33**, 3422 (1968).
17. T. B. R. A. Chen, J. J. Burger, and E. R. de Waard. Tetrahedron Lett. 4527 (1977).
18. B. B. Jarvis and W. P. Tong. J. Org. Chem. **41**, 1557 (1976).
19. R. Otto and W. Otto. J. Prakt. Chem. [2] **36**, 26 (1887); J. Troeger and W. Muller. Arch. Pharm. **252**, 32 (1914).
20. D. N. Harpp and T. G. Back. J. Org. Chem. **38**, 4328 (1973).
21. M. Jautelat, J. B. Grutzner, and J. D. Roberts. Proc. Natl. Acad. Science. U.S.A. **65**, 288 (1970).
22. H. Bredereck, A. Wagner, H. Beck, and R.-J. Klein. Ber. **93**, 2736 (1960).
23. E. Knoevenagel and L. Polack. Ber. Dsch. Chem. Ges. **41**, 3323 (1908).
24. M. Kobayashi M. Terao. Bull. Chem. Soc. Jpn. **39**, 802 (1966); **39**, 1292 (1966).
25. J. L. Kice and A. R. Puls. J. Am. Chem. Soc. **99**, 3455 (1977), and references therein.
26. R. B. Boar and A. C. Patel. Synthesis, 584 (1982).
27. E. P. Kohler and M. B. MacDonald. Am. Chem. J. **22**, 219 (1899).
28. W. Müller and K. Schank. Ber. **111**, 2870 (1978).

Synthesis and crystal structure of 17-deaza-17-methyl thionium isomorphinan (isosulforphanol) perchlorate, an isostere of the opiate isolevorphanol

BERNARD BELLEAU, UGO GULINI,[1] AND BARBARA GOUR-SALIN
Department of Chemistry, McGill University, Montreal (Que.), Canada H3A 2K6

AND

F. R. AHMED
Division of Biological Sciences, National Research Council, Ottawa, Ont., Canada K1A 0R6

Received August 7, 1984

BERNARD BELLEAU, UGO GULINI, BARBARA GOUR-SALIN, and F. R. AHMED. Can. J. Chem. **63**, 1268 (1985).

No morphinan analog carrying a heteroatom other than nitrogen at position 17 has yet been synthesized. The synthesis of the position 17 sulfur analog of the perchlorate salt of (±)-isolevorphanol is described. The strategy adopted is based on the classical Grewe synthesis of morphinans and, under narrowly defined conditions, the title compound isosulforphanol (**3***a*) and an intermediate by-product **13** resulting from an unusual non-bridged head ring closure of **11***a* were obtained. The X-ray structures of both **3***a* and **13** were determined. Crystals of **13** ($C_{17}H_{22}OS$) are monoclinic, space group $P2_1/a$, $a = 17.080(2)$, $b = 9.372(1)$, $c = 9.327(1)$ Å, $\beta = 108.67(1)$, $V = 1414.4$ Å^3, $Z = 4$. Final $R = 0.034$ for 2545 reflections. The crystals of **3***a* ($C_{17}H_{23}OS^+ \cdot ClO_4^-$) are orthorhombic, space group $Pna2_1$, $a = 10.934(1)$, $b = 9.219(1)$, $c = 17.131(2)$ Å, $V = 1726.8$ Å^3, $Z = 4$. Final $R = 0.053$ for 1018 reflections. The $C_{17}H_{23}OS^+$ molecule has been identified by this X-ray analysis as *S*-methyl isosulforphanol (Fig. 2). The structure of **13** is shown in Fig. 1. The stereochemical outcome of the Grewe-like synthesis is thus established as proceeding in a reversed manner when sulfur replaces the nitrogen in the final cyclization step. Preliminary pharmacological studies showed that **3***a* is a potent agonist in the central nervous system but a potent antagonist on the guinea-pig ileum.

BERNARD BELLEAU, UGO GULINI, BARBARA GOUR-SALIN et F. R. AHMED. Can. J. Chem. **63**, 1268 (1985).

Jusqu'à maintenant, aucun analogue de la morphinane portant un hétéroatome autre que l'azote en position 17 n'a été synthétisé. On décrit la synthèse d'un analogue portant un atome de soufre en position 17; il s'agit du perchlorate du (±)-isolévorphanol. La stratégie adoptée se base sur la synthèse classique des morphinanes développée par Grewe et, utilisant des conditions étroitement définies, on a obtenu le composé isosulforphanol (**3***a*) mentionné dans le titre ainsi qu'un sous-produit intermédiaire (**13**) provenant d'une cyclisation inhabituelle du composé **11***a* à une position différente de la tête de pont. Faisant appel à la diffraction des rayons-X. On a déterminé les structures des deux composés **3***a* et **13**. Les cristaux du composé **13** ($C_{17}H_{22}OS$) sont monocliniques et appartiennent au groupe d'espace $P2_1/a$ avec $a = 17{,}080(2)$, $b = 9{,}372(1)$, $c = 9{,}327(1)$ Å, $\beta = 108{,}67(1)$, $V = 1414{,}4$ Å^3, $Z = 4$. On a obtenu une valeur de R de 0,034 pour 2545 réflexions. Les cristaux du composé **3***a* ($C_{17}H_{23}OS^+ \cdot ClO_4^-$) sont orthorhombiques et appartiennent au groupe d'espace $Pna2_1$ avec $a = 10{,}934(1)$, $b = 9{,}219(1)$, $c = 17{,}131(2)$ Å, $V = 1726{,}8$ Å^3 et $Z = 4$. On a obtenu une valeur finale de R de 0,053 pour 1018 réflexions. L'analyse par rayons-X de la molécule de $C_{17}H_{23}OS^+$ a permis de l'identifier comme étant le *S*-methyl isosulforphanol (fig. 2). La figure 1 illustre la structure du composé **13**. On a ainsi établi que le résultat stéréochimique de la synthèse de Grewe est inversé lorsqu'on remplace l'azote par le soufre dans l'étape finale de cyclisation. Des études pharmacologiques préliminaires indiquent que le composé **3***a* est un agoniste potentiel dans le système nerveux central mais un antagoniste potentiel dans l'iléum du cochon d'inde.

[Traduit par le journal]

Introduction

A decade ago we reported the surprising observation that structurally induced pyramidal inversion about the basic nitrogen of the potent narcotic analgesic levorphanol (**1**) suppressed its in vivo activity (1). The idea that the nitrogen lone-pair directionality in levorphanol (**1**) and analogous narcotic analgesics is a stereoselective determinant of productive interaction with the morphine receptor was put forward, and the most obvious implication of this stereoelectronic parameter centers on the ability of the N lone pair to act as a proton acceptor and (or) donor at physiological pH (1), the rest of the molecule serving as a selective carrier of this pivotal atom (2). Although the quality of the receptor response can sometimes be modulated by geometrical inversion to the isomeric planar stereochemistry as in **2**, the available evidence based on studies with several analogs (3) allows the firm conclusion that affinity for the receptor can be favoured equally well by the flattened main skeleton of the isomorphinans (**2**).

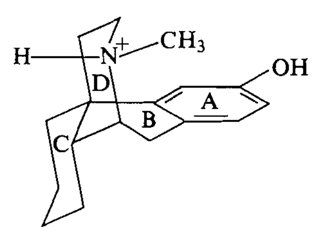

1

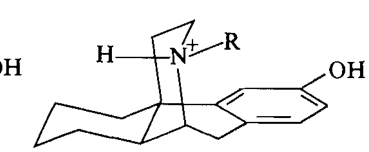

2

In recent years, a number of publications have appeared which purport to demonstrate that the N lone-pair directionality as we perceived it (1) would be unimportant in the receptor recognition process (4–6). However, in all these cases the morphinan analogs studied either exhibited very weak activity (5, 6) or were "so toxic that the observed activity was equivocal" (4).

In an effort to clarify further the stereoelectronic role on activity of the N lone pair of morphinan related compounds, we undertook the synthesis of the sulfonium analogs **3***a* and **3***b* which, for convenience, shall be referred to as *S*-methyl isosulforphanol and *S*-methyl sulforphanol respectively. In the

[1] Permanent address: Dipartimento di Scienze Chimiche, University of Camerino, Camerino, Italy.

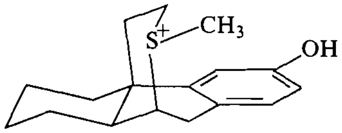

3*a*

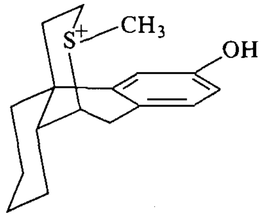

3*b*

stereoelectronic and physico-chemical sense, sulfonium ions are, for the purpose of electrostatic pairing, close relatives of protonated tertiary amines and not of quaternary nitrogen compounds. Therefore, we hoped that pharmacological studies with the sulfonium analogs 3*a* and 3*b* would help in the clarification of the separate roles of ion pairing and of hydrogen bond complex formation at the counter-acceptor site level of the morphine receptor.

The purpose of this report is to describe a synthetic route leading exclusively to stereochemistry 3*a*. A non-morphinan-like side product of structure **13** was also obtained. A following paper will describe an alternate methodology allowing the generation of both 3*a* and 3*b*.

The commercial Grewe synthesis (7) of levorphanol (8–10) (**1**) provides a conceptual basis for the construction of the ring system of **3**. However, the scheme as applied to levorphanol (**1**) has not been previously tested with a relevant sulphur analog and special experimental methodologies had to be introduced for the successful production of the sulphur-containing ring system.

Results and discussion

The synthesis of *S*-methyl isosulforphanol (3*a*) was carried out as summarized in Scheme 1.

The nitrile group of 1-cyclohexen-1-yl acetonitrile (**4**) (11) was hydrolyzed with aqueous sodium hydroxide to yield the known acid (**5**) in 85% yield. Lithium aluminum hydride reduction of the acid functionality led cleanly to the alcohol (**6**) which was treated with *p*-toluenesulfonyl chloride to yield **7** in 72% yield. The latter tosylate was reacted with potassium thioacetate in dry THF to give 2-(cyclohexen-1-yl)ethanethiol acetate (**8**) in 85% yield after purification by distillation. The thiol acetate functionality of **8** was cleaved with sodium methoxide in methanol at room temperature to yield the free thiol **9**, which was reacted with *p*-methoxyacetaldehyde (**10**) (12) in a mixture of trifluoroacetic acid and acetic acid at room temperature to yield a mixture of double bond isomers of intermediate **11** in 37% yield. These experimental conditions appeared critical and are unlike those employed in the nitrogen series. Reaction of the latter with anhydrous hydrogen fluoride at −78°C, followed by chromatographic purification of the crude product, afforded a 34% yield of 3-methoxy-17-deaza-17-thiaisomorphinan (**12**) and a 5% yield of the isomeric ring structure (**13**). It is worth noting that, in our hands, the success of this reaction was critically dependent on the use of hydrogen fluoride as solvent and catalyst. Boron tribromide treatment of **12** at −78°C led to 3-hydroxy-17-deaza-17-thiaisomorphinan (**14**), which was converted to the methyl iodide salt (**15**) in 88% yield by reaction with methyl iodide in acetonitrile at room temperature. Anion exchange processing yielded (±)*S*-methyl isosulforphanol perchlorate (3*a*) whose nmr spectrum in chloroform indicated that only one geometrical isomer was present. The assigned structure 3*a* and that of the by-product **13** were elucidated by X-ray diffraction analysis.

Crystal structure analysis

(a) *Data measurement (Tables 1–4)*

Crystal data for $C_{17}H_{22}OS$ (**13**) and the *S*-methyl isosulforphanol perchlorate, $C_{17}H_{23}OS^+ \cdot ClO_4^-$ (3*a*), are presented in Table 1. The X-ray measurements were carried out on a Nonius

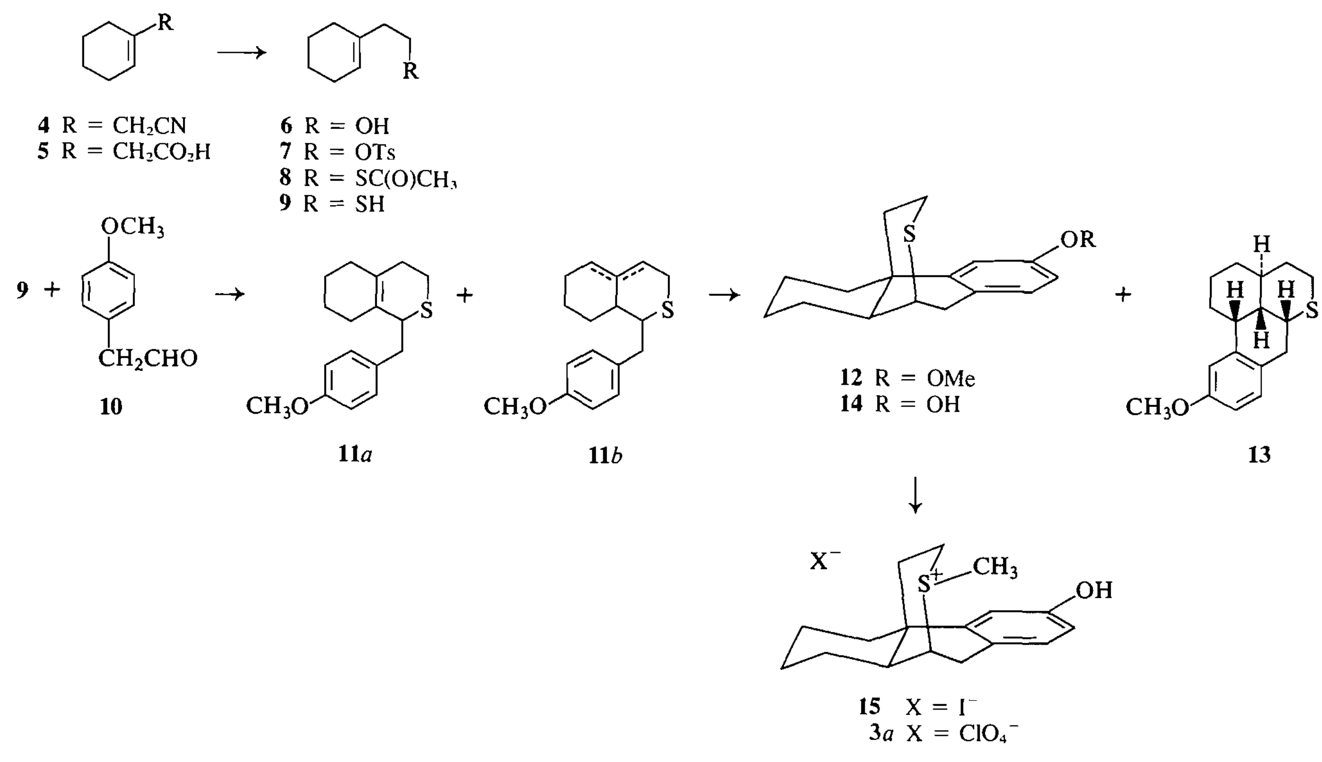

SCHEME 1

TABLE 1. Crystal data

Parameter	13	3*a*
Formula	$C_{17}H_{22}OS$	$C_{17}H_{23}OS^+ \cdot ClO_4^-$
M_r	274.4	374.9
System	Monoclinic	Orthorhombic
Space group	$P2_1/a$	$Pna2_1$
a (Å)	17.080(2)	10.934(1)
b	9.372(1)	9.219(1)
c	9.327(1)	17.131(2)
β (°)	108.67(1)	—
V (Å^3)	1414.4	1726.8
Z	4	4
F(000)	592	792
D_x (g cm^{-3})	1.288	1.442
Crystal dimensions (mm)	0.60×0.60×0.10	0.03×0.07×0.57
ω-scan range (°)	1.10+0.14 tan θ	0.80+0.14 tan θ
ω-speed (° min^{-1})	0.65–3.35	0.46–1.68
No. of unique reflections	2915	1522
Threshold limit	$2.0\sigma(I)$	$1.5\sigma(I)$
No. of obs. reflections	2545	1018
$R = \Sigma\|\|F_o\| - \|F_c\|\|/\Sigma\|F_o\|$	0.034	0.053
$R_w = [\Sigma w(\Delta F)^2/\Sigma w\|F_o\|^2]^{1/2}$	0.042	0.071
$s = [\Sigma w(\Delta F)^2/(m-n)]^{1/2}$	0.43	1.37
Max. (shift/esd)	0.39	0.48
Mean (shift/esd)	0.09	0.10

TABLE 2. Fractional atomic coordinates (×10^4; ×10^5 for S) and equivalent temperature factors (Å^2) for $C_{17}H_{22}OS$ **13**. Estimated standard deviations are in parentheses

Atom	*x*	*y*	*z*	*B*(eq)
C(1)	4071(1)	5899(2)	−27(2)	3.2
C(2)	4407(1)	6142(2)	1497(2)	3.3
C(3)	3944(1)	5845(2)	2440(2)	3.0
C(4)	3150(1)	5299(2)	1842(1)	2.9
C(5)	1344(1)	4807(2)	501(2)	3.6
C(6)	1110(1)	6380(2)	333(2)	4.2
C(7)	727(1)	6779(2)	−1322(2)	4.1
C(8)	1281(1)	6399(2)	−2267(2)	3.2
C(9)	2118(1)	4391(2)	−2933(2)	3.3
C(10)	2947(1)	5152(2)	−2354(2)	3.6
C(11)	3273(1)	5354(2)	−660(2)	2.9
C(12)	2804(1)	5053(1)	282(1)	2.6
C(13)	1938(1)	4418(1)	−375(2)	2.9
C(14)	1536(1)	4820(2)	−2056(2)	2.9
C(15)	838(1)	6754(2)	−3932(2)	4.3
C(16)	1344(1)	6480(2)	−4976(2)	4.9
S(17)	16500(3)	46275(5)	−49683(4)	4.3
O(18)	4327(1)	6141(1)	3934(1)	4.3
C(19)	3906(1)	5827(2)	4981(2)	4.0

CAD-4 diffractometer using Ni-filtered Cu radiation. While crystals of **13** were well formed and of good size, those of **3*a*** were minute and poorly formed; hence, data collection for **13** was taken to 2θ = 150° while that for **3*a*** was limited to 2θ = 130°. The cell parameters were derived by a least-squares fit to the angular settings of 22 reflections with 84 < 2θ < 148° for **13**, and 20 reflections with 52 < 2θ < 88° for **3*a***. The intensities were measured in the ω–2θ scan mode for the ranges stated in Table 1, and extended by 25% at each side for the background measurements. Three standard reflections measured after every hour of exposure time varied within ±1.3% of their mean values. The net intensities were corrected for scale variations, Lorentz and polarization effects, and for absorption by Gaussian integration. The absorption corrections were in the range 1.206–2.597 for **13** and 1.109–2.467 for **3*a***.

TABLE 3. Fractional atomic coordinates (×10^4) and equivalent temperature factors (Å^2) for $C_{17}H_{23}OS^+ \cdot ClO_4^-$ **3*a***. Estimated standard deviations are in parentheses

Atom	*x*	*y*	*z*	*B*(eq)
Cl	1074(2)	376(3)	0	4.5
O(1)	2243(9)	1035(13)	−129(6)	8.2
O(2)	963(8)	−46(15)	799(5)	9.3
O(3)	959(10)	−868(10)	−470(6)	7.9
O(4)	98(14)	1288(18)	−145(10)	13.6
C(1)	2115(9)	4127(10)	1320(5)	3.3
C(2)	3194(8)	4073(10)	1742(6)	3.7
C(3)	3152(8)	4379(11)	2520(6)	3.8
C(4)	2090(8)	4710(10)	2904(5)	3.1
C(5)	−222(9)	4693(12)	3743(5)	3.6
C(6)	−1465(9)	4918(13)	4141(6)	4.4
C(7)	−2527(8)	4215(13)	3689(6)	4.2
C(8)	−2530(9)	4827(12)	2856(6)	4.2
C(9)	−1272(8)	4979(10)	1587(5)	3.3
C(10)	−145(9)	4409(10)	1174(5)	3.6
C(11)	998(9)	4430(10)	1683(5)	3.5
C(12)	979(8)	4778(9)	2487(5)	2.6
C(13)	−204(8)	5213(9)	2893(5)	2.8
C(14)	−1307(8)	4555(11)	2459(5)	3.2
C(15)	−219(8)	6905(11)	2877(6)	3.6
C(16)	−193(10)	7549(11)	2061(6)	4.1
S(17)	−1522(2)	6937(3)	1530(2)	3.7
O(18)	4271(6)	4301(8)	2911(4)	4.7
C(19)	−1264(11)	7389(12)	543(7)	5.2

(b) *Structure determination*

Structure **13** was determined by the direct method of symbolic addition (13). All the non-hydrogen atoms were observed in the *E* map and, after partial refinement of their parameters, the H atoms were located from a difference Fourier map. Refinement of the atomic coordinates and anisotropic thermal parameters (isotropic for H) and a scale factor, constituting a total of 260 parameters, was by block-diagonal least squares, minimizing $\Sigma w(F_o - F_c)^2$ with $w = \{1 + [(|F_o| - 3)/25]^2\}^{-1}$ and excluding the unobserved reflections as well as four strong ones (020, 320, 400, and 20$\bar{1}$) showing extinction effect.

Structure **3*a*** was determined by the heavy atom method, using a Patterson and three Fourier syntheses for location of the non-hydrogen atoms. The H atoms were located from a difference map at a later stage. Refinement was as described for **13**, except that the weights were calculated according to the expression $w = \{1 + [(|F_o| - 10/30]^2\}^{-1}$; the *z* coordinate for Cl was fixed to define the origin along the *z* axis, and the H parameters were not refined, so that the number of refined parameters was 216. The (020) reflection which showed an extinction effect was excluded.

The scattering factor curves were from refs. 14 and 15, and all calculations were performed with the aid of the NRC program system (16) and ORTEP (17). The final atomic coordinates and equivalent isotropic thermal parameters are listed in Tables 2 and 3.[2]

[2] The structure factor tables, parameters for the H atoms, and anisotropic thermal parameters for the non-hydrogen atoms are available, at a nominal charge, from the depository of unpublished data, CISTI, National Research Council of Canada, Ottawa, Ont., Canada K1A 0S2.

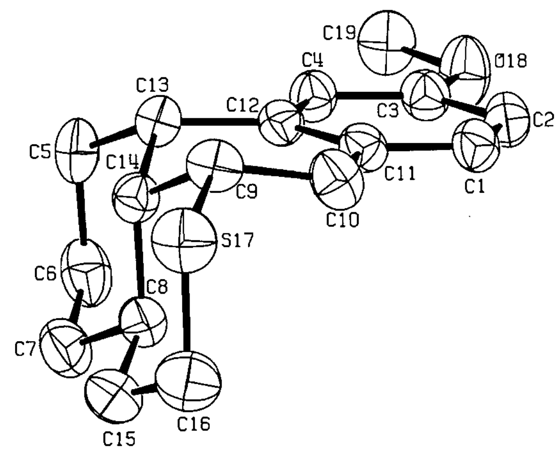

FIG. 1. A view of the molecular structure of $C_{17}H_{22}OS$ (**13**) showing the conformation and atom numbering. The thermal ellipsoids are drawn at 50% probability and the H atoms have been omitted.

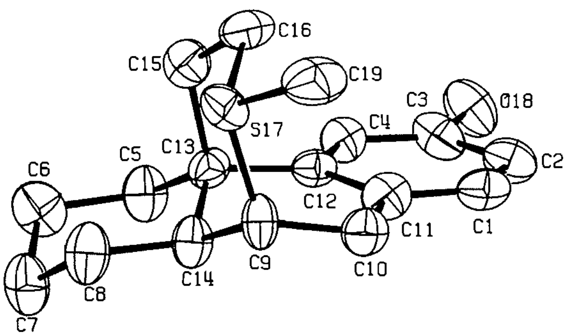

FIG. 2. A view of the molecular structure of $C_{17}H_{23}OS^+$ (*3a*) showing the conformation and atom numbering. The thermal ellipsoids are drawn at 50% probability and the H atoms have been omitted. This view is for the opposite enantiomorph of the coordinates listed in Table 3.

Structural analyses

The molecular conformations and atom numbering for compounds **13** and **3***a* are presented in Figs. 1 and 2, respectively. Whereas the piperidine ring in levorphanol is fused along the C(9)—C(14) and C(13)—C(14) bonds, the $C_{17}H_{22}OS$ product shown in Fig. 1 has the corresponding ring fused at C(9)—C(14) and C(8)—C(14). Also, the methyl group which is substituted at N(17) in levorphanol is found to be substituted instead at O(18). These anomalies, however, are not present in molecule **3***a* (Fig. 2), which is shown to possess the correct *S*-methyl isosulforphanol structure.

The bond lengths and valence angles for compounds **13** and **3***a* are listed in Table 4. Equivalent bond lengths in the two molecules are comparable, with the largest difference of 0.032(11) Å in the C(3)—O(18) bond being insignificant at the 0.1% probability level. However, six pairs of equivalent valence angles show significant differences of 3.3(8)–5.2(6)° with the largest difference occurring at C(10)—C(9)—S(17) and C(14)—C(9)—S(17), probably as a result of the differences in molecular conformations. In both molecules the endocyclic angle C(9)—S(17)—C(16) is 99.0 ± 0.4°, which is considerably smaller than the normal tetrahedral angle of 109.7°.

The aromatic ring is planar; χ^2 (= $\Sigma\Delta^2/\sigma^2$) is 7.7 for molecule **13** and 11.1 for **3***a*. The adjacent ring has nearly the same conformation in both molecules with insignificant differences (within ±1.3°) in the corresponding torsion angles. The absolute values of the torsion angles in the sulfonium ring and the remaining ring are 52.5(2)–61.1(2)° and 53.4(2)–57.1(s)° for molecule **13**, compared to 58.7(7)–67.0(8)° and 50.6(10)–58.2(11)° for molecule **3***a*, respectively.

While there are no short intermolecular interactions in the crystals of compound **13**, there is a short contact in **3***a* of 2.789(12) Å between the hydroxyl O(18) and O(3) of the perchlorate group, indicative of a possible hydrogen bond between them.

These structural analyses establish that the substitution of a basic nitrogen by a sulfur in a Grewe-like process for morphinan synthesis unexpectedly leads to a complete reversal of the B/C ring junction stereochemistry of the product. The *trans*-geometry of the resulting sulforphan **12** can hardly be attributed to the different nature of the Friedel–Crafts catalyst (hydrogen fluoride); rather, it is likely that the longer C—S bonds (>1.8 Å) relative to the C—N bonds of morphinans serve to relieve 1,3-axial compressions between the ring D sulfur atom and the ring C hydrogens, thus reversing the thermodynamic stability of the transition states leading respectively to morphinans and sulforphans.

The unexpected formation of the polyhydro-thiabenzanthracene by-product **13** is best explained by the involvement of a double bond isomerization of **11***a* followed by direct electrophilic attack of the phenyl ring. This implies the intermediacy of a secondary carbonium ion intermediate which probably accounts for the very low yield (~5%) of product.

The sulfonium analog **3***a* (isosulforphanol) was tested as the perchlorate salt for its effect on the opiate receptors of the guinea-pig ileum (GPI) longitudinal muscle, the mouse *vas deferens*, and the central nervous system (CNS) of hooded rats by the intracerebroventricular route of administration. The results, which have been recently reported in preliminary form (18), showed that analog **3***a* displays marked affinity for the opiate receptor while inducing divergent effects in the GPI and the CNS respectively. The mechanistic significance of these observations is under active investigation.

Experimental

General

Melting points and distillation temperatures are uncorrected. Infrared spectra were recorded on a Perkin–Elmer model 297 spectrophotometer. Proton nuclear magnetic resonance (^1H nmr) spectra were measured using a Varian XL-200 spectrometer. Tetramethylsilane was employed as the internal standard for all compounds. Mass spectrometric measurements were recorded on Dupont 21-492B or LKB 9000 mass spectrometers.

2-(1-Cyclohexen-1-yl) acetic acid (5)

1-Cyclohexen-1-yl acetonitrile (**4**) (50 g, 0.415 mol) and sodium hydroxide (30 g, 0.075 mol) were dissolved in H_2O (300 mL) and heated at reflux for 20 h. The reaction mixture was extracted with chloroform (3 × 75 mL) to remove any unwanted side products. The remaining aqueous layer was acidified and again extracted with chloroform (3 × 75 mL). The combined extracts were dried and solvent removed *in vacuo* to yield a green oil which was distilled (bp 155–157°C/20 Torr; 1 Torr = 133.3 Pa) to give 49 g (0.35 mol, 85% yield) of a white waxy solid, mp ≈ 26°C; ir ($CHCl_3$): 2920, 1700 cm^{-1}; ^1H nmr ($CDCl_3$) δ: 1.56–1.92 (m, 4H), 2.00–2.18 (m, 4H, allylic), 3.00 (s, 2H, CH_2COO), 5.71 (s, 1H, C=CH), 8.00 (br s, 1H, COOH); *m/e*: 111 (M^+ − COOH, base peak).

2-(1-Cyclohexen-1-yl)ethanol (6)

A solution of 2-(1-cyclohexen-1-yl) acetic acid (10 g, 0.071 mol)

TABLE 4. Bond lengths and valence angles and their estimated standard deviations in parentheses, for **13**: $C_{17}H_{22}OS$ and **3*a***: $C_{17}H_{23}OS^{+} \cdot ClO_4^{-}$

Bond	Bond length (Å)	
	13	**3*a***
C(1)—C(2)	1.371(3)	1.385(13)
C(1)—C(11)	1.397(3)	1.399(13)
C(2)—C(3)	1.386(3)	1.363(14)
C(3)—C(4)	1.387(3)	1.369(13)
C(3)—O(18)	1.365(2)	1.397(11)
C(4)—C(12)	1.403(3)	1.411(12)
C(5)—C(6)	1.522(3)	1.535(14)
C(5)—C(13)	1.536(3)	1.533(12)
C(6)—C(7)	1.518(3)	1.539(14)
C(7)—C(8)	1.527(3)	1.534(15)
C(8)—C(14)	1.537(3)	1.521(13)
C(8)—C(15)	1.531(3)	—
C(9)—C(10)	1.521(3)	1.515(13)
C(9)—C(14)	1.530(3)	1.543(12)
C(9)—S(17)	1.821(2)	1.828(10)
C(10)—C(11)	1.510(3)	1.524(13)
C(11)—C(12)	1.394(3)	1.414(12)
C(12)—C(13)	1.529(3)	1.522(12)
C(13)—C(14)	1.543(3)	1.542(12)
C(13)—C(15)	—	1.560(12)
C(15)—C(16)	1.517(3)	1.519(14)
C(16)—S(17)	1.812(2)	1.805(11)
S(17)—C(19)	—	1.764(11)
O(18)—C(19)	1.417(2)	—
Cl—O(1)	—	1.432(10)
Cl—O(2)	—	1.428(9)
Cl—O(3)	—	1.407(10)
Cl—O(4)	—	1.381(16)

Bond	Valence angle (deg)	
	13	**3*a***
C(2)—C(1)—C(11)	121.8(2)	121.3(8)
C(1)—C(2)—C(3)	119.3(2)	118.3(9)
C(2)—C(3)—C(4)	120.1(2)	123.0(9)
C(2)—C(3)—O(18)	115.0(2)	115.4(8)
C(4)—C(3)—O(18)	124.9(2)	121.6(8)
C(3)—C(4)—C(12)	120.8(2)	119.8(8)
C(6)—C(5)—C(13)	111.8(1)	113.0(8)
C(5)—C(6)—C(7)	110.9(1)	112.8(9)
C(6)—C(7)—C(8)	112.6(1)	108.3(8)
C(7)—C(8)—C(14)	110.7(1)	110.8(8)
C(7)—C(8)—C(15)	109.8(1)	—
C(14)—C(8)—C(15)	111.5(1)	—
C(10)—C(9)—C(14)	112.2(1)	112.6(7)
C(10)—C(9)—S(17)	111.2(1)	116.1(6)
C(14)—C(9)—S(17)	112.5(1)	107.3(6)
C(9)—C(10)—C(11)	114.9(2)	113.3(8)
C(1)—C(11)—C(10)	118.1(2)	117.3(8)
C(1)—C(11)—C(12)	119.2(2)	119.4(8)
C(10)—C(11)—C(12)	122.7(2)	123.2(8)
C(4)—C(12)—C(11)	118.9(2)	118.1(8)
C(4)—C(12)—C(13)	120.9(1)	120.8(8)
C(11)—C(12)—C(13)	120.2(1)	121.1(8)
C(5)—C(13)—C(12)	114.4(1)	111.3(7)
C(5)—C(13)—C(14)	109.1(1)	109.0(7)
C(5)—C(13)—C(15)	—	109.2(7)
C(12)—C(13)—C(14)	111.8(1)	109.9(7)
C(12)—C(13)—C(15)	—	105.3(7)
C(14)—C(13)—C(15)	—	112.1(7)

TABLE 4. (*Continued*)

Bond	Valence angle (deg)	
	13	**3*a***
C(8)—C(14)—C(9)	112.9(1)	114.4(8)
C(8)—C(14)—C(13)	112.4(1)	113.9(8)
C(9)—C(14)—C(13)	109.0(1)	110.4(7)
C(8)—C(15)—C(16)	114.6(2)	—
C(13)—C(15)—C(16)	—	114.0(8)
C(15)—C(16)—S(17)	112.5(1)	109.1(7)
C(9)—S(17)—C(16)	98.6(1)	99.3(5)
C(9)—S(17)—C(19)	—	105.1(5)
C(16)—S(17)—C(19)	—	106.3(5)
C(3)—O(18)—C(19)	118.6(1)	—
O(1)—Cl—O(2)	—	109.8(6)
O(1)—Cl—O(3)	—	109.7(6)
O(1)—Cl—O(4)	—	113.8(8)
O(2)—Cl—O(3)	—	108.6(6)
O(2)—Cl—O(4)	—	105.8(8)
O(3)—Cl—O(4)	—	108.9(8)

in dry ether (30 mL) was added dropwise to a suspension of $LiAlH_4$ (2.8 g, 0.074 mol) in dry ether (20 mL) under N_2. After the addition had been completed the reaction mixture was allowed to stir under N_2 for an additional 1.5 h. The remaining unreacted $LiAlH_4$ was decomposed by the dropwise addition of water. The reaction mixture was slowly added to a 1 *N* aqueous solution of HCl (100 mL). The ether layer was removed and the remaining aqueous layer extracted with ether (3 × 75 mL). The combined organic extracts were dried and the ether removed *in vacuo*. The residue was distilled (bp 101–102°C/20 Torr) to yield 7.16 g (0.57 mol, 80% yield) of a colorless oil; ir ($CHCl_3$): 3610 cm^{-1}; ^1H nmr ($CDCl_3$) δ: 1.58–1.80 (m, 4H), 1.96–2.15 (m, 4H, allylic), 2.26 (m, 2H, = —CH_2), 3.54 (s, 1H, OH), 3.68 (t, 2H, *J* = 4 Hz, CH_2O), 5.56 (s, 1H, C=CH); *m/e*: 126 (M^+), 108, 79 (base peak).

2-(1-Cyclohexen-1-yl)ethanol tosylate (7)

2-(1-Cyclohexen-1-yl)ethanol (**6**) (9.0 g, 0.071 mol) was dissolved in dry pyridine (50 mL) and cooled to 0°C. A solution of *p*-toluenesulfonyl chloride (15 g, 0.079 mol) in dry pyridine (75 mL) was added at 0°C and the reaction mixture was sitrred at 0°C for 2 h. After a further 24 h at 0°C the solution was poured into a solution of ice-water (300 g) and extracted with methylene chloride (3 × 75 mL). The combined organic extracts were washed with cold 10% aqueous HCl (6 × 50 mL) to remove any pyridine. The organic layer was dried and the solvent removed *in vacuo*. Low temperature recrystallization yielded 14.2 g (0.051 mol, 72.3% yield) of a white solid; mp ≈ 23°C; ir ($CHCl_3$): 2940, 1600, 1360, 1170, 970, 930 cm^{-1}; ^1H nmr ($CDCl_3$) δ: 1.4–1.5 (m, 4H), 1.53–1.9 (m, 4H, allylic), 2.2–2.3 (m, 2H, = —CH_2), 2.41 (s, 3H, $ArCH_3$), 4.05 (t, 2H, *J* = 2 Hz, CH_2O), 5.37 (br s, 1H, =CH), 7.33, 7.75 (ABq, 4H, *J* = 4 Hz, ArH); *m/e*: 280 (M^+), 200, 155, 109 (base peak).

2-(1-Cyclohexen-1-yl)ethanethiol acetate (8)

2-(1-Cyclohexen-1-yl)ethanol tosylate (**7**) (16 g, 0.057 mol) was dissolved in dry THF (150 mL) and a solution of potassium thioacetate (25 g, 0.23 mol) in dry THF (200 mL) was added. The reaction mixture was heated at reflux for 2 h and the THF was removed *in vacuo*. The residue was dissolved in H_2O (100 mL) and extracted with methylene chloride (3 × 75 mL). The combined organic extracts were dried and the solvent removed *in vacuo*. The yellow oil was purified by distillation (bp 113°C/5 Torr) to yield 8.97 g (0.049 mol, 85.5% yield) of a pale yellow oil; ir (neat): 1690, 1435, 1350, 1120, 950, 620 cm^{-1}; ^1H nmr ($CDCl_3$) δ: 1.4–1.64 (m, 4H), 1.94–1.98 (m, 4H, allylic), 2.12–2.20 (m, 2H, = —CH_2), 2.28 (s, 3H, $C(O)CH_3$), 2.91 (t, 2H, *J* = 4 Hz, CH_2S), 5.44 (s, 1H, =CH); *m/e*: 184 (M^+), 108 (base peak). *Anal.* calcd. for $C_{10}H_{16}OS$: C 65.17, H 8.75; found: C 65.39, H 8.75.

2-(1-Cyclohexen-1-yl)ethanethiol (9)

Methanol (50 mL) was degassed by passing N_2 through the solution. Sodium (1.44 g, 0.063 mol) was added and the solution stirred until all the sodium had dissolved. A solution of 2-(1-cyclohexen-1-yl)-ethanethiol acetate (4.4 g, 0.024 mol) in dry THF (10 mL) was added and the reaction mixture was stirred under N_2 for 4 h. The solution was diluted with saturated aqueous NaCl (100 mL) and the pH adjusted to 4 with 10% aqueous citric acid. The aqueous layer was extracted with ether (4 × 75 mL). The combined organic extracts were dried and the solvent removed *in vacuo*. The residue was distilled (bp 116°C/45 Torr) to give 0.065 g (0.0455 mol, 72.3% yield) of a colorless oil; ir (neat): 2900, 1440, 720 cm^{-1}; ^1H nmr ($CDCl_3$) δ: 1.34–1.39 (m, 1H, SH), 1.51–1.65 (m, 4H, CH_2CH_2), 2.53–2.59 (m, 2H, CH_2S), 5.46 (br s, 1H, C=CH); *m/e*: 142 (M^+, base peak), 126, 108. *Anal.* calcd. for $C_8H_{14}S$: C 67.54, H 9.91; found: C 67.32, H 9.80.

p-*Methoxyacetaldehyde (10) (ref. 12)*[3]

4-Allylanisole (5 mL) was added to a vigorously stirred solution of aqueous H_2O_2 (30%, 37 mL, 1.2 mol) and aqueous formic acid (90%, 160 mL, 4.2 mol) and the reaction mixture was heated to 40°C. The temperature was maintained between 40 and 45°C by heating or cooling as necessary while a further 35 mL of 4-allylanisole (0.26 mol) was added dropwise. The reaction mixture was stirred overnight at room temperature and evaporated to dryness *in vacuo*. To the remaining red residue was added aqueous NaOH (37%, 45 mL), at 45°C, and H_2O (65 mL). The solution was heated to 50°C for 1 h. After cooling, concentrated HCl (33 mL) was added and the aqueous layer extracted with $CHCl_3$ (3 × 75 mL). The combined organic extracts were dried, filtered, and the solvent removed *in vacuo*. The residue was purified by distillation (bp 150–152°C/25 Torr) through an air-cooled condenser to afford 29.8 g (0.16 mol, 63% yield) of 1,2-dihydroxy-3-(4-methoxyphenyl)propane; ir ($CHCl_3$): 3400, 2930, 1610, 1505 cm^{-1}; ^1H nmr ($CDCl_3$) δ: 2.6 (d, 2H, J = 4 Hz, CH_2Ar), 3.4 (m, 1H, CHO), 3.5–3.8 (m, 2H, CH_2O), 3.7 (s, 3H, OCH_3), 4.1 (br s, 1H, OH), 6.78 (d, 2H, J = 4 Hz, ArH), 7.1 (d, 2H, J = 4 Hz, ArH); *m/e*: 182 (M^+), 148, 121 (base peak).

1,2-Dihydroxy-3-(4-methoxyphenyl)propane (22.3 g, 0.12 mol) was dissolved in dry benzene (1250 mL). One-tenth of the solvent (125 mL) was distilled off under N_2 and, after cooling, one equivalent of lead tetraacetate (55.4 g, 0.12 mol) was added and the mixture stirred at room temperature overnight. The suspension was poured onto H_2O (1000 mL) and the lead oxides removed by filtration through Celite. The aqueous layer was separated, the organic layer washed with H_2O (2 × 500 mL), saturated $NaHCO_3$ (1 × 500 mL), and then dried, filtered, and concentrated *in vacuo*. The residue was distilled (bp 76–77°C/0.25 Torr) to yield 8.3 g (0.06 mol, 45% yield) of *p*-methoxyacetaldehyde as a yellow liquid; ir (neat): 1720, 1670, 1580, 1510 cm^{-1}; ^1H nmr (CD_2Cl_2) δ: 3.48 (br s, 2H, CH_2O), 3.7 (s, 3H, OCH_3), 6.8–7.1 (m, 4H, ArH), 9.6 (br s, HCO); *m/e*: 150 (M^+), 121 (base peak).

*1-(*p*-Methoxybenzyl)-3,4,5,6,7,8-hexahydro-1*H*-isobenzothiapyran (11*a*)*

2-(Cyclohexen-1-yl)ethanethiol (**9**) (3.5 g, 0.025 mol) was dissolved in acetic acid (6 mL) and the solution added dropwise to a stirred solution of the preceding *p*-methoxyphenylacetaldehyde (9.2 g, 0.061 mol) in trifluoroacetic acid (12 mL) and acetic acid (6 mL) under argon at room temperature. The reaction mixture was stirred for 20 h and then poured onto ice-water (50 mL) and the mixture neutralized with saturated sodium bicarbonate solution. The aqueous layer was extracted with ether (3 × 75 mL), the combined extracts dried, and the solvent removed *in vacuo* to yield a yellow oil which was purified by flash chromatography (8 in. × 1 in. silica gel 60 (230–400 mesh)) using petroleum ether/ethyl acetate 50:1 (v/v) as the eluent to give 1.2 g (4.69 mmol) of **11***a* and 0.6 g (2.34 mmol) of **11***b* (28.1% yield overall); ir (**11***a*) (neat): 2920, 1610, 1510, 1240, 750 cm^{-1}; ^1H nmr (**11***a*) ($CDCl_3$) δ: 1.0–3.0 (complex m, 15H), 3.75 (s, 3H, OCH_3), 6.8 (d, 2H, J = 4 Hz, ArH), 7.1 (d, 2H, J = 4 Hz, ArH); *m/e* (**11***a*): 274 (M^+), 153, 83 (base peak). *Anal.* calcd. for $C_{17}H_{22}OS$: C 74.40, H 8.08; found: C 74.36, H 8.01. Infrared (**11***b*) (neat): 2920, 1610, 1510, 1240, 750 cm^{-1}; ^1H nmr (**11***b*) ($CDCl_3$) δ: 1.0–3.0 (complex m, 14H), 3.75 (s, 3H, OCH_3), 5.6 (br s, 1H, =CH), 6.8 (d, 2H, J = 8.6 Hz, ArH), 7.1 (d, 2H, J = 8.55 Hz, ArH); *m/e* (**11***b*): 274 (M^+), 83 (base peak).

3-Methoxy-17-deaza-17-isothioamorphinan (12)

The isomers of **11** (1.8 g, 7.03 mmol) were dissolved in anhydrous HF at −78°C. The reaction mixture was allowed to warm to room temperature and stirred for an additional 24 h. The HF was evaporated and the remaining residue dissolved in ether. The ethereal solution was washed several times with water, dried, and the solvent removed *in vacuo*. The red-colored residue was purified by flash chromatography (8 in. × 1 in. silica gel 60 (230–400 mesh)) using petroleum ether/ethyl acetate 50:1 (v/v) to give 0.61 g (2.2 mmol), 34% yield of **12** (mp 73–74°C) and 0.1 g (0.36 mmol), 5.1% yield of **13**; mp 134–135°C; ir (**12**) (KBr disc): 1610, 1570, 1490, 1420, 1280, 1040, 800, 590 cm^{-1}; ^1H nmr (**12**) ($CDCl_3$) δ: 1.2–2.8 (complex m, 14H), 3.24 (d, 1H, J = 8 Hz, CHAr), 3.8 (s, 3H, OCH_3), 6.7–7.0 (m, 4H, ArH); *m/e* (**12**): 274 (M^+), 213 (base peak). *Anal.* calcd. for $C_{17}H_{22}OS$: C 74.40, H 8.08; found: C 74.61, H 8.17. Infrared (**13**) (KBr disc): 2930, 1610, 1500, 1260, 1230, 1040, 800 cm^{-1}; ^1H nmr (**13**) ($CDCl_3$) δ: 0.8–3.2 (complex m, 16H), 3.7 (s, 3H, OCH_3), 6.8–7.2 (m, 3H, ArH); *m/e* (**13**): 274 (M^+, base peak). The X-ray of this compound is shown in Fig. 1.

3-Hydroxy-17-deaza-17-isothiamorphinan (14)

3-Methoxy-17-deaza-17-isothiamorphinan (**12**) (0.59 g, 2.14 mmol) was dissolved in dry methylene chloride (20 mL) at −78°C under argon. A solution of BBr_3 (0.342 mL in 3 mL CH_2Cl_2) was added at −78°C and the reaction allowed to warm to room temperature. After 17 h the solution was poured onto H_2O (50 mL) and the organic layer collected. The aqueous layer was extracted with methylene chloride (3 × 50 mL) and the combined organic extracts were dried and the solvent removed *in vacuo*. The residue was purified by flash chromatography (1 in. × 4 in. silica gel 60 (230–400 mesh)) using chloroform as the eluent to yield 0.47 g (1.82 mmol, 85.6% yield) of white crystals; mp 177–178°C; ir (KBr disc): 3290, 2910, 1620, 1580, 1500, 1285 cm^{-1}; ^1H nmr ($CDCl_3$) δ: 1.1–2.8 (m, 14H), 3.25 (d, 1H, J = 8 Hz, J = 3 Hz, CHAr), 4.6 (s, 1H, OH), 6.6–7.1 (m, 3H, ArH); *m/e*: 260 (M^+), 57 (base peak). *Anal.* calcd. for $C_{16}H_{20}OS$: C 73.80, H 7.74; found: C 73.98, H 7.70.

3-Hydroxy-17-deaza-17-isothiamorphinan-17-methyl onium iodide (15)

3-Hydroxy-17-deaza-17-isothiamorphinan (0.155 g, 0.596 mmol) was dissolved in CH_3CN (1.5 mL) containing methyl iodide (4 mL). The reaction mixture was allowed to stand for 20 h and dry ether was added to maximum precipitation of white crystals of the iodide salt. These were collected, washed with dry ether, and dried *in vacuo* to yield 0.210 g (5.22 × 10^{-1} mmol, 88% yield) of white crystals; ir (KBr disc): 3260, 2930, 1615, 1490, 1290 cm^{-1}; ^1H nmr ($CDCl_3/CF_3COOH$) δ: 1.0–4.0 (m, 16H), 2.95 (s, 3H, SCH_3), 6.7–7.2 (m, 3H, ArH); *m/e*: 260 ($M^+ - CH_3I$), 142 (CH_3I, base peak). *Anal.* calcd. for $C_{17}H_{23}IOS$: C 50.75, H 5.76; found: C 50.61, H 5.57.

S-*Methyl isosulforphanol perchlorate (3a)*

A methanol solution of the preceding salt (**15**) (0.210 g, 0.52 mmol) was passed through an anion exchange column in the perchlorate form (prepared as described below) to yield a methanol solution of *S*-methyl isosulforphanol perchlorate. Removal of the solvent yielded 0.154 g (0.412 mmol, 79% yield) of white crystals. The product was recrystallized from CH_3CN/hexane to give 0.132 g (0.352 mmol, 67.5% yield) of long white needles. Nuclear magnetic resonance analysis indicated only one type of methyl group was present; ir (KBr disc): 3350, 1610, 1100 (ClO_4^-), 620 (ClO_4^-) cm^{-1}; ^1H nmr (CD_3CN)

[3] Experimental details previously unreported in this reference.

δ: 1.1–4.0 (m, 16H), 2.9 (s, 3H, SCH_3), 6.7–7.1 (m, 3H, ArH); *m*/*e*: 260 ($M^+ - MeClO_4$), 28 (base peak). The X-ray structure of the compound is shown in Fig. 2.

The anion exchange column was prepared using analytical grade resin AG1-X8 from B10-RAD (100–200 mesh) in the chloride form. The resin was washed with aqueous NaOH (1 *N*) and then to neutrality with distilled water, followed by washing with dilute aqueous perchloric acid (5%). The resin was again washed to neutrality with distilled water and then methanol. It was packed into a small column (1/2 in. × 2 in.), a methanol solution of **15** applied to the top of the column, and the product eluted under a low pressure of nitrogen.

Acknowledgements

We are grateful to the Natural Sciences and Engineering Research Council of Canada and the Government of Quebec (Fonds F.C.A.C.) for their financial support and to Mrs. M. E. Pippy for assistance with the X-ray computations.

1. B. BELLEAU, T. CONWAY, F. R. AHMED, and A. D. HARDY. J. Med. Chem. **17**, 907 (1974).
2. J. DIMAIO, F. R. AHMED, P. SCHILLER, and B. BELLEAU. *In* Recent advances in receptor chemistry. *Edited by* F. Gualtieri, M. Giannella, and C. Melchiorre. Elsevier/North Holland, Amsterdam, New York, Oxford. 1979. pp. 221–234.
3. B. BELLEAU. *In* The chemical regulation of biological mechanisms. *Edited by* A. M. Creighton and S. Turner. The Royal Society of Chemistry Special Publication No. 42. Burlington House, London. 1982, pp. 200–221; A. F. Casy. *In* Progress in drug research. *Edited by* E. Jucker. Birkhauser. 1978. pp. 149–226.
4. K. OPHEIM and B. M. COX. J. Med. Chem. **19**, 857 (1976).
5. S. SHIOTANI, T. KOMETANI, Y. IITAKA, and A. ITAI. J. Med. Chem. **21**, 153 (1978).
6. R. J. KOBYLECKI, A. C. LANE, C. F. C. SMITH, L. P. G. WAKELIN, W. B. T. CRUSE, E. EGERT, and O. KENNARD. J. Med. Chem. **25**, 1278 (1982).
7. R. GREWE and A. MONDON. Chem. Ber. **81**, 279 (1948).
8. O. SCHNIDER and J. HELLEBACK. Helv. Chim. Acta, **33**, 1437 (1950).
9. N. B. EDDY, J. G. MURPHY, and E. L. MAY. J. Org. Chem. **22**, 1370 (1957).
10. M. ONDA, Y. SUGAMA, H. YOKOYAMA, and F. TADA. Chem. Pharm. Bull. (Japan), **21**, 2359 (1973).
11. A. C. COPE, A. A. ADDIECO, D. E. WHYTE, and A. GLICKMAN. Org. Synth. Coll. Vol. 4, 1963. p. 234.
12. B. BELLEAU and J. BURBA. J. Am. Chem. Soc. **82**, 5751 (1960).
13. I. L. KARLE and J. KARLE. Acta Crystallogr. **16**, 969 (1963).
14. International tables for X-ray crystallography. Vol. IV. Kynoch Press, Birmingham. 1974. p. 72.
15. R. F. STEWART, E. R. DAVIDSON, and W. T. SIMPSON. J. Chem. Phys. **42**, 3175 (1965).
16. F. R. AHMED, S. R. HALL, M. E. PIPPY, and C. P. HUBER. J. Appl. Crystallogr. **6**, 309 (1973).
17. C. K. JOHNSON. ORTEP II, Report ORNL-3794, 2nd rev. Oak Ridge National Laboratory, Tennessee. 1971.
18. B. BELLEAU, U. GULINI, B. GOUR-SALIN, R. CAMICIOLI, S. LEMAIRE, and F. JOLICOEUR. *In* Highlights in receptor chemistry. *Edited by* C. Melchiorre and M. Giannella. Elsevier Science Pub., New York. 1984. pp. 135–148.

Oxidation of hydrocarbons.14.Autocatalysis during the oxidation of 1-tetradecene by methyltributylammonium permanganate

DONALD G. LEE[1] AND JOAQUIN F. PEREZ-BENITO
Department of Chemistry, University of Regina, Regina, Sask., Canada S4S 0A2

Received August 27, 1984

DONALD G. LEE and JOAQUIN F. PEREZ-BENITO. Can. J. Chem. **63**, 1275 (1985).

Autocatalysis has been detected during the reaction of methyltributylammonium permanganate with 1-tetradecene in methylene chloride solutions. Activation of permanganate by adsorption on colloidal particles of the product, manganese dioxide, appears to be responsible for the observed autocatalysis. Permanganate so activated can then be reduced either by reaction with the alkene or by thermal decomposition.

DONALD G. LEE et JOAQUIN F. PEREZ-BENITO. Can. J. Chem. **63**, 1275 (1985).

On a pu détecter de l'autocatalyse au cours de la réaction, en solution dans le chlorure de méthylène, du permanganate de méthyltributylammonium avec le tétradécène-1. Il semble qu'une activation du permanganate par adsorbtion sur des particules colloïdales du produit de la réaction (le bioxyde de manganèse) serait responsable de l'autocatalyse observée. Le permanganate qui est ainsi activé peut alors provoquer une réduction soit par réaction avec l'alcène soit par décomposition thermique.

[Traduit par le journal]

Introduction

It is well known that certain permanganate reactions are autocatalytic. For example, the oxidation of amines (1, 2), hydrogen peroxide (3), and oxalic acid (4), as well as the thermal decomposition of aqueous potassium permanganate (5), have been observed to be autocatalytic.

Despite its extensive occurrence in other reactions, evidence for autocatalysis during the reduction of permanganate by alkenes has not previously been reported. However, we have now obtained results which establish the importance of this phenomenon during the oxidation of 1-tetradecene by methyltributylammonium permanganate. In this paper we wish to describe these results and attempt to identify the mechanism of the autocatalytic reactions.

Experimental

Reaction rates were determined by periodic scanning of the uv–vis absorption spectrum using an HP 8450A spectrophotometer equipped with a temperaure controlled cuvette holder. The good isosbestic point observed when sequential spectra are plotted as in Fig. 1 indicates that no long-lived intermediates are formed during the course of the reaction. The concentration of permanganate corresponding to any spectrum can therefore be determined by noting the absorbance at 526 nm (A^{526}), and subtracting from it that portion due to absorption by the product. The latter can be obtained from the absorbance at 418 nm (A^{418}), where permanganate is transparent. As indicated by eqs. [1]–[3], where the product is denoted by the symbol "P", the superscripts indicate wavelengths, and the subscripts i, f, and t stand for initial, final, and variable times respectively, it is possible to calculate the permanganate concentration from absorbance measurements at 526 nm and 418 nm.

[1] $$[QMnO_4]_t = (A_t^{526} - \epsilon_P^{526}[P]_t)/\epsilon_{QMnO_4}^{526}$$

[2] $$[QMnO_4]_t = (A_t^{526} - \epsilon_P^{526}A_t^{418}/\epsilon_P^{418})([QMnO_4]_i/A_i^{526})$$

[3] $$[QMnO_4]_t = (A_t^{526} - A_f^{526}A_t^{418}/A_f^{418})([QMnO_4]_i/A_i^{526})$$

Permanganate solutions were prepared by dissolving weighed amounts of methyltributylammonium permanganate in anhydrous methylene chloride that had been carefully distilled from molecular sieves. Since permanganate reacts slowly with the solvent under these conditions, the solutions were freshly prepared prior to each experiment and the calculated rate constants were all appropriately corrected

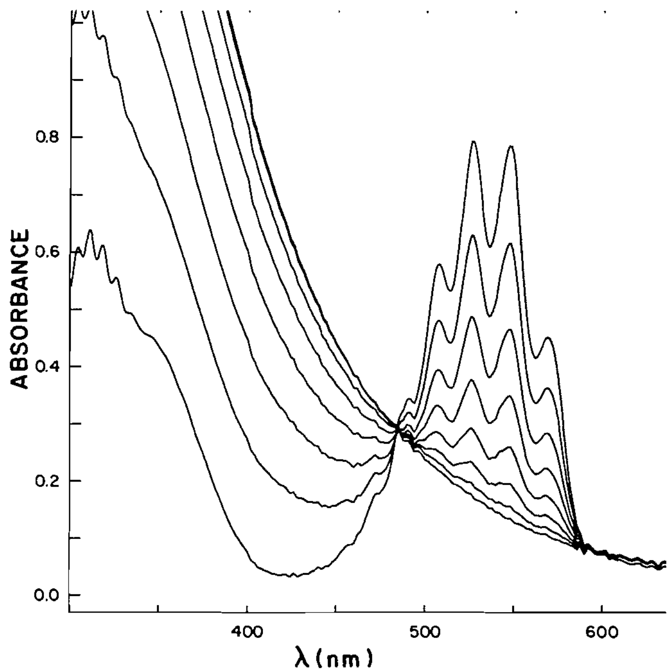

FIG. 1. Successive scans obtained during the oxidation of 1-tetradecene (7.89 × 10^{-3} M) by methyltributylammonium permanganate (3.02 × 10^{-4} M) in methylene chloride at 25.0°C. Isosbestic point at 484 nm.

by subtracting the rate of reduction of the oxidant by the solvent.

In a typical experiment, a 50-mL volumetric flask containing a solution of the desired concentration of 1-tetradecene in methylene chloride was thermostated in an ethylene glycol/water bath for about 20 min. Then, solid methyltributylammonium permanganate (0.0049 g) was added and the solution stirred until homogeneous. A portion of this solution (~2 mL) was then transferred to a cuvette in the thermostated cell compartment of the spectrophotometer, absorbances were measured at intervals, and the concentration of permanganate calculated using eq. [3].

At the conclusion of the reaction the oxidation state of the product was determined iodometrically using the following procedure. A solution of methyltributylammonium permanganate (2.98 × 10^{-4} M) in methylene chloride was allowed to react until no trace of permanganate could be seen in the absorption spectrum. An aliquot (2.0 mL) of the resulting brown-yellow solution was titrated by adding

[1]Author to whom correspondence may be addressed.

TABLE 1. Initial reaction rates

$[MnO_4^-]_i(M \times 10^4)$[a]	$r_T(M\ s^{-1} \times 10^7)$[b]	$r_s(M\ s^{-1} \times 10^8)$[c]	$r_i(M\ s^{-1} \times 10^7)$[d]	$k_1(s^{-1} \times 10^3)$[e]
0.82	2.47	0.37	2.43	2.96
1.54	4.76	0.72	4.69	3.05
2.36	7.11	1.11	7.00	2.97
3.17	9.89	1.50	9.74	3.07
3.80	11.66	1.81	11.48	3.02

[a]Initial $[MnO_4^-]$, [1-tetradecene] = 7.89×10^{-2} M, temperature = 25.0 ± 0.1°C.
[b]Observed initial rate.
[c]Rate of reaction of permanganate with solvent.
[d]Corrected initial rate.
[e]$k_1 = r_i/[MnO_4^-]_i$.

TABLE 2. Dependence of initial rates on alkene concentration[a]

$[MnO_4^-]_i(M \times 10^4)$	[1-Tetradecene]$(M \times 10^2)$	$r_i(M\ s^{-1} \times 10^7)$	$k_1(s^{-1} \times 10^3)$	$k_2(M^{-1}\ s^{-1} \times 10^2)$[b]
2.72	0.79	0.80	0.29	3.72
2.97	1.58	1.83	0.62	3.90
2.97	2.37	2.75	0.93	3.91
2.96	3.16	3.77	1.27	4.02
2.39	3.95	3.76	1.57	3.99
3.07	4.74	5.70	1.86	3.92
3.20	5.53	6.91	2.16	3.91
2.88	6.31	7.17	2.49	3.95
3.07	7.10	8.52	2.78	3.91
3.03	7.89	9.40	3.10	3.93

[a]Temperature = 25.0 ± 0.1°C. Symbols defined in Table 1.
[b]$k_2 = k_1/$[1-tetradecene].

2.0 mL of tetrabutylammonium iodide (3.00×10^{-2} M) in methylene chloride and 5.0 mL of glacial acetic acid, followed by dilution with CH_2Cl_2 to 50.0 mL. The amount of iodine liberated was then determined spectrophotometrically by measuring absorbances at 365 nm ($\epsilon = 2.62 \times 10^4$). These were found to be 0.318 and 0.316 in duplicate determinations.

Results

The oxidation state of the final product was determined by iodometric titration to be 4.01 ± 0.04.

The order of the reaction with respect to oxidant was determined by measuring the initial reaction rate at several different permanganate concentrations while the concentration of 1-tetradecene was held in a constant, large excess. As the data in Table 1 indicate, the order of the reaction with respect to permanganate is unity. The observation that the pseudo-first-order rate constants so obtained are directly proportional to the concentration of 1-tetradecene (Table 2) indicates that the rate of reaction is also first order in alkene.

Therefore, in the absence of complications, it would be expected that plots of ln $[QMnO_4]$ vs. time should be linear. However, all of the plots obtained were found to exhibit a definite concave upward curvature. Typical examples (which have been reproduced in Fig. 2) indicate that the reaction is obviously more complicated than suggested from the initial reaction rate studies.

The activation energies obtained from plots of ln k vs. $1/T$ (Fig. 3) have been summarized in Table 3.

Discussion

Evidence available in the literature indicates that alkenes react with permanganate to form cyclic manganate(V) diesters as in eq. [4] (6).

[4] 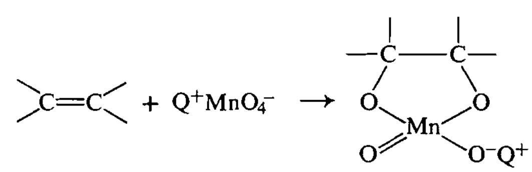

The results of isotopic labelling experiments (7) as well as several product studies (8) are consistent with this conclusion. For example, Wagner (9) converted 3-methyl-1-butene into 1,2-dihydroxy-3-methylbutane by use of alkaline permanganate, and Ogino and Mochizuki (10) found that 1,2-dihydroxyoctane was formed by basic hydrolysis of the product obtained when 1-octene was oxidized under conditions similar to those used in these experiments.

Since the oxidation state of the product appears to be +4 and since no long-lived intermediate could be detected, this initial reaction must be followed by a very fast reaction in which the manganate(V) diester is reduced to manganate(IV), possibly by abstraction of a hydrogen atom from the solvent as in eq. [5].

[5] 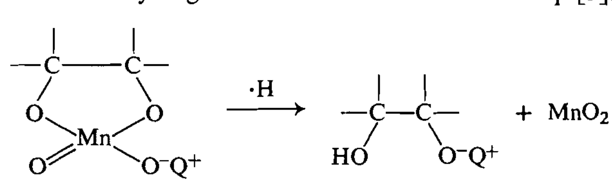

Two properties of the product suggest that it must be colloidal in nature. Firstly, the intensity of its absorption spectrum increases with time, presumably because flocculation is slowly occurring. If traces of moisture are added, the rate of flocculation increases and a brown solid eventually precipitates. Secondly, the logarithm of the absorption of the product is linearly related to the logarithm of the wavelength, a property

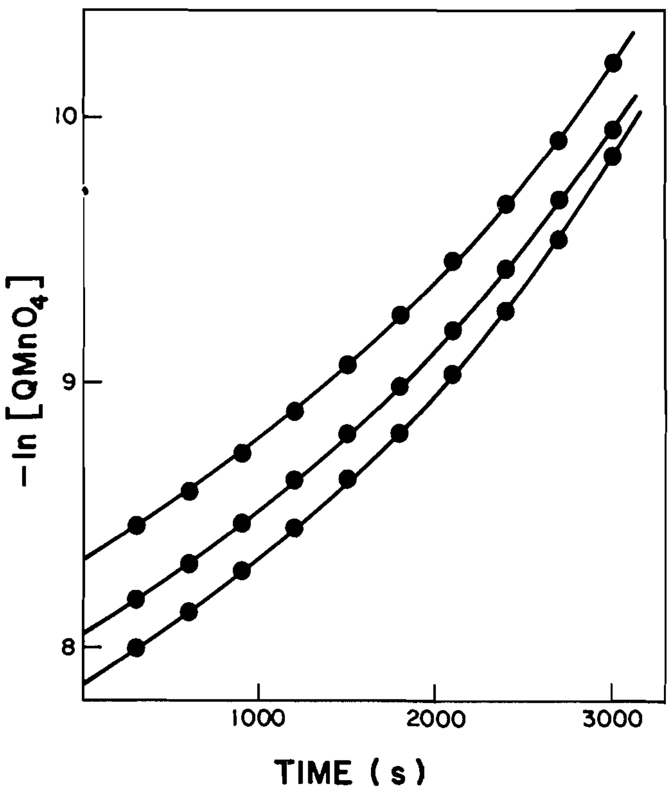

FIG. 2. Attempted pseudo-first-order plots.

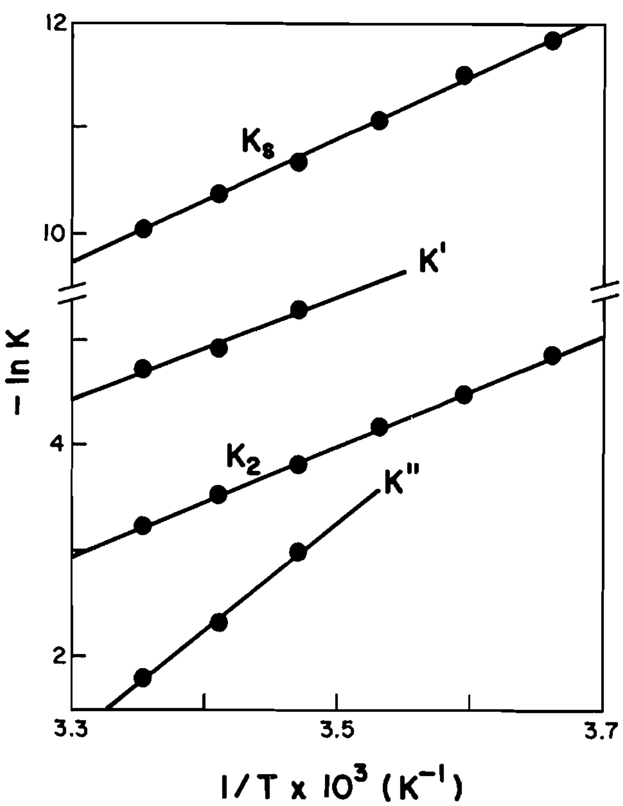

FIG. 3. Arrhenius plots. Symbols defined in text. For k_s plot, $[QMnO_4]_i = 3.00 \times 10^{-4}\ M$. For k_2 plot, $[QMnO_4]_i = 3.00 \times 10^{-4}\ M$, [1-tetradecene] = 7.9×10^{-3} to $7.9 \times 10^{-2}\ M$. For k' and k'' plots, $[QMnO_4]_i = 3.00 \times 10^{-4}\ M$, $[MnO_2]_i = 2.96 \times 10^{-4}\ M$, [1-tetradecene] = 6.3×10^{-3} to $8.5 \times 10^{-2}\ M$.

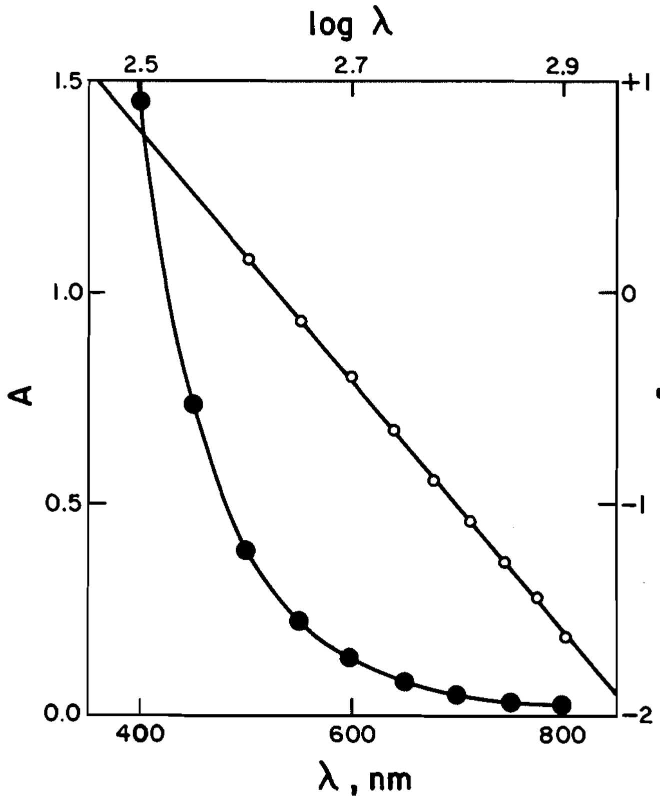

FIG. 4. Closed circles: spectrum of the product formed from the reaction of 1-tetradecene ($4.74 \times 10^{-2}\ M$) with methyltributylammonium permanganate ($5.56 \times 10^{-4}\ M$) in methylene chloride at 25.0°C. Open circles: log (absorbance) vs. log (λ) calculated from this spectrum. Slope = −5.90, r = 1.000.

TABLE 3. Activation energies

Rate constant[a]	E_a(kJ/mol)
k_s	49.0
k_2	43.8
k'	40.7
k''	85.1

[a]The rate constants are defined in eqs. [8]–[10].

exhibited by most colloids (11*a*). See Fig. 4.

The observance of concave rate plots, as in Fig. 2, suggests that the reaction may be autocatalytic. This was confirmed by determining initial rates in solutions that contained varying concentrations of product obtained from a previous experiment. When fresh methyltributylammonium permanganate was added to solutions in which the permanganate had been completely reduced, the rate of reaction was found to increase with the concentration of manganese(IV) in the solutions (Fig. 5). Consequently, it appears as if the autocatalysis may be associated with the formation of a manganese(IV) colloid, most likely MnO_2, that would provide a surface on which the catalyzed reaction could take place.

On the basis of these results it can be seen that the total rate law for the disappearance of permanganate should take the form of eq. [6],

$$[6] \quad \text{Rate}_{obs} = \text{rate}_{solvent} + \text{rate}_{alkene} + \text{rate}_{cat}$$

where

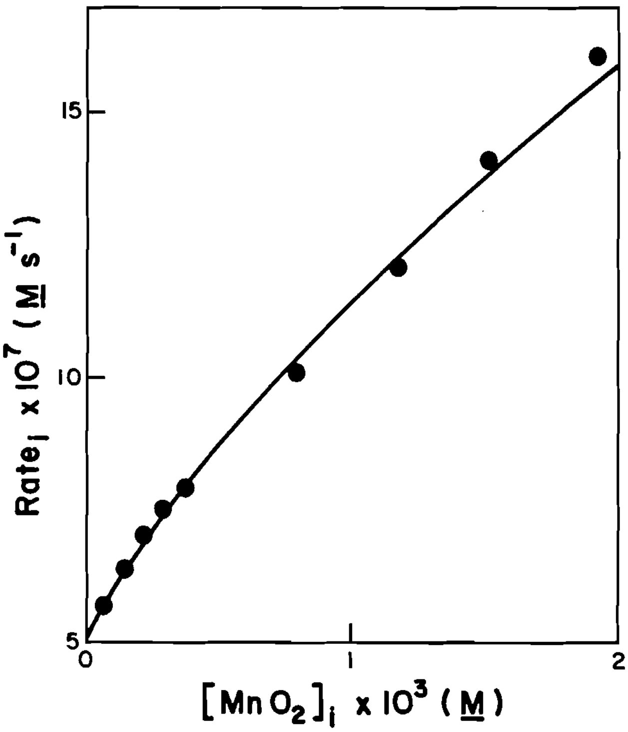

FIG. 5. Dependence of initial rates on manganese dioxide concentrations.

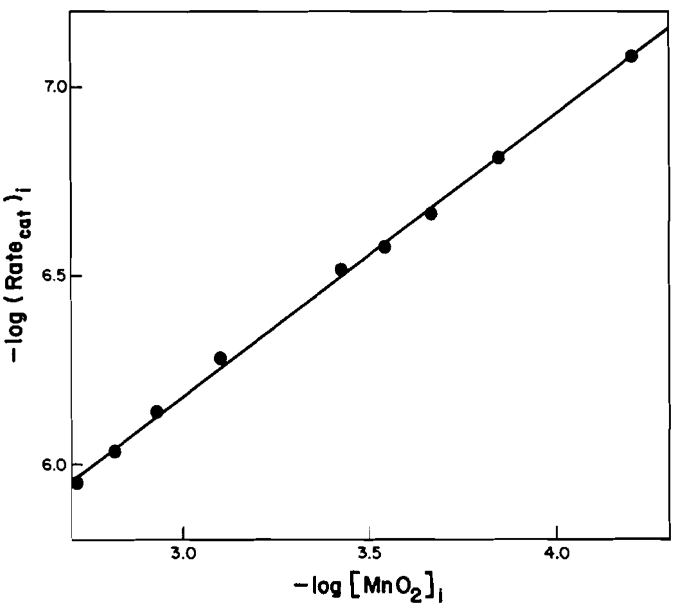

FIG. 6. Dependence of the rate of the catalytic reaction on the apparent concentration of MnO_2 present in the solution. $[QMnO_4]_i$ = 3.00×10^{-4} *M*, [1-tetradecene] = 3.95×10^{-2} *M*, 25°C, slope = 0.75, r = 0.999.

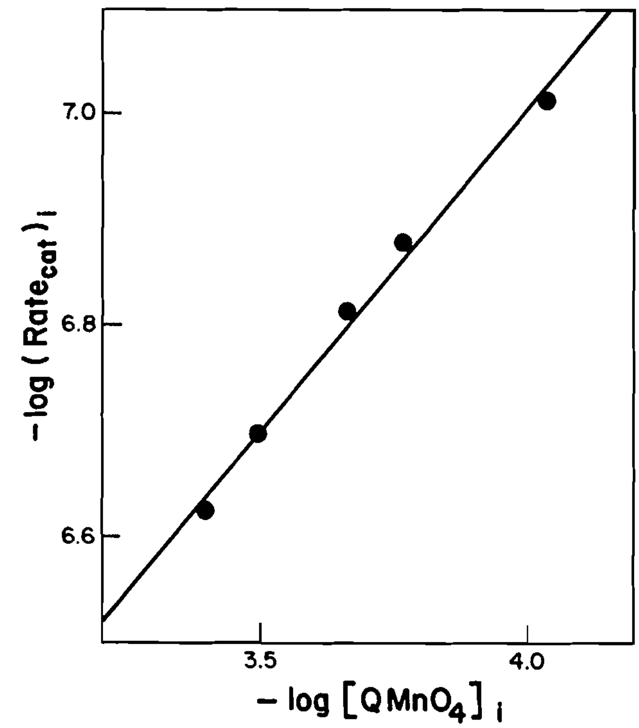

FIG. 7. Dependence of the rate of the catalytic reaction on the permanganate concentration. $[MnO_2]_i$ = 3.01×10^{-4} *M*, [1-tetradecene] = 7.89×10^{-3} *M*, 25°C, slope = 0.61, r = 0.996.

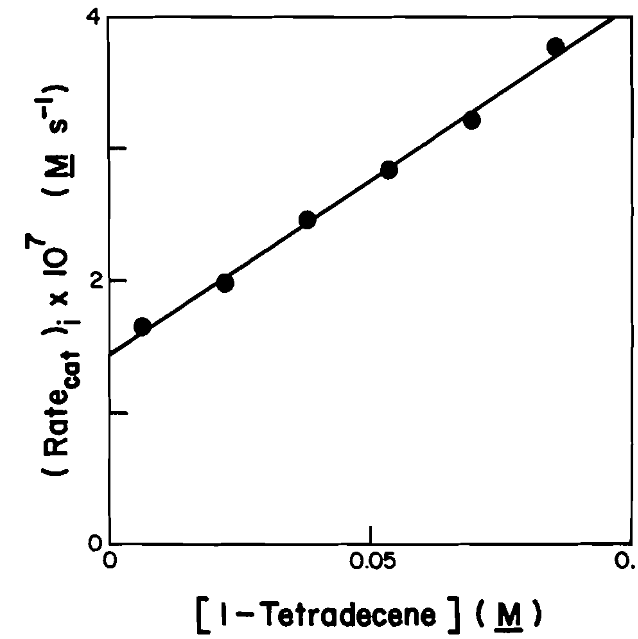

FIG. 8. Dependence of the rate of the catalytic reaction on the concentration of 1-tetradecene. $[QMnO_4]_i$ = 3.00×10^{-4} *M*, $[MnO_2]_i$ = 2.96×10^{-4} *M*, 25°C, slope = 2.68×10^{-6} s^{-1}, intercept = 1.43×10^{-7} *M* s^{-1}, r = 0.997.

$$[7] \quad \text{Rate}_{\text{obs}} = -\frac{d[MnO_4^-]_t}{dt}$$

$$[8] \quad \text{Rate}_{\text{solvent}} = k_s[MnO_4^-]$$

$$[9] \quad \text{Rate}_{\text{alkene}} = k_2[MnO_4^-][\text{1-tetradecene}]$$

Since k_s and k_2 can be independently determined, as described above, it is possible to investigate the catalytic portion of the rate law by subtracting the rate due to solvent oxidation plus the rate due to alkene oxidation from the observed reaction rates (eq. [6]). When this is done it is found empirically that the catalytic rate conforms to eq. [10] (Figs. 6, 7, and 8).

$$[10] \quad \text{Rate}_{\text{cat}} = (k' + k''[\text{1-tetradecene}])[MnO_2]^{0.75}[QMnO_4]^{0.61}$$

The nonintegral order of the reaction with respect to MnO_2 is not surprising since the rate of reaction would be dependent on the number of colloidal particles in solution rather than on the number of moles of MnO_2 present. Consequently, if the extent of flocculation is greater at higher MnO_2 concentrations, the apparent order, based on absorbance measurements, will appear to be less than unity.

Similarly, the apparent nonintegral order with respect to permanganate must arise because the rate of reaction is proportional to the amount of permanganate adsorbed rather than the amount in solution. According to the empirical isotherm of Freundlich the amount of permanganate adsorbed (y) is related to the amount in solution (c) by eq. [11], where a and b are constants (11*b*). Since b is always less than unity the observed

$$[11] \quad y = ac^b$$

order with respect to the concentration of permanganate in solution would also be fractional.

The part of eq. [10] that is independent of alkene concentration probably arises from the thermal decomposition of permanganate, which is known to take place readily in the presence of manganese dioxide (5). The total catalytic contribution to the rate of reaction can therefore be visualized as resulting from an activation of permanganate by adsorption on the surface of colloidal MnO_2 particles. These "activated" MnO_4^- ions can then be reduced by reaction with alkene or by the thermal explusion of oxygen (12). In fact, at low alkene concentrations, thermal decomposition of the activated permanganate appears to be the primary autocatalytic mechanism (see Fig. 8). As expected, the activation energy for this process (40.7 kJ/mol) is substantially less than for the decomposition of unactivated $KMnO_4$, which is known to have an activation energy of approximately 150 kJ/mol (12).

Acknowledgments

Financial assistance from the Natural Sciences and Engineering Research Council of Canada is gratefully acknowledged. J. F. Perez-Benito wishes to thank the Spanish Ministry of Education and Science for a grant to study in Canada, thus making possible his participation in this project.

1. F. Mata, J. Perez-Benito, and A. Arranz. Z. Phys. Chem. (Neue Folge), **135**, 141 (1983).
2. M.-M. Wei and R. Stewart. J. Am. Chem. Soc. **88**, 1974 (1966).
3. F. Fouinat and M. Magat. J. Chim. Phys. **47**, 514 (1950).
4. D. A. Skoog and D. M. West. Fundamentals of analytical chemistry. 2nd ed. Holt, Rinehart and Winston, Toronto. 1969. p. 422.
5. R. Stewart. *In* Oxidation in organic chemistry. Part A. *Edited by* K. B. Wiberg. Academic Press, New York. 1965. p. 20.
6. R. Stewart. Oxidation mechanisms, applications to organic chemistry. W. A. Benjamin, New York. 1964. pp. 62–63.
7. K. B. Wiberg and K. A. Saegebarth. J. Am. Chem. Soc. **79**, 2822 (1957).
8. D. Arndt. Manganese compounds as oxidizing agents in organic chemistry. Open Court, La Salle, Illinois. 1981. pp. 208–209.
9. G. Wagner. Chem. Ber. **21**, 1230 (1888); **21**, 3347 (1888).
10. T. Ogino and K. Mochizuki. Chem. Lett. 443 (1979).
11. G. M. Barrow. Physical chemistry. 2nd ed. McGraw–Hill, New York. 1966. (*a*) p. 803, (*b*) p. 766.
12. E. G. Prout and F. C. Tompkins. Trans. Faraday Soc. **40**, 488 (1944).

Tetracyclic triterpenes. VIII. The skeletal rearrangement of 3β-acetoxy-9α,11α-epoxy-5α-lanostan-7-one: 13- and 10-methyl group migration[1]

ZDZISŁAW PARYZEK AND ROMAN WYDRA
Department of Chemistry, Adam Mickiewicz University, 60-780 Poznań, Poland

Received March 27, 1984[2]

ZDZISŁAW PARYZEK and ROMAN WYDRA. 1985. Can. J. Chem. **63**, 1280 (1985).

The boron trifluoride etherate catalyzed rearrangement of 3β-acetoxy-9α, 11α-epoxy-5α-lanostan-7-one (**1**) in acetic anhydride resulted in formation of 19(10 → 9β)*abeo* compounds **2** and **4** along with 18(13 → 12β)*abeo* compound **5**, as the major product. These structures are supported by spectral data and chemical transformations. The possible mechanism of the rearrangement is discussed.

ZDZISŁAW PARYZEK et ROMAN WYDRA. 1985. Can. J. Chem. **63**, 1280 (1985).

La transposition, catalysée l'éthérate du fluorure de bore, de l'acétoxy-3β époxy-9α, 11α 5α-lanostanone-7 (**1**) en solutiion dans l'anhydride acétique conduit à la formation des composés 19(10 → 9β)*abeo* (**2** et **4**) en plus du composé 18(13 → 12β)*abeo* (**5**) qui se forme comme produit principal. Les structures proposées sont en accord avec les données spectrales et les transformations chimiques. On discute du mécanisme possible de cette transposition.

[Traduit par le journal]

The rearrangement of lanostane derivatives which possess the oxirane fragment in ring C has been a subject of several studies in recent years (1). These investigations were undertaken in connection with the possible transformation of the lanostane skeleton into the related, biologically important, skeletons of cycloartane, cucurbitane, and protostane. Indeed, by this approach effective transformations into the last two types have been achieved (1*b*, 2–4).

Our interest in the rearrangement of 3β-acetoxy-9,11-epoxy-5α-lanostan-7-ones was based on the assumption that the carbonyl group, due to its electronic effect, might suppress the rearrangement to a protostane skeleton. Consequently, formation of compounds with cucurbitane and (or) cycloartane skeletons was expected. This was the case when 9β,11β-epoxy-7-ketone was treated with boron trifluoride in acetic anhydride at room temperature (3) or at 0°C (4). However, the 9α,11α-epimer has been reported to react under similar conditions (0°C) with exclusive migration of the 13-methyl group to position 12 (4). This result was rather unexpected if one takes into account the 1,2-*trans* relationship of the oxirane oxygen and the 10-methyl group. Indeed, we found this rearrangement to be a more complex reaction than had been reported. Reinvestigation of the rearrangement of 3β-acetoxy-9α,11α-epoxy-5α-lanostan-7-one (5) is now presented in full.

The rearrangement of epoxide **1** catalyzed by boron trifluoride etherate in acetic anhydride at room temperature gave a complex mixture. By combining repeated column chromatography and tlc separations, four compounds **2**, **4**, **5**, and **6** were isolated in yields of 13, 10, 44, and 12%, respectively.

The structure assignment of compound **2** was based on spectral data. Its uv (λ_{max}: 244 nm, ϵ 11 600) and ir (ν_{max}: 1658 cm^{-1}) spectra agreed with an α,β-unsaturated ketone moiety with the double bond in position 5,6. This was supported by its ^{1}H nmr spectrum, in which all characteristic signals were present: singlet from the 6-H (δ 6.06), triplet from the 11β-H (δ 5.18, J = 8 Hz), and singlet from the 3α-H (δ 4.85). The comparison of its ^{13}C nmr spectrum with those of compounds with a different substitution pattern, **7**, **8**, and **9** (see Table 1), has also been valuable. The carbon resonances in these compounds were assigned on the basis of the residual splittings in

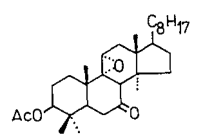

1

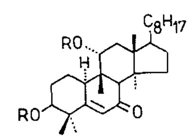

2 R=Ac
3 R=H

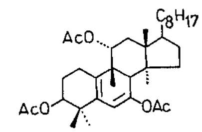

4

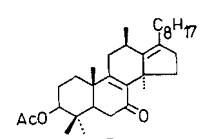

5

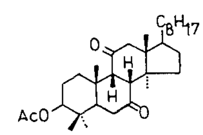

6

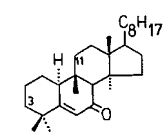

7 3β-OAc, 11-oxo
8 3β-OAc, 11β-OAc
9 3-oxo, 11β-OAc
10 3-oxo, 11-oxo

off-resonance decoupled spectra, chemical shift rules (6), chemical shift comparison from compound to compound, correlation with values for related compounds from our collection, and low power selective enhancement of signals from quaternary carbon atoms (7). Besides the readily assigned signals (C-3, C-5, C-6, C-7, C-11, and the side chain carbons (8)) the most characteristic resonances in this series are those of carbon atoms 8, 9, and 10.

Confirmation of the structure of compound **2** came from its mild basic hydrolysis to the amorphous 3,11-dihydroxy compound **3** followed by oxidation with Jones reagent to the crystalline triketone **10**, identical with the product obtained from the 3β,11β-diacetoxy compound **8** (3*a*) by similar transformations.

The second product isolated as an oil was assigned structure **4** on the basis of the following spectral properties. The ^{1}H nmr spectrum revealed three separate singlets for the acetate methyl groups at δ 2.09, 2.06, 2.02, and a sharp singlet arising from one olefinic proton at δ 5.86. The presence of a sharp singlet at δ 2.27 ascribed to the 8β-proton confirms the absence of protons in the 7 and 9 positions and is characteristic of all cucurbitane derivatives which lack hydrogen atoms in position 7 (3). Its uv spectrum had the maximum expected for the 5(10),6-diene system at 275 nm. Compound **4** was most

[1] For a preliminary account of this work see ref. 5*c*.
[2] Revision received October 29, 1984.

TABLE 1. ^{13}C Chemical shifts of cucurbitanes[a]

Carbon atom	2	7	8	9
C-1	25.78	27.97	22.54	24.51
C-2	26.37	25.63	26.25	38.12
C-3	78.46	77.66	78.18	210.69
C-4	39.68	41.44	41.38	51.42
C-5	167.82	165.88	166.45	166.18
C-6	125.26	125.08	125.24	125.34
C-7	200.79	199.97	201.89	201.47
C-8	59.33	59.38	58.58	58.10
C-9	38.70	49.07	40.68	41.66
C-10	41.78	37.35	41.04	42.04
C-11	79.12	211.66	72.62	72.57
C-12	35.90	49.21	36.01*	36.05*
C-13	46.80	48.40*[b]	44.55	44.73
C-14	48.17	48.96*	48.49	48.61
C-15	33.61	34.25	34.39	34.50
C-16	27.94	27.97	27.99	28.02
C-17	50.00	48.27	50.35	50.43
C-18	16.32	16.87	17.01	17.03
C-19	25.58	21.14	21.74	21.11
C-20	36.25	36.27	36.37	36.42
C-21	18.80	18.54	18.84	18.89
C-22	35.90	35.92	36.10*	36.23*
C-23	24.02	23.93	24.00	24.05
C-24	39.42	39.40	39.45	39.50
C-25	27.94	27.83	27.62	27.58
C-26	22.78	22.78	22.82	22.81
C-27	22.52	22.51	22.54	22.55
C-28	19.19	18.54	18.01	17.94
C-29	26.82	27.83	27.43	28.36
C-30	24.80	24.47	24.48	23.09

[a]CH_3COO signals appear at 21.02 to 21.70 and CH_3COO signals at ca. 170 ppm.
[b]Chemical shifts marked with asterisks may be interchanged.

probably formed via 3β-aceotxy-19(10 → 9β*abeo*-lanost-5(10)-en-7-one, since compound **2** did not give the dienol acetate **4** under the rearrangement conditions.

Pure compound **4**, when left for several weeks, gave after tlc purification an oily substance, whose uv spectrum showed λ_{max} at 249 nm suggesting the presence of a Δ^5-7-ketone chromophore. This was confirmed by ν_{max}: 1660 cm^{-1} in the ir spectrum. In the ^{1}H nmr spectrum the following signals were important: sharp singlet from one proton at δ 6.33, multiplet from one proton at δ 5.08, triplet at δ 4.86, doublet at δ 4.25, and two acetate methyl group singlets at δ 2.10 and 2.00. The high resolution mass spectrum showed molecular ion corresponding to the formula $C_{34}H_{52}O_6$. All these data were in accordance with formula **11**. In the mass spectrum, fragments m/z 121, 135, and 162 confirmed the presence of the oxirane oxygen atom in position 1,10 assuming that fragmentation *a*, *b*, and *c* occurs, respectively:

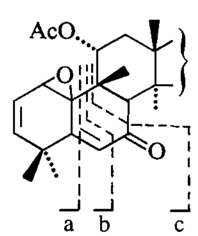

The accurate mass measurement was in agreement with the constitution of these fragments. The mechanism of the trans-

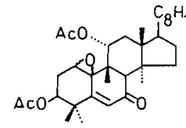
11

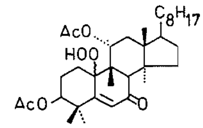
12

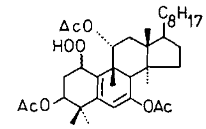
13

formation **4** → **11** is unknown; however, the intermediacy of hydroperoxides **12** or **13** is considered (9). Allylic hydroperoxides are known to give the respective α,β-unsaturated ketones (10), but we are not aware of the formation of an epoxide which, in this case, would involve abstraction of a hydrogen atom from C-1 in **12**. More probably, compound **11** arose by the sequence shown in eq. [1].

[1] 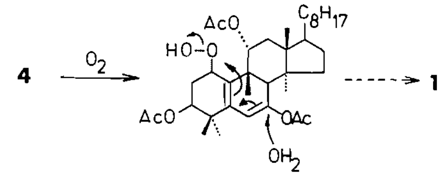

Compound **5** has been reported previously (4); however, the 18(13 → 12β)*abeo* structure was proposed solely on the basis of spectral data. Since rearrangement which involved the 13-methyl group migration to position 12 was rather unusual, we sought further evidence in favour of structure **5**.

Epoxidation of **5** with *m*-chloroperbenzoic acid gave epoxide **14**, whose uv spectrum showed λ_{max} at 251 nm and whose ir spectrum showed ν_{max} at 1658 cm^{-1}, equally characteristic of a Δ^8-7-ketone chromophore. Reaction of compound **5** with chromium trioxide in acetic acid gave a complex mixture from

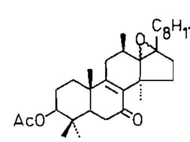
14 R=H_2

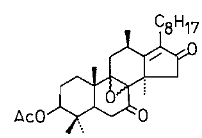
15

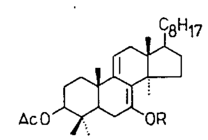
16 R=$COCH_3$
17 R=$COCF_3$

which a major compound could be isolated in pure form. Its elemental analysis and molecular ion at m/z 512 suggested incorporation of two oxygen atoms into **5**. Its ir spectrum did not contain absorption associated with the Δ^8-7-ketone moeity. However, a strong band indicating two carbonyl groups was present at 1710 cm^{-1} with a shoulder at 1728 cm^{-1}. The uv maximum at 253 nm was in agreement with the presence of a 16-carbonyl group conjugated with a 13,17-double bond. A weak absorption around 290 nm suggested the presence of the saturated carbonyl group in position 7. These data were in agreement with structure **15** resulting from allylic oxidation of position 16 and an unusual epoxidation of the conjugated 8,9-double bond in compound **5**. Substantial oxidation of the allylic 11-carbon atom in compound **5** was not observed, in contrast to the easy oxidation of 3β-acetoxy-5α-lanost-8-en-7-one (11) to 3β-acetoxy-5α-lanost-8-ene-7,11-dione (12) under similar conditions.

Compound **5** was found to behave abnormally in enol acetylation reactions. It formed 3β,7-diacetoxy-18(13→ 12β)*abeo*-lanosta-6,8,13(17)-triene on action of sulfuric acid and isopropenyl acetate (4) and did not give enol trifluoroacetate with trifluoroacetic acid anhydride. Contrary to the behaviour of compound **5**, 3β-acetoxy-5α-lanost-8-en-7-one gave heteroannular dienol acetate **16** on the action of *p*-toluenesulfonic

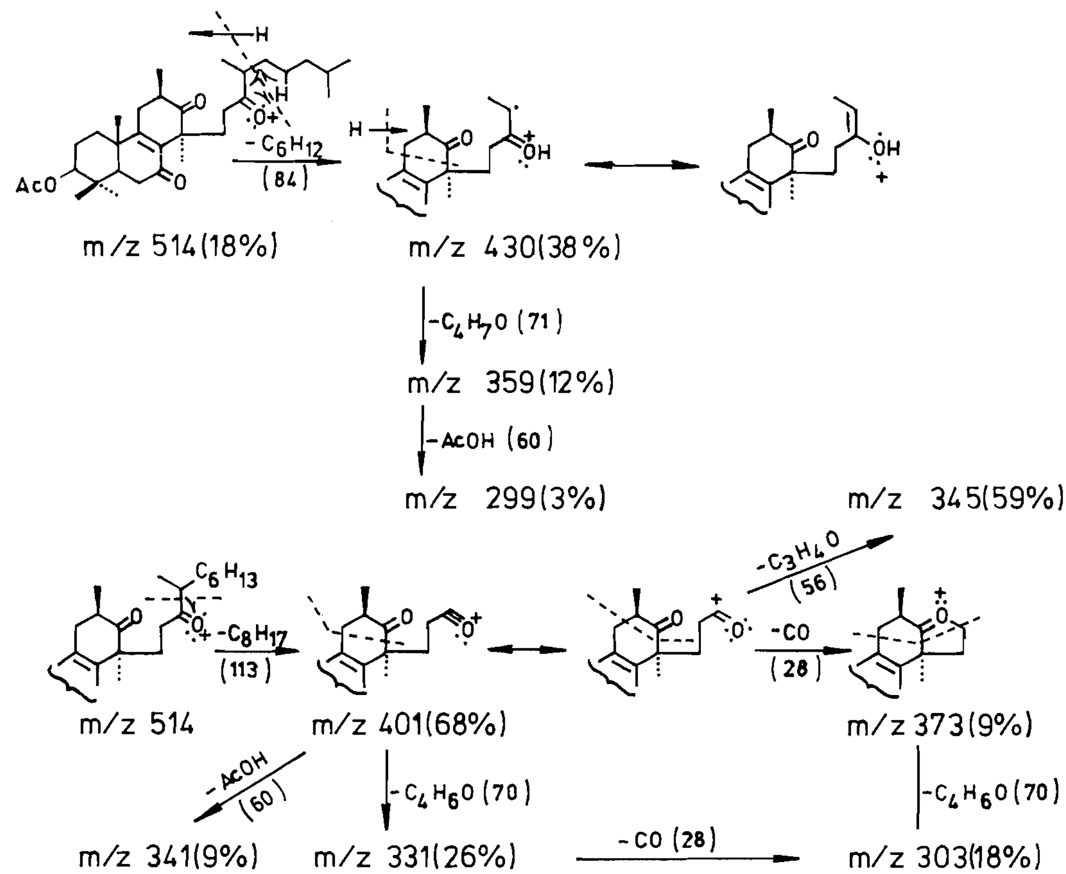

SCHEME 1

acid in acetic anhydride (13) and was very easily transformed to the dienol trifluoroacetate **17** upon dissolving in trifluoroacetic acid anhydride. The last reaction seems to be specific for the 8-ene-7-one functionality in lanostane since, for example, cholest-4-en-3-one does not react under similar conditions.

Finally, ruthenium tetraoxide – sodium metaperiodate oxidation of compound **5** afforded the seco compound **18** as an oil. Its ^{1}H nmr spectrum had two broadened signals ascribed to the 11β- and 11α-protons at δ 3.12 and 3.02, which were well

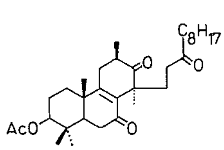

18

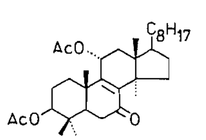

19

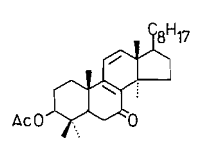

20

separated from signals of protons α to carbonyl groups in the region 2.75 and 2.45. The ir spectrum showed the presence of both conjugated (1663 cm^{-1}) and unconjugated (1715 cm^{-1}) carbonyl groups. Its uv spectrum had λ_{max}: 248 nm (ε 8200). Very important information came from mass spectral fragmentation of the seco compound **18** shown in Scheme 1. The fragmentation pattern confirms the presence of a methyl group in position 12.

The formation of compounds **2** and **4** having the cucurbitane skeleton results from the opening of the oxirane ring in **1**, probably in a concerted process involving migration of the 10-methyl group to position 9. However, this is not a predominant pathway despite the favourable *trans* relationship between the migrating group and the breaking carbon–oxygen bond. The carbonyl group in position 7 clearly prevents formation of a transient carbocation at C-8. For example, in the rearrangement of 9,11-epoxylanostanes without a 7-carbonyl group, compounds with the protostane skeleton are formed (1*b*, 2).

To find an explanation for the formation of the 18(13 → 12β)*abeo* compound **5** from **1** it was of interest to test the possible intermediacy of compounds **19** or **20** in the rearrangement. It was hoped to obtain dienone **20** from 3β-acetoxy-11β-hydroxy-5α-lanost-8-en-7-one (**21**) according

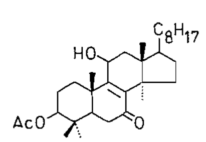

21

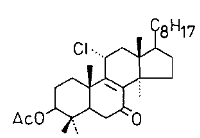

22

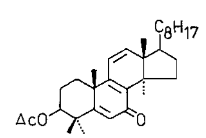

23

to the procedure described by Dias (14). Thus, sodium borohydride reduction of 3β-acetoxy-5α-lanost-8-ene-7,11-dione was carried out. The reaction was reported to give either 3β-acetoxy-7β-hydroxy-5α-lanost-8-en-11-one (15) or a mixture of the same compound and 3β-acetoxy-11β-hydroxy-5α-lanost-8-en-7-one in the ratio 3:1 (14, 16). We have identified three products of the reduction carried out under similar conditions. 3β-Acetoxy-11β-hydroxy-5α-lanost-8-en-7-one (**21**) (14, 16), 3β-acetoxy-7α-hydroxy-5α-lanost-8-en-11-one, and 3β-acetoxy-7β-hydroxy-5α-lanost-8-en-11-one (15) were formed in the yield 3, 10, and 76%, respectively. Hence, the desired 11β-alcohol **21** was obtained in only minute amounts. However, it was formed with 3β-acetoxy-9β,11β-epoxy-5α-lanostan-7-one (**5*a***) was treated with a solution of potassium

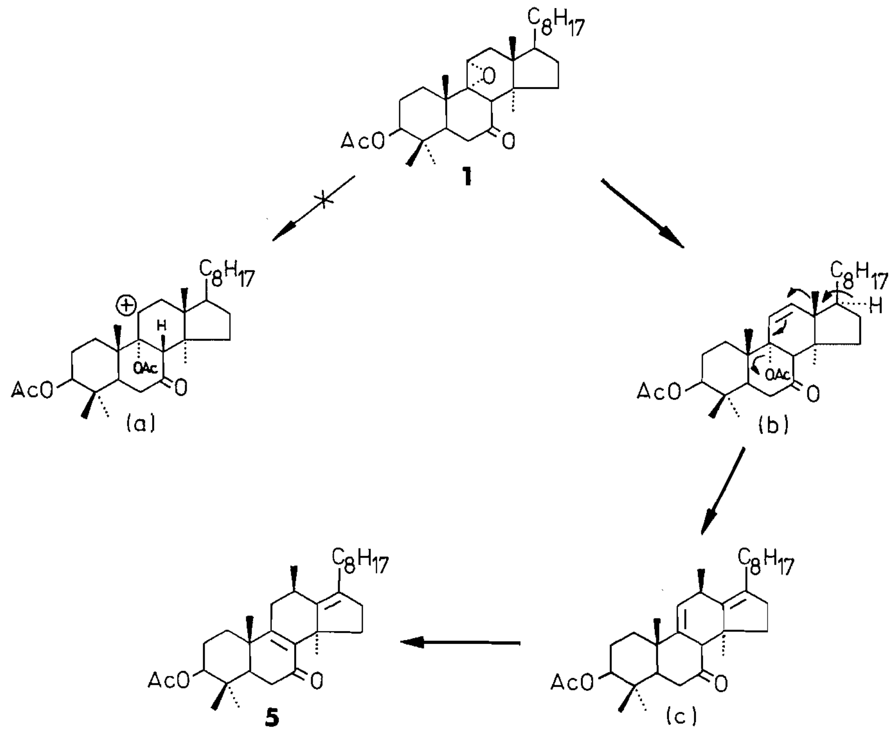

SCHEME 2

carbonate in methanol to give 3β,11β-dihydroxy-5α-lanost-8-en-7-one, which upon acetylation gave compound **21**.

The attempts to prepare dienone **20** from **21**, according to the described procedure (14, 16), failed. Reaction of **21** with *p*-toluenesulfonyl chloride in benzene gave 3β-acetoxy-5α-lanostane-7,11-dione (17). When a mixture of benzene–pyridine was used as the solvent the above reaction gave 3β-acetoxy-5α-lanost-8-ene-7,11-dione (17) and 3β-acetoxy-5α-lanostane-7,11-dione in the ratio 1:2. In pyridine itself, the ratio was close to 2:1. Compound **21** could not be dehydrated by action of thionyl chloride in pyridine. Instead, 3β-acetoxy-11α-chloro-5α-lanost-8-en-7-one (**22**) was formed in 55% yield. It had ν_{max}: 1668 cm^{-1} and λ_{max}: 256 nm (ε 9200). Its ^{1}H nmr spectrum had signals due to an 11-proton at δ 4.66 and a 3α-proton at δ 4.49. The ^{13}C nmr spectrum showed all expected low field signals and, in the off-resonance spectrum, a doublet centered at δ 53.4 of the 11-carbon atom. The proof of the configuration of the chlorine atom was based on the comparison of the shape of the 11-proton signal in compounds **19**, **21**, and **22**. Also, the region of methyl group signals (δ 1.3–0.5) had a similar pattern for compounds **19** and **22** in contrast to compound **21** and its 3-hydroxy derivative. Similar replacement of a hydroxy group has been reported (18). Bromination of 3β-acetoxy-5α-lanost-8-en-7-one followed by dehydrobromination of the crude reaction product with calcium carbonate in dimethylacetamide gave 3β-acetoxy-5α-lanosta-8,11-diene-7-one (**20**) (19) and 3β-acetoxylanosta-5,8,11,trien-7-one (**23**) (20).

When the dienone **20** was treated with boron trifluoride – ether complex in acetic anhydride (conditions used in the rearrangement of the title epoxide) a complex mixture was formed. Careful tlc examination showed the absence of compound **5**, therefore excluding the intermediacy of the dienone **20** in the rearrangement. Similarly, 3β,11α-diacetoxy-5α-lanost-8-en-7-one (**19**) (5*a*) was excluded as an intermediate since it remained unchanged when it was treated with boron trifluoride – ether complex in acetic anhydride for 10 min.

On the basis of the above results two alternatives seem to remain for the mechanism of formation of **5**. One is the opening of the epoxide to give the secondary cation (Scheme 2, (a)) followed by elimination to the 9α-acetoxy-11-ene (b). The formation of the allylic cation from (b) could then initiate the migration of C-18 and loss of the 17-hydrogen to give (c). Final conjugation of the 9(11) double bond with the carbonyl would give **5**. However, the secondary cation (a) is undoubtedly around 10 kcal/mol less stable[3] than the tertiary cation on C-9. It thus seems probable that the acetylium ion opens the epoxide with elimination of the 12β-hydrogen, giving (b) directly, the subsequent steps being as indicated above.

The present and previous results clearly indicate that in these rigid triterpenoid epoxides a delicate balance between electronic and steric factors determines the main pathway of a particular rearrangement leading to various structurally important products. These reactions are also sensitive to small variations in reaction conditions.

Experimental

Melting points were determined on a Kofler hot-stage apparatus and are uncorrected. The ir spectra were determined with a Perkin Elmer 580 spectrophotometer for solutions in chloroform. The uv spectra were recorded with a Zeiss Specord uv–vis spectrophotometer for solutions in ethanol. The ^{1}H nmr spectra were recorded with Varian EM-360 or Tesla BS 467 60-MHz spectrometers for solutions in deuteriochloroform with tetramethylsilane as an internal standard. The ^{13}C nmr spectra were recorded on a Varian XL-100-15 spectrometer operating at 25.2 MHz and (or) on a JEOL FX 900 spectrometer operating at 22.5 MHz, in the Fourier transform mode, using approximately 0.5 *M* solutions in deuteriochloroform. Solvent signal (δ 77.0) was used as an internal standard. The chemical shifts (δ) are expressed

[3]We thank the referees for critical comment on the mechanism.

in ppm relative to tetramethylsilane. Mass spectra were recorded with a JEOL JMS-D 100 spectrometer using electron impact.

Rearrangement of epoxide 1

To a solution of epoxide **1** (864 mg) in acetic anhydride (30 mL), boron trifluoride – diethyl ether complex (0.86 mL) was added at room temperature. After 1 min the solution was poured on ice and the product was extracted with a benzene–ether (1:1) mixture. The organic layer was washed with a pyridine–water mixture, hydrochloric acid (5%), water, sodium hydroxide solution (2%), and finally with water. After drying with magnesium sulfate and evaporation, the residue was chromatographed on a silica column eluted with benzene – methylene chloride mixtures. The appropriate fractions were combined and were rechromatographed on preparative silica gel tlc plates with methylene chloride as eluent. Four substances were isolated in order of increasing polarity, as follows.

*3β-Acetoxy-18(13→12β)*abeo*-5α-lanosta-8,13(17)-dien-7-one* (**5**) (366 mg, 44% yield); mp 136–138.5°C (lit.(4) mp 135–136°C); ^{1}H nmr, ir, and uv spectra were in accord with the reported data.

3β,7,11α-Triacetoxy-cucurbita-5(10),6-diene (**4**) (oil, 101 mg, 10% yield); λ_{max}: 275 nm; δ: 5.86 (s, 6-H), 5.15 (m, 11β-H), 4.71 (t, J = 6.5 Hz, 3α-H), 2.09, 2.06, and 2.02 (3 s, acetate methyl groups), 1.19, 1.02, 0.97, 0.89, and 0.81 (methyl groups); m/z: 584 (M^+). *Anal.* calcd. for $C_{36}H_{56}O_6$: C 73.93, H 9.65; found: C 74.16, H 9.80.

3β-Acetoxy-5α-lanostan-7,11-dion (**6**) (104 mg, 12% yield); mp 208–210°C; ir, ^{1}H nmr, and mass spectra were in agreement with those of an authentic sample (5*a*).

3β,11α-Diacetoxy-10α-cucurbit-5-en-7-one (**2**) (122 mg, 13% yield); mp 151–153°C; ν_{max}: 1730 and 1658 cm^{-1}; λ_{max}: 244 nm (ε 11 600); δ: 6.06 (br s, 6-H), 5.18 (t, J = 8 Hz, 11β-H), 4.85 (br s, $w_{1/2}$ = 6 Hz, 3α-H), 2.47 (s, 8β-H), 2.06 and 2.00 (2 s, acetate methyl groups), 1.24, 1.14, 1.07, 1.00, 0.84, and 0.79 (methyl groups; m/z: 542 (M^+), 482, 422, 407, 343, 261, and 189. *Anal.* calcd. for $C_{34}H_{54}O_5$: C 75.23, H 10.03; found: C 75.01, H 10.20.

Hydrolysis of 2

Compound **2** (60 mg) was treated with a methanolic solution of potassium carbonate (5 mL) at room temperature for 5 days. Dilution with water and extraction with benzene gave dihydroxy derivative **3** as an oil; λ_{max}: 248 nm; δ: 6.06 (s, 6-H), 3.90 (t, J = 8 Hz, 11β-H), 3.58 (br s, 3α-H); m/z: 458 (M^+). *Anal.* calcd. for $C_{30}H_{50}O_3$: C 78.55, H 10.99; found: C 78.28, H 10.72.

Oxidation of 3 to triketone 10

Compound **3** (40 mg) was dissolved in acetone (1 mL) and oxidized with Jones reagent. The reaction mixture was poured onto ice, the precipitate filtered off, washed with water, and dried. The crude product was crystallized from heptane–benzene mixture to give 10α-cucurbit-5-ene-3,7,11-trione (**10**) (26 mg); mp 175–178°C; ν_{max}: 1718, 1698, 1658, and 1620 cm^{-1}; λ_{max}: 248 nm (ε 8800); m/z: 454 (M^+), 439, 411, 291, and 205. *Anal.* calcd. for $C_{30}H_{46}O_3$: C 79.25, H 10.20; found: C 79.50, H 10.32. Compound **10** was identical in all respects with the product obtained from 3β,11β-diacetoxy-10α-cucurbit-5-en-7-one (**8**) (3*b*) by hydrolysis and oxidation procedures similar to those described above.

Air oxidation of dienol acetate 4

Compound **4** (58 mg) was stored for several weeks at room temperature. Then it was chromatographed on a silica tlc plate developed twice with methylene chloride. Compound **11** (24 mg) was separated as an oil, which had ν_{max}: 1735, 1660, and 1623 cm^{-1}; λ_{max}: 249 nm (ε 8200); δ: 6.33 (s, 6-H), 5.08 (dd, J = 12 Hz, J = 4 Hz, 11β-H), 4.86 (*t*, J = 4 Hz, 3α-H), 4.25 (br d, J = 3.5 Hz, 1-H), 2.52 (s, 8β-H), 2.10 and 2.00 (2 s, acetate methyl groups), 1.22, 1.15, 1.04, 0.88, and 0.81 (methyl groups); m/z: 556 (M^+), 514, 496, 481, 454, 436, 348, 335, 322, 275, 162, 135, and 121; HR mass measurements: calcd. for C_8H_9O: 121.0653; found: 121.0655; calcd. for $C_9H_{11}O$: 135.0809; found; 135.0809; calcd. for $C_{10}H_{10}O_2$: 162.0680; found: 162.0671; calcd. for $C_{34}H_{52}O_6$: 556.3761; found: 556.3771 (M^+). *Anal.* calcd. for $C_{34}H_{52}O_6$: C 73.35, H 9.41; found: C 73.06, H 9.35.

Epoxidation of compound 5

Compound **5** (50 mg) was oxidized with *m*-chloroperbenzoic acid in methylene chloride (3 mL) at room temperature for 45 min. After work-up, a crude product was crystallized from heptane to give epoxide **14** (41 mg), mp 162–164°C; ν_{max}: 1728 and 1658 cm^{-1}; λ_{max}: 251 nm (ε 10 000); δ: 4.49 (br s, 3α-H), 2.49 (m, protons α to carbonyl and in allylic position), 2.05 (s, acetate methyl group), 1.26, 1.08, 1.00, 0.95, 0.92, and 0.82 (methyl groups); m/z: 498 (M^+), 385, 372, 330, 164, and 149. *Anal.* calcd. for $C_{32}H_{50}O_4$: C 77.06, H 10.10; found: C 76.92, H 10.40.

Oxidation of compound 5 with chromium trioxide

To a stirred solution of **5** (43 mg) in acetic acid (4.3 mL) a solution of chromium trioxide (43 mg) in 90% acetic acid (0.43 mL) was added and the reaction mixture was stirred at room temperature for 15 min. Then it was poured into water, and extracted with a 1:1 mixture of benzene–ether. The organic layer was washed with water and dried over magnesium sulfate. The crude product was purified on a silica gel tlc plate developed four times with benzene – ethyl acetate 10:1 mixture to give 3β-acetoxy-8α,9α-epoxy-18(13→12β)*abeo*-5α-lanost-13(17)-ene-7,16-dione (**15**) (12.4 mg, 27% yield) which had mp 203–205°C (from ethanol); ν_{max} 1728 sh, 1710 (very intense absorption); λ_{max}: 253 nm (ε 11 200); m/z: 512 (M^+), 496, 481, 301. *Anal.* calcd. for $C_{32}H_{48}O_5$: C 74.96, H 9.44; found: C 75.12, H 9.52.

Oxidation of 3β-acetoxy-5α-lanost-8-en-7-one with chromium trioxide

To a solution of the substrate (40 mg) in acetic acid (4 mL) a solution of chromium trioxide (40 mg) in acetic acid (90%, 0.4 mL) was added at room temperature. After 20 min, the reaction mixture was poured into water and the product extracted with benzene. The organic layer was washed with water, then with sodium carbonate solution, dried over magnesium sulfate, and the solvent evaporated to give 38 mg of the residue, which on two crystallizations from methanol–chloroform gave 3β-acetoxy-5α-lanost-8-ene-7,11-dione, mp 155–158°C (lit. (12) mp 155–157°C), whose spectra (ir, uv, and ^{1}H nmr) were identical with those of an authentic sample (12).

Action of trifluoracetic acid anhydride on conjugated enones

(a) *Reaction with 3β-acetoxy-5α-lanost-8-en-7-one(11)*

The substrate (133 mg) was dissolved in trifluoracetic acid anhydride (0.8 mL) at room temperature. After 40 min the solvent was evaporated and the residue was crystallized from methanol to give 3β-acetoxy-7-trifluoroacetoxy-5α-lanosta-7,9(11)-dien (**17**) (135 mg, 85% yield), which had mp 97–99°C; λ_{max}: 238 nm (ε 13 400); δ: 5.44 (t, J = 4 Hz, 11-H), 4.49 (m, $W_{1/2}$ = 14 Hz, 3α-H), 2.03 (s, acetate methyl group), 1.06, 0.93, 0.91, 0.86, 0.83, 0.80, and 0.63 (methyl groups); m/z: 580 (M^+), 565 365, 352. *Anal.* calcd. for $C_{34}H_{51}F_3O_4$: C 70.31, H 8.85; found: C 70.68, H 8.96.

(b) *Reaction with compound 5*

Compound **5** when treated as above for 1 h gave only the substrate. Reaction in the presence of a catalytic amount of *p*-toluenesulfonic acid gave the same negative result.

(c) *Reaction with cholest-4-en-3-one (21)*

Cholest-4-en-3-one was treated as in (a) and only the substrate was recovered.

Oxidation of compound 5 to seco-compound 18

To a stirred solution of compound **5** (50.5 mg) in chloroform (5 mL), ruthenium dioxide (5.5 mg) and a 5% aqueous solution of sodium metaperiodate (3 mL) were added at room temperature. The reaction mixture was stirred for 11 h. Ethanol (2 mL) was added and the mixture diluted with ether. The organic layer was washed with water, dried with magnesium sulfate, and evaporated. The crude product was chromatographed on a silica gel tlc plate developed three times with benzene – ethyl acetate (3:1) mixture. This gave 3β-acetoxy-13,17-seco-18(13→12β)*abeo*-5α-lanost-8-ene-7,13,20-trione (**18**) as an oil (31 mg, 57% yield) which had ν_{max}:

1728 sh, 1715, 1663, and 1620 cm^{-1}; λ_{max}: 248 nm (ϵ 8200); δ: 4.53(m, $W_{1/2}$ = 20 Hz, 3α-H), 3.12 (br s, $W_{1/2}$ = 4 Hz, 11β-H), 3.02 (br s, $W_{1/2}$ = 4 Hz, 11α-H), 2.75–2.45 (protons α to carbonyls), 2.07 (s, acetate methyl group), 1.31, 1.12, 1.01, 0.91, and 0.70(methyl groups); m/z: 514(M$^+$), 430, 401, 373, 359, 345, 341, 331, 303, and 164. *Anal.* calcd. for $C_{32}H_{50}O_5$: C 74.67, H 9.79; found: C 74.42, H 9.93.

Sodium borohydride reduction of 3β-acetoxy-5α-lanost-8-ene-7,11-dione

3β-Acetoxy-5α-lanost-8-ene-7,11-dione (12) (1 g) was dissolved in a mixture of tetrahydrofuran (2 mL), methanol (2.65 mL), and ethyl acetate (0.65 mL). To this stirred solution sodium borohydride (0.065 g) was added gradually at 0°C. After being stirred at room temperature for a further 2 h the reaction mixture was poured into water and the precipitate filtered and dried. The solid, consisting of three components, was crystallized thrice form chloroform–methanol to give 503 mg (50% yield) of 3β-acetoxy-7β-hydroxy-5α-lanost-8-en-11-one, which had mp 210–212°C (lit.(16) mp 213–215°C); λ_{max}: 256 nm (ϵ 9600). The ^{1}H nmr and mass spectra of this compound were in agreement with those reported (16). The combined mother liquors were evaporated and chromatographed on a silica gel column eluted with benzene or a benzene – ethyl acetate 50:1 mixture. Three compounds were separated: 3β-acetoxy-11β-hydroxy-5α-lanost-8-ene-7-one (**21**) (33 mg, 3% yield), which had physical and spectral properties identical with compound **21** obtained from 3β-acetoxy-9β,11β-epoxy-5α-lanostan-7-one; 3β-acetoxy-7α-hydroxy-5α-lanost-8-en-11-one (101 mg, 10% yield), which had mp 214–215°C; δ: 4.63–4.23 (m, 3α-H and 7β-H), 2.60 (d, 12 -H$_2$), 2.00 (s, acetate methyl group), 1.21, 1.11, 0.84, and 0.77 (methyl groups); m/z: 500 (M$^+$), 485, 319, and 293. *Anal.* calcd. for $C_{32}H_{52}O_4$: C 76.75, H 10.47; found: C 76.80, H 10.57; and an additional crop of 3β-acetoxy-7β-hydroxy-5α-lanost-8-en-11-one (259 mg, 26% yield).

3β-Acetoxy-11β-hydroxy-5α-lanost-8-en-7-one (21)

3β-Acetoxy-9β,11β-epoxy-5α-lanostan-7-one (702 mg) was dissolved in a methanol (28 mL) and benzene (14 mL) mixture. Saturated potassium carbonate solution in methanol (3 mL) was added and the reaction mixture was left at room temperature for 70 h. Work-up gave crude 3β,11β-dihydroxy-5α-lanost-8-en-7-one (640 mg) which was acetylated in a pyridine (5 mL) and acetic anhydride (2.5 mL) mixture at room temperature for 5 h. The reaction mixture was poured into water and the precipitate was filtered off and dried. Two crystallizations from chloroform–methanol gave 3β-acetoxy-11β-hydroxy-5α-lanost-8-en-7-one (**21**) (366 mg), which had mp 211–214°C (lit.(14, 16) mp 217–218°C); λ_{max}: 256 nm (ϵ 9900). The ^{1}H nmr and ir spectra of this sample were in agreement with those reported (16).

3β-Acetoxy-11α-chloro-5α-lanost-8-en-7-one (22)

To a solution of compound **21** (243 mg) in pyridine (5 mL), thionyl chloride (0.2 mL) was added and the reaction mixture was stirred at room temperature for 20 min. Then it was poured into water and the product extracted with a benzene–ether 1:1 mixture. The organic layer was washed with water and dried with magnesium sulfate. The crude product was crystallized from chloroform–methanol to give 3β-acetoxy-11α-chloro-5α-lanost-8-en-7-one (**22**) (139 mg, 55% yield), which had mp 173–175°C; ν_{max}: 1728 and 1668 cm^{-1}; λ_{max}: 256 nm (ϵ 9200); δ: 4.66 (t, J = 5.5 Hz, 11β-H), 4.49 (t, J = 6 Hz, 3α-H), 2.00 (s, acetate methyl group), 1.18, 0.91, 0.86, 0.77, and 0.59; ^{13}C nmr δ 198.8 (C-7), 170.5 (CH_3COO), 157.9(C-9), 143.4(C-8), 79.5(C-3), and 53.4(C-11); m/z: 482 (M$^+$ − HCl), 467, and 407. *Anal.* calcd. for $C_{32}H_{51}O_3Cl$: C 74.03, H 9.90; found: C 73.94, H 10.04.

Action of p*-toluenesulfonic acid chloride on 3β-acetoxy-11β-hydroxy-5α-lanost-8-en-7-one (21)*

(a) *In pyridine*

To a solution of compound **21** (53 mg) in pyridine (5 mL), *p*-toluenesulfonic acid chloride (320 mg) was added and the mixture refluxed under argon for 3 h. Then it was poured into water, the precipitate filtered off, washed with water, and dried. The resulting mixture of two components was separated on a preparative silica gel plate developed with benzene – ethyl acetate 50:1. Two compounds were isolated: 3β-acetoxy-5α-lanost-8-ene-7,11-dione (35 mg, 67% yield), which had mp 155–158°C (from methanol) and λ_{max} 272 nm (ϵ 9000) (lit. (12*b*) mp 155–157°C, λ_{max}: 272 nm (log ϵ 3.96), and 3β-acetoxy-5α-lanostane-7,11-dione (16 mg, 30% yield), which had mp 223–225°C (from methanol–chloroform) (lit. (17*b*) mp 222–224°C) and all spectral properties of the authentic specimen.

(b) *In benzene*

Refluxing a benzene solution of compound **21** and *p*-toluenesulfonyl chloride (6.5 molar excess) in an argon atmosphere for 2.5 h gave only one product, 3β-acetoxy-5α-lanost-8-ene-7,11-dione.

(c) *In benzene–pyridine (10:1) mixture*

Refluxing of compound **21** and *p*-toluenesulfonyl chloride dissolved in the above mixture of solvents in an argon atmosphere for 8 h gave a mixture of 3β-acetoxy-5α-lanost-8-ene-7,11-dione and 3β-acetoxy-5α-lanostane-7,11-dione in the ratio 1:2.

Bromination–dehydrobromination of 3β-acetoxy-5α-lanost-8-en-7-one

To a solution of 3β-acetoxy-5α-lanost-8-en-7-one (150 mg) in acetic acid (5.6 mL), a solution of bromine (50 mg) in acetic acid (0.75 mL) was added dropwise. When the reaction mixture became colorless a few milliliters of water were added and the resulting precipitate was filtered off and dried. The crude product (189 mg) was dissolved in dimethylacetamide (3.25 mL) and this solution was added dropwise to a boiling solution of calcium carbonate (161 mg) in dimethylacetamide (1.6 mL). Refluxing was continued for 15 min. The reaction mixture was cooled down, water was added, and the product was extracted with ether. The organic layer was washed with water, dried with magnesium sulfate, and evaporated. The crude product was chromatographed on a preparative silica gel plate developed with benzene – ethyl acetate (20:1) mixture to give two compounds. The one with higher R_f was 3β-acetoxy-5α-lanosta-8,11-dien-7-one (**20**) (89 mg, 60% yield), which had mp 134–136°C, (from methanol) λ_{max}: 318 nm (ϵ 7400) (lit.(18) mp 150°C, λ_{max}: 315 nm (log ϵ 3.52); lit.(14) mp 120–123°C). Its ^{1}H nmr spectrum contained all important signals reported in refs. 14 and 18 and its mass spectrum was in agreement with data reported by Dias (14). The product with lower R_f was 3β-acetoxy-lanosta-5,8,11-trien-7-one (**23**) (49 mg, 33% yield), which had mp 192–194°C (from methanol); λ_{max}: 256 nm (ϵ 7800) and 327 nm (ϵ 7000); δ: 6.67(d, J = 10 Hz, 11-H), 6.26(br s, 6-H), 6.06(d, J = 10 Hz, 12-H), 4.56(m, 3α-H), 2.11(s, acetate methyl group), 1.38, 1.28, 1.17, 0.97, 0.90, and 0.82(methyl groups); m/z: 480(M$^+$), 465, 405, and 240 (lit.(19) mp 195–196°C, λ_{max}: 256 and 327 nm (log ϵ 3.9)).

*Treatment of 3β,11α-diacetoxy-5α-lanost-8-en-7-one (**19**) with boron trifluoride – ether complex in acetic anhydride*

Compound **19** (50 mg) was dissolved in acetic anhydride (2.5 mL) and boron trifluoride – ether complex (0.05 mL) was added. The solution was kept for 10 min at room temperature. After work-up the residue was carefully examined by tlc which showed no spot of other substance than that of the substrate. This was confirmed by the ^{1}H nmr spectrum.

*Treatment of 3β-acetoxy-5α-lanosta-8,11-dien-7-one (**20**) with boron trifluoride – ether complex in acetic anhydride*

Dienone **20** (38 mg) dissolved in acetic anhydride (2 mL) was treated with boron trifluoride – ether complex (0.038 mL) at room temperature for 5 min. After work-up, 34 mg of the complicated mixture was isolated. It showed at least seven spots on the tlc plate, most of them having lower R_f than the substrate. Careful tlc examination of the reaction product using various solvent systems showed no presence of compound **5**. The mixture was not further examined.

Acknowledgements

We thank Professor M. A. Battiste, University of Florida, Gainesville, for access to the Varian XL-100-15 spectrometer and Professor W. C. Brey for competent experimental assistance. Financial support of the work from the Polish Academy of Sciences is gratefully acknowledged.

1. (*a*) E. C. LEVY and D. LAVIE. Israel J. Chem. **8**, 677 (1970); (*b*) I. G. GUEST and B. A. MARPLES. J. Chem. Soc. (C), 1468 (1971).
2. (*a*) R. KAZLAUSKAS, J. T. PINHEY, and J. J. H. SIMES. J. Chem. Soc. Perkin Trans. 1, 1243 (1972); (*b*) Z. PARYZEK and R. WYDRA. Bull. Acad. Polon. Sci. Ser. Sci. Chim. **26**, 591 (1979).
3. (*a*) Z. PARZEK. Tetrahedron Lett. 4761 (1976); (*b*) J. Chem. Soc. Perkin Trans. 1, 1222 (1979); (*c*) Z. PARYZEK and R. WYDRA. Steroids, **38**, 141 (1981).
4. G. V. BADDELEY, H. J. SAMAAN, J. J. H. SIMES, and TU HOA AI. J. Chem. Soc. Perkin Trans. 1, 7 (1979).
5. (*a*) Z. PARYZEK. J. Chem. Soc. Perkin Trans. 1, 329 (1978); (*b*) Bull. Acad. Polon. Sci. Ser. Sci. Chim. **26**, 583 (1978); (*c*) Z. PARYZEK and R. WYDRA. Chem. Lett. 1171 (1983).
6. F. W. WEHRLI and T. WIRTHLIN. Interpretation of carbon-13 NMR spectra. Heyden, London. 1976. Chapt. 2.
7. I. H. SADLER. Chem. Commun. 809 (1973).
8. F. W. WEHRLI and T. NISHIDA. *In* Progress in the chemistry of organic natural products. Vol. 36. *Edited by* W. Herz, H. Grisebach, and G. W. Kirby. Springer Verlag, Wien. 1979. p. 104.
9. E. L. SHAPIRO, T. LEGATT, and E. P. OLIVETO. Tetrahedron Lett. 663 (1964); K. CROWSHAW, R. C. NEWSTEAD, and N. A. J. ROGERS. Tetrahedron Lett. 2307 (1964); A. A. GORMAN. Chem. Soc. Rev. **10**, 205 (1981).
10. J. E. FOX, A. I. SCOTT, and D. W. YOUNG. J. Chem. Soc. Perkin Trans. 1, 799 (1972).
11. J. T. PINHEY, B. J. RALPH, J. J. H. SIMES, and M. WOOTTON. Aust. J. Chem. **23**, 2141 (1970).
12. (*a*) J. F. CAVALLA and J. F. MCGHIE. J. Chem. Soc. 834 (1951); (*b*) C. W. SHOPPEE, N. W. HUGHES, and R. E. LACK. J. Chem. Soc. (C), 2359 (1966).
13. M. V. MIJOVIC, W. VOSER, H. HEUSSER, and O. JEGER. Helv. Chim. Acta, **35**, 964 (1952).
14. J. R. DIAS. Org. Mass Spectrom. **11**, 333 (1976).
15. D. H. R. BARTON, A. HAMEED, and J. F. MCGHIE. Tetrahedron Lett. 4343 (1965).
16. J. R. DIAS. J. Org. Chem. **39**, 1767 (1974).
17. (*a*) L. RUZICKA, E. RAY, and A. C. MUHR. Helv. Chim. Acta, **27**, 472 (1944); (*b*) C. DOREE, J. F. MCGHIE, and F. KURZER. J. Chem. Soc. 988 (1948).
18. D. H. R. BARTON and Y. HOUMINER. J. Chem. Soc. Perkin Trans. 1, 919 (1972).
19. P. S. COOPER, C. M. CULSHAW, R. E. GALL, and J. E. NEMORIN. Aust. J. Chem. **32**, 179 (1979).
20. J. M. BIRCHENOUGH and J. F. MCGHIE. J. Chem. Soc. 1249 (1950); J. F. CAVALLA and J. F. MCGHIE. J. Chem. Soc. 744 (1951).
21. L. F. FIESER. J. Am. Chem. Soc. **75**, 5421 (1953).

Enantioselective ester hydrolyses using *Rhizopus nigricans*: stereoselective synthesis and absolute stereochemistry of (−)-*cis*- and (−)-*trans*-1-hydroxy-4-methyl-1,2,3,4-tetrahydronaphthalene

MASAJI KASAI[1] AND HERMAN ZIFFER

Laboratory of Chemical Physics, National Institute of Arthritis, Diabetes, and Digestive and Kidney Diseases, National Institutes of Health, Bethesda, MD 20205, U.S.A.

AND

J. V. SILVERTON

Laboratory of Chemistry, National Heart, Lung, and Blood Institute, National Institutes of Health, Bethesda, MD 20205, U.S.A.

Received August 14, 1984

MASAJI KASAI, HERMAN ZIFFER, and J. V. SILVERTON. Can. J. Chem. **63**, 1287 (1985).

Enantioselective hydrolysis of racemic acetates of *cis*- and *trans*-1-hydroxy-4-methyl-1,2,3,4-tetrahydronaphthalene using *Rhizopus nigricans* yields chiral alcohols. The *absolute stereochemistry* of these compounds, and that of a key intermediate in their stereoselective synthesis, r-1-hydroxy-2,*t*-bromo-4,*c*-methyl-1,2,3,4-tetrahydronaphthalene, were determined by chemical transformations to 1-oxo-4-methyl-1,2,3,4-tetrahydronaphthalene of known absolute stereochemistry. The *relative stereochemistry* of the acetate of the key intermediate was established by X-ray crystallography.

MASAJI KASAI, HERMAN ZIFFER et J. V. SILVERTON. Can. J. Chem. **63**, 1287 (1985).

L'hydrolyse énantiosélective des acétates racémiques des hydroxy-1 méthyl-4 tétrahydro-1,2,3,4 naphtalènes-*cis* et *trans*, effectuée en présence de *Rhizopus nigricans*, conduit à des alcools chiraux. On a déterminé la *stéréochimie absolue* de ces composés ainsi que celle d'un intermédiaire clé dans leur synthèse stéréosélective, le hydroxy-1-r bromo-2,*t* méthyl-4,*c* tétrahydro-1,2,3,4 naphtalène, en leur faisant subir des transformations chimiques conduisant à l'oxo-1 méthyl-4 tétrahydro-1,2,3,4 naphtalène de stéréochimie absolue connue. On a déterminé la *stéréochimie relative* de l'acétate de l'intermédiaire clé en faisant appel à la diffraction des rayons-X.

[Traduit par le journal]

We recently reported (1) on a method for preparing chiral alcohols of a predictable absolute stereochemistry using the mold, *Rhizopus nigricans*, by enantioselective hydrolysis of the corresponding racemic acetates. The absolute stereochemistry of the alcohols formed was accounted for by a suggested rule (1*a*) which states that the enantiomer shown in Fig. 1 is the one more rapidly hydrolyzed. The relative sizes of R_1 and R_2 required to account for our results in these hydrolyses are identical to those employed in Horeau's method (2). For example, an aromatic group (R_1) is always larger than an alkyl group (R_2) and, in cyclic carbinols, a substituted methylene group is larger than an unsubstituted one, etc. This simple concept and the associated empirical observations (1) account for the configurations of some fifty acyclic and cyclic carbinols, several of which required special explanations in order to reconcile their known absolute stereochemistry with data from Horeau's method. Since knowledge of the relative sizes of substituents is critical in predicting the absolute stereochemistry of carbinols formed in these hydrolyses, we needed to establish the influence of distant groups on the relative sizes of substituents on the carbinol carbon. Many data (1*c*) have been collected on 2-substituted 1-acetoxy-1,2,3,4-tetrahydronaphthalenes, and it has been established that a fused benzene ring is effectively larger than a saturated carbon bearing two hydrogens, but smaller than one in which one or both of the hydrogens has been replaced by a chlorine or bromine atom or a methyl or hydroxyl group. In order to examine the influence of distant groups, we have therefore investigated the effects associated with replacing a hydrogen on C-4 by a *cis*- or *trans*-methyl group. Since the presence of the methyl on C-4 could

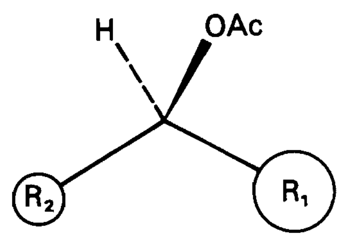

FIG. 1. Enantiomer more rapidly hydrolyzed (where R_1 is effectively larger than R_2).

increase the relative size of the fused aromatic ring in both compounds, the hydrolysis of **2***b* was also examined, where the fused aromatic ring was the smaller substituent and an increase in its size might alter the effective sizes of a fused aromatic ring and a saturated carbon with an additional substituent.

Finally, we also tested the ability of a chiral Pirkle hplc (high performance liquid chromatography) column ((*R*)-*N*-(3,5-dinitrobenzoyl)phenylglycine ionically bonded to γ-aminopropyl-silanized silica) to resolve **4***a* and **5***b*. Earlier studies (3) focused on the relation between the absolute stereochemistry of an enantiomer and the order, relative to its antipode, in which it is eluted from the chiral column. However, many 2-substituted 1-hydroxy-1,2,3,4-tetrahydronaphthalenes were not resolved by this column and, in an attempt to understand the relation between the structure of these cyclic carbinols and the ability of a Pirkle column to separate enantiomers, the chromatographic behavior of **4***a* and **5***b* was examined.

Synthesis

There are literature reports (4) describing the preparation of mixtures of *cis*- and *trans*-1-hydroxy-4-methyl-1,2,3,4-tetrahydronaphthalene (**4***a* and **5***b*). However, we were unable to

[1]On leave from Kyowa Hakko Kogyo Co., Ltd., Tokyo Research Laboratory, 3-6-6 Asahi-machi Machida-shi, Tokyo 194, Japan.

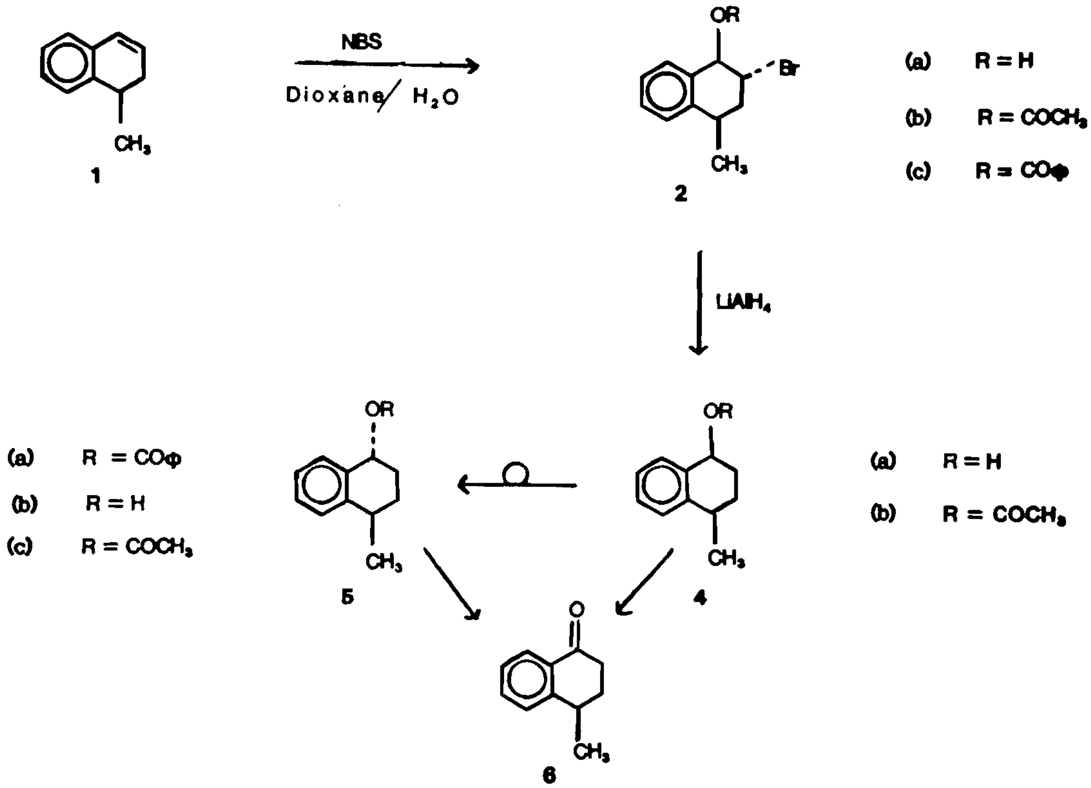

SCHEME 1

locate a description of a stereoselective synthesis of either isomer. Furthermore, an examination of the ^{1}H nmr spectrum of a mixture of isomers prepared by lithium aluminum hydride reduction of 1-oxo-4-methyl-1,2,3,4-tetrahydronaphthalene, **6**, indicated that it would be extremely difficult to assign relative stereochemistry with confidence from data on coupling constants and chemical shifts. A stereoselective synthesis was therefore designed in which the methyl group was used to affect the stabilities of two possible bromonium intermediates **3***a* and **3***b*. Thus the relative concentration of these species and the relative rates of attack by water on C-1 controlled the amount

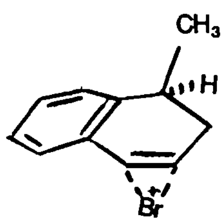

3a

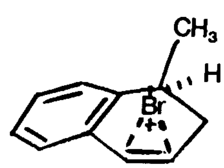

3b

of each bromohydrin formed. Reaction of **1** with *N*-bromosuccinimide in dioxane–water yielded a mixture of bromohydrins in which one isomer predominated (16:1). The major isomer was readily purified by crystallization of the acetyl derivative. Neither its ^{1}H nmr spectrum nor that of the free alcohol could be used to assign relative stereochemistry. However, a series of decoupling experiments on a benzoate derivative suggested the stereochemistry shown in **2***c*. Since **2***b* was to be used for preparation of **4***a* and **5***b*, the relative stereochemistry was verified by an X-ray crystallographic structure determination.

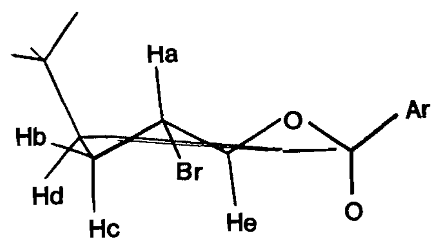

2c

The crystal structure of **2***b* was determined as described in the experimental section. The final bond lengths and angles are given in Fig. 2 and appear unexceptional.

The reactions employed for converting **2***b* to the *cis*-isomer, **4***a*, and the *trans*-isomer, **5***b*, are outlined in Scheme 1. Our expectation that the use of the Misunobu reaction would cleanly invert the configuration at C-1 was based, in part, on results of an earlier study (5) in which we had shown that this reaction on (1*R*)-phenylethanol yielded the *S*-enantiomer with an optical purity of better than 95%.

Preparation of chiral alcohols and a determination of their absolute stereochemistry

Microbial hydrolysis of **4***b* yielded (−)-**4***a* whose specific rotation was surprisingly small (see summary of results in Table 1). In order to estimate the enantiomeric excess (e.e.) and to establish its absolute stereochemistry, (−)-**4***a* was oxidized with Jones' reagent to 4*S*-methyl-1-tetralone, (−)-**6**, of known absolute stereochemistry (6). The sign and magnitude of the specific rotation of the (−)-**6** obtained and its cd (circular dichroism) spectrum was used to assign the absolute stereochemistry of (−)-**4***a* (e.e. 33%) as 1*R*,4*S*. Thus, the presence

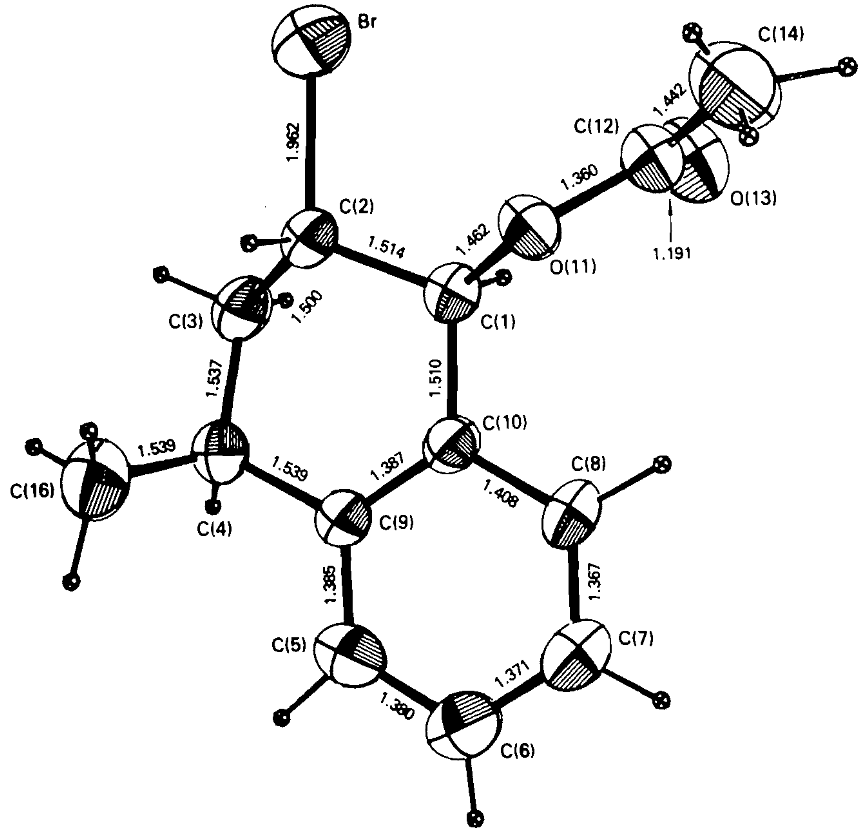

FIG. 2. Crystal conformation of **2***b* showing bond lengths.

TABLE 1. A summary of data on the enantioselective hydrolyses of acetates

Compound	Absolute stereochemistry of alcohol formed (enantiomeric excess)	Percent hydrolysis	Specific rotation: Acetate	Specific rotation: Alcohol
4*b*	1*R*,4*S* (33%)	37%	−18.0° (c 5.1, $CHCl_3$)	−1.9° (c 4.8, $CHCl_3$)
5*c*	1*R*,4*R* (15%)	81%	−14.0° (c 1.6, $CHCl_3$)	−10.9° (c 3.9, $CHCl_3$)
2*b*	1*R*,2*R*,4*R* (53%)	8%	+4.9° (c 5.9, $CHCl_3$)	+12.2° (c 1.3, $CHCl_3$)

of a *cis*-methyl group on C-4 did not alter the absolute stereochemistry at the carbinol carbon; however, the e.e. of the alcohol was smaller (33%) than that obtained for 1-tetralol (71%).

Data on the hydrolysis of the *trans*-isomer, **5***c*, is summarized in Table 1. The absolute stereochemistry of (−)-**5***b* formed in the hydrolysis was established as 1*R*,4*R* by oxidation to the 4*R*-ketone (6). Thus the presence of a *trans*-methyl group again did not alter the stereochemical course of the hydrolysis.

Hydrolysis of **2***b* by *R. nigricans* yielded (+)-**2***a* and its absolute stereochemistry was established by chemical transformation to (+)-**4***a*. A sample of (+)-**2***b* recovered from the microbially mediated hydrolysis (the *antipode* of the alcohol formed) was reduced with lithium aluminum hydride to (−)-**4***a*. Since the specific rotation of the alcohol obtained was small, the stereochemical assignment was confirmed by acetylation to yield a sample of (+)-**4***b* with a larger specific rotation. These transformations established the absolute stereochemistry at the carbinol carbon as *S*, i.e. the presence of the 4-methyl group *did not alter* the relative sizes of the fused aromatic ring and C-2. The e.e. of the alcohol was essentially identical (53 vs. 56) with that reported for the des-methyl compound. While it may be tempting to try to relate the observed e.e. with steric and electronic factors, it is important to remember that these are kinetic resolutions and the e.e. depends upon the quantity of substrate hydrolysed. Furthermore, the culture of *R. nigricans* contains a variety of other enzymes that oxidize varying amounts of substrate and product. Thus, although a considerable effort was made to standardize the cultures employed, there were significant variations in the rates of hydrolysis of different substrates.

The major advantages of using *R. nigricans* to assign the absolute stereochemistry of a secondary alcohol are: (*1*) The enzyme system responsible for the hydrolyses does not appear to be sensitive to the presence of groups some distance from the carbinol carbon, i.e. the stereochemistry of the alcohol formed is primarily dependent on the relative size of substituents on the carbinol carbon. (*2*) This method provides chiral material that can be used to verify assigned configurations. This latter point is important, since absolute stereochemistries assigned by this method, that of Horeau, and other proposed methods (3) are not completely certain. However, since each general method depends on a different property or reaction of the alcohol, one can be more confident of assignments based on data from several methods.

Experimental

General procedure

Melting points were determined by using a hot-stage apparatus; they are uncorrected. Proton magnetic resonance spectra were recorded on a Varian HR-220 MHz instrument; chemical shifts are reported in parts per million (δ) downfield from tetramethylsilane as an internal standard, with coupling constants (J) in hertz. Optical rotations were recorded on a Perkin–Elmer 241MC polarimeter, mass spectra on an LKB instrument. Microbial hydrolyses were carried out as described earlier (ref. 1), using *Rhizopus nigricans* (ATCC 6227b).

Synthesis

*1-Methyl-1,2-dihydronaphthalene (**1**)*

A solution of 4-methyl-1-tetralone (5.0 g) in anhydrous ether (5 mL) was added dropwise to a slurry of $LiAlH_4$ (0.408 g) in anhydrous ether (50 mL) with stirring at room temperature. When the addition was complete, the solution was refluxed for 1 h and worked up in the usual manner. The crude mixture of alcohols was dissolved in benzene (100 mL), *p*-toluene sulfonic acid (50 mg) was added, and the solution was refluxed for 4 h. The reaction mixture was cooled, washed with aqueous sodium bicarbonate, then with water, and dried. The solvent was removed *in vacuo* and the residue distilled under reduced pressure to give **1** as a colorless liquid (3.44 g), bp 59–61°C/1.4 Torr (1 Torr = 133.3 Pa), in 77% yield (lit. (7) bp 70–85°C/0.07 Torr).

*2-Bromo-4-methyl-1,2,3,4-tetrahydronaphth-1-yl acetate (**2**b)*

N-Bromosuccinimide (7.95 g) was added to a solution of **1** (6.3 g) in 51 mL of dioxane–water (44:7.3) and the solution was stirred overnight at room temperature. It was poured into water (330 mL) and the mixture was extracted with methylene chloride (3 × 100 mL). The combined organic layers were washed with water, brine, and dried. The solvent was removed under reduced pressure and the reaction products were acetylated with acetic anhydride (8.3 mL) and pyridine (35 mL) at room temperature. An estimate of the stereoselectivity of the reaction (~16:1) of the *cis* and *trans*-4-methyl bromohydrins was made from an nmr spectrum of the crude acetylation mixture, which was worked up in the usual manner and chromatographed on silica gel to give crude **2***b*, which was crystallized from hexane to yield pure **2***b* (8.64 g) in 70% yield, mp 85–86°C; ^1H nmr ($CDCl_3$) δ: 1.36 (d, 3H), 2.08 (s, 3H), 2.23 (m, 2H), 3.16 (q, 1H), 4.50 (m, 1H), 6.11 (d, 1H), 7.15–7.27 (m, 4H). *Anal.* calcd. for $C_{13}H_{15}O_2Br$: C 55.14, H 5.34; found: C 55.29, H 5.51.

A sample of **2***a* was treated with benzoyl chloride and pyridine in the usual manner to yield **2***c*; ^1H nmr ($CDCl_3$) showed peaks at δ (ppm): 1.42 (d, 3H), 2.26–2.47 (m, 2H), 3.22 (m, 1H), 4.66 (m, 1H), 6.38 (d, 1H), 7.23–8.28 (m, 9H).

The coupling constants H_A-H_E (**2***c*) were determined by decoupling experiments on the 300 MHz Bruker spectrometer.

J_{AB} = 3.2 Hz	J_{BD} = 6.0 Hz
J_{AC} = 6.9 Hz	J_{BC} = 14.5 Hz
J_{AE} = 5.0 Hz	J_{CD} = 7.9 Hz

*cis-1-Hydroxy-4-methyl-1,2,3,4-tetrahydronaphthalene (**4**a)*

A solution of **2***b* (2.83 g) in THF (10 mL) was added dropwise over 10 min to a stirred slurry of $LiAlH_4$ (0.570 g) in anhydrous THF (10 mL). The reaction mixture was then refluxed for 4 h and worked up in the standard manner. The product was chromatographed on silica gel (hexane/ethyl acetate 9:1) to afford **4***a* (1.35 g, 83% yield) as a colorless solid, mp 66–68°C; ^1H nmr ($CDCl_3$) showed peaks at δ (ppm): 1.31 (d, 3H), 1.66–1.95 (m, 4H), 2.22 (s, 1H), 2.81 (q, 1H), 4.67 (bs, 1H), 7.19–7.39 (m, 4H).

*cis-4-Methyl-1,2,3,4-tetrahydronaphth-1-yl acetate (**4**b)*

A sample of **4***a* was acetylated with acetic anhydride/pyridine in the usual manner to yield **4***b* as a colorless oil; ^1H nmr ($CDCl_3$) showed peaks at δ (ppm): 1.33 (d, 3H), 1.60–1.99 (m, 4H), 2.04 (s, 3H), 2.80 (q, 1H), 5.94 (t, 1H), 7.12–7.28 (m, 4H).

*trans-1-Hydroxy-4-methyl-1,2,3,4-tetrahydronaphthalene (**5**b)*

A mixture of diisopropyl azodicarboxylate (1.62 g) and triphenylphosphine (2.10 g) in freshly distilled THF (20 mL) was stirred at 0°C for 30 min. To this solution was added a solution of **4***a* (0.648 g) and benzoic acid (0.976 g) in THF (7.5 mL) dropwise over 5 min. The reaction mixture was stirred at 0°C for 1 h and left in the refrigerator overnight. The solvent was removed *in vacuo* and the residue chromatographed on silica gel to give **5***a* (1.02 g) as a colorless oil in 96% yield; ^1H nmr ($CDCl_3$) showed peaks at δ (ppm): 1.27 (d, 3H), 1.57 (m, 2H), 1.98 (m, 1H), 2.23 (m, 1H), 2.99 (m, 1H), 6.06 (d, 1H), 6.95–7.41 (m, 3H), 7.89 (d, 1H). The benzoate was hydrolyzed by refluxing for 1 h in methanol–water (25 mL) containing sodium hydroxide (1.3 g). The reaction mixture was diluted with water (100 mL) and extracted with ethyl acetate (3 × 100 mL). The combined extracts were washed with brine, and dried and concentrated *in vacuo*. The residue was chromatographed on silica gel to give **5***b* as a colorless solid (0.611 g) in 98% yield, mp 35–37°C; ^1H nmr ($CDCl_3$) showed peaks at δ (ppm): 1.22 (d, 3H), 1.45 (m, 1H), 1.73 (m, 1H), 2.08 (m, 2H), 2.36 (s, 1H), 2.91 (q, 1H), 4.66 (bs, 1H), 7.15–7.38 (m, 4H).

Microbial hydrolyses

The potato-dextrose medium for growing *R. nigricans* was prepared as previously described (1). A 1-L Erlenmeyer flask containing 250 mL of this medium was inoculated with *Rhizopus nigricans* (ATTC 6227b) grown in liquid culture, and shaken for 6–7 days at 25°C. The substrate (~450 mg) in 1 mL of THF was added and the flask was shaken for 26 h. The mycelium and medium were extracted with ethyl acetate (3 × 100 mL) and the combined extracts were dried and concentrated. An nmr spectrum of the crude product was used to determine percent hydrolysis. The recovered acetate and the alcohol formed were separated by column chromatography on silica gel with *n*-hexane and ethyl acetate as eluants. Results for the hydrolysis of **2***b*, **4***b*, and **5***c* are given in Table 1.

*Absolute stereochemistry of (−)-**4**a*

Jones' reagent was added dropwise with stirring to a solution of (−)-**4***a* (22.7 mg, $[\alpha]_D^{25}$ −1.9° (c 4.75, $CHCl_3$)) in acetone (4 mL) at 0°C. After 30 min the reaction mixture was diluted with water (50 mL) and the solution was extracted with ethyl acetate (3 × 30 mL). The ethyl acetate extract was washed with aqueous sodium bicarbonate and brine. The solvent was removed *in vacuo* and the residue was purified by column chromatography on silica gel to yield (−)-4-methyl-1-tetralone, (−)-**6** (22.4 mg, $[\alpha]_D^{25}$ −6.4° (c 1.5, $CHCl_3$)). The optical purity of (−)-4-methyl-1-tetralone was determined as 33% by averaging a comparison of the measured values with those reported in the literature (6): 376 nm (−72.2, reported −214.5), 367 nm (+51.0, reported 161.7), 359 nm (−118.8, reported −363), 351 nm (+137.2, reported 429), 344 nm (−88.4, reported −277), 337 nm (+189.4, reported 594), 330 nm (−20.3, reported −52.8), 323 nm (+196.9, reported 528), 312 nm (+133.6, reported +429).

*Conversion of (−)-**4**a to (+)-**4**b*

A sample of (−)-**4***a* (24.3 mg, $[\alpha]_D^{25}$ −1.9° (c 4.75, $CHCl_3$)) was acetylated in the usual manner to yield (+)-**4***b* (27.3 mg, 89% yield); $[\alpha]_D^{25}$ +37.6° (c 1.8, $CHCl_3$). The ^1H nmr spectrum of (+)-**4***b* was identical with that of racemic material described above.

*Absolute stereochemistry of (−)-**5**b*

A sample of (−)-**5***b* (38.8 mg, $[\alpha]_D^{25}$ −10.9° (c 3.9, $CHCl_3$)) was oxidized as described for (−)-**4***a* to give an oil, (+)-4-methyl-1-tetralone (37.1 mg, $[\alpha]_D^{25}$ +2.9° (c 3.1, $CHCl_3$)), e.e. 15%.

*Absolute stereochemistry of (+)-**2**a*

A sample of (−)-**2***a* (19.0 mg, $[\alpha]_D^{25}$ + 12.2° (c 1.3, $CHCl_3$)) was acetylated in the usual manner to yield (−)-**2***b* (20.0 mg, $[\alpha]_D^{25}$ −90.0°

(c 1.3, $CHCl_3$)), e.e. 53%.

The absolute stereochemistry of (−)-**2***a* was established by reduction of a sample of (+)-**2***b* (85.1 mg, $[\alpha]_D^{25}$ +10.2° (c 5.14, $CHCl_3$)) with excess $LiAlH_4$ in THF to yield (−)-**4***a* (27.5 mg, $[\alpha]_D^{25}$ −0.16° (c 1.83, $CHCl_3$). The observed rotation was very small so the compound was acetylated in the usual manner to yield (+)-**4***b*, 32.0 mg $[\alpha]_D^{25}$ +6.90° (c 2.13, $CHCl_3$). The absolute stereochemistry of this material is therefore 1*R*,4*S* and that of (+)-**2***a* formed in the hydrolysis 1*R*,2*R*,4*R*.

High performance liquid chromatography studies with Pirkle column

The hplc measurements were made using a column purchased from the Regis Chemical Co., Martin Grove, IL 60053. The column consists of (*R*)-*N*-(3,5-dinitrobenzoyl)phenylglycine ionically bonded to a γ-aminopropyl-silanized silica column. The solvent system was 0.5% isopropanol in hexane. No separation was observed for **4***a* or **5***b* under these conditions.

X-ray crystal structure determination of **2b**

Crystal data for compound **2***b* are:
Molecular formula: $C_{13}H_{15}O_2Br$ Mol. wt. 283.16
Habit: elongated plates; radiation: Cu Kα (graphite monochromator); wavelength: 1.5418 Å; space group: $P2_12_12_1$ (No. 19); cell dimensions (from LS reft. of ±θ data), a = 8.810(1) Å, b = 9.661(1) Å, c = 14.852(1) Å, V = 1264.10 Å^3, Z = 4, D_x = 1.488 g cm^{-3}. Crystal size: ca. 0.3 × 0.1 × 0.05 mm; reflections: 1468 (193 < 1σ); maximum sin θ/λ: 0.6229 Å^{-1}. Diffractometer: Nonius CAD-4; function minimized: $\Sigma w\Delta^2$; anisotropic temperature factor: exp $(-2\pi^2(\Sigma_i\Sigma_j U_{ij}a_i^* a_j^* h_ih_j))$. Final R-factor (observed reflections only): 4.9%.

The crystals were very thin elongated plates but by careful selection it was possible to obtain adequate samples for crystallographic work. Interestingly, the crystal habit was not centrosymmetric and the plates had a triangular cross section when viewed perpendicular to the smallest face. It is possible that spontaneous resolution has taken place in view of the chiral space group but hand sorting would not be practical in view of the small size of the crystals. The compound is sensitive to X-radiation and a preliminary experiment indicated a fall-off of 33% in the intensities of standard reflections after only 10 h of exposure. Five crystals were used to collect the X-ray intensity data; each crystal was replaced when the periodically measured standard intensities had fallen to 90% of their initial values. The dimensions of all crystals used were as indicated in the crystal data section except for the last one which was somewhat thicker. Two scale factors were used for each group of data except for the last group whose standards had only dropped 5% at the end of the data collection. Since several crystals were used to collect the X-ray data, no attempt was made to determine absolute configuration nor was anomalous dispersion taken into account in the refinement.

The structure was solved using a Patterson map to find the Br atom and then by use of the programs of MULTAN 78 (8). The structure was refined using XRAY 72 (9). After anisotropic refinement of the heavier atoms, a difference map gave evidence for all H atoms. The positional parameters of the H atoms were refined but not the temperature factors, which were estimated from the isotropic thermal parameters of the heavier atoms.

The diagram showing the X-ray results was drawn by ORTEP (10).

1. (*a*) K. KAWAI, M. IMUTA, and H. ZIFFER. Tetrahedron Lett. 2527 (1981); (*b*) H. ZIFFER, K. KAWAI, M. KASAI, M. IMUTA, and C. FROUSSIOS. J. Org. Chem. **48**, 3017 (1983); (*c*) M. KASAI, K. KAWAI, M. IMUTA, and H. ZIFFER. J. Org. Chem. **49**, 675 (1984).
2. A. HOREAU. Stereochemistry: fundamentals and methods. Vol. 2. George Thieme, Stuttgart. 1977. pp. 52−94.
3. (*a*) W. H. PIRKLE, and J. M. FINN. J. Org. Chem. **46**, 2935 (1981); (*b*) M. KASAI, C. FROUSSIOS, and H. ZIFFER. J. Org. Chem. **48**, 459 (1983).
4. (*a*) G. NEURATH, and W. LUETTICH. J. Chromatogr. **34**, 253 (1968); (*b*) P. PERRUS, J. P. MORIZUR, J. KOSSANJI, and A. M. DUFFIELD. Bull. Soc. Chim. Fr. 2105 (1973).
5. K. KABUTO, M. IMUTA, E. S. KEMPNER, and H. ZIFFER. J. Org. Chem. **43**, 2357 (1978).
6. J. BARRY, H. B. KAGAN, and G. SNATZKE. Tetrahedron, **27**, 4737 (1971).
7. H. HEIMGARTNER, L. ULRICH, H. J. HANSEN, and H. SCHMID. Helv. Chim. Acta, **54**, 2313 (1971).
8. P. MAIN, S. E. BULL, L. LESSINGER, G. GERMAIN, J.-P. DECLERCQ, and M. M. WOOLFSON. MULTAN 78, a system of computer programs for the solution of crystal structures from X-ray diffraction data. Universities of York and Louvain. 1978.
9. J. M. STEWART, G. J. KRUGER, H. L. AMMON. C. DICKINSON, and S. R. HALL. XRAY 72, Tech. Report TR-192, Computer Center, The University of Maryland, College Park, MD. 1972.
10. C. K. JOHNSON. ORTEP, Oak Ridge National Laboratory Report ORNL-3794. 1965.

Inter-ring dihedral angles in polychlorinated biphenyls from photoelectron spectroscopy

J. J. DYNES, F. L. BAUDAIS,[1] AND R. K. BOYD
Guelph–Waterloo Centre for Graduate Work in Chemistry, University of Guelph, Guelph, Ont., Canada N1G 2W1

Received August 30, 1984

J. J. DYNES, F. L. BAUDAIS, and R. K. BOYD. Can. J. Chem. **63**, 1292 (1985).

A proposal that the physiological activity of a chlorinated biphenyl is related to its degree of molecular planarity is explored through experimental measurements of inter-ring dihedral angles in the gas phase. A known correlation between the difference between fourth and first ionization energies of substituted biphenyls (via photoelectron spectroscopy), and the thermally averaged inter-ring dihedral angle as established by electron diffraction techniques, is confirmed and exploited for the present purpose. The expectation, based on both qualitative and quantitative theoretical considerations, that increased *ortho* substitution causes an increase in inter-ring angle, is confirmed. However, the observation that, for 2,2′-substituted halobiphenyls the only observed conformation is the near-*syn* form, is not easy to explain, and is discussed in terms of a non-bonding attractive force between halogen atoms.

J. J. DYNES, F. L. BAUDAIS et R. K. BOYD. Can. J. Chem. **63**, 1292 (1985).

Faisant appel aux mesures expérimentales effectuées en phase gazeuse des angles dièdres entre les cycles, on a étudié l'hypothèse suggérant que l'activité physiologique des biphényles chlorés est reliée à son degré de planéarité moléculaire. Dans cette étude, on a confirmé et exploité la corrélation connue qui existe entre les quatrième et première énergies d'ionisation des biphényles susbtitués telles que mesurées (via la spectroscopie photoélectronique) et l'angle dièdre inter-cycle pondéré thermiquement tel qu'établi par les techniques de diffraction électronique. En se basant sur des considérations théoriques tant qualitatives que quantitatives, on peut prévoir qu'une augmentation de la substitution en position *ortho* provoquera une augmentation de l'angle inter-cycle; nos résultats confirment cette hypothèse. Cependant, on ne peut pas expliquer facilement le fait que, dans le cas des biphényles halogénés substituées en positions 2,2′, la forme quasi-*syn* est la seule conformation observée. On en discute en fonction d'une force attractive non liée entre les atomes d'halogènes.

[Traduit par le journal]

Introduction

Maier and Turner (1) showed how the dihedral angle between the two rings of a series of gaseous biphenyls is related to the difference in ionization energies for electrons in the π_3 and π_6 molecular orbitals. This difference between fourth and first ionization energies was shown (1) empirically to vary linearly with cos θ, where θ is the inter-ring dihedral angle determined by electron diffraction. The qualitative trends observed were satisfactorily accounted for (1) by simple analogies drawn with the molecular orbitals (MO's) of substituted benzenes, as determined (2) by photoelectron spectroscopy (PES). The linear correlation between $\Delta E(\pi_3 - \pi_6)$ and cos θ was satisfactorily accounted for (1) by an ingenious analysis of the π-MO's described by a Huckel approach using as basis set the semi-localized π-MO's of the phenyl moieties, in place of the more usual atomic orbitals. Together with a frozen-orbital (Koopmans' theorem) assumption to permit identification of an orbital energy with the negative of the corresponding experimental ionization energy (I.E.), this approach was shown by Maier and Turner (1) to lead to the following prediction:

$$[1] \quad \Delta E(\pi_3 - \pi_6) = B \cos \theta$$

where B is related to the standard Huckel resonance integral. Not surprisingly, this Huckel formalism predicts the correct qualitative relationship, but fails to predict quantitatively the values of the parameters, e.g. the experimental intercept at $\theta = 90°$ is non-zero (1).

Apart from these and other considerations of the more fundamental aspects of the PES results, the empirically determined linear relationship between $\Delta E(\pi_3 - \pi_6)$ and cos θ was used (1) to determine the inter-ring dihedral angles θ for several substituted biphenyls which had not been subjected to electron diffraction analysis.

Recently a theoretical investigation of the conformations of some polychlorinated biphenyls (PCB's) was published (3). Rotation potentials (potential energy as a function of θ) were determined for biphenyl itself and for three dichloro isomers as well as one tetrachloro and one hexachloro isomer (3). The experimentally determined inter-ring angles θ presumably correspond to the minima in these potential profiles (3). The motivation behind this theoretical study (3) lies in the strong isomer dependence of physiological activity of different PCB congeners. For example, it was shown (4) that the induction by PCB's of aryl hydrocarbon hydroxylase (AHH) and ethoxyresorufin (OR) O-deethylase activity in rat hepatoma H-4-II-E cells was strongly dependent on substitution pattern in the PCB's. Chlorine substitution at both *para* and at least two *meta* positions was shown (4) to result in maximum activity, whereas *ortho* chlorines resulted in appreciably decreased activities. *Ortho*-substituted PCB's are more soluble in water, and thus have lower octanol–water partition coefficients (5) than do their non-*ortho*-substituted isomers. This and similar evidence has led to the suggestion (6) that the degree of planarity of the PCB molecule is a major determinant of its lipid solubility and thus its physiological activity. *Ortho*-substituted PCB's are expected to exhibit the largest values of θ, thus accounting for the lower activities.

The motivation for the present work was similar to that for the theoretical study cited (3), viz. to investigate the relationship between molecular planarity and physiological activity. The dihedral angles for a series of PCB congeners have been determined from PES, using the correlation described previously (1). In this work we concentrated upon the more volatile lower congeners (mono, di, and trichlorobiphenyls), although examples of compounds of more immediate toxicological interest are also included. In addition, some other

[1] Present address: Bomem Inc., 625 Rue Marier, Vanier, Ont., Canada G1M 2Y2.

biphenyls were investigated, both to test our experimental technique against the original work (1) and to investigate the effect of methyl groups as replacement substituents for chlorine atoms.

Experimental

The electron energy spectrometer is of the differential retarding field type first described by Lindau *et al.* (7), and more recently by Hotop and Hubler (8). In its present configuration, resolution has been sacrificed for sensitivity since many of the compounds to be studied are of low volatility.

The light source (He I line) is a sealed helium discharge lamp, based on the design of Kinsinger *et al.* (9). The aluminum filter window was constructed from metal film purchased from Luxel Corporation, Santa Barbara, CA. The discharge was maintained by a Raytheon Model PGM 10 × 1 microwave generator. Titanium getter wires (Vacuum Instrument Co., New York) were used in a manner similar to that described previously (9).

The electron multiplier used was a SEM Model 4219 spiraltron (Galileo Inc., Sturbridge, MA). Signal detection and amplification was achieved via a pulse amplifier/discriminator and counter, based on the design of Borders *et al.* (10). A Rockwell AIM 65 microprocessor (Rockwell International, Aneheim, CA) with Dram Plus Expansion Board (Computerist Inc., Chelmsford, MA), was programmed to control spectrometer scan functions and to acquire and store data on conventional magnetic tape cassetes. Multiple-scan accumulation permitted a considerable increase in attainable signal/noise ratios.

The high vacuum was maintained by an Edwards EO 6 diffusion pump (1350 L/s for air). Ultimate vacuum better than 2×10^{-7} Torr (1 Torr = 133.3 Pa) could be achieved.

Most of the polychlorinated biphenyl samples were obtained from Ultra Scientific Inc. (Hope, RI). The samples of the 2,2′,5,5′ and 2,2′,4,4′,5,5′ congeners were gifts from Dr. S. Safe, Texas A and M University. All other samples used were purchased from Aldrich or Chemicals Procurement Labs, Inc. and were used as received. The helium used in the discharge lamp was Matheson 99.9999% purity.

Results

A photoelectron spectrum of nitrogen was always taken just prior to each biphenyl compound, in order to check on instrument performance, energy-scale calibration, etc. The inherent instrumental energy resolution is of the order of 0.1 eV. This is less than that ultimately obtainable on an instrument of this type (7, 8) by a factor of about 5, but is adequate for the present purpose.

The spectra of the compounds studied in the present work are shown in Figs. 1–3. The signal-to-noise ratio is somewhat variable due partly to differences in sample volatility, and also to deterioration of the aluminum foil window on the helium discharge source. In those cases where comparisons are pertinent, the present results are in good agreement with those of Maier and Turner (1).

Table 1 summarizes the data obtained for:

$$[2] \quad \Delta E \equiv (\mathrm{IE}_4 - \mathrm{IE}_1) = E(\pi_6) - E(\pi_3)$$

for those compounds for which gas-phase electron-diffraction data on inter-ring angles θ are available. This list contains one compound (4,4′-difluorobiphenyl) which was not included in the corresponding table of Maier and Turner (1), even though this compound was indeed studied in the original work (1). In fact, the value of ΔE for this compound is extremely close to that for 2-fluorobiphenyl and to that for biphenyl itself, so that its omission from the calibration table makes little difference to the final correlation. In addition, 2,2′-dichlorobiphenyl was studied here, but not previously (1). Figure 4 shows the data of Table 1 plotted as ΔE vs. cos θ, as proposed previously (1). Least-squares linear regression analysis of the combined data of Table 1 yields:

$$[3] \quad \Delta E = 1.60 \cos \theta + 0.31$$

The status of the electron-diffraction measurements in the gas phase has been reviewed (16). A general review of principles and applications of conformational analysis by PES has been published (17).

Table 2 lists the experimental data for those compounds, studied in the present work, for which no electron-diffraction data are available. The values of inter-ring angle θ quoted for these compounds are those calculated from the experimental value for ΔE together with eq. [3]. The main uncertainty in the measurement of θ, in most cases, arose from difficulties in identifying ΔE from the spectra. The uncertainties in the present values of θ (Tables 1 and 2) are standard deviations calculated for four independent estimates of ΔE for each spectrum, made by two different observers. In Table 3 are listed more complete data for all ionization energies which could be determined reasonably unambiguously from the spectra.

In the spectra of a few of the compounds which were of low volatility, a rather sharp peak appears at an ionization energy of around 13.8 eV. No such feature is apparent in any other of the spectra, and it is believed that this corresponds to an impurity resulting from thermal decomposition of the sample at the high temperatures used.

Discussion

The general trends observed in the photoelectron spectra appear to agree well with those observed in the original work of Maier and Turner (1), and thus require little additional comment here. Some of the inter-ring angles listed in Table 2 are of the order of 80°, which corresponds to the angle at which the energies of the π_4 and π_6 MO's (and also of the π_3 and π_5 MO's) cross over (1). Thus, these estimates are subject to uncertainties of interpretation, quite apart from those arising from difficulties in estimating ΔE. A similar comment applies to a recent PES measurement of the conformation of 2,2′-diethynylbiphenyl (18), which indicated an inter-ring dihedral angle in the range 80–90°.

The present discussion will concentrate upon the values found for the inter-ring angles. In general, these follow the expected pattern, with increased *ortho* substitution causing an increase in θ. Of course, such angles represent some appropriate thermal average over the inter-ring twisting motion, as has been emphasized (16) in the review of the electron diffraction work upon which the present measurements are ultimately based. The existence of a potential well which is broad with respect to twist angle θ, deduced from the electron diffraction data for biphenyls (16), is confirmed by theoretical calculations (3, 14, 19, 20). However, none of these calculations which considered halobiphenyls (3, 14) was able to account for the observation (16) that the prevailing conformer in all the 2,2′-dihalobiphenyls is that with the two halogen atoms on the same side, i.e. close to the *syn* rather than the *anti* conformation. In terms of the definition of inter-ring angle used in the most recent theoretical work (3), (θ = 0 for 2,2′-dichlorobiphenyl defined as the planar molecule with the chlorine atoms in the *transoid* configuration), experiment (13, 15) finds that the preferred value of θ lies between $\pi/2$ and π rather than

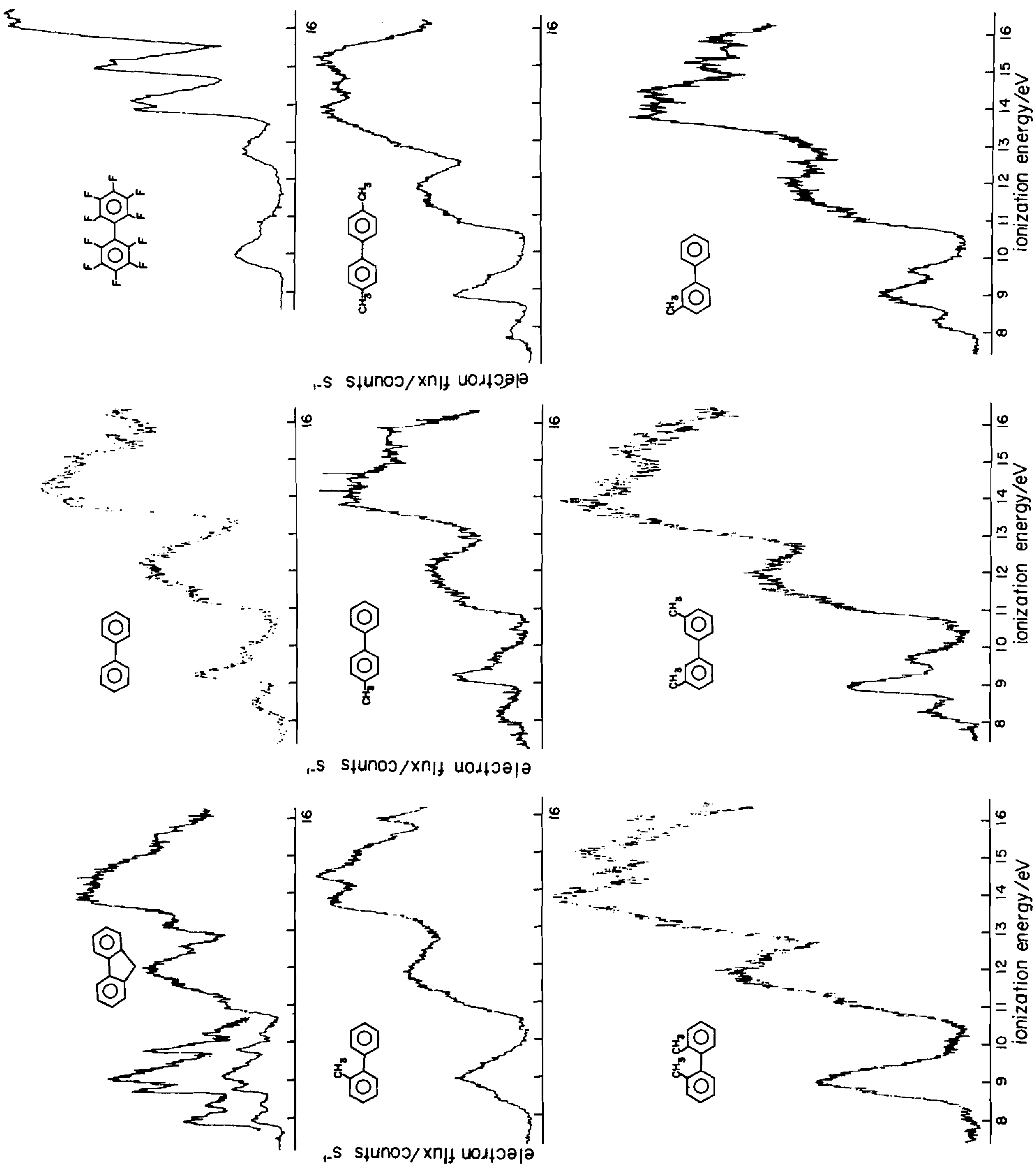

FIG. 1. Photoelectron spectra (He I line, 21.22 eV) of substituted biphenyls.

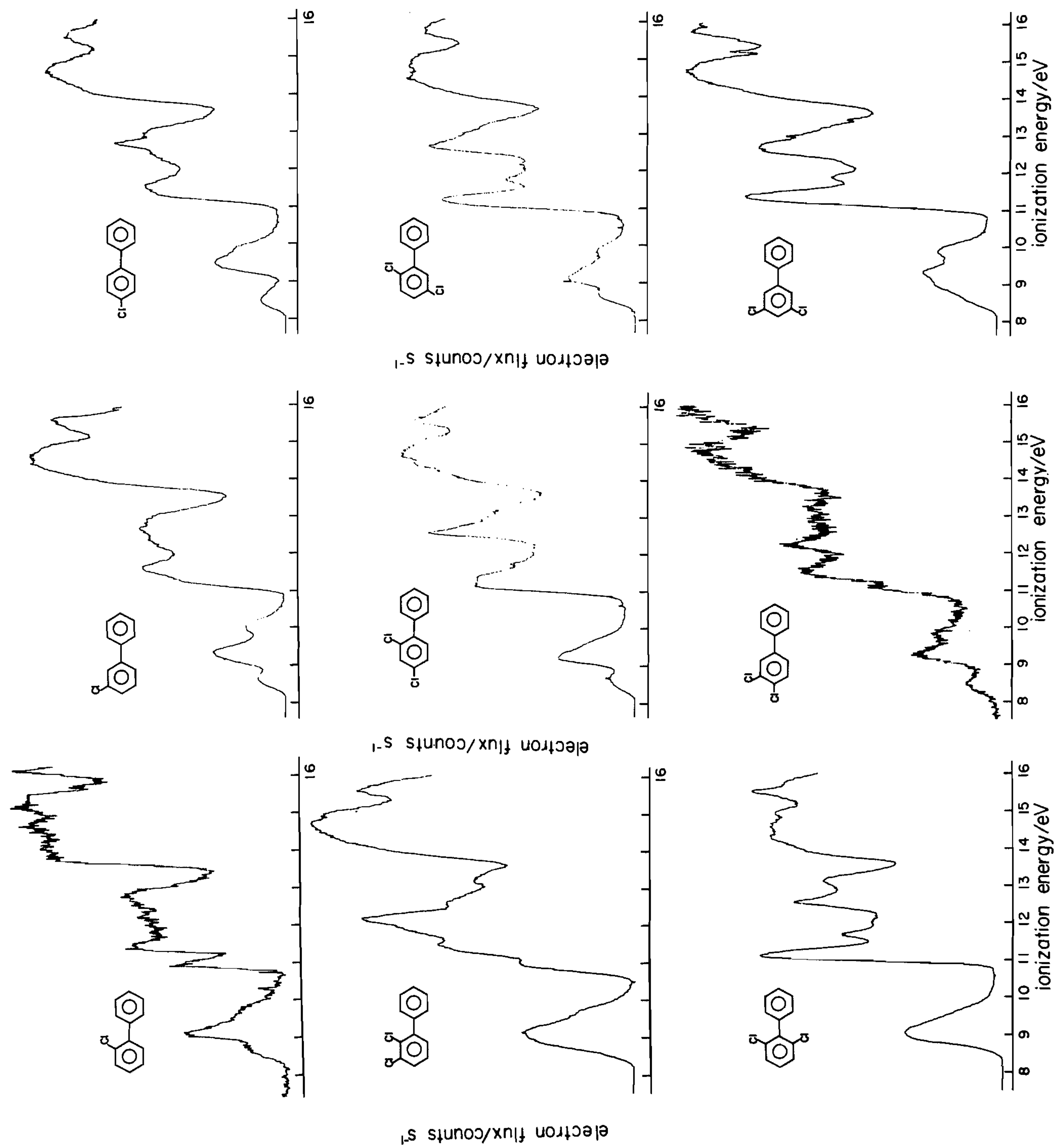

FIG. 2. Photoelectron spectra (He I line, 21.22 eV) of chloro-substituted biphenyls.

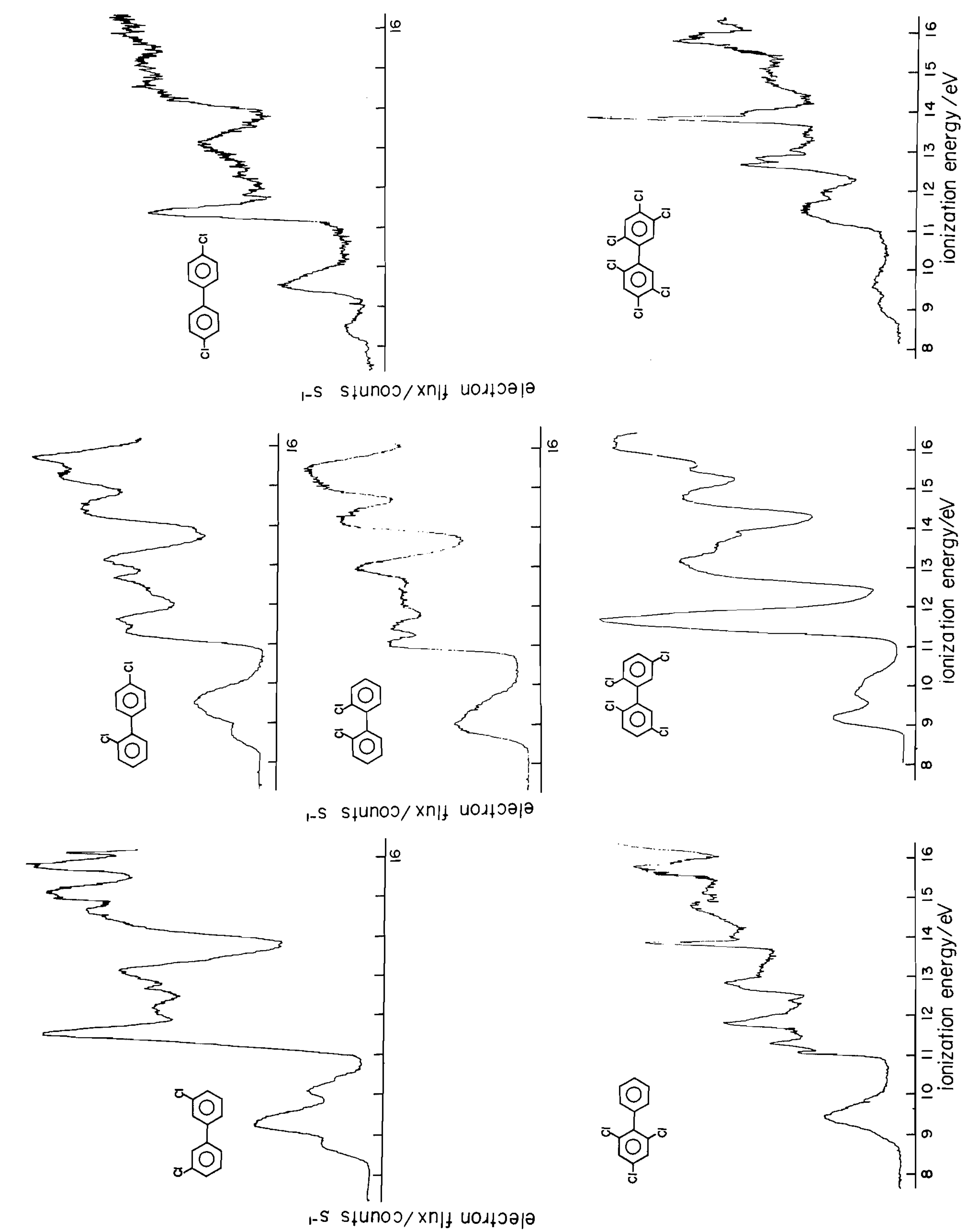

FIG. 3. Photoelectron spectra (He I line, 21.22 eV) of chloro-substituted biphenyls.

TABLE 1. Experimental data on ΔE for biphenyl compounds for which the inter-ring angle θ is known from electron diffraction

Compound	ΔE (eV), present work	ΔE (eV), ref. 1	θ (deg)	Reference
Fluorene	1.92 ± 0.03	1.98 ± 0.02	0	
Biphenyl	1.43 ± 0.05	1.46 ± 0.02	42 ± 2	11
4,4′-Difluorobiphenyl		1.42 ± 0.02	44 ± 5	12
2-Fluorobiphenyl		1.40 ± 0.02	49 ± 5	12
2,2′-Difluorobiphenyl		1.15 ± 0.02	60 ± 5	13
Perfluorobiphenyl	0.94 ± 0.07[a]	0.90 ± 0.02	70 ± 2	14
2,2′-Dichlorobiphenyl	0.7 ± 0.1		74 ± 2	13, 15
2,2′-Dibromobiphenyl		0.7 ± 0.1	75 ± 10	13

[a] One band poorly resolved.

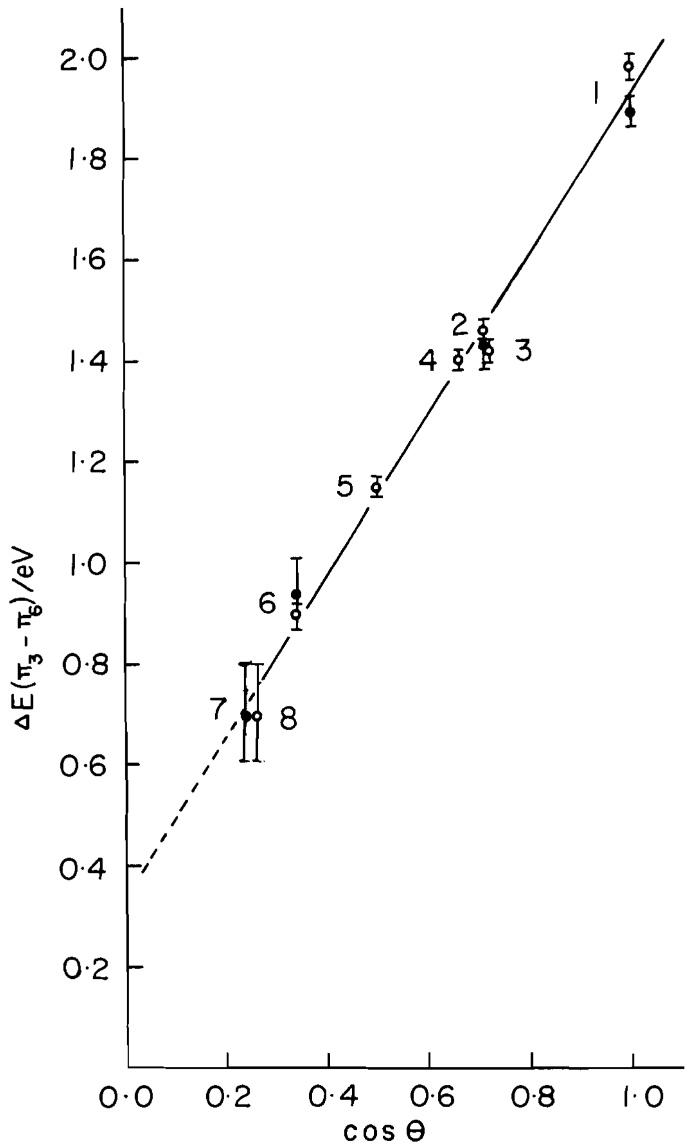

FIG. 4. Plot of ΔE (I.E.$_4$ − I.E.$_1$) vs. cos θ (from electron diffraction); data of Table 1. Full symbols, ref. 1; open symbols, present work.

between 0 and $\pi/2$. On the other hand, theory predicts the opposite to be the case; e.g. in the more recent work (3), the potential minimum occurs at approximately 75° from the zero defined as above, i.e. the near-*anti* configuration. It was a similar discrepancy between early experimental (13) and theoretical (14) results which led to a careful re-examination of the electron diffraction experiment on 2,2′-dichlorobiphenyl (15). This study (15), which essentially confirmed the earlier experimental work on this compound (13), used a rather high temperature of 300°C in a (fruitless) search for the other conformer. As was clearly shown (15) by X-ray diffraction, this compound in the crystalline state also exists exclusively as the near-*syn* form.

As was shown previously (16), the electron-diffraction results for 2,2′-dihalobiphenyls fall into a general pattern in which the dihedral angle increases with increasing size of the halogen substituents. More interestingly, however, the near-*syn* configuration is always that observed. Further, the experimental X—X distances (X ≡ halogen, except for F) are shorter than those predicted on the basis of Pauling's van der Waals radii (21), the discrepancy increasing with increasing atomic number of X. In the case of X = F the X—X distance is actually slightly larger than that predicted on the basis of van der Waals radii (21), but values are shorter by 14, 28, and 48 pm for X = Cl, Br, and I respectively (16).

These observations (16) strongly suggest the existence of some halogen–halogen non-bonded attraction force, which was not taken into account in the theoretical work (3, 14). A similar conclusion can be reached from the results of the present work, through comparison of inter-ring angles for corresponding methyl and chloro-substituted biphenyls. The relevant data are drawn together in Table 4. The point of comparing X = CH_3 with X = Cl is that the steric requirements of these two substituents are essentially identical (22) provided that the CH_3 groups are freely rotating. While the differences in Table 4 are not large, barely statistically significant, it is interesting that the 3,3′- and 4,4′-disubstituted compounds show $\theta(CH_3) < \theta(Cl)$, while the reverse is true for the 2,2′-disubstituted biphenyls. This trend is thus also consistent with the existence of an attractive force between two nonbonded Cl atoms, which is absent if X = CH_3.

Table 2 also shows that further substitution at sites well removed from the *ortho* positions induces small but significant decreases in θ from the value for 2,2′-dichlorobiphenyl itself.

With the exception of 2,2′-difluorobiphenyl, for which electrostatic repulsion between highly electronegative fluorine atoms could be expected to dominate, the existence of an intramolecular attractive force between nonbonded halogen atoms seems to be established for 2,2′-dihalobiphenyls. A corresponding intermolecular attractive force underlies the so-called "chlorine atom effect" of Schmidt and Green (23–25). This effect manifests itself via the production of close-packed, highly overlapped parallel molecules in the crystal structures of

TABLE 2. Experimental data on ΔE, and values for inter-ring angle θ calculated from eq. [3]

Compound	ΔE (eV), present work	θ (deg)	ΔE (eV), ref. 1	θ (deg)
2-Methylbiphenyl	0.90 ± 0.05	69 ± 2	0.90 ± 0.02	69
3-Methylbiphenyl	1.41 ± 0.03	47 ± 1	1.45 ± 0.02	45
4-Methylbiphenyl	1.50 ± 0.03	42 ± 1	1.45 ± 0.02	45
2,2′-Dimethylbiphenyl	0.67 ± 0.08	78 ± 3	0.70 ± 0.02	76
3,3′-Dimethylbiphenyl	1.43 ± 0.03	46 ± 1	1.38 ± 0.02	48
4,4′-Dimethylbiphenyl	1.43 ± 0.03	46 ± 1		
2-Chlorobiphenyl	1.06 ± 0.05	62 ± 2	1.00 ± 0.02	65
3-Chlorobiphenyl	1.41 ± 0.03	47 ± 1		
4-Chlorobiphenyl	1.34 ± 0.03	50 ± 1	1.30 ± 0.02	52
2,3-Dichlorobiphenyl	0.80 ± 0.05	72 ± 2		
2,4-Dichlorobiphenyl	0.90 ± 0.08	68 ± 3		
2,5-Dichlorobiphenyl	1.14 ± 0.03	60 ± 1		
2,6-Dichlorobiphenyl	≤ 0.6	≥ 80		
3,4-Dichlorobiphenyl	1.37 ± 0.03	49 ± 1		
3,5-Dichlorobiphenyl	1.17 ± 0.07	58 ± 3		
2,4′-Dichlorobiphenyl	1.01 ± 0.07	64 ± 3		
3,3′-Dichlorobiphenyl	1.37 ± 0.03	49 ± 1		
4,4′-Dichlorobiphenyl	1.34 ± 0.07	50 ± 3		
2,4,6-Trichlorobiphenyl	≤ 0.65	≥ 78		
2,2′,5,5′-Tetrachlorobiphenyl	0.93 ± 0.05	67 ± 2		
2,2′,4,4′,5,5′-Hexachlorobiphenyl	0.88 ± 0.07	69 ± 3		

TABLE 3. Observed ionization energies (eV)[a]

Biphenyl compound	I_1	I_2, I_3[b]	I_4	I_5
Biphenyl	8.35 (8.05)	9.1, 9.25	9.80	11.25 (10.9)
Fluorene[c]	7.95 (7.75)	8.85, 9.15	9.90	11.0 (10.65)
2-Methyl	8.55 (8.05)	9.0	9.45	11.15 (10.6)
3-Methyl	8.30 (7.90)	8.90, 9.05	9.70	11.25 (10.75)
4-Methyl	8.15 (7.75)	9.1 (8.80)	9.65	11.05 (10.80)
2,2′-Dimethyl	8.7 (8.15)	9.0	9.4	11.15 (10.5)
3,3′-Dimethyl	8.20 (7.90)	8.9	9.60	11.10 (10.6)
4,4′-Dimethyl	7.80 (7.35)	8.85 (8.60), 9.05	9.25	10.90 (10.45)
Perfluoro	9.8 (9.45)	9.95, 10.10	10.75	12.8 (12.3)
4,4′-Difluoro				
2-Chloro	8.70 (8.25)	9.20	9.75	11.0 (10.7)
3-Chloro	8.60 (8.20)	9.25	10.00	11.30 (10.90)
4-Chloro	8.45 (8.05)	9.50	9.80	11.25 (10.85)
2,3-Dichloro	8.85 (8.25)	9.15	9.65	11.00 (10.50)
2,4-Dichloro	8.65 (8.15)	9.2	9.55	11.30 (10.80)
2,5-Dichloro	8.65 (8.20)	9.15, 9.35	9.80	11.20 (10.75)
2,6-Dichloro	(8.3)	9.1	9.6	11.15 (10.80)
3,4-Dichloro	8.40 (8.05)	9.25, 9.45	9.80	11.10 (10.75)
3,5-Dichloro	8.65 (8.15)	9.0, 9.3	9.85	11.25 (10.80)
2,4′-Dichloro	8.75 (8.25)	9.4	9.75	11.30 (10.85)
2,2′-Dichloro	8.85 (8.35)	9.05, 9.25	9.55	11.05 (10.7)
3,3′-Dichloro	8.75 (8.25)	9.2	10.15	11.55 (10.95)
4,4′-Dichloro	8.40 (8.05)	9.5 (9.2)	9.75	11.35 (11.0)
2,4,6-Trichloro	9.05 (8.75)	9.3	9.7	11.05 (10.85)
2,2′,5,5′-Tetrachloro	9.15 (8.80)	9.8	10.1	11.65 (11.15)
2,2′,4,4′,5,5′-Hexachloro	9.05 (8.7)	9.6	9.93	11.50 (10.9)

[a] Threshold values, where available, given in parentheses.
[b] In some cases, I_2 and I_3 were not resolved, and value given corresponds to unresolved maximum.
[c] Spectrum corresponds closely to that given in ref. 1, but with two extra peaks at I.E. values of 8.35 and 10.20 eV, probably due to an impurity.

aromatic molecules, induced by halogen (and particularly dichloro) substitution on phenyl rings. This is a dramatic change from the highly characteristic herring-bond structure of alternate layers of phenyl rings in the crystalline state, and has been exploited (23–25) in the engineering of crystal structures for stereospecific photodimerization reactions in the solid state.

The intramolecular effect observed (16) for 2,2′-dihalobiphenyls may also be related to the relative stabilities of *cis* and *trans* isomers of 1,2-dihaloethylenes. In the gas-phase, the *cis* forms are generally more stable than the *trans*, again in opposition to predictions based only on van der Waals effects. This observation has been investigated theoretically by Epiotis *et al.* (26, 27), and characterized as due to a through-space interaction of lone pair orbitals, akin to a charge-transfer inter-

TABLE 4. Inter-ring dihedral angles (degrees) for corresponding methyl and chloro-substituted biphenyls (values in parentheses for ref. 1)

Substitution	θ, X = CH_3	θ, X = Cl	[θ(CH_3) − θ(Cl)]
2,2′	78(76)	74[a]	+4
3,3′	46(48)	49	−3
4,4′	46	50	−4

[a] Value for electron diffraction, ref. 15.

action. Such an interaction could also be responsible for difficulties in accounting for the observed crystal structure of Cl_2 (28).

The broad implications of the present work, for the relative toxicities of different PCB congeners, is based upon the proposal (6) that it is the planar conformations which are the most active in this respect. Certainly the experimental evidence (4) bears out the implication that *ortho* chlorine substitution should decrease physiological activity. The present work, which in this one respect is best viewed as an extension of the electron diffraction work (16), confirms that increasing *ortho* substitution drives the preferred conformation further from planarity. The failure to observe both conformers in gaseous 2,2′-dichlorobiphenyl (15) suggests that the barrier to rotation from the near-*syn* to the near-*anti* conformation must be much higher than the value of RT ($\approx$5 kJ mol^{-1}) at the experimental temperature (15). This observation (15) is difficult to understand in terms of either qualitative intuition or of quantitative theoretical estimates (3, 14) of the potential energy profile for inter-ring rotation. It is clear that understanding of the problem of conformation of substituted biphenyls still leaves much to be desired.

Acknowledgements

We are indebted to Dr. Stephen Safe for the gift of the tetrachloro and hexachloro biphenyls, and to Dr. Giacinto Scoles for the loan of the microwave generator. The criticisms of Dr. N. Westwood greatly improved the final manuscript. Financial support by NSERC is acknowledged.

1. J. P. MAIER and D. W. TURNER. Disc. Faraday Soc. **54**, 149 (1972).
2. A. D. BAKER, D. P. MAY, and D. W. TURNER. J. Chem. Soc. B, 22 (1968).
3. J. D. MCKINNEY, K. E. GOTTSCHALK, and L. PEDERSEN. J. Mol. Struct. Theochem. **104**, 445 (1983).
4. T. SAWYER and S. SAFE. Toxicol. Lett. **13**, 87 (1982).
5. W. A. BRUGGEMAN, J. VAN DER STEEN, and O. HUTZINGER. J. Chromatogr. **238**, 335 (1982).
6. J. D. MCKINNEY and P. SINGH. Chem.-Biol. Interact. **33**, 271 (1980).
7. I. LINDAU, J. C. HELMER, and J. UEBBING. Rev. Sci. Instrum. **44**, 265 (1973).
8. H. HOTOP and G. HUBLER. J. Electron Spectrosc. Relat. Phenom. **11**, 101 (1977).
9. J. A. KINSINGER, W. L. STEBBINGS, R. A. VALENZI, and J. W. TAYLOR. Anal. Chem. **44**, 773 (1972).
10. R. A. BORDERS, J. W. BIRKS, and J. A. BORDERS. Anal. Chem. **52**, 1273 (1980).
11. A. ALMENNINGEN and O. BASTIANSEN. K. Norske Vidensk. Selsk. Skr. No. 4 (1958).
12. O. BASTIANSEN and L. SMEDVIK. Acta Chem. Scand. **8**, 1593 (1954).
13. O. BASTIANSEN. Acta Chem. Scand. **4**, 926 (1950).
14. A. ALMENNINGEN, A. O. HARTMANN, and H. M. SEIP. Acta Chem. Scand. **22**, 1013 (1968).
15. C. ROMMING, H. M. SEIP, and I.-M. AANESEN OYMO. Acta Chem. Scand. Ser. A, **28**, 507 (1974).
16. O. BASTIANSEN, K. KVESETH, and H. MOLLENDAL. *In* Large-amplitude motion in molecules, I. Topics in Current Chemistry 81. Springer Verlag, New York. 1979.
17. M. KLESSINGER and P. RADEMACHER. Angew. Chem. Int. Ed. Engl. **18**, 826 (1979).
18. R. GLEITER, W. SCHAFER, and M. ECKERT. Chem. Ber. **114**, 2309 (1981).
19. A. IMAMURA and R. HOFFMAN. J. Am. Chem. Soc. **90**, 5379 (1968).
20. J. ALMLÖF. Chem. Phys. **6**, 135 (1974).
21. L. PAULING. The nature of the chemical bond. Cornell University Press, Ithaca, NY. 1960.
22. C. P. SMYTH. *In* Physics and chemistry of the organic solid state. *Edited by* D. Fox, M. M. Labes, and A. Weissbeger. Wiley–Interscience, New York. 1963. Chapt. 12.
23. B. S. GREEN and G. M. J. SCHMIDT. Tetrahedron Lett. 4249 (1970).
24. G. M. J. SCHMIDT. Pure Appl. Chem. **27**, 647 (1971).
25. A. ELGAVI, B. S. GREEN, and G. M. J. SCHMIDT. J. Am. Chem. Soc. **95**, 2058 (1973).
26. N. D. EPIOTIS. J. Am. Chem. Soc. **95**, 3087 (1973).
27. N. D. EPIOTIS, R. L. YATES, J. R. LARSON, C. R. KIRMAIER, and F. BERNARDI. J. Am. Chem. Soc. **99**, 8379 (1977).
28. S. C. NYBURG. J. Chem. Phys. **40**, 2493 (1964).

An exciplex probe for end-to-end cyclization of polystyrene. Cyclization dynamics of polymers. 15[1]

MITCHELL A. WINNIK[2] AND ANDREW M. SINCLAIR
Lash Miller Laboratories, Department of Chemistry and Erindale College, University of Toronto, Toronto, Ont., Canada M5S 1A1

AND

GÉRARD BEINERT
Centre de Recherches sur les Macromolécules, 6 rue Boussingault, 67083, Strasbourg, France

Received June 19, 1984

MITCHELL A. WINNIK, ANDREW M. SINCLAIR, and GÉRARD BEINERT. Can. J. Chem. **63**, 1300 (1985).

An asymmetrically end-labelled polystyrene of low polydispersity has been synthesized. The labels are pyrene and dimethylaniline, which can form an emissive exciplex from excited pyrene. End-to-end cyclization rate constants $\langle k_1 \rangle$ have been calculated from fluorescence decay data in a variety of solvents. Steady-state measurements are also presented. Correction of the $\langle k_1 \rangle$'s for differences in solvent viscosity yields cyclization rate constants of $0.7 \times 10^6\ s^{-1}$ in good solvents and about twice this in poor (sub-θ) solvents. Cyclization rate constants $\langle k_1 \rangle$ in toluene and cyclohexane at 22°C obtained using this pyrene/dimethylaniline exciplex probe are compared with those obtained previously using a pyrene/pyrene excimer probe.

MITCHELL A. WINNIK, ANDREW M. SINCLAIR et GÉRARD BEINERT. Can. J. Chem. **63**, 1300 (1985).

On a synthétisé un polystyrène de faible polydispersité et marqué de façon asymétrique aux extrémités. Les marqueurs sont le pyrène et la diméthylaniline qui peuvent former un exciplex émissif à partir du pyrène excité. On a calculé les constantes de vitesse $\langle k_1 \rangle$ de la cyclisation bout à bout, à partir des données de décroissance de la fluorescence dans divers solvants. On présente également des mesures effectuées dans l'état stationnaire. Les corrections apportées aux valeurs de $\langle k_1 \rangle$, pour tenir compte des différences de viscosités des solvants, donnent des constantes de vitesse de cyclisation de $0{,}7 \times 10^6\ s^{-1}$ dans les bons solvants et environ le double dans les solvants (sub-θ) pauvres. On compare les constantes de vitesse de cyclisation $\langle k_1 \rangle$ dans le toluène et le cyclohexane, obtenues à 22°C en utilisant cette sonde d'exciplex pyrène/diméthylaniline, avec celles obtenues antérieurement en utilisant comme sonde d'excimère le couple pyrène/pyrène.

[Traduit par le journal]

Introduction

Since the seminal papers by Wilemski and Fixman (1) (WF) on the theory of cyclization dynamics of polymers, various experimental methods have been used to try to measure these rates. Cuniberti and Perico (2) used steady-state measurements of pyrene excimer formation to study poly(ethylene oxide). Mita, Horie *et al.* (3) examined triplet–triplet (TT) annihilation between anthracene groups to study polystyrene. Redpath, Winnik, and co-workers used a combination of fluorescence decay and steady state of pyrene excimer formation to study polystyrene (4, 5) poly(ethylene oxide) (6), and polydimethylsiloxane (7). Each of these experiments required the synthesis of polymers of narrow molecular weight distribution, specifically substituted on both chain ends with spectroscopically appropriate (anthracene or pyrene) luminescent groups.

The important questions addressed, for polymer cyclization in dilute solution, have been the chain length (N) dependence of the cyclization rate constant k_{cy}, and the effect of solvent on these rates. Chain length enters the problem because the mean-squared separation of the chain ends R_F^2 increases with chain length, as do the low frequency relaxation times of the chain. Solvent viscosity retards dynamic motion of the chain, whereas solvent quality (good solvent, poor solvent, θ-solvent for the polymer) affects the degree of chain swelling, and hence R_F (8).

WF theory addresses these features in terms of the bead-and-spring model, Fig. 1 (9). In this model one views the chain as

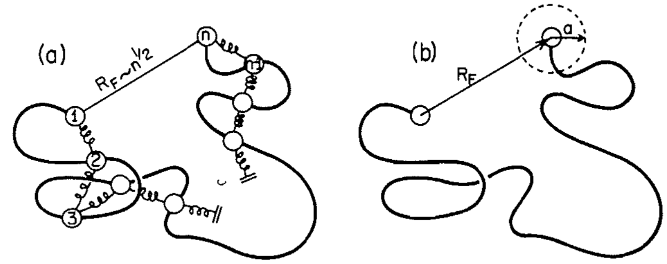

FIG. 1. (a) Depiction of the bead-and-spring (Rouse–Zimm) model for a polymer chain. (b) Depiction of the root-mean-squared end-to-end distance R_F and the quenching radius a for a polymer chain.

a sequence of beads (mass and friction centers) connected by harmonic springs. In the Rouse model, the beads act as independent friction centers, whereas in the Zimm model the solvent is viewed as being trapped (non-draining) inside the coil. Finite chains are partially draining: one must take account of the extent of hydrodynamic coupling between beads which, separated along the chain contour, happen to be in proximity (8).

The original WF papers raised a number of important theoretical issues which were subsequently examined in detail by Doi (10), by Perico and co-workers (11*a*–*c*; see also 11*d*), and by Perico and Cuniberti (12). This subject was recently reviewed in some detail (8).

One of the central predictions of the theory is that $k_{cy} \propto N^{\alpha}$, with α taking he value of $-3/2$ for very long chains in a θ-solvent. For long chains in a good solvent α should approach the value $-9/5$ because of excluded volume effects (4*a*, 8). Furthermore, k_{cy}^{-1} for these long chains should be almost equal

[1] This and the following papers are dedicated to the memory of Li Xiao-Bai of Nankai University, Peoples Republic of China, who died of a sudden illness after returning home from two fruitful years of research in the laboratories of M.A. Winnik and J.E. Guillet at the University of Toronto.

[2] Author to whom correspondence may be addressed.

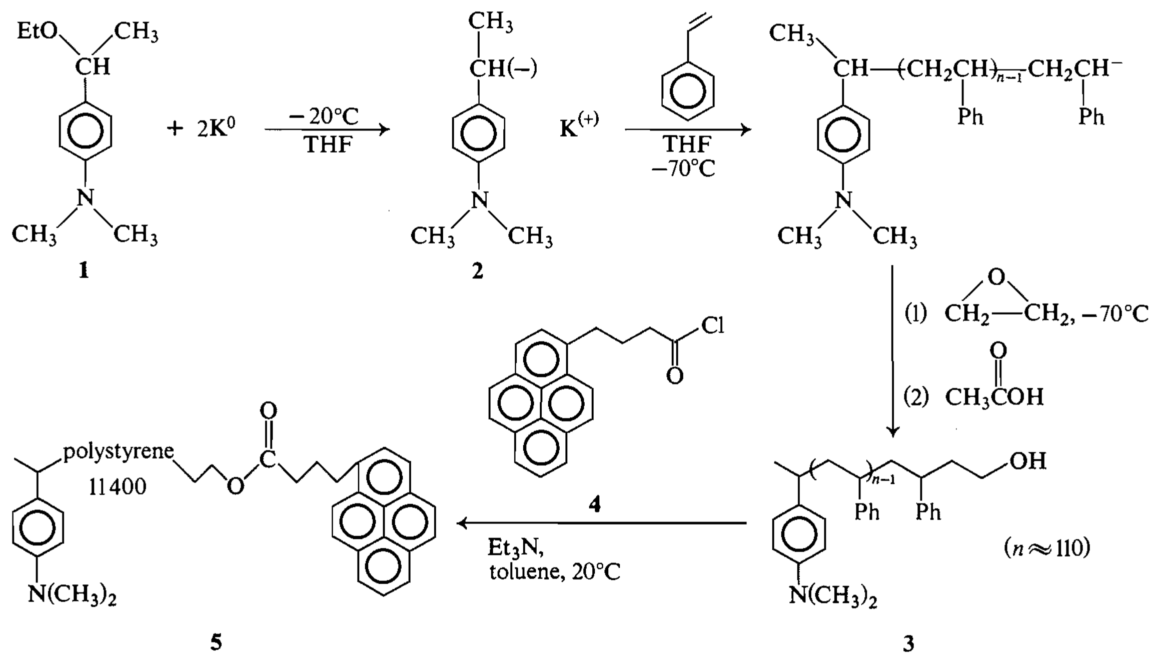

SCHEME 1

to τ_1, the slowest internal relaxation time of the chain, as determined, for example, by viscoelastic relaxation experiments (13).

For shorter chains, other features appear. Cyclization is no longer dominated exclusively by τ_1; all the higher order relaxation modes contribute to k_{cy}. In addition, and of particular importance here, the size of the capture (or quenching) radius a enters into the magnitude of k_{cy} as the ratio of a/R_G, where R_G is the radius of gyration of the chain. Since R_G changes with chain length, but a does not, the value of α is affected. This effect is quite subtle. It has been examined in some detail by Perico and Cuniberti (8, 12) who showed that as $N \rightarrow \infty$, $a/R_G \rightarrow 0$, and k_{cy} becomes independent of a.

One of the curious features of the experimental determinations of the cyclization rate constants has been the discrepancies that exist between results reported by different laboratories. Gross features of the theory have been confirmed in all experiments (2–8). Thus where sufficient data exist, one can quite reasonably draw straight lines through plots of log k_{cy} vs. log N. The slopes frequently differ (although they fall in the range -1 to -1.8) and the magnitudes of k_{cy} sometimes differ for the same polymer–solvent – chain length combination by more than one might anticipate from the precision of the individual experiments.

A notable case concerns the cyclization of polystyrene chains of M = 30 000 to 100 000 in cyclohexane at 34.5°C, the θ-temperature. Rates determined by the study of intramolecular excimer formation of pyrene-end-capped polymers (4, 5) are more than an order of magnitude faster than rates determined by TT annihilation of chains terminated by anthracene groups (3).

In order to test the idea that *measured cyclization rates* might depend upon the spectroscopic technique used to detect cyclization, we decided to examine exciplex formation in a polystyrene polymer containing an aromatic amine at one end and a pyrene group at the other. We chose a chain length ($\bar{M}_n$ = 11 400) sufficiently small that a/R_G was significant, with a value of ca. 0.2. Since a for exciplex formation is larger than for excimer formation (see below), at least in polar solvents, we felt that we would have the means to examine the probe dependence of the cyclization process. We also recognized that exciplexes themselves are sensitive to solvent polarity, whereas pyrene excimers are not (14). We therefore were curious to see whether changes in solvent polarity had significant effects on the rates of polystyrene cyclization as measured by exciplex formation.

Results and discussion

Design and synthesis

Both spectroscopic and synthetic considerations enter into the choice of end groups to be incorporated into the polymer. Our philisophy was to choose a derivative of one of these groups (D) as an initiator for anionic polymerization of styrene, and to terminate the polymerization with ethylene oxide. In this way we could produce a polymer of the form D∿∿OH, and a variety of chromophores could be attached to the other end via the hydroxy group. If D had several spectroscopic properties of interest, quite a broad range of experiments could be carried out on one polymeric starting material. For example, if D could form an exciplex with pyrene and also serve as an effective triplet quencher, two quite different experiments could be performed on polymers to which pyrene groups or aromatic ketone groups could be attached.

From a spectroscopic point of view, the *N,N*-dimethylaminophenyl (DMAP) group serves all of these functions. Dimethylaniline and dimethyltoluidine form exciplexes with pyrene and with a variety of other polycyclic aromatic groups. These amines quench ketone triplet states by an electron-transfer process, and they are compatible chemically with the conditions of anionic polymerization. Worsfold, for example, has initiated anionic polymerization using lithiated aliphatic species containing the Me_2N— group (15).

Our initial attempt to add *sec*-butyllithium to 4-isopropenyl-*N,N*-dimethylaniline did not provide useful polymers. Instead we generated the initiator **2** by treatment of 1-[4′-(*N,N*-dimethylaminophenyl)phenyl]ethyl ethyl ether (**1**) with potassium metal in tetrahydrofuran, Scheme 1. The reaction was terminated with ethylene oxide in keeping with our philosophy that

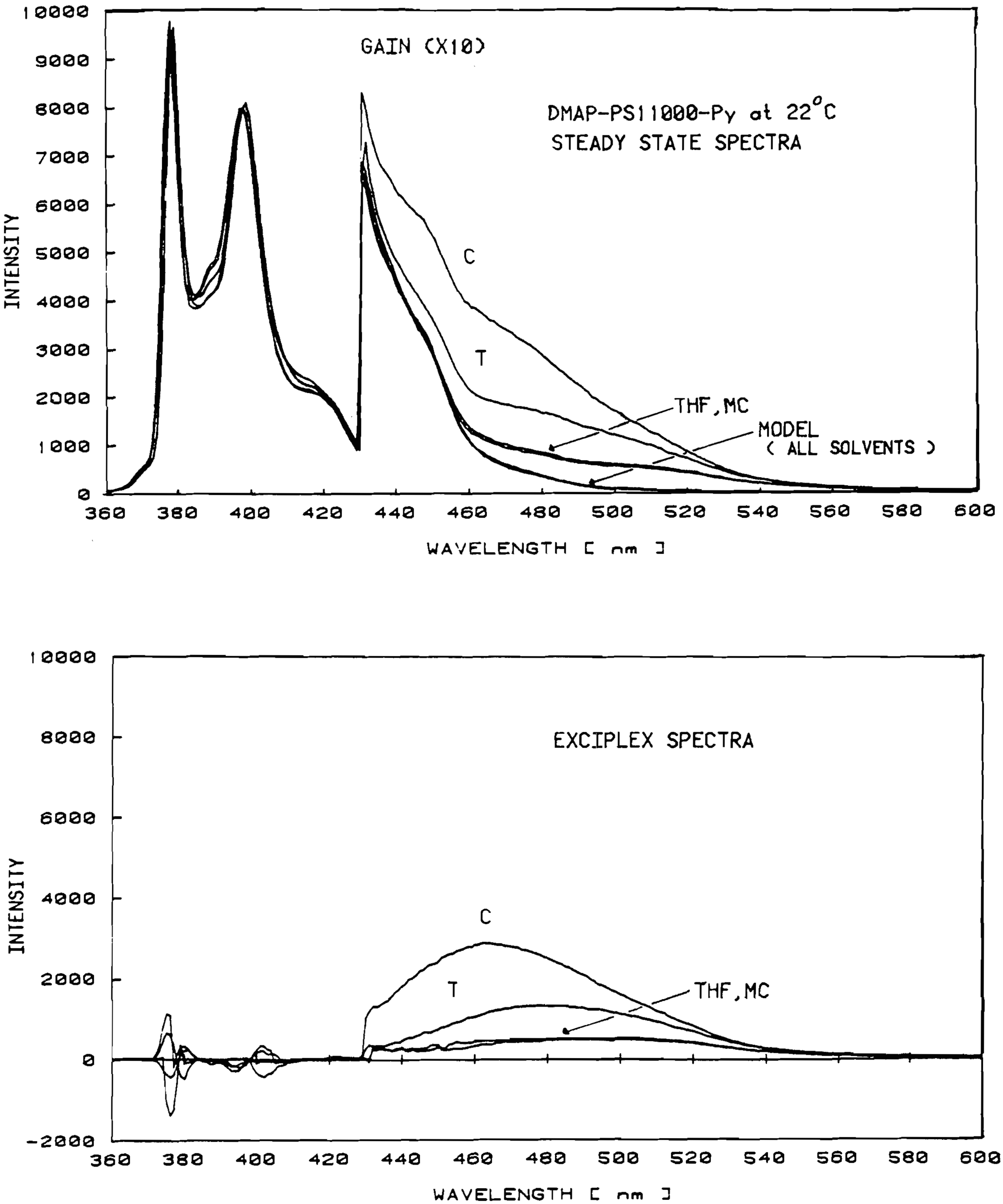

FIG. 2. Fluorescence spectra of DMAP-PS11000-Py **5** and PS5900-Py (Model, *b*) at 22°C in several solvents. Intensities are arbitrarily normalized at 398 nm. The model polymer **6** had nearly identical spectra in all solvents. For **5**, spectra are shown in cyclohexane (C), toluene (T), tetrahydrofuran (THF), and methylene chloride (MC). The lower curves are exciplex spectra obtained by subtracting the normalized spectrum of **6** from that of **5**.

functional group manipulation on polymer termini is much less onerous than synthesis of the polymers themselves. Small amounts of the polymer $Me_2N—C_6H_4—CH(CH_3)$-polystyrene-CH_2CH_2OH (DMAP-PS-OH, **3**) were treated at a later stage with $PyCH_2CH_2CH_2C(O)Cl$ (**4**) in order to obtain the final polymer DMAP-PS-Py (**5**).

Ultraviolet analysis of the polymer **3** indicated 1.0 ± 0.1 $Me_2N—C_6H_4—$ groups per chain based upon M_n = 11 400 for the polymer. Corresponding analysis of **5** showed only 0.8 ± 0.1 pyrenes per chain. The reason for incorporation of less than one pyrene per chain is not yet clear. One possibility may be incomplete esterification. Since the fluorescence experiments at high dilution examine only those chains with excited pyrene groups, our results do not require that every chain carry a pyrene.

Spectroscopy

In order to interpret fluorescence studies of exciplex formation in **5**, one must compare the data to the fluorescence of a model polymer in which no intramolecular exciplex can be formed. For example, in Fig. 2 we show the fluorescence spectra of **5** in four solvents: cyclohexane, toluene, tetrahydrofuran (THF), and methylene chloride. In the same figure we also show the fluorescence of **6** in these same four solvents. These spectra have been normalized in intensity at the

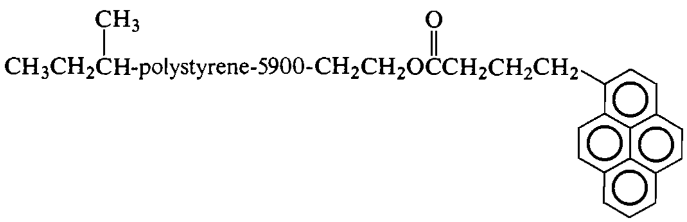

PS5900-Py, **6**

(0,2) band at 398 nm. One sees that the change in solvent or the presence of the terminal DMAP group has little effect on the emission spectrum of the locally excited pyrene.

At longer wavelengths, exciplex emission can be seen in samples of **5** at a Py group concentration of ca. 6 × 10^{-6} *M*. The exciplex emission from **5** was quite weak; therefore the gain was increased by a factor of 10 above 430 nm to increase sensitivity. Exciplex spectra, Fig. 2b, were obtained by subtracting spectra of the model polymer **6** from those of **5** in the same solvent. There are two important features to note in Fig. 2b. First, exciplex intensity I_E decreases, relative to that of the locally excited pyrene intensity I_M, with increasing solvent polarity. In addition, the exciplex emission maximum shifts to the red, as the solvent polarity increases.

The red shift is consistent with the charge-transfer nature of the exciplex, which is stabilized relative to the ground state in polar solvents (14). It is also known that radiationless decay rates of exciplexes increase in polar solvents. Their emission quantum yields decrease and therefore I_E/I_M values should decrease with increasing solvent polarity. Since the rate and extent of cyclization will also affect I_E/I_M values, a simple interpretation of these relative intensities is not possible at this time.

Fluorescence decay profiles were measured using the time-correlated single photon counting technique. An example is shown in Fig. 3 where we present both pyrene ($I_M(t)$) and excimer ($I_E(t)$) fluorescence profiles for the DMAP-PS11000-Py sample in cyclohexane. Lifetimes are obtained by iterative reconvolution of a trial function with the lamp profile. The $I_M(t)$ decays gave good fits to a single exponential decay func-

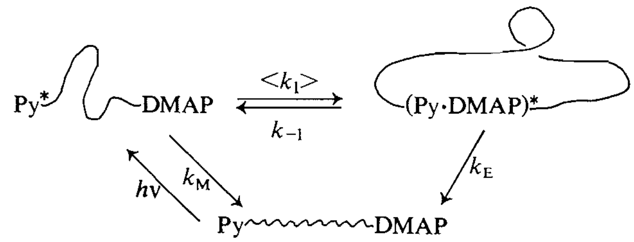

SCHEME 2

tion, whereas the growing-in and decay of the exciplex had to be fit to a difference of two exponential terms.

In the experiments reported here, the $I_M(t)$ decay times were always 3% to 5% longer than the corresponding long component of the $I_E(t)$ decays. We note that our polymer samples with $\bar{M}_w/\bar{M}_n$ = 1.08 have a finite polydispersity. The decay constants obtained from the measurements and the calculated rate constants are therefore averages over that distribution. On the other hand, the longer value of the $I_M(t)$ decay times could arise from a small fraction of polymer containing Py but no DMAP groups. In this case, using the $I_E(t)$ values to calculate rate constants should avoid any complications due to incomplete chain functionalization.

Data and data analysis

Exciplex formation is normally diffusion controlled. In Scheme 2, the rate constant $\langle k_1 \rangle$ describes cyclization leading to intramolecular exciplex formation. The angle brackets $\langle\rangle$ emphasize that k_1 should vary sensitively with chain length, and that values obtained from the study of polymers with a finite polydispersity represent averages over the molecular weight distribution in the sample. We denote exciplex dissociation (ring opening) by k_{-1}; k_M and k_E describe the reciprocal lifetimes of the locally excited pyrene ("monomer") and exciplex lifetimes, respectively.

Scheme 2 predicts the fluorescence decay laws

$$[1] \quad I_M(t) = a_1 \exp(-\lambda_1 t) + a_2 \exp(-\lambda_2 t)$$

$$[2] \quad I_E(t) = a_3 [\exp(-\lambda_1 t) - \exp(-\lambda_2 t)]$$

where the decay constants λ_1, λ_2 are related to the rate constants by the expression

$$[3] \quad 2\lambda_1, \lambda_2 = (k_M + \langle k_1 \rangle + k_E + k_{-1}) \mp \{[(k_E + k_{-1}) - (k_M + \langle k_1 \rangle)]^2 + 4\langle k_1 \rangle k_{-1}\}^{1/2}$$

Note that when $4\langle k_1 \rangle k_{-1}$ is small compared to the squared term in brackets, eq. [3] simplifies to

$$[4] \quad \lambda_1 = \langle k_1 \rangle + k_M$$

$$[5] \quad \lambda_2 = k_{-1} + k_E$$

Values of $\langle k_1 \rangle$ were calculated from eq. [4], using λ_1 values from the pyrene decay, with k_M taken to be the exponential decay rate of the model polymer **6**. One should note that all the rate constants in Scheme 2 might be expected to vary with solvent. This is emphasized by the variation of λ_M^{-1} values from solvent to solvent, Table 1, where, for example, one sees that λ_M^{-1} (cyclopentane) = 243 ns and λ_M^{-1} (benzene) = 156 ns. Cyclization rate constants obtained in this way are collected in Table 1.

Cyclization rates

Values of $\langle k_1 \rangle$ for DMAP-PS11000-Py at 22°C vary from

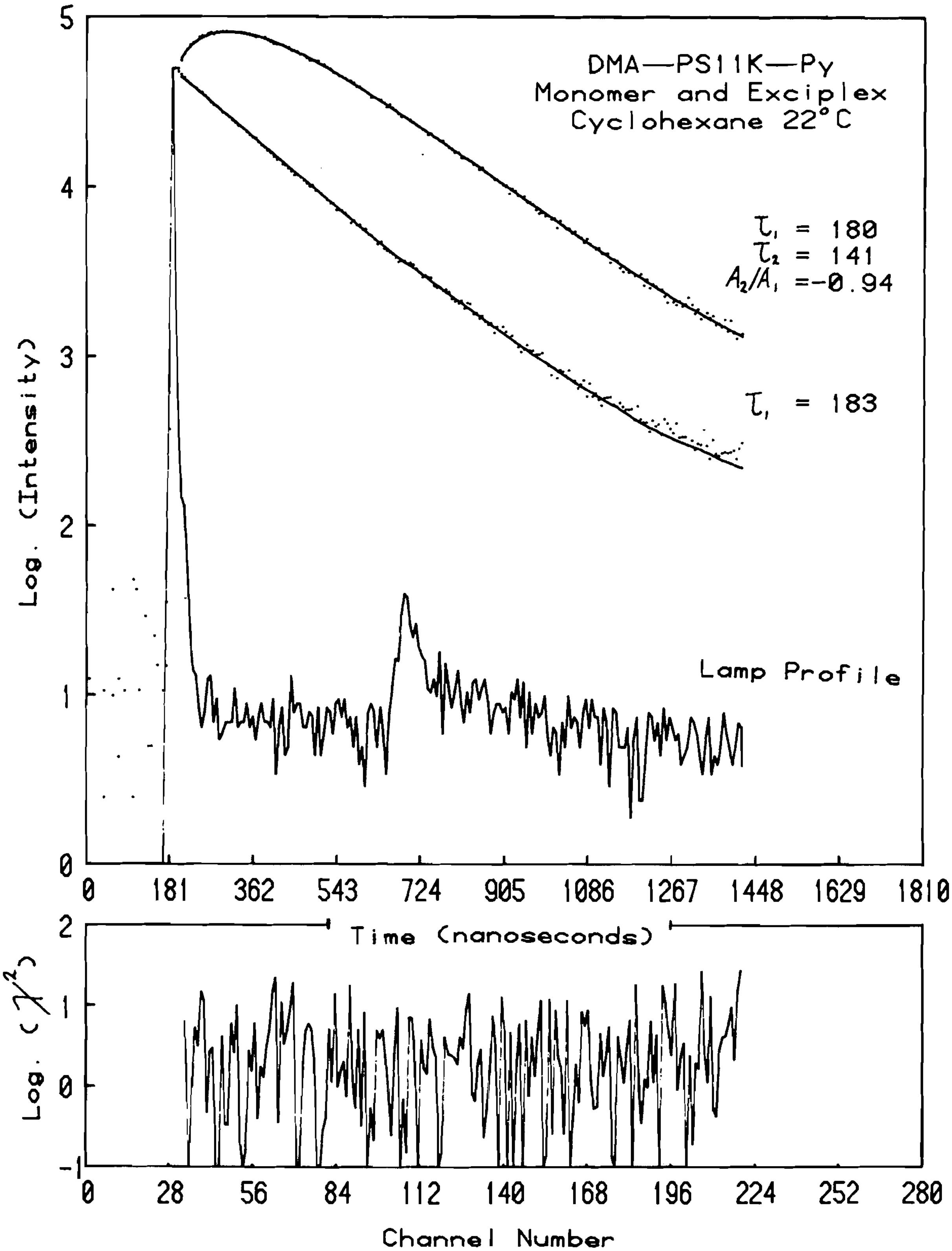

FIG. 3. Fluorescent decay profiles of DMAP-PS11000-Py in cyclohexane at 22°C. The upper curve is the exciplex emission ($\lambda_{EM} > 500$ nm). The middle curve is the monomer emission (370 nm $> \lambda_{EM} >$ 400 nm) and the lower curve is the excitation lamp profile ($\lambda_{EM} = \lambda_{EX} = 345$ nm). Both spectra are normalized to the lamp maximum of 50 000 counts for presentation. The lower graph is a representative plot of the log of the point by point χ^2 versus channel number.

1.01×10^6 s^{-1} in benzene to 2.67×10^6 s^{-1} in cyclopentane. Two factors affect the magnitude of the cyclization rates; the polymer dimensions in the solvent, and the solvent viscosity. Since diffusion rates vary as T/η, where η is the solvent viscosity, we define $\eta_{rel} = \eta/\eta_{cyclohexane}$ and calculate values of $\langle k_1\rangle_{corr} = \eta_{rel}\,\langle k_1\rangle$. These are plotted in Fig. 4 as a function of solvent viscosity. Figure 4 emphasizes that for benzene, toluene, and THF, the viscosity corrected cyclization rates are

TABLE 1. Lifetimes and rate constants

	Cyclohexane	Cyclopentane	Toluene	Benzene	THF
$\tau_1{}^a$ (6) (ns)	242	243	189	185	213
$\tau_1{}^a$ (5) (ns)	183	147	155	156	166
$\tau_1{}^b$ (5) (ns)	180	149	151	147	143
$\tau_2{}^b$ (5) (ns)	141	133	130	136	135
$A_2/A_1{}^b$ (5)	−0.94	−0.94	−0.94	−0.96	−0.94
$10^{-6}\ \langle k_1\rangle^c$ (s^{-1})	1.33	2.67	1.15	1.01	1.33
$10^{-6}\ \langle k_1\rangle$ corr (s^{-1})	1.33	1.21	0.70	0.68	0.67
η (cP)^d	0.945	0.429	0.573	0.630	0.475
$\delta_H{}^e$	8.2	8.7	8.9	9.2	9.1
ϵ^f at 25°C	$2.02^{20°C}$	$1.97^{20°C}$	2.38	2.28	7.58

[a] $I_M(t)$ decay measured at 380–400 nm. Uncertainties are typically ±1 ns.
[b] Exciplex data measured above 500 nm. Fits are somwhat soft, especially in THF where the intensity is very low.
[c] Calculated from $I_M(t)$ data. Uncertainties are ca. $\pm 0.1 \times 10^6$ s^{-1}.
[d] Viscosity at 22°C (1 cP = 10^{-3} Pa s).
[e] Hildebrand solubility parameter (22*a*, *b*). Note that δ_H for polystyrene is ca. 9.1 (see footnote 3).
[f] Dielectric constant at the temperature indicated (21).

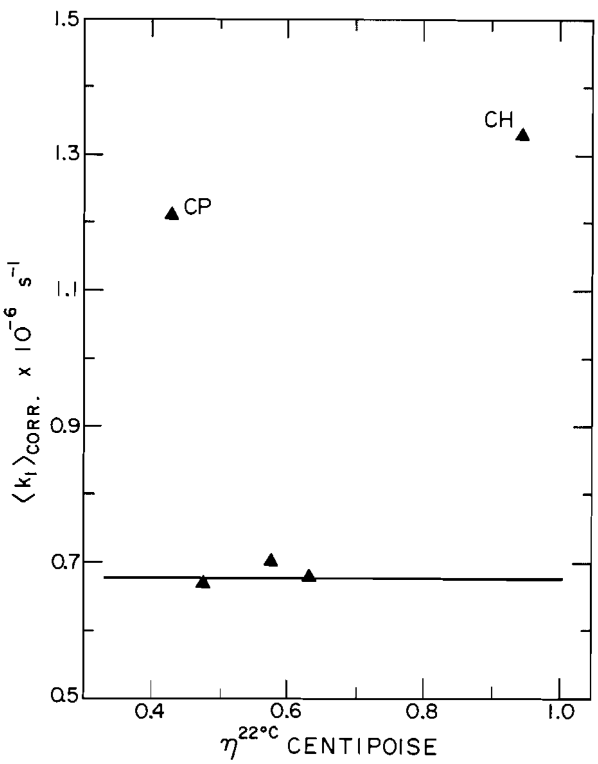

FIG. 4. Viscosity corrected cyclization rate constant versus solvent viscosity at 22°C for DMAP-PS11000-Py in four solvents. $\eta_{rel} = \eta_{solvent}/\eta_{cyclohexane}$.

indistinguishable. Cyclization in cyclohexane and cyclopentane are significantly faster.

Benzene, toluene, and THF are good solvents for PS. For a polymer as short as M = 11 000 one anticipates similar values of the root-mean-square radius of gyration R_G or end-to-end distance R_F for the polymer in each of these solvents. Cyclopentane at 23°C is a θ-solvent for polystyrene. The θ-temperature for PS in cyclohexane is 34.5°C; thus in our experiments at 22°C, cyclopentane represents θ-conditions, and cyclohexane, sub-θ-conditions. R_F and R_G values here are smaller than for the polymer in the good solvents. In addition, attractive interactions between chain elements distort the end vector distribution function to enhance the probability of the two chain ends being in proximity.

Comparison with excimer probes of cyclization

The extensive studies of Redpath and co-workers (4, 5) on excimer formation in Py-PS-Py provide cyclization rate constants with which our values can be compared. In the discussion which follows, we denote these values obtained from excimer studies as $\langle k_1\rangle_{exm}$. The Redpath experiments in toluene were carried out at 22°C for polymers of M = 3000 to 10^5. Experiments in cyclohexane for this span of molecular weights were carried out at the θ-temperature. Three samples with M = 3000 to 9200 were examined as a function of temperature, from 34 to 84°C. Activation energies were obtained; with these data a value for cyclization at 22°C of a Py-PS-Py sample of M = 11 400 can be estimated. We also remeasured the decay parameters at 22°C and 34.5°C for Redpath's samples in cyclohexane and toluene for Py-PS-Py of $\bar{M}_n$ = 9200 and $\bar{M}_n$ = 15 500.[3] These data provide an alternative estimate of $\langle k_1\rangle_{exm}$ for a sample of M = 11 400.

The interpolated value of the cyclization rate constant using $I_M(t)$ data in toluene at 22°C for Py-PS11400-Py (excimer formation) is 0.79×10^6 s^{-1}. This compares, Table 2, with a value of 1.15×10^6 s^{-1} for DMAP-PS11400-Py (exciplex formation). In toluene at 22°C, exciplex formation occurs 1.5 times faster than excimer formation, suggesting that the end group or the spectroscopic technique may affect the measured rate of diffusion controlled cyclization. If the $I_E(t)$ data are used to calculate $\langle k_1\rangle$, we obtain values 0.2×10^6 s^{-1} larger.

In cyclohexane, the interpolated best-fit value at 34.5°C for $\bar{M}_n$ is 11 400 (2.2×10^6 s^{-1}) and, correcting it to 22°C using the value of 3.1 kcal/mol determined from $\langle k_1\rangle_{exm}$ for several chain lengths of Py-PS-Py,[4] we obtain a value of 1.78×10^6 s^{-1}. On the other hand, reexamining two of Redpath's original samples at 22°C led to an interpolated $\langle k_1\rangle_{exm}$ value of 1.56×10^6 s^{-1}.

Our value $\langle k_1\rangle$ for DMAP-PS11400-Py is 1.33×10^6 s^{-1} in cyclohexane at 22°C. This value increases to 1.70×10^6 s^{-1} if

[3] It is worth noting that, three years after sample preparation, virtually identical lifetimes are obtained for the samples prepared by Redpath.

[4] A. E. Redpath and M. A. Winnik. Unpublished results.

TABLE 2. Comparison of cyclization rates for PS11400 obtained by pyrene excimer $\langle k_1\rangle_{exm}$ and DMAP/Py exciplex $\langle k_1\rangle_{exp}$ measurements

Cyclization: Probe		Cyclization: Data	$10^{-6}\langle k_1\rangle^a$ Toluene 22°C	$10^{-6}\langle k_1\rangle^a$ Cyclohexane 22°C	
DMAP	Py	Monomer	1.15	1.33	
		Exciplex	1.35	1.70	
Py	Py[b]	Monomer	0.79	1.56	
		Excimer	0.99	1.79	1.78[c]

[a] From $\langle k_1\rangle = \lambda_1 - k_M$ for the monomer λ_1 from single exponential fits and for the excimer/exciplex λ_1 from double exponential fits.

[b] Estimated by log–log interpolation between the $\langle k_1\rangle$ values of Py-PS9600-Py and Py-PS15600-Py.

[c] By correcting the least-squares best fit data of Redpath and co-workers (4*c*), reported at 34.5°C, to 22°C using $E_a(k_1) = 3$ kcal/mol.

the $I_E(t)$ data are used to calculate $\langle k_1\rangle$.

Figure 3 shows typical monomer and exciplex decay profiles for DMAP-PS11400-Py in cyclohexane at 22°C. In all the cases examined, for this molecular weight, the monomer decays fit well to single exponential decay laws to yield λ_1. The excimer and exciplex fit to a difference of two exponentials with a λ_2 growing-in component and a λ_1 decaying component. It is found in all cases that the monomer λ_1 is always 2 to 5% larger than the excimer or exciplex λ_1. This may be due, in the case of excimers (Py-PS-Py), to a small percentage of monofunctionalized polymer, or, in the case of exciplexes (DMAP-PS-Py), to polymers with no dimethylamino end group. In either case the small impurity would give rise to the model compound **6** decay lifetime which would increase the apparent monomer lifetime. The excimer or exciplex would not form from the impurity and thus would give rise to the better data.

The difference is magnified when calculating $\langle k_1\rangle$, obtained as the difference of two large numbers. Thus we find that $\langle k_1\rangle$ values calculated from $I_E(t)$ data are 10% to 20% larger than those calculated from $I_M(t)$ data. These data are summarized in Table 2. The conclusions we draw are independent of which set of data are compared.

From the data in Table 2 it appears that in toluene the exciplex probe (DMAP-PS-Py) gives a $\langle k_1\rangle$ value 1.5 times larger than that obtained from the excimer probe (Py-PS-Py). In cyclohexane, the $\langle k_1\rangle$ values agree to within 10%. If anything, exciplex formation is a bit slower.

Mechanism of exciplex formation

Long range interactions are not thought to be important in *excimer* formation. Py/Py separation in the excimer is ca. 3.5 Å (14), and the reactive radius for excimer formation is probably not much larger than 5 Å. *Exciplexes* are formed by a different mechanism. There is compelling evidence that electron transfer occurs between the donor (here DMAP-) and the acceptor (here Py-) to form a solvent-separated ion pair (16, 17). Under the force of the coulombic attraction, the ions come together to form the exciplex. This is sometimes referred to as a "harpooning" mechanism. While there are no rigorous measurements, the reactive distance for electron transfer is commonly taken to be 7 Å. In very polar solvents, the ion pair dissociates into free ions; no exciplex emission is seen (14).

The free energy of ion pair formation can be estimated from the oxidation potential of the donor ($E_{1/2}$(ox)), the reduction potential of the acceptor ($E_{1/2}$(red)), and the excitation energy of the excited state species (here E_{00}(py)) (18). For DMAP- and Py- one calculates from

$$[6]\quad \Delta G = E_{1/2}(\mathrm{ox}) - E_{1/2}(\mathrm{red}) - E_{00}(\mathrm{py})$$

that $\Delta G = -10$ kcal/mol. For electron transfer reactions of such exergonicity, solvent effects on the electron transfer rate are expected to be small (18*a*). Thus we see no important differences in $\eta_{rel}\langle k_1\rangle$ values determined in benzene, THF, or toluene. It may well be that ΔG is not sufficiently exergonic to allow a harpooning mechanism in cyclohexane or cyclopentane.

Reactive radius effects on the cyclization process

Calculations carried out by Perico and Cuniberti (12) on the cyclization of partially draining finite chains within the framework of the bead-band-spring model indicate that the magnitude of the reactive radius a can affect the rate of cyclization. The ratio a/R_G enters into the calculation of k_{cy} in a complicated way. For example, the dependence of k_{cy} upon a/R_G disappears for chains of sufficient length (large R_G) and appears to be relatively unimportant for $a/R_G < 0.1$. One can estimate from literature data (19) that R_G for PS11400 in toluene is ca. 32 Å. Taking $a = 5$ Å for excimer formation and $a = 7$ Å for exciplex formation, one obtains values of 0.16 and 0.22 respectively for a/R_G. Thus we can rationalize the faster cyclization rate for exciplex formation vs. excimer formation in toluene in terms of the larger reactive radius of the former process.

In cyclohexane the results are less clear and hence more difficult to intepret. One knows from studies of molecules substituted with bulky groups that exciplex formation in aliphatic hydrocarbon solvents is less sensitive to steric effects than is excimer formation (20). Thus there is no evidence to suggest that reactive distances for the two processes become comparable in nonpolar solvents. In the absence of further results, further speculation seems unwarranted.

Experimental

Synthesis

The unsymmetrical difunctional polymer DMAP-PS11000-OH **3** was prepared by anionic polymerization in THF at −70°C under argon. The polymerization was initiated by the anion **2**, formed from the treatment of 1-[4′-(*N*,*N*-dimethylamino)phenyl]ethyl ethyl ether **1** with potassium metal in THF at −20°C. The solution was cooled to −70°C and styrene was added. After completion of the reaction the living polymer was reacted with a large excess of ethylene oxide. Decoloration of the solution due to quenching of the living anion occurs at ca. −50°C. After addition, first, of aqueous hydrochloric acid and then ammonium hydroxide, the potassium chloride produced is filtered off. The hydroxy-terminated polymer **3** is precipitated by addition of the solution to a large excess of methanol. Polymer **3** was further purified by reprecipitation of a concentrated THF solution in methanol containing a small amount of ammonium hydroxide that facilitated decantation. Further details of the polymerization will be reported elsewhere.

4-(1′-Pyrene)butyryl chloride **4** was prepared from the corresponding acid by treatment with excess oxalyl chloride in benzene. It was recrystallized from a toluene–hexane mixture to give pale yellow crystals, mp 80–81°C.

Functionalization of the polymer **3** with **4** to yield DMAP-PS11000-Py **5** was effected by mixing 1.0 g (0.09 mmol) of **3** with 0.1 g (0.36 mmol) of **4** in 20 mL of toluene that was freshly distilled under nitrogen from sodium metal. Triethylamine (1.0 mL, 7.2 mmol; distilled under nitrogen from CaH_2) was then added. The reaction mixture was then outgassed with nitrogen and stirred under N_2 in the dark for 12 days. To terminate the reaction, 0.2 g of dry silica gel was added. After stirring for an hour, the solution was filtered through a glass wool plug into 200 mL of vigorously stirred methanol. The precipitated polymer was collected, redissolved in toluene, and then reprecipitated twice in methanol. The yield of polymer **5** was effectively quantitative.

The synthesis of the model polymer PS5900-Py **6** has been described previously (4*c*).

Characterization

The molecular weight of the polymer **3** was obtained using a Waters associates high pressure liquid chromatograph (hplc) with a pair of Shodex A 80M gpc columns in THF solution using a Waters R401 refractive index detector. The 2-(4′-*N*,*N*-dimethylaminophenyl)-propane end group could be detected by its absorbance at 304 nm ($\epsilon = 2050$). The M_n and M_w were found to be 11 400 and 12 300 respectively.

Polymer **5** was also analyzed by hplc. By examining the uv absorbance at 345 nm it was found that all of the pyrene in the sample was attached to the polymer. End group analysis showed that about 80% of the polymers had a pyrene end group. It should be pointed out that, as these measurements involve only intrapolymer exciplex formation, polymers with no pyrene end group will not enter into the results.

Sample preparation

Polymer samples were weighed on a microbalance, dissolved in the appropriate solvent, and diluted to 10 mL in a volumetric flask. Toluene, benzene, and cyclohexane were distilled from sodium, cyclopentane and tetrahydrofuran from $LiAlH_4$ and dichloromethane from P_2O_5. The solutions (2×10^{-6} *M*) were then degassed by five freeze–pump–thaw cycles to lower than 10^{-5} Torr (1 Torr = 133.3 Pa) and then sealed under vacuum. Two sets of samples were prepared, one in cylindrical Pyrex cells for lifetime measurements and another in 10 mm × 10 mm rectangular cells for steady-state measurements.

Steady-state spectra

Emission spectra (see Fig. 1) were measured on a SLM model 4800 fluorescence spectrometer. The excitation wavelength was 345 nm and the emission was scanned from 360–600 nm in 1-nm steps. The output was digitally recorded on a Tektronix 4051 computer and stored on disc. All manipulations of the spectra, integrations, normalizations, and subtractions were performed by the computer.

Lifetime measurements

Fluorescent lifetimes were measured by the time correlated single photon counting technique (4). Decays were fit from two channels after the lamp maximum to the end of the measured decay and in all cases the χ^2 values were less than 2.0. The excitation wavelength for all samples was 345 nm. Pyrene monomer decays were measured from emission between 370 nm and 400 nm collected through filters. The pyrene monomer decays were fit to single exponential decay laws by a process of iterative reconvolution with the excitation lamp profile. Pyrene–dimethylaniline exciplex decays were measured above 500 nm using a cutoff filter, and were fit to the difference of two exponential terms.

Acknowledgments

The authors thank NSERC Canada and the Petroleum Research Fund administered by the American Chemical Society for their contribution to the support of this work. We would also like to thank Dr. François Isel for his assistance in synthesizing the polymers. We acknowledge the contribution of Mr. Li Xiao Bai to the early stages of this research, noting that his efforts led to the previous three papers in this series (5*b*, 22).

1. G. WILEMSKI and M. FIXMAN. J. Chem. Phys. **58**, 4009 (1973); **60**, 866 (1974); **60**, 878 (1974).
2. C. CUNIBERTI and A. PERICO. Eur. Polym. J. **13**, 369 (1977); **16**, 887 (1980).
3. K. HORIE, W. SCHNABLE, I. MITA, and H. USHIKI. Macromolecules, **14**, 1422 (1981); H. USHIKI, K. HORIE, A. OKAMOTO, and I. MITA. Polymer J. **12**, 35 (1980).
4. (*a*) M. A. WINNIK, A. E. REDPATH, and D. H. RICHARDS. Macromolecules, **13**, 328 (1980); (*b*) A. E. REDPATH and M. A. WINNIK. Ann. N.Y. Acad. Sci. **366**, 75 (1981); (*c*) M. A. WINNIK, A. E. REDPATH, K. PATON, and J. DANHELKA. Polymer, **25**, 91 (1984).
5. (*a*) A. E. REDPATH and M. A. WINNIK. J. Am. Chem. Soc. **104**, 5604 (1982); (*b*) M. A. WINNIK, X. B. LI, and J. E. GUILLET. J. Polym. Sci. Poly. Symp. In press (1985); (*c*) A. E. REDPATH and M. A. WINNIK. Polymer, **24**, 1286 (1983).
6. S. T. CHEUNG, M. A. WINNIK, and A. E. REDPATH. Makromol. Chem. **183**, 1815 (1982).
7. P. SVIRSKAYA, J. DANHELKA, A. E. REDPATH, and M. A. WINNIK. Polymer, **24**, 319 (1983).
8. C. CUNIBERTI and A. PERICO. Prog. Polym. Sci. **10**, 271 (1984).
9. H. YAMAKAWA. Modern theory of polymer solutions. Harper and Row, New York. 1970.
10. M. DOI. Chem. Phys. **9**, 455 (1975); **11**, 107 (1975); **11**, 115 (1975).
11. (*a*) M. BATTEZZATI and A. PERICO. J. Chem. Phys. **74**, 4527 (1981); (*b*) **75**, 886 (1981); (*c*) A. PERICO and M. BATTEZZATI. J. Chem. Phys. **75**, 4430 (1981); See also: (*d*) A. SZABO, K. SCHULTEN, and Z. SCHULTEN. J. Chem. Phys. **72**, 4350 (1980).
12. A. PERICO and C. CUNIBERTI. J. Polym. Sci. Phys. Ed. **15**, 1435 (1977).
13. J. D. FERRY. Viscoelastic properties of polymers. J. Wiley and Sons, New York. 1980.
14. J. B. BIRKS. Photophysics of aromatic molecules. J. Wiley and Sons, New York. 1970.
15. D. J. WORSFOLD. J. Polym. Sci. Chem. Ed. **21**, 2237 (1983).
16. (*a*) J. D. SIMON and K. S. PETERS. J. Am. Chem. Soc. **103**, 6403 (1981); **104**, 6542 (1982); (*b*) L. E. MANRING and K. S. PETERS. J. Am. Chem. Soc. **105**, 5708 (1983); (*c*) K. S. PETERS, E. PANG, and J. RUDZKI. J. Am. Chem. Soc. **104**, 5535 (1982).
17. W. HUB, S. SCHNEIDER, F. DÖRR, J. D. OXMAN, and F. D. LEWIS. J. Am. Chem. Soc. (*a*) **106**, 701 (1984); (*b*) **106**, 708 (1984).
18. (*a*) D. REHM and A. WELLER. Isr. J. Chem. **8**, 259 (1970); (*b*) A. WELLER. Z. Phys. Chem. (Wiesbaden), **101**, 371 (1976); **130**, 129 (1982); **133**, 93 (1982); (*c*) H. KNIBBE. Ph.D. Thesis, University of Amsterdam, The Netherlands. 1969.
19. J. RACZEK and G. MEYERHOFF. Abstracts 27th Int. Symp. Macromolecules. Vol. II. Strasbourg. July, 1981. p. 700.
20. S. T. CHEUNG and W. R. WARE. J. Phys. Chem. **87**, 466 (1983).
21. (*a*) J. H. HILDEBRAND and R. L. SCOTT. The solubility of nonelectrolytes. 3rd ed. Dover Pub., New York. 1964; (*b*) J. BRANDRUP and E. H. IMMERGUT (*Editor*). Polymer handbook. 2nd ed. Wiley, New York. 1975; (*c*) J. A. RIDDICK and W. B. BUNGER. Organic solvents. 3rd ed. Wiley–Interscience, New York. 1970.
22. (*a*) X. B. LI, M. A. WINNIK, and J. E. GUILLET. Macromolecules, **16**, 992 (1983); (*b*) M. A. WINNIK, X. B. LI, and J. E. GUILLET. Macromolecules, **17**, 699 (1984).

Intrazeolite photochemistry. II. Evidence for site inhomogeneity from studies of aromatic ketone phosphorescence[1]

H. L. CASAL AND J. C. SCAIANO
Division of Chemistry, National Research Council of Canada, Ottawa, Ont., Canada K1A 0R6

Received June 14, 1984

This paper is dedicated to the memory of Li Xiao-Bai

H. L. CASAL and J. C. SCAIANO. Can. J. Chem. **63**, 1308 (1985).

The luminescent properties of several aromatic ketones included in the hydrophobic zeolite Silicalite have been examined. Acetophenone, benzophenone, and β-phenylpropiophenone show readily detectable phosphorescence; by contrast, valerophenone does not luminesce, but undergoes the Norrish Type II reaction. Thus, irradiated samples of valerophenone in Silicalite show phosphorescence due to the accumulation of acetophenone. In the case of β-phenylpropiophenone the triplet lifetime is ca. 100 000 times longer than the solution value, suggesting severe conformational restrictions. Co-inclusion of acetophenone with various substrates and oxygen quenching studies indicate that Silicalite has at least two distinct classes of inclusion sites. In one of them energy transfer processes are rapid and efficient, suggesting a cooperative effect in the inclusion of ketones in these regions of the Silicalite framework.

H. L. CASAL et J. C. SCAIANO. Can. J. Chem. **63**, 1308 (1985).

On étudie les propriétés luminescentes de plusieurs cétones aromatiques contenues dans la zéolite hydrophobe Silicalite. L'acétophénone, la benzophénone et la β-phénylpropiophénone présentent une phosphorescence que l'on peut déceler facilement; par ailleurs, la valérophénone n'est pas luminescente, mais elle subit une réaction de type Norrish II. Ainsi, les échantillons irradiés de valérophénone dans la Silicalite ont une phosphorescence qui provient d'une accumulation d'acétophénone. Dans le cas de la β-phénylpropiophénone, le temps de vie du triplet est environ 100 000 fois plus long que la valeur en solution et ceci suggère la présence d'importantes contraintes conformationnelles. La co-inclusion de l'acétophénone avec différents substrats et des études de piégage d'oxygène indiquent que la Silicalite a au moins deux classes distinctes de sites d'inclusion. Dans l'un d'eux, le processus de transfert d'énergie est rapide et efficace; ceci suggère un effet d'ensemble lors de l'inclusion des cétones dans ces régions du squelette de la Silicalite.

[Traduit par le journal]

Introduction

Photoprocesses in solid systems, including surfaces, crystals, and inclusion compounds, have been the subject of several recent reports (1–3). In spite of the extensive and varied use that zeolites receive in industry, organic photoprocesses have received very limited attention in these media (4–6).

In a preliminary report (7), we showed that the triplet lifetime of β-phenylpropiophenone in Silicalite is enhanced by five orders of magnitude, by comparison with the value in solution under otherwise comparable conditions. This enhancement was attributed to restrictions to mobility that prevent the intramolecular quenching process.

Silicalite forms part of a recently developed class of zeolites with a new topologic type of tetrahedral framework (8). The channel system of this zeolite consists of near-circular zig-zag channels defined by 10 oxygen centres, which are cross-linked by elliptical straight channels. The diameter of the circular channels is 5.4 ± 0.2 Å, and the free cross-section of the elliptical ones is 5.75×5.15 Å^2. One of the remarkable properties of this zeolite is its high hydrophobicity which ensures no deactivation effect due to water, and allows the selective extraction of organic materials from their aqueous solutions (9).

We have examined the possibility of using the luminescence of aromatic ketones in zeolites to probe their dynamics and concurrently to examine the properties of the various sites available to the guest molecules. This report deals with the phosphorescence properties of several aromatic ketones included in the channel structure of Silicalite. We conclude that there are several classes of sites accessible to the guest molecules. The geometry of the Silicalite channels has preferential adsorption of the different aromatic ketones. While it seems that all sites are probably accessible to acetophenone, β-phenylpropiophenone, and valerophenone, benzophenone cannot reach at least one class of sites. This particular class is not readily accessible to oxygen.

Experimental

Silicalite S-115 was purchased from Union Carbide Canada and calcined at 500°C for 24 h and kept under vacuum for 12 h prior to use. Acetophenone and valerophenone (Aldrich) were distilled prior to use, while benzophenone (Eastman Kodak) had been recrystallized from ethanol. β-Phenylpropiophenone was prepared and purified according to literature procedures (10). 1-Phenylhexane (Aldrich) was distilled under reduced pressure, and 1,4-cyclohexadiene (Aldrich) and 2,2,4-trimethylpentane (isooctane, Aldrich Gold Label) were used as received. 1-Phenyl-3-pentanone (Wiley) was used as received. Silica gel was from Merck (70–230 mesh) and Mordenite was obtained from Norton.

The phosphorescence emission spectra (uncorrected, front face) were recorded using a computer controlled Perkin–Elmer LS-5 fluorescence spectrometer. Sample excitation was at 254 or 313 nm, using the appropriate monochromator setting plus suitable interference filters, while a microscope slide was used as a ~300-nm emission cut-off. Excitation and emission bandpasses were <10 nm. The samples were contained in cells made of 3×7 mm^2 Suprasil tubing, and were continuously flushed with N_2, O_2, or appropriate mixtures delivered through a Matheson model 610 gas mixing system. The LS-5 is a gated instrument, its excitation source providing 10-μs pulses at 60 Hz. The design of this instrument is such that Stern–Volmer phosphorescence plots require a more elaborate interpretation than in conventional steady-state spectrometers (*vide infra*).

Inclusion in Silicalite was achieved using the following procedure, illustrated here for the case of β-phenylpropiophenone: 3 g of Silicalite were mixed with a solution of 80 mg of β-phenylpropiophenone in 5 mL of 2,2,4-trimethylpentane (isooctane) in air at room temperature. The molecules of this solvent are sufficiently large that

[1]Issued as NRCC 23702.

TABLE 1. Composition of the samples examined

No.	Substrates	Nominal occupancy[a]	% C Expected	% C Found[b]
1	Acetophenone	20%	3.1	3.3
2	Acetophenone	80%	12.5	11.0
3	β-Phenylpropiophenone	20%	3.3	2.8
4	Benzophenone	20%	3.3	0.92
5	{Acetophenone (5%) Valerophenone (95%)	40%	6.3	6.6
6	{Acetophenone (<1%)[c] Valerophenone	40%	6.3	6.2
7	{Acetophenone (5%) 1-Phenylhexane (95%)	40%	6.8	7.9
8	{Acetophenone (5%) 1-Phenyl-3-pentanone (95%)	40%	6.1	6.83

[a]Based on a void volume of 0.19 mL/g (see ref. 8).
[b]%C determined by microanalysis.
[c]Generated *in situ*, see text.

reportedly (11) they cannot enter the channels of Silicalite. The resulting slurry was stirred for 3 h. The excess solvent was then removed by filtration and the solid washed with a further 4 mL of isooctane and allowed to dry for 10–16 h in a current of dry air at room temperature.

The actual yield of inclusion was also determined by elemental analysis (C, H, and inorganic residue) of the zeolite substrate samples (see Table 1).

The sample of Silicalite used (empty) was also examined using X-ray fluorescence, which, in addition to silicon, only showed a small amount of aluminum (<0.5%) and traces of potassium and calcium or indium (probably the former). Potassium and calcium could be impurities introduced through sample handling and preparation in our laboratory or at the manufacturer's. The presence of aluminum (presumably as AlO_2^-) as impurity is consistent with the results of nmr studies (12).

Results

Phosphorescence of aromatic ketones under nitrogen

The phosphorescence emission spectra of acetophenone, β-phenylpropiophenone, and benzophenone in Silicalite are shown in Fig. 1. The spectrum in Fig. 1D shows the luminescence from Silicalite with no guests. The ordinate scales have been expanded for presentation and no direct comparison of the relative intensities can be made from this figure. The emission from Silicalite is much weaker than that from any of the others (λ_{max} ~405 nm) and a correction for this background signal is not essential. No phosphorescence could be observed in the case of fresh samples (*vide infra*) of valerophenone in Silicalite.

The spectra obtained in Silicalite are in good agreement with those obtained in glasses, or with solution spectra in the case of acetophenone and benzophenone (β-phenylpropiophenone does not phosphoresce in solution (13)). The vibrational structure is evident in the cases of acetophenone and β-phenylpropiophenone, while no structure is apparent in the case of benzophenone (Fig. 1). It should be noted that in the case of benzophenone the elemental analysis showed very poor inclusion (see Table 1).

The phosphorescence decay of ketones in Silicalite was typically nonexponential. This is common to the decay law of other luminescent probes in heterogeneous media (ref. 14 and refs. therein). Table 2 includes several phosphorescence lifetimes obtained at room temperature; these refer to the first

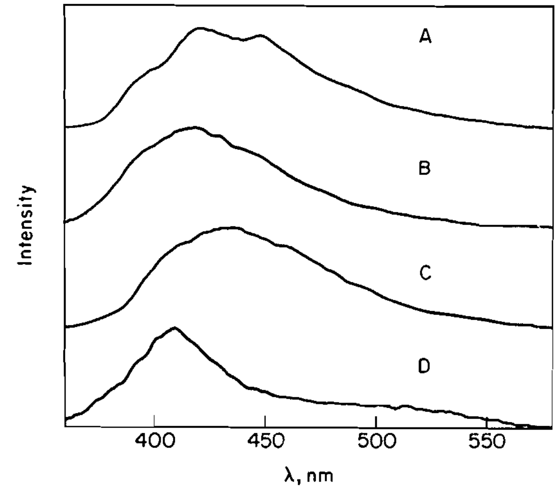

FIG. 1. Phosphorescence emission spectra (λ_{ex} = 254 nm) of acetophenone (A), β-phenylpropiophenone (B), and benzophenone (C) included in Silicalite at room temperature, and (D) luminescence of Silicalite (no guests) recorded under the same conditions. The intensity scales have been arbitrarily expanded, and no intensity comparisons can be made.

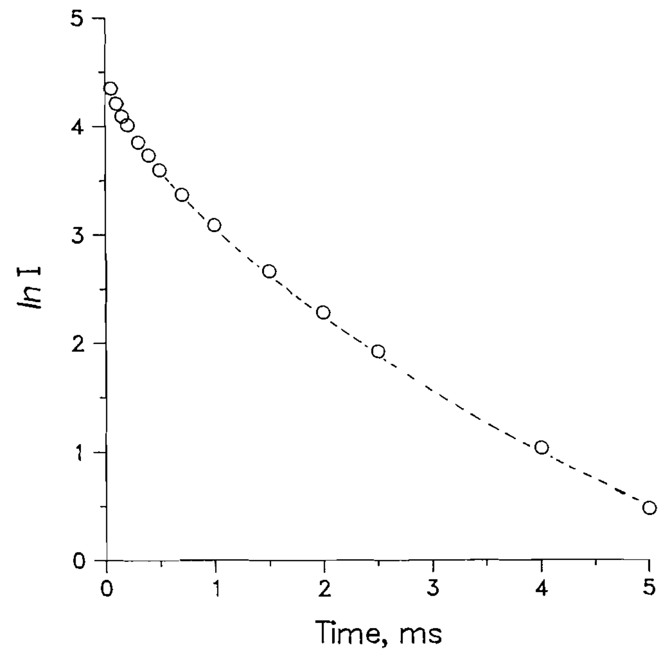

FIG. 2. Luminescence (ln I) intensity of acetophenone in Silicalite as a function of time.

lifetime monitored following a 20-μs delay after a 10-μs excitation pulse. Substantially longer lifetimes can be obtained by monitoring the emission after a longer delay between the excitation pulse and the beginning of the monitoring period. Figure 2 shows a logarithmic plot of the luminescence intensity from acetophenone as a function of time; similar plots were obtained for the other substrates.

Plots similar to that of Fig. 2 show a much better linear correlation when plotted against $t^{\frac{1}{2}}$ rather than t. This is frequently indicative of reaction (emission in this case) from multiple sites of an inhomogeneous matrix (15). Further work in this area is continuing, in an attempt to monitor the phosphorescence over several decades in emission intensity.

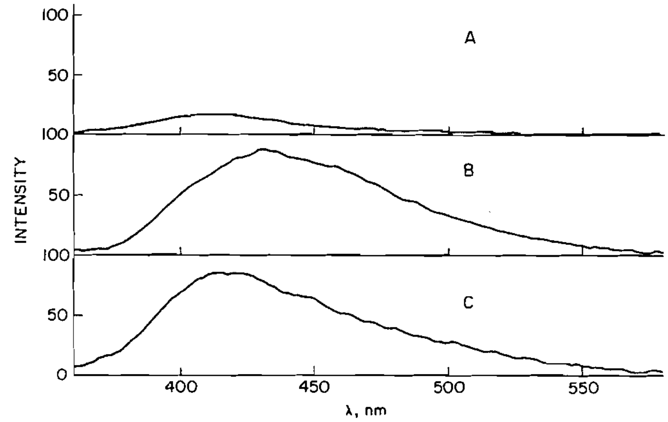

FIG. 3. Phosphorescence emission spectra (λ_{ex} = 254 nm) of (A) valerophenone in Silicalite (kept in the dark before the measurement), (B) same sample as in A but after 3 min irradiation at 300 nm (the intensity scale of parts A and B is the same), (C) valerophenone and acetophenone (co-included in the ratio 95:5 mol/mol).

TABLE 2. Phosphorescence of the various samples

No.	Substrate	τ, ms[a]	(Φ^0/Φ), (O_2)[b]
1	Acetophenone (20%)	0.18	4
2	Acetophenone (80%)	0.18	4
3	β-Phenylpropiophenone	0.14	5
4	Benzophenone	0.30	>10
5	Acetophenone/valerophenone	0.20	>15
6	Acetophenone[c]/valerophenone	0.19	>15
7	Acetophenone/1-phenylhexane	0.25	1.9
8	Acetophenone/1-phenyl-3-pentanone	0.04	4

[a]Based on the first lifetime, see text.
[b]Approximate intensity ratio in the absence of, and under 1 atm of, oxygen.
[c]Generated *in situ* via irradiation, see text.

Effect of co-inclusion on phosphorescence

In a reference to valerophenone above, we have emphasized that no phosphorescence is observed in *fresh* samples; i.e., samples prepared and kept in the dark. If valerophenone is exposed to uv radiation, analysis of the organic fraction following extraction reveals the presence of products of the Norrish Type II reaction (16), i.e.

[1] 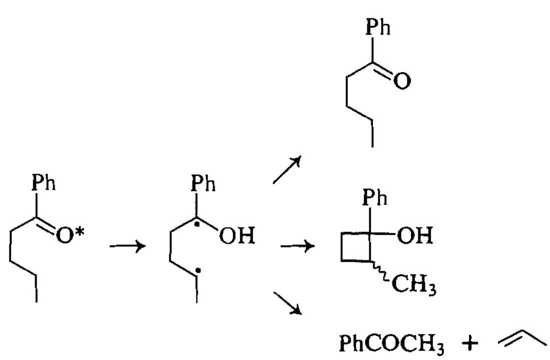

After even very short irradiation periods (2–3 min) the emission from the acetophenone formed becomes readily observable, and the intensity of the resulting phosphorescence increases with irradiation time. Alternatively, it is possible to prepare acetophenone–valerophenone samples by direct co-inclusion of a mixture of the two ketones, rather than *in situ* generation of acetophenone. The spectrum obtained following co-inclusion is similar, but not identical to that obtained by *in situ* generation; Fig. 3 shows the various spectra in the valerophenone-containing samples. The vibrational structure in co-included acetophenone samples also appears to be somewhat different from that obtained from acetophenone itself (compare Fig. 3 with Fig. 1A). It should also be noted that the samples used have different levels of occupancy (see Table 1).

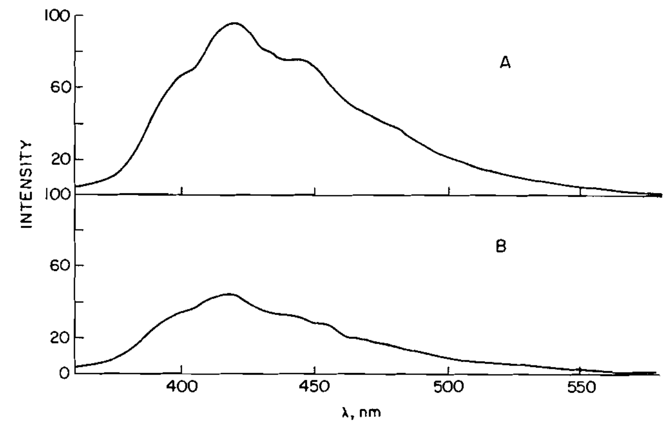

FIG. 4. Phosphorescence emission spectrum (λ_{ex} = 254 nm) of acetophenone and 1-phenylhexane (co-included in the ratio 5:95 mol/mol); (A) under 1 atm of N_2; (B) under 1 atm of O_2.

Studies involving co-inclusion of two ketones raise questions relating to energy transfer and (or) questions of preferential adsorption (*vide infra*). In order to be able to address these questions we carried out control experiments by co-inclusion of acetophenone and 1-phenylhexane as well as acetophenone and 1-phenyl-3-pentanone (5:95 molar ratio) in Silicalite. These cosubstrates were selected because their kinetic diameter and volume are comparable to those of valerophenone. The phosphorescence spectrum from acetophenone in the mixture with 1-phenylhexane is shown in Fig. 4; the spectrum under these conditions is quite strong and well resolved.

Phosphorescence quenching by oxygen

Oxygen was found to quench the phosphorescence of aromatic ketones to a different degree, depending on the ketone and its inclusion partners. All quenching experiments were performed by flowing oxygen through the samples while these remained in the spectrofluorimeter. Figure 5 shows the time dependence of the phosphorescence emission from included acetophenone (Fig. 5A) and benzophenone (Fig. 5B) with changing conditions. In both cases we observe luminescence quenching upon addition of oxygen. Quenching occurs over a few seconds, and is apparently controlled by the rate at which the composition of the gas in contact with the sample can be changed. When nitrogen is flowed again through the sample, the phosphorescence recovers; however, this process takes place over a longer period (~100 s) than that required for oxygen quenching. In these experiments the delay between excitation and monitoring was kept constant at 60 μs and the detection gate was 10 μs.

In the case of the sample of acetophenone co-included with 1-phenylhexane, 1 atm of pure oxygen quenched only 45% of the emission observed under nitrogen (see Figs. 4A and 4B). The vibrational structure of the acetophenone emission remains well resolved even in the spectrum recorded under an oxygen atmosphere. The quenching process for this sample was slow compared with all other samples examined; i.e. it was not controlled by the rate at which the gas was replaced. This is

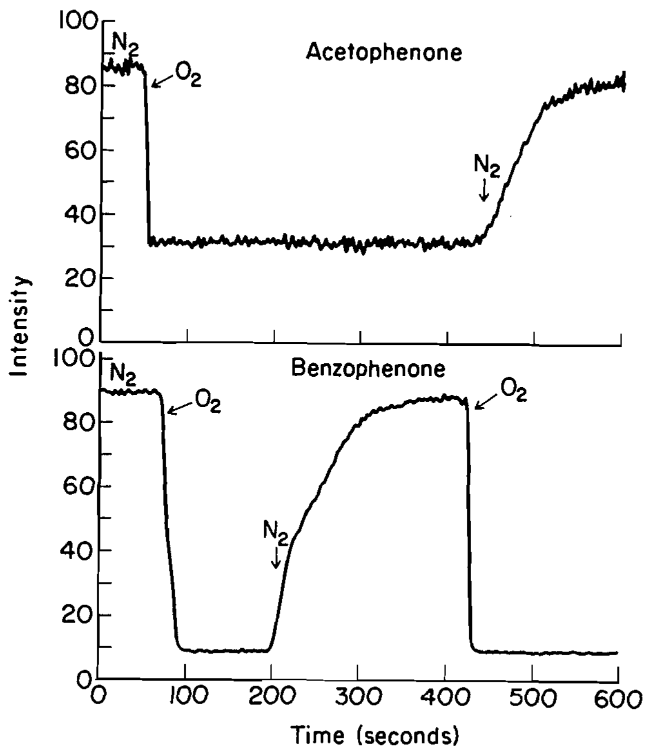

FIG. 5. Effect of changing the atmosphere of the sample cell on the phosphorescence emission (measured at 430 nm) of (A) acetophenone and (B) benzophenone in Silicalite.

illustrated in Fig. 6; oxygen takes ~50 s to quench the initial emission, and nitrogen takes ~150 s to restore it.

We have also monitored the dependence of the phosphorescence intensity with the composition of oxygen–nitrogen mixtures. It should be noted that the equivalent of Stern–Volmer plots takes a different form in the case of gated spectrometers. If the luminescence intensity is monitored at a constant preselected time (t_d) following pulsed excitation, the ratio I_t^0/I_t of the luminescence intensities in the absence and presence of quencher, respectively, is given by:

$$[2] \quad (I_t^0/I_t) = \exp\,(k_q t_d[Q])$$

Thus, eq. [2] contains the delay, t_d, rather than the triplet lifetime (which cancels out), and assumes an exponential form. Analysis of the luminescence yield according to the log form of eq. [2] as a function of the mole fraction of oxygen (total pressure = 1 atm) leads to nonlinear plots (for representative examples see Figs. 7–9). This behaviour can be approximated on the basis of (at least) two sites of different accessibility. This analysis, for t_d = 60 μs, has been included in Table 3 for several samples, in terms of a fast and a slow rate constant and the percent contribution from each process. Note that the rate constants (already divided by t_d) have units of s^{-1}, since they are based on mole fractions, not actual concentrations.

β-Phenylpropiophenone on other materials

This ketone does not phosphoresce in solution at ambient temperatures as a result of its efficient intramolecular deactivation which leads to a triplet lifetime in the neighborhood of 1 ns (13). This lifetime increases by about five orders of magnitude when β-phenylpropiophenone is included in Silicalite, and results in readily observable phosphorescence. In order to explore further the nature of this remarkable phosphorescence

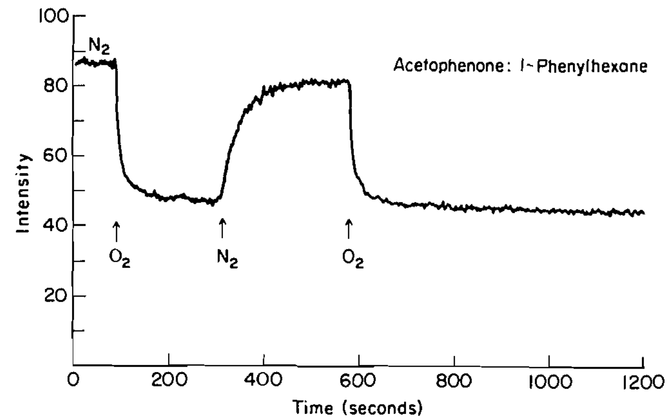

FIG. 6. Effect of changing the atmosphere of the sample cell on the phosphorescence emission (measured at 430 nm) of a mixture of acetophenone and 1-phenylhexane (5:95 mol/mol) co-included in Silicalite.

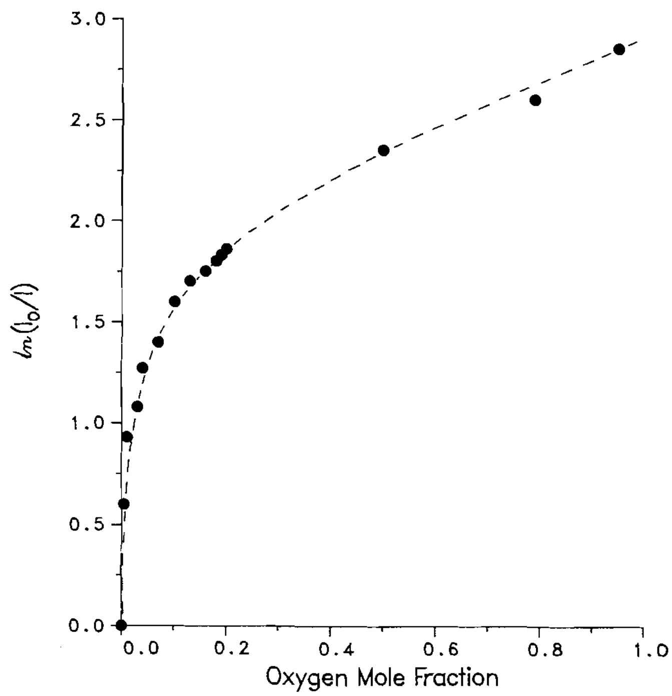

FIG. 7. Quenching of benzophenone phosphorescence by O_2 according to eq. [2]. Excitation: 254 nm; emission: 450 nm.

enhancement, we examined the luminescence of β-phenylpropiophenone in other two materials. A sample of silica gel (70–230 mesh) was subjected to the same protocol as Silicalite and no phosphorescence could be detected. Similarly, a sample of Mordenite, which has a much larger pore diameter (~9 Å) (17) gave no phosphorescence after treatment to include β-phenylpropiophenone.

Discussion

It seems clear from the results presented in the previous sections that the behaviour of aromatic ketones cannot be fully interpreted from the assumption of a single class of sites. The channel structure of Silicalite imposes a considerable restriction on some types of molecular motion. For example, in the case of β-phenylpropiophenone in solution, its lifetime at room temperature is around 1 ns (13); this short lifetime reflects intramolecular quenching by the aromatic ring, in a process that

TABLE 3. Stern–Volmer slopes for the quenching of phosphorescence by oxygen

No.	Substrate	λ_{ex}(nm)	k_q (slow)[a]	k_q (fast)[a]	% Fast[b] quenching
1	Acetophenone (20%)	254	1.6×10^4	$\sim10^6$	8
2	Acetophenone (80%)	254	2.2×10^4	2.6×10^6	13
4	Benzophenone	254/313	2.9×10^4	2.6×10^6	[c]
5	Acetophenone/valerophenone	254	$<3\times10^4$	8×10^5	[c]
7	Acetophenone/1-phenylhexane	254	6×10^3	8×10^5	30
		313	6×10^3	8.3×10^5	70
8	Acetophenone/1-phenyl-3-pentanone	254	2×10^4	$(1-3\times10^5)$	19
		313	2×10^4	3×10^5	45

[a]In units of s^{-1} (see text).
[b]Contribution of fast quenching to the total of quenching events.
[c]Continuous variation does not allow a proper separation of the two components. Quenching is essentially complete for 1 atm of oxygen.

with less efficiency also takes place in the case of other carbonyl triplets in aromatic solvents (see, for example, ref. 18). We have shown (13) that quenching occurs from the following conformation:

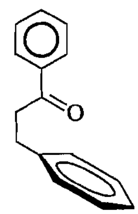

Not only does quenching require this conformation, but in fact triplet lifetimes are largely determined by the rate at which this conformation can be achieved (13). The strong phosphorescence from β-phenylpropiophenone and the fact that its triplet lifetime is comparable to that for acetophenone in Silicalite indicates that this molecule phosphoresces from regions where the conformation required for deactivation cannot be achieved. This should not be taken to mean that other sites where deactivation would be permitted are not populated as well, since those sites would not be observable using phosphorescence techniques. We suggest that β-phenylpropiophenone is mainly included within the channel structure of Silicalite (as opposed to the surface), where folding cannot occur. This conclusion is further supported by the absence of phosphorescence on silica gel, where only surface-adsorbed species are found, as well as in the case of Mordenite, where the cavities are much larger than in Silicalite (17). It should, however, be noted that these comparisons do leave room to some reservations, since the surface of silica gel is quite hydrophilic (19), in contrast with the hydrophobicity of the Silicalite channels. A critical dependence of the phosphorescence emission intensity of β-phenylpropiophenone and its derivatives on cavity size has also been observed in recent experiments in which this ketone was complexed with cyclodextrins.[2]

Deactivation in the case of valerophenone (see reaction [1]) requires a conformation similar to that required in the case of β-phenylpropiophenone; however, the absence of an aromatic ring on the hydrocarbon chain permits larger mobility, thus making the process possible, even if kinetically it may be slower than in solution, where triplet valerophenone lives less than 10 ns (20). Quite clearly, spatial requirements in the case of valerophenone are less stringent than for β-phenylpropiophenone. The occurrence of the Norrish Type II reaction in the case of valerophenone was also confirmed by product studies, and in fact is not unexpected in view of results from this laboratory showing that the reaction also occurs in other phenyl alkyl ketones when they are included in urea clathrates, where the diameter of the channel is ~5.5 Å (ref. 21).

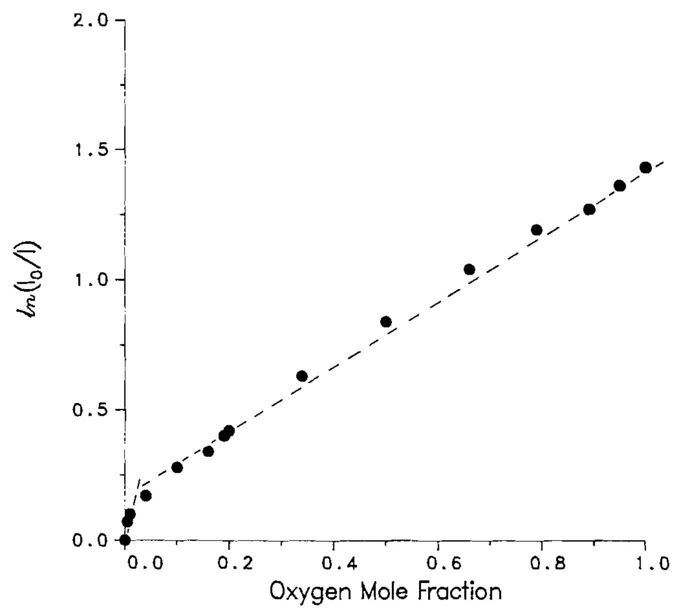

FIG. 8. Quenching of acetophenone phosphorescence by O_2 according to eq. [2]. Excitation: 254 nm; emission: 450 nm; nominal occupancy: 80%.

Phosphorescence from other ketones, such as acetophenone and benzophenone, is not surprising, since emission from these is readily observable in solution at room temperature in inert solvents (22).

Oxygen quenching experiments are quite useful in trying to understand the accessibility of different types of sites available in Silicalite. Thus, acetophenone an β-phenylpropiophenone are only partially quenched by 1 atm of oxygen. In the case of acetophenone, co-inclusion with 1-phenylhexane changes the rate and fraction of quenching, but not the qualitative observation that only partial quenching can be achieved under these conditions. By contrast, when acetophenone is generated *in situ* by photodecomposition of valerophenone, over 95% of its

[2]J. C. Netto-Ferreira, H. L. Casal, and J. C. Scaiano. Unpublished results.

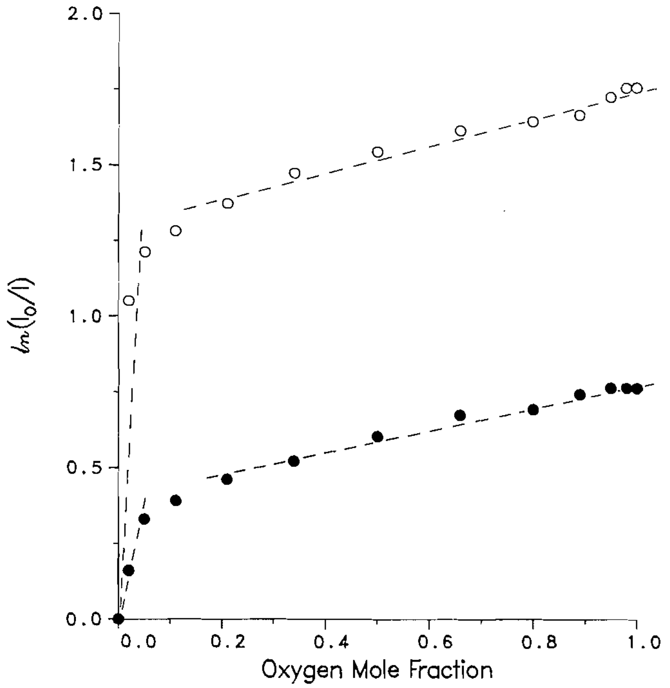

FIG. 9. Plots for the quenching of acetophenone phosphorescence by O_2 in a sample consisting of a mixture (5:95 mol/mol) of acetophenone and 1-phenylhexane in Silicalite (occupancy: 40%). Excitation: 254 nm (●); 313 nm (○). In both cases the emission was measured at 450 nm.

phosphorescence is quenched by 1 atm of oxygen. In principle, this observation could be the result of the occurrence of the Norrish Type II reaction in only one type of site (i.e. that which is readily accessible to oxygen). However, the phosphorescence of acetophenone is also suppressed by oxygen when acetophenone and valerophenone are co-included from a mixture of the two substrates. Here it is reasonable to assume that acetophenone is included in all types of sites, even if not necessarily with equal probability, and is supported by the result using acetophenone – 1-phenylhexane and acetophenone – 1-phenyl-3-pentanone mixtures, where their sizes are comparable to that of valerophenone; in these cases only partial quenching is observed.

From the analysis above, we conclude that the Norrish Type II reaction of valerophenone must occur in sites of all types. Why is acetophenone phosphorescence, observable only from the same sites that are accessible to oxygen? We believe that, in the more protected sites, the triplet state of acetophenone is quenched by valerophenone (reaction [3]), thus leading to a sensitized Norrish Type II reaction. Quasi-isoenergetic energy transfer between phenyl alkyl ketones has been shown to occur in solution with rate constants in the neighborhood of $10^9\ M^{-1}\ s^{-1}$ (23), while in polymer systems typical frequencies for energy hopping between nearby chromophores are in the $10^{10}-10^{12}\ s^{-1}$ range (24).

[3]
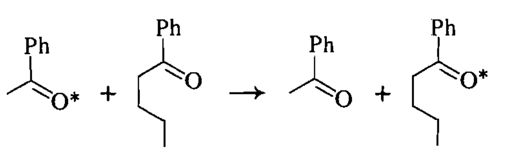

Thus, the evidence presented above indicates the presence of *at least* two different types of sites, which for convenience we will call A and B. Class A represents the more protected type of sites, which are not readily accessible to oxygen as shown by the only partial quenching observed in several of the examples examined. The guest molecules in sites of type A must be in close proximity, since no luminescence from these sites is observed when acetophenone is co-included with valerophenone, the result being the same regardless of the mode of co-inclusion (*in situ* generation of acetophenone or using substrate mixtures). Since quenching of acetophenone by valerophenone takes place even when the guest molecules occupy only 20% of the void volume of Silicalite, it is interesting to speculate that inclusion in these sites may involve a considerable degree of cooperative effect.

In the second class of sites (B), quenching by oxygen occurs efficiently and rapidly, implying fast diffusion in these regions. Further, the molecules must be well separated, since valerophenone is unable to quench acetophenone in these regions. In spite of the apparent separation between molecules and the rapid quenching by oxygen, molecular motion is sufficiently limited as to prevent intramolecular quenching in the case of β-phenylpropiophenone.

The phosphorescence of β-phenylpropiophenone must arise from sites located within the channel structure of Silicalite and not on its surface. Some β-phenylpropiophenone may be adsorbed on the surface, but (assuming that surface-adsorbed species are not immobilized) this fraction is not expected to show phosphorescence.

An analysis of the luminescence quenching data (Table 3) provides further information on the nature and characteristics of the various sites in Silicalite. Benzophenone shows a continuous variation of the slope, suggesting many sites. It is important to note (see Table 1) that this is the only substrate for which the experimental carbon content of the sample is much lower than the value calculated on the basis of the amount of material used during sample preparation. This suggests that most of the benzophenone is adsorbed in areas readily accessible to isooctane, which does not enter the Silicalite channel framework (11) and washes surface-absorbed species during preparation. Thus, most of the benzophenone may actually be on the surface of Silicalite or, perhaps, in structural defects. The kinetic diameter and shape of benzophenone probably make it a borderline case for inclusion in Silicalite.

The samples of acetophenone co-included with various substrates are particularly interesting. The marked differences in k_q (particularly for 1-phenylhexane) probably reflect differences in accessibility, since the triplet lifetimes do not enter in eq. [2], and in any event do not seem to change much (see Table 2). Thus, in the samples with valerophenone (No. 5 and No. 6) the luminescence is readily quenched by oxygen (Tables 2 and 3). The situation contrasts with that for samples No. 7 and No. 8 where a large fraction of the luminescence arises from the better protected triplet. We believe that this is due to the quenching of acetophenone triplets by valerophenone, which occcurs efficiently in the "slow" A sites. It would thus seem that in this class of sites the two ketones are in close proximity, further suggesting a cooperative binding effect.

These ideas are further supported by the data for the sample containing acetophenone and 1-phenylhexane (No. 7). Note that the same two triplets are produced in different ratio (Table 3) depending on the excitation wavelength. A simple explanation of this effect is that, while at 313 nm the light is almost exclusively absorbed by the ketone, at 254 nm about 90% of the radiation will be absorbed by 1-phenylhexane. In sites "A", where the substrates are in close proximity, sensitization via energy transfer takes place efficiently; by contrast, in sites "B", a larger separation minimizes energy transfer. As a result, luminescence from sites of type "A" is favoured at 254 nm. The same ideas apply to sample No. 8. A related example has been published in a recent report showing very efficient sensitization of the fluorescence from anthracene on filter paper, coadsorbed with naphthalene, used as a sensitizer (25).

In the case of acetophenone most of the luminescence seems to arise from well-protected sites. This probably reflects the easy access of acetophenone to the channel framework of Silicalite. Further, it is also possible that energy migration and self-quenching processes that are well established in micellar solution (26) may play an important role.

We would like to note that we have referred to sites A, B, and the surface as "classes or types" of sites in an attempt to emphasize that each group may include several locations within the framework of Silicalite; these locations have common properties in the case of phosphorescent aromatic ketones and their quenching by oxygen; the latter probably reflects differences in accessibility. Recent work by Fyfe *et al.* (12) suggests the presence of numerous sites in the case of Silicalite, an observation that seems consistent with our preliminary observation of a $t^{\frac{1}{2}}$ dependence of the phosphorescence intensity.

Finally, while the data in Table 3 have been obtained taking into account the values of t_d (see eq. [2]), we have not varied this parameter systematically. Current work is concentrating on this particular aspect, i.e. the time dependence of the luminescence quenching data, in the hope that this will help to understand better the nature of the different classes of sites.

Acknowledgements

Thanks are due to Mr. S. E. Sugamori for technical assistance and to Dr. A. P. Roth for recording the X-ray fluorescence of Silicalite.

1. P. DE MAYO. Pure Appl. Chem. **54**, 1623 (1982); R. FARWAHA, P. DE MAYO, and Y. C. TOONG. J. Chem. Soc. Chem. Commun. 739 (1983); M. E. ZAWADSKI and A. B. ELLIS. J. Org. Chem. **48**, 3156 (1983).
2. J. R. SCHEFFER. Acc. Chem. Res. **13**, 283 (1980); J. TROTTER. Acta Crystallogr. Sect. B, **39**, 373 (1983).
3. H. L. CASAL, P. DE MAYO, J. F. MIRANDA, and J. C. SCAIANO. J. Am. Chem. Soc. **105**, 5155 (1983); H.-G. LÖHR, F. VÖGTLE, W. SCHUH, and H. PUFF. J. Chem. Soc. Chem. Commun. 924 (1983); H. AOYAMA, K. MIYAZAKI, M. SAKAMOTO, and Y. OMOTE. J. Chem. Soc. Chem. Commun. 333 (1983); Y. HUI, J. R. WINKLE, and D. G. WHITTEN. J. Phys. Chem. **87**, 23 (1983).
4. G. A. OZIN and F. HUGHES. J. Phys. Chem. **86**, 5174 (1982); G. A. OZIN, F. HUGUES, S. M. MATTAR, and D. F. MCINTOSH. J. Phys. Chem. **87**, 3445 (1983).
5. B. H. BARETZ and N. J. TURRO. J. Photochem. **24**, 201 (1984).
6. K. CHANDRASEKARAN, T. K. FOREMAN, and D. G. WHITTEN. Nouv. J. Chim. **5**, 275 (1981); S. LEUTWYLER and E. SCHUMACHER. Chimia, **31**, 475 (1977).
7. H. L. CASAL and J. C. SCAIANO. Can. J. Chem. **62**, 628 (1984).
8. E. M. FLANIGEN, J. M. BENNETT, R. W. GROSE, J. P. COHEN, R. L. PATTON, R. M. KIRCHNER, and J. V. SMITH. Nature, **271**, 512 (1978).
9. N. B. MILESTONE and D. M. BIBBY. J. Chem. Tech. Biotechnol. **31**, 732 (1981); G. M. W. SHULTZ-SIBBEL, D. T. GJERDE, C. D. CHRISWELL, J. S. FRITZ, and W. E. COLEMAN. Talanta, **29**, 447 (1982).
10. E. F. PRATT and A. P. EVANS. J. Am. Chem. Soc. **78**, 4950 (1956).
11. P. A. JACOBS, J. A. MARTENS, J. WEIKAMP, and H. K. BEYER. Faraday Disc. Chem. Soc. **72**, 353 (1981).
12. C. A. FYFE, G. C. GOBBI, J. KLINOWSKI, J. M. THOMAS, and S. RANDAS. Nature, **296**, 530 (1982).
13. J. C. SCAIANO, M. J. PERKINS, J. W. SHEPPARD, M. S. PLATZ, and R. L. BARCUS. J. Photochem. **21**, 137 (1983).
14. A. HABTI, D. KERAVIS, P. LEVITZ, and H. VAN DAMME. J. Chem. Soc. Faraday Trans. 2, **80**, 67 (1984).
15. T. DOBA, K. U. INGOLD, and W. SIEBRAND. Chem. Phys. Lett. **103**, 339 (1984).
16. J. C. SCAIANO, E. A. LISSI, and M. V. ENCINA. Rev. Chem. Intermed. **2**, 139 (1978).
17. R. M. BARRER. Zeolites and clay minerals as sorbents and molecular sieves. Academic Press, New York. 1978.
18. M. W. WOLF, R. E. BROWN, and L. A. SINGER. J. Am. Chem. Soc. **99**, 526 (1977); J. A. BELL and H. LINSCHITZ. J. Am. Chem. Soc. **85**, 828 (1963); J. SALTIEL, H. C. CURTIS, L. METTS, J. W. MILEY, J. WINTERLE, and M. WRIGHTON. J. Am. Chem. Soc. **92**, 410 (1970); D. I. SCHUSTER, T. M. WEIL, and M. R. TOPP. Chem. Commun. 1212 (1971).
19. P. DE MAYO, A. SAFARZADEH-AMIRI, and S. K. WONG. Can. J. Chem. **62**, 1000 (1984).
20. M. V. ENCINA, E. A. LISSI, E. LEMP, A. ZANOCCO, and J. C. SCAIANO. J. Am. Chem. Soc. **105**, 1856 (1983).
21. L. C. FETTERLY. *In* Nonstoichiometric compounds. *Edited by* L. Mandelcorn. Academic, New York. 1964. Chapt. 8.
22. N. J. TURRO. Modern molecular photochemistry. Benjamin-Cummings, Menlo Park, CA. 1978. pp. 129–130.
23. M. V. ENCINA and J. C. SCAIANO. Chem. Phys. Lett. **63**, 305 (1979).
24. M. V. ENCINAS, K. FUNABASHI, and J. C. SCAIANO. Macromolecules, **12**, 1167 (1979); J. C. SCAIANO and J. C. SELWYN. Macromolecules, **14**, 1723 (1981).
25. P. G. SEYBOLD, D. A. HINCKLEY, and T. A. HEINRICHS. Anal. Chem. **55**, 1996 (1983).
26. J. C. SCAIANO and J. C. SELWYN. Can. J. Chem. **59**, 2368 (1981); Photochem. Photobiol. **34**, 29 (1981).

Photochemical reactions in organized assemblies. 40.[1] Amylose and carboxymethylamylose inclusion complexes with photoreactive molecules

BRIAN R. SUDDABY, RAYMOND N. DOMINEY, Y. HUI,[2] AND DAVID G. WHITTEN
Department of Chemistry, University of Rochester, Rochester, NY 14627, U.S.A.

Received June 14, 1984

This paper is dedicated to the memory of Li Xiao-Bai

BRIAN R. SUDDABY, RAYMOND N. DOMINEY, Y. HUI, and DAVID G. WHITTEN. Can. J. Chem. **63**, 1315 (1985).

This paper focuses on a study of unimolecular and bimolecular photoreactions occurring with reactants which can be incorporated into the linear polysugars amylose and carboxymethylamylose. Hydrophobic and surfactant *trans* (E) stilbene derivatives form complexes in which the stilbene chromophore shows enhanced fluorescence and reduced *trans* → *cis* isomerization efficiencies. The reactivity of the excited surfactant–stilbene singlet towards the quencher iodide ion has been compared in water/dimethylsulfoxide in the presence and absence of amylose under conditions where complex formation is nearly complete. Some relatively hydrophobic viologen dications have also been found to form complexes with the water soluble carboxymethylamylose. Although the dications complex relatively weakly, the partially reduced monocations complex more strongly. This results in selective retardation of back electron transfer rates when the viologens are used as electron transfer quencher-oxidants for certain luminescent ruthenium polypyridine complexes.

BRIAN R. SUDDABY, RAYMOND N. DOMINEY, Y. HUI et DAVID G. WHITTEN. Can. J. Chem. **63**, 1315 (1985).

On étudie les photoréactions uni- et bi-moléculaires qui se manifestent dans le cas de réactifs que l'on peut incorporer dans les polysucres linéaires de l'amylose et du carboxyméthylamylose. Les dérivés hydrophobes et tensioactifs du *trans* (E) stilbène forment des complexes dans lesquels le chromophore stilbène présente des efficacités accrue de fluorescence et réduite d'isomérisation *trans* → *cis*. Opérant dans un mélange eau/diméthylsulfoxyde, en présence ou en l'absence d'amylose et dans des conditions où la formation du complexe est pratiquement totale, on a comparé la réactivité du singulet du stilbène tensioactif excité vis-à-vis d'un ion iodure, agissant comme piège. On a aussi trouvé que quelques dications viologènes relativement hydrophobes forment des complexes avec le carboxyméthylamylose soluble dans l'eau. Bien que les dications forment des complexes relativement faibles, les monocations partiellement réduits se complexent plus fortement. Ceci conduit à des retards sélectifs dans les vitesses de transfert en retour d'électrons lorsqu'on utilise les viologènes comme oxydants pièges de transfert d'électrons pour certains complexes luminescents de ruthénium polypyridine.

[Traduit par le journal]

Introduction

The interaction of small molecules dissolved as solutes in solution with various sorts of interfaces, the binding of small molecules to reactive sites in soluble and insoluble polymers, and the formation of inclusion complexes between small molecules or ions and various types of "hosts" such as zeolites, cyclodextrins, cryptates, and crown ethers represent seemingly disparate but often closely related studies of what might best be grouped under the broad title of interfacial chemistry (1–9). When small molecules are bound or sequestered at the various interfacial sites described above, their behavior and reactivity is often modified compared to that in fluid solution. The modified reactivity encountered in such situations is of wide interest both due to its possible utility and to its frequent apparent relationship to biochemical and biophysical phenomena.

Among the various kinds of inclusion complexes studied, those with cyclodextrins as hosts and relatively small, nonpolar molecules as guests have been widely and thoroughly investigated (10–16). The cyclodextrin host is generally water soluble and presents a "cavity" into which small molecules can be imbedded. Molecular models indicate that this cavity is relatively hydrophobic and it has been found indeed that association is often very strong between nonpolar "guests" and the cyclodextrin host (14, 15). When the cyclodextrin incorporates specific molecules it is frequently observed that the reactivity of the incorporated molecule is substantially modified both with respect to unimolecular and biomolecular reactivity (10–16). In some cases conformationally flexible molecules give evidence that incorporation into a cyclodextrin complex leads to preferential "locking" into specific configuration. In other cases it has been found that bimolecular reactions of the guest are either retarded or, in some examples, completely inhibited (17). While rigid cyclodextrins can specifically incorporate molecules depending upon their size and hydrophobicity, it has also been found that the much more flexible glucose polymer amylose can also incorporate a variety of small molecules in what appear to be relatively similar inclusion complexes (18–23). Studies of binding constants for various molecules indicate that the amylose host provides a "cavity" with at least some characteristics similar to those of the cyclodextrins. However, in the case of the amylose it appears clear that there is considerably more flexibility in the size and length of the guest binding sites. Studies of the behavior of incorporated molecules have suggested that at least in some cases the binding sites are, like the cyclodextrins, relatively hydrophobic; for example, investigation with the fluorescent probe 2-(p-toluidinyl)-naphthalene-6-sulfonate, which shows unusual sensitivity to environment polarity, indicates that in low molecular weight amylose–water the fluorescence of the complex probe is similar to that observed in organic solvents or relatively hydrophobic sites of proteins (19). A number of investigations have suggested that amylose can exist in a variety of conformations in the absence of guests; it has been proposed that these conformations can easily rearrange to helical segments which are the site for inclusion complex formation (20). For both amylose and the somewhat more polar carboxymethylamylose it appears that the conformation of the macromolecule and its binding properties are strongly influenced by the solvent composition (22).

As par of our investigations of the properties in reactivity of

[1] Paper 39 is ref. 36.

[2] Permanent address: Shanghai Institute of Organic Chemistry, Academia Sinica, People's Republic of China.

organized assemblies and small molecules incorporated therein, we have recently examined the photochemical and photophysical behavior of functionalized surfactant molecules containing reactive chromophores in a number of different media; recently we found that a series of surfactant ketones and stilbenes form inclusion complexes with amylose and carboxymethylamylose (24, 25). In both studies we found evidence that the chromophore experiences a moderately hydrophobic environment in which there is reduced conformational flexibility. In the present paper we report an extension of these studies to include both a more detailed study of the various kinds of complexes formed from substituted stilbenes, as well as new investigations of bimolecular photoreactions in which one of the partners can be complexed or at least partially associated with carboxymethylamylose.

Experimental

Materials

Amylose (Aldrich, mol. wt. over 150 000) was used as received. Carboxymethylamylose was prepared as described below. The surfactant *trans*-stilbene probes were prepared by procedures described elsewhere (26). Distilled water was used in all studies and dimethylsulfoxide (Mallinckrodt) was spectrophotometric grade. The viologen derivatives were commercial (Aldrich) samples while the tris(2,2′-bipyridine) ruthenium hexafluorophosphate was prepared from a commercial (Aldrich) sample of the dichloride hexahydrate.

Carboxymethylamylose

Ten grams of amylose (Aldrich mol. wt. $\sim 1.5 \times 10^5$) is dissolved in 200 mL of 20% aqueous NaOH (40 g NaOH/200 mL H_2O). Dissolution is accomplished by *small* batch additions of the amylose to the continuously stirred NaOH solution while holding the temperature of solution at ~60°C (*T* must be <80°C to prevent decomposition which produces a yellow coloration). This may take 1–2 h. After complete dissolution, 7.5 g of $ClCH_2COOH$ is added and the mixture stirred for 15–24 h at room temperature. While stirring, the solution is diluted with ~600 mL 95% EtOH to produce a white precipitate. After decanting the liquid phase the Na-CMA can be purified by redissolving in 150–250 mL H_2O. Reprecipitation is then effected by *slow* addition to a *vigorously* stirred volume (~1 L) of EtOH (95%). After filter collection, the Na-CMA is vacuum dried and ground to a powder. The measurement of the degree of substitution (DS) is based on a conductometric procedure. Dried CMA (200 mg) is dissolved in 175 mL of distilled H_2O and 1.5 mL of 0.4 *N* NaOH solution is added. The solution is titrated with 0.14 *N* aqueous HCl, followed by conductivity measurements. Calculation of DS is made according to the following equation:

$$\mathrm{DS} = \frac{A \times 0.162}{1 - 0.080 \times A}$$

where $A = (V_2 - V_1)N/(\text{g sample})$, V_2 and V_1 are obtained from the titration curve, and N is the normality of the HCl solution (27).

Spectroscopic measurements

Luminescence spectra were recorded on an SLM 800 or a SPEX Fluorolog2 digital, photon-counting spectrofluorimeter. Absorption spectra were obtained using a Perkin–Elmer 576ST spectrophotometer.

Results and discussion

Complexes between functionalized trans-*stilbene derivatives and amylose*

As reported previously (24), we have found that while *trans*-stilbene itself gives no evidence for association with low or moderate molecular weight amylose in 1:1 dimethylsulfoxide (DMSO)/water, the substituted *trans*-stilbene derivatives S_nA, where n = 4, 6, and 12, form complexes in which there is a

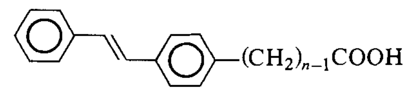

modest increase in fluorescence with a concomitant decrease in the quantum yield for *trans–cis* isomerization. For all three of these stilbenes the quantum yield within the inclusion complex shows an approximate four-fold increase to a value of ϕ_f = 0.23. The increase in fluorescence upon addition of amylose to the DMSO/water solution can be used to evaluate the association constants for the different stilbenes with amylose. It is found, in accord with other studies (17–22), that the association constants increase with effective increases in the chain length or hydrophobicity of the surfactant stilbene. In recent investigations we have prepared additional substitute stilbenes including both surfactant and hydrophobic derivatives which contain the *trans*-stilbene chromophore in the middle of a long alkyl chain (26). Compounds we have studied with amylose include ${}_4S_4$ and ${}_6S_4A$. These structures are shown below.

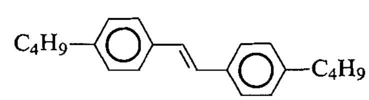

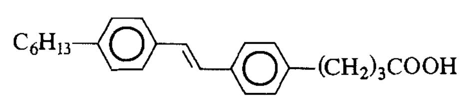

These stilbenes exhibit modest solubility in DMSO/water but at even relatively low or moderate concentrations they show evidence of aggregation to form what are apparently H-aggregates (26). Our investigations have revealed that addition of amylose to solutions of the stilbenes in DMSO/water results in a sharp decrease in the fluorescence spectrum of the H-aggregated species in both cases, concurrent with an appearance of a sharp fluorescence attributable to the monomeric species (Fig. 1). The effect is especially striking with ${}_6S_4A$ where the two species have quite different fluorescence spectra. Although both ${}_4S_4$ and ${}_6S_4A$ show aggregates at low concentrations, dilution of DMSO/water solutions of the latter leads to monomeric absorption and fluorescence spectra at low concentrations. Under these conditions the ratio of fluorescence quantum yields in the presence and absence of amylose (1%) is 5.06 (Fig. 2). Since the quantum yield of fluorescence of ${}_6S_4A$ in the absence of amylose is 0.20 ± 0.01, this indicates that the presence of amylose raises ϕ_f to ~1.0 and further indicates that virtually all of the ${}_6S_4A$ is complexed. The effect with the intrachain stilbene is thus considerably greater than with the previously studied hydrophobic compounds in which the chromophore is at the end of the chain. For example, $S_{12}A$, which has an effectively "longer" hydrophobic chain, gives a fraction complexed at the same concentration of amylose of 0.70 and a limiting quantum yield of ϕ_f = 0.23; for this compound, as well as with S_4A and S_6A, an appreciable fraction of included stilbene molecules activated by light undergo *trans* → *cis* isomerization. In contrast, for complexes ${}_6S_4A$ there is effectively no photoisomerization. Iodide ion, which has been previously shown to quench *trans*-stilbene in 2:3 acetonitrile/water with a rate constant $k_q = 2.2 \times 10^{10}\ M^{-1}\ s^{-1}$ (28), has been examined as a quencher of the luminescence of ${}_6S_4A$ in the presence and absence of amylose. Preliminary studies indicate that amylose incorporation substantially reduces, but does not eliminate, quenching of the stilbene chro-

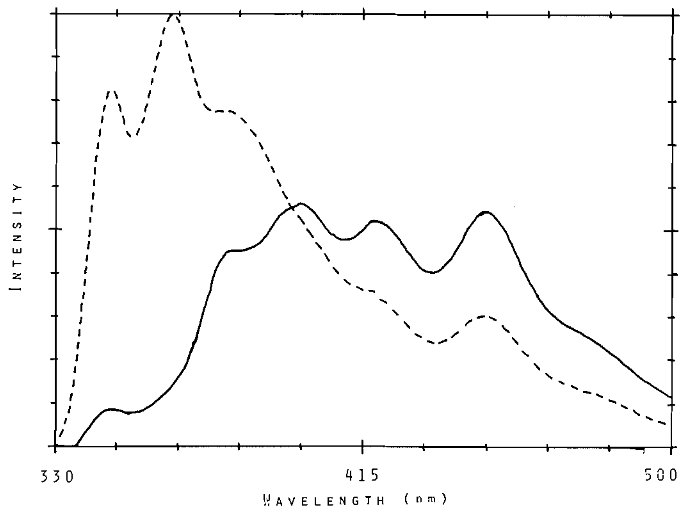

FIG. 1. Fluorescence spectra of $_6S_4A$ 5.0 × 10^{-5} M in 1:1 DMSO/H_2O (—) and 1% amylose in 1:1 DMSO/H_2O (- - -). λ_{ex} = 300 nm.

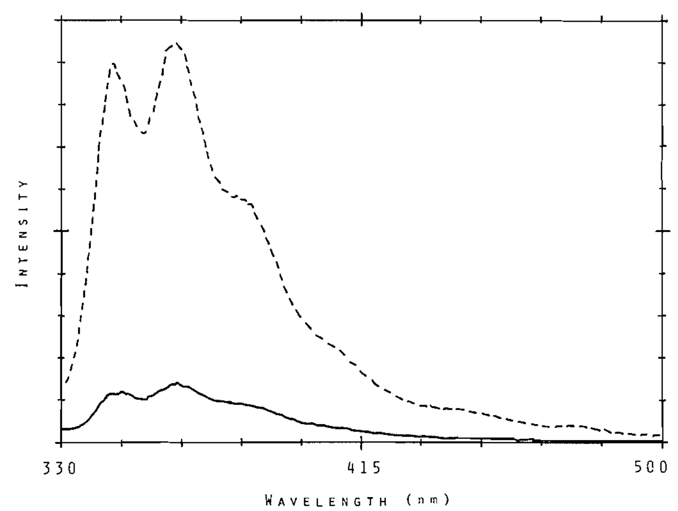

FIG. 2. Fluorescence spectra of $_6S_4A$ 5 × 10^{-7} M in 1:1 DMSO/H_2O (—) and 1% amylose in 1:1 DMSO/H_2O (- - -). λ_{ex} = 300 nm.

mophore singlet. Thus we find the Stern–Volmer quenching constants are 2.5 and 0.5 for $_6S_4A$ in the absence and presence of amylose respectively. Using lifetimes estimated from fluorescence efficiencies, we obtain k_q values of 4.4 × 10^8 M^{-1} s^{-1} and 1.3 × 10^{10} M^{-1} s^{-1} in DMSO/water in the presence and absence of amylose. Thus quenching is reduced about thirty-fold for iodide by amylose incorporation of the stilbene chromophore. It has been suggested that quenching of stilbene by iodide is a "charge-transfer" interaction since the quenching constants for several inorganic ions correlated with oxidation potentials (28); however, since fluorescence quenching is accompanied by an increase in *trans* → *cis* isomerization, heavy atom effects may also be important (28). The latter should require relatively close approach between the iodine nucleus and the stilbene chromophore and thus would explain in part the reduction in quenching rate. This seems not unreasonable in view of the presumed structure of the complex, in which any kind of major rotation of the stilbene chromophore around the ethylenic bond should be difficult, if not entirely forbidden, during the lifetime of excited singlet or triplet states. Studies on the photoreactivity of bound and free $_6S_4A$ also reveal sharp differences between the H-aggregated and amylose-incorporated species. Thus we find that the H-aggregate undergoes rapid photobleaching while the $_6S_4A$ shows relatively low photoreactivity. At the present time we have not established whether the photobleaching of the H-aggregated species is due to *trans* → *cis* isomerization or, perhaps, dimerization.

We are currently examining reactivity of amylose-incorporated $_6S_4A$ with a variety of potential quenchers of its excited singlet state. These studies should provide further insights into how reactions such as photoaddition, light induced electron transfer, or other processes can be modified by formation of the inclusion complexes.

Modification of rates of light induced electron transfer reactions by carboxymethylamylose host–guest interactions

As described above, we and others have found that organic chromophores, especially relatively linear or rod-like molecules that are more or less compatible with polymethylene chains, frequently form complexes with amylose and carboxymethylamylose. A very well-studied class of redox active molecules which might appear to belong in this category are the dialkyl viologens, R_2V^{2+},

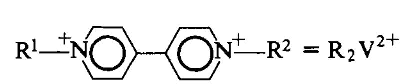

whose basic 4,4′-bipyridinium structure can be easily modified by varying structure of the N and N′ alkyl groups. Thus it would seem that dialkyl viologens having one or two long alkyl chains should form reasonably good complexes with amylose derivatives in either their oxidized (dication) or mono reduced (cation-radical) forms. Towards this end we have investigated both complex formation with various viologen derivatives as well as their participation in light induced electron transfer reactions.

Unlike the previously described stilbene derivatives, which show pronounced absorption and fluorescent spectral changes upon incorporation into amylose, the viologen cations undergo no discernible spectral changes and are not easy to detect if they are complexed. To assay the binding of various viologen derivatives to carboxymethylamylose in water, we have taken advantage of the fact that the amylose and carboxymethylamylose form intensely blue colored complexes with polyiodide ions (29–31). This complex evidently consists of linear I_x^- (x = 3 or 5) incorporated into helical cavities formed by the amylose chain (29). The complex has a reasonably sharp absorption with λ_{max} = 600 nm, an absorbance which is relatively stable over time. The 600-nm band is discharged by the addition of long chain alcohols such as decanol or surfactants such as dodecyltrimethylammonium ion but not by small ions such as tetramethylammonium or shorter chain alcohols such as 1-hexanol. Examination of the viologen derivatives shows that dimethyl viologen (R^1, R^2 = CH_3) has no effect on the iodide absorption at 600 nm while, in contrast, addition of heptyl viologen (R^1, R^2 = C_7H_{15}) causes rapid bleaching of the band at 600 nm. In fact, there is a linear decrease in the absorbance at 600 nm as the concentration of heptyl viologen increases. From the degree of bleaching it can be ascertained that there are approximately 35 binding sites for heptyl viologen molecules per unit of carboxymethylamylose used. Thus, with the viologens as with the stilbenes, we find evidence that formation of the inclusion complexes can be correlated quite well with apparent chain length or overall hydrophobicity.

Since the monoreduced viologen derivatives should be substantially more hydrophobic than the dications, it might be expected that reduction would result in increased facility to form host–guest inclusion complexes. This is not easy to ascertain with dimethyl viologen; however, some evidence that this is the case can be obtained by studying reduced heptyl viologen. For the latter compound it has been established that the monocation reversibly dimerizes in aqueous solutions for $[H_2V^+] = 1 \times 10^{-5}$ *M*. This is accompanied by a decrease in the absorbance at 605 nm, the λ_{max} for the heptyl viologen cation radical monomer, and a corresponding increase at 565 nm, where the dimer absorbs. Thus we find that independent preparation of the radical cation in the absence of CMA leads to dimerization at these concentrations, and the addition of 1% CMA results in detection of only monomer until concentrations of the radical cation greater than 10^{-4} *M* are reached. This affirms once again that the radical cation readily forms an inclusion complex with CMA.

A reaction of various viologen derivatives which has been particularly well studied involves light induced oxidation of the tris(2,2′-bipyridine) ruthenium(II) dication (32–35). In this reaction (eq. [1]) the excited state of the ruthenium complex is quenched by single electron transfer to viologens such as dimethyl viologen.

[1] $Ru(bpy)_3^{2+*} + RV^{2+} \rightarrow Ru(bpy)_3^{3+} + RV^{\dot{+}}$

[2] $Ru(bpy)_3^{3+} + RV^{\dot{+}} \rightarrow Ru(bpy)_3^{2+} + RV^{2+}$

This reaction, which occurs at rates very close to diffusion controlled, involves efficient oxidation of the metal complex excited state; however, it is followed almost immediately by a back electron transfer process (eq. [2]) which regenerates the starting materials in their ground states. Rates of reaction [1] and analogous quenching processes are easily measured by examining either quenching of the phosphorescence of the luminescent ruthenium complex or reduction of the phosphorescent lifetime, while rates of the second reaction (eq. [2]) are easily studied by flash photolysis techniques. Interestingly, we find with $Ru(bpy)_3^{2+}$ there is *no effect* upon addition of CMA of quenching by either methyl viologen or heptyl viologen (Table 1). Replacement of $Ru(bpy)_3^{2+}$ with the anionic complex RuL_3^{4-} (where L = 4,4′-dicarboxy-2,2′-bipyridine) results once again in no effect upon addition of CMA on the quenching process by methyl viologen. Here, however, a Stern–Volmer quenching plot with heptyl viologen shows a curvature consistent with at least some intial sequestering of the viologen at very low concentrations. Nonetheless the overall effect observed on bimolecular quenching by both viologens upon addition of CMA is essentially negligible. This is surprising for several reasons. First of all, one might expect that a sequestered viologen would have considerably lowered reactivity as a quencher for an excited state and a process such as eq. [1]. Secondly, addition of CMA to aqueous solutions would surely be expected to increase the bulk viscosity of the solution. In fact, viscosity measurements indicate that at the levels of CMA used (1%) there is an apparent increase in viscosity of a factor of 1.5. This indicates that a diffusion controlled reaction should experience a change in rate constant of about 0.67; such a change is clearly not observed even under conditions where a significant fraction of the heptyl viologen should be complexed. With regard to the present results, the most reasonable explanation seems to be that with methyl viologen (which does not complex with CMA), although the bulk viscosity is increased, the microviscosity of the solution where the quenching process (eq. [1]) occurs is effectively unaffected. It is more difficult to come up with an explanation for the lack of effect noted with heptyl viologen; however, one possible explanation is that the equilibrium between complexed and uncomplexed viologen is rapid and favors the uncomplexed form at the concentration used in the quenching experiments; thus the effect is minimal and difficult to detect. An alternative explanation, that complexed and uncomplexed heptyl viologen react at similar rates, appears relatively unattractive.

In contrast to the lack of effect of CMA on the quenching processes, examination of the rates of back electron transfer (eq. [2]), as measured by the disappearance of the viologen radical cation absorption at 605 nm, shows that substantial effects are observed for both methyl and heptyl viologens (Table 2). The back reaction rates are retarded by factors of 3 to 5 for heptyl viologens (depending upon pH) and by factors of 2 to 3 for methyl viologens. These retardations are clearly greater than would be predicted simply on the basis of the change in bulk viscosity mentioned above. The reactions follow clean second-order equal concentration kinetics and suggest that the reaction involves almost exclusively viologen cation contained within the inclusion complex.

Results obtained in the study are interesting in that they point out the degree of control or selectivity which may be possible in modification of bimolecular reactions. Thus in the electron transfer overall sequence the difference in hydrophobicity of the viologen monocations compared to the dications allows selective, although modest, retardation of the back electron transfer process. However, the relatively modest extent of the retardation on the exothermic back electron transfer reaction raises questions as to just how "sequestered" an amylose-incorporated molecule is for different kinds of reactions. There is increasing evidence that exothermic electron transfer reactions can occur over distances of several angstroms; one possibility is that the net retardation observed is due to a combination of the viscosity effect noted above and reasonably close

TABLE 1. Stern–Volmer quenching of $Ru(bpy)_3^{2+*}$ [a]

[CMA] (%)	Viologen	k_q (M^{-1} s^{-1})
0	Heptyl	2.5×10^9
1	Heptyl	2.5×10^9
0	Methyl	1.9×10^9
1	Methyl	1.8×10^9

[a] Aqueous solution.

TABLE 2. Back reaction rates $Ru(bpy)_3^{3+} + RV^{\dot{+}} \xrightarrow{k_{Bk}} Ru(bpy)_3^{2+} + RV^{2+}$ as determined by flash photolysis[a]

[CMA] (%)	Viologen	pH	k_{Bk} (M^{-1} s^{-1})	$k_{Bk}^{(0)}/k_{Bk}^{(CMA)}$
0	Heptyl	2.8	8.4×10^9	4.6
1	Heptyl	3.7	1.8×10^9	
0	Heptyl	5.6	3.3×10^9	3.5
1	Heptyl	6.2	9.3×10^8	
0	Heptyl	8.0	2.4×10^9	2.7
1	Heptyl	9.5	9.6×10^8	
0	Methyl	6.2	7.2×10^9	2.3
1	Methyl	6.2	3.1×10^9	

[a] $[Ru(bpy)_3^{2+}] = 2 \times 10^{-5}$ *M*, [NaCl] = 0.3 *M* [viologen] = 10 m*M*, 0.1 *M* phosphate buffer.

contact permitted between the complexed viologen and oxidized metal complex. Subsequent studies will be performed to indicate whether greater sequestering can be obtained in related electron transfer reactions. Of additional interest, of course, is a comparison of electron transfer reactions with other bimolecular processes involving these apparently sequestered molecules. It is clearly reasonable that processes which involve specific bond formation – bond breaking interactions should be much more sensitive to molecular separation than simple electron transfer reactions. The relatively larger retardation observed for stilbene quenching may either be an example of this effect or it may reflect differences in the type of interaction among different host–guest combinations. We are currently extending these studies to better define the range of interactions that can occur with these complexes.

Acknowledgement

We are grateful to the U.S. Department of Energy (Contract Number DE-AC02-84ER 13151) for support of this research.

1. J. EMERT and R. BRESLOW. J. Am. Chem. Soc. **97**, 670 (1975).
2. L. MANDELCORN (*Editor*). Non stoichiometric compounds. Academic Press, New York. 1964.
3. H. R. ALLCOCK. Acc. Chem. Res. **11**, 81 (1978).
4. J.-M. LEHN. Acc. Chem. Res. **11**, 49 (1978).
5. J. C. RUSSELL and D. G. WHITTEN. J. Am. Chem. Soc. **103**, 3219 (1981).
6. M. W. GEIGER and N. J. TURRO. Photochem. Photobiol. **26**, 221 (1977).
7. J. C. RUSSELL, S. B. COSTA, R. P. SEIDERS, and D. G. WHITTEN. J. Am. Chem. Soc. **102**, 5678 (1980).
8. N. J. TURRO, K. C. LIU, and M. F. CHOW. Photochem. Photobiol. **26**, 413 (1977).
9. P. R. WORSHAM, D. W. EAKER, and D. G. WHITTEN. J. Am. Chem. Soc. **100**, 7091 (1978).
10. M. L. BENDER and M. KOMIYAMA. Cyclodextrin chemistry. Springer Verlag, New York. 1978.
11. S. HARATA. Bull. Chem. Soc. Jpn. **48**, 2409 (1975).
12. R. L. VANETTEN, J. F. SEBASTIAN, G. A. CLOWES, and M. L. BENDER. J. Am. Chem. Soc. **89**, 3242 (1967).
13. P. C. MANOR and W. SAENGER. J. Am. Chem. Soc. **96**, 3630 (1974).
14. I. TABUSHI, Y. KIYOSUKE, and K. YAMAMUNA. J. Am. Chem. Soc. **100**, 916 (1978).
15. I. TABUSHI. Acc. Chem. Res. **15**, 66 (1982).
16. I. TABUSHI and L. C. YUAN. J. Am. Chem. Soc. **103**, 3574 (1981).
17. N. J. TURRO, G. S. COX, and X. LI. Photochem. Photobiol. **37**, 149 (1983).
18. N. NISHIMURA and M. JANADO. J. Biochem. **77**, 421 (1975).
19. H. NAKATANI, K.-I. SHIBATA, H. KONDO, and K. HIROMI. Biopolymers, **16**, 2363 (1977).
20. Y. HUI and J. GU. Acta Chim. Sin. **39**, 309 (1981).
21. Y. HUI, J. GU, and X. JIANG. Acta Chim. Sin. **39**, 376 (1981).
22. Y. HUI, X. CHEN, J. GU, and X. JIANG. Sci. Sin. (Engl. ed.) Ser. B, **25**, 698 (1982).
23. Y. HUI, S. WANG, and X. JIANG. J. Am. Chem. Soc. **104**, 347 (1982).
24. Y. HUI, J. C. RUSSELL, and D. G. WHITTEN. J. Am. Chem. Soc. **105**, 1347 (1983).
25. Y. HUI, J. R. WINKLE, and D. G. WHITTEN. J. Phys. Chem. **87**, 23 (1983).
26. W. M. MOONEY III, P. E. BROWN, J. C. RUSSELL, S. B. COSTA, L. G. PEDERSEN, and D. G. WHITTEN. J. Am. Chem. Soc. **106**, 5659 (1984).
27. R. W. EYLER, E. D. KLUG, and F. DIEPHUIS. Anal. Chem. **19**, 24 (1947).
28. U. MAZZUCATO, G. G. ALOISI, and F. MASETTI. J. Photochem. **18**, 211 (1982).
29. R. C. TEITELBAUM, S. L. RUBY, and T. J. MARKS. J. Am. Chem. Soc. **100**, 3215 (1978).
30. J. M. REDDY, K. KNOX, and M. B. ROBBIN. J. Chem. Phys. **40**, 1082 (1964).
31. R. RUNDLE and R. BALDWIN. J. Am. Chem. Soc. **65**, 544 (1943).
32. C. R. BOCK, T. J. MEYER, and D. G. WHITTEN. J. Am. Chem. Soc. **96**, 4710 (1974).
33. D. G. WHITTEN. Acc. Chem. Res. **13**, 83 (1980).
34. Y. MOROI, A. M. BRAUN, and M. GRÄTZEL. J. Am. Chem. Soc. **101**, 56 (1979).
35. T. K. FOREMAN, W. M. SOBOL, and D. G. WHITTEN. J. Am. Chem. Soc. **103**, 5333 (1981).
36. M. KRIEG and D. G. WHITTEN. J. Photochem. **25**, 235 (1984).

Photon harvesting polymers: intracoil energy transfer in anthryl- and fluorescein-tagged polystyrene

J. S. HARGREAVES[1] AND S. E. WEBBER[2]

Department of Chemistry and Center for Polymer Research, University of Texas at Austin, Austin, TX 78712, U.S.A.

Received June 14, 1984

This paper is dedicated to the memory of Li Xiao-Bai

J. S. HARGREAVES and S. E. WEBBER. Can. J. Chem. **63**, 1320 (1985).

Polystyrene containing small mole fractions of pendent 9,10-diphenylanthracene (DPA) and fluorescein (F) was prepared. Absorption of light by DPA results in very efficient intracoil sensitization of the ^{1}F* state. The quantum efficiency (χ) of this process has been estimated as 0.75 in dimethylformamide (DMF) and 0.95 in 5:1 DMF/H_2O. The increase in χ in this latter solvent mixture is ascribed to the diminished polymer coil size in this poorer solvent. Analysis of the time dependence of fuorescence suggests a combined static and dynamic quenching of ^{1}(DPA)* by energy transfer. Studies of ^{1}(DPA)* and ^{1}(F)* fluorescence quenching by DABCO corroborate this model.

J. S. HARGREAVES et S. E. WEBBER. Can. J. Chem. **63**, 1320 (1985).

On a préparé du polystyrène contenant de faibles fractions molaires de diphényl-9,10 anthracène (DPA) et de fluoresceine (F). L'absorption de la lumière par le DPA est dûe à une sensibilisation très efficace et intraréseau de l'état ^{1}F*. On a évalué que l'efficacité quantique (χ) de ce processus est égale à 0,75 dans le diméthylformamide (DMF) et à 0,95 dans un mélange 5:1 de DMF/H_2O. On attribue l'augmentation de χ dans ce dernier mélange de solvants, à une diminution de la taille de l'enroulement du polymère dans ce solvant plus pauvre. Une analyse de l'influence du temps sur la fluorescence suggère l'existence de piégeages combinés statique et dynamique du ^{1}(DPA)* par transfert d'énergie. Des études de piégeage de fluorescence ^{1}(DPA)* et ^{1}(F)* par le DABCO corroborent ce modèle.

[Traduit par le journal]

Introduction

Energy migration within isolated polymer coils has been studied extensively by a number of groups in the last few years (for reviews see ref. 1). Energy transfer phenomena can be expected to play an important role in polymer photodegradation and in the utilization of polymers as photon collection moieties. In all previous cases it has been difficult to distinguish between "excitonic" (down-chain) energy transfer and cross-chain energy transfer since both mechanisms may be reasonably expected to occur.

The present study is motivated by the following: (1) elucidation of a polymeric energy transfer system in which the extent of the excitonic mechanism can be varied, (2) characterization of some of the photophysical properties of polymer-bound dyes, and (3) demonstration that effective energy transfer can extend the response function of a polymer-bound dye.

The system discussed herein is composed of three components: (1) a polystyrene chain, spectroscopically inert in the present context, (2) polymer-bound 9,10-diphenylanthracene (DPA), which is a very efficient fluorophore, and (3) polymer-bound fluorescein, one of the most studied of the xanthene dyes, itself an efficient fluorophore and also efficiently sensitized by DPA via the Forster mechanism. Soluble polymers containing fluorescein have been prepared but very little spectroscopic work has been carried out on them (2, 3). Insoluble polymers of rose bengal covalently bound to an inert polymer support have been used by Neckers to produce singlet oxygen, which in turn acts as a photooxidizer (4). The polymer-bound photosensitizer has several advantages over the unbound dye. As will be shown, the quantum efficiency of sensitization of the fluorescein by DPA is ca. 75% in "good" polymer solvent (pure dimethylformamide, DMF) and ca. 95% in a "poor" polymer solution (5:1 DMF/H_2O). This solvent effect is interpreted in terms of the change in the coil size of a polymer containing at least one DPA–fluorescein pair. Fluorescence decay measurements demonstrate that most of the sensitization in pure DMF is static in nature, i.e. with little effect on the decay of the residual DPA fluorescence. In DMF/H_2O the DPA fluorescence lifetime is shortened, indicative of dynamic quenching. This implies that in DMF/H_2O essentially all DPA moieties are within the Forster radius (R_0) of a fluorescein.

Experimental

(a) *Chemical*

9-(*p*-Ethenylphenyl)-10-phenylanthracene was synthesized and purified as previously described (5). Styrene (Aldrich) and chloromethylstyrene (Polysciences) were purified by column chromatography using activated alumina immediately before use.

Dibenzylfluorescein (DPF) (IUPAC name: benzoic acid, 2-(6-benzyloxy-3-oxo-3*H*-xanthen-9-yl)-benzyl ester) was prepared by refluxing 0.05 mol of the disodium salt of fluorescein in 100 mL of dimethylformamide (DMF) with excess of α-chlorotoluene (MCB) for 3 h. After cooling, the solution was poured into water and the precipitate filtered. As much of this solid as possible was dissolved in methylene dichloride (CH_2Cl_2), the solution filtered, and the solvent removed under vacuum to give a brown material. The solid was repeatedly washed with NaOH solution until thin layer chromatographic analysis using activated silica and 4:1 Skelly B – ethyl acetate as eluent showed only one spot (R_f = 0.26). Finally, the solid was precipitated from a DMF solution by addition of acidified water, washed thoroughly with distilled water, and dried to give an orange powder: mp 185–187°C; ir (KBr): 1740 cm^{-1} (ester[3]); λ_{max} (C_6H_6): 460 nm, $\epsilon = 2 \times 10^4$ L M^{-1} cm^{-1}; nmr ($CDCl_3$) δ: 4.9 (s, 2H), 5.1 (s, 2H), 6.2–8.3 (m, 20H); m/e = 512.

Terpolymers of 9-(*p*-ethenylphenyl)-10-phenylanthracene, styrene, and chloromethylstyrene were prepared by dissolving selected mole ratios of the monomers (see Table 1), along with 1% by weight of 2,2′-azobis(isobutyronitrile) (AIBN), in 10 mL of benzene in a polymerization tube. After thoroughly degassing the solution by three

[1]Present address: Hewlett–Packard, Palo Alto, California.
[2]Author to whom correspondence may be addressed.

[3]This band is not present in normal fluorescein (see ref. 6). The detection of the ether linkage by ir was difficult because of the complexity of the spectrum.

freeze–pump–thaw cycles, the tubes were sealed under vacuum and maintained at 70°C for 60 h.

The polymers were then purified by repeated precipitation of toluene solutions by methanol. After drying under vacuum the diphenylanthracene content in the polymer were determined by visible absorption spectroscopy (5).

Fluorescein was attached to the methyl chloride group on the polymer support by the method described by Neckers and co-workers (7) using the chemistry of Merrifield (8). To a solution of 1 g of the above polymer in about 50 mL DMF, disodium fluorescein was added in excess. The solution was refluxed for 3 h, after which it was cooled, filtered, and poured into water. The solid was filtered off and the above purification repeated three times. After drying, the polymer was dissolved in CH_2Cl_2, filtered, precipitated out with methanol, and refiltered. As a final precaution, and to remove traces of sodium, a DMF solution of the polymer was precipitated out with acidified water. After thoroughly washing with distilled water the polymer was dried under vacuum to give a yellow powder.

Polymers were prepared that contained, apart from the inert polystyrene backbone, diphenylanthracene only, fluorescein only, or both diphenylanthracene and fluorescein. For convenience these polymers will be designated as PA, PF, or PAF respectively.

Molecular weights of the polymers were determined using a Waters hplc chromatograph (with Waters μ-Styragel columns, 500, 10^3, 10^4, and 10^5 Å pore size and CH_2Cl_2 or THF as the mobile phase) calibrated with polystrene standards. This also provided a final means of purification and, in fact, all emission spectra were taken only on polymers that had been purified by this method. The molecular weights determined from gpc traces agreed with those determined from viscosity measurements (using the Mark–Houwink parameters for polystyrene) (9).

The fluorescein content in the polymers was determined by visible absorption spectroscopy using solutions in DMF made basic by the addition of 0.1 *M* triethylamine. Extinction coefficients for fluorescein in this solvent were taken from this work and that of Martin (10).

1,4-Diazabicyclo[2.2.2]octane (DABCO, Aldrich) was purified by sublimination before use. Dimethylformamide (DMF) was purified by fractional distillation. Water was similarly purified. The ratio of DMF/H_2O used as a polymer solvent was 5:1 (by volume) in all cases, and the concentration of polymer in this solvent mixture was always less than 0.01% by weight. Increasing the water content by a small amount above the 5:1 ratio did not further alter the absorption and fluorescence spectra. Addition of a larger amount of water (~5:2) resulted in precipitation of the polymer. Increasing the concentration of polymer above 0.01% resulted in the precipitation of the polymer at lower H_2O content. As will be pointed out in the next section, the fluorescein photophysics is very sensitive to a polar solvent like H_2O. For that reason we did not study these polymers extensively in solvents like THF or CH_2Cl_2 because significant variations might be observed according to the adventitious H_2O content (which will be low in any case).

(b) *Optical*

All steady state fluorescence spectra were taken on a SPEX 1905 Fluorolog as previously described. All solutions for fluorescence work were thoroughly degassed and had an optical density of <0.1 at the absorption maximum. Absorption spectra were taken on a Cary 17 spectrophotometer.

Fluorescence decay curves were measured several different ways. At the Center for Fast Kinetics Research a 30-ps tripled Nd:YAG pulse (355 nm) was used for excitation and the fluorescence signal was digitized by either a Tektronix R7912 digitizer or a Hammamatsu streak camera. In our own labs a home-built correlated single-photon apparatus was used. In this system a Photochemical Research Associates nanosecond lamp is the excitation source, which when air filled at ~400 Torr (1 Torr = 133.3 Pa) has a half-width on the order of 4.8 ns. In this case excitation was at 358 nm. Standard ORTEC pulse shaping modules and an ORTEC model 457 time-to-amplitude (TAC) was used. The photomultiplier was a RCA 8850, wired for photon counting. A LeCroy model 3501 24 bit analog-to-digital converter was used to digitize the TAC output into the histogram memory of a LeCroy 3500M multichannel analyzer. These data were transferred to the University of Texas Cyber system and fit to exponential decay functions using reconvolution techniques (see, for example, ref. 11) in this technique the value of Δ is minimized for the quantity

$$[1] \qquad \Delta(k) = \int_0^{t_{max}} \left| I_{obs}(t) - \int_0^t F(t-\tau;\, k) R_{obs}(\tau)\mathrm{d}\tau \right|^2 \omega(t)\mathrm{d}t$$

where $I_{obs}(t)$ is the experimentally observed fluorescence at time t, $R_{obs}(t-\tau)$ is the experimentally observed response function of the excitation lamp and detector combination, and $F(t-\tau;\, k)$ is a proposed fluorescence decay function with parameter(s) k. We have taken the weighting function, $\omega(t)$, to be $I_{obs}(t)^{-1}$. The integral in eq. [1] is actually a summation over all the data channels (corresponding to 0–50 ns for these experiments). In addition to minimizing the quantity $\Delta(k)$ with respect to variations in k, the residuals

$$[2] \qquad D(t) = \left(I_{obs}(t) - \int_0^t F(t-\tau;\, k') R_{obs}(\tau)\mathrm{d}\tau \right) \omega(t)$$

were inspected for randomness. Based on the appearance of $D(t)$ it would seem that there is a systematic time shift between photons detected at the excitation wavelength (358 nm) and the two observation wavelengths (at 440 nm, ~ +0.4 ns and at 540 nm, ~ +0.6 ns) that has nothing to do with the normal shift between excitation and fluorescence maxima. If the fluorescence decay data were shifted by ca. −0.4 and −0.6 ns at 440 and 540 nm respectively, the best fits by the Δ criterion and the appearance of $D(t)$ are frequently obtained. This time shift always shortens the single exponential lifetimes obtained by 0.3–0.5 ns and slightly worsens the fit at longer times. Thus our estimated error for fluorescence lifetimes is ca. 0.3–0.5 ns based on this analysis.

Fluorescence quantum yields of polymeric fluorescein were taken as previously described (12), using an alkaline aqueous solution of fluorescein (purified by the method similar to that of Cramer and Spears, ref. 13) as the standard. Fluorescence quantum yield, lifetimes, and λ_{max} for fluorescence for compounds relevant to this paper are compiled in Table 2. For the sake of comparison, quantum yield, lifetime, and λ_{max} data for several fluorescein derivatives have also been collected in this table.

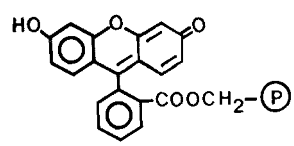

DYE I

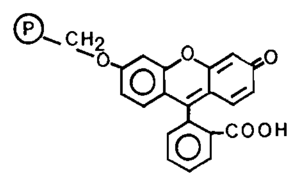

DYE II

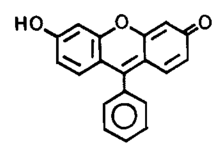

HPF

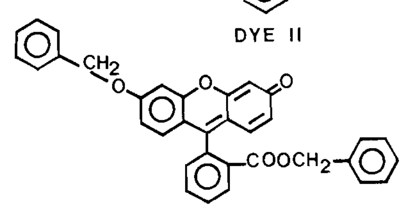

DBF

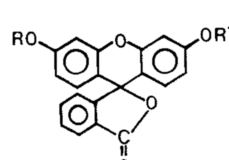

FMGB·HCl R = H, R′ = X

FDGB·2HCl R = R′ = X

X = 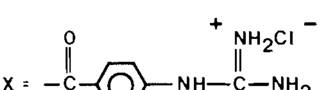

χ values were obtained by comparing PAF samples with optically matched solutions of PF at 430 nm. Fluorescence and absorption spectra are easily resolvable into their various components because large portions of these spectra result from only one species.

TABLE 1. Relative mole ratios of the various components used in the polymer feeds

Polymer	Styrene	Chloromethyl styrene	Vinyl DPA
PA	1	3.4×10^{-2}	3×10^{-3}
PF	1	3.4×10^{-2}	—
PAF-1	1	3.4×10^{-2}	3×10^{-3}
PAF-2	1	3.4×10^{-2}	29×10^{-3}
PAF-3	1	3.4×10^{-2}	57×10^{-3}

Results

(a) *Absorption, steady-state fluorescence*

The absorption and fluorescence properties of fluorescein depend strongly on the degree of ionization and the polarity of the solvent (14). An example of this effect can be found in the recent study by Lamberts and Neckers (15) on substituted rose bengal, which is also a dye in the xanthene group. The method of fluorescein attachment to our copolymers can lead to either of the species, dye I or dye II. Ionization of the phenol group in dye I is expected to lead to the usual dianion fluorescein absorption and fluorescence. Ionization of the carboxylic group in dye II is expected to have relatively little effect on the dye absorption and fluorescence since the phenyl group is only weakly conjugated with the main xanthene ring. This is illustrated by the work of Martin and Lindquist on 6-hydroxy-9-phenyl fluoran (HPF) in which the absorption properties of HPF are virtually identical to the fluorescein dianion (14*d*). In Fig. 1 the absorption spectra of HPF, DBF, and PF in DMF are compared. The polymer, PF, is a clear superposition of "HPF" and "DBF" which we take to indicate the presence of dye I and dye II respectively. Also presented in Fig. 1 is the fluorescence excitation spectrum (λ_{obs} = 560 nm) for the range 420–550 nm. Clearly it is primarily the "HPF" (dye I) component of the polymer-bound fluorescein that is contributing to the fluorescein fluorescence. We will return to this point in the Discussion. We do not believe that there is any significant amount of intracoil doubly substituted fluorescein in PF because (1) the mole fraction of chloromethylstyrene in the polymer is very low, (2) there is no evidence for cross-linking upon reacting the fluorescein with the polymer, and (3) the hplc traces before and after fluorescein attachment are virtually identical. In addition,

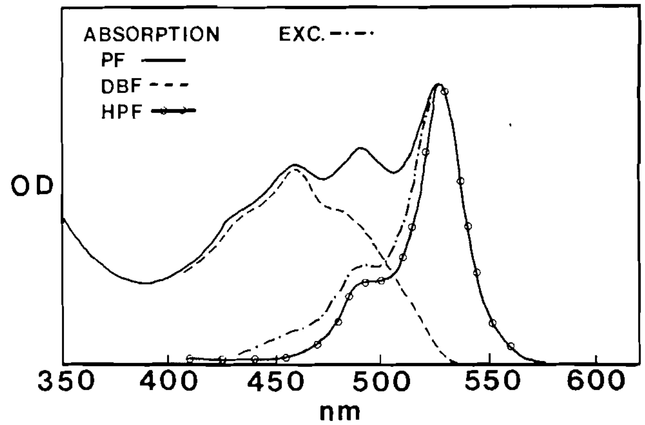

FIG. 1. Absorption spectra of PF (—), DBF (––), and HPF (ref. 14*d*) (⊖), (–·–) excitation spectra of PF or PAF (λ_{obs} = 560 nm) (all in DMF) scaled to match at long wavelength peak).

the fluorescence spectrum of doubly substituted fluorescein (DBF) is distinctly different from that of the PS-bound fluorescein (see Fig. 2 and cf. fluorescence lifetimes for PF and DBF in Table 2). In the present set of experiments the same ratio of styrene/chloromethylstyrene was used for all polymers and the degree of polymerization was very similar in all cases such that the average number of fluorescein moieties per chain was nearly identical (see Table 3). The relative fraction of dye I and II could be estimated from the long wavelength part of the absorption spectrum (see Fig. 1), i.e. the optical density at 460 nm is primarily due to dye II while that at 526 nm is primarily from dye I. Dye II was favored for PAF-2 and PAF-3 whilst dye I was favored for PAF-1 (Table 3). We defer to the Discussson our analysis of the effect of having two types of fluorescein moieties.

The effect of solvent polarity on fluorescein photophysics cannot be overemphasized (14). In Fig. 3 the absorption spectra of PF in DMF and CH_2Cl_2 are compared. In the latter solvent the spectrum looks like that of DBF, i.e. unionized fluorescein. Similarly we expect the fluorescein emission intensity to depend on solvent polarity (see below). The Forster R_0 value for DPA–fluorescein energy transfer might also be expected to depend on solvent because of this spectral change. In Fig. 3

TABLE 2. Fluorescence quantum yields and emission maxima

Chromophore	Solvent	ϕ_f (±5%)	τ (ns)	λ^{n}_{max} (nm)	Reference
Fluorescein	DMF	0.55	4.4[d]	543	10
Fluorescein	DMF/H_2O (5:1)	0.83	—	526	This work
HPF	DMF	0.045	0.18[c]	553	10
FMGB·HCl	PBS[e]	0.03	1.7	557	20
FDGP·2HCl	PBS[e]	0.02	2.1	527	20
DBF	Methanol	0.27	0.6	520	This work
PS-bound fluorescein[a]	DMF	0.05	4.8	553	This work
PS-bound fluorescein[a]	DMF/H_2O (5:1)	0.14	2.2	543	This work
DPA	—[b]	0.93	6.8	440	21

[a]Determined using fluorescein in DMF as a standard and exciting at 520 nm. This quantum yield is independent of the presence of DPA and is the same for PF or PAF samples.

[b]The quantum yield of DPA fluorescence does not depend significantly on solvent. Equation [12] is derived considering only one kind of energy transfer mechanism per fluorescein. We have argued that the bulk of the energy transfer can be thought of as a static mechanism (i.e. no lifetime shortening). Stricttly speaking, each χ_i in eq. [12] should be replaced by $(\chi_i^{static} + \chi_i^{dynamic})$.

[c]Estimated from quantum yield data in ref. 10.

[d]This work, using single photon method.

[e]Phosphate buffered saline solution, pH = 7.2.

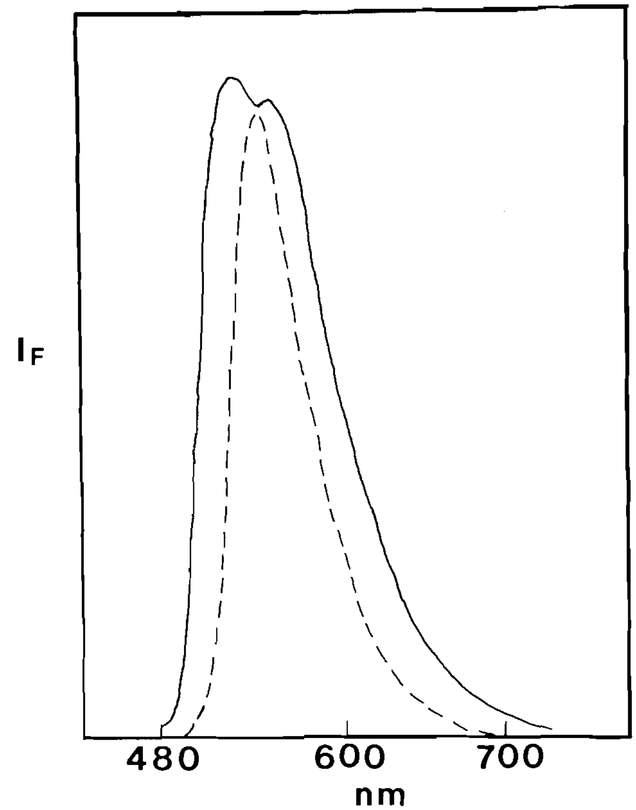

FIG. 2. Fluorescence spectra of PF (--) and DBF (—) in 5:1 DMF/H_2O, λ_{ex} = 475 nm (in arbitrary units, scaled for ease of comparison; uncorrected for PM response).

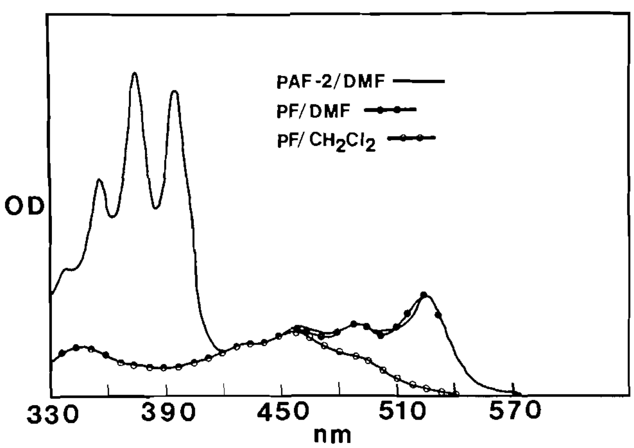

FIG. 3. Absorption spectra of PAF-2 in DMF (—), PF in DMF (●), and PF in CH_2Cl_2 (○) (equal concentrations of fluorescein).

we have also presented the absorption spectrum of PAF-2 in DMF at a concentration such that the fluorescein absorption is equal to that of PF. The DPA component at wavelengths below 420 nm is obvious.

The primary observation that we wish to discuss in this section is presented in Fig. 4 for PAF-2 and PF solutions optically matched in the fluorescein absorption region. Excitation light at 375 nm is absorbed primarily by DPA moieties in the case of PAF-2, yet the fluorescein component in the total steady-state fluorescence spectrum for PAF-2 is much larger than PF directly excited at 375 nm. Clearly very efficient energy transfer from DPA to fluorescein is occurring. This effect is

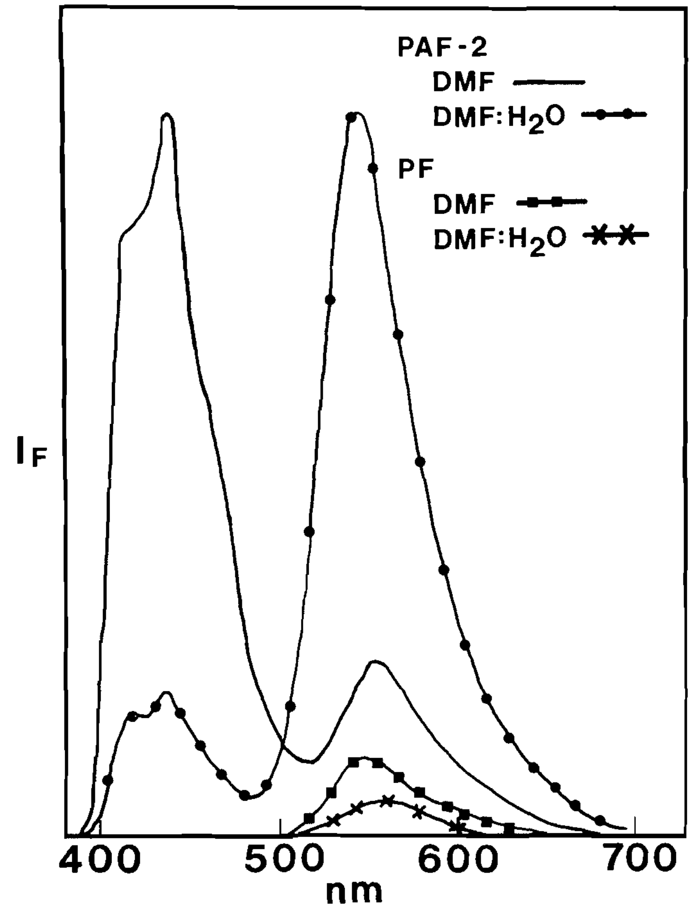

FIG. 4. Fluorescence spectra excited at 375 nm: (1) PAF-2 in DMF (—); (2) PAF-2 in 5:1 DMF/H_2O (●); (3) PF in DMF (×); (4) PF in 5:1 DMF/H_2O (■). The OD of the PF and PAF-2 solutions are matched at 430 nm (uncorrected for PM response).

especially pronounced in 5:1 DMF/H_2O, where the fluorescein component dominates the total fluorescence spectrum. This solvent effect is much larger than can be rationalized by the effect of solvent on the fluorescence quantum yield of PF or on the solvent shift of the fluorescein absorption spectrum. We interpret this very large enhancement to be the result of the diminution of the coil size of PAF by the more polar solvent, which decreases the average DPA–fluorescein separation (see Discussion) (16).

The efficiency of energy transfer can be quantified by means of the following equation (12, 17):

$$[3] \qquad \chi/(1-\chi) = (\phi_{DPA}/\phi_F)(I_F/I_{DPA})$$

In eq. [3] ϕ and I are respectively the quantum yield of fluorescence and the relative fluorescence intensity (as measured by relative areas in the total corrected fluorescence spectrum) for a given species. The subscripts DPA and F correspond to diphenylanthracene and fluorescein. One may interpret χ as the fraction of photons absorbed by the sensitizer (DPA) that are transferred to the fluorescein acceptor. Using ϕ_F for PS-bound fluorescein in Table 2, the χ values were identical within experimental error for all PAF samples and go from ca. 0.75 for DMF to ca. 0.95 for 5:1 DMF/H_2O. We will argue in the next subsection that most of this energy transfer is equivalent to static (i.e. contact) quenching of the DPA fluorescence.

It should be emphasized that, within experimental error, the

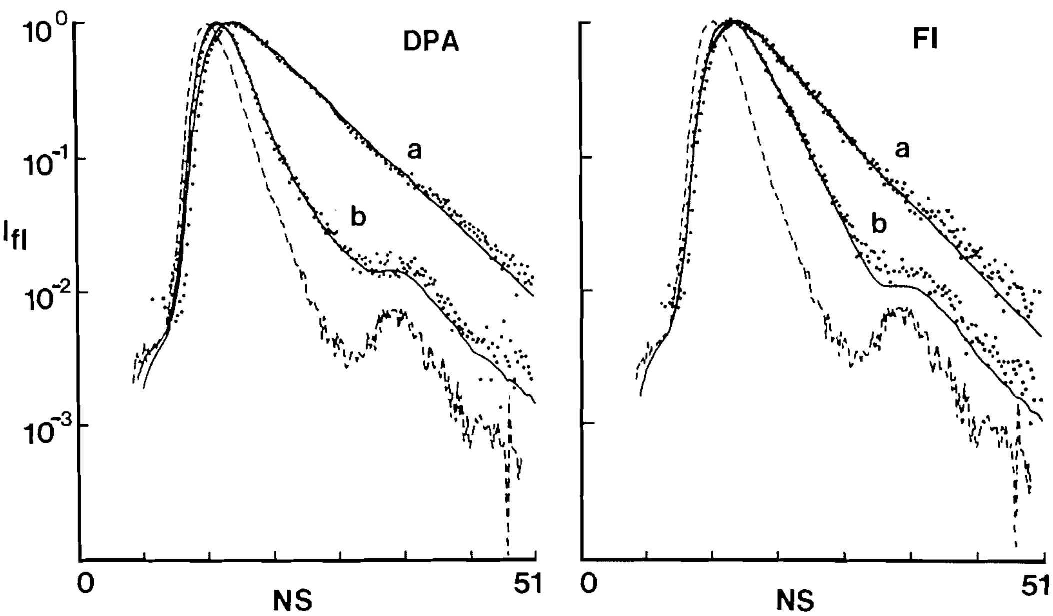

FIG. 5. Fluorescence decay curves for DPA and fluorescein (Fl); (––) instrumental resonse function; (···) raw data; (—) best fit curve. Curve a, DMF; curve b; 5:1 DMF/H_2O. Except for curve b, DPA, all best fits are a single exponential (see text).

value of χ does not depend on the average number of anthracenes per coil. This implies that the fluorescein sensitization occurs primarily by a single-step transfer with minimal contribution from DPA–DPA self-transfer. Furthermore, the average DPA–fluorescein separation must be on the order of R_0. R_0 for DPA–fluorescein in ethanol has been calculated as 41 Å (18), which is the same order of magnitude as the polymer coil dimension (estimated as 52 Å for polystyrene of comparable molecular weight in toluene).

We should also mention the striking effect of pendent fluorescein moieties on the solubility properties of PAF. PA is soluble in pure DMF but only very sightly soluble in 5:1 DMF/H_2O. Reaction of a PA polymer (these polymers always contain chloromethylstyrene groups) with fluorescein renders the resultant PAF soluble in DMF/H_2O to reasonable concentrations (0.01 wt.%), despite the fact that there is on the average approximately one fluorescein per polymer chain (Table 3). It was not possible to dissolve 0.01 wt.% PAF in DMF with higher mole fractions of added H_2O.

(b) *Fluorescence decay measurements*

The values of the fluorescence lifetime measured in DMF or DMF/H_2O at 440 nm (DPA) or 543 nm and 553 nm (fluorescein) are tabulated in Table 4. The fluorescence lifetime (τ_{fl}) of PA in DMF was typical of DPA (as noted in the previous section, it is not possible to dissolve PA in DMF/H_2O). The fluorescence lifetimes for the anthracene emission in all the PAF samples in DMF were slightly shortened (~1 ns) but were fit adequately by a single exponential (see Fig. 5 for PAF-2 data). Likewise, the fluorescence decay of the fluorescein was adequately fit by a single expontential for either DMF or DMF/H_2O, but the τ_{fl} value is slightly *longer* in the PAF samples than PF. We attempted to detect differences in the fluorescence build-up rate constant using 30-ps excitation at 353 nm, a 500-nm cut-off filter, and a streak camera. Within experimental error, there was no difference in these rate constants between PF and PAF-3 in DMF (4.4×10^{10} s^{-1} and 4.9×10^{10} s^{-1} respectively). This is consistent with the existence of significant static quenching of $^1(DPA)^*$ by the fluorescein.

TABLE 3. Mole ratios of components of polymers[a]

Polymer	DPA/S	DPA/(I+II)	I/II	(I+II)/S
PA	0.0038 (1.1)	—	—	—
PF	—		0.31	0.0032 (0.96)
PAF-1	0.0038 (1.1)	1.3	1.26	0.0029 (0.87)
PAF-2	0.026 (7.8)	8	0.37	0.0032 (0.96)
PAF-3	0.077 (23.1)	25	0.42	0.0030 (0.90)

[a]DPA = 9,10-diphenylanthracene; S = styrene; I and II = dye I and dye II. Degree of polymerization for all polymers ca. 300 ($M_N/M_n \cong 1.8$). Values in parentheses are the average number of DPA and fluorescein moieties per chain (columns 2 and 5 respectively).

The most important effect illustrated by the data presented in Table 4 or Fig. 5 is the drastic shortening of the anthracene fluorescence lifetime in going to DMF/H_2O. The shortening is especially noticeable for PAF-3, which contains the highest mole fraction of anthracene. We interpret this as the result of dynamic (i.e. diffusive) quenching of $^1(DPA)^*$ via energy transfer to the fluorescein. Furthermore, we take the fact that PAF-3 has the most shortened lifetime to imply the presence of energy migration between DPA groups which further enhances dynamic quenching of $^1(DPA)^*$. For PAF-1 and PAF-2 the anthracene fluorescence decay could not fit satisfactorily to a single exponential. The fit to a biexponential decay function of the following form was satisfactory, even if the slow component lifetime (τ_2) was constrained to be that of unquenched anthracene (τ_2 = 6.8 ns).

$$[4] \qquad I(t) = a_1 e^{-t/\tau_1} + a_2 e^{-t/\tau_2}$$

For these constrained biexponential fits $a_1/(a_1 + a_2) \geqq 0.98$ (see Table 4). This implies that in DMF/H_2O $\leqq$2% of the DPA moieties are outside the range of dynamic energy transfer (these could be the DPA groups that reside on a polymer coil without a pendent fluorescein). The remaining DPA's must be located either much less than R_0 from the fluorescein (equivalent to static quenching) or on the order of R_0 from the fluorescein, leading to lifetime shortening. The fluorescence decay

TABLE 4. Fluorescence lifetime data (ns)[a]

Sample	DMF/H_2O (5:1)		DMF	
	DPA	F	DPA	F
PA	—	—	6.8 [6.5]	—
PF	—	2.2 [1.6] (2.7)[b]	—	4.8 [4.3] (4.0)[b]
PAF-1	1.0 (0.98)[c]	2.2 [1.7]	5.5 [5.2]	5.5 [5.0][d]
PAF-2	1.1 (0.98)[c]	3.0 [2.6]	6.0 [5.7]	5.5 [5.0][d]
PAF-3	0.8 (~1.0)[c]	3.3 [2.9]	5.9 [5.5]	6.0 [5.5][d]

[a]Solutions outgassed. Values in brackets result from fit to time-shifted decay curve (see experimental section). We estimate our error in best fit lifetimes to be approximately 0.5 ns. For DPA λ_{obs} is 440 nm, and for F λ_{obs} is 543 nm for DMF/H_2O and 553 nm for DMF.

[b]Determined for very dilute solutions to minimize apparent lifetime lengthening by self-absorption. Because of poor S/N the quality of the raw data and subsequent fit is diminished.

[c]A single exponential fit for PAF-1, PAF-2 is unsatisfactory. The data were fit to a constrained biexponential with one lifetime at 6.8 ns (unquenched DPA). Value in parentheses is the fraction of the short lifetime component in the best fit.

[d]These lifetimes are observed from sensitized fluorescence. The lifetimes obtained by direct excitation are like PF.

of PAF-3 was fit in the same way but was almost a pure exponential.

A rough calculation shows that these results are consistent with our χ values. For this calculation we assume that the DPA's can be divided into two independent groups, those statically quenched and those uniformly dynamically quenched. We assume that 0.75 of all DPA's are quenched statically (from the DMF data), and the remaining DPA's are quenched dynamically in DMF/H_2O. For this latter group

$$[5] \qquad \chi_{\text{dynamic}} = k_T/(k_0 + k_T)$$

where k_0 is the rate constant for all excited state relaxation processes other than energy transfer and k_T is the energy transfer rate. We take k_0 to be equivalent to the rate constant for PA in DMF and k_T may be calculated by

$$[6] \qquad k_T = k_{PAF} - k_0$$

From the observed lifetimes in Table 4 χ_{dynamic} is estimated as 0.86. Thus summing 0.75 (static transfer) plus (0.86)(0.25) = 0.22 (dynamic transfer) the net transfer efficiency is calculated as 0.97, within the experimental error of 0.95 determined by steady-state methods. In this calculation we are neglecting enhanced static quenching that results from coil contraction. Despite the crudeness of this calculation we feel it illustrates the overall consistency of our steady-state and time-dependent data.

(c) *Fluorescence quenching of PAF-3 by DABCO*

These experiments were designed to further elucidate the effect of rapid energy transfer from ^{1}(DPA)* to fluorescein. In order to minimize direct absorption by fluorescein only PAF-3 was studied. The quencher chosen was DABCO (1,4-diazabicyclo[2.2.2]octane) which is known to be an efficient singlet-state quencher, presumably by an electron transfer mechanism (19). The quenching of the steady-state fluorescence of the anthracene or the fluorescein could be fit satisfactorily to a Stern–Volmer plot.

$$[7] \qquad I_0/I_Q = I + K_{SV}[Q] = 1 + k_q\tau_0[Q]$$

In the case of fluorescein the fit was satisfactory for either direct excitation at 500 nm or sensitized by DPA absorption at 375 nm. The data are collected in Table 5.

TABLE 5. DABCO quenching data[a]

Polymer	λ_{obs} (nm)	λ_{exc} (nm)	K_{sv} (M^{-1})	τ_0 (ns)	$k_q \times 10^{-9}$ (M^{-1} s^{-1})
PA	440	375	18[b]	6.8[b]	2.6
PAF-3	440	375	1.6	0.8	2.0
	545	375	1.1	3.3	0.33
PAF-3	545	500	0.48	2.2	0.22

[a]All data for 5:1 DMF/H_2O except where noted.

[b]From PA in DMF. There are no data for PA in DMF/H_2O because of poor solubility. However, in separate experiments, DPA bound to water-soluble polymers exhibits a normal fluorscence lifetime of ~6.8 ns.

For the ^{1}(DPA)* fluorescence quenching the k_q value was very similar in DMF and DMF/H_2O (note that there is a very large effect of τ_0 in the calculation of k_q). Alternatively, the change in K_{SV} could be used to estimate τ_0 for the quenched ^{1}(DPA)* in DMF/H_2O. The estimated value of τ_0 is 0.53 ns, in reasonable agreement with the experimentally measured 0.8 ns. The conclusion from these results is that the DPA moieties that do fluoresce are equally well quenched by DABCO in DMF and DMF/H_2O, which implies that they remain accessible to the DABCO (i.e. the DPA are not protected by a partially collapsed coil).

Perhaps of more importance is the fact that the quenching rate of fluorescein emission is essentially the same for direct or sensitized excitation and this quenching is fit satisfactorily by a Stern–Volmer plot. One can easily show that the quenching of sensitized fluorescein fluorescence also reflects the quenching of the precursor state, i.e. ^{1}(DPA)*, leading to the following equation:

$$[8] \qquad I_0^F/I_Q^F = (1 + K_{SV}^{DPA}[Q])(1 + K_{SV}^F[Q]) = 1 + (K_{SV}^{DPA} + K_{SV}^F)[Q] + K_{SV}^{DPA}K_{SV}^F[Q]^2$$

where K_{SV}^{DPA}, K_{SV}^F are the products $k_q\tau_0$ for DPA and fluorescein respectively. While it is not surprising that the quadratic dependence on $[Q]$ has not shown up in our data (i.e. the product $K_{SV}^{DPA}K_{SV}^F$ is not large), clearly the experimental K_{SV}^F value is much smaller than predicted in eq. [8]. We conclude that the DPA's monitored by fluorescence are not the primary precursors of the fluorescein singlet state, ^{1}F*. This is consistent with our model of this system in which a large fraction of the ^{1}(DPA)* species are quenched statically. The remaining ^{1}(DPA)* are quenched dynamically, i.e. fluorescence lifetime and yield nearly equally decreased.

Discussion

In this work we have demonstrated that very efficient energy transfer can occur between ^{1}(DPA)* and fluorescein moieties, thereby enhancing the action spectrum of fluorescein into the uv. Based on our mole fraction data, we find that high quantum efficiencies (χ) can exist even if there is on the average only one DPA–fluorescein pair per polymer coil (e.g. PAF-1, Table 3).

In a good solvent (DMF) the energy transfer mechanism is largely equivalent to static quenching since the lifetime shortening of ^{1}(DPA)* in the PAF samples is much less than expected for a χ value of 0.75 (see the discussion below concerning the χ value calculation for this system). Furthermore, the ^{1}(DPA)* fluorescence decay can be fit by a single exponential within experimental error. This implies that there is not a significant population of ^{1}(DPA)* species that resides on polymers without a pendent fluorescein[4] (but see the next paragraph). We note that the fluorescence lifetime of *sensitized* ^{1}(F)* is longer than directly excited ^{1}(F)*, which is what is to be expected if there exists a relatively long-lived precursor state (^{1}(DPA)*). We conclude that in DMF all energy transfer processes are intracoil and that all ^{1}(DPA)* species are affected by energy transfer to some extent. There is no systematic effect of DPA mole fraction, such that DPA–DPA energy transfer does not seem to play a major role in the value of χ.

Reducing the solvent quality by the addition of H_2O drastically alters the ^{1}(DPA)* fluorescence properties. The χ value increases to ca. 0.95 and the ^{1}(DPA)* fluorescence lifetime is greatly shortened. In this case a biexponential fit is possible and the two lifetimes obtained are quite different. The mole fraction of ^{1}(DPA)*'s with an unchanged fluorescence lifetime (i.e. fluorescein-free polymers) is estimated to be $\leqq 0.02$ (see Table 4). Our interpretation is as follows: the addition of the H_2O nonsolvent reduces the coil dimensions to the point that essentially all DPA's are within the Forster R_0 distances of a fluorescein moiety (R_0 is estimated as 41 Å for ^{1}(DPA)*–fluorescein in ethanol). Addition of a nonsolvent can encourage polymer aggregation, which also would serve to reduce the average DPA–fluorescein separation. There is no evidence for aggregation for our 0.01 wt.% polymer in DMF/H_2O solutions since: (1) there is no measurable turbidity, either immediately after addition of H_2O or after standing for days, and (2) the spectral properties of these solutions do not change upon standing. However, the presence of some degree of aggregation cannot be completely eliminated based on direct experimental evidence.

We must now consider the complications in the present system because of the existence of two different fluorescein derivatives on the polymer chain (dye I and II). Equation [3] is obtained from a classical kinetic scheme in which ^{1}(DPA)* is the sole precursur of ^{1}(F)*, the fluorescein singlet state. Under steady-state conditions

$$[9a]\quad [^1(\mathrm{DPA})^*] = I_{\mathrm{ex}}(k_{\mathrm{DPA}} + k_{\mathrm{T}})^{-1}$$

$$[9b]\quad [^1(\mathrm{F})^*] = [^1(\mathrm{DPA})^*](k_{\mathrm{T}}/k_{\mathrm{F}}) = (I_{\mathrm{ex}}/k_{\mathrm{F}})\chi$$

where

$$[10]\quad \chi = k_{\mathrm{T}}(k_{\mathrm{DPA}} + k_{\mathrm{T}})^{-1}$$

In eqs. [9] and [10] I_{ex} is the rate of DPA excitation, k_{DPA} and k_F are the normal first-order decay rates, and k_T is the energy transfer rate for ^{1}(DPA)* $\rightarrow$ ^{1}(F)*. The intensity of fluorescence for each species is given by

$$[11]\quad \begin{aligned} I_{\mathrm{DPA}} &= \phi_{\mathrm{DPA}}(1-\chi)I_{\mathrm{ex}} \\ I_{\mathrm{F}} &= \phi_{\mathrm{F}}\chi I_{\mathrm{ex}} \end{aligned}$$

where ϕ_{DPA} and ϕ_F are the fluorescence quantum yields for each species for direct excitation and in the absence of energy transfer. If we have two types of fluorescein moieties, but only one per polymer chain, then eq. [11] can be extended as follows (19):

$$[12]\quad (I_{\mathrm{F}}/I_{\mathrm{DPA}})(\bar{\phi}_{\mathrm{F}}/\phi_{\mathrm{D}}) = [X_1\chi_1(\phi_{\mathrm{F}_1}/\bar{\phi}_{\mathrm{F}}) + X_2\chi_2(\phi_{\mathrm{F}_2}/\bar{\phi}_{\mathrm{F}})]/[X_1(1-\chi_1) + X_2(1-\chi_2)]$$

where

$$[13]\quad \bar{\phi}_{\mathrm{F}} = X_1\phi_{\mathrm{F}_1} + X_2\phi_{\mathrm{F}_2}$$

In eqs. [12] and [13] X_1 and X_2 are the mole fraction of each type of fluorescein, ϕ_{F_1} and ϕ_{F_2} the appropriate fluorescence quantum yields, and χ_1 and χ_2 the quantum efficiency of sensitization for each species (the subscripts 1, 2 refer to dye I and II respectively). In deriving eq. [12] it is assumed that the DPA's are spectroscopically equivalent for both types of coils. I_F is taken to be the total "fluorescein" fluorescence. This is strictly appropriate only if the fluorescence of F_1 and F_2 overlap extensively. In eq. [12] we experimentally determine $\bar{\phi}_F$ (Table 2) and X_1 and X_2 (Table 3).

Obviously eq. [12] is more complex to analyze than eq. [3]. The only simple cases are

$$[14a]\quad 1.\ \phi_{\mathrm{F}_2} = 0 \text{ and } \chi_2 = 1;\ \chi = X_1$$

$$[14b]\quad 2.\ \phi_{\mathrm{F}_2} = 0 \text{ and } \chi_2 = 0;\ \chi = X_1\chi_1$$

$$[14c]\quad 3.\ \phi_{\mathrm{F}_1} = \phi_{\mathrm{F}_2};\ \chi = X_1\chi_1 + X_2\chi_2 = \bar{\chi}$$

In general the spectroscopic properties of fluorescein derivatives are sensitive to solvent and substitution (see Table 2). While we were able to prepare a doubly substituted fluorescein derivative (DBF), we were not able to prepare separate analogs of dye I and II using methods analogous to our polymer modification scheme. However, other experimental evidence exists that suggests $\phi_{F_2} = 0$, as follows.

(1) The "fluorescein" fluorescence spectrum does not change with excitation wavelength, despite the very striking difference in dye I and II absorption spectra (Fig. 1). (Note, for example, that the fluorescence of DBF is significantly broader than PF (Fig. 2).)

(2) There is no evidence for biexponentiality in the fluorescein fluorescence decay, nor was any significant effect of observation wavelength found in the fluorescence lifetime.

(3) The excitation spectrum for PF or PAF fluorescence is very different from the absorption spectrum and is essentially identical to the HPF absorption spectrum (see Fig. 1).

4) The spectral overlap of ^{1}(DPA)* fluorescence with DBF or dye II moieties is much more favorable for Forster energy transfer than ^{1}(DPA)* – dye I. The absorption strength of these two moieties is similar, hence it is reasonable to suppose $\chi_2 > \chi_1$.

Taking all these facts into account we believe that our system is an example of case (1) (eq. [14*a*]), i.e. $\phi_{F_2} \approx 0$, $\chi_2 \approx 1$, such that our χ value actually is χ_1 and all our photophysical observations are for the part of our polymer ensemble for which there is one dye I fluorescein per chain in addition to some number of DPA's. The copolymers with dye II fluorescein make no contribution to our observations because the net fluorescence yield from either DPA or dye II is essentially zero.

In addition to enhancing the spectral response of a pendent dye, polymers of the type discussed herein provide a very nice model for theories of energy transfer in disordered media. In particular there is the possibility of simultaneous down-chain transfer and single-step transfer to the dye trapping site. The use of DPA is advantageous because excimer formation is avoided. However, a detailed theoretical analysis of the present results may not be justified because of the complication that two types of fluorescein moieties exist. Future studies will be directed toward alternative dye systems and (or) attachment methods that avoid this complication.

[4]A biexponential fit is not very accurate if the two lifetimes are very close (see ref. 11). This biexponential analysis is much more accurate in the case of DMF/H_2O.

Acknowledgements

This work has been sponsored by the national Science Foundation (DMR8013709) and a grant from the 3M Corporation. The single-photon lifetime apparatus was purchased with NSF equipment grant DMR8211353. We gratefully acknowledge this financial support. We also acknowledge the help of the staff and the use of the facilities of the Center for Fast Kinetics Research, which is supported jointly by the Biotechnology Branch of the Division of Research Resources of the NIH (grant RR00886) and The University of Texas at Austin. We would like to thank Edward Gaffney for his help with the fluorescence lifetime measurements.

1. (*a*) GUILLET, J. E. Polymer photophysics and photochemistry. Cambridge University Press. In press. 1984–85; (*b*) S. N. SEMERAK and C. W. FRANK. Photophysics of excimer formation in aryl vinyl polymers. Adv. Polym. Sci. **54**, 33 (1983).
2. M. TAHAN, D. PEREZ, and A. ZILKHA. Isr. J. Chem. **9**, 191 (1971).
3. H. KAMOGAWA. J. Polym. Sci. **A1**, 2458 (1969).
4. D. C. NECKERS. Nouv. J. Chim. **6**, 645 (1982), and references therein.
5. J. S. HARGREAVES, and S. E. WEBBER. Macromolecules, **17**, 1741 (1984).
6. R. MARKUSZEWSKI and H. DIEHL. Talanta, **27**, 937 (1980).
7. E. C. BLOSSEY, D. C. NECKERS, A. P. SCHAAP, and A. L. THAYER. J. Am. Chem. Soc. **97**, 3741 (1975).
8. R. B. MERRIFIELD. J. Am. Chem. Soc. **85**, 2149 (1963).
9. J. BRANDRUP and E. M. IMMERGUT. Polymer handbook. John Wiley and Sons, New York. 1975.
10. M. M. MARTIN. Chem. Phys. Lett. **35**, 105 (1975).
11. J. N. DEMAS. Excited state lifetime measurements. Academic Press, New York. 1983.
12. J. S. HARGREAVES and S. E. WEBBER. Macromolecules, **15**, 424 (1982).
13. L. E. CRAMER and K. G. SPEARS. J. Am. Chem. Soc. **100**, 221 (1978).
14. (*a*) V. ZANKER and W. PETER. Chem. Ber. **91**, 572 (1958); (*b*) L. LINDQUIST. Ark. Kemi. **16**, 79 (1960); (*c*) F. M. ABDEL-HALIM, R. M. ISSA, and A. A. HASANEIN. U.A.R.J. Chem. **14**, 275 (1971); (*d*) M. M. MARTIN and L. LINDQUIST. J. Lumin. **10**, 381 (1975); (*e*) S-C. CHEN, H. NAKAMURA, and Z. TAMURA. Chem. Pharm. Bull. **27**, 475 (1979).
15. J. J. M. LAMBERTS and D. C. NECKERS. J. Am. Chem. Soc. **105**, 7465 (1983).
16. (*a*) J. S. ASPLER, C. E. HOYLE, and J. E. GUILLET. Macromolecules, **11**, 925 (1978); (*b*) D. A. HOLDEN, W. A. RENDALL, and J. E. GUILLET. Ann. N.Y. Acad. Sci. **366**, 11 (1981).
17. D. A. HOLDEN and J. E. GUILLET. Macromolecules, **13**, 289 (1980).
18. I. B. BERLMAN. Energy transfer parameters of aromatic compounds. Academic Press, New York. 1973.
19. (*a*) D. G. LISHAN, G. S. HAMMOND, and W. A. YEE. J. Phys. Chem. **85**, 3435 (1981); (*b*) A. R. WATKINS. Aust. J. Chem. **33**, 177 (1980); (*c*) S. R. DAVIDSON and K. R. TRETHEWEY. J. Chem. Soc. Perkin Trans. 2, 178 (1977).
20. L. L. MELHADO, S. W. PELTZ, S. P. LEYTUS, and W. F. MANGEL. J. Am. Chem. Soc. **104**, 7299 (1982).
21. S. R. MEECH, and D. PHILLIPS. J. Photochem. **23**, 193 (1983).

Energy migration in the aromatic vinyl polymers. 5. Poly(2-vinyl naphthalene) and polystyrene

STEVEN N. SEMERAK AND CURTIS W. FRANK

Department of Chemical Engineering, Stanford University, Stanford, CA 94305, U.S.A.

Received August 1, 1984

This paper is dedicated to the memory of Li Xiao-Bai

STEVEN N. SEMERAK and CURTIS W. FRANK. Can. J. Chem. **63**, 1328 (1985).

Electronic energy migration in pure poly(2-vinyl naphthalene) (P2VN) is analyzed in terms of a theory for three-dimensional transport and trapping in a homogeneous system of randomly distributed chromophores. A simpler theory for 3-D transport on a spatially periodic lattice, which was applied previously to polystyrene (PS) gave self-contradictory results for P2VN because of higher transport rates in P2VN. The fraction of rings in excimer-forming sites (EFS) in pure P2VN, analyzed by the former theory, is found to be 0.072 – moderately larger than the single-chain fraction of 0.026. In contrast, the EFS ring fraction in pure PS was 0.33, much larger than the single-chain fraction of 0.051. This reflects the reduced probability, relative to a phenyl ring pair, of packing a naphthyl ring pair into the necessary sandwich arrangement in the pure polymers. Energy migration in very dilute, miscible blends containing P2VN is analyzed by a one-dimensional transport model, which was applied previously to similar blends containing PS. The nearest-neighbor migration rates obtained from the data for both P2VN and PS are about one hundred times higher than the expected dipole–dipole rates. This suggests that (1) migration is not limited to nearest-neighbor rings, (2) the morphology of the dilute blends does not consist of isolated chains of the aromatic vinyl polymers, or (3) short-range electronic interactions other than dipole–dipole are involved in energy migration.

STEVEN N. SEMERAK et CURTIS W. FRANK. Can. J. Chem. **63**, 1328 (1985).

Faisant appel à une théorie de transport tridimensionnel et de piégage dans un système homogène de chromophores distribués au hasard, on analyse la migration de l'énergie électronique dans le poly(vinyl-2 naphtalène) (PV2N) à l'état pur. Une théorie plus simple pour le transport 3-D sur un réseau périodique dans l'espace, qui a été utilisée antérieurement pour le polystyrène (PS), donne des résultats auto-contradictoires avec le PV2N; ceci est du à des vitesses de transport plus grandes dans le PV2N. Si l'on se base sur la première théorie, on trouve que la fraction des cycles dans les sites de formation des excimères (SFE) du PV2N à l'état pur est égale à 0,072 et cette valeur est modérément plus élevée que la valeur de 0,026 obtenue pour la fraction de chaîne unique. Par ailleurs, la fraction de cycle dans les SFE d'une fraction de cycle dans le PS à l'état pur est égale à 0,33 et cette valeur est beaucoup plus grande que la valeur de 0,051 obtenue pour la fraction de chaîne unique. Ces résultats reflètent une probabilité réduite, par rapport à une paire de cycles phényles, d'entassement d'une paire de cycles naphtyles dans l'arrangement nécessaire en sandwich dans le polymère à l'état pur. Utilisant un modèle de transport unidimensionnel, utilisé antérieurement dans le cas de mélanges analogues contenant du PS, on a analysé la migration d'énergie dans des mélanges très dilués et miscibles contenant du PV2N. Les vitesses de migration du voisin le plus proche, obtenues à partir de données relatives au PV2N ainsi qu'au PS, sont environ 100 fois plus élevées que les vitesses de dipôle–dipôle attendues. Ceci suggère que: (1) la migration n'est pas limitée aux cycles les plus voisins, (2) la morphologie des mélanges dilués n'est pas constituée de chaînes isolées de polymères vinyl-aromatiques ou (3) des interactions électroniques à courte distance, autres que les interaction dipôle–dipôle, sont impliqués dans la migration d'énergie.

[Traduit par le journal]

Introduction

Photophysical phenomena exhibited by the aryl vinyl polymers in the solid state include, among others, "monomer" fluorescence from an individual pendant aromatic ring in its excited singlet state, "excimer" fluorescence resulting from trapping of incident excitation energy at the conformational structure formed between two coplanar, opposed pendant rings on the same or different chains (termed an "excimer-forming-site" or EFS), and energy migration among the individual chromophores. A recent review (1) has discussed the photophysics of excimer formation in some detail. The purpose of the present paper is to investigate the rate of singlet energy migration and the number of excimeric traps occurring in poly(2-vinyl naphthalene) (P2VN) and polystyrene (PS), in dilute and concentrated blends with nonfluorescent host polymers and in the pure state.

Previous work on energy migration in dilute solution or solid miscible blends in which the fluorescent polymer may be considered to be isolated has involved application of a strictly one-dimensional random walk analysis to toluene solutions of P2VN (2), miscible blends of PS with poly(vinyl methyl ether) (PVME) (3), and miscible blends of P2VN with poly(cyclohexyl methacrylate) (4). At sufficiently high concentrations of the aryl vinyl polymer, energy migration in miscible PS/PVME blends has been treated approximately as a three-dimensional random walk on a spatially periodic lattice (5).

These studies are extended in two ways in this paper. First, the three-dimensional migration process in pure P2VN and PS is treated successfully under a recent theory of exciton transport in homogeneous systems containing donors and traps (6). We show, after making a slight correction to the 3-D lattice model (5), that it cannot be accurately applied to P2VN because of the higher migration rates in P2VN relative to PS. Second, the 1-D migration model (2–4) is presented graphically, and the nearest-neighbor migration rates in dilute, miscible blends containing P2VN or PS are extracted from published data. Implications for the 1-D model and for the morphology of the dilute blends are briefly discussed.

Experimental

All P2VN/PS blends and pure films were cast from toluene solution and dried at room temperature. The spectrofluorimeter and solvent casting procedure have been described previously, as have the sources of the P2VN(70 000) and P2VN(265 000) samples and the PS(2200) sample with which they were blended (7). Pure P2VN and the 35% blend were examined by front face excitation, and the 0.3% blend by back face excitation. The excitation wavelength was 290 nm. Spectral data for the 0.3% and 35% P2VN blends have been published in refs. 7 and 8, respectively. The pure P2VN(70 000) and P2VN(265 000) samples examined in this work had spectra which were identical at room temperature, and were similar to published P2VN spectra, e.g. ref. 21.

The 60% PS(100 000)/poly(vinyl methyl ether) blend and the pure PS(100 000) film were described previously (5), as was the 5% PS(100 000)/PVME blend (3). Spectra were taken under front face excitation.

Results and discussion

A. *Three-dimensional energy migration and photophysics of undiluted P2VN and PS*

1. *Spatially periodic lattice model*

Gelles and Frank (5) (GF) have proposed a three-dimensional migration model for pure PS and miscible PS/PVME blends containing more than 60% PS. Only nearest-neighbor migration or transfer is allowed at a uniform rate W per neighbor in a lattice with N nearest neighbors. Each lattice point represents a phenyl ring. In the blends, the value of N is reduced to $N\nu_{PS}$, where ν_{PS} is the volume fraction of PS; $1 - \nu_{PS} \ll 1$. The EFS ring fraction, q, is expressed as the sum of an intramolecular part arising from *tt meso* rotational dyads, q_{intra}, and an intermolecular portion due to segmental association between different chains, q_{inter}. The latter part was taken to be proportional to ν_{PS}. In the analysis, the migrating singlet was assumed not to resample chromophores. That is, the number of steps from the point of absorption to the excimer trap should be small, so that there is no backtracking.

There is a slight error in the GF analysis which concerns the fact that an EFS contains two rings. Because of this, the migrating singlet excitation samples the state of the neighboring *dyad* at each step. However, the EFS are not randomly distributed over the ring pairs in the system due to the strict requirements for coplanar overlap of the aromatic rings (1). For example, one ring in a lattice site oriented with the normal to the ring plane along the, e.g., *x*-axis, could form an EFS only with a second ring placed in a lattice site along that same axis. The mutually perpendicular axes would not provide the necessary overlap.

This problem can be handled by considering that any migrating singlet excitation samples a one-dimensional string of chromophores within the three-dimensional system. We will assume that the EFS are randomly distributed among the dyads of the sampling string with the quasi-dyad fraction

$$[1] \quad q_D = 1 - (1 - q)^{1/2}$$

where q is the ring fraction of EFS. Rearrangement gives the relation

$$[2] \quad q = q_D(2 - q_D)$$

Following the lines of the GF model with this correction, M, the probability of ultimate decay of the excitation through a monomer radiative or nonradiative process, is given by

$$[3] \quad M = \frac{(\alpha - q\alpha)}{\left[\alpha + q\left[\dfrac{1-\alpha}{2-q_D}\right]\right]}$$

in which

$$[4] \quad q_D = q_{D,\text{intra}} + (N-2)\Omega_D\nu$$

and

$$[5] \quad \alpha = (1 + N\nu W\tau)^{-1}$$

TABLE 1. Excimer-to-monomer fluorescence ratio, R, of pure P2VN, PS, and concentrated blends

Guest/host polymers	Fluorescent polymer concentration (wt.%)	R	Φ_D/Φ_M[b]	$1/M - 1$
P2VN	100	45 ± 2[a]	47	85 ± 5[c]
P2VN/PS	35	7.6[a,d]	7.9	14.4[c]
PS	100	12.6[e]	—	30
PS/PVME	60	4.3[e]	—	10.2

[a] Ratio of fluorescence envelope intensities, I_{398}/I_{337}, measured under front face illumination and corrected for spectral overlap.
[b] Obtained from R after multiplying by the front face spectrometer instrumental calibration constant of 1.04.
[c] Given by $(\Phi_D/\Phi_M)/(Q_D/Q_M)$, where Q_D/Q_M is taken to be 0.55 ± 0.15 (1).
[d] Reference 8.
[e] Ratio of fluorescence envelope intensities, I_{332}/I_{280}, measured under front face illumination (5). No overlap correction was necessary.

TABLE 2. Parameters of the modified Gelles–Frank three-dimensional migration model for undiluted P2VN and PS

Polymer	$NW\tau$	$(N-2)\Omega_D$	q[a]	E[b,c]	Ω_D[c]
P2VN	1440 ± 100	0.04 ± 0.005	0.10	144	0.005
PS	105	0.16	0.34	10.5	0.02

[a] For undiluted polymer.
[b] $E = W\tau$.
[c] Computed assuming $N = 10$.

The quantity α is the probability of monomer decay during each energy migration step, τ is the measured lifetime of the excitation in the absence of transfer, ν is the volume fraction of the fluorescent polymer, and Ω_D is the probability that two adjacent chromophores are in an intermolecular EFS. The excimer-to-monomer quantum yield ratio for the system is then given by

$$[6] \quad \frac{\Phi_D}{\Phi_M} = \frac{Q_D}{Q_M}\left[\frac{1-M}{M}\right]$$

Q_D and Q_M are the intrinsic quantum yields for excimer and monomer fluorescence, respectively.

By combining eqs. [1]–[6], the fluorescence ratio of undiluted aryl vinyl polymers or concentrated blends may be predicted from the parameters of the modified GF model. Experimental values of the fluorescence ratio of P2VN and PS are given in Table 1; the fitted parameters $NW\tau$ and $(N-2)\Omega_D$ appear in Table 2. If $N = 10$ is arbitrarily assumed, the three-dimensional migration parameter $E = W\tau$ is found to be 144 and 10.5 for P2VN and PS, respectively.

To evaluate whether the assumption of no resampling in the P2VN systems is valid, the expected number of steps $\langle S\rangle$ made by the migrating singlet exciton must be computed. After making the same corrections as before, $\langle S\rangle$ becomes

$$[7] \quad \langle S\rangle = \frac{1-q}{\left[\alpha + q\left[\dfrac{1-\alpha}{2-q_D}\right]\right]}$$

where q_D is again defined by eq. [1]. The corrected values of $\langle S\rangle$ for pure PS and 60% PS/PVME are 3.4 and 5.7, respectively. Values of $\langle S\rangle$ for pure P2VN and 35% P2VN/PS are 17 and 33, respectively. The approximation of no resampling in P2VN systems is, thus, poor, since $\langle S \rangle$ is larger than the number of nearest neighbors N.

2. *Self-consistent two-body model for random systems*

Because the assumption of no resampling in the three-dimensional nearest-neighbor lattice model (5) does not seem valid for P2VN, we will consider a second model that does not restrict either resampling or migration to more distant chromophores. Loring, Andersen, and Fayer (6) have recently solved the Förster problem in which energy migration among the donors is allowed. The solution was given in terms of the Laplace transform of the donor response function, $G_d(s)$. Moreover, $G_d(s)$ has been shown to be directly related to M, the probability that an excited chromophore decays through a donor, or monomer, pathway (9). M is thus related to the chromophore density, the donor–donor and donor–acceptor Förster radii, and the fraction of excimer forming sites acting as exciton traps (10). This model is best applied to undiluted polymers, however, since the assumption of a random isotropic distribution of chromophores is less accurate in dilute polymer blends.

The probability of ultimate monomer decay M according to the LAF model is[1]

$$[8] \quad M = \frac{(1-q)X^2}{(1-YX)}$$

where

$$[9] \quad X = (Z^2+1)^{1/2} - Z$$

$$[10] \quad Y = \frac{\pi}{2\sqrt{2}} C_d$$

$$[11] \quad Z = \frac{\pi}{4\sqrt{2}} (C_d + \sqrt{2}\, C_a)$$

$$[12] \quad C_d = \frac{4\pi}{3} n_d R^3_{0,d-d}$$

$$[13] \quad C_a = \frac{4\pi}{3} n_a R^3_{0,d-a}$$

The quantities n_d and n_a are the number densities of donor and acceptor, respectively, and have units of Å^{-3}. The subscripts d–d and d–a on R_0 indicate the donor–donor and donor–acceptor Förster radii, in Å. The above relations were obtained by a combination of eq. 33 in ref. 9 and eqs. 40, 48, and 54 in ref. 6. The latter three equations (6) were based on the two-body approximation, which has been shown to be a physically realistic approximation. The more exact solutions of the problem (6) were not considered here, in the interest of simplicity.

In applying eqs. [8]–[13] to determine the fluorescence ratio of undiluted aryl vinyl polymers, both n_a and n_d may be related to the chromophore density of the polymer n. Utilizing the same quasi-dyad approximation discussed earlier, we have (d = monomer, a = excimer forming site)

$$[14] \quad n_a = \frac{nq}{(2-q_D)}$$

and

$$[15] \quad n_d = n(1-q)$$

where q_D is given by eq. [1]. By the same token, the migration and transfer Förster radii are related by the expression

[1] G. H. Fredrickson, personal communication.

TABLE 3. Parameters of the Loring–Andersen–Fayer three-dimensional migration model for undiluted P2VN and PS

Polymer	q_{intra} (Å)	$R_{0,max}$	E_{max}[a]	$R_{0,Förster}$	$E_{Förster}$[b]	q_{max}
P2VN	0.026	14.0	147	11.75[c]	51	0.072
PS	0.051	9.45	26	6.47[d]	2.7	0.33

[a] $E_{max} = W_T = (R_{0,max}/r)^6$; r = 6.11 Å for P2VN and 5.48 Å for PS (1).
[b] As in note a, except $R_{0,Förster}$ replaces $R_{0,max}$.
[c] Value for 2-methyl naphthalene/2-methyl naphthalene (20).
[d] Value for isopropyl benzene/isopropyl benzene (20).

$$[16] \quad R^6_{0,d-a} = (2-q_D)R^6_{0,d-d}$$

Combination of eqs. [1]–[16] and elimination of the d–d subscript yields the following expressions for Y and Z

$$[17] \quad Y = \frac{\sqrt{2}\,\pi^2}{3} nR_0^3(1-q)$$

$$[18] \quad Z = \frac{\sqrt{2}\,\pi^2}{6} nR_0^3[(1-q) + q(1-0.5q_D)^{-1/2}]$$

Analysis of the experimental results requires that the Förster radius R_0 and the EFS trap concentration q be known. Although R_0 values are available for the low molecular weight aromatic chromophores, it is not clear whether the same values should apply when the chromophores are bound to the polymer backbone. In addition, whereas the intramolecular contribution to the trap concentration arising from the *tt meso* dyads may be calculated, there is some evidence that the intermolecular EFS concentration may depend upon the degree to which residual casting solvent is removed from the sample.[2] Nevertheless, it is possible to use the LAF model to set limits on R_0 and q.

Two limits will be examined. First, the apparent maximum value of the donor–donor Förster radius, $R_{0,d-d}$, will be obtained by assuming that there are only intramolecular contributions to the EFS ring fraction, q. Second, q for pure P2VN will be determined by taking $R_{0,d-d}$ equal to the Förster value for 2-methylnaphthalene/2-methylnaphthalene. The fluorescence ratio of pure PS (5) will also be examined under the LAF model to complete the earlier work in which the GF model was applied to PS and PS/PVME blends (5).

The limiting parameters, which were calculated for the fluorescence ratios of pure P2VN and PS taken from Table 1, are collected in Table 3. For q = 0.33 in PS, E takes its Förster value of 2.7 in the LAF model, whereas E = 10.5 (and N = 10 neighbors) in the GF model. To achieve E = 2.7 with the GF model requires that N = 40 neighbors in PS, which is unreasonable. The inclusion of migration steps other than to nearest neighbors, as in the LAF model, yields an energy migration parameter which is lower and thus more realistic. The same trend holds for P2VN, although the GF parameters are less meaningful because of the breakdown of that model.

The ring fraction of EFS in pure P2VN, given by the LAF model, is 0.072 for the Förster value of E = 51. This is rather small, considering that q = 0.33 for PS, but seems plausible, given the lower symmetry of the naphthyl pair. The difference in the EFS fraction between PS and P2VN is lower for isolated polymer chains, as shown in Table 3. The values of q_{intra} have been determined for PS (3) and P2VN (1) assuming an atactic (45% *meso*) polymer. It would be useful to examine the photophysics of isotactic samples of PS and P2VN in the pure state,

[2] J. W. Thomas and C. W. Frank, unpublished results.

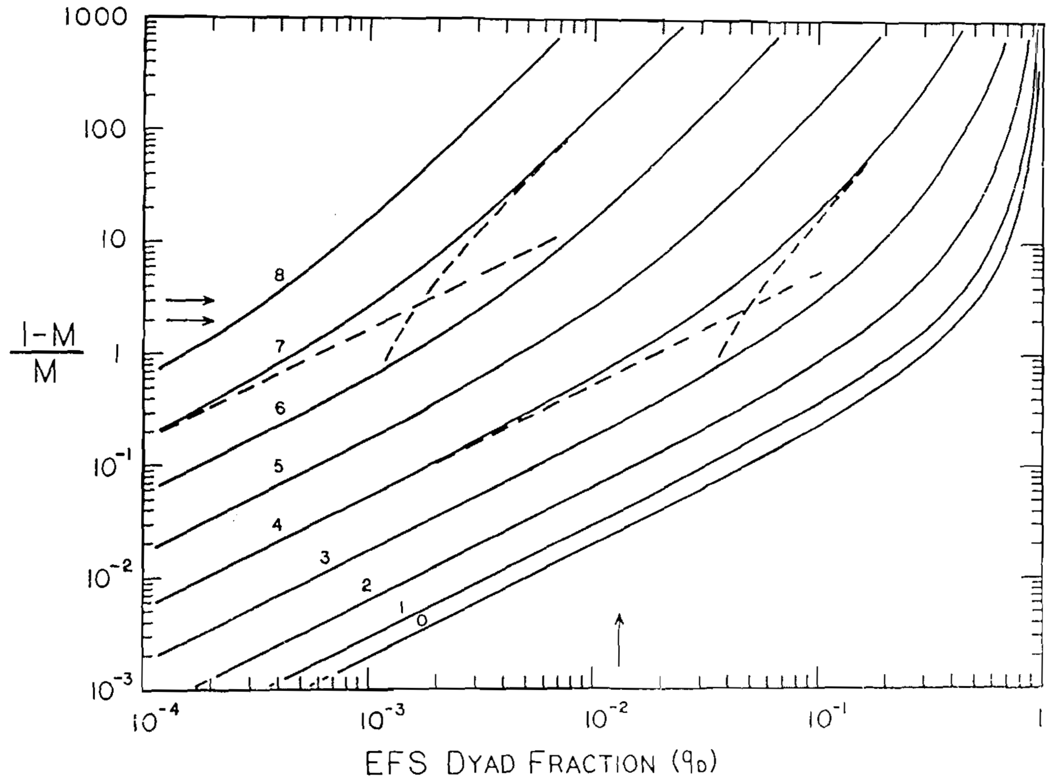

FIG. 1. Relationship between the dyad fraction of traps, q_d, and the probability ratio $(1 - M)/M$ for photons absorbed on an infinite one-dimensional lattice. The relative energy migration rates $E = W\tau$ for the solid curves numbered 0 to 8 are E = 0, 0.7, 7, 70, 700, 7 000, 70 000, 700 000, and 7 000 000, respectively. The dashed curves are the asymptotes given by eqs. [21] and [22] for curves 4 and 7. The vertical arrow indicates the value $q_D = 0.013$, while the horizontal arrows indicate values of the ratio $(1 - M)/M$ = 2 and 3.

to see whether the number of EFS traps would change. Also, the effect of low molecular weights on the fluorescence of pure films would provide an interesting study, if the foreign end groups which can cause spurious fluorescence could be removed.

B. *One-dimensional energy migration in dilute miscible blends*

The statistical model for strictly one-dimensional migration on an isolated polymer chain employed in this and previous (2, 3) studies is based on the original analysis for an infinite lattice by Levinson (11). If the EFS traps are completely effective in removing the captured photons, each sequence of nontrap sites can be analyzed without regard to the neighboring sequences. The probability M that an absorbed photon ultimately decays from the nontrap sites was computed (2) by averaging the value of M for each sequence length over the distribution of nontrap sequence lengths. As a result, Levinson's analysis was extended to the one-dimensional lattice of finite extent, and the fact that excimer-forming sites acting as traps consist of two adjacent trapping chromophores was taken into account.

The probability of ultimate monomer decay, M, of an infinite molecular weight aryl vinyl polymer is given by (2, 11).

$$[19] \quad M = 1 - q_D - \frac{q_D^2}{\tanh(\Gamma)} \sum_{x=1}^{\infty} (1 - q_D)^x \tanh(\Gamma x)$$

where

$$[20] \quad \Gamma = 0.5 \ln \left[\frac{1 + 2E + (1 + 4E)^{1/2}}{2E}\right]$$

In eq. [20], $E = W\tau$ and q_D is the dyad fraction of EFS. While eq. [19] must generally be evaluated numerically, there are two analytical expressions (11) in the limit when $E \gg 1$ and, hence $\Gamma \approx 0.5\, E^{-1/2}$. The first case, $q_D \ll \Gamma$, yields

$$[21] \quad M \approx 1 - 2q_D(E^{1/2} + 1)$$

while the second case, $q_D \gg \Gamma$, yields

$$[22] \quad M \approx \frac{[1 + q_D]^2}{2q_D^2 E}$$

Equation [21] has also been obtained by Fredrickson and Frank (10).

Because the asymptotes fail for $(1/M - 1) = 0.3$ to 30, the quantity $(1/M - 1)$ has been numerically evaluated from eq. [19] and plotted as a function of q_D for various discrete values of E. The results are presented in log–log form in Fig. 1. The dashed lines illustrate the asymptotic expressions, eqs. [21] and [22], for $E = 700$ and 7×10^5.

In this work, we wish to evaluate W for P2VN in 0.3% P2VN/PS(2200) blends, which were earlier determined to be miscible (7, 8). While Q_D/Q_M and the instrument factor relating I_D/I_M to the quantum yield ratio Φ_D/Φ_M are known (1), only an upper bound of $q_D = 0.013$ has been estimated for the dyad fraction of EFS in P2VN (1). Moreover, only three P2VN samples having broad and poorly characterized molecular weight distributions were studied. Thus, we will deduce W by comparing the fluorescence ratio of the miscible P2VN(70 000) and P2VN(265 000) guests (7) with the infinite molecular weight limit given by eq. [19].

In order to obtain a value of E from Fig. 1, both q_D and $(1/M - 1)$ must be known for the infinite molecular weight polymer. The fluorescence intensity ratios of dilute miscible blends con-

TABLE 4. Energy migration parameter, E, calculated from the excimer-to-monomer fluorescence ratio, R, of 0.3% P2VN/PS (2200) blends and of a 5% PS/PVME(44 600) blend

P2VN Mol.Wt.	R^a	$\Phi_D/\Phi_M{}^b$	$1/M - 1$	E
70 000	0.895	1.07	2 ± 0.5^c	2400^d
265 000	1.42	1.70	3 ± 0.8^c	4500^d
PS(100 000)^e	0.9^e	0.85^e	2.1^e	660^e

[a] Ratio of fluorescence envelope intensities, I_{398}/I_{337}, measured under back face illumination and corrected for spectral overlap (7).

[b] Obtained from the overlap-corrected value of R after multiplying by the back face spectrometer instrumental calibration constant of 1.2.

[c] Given by $(\Phi_D/\Phi_M)/(Q_D/Q_M)$, where Q_D/Q_M is taken to be 0.55 $\pm$ 0.15 (1).

[d] Obtained from Fig. 1, given that $q_D = 0.013$.

[e] Data from ref. 3. See Note e in Table 1. Take $Q_D/Q_M = 0.4$ and $q_D = 0.026$.

taining P2VN of molecular weights 70 000 and 265 000 and the calculations that transform this ratio into $(1/M - 1)$ are collected in Table 4. If the excimer dyad fraction, q_D, is taken to be 0.013, the values of $E = 2400$ and 4500 may be interpolated from Fig. 1 for P2VN(70 000) and P2VN(265 000), respectively. Thus, W for P2VN is about 4×10^{10} to 8×10^{10} s^{-1}, if we choose a rate constant of $\tau^{-1} = 1.8 \pm 0.2 \times 10^7$ s^{-1} for the 2-naphthyl group (1). By comparison, the energy migration parameter for PS, evaluated as described in Table 4 from the fluorescence ratio of dilute PS/PVME blends (3), was $E = 660$ at 298 K. If τ^{-1} for PS is taken (12) to be 4.5×10^7 s^{-1}, then $W = 3 \times 10^{10}$ s^{-1} for PS.

The Förster dipole–dipole expression (13) was used earlier (1) to estimate E for PS and P2VN, based on average distances between chromophores of 6.11 Å for P2VN and 5.48 Å for PS. The results were $E = 51$ for P2VN and 2.7 for PS. Comparison of the Förster prediction with the one-dimensional random walk model leads to two observations. The most significant is the dramatic disagreement between the values for W for each polymer. For P2VN, the 1-D random walk model predicts migration rates from 47 (for P2VN(70 000)) to 88 (for P2VN(265 000)) times faster than the Förster expression. For PS, the predictions differ by a factor of 244. Secondly, we note that both the Förster model and the 1-D random walk model indicate that excitation migration in P2VN is much faster than in PS.

There are three problems which could explain why the Förster migration rates are lower than those derived by the 1-D random walk analysis. First, we note that the 1-D migration rate for P2VN is only 1/15th the rate of migration observed experimentally in crystalline naphthalene (14). In fact, the Förster mechanism is strictly dipole–dipole, whereas the dipole–dipole term is only one of a variety of short-range interactions (such as octupole–octupole (15)) that may come into play when the 2-naphthyl chromophores are only 5 or 6 Å apart. Second, the occurrence of "cross-loop" migration steps would increase the efficiency of sampling the EFS traps. The apparent migration rate derived from the 1-D model would thus be too high. Finally, the PS or P2VN chains in the dilute blends may not be isolated, despite the fact that these blends have been determined to be miscible.

An improved model of energy migration in "quasi-one-dimensional" systems has not yet appeared. There are analytical techniques for treating excitation transport and trapping on polymer chains that contain a small concentration or randomly distributed chromophores along the chain contour (16–19). It is hoped that such techniques can eventually be extended to cover the dilute aryl vinyl polymer blends in this study.

Acknowledgements

This work was supported by the Polymers Program of the National Science Foundation. The authors wish to thank Glenn H. Fredrickson for extensive discussion and assistance with this study.

1. S. N. SEMERAK and C. W. FRANK. Adv. Polym. Sci. **54**, 31 (1983).
2. P. D. FITZGIBBON and C. W. FRANK. Macromolecules, **15**, 733 (1982).
3. R. GELLES and C. W. FRANK. Macromolecules, **15**, 741 (1982).
4. J. W. THOMAS, JR. and C. W. FRANK. Macromolecules. In press.
5. R. GELLES and C. W. FRANK. Macromolecules, **15**, 747 (1982).
6. R. F. LORING, H. C. ANDERSEN, and M. D. FAYER. J. Chem. Phys. **76**, 2015 (1982).
7. S. N. SEMERAK and C. W. FRANK. Macromolecules, **14**, 443 (1981).
8. S. N. SEMERAK and C. W. FRANK. Adv. Chem. **203**, 757 (1983).
9. G. H. FREDRICKSON and C. W. FRANK. Macromolecules, **16**, 1198 (1983).
10. G. H. FREDRICKSON and C. W. FRANK. Macromolecules, **16**, 572 (1983).
11. N. J. LEVINSON. Soc. Indust. Appl. Math. **10**, 442 (1962).
12. J. B. BIRKS. Photophysics of aromatic molecules. Wiley–Interscience, New York. 1970. p. 126.
13. TH. FÖRSTER. Compr. Biochem. **22**, 61 (1967).
14. R. C. POWELL and Z. G. SOOS. J. Lumin. **11**, 1 (1975).
15. D. C. CRAIG and S. H. WALMSLEY. *In* Physics and chemistry of the organic solid state. Vol. 1. *Edited by* D. Fox, M. M. Labes, and A. Weissberger. Interscience, New York. 1963. p. 585.
16. G. H. FREDRICKSON, H. C. ANDERSEN, and C. W. FRANK. Macromolecules, **16**, 1456 (1983).
17. G. H. FREDRICKSON, H. C. ANDERSEN, and C. W. FRANK. Macromolecules, **17**, 54 (1984).
18. G. H. FREDRICKSON, H. C. ANDERSEN, and C. W. FRANK. Macromolecules, **17**, 1496 (1984).
19. G. H. FREDRICKSON, H. C. ANDERSEN, and C. W. FRANK. J. Polym. Sci. Polym. Phys. Ed. In press.
20. I. B. BERLMAN. Energy transfer parameters of aromatic compounds. Academic Press, New York. 1973.
21. L. A. HARRAH. J. Chem. Phys. **56**, 385 (1972).

Prospects for solar synthesis. II. Study of the photocyclization of α-(*o*-tolyl)acetophenone in solution and in crosslinked ethylene – vinyl acetate beads[1]

J. E. GUILLET, W. K. MACINNIS, AND A. E. REDPATH
EcoPlastics Limited, 518 Gordon Baker Road, Willowdale, Ont., Canada M2H 3B4

Received September 13, 1984

This paper is dedicated to the memory of Li Xiao-Bai

J. E. GUILLET, W. K. MACINNIS, and A. E. REDPATH. Can. J. Chem. **63**, 1333 (1985).

Studies of the photocyclization of α-(*o*-tolyl)acetophenone dissolved in crosslinked ethylene – vinyl acetate beads show that quantum yields close to unity can be achieved, even in the solid polymer matrix. In preliminary experiments using solar radiation it was demonstrated that the rates of photochemical transformations are close to those calculated from the photon energy distribution of the solar spectrum.

J. E. GUILLET, W. K. MACINNIS et A. E. REDPATH. Can. J. Chem. **63**, 1333 (1985).

Des études sur la photocyclisation de l'α-(*o*-tolyl)acétophénone dissoute dans des billes d'un polymère réticulé d'éthylène et d'acétate de vinyle ont permis de montrer que l'on peut obtenir des rendements quantiques qui s'approchent de l'unité, même dans la matrice solide d'un polymère. Dans des expériences préliminaires faisant appel à la radiation solaire, on a pu démontrer que les vitesses des transformations photochimiques se rapprochent de celles que l'on peut calculer en utilisant la distribution des énergies des photons du spectre solaire.

[Traduit par le journal]

Introduction

The study of organic photochemistry has been an active field of research for many years. As a result of this work there is a wide variety of synthetic photochemical routes to the synthesis of novel organic compounds and intermediates. Surprisingly, very few applications of these synthetic routes have reached commercial practice, probably because of the high cost of using electrically driven lamps to provide the necessary photon energy. For a number of years, we have been interested in exploring the possible use of polymeric devices which could utilize natural sunlight to carry out photochemical processes in a manner which could be easily expanded to large-scale commercial production. In this paper we report a method of carrying out photochemical reactions in small crosslinked polymer beads. The beads can be supported on water which provides both a self-levelling support and a means of transporting the beads from the exposure area to a collection device.

The sun as a photochemical light source

In principle, the sun is an excellent source of photon energy for initiating the synthesis of organic compounds. An obvious example of this is the relatively high efficiency of plant photosynthesis and the myriad of biochemical reactions which flow from it. However, sunlight is much less intense, in certain photon ranges, than electrically driven lamps and so exposure must usually be carried out over much larger areas. Figure 1 shows the distribution of solar photon energy at the earth's surface for air mass 1, i.e., with the sun directly overhead at sea level. This distribution is slightly affected by both air mass and latitude, but can be considered to be relatively independent of geographic location to a first approximation. However, seasonal variations in intensity do occur because of latitude and cloud cover. The total daily energy ranges from about 110 W/m^2 in southern Sweden to about 300 W/m^2 in arid equatorial zones. Thus the energy input on a 1-hectare area (10^4 m^2) ranges from 26 400 to 72 000 kW h/day. As shown in Fig. 1 the photon flux remains relatively constant from about 450-nm to 850-nm wavelengths, but even below 450 nm a substantial number of photons is available (1). Using the data in Fig. 1, one can calculate the solar power available over different wavelength ranges. These are summarized in Table 1 along with the theoretical production of a 1-hectare solar chemical reactor. The latter data are calculated assuming that the product has a molecular weight of 400 and a quantum yield of unity. Even for short-wavelength uv, $\lambda < 300$ nm, theoretical yields of several metric tonnes a day are calculated. If visible light can be used (i.e., λ = 400–700), the yield might be as much as several hundred tonnes per day. Of course these calculations represent an upper maximum because of inefficiencies due to absorption and reflection losses as well as side reactions and other chemical causes of reduced efficiency. Nonetheless, the potential of

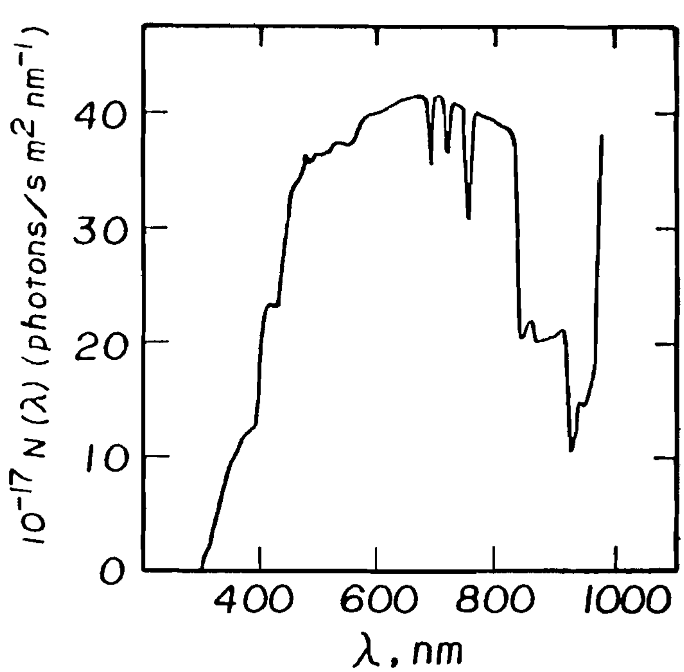

FIG. 1. Air mass 1 solar radiation: spectral photonic flux density (photons/s m^2 nm) (see ref. 1).

[1] This paper was presented (in part) at the Li Xiao-Bai Memorial Symposium (April 16–17, 1984; Department of Chemistry, University of Toronto) as a tribute to a respected friend and distinguished colleague from the People's Republic of China.

TABLE 1. Theoretical production of a 1-hectare solar plant

Wavelength range, nm	kW/hectare, noon	Einstein/kW h	Metric tonnes/day[a]
<300	120	9.02	3.5
300–350	340	10.5	11.4
350–400	440	12.0	16.9
400–700	3980	21.0	267
700–1000	2210	30.0	212
>1000	2910	>30	279

[a] Assumes product GMW = 400; average solar input = 300 W/m^2; quantum yield = 1.0.

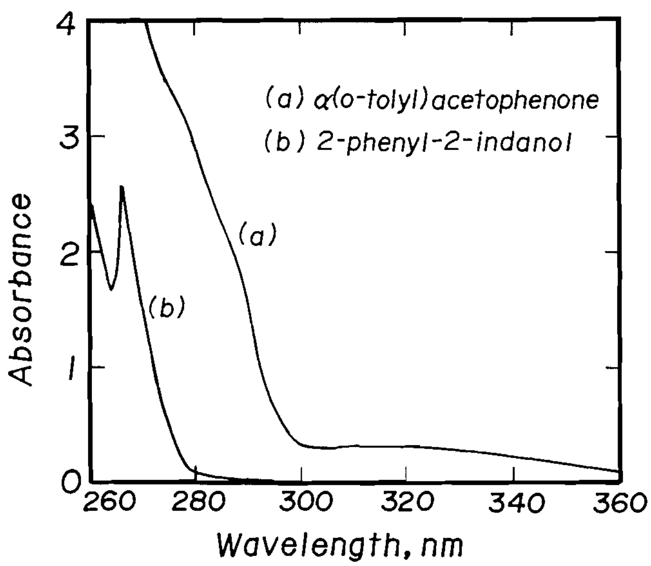

FIG. 2. Ultraviolet absorption spectra of α-(*o*-tolyl)acetophenone and 2-phenyl-2-indanol (2.8 × 10^{-3} *M* in EtOAc).

solar synthesis for producing large quantities of organic compounds is obvious, provided a suitable means of exposure and collection is possible.

Principles of reactor design

The most successful reactor design so far achieved is that of the leaf of a green plant. The photons are strongly absorbed by thin layers of organic pigments in a relatively thin flat membrane containing mechanical devices to assure access to the reagents, and removal or storage of the products. Leaves also contain photon-harvesting devices (antenna chlorophyll) which absorb photons and transfer the photon energy to active sites where the photochemical energy conversion process takes place. In recent studies in our laboratories we have shown how to construct polymeric macromolecules which can mimic this essential feature of plant photosynthesis (2–4). These antenna polymers have the property of being able to collect photon energy by absorption in chromophores attached to a polymer chain. This energy is transferred by one or more energy-transfer steps to a trap at the middle or end of the chain where photochemical reactions can be induced to take place. The "antenna effect" is believed to be required for processes involving multiphoton reactions but may not contribute to the efficiency of simple one-step single-photon photochemistry.

In a previous paper (5) we have described the initiation of photochemical reactions in crosslinked plastic beads or platelets which are floated on water for exposure to sunlight. The design was to imitate the highly efficient photochemical collection system of the aquatic plant *Lemna minor* (duckweed). In the early work we showed that a variety of photochemical reactions, including the Norrish type I and type II processes in aliphatic ketones, and the addition of singlet oxygen to olefins could be carried out in these polymeric devices. In this paper we wish to report studies on a model photochemical reaction which can be used to illustrate the potential for commercial synthesis.

Recently, Meador and Wagner (6) have reported that α-(*o*-tolyl)acetophenone undergoes a photocyclization reaction via the intramolecular abstraction of the γ-hydrogen, eq. [1],

[1] 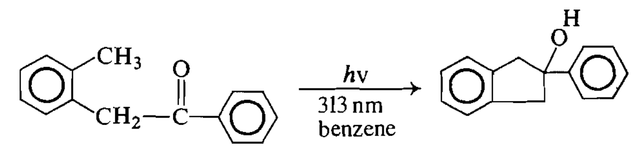

with a quantum yield close to unity. The ketone absorbs available solar energy in the 280–360 nm region but the product 2-phenyl-2-indanol is transparent above 280 nm, as shown in Fig. 2. This is of particular value because the reaction can be run to a high degree of conversion with no interference by light absorption by the product. This then represents an ideal actinometer system to study potential yields of solar photochemical processes in this wavelength region.

Experimental

α-(*o*-Tolyl)acetophenone was synthesized by the procedure described in a previous publication (5). Analytical determinations were made in early runs by gas chromatography using a flame ionization detector and a 5% Carbowax 1540 on a Chromosorb WHP 80–110 column at 212°C. Later analytical data were obtained by hplc using a μ Porosil column with chloroform/hexane/ethyl acetate 70:30:2 solvent system and a 254-nm uv detector. The system was calibrated in both cases with known amounts of the pure components, using 9-fluorene methanol as an internal standard for the gc work and benzyl alcohol as the internal standard for hplc. The bead reactors were prepared by crosslinking a commercially available ethylene – vinyl acetate copolymer (Elvax 150N) which contains about 20% vinyl acetate. The beads were sealed in a glass jar under nitrogen and exposed in an AECL Gammacel 220 to 60 Mrad of γ-radiation from ^{60}Co. Before use the beads were extracted for 16 h with diethyl ether, thus removing all uncrosslinked polymer. They were then dried in the air at 35°C.

For calibration purposes the exposure of the beads was compared with exposures in solution in the absence of air. The bead samples were prepared as follows. The starting material (100 mg) was dissolved in ether and loaded onto 2 g of crosslinked EVA beads. The beads swell in a few minutes with the ether solution, after which they are dried in air to remove the ether. They were then placed in a single layer in quartz tubes which were flushed with nitrogen. In a control experiment, a solution of 150 mg of α-(*o*-tolyl)acetophenone was dissolved in 15 mL of ethyl acetate. The samples were exposed in similar quartz tubes under nitrogen.

During exposure to solar uv radiation the intensity was monitored as hourly integrated totals using a detector (Optical Associates Inc., Santa Clara, Calif.) with a peak sensitivity at 313 nm. The band-pass of the filter was ca. 40 nm. Bead samples and solution aliquots were removed periodically for work-up. The ethyl acetate solution was analyzed as received; the beads were extracted three times with ether (3 × 20 mL) to remove the product. (In an earlier experiment, gc analysis indicated that a mass balance of 90% was achieved by one extraction of the beads with solvent.) Each sample was analyzed by hplc to determine product yields and by uv to monitor changes in the absorbance spectrum.

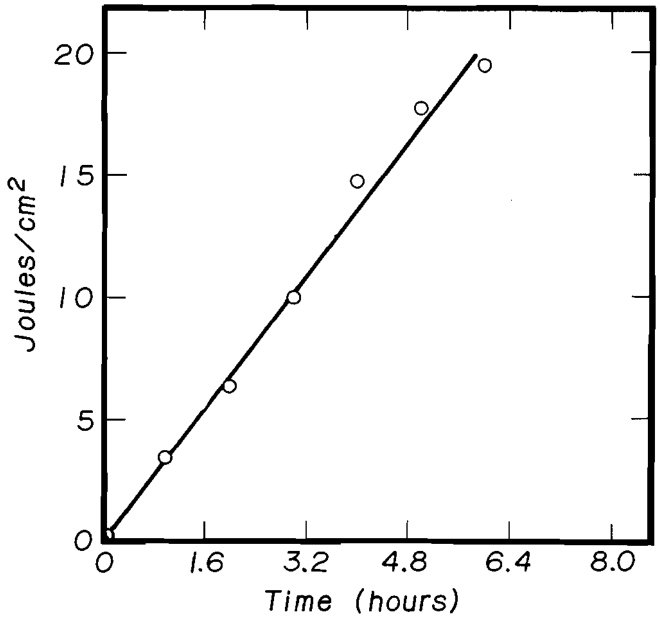

FIG. 3. Integrated exposure (OAI actinometer) vs. time.

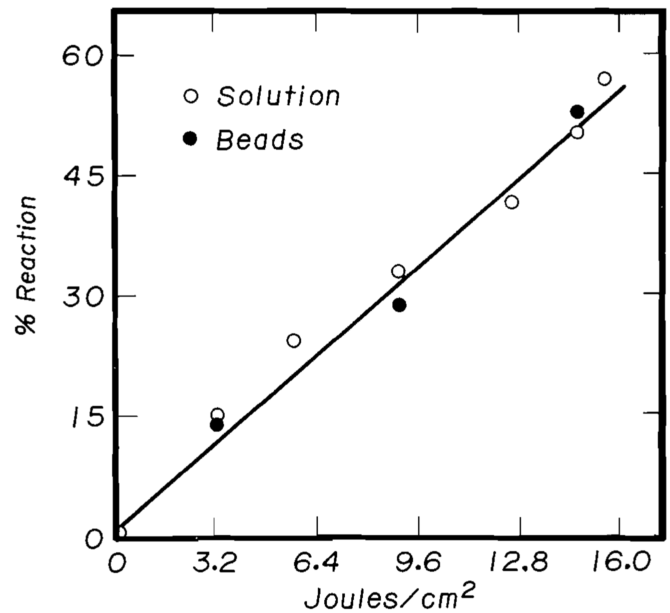

FIG. 5. Percent reaction vs. exposure (corrected).

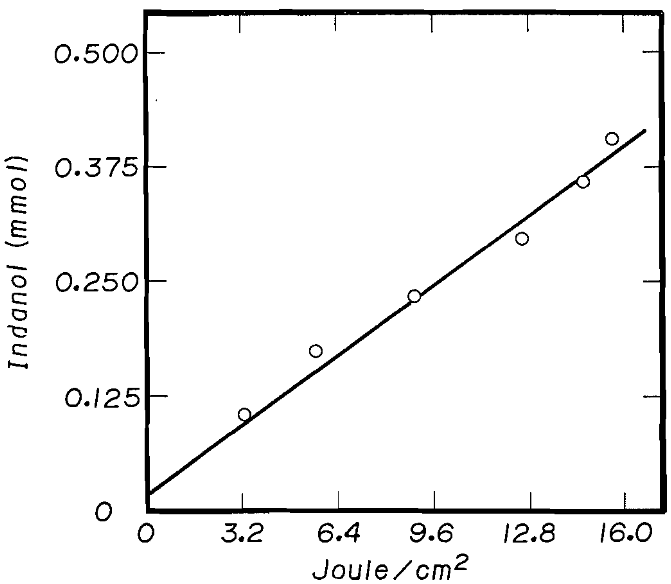

FIG. 4. Millimoles of product vs. corrected exposure (reaction in solution).

Results

Figure 3 shows the solar intensity as a function of time for exposure for daylight hours in the middle of May 1984 in Toronto. Exposures were initiated at 10:00 and terminated at 17:00 hours. An approximately linear relationship exists between intensity at 313 nm and exposure time in hours over most of the time period. These data form the basis of our calculation of the rate of conversion of the α-(*o*-tolyl)acetophenone as a function of photon exposure, as shown in Fig. 4 for reactions in ethyl acetate solution. However, the uv spectra of the product solutions showed evidence not only for the disappearance of the α-(*o*-tolyl)acetophenone starting material, but also for the appearance of a uv absorbing by-product. In our earlier work this problem was considered and attributed to 2-phenylindene formation. Although gc and hplc analyses show this by-product to be present in very small quantities, its uv absorbance in the 280–360 nm region is not negligible. This has the effect of reducing the photon flux available to the ketone. Since the hplc analysis permits us to calculate the amount of ketone present in any solution, and thus the uv absorbance due to the ketone, the absorbance due to the by-product could be estimated. The ratio of these absorbance values was used to correct the incident photon flux over each successive sample interval. This correction factor increased over time to a maximum of 25–30% at the longest times of the experiment. Figure 5 shows the percent conversion in solution and in the beads as a function of photon energy absorbed, corrected as described above for both bead and solution experiments. the results are essentially identical.

From these data, the apparent quantum yield can be estimated if the actual exposure areas are known. This is most readily done for the solution experiments from which we calculate a quantum yield of close to unity (and, as shown in Fig. 5, similarly so in the beads), in good agreement with the literature value (6).

The data in Fig. 5 also lead to the conclusion that the production rates estimated in Table 1 can indeed be approached in a practical photochemical reaction. In these exposures 0.05 mmol of product were made in one day with beads covering 2 cm^2. Thus for a 1-hectare reactor area, 10^8 cm^2, we should obtain 2.5×10^3 mol or 525 kg of product. This amounts to about 0.5 metric tonnes per day, which is lower than, but of the same order of magnitude as, the values listed in Table 1 for reactions sensitized by uv light, $\lambda < 350$ nm, once correction is made for our lower light intensity and the lower molecular weight of our product.

Conclusions

From these experiments we conclude that the higher internal viscosity of the crosslinked plastic beads does not interfere with the photochemical efficiency of intramolecular photocyclization reactions of the type described here, and that the bead reactors may well be useful for carrying out a variety of photochemical reactions by means of solar radiation.

1. S. CLAESSON and L. ENGSTROM (*Editors*). Solar energy – photochemical conversion and storage. National Swedish Board for Energy Source Development, Stockholm. 1977. p. II.6.
2. J. S. ASPLER, C. E. HOYLE, and J. E. GUILLET. Macromolecules, **11**, 925 (1978).
3. D. A. HOLDEN, W. A. RENDALL, and J. E. GUILLET. Ann. N.Y. Acad. Sci. **366**, 11 (1981).
4. J. GUILLET. Polymer photophysics and photochemistry. Cambridge University Press, Cambridge. 1985. Chapt. 9.
5. J. E. GUILLET, J. SHERREN, H. M. GHARAPETIAN, and W. K. MACINNIS. J. Photochem. **25**, 501 (1984).
6. M. A. MEADOR and P. J. WAGNER. J. Am. Chem. Soc. **105**, 4484 (1983).

Polymérisation du chloroformiate de vinyle et de ses dérivés

SYLVIANE BOIVIN, PATRICK HEMERY ET SYLVIE BOILEAU[1]
Collège de France, 11 place Marcelin Berthelot, 75231 Paris Cédex 05, France

Reçu le 19 juin 1984

Cet article est dédié à la mémoire de Monsieur Li Xiao-Bai

SYLVIANE BOIVIN, PATRICK HEMERY et SYLVIE BOILEAU. Can. J. Chem. **63**, 1337 (1985).

La polymérisation radicalaire du chloroformiate de vinyle a été étudiée dans le chlorure de méthylène à 35°C, avec le peroxydicarbonate de dicyclohexyle comme amorceur. Des mesures cinétiques ont été effectuées par dilatométrie dans des appareils entièrement scellés sous vide poussé. L'ordre de la réaction de polymérisation par rapport à la concentration en monomère est égal à 1 et celui relatif à la concentration en amorceur est égal à 0,5.

Par ailleurs, des polymères nouveaux ont été préparés soit par polymérisation radicalaire de monomères dérivés du chloroformiate de vinyle, soit par modification chimique du polychloroformiate de vinyle par des amines, des alcools, des thiols, des acides carboxyliques, KCN . . . , par catalyse par transfert de phase. La structure de ces polymères ainsi que leur comportement thermique ont été examinés.

SYLVIANE BOIVIN, PATRICK HEMERY, and SYLVIE BOILEAU. Can. J. Chem. **63**, 1337 (1985).

The free-radical polymerization of vinyl chloroformate has been studied in methylene chloride at 35°C using dicyclohexyl peroxydicarbonate as initiator. Kinetic measurements performed by dilatometry under high vacuum have shown that the reaction order in monomer is equal to one whereas that in catalyst is equal to 0.5.

New polymers have been prepared either by free-radical polymerization of monomers derived from vinyl chloroformate or by chemical modification of poly(vinyl chloroformate) with amines, alcohols, thiols, carboxylic acids, KCN . . . using phase transfer catalysis. The structure of these polymers as well as their thermal behaviour have been studied.

Introduction

L'intérêt croissant suscité par le chloroformiate de vinyle (CH_2=CHOCOCl : VOCCl) provient du fait qu'il sert de matière première pour la préparation de nombreux médicaments ainsi que pour la synthèse de monomères vinyliques variés. Toutefois, la polymérisation du chloroformiate de vinyle (1) et de certains de ses dérivés – carbamates vinyliques (1–3), carbonates vinyliques (1, 4) et cyanoformiate de vinyle (1) – a été très peu étudiée jusqu'à ces dernières années, en raison des difficultés de préparation et de purification de ce monomère.

Un nouveau procédé de synthèse de chloroformiate de vinyle quasiment exempt d'impuretés, avec un rendement de 80% a été mis au point récemment (5). Ceci nous a incités à examiner en détail la polymérisation de ce monomère (6–8) et de quelques dérivés (6, 8, 9) ainsi que la modification chimique du polychloroformiate de vinyle (6, 10–12).

L'emploi de peroxydicarbonates comme amorceurs de la polymérisation radicalaire du chloroformiate de vinyle, en masse et en solution, conduit à des polymères de masses molaires élevées (7, 8). Les résultats de l'étude cinétique effectuée dans le chlorure de méthylène à 35°C, en présence de peroxydicarbonate de dicyclohexyle, sont exposés dans le présent article.

Par ailleurs, de nouveaux polymères ont été préparés soit par polymérisation radicalaire de monomères dérivés du chloroformiate de vinyle, soit par modification chimique du PVOCCl par des amines, des alcools, des phénols, des thiols, des acides carboxyliques et leurs sels alcalins, KCN ... en utilisant la catalyse par transfert de phase. Les résultats récents obtenus dans ce domaine sont mentionnés dans cet article.

Partie expérimentale

La pureté du VOCCl (Société Nationale des Poudres et Explosifs) est généralement supérieure à 99%. Ce monomère est introduit dans un ballon scellé sous vide poussé; il est conservé dans des tubes gradués munis de joints fragiles, à −35°C, à l'obscurité. Il est débarrassé de son stabilisant juste avant emploi.

Les carbamates vinyliques tels que le carbamate de vinyle et de *N*-diéthyle ($VOCNEt_2$ où VOC: CH_2=CH—O—C(O)—) et le carbamate de vinyle et de *N*-pipéridine ($VOCNC_5H_{10}$) sont obtenus par réaction du VOCCl avec la triéthylamine et la *N*-éthylpipéridine respectivement, selon le procédé général de déalkylation des amines tertiaires développé par Schnur et Olofson *et al.* (13–15). Les autres carbamates vinyliques comme le carbamate de vinyle et de n-butyle (VOCNHBu) et le carbamate de vinyle et de *N*-méthyl cyclohexyle ($VOCN(CH_3)C_6H_{11}$) sont préparés par réaction du VOCCl avec les amines correspondantes en présence d'un capteur d'acide chlorhydrique (8, 13).

La réaction du VOCCl avec le phénol et le menthol en présence de soude ou de pyridine conduit aux carbonates vinyliques correspondants (VOCOPh, VOCOMenthyle) (8, 13). Le thiocarbonate de vinyle et de phényle (VOCSPh) est préparé selon une méthode déjà décrite (16).

Le chlorure de méthylène est purifié sur P_2O_5 puis sur des miroirs de sodium successifs, selon la méthode mise au point au laboratoire (17). L'azobisisobutyronitrile (AIBN) et le peroxydicarbonate de dicyclohexyle (DCPD) sont séchés sous vide avant emploi.

La plupart des polymérisations sont effectuées dans des appareils en verre entièrement scellés sous vide poussé, selon la technique utilisée pour les polymérisations anioniques (18). Le monomère (VOCCl) est condensé dans un tube annexe afin d'éliminer l'inhibiteur, avant d'être introduit par distillation sur paroi froide, ainsi que le solvant, dans un ballon contenant l'amorceur. Les polymérisations des dérivés du VOCCl sont effectuées sous azote, dans des appareils reliés à une ligne à vide. Le monomère est introduit avec une seringue à travers un bouchon de caoutchouc à jupe rabattable, dans un ballon contenant le catalyseur qui est séché sous vide au préalable. Dans tous les cas, l'agitation du milieu est assurée par un barreau aimanté enrobé de verre, à une température donnée. Les polymères sont récupérés après dissolution dans le chlorure de méthylène et précipitation dans l'éther de pétrole. Ils sont ensuite séchés sous vide poussé.

Nous avons utilisé une méthode dilatométrique comme moyen d'étude cinétique selon la technique expérimentale mise au point au laboratoire (19). Les masses spécifiques du monomère (VOCCl) et du

[1]Laboratoire de Chimie Macromoléculaire associé au C.N.R.S. n° 24.

TABLEAU 1. Résultats cinétiques de la polymérisation radicalaire du chloroformiate de vinyle amorcée par le peroxydicarbonate de dicyclohexyle, dans CH_2Cl_2 à 35°C

Essai	$[M]_0$ (mol L^{-1})	$[A]\times 10^3$ (mol L^{-1})	$V_p/[M]\times 10^3$ (min^{-1})	$k_{app} = \frac{V_p}{[M][A]^{1/2}} \times 10^2$ ($L^{1/2}$ $mol^{-1/2}$ min^{-1})
1	1,98	3,99	0,82	1,3
2	1,98	5,98	1,08	1,4
3	1,98	7,15	1,22	1,4
4	1,96	7,83	1,34	1,5
5	2,84	7,93	1,35	1,5
6	4,71	7,96	1,35	1,5
7	1,98	9,98	1,52	1,5

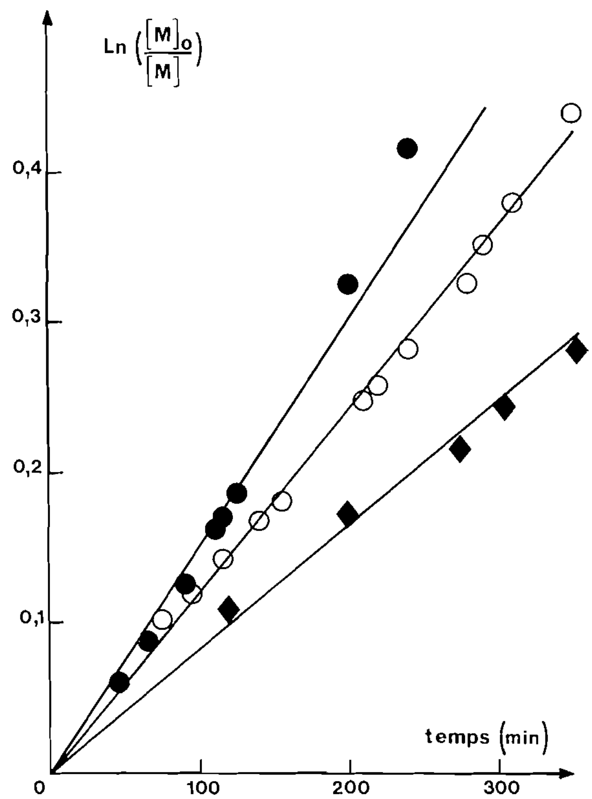

FIG. 1. Variations de ln $[M]_0/[M]$ en fonction du temps lors de la polymérisation radicalaire du VOCCl amorcée par le DCPD dans CH_2Cl_2 à 35°C: ● $[M]_0 = 1{,}98$ mol L^{-1}, $[A] = 9{,}98 \times 10^{-3}$ mol L^{-1}; ○ $[M]_0 = 1{,}98$ mol L^{-1}, $[A] = 7{,}15 \times 10^{-3}$ mol L^{-1}; ◆ $[M]_0 = 1{,}98$ mol L^{-1}, $[A] = 3{,}99 \times 10^{-3}$ mol L^{-1}.

polymère en solution dans CH_2Cl_2 à 35°C ont été mesurées avec un densimètre électronique à tube vibrant (PAAR DMA 45).

La technique de modification chimique du PVOCCl a été décrite précédemment (10). Les substituants sont des produits commerciaux utilisés sans purification spéciale à l'exception des amines qui sont redistillées avant emploi. Les catalyseurs: dicyclohexyl-18 couronne-6 (DCHE); sulfate acide de tétrabutylammonium (TBAH); Kryptofix [222] sont des produits commerciaux séchés sous vide poussé. Le degré de substitution est déterminé d'après l'analyse élémentaire des polymères modifiés. Ceux-ci sont conservés à −30°C dans des tubes scellés sous vide poussé.

Les polymères sont examinés par spectrophotométrie ir et par rmn du carbone 13. Dans ce dernier cas, les spectres de solutions de polymères dans un mélange 90:10 de trichloro-1,2,4 benzène et de nitrobenzène deutérié sont enregistrés à 100°C sur un appareil Brucker WP 250 à 62,5 MHz. Les masses molaires moyennes en nombre des polymères sont mesurées par osmométrie dans le toluène à 37°C. Les températures de transition vitreuse sont déterminées grâce à un analyseur thermique du Pont 1090 et la stabilité thermique des polymères est examinée par thermogravimétrie en chauffant les échantillons de 20 à 700°C à 5°C/min à l'air (9).

Résultats et discussion

1. *Polymérisation du chloroformiate de vinyle*

Nous avons montré que la polymérisation radicalaire du chloroformiate de vinyle donne des polymères de masses molaires élevées, avec des rendements quantitatifs (7, 8). Les meilleurs systèmes catalytiques sont les peroxydicarbonates, en solution dans le chlorure de méthylène, car ils permettent d'opérer à des températures n'excédant pas 40°C. Dans ces conditions, on n'observe pas de dégradation des polymères.

Nous avons donc effectué une étude cinétique de la polymérisation du VOCCl amorcée par le peroxydicarbonate de dicyclohexyle, dans CH_2Cl_2 à 35°C. Nous avons utilisé une technique dilatométrique et nous avons effectué toutes les mesures à partir d'un même lot de monomère afin d'avoir des résultats reproductibles.

Le facteur de contraction α correspondant à la variation de volume spécifique lorsqu'on passe du monomère au polymère a été déterminé par deux méthodes. La première consiste à conduire une réaction de polymérisation, dans un dilatomètre, jusqu'à conversion totale. La mesure des différences de niveau dans le capillaire, entre le début et la fin de la réaction, permet de calculer α. La deuxième technique consiste à mesurer les masses spécifiques du monomère, m_{35} (VOCCl), et du polymère, m_{35}(PVOCCl), dans CH_2Cl_2 à 35°C. Le facteur de contraction, α_{35}, est calculé d'après la relation:

$$[1] \quad \alpha_{35} = \frac{1}{m_{35}(\text{VOCCl})} - \frac{1}{m_{35}(\text{PVOCCl})}$$

On obtient ainsi $\alpha_{35} = 0{,}229$ mL g^{-1} pour des concentrations en monomère et en polymère ($\overline{M}_n = 18\,500$) égales à 1,96 mol L^{-1}. Cette valeur est en excellent accord avec celles déterminées lors de deux expériences dilatométriques (essais 3 et 7 du tableau 1): $\alpha = 0{,}23$ mL g^{-1}.

Les résultats cinétiques sont indiqués dans le tableau 1. Sur la fig. 1, nous avons porté les variations de ln$[M]_0/[M]$ en fonction du temps, où $[M]_0$ et $[M]$ sont les concentrations en monomère respectivement au temps zéro et à l'instant *t*, pour les essais 1, 3 et 7. On obtient des droites passant par l'origine jusqu'à des taux de conversion de 30 à 50%, ce qui montre que l'ordre interne de la réaction de polymérisation par rapport à la concentration en monomère est égal à 1. Les pentes de ces droites sont égales à $V_p/[M]$.

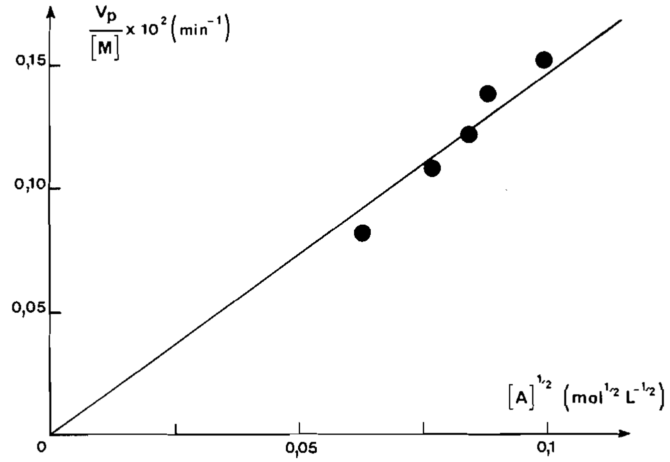

FIG. 2. Variations de $V_p/[M]$ en fonction de $[A]^{1/2}$ lors de la polymérisation radicalaire du VOCCl amorcée par le DCPD dans CH_2Cl_2 à 35°C.

Si l'on admet que l'hypothèse de l'état stationnaire est vérifiée pour ce système, la vitesse de polymérisation V_p est donnée par la relation suivante:

$$[2] \quad V_p = -\frac{d[M]}{dt} = k_p\left(f\frac{k_d}{k_t}[A]\right)^{1/2}[M]$$

où [M] et [A] sont les concentrations en monomère et en amorceur; k_p, k_d et k_t sont respectivement les constantes de propagation, de dissociation de l'amorceur et de terminaison et où f représente l'efficacité de l'amorceur.

Nous avons vérifié que la vitesse de polymérisation est proportionnelle à [M] et à $[A]^{1/2}$ car on observe bien des relations linéaires entre $V_p/[M]$ et $[A]^{1/2}$ d'une part et entre $V_p/[A]^{1/2}$ et [M] d'autre part, ainsi qu'en témoignent les figures 2 et 3. La valeur de la constante apparente de vitesse

$$k_{app} = \frac{V_p}{[M][A]^{1/2}}$$

est égale à $1{,}4 \times 10^{-2} \pm 0{,}1 \times 10^{-2}\ L^{1/2}\ mol^{-1/2}\ min^{-1}$.

2. *Polymères dérivés du polychloroformiate de vinyle*

Deux voies d'accès aux polymères dérivés du PVOCCl ont été examinées: d'une part, la polymérisation radicalaire de composés provenant du VOCCl et d'autre part, la modification chimique du PVOCCl par des substituants appropriés.

Le tableau 2 rassemble les résultats les plus significatifs de la polymérisation radicalaire, en masse, de quelques dérivés du chloroformiate de vinyle tels que des carbonates, thiocarbonates et carbamates vinyliques. On obtient des polymères de masses molaires élevées avec de bons rendements. Les résultats sont améliorés lorsqu'on opère dans des conditions rigoureuses de pureté (essais 15 et 16).

La modification chimique du PVOCCl par des amines et des alcools a été décrite par Schaefgen (1). Cependant, cet auteur a généralement observé des réactions secondaires d'hydrolyse conduisant à des polymères réticulés dont le degré de substitution ne dépasse pas 30%. Nous avons mis au point des conditions opératoires qui permettent d'éviter les réactions de dégradation (6, 10–12). Les polymères ainsi modifiés sont solubles et les degrés de substitution sont excellents. Les rendements en polymères solubles sont de l'ordre de 80%. Les résultats concernant la modification chimique du PVOCCl par les amines, les alcools, thiols et phénols, les acides carboxyliques et les sels alcalins (carboxylates et cyanures) sont rassemblés dans les tableaux 3 à 7.

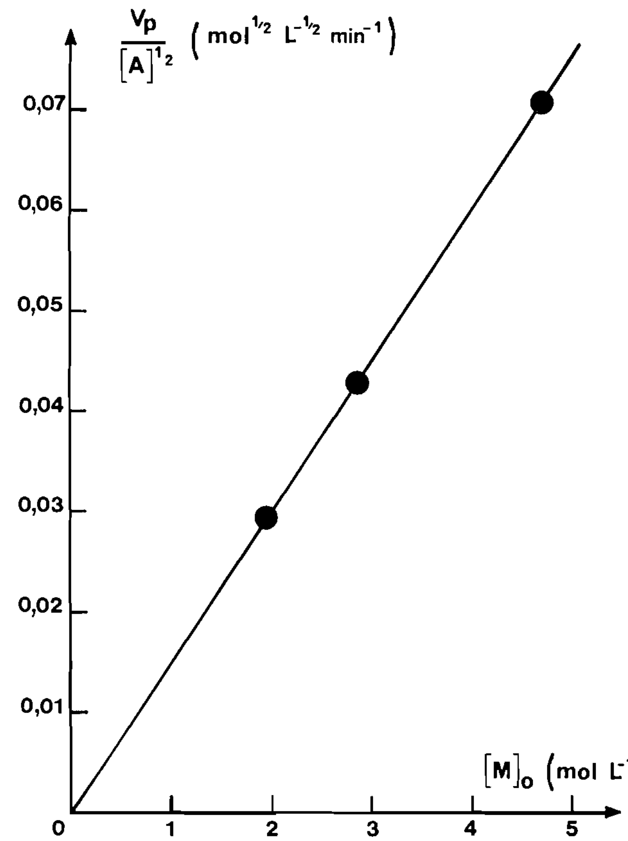

FIG. 3. Variations de $V_p/[A]^{1/2}$ en fonction de $[M]_0$ lors de la polymérisation radicalaire du VOCCl amorcée par le DCPD dans CH_2Cl_2 à 35°C.

Les amines aliphatiques conduisent à des degrés de substitution voisins de 100% (essais 17 à 24, tableau 3) selon un mécanisme faisant intervenir une attaque nucléophile du carbonyle par ces amines. Parmi les différents capteurs d'acide chlorhydrique utilisés, c'est la soude à 50% qui est le plus efficace comme le montrent les essais 18 et 19 effectués avec la *N*-méthylbenzylamine. Les amines primaires réagissent aussi bien que les amines secondaires. De plus, dans le cas de l'éthyléthanolamine (essai 23), la réaction s'effectue de façon sélective par l'intermédiaire de la fonction amine ainsi qu'en témoigne le spectre ir du polymère modifié. Le faible caractère nucléophile présenté par les amines aromatiques telles que le carbazole ou le diméthyl-2,3 indole nécessite l'emploi de la catalyse par transfert de phase. Les essais 25 et 26 montrent qu'en absence d'un sel d'ammonium quaternaire, la réaction des groupements chloroformiate avec le carbazole n'a pas lieu alors qu'elle s'effectue avec 100% de rendement après 3 h à 20°C, en présence de SO_4HNBu_4.

Il n'est pas possible de mesurer directement les masses molaires des échantillons de PVOCCl, par osmométrie ou par gpc, en raison de la grande réactivité des fonctions chloroformiate. Elles ont donc été déterminées indirectement à partir des masses molaires des polymères modifiés, en tenant compte du degré de substitution. Quelques résultats significatifs obtenus avec trois lots différents de PVOCCl sont rassemblés dans le tableau 4. On observe un excellent accord entre les valeurs de $\overline{M}_n$ pour un même échantillon de PVOCCl quelle que soit la nature du substituant (essais 29 et 20; essais 31, 22 et 32) et

TABLEAU 2. Polymérisation en masse de carbamates, carbonates et thiocarbonates vinyliques ([amorceur]/[monomère] = 0,5%)

Essai	Monomère	Amorceur[a]	T (°C)	Temps (h)	Rdt. (%)	$\bar{M}_n$ osm.
8	VOCOPh	DCPD	35	20	65	92 000
9	VOCOPh	AIBN[b]	65	6	30	42 000
10	VOCO Menthyle	DCPD	35	16	44	73 000
11	VOCSPh	AIBN	60	18	57	43 000
12	VOCNEt$_2$	AIBN	60	18	84	79 000
13	VOCNHBu	AIBN	60	18	65	35 000
14	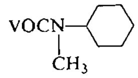	AIBN	60	18	70	80 000
15	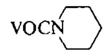	AIBN	60	18	63	46 500
16	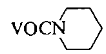	AIBN[c]	65	3	53	53 000

[a]DCPD: peroxydicarbonate de dicyclohexyle; AIBN: azobisisobutyronitrile.
[b][A]/[M] = 1%.
[c][A]/[M] = 1%; essai effectué dans un appareil entièrement scellé sous vide poussé.

TABLEAU 3. Réaction des amines avec le PVOCCl dans CH_2Cl_2 (PVOCCl: 5×10^{-3} mol; CH_2Cl_2: 35 mL)

Essai	Amine	[Amine]/[PVOCCl]	Base ([Base]/[Cl])	TBAH[a] (mol. %)	T (°C)	Temps	Degré de substitution (%)
17	n-$C_4H_9NH_2$	1,5	Na_2CO_3(2)	—	42	2 h	96
18	$C_6H_5CH_2NHCH_3$	1,5	K_2CO_3(2)	—	40	3 h	100
19	$C_6H_5CH_2NHCH_3$	2,3	NaOH 50%(1,5)	—	20	10 min	100
20	(n-$C_4H_9)_2NH$	1,5	Na_2CO_3(2)	—	40	2,75 h	94
21	$H_2NCH_2COOC_2H_5$,HCl	1,2	Et_3N(2)	—	40	3 h	100
22	$C_6H_5NHCH_3$	2,5	NaOH 50%(1,5)	—	20	20 min	100
23	$C_2H_5NHCH_2CH_2OH$	1,5	Na_2CO_3(2)	—	42	2 h	84
24	Amino-3 éthyl-9 carbazole	1,1	NaOH 50%(2)	—	20	5 h	98
25	Carbazole	2,5	NaOH 50%(1,5)	—	20	30 min	0
26	Carbazole	2,5	NaOH 50%(1,5)	5	20	3 h	100
27	Carbazole	1	NaOH 50%(1,5)	5	20	5 h	100
28	Diméthyl-2,3 indole	2,5	NaOH 50%(1,5)	5	20	7 h	90

[a]Sulfate acide de tétrabutylammonium, pourcentage molaire par rapport au chlore du PVOCCl.

TABLEAU 4. Masses molaires des échantillons de PVOCCl

Essai	Substituant	Base	T (°C)	Temps	D.S.[a] (%)	$\bar{M}_n$ PVOCCl[b]
29	$C_6H_5CH_2NHCH_3$	Na_2CO_3	40	2,5 h	98	76 000
20	(n-$C_4H_9)_2NH$	Na_2CO_3	40	2,75 h	94	77 000
30	$C_6H_5CH_2NHCH_3$	Na_2CO_3	40	2,5 h	98	18 000
19	$C_6H_5CH_2NHCH_3$	NaOH 50%	20	10 min	100	18 500
31	$C_6H_5CH_2NHCH_3$	NaOH 50%	20	15 min	97	33 000
22	$C_6H_5NHCH_3$	NaOH 50%	20	20 min	100	35 000
32	C_6H_5OH[c]	NaOH 50%	20	1,5 h	96	34 500

[a]Degré de substitution déterminé d'après la microanalyse.
[b]Calculée d'après la valeur de $\bar{M}_n$ du polymère modifié mesurée par osmométrie dans le toluène à 37°C et d'après le degré de substitution.
[c]+5 mol. % TBAH.

quelles que soient les conditions opératoires pour un substituant donné (essais 30 et 19). En particulier, on peut conclure que la modification chimique du PVOCCl en solution dans CH_2Cl_2, en présence de NaOH 50% et d'un catalyseur de transfert de phase (essai 32) ne provoque pas de dégradation du polymère avec un substituant comme le phénol.

Les résultats de la modification chimique du PVOCCl par des alcools, des phénols et un thiol sont rassemblés dans le tableau 5. Les phénols et les alcools sont moins réactifs que les amines aliphatiques vis-à-vis des chloroformiates (20). La catalyse par transfert de phase donne d'excellents résultats en ce qui concerne le phénol et la mercapto-2 pyrimidine (essais 32 et 38). D'une façon générale, il faut noter que, contrairement à certains résultats publiés récemment (21), les conditions opé-

TABLEAU 5. Réaction des alcools, des phénols et des thiols avec le PVOCCl dans CH_2Cl_2 ([substituant]/[Cl] = 1,5; [base]/[Cl] = 2)

Essai	Substituant	Base	Catalyseur[a] (mol. %)	T (°C)	Temps (h)	D.S. (%)
33	$NO_2C_6H_4OH$	K_2CO_3	DCHE (1,5)	40	2	23
34[b]	Quinine	K_2CO_3	DCHE (1,5)	20	1,25	45[c]
35	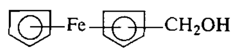	Pyridine	—	0	3	69
36	$CH_3OC_6H_4CH_2OH$	Pyridine	—	0	3	93
37	C_6H_5OH	Pyridine	—	−10	3	88
32	C_6H_5OH	NaOH 50%	TBAH (5)	20	1,4	96
38	Mercapto-2 pyrimidine	NaOH 50%	TBAH (5)	20	4	98

[a]DCHE: dicyclohexyl-18 couronne-6; TBAH: SO_4HNBu_4; pourcentage molaire par rapport au chlore du PVOCCl.
[b]Solvant: THF.
[c]Polymère insoluble.

TABLEAU 6. Réaction des acides carboxyliques avec le PVOCCl dans les conditions de la catalyse par transfert de phase à 20°C (PVOCCl: 4,7 × 10^{-3} mol; RCOOH: 5 × 10^{-3} mol; CH_2Cl_2: 100 mL)

Essai	RCOOH	$[K_2CO_3]$/[PVOCCl]	TBAH[a] (mol. %)	Temps	D.S. (%)
39	C_6H_5COOH	0	0	19 h	0
40	C_6H_5COOH	3,2	0	5 h	90[b]
41	C_6H_5COOH	3,5	5	20 min	94
42	$CH_2{=}CH{-}COOH$	3,2	5	10 min	97
43	Acide acétylsalicylique	3,2	0	5 h	54[b]
44	Acide acétylsalicylique	3,2	5	40 min	81
45	$CH_3(CH_2)_5COOH$	3,2	5	10 min	80

[a]TBAH: SO_4HNBu_4; pourcentage molaire par rapport au chlore du PVOCCl.
[b]Référence 22.

ratoires que nous avons utilisées conduisent à l'obtention de polymères solubles possédant des degrés de substitution élevés.

La catalyse par transfert de phase constitue une excellente méthode pour modifier le PVOCCl par les acides carboxyliques ainsi qu'en témoignent les résultats du tableau 6 (essais 41, 42, 44 et 45). On obtient des polymères solubles porteurs de fonctions anhydride mixte —OCOOCOR latérales (12). Ces polymères sont également préparés par réaction de carboxylates alcalins avec le PVOCCl au moyen de la catalyse par transfert de phase solide–liquide. Les résultats sont indiqués dans le tableau 7. En l'absence de catalyseur, on n'observe aucune réaction entre le benzoate de sodium et le PVOCCl dans le chlorure de méthylène même après 17 h à 20°C (essai 46). Par contre, on obtient des degrés de substitution voisins de 100% en présence d'un catalyseur de transfert de phase comme le sulfate acide de tétrabutylammonium (essai 48 et 49), un éther-couronne (essai 47) ou un cryptand (essai 50). La réaction avec le benzoate de tétraéthylammonium est extrêmement rapide (essai 51); ceci montre que l'intermédiaire réactionnel dans le cas des benzoates de sodium et de potassium, en présence de TBAH, est un carboxylate de tétraalkylammonium. Une étude cinétique détaillée de ce type de réaction est actuellement en cours.

Nous avons également fait figurer, dans le tableau 7, quelques résultats relatifs à la réaction de KCN avec le PVOCCl (8). Un sel d'ammonium quaternaire comme le TBAH est un catalyseur plus efficace qu'un éther-couronne, dans CH_2Cl_2 à 20°C (essais 52 et 53).

En conclusion, nous avons montré les avantages de la catalyse par transfert de phase lors de la modification chimique du

TABLEAU 7. Réaction des carboxylates et du cyanure de potassium avec le PVOCCl dans les conditions de la catalyse par transfert de phase à 20°C ([substituant]/[PVOCCl] = 1 sauf pour l'essai 54 (1,5))

Essai	Substituant	Catalyseur[a] (mol. %)	Temps	D.S. (%)
46	C_6H_5COONa	—	17 h	0
47	C_6H_5COONa	DCHE (10)	3 h	98
48	C_6H_5COONa	TBAH (5)	1,5 h	85
49	C_6H_5COOK	TBAH (5)	3 h	97
50	C_6H_5COOK	[222] (5)	5,5 h	85
51	$C_6H_5COONEt_4$	—	5 min	94
52[b]	KCN	TBAH (5,3)	3,7 h	92
53	KCN	DCHE (5)	5 h	29
54[c]	KCN	DCHE (2,2)	3 h	79

[a]DCHE: dicyclohexyl-18 couronne-6; TBAH: SO_4HNBu_4; Kryptofix [222]; pourcentage molaire par rapport au chlore du PVOCCl.
[b]+0,1 mL d'eau.
[c]Solvant: acétonitrile.

PVOCCl par des substituants variés. Cette méthode permet d'obtenir des polymères solubles possédant des degrés de substitution élevés, à la température ordinaire.

3. *Propriétés des dérivés du polychloroformiate de vinyle*

Les polymères obtenus soit à partir de dérivés du VOCCl, soit par modification chimique du PVOCCl ont été caractérisés par spectrophotométrie ir et par rmn du carbone 13. La bande d'absorption du groupe carbonyle est située à 1770 cm^{-1} pour le PVOCCl. Elle apparaît à 1690 cm^{-1} pour les polycarbamates vinyliques, à 1735 cm^{-1} pour le polycyanoformiate de vinyle,

TABLEAU 8. Déplacements chimiques des atomes de carbone de la chaîne principale et du groupe carbonyle de quelques dérivés du PVOCCl: $-[-CH_2-CH-(O-\overset{\displaystyle O}{\underset{\|}{C}}-R)-]_n-$ (ppm; réf.: HMDS; 100°C; $C_6H_3Cl_3/C_6D_5NO_2$ = 90: 10; 62,5 MHz; m: multiplet)

Essai	R	>C=O	—CH—	—CH_2—
12	—NEt_2	157,2	67,4 67,1 66,8	(m)38,7
13	—NHBu	154,4	67,6 67,3	(m)37,9
16	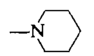	153,1	67,8 67,5 67,2	(m)38,7
14	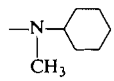	153,5	67,5 67,2 67,0	(m)38,6
31	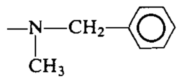	154,2	68,1 67,6 67,3	(m)38,8
22	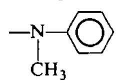	153,1 153,0 152,9	68,3 67,7 67,4	(m)38,4
27	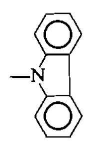	149,8 149,7	70,8 69,9 69,4	(m)38,1
11	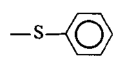	167,1 166,9	70,8 69,9 69,3	(m)38,0
9	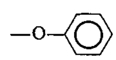	151,2 151,5 151,7	71,9 70,7 69,6	(m)37,9

à 1730 cm^{-1} pour le polythiocarbonate de vinyle et de phényle et à 1750 cm^{-1} pour le polycarbonate de vinyle et de phényle. Les polymères porteurs de fonctions anhydride mixte présentent deux bandes d'absorption des groupements carbonyle situées vers 1810 et 1745 cm^{-1}. Ces bandes sont suffisamment distinctes de celle correspondant au PVOCCl si bien que l'on peut suivre la cinétique de la réaction de ce polymère avec les acides carboxyliques par spectrophotométrie ir.

Les déplacements chimiques des atomes de carbone de la chaîne principale et du groupement carbonyle sont indiqués dans le tableau 8, pour quelques polymères dérivés du PVOCCl. Dans tous les cas, on observe une stéréosensibilité des carbones de la chaîne principale. Les carbones méthyléniques sont sensibles à des effets de diades, de tétrades et parfois même d'hexades. On observe des effets de triades pour les carbones tertiaires. Les surfaces des trois pics correspondent approximativement au rapport 1:2:1. On peut en déduire que tous les polymères sont atactiques et qu'ils obéissent probablement à une statistique de Bernouilli comme attendu pour des échantillons préparés par polymérisation radicalaire. Pour quelques polymères, on observe une stéréosensibilité du carbone du groupement carbonyle. Il faut remarquer que ces polymères possèdent des valeurs de T_g plus élevées que les autres ce qui correspond à une moins grande mobilité des groupements latéraux (tableau 9).

Les températures de transition vitreuse et la stabilité

TABLEAU 9. Propriétés thermiques de quelques dérivés du PVOCCl: $-[-CH_2-CH(O-\overset{\displaystyle O}{\underset{\|}{C}}-R)-]_n-$

Essai	R	T_g (°C)	T décomposition[a] (°C)	$\bar{M}_n$
16	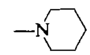	45	285	53 000
14	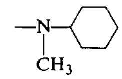	37	270	80 000
31	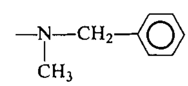	40	273	58 000
22	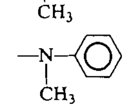	62	264	58 000
27	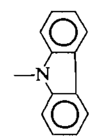	65	247	≃78 000[b]
38	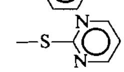	35	219	≃60 000[b]
11	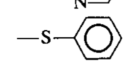	74	240	43 000
9	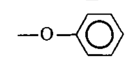	82	257	42 000

[a]Maximum de la dérivée du thermogramme.
[b]Calculée à partir de la valeur de $\bar{M}_n$ du PVOCCl (34 000) car le polymère est insoluble dans le toluène.

thermique de quelques polymères ont été déterminées. Les résultats sont rassemblés dans le tableau 9. La stabilité thermique des polymères semble décroître légèrement selon l'ordre suivant: polycarbamates > polycarbonates > polythiocarbonates. Par ailleurs, les valeurs de T_g des polymères $-[-CH_2-CH-(O-\overset{\displaystyle O}{\underset{\|}{C}}-R-)-]_n-$ décroissent selon l'ordre suivant pour R: —O—Ph > —S—Ph > —$N(CH_3)$—Ph. Les légères différences observées parmi les valeurs de T_g des polycarbamates vinyliques peuvent être expliquées par la structure des groupements latéraux qui influence la mobilité de la chaîne principale (23).

En conclusion, nous avons déterminé les paramètres cinétiques de la polymérisation radicalaire du chloroformiate de vinyle amorcée par le peroxydicarbonate de dicyclohexyle, à 35°C dans CH_2Cl_2. Ceci nous a permis de préparer des échantillons de polychloroformiate de vinyle bien définis dont nous avons examiné la modification chimique. La catalyse par transfert de phase est une méthode de choix pour obtenir des polymères solubles possédant des degrés de substitution très élevés. Par ailleurs de nouveaux polymères ont été préparés par polymérisation radicalaire de monomères dérivés du chloroformiate de vinyle. Les capacités réactionnelles remarquables du chloroformiate vinylique ainsi que du polymère correspondant ou de ses copolymères ouvrent un champ d'investigations très vaste et permettent d'envisager des applications très variées.

Remerciements

Nous remercions la Société Nationale des Poudres et Explosifs pour son aide matérielle. Nous remercions également le Professeur R. Olofson et le Docteur G. Wooden pour la préparation de certains monomères, le Professeur H. Chéradame et Madame E. Rousset pour leur contribution à l'analyse des polymères par rmn du carbone 13 ainsi que Madame C. Noël pour son aide dans l'interprétation des thermogrammes.

1. J. R. SCHAEFGEN. U. S. Patent n° 3 118 862 (1964); Am. Chem. Soc. Polym. Prepr. **8**, 723 (1967); J. Polym. Sci. C, **24**, 75 (1968).
2. C. G. OVERBERGER, H. RINGSDORF et N. WEINSHENKER. J. Org. Chem. **27**, 4331 (1962).
3. Dow Chemical Co. Fr. Patent n° 1 478 633 (1966).
4. F. E. KÜNG. U. S. Patent n° 2 370 549 (1945).
5. T. MALFROOT et M. PITEAU. Fr. Patents n^{os} 2 381 739 (1977) et 2 421 866 (1977).
6. G. MEUNIER, P. HEMERY, J. P. SENET et S. BOILEAU. Polym. Bull. **1**, 809 (1979).
7. S. BOILEAU, S. JOURNEAU et G. MEUNIER. Fr. Patent n° 2 475 558 (1980).
8. G. MEUNIER, P. HEMERY, S. BOILEAU, J. P. SENET et H. CHERADAME. Polymer, **23**, 849 (1982).
9. F. KASSIR, S. BOIVIN, S. BOILEAU, H. CHERADAME, G. WOODEN et R. A. OLOFSON. Polymer, **26**, 443 (1985).
10. G. MEUNIER, S. BOIVIN, P. HEMERY, S. BOILEAU et J. P. SENET. Polymer, **23**, 861 (1982).
11. S. BOIVIN, A. CHETTOUF, P. HEMERY et S. BOILEAU. Polym. Bull. **9**, 114 (1983).
12. S. BOIVIN, P. HEMERY, J. P. SENET et S. BOILEAU. Bull. Soc. Chim. Fr. II, 201 (1984).
13. R. C. SCHNUR. Ph.D. Thesis, Pennsylvania State Univ., (1973).
14. R. A. OLOFSON, R. C. SCHNUR et L. BUNES. U.S. Patent n° 3 905 981 (1973).
15. R. A. OLOFSON, R. C. SCHNUR, L. BUNES et J. P. PEPE. Tetrahedron Lett. 1567 (1977).
16. R. A. OLOFSON et J. CUOMO. J. Org. Chem. **45**, 2538 (1980).
17. H. CHERADAME et P. SIGWALT. Bull. Soc. Chim. Fr. 843 (1970).
18. S. BOILEAU, G. CHAMPETIER et P. SIGWALT. Makromol. Chem. **69**, 180 (1963).
19. J. C. FAVIER, S. BOILEAU et P. SIGWALT. Eur. Polym. J. **4**, 3 (1968).
20. M. MATZNER, R. P. KURKJY et R. J. COTTER. Chem. Rev. **64**, 67 (1964).
21. J. P. PAYAN, S. RAYNAL, J. P. MARTY, C. JACQUOT et E. LEPAIN-PAYAN. Eur. Polym. J. **20**, 487 (1984).
22. J. P. SENET. Fr. Patent n° 81/85 873 (1981).
23. H. R. ALLCOCK et F. W. LAMPE. Contemporary polymer chemistry. Prentice–Hall Inc., Englewood Cliffs, New Jersey. 1981.

ADDITIONS AND CORRECTIONS / AJOUTS ET CORRECTIONS

Vol. 61, 1983

Marek J. Wójcik and Czeslawa Paluszkiewicz. Infrared spectra of hydrogen-bonded salicylic acid and its derivatives. Methyl salicylate

Page 1449. The captions of Figs. 2–4 have been mistakenly exchanged. The caption under Fig. 2 should appear under Fig. 3, the caption under Fig. 3 should appear under Fig. 4, and the caption under Fig. 4 should appear under Fig. 2.

Charge transfer electron–exciton complexes in single crystals[1]

CONSTANTINE MAVROYANNIS
Division of Chemistry, National Research Council of Canada, Ottawa, Ont., Canada K1A 0R6

Received March 8, 1984

This paper is dedicated to Professor Camille Sandorfy on the occasion of his 65th birthday

CONSTANTINE MAVROYANNIS. Can. J. Chem. **63**, 1345 (1985).

We have considered the excitation spectrum arising from the coherent electron–exciton pairing in crystals at low temperatures. For the pairing processes, three different types of excitons have been considered: Frenkel excitons (tightly bound), Wannier–Mott excitons (loosely bound), and excitons of the intermediate binding. Expressions for the gap functions and transition temperatures at which metal-to-nonmetal phase transitions occur have been derived and discussed for each type of pairing. In the electron pairing with the intermediate exciton, the dispersion relations which determine the exciton and the electron–exciton modes are solved numerically and the derived results are graphically presented. The physical picture for the electron–exciton coupled modes is analogous to that for polaritons and magnon–phonon modes in crystals.

CONSTANTINE MAVROYANNIS. Can. J. Chem. **63**, 1345 (1985).

Nous avons étudié les spectres d'excitation provenant de l'appariement cohérent électron–exciton dans des cristaux à basse température. Pour le processus d'appariement, nous avons considéré les trois types d'exciton suivants: les excitons de Frenkel (fortement liés), les excitons de Wannier–Mott (faiblement liés) et des excitons ayant des forces de liaisons intermédiaires. On a déduit des expressions pouvant représenter les fonctions d'intervalle et les températures de transition auxquelles les transitions de la phase métal à la phase non-métal se produisent et on en discute pour chaque type d'appariement. Dans le cas de l'appariement de l'électron avec l'exciton intermédiaire, on a résolu les relations de dispersion qui déterminent les modes de l'exciton et du couple électron–exciton d'une façon mathématique et on présente les résultats obtenus d'une façon graphique. La représentation physique des modes pour l'électron–exciton couplés est analogue à celle des modes des polaritons et du couple magnon–phonon dans les cristaux.

[Traduit par le journal]

I. Introduction

Considerable interest has been recently given to the existence of charged excitons in insulating and semiconducting crystals. A charged exciton is a quasiparticle consisting of a bound state of an exciton and either an electron in the conduction band or a hole in the valence band, which moves with definite energy and wave vector through the crystal (1–3). At the present time, experimental evidence for the existence of such conducting states is limited (4, 5) but these types of excitations may play an important role in the metal–insulator transitions at high excitation intensities (6). Theoretical calculations have been done so far when conduction electrons interact with Frenkel excitons (1, 2, 7, 8) and Wannier–Mott excitons (3), which are the appropriate collective excitations for molecular crystals and semiconductors, respectively. However, excitons with intermediate binding have also been found to exist in rare-gas solids (9, 10). We shall describe here our recent work (11) concerning the formation of a bound state consisting of an exciton of the intermediate binding and an electron which is excited into the conduction band. The derived results will be compared with those obtained when the pairing process takes place with a Frenkel exciton (1, 7, 8) and a Wannier–Mott exciton (3), respectively.

II. Intermediate exciton–electron pairing

We consider a simple model for the crystal consisting of N identical atoms on a rigid cubic lattice with one atom per unit cell and lattice spacing a_0. Each atom is assumed to have two nondegenerate levels corresponding to the valence and conduction bands and all effects due to electron spin are discarded. At $T = 0$ K, the valence band is full of electrons while the conduction band is empty. The exciton (electron–hole pair) under consideration is formed when an electron from the valence band is excited into the conduction band, leaving behind a hole in the valence band at the same lattice site. In addition, the usual band motions of electrons and holes from one lattice site to another without creating excitons are included. The Hamiltonian of such a system may be taken as (11–13)

$$[1] \quad H = \sum_{\langle ll'\rangle} T_\alpha(ll')\alpha_{l'}^{+}\alpha_l - \sum_{\langle ll'\rangle} T_\beta(ll')\beta_{l'}^{+}\beta_l + E_\alpha \sum_l \alpha_l^{+}\alpha_l - E_\beta \sum_l \beta_l^{+}\beta_l + u_0 \sum_l \beta_l^{+}\beta_l\alpha_l^{+}\alpha_l - \sum_{\langle ll'\rangle} u(ll')\beta_l^{+}\alpha_l\alpha_{l'}^{+}\beta_{l'} + \sum_{\langle ll'\rangle} v(ll')\alpha_l^{+}\alpha_l\beta_{l'}^{+}\beta_{l'}$$

where α_l^{+}, α_l are the creation and destruction operators for electrons at the lattice site $\boldsymbol{R}_l^0$ in the conduction band, and β_l^{+}, β_l are the corresponding operators for electrons in the valence band. E_α, E_β denote the on-site energy of the electron in the conduction and valence bands, respectively, and $\langle ll'\rangle$ denotes that the sum is to be done over nearest-neighbor pairs $\boldsymbol{R}_l^0$ and $\boldsymbol{R}_{l'}^0$. T_α and T_β are the hopping energies for electrons in the respective bands, u_0 is the on-site Coulomb interaction, and $u(ll')$, $v(ll')$ are the exchange and direct Coulomb interactions between electrons on neighboring lattices sites.

Let us introduce the exciton operator $b_l \equiv \beta_l^{+}\alpha_l$. For the two level system, we have $\beta_l^{+}\beta_l + \alpha_l^{+}\alpha_l = 1$. Using this and the usual anticommutation relations for the electron operators, we have $\beta_l^{+}\beta_l = b_l b_l^{+}$ and $\alpha_l^{+}\alpha_l = b_l^{+}b_l$. Making use of these results in eq. [1], we find that the exchange Coulomb term is quadratic in the exciton operators. We also find that the direct Coulomb term is quartic in (a) the exciton operators and (b) the exciton and electron operators. When written in the form (a), we find that the direct Coulomb term describes an exciton density interacting with an exciton density at a neighbouring lattice site. The form (b) describes an electron density interacting with an exciton density on a neighbouring lattice site.

[1]NRCC No. 23963.

The excitation energy of the conduction electron–exciton complex is obtained by making use of the Green function method. The two Green functions which we are going to evaluate are defined as $G(ll';t) = \langle\langle b_l(t);b_{l'}^+(0)\rangle\rangle$ and $F(ll';t) = \langle\langle \alpha_l(t);b_{l'}^+(0)\rangle\rangle$, where the operators are in the Heisenberg representation and use has been made of the notation, $\langle\langle A(t);B(0)\rangle\rangle = -i\theta(t)\,\langle[A(t),B(0)]_+\rangle$ for the operators A and B. The diamond brackets stand for an ensemble average. The properties of the Green functions can be found elsewhere (14).

Commuting the operators b_l and α_l in turn with the Hamiltonian in eq. [1] and then decoupling the resulting equations of motion, we find that the Green functions $G(ll';t)$ and $F(ll';t)$ are solutions of the two sets of coupled equations, whose Fourier transforms with respect to $(l - l')$ and the time, are given by ($\hbar = 1$)

$$[2] \quad G(k,\omega) = G^{\mathrm{HF}}(k,\omega) - G^{\mathrm{HF}}(k,\omega)\Delta(k)F(k,\omega)$$

$$[3] \quad [\omega - E_\alpha(k) - u_0 - v(k=0)]F(k,\omega) = -\Delta^*(k)G(k,\omega)$$

where

$$[4] \quad \Delta(k) = \frac{1}{N}\sum_{k'} v(k-k')\,\langle b_{k'}\alpha_k^+\rangle$$

$$[5] \quad G^{\mathrm{HF}}(k,\omega) = \frac{G_0(k,\omega)}{\epsilon_+(k,\omega)}$$

with the single-particle Green function given by

$$[6] \quad G_0(k,\omega) = \frac{1}{N}\sum_q \frac{1}{\omega - E_\beta^0 - E_\alpha(q-k) - E_\beta(q)}$$

and $\epsilon_+(k,\omega)$ is defined by

$$[7] \quad \epsilon_+(k,\omega) = 1 + [u(k)G_0(k,\omega) - v(k=0)G_0(k=0,\omega)]$$

$E_\alpha(k)$ and $E_\beta(k)$ are the energy bands (13) and we have chosen $E_\beta = E_\beta^0 + 6T_\beta$ and $E_\alpha = 6T_\alpha$ where $T_{\alpha,\beta}(ll') = -T_{\alpha,\beta}$ for nearest-neighbour lattice sites. $u(k)$ and $v(k)$ are the Fourier transforms for the nearest neighbour exchange and direct Coulomb interactions of strength u and v, respectively. In eqs. [2]–[7], $G^{\mathrm{HF}}(k,\omega)$ is the exciton–exciton Green function which is correct in the Hartree–Fock (HF) approximation, $G_0(k,\omega)$ is the noninteracting Green function (13) while $\Delta(k)$ is the coupling parameter describing the pairing of an exciton at the lattice site $\boldsymbol{R}_l$ with an electron, which is excited into the conduction band, at the nearest-neighbour lattice site $\boldsymbol{R}_{l'}$.

Solving eqs. [2] and [6], we obtain

$$[8] \quad G(k,\omega) = [\omega - E_\alpha(k) - u_0 - v(k=0)]\frac{G_0(k,\omega)}{D^{\mathrm{B}}(k,\omega)}$$

$$[9] \quad F(k,\omega) = -\Delta^*(k)\frac{G_0(k,\omega)}{D^{\mathrm{B}}(k,\omega)}$$

where

$$[10] \quad D^{\mathrm{B}}(k,\omega) = [\omega - E_\alpha(k) - u - v(k=0)]\epsilon_+(k,\omega) - |\Delta(k)|^2G_0(k,\omega)$$

Singularities of $G(k,\omega)$ and $F(k,\omega)$ are located at the solutions of $D^{\mathrm{B}}(k,\omega) = 0$. These correspond to the bound states of the electron–exciton complex, provided the roots of $D^{\mathrm{B}}(k,\omega) = 0$ are separated from the solution of the equation $\epsilon_+(k,\omega) = 0$ which determine the frequencies of the exciton band. They must also be different from $\omega = E_\alpha(k) + u_0 + v(k=0)$ which corresponds to the band energies of the conduction electron renormalized by the screened Coulomb interactions. Referring to eq. [10], we see that a finite value of $\Delta(k)$ may produce a bound state for the electron–exciton complex.

In the denominator of eq. [6], E_β^0 is the separation between the valence and conduction bands for zero wave vector and it also corresponds to the value of the lower bound of the electron-hold excitations for $k = 0$. For a stable electron–exciton complex, we therefore require that E_β^0 should satisfy the relation $E_\beta^0 > u_0 + 6v$. For a simple cubic lattice, since we have $\Delta(k) = [v(k)/6v]\Delta_0$, where $\Delta_0 = \Delta\ (k=0)$, it is straightforward to calculate the frequency of the (electron–exciton) mode in the long wavelength limit. In particular, the frequency of the mode for $k = 0$ is

$$[11] \quad \omega_0 = E_\beta^0 - 2x_0(T_\alpha + T_\beta)$$

where x_0 is the solution of the nonlinear equation

$$[12] \quad [E_\beta^0 - u_0 - 6v - 2x_0(T_\alpha + T_\beta)][3(u-v)J(x_0) - (T_\alpha + T_\beta)] = \tfrac{1}{2}\Delta_0^2 J(x_0)$$

Here, $J(x_0)$ is a one-dimensional integral:

$$[13] \quad J(x_0) = \int_0^\infty \mathrm{d}s\,[\exp(-s(3+x_0))]I_0^3(S)$$

where $I_0(S)$ is the modified Bessel function of the first kind, of order zero.

We have evaluated $D^{\mathrm{D}}(k,\omega)$ numerically, assuming for simplicity that the coupling parameter $\Delta(k)$ is a constant Δ. We have chosen the bandwidth of the conduction band ($12T_\alpha$) and that of the valence band ($12T_\beta$) to be 0.6 eV. The nearest-neighbour exchange interaction (u) and the nearest-neighbour direct interaction (v) are set equal to 0.3 and 0.01 eV, respectively. The energy gap between the valence and conduction bands at zero wave vector is $\epsilon_\beta^0 = 1.5$ eV and the coupling parameter Δ is chosen as 0.1 eV. A schematic plot of $D^{\mathrm{B}}(k,\omega)$ is shown in Fig. 1. There we see that, for a given value of k, there are two coupled mode frequencies below the electron-hold continuum so that there are two branches to the dispersion relation. In Fig. 2, we have plotted the dispersion relation for the electron–exciton complex in the (100) direction. The dispersion relation for the coupled mode has a form similar to that for polaritons and magnon–phonon modes in ferromagnets. Referring to Fig. 2, we find that as $k \rightarrow \pi/a_0$, the upper branch approaches the exciton band and the lower branch approaches the conduction band. However, as k decreases the separation between these modes becomes larger.

III. Frenkel exciton–electron pairing

For the process of coherent pairing of a Frenkel exciton with an excited electron, the fifth term in the Hamiltonian [1], which describes the Coulomb interaction u_0 between the electron and hole densities located on the same lattice site in the crystal, does not make any contribution and, therefore, is discarded. Such a model is appropriate for excitations occurring in molecular crystals where van der Waals interactions between the atoms are prevailing. Then using the Hamiltonian [1] and the Green function formalism, which is analogous to that used in the theory of superconductivity (15), the gap functions $\Delta(k)$ describing the Frenkel exciton–electron pairing (1, 8) is found to be

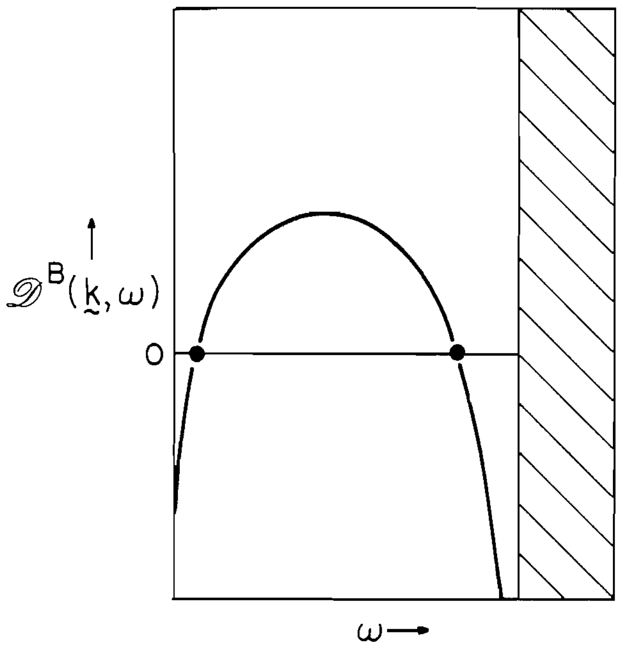

FIG. 1. Schematic of $D^B(k,\omega)$ as a function of frequency, for a fixed wave vector. The two solutions of $D^B(k,\omega) = 0$ correspond to the coupled conduction electron–exciton modes. The hatched area corresponds to the single-particle excitons of electrons and holes.

$$[14]\quad \Delta(k) = \frac{\bar{\omega}}{\sinh(1/\rho)} \approx 2\bar{\omega}e^{-1/\rho}$$

where

$$[15]\quad \bar{\omega} = \xi^2\sigma/4m, \qquad \xi = (6\pi^2 n)^{1/3}$$

$$[16]\quad \rho = N(0)v(k) = 3v(k)/2\bar{\omega}, \qquad \sigma = m\left|\frac{1}{m_e} - \frac{1}{m_{exc}}\right|$$

with $n = N/V$ is the exciton (electron) density, $N(0)$ is the density of states, m_e and m_{ex} are the effective masses for the electron and exciton, respectively; m is the mass of the free electron and $v(k)$ is the Fourier transform of the interaction energy $v(ll')$. In deriving eq. [14], use has been made of the effective mass approximation for the Frenkel exciton and excited electron spectra, respectively. The transition temperature T_c may be found by the relation

$$[17]\quad T_c = 0.57\Delta(k)/k_B$$

where k_B is Boltzmann's constant. The coherent energy W_0, which describes the binding energy corresponding to the electron–exciton pairing, has been calculated by averaging the Hamiltonian (1) to obtain the ground-state energy of the system (1, 7, 8) and it is found to be

$$[18]\quad W_0 = -\frac{N(0)\bar{\omega}^2}{\tanh(1/\rho)} = -\frac{3\bar{\omega}}{2\tanh(1/\rho)}$$

Estimates for the gap function $\Delta(k)$, transition temperature T_c, binding energy W_0 divided by σ are given in Table 1 as a function of the exciton (electron) density n. The data in Table 1 indicate that for exciton concentrations $n \geq 2 \times 10^{18}$ cm^{-3}, the energy-gap function is a measurable quantity provided that we are dealing with the strong coupling limit which occurs when the average interaction energy is equal or greater than the average kinetic energy, $v(k) \geq \bar{\omega}$. The last column in Table 1 gives the values $\bar{\omega}/\sigma$ for different exciton densities which indicate the condition of strong coupling limit $v(k) \geq \bar{\omega}$ can be easily fulfilled with a reasonable strength of the required interaction $v(k)$. The results of the present study imply that at exciton densities $n \geq 2 \times 10^{18}$ cm^{-3}, the obser-

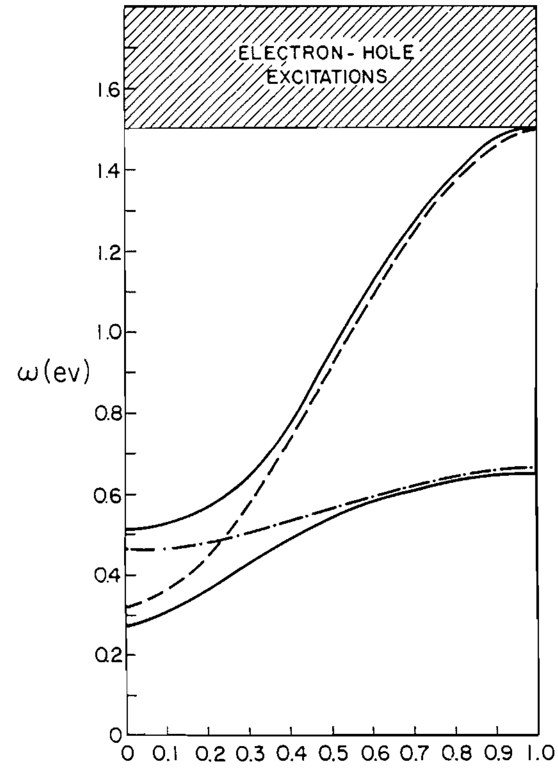

FIG. 2. Dispersion relation for coupled electron–exciton modes (—) in an insulator, with intermediate binding for the excitons. Also shown are the exciton band (- - -) and the conduction electron band (-·-·-) from which the coupled mode is formed. The parameters used in the calculation are given in the text.

TABLE 1. Computed values for the gap funtion Δ/σ, transition temperature T_c, binding energy W_0/σ, and average kinetic energy $\bar{\omega}/\sigma$

n (cm^{-3})	ρ	$v(k)/\bar{\omega}$	Δ/σ (cm^{-1})	T_c/σ (°K)	$-W_0/\sigma$ (cm^{-1})	ω/σ (cm^{-1})
2×10^{18}	1.5	1.0	52	43	96	37
	2.0	1.3	74	61	121	37
	2.5	1.6	93	76	146	37
	3.0	2.0	111	91	174	37
4×10^{18}	1.5	1.0	83	68	152	59
	2.0	1.3	117	96	191	59
	2.5	1.6	146	120	232	59
	3.0	2.0	167	137	277	59
6×10^{18}	1.5	1.0	109	89	200	77
	2.0	1.3	154	126	250	77
	2.5	1.6	193	158	304	77
	3.0	2.0	231	189	363	77
8×10^{18}	1.5	1.0	132	108	242	93
	2.0	1.3	187	153	303	93
	2.5	1.6	234	192	369	93
	3.0	2.0	281	230	440	93
1×10^{19}	1.5	1.0	153	125	281	108
	2.0	1.3	217	188	352	108
	2.5	1.6	271	222	428	108
	3.0	2.0	326	267	511	108

vation of the charge carrying electron–exciton states is feasible in molecular organic solids.

IV. Wannier–Mott exciton–electron pairing

For the process under consideration, the sixth term in the Hamiltonian [1], which describes the interaction between two Frenkel excitons, does not contribute and, hence, it is neglected. Then the Hamiltonian [1] is appropriate to describe excitations occurring in semiconducting crystals which are characterized by small energy gaps between the valence and conduction bands and large dielectric constants. In this case, a similar calculation (3) to that used before gives the following expression for the gap function

$$[19]\quad \Delta(k) = \frac{\bar{\omega}}{\sinh(1/\rho)}\left[1 - \frac{2d}{\bar{\omega}}\left(1 + \frac{d}{\bar{\omega}}\right)\left(\cosh\frac{1}{\rho} - 1\right)\right]^{1/2}$$

$$[20]\quad \simeq \frac{\bar{\omega}}{\sinh(1/\rho)} \quad \text{for either } \frac{d}{\bar{\omega}} \ll 1 \text{ or } \frac{d}{\bar{\omega}} \approx 1$$

where $d = \mu e^4/4$ is one-half of the energy of the exciton Rydberg and μ is the reduced mass of the electron–hole pair. The binding energy W_0 is found to be

$$[21]\quad W_0 = \frac{N(0)\bar{\omega}^2}{\tanh(1/\rho)}\left[\left(1 + \frac{d}{\bar{\omega}}\right)^2 + \left(\frac{d}{\bar{\omega}}\right)^2 - \frac{2d}{\bar{\omega}}\left(1 + \frac{d}{\bar{\omega}}\right)\Big/\cosh(1/\rho)\right]$$

$$[22]\quad \simeq \frac{-N(0)\bar{\omega}^2}{\tanh(1/\rho)} = \frac{-3\bar{\omega}}{2\tanh(1/\rho)} \quad \text{for either } \frac{d}{\bar{\omega}} \ll 1 \text{ or } \frac{d}{\bar{\omega}} \approx 1$$

For most semiconducting solids $\nu(k)$ is expected to be of the order of the energy of the exciton Rydberg. Then considering eq. [16] for ρ, the limit $d \ll \bar{\omega}$ also implies that $\rho \ll 1$ provided that $\nu(k) \approx 2d$, which is the weak coupling limit. In the limiting case when $d \approx \bar{\omega}$ then $\rho \geq 1$ which may be considered as the intermediate or strong coupling limit. In both cases, $\Delta(k)$ and W_0 are determined by eqs. [20] and [22], respectively. Finally, when $d \gg \bar{\omega}$, $\Delta(k)$ is given by eq. [19] provided that the relation

$$\frac{2d}{\bar{\omega}}\left(1 + \frac{d}{\bar{\omega}}\right)\left(\cosh\frac{1}{\rho} - 1\right) < 1$$

is satisfied. This corresponds to the extreme strong coupling limit where $\rho \gg 1$ provided that $\nu(k) \approx d$. In this case an enhancement of the binding energy of the complex is anticipated to occur.

V. Summary

In conclusion, we have discussed the excitation spectra arising from the interaction of Frenkel, Wannier–Mott, and intermediate type excitons with conduction electrons to form bound states at low temperatures; such conducting states are appropriate to occur in molecular crystals, semiconductors and rare-gas solids, respectively. We hope that the present discussions will stimulate experimental interest on the spectroscopic properties of electron–exciton complexes and their transport properties as well.

1. C. MAVROYANNIS. Physica, **77**, 373 (1974).
2. E. L. NAGAEV and E. B. SOKOLOVA. Phys. Status Solidi (*b*) **64**, 441 (1974).
3. C. MAVROYANNIS. J. Low Temp. Phys. **20**, 285 (1975).
4. B. STEBE, T. SAUDER, M. CERTIER, and C. COMTE. Solid State Commun. **26**, 637 (1978).
5. G. BADER, L. CARON, and L. SANCHE. Solid State Commun. **38**, 849 (1981).
6. G. A. THOMAS and T. M. RICE. Solid State Commun. **23**, 359 (1977).
7. C. MAVROYANNIS. Phys. Rev. B**15**, 1906 (1977).
8. C. MAVROYANNIS. Phys. Rev. B**16**, 2863 (1977).
9. J. HERMANSON. Phys. Rev. **150**, 660 (1966).
10. M. ALTARELLI and F. BASSANI. J. Phys. C**4**, L328 (1971).
11. G. GUMBS and C. MAVROYANNIS. Solid State Commun. **41**, 237 (1982).
12. G. GUMBS and C. MAVROYANNIS. J. Phys. C: Solid State, **14**, 2199 (1981).
13. G. GUMBS and C. MAVROYANNIS. Phys. Rev. B**24**, 7258 (1981).
14. E. N. ECONOMOU. Green's functions in quantum physics. Vol. 7. Springer-Verlag, New York. 1979.
15. J. R. SCHRIEFFER. Theory of superconductivity. Benjamin, Reading. 1964.

The multiphoton spectra of all-*trans* 1,3,5-hexatriene in the region of 6.0 eV

MARCO ANTONIO CHAER NASCIMENTO

Instituto de Química, Departamento de Físico-Química, Universidade Federal do Rio de Janeiro, Rio de Janeiro, RJ 21910, Brasil

Received March 12, 1984

This paper is dedicated to Professor Camille Sandorfy on the occasion of his 65th birthday

MARCO ANTONIO CHAER NASCIMENTO. Can. J. Chem. **63**, 1349 (1985).

The multiphoton spectra of all-*trans* 1,3,5-hexatriene, in the region of 6.0 eV, is investigated using highly correlated wavefunctions. On the basis of the computed transition energies, intensities, and polarization ratios, an attempt is made to explain the experimentally observed spectra.

MARCO ANTONIO CHAER NASCIMENTO. Can. J. Chem. **63**, 1349 (1985).

Opérant dans la région de 6,0 eV et faisant appel à des fonctions d'ondes très coordonnées, on a étudié le spectre multiphoton de l'hexatriène-1,3,5 qui est complètement trans. En se basant sur les énergies de transition, les intensités et les rapports de polarisation calculés, on essaye d'expliquer le spectre obtenu expérimentalement.

[Traduit par le journal]

1. Introduction

The electronic spectra of linear polyenes has been the subject of intensive experimental and theoretical studies since they were first prepared in the early 1930's. Recently there has been a revival of interest in the subject (1). By forming the basic chromophore of important photobiological systems, such as visual pigments (2) and bacteriorhodopsin (3), the longer polyenes (for which hexatriene serves as a model) have become the subject of numerous photochemical, spectroscopic, and theoretical studies (1).

Several experimental techniques (4–6) have been applied to all-*trans* 1,3,5-hexatriene (hereafter hexatriene). Despite the numerous studies, there are still uncertainties concerning the character, location, and assignment of the excited states. Most important is the characterization of the low-lying excited states which could be involved in the photochemistry of the visual process.

There have been suggestions that the first excited state of all polyenes is a symmetry-forbidden ^1A_g state (7). For both butadiene and hexatriene, extensive *ab initio* calculations (8) have placed the $2\,^1A_g$ state above the experimentally observed strong dipole-allowed ^1B_u state. For butadiene the $2\,^1A_g$ state is calculated at 7.06 eV and 5.87 eV for hexatriene. The experimentally observed ^1B_u states are at 5.92 eV for butadiene and at 4.95 eV for hexatriene. Since the ^1A_g states are dipole-forbidden, they would appear in the one-photon spectra as weak vibronic transitions. Therefore, they should be more easily observed in the two-photon spectra of the polyene compounds. Electron impact spectroscopy can also be used to reveal optically-forbidden states.

Johnson (9) has looked at the two-photon spectra of butadiene and did not detect any ^1A_g state below 5.92 eV as has been suggested (7). Unfortunately, he was not able to record the spectra for energies above 6.79 eV and, therefore, was unable to verify the state at 7.06 eV. Doering and McDiarmid (5*b*) examined the electron impact spectra of butadiene and concluded that the $2\,^1A_g$ state should correspond to the band observed at 7.3 eV in the spectra. There are, therefore, no experimental evidences for the occurrence of a $2\,^1A_g$ valence state below the ^1B_u, in butadiene.

For the hexatriene molecule the work of Flicker *et al.* (5*a*) does not show the presence of any ^1A_g state below 4.95 eV. More recently, El-Sayed (10) investigated the two-photon spectra of hexatriene in the region of 6.0 eV (6.0–6.7 eV). In this region, he observed a single transition at 6.23 eV (and its vibronic structure). From polarization studies (11, 12) he concluded that the excited state should have A_g symmetry.

From our previous calculations (8), the $2\,^1A_g$ valence state should be at 5.87 eV. The fact that the 3*s* Rydberg state is two-photon forbidden leaves the 3*p* Rydbergs as possible candidates for the observed state. From the present calculations both the ^1A_g (π-$3p_x$) and the two ^1B_g ($\pi \rightarrow 3p_y, 3p_z$) Rydberg states occur in this region of the spectra (6.0–6.3 eV).

Comparing the experimental and theoretical results, one sees that some questions remain to be answered. First of all, what is the nature of the observed ^1A_g state? Would it be the theoretically predicted $3p_x$ Rydberg state or the $2\,^1A_g$ valence state, placed at 5.87 eV by the *ab initio* calculation (8)? If the theoretical predictions are correct, why the ^1B_g states were not observed in the two-photon experiment of El-Sayed (10)?

To answer these questions, we calculated the intensities for the transitions from the $X\,^1A_g$ state of the hexatriene molecule to all of the above mentioned states, for both linearly and circularly polarized light. We also computed Ω (the polarization ratio (12)) as an internal check to our calculations.

2. Computational details

All the calculations were carried out using the Dunning (13) valence double-ζ (DZ) contraction of Huzinaga (14) double-ζ ($9s/5p$, $4s$) gaussian basis set, augmented with diffuse basis functions of $3p_\sigma$ and $3p_\pi$ character ($\zeta = 0.021$), in order to provide adequate description of the Rydberg excited states.

With the molecule in the *yz* plane, we used the experimentally-determined ground-state geometry (15) in all the calculations.

The ground state, $X\,^1A_g$, was solved self-consistently at the GVB(3/PP) level (correlating the three π bonds) and the orbitals of this calculation used for the CI calculations of the valence ^1A_g states. These calculations have been extensively discussed in a previous publication (8). The natural orbitals of the GVB calculation were recombined into symmetry orbitals, to be used as starting guesses in the SCF calculations of the Rydberg states.

For the σ Rydberg states we used the IVO's (for Improved Virtual Orbitals, see ref. 16) obtained from the ground state orbitals, and with the basis set augmented with one $3p_\sigma$ basis on each carbon atom, as starting guesses for the excited orbital. Using the first IVO of b_u ($3p_\sigma$) symmetry, we solved self-

TABLE 1. Transition energies (ΔE), two-photon transition rates (τ) and polarization ratios (Ω) for some electronic transitions of the hexatriene molecule

State	ΔE (eV)[a]	τ_c[b]	τ_l[b]	Ω[c] (τ_c/τ_l)
2^1A_g ($\pi \rightarrow \pi^*$)	5.87	3.40(−50)	4.90(−50)	0.69
3^1A_g ($3p_x$)	6.26	0.90(−52)	1.90(−52)	0.47[d]
1^1B_g ($3p_y$)	6.00	4.82(−54)	3.83(−54)	1.26
2^1B_g ($3p_z$)	6.20	7.46(−54)	6.06(−54)	1.23

[a]Transition energies relative to the ground state (X^1A_g) energy of −231.81913 hartrees.

[b]In units of F^2 s^{-1}, where F is the photon flux in photons/cm^2 s.

[c]$\Omega < 1$ for $A_g \leftrightarrow A_g$ transitions and equal 3/2 for $A_g \leftrightarrow B_g$ transitions. See ref. 12.

[d]Ω observed = 0.25−0.40. See ref. 10.

consistently for the ^1B_g ($3p_\sigma$) Rydberg state. At this level of calculation we obtained a transition energy (referred to a ground-state energy of −271.72322 hartree) of 5.29 eV. The CI calculation was performed in the following way. The π space was formed by the orbitals generated by SCF calculation. The σ space was formed by the $3p_\sigma$ self-consistently optimized orbital plus five σ IVO's (three a_g + two b_u), properly reorthogonalized to the HF orbitals. Using this space, we allowed up to triple excitations among the twelve π MO's simultaneously allowing the σ electrons the readjust among the six σ orbitals. The first two roots of this calculation correspond to the $3p_y$ and $3p_z$ Rydberg states.

For the π Rydberg state, the IVO's were obtained with DZ basis augment with one $3p_\pi$ basis on each carbon atom. The first IVO of a_u ($3p_\pi$) symmetry was used in the HF calculation of the ^1A_g ($3p_\pi$) Rydberg state. At this level of calculation the transition energy to the X^1A_g state is meaningless since the Rydberg state is not yet a pure state. For the CI calculations the π space was composed of the HF π orbitals plus six π IVO's (three a_u + three b_g), properly reorthogonalized. Using this space we allowed up to quadruple excitations in the CI calculation. The first root corresponds to the X^1A_g ground state. The second root is also a valence state and exhibits the doubly-excited dominant configuration characteristic of the $2^1A_g(\pi \rightarrow \pi^*)$ state (8). Finally, the third root corresponds to a diffuse state and it is assigned to the ^1A_g ($3p_x$) Rydberg state.

With these wavefunctions we computed the two-photon transition rates, and polarization ratios (12). The virtual intermediate states (12) were generated at the same level of excitation.

3. Results and discussion

Table 1 shows the results of these calculations. From the results, we assign the transition at 6.23 eV to the $\pi \rightarrow 3p_x$ (π^*) ^1A_g state, because of the excellent agreement between the theoretical and experimental result for the transition energy and for Ω.

One also sees from Table 1 that the two-photon intensities of the transition to the ^1A_g ($3p_{\pi_x}$) state relative the ^1B_g states ($\pi \rightarrow \sigma^*$) ($W_{A_g \rightarrow A_g}/W_{A_g \rightarrow B_g}$) are 18.65 ($3p_y$) and 12.05 ($3p_z$), respectively, for circularly polarized light and 49.60 ($3p_y$) and 31.35 ($3p_z$), respectively, for linearly polarized light. Thus, the ^1B_g states should be much more difficult to detect in the El-Sayed experiment (10).

Finally, with respect to the 2^1A_g valence state, one sees from Table 1 that its transition rate is much larger than the one for Rydberg states, implying that it should be easily detected by El-Sayed, would it occur in the 6.0−6.7 eV region of the spectra. Our calculations suggest that an experiment conducted at lower energies should reveal the presence of the 2^1A_g valence state.

4. Acknowledgment

The author acknowledges Conselho Nacional de Desenvolvimento Científico e Tecnológico (CNPq-Brasil) for financial support.

1. B. KOHLER, B. HUDSON, and K. SCHULTEN. *In* Excited states. Vol. 6. *Edited by* E. Lim. Academic Press, New York. 1983. p. 1 and references therein.
2. B. HONIG and T. EBREY. Ann. Rev. Biophys. Bioeng. **3**, 151 (1974).
3. D. OESTERHELT. Angew. Chem. Intern. Ed. **15**, 17 (1976).
4. R. M. GAVIN JR. and S. A. RICE. J. Chem. Phys. **60**, 3231 (1974).
5. (*a*) W. M. FLICKER, O. A. MOSHER, and A. KUPPERMANN. Chem. Phys. Lett. **45**, 492 (1977); (*b*) J. P. DOERING and R. MCDIARMID. J. Chem. Phys. **73**, 3617 (1980).
6. D. H. PARKER, S. J. SHENG, and M. A. EL-SAYED. J. Chem. Phys. **65**, 5534 (1976).
7. B. S. HUDSON and B. E. KOHLER. Chem. Phys. Lett. **14**, 299 (1972); K. SCHULTEN and M. KARPLUS. Chem. Phys. Lett. **14**, 305 (1972).
8. M. A. C. NASCIMENTO and W. A. GODDARD, III. Chem. Phys. **36**, 147 (1979).
9. P. M. JOHNSON. J. Chem. Phys. **64**, 4638 (1976).
10. D. H. PARKER, J. O. BERG, and M. A. EL-SAYED. Chem. Phys. Lett. **56**, 197 (1978).
11. W. M. MCCLAIN. J. Chem. Phys. **55**, 2789 (1971).
12. M. A. C. NASCIMENTO. Chem. Phys. **74**, 51 (1983).
13. T. H. DUNNING JR. and P. J. HAY. *In* Modern theoretical chemistry. Vol. 3. *Edited by* H. F. Schaefer. Plenum Press, New York. 1977. p. 1.
14. S. HUZINAGA. J. Chem. Phys. **42**, 1293 (1965).
15. M. TRAETEBERG. Acta Chem. Scand. **22**, 628 (1968).
16. W. J. HUNT and W. A. GODDARD, III. Chem. Phys. Lett. **3**, 414 (1969).

Raman spectral studies of solutions of alkali metal perchlorates in dimethyl sulfoxide and water

M. I. S. SASTRY AND SURJIT SINGH
Structural Chemistry Group, Department of Chemistry, Indian Institute of Technology, Madras 600036, India

Received April 19, 1984

This paper is dedicated to Professor Camille Sandorfy on the occasion of his 65th birthday

M. I. S. SASTRY and SURJIT SINGH. Can. J. Chem. **63**, 1351 (1985).

Raman spectra of solutions of alkali metal perchlorates in dimethyl sulfoxide (DMSO) in the Cl—O, C—S, and S=O stretching regions, as well as of perchlorates in aqueous solutions in the Cl—O stretching region are reported. The results are discussed in terms of half-bandwidths, relative intensities, and depolarization ratios. For H_2O the half-bandwidth of the Cl—O stretching band at ~935 cm^{-1} is almost double the value in DMSO solutions. Solutions of perchlorates in DMSO show two symmetric bands in the Cl—O stretching region, whereas in aqueous solutions only one band is observed. The half-bandwidths in perchlorate solutions in DMSO for the C—S stretching band increase with increase in concentration of perchlorate compared to that of liquid DMSO. The band contours in the S=O stretching region in DMSO solutions also show significant changes. These observations are explained on the basis of formation of ion pairs of metal perchlorates in solutions of DMSO and ion hydrates in the case of aqueous solutions.

M. I. S. SASTRY et SURJIT SINGH. Can. J. Chem. **63**, 1351 (1985).

On rapporte les spectres Raman de perchlorates de métaux alcalins en solution dans le diméthylsulfoxyde (DMSO) dans les régions d'élongation du Cl—O, du C—S et du S=O ainsi que ceux de solutions aqueuses de perchlorates dans la région d'élongation du Cl—O. On discute des résultats en fonction de la largeur à mi-hauteur des bandes, des intensités relatives et des rapports de dépolarisation. Dans l'eau, la largeur à mi-hauteur de la bande d'élongation du Cl—O à 935 cm^{-1} est à peu près le double de la valeur dans le DMSO. Les solutions de perchlorate dans le DMSO montrent deux bandes symétriques dans la région d'élongation du Cl—O alors qu'on n'en observe qu'une seule en solution aqueuse. La largeur à mi-hauteur de la bande d'élongation du C—S des solutions de perchlorate dans le DMSO augmente avec une augmentation de la concentration de perchlorate par rapport à celle du DMSO liquide. Les contours des bandes dans la région d'élongation du S=O dans les solutions de DMSO changent d'une façon importante. On explique ces observations par la formation de paires d'ions dans les perchlorates métalliques en solution dans le DMSO et par la formation d'hydrate d'ions dans le cas de solutions aqueuses.
[Traduit par le journal]

Introduction

In the past two decades vibrational spectral studies of electrolytes have attracted considerable attention. Several reports (1–13) on this subject have appeared, dealing with various aspects of aqueous and nonaqueous solutions of electrolytes, molten salts, effect on solvent vibrational bands in aqueous and non-aqueous solutions of electrolytes, etc. While studying the vibrational spectra of solutions of electrolytes several effects, such as ion solvation, ion association, as well as the effect of dissolved electrolytes on the vibrational spectra of the solvent bands, are considered. Ionic and molecular associates found in solutions are often short-lived and may have a well-defined identity on the vibrational time scale only. Since Raman spectra can be recorded for the solute and solvent bands simultaneously for the same concentration of the solution with varying photon count and other such parameters, this branch of vibrational spectroscopy has been widely used for the study of electrolyte solutions. Several papers have appeared on the studies of ion association by vibrational spectroscopy. Alkali metal perchlorates have not been found to show any detectable ion pairs in aqueous solutions (14). The perchlorate band is often used in Raman spectra as an internal standard because of an apparent inability of ClO_4 ions to form inner-sphere ion pairs with most cations. No definite evidence has been reported to indicate the splitting of the $\nu_3(f_2)$ band of ClO_4^- in dilute aqueous solutions. Metal perchlorates in matrix isolation spectra show pronounced splitting of the ν_3 band (14), indicating the formation of ion pairs. Raman spectral studies of aqueous metal chlorates show $\nu_3(e)$ doublets even in the spectra of dilute solutions, similar to the doublets in aqueous metal nitrate solutions (15–17). A possible explanation for the difference between the ν_3 region of ClO_4^- (aq) and ClO_3^- (aq) is that the ClO_4^- (aq) is less strongly hydrogen bonded to the water (1). Symons and Waddington (18) studied the ir spectra of aqueous perchlorate solutions and assigned a new band at a frequency higher than that of the stretching modes of pure water to the $ClO_4^- \ldots H_2O$ complex and computed a hydration number of 4 from intensity measurements. Sodium perchlorate in acetonitrile, tetrahydrofuran, and pyridine was found to show ion association by ^{23}Na nmr chemical shift and vibrational spectral studies (19). Similarly lithium, sodium, and magnesium perchlorates in acetone (20, 21), and lithium and sodium perchlorates in pyridine (22) show splittings. Definite support for the presence of ion pairs in solutions comes from analogous splittings observed in matrices (14) and crystalline perchlorate complexes (23).

All the above studies on vibrational spectra of solutions of ClO_4^- are confined to the splitting of the $\nu_3(f_2)$ Cl—O stretching vibrational band. A survey of the perchlorate vibrations under T_d, C_{3v}, and C_{2v} symmetries shows that for an equilibrium between free perchlorates (T_d) and singly (C_{3v}) or doubly (C_{2v}) associated perchlorates, additional bands should also be observed in the totally symmetric Cl—O stretching (A_1) region. In addition to these effects, the solvent bands may also show certain changes in the band profiles, in case the solvent structure changes during the equilibrium. We have recently reported results on the Raman spectral studies of the structure of DMSO and the effect of dilution when its solutions in water and CCl_4 (24, 25) are considered. We report here Raman spectra of solutions of alkali metal perchlorates in DMSO with a view to understanding the ion association and ion–solvent interactions. For comparison, spectra of aqueous solutions of perchlorates in the Cl—O stretching region are also included.

Experimental

Analar DMSO (Merck) was purified by vacuum distillation and kept on 4A Linde sieves. Sodium perchlorate monohydrate (Fluka), lithium perchlorate monohydrate (BDH), and potassium perchlorate (Reidel) were used as such without further purification. They were kept in a desiccator over calcium chloride. Vacuum distilled DMSO, and triple distilled water were used for preparation of solutions. The solutions were separately prepared in 25-mL standard flasks.

Raman spectral measurements were made at room temperature, on a Cary 82 laser Raman spectrometer equipped with a Spectra Physics argon ion laser (Model 165), with the sample contained in a glass cell. All the spectra were recorded employing a 514.5-nm exciting line, varying in the range 300–500 mW power. A 90° scattering geometry was employed. Slit widths of 1.2–2 cm^{-1} were used for different concentrations, with 2–5 s time constant. Spectra were recorded with 0.10 cm^{-1}/s monochromator speed. Both parallel and perpendicularly polarized spectra were recorded at the same instrumental settings. The spectra are reproducible to within ±1 cm^{-1}.

Results and discussion

Raman spectra of solutions of lithium, sodium, and potassium perchlorates were recorded in solutions of varying concentrations in DMSO and water. The results are presented below.

Cl—O stretching region

In Figs. 1 to 4 are given Raman spectra of DMSO and solutions of metal perchlorates in the 900–1100 cm^{-1} region. Pure DMSO shows band due to CH_3 rocking at ~953 cm^{-1}. The ClO_4^- ion in its T_d symmetry is known (2) to show a totally symmetric Raman band at ~935 cm^{-1}. In Figs. 2 to 4 perchlorates are found to show a sharp band in this region. In addition to this strong and sharp band, a low frequency band is observed in all the solutions of perchlorates in DMSO at ~910 cm^{-1}. Raman spectra of aqueous solutions of lithium and sodium perchlorates given in Figs. 5 and 6 do not show flow frequency bands as observed in the respective solutions in DMSO. Matrix isolation studies on metal perchlorates were carried out by Smyrl and Devlin (14). Perchlorates when deposited in argon matrices only have ion pairs with definite dipole moments. Such ion pairs are assumed to have the perchlorate ions in C_{3v} symmetry, in contrast to free perchlorate ions which have T_d symmetry. In a system where both free perchlorate ions as well as their ion pairs are present, it is expected to observe separate bands because of totally symmetric Cl—O stretchings for the free ClO_4 ion under the T_d symmetry, as well as for the ion-paired ClO_4 ion under the C_{3v} symmetry. The low frequency band at ~910 cm^{-1} may be assigned to the totally symmetric stretching vibration of the ion-paired ClO_4^-. Weak bands in the ir spectra of matrix-isolated perchlorates have been reported in this region by Smyrl and Devlin (14). Neither of the two bands at ~910 cm^{-1} and ~935 cm^{-1} are shown in the Raman spectra in the perpendicular polarized mode. This shows that both the bands are totally symmetric. The lower frequency Cl—O stretching band was reported in the Raman spectra of perchlorates in acetonitrile, THF, and pyridine by Greenberg and Popov (19), and in acetone by James and Mayes (21), in the figures included in these reports, without giving any proper assignments for such bands. However, appearance of a weak band in this region in the matrix-isolated ir spectra of perchlorates may justify the assignment of this band to the ion-paired perchlorates. In the early reports (19, 21), components of the main Cl—O stretching band contour at frequencies higher than the 935 cm^{-1} band are assigned to ion pairs. Since the Cl—(OH) stretching band in

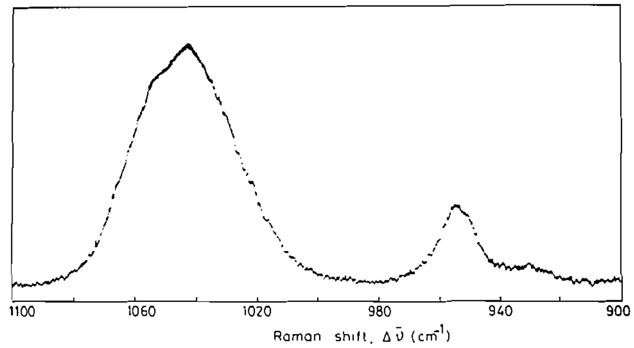

FIG. 1. S=O stretching band in Raman spectra of pure DMSO ($I_{\parallel}$).

$HClO_4$ is assigned to the 734 cm^{-1} band (26, 27), which is lower than the 935 cm^{-1} band, as an analogy we believe the Cl—(OM^+) stretching should be assigned to the lower frequency band at ~910 cm^{-1} as reported in the present work. As mentioned above, in aqueous solutions of perchlorates no band is seen in this region. This is not surprising as ion pairs cannot be formed in aqueous solutions of perchlorates because of the greater possibility of hydration of M^+ and ClO_4^- ions (1, 18). In Tables 1 and 2, spectral parameters of the Cl—O stretching bands in terms of band positions, half-bandwidths, and band heights are given for the various systems considered. The ratios of the intensities of the high frequency band to the low frequency band are shown in the last columns of Table 1. It is noticed that positions of the two bands do not change from system to system and from one concentration to another. The intensity ratio is found to decrease with higher concentrations of perchlorate, indicating greater possibility of association at higher perchlorate concentrations. It is noticed (Tables 1 and 2) that the half-bandwidth of the Cl—O stretching band at ~935 cm^{-1} is about twice as great when ClO_4^- is in aqueous solution compared to when in DMSO solutions. For example, for a 1.0 *M* solution of sodium perchlorate in DMSO the $\Delta\nu_{1/2}$ is 4.0 cm^{-1}, whereas for the same concentration of sodium perchlorate in aqueous solution the value is found to be 8.5 cm^{-1}. It is further noticed that the half-bandwidth increases considerably with increasing concentration of perchlorate in aqueous solutions (varying from 8.5 cm^{-1} for a 1.0 *M* solution to 14.5 cm^{-1} for a 5.0 *M* solution). These observations support the possibility of hydration of ClO_4^- as suggested by Symons and Waddington (18), though the broadening of the Cl—O stretching bands can also be explained in part by the dynamics of the spherical perchlorate ions in aqueous solutions. Dean and Wilkinson have recently reported (28) that the A_1 stretching bands for SO_4^{2-}, WO_4^{2-}, and MoO_4^{2-} ions in aqueous solutions shift to higher frequencies with increasing concentrations of the solutions. We have obtained similar results in sodium perchlorate solutions: the Cl—O stretching band is found to shift from 933.5 cm^{-1} for a 1 *M* solution to 936 cm^{-1} for a 5 *M* solution. In the case of $LiClO_4$, however, no significant shift is observed. The ν_0 value extrapolated to infinite dilution is approximately 933.5 cm^{-1} in both cases.

S=O Stretching region

Figure 1 shows the band contour for the S=O stretching mode of pure liquid DMSO. In earlier publications from this group (24, 25) it was shown that this band is made up of at least four bands at ~1070 cm^{-1}, ~1058 cm^{-1}, ~1040 cm^{-1}, and ~1025 cm^{-1}. It was suggested (25) that the high frequency

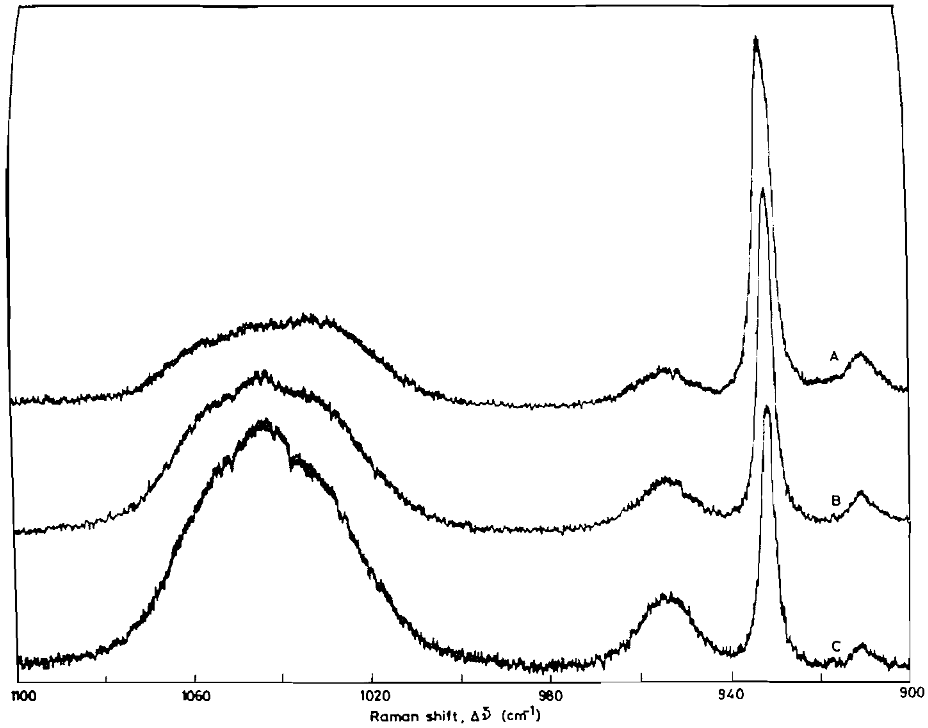

FIG. 2. S=O and Cl—O stretching bands in Raman spectra of solutions of lithium perchlorate in DMSO ($I_{\parallel}$) with concentrations: A, 2.0 *M*; B, 1.0 *M*; C, 0.5 *M*.

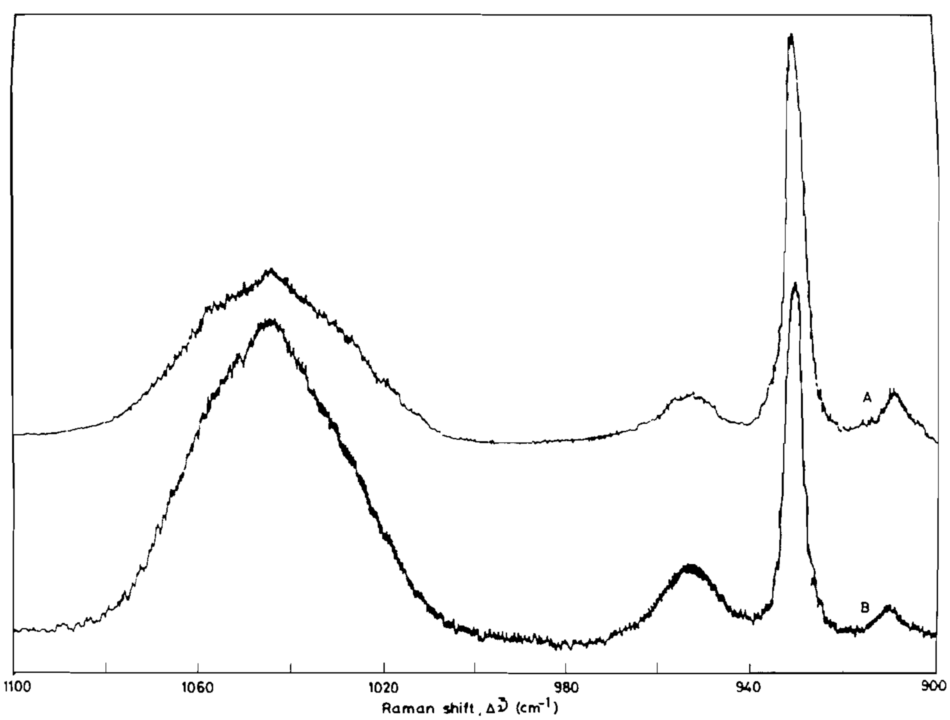

FIG. 3. S=O and Cl—O stretching bands in Raman spectra of solutions of sodium perchlorate in DMSO ($I_{\parallel}$) with concentrations: A, 1.0; B, 0.5 *M*.

band belongs to free S=O stretching, whereas the low frequency bands at ~1058 cm^{-1} and ~1040 cm^{-1} belong to a cyclic dimer and at ~1025 cm^{-1} to a linear dimer and other open-chain polymers. Addition of perchlorates clearly shows perturbation in the structure of the S=O stretching band (Figs. 2–4). The half-bandwith is found to increase with the addition of perchlorates. The increase is of the order of 10–20% for 1.5 molar solutions of perchlorates. It is also noticed that the relative intensity of the low frequency band at ~1025 cm^{-1}, with respect to higher frequency bands, increases considerably with increasing concentration of perchlorates. This may well indicate the presence of ion pairs and the structure making character of perchlorates for liquid DMSO. If the ions were to be solvated by DMSO one would expect structure breaking of

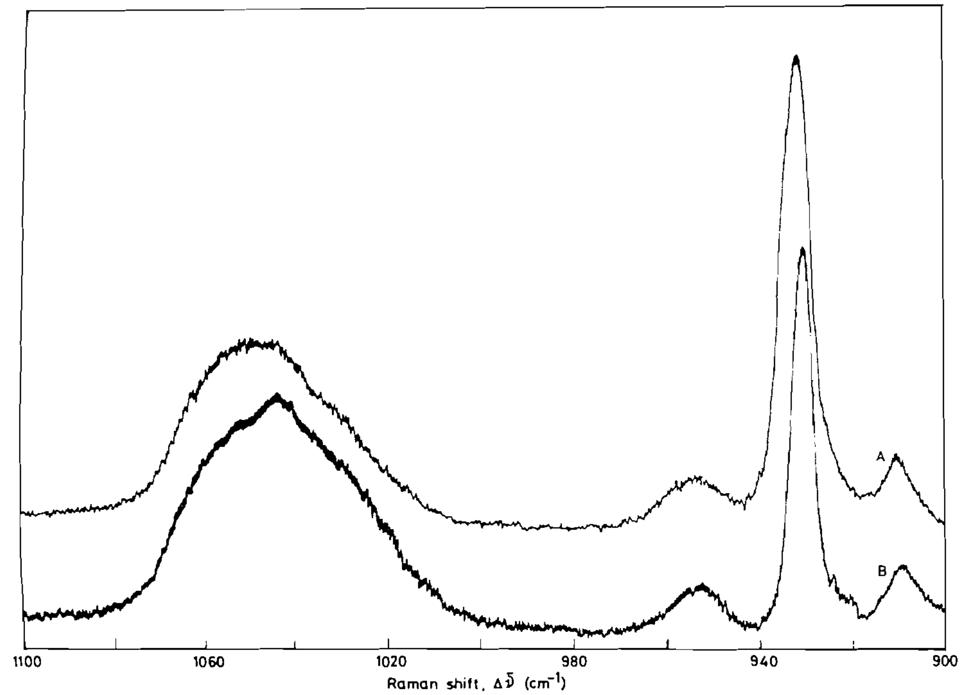

FIG. 4. S=O and Cl—O stretching bands in Raman spectra of solutions of potassium perchlorate in DMSO ($I_{\parallel}$) with concentrations: A, 2.0 M; B, 1.0 M.

TABLE 1. Raman spectral parameters for the Cl—O stretching band of alkali metal perchlorates in DMSO

System	Concentration (M)	$\bar{\nu}$(cm^{-1})	$\Delta\bar{\nu}_{1/2}$ (cm^{-1})	Band heights, I	$A = I \times \Delta\bar{\nu}_{1/2}$	I_{935}/I_{910}	A_{935}/A_{910}
$LiClO_4$	0.5	932.0	4.0	5.50	22.0	15.71	11.89
		911.5	5.0	0.35	1.85		
	1.0	932.0	4.0	7.10	28.4	11.83	8.61
		911.0	5.5	0.60	3.3		
	2.0	931.5	5.0	7.50	37.5	10.00	7.14
		911.0	7.0	0.75	5.25		
$NaClO_4$	0.5	931.0	4.0	7.25	29.0	14.50	9.67
		910.5	6.0	0.50	3.0		
	1.0	931.5	4.0	8.40	33.6	9.33	6.22
		910.5	6.0	0.90	5.4		
	1.5	932.0	5.0	7.30	36.5	9.13	7.60
		910.5	6.0	0.80	4.8		
$KClO_4$	1.0	931.0	5.0	7.70	38.5	7.33	6.11
		910.0	6.0	1.05	6.3		
	2.0	933.0	5.0	7.8	39.0	8.66	4.33
		911.0	10.0	0.9	9.0		

liquid DMSO leading to decrease of intensity of the low frequency band (~1025 cm^{-1}) which is assigned to various associated species of DMSO. In all the perchlorate solutions, concentrations more than 1.5 mol L^{-1} could not be considered because of the solubility limitation, except for $KClO_4$, where the spectra were also recorded for a 2 M solution. In the case of a 2 M solution of potassium perchlorate in DMSO it is further observed that the relative intensities of the 1040 cm^{-1} and ~1050 cm^{-1} components are nearly similar, unlike the case in dilute solutions, as well as in pure DMSO, where the relative intensity of the ~1040 cm^{-1} band is slightly higher than that of the ~1050 cm^{-1} band. This effect may be brought about by the lowering of the concentration of cyclic dimers and

TABLE 2. Raman spectral paprameters for alkali metal perchlorates in water in the Cl—O stretching region

System	Concentration	$\bar{\nu}$ (cm^{-1})	$\Delta\bar{\nu}_{1/2}$ (cm^{-1})
$LiClO_4$	1.0	933.5	9.0
	2.0	933.5	8.5
	3.0	934.0	11.0
	4.0	933.0	10.0
$NaClO_4$	1.0	933.5	8.5
	2.0	934.5	9.5
	3.0	935.0	11.5
	4.0	935.0	13.0
	5.0	936.0	14.5

TABLE 3. Raman spectral parameters for DMSO – perchlorate systems in the C—S stretching region

System	Concentration (mol)	$\bar{\nu}$ (cm^{-1})	$\Delta\bar{\nu}_{1/2}$ (cm^{-1})	$I_{\parallel}$	$I_{\perp}$	$\rho = I_{\perp}/I_{\parallel}$
Pure		669.0	13.0	8.0	0.70	0.09
DMSO		698.5	15.0	1.85	1.20	0.65
$LiClO_4$	0.5	670.0	13.0	7.30	0.55	0.08
+ DMSO		699.5	18.0	2.00	1.03	0.51
	1.0	671.0	18.0	9.40	0.90	0.09
		701.0	20.0	3.05	1.65	0.54
	2.0	673.5	18.0	8.30	0.75	0.09
		705.5	19.0	2.05	1.30	0.63
$NaClO_4$	0.5	670.0	15.0	8.80	0.80	0.09
+ DMSO		700.0	17.0	2.55	1.50	0.59
	1.0	670.5	15.0	8.10	0.70	0.09
		700.0	18.0	2.00	1.30	0.65
	1.5	673.0	16.0	8.10	0.60	0.07
		702.0	19.0	2.10	1.15	0.55
$KClO_4$	1.0	670.0	15.0	8.50	0.70	0.08
+ DMSO		699.5	17.0	2.35	1.35	0.57
	2.0	672.5	15.0	7.70	0.83	0.11
		702.0	16.0	1.90	1.15	0.61

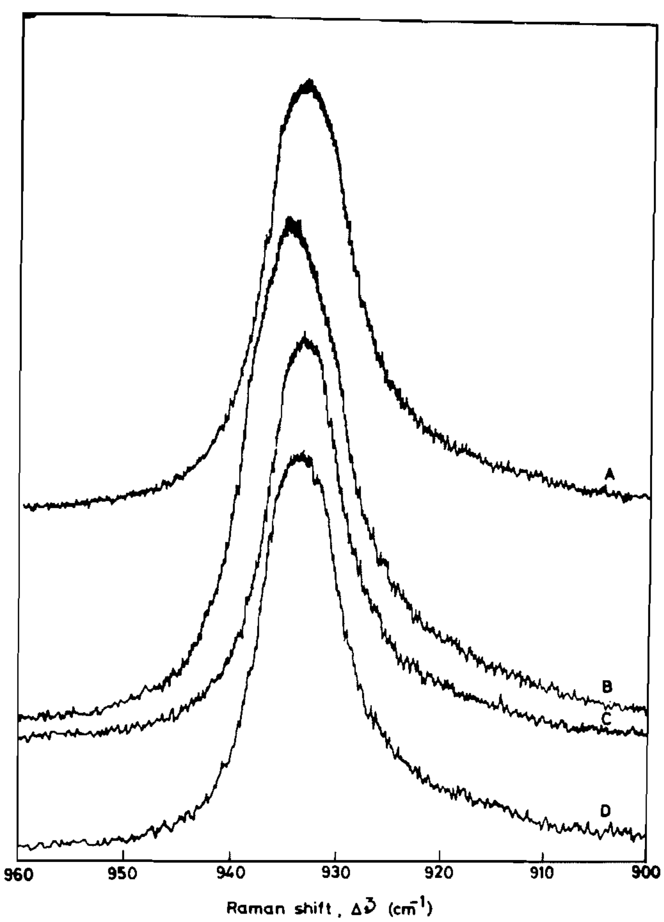

FIG. 5. Cl—O stretching bands in Raman spectra of aqueous solutions of lithium perchlorate ($I_{\parallel}$) with concentrations: A, 4.0 *M*; B, 3.0 *M*; C, 2.0 *M*; D, 1.0 *M*.

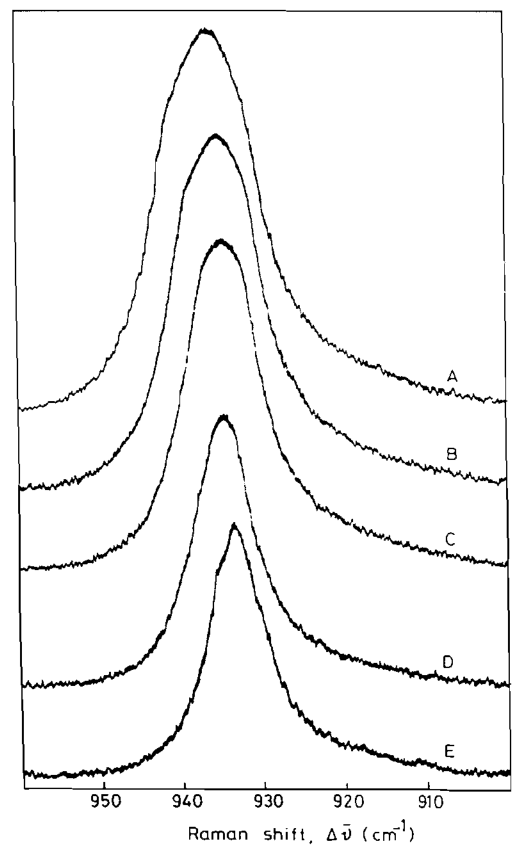

FIG. 6. Cl—O stretching bands in Raman spectra of aqueous solutions of sodium perchlorate ($I_{\parallel}$) with concentrations: A, 5.0 *M*; B, 4.0 *M*; C, 3.0 *M*; D, 2.0 *M*; E, 1.0 *M*.

free DMSO molecules with increasing concentration of perchlorates, which is in conformity with the above observations on corresponding increase in intensity of the low frequency component of the S=O stretching band.

C—S Stretching region

The spectral parameters of the C—S symmetric and asymmetric stretching bands are given in Table 3. The depolarization ratios for the low frequency band are in the range of 0.08 to 0.10; whereas for the high frequency band they range between 0.50 and 0.65. It is noticed that the half-bandwidth of the high frequency band increases wih increasing concentration of perchlorates, being 15 cm^{-1} for pure DMSO and nearly 20 cm^{-1} for a 1 *M* solution of $LiClO_4$. Similar increases are observed in the half-bandwidths for other solutions as well. The low frequency symmetric stretching band for solutions of $LiClO_4$ shows a considerable increase in the bandwidth, whereas those for the solutions of potassium and sodium perchlorates have similar bandwidths for the concentration range of 0.5–2 *M*, which is about 2 cm^{-1} higher than the pure DMSO band. Since the spectral parameters were different for different concentrations for recording the Raman spectra, the intensities of the bands cannot be accurately compared for the same system over a range of concentrations. However, the variation in half-bandwidths as well as depolarization ratios with varying concentrations of perchlorates definitely shows reordering of the DMSO molecules in the perchlorate solutions, when compared with pure liquid DMSO. Fourier transform of these bands may be helpful in determining the vibrational relaxation times, which may give extra support to the proposed structure-making properties of perchlorates for liquid DMSO. Work in this direction is under progress and will be published elsewhere.

Conclusions

Raman spectra of perchlorate solutions in DMSO suggest the presence of ion pairs in the solutions of DMSO on the basis of the Cl—O stretching bands. The band contours in the S=O stretching region also show significant changes. The bands in the C—S stretching region show increase in the half-bandwidths, and decrease in the depolarization ratio of the higher frequency asymmetric stretching bands. Raman spectra of aqueous perchlorate solutions do not show the low frequency Cl—O stretching band due to ion-paired ClO_4^- species with the C_{3v} point group observed in the case of solutions in DMSO, which is in accordance with earlier conclusions that ClO_4^- ions do not show evidence of ion association in aqueous solutions.

Acknowledgements

One of us (M.I.S.S) is grateful to I.I.T., Madras, for providing a Research Fellowship. This work was carried out under a joint Project from the Volkswagen Foundation with Prof. W.A.P. Luck of Uni-Marburg (W.-Germany), which is gratefully acknowledged.

1. D. E. IRISH and M. H. BROOKER. Adv. Infrared Raman Spectrosc. **2**, 212 (1976).
2. D. E. IRISH. *In* Ionic interactions. Vol. 2. *Edited by* S. Petrucci. Academic Press, New York. 1971. p. 188.
3. R. S. TOBIAS. *In* The Raman effect. Vol. 2. *Edited by* A. Anderson. Marcel Dekker, Inc., New York. 1973. p. 405.
4. R. E. VERRALL. *In* Water, a comprehensive treatise. Vol. 3. *Edited by* F. Franks. Plenum Press, New York/London. 1973. p. 211.
5. T. H. LILLEY. *In* Water, a comprehensive treatise. Vol. 3. *Edited by* F. Franks. Plenum Press, New York/London. 1973. p. 265.
6. D. E. IRISH. *In* Physical chemistry of organic solvent systems. *Edited by* A. K. Covington and T. Dickinson. Plenum Press, London/New York. 1973. p. 433.
7. A. K. COVINGTON and T. H. LILLEY. *In* Electrochemistry, a specialist periodical report. Vol. 1. The Chemical Society, Burlington House, London. 1969. p. 1.
8. R. E. HESTER. Anal. Chem. **44**, 490R (1972).
9. W. E. L. GROSSMAN. Anal. Chem. **46**, 345R (1974).
10. D. N. WATERS. *In* Molecular spectroscopy, a specialist periodical report. Vol. 6. The Chemical Society, Burlington House, London. 1979. p. 46.
11. M. C. R. SYMONS. Chem. Soc. Rev. **12**, 1 (1983).
12. D. J. GARDINER. Adv. Infrared Raman Spectrosc. **3**, 167 (1977).
13. M. C. R. SYMONS. *In* Electron–solvent and anion–solvent interactions. *Edited by* L. Kevan and B. C. Webster. Elsevier, Amsterdam. 1976. p. 311; Annu. Rep. Chem. Soc. **73**A, 91 (1976).
14. N. SMYRL and J. P. DEVLIN. J. Chem. Phys. **62**, 1982 (1975).
15. B. G. OLIVER and G. J. JANZ. J. Phys. Chem. **75**, 2948 (1971).
16. D. J. GARDINER, R. B. GIRLING, and R. E. HESTER. J. Mol. Struct. **13**, 105 (1972).
17. D. J. GARDINER, R. B. GIRLING, and R. E. HESTER. J. Phys. Chem. **77**, 640 (1973).
18. M. C. R. SYMONS and D. WADDINGTON. J. Chem. Soc. Faraday Trans. 2, **71**, 22 (1975).
19. M. S. GREENBERG and A. I. POPOV. J. Solution Chem. **5**, 653 (1976).
20. I. S. PERELYGIN and M. A. KLIMCHUK. Russ. J. Phys. Chem. **49**, 76 (1975).
21. D. W. JAMES and R. E. MAYES. Aust. J. Chem. **35**, 1775 (1982).
22. I. S. PERELYGIN and M. A. KLIMCHUK. Russ. J. Phys. Chem. **50**, 1857 (1976).
23. D. L. LEWIS, E. D. ESTES, and D. J. HODGSON. J. Cryst. Mol. Struct. **5**, 67 (1975).
24. SURJIT SINGH and P. K. KRUEGER. J. Raman Spectrosc. **13**, 178 (1982).
25. M. I. S. SASTRY and SURJIT SINGH. J. Raman Spectrosc. **15**, 80 (1984).
26. P. A. GIGUERE and R. SAVOIE. Can. J. Chem. **40**, 495 (1962).
27. M. KINUGASA, K. KISHI, and S. IKEDA. J. Phys. Chem. **77**, 1914 (1973).
28. K. J. DEAN and G. R. WILKINSON. J. Raman Spectrosc. **14**, 130 (1983).

Reactions of lumiflavin with amine radicals

PARMINDER S. SURDHAR, DOUGLAS E. BADER, AND DAVID A. ARMSTRONG
Department of Chemistry, University of Calgary, Calgary, Alta., Canada T2N 1N4

Received April 26, 1984

This paper is dedicated to Professor Camille Sandorfy on the occasion of his 65th birthday

PARMINDER S. SURDHAR, DOUGLAS E. BADER, and DAVID A. ARMSTRONG. Can. J. Chem. **63**, 1357 (1985).

The amino radicals ($\cdot$AH) formed by the ^{60}Co radiolysis of N_2O-saturated 0.05 *M* solutions of ethylene diamine tetraacetate (EDTA) at pH 7 and 11.2 and of glycine at pH 11.2 brought about an efficient two-electron reduction of lumiflavin (Fl). The spectra of the products were identical to those formed by photolysis of the same solutions and by reduction of the lumiflavin with $\cdot CO_2^-$ radicals. The products were reoxidised to flavin by oxygen. The quantum yield for flavin disappearance was 0.52 $\pm$ 0.07 and 0.17 $\pm$ 0.01 in the presence of EDTA at pH 7 and 11.2 and 0.065 $\pm$ 0.008 and 0.17 $\pm$ 0.01 for glycine at the same pHs, respectively.

The overall two-electron reduction can be explained by the mechanism:

[4] $\cdot AH + Fl \rightarrow \cdot FlH + A$

[5] $\cdot FlH + \cdot FlH \rightarrow Fl + FlH^- + H^+$

[6] $\cdot FlH + \cdot AH \rightarrow FlH^- + A + H^+$

The rate constants of reaction [4] were found by pulse radiolysis to be $1.8 \pm 0.3 \times 10^9$ and $1.5 \pm 0.3 \times 10^9$ M^{-1} s^{-1} for the radicals of glycine and EDTA at pH 7 and $3.6 \pm 0.3 \times 10^8$ M s^{-1} for glycine radicals at pH 11.2. The spectrum of $\cdot$FlH formed by glycine radicals at pH 7 is similar to that produced by $\cdot CO_2^-$, but there was some perturbation, which is apparently due to interaction with the amine.

The radicals formed from the secondary amines piperazine and diethylamine at pH 11.8 also effected reversible two-electron reduction. However, the radicals from glycine anhydride and the primary amine ethylamine yielded significant amounts of non-oxidisable products. The reaction mechanisms are discussed and effects of pH are considered.

PARMINDER S. SURDHAR, DOUGLAS E. BADER et DAVID A. ARMSTRONG. Can. J. Chem. **63**, 1357 (1985).

Les radicaux aminés ($\cdot$AH) issus de la radiolyse au ^{60}Co de solutions saturées en N_2O, contenant 0,05 *M* de tétraacétate d'éthylène diamine (TAED) at maintenues à des pH de 7 ou 11,2 ou contenant de la glycine à un pH 11,2, provoquent une réduction à deux électrons efficace de la lumiflavine (Fl). Les spectres des produits sont identiques à ceux des produits obtenus par la photolyse des mêmes solutions et par la réduction de la lumiflavine par les radicaux $\cdot CO_2^-$. L'oxygène provoque une réoxydation des produits en flavine. A des pH de 7 et 11,2 et en présence du TAED, les rendements quantiques pour la disparition de la flavine sont respectivement égaux à 0,52 $\pm$ 0,07 et de 0,17 $\pm$ 0,01 alors qu'en présence de glycine et aux mêmes pH ces rendements sont égaux à 0,065 $\pm$ 0,008 et 0,17 $\pm$ 0,01.

On peut ilustrer la réduction globale à deux électrons, par le mécanisme suivant:

[4] $\cdot AH + Fl \rightarrow \cdot FlH + A$

[5] $\cdot FlH + \cdot FlH \rightarrow Fl + FlH^- + H^+$

[6] $\cdot FlH + \cdot AH \rightarrow FlH^- + A + H^+$

Faisant appel à la radiolyse à pulsation, on a pu établir que les constantes de vitesse de la réaction [4] sont égales à $1,8 \pm 0,3 \times 10^9$ et à $1,5 \pm 0,3 \times 10^9$ M^{-1} s^{-1} respectivement pour les radicaux glycine et TAED à un pH de 7 et à $3,6 \pm 0,3 \times 10^8$ M^{-1} s^{-1} pour les radicaux glycine à un pH de 11,2. Le spectre du $\cdot$FlH formé par les radicaux glycine à pH de 7 est semblable à celui produit par le $\cdot CO_2^-$, mais il y a une certaine perturbation qui provient apparemment d'une interaction avec l'amine.

Les radicaux formés à un pH de 11,8, à partir des amines secondaires comme la pipérazine et la diéthylamine, provoquent également une réduction réversible impliquant deux électrons. Cependant, les radicaux provenant de l'anhydre de la glycine ainsi que de l'amine primaire l'éthylamine donnent des quantité importantes de produits qui ne sont pas oxydables. On discute du mécanisme de la réaction et on considère l'influence du pH.

[Traduit par le journal]

Introduction

Apart from their intrinsic interest in the chemistry of organic free radicals, the reactions of amine radicals with flavins are of potential relevance to the mechanism of action of monoamine oxidase enzymes (1, 2), and to the important area of pharmacology which is based on monoamine oxidase inhibition (1–4). This study is concerned with the one and two electron reduction of lumiflavin (Fl) by amino radicals ($\cdot$AH) formed from glycine and ethylene diamine tetraacetate (EDTA), and with certain other types of reaction which occur for radicals formed from ethylamine, diethylamine, piperazine, and glycine anhydride.

The radicals were produced by radiolysis or by photolysis. In the former technique the following well-established sequence of reactions occurs in nitrous oxide-saturated solutions (5, 6):

[1] $$4.2\ H_2O \rightsquigarrow 2.7\ e_{aq}^- + 0.6\ \cdot H + 2.8\ \cdot OH + 2.7\ H^+ + 0.5\ H_2 + 0.7\ H_2O_2$$

[2] $$e_{aq}^- + N_2O + H_2O \rightarrow OH^- + \cdot OH + N_2$$

[3] $$\cdot OH\ (\text{or}\ \cdot H) + AH_2 \rightarrow H_2O\ (\text{or}\ H_2) + \cdot AH$$

Concentrations of AH_2 and Fl were chosen so that the time scale of reactions [1] to [3] was much shorter ($\lesssim 10^{-7}$ s) than that for the reaction of Fl with any of the primary radicals. Depending on its rate constant, reaction [4]

[4] $$\cdot AH + Fl \rightarrow A + \cdot FlH$$

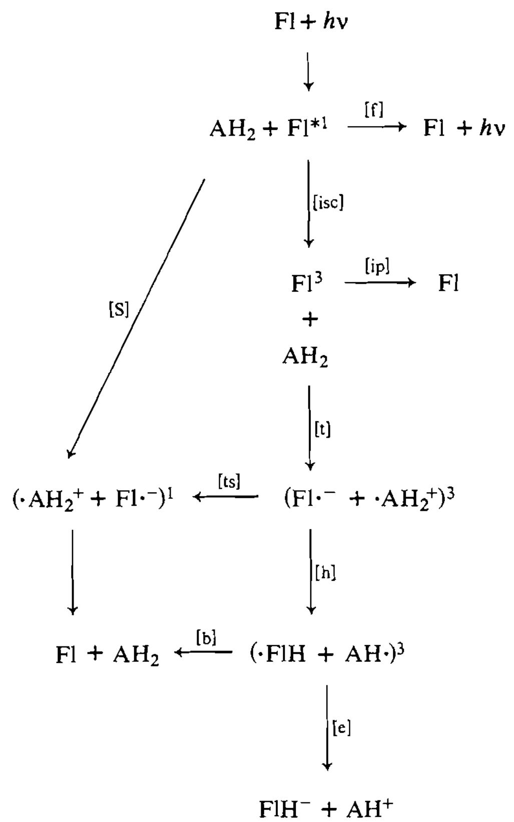

Glycine (15, 19)

Glycine $pK = 9.77$

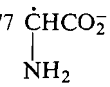

EDTA (18)

(a)

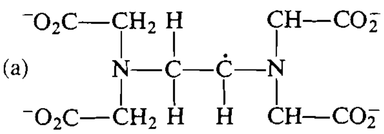

Glycine anhydride (16, 17)

Radical $pK = 9.6$

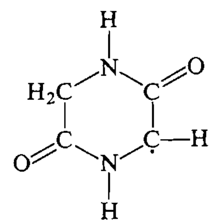

(b)

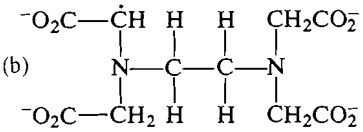

Piperazine (19)

Amine $pK_2 = 9.73$

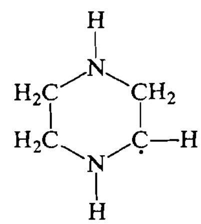

Ethylamine[2] (19, 20)

Amine $pK_b = 10.14$

(β) $\cdot CH_2—CH_2—NH_2$

(α) $CH_3—\dot{C}H—NH_2$

Radical $pK = 10.6$

Diethylamine[2] (19, 20)

Amine $pK_b = 10.19$

(β) $\cdot CH_2—CH_2—NH—C_2H_5$

(α) $CH_3—\dot{C}H—NH—C_2H_5$

SCHEME 1. [f] = fluorescence,
[isc] = Intersystem crossing,
[ip] = triplet decay via isc and phosphorence,
[s] = singlet quenching,
[t] = triplet quenching,
[ts] = triplet → singlet,
[h] = proton transfer,
[b] = back donation,
[e] = electron transfer.

would then occur on a 1 μs or longer time scale. Its kinetics can be followed directly in pulse radiolysis experiments (6). Alternatively, in continuous γ radiolysis experiments at low intensity, the product[1] FlH^- produced by the disproportionation of ·FlH (reaction [5] (7, 8)) can be detected by spectro-

[5]/[−5] $2\ \cdot FlH \rightleftarrows Fl + FlH^- + H^+$

photometry (9). Analogy with reaction of *reducing* radicals formed from alcohols (9) would suggest that the sequence [4]–[5], and possibly also reaction [6], would continue until all

[6] $\cdot FlH + \cdot AH \rightarrow FlH^- + A + H^+$

Fl have been converted to FlH^-, at which point the disproportionation *cum* combination of ·AH would become the dominant

[7] $2\ \cdot AH \rightarrow A + AH_2$ or $(AH)_2$

mode of radical loss. This of course assumes that FlH^- is inert to ·AH.

The photochemical technique produces equal yields of ·FlH and ·AH through the sequence of reactions shown in Scheme 1.

The values of many of the rate constants for the photophysical steps are known for representative flavins (2, 10–14), and the overall quantum yield for ·FlH formation has been reported for several amines (11, 12). Reactions [b] and [e] are favoured by the cage effect for the geminate radical pair. However, one study has shown that the radicals may diffuse appart before reacting (14). In flash experiments radical–radical reactions are rapid, and ·FlH + ·AH reactions may occur preferentially (12) with diffusing radicals. Thus reactions [5], [6], and [7] cannot be excluded. However, for the low intensity continuous photolysis procedure used here ·AH should disappear mainly via reaction [4], which should be followed by [5]. The yield of FlH^- would therefore be equal to the yield of ·FlH and ·AH, assuming [b] is negligible.

The structures of the radicals, which should be produced in reaction [3] at pH 7 are shown below for each of the amines. Where there is evidence for pKs of AH_2 and ·AH in the pH 7 to 12 range these are also given, along with references (in parentheses) to both the structures and the pKs. Spin resonance and other studies show that when the amine is deprotonated, hydrogen atom abstraction is primarily from the α-carbon. Thus far the ethylamines α-type radicals dominate at pH ≥ 11

[1] The pK of FlH_2 is ~6.7 and that of ·FlH is ~8.3 (7). Our equations have been written for pH just above 7.

[2] Abstraction of ·H by ·OH is mainly from β carbon for protonated amine and from α carbon for unprotonated amine (20). Thus (β) should be the main radical species below pK_b and (α) the main one above pK_b.

although some β-radicals must be anticipated (15–18, 20). Two types of radicals are also possible for EDTA, and the p*K*s are not known. For glycine and probably for piperazine one radical type should be dominant at pH 7 or 11.8. For glycine anhydride at pH 11.8, the radical structure will differ from that shown by the loss of the proton from the N atom adjacent to the radical sight.

Experimental

Materials

Chemicals obtained were EDTA and lumiflavin (Sigma Chemical Co.), analar grade diethylamine and glycine (British Drug Houses), ethylamine and piperazine (Eastman Kodak Co.). All other chemicals were the purest available grade and used as supplied.

Apparatus

The pulse radiolysis experiments were performed by utilizing 2 μs pulses of electrons with a dose of 2 to 4 gray per pulse from the 1.5 MeV Van de Graaff generator described earlier (21). A 1.0 cm path length optical cell was used with a fresh solution for each pulse. Dosimetry was based on absorbance changes in N_2O-saturated 1×10^{-2} *M* potassium ferrocyanide solutions with ($G \times \epsilon_{420}$) taken as 6.4×10^3 molecules $(100 \text{ eV})^{-1}$ M^{-1} cm^{-1} (22). Here *G* is the yield of the product (ferricyanide) in molecules per 100 eV of radiation energy and ϵ_{420} the difference in molar absorbance co-efficients of ferri- and ferrocyanide at 420 nm.

Values of ΔA, the change in absorption per unit dose observed at any given time after the radiation pulse, were converted to [ε(Fl radical) − ε(Fl)] at each wavelength by dividing ΔA by the concentration of radicals produced per kilogray. Values of ε(Fl radical) were then obtained by adding values of ε(Fl), which were measured on a Cary-219 spectrophotometer. Radical yields per kGy were 5.6×10^{-4} *M* for 0.05–0.1 *M* glycine at pH 7, 7.0×10^{-4} *M* for 0.05 *M* glycine at pH 11.2, and for 0.05 *M* EDTA 6.4×10^{-4} *M* and 7.0×10^{-4} *M* at pH 7 and 11.2, respectively. The differences reflect the different reactivities towards ·OH (5, 23).

Steady state radiolyses were performed in an AECL ^{60}Co γ cell with a steady dose rate of 10.0 Gy min^{-1}. The dose rate was determined by ferrous sulphate dosimetry, assuming $G(Fe^{3+}) = 15.6$ molecules per 100 eV (5), and checked periodically.

All solutions were prepared from triply distilled water and purged with N_2O or argon as indicated. The gases were first passed through a column of ridox (Fisher Scientific Co.) to remove traces of oxygen. All solutions were buffered with 10 m*M* phosphate and protected from light as much as possible. Experiments were performed at 23 ± 2°C. The net number of moles of radicals produced per litre of solution for a given radiation dose, e_{red}, was calculated by means of eq. [12] of ref. 9.

The photolysing lamp consisted of a 250W Halogen Bellophot fitted with a water filter. The light was collimated through filters with maximum and minimum transmissions of λ445 and λ420 nm, respectively. Light intensities at various distances were determined chemically using ferrioxalate actinometry (24). The actinometer solution was 0.15 *M* potassium ferrioxalate in 0.1 *N* sulphuric acid. A molar extinction coefficient of 1.05×10^4 M^{-1} cm^{-1} at 510 nm for the 1,10-phenanthroline complex was determined experimentally by procedures of Hatchard and Parker (24). The spectrum incident on the 1 cm square quartz photolysis cell was calculated from the emission spectrum of the lamp and the percentage transmissions of the filters. The fraction of light absorbed over the band of wavelengths was calculated from the absorption spectrum for each irradiated solution.

Results

Pulse radiolysis

The solid line, the mean of four determinations, in Fig. 1 shows the spectrum at pH 7 produced by the reaction of the glycine radical with 40 μm Fl at 60 μs after the pulse in N_2O-saturated solutions, while the dashed line is the spectrum

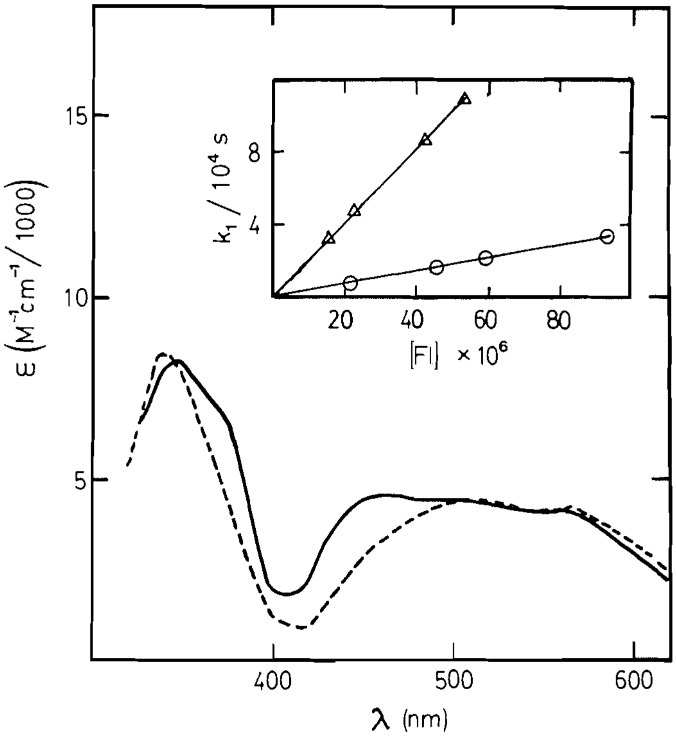

FIG. 1. Absorption spectra 60 μs after pulse radiolysis of 40 μ*M* Fl at pH 7, in phosphate buffer. Reacting radicals: (- - -) $\cdot CO_2^-$ in formate solutions (20×10^{-3} *M*) and N_2O-saturated; $\dot{C}H(NH_2)CO_2^-$ in 0.05 *M* – 0.1 *M* glycine solution, argon, and N_2O-saturated. Inset: plots of pseudo first order rate constants vs. concentration of Fl for pH 11.2 (○) and 7 (△).

of ·FlH produced by the reaction of $\cdot CO_2^-$ with Fl. The main features of the spectrum produced by $\cdot CO_2^-$ were a minimum at 415 nm, maxima at 340 and 510 nm, and a broad shoulder at 570 nm. The spectrum produced by the glycine radical is somewhat different. In addition to the maximum at 345 nm it has a shoulder around 380 nm and there is an increase in absorption in the 400–500 nm region. A similar spectrum was obtained in argon-saturated solutions indicating that the radical species produced by glycine in argon or N_2O-saturated solutions are the same. The spectrum was independent of glycine concentration in the range 0.05 to 0.1 *M*. The growth in absorbance above 500 nm and the change in absorbance at other selected wavelengths exhibited a pseudo-first order behaviour when plotted as a function of time.

The slope of the plot of the pseudo-first order rate constant versus [Fl] for four concentrations in the range 10–100 μ*M* gave a k_4 value of $1.8 \pm 0.3 \times 10^9$ M^{-1} s^{-1}. The rate constant for reaction of the glycine radical with Fl was similarly determined at pH 11.2 and found to be $3.6 \pm 0.3 \times 10^8$ M^{-1} s^{-1}. The plots are shown in the inset of Fig. 1. Likewise the observed value of k_4 for EDTA radicals at pH 7 was $1.5 \pm 0.3 \times 10^9$ M^{-1} s^{-1}. Absorption spectra for the flavin species formed by the radicals of EDTA and of glycine at pH 11.2 will be discussed separately in a future publication.

^{60}Co γ radiolysis and photolysis of glycine and EDTA solutions of Fl

Spectral changes resulting from the reduction of 20 μ*M* Fl with radicals from 0.1 *M* glycine in N_2O-saturated solutions at pH 7 and 11.2 are shown in Figs. 2 and 3, respectively. The initial spectrum of Fl was suppressed by each successive dose

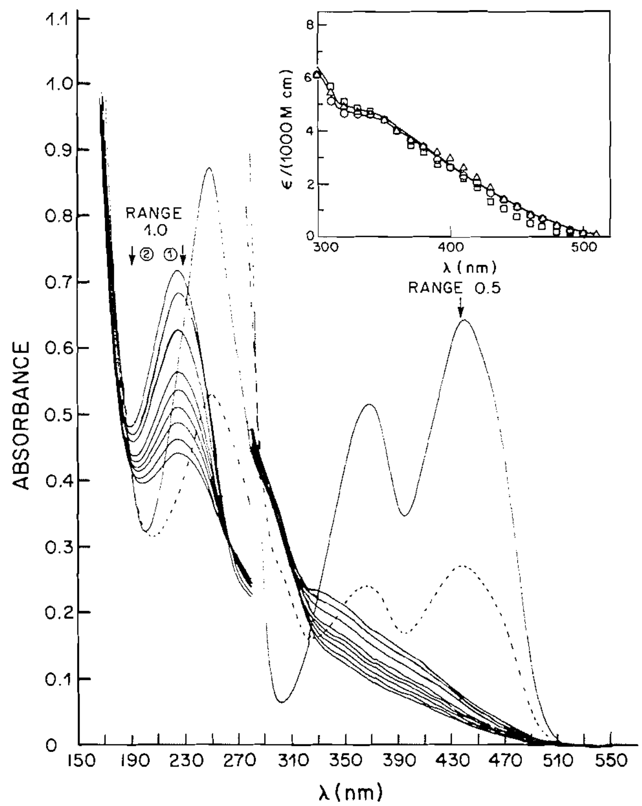

FIG. 2. Spectra obtained from N_2O-saturated solutions of 20 μM LF in 0.1 M glycine and 10 mM phosphate buffer at pH 7 before irradiation, and after 16, 20, 28, 36, 40, 44, 48, 52, and 56 min of γ irradiation at 10 gray min^{-1}. Dashed line: spectrum after reaeration of the irradiated solution. Inset shows spectrum of the reduced species formed by the reacting radicals produced from: photolysis in 0.05 M EDTA (△), 0.05 M Glycine (○); and γ radiolysis of 0.1 M EDTA (□) in buffered solutions containing 20–40 μM Fl. Lines: error limits for species produced by the $\cdot CO_2^-$ radicals in irradiated formate solutions.

of radiation at pH 11.2 and there was no further change in the spectrum after 20 min of radiation. The original spectrum of Fl was regenerated on aeration as shown by the dotted lines in Fig. 3. At pH 7.0, however, the spectrum did not reach a steady state. On addition of air the original spectrum of Fl was not regenerated as shown by the dotted lines in Fig. 2, indicating the formation of a new product. The identification of this new product was not pursued.

In the case of reduction of 20 μm Fl irradiated in 0.1 M EDTA the spectra reached a steady state and the original spectrum of Fl was regenerated at both pH 7 and 11.2 on addition of air.

The insets of Figs. 2 and 3 show that the spectra of the species produced from Fl by γ-radiolysis and photolysis of 0.05–0.1 M glycine and EDTA and by $\cdot CO_2^-$ are identical. There are small differences between pH 7 and 11.2, due to the more complete ionisation of FlH_2 at the higher pH.

Figure 4 shows a plot of $\Delta[Fl] \times 10^6$ M versus $e_{red} \times 10^5$ M. From the initial slopes values of η, the number of moles of reducing equivalents taken up per mole of flavin were calculated. They were 2.28 and 2.34 for EDTA, and 2.25 and 2.42 for glycine at pH 7.0 and 11.2, respectively. These values were consistent with the overall two-electron reduction, viz.

[8] $2AH\cdot + Fl \rightarrow FlH_2 + 2A$

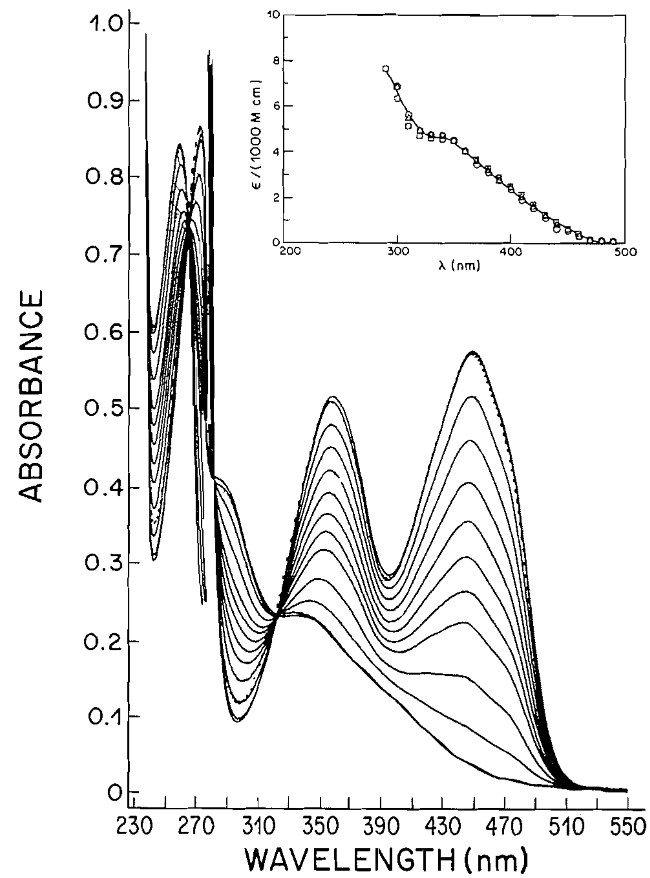

FIG. 3. Spectra obtained from N_2O-saturated solutions of 20 μM Fl in 0.1 M glycine and 10 mM phosphate buffer at pH 11.2 before irradiation and after 2, 3, 4, 5, 6, 7, 8, 10, 12, 16, and 20 min of γ irradiation at 10 gray min^{-1}. Dotted line: spectrum after reaeration of the irradiated solution. Inset shows spectrum of the reduced species formed by the reacting radicals produced from photolysis in 0.05 M glycine (□); and γ radiolysis of 0.1 M EDTA (○) and 0.1 M Glycine (△) at pH 11.2 in buffered solutions containing 20–40 μM Fl. The line shows the species produced by $\cdot CO_2^-$ in formate solutions.

Quantum yields for the photoreduction of 20–40 μM Fl in 0.05 M EDTA and glycine at pH 7 and 11.2 were 0.52 ± 0.07, 0.17 ± 0.01, and 0.065 ± 0.008 and 0.17 ± 0.01, respectively. These are average values determined at several light intensities from the initial slopes of Δ[Fl] versus time over a small period of time or by using the integrated rate law $\ln[10^{A_0} - 1)/(10^{A_t} - 1)] = \Phi\bar{\epsilon}I_0t$ (11). Here I_0 is the incident light intensity, A is the absorbance at time t, Φ the quantum yield of photoreduction, and $\bar{\epsilon}$ the molar extinction coefficient of Fl weighted for the overall spectrum transmitted by the filters. This was determined to be 8459 M^{-1} cm^{-1}. Both methods gave the same values of Φ. The integrated plots for three different light intensities are shown in Fig. 5. The average quantum yield for EDTA at pH 7 was made for six different intensities with I_0 covering the range 1 to 226 × 10^{-7} einsteins cm^{-2} s^{-1}.

^{60}Co γ radiolysis and photolysis of Fl solutions containing other amines

Spectral changes resulting from the gamma radiolysis or photolysis of 20–40 μM Fl in the presence of the amines listed in Table 1, other than EDTA and glycine, were followed in the same way as those described above for glycine and EDTA. In most cases γ radiolysis experiments were carried out in argon-

TABLE 1. Quantum yields for Fl disappearance

Amine*	pH 7			pH 11.2–11.8		
	$2/\eta_{N_2O}$	$2/\eta_{Ar}$	Φ/Φ EDTA	$2/\eta_{N_2O}$	$2/\eta_{Ar}$	Φ/Φ EDTA
EDTA	0.89(99+)	—	1.00(99+)	0.83(99+)	—	1.00(99+)
Diethylamine	0.74(17)	0.64(23)	0.21(80)	0.64(87)	0.80(93)	0.035(100)
Piperazine	—	0.38(91)	0.03(85)	0.18(96)	0.56(98)	0.0057(95)
Ethylamine	0.75(13)	0.77(32)	0.011(60)	0.37(58)	0.69(46)	0.056(64)
Glycine	0.88(99+)	—	0.13(99+)	0.85(99+)	—	1.00(99+)
Glycine anhydride	0.37(42)	—	0.008(6)	0.98(21)	—	0.18(90)

*[Amine] = 0.1 *M* and 0.05 *M*, respectively, for γ-radiolysis and photolysis, except for glycine anhydride where the concentration in radiolysis was 20 m*M*. [Fl] is 20 μ*M* and 40 μ*M* for γ-radiolysis and photolysis, respectively. Photolysis was carried out in N_2O purged solutions. The subscript only indicates purging gas for radiolysis method. Standard deviations are typically ±5%.

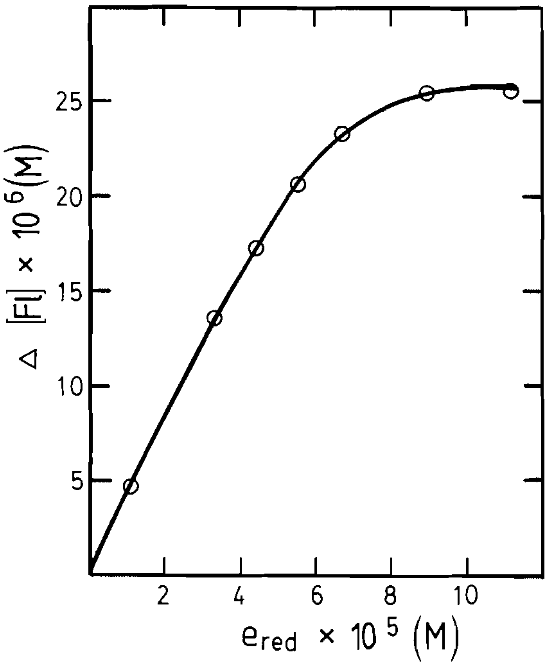

FIG. 4. Change in Δ[Fl] versus e_{red}, number of equivalents of reducing species reacted, for Fl + $H\dot{C}(NH_2)CO_2^-$ at pH 11.2.

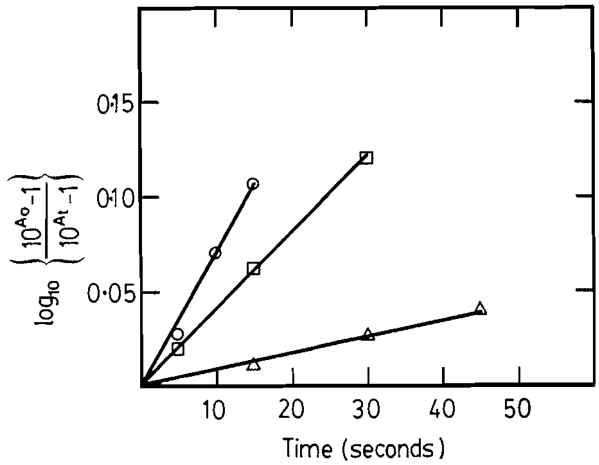

FIG. 5. Plot of $\log_{10}\{(10^{A_0} - 1)/(10^{A_t} - 1)\}$ versus time for three different light intensities. The I_0 values are 1.08×10^{-7} (△), 4.82×10^{-7} (□), and 8.12×10^{-7} (○) einsteins cm^2 s^{-1}.

purged, as well as N_2O-saturated solutions.

The purpose of these experiments was to examine the efficiency of two electron reduction of Fl by different kinds of amine radicals and to determine whether any products, which were not oxidisable by oxygen, were formed. Values of η for the radiolysis were determined from initial slopes of plots of Δ[Fl] versus e_{red}, as in Fig. 4. The efficiencies, given as 2/η have been presented in Table 1. Quantum yields for the photolysis, determined as for EDTA and glycine, were for diethylamine, piperazine, ethylamine, and glycine anhydride 0.01_1, 0.016, 0.055, and 0.043 at pH 7 and 0.0059, 0.0010, 0.0096, and 0.03_1 at pH 11.8, respectively. These have been expressed in Table 1 relative to those of EDTA at the same pH. The reversible reduction was determined by expressing the increase in absorbance at 440–447 nm on addition of air as a percentage of the total loss of absorbance. In cases like that of glycine at pH 7, where the spectrum did not reach a steady state, reoxidation was carried out well before the stoichiometric equivalence point. Those cases were glycine, ethylamine, and diethylamine. The percentages of reoxidation by air have been given in italics in Table 1.

It should be noted that for ethylamine and diethylamine at pH 7, if radiolytic reduction was taken beyond the stoichiometric equivalence point, there was less than 5% reoxidation. The products of the radical plus flavin reactions exhibited maxima at 310 nm and lower absorbance in the region from 330 to 470 nm than the reduced flavins formed by $\cdot CO_2^-$ or EDTA radicals. This was true for both N_2O- and argon-saturated solutions.

Discussion

Formation of ·FlH by glycine and EDTA radicals

As shown in eq. [2], in nitrous oxide-saturated solutions e_{aq}^- is converted to ·OH. Glycine radicals produced via reaction [3] are then the only significant species reacting with Fl. On the other hand, in argon-purged solutions e_{aq}^- reacts directly with Fl (reaction [9] (8)) in a yield comparable to that of the glycine

$$[9] \quad e_{aq}^- + Fl + H^+ \rightarrow \cdot FlH$$

radical ($G_{e_{aq}^-} = 2.7$ and $G_{\cdot OH} = 2.8$ from eq. [1]). Since the spectra were the same in N_2O- and argon-purged solutions, one must conclude that the species produced by glycine radicals and e_{aq}^- were the same. Also, since in the absence of glycine the spectrum of ·FlH produced in reaction [9] is the same as that formed by $\cdot CO_2^-$ and other reducing radicals (8, 25), it would appear that the difference between the two ·FlH spectra in Fig. 1 was caused by the presence of glycine and not by the different reducing radicals $\cdot CO_2^-$ and $H_2N\dot{C}HCO_2^-$. Similar experiments performed at pH 10 showed that addition of glycine to formate solutions, in which Fl^- was formed by reaction of Fl with $\cdot CO_2^-$ and e_{aq}^-, again caused perturbation of the $\cdot Fl^-$ spectrum. Furthermore at pH 7 several of the other amines used here created an even stronger enhancement of the ·FlH absorbance in the region near 450 nm than that seen in Fig. 1. A systematic study of these effects will be reported in detail elsewhere. However, it is evident that several amines interact relatively strongly with ·FlH and $\cdot Fl^-$, causing significant alterations in their absorption spectra. Some evidence for interactions between flavin radicals and certain amino acids has been reported previously (26).

The rate constants for reaction of glycine and EDTA radicals with Fl at pH 7 were $1.8 \pm 0.3 \times 10^9$ and $1.5 \pm 0.3 \times 10^9\ M^{-1}\ s^{-1}$, respectively. These may be compared with 3.6 ± 0.3, 2.6 ± 0.3, and $2.0 \pm 0.3 \times 10^9\ M^{-1}\ s^{-1}$ for $\cdot CO_2^-$, $CH_3\dot{C}(OH)H$, and $(CH_3)_2\dot{C}OH$, respectively. All of these radical reduction processes appear to be close to the diffusion-controlled limit. The smaller rate constant for glycine radicals and Fl at pH 11.2, $3.6 \times 10^8\ M^{-1}\ s^{-1}$, is probably due to the development of a negative charge on the lumiflavin, which has a pK of about 10 (7), and the consequent interaction with the negatively charged glycine radical. The present value of $k_4 = 1.5 \times 10^9\ M^{-1}\ s^{-1}$ for EDTA radicals plus lumiflavin at pH 7 may be compared with published rate constants of 2×10^8 and $5 \times 10^8\ M^{-1}\ s^{-1}$, respectively, for the corresponding reaction of EDTA radicals with flavin mononucleotide (27) and 3-methyllumiflavin (14), which are slightly smaller.

The formation of FlH^- by glycine and EDTA radicals

The spectra of the products formed in γ radiolysis from EDTA radical at pH 7 and 11.2 and from glycine radicals at pH 11.2 were identical to those produced by photolysis of the same solutions and by $\cdot CO_2^-$ (9) (see Figs. 2 and 3). This feature and the fact that all of these products can be reoxidised to Fl by air are consistent with FlH^- as the only significant compound formed by these radicals.

The case of the glycine radical at pH 7 is interesting, since the spectrum did not reach a steady state. The spectral changes in the 310 to 510 nm region of Fig. 2 for the addition of the first 5 mol of $H_2N\dot{C}HCO_2^-$ radical per mole of flavin demonstrates that reduction to FlH^- did occur (cf. the data in the inset). The stepwise spectral changes for added radical concentration up to this point were quite similar to those in Fig. 3 and have been omitted for clarity. However, beyond that point there was a reduction in the absorbance at the 220 nm peak and in the 310 to 510 nm region. Also, after prolonged irradiation such as the one shown in the Fig. 2, the initial concentration of Fl was not recovered on addition of air. These observations demonstrate that at pH 7 glycine radicals react with FlH^-, causing an irreversible change and producing a product, which cannot be oxidised to Fl by oxygen. The effect of this process will obviously be less apparent when glycine radicals are produced by photolysis, since the rate of formation of glycine radicals becomes zero when all Fl has been converted to FlH^-. In contrast, in γ radiolysis the rate of radical production is independent of [Fl] and [FlH^-]. The only other radical for which similar behaviour has been observed thus far is e_{aq}^- (9).

As stated in the Results section, the initial slopes of plots of Δ[Fl] versus e_{red} as in Fig. 4 yield values of $\eta = 2.2$ to 2.4 for both glycine and EDTA radicals at pH 7 and 11.2. This feature indicates a relatively efficient two radical per flavin reduction process as in eq. [8]. Thus reaction [7] cannot be of very great significance, certainly not in the initial phases of the reduction. The reactions contributing to reduction may be taken to be [4] and [5] with some possible contribution from [6]. The present study is a necessary prelude to a determination of the rate of this reaction by the technique of long pulses (28).

Interpretation of the quantum yields for flavin disappearance is not as easy as for the values of η. However, the values of Φ_{ISC} (= $k_{ISC}(k_{ISC} + k_f)^{-1}$, if other singlet loss processes are neglected) lie between 0.5 and 0.7 at pH 7 and fall off at high pH to about 0.17 at pH 10.3 (10–13). Thus the quantum yields for EDTA reduction at both pHs and for glycine at pH 11.2 are equal or close to the maximum values, which can be obtained from reactions [t], [h], [e] and [6] or [4] + [5]. Actually the present quantum yields at pH 7 are in gratifyingly good agreement with those reported for the photoreduction of riboflavin (11) and of FMN (13) by EDTA at pH 7. One may note that the data of ref. 13, indicate a quantum yield of 0.67 ± 0.09 for ·FlH from a flash experiment, while $\Phi(FlH_2)$ was 0.54 ± 0.05 in steady-state photolysis and 0.61 ± 0.12 in the flash experiment. These results suggest that slightly fewer radicals produce FlH^- at low intensity, but in both cases the conversion of ·FlH + ·AH radicals pairs to FlH^- was ≥70%. For comparison the efficiencies for the two-radical reductions, which can be calculated from the η values for the γ radiolysis (= $2\ \eta^{-1} \times 100\%$) reported above are ≥80%. These figures are presented in Table 1 as fractions.

The much smaller quantum yield for photosensitised reduction in the presence of glycine at pH 7 ($\Phi(FlH_2) = 0.065$) may be attributed to the small value of k_t (<$10^5\ M^{-1}\ s^{-1}$ for FMN[3] at pH 7 (12)), which has been reported for the amino acid. For EDTA k_t is apparently much larger (6.2×10^8 for 3-methyllumiflavin (14)).

The products derived from EDTA for radical reductions of Fl to FlH^- have been discussed by Armstrong, Hemmerich, and Traber (29). In the absence of metal ions 1 mol of glyoxalate and of CO_2 were formed per mol of flavin reduced. The reactions which they propose are shown in Scheme 2. The major ·AH radical is seen to be $-\overset{|}{N}-\dot{C}HCOOH$, which is the type b radical expected from ·OH abstraction. This radical probably dominates over the (*a*) radical in γ radiolysis, since there are twice as many C—H bonds from which it may be produced. Support for that comes from the observation that glyoxalic acid is also the main product of the radiolysis of EDTA in air-free solutions (18). This product plus the amine formed with it correspond to A in reaction [4]. In the case of glycine, electron transfer from $H_2N\dot{C}HCO_2^-$ produces $H_2\overset{+}{N}{=}CHCO_2^-$, which hydrolyses to ammonia plus glyoxylic acid and a smaller amount of formaldehyde (30, 31).

Reactions of other amine radicals

The experiments reported here were carried out to determine whether the reversible two electron reductions observed with glycine and EDTA radicals occurred with other amine radicals. The quantum yields for Fl disappearance are seen (Table 1) to be much smaller than those for EDTA, which probably represent the values of the yields for Fl^{*1} intersystem crossing in the two pH regimes. Evidently with the other amines there is more singlet quenching (without product formation) and/or the values of k_t are significantly lower. In addition, the γ radiolysis results imply that the reactions of ·AH may now be slightly less effective in forming FlH^- (see below).

The results in Table 1 at pH 11.8, where the amines are

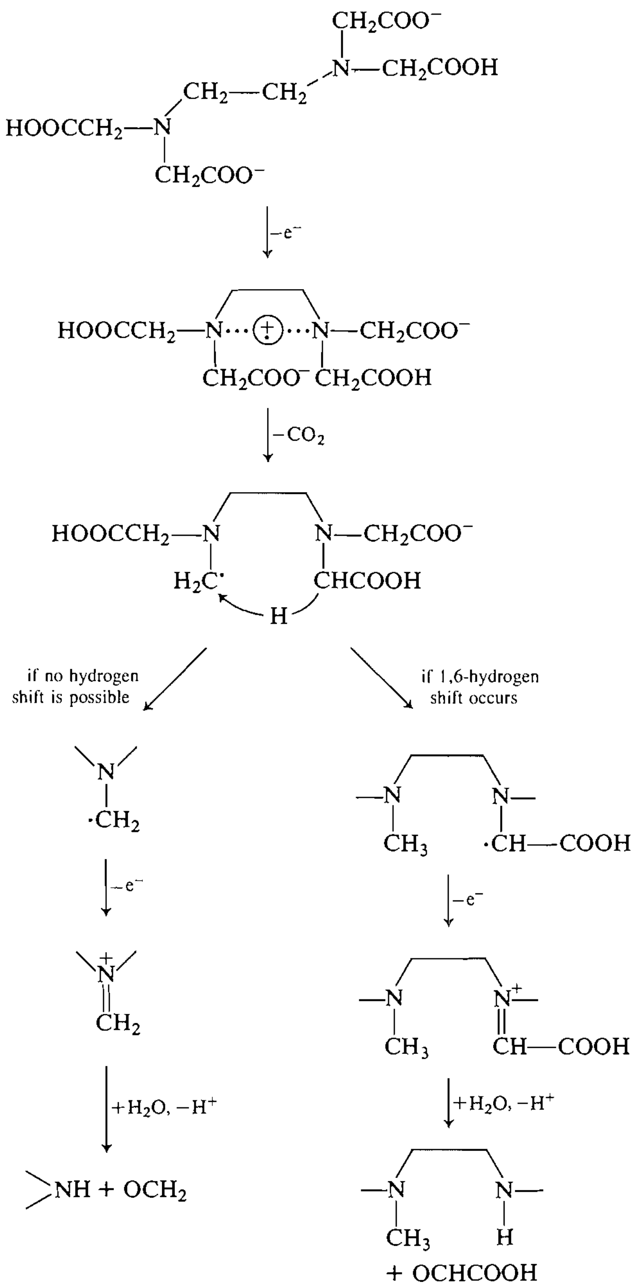

SCHEME 2. Reaction pathways of Fl_{ox} sensitised photooxidation of EDTA (29).

deprotonated, will be considered in detail first. In the case of piperazine both photolysis and radiolysis led to products, which could be reoxidised to flavin to the extent of 95+%. In this regard it was probably significant that only one type of radical could be formed by ·OH abstractions of H from CH_2 groups, which is expected to be the main site of ·OH attack (32). From published mechanisms for flavin-catalysed amine oxidations, one may reasonably expect this to be the same as the radical arising from photolysis (Scheme 1). For the other secondary amine, diethylamine, one sees on the other hand the percentage of reoxidisable product fall to 87 in going from the photolysis to the radiolysis in N_2O-saturated solutions. Here some ·OH abstraction of H from β-carbon atoms may occur, and from studies with alcohols it has been found that such radicals form non-oxidisable products via reaction [10] (9). Thus it seems probable that the α-amine radicals of diethylamine reacted similarly to those of piperazine and the non-

[10] ·FlH + ·AH → HFl—AH

oxidisable product was due primarily to the presence of some 10% or so of β radicals. Evidently these species are not found in the photolysis at all. The above results with secondary amines are in contrast to the behaviour for the primary amine ethylamine. Here, both photolysis and radiolysis yielded large percentages of non-oxidisable product. These results could be explained if reaction [h] and [t] in Scheme 1 were in competition with a β-hydrogen abstraction by Fl^3 and this and the ·OH in the N_2O-saturated irradiated solutions produced roughly 40% of β-amine radicals. However, based on conclusions from pulse radiolysis (20) this seems to be a rather high proportion of β-radicals, and the alternative hypothesis, that α-amine radicals of ethylamine form oxygen-stable products, must be considered. Rather interestingly, substitution of the —CO_2^- group of glycine for the β-CH_3 of ethylamine completely altered the situation and only reoxidisable product was seen (Table 1).

At pH 7 the proportion of ·OH abstraction of H from the β-carbon rises, due to protonation of the amine (20). Reference to Table 1 shows that the percentages of flavin product reoxidised by air after irradiation of N_2O-saturated solutions of diethylamine and ethylamine fell dramatically, which is in accord with the formation of β-radical adducts in reaction [10]. Based on earlier studies these were probably C-4*a*-alkylated 4*a*,5-dihydroflavins (9), but we did not attempt to identify them here.

It is interesting that the percentage of reversible reduction also fell off for the photolysed solutions, although by a much smaller amount. Evidently for these primary and secondary amines either pH influences the photochemical reactions or the mechanism of reaction between ·FlH and ·AH is different from that between $Fl^{\cdot -}$ and ·AH. This is in contrast to the pH independent yield of reduction for the tertiary amine EDTA. One may note that other tertiary amines, Et_3N and Me_2NCH_2Ph, have been reported to produce 100% oxygen reversible reduction on photolysis (2) at pH 7.

The percentages of reoxidation for glycine anhydride are different from those for the other two secondary amines. Clearly the reactions which occur are altered quite drastically by the replacement of CH_2 by CO (cf. piperazine).

The values of $2/\eta$ for the other amines are also different from those of EDTA. As stated earlier ·AH and ·FlH are produced from ·OH and e^-_{aq} in approximately equal yields in argon-purged solutions. The values of $2/\eta_{Ar}$ in Table 1 are therefore a measure of the efficiency of conversion of the ·AH plus ·FlH mixtures to products. The fact that these were significantly less than unity for diethylamine, piperazine and ethylamine implies that reaction [7] and/or the back donation [b] are important. The even lower efficiencies in N_2O-saturated solutions, where there was no source of ·FlH apart from reaction [4], is an indication that some ·AH radicals *were lost* via reaction [7].

Finally it is interesting that the percentage of reversible oxidation fell off when the number of radicals reacted per flavin at pH 7 was taken beyond the stoichiometric equivalence point. This implies that oxidisable product formed in the initial stages may be converted to an oxygen stable form. In this connection one may recall that there is an equilibrium between Fl, FlH^-, and ·FlH (reactions [5] and [−5]). This provides an avenue for the conversion of FlH^- to HFl—AH through reactions [−5]–[10]. Further work on this aspect is desirable. Also needed is a more quantitative assessment of the proportion of

>N· radicals produced by ·OH and Fl^3 reactions both above and below the amine pK. It is not possible at present to say whether that type of radical undergoes addition or electron transfer.

Acknowledgements

The authors appreciate the financial assistance provided to D.E.B. by the Alberta Heritage Foundation for Medical Research in the form of a summer studentship in 1983 and the support of NSERCC under grant A3571. They are also grateful to D. Malinsky and S. Przepiora for technical assistance.

1. R. B. SILVERMAN and S. S. HOFFMAN. J. Am. Chem. Soc. **102**, 884 (1980).
2. J. T. SIMPSON, A. KRANTZ, F. D. LEWIS, and B. KOKEL. J. Am. Chem. Soc. **104**, 7155 (1982).
3. B. T. HO. J. Pharm. Soc. 61 (1972).
4. T. P. SINGER, R. W. VAN KORFF, and D. L. MURPHY (*Editors*). Monoamine oxidase: structure, function, and altered functions. Academic Press, New York. 1979.
5. I. G. DRAGANIĆ and Z. D. DRAGANIĆ. The radiation chemistry of water. Academic Press, New York. 1971.
6. G. D. ADAMS and P. WARDMAN. Free radicals in biology. Vol. 3. *Edited by* M. Pryor. Academic Press, New York. 1977. pp. 2–48.
7. T. C. BRUICE. Prog. Bioorg. Chem. **4**, 1 (1979).
8. E. L. LAND and A. J. SWALLOW. Biochemistry, **8**, 2117 (1969).
9. R. AHMAD and D. A. ARMSTRONG. Biochemistry, **21**, 5445 (1982).
10. M. S. GRODOWSKI, B. VEYRET, and K. WEISS. Photochem. Photobiol. **26**, 341 (1977).
11. D. J. FIFE and W. M. MOORE. Photochem. Photobiol. **29**, 43 (1979).
12. P. F. HEELIS, B. J. PARSONS, and G. O. PHILLIPS. Biochim. Biophys. Acta, **587**, 455 (1979).
13. P. F. HEELIS, B. J. PARSONS, G. O. PHILLIPS, and J. F. MCKELLAR. Photochem. Photobiol. **30**, 343 (1979).
14. R. TRABER, H. E. A. KRAMER, and P. HEMMERICH. Biochemistry, **21**, 1687 (1982).
15. P. NETA and R. W. FESSENDEN. J. Phys. Chem. **75**, 738 (1971).
16. E. HAYON and M. SIMIC. J. Am. Chem. Soc. **93**, 6781 (1971).
17. P. S. RAO and E. HAYON. Biochim. Biophys. Acta, **292**, 516 (1973).
18. S. M. BHATTACHARYYA and K. P. KUNDU. Radiat. Phys. Chem. **4**, 31 (1972).
19. Hand book of biochemistry. 2nd ed. 1973.
20. M. SIMIC, P. NETA, and E. HAYON. Int. J. Radiat. Phys. Chem. **3**, 309 (1971); N. GETOFF and F. SCHWORER. Int. J. Radiat. Phys. Chem. **5**, 101 (1973).
21. A. J. ELLIOT, F. WILKINSON, and D. A. ARMSTRONG. Int. J. Rad. Biol. **38**, 1 (1980).
22. R. H. SCHULER, L. K. PATTERSON, and E. JANATA. J. Phys. Chem. **84**, 2089 (1980).
23. Z. D. DRAGANIĆ and I. G. DRAGANIĆ. J. Phys. Chem. **75**, 3950 (1971); **77**, 765 (1973).
24. C. G. HATCHARD and C. A. PARKER. Proc. R. Soc. A **235**, 518 (1956).
25. P. S. SURDHAR, R. AHMAD, and D. A. ARMSTRONG. Can. J. Chem. **62**, 580 (1984), and unpublished results.
26. L.-S. L. YEH and L. L. INGRAM. Flavins and flavoproteins. *Edited by* T. P. Singer. Elsevier, Amsterdam. 1976. p. 765.
27. C. SALET, E. J. LAND, and R. SANTUS. Photochem. Photobiol. **33**, 753 (1981).
28. R. AHMAD, WU ZHENNAN, and D. A. ARMSTRONG. Biochemistry, **22**, 1806 (1983).
29. J. S. ARMSTRONG, P. HEMMERICH, and R. TRABER. Photochem. Photobiol. **35**, 747 (1982).
30. W. M. GARRISON. Reaction mechanism in the radiolysis of peptides, polypeptides and proteins I reaction of the peptide main-chain in model systems. Technical Information Department, Lawrence Berkeley Laboratory, University of California, Berkeley, CA.
31. C. L. GREENSTOCK. The chemistry of amine, nitroso and nitro compounds and their derivative. *Edited by* S. Patai. John Wiley and Sons, New York. 1982.
32. A. S. NAZRAN and D. GRILLER. J. Am. Chem. Soc. **105**, 1970 (1983).

Raman intensity calculations with the CNDO method. Part III: *N*,*N*-dimethylamide – water complexes

EDUARD D. SCHMID AND ELEONORE BRODBEK

Institut für Physikalische Chemie der Universität Freiburg, Albertstrasse 23a, 7800 Freiburg, Federal Republic of Germany

Received June 1, 1984

This paper is dedicated to Professor Camille Sandorfy on the occasion of his 65th birthday

EDWARD D. SCHMID and ELEONORE BRODBEK. Can. J. Chem. **63**, 1365 (1985).

Absolute differential Raman scattering coefficients of hydrogen bonded *N*,*N*-dimethylformamide (DMF) – water complexes and a *N*,*N*-dimethylacetamide (DMA) – water complex are calculated with a variational method within the CNDO approximation using an extended basis set. Changes of Raman intensities caused by intermolecular interactions are modeled in our Raman intensity calculations and the calculated intensities of the amide I (C=O stretching), OCN bending, and N—(Me)$_2$ stretching vibration of the DMF (and DMA) – water complexes are compared with the experimental absolute Raman intensities of DMF and DMA dissolved in water. The calculated Raman intensities of characteristic normal modes of DMF and DMA and their 1:2 amide–water model are in good agreement with the experimental data. The results show that it is possible to obtain qualitative information on solute–solvent interactions from Raman intensity calculations of complex molecular systems like hydrated DMF and DMA.

EDWARD D. SCHMID et ELEONORE BRODBEK. Can. J. Chem. **63**, 1365 (1985).

Faisant appel à une méthode variationnelle, dans les limites de l'approximation DNDO et à l'aide d'un ensemble de base étendu, on a calculé les coefficients absolus de dispersion Raman différentielle des complexes de *N*,*N*-diméthylformamide (DMF) – eau et d'un complexe de *N*,*N*-diméthylacétamide (DMA) – eau comportant des liaisons hydrogènes. Les changements dans les intensités Raman qui sont causés par des interactions intermoléculaires sont insérés dans notre modèle de calculs des intensités Raman; on compare les intensités calculées pour l'amide I (élongation C=O), la déformation OCN et vibration d'élongation N—(CH$_3$)$_2$ des complexes DMF (et DMA) – eau avec les intensitiés expérimentales Raman absolues de la DMF et de la DMA dissoutes dans l'eau. Les intensités Raman calculées pour les modes normaux caractéristiques de la DMF, de la DMA et de leur modèle 1:2 amide–eau sont en bon accord avec les données expérimentales. Les résultats montrent qu'il est possible d'obtenir des informations qualitatives sur les interactions soluté–solvant à partir de calculs d'intensité Raman sur des systèmes comme la DMF et la DMA hydratées.

[Traduit par le journal]

I. Introduction

Recently it has been shown that it is possible to predict with considerable accuracy absolute Raman intensities of diatomic molecules like H_2, N_2, CO, Cl_2, HCl, and HF (1, 2). These predictions are made by using normal coordinate analysis based on empirical or *ab initio* calculated force constants and intensity parameters calculated by *ab initio* methods. Absolute Raman intensities for molecules larger than diatomic molecules are also calculated with *ab initio* methods for H_2O, NH_3, CH_4, C_2H_4 (2–5). Since the experimental data are often incompletely determined, only a part of the predicted spectra can be compared with the experiment. It is important to realize that the predicted Raman intensities of these small molecules are in agreement with the experimental intensities of the isolated molecule within a factor of two.

The aim of our Raman studies is to comprehend molecular interactions via a comparison of predicted and experimental absolute Raman intensities. Our experimental investigations of substituent effects on benzene derivatives (6, 7) and solvent effects on the Raman intensities of numerous substrate molecules (8) have shown that the Raman intensity is very sensitive to molecular interactions. These studies represent a challenge with respect to extension of Raman intensity calculations to larger molecules (>6 atoms) and with respect to elucidation of effects of intermolecular interactions with these computations. In order to understand the effect of intermolecular interactions on the spectrum of a molecule it is important first to understand the spectrum of the isolated molecule. Calculations of absolute Raman intensities of larger molecules were performed for benzene (9), but only within the semiempirical CNDO approximation (10) with an extended basis set. *Ab initio* calculations of Raman intensities for this type of molecule are at present too extensive. The experimental intensities of benzene in the gas phase and the calculated non-resonant absolute Raman intensities of the 3032 cm^{-1} and 992 cm^{-1} vibrations are in good agreement. This might be an indication that Raman intensities of larger molecules (>6 atoms) can be calculated with the CNDO method with an extended basis set. We adopted this CNDO program developed by E. N. Svendsen *et al.* (11, 12) without changing any parameter of the CNDO method, and calculated the absolute intensities of the in-plane vibrations of formamide (13), and of DMF, and DMA (14). The predicted Raman intensities were compared with experimental intensities of these amides dissolved in an "inert" solvent (carbon tetrachloride) and the agreement is within a factor of two. Raman intensities of the gas phase or of matrix isolated molecules are not available.

Encouraged by this success, we extend our Raman intensity calculations to study intermolecular interactions. We have two reasons to calculate Raman intensities of amide–water complexes. First, we know from our experimental Raman studies that water as a solvent shows the most pronounced intensity change relative to an inert solvent. Second, the amide–water interaction is predominantly determined by hydrogen bonding and this specific interaction can be more easily taken into account in the calculation than the numerous solvent polarity–polarizability effects. The Raman intensity calculations of the DMF (DMA) – water complexes are compared with experimental data for the characteristic modes of DMF (DMA) dissolved in water: the amide I (C=O stretching), δOCN bending, and νN—(Me)$_2$ stretching vibrations. The results of these investigations are reviewed in this paper.

II. CNDO calculations

The polarizabilities and absolute differential Raman scattering coefficients are computed with a variational method which has been applied in previous calculations (9, 11, 13, 14). The valence basis set of the CNDO approximation is extended with polarization functions. The hydrogen atoms are defined with *s*- and *p*-functions. Similarly, *d*-functions are added to the first row elements. A description of this Raman intensity calculation method has been given in previous papers (9, 11, 13).

The absolute differential scattering coefficient for observation at right angles to the laser beam using linear polarized light is defined (17) as:

$$[1] \quad \frac{d\sigma}{d\Omega} = \frac{(2\pi)^4}{45} \cdot \frac{(\nu_0 - \nu_j)^4 g_j}{1 - \exp(-hc\nu_j/kT)} \cdot \frac{h}{8\pi^2 c\nu_j} \times (45\bar{\alpha}_j'^2 + 7\gamma_j'^2)$$

$\bar{\alpha}_j'$ and γ_j' are the derivatives of the mean polarizability and the anisotropy with respect to the *j*'th normal coordinate. Here, g_j denotes the degree of degeneracy of the normal mode ν_j, h Planck's constant, c the velocity of light in a vacuum, k Boltzmann's constant, and T the absolute temperature.

The experimental Raman intensities are determined relative to the ν_1 band of CCl_4 at 469 cm^{-1}. The conversion of the relative Raman intensities S_j into absolute differential Raman scattering coefficients $d\sigma/d\Omega$ is performed with the absolute value of $\frac{d\sigma}{d\Omega}(\nu_0 - \nu_1)^{-4} = 137 \times 10^{-48}$ cm^6 for the ν_1 band of CCl_4 measured by Kato and Takuma (27):

$$[2] \quad \left(\frac{d\sigma}{d\Omega}\right)_j = S_j \cdot 137 \cdot 10^{-48}\ \text{cm}^6\ (\nu_0 - \nu_j)^4 \cdot \frac{\nu_1}{\nu_j} \cdot \frac{g_j}{g_1} \cdot \frac{1 - \exp(-hc\nu_1)/kT}{1 - \exp(-hc\nu_j/kT}$$

The electron densities and the dipole moments for the equilibrium geometries are calculated with the CNDO method (9) with only a valence basis set, since this method already gives reliable results for first-order quantities. We have not fitted any parameter in the CNDO method to our problems. The empirical parameters defined by Pople and Beveridge (10) are used.

III. *N,N*-Dimethylformamide – water complexes

(a) *Equilibrium geometry*

Structural studies of amide–water complexes predict that the oxygen atom in amides can accommodate two water molecules (16, 19–22). *Ab initio* calculations of hydrogen bond energies (20, 21) show that the hydrogen bond is formed between the directed lone pairs of electrons on the oxygen atom in amides and two water molecules. This model of a 1:2 amide–water complex seems to reflect an important part of the amide–water interaction. Pullman *et al.* (20, 23) made explicit computations with a third H_2O molecule and found that it is bound to one of the two water molecules of such a 1:2 amide–water complex. The interaction of water with amide molecules through the intermediacy of a second water molecule reflects effects from the second hydration shell.

There is also a possibility of water hydrogen bonding to the π-system of amides. Calculations of Kollmann and co-workers (21) and Schreiner and Kern (22) indicate that the interaction with the π-system would occur when the water molecule is located perpendicular to the OCN plane at the oxygen atom of the amide molecule. But inclusion of further water molecules at the oxygen atom of the amide molecule weakens the interaction between the π-system and H_2O.

A 1:1 amide–water complex can also be considered as an interaction model complex (18).[1] But this complex seems not to exist actually in nature, since the binding energy between one water molecule and the amide molecule is much smaller than in the 1:2 amide–water complex. The O—H bond of a H_2O molecule would be directed along the C═O bond of the amide molecule bisecting the angle of the lone pairs of the C═O bond. This 1:1 amide–water complex can be considered as a test of the sensitivity of the Raman intensity calculation to distinguish between different interaction models.

All these studies on amide–water complexes were performed with formamide, *N*-methylformamide (NMF), and *N*-methylacetamide (NMA). No explicit models for DMF–water complexes or DMA–water complexes are available. Therefore we constructed three DMF–water complexes which are based on the results of the discussed amide–water models.

(1) A 1:2 DMF–water complex (Fig. 1*c*) where two water molecules take part in the formation of linear hydrogen bonds with the oxygen atom of DMF. The hydrogen bond lengths and the orientation of the two water molecules are taken from an *ab initio* study of *N*-methylformamide (NMF) – water complexes (19).

(2) A 1:3 DMF–water complex (Fig. 1*d*) which is based on a study of Pullman *et al.* (20) of formamide–water complexes. The third H_2O molecule is located at one of the water molecules of the 1:2 DMF–water complex.

(3) A 1:1 DMF–water complex (Fig. 1*b*) with a linear hydrogen bond between the O—H bond of H_2O and the C═O bond of DMF. The hydrogen bond length has been taken from *ab initio* calculations of a formamide–water comlex.[1]

Experimental geometries determined by electron diffraction were used for DMF (24) and H_2O (25). The methyl group "*cis*" to the C═O bond must be rotated in a staggered conformation with respect to the H_2O molecule at the oxygen atom of DMF to avoid steric interaction with water (22). The structural parameters of these complexes are listed in Table 1.

(b) *Normal coordinate analysis*

The normal coordinates are calculated with Wilson's GF-matrix method (15). The methyl groups and water molecules are considered as point masses. The approximation to consider H_2O as a point mass is justified, since the intramolecular vibrations of H_2O are not the subject of this study. We are interested in the effect of the hydrogen bond between DMF and the water molecules on the vibrations of DMF.

As a first step in our normal coordinate analysis of the 1:2 DMF–water complex we use the valence force field of the isolated DMF, which is reported in a previous paper (14), and an assumed hydrogen bond stretching force constant of 0.1 mdyne/Å. This force field is refined with experimental frequencies of DMF dissolved in water.[2] The fitted hydrogen bond stretching force constant of 0.23 mdyne/Å is in agreement with an *ab initio* calculated value of 0.27 mdyne/Å of a formamide–water hydrogen bond stretching force constant (16). This might be an indication that our force field is not far from the actual force field, which could be calculated by quantum mechanical procedures. The internal coordinate definitions

[1] R. Topsom, private communication.
[2] U. Hnida, private communication.

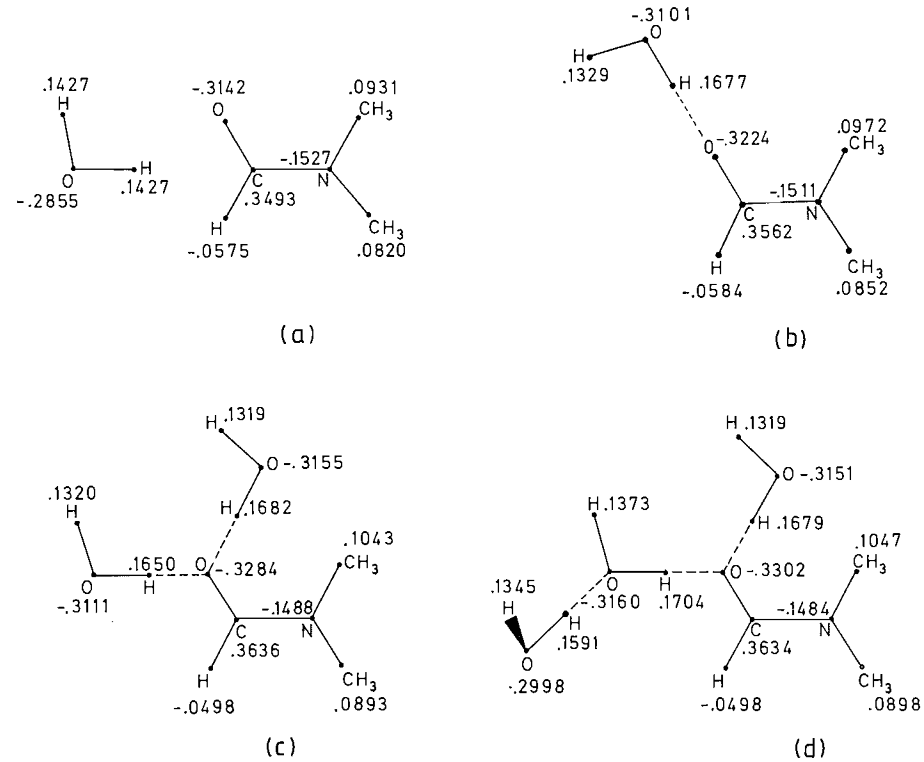

FIG. 1. Equilibrium geometries and electron densities of DMF and the DMF−water complexes. (a) Non-interacting DMF and H_2O molecules; (b) 1:1 DMF−water complex; (c) 1:2 DMF−water complex; (d) 1:3 DMF−water complex.

TABLE 1. Structural parameters of the DMF−water and DMA−water complexes

	DMF[a]		DMA[a]
rC—N	1.366		1.386
rC=O	1.291		1.225
rC—H	1.125		1.520
rN—Me[b]	1.459		1.469
∠OCN	124.600		121.800
∠HCN	112.700		114.100
∠CNMe[b]	121.400		119.700
Methyl group parameters[b]			
rC′—H	1.080		
∠NC′H	109.470		
Hydrogen bond parameters			
	DMF + H_2O[c]	DMF + $2H_2O$[d]	DMA + $2H_2O$[d]
$r(CH_3)_2NHCO{-}{-}H_1$	1.867	1.820	1.810
$r(CH_3)_2NHCO{-}{-}H_2$		1.850	1.840
$\angle COH_1$	180.000	117.000	121.000
$\angle COH_2$		135.000	138.000
Water parameters[e]			
rO—H	0.96		
∠HOH	104.50		
rO−−H[f]	2.00		

[a]Bond length in Å, angles in degrees, data from refs. 24 and 29.
[b]C_{3v} symmetry assumed; Me = methyl group.
[c]Data from footnote 1.
[d]Data from ref. 19.
[e]Data from ref. 25.
[f]Reference 30.

TABLE 2. Internal coordinate definitions[a]

1	νC—N	C—N stretching
2	νC=O	C=O stretching
3	νC—H	C—H stretching
4, 5	νN—Me	N—Me stretching
6, 7	νO- -H	Hydrogen bond stretching
8	δOCH	OCH deformation
9	δOCN	OCN deformation
10	δHCN	HCN deformation
11, 12	δCNMe	CNMe deformation
13	δMeNMe	MeNMe deformation
14	γC—H	C—H out-of-plane deformation
15, 16	γN—Me	N—Me out-of-plane deformation
17	τC—N	C—N torsion

[a]Me: methyl group.

TABLE 3. Valence force constants[a]

Force constant	DMF	DMF−water complex	DMA	DMA−water complex
$F_{1,1}$	6.200	6.017	6.050	6.050
$F_{2,2}$	8.060	7.909	8.060	7.303
$F_{3,3}$	4.400	4.400	4.500	4.353
$F_{4,4}$, $F_{5,5}$	5.000	4.963	4.800	4.800
$F_{6,6}$, $F_{7,7}$		0.230		0.230
$F_{2,6}$, $F_{2,7}$	—	−0.043	—	−0.043
$F_{8,8}$	0.700	0.924	0.800	0.792
$F_{9,9}$	1.700	1.673	1.770	1.600
$F_{10,10}$	0.954	0.562	1.270	1.100
$F_{11,11}$, $F_{12,12}$	1.750	1.727	1.000	1.000
$F_{13,13}$	0.440	0.446	0.440	0.440
$F_{14,14}$	0.430	0.430	—	—
$F_{15,15}$, $F_{16,16}$	0.004	0.004	0.004	0.004
$F_{17,17}$	0.490	0.490	0.490	0.490
$F_{1,2}$	−0.061	−0.061	−0.026	−0.016
$F_{1,9}$	−0.155	−0.112	0.150	0.150
$F_{1,10}$	0.818	0.749	0.788	0.788
$F_{1,11}$, $F_{1,12}$	0.053	0.065	0.036	0.036
$F_{8,9}$	0.061	0.052	−0.043	−0.043
$F_{8,10}$	0.053	0	0.046	0.069
$F_{11,13}$, $F_{12,13}$	0.320	0.305	0.027	0.027

[a]Force constants in internal coordinates. Units: stretch in mdyne/Å, bend in mdyne Å/rad^2, stretch−bend interaction in mdyne/rad, torsion in mdyne Å/rad^2.

(Table 2), the fitted force field (Table 3), and the assignments of the normal vibrations of the DMF−water complex which are considered in the Raman intensity calculations are listed in Table 4.

(c) *Results and discussion of the normal coordinate analysis and the Raman intensity calculation*

The valence force field (Table 3) of DMF changes in some force constants when an intermolecular stretching force constant between DMF and water is assumed. The C=O stretching and the HCN bending force constants decrease due to hydrogen bonding and the calculated frequency of the amide I (C=O stretching) vibration shifts from 1712 cm^{-1} in DMF to 1658 cm^{-1} in the DMF−water complexes. This corresponds to the experimental frequency shift of the amide I mode of DMF from 1684 cm^{-1} to 1655 cm^{-1} when the solvent varies from carbon tetrachloride to water. The experimental frequencies of the δ OCN bending and νN—(Me)$_2$ symmetrical stretching vibrations remain almost unchanged in these two solvents. This is also confirmed by the normal coordinate analysis where considerable changes are calculated only for the frequency and potential energy distribution (PED) of the amide I vibration (Table 4).

Based on our normal coordinate analysis and the intensity calculation with the variational method, we predict Raman intensities of DMF−water complexes for three amide vibrations. The predicted and experimental values are listed in Table 5. The predicted intensities of the isolated DMF molecule and measured intensities of DMF dissolved in CCl_4 are in agreement within a factor of two (Table 5). Calculated and experimental Raman intensities can be directly compared, since both of them are independent of the resonance denominator of the polarizability tensor.

The same agreement as for the isolated molecules has been obtained between predicted intensities of the 1:2 DMF−water complex and the experimental Raman intensities of DMF dissolved in H_2O (Table 5). Considerable changes in the Raman intensities of DMF due to the DMF−water interaction are observed for the amide I band. If we compare the intensity of the amide I vibration of the isolated DMF, or rather DMF dissolved in CCl_4, with the 1:2 DMF−water complex, or rather DMF dissolved in water, there exists a pronounced decrease of the Raman intensity by a factor larger than 4. The predicted intensities of the amide I mode of the 1:2 DMF−water and 1:3 DMF−water complexes are equal within the accuracy of the calculation.

To check the sensitivity of the Raman intensity calculation with respect to the intermolecular interaction models we predicted the force field and the Raman intensity of the amide I vibration of the 1:1 DMF−water complex. The result of the normal coordinate analysis shows that the calculated force field and PED for the 1:1 complex are the same as for the 1:2 complex. As shown in Table 5, the calculated Raman intensity of the amide I vibration of the 1:1 DMF−water complex is smaller by 1/10 than that of the 1:2 DMF−water complex, and a factor 1/6 smaller than the experimental value. Though the accuracy of such a small value is not assessible, it could be concluded at least qualitatively that the 1:1 complex is not favoured to describe the intermolecular interaction between amide and water.

The experimental and calculated Raman intensity of the νN—(Me)$_2$ stretching vibration increases slightly. Because the normal coordinate and frequency are nearly identical for DMF and the DMF−water complex, a possible explanation of this intensity shift is the decrease of negative charge in the N—Me bond of the complex, caused by an electron loss at the nitrogen atom (Fig. 1).

The calculated δ OCN band intensity remains unchanged when intermolecular interaction between DMF and water is assumed. The normal coordinate of this mode, as well as the derivatives of the polarizabilities with respect to the normal coordinate, show no evident changes compared to the DMF monomer.

Because of the approximations of the CNDO method and the arbitrariness of the experimental force constants used in the Raman intensity calculation, the absolute values of our calculated Raman scattering coefficients have predominantly qualitative significance. But the results suggest that the simplest interaction model has to consider two H_2O molecules at the oxygen of DMF. The following discussion will show that our findings are consistent with other physical properties of

TABLE 4. Normal modes of DMF and DMF−water complex (cm^{-1})

	ν_{obs}	ν_{cal}	PED (%)	Assignment
DMF	1684	1712	$F_{10,10}$ (36), $F_{2,2}$ (32), $F_{8,8}$ (15)	amide I
	866	880	$F_{4,4}$ (71), $F_{9,9}$ (16)	ν_sN—(Me)$_2$
	660	615	$F_{4,4}$ (33), $F_{1,1}$ (24), $F_{11,11}$ (23), $F_{9,9}$ (13)	δOCN
DMF+H_2O	1655	1659	$F_{2,2}$ (40), $F_{8,8}$ (24), $F_{10,10}$ (20), $F_{1,1}$ (10)	amide I
	864	868	$F_{4,4}$ (70), $F_{9,9}$ (16)	ν_sN—(Me)$_2$
	663	609	$F_{4,4}$ (33), $F_{1,1}$ (24), $F_{11,11}$ (25), $F_{9,9}$ (12)	δOCN
DMF+2H_2O[a]	1655	1658	$F_{2,2}$ (39), $F_{8,8}$ (25), $F_{10,10}$ (21), $F_{1,1}$ (10)	amide I
	864	869	$F_{4,4}$ (70), $F_{9,9}$ (16)	ν_sN—(Me)$_2$
	663	606	$F_{4,4}$ (33), $F_{1,1}$ (25), $F_{11,11}$ (24), $F_{9,9}$ (12), $F_{2,2}$ (11)	δOCN

[a]The results DMF+3H_2O are identical with those of DMF+2H_2O.

TABLE 5. Absolute differential Raman scattering coefficients

Mode	ν_{obs} (cm^{-1})	Calcd. model	$\left(\frac{d\sigma}{d\Omega}\right)_{calc}$ (10^{-30} cm^2)	Solute/solvent	$\left(\frac{d\sigma}{d\Omega}\right)_{exp}$ (10^{-30} cm^2)
Amide I	1684	DMF	3.816	DMF/CCl_4	3.813
ν_sN—(Me)$_2$	865		1.037		2.262
δOCN	660		2.007		2.320
Amide I	1655	1:2 DMF−water	1.021	DMF/H_2O	0.675
ν_sN—(Me)$_2$	864		3.822		3.655
δOCN	663		2.283		2.725
Amide I	1655	1:3 DMF−water	0.858	DMF/H_2O	0.675
Amide I	1655	1:1 DMF−water	0.102	DMF/H_2O	0.675
Amide I	1660	DMA	3.297	DMA/CCl_4	4.069
ν_sN—(Me)$_2$	730		3.707		7.223
δOCN	590		0.609		0.635
Amide I	1605	1:2 DMA−water	0.629	DMA/H_2O	0.324
ν_sN—(Me)$_2$	743		3.886		5.794
δOCN	595		0.488		0.619

TABLE 6. Binding energies, dipole moments, and polarizabilities

	ΔE^a	μ^b	α_{xx}	α_{yy}	α_{zz}	$\bar{\alpha}^c$
DMF		3.45	11.190	7.684	10.367	9.747
DMF+H_2O	6.270	4.92	12.696	8.270	10.871	10.612
DMF+2H_2O	6.803	2.99	13.598	8.508	12.421	11.509
DMF+3H_2O	6.082	3.61	13.788	8.586	12.884	11.752
DMA		3.61	13.167	9.082	12.277	11.509
DMA+2H_2O	6.866	3.28	15.669	10.510	14.649	13.609

[a]ΔE: Binding energy per H_2O. Unit: kcal/mol.
[b]Calculated with the finite field perturbation (FFP) method and a valence basis set. Unit: Debye.
[c]Calculated with the variational method (VM) and an extended basis set. Unit: Å^3. $\bar{\alpha} = 1/3(\alpha_{xx} + \alpha_{yy} + \alpha_{zz})$.

amide−water complexes.

In the models of the 1:2 and 1:3 DMF−water complexes, hydrogen bonds arise between the lone pairs of electrons on the oxygen atom of DMF and the water molecules (Fig. 1*c*, 1*d*). Our electron density calculation shows that negative charge is moved through the DMF molecule to the oxygen atom in DMF. The nitrogen and carbon atoms of DMF and the hydrogen bonded H-atoms of water lose electrons and this negative charge is moved to all oxygens of the complex and the non-bonded H atoms of water. This is in agreement with the "pileup effect" of negative charge to the donor atom and the "spillover effect" of negative charge from the acceptor atom (26).

The additional water molecule in the 1:3 DMF−water complex acts as proton donor to a H_2O molecule, which in turn acts as proton donor to the C═O bond of DMF (Fig. 1*d*). The charge transfer from the DMF molecule to the water dimer increases, compared to the charge transfer induced by one water molecule.

The polarizabilities of the 1:2 and 1:3 DMF−water complexes increase, compared to the DMF monomer (Table 6). The calculated dipole moments of the 1:2 and 1:3 DMF−water complexes are smaller than the dipole moment of DMF (Table 6). The partial C═O bond order decreases with growing number of H_2O molecules in the complex. The smaller overlap of $2p\pi$ atomic orbitals of the C═O bond of the complexes, compared with the $2p\pi$ atomic orbital overlap of the C═O bond of DMF, is responsible for the decreasing bond order. These results are consistent with other calculations of electron density distributions of amide−water complexes (16, 19−22).

The decrease of C═O bond order indicates that the polarizability in the carbonyl group is reduced. Moreover, the normal coordinate of the amide I vibration which is located in the OCN group is influenced by hydrogen bonding. Both effects are responsible for the smaller Raman intensity of the amide I (C═O stretching) band of the DMF−water complex. This is consistent with the empirical rule that bond order and Raman intensity of a vibration which is located in this bond behave in the same way (28).

TABLE 7. Normal modes of DMA and the DMA−water complex (cm^{-1})

	ν_{obs}	ν_{cal}	PED (%)	Assignment
DMA	1660	1666	$F_{2,2}$ (49), $F_{3,3}$ (16), $F_{9,9}$ (11)	νC=O amide I
	730	682	$F_{4,4}$ (32), $F_{3,3}$ (31), $F_{1,1}$ (21), $F_{2,2}$ (10)	νN—(Me)$_2$
	590	568	$F_{9,9}$ (33), $F_{4,4}$ (19), $F_{3,3}$ (15)	δOCN in-plane bending
DMA+2H_2O	1605	1609	$F_{2,2}$ (50), $F_{3,3}$ (14), $F_{9,9}$ (9)	νC=O amide I
	743	685	$F_{4,4}$ (48), $F_{3,3}$ (19), $F_{1,1}$ (18), $F_{2,2}$ (9)	νN—(Me)$_2$
	595	537	$F_{9,9}$ (36), $F_{4,4}$ (16), $F_{3,3}$ (19), $F_{11,11}$ (18)	δOCN in-plane bending
		169	$F_{6,6}$ (85), $F_{9,9}$ (7)	ν_{σ}^{s} hydrogen bond stretching
		151	$F_{6,6}$ (87), $F_{9,9}$ (5)	ν_{σ}^{as} hydrogen bond stretching

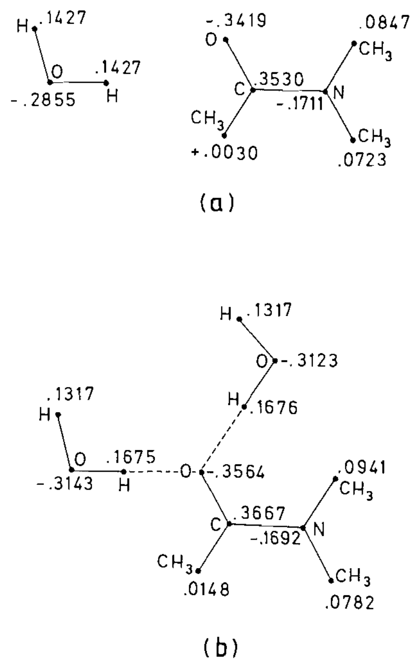

FIG. 2. Equilibrium geometries and electron densities of DMA and the DMA−water complex. (a) Non-interacting DMA and H_2O molecules; (b) 1:2 DMA−water complex.

IV. *N,N*-Dimethylacetamide − water complexes

(a) *Equilibrium geometry*

In the 1:2 DMA−water model considered (Fig. 2), two H_2O molecules form hydrogen bonds with the oxygen of the DMA analog to the 1:2 DMF−water complex. The hydrogen bond length and the orientation of the two water molecules are taken from *ab initio* calculations (19). These structural parameters are different from those of the 1:2 DMF−water complex. The experimental geometries of DMA (29) and H_2O (25), determined by electron diffraction, are chosen and have not been modified through the calculation. The methyl groups of the DMA−water complex are staggered to the C=O bond to avoid steric interaction with the two water molecules (22). All structural parameters are listed in Table 1.

(b) *Normal vibrations and Raman intensities*

The force constants of the isolated DMA (14) and the hydrogen bond stretching force constant predicted for the DMF−water complex are taken as the force field for the normal coordinate analysis of the 1:2 DMA−water complex. Only the force constants of the DMA part of the force field are fitted with experimental frequencies of DMA dissolved in water.[2]

Essential wavenumber shifts of 55 cm^{-1} are observed for the amide I mode of DMA if the solvent changes from carbon tetrachloride to water (Table 7). The normal coordinate analysis also shows a decrease of the amide I wavenumber of 57 cm^{-1} and no important changes for the other vibrations of the DMA−water complex. Since the potential energy distribution (PED) remains nearly unchanged for all considered modes of the DMA−water complex, compared to the DMA monomer (Table 7), the reason for the wavenumber shift of the amide I vibration is the decrease of the C=O stretching force constant by about 10% (Table 3). The C=O stretching force constant does not contribute to the PED of the δOCN bending and νN—Me stretching vibration.

The measured Raman intensity of the amide I mode of the DMA decreases from 4.069×10^{-30} cm^2 in carbon tetrachloride to 0.324×10^{-30} cm^2 in water (Table 5). Hydrogen bonding at the oxygen of DMA contributes to a decrease of C=O bond order and C=O stretching force constant. This indicates a loss of double bond character of the C=O bond and is also reflected in the smaller wavenumber and Raman intensity of the amide I vibration of the DMA−water complex, compared to the DMA molecule (Table 5).

The absolute differential scattering cross sections of the δOCN bending and νN—(Me)$_2$ stretching vibrations are not changed if DMA is dissolved in water (Table 5). This is in agreement with the normal coordinate analysis and the Raman intensity calculation of these two vibrations of DMA and the 1:2 DMA−water complex.

V. Conclusions

Hydrogen bonding between *N,N*-disubstituted amides (DMF, DMA) and water causes a charge transfer in the amide molecule which can be described with the resonance structures:

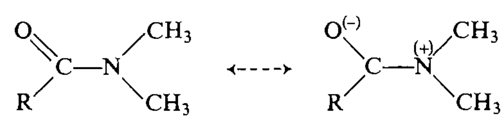

If one compares the gross electronic charges of the atoms of DMF and DMA in the 1:2 amide−water complex (Figs. 1 and 2) it is found that the carbon methyl group of DMA supplies electrons to the complex, and therefore the average binding energy per H_2O molecule is larger than in the DMF−water complex (Table 6). The stronger interaction between DMA and water causes a larger decrease of the C=O bond order and the absolute differential Raman scattering coefficient of the amide I (C=O stretching) mode in the DMA−water complex, compared to the DMF−water complex (Table 5).

The results of the Raman intensity calculation of amide−water complexes show that the variational method and the

CNDO approximation supply reliable absolute Raman intensities of complex molecular systems. The agreement between measured and calculated Raman intensities makes it possible to correlate the changes in Raman intensities with intermolecular interactions which are considered in a 1:2 amide–water model complex. But the limitations of the CNDO method and the arbitrariness inherent in any force field not supported by accurate quantum mechanical force constant calculations permit only a qualitative, rather than a quantitative, description of the solute–solvent interactions. An improvement of the Raman intensity calculation can surely be achieved by quantum mechanical force field methods.

This is a first investigation of intermolecular interactions by means of Raman intensity calculations. Such studies of intermolecular interaction via Raman intensity calculations have not been published up to now.

Acknowledgements

We are grateful to Ulrich Hnida for experimental work and the Deutsche Forschungsgemeinschaft for financial support.

1. E. N. SVENDSEN and J. ODDERSCHEDE. J. Chem. Phys. **71**, 3000 (1979).
2. C. V. HEMERT and C. E. BLOM. Mol. Phys. **43**, 229 (1981).
3. C. E. BLOM and C. ALTONA. Mol. Phys. **34**, 177 (1977).
4. A. KORMORNICKI and J. W. MCIVER. J. Chem. Phys. **70**, 2014 (1979).
5. D. R. FREDKIN, A. KORMORNICKI, S. R. WHITE, and K. R. WILSON. J. Chem. Phys. **78**, 7077 (1983).
6. E. D. SCHMID and R. D. TOPSOM. J. Am. Chem. Soc. **103**, 1628 (1981).
7. E. D. SCHMID and R. D. TOPSOM. J. Raman Spectrosc. **14**, 191 (1983).
8. M. MOSCHALLSKI. Dissertation, Freiburg. 1984.
9. E. N. SVENDSEN. Proc. VIIth Int. Conf. Raman. Spectroscopy, Ottawa, Canada. 1980. p. 284.
10. J. A. POPLE and D. A. BEVERIDGE. Approximate molecular orbital theory. McGraw–Hill, New York. 1970.
11. E. N. SVENDSEN and H. F. HAMEKA. J. Chem. Phys. **62**, 2760 (1975); Int. J. Quant. Chem. **10**, 249 (1976); **11**, 129 (1977).
12. E. N. SVENDSEN and T. STROYER-HANSEN. Theor. Chem. Acta, **45**, 53 (1977); Int. J. Quant. Chem. **13**, 235 (1978); E. N. SVENDSEN, T. STROYER-HANSEN, and J. TANGAA. J. Mol. Spectrosc. **77**, 244 (1979).
13. E. D. SCHMID and E. BRODBEK. J. Chem. Phys. **78**, 1117 (1983).
14. E. D. SCHMID and E. BRODBEK. Theochem. **108**, 17 (1984).
15. H. FUHRER, K. B. KARTHA, K. G. KIDD, P. J. KRÜGER, and H. H. MANTSCH. N.R.C.C. Bulletin No. 15 (1976).
16. T. OTTERSEN and H. H. JENSEN. J. Mol. Struct. **26**, 375 (1975); **28**, 223 (1975); T. OTTERSEN and A. HEIBERG. Adv. Mol. Relaxation Processess, **8**, 305 (1976).
17. A. D. LONG. Raman spectroscopy. McGraw–Hill, New York. (1977).
18. C. N. RAO, P. C. DURIVEDI, A. GUPTA, H. S. RANDHAWA, H. RATAJCZAK, M. M. SZCZESNIAK, K. ROMANOWSK, and W. J. ORVILLE-THOMAS. J. Mol. Struct. **30**, 271 (1976).
19. J. E. DEL BENE. J. Am. Chem. Soc. **100**, 1387 (1978).
20. A. PULLMAN, H. BERTHOD, C. GIESSNER-PRETTRE, J. F. HINTON, and D. HARPOOL. J. Am. Chem. Soc. **100**, 3991 (1978).
21. A. JOHANSSON, P. KOLLMAN, S. ROTHENBERG, and J. MCKELVEY. J. Am. Chem. Soc. **96**, 3794 (1974).
22. S. SCHREINER and C. W. KERN. J. Am. Chem. Soc. **99**, 7042 (1977).
23. A. PULLMAN. Bull. Soc. Chim. Belg. **85**, 963 (1976).
24. M. KITANO and K. KUCHITSU. Bull. Chem. Soc. Jpn. **47**, 631 (1974).
25. S. SHIBATA and L. S. BARTELL. J. Chem. Phys. **42**, 1147 (1965).
26. V. GUTMANN. The donor–acceptor approach to molecular interactions. Plenum Press, New York. (1978).
27. Y. KATO and H. TAKUMA. J. Chem. Phys. **54**, 5398 (1971).
28. R. E. HESTER. *In* Raman spectroscopy. *Edited by* H. A. Szymanski. Plenum Press, New York. 1967.
29. M. KITANO, T. FUKUYAMA, and K. KUCHITSU. Bull. Chem. Soc. Jpn. **46**, 384 (1973).
30. E. CLEMENTI and P. HABITZ. J. Am. Chem. Soc. **87**, 2815 (1983).

A blind chemist's approach to automated scientific information

JEAN-PIERRE CARTIER[1,2] AND FRANCINE PAQUIN
Département de chimie, Université du Québec à Montréal, Montréal (Qué.), Canada H3C 3P8

Received June 12, 1984

This paper is dedicated to Professor Camille Sandorfy on the occasion of his 65th birthday

JEAN-PIERRE CARTIER and FRANCINE PAQUIN. Can. J. Chem. **63**, 1372 (1985).

Computer access to chemical information by a blind chemist is made possible with a VersaBraille system (Braille Information Processor). The CAS database of the DIALOG system is used in this updating assay. Preliminary trials showed the need to establish a rigorous procedure to avoid loss of data. In this study, a functional method is suggested as a substratum to circumvent costly problems.

JEAN-PIERRE CARTIER et FRANCINE PAQUIN. Can. J. Chem. **63**, 1372 (1985).

Grâce au VersaBraille (Processeur d'Information en Braille), l'accès aux bases de données est maintenant devenu possible pour le chimiste handicapé de la vue. Les séances de mise à jour, sont ici faites en utilisant le fichier CAS du réseau DIALOG. Des tentatives préliminaires ont démontré la nécessité d'utiliser une procédure rigoureusement définie, afin d'éviter la perte de données. La présente étude veut proposer une méthode fonctionnelle, dont le substratum tend à circonvenir des problèmes coûteux.

[Traduit par le journal]

Introduction

The time-consuming task of updating bibliography has long been an accepted fact of a chemist's life. In a certain way, the printed form of the Chemical Abstracts facilitates access to scientific information. In 1970, more than 3×10^7 printed pages (1) of scientific papers were published. The chemist, who wishes then to be informed of the latest scientific results, faces an almost impossible task. Today, certain computer networks (2) offer a personal and instantaneous access to chemical data.

Now, consider what would happen if the researcher is blind. Years ago, for many, blindness would have been treated as a catastrophe. However, technological developments (3, 4) may favor a "detour" (5) and allow for successful achievement (6). The advent of braille information processors places this chemist in a "quasi-normal" state of endeavor.

The objectives of this paper are twofold: to illustrate the facility of communication between the VersaBraille system (7) and the DATAPAC/DIALOG network; to emphasize the necessity of a procedure to avoid loss of data.

Experimental

The apparatus used in this updating experiment consists of a braille information processor, a teleprinter with a keyboard, and an acoustic coupler or MODEM. The braille information processor is a model P2 VersaBraille, version C2. The procedure described below worked equally well with earlier versions, which are presented elsewhere (3, 8). Both the VersaBraille and the teleprinter are connected to the MODEM by a "Y" cable (9). This provides a means to verify the "loss of data" and allows each unit to be enabled separately or simultaneously. Once the configuration control parameters are fixed for compatibility with the DIALOG system, the VersaBraille is then set in remote mode. It is understood that the operator, being blind, is at ease with the remote mode and computer braille (10). On some occasions, a knowledge of the teleprinter's keyboard did appear helpful. In this case, the important keys were marked with transparent braille-embossed DYMO tape.

Results

The experimental assays on bibliographic updating with a database gave rise to the following procedure. In this procedure, the commands and search expressions are exactly the same as specified in the GUIDE TO DIALOG SEARCHING (2). The difference resides only in their written form, which the blind operator enters in computer braille on the VersaBraille. Each element of the sequence (SIGNON, SEARCH, TYPE LOGOFF) has its own chapter on the braillecassette.

GETTING ONLINE or SIGNON needs no special action, except for the detection of the carrier light on the acoustic coupler or on the MODEM. This is accomplished with a light sensor (11) or with the Optacon (12). Once the network is chosen and the password entered, the operator may read rapidly the news and status messages. Normally, this information adds up to less than 1000 characters (a full page buffer in the VersaBraille). By pressing occasionally the "LOCATE" key, the operator can verify the fullness of the page buffer. When about 800 characters have been transmitted, he then saves the output on a new page of the braillecassette. The appearance of the prompt character indicates the end of this first chapter.

SEARCH is the title of the newly opened second chapter. It includes the request for connection to a specific file. In this case, chemical information is sought by the command BEGIN 311 (b 311). After the unit cost and the latest update, the prompt character reappears. Moving to the next blank page in this SEARCH chapter, the operator enters a maximum of five words chosen from his keyword strategy. These keywords were previously written on a paperbraille list. It is on this list that the set number and the number of records are assigned to each keyword as they are given. Here again, the operator verifies the character count. Using the "word" key, he scans the page and constructs a search expression. Returning to the current cursor position, the search expression is then entered. At this point, the user verifies the first records of this retrieval by writing the command: T Si/6/X (where T = TYPE; i = set number; 6 = format option; X = first records). If these records are not relevant, he then forms a different keyword combination. If the results of the search are pertinent, they are stored in a chapter called TYPE.

A new chapter, TYPE, is opened on the VersaBraille unit. The command, T Si/5/1 $- x$ (where x = number of the last record), lists the selected records. As the first lines are displayed, the received data are stored on the VersaBraille tape.

[1]Author to whom correspondence may be addressed.
[2]Operator of the VersaBraille unit.

During the automatic transfer, no scrolling occurs. The "LOCATE" key is then used to see if the data characters are still coming in. When the output is completed, the VersaBraille system is switched to operative function. If the search is continued, new chapters would be opened and executed: SEARCH2, TYPE2 as describd above.

LOGOFF is the name of the fourth and last chapter of the CA retrieval. It is also the command used to terminate the search session. Furthermore, if desired, the END/SAVE command is utilised to store the search strategy.

Discussion and conclusion

Two facts should be kept in mind as one reads through these lines. First, the operator types the entries in braille code, e.g., computer braille, which is translated to the ASCII data communication code. Thus, the VersaBraille system produces the same electronic signals as those from a standard terminal. Secondly, the display appears on a tactile array which is a 20-character window that can be moved through the page buffer.

The sequence described in the procedure is based on the methods for simulation (13). Obviously, online communication with a database requires careful planning. Therefore, it is necessary to inscribe the keywords and their priority in the SEARCH on a paperbraille list. This list is organized in such a way as to permit the subsequent inscription of the set numbers and their corresponding number of records.

The critical point, at which scrolling occurs most frequently, is the SEARCH section. The use of more than five keywords will also result in scrolling of information. And the operator is confronted with a large amount of data that causes confusion. Consequently, the utilization of the paperbraille list demands less concentration on his part, therefore, reducing the online cost of the search. However, the operator must be cautious to write and form the final search expression on his paperbraille list. This step eliminates the need to back scan the set combinations on the braillecassette.

If a pause is needed, the database offers certain options, such as a ten-minute hold or a temporary save. During this break, the paperbraille list can be reviewed with ease.

It was found in the TYPE section that an average of 75 lines at 30 cps were lost when the operator does a manual page advance. The change to automatic transfer mode prevents any loss of data.

Personal online searching of literature is an indispensable and powerful tool (14) to retrieve and update scientific information. During the past year, the CA SEARCH was done entirely with a VersaBraille unit and the DIALOG Information Retrieval Services. This automated method proved to be more efficient and more rapid than the search in the printed form of the CA. Nonetheless, the updating procedure is but one of the many applications of the VersaBraille system in the field of chemical research and education (15).

In the last ten years, many technological tools have enhanced the capabilities of the physically handicapped to fulfill the duties of a normal work load. Braille information processors, in this case the VersaBraille, offer a means for the blind worker to succeed on the same basis as his sighted colleagues. Recent developments in computer technology have broadened the horizon for many visually impaired individuals. Technology may resolve the numerous problems inherent in a physical handicap. However, a huge problem still remains unsolved; it concerns the discrimatory attitude as pointed out in the manual (16) of the ACS Committee on the Handicapped.

Acknowledgements

This work was financially supported by a grant from the FCAC (Formation de Chercheurs et Actions Concertées). The authors wish to acknowledge the support of the Département de chimie (UQAM). We also wish to thank Betacom, Mrs. Ulla de Stricker (DIALOG), and Mr. Serge Gagné for their technical support.

One of the authors (J.P.C.) is deeply grateful and indebted to Dr. Camille Sandorfy, to whom this article is dedicated. In 1960, in spite of his aquired blindness, J.P.C. was accepted as a graduate student under the tutorship of Dr. Sandorfy. His countless hours of discussion and encouragement became a stimulating factor in the pursuit of J.P.C.'s career.

1. Documentation et bibliothèque. Université Laval. **22**, 5 (1976).
2. DIALOG Information Retrieval Service. DIALOG Information Services, Palo Alto, CA. March, 1984.
3. B. GILBETT. Interface Age (USA), **4**, 44 (1979).
4. C. M. MELLOR. J. Visual Impairment Blindness, **73**, 339 (1979).
5. J. P. CARTIER. Moyens techniques et l'expertise dans le développement des qualités de l'handicapé de la vue. Annexe au Rapport Comité Consultatif SAS/MEQ, mars 1977. pp. 1–51.
6. R. L. RAWLS. Chem. Eng. News, **23**, 25 (1978).
7. Telesensory Systems Inc. The VersaBraille system. Mountain View, CA. 1983. pp. 1–31.
8. DIALOG Information Services, Monolog 2, Sept 1982.
9. P. JONES. Services de l'information (UQAM), 1982.
10. Telesensory Systems Inc. The VersaBraille system for the blind. Palo Alto, CA. 1983. Section V, p. 11.
11. D. TOMBAUGH. J. Chem. Educ. **58**, 222 (1981)
12. Telesensory Systems Inc. Optacon, A reading system for the blind. Palo Alto, CA. 1976 p. 5.
13. W. J. GRAYBEAL and UDO W. POOCH. Simulation: principal and methods. Winthrop, Cambridge. 1980 p. 249.
14. T. L. ISENHOUR (*Editor*). J. Chem. Inf. Comput. Sci. **23**, 2A (1983).
15. P. LYKOS (*Editor*). Personal computers in chemistry. John Wiley and Sons Inc., Toronto. 1981.
16. K. M. REESE (*Editor*). Teaching chemistry to physically handicapped students. Introduction. ACS. May 1981.

A note on the temperature dependence of the yield and range of photoejected electrons from *N,N,N',N'*-tetramethyl-*p*-phenylenediamine in 2,2,4-trimethylpentane

KAIDEE LEE[1] AND SANFORD LIPSKY

Department of Chemistry, University of Minnesota, Minneapolis, MN 55455, U.S.A.

Received June 27, 1984

This paper is dedicated to Professor Camille Sandorfy on the occasion of his 65th birthday

KAIDEE LEE and SANFORD LIPSKY. Can. J. Chem. **63**, 1374 (1985).

The photocurrent of *N,N,N',N'*-tetramethyl-*p*-phenylenediamine (TMPD) in 2,2,4-trimethylpentane (isooctane) excited at 5.90 eV has been studied as a function of temperature from 195 to 298 K both in the absence and presence of the electron scavengers *n*-perfluoroheptane and perfluoromethylcyclohexane. Using an exponential radial distribution function for geminate pair separation distances with range parameter corrected to accommodate its change with temperature, it is found that the photoejection quantum yield of TMPD is essentially independent of temperature from 298 K to ≃250 K and then increases slightly (by ≃20%) on further cooling to 195 K. In the presence of electron scavengers there is a contribution to the magnitude of the range parameter from the action of the scavenger to pre-thermalize the epithermal electron. The temperature dependence of this contribution is analyzed and found to increase with decreasing temperature.

KAIDEE LEE et SANFORD LIPSKY. Can. J. Chem. **63**, 1374 (1985).

Opérant à des températures allant de 195 à 298 K, tant en présence qu'en l'absence de pièges à électrons comme le *n*-perfluoroheptane et la perfluorométhylcyclohexane, on a étudié le photocourant de la *N,N,N',N'*-tétraméthyl *p*-phénylènediamine (TMPD) dans le triméthyl-2,2,4 pentane (isooctane) excité à 5,90 eV. On a utilisé une fonction de distribution radiale exponentielle pour les distances qui séparent les paires géminées et, à l'aide de cette fonction qui inclut un paramètre de correction des intervalles permettant d'accomoder sa variation avec la température, on a pu établir que le rendement quantique pour la photoéjection de la TMPD est pratiquement indépendant de la température de 298 K jusqu'à environ 250 K et que, si la température est abaissée jusqu'à 195 K, ce rendement n'augmente que légèrement (environ 20%). En présence de pièges à électrons, il existe une contribution à l'amplitude du paramètre d'intervalle qui provient de l'action des pièges à électrons qui pré-thermalisent les électrons épithermaux. On a analysé la variation de cette contribution avec la température et on a trouvé qu'elle augmente avec une diminution de la température.

[Traduit par le journal]

Introduction

Tetramethyl-*p*-phenylenediamine (TMPD) photoionizes in 2,2,4-trimethylpentane (isooctane) at 25°C at a threshold energy of 4.66 eV (1). Above this energy a photocurrent is observed, the quantum yield of which, ψ_J can be expressed as

$$[1]\quad \psi_J = \phi_{\pm}\int_0^{\infty} P_{esc}(r)f(r)r^2\mathrm{d}r$$

where $\phi_{\pm}$ is the primary quantum yield for electron ejection, $P_{esc}(r)$ is the Coulomb escape probability of the thermalized geminate ion-pair at a separation distance, r, and $f(r)$ is the radial probability density of ion-pair separation distances.

From measurement of the temperature dependence of ψ_J, Holroyd and Russell (1) in their early work on TMPD photoionization, estimated that $\phi_{\pm}$ increased with increasing temperature (over the range $T \simeq 196-298$ K) with an activation energy of ≃870 cal/mol. This estimate was based on the assumption that $r^2f(r)$ could be represented by a Dirac delta function, $\delta(r-b)$ with range b, independent of temperature. Our purpose in this Note is to attempt to improve on this estimate.

We utilize a radial distribution function

$$[2]\quad f(r) = \frac{\alpha^3}{2}\mathrm{e}^{-\alpha r}$$

which has been demonstrated to predict well the observed dependence of ψ_J on electric field strength (2, 3). The range parameter, α, in eq. [2] is also corrected to accommodate its change with temperature due to an implicit dependence on the liquid density. This latter dependence derives, in part, from the effect of density on the "stopping power" of the liquid and, in part, from the effect of density on the vertical polarization energy of the ion-pair. By changing this polarization energy, there is effected a change in the threshold energy for photoejection and, therefore, a change in the kinetic energy with which the electron is ejected.

As will be documented in what follows, we find that the temperature dependence of $\phi_{\pm}$ is much weaker than estimated by Holroyd and Russell (1) and, in fact, $\phi_{\pm}$ increases slightly at low temperatures. Also we have utilized this temperature dependence of $\phi_{\pm}$ to extract the temperature dependence of α when electron scavengers are present that act to pre-thermalize the epithermal geminate electron. In the presence of such scavengers, eq. [2] has been shown to continue to predict the field dependence of ψ_J and also the dependence of ψ_J on scavenger concentration, c, when α is given the empirical form:

$$[3]\quad \alpha = (\gamma_0 + \gamma_1 c)^{1/3}$$

where $\gamma_0^{1/3}$ is the range parameter at $c = 0$ and γ_1 is a measure of the epithermal electron-scavenger thermalization cross-section (3, 4).

Experimental

A D_2 lamp (Bausch & Lomb, DE50A) was used as a light source. The light was dispersed through a 0.3 m f/5.3 monochromator (McPherson, Model 218) operating at bandpasses ranging from 1.86 nm to 4.77 nm. The light from the monochromator was focused by an f/1.8 LiF lens into a temperature-controlled cell consisting of three concentric cylinders to each of which was fused a 0.16 cm thick Supersil quartz window. Two 1 × 2 cm stainless steel electrodes, parallel to and separated from each other by 0.533 cm were situated in the innermost cylinder with their edges in close contact with the

[1]Present address: Physics Division, Argonne National Laboratory, 9700 South Cass Avenue, Argonne, IL 60439, U.S.A.

quartz window (clearance ca. 0.01 cm). The electrodes were welded under He-arc, each to a Kovar rod, to which was spot-welded, under He, a braided molybdenum wire extending through the feedthrough tube to external electrical connections. Temperature control of the cell solution was achieved by varying the flow rate of precooled nitrogen, directed through a capillary to the space between the middle and the innermost cylinders. The temperature was monitored by thermocouples. The solution temperature was calibrated by the difference in temperatures recorded in the solution and in the nitrogen jacket when the electric field was absent. The solution temperature, thus determined, is accurate to within ±1 K. Thermal insulation of the cell was provided by a vacuum jacket formed by the outermost and middle cylinders.

TMPD (Aldrich) was purified by vacuum sublimation followed by zone refining. Isooctane (Aldrich), perfluoroheptane (kindly donated by the 3M Company), and perfluoromethylcyclohexane (PCR Research Chemicals) were purified by passing through silica gel which had been activated at 150°C for 24 h.

The TMPD concentrations were $2-3 \times 10^{-4}$ *M*. The quencher concentrations were within the range of 0.0090–0.07 *M*, the upper limit being set by the quencher solubility at the lowest temperature employed in each case. All the solutions were carefully purged with N_2. The excitation energy was 5.90 eV (210 nm) and the applied electric field strength, 3.75 kV/cm in all experiments reported here.

Results and discussion

According to the Onsager theory (5), at low field strenghts, E, the geminate pair escape probability, $P_{esc}(r)$, approaches

$$[4] \quad P_{esc}(r) = [\exp(-r_0/r)]\left(1 + \frac{\epsilon r_0^2}{2|e|}E\right)$$

where $r_0 = e^2/\epsilon kT$, e is the electron charge, ϵ is the dielectric constant, and k the Boltzmann constant. The next highest term in the expansion of P_{esc} in powers of E (6) contributes less than 1% at the applied field strength of E = 3.75 kV/cm and at all temperatures studied and can be safely ignored. Substitution of eqs. [2] and [4] into eq. [1] gives

$$[5] \quad \psi_J = \phi_{\pm}\left(1 + \frac{\epsilon r_0^2}{2|e|}E\right)(\alpha r_0)^{3/2}\, K_3(2\sqrt{\alpha r_0})$$

where K_3 is the modified Bessel function of order 3 (4, 7).

The dashed curve in Fig. 1 represents a least-square fit of the right hand side of eq. [5] to the experimental dependence of ψ_J on T (shown as open circles and normalized to unity at T = 298 K), using α as a least-square parameter and assuming that $\phi_{\pm}$ and α are temperature independent (i.e., that the entire temperature dependence of ψ_J resides in ϵ and r_0). The failure of this assumption is clearly indicated by the poorness of the fit and the large discrepancy between the least-square estimate of α (0.0563 Å^{-1}) and the more reliable value obtained from the field dependence of ψ_J (0.0361 Å^{-1}) (3).[2]

To correct for the temperature dependence of α at a fixed initial kinetic energy, K, of the ejected electron, we presume α to be proportional to the isooctane density, ρ. This approximation, which assumes a temperature invariant thermalization cross-section, has been successfully applied in predicting the temperature dependence of the free-ion yield in high-energy radiation experiments (8–10). Next, in order to accommodate the dependence of K on temperature (at a fixed excitation energy) we utilize the connection between the TMPD ioniz-

[2]In ref. 3, α is reported as 0.0370 Å^{-1} at an excitation energy of 5.80 eV. The value 0.0361 Å^{-1} at 5.90 eV is obtained by interpolation and normalization of the data of Choi *et al.* (2).

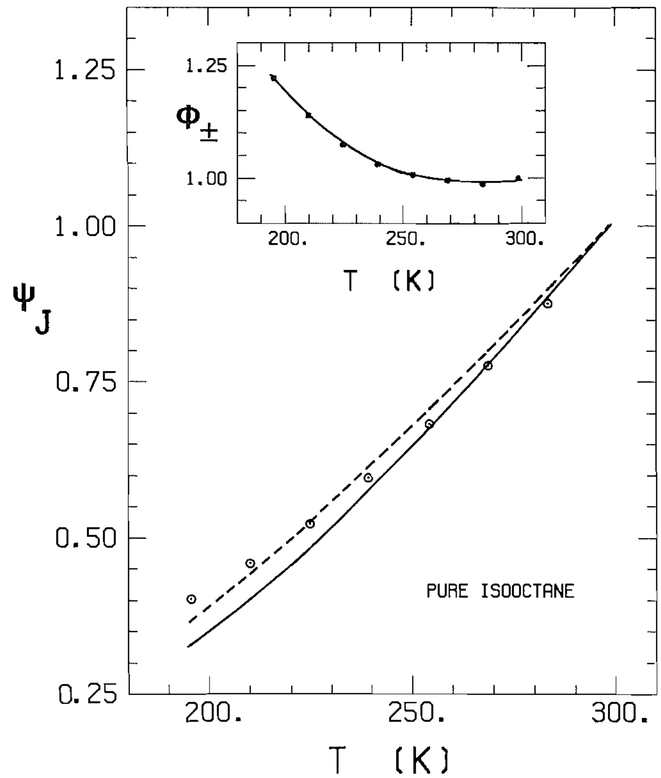

FIG. 1. The dependence of the yield of photocurrent, ψ_J, on temperature T, for TMPD in pure isooctane excited at 5.90 eV. The yield is normalized to unity at T = 298 K. Open circles: experimental data; dashed curve: least-square fit of eq. [5] with α as least-square parameter and assuming α and $\phi_{\pm}$ to be independent of T; solid curve: eq. [5] with α corrected for temperature variation but assuming $\phi_{\pm}$ independent of T. Insert: variation of $\phi_{\pm}$ with T (normalized to unity at 298 K).

ation potentials in liquid (I_l) and gas (I_g) phases and the "vertical" polarization energies of TMPD$^+$ (P_+) and e$^-$ (V_0), i.e.,

$$[6] \quad I_l = I_g + P_+ + V_0$$

The temperature dependence of P_+ was obtained from the Born equation:

$$[7] \quad P_+ = \frac{-e^2}{2r_i}\left(1 - \frac{1}{\epsilon}\right)$$

using Holroyd's value of $e^2/2r_i$ = 2.89 eV (1) and the temperature dependence of the isooctane dielectric constant, ϵ. To evaluate the temperature dependence of V_0, we have adopted the model of Springett, Jortner, and Cohen (11) which has previously been successfully applied by Fueki, Feng, and Kevan (12) and by Holroyd and Russell (1). Our results for both P_+ and V_0 are given in Table 1 and show that from 298 K to 195 K the ionization potential of TMPD increases by 0.083 eV. The effect of this on α was then deduced from the experimental dependence of α on excitation energy, ϵ_{exc}, as determined at 25°C by Choi, Sethi, and Braun (2). Normalizing their results to a value of α = 0.0361 Å^{-1} at ϵ_{exc} = 5.90 eV (3), the change in α with a small change in temperature, ΔT, is obtained by simply incrementing α by $(d\alpha/d\epsilon_{exc})\Delta K$ where $\Delta K = -\Delta I_l$.

The total change in α with temperature was therefore constructed from

TABLE 1. Temperature dependence of the range parameter, α, of photoejected electrons from TMPD in isooctane at ϵ_{exc} = 5.90 eV and of some parameters that determine this dependence in the absence of scavengers

T (K)	ρ (g cm^{-3})	P_+ (eV)	V_0 (eV)	α ($Å^{-1}$)
298	0.689	−1.395	−0.17	0.0361
283	0.700	−1.411	−0.15	0.0368
269	0.712	−1.427	−0.12	0.0375
254	0.724	−1.442	−0.099	0.0382
239	0.736	−1.457	−0.071	0.0390
225	0.748	−1.471	−0.043	0.0397
210	0.760	−1.486	−0.013	0.0405
195	0.772	−1.500	+0.018	0.0413

$$[8] \quad \alpha(T + \Delta T) = \left[\alpha(T) + \left(\frac{d\alpha}{d\epsilon_{exc}}\right)_T \Delta K\right] \frac{\rho(T + \Delta T)}{\rho(T)}$$

where α (T = 298 K) is the range parameter at ϵ_{exc} = 5.90 eV. The results of this calculation are displayed in Table 1. Using these values of α, the right hand side of eq. [5] was reevaluated and is shown plotted as the solid line in Fig. 1 (again normalized to unity at T = 298 K). The discrepancy between this solid line and the experimental points (open circles) we presume now to derive mainly from the variation of $\phi_\pm$ with temperature. The insert in Fig. 1 shows this variation to be less than 1% from 298 K to 250 K and to increase by about 20% from 250 K to 195 K. Since the photoejection process appears to be an autoionization (13), this relatively small increase in $\phi_\pm$ may be attributed to the competition between electron ejection and neutral decay channels of the autoionizing state that are temperature activated.

The temperature dependence of ψ_J has also been measured in the presence of various concentrations of n-perfluoroheptane and perfluoromethylcyclohexane. Figure 2 shows some of this data (normalized to unity at T = 298 K) for six concentrations, c, of n-perfluoroheptane. It will be noted that as c increases, ψ_J becomes increasingly sensitive to T. This has also been observed for perfluoromethylcyclohexane (4). Since most of the temperature dependence of ψ_J resides in r_0, this increased sensitivity can be simply explained as due to the effect of the scavenger to make the distribution function, $f(r)$, more spatially compact. This consequence of epithermal "scavenging" has already been established, and more definitively, from the effect of scavengers to alter the field dependence of ψ_J (3).

Using the variation of $\phi_\pm$ with temperature, we can now, via eq. [5], extract from the data of Fig. 2, the range parameter α as a function of both temperature and scavenger concentration. According to eq. [3], α^3 should be linear on c with intercept of γ_0 and slope of γ_1. Such plots are shown at various temperatures in the insert of Fig. 2. The solid lines are linear least-square fits. The cube roots of the intercepts at the four temperatures of 298 K, 268 K, 240 K, and 207 K are, respectively, 0.037 $Å^{-1}$, 0.039 $Å^{-1}$, 0.040 $Å^{-1}$, and 0.042 $Å^{-1}$, all of which agree reasonably well with the range parameters obtained at c = 0 (see Table 1). The slopes, γ_1, increase monotonically with decrease in temperature, i.e., 1.0 × 10^{-3} at 298 K, 1.1 × 10^{-3} at 268 K, 1.2 × 10^{-3} at 240 K, and 1.5 × 10^{-3} at 207 K. Similar results are obtained for perfluoromethylcyclohexane, but γ_1 increases about half as fast over the same temperature range. Some of the temperature dependence of γ_1 may be attributed to the dependence on density of the electron mean free path (which is implicitly contained in γ_1 as is suggested by dimensional arguments (4)). The remaining change is associated with the effect of temperature on the cross-section, σ, of the epithermal scavenging process via its dependence on both the kinetic energy, K, of the ejected electron and on the electron affinity, $-V_0$, of the fluid. The kinetic energy effect, as has been previously discussed (4), should increase σ as T (and, therefore, K), declines whereas increase in V_0 with decreasing T (see Table 1) will, through Franck–Condon factors, increase or decrease σ depending on the nature of the scavenger (14–16). It is this latter effect which we presume to be responsible for the relatively small difference between n-perfluoroheptane and perfluoromethylcyclohexane.

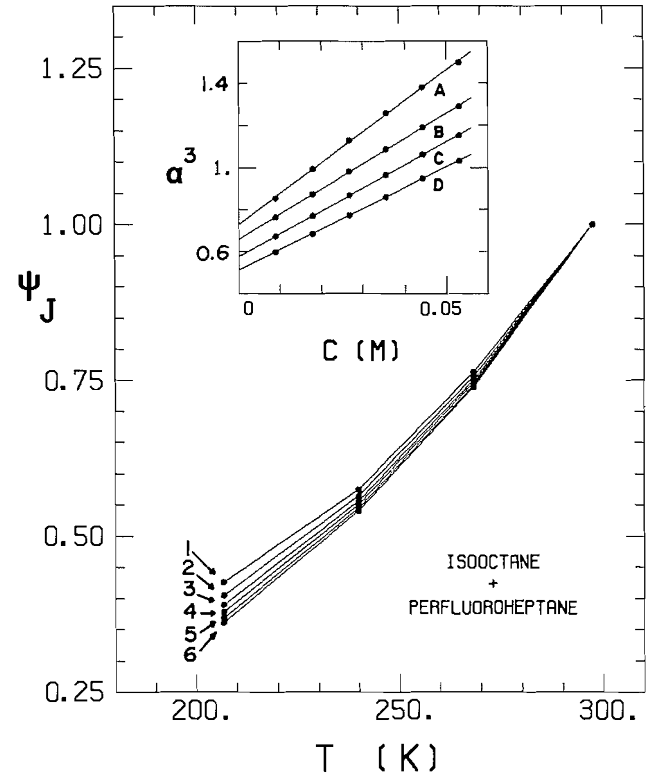

FIG. 2. The dependence of the yield of photocurrent, ψ_J, on temperature, T, for TMPD in isooctane at various concentrations, c, of n-perfluoroheptane and excited at 5.90 eV. The yields are all normalized to unity at T = 298 K. Closed circles: experimental data at 0.00892 M (*1*), 0.0178 M (*2*), 0.0266 M (*3*), 0.0355 M (*4*), 0.0442 M (*5*), and 0.0530 M (*6*). The solid lines merely connect the data points. Insert: plot of α^3 (units of 10^{-4} $Å^{-3}$) vs. c at various temperatures 207 K (*A*), 240 K (*B*), 268 K (*C*), 298 K (*D*). The solid lines are linear least-square fits to eq. [3].

Acknowledgments

This research was supported in part by the U.S. Department of Energy, Divison of Chemical Sciences, Office of Basic Energy Sciences. We are also very grateful to Mr. D. B. Johnston for his technical assistance.

1. R. A. HOLROYD and R. L. RUSSELL. J. Phys. Chem. **78**, 2128 (1974).
2. H. T. CHOI, D. S. SETHI, and C. L. BRAUN. J. Chem. Phys. **77**, 6027 (1982).
3. K. LEE and S. LIPSKY. J. Phys. Chem. **88**, 4251 (1984).
4. K. LEE and S. LIPSKY. J. Phys. Chem. **86**, 1985 (1982).
5. L. ONSAGER. Phys. Rev. **54**, 554 (1938).

6. A. MOZUMDER. J. Chem. Phys. **60**, 4300 (1974).
7. M. ABRAMOWITZ and I. A. STEGUN. Handbook of mathematical functions. Dover Publications, New York. 1970. Chapt. 9.
8. W. F. SCHMIDT and A. O. ALLEN. J. Phys. Chem. **72**, 3730 (1968).
9. W. F. SCHMIDT and A. O. ALLEN. J. Chem. Phys. **52**, 2345 (1970).
10. K. SHINSAKA, J-P. DODELET, and G. R. FREEMAN. Can. J. Chem. **53**, 2714 (1975) and references therein.
11. B. E. SPRINGETT, J. JORTNER, and M. H. COHEN. J. Chem. Phys. **48**, 2720 (1968).
12. K. FUEKI, D-F. FENG, and L. KEVAN. Chem. Phys. Lett. **13**, 616 (1972).
13. K. C. WU and S. LIPSKY. J. Chem. Phys. **66**, 5614 (1977).
14. K. FUNABASHI and J. L. MAGEE. J. Chem. Phys. **62**, 4428 (1975).
15. A. HENGLEIN. Can. J. Chem. **55**, 2112 (1977).
16. S. LIPSKY. J. Chem. Educ. **58**, 93 (1981) and references therein.

The conformational changes accompanying the $\tilde{a}^3A'' \leftarrow \tilde{X}^1A'$ triplet–singlet electronic excitation of acetaldehyde, CH_3CHO

D. C. MOULE AND K. H. K. NG
Department of Chemistry, Brock University, St. Catharines, Ont., Canada L2S 3A1

Received July 4, 1984

This paper is dedicated to Professor Camille Sandorfy on the occasion of his 65th birthday

D. C. MOULE and K. H. K. NG. Can. J. Chem. **63**, 1378 (1985).

The first electronic absorption system of acetaldehyde was recorded in the vapour phase at room temperature. The many-banded spectrum proved to be very complex and it was only at the extreme red edge of the absorption that the pattern became simple enough to analyze. The major experimental requirement was a high pressure × path length (500 Torr × 168 m). Spectra were interpreted in terms of the torsional mode ν'_{15} and ν''_{15} attached to the ν'_{14} out-of-plane bending mode. Both modes were highly Franck–Condon active and the 0^0_0 band at 27240.4 cm^{-1} was not directly observed. The barrier to rotation of the methyl group was 618.5 cm^{-1}. More surprising was the observation that the methyl group undergoes a rotation from a $\tilde{X}$ eclipsed configuration to a staggered configuration. The intensity of the ν'_{14} quantum addition and its position in the spectrum suggest that the aldehydic hydrogen is nonplanar in the $\tilde{a}$ state.

D. C. MOULE and K. H. K. NG. Can. J. Chem. **63**, 1378 (1985).

Opérant en phase gazeuse et à la température ambiante, on a enregistré le spectre de la première absorption électronique de l'acétaldéhyde. Le spectre comporte plusieurs bandes, il est très complexe et ce n'est que l'extrémité du spectre qui absorbe dans le rouge que l'on a pu analyser. L'exigence expérimentale principale est une valeur élevée pour la pression × la longueur de parcours (500 Torr × 168 m). On a interprété les spectres en fonction des modes de torsion ν'_{15} et ν''_{15} attachés au mode de vibration angulaire hors-plan ν'_{14}. Les deux modes sont très actifs dans la région de Franck–Condon et on n'a pas pu observer la bande 0^0_0 à 27240,4 cm^{-1}. La barrière à la rotation du groupe méthyle est égale à 618,5 cm^{-1}. Le résultat le plus surprenant est l'observation que le groupe méthyle subit une rotation qui le fait passer de la configuration éclipsée $\tilde{X}$ vers une configuration décalée. L'intensité de l'addition du quantum ν'_{14} ainsi que sa position dans le spectre suggèrent que, dans l'état $\tilde{a}$, l'hydrogène aldéhydique n'est pas dans le plan.

[Traduit par le journal]

Introduction

The banded absorption system of acetaldehyde at 330 nm has been the subject of a number of studies. The assignment of the vibrational fine structure has been hampered by a spectral congestion which extends throughout this system and progress has been slow. Rao and Rao (1), the first investigators to attempt a complete vibrational assignment, placed the singlet–singlet system origin at 320.4 nm. Somewhat later, Giddings and Innes (2) revised this value upwards to 348.4 nm. More recently, Hubbard, Bocian, and Birge (3) combined a medium resolution absorption study with resolved laser fluorescence to place the origin at 346.4 nm. This problem has been solved by the powerful technique of supersonic jet spectroscopy. Noble, Apel, and Lee (4) observed the excitation spectrum of a sample of jet cooled CH_3CHO which was free from the complications of thermally induced vibration–rotation fine structure. They were able to unequivocally fix the origin at 29771 cm^{-1} (335.9 nm), the V'_3 three-fold barrier to 653 cm^{-1} and the O^-—O^+ inversion splitting to 33 cm^{-1}.

Ng (5) has made a study of this system in absorption at path lengths up to 168 m and temperatures down to −90°C. He established that a large number of bands in the 363–351 nm region were temperature insensitive. It follows from the jet studies that these bands must result from the spin forbidden triplet–singlet $\tilde{a}^3A'' \leftarrow \tilde{X}^1A'$ electronic transition. The other information which is available for the $\tilde{a}$ state comes from emission spectroscopy. CH_3CHO is known to fluoresce as well as phosphoresce, and a difficulty has been to resolve contributions of each from the total emission spectrum. Schuh *et al.* (6) optically excited the $\tilde{A}$ singlet system at 320 nm with a YAG laser-pumped dye laser system. They observed that the resulting emission could be resolved into a very short-lived 5 ns component and a much longer 25 μs emission. These they attributed to the separate $\tilde{A} \rightarrow \tilde{X}$, S–S and $\tilde{a} \rightarrow \tilde{X}$, T–S fluorescence and phosphorescence emissions. From the onset of the phosphorescence, the origin of the T–S system may be estimated to lie in the region of 369 nm.

Recently (7), we have made a vibronic assignment of the $\tilde{a} \leftarrow \tilde{X}$ and $\tilde{A} \leftarrow \tilde{X}$ transitions in CH_3CHS. We felt that we might be able to combine the $E(\tilde{A}) - E(\tilde{a})$ intervals from this work with the corresponding values for CH_2S and CH_2O and arrive at an estimate for CH_3CHO. Also, the vibronic fine structure of the T–S system is expected to be simplified as a result of the more stringent vibronic–spin–orbit selection rules. That is, the inversion doublets which greatly complicate the S–S system are expected to be absent in the T–S spectrum.

Experimental

Acetaldehyde, CH_3CHO, was obtained from B.D.H. Chemicals, Ltd., and was purified by trap-to-trap distillation. The spectra at room temperature were recorded at a path length of 168 m which was obtained from 28 traversals of a 6 m multiple reflection cell. The pressures of the vapour in these experiments varied from 25 to 500 Torr. A total of 250 mL of acetaldehyde was required to fill the cell at its highest pressure which made it impractical to record the spectrum of the D compounds in the region of the origin. The temperature effect was observed with a 2 m multiple reflection cell (8) which could be thermostated at temperatures down to −90°C. Spectra were recorded under conditions of modest resolution with a Bausch and Lomb 1.5 m grating spectrograph. The plate holder on this instrument is fixed so that wavelengths shorter than 375 nm are recorded in the second order and those greater than 375 nm in the first order. A 450 W Xe arc was used as a source of continuous radiation and a Fe–Ne hollow cathode lamp for the iron standard lines. Spectra were calibrated from 10-fold enlargements of the photographic film.

Results and discussion

The starting point for the assignment of the bands in the T–S came from the jet-laser studies of the S–S system which place the origin of the $\tilde{A} \leftarrow \tilde{X}$ system at 29771 cm^{-1}. The separation between the $\tilde{A}$ singlet and $\tilde{a}$ triplet states $\Delta E = E(\tilde{A}) - E(\tilde{a})$ was estimated from CH_2O (9), CH_2S (9), and CH_3CHS (10). The data were combined as follows: $\Delta E(CH_3CHO) = \Delta E(CH_2O)$. $\Delta E(CH_3CHS)/\Delta E(CH_2S) = (2996)(1522)/(1853) = 2461$ cm^{-1}. The origin band for the $\tilde{a} \leftarrow \tilde{X}$ transition therefore should lie at $29771 - 2461 = 27310$ cm^{-1}. A second estimate comes from the phosphorescence of Schuh *et al.* (6) who placed the origin at 27100 cm^{-1}.

The temperature effect showed that the bands in the 26900–28200 cm^{-1} region do not bear ground state excitation energies of 1571 cm^{-1} or greater and they are assigned to the T–S system. The key to the analysis was the recognition that the ν_{15} torsional mode was highly active and formed long progressions in the spectrum. As a consequence of the large Boltzmann populations, the hot bands bearing ground state excitation of ν''_{15} should be present in the spectrum. Sequences and progressions in ν''_{15} should be among the first bands encountered at the red edge of the spectrum.

The bands at 27098.5 and 26985.3 are free from congestion and are among the few simple bands that were observed. It was felt that these were hot bands and that their assignments could be obtained by comparing their frequency difference of 113.2 cm^{-1} against ground state energy levels derived from microwave data (11). From a combination of all pairs of levels in ν''_{15} the difference $15_{2A} - 15_{1E} = 111.5$ cm^{-1}. This would give the lower frequency band the assignment 15^{0A}_{2A} and the higher band 15^{0E}_{1E}. These bands would fix the 0^{0A}_{0A} origin at $27098.5 + 140.1 = 27238.6$ or alternatively $26985.3 + 251.6 = 27236.9$ cm^{-1}. The assignment of the S–S bands at higher frequencies by Noble *et al.* (4) was used as an aid in establishing the quantum numbering for the $\tilde{a}$ state. For the S–S system the ν'_{15} torsional frequency is $15^{1E} - 15^{0A} = 185.5$. With this interval as a guide, we assigned the bands at 27278.3 and 27148.1 cm^{-1} to the transitions 15^{1A}_{1A} and 15^{1E}_{2E}. The other assignments locked into the vibrational pattern. A strong band at 27474.4 cm^{-1} is +334.0 cm^{-1} above the 0^{0A}_{0A} origin. It is assigned to the transition 15^{2A}_{0A}. The identification of the band at 26967.3 as 15^{0E}_{2E} completed the assignment of the pure torsional transitions.

Many bands are found in this region which could not be fitted into the above assignments. These bands were too close to the origin to be classified as fundamentals and they were attributed to hot bands derived from higher vibrational states. The pattern of the vibrational fine structure at energies in excess of +300 cm^{-1} from the T–S origin can be inferred from the jet spectra of Noble *et al.* (4). These authors observed the low frequency quanta of the out-of-plane bending mode 14^1_0 and 14^2_0 as well as the single quantum addition 10^1_0. As the quanta were attached to each other and to quanta of the torsional mode they found that the spectrum became complex very quickly. Even though the vibronic–spin–orbit selection rules (12) do not allow for 14^1_0 here we felt that a detailed analysis of our room temperature spectrum would not be realistic. Instead we made a search for the two strongest members of the progression $14^2_0\ 15^{2A}_{0A}$ and $10^1_0\ 15^{2A}_{0A}$. Bands were found at 27934.6 and 28074.6 cm^{-1} which lead to $2\nu'_{14} = 500.2$ and $\nu'_{10} = 360.2$ cm^{-1}. These values are to be compared to the 487 and 373 cm^{-1} set obtained for the $\tilde{A}$ state. While in principle it should be possible to verify these assignments by identifying other members of the ν'_{15} progression, the complexity of the absorption allows for too many alternatives. Rather, a detailed analysis of this region will have to await methods more powerful than absorption spectroscopy.

TABLE 1. Assignment of the main vibrational features in the 362–371 region of acetaldehyde

Assignment	Observed	Calculated[a]
15^{2A}_{0A}	27574.4	27576.21
15^{1A}_{1A}	27278.3	27273.66
15^{1E}_{2E}	27148.1	27150.66
15^{0E}_{1E}	27098.5	27096.57
15^{0A}_{2A}	26985.3	26986.57
15^{0E}_{2E}	26967.3	26971.92
15^{0E}_{3E}	26899.7	26896.43

[a]From the constants of the $\tilde{a}$ and $\tilde{X}$ states given in Table 2.

TABLE 2. Comparison of the torsional constants for the $\tilde{X}$, $\tilde{a}$, $\tilde{A}$, and $\tilde{B}$ states of acetaldehyde (cm^{-1})

	Barrier height	F	T_0
$\tilde{X}$ state[a]	398.4±8.1	7.48±0.17	0.0
$\tilde{a}$ state[b]	624.8±21.5	6.81±0.58	27240.4 ±2.8
$\tilde{A}$ state[c]	653	6.6	29771
$\tilde{B}$ state[d]	755±10	7.696	55039

[a]Parameters refined from the data of ref. 11.
[b]This work.
[c]From ref. 4.
[d]From ref. 14.

Discussion

When interaction with others vibrational modes is neglected, the torsional motion in acetaldehyde is governed by the Hamiltonian

$$[1]\quad H = -\frac{Fd^2}{d\phi^2} + \frac{V_3}{2}(1 - \cos 3\phi)$$

where F is the reduced rotational constant, V_3 is the height of the barrier to internal rotation, and ϕ the torsional angle. Following the method of Lewis *et al.* (13), the Hamiltonian matrix corresponding to eq. [1] was set up in terms of sine and cosine basis functions and diagonalized to yield the eigenvalues and wavefunctions. The energies of the transitions allowed by the selection rules $A_1 \leftrightarrow A_1$, $A_2 \leftrightarrow A_2$, $E \leftrightarrow E$ were calculated by combining levels of the upper $\tilde{a}$ state with the lower $\tilde{X}$ ground state. The V''_3 and F'' parameters of the lower state were recalculated from the levels derived from the microwave spectrum (11) using the model function of eq. [1]. The calculated transition energies were fitted to the torsional data by a least squares procedure in which the electronic origin V'_3 and F' were refined. The fit to the data is illustrated in Table 1 and the resulting spectroscopic parameters are given in Table 2. An inspection of the spectrum at 27240.4 cm^{-1} indicates that this region does not contain bands which can be assigned to the 0^{0A}_{0A} origin. The two estimates for the position of the origin do bracket the value observed here in that the correlation between CH_3CHS, CH_2S, and CH_2O gave 27310 cm^{-1} while the phosphorescence measurements gave 27100 cm^{-1}.

Torsional dynamics for CH_3CHO have been determined for the 4 states $\tilde{X}$, $\tilde{a}$, $\tilde{A}$, and $\tilde{B}$. The parameters are tabulated in Table 2. It is not too surprising that the V_3 and F constants of

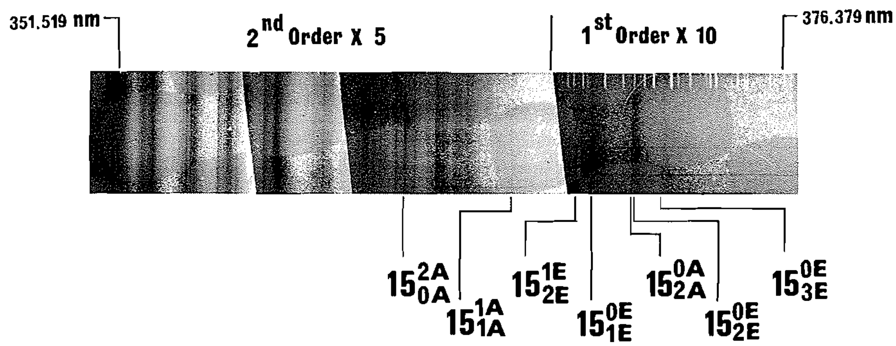

FIG. 1. Low resolution absorption spectrum of acetaldehyde CH_3CHO recorded at a pressure × path length of 500 Torr × 168 m.

the $\tilde{a}$ and $\tilde{A}$ states resemble each other since the states are derived from the same nπ^* electron configurations. What is unusual is that the gross features of the torsional structure in the $\tilde{B} \leftarrow \tilde{X}$ Rydberg transition are very different from those of the two lower $\tilde{a}$, $\tilde{A} \leftarrow \tilde{X}$ valence transitions. That is, the n $\rightarrow$ 3s transition is characterized by a 0^0_0 band which is very strong and dominates the spectrum whereas in the n $\rightarrow \pi^*$ transitions this band is too weak to be observed. A simple explanation for these results is to assume that on excitation to the $\tilde{B}$ state the methyl group does not change its conformation. The three-fold barriers would be in phase (eclipsed conformations in both states). The strongest transitions are found in Δv sequences in which successive members decrease rapidly because of their increasing Boltzmann factors. Indeed, Gordon (16) has been able to replicate the intensity patterns in the $\tilde{B} \leftarrow \tilde{X}$ spectrum from a Franck–Condon calculation based on this model. On the other hand, the intensity profiles of the torsional transitions in the near uv systems would be rationalized by a change in conformation. On electronic excitation, the methyl hydrogens would undergo a rotation from their eclipsed ground state configuration to a staggered configuration in the upper state. In this case the strongest transitions in absorption would come from the $v'' = 0$ level and terminate on levels just below the top of the upper barrier. Noble and Lee (15) used this model to explain the observed intensities in the torsional progressions in the $\tilde{A} \leftarrow \tilde{X}$ spectrum. The problem here is compounded by the inversion motion of the aldehyde wagging mode.

A major question which emerges from this analysis is why the methyl group undergoes a torsional distortion on excitation to the nπ^* state yet retains its conformation on excitation to the n3s state. A somewhat simplistic viewpoint is to break the structural changes into two parts: those arising from the removal of the electron from the n orbital and those resulting from the addition of the electron to either the 3s or π^* orbitals. Information about the first process comes from a comparison of the Rydberg spectrum (14) with the first transition in the photoelectron spectrum (17). Both of these transitions have in common the loss of the n electron. Also, they have torsional transitions which are Franck–Condon allowed. It follows that the removal of the n electron in the n $\rightarrow \pi^*$ process is not responsible for the observed torsional distortion. Rather, the source for this effect comes from the addition of the electron to the π^* orbital. The effects of the methyl group on the out-of-plane electronic structure of a molecule can be treated by simple Hückel MO theory. If the methyl group is assumed to have a three-fold symmetry, the σ MO's can be decomposed into the representations $2a' + a''$ of the C_s point group. This means that one of the σ orbitals transforms as a''. It is constructed from a set of 1s orbitals at the non-planar methyl hydrogens and has a node at the molecular plane. It has the resemblance of a p orbital. Three other p orbitals are required to complete the description of the π network. Two of these are located in the CHO frame, at the carbonyl carbon and oxygen atoms while the fourth is at the methyl carbon. Figure 2 shows the arrangement. This model is not unlike that of the butadiene system in which 4π MO's are derived from 4p type AO's. The order of these orbitals in decreasing stability would be (a) + + + +, (b) + + − −, (c) + − − +, and (d) + − + −. In the $\tilde{X}$ state of the molecule, the lowest orbitals (a) and (b) would be fully occupied. The $\tilde{a}$ or $\tilde{A}$ states which are arrived at by n $\rightarrow \pi^*$ excitation have the configuration $(a)^2(b)^2(c)^1$. If weak interactions were postulated between the terminal orbitals it is clear that (a) and (c) would give bonding end-to-end contribution whereas (b) and (d) would be antibonding. Simple MO theory predicts that the *trans* isomer would be the preferred conformer for the $\tilde{X}$ and $\tilde{B}$ states and that the $\tilde{a}$ and $\tilde{A}$ states should adopt a *cis* conformation.

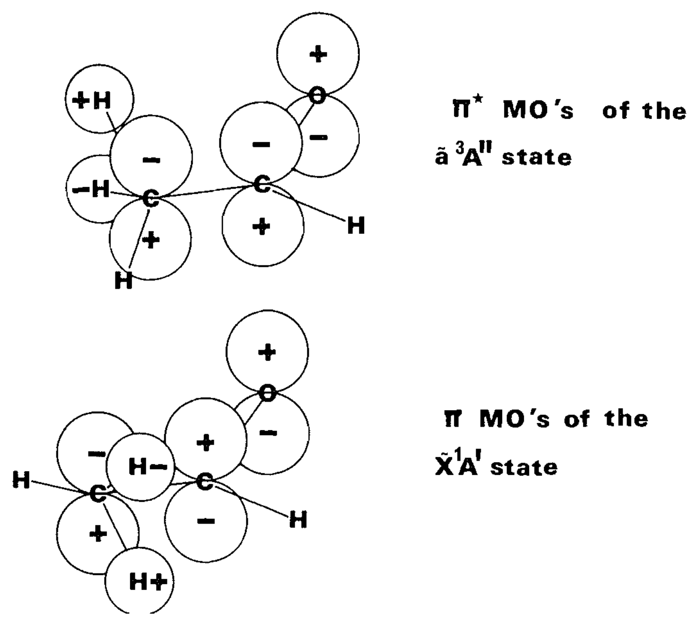

FIG. 2. Conjugative Hückel MO model for the second and third MO's of acetaldehyde. The AO's on the C_1, C_2, and O centers are p-type while the AO on the hydrogens are s-type.

The microwave spectrum (11) clearly shows that the methyl group eclipses the carbonyl double bond. That is, acetaldehyde adopts a configuration in the $\tilde{X}$ state which minimizes the antibonding repulsions between the p-type terminal orbitals. As n $\rightarrow$ 3s Rydberg excitation does not directly involve the π network, the model predicts that the methyl group would retain its conformation in the $\tilde{B}$ state, and that the torsional transitions would be Franck–Condon allowed in the spectrum. This is precisely what is observed in the multiphoton ionization spectrum of Heath *et al.* (14). The results obtained here for the T–S transition and those of Noble *et al.* (4) for the S–S transition can best be explained by a gross displacement of the torsional angle on excitation. The MO model predicts that the angle would be 60°. A complication here is that on $n \rightarrow \pi^*$ excitation the molecule undergoes a second out-of-plane distortion. This is the well-known tendency for the aldehyde hydrogen to assume a pyramidal geometry. In the $\tilde{A}$ state this leads to the inversion manifold of 0, 33, 487 cm^{-1}. While selection rules do not allow for the observation of the first quantum, we do see the 14^2 interval of 500.2 cm^{-1}. In the carbonyl series of molecules the $\tilde{a}$ states in general are known to have higher inversion barriers than the $\tilde{A}$ states. Certainly, the planarity of the CHO frame would be lost in the $\tilde{a}$ state of acetaldehyde and it is doubtful if the displacement of the torsional angle is a full 60°. In any case, a complete description of the dynamics of either the $\tilde{A}$ or the $\tilde{a}$ states would have to involve a set of coupled large amplitude oscillators, one of which would be described as an inversion doubling of the aldehyde hydrogen and the other would be methyl group internal rotation.

A survey of the molecules which have methyl groups next to chromophores which undergo $n \rightarrow \pi^*$ excitation shows that the phenomena observed here for acetaldehyde may be quite widespread. Ernsting *et al.* (18) and Gordon (19) have conclusively demonstrated that the torsional fine structure in the 675 nm band system of CH_3NO can only be explained by a *trans–cis* displacement on electronic excitation. Under supersonic jet conditions (20), the methyl-substituted glyoxals $CHOCCH_3O$ and $(CH_3CO)_2$ give rise to an excitation spectrum which displays progressions in the torsional mode. The spectra would be interpreted in terms of the model used here. Finally, we have recently observed the S–S and T–S transitions resulting from $n \rightarrow \pi^*$ excitations in thioacetone (7) and thioacetaldehyde (10). Again, the spectra are assigned on the basis of a *trans–cis* change in conformation. In all of the examples cited here the molecular frame is either rigidly planar or it is slightly flexible at the aldehydic carbon. None of these molecules undergo the pyramidal distortion which is observed for acetaldehyde yet they all display the same conformational displacements. The above analysis does suggest a generalization, namely, that the conformation of a methyl group attached to a frame undergoing $n \rightarrow \pi^*$ excitation adopts a 60° staggered configuration in the upper state.

Conclusions

The majority of bands in the room temperature absorption spectrum of acetaldehyde are too complex and too congested for a vibronic analysis. It was found that the extreme red edge of the spectrum, under conditions of a very long path of 168 m and a high pressure of 500 Torr, was sufficiently simple that an assignment could be made. The bands observed here were assigned to the spin-forbidden $\tilde{a}^3A'' \leftarrow \tilde{X}^1A'$, $n \rightarrow \pi^*$ transition. A correlation with the recent (4) jet spectrum fixed the 0_0^0 origin at 27240.4 cm^{-1} and the barrier in the triple-minimum torsional potential function to 618.5 cm^{-1}. The strength of the progression in the torsional mode was attributed to a change in the conformation of the methyl group on electronic excitation. The displacement was accounted for by a simple Hückel model in which the 1*s* AO's of the methyl group were conjugated into the 2*p* AO's which formed the π and π^* MO's. The equilibrium conformation was determined by the antibonding repulsions between the end orbitals with the $\tilde{X}$ and $\tilde{B}$ states favouring the *trans* form and the $\tilde{a}$ and $\tilde{A}$ states the *cis* form.

1. V. R. RAO and I. A. RAO. A. Indian J. Phys. **28**, 491 (1954).
2. K. K. INNES and L. E. GIDDINGS. J. Mol. Spectrosc. **7**, 435 (1961).
3. L. M. HUBBARD, D. F. BOCIAN, and R. R. BIRGE. J. Am. Chem. Soc. **103**, 3313 (1981).
4. M. NOBLE, E. C. APEL, and E. K. C. LEE. J. Chem. Phys. **78**, 2219 (1983).
5. K. H. K. NG. M.Sc. thesis. Brock University, St. Catharines, Ont., Canada. 1978.
6. M. D. SCHUH, S. SPEISER, and G. H. ATKINSON. Private communication.
7. R. H. JUDGE, D. C. MOULE, A. E. BRUNO, and R. P. STEER. Chem. Phys. Lett. **102**, 385 (1983).
8. A. BIERNACKI, D. C. MOULE, and J. L. NEALE. Appl. Spectrosc. **26**, 648 (1972).
9. R. P. STEER. Res. Chem. Intermed. **4**, 1 (1981).
10. R. H. JUDGE and D. C. MOULE. To be published.
11. A. BAUDER and H. H. GUNTHARD. J. Mol. Spectrosc. **60**, 290 (1976).
12. G. HERZBERG. Electronic spectra of polyatomic molecules. Van Nostrand, New York, 1966.
13. J. D. LEWIS, T. B. MALLOY, T. H. CHAO, and J. LAANE. J. Mol. Struct. **12**, 427 (1972).
14. B. A. HEATH, M. B. ROBIN, N. A. KUEBLER, G. J. FISANICK, and T. S. EICHELBERGER. J. Chem. Phys. **72**, 5565 (1980).
15. M. NOBLE and E. K. C. LEE. Private communication.
16. R. D. GORDON. J. Chem. Phys. **73**, 5907 (1980).
17. D. W. TURNER, C. BAKER, A. D. BAKER, and C. R. BRUNDLE. Molecular photoelectron spectroscopy. Wiley Interscience. 1970.
18. N. P. ERNSTING, J. PFAB, and J. RÖMELT. J. Chem. Soc. Faraday II, **74**, 2286 (1978).
19. R. D. GORDON and P. LUCK. Chem. Phys. Lett. **65**, 480 (1979).
20. M. GURNICK, J. CHAIKEN, T. BENSON, and J. D. MCDONALD. J. Chem. Phys. **74**, 99 (1981).

Intermolecular perturbation approach to specific solvent effects

Ottó B. Nagy

Laboratoire de Chimie Organique Physique, Université Catholique de Louvain, Bâtiment Lavoisier, 1, Pl. L. Pasteur, 1348-Louvain-la-Neuve, Belgium

Received July 13, 1984

This paper is dedicated to Professor Camille Sandorfy on the occasion of his 65th birthday

Ottó B. Nagy. Can. J. Chem. **63**, 1382 (1985).

One possible specific solvent effect, namely, the π-donor ability is considered in the light of simple intermolecular second order perturbation theory. By using the Polányi–Evans–Bell principle this theory predicts that increasing π-donor ability of solvent should decrease the reaction rate. This prediction is fully borne out by experimental data observed for the solvent effect on 4 + 2 cycloaddition of tetracyanoethylene to anthracene.

Ottó B. Nagy. Can. J. Chem. **63**, 1382 (1985).

Un effet de solvant spécifique possible, à savoir la capacité π-donneur, est considéré à la lumière d'une simple théorie perturbationnelle intermoléculaire de deuxième ordre. En utilisant le principe de Polányi–Evans–Bell, cette théorie prédit que l'augmentation de la capacité π-donneur du solvant doit diminuer la vitesse réactionnelle. Cette prédiction est complètement corroborée par les données expérimentales observées pour l'effet de solvant sur la cycloaddition 4 + 2 du tétracyanoethylène à l'anthracène.

Solute–solvent interactions are ubiquitous in most fields of chemistry and their importance in influencing the physico-chemical properties of molecules needs no further comments.

The complexity of the phenomena involved is quite appropriately reflected by the overwhelming literature on the subject. The approaches to the solution of this problem used by various authors range from purely empirical to highly sophisticated theoretical considerations (1, 2).

In this paper an intermolecular perturbational approach will be presented to account for specific solvent effects observed in reactions between neutral molecules. The astonishing success achieved by simple perturbation theory (3) especially in the frontier molecular orbital (FMO, which should mean, more appropriately, Fukui molecular orbitals) approximation (4) suggests that some aspects of solute–solvent interactions might be handled along the same line (6).

Solvent effects may be general or specific. General solvent effects are based on polarity and polarizability of solvent molecules while specific solvent effects stem from their n-donor, π-donor, and hydrogen bond forming abilities.

The hydrogen bond problem has been dealt with recently by Sandorfy and co-workers (7) who ably demonstrate the subtleties responsible for the therapeutic action of some anesthetic agents.

In the present paper only aprotic solvents will be examined. These must be divided into various classes (8) in which the specific and general effects intervene to different extents. Both spectroscopic and kinetic studies show, as a general rule, that wherever specific solvent effects are present they dominate the overall effects (8–13). This is clearly demonstrated also by the solvent effects observed for cycloaddition reactions. It is well known that 2 + 2 cycloaddition reactions usually involve a zwitterionic intermediate (14). This highly charged species is very sensitive to solvent polarity (general effect) and it is not surprising that one single straight line is observed when the logarithm of the second order rate constant (log k) is plotted against a general solvent effect parameter (E_T (2) or S_M (9)).

On the other hand, 4 + 2 cycloadditions are concerted reactions involving only uncharged species (15). The latter are especially sensitive to the n-donor or π-donor ability of the solvent (specific effects). Therefore a log k vs. S_M plot reveals the same solvent classes that have been observed previously (16), namely, halogenated, n-donor, and π-donor solvents.

Table 1. Reaction of tetracyanoethylene (A) with anthracene (D) in π-donor solvents (S) at T = 20 ± 0.1°C

Solvent	k^a ($dm^3\ M^{-1}\ min^{-1}$)	$I_S{}^b$ (eV)	$E_{ho}^{S\ c}$ (β)
1. *o*-Dichlorobenzene	207.34	9.06	1.083
2. Bromobenzene	110.4	8.98	1.0
3. Chlorobenzene	86.0	9.07	1.0
4. Benzene	15.9	9.24	1.0
5. α-Methylnaphthalene	9.13	7.96	0.528
6. Toluene	5.5	8.82	0.833
7. *o*-Xylene	2.57	8.58	0.750
8. *m*-Xylene	1.79	8.6	0.750
9. Mesitylene	0.458	8.14	0.750

[a]The data for solvents **1**, **2**, **3**, and **7** are taken from ref. 17.
[b]Solvent ionization potential (18).
[c]Highest occupied Hückel molecular orbital energy of solvent relative to the α = 0 level. These values have been calculated by perturbation theory (25, 26) using the following perturbation parameters: $\delta\alpha_r$ = −0.5β, + 0.5β, and +0.2β for —CH_3, —Cl, and —Br respectively (r designates the substituent bearing atom).

The results for the reaction of tetracyanoethylene with anthracene in π-donor solvents are given in Table 1.

They suggest that the monotonic decrease of reactivity when going from *o*-dichlorobenzene to mesitylene might be due to the increasing electron donor character of the solvent as reflected roughly by their ionization potentials (I_S). This seems reasonable in light of the detailed mechanism of this reaction. The very first step is the formation of a charge-transfer molecular complex (C) between the electron acceptor tetracyanoethylene (A) and the electron donor anthracene molecules (D). It has been suggested (10) that such complexes are true reaction intermediates sitting on the reaction path and their presence in any reaction must be quite general. It turned out that this is really so (19) and evidence was put forward demonstrating the intermediacy of these complexes (20, 21). We have therefore the following reaction scheme:

$$\mathrm{A} + \mathrm{D} \overset{K}{\rightleftharpoons} \mathrm{C} \overset{k}{\rightarrow} \text{product}$$

where C is a binary complex AD. If the solvent can also form

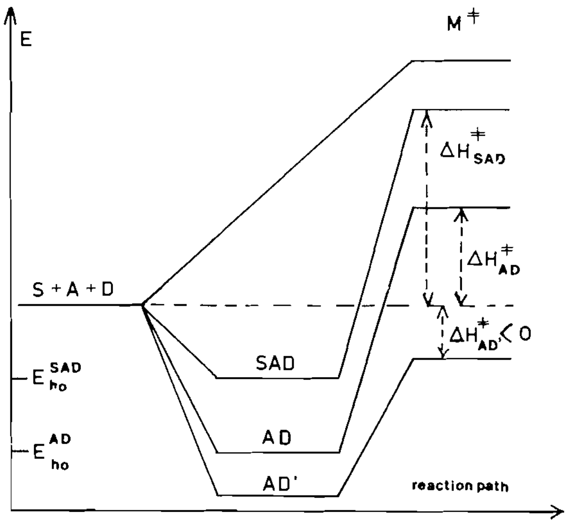

FIG. 1. Energetics of activation processes in bimolecular reaction. The energy of transition state ($M^{\ddagger}$) is strongly depending on the stability of the intermediate complex (AD, AD', or SAD).

molecular complexes with A, the solvent molecules (S) will compete with D and the formation of C will be more difficult:

$$A + D + S \rightleftharpoons AS + D \rightleftharpoons C' \rightarrow \text{product}$$

where C' is a ternary complex SAD. This reduces the reaction rate since the stability of C favours the reaction leading even to negative activation energies in favorable cases (20, 21) (Fig. 1).

Let us now see how this qualitative conclusion can be supported quantitatively by simple intermolecular perturbation theory.

Since the perturbation is an intermolecular one it is necessary to use second or higher order perturbation theory. The following treatment will be limited to second order.

According to standard perturbation theory (24, 25) the interaction of two energy levels E_i and E_j brings about a second order energy variation which is directly proportional to the perturbation matrix element and inversely proportional to the energy separation of the two interacting levels. In the present case the π-donor solvent molecules (S) interact with the π-acceptor substrate (A) leading to a new species AS. In the FMO approximation (Fig. 2) the energy of its lowest unoccupied orbital (E^{AS}_{lu}) is

$$[1] \quad E^{AS}_{lu} = E^{A}_{lu} + \frac{\langle l_A|H^S|h_S\rangle^2}{E^{A}_{lu} - E^{S}_{ho}}$$

It is directly related to the corresponding energy (E^{A}_{lu}) of the isolated acceptor molecule. The corresponding wave function (to first order, unnormalized) is

$$[2] \quad |l_{AS}\rangle = |l_A\rangle + \frac{\langle l_A|H^S|h_S\rangle}{E^{A}_{lu} - E^{S}_{ho}}|h_S\rangle$$

H^S is the solute–solvent interaction Hamiltonian; $|l_A\rangle$ and $|h_S\rangle$ are the zeroth order lowest unoccupied orbital of the acceptor and the highest occupied orbital of the solvent (donor), respectively; E^{A}_{lu} and E^{S}_{ho} are the corresponding energies. The interaction between the levels E_{ho} of the acceptor and E_{lu} of the donor will be neglected. On the other hand, the donor reagent (D) attacks the species AS to form a new intermediate SAD. The lowest unoccupied level of the AS complex of energy E^{AS}_{lu} and wave function $|l_{AS}\rangle$, interacts with the highest occupied

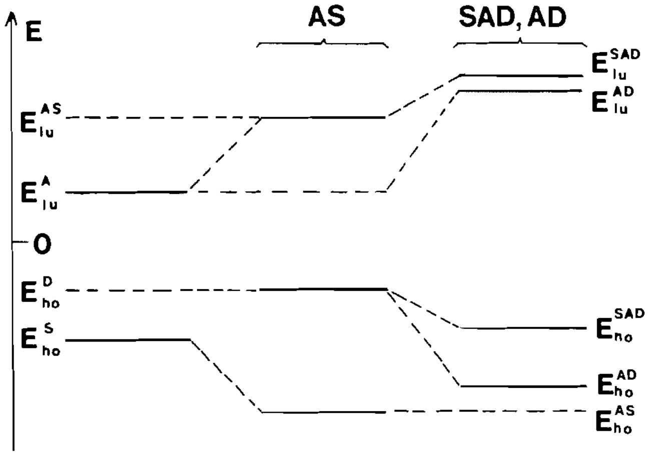

FIG. 2. Variation of energies of the highest occupied (E^{i}_{ho}) and lowest unoccupied (E^{i}_{lu}) orbitals of the interacting partners according to second order perturbation theory.

molecular orbital (E^{D}_{ho}, $|h_D\rangle$) of the donor reagent (D). The energy of the highest occupied level of the actual intermediate (E^{SAD}_{ho}) is given by

$$[3] \quad E^{SAD}_{ho} = E^{D}_{ho} + \frac{\langle l_{AS}|H^D|h_D\rangle^2}{E^{D}_{ho} - E^{AS}_{lu}}$$

where H^D is the perturbing Hamiltonian. Substituting eqs. [1] and [2] (normalized) into eq. [3] and remembering that $\langle h_S|H^D|h_D\rangle = 0$ in the zero differential overlap approximation (i.e., the donor reagent is not influenced by donor solvents) one obtains:

$$[4] \quad E^{SAD}_{ho} = E^{D}_{ho} + \langle l_A|H^D|h_D\rangle^2 \left[(E^{D}_{ho} - E^{A}_{lu}) - \frac{\langle l_A|H^S|h_S\rangle^2}{E^{A}_{lu} - E^{S}_{ho}} + \left(\frac{\langle l_A|H^S|h_S\rangle}{E^{A}_{lu} - E^{S}_{ho}}\right)^2 (E^{D}_{ho} - E^{A}_{lu}) - \left(\frac{\langle l_A|H^S|h_S\rangle}{E^{A}_{lu} - E^{S}_{ho}}\right)^4 (E^{A}_{lu} - E^{S}_{ho})\right]^{-1}$$

The last two higher order terms in the denominator may be safely neglected except when $(E^{A}_{lu} - E^{S}_{ho}) = (E^{A}_{lu} - E^{D}_{ho})$ in which case the third term becomes identical to the second one and it will be no longer negligible. The matrix element $\langle l_A|H^D|h_D\rangle \equiv K_1$ is constant throughout since it involves the same interacting partners, i.e., the two reagents. For the same reason $(E^{D}_{ho} - E^{A}_{lu}) \equiv K_2$. Since the solvents used are quite similar it is supposed that the matrix element $\langle l_A|H^S|h_S\rangle \equiv K_3$ does not vary much in the class of π-donor solvents and it may safely be considered as constant. Hence

$$[5] \quad E^{SAD}_{ho} = E^{D}_{ho} + \frac{K_1^2}{K_2 - K_3^2(E^{A}_{lu} - E^{S}_{ho})^{-1}}$$

This equation shows that when $(E^{A}_{lu} - E^{S}_{ho})$ decreases the acceptor–solvent interaction increases leading to a reduced absolute value of $(E^{SAD}_{ho} - E^{D}_{ho})$ (Fig. 2). This means that the intermediate charge transfer complex C' involving the solvent is less stabilized than the complex C which contains only the reagents.

The change in reagent (i.e., intermediate complex C') stability is directly related to the activation enthalpy $\Delta H^{\ddagger}$ through the Polányi–Evans–Bell principle (22, 23):

$$[6] \quad \Delta H^{\ddagger} = a + bE^{SAD}_{ho}$$

where a and b are constants (see also Fig. 1). This relation is valid in a homologous series if the various potential hyper-

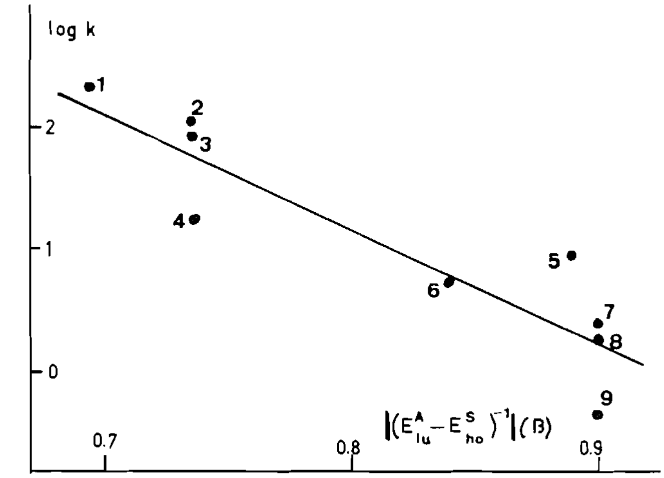

FIG. 3. Dependence of rate constants on the energy separation of interacting orbitals (eq. [7]).

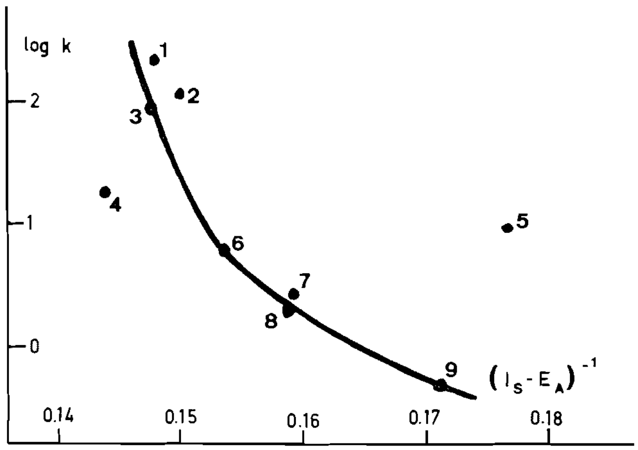

FIG. 4. Influence of solvent ionization potential on the reaction rate (eq. [8]).

surfaces do not cross and if the activation entropy remains reasonably constant. Therefore we have $\log k \sim -\Delta H^{\ddagger}$. Using eqs. [5] and [6] a new relationship is obtained which relates the experimental rate constants to the stabilization energy of the intermediate complex:

$$[7] \quad \log k = P + Q[1 - K(E^{A}_{lu} - E^{S}_{ho})^{-1}]^{-1}$$

where P, Q, and K are composite constants. By substituting the data of Table 1 into eq. [7] together with the value (Hückel approximation) $E^{A}_{lu} = -0.36\beta$ (27) of tetracyanoethylene one obtains Fig. 3 when $\log k$ is plotted as a function of $|(E^{A}_{lu} - E^{S}_{ho})^{-1}|$: $\log k = 8.63(\pm 1.32) - 9.29(\pm 1.62)|(E^{A}_{lu} - E^{S}_{ho})^{-1}|$, $r = 0.91$, $\sigma = 0.40$. It can be seen that the prediction of our model is corroborated by experiment: the reaction rate diminishes when the solvent–tetracyanoethylene interaction increases. It seems that the dispersion of certain points might be due to the simple first order approach used to calculate the E^{S}_{ho} values. As a consequence some solvents cannot be differentiated from each other (see Table 1). However, going to second order intramolecular perturbation does not much improve the situation (26).

A much better correlation is obtained when the theoretical energies are replaced by experimental values. According to Koopmans' theorem the energy of the highest occupied molecular orbital is directly related to the ionisation potential and by extension that of the lowest unoccupied orbital is given by the electron affinity. Therefore we have

$$E^{S}_{ho} = -I_S \text{ and } E^{A}_{lu} = -E_A$$

Using this substitution together with $E_A = 2.3$ eV (5), one obtains eq. [8] and Fig. 4:

$$[8] \quad \log k = P + Q[1 - K(I_S - E_A)^{-1}]^{-1}$$

It can be seen that both the monotonic decrease of reactivity with increasing $(I_S - E_A)^{-1}$ and the curved behaviour are correctly represented as required by eq. [7]. It should be noted that α-methylnaphthalene deviates considerably from the observed correlation. However, this behaviour disappears when empirical solvent effect parameters are used to account for specific effects (12).

In conclusion, it appears that simple intermolecular perturbation theory can successfully account for the specific solvent effect stemming from the π-donor ability of solvent molecules shedding new light on the behaviour of intermediate molecular complexes.

Experimental

Tetracyanoethylene (UCB) was purified by several sublimations while anthracene (UCB) was recrystallized from ethanol. All the solvents (Aldrich) used have been refluxed over P_2O_5 for 24 h and freshly distilled before use. The kinetic measurements have been carried out using a CARY 16 spectrophotometer according to standard procedure described in the literature (17, 21). The temperature was kept constant at 20 ± 0.1°C.

1. J. A. PRYDE. The liquid state. Hutchinson, London. 1969.
2. CHR. REICHARDT. Lösungsmittel-Effecte in der Organischen Chemie. Verlag Chemie, Weinheim, Bergstrasse. 1969.
3. M. J. DEWAR and R. C. DOUGHERTY. The PMO theory in organic chemistry. Plenum Press, New York. 1975.
4. K. FUKUI, T. YONEZAWA, and C. NAGATA. Bull. Chem. Soc. Jpn. **27**, 423 (1954).
5. L. E. LYONS and L. D. PALMER. Aust. J. Chem. **29**, 1919 (1976).
6. R. C. DOUGHERTY. Tetrahedron Lett. **6**, 385 (1975).
7. C. SANDORFY, R. BUCHET, P. HOBZA, and P. RUELLE. J. Mol. Struct., Theochem. **107**, 251 (1984).
8. O. B.NAGY, J. B.NAGY, and A. BRUYLANTS. J. Chem. Soc. Perkin Trans. II, 968 (1972).
9. S. DUPIRE, J. M. MULINDABYUMA, J. B.NAGY, and O. B.NAGY. Tetrahedron, **31**, 135 (1975).
10. J. B.NAGY, O. B.NAGY, and A. BRUYLANTS. Bull. Soc. Chim. Belg. **82**, 539 (1973).
11. O. B.NAGY and J. B.NAGY. *In* Environmental effects on molecular structure and properties. *Edited by* B. Pullman. D. Reidel Publishing Co., Dordrecht, Holland. 1976. p. 179.
12. O. B.NAGY, M. WA MUANDA, and J. B.NAGY. J. Phys. Chem. **83**, 1961 (1979).
13. O. B.NAGY, M. WA MUANDA, and J. B.NAGY. J. Chem. Soc. Faraday Trans. I, **74**, 2210 (1978).
14. R. HUISGEN, L. A. FEILER, and P. OTTO. Tetrahedron Lett. **43**, 4485 (1968).
15. J. SAUER and R. SUSTMANN. Angew. Chem. Int. Ed. Engl. **19**, 779 (1980).
16. O. B.NAGY and A. VANDERMENSBRUGGHE. To be published.
17. P. BROWN and R. C. COOKSON. Tetrahedron, **21**, 1977 (1965).
18. V. I. VEDENEYEV, L. V. GURVICH, V. N. KONDRATYEV, V. A. MEDVEDEV, and YE. L. FRANKEVICH. Bond energies, ionization potentials and electron affinities. E. Arnold, London. 1966.
19. P. RYS. Acc. Chem. Res. **9**, 345 (1976).
20. D. MUKANA, J. B.NAGY, O. B.NAGY, and A. BRUYLANTS. Bull.

Soc. Chim. Belg. **83**, 201 (1974).
21. V. D. KISELEV and J. G. MILLER. J. Am. Chem. Soc. **97**, 4036 (1975).
22. M. G. EVANS and M. POLANYI. Trans. Faraday Soc. **32**, 1340 (1936).
23. R. P. BELL. Proc. R. Soc. London, A**154**, 414 (1936).
24. H. F. HAMEKA. Advanced quantum chemistry. Addison Wesley, Reading, USA. 1965.
25. E. HEILBRONNER and H. BOCK. Das HMO-Modell und seine Anwendung. Verlag Chemie, Weinheim/Bergstrasse. 1970.
26. O. B.NAGY, S. DUPIRE, and J. B.NAGY. Tetrahedron, **31**, 2453 (1975).
27. W. M. MOREAU and K. WEISS. J. Am. Chem. Soc. **88**, 204 (1966).

The search for fluorescence and the study of radiationless transitions of electronic excited states of NH_3^+

GÉRALD DUJARDIN AND SYDNEY LEACH

Laboratoire de Photophysique Moléculaire du C.N.R.S., Bâtiment 213, Université Paris-Sud, 91405 Orsay Cédex, France

Received July 16, 1984

This paper is dedicated to Professor Camille Sandorfy on the occasion of his 65th birthday

GÉRALD DUJARDIN and SYDNEY LEACH. Can. J. Chem. **63**, 1386 (1985).

Photoion – fluorescence photon coincidence experiments were carried out in order to detect the fluorescence of NH_3^+ which is expected to occur from that part of its $\tilde{A}$ electronic state that lies below the lowest dissociation limit. HeI and NeI sources were used to produce the ions. No NH_3^+ fluorescence was detected and upper limits for its quantum yield under our experimental conditions are given. We show that the lifetime of the $\tilde{A}$ state is probably very long, making it difficult to observe fluorescence. Furthermore, we argue that the molecular parameters and potential energy surfaces of the $\tilde{A}$ and $\tilde{X}$ states are such that resonance limit nonradiative coupling to high rovibrational levels of the $\tilde{X}$ state could be an efficient process for apparent intramolecular quenching of NH_3^+ $\tilde{A}$ state fluorescence.

GÉRALD DUJARDIN et SYDNEY LEACH. Can. J. Chem. **63**, 1386 (1985).

Une partie de l'état électronique $\tilde{A}$ de NH_3^+ se trouve en dessous de la limite de dissociation de cet ion. On a essayé de détecter la fluorescence de l'état $\tilde{A}$ par la technique de coincidences entre photoion et photon de fluorescence, en utilisant des sources HeI et NeI pour former les ions. Aucune fluorescence de NH_3^+ n'a été détectée; on donne des valeurs limites supérieures pour le rendement quantique dans nos conditions expérimentales. On montre que la durée de vie de l'état $\tilde{A}$ est probablement très longue, ce qui rend difficile l'observation de la fluorescence. De plus, on montre que les paramètres moléculaires et les surfaces d'énergie potentielle des états $\tilde{A}$ et $\tilde{X}$ devraient permettre un couplage non radiatif, de type limite de résonnance, aux niveaux rovibrationnels élevés de l'état $\tilde{X}$. Ceci correspond à un processus efficace pour l'extinction intramoléculaire apparente de la fluorescence de l'état $\tilde{A}$ de NH_3^+.

1. Introduction

Previous studies of the relaxation of excited electronic states of the gas phase ammonia cation have essentially been concerned with the dissociative mode (1).

The threshold of the lowest dissociative channel, $NH_3 + h\nu \rightarrow NH_2^+ + H + e^-$, is at 15.768 ± 0.008 eV as determined by photoionization mass spectrometry (2). This corresponds to an energy within the second photoelectron band (3, 4), forming the $\tilde{A}^2E'$ state of NH_3^+, which extends approximately from 14.98 to approximately 18 eV. Predissociation appears to be 100% above the threshold (5). However, since the origin of the first excited electronic state of NH_3^+, at 14.98 eV, lies below the first dissociation limit, radiative relaxation to the ground state of the ion at 10.15 eV is conceivable. Indeed Herzberg and Lew (6, 7) have observed an emission spectrum in the 2200–2400 Å region by electron beam excitation of a low pressure jet of ammonia gas. A band near 2338 Å was provisionally assigned to NH_3^+, whereas other features in this spectral region are possibly due to NH_2 or NH_2^+ (7). Electronic spectra of these species are of astrophysical interest, especially for cometary science.

In the present work we investigate whether NH_3^+ emits photons, by measurement of the fluorescence quantum yield of this ion using a photoion – fluorescence photon coincidence (PIFCO) (8, 9) technique. In an earlier attempt to measure this quantum yield, Devoret failed to find NH_3^+ fluorescence (10), but his experiment was carried out with a PIFCO apparatus of much lesser sensitivity (8) than the one used here (9).

The photoions are produced by excitation of NH_3 with HeI (21.22 eV) or NeI (16.85, 16.67 eV) radiation. In this excitation range, only two electronic states of the ammonia ion can be formed, the $\tilde{X}^2A_2''$ ground state and $\tilde{A}^2E'$ excited state, whose electron configurations and adiabatic ionization potentials (IP) (3, 4) are as follows:

$$(1a_1')^2\,(2a_1')^2\,(1e')^4\,(1a_2'')^1\ \tilde{X}^2A_2''\ \text{IP (adiab.)} = 10.15\ \text{eV}$$

$$(1a_1')^2\,(2a_1')^2\,(1e')^3\,(1a_2'')^2\ \tilde{A}^2E'\ \text{IP (adiab.)} = 14.98\ \text{eV}$$

The ion is assumed to have a D_{3h} planar geometry, at least in its ground state (see later), in conformity with the quasi-planar structure of the isoelectronic species CH_3 (11, 12).

2. Experimental and results

The photoion – fluorescence photon coincidence (PIFCO) technique has been described in detail elsewhere (8, 9) and only a short outline will be given here. NH_3 molecules are photoionized in a gas jet issuing from a hypodermic needle, using dc rare gas lamp sources (HeI, 21.22 eV; NeI, 16.85, 16.67 eV) mounted on a VUV monochromator. In our experiments the pressure of NH_3 was in the range 10^{-3} – 10^{-4} Torr (1 Torr = 133.3 Pa). Photoions and photoelectrons are accelerated away from the region of formation by an electric field ($\cong$100 V cm^{-1}) towards microchannel plates and a channeltron respectively. Fluorescence photons emitted from excited ions or molecules are detected at right angles by an EMI 9635QB photomultiplier (NeI excitation) or via a glass lens system and a cooled Hamamatsu R943 photomultiplier (HeI excitation). The fluorescence wavelength detection range was 175–360 nm and 380–910 nm with the respective photomultipliers.

Photoion–photoelectron coincidences are first recorded and give a time-of-flight mass analysis of parent and fragment photoions. After this analysis, which enabled us to identify the NH_3^+ time-of-flight, coincidences between fluorescnce photons and NH_3^+ photoions were counted as a function of delay time, together with the total number of photoions.

The fluorescence efficiency $\eta_F(NH_3^+)$ of the NH_3^+ ion can be deduced from the ratio N_c/N_i where N_c is the number of NH_3^+ photoion – fluorescence photon coincidences and N_i the number of photoions detected in the same time interval. Instrumental factors are determined and calibration carried out by experiments with N_2^+ $B^2\Sigma_u^+ - X^2\Sigma_g^+$ emission, which has unit fluorescence quantum yield (8, 9).

Coincidence counts between NH_3^+ ions and fluorescence photons were made under the following experimental conditions for HeI excitation: photon count rate, 10 photons/s; ion count rate, 6500 ions/s; cumulative count time, 120 h; photon detection region 380–910 nm with a Hamamatsu R943 photomultiplier. Experiments were also carried out with NeI excitation, using an EMI 9635QB photomultiplier (175–630 nm), which is several times more sensitive than the Hamamatsu photomultiplier over the common spectral detection range; cumulative count time was 13 h.

The PIFCO signal showed no evidence for NH_3^+ fluorescence. From the noise level in the false coincidence spectrum, using a coincidence gate open time of 500 ns, we determine the following upper limiting values of the fluorescence efficiency $\eta_F(NH_3^+)$:

HeI excitation, 380–910 nm detection range:

$$\eta_F(NH_3^+) < 4 \times 10^{-5}$$

NeI excitation, 175–630 nm detection range:

$$\eta_F(NH_3^+) < 2.5 \times 10^{-4}$$

The fluorescence quantum yield of an ion M^+ in the jth electronic state, averaged over accessible vibrational levels of this state, is given by the relation:

$$\bar{\Phi}_F(M^+, j) = \eta_F(M^+, j)/f(j)$$

where $f(j)$ is the branching ratio for forming the jth state with the particular excitation source used.

In the case of the $\tilde{A}(^2E')$ state of NH_3^+, a value of $f(\tilde{A}) \approx 0.75$ is obtained for HeI excitation (13, 14); electron impact dipole (e, 2e) coincidence measurements give $f(\tilde{A}) \approx 0.8$ for an excitation energy of 21.22 eV (15). NeI photons (16.85, 16.67 eV) are in the same energy range as the $\tilde{A}^2E'$ state of NH_3^+, which is moreover a region of incomplete ionization (1, 15). Thus it is difficult to obtain reliable $f(\tilde{A})$ values for NeI excitation. A calculated value $f(\tilde{A}) = 0.52$ has been given for 16.85 eV excitation energy (13).

The upper limiting value for the fluorescence quantum yield under our experimental conditions is:

$$\text{HeI excitation: } \bar{\Phi}_F(NH_3^+\ \tilde{A}^2E') < 5 \times 10^{-5}$$

Using the theoretical value of $f(\tilde{A}) = 0.52$ for NeI excitation, one obtains in this case:

$$\bar{\Phi}_F(NH_3^+\ \tilde{A}^2E') < 5 \times 10^{-4}$$

We recall that the fluorescence efficiency, and thus the $\bar{\Phi}_F$ values, were determined using a coincidence gate open time of 500 ns.

3. Discussion

The very low upper limiting value for NH_3^+ $\tilde{A}^2E'$ fluorescence indicates that it would be extremely difficult to observe a dispersed emission spectrum of NH_3^+. It is therefore highly unlikely that any of the observed features in the emission spectrum in the 2200–2400 Å region reported by Herzberg (6, 7) is due to NH_3^+.

The absence of $\tilde{A}^2E'$ state fluorescence from NH_3^+ vibronic levels between 14.98 and 15.77 eV could result from one, or the conjunction of a number of causes. Before presenting the relevant arguments, it is necessary to discuss the geometry of the $\tilde{A}$ and $\tilde{X}$ electronic states of NH_3^+.

From calculations and analysis of the first band in the photoelectron spectrum of NH_3, the ground state of the ion has been shown to be planar (13, 16, 17), as is the corresponding state of the isoelectronic species CH_3 whose optical spectrum has been analyzed (11, 12). However, although the $\tilde{A}^2E'$ state is usually expected to be pyrimidal (13), there is no direct evidence for this structure. On the basis of SCF calculations, Köppel *et al.* (18) do derive a C_{3v} structure for this state. However, it should be stated that for the analogous state of the isoelectronic species CH_3, calculations also predict a C_{3v} structure (19), but that a search for the $\tilde{A}^2E' - \tilde{X}^2A_1$ (C_{3v} notation) transition, which is optically allowed for a C_{3v} upper state, has been fruitless (11); we remark that this transition is forbidden in strict D_{3h} symmetry (see later).

Whether an XH_3 species will be pyrimidal or planar depends on a critical balance of opposing forces (20–22). Furthermore, existing calculations on the electronic states of NH_3^+ were made in order to interpret photoelectron spectra. In these calculations, a planar structure was imposed on the $\tilde{X}$ state (17), a pyrimidal structure on the $\tilde{A}$ state (18). The existence of a Jahn–Teller effect in the $\tilde{A}$ state adds to the complications of interpretation (13). Thus although one can advance reasonable theoretical arguments in favour of a pyrimidal structure for the $\tilde{A}$ state, we consider it best to retain an open mind on this question. The discussion which follows will therefore consider both possible structures, D_{3h} and C_{3v}, for the $\tilde{A}$ state of NH_3^+.

A. *The strength of the* $\tilde{A} \rightarrow \tilde{X}$ *radiative transition*

The $\tilde{A}^2E' - \tilde{X}^2A_2''$ transition is electric dipole forbidden if both electronic states are planar. In principle, the excitation of an a_2'' or an e' vibration in either upper or lower state could create a vibronically (Herzberg–Teller) (24) induced transition. The strength of the vibronic interaction depends on the proximity of a third electronic state having an allowed dipole transition to either the $\tilde{A}^2E'$ or $\tilde{X}^2A_2''$ states. The closest known state of this type is the $(2a_1'^{-1})\ ^2A_1'$ level which is at about 12 eV above $\tilde{A}^2E'$ and 17 eV above $\tilde{X}^2A_2''$ (3, 15, 23). For the large energy intervals, ΔE, involved, we predict that any Herzberg–Teller induced transition strength, which is a function of $(\Delta E)^{-2}$ (24), will be small. Thus we expect $\tau(\tilde{A})$, the lifetime of the $\tilde{A}^2E'$ state, to be long. If $\tau(\tilde{A})$ is greater than $\approx 50\ \mu s$, a true coincidence PIFCO signal would not be detectable unless the cumulative count time was impracticably long, i.e. one or more orders of magnitude greater than in the present experiments. If this is indeed the case, the true fluorescence quantum yield could be of the order of unity, our low value of $\bar{\Phi}_F$ being an effective value under our experimental conditions. Indeed, we estimate that under our experimental conditions $\tau(\tilde{A}) > 400\ \mu s$ if $\bar{\Phi}_F = 1$.

We remark, however, that this discussion posits a D_{3h} symmetry for both the $\tilde{A}$ and $\tilde{X}$ states. In the event that one of these states has a lesser symmetry, one must consider the common symmetry elements of the two states. If the $\tilde{A}$ state belongs to the C_{3v} point group, the $\tilde{A}$–$\tilde{X}$ transition would then become formally allowed and one would expect both ν_1 and ν_2 to be active vibrations since they become totally symmetric in the reduced point group. Thus, the $\tilde{A}$–$\tilde{X}$ transition may be considerably stronger, and the lifetime of the $\tilde{A}$ state considerably shorter, than would occur if a rigorous D_{3h} group symmetry applied.

B. *Intramolecular radiationless coupling*

B.1. *Coupling with the* $\tilde{X}$ *state*

Since no emission is observed, relaxation of the $\tilde{A}$ state below the dissociation limit must occur via an intramolecular process and implies, in the first instance, coupling of $\tilde{A}$ with isoenergetic levels of the $\tilde{X}$ state. In this case, not only the electronic matrix element coupling the two states must be nonzero but also the Franck–Condon vibrational overlap integrals $\langle\psi_v(\tilde{A})|\psi_v(\tilde{X})\rangle$. For the latter condition to be met requires that the potential energy surfaces of the $\tilde{A}$ and $\tilde{X}$ states approach each other or even intersect at energies in the 15-eV region.

Before examining the situation of the potential energy surfaces we will first consider another parameter, the density of vibrational levels ρ_v of the $\tilde{X}$ state in the $\tilde{A}$ state region. The order of magnitude of ρ_v provides an indication as to the particular case of the radiationless transition to be expected, each case having its own physical characteristics: resonance limit ($\rho_v \lesssim 10^2$ states/cm^{-1}), intermediate case ($\rho_v \approx 10^4 - 10^5$ states/cm^{-1}), or statistical limit ($\rho_v \gg 10^5$ states/cm^{-1}) (25). The density of states ρ_v was calculated by Haarhoff's approximation (26) to the harmonic density of states, using the following vibrational frequencies (in cm^{-1}), $\nu_1(a_1') = 3340$, $\nu_2(a_2'') = 950$, $\nu_3(e') = 3445$, $\nu_4(e') = 1630$, which were assumed to be the same in NH_3 (27) and NH_3^+. This calculation gave the following values: $\rho_v = 18$ states/cm^{-1} at the $\tilde{A}$ state origin level energy, and $\rho_v = 33$ states/cm^{-1} at the dissociation threshold. In spite of the approximations involved, these results should provide reliable order of magnitude values for ρ_v. The values obtained indicate that intramolecular coupling, if it exists, between the $\tilde{A}$ and $\tilde{X}$ states would correspond to the resonance limit of radiationless transitions. In this case one would expect lifetime lengthening of the $\tilde{A}$ state with respect to what might be expected on the basis of the integrated absorption intensity (apparent oscillator strength), i.e. manifestations of the Douglas effect (28). This would enhance the possibility of the existence and consequences of a long radiative lifetime, discussed in a previous section.

In discussing now the vibrational parameters involved in an $\tilde{A}$, $\tilde{X}$ intramolecular coupling process we first pay attention to the promoter modes. The D_{3h} symmetry selection rule for intramolecular radiationless coupling between the $\tilde{A}^2E'$ and $\tilde{X}^2A_2''$ states induced by vibrations (we neglect Coriolis coupling) is that the product $A_2'' \times E' \times \Gamma_v = A_1'$, where Γ_v is the representation of the vibrational mode(s) excited. This is satisfied by the condition $\Gamma_v = e''$; however, NH_3^+ is a "symmetry deficient" molecule in the Kasha sense (29), in that there is no vibrational mode of e'' symmetry. Therefore single one-quantum vibrations cannot correspond to promoting modes. Two quantum combinations $\nu_2(a_2'') + \nu_3(e')$ or $\nu_2(a_2'') + \nu_4(e')$ could give $\Gamma_v = e''$; however, these would be of second-order strength in inducing the $\tilde{A} \rightsquigarrow \tilde{X}$ radiationless transition. If the $\tilde{A}$ state has a C_{3v} structure, then each and any of the four vibrational modes could be single quantum promoting modes.

We now consider the relevant potential energy functions of the $\tilde{A}$ and $\tilde{X}$ states in order to investigate other parameters involved in both radiative and nonradiative transitions. Excitation of NH_3 with HeI or NeI radiation will form a progression of ν_2 vibrational levels in the $\tilde{A}$ state, and will also excite one or both of the e' vibrations (ν_3, ν_4) which induce Jahn–Teller coupling in this state (3, 4). Furthermore, because of the bonding nature of the $1e'$ orbital, there will be an important change of the r(NH) distance in forming the $\tilde{A}$ state, thus the a_1' vibration is also expected to be excited (18). We consider first the bending potential.

In Fig. 1 are shown potential energy functions of the ν_2 bending mode for NH_3^+ in the $\tilde{X}$ and $\tilde{A}$ states; the curves are adapted from published figures (17, 18) resulting from theoretical calculations made in order to interpret the vibrational

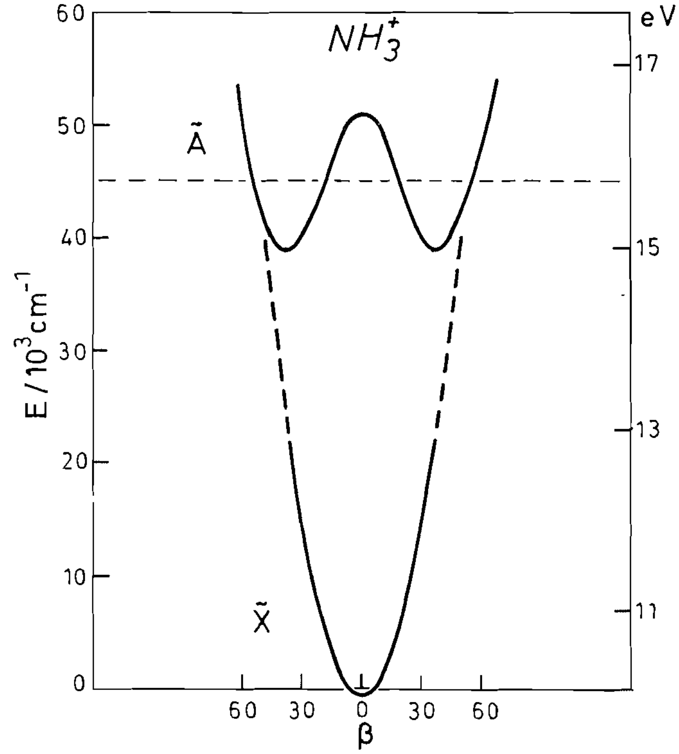

FIG. 1. Potential energy functions of the ν_2 bending mode of NH_3^+ in its $\tilde{X}$ ground state and $\tilde{A}$ first excited electronic state. β is the angle (in degrees) between an N—H bond and the plane vertical to the C_3 rotation axis. The horizontal dashed line at 15.77 eV coresponds to the threshold energy of the lowest dissociation channel $NH_3 + h\nu \rightarrow NH_2^+ + H + e^-$.

structure in the photoelectron spectrum of ammonia. The abscissa represents the angle β between the N—H bonds and the plane vertical to the C_3 rotation axis. The $v = 0$ energies of the states have been adjusted to their experimental values. We use this figure to make some qualitative statements, as follows.

(*i*) *Radiative transitions*: the equilibrium structure of the $\tilde{A}$ state is apparently pyrimidal, that of the $\tilde{X}$ state is planar. However, no geometry optimization was carried out for different bond angles (17, 18). On the basis of the equilibrium structures in Fig. 1, the D_{3h} symmetry selection rules for both radiative and nonradiative transitions between the $\tilde{A}^2E'$ and $\tilde{X}^2A_2''$ states will be somewhat relaxed. However, we note that radiative transitions from occupied vibrational levels in the $\tilde{A}$ state below the dissociation limit will have very high vibrational levels of the $\tilde{X}$ state as their final states. Thus the individual Franck–Condon factors for the vibrational components of an $\tilde{A} \rightarrow \tilde{X}$ transition will tend to be small, so that any emission from the $\tilde{A}$ state will be spread out over a very wide spectral region, rendering more difficult its detection.

(*ii*) *Nonradiative transitions*: extrapolation (thick dashed line) of the $\tilde{X}$ potential energy curve to higher energies indicates that it approaches close to the $\tilde{A}$ surface. This is conducive to intramolecular radiationless coupling between $\tilde{A}$ and $\tilde{X}$. The possibility of $\tilde{A}$, $\tilde{X}$ interaction might be amplified by concomitant Jahn–Teller effects involving e' vibration excitation. Furthermore, Köppel[1] has recently taken into account simultaneous shortening of the N—H bond in going from $\tilde{A}$ to $\tilde{X}$. He finds that the energy of the crossing between $\tilde{A}$ and $\tilde{X}$ is strong-

[1] H. Köppel, private communication (1983).

ly lowered and concludes that consideration only of the pure bending potential energy curves underestimates the importance of the $\tilde{A}-\tilde{X}$ conical intersection. The latter will, of course, give rise to strong non-adiabatic effects which would reinforce the Franck–Condon factors in $\tilde{A}-\tilde{X}$ coupling.

B.2. *Coupling with other states*

We now consider the possibility of states other than the $\tilde{X}$ state as final (or intermediate) states in intramolecular coupling with the $\tilde{A}$ state.

Low-lying $^2A_1'$ *Rydberg state*

Based on Walsh-rules arguments one can predict that the lowest Rydberg state of NH_3^+ should be planar and have the electron configuration $(1a_1')^2\,(2a_1')^2\,(1e')^4\,(3a_1')^1$ and electronic symmetry $^2A_1'$. The analogous state has been observed in optical absorption of the isoelectronic species CH_3 (11). According to Walsh-type diagrams (22), for a planar configuration, the vertical transition energy $(1e')^3\,(2a_2'')^2\,{}^2E' \leftarrow (1e')^4\,(2a_2'')^1\,{}^2A_2''$ would be expected to be greater than $(1e')^4\,(3a_1')^1\,{}^2A_1' \leftarrow (1e')^4\,(2a_2'')^1\,{}^2A_2$. Calculations of the Rydberg state have not been made, but for CH_3, *ab initio* SCF calculations (19) of vertical energies have been carried out for both the $^2E'$ and $^2A_1'$ states. For the $^2A_1'$ state the calculated energy agrees well with that observed; it is predicted to have an energy 71% of that of the $^2E'$ state. The $(3a_1')^1\,{}^2A_1'$ state of NH_3^+ is not accessible by photoelectron spectroscopy of NH_3 since its formation would involve a two-electron transition. If we assume that this state lies lower than $^2E'$ by the same proportion as that calculated for CH_3, then we would expect the vertical energy of the $3a_1'\,{}^2A_1'$ state of NH_3^+ to lie at $\approx$14.3 eV. Let us call this Rydberg state $\tilde{R}(^2A_1')$.

If the $\tilde{R}(^2A_1')$ state does indeed lie in this energy region, one would expect Herzberg–Teller interaction to occur since $^2A_1' - {}^2A_2''$ corresponds to an allowed dipole transition. If $\tilde{R}(^2A_1')$ and $\tilde{A}(^2E')$ are close in energy, mixed $\tilde{R}$, $\tilde{A}$ states resulting from vibronic close coupling (via e' promoter modes) could have a non-negligible dipole transition moment for radiative coupling with the $\tilde{X}$ state. The absence of observed emission for NH_3^+ implies that the $\tilde{R}(^2A_1')$ state lies well above A^2E', or that it lies considerably below the estimated 14.3 eV energy.[2]

Low-lying quartet state

The lowest quartet state of NH_3^+ would have the (single) electron configuration $(1e')^3\,(1a_2'')^1\,(2a_1')^1$ and thus be doubly excited with respect to the ground state of the ion. Its vertical energy would therefore be greater than either the $(1e')^4\,(2a_1')^1\,\tilde{R}(^2A_1')$ or the $(1e')^3\,(1a_2'')^2\,\tilde{A}(^2E')$ state. Thus we can discount coupling of the optically excited $\tilde{A}^2E'$ state with a low-lying quartet state as a source of intramolecular quenching of NH_3^+ fluorescence.

Conclusion

Although a significant proportion of the $\tilde{A}$ state of NH_3^+ lies below the dissociation limit, our PIFCO measurements have demonstrated that the fluorescence quantum yield of this state is effectively zero under our experimental conditions. We have examined various possible reasons for apparent intramolecular fluorescence quenching. From our discussion we conclude that the lifetime of the $\tilde{A}$ state could be very long, making it difficult to observe fluorescence. Furthermore, the molecular parameters and potential energy surfaces of the $\tilde{A}$ and $\tilde{X}$ states are such that resonance limit nonradiative coupling of the $\tilde{A}$ state to high rovibrational levels of the $\tilde{X}$ state of NH_3^+ is likely to be an efficient intramolecular quenching process. On the other hand we argue that neither the $(1e')^4\,(2a_1')^1\,{}^2A_1'$ Rydberg state, nor a low-lying quartet state of NH_3^+ is involved in the $\tilde{A}$ state relaxation process. Our results show that the emission band near 2338 Å observed in an electron impact experiment in ammonia is unlikely to be due to NH_3^+, as tentatively assigned by Herzberg (6, 7). Detailed information on this potentially important astrophysical species must be sought by experiments other than optical emission spectroscopy.

[2] NOTE ADDED IN PROOF: A recent calculation by A. R. Rossi and P. Avouris (ref. 30) predicts that the $\tilde{R}$ state lies 5–6 eV above the $\tilde{A}$ state.

1. J. BERKOWITZ. Photoabsorption, photoionization and photoelectron spectroscopy. Academic Press, New York. 1979. p. 128.
2. K. E. MCCULLOH. Int. J. Mass Spectrom. Ion Phys. **21**, 333 (1976).
3. A. W. POTTS and W. C. PRICE. Proc. R. Soc. London Ser. A, **326**, 181 (1972).
4. J. W. RABALAIS, L. KARLSSON, L. O. WERME, T. BERGMARK, and K. SIEGBAHN. J. Chem. Phys. **58**, 3370 (1973).
5. B. BREHM and E. VON PUTTKAMER. Adv. Mass Spectrom. **4**, 591 (1968).
6. G. HERZBERG. *In* Interstellar molecules. *Edited by* B. H. Andrew. IAU Symposium 87. 1980. p. 231.
7. G. HERZBERG. J. Phys. Chem. **84**, 2095 (1980).
8. J. H. D. ELAND, M. DEVORET, and S. LEACH. Chem. Phys. Lett. **43**, 97 (1976).
9. G. DUJARDIN, S. LEACH, and G. TAIEB. Chem. Phys. **46**, 407 (1980).
10. M. DEVORET. Thèse 3ème cycle, Université Paris-Sud, 1976.
11. G. HERZBERG. Proc. R. Soc. London Ser. A, **262**, 291 (1961).
12. G. B. ELLISON, P. C. ENGELKING, and W. C. LINEBURGER. J. Am. Chem. Soc. **100**, 2556 (1978), and references therein.
13. J. W. RABALAIS. Principles of ultraviolet photoelectron spectroscopy. Wiley, New York. 1977.
14. Y. ACHIBA, T. YAMAZAKI, and K. KIMURA. J. Electron Spectrosc. Relat. Phenom. **22**, 187 (1981).
15. C. E. BRION, A. HAMNETT, G. R. WIGHT, and M. J. VAN DER WIEL. J. Electron Spectrosc. Relat. Phenom. **12**, 323 (1977); G. R. WIGHT, M. J. VAN DER WIEL, and C. E. BRION. J. Phys. B, **10**, 1863 (1977).
16. W. R. HARSHBURGER. J. Chem. Phys. **56**, 127 (1972); P. AVOURIS, A. R. ROSSI, and A. C. ALBRECHT. J. Chem. Phys. **74**, 5516 (1981).
17. H. ÅGREN, I. REINECK, H. VEENHUIZEN, R. MARIPU, R. ARNEBERG, and L. KARLSSON. Mol. Phys. **45**, 477 (1982).
18. H. KÖPPEL, L. S. CEDERBAUM, W. DOMCKE, and W. VON NIESSEN. Mol. Phys. **35**, 1283 (1978).
19. Y. ISHIKAWA and R. C. BINNING, JR. Chem. Phys. Lett. **40**, 342 (1976).
20. H. NAKATSUJI. J. Am. Chem. Soc. **95**, 354 (1973).
21. B. M. DEB. J. Am. Chem. Soc. **96**, 2030 (1974).
22. J. K. BURDETT. Chem. Soc. Rev. **7**, 507 (1978).
23. M. S. BANNA and D. A. SHIRLEY. J. Chem. Phys. **63**, 4759 (1975).
24. G. HERZBERG and E. TELLER. Z. Phys. Chem. Abt. B, **21**, 410 (1933).
25. S. LEACH, G. DUJARDIN, and G. TAIEB. J. Chim. Phys. **77**, 705 (1980).
26. P. C. HAARHOFF. Mol. Phys. **7**, 101 (1963).
27. G. HERZBERG. Electronic spectra of polyatomic molecules. Van Nostrand, New York. 1966.
28. A. E. DOUGLAS. J. Chem. Phys. **45**, 1007 (1966).
29. P. J. GARDNER and M. KASHA. J. Chem. Phys. **50**, 1543 (1969).
30. A. R. ROSSI and P. AVOURIS. J. Chem. Phys. **79**, 3413 (1983).

Phospholipid–protein molecular interactions. 2. Raman spectroscopic and calorimetric studies of phospholipid–polylysine and phospholipid–histones interactions in model membranes

A. BERTOLUZZA,[1,2] S. BONORA,[1] G. FINI,[1] AND M. A. MORELLI[3]

Centro di Studio Interfacoltà sulla Spettroscopia Raman, Istituto Chimico "G. Ciamician", Università di Bologna, via Selmi 2, 40126 Bologna, Italy

Received July 17, 1984

This paper is dedicated to Professor Camille Sandorfy on the occasion of his 65th birthday

A. BERTOLUZZA, S. BONORA, G. FINI, and M. A. MORELLI. Can. J. Chem. **63**, 1390 (1985).

Dimyristoylphosphatidylcholine (DMPC) – polylysine and DMPC–histones systems have been studied by Raman spectroscopy and differential scanning calorimetry. The results of both techniques indicate that the interactions are mainly confined to the lipid–water interface. The protein fraction of histones giving rise to a partial penetration into the bilayer is not the lysine-rich fraction but rather the non-polar component of the proteins. On the basis of the results obtained, the formation of lipoprotein complexes between histones and DMPC appears to be ruled out.

A. BERTOLUZZA, S. BONORA, G. FINI et M. A. MORELLI. Can. J. Chem. **63**, 1390 (1985).

Faisant appel à la spectroscopie Raman ainsi qu'à la calorimétrie à balayage différenciel, on a étudié les systèmes dimyristoylphosphatidylcholines (DMPC) – polylysine et DMPC–histones. Les résultats obtenus par chacune des techniques indiquent que les interactions sont principalement confinées à l'interface lipide–eau. La fraction de la protéine des histones qui donne lieu à une pénétration partielle de la double couche n'est pas la fraction qui est riche en lysine; il s'agit plutôt de la portion des protéines qui n'est pas polaire. Sur la base des résultats obtenus, il semble que l'on doive exclure la possibilité de formation de complexes entre les histones et le DMPC.

[Traduit par le journal]

Introduction

Molecular interactions between proteins and phospholipids in biomembranes have been shown to play an important role in the regulation of both the structural and dynamical properties of biomembranes and of the biological function of membrane proteins. Intrinsic proteins show non-specific hydrophobic interactions with the hydrocarbon moiety of lipid molecules and the changes in the lipid environment are reflected in the protein activity. On the contrary, extrinsic proteins are bound by means of specific H-bond interactions with the polar head of lipid molecules on the surface of the bilayer. A previous paper (1) was devoted to a characterization of different types of surface binding of polypeptides on the lipid bilayer by means of differential scanning calorimetry and Raman spectroscopy. These interactions on the one hand can display a well-defined topography (which is important in determining the specific local interactions between lipid and extrinsic protein molecules), on the other hand can bring about a change in the core of the lipid membrane.

In an attempt to characterize the interactions between dimyristoylphosphatidylcholine (DMPC) and extrinsic proteins, the binding of polylysine and some basic proteins to DMPC liposomes has been investigated. Histones, which enter in the composition of chromatin, have been chosen as representatives of basic protein; it is known that the nucleohistone component of eukaryotic chromatin is organized as a string of closely packed subunits, called nucleosomes. Histones H4, H3, H2A, and H2B ("inner histones") are present in the core of nucleosomes. Lysine-rich histones H1 and H5 are located outside of the core particle, on the internucleosomal linker region, and are bound to DNA; they modulate the interactions between chromatin and phospholipids (2, 3). The importance of these interactions in the control of the genome activities has been frequently pointed out (4). This work was undertaken as a contribution to the study of the specific interactions between histones with different content of lysine and arginine, and lipidic multilayers.

This work is part of a research programme involving Raman and ir spectroscopic studies of the physico-chemical characterization and biological function of the phospholipids, as the more significant component of biological membranes. It follows previous papers devoted to the nature and strength of the hydrogen bond between phospholipids and proton donors (5), to the interactions between polyglycine and phospholipids (1), and to the interactions between water and cholesterol–phospholipid mixed liposomes and between water and phospholipid in an inert solvent (6).

Experimental

L-α-Dimyristoylphosphatidylcholine (DMPC), polylysine hydrobromide type II (average molecular weight 4000) (PL), histone type III-S from calf thymus (lysine rich, H1), and histone type VI-S from calf thymus (slightly lysine rich and H2A–H4 mixture) were obtained from Sigma Chemical Company; they were used without further purification. The average compositions of histones in lysine and arginine are: lysine 11.8 wt.% and arginine 17.6 wt.% for histone VI-S, lysine 25.6 wt.% and arginine 1.6 wt.% for histone III-S.

DMPC liposomes were prepared by adding the appropriate amount of aqueous solutions of PL or histones and twice-distilled water to a final lipid concentration of about 25 wt.%. The suspensions were incubated overnight at 10°C above the main phase transition temperature and then transferred into glass capillaries (1.5 mm) for Raman measurements.

Vibrational Raman spectra were recorded with a Jasco R-500 spectrometer equipped with a Lexel Ar^+ laser; typical laser power at sample was 300 mW at 488 nm. The spectral resolution was 3–5 cm^{-1}. All samples were contained in a cell holder regulated thermostatically to ±1°C. Eight repeated scans of the C—H and of the C—C

[1] Cattedra di Chimica e Propedeutica Biochimica, Facoltà di Medicina e Chirurgia, Istituto Chimico "G. Ciamician", Università di Bologna, via Selmi 2, 40126 Bologna, Italy.

[2] Author to whom correspondence may be addressed.

[3] Istituto di Scienze Chimiche, Facoltà di Farmacia, Università di Bologna, via S. Donato 15, 40126 Bologna, Italy.

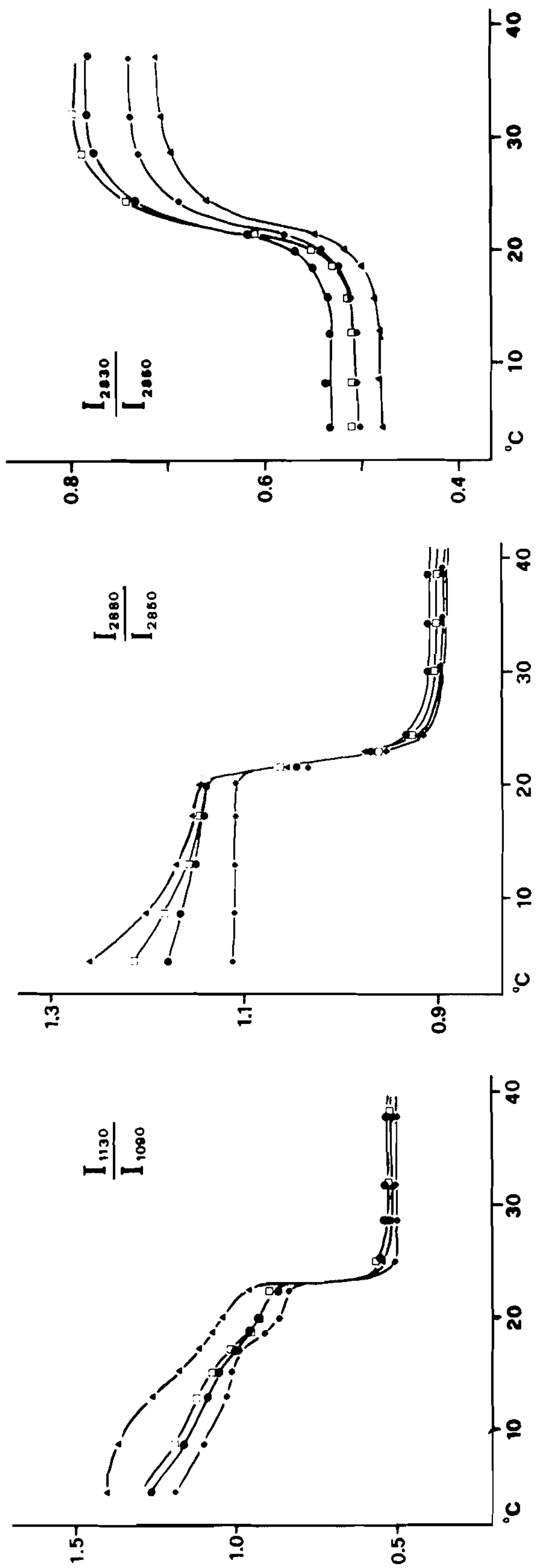

FIG. 1. Melting curves for dispersions of dimyristoylphosphatidylcholine: (▲) DMPC; (●) DMPC + 15% polylysine; (*) DMPC + 15% histone III-S; (□) DMPC + 15% histone VI-S.

stretching mode regions were computer averaged for each temperature to provide high quality spectra. Raman intensities were measured from peak heights (7).

Differential scanning calorimetry (DSC) measurements were obtained on a Mettler DSC 20 calorimeter. The heating rate was 2°C per min. To calibrate the temperature and enthalphy scales, indium samples were used; the temperature scale in the range studied was also calibrated with caprylic acid.

Results and discussion

The structure of the lipid bilayer and the modification induced by the interaction with polypeptides can be described in terms of various kinds of parameters. S_T and S_L order parameters are derived empirically from the $I_{1130\ \mathrm{cm}^{-1}}/I_{1090\ \mathrm{cm}^{-1}}$ and $I_{2880\ \mathrm{cm}^{-1}}/I_{2850\ \mathrm{cm}^{-1}}$ peak height intensity ratios of Raman spectra in the C—C and in the C—H stretching mode regions respectively (8). These parameters are widely used in the analysis of membrane structure by means of Raman spectroscopy, although they are of value only in qualitative analysis (9, 10). More recently Vogel and Stockburger (11) introduced a new order parameter

$$\frac{I_{1130\ \mathrm{cm}^{-1}}}{I_{1090\ \mathrm{cm}^{-1}}} = \frac{c_t P_t}{c_g(1 - P_t) + 0.45}$$

whereby the conformational order is expressed in terms of the probability of finding a C—C bond in a *trans* conformation (P_t) and is related to the $I_{1130\ \mathrm{cm}^{-1}}/I_{1090\ \mathrm{cm}^{-1}}$ intensity ratio. For the systems considered by us, the constant values which appear in the P_t expression have been calculated by assuming $P_t = 1$ in the solid phase at a low temperature (−30°C), and $P_t = 0.62$ for the fluid membrane, according to Vogel and Jänig (12). The assumption that $P_t = 1$ at −30°C is arbitrary because a gel–gel phase transition was observed at −60°C (13); however, P_t does not vary very much in the gel phase when the measured peak intensity ratios are higher than 1 and, consequently, we suppose that our assumption does not introduce a significant error.

Figure 1 shows the $I_{1130\ \mathrm{cm}^{-1}}/I_{1090\ \mathrm{cm}^{-1}}$, $I_{2880\ \mathrm{cm}^{-1}}/I_{2850\ \mathrm{cm}^{-1}}$, and $I_{2930\ \mathrm{cm}^{-1}}/I_{2850\ \mathrm{cm}^{-1}}$ intensity ratios as a function of temperature. The shape of the plot does not change noticeably when PL and proteins are added. In the gel phase some levelling of the curves is noted; this indicates a lowering of the number of C—C bonds in a *trans* conformation and a decrease of the lateral packing in the gel phase. This structure buffering effect has been noted also in the gel phase of DMPC liposomes when polyglycine is added (1).

S_T and S_L order parameters behave similarly to the intensity ratios shown in Fig. 1. The presence of PL and histones decreases both parameters below T_m. The greatest decrease is observed in the presence of histone III-S: S_T decreases by about 5% and S_L by about 30%.

The same conclusions can be drawn on the basis of the previously defined P_t order parameter. In this case the changes are smaller, actually about 2%. According to the order parameter of Vogel (11), the effect of PL and histones is so small that it cannot decrease appreciably the number of C—C bonds in a *trans* configuration in the acylic chains of lipid molecules below T_m ($P_t = 0.90 \pm 0.02$). Likewise, at a temperature above T_m, the behaviour of the P_t order parameter suggests that the number of C—C bonds remaining in a *trans* configuration after the melting does not change by addition of PL and histones ($P_t = 0.63 \pm 0.02$).

Figure 1 shows that the decrease of the lateral packing in the gel phase is maximum for the systems DMPC – histone III-S;

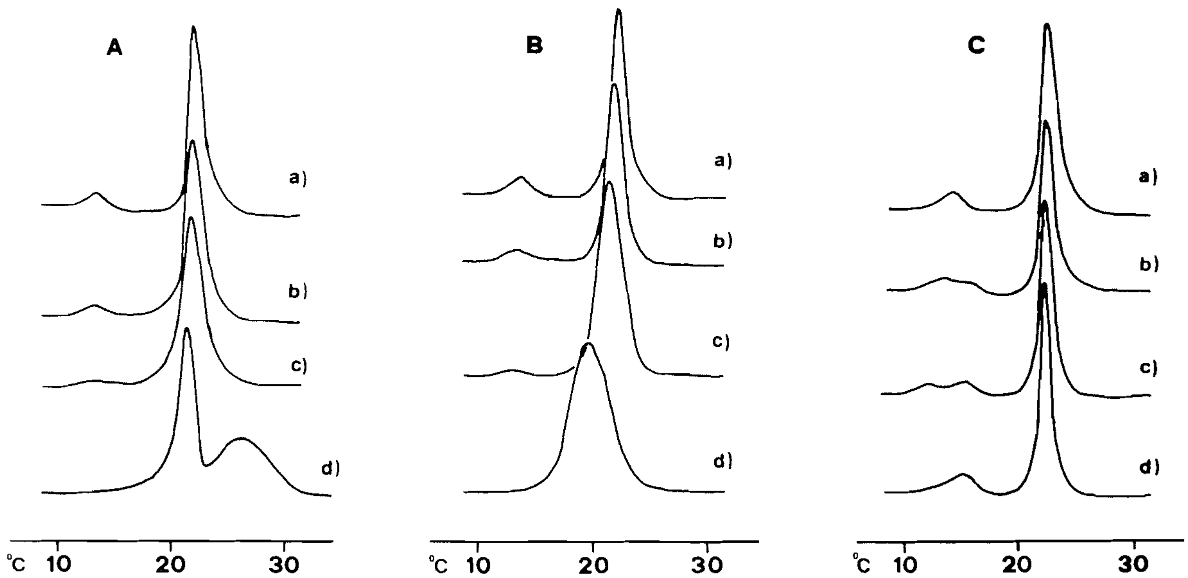

FIG. 2. Differential scanning calorimetry of dimyristoylphosphatidylcholine dispersions with increasing amount of (A) polylysine, (B) histone III-S, and (C) histone VI-S: (a) O wt.%; (b) 10 wt.%; (c) 25 wt.%; (d) 50 wt.%.

TABLE 1. Effects of polylysine and histones on the thermal data for dispersions of dimyristoylphosphatidylcholine

Dispersion	T_m(°C)	ΔH (kcal mol^{-1})
DMPC	22.5	5.4
+ 10% PL	22.3	4.9
+ 25% PL	22.1	4.7
+ 50% PL	21.9	5.4
+ 10% Hist. VI-S	22.8	5.6
+ 25% Hist. VI-S	22.6	5.9
+ 50% Hist. VI-S	22.5	6.3
+ 10% Hist. III-S	21.8	5.6
+ 25% Hist. III-S	21.3	5.9
+ 50% Hist. III-S	19.3	6.1

on the contrary, the effects of PL and histone VI-S are similar. This leads us to conclude that the observed structural modifications induced by histone III-S on the lipid bilayers are not due to the lysine fraction, but rather to the domains containing hydrophobic residues (14).

The $I_{2930\ cm^{-1}}/I_{2850\ cm^{-1}}$ intensity ratios increase both in the gel and in the liquid-crystalline phase when PL or histones are added to the lipid bilayers. PL and histone VI-S show similar effects above T_m; on the contrary, histone III-S induces only a slight enhancement of the measured intensity ratios in the liquid-crystalline phase. Similar effects were observed in DMPC–polyglycine systems and attributed to an increase of the mobility of —CH_3 terminal groups or to a lowering of the symmetry arising from the increased mobility of the acyl chains (1). Nevertheless, the increase observed in the systems actually considered might be far from meaningful because of the overlapping effect due to the strong bands of PL and histones over the 2900–3000 cm^{-1} spectral range (15, 16).

The systems DMPC–PL and DMPC–histones were studied up to a 0.5 w/w polypeptide/lipid weight ratio by means of differential scanning calorimetry. Raman investigations of the systems with the amount of PL and histones greater than 15% were not possible because of the overlapping of the spectra.

Figure 2 shows DSC heating curves of lipid bilayers with increasing amounts of added PL and histones. The presence of PL does not noticeably change T_m, whereas the associated ΔH decreases (Table 1). When a greater amount of PL is present (0.5 w/w) a doubling of the transition is observed, and a broad heat absorption appears at about 27°C. A similar behaviour observed in lipid–cholesterol mixed liposomes has been attributed to a lateral phase separation followed by melting, first of free lipid and then of a lipid–cholesterol complex (14). The presence of this broad absorption and the existence of a phase separation could explain the observed increase of ΔH. DSC heating curves of lipid bilayers with an increasing amount of histone III-S show a decrease of T_m with a broadening of the transition. On the contrary, in the system DMPC – histone VI-S, T_m and the width of the transition do not change, and a weak broad transition appears at about 16°C, its intensity increasing with the amount of histone present. Both histones increase ΔH of the main transition by about 15% for the systems with a 0.5 w/w ratio.

Conclusions

Polylysine exhibits mainly superficial interactions with dimyristoylphosphatidylcholine bilayers, as our Raman and DSC results suggest, both through the persistence of the pretransition, at least in the systems with a low amount of PL, and through the unaltered cooperativity of the melting processes as deduced from the width of the main transition. The presence of a broad transition at 27°C could be attributed to a phase separation induced by the great quantity of PL. The double melting process should indicate the setting up of regions with different amounts of bound PL on the bilayer surface.

PL–lipid molecular interactions are mainly due to the electrostatic binding between the polar groups of phospholipid and PL molecules, according to the literature data (17, 18). As a consequence of these superficial interactions, interchain interactions decrease, the rotational freedom of acyl chains increases in the gel phase, and the polarity of the hydrocarbon chain environment also increases, probably because of the penetration of water into the bilayers. A proof of the increased polarity can be deduced by the increase of the $I_{2930\ cm^{-1}}/I_{2850\ cm^{-1}}$ intensity ratio (9), provided we disregard overlapping effects, at least in the presence of small amounts of PL and histones.

Alternatively, a partial penetration of PL into the DMPC bilayers could be supposed, but this hypothesis seems to be less probable, because PL has been used as a model for an extrinsic protein (17, 18).

Histone VI-S (slightly lysine rich) behaves similarly to PL; indeed it does not affect the T_m of the main transition nor the cooperativity of the melting.

On the contrary, the addition of histone III-S (lysine rich) to DMPC bilayers decreases both T_m and the cooperativity of the melting process, as DSC data show. Moreover, in the gel phase, the protein exhibits a noticeable structure buffering effect, analogous to that observed with certain intrinsic proteins. The results suggest that partial penetration together with surface adsorption takes place and the behaviour is different from that of PL and similar to that of a few other basic proteins (18, 19). The different behaviour of PL and histone III-S, and the analogies between PL and histone VI-S, lead to the conclusion that the protein fraction giving rise to the partial penetration into the DMPC bilayers may not be the lysine-rich fraction present in the protein. Therefore, to explain the different behaviour of the two histones considered, the different content of non-polar aminoacids and the domain distribution into the protein molecule should be taken into account. In determining the bilayer properties, hydrophobic interactions between lipid and protein fraction may be, in this case, more important than the electrostatic interactions. According to this hypothesis, the partial penetration of a few basic proteins, such as for example myelin (18, 20), could be due to the non-polar component of the proteins, since no specific interactions between DMPC and basic aminoacids have been found.

For the systems examined we can conclude that the hydrophobic interactions of the non-polar domains of histone molecules have a more important role than the electrostatic binding between the polar groups in determining the structural and dynamical properties of biomembranes. Moreover, the formation of lipoprotein complexes between histones and DMPC can be ruled out.

Acknowledgements

This work was supported by financial aid from the Consiglio Nazionale delle Ricerche. We are grateful to Prof F. A. Manzoli for some helpful discussions on this work that extends an interdisciplinary research subject studied by means of complementary experimental techniques.

1. A. BERTOLUZZA, S. BONORA, G. FINI, M. A. MORELLI, and R. SIMONI. J. Raman Spectrosc. **14**, 395 (1983).
2. J. D. MCGHEE and G. FELSENFELD. Annu. Rev. Biochem. **49**, 1115 (1980).
3. I. ISENBERG. Annu. Rev. Biochem. **48**, 159 (1979).
4. F. A. MANZOLI, S. CAPITANI, N. M. MARALDI, L. COCCO, and O. BERNABEI. *In* Advances in enzyme regulation. Vol. 17. *Edited by* G. Weber. Pergamon Press, Oxford. 1979. p. 175.
5. A. BERTOLUZZA, S. BONORA, G. FINI, and M. A. MORELLI. J. Raman Spectrosc. **11**, 225 (1981).
6. A. BERTOLUZZA, S. BONORA, G. FINI, and M. A. MORELLI. Can. J. Spectrosc. In press.
7. C. HUANG, J. T. MASON, and I. W. LEVIN. Biochemistry, **22**, 2775 (1983).
8. B. GABER and W. L. PETICOLAS. Biochim. Biophys. Acta, **465**, 260 (1977).
9. D. F. H. WALLACH, S. P. VERMA, and J. FOOFSON. Biochim. Biophys. Acta, **559**, 153 (1979).
10. P. CAREY. Biochemical applications of Raman and resonance Raman spectroscopies. Academic Press, London. 1982.
11. H. VOGEL and M. STOCKBURGER. Chem. Phys. Lipids, **32**, 91 (1983).
12. H. VOGEL and F. JÄNIG. Chem. Phys. Lipids, **29**, 83 (1981).
13. P. T. T. WONG and H. H. MANTSCH. Can. J. Chem. **60**, 2137 (1982).
14. T. J. O'LEARY. Biochim. Biophys. Acta, **731**, 47 (1983).
15. G. J. THOMAS JR., B. PRESCOTT, and D. E. OLINS. Sciences, **197**, 385 (1977).
16. J. J. JUTIER, R. SAVOIE, M. PIGEON-GOSSELIN, P. NADEAU, and P. N. LEWIS. J. Raman Spectrosc. **15**, 29 (1984).
17. H. SUSI, J. SAMPUGNA, J. W. HAMPSON, and J. S. ARD. Biochemistry, **18**, 297 (1979).
18. D. PAPAHADJOPOULOS, M. MOSCARELLO, E. H. EYLAR, and T. ISAC. Biochim. Biophys. Acta, **401**, 317 (1975).
19. R. SMITH, B. A. CORNELL, M. A. KENIRY, and F. SEPAROVIC. Biochim. Biophys. Acta, **732**, 492 (1983).
20. E. H. EYLAR, S. BROSTOFF, G. HASHIM, J. CACCAM, and P. BURNETT. J. Biol. Chem. **246**, 5770 (1971).

Étude vibrationnelle des acides deltiques $C_3O_3H_2$ et $C_3O_3D_2$

ALAIN LAUTIÉ, MARIE-FRANCE LAUTIÉ ET ALEXANDRE NOVAK
Laboratoire de Spectrochimie Infrarouge et Raman, C.N.R.S., 2, rue Henry Dunant, 94320-Thiais, France

Reçu le 17 juillet 1984

Cet article est dédié au Professeur Camille Sandorfy à l'occasion de son 65^e anniversaire

ALAIN LAUTIÉ, MARIE-FRANCE LAUTIÉ et ALEXANDRE NOVAK. Can. J. Chem. **63**, 1394 (1985).

Les spectres infrarouges et Raman de l'acide deltique et de son dérivé deutérié cristallisés ont été étudiés entre 4000 et 20

cm^{-1}. Les 18 vibrations intramoléculaires ont été attribuées sur la base d'une symétrie moléculaire C_{2v}. Le groupe d'espace cristallin doit être $P\bar{1}$ ou $P2/m$ avec Z = 2. Les molécules sont associées entre elles par deux liaisons hydrogène OH...O différentes, très fortes et asymétriques, en formant probablement des chaînes infinies; les distances O...O sont estimées à 2,49 et 2,56 Å.

ALAIN LAUTIÉ, MARIE-FRANCE LAUTIÉ, and ALEXANDRE NOVAK. Can. J. Chem. **63**, 1394 (1985).

The infrared and Raman spectra of crystalline deltic acid and its deuterated derivative have been investigated in the 4000–20

cm^{-1} range. An assignment of all the intramolecular fundamentals has been proposed assuming a C_{2v} molecular symmetry. The crystal symmetry is likely to be described by the $P\bar{1}$ or $P2/m$ space group with Z = 2. Deltic acid molecules probably form infinite chains linked with two very strong, asymmetric, and different OH...O hydrogen bonds, with O...O distances estimated at 2.49 and 2.56 Å.

Introduction

A la suite d'une étude de l'acide carré $C_4O_4H_2$ (1), dont le cristal subit une transition de phase para-ferroélectrique, nous nous sommes intéressés à l'acide deltique $C_3O_3H_2$ (dihydroxy-2,3 cyclopropènone). Ce composé a été synthétisé récemment (2,3) et contient le cycle cyclopropènone dont le spectre de vibration présente de nombreuses particularités (4–7). Le but principal de notre travail était de préciser la structure cristalline de cet acide en déterminant notamment son mode d'association ainsi que le type et la force des liaisons hydrogène OH...O.

A notre connaissance, aucune étude spectroscopique antérieure n'a encore été publiée. Par contre, son anion $C_3O_3^{2-}$ a fait l'object de travaux tant à l'état solide qu'en solution aqueuse (8). Nous avons donc enregistrée, à température ambiante et à celle de l'azote liquide, les spectres infrarouges et Raman de l'acide deltique et de son dérivé deutérié entre 4000 et 20 cm^{-1}.

Conditions expérimentales

L'acide deltique a été synthétisé par l'intermédiaire du diester de tertiobutyle (3). Bien que cette méthode donne des rendements en acide aléatoires, elle est plus fiable que celle précédemment décrite (2). Le produit cristallisé dans CF_3COOH (CF_3COOD pour le dérivé deutérié) a été utilisé sans purifications ultérieures.

Les spectres infrarouges de suspensions dans le Nujol et le Fluorolube ont été enregistrés sur les spectromètres Perkin–Elmer 180 et Bruker IFS113V. Des faces de CaF_2, CsI ou TPX ont été utilisées. Les spectres Raman ont été obtenus avec la microsonde Raman MOLE (Jobin–Yvon) sur des microcristaux d'une dizaine de µm. La puissance de la raie excitatrice à 514,5 nm d'un laser à Ar^+ Spectraphysics 164 était de 10 mW au niveau de l'échantillon. Le spectre du dérivé deutérié est difficilement exploitable à cause d'une fluorescence importante. Seules les raies les plus intenses ont pu être identifiées et aucune n'a été mise en évidence au-dessus de 1000 cm^{-1}. Les spectromètres ont été étalonnés à partir des spectres des composés gazeux habituels (infrarouge) et des raies parasites du plasma (Raman). La précision sur les fréquences est de ±1 cm^{-1} pour les raies fines; par contre, les vibrations ν OH, apparaissant sous forme de massifs complexes, ne sont déterminées qu'à 50 cm^{-1} près.

Interprétation des spectres

En l'absence de données structurales, nous supposerons que la molécule est plane et possède, en première approximation, la symétrie C_{2v}. Dans ce cas, ses 18 vibrations fondamentales se répartissent en 13 vibrations planes (7 A_1 et 6 B_1) et cinq vibrations hors du plan (2 A_2 et 3 B_2). Toutes sont actives en diffusion Raman et seules celles de type A_2 sont interdites en absorption. D'un autre côté, il est commode d'utiliser la représentation en terme de vibrations de groupe reportée dans le tableau 1.

Les spectres infrarouges et Raman des acides deltiques $C_3O_3H_2$ et $C_3O_3D_2$ à 35°C sont représentés sur la fig. 1. Les fréquences, les intensités relatives et l'attribution proposée sont réunies dans le tableau 2. Cette dernière est basée sur la substitution isotopique, les intensités relatives en infrarouge et en Raman et les analogies avec les spectres des composés contenant le cycle cyclopropènone.

Vibrations des groupements OH

Les deux vibrations ν OH de l'acide deltique apparaissent en absorption sous la forme de bandes larges et intenses centrées vers 2360 et 1450 cm^{-1} sur lesquelles d'autres bandes sont superposées; elles sont peu sensibles à la température entre 300 et 90 K. La contrepartie Raman n'est observée clairement que pour celle de haute fréquence vers 2500 cm^{-1} (fig. 1). La

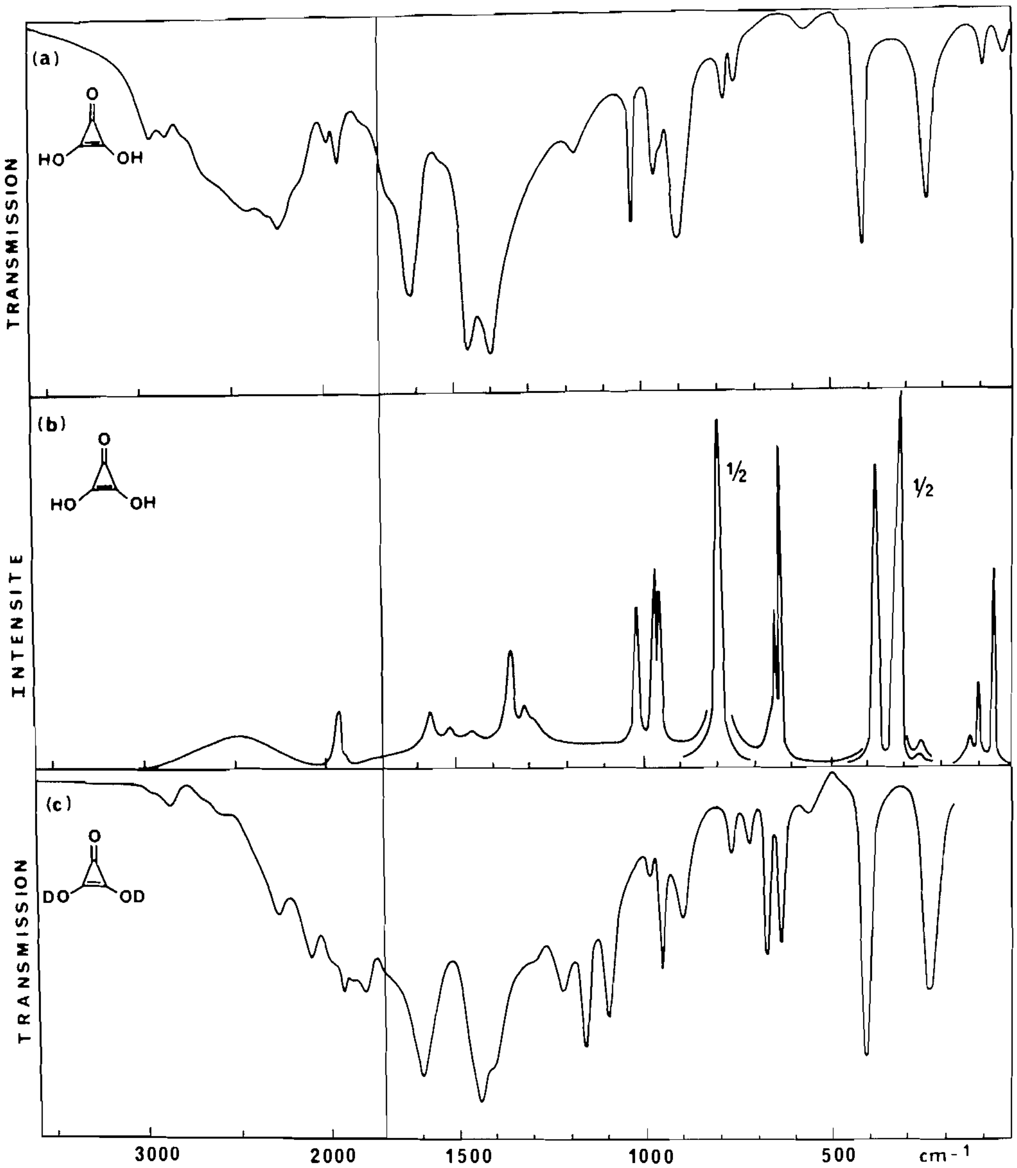

FIG. 1. Spectres infrarouge ((a) et (c)) et Raman (b) de l'acide deltique ((a) et (b)) et de son dérivé deutérié (c).

TABLEAU 1. Dénombrement des vibrations de la molécule d'acide deltique en admettant la symètrie C_{2v}*

C_{2v}	n	Cycle	C=O	C—OH	O—H	Infrarouge	Raman
A_1	7	2	ν	$\nu + \delta$	$\nu + \delta$	a	a
B_1	6	1	δ	$\nu + \delta$	$\nu + \delta$	a	a
A_2	2	0	—	γ	γ	in	a
B_2	3	0	γ	γ	γ	a	a

* Abréviations: a, active; in, inactive; ν, δ et γ sont les vibrations de valence et de déformation dans le plan et hors du plan.

substitution isotopique de l'hydrogène par le deutérium déplace la bande vers 2360 cm^{-1} à 1920 cm^{-1} alors que la fréquence de l'autre ne varie pratiquement pas. Les rapports isotopiques ν OH/ν OD sont donc très différents: 1,23 et 1,00 respectivement. Ce comportement indique l'existence de deux groupements OH engagés dans deux liaisons hydrogène fortes différentes. En aucun cas, l'existence de ces deux bandes ν OH ne peut correspondre à un couplage intra ou intermoléculaire de groupements OH similaires.

Leurs déplacements isotopiques permettent d'identifier les déformations planes δ OH et hors du plan γ OH (tableau 2). Comme dans le cas des vibrations de valence, l'écart important des fréquences de déformation montre que chacun de ces modes correspond plutôt à un groupement OH donné qu'à un effet de couplage. Nous faisons donc correspondre les fréquences élevées δ OH à 1660 cm^{-1} et γ OH à 1169 cm^{-1} à la liaison hydrogène la plus forte (notée $O_{(2)}H_{(2)}$ sur le tableau 2 et la fig. 2) responsable de la bande ν OH à 1450 cm^{-1} et les plus

TABLEAU 2. Fréquences, intensités relatives et attribution des bandes infrarouges et Raman des acides deltiques $C_3O_3H_2$ et $C_3O_3D_2$ cristallisés à 35°C*

$C_3O_3H_2$		$C_3O_3D_2$			
Infrarouge	Raman	Infrarouge	Raman	ν/ν'†	Attribution‡
2360		1920		1,23	ν $O_{(1)}H_{(1)}$
1450		1450		1,00	ν $O_{(2)}H_{(2)}$
1976 m 1931 m	1940(1)	1925 m 1809 m		1,05	ν C=O A_1
1660 ép (1696 TF)		1221 m (1242 TF)		1,36	δ $O_{(2)}H_{(2)}$ B_1
1616 TF	1569(0)	1605 TF		1,01	Cycle B_1
1465 TF (1477 TF)	1458(0)	1093 F (1100 TF)		1,34	δ $O_{(1)}H_{(1)}$ A_1
1406 TF		1447 TF		0,97	ν C—OH B_1
1350 ép	1350(1,5)	1300 ép		1,04	ν C—OH A_1
1169 m (1170 f)		893 m (906 m)		1,31	γ $O_{(2)}H_{(2)}$ A_2
1025 F	1015(2)	1161 F		0,88	Cycle A_1
965 m 956 ép	964(2,5) 957(2,5)	955 m	955(1)	1,01	δ C=O B_1
906 F (916 F)		668 F (674 F)		1,36	γ $O_{(1)}H_{(1)}$ B_2
781 f	799(9,2)	770 f	785(9)	1,02	Cycle A_1
	653(2) 641(4)	635 F	648(3)		γ C=O B_2
562 f		560 f			γ C—OH B_2
413 TF		408 TF		1,01	δ C—OH B_1
	379(8)		370(8)	1,02	γ C—OH A_2
311 tf	315(10)		303(10)	1,04	δ C—OH A_1
	269(0)		269(0)		ν OH...O T'
247 F (253 F)		239 F (246 F)		1,03	ν OH...O R'_y
	133(0)		130(0)	1,03	
	109(1)		108(1)		
91 f		90 f		1,01	R'_x
	63(2,6) 60 ép				
36 tf					R'_z

*Les fréquences entre parenthèses correspondent aux vibrations δ OH, γ OH et ν OH...O à 90 K.
†ν/ν' est le rapport des fréquences des molécules $C_3O_3H_2$ et $C_3O_3D_2$.
‡Les souscrits (1) et (2) correspondent aux deux liaisons hydrogène différentes.

basses à 1465 et 906 cm^{-1} à la liaison hydrogène la plus faible ($O_{(1)}H_{(1)}$) caractérisée par la vibration ν OH à 2360 cm^{-1}. Contrairement aux vibrations de valence, celles de déformation sont sensibles à la température; leurs fréquences s'élèvent d'une dizaine de cm^{-1} à 90 K. Les vibrations δ $O_{(2)}H_{(2)}$ et δ $O_{(2)}D_{(2)}$ présentent une élévation encore plus importante en même temps qu'une exaltation d'intensité.

Les rapports isotopiques ν/ν' des modes de déformation varient entre 1,31 et 1,36 indiquant que leur energie potentielle est concentrée principalement dans les mouvements correspondant aux vibrations δ OH ou γ OH. Cependant, certains couplages avec des vibrations du squelette peuvent être mis en évidence. C'est ainsi que la vibration δ $O_{(2)}H_{(2)}$ à 1660 cm^{-1} apparaît couplée avec la vibration ν C—OH de type B_1 dont la fréquence monte de 1406 à 1447 cm^{-1} après la deutériation. Il en est de même des vibrations δ $O_{(1)}H_{(1)}$ à 1465 cm^{-1} et du cycle vers 1025 cm^{-1} de symétrie A_1. Il faut souligner ici le caractère approximatif des types de symétrie de l'acide deltique. En effet, la mise en évidence de deux liaisons hydrogène différentes implique que la symétrie C_{2v} moléculaire ne peut exister en toute rigueur dans le cristal et que la symétrie maximale est C_s. C'est ainsi que la vibration γ OH de type A_2 apparaît en absorption, mais son intensité est cependant beaucoup plus faible que celle de type B_2.

Les deux composantes qui apparaissent sur le spectre infrarouge de $C_3O_3D_2$ (fig. 1) vers 640 cm^{-1} sont attribuées à deux vibrations différentes car l'intensité de celle de plus haute fréquence augmente quand la température s'abaisse alors que l'autre subit l'effet inverse. La première est donc attribuée à γ $O_{(1)}D_{(1)}$, alors que la seconde correspond à la vibration γ C=O, non détectée en infrarouge pour $C_3O_3H_2$, dont l'intensité se trouve renforcée par un mécanisme de résonance.

Vibrations du squelette

Les vibrations du squelette sont attribuées par comparaison avec l'ion deltate (8) et les cyclopropènones substituées (6, 7); dans les spectres de ces dernières, on attend en particulier deux vibrations vers 1900 et 1600 cm^{-1} (6). La première, correspondant principalement à ν C=O, apparaît pour l'acide deltique à 1940 cm^{-1} en Raman et comme un doublet à 1976–1931 cm^{-1} en infrarouge. Ce doublet est interprété en terme de résonance de Fermi entre ν C=O et une combinai-

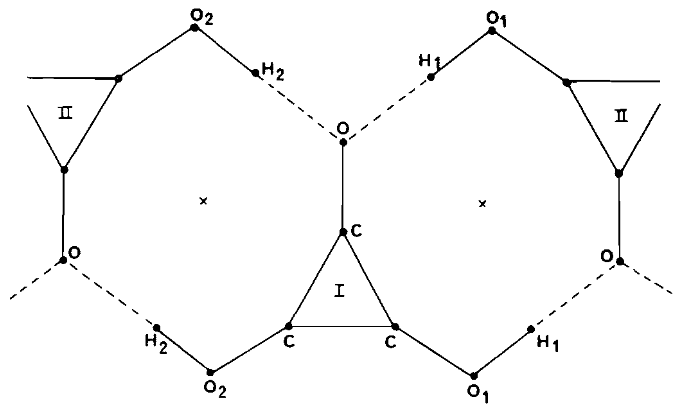

FIG. 2. Structure cristalline de l'acide deltique compatible avec les données spectroscopiques.

son, probablement l'harmonique de la vibration de déformation δ C═O à 965 cm^{-1} ou de la vibration du cycle à 1025 cm^{-1}. La vibration ν C═O du dérivé deutérié est plus difficile à localiser car elle est masquée par la forte absorption d'une des vibrations ν OD; nous lui faisons correspondre le doublet, encore attribué à une résonance de Fermi, avec 2 δ C═O, à 1925–1809 cm^{-1}. Quant à la vibration du cycle de plus haute fréquence, elle absorbe fortement vers 1610 cm^{-1} (fig. 1). Signalons que nous avons observé ces deux vibrations respectivement à 1877 et 1640 cm^{-1} sur le spectre infrarouge du deltate de tertiobutyle.

Les autres vibrations de fréquences supérieures à 600 cm^{-1} sont attribuées sans difficulté. Ainsi, la raie Raman très intense à 799 cm^{-1} correspond vraisemblablement à la respiration du cycle. Les fréquences de déformation δ C═O et γ C═O sont légèrement supérieures à celles de l'acide carré (9); ceci peut s'intepréter par le fait que le groupement C═O de l'acide deltique est engagé dans deux liaisons hydrogène au lieu d'une.

Entre 600 et 300 cm^{-1}, les seules vibrations intramoléculaires attendues sont celles de déformation des liaisons C—OH que nous attribuons donc aux quatre bandes observées dans cette région. Comme pour l'ion $C_3O_3^{2-}$ (8), les fréquences des déformations hors du plan γ OH sont supérieures à celles des déformations planes.

En résumé, toutes les vibrations fondamentales de l'acide deltique ont été identifiées sur la base d'une symétrie moléculaire C_{2v}. Bien que ses distances interatomiques n'aient pas encore été déterminées, nous avons tenté d'appliquer la règle du produit des rapports (10) en considérant une structure moyenne: C—C = 1,40 Å; C═O = 1,24 Å; C—O = 1,27 Å et O—H = 1,00 Å. En ne faisant pas intervenir les vibrations ν OH dont l'anharmonicité importante conduit à des rapports isotopiques faibles, les valeurs expérimentales sont proches de celles calculées: 1,37 pour 1,40 (A_1); 1,36 pour 1,39 (B_1); 1,34 pour 1,35 (A_2) et 1,36 pour 1,36 (B_2).

Discussion

Structure cristalline

Aucune vibration intramoléculaire n'étant attendue endessous de 300 cm^{-1}, nous attribuons les trois bandes infrarouges, et les cinq raies Raman observées dans cette région aux vibrations de réseau. En l'absence de données sur la structure cristalline, une analyse rigoureuse paraît difficile. Cependant, le nombre réduit de vibrations externes est en faveur d'une maille primitive ne contenant que deux molécules. Celleci doit être centrée car aucune fréquence Raman ne coïncide avec une fréquence infrarouge. Le groupe ponctuel isomorphe du groupe spatial est donc C_i ou C_{2h} avec $Z = 2$. Ceci est compatible avec le comportement des vibrations intramoléculaires qui montrent généralement deux composantes, une en infrarouge et une en Raman, dont les écarts de fréquence, compris entre 10 et 37 cm^{-1}, sont bien supérieurs aux erreurs expérimentales. Seules les trois vibrations du groupement C═O présentent des doublets en absorption ou en diffusion. Celui de la vibration de valence a été attribué à une résonance de Fermi et un phénomène analogue doit probablement être invoqué pour les vibrations de déformation.

D'un autre côté, nous avons vu que les deux groupements OH de l'acide deltique sont engagés dans des liaisons hydrogène fortes; celles-ci doivent donc être pratiquement linéaires. Les trois seules structures cristallines compatibles avec une molécule plane sont alors $P\bar{1}$, $P2/m$ (groupe de site C_s) ou $P2/b$ (groupe de site C_2). La non équivalence des liaisons hydrogène est en faveur des deux premières et l'arrangement des molécules serait alors celui représenté sur la figure 2. Signalons que nous n'avons observé aucune transition de phase entre 90 et 300 K; à une température supérieure, le produit se décompose assez rapidement.

Vibrations externes

A partir de ces résultats, nous pouvons préciser l'attribution des vibrations externes. Les trois librations R' actives en absorption ont été observées à 247, 91 et 36 cm^{-1}. Celle de plus haute fréquence, qui est aussi la plus intense, correspond probablement à un mouvement de valence des liaisons hydrogène OH...O; sa fréquence est voisine de celle relevée pour l'acide carré: 230 cm^{-1} (1). Elle est attribuée à un mouvement de rotation autour de l'axe perpendiculaire au plan de la molécule R'_y, car son rapport isotopique est égal à la racine carrée du rapport des moments d'inertie autour de cet axe: $(I_D/I_H)_y^{1/2} = 1{,}03$. Pour les deux autres axes, les valeurs sont nettement différentes: 1,01 et 1,05.

En diffusion Raman, cinq (tableau 2) des six vibrations attendues ($3R' + 3T'$) sont mises en évidence, mais la distinction entre les mouvements T' et R' est difficile. Cependant, les premières impliquent nécessairement une modification des distances O...O et mettent donc en jeu, contrairement à ce qui se passait pour l'acide carré (1), les liaisons hydrogène. D'autre part, la libration R'_y correspondant ici à une rotation des molécules dans le même sens ne joue pratiquement pas sur la distance O...O et doit donc se trouver à plus basse fréquence que celle qui lui correspond en infrarouge. Nous attribuons alors la faible raie Raman à 269 cm^{-1} à une antitranslation T'; son rapport isotopique, voisin du rapport de la racine carrée des masses $(M_D/M_H)^{1/2} = 1{,}01$, est compatible avec cette interpretation.

Liaisons hydrogène

Comme en témoignent leurs vibrations de valence et de déformation, les groupements OH de l'acide deltique sont engagés dans deux liaisons hydrogène fortes OH...O différentes, ($O_{(1)}H_{(1)}$...O et $O_{(2)}H_{(2)}$...O sur la figure 2). La longueur de la plus faible, déterminée à partir de la fréquence ν OH (11) à 2360 cm^{-1}, est $R_{O...O} = 2{,}56$ Å; la distance R_{O-H} peut être estimée de la même façon (11) à 1,10 Å. Ces caractéristiques montrent que la force de cette liaison hydrogène est sensiblement équivalente à celle existant dans le cristal de $RbHCO_3$ (11). La fréquence ν OH de l'autre vibrateur, 1450 cm^{-1}, conduit à des distances $R_{O...O} = 2{,}49$ Å et $R_{O-H} = 1{,}16$ Å; il est donc engagé dans une liaison hydrogène comparable à celle observée pour $KH(CH_3COO)_2$ (11). Bien que fortes, ces deux liaisons hydrogène sont donc asymétriques. Ceci est confirmé par les faibles rapports isotopiques ν OH/ν OD égaux respectivement à 1,23 et 1,00. Ces valeurs sont très proches de celles obtenues à l'aide de la relation $\nu \text{ OH}/\nu \text{ OD} = 2/[(\sqrt{2} - 1)\nu^0 \text{ OH}/\nu \text{ OH} + 1]$ (12): 1,22 et 0,98 pour une fréquence ν^0 du vibrateur non perturbé estimée voisine de 3600 cm^{-1}.

Deux modes externes ont été interprétés comme des vibrations de valence des liaisons hydrogène. Dans l'approximation du modèle diatomique, leur constante de force F_h peut être évaluée à partir de l'antitranslation T' à 269 cm^{-1} en utilisant la géométrie de la figure 2. Elle est comprise entre 60 et 70 N m^{-1} suivant l'orientation de T'. Ce résultat est compatible avec les valeurs obtenues pour d'autres liaisons hydrogène de force voisine (11).

Remerciements

Nous tenons à remercier le professeur F. Serratosa (Université de Barcelone) pour les précisions qu'il nous a données sur la synthèse de l'acide deltique et pour l'échantillon du diester de tertiobutyle qu'il nous a aimablement fourni.

1. D. BOUGEARD et A. NOVAK. Solid State Commun. **27**, 453 (1978).
2. D. EGGERDING et R. WEST. J. Am. Chem. Soc **98**, 3641 (1976).
3. F. SERRATOSA. Acc. Chem. Res. **16**, 170 (1983).
4. R. W. MITCHELL et J. A. MERRIT. Spectrochim. Acta Part A, **27**, 1643 (1971).
5. F. R. BROWN, D. H. FINSETH, F. A. MILLER et K. H. RHEE. J. Am. Chem. Soc. **97**, 1011 (1975).
6. E. C. TUAZON, D. H. FINSETH et F. A. MILLER. Spectrochim. Acta Part A, **31**, 1133 (1975).
7. R. SCHUBERT, A. ANSMAN, P. BLECKMANN et B. SCHRADER. J. Mol. Struct. **26**, 429 (1975).
8. R. WEST, D. EGGERDING, J. PERKINS, D. HANDY et E. C. TUAZON. J. Am. Chem. Soc. **101**, 1710 (1979).
9. F. G. BAGLIN et C. B. ROSE. Spectrochim. Acta Part A, **26**, 2293 (1970).
10. G. HERZBERG. Infrared and Raman spectra of polyatomic molecules. D. Van Nostrand Company, New York. 1964. p. 232.
11. A. NOVAK. Struct. Bonding, **18**, 177 (1974).
12. N. D. SOKOLOV et V. A. SAVEL'EV. Chem. Phys. **22**, 383 (1977).

The hydrogen bond energies of the bihalide ions XHX^- and YHX^-

G. CALDWELL AND P. KEBARLE
Department of Chemistry, University of Alberta, Edmonton, Alta., Canada T6G 2G2

Received July 17, 1984

This paper is dedicated to Professor Camille Sandorfy on the occasion of his 65th birthday

G. CALDWELL and P. KEBARLE. Can. J. Chem. **63**, 1399 (1985).

Experimental measurements of the gas phase ion equilibria $X^- + HX = XHX^-$, $X^-(HX)_{n-1} + HX = X^-(HX)_n$, and $X^- + HY = XHY$ where X, Y = Cl, Br, I, with a high pressure mass spectrometer, combined with the recent determination of $F^- + HF = FHF^-$ by Larson and McMahon, provide a very complete set of hydrogen bond dissociation enthalpies and free energies for the hydrogen bihalide ions. The bond energy trends in the different XHX^- and XHY^- are discussed. The data can be used also for the evaluation of lattice energies of salts containing the bihalide ions and for determinations of the solvation energies of these ions.

G. CALDWELL et P. KEBARLE. Can. J. Chem. **63**, 1399 (1985).

Utilisant un spectromètre de masse à haute pression, on a obtenu des mesures expérimentales pour les équilibres ioniques en phase gazeuse $X^- + HX = XHX^-$; $X^-(HX)_{n-1} + HX = X^-(HX)_n$ et $X^- + HY = XHY$ où X, Y = Cl, Br, I. On a combiné ces résultats avec ceux obtenus récemment par Larson et McMahon, pour l'équilibre $F^- + HF = FHF^-$, pour développer un ensemble complet des enthalpies et des énergies libres de dissociation des liaisons hydrogènes des ions hydrogènes bihalogénés étudiés. On discute des tendances observées dans les énergies de liaisons des différents ions XHX^- et XHY^-. On peut également utiliser les données pour évaluer les énergies du réseau des sels contenant des ions bihalogénés et pour déterminer les énergies de solvatation de ces ions.

[Traduit par le journal]

Introduction

The bihalide ions XHX^- and YHX^- where (X, Y) = F, Cl, Br, and I, are of particular interest since they contain only the three atoms normally considered to constitute the hydrogen bond. The strong ion–neutral hydrogen bonds are distinctly different from the weaker neutral–neutral interactions and usually merit a classification of their own (for a review, see ref. 1). Consequently, the hydrogen bihalide ions have been made the subject of numerous theoretical investigations (2) and spectroscopic studies (3) including ir spectroscopy (3*a*), X-ray (3*b*), and neutron (3*c*) diffraction and nmr spectroscopy (3*d*).

Although the homobihalides (XHX^-) and heterobihalides (XHY^-) ions have been studied for many years, no reliable data for the hydrogen bond energies X^-HX and X^-HY were available until the advent of gas phase ion equilibria measurements (4). The hydrogen bond energies were originally estimated from Born cycles which relied on calculations of alkali metal bihalide $M^+(HX_2^-)$ crystal lattice energies (5) or assumptions (6) that the lattice energies of tetrabutylammonium halides and tetrabutylammonium hydrogen bihalides were similar. Martin and co-workers (7), using a simple electrostatic model, estimated the binding energies of several bihalide ions.

Over a decade ago, Yamdagni and Kebarle (8) measured the gas phase ion–molecule equilibria [1] and [2] for X = Cl, with a high pressure mass spectrometer (HPMS).

$$[1] \quad X^- + HX = XHX^- \qquad (0, 1)$$

$$[2] \quad X^-(HX)_{n-1} + HX = X^-(HX)_n \qquad (n-1, n)$$

The bond energy, $D(Cl^-—HCl)$ = 23.7 kcal/mol, determined in that work was 10 kcal/mol greater than that obtained with McDaniel's assumption (6). Recently, Larson and McMahon (9, 10), using ion cyclotron resonance (ICR) to measure the gas phase exchange equilibria [3], were able to determine the very important bond

$$[3] \quad X^-HR + HB = X^-HB + HR$$

energy $D(F^-—HF)$ = 38.6 kcal/mol (9). These authors also obtained $D(Cl^-—HF)$ = 21.8 kcal/mol and $D(Cl^-—HCl)$ = 23 kcal/mol, the latter value being very close to the HPMS value from this laboratory (8).

Larson and McMahon (10) were also able to predict some bond energies, which are not yet experimentally available, from a correlation of the hydrogen bond energy in the bihalide ions with spectroscopically measured frequency shifts ($\Delta\nu$) of the hydrogen bond frequencies relative to the frequencies of the free halogen acids. From such $\Delta\nu$ vs. ΔH plots, the following binding energies were estimated: $Br^-—HCl$ (19 kcal/mol), $I^-—HCl$ (13 kcal/mol), $Br^-—HF$ (17 kcal/mol), and $I^-—HF$ (15 kcal/mol) (10).

In view of the importance of the bihalide ions and past uncertainty concerning their bond energies we have experimentally determined, using HPMS, the temperature dependence for several gas-phase equilibria [1] and [2] where X = Cl, Br, and I. These measurements permit the evaluation of $D(X^-—HX) = \Delta H^0_{1,0}$ and also binding energies for the higher order clusters, $X^-(HX)_n$. Similar measurements involving the heterobihalides $X^-(HY)_n$ were also performed.

It will be shown that the thermodynamic quantities obtained in the present work support the bihalide binding energies predictions made by McMahon (10). The new data also permit evaluation of the lattice energy of alkali bihalides and other thermochemical data of interest.

Experimental

The high-pressure ion source mass spectrometer with which the measurements were made has been described previously (8, 12). Briefly, a 2000 eV electron beam was pulsed "on" for 10–50 μs and "off" for 2–4 ms through the high pressure ion source. The ion source contains a suitable reaction mixture. The resulting ions react with the gas molecules and under suitable conditions the desired ion–molecule equilibria establish themselves. Some of the ions escape, through a very small sampling slit, into an evacuated region where they are mass analyzed, counted, and by means of a multiscaler recorded as a function of their arrival time after the electron pulse. The arrival times are equal to the residence times in the ion source, since the time required for mass analysis is very short. The gas mixture supplied to the ion source consisted of methane as major gas (2–3 Torr) containing mix-

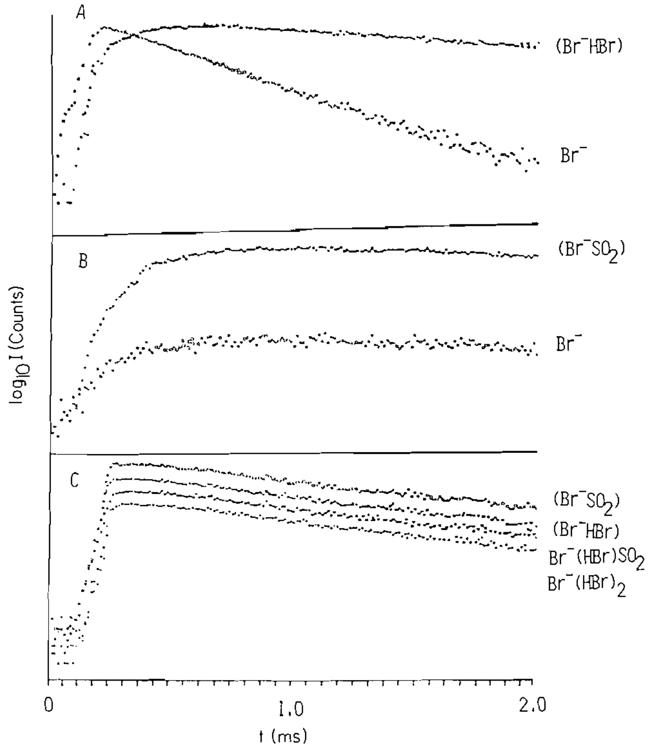

FIG. 1. (*a*) Plot of log (ion counts) vs. time. Concentration used: HBr 270 mTorr, CH_2Br_2 2 mTorr, third gas CH_4 at 4.3 Torr. Temperature 424 K. Br^- is produced by rapid dissociative capture of near thermal electrons by CH_2Br_2. The observed first order disappearance of Br^- is due to the termolecular association: $Br^- + HBr + CH_4 \rightarrow BrHBr^- + CH_4$ (1). Rate constant $k_1 = 7 \times 10^{-30}$ molecule^{-2} cm^6 s^{-1} obtained from slope $\nu_1 = k_1[CH_4][HBr]$ is very low. This must be due to termolecular complex being only triatomic. (*b*) Same conditions as in (*a*) but HBr has been replaced with SO_2 at the same pressure. Termolecular association with SO_2 is much faster and system is in equilibrium: $Br^- + SO_2 = BrSO_2^-$. (*c*) Rapid association with SO_2 used as catalyst for attainment of clustering equilibrium Br^- + HBr = $(BrHBr)^-$. The $BrSO_2^-$ produced rapidly as in (*b*) undergoes the rapid switching reaction $BrSO_2^- + HBr = BrHBr^- + SO_2$. Higher clusters $Br(HBr)_2^-$ and $Br^-(HBr)SO_2$ are also present. Constant difference between log (ion counts) plots observed after about 0.3 ms indicates equilibrium. SO_2 1.1 Torr, HBr 0.17 Torr, CH_4 3 Torr, T = 328 K.

tures of HX in the 0.03 to 0.2 Torr range. Electron capture agents (CCl_4, CH_2Br_2, and CH_3I) were also added at some 0.001 Torr in order to produce the desired ions Cl^-, Br^-, and I^-. Some of the equilibria measurements were performed in the presence of SO_2, which was found to speed up the attainment of the equilibria (see next section). All chemicals used were commercially available and were used without further purification.

Reaction mechanisms in equilibria measurements and thermodynamic results

The reactions occurring in a typical experiment are summarized below:

[4] $AX + e \rightarrow X^- + A$

[1] $X^- + HX = X^-HX$

[2] $X^-(HX)_{n-1} + HX = X^-(HX)_n$

Secondary near thermal electrons produced by the primary electron pulse are captured by traces of AX (= CCl_4 for Cl^-, CH_2Br_2 for Br^-, and CH_3I for I^-) introduced in the ion source

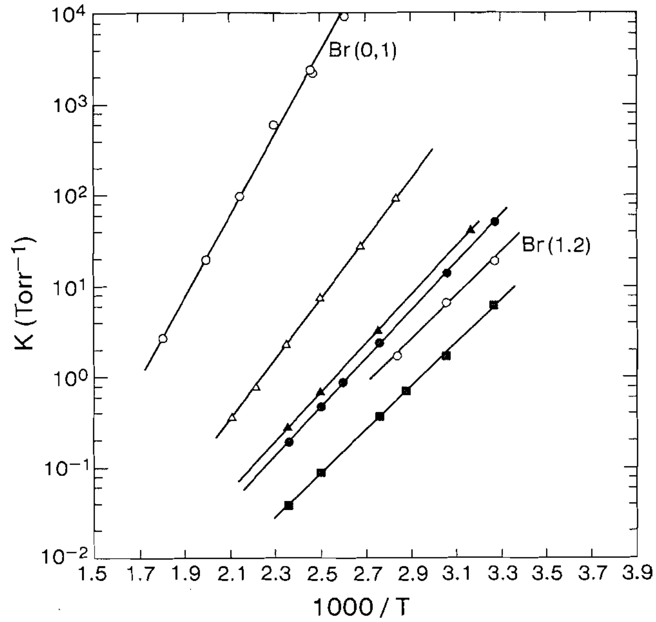

FIG. 2. van't Hoff plots of equilibrium constants $K_{n-1,n}$ for the clustering reaction: ○, $Br^-(HBr)_{n-1} + HBr = Br^-(HBr)_n$; △, I^- + HCl = I^-HCl; ●, $Br^-HCl + SO_2 = Br^-(HCl)SO_2$; ▲, $Cl^-HCl + SO_2 = Cl^-(HCl)SO_2$; ■, $Br^-HBr + SO_2 = Br^-(HBr)SO_2$.

with the reaction mixture. The desired ion X^- is created by the dissociative electron capture reaction [4]. In the presence of the clustering gas HX clustering reactions [1] and [2] occur. For HBr and HI, the first step [1] in the clustering sequence proved to be very slow, particularly at the high temperatures at which the equilibrium [1] was to be measured. The results from such an experiment involving the (0, 1) clusters of Br^- + HBr are shown in Fig. 1*a*. The disappearance of Br^- is clearly too slow under these conditions to lead to the equilibrium [1].

The rate constant k_1 for the forward clustering reaction is third order for the conditions of the experiments and decreases with temperature increase (13). The magnitude of the rate constant in an ion molecule association reaction $A^{\pm} + B \rightarrow (AB^{\pm})^* \rightarrow AB^{\pm}$ increases with the number of internal degrees of freedom of the complex $AB^{\pm}$ and the binding energy ($A^{\pm}$—B) (13). For the triatomic complexes XHX^-, the available degrees of freedom are very few and this leads to a very small k_1.

The k_1 determined from the observed concentration changes in Fig. 1*a* is 7×10^{-30} cm^2 molecule^{-1} s^{-1}. This value is two to three orders of magnitude smaller than the rate constant for an association reaction involving polyatomic reactants $A^{\pm}$ and B and an $A^{\pm}$—B binding energy similar to the Br^-—HBr bond energy (for other references for third order and temperature dependence kinetics see ref. 13*b*). Increase of the HX concentration speeds up the rate of [1]. The equilibria results in Fig. 2 and 3 were obtained from experiments where the HX pressure was increased to the 1 Torr range. However, the high HX pressure led, for reasons that we do not fully understand, to a more rapid decrease of the total X^- and X^-HX signal with time. Better conditions for the equilibria measurements were created with the introduction of SO_2 gas in the reaction mixture. The presence of SO_2 led to the clustering reactions [5] and [6].

[5] $X^- + SO_2 = X^-(SO_2)$

[6] $X^-(SO_2)_{n-1} + SO_2 = X^-(SO_2)_n$

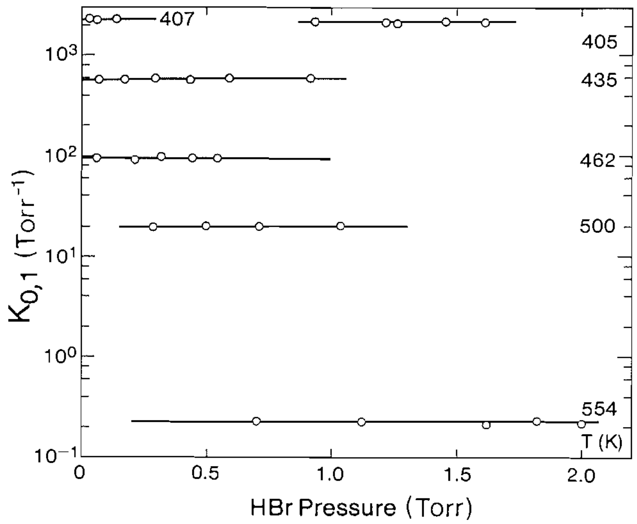

FIG. 3. Equilibrium constants $K_{0,1}$ for reaction: $Br^- + HBr = Br^-HBr$ as a function of temperature and HBr pressure. Measurements in the presence of 3–4 Torr CH_4. Standard state 1 Torr.

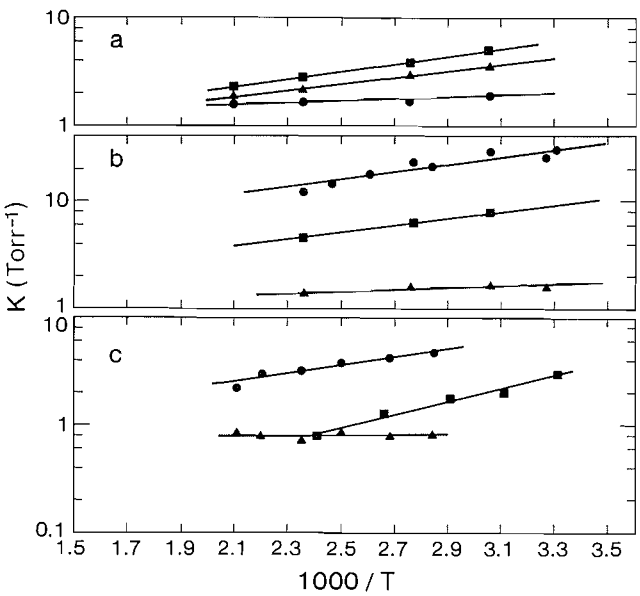

FIG. 4. van't Hoff plots of equilibrium constants $K_{n-1,n}$ for the exchange reactions: Plot *a*: ■, $Cl^-(HCl)SO_2 + HCl = Cl^-(HCl)_2 + SO_2$; ▲, $Br^-(HBr)SO_2 + HBr = Br^-(HBr)_2 + SO$; ●, $Br^-(HCl)SO_2 + HCl = Br^-(HCl)_2 + SO_2$. Plot *b*: ●, $Br^-SO_2 + HBr = Br^-HBr + SO_2$; ■, $Cl^-SO_2 + HCl = Cl^-HCl + SO_2$; ▲, $Br^-SO_2 + HCl = Br^-HCl + SO_2$. Plot *c*: ●, $I^-SO_2 + HBr = I^-HBr + SO_2$; ■, $I^-SO_2 + HI = I^-HI + SO_2$; ▲, $I^-SO_2 + HCl = I^-HCl + SO_2$.

[7] $X^-(SO_2)_n + HX = X^-(SO_2)_{n-1}HX + SO_2$

[8] $X^-(HX)_{n-1}SO_2 + HX = X^-(HX)_n + SO_2$

The clustering reaction [5] involving Br^- and SO_2 was much faster than the corresponding reaction of Br^- and HBr. This fact is demonstrated by the results shown in Fig. 1*b*. Evidently the additional vibrations in the triatomic SO_2 molecule lead to a much higher termolecular rate constant. When both SO_2 and HX are present, as in Fig. 1*c*, the rapid X^-SO_2 clustering is followed by the switching reactions [7] and [8] in which the stronger bonding HX displaces the SO_2 molecules from the ion X^-. Measurement of the exchange equilibria [7] and [8] from

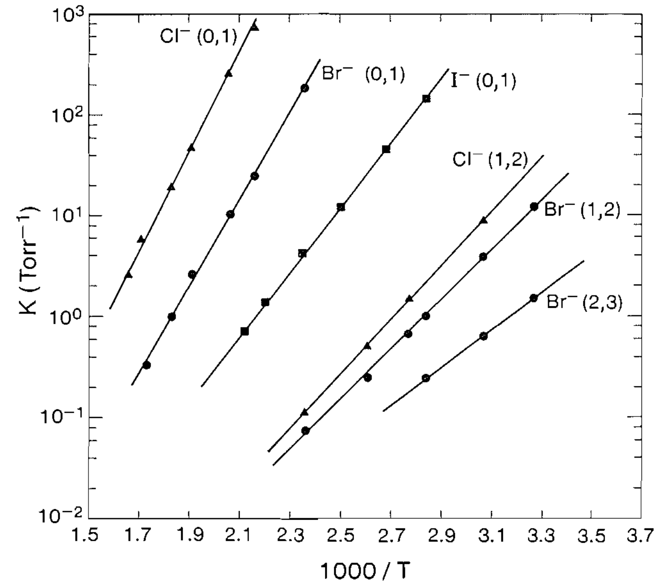

FIG. 5. van't Hoff plots of equilibrium constants $K_{n-1,n}$ for reactions ▲, $Cl^-(SO_2)_{n-1} + SO_2 = Cl^-(SO_2)_n$; ●, $Br^-(SO_2)_{n-1} + SO_2 = Br^-(SO_2)_n$; ■, $I^-(SO_2)_{n-1} + SO_2 = I^-(SO_2)_n$.

runs like that shown in Fig. 1*c* led to the exchange equilibria van't Hoff plots shown in Fig. 4. In addition to these exchange reactions, the X^-, SO_2 clustering equilibria [5] and [6] were measured in the absence of HX. The van't Hoff plots for these results are shown in Fig. 5. Combining the SO_2 clustering equilibria [5] and [6] with the HX exchange equilibria [7] and [8] in a thermodynamic cycle leads to the $X^-(HX)_n$ or $X^-(HY)_n$ equilibria and associated thermochemical quantities.

The thermochemical data from measurements involving SO_2, association and exchange are given in Table 2. Table 1 contains data from the direct X^-HX association equilibria measurements and also association equilibria data derived from the SO_2 cycles described above.

Data from the literature are also included in Table 1. All determinations involving F^- are due to McMahon and co-workers (9, 10). Included are also the results of Castleman and co-workers (14) for X^-SO_2 association reactions. There is generally good agreement between determinations from different laboratories. Thus, the Cl^-—SO_2 and Cl^-—HCl bond enthalpies from three different determinations are within 1 kcal/mol (Table 1).

Discussion of results

(*a*) *The dissociation energies in* $(XHX)^-$ *and* $(XHY)^-$

The hydrogen bond energies corresponding to dissociations $(XHX)^- \rightarrow X^- + HX$ and $(XHY)^- \rightarrow X^- + HY$ are summarized in Table 3. First we consider the XHX^-, which lie on the diagonal in Table 3. The bond enthalpy values are 38.6, 23.5, 20.9, and 17.0 kcal/mol for X = F, Cl, Br, I. Prior to the experimental determination of $D(F^-$—$HF)$ = 38.6 kcal/mol due to Larson and McMahon (9), theoretical MO calculations (2) had not provided a reliable or consistent result for this bond energy. In retrospect only the calculation of Noble and Kortzeborn (2*h*) with 40 kcal/mol has turned out to be a result close to the experimental value. Emsley and co-workers (2*d*) have discussed the reasons for the theoretical difficulties and the special need for a large flexible Gaussian basis set when dealing with the F^-HF system. Theoretical calculations for

TABLE 1. Thermochemistry of clustering reaction $(n-1, n)$ $XL_{n-1}^{-} + L = X^{-}L_n$ from gas phase equilibria[a]

Ligand (L)	Ion (X^-)	$(n-1,n)$ $-\Delta H^0$ (0, 1)	(1, 2)	(2, 3)	(3, 4)	$(n-1,n)$ $-\Delta G^0$ (300 K) (0, 1)	(1, 2)	(2, 3)	(3, 4)	$(n-1,n)$ $-\Delta S^0$ (0, 1)	(1, 2)	(2, 3)	(3, 4)
SO_2	F^-	43.8^b				36.6^b				24^b			
	Cl^-	22.2	12.3			15.7	6.2			21.6	20.2		
		21.8^c	12.3^c	10.0^c	8.6^c	14.8^c	5.5^c	3.1^c	1.6^c	23.2^c	22.7^c	23.1^c	23.2^c
		20.9^b				14.7^b				21^b			
	Br^-	19.3	11.2	8.5		12.7	5.6	4.4		22.0	18.7	13.8	
	I^-	14.3				9.0				17.6			
		12.9^c	10.1^c	9.2^c		6.8^c	3.6^c	1.8^c		20.2	21.6	24.7	
HF	F^-	38.6^b				30.9^b				25.7^b			
	Cl^-	21.8^b				15.1^b				22.5^b			
HCl	Cl^-	23.8^d	14.0^d			17.1^d	7.9^d			22.3^d	20.4^d		
		23.7^e	15.2^e	11.7^e	10.3^e	16.7^e	7.9^e	4.7^e	2.4^e	23.5^e	24.4^e	23.4^e	26.7^e
		23.1^b				15.8^b				24.2^b			
	Br^-	19.6^d	12.5^d			13.0^d	7.0^d			22.0^d	18.4^d		
	I^-	14.8				8.8				20.0			
		14.3^d				8.9^d				18.0^d			
		14.2^e				7.4^e				22.7^e			
HBr	Br^-	20.6	11.0			13.9	5.9			22.3	17.0		
		21.1^d	12.3^d			14.8^d	6.1^d			21.0^d	20.8^d		
	I^-	16.1^d				10.2^d				19.6^d			
HI	I^-	17.0^d				9.7				24.4^d			

[a] ΔH^0 and ΔG^0 (300 K) in kcal/mol; ΔS^0 in cal deg^{-1} mol^{-1} (standard state 1 atm). Thermochemical data taken from Fig. 2 and 5 unless otherwise indicated. Estimated error: ± 1 kcal/mol for ΔH and ΔG^0 (300 K), ±4 cal deg^{-1} mol^{-1} for ΔS^0.
[b] From McMahon and co-workers (9, 10).
[c] From Keesee and Castleman (14).
[d] From Table 2.
[e] From Yamdagni and Kebarle (8).

TABLE 2. Thermochemical data[a] from equilibria involving SO_2

	Reaction	$-\Delta H$	$-\Delta S$	$-\Delta G$
[1]	$Cl^- + SO_2 = Cl^-SO_2$	22.2	21.6	15.7
[2]	$Cl^-SO_2 + HCl = Cl^-HCl + SO_2$	1.6	0.7	1.4
[3]	$Cl^-HCl + SO_2 = Cl^-(HCl)SO_2$	12.3	18.5	6.8
[4]	$Cl^-(HCl)SO_2 + HCl = Cl^-(HCl)_2 + SO_2$	1.7	1.9	1.1
[5]	$Br^- + SO_2 = Br^-SO_2$	19.3	22.0	12.7
[6]	$Br^-SO_2 + HBr = Br^-HBr + SO_2$	1.8	−1.0	2.1
[7]	$Br^-HBr + SO_2 = Br^-(HBr)SO_2$	10.9	18.9	5.2
[8]	$Br^-(HBr)SO_2 + HBr = Br^-(HBr)_2 + SO_2$	1.4	1.9	0.8
[9]	$Br^-SO_2 + HCl = Br^-HCl + SO_2$	0.3	0.0	0.3
[10]	$Br^-HCl + SO_2 = Br^-(HCl)SO_2$	12.1	18.6	6.5
[11]	$Br^-(HCl)SO_2 + HCl = Br^-(HCl)_2 + SO_2$	0.4	−0.2	0.5
[12]	$I^- + SO_2 = I^-SO_2$	14.3	17.6	9.0
[13]	$I^-SO_2 + HCl = I^-HCl + SO_2$	0.0	0.4	−0.1
[14]	$I^-SO_2 + HBr = I^-HBr + SO_2$	1.8	2.0	1.2
[15]	$I^-SO_2 + HI = I^-HI + SO_2$	2.7	6.8	0.7

[a] All values are in kcal/mol, ΔG^0 values for 300 K, ΔS^0 in eu, standard state 1 atm.

$D(Cl^-—HCl) = 20$ kcal/mol were obtained by Almlöf (2*g*) in fairly good agreement with the experimental result of 23.5 kcal/mol from this laboratory (8). MO calculations for Br^-HBr and I^-HI have not been performed.

Martin and Fujiwara (3) have published results from some very simple electrostatic calculations for the bond energies X^-HX and X^-HY. These authors obtained the binding energy U by considering the ion dipole and the ion-induced dipole interaction as shown in eq. [9].

[9*a*] $$U = U_{dip} + U_{pol}$$

[9*b*] $$U_{dip} = -\frac{69.1}{r^2}\mu \text{ (kcal/mol)}$$

[9*c*] $$U_{pol} = -\frac{165.6}{r^4}\alpha \text{ (kcal/mol)}$$

[9*d*] $$r = r_{X^-} + (1/2)r_{HX}$$

μ and α are the dipole moment and the polarizability (along the bond axis) of HX and the numerical factors in [9*b*] and [9*c*] are adjusted for use with μ in Debye and α in Å^3 units. A rigid sphere approach was used where the distance r between the ion and the point dipole and polarizability was taken as the sum of the Pauling ion radius and half of the HX bond distance r_{HX}. The values for α, μ, and r_{HX} and the resulting bonding energy $-U$ are shown in Table 4. Apart from the too high value for $-U(F^-HF) = 51$ kcal/mol, there is good agreement with the

TABLE 3. Hydrogen bond cleavage enthalpy change; $(XHY)^- \rightarrow X^- + HY$ and $(XHY)^- \rightarrow Y^- + HX$[a]

	Enthalpy change for HY =			
X^-	HF	HCl	HBr	HI
F^-	38.6[b]	59.9[c]	(65.0)[c,e]	(72.0)[c,e]
Cl^-	21.8[b]	23.5[d]	29.4[c]	30.7[c]
Br^-	(17.0)[c]	19.6	20.9[d]	25.4[c]
I^-	(15.0)[c]	14.4	16.1	17.0

[a]All ΔH^0 and ΔG^0 values in kcal/mol from Table 1. Unless otherwise indicated bond energies for the reaction $(XHY)^- \rightarrow X^- + HY$ where HY is a weaker acid than HX. For free energy changes see Table 1.
[b]From McMahon and co-workers (9) and (10).
[c]Estimated from $\Delta\nu$ vs. ΔH plot, see text and refs. 10 and 11.
[d]Value based on an average from Table 1.
[e]Values obtained for reaction $(XHY) \rightarrow Y^- + HX$ by addition of halide binding energy to the difference in gas phase acidities of HX and HY, see text.

experimental values. Electrostatic calculations like [9] depend critically on the choice of the radius r. The choice of r in Martin's calculation is arbitrary since the radius of the H atom was not taken into consideration. Increasing the value of r by adding r_H would lead to much too low binding energies for all X^-HX, particularly the higher members. While the evaluation of quantitative data via [9] is not truly meaningful, the qualitative features are of interest. Thus, the binding energy in the series F $\rightarrow$ I decreases because of the increasing radius of X which leads to an increase of r_{X^-} and r_{HX}. An additional decrease of bonding is due to the large (factor of 5) decrease of the HX dipole from HF to HI (see Table 4). The combined effects of the r and μ changes lead to a tenfold decrease of U_{dip} from F^-HF to I^-HI. On the other hand, the rapidly increasing polarizability of X leads to an almost constant U_{pol} term for the whole series.

The results in Table 3 also provide information on the bond energy changes in X^-HY where X^- is kept constant and HY is changed. The general trend observed is that the bond energy increases as HY is changed from HF to HI. For example, in Br^-—HF, Br^-—HCl, and Br^-—HBr the energies are 17, 19.6, and 20.9 kcal/mol. The bond energies obtained with the electrostatic calculations (9) using the parameters from Table 5 are 25, 23, and 22 kcal/mol (see also Table IV in ref. 7*c*). Thus, numerically the electrostatic results are not too far off, but the predicted trend, i.e. a decrease of bonding from HF to HBr, is incorrect. It should be noted that the gas phase acidity of HY increases from HF to HI, which means that the observed hydrogen bond energy in X^-HY increases with the acidity of HY. This type of dependence has been observed for many systems B^-HA. Yamdagni and Kebarle (4, 15) were the first to document that the hydrogen bond energy in B^-HA increases with the gas phase acidity of AH and the gas phase basicity of B^-. For systems where AH are series of related compounds, a linear relationship between the bond energy and the acidity of AH is found. Examples of such behavior were obtained for $B^- = Cl^-$ and AH = substituted phenols (16) and Cl^- and a variety of acids (17). More recently Larson and McMahon (9) in a comprehensive examination of the hydrogen bonding in F^-HA have demonstrated the existence of such a linear relationship for HA corresponding to a variety of alcohols. The observed increase of binding energy of B^-HA with acidity of AH suggests the reason for the failure of the electrostatic approach (eq. [9]) to predict the correct trend of binding energies in $Br^-.HY$ and generally $X^-.HY$. In a series like

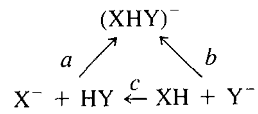

SCHEME 1

Br^-HF, Br^-HCl, Br^-HBr on formation of the hydrogen bond from Br^- and HY there is increasing proton donation from HY to Br^-. Thus, while in Br^-HF the proton is associated largely with HF in Br^-HBr the proton is already shared equally. The electrostatic calculation which treats HY as rigid fails to take this progressive proton shift into account. The largest exothermicity for the series $Br^- + HY = (BrHY)^-$ is observed for HI. (See Table 3). Of the two association reaction exothermicities shown in Scheme 1, by convention, only one is considered as a hydrogen bond energy. This would be ΔH_a assuming that X^- is a weaker base than Y^-. ΔH_b is not considered as representing the energy for the formation of a hydrogen bond since a large part of the exothermicity of [*b*] is due to proton transfer [*c*] from XH to Y^-, the product $(XHY)^-$ being (largely) $X^-.HY$. While the convention may be meaningful for a classification of hydrogen bonds, there is some degree of proton transfer on formation of all XHY^- hydrogen bonds as was shown above for the series Br^- + HF, HCl, HBr. Therefore, the inclusion of HI into the series is natural and extends the illustration of the progressively increasing proton transfer. All horizontal rows in Table 3 represent series with proton transfer and exothermicities increasing from left to right. A theoretical analysis of the role of proton transfer (proton drift) in hydrogen bonds has been given by Desmeules and Allen (18).

It is interesting to note that the proton transfer discussed above can be reversed by the presence of the cationic counter ion. In the matrix isolation studies of Ault (3), the alkali halides MX and the halogen acids HY were codeposited from the gas phase in an argon matrix to produce the unsymmetrical ions XHY^- together with M^+ as counterion. Evidence from the vibrational spectra obtained showed the presence of two isomers $X^-.HY$ and $XH.Y^-$ whose abundance depended on the nature of the counterion M^+. If X^- is the larger halide ion (i.e. the weaker base) then $X^-.HY$ will be more stable than $XH.Y^-$ in the absence of M^+. The interactions being largely electrostatic, the cations M^+ will bond preferentially to the smaller anion, i.e. the presence of M^+ will promote a proton transfer in $X^-.HY$ leading to $XH.Y^-M^+$. This tendency will increase if the size of M^+ is decreased. This corresponds exactly to the findings in the matrix isolation studies of Ault (3) where the abundance of the $XH.Y^-M^+$ species was observed to increase as the radius of M^+ was decreased.

A discussion of the potential energy changes in the (gaseous) XHY^- with proton transfer from X to Y has been given by Larson and McMahon (10).

The enthalpies for the reaction [10] have been measured (19, 20) in solution of the aprotic solvents, sulfolane (SF) (19), and propylene carbonate (PC) (20).

[10] $X^- + HCl = X^-HCl$

The gas phase and solution data are shown in Table 5. The exothermicities for [10] in solution are seen to be much lower. One factor decreasing the exothermicity is the solvation energy of HCl. The solvation energy of gaseous HCl in SF has been quoted by Benoit *et al.* (19) as ΔH_S (HCl) = −5.8 kcal/mol. The other factor decreasing the exothermicities of reaction [1]

TABLE 4. Calculated bond energies of X^-HX

Ion	rHX^a (Å)	X^{-b} (Å)	$\alpha_\parallel{}^c$ (symm. axes)	μ^d (D)	r^e (Å)	$-U_{dip}{}^f$ (kcal/mol)	$-U_{pol}{}^f$ (kcal/mol)	$-U^f$ (kcal/mol)	ΔE^g (kcal/mol)	ΔH^h (kcal/mol)
F^-HF	.917	1.36	.96	1.74	1.82	36.3	14.5	50.8	40.4	38.6
Cl^-HCl	1.275	1.81	3.13	1.07	2.45	12.3	14.4	26.7	20.0	23.5
Br^-HBr	1.414	1.95	4.22	0.79	2.66	7.7	14.0	21.7	—	20.9
I^-HI	1.604	2.16	6.58	0.38	2.96	3.0	14.2	17.2	—	17.0

[a]HX bond lengths, ref. 24.
[b]Crystal radii, ref. 25.
[c]Polarizability along symmetry axis of HX ($\times 10^{24}$ cm^3), ref. 26.
[d]Dipole moment, ref. 27.
[e]Radius (r) taken as half the HX distance plus the Pauling radius of X^-.
[f]Electrostatic estimate of binding energy $U = U_{dip} + U_{pol}$ (see eq. [9]).
[g]*Ab initio* results, FHF^-, refs. 2*d* and 2*h*, $ClHCl^-$ ref. 2*g*.
[h]Experimental data, see Table 3.

TABLE 5. Comparison of enthalpies for the reaction [10] $X^- + HCl = X^-HCl$ in gas phase and solution[a]

Parameter	Value when X^- = Cl$^-$	Br$^-$	I$^-$
$-\Delta H_{10(g)}$	23.5	19.6	14.4
$-\Delta H_{10}(SF)^b$	8.1	4.9	2.2
$-\Delta H_{10}(PC)^c$	2.5	1.2	0.9
$\delta\Delta H_S(X^-HCl)(SF)^d$	9.6	8.9	6.4
$\delta\Delta H_S(X^-HCl)(PC)^e$	~14.0	~11.4	~6.5

[a]All values in kcal/mol.
[b]In sulfolane, Benoit *et al.* (19).
[c]In propylene carbonate, Bates and co-workers (20).
[d]$\Delta H_S(X^-HCl) - \Delta H_S(X^-)$ from cycle (11) and $\Delta H_S(HCl) = -5.8$ kcal/mol (19).
[e]Same as *d* but solvation of HCl in PC, for which an experimental value is not available, assumed $\Delta H_S(HCl) = -7$ kcal/mol.

in solution is the solvation energy difference $\Delta H_S(X^-) - \Delta H_S(X^-HCl)$. This difference can be evaluated from cycle

$$[11] \qquad \begin{array}{ccc} X^-_{(g)} + HCl_{(g)} & \xrightarrow{\Delta H_{10(g)}} & X^-HCl_{(g)} \\ \uparrow {\scriptstyle -\Delta H_S(X^-) \atop -\Delta H_S(HCl)} & & \downarrow {\scriptstyle \Delta H_S(X^-HCl)} \\ X^-_{(s)} + HCl_{(s)} & \xrightarrow{\Delta H_{10(s)}} & X^-HCl_{(s)} \end{array}$$

$$\Delta H_S(X^-HCl) - \Delta H_S(X^-) = \Delta H_{10(s)} - \Delta H_{10(g)} + \Delta H_S(HCl)$$

[11]. The results obtained are given in Table 5. Dipolar aprotic solvents like SF and PC are known to solvate negative ions inefficiently. What is more significant for reaction [10] is that in these liquids the solvation of negative ions decreases less with increasing size of the negative ion than is the case for protic solvents (21). Examining the data in Table 5 we conclude that in sulfolane, solvation decreases less with increasing size of the negative ion than is the case for PC. Thus, propylene carbonate is, in this respect, closer to protic solvents. In protic solvents reaction (10) does not occur at all, exactly because negative ion solvation in these solvents decreases so much more with increasing size of the ion, i.e., the large, unfavorable energy difference for the solvation X^- and X^-HY leads to an unfavorable free energy change for [10] in protic solvents.

(*b*) *Binding energies and structure of the polyhalide ions* $X^-(HX)_n$

The changes of $\Delta H_{n-1,n}$ with n are shown in Fig. 6. The data used are from Table 1 except the $F^-(HF)_n$ data which represent results from MO calculations by Emsley *et al.* (2*c*, 2*d*). No experimental data for $F^-(HF)_n$ are available. Emsley's results are of interest because they provide structural information on the clusters. Thus while FHF^- is linear (as are the other XHX^-), $F^-(HF)_2$ is bent (C_{2v} symmetry, see structure **I**). This appears to result from a compromise between the covalent bonding angle of 109° and the 180° angle expected on electrostatic grounds due to the repulsion between the two HF dipoles. $F^-(HF)_3$ is found to be planar with the three HF molecules pointing towards F^-, D_{3h} symmetry (see structure **II**). This structure was found to be more stable than the chain structure $H_3F_7^-$ (**III**), expected, on the basis of covalent bonding.

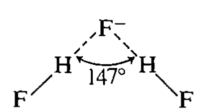

I

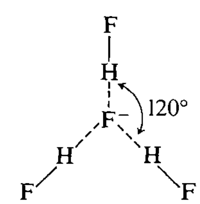

II

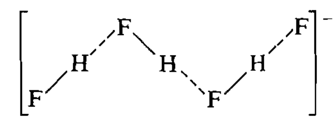

III

The stable structure for $F^-(HF)_4$ was tetrahedral with F^- in the centre and four HF pointing towards it (T_d symmetry). Evidently, as n in $F^-(HF)_n$ increases, the structures become increasingly determined by electrostatic type forces. For $Cl^-(HCl)_n$ and other $X^-(HX)_n$ we expect that electrostatic demands will dominate even more. Therefore we expect that the tendency for $X^-(HX)_2$ to become linear will increase from X = F to X = I.

The $-\Delta H_{n-1,n}$ in Fig. 5 are seen to decrease with n for all $X^-(HX)_n$. However, the pattern for $F^-(HF)_n$ is somewhat different. The largest drop off occurs for the addition of the third HF in $F^-(HF)_n$. For the other $X^-(HX)_n$ the largest drop off occurs between $\Delta H_{0,1}$ and $\Delta H_{1,2}$, i.e., already for the addition of the second HX. Assuming that the theoretical HF and experimental HX results are reliable, the above difference may be rationalized by the stronger covalent contribution to the bonding in $F^-(HF)_2$. Thus, covalent bonding stabilizes

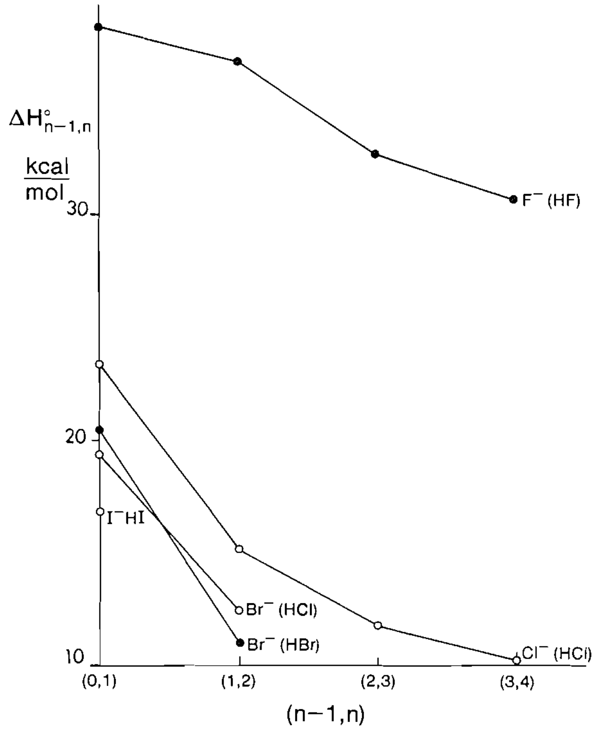

FIG. 6. Plot of $\Delta H^0_{n-1,n}$ for solvation reaction in the gas-phase: $X^-(HX)_{n-1} + HX = X^-(HX)_n$. $F(HF)_n$ data from refs. 2*c* and *d*.

$F^-(HF)_2$ (structure **II**) but probably plays no role in the other $X^-(HX)_2$ and $X^-(HX)_n$ whose fall off of binding energy with n is characteristic of electrostatic type bonding (see for example $Br^-(H_2O)_n$ and other similar systems (4).

(*c*) *Lattice energies of* $M^+.X_2H^-$

As mentioned in the Introduction, lattice energies of $M^+X_2H^-$ and the binding energies X^-—HX can be related by means of a Born type cycle (see [12])

[12]
$$\begin{tikzcd} M^+_{(g)} + X^-_{(g)} + HX_{(g)} \arrow[r, "\Delta H_{0,1}"] \arrow[d, "-\Delta H_L(MX)"] & M^+_{(g)} + HX_2{}^-_{(g)} \\ MX_{(s)} + HX_{(g)} \arrow[r, "\Delta H_r"] & MHX_{2(s)} \arrow[u, "\Delta H_L(MHX_2)"'] \end{tikzcd}$$

[12*a*] $\Delta H_{0,1} = \Delta H_L(MHX_2) - \Delta H_L(MX) + \Delta H_r$

[12*b*] $\delta\Delta H_L = \Delta H_L(MX) - \Delta H_L(MHX_2)$

where ΔH_L stands for lattice energy. $\Delta H_L(MX)$ can be evaluated from experimental data and ΔH_r can be obtained from the experimentally available heats of formation of the reactants. $\Delta H_{0,1}$ can be obtained if $\Delta H_L(MHX_2)$ is available or vice versa. In the early work (2*e*) classical lattice energy calculations for MHX_2 were used in [12*a*] to estimate $\Delta H_{0,1}$ for X = F. These led to $-\Delta H_{0,1}$ which were much higher than the experimental value given in Table 3. Now, using the experimental $\Delta H_{0,1}$ from Table 3 we can reverse the procedure and provide experimental lattice energies $\Delta H_L(MHX_2)$. The data for MHF_2 are summarized in Table 6. Lattice energies for the other MHX_2 can be also evaluated provided that the ΔH_r are available. Comparing the $\Delta H_L(MHF_2)$ in Table 6 with recent lattice energy calculations of Jenkins and Pratt (23) one finds that the classically calculated values are, on the average, too small by some 13 kcal/mol.

TABLE 6. Lattice energies of MHF_2 salts[a]

	Value				
Parameter	$LiHF_2$	$NaHF_2$	KHF_2	$RbHF_2$	$CsHF_2$
ΔH_r[a]	13.2	18.0	21.3	22.4	23.7
$\Delta H_L(MF)$[b]	250.0	221.7	197.5	189.3	180.7
$\Delta H_L(MHF_2)$[c]	224.6	201.1	180.2	173.1	165.8

[a]All values in kcal/mol at ~300 K. For symbols used and evaluation see eq. [12].
[b]Lattice energy of MHF_2 from Wagman *et al.* (22).
[c]From eq. [12*a*], $\Delta H_{0,1} = -38.6$ kcal/mol (for X = F), Larson and McMahon (9, 10). Estimated error of $\Delta H_L(MHF_2)$, +4 kcal/mol.

Previous estimates of hydrogen bond energies for $HF_2{}^-$, $HCl_2{}^-$, $HBr_2{}^-$, and $HI_2{}^-$ based on lattice energies considerations were made by McDaniel and co-workers (6). These authors determined experimentally the enthalpy changes (ΔH_r) for reaction [13].

[13] $R_4NX(s) + HX(g) = R_4NHX_2(s)$

They argued that as the size of R_4N^+ is increased the lattice energy of R_4NHX_2 should gradually approach that of R_4NX. When the quantities become equal, it follows from eq. [12*a*] that $\Delta H_{0,1}$ will become equal to $\Delta H_r = \Delta H_{13}$, i.e., ΔH_{13} should give the desired hydrogen bond energy. McDaniel and co-workers (6) were able to measure ΔH_{13} for (Cl, Br, I) and gradually increasing R (Me, Et, *n*-Bu). They found, as expected, that $-\Delta H_{13}$ increases with increasing size of the alkyl group and that it seems to reach a limiting value. The approach to the limiting value was fastest for Cl and slowest for I (see Fig. 7 in ref. 6*b*). The limiting values for $-\Delta H_{13}$ were: ~14 (Cl), 12.8 (Br), 12.4 (I) while the corresponding $-\Delta H_{0,1}$ from Table 3 are 23, 21, and 17 kcal/mol. Only a single $-\Delta H_{13}$ (R = Me) experimental value could be obtained for F. This value was 37 kcal/mol while $-\Delta H_{0,1}$ is 38.6 kcal/mol. Evidently, McDaniel *et al.* provide legitimate lower limits for the hydrogen bond energies of all the XHX^-. However, the results are somewhat confusing. For $ClHCl^-$ where a limiting value seemed to have been reached, the $-\Delta H_{13}$ shows the largest deviation from the $\Delta H_{0,1}$, while for FHF^- where attainment of the limiting value already for R = Me could be in doubt, closest agreement with the $\Delta H_{0,1}$ is observed. It is not clear whether these complexities result from experimental error or are due to intricate changes of the lattice energies of the compounds involved.

Acknowledgements

This work was generously supported by a Grant from the Canadian Natural Sciences and Engineering Research Council of Canada. We are also grateful to Professor T. B. McMahon for supplying us with preprints of this recent work (10).

1. J. EMSLEY. Chem. Soc. Rev. **9**, 91 (1980) and references therein.
2. (*a*) A. STØGARD, A. STRECH, J. ALMHÖF, and B. ROOS. Chem. Phys. **8**, 405 (1975); (*b*) F. KEIL and R. AHLRICKS. J. Am. Chem. Soc. **98**, 4787 (1976); (*c*) J. H. CLARK, J. EMSLEY, D. J. JONES, and R. E. OVERILL. J. Chem. Soc. Dalton Trans. 1219 (1981); (*d*) J. EMSLEY, R. J. PARKER, and R. E. OVERILL. J. Chem. Soc. Faraday Trans. **2**, 198 (1982); 1347 (1982); (*e*) C. THOMSON, D. T. CLARK, T. C. WADDINGTON, and H. D. B. JENKINS. J. Chem. Soc. Faraday II. **71**, 1942 (1975); (*f*) M. DIXON and R. E. OVERILL. J. Mol. Struct. **48**, 115 (1978); (*g*)

J. ALMLÖF. J. Mol. Struct. **85**, 179 (1981); (*h*) P. N. NOBLE and R. N. KORTZEBORN. J. Chem. Phys. **52**, 5375 (1970).
3. (*a*) K. M. HARMON and R. R. LOVELACE. J. Phys. Chem. **86**, 900 (1982); (*b*) R. KRUH, K. FUWO, and T. E. MCEVER. J. Am. Chem. Soc. **78**, 4256 (1956); T. R. R. MCDONALD. Acta Crystallogr. **13**, 113 (1960); (*c*) J. A. IBERS. J. Chem. Phys. **40**, 402 (1964); J. M. WILLIAMS and L. F. SCHNEEMEYER. J. Am. Chem. Soc. **95**, 5780 (1973); (*d*) J. C. EVANS and G. Y.-S. LO. J. Phys. Chem. **70**, 11 (1966), **71**, 3942 (1967), **73**, 448 (1969); (*e*) F. Y. FUJIWARA and J. S. MARTIN. Can. J. Chem. **49**, 3071 (1971); J. Am. Chem. Soc. **96**, 7632 (1974); (*f*) B. S. AULT. Acc. Chem. Res. **15**, 103 (1982) and references therein.
4. P. KEBARLE. Ann. Rev. Phys. Chem. **28**, 445 (1977).
5. (*a*) J. A. A. KETELAAR. Rec. Trav. Chim. **60**, 523 (1941); (*b*) T. C. WADDINGTON. Trans Faraday Soc. **54**, 25 (1958); (*c*) H. P. DIXON, H. D. B. JENKINS, and T. C. WADDINGTON. J. Chem. Phys. **57**, 4388 (1972); (*d*) H. D. B. JENKINS and K. F. PRATT. J. Chem. Soc. Faraday Trans II. **73**, 872 (1977).
6. (*a*) S. A. HARRELL and D. H. MCDANIEL. J. Am. Chem. Soc. **86**, 4497 (1964); D. H. MCDANIEL and R. E. VALLEÉ. Inorg. Chem. **2**, 996 (1963).
7. (*a*) R. D. GREEN and J. S. MARTIN. J. Am. Chem. Soc. **90**, 3659 (1968); (*b*) J. S. MARTIN and F. Y. FUJIWARA. J. Chem. Phys. **56**, 4098 (1972); (*c*) J. S. MARTIN and F. Y. FUJIWARA. J. Am. Chem. Soc. **96**, 7625 (1974).
8. R. YAMDAGNI and P. KEBARLE. Can. J. Chem. **52**, 2249 (1974).
9. J. W. LARSON and T. B. MCMAHON. J. Am. Chem. Soc. **105**, 2944 (1983).
10. J. W. LARSON and T. B. MCMAHON. Inorg. Chem. To be published.
11. M. D. JOESTEN and L. J. SCHAAD. Hydrogen bonding. Marcel Dekker, Inc., New York. Chapt. 4.
12. J. D. PAYZANT, R. YAMDAGNI, and P. KEBARLE. Can. J. Chem. **49**, 3308 (1971); R. YAMDAGNI, J. D. PAYZANT, and P. KEBARLE. Can. J. Chem. **51**, 2507 (1973); A. J. CUNNINGHAM, J. D. PAYZANT, and P. KEBARLE. J. Am. Chem. Soc. **94**, 7627 (1972).
13. (*a*) J. D. PAYZANT and P. KEBARLE. J. Chem. Phys. **56**, 3482 (1972); (*b*) Y. K. LAU, S. IKUTA, and P. KEBARLE. J. Am. Chem. Soc. **104**, 1462 (1982).
14. R. G. KEESEE and A. W. CASTLEMAN, JR. J. Am. Chem. Soc. **102**, 1446 (1980); R. G. KEESEE, N. LEE, and A. W. CASTLEMAN, JR. J. Chem. Phys. **73**, 2195 (1980).
15. R. YAMDAGNI and P. KEBARLE. J. Am. Chem. Soc. **93**, 7139 (1971); J. D. PAYZANT, R. YAMDAGNI, and P. KEBARLE. Can. J. Chem. **49**, 3308 (1979).
16. J. B. CUMMING, M. A. FRENCH, and P. KEBARLE. J. Am. Chem. Soc. **99**, 6999 (1977).
17. M. A. FRENCH, S. IKUTA, and P. KEBARLE. Can. J. Chem. **60**, 1907 (1982).
18. P. J. DESMEULES and L. C. ALLEN. J. Chem. Phys. **72**, 4731 (1980).
19. R. L. BENOIT, M. RINFRET, and R. DOMAIN. Inorg. Chem. **11**, 2603 (1972).
20. Z. PAWLAK, L. M. MUKHERJEE, A. A. HAMPTON, and R. G. BATES. J. Chem Thermodyn. **15**, 189 (1983).
21. T. F. MAGNERA, G. CALDWELL, J. SUNNER, S. IKUTA, and P. KEBARLE. J. Am. Chem. Soc. To be published.
22. D. D. WAGMAN, W. H. EVANS, I. HALOW, S. M. BAILEY, V. B. PARKER, R. M. SCHUMM, K. L. CHURNEY, and R. L. NUTTALL. J. Phys. Chem. Ref. Data, Supp. **2**, 11 (1982).
23. H. D. B. JENKINS and K. F. PRATT. J. Chem. Soc. Faraday Trans. **73**, 872 (1977) and references therein.
24. G. HERZBERG. Spectra of diatomic molecules. Van Nostrand, New York. 1950.
25. L. PAULING. The nature of the chemical bond. 3rd. ed. Cornell University Press, Ithaca, NY. 1960.
26. LANDOLT-BORNSTEIN. Zahlenwerten und Funktionen. Vol. 1. Springer, Berlin. 1951. Part 3.
27. A. L. MCCLELLAN. Tables of experimental dipole moments. Freeman, San Francisco. 1963.

Ligand field and Rydberg assignments of the $PtCl_4^{2-}$ spectrum: a relativistic MS-Xα study

A. GOURSOT
Laboratoire de Photochimie Générale, ERA du CNRS N° 386, E.N.S.C.Mu., 3 rue Alfred Werner, 68093 Mulhouse Cedex, France

AND

H. CHERMETTE
Institut de Physique Nucléaire (et IN2P3), Université Lyon-1, 43 Bd du 11 Novembre 1918, 69622 Villeurbanne Cedex, France

Received July 19, 1984

This paper is dedicated to Professor Camille Sandorfy on the occasion of his 65th birthday

A GOURSOT and H. CHERMETTE. Can. J. Chem. **63**, 1407 (1985).

Relativistic MS-Xα calculations are reported for a $PtCl_4^{2-}$ cluster. Good agreement with experiment is obtained for the optical spectrum. A ligand field approach has been used to evaluate the $d-d$ transitions through the use of a strong field matrix, where the crystal field parameters have been replaced by values derived from the Xα calculation. The high intensity spectrum is clearly interpreted in terms of Rydberg Pt $5d \rightarrow 6p$ transitions.

A GOURSOT et H. CHERMETTE. Can. J. Chem. **63**, 1407 (1985).

On rapporte des calculs relativistes MS-Xα pour le cluster $PtCl_4^{2-}$. Pour le spectre optique, on obtient une bonne corrélation avec l'expérience. Dans le but d'évaluer les transitions $d-d$, on a utilisé une approche par la théorie du champ de ligand pour laquelle on fait appel à une matrice champ fort, dans laquelle on a remplacé les paramètres de champ cristallin par des valeurs obtenues par les calculs Xα. On interprète facilement le spectre de forte intensité sur la base de transitions de Rydberg Pt $5d \rightarrow 6p$.

[Traduit par le journal]

Introduction

The electronic absorption spectra of transition metal complexes are generally interpreted as displaying a low-intensity part attributed to the ligand field transitions, and intense absorption bands referred to as charge transfer (CT) transitions.

The $d-d$ spectra have been extensively studied by application of the ligand field theory. On the other hand, CT bands are generally assigned with the aid of energy levels diagrams. Quantitative analyses of the CT spectra through molecular orbital (MO) methods require a realistic description of the relative energies of the metal and ligand orbitals, together with a satisfactory representation of the metal–ligand interactions. Moreover, a quantitative description of CT transitions requires ΔSCF Hartree–Fock calculations in order to account for orbital relaxation. These requirements explain that such transitions are not extensively studied, although they represent an interesting characteristic part of the absorption spectra of transition metal complexes, often involved in their photochemical properties.

Moreover, the high-intensity absorptions could also be due to transitions from the metal nd orbitals to mainly metal $(n+1)s$ or $(n+1)p$ orbitals. This possibility of encountering Rydberg transitions, in a wavelength region generally assigned to CT bands, has already been mentioned, particularly in the case of square planar complexes (1). In this paper, we want to put some emphasis upon the assignment of the high-intensity bands of $PtCl_4^{2-}$, and more specifically upon the Rydberg alternative to the CT assignment.

Considerable experimental work has been devoted to the elucidation of the absorption spectrum of $PtCl_4^{2-}$. However, most of the experimental studies as well as the previous theoretical works are principally interested in the ligand field transitions. Even though some of them mention Rydberg $5d \rightarrow 6p$ transitions as possible assignments for the high-intensity bands, no quantitative analysis has been presented to support these proposals. This is why we have chosen to perform relativistic MS-Xα calculations in order to assign the main features of the $PtCl_4^{2-}$ absorption spectrum and to assess their ligand field, CT, or Rydberg origin. The relativistic Xα method (2) is based on the Cowan and Griffin (3) approximation of the Dirac–Hartree–Fock equations. The effects of the mass–velocity and Darwin corrections are included self-consistently, while those of the spin–orbit operator are thus neglected. The spin–orbit effects may then be taken into account after self-consistency, by first order perturbation theory.

Calculation parameters

The Pt—Cl bond length is taken as 2.30 Å (4). The atomic α value for Pt (0.69306) and Cl (0.72325) are taken from the compilation of Schwarz (5, 6). A weighted average of these atomic values is chosen for the interatomic and extramolecular regions (0.71721). As for previous calculations on halide complexes (7–9), the Pt and Cl spheres are allowed to overlap by an amount of 20% (r(Pt) = 2.58951; r(Cl) = 2.62613). An external tangent outer sphere is used ($r_{OUT} = 6.97250$), which also serves as a "Watson Sphere" (10) on which a positive charge +2.5 is distributed. This +2.5 value has been used to push down the valence levels and thus to find the upper virtual levels with negative energies. It has been shown extensively that such a small increase of the Watson Sphere charge (usually 0.5) involves only a uniform stabilization of the eigenvalues, thus providing the ability of finding more virtual levels.

Partial waves up to $l = 4$ are included in the multiple scattering expansion in the platinum sphere and extramolecular region, and up to $l = 1$ in the chlorine spheres.

All calculations of transition energies have been performed with the use of Slater's transition-state method (11).

The use of the Slater's transition state (TS) procedure in MS Xα calculations has been criticized by Oliveira and Maffeo (12), who concluded that the best estimate of the excitation energy is indeed given by the TS procedure, only when both occupied and virtual orbitals involved in the transition are con-

TABLE 1. Ground state energy levels[a] (Ry) and charge distribution of $PtCl_4^{2-}$

		Pt								Cl				
MO	Energy	s	p_σ	p_π	d_{z^2}	$d_{x^2-y^2}$	d_{xy}	$d_{xz,yz}$	f	s	p_σ	p_π	INT	OUT
$5e_u$	−0.029												3	97 (98% p)
$3a_{2u}$	−0.036												7	93 (98% p)
$5a_{1g}$	−0.055												13	86 (37% s, 63% d)
$4e_u$	−0.098									1	2		26	71 (95% p)
$2a_{2u}$	−0.163			1								6	51	42 (95% p)
$4a_{1g}$	−0.178				5					3			42	50 (93% s)
$3b_{1g}$	−0.188					56				4	26		8	6
$2b_{2g}$	−0.430						74					17	8	1
$2e_g$	−0.456							72				19	8	1
$3a_{1g}$	−0.510	9			69						1		20	1
$1a_{2g}$	−0.586											89	10	1
$3e_u$	−0.623		1						1		25	51	10	2
$1b_{2u}$	−0.630								1			85	12	2
$1a_{2u}$	−0.673			1								78	19	2
$1e_g$	−0.691							20				64	15	1
$2e_u$	−0.701		7						1		60	22	7	3
$1b_{2g}$	−0.751						19					63	17	1
$2b_{1g}$	−0.813					37					62		—	1
$2a_{1g}$	−0.833	14			11					4	68		2	1
$1e_u$	−1.510		2						1	94			3	—
$1b_{1g}$	−1.513					5				93			2	1
$1a_{1g}$	−1.545				1					90	1		3	1

[a]The highest occupied level is $2b_{2g}$.

centrated in the same atomic sphere. In the case of different atomic spheres (CT transitions), they concluded that a TS calculation may not necessarily provide an improvement over the "Koopmans" difference of the ground state (GS) eigenvalues. In our opinion, even though it does not provide the exact ΔSCF energies,[1] the TS procedure allows one to take into account the major portion of the relaxation effect, leading to good estimates of the CT spectra and particularly of the differences between metal−metal and ligand−metal transition energies. This point has been verified by the authors in various studies (7−9, 13−15). In those cases, and in the present one, the relaxation of the orbitals involved in the TS procedure imply some redistribution of the electronic density inside the atomic spheres, but without altering the intersphere contribution by more than 1%, with respect to the GS structure. Moreover, when the virtual orbital is located in the outersphere region, previous work (16, 17) has shown that the calculated relaxation energies are substantial, requiring the use of the TS procedure rather than the Koopmans one.

Ground state electronic structure

The GS valence levels of $PtCl_4^{2-}$ and the corresponding charge distribution are reported in Table 1 (spin-restricted calculation).

Previous SCF-Xα calculations (18−21) have already been performed on this complex, but without introducing relativistic corrections. As described previously for Ir or Pt halides (7−9), the main effect of the relativistic contraction of the metal s and p orbitals, which increases the nuclear shielding, is to allow the expansion of the d and f orbitals. The valence molecular orbitals (MOs), which display a preponderant metal $5d$ character are thus all shifted upwards. Moreover, with respect to non-relativistic results, the upper occupied antibonding MOs, namely, $3a_{1g}$, $2e_{2g}$, $2b_{2g}$, have substantially increased contributions, while their bonding counterparts ($2a_{1g}$, $1e_g$, $1b_{2g}$) have a decreased Pt $5d$ participation. This upwards energy shift of the Pt $5d$ levels moves them away from the pure ligand π levels ($1a_{2g}$, $3e_u$, $1b_{2u}$, $1a_{2u}$) which remain nearly unchanged, while the energy separations between the Pt $5d$ levels themselves are not so much perturbed. The same tendency is obtained from a relativistic extended Hückel (REX) calculation (22), while the Dirac−Slater (DS) method (22) leads to a somewhat different situation, where the upward energy shift concerns only the $3a_{1g}$ level and the $2e_g$ (3/2) component (calculation performed in the double group D^*_{4h}).

In our case, the metal levels ordering is maintained, with respect to the non-relativistic case. This will lead to roughly comparable ligand field transitions. On the contrary, the ligand-to-metal or metal-to-ligand CT transitions will undergo substantial modifications. The calculated ordering of the "$5d$-like" MOs is

$$3b_{1g}(d_{x^2-y^2}) > 2b_{2g}(d_{xy}) > 2e_g(d_{xz}, d_{yz}) > 3a_{1g}(d_{z^2})$$

This ordering is consistent with the experimental observations on the basis of MCD data (23), of spectra recorded with polarized light (24). It was also obtained from EH calculations (25, 26). However, a comparison with these earlier theoretical results shows some important differences in the values of the energy separations: Δ1 ($3b_{1g} - 2b_{2g}$), Δ2 ($2b_{2g} - 2e_g$), and Δ3 ($2e_g - 3a_{1g}$) which are calculated as 26 550, 2 950, and 5 950 cm^{-1} in the present work. The virtual MOs, except $3b_{1g}$, are essentially localized outside of the atomic spheres and may be considered as Rydberg orbitals, which are considered as one-center expansions about the molecular center. Their charge analysis shows that $2a_{2u}$, $3a_{2u}$, $4e_u$, and $5e_u$ have predominant contributions of the outersphere (sphere surrounding the whole

[1]For example, the ΔSCF energy of the LMCT transition $3e_u \rightarrow 3b_{1g}$ of $PtCl_4^{2-}$ is 51 300 cm^{-1}, which compares very well with the TS value of 51 000 cm^{-1} (cf. Table 3).

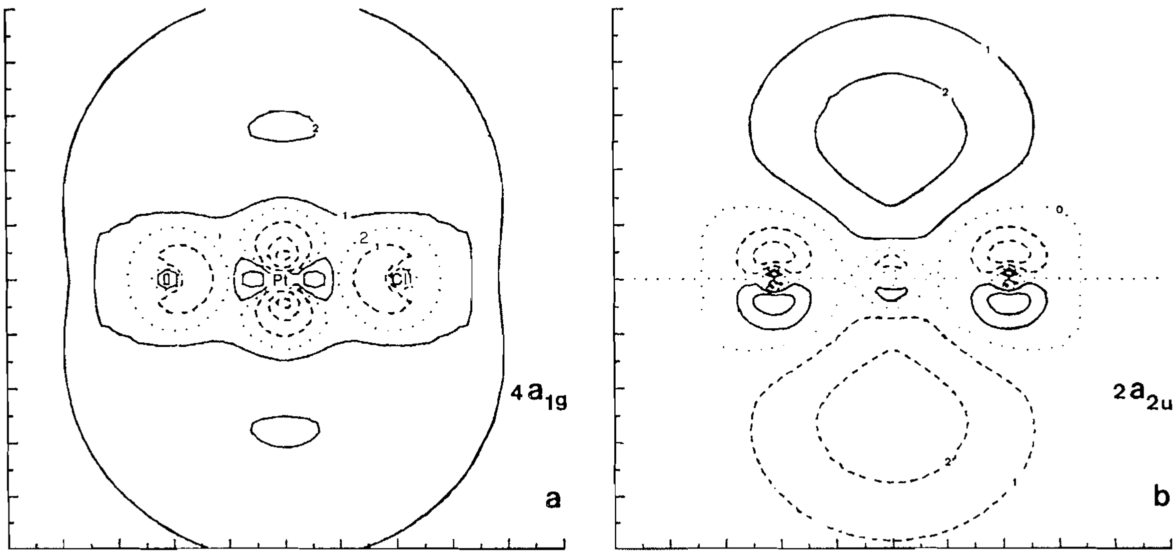

FIG. 1. Contours labelled 0, 1, 2 are equal to 0, 0.019, and 0.038 (electrons/bohr^3)$^{1/2}$ for case *a* and 0, 0.066, and 0.132 (electrons/bohr^3)$^{1/2}$ for case *b*. Positive wavefunction contours are represented by a solid line, negative contours by a dashed line, and dotted lines are related to the contour 0.

molecule), which corresponds essentially to a *p* partial wave (for 95% p_z, 98% p_z, 95% p_{xy}, and 98% p_{xy}, respectively). For the $4a_{1g}$ and $5a_{1g}$ MOs, the principal component in the outer sphere region is an *s* partial wave for the former (93%) and a *d* partial wave for the latter (63% *d*, 37% *s*). The low-lying $4a_{1g}$ and $2a_{2u}$ MOs have a substantial intersphere contribution. This is certainly due to the use of the Xα division of space in the case of a square planar structure, providing a strong intersphere participation to the diffuse *s* and p_z metal orbitals. The diffuseness of these MOs is illustrated in Fig. 1, which gives a clear indication of their 4*s* ($4a_{1g}$) and $4p_z$ ($2a_{2u}$) Rydberg character.

Ligand field spectrum

As reported previously (7, 8, 18), Xα spin polarized calculations in D_{4h} symmetry would lead to the complete determination of the multiplet states corresponding to the excited configurations ($3a_{1g}^2 2e_g^2 2b_{2g}^1 3b_{1g}^1$), ($3a_{1g}^2 2e_g^1 2b_{2g}^2 3b_{1g}^1$), and ($3a_{1g}^1 2e_g^2 2b_{2g}^2 3b_{1g}^1$). The spin–orbit parameters ζ_{nl} may be calculated for every radial function $R_{nl}(r)$ through the use of the spin–orbit operator

$$\zeta(r) = 2(\alpha^2/4)[1 + \alpha^2/4(\epsilon - V)]^{-1} \frac{1}{r} \frac{dV}{dr}$$

(for details see refs. 2, 8). The ζ_{5d}(Pt) parameters, related to the MOs involved in the *d–d* transitions, have large calculated values (around 6500 cm^{-1}). Thus it seems desirable to take into account the spin–orbit interaction which mixes the ligand field excited states and the ground state $^1A_{1g}$ with the triplet $^1A_{2g}$ and ^3E_g. As in previous works (7, 8), we are thus led to use a ligand field approach on the basis of parameters derived from the Xα calculation for the ground-state. The energies of the ground and excited states have been evaluated through the strong field matrix elements for square planar d^8 systems (27, 28) where the crystal field parameters have been replaced by the Δ1, Δ2, Δ3 values obtained from our Xα calculation, so as the spin–orbit coupling parameter $\alpha = (1/2)\ \zeta_{5d}(\text{eff}) = 1850$ cm^{-1}. ζ_{5d}(eff) is calculated as the average value over $3a_{1g}$, $2e_g$, $2b_{2g}$, and $3b_{1g}$ of the products $\rho_M \times \zeta_{5d}$(Pt), specific to each MO, where ρ_M is the fraction of the 5*d* Pt charge involved in this MO. The two Slater–Condon parameters F_2 and F_4 can then be treated as arbitrary parameters, kept within reasonable limits. The better agreement with the observed spectra is obtained for F_4 = 65 cm^{-1} and F_2 = 775 cm^{-1}.

Table 2 presents a comparison between the calculated ligand field transition energies and the experimental peak positions. These g–g transitions are forbidden according to the symmetry selection rules. They correspond to the low-intensity part of the spectrum (up to 34 000 cm^{-1}).

The spin–orbit interaction allows transitions from the ground state to excited states derived from triplet states, which may appear as very low intensity absorptions. The assignment presented in Table 2 is consistent with the experimental intensities and peak positions, as well as with the indications provided by the spectra in polarized light and MCD data. In agreement with the results of Martin *et al.* (24) and McCaffery *et al.* (23), the bands around 27 000 and 30 000 cm^{-1} are assigned to the $A_{1g}(^1A_g) \rightarrow A_{2g}(^1A_{2g})$ and $A_{1g}(^1A_{1g}) \rightarrow E_g(^1E_g)$, respectively. In fact, the two corresponding excited states keep a preponderant singlet character (cf. Table 2). The $A_{1g}(^1A_{1g}) \rightarrow B_{1g}(^1B_{1g})$ transition is calculated to occur at 34 200 cm^{-1}, that is on the low-energy side of the first high-intensity band. These assignments are at variance with CI + spin–orbit results obtained with the use of relativistic effective core potentials (29). This technique (RECP) yields a different singlet state ordering ($^1A_{2g} > {}^1E_g > {}^1B_{1g}$) from ours, which implies that, after diagonalizing the spin–orbit matrix, the $A_{1g}(^1A_{1g}) \rightarrow A_{2g}(^1A_{2g})$ and $A_{1g}(^1A_{1g}) \rightarrow E_g(^1E_g)$ transitions are correlated respectively with the 30 000 cm^{-1} and 27 000 cm^{-1} absorptions. This result is in full disagreement with the MCD (23) and polarized crystal data (24, 30). Our results are in agreement with previous assignments based on MO calculations (19, 26) or on ligand field calculations using substantial Δ3 values (24, 25, 28) particularly as alternative A proposed by Martin *et al.* (28). Elding and Olsson (31), following the proposal of alternative B by Martin *et al.* (28), suggested that the a_{1g} (d_{z^2}) and e_g ($d_{xz,yz}$) MOs might have very similar energies, leading to quasi degenerate $A_{1g}(^1A_{1g}) \rightarrow E_g(^1E_g)$ and $A_{1g}(^1A_{1g}) \rightarrow B_{1g}(^1B_{1g})$ transitions near 30 000 cm^{-1}. This assignment would imply Δ3 <

TABLE 2. Calculated ligand field excitation energies (cm^{-1}) and experimental peak positions (K_2PtCl_4 crystal spectrum)

Ligand field excited state	Calculated energies and singlet or triplet major participations	Observed peak positions (from ref. 20)
B_{1g}	34 300 ($^1B_{1g}$ 86)	
E_g	30 400 (^1E_g 54; $^3B_{1g}$ 33)	30 000
B_{2g}	28 500 ($^3B_{1g}$ 62; ^3E_g 36)	27 100
A_{2g}	27 250 ($^1A_{2g}$ 86)	
E_g	24 800 ($^3A_{2g}$ 34; $^3B_{1g}$ 23; ^3E_g 20; ^1E_g 21)	24 500
A_{1g}	23 750 ($^3A_{2g}$ 66; ^3E_g 25)	
E_g	21 100 ($^3A_{2g}$ 41; $^3B_{1g}$ 32; ^1E_g 18)	21 300
B_{1g}	20 700 (^3E_g 83)	
B_{2g}	18 800 (^3E_g 62; $^3B_{1g}$ 36)	18 000–19 000
E_g	17 450 (^3E_g 64; $^3A_{2g}$ 22)	
A_{2g}	17 100 ($^3A_{2g}$ 90)	
A_{1g}	16 400 (^3E_g 72)	

TABLE 3. Calculated Rydberg-type and CT-type transitions (cm^{-1}) compared with the available experimental peak positions

Transition[a]	Type[b]	Calculated value	Experimental value[c]
$2b_{2g} \rightarrow 2a_{2u}$ (F)	R $5d_{xy} \rightarrow 6p_z$	37 300	37 600
$2e_g \rightarrow 2a_{2u}$ (A)	R $5d_{xz,yz} \rightarrow 6p_z$	39 150	42 600 – 43 700
$2b_{2g} \rightarrow 4e_u$ (A)	R $5d_{xy} \rightarrow 6p_{x,y}$	44 300	
$3a_{1g} \rightarrow 2a_{2u}$ (A)	R $5d_{z^2} \rightarrow 6p_z$	45 200	45 050 – 46 300
$2e_g \rightarrow 4e_u$ (A)	R $5d_{xz,yz} \rightarrow 6p_{x,y}$	46 400	
$3e_u \rightarrow 4a_{1g}$ (A)	$L_\pi \rightarrow R_{\sigma s}$	51 000	
$3e_u \rightarrow 3b_{1g}$ (A)	L → M	51 300	
$3a_{1g} \rightarrow 4e_u$ (A)	R $5d_{z^2} \rightarrow 6p_{x,y}$	52 600	

[a]F: forbidden; A: allowed transitions according to the symmetry selection rules.
[b]R: Rydberg; L: ligand; M: metal.
[c]From refs. 27 and 31.

1000 cm^{-1}. This assumption disagrees with MO calculations and, particularly, with the present one, which yields a separation of 5950 cm^{-1} between the $3a_{1g}$ and $2e_g$ MOs. The low-intensity band around 17 000 – 18 000 cm^{-1} is assigned to the $A_{1g}(^1A_{1g}) \rightarrow A_{1g}(^3E_g)$, $A_{1g}(^1A_{1g}) \rightarrow A_{2g}(^3A_{2g})$, and $A_{1g}(^1A_{1g}) \rightarrow E_g(^3A_{2g})$ transitions. The broad absorption near 20 000 – 21 000 cm^{-1} and the shoulder at 24 000 cm^{-1} are assigned to the superposition of several transitions to states derived from triplet states.

High intensity spectrum

It consists of a moderately intense absorption band with a maximum peak at 46 200 cm^{-1} and a pronounced shoulder at 43 400 cm^{-1} (ϵ = 8 500) (23, 32). A weak shoulder ($\epsilon \simeq 400$) appears on its low-energy edge, near 37 500 cm^{-1}.

Most MO calculations have considered these intense bands as ligand-to-metal CT transitions (19, 25, 33–35), with the exception of Cotton and Harris (26), who proposed a metal $5d \rightarrow 6p$ assignment, in agreement with an earlier suggestion by Chatt *et al.* (36).

Later, the analysis of the polarized single-crystal spectra of K_2PtCl_4 (32) supported the suggestion that the 46 000 cm^{-1} band contains a low-lying Pt $5d_{z^2} \rightarrow 6p_z$ component. In their comparative study of the solution spectra of $PtX_n(H_2O)_{4-n}^{2-n}$ (X = Cl, Br), Elding and Olsson (31) have described the high intensity bands as the superposition of the metal-to-ligand CT transitions $3a_{1g} \rightarrow 2a_{2u}$ and $2e_g \rightarrow 2a_{2u}$. This assignment retains the $5d \rightarrow a_{2u}$ proposal (26, 32) but considers now a_{2u} as a predominantly ligand level instead of a Pt $6p$ one, on the basis of arguments drawn from the comparison of $PtCl_4^{2-}$ and $PdCl_4^{2-}$ spectra. Very recently, Larsson *et al.* (22) concluded to a $5d \rightarrow 6p$ assignment for the $2e_g \rightarrow 2a_{2u}$ transition, on the basis of their REX calculation, while their DS results show a strongly underestimated value for this transition energy.

As underlined previously, the relativistic corrections used in the present calculation have induced an increased separation between the upper occupied ligand $p\pi$ levels ($1b_{2u}$, $3e_u$) and the Pt $5d$ levels ($3a_{1g}$, $2e_g$, $2b_{2g}$) with respect to non relativistic MO results. Consequently, the ligand-to-metal CT transitions from ($1b_{2u}$, $3e_u$) to $3b_{1g}$ are calculated at higher energies than the $5d \rightarrow 6p$ transitions of Rydberg type, from ($3a_{1g}$, $2e_g$, $2b_{2g}$) to ($2a_{2u}$, $4e_u$).

As Table 3 shows, the orbitally forbidden $^1A_{1g} \rightarrow {}^1B_u$ ($2b_{2g} \rightarrow 2a_{2u}$) Rydberg transition is the lowest one and its calculated value compares very well with the shoulder of weak intensity located near 37 600 cm^{-1}.

In the same way, the structured band that peaks at 46 300 cm^{-1} is assigned to the superposition of absorption bands related to the transitions from the $^1A_{1g}$ ground state to the Rydberg-type excited states of configuration $5d^76p$, with the exception of the ^1E_u state which is calculated at a higher energy (52 600 cm^{-1}).

The results presented in Table 3 correspond to non spin-polarized calculations. They have been obtained without including configuration interaction, via the spin–orbit coupling, between the singlet and triplet $5d^7\,6p$ excited states. The intense absorption bands are related to singlet–singlet transitions and in this case, the spin–orbit coupling vanishes in a first-order approximation.

Relativistic MS-Xα calculations, performed in the double group D_{4h}^* symmetry would certainly lead to a more precise description of the fine structure of the 43 000 – 46 000 cm^{-1} band. Further work in this direction is in progress. Nevertheless, the present work does support unambiguously the assignment of the high intensity bands of the $PtCl_4^{2-}$ spectrum as Rydberg Pt $5d \rightarrow 6p$ transitions.

1. H. L. SCHLÄFER and G. GLIEMAN. *In* Basic principles of ligand field theory. Wiley Interscience, New York. 1969.
2. H. J. WOOD and M. BORING. Phys. Rev. B**18**, 2701 (1978).
3. R. D. COWAN and D. C. GRIFFIN. J. Opt. Soc. Am. **66**, 1010 (1976).
4. L. E. SUTTON. Chem. Soc. Sp. Publ. No. 18 (1965).
5. K. SCHWARZ. Phys. Rev. B**5**, 2466 (1972).
6. K. SCHWARZ. Theorit. Chim. Acta, **34**, 225 (1974).
7. A. GOURSOT, H. CHERMETTE, and C. DAUL. Inorg. Chem. **23**, 305 (1984).
8. A. GOURSOT and H. CHERMETTE. Chem. Phys. **69**, 329 (1982).
9. A. GOURSOT, E. PENIGAULT, and H. CHERMETTE. Chem. Phys. Lett. **97**, 215 (1983).
10. R. E. WATSON. Phys. Rev. III, 1108 (1958).
11. J. C. SLATER. Quantum theory of molecules and solids. McGraw-Hill, New York. 1974.
12. P. M. OLIVEIRA and B. MAFFEO. Int. J. Quantum Chem. **20**, 1127 (1981).
13. A. GOURSOT, H. CHERMETTE, E. PENIGAULT, M. CHANON, and W. L. WALTZ. Inorg. Chem. **23**, 3618 (1984).
14. C. DAUL, C. W. SCHLÄPFER, A. GOURSOT, E. PENIGAULT, and J. WEBER. Chem. Phys. Lett. **78**, 304 (1981).
15. A. GOURSOT, E. PENIGAULT, and J. WEBER. Nouv. J. Chim. **3**, 675 (1979).
16. R. ROBERGE and D. R. SALAHUB. J. Chem. Phys. **1**, 1177 (1979).
17. L. S. LUSSIER, C. SANDORFY, A. GOURSOT, E. PENIGAULT, and J. WEBER. J. Phys. Chem. **88**, 5492 (1984).
18. R. P. MESSMER, U. WAHLGREN, and K. H. JOHNSON. Chem. Phys. Lett. **18**, 7 (1973).
19. R. P. MESSMER, L. V. INTERRANTE, and K. H. JOHNSON. J. Am. Chem. Soc. **96**, 3847 (1974).
20. M. BARBER, J. D. CLARK, and A. HINCHCLIFFE. J. Mol. Struct. **57**, 305 (1979).
21. J. A. HORSLEY. J. Chem. Phys. **76**, 1451 (1982).
22. S. LARSSON, L. F. OLSSON, and A. ROSEN. Int. J. Quantum Chem. **25**, 201 (1984).
23. A. J. MCCAFFERY, P. N. SCHATZ, and P. J. STEPHENS. J. Am. Chem. Soc. **90**, 5730 (1968).
24. D. S. MARTIN, M. A. TUCKER, and A. J. KASSMAN. Inorg. Chem. **4**, 1682 (1965).
25. H. BASCH and H. B. GRAY. Inorg. Chem. **6**, 365 (1967).
26. F. A. COTTON and C. B. HARRIS. Inorg. Chem. **6**, 369 (1967).
27. R. F. FENSKE, D. S. MARTIN, and K. RUEDENBERG. Inorg. Chem. **1**, 441 (1962).
28. D. S. MARTIN, M. A. TUCKER, and A. J. KASSMAN. Inorg. Chem. **5**, 1298 (1966).
29. P. J. HAY. *In* Relativistic effects in atoms, molecules and solids. *Edited by* G. Malli. Plenum. 1983.
30. P. DAY, A. F. ORCHARD, A. J. THOMSON, and R. J. P. WILLIAMS. J. Chem. Phys. **42**, 1973 (1965).
31. L. I. ELDING and L. F. OLSSON. J. Phys. Chem. **82**, 69 (1978).
32. B. G. ANEX and N. TAKEUCHI. J. Am. Chem. Soc. **96**, 4412 (1974).
33. C. K. JØRGENSEN. Halogen chemistry. Vol. 1. Academic Press, London. 1967.
34. H. B. GRAY and C. J. BALLHAUSEN. J. Am. Chem. Soc. **85**, 260 (1963).
35. W. R. MASON and H. B. GRAY. J. Am. Chem. Soc. **90**, 5721 (1968).
36. J. CHATT, G. A. GAMLEN, and L. E. ORGEL. J. Chem. Soc. 486 (1958).

Substituent effects in alkynes and cyanides: a momentum density perspective[1]

ALFREDO M. SIMAS AND VEDENE H. SMITH, JR.
Department of Chemistry, Queen's University, Kingston, Ont., Canada K7L 3N6

AND

AJIT J. THAKKAR[2]
Department of Chemistry, University of New Brunswick, Fredericton, N.B., Canada E3B 5A3

Received July 19, 1984

This paper is dedicated to Professor Camille Sandorfy on the occasion of his 65th birthday

ALFREDO M. SIMAS, VEDENE H. SMITH, JR., and AJIT J. THAKKAR. Can. J. Chem. **63**, 1412 (1985).

A priori quantum mechanical calculations are made for the alkynes XCCH (X = H, Li, F, Cl, and NC), and the cyanides XCN (X = H, F, Cl, O^-, S^-, and NC) in order to examine how substituent effects in these homologous series are reflected by changes in the three-dimensional one-electron momentum density. Our qualitative analysis is based on a partial wave decomposition of the momentum density, and is in harmony with analogous studies of the position space charge density. Our quantitative analysis is based on various properties of the isotropic momentum density and on the kinetic energy anisotropy. Values of the latter quantity relative to the parent unsubstituted molecule of the pertinent homologous series are found to correlate with the Taft resonance and Dewar–Grisdale mesomeric substituent constants.

ALFREDO M. SIMAS, VEDENE H. SMITH, JR. et AJIT J. THAKKAR. Can. J. Chem. **63**, 1412 (1985).

Dans le but d'évaluer si les effets de substituants dans ces séries se réflètent par des changements dans la densité tri-dimentionnelle du moment d'un électron, on a effectué des calculs a priori de mécanique quantique sur les alcynes XCCH (X = H, Li, F, Cl et NC) et sur les cyanures XCN (X = H, F, Cl, O^-, S^- et NC). Notre analyse qualitative est basée sur une décomposition par ondes partielle de la densité du moment et elle est en harmonie avec des études analogues sur la densité de charge dans l'espace de la position. Notre analyse quantitative est basée sur diverses propriétés de la densité du moment isotrope et sur l'anisotropie de l'énergie cinétique. On a trouvé que l'on peut établir une corrélation entre la valeur de cette dernière quantité, relative à celle de la molécule de base non substituée des séries homologues pertinentes, et les constantes de résonance de Taft et mésomérique de Dewar et Grisdale relatives aux substituants.

[Traduit par le journal]

Introduction

Compton scattering provides a powerful experimental probe of electronic momentum distributions in atoms, molecules, and solids. Hence, much effort has been expended (1) to correlate chemical properties with the usual gas-phase isotropic Compton profiles $\bar{J}(q)$ and their parent spherically averaged one electron momentum densities $\bar{\Pi}(p)$. Unfortunately detailed correlations have not been easy to find because the numerous integrations necessary to obtain $\bar{J}(q)$ from a wave function seem to wash the chemical information away. Nevertheless, some progress has been made with the help of bond difference profiles (2). However, the most promising avenue for obtaining chemistry from Compton scattering seems to be via directional Compton profiles $J(\mathbf{q})$ and their parent three-dimensional one-electron momentum densities $\Pi(\mathbf{p})$.

A few studies of the anisotropic $\Pi(\mathbf{p})$ and $J(\mathbf{q})$ have already been made (for extensive bibliographies, see refs. 3 and 4) and attempts to gain insight into their structure have been based on contour maps, difference contours with respect to prepared atoms, and partitioning into orbital contributions. Since the isotropic momentum density $\bar{\Pi}(p)$ has already been studied extensively, it seems that a useful partitioning scheme should first separate $\bar{\Pi}(p)$ from $\Pi(\mathbf{p})$, and then separate the anisotropic remainder into appropriately chosen components. We have shown recently (3, 4) that a partial wave decomposition of $\Pi(\mathbf{p})$ provides such a partitioning. This analysis takes a particularly simple form for linear molecules, and our studies (3–5) on 21 linear molecules, with occupied σ and π MO's only, show that if attention is restricted to the valence region then all qualitative features of the momentum density are described by merely four partial waves. The purpose of this paper is to examine how substituent effects in alkynes and cyanides are reflected by changes in these four chemically dominant partial waves of the momentum density.

Review of theory

In the case of linear molecules with the molecular axis aligned along the polar axis, which will be the sole concern of this paper, $\Pi(\mathbf{p})$ has $D_{\infty h}$ symmetry irrespective of whether the molecular skeleton has $C_{\infty v}$ or $D_{\infty h}$ symmetry (3). Thus the momentum density of a linear molecule may be expanded as follows:

$$\Pi(\mathbf{p}) = \Pi_0(p) + \Pi_2(p)P_2(\cos\theta_p) + \Pi_4(p)P_4(\cos\theta_p) + \ldots$$

where the $P_L(\cos\theta_p)$ are Legendre polynomials, $\Pi_0(p)$ is precisely equal to the spherically averaged momentum density $\bar{\Pi}(p)$, and the higher partial waves $\Pi_2, \Pi_4, \ldots$, represent the anisotropy. We call this partitioning process a *partial wave analysis of the momentum density* (3, 4). Such an analysis is well suited to the momentum density because it is essentially a monocentric function. Clearly all expectation values of the form $\langle\Sigma_i f(p_i)\rangle$ are determined by $\Pi_0(p)$ alone:

$$\langle\Sigma_i f(p_i)\rangle = \int\Pi(\mathbf{p})f(p)\,d\mathbf{p} = 4\pi\int_0^\infty\Pi_0(p)\,f(p)\,p^2\,dp \equiv \langle f(p)\rangle$$

An example of the above is the total kinetic energy T which corresponds to $f(p) = p^2/2$. Hartree atomic units (6) are used throughout this section. An illustration of the power of partial wave analysis is provided by the fact that the anisotropy of the kinetic energy tensor is determined by Π_2 alone. Thus

$$T_\parallel - T_\perp = (2\pi/5)\int_0^\infty\Pi_2(p)p^4\,dp$$

[1] Based in part on the Ph.D. dissertation of A.M.S.
[2] NSERCC University Research Fellow.

where $T_{\|}$ and $T_{\perp}$, respectively, are the components of the kinetic energy parallel and perpendicular to the molecular axis. Of course $T = T_{\|} + 2T_{\perp}$. These components of the kinetic energy are important because they are experimentally accessible (7) through directional Compton profiles, and because they play a pivotal role in certain types of analyses of chemical bonding (8).

Convergence studies (3, 4) on 21 linear molecules (including all those considered in this paper) have indicated that such an expansion converges particularly rapidly for small momentum, p, and less rapidly for large momentum. However, we have shown (3) for these 21 molecules, that the region $0 \le p \le 3\hbar a_0^{-1}$ is essentially the valence region and that the anisotropic momentum density $\Pi(\boldsymbol{p})$ in this region can be studied satisfactorily from a chemical point of view by considering merely four partial waves: $\Pi_0(p)$, $\Pi_2(p)$, $\Pi_4(p)$, and $\Pi_6(p)$.

Evaluation of the partial waves of the momentum density from a wave function constructed from an orbital basis set is not difficult. Analytic formulae for these purposes are implicit in eqs. (129)–(133) and eqs. (145)–(147) of ref. 9 for spherical harmonic and cartesian Gaussian-type basis functions, respectively. All the wavefunctions that are employed in this paper are built from Slater type orbital (STO) basis sets which are a special case of spherical harmonic basis sets. Hence all partial waves displayed in this paper were obtained via analytic formulae. It is worth noting that STO basis sets provide a reasonable balance between accuracy in position space and accuracy in momentum space (10).

It has been pointed out (3) that the partial wave $\Pi_L(p)$ behaves as p^L for small p, and that $\Pi_L(p)$ decays to zero as $p^{\delta(L,0)-9}$ where $\delta(L,0)$ is the Kronecker delta, for all STO basis sets that include at least one $1s$ STO — a condition fulfilled in an overwhelming majority of STO basis sets including all those considered in this paper. Moreover, empirical rules outlined earlier (3–5) enable one to predict the qualitative valence region (small p) behaviour of the contributions of various types of canonical molecular orbitals (MO's) to the chemically dominant partial waves. These rules are summarized in Table 1 for the reader's convenience.

Qualitative substituent effects

Momentum densities and pertinent partial wave expansions were calculated for two homologous series: the cyanides XCN with X = H, F, Cl, O^-, S^-, and NC, and the alkynes XCCH with X = H, Li, F, Cl, and NC. These two series have been considered together because the ethynil and cyano groups are isoelectronic, have very similar electronic structures, and both contain a nominal triple bond. The self consistent field (SCF) wavefunctions used were those of McLean and Yoshimine (11) at the geometries corresponding to the lowest computed energies and are built from atom optimized STO basis sets of double-ζ plus polarization quality or better.

Politzer and co-workers (12) used exactly the same wavefunctions for their position space studies of these molecules. Their studies indicate that the ethynil and cyano groups maintain their properties across their respective homologous series. Thus the lengths and force constants of the CC and CN bonds are virtually independent of the substituent in the alkynes and cyanides, respectively. Moreover, Politzer and Kasten (12*d*) have demonstrated that the charge densities of the ethynil and cyano fragments are relatively little affected by the nature of the substituent.

Figures 1 and 2 show partial waves of the momentum density for the cyanides and alkynes, respectively. Note that all quantities are per electron (i.e. divided by the number of electrons) to facilitate comparisons between molecules. Moreover, all the spherically averaged momentum densities $\Pi_0(p)$ are shown to the same scale, and all the higher order partial waves, except those for HCCH and LiCCH, are shown to another uniform scale. In view of some recent interest (13) in the monotonicity or otherwise of $\bar{\Pi}(p)$, note that the vast majority of the alkynes and cyanides shown in Figs. 1 and 2 have *nonmonotonic* isotropic momentum densities.

TABLE 1. Empirical rules (3) governing the valence region (small p) behaviour of the contributions from various types of canonical MO's to the partial waves of the momentum density

L/MO	σ bonding	σ antibonding	π bonding	π antibonding
2	−	+	−	~0
4	~0	~0	+	−
6	~0	~0	−	+

First consider only those substituents (X = H, F, Cl, and CN) for which partial waves are shown for both the cyanide and alkyne. The figures show that, for fixed X, the partial waves of the isoelectronic XCCH and XCN molecules are rather similar. This is the momentum density analog of Politzer and Kasten's observation (12*d*) that the charge densities of the XC fragments in the XCCH and XCN molecules are very similar for fixed X. Proceeding further, the interpretation of the curves is straightforward. The extrema of the non-zero L $\Pi_L(p)$'s for XCCH occur at a smaller p value than the corresponding extrema for XCN for the same X. This is a result of the fact that XCCH is longer than XCN. Furthermore, the amplitudes of the non-zero L $\Pi_L(p)$'s for X = H, F, and Cl are larger for XCCH as compared to the corresponding XCN indicating that the position space representation of the highest occupied molecular orbital (HOMO), which in all cases is a π orbital, is more delocalized in XCCH. This is consistent with the finding of Politzer and Harris (12*a*) that a very significant portion of the π electronic charge density is not in the bonding region but spread in regions adjacent to it resulting in a very significant degree of π bonding with the neighbouring atoms even if one of them is a hydrogen. On the other hand, the non-zero L $\Pi_L(p)$'s of NCCN have a larger amplitude than their NCCCH counterparts indicating, as expected, that the higher symmetry in the former enhances the position space delocalization of the π orbitals. On the other hand the partial waves are very different for different X implying that a substituent can indeed substantially modify the momentum density (per electron) of a compound. The partial waves of HCCH and HCN, especially the negative Π_6's, clearly indicate (see Table 1) that the HOMO for these molecules is a π bonding orbital as opposed to the other molecules, with X = F, Cl, and CN, where the HOMO is an antibonding π orbital which leads to a positive $\Pi_6(p)$.

Thus substituent effects in these small series are seen to be strongly correlated with the electronic structure of the substituent and its interaction with the electronic structure of the functional group. On the basis of the partial waves it is possible to separate the molecules into three clusters. One defined by X = H and characterized by a negative $\Pi_6(p)$, another defined by X = F, Cl and characterized by a negative small amplitude $\Pi_4(p)$ and a positive $\Pi_6(p)$, and the last one defined by X = CN and characterized by a positive Π_6 and a clearly oscillating $\Pi_4(p)$ starting from negative values at low p. These last two clusters

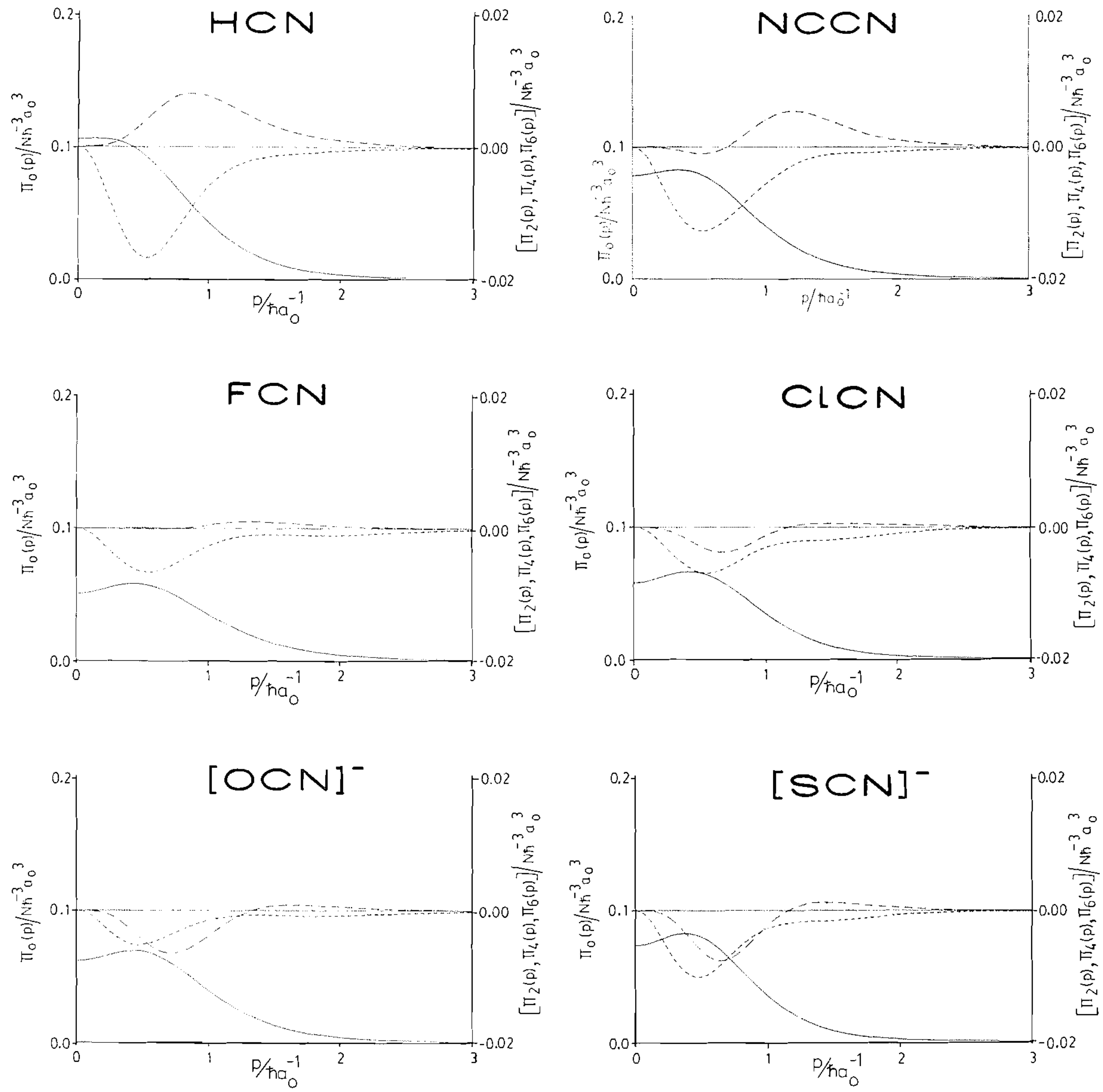

FIG. 1. Partial waves of the momentum density (per electron) for the cyanides XCN with X = H, NC, F, Cl, O^-, and S^-. Note that the left hand scale for $\Pi_0(p)$ is different from the right hand scale for the higher partial waves. — $\Pi_0(p)$; ---- $\Pi_2(p)$; -·-·-·- $\Pi_4(p)$; ···· $\Pi_6(p)$.

TABLE 2. Properties of the isotropic momentum density

Molecule	$\Pi(0)/\hbar^{-3}a_0^3$	$\langle p^{-2}\rangle/\hbar^{-2}a_0^2$	$\langle p^{-1}\rangle/2\hbar^{-1}a_0$	$\langle p\rangle/\hbar a_0^{-1}$	T/E_h	$\langle p^3\rangle/\hbar^3 a_0^{-3}$	$\langle p^4\rangle/\hbar^4 a_0^{-4}$
HCCH	1.7401	42.653	6.3306	31.622	76.713	1370	2.32E4*
HCN	1.4880	36.477	5.7815	34.862	92.727	1814	3.39E4
LiCCH	2.5421	52.116	7.2813	35.857	83.795	1441	2.39E4
FCCH	1.4725	45.084	8.1279	60.139	175.51	3905	8.63E4
FCN	1.1051	38.433	7.5803	63.330	191.46	4350	9.70E4
[OCN]$^-$	1.3568	44.152	8.1750	58.885	167.24	3542	7.25E4
NCCCH	2.3002	64.317	10.609	64.643	168.37	3181	5.71E4
NCCN	2.0318	58.303	10.066	67.876	184.29	3624	6.77E4
ClCCH	2.0759	60.594	10.442	111.72	535.56	2.156E4	9.16E5
ClCN	1.7365	54.425	9.9165	114.91	551.54	2.200E4	9.27E5
[SCN]	2.1965	62.822	10.604	108.23	489.87	1.839E4	7.28E5

*2.32E4 means 2.32×10^4.

have in common the fact that antibonding π orbitals are occupied.

Consider now the partial waves of LiCCH in Fig. 2. Clearly the negative $\Pi_6(p)$, evidence of only bonding π orbitals, places it into the X = H cluster. The large amplitudes of the non-zero $L\,\Pi_L(p)$'s indicate a large degree of π electronic interaction in HCCH and LiCCH. On the other hand, Fig. 1 clearly shows that $[OCN]^-$ and $[SCN]^-$ belong to the X = F, Cl cluster. In

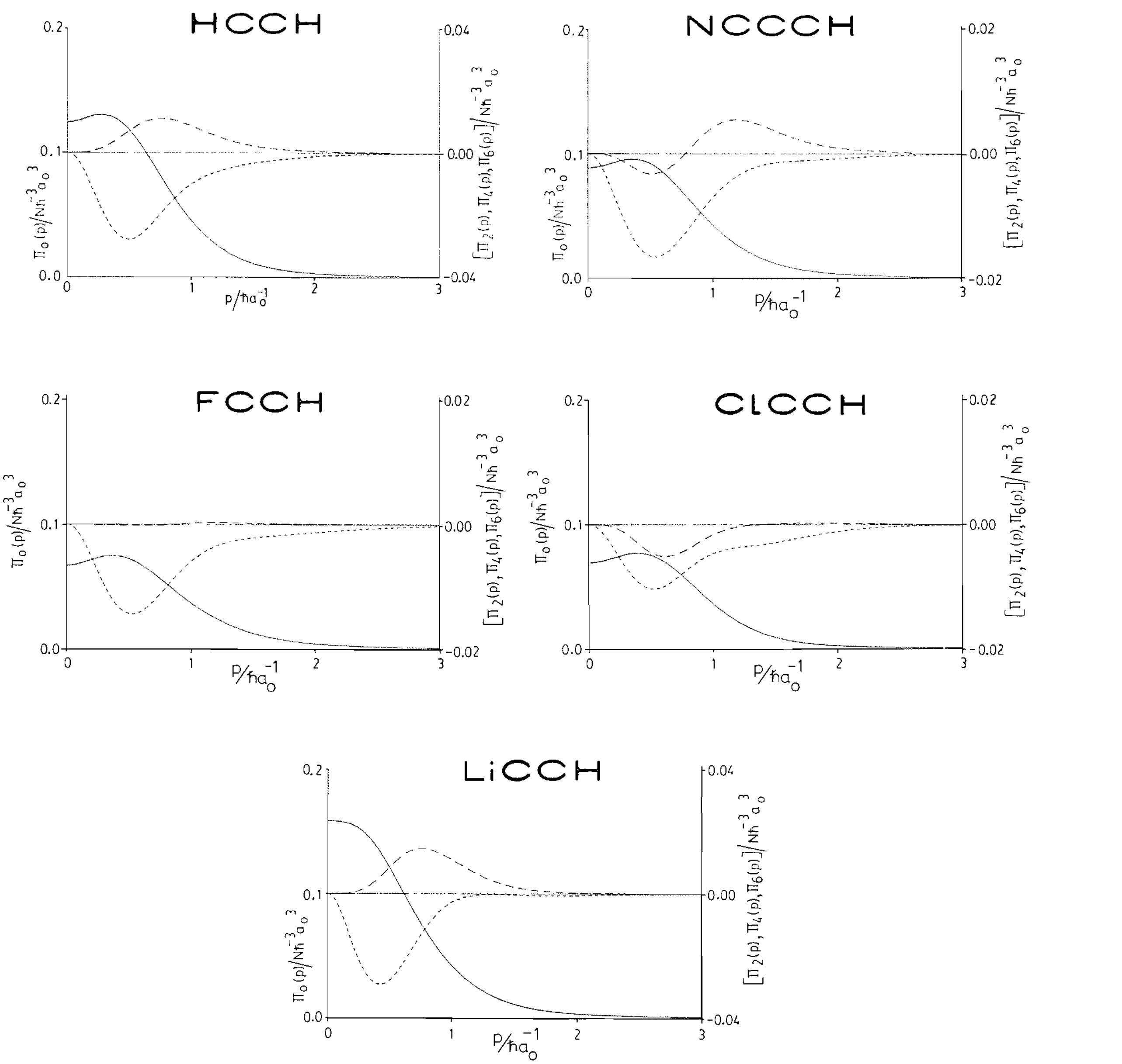

FIG. 2. Partial waves of the momentum density (per electron) for the alkynes XCCH with X = H, NC, F, Cl, and Li. See the caption to Fig. 1. Also note that the higher order partial waves for HCCH and LiCCH are shown on a scale that is one-half of that to which the $\Pi_L(p)$ ($L \neq 0$) for the remaining alkynes are shown.

fact, there is such a strong similarity between the partial waves of the isoelectronic pairs $[OCN]^-$ and FCN, and $[SCN]^-$ and ClCN that the only means of deciding which one is which is comparison of $\Pi_0(0)$; the latter is larger in the negative molecular ions than in their isoelectronic neutral counterparts.

Quantitative substituent effects

Quantitative results are considered next. Table 2 lists values of $\bar{\Pi}(0)$ and the well-defined moments $\langle p^k \rangle$ ($-2 \leq k \leq 4$) for each of the 11 molecules considered in this study while Table 3 lists their characteristic momenta defined (7*c*) by

$$p^* = [\bar{J}(0)/2\pi\bar{\Pi}(0)]^{1/2}$$

where $\bar{J}(0) = \langle p^{-1} \rangle/2$. The characteristic momentum is related to the valence momentum density. Like the characteristic momenta of the atoms which correlate, within a period, with the electronic saturation of the valence shell (7*c*, 13*c*), the characteristic momenta of the molecules increase with increasing electron sharing and number of valence electrons. Thus, of the molecules considered, FCN possesses the largest and LiCCH the smallest p^*.

TABLE 3. Characteristic momenta

	$p^*/\hbar a_0^{-1}$	
X	For XCCH	For XCN
Li	0.675	—
H	0.761	0.786
S^-	—	0.877
NC	0.857	0.888
Cl	0.895	0.953
O^-	—	0.979
F	0.937	1.045

TABLE 4. Differences of properties of the spherically averaged momentum density

System	$\Pi(0)/\hbar^{-3}a_0^3$	$\langle p^{-2}\rangle/\hbar^{-2}a_0^2$	$\langle p^{-1}\rangle/2\hbar^{-1}a_0$	$\langle p\rangle/\hbar a_0^{-1}$	T/E_h
HCCH − H − {CCH}	0	0	0	0	0
HCN − H − {CN}	0	0	0	0	0
LiCCH − Li − {CCH}	−12.683	−25.616	−1.0571	0.196	0.139
FCCH − F − {CCH}	0.1985	0.021	−0.0817	0.171	−0.11
FCN − F − {CN}	0.0832	−0.218	−0.0802	0.122	−0.18
$[OCN]^-$ − O^- − {CN}	0.0946	−1.795	−0.3211	0.472	0.22
NCCCH − {CN} − {CCH}	0.6933	2.529	0.195	−0.143	−0.07
NCCN − 2{CN}	0.6770	2.611	0.201	−0.150	−0.16
ClCCH − Cl − {CCH}	0.1921	−0.055	−0.060	0.07	−0.05
ClCN − Cl − {CN}	0.1048	4.184	−0.0365	0.02	−0.27
$[SCN]^-$ − S^- − {CN}	−0.1012	−8.127	−0.483	0.37	0.10
{CCH} = HCCH − H	0.9295	16.512	5.4818	30.773	76.213
{CN} = HCN − H	0.6774	13.397	4.9327	34.013	92.227

Since substituent effects are of interest in this paper, Table 4 lists differences between the molecular properties and those of isolated ground state atoms and fragments. The higher moments $\langle p^3\rangle$ and $\langle p^4\rangle$ are not considered since they are primarily large momentum, and hence core electron, properties. The atomic properties used in Table 4 were computed from atomic SCF wavefunctions built from STO basis sets of a quality comparable to the pertinent molecular basis sets. These atomic properties have been listed elsewhere (4). Table 4 shows a high correlation between the various difference properties of XCCH and XCN when X is the same implying that substituent effects in momentum space can, within reasonable limits, be transferred across different homologous series. The largest differences in Table 4 occur for LiCCH due not to the molecule itself, but to the momentum space properties of the lithium atom which has a huge value for $\Pi(0)$ that is highly dependent on the quality of the basis set employed. Unfortunately, each of the difference properties orders the various substituents in different ways.

Substituent effects are often described in terms of substituent constants (14, 15). Of these σ_P is the relative effect of a substituent in the *para* position on benzoic acid dissociation in water at 25°C. It is interpreted as the ability of the substituent to withdraw electronic charge from the rest of the molecule. It can be divided into an inductive part, σ_I, and a resonance part, σ_R, such that $\sigma_P = \sigma_I + \sigma_R$. The constant σ_I is interpreted as the ability to withdraw charge through "inductive" interactions which occur in the electronic σ system while the Taft resonance constant σ_R is interpreted as a measure of the tendency of a substituent to withdraw electronic charge through some sort of conjugative or resonance effect which should occur mainly in the electronic π system. These constants, despite being obtained from substituent effects on acid dissociation, have proven to be useful in a wide range of other equilibria and rate processes. We tried to find correlations between the various difference properties in Table 4 and the substituent constants. None could be found for σ_I. On the other hand the difference $\bar{J}(0) = \langle p^{-1}\rangle/2$ could correlate with σ_P for the XCN series because for O^- it is equal to $-0.3211/\hbar^{-1}a_0$ and σ_P is −0.5 (14) while for CN it is $0.201/\hbar^{-1}a_0$ and σ_P is 0.69 (14). Such correlation, however, predicts F and Cl to be overall weak electron-releasing substituents which is clearly wrong.

So far we have only considered difference properties of the isotropic momentum density Π_0. Let us now turn to the anisotropy of the kinetic energy tensor – a property of Π_2 alone (see theory section). Table 5 lists values of $T_\| - T_\perp$ relative to HCCH and HCN for the alkynes and cyanides, respectively. Table 5 shows that the substituent constant σ_R correlates in a consistent way with the *relative* $T_\| - T_\perp$. The correlation is better for the XCCH series which is not surprising given the definition of σ_R. The implication is that if the relative $T_\| - T_\perp > 0$ then X is a conjugative electron-withdrawing substituent, while if the relative $T_\| - T_\perp < 0$ then X is a conjugative electron-releasing substituent. The Dewar–Grisdale mesomeric constant M (14), which is supposed to include the π-inductive as well as the resonance polar effect, also correlates well with the relative $T_\| - T_\perp$ as indicated by Table 5. At the moment it is not safe to try an interpretation of this correlation because of the small number of substituents involved.

TABLE 5. Comparison between the relative kinetic energy anisotropy, $(T_\| - T_\perp)$, and the Taft resonance, σ_R, and Dewar–Grisdale mesomeric, M, substituent constants[a] for the XCCH and XCN series[b]

	$(T_\| - T_\perp)/E_h$			
X	XCCH − HCCH	XCN − HCN	σ_R	−M
Li	0.45			
NC	0.33	−0.01	0.10	1.60
H	0	0	0	0
Cl	−0.89	−0.50	−0.24	−0.91
O^-		−0.62		
S^-		−0.98		
F	−1.07	−1.16	−0.46	−2.10

[a] From ref. 14, p. 19.
[b] $(T_\| - T_\perp)/E_h = -0.547$ and −0.22 for HCCH and HCN, respectively.

Concluding remarks

In this paper we have examined how substituent effects in alkynes and cyanides are reflected in the three-dimensional one-electron momentum density $\Pi(\mathbf{p})$. Qualitative studies, based on the four chemically dominant partial waves (3, 4) of the momentum density, were in harmony with previous studies (12) of the position space charge densities. Quantitative correlations between properties of the isotropic momentum density and chemical indices could not be found as in many other studies (1). However, a correlation *was* found between the usual substituent constants of physical organic chemistry (14,

15) and the values of the kinetic energy anisotropy $T_\parallel - T_\perp$ relative to the hydrogen-containing (or non-substituted) parent of the pertinent homologous series. This correlation, meagre as it may seem to the reader unfamiliar with momentum density studies (1), is, in our opinion, a significant step towards locating the elusive chemical information content of momentum densities.

Acknowledgments

The support of the Natural Sciences and Engineering Research Council of Canada is gratefully acknowledged. One of us (A.M.S.) wishes to thank the Conselho Nacional de Desenvolvimento Científico e Tecnológico – CNPq (Brazil) for a graduate fellowship.

1. B. G. WILLIAMS (*Editor*). Compton scattering: the investigation of electron momentum distributions, McGraw-Hill, New York. 1977.
2. (*a*) P. KAIJSER, V. H. SMITH, JR., and A. J. THAKKAR. Mol. Phys. **41**, 1143 (1980); (*b*) B. S. SHARMA, A. N. TRIPATHI, and A. J. THAKKAR. J. Chem. Phys. **79**, 3164 (1983); (*c*) A. J. THAKKAR. Int. J. Quantum Chem. **23**, 227 (1983).
3. A. J. THAKKAR, A. M. SIMAS, and V. H. SMITH, JR. J. Chem. Phys. **81**, 2953 (1984).
4. A. M. SIMAS. Ph.D. dissertation, Queen's University at Kingston, Canada, 1982; University Microfilms Publication No. 82-15, 185.
5. A. M. SIMAS, V. H. SMITH, JR., and A. J. THAKKAR. Int. J. Quantum Chem. Quantum Chem. Symp. In press.
6. D. G. WHIFFEN. Pure Appl. Chem. **50**, 75 (1978).
7. (*a*) W. WEYRICH. Ber. Bunsenges. Phys. Chem. **83**, 797 (1979); (*b*) A. M. NYANDA and B. G. WILLIAMS. Phil. Mag. B **40**, 97 (1979); (*c*) A. J. THAKKAR, A. M. SIMAS, and V. H. SMITH, JR. Chem. Phys. **63**, 175 (1981).
8. (*a*) M. J. FEINBERG, K. RUEDENBERG, and E. L. MEHLER. Adv. Quant. Chem. **5**, 27 (1970); (*b*) M. J. FEINBERG and K. RUEDENBERG. J. Chem. Phys. **54**, 1495 (1971); **55**, 5804 (1971); (*c*) K. RUEDENBERG. *In* Localization and delocalization in quantum chemistry. Vol. 1. *Edited by* O. Chalvet, R. Daudel, S. Diner, and J. M. Malrieu. Reidel, Dordrecht. 1975. p. 223.; (*d*) F. DRIESSLER and W. KUTZELNIGG. Theoret. Chim. Acta, **43**, 1 (1976); (*e*) W. BUTSCHER and H. H. SCHMIDTKE. Chem. Phys. **23**, 87 (1977); (*f*) T. KOGA and M. MORITA. Theoret. Chim. Acta, **59**, 423 (1981).
9. P. KAIJSER and V. H. SMITH, JR. Adv. Quant. Chem. **10**, 371 (1977).
10. A. M. SIMAS, A. J. THAKKAR, and V. H. SMITH, JR. Int. J. Quantum Chem. **21**, 419 (1982); **24**, 527 (1983).
11. A. D. MCLEAN and M. YOSHIMINE. Tables of linear molecule wave functions. IBM, San Jose. 1967; a supplement to the paper by A. D. McLean and M. Yoshimine, IBM J. Res. Dev. **12**, 206 (1968).
12. (*a*) P. POLITZER and R. R. HARRIS. Tetrahedron, **27**, 1567 (1971); (*b*) P. POLITZER and P. H. REGGIO. J. Am. Chem. Soc. **94**, 8308 (1972); (*c*) P. POLITZER and J. W. TIMBERLAKE. J. Org. Chem. **37**, 3557 (1972); (*d*) P. POLITZER and S. D. KASTEN. J. Phys. Chem. **80**, 283 (1976).
13. (*a*) A. J. THAKKAR. J. Chem. Phys. **76**, 747 (1982); (*b*) S. R. GADRE and R. L. MATCHA. J. Chem. Phys. **76**, 748 (1982); (*c*) A. HARMALKAR, A. M. SIMAS, V. H. SMITH, JR., and W. M. WESTGATE. Int. J. Quantum Chem. **23**, 811 (1983).
14. P. R. WELLS. Linear free energy relationships. Academic Press, New York. 1968.
15. C. D. JOHNSON. The Hammett equation. University Press, Cambridge, England. 1973.

Vibronic analysis of the $\tilde{A}(^1A_2) \leftarrow \tilde{X}(^1A_1)$ spectrum of Br_2CS

B. SIMARD AND R. P. STEER[1]

Department of Chemistry, University of Saskatchewan, Saskatoon, Sask., Canada S7N 0W0

Received July 20, 1984

This paper is dedicated to Professor Camille Sandorfy on the occasion of his 65th birthday

B. SIMARD and R. P. STEER. Can. J. Chem. **63**, 1418 (1985).

$\tilde{A}(^1A_2)-\tilde{X}(^1A_1)$ fluorescence excitation and emission spectra of Br_2CS have been recorded. A vibronic analysis shows that the molecule is non-planar in the $\tilde{A}$ state with an equilibrium out-of-plane angle of 13° and a barrier to inversion of 164 cm^{-1}. Upper state vibrational frequencies of modes 1, 2, 3, 4, and 6 have been obtained. Comparisons with other tetraatomic thiocarbonyls support the assignments. A ground state C—Br dissociation energy of 52.3 kcal mol^{-1} has been obtained from the onset of diffuseness in the $\tilde{A}-\tilde{X}$ spectra. A search for phosphorescence proved unsuccessful.

B. SIMARD et R. P. STEER. Can. J. Chem. **63**, 1418 (1985).

Les spectres d'excitation et d'émission de la transition $\tilde{A}(^1A_2)-\tilde{X}(^1A_1)$ du Br_2CS ont été enregistrés. L'analyse vibrationnelle indique que la molecule est non-planaire avec une barrière d'inversion de 164 cm^{-1} et d'un angle d'équilibre hors du plan de 13°. Les fréquences vibrationnelles des modes 1, 2, 3, 4 et 6 dans l'état excité ont aussi été evaluées. Des comparaisons avec d'autre thiocarbonyles tétra-atomiques appuient les attributions vibrationnelles apportées. Une energie de dissociation de 52.3 kcal/mol a été calculée pour la liaison C—Br à partir du seuil de diffusion du spectre. La recherche de la phosphorescence s'est avérée négative.

[Traduit par le journal]

Introduction

The spectroscopy of tetraatomic molecules containing the thiocarbonyl group has been extensively studied for the last two decades. Two electronic transitions involving $n \rightarrow \pi^*$ electron promotions are found in the visible whereas at least four transitions, three Rydberg and one $\pi \rightarrow \pi^*$ intravalence, have been observed in the near uv. Unlike most of their carbonyl counterparts, these compounds are photostable when excited to low-lying vibrational levels of their $\tilde{a}$, $\tilde{A}$, and in some cases $\tilde{B}$ states (1). As a result linewidths are narrow so that vibronically resolved absorption and emission spectra can be recorded and the structures of the excited states elucidated. The spectra of H_2CS (2), D_2CS (2), F_2CS (1), ClFCS (1), and Cl_2CS (3) have been examined to date, but little is known about the heavier, Br and I substituted compounds, including Br_2CS.

The structure of the ground state of Br_2CS has been determined by electron diffraction (4) and ir—Raman force field (5) methods. The microwave spectrum has not been reported and the ground state rotational constants therefore remain unknown. No electronic spectra have been measured so that no information at all about any of its upper states is presently available. We report here a partial vibrational analysis of the $\tilde{A}(^1A_2)-\tilde{X}(^1A_1)$ band system and extract from it several parameters which characterize the structure of its $\tilde{A}$ state.

Experimental

Br_2CS was prepared by the reaction of thiophosgene (Aldrich) with boron tribromide (Aldrich) at 60°C according to the method of Diderrich and Hass (6). Purification was achieved by trap-to-trap vacuum distillation. Mass spectral analysis showed that traces of BBr_3 and BCl_3 (both non-emissive) were the main contaminants; there was no evidence of residual Cl_2CS. When not in use the product was kept in the dark at about −10°C to prevent dimerization. Before recording a spectrum, the sample was thoroughly degassed by freeze—pump—thaw cycles to remove traces of oxygen.

The experimental arrangement used for recording emission and excitation spectra is shown schematically in Fig. 1. Sample fluorescence was excited in a double pass cell by a Spectra-Physics argon-ion pumped dye laser equipped with a three-plate birefringent filter. The output linewidth was about 40 GHz (1.3 cm^{-1}). Disodium fluorescein, rhodamine-6G, and DCM dyes were used to cover the 535—700 nm spectral region.

Emission was collected at right angles to the excitation axis by a telescope lens and reflecting mirror system and was focussed onto the entrance slit of a Jarrell-Ash 0.75 m f/6.5 monochromator fitted with an 1800 line/mm holographic grating. Emission was detected by single photon counting with a red-sensitive RCA 31034A photomultiplier tube coupled to a Tracor Northern Model 7200 multichannel analyzer operating in the multichannel scaling mode. Data were transferred from the MCA to a time-shared DEC 2060 computer for background subtraction, correction for spectral sensitivity of the detection system and correction for the variation in laser power with wavelength. First order diffraction was observed when emission spectra were measured. When excitation spectra were recorded the birefringent filter of the dye laser was coupled to a stepping motor drive system and zero order diffraction was viewed through a single cut-off filter (Corning 26-4424 or 26-4416 or CS-1-69) to eliminate scattered exciting light. Wavelength calibration was effected by interpolation between lines in the Ne arc spectrum; spectral bands could be determined to an accuracy of ± 15 cm^{-1}.

Low resolution absorption spectra were recorded with a Cary 118 double beam spectrophotometer. Gas phase spectra were obtained by filling a 10 cm long fused quartz absorption cell with Br_2CS at its room temperature vapor pressure, ca. 6 Torr, using a grease and mercury-free vacuum line equipped with a Wallace and Tiernan metallic membrane manometer. Background pressures, measured with an ionization gauge, were $<10^{-3}$ Torr. All experiments were carried out at a room temperature of 22 ± 2°C.

Results and discussion

A low resolution absorption spectrum of Br_2CS taken in the gas phase at a pressure—path of ca. 60 Torr—cm is shown in Fig. 2. Under these conditions measurable absorption in the visible occurs between approximately 620 and 380 nm and exhibits a maximum at 480 nm, at which the molar extinction coefficient is 5.6 M^{-1} cm^{-1}. Similar spectra taken in $CHCl_3$ or CCl_4 solution reveal that the absorption in the visible has an onset which lies near 630 nm and increases monotonically to the maximum with very little evidence of gross vibronic structure. On the other hand a spectrum of pure Br_2CS (l) in a

[1]To whom all correspondence should be addressed.

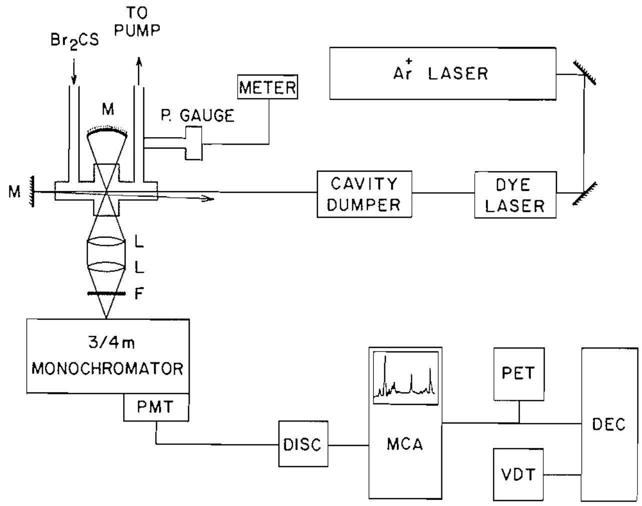

FIG. 1. Experimental apparatus. M, mirror; L, lens; F, filter; PMT, photomultiplier tube; DISC, discriminator; MCA, multichannel analyzer; DEC, DEC 2060 computer; PET, microcomputer; VDT videodisplay terminal.

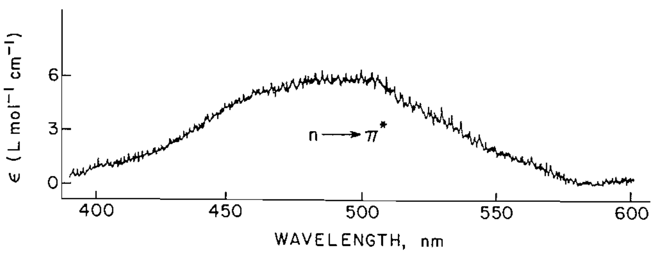

FIG. 2. Low resolution gas phase absorption spectrum of Br_2CS at a pressure–path of 60 Torr–cm and room temperature.

1 cm cell exhibits an absorption onset at ca. 660 nm. By analogy with the previous analyses of similar molecules (1), the absorption in this region is attributed to forbidden transitions of largely n → π* character.

A major problem concerns the separation of absorptions due to the $\tilde{A}(^1A_2) \leftarrow \tilde{X}(^1A_1)$ system from those due to the $\tilde{a}(^3A_2) \leftarrow \tilde{X}(^1A_1)$ system in this region. In Cl_2CS both the $\tilde{A} \leftarrow \tilde{X}$ (3) and $\tilde{a} \leftarrow \tilde{X}$ (7, 8) systems have been identified; their origins are separated by only 1224 cm^{-1}, and their oscillator strengths probably differ by no more than a factor of ten. The difference in the frequencies of the $\tilde{A} \leftarrow \tilde{X}$ and $\tilde{a} \leftarrow \tilde{X}$ origins in Br_2CS should be similar to that of Cl_2CS, so that extensive overlap of the two absorption systems is inevitable. Compounding the problem, the oscillator strength of the triplet system is expected to be greater (relative to the singlet system) in Br_2CS than in Cl_2CS due to the more effective induction of spin–orbit coupling resulting from the presence of heavy Br atoms in the former. Such expectations are realized in the tetraatomic carbonyls in which the $\tilde{a} \leftarrow \tilde{X}$ oscillator strength of Br_2CO is calculated to be ca. 100 times greater than that of Cl_2CO (9). On these grounds the visible absorption spectrum of Br_2CS is expected to be complex and the unequivocal assignment of bands difficult, especially in the region of overlap of the two systems.

Fortunately, the identification of bands which are part of the singlet system in the presence of those which belong to the triplet may be achieved using laser-induced emission excitation spectroscopy if the photophysical behaviors of the $\tilde{a}$ and $\tilde{A}$ states are significantly different. Differences in the radiative lifetimes of the two states are not expected to be large, for the same reasons that the oscillator strengths of the two absorption systems are expected to be comparable. On the other hand, both intramolecular nonradiative decay and collisional quenching processes could occur at greatly different rates in the two states. Thus, under appropriate conditions, the quantum yield of emission from the $\tilde{A}$ state could differ from that of the $\tilde{a}$ state by a large factor, so that the emission excitation spectrum of one system would be much more intense than the emission excitation spectrum of the other. This is certainly the case in Cl_2CS in which fluorescence from the $\tilde{A}(^1A_2)$ state (with quantum yield approaching unity in the collision-free limit (10)) can be observed very easily using laser excitation methods (11), whereas phosphorescence from the $\tilde{a}(^3A_2)$ state has never been observed despite repeated attempts to find it (12). Although the excited state dynamics of Br_2CS will be the subject of a separate investigation, we assume here that Br_2CS and Cl_2CS will exhibit similar photophysical properties; namely, the $\tilde{A}$ states will emit with relatively large quantum yields whereas the $\tilde{a}$ states will be "dark" (or nearly so) under the experimental conditions ($P \sim 0.1-6$ Torr) which we have employed. We therefore assume that emission from Br_2CS excited in the 630–535 nm region originates largely in the $\tilde{A}(^1A_2)$ state. The ability to analyze both the excitation and emission spectra and to assign all of the strong and most of the weak bands on this basis would appear to justify the assumption.

Laser excitation spectra have been recorded from 630 to 535 nm. Figure 3 shows that portion from 630 to 570 nm (taken with R6G dye). This spectrum is uncorrected for the variation in laser output power with wavelength so that quantitative comparisons of the relative intensities of bands which are not adjacent is inappropriate. A search for additional emission to the red (610–700 nm) using DCM as a laser dye proved unsuccessful. The observed band system is highly structured from 628 to 547 nm. The spectrum becomes much more congested near 547 nm and to the blue consists of a series of crowded sharp features superimposed on what appears to be a diffuse continuum at the resolution employed. To the red of 547 nm, bands are well-resolved (although their frequencies could not be measured with an absolute accuracy of better than ±15 cm^{-1} with the experimental arrangement employed).

The emission excitation spectrum was analyzed within the following theoretical framework. First, using vibrational frequencies determined by Willner and Hauswirth (5) from infrared and Raman spectra (Table 1), room temperature Boltzmann populations of the ground state levels were calculated. Accordingly, only cold bands ($v_i'' = 0$) and hot bands originating from $v_i'' = 1$ were considered to contribute significantly to the spectrum on relative intensity grounds. It is important to note that $v_4'' = 1$ has a population which is 13% of that of $v_4'' = 0$ at room temperature, so that hot bands originating in mode 4, an important promoting mode (vide infra), should be observable. Second, Herzberg–Teller vibronic coupling (13) was assumed to be the mechanism whereby intensity is acquired by the symmetry forbidden $^1A_2 \leftarrow {}^1A_1$ transition, similar to the cases of the analogous molecules, Cl_2CS (3) and H_2CO (14). According to the Herzberg–Teller mechanism the orbitally forbidden transition "borrows" intensity from nearby electric-dipole allowed transitions to valence or Rydberg states of B_1 or B_2 symmetry via non-totally symmetric vibrations. In the case of tetraatomic molecules exhibiting C_{2v} ground state symmetry but having non-planar excited state geometries, the most active symmetry-breaking vibration is $\nu_4(b_1)$, the out-of-plane ben-

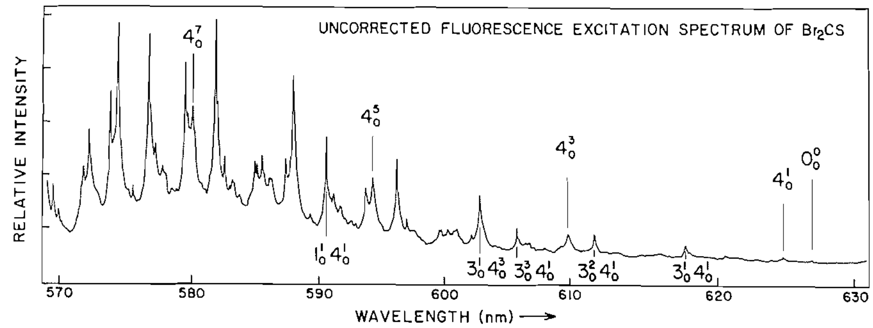

FIG. 3. Laser-induced fluorescence excitation spectrum of Br_2CS at a pressure of 6 Torr and room temperature.

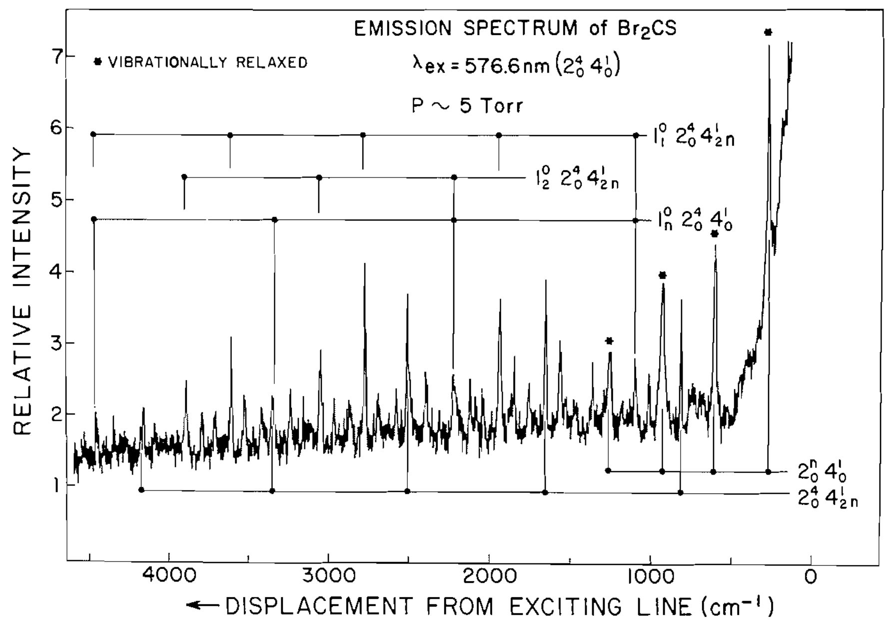

FIG. 4. Emission spectrum recorded by exciting 5 Torr of Br_2CS in the strong absorption feature at 576.6 nm ($2^4_0 4^1_0$). Important progressions are noted.

TABLE 1. Fundamental frequencies of Br_2CS in the ground state[a]

Mode	Symmetry	Description	Frequency (cm^{-1})
1	a_1	C—S stretch	1116
2	a_1	C—Br sym. stretch	367
3	a_1	Br—C—Br scissor	183
4	b_1	out-of-plane bend	415
5	b_2	C—Br antisym. stretch	697
6	b_2	Br—C—Br rock	230

[a]Reference 5.

ding mode. Vibronic bands characterized by odd quantum number changes in v_4 are expected to be intense; cold and hot band progressions converge on the false origins 4^1_0 and 4^0_1, respectively. Bands involving unrestricted quantum number changes in the totally symmetric modes (ν_1, ν_2, and ν_3; cf. Table 1) in combination with odd quantum number changes in mode 4 are also expected to be prominent.

Experimentally, measurement of the emission spectrum excited in the strong band at 576.6 nm proved very useful in the analysis. This spectrum, shown in Fig. 4, exhibits three resonance fluorescence progressions in which members are separated by $2\nu_4''$ and one resonance fluorescence progression in which members are separated by ν_1''. From the band spacing in these progressions one obtains vibrational frequencies of $\nu_4'' = 412$ cm^{-1} and $\nu_1'' = 1110$ cm^{-1}, which compare very favorably with values of 415 cm^{-1} and 1116 cm^{-1} obtained by ir and Raman measurements (cf. Table 1). One prominent progression of four members in the emission spectrum, identified by asterisks in Fig. 4, could not be assigned to resonance emission. These bands are wider than any other bands in the spectrum, and the distribution of their intensities is different. Their peak-to-peak spacing, ca. 320 cm^{-1}, does not fit any ground state vibrational frequency. The only reasonable course was to assign these bands to non-resonant emission resulting from collisional vibrational relaxation in the excited state. Since upper state frequencies are almost certain to be more or less smaller than those of the corresponding modes in the ground state, and since only modes 1–4 are likely to be prominent, reasonable deduction led to a tentative assignment of the 576.6 nm band as $2^4_0 4^1_0$. Using this band as a starting point, the 4^1_0 false origin in the excitation spectrum could easily be identified and most of the bands assigned.

Reasonable assignments of all bands in the $\tilde{A}-\tilde{X}$ system having intensities $\geq 10\%$ of those of the strongest nearby bands are listed in Table 2. Figure 5 shows graphically the convergence of members of prominent progressions to the 4^1_0 false origin. The convergences of other progressions are shown in Fig. 6. Assignments of many of the weaker bands should be

TABLE 2. Assignment of prominent vibronic bands

Frequency (cm^{-1})	Intensity[a]	Assignment	Frequency (cm^{-1})	Intensity[a]	Assignment
15930	W	0^0_0	17161	S	$2^1_0 3^5_0 4^1_0$, $2^2_0 3^3_0 4^1_0$, $2^3_0 3^1_0 4^1_0$
16005	W	4^1_0	17221	S	4^7_0, $3^5_0 4^3_0$
16088	W	6^1_0	17242	S	$1^1_0 2^1_0 4^1_0$
16176	W	$3^1_0 4^1_0$, 4^4_1, $2^2_0 4^0_1$	17249	S	$1^1_0 3^2_0 4^1_0$
16331	W	$2^1_0 4^1_0$, $3^2_0 4^1_0$, $3^1_0 4^4_1$	17305[b]	W	$2^1_0 3^1_0 4^5_0$
16395	W	4^3_0	17311	W	$1^2_0 4^0_1$, $1^1_0 4^5_1$
16416[b]	W	$1^1_0 4^0_1$	17328	M	$2^1_0 3^6_0 4^1_0$, $2^2_0 3^4_0 4^1_0$, $2^3_0 3^2_0 4^1_0$
16477[b]	W	$3^4_0 4^2_1$	17343	S	$2^4_0 4^1_0$, $2^1_0 4^8_1$
16503	W	$2^1_0 3^1_0 4^1_0$, $3^3_0 4^1_0$, $2^3_0 4^0_1$, $2^1_0 4^4_1$, $3^2_0 4^4_1$	17373	W	$2^3_0 4^3_0$
16565	M	$3^1_0 4^3_0$	17403	S	$1^1_0 2^1_0 3^1_0 4^1_0$
16581	W	$1^1_0 3^1_0 4^0_1$	17418	S	$1^1_0 3^3_0 4^1_0$
16613	W	4^6_1	17465	M	$1^1_0 3^1_0 4^3_0$, $2^2_0 4^5_0$
16637	W	$3^5_0 4^2_1$	17478	M	4^{10}_1
16664	W	$2^2_0 4^1_0$, $3^4_0 4^1_0$, $2^1_0 3^2_0 4^1_0$, $3^3_0 4^4_1$	17551	W	$2^1_0 4^7_0$
16728[b]	W	$2^1_0 4^3_0$	17572	W	$1^1_0 2^2_0 4^1_0$
16748[b]	M	$3^2_0 4^3_0$, $1^1_0 2^1_0 4^0_1$, $1^1_0 3^2_0 4^0_1$	17592	S	$1^1_0 3^4_0 4^1_0$
16808	M	4^5_0, $3^6_0 4^2_1$	17663	S	4^9_0, $2^5_0 4^1_0$
16820	M	$3^5_0 4^1_0$, $2^2_0 3^1_0 4^1_0$, $2^1_0 3^3_0 4^1_0$	17735	M	$1^1_0 2^2_0 3^1_0 4^1_0$
16837[b]	W	$3^4_0 4^4_1$	17767	M	$1^1_0 3^5_0 4^1_0$
16848[b]	W	$2^2_0 4^4_1$	17809	M	$1^2_0 4^1_0$, $2^3_0 4^5_0$, $1^1_0 2^1_0 3^1_0 4^3_0$, $2^1_0 4^{10}_1$, $3^2_0 4^{10}_1$
16872	W	$1^1_0 3^1_0 4^2_1$	17832	S	$3^1_0 4^9_0$, $2^5_0 3^1_0 4^1_0$
16886	W	$2^1_0 3^1_0 4^3_0$	17908	M	$1^1_0 2^2_0 3^2_0 4^1_0$
16905	M	$1^1_0 4^1_0$, $3^3_0 4^3_0$	17917	W	$1^1_0 3^6_0 4^1_0$
17004	S	$2^3_0 4^1_0$, $2^1_0 3^4_0 4^1_0$, $2^2_0 3^2_0 4^1_0$, $3^5_0 4^4_1$	17935	W	$1^2_0 3^2_0 4^2_1$
17016	M	4^8_1	17973	M	$1^2_0 3^1_0 4^1_0$, $1^1_0 2^1_0 3^2_0 4^3_0$, $1^2_0 4^4_1$
17050	W	$2^2_0 4^3_0$, $2^1_0 3^2_0 4^3_0$	17997	S	$2^6_0 4^1_0$, $2^1_0 4^9_0$, $3^2_0 4^9_0$, $2^5_0 3^2_0 4^1_0$
17066	M	$3^4_0 4^3_0$	18037	S	4^{11}_0
17079	M	$1^1_0 3^1_0 4^1_0$	18065	S	$1^1_0 2^3_0 3^1_0 4^1_0$
17081	M	$3^4_0 4^3_0$, $1^1_0 4^4_1$	18099	M	$1^2_0 3^3_0 4^2_1$
17139	M	$2^1_0 4^5_0$	18150	S	$1^2_0 2^1_0 4^1_0$, $1^2_0 3^2_0 4^1_0$, $2^5_0 3^3_0 4^1_0$, $3^3_0 4^9_0$, $1^1_0 2^1_0 3^3_0 4^3_0$

[a]w = weak, m = medium, s = strong.
[b]Extrapolated value.

regarded as highly tentative since the errors in measuring band frequencies are relatively large and there was no reasonable way, using the present data, to distinguish between weak cold bands and sequence bands which might be observable due to favorable Boltzmann factors for ν_3'' and ν_6''. With the exception of bands originating in the ν_4'' stack (which are expected to be prominent on Franck–Condon grounds), weak bands were arbitrarily assigned as cold in cases where hot sequence bands were reasonable alternatives.

As will be discussed later, it was quite reasonable to locate the origin of the $\tilde{A}-\tilde{X}$ system 75 cm^{-1} to the red of the 4^1_0 band, i.e. at 15930 cm^{-1}. If vibronic intensity borrowing were the only mechanism whereby bands in the $\tilde{A}-\tilde{X}$ spectra acquired intensity, the 0^0_0 band would be completely absent. In fact a very weak band is observed at the calculated origin frequency (vide infra). The origin band has been observed in the $\tilde{A}-\tilde{X}$ transitions of H_2CS and D_2CS (15, 16) in which cases the observed intensity was attributed to magnetic dipole transitions similar to that seen in H_2CO (17). However, the origin band has never been observed in the $\tilde{A}-\tilde{X}$ system of Cl_2CS (3, 11). If the band at 15930 cm^{-1} is the origin, the magnetic-dipole allowed 4^2_0 band ca. 280 cm^{-1} to the blue should also be observable on Franck–Condon grounds. A broad, weak feature is found in the required spectral region, but lack of sufficient intensity and resolution precluded its assignment. The nature of this and the origin band of the $\tilde{A}-\tilde{X}$ system in Br_2CS remains uncertain.

The experimental and calculated energy levels of ν_4' are shown schematically in Fig. 7. The calculations were performed by modelling the excited state double minimum potential-energy along the inversion vibration coordinate by a harmonic function perturbed by a Gaussian barrier, following the method of Coon *et al.* (18). This model has previously been used successfully to calculate the inversion vibrational energies and the equilibrium out-of-plane angles of the lowest triplet and excited singlet states of a number of tetraatomic carbonyls (19) and thiocarbonyls (3, 20). The function has the form

$$[1] \quad V(Q) = (1/2)\lambda Q^2 + \delta e^{\rho} \exp\{-\lambda Q_2/2\delta\}$$

where $\lambda = (2\pi c \nu_0)^2$ is the harmonic force constant and $\delta = Bhc\nu_0/(e^{\rho} - \rho - 1)$. $B\nu_0$ is the inversion barrier height in

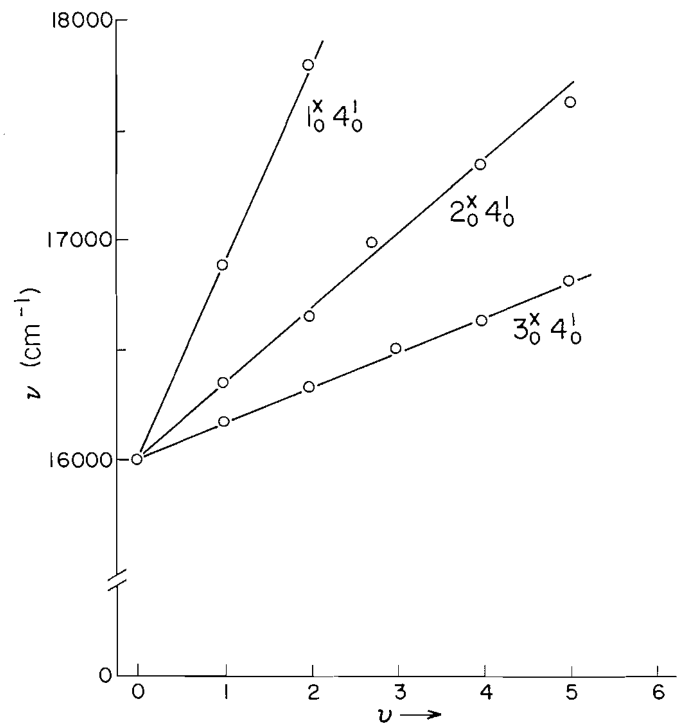

FIG. 5. Convergence of strong progressions in the excitation spectrum to the false origin at 16005 cm^{-1} (4^1_0).

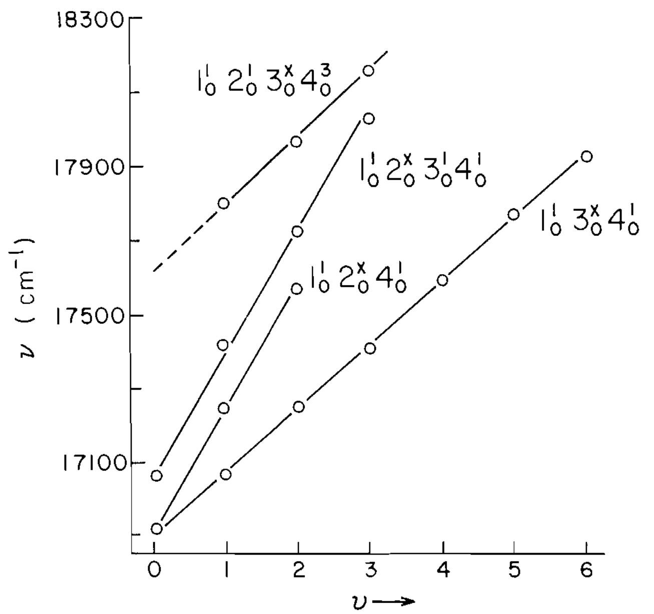

FIG. 6. Progressions in modes 2 and 3 in the excitation spectrum.

wavenumbers, and ρ is a shape factor related to the relative steepness of the inner and outer sides of the double minimum surface. Using the linear variation method the final vibrational eigenvalues are given in the form

$$[2]\quad \frac{G}{\nu_0} = \frac{E}{hc\nu_0} - \frac{B(\rho + 1)}{e^{\rho} - \rho - 1}$$

These eigenvalues have been tabulated by Coon *et al.* (18) for values of ρ from 0.6 yo 2.4 and values of B from 0 to 5. Values of B and ν_0 were calculated for each fixed value of ρ and the iteration continued until the best fit between the calculated and

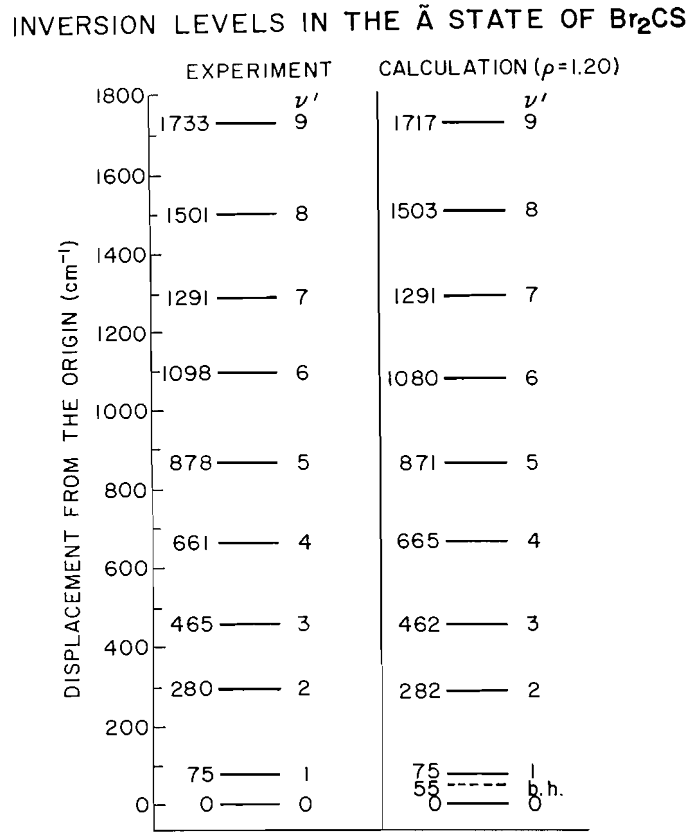

FIG. 7. Experimental and calculated energies of ν_4' in the $\tilde{A}$ state of Br_2CS. The dashed line indicates the position of the top of the barrier to inversion.

observed values of ν_4' was found. In the case of Br_2CS in its $\tilde{A}$ state the best fit was obtained with $\rho = 1.20$, $\nu_0 = 218$ cm^{-1} and a barrier height of 164 cm^{-1}. The agreement between calculated and experimental values of ν_4' is reasonably good, taking into account the fact that the experimental frequencies could be determined to no better than ± 15 cm^{-1}.

A barrier height of the order of 164 cm^{-1} is reasonable on qualitative, comparative grounds. It has been established empirically that the inversion barrier heights in the $\tilde{a}$ states of tetraatomic thiocarbonyl halides increase with increasing electronegativities of the substituent atoms (20). (This observation is rationalized by the fact that, in accord with Walsh's postulate (21), the p electron density on the central carbon atom in the excited state governs the barrier height (22).) Since the electronegativities of the halogens decrease in the order F > Cl > Br, the inversion barrier heights in the $\tilde{A}$ states should be in the order F_2CS > ClFCS > Cl_2CS > Br_2CS, as observed (1).

The equilibrium out-of-plane angle for Br_2CS in the $\tilde{A}$ state was calculated using the relation

$$[3]\quad \theta_{min} = Q_{min}/(\mu^{1/2}r)$$

where Q_{min} is the mass weighted coordinate at θ_{min}, r is the C—S bond distance, and μ is the reduced mass (18). The equilibrium geometry of Br_2CS in its $\tilde{A}$ (or any other excited) state has not been determined so that μ and r are not known. Fortunately both parameters can be estimated reasonably closely by extrapolation from the ground state geometry using the changes in vibrational frequencies and the behavior of other thiocarbonyl halides on $\tilde{A} \leftarrow \tilde{X}$ excitation as guides. The C—S bond lengths of H_2CS, F_2CS, and Cl_2CS all increase by ca.

TABLE 3. Geometry of Br_2CS

Parameter	Value	
	$\tilde{X}$[a]	$\tilde{A}$[b]
d(C—S)(Å)	1.60	1.70
d(C—Br)(Å)	1.92	1.92
∠Br—C—Br (deg)	112	114

[a]References 4 and 5.
[b]Estimated.

TABLE 4. Ratios of the $\tilde{X}:\tilde{A}$ frequencies of vibrational modes of several thiocarbonyls

Compound	Ratio			
	C—S stretch	CX_2 symmetric stretch	CX_2 bend	CX_2 rock
H_2CS[a]	1.29	0.98	1.11	—
D_2CS[a]	1.21	1.01	1.16	—
F_2CS[b]	1.24	1.07	1.37	—
Cl_2CS[b]	1.26	1.05	1.20	1.46
Br_2CS	1.24	1.10	1.10	0.80

[a]Reference 2.
[b]Reference 1.

0.1 Å on $n \rightarrow \pi^*$ excitation whereas the C—X (X ≡ F, Cl, H, D) bond lengths remain approximately constant (1). Using estimated equilibrium bond lengths and angles for Br_2CS $\tilde{A}(^1A_2)$ given in Table 3, an equilibrium out-of-plane angle of 13° was obtained. This angle is substantially smaller than those of F_2CS, ClFCS, and Cl_2CS (1), possibly due to repulsive electronic interactions between the large substituent bromine atoms in Br_2CS.

Modes 1, 2, and 3 are totally symmetric and appear with no restrictions in quantum number change when combined with odd quantum number changes in mode 4. The frequencies of these modes can be extracted from the slopes of the lines in Figs. 5 and 6 (or from averaging combination differences). Frequencies of 902 cm^{-1}, 332 cm^{-1}, and 168 cm^{-1} are obtained for ν_1', ν_2', and ν_3' respectively. As shown in Table 4, the ratio of the frequencies of the C—S stretching mode in the $\tilde{X}:\tilde{A}$ states is almost constant for all the tetraatomic thiocarbonyls examined to date. We take this as an indication that the change in electron distribution in the C—S bond resulting from $n \rightarrow \pi^*$ excitation is approximately the same for all of these molecules, a notion which is reasonable, given that the excitation is primarily localized in the C—S moiety. An approximately constant ratio is also obtained for the frequencies of the C—X_2 symmetric stretching mode. However substantial differences occur in the X—C—X symmetric bending mode frequency changes.

A single weak band located 158 cm^{-1} to the blue of the origin could not be assigned reasonably as either a hot band or as part of a progression involving modes 1−4 in the upper state. It might reasonably be assigned as 6_0^1. This mode is weakly active in Cl_2CS (3, 11) and a frequency for ν_6' of 158 cm^{-1} is not unreasonable for Br_2CS. However, such an assignment should be considered as highly tentative.

The fluorescence excitation spectrum also exhibits diffuseness with an onset near 547 nm. By analogy with Cl_2CS (10, 23), it is reasonable to assume that predissociation of the $\tilde{A}$ state by unbound levels of the ground state is responsible. Using a frequency of ca. 18300 cm^{-1} for the onset of predissociation, a value of 52.3 kcal mol^{-1} is calculated for the ground state C—Br dissociation energy of Br_2CS. The ground state C—Cl dissociation energy is a factor of 1.258 larger in CH_2Cl_2 than in $CSCl_2$ (24). A similar factor should apply when comparing CH_2Br_2 and $CSBr_2$. Given that D_0(Br—CH_2Br_2) = 66.9 kcal mol^{-1} (24), a value of D_0(Br—CSBr) = 53.2 kcal mol^{-1} is obtained which compares very well with that calculated from the onset of spectral diffuseness.

Acknowledgements

The authors gratefully acknowledge the continuing financial support of the Natural Sciences and Engineering Research Council of Canada. One of us (B.S.) is grateful for the award of an NSERC Postgraduate Scholarship. We also thank Dr. A. Bruno for valuable discussions and helpful technical assistance.

1. R. P. STEER. Rev. Chem. Intermed. **4**, 1 (1981), and references therein.
2. D. J. CLOUTHIER and D. A. RAMSAY. Ann. Rev. Phys. Chem. **34**, 31 (1983).
3. J. C. D. BRAND, J. H. CALLOMON, D. C. MOULE, J. TYRRELL, and T. H. GOODWIN. Trans. Faraday Soc. **61**, 2365 (1965).
4. D. CHRISTEN. J. Mol. Struct. **66**, 211 (1980).
5. W. HAUSWIRTH and H. WILLNER. Spectrochim. Acta, **35A**, 263 (1979).
6. G. DIDERRICH and A. HASS. Chem. Ber. **109**, 3432 (1976).
7. D. C. MOULE and C. R. SUBRAMANIAM. Chem. Commun. 1340 (1969).
8. D. C. MOULE and C. R. SUBRAMANIAM. J. Mol. Spectrosc. **48**, 336 (1973).
9. D. G. CARROLL, L. G. VANQUICKENBOURNE, and S. P. MCGLYNN. J. Chem. Phys. **45**, 2777 (1966).
10. L. E. BRUS and J. R. MCDONALD. Chem. Phys. Lett. **16**, 587 (1972).
11. D. J. CLOUTHIER and D. C. MOULE. J. Mol. Spectrosc. **87**, 471 (1981).
12. P. F. BERNATH, P. G. CUMMINS, R. W. FIELD, and J. RL LOMBARDI. J. Mol. Spectrosc. **69**, 166 (1978).
13. G. HERZBERG. Electronic spectra of polyatomic molecules. Van. Nostrand-Reinhold Co., New York. 1966.
14. J. R. HENDERSON. J. Chem. Phys. **44**, 3496 (1966). K. K. INNES. J. Mol. Spectrosc. **99**, 294 (1983).
15. R. H. JUDGE and G. W. KING. Can. J. Phys. **53**, 1927 (1975).
16. R. N. DIXON, D. A. HANER, and C. R. WEBSTER. Chem. Phys. **22**, 199 (1973).
17. D. C. MOULE and A. D. WALSH. Chem. Rev. **75**, 67 (1975).
18. J. B. COON, N. W. NAUGLE, and R. D. MCKENZIE. J. Mol. Spectrosc. **20**, 107 1966).
19. A. KAPUR, R. P. STEER, and P. G. MEZEY. Can. J. Chem. **60**, 100 (1982).
20. A. KAPUR, R. P. STEER, and P. G. MEZEY. J. Chem. Phys. **70**, 745 (1979).
21. A. D. WALSH. J. Chem. Soc. London. 2306 (1953).
22. D. C. MOULE and D. A. CONDIRSTON. Theoret. Chim. Acta, **29**, 133 (1973).
23. H. OKABE. J. Chem. Phys. **66**, 2058 (1977).
24. H. OKABE. Photochemistry of small molecules. John Wiley and Sons, New York. 1978. p. 304.

The high pressure photochemistry of alkenes. III. The 184.9 nm photoisomerization processes in acyclic alkenes

Guy J. Collin[1] and Hélène Deslauriers

Département des sciences fondamentales, Université du Québec à Chicoutimi, Chicoutimi (Qué.), Canada G7H 2B1

Received July 19, 1984

This paper is dedicated to Professor Camille Sandorfy on the occasion of his 65th birthday

Guy J. Collin and Hélène Deslauriers. Can. J. Chem. **63**, 1424 (1985).

We have made a systematic study of the 184.9 nm photoisomerization of the gaseous acyclic alkenes. Apart from the *cis–trans* isomerization (geometric isomerization), we have also observed the formation of products arising from the 1,3-hydrogen and methylene shifts (structural isomerization). 1-Alkenes do not show evidence of structural isomerization. This kind of isomerization increases with an increase in the number of alkyl substituents around the double bond. These observations, combined with those from the literature, may be explained on the basis of the following: (*a*) the $^1\pi,\pi^*$ state is involved in the *cis–trans* isomerization process; (*b*) the $^1\pi$,R(3*s*) state is responsible for the methylene shifts; (*c*) another singlet state is required for the 1,3-hydrogen shift; (*d*) this last state is either at an energy level higher than that of the Rydberg state or the hot ground state. Finally, the photoexcited molecules, through internal conversion, may convert from one state to another, and their lifetime is long enough to be stabilized by collision.

Guy J. Collin et Hélène Deslauriers. Can. J. Chem. **63**, 1424 (1985).

Nous avons entrepris une étude systématique de la photoisomérisation des alcènes non-cycliques à 184,9 nm en phase gazeuse. Outre l'isomérisation *cis–trans* (isomérisation géométrique) nous avons pu observer la formation d'isomères résultant d'un transfert interne soit d'un atome d'hydrogène, soit d'un groupe méthylène (isomérisation structurale). Alors que les oléfines terminales ne montrent pas d'isomérisation structurale évidente, celle-ci semble de plus en plus importante, au fur et à mesure que s'accroît le nombre de substituants autour de la double liaison. L'ensemble de ces observations, combinées à celles relevées dans la littérature, peuvent être expliquées par l'intervention: (*a*) de l'état $^1\pi,\pi^*$ dans l'isomérisation *cis–trans*; (*b*) de l'état $^1\pi$,R(3*s*) dans le transfert d'un groupe méthylène; (*c*) d'un autre état singulet excité dans le transfert d'un atome d'hydrogène. Ce dernier état excité est soit situé à un niveau d'énergie plus haut que celui de l'état Rydberg ou est l'état fondamental vibrationnellement excité. En outre il semble que la molécule puisse passer d'un état à l'autre par conversion interne et que le temps de vie de ces états électroniques est suffisamment long pour que ceux-ci soient stabilisés par collision.

Introduction

The isomerization of alkenes was observed under various conditions. Of course, in ethylene (for a review and a theoretical approach, see ref. 1) the isomerization process involves isotopic scrambling of hydrogen atoms in the direct photolysis of various dideuterioethylenes in condensed phases (2, 3). Similar behavior was reported in triplet-sensitized gas-phase chemistry (1, 4–6). Direct or sensitized higher alkene photoisomerization was also observed in various systems. For example, the *cis–trans* isomerization of partially deuterated propene was observed in sensitized systems (7). Of course, 2-butene is a "test case": the geometric *cis–trans* isomerization process was observed by several authors and is described in textbooks (see, for example, ref. 8*a*). Direct photoisomerization results are relatively scarce. However, the *cis–trans* isomerization of 2-butene was observed at 202.6–206.2 nm (9) as well as at 184.9 nm (10). Moreover, structural isomerization was also observed either in the gas (11) or liquid phases (12–14). Some of these reports tried to link the nature of the excited state(s) with the product formation (1, 10, 12*b*, 14*b*). Although it is well known that the *cis–trans* isomerization process involves the formation of the $^1\pi,\pi^*$ electronic singlet state (the V state), the formation of other isomers is not unambiguously linked to other excited state(s) (14*b*).

In this report we shall describe a systematic study of the 184.9 nm photochemistry of gaseous acyclic alkenes, and, with results taken from the literature, we shall try to throw more light on the relationship linking the available excited states to the formation of isomers.

[1] To whom all correspondence should be addressed.

Experimental

Experimental details were the same as those reported in previous studies from this laboratory (11, 15, 16).

Materials

All the alkenes are API products (Table 1): they are used after being degassed under high vacuum and at low temperature in a mercury-free Pyrex line (Teflon stopcocks, Wallace and Tiernan membrane manometers). Propane (99.99%) and oxygen (99.98%) — Research purity materials — are from Matheson and are used as received.

Photolysis

All the photolyses are performed in two different cells. The first one (a 90.3 cm^3 Pyrex one) is used at pressures lower than 1 atm, the second one (a 4.2 cm^3 brass one) is used at higher pressures (16). They have quartz windows. All the experiments are made with a mixture of alkene : oxygen (100 : 10) in order to prevent the formation of isomers through radical recombination reactions. The standard pressures of the alkene are as follows: (*1*) in the Pyrex cell the alkene pressure is 5 Torr (665 N m^{-2}); (*2*) in the brass cell the alkene pressure is 50 Torr (6650 N m^{-2}). In each case propane is added in order to obtain the desired total pressure. The incident photon beam is completely absorbed by the starting alkene material due to its very high absorption coefficient. The actinometry has also been described elsewhere (11, 15, 16). Ethylene ($\Phi(C_2H_2) = 0.50$) is used to determine the quantum yields. The conversion percentage of the starting alkene is kept below 1% in order to avoid back reactions.

Analysis

All analyses are done chromatographically. A squalane column (25% on firebrick) is used at room temperature. The gas-chromatograph is equipped with a dual flame ionisation detector.

Results

The quantum yields of isomers formed in the photolytic

TABLE 1. Starting materials

Alkenes	Abbreviation[a]	Stated impurity (mol%)	Main C_5 or C_6 analyzed impurities[b] (ppm)
2-Methyl-2-butene	2M2B	0.06±0.04	2M1B: 14–16; 3M1B: 11
4-Methyl-*trans*-2-pentene	4M*t*2P	0.14±0.07	4M*c*2P: 50; 2,3dM2B: 210; 3M*t*2P: 2–5
4-Methyl-*cis*-2-pentene	4M*c*2P	0.08±0.07	4M1P: 130–160; 3,3DM1B: 2–4
cis-3-Hexene	*c*3H	0.086±0.013	1H: 11–13; 4M*t*2P: 2–4
3-Methyl-*trans*-2-pentene	3M*t*2P	0.15±0.08	3M*c*2P: 1000–1700; 3H: 31
3-Methyl-*cis*-2-pentene	3M*c*2P	0.03±0.01	2E1B: 35–70; 4M*c*2P: 200; 3,3DM1B: 20
2,3-Dimethyl-2-butene	2,3dM2B	0.03±0.02	None

[a] Symbols are as follows: M ≡ methyl, E ≡ ethyl, B ≡ butene, P ≡ pentene. H ≡ hexene, cyPr ≡ cyclopropane; for example, 4M*t*2P stands for 4-methyl-*trans*-2-pentene.
[b] Analysis of the starting material may vary from one sample to another.

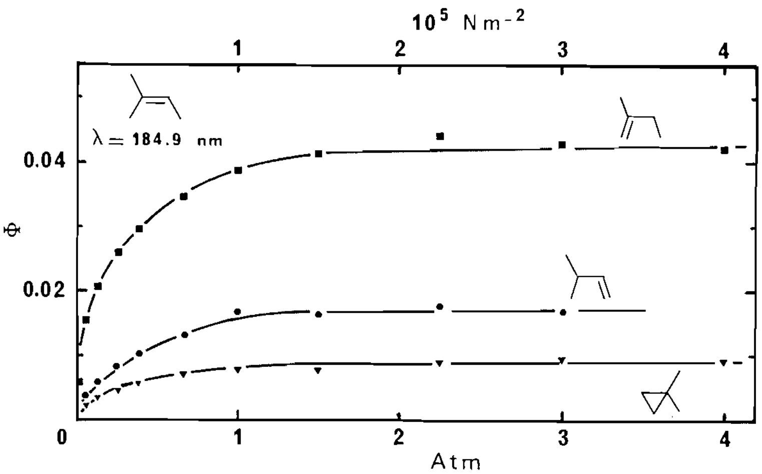

FIG. 1. Plot of product quantum yields vs. pressure in the photolysis of 2-methyl-2-butene at 184.9 nm. *cis*-1,2-Dimethylcyclopropane (c1,2,dMcyPr) is also formed and its quantum yield is similar to that of the 1,1-dimethylcyclopropane (1,1dMcyPr) — see Table 2.

experiments are reported in Figs. 1–5. For example, Fig. 1 shows the quantum yields of 2-methyl-1-butene, 3-methyl-1-butene, and dimethyl-1,1-cyclopropane measured in the 184.9 nm photolysis of 2-methyl-2-butene (trimethylethylene). In all cases, the quantum yields increase from the lower pressure regimes to plateau values obtained at pressures higher than 1 atm. Table 2 shows the quantum yields measured at higher pressures. In fact, they are measured in the plateau regions that can be identified from the previous figures. Other results from this laboratory also appear in Table 2. Table 3 gives other results taken from the literature.

Discussion

(A) The isomerization processes

(a) The cis–trans *isomerization process*

Table 2 lists the photochemical quantum yields of isomer formation from various acyclic alkenes. In the case of 1-alkenes, the *cis–trans* isomerization process could not be oserved in this work. In fact, it is known from the literature that it is an efficient one, and was observed in the direct photolysis of ethylene at 184.9 nm in nitrogen solution at 77 K (3); it probably involves the relaxation of either an excited ethylene molecule to an ethylidene structure or an excited $^1\pi,\pi^*$ state (see later) or both (1, 3).

Of course, the *cis–trans* isomerization process in the direct photolysis of 2-alkenes has been observed in several laboratories. For example, Borrell *et al.* measured the following quantum yields (Table 3): $\Phi(cis \rightarrow trans) \simeq \Phi(trans \rightarrow cis) \simeq 0.1$ at a pressure lower than 80 Torr. Moreover, *trans*-2-butene also appears to be the major product at 202.6–206.2 nm provided that the pressure is high enough to stabilize the excited intermediate (9). The 2-pentene case has been published recently (16). At 184.9 nm the *cis–trans* interconversion has a high quantum yield ($\Phi \simeq 0.40$) in the pressure region higher than 3 atm. Similar results were obtained for the case of 4-methyl-*trans*-2-pentene (Fig. 5). Finally, 3-methyl-2-pentene undergoes *cis–trans* isomerization with peculiar quantum yields: it appears that the formation of the *cis*-structure is preferentially formed. Some steric effect may be responsible for such behavior (17).

(b) The [1,3]-sigmatropic hydrogen shift

In addition to the *cis–trans* isomerization process, 1,3-hydrogen internal atom transfer (a 1,2-double bond migration) was recognized very early. However, in several studies from this laboratory, it was impossible to observe this internal shift in 1-alkenes (18, 19), i.e. the quantum yield of 2-alkene formation is smaller than 0.005. Conversely, this transfer was observed in various liquid 2-alkene systems (9, 12). In the gas phase, this transfer is a general occurrence (Table 2). Although not all the pertinent products have been analyzed due to chromatographic difficulties, the quantum yields for such a process are between 0.02 and 0.10 in disubstituted alkenes. It must also be realized that in 2-pentene, for example, 1,3-hydrogen shift gives rise to the formation of either 1-pentene or 2-pentene. Thus, the Φ(1-pentene) value is a lower limit of the total Φ(1,3-hydrogen shift) value.

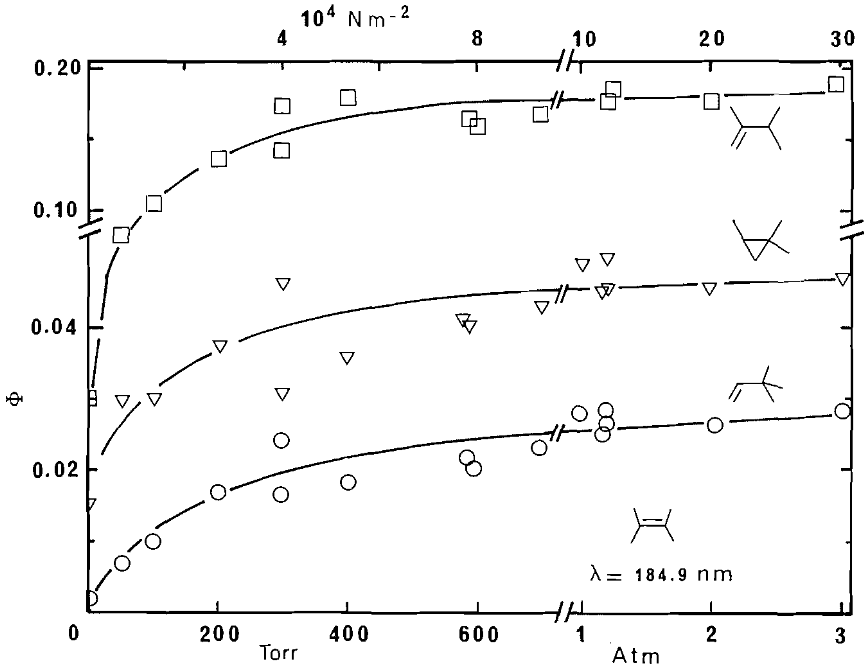

FIG. 2. Plot of product quantum yields vs. pressure in the photolysis of 2,3-dimethyl-2-butene at 184.9 nm.

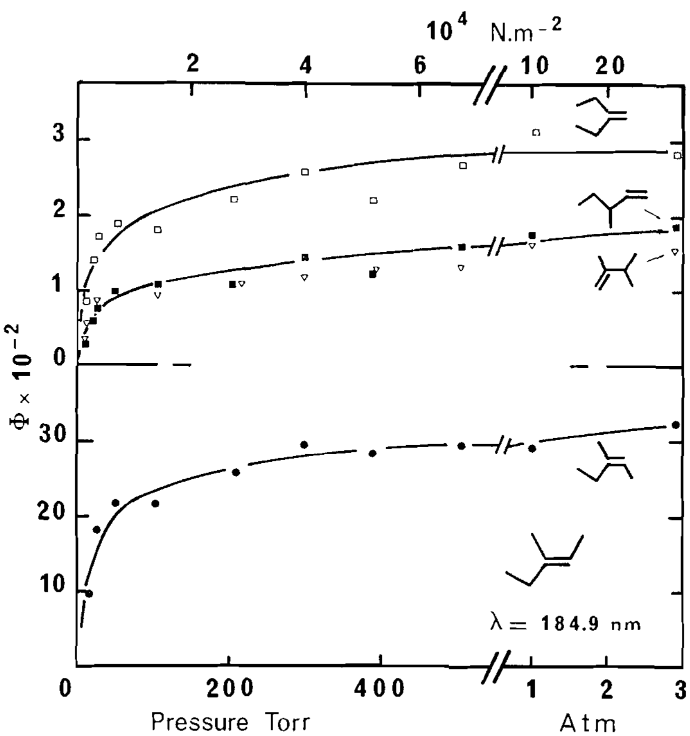

FIG. 3. Plot of product quantum yields vs. pressure in the photolysis of 3-methyl-*cis*-2-pentene at 184.9 nm.

Again in the 3-methyl-2-pentene case, the starting material is among the products for such a process, and part of the hydrogen transfer is embedded in the *cis–trans* isomerization process. Thus, the Φ(3-methyl-1-pentene + 2-ethyl-1-butene) value is smaller than the true Φ(1,3-Hydrogen shift) value. Finally, for the tetramethylethylene case, the extent of this process undergoes a drastic increase.

(c) The methylene shift

Again, there is no indication of an additional structural isomerization process for the case of 1-alkenes. Conversely, small quantities of isomers, requiring extensive rearrangement, are formed in the case of 2-alkenes. For example, 2-methyl-1-butene is a product of the *cis*-2-pentene photolysis: Φ(2-methyl-1-butene) $\simeq$ 0.01_5. Alkyl-substituted cyclopropanes are found in this category of reactions (12, 13). Again, it must be recalled that the chromatographic separations of the pertinent products from the starting materials are often very bad. Thus, the given quantum yields represent lower values for these methylene shift reactions. However, one can say that the quantum yields of such a process increase with an increase in the number of alkyl substituents on the double bond.

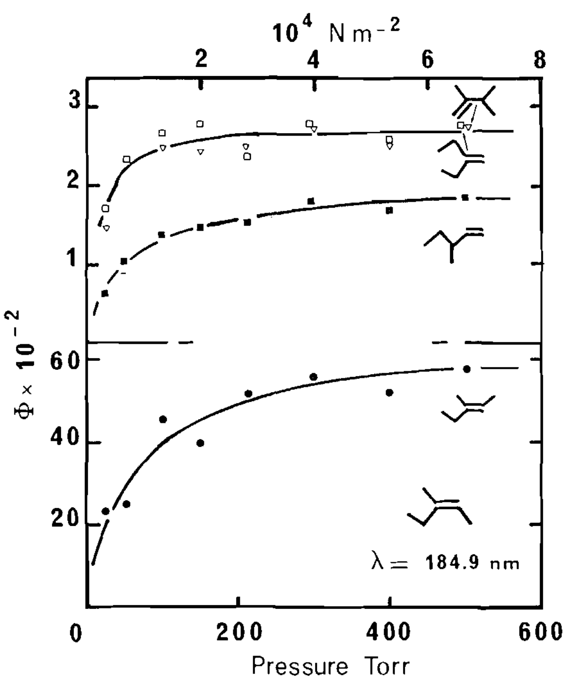

FIG. 4. Plot of product quantum yields vs. pressure in the photolysis of 3-methyl-*trans*-2-pentene at 184.9 nm.

TABLE 2. Photoisomerization of various alkenes at 184.9 nm, quantum yields measured at high pressures

Alkenes[a]	*cis* ⇄ *trans*	1,3-H transfer	CH_2 transfer	Reference
1-alkene	?	Not observed	Not observed	18, 19
*c*2P	$c \rightarrow t$: 0.40	1P: 0.02_5	2M1B: 0.01_5	16
*t*2P	$t \rightarrow c$: 0.38			16
4M*t*2P	$t \rightarrow c$; 0.41	4M1P: 0.06_5		This work
		2M2P: 0.03		This work
4M*c*2P	Not measured	4M1P: 0.04	iPrcyPr: 0.01	This work
*c*3H	Not measured	*c*2H: 0.02	4M*t*2P: 0.01	25
2M2B	?	2M1B: 0.045	*c*1,2dMcyPr: 0.01	This work, 11*a*
		3M1B: 0.01_7	dM1,1cyPr: 0.00_9	This work, 11*a*
3M*t*2P	$t \rightarrow c$: 0.57	3M1P: 0.02	2,3dM1B: 0.02_7	This work
		2E1B: 0.02_7		
3M*c*2P	$c \rightarrow t$: 0.33	3M1P: 0.02	2,3dM1B: 0.01_7	This work
		2E1B: 0.02_8		
2,3dM2B	?	2,3dM1B: 0.18	3,3dM1B: 0.03	This work, 11*b*
			tM1,1,2cyPr: 0.05	This work, 11*b*

[a] See Table 1 for explanation of the symbols: $t \equiv$ *trans*, $c \equiv$ *cis*, t $\equiv$ tri. Results are $\pm$ 10%.

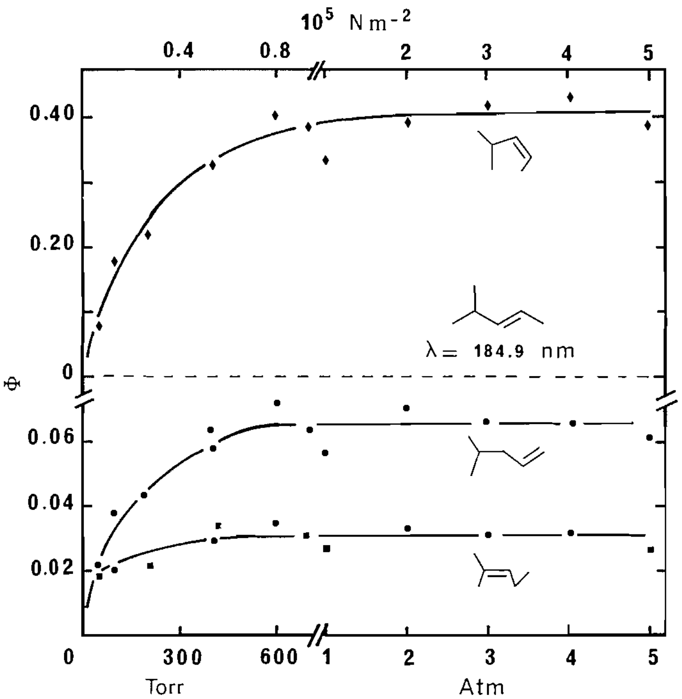

FIG. 5. Plot of product quantum yields vs. pressure in the photolysis of 4-methyl-*trans*-2-pentene at 184.9 nm.

(B) The nature of the excited states

(a) The absorption spectra

The obvious question arising at this point is pertinent to the nature of the excited states leading to each of the previously reported processes. The absorption spectra of this class of molecules are well known and a full description of the transitions involved has been given (20) although a large number of details are evidently lacking (21, 22). However, definite trends may be observed from these spectra. At 184.9 nm, all these C_4, C_5, and C_6 alkenes have a very strong absorption band corresponding to the formation of a $^1\pi,\pi^*$ electronic excited state (the V State). The stable configuration of this excited state has a skew structure as shown for the example of ethylene in Fig. 6. On its way back to the electronic ground state the molecule has an equal probability of finding either its original structure or its geometric isomer. On the red side of this strong $^1\pi,\pi^*$ absorption band, a much smaller, not resolved one, appears in the 2M2B spectrum. This band is also badly resolved in the 2,3dM2B case (2) and was attributed to the formation of the Rydberg — $^1\pi$,R(3*s*) — excited state (20). This electronic state is thought to be responsible for the formation of a carbene intermediate (23) leading to the observed methylene shifts (8*b*). The increase in the quantum yields for methylene shifts with increasing alkyl substitution on the double bond has been linked to the probably greater stability of the Rydberg state of tetramethylethylene as compared to that of the V State (23). The correlation between the electronic states and the [1,3]-sigmatropic hydrogen shift, however, is not so evident. Kropp has proposed that the $^1\pi,\sigma^*$ state is the one involved in such a transfer (23) although some controversy exists (14*b*).

(b) The photofragmentation

From the Stern–Volmer plots of the methyl radical formation (a product of the primary β(C—C) bond rupture) we have been able to measure the rate constant for β(C—C) bond rupture. These experimentally derived rate constants are in the 0.5–5 $\times$ 10^9 s^{-1} range for the C_6 1-alkene (19) and 2-alkene groups (25). Moreover, the rate constants of these processes have also been estimated using the RRKM method, assuming that all the photon energy is redistributed in the vibrational framework of the molecule. The rate constants of the fragmentation process calculated in this way are again in the 10^9 s^{-1} range. Thus it is quite reasonable to assume that the fragmentation products arise from the vibrationally excited ground state. In the case of 4-methyl-*cis*-2-pentene, the lifetime of this excited precursor has been determined from the Stern–Volmer plot and is around 3 ns (24). From Fig. 7, the lifetime of the precursor of the *trans–cis* process may be estimated to be around 0.3 ns. Except for some unlikely difference between the *cis*- and the *trans*-compounds, it appears that the precursors of the isomerization and of the fragmentation processes are not the same.

(c) The dynamics of the excited states

Thus, at 184.9 nm it is relatively safe to assume that the absorption of a photon by monoalkenes leads to the population of the V state. This $^1\pi,\pi^*$ excited state is the one involved in the *cis–trans* process. On its way to its skew structure, the

TABLE 3. Photolysis of acyclic alkene at 184.9 nm: quantum yields of isomerization and results from the literature

Alkene[a]	Isomer		Pressure range	Reference
2B	$c \rightarrow t$	: 0.10	1–80 Torr	10*a*
	$t \rightarrow c$	: 0.10	1–80 Torr	
1B	2B	: 0.01	?	30
*c*2P	$c \rightarrow t$	: 0.36	150 Torr	31
2,3dM2B	2,3dM1B	: 0.23	Pentane solutions	14*b*
	3,3dM1B	: 0.016	Pentane solutions	
	tM1,1,2cyPr	: 0.023	Pentane solutions	
2,3dM2B	2,3dM1B	: 0.24_3[b]	50–400 Torr of propane	11*b*
	3,3dM1B	: 0.03_5[b]	50–400 Torr of propane	
	tM,1,1,2cyPr	: 0.06_0[b]	50–400 Torr of propane	

[a] See Table 1 for symbols.
[b] Values obtained from extrapolation to "infinite" pressure.

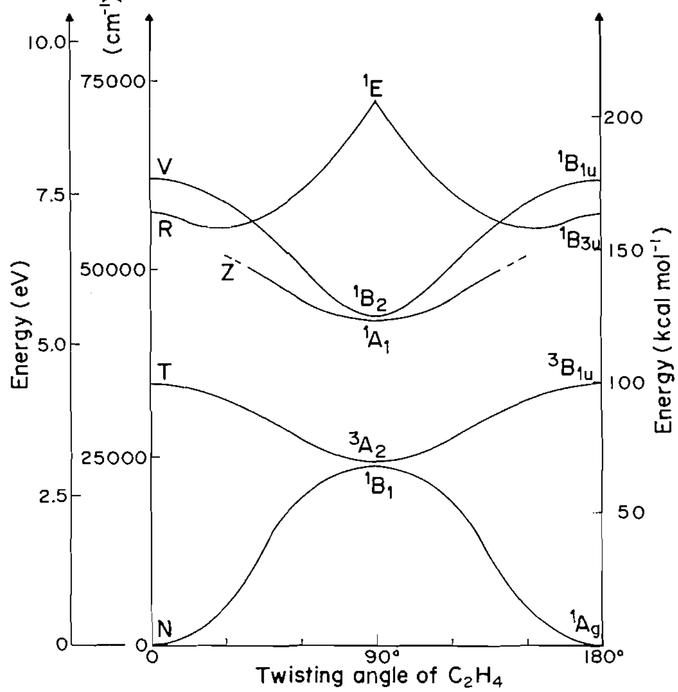

SCHEMATIC POTENTIAL ENERGY DIAGRAM

FIG. 6. Schematic potential energy diagram of ethylene, see refs. 22 and 29.

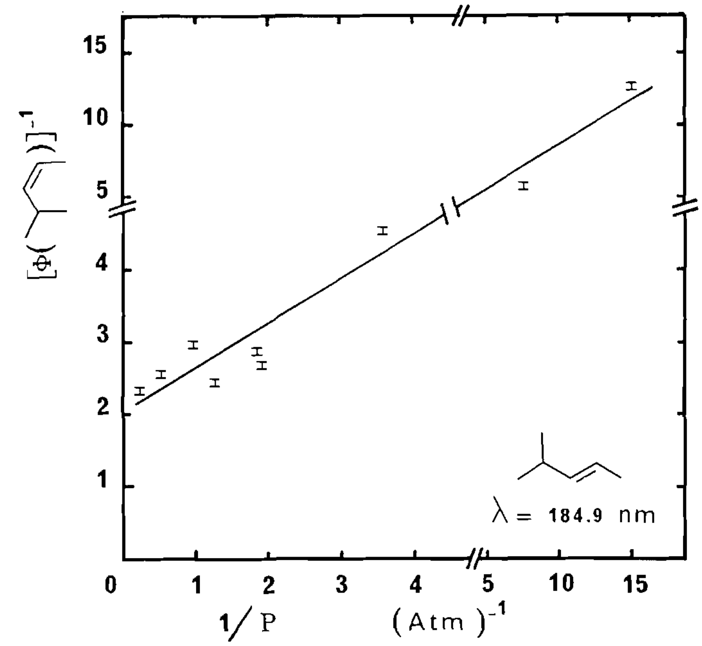

FIG. 7. Stern–Volmer plot for the formation of the *cis* isomer in the photolysis of 4-methyl-*trans*-2-pentene at 184.9 nm.

molecule, on the V surface, crosses the Rydberg energy surface, and it may remain on the V surface or, by internal conversion, cross to the ^{1}R state. (Fig. 8).[2] The relative energy levels of the two states determine the equilibrium (?) ratio of the two exit channels. Since the relative position of the two states is dependent on the number of alkyl substituents, this ratio is also affected (12). Again, it may be assumed that the excited ^{1}R state of the starting alkene is in equilibrium with the ^{1}R state of the isomers (25) (Fig. 8). The situation is even more complex since some of the isomers are alkenic in nature and their ^{1}R state is also, by the same token, in equilibrium with their ^{1}V state. Of course, one may assume that the excited states of 2,3dM2B have lower energy levels, so that their concentrations are higher than those of the other isomers. The lifetimes of the excited isomers are long enough to be stabilized by collisions. Obviously, the resulting products depend on the structure of the excited intermediate.

The same argument may be used to explain the formation of 2,3-dM1B from 2,3-dM2B. However, the nature of the excited state of the intermediate involved in the formation of this product is different from the one involved in the methylene shift processes. With regard to the latter, it is known that the 3,3-dimethyl-1-butene/1,1,2-trimethylcyclopropane ratio is independent of temperature (11*b*) and incident wavelength (11*b*, 14*b*). On the other hand, the 2,3-dimethyl-1-butene/3,3-dimethyl-1-butene ratio is not constant. Moreover, since the latter ratio decreases with an increase in the wavelength from 184.9 to 228.8 nm, it is reasonable to assume that the energy level of the state involved in the 1,3-hydrogen shift is higher than that involved in the methylene shifts. This observation does not favor the involvement of the $^1\pi,\sigma^*$ state, since it is accepted that this state is the lowest in energy (ref. 14*b* and references therein). Another argument in favor of internal conversion between these excited singlet states may be seen in

[2] In this kind of study, no reference is made to triplet states. For different reasons it is thought that triplet states are not involved in the direct photolysis. However, definite proof would be helpful.

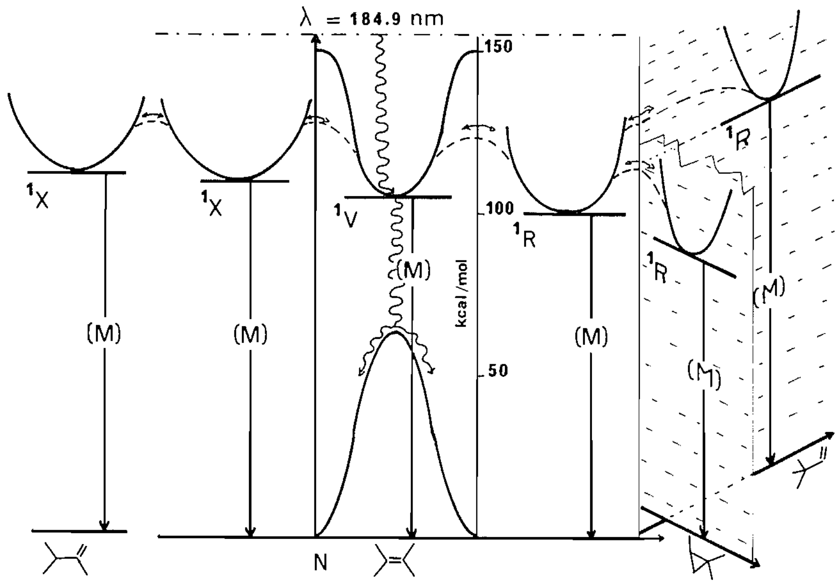

FIG. 8. Schematic representation of the tetramethylethylene excited singlet-state surface.

Figs. 1–5 where it appears that, in each case, the magnitudes of the pressure dependence of the various isomer quantum yields are similar. Although this similarity may be fortuitous, we would expect different pressure behavior in the absence of internal conversion.

Of course, the hot or vibrationally excited ground state cannot be ruled out. We have recently shown that the thermal isomerization of 2,3dM2B to 3,3dM1B and 2,3dM1B is efficient (26). However, 1,1,2tMcyPr is not formed and the ratio 3,3dM1B/2,3dM1B is close to 15, contrary to what is observed in photochemical experiments (Table 3). Thus, it can be said that the lower vibrationally excited levels of the ground state are not involved in the photoisomerization processes, although part of 3,3dM1B may be formed from the hot ground state.

(d) Fluorescence

Fluorescence of monoalkenes was observed either in the gas or in the liquid phases by Hirayama and Lipsky (27). They measured very low quantum yields: $\Phi(\text{fluor}) \simeq 10^{-6}$; and indicated that this could be due to the presence of a very efficient channel for non-radiative decay (27). The other main characteristics are the following: the quantum yield increases with an increase in (*a*) the number of substituents on the double bond; (*b*) the concentration of the alkene, i.e. on going from 1 atm (gas) to the neat liquid. The authors conclude that their "...entire...discussion has been able to argue only for the reasonableness of the Rydberg assignment" to fluorescence (14*b*).

Since we know that the molecule photoexcited in this region of the spectrum may isomerize, an alternative to the assignment of the fluorescence may be found for the case of 2,3dM2B in one or several excited isomers. It is known that the fluorescence quantum yields of saturated hydrocarbons are around two orders of magnitude greater than those of the monoalkenes (28). Thus, it is not unlikely that some of the initially formed excited cyclopropane derivatives are responsible for the observed fluorescence. Unfortunately, the authors have no indication whether the cyclopropanes fluoresce.

NOTE ADDED IN PROOF: After this study was submitted, the 193 nm laser photolysis of two C_7 alkenes appeared in literature. The results show an important β(C—C) split and, using absorption spectroscopy, the authors were able to follow the increase in the trimethally radical concentration with time. The lifetime of the photoexcited molecules were found in the 50–70 ns range (32). The longer lifetimes observed in this study are in line with the ones mentioned above of the C_6 photoexcited alkene molecules. The RRKM calculations show that the addition of one CH_2 group decreases the probability to find the needed energy in the right β(C—C) bond (33).

Acknowledgments

We would like to express our gratitude to the University of Quebec at Chicoutimi for the supporting salary given to one of us (H.D.) and the Natural Sciences and Engineering Research Council of Canada for financial assistance throughout this work.

1. E. M. EVLETH and M. SEVIN. J. Am. Chem. Soc. **103**, 7414 (1981).
2. R. GORDON, JR., and P. AUSLOOS. J. Res. Natl. Bur. Stand. **75**a, 141 (1971).
3. S. HIROKAMI and R. J. CVETANOVIĆ. J. Phys. Chem. **78**, 1254 (1974).
4. S. HIROKAMI and S. SATO. Can. J. Chem. **45**, 3181 (1967).
5. S. TSUNASHIMA, S. HIROKAMI, and S. SATO. Can. J. Chem. **46**, 995 (1968).
6. H. E. HUNZIKER. J. Chem. Phys. **50**, 1288 (1969).
7. S. HIROKAMI and S. SATO. Bull. Chem. Soc. Jpn. **43**, 2389 (1970).
8. N. J. TURRO. *In* Modern molecular photochemistry. The Benjamin/Cummings Publishing Co., Inc. Menlo Park, CA. 1978. (*a*) pp. 474–480; (*b*) pp. 486–487.
9. J. P. CHESICK. J. Chem. Phys. **45**, 3934 (1966).
10. (*a*) P. BORRELL and F. C. JAMES. Trans. Faraday Soc. **62**, 2452 (1966); (*b*) P. BORRELL and P. CASHMORE. Trans. Faraday Soc. **68**, 345 (1972).
11. (*a*) G. J. COLLIN and H. DESLAURIERS. Nouv. J. Chim. **5**, 447 (1981); (*b*) G. J. COLLIN and H. DESLAURIERS. Can. J. Chem. **61**, 1510 (1983).
12. (*a*) P. J. KROPP, E. J. REARDON, JR., Z. L. F. GAIBEL, K. F. WILLIARD, and J. H. HATTAWAY, JR. J. Am. Chem. Soc. **95**, 7058 (1973); (*b*) P. J. KROPP, H. G. FRAVEL, JR., and T. R.

FIELDS. J. Am. Chem. Soc. **98**, 840 (1976).
13. R. SRINIVASAN and K. H. BROWN. J. Am. Chem. Soc. **100**, 4602 (1978).
14. (*a*) Y. INOUE, T. MUKAI, and T. HAKUSHI. Chem. Lett. 1045 (1982); (*b*) Y. INOUE, T. MUKAI, and T. HAKUSHI. Chem. Lett. 1665 (1983).
15. G. J. COLLIN, H. DESLAURIERS, and A. WIĘCKOWSKI. J. Phys. Chem. **85**, 944 (1981).
16. G. R. DE MARÉ, G. J. COLLIN, H. DESLAURIERS, and J. GAWLOWSKI. J. Photochem. To be published.
17. P. J. KROPP and F. P. TISE. J. Am. Chem. Soc. **103**, 7293 (1981).
18. H. DESLAURIERS, G. J. COLLIN, and B. SIMARD. J. Photochem. **21**, 19 (1983).
19. H. DESLAURIERS and G. J. COLLIN. Can. J. Chem. **63**, 62 (1985).
20. M. B. ROBIN. *In* Higher excited states of polyatomic molecules. Vol. 2. Academic Press, New York. 1975. and references cited therein. pp. 2–50.
21. R. S. MULLIKEN. J. Phys. Chem. **66**, 2448 (1977); R. S. MULLIKEN. J. Chem. Phys. **71**, 556 (1979).
22. R. MCDIARMID. J. Phys. Chem. **84**, 64 (1980).
23. P. J. KROPP. ARO-report, ARO-12810-2C (1978).
24. H. DESLAURIERS and G. J. COLLIN. Can. J. Chem.
25. C. PETRONGOLO, R. J. BUENKER, and S. D. PEYERIMHOFF. J. Chem. Phys. **76**, 3655 (1982).
26. G. J. COLLIN et H. DESLAURIERS. J. Photochem. **27**, 387 (1984).
27. F. HIRAYAMA and S. LIPSKY. J. Chem. Phys. **62**, 576 (1975).
28. W. ROTHMAN, F. HIRAYAMA, and S. LIPSKY. J. Chem. Phys. **58**, 1300 (1973).
29. Y.-P. LEE and G. C. PIMENTEL. J. Chem. Phys. **75**, 4241 (1981).
30. P. BORRELL and P. CASHMORE. Ber. Bunsen. Phys. Chem. **72**, 182 (1968).
31. P. BORRELL and P. CASHMORE. Trans. Faraday Soc. **65**, 2412 (1969).
32. N. NAKASHIMA, N. SHIMO, N. IKEDA, and K. YOSHIHARA. J. Chem. Phys. **81**, 3738 (1984).
33. J. GAWLOWSKI and G. J. COLLIN. J. Photochem. **23**, 241 (1983).

Synthesis of 8-, 9-, 12-, and 13-mono-^{13}C-retinal

J. A. PARDOEN, P. P. J. MULDER, E. M. M. VAN DEN BERG, AND J. LUGTENBURG
Gorlaeus Laboratory, Department of Chemistry, Leiden University, 2300 RA Leiden, The Netherlands

Received July 24, 1984

This paper is dedicated to Professor Camille Sandorfy on the occasion of his 65th birthday

J. A. PARDOEN, P. P. J. MULDER, E. M. M. VAN DEN BERG, and J. LUGTENBURG. Can. J. Chem. **63**, 1431 (1985).

The 8-, 9-, 12-, and 13-mono-^{13}C-retinals were synthesized with >98% chemical purity and 93% ^{13}C incorporation from ^{13}C-labelled acetonitrile. Their ^{13}C$-$^{13}C and ^{13}C$-$^{1}H nmr coupling constants were determined.

J. A. PARDOEN, P. P. J. MULDER, E. M. M. VAN DEN BERG et J. LUGTENBURG. Can. J. Chem. **63**, 1431 (1985).

Les 8-, 9-, 12- et 13-mono-^{13}C rétinènes ont été synthétisés avec plus de 98% de pureté chimique et 93% d'incorporation de ^{13}C à partir d'acetonitrile marqué au ^{13}C. Leurs constants ^{13}C$-$^{13}C et ^{13}C$-$^{1}H de couplage de rmn ont été déterminées.

[Traduit par le journal]

Introduction

The retinylidene group occurs as the chromophoric part of the membrane proteins bacteriorhodopsin and rhodopsin, and is formed by reaction of all-*trans* or 11-*cis* retinal with a lysine ε-amino group of the peptide chain under formation of a protonated Schiff base bond as shown in Fig. 1 (1, 2). We have synthesized a number of ^{13}C-labelled retinals (3, 4) and prepared ^{13}C-labelled bacteriorhodopsins from these materials. Recently we obtained solid state cross polarization magic angle spinning ^{13}C nmr (CP$-$MAS ^{13}C nmr) spectra of bacteriorhodopsins with the ^{13}C-enriched chromophore (5, 6). These spectra gave the first *in situ* ^{13}C nmr information of the chromophore within a protein, establishing that in dark-adapted bacteriorhodopsin the chromophore occurs in a 40% all-*trans* protonated Schiff base and 60% 13-*cis*, 15-*cis* protonated Schiff base structure which are not interconverting on the ^{13}C nmr time scale. These results were strongly supported by resonance Raman (RR) (7, 8) and Fourier transform infrared difference (FTIR diff.) (9) vibrational studies of the ^{13}C-labelled bacteriorhodopsins and further detailed information concerning the chromophore structure was obtained. In order to extend these studies we needed bacteriorhodopsins with a ^{13}C-label at positions 9 and 13. These are quaternary positions with a substantial positive charge in a protonated Schiff base structure (10). ^{13}C nuclear magnetic resonance spectroscopy may give insight into how these positions of the chromophore interact with the protein part. Position 8 can give us information on how the 7,8 double bond interacts with the peptide, since this interaction is essential for the colour of light- and dark-adapted bacteriorhodopsin (11). In the rhodopsin bleaching sequence, isomerization takes place around the 11,12 double bond, and to investigate this isomerization process by CP$-$MAS ^{13}C nmr, RR and FTIR diff. studies we needed retinal with a ^{13}C-label at position 12.

In this paper we describe the synthetic schemes by which we prepared retinal ^{13}C-labelled at positions 8 and 9 and at positions 12 and 13 with a level of ^{13}C-enrichment of more than 90%.

Synthesis and spectroscopic characterization

For the preparation of 8-^{13}C and 9-^{13}C retinal, we used the reaction sequence as presented in Scheme 1. The starting aldehyde β-cyclocitral **3** necessary for this synthesis is obtained by cyclization of the *N*-phenylimine of citral **2** with 95% sulfuric acid at -20°C by the method of Gedye *et al.* (12). Addition at -60°C of ^{13}C lithioacetonitrile, obtained by the

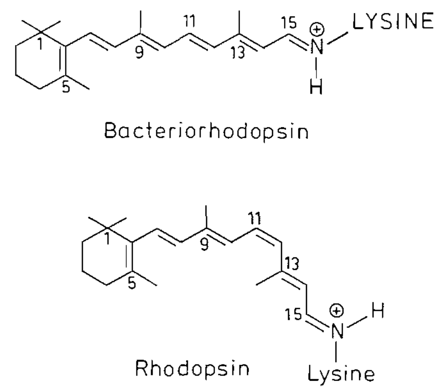

FIG. 1. Chromophoric groups of bacteriorhodopsin and rhodopsin.

reaction of 1 equiv. of n-butyllithium with ^{13}C acetonitrile, to β-cyclocitral **3** gives the alcohol-nitrile **4***a*,*b* in 95% yield. Starting with 2-^{13}C-acetonitrile introduces the label at position 8 (**4***a*) and with 1-^{13}C-acetonitrile at position 9 (**4***b*). For the dehydration we used a two-step method under basic conditions. Quantitative conversion of the alcohol **4***a*,*b* into its acetate with acetic anhydride (Ac_2O) and 4-dimethylaminopyridine (DMAP) is followed by deacetylation using diazabicyclononene (DBN) in toluene. Performing the deacetylation at room temperature $-$ which is completed in 3 days $-$ the nitrile **5***a*,*b* is obtained in 80% yield as a 7-*E*/*Z* (3:1) mixture (determination by ^{1}H nmr spectroscopy), which is converted to ^{13}C-labelled β-ionone **6***a*,*b* in three steps. The nitrile is reduced with diisobutylaluminium hydride (Dibal) to the aldehyde, after which conversion the complete double bond isomerization has taken place, leading to the 7-*E* aldehyde only. Reaction with excess methyl magnesium iodide (CH_3MgI) and oxidation of the α,β-unsaturated alcohol with active manganese dioxide (MnO_2) yields the ^{13}C-labelled β-ionone **6***a*,*b* in 60% overall yield from **5***a*,*b*. The β-ionone ^{13}C-labelled at position 8 or 9 is transformed to the C15-aldehyde **7***a*,*b* with high 9-*E* content, in 80% yield, in two steps by reaction with the anion of diisopropylphosphonoacetonitrile (13) followed by Dibal reduction of the nitrile. The C15-aldehyde **7***a*,*b* is converted into retinal **1***a*,*b* by Horner$-$Emmons coupling with the C5-synthon **8** (14), leading to retinonitrile, followed by Dibal reduction, providing 8-^{13}C-retinal **1***a* and 9-^{13}C-retinal **1***b* in 80% yield from the C15-aldehyde **7***a*,*b*.

For the synthesis of 12-^{13}C (**1***c*) and 13-^{13}C-retinal (**1***d*) an analogous reaction scheme is used, with the C15-aldehyde **7** as the starting aldehyde (Scheme 2). Addition of 9-*E* C15-

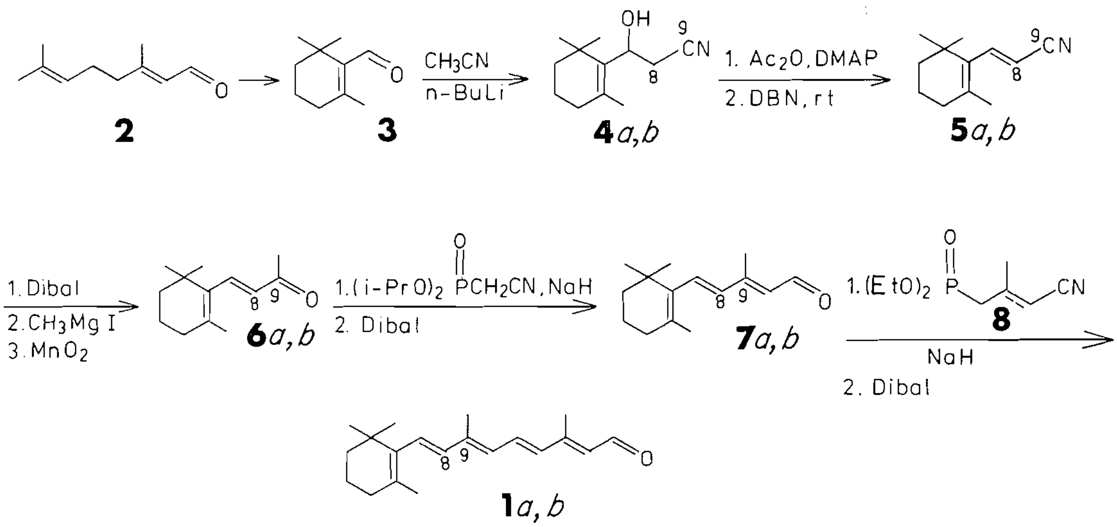

SCHEME. 1. Synthesis of (8-^{13}C) **1***a* and (9-^{13}C) retinal **1***b*; *a*, $^{13}CH_3CN$; *b*, $CH_3{}^{13}CN$.

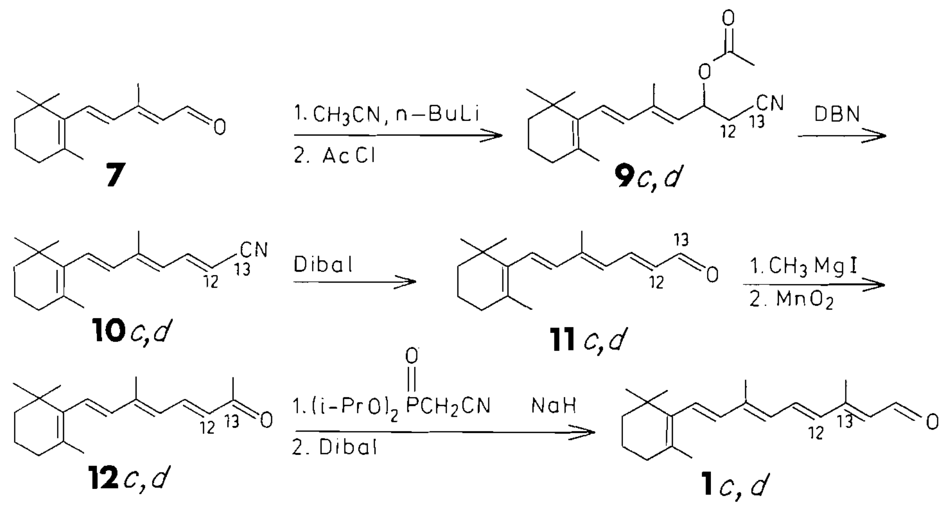

SCHEME 2. Synthesis of (12-^{13}C) **1***c* and (13-^{13}C) retinal **1***d*; *c*, $^{13}CH_3CN$; *d*, $CH_3{}^{13}CN$.

aldehyde **7** to lithioacetonitrile is followed by quenching the reaction mixture with acetyl chloride, leading to the secondary acetate **9***c*,*d* in a one-pot reaction. The addition of the C15-aldehyde **7** to lithioacetonitrile has to be performed at −90°C to prevent base-catalyzed side reactions of the aldehyde (15). The quenching is then performed at −60°C to give **9***c*,*d* in 85% yield after column chromatography. Base-induced acetic acid elimination with DBN in refluxing toluene gives the tetraenenitrile **10***c*,*d* in 88% yield. Dibal reduction leads to the C17-aldehyde **11***c*,*d* (95%) and reaction with excess methyl magnesium iodide (CH_3MgI) and subsequent MnO_2 oxidation gives the desired C18-ketone **12***c*,*d* in 60% yield. Horner–Emmons coupling of **12***c*,*d* with diisopropylphosphonoacetonitrile followed by Dibal reduction of the resulting retinonitrile affords the ^{13}C-labelled retinal in 90% yield, with 85% 13-*E* configuration. Starting with 2-^{13}C-acetonitrile leads to 12-^{13}C-retinal **1***c* and with 1-^{13}C-acetonitrile leads to 13-^{13}C-retinal **1***d* in 38% overall yield from the ^{13}C-labelled acetonitriles. From 0.25 g labelled acetonitrile, 0.64 g ^{13}C-labelled retinal is obtained in eight steps.

The all-*trans* isomers of the labelled retinals **1***a*–*d* can be separated by column chromatography. Irradiation of the all-*trans* isomer with visible light in acetonitrile gives an isomeric mixture which is separated by preparative hplc to yield pure 9-*cis*, 11-*cis*, 13-*cis*, and all-*trans* isomers. The uv–vis spectra of these retinals are identical with those of the unmodified retinal isomers. The mass spectra of the ^{13}C-labelled retinals **1***a*–*d* show the expected 92–93% ^{13}C-incorporation, based on the incorporation of the starting materials.

From the multiplet splittings in the 300-MHz ^{1}H nmr spectra of **1***a*–*d* the location of the ^{13}C is immediately evident. For 8-^{13}C (**1***a*) and 12-^{13}C-retinal (**1***c*) the signals of the H-atoms directly bonded to the labelled position show large splittings with the ^1J(C–H) values of 155.7 Hz for position 8 and 154.6 Hz for position 12. The intensity ratio is 93% ^{13}C-enriched to 7% non-enriched retinal, as has been found by mass spectrometery. For 9-^{13}C (**1***b*) and 13-^{13}C-retinal (**1***d*), containing a quaternary ^{13}C-atom, no one-bond C—H couplings occur. For all four ^{13}C-retinals two- and three-bond C—H couplings are determined from the spectra and these values are presented in Table 1.

The ^{1}H noise-decoupled ^{13}C nmr spectra of the ^{13}C-labelled retinals clearly show the position of ^{13}C-enrichment. They display one strong single line due to the labelled carbon atom at the chemical shift value known from the natural abundance ^{13}C nmr spectrum of unmodified retinal (16). The enriched

TABLE 1. ^{13}C-^{1}H nuclear magnetic resonance coupling constants in all-*trans* retinal as obtained from **1***a*–*d*. Signs not determined

$^{1}J(^{13}C-^{1}H)$		$^{2}J(^{13}C-^{1}H)$		$^{3}J(^{13}C-^{1}H)$	
C(8)–H(8)	155.7	C(8)–H(7)	N.d.*	C(8)–H(10)	8.5
C(12)–H(12)	154.6	C(9)–H(8)	3.2	C(8)–H(19)	3.8
		C(9)–H(10)	0	C(9)–H(7)	6
		C(9)–H(19)	6.2	C(9)–H(11)	3.3
		C(12)–H(11)	0	C(12)–H(10)	5.0
		C(13)–H(12)	2.7	C(12)–H(14)	8.0
		C(13)–H(14)	0	C(12)–H(20)	4.0
		C(13)–H(20)	6.1	C(13)–H(11)	5.7
				C(13)–H(15)	0

*Not determined due to complex signal because of long-range proton–proton couplings.

TABLE 2. $^{13}C-^{13}C$ nuclear magnetic resonance coupling constants in all-*trans* retinal as obtained from **1***a*–*d*. Signs not determined.

$^{1}J(^{13}C-^{13}C)$		$^{2}J(^{13}C-^{13}C)$		$^{3}J(^{13}C-^{13}C)$	
C(7)–C(8)	71.1	C(6)–C(8)	Obsc.*	C(1)–C(8)	0
C(8)–C(9)	56.0	C(7)–C(9)	0	C(5)–C(8)	0
C(9)–C(10)	70.4	C(8)–C(10)	2.4	C(6)–C(9)	5.4
C(9)–C(19)	43.3	C(8)–C(19)	1.9	C(8)–C(11)	7.1
C(11)–C(12)	69.8	C(9)–C(11)	0	C(9)–C(12)	9.4
C(12)–C(13)	54.2	C(10)–C(12)	0	C(10)–C(13)	7.5
C(13)–C(14)	66.7	C(11)–C(13)	0	C(12)–C(15)	7.2
C(13)–C(20)	40.4	C(12)–C(14)	0		
		C(12)–C(20)	1.9		
		C(13)–C(15)	3.0		

*Obscured by the enriched signal.

materials also contain the natural abundance (1.1%) of ^{13}C at each of the non-enriched positions. The singly labelled materials therefore contain two ^{13}C isotopes at the 1.0% level (0.93 × 1.1%), in which one position is enriched and the other is at the natural abundance level. From the ^{1}H noise-decoupled ^{13}C nmr spectra the $^{13}C-^{13}C$ coupling constants are obtained, as shown in Table 2.

Discussion

The four ^{13}C-labelled retinals with the required purity were prepared in high yield by the methods shown in Schemes 1 and 2. In both reaction schemes, by choosing the appropriately ^{13}C-labelled acetonitrile, we can label two different polyene carbon positions. This, together with the fact that in our syntheses we get a high percentage of the all-*trans* isomer, is an advantage over the published synthesis of 9-^{13}C-retinal (17). A further advantage of our methods is that in the first step a simple synthon is added to a higher molecular weight compound in high yield. As after coupling the product has in general only to undergo a number of high yield conversions, the ^{13}C-labelled material is put to an efficient use.

For the introduction of a sp^2-^{13}C label at all retinal chain positions 8 to 15, we used ^{13}C-labelled acetonitrile, whose anion, obtained with n-butyllithium, is coupled in an aldol-type reaction with ketones (3, 4) as well as aldehydes in good yield. To obtain good yields low temperatures have to be used for this addition reaction, especially in the case of the C15-aldehyde **7** (−90°C, Scheme 2). After introduction of the labelled synthon by the aldol-type reaction, dehydration is the first step to be performed. To prevent dehydration taking place in the direction of the trimethylcyclohexyl ring, with formation of retro compounds (18), we needed to use the basic reaction conditions described.

From these labelled retinals, nmr parameters such as $J(^{13}C$-$^{1}H)$ and $J(^{13}C-^{13}C)$ are easily obtained from the high-field nmr spectra. The $J(^{13}C-^{1}H)$ values found are in agreement with values known for sp^2 bonded hydrogens in a hydrocarbon chain (19) and those we found before for the other retinal chain positions (3, 4). The $^{1}J(^{13}C-^{13}C)$ values in particular show a good relation to the double or single bond character of the bond between two carbon atoms. The values found for the various types of bonds in this large polyene chain are around 70 Hz for carbons bonded via a double bond, around 55 Hz for a single bond in the chain, and 40 Hz for the sp^2-sp^3 single bonds to the 9- and 13-methyl group (Table 2). These values are in good agreement with values known for small systems like butadiene and 1-methyl-cyclohexene (20) and are a measure of the hybridization and bond lengths of the C—C bond in question.

From the ^{13}C-labelled retinals, specifically ^{13}C-labelled visual pigments and bacteriorhodopsin can be obtained. The isotopic substitution does not introduce ambiguities due to changes in the electronic structure of the chromophore or protein–chromophore interaction, nor are changes in quantum yields and photostationary state compositions to be expected. These highly ^{13}C-labelled retinals serve as the basic materials both for the solid state CP–MAS ^{13}C nmr studies of the chromophore of the retinylidene pigments as well as for the unambiguous assignments of the resonance Raman and FTIR difference vibrational spectra. Some of the spectroscopic results obtained from the isotopically labelled rhodopsins and bacteriorhodopsins have been published (8, 21, 22).

Experimental

All experiments were carried out in a dry nitrogen atmosphere, and the purified polyenes were handled in dim red light. Distilled dry solvents were used; pet. ether refers to low boiling petroleum ether 40–60°C. Unless otherwise stated, purification was performed by flash chromatography (23) (Merck silica gel 60, 230–400 mesh) using ether/pet. ether mixtures. The tlc analyses were performed on Schleicher & Schüll F 1500/LS 254 silica gel plates using ether/pet. ether mixtures. Evaporation of the solvents was carried out *in vacuo* (10 Torr; 1 Torr = 133.3 Pa).

The ^{1}H nmr spectra were recorded on a Brucker WM-300 or on a JEOL PS-100 spectrometer using tetramethylsilane (TMS; δ 0 ppm) as internal standard. The ^{13}C nmr spectra were recorded on a Brucker WM-300 spectrometer at 75.5 MHz or on a JEOL PFT system at 25 MHz using tetramethylsilane (TMS; δ 0 ppm) as internal standard. The mass spectra were recorded using an AEI MS 902 instrument. The ir spectra were obtained using a Pye–Unicam SP3-200 and the uv–vis spectra using a Cary 219 spectrophotometer. The hplc separations were performed using a Dupont 830 equipped with a Dupont spectrophotometer (360 nm) and a 25 cm × 22.5 mm Zorbax Sil column. Elution was effected using 10% ether in pentane at a flow rate of 20 mL/min. The glc analyses were performed using a Hewlett–Packard 5700 with a 50-m OV101 capillary column at 160°C. The experimental conditions and spectral assignments are given for the unlabelled compounds. For the labelled compounds only the changes relative to the unlabelled compounds are given. Spectra signal designations were based on the retinoid numbering system (24). (1-^{13}C) Acetonitrile and (2-^{13}C) acetonitrile (90% ^{13}C enrichment) were purchased from Merck Sharp and Dohme Isotopes.

*C12-Alcohol-nitrile **4**: 3-hydroxy-3(2,6,6-trimethyl-1-cyclohexenyl)-propanenitrile*

To a stirred solution of 6 mmol of acetonitrile (0.25 g) in 20 mL dry THF, 6 mmol of n-butyllithium (4.3 mL of a 1.4 *M* solution in hexane) were added dropwise at −60°C and warmed to −20°C. After 15 min, 6 mmol of β-cyclocitral **3** (12) (0.9 g) in 5 mL dry THF were added dropwise at −60°C. The mixture was warmed to 0°C in 1 h, poured into half-saturated NH_4Cl, and extracted with ether. The organic layer was washed with water followed by brine, and then dried ($MgSO_4$). Evaporation of the solvent afforded 1.1 g (95%) of pure C12-alcohol-nitrile **4**; ir (KBr): 3470 cm^{-1} (OH stretch), 2250 cm^{-1} (C≡N stretch); ^{1}H nmr (100 MHz, $CDCl_3/CCl_4$ 1:1), δ: 0.98−1.09 (2s, $(CH_3)_2C$), 1.79 (s, 5-CH_3), 2.44 (dd, *J* 17 Hz, *J* 4.5 Hz, H8), 2.87 (dd, *J* 17 Hz, *J* 10 Hz, H8), 3.04 (s, OH), 4.60 (dd, *J* 10 Hz, *J* 4.5 Hz, H7).

C12-Acetate-nitrile: 3-acetoxy-3-(2,6,6-trimethyl-1-cyclohexenyl)-propanenitrile

To a solution of 5.7 mmol of the C12-alcohol-nitrile (1.1 g) in 30 mL dry toluene and 10 mL pyridine were added 11.4 mmol of acetic anhydride (2 equiv., 1.2 g) and a catalytic amount of 4-(dimethylamino)pyridine and the mixture stirred at room temperature. After 20 h, when the reaction was complete according to glc, the solids were filtered and washed with ether. The organic filtrates were washed with water, followed by brine, and then dried ($MgSO_4$). Evaporation of the solvents afforded the acetate in quantitative yield; ir (KBr): 2250 cm^{-1} (C≡N stretch), 1745 cm^{-1} (C=O stretch); ^{1}H nmr (100 MHz, $CDCl_3/CCl_4$ 1:1), δ: 1.03−1.08 (2s, $(CH_3)_2C$), 1.79 (s, 5-CH_3), 2.04 (s, CO—CH_3), 2.61 (dd, *J* 17.3 Hz, *J* 5.2 Hz, H8), 2.94 (dd, *J* 17.3 Hz, *J* 10.0 Hz, H8), 5.75 (dd, *J* 10.0 Hz, *J* 5.2 Hz, H7).

β-Cyclocitrylideneacetonitrile 5: 3-(2,6,6-trimethyl-1-cyclohexenyl)-2-propenenitrile

Two equivalents of diazabicyclononene (DBN) (11 mmol, 1.4 g) were added to a solution of 5.5 mmol C12-acetate-nitrile (1.3 g) in toluene and the mixture stirred at room temperature for 72 h, when the reaction according to glc was complete, and then poured into water. The aqueous layer was washed with ether and the organic layers were washed with water until neutral, followed by brine, and then dried ($MgSO_4$) and concentrated. The residue was purified by chromatography using 5% ether/pet. ether to yield 0.8 g (80%) of a 3:1 *E*/*Z* mixture of **5**; ir (KBr): 2210 cm^{-1} (C≡N stretch); ^{1}H nmr (100 MHz, $CDCl_3/CCl_4$ 1:1), 7-*E*, δ: 1.08 (s, $(CH_3)_2C$), 1.75 (s, 5-CH_3), 5.27 (d, *J* 17.5 Hz, H8), 7.08 (d, *J* 17.5 Hz, H7); 7-*Z*, δ: 5.48 (d, *J* 12.0 Hz, H8), 6.72 (d, *J* 12.0 Hz, H7).

5*a*: ^{1}H nmr, 7-*E*, δ: 5.27 (dd, ^1J(C8−H8) 172 Hz, *J* 17.5 Hz, H8), 7.08 (dd, *J* 17.5 Hz, ^2J(C8−H7) 1.9 Hz, H7); 7-*Z*, δ: 5.48 (dd, ^1J(C8−H8) 172 Hz, *J* 12.0 Hz, H8), 6.72 (dd, *J* 12.0 Hz, ^2J(C8−H7) 1.6 Hz, H7).

5*b*: ^{1}H nmr, 7-*E*, δ: 5.27 (dd, *J* 17.5 Hz, ^2J(C9-H8) 3.0 Hz, H8), 7.08 (dd, *J* 17.5 Hz, ^3J(C9−H7) 8.0 Hz); 7-*Z*, δ: 5.48 (dd, *J* 12.0 Hz, ^2J(C9−H8) 3.0 Hz, H8), 6.72 (dd, *J* 12.0 Hz, ^3J(C9−H7) 12.0 Hz, H7).

β-Ionone 6

A 1 *M* solution (1.5 equiv.) of diisobutylaluminium hydride (Dibal) in hexane (6.9 mL) was added dropwise by syringe to a solution of 4.6 mmol **5** (0.8 g) in dry pet. ether at −60°C and the mixture warmed to −20°C in 1 h. A suspension of 1:5 water/silicagel in ether/pet. ether 1:1 was added and the mixture stirred at room temperature for 1 h. After drying with $MgSO_4$, the solids were filtered off and washed with dry ether. Evaporation of the solvents yielded the C12-aldehyde in 95% yield; ^{1}H nmr (100 MHz, $CDCl_3/CCl_4$ 1:1), δ: 6.14 (dd, *J* 16.0 Hz, *J* 8.0 Hz, H8), 7.27 (d, *J* 16.0 Hz, H7), 9.52 (d, *J* 8.0 Hz, H9). The C12-aldehyde (4.2 mmol, 0.75 g) in dry ether was added dropwise to a solution of 2 equiv. of methyl magnesium iodide in dry ether, freshly prepared from methyl iodide (1.2 g) and magnesium (0.2 g). The solution was refluxed for 1 h, poured into half-saturated NH_4Cl, and extracted with ether. The organic layer was washed with water followed by brine, and then dried ($MgSO_4$). Evaporation of the solvent afforded the β-ionol in 90% yield. The β-ionol dissolved in hexane was added to an 8-fold excess of active manganese dioxide in hexane and stirred at room temperature until no further β-ionol could be detected by tlc. The solids were filtered off through Celite, washed with ether, and the filtrates concentrated to afford an oil which was purified by preparative hplc to give the β-ionone in 70% yield; ^{1}H nmr (100 MHz, $CDCl_3/CCl_4$ 1:1), δ: 1.09 (s, $(CH_3)_2C$), 1.76 (s, 5-CH_3), 2.26 (s, 9-CH_3), 6.09 (d, *J* 17.0 Hz, H8), 7.28 (d, *J* 17.0 Hz, H7).

6*a*: ^{1}H nmr, δ: 6.09 (dd, ^1J(C8−H8) 156 Hz, *J* 17.0 Hz, H8).

6*b*: ^{1}H nmr, δ: 2.26 (d, ^2J(C9−(9-CH_3)) 6 Hz, 9-CH_3), 6.09 (dd, *J* 17.0 Hz, ^2J(C9−H8) 3.3 Hz, H8), 7.28 (dd, *J* 17.0 Hz, ^3J(C9−H7) 6.5 Hz, H7).

*β-Ionylidene acetaldehyde 7: (4*E*)-3-methyl-5-(2,6,6-trimethyl-1-cyclohexenyl)-2,4-pentadienal*

Sodium hydride (NaH, 120 mg, 2.7 mmol, 55% in mineral oil) was washed three times with dry pet. ether to remove the mineral oil, and suspended in 10 mL dry THF. A solution of 3.1 mmol of diisopropylphosphonoacetonitrile (0.65 g) in dry THF was added dropwise and stirred for 30 min at room temperature. After cooling to 0°C a solution of 2.1 mmol β-ionone (0.4 g) in dry THF was added dropwise and the mixture stirred and warmed to room temperature. After 2 h the solution was poured into half-saturated NH_4Cl and extracted with ether. The organic layers were washed with water followed by brine, and dried ($MgSO_4$). After filtration through a layer of silica gel the solvents were evaporated to afford β-ionylidene acetonitrile which was reduced with Dibal as described for the reduction of **5** to yield 0.36 g (80%) of β-ionylidene acetonitrile **7** as a 9-*E*/*Z* 85:15 mixture; ^{1}H nmr (100 MHz, $CDCl_3/CCl_4$ 1:1), 9-*E*, δ: 1.01 (s, $(CH_3)_2C$), 1.70 (s, 5-CH_3), 2.28 (s, 9-CH_3), 5.87 (d, *J* 8.0 Hz, H10), 6.15 (d, *J* 16.0 Hz, H8), 6.68 (d, *J* 6.0 Hz, H7), 10.19 (d, *J* 8.0 Hz, H11); 9-*Z*, δ: 1.03 (s, $(CH_3)_2$), 1.75 (s, 5-CH_3), 2.09 (s, 9-CH_3), 5.80 (d, *J* 8.0 Hz, H10), 6.56 (d, *J* 16.0 Hz, H7), 7.11 (d, *J* 16.0 Hz, H8), 10.23 (d, *J* 8.0 Hz, H11).

7*a*: ^{1}H nmr, 9-*E*, δ: 5.87 (dd, *J* 8.0 Hz, ^3J(C8−H10) 6.0 Hz, H10), 6.15 (dd, ^1J(C8−H8) 162 Hz, *J* 16.0 Hz, H8).

7*b*: ^{1}H nmr, 9-*E*, δ: 2.28 (d, ^2J(C9−(9-CH_3)) 6.0 Hz, 9-CH_3), 5.87 (dd, *J* 8.0 Hz, ^2J(C9−H10) 1.0 Hz, H10), 6.15 (dd, *J* 16.0 Hz, ^2J(C9−H8) 3.2 Hz, H8), 6.68 (dd, *J* 16.0 Hz, ^3J(C9−H7) 6.4 Hz, H7).

*Retinal 1*a,b

Sodium hydride (NaH, 80 mg, 1.8 mmol, 55% in mineral oil) was washed three times with dry pet. ether to remove the mineral oil, and suspended in 10 mL dry THF. A solution of 2.1 mmol diethyl-3-cyano-2-methylprop-2-enylphosphonate **8** (14) (0.45 g) in dry THF was added dropwise and stirred for 30 min at room temperature. After cooling to 0°C a solution of 1.4 mmol β-ionylidene acetaldehyde **7** (0.3 g) in dry THF was added dropwise and the mixture stirred and warmed to room temperature. After 2 h the solution was poured into half-saturated NH_4Cl and extracted with ether. The organic layers were washed with water followed by brine, dried ($MgSO_4/K_2CO_3$), and then concentrated. The residue was purified by chromatography using 5% ether/pet. ether to yield the pure retinonitrile, which was reduced with Dibal as described for the reduction of **5** to provide the crude retinal in 80% yield (0.3 g). The all-*trans* isomer **1** was separated by column chromatography (silica gel >230 mesh, 4% ether/pet. ether) and further purified by prep. hplc. The 300-MHz ^{1}H nmr spectra of **1***a*,*b* are identical to those described by Patel (25) except for the additional ^{13}C-^{1}H coupling constants as shown in Table 1. The 75.5-MHz ^{13}C nmr spectra of **1***a*,*b* display the enriched signals and are further identical to those described by Englert (16) except for the additional ^{13}C−^{13}C coupling constants as shown in Table 2; ms: **1***a* and **1***b* *m*/*z* 285 (M^+); level of ^{13}C enrichment calculated from the mass spectra: 93%.

*C17-Acetate-nitrile 9: (4*E*,6*E*)-3-acetoxy-5-methyl-7-(2,6,6-trimethyl-1-cyclohexenyl)-4,6-heptadienenitrile*

To a stirred solution of 6 mmol of acetonitrile (0.25 g) in 20 mL dry THF, 6 mmol of n-butyllithium (4.3 mL of a 1.4 *M* solution in hexane) were added dropwise at −60°C and stirred at −20°C for 15 min. The reaction mixture was cooled to −90°C and 6 mmol of 7*E*,9*E*-β-ionylidene acetaldehyde (1.3 g) in 10 mL dry THF were slowly added dropwise. The mixture was warmed to −60°C in 30 min and 12 mmol acetyl chloride (0.9 g) was added dropwise. After warming to 10°C, 20 mL of half-saturated $NaHCO_3$ solution was added and the mixture extracted with ether. The organic layer was washed with water followed by brine, and then dried ($MgSO_4$). Evaporation of the solvent afforded an oil which was purified by chromatography using 15% ether/pet. ether to yield 1.5 g (85%) of C17-acetate-nitrile **9**; ir (KBr): 2250 cm^{-1} (C≡N stretch), 1745 cm^{-1} (C=O stretch); ^1H nmr (100 MHz, $CDCl_3/CCl_4$ 1:1), δ: 0.99 (s, $(CH_3)_2C$), 1.65 (s, 5-CH_3), 1.90 (s, 9-CH_3), 2.06 (s, CO—CH_3), 2.64 (d, *J* 6.0 Hz, H12), 5.35 (d, *J* 10.0 Hz, H10), 5.80 (dt, *J* 10.0 Hz, *J* 6.0 Hz, H11), 5.94 (d, *J* 16.5 Hz, H8), 6.22 (d, *J* 16.5 Hz, H7); ^{13}C nmr (25 MHz, $CDCl_3$), δ: 13.1, 19.2, 21.0, 21.6, 24.0, 28.8, 32.9, 34.2, 39.5, 66.0, 116.2, 123.7, 129.5, 129.7, 135.6, 137.1, 140.1, 169.8.

9*c*: ^1H nmr, δ: 2.64 (dd, ^1J(C12−H12) 137.0, *J* 6.0 Hz, H12), 5.80 (dtd, *J* 10.0 Hz, *J* 6.0 Hz, ^2J(C12−H11) 1.9 Hz, H11); ^{13}C nmr, 92% enriched signal, δ: 24.0.

9*d*: ^1H nmr, δ: 2.64 (dd, ^2J(C13−H12) 9.0 Hz, *J* 6.0 Hz, H12); ^{13}C nmr, 92% enriched signal, δ: 116.2.

*C17-Nitrile **10**: 5-methyl-7-(2,6,6-trimethyl-1-cyclohexenyl)-2,4,6-heptatrienenitrile*

Two equivalents of diazabicyclononene (DBN) were added to a solution of the C17-acetate-nitrile **9** in toluene and the mixture was brought to a gentle reflux. After 90 min (no acetate left by tlc) the mixture was cooled, poured into water, and extracted with ether. The organic layers were washed with water until neutral, followed by brine, and then dried ($MgSO_4$) and concentrated. The residue was purified by chromatography using 5% ether/pet. ether. Yield: 88% of a 11-*E*/*Z* mixture which was used in the next step.

*β-C18-ketone **12**: 6-methyl-8-(2,6,6-trimethyl-1-cyclohexenyl)-3,5,7-octatriene2-one*

The β-C18-ketone **12** was prepared in two steps from the C17-nitrile **10** in 60% yield as described for the preparation of **6** from **5**; ^1H nmr (300 MHz, $CDCl_3$), δ: 1.04 (s, $(CH_3)_2C$), 1.72 (s, 5-CH_3), 2.07 (s, 3H, 9-CH_3), 2.30 (s, 13-CH_3), 6.16 (d, *J* 11.7 Hz, H10), 6.17 (d, *J* 15.4 Hz, H12), 6.17 (d, *J* 16.1 Hz, H8), 6.42 (d, *J* 16.1 Hz, H7), 7.55 (dd, *J* 15.4 Hz, *J* 11.7 Hz, H11).

*Retinal **1**c,d*

The retinal **1***c,d* was prepared in two steps from the β-C18-ketone **12***c,d* in 85% yield as described for the synthesis of **7** from **6**. The all-*trans* isomer **1** was separated by column chromatography (silicagel >230 mesh, 4% ether/pet. ether) and further purified by preparative hplc; ms: **1***c* and **1***b* *m*/*z* 285 (M^+); level of ^{13}C enrichment calculated from the mass spectra: 93%. For ^1H nmr, compare **1***a,b*.

Acknowledgements

This investigation was supported by the Netherlands Foundation for Chemical Research (SON) with financial aid from the Netherlands Organization for the Advancement of Pure Research (ZWO). The authors wish to thank Drs. C. Erkelens and Mr. F. Lefeber for recording the nmr spectra and Mr. J. J. van Houte for recording the mass spectra. The manuscript was reviewed by Miss S. Amadio.

1. R. R. BIRGE. Annu. Rev. Biophys. Bioeng. **10**, 315 (1981).
2. W. STOECKENIUS and R. A. BOGOLMOLNI. Annu. Rev. Biochem. **52**, 587 (1982).
3. J. A. PARDOEN, H. N. NEIJENESCH, P. P. J. MULDER, and J. LUGTENBURG. Recl. Trav. Chim. Pays-Bas, **102**, 341 (1983).
4. J. A. PARDOEN, C. WINKEL, P. P. J. MULDER, and J. LUGTENBURG. Recl. Trav. Chim. Pays-Bas, **103**, 135 (1984).
5. G. S. HARBISON, S. O. SMITH, J. A. PARDOEN, C. WINKEL, J. LUGTENBURG, J. HERZFELD, R. MATHIES, and R. G. GRIFFIN. Proc. Natl. Acad. Sci. USA, **81**, 1706 (1984).
6. G. S. HARBISON, S. O. SMITH, J. A. PARDOEN, P. P. J. MULDER, J. LUGTENBURG, J. HERZFELD, R. MATHIES, and R. G. GRIFFIN. Biochemistry, **23**, 2662 (1984).
7. S. O. SMITH, A. B. MYERS, J. A. PARDOEN, C. WINKEL, P. P. J. MULDER, J. LUGTENBURG, and R. MATHIES. Proc. Natl. Acad. Sci. USA, **81**, 2055 (1984).
8. S. O. SMITH, A. B. MYERS, M. BRAIMAN, J. A. PARDOEN, C. WINKEL, P. P. J. MULDER, J. LUGTENBURG, and R. MATHIES. Biophys. J. **45**, 209a (1984).
9. K. J. ROTHSCHILD, P. ROEPE, J. LUGTENBURG, and J. A. PARDOEN. Biochemistry. In press.
10. J. W. SHRIVER, E. W. ABRAHAMSON, and G. D. MATEESCU. J. Am. Chem. Soc. **98**, 2407 (1976).
11. M. MURADIN-SZWEYKOWSKA, J. A. PARDOEN, D. DOBBELSTEIN, L. J. P. VAN AMSTERDAM, and J. LUGTENBURG. Eur. J. Biochem. **140**, 173 (1984).
12. R. N. GEDYE, P. C. ARORA, and K. DECK. Can. J. Chem. **49**, 1764 (1971).
13. R. W. DUGGER and C. H. HEATHCOCK. Synth. Commun. **10**, 509 (1980).
14. K. FUJIWARA, H. TAKAHASHI, and M. OHTA. Bull. Chem. Soc. Jpn. **35**, 1743 (1962).
15. A. F. THOMAS and R. GUNTZ-DUBINI. Helv. Chim. Acta, **59**, 2261 (1976).
16. G. ENGLERT. Helv. Chim. Acta, **58**, 2367 (1975).
17. G. D. MATEESCU, W. G. COPAN, D. D. MUCCIO, D. V. WATERHOUS, and E. W. ABRAHAMSON. Synth. Appl. Isot. Labeled Compd. Proc. Int. Symp. 1982 (Publ. 1983).
18. K. EITER, E. TRUSCHEIT, and H. OEDIGER. Angew. Chem. **72**, 948 (1960).
19. J. B. STOTHERS. Carbon-13 NMR spectroscopy. Academic Press, New York. 1972. Chapt. 10.
20. V. WRAY. Prog. Nucl. Magn. Reson. Spectrosc. **13**, 177 (1979).
21. B. CURRY, I. PALINGS, A. BROEK, J. A. PARDOEN, P. P. J. MULDER, J. LUGTENBURG, and R. MATHIES. J. Phys. Chem. **88**, 688 (1984).
22. S. O. SMITH, A. B. MYERS, R. A. MATHIES, J. A. PARDOEN, C. WINKEL, E. M. M. VAN DEN BERG, and J. LUGTENBURG. Biophys. J. Submitted.
23. W. C. STILL, M. KAHN, and J. MITRA. J. Org. Chem. **43**, 2923 (1978).
24. IUPAC−IUB Joint Commision on Biochemical Nomenclature. Eur. J. Biochem. **129**, 1 (1982).
25. D. PATEL. Nature, **221**, 825 (1969).

Infrared spectra of vitreous lithium and cadmium mixed phosphates

C. GARRIGOU-LAGRANGE
Centre de recherches Paul Pascal, Domaine Universitaire, 33405 Talence Cedex, France

AND

M. OUCHETTO AND B. ELOUADI
Applied Solid State Chemistry Laboratory, Department of Chemistry, Faculty of Sciences, Avenue Ibn Batota, Rabat, Morocco

Received July 27, 1984

This paper is dedicated to Professor Camille Sandorfy on the occasion of his 65th birthday

C. GARRIGOU-LAGRANGE, M. OUCHETTO, and B. ELOUADI. Can. J. Chem. **63**, 1436 (1985).

Infrared reflection spectra of vitreous phosphates $(1 - x - \chi)Li_2O - xCdO-\chi P_2O_5$ are analysed in relation to the conformation when it is known. The evolution of the spectra with the different constituents is studied and the oxide forming-character of CdO is discussed.

C. GARRIGOU-LAGRANGE, M. OUCHETTO et B. ELOUADI. Can. J. Chem. **63**, 1436 (1985).

Les spectres de réflexion infrarouges de verres de phosphate de composition $(1 - x - \chi)Li_2O - xCdO-\chi\ P_2O_5$ ont été analysés et reliés à leur conformation lorsque celle-ci était connue. L'évolution des spectres avec les différents constituants a été étudiée et le caractère "oxyde formateur" du CdO discuté.

Introduction

The glass region of the binary systems $A_2O-P_2O_5$ and $BO-P_2O_5$ (A = monovalent cation; B = bivalent cation) has been widely studied, but no complete vibrational survey is actually available for the ternary diagram $Li_2O-CdO-P_2O_5$ (1, 2).

The purpose of this paper is to complete our earlier Raman studies, by giving the interpretation of the evolution of the infrared spectra inside the vitreous domain of this ternary system (3, 4).

Experimental

The glass samples were prepared by the same procedure as described in ref. 3. Figure 1 and Table 1 give the chemical compositions of the specimens studied. Any point of the glass-forming region in the ternary system can be characterized by the general formula:

$$(1 - x - \chi)Li_2O.xCdO.xP_2O_5 \qquad (0 < x < 1; 0 < \chi < 1)$$

where x = CdO molar fraction ratio; χ = P_2O_5 molar fraction ratio.

Infrared reflection spectra were recorded with the P.E.599 spectrometer, and Nicolet MX1 and 7000 and Polytec IR30 interferometers. The Kramers–Kronig method was used for spectra analysis using a Vax computer.

The results of the infrared spectroscopic measurements are presented in Figs. 2–10. The absorption band frequencies are given in Tables 2–10.

Results and discussion

The structural modifications are widely dependent upon the forming oxide (P_2O_5) molar ratio which is decreasing as the glass region extends (from P_2O_5) inside the ternary system $Li_2O-CdO-P_2O_5$ (3). Furthermore, the modifier character of the alkaline oxides is well established, but, for CdO, this is not definitely clear.

With a rough approximation, the spectrum of a compound can usually be considered as the sum of the absorption peaks arising from individual group vibrations. In order to clear up the role of each component in the phosphate glasses studied, the present infrared study has been carried out in the following order (Fig. 1).

1. Pure P_2O_5.
2. Metaphosphates region (χ = 0.5) situated along the line $Li_2O.P_2O_5$ N $CdO.P_2O_5$.

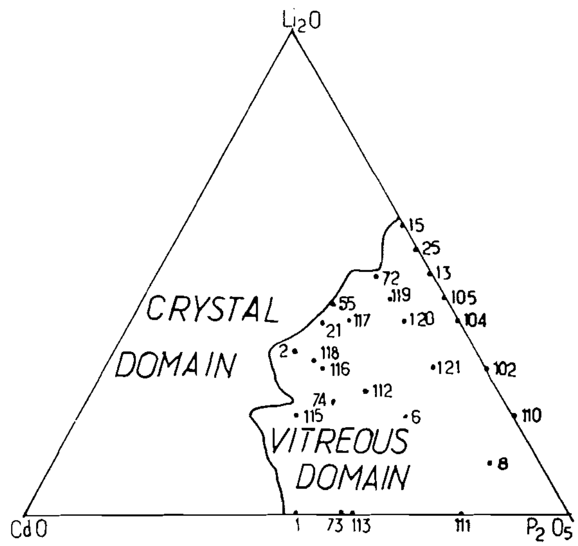

FIG. 1. Vitreous domain inside the system $Li_2O.CdO.P_2O_5$ at 1000°C (cf. Table 1 for the correspondence between the numbers of samples and their composition).

3. Ultraphosphates (lines χ = 0.6 and 0.8) extending on the surface of the triangle $P_2O_5-Li_2O.P_2O_5-CdO.P_2O_5$.
4. Oligophosphates (lines χ = 0.4 and 0.33) included inside the trapezium $Li_2O.P_2O_5-CdO.P_2O_5-2Li_2O.P_2O_5-CdO.P_2O_5$.
5. Lines with a constant ratio Li_2O/CdO and variable χ (lines $P_2O_5-Li_2O$; $CdO-P_2O_5$; $(1 - x)/2\ Li_2O.(1 - x)/2\ CdO-\chi P_2O_5$; $xLi_2O.xCdO.(1 - 2x)P_2O_5$.

This order of investigation has been adopted so that some simple and well-established structural types can be used to approach the more complicated ones. For example: (*i*) infrared spectra of pure P_2O_5 (built up as a tridimensional disordered network of PO_4 tetrahedra sharing three of their oxygens) and those of the metaphosphates (built up as infinite PO_4 tetrahedral chains) will allow the interpretation of the structural evolution inside the ultraphosphate domain. (*ii*) Infrared spectra of metaphosphates (infinite chain structure) and pyrophosphate (two linked tetrahedra) will permit the interpretation of the

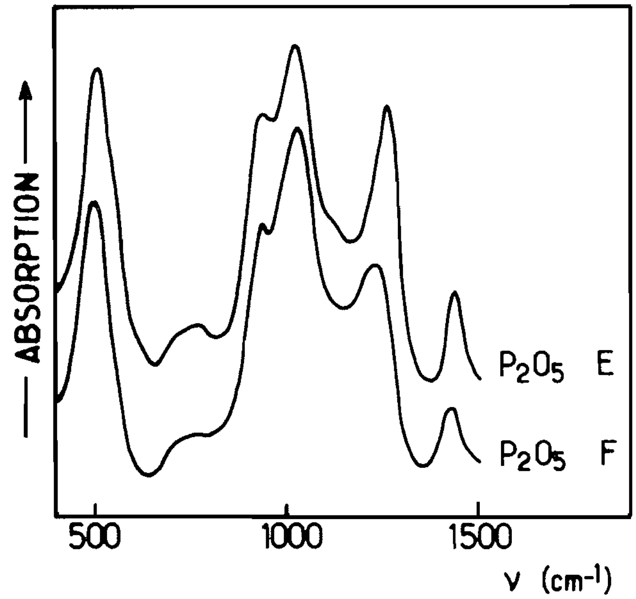

FIG. 2. Infrared spectra of vitreous P_2O_5 (sample F is more hydrated than sample E).

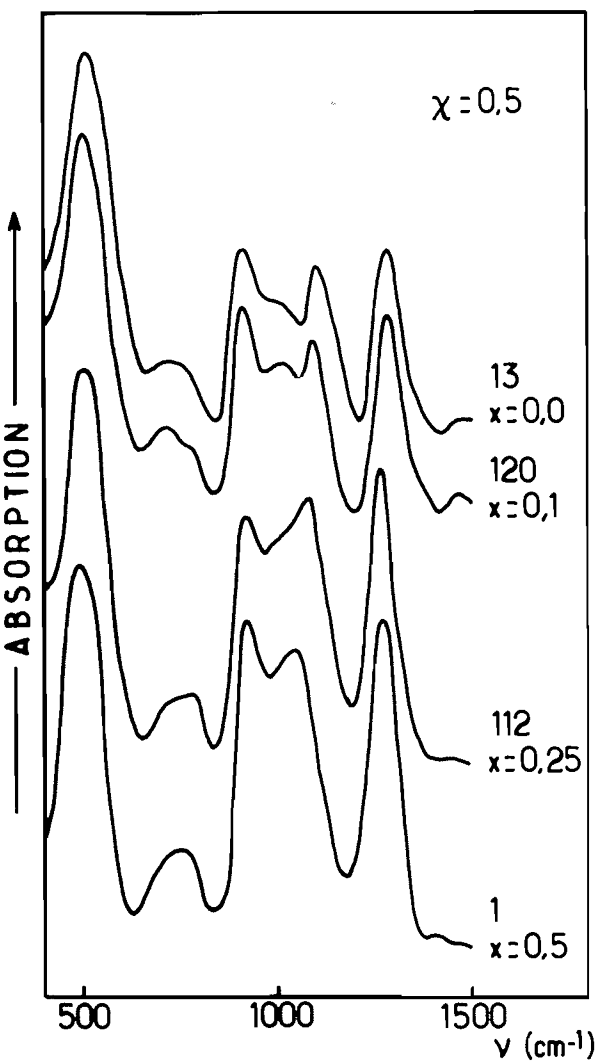

FIG. 3. Infrared spectra of metaphosphates $(0.5 - x)Li_2O - xCdO - 0.5P_2O_5$.

TABLE 1. Chemical composition of the samples studied (Fig. 1)

	Composition		
Order number	χ (P_2O_5)	x(CdO)	$(1-x-\chi)Li_2O$
1	0.50	0.50	0.00
2	0.33	0.33	0.33
6	0.60	0.20	0.20
8	0.80	0.10	0.10
13	0.50	0.00	0.50
15	0.40	0.00	0.60
21	0.35	0.25	0.40
25	0.45	0.00	0.55
55	0.35	0.215	0.435
72	0.405	0.105	0.49
73	0.58	0.42	0.00
74	0.45	0.32	0.23
102	0.70	0.00	0.30
103	0.65	0.00	0.35
104	0.60	0.00	0.40
105	0.55	0.00	0.45
110	0.80	0.00	0.20
111	0.80	0.20	0.00
112	0.50	0.25	0.25
113	0.60	0.40	0.00
115	0.40	0.40	0.20
116	0.40	0.30	0.30
117	0.40	0.20	0.40
118	0.37	0.315	0.315
119	0.45	0.10	0.45
120	0.50	0.10	0.40
121	0.60	0.10	0.30

TABLE 2. P_2O_5 attribution of Raman and infrared spectra

	P_2O_5 dry	P_2O_5 (E)
	Spectroscopy	
Attribution	Raman	Infrared
δ skeleton	190 w	
	493 w	
		516 S
ν_s POP	648 SP	
ν_s' POP		772 w
	790 sh	
	860 w	
ν_a POP	935 w	946 S
		1030*
Combination	1085 w	
δ OH	1147* w	
ν P=O*	1275 sh	1270 M
ν P=O	1363 SP	
Combination		1450 w

*See text.

oligophosphate spectra.

All these results will be used to follow the evolution of infrared spectra along the lines with variable χ.

1. *Pure P_2O_5*

The infrared spectra we recorded (Fig. 2) correspond to slightly hydrated samples because the recording was done in the presence of dried air. They show three wide bands: the one

TABLE 3. Metaphosphates (χ = 0.5). Attribution of Raman and infrared spectra

Sample no.:	13		120		112		1	
Composition:	$x = 0$		$x = 0.1$		$x = 0.25$		$x = 0.5$	
	Spectroscopy							
Attribution	Raman	Infrared	Raman	Infrared	Raman	Infrared	Raman	Infrared
	335		325		~350		~350	
δ skeleton		514 S		502 S		508 S		490 S
ν_s POP	703 SP		700 SP		700 SP		700 SP	
		718		736		742		746
			~800 sh		~810 sh		~790 sh	
ν_a POP	920	916 S		912 S		920 S		924 S
	1026	1016 sh		1010		~1000		
		1106 S		1100 S		1080 S		1046 S
ν_s PO_2	1179 SP		1176 SP		1177 SP		1170 SP	
ν_a PO_2	1255	1290	1255	1288	1260	1268	1260	1274
			1325 sh					

TABLE 4. Ultraphosphates (χ = 0.6). Attribution of Raman and infrared-spectra

Sample no.:	104		121		6		113	
Composition:	$x = 0$		$x = 0.1$		$x = 0.2$		$x = 0.4$	
	Spectroscopy							
Attribution	Raman	Infrared	Raman	Infrared	Raman	Infrared	Raman	Infrared
					235 sh		250 sh	
	300		300		310		323	
δ skeleton		472 S		484 S		482 S		488 S
								520 S
ν_s POP	672 SP		675 SP		675 SP		675 SP	
ν POPO		746		750		736		746
	790 sh		800 sh		800 sh		790 sh	
ν_a POP		934		944		920		934
		1024		1040		1040		1038
		1094						
ν_s PO_2	1175 SP		1179 SP		1172 SP		1172 SP	
ν_a PO_2	1312	1306	1315	1322	1290	1316	1285	1310

TABLE 5. Ultraphosphates (χ = 0.8). Attribution of Raman and infrared spectra

Sample no.:	110		8		111	
Composition:	$x = 0$		$x = 0.1$		$x = 0.2$	
	Spectroscopy					
Attribution	Raman	Infrared	Raman	Infrared	Raman	Infrared
	220		220		220	
	284		300		300	
δ skeleton		484 S		470 S		500 S
ν_s POP	670 SP		670 SP		670 SP	
		766		760		758
	790		790		780	
ν_a POP	950	956 S	950	940 S	950	952 S
		1050		1050		1032
	1087		1075		1070	
ν_s PO_2	1155 S		1155 S		1156 S	
ν P=O, ν_a PO_2	1337 S	1332 S	1342 S	1322 S	1322 S	1310 S

TABLE 6. Phosphates $\frac{1-\chi}{2}\cdot Li_2O - \frac{1-\chi}{2}\cdot CdO-\chi P_2O_5$. Attribution of Raman and infrared spectra

Sample no.:	2		118		116		112		6		8		P_2O_5	
Composition:	$\chi = 0.33$		$\chi = 0.37$		$\chi = 0.4$		$\chi = 0.5$		$\chi = 0.6$		$\chi = 0.8$		$\chi = 1$	
	Spectroscopy													
Attribution	Raman	Infrared	Raman	Infrared	Raman	Infrared	Raman	Infrared	Raman	Infrared	Raman	Infrared	Raman	Infrared
			345		352				235 sh		220		190	
		420					350		310		300			
			500											
δ skeleton	550	574 S	550	560 S	540	546		508		482 S		470 S	493	516 S
	605													
ν_s POP	752 SP		710 SP		705 SP		700 SP		675 SP		670 SP		648 SP	
		738	745 SP	736	750 sh	740		742		736		760		772
							810 sh	788	800 sh		790		790 sh	
													860	
ν_a POP	952	934	927 sh	930		920		920		920	950	940 S	935	946
	994		1000	990	990	984								
														1030
ν_s PO_3	1046 S	1038	1040 S	1036	1040	1034								
	1092							1080		1040	1075	1050	1085	
$\nu_a PO_3$		1144 S		1124 S	1110 sh	1120 M								
ν_s PO_2			1130 MP		1165 SP		1177 SP		1172 SP		1155 SP		1147	
	1200													
ν_a PO_2			1240	~1260	1260	~1270	1260	1268	1290	1316				
													1275	1270
νPO											1342 S	1322	1363 S	
										1462		1440		1450

TABLE 7. Oligophosphates (χ = 0.4). Attribution of Raman and infrared spectra

Sample no.:	15		72		117		116		115	
Composition:	x = 0		x = 0.1		x = 0.2		x = 0.3		x = 0.4	
	Spectroscopy									
Attribution	Raman	Infrared	Raman	Infrared	Raman	Infrared	Raman	Infrared	Raman	Infrared
	330		338		335		352		340	
δ skeleton	505	500 S	507	520 S	560	546 S	~540	546 S	530	530 S
	585									
ν_s POP	703 SP	706	705 SP		700 SP		705 SP		700 SP	
				732		732		740		~748
ν_a POP		916 S	910	918 S		922 S		922 S		924 M
									960	
	1010	990	1000	980	1000 sh	990	990	984		994
ν_s PO_3	1045		1038	1030	1040	1036	1040	1034	1020	
ν_a PO_3		1146 S		1124 S	1110 sh	1120 S	1110 sh	1120 S		1080 S
ν_s PO_2	1160 SP		1160 SP		1160 SP		1165 SP		1175 SP	
ν_a PO_2	1255	1260	1252	1252	1249	1244	1260	~1270	1242	1260 S

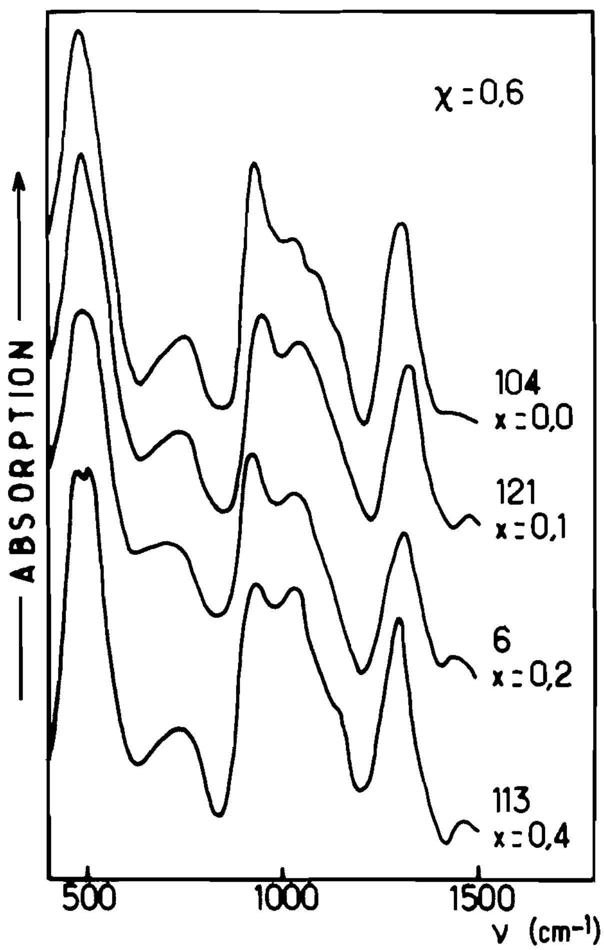

FIG. 4. Infrared spectra of ultraphosphates $(0.4 - x)Li_2O - xCdO-0.6P_2O_5$.

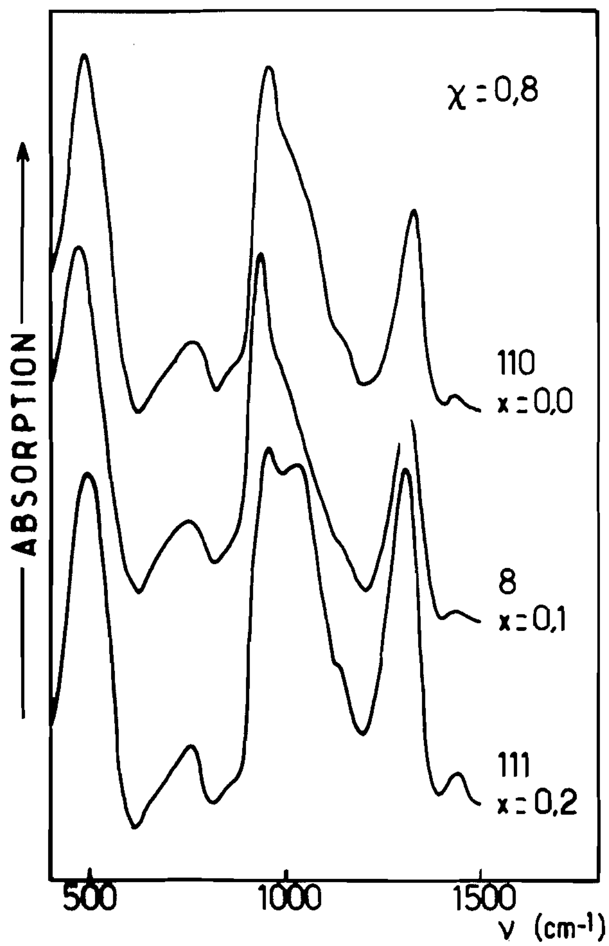

FIG. 5. Infrared spectra of ultraphosphates $(0.2 - x)Li_2O - xCdO-0.8P_2O_5$.

near 1270 cm^{-1} attributed to ν P=O is lower than the one observed by Raman spectroscopy (1) because of the association with water. Two absorptions near 946 and 780 cm^{-1} are due to the ν_a POP and ν_s' POP vibrations. The comparison between the spectra of the two samples noted E and F in Fig. 2, each having a different quantity of water, shows that the absorption at 1030 cm^{-1} is due to hydration.

2. *Metaphosphate glasses*

2.1. *Previous results*

Infrared spectra of metaphosphate glasses have been studied by several authors (1−13). It is also well established that metaphosphate glasses are composed of linear chains of polyphosphate anions with the cations situated between the chains. Shih and Su have discussed two models of the chain arrange-

TABLE 8. Binary phosphates $(1 - \chi)Li_2O - \chi P_2O_5$. Attribution of Raman and infrared spectra

Sample no.:	15		25		13		104		103		102		110		P_2O_5	
Composition:	$\chi = 0.4$		$\chi = 0.45$		$\chi = 0.5$		$\chi = 0.6$		$\chi = 0.65$		$\chi = 0.7$		$\chi = 0.8$		$\chi = 1$	
	Spectroscopy															
Attribution	Raman	Infrared	Raman	Infrared	Raman	Infrared	Raman	Infrared	Raman	Infrared	Raman	Infrared	Raman	Infrared	Raman	Infrared
											210		220		190	
	330		326		335		300		291		290		284			
δ skeleton	505	500 S		496 S		514 S		472 S		476 S		486 S		484 S	493	516 S
	585															
ν_s POP	703 SP	706	700 SP		703 SP		672 SP		668 SP		664 SP		670 SP		648 SP	
				728		718		746		746		740		766		772
			800 sh	~790			790 sh		795 sh		805		790		790 sh	
															860	
ν_a POP		916 S		916 M	920	916 M	945?	934 M	955 sh	956 M	950	948 S	950	956 S		944
			950													1030
				984												
	1010	990	1029		1026	1016 sh		1024		1050		1024		1050		
ν_s PO_3	1045												1087		1085	
ν_a PO_3		1146 S		1106 M												
						1106 M		1094							1147	
ν_s PO_2	1160 SP		1174 SP		1179 SP		1175 SP		1175 SP	1160	1170 SP	1154	1170 SP			
ν_a PO_2	1255	1260	1259	1266 M	1255	1290 M	1312	1306 S	1325	1340 S	1333	1326				
ν PO													1377 S	1332 S	1363 S	1270 S
										1476		1432				1450

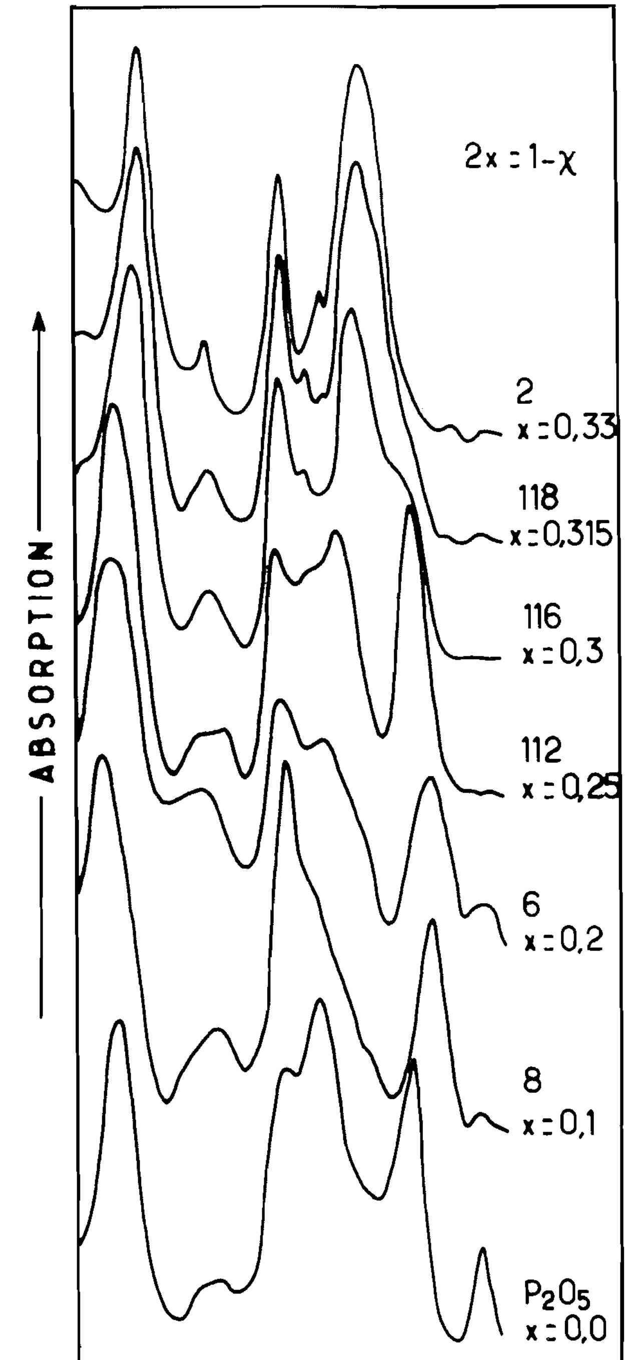

FIG. 6. Infrared spectra of some phosphates $x\text{Li}_2\text{O}-x\text{CdO}-(1-2x)\text{P}_2\text{O}_5$.

ment, viz. the straight chain and the zigzag chain models (2).

(a) *Straight chain model* (Fig. 11a)

According to this model, the PO_4 tetrahedra are disposed in such a way that all phosphorus should stand in a straight line (chain axis). The straight-chain symmetry is C_{2v}. Eight vibrational modes can thus be predicted, if a translation unit —$OP(O_2)O$— is admitted:

$$[1] \quad \Gamma_s = 3A_1 + A_2 + 2B_1 + 2B_2 = 8$$

According to the selection rules, the A_2 mode should be

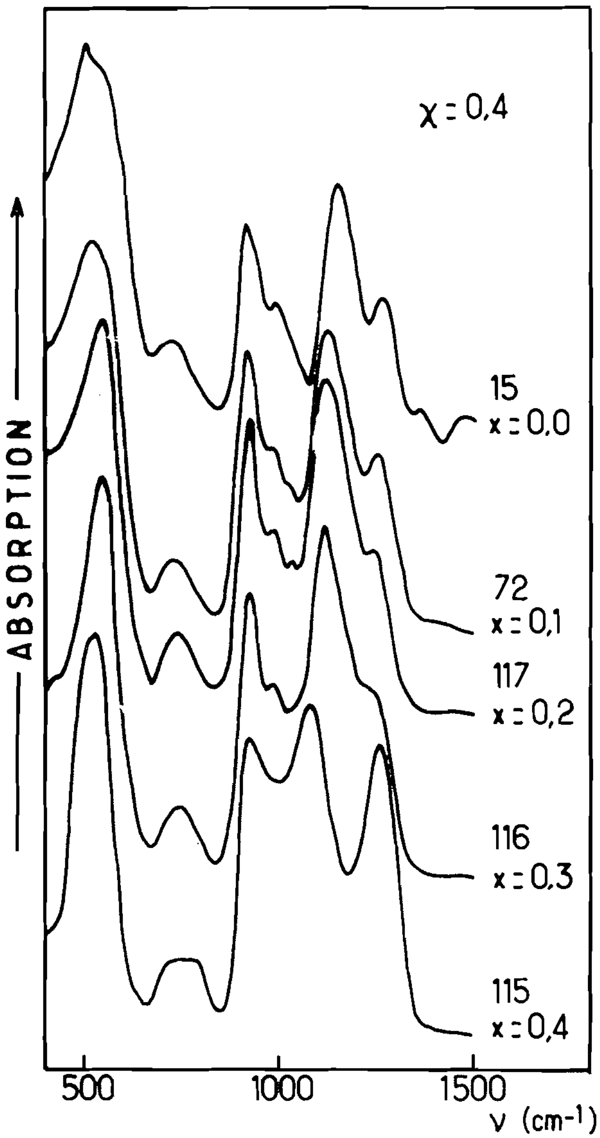

FIG. 7. Infrared spectra of oligophosphates $(0.6-x)\text{Li}_2\text{O}-x\text{CdO}-0.4\text{P}_2\text{O}_5$.

active in Raman and forbidden in infrared. The other modes are active in both spectroscopies.

Since more than seven absorption bands were observed in the recorded spectra, this model was rejected by Shih and Su.

(b) *Zigzag chain model* (Fig. 11b)

In this case, all the phosphorus and bridging oxygen atoms are localized in a plane passing through the chain axis; the identical PO_4 tetrahedra are aligned in a zigzag manner. The resulting point group symmetry is C_s. Twenty vibrational modes can be predicted; they all are active in both spectroscopies:

$$[2] \quad \Gamma_s = 12A' + 8A'' = 20$$

According to SHIH and SU (2), the calculated results (on the basis of the Wilson F−G matrix) seem to agree with the observed infrared spectra.

2.2. *Analysis of our results*

In the frequency domain explored (200−1600 cm^{-1}), we expect to observe the following vibrational modes: ν_s POP, ν_a POP, ν_s PO_2, ν_a PO_2, ν(OPOP), and the skeleton

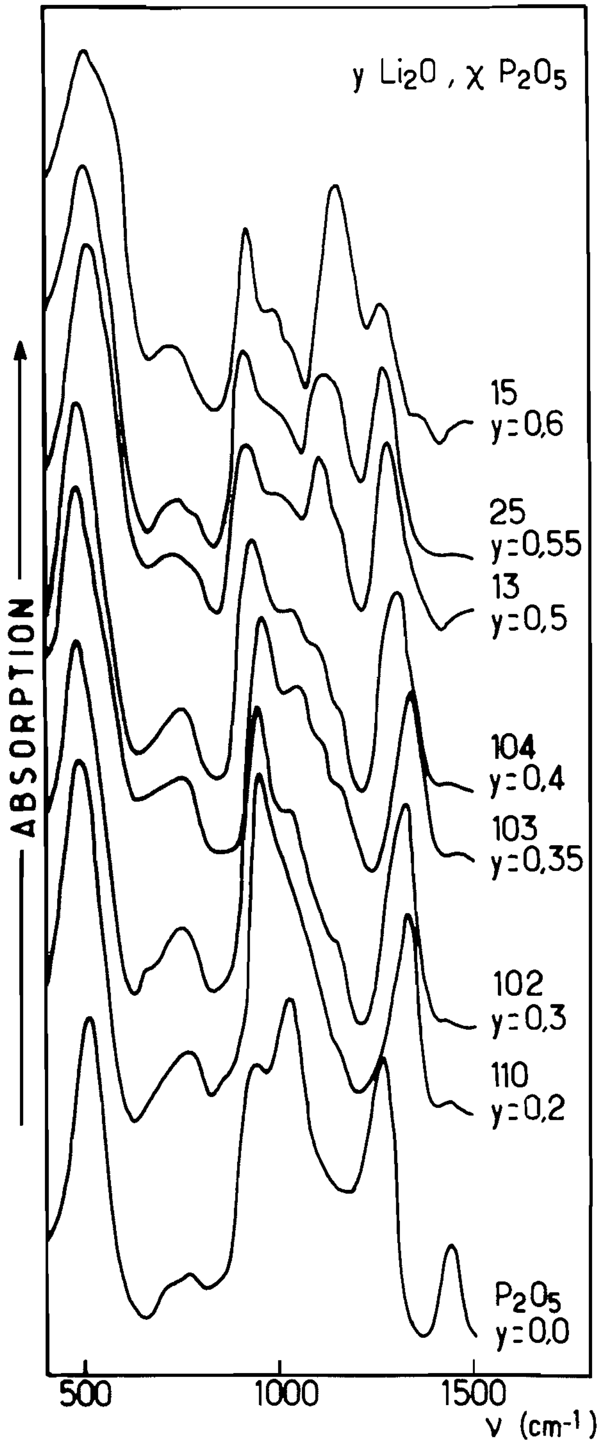

FIG. 8. Infrared spectra of binary phosphates $y\mathrm{Li_2O}-\chi\mathrm{P_2O_5}$.

deformations.

Let us remember that the recorded Raman spectra are relatively simple: two intense and polarized bands are observed at 700 and 1170 cm^{-1}; they were respectively attributed to ν_s POP and ν_s PO_2 (3) (Table 3). Furthermore, four strong absorption bands have been observed in the infrared spectra; the corresponding frequencies are 520, 920, 1100, and 1270 cm^{-1} (Fig. 3).

The bands at 500, 920, and 1270 cm^{-1} were respectively attributed to the skeleton deformation and the ν_a POP and ν_a PO_2 vibrations.

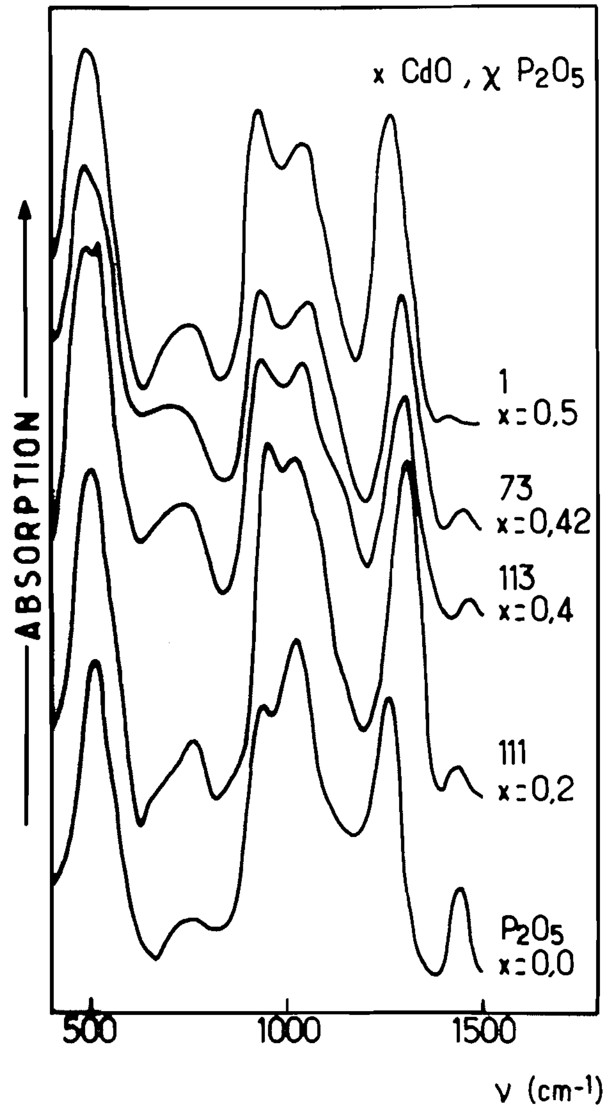

FIG. 9. Infrared spectra of binary phosphates $x\mathrm{CdO}-\chi\mathrm{P_2O_5}$.

The band near 1100 cm^{-1} is more difficult to explain. In Fig. 12, we compare the Raman spectra of some crystalline and vitreous compounds. It can be seen that the spectra of vitreous compounds can be described as the envelope of the crystalline ones. Thus we consider that, in the glasses containing lithium, this infrared absorption corresponds to a component of the ν_s PO_2, the displacement viz. the Raman frequency being due to a correlation effect.

This band is not seen in the pure cadmium metaphosphate, but a new strong band appears at 1046 cm^{-1}. We note that, in the Raman spectrum of the crystallized $CdPO_3$ (Fig. 12), the Davydov splitting is less pronounced than in $LiPO_3$. We think that the 1046 cm^{-1} absorption in the glass is due to the ν_a POP vibration, split because the Cd^{2+} ion introduces a dissymmetry in the skeleton.

The weak bands observed at about 750–800 cm^{-1} are probably due to a third normal mode called ν(OPOP).

All the observed infrared and Raman bands of metaposphate glasses inside the ternary system $Li_2O-CdO-P_2O_5$ have been assigned according to the hypothesis that metaphosphates adopt infinite zigzag chain models: $(PO_3)_\infty$. No vibration mode corresponding to ν P=O has been observed in this case.

TABLE 9. Binary phosphates $(1 - \chi)CdO - \lambda P_2O_5$. Attribution of Raman and infrared spectra

Sample no.:	1		73		113		111		P_2O_5	
Composition:	$\chi = 0.5$		$\chi = 0.58$		$\chi = 0.6$		$\chi = 0.8$		$\chi = 1$	
	Spectroscopy									
Attribution	Raman	Infrared	Raman	Infrared	Raman	Infrared	Raman	Infrared	Raman	Infrared
					250		220		190	
	~350				323		310			
					400 sh					
δ skeleton		490 S		482 S		488 S		500 S	493	516 S
	~545					520 S				
ν_s POP	700 SP		694 SP		675 SP		657 SP		648 SP	
		746		726		746		758		772
	790 sh		797 sh		790 sh		790		790 sh	
							880		860	
ν_a POP		924 S		932 S		934 S		952 S		944
		1046		1058 S		1038 S		1032 S		
										1030
							1090		1085	
									1147	
ν_s PO_2	1170 SP		1174 SP		1172 SP		1160 SP			
ν_a PO_2	1260	1274 S	1272	1302 S	1285	1310 S				
									1275 sh	
ν PO							1330 S	1310 S	1363 S	1270 S
						1462		1440		1450

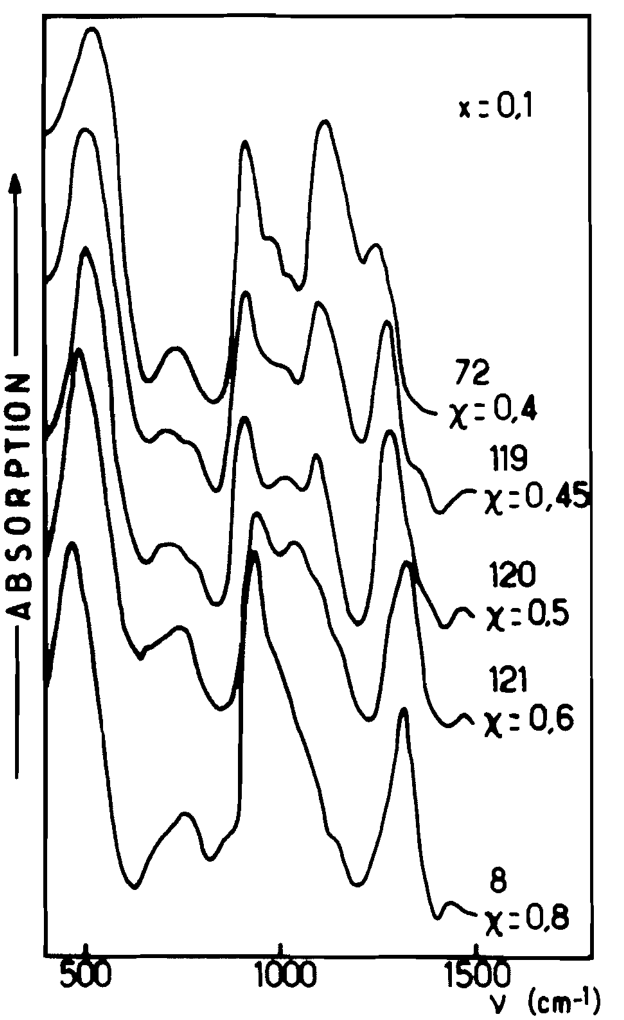

FIG. 10. Infrared spectra of some phosphates $(0.9 - x)Li_2O - 0.1CdO{-}\chi P_2O_5$.

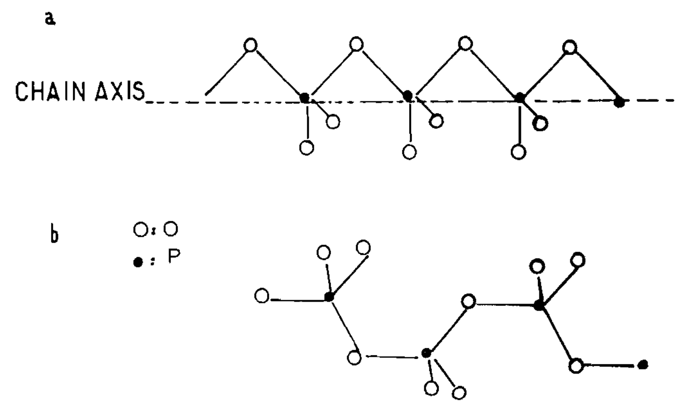

FIG. 11. Model of linear chains (a) and zigzag chains (b).

3. *Ultraphosphate domain*

In order to approach the glass structure in this domain, two lines have been studied: the one corresponds to $0.6P_2O_5(2Li_2O.3P_2O_5 - 2CdO.3P_2O_5)$ and the other one to $0.8P_2O_5(Li_2O.4P_2O_5 - CdO.4P_2O_5)$.

The bands observed in Raman and infrared are given in Tables 4 and 5. In all infrared spectra of these compounds (Figs. 4 and 5), a weak shoulder and a band have been respectively observed at 1100 and 1040 cm^{-1}. The latter becomes stronger as the amount of CdO increases. We adopt here the interpretation given formerly for metaphosphate glasses. The band at 1300 cm^{-1} was attributed to ν_a PO_2 superposed with ν P=O.

4. *Oligophosphate region*

The compounds studied are those situated on the line ($\chi = 0.4P_2O_5$) and the point corresponding to the composition $Li_2O.CdO.P_2O_5$ ($Li_2CdP_2O_7$).

The infrared spectrum of $Li_2CdP_2O_7$ is given in Fig. 6 (N2; $\chi = 0.33$). Twenty-one vibrations are expected for this compound: 3 vibrations due to POP bonds: ν_s POP, ν_a POP, POP;

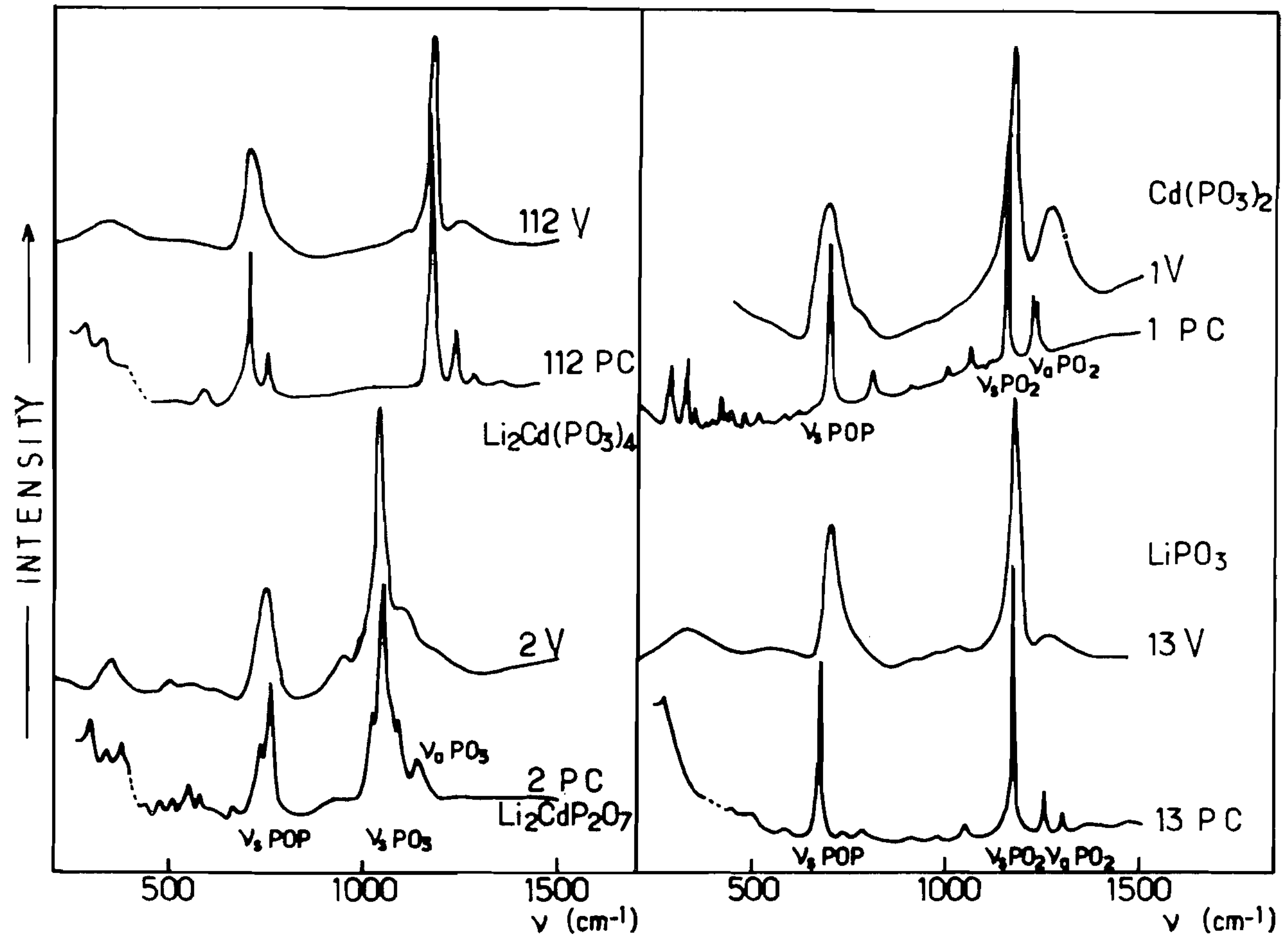

FIG. 12. Raman spectra of some crystallized (PC) and vitreous (V) compounds.

TABLE 10. Phosphates $(0.9 - \chi)Li_2O - 0.1CdO - \chi P_2O_5$. Attribution of Raman and infrared spectra

Sample no.: Composition:	72 $\chi = 0.4$		119 $\chi = 0.45$		120 $\chi = 0.5$		121 $\chi = 0.6$		8 $\chi = 0.8$	
	Spectroscopy									
Attribution	Raman	Infrared	Raman	Infrared	Raman	Infrared	Raman	Infrared	Raman	Infrared
									220	
	338		325		325		300		300	
δ skeleton	507	520 S		500 S		502 S		484 S		470 S
ν_s POP	705 SP		700 SP		700 SP		675 SP		670 SP	
		732		716		736		750		760
				776	800 sh		~800 sh		790	
ν_a POP	910	918 S		916 S		912 S		944 S	950	940 S
	1000	980		984		~1010		1040		1050
ν_s PO_3	1038	1030	1030	1036		1100 S			1075	
ν_a PO_3		1124 S		1112 S						
ν_s PO_2	1160 SP		1175 SP		1176 SP		1179 SP		1155 S	
ν_a PO_2	1252	1252	1250	1275 S	1255	1288	1315	1322		
ν PO									1342 S	1322 S
					1325 sh					
						1450				

and 18 vibrations due to the PO_3 groups.

The interpretations of the Raman and infrared spectra are given in Table 6, according to this assignment.

Fig. 7 shows infrared spectra of some glasses situated on the line $\chi = 0.4P_2O_5$. Their attributions (Table 7) are based on a comparison with metaphosphate and pyrophosphate spectra.

The ν PO_3 bands are observed in both infrared and Raman spectra. Raman ν_s PO_3 intensity decreases when xCdO increases, while ν_a PO_3 intensity (ir) remains strong for all the values of x, the corresponding frequency decreasing from 1144 to 1080 cm^{-1}. This can be explained if we admit that an oxygen atom of the PO_3 group is partially linked to the Cd^{2+} ion, due to the electronegativity of this ion (1.69), very close to that of the phosphorus (2.19) (ref. 14). Other techniques like nmr, epr, etc. should be useful in verifying this assumption.

5. *Vibrational spectra of glass regions existing along lines with a variable amount of P_2O_5*

5.1. *Binary systems $Li_2O-P_2O_5$ and $CdO-P_2O_5$*

Infrared spectra recorded along the lines $(1 - \chi)Li_2O - \chi P_2O_5$ and $(1 - \chi)CdO - \chi P_2O_5$ are shown in Figs. 8 and 9. Tables 8 and 9 give the interpretation of the infrared and Raman spectra.

The Raman spectra are very similar to those recorded by other authors for various binary systems $Na_2O-P_2O_5$, $CaO-P_2O_5$, etc. (15, 16). The infrared spectra of the Cd glasses contain a doublet (920−1050 cm^{-1}) which does not exist in Li glasses. It can be explained by a doubling of the vibration ν_a POP due to the dissymmetry of the bands introduced locally by Cd^{2+}.

5.2. *The medium line of the triangle $Li_2O-CdO-P_2O_5$ crossing the point P_2O_5*

The composition along this line can be written:

[3] $(1 - \chi)/2Li_2O.(1 - \chi)/2CdO.\chi P_2O_5$

or

[4] $xLi_2O.xCdO.(1 - 2x)P_2O_5$

Both Raman (3, 4) and infrared spectra (Fig. 6) recorded are similar to those of the previously discussed binary systems $Li_2O-P_2O_5$ and $CdO-P_2O_5$.

The frequency of ν_s POP decreases substantially when χ increases:

ν_s POP = 752 cm^{-1} for $\chi = 0.33$ (pyrophosphate P_2O_7) containing only one POP bond.

ν_s POP = 700 cm^{-1} for $\chi = 0.50$ (metaphosphates containing infinite chains and two POP bonds by P atom).

ν_s POP = 648 cm^{-1} for $\chi = 1$ (pure P_2O_5 containing a 3-dimensionally bounded PO_4 and three POP bonds on each P atom).

The value of this frequency may give an indication of the nature of the bonds between phosphorus and oxygen in the glass region.

Conclusion

Vibrational spectroscopy has allowed us to follow the evolution of the glass structure inside the ternary system $Li_2O-CdO-P_2O_5$. In glasses containing a high Li_2O ratio CdO, the oxide LiO_2 acts as a modifier, like all the alkali oxides. When the proportion of CdO increases in the vitreous domain, the dissymmetry introduced by this oxide in the PO_4 network could be consistent with an oxide-forming character. The ν_s POP frequency can given an indication of the dimensionality of the phosphate skeleton.

Acknowledgments

The authors are grateful to Drs. Davidovics and Pourcin, University of Provence, and to Professor Lascombe and Dr. Marchand, University of Bordeaux I, for having allowed them to record some spectra on their ir spectrometers and interferometers.

1. M. OUCHETTO. Diplôme d'Etudes Superieures de troisième cycle, Faculte des Sciences, Rabat. 1983.
2. C. K. SHIH and G. J. SU. 7th Int. Congress on Glass, Brussels. 1965.
3. B. ELOUADI, M. OUCHETTO, and C. GARRIGOU-LAGRANGE. Mater. Lett. **1**, 5 (1982).
4. C. GARRIGOU-LAGRANGE, M. OUCHETTO, and B. ELOUADI. *In* Raman spectroscopy, linear and non-linear. *Edited by* Lascombe and Huong. John Wiley and Sons, New York. 1982.
5. R. F. BARTHOLOMEW. J. Non-Cryst. Solids, **7**, 221 (1972).
6. D. E. C. CORBRIDGE and E. J. LOWE. J. Chem. Soc. 493 (1954); 4555 (1954).
7. W. BUES and H. W. GEHRKE. Z. Anorg. Allgem. Chem. **288**, 291 (1956).
8. V. A. KOLESOVA. Opt. Spektrosk. (USSR), **2**, 165 (1957).
9. D. J. WILLIAM, B. T. BRADBURG, and W. R. MADDOCKS. J. Soc. Glass Technol. **43**, 337T (1959).
10. K. P. MULLER. Glastechn. Ber. **42**, 83 (1969).
11. M. E. MILBERG and M. C. DALY. J. Chem. Phys. **39**, 2966 (1963).
12. W. A. WEYL and E. C. MARBOE. The constitution of glasses, a dynamic interpretation. Vol. II. Part I. Interscience, New York. 1964. p. 569.
13. D. J. WILLIAMS. J. Soc. Glass Technol. **43**, 352T (1959).
14. F. A. COTTON and G. WILKINSON. Advanced inorganic chemistry. 3rd ed. Interscience, New York. 1972. p. 115.
15. V. FAWCETT, D. A. LONG, and L. H. TAYLOR. Proc. 5th Int. Conf. on Raman spectroscopy, Freiburg. 1976. p. 112.
16. YA. BOBOVITCH. Opt. Spectrosk. **13**, 274 (1962).

Étude théorique des réactions d'abstraction d'hydrogène RH + X $\rightleftharpoons$ R + HX, avec R, X$\equiv$H, CH_3, NH_2, OH et F

GEORGES LEROY,[1] MICHEL SANA[2] ET ANNE TINANT
Université Catholique de Louvain, Laboratoire de Chimie Quantique, Place Louis Pasteur, 1, B-1348 Louvain-la-Neuve, Belgique

Reçu le 27 juillet 1984

Cet article est dédié au Professeur Camille Sandorfy à l'occasion de son 65ᵉ anniversaire

GEORGES LEROY, MICHEL SANA et ANNE TINANT. Can. J. Chem. **63**, 1447 (1985).

Nous avons étudié théoriquement les réactions d'abstraction d'hydrogène RH + X $\rightleftharpoons$ R + HX avec R, X$\equiv$H, CH_3, NH_2, OH et F. Tous les calculs *ab initio* ont été effectués par la méthode UHF avec la base 6-31G. Cependant, les grandeurs énergétiques ont été recalculées au niveau CI. Les constantes de vitesse et les paramètres d'Arrhénius ont été obtenus par la théorie de l'état de transition avec une correction d'effet tunnel basée sur le potentiel d'Eckart. L'accord peu satisfaisant entre résultats théoriques et expérimentaux nous a conduit à élaborer un procédé semi-empirique de calcul des barrières d'activation dans lequel les liaisons en évolution sont représentées par des courbes de Morse. Les résultats obtenus dans cette optique sont en bon accord avec l'expérience. Ils mettent en évidence le comportement "non-Arrhénius" de toutes les réactions étudiées et permettent de rationaliser un ensemble important de faits expérimentaux

GEORGES LEROY, MICHEL SANA, and ANNE TINANT. Can. J. Chem. **63**, 1447 (1985).

Hydrogen abstraction reactions RH + X $\rightleftharpoons$ R + HX with R, X$\equiv$H, CH_3, NH_2, OH, and F have been studied at the *ab initio* 6-31G − UHF level. However, energetic properties were computed at the CI level. Rate constants and Arrhenius parameters have been obtained using the transition state theory formalism with Eckart's tunneling correction. The discrepancy between theoretical and experimental results led us to elaborate a semi-empirical procedure to calculate activation barriers, in which the bonds R—H and X—H are represented by Morse curves. Thus, the agreement between theory and experiment is much better. Moreover, the results obtained by this procedure demonstrate the non-Arrhenius behavior of all the reactions under consideration and allow us to rationalize a large number of experimental facts.

Introduction

Dans le cadre de nos travaux théoriques sur les radicaux libres (1−13), nous avons étudié un ensemble de réactions d'abstraction d'hydrogène décrites par l'équation générale:

$$RH + X \rightleftharpoons R + HX$$

dans laquelle R et X désignent l'un des atomes ou groupes suivants: H, CH_3, NH_2, OH et F.

Tous les calculs théoriques ont été effectués suivant une démarche décrite par ailleurs (12) et dont nous rappelons schématiquement les points essentiels:

Utilisation de la méthode UHF de Pople−Nesbet (14) avec la base 6-31G de Hehre *et al.* (15) grâce au programme GAUSSIAN-70 (16) complété par le programme FORCE de Schlegel (17).

Recherche des points stationnaires (réactifs, points de transition et produits) grâce à la construction de formes analytiques locales de la surface de potentiel, dans l'espace des paramètres de structure comportant $3N - 6$ degrés de liberté (N: nombre d'atomes de la supermolécule).

Détermination des modes normaux de vibration et des fréquences correspondantes, dans l'approximation quadratique.

Calcul des corrections thermiques, des capacités calorifiques et des entropies grâce au formalisme de la thermodynamique statistique.

Calcul des énergies totales des points stationnaires en méthode d'interaction de configurations avec: (*i*) sélection itérative, par perturbation, des configurations importantes; (*ii*) traitement en orbitales naturelles; (*iii*) extrapolation pour un nombre infini de déterminants.

Calcul des constantes de vitesse selon le formalisme de la théorie de l'état de transition, avec correction d'effet tunnel:

$$[1] \quad k(T) = x(T)\cdot k^{\mathrm{TST}}(T)$$

$$[2] \quad k(T) = x(T)\cdot\frac{N(\chi T)^2}{h}\exp\left(-\frac{\Delta G_0^{\ddagger}}{RT}\right)$$

Résultats théoriques

I. *Structures géométriques*

Les paramètres géométriques de la supermolécule sont définis sur la fig. 1. Leurs valeurs à l'état de transition sont réunies dans le tableau 1. Les résultats relatifs aux réactifs et produits sont donnés par ailleurs (12).

On notera que, dans la plupart des structures de transition, les atomes A_1, H_2 et B_6 sont pratiquement sur une droite. Pour analyser les paramètres de structure r_1 et r_2, à l'état de transition, nous définissons les rapports suivants:

$$[3] \quad r_1(\text{rel.}) = \frac{r_1^{\ddagger}}{r_1(AH_{n+1})}$$

et

$$[4] \quad r_2(\text{rel.}) = \frac{r_2^{\ddagger}}{r_2(BH_{m+1})}$$

On constate aisément qu'ils varient relativement peu d'une réaction à l'autre comme l'illustrent également les résultats ci-dessous:

$$[5] \quad \left\langle\frac{r_1(\text{rel.}) + r_2(\text{rel.})}{2}\right\rangle = 1{,}25 \text{ (écart type: 0,03)}$$

et

$$[6] \quad \langle r_1(\text{rel.})/r_2(\text{rel.})\rangle = 0{,}99 \text{ (écart type: 0,04)}$$

Au total, dans les réactions d'abstraction d'hydrogène, la liai-

[1]Auteur à qui adresser la correspondance.
[2]Chercheur Qualifié du Fonds National de la Recherche Scientifique Belge.

TABLEAU 1. Géométrie optimisée des structures de transition, au niveau SCF en base 4-31G (distances en Å et angles en deg)

Système	r_1	r_2	d_3	d_4	d_5	d_7	d_8	d_9	α_3	α_4	α_5	α_7	α_8	α_9	β_4	β_5	β_8	β_9	δ	ϕ	Ω
HHH	0,936	0,936	—	—	—	—	—	—	—	—	—	—	—	—	—	—	—	—	180,0	—	—
$HHCH_3$	0,934	1,363	—	—	—	1,077	1,077	1,077	—	—	—	104,3	104,3	104,3	—	—	114,1	114,1	180,0	180,0	—
$HHNH_2$	0,943	1,246	—	—	—	1,009	1,009	—	—	—	—	104,2	104,2	—	—	—	115,8	—	163,3	57,9	—
HHOH	0,944	1,168	—	—	—	0,962	—	—	—	—	—	104,8	—	—	—	—	—	—	168,5	0,0	—
HHF	0,913	1,144	—	—	—	—	—	—	—	—	—	—	—	—	—	—	—	—	180,0	—	—
H_3CHCH_3	1,357	1,357	1,079	1,079	1,079	1,079	1,079	1,079	105,1	105,1	105,1	105,1	105,1	105,1	113,5	113,5	113,5	113,5	180,0	180,0	180,0
H_3CHNH_2	1,341	1,261	1,078	1,079	1,079	1,008	1,008	—	108,4	103,4	103,4	104,8	104,8	—	113,6	113,6	110,4	—	187,7	180,0	58,1
H_3CHOH	1,334	1,192	1,078	1,077	1,077	0,962	—	—	106,5	102,7	102,7	104,6	—	—	114,3	114,3	—	—	186,5	180,0	180,0
H_3CHF	1,282	1,179	1,077	1,077	1,077	—	—	—	104,1	104,1	104,1	—	—	—	114,3	114,3	—	—	180,0	180,0	—
H_2NHNH_2	1,253	1,253	1,009	1,009	—	1,009	1,009	—	102,4	102,4	—	102,4	102,4	—	113,4	—	113,4	—	180,0	—	180,0
H_2NHOH	1,213	1,211	1,008	1,008	—	0,962	—	—	104,0	104,0	—	101,2	—	—	110,0	—	—	—	169,3	166,9	112,1
HOHOH	1,175	1,175	0,962	—	—	0,962	—	—	103,2	—	—	103,2	—	—	—	—	—	—	180,0	—	180,0
HOHF	1,109	1,199	0,959	—	—	—	—	—	109,9	—	—	—	—	—	—	—	—	—	144,9	0,0	—
FHF	1,126	1,126	—	—	—	—	—	—	—	—	—	—	—	—	—	—	—	—	180,0	—	—

son qui se rompt subit un allongement d'environ 25%, à l'état de transition, par rapport à sa valeur initiale. De même, la liaison en formation est plus longue d'environ 25% dans le complexe activé que dans la molécule-produit. Il est intéressant de noter que, dans les réactions en couches fermées que nous avons étudiées précédemment (18−34), l'allongement des liaisons à l'état de transition est généralement de l'ordre de 50%.

II. *Surfaces de potentiel locales*

Au voisinage de chaque point stationnaire, nous avons construit une forme analytique locale de la surface de potentiel. Il s'agit d'un développement polynomial d'ordre deux, paramétrisé par régression linéaire sur les gradients de potentiel calculés pour $2k + 1$ ($k = 3N - 6$) structures moléculaires judicieusement choisies (35). Ceci nous a permis d'effectuer l'analyse vibrationnelle de Wilson et de calculer les modes normaux de vibration dans l'approximation harmonique en négligeant le couplage de Coriolis. Comme nous l'avons montré par ailleurs (12), l'approximation quadratique est tout à fait satisfaisante dans le cas des composés polyatomiques. Les fréquences obtenues pour les points de transition sont réunies dans le tableau 2. Ces résultats permettront le calcul des corrections thermiques et des entropies grâce aux équations de la thermodynamique statistique.

III. *Grandeurs énergétiques*

Les énergies totales des points stationnaires ont été calculées en méthode d'interaction de configurations en utilisant les géométries optimisées au niveau SCF.

Dans le tableau 3, différentes énergies théoriques des structures d'équilibre sont comparées aux valeurs expérimentales correspondantes. Nous y donnons également les énergies UHF et CI des structures de transition. Ces données permettent d'évaluer les effets thermiques à 0 K et les barrières d'activation des différentes réactions considérées. Nous les donnons dans le tableau 4 avec quelques résultats théoriques plus précis obtenus par d'autres auteurs.

Les valeurs de ΔE_0^0 (CI extr.) sont souvent très sous-estimées. Ceci révèle l'existence d'erreurs plus ou moins importantes au niveau des barrières d'activation des réactions correspondantes. La comparaison de celles-ci à des données expérimentales nécessite l'introduction d'un modèle tel que celui de l'état de transition, avec ou sans effet tunnel. Cependant, en comparant certaines d'entre elles à des résultats théoriques plus précis, on s'aperçoit qu'elles peuvent être assez fortement surestimées.

IV. *Constantes de vitesse et énergies d'activation*

En vue de tester la fiabilité de nos résultats théoriques, nous avons calculé les constantes de vitesse et les énergies d'activation des réactions considérées en utilisant la théorie de l'état de transition avec correction d'effet tunnel. Rappelons qu'en l'absence de celle-ci, la constante de vitesse d'un processus bimoléculaire s'écrit, dans le cadre de la théorie de l'état de transition:

$$[7] \qquad k(T) = \frac{N(\chi T)^2}{h} \exp\left(-\frac{\Delta G_0^{\ddagger}}{RT}\right)$$

où:

$$[8] \qquad \Delta G_0^{\ddagger} = \Delta H_0^{\ddagger} - T\Delta S_0^{\ddagger}$$

$\Delta H_0^{\ddagger}$ est l'enthalpie d'activation à la température T.

La dépendance thermique de la constante de vitesse s'exprime par la relation:

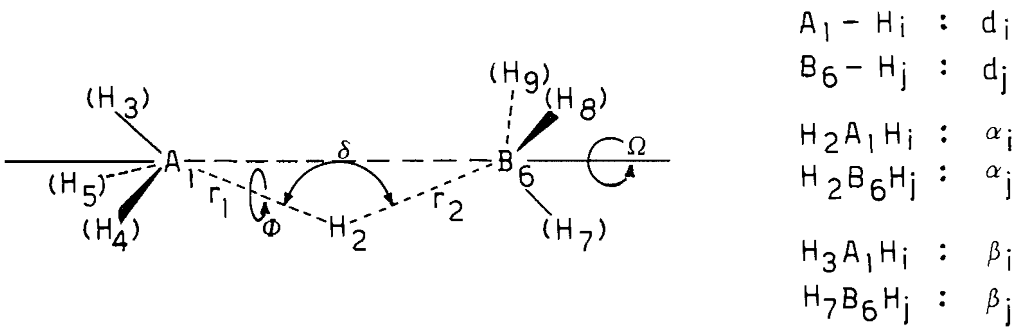

FIG. 1. Paramètres géométriques de la supermolécule.

TABLEAU 2. Fréquences des structures de transition (cm^{-1})

HHH	2014,5	H_3CHCH_3	3382,2	H_3CHOH	3945,0	H_2NHOH	3903,1
	1121,6		3382,2		3375,0		3775,6
	1121,6		3380,8		3369,0		3650,8
	i 2469,0		3380,8		3220,0		1710,7
$HHCH_3$	3383,5		3246,3		1631,0		1501,4
	3383,5		3243,7		1597,0		1462,6
	3238,7		1603,7		1542,0		1017,0
	1709,6		1603,7		1468,0		614,1
	1579,0		1584,5		1281,0		511,7
	1579,0		1584,5		922,0		454,3
	1330,7		1501,2		603,0		234,5
	1330,7		1501,2		508,0		i 5353,9
	1247,6		1330,1		367,0	HOHOH	3912,1
	630,6		1277,6		i 3172,0		3909,7
	630,6		784,6	H_3CHF	3394,4		1625,9
	i 1922,0		784,6		3394,4		1095,0
$HHNH_2$	2357,0		489,4		3247,2		705,5
	3623,7		373,8		1571,7		576,2
	1692,0		373,8		1571,7		411,3
	1588,9		37,8[a]		1360,2		i 4757,2
	1502,8		i 2457,5		1221,6	HOHF	3949,1
	1173,8	H_3CHNH_2	3668,0		1221,3		1676,2
	744,5		3386,0		514,4		906,1
	i 2851,8		3381,0		351,2		448,9
HHOH	3932,9		3245,0		351,2		392,2
	1574,1		1758,0		i 2893,0		i 4462,2
	1448,7		1739,0	H_2NHNH_2	3823,7	FHF	2014,5
	705,8		1682,0		3778,9		1121,6
	354,5		1655,0		3701,9		1121,6
	i 2131,9		1574,0		3678,1		i 2469,0
HHF	1570,8		1475,0		1773,2		
	777,8		1060,0		1671,6		
	777,8		981,0		1627,4		
	i 3222,7		540,0		1330,0		
			440,0		1055,1		
			389,0		815,9		
			i 2886,5		593,3		
					558,4		
					360,1		
					57,4[a]		
					i 1709,5		

[a] Rotateur libre.

$$[9] \quad RT^2 \left(\frac{d\ln k}{dT}\right)_P = \Delta H_0^{\ddagger} + 2\,RT$$

Cette expression s'identifie à l'énergie d'activation classique d'Arrhénius:

$$[10] \quad E_a = \Delta H_0^{\ddagger} + 2\,RT$$

Pour tenir compte de l'effet tunnel, on multiplie la constante de vitesse [7] par un terme correctif supérieur à un, $x(T)$, qui mesure la perméabilité de la surface aux trajectoires réactives. On écrit donc:

$$[11] \quad k^*(T) = x(T)\,k(T)$$

où:

$$[12] \quad x(T) = \int_a^{\infty} W(t)\,\exp(-t)\mathrm{d}t$$

TABLEAU 3. Energies totales des points stationnaires (ua)

	E(UHF) (36)	E(HF lim.) (37)	E(CI)	E(CI extr.)	E(exp.) (37)
H_2	−1,12683	−1,1336	−1,15152	−1,15152	−1,1744
H	−0,49823	−0,500	—	—	−0,500
CH_4	−40,18055	−40,219	−40,29069	−40,29260	−40,526
CH_3	−39,54666	−39,584	−39,63790	−39,63947	−39,846
NH_3	−56,16552	−56,226	−56,28537	−56,28750	−56,588
NH_2	−55,53136	−55,591	−55,61463	−55,63231	−55,911
H_2O	−75,98536	−76,068	−76,11729	−76,11736	−76,483
OH	−75,36318	−75,426	−75,46154	−75,46154	−75,783
HF	−99,98343	−100,072	−100,11222	−100,11222	−100,533
F	−99,36086	−99,415	−99,44823	−99,44823	−99,809
HHH	−1,59649		−1,61022	−1,61022	
$HHCH_3$	−40,63998		−40,75229	−40,76502	
$HHNH_2$	−56,62058		−56,75191	−56,75566	
HHOH	−76,44587		−76,58505	−76,58843	
HHF	−100,43859		−100,57571	−100,57797	
H_3CHCH_3	−79,67990		−79,80034	−79,90067	
H_3CHNH_2	−95,66352		−95,82929	−95,89932	
H_3CHOH	−115,49267		−115,67862	−115,73600	
H_3CHF	−139,49924		−139,69512	−139,72906	
H_2NHNH_2	−111,64641		−111,82615	−111,83711	
H_2NHOH	−131,47677		−131,69193	−131,70488	
HOHOH	−151,29995		−151,49824	−151,52008	
HOHF	175,29985		−175,51794	−175,53196	
FHF	−199,28487		−199,51184	−199,51778	

TABLEAU 4. Chaleurs de réaction et barrières d'activation (0 K, kcal/mol)

Réaction	ΔE_0^0 (CI extr.)	ΔE_0^0 (exp.)	$\Delta E^{\neq}$ (CI extr.)	$\Delta E^{\neq}$ (autres auteurs)
H_2 + H	0,00	0,00	24,80	10,1 (38)
				13,2 (39)
H_2 + CH_3	0,10	−3,51	16,29	9,9 (39)
				16,1 (40)
H_2 + NH_2	−1,19	−1,63	17,67	11,2 (39)
H_2 + OH	−1,58	−16,06	15,45	6,2 (41)
H_2 + F	−6,71	−31,12	13,66	1,7 (42)
CH_4 + H	−0,10	3,51	16,19	—
CH_4 + CH_3	0,00	0,00	19,69	—
CH_4 + NH_2	−1,29	1,88	16,05	—
CH_4 + OH	−1,68	−12,55	11,38	—
CH_4 + F	−6,81	−27,60	7,38	—
NH_3 + H	1,19	1,63	18,86	—
NH_3 + CH_3	1,29	−1,88	17,35	—
NH_3 + NH_2	0,00	0,00	51,88	—
NH_3 + OH	−0,39	−14,43	27,70	—
NH_3 + F	−5,52	−29,48	—	—
H_2O + H	1,58	16,06	17,04	—
H_2O + CH_3	1,68	12,55	13,07	—
H_2O + NH_2	0,39	14,43	28,10	—
H_2O + OH	0,00	0,00	36,90	—
H_2O + F	−5,12	−15,06	21,10	—
HF + H	6,71	31,12	20,38	—
HF + CH_3	6,81	27,60	14,20	—
HF + NH_2	5,52	29,48	—	—
HF + OH	5,12	15,06	26,22	—
HF + F	0,00	0,00	26,77	—

avec:

$$[13] \quad a = \frac{Q - P}{\chi T}$$

Les termes Q et P désignent respectivement l'effet thermique (à 0 K) et la barrière d'activation de la réaction considérée dans le sens endothermique ($Q \geq 0$; $P > 0$). La fonction $W(t)$ dépend de la température et de la forme de la surface de potentiel au voisinage du point selle. On adopte, en général, un potentiel à une dimension pour exprimer $W(t)$. Dans ce travail, nous avons choisi le potentiel d'Eckart (43) plus réaliste que le potentiel parabolique de Christov (44). Cependant, sa forme

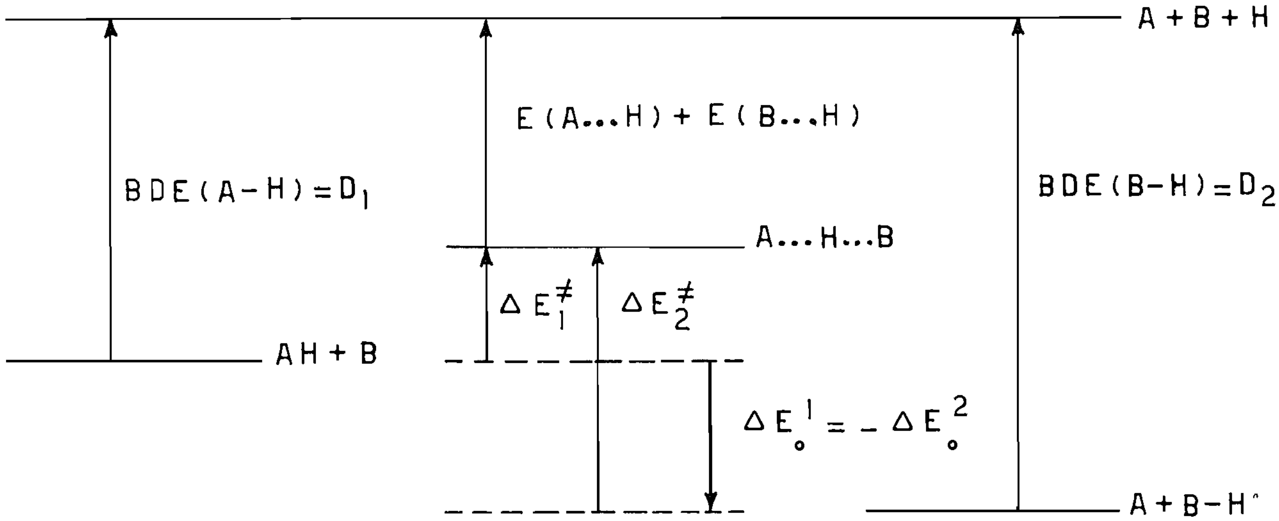

FIG. 2. Diagramme énergétique des réactions d'abstraction d'hydrogène.

TABLEAU 5. Comparaison des énergies d'activation théoriques et expérimentales (kcal/mol)

Réaction	T(K)	E_a (exp.)	E_a (théo.)
H_2 + H	873	6,86 (46)	23,37
H_2 + CH_3	897	14,0 (47)	17,77
H_2 + OH	1136	5,9 (45)	15,54
CH_4 + H	587	11,8 (45)	12,32
CH_4 + CH_3	625	14,0 (45)	18,21
CH_4 + OH	1500	6,0 (45)	18,81
NH_3 + H	913	13,7 (45)	13,79
H_2O + H	613	20,4 (45)	12,19
H_2O + CH_3	1523	24,7 (45)	16,53

TABLEAU 6. Paramètres des courbes de Morse

Liaison	D_i (kcal/mol) (37)	a_i (Å^{-1})[a]	r_{ie} (Å) (49)
H—H	109,405	1,947	0,742
H_3C—H	112,918	1,784[b]	1,094
H_2N—H	111,036	2,063[b]	1,012
HO—H	125,464	2,126[b]	0,957
F—H	140,520	2,224	0,917

[a]Calculés avec les fréquences théoriques de la réf. 36.
[b]On a utilisé la fréquence de "stretching" asymétrique R—H pour obtenir ce résultat.

particulière ne permet pas la résolution analytique de l'intégrale [12]. Celle-ci a donc dû être calculée par intégration numérique.

A basse température, les corrections d'effet tunnel deviennent très importantes et cessent d'être valables. On peut admettre qu'en dessous de la température caractéristique de Christov (44) définie par la relation:

$$[14] \quad T_c = \frac{h\nu^{\neq}}{\pi\chi}$$

où $\nu^{\neq}$ désigne la fréquence imaginaire associée à la courbure négative du point de transition, un calcul quantique complet devrait être effectué.

Connaissant numériquement la fonction k^* (T) [11] il est aisé de calculer les paramètres d'Arrhénius A^* et E_a^* à toute température supérieure à $T_c/2$ (dans la suite, l'astérisque sera systématiquement omis).

La comparaison théorie–expérience peut s'effectuer au niveau de log k, log A et E_a. Elle n'est possible que dans un nombre relativement restreint de cas. En effet, les calculs théoriques ne sont valables qu'à des températures supérieures à $T_c/2$ auxquelles il est assez rare que des données expérimentales existent. Par ailleurs, celles-ci sont très disparates ce qui rend difficile un choix cohérent de valeurs. Le tableau 5 permet de comparer nos énergies d'activation théoriques à des données expérimentales de la littérature.

L'accord théorie–expérience est loin d'être excellent. De plus, la surestimation de certaines barrières d'activation signalée plus haut (voir tableau 4) est confirmée au niveau des énergies d'activation proprement dites.

La qualité médiocre de nos résultats théoriques trouve essentiellement son origine dans la limitation des calculs d'interaction de configurations qui découle elle-même de la troncature de la base atomique utilisée. L'introduction d'orbitales de polarisation aurait sans conteste un effet bénéfique sur les résultats CI mais nous ne pouvions pas l'envisager systématiquement dans ce travail vu la taille des systèmes étudiés. D'autre part, nous n'avons pas effectué la correction dite de contrepoids sur les énergies des réactifs et des produits car nous lui trouvons un caractère très arbitraire non seulement au niveau SCF où plusieurs méthodes ont été proposées pour l'évaluer mais encore, a fortiori, au niveau CI où elle n'est généralement pas effectuée. Notons d'ailleurs que les énergies de réaction calculées à la limite Hartree–Fock, où tous les effets de base ont disparu, restent très sous-estimées.

V. *Calcul simplifié des barrières d'activation*

En vue d'obtenir des résultats théoriques plus précis que ceux du tableau 5, nous avons élaboré un modèle original permettant de calculer très simplement les barrières d'activation des réactions d'abstraction d'hydrogène et, par là, de vérifier et de rationaliser un ensemble important de faits expérimentaux. Soit le processus réversible:

$$AH + B \underset{2}{\overset{1}{\rightleftharpoons}} A + HB$$

Le diagramme énergétique repris sur la fig. 2 permet d'exprimer la barrière d'activation de la réaction directe (notée 1) par la relation:

TABLEAU 7. Barrières d'activation modifiées (kcal/mol)

Réaction	$r_1^\ddagger$	$u_1(r_1^\ddagger)$	$r_2^\ddagger$	$u_2(r_2^\ddagger)$	$\Delta E^\ddagger$
H − H + H	0,936	10,83	0,936	10,83	10,83
H − H + CH_3	0,934	10,64	1,363	16,41	11,77
H − H + NH_2	0,943	11,47	1,246	16,28	13,06
H − H + OH	0,944	11,57	1,168	16,37	5.94
H − H + F	0,913	8,77	1,144	22,07	~0,00
H_3C − H + H	1,363	16,41	0,934	10,64	15,28
H_3C − H + CH_3	1,357	15,84	1,357	15,84	15,84
H_3C − H + NH_2	1,341	14,34	1,261	17,92	17,07
H_3C − H + OH	1,334	13,70	1,192	19,38	10,27
H_3C − H + F	1,282	9,17	1,179	27,40	4,48
H_2N − H + H	1,246	16,28	0,943	11,47	14,69
H_2N − H + CH_3	1,261	17,92	1,341	14,34	15,19
H_2N − H + NH_2	1,253	17,05	1,253	17,05	17,05
H_2N − H + OH	1,213	12,80	1,211	21,82	10,09
HO − H + H	1,168	16,37	0,944	11,57	22,00
HO − H + CH_3	1,192	19,38	1,334	13,70	22,81
HO − H + NH_2	1,211	21,82	1,213	12,80	24,52
HO − H + OH	1,175	17,24	1,175	17,24	17,24
HO − H + F	1,109	14,07	1,199	30,49	14,76
F − H + H	1,144	22,07	0,913	8,77	30,98
F − H + CH_3	1,179	27,40	1,282	9,17	32,08
F − H + OH	1,199	30,49	1,109	14,07	29,81
F − H + F	1,126	19,41	1,126	19,41	19,41

[15] $\Delta E_1^\ddagger = D_1 - [E(A\cdots H) + E(B\cdots H)]$

Représentons par des courbes de Morse les énergies potentielles des liaisons A—H et B—H:

[16] $u_1 = D_1[1 - e^{-a_1(r_1 - r_{1e})}]^2$

[17] $u_2 = D_2[1 - e^{-a_2(r_2 - r_{2e})}]^2$

Les paramètres des différentes courbes de Morse sont données dans le tableau 6.

Nous admettons que la somme des énergies de liaison $E(\mathrm{A}\cdots\mathrm{H}) + E(\mathrm{B}\cdots\mathrm{H})$ peut se mettre sous la forme:

[18] $E(\mathrm{A}\cdots\mathrm{H}) + E(\mathrm{B}\cdots\mathrm{H}) = \frac{1}{2}[D_1 - u_1(r_1^\ddagger) + D_2 - u_2(r_2^\ddagger)]$

Les barrières d'activation des réactions 1 et 2 s'écrivent alors simplement:

[19] $\Delta E_1^\ddagger = D_1 - \frac{1}{2}[D_1 - u_1(r_1^\ddagger) + D_2 - u_2(r_2^\ddagger)]$

[20] $\Delta E_2^\ddagger = D_2 - \frac{1}{2}[D_1 - u_1(r_1^\ddagger) + D_2 - u_2(r_2^\ddagger)]$

et les chaleurs de réaction à 0 K:

[21] $\Delta E_0^1 = \Delta E_2^\ddagger - \Delta E_1^\ddagger = D_2 - D_1 = -\Delta E_0^2$

Dans le cas de réactions thermoneutres, les barrières d'activation s'obtiennent par l'équation:

[22] $\Delta E_1^\ddagger = u_1(r_1^\ddagger) = u_2(r_2^\ddagger) = \Delta E_2^\ddagger$

Dès lors, il est aisé de recalculer tous les $\Delta E_i^\ddagger$ en utilisant les géométries optimisées des structures de transition données dans le tableau 1. On obtient ainsi les résultats repris au tableau 7. On constate qu'ils se rapprochent des valeurs correspondantes obtenues par des calculs théoriques plus élaborés (voir tableau 4). Ils nous ont permis de repréciser les paramètres cinétiques et thermodynamiques de toutes les réactions étudiées, à différentes températures.

Dans le tableau 8, nous les comparons à des données expérimentales disponibles. Dans l'ensemble, l'accord théorie–expérience peut être considéré comme très satisfaisant. Ceci constitue une justification du modèle simple qui nous a permis de déterminer les barrières d'activation. Nous pouvons donc aussi l'utiliser pour interpréter la cinétique des réactions d'abstraction d'hydrogène.

VI. *Utilisation des barrières d'activation*

Passons brièvement en revue quelques applications concrètes de nos résultats théoriques.

Tout d'abord, les énergies d'activation calculées à partir des barrières correspondantes permettent d'analyser la cohérence des résultats expérimentaux concernant les processus d'abstraction d'hydrogène. Sans insister sur ce point, relevons cependant que, dans cette optique, certaines énergies d'activation mesurées pour les réactions $CH_4 + H \rightleftharpoons CH_3 + H_2$ semblent contestables.

Ensuite, nos barrières d'activation permettent de préciser les limites d'applicabilité de la relation d'Evans–Polanyi (à 0 K). Nous avons constaté que, pour toute série de réactions faisant intervenir le même radical abstracteur, la barrière d'activation est une fonction linéaire de l'énergie de réaction. C'est ce que montrent les résultats repris dans le tableau 9.

On peut trouver la signification des paramètres α et β en identifiant la relation d'Evans–Polanyi à l'équation [19] écrite sous la forme:

[23] $\Delta E^\ddagger = \left(\frac{1 + a}{2}\right) \Delta E_0^0 + \left(\frac{a + b}{2}\right) D_2$

où a et b sont respectivement définis par les formules:

[24] $a = \frac{u_1(r_1^\ddagger)}{D_1}$

[25] $b = \frac{u_2(r_2^\ddagger)}{D_2}$

TABLEAU 8. Comparaison des paramètres cinétiques théoriques et expérimentaux (cm^3/mol s et kcal/mol)

Réaction	T(K)[a]	log k		log A		E_a	
		Théo.	Exp.	Théo.	Exp.	Théo.	Exp.
H_2 + H	650 (46)	10,69	11,34	13,04	13,66	6,98	6,86
	653 (46)	10,70	11,18	13,04	13,7	7,00	7,50
	653 (46)	10,70	11,37	13,04	14,06	7,00	8,00
	873 (46)	11,35	12,23	13,45	13,96	8,40	6,86
	948 (46)	11,52	12,38	13,55	13,91	8,81	6,61
H_2 + CH_3	490 (46)	6,97	6,97	11,66	11,1	10,52	9,2
	506 (47)	7,11	7,27	11,73	11,75	10,68	10,3
	522 (47)	7,26	7,12	11,80	11,59	10,84	10,6
	897 (47)	9,35	9,67	12,58	13,1	13,29	14,0
	1135 (46)	10,06	10,52	12,88	12,5	14,64	10,2
H_2 + NH_2	650	9,30	—	12,30	—	8,91	—
H_2 + OH	1020 (45)	12,81	12,79	14,00	14,17	5,55	6,4
	1076 (45)	12,87	12,32	14,07	14,08	5,87	8,6
	1400 (45)	13,19	12,52	14,38	14,34	7,66	5,2
	2050 (45)	13,64	12,99	14,82	13,6	11,04	5,7
H_2 + F	530 (50)	—	13,64	—	14,13	—	1,18
	1000	14,12	—	14,12	—	0,00	—
CH_4 + H	548 (45)	8,93	8,89	13,39	12,5	11,18	9,0
	587 (45)	9,23	9,42	13,54	13,84	11,66	11,8
	644 (45)	9,62	9,27	13,71	11,8	12,06	7,4
	713 (45)	10,03	9,88	13,88	14,53	12,59	15,1
	785 (45)	10,39	10,36	14,03	12,6	13,08	8,00
	1413 (45)	12,19	12,51	14,73	14,3	16,46	11,5
CH_4 + CH_3	625 (45)	7,78	6,68	12,26	11,6	12,81	14,0
	711 (47)	8,34	7,00	12,63	11,36	13,92	14,1
CH_4 + NH_2	410 (48)	—	6,06	—	11,69	—	10,5
	700	7,90	—	12,36	—	14,29	—
CH_4 + OH	1500 (45)	12,89	12,6	14,60	13,48	11,75	6,0
	1503 (45)	12,89	13,2	14,61	14,15	11,77	6,5
	1550 (45)	12,95	13,26	14,65	14,54	12,07	9.00
CH_4 + F	350 (51)	—	13,74	—	14.25	—	0,8
	700	14,13	—	14,08	—	−0,16	—
NH_3 + H	618 (45)	—	9,04	—	12,6	—	10,00
	913 (45)	11,48	10,31	13,85	13,61	9,87	13,7
NH_3 + CH_3	533 (45)	—	6,7	—	11,28	—	11,1
	700	7,73	—	11,67	—	12,65	—
NH_3 + NH_2	500	5,12	—	11,58	—	14,79	—
NH_3 + OH	484 (45)	—	10,6	—	12,51	—	4,2
	1250	11,94	—	13,27	—	7,65	—
NH_3 + F[b]	—	—	—	—	—	—	—
H_2O + H	613 (45)	7,31	6,64	13,73	13,96	18,00	20,4
	1020 (45)	10,03	10,19	14,39	14,84	20,39	21,6
	1148 (45)	10,52	10,23	14,53	14,04	21,05	19,9
	1150 (45)	10,53	10,45	14,53	14,48	21,06	21,1
	1400 (45)	11,26	10,77	14,74	13,97	22,29	20,39
	1648 (45)	11,80	11,49	14,90	14,25	23,42	20,66
H_2O + CH_3	1523 (45)	9,63	10,01	13,41	13,57	26,34	24,7
H_2O + NH_2	350	—	—	—	—	—	15,8[c]
	1250	8,63	—	12,84	—	24,12	—
H_2O + OH	1100	10,52	—	12,82	—	11,60	—
H_2O + F	304 (51)	—	12,84	—	13,12	—	0,39
	1050	11,98	—	13,66	—	8,05	—
HF + H	300	—	—	—	—	—	34,4[c]
	750	4,63	—	13,51	—	30,49	—
HF + CH_3	300	—	—	—	—	—	33,6[c]
	650	1,61	—	12,03	—	30,98	—
HF + NH_2[b]	—	—	—	—	—	—	—
HF + OH	300	—	—	—	—	—	17,19[c]
	1000	7,43	—	12,78	—	24,46	—
HF + F	550	5,64	—	11,16	—	13,90	—

[a]Moyenne des températures extrêmes de l'intervalle où les mesures ont été effectuées.
[b]Aucune structure de transition n'a pu être obtenue au niveau SCF.
[c]Valeurs obtenues à partir des paramètres de la réaction inverse.

TABLEAU 9. Relations d'Evans–Polanyi

Réaction	$\Delta E^{\neq} = \alpha \Delta E_0^0 + \beta$(kcal/mol)	r
AH + H	$\Delta E^{\neq} = 0{,}596\ \Delta E_0^0 + 12{,}512$	0,990
AH + CH_3	$\Delta E^{\neq} = 0{,}609\ \Delta E_0^0 + 15{,}301$	0,994
AH + NH_2	$\Delta E^{\neq} = 0{,}632\ \Delta E_0^0 + 15{,}605$	0,967
AH + OH	$\Delta E^{\neq} = 0{,}705\ \Delta E_0^0 + 18{,}618$	0,990
AH + F	$\Delta E^{\neq} = 0{,}616\ \Delta E_0^0 + 21{,}017$	0,968

Les barrières d'activation peuvent encore s'exprimer en fonction de D_1 et D_2, selon la relation:

$$[26] \quad \Delta E^{\neq} = \left(\frac{1+a}{2}\right) D_1 - \left(\frac{1-b}{2}\right) D_2$$

Les formes explicites des équations [23] et [26] sont données dans le tableau 10 pour les différentes classes de réactions considérées.

Comme le montrent les relations [24] et [25], les constantes a et b et, dès lors, α et β dépendent de la structure des complexes activés ($r_1^{\neq}$, $r_2^{\neq}$) et des paramètres des courbes de Morse. En principe, seul un calcul théorique permet de déterminer $r_1^{\neq}$ et $r_2^{\neq}$. Cependant, nous avons constaté qu'en adoptant pour $r_1^{\neq}$ ($r_2^{\neq}$) les valeurs trouvées dans les complexes activés symétriques, on pouvait obtenir des barrières d'activation très correctes grâce à la formule [19]. Il est, par ailleurs, intéressant de noter que ces valeurs "standards" de $r_1^{\neq}$ ($r_2^{\neq}$) sont systématiquement égales à 80% du "rayon" de l'atome lié à l'hydrogène transféré.

Les données nécessaires pour effectuer ces calculs ainsi que les résultats obtenus sont respectivement rassemblés dans les tableaux 11 et 12.

On peut dès lors imaginer une démarche très simple pour estimer la barrière d'activation d'une réaction d'abstraction d'hydrogène. Nous l'illustrons par un exemple. Soit à calculer $\Delta E^{\neq}$ pour le processus:

$$H - H + Cl \rightarrow H + HCl$$

Posant:

$$[27] \quad r^{\neq}(H \cdots H) = 0{,}936\ Å$$

et

$$[28] \quad r^{\neq}(H \cdots Cl) = 0{,}80\ r(Cl) = 1{,}416\ Å$$

et utilisant la courbe de Morse (49):

$$[29] \quad u(HCl) = 106{,}515\ [1 - e^{-1{,}868(r_2 - 1{,}275)}]^2$$

on trouve aisément, en utilisant la relation [19]

$$[30] \quad \Delta E_1^{\neq} = 109{,}405 - \frac{1}{2}[109{,}405 - 10{,}83 + 106{,}515 - 5{,}711]$$

TABLEAU 11. Valeurs standards de $r_i^{\neq}$ et $u_i(r_i^{\neq})$

Atome (A)	r(Å) (52)	$r^{\neq}$(A···H) (Å)	$u(r^{\neq})$ (kcal/mol)
H	1,17	0,936	10,83
C	1,70	1,357	15,84
N	1,40	1,253	17,05
O	1,47	1,175	17,24
F	1,41	1,126	19,41

soit encore:

$$[31] \quad \Delta E_1^{\neq} = 9{,}72\ \text{kcal/mol}$$

Un calcul semblable fournit la barrière d'activation du processus inverse:

$$[32] \quad \Delta E_2^{\neq} = 6{,}83\ \text{kcal/mol}$$

Les énergies d'activation expérimentales à 300 K, soit respectivement $E_a^1 = 4{,}5$ à 5,3 et $E_a^2 = 3{,}2$ kcal/mol (45), ne sont pas directement comparables à nos résultats mais elles se classent dans le même ordre.

Au total, les barrières d'activation des réactions d'abstraction d'hydrogène se rationalisent bien à partir des propriétés des espèces isolées et des atomes directement impliqués dans le processus.

Enfin, la relation [26] permet d'étudier l'influence des substituants sur ces barrières d'activation. Considérons, par exemple, les réactions d'arrachement d'hydrogène de méthanes disubstitués:

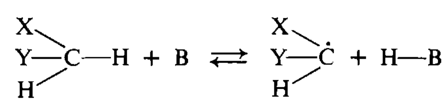

Comme l'un de nous l'a montré par ailleurs (53), D_1 dépend de la nature des substituants X et Y comme indiqué ci-dessous (c≡capteur; d≡donneur):

X	Y	BDE(C—H) = D_1
d	d	Très élevé
c	c	Très petit
c	d	Relativement petit

Dès lors, pour un radical abstracteur donné, la barrière d'activation de la réaction précédente sera plus importante pour les composés ddCH_2 que pour les espèces cdCH_2 et, a fortiori, ccCH_2.

Conclusion

Les résultats énergétiques obtenus dans ce travail au niveau 6-31G – SCF-CI fournissent des paramètres thermodyna-

TABLEAU 10. Expressions des barrières d'activation (kcal/mol)

Réaction	Equation [23]	Equation [26]
AH + H	$\Delta E^{\neq} = 0{,}596\ \Delta E_0^0 + 0{,}114\ D_2$	$\Delta E^{\neq} = 0{,}596\ D_1 - 0{,}482\ D_2$
AH + CH_3	$\Delta E^{\neq} = 0{,}609\ \Delta E_0^0 + 0{,}136\ D_2$	$\Delta E^{\neq} = 0{,}609\ D_1 - 0{,}473\ D_2$
AH + NH_2	$\Delta E^{\neq} = 0{,}632\ \Delta E_0^0 + 0{,}140\ D_2$	$\Delta E^{\neq} = 0{,}632\ D_1 - 0{,}492\ D_2$
AH + OH	$\Delta E^{\neq} = 0{,}705\ \Delta E_0^0 + 0{,}148\ D_2$	$\Delta E^{\neq} = 0{,}705\ D_1 - 0{,}557\ D_2$
AH + F	$\Delta E^{\neq} = 0{,}616\ \Delta E_0^0 + 0{,}150\ D_2$	$\Delta E^{\neq} = 0{,}616\ D_1 - 0{,}466\ D_2$

TABLEAU 12. Barrières d'activation estimées en utilisant des géométries standards d'état de transition (kcal/mol)

Réaction	$r_1^{\neq}$	$u_1(r_1^{\neq})$	$r_2^{\neq}$	$u_2(r_2^{\neq})$	$\Delta E^{\neq}$ estimé	$\Delta E^{\neq}$ correct
H − H + H	0,936	10,83	0,936	10,83	10,83	10,83
H − H + CH_3	0,936	10,83	1,357	15,84	11,58	11,77
H − H + NH_2	0,936	10,83	1,253	17,05	13,12	13,06
H − H + OH	0,936	10,83	1,175	17,24	6,01	5,94
H − H + F	0,936	10,83	1,126	19,41	~0,00	~0,00
H_3C − H + H	1,357	15,84	0,936	10,83	15,09	15,28
H_3C − H + CH_3	1,357	15,84	1,357	15,84	15,84	15,84
H_3C − H + NH_2	1,357	15,84	1,253	17,05	17,39	17,07
H_3C − H + OH	1,357	15,84	1,175	17,24	10,27	10,27
H_3C − H + F	1,357	15,84	1,126	19,41	3,82	4,48
H_2N − H + H	1,253	17,05	0,936	10,83	14,76	14,69
H_2N − H + CH_3	1,253	17,05	1,357	15,84	15,50	15,19
H_2N − H + NH_2	1,253	17,05	1,253	17,05	17,05	17,05
H_2N − H + OH	1,253	17,05	1,175	17,24	9,93	10,09
H_2N − H + F	1,253	17,05	1,126	19,41	3,49	—
HO − H + H	1,175	17,24	0,936	10,83	22,06	22,00
HO − H + CH_3	1,175	17,24	1,357	15,84	22,81	22,81
HO − H + NH_2	1,175	17,24	1,253	17,05	24,36	24,52
HO − H + OH	1,175	17,24	1,175	17,24	17,24	17,24
HO − H + F	1,175	17,24	1,126	19,41	10,80	14,76
F − H + H	1,126	19,41	0,936	10,83	30,68	30,98
F − H + CH_3	1,126	19,41	1,357	15,84	31,43	32,08
F − H + NH_2	1,126	19,41	1,253	17,05	32,97	—
F − H + OH	1,126	19,41	1,175	17,24	25,85	29,81
F − H + F	1,126	19,41	1,126	19,41	19,41	19,41

miques et cinétiques peu réalistes pour les réactions d'abstraction d'hydrogène, dans le cadre de la théorie de l'état de transition avec correction d'effet tunnel. On peut pallier cette difficulté en utilisant des barrières d'activation semiempiriques dont la forme découle d'une expression intuitive de la somme des énergies de liaison $E(A \cdots H) + E(B \cdots H)$, à l'état de transition.

Les résultats obtenus avec ces nouvelles barrières sont en bon accord avec les données expérimentales correspondantes. Ils mettent en évidence le comportement "non-Arrhénius" des réactions d'abstraction d'hydrogène considérées. En outre, ils permettent de tester la cohérence des résultats expérimentaux, d'analyser de façon critique la relation d'Evans−Polanyi et de préciser la signification des paramètres qu'elle renferme.

Des barrières d'activation très satisfaisantes peuvent aussi s'obtenir à partir de valeurs standards de longueurs de liaison à l'état de transition. Celles-ci se rencontrent dans les complexes activés symétriques. Elles peuvent également se déduire de rayons des sphères atomiques. Des barrières d'activation sont ainsi accessibles sans effectuer de calculs *ab initio*.

Enfin, l'influence de substituants sur la cinétique des réactions d'échange d'hydrogène peut être, en principe, rationalisée grâce aux expressions de barrières d'activation que nous avons déduites.

Au total, ce travail montre que l'utilisation conjointe de résultats théoriques et expérimentaux, dans le cadre d'un modèle approprié, permet non seulement d'interpréter de nombreux faits connus mais aussi d'effectuer certaines prévisions originales.

1. G. LEROY, D. PEETERS, C. WILANTE et M. KHALIL. Nouv. J. Chim. **4**, 403 (1980).
2. M. SANA et G. LEROY. Theochem. **76**, 259 (1981).
3. G. LEROY. Structure and properties of free radicals. *Dans* Computational theoretical organic chemistry. *Edité par* I. G. Csizmadia et R. Daudel. Reidel, Dordrecht. 1981. p. 253.
4. G. LEROY et D. PEETERS. Theochem. **85**, 133 (1981).
5. G. LEROY, C. WILANTE, D. PEETERS et M. KHALIL. Ann. Soc. Sci. Bruxelles, **95**, 157 (1981).
6. G. LEROY. Structure and properties of free radicals. A theoretical contribution. *Dans* New concepts of free radicals in chemistry and biology. Table Ronde Roussel Uclaf n°41, 1981, p. 42.
7. M. SANA et G. LEROY. Bull. Soc. Chim. Belg. **91**, 663 (1982).
8. G. LEROY, D. PEETERS et C. WILANTE. Theochem. **88**, 217 (1982).
9. G. LEROY. Int. J. Quantum Chem. **23**, 271 (1983).
10. G. LEROY. Theochem, **93**, 175 (1983).
11. D. PEETERS, G. LEROY et C. WILANTE. Theochem. **107**, 157 (1984).
12. M. SANA, G. LEROY et J. L. VILLAVECES. Theor. Chim. Acta, **65**, 109 (1984).
13. G. LEROY. The theoretical approach to some chemical problems. *Dans* Advances in quantum chemistry. *Edité par* P. O. Löwdin. Academic Press, New York. Sous presse.
14. J. A. POPLE et K. NESBET. J. Chem. Phys. **22**, 571 (1954).
15. W. J. HEHRE, R. DITCHFIELD et J. A. POPLE. J. Chem. Phys. **56**, 2257 (1972).
16. W. J. HEHRE, W. A. LATHAN, R. DITCHFIELD, M. D. NEWTON et J. A. POPLE. Quantum Chemistry Program Exchange 236, Indiana University, Bloomington, Indiana.
17. H. B. SCHLEGEL. *Ab initio* energy derivatives calculated analytically. *Dans* Computational theoretical organic chemistry. *Edité par* I. G. Csizmadia et R. Daudel. Reidel, Dordrecht. 1981. p. 129.
18. G. LEROY et M. SANA. Tetrahedron, **31**, 2091 (1975).
19. L. A. BURKE, G. LEROY et M. SANA. Theor. Chim. Acta, **40**, 313 (1975).
20. G. LEROY et M. SANA. Tetrahedron, **32**, 709 (1976).
21. L. A. BURKE, J. ELGUERO, G. LEROY et M. SANA. J. Am. Chem. Soc. **98**, 1685 (1976).
22. G. LEROY et M. SANA. Tetrahedron, **32**, 1379 (1976).
23. G. LEROY, M. T. NGUYEN et M. SANA. Tetrahedron, **32**, 1529 (1976).

24. G. LEROY, M. T. NGUYEN et M. SANA. Tetrahedron, **34**, 2459 (1978).
25. L. A. BURKE, G. LEROY, M. T. NGUYEN et M. SANA. J. Am. Chem. Soc. **100**, 3668 (1978).
26. G. LEROY et M. SANA. Ann. Soc. Sci. Bruxelles, **92**, 79 (1978).
27. G. LEROY, M. SANA, L. A. BURKE et M. T. NGUYEN. Contribution to the theoretical study of reaction mechanisms. *Dans* Quantum theory of chemical reactions. Vol. 1. *Edité par* R. Daudel, A. Pullman, L. Salem et A. Veillard. Reidel, Dordrecht. 1979. p. 91.
28. G. LEROY, M. T. NGUYEN, M. SANA, K. J. DIGNAM et A. F. HEGARTY. J. Am. Chem. Soc. **101**, 1988 (1979).
29. M. T. NGUYEN, M. SANA, G. LEROY, K. J. DIGNAM et A. F. HEGARTY. J. Am. Chem. Soc. **102**, 573 (1980).
30. G. LEROY, M. T. NGUYEN, M. SANA et J. L. VILLAVECES. Bull. Soc. Chim. Belg. **89**, 1023 (1980).
31. M. T. NGUYEN, M. SANA et G. LEROY. Bull. Soc. Chim. Belg. **90**, 681 (1981).
32. M. T. NGUYEN, G. LEROY, M. SANA et J. ELGUERO. J. Heterocycl. Chem. **19**, 943 (1982).
33. M. SANA, G. LEROY, G. DIVE et M. T. NGUYEN. Theochem. **89**, 147 (1982).
34. M. T. NGUYEN, M. SANA, G. LEROY et J. ELGUERO. Can. J. Chem. **61**, 1435 (1983).
35. M. SANA. Theor. Chim. Acta, **60**, 543 (1982).
36. J. L .VILLAVECES. Contribution to the theoretical study of hydrogen abstraction reactions by free radicals. Thèse de Doctorat. Louvain-la-Neuve, 1981.
37. J. A. POPLE et J. S. BINKLEY. Mol. Phys. **29**, 599 (1975).
38. B. LIU. J. Chem. Phys. **58**, 1925 (1973).
39. M. S. GORDON, D. R. GANO et J. A. BOATZ. J. Am. Chem. Soc. **105**, 5771 (1983).
40. K. NIBLAEUS, B. O. ROOS et P. E. M. SIEGBAHN. Chem. Phys, **26**, 59 (1977).
41. G. C. SCHATZ et S. P. WALCH. J. Chem. Phys. **72**, 776 (1980).
42. C. F. BENDER, S. V. O'NEIL, P. K. PEARSON et H. F. SCHAEFER III. Science, **176**, 1412 (1972).
43. S. G. CHRISTOV. Dokl. Akad. Nauk SSSR. **136**, 663 (1960).
44. S. G. CHRISTOV. Collision theory and statistical theory of chemical reactions. Lecture Notes in Chemistry 18. Springer Verlag, Berlin. 1980.
45. J. A. KERR et S. J. MOSS. Handbook of bimolecular and termolecular gas reactions. Vol. 1. C. R. C. Press, Boca Raton. 1981.
46. V. N. KONDRATIEV. Rate constants of gas phase reactions. *Traduit par* L. J. Holtschlog. *Edité par* R. M. Fristrom. U.S. Dept. of Commerce, NBS, COM-72-10014.
47. J. A. KERR et M. J. PARSONAGE. Evaluated kinetic data of gas phase hydrogen transfer reactions of methyl radicals. Butterworth, London. 1976.
48. M. DEMISSY et R. LESCLAUX. J. Am. Chem. Soc. **102**, 2898 (1980).
49. K. P. HUBER et G. HERZBERG. Constants of diatomic molecules. Van Nostrand Reinhold, New York. 1979.
50. R. F. HEIDNER, J. F. BOTT, C. E. Gardner et J. E. METZGER. J. Chem. Phys. **72**, 4815 (1980).
51. D. L. BAULCH, R. A. COX, R. F. HAMPSON JR., J. A. KERR, J. TROE et R. T. WATSON. J. Phys. Chem. Ref. Data. Vol. 9, n°2, 295 (1980).
52. A. GAVEZZOTI. J. Am. Chem. Soc. **105**, 5220 (1983) et références citées.
53. G. LEROY. Proceedings of the 15th Conference of the Theoretical Chemists of Latin Expression. A paraître.

Synthesis and vibrational spectra of complexes of small carboxylic acids with 18-crown-6

RODRIQUE SAVOIE,[1] ANDRÉ RODRIGUE, MARIE PIGEON-GOSSELIN, AND ROBERT CHÊNEVERT[1]
Département de Chimie et Centre de recherches sur les atomes et les molécules, Université Laval, Québec (Qué.), Canada G1K 7P4

Received July 27, 1984

This paper is dedicated to Professor Camille Sandorfy on the occasion of his 65th birthday

RODRIGUE SAVOIE, ANDRÉ RODRIGUE, MARIE PIGEON-GOSSELIN, and ROBERT CHÊNEVERT. Can. J. Chem. **63**, 1457 (1985).

The neutral-component complexes $(HCOOH)_3 \cdot (18\text{-crown-}6)_2$, $(CH_3COOH)_2 \cdot 18$-crown-6, and various halogenated CH_3COOH/18-crown-6 adducts have been isolated and studied by infrared and Raman spectroscopy. The halogenated (F, Cl, and Br) derivatives, which occur as $(\text{acid} \cdot \text{water})_x \cdot 18$-crown-6($x = 1$ or 2) adducts, probably have a structure which is similar to that of the known $CH_2(CN)COOH \cdot H_2O \cdot 18$-crown-6 complex.

RODRIGUE SAVOIE, ANDRÉ RODRIGUE, MARIE PIGEON-GOSSELIN et ROBERT CHÊNEVERT. Can. J. Chem. **63**, 1457 (1985).

Les complexes à composantes neutres $(HCOOH)_3 \cdot (18\text{-couronne-}6)_2$, $(CH_3COOH)_2 \cdot 18$-couronne-6, de même que plusieurs autres obtenus à partir de dérivés halogénés de l'acide acétique, ont été isolés et étudiés par spectroscopie infrarouge et Raman. Les complexes halogénés (F, Cl et Br), qui ont une stoechiométrie acide/eau/18-couronne-6 égale à 2:2:1 ou 1:1:1, semblent avoir une structure similaire à celle du composé d'addition connu $CH_2(CN)COOH \cdot H_2O \cdot 18$-couronne-6.

Introduction

The macrocyclic polyether 18-crown-6 (hereafter referred to as 18C6) readily forms complexes with hydrates of very strong acids, which exist as hydronium salts (1–3). In these complexes, the hydronium ion is retained within the ether cavity by electrostatic interactions as well as by hydrogen bonds of the $OH_3^+ \cdots$ ether type, with a resulting noticeable lowering of the crown D_{3d} symmetry. Neutral-component complexes have been reported with hydrates of weaker acids. With nitric acid, the $(HNO_3 \cdot H_2O)_2 \cdot 18C6$ complex was obtained (2), whereas a 1:1:1 stoichiometry was determined in the case of the adduct $CH_2(CN)COOH \cdot H_2O \cdot 18C6$ (4, 5).

In this paper we report the synthesis of a number of new complexes of 18C6, with formic, acetic, and halogenated acetic acids. The infrared and Raman spectra of these adducts have been recorded in an attempt to characterize their structure.

Experimental

The complexes were prepared by the following methods.

Method A

The 18C6 (1.057 g, 4 mmol) and the carboxylic acid (13.3 mmol) are dissolved in a specified volume of diethyl ether. Petroleum ether (30–60°C) is added and the complex crystallizes after lowering the temperature.

Method B

The concentrated acid (0.5 mL) is slowly added to a solution of the crown (528 mg, 2 mmol) in diethyl ether (40 mL). If needed, the temperature of the resulting solution is lowered to allow for the crystallization of the complex.

The complexes were filtered under reduced pressure, washed with petroleum ether (30–60°C), and dried. Their stoichiometry was determined from the integrated intensity of the ^{1}H nmr peaks (in $CDCl_3$, using a Bruker HX-90 instrument), from elemental analysis, or from titration by 0.1 *N* NaOH (complexes with CF_3COOH and CCl_3COOH). The ^{13}C nmr spectra were recorded in $CDCl_3$, on a Bruker WP-80 spectrometer working at 20 MHz. Details pertaining to the individual complexes are given below.

$(HCOOH)_3 \cdot (18C6)_2$

Prepared by method A, using 20 mL diethyl ether and 40 mL petroleum ether. Precipitation starts at room temperature and is further favored by lowering the temperature to 0°C. The solid is dried 30 min under vacuum. This complex can also be prepared by method B. Yield: 96%; mp: 79–80°C; ^{1}H nmr δ: 10.24 (s, 3H, COOH), 8.30 (s, 3H, H—C), 3.69 (s, 48H, 18C6); ^{13}C nmr δ: 164.121 (3C, COOH), 70.463 (24C, 18C6). *Anal.* calcd.: C 48.64, H 8.16; found: C 48.34, H 7.43%.

$(CH_3COOH)_2 \cdot 18C6$

Prepared by method A, using 20 mL diethyl ether and 40 mL petroleum ether. This complex can also be prepared by method B. It decomposes slowly at room temperature. It is dried in air during approximately 1 h and kept in a closed container at low temperature. Yield: 92%; mp: 45–50°C; ^{1}H nmr δ: 10.86 (multiplet, 2H, COOH), 3.70 (s, 24H, 18C6), 2.10 (s, 6H, CH_3); ^{13}C nmr δ: 175.755 (2C, COOH), 70.755 (12C, 18C6), 20.634 (2C, CH_3).

$CF_3COOH \cdot H_2O \cdot 18C6$

Prepared by method A, using 20 and 50 mL, respectively, of diethyl ether and petroleum ether. (The complex can also be obtained by dissolving the acid and 18C6 in 5 mL diethyl ether.) The complex precipitates at −20°C. It is dried under vacuum for a few minutes. This adduct is not stable under vacuum, and it decomposes slowly at atmospheric pressure and room temperature. Yield: 69%; mp: 53–54°C; ^{1}H nmr δ: 8.00 (s, 3H, H_2O and COOH), 3.69 (s, 24H, 18C6); ^{13}C nmr δ: 162.517, 160.513, 158.509, and 156.565 (q, 1C, COOH), 137.192, 122.859, 108.648, 94.376 (q, 1C, CF_3), 70.266 (12C, 18C6). *Anal.* calcd.: C 42.42, H 6.86; found: C 41.85, H 6.13%. Titration of the complex dissolved in H_2O by 0.1 *N* NaOH confirmed the 1:1:1 stoichiometry (within 1.5%). We have had indications that under certain conditions a complex of 2:2:1 stoichiometry can be formed. The crystals then have a globular shape instead of the fine needles characteristic of the 1:1:1 complex.

$(CCl_3COOH \cdot H_2O)_2 \cdot 18C6$

Prepared by method A, using 20 and 40 mL of diethyl ether and petroleum ether, respectively. The crystallization temperature is −20°C (a stoichiometry intermediate between 1:1:1 and 2:2:1 is obtained at lower temperatures). The solid is dried under vacuum for 30 min. Yield: 73%; mp: 72–73°C; ^{1}H nmr δ: 8.10 (s, 6H, H_2O and COOH), 3.71 (s, 24H, 18C6); ^{13}C nmr δ: 163.087 (2C, COOH), 91.316 (2C, CCl_3), 70.097 (12C, 18C6). *Anal.* calcd.: C 30.64, H 4.82; found: C 30.14, H 4.40%. Titration of the complex dissolved in water by 0.1 *N* NaOH indicated 6% acid missing for a 2:2:1 stoichiometry.

$(CHCl_2COOH \cdot H_2O)_2 \cdot 18C6$

Prepared as the complex above. This complex slowly decomposes

[1]Authors to whom correspondence should be addressed.

under vacuum. It is dried in air at room temperature. Yield: 81%; mp: 41.0–41.5°C; ^{1}H nmr δ: 7.37 (s, 6H, H_2O and COOH), 6.00 (s, 2H, $CHCl_2$), 3.70 (s, 24H, 18C6); ^{13}C nmr δ: 166.023 (2C, COOH), 70.097 (12C, 18C6), 65.121 (2C, $CHCl_2$).

$CH_2ClCOOH \cdot H_2O \cdot 18C6$

Prepared by method A, using 20 mL of diethyl ether and 40 mL of petroleum ether. The complex is crystallized at 0°C. (An intermediate stoichiometry, 1:1:1 – 2:2:1, is obtained with this complex, as well as with the one with monobromoacetic acid, when the temperature of crystallization is higher than 0°C.) The solid is dried under vacuum for 30 min. Yield: 57%; mp: 51.5–52°C; ^{1}H nmr δ: 6.70 (s, 3H, H_2O and COOH), 4.10 (s, 2H, CH_2Cl), 3.70 (s, 24H, 18C6); ^{13}C nmr δ: 169.023 (1C, COOH), 70.536 (12C, 18C6), 41.194 (1C, CH_2Cl). *Anal.* calcd.: C 44.62, H 7.76; found: C 44.33, H 7.21%.

$CH_2BrCOOH \cdot H_2O \cdot 18C6$

Prepared as the complex above, using 30 and 10 mL, respectively, of diethyl ether and petroleum ether. Yield: 75%; mp: 65–66°C; ^{1}H nmr δ: 6.70 (s, 3H, H_2O and COOH), 3.87 (s, 2H, CH_2Br), 3.69 (s, 24H, 18C6); ^{13}C nmr δ: 168.877 (1C, COOH), 70.390 (12C, 18C6), 26.707 (1C, CH_2Br). *Anal.* calcd.: C 39.91, H 6.93; found: C 40.37, H 6.40%.

$CH_2(CN)COOH \cdot H_2O \cdot 18C6$

This complex was prepared as described by Elbasyouny *et al.* (4).

Vibrational spectra

The infrared spectra, obtained from Nujol and hexachlorobutadiene mulls pressed between Irtran-4 (ZnSe) or silver chloride windows, were recorded on a Beckman IR 4250 spectrophotometer. The Raman spectra were obtained from the solids contained in sealed glass capillary cells. For the low temperature measurements, the glass cell was placed inside a cavity in the copper tail section of a liquid nitrogen cryostat. The spectra were recorded on a microcomputer-controlled Spex Model 1400 spectrometer (6), using the 514.5-nm exciting line from a Spectra Physics Model 165 argon ion laser. The spectra were usually obtained at 300 mW laser power at the sample, 2 cm^{-1} spectral slit width, an integration time of 2 s, and a frequency increment of 2 cm^{-1} at room temperature (1 cm^{-1} at liquid nitrogen temperature).

Results and discussion

Except for the ν(C=O) and ν(CH_2) regions, at 1750 and 2900 cm^{-1} respectively, the high-frequency region of the infrared spectra of the complexes described here mostly contains bands due to O—H vibrations. As can be seen in Fig. 1, a number of weaker peaks, attributable to overtones and combination modes, are also present in the spectra. The O—H vibrations are also seen in the Raman spectra, but they are comparatively very weak. At frequencies lower than 1500 cm^{-1} (see, for example, Fig. 2), both the infrared and Raman spectra mostly reveal the vibrational bands of the crown ether, although some of the bands of the acid can also be indentified in both types of spectra.

Both the frequencies and spectral activity of the crown ether bands in the infrared and Raman spectra of the complexes are comparable to those found in various complexes (7) in which the 18C6 crown is known to have a highly regular D_{3d} symmetry. It is therefore concluded that the crown essentially retains this high symmetry in the complexes involving carboxylic acids. This contrasts with the situation found in complexes involving the hydronium ion, such as with very strong acids, where distortion of the crown occurs, causing a splitting of many of the vibrational bands of the ether (1–3). This type of splitting, which is particularly evident in the 850 and 950 cm^{-1} regions of the infrared spectrum, does not occur in the spectra of the complexes reported here. The structures of the acid·18C6 and acid·water·18C6 basic units found in those complexes are discussed separately below.

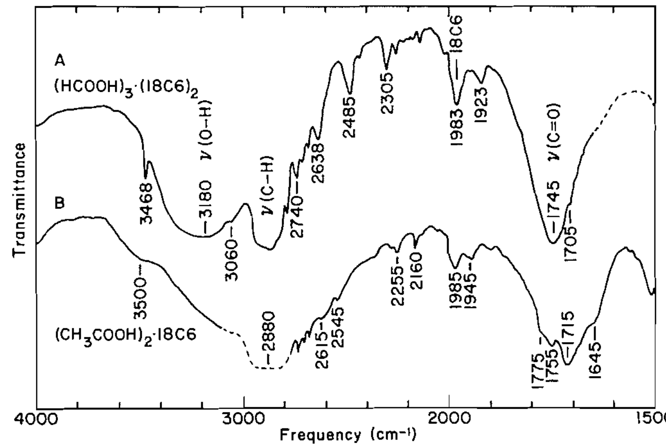

FIG. 1. Infrared spectra of (A) $(HCOOH)_3 \cdot (18C6)_2$ and (B) $(CH_3COOH)_2 \cdot 18C6$ in Nujol or hexachlorobutadiene mulls. The dotted sections refer to the spectrum in the complementary mulling agent.

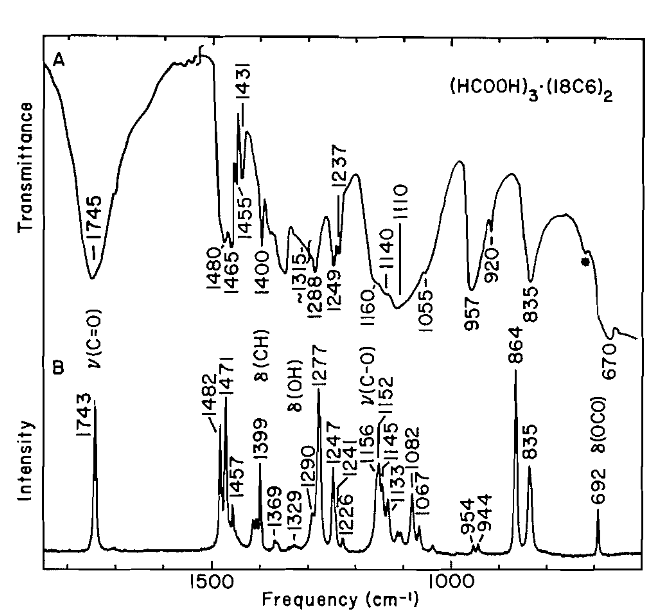

FIG. 2. (A) Infrared and (B) Raman spectra of the $(HCOOH)_3 \cdot (18C6)_2$ in the 600–1850 cm^{-1} region. The infrared spectrum was obtained in Nujol, except for the 1300–1520 cm^{-1} region (C_4Cl_6).

$(HCOOH)_3 \cdot (18C6)_2$

This complex is particularly stable as compared to the other adducts involving carboxylic acids, and it is much more resistant to decomposition under vacuum. This stability is reflected in its melting point (79–80°C), which is higher than those of the other adducts in the same series.

The high-frequency region of the infrared spectrum of the complex (Fig. 1) clearly indicates that the acidic proton of HCOOH is rather weakly hydrogen bonded (ν(O—H) = 3180 cm^{-1}). The spectrum is very similar to that of the acid associated with acetonitrile in CCl_4 solution (ν(O—H) = 3200 cm^{-1}) (8), and it also contains many of the weaker bands due to overtones and combination modes present in the latter. The fundamentals are identified in the Raman and infrared spectra (700–1800 cm^{-1} region) reproduced in Fig. 2.

Among the various structures which can be considered for the complex, many can be eliminated from characteristic features in the vibrational spectra. For example, the possibility of having hydrogen-bonded molecular chains of HCOOH, similar to those in the pure solid (9), intercalated between 18C6 molecules in the complex is not borne out by experiment, as in such a case one should get a ν(O—H) absorption band in the 2500–2800 cm^{-1} region (10, 11). Similarly, the presence of cyclic dimers is not consistent with the spectroscopic results. Normal coordinate analyses (12, 13) have shown that intermolecular vibrational coupling in such dimers causes an appreciable splitting of the vibrational energy levels, the infrared and Raman active modes having sometimes widely different frequencies. The ν(C═O) mode is particularly characteristic on that account, as it shows a splitting of more than 60 cm^{-1}. In the present case, both the infrared and Raman components have essentially identical frequencies (1745 cm^{-1}).

One of the most striking features in the Raman spectrum of the $(HCOOH)_3\cdot(18C6)_2$ complex in the crystalline state is the sharpness of the bands of the acid and the lack of noticeable splitting of these bands. With the exception of the weak doublet at 1329/1335 cm^{-1} (1335/1341 cm^{-1} at −189°C), which is tentatively assigned to the δ (C—O—H) mode, all the other HCOOH peaks occur as singlets, whose width at half-intensity is less than 4 cm^{-1} at −189°C (for a 2 cm^{-1} spectral slit width). This suggests that (*i*) the HCOOH molecules interact only weakly with each other in the complex, and (*ii*) that the three acid molecules in each basic unit are symmetrically equivalent.

The model proposed in Fig. 3 is consistent with the above interpretation and the 3:2 stoichiometry of the complex. In this model, three HCOOH molecules related by a threefold symmetry axis are linked to alternate oxygen atoms of the crown by hydrogen bonds, with an O···O distance estimated at 2.73 Å from the observed ν(O—H) frequency (14). The CH tail section of each acid molecule is assumed to interact weakly with the oxygen atoms of a second 18C6 molecule. The HCOOH molecules in this structure are equivalent in the sense that each is linked to two different 18C6 molecules in the same manner. They are not strongly bonded to each other, so that they are not expected to give rise to any appreciable intermolecular vibrational coupling. Obviously, variants of this simple model could also be considered, and disorder could be introduced by interchanging the relative orientation of some of the acid molecules. However, the sharpness of the Raman lines is not indicative of such disorder, even though the ν(O—H) band in the infrared spectrum appears to be abnormally broad, given its relatively high frequency.

$(CH_3COOH)_2\cdot 18C6$

This complex (mp: 45–50°C) is not nearly as stable as the 3:2 adduct obtained with formic acid. It decomposes rapidly under normal conditions and it has to be kept in an inert atmosphere and at low temperature. Some of the secondary features in the infrared spectrum (Fig. 1) suggest the presence in the sample of a small amount of H_2O (~3500 and 1645 cm^{-1}) and possibly of unbound acid (1775 cm^{-1}). Otherwise, the spectrum is characterized by a broad ν(O—H) band centered at ~2880 cm^{-1}, a frequency which is comparable to that in crystalline CH_3COOH (14, 15) but significantly lower than the average calculated for the $(CH_3COOH)_2$ dimer (~3100 cm^{-1}) (12). On the other hand, the strong ν(C═O) band with maximum at 1715 cm^{-1} has a frequency which is much higher than in the crystalline acid (1657 cm^{-1}) (15). These observations indicate that the C═O group of each acid molecule in the complex is not an acceptor of a strong hydrogen bond and, consequently, that the OH groups are bonded to the oxygen

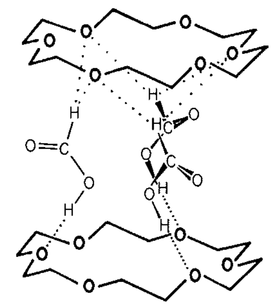

FIG. 3. Structural model for the $(HCOOH)_3\cdot(18C6)_2$ complex.

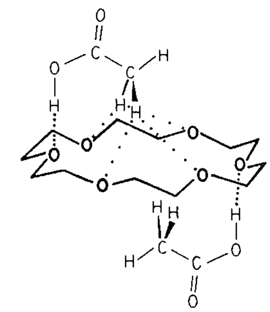

FIG. 4. Structural model for the $(CH_3COOH)_2\cdot 18C6$ complex.

atoms of the crown ether.

Two different types of structure are consistent with the above deductions. One can first consider a structure somewhat similar to that proposed for the HCOOH complex, in which stacked 18C6 molecules are linked to each other by two molecules of CH_3COOH. These acid molecules (disposed in a parallel or antiparallel manner) would be linked to one of the 18C6 units through an O—H···O bond, with O···O distance of ~2.65 Å (14), and to the other unit by weak CH_3···O interactions. In the second model, the two ends of each CH_3COOH molecule are linked to the same crown molecule, as illustrated in Fig. 4. This second model is perhaps to be favored, as this complex differs from that with formic acid in that it contains stronger XOH···O bonds, which suggests that the two compounds have different basic structures. Furthermore, it is generally observed that in 1:2 host/guests complexes of this type the guest molecules approach the crown ring from both sides of the plane (16). Whatever the model chosen, it is not surprising that this complex is much less stable than the corresponding 3:2 adduct with HCOOH: it contains proportionally fewer acid linkers in the 18C6 supporting matrix, and the CH···O interactions are certainly weaker with CH_3COOH than with HCOOH, due to the lower relative acidity of the methyl substituent.

Substituted $CH_3COOH/H_2O/18C6$

Spectroscopic data are available in the literature for the substituted acetic acids involved in the complexes reported here: CF_3COOH (17–19), CCl_3COOH (20, 21), $CHCl_2COOH$ (21, 22), $CH_2ClCOOH$ (20, 23), $CH_2BrCOOH$ (24), and $CH_2(CN)COOH$ (25). Two different types of complexes are formed with these acids and 18C6. In general, they have an acid/water/18C6 stoichiometry of 1:1:1, such as with CF_3COOH, $CH_2ClCOOH$, $CH_2BrCOOH$, and $CH_2(CN)COOH$, but the complexes with the trichloro and dichloroacetic acids were obtained as 2:2:1 adducts. The high-frequency regions of the infrared spectra of these complexes are

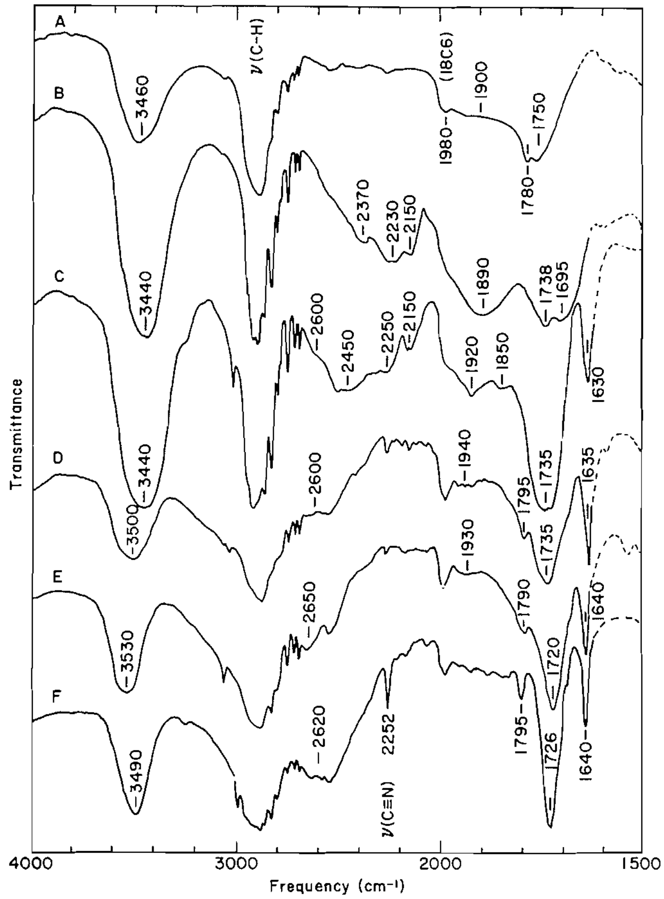

FIG. 5. Infrared spectra of (A) $CF_3COOH \cdot H_2O \cdot 18C6$, (B) $(CCl_3COOH \cdot H_2O)_2 \cdot 18C6$, (C) $(CHCl_2COOH \cdot H_2O)_2 \cdot 18C6$, (D) $CH_2ClCOOH \cdot H_2O \cdot 18C6$, (E) $CH_2BrCOOH \cdot H_2O \cdot 18C6$, and (F) $CH_2(CN)COOH \cdot H_2O \cdot 18C6$ in hexachlorobutadiene (—) or Nujol (- - -).

reproduced in Fig. 5. The synthesis of the complex with $CH_2(CN)COOH$, whose spectrum is also included in the figure, has been reported earlier (4) and its crystal structure has been determined by X-ray crystallography (5). As shown schematically in Fig. 6, the H_2O molecule in this adduct acts as a linker between the acid and 18C6 molecules. Each H_2O molecule interacts weakly with two oxygen atoms of a crown (O···O distance ≃ 2.92 Å), and it acts as a strong hydrogen bond acceptor from the acid (O···O distance of 2.6 Å). The CH_2 group of the acid also interacts weakly with oxygen atoms from the next 18C6 unit.

The likeness of the spectra in Fig. 5 strongly suggests that all of the complexes in this series have similar structures. It can be assumed that the 2:2:1 adducts differ from the 1:1:1 complexes only in that they contain one water·acid unit on both sides of a crown, instead of only on one side as in the latter. Therefore, the structures of the 2:2:1 complexes obtained here are probably similar to those of diaquo complexes of 18C6, such as those with 3-nitrophenol and *p*-nitrobenzaldehyde oxime (16). The similarity of structure between the 1:1:1 and 2:2:1 complexes obtained with the halogenated acetic acids probably explains why adducts of intermediate composition are commonly obtained with these compounds when they are recrystallized at an improper temperature (e.g. below −20°C or above 0°C).

The spectra in Fig. 5 are best interpreted by comparison with

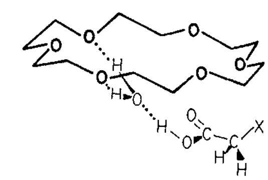

FIG. 6. Basic structure of the $CH_2(CN)COOH \cdot H_2O \cdot 18C6$ complex.

that of the $CH_2(CN)COOH$ complex, whose molecular and crystal structures are known (5). In this complex, the very weak bonding of the water molecules to the crown leads to a relatively high frequency of the stretching fundamentals of water, which occur in the 3440–3530 cm^{-1} range for all the complexes. These values are consistent with the 2.9 Å O···O distances of the OH_2···crown hydrogen bonds determined by X-ray diffraction (5). Note that this frequency in the 2:2:1 complexes is slightly lower than in the 1:1:1 adducts, but this could be fortuitous as the difference is quite small. The ν(OH) band of H_2O is also present in the Raman spectra. In the $CH_2(CN)COOH$ complex, the maximum is found at 3460 cm^{-1}, with shoulder at ~3500 cm^{-1} where the maximum of the infrared band occurs. At liquid nitrogen temperature, the two Raman peaks (width at half-intensity ≃ 12 cm^{-1}) are well separated at 3438 and 3475 cm^{-1}. These two peaks most likely belong to the ν_1 and ν_3 vibrations of H_2O, as their separation (37 cm^{-1}) is close to that expected from the established relation between ($\nu_1 - \nu_3$) and the average ν_{OH} frequency (47 cm^{-1}) (26). This interpretation is also supported from the fact that the corresponding ν_{OH} vibration from HOD species gives a single peak at an intermediate frequency in the spectra of partly deuterated samples.

In most spectra, the bending mode of water $\delta(OH_2)$ gives a very sharp peak at 1635 cm^{-1}, on the low-frequency side of the strong ν(C=O) band. The absence of such a peak from the spectra of the complexes with CF_3COOH and CCl_3COOH will be discussed below. In the case of the complex with $CHCl_2COOH$, the frequency of this band is comparable to that of the $\nu_{as}(CO_2^-)$ mode of the corresponding carboxylate ion ($CHCl_2COO^-$) (27), which could be taken as an indication of the presence of this anion in the sample. However, such an hypothesis does not hold, as the $\nu_{as}(CO_2^-)$ frequency differs appreciably from 1635 cm^{-1} for the other acids (e.g. 1596 cm^{-1} for CH_2BrCOO^-) (27). It should be noted that the occurrence of a very sharp peak for the ν_2 vibration of water is not uncommon. For example, it has been observed in various crystalline hydrates, such as $NaClO_4 \cdot H_2O$ (28), in which the O···O distance between the weakly bound water molecules and ClO_4^- ions is ~2.96 Å long. In this case the ν_2 mode of water gives a sharp singlet at 1628 cm^{-1} in the infrared spectrum.

The 2620 cm^{-1} ν(OH) frequency of the acid in $CH_2(CN)COOH \cdot H_2O \cdot 18C6$ (Fig. 5-F) reflects the short XOH···OH_2 hydrogen bond linking this molecule to water (O···O = 2.6 Å) in the complex. Approximately the same frequency is observed in the adducts with the monochloro and monobromoacetic acids. These three complexes probably have isomorphous crystal structures, with very similar lattice parameters. The strength of the XOH···OH_2 bond increases with acid strength, and the ν(OH) frequency of the acid decreases appreciably, to 2450 and 2230 cm^{-1}, in the complexes with dichloro and trichloroacetic acid, respectively. The infrared spectra of these adducts are characteristic of strongly hydrogen-bonded systems, and they are very similar to those of complexes of these same acids with strong hydrogen bond acceptors, such as trioctylphosphine oxide (20, 22). The subbands associated with the main transition appear to be similar to those observed in the spectra of HCl–ether systems, where they were interpreted as sum and difference bands arising from combinations of the acid stretching vibration with the hydrogen bond stretching motion (29, 30).

Another characteristic feature linked to the increase in hydrogen bond strength in the complexes studied is the increased intensity of the band in the 1900 cm^{-1} region, which is normally attributed to the overtone of the (out-of-plane) γ(OH) mode. Part of the intensity increase is probably caused by electrical anharmonicity (31), but Fermi resonance with ν(OH) is also involved (20, 22). This latter effect is evident in Fig. 5, where it is seen that the 1900 cm^{-1} band decreases in frequency with increased hydrogen bond strength, whereas the frequency of the γ(OH) mode itself is expected to increase slightly under the same conditions (14). Note that the ν(OH) band, at ~2230 cm^{-1} in the CCl_3COOH complex, is displaced to higher frequency on account of this resonance interaction. Were it not for this effect, it would probably occur near 2150 cm^{-1}, a value which normally reflects an O···O distance of ~2.55 Å and a very strong hydrogen bond of energy ~11 kcal/mol (14, 32).

The spectrum of the CF_3COOH complex (Fig. 5-A) is unique among the series shown, as it apparently contains no band attributable to the ν(OH) mode of the acid. However, if one correlates the strength of the acids contained in the complexes (pK_a = 2.85 ($CH_2ClCOOH$), 1.00 (CCl_3COOH), and −0.25 (CF_3COOH)) (21) with the observed ν(OH) frequency in the spectra, extrapolation to the CF_3COOH complex suggests a ν(OH) frequency of less than 2000 cm^{-1}. Therefore, it is likely that both the ν(OH) frequency an the 2 γ(OH) overtone overlap at ~1900 cm^{-1} in the spectrum of this complex.

The low frequency of the ν(OH) mode in the CF_3COOH and CCl_3COOH complexes is probably responsible for the disappearance of the ν_2 band of water near 1640 cm^{-1} in the infrared spectra of these compounds. As the ν(OH) frequency gets close to that of the $\delta(OH_2)$ vibration of water, coupling is likely to occur between these two vibrations. An in-phase induced stretching of the acid O—H group by the $\delta(OH_2)$ motion of water could give rise to a dipole change opposed to that caused by the latter vibration, with very small resulting value of the dipole derivative associated with the overall motion, and consequent reduction of the intensity of the $\delta(OH_2)$ infrared band. It is also possible that the coupling of the acid ν(OH) mode with the $\delta(OH_2)$ vibration of water could give rise to a splitting of the $\delta(OH_2)$ mode, the two components having appreciably different frequencies and infrared intensities, as they involve inphase and out-of-phase motions, with corresponding addition and subtraction of the dipole changes associated with each individual mode. In the CCl_3COOH complex, the two modes could occur at 1695 cm^{-1} (strong) and 1605 cm^{-1} (very weak). The 1738 cm^{-1} band in the spectrum is attributed to the ν(C=O) mode in view of the 1742 cm^{-1} frequency of this vibration of the free acid in the liquid state (21). In the CF_3COOH complex, the two $\delta(OH_2)$ modes would be further apart, and the high-frequency component could overlap the ν(C=O) mode in the 1750 cm^{-1} region, whereas its low-frequency counterpart could be responsible for the weak and broad band centered at 1613 cm^{-1} in the Raman spectrum. Whatever the exact mechanism responsible for the disappearance of the $\delta(OH_2)$ band of water in the infrared spectra of the CF_3COOH and CCl_3COOH complexes, the very low frequency of the acid ν(OH) vibration suggests that the XOH···OH_2 bond is very short, with the acidic proton located near the center of the O···O bond, in an asymmetric potential well.

Although the various adducts involving substituted acetic acids were not systematically studied at low temperature, the $CH_2(CN)COOH$ complex was investigated by Raman spectroscopy at temperatures down to −185°C. Splitting of the vibrational bands of the acid by ~5 cm^{-1} was found to occur at low temperature, an effect which is not observed at room temperature. It is unlikely that this splitting results from intermolecular vibrational coupling, as the molecules of the acid are well isolated from each other in the solid. More likely, the observed splitting is caused by the presence of two crystallographically nonequivalent acid molecules in the primitive cell of the crystal. This interpretation is also suggested from the fact that the two components of the observed doublets have nearly equal intensities in all cases.

Other complexes

The stoichiometric complexes isolated as solids using the substituted acetic acids all contained water, with a ratio of one water per acid molecule. Attempts to isolate water-free complexes with these acids failed. However, we have had indications that adducts with approximate 2:1 and 6:1 acid/18C6 stoichiometry are formed by direct mixing of the acid and crown ether in rigorously anhydrous solvents such as dichloromethane and diethyl ether, although it was not possible to crystallize the oily material resulting from such mixtures. Of particular interest was the 6:1 complex with CF_3COOH, obtained using an excess of acid in the preparation procedure. After evaporation of the solvent and excess acid, this complex proved to be very stable, showing a loss of acid of ~5% only after 3 h at 1 Torr pressure (1 Torr = 133.3 Pa). Presumably, in such a 6:1 adduct there is one acid molecule hydrogen bonded to each of the oxygen atoms of the cyclic ether, giving a complex with three acid molecules on each face of the crown. The 2:1 corresponding binary adduct would have a structure similar to that of the $(CH_3COOH)_2$·18C6 complex, with one acid molecule bonded on each side of the crown. The infrared and Raman spectra of these ill-defined complexes are consistent with this type of bonding, as the acid ν(OH) region is quite similar for the 2:1 and 6:1 adducts, showing generally two main peaks at ~2700 and 2550 cm^{-1}, irrespective of the acid involved.

The way in which the complexes studied are formed, be it by direct hydrogen bonding of the acid COOH group to an oxygen of the crown or by the use of a water molecule as a linker between the acid and the ether, is quite straightforward. Although our study has been limited to a few small carboxylic acids, it is likely that larger acids of this type could also form stoichiometric adducts with 18C6. As is generally observed in neutral-component complexes containing one hydrogen bond donor only, these adducts are expected to be of the aquo type, similar to those obtained with the halogenated acetic acids.

Acknowledgements

Financial support of this work by the Natural Sciences and Engineering Research Council of Canada and the Ministère de l'Education du Québec is gratefully acknowledged.

1. R. Chênevert, A. Rodrigue, M. Pigeon-Gosselin, and R. Savoie. Can. J. Chem. **60**, 853 (1982).
2. G. S. Heo and R. A. Bartch. J. Org. Chem. **47**, 3557 (1982).

3. R. Chênevert, A. Rodrigue, P. Beauchesne, and R. Savoie. Can. J. Chem. **62**, 2293 (1984).
4. A. Elbasyouny, J. Klimes, A. Knöchel, J. Oehler, and G. Rudolph. Z. Naturforsch. Teil B, **31**, 1192 (1976).
5. A. Elbasyouny, H. J. Brügge, K. von Deuten, M. Dickel, A. Knöchel, K. U. Koch, J. Kopf, D. Melzer, and G. Rudolph. J. Am. Chem. Soc. **105**, 6568 (1983).
6. R. Savoie, B. Boulé, G. Genest, and M. Pézolet. Can. J. Spectrosc. **24**, 112 (1979).
7. M. Fouassier and J.-C. Lassègues. J. Chem. Phys. **75**, 865 (1978).
8. H. Wolf, H. Müller, and E. Wolf. J. Chem. Phys. **64**, 2192 (1976).
9. I. Nahringbauer. Acta Crystallogr. Sect. B, **34**, 315 (1978).
10. H. R. Zelsmann, F. Bellon, Y. Maréchal, and B. Bullemer. Chem. Phys. Lett. **6**, 513 (1970).
11. H. R. Zelsmann, Y. Maréchal, A. Chosson, and P. Faure. J. Mol. Struct. **29**, 357 (1975).
12. S. Kishida and K. Nakamoto. J. Chem. Phys. **41**, 1558 (1964).
13. K. Nakamoto and S. Kishida. J. Chem. Phys. **41**, 1554 (1964).
14. A. Novak. Struct. Bonding, **18**, 177 (1974).
15. R. Foglizzo and A. Novak. J. Chim. Phys. **71**, 1322 (1974).
16. W. H. Watson, J. Galloy, D. A. Grossie, F. Vögtle, and W. M. Müller. J. Org. Chem. **49**, 347 (1984).
17. J. R. Barceló and C. Otero. Spectrochim. Acta, **18**, 1231 (1962).
18. R. L. Redington and K. C. Lin. Spectrochim. Acta Part A, **27**, 2445 (1971).
19. M. Leuchs and G. Zundel. J. Chem. Soc. Faraday Trans. 2, **76**, 14 (1980).
20. D. Hadži. Pure Appl. Chem. **11**, 435 (1965).
21. S. Bratož, D. Hadži, and N. Sheppard. Spectrochim. Acta, **8**, 249 (1956).
22. D. Hadži and N. Kobilarov. J. Chem. Soc. (A) 439 (1966).
23. D. Sinha, J. E. Katon, and R. J. Jakobsen. J. Mol. Struct. **24**, 279 (1975).
24. J. E. Katon and R. L. Kleinklein. Spectrochim. Acta Part A, **29**, 791 (1973).
25. D. Sinha and J. E. Katon. Appl. Spectrosc. **26**, 599 (1972).
26. J. Schiffer, M. Intenzo, P. Hayward, and C. Calabrese. J. Chem. Phys. **64**, 3014 (1976).
27. E. Spinner. J. Chem. Soc. 4217 (1964).
28. G. Brink and M. Falk. Can. J. Chem. **48**, 2096 (1970).
29. J. E. Bertie and J. E. Millen. J. Chem. Soc. 497 (1965).
30. J.-C. Lassègues and P. V. Huong. Chem. Phys. Lett. **17**, 444 (1972).
31. C. Sandorfy. *In* Infrared and Raman spectroscopy of biological molecules. NATO Advanced Study Institutes Series, Series C, V. 43. *Edited by* T. M. Theophanides. D. Reidel Pub. Co., Holland. 1979.
32. E. R. Lippincott and R. Schroeder. J. Chem. Phys. **23**, 1099 (1955).

Photofrins: a spectral study

ROY POTTIER,[1] JEAN PIERRE LAPLANTE, AND YING-FUN ADA CHOW
Department of Chemistry and Chemical Engineering, Royal Military College of Canada, Kingston, Ont., Canada K7L 2W3

AND

JAMES KENNEDY[2]
Department of Radiation Oncology, Queen's University, Kingston, Ont., Canada K7L 2V7

Received July 27, 1984

This paper is dedicated to Professor Camille Sandorfy on the occasion of his 65th birthday

ROY POTTIER, JEAN PIERRE LAPLANTE, YING-FUN ADA CHOW, and JAMES KENNEDY. Can. J. Chem. **63**, 1463 (1985).

The absorbance and fluorescence spectra of Hematoporphyrin IX, Photofrin, and Photofrin II are measured as a function of pH, concentration, and temperature, in order to isolate the ionic equilibria from the monomer/dimer/aggregate equilibria. Based on photometric and volumetric titrations, the distribution diagram for four ionic species is presented, with pK_a values of 2.7, 5.2, and 9.1. Protonation sites for these pK_a's are assigned.

ROY POTTIER, JEAN PIERRE LAPLANTE, YING-FUN ADA CHOW et JAMES KENNEDY. Can. J. Chem. **63**, 1463 (1985).

Les spectres d'absorption et de fluorescence de l'Hématoporphyrine IX, du Photofrin et Photofrin II ont été mesurés en fonction du pH, de la concentration et de la température, dans le but d'isoler les équilibres ioniques des équilibres monomères/dimères/aggrégats. A partir des titrages photométriques et volumiques, les courbes de distribution contenant quatre espèces ioniques sont présentées, avec des pK_a de 2,7, 5,2 et 9,1. Les sites de protonation pour ces pK_a sont discutés.

Introduction

Hematoporphyrin derivatives (Hpd) are a complex mixture of porphyrins that are used for photochemotherapy of cancer. This technique is based on two properties that are at present only partially understood. The first is that of selective biodistribution, whereby most types of malignant tissue preferentially retain one or more of the components of Hpd. The second is that of photosensitization, sometimes referred to by photobiologists as photodynamic action, which is believed to occur via the type II mechanism involving singlet oxygen. The photophysics, photochemistry, and phototherapy of Hematoporphyrin and Hpd have recently been reviewed by Kessel (1). More comprehensive background can be obtained in refs. 2, 3, and 4.

A fuller understanding of the selective biodistribution mechanism has been hampered mainly by two complications. First, most investigations have been carried out on solutions of Hpd in which the true composition of these solutions was unknown. The information obtained could only be termed semiquantitative at best. Second, two basic sets of equilibria are simultaneously involved in porphyrin derivatives: the ionic equilibria, dependent on pH, and the monomer/dimer/aggregate equilibria for each ionic species present. Because each set of equilibria is interlinked, a variation in pH will not only affect the ionic species present, but will also affect the proportion of monomers, dimers, and aggregates of each ionic species present. Results obtained at different pH's thus become very difficult to compare. Buffering the solutions to fix the pH has its drawbacks also, since the buffer tends to modify the results, as has been observed in the singlet oxygen production in thiazine photosensitization studies (5). If one adds to this the fact that tumor cells have a lower pH than normal cells, it clearly becomes apparent that knowledge of the ionic distribution diagrams, along with quantitative information on any dimerization/aggregation process, becomes a prerequisite to any detailed understanding of the operative mechanism of selective biodistribution of Hpd in cells.

In an attempt to shed some light on this problem, we have undertaken a spectroscopic study of commercially available preparations of Hpd, known as Photofrins.

Experimental

Chemicals and solutions

Photofrin (PF) and Photofrin II (PFII) were obtained from Photofrin Medical Inc., Cheektowaga, N.Y. Hematoporphyrin IX dihydrochloride (HP) was obtained from Porphyrin Products, Logan, UT. All materials were prepared in 0.9% aqueous NaCl solutions. Solutions at different pH's were prepared by two different methods:

(*a*) A measured amount (volume for the Photofrins, mass for Hematoporphyrin IX) was dissolved in a dark volumetric flask, and sufficient saline solvent was added to obtain the required porphyrin concentration. Just prior to making the spectral measurements, the pH was measured and adjusted to the required pH value by adding the required amount of concentrated HCl (for low pH values) or by dipping a wetted sodium hydroxide pellet (for high pH values). This technique introduced a slight error due to dilution by the HCl solution or the NaOH pellet, but this effect was quite small. On the other hand, this method has the advantage that one can adjust the pH just prior to the actual measurement. This is especially important if the composition of the strongly acidic or strongly basic solutions changes with time.

(*b*) A series of solutions, all containing the same Photofrin concentrations, were prepared at different pH's. Any pH could thus be obtained by mixing appropriate solutions of lower and higher pH's. This method has the advantage that the concentration of the Photofrin is held constant, but suffers from the disadvantage that the Photofrin remains in the presence of the hydronium or hydroxide ions longer than in method (*a*). Method (*a*) was preferred for the strongly acidic or strongly basic solutions, in order to reduce the time that the solution was in contact with the acid or base, whereas method (*b*) was preferred for intermediate pH values, since these solutions were relatively stable. All solutions were kept in dark bottles and fresh solutions were prepared daily.

Spectrophotometry

The effect of concentration on absorbance was studied with the use of a Varian DMS-100 double beam ratio recording spectrophotometer. The scanning rate was 100 nm min^{-1} and the time to record one

[1] To whom all correspondence should be addressed.
[2] Cancer Scientist of the Ontario Treatment and Research Foundation.

spectrum was approximately 1.5 min. The path length of matched quartz cells was varied from 0.01 to 100 mm with the concentration of the Porphyrin being varied inversely. Temperature and pH effects were done on a Tracor-Northern 1710 spectrophotometer. This instrument is a single beam system, with a photodiode array containing 1024 photodiodes that allows the full spectrum to be recorded simultaneously. The exposure time of the analyzing light on the solution was typically of the order of 3 s, during which 200 spectra were accumulated. The average (for absorbance) or sum (for fluorescence) was stored in digitalized form on diskettes for future analysis. The grating used for absorbance studied is blazed at 300 nm, and the spectral range studied was from 225 to 525 nm. For emission studied, the spectral range studied was between 500 and 800 nm.

For the temperature measurements, a series of solutions at fixed pH were brought to a fixed temperature in an ice bath or warm water bath, then placed in the instrument sample holder and the spectrum was recorded. The actual temperature of the solution was recorded at the time of spectral measurement. Temperature changes during measurement time (3 s) were negligible.

Quartz cells were used in all measurements, and were cleaned in 3 *M* nitric acid overnight prior to any series of measurements. Before any specific measurement was done, the cells were further washed with methanol, distilled water, and rinsed with the analytical solution.

Titrations

The commercial solutions of PF and PFII had been pre-adjusted to pH 7 (unbuffered). Titrations of these solutions had to be done in two parts; above pH 7 using freshly prepared NaOH solutions, and below pH 7 using standardized HCl. The titrated solutions were then back-titrated, and this procedure was repeated several times using a variety of relative concentrations of the Photofrin solutions and the acid/base solutions. HP was prepared by a standard weighing procedure. A Fisher Accumet digitalized pH meter, Model 810, was used with a combination Ag/AgCl reference electrode (Canadawide Scientific No. 6471-06).

Results and discussion

Absorbance and fluorescence spectra

A parallel study was carried out on HP, PF, and PFII at various conditions of concentration, temperature and pH. Sample data are presented in Fig. 1, showing the absorbance and fluorescence feature of all three solutions at low, neutral, and high pH. By using HP as a reference, with a sharp soret peak at 399.5 nm in acidic solutions and 392.9 nm in both neutral and basic solutions, several salient features of the Photofrins can be pointed out. First and foremost is the presence of a broad band in both PF and PFII, having a λ_{max} near 370 nm in acidic solutions, 365 nm in neutral solutions, and 375 nm in basic solutions. This new band clearly reflects a different type of Hpd. PFII is specified to contain mainly Dihematoporphyrin IX ether. Dougherty has proposed that the structure of this compound consists of isomers of bis-1-[8-(1-hydroxyethyl)deuteroporphyrin-3-yl] ester ether, which he calls DHE, containing two HP rings attached by an ether link (6). In fact, an ether-linked polymer had previously been proposed by Bonnett (7), on the basis of HPLC data. Grossweiner has recently proposed that the 570 nm band is due to a "folded over" dihematoporphyrin, which he refers to as Hpd-A (8). Ward has also recently proposed a small polymeric structure for the main component of the Photofrins (9). On the basis of separation data, he extends the structure proposed by Dougherty to include approximately 20 Porphyrin rings.

The fluorescence spectra of PF and PFII are identical to that of HP, except for an intensity factor. At low pH, two maxima, with near equal intensity, are observed at 595 nm and 654 nm. When the pH is greater than 3.5, the maxima are red shifted to 614 nm and 675 nm, with relative intensities of 2.5 and 1, respectively. The change in relative intensities upon change of pH is probably related to a change in symmetry of the different ionic species responsible for the emission (10).

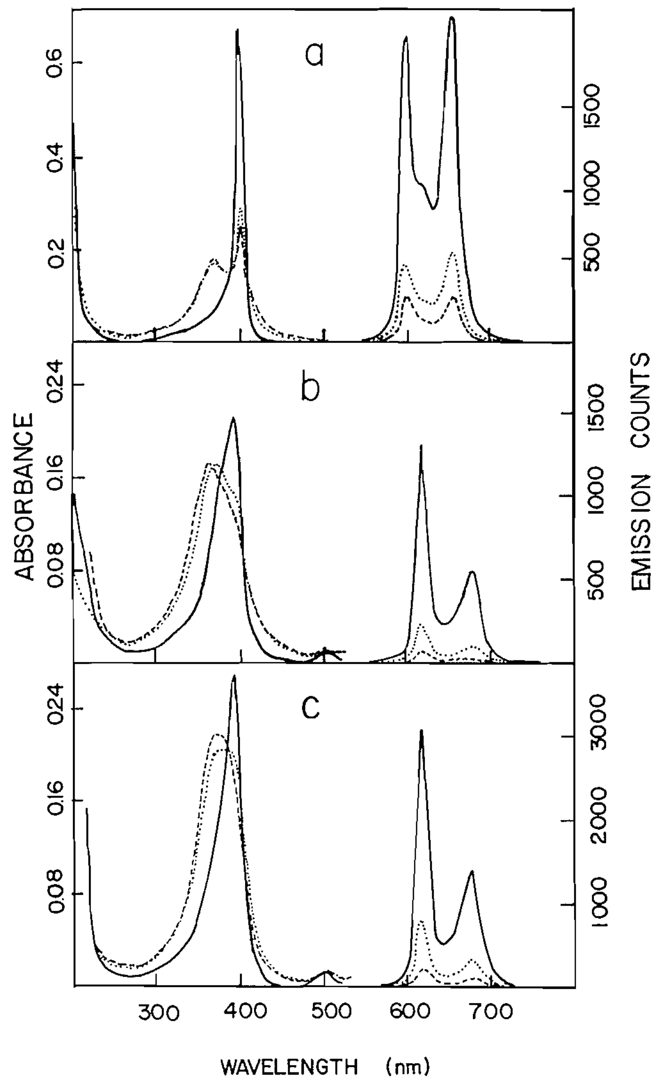

FIG. 1. Absorbance and fluorescence of Hematoporphyrin IX (—), Photofrin (······), and Photofrin II (---). (*a*) pH = 1.1, (*b*) pH = 7.0, (*c*) pH = 11.6. Concentration is 1 μM and path length is 1.00 cm. Temperature is 22°C.

The relative intensity of the entire spectrum of HP:PF:PFII emission is roughly 10:3:1. This ratio observed is for all pH values between 0 and 14. It is important to note that no other fluorescence was observed in PF and PFII. We are thus led to the conclusion that attempts to study the main component of the Photofrins by fluorescence lead to an observation of its HP or similar impurities. This being the case, one can easily estimate the percentage of HP or similar impurities present in PF and PFII as being approximately 30% and 10%, respectively.

The concentration and temperature effects are much more pronounced on HP than on PF or PFII. Sample data comparing the concentration effects on HP and PFII are shown in Fig. 2. Concentration studies on HP have been reported by Karns (11) and Brown (12). Both authors observed a rapid λ_{max} shift as a function of concentration, this drop occurring in the vicinity of 4 μM. They have attributed this effect as being due to aggregation of HP. Our data show that at high pH (11.6) two such

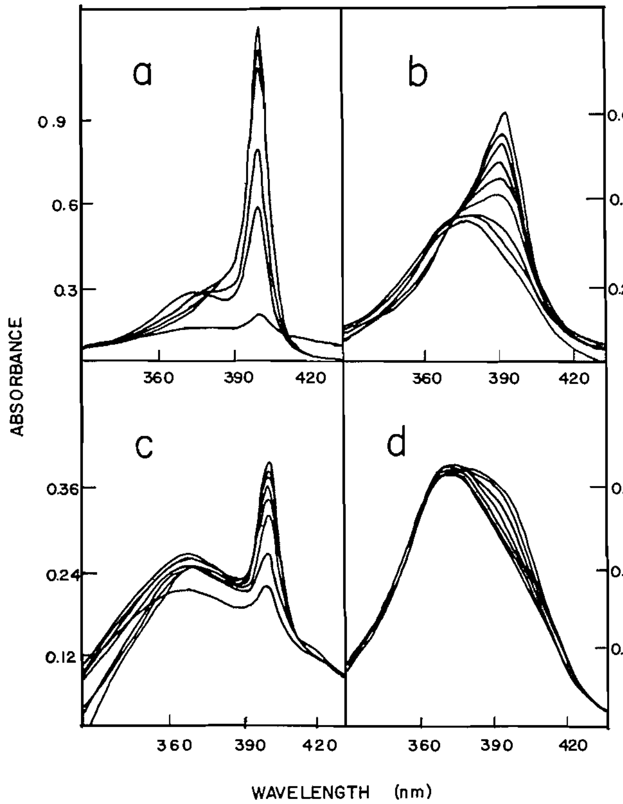

FIG. 2. Concentration effect on Hematoporphyrin IX and Photofrin II. (*a*) HP, pH = 1.9, concentration from 0.04 to 2000 μM; (*b*) HP, pH = 11.6, concentration from 0.04 to 2000 μM; (*c*) PFII, pH = 1.9, concentration from 0.4 to 400 μM; (*d*) PFII, pH = 11.7, concentration from 0.4 to 400 μM.

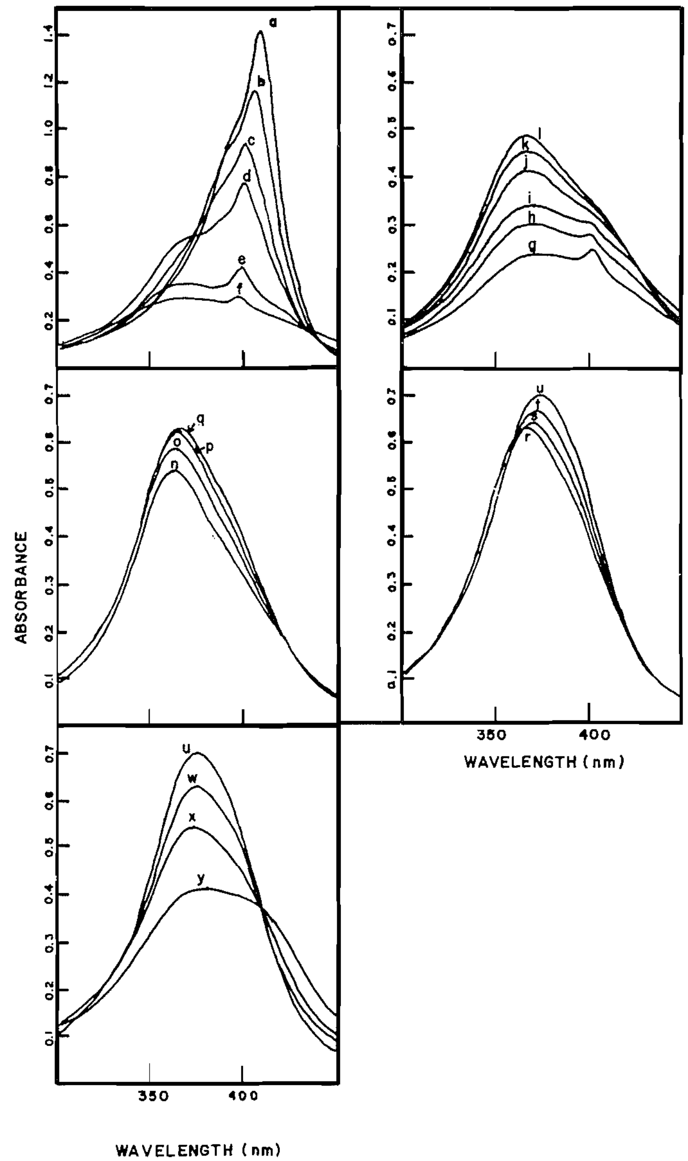

FIG. 3. Absorbance spectra of Photofrin II as a function of pH. Values of pH are *a* to *y* (with the omission of *m* and *v*) respectively: −1, −0.7, 0.2, 0.65, 1.8, 2.38, 2.68, 2.82, 3.17, 3.61, 4.20, 4.80, 5.75, 6.25, 7.25, 8.10, 8.65, 9.31, 10.20, 11.70, 14.0, 14.7, 15.0. Concentration is 4 μM and pathlength is 1.00 cm.

change in spectra occur, one λ_{max} change in the range 2–4 μM, and another in the 15–25 μM concentration range, possibly reflecting the dimerization and aggregation processes, respectively. This would place the λ_{max} values for the monomer, dimer and, aggregates at 392.7 nm, 390.7 nm, and 370.0 nm, respectively, for alkali solutions. PF and PFII, on the other hand, showed much less sensitivity to changes in concentration. The effects observed can be attributed to the HP type impurities. In fact, if one subtracts the contribution of HP from the spectra of PF and PFII, one finds that the remaining spectrum is not effected by a 500-fold increase in concentration (range, 0.4 to 200 μM). This is in agreement with the recent published results of Grossweiner (8), who reported that Beer's law is observed over a 100-fold increase in concentration for purified Hpd-A.

Results obtained by an increase in concentration were also obtained by a decrease in temperature. Spectra observed at 4°C compared well with those at high concentration, and those obtained at 35°C are similar to the ones obtained at low concentrations.

Titrations

Absorbance photometric titrations (pH 0 to 15) were carried out at low concentration (4 μM) in order to keep the interference from dimers or aggregates as low as possible while still retaining sufficient sensitivity on the absorbance measurements. The spectra at the various pH studied are shown in Fig. 3, and have been separated in five subsections to show more clearly the various changes that occur in the spectra as the pH is varied. A plot of the 400 nm absorbance versus pH shows minima at pH 2.5 and 5.5 (see Fig. 4(*a*)). In an attempt to remove the interference from spectral overlap at a fixed wavelength, we used the entire spectrum from 300 to 600 nm (1024 data points) and mixed coefficients of observed spectra at different pH values in order to generate a composite spectrum at another intermediate pH. The distribution diagram thus obtained is presented in Fig. 5(*a*), and represents our best fit. This gives three pK_a values at 2.7, 5.2, and 9.1.

Fluorescence, photometric titrations between pH 1 and 13 were carried out at low concentration (1 μM), and, except for an intensity factor, both HP and PFII gave the same results. See Fig. 4(*b*).

Volumetric titrations on HP, PF, and PFII were carried out and typical results obtained are shown in Fig. 6. All the titration curves have two inflection points. These titrations were repeated several times, using concentrations 5 to 20 μM of Porphyrins, and different concentrations of acid and base ti-

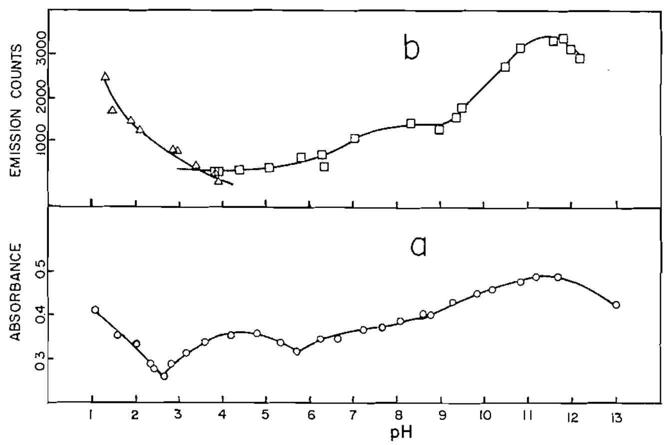

FIG. 4. Effect of pH on Photofrin II. (*a*) Absorbance, λ = 399.0 nm concentration, 4 μM; (*b*) Emission, λ_{ex} = 400 nm, λ_{anal} = 595 nm ($\triangle$) and 616 nm ($\square$). Concentration, 1 μM.

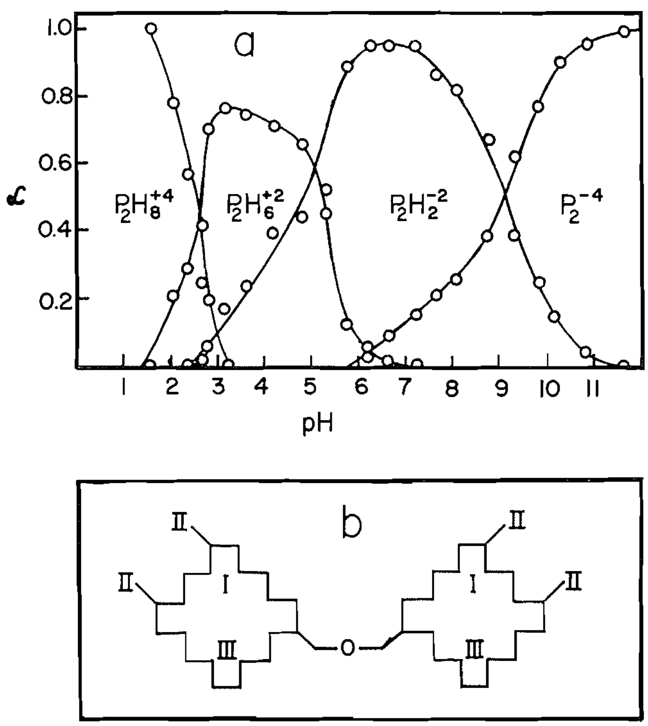

FIG. 5. (*a*) Distribution diagram of Photofrin II, as calculated from the absorbance data. (*b*) Protonation sites on Dihematoporphyrin ether.

trant. As mentioned above, one would expect more aggregate formation at higher concentrations and the first inflection point in the vicinity of pH 5 could possibly be interpreted as being an artifact due to aggregate formations. If this were the case, one would expect a diminution of this inflection point at lower Porphyrin concentrations, but this was not observed. For HP, the analytical mass and the original pH could be measured, and one can calculate the two pK_a's as 3.7 and 6.0. However, the original pH of PF and PFII (prior to being adjusted to pH 7 by manufacturer) is unknown, and one cannot calculate a reliable value for the first pK_a from the volumetric titrations. The second pK_a, located halfway between the two inflection points, gives a pK_a of ~6.

If one adopts the Dihematoporphyrin ether (DHE) as the

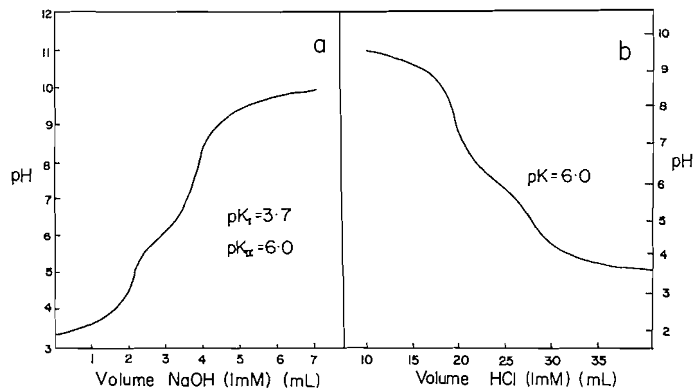

FIG. 6. Volumetric titration curves for Hematoporphyrin IX (*a*) and Photofrin II (*b*).

structure of the main component of the Photofrins (6), then tentative assignments of the protonation sites for PFII at 4 μM concentration can be made. The monomeric ionic equilibria can be represented as:

$$P_2H_8^{4+} \rightleftarrows P_2H_6^{2+} + 2H^+ \qquad pK_a(I) = 2.7$$

$$P_2H_6^{2+} \rightleftarrows P_2H_2^{2-} + 4H^+ \qquad pK_a(II) = 5.2$$

$$P_2H_2^{2-} \rightleftarrows P_2^{4-} + 2H^+ \qquad pK_a(III) = 9.1$$

where $P_2H_8^{4+}$ represents the DHE with four protons on the ring nitrogens and four protons on the carboxylic acid groups. pK_a(I) is believed to involve the protons on the double bonded nitrogen atoms, one proton on each Porphyrin ring. pK_a(II) is assigned to the carboxylic group protons, whereas pK_a(III) is assigned to the removal of the last two protons on the Porphyrin rings. These protonation sites are illustrated in Fig. 5(*b*).

It is interesting to note that the polymeric model proposed by Ward (9), including ~20 Porphyrin rings, can also be fitted to this scheme. Each ring would contain the same number of protons, and all the carboxylic acid groups would also be in the same ratio. One need only rewrite the ionic equilibria, starting with nPH_4^{2+} instead of $P_2H_8^{4+}$, n being the number of Porphyrin rings.

It must be emphasized that, although solutions at 4 μM looked clear, they undoubtedly contain some dimers and possibly aggregates in the pH range 2–5. The asymmetric nature of the distribution diagram (Fig. 5(*a*)) is possibly the result of interference from dimers or aggregates. Thus, Fig. 5(*a*) should be considered with caution, until independent measurements can be made that will distinguish unambiguously between the various monomeric ionic species and their corresponding dimers or aggregates. Moan has recently reported that although both aggregated and non aggregated components of PFII bind to human cells, only the non-aggregated porphyrins contribute significantly to the photosensitivity of the cells (15). Our results lead us to infer that what is sometimes referred to as properties of dimers could be due to a different ionic species in its monomeric form. Keeping in mind the lower pH of cancer cells, such a finding could possibly play a role in the selective biodistribution of Porphyrins in tumors.

Summary and conclusions

The absorbance data can be fitted to three ionic equilibria, involving four monomeric species. The interfering effects of dimers or aggregates, especially in the pH range 2–5, cannot be totally ignored.

Fluorescence emission from the Photofrin solutions is believed to be solely from impurities, and spectral changes in these impurities reflect their various monomeric species. This is to be contrasted with the assignment of two fluorescence decay lifetimes as being due to the monomeric and dimeric species in HP and PFII (13, 14). We present an alternative view whereby the different fluorescence lifetimes could be assigned to different monomeric species, the relative concentration of each species being dependent on the pH.

We have recently initiated a series of laser light scattering on the Photofrins. Until more experiments of this nature are carried out, the question of the ionic species present at various pH's, along with their different states of aggregation, remains a topic of open controversy.

Acknowledgements

This project was supported by DND ARP Grant No. 3610-625 and MRC Grant MA-8124.

1. D. KESSEL. Photochem. Photobiol. **39**, 851 (1984).
2. K. C. SMITH (*Editor*). Photochemical and photobiological reviews. Vol. 7. Plenum Press, NY. 1983.
3. D. KESSEL and T. J. DOUGHERTY (*Editors*). Porphyrin photosensitization. Plenum Press, NY. 1982.
4. K. C. SMITH (*Editor*). Topics in photomedicine. Plenum Press, NY. 1984.
5. R. BONNEAU, R. POTTIER, O. BAGNO, and J. JOUSSOT-DUBIEN. Photochem. Photobiol. **21**, 159 (1975).
6. T. J. DOUGHERTY, W. R. POTTER, and K. R. WEISHAUPT. *In* Porphyrins in tumor phototherapy. *Edited by* A. Andreoni and R. Cubeddu, Plenum Press, NY. 1984. pp. 23–35.
7. R. BONNETT, M. C. BERENBAUM, and P. A. SCOURIDES. Br. J. Cancer, **45**, 571 (1982).
8. L. I. GROSSWEINER and G. C. GOYAL. Photochem. Photobiol. **40**, 1 (1984).
9. A. D. WARD and A. G. SWINCER. Abstract of Porphyrin Photosensitization Workshop, Philadelphia. July, 1984.
10. M. GOUTERMAN. *In* The porphyrins. *Edited by* D. Dolphin. Academic Press, NY. 1978. pp. 1–165.
11. G. A. KARNS, W. A. GALLAGHER, and W. B. ELLIOTT. Bioorg. Chem. **8**, 69 (1979).
12. S. B. BROWN, M. SHILLOCK, and P. JONES. Biochem. J. **153**, 279 (1976).
13. A. R. ANDREONI, R. CUBBEDU, S. DESILVESTRI, G. JORI, P. LAPORTA, and E. REDDI. Zeit. Natur. **386**, 83 (1983).
14. A. ANDREONI, S. DESILVESTRI, P. LAPORTA, G. JORI, and E. REDDI. Chem. Phys. Lett. **88**, 33 (1982).
15. J. MOAN and S. SOMMER. Photochem. Photobiol. **40**, 631 (1984).

A theoretical investigation of energetics and structures of $CH_5^+(CH_4)_n$ clusters for $n = 1-4$

ETTORE FOIS, ALDO GAMBA, AND MASSIMO SIMONETTA[1]
Dipartimento di Chimica Fisica ed Elettrochimica, Università di Milano, V. Golgi 19-I-20133 Milano, Italy

Received July 27, 1984

This paper is dedicated to Professor Camille Sandorfy on the occasion of his 65th birthday

ETTORE FOIS, ALDO GAMBA, and MASSIMO SIMONETTA. Can. J. Chem. **63**, 1468 (1985).

The structures of $CH_5^+(CH_4)_n$ ($n = 1-4$) are determined by semiempirical and *ab initio* MO calculations. The results of the present calculations are in fair agreement with the values of $-\Delta H$ obtained in mass spectrometric experiments. It appears that a three-center–two-electron bond has the most efficient attractive power for the incoming methane molecules.

ETTORE FOIS, ALDO GAMBA et MASSIMO SIMONETTA. Can. J. Chem. **63**, 1468 (1985).

On a déterminé les structures des ions $CH_5^+(CH_4)_n$ ($n = 1-4$) en faisant appel à des calculs d'OM *ab initio* ainsi que semi-empiriques. Les résultats obtenus à l'aide de ces calculs sont en bon accord avec les valeurs de $-\Delta H$ qui ont été obtenues à l'aide d'expériences de spectroscopie de masse. Il semble qu'une liaison à trois centres et à deux électrons présente le pouvoir d'attraction le plus efficace pour les molécules incidentes de méthane.

[Traduit par le journal]

Introduction

Strong interest on alkane protonation was provoked by the work of Olah (1, 2), who investigated the reaction in superacid solutions. A three-center bond structure with C_s symmetry (**1** in Fig. 1) was proposed for the methonium ion (CH_5^+) on the basis of these studies, and several theoretical calculations performed at different levels of approximation have provided independent evidence that the lowest energy structure of CH_5^+ in the gas phase has C_s symmetry, corresponding to a three-center–two-electron (3c–2e) bond complex between CH_3^+ and H_2 (3–10). However, when energy correlation corrections are included in the calculations, the energies of C_s, C_{2v}, C_{4v}, and D_{3h} structures are compressed in a small range (10).

On the other hand, there is a continuing refinement in the study of energies and structures of carbocations by gas phase experimental methods, and measurements of clustering ion equilibria of the methonium ion were performed for the reaction with methane itself (11, 12):

[1] $CH_5^+(CH_4)_{n-1} + CH_4 \rightarrow CH_5^+(CH_4)_n$ ($n = 1-4$)

Binding energies obtained by these investigations are of general thermochemical interest and can also provide information on the structure of CH_5^+. The measured enthalpy changes for the (n, $n-1$) reactions ($n = 1-4$) showed a decrease with n, expected in the case of ion clusters because of the gradual charge dispersion with the addition of new methane units. The observed decrease is not regular: the fall-off between the first two interactions ($\Delta H_{1,0}$, $\Delta H_{2,1}$) is relatively small; a comparable but slightly higher decrease occurs between $\Delta H_{2,1}$ and $\Delta H_{3,2}$, followed by a very low decrease to $\Delta H_{4,3}$. This trend is interpreted as due to the relatively strong interaction with CH_5^+ of the first two incoming CH_4 molecules, while the next units experience weaker and quite different interactions (12).

The fact that experimental information on these compounds is available makes it tempting to investigate theoretically their structures and stabilities. It is also of interest to examine the accuracy of theoretical methods applied at different levels of approximation to reproduce experimental data. In the present study *ab initio* HF SCF MO and semi-empirical CNDO/2 methods are employed to calculate optimized geometries and energies of the clusters $CH_5^+(CH_4)_n$ formed by one methonium ion and a number ($n = 1-4$) of methane molecules.

Methods of calculation

Total energies and stabilization energies $\Delta E_{n,n-1}$ were computed by the *ab initio* spin-restricted Hartree–Fock method, using the GAUSSIAN 80 series of programs (13, 14). The geometry of the smallest cluster $CH_5^+CH_4$ was fully optimized using the standard 3-21G basis set. For the larger clusters ($n > 1$), complete optimization was performed on C_s symmetry constrained structures. Single point calculations with 6-31G** basis set were carried out on the 3-21G optimized geometries ($n = 1, 2$), and they are designated as HF/6-31G**//3-21G.

The analysis of the force constant matrix was performed for $CH_5^+CH_4$ to ensure a complete characterization of the potential energy surface (15, 16). In CNDO/2 calculations (17) the parametrization of Wiberg (18) was adopted, which was the first to predict a C_s structure (3) for CH_5^+. The geometry of the smallest cluster ($n = 1$) was fully optimized. For larger clusters the geometry of the methane units was kept rigid. The Powell technique (19) was employed in the optimization process.

Results and discussion

The total energy calculated by the different methods for methonium ion/methane clusters are collected in Table 1, where enthalpy changes $\Delta H_{n,n-1}$ are also reported.

$CH_5^+CH_4$

The most interesting geometrical parameters of the fully optimized ground-state structure are reported in Table 2, referring for atom numbering to Fig. 1.

It appears that CH_5^+ retains in the 1:1 complex the C_s structure of the isolated ion, and in particular the geometry of the characteristic 3c–2e bond is slightly affected by the interaction with methane: H1—H2 = 0.86 Å (0.85); ∠H1—C1—H2 = 41° (40°); C1—H1 = 1.24 Å (1.24); C1—H2 = 1.22 Å (1.24), values in parentheses referring to isolated CH_5^+. The lengthening of C1—H2 bond is negligible and H1 lies very near to the line connecting C1 and C2 atoms (∠C2—C1—H1 = 4.2°).

The presence of a 3c–2e stabilizing interaction in all the clusters is not surprising as one or more 3e–2c bonds have

[1]To whom all correspondence should be addressed.

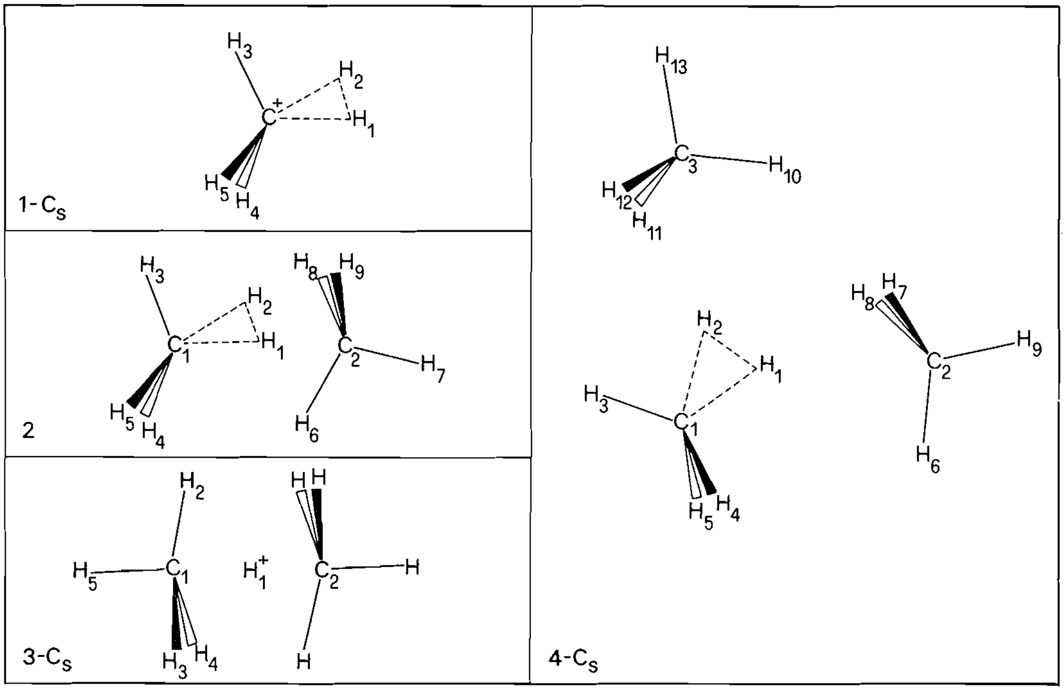

FIG. 1. Optimized structures and atom numbering for free CH_5^+ and $CH_5^+(CH_4)_n$ clusters (n = 1−2).

TABLE 1. *Ab initio* and semiempirical total energies and enthalpies ($\Delta H_{n,n-1}$) for $CH_5^+(CH_4)_n$ systems (n = 0−4)

System		Symmetry	−E (au) (a)	−E (au) (b)	−E (au) (c)	$-\Delta E_{n,n-1}$ (kcal mol^{-1}) (a)	$-\Delta E_{n,n-1}$ (kcal mol^{-1}) (b)	$-\Delta E_{n,n-1}$ (kcal mol^{-1}) (c)	$-\Delta H_{n,n-1}$ (kcal mol^{-1})[d]
CH_5^+	1	C_s	40.405665	40.160564	10.20243	—	—	—	—
$CH_5^+CH_4$	2		80.612576	80.143010	20.03709	3.27	3.48	11.95	7.4
	3	C_s	80.574259	80.120746	20.03461				
$CH_5^+(CH_4)_2$	4	C_s	120.818989	120.124690	29.85909	2.95	3.01	3.9	5.9
$CH_5^+(CH_4)_3$	5	C_s		160.104056	39.68598		1.56	7.0	4.1
$CH_5^+(CH_4)_4$	6			200.083024	49.50901		1.31	4.7	3.9

[a]HF/6-31G**//3-21G.
[b]HF/3-21G.
[c]CNDO/2.
[d]Reference 12.

been predicted by refined HF calculations performed on different carbo and dicarbo cations, such as CH_6^{2+}, $C_2H_6^{2+}$, and $C_2H_8^{2+}$ (20, 21). The presence of a two 3c−2e bond structure, suggested by Hiraoka and Kebarle (12) by analogy with the H_5^+ structure, was accurately checked. The potential energy surface was fully investigated using the 3-21G basis set. Numerical second derivatives with respect to all nuclear coordinates were evaluated. Only two stationary points were found; one was characterized by no imaginary frequency corresponds to the minimum energy structure **2** with one 3c−2e bond while the other (one imaginary frequency) is associated with structure **3** (saddle point), showing no 3c−2e bond. The latter probably represents the transition state for proton transfer between methonium ion and methane. It appears that one proton is symmetrically coordinated by two methane molecules (C—H1 = 1.46 Å, Q(H) = 0.475 e in HF/6-31G**//3-21G calculations) and C1—C2 distance (2.92 Å) is significantly shorter than in the ground state (3.60 Å). The energy barrier predicted by HF/3-21G calculations is 14.6 kcal mol^{-1}, which raises to 24.04 kcal mol^{-1} in HF/6-31G**//3-21G calculations.

Also the CNDO/2 method predicts correctly two structures only, whose geometries are very similar to the *ab initio* ones; however, the energy barrier is lower and corresponds to 1.55 kcal mol^{-1}, and the C1—C2 distances are 3.2 and 2.7 Å in the ground and transition states, respectively.

$CH_5^+(CH_4)_n$, n = 2−4

A complete *ab initio* geometry optimization was allowed using the 3-21G basis set, with the only constraint of C_s symmetry conservation. The optimized structures are shown in Figs. 1 and 2, and the values of the most relevant geometrical parameters are reported in Table 2. The typical structure of isolated CH_5^+ is retained in the clusters, and the CH_4 units coordinate progressively to the different hydrogens of the ion, the first two methanes interacting with the two protons of the 3c−2e bond, as shown in Fig. 1. The structure of this bond is also slightly modified by clustering methanes. CNDO/2 calculations predict similar structures, but C—C distances are shorter by about 0.5 ~ 0.6 Å with respect to the *ab initio* optimized values. This finding is expected if one considers that

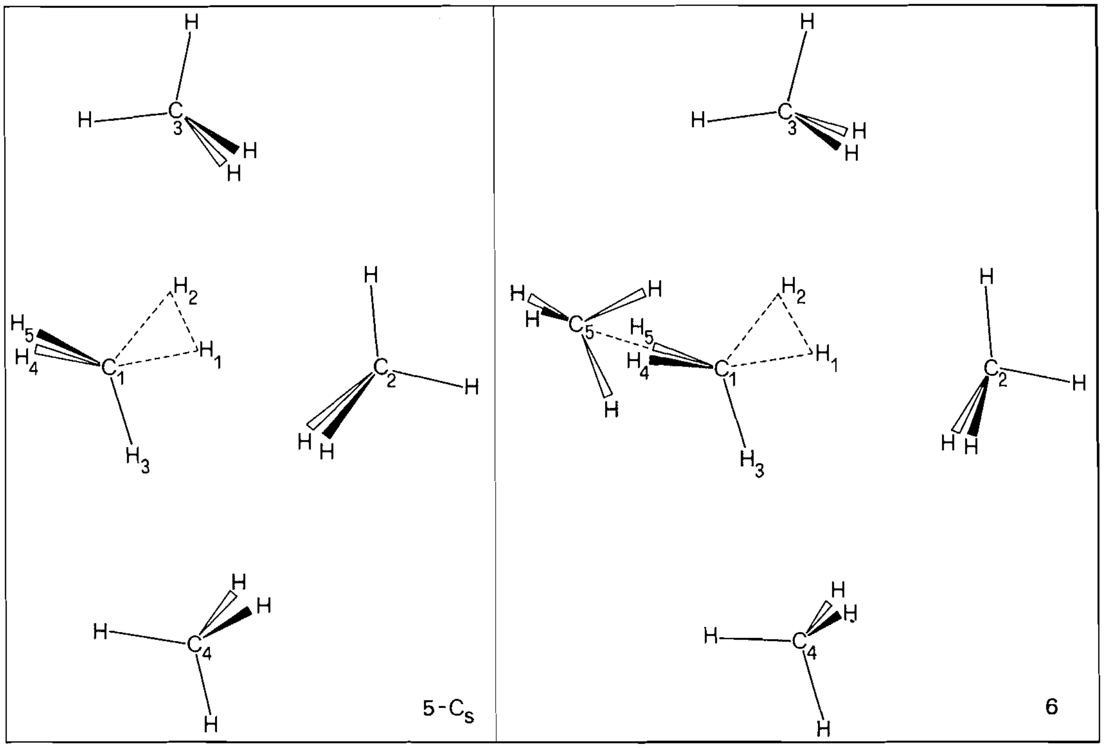

FIG. 2. Optimized structures and atom numbering for $CH_5^+(CH_4)_n$ clusters (n = 3–4).

TABLE 2. *Ab initio* HF/3-21G optimized geometrical parameters for $CH_5^+(CH_4)_n$ systems (n = 0–4)

n	0		1		1		2		3[a]		4[a]	
Symmetry	C_s		—		C_s		C_s		C_s		C_s	
Structure	**1**		**2**		**3**		**4**		**5**		**6**	
[b]	C—H1	1.241	C1—C2	3.595	C1—H1	1.458	C1—C2	3.573	C1—C2	3.602	C1—C2	3.616
	C—H2	1.243	H1—C2	2.359	C1H1C2	180.	C1—C3	3.514	C1—C3	3.522	C1—C3	3.536
	C—H3	1.091	C1—H1	1.243	C1—H2	1.092	C2C1C3	75.5	C1—C4	3.778	C1—C4	3.784
	C—H4	1.079	C1—H2	1.223	C1—H3	1.092	C1—H1	1.229	C2C1C3	74.7	C1—C5	3.802
	C—H5	1.079	C1—H3	1.090	C1—H4	1.101	C1—H2	1.230	C2C1C4	73.9	C2C1C3	75.7
	H1—H2	0.854	C1—H4	1.079	C1—H5	1.101	C1—H3	1.089	C1—H1	1.229	C2C1C4	73.2
			C1—H5	1.079	H1C1H2	80.4	C1—H4	1.079	C1—H2	1.226	C2C1C5	114.6
			H1—H2	0.863	H1C1H3	80.4	C1—H5	1.079	C1—H3	1.090	C1—H1	1.234
			C2—H6	1.090	H1C1H5	180.	C3—H6	1.085	C1—H4	1.079	C1—H2	1.231
			C2—H7	1.082			C3—H7	1.087	C1—H5	1.079	C1—H3	1.090
			C2—H8	1.085			C3—H8	1.087	C2C1H1	10.9	C1—H4	1.079
			C2—H9	1.085			C3—H9	1.082	C2C1H2	52.4	C1—H5	1.079
			C2C1H1	4.2			C2—H10	1.085	C2C1H4	119.8	C2C1H1	12.0
			C2C1H2	45.2			C2—H11	1.086	C2C1H5	119.8	C2C1H2	53.2
			C2C1H3	130.9			C2—H12	1.086	C2C1H3	73.9	C2C1H3	72.7
			C2C1H4	94.9			C2—H13	1.082	H1—H2	0.870	C2C1H4	119.2
			C2C1H5	94.4			C2C1H1	55.1			C2C1H5	119.2
			C2C1H6	58.7			C2C1H2	13.8			H1—H2	0.867
			C1C2H7	165.4			C2C1H3	71.				
			C1C2H8	79.9			C2C1H4	119.8				
			C1C2H9	79.9			C2C1H5	119.8				
			H1—H2	0.863			C1C3H6	67.9				
							C1C3H7	74.7				
							C1C3H8	74.7				
							C1C3H9	184.1				
							C1C2H10	84.0				
							C2C1H11	67.1				
							C1C2H12	67.1				
							C1C2H1	168.0				
							H1—H2	0.868				

[a]The geometries of methane molecules remains practically unchanged; their geometrical parameters are available from the author upon request.
[b]"$i-j$" represents a distance and "ijk" represents an angle.

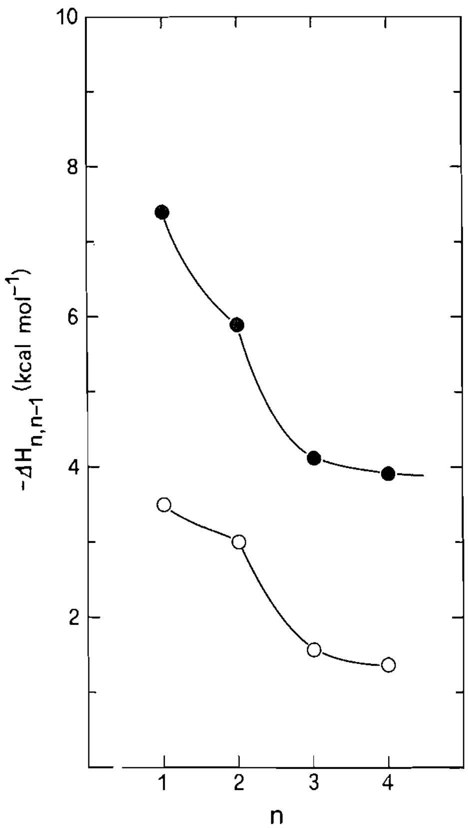

FIG. 3. Plots of experimental $\Delta H_{n,n-1}$ (full circles) and calculated (empty circles) $\Delta E_{n,n-1}$ by HF/3-21G basis set.

the semiempirical method systematically overestimates the bonding properties.

The plot of the experimental $\Delta H_{n,n-1}$ value for reaction [1] is shown in Fig. 3, where the corresponding plot of *ab initio* computed $\Delta E_{n,n-1}$ are also reported. The qualitative agreement is excellent, and the anomaly observed at $n = 2$ is correctly reproduced. The corresponding values calculated for the smallest clusters at the HF/6-31G**//3-21G level are slightly lower and confirm the decrease of $\Delta E_{n,n-1}$ as n increases. It appears that each added CH_4 (at least till $n = 4$) interacts with each free hydrogen of CH_5^+ to form a regular cluster around the methonium ion, so that polymer structures appear less favoured. The finding is expected because of the relatively small interaction energy involved. In contrast, the interaction is stronger for ammonia cluster ions ($NH_4^+(NH_3)_n$) where hydrogen bonds are formed. The larger enthalpies measured by molecular-beams mass spectrometry (22) and confirmed by HF calculations (23), put in evidence the different extent of the interaction for the two types of ion clusters. The analysis of the ordering and the relative stabilities of the most relevant MO's can explain the anomaly present at $n = 2$ in the experimental $\Delta H_{n,n-1}$ plot, well reproduced by HF/3-21G calculations. The occupied MO energy levels for the different clusters are collected in Fig. 4 where those of CH_4 and CH_5^+ are also reported for reference. It is noteworthy that the ordering is independent of the basis set (3-21G and 6-31G**) at least in the case where comparison was possible. It emerges that all MO's of CH_5^+ are slightly destabilized in each of the clusters considered, while CH_4 MO's are always stabilized by the interaction. Moreover the MO stabilization of the first two methanes, localized in the region of the 3c−2e bond, is stronger than that of the subsequently added CH_4 units which interact with the remaining less acidic hydrogen of CH_5^+.

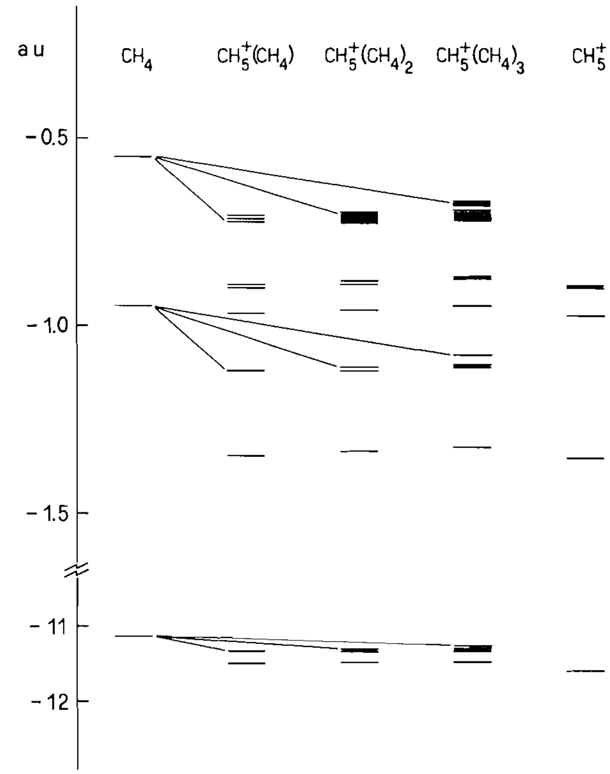

FIG. 4. Occupied MO's energy levels (HF/3-21G) for structures **1**, **2**, **4**, **5**, and free methane.

The irregular decrease of the enthalpy vs. n in the gas phase clustering of methonium ions by methane can therefore be unequivocally explained by the different extent of the interaction of methane molecules with the two kinds of protons of the methonium ion.

1. G. A. OLAH, G. K. KLOPMAN, and R. H. SCHLOSSBERG. J. Am. Chem. Soc. **91**, 3261 (1969).
2. G. A. OLAH. Chem. Ber. **8**, 281 (1972).
3. A. GAMBA, G. MOROSI, and M. SIMONETTA. Chem. Phys. Lett. **3**, 20 (1969).
4. W. A. LATHAN, W. J. HEHRE, and J. A. POPLE. J. Am. Chem. Soc. **93**, 808 (1971).
5. W. A. LATHAN, W. J. HEHRE, and J. A. POPLE. Tetrahedron Lett. **31**, 2699 (1970).
6. W. A. LATHAN, W. J. HEHRE, L. A. CURTISS, and J. A. POPLE. J. Am. Chem. Soc. **93**, 6377 (1971).
7. P. C. HARIHARAN, W. A. LATHAN, and J. A. POPLE. Chem. Phys. Lett. **14**, 385 (1972).
8. V. DYCZMONS, V. STAEMMLER, and W. KUTZELNIGG. Chem. Phys. Lett. **5**, 361 (1970).
9. V. DYCZMONS and W. KUTZELNIGG. Theor. Chim. Acta, Berlin, **33**, 239 (1974).
10. K. RAGHAVACHARI, R. A. WHITESIDE, J. A. POPLE, and P. v. R. SCHLEYER. J. Am. Chem. Soc. **103**, 5649 (1981).
11. F. H. FIELD and D. P. BEGGS. J. Am. Chem. Soc. **93**, 1585 (1971).
12. K. HIRAOKA and P. KEBARLE. J. Am. Chem. Soc. **97**, 4179 (1975).
13. J. S. BINKLEY, R. A. WHITESIDE, R. KRISHNAN, R. SEEGER, D. J. DEFREES, H. B. SCHLEGEL, S. TOPIOL, L. R. KAHN, and J. A. POPLE. QCPE, **13**, 406 (1981).
14. P. N. VANKAMPEN, G. F. SMITS, F. A. A. M. DELEEUW, and C. ALTONA. QCPE, **14**, 437 (1982).

15. K. FUKUI. Acc. Chem. Res. **14**, 36 (1981).
16. M. SANA, G. RECKINGER, and G. LEROY. Theor. Chim. Acta, Berlin, **58**, 145 (1981).
17. J. A. POPLE and D. L. BEVERIDGE. Approximate molecular orbital theory. McGraw-Hill, New York. 1970.
18. K. B. WIBERG. J. Am. Chem. Soc. **90**, 59 (1968).
19. M. J. D. POWELL. Comput. J. **7**, 303 (1965).
20. K. LAMMERTSMA, M. BARZAGHI, G. A. OLAH, J. A. POPLE, P. v. R. SCHLEYER, and M. SIMONETTA. J. Am. Chem. Soc. **105**, 5258 (1983).
21. K. LAMMERTSMA, G. A. OLAH, M. BARZAGHI, and M. SIMONETTA. J. Am. Chem. Soc. **104**, 6851 (1982).
22. K. D. COOK and J. W. TAYLOR. Intern. J. Mass Spectrom. Ion Phys. **30**, 345 (1979).
23. K. HIRAO, T. FUJIKAWA, H. KONISHI, and S. YAMABE. Chem. Phys. Lett. **104**, 184 (1984).

Vibrational spectra and structure of *N*-methylacetamide in some solid complexes with neutral salts

M. H. BARON AND F. FILLAUX

Laboratoire de Spectrochimie Infrarouge et Raman, Centre National de la Recherche Scientifique, 2 rue Henri-Dunant, 94320 Thiais, France

Received July 27, 1984

This paper is dedicated to Professor Camille Sandorfy on the occasion of his 65th birthday

M. H. BARON and F. FILLAUX. Can. J. Chem. **63**, 1473 (1985).

Infrared spectra of crystalline complexes of *N*-methylacetamide ($CH_3CONHCH_3$) and of its ND analog with alcaline perchlorates, tetrabutylammonium halogenides, and alcaline halogenides have been investigated in NH stretching (3500–3050 cm^{-1}), CO stretching (amide **I**, 1750–1500 cm^{-1}), and NH bending (800–400 cm^{-1}) regions. Possible structures for the complexes are proposed and the non-planarity of the amide group is discussed.

M. H. BARON et F. FILLAUX. Can. J. Chem. **63**, 1473 (1985).

Les spectres infrarouge de complexes cristallins formés à partir de *N*-méthylacétamide (NH ou ND) et des perchlorates alcalins, ou des halogénures de tétrabutylammonium, ou des halogénures alcalins, sont étudiés dans les régions spectrales 3500–3050 cm^{-1}(νNH), 1750–1500 cm^{-1} (amide **I**) et 800–400 cm^{-1} (γNH). Les différentes structures possible et la non planéarité du groupement peptidique sont discutés.

I. Introduction

N-Methylacetamide (NMA) has been shown to be non-planar in the crystalline state as well as in solution (1–4) and new assignments have been proposed for infrared and Raman bands corresponding to the torsion (τ_{CN}) around the CN central bond, to the $\gamma_{NH(ND)}$ bending and to the $\nu_{NH(ND)}$ stretching modes.

We were interested in complexes formed between NMA and neutral salts (5–7) and wanted to find out the influence of various interactions between the amide group and ions on the structure of the CONH entity.

II. Experimental

Two different methods have been used to obtain the complexes.

In the first one the salts were dissolved in NMA heated at 60–70°C in order to obtain the desired amide/salt ratio. Complexes were crystallized at room temperature for the following compositions: amide/$Ba(ClO_4)_2$ = 6 or 5, amide/$LiClO_4$ = 4, 3, or 2, amide/Bu_4NBr = 4 or 2, (Bu_4N^+ is the tetrabutylammonium anion), amide/LiBr = 4.

In the second route the salts were added to a solution of amide in methanol or pyridine with the desired amide/salt ratio. The solvent was then slowly pumped out under vacuum.

Infrared spectra were recorded with a Perkin-Elmer 225 spectrometer with a slit width of 2 cm^{-1}. The uncertainty on frequency was about ±2 cm^{-1}. Thin films of Nujol or Fluorolube mulls were examined between KBr or CsI windows.

For each complex the infrared spectrum of the NH and ND derivatives were recorded in order to settle the NH bending assignment.

II. Results and discussion

II.1. Spectral ranges and band assignment

Interactions of the CONH group manifest themselves in infrared as frequency shifts of the normal modes involving mainly the CO and NH bonds. Due to tunnel effect, the mean structure of NMA has the C_s symmetry and the denomination for the normal modes proposed by Miyazawa (8) can be kept. Three spectral regions are selected where the most localized modes appear (8–15): 400–800 cm^{-1} ($\gamma_{NH(ND)}$), 1500–1700 cm^{-1} (amide **I** and **II**) and 3050–3600 cm^{-1} (ν_{NH}). The spectra of pure NMA at room and liquid nitrogen temperature are given in Fig. 1*a* and 1*b*, respectively.

TABLE 1. Schematic representation and related frequencies (in cm^{-1}) for the various types of interaction in self-associated NMA and complexes with salts

		Amide I	ν_{NH}	γ_{NH}	
I	—CO···NH—CO···HN—	1654	3300	725	601
II	ClO_4^-···HN—CO···Ba^{2+}	1652	3405	666	582
II	ClO_4^-···HN—CO···Li^+	1663	3405	~670	582
III	ClO_4^-···HN—CO<(Li^+)(Li^+)	1625	~3400	700	598
IV	ClO_4^-···HN—CO<(Li^+)(HN—)[a]	1630	3300–3258 3300–3356	728 672	711 590
II	Br^-···HN—CO···NBu_4^+ [b]	1667	3258	720	593
II	Br^-···HN—CO···Li^+ [d]	1665 1632	3277	715	598
	Br^- HN—CO(Li^+)···Li^+ [d]	1632	3380	—	580

[a]Observed only at low temperature.
[b]Bu_4N^+ represents the tetrabutylammonium entity.
[c]Complex obtained from a mixture of amide and salt.
[d]Complex obtained from a mixture of amide and salt in methanol. In this case, some of the interactions cannot be localized definitively.

II.2. Interactions with neutral salts

Depending on the amide/salt ratio four different types of local structures have been identified (5) (Table 1): self-associated chains (**I**), complexes of a single molecule with ions (**II** and **III**), and self-associated chains interacting with ions (**IV**). These representations are quite schematic since they do not account for the real coordination of the ions.

II.2.1. Interactions with perchlorate salts

Infrared spectra corresponding to NMA interacting with barium perchlorate ($Ba(ClO_4)_2$, amide/salt = 5 or 6) are typical of a complex of type **II** (5) with an amide A band at 3405 cm^{-1} and amide **V** and **VI** bands at 666, 582 cm^{-1} due to weak NH···ClO_4^- interaction. The amide **I** at 1652 cm^{-1} corre-

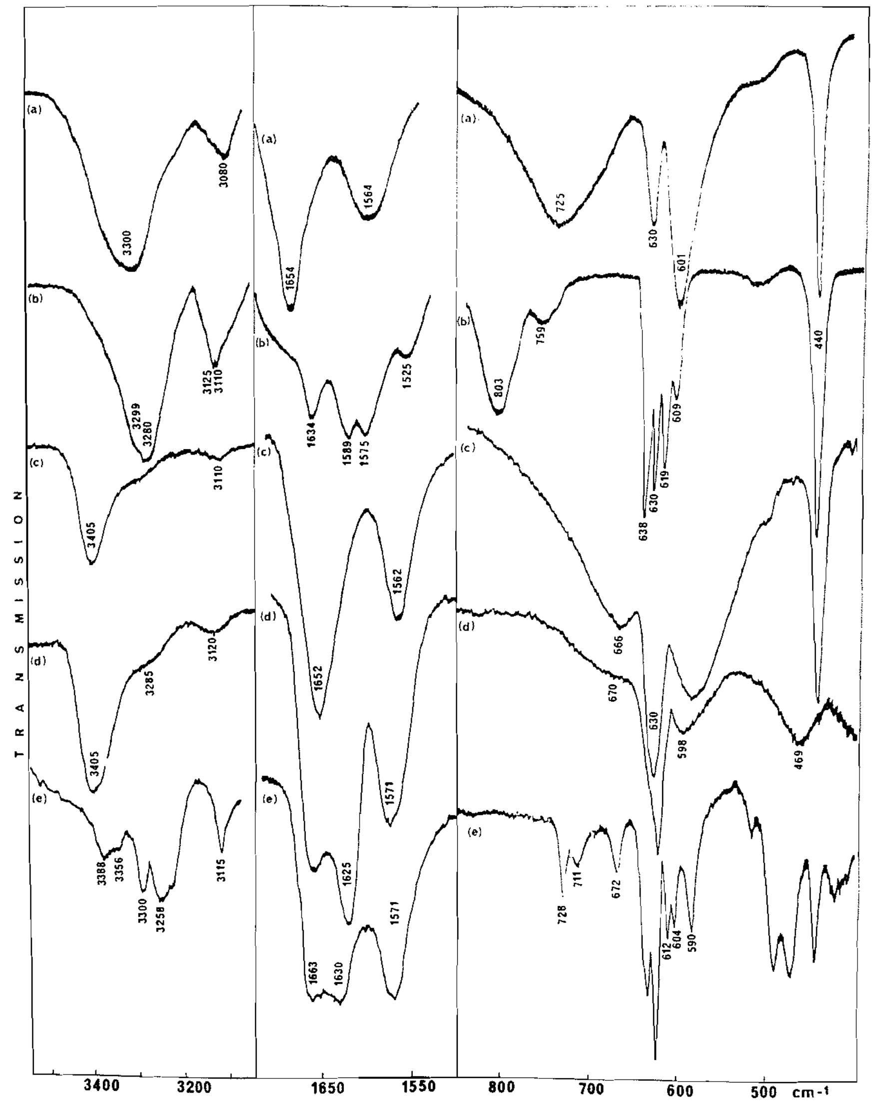

FIG. 1. Infrared spectra in the γ_{NH}, ν_{CO}, and ν_{NH} regions of NMA and its complexes in Nujol or Fluorolube mulls: (*a*) pure liquid NMA at room temperature; (*b*) pure NMA crystallized at liquid nitrogen temperature; (*c*) NMA with barium perchlorate (amide/salt = 5) at room temperature; (*d*) NMA with lithium perchlorate (amide/salt = 2) at room temperature; (*e*) NMA with lithium perchlorate (amide/salt = 2) at liquid nitrogen temperature.

sponds to $CO\cdots Ba^{2+}$ contacts (Fig. 1*c* and Table 1). It must be noticed that the strong band at 630 cm^{-1} is due to the overlapping of the ClO_4^- stretching with the bending of the carbonyl group.

The situation is quite similar for $LiClO_4$ salt at room temperature but depending on the amide/salt ratio the amide **I** band shows one or two components corresponding to one or two Li^+ interacting with the carbonyl group (1663 and 1625 cm^{-1}, respectively) indicating the existence of complexes **II** and **III** (Table 1). Figure 1*d* shows an example of a mixture of the two complexes. In this case the Li^+ vibration is observed at 469 cm^{-1}. At low temperature (Fig 1*e*), the amide A band splits in several components (3258, 3300, 3356, 3388 cm^{-1}) and three amide **V–VI** doublets (728–612, 711–604, and 672–590 cm^{-1}) are well resolved in the NH bending region, which suggest that there may be several different interactions acting simultaneously. A tentative interpretation is given (Table 1) on the ground of the relationship between frequencies and the strength of the interactions previously discussed (3–7, 14, 15).

II.2.2 Interactions with tetrabutylammonium bromide

Infrared spectrum of a mixture of NMA with tetrabutylammonium bromide (Fig. 2) shows that self-association is destroyed while rather strong $NH\cdots Br^-$ (amide A at 3258 cm^{-1}) interactions appear. The observed frequencies are all consistent with type **II** complex (Table 1) (5). Amide **V** and **VI** bands appear at 593 and 720 cm^{-1}, respectively, the latter overlapping with a band at 738 cm^{-1} due to the tetrabutylammonium ion.

II.2.3. Interactions with lithium bromide

In this case the spectrum depends on the sample preparation method.

When the salt is dissolved in pure NMA the spectra in the NH stretching and bending regions are similar to those observed for the complex with tetrabutylammonium bromide, while the amide **I** frequency corresponds to that observed for $CO\cdots Li^+$ interactions (Fig. 3*a*). These results support the existence of type **II** and **III** complexes in which one or two Li^+ ions interact with the carbonyl group. Crystallographic data (16) indicate that the carbonyl group interacts with only one lithium but there are two different $CO\cdots Li^+$ distances in the

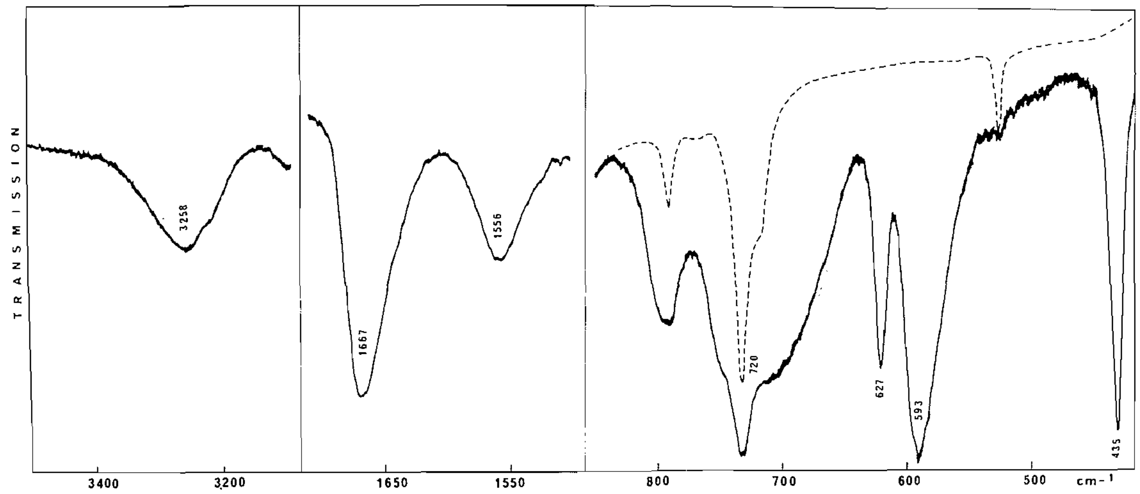

FIG. 2. Infrared spectra in the γ_{NH}, ν_{CO}, and ν_{NH} regions of (——) NMA with tetrabutylammonium bromide (amide/salt = 4); (----) tetrabutylammonium bromide; in Nujol or Fluorolube mulls at room temperature.

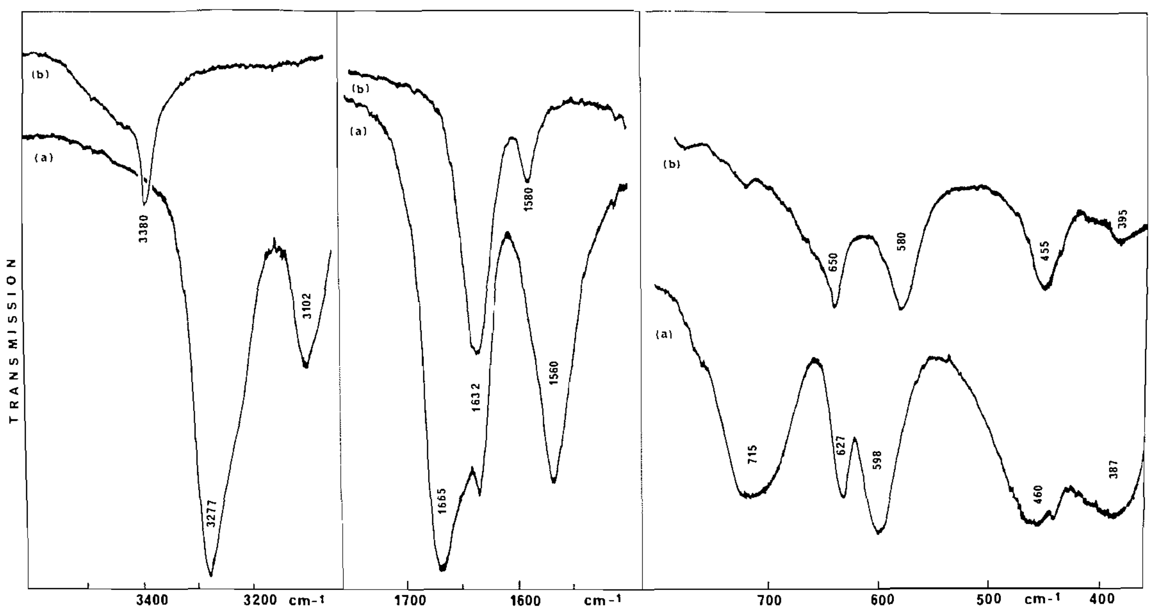

FIG. 3. Infrared spectra in the γ_{NH}, ν_{CO}, and ν_{NH} regions of NMA with LiBr in Nujol or Fluorolube mulls: (*a*) complex obtained from a simple mixture of amide and salt; (*b*) complex obtained from a mixture of amide and salt in methanol.

unit cell which may account for the two observed amide **I** bands. Amide **V** and **VI** are at 598 and 715 cm^{-1}, respectively. The strong bands near 400 and 460 cm^{-1} are ascribed to Li^+ vibrations.

If NMA and LiBr are dissolved with the same amide/salt ratio in methanol which is then removed slowly, a completely different spectrum is observed (Fig. 3*b*): the amide A band appears at 3380 cm^{-1} indicating a very weak interaction of the NH group, while the frequency of the amide **I** band (1633 cm^{-1}) is rather low. The amide B band is very weak. There is only one NH bending mode at 580 cm^{-1} which can be clearly identified upon deuteration but there may be a weak component about 650 cm^{-1} overlapping with the amide **IV** band at 630 cm^{-1}.

Frequencies of the amide A and of the NH bending appear too high and too low, respectively, to be ascribed to $NH\cdots Br^-$ or self associated species alone (5). A possible interpretation could be to consider some additional interactions between the nitrogen atom or π electrons and the Li^+ ion.

II.3 Discussion

In pure NMA (Fig. 1*a*) amide **V** and **VI** bands observed between 600–620 and 700–800 cm^{-1}, respetively (Fig. 1*a* and *b*) have been ascribed to a tunnel effect due to the inversion of the NH bond (3). These bands are hydrogen bond sensitive: the frequencies and the splitting decrease when the $NH\cdots X$ bond strength decreases (3). Amide **V** and **VI** bands are clearly identified in complexes with neutral salts which suggests a non-planar structure of the nitrogen atom. The complex with LiBr (Fig. 3*b*) is the only case where there is no clear-cut evidence for tunnel effect and it is difficult to decide whether the structure is planar or not.

Amide A and B bands for pure NMA appear in the 3050–3150 and 3250–3300 cm^{-1} ranges (Fig. 1*a* and *b*).

They have been ascribed to the fundamental ν_{NH} transition (amide B) and to the combination $\nu_{NH} + \gamma^{*}_{NH}$ (amide A, γ^{*}_{NH} representing the frequency of the bending mode in the excited state of the NH stretching (4)). According to this interpretation, the amide A and B bands depend on the strength of the interaction in which the NH group is engaged and their relative intensities are related to the non-planarity of the nitrogen atom in the fundamental state (4). In complexes with neutral salts the amide B band remains always weak relatively to the amide A band which is consistent with a pyramidal structure of the nitrogen atom.

III. Conclusion

Infrared spectra of complexes of NMA with neutral salts give evidence for various interactions of the CO and NH groups with the ions and schematic structures are proposed in agreement with previous results (5). In every case, much in the same way as for NMA in solutions (3), the NH bending mode gives one or several doublets which may be ascribed to tunnel effect indicating a non-planar structure of the nitrogen atom and a fast inversion of the NH bond. This interpretation is consistent with the fact that the amide B band remains weak relatively to the amide A band in every case (4) and confirms that the pyramidal structure is but not too sensitive to the strength and to the nature (hydrogen bond or ionic) of the interactions of the CONH entity with the surrounding medium.

1. F. FILLAUX and J. TOMKINSON. Chem. Phys. **26**, 295 (1977).
2. F. FILLAUX, M. H. BARON, C. DE LOZÉ, and G. SAGON. J. Raman Spectrosc. **7**, 246 (1978).
3. F. FILLAUX and M. H. BARON. Chem. Phys. **62**, 275 (1981).
4. F. FILLAUX. Chem. Phys. **62**, 287 (1981).
5. M. H. BARON and C. DE LOZÉ. J. Chim. Phys. **69**, 1084 (1972).
6. M. H. BARON. Thèse d'Etat, Paris. 1973.
7. C. DE LOZÉ, M. H. BARON, and F. FILLAUX. J. Chim. Phys. **75**, 631 (1978).
8. T. MIYAZAWA. J. Mol. Spectrosc. **5**, 155 (1960).
9. H. PIVCOVA, B. SCHNEIDER, and J. ŠTOKE. Coll. Czech. Chem. Commun. **30**, 2215 (1965).
10. B. SCHNEIDER, B. HORENI, H. PIVCOVA, and J. HONŽL. Coll. Czech. Chem. Commun. **30**, 2196 (1965).
11. J. JAKEŠ and S. KRIMM. Spectrochim. Acta, **27**A, 19 (1971).
12. M. REY-LAFON, M. T. FOREL, and C. GARRIGOU-LAGRANGE. Spectrochim. Acta, **29**A, 471 (1973).
13. E. M. BRADBURY and A. ELLIOTT. Spectrochim. Acta, **19**, 995 (1963).
14. F. FILLAUX and C. DE LOZÉ. J. Chim. Phys. **69**, 36 (1972).
15. M. REY-LAFON, J. LASCOMBE, and M. L. JOSIEN. Ann. Chim. **8**, 493 (1963).
16. D. J. HAAS. Nature, **201**, 64 (1964).

Determination of stretching force constants of weakly bound dimers from centrifugal distortion constants

D. J. MILLEN

Christopher Ingold Laboratories, Department of Chemistry, University College London, 20 Gordon Street, London WC1H 0AJ, England

Received July 27, 1984

This paper is dedicated to Professor Camille Sandorfy on the occasion of his 65th birthday

D. J. MILLEN. Can. J. Chem. **63**, 1477 (1985).

Expressions are derived from which stretching force constants for the weak bond in weakly bound dimers may be evaluated directly from observed rotational constants and centrifugal stretching distortion constants.

D. J. MILLEN. Can. J. Chem. **63**, 1477 (1985).

On a dérivé des expressions à partir desquelles on peut évaluer les constantes de force d'élongation pour la faible liaison dans des dimères faiblement liés; cette évaluation peut se faire directement à partir des constantes rotationnelles observées et des constantes de distortion lors de l'élongation des liaisons par force centrifuge.

[Traduit par le journal]

Introduction

In recent years stretching force constants have been obtained for many weakly bound dimers. In some cases such force constants have been determined in the well-established way from vibrational wavenumbers associated with the stretching modes of the weakly bound dimer (1). In the majority of cases, however, they have been determined from the centrifugal distortion constant D_J since the information available is limited, by the experimental technique employed, to properties of the vibrational ground state (2, 3). Often a pseudo-diatomic model, which is equivalent to regarding each monomer as a point mass, has been used although it has been pointed out that this model is found to be satisfactory only when moments of inertia of the constituent monomers are small (4). Expressions have been obtained when this restriction is relaxed and allowance made for the inertial properties of the monomers for the specific case of a linear triatomic dimer (5) and for other particular cases (4), although these latter expressions contain a geometrical parameter which refers to the distance between the monomer units in the dimer. The present paper derives expressions in a general manner, for various classes of dimer, in a form which can be used for the evaluation of force constants directly from centrifugal distortion constants and rotational constants without introducing any structural parameters or indeed any assumption about internuclear distances in the dimer. It is clearly advantageous for such purposes as the comparison of force constants for series of hydrogen bonded dimers if force constants are evaluated from expressions not limited by the pseudo-diatomic approximation. Indeed, in some cases force constants free of this limitation have already been reported (4, 6).

Results and discussion

Dimers of the general type to be examined are conveniently denoted as B···H—A. The proton donor H—A may be a diatomic molecule, e.g. HF, HCl, or a polyatomic linear molecule, e.g., HCN, H—C≡C—H. The acceptor B is taken in turn to be a linear molecule, a symmetric top, and then cases are examined where B is a planar asymmetric top, first with HA in the plane of the asymmetric top and then with HA perpendicular to the plane of the asymmetric top. The model employed throughout regards force constants for distortions which contribute to D_J, other than the force constant for the stretching of the weak bond, to be so large by comparison with the stretching force constant of the weak bond that all distortions other than stretching of the weak bond can be neglected. Thus for a linear dimer where D_J, measured as a frequency, is given by

$$[1] \quad D_J h = \frac{\hbar^4}{8I^4} \sum_{ij} J_{xx}^{(i)} (f^{-1})_{ij} J_{xx}^{(i)}$$

in which I is the principal moment of inertia, $J_{xx}^{(i)} = \partial I_{xx}/\partial R_i$, where R_i is the ith internal co-ordinate and $(f^{-1})_{ij}$ is the ijth compliance constant, all the $(f^{-1})_{ij}$ which contribute to D_J are put to zero except for the compliance constant which refers to the stretching of the weak bond.

The derivations use relationships between moments of inertia of dimer and monomers as for rigid bodies and so the expressions obtained will be strictly applicable to equilibrium rotational constants. The use of ground state rotational constants may lead to significant deviation where vibration–rotation constants α arise which are significant by comparison with rotational constants, as for example for large amplitude bending or stretching modes of very weakly bonded dimers.

Triatomic linear dimers B···H—A

A number of dimers of this class have been studied, including for example Ar···HF (7) and also Kr···ClF (8). Geometrical parameters and masses for such a dimer are defined in Fig. 1. B is represented by the mass m_B while D and d refer to the distances of B from centres of masses of dimer and H—A monomer, respectively. The principal moment of inertia of the dimer is given by

$$[2] \quad I_D = m_B D^2 + I_{HA} + m_{HA}(d - D)^2$$

where m_{HA} and I_{HA} refer to the mass and principal moment of inertia of HA. Substituting for D from the centre of mass condition we obtain

$$[3] \quad I_D = I_{HA} + \mu_D d^2$$

where

$$[4] \quad \frac{1}{\mu_D} = \frac{1}{m_B} + \frac{1}{m_{HA}}$$

Now if we use eq. [3] to insert into eq. [1] the single term that arises in the model, namely, that for stretching the weak intermolecular bond for which the force constant is k, the result is

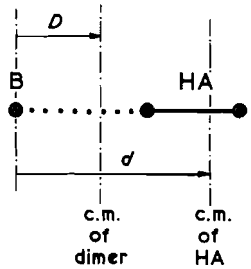

FIG. 1. Geometrical parameters and masses for triatomic linear dimers.

$$[5] \quad D_J h = \frac{\hbar^4}{2I_D^4}\frac{\mu_D^2 d^2}{k}$$

Finally eliminating d from this equation by using eq. [3] leads to

$$[6] \quad k = \frac{16\pi^2 \mu_D B_D^3}{D_J}\left(1 - \frac{B_D}{B_{HA}}\right)$$

where B_D and B_{HA} are the rotational constants for the dimer B···HA and for the monomer HA, respectively. If the stretching frequency ω of the dimer is assumed to be given as for a diatomic molecule, that is, if coupling with the H—A stretching motion through the stretching force constant for this bond and the cross term in the potential function are ignored, then eq. [6] leads to

$$[7] \quad D_J = \frac{4B_D^3}{\omega^2}\left(1 - \frac{B_D}{B_{HA}}\right)$$

an equation which has been obtained by Novick (5) using an alternative derivation for the particular case of the triatomic dimer. The equation reduces to the well known expression for the pseudo-diatomic case

$$[8] \quad D_J = \frac{4B_D^3}{\omega^2}$$

when $B_{HA} >> B_D$.

Polyatomic linear dimer

The geometrical parameters required for discussion of the general case are defined in an analogous way to those for the triatomic dimer and are shown in Fig. 2. In this case the principal moment of inertia of the dimer is given by

$$[9] \quad I_D = I_B + m_B D^2 + I_{HA} + m_{HA}(d - D)^2$$

where m_B and I_B are the mass and principal moment of inertia of B. Proceeding as before we obtain

$$[10] \quad D_J h = \frac{\hbar^4}{2I_D^4}\frac{\mu_D^2 d^2}{k}$$

In this case $\mu_D d^2$ is given by

$$[11] \quad \mu_D d^2 = I_D\left(1 - \frac{I_{HA} + I_B}{I_D}\right)$$

and hence the force constant k is given by

$$[12] \quad k = \frac{16\pi^2 \mu_D B_D^3}{D_J}\left(1 - \frac{B_D}{B_{HA}} - \frac{B_D}{B_B}\right)$$

When B is a point mass eq. [12] reduces to eq. [6]. The conditions under which this expression reduces to that for the pseudo-diatomic model are seen to be $B_{HA} >> B_D$ and $B_B >> B_D$.

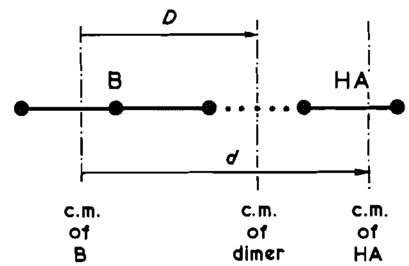

FIG. 2. Geometrical parameters and masses for polyatomic linear dimers.

Symmetric top dimers

Numerous examples of symmetric top dimers such as CH_3CN···HF (9), PH_3···HCl (10), and H_3N···H—C≡C—H (11) have been examined. The parameters D and d are defined again as in Fig. 2. D and d are related through the centre of mass condition.

$$[13] \quad \sum_{B} m_i(z_i - D) + \sum_{HA} m_j(z_j + d - D) = 0$$

where z refers to the symmetry axis of the top. These lead to

$$[14] \quad D = \frac{m_{HA} d}{m_B + m_{HA}}$$

and making use of the expression for a symmetric rotor (16)

$$[15] \quad D_J h = -\frac{\hbar^4}{4}\tau_{xxxx}$$

we obtain

$$[16] \quad k = \frac{16\pi^2 \mu_D B_D^3}{D_J}\left(1 - \frac{B_D}{B_{HA}} - \frac{B_D}{B_B}\right)$$

An alternative expression (4) has been obtained by a similar derivation for symmetric tops, but the present expression has the advantage of allowing calculation of k directly from the centrifugal distortion constants and rotational constants without requiring the evaluation of any structural parameter of the dimer.

Asymmetric top dimers

Planar asymmetric top dimers with C_{2v} symmetry

Examples of this group of dimer are formed by H—C≡C—H with HF (12) and HCl (13), and the group may be extended to include H_2O···HF (14) and H_2O···HCl (15), which are effectively planar. The parameters D and d are defined in an analogous way to that in Fig. 2. If we take the case where the symmetry axis z is the a-axis, we have for the principal moments of inertia about the b- and c-axes

$$[17] \quad I_D^b = I_B^b + I_{HA} + \mu_D d^2$$

and

$$[18] \quad I_D^c = I_B^c + I_{HA} + \mu_D d^2$$

In this case it has been shown (16)

$$[19] \quad D_J h = -\frac{\hbar^4}{32}(3\tau_{bbbb} + 3\tau_{cccc} + 2\tau_{ccbb})$$

Following the procedure as before we obtain

$$[20] \quad D_J h = 16\pi^4 \mu_D^2 d^2 k^{-1}[4B_D^4 + 4C_D^4 - (B_D - C_D)^2(B_D + C_D)^2]$$

which, when combined with eqs. [17] and [18], leads to

$$[21] \quad k = \frac{8\pi^2\mu_D}{D_J}[B_D^3(1-b) + C_D^3(1-c) - \tfrac{1}{4}(B_D - C_D)^2(B_D + C_D)(2-b-c)]$$

where

$$[22] \quad b = \frac{B_D}{B_B} + \frac{B_D}{B_{HA}}$$

and c is given by an analogous expression. In the case when $B_D = C_D$ eq. [21] reduces to eq. [12].

Asymmetric top dimers with hydrogen bond perpendicular to planar momomer

Dimers of this kind include hydrogen bonded complexes formed by $H_2C{=}CH_2$ with HF (17) and HCl (18). The parameters D and d now refer to the distance along the z-direction of the molecular plane of B from the centres of mass of dimer and HA respectively. I_D^b and I_D^c are again given by eqs. [17] and [18]. The centrifugal distortion constant Δ_J is given by (19).

$$[23] \quad \Delta_J h = -\frac{\hbar^4}{8}(\tau_{xxxx} + \tau_{yyyy})$$

and following the procedures used previously we obtain

$$[24] \quad \Delta_J h = 64\pi^4\mu_D^2 d^2 k^{-1}[B_D^4 + C_D^4]$$

Substituting for $\mu_D d^2$ from eqs. [17] and [18] leads to

$$[25] \quad k = \frac{8\pi^2\mu_D}{\Delta_J}[B_D^3(1-b) + C_D^3(1-c)]$$

where b and c are defined as before. This expression is generally applicable to asymmetric rotor dimers with HA along a principal axis of inertia and thus also applies to planar dimers. It is seen from eq. [25] that significant deviations from the pseudo-diatomic model will arise when rotational constants for the dimer, B_D and C_D, are not small by comparison with B and C values for either of the constituent monomers of the dimer.

Discussion

Expressions have been obtained which relate stretching force constants for the weak bond in weakly bound dimers to centrifugal stretching distortion constants. The expressions, which are free of limitations of the pseudo-diatomic model, are in a convenient form for direct application to dimers B···HA of linear and symmetric rotor types and also to certain asymmetric rotor types. Calculations have already been made (4) which show that use of the pseudo-diatomic model can lead to significant error in the force constant k as a consequence of neglecting the inertial properties of the components which constitute the dimer. Other calculations have been made which show that the expressions obtained lead to consistent results when applied to a series of molecules (6), to series of several isotopic species of a linear dimer, $N_2\cdots HCN$ (20), and to a series of several isotopic species of an asymmetric rotor dimer, $H_2O\cdots HCN$ (21). Recent applications have also been made to the linear dimer $HC{\equiv}C{-}C{\equiv}N\cdots HF$ (22) and to the symmetric rotor $(CH_3)_3P\cdots HCN$ (23).

1. A. C. Legon, D. J. Millen, and S. C. Rogers. Proc. R. Soc. Ser. A, **370**, 213 (1980).
2. A. C. Legon. Ann. Rev. Phys. Chem. **34**, 275 (1983).
3. T. R. Dyke. Top. Curr. Chem. **120**, 86 (1984).
4. W. G. Read, E. J. Campbell, and G. Henderson. J. Chem. Phys. **78**, 3501 (1983).
5. S. E. Novick. J. Mol. Spectrosc. **68**, 77 (1977).
6. A. C. Legon and L. C. Willoughby. Chem. Phys. Lett. **109**, 502 (1984).
7. M. R. Keenan, L. W. Buxton, E. J. Campbell, A. C. Legon, and W. H. Flygare. J. Chem. Phys. **74**, 2133 (1981).
8. S. E. Novick, S. J. Harris, K. C. Janda, and W. Klemperer. Can. J. Phys. **53**, 2007 (1975).
9. J. W. Bevan, A. C. Legon, D. J. Millen, and S. C. Rogers. Proc. R. Soc. Ser. A, **370**, 239 (1980).
10. A. C. Legon and L. C. Willoughby. J. Chem. Soc. Chem. Commun. 997 (1982).
11. G. T. Fraser, K. R. Leopold, and W. Klemperer. J. Chem. Phys. **80**, 1423 (1984).
12. W. G. Read and W. H. Flygare. J. Chem. Phys. **76**, 2238 (1982).
13. A. C. Legon, P. D. Aldrich, and W. H. Flygare. J. Chem. Phys. **75**, 625 (1981).
14. J. W. Bevan, Z. Kisiel, A. C. Legon, D. J. Millen, and S. C. Rogers. Proc. R. Soc. Ser. A, **372**, 441 (1980).
15. A. C. Legon and L. C. Willoughby. Chem. Phys. Lett. **95**, 449 (1983).
16. D. Kivelson and E. B. Wilson. J. Chem. Phys. **20**, 1575 (1952).
17. J. A. Shea and W. H. Flygare. J. Chem. Phys. **76**, 4857 (1982).
18. P. D. Aldrich, A. C. Legon, and W. H. Flygare. J. Chem. Phys. **75**, 2126 (1981).
19. J. K. G. Watson. J. Chem. Phys. **46**, 1935 (1967).
20. E. J. Goodwin and A. C. Legon. Chem. Phys. Lett. In press.
21. A. Fillery-Travis, A. C. Legon, and L. C. Willoughby. Proc. R. Soc. Ser. A. **396**, 405 (1984).
22. K. Georgiou, A. C. Legon, D. J. Millen, H. M. North, and L. C. Willoughby. Proc. R. Soc. Ser. A, **394**, 387 (1984).
23. H. L. Hirani, A. C. Legon, D. J. Millen, and L. C. Willoughby. J. Mol. Struct. **125**, 171 (1984).

Étude d'un modèle simplifié de la rhodopsine: la toute *trans*-rétinylidène *tert*-butylamine en présence de divers acides carboxyliques

MARTINE BISSONNETTE, HOA LE THANH ET DANIEL VOCELLE[1]

Département de chimie, Université du Québec à Montréal, C.P. 8888 succ. A, Montréal (Qué.), Canada H3C 3P8

Reçu le 29 juillet 1984

Cet article est dédié au Professeur Camille Sandorfy à l'occasion de son 65e anniversaire

MARTINE BISSONNETTE, HOA LE THANH et DANIEL VOCELLE. Can. J. Chem. **63**, 1480 (1985).

Un système modèle du chromophore de la rhodopsine consistant en une base de Schiff (la toute *trans*-rétinylidène *tert*-butylamine) et divers acides carboxyliques a été étudié par les spectroscopies ultraviolette–visible (uv–vis) et par résonance magnétique nucléaire du proton. Dans le méthanol, un solvant polaire, les résultats montrent que les acides faibles sont capables de protoner complètement la fonction imine, que les doubles liaisons sont perturbées par la protonation, qu'un effet de nivellement est présent et que finalement, il existe un échange de protons entre l'imine protonée et le solvant. Dans le chloroforme, les résultats indiquent que les acides faibles ne peuvent pas protoner complètement la base de Schiff et qu'un équilibre existe entre une paire d'ions ($—\overset{+}{N}H$----$\overset{-}{O}_2C—$) et sa contre-partie neutre ($—N$:----$HO_2C—$). De plus, une interaction similaire à celle proposée par Nakanishi (théorie de l'effet de charges externes) semble se produire entre la chaîne polyénique de la base de Schiff et une fonction polaire localisée sur l'acide. Finalement, deux comparaisons sont faites: l'une utilise une base de Schiff similaire (la *trans,trans*-heptadiénylidène-2,4 *tert*-butylamine), l'autre se réfère à la rhodopsine.

MARTINE BISSONNETTE, HOA LE THANH, and DANIEL VOCELLE. Can. J. Chem. **63**, 1480 (1985).

A model system of the chromophore of rhodopsin consisting of a Schiff base (all-*trans*-retinylidene *tert*-butylamine) and several carboxylic acids has been studied by uv–vis and ^1H nmr spectroscopy. In methanol, a polar solvent, results indicate that weak acids are able to protonate fully the imine function, that all the double bonds are perturbed by protonation, that a leveling effect is present, and, finally, that a proton exchange between the protonated Schiff base and the solvent is also present. In chloroform, results indicate that weak acids cannot fully protonate the Schiff base and that an equilibrium exists between an ion pair ($—\overset{+}{N}H$----$\overset{-}{O}_2C—$) and a neutral species ($—\dot{N}$----$HO_2C—$). Furthermore, an interaction similar to Nakanishi's external point charge seems to exist between the polyenic chain of the Schiff base and a polar function on the acid. Finally, two comparisons are established: one with a similar Schiff base – the *trans,trans*-2,4-heptadienylidene *tert*-butylamine – the other with rhodopsine.

Introduction

Le mécanisme moléculaire de la vision est encore mal connu même si de multiples travaux ont été faits au cours des vingt dernières années. Plusiers excellentes revues et monographies ont été publiées récemment (1). La structure exacte de la rhodopsine, le pigment visuel, fait encore l'objet de controverse, surtout au niveau de la protonation de la fonction imine et de la nature des interactions protéine–chromophore. Suite aux travaux de Kropf et Hubbard (2*a*), de Wiesenfeld et Abrahamson (2*b*) et de Kakitani et Kakitani (2*c*) sur la régulation de l'absorption maximale (λ_{max}) de la rhodopsine, Nakanishi et coll. (2*d*, *e*, *f*) ont présenté, sur la base de modèles expérimentaux, une proposition qui fait appel à deux interactions principales: la première résulte de la protonation de la fonction imine tandis que la seconde provient de charges situées près des doubles liaisons $C_{11}—C_{12}$ et $C_{13}—C_{14}$. Tout récemment, Mateescu et Igbal (2*g*) ont décrite des modèles qui, eux aussi, font appel à des interactions dues à un azote chargé positivement et à un ion carboxylate. Toutefois, des études en résonance magnétique nucléaire du ^{13}C et ^{15}N tendent à démontrer que la protonation est très variable et que celle-ci semble dépendre pour beaucoup de la préparation de l'échantillon (3) (voir aussi la réf. 3*e* au sujet de la bactériorhodopsine).

Afin d'approfondir ces deux questions, il est impérieux de connaître quel acide de l'opsine peut servir d'agent de protonation de la base de Schiff et quelle est la nature du milieu environnant le chromophore. Maintenant que la structure primaire de l'opsine est mieux connue (4), il est vraisemblable de penser que le chromophore puisse être protoné par les fonctions carboxyles terminales des acides glutamique ou aspartique tandis que les charges responsables du déplacement dû à l'opsine puissent provenir également d'une fonction carboxylate. Le milieu entourant le chromophore se doit d'être aussi évalué car il influe beaucoup sur ces interactions électrostatiques. Ainsi Honig *et al.* (5), afin d'expliquer le grande différence d'énergie entre la rhodopsine et la bathorhodopsine (tout près de 35 kcal/mol, réf. 6), ont proposé une séparation de charge entre l'imine protonée et son contre-ion carboxylate. Pour ce faire, ils ont suggéré un environnement hydrophobe (de faible constante diélectrique) afin d'avoir une paire d'ions de type $—\overset{+}{N}H$----$\overset{-}{O}_2C—$. Toutefois, Rafferty et Shichi (7) ont montré la présence d'eau autour du chromophore tandis que Warshel et Barboy (8) doutent de la présence d'un environnement non polaire car les paires d'ions n'y seraient pas stables. Les problèmes concernant les interactions du chromophore de la rhodopsine avec son milieu protéinique ne sont donc pas résolus ce qui retarde d'autant plus la solution du mécanisme moléculaire de la vision, du moins dans son étape initiale.

Afin de jeter quelques lumières sur la nature de ces interactions, nous avions imaginé, dans un premier temps, un modèle très simplifié de la rhodopsine. Ce modèle consistait en une base de Schiff trois fois conjuguées, la *trans,trans*-heptadiénylidène-2,4 *tert*-butylamine (HBA), et divers acides carboxyliques servant à la fois d'agent de protonation et d'agent de perturbation des doubles liaisons. La figure 1(a) montre ce modèle et la nature des interactions espérées. Pour explorer le rôle du milieu environnant le chromophore dans la rhodopsine, deux solvants – le chloroforme et le méthanol – ont été utilisés dans notre modèle. Puisque Honig *et al.* (5) préconisent l'existence d'un environnement peu polaire, de faible constante diélectrique, nous avons pensé utiliser le chloroforme afin d'imiter ce milieu. Quoique ce solvant ressemble peu au milieu biologique, notre choix s'explique par les faits suivants: le

[1] Auteur à qui adresser la correspondance.

(a)

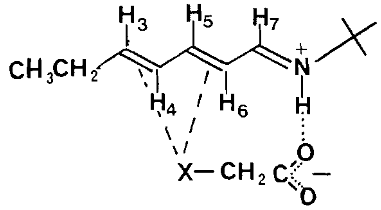

(b)

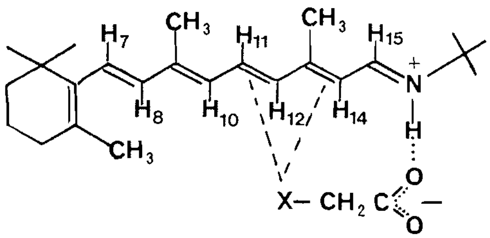

FIG. 1. Modèle simplifié de la rhodopsine; (a) la *trans,trans*-heptadiénylidène-2,4 *tert*-butylamine en présence d'un acide carboxylique; (b) la toute *trans*-rétinylidène *tert*-butylamine.

solvant doit être hydrophobe, les acides carboxyliques de même que leurs sels choisis pour notre étude doivent y avoir une solubilité assez grande pour que des spectres de ^{1}H rmn puissent être pris (il faut aussi que l'analogue deutérié existe) et finalement, le solvant utilisé doit permettre des recoupements avec d'autres études faites sur ce sujet. Le chloroforme remplit ces trois conditions et a donc été retenu. Le choix du méthanol repose sur les mêmes conditions que précédemment sauf que nous voulions un milieu plus hydrophile, l'eau étant exclue puisque l'imine protonée y réagit instantanément pour donner l'heptadiénal et la *tert*-butylamine. L'étude spectroscopique (uv – ^{1}H rmn) de ce modèle (9) a permis de mettre en évidence les points suivants. 1. Les acides carboxyliques modérément acides (pK_a (H_2O) entre 2 et 4) ne parviennent à protoner que partiellement la base de Schiff dans le chloroforme. 2. Également dans le chloroforme, un équilibre est établi entre une paire d'ions et la paire non-ionisée tel que montré ci-dessous (éq. [1]):

$$[1] \quad \mathrm{RCH{=}\overset{\displaystyle R'}{\underset{+}{N}}{-}H{-}{-}{-}{-}\underset{-}{O_2}C{-}R''} \rightleftharpoons \mathrm{RCH{=}\overset{\displaystyle R'}{N}{-}{-}{-}{-}H{-}O_2CR''}$$

3. Dans le méthanol, la protonation est cette fois-ci complète et aucune paire d'ions ne semble exister. Un effet de nivellement (tous les résultats sont les mêmes) est créé par le solvant.

Comme ces données sont fort importantes en regard de leur implication dans le mécanisme moléculaire de la vision, nous avons voulu les vérifier à l'aide d'un modèle s'apparentant encore mieux avec la rhodopsine où le chromophore est une rétinylidène amine de configuration 11 *cis*. Le modèle retenu consiste en la toute-*trans*-rétinylidène *tert*-butylamine (RBA) et en les mêmes acides et solvants qu'auparavant. La figure 1(b) montre notre modèle. La similitude de ce modèle avec celui de la fig. 1(a) est très grande de telle sorte que d'utiles comparaisons pourront être établies.

Méthode et procédure

La toute-*trans*-rétinylidène *tert*-butylamine a été synthétisée de la manière usuelle en suivant les indications fournies par Blatz *et al.* (10). Pour ce faire, le tout *trans*-rétinal (Aldrich Chemical Co.) est ajouté à la *tert*-butylamine fraîchement distillée, sous atmosphère d'azote et à l'obscurité. Du méthanol anhydre est utilisé comme solvant et quelques billes de tamis moléculaire (4A) sont ajoutées au mélange afin d'enlever l'eau produite par la réaction. Le tout est gardé à 0°C et un solide jaunâtre est obtenu. Plusieurs lavages à l'éther éthylique puis une évaporation poussée ont conduit à la *trans*-rétinylidène *tert*-butylamine. La pureté du produit a été évaluée par rmn et par uv–vis. Les acides utilisés étaient des produits commerciaux qui ont été séchés soit par distillation sur tamis moléculaire soit sous vide en présence de P_2O_5. Le chloroforme a été chromatographié sur une colonne d'alumine basique puis distillé sur du tamis moléculaire tandis que le méthanol a été rendu anhydre par la méthode de Perrin *et al.* (11).

Les spectres électroniques ont été obtenus en utilisant un spectrophotomètre Cary 17 et des solutions de RBA et d'acides à des concentrations de 10^{-5} *M*. Les spectres de rmn du proton ont été obtenus à l'aide d'un instrument Brucker WH/DS (400 MHz). Les concentrations dans ces cas étaient de l'ordre de 10^{-2} *M*. L'attribution des pics aux différents hydrogènes va de soi pour H_{15} et H_{11} qui sont les deux hydrogènes les plus déblindés mais est plus complexe pour les autres hydrogènes éthyléniques. L'attribution des pics à H_{14} et aux couples H_7, H_8 et H_{10}, H_{12} a été faite en utilisant la technique de la double résonance. Cette technique a été utilisée pour tous les spectres de mélange de RBA et d'acides. L'identification des pics pour H_7 et H_8 de même que pour H_{10} et H_{12} a été possible en se référant au spectre du tout *trans*-retinal et des attributions faites par Patel (12). Sur la base de ces travaux, H_7 est plus déblindé que H_8 et H_{12} est plus déblindé que H_{10} (voir plus loin dans le texte pour une discussion plus approfondie). Les solvants deutérés: $CDCl_3$, CD_3OD et CD_3OH ont été utilisés sans autre purification (MSD-Isotopes).

Résultats et discussion

Étude des spectres électroniques

La toute *trans*-rétinylidène *tert*-butylamine a été mélangée dans un rapport 1:1 avec différents acides carboxyliques en utilisant le chloroforme et le méthanol comme solvants. L'étude des spectres électroniques de ces systèmes est présentée au tableau 1. Dans le méthanol, les résultats sont simples: les spectres ne montrent qu'une seule bande à 440 nm. La figure 2 montre le spectre électronique de RBA avec l'acide chloroacétique dans le méthanol. Comme la RBA seule absorbe à 365 nm, les acides carboxyliques ont par conséquent exercé un effet bathochrome d'environ 75 nm. En se servant des travaux de Blatz *et al.* (10, 13) comme référence, l'interprétation des résultats est aisée: la bande à 440 nm représente la transition $\pi^* \leftarrow \pi$ de RBA protonée. La protonation est complète et puisque tous les spectres obtenus sont à toutes fins pratiques superposables, le méthanol a aussi créé un effet de nivellement (leveling effect). Ce nivellement des données implique que l'ion immonium est solvaté par le méthanol ce qui sépare ainsi le cation de son anion. Dans le méthanol, il n'existe donc pas de paire d'ions formée de l'ion rétinylidène immonium et de son contre-ion carboxylate. De plus, dans ce solvant, l'interaction du groupe polaire (l'atome d'halogène dans les acides acétiques halogénés) avec les doubles liaisons éthyléniques n'est pas présente car alors les résultats divergeraient selon l'acide utilisé.

Dans le chloroforme, les spectres électroniques varient selon l'acide utilisé. Sauf pour l'acide trichloroacétique qui n'induit qu'une seule bande (λ_{max} 453 nm), les autres systèmes présentent deux bandes: l'une à 366 nm, l'autre bande varie de 445 à 453 nm. Le spectre électronique de RBA en présence d'acide chloroacétique dans le chloroforme est représenté à la fig. 3. Lorsque la proportion d'acide est augmentée de telle sorte que le rapport imine–acide passe de 1:1 à 1:100, les

TABLEAU 1. Pourcentage d'espèces protonées pour les systèmes RBA/RCO_2H dans le chloroforme et le méthanol.

Systèmes	$CHCl_3$ λ_{max} (nm)	$CHCl_3$ % protonation	MeOH λ_{max}	MeOH % protonation
RBA/$CH_3CH_2CO_2H$	445	0	440	100
RBA/ICH_2CO_2H	445	18	440	100
RBA/$BrCH_2CO_2H$	445	19	440	100
RBA/FCH_2CO_2H	445	27	440	100
RBA/$ClCH_2CO_2H$	445	20	440	100
RBA/Cl_2CHCO_2H	448	82	440	100
RBA/Cl_3CCO_2H	453	100	440	100
RBA/$O_2NCH_2CH_2CO_2H$	448	31	440	100
RBA/$N{\equiv}CCH_2CO_2H$	447	47	440	100
RBA/$HC{\equiv}CCO_2H$	445	47	440	100

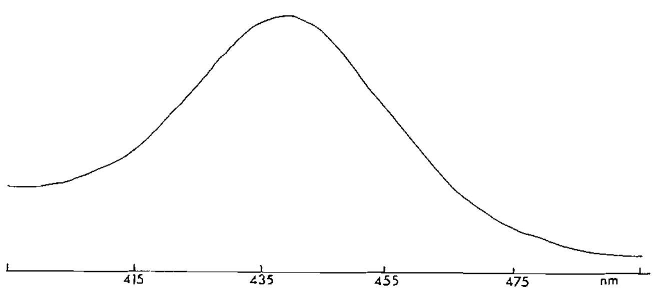

FIG. 2. Le spectre électronique de la toute *trans*-rétinylidène *tert*-butylamine en présence d'acide chloroacétique dans des concentrations équimolaires dans le méthanol.

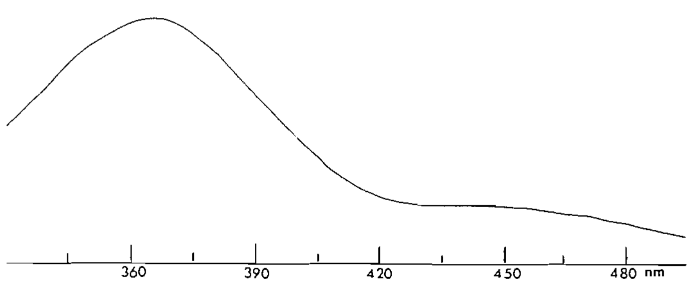

FIG. 3. Le spectre électronique de la toute *trans*-rétinylidène *tert*-butylamine en présence d'acide chloroacétique dans des concentrations équimolaires dans le chloroforme.

spectres électroniques n'indiquent plus qu'une seule bande et cela pour tous les acides utilisés. Ainsi, par exemple, l'acide chloroacétique dans des concentrations équimolaires avec RBA réussit à perturber la base de Schiff de telle sorte que deux bandes sont obtenues: l'une n'ayant pas bougé (λ_{max} 366 nm), l'autre ayant un λ_{max} de 445 nm. La première bande disparaît au profit de la deuxième dès qu'un large excès d'acide est utilisé et celle-ci a une absorption maximale à 450 nm et une absorptivité de 32 600. Cette dernière a servi à quantifier la proportion de la bande à 445 nm pour un rapport imine–acide de 1:1. Cette façon de faire a été suivie pour tous les autres acides. Dès qu'une seule bande apparaît, celle-ci a un λ_{max} qui ne varie que légèrement (maximum de variation: 9 nm pour l'acide dichloroacétique) par rapport à la première indiquant ainsi qu'un large excès d'acide a peu d'influence sur le λ_{max} de RBA. Considérant que la bande à 445 nm est due à la transition $\pi^* \leftarrow \pi$ de RBA protonée tandis que la bande à 366 nm est due à l'imine non protonée, on doit donc conclure que la plupart des

TABLEAU 2. Comparaison des pourcentages de protonation dans le $CHCl_3$, entre HBA et RBA en présence des mêmes acides

Acides utilisés	RBA % protonation	HBA % protonation
$CH_3CH_2CO_2H$	0	0
ICH_2CO_2H	18	17
$BrCH_2CO_2H$	19	17
FCH_2CO_2H	27	18
$ClCH_2CO_2H$	20	22
Cl_2CHCO_2H	82	100
Cl_3CCO_2H	100	100
$O_2NCH_2CH_2CO_2H$	31	10
$N{\equiv}CCH_2CO_2H$	47	51
$HC{\equiv}CCO_2H$	47	49

acides du tableau 1 ne réussissent à protoner que partiellement la base de Schiff et un équilibre tel que préconisé auparavant (éq. [1]) pour le système HBA, est aussi valable pour le système rétinylidène. D'ailleurs, les résultats obtenus à partir du système rétinylidène offrent une assez grande similitude avec le système heptadiénylidène. Le tableau 2 établit cette comparaison. Deux acides montrent des résultats divergents (les acides dichloroacétique et nitro-3 propanoïque) mais généralement les données de l'un ou de l'autre système concordent assez bien. Cette similitude dans les résultats implique que dans le système du rétinal, la partie de la molécule comprenant le cycle hexénique ainsi que les doubles liaisons situées sur les carbones C_7—C_8 et C_9—C_{10} n'interagissent pas avec les acides. Ces derniers exercent leur action surtout au niveau des atomes C_{11} jusqu'à N_{16}. Tout comme pour HBA, le pourcentage de protonation de RBA n'est pas linéairement relié avec le pK_a, mesuré dans l'eau, des acides carboxyliques. Toutefois, plus l'acide est fort plus grande est la protonation de RBA.

En conclusion, l'étude des spectres uv–vis de RBA en présence de divers acides confirme ce qui avait été trouvé précédemment pour HBA (9), à savoir que dans un solvant peu polaire comme le chloroforme, les acides carboxyliques ressemblant à ceux du tableau 1 ne peuvent pas protoner complètement l'imine conjuguée et un équilibre existe entre l'imine non protonée et protonée (voir éq. [1]). Extrapolée à la rhodopsine, cette conclusion porte à croire que si le milieu a une constante diélectrique faible (milieu hydrophobe), les acides glutamique ou aspartique ne pourront pas protoner le chromo-

TABLEAU 3. Déplacements chimiques exprimés en ppm de RBA dans le $CDCl_3$ et CD_4OD et valeurs de déblindage des hydrogènes H_7 à H_{15} du système rétinylidène en présence de divers acides carboxyliques

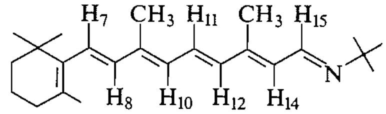

Déplacements	H_{15}*	H_{14}	H_{12}	H_{11}	H_{10}	H_8	H_7	C_{13}—CH_3	C_9—CH_3
Dans $CDCl_3$	8,33	6,24	6,36	6,83	6,16	6,13	6,22	2,10	1,99
Dans CD_3OD	8,50	6,27	6,51	7,06	6,26	6,23	6,36	2,24	2,09

Valeurs de déblindage†

Acides utilisés	H_{15}		H_{14}		H_{12}		H_{11}		H_{10}		H_8		H_7		C_{13}—CH_3		C_9—CH_3	
$CH_3CH_2CO_2H$	−0,01	−0,12	0,04	0,16	0,02	0,10	0,01	0,32	0,00	0,10	0,00	0,07	0,01	0,14	0,01	0,07	0,00	0,02
$O_2NCH_2CH_2CO_2H$	−0,19	−0,17	0,54	0,24	0,20	0,06	0,43	0,45	0,12	0,13	0,09	0,09	0,21	0,19	0,15	0,20	0,07	0,09
ICH_2CO_2H	−0,14	−0,21	0,56	0,29	0,16	0,19	0,28	0,57	0,06	0,17	0,05	0,11	0,14	0,25	0,10	0,26	0,05	0,12
$BrCH_2CO_2H$	−0,11	−0,22	0,50	0,29	0,11	0,19	0,24	0,56	0,04	0,17	0,04	0,11	0,12	0,24	0,08	0,26	0,03	0,12
$ClCH_2CO_2H$	−0,11	−0,21	0,47	0,33	0,08	0,19	0,22	0,50	0,04	0,16	0,02	0,10	0,09	0,21	0,11	0,25	0,05	0,10
FCH_2CO_2H	−0,07	−0,21	0,30	0,27	0,07	0,19	0,14	0,57	0,02	0,17	0,02	0,11	0,07	0,24	0,05	0,26	0,02	0,11
$N{\equiv}C$—CH_2CO_2H	−0,03	−0,06	0,14	0,07	0,04	0,05	0,07	0,16	0,02	0,05	0,01	0,03	0,04	0,07	0,03	0,07	0,01	0,03
$HC{\equiv}C$—CO_2H	0,00	−0,10	0,04	0,12	0,02	0,09	0,02	0,27	0,04	0,08	0,00	0,05	0,03	0,12	0,01	0,12	0,00	0,05
Cl_2CHCO_2H	−0,17	−0,22	0,60	0,28	0,19	0,20	0,47	0,59	0,12	0,18	0,10	0,12	0,24	0,25	0,18	0,27	0,08	0,12
Cl_3C—CO_2H	−0,09	−0,24	0,46	0,29	0,07	0,20	0,27	0,58	0,04	0,18	0,04	0,12	0,12	0,25	0,10	0,26	0,04	0,12

*Un signe négatif indique que l'hydrogène est blindé.
†Colonne de gauche, le solvant est le $CDCl_3$; à droite, le CD_3OD.

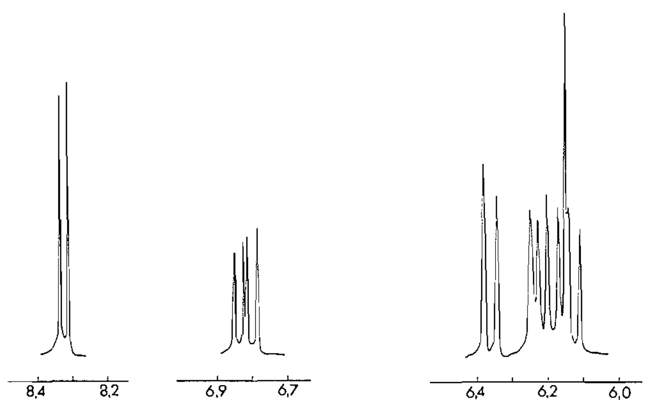

FIG. 4. Spectre de rmn du proton (400 MHz) de la toute *trans*-rétinylidène *tert*-butylamine dans le $CDCl_3$.

phore. Si le milieu est plus polaire la protonation pourra être complète mais le cation immonium devrait être alors solvaté par le milieu.

Étude en résonance magnétique nucléaire

Les mêmes systèmes que précédemment ont été étudiés par résonance magnétique nucléaire du proton (^1H rmn). Les données paraissent au tableau 3. Elle montre dans un premier temps les déplacements chimiques de tous les hydrogènes éthyléniques de RBA en plus de ceux des deux groupes méthyles (C_{13}—CH_3 et C_9—CH_3). Dans un second temps, le tableau 3 montre les valeurs de déblindage de ces hydrogènes lorsque RBA est mis en présence d'acides carboxyliques dans des concentrations équimolaires. La partie éthylénique du spectre de rmn de RBA est présentée à la fig. 4. L'attribution des différents pics aux hydrogènes éthyléniques s'est faite à l'aide de découplage spin–spin et par correlation avec les données fournies par Patel (12) pour le tout *trans*-retinal. L'attribution paraît logique car H_7 étant situé sur un carbone porteur d'une charge positive résiduelle par résonance, devrait être plus déblindé que H_8 qui lui, n'en porte pas. H_{10} et H_{12} sont situés sur des carbones qui ne portent pas de charge positive résiduelle mais comme H_{12} est plus près de la fonction imine que H_{10}, il devrait être plus déblindé. La délocalisation des électrons dans le système RBA se fait comme suit:

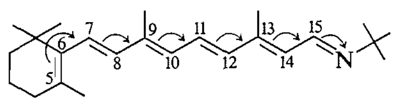

Les carbones 5, 7, 9, 11, 13 et 15 ont une charge positive résiduelle tandis que les atomes de carbone 6, 8, 10, 12 et 14 n'en ont pas. En présence d'acide, la délocalisation des électrons du système rétinylidène s'accroît et ainsi, la présence d'acide conduit à un déblindage de tous les hydrogènes, ce déblindage étant plus important là où réside une charge positive partielle. Ce n'est toutefois pas le cas de H_{15} car cet hydrogène varie que peu lorsque RBA est protoné. Ceci est montré au tableau 3 et est en tous points similaires aux résultats obtenus précédemment par nous (9) et par d'autres (13, 14). Sharma et Roels (14) ont expliqué le peu de changement subi par H_{15} lors de la protonation de l'azométhine par le fait que le déblindage normalement attendu, à cause de la présence d'une charge positive résiduelle sur ce carbone, est contrebalancé par la diminution du caractère de double liaison de la fonction imine ce qui diminue d'autant l'anisotropie du lien C—N. Le tableau 3 indique que H_{15} est blindé plutôt que déblindé; l'effet inverse est donc obtenu.

Dans le méthanol

L'examen des colonnes de droite du tableau 3 indique qu'à l'exception des acides cyanoacétique et propiolique (et de façon moindre, de l'acide propionique), les sept autres acides ont des déblindages très semblables. Cela implique un effet de nivellement tel que préconisé déjà par Blatz (13) pour le méthanol. Ce nivellement des valeurs de déblindage est encore perçu par le fait que H_{14} est peu déblindé (dans le chloroforme H_{14} l'est beaucoup plus) ce qui implique que le contre-ion carboxylate est remplacé par des molécules de solvant. De plus, le tableau 3 révèle que l'action des acides sur RBA se répercute tout le long de la chaîne polyénique. Pour le moment, les résultats obtenus à partir des acides cyanoacétique et propiolique paraissent incohérents. Dans le système heptadiénylidène, leur comportement était aligné aux autres acides.

En conclusion, les données obtenues par rmn confirment les résultats obtenus en uv–vis: le méthanol a un efffet de nivellement.

Dans le chloroforme

Le spectre de RBA et de l'acide chloroacétique dans le $CDCl_3$ est représenté à la fig. 5 et il montre bien le déblindage subi par les hydrogènes par la présence de l'acide. Les résultats paraissent au tableau 3, colonne de gauche. On notera que dans ce solvant, les données diffèrent sensiblement selon l'acide utilisé. C'est l'acide dichloroacétique qui perturbe le plus le système rétinylidène et pourtant, les résultats en uv–vis indiquent que cet acide ne réussit à protoner RBA qu'à 82%. L'acide nitro-3 propanoïque vient en second suivi par l'acide trichloroacétique. Il est visible qu'il n'existe pas de relation linéaire entre ces valeurs de déblindage et le pK_a des acides mesuré dans l'eau.

On peut expliquer les résultats obtenus en recourant à la théorie de Nakanishi sur l'intéraction causée par la présence de charges externes ("external point charge theory" – réf. 2*a*). La présence d'un groupe polaire en bout de chaîne de l'acide peut stabiliser la charge positive partielle générée par la protonation. Cet effet de pince est illustré ci-dessous:

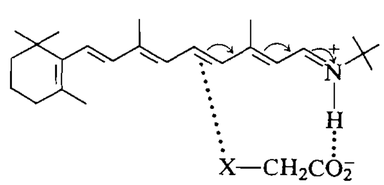

Cette explication semble être vérifiée par le fait que l'acide propionique qui n'a pas de groupe polaire terminal ne réussit pas à déblinder de façon sensible les hydrogènes de RBA (le tableau 1 montre par contre, que cet acide est incapable de protoner RBA). Plus important est le fait que les valeurs des déblindages des hydrogènes H_7, H_{11}, H_{12}, H_{14} varient selon le caractère nucléophile des atomes d'hydrogènes: l'iode causant un déblindage plus important que le brome, que le chlore et que le fluor. À noter que le déblindage est à l'inverse de la force des acides. Lorsque l'acide porte deux chlores (acide dichloroacétique), le maximum de déblindage est obtenu. Même si l'acide trichloroacétique est un acide plus fort que l'acide di-

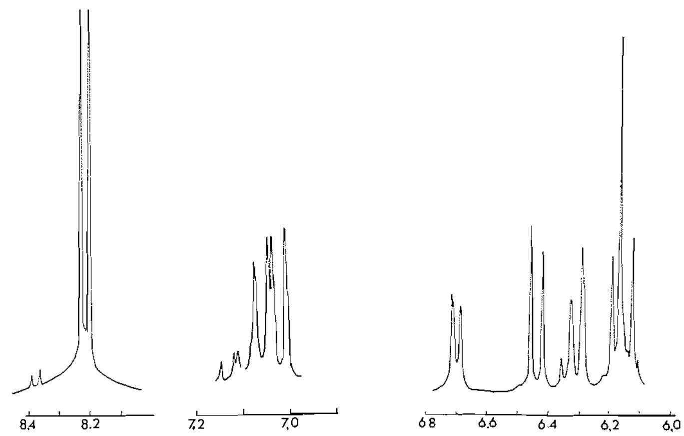

FIG. 5. Spectre de rmn du proton (400 MHz) de la toute *trans*-rétinylidène *tert*-butylamine en présence d'acide chloroacétique dans des concentrations équimolaires dans le $CDCl_3$.

chloroacétique, il cause un déblindage moindre. Tout ceci semble donc aller dans le sens indiqué: à savoir, que le groupe polaire de l'acide interagit avec la chaîne polyénique du système rétinylidène. Dans le chloroforme, les acides cyanoacétique et propiolique continuent à avoir un comportement différent des autres acides.

La présence d'une interaction entre les groupes polaires et la RBA présuppose l'existence d'une paire d'ions car il faut nécessairement que l'acide soit très près des doubles liaisons pour que l'interaction soit présente. L'existence ou non de paires d'ions dans ce système est un point fort important car, il faut le rappeler, Nakanishi et Honig (2, 5) préconisent l'existence de paires d'ions semblables dans la rhodopsine où elles jouent un rôle fondamental lors de la transformation photochimique du pigment visuel en bathorhodopsine. Les résultats du tableau 3, dans le chloroforme, montrent que cette paire d'ions existent car l'important déblindage de H_{14} résulte fort probablement de la présence du contre-ion carboxylate près de cet hydrogène. Si une paire d'ions existe, la fig. 1(b) montre que l'anion carboxylate devrait être près près de H_{14}; l'anisotropie causée par cette fonction devrait donc être responsable de l'important déblindage subi par H_{14}.

Le couplage de H_{15} est aussi très important car il indique ce qui se passe au niveau de l'azote de l'imine. En effet, H_{15} est un doublet lorsque la base de Schiff n'est pas protonée et devient un doublet de doublets si celle-ci est protonée (14). Or, tous les spectres indiquent un doublet pour H_{15}, même dans le cas où l'agent de protonation est l'acide trichloroacétique. Ceci ne signifie pas que RBA ne soit pas protonée (tous les hydrogènes, sauf H_{15}, sont largement déblindés) mais plutôt vérifie le fait, déjà trouvé par l'étude en uv–vis, qu'un équilibre semblable à celui montré à l'éq. [1] existe dans le chloroforme. Ce comportement de H_{15} est tout à fait conforme à celui trouvé pour le proton aldimine dans le système heptadiénylidène (9). Dans ce dernier cas, en utilisant un large excès d'acide, l'équilibre était déplacé en faveur de la paire d'ions et un doublet de doublets en résultait dès lors.

En conclusion, dans un solvant peu polaire comme le chloroforme, les données obtenus par rmn du proton indiquent que l'effet de charges externes tel que préconisé par Nakanishi peut expliquer les déblindages des hydrogènes éthyléniques mais que la question de la protonation de la fonction imine est plus complexe que prévue car les résultats montrent fort bien l'exis-

TABLEAU 4. Comparaison des données de résonance magnétique nucléaire dans le $CDCl_3$ entre les systèmes rétinylidène et heptadiénylidène

Acides utilisés	H_{15}/H_7	H_{14}/H_6	H_{12}/H_4	H_{11}/H_3
$CH_3CH_2CO_2H$	−0,01/−0,03	0,04/0,38	0,02/0,09	0,01/0,19
$NO_2CH_2CH_2CO_2H$	−0,19/−0,06	0,54/0,46	0,20/0,18	0,43/0,32
ICH_2CO_2H	−0,14/−0,06	0,56/0,53	0,16/0,17	0,28/0,32
$BrCH_2CO_2H$	−0,11/−0,05	0,50/0,59	0,11/0,15	0,24/0,38
$ClCH_2CO_2H$	−0,11/+0,03	0,47/0,59	0,08/0,26	0,22/0,49
FCH_2CO_2H	−0,07/−0,03	0,30/0,64	0,07/0,19	0,14/0,43
$N{\equiv}C{-}CH_2CO_2H$	−0,03/−0,03	0,14/0,62	0,04/0,17	0,07/0,40
$HC{\equiv}C{-}CO_2H$	−0,00/+0,05	0,04/0,74	0,02/0,22	0,02/0,39
Cl_2CHCO_2H	−0,17/+0,06	0,60/0,64	0,19/0,19	0,47/0,52
Cl_3CCO_2H	−0,11/+0,10	0,49/0,68	0,10/0,17	0,28/0,49

tence d'un équilibre entre une paire d'ions ($R_2{-}\overset{+}{N}H{-}{-}{-}{-}\bar{O}_2R$) et une association de molécules neutres ($R_2N{-}{-}{-}{-}HO_2C{-}R$).

Comparaison entre les systèmes rétinylidène et heptadiénylidène

Tout au long de ce travail, d'utiles recoupements avec la *trans,trans*-heptadiénylidène-2,4 *tert*-butylamine (HBA) ont été invoqués. Une comparaison entre les données de rmn obtenues dans le chloroforme pour ces deux bases de Schiff pouvait être fort intéressante. À partir des données fournies par la réf. 9, le tableau 4 a pu être établie. On notera la correspondance des hydrogènes H_{15} pour RBA et H_7 pour HBA et ainsi de suite (voir figures 1(a) et 1(b)) qui existe entre les deux systèmes. Le tableau 4 montre que quatre des dix acides perturbent les bases de Schiff de façon fort semblable. Les acides nitro-3 propanoïque, iodoacétique, bromoacétique et dichloroacétique exercent donc leurs effets surtout au niveau des trois premières doubles liaisons dans le système RBA. Par contre, les six autres acides causent des déblindages dont la valeur varie selon l'un ou l'autre système. Le tableau 4 indique, pour ces acides, une valeur de déblindage toujours plus basse pour les hydrogènes de RBA. Pour ces six acides, leur action est moins localisée et comme RBA est beaucoup plus conjuguée que HBA, la perturbation causée par ces acides peut dès lors s'étendre sur un plus grand nombre de liaisons.

Dans le méthanol, les résultats offrent des similitudes plus frappantes. Les deux systèmes montrent l'effet de nivellement du méthanol; H_{14} pour RBA et H_6 pour HBA ont un déblindage très voisin (0,3 ppm) mais comme RBA est une imine plus conjuguée que HBA, les autres hydrogènes ont des valeurs de déblindage moindres. L'emploi comme solvant de CD_3OD ne permet pas de noter la présence d'un échange de proton entre la base Schiff et le solvant; aussi, pour obvier à ce problème et puisque cette question est fort importante, les systèmes RBA – acide chloroacétique et RBA – acide trichloroacétique ont été aussi étudiés dans le CD_3OH. Les valeurs de déblindage sont bien sûr les mêmes que précédemment mais H_{15} est toujours un doublet. HBA a donné aussi ce résultat et les deux imines indiquent bien qu'un échange de proton s'établit entre la base de Schiff protonée et le solvant.

De cette étude comparative il ressort que le système heptadiénylidène est un modèle fort approprié de celui du rétinal et a comme avantage d'être facilement disponible, d'être économique, et surtout de présenter en rmn des données facilement interprétables.

Comparaison du système RBA avec la rhodopsine

Des résultats obtenus en uv–vis et rmn, il est possible de faire plusieurs hypothèses concernant la rhodopsine. En premier lieu, si le milieu environnant le chromophore est polaire, on peut prévoir une protonation complète du chromophore par les acides glutamique ou aspartique. Par contre, une paire d'ions de type $-\overset{+}{N}H{-}{-}{-}{-}\bar{O}_2C-$ apparaît comme peu probable à cause de l'effet de nivellement. De même, l'interaction directe entre une charge et les doubles liaisons selon la théorie de Nakanishi paraît aussi improbable. Il demeure possible, toutefois, qu'un système d'interactions par l'intermédiaire de l'eau puisse exister mais cela ne peut être montré par nos résultats. Dans un second temps, si le milieu protéinique entourant le chromophore a une constante diélectrique basse s'approchant de celle du chloroforme (dont la valeur est de 4,8), alors il est à prévoir que les acides glutamique ou aspartique ne pourront protoner que partiellement (voir même, pas du tout) le chromophore. De plus, une paire d'ions ($-\overset{+}{N}H{-}{-}{-}{-}\bar{O}_2C-$) sera en équilibre avec l'espèce neutre ($-N{:}{-}{-}{-}{-}HO_2C$) et l'interaction directe de charges avec les doubles liaisons pourra se faire.

Quelle que soit la polarité du milieu, un échange de proton existera entre la base de Schiff protonée et le contre-ion (milieu hydrophobe) ou l'eau (milieu polaire).

Remerciements

Cette étude a bénéficié des conseils judicieux du professeur C. Sandorfy que nous désirons remercier vivement. Les spectres de rmn ont été obtenus grâce aux bons offices du Centre régional de rmn à haut champ de l'Université de Montréal. Nous désirons remercier également Madame Sylvie Pepin pour la dactylographie de ce texte. Finalement, ce travail a reçu le secours financier du CRSNG (A0943) et de l'Université du Québec à Montréal.

1. (*a*) V. BALOGH-NAIR et K. NAKANISHI. *Dans* New comprehensive biochemistry. Vol. 3. *Édité par* Ch. Tamm. Elsevier Biomedical Press, New York. 1982; (*b*) B. HONIG. Curr. Top. Memb. Transp. **16**, 371 (1982); (*c*) R. R. BIRGE. Ann. Rev. Biophys. Bioeng. **10**, 315 (1981); (*d*) M. OTTOLENGHI. Adv. Photochem. **12**, 97 (1980); (*e*) H. SHICHI. Biochemistry of vision. Academic Press, New York. 1983.
2. (*a*) A. KROPF et R. HUBBARD. Ann. N.Y. Acad. Sci. **74**, 266 (1958); (*b*) J. R. WIESENFELD et E. W. ABRAHAMSON. Photochem. Photobiol. **8**, 487 (1968); (*c*) T. KAKITANI et H. KAKITANI. J. Phys. Soc. Jpn. **42**, 996 (1977); **44**, 1403 (1978); (*d*) B. HONIG, U. DINUR, K. NAKANISHI, V. BALOGH-NAIR, M. A. GAWINOWICZ, M. ARNABOLDI et M. G. MOTTO. J. Am. Chem. Soc. **101**, 7084 (1979); (*e*) K. NAKANISHI, V. BALOGH-NAIR, M. ARNABOLDI, K. TSUJIMOTO et B. HONIG. J. Am. Chem. Soc. **102**, 7945 (1980); (*f*) S. MORDECHAI et K. NAKANISHI. J. Am. Chem. Soc. **105**, 4033 (1983); (*g*) G. D. MATEESCU et M. IGBAL.

Biochemistry, **23**, 3357 (1984).

3. (*a*) J. SHRIVER, G. MATEESCU, R. FAGER, D. TORCHIA et E. W. ABRAHAMSON. Nature (London), **270**, 271 (1977); (*b*) G. D. MATEESCU, D. D. MUCCIO, W. G. COPAN et E. W. ABRAHAMSON. J. Photochem. **17**, 63 (1981); (*c*) J. SHRIVER, G. D. MATEESCU et E. W. ABRAHAMSON. Methods Enzymol. **81**, 698 (1982); (*d*) G. D. MATEESCU, W. G. COPAN, D. D. MUCCIO, D. V. WATERHOUS et E. W. ABRAHAMSON. *Dans* Proceedings of the International Symposium on Synthesis and Applications of Isotopically Labeled Compounds. Elsevier, Amsterdam. 1983. pp. 123–132; (*e*) G. D. HARBISON, S. O. SMITH, J. A. PARDOEN, P. P. J. MULDER, J. LUGTENBURG, J. HERZFELD, R. MATHIES et R. G. GRIFFIN. Biochemistry, **23**, 2662 (1984).
4. (*a*) Y. A. OVCHINNIKOV, N. G. ABDULAEV, M. Y. FEIGINA, I. D. ARTAMONOV, A. S. ZOLOTAREV, M. B. KOSTINA, A. S. BOGACHUK, A. I. MOROSHNIKOV, V. I. MARTINOV et A. B. KUDELIN. Biorg. Khim. **8**, 1011 (1982); (*b*) P. A. HARGRAVE, J. H. MCDOWELL, D. R. CURTIS, J. K. WANG, E. JUSZCZAK, S. L. FONG, J. K. MOHANA RAO et P. ARGOS. Biophys. Struct. Mech. Sous presse; (*c*) E. A. DRATZ et P. HARGRAVE. Trends Biochem. Sci. **8**, 128 (1983).
5. B. HONIG, T. EBREY, R. H. CALLENDER, U. DINUR et M. OTTOLENGHI. Proc. Natl. Acad. Sci. U.S.A. **76**, 2503 (1979).
6. A. COOPER. Nature (London), **282**, 531 (1979).
7. C. N. RAFFERTY et H. SHICHI. Photochem. Photobiol. **33**, 229 (1981).
8. (*a*) A. WARSHEL et N. BARBOY. J. Am. Chem. Soc. **104**, 1469 (1982); (*b*) A. WARSHEL. Biochemistry, **20**, 3167 (1981).
9. (*a*) M. BISSONNETTE et DANIEL VOCELLE. Spectros. Int. J. **2**, 120 (1983); (*b*) M. BISSONNETTE, H. LE THANH et D. VOCELLE. Can. J. Chem. **62**, 1459 (1984).
10. P. E. BLATZ, J. H. MOHLER et H. V. NAVANGUL. Biochemistry, **11**, 848 (1972).
11. D. D. PERRIN *et al. Dans* Purification of laboratory chemicals. 2[e] éd. Pergamon Press, Toronto. 1980.
12. (*a*) D. J. PATEL. Nature **224**, 799 (1969); (*b*) Nature **221**, 825 (1969).
13. (*a*) P. E. BLATZ et J. H. MOHLER. Biochemistry, **14**, 2304 (1975); (*b*) P. E. BLATZ et P. A. LIEBMAN. Exp. Eye Res. **17**, 543 (1973); (*c*) P. E. BLATZ et J. H. MOHLER. Biochemistry, **11**, 2340 (1972); (*d*) J. O. ERICKSON et P. E. BLATZ. Vision Res. **8**, 1367 (1968).
14. G. M. SHARMA et O. A. ROELS. J. Org. Chem. **38**, 3648 (1973).

Net charges and valence AO's in the methylamines; the hydrogen basis set and the properties of nitrogen

GIUSEPPE DEL RE[1]
Département de Chimie, Université de Montréal and Department of Applied Mathematics, University of Waterloo, Waterloo, Ont., Canada N2L 3G1

AND

SÁNDOR FLISZÁR, MICHEL COMEAU, AND CLAUDE MIJOULE[2]
Département de Chimie, Université de Montréal, C.P. 6210, Succ. A, Montreal, Qué., Canada H3C 3V1

Received July 30, 1984

This paper is dedicated to Professor Camille Sandorfy on the occasion of his 65th birthday

GIUSEPPE DEL RE, SÁNDOR FLISZÁR, MICHEL COMEAU, and CLAUDE MIJOULE. Can. J. Chem. **63**, 1487 (1985).

Net charges and valence AO's for ammonia, methylamine, dimethylamine, and trimethylamine were calculated using extended basis sets. Superposition effects, evaluated by replacing Pople's standard 6-31G* basis by an extended form in which the basis of the ammonia H atoms and of the methyl groups of trimethylamine are retained in the treatment of each molecule, indicate that the quality of the treatment of amine nitrogen atoms is strongly dependent on the number of methyl groups. A new, augmented basis is proposed for the hydrogens, which appears to be reasonably well balanced: comparison with familiar (e.g., 6-31G*) calculations illustrates in what manner the treatment of nitrogen is worsened when even just one methyl group is replaced by hydrogen unless the impoverishment of the basis is suitably taken care of.

GIUSEPPE DEL RE, SÁNDOR FLISZÁR, MICHEL COMEAU et CLAUDE MIJOULE. Can. J. Chem. **63**, 1487 (1985).

Faisant appel à des ensembles de base élargis, on a effectué des calculs sur l'ammoniac, la méthylamine, la diméthylamine et la triméthylamine. Si on remplace la base normale 6-31G* de Pople par une forme élargie dans laquelle on conserve la base des atomes d'hydrogène de l'ammoniac et des groupes méthyles de la triméthylamine dans le traitement de chaque molecule, on peut évaluer les effets de superposition; ces effets indiquent que la qualité du traitement des atomes d'hydrogène de l'amine dépend fortement du nombre de groupes méthyles. Pour l'hydrogène, on propose une nouvelle base encore plus élargie qui semble être bien balancée; une comparaison avec des calculs familiers comme 6-31G* permet d'illustrer les complications qui interviennent dans l'étude de l'azote même lorsqu'on ne substitue qu'un seul groupe méthyle par un hydrogène si on ne fait pas les corrections qu'impose l'appauvrissement de la base.

[Traduit par le journal]

Introduction

It has been known for a long time, but seldom duly emphasized, that the properties of atoms carrying one or more hydrogens may differ significantly from those of the same atoms when linked only to atoms other than hydrogen. The debate on the electric dipole moment of the CH bond (1) and the pioneering discussion by Parks and Parr (2) do not seem to have been followed by much *ad hoc* theoretical work. Yet, even the special parametrization required by hydrogen in the empirical method proposed by one of us (3) pointed to the need for further theoretical investigations.

Quite recently, the treatment of hydrogen in *ab initio* computations has been investigated in connection with small molecules (4*a*) and with hydrogen-bonded dimers (4*b*). These papers point to the conclusion that *ad hoc* scaling of hydrogen may be equivalent to an important basis extension with counterpoise correction (4*c*). These exhaustive studies, however, have left open the case of larger molecules, where the interplay of hydrogen polarization and superposition effects may affect the results for ordinary chemical bonds.

We have come across this question in connection with an attempt to extend previous work on the relationships between Mulliken net charges and nuclear magnetic resonance shifts (5) to the alkylamines (6): the behavior of trialkylamines appeared to follow a trend differing from that of mono- and dialkylamines.

As is well known, not only are Mulliken net charges just one of the possible definitions of atomic net charges (7), but widely different values are produced with comparatively small changes in a basis set even in *ab initio* SCF calculations (5*a*, 8). Since trends within similar series are generally little affected by the computational scheme (5*a*, 8), this has not received great attention so far in applications to chemical problems. But our present problem is one where the choice of the basis could play a very important role.

Indeed, the superposition effect in a standard treatment of a series of amines certainly depends on the number and geometrical arrangement of the alkyl groups. Consideration of the local symmetry about the nitrogen atom suggests that two or three hydrogens (or two alkyl groups) should have roughly the same effect on nitrogen as one, whereas tertiary amines, where there is no N-bonded hydrogen at all, could differ significantly in the importance of superposition. Most important is also that the replacement of alkyl groups by hydrogens greatly impoverishes the basis, so that nitrogen is treated in a very special way when the presence of alkyl groups makes superposition effects likely to be very marked.

With these considerations in mind, we have first of all carried out a calculation of ammonia and its methyl-substituted derivatives using one and the same extended basis, 6-31G*, including the hydrogen basis set used for ammonia as well as the carbon and hydrogen orbitals used for trimethylamine. Then we have studied the possibility, usefulness, and physical significance of an improved basis set for hydrogen, following

[1] Visiting scientist. Permanent address: Cattedra di Chimica Teorica della Facoltà di Scienze, Via Mezzocannone 4, I-80134, Napoli, Italia.

[2] Visiting scientist, on leave from the "Centre de Mécanique Ondulatoire Appliquée", Paris, France.

TABLE 1. Superposition effect (SE) on calculated energies, electric dipole moments, and Mulliken N net charges in the 6-31G* basis[a]

Molecule	Energy (au)		μ (debyes)		q_N (me)	
	No SE	With SE	No SE	With SE	No SE	With SE
NH_3	−56.1844	−56.1961	1.92	1.58	−996	−940
NH_2CH_3	−95.2087	−95.2167	1.65	1.47	−832	−812
$NH(CH_3)_2$	−134.2360	−134.2404	1.34	1.26	−680	−701
$N(CH_3)_3$	−173.2654	−173.2664	1.02	1.00	−546	−590

[a] NH_3, $N(CH_3)_3$, (C_{3v}) and NH_2CH_3, $NH(CH_3)_2$ (C_s symmetry) were calculated in all cases using "standard" geometries closely copying optimized STO-3G results, namely (Å, viz. decimal degrees), r(NH) = 1.0032, r(CN) = 1.4900, $r(CH_t)$ = 1.0938, r(CH) = 1.0880, ∠HNH = 107.15, ∠CNH = 108.60, ∠H_tCN = 112.34, ∠HCN = 109.84, ∠HCH = 109.10, ∠H_tCH = 107.82, and ∠CNC = 109.94, where H_t is the hydrogen *trans* with respect to the nitrogen lone pair.

the line of reasoning explained below, and analyzing the MO's in terms of localized orbitals and of the procedure proposed by Del Re and Barbier (9).

Superposition effect

Table 1 indicates the results obtained when the standard 6-31G* basis set is replaced by the extended form 6-31G*-super, in which the basis set of the H atoms of ammonia and of the methyl groups of $N(CH_3)_3$ are all retained in the treatment of any of the four molecules listed.[3]

As expected, it is ammonia which benefits most from the presence of the "dummy" centers: the energy improvement is of the order of 30 kJ mol^{-1}, which is quite significant. On the other hand, the influence of the dummy ammonia hydrogen on the predicted SCF energy of trimethylamine only produces a ~3 kJ mol^{-1} decrease in total energy. This confirms that the quality of the treatment of nitrogen obtained by the standard basis is strongly dependent on the number of methyl groups.

In contrast with the trend suggested in the introduction, the energy corrections appear to decrease practically linearly with the number of methyl groups. However, this is not the case for dipole moments. The dipole moment of ammonia is reduced by 0.34 D, those of NH_2CH_3 and $NH(CH_3)_2$ by 0.18 and 0.08 D, respectively, and that of $N(CH_3)_3$ by 0.02 D. This suggests that, in addition to the slight improvement of the energy, the superposition effect leads to a reduction in polarization which corresponds to restoring electrons on the hydrogens – the greatest change being associated with axial symmetry.

The results for the net charge of nitrogen, q_N, suggest that inclusion of dummy centers produces two effects. In ammonia, nitrogen as well as the hydrogens lose electrons which move to the dummy centers beyond the hydrogens: there is a buildup of electronic charge in the outer sphere of the molecule. In trimethylamine, nitrogen gains electrons, as well as the three carbons and the dummy hydrogens: the electrons all come from the methyl hydrogens. The other two amines appear to be intermediate cases.

Since in trimethylamine the energy and dipole moment changes in going from 6-31G* to 6-31G*-super are minor, indeed, we infer tentatively that the internal charge redistribution is not physically very significant. The case of ammonia is quite different: not only are the energy and the electric dipole moment changes very important, but the reduction in electron population of nitrogen takes place with a basis set which certainly describes the correct situation about nitrogen in a more detailed way.

TABLE 2. Summary of results obtained for NH_3 from different basis sets

Basis set	Energy (au)	μ (debyes)	q_N (me)
1 6-31G*	−56.1844	1.92	−996
2 6-31G*+SE	−56.1961	1.58	−940
3 6-31G**	−56.1955	1.86	−790
4 6-31G*; 6-31 H	−56.2031	1.66	−533
5 6-311G**	−56.2104	1.74	−563
6 6-311 H	−56.2177	1.62	−556
7 6-311G** Opt.	−56.2104	1.73	−564
8 6-311 H Opt.	−56.2178	1.61	−556
9 6-311++G(3*df*, 3*pd*)	−56.2184		

Note: basis **9**, studied by Frisch, Pople, and Binkley (11) is the best result obtained by those authors in an instructive comparison of a variety of basis sets. Our result **8** is marginally better than that deduced from the 6-311++G(2*df*, 2*p*) set described in ref. 11 (E = −56.2176 au).

Of course, results obtained by means of a somewhat artificial and clumsy basis such as 6-31G*-super are subject to doubts, particularly as regards net charges. For instance, one may wonder if the reduced nitrogen charge in ammonia is not a purely artificial result: additional contributions to the electron density near that atom could be associated with basis functions protruding from the dummy centers. It is difficult to construct a logically consistent argument in this direction, but the awkwardness of a basis involving dummy centers is sufficient reason for not insisting on its use. We have tried to proceed in our study by constructing a basis that would take into account the lessons taught by Table 1 without introducing dummy centers. Indeed, our purpose will be to use the new basis in an attempt to recover a chemical description of valence effects in the molecules under consideration.

Optimized bases 6-31 H and 6-311 H

The fact that the presence of a NH bond seems to make a lot of difference as concerns superposition effects suggests that the treatment of hydrogen should be improved. Also the need for improvement in the treatment of nitrogen should be explored lest the extension of the hydrogen basis should be used to the benefit of the nitrogen electron density. Therefore, we have started from the two well-known 6-31G* and 6-311G* basis sets (10) and optimized an extended basis on hydrogen (Tables 2 and 3). The relevant results are indicated in Table 4.

[3] We use here the term superposition only because the basis is that typically used to estimate superposition errors. Actually, within the scope of this study, the floating part of the basis can be interpreted to some extent as a set of off-center polarization functions; its role should be compared with results obtained from a standard basis saturated on all centers.

TABLE 3. Optimized extensions of the 6-31G* and 6-311G* basis sets for H of NH_3

Basis	Type	α_K[a]	$d_{K,2s}$	$d_{K,2p}$
6-31 H	*sp*	4.3682724	−1.2416719 E-1	6.6105642 E-2
		1.3312885	−1.6737118 E-1	3.0315498 E-1
		5.4424926 E-1	1.1897837	7.1309634 E-1
	(*sp*)′	7.8714480 E-2		
6-311 H	*sp*	3.8682724	−1.2100128 E-1	6.8157767 E-2
		1.3012885	−1.6310369 E-1	3.1256586 E-1
		3.9424926 E-1	1.1594476	7.3523307 E-1
	(*sp*)′	6.3714480 E-2	1.0	1.0
	(*sp*)″	2.5000000 E-1	1.0	1.0

[a] All scale factors are 1.0.

TABLE 4. Effect of augmented bases for H attached to N

	Energy (au)		μ (debyes)		q_N (me)	
Molecule	6-31 H	6-311 H	6-31 H	6-311 H	6-31 H	6-311 H
NH_3	−56.2031	−56.2177	1.66	1.62	−533	−556
NH_2CH_3	−95.2209	−95.2234	1.59	1.56	−532	−670
$NH(CH_3)_2$	−134.2422	−134.2320	1.38	1.38	−528	−667
$N(CH_3)_3$	−173.2654	−173.2422	1.02	1.05	−546	−619

Table 2 presents a familiar picture: small improvements in energy are associated with large oscillations in the values of expected electric dipole moments. The nitrogen net charge seems to follow a more regular trend. However, optimization of an enlarged hydrogen basis at the 6-31G* level (basis 6-31 H) leads to a sharp decrease of the nitrogen charge; this is slightly compensated by further extension of the nitrogen basis and it would seem that, as far as charges on ammonia are concerned, the saturation limit is reasonably well approached already with 6-311G*. However, the importance of an extended treatment of hydrogen (basis 6-31 H) is clear from the sudden jump between case **3** and case **4** (Table 2). Moreover, as can be seen in Table 4, the 6-311 H basis is really not very good for dimethyl- and trimethylamine. Thus, it appears that the 6-31 H basis actually represents the basis of choice for treating alkylamines, both because of the quality of the energy and dipole moments and because, in contrast with more extended bases (11), we can use it for the whole $NH_m(CH_3)_{3-m}$ series.

A few comments are in order. The hydrogen basis has been extended here to include not only polarization but radial distortion as well. This approach has been followed only for hydrogens linked to nitrogen because here we are only interested in improving the description of that atom.[4] The importance of the radial distortion of the hydrogen 1*s* orbital in bond formation will be discussed below. At this stage, we only point out that the analysis of Boys' localized orbitals indicates that the long-range components seem especially important in order to reproduce correctly the hydrogen–hydrogen interactions, but also carry a non-negligible weight in the bonding orbitals. In fact, due to the large overlap values, the additional 2*sp* component goes to improve the quality of the standard 6-31G* 1*s* component: its weight is roughly 30%, 20%, and 10% of the latter in NH_3, NH_2CH_3, and $NH(CH_3)_2$, respectively. These results confirm that, as expected, the higher flexibility in the hydrogen basis set is largely used to improve the description of the electron density about the nitrogen. This conclusion is certainly relevant in any assessment of calculated net charges which reveal, indeed, surprising features (Table 4).

Discussion

(a) *Energies and dipole moments*

The energy values shown in Tables 1 and 4 have already been discussed. Let us only emphasize here that the poor quality of the 6-311G* set for trimethylamine indicates that a mere increase in the flexibility of the basis is not sufficient to improve the results. On the other hand, the great improvement obtained for ammonia is sufficient proof that the poor quality of the 6-31G* set depends on an insufficient allowance for polarization and radial distortion in the hydrogen basis. The predicted electric dipole moments are also in line with the suggestion that the 6-31 H basis is well balanced: note that once again the 6-31G* result is better than that given by the 6-311G* basis.

(b) *Charges*

The most striking feature of the nitrogen net charges, q_N, obtained from the 6-31 H basis is that the presence of at least one hydrogen atom is sufficient to lower q_N to a "standard" value of ~ -0.53 e; in turn, this value is very close to that given for trimethylamine by the 6-31G* set. The trend is thus entirely different from that obtained with the 6-31G* and 6-311 H sets. It is in line with the thesis that the treatment of nitrogen is greatly worsened when even just one methyl group is replaced by hydrogen unless the impoverishment of the basis is suitably taken care of.

[4] The fact that we have combinations of three Gaussians for the additional *sp* basis functions is a purely technical detail, which is probably a superfluous feature. In fact, the exponents (whose original choice was the standard one for carbon atoms) include one value practically unaffected by optimizations. This is indirectly confirmed by the triple-ζ optimized basis of 6-311 H, where the additional (*s*,*p*) gaussian turns out to have a width close to the leading gaussian of the 3G group, so as to give something quite close to the (2*sp*) group of 6-31 H.

TABLE 5. The orbitals of the nitrogen and hydrogen atoms, from Boys localized MO's

(a) Overall coefficients of N									
	N—H bond			N—C bond			Lone pair		
Molecule	6-31G*	6-31 H	6-311 H	6-31G*	6-31 H	6-311 H	6-31G*	6-31 H	6-311 H
NH_3	0.687	0.644	0.660				1.031	0.960	0.940
NH_2CH_3	0.690	0.655	0.651	0.674	0.660	0.837	1.028	0.977	0.943
$NH(CH_3)_2$	0.694	0.666	0.648	0.680	0.674	0.746	1.024	0.993	0.978
$N(CH_3)_3$				0.687	0.687	0.712	1.021	1.021	1.012
(b) *p*-characters of N									
NH_3	2.92	2.96	1.92				1.73	1.61	1.78
NH_2CH_3	2.78	2.80	2.56	2.67	2.47	0.85	1.82	1.66	2.64
$NH(CH_3)_2$	2.56	2.64	3.05	2.56	2.40	1.53	1.84	1.73	2.32
$N(CH_3)_3$				2.38	2.38	2.22	1.77	1.77	2.09
(c) Overall coefficients of H in NH bonds				(d) c_s	c_p	d_H (NH bonds)			
NH_3	0.425	0.415	0.479	−0.92037	0.39104	−0.12170			
NH_2CH_3	0.427	0.432	0.463	−0.86182	0.50722	−0.08007			
$NH(CH_3)_2$	0.428	0.455	0.474	0.44392	0.89607	0.03822			

One question still remains open: are the 6-31 H charges really representative of the electron density around nitrogen? The fact that they are quite independent of the molecule suggests at first sight that all the difference in bond polarization due to substitution of H with C is taken up by the atomic orbital assigned to other atoms. This is not the case, at least in a first approximation: the Mulliken net charges of the hydrogen atoms linked to N are 178, 185, and 175 me from ammonia on, those of the methyl groups are 162, 175, and 181 me from methylamine on. Note also that the methyl groups are slightly less charged than the hydrogen atoms, when both are present. Thus, there are reasons to believe (*cum grano salis*) that the major features revealed by Mulliken net charges computed by the 6-31 H basis set are physically significant, in particular as concerns nitrogen. One last argument concerns the point charge approximation based on the experimental dipole (1.48 D), which gives $|q_N| \simeq 0.3$ e for ammonia and even smaller values for the amines (3).

(c) *Orbital energies*

Assuming now that the new basis is reasonably reliable, additional information can be obtained by analyzing suitable molecular orbitals in terms of the simple valence theory (9). This requires assigning to each atom A a single contribution to a given MO, $|j\rangle$, so that

$$|j\rangle = \Sigma\, c_A |h_{Aj}\rangle$$

where $|h_{Aj}\rangle$ is a fully contracted *in situ* atomic orbital (CAO), i.e., a normalized hybrid AO characterized by: (*i*) a *p* character *n* (defined as $(c_p/c_s)^2$, c_s, c_p being the coefficients of the *s* and *p* components in the expansion of the hybrid) and (*ii*) radially distorted *s*, *p*, and *d* parts, where by radial distortion we mean a change in the radial part of the AO with respect to the free-atom (or some similar) standard. The radial distortion is difficult to represent by a single number but can be measured to some extent by overlap values.

The choice of the molecular orbitals for use in this analysis is difficult whenever equivalent bonds appear. In this paper we shall refer to Boys' localized MO's such as they are produced by the library MONSTERGAUSS program (12). These orbitals have serious shortcomings: for one thing, they yield, in general, overlapping hydrids of the same atom – a mathematically unobjectionable but a chemically unpleasant result. The adoption of a localization criterion more in line with the tenets of the elementary theory of valency is the subject of work in progress.

The coefficients c_N of the CAO's of nitrogen are listed in the first part of Table 5 for the three relevant bases. In all cases, the c_N values for a given Boys bond orbital are fairly close to one another. This is satisfactory because it confirms first-order transferability of at least the atomic orbital coefficients. That the 6-311 H basis should give the least transferable values is in line with the claim that it is not well balanced.

Of course, complete transferability would be in contrast with the well-known existence of inductive effects: thus, the modest and quite regular changes in the c_N's along the series are acceptable. It is also interesting that the weights of nitrogen in the NH and NC bonds are very close to one another, except in the unbalanced basis 6-311 H. This supports to some extent the naïve idea that the coefficients with which atoms enter bonds are related to electronegativities. The electronegativities of carbon and hydrogen being close to each other, the c_N's must also be close.

The lone pair AO's should carry weight 1. That this is not the case depends, of course, on "non-bonding" couplings. We can, in a way, see in the deviation a measure of the transferability to be expected in the coefficients of AO's: in the best basis it is of the order of 4%, which corresponds to the dispersion of the values for the NH and NC bonds.

The third part of Table 5 shows the overall coefficients of H. The greater flexibility of the hydrogen subset in 6-31 H and 6-311 H is evident from the variation of the coefficients along the series but, once again, 6-31 H is physically much more satisfactory. Note also that with 6-31 H the coefficients of H (as well as those of N) increase as the *p*-characters, *n*, of the nitrogen hydrids (discussed below) decrease. This should correspond to a slight decrease in the "bond charge" due to the inductive effect of the methyl group.

We come now to hybridization. The *p*-characters indicated in Table 5 are particularly instructive. On the one hand, the 6-31 H basis yields the most regular set of values, thus indicating that the extension of the hydrogen basis has cured 6-31G* of its main shortcomings. It is also evident that the values deduced from 6-311 H are ill-behaved. On the other hand, the hybrids obtained are obviously not orthogonal. Indeed, the property that the sum of $1/(1 + n)$ for the four hybrids should give unity is certainly not satisfied with any basis. Now, even though a theoretical justification of the orthogonality requirement on hybrids is not immediate, the importance of that requirement in determining the direction of, say, equivalent hybrids is well known. The difficulty, of course, lies with Boys' localization criterion, which should be replaced by another one if the scheme of the elementary theory of valence is to be followed. At any rate, the 6-31 H basis does give the expected results for the binding orbitals of nitrogen (almost tetrahedral hybrids) and consistently with the other bases indicates that nitrogen polarization is slightly higher in the NH bond than in the NC bond. Also the lower *p*-character of the lone-pair hybrids is in line with results from hybridization theory (13).

In addition to the orthogonality problem, the difference in the radial parts of the *s* and *p* components also makes somewhat delicate the application of the standard concept of hybridization (9). In any case, all the considerations given here hold for distances where the radial parts of the components are approximately equal – which is well within the physically significant range.

Finally, the last part of Table 5 (d) contains information concerning the role of the basis set added to hydrogen in passing from 6-31G* to 6-31 H (on NH bonds only). They are the coefficients c_s, c_p of the normalized additional *sp* hybrids contracted to a single *s* orbital and a single *p* orbital, and the overall coefficient d_H of the distortion–polarization subset in question. Whereas d_H decreases regularly in the series, the interplay of polarization and distortion is less regular. This is obviously due to the combination of the inductive and through-space effects of the methyl groups.

Conclusion

The above discussion shows first of all that an adequate treatment of hydrogen is much more important than brute force basis extension in the description of organic molecules. This is a comforting conclusion because it confirms other indications that a physically satisfactory basis need not necessarily be too large.

Secondly, the comparatively small 6-31 H basis optimized with respect to hydrogen yields a description of the valence orbitals of nitrogen that is clearly in line with customary chemical intuition.

Of course, additional work is necessary. In particular, the hydrogen basis set can probably be further simplified while retaining its flexibility and the localized orbitals used to obtain the valence orbitals should satisfy criteria other than that of Boys. A detailed analysis of the radial distortion could also yield information about the optimal way of improving the basis sets.

It seems to us, at any rate, that the results and the type of analysis described in this paper should be kept in mind by all those trying to use *ab initio* SCF calculations for interpreting the chemical properties of relatively large molecules.

As concerns the methylamines, in particular, we emphasize, among other things, the result that the net charges of nitrogen appear to be almost invariant under substitution of hydrogen with a methyl group – a situation somewhat reminiscent of similar findings for alkane carbon atoms (5*a*).

Acknowledgements

This article is dedicated to Professor Camille Sándorfy for his 65th birthday. It is a welcome opportunity for Sándor Fliszár and Giuseppe Del Re to express to him their gratitude for the constant encouragement and invaluable advice received from him for many years. We are also greatly indebted to Dr. J. Andzelm for extremely useful advice on Gaussian basis sets and thank Dr. J. Bridet for assistance in the computations. G. DR. acknowledges the hospitality of the Departments of Chemistry, Université de Montréal and of Applied Mathematics, University of Waterloo. Support received from the National Research Council of Canada, the France-Québec exchange program, and from the Italian Research Council, CNR, (G. DR) is also gratefully acknowledged, as well as the cooperation offered by Le Centre de Calcul de l'Université de Montréal.

1. R. S. MULLIKEN and C. C. ROOTHAAN. Chem. Rev. **41**, 219 (1947).
2. J. M. PARKS and R. G. PARR. J. Chem. Phys. **28**, 335 (1958).
3. G. DEL RE. J. Chem. Soc. 4031 (1958).
4. (*a*) W. KOLOS. Theor. Chim. Acta, **54**, 187 (1980); (*b*) W. A. SOKALSKI. J. Chem. Phys. **77**, 4529 (1982); (*c*) J. G. M. VAN DUIJNEVELDT-VAN DE RIJDT and F. B. VAN DUIJNEVELDT. J. Mol. Struct. Theochem. **89**, 185 (1982).
5. (*a*) S. FLISZÁR, G. CARDINAL, and M.-T. BÉRALDIN. J. Am. Chem. Soc. **104**, 5287 (1982); (*b*) E. VAUTHIER, S. FLISZÁR, F. TONNARD, and S. ODIOT. Can. J. Chem. **61**, 1417 (1983).
6. M. COMEAU, M.-T. BÉRALDIN, E. VAUTHIER, and S. FLISZÁR. To be published.
7. V. H. SMITH. Phys. Scr. **15** 147 (1977); A. JULG. Top. Curr. Chem. **58**, 1 (1975).
8. S. FLISZÁR, G. KEAN, and R. MACAULAY. J. Am. Chem. Soc. **96**, 4354 (1974).
9. G. DEL RE and C. BARBIER. Croatica Chem. Acta. In press.
10. P. C. HARIHARAN and J. A. POPLE. Theor. Chim. Acta, **28**, 213 (1973); W. J. HEHRE, R. DITCHFIELD, and J. A. POPLE. J. Chem. Phys. **56**, 2257 (1972); R. KRISHNAN, J. S. BINKLEY, and J. A. POPLE. J. Chem. Phys. **72**, 650 (1980).
11. M. J. FRISCH, J. A. POPLE, and J. S. BINKLEY. J. Chem. Phys. **80**, 3265 (1984).
12. M. R. PETERSON and R. A. POIRIER. Monstergauss program, University of Toronto, Toronto, Ont., Canada. 1981.
13. G. DEL RE. Theor. Chim. Acta, **1**, 188 (1963); G. DEL RE, U. ESPOSITO, and M. CARPENTIERI. Theor. Chim. Acta, **6**, 36 (1966).

Étude, par spectroscopie de vibration, de l'autoprotolyse de l'acide nitrique absolu. Nouvelle interprétation

MARIE-HÉLÈNE HERZOG-CANCE, ANTOINE POTIER ET JACQUELINE POTIER[1]
Laboratoire des Acides Minéraux, LA 79, Université des Sciences et Techniques du Languedoc, Place E. Bataillon, 34060 Montpellier Cédex, France

Reçu le 30 juillet 1984

Cet article est dédié au Professeur Camille Sandorfy à l'occasion de son 65^e anniversaire

MARIE-HÉLÈNE HERZOG-CANCE, ANTOINE POTIER et JACQUELINE POTIER. Can. J. Chem. **63**, 1492 (1985).

L'étude spectroscopique ir et Raman de HNO_3 dans les états cristallisé et liquide a été entreprise afin de régler le problème de l'autodissociation de cet acide. On a ainsi identifié l'oligomère en chaîne $(HNO_3)_x$, des ions NO_2^+ et $(NO_3 \cdot 3HNO_3)^-$, du monohydrate sous deux formes: la paire ionique $H_2OH^+ \ldots ONO_2^-$ et l'association moléculaire $H_2O \ldots HONO_2$ et enfin très peu d'ions H_3O^+.

MARIE-HÉLÈNE HERZOG-CANCE, ANTOINE POTIER, and JACQUELINE POTIER. Can. J. Chem. **63**, 1492 (1985).

The ir and Raman spectra of solid and liquid anhydrous HNO_3 have been investigated for the purpose of solving the self-dissociation problem. Identified species are: the oligomer $(HNO_3)_x$ (chains), NO_2^+ and $(NO_3 \cdot 3HNO_3)^-$ ions, two monohydrate forms: the ionic pair $H_2OH^+ \ldots ONO_2^-$ and the molecular association $H_2O \ldots HONO_2$, and, finally, some free H_3O^+ ions.

Introduction

Le problème de l'autoprotolyse de l'acide nitrique absolu liquide a fait, il y a bien longtemps, l'objet de nombreux travaux et en particulier, ceux de Gillespie *et al.* (1) et de Lee et Millen (2). Il a été établi que l'autodissociation thermodynamique pouvait s'écrire:

[1] $2HNO_3 \rightleftharpoons NO_2^+ + NO_3^- + H_2O$

De plus la cryoscopie autour de l'acide nitrique (2) a conduit à considérer que les ions nitrate et nitryle (nitronium) étaient solvatés par un total de 4 molécules d'acide nitrique et que l'eau l'était par 2 autres. Des considérations basées sur les connaissances du moment ont permis de proposer une solvatation de 2 pour NO_3^- et donc de 2 pour NO_2^+.

En 1956, Wyatt (3) a préféré proposer un équilibre d'autodissociation faisant apparaître $HNO_3 \cdot H_2O$, NO_2^+ et $NO_3^-(HNO_3)_2$.

Cependant à l'époque le manque normal de données spectroscopiques n'avait pas permis d'aller plus loin et il est bien clair que la cryoscopie, si elle permet de dénombrer le degré de solvatation des espèces d'une solution, est d'un intérêt limité pour l'identification des espèces réellement présentes. D'ailleurs l'équilibre [1] lui-même n'avait été écrit qu'après reconnaissance spectroscopique des espèces par Ingold et Millen (4).

Belin et Potier (5) ont étudié l'autoassociation de HNO_3 en solvant inerte par spectroscopie de vibration ir et abaissement cryoscopique, ils ont montré ainsi la formation unique de polymères $(HNO_3)_x$ ouverts.

Les études spectroscopiques faites récemment sur les composés $HNO_3 \cdot H_2O$[2] (6) et $4HNO_3 \cdot H_2O$[2] (7) dans le verre et le liquide ont permis de trouver les espèces existantes dans ces deux états désordonnés, les interprétations n'ont été possibles pour le 4:1 qu'après avoir montré que le cristal est le trihydrogénotétranitrate d'oxonium: $H_3O^+(NO_3 \cdot 3HNO_3)^-$. On peut donc penser que les mêmes techniques permettraient de faire avancer le problème des espèces réellement présentes dans l'acide nitrique absolu. Dans cette optique, il est clair que les recherches précédentes (6, 7), devraient être d'un précieux secours ne serait-ce que parce que l'ion $(NO_3 \cdot 3HNO_3)^-$ présent dans des solutions très concentrées en acide nitrique peut être soupçonné d'exister encore dans l'acide absolu.

Par ailleurs, depuis les travaux de l'école d'Ingold, peu de progrès ont été faits sur le spectre de l'espèce HNO_3 dans l'acide absolu puisqu'on ne peut citer que le travail de MacGraw *et al.* (8) sur la vapeur, leur exploration très partielle du liquide et du solide, et le travail de Guillory et Bernstein (9) sur HNO_3 isolé en matrice. Il est donc apparu nécessaire de commencer la présente étude par l'acide nitrique cristallisé dont une image plus ou moins déformée pouvait apparaître dans le liquide. Pour cette raison nous avons malgré l'ancienneté de la structure établie par Luzzati (10) tenté de la concilier avec les spectres que nous avons obtenus.

Il faut souligner que, comme les précédentes (6, 7), cette recherche est en grande partie une étude du comportement de la liaison hydrogène en relation avec les propriétés de donneur ou d'accepteur des molécules constituant les supermolécules recontrées.

Ceci doit permettre d'avoir une idée plus nette de la nature de l'autoprotolyse de la molécule amphiprotique HNO_3.

L'acide nitrique cristallisé

La seule détermination structurale est celle de Luzzati (10) en 1951. Ce travail ancien a été, avec les possibilités de l'époque, réalisé sur un monocristal mâclé, cependant son auteur a pu proposer le groupe d'espace $P2_1/c(C_{2h}^5)$ avec les paramètres suivants: a = 16,23; b = 8,57; c = 6,31 Å et β = 90°. Ceci impose 16 molécules dans la maille tandis que l'unité asymétrique n'en comporte que quatre.

Les différentes distances NO obtenues dans ces conditions sont $d_{N-OH} = 1{,}30 \pm 0{,}045$ Å et $d_{N-O} = 1{,}24 \pm 0{,}025$ Å. Les molécules d'acide nitrique s'organisent en chaîne qui se correspondent par un centre d'inversion. Cette structure est à rapprocher de celle trouvée pour CH_3COOH (11) ou $NaHCO_3$ (12, 13) par exemple.

Les travaux de spectroscopie de vibration ont été plus nombreux (8, 9, 14, 15) mais aucun n'a été fait en s'appuyant sur la structure proposée par Luzzati.

Sur les figures 1 et 2 sont représentés les spectres ir des acides hydrogéné et deutérié et les tracés de certains domaines

[1] Auteur à qui toute correspondance doit être adressée.
[2] Appelés respectivement 1:1 et 4:1 dans ce travail.

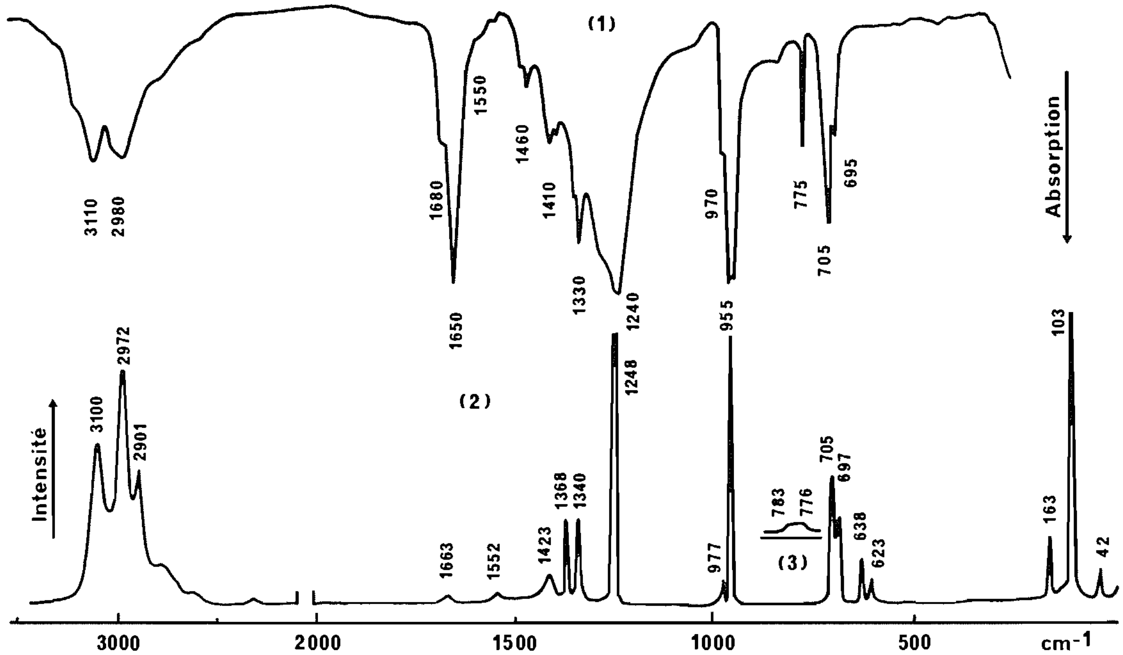

FIG. 1. HNO_3 cristal: spectres ir (1) et Raman (2).

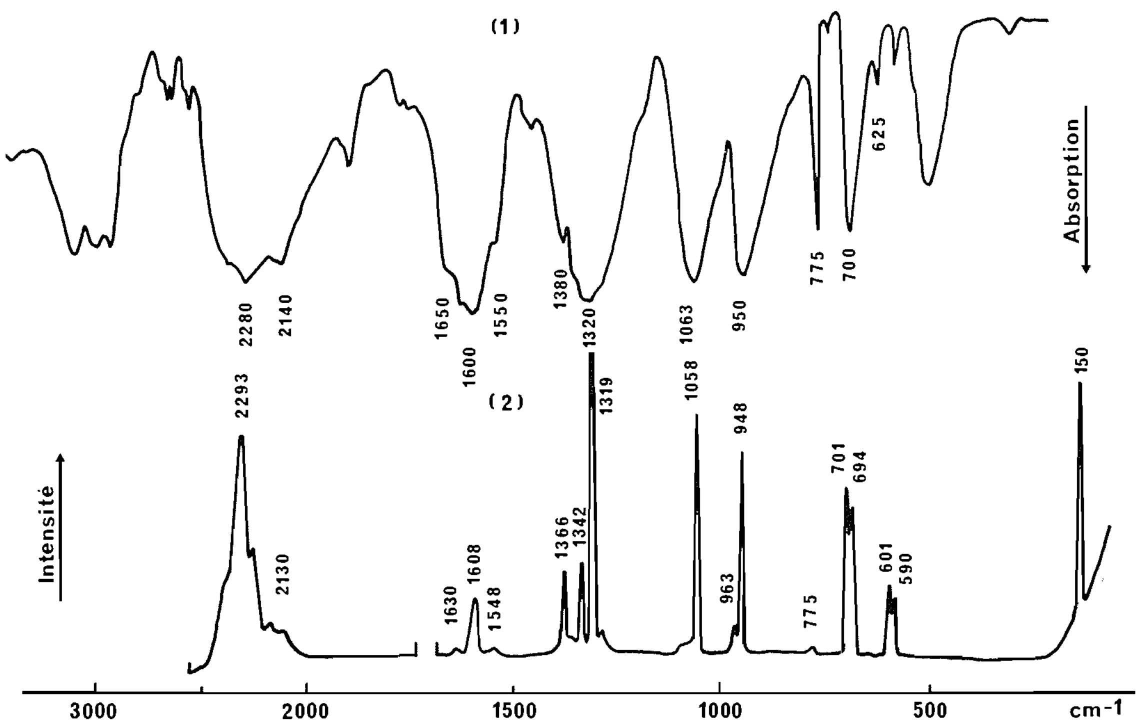

FIG. 2. DNO_3 cristal: spectres ir (1) et Raman (2).

les plus caractéristiques observés en Raman. On remarque leur complexité.

Pour la molécule HNO_3 de symétrie C_s on attend 9 vibrations (7 A' et 2 A''). Si on tient compte des 16 molécules par maille on attend 237 modes de vibration soit:

pour les vibrations internes: 32 Ag + 39 Au + 40 Bg + 30 Bu

pour les rotations: 16 Ag + 8 Au + 8 Bg + 16 Bu

pour les translations: 16 Ag + 8 Au + 8 Bg + 16 Bu

La complexité du spectre ne permet pas de prévoir l'ensemble, ce qui paraît d'ailleurs peu raisonnable.

Si on essaie de raisonner avec l'unité asymétrique proposée par Luzzati, et de symétrie C_{2h}, on arrive à 57 vibrations:

pour les vibrations internes: 12 Ag + 6 Au + 6 Bg + 12 Bu

pour les rotations: 4 Ag + 2 Au + 2 Bg + 4 Bu

pour les translations: 4 Ag + 1 Au + 2 Bg + 2 Bu

ce qui paraît être plus abordable.

Avec ce mode de raisonnement, on voit que chaque vibration de HNO_3 donnera deux composantes actives en ir et deux en Raman.

On peut cependant proposer une autre analyse basée sur l'analogie avec $(HCO_3^-)_x$ dans le sel de sodium (12).

Cette dernière repose sur l'hypothèse que les couplages interchaînes seront faibles voire non existants. Dans ces conditions on analyse les spectres en ne prenant en compte qu'une chaîne $(HNO_3)_x$ de symétrie C_{2v}. Par ailleurs si on prend en compte les éléments de symétrie du cristal on peut décrire les mouvements de ce polymère (16) en analysant ceux du dimère $(HNO_3)_2$ comme cela a été fait pour $(HCO_3)_x$ dans $NaHCO_3$ par la réf. 12.

On attend alors, en ir et en Raman, deux composantes pour chaque vibration interne sauf pour les vibrations d'espèce A'' qui ne donnent qu'une composante en ir.

Le choix entre ces deux modes de raisonnement n'est pas que subjectif puisque, dans la première analyse, on doit noter une activité sélective ir et Raman et que de ce fait les fréquences observées doivent être, au moins dans la majorité des cas, différentes.

Dans une première étape, on peut retenir que, quelle que soit l'hypothèse choisie, on attend deux composantes pour les vibrations d'espèce A'.

On peut donc essayer d'interpréter le spectre.

Domaine des vibrations de valence: ν OH (2000–4000 cm⁻¹)

On relève sur le spectre ir du composé hydrogéné deux bandes importantes à 3110 et 2980 cm^{-1} tandis qu'en Raman on observe essentiellement deux raies à 3100 et 2972 cm^{-1}. Les composantes de DNO_3 sont relevées en ir à 2280 et 2140 cm^{-1} (avec des rapports isotopiques de 1,36 et 1,39) et en Raman à 2293 et 2130 cm^{-1} (avec ρ = 1,36 et 1,39).

On note au passage la différence d'intensité pour la seconde composante en Raman.

Par ailleurs, il ne faut pas négliger les différents épaulements observés tant en ir qu'en Raman et attribuables tout au moins partiellement à des harmoniques ou des combinaisons.

Sur le spectre partiellement deutérié, on remarque la présence de trois bandes de même intensité sur lesquelles nous reviendrons un peu plus loin. La fréquence moyenne de ν OH (≃3050 cm^{-1}) conduit, en référence à la courbe de Novak (17), à une distance $d_{O\ldots O}$ comprise entre 2,64 et 2,66 Å alors que Luzzati indique $d_{O\ldots O}$ = 2,87 Å en moyenne.

Domaine des vibrations de valence asymétriques: ν_{as} NO_2 (1500–1700 cm⁻¹)

On observe dans ce domaine sur le spectre ir de HNO_3 cristallisé une composante à 1650, un épaulement à 1680 cm^{-1} et une autre composante très faible à 1550 cm^{-1} tandis qu'en Raman apparaissent une raie à 1663 cm^{-1} avec un épaulement à plus haute fréquence et une raie d'intensité plus faible (mais toutefois plus intense qu'en ir) à 1542 cm^{-1}.

Pour l'homologue deutérié, on observe les mêmes composantes avec un déplacement vers les basses fréquences dû à un effet secondaire de la deutériation.

Si on ne tient compte que des raies et bandes les plus importantes, les deux modes d'analyses envisagés sont corrects.

Domaine des vibrations de valence symétriques: ν_s NO_2 (1200–1500 cm⁻¹)

Ce domaine est très sensible à la deutération puisque la bande (ou raie) la plus intense (1240 cm^{-1}) se déplace alors de +70 cm^{-1} (tableau 1). Cette évolution est la preuve d'un couplage entre la vibration ν_s NO_2 et la vibration du mode de déformation δ OH dû à la formation de la chaîne. On observe effectivement dans le spectre de DNO_3 la disparition de la bande (ou raie) à 1410 cm^{-1} (1423 cm^{-1}) tandis qu'apparaissent à 1058 cm^{-1} (Raman) et 1063 cm^{-1} (ir) une raie et une bande relativement intenses. Au passage signalons que ce mode de vibration est observé par Guillory et Bernstein (9) à 1343 cm^{-1} dans le monomère et à 1398 cm^{-1} dans le dimère. Ce glissement de +67 cm^{-1} semble logique et correspond au glissement de −440 cm^{-1} observé pour ν OH.

Pour éviter l'interférence δ OH − ν_s NO_2, on peut analyser le spectre de DNO_3; on y relève, en Raman, quatre raies d'inégales intensités à 1297; 1319; 1342 et 1366 cm^{-1} (en ir à 1320; 1350 et 1380 cm^{-1}). Les composantes supplémentaires sont dues soit à des harmoniques soit à des combinaisons avec les modes de vibration par effet de corrélation; dans ce dernier cas il convient d'espérer une autre détermination structurale.

Domaine 800–1200 cm⁻¹

Dans ce domaine, on attend pour $(HNO_3)_x$ essentiellement ν N(OH) (= ν NO').

Nous ne reviendrons pas ici sur le choix d'attribution proposé par Diop et Potier (18) et confirmé par Guillory et Bernstein (9).

Cette bande apparaît à 955 cm^{-1} (953 en Raman) mais cependant elle n'est pas unique comme on le voit sur la figure 1. La deutériation simplifie la bande ir; on n'observe qu'une composante principale à 950 cm^{-1} mais simultanément apparaît une bande à 740 cm^{-1}. Ceci conduit à attribuer une des deux bandes autour de 950 cm^{-1} à γ OH $(HNO_3)_x$. (On note un glissement de fréquence de −5 cm^{-1} dû à l'effet de la deutériation (Fig. 2).)

Pour ν NOH la présence d'une raie intense et d'une plus faible à 977 cm^{-1} (Raman) est toujours compatible avec le mode de raisonnement adopté.

Domaine 800–700 cm⁻¹

On doit trouver essentiellement, dans ce domaine, les vibrations de déformations de NO_2 et de l'angle ON(OH). Les éclatements y sont plus faibles, ils apparaissent cependant en Raman où la résolution est meilleure. Pour ρ NO_2 (783–776 cm^{-1} en Raman; 775 en ir), il semble qu'on ait la preuve que dans le cristal HNO_3 tout se passe comme si, seul intervenait dans le dénombrement des modes de vibration, le motif $(HNO_3)_2$.

Il n'est pas utile de discuter de façon détaillée les attributions; elles sont reportées dans le tableau 1 et ne s'écartent pas des attributions classiquement proposées.

Domaine des vibrations de réseau

On observe en Raman trois vibrations de réseau à 42,103 et 163 cm^{-1}. On peut penser comme Hadzi *et al.* (19) que la vibration à 163 cm^{-1} correspond à un mode de liaison hydrogène.

En conclusion, il semble que l'analyse des données spectroscopiques ne prenant en compte que l'unité asymétrique soit correcte. Cependant il reste le problème des trois composantes ν OH d'égale intensité observées en ir dans le composé partiellement deutérié et la présence en Raman de trois composantes dans $(HNO_3)_x$ ou $(DNO_3)_x$. Il n'est guère possible d'attribuer une de ces trois bandes à une combinaison. L'égalité de leur intensité conduirait à les attribuer à 3 vibrations O—H—O d'inégale longueur ainsi que le propose Luzzati. Ce dernier a trouvé des liaisons hydrogène de 2,84 à 2,98 Å, ce qui correspondrait selon la courbe de Novak (17) à des fréquences ν OH de 3400 à 3500 cm^{-1}. Les différentes fréquences observées ici conduisent à des distances de 2,66 à 2,64 Å, soit des différences de distances O...O comparables. Signalons que Rozière *et al.* (20, 21) ont réinterprété pour $[NO_3 . HNO_3]^-$ les

TABLEAU 1. Fréquences et attributions des divers modes de vibration pour HNO_3 cristal

HNO_3		DNO_3		
Infrarouge	Raman	Infrarouge	Raman	Attributions
		3110 m		
		3000 m		
		2930 m		
		2790 ép.		
		2660 f		
		2640 f		
		2550 f		
3110 F	3100 m	2280 F	2293 F	
		2265 ép.		ν OH
2980 F	2972 F	2140 F	2130 ép.	
	2901 m			
		1940 ép.		
2780 ép.	2792 f	1900 m		2 δ OH
2620 ép.	2622 m			
		1780 ép.		
		1750 ép.		
1680 ép.	1680 f	1650 ép.	1630 f	
1650 F	1663 f	1600 F	1608 f	ν_{as} NO_2
1550 ép.	1552 f	1550 ép.	1548 f	
1460 f		1450 f		
1410 m	1423 m			δ OH
1345 ép.	1368 m	1380 ép.	1366 m	
1330 m	1340 m	1350 ép.	1342 m	ν_s NO_2
1240 F	1248 F	1320 F	1319 F	
			1297 f	
		1063 F	1058 F	δ OD
970 ép.	977 f		963 f	
955 F	955 F	950 F	948 F	ν NOH(HNO_3)
950 F				γ OH$(HNO_3)_x$
	783 f			
775 m		775 F	775 f	ρ NO_2
	776 f			
		740 f		γ OD$(DNO_3)_x$
705 F	705 m	700 F	701 m	
695 ép.	697 m		694 m	δ_s NO_2
	638 f		601 f	
	623 f	625 f	590 f	δ ONOH
	163 m		150 F	
	103 F			Vibration de réseau
	42 f			

analyses structurales et, en introduisant un désordre ont amené la distance O...O de 2,85 (22) à 2,44 Å.

L'acide nitrique liquide

Comme nous l'avons vu en introduction, l'équilibre d'auto-dissociation de l'acide proposé par Ingold et coll. (1) fait apparaître des ions NO_2^+ (solvatés par deux molécules d'acide nitrique), l'ion dihydrogénotrinitrate et de l'eau elle aussi solvatée par deux molécules d'acide.

Depuis ce travail, Leuchs et Zundel pour HNO_3-H_2O (23) et nous mêmes pour $HNO_3 \cdot H_2O$ et $4HNO_3 \cdot H_2O$ (6, 7) avons montré que l'interaction H_2O – acide nitrique correspondait à la réaction acide–base sans transfert de proton: $H_2O \cdots HONO_2$ avec l'oxygène de la molécule d'eau comme centre basique plutôt qu'à la création de l'entité $H_2O(HNO_3)_2$.

Il faut aussi rappeler que HNO_3 dans un solvant neutre (5) est dissocié à grande dilution en donnant le monomère caractérisé par une bande à 3484 cm^{-1} avec une constante d'anharmonicité selon Sandorfy (24) $X_{12} = 64$; $X_{23} = 80$; $X_{13} = 72$ tandis que pour HNO_3 anhydre on observe $X_{12} = 43$; $X_{23} = 93$ et $X_{13} = 68$ ce qui permet d'éliminer l'hypothèse de la présence unique de monomère. Et ce d'autant plus que la vibration OH du polymère ouvert est observée à la même fréquence que le monomère (25).

Par ailleurs, une étude des abaissements cryoscopiques en solvant inerte avait conduit Belin et Potier (5) à n'admettre que la présence de polymères ouverts. Notons également que ces auteurs n'ont pas envisagé pour HNO_3 liquide la présence possible de plusieurs espèces liées à la formation de l'équilibre d'auto déshydratation.

Présence de l'ion NO_2^+

Ce travail confirme sans ambiguïté la présence de l'ion NO_2^+ (avec ν_s = 1399 cm^{-1} en Raman et ν_{as} = 2330–2360 cm^{-1}; δ_{deg} = 550 cm^{-1} et $\nu_s + \nu_{as}$ = 3740 cm^{-1} en ir).

Sur la figure 3 on voit que les fréquences relevées pour cet ion s'intègrent parmi les fréquences relevées pour des ions NO_2^+ libres comme l'ont montré des études structurales. L'absence de tout abaissement de fréquence notamment pour ν_s

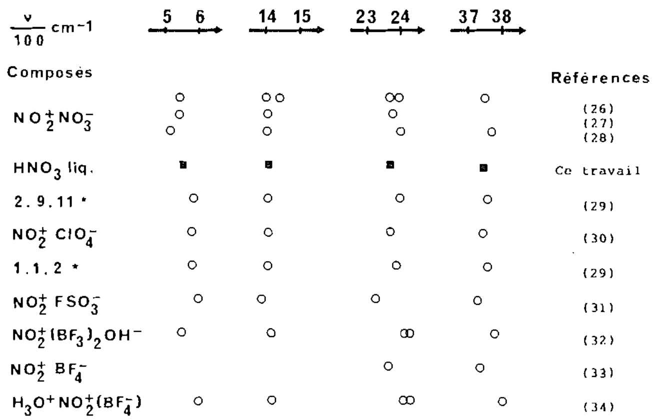

FIG. 3. Evolution des fréquences caractéristiques de l'ion NO_2^+ dans différents sels de nitryle (× 2.9. 11 = $(H_3O^+)_2(NO_2^+)_9(ClO_4^-)_{11}$ et 1.1.2 = $H_3O^+ NO_2^+(ClO_4^-)_2$).

(NO_2^+) **permet de ne pas retenir l'hypothèse d'une solvatation de ce cation par deux molécules d'acide nitrique.**

Recherche de l'ion $(NO_3 \cdot 2HNO_3)^-$

Il apparaît normal de rechercher la présence potentielle de cet anion qui a été caractérisé tant par diffraction de rayons X (35) que par spectroscopie de vibration (18) dans la série des dihydrogénotrinitrates, $MNO_3 \cdot 2HNO_3$ (M = K^+, NH_4^+, Cs^+, Rb^+...).

Sur les spectres de Potier et Diop (18) on peut noter quelques bandes ou raies caractéristiques de l'anion $(NO_3 \cdot 2HNO_3)^-$ en particulier, la présence de la liaison hydrogène de 2,60 Å entraîne celle d'une bande large à 2500 cm^{-1}. Un autre fait spécifique de cet anion est l'existence à côté de la raie à 1312 cm^{-1} d'une raie d'égale importance à 1367 cm^{-1} liée à la solvatation de l'ion nitrate par deux molécules HNO_3 et à la présence d'un vibrateur NO libre.

L'absence de la bande à 2500 cm^{-1} et de la raie à 1367 cm^{-1} dans les spectres de HNO_3 dans l'état liquide permet sans ambiguïté de réfuter la formation de cet anion dans l'acide nitrique anhydre. Une conclusion semblable avait été proposée lors de l'analyse des spectres du 4:1 et de 1:1 dans les états désordonnés (6, 7).

Domaine des vibrations de valence ν NOH (ν NO′)

Ayant montré la présence d'un ion NO_2^+ non solvaté et l'absence de $(NO_3 \cdot 2HNO_3)^-$, il reste à rechercher les espèces responsables de la complexité des spectres. Comme cela a été fait pour le 4:1 et le 1:1 (6, 7), on étudie en premier lieu le domaine des vibrations ν NO′ où peuvent apparaître différents types de vibrateurs.

Une première analyse du spectre Raman (Fig. 4) montre que HNO_3 liquide a un comportement comparable à celui de 4:1 liquide et que la raie centrée autour de 940 cm^{-1} est complexe. Il semble logique de lier ici l'apparition des différentes composantes, à l'existence de divers vibrateurs ν NO′. On remarque toutefois des variations d'intensité quand on passe de HNO_3 au 4:1.

On peut penser que dans les deux cas, les mêmes modes de vibrations sont responsables des raies ou bandes observées à des fréquences proches. Dans le tableau 2, on a rassemblé les attributions proposées en fonction de cette hypothèse de travail; ceci permet d'envisager la présence:

de l'ion trihydrogénotétranitrate $(NO_3 \cdot 3HNO_3)^-$

de l'association moléculaire $H_2O \cdots HONO_2$

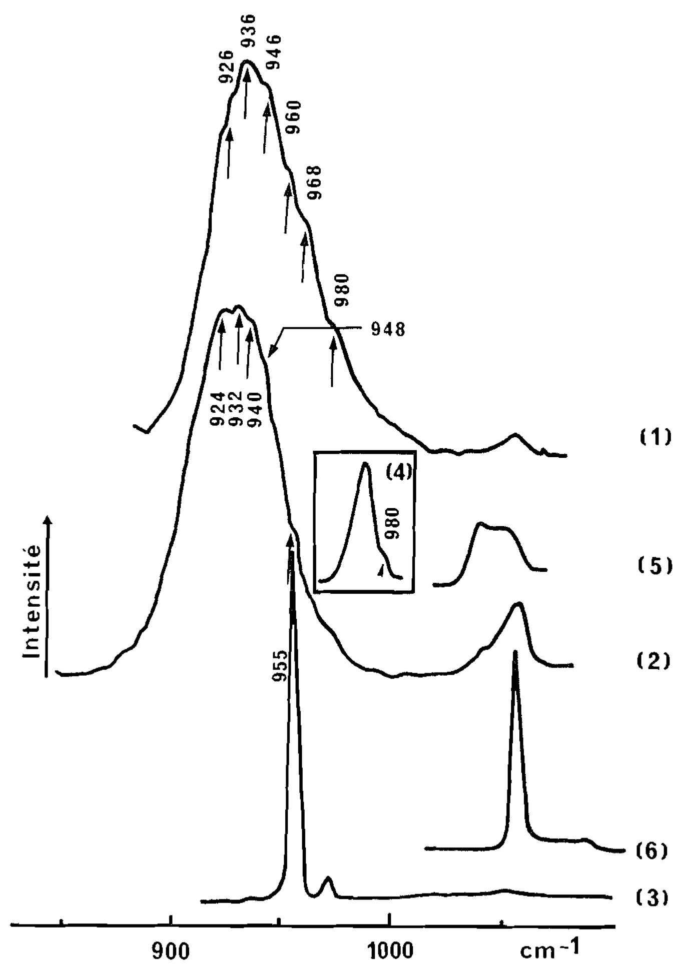

FIG. 4. Spectres Raman entre 850 et 1050 cm^{-1}: (1) $4HNO_3 \cdot H_2O$ liquide, (2) HNO_3 liquide, (3) HNO_3 cristal, (4) HNO_3 liquide: épaulement à 980 cm^{-1}, (5) DNO_3 liquide autour de 1050 cm^{-1}, (6) HNO_3 cristal autour de 1050 cm^{-1}.

d'acide nitrique "libre"

(Bien entendu il faut que l'analyse des autres domaines de fréquence corrobore ces attributions.)

Plus précisément on relève sur la spectre Raman enregistré à −35°C (liquide froid) un épaulement à 980 cm^{-1} noyé dans la plupart des autres spectres, dans le pied de la raie autour de 940 cm^{-1} (fig. 4(4)). Cette composante est à rapprocher de celle attribuée à ν NO′ de la liaison hydrogène centrale de $(NO_3 \cdot 3HNO_3)^-$. Ceci est une des premières indications de la présence de cette espèce dans HNO_3 liquide et justifie la recherche des autres espèces susceptibles d'exister (tableau 2).

En plus de ces composantes, on trouve pour HNO_3 liquide, une vibration ν NO′ à 950 cm^{-1} absente dans le 4:1 et le 1:1. Cette fréquence est à rapprocher de celle observée dans le cristal où les molécules d'acide nitrique forment le polymère ouvert $(HNO_3)_x$. Le déplacement de fréquence traduit un affaiblissement de la liaison hydrogène qui peut être lié à un effet de température.

Domaine des vibrations de valence ν OH (4000–2000 cm^{-1})

Sur la figure 5 on a regroupé les tracés ir du 4:1, de HNO_3 et DNO_3 liquide. On note, mis à part des différences au niveau des fréquences des ν OH, une allure similaire avec apparition des bandes A, B et C caractéristiques des liaisons hydrogène. Il semble logique d'attribuer ce comportement, comme dans le

TABLEAU 2. Fréquences et attributions des divers vibrateurs ν NO′ pour HNO_3 et DNO_3 liquides. Comparaison avec $4HNO_3 \cdot H_2O$

Infrarouge		Raman			Raman	
HNO_3	DNO_3	HNO_3	DNO_3	Attribution	$4HNO_3 \cdot H_2O$ (7)	$4DNO_3 \cdot D_2O$ (7)
920	920	924	920	ν NO′ HNO_3 libre	926	
	930	932	932	ν NO′ term.	936	935
940	—	940	939	anion complexe	946	945
950	—	948	949	ν NO′ $(HNO_3)_x$		
955	—	955	962	ν NO′ HNO_3 assoc. mol.	960	960
980	980	980	980	ν NO′ centraux	968	970
				anion complexe	982	980

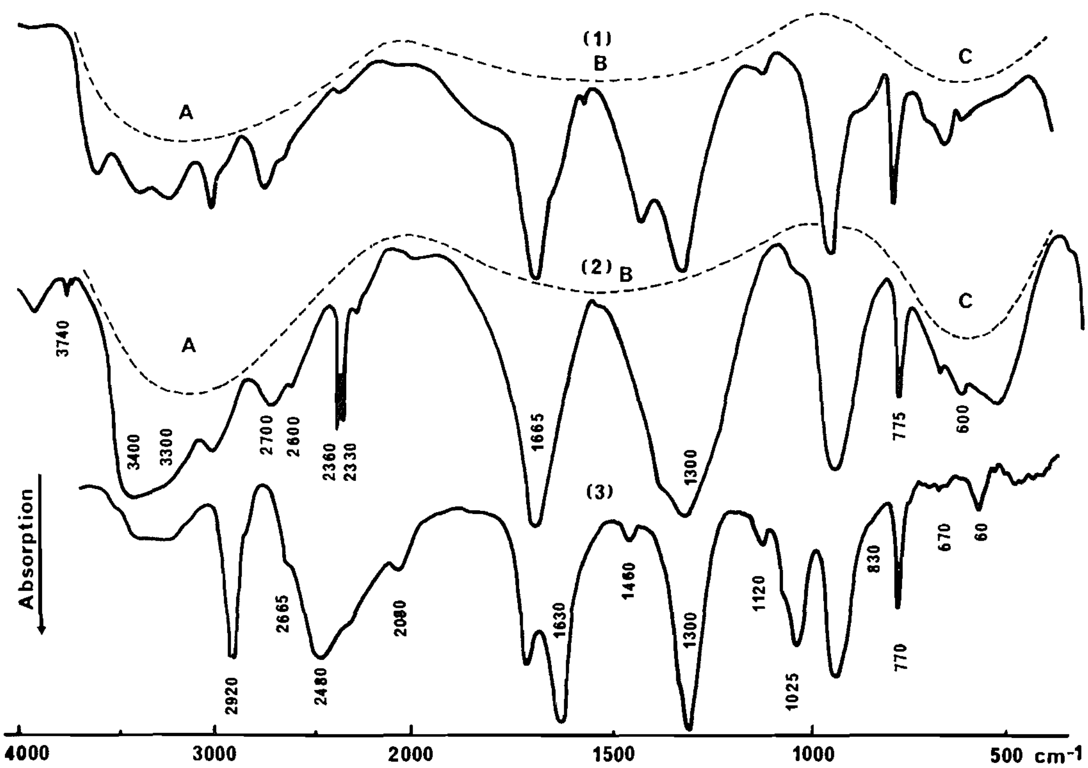

FIG. 5. Spectres ir de $4HNO_3 \cdot H_2O$ liquide (1), HNO_3 liquide (2) et DNO_3 liquide (3).

4:1, à la présence d'une liaison hydrogène moyennement forte centrée autour de 1500 cm^{-1} due à la même espèce: l'ion $(NO_3 \cdot 3HNO_3)^-$ dont la vibration ν NO′ est observée à 980 cm^{-1}.

Cependant, traditionnellement la recherche des autres espèces est effectuée sur les spectres Raman souvent mieux résolus. Sur la figure 6 sont reportés les spectres Raman de HNO_3 et du 4:1 dans l'état liquide. On y relève trois domaines principaux de vibration autour de 3350, 3050 et 2650 cm^{-1}, les intensités des deux derniers sont plus faibles que dans le 4:1.

Comme pour le 4:1, le massif large centré autour de 2650 cm^{-1} correspond aux vibrations ν OH (H_3O^+) de la paire ionique. De même on retrouve ν OH (HNO_3) de l'association moléculaire $H_2O\ldots HONO_2$ autour de 3020 cm^{-1} tandis que ν_s et ν_{as} (H_2O) de cette association apparaissent à 3545 cm^{-1} en épaulement au massif large entre 3100 et 3500 cm^{-1} (il convient de noter que dans le 1:1 (6) l'intensité de cette raie est particulièrement importante).

En ir (fig. 5) sur le spectre de HNO_3 deutérié, on observe comme pour le 4:1, la présence d'une bande fine à 2920 cm^{-1} qui glisse par deutériation à 2080 cm^{-1}. Cette bande n'existe pas sur le spectre ir de HNO_3; à sa place on observe une fenêtre de transmission d'Evans (due à 2 δ OH) comme nous l'avions déjà noté et discuté pour le 4:1.

Bien qu'une analyse quantitative des variations d'intensité ne soit pas possible, on peut remarquer cependant, comme sur les spectres Raman, une diminution des intensités des bandes caractéristiques des espèces $H_2O\ldots HONO_2$ et $H_2OH^+\ldots ONO_2^-$ quand on passe de 4:1 à HNO_3; en particulier le rapport ν OH $(H_2OHONO_2)/\nu_{as}NO_2$ est de 0,45 dans le 4:1 et n'est que de 0,33 pour HNO_3.

Dans le 4:1 on a attribué à HNO_3 "libre", une raie à 3280 cm^{-1}, ici on retrouve une raie à 3330 cm^{-1}; on peut penser qu'elle provient de la présence d'acide nitrique "libre", sa

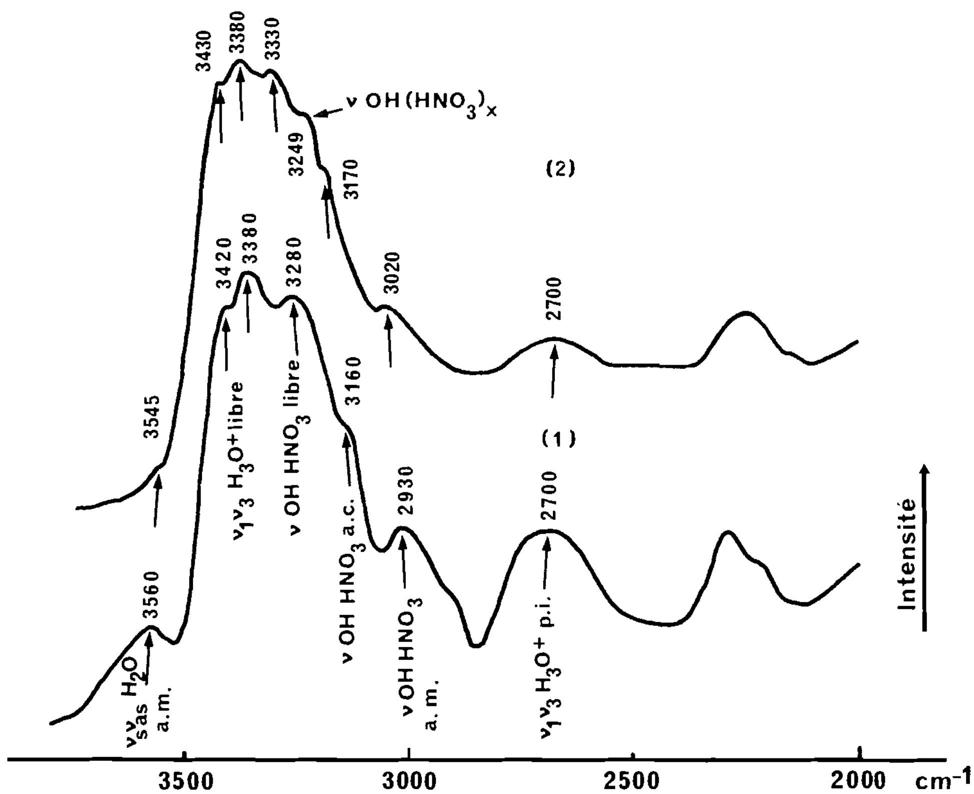

FIG. 6. Spectres Raman de $4HNO_3 \cdot H_2O$ liquide (1) et HNO_3 liquide (2) entre 2000 et 4000 cm^{-1} (a.c. = anion complexe; a.m. = association moléculaire; p.i. = paire ionique).

fréquence est plus élevée à cause de l'affaiblissement des liaisons hydrogène par rapport à celles du cristal. On remarque que dans le spectre HNO_3 liquide, la raie relative à ν OH (HNO_3) libre est plus intense que dans le 4:1 ce qui est tout à fait logique et que sa fréquence y est plus élevée (+50 cm^{-1}). Ce glissement de fréquence de 50 cm^{-1}, général quand on passe de 4:1 à HNO_3 amène quelques commentaires. Dans le gaz en matrice Bernstein a observé ν OH à 3490 cm^{-1} tandis qu'il a noté pour le dimère 3280 cm^{-1} (9). Il semble que ce que nous appelons acide nitrique "libre" est en réalité **un acide déjà engagé dans une liaison hydrogène très faible**; comme Belin et Potier l'on déjà indiqué (5) pour la suite de ce mémoire, nous garderons le terme "HNO_3 libre".

La raie à 3170 cm^{-1} qui se déplace à 2336 cm^{-1} par deutération est comparable à celle qui est observée à 3160 cm^{-1} dans le 4:1 et est attribuée à ν OH (HNO_3) terminal de l'anion complexe.

Ayant confirmé la présence de l'anion complexe $(NO_3 \cdot 3HNO_3)^-$ il importe de rechercher l'existence d'ions H_3O^+ libres. Il semble que l'on puisse attribuer à ν_1 et ν_3 H_3O^+ les vibrations observées à 3380 et 3430 cm^{-1} en Raman (3380 et 3420 cm^{-1} en ir) qui se déplacent par deutération (ρ = 1,37). Dans ce domaine de fréquences sont également attendus les vibrateurs ν OH de HNO_3 monomère et ν OH terminaux du polymère ouvert.

Reste à examiner le cas du vibrateur ν OH à 3250 cm^{-1}, ce vibrateur est absent dans le 4:1; il semble justifié de l'attribuer au vibrateur OH engagé du polymère $(HNO_3)_x$ observé dans HNO_3 cristal. Sa fréquence supérieure à celle relevée dans ce dernier (3110 cm^{-1}) indique un affaiblissement des liaisons hydrogène de ce polymère ou une dépolymérisation partielle mais est aussi lié à un effet de température.

La variation des fréquences des diverses vibrations ν NO′ et ν OH quand on passe de HNO_3 à $4HNO_3 \cdot H_2O$ et $HNO_3 \cdot H_2O$ est reportée sur la figure 7.

Domaine des vibrations de valence ν_s et ν_{as} NO_2

L'ensemble des attributions proposées dans le domaine des vibrations de valence ν_s et ν_{as} NO_2 est reporté dans le tableau 3. On doit souligner qu'en ir on observe deux composantes à 1300 et 1350 cm^{-1}. De plus on remarque la disparition du déplacement de ν_s NO_2 sous l'effet de la deutération.

La présence de la raie à 1380 cm^{-1} dans DNO_3, absente sur le spectre du 4:1 semble difficilement attribuable à une harmonique mais paraît plutôt due à une des composantes du polymère $(HNO_3)_x$.

Domaine entre 1000 et 700 cm^{-1}

Si les espèces apparemment détectées jusqu'à maintenant sont réellement présentes, on attend dans HNO_3 autour de 1000 cm^{-1} ν_2 (H_3O^+) et en plus en Raman ν_1 NO_3^- de la paire ionique, tandis que pour DNO_3 on doit retrouver les déformations δ OD de HNO_3 "libre", δ OD du (ou des) polymères et enfin ν_1 NO_3^-.

En ir, si on compare au spectre de HNO_3 cristal, on observe ici une bande de très faible intensité (1050 cm^{-1}). Tandis que, si dans DNO_3 cristal on note une bande à 1065 cm^{-1}, pour DNO_3 liquide on n'observe qu'une bande large à 1025 cm^{-1} avec un épaulement à 1055 cm^{-1} et par ailleurs un épaulement à 830 cm^{-1}, épaulement absent sur le spectre de HNO_3 liquide ce qui conduit à y voir ν_2 H_3O^+ et ν_2 D_3O^+ (ρ = 1,27).

En Raman (fig. 4), les modifications rencontrées quand on passe de HNO_3 à DNO_3 sont plus importantes (on rappelle que dans HNO_3 cristal il n'y a qu'une raie dans ce domaine, fig. 4 (6)). On voit pour HNO_3 une raie fine à 1055 cm^{-1} avec un

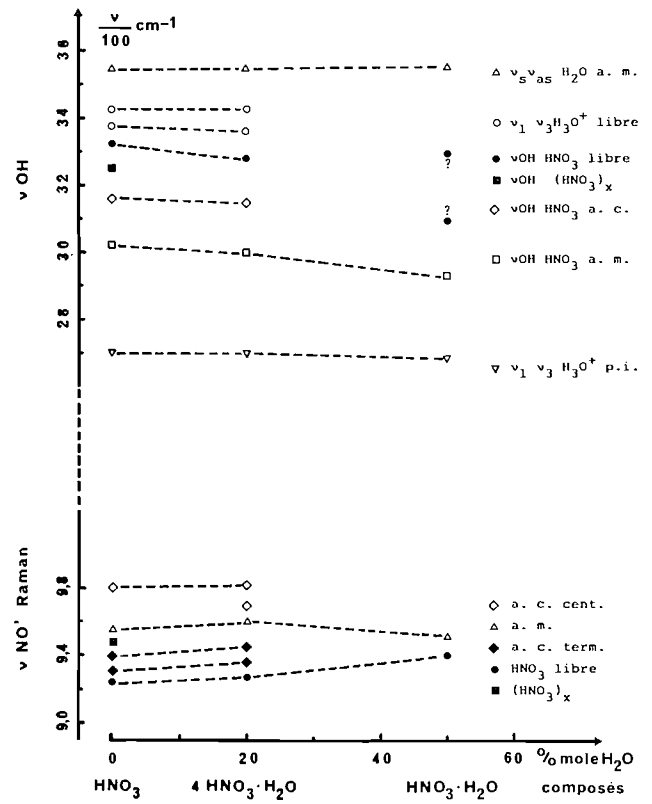

FIG. 7. Variation des fréquences des vibrateurs ν NO' et ν OH entre HNO_3, $4HNO_3 \cdot H_2O$ et $HNO_3 \cdot H_2O$.

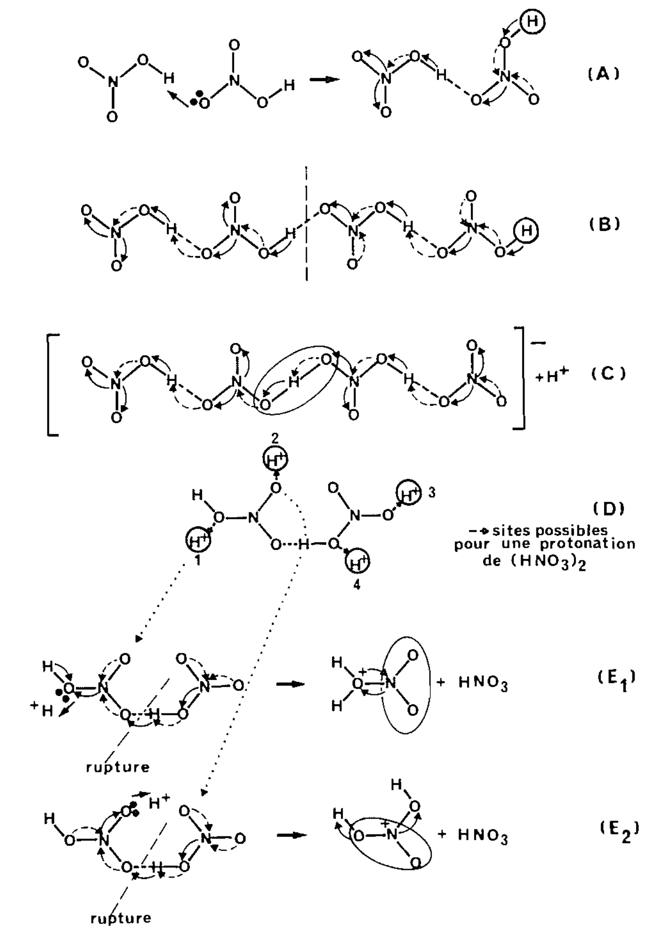

FIG. 8. (A) Formation du dimère; (B) formation du tétramère; (C) l'ion trihydrogénotétranitrate; (D) possibilités d'attaque du dimère; (E) réaction résultante (la direction des flèches indique le sens du transport des électrons – flèche en trait plein = allongement de la liaison, en tireté = raccourcissement).

épaulement à 1040 cm^{-1} (fig. 4 (2)) tandis que pour DNO_3, la raie à 1055 cm^{-1} diminue d'intensité et qu'apparaît une raie plus intense à 1034 cm^{-1} (fig. 4 (5)).

Ces faits semblent rendre compte de la présence de ν_2 H_3O^+ (diminution de la raie à 1055 cm^{-1} et apparition de l'épaulement à 830 cm^{-1} sur le spectre de DNO_3) tandis que les deux raies de DNO_3 seraient attribuables aux vibrateurs δ OD des polymères et de HNO_3 "libre" attendus.

L'épaulement à 1040 cm^{-1} dans HNO_3 liquide indique la présence de ν_1 NO_3^- de la paire ionique. Il semble que les liaisons hydrogène sont affaiblies (la fréquence de ν_1 NO_3^- est supérieure à celle observée dans le 4:1).

La fréquence relevée à 1034 cm^{-1} sur le spectre Raman de DNO_3 peut être attribuée à δ OD de HNO_3 "libre"; rappelons que pour HNO_3 gaz en matrice Bernstein (9) avec ν OH = 3490 cm^{-1} observe δ OD à 1031 cm^{-1}, il est donc logique avec ν OH = 3300 cm^{-1} de retrouver δ OD à 1034 cm^{-1} compte tenu des effets de température (−180°C pour la réf. 9 et 0°C dans ce travail). La raie à 1055 cm^{-1} serait due à δ OD du polymère.

En dessous de 800 cm^{-1} apparaissent classiquement, les déformations des groupes NO_2 et des angles ON(OH) comme on le voit sur le tableau 3. On doit rappeler le comportement similaire noté en ir au niveau de la bande large autour de 600 cm^{-1} pour le 4:1.

Le tableau 3 rassemble l'ensemble des fréquences et attributions proposées pour les espèces présentes dans HNO_3 et DNO_3 liquide.

Conclusion. Proposition pour une autoprotolyse de l'acide nitrique absolu

Les résultats précédents conduisent à préciser l'équation thermodynamique de Ingold et coll. (1) en:

$$[a] \quad \frac{6}{x}(HNO_3)_x \rightleftharpoons NO_2^+ + (NO_3 \cdot 3HNO_3)^- + H_2O \ldots HONO_2$$

qui est l'équilibre principal auquel on doit ajouter:

$$H_2O \ldots HONO_2 \rightleftharpoons H_2OH^+ \ldots ONO_2^-$$

déjà écrit pour le quart et le monohydrate (6, 7) et:

$$\frac{4}{y}(HNO_3)_y + H_2O \rightleftharpoons (NO_3 \cdot 3HNO_3)^- + H_3O^+$$

avec $y \leq 4$.

Ceci rend compte de l'identification spectroscopique: (*i*) de l'oligomère en chaîne $(HNO_3)_x$ peu condensé; (*ii*) des espèces NO_2^+ et $(NO_3 \cdot 3HNO_3)^-$, (*iii*) des deux formes du monohydrate (association moléculaire et paire ionique), et (*iv*) de la présence de très peu d'ions oxonium.

On doit alors noter que l'acidité protonique est celle du polymère nitrique, a priori plus acide que la molécule isolée. Mais cette acidité est réduite par ionisation du tétramère qui créée l'ion $(NO_3 \cdot 3HNO_3)^-$ en libérant un proton qui, cherchant un accepteur protonique ne peut le trouver que sur une espèce existante c'est-à-dire un autre oligomère nitrique ($x < 4$ peut être 3 ou 2) plus basique que le tétramère. Cette attaque conduit à $H_2NO_3^+$ qui se déshydrate facilement donnant alors l'ion NO_2^+ et la base H_2O qui se recombine avec $(HNO_3)_x$ en donnant le monohydrate. Ceci peut être présenté dans le contexte des lois

TABLEAU 3. Fréquences et attributions des modes de vibration pour HNO_3 liquide

HNO_3		DNO_3'		
Infrarouge	Raman	Infrarouge	Raman	Attributions
3550 ép.	3545 f	2665 ép.	2650 ép.	ν_s, ν_{as} (H_2O). ass. mol.
	3430 F			
3400 F		2480 F	2492 F	ν_1, ν_3 H_3O^+ libre
	3380 F			
3300 F	3330 F	—	2454 F	ν OH HNO_3 libre
	3249 F		2400 F	ν OH $(HNO_3)_x$
	3170 ép.		2346 m	ν OH (HNO_3) anion complexe
2920 F	3020 m	2080 m	2107 f	ν OH (HNO_3) ass. mol.
2700 m				
	2700 m	1980 f		$\nu_1 \nu_3$ (H_3O^+) p. ionique
2600 m				
	2200			
2010				
		1715 m		
	1692 ép.			
1665 F	1675 f	1630 F	1645 f	ν_{as} NO_2
	1670 f		1615 f	
1540 ép.	1541 f		1540 f	
1460 f		1450 m		ν_1 NO_3^- p. ionique
1380 ép.		1380 ép.	1383 m	
1350 ép.	1365 ép.	1360 ép.		
			1338 ép.	ν_s NO_2
1300 F	1300 F	1300 F	1307 F	
	1287 ép.		1278 ép.	
1250 ép.		1270 ép.		ν_3 NO_3^- p. ionique
		1180 ép.		ν_4 D_3O^+ libre
		1120 m		δ OD (D_2O) ass. mol.
1050 f	1055 m	1055 ép.	1055 ép.	δ OD $(DNO_3)_x$ et ν_2 H_3O^+
				ν_1 NO_3^- p. ionique et
	1040 ép.	1025 m	1034 m	δ OH HNO_3 "libre"
		830 ép.	830 ép.	ν_2 D_3O^+
770 m	767 f	760 m	775 f	ρ NO_2
		740		γ OD $(DNO_3)_x$
710 ép.	700 ép.	710 ép.	705 ép.	δ_s NO_2
670 f	676 m	670	681 m	
	644		603	δ ONOH
600 f	614 m	560	580 m	

de Gutmann (36).

La figure 8(A) montre les effets dus à la formation du dimère. Les faits notables sont le raccourcissement des liaisons N—(OH), l'allongement de (NO)—H dans la formation de la liaison hydrogène et surtout l'allongement du OH terminal (affaiblissement et transport simultané d'électrons de H à O) c'est à dire **l'augmentation d'acidité de l'hydrogène terminal** par rapport à l'acide monomère.

La figure 8(B) présente la formation du tétramère conduisant à celle du trihydrogénotétranitrate. A l'allongement d'une liaison O—H et au raccourcissement d'une liaison H...O correspond (lois de Gutmann) un raccourcissement de la liaison hydrogène O—H...O. Mais on note surtout l'augmentation de l'acidité de l'hydrogène terminal (entouré).

Plus la chaîne d'oligomère s'allonge, plus elle est acide et a tendance à "relarguer" H^+. Ici, ceci conduit à l'ion trihydrogénotétranitrate représenté sur la figure 8(C).

On comprend que les liaisons hydrogène doivent se raccourcir et surtout que la liaison hydrogène centrale peut devenir symétrique.

La figure 8(D) correspond à la suite de la réaction [a]. On considère que le tétramère (fig. 8(B)) "relargue" son proton en donnant $(NO_3 \cdot 3HNO_3)^-$ (fig. 8(C)). Le proton disponible attaque, par exemple, un dimère.

A priori, il est difficile de localiser l'oxygène de protonation puisque lors de la formation du dimère (fig. 8(A)), tous les oxygènes se sont chargés. Parmi les quatre positions, la troisième et la quatrième apparaissent les moins favorables (fig. 8(E)).

Dans les deux premiers cas, les liaisons NO pouvant conduire à NO_2^+ sont effectivement raccourcies et les liaisons NO dont il faut envisager la rupture sont allongées.

En tout état de cause la réaction résultante est:

$$NO_3H_2^+ \rightarrow NO_2^+ + H_2O$$

L'eau libérée vient attaquer une molécule HNO_3 et donne l'association moléculaire $H_2O \cdots HONO_2$.

Remarque 1:

Le processus d'oligomérisation de l'acide nitrique conduit à une raccourcissement des liaisons hydrogène de chaînes à condensation croissante. Ceci confirme l'inteprétation de nos données spectroscopiques et conduit à une révision probable des distances données par Luzzati dans le cristal HNO_3.

Remarque 2:

En plus des règles de Gutmann on est conduit à ajouter **la**

règle sur la liaison hydrogène: tout allongement de la liaison O—H, la plus courte de O—H...O, conduit à un raccourcissement de la liaison O...O, tout allongement de H...O provoque un allongement de O...O.

Partie expérimentale

Echantillons

L'acide nitrique est obtenu selon la méthode mise au point par Potier (37).

L'acide deutéronitrique est obtenu à partir de l'anhydride nitrique N_2O_5 dont la méthode de préparation mise au point au laboratoire (30) est une adaptation de celle de Hackspill et Besson (38).

Pour les études Raman, les échantillons sont introduits, en boîte à gants, dans des tubes de verre Pyrex de 5 mm de diamètre qui sont ensuite scellés sous vide. La cristallisation des échantillons nécessite des traitements thermiques. Le cycle est le suivant: on fait une trempe à 90 K suivie d'un réchauffement lent jusqu'à l'apparition des premiers cristaux puis de nouveau trempe et réchauffement et ce jusqu'à cristallisation totale.

Appareillage

Les spectres ir ont été enregistrés sur un spectromètre Perkin Elmer 180. La cellule à température variable est de type conventionnel (VLT2). Les échantillons sont placés en boîte à gants entre des faces en AgCl.

Les spectres Raman sont enregistrés sur un spectromètre Raman Dilor couplé à un analyseur modulaire multicanaux Tracor (Northern Instrument). Le laser à argon ionisé Spectra Physics a une puissance maximale de 1 W sur la raie à 5145 Å. Le refroidissement des échantillons est assuré par un ensemble cryostat et régulation de température Coderg.

1. R. J. GILLESPIE, E. D. HUGHES et C. K. INGOLD. J. Chem. Soc. **36**, 2552 (1950).
2. W. H. LEE et D. J. MILLEN. J. Chem. Soc. 4463 (1956).
3. P. A. H. WYATT. Trans. Faraday Soc. **52**, 806 (1956).
4. C. K. INGOLD et D. J. MILLEN. J. Chem. Soc. 2612 (1950).
5. C. BELIN et A. POTIER. J. Chim. Phys. **68**, 963 (1971).
6. M. H. HERZOG-CANCE, J. POTIER, A. POTIER, P. DHAMELINCOURT, B. SOMBRET et F. WALLART. J. Raman Spectrosc. **7**, 303 (1978).
7. M. PHAM THI, M. H. HERZOG-CANCE, A. POTIER et J. POTIER. J. Raman Spectrosc. **11**, 96 (1981).
8. G. E. MACGRAW, D. L. BERNITT et I. C. HISATSUNE. J. Chem. Phys. **42**, 237 (1965).
9. W. A. GUILLORY et M. L. BERNSTEIN. J. Chem. Phys. **62**, 1058 (1975).
10. V. LUZZATI. Acta Crystallogr. **4**, 120 (1951).
11. R. E. JONES et D. H. TEMPLETON. Acta Crystallogr. **11**, 484 (1958).
12. A. NOVAK, P. SAUMAGNE et L. D. C. BOK. J. Chim. Phys. **60**, 1385 (1960).
13. A. NOVAK. J. Chim. Phys. **72**, 981 (1975).
14. C. BELIN. Thèse Montpellier (1974).
15. L. DIOP. Thèse Montpellier (1976).
16. S. KRIMM. Adv. Polym. Sci. **2**, 51 (1960).
17. A. NOVAK. Struct. Bonding, **18**, 177 (1974).
18. L. DIOP et J. POTIER. J. Mol. Struct. **36**, 191 (1977).
19. D. HADZI, B. OREL et A. NOVAK. Spectrochim. Acta Part A, **29**, 1745 (1973).
20. J. ROZIÈRE, M. T. ROZIÈRE-BORIES et J. WILLIAMS. Inorg. Chem. **15**, 2490 (1976).
21. J. ROZIÈRE, M. S. LEHMAN et J. POTIER. Acta Crystallogr. Sect. B, **35**, 1099 (1979).
22. G. C. ROBINSON, R. MASSON et D. RUSSEL. Chem. Commun. 62 (1967).
23. M. LEUCHS et G. ZUNDEL. J. Phys. Chem. **82**, 1632 (1978).
24. C. SANDORFY. *Dans* Molecular spectra and molecular structure. I. Spectra of diatomic molecules. Section III-2. *Edité par* G. Herzberg. Van Nostrand, Princeton, NJ. 1950.
25. M. L. JOSIEN, J. DOS SANTOS et P. PINEAU. J. Chim. Phys. **62**, 628 (1965).
26. I. C. HISATSUNE, J. P. DEVLIN et Y. WADA. Spectrochim. Acta, **18**, 1641 (1962).
27. R. TERANISCHI et J. C. DECIUS. J. Chim. Phys. **22**, 896 (1954).
28. P. VITSE. Bull. Soc. Chim. Fr. **1**, 92 (1972).
29. A. M. MAJOU-DEUMIÉ. Thèse Montpellier (1969).
30. D. ROUSSELET. Thèse Montpellier (1968).
31. P. VAST. Thèse Lille (1969).
32. R. FOURCADE. Bull. Soc. Chim. Fr. **12**, 4493 (1972).
33. D. COOK, S. J. KUHN et G. A. OLAH. J. Chem. Phys. **33**, 1669 (1960).
34. J. F. HERZOG. Thèse Montpellier (1982).
35. J. R. C. DUKE et F. J. LLEWELYNN. Acta Crystallogr. **3**, 305 (1950).
36. V. GUTMANN. The donor–acceptor approach to molecular interactions. Plenum Press, New York, Londres. 1978.
37. A. POTIER. C. R. Acad. Sci. Paris, **233**, 1113 (1951).
38. L. HACKSPILL et J. BESSON. Bull. Soc. Chim. **16**, 479 (1949).

Supersonic beam investigations of indole and indole–halomethane complexes: intermolecular interactions

JAMES HAGER AND STEPHEN C. WALLACE
Department of Chemistry, University of Toronto, Toronto, Ont., Canada M5S 1A1

Received July 31, 1984

This paper is dedicated to Professor Camille Sandorfy on the occasion of his 65th birthday

JAMES HAGER and STEPHEN C. WALLACE. Can. J. Chem. **63**, 1502 (1985).

We report the findings of a supersonic beam investigation of the 1:1 gas phase complexes of indole with various halomethanes. The unique environment of the supersonic jet provides a method by which the pairwise intermolecular interactions of these complexes can be studied without the complications of condensed media effects. The behavior of argon and methane van der Waals molecules is described first in order to provide examples of simple dispersive interactions. These are then contrasted with complexing species such as CF_4 and CCl_4 where repulsive interactions offset the stabilization due to dispersive and dipole – induced dipole forces. Finally, we show that the interaction between the probe molecule and $CHCl_3$ and CH_2Cl_2 is apparently hydrogen bonding with the indole π electronic system. The implications of these intermolecular interactions on the area of general anesthesia are discussed in terms of a picture in which both the hydrophobic and polar portions of cell membrane may be reversibly affected.

JAMES HAGER et STEPHEN C. WALLACE. Can. J. Chem. **63**, 1502 (1985).

On rapporte les résultats obtenus au cours d'une étude, effectuée en phase gazeuse et à l'aide d'un faisceau supersonique, de complexes 1:1 d'indole avec divers halométhanes. L'environnement unique du jet supersonique fournit une méthode par laquelle les interactions intermoléculaires pairées de ces complexes peuvent être étudiées sans les complications inhérentes aux effets des milieux condensés. Dans le but d'avoir des exemples d'interactions dispersives simples, on décrit en premier le comportement des molécules de van der Waals entre l'argon et le méthane. On met ensuite ces molécules en opposition avec des espèces complexantes comme le CF_4 et le CCl_4 dans lesquelles les interactions répulsives compensent la stabilisation qui provient des forces dispersives et des forces dipolaires induites par des dipôles. Enfin, on démontre que l'interaction entre la molécule qui sert de sonde et le $CHCl_3$ ou le CH_2Cl_2 est apparemment due à une liaison hydrogène avec le système électronique π de l'indole. On discute des implications de ces interactions intermoléculaires sur le domaine de l'anesthésie générale en fonction d'une hypothèse par laquelle les portions tant hydrophobes que polaires de la membrane cellulaire peuvent être affectées d'une façon réversible.

[Traduit par le journal]

Introduction

Supersonic beams technology has enabled the synthesis of a wide variety of van der Waals molecules in which a "probe" molecule is embedded in a well-characterized "solvent" of finite extent (1–4). This has opened the way for the comparison of isolated molecule behavior with that of the same molecule associated with a chemical interesting ligand. The versatility of this technique can be seen by examining the enormous range of atoms and molecules that have been investigated in this way. These systems include rare gas dimers and clusters (2), hydrogen bonding species (3), and even bio-molecules such as tetraporphyrins and their associated van der Waals molecules (4). In this paper we examine the excited state behavior of indole van der Waals complexes with a series of halocarbons that are of interest in the area of general anesthesia. Supersonic expansions provides a unique medium in which to study the *pairwise* intermolecular interactions that are of great interest with respect to these weak forces.

General anesthetics encompass a group of atoms and molecules of widely differing chemical behavior. Substances such as molecular hydrogen and nitrogen as well as CF_4 and SF_6 exhibit limited anesthetic activity (5). Other more potent anesthetics include ether, chloroform, halothane ($CF_3CHClBr$), and methoxyflurane ($CH_3OCF_2CHCl_2$). The molecular view of the way in which this diverse group of chemical substances can reversibly affect the nerve cell membrane indicates that weak molecular associations are the physical interactions responsible for their anesthetic action (5). It has been suggested (6) that the study of weak molecular interactions can shed light on the perturbations of the optimum conditions for ion transport in and out of the nerve cells. Due to the good relationship between anesthetic potency and lipid solubility it has been routinely assumed that anesthetics are involved almost exclusively with interactions at the hydrophobic parts of the membrane lipids. The universality of this point has recently been questioned by Sandorfy and co-workers (6, 7) based on their infrared spectroscopic investigations of intermolecular associations between various functionalities and a wide variety of anesthetic molecules.

Briefly, the results of these investigations indicate that polar interactions may be very important in determining the anesthetic potency of a given molecule. A classification scheme based on the types of intermolecular interactions through which a given anesthetic molecule can affect molecular associations has been proposed by Sandorfy (6, 7). First there are those anesthetics that are non-polar and can associate only through dispersion forces, ion – induced dipole interactions, and dipole – induced dipole interactions. These anesthetics would be expected to interact primarily with the membrane lipids or proteins. Examples of these include Xe, SF_6, C_2F_6, and C_2H_4. Highly polarizable anesthetics in this class may also associate with the ionic and polar sites. Secondly, there are anesthetics that interact through charge transfer complex formation, though there are no confirmed examples of this as of yet. Thirdly, there are the anesthetics with an appreciable dipole moment, and consequently, can enter into electrostatic ion–dipole and dipole–dipole interactions. This group also contains those anesthetics that participate in hydrogen bonding as either a proton donor or proton acceptor.

The studies of the Sandorfy group have clearly shown, both

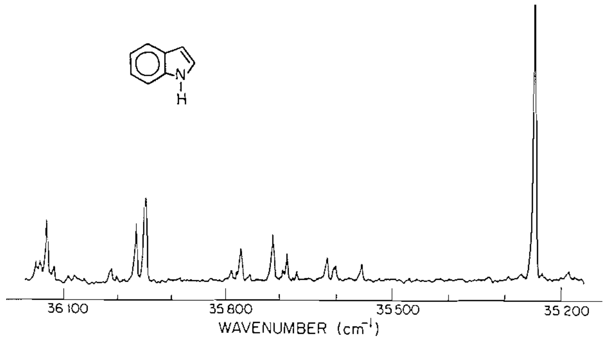

FIG. 1. Fluorescence excitation spectrum of bare indole.

experimentally and theoretically, that certain halogenated anesthetics perturb hydrogen bonds, shifting the equilibrium away from associated molecules toward the free species. In addition it appears that the degree to which a given fluorocarbon molecule perturbs this equilibrium is directly proportional to its anesthetic potency. Especially interesting is that the presence of a hydrogen atom in the halocarbon anesthetic greatly increases the hydrogen-bond perturbing potency and anesthetic activity.

We have undertaken a supersonic beam investigation of van der Waals complexes of indole with a variety of molecules of anesthetic interest in order to try to identify the relevant intermolecular interactions under isolated cluster conditions. The technique involves the *in situ* synthesis of a given indole – van der Waals complex and then probing the complex via laser-induced fluorescence excitation spectroscopy. Due to the very low vibrational and rotational temperatures in the jet, the complicated ultraviolet spectrum of the indole probe molecule is greatly simplified (1). Most vibronic hot bands are completely eliminated and the rotational envelope of the S_1 0–0 transition is reduced to ≤ 1.8 cm^{-1} as shown in Fig. 1. That this technique is useful for investigating weak molecular interactions has been demonstrated by many workers (1, 8, 9). Upon electronic excitation of a mixture of bare probe molecule and associated van der Waals complexes, one observes a spectral feature displaced from the bare molecular origin by a frequency interval that is a direct measure of the difference in the ground state binding energies of the complex. This energy difference is referred to as the spectral shift. From the direction and magnitude of this frequency shift for a given probe molecule and a series of complexing partners, one can often identify the relevant intermolecular forces of a van der Waals molecule. Based on the above discussion, this would yield particularly important results for the anesthetic halocarbons.

First, we present excited state results of isolated, uncomplexed indole spectral positions and fluorescence lifetimes. With this characterization of the probe molecule, we then proceed to the results of van der Waals molecule formation with a series of halogen-substituted methanes.

Experimental

Details of the molecular beam apparatus have been provided in previous publications (9). The Quanta Ray Nd:YAG (DCR-1) pumped dye (PDL-1) pulsed laser system was operated with rhodamine 590 and frequency doubled in a KD*P crystal for the entire spectral region of this study. Typical uv pulse energies were ≥ 5 mJ with a resulting linewidth in the uv of 0.2 cm^{-1}. For all fluorescence lifetime measurements this linewidth was further reduced to 0.01 cm^{-1}, as measured by a 0.25 cm^{-1} spectral free energy Fabry-Perot, by introducing an intracavity etalon in the dye laser.

Fluorescence was detected with a high-quality collection lens (f/1, quartz doublet), a spectral mask to exclude hot background signal and an RCA 4840 photomultiplier. Lifetime measurements were made with a Tektronix 7912AD transient digitizer with a dedicated 4052 microcomputer. All fluorescence decays were averaged a minimum of 400 times and are corrected for small (<1%) baseline wrinkles intrinsic to the oscilloscope. The dynamic linearity was verified over a range of two decades.

Indole was obtained from Aldrich (99+%) and was used without further purification. The liquid complexing partners were of spectrograde quality. The complexing gases Ar, CH_4, CF_4, and CF_2Cl_2 were all obtained from Matheson. The principle carrier gas was He, and van der Waals complexes were then prepared by introducing a few percent of the complexing species in a flow system. The liquid complexing partners were placed in a stainless steel vessel attached to a separate helium flow line monitored by one of two Hastings linear mass flow meters. The other mass flow meter monitored the total flow of the expansion mixture. A similar procedure was used for the gaseous complexing species as described in a previous publication (8).

Results

A. *Indole spectroscopy*

Indole is an aromatic molecule of C_s symmetry that has been investigated by several groups (8, 10, 13). Despite these investigations there is still no normal mode analysis available in either the ground or excited states. In 1964 Hollas investigated the ultraviolet absorption spectrum of indole vapor (10). His studies show that electronic excitation to the first excited electronic state is an allowed $\pi^* \leftarrow \pi$ transition ($A' \leftarrow A'$) with only totally symmetric (a') vibrations active. This work also shows complex vibrational structure to approximately 2500 cm^{-1} above the origin with no strong progressions and with more than two members, indicating little change in shape or size upon electronic excitation. Mani and Lombardi (13) have interpreted the high resolution spectrum of the rotational fine structure at the indole origin in terms of a general loosening of the electronic structure upon excitation. The magnitude of this ring expansion is approximately one quarter of that of benzene. The electronic transition moment of indole is oriented at $\pm 26 \pm 7°$ relative to the long axis of the molecule.

The jet-cooled fluorescence excitation spectrum of the isolated indole molecule is shown in Fig. 1. As one can readily see that the 0–0 transition is by far the most intense feature in this spectrum. This confirms the suggestion by Hollas (10) and Mani and Lombardi (13) that there is only a small change in geometry upon electronic excitation with $\Delta v = 0$ transitions being favored. The excited state vibrational line positions are listed in Table 1. These values are in good agreement with Hollas' spectrum, though we have observed many more weak cold vibronic bands as expected. Since our earlier published work on the indole spectrum (8) two other supersonic jet studies have appeared (11, 12). Nibu *et al.* (11) have investigated the dispersed fluorescence of major vibronic bands below 1300 cm^{-1} and have clearly shown that in all cases the excited state vibrational bands exhibit relatively small decrease in frequency over their ground state counterparts. This, again, is indicative of the small expansion of the molecular dimensions in the excited state.

Bersohn *et al.* (12) have examined the indole fluorescence excitation spectrum and a few selected fluorescence decay times. Our line position data agree quite well with theirs, however, a comparison of the fluorescence lifetimes between the two studies shows a systematic difference between the two sets of results, even including the error bars of ±10% in the work

TABLE 1. Band positions and fluorescence lifetimes for the indole S_1 transition

Band position (cm^{-1})	Lifetime (ns)
0–0 (35 239 cm^{-1})	17.5 ± 0.5
0 + 316	14.7
0 + 365	13.2
0 + 380	15.8
0 + 456	14.6
0 + 480	15.2
0 + 540	13.8
0 + 718	13.1
0 + 720	13.9
0 + 738	11.0
0 + 909	12.7
0 + 920	11.3
0 + 969	12.3
0 + 990	10.2

of Bersohn *et al.* (12). Our value of 17.5 ± 0.5 ns for the bare indole origin is substantially different from the 30 ns ± 10% reported by Bersohn *et al.* (12). We have reexamined the fluorescence decay behavior of bare indole in light of this difference and have found the 17.5 ns lifetime to be independent of carrier gas and interrogation distance downstream from the expansion orifice.

Table 1 also lists the remaining fluorescence decay times of the vibronic transitions below 1000 cm^{-1}. The monotonic decrease in fluorescence lifetime is indicative of an increase in nonradiative rate due to coupling with a dense manifold of triplet electronic states isoenergetic with the S_1 state. Glasser and Lami (14) have shown that the fluorescence quantum yield of indole and substituted indoles decreases in a similar fashion as a function of excess energy above the S_1 origin. Calculations (15) have put T_1 at 1.3 eV below S_1, T_2 and T_3 at lower energies than S_1, and T_4 and T_5 approximately isoenergetic with S_1. Thus, the high density of triplet electronic levels in the S_1 spectral region provide the necessary acceptor states to explain the monotonic decrease in fluorescence quantum yield as being due to intersystem crossing.

B. Molecular interactions of indole with selected halomethanes

Since dispersion forces will always be present in the van der Waals molecules we are investigating, it is useful to consider the behavior of a system in which this is the major interaction present. To this end the indole–Ar van der Waals molecule spectrum and its interpretation will be presented first. In the simplest form the expression for dispersion interactions between two species is given by (16)

$$u(r) = -\frac{3}{2}\frac{h}{r^6}\left(\frac{\nu_1\nu_2}{\nu_1+\nu_2}\right)\alpha_1\alpha_2$$

where r is the separation distance of the two species of the complex, α_1 and α_2 are the polarizabilities of the two molecules in the complex, and ν_1 and ν_2 are the transition frequencies to the respective ionization potentials. Argon is a fairly polarizable complexing partner, and thus based on theoretical treatments of intermolecular forces, should give rise to an attractive excited state interaction and a shift to lower energies of the associated electronic transition. This is indeed what is observed experimentally as shown in Fig. 2 where the indole–argon 0–0 electronic transition is shifted 25 cm^{-1} to lower energy than that of complexed indole. Since the polarizability of argon (17) is

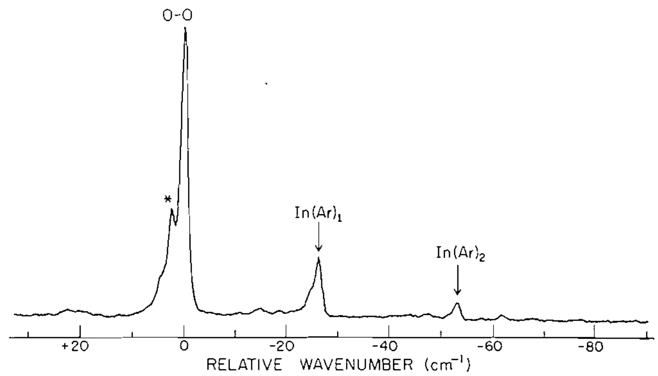

FIG. 2. Fluorescence excitation spectrum of the indole–argon van der Waals molecule in the region of the bare indole origin. The starred feature is due to the indole–helium van der Waals complex.

0.18×10^{-23} cm^3, one would expect any complexing partner with a polarizability of this value or greater to lead to a stabilization of the excited state well over that of the ground state of 26 cm^{-1} or more if dispersion interactions are dominant.

This turns out to be a useful relationship since the difference between the excited state binding energy over that in the ground state of the van der Waals molecules with a nonpolar complexing partner can be approximately written as the sum of three terms (18).

$$\Delta\nu_{TOT} = \Delta\nu_{REP} + \Delta\nu_{DISP} + \Delta\nu_{DIDI}$$

Here $\Delta\nu_{REP}$ is due to short range repulsive interactions, $\Delta\nu_{DISP}$ is the dispersion contributions, and $\Delta\nu_{DIDI}$ is due to dipole-induced interactions. Of these three terms, only that arising from short range repulsive interactions will be reflected in a destabilization of the excited state complex and is most often observed with helium van der Waals molecules. The other two terms are due to attractive forces, and without the presence of any repulsive interactions, will lead to a spectral shift to lower energies (i.e. to the red of the associated bare molecule transition). Amirav *et al.* (19) have shown that for the aniline–Ar van der Waals system, the contribution of dipole – induced dipole interactions to the total excited spectral shift is approximately 5%. The simplest expression for this dipole – induced dipole stabilization energy using a point dipole approximation is given by (16),

$$u(r) = -4\alpha\mu^2/r^6$$

where μ is the dipole moment of the polarizer (in this case indole) and α is the polarizability of the complexing partner in the van der Waals molecule. Thus, one can see that the total interaction energy (neglecting repulsive terms) in this case can also be directly related to the polarizability of the complexing partner. A more rigorous treatment is given in the appendix of ref. 19.

Turning to the spherically symmetric molecule methane, one would expect similar behavior to that of argon in an indole – van der Waals molecule with a dominating excited state dispersive stabilization. Experimentally, we have observed a red spectral shift of 36 cm^{-1} from the indole origin. Figure 3 shows the associated fluorescence excitation spectrum in the lowest energy spectral region. The polarizability (19) of CH_4 is 0.29 $\times 10^{-23}$ cm^3 which is greater than that of Ar and thus, based on the above discussion, dispersion interactions again appear to be the major source of the excited state stabilization. This is illus-

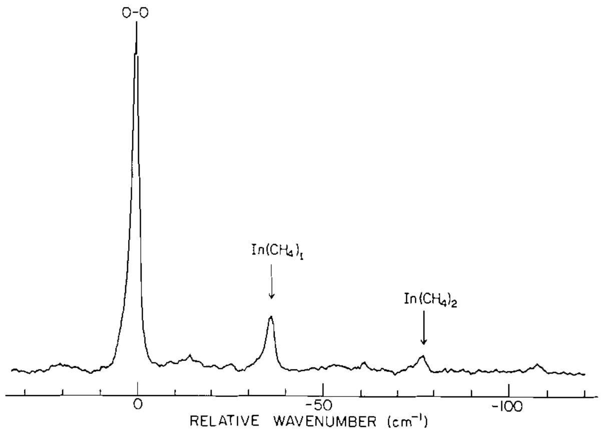

FIG. 3. Fluorescence excitation spectrum of the indole–methane van der Waals molecule in the region of the bare indole origin.

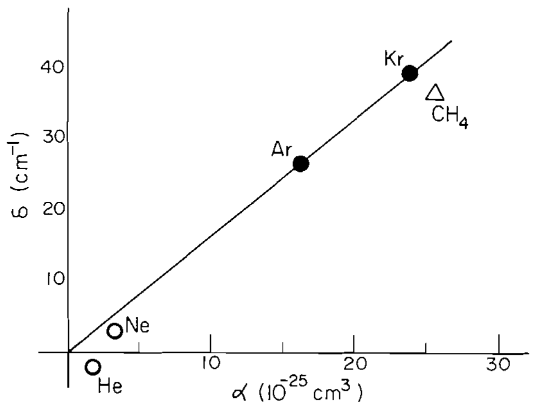

FIG. 4. The relationship between the observed spectral shift and the static polarizability of the complexing partner for indole van der Waals molecules.

trated in Fig. 4 where a linear relationship between the rare gas polarizability and the observed spectral shift is observed for the rare gases where dispersion interactions are dominant (1). There is only a slight deviation for indole–methane. Two additional features of this figure should be noted. First, for rare gas atoms such as He and Ne with small polarizabilities, repulsive interactions largely off-set the attractive contributions. Secondly, the reasonably good agreement of indole–methane within this picture indicates that the behavior of argon and methane as complexing partners is quite similar, reflecting the importance of dispersion interactions for these systems.

From this examination of these relatively simple interactions with fairly polarizable nonpolar molecules, we expanded our investigations to the halomethanes CF_4 and CCl_4. These two systems should help provide a starting point for the studies of the halomethanes of anesthetic interest.

Both CF_4 and CCl_4 are fully substituted methanes and have isotropic polarizabilities substantially greater than those of argon and methane ($\alpha(CF_4) = 0.43 \times 10^{-23}$ cm^3 and $\alpha(CCl_4) = 1.25 \times 10^{-23}$ cm^3). Consequently, one might expect that the experimental spectral shift to be at least as large as that observed for indole–methane. In fact, assuming that the spectral shifts and polarizabilities do follow the linear relationship put forward, a rough estimate would lead to the prediction of a ~ -55 cm^{-1} spectral shift for indole–CF_4 and ~ -180 cm^{-1} for indole–CCl_4. These estimates will only be approximately correct ($\sim \pm 20\%$) if the major interactions terms are due to dispersive forces and dipole – induced dipole forces under the assumptions mentioned above. The actual experimentally observed spectral shifts are $+10$ cm^{-1} for indole–CF_4 (see Fig. 5*a*) and 0 cm^{-1} for indole–CCl_4.

We are confident that the indole–CCl_4 van der Waals molecule does indeed have a 0 cm^{-1} spectral shift at the bare molecule origin for two reasons. First, we can indirectly observe the formation of van der Waals complexes by monitoring the intensity of the bare molecule features as a function of CCl_4 concentration. As this concentration is increased there is an associated decrease in the intensity of the bare molecule band. Second, at several higher energy spectral features, where we have observed a general trend of spectral shifts slightly to the blue of their position at the origin regardless of complexing partner, we were able to locate two indole–CCl_4 features. These two features are blue shifted from the associated bare molecule bands (see Fig. 5*b*) confirming our assignment of a 0 cm^{-1} spectral shift at the origin.

These results indicate that in some fashion the normally dominant polarizability-induced dispersive and dipole – induced dipole interactions are offset by excited state destabilizing interactions. A possible source of this destabilization, short-range repulsive interactions, has already been mentioned. This has almost exclusively been seen in the cases of helium and neon van der Waals molecules. Electrostatic potential interaction calculations by Ruelle and Sandorfy (20) demonstrate that for CF_4, there is a considerable repulsive effect for the short range interaction with a complexing partner due to the fluorine lone pair electrons. This appears to be a satisfactory explanation for the excited state energetics of indole–CF_4.

It seems surprising, however, that the indole–CCl_4 van der Waals complex spectral shift can be due to these short range interactions. Previous workers investigating aromatic – CCl_4 van der Waals molecules have reported quite large spectral shifts; tetracene – CCl_4 = -176 cm^{-1} (21), fluorobenzene – CCl_4 = -89 cm^{-1} (22), and 2-aminopyridine – CCl_4 = -195 cm^{-1} (23). In these systems, dispersive interactions have been found to give the major contribution to the electronic spectral shifts resulting in the most likely structures involve a CCl_4 molecule above the molecular plane. In the case of indole–CCl_4, we find that the binding energies in the ground and excited state are approximately the same (within 2 cm^{-1}), and thus, some excited state interaction has offset the normally attractive dispersive forces. As mentioned above, it seems surprising that short-range repulsive interactions can be responsible for the entire effect. A possible explanation is that, upon electronic excitation, the more bulky CCl_4 molecule is no longer in the optimum geometry for maximum complex stabilization, but rather in a local minimum on the potential energy surface. In this case the full effect of the dispersion stabilization interaction is not experienced by the van der Waals molecule. Further investigations of this system are currently underway in our laboratory.

The next system to be studied is the indole–CF_2Cl_2 van der Waals molecule. In this case the polarizability of the complexing partner is anisotropic and there is a small dipole moment present. The interaction of a polar indole molecule with a polar van der Waals partner complicates the simple picture presented for nonpolar ligands. Previous studies (21) indicate that these polar forces can result in either an attractive or repulsive interaction. Also, it is not clear whether even the approximately

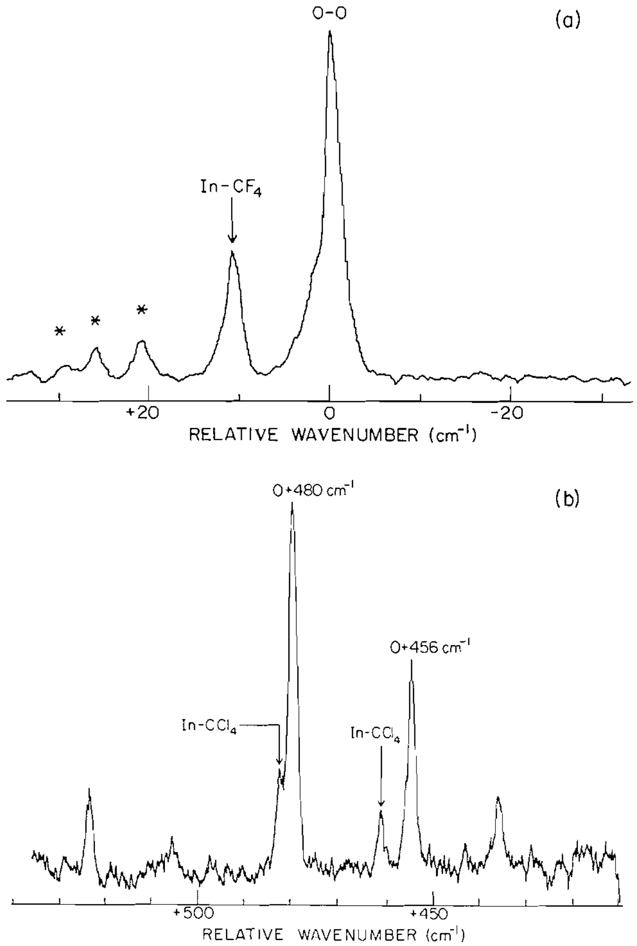

FIG. 5. (*a*) The fluorescence excitation spectrum of the indole–CF_4 van der Waals molecule in the region of the bare indole origin. The starred features are due to vibrational excitation of the van der Waals molecule in the first excited state. (*b*) The fluorescence excitation spectrum of the indole–CCl_4 van der Waals molecule in the $0 + 456$ cm^{-1} and $0 + 480$ cm^{-1} bare indole spectral region.

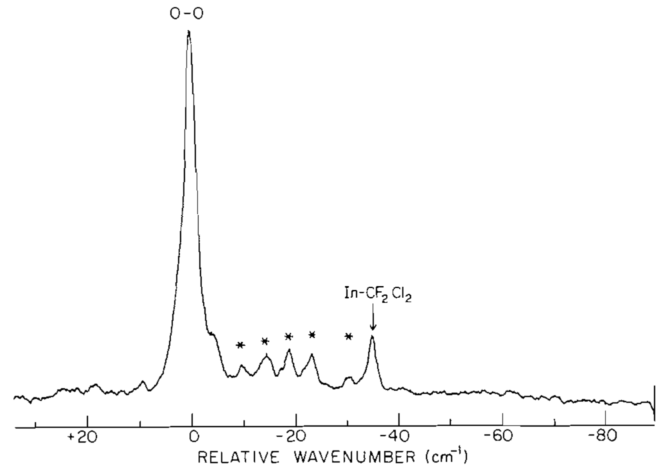

FIG. 6. The fluorescence excitation spectrum of the indole–CF_2Cl_2 van der Waals molecule in the region of the bare indole origin. The starred features are due to vibrational excitation of the van der Waals molecule in the first excited state.

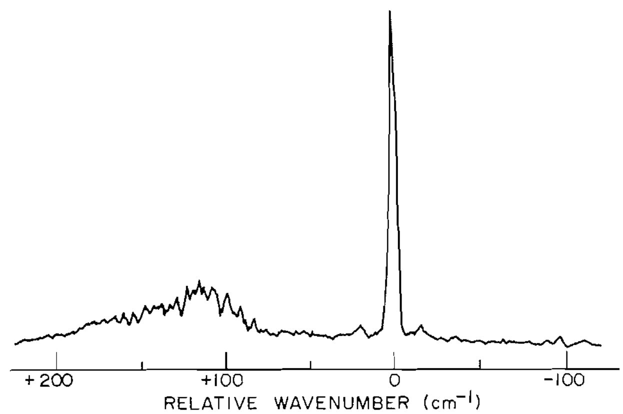

FIG. 7. The fluorescence excitation spectrum of the indole–$HCCl_3$ complex near the bare indole origin.

additive relationship between the various interaction contributions remains valid. However, though indole is a polar molecule, the change of dipole moment upon excitation is small (24) ($|\Delta\mu| = 0.14 \pm 0.05$ D), and thus we do not expect much deviation from the simple picture presented.

The experiment fluorescence excitation spectrum of indole–CF_2Cl_2 in the region of the bare molecule origin is shown in Fig. 6. There are two points to note regarding this spectrum, first, the spectral shift is to the red (-36 cm^{-1}) showing that the excited state is stabilized to a greater degree than the ground state. This suggests that a treatment based on dispersive and polar interactions is appropriate. Secondly, there is a prominant 4 cm^{-1} vibrational progression in the van der Waals molecule spectrum. This vibrational activity does not arise from hot band excitation because of the low rotational and vibrational temperatures in the jet. From the very low frequency of this motion it may be due to a van der Waals bending-type motion or movement of the CF_2Cl_2 parallel to the indole molecular plane. The possibility of several of these features arising from different chemical isomers also exists.

The remaining two halocarbon van der Waals molecules in this family that we have investigated are dichloromethane and chloroform. The chloroform–indole results will be discussed first. Chloroform is commonly known as a general anesthetic. A major reason for its anesthetic potency has been suggested to be due to the presence of the lone acidic hydrogen (7). When methane hydrogens are successively replaced by chlorine atoms there is an associated increase in the acidity of the remaining hydrogens. Consequently, one intuitively expects that chloroform is a better proton donor than dichloromethane. Electrostatic potential calculations (20) show that the region of positive potential for the remaining hydrogens reaches farther for chloroform and dichloromethane than for methylchloride. In addition this larger positive region helps to offset the chlorine lone pair repulsive interactions. These considerations suggest that the interaction between indole and chloroform and dichloromethane will be highly directional in nature and that the possibility of hydrogen bond formation exists.

The experimental fluorescence excitation spectrum of indole–$HCCl_3$ near the indole origin is shown in Fig. 7. Here the maximum of the complex features is located at approximately 120 cm^{-1} to the blue of the bare molecule band. The structure associated with this relatively broad feature is initially quite regular with a spacing of approximately 8 cm^{-1}. Beyond this point, however, the spectrum becomes quite complex. The nature of the spectral shift and considerations of the most likely directionality of the interaction has led us to the interpretation that the chloroform molecule is the proton donating moiety in

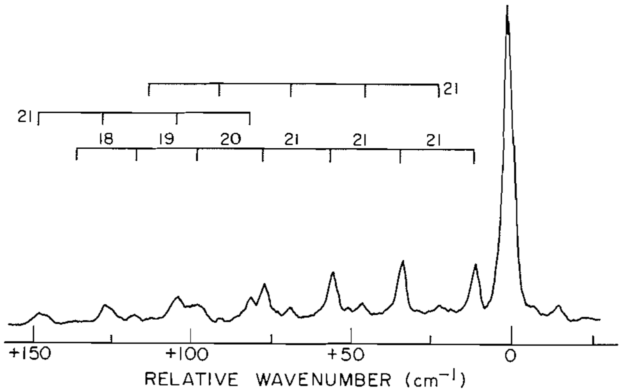

FIG. 8. The fluorescence excitation spectrum of the indole–H_2CCl_2 complex near the bare indole origin.

a π-hydrogen bond (3). Gonohe *et al.* (22) have proposed a similar explanation for the behaviour of the fluorobenzene–$HCCl_3$ complex which shows a blue shift of 117 cm^{-1} from the fluorobenzene origin. This type of π-hydrogen bonding interaction has also been proposed as the mechanism for indole auto-association (25). The fact that, from the direction and magnitude of the electronic spectral shift, one can identify hydrogen bonded species in a supersonic molecular beam makes this technique very useful.

The lowest energy portion of the indole–CH_2Cl_2 fluorescence excitation spectrum is shown in Fig. 8. The most striking feature of this spectrum is the great amount of excited state vibrational activity. There is a well developed progression that begins at +12 cm^{-1} from the bare indole origin and finally dies out at approximately +160 cm^{-1}. In all we have identified three progressions with spacings of ~21 cm^{-1} one of which is comprised of seven members. The prominence of these low frequency excited state vibrations in both this spectrum and that of indole–$HCCl_3$ indicates a substantial change in equilibrium geometry of these binary clusters upon electronic excitation.

Our spectral results show that the net effect of the indole–CH_2Cl_2 interactions lead to a destabilization of the first excited electronic state with respect to the ground state. This suggests that the relevant intermolecular interactions for the indole–CH_2Cl_2 arise from either (*a*) van der Waals interactions or (*b*) π-hydrogen bonding. As discussed above, recent investigations of van der Waals molecules containing a highly polarizable complexing partner such as dichloromethane demonstrate a substantial stabilization of the excited state relative to the ground state of the complex in the absence of a large dipole moment change of the probe molecule (21). In addition, we have found that when indole forms a one-to-one complex with the fluorine-substituted analogue of dichloromethane, CF_2Cl_2, there is a red electronic spectral shift as expected from simple van der Waals interaction arguments. Thus, the replacement of the hydrogen atoms by inert fluorine atoms in this halomethane complexing partner leads to dramatic spectroscopic changes reflecting the differences in interaction potentials between these two indole complexes. This spectroscopic evidence indicates that the highly directional nature of the electrostatic potential around dichloromethane molecule plays a crucial role in the pairwise interaction of the complex. We therefore favor the view of the π-hydrogen bonding is the appropriate explanation for the indole–dichloromethane intermolecular interaction.

We have also investigated the fluorescence decay behavior of all of these binary indole complexes near the bare molecule origin and have observed a wide range of behavior. One expects that for a sufficiently inert complexing partner there will be no change in the fluorescence lifetime of the van der Waals molecule relative to the bare probe molecule (1). In this case there is minimal modification of the energy levels due to the weak nature of the intermolecular interactions. For stronger interactions such as hydrogen bonding other investigators have shown that one can expect rather large changes in the measured fluorescence lifetimes upon complexation (3, 27).

TABLE 2. Fluorescence decay times for indole complexes

Species	Lifetime (ns)
Indole, $S_1(0-0)$	17.5 ± 0.5
In–He_1	18.1 ± 0.5
In–Ne_1	18.2 ± 0.5
In–Ar_1	16.7 ± 0.5
In–Kr_1	≤ 1
In–$(CH_4)_1$	21.9 ± 0.5
In–$(CF_4)_1$	18.0 ± 0.5
In–$(CF_2Cl_2)_1$	17.1 ± 0
In–$(CCl_4)_1$[a]	≤ 1
In–$(CHCl_3)_1$	5 – 8
In–$(CH_2Cl_2)_1$	7 ± 1

[a]The fluorescence decay times for this complex was measured at the van der Waals features associated with the 0 + 456 cm^{-1} and 0 + 480 cm^{-1} bare indole features (see Fig. 5*b*).

For van der Waals complexes of indole and species such as the rare gases He, Ne, and Ar, methane, CF_4, and CF_2Cl_2 we do indeed observe fluorescence decay times very close to that of the bare indole origin (Table 2). This is indicative of the weak nature of interaction potential between the indole probe molecule and the van der Waals partner. Thus, these inert partners do not modify either the radiative rate or the nonradiative rate characteristic of bare indole.

This simple picture of the absence of one-solvent molecule perturbations of the indole fluorescence lifetime is no longer valid when one looks at the behavior of the indole–krypton van der Waals molecule. Here the measured fluorescence decay time is much shorter than that of the bare probe molecule owing to a substantial modification of the spin–orbit coupling between S_1 and the triplet manifold (1, 8). Thus, the external heavy atom effect leads to a large change in the nonradiative rate from the vibrationless level of the first excited singlet state of the van der Waals complex relative to that for bare indole. We have also measured the fluorescence lifetimes of the indole–CCl_4 van der Waals molecule at the spectral region indicated in Fig. 5*b*. These features also show a dramatic lifetime shortening similar to that observed for indole–krypton.

Measurements of the fluorescence decay times for the π-hydrogen bonded systems indole–CH_2Cl_2 and indole–$CHCl_3$ also indicate a substantial perturbation of bare molecules radiative and/or nonradiative rates (see Table 2). Felker and Zewail (26) have shown for hydrogen bonded isoquinoline that the fluorescence lifetimes of these complexes approach those found for liquid phase behavior in hydrogen bonding solvents. We have also demonstrated similar behavior for indole hydrogen bonded to a series of alcohols and amines investigated in a supersonic jet (3). Thus the radiative behaviour of indole is quite susceptible to changes in energy levels induced by hydrogen bond formation. We are unaware of any solution phase lifetime measurements of unsubstituted indole in dichloromethane or chloroform and therefore cannot make any direct comparisons with our jet data. However, the values for these supersonic jet complexes are similar to those found (27) for indole in various other hydrogen bonding solvents (3–6 ns).

Discussion

Since our investigation is specifically based on the study of individual indole van der Waals complexes in the more general context of anesthesia, this discussion will relate the observed excited state spectral features with anesthetic potency. The excited state spectral shifts reflects the sensitivity of the weak intermolecular forces to the electronic transition moment making *changes* in these interactions experimentally observable. As discussed earlier both a stabilized and a destabilized excited state of the complex (with respect to the ground state) have been observed. It is the direction and magnitude of this change in binding energies that is of interest in the following discussion. In addition fluorescence lifetime measurements provide an indication of the absolute strength of the intermolecular interactions. Relatively weak interactions results in little modification of the observed decay time relative to that of the incomplexed molecule while stronger interactions are reflected by greater changes in the time-resolved behavior.

The investigations of the indole–Ar and indole–CH_4 van der Waals complexes were undertaken to exemplify the effects of complexing species that can only interact through dispersion forces and provide a measure of the effects of the presence of other types of intermolecular interactions. Deviations from the spectral shifts expected based on dispersion interactions alone can be attributed to repulsive interactions and/or dipole–induced dipole interactions. The fluorescence lifetimes of these van der Waals molecules indicate a negligible modification of the indole radiative behavior due to complex formation, putting them in the weakly interacting category.

The results for indole–CF_4 and indole–CCl_4 illustrate the usefulness of this comparative technique. In both cases the stabilizing dispersion and dipole – induced dipole forces were found to be offset by some excited state repulsive interaction. This is not unexpected in the case of CF_4 based on the electrostatic potential calculations of Ruelle and Sandorfy (20) where the fluorine lone pairs tend to hinder interaction with a negative site such as benzene ring of an aromatic molecule. However, based on other studies of carbon tetrachloride van der Waals complexes (21–23), one would not expect this behavior for indole–CCl_4. This might indicate that the indole probe molecule is much more sensitive to repulsive interactions with complexing partners of the form CX_4, where X is a halogen atom, than previously studied systems.

The lifetime studies of these two van der Waals molecules show that CF_4 behaves similarly to argon and methane in that it does not alter the radiative rates of the indole probe molecule. Carbon tetrachloride, on the other hand, must be more strongly interacting as can be seen from the fluorescence lifetime measurements reflecting the propensity of this complexing molecule to lead to more efficient spin–orbit coupling.

The van der Waals molecules mentioned above deal with complexing species that have negligible anesthetic potency. These halocarbons can only interact through dispersive and dipole – induced dipole forces. On the other hand, the molecule CF_2Cl_2 (weakly anesthetic) can associate through the additional interaction of polar forces. The lack of a large repulsive contribution to the observed spectral shift, unlike that observed for indole–CF_4 and indole–CCl_4 may indicate that anesthetic action in fully halogenated methanes is related to this additional mechanism of association. Time-resolved measurements of the indole–CF_2Cl_2 van der Waals molecule illustrate behavior indicative of weak intermolecular interactions. This observation may be related to the fact that CF_2Cl_2 is only weakly anesthetic in nature.

The anesthetic potency of halocarbons is greatly increased with the presence of a lone "acidic" hydrogen (7). Electrostatic potential calculations (20) on these anesthetic species reveal that the region of positive potential is quite extensive extending to greater range of $CHCl_3$ than CHF_3. In addition, this positive region helps to shield the halogen lone pairs reducing repulsive interactions with an approaching nucleophile. Thus, one would not be surprised at the formation of hydrogen bonds with these complexing partners and a proton acceptor such as a π system of an aromatic molecule. This is indeed what we have observed in the case of indole–$HCCl_3$ and to a lesser extent for indole–H_2CCl_2. The implications of this finding can be seen by considering some proposed mechanisms of anesthetic action. Recently, the suggestion (6, 9) that, for more potent anesthetics, polar interactions can be quite important in determining activity has been put forward. In this picture these potent anesthetics act in the polar, rather than hydrophobic, portions of the membrane lipids. Thus, anesthetics containing an acidic hydrogen can be expected to perturb the existing intermolecular associations or actually break hydrogen bands (6). This is in contrast to those anesthetic molecules that are either nonpolar or weakly polar that mainly effect the hydrophobic network in lipids. Our studies on indole–$HCCl_3$ and indole–H_2CCl_2 show that π-hydrogen bonding is an important mechanism for the association of these halocarbons with aromatic molecules. The mechanism of π-hydrogen bonding is also responsible for indole autoassociation in solution, and consequently, indole–$HCCl_3$ formation would be expected to directly compete with indole dimerization reducing the concentration of the dimer. This stronger type of intermolecular interaction would have profound consequences if it took place in the cell membrane of ionic channels due to a disruption of optimum conditions for ion transport in and out of the nerve cells.

Conclusions

Supersonic beam technology has been proven useful in directly measuring the type of intermolecular associations operative for indole–halomethane excited state complexes. Though this is a gas phase technique, it is of great interest to investigate these associations in an environment in which only pairwise interactions are present and extend the results to the solution phase studies in the area of general anesthesia. Species such as CF_4 and CCl_4 exhibit an unusually strong repulsive interaction under these experimental conditions which may be attributable to the repulsion between the halogen lone pair electrons and the aromatic π-electrons. Indole–CF_2Cl_2 illustrates a system in which dispersive and induction forces are the main contributions to the intermolecular association. Based on this one would expect this weakly anesthetic molecule to interact with the hydrophobic parts of the membrane lipids. On the other hand, species such as chloroform and dichloromethane choose to interact with the indole probe molecule by means of hydrogen bonding rather than through van der Waals complex formation. This supports the proposal of Sandorfy and co-workers (6, 7) that the hydrophobic portions of the cell membrane may not be the major interaction sites for polar anesthetics of this type.

Acknowledgements

The financial support of the Natural Sciences and Engineering Research Council of Canada and the Petroleum Research Fund administered by the American Chemical Society is gratefully acknowledged.

1. A. AMIRAV, U. EVEN, and J. JORTNER. J. Chem. Phys. **75**, 2489 (1981).
2. A. DING and J. HESSLICH. Chem. Phys. Lett. **94**, 54 (1983).
3. J. HAGER and S. C. WALLACE. J. Phys. Chem. **88**, 5513 (1984).
4. U. EVEN and J. JORTNER. J. Phys. Chem. **87**, 28 (1983).
5. K. W. MILLER and E. B. SMITH. *In* A guide to molecular pharmacology — toxicology. Part 2. *Edited by* R. M. Featherstone. Dekker, New York. 1973. pp. 427–475.
6. C. SANDORFY. *In* Progress in anesthesiology. Vol. 2. Mechanisms of anesthesia. *Edited by* B. R. Fink. Raven, New York. 1980. pp. 353–359.
7. G. TRUDEAU, J.-M. DUMAS, P. DUPUIS, M. GUERIN, and C. SANDORFY. Top. Curr. Chem. **93**, 91 (1980).
8. J. HAGER and S. C. WALLACE. J. Phys. Chem. **87**, 2121 (1983).
9. W. SHARFIN, P. KROGER, and S. C. WALLACE. Chem. Phys. Lett. **85**, 81 (1982).
10. J. M. HOLLAS. Spectrochim. Acta, **19**, 753 (1963).
11. Y. NIBU, H. ABE, N. MIKAMI, and M. ITO. J. Phys. Chem. **87**, 3898 (1983).
12. R. BERSOHN, U. EVEN, and J. JORTNER. J. Chem. Phys. **80**, 1050 (1984).
13. A. MANI and J. R. LOMBARDI. J. Mol. Spectrosc. **31**, 308 (1969).
14. N. GLASSER and H. LAMI. J. Chem. Phys. **74**, 6526 (1981).
15. D. A. LERNER, P. M. HOROWITZ, and E. M. EVLETH. J. Phys. Chem. **81**, 12 (1977).
16. (*a*) J. O. HIRSCHFELDER, C. F. CURTISS, and R. B. BIRD. Molecular theory of gases and liquids. Wiley, New York. 1964. Chapt. 13; (*b*) M. M. DAVIES. Some electrical and optical aspects of molecular behavior. Pergamon, Oxford. 1965. Chapt. 7.
17. A. DALGARNO and A. E. KINGSTON. Proc. R. Soc. London, Ser. A, **259**, 424 (1961).
18. E. R. CHAN. *In* A guide to molecular pharmacology — toxicology. Part 2. *Edited by* R. M. Featherstone. Dekken, New York. 1973. pp. 697–734.
19. A. AMIRAV, U. EVEN, J. J. JORTNER, and B. DICK. Mol. Phys. **49**, 899 (1983).
20. P. RUELLE and C. SANDORFY. Int. J. Quant. Chem. **21**, 691 (1982).
21. U. EVEN and J. JORTNER. J. Chem. Phys. **78**, 3445 (1983).
22. N. GONOHE, H. ABE, N. MIKAMI, and M. ITO. J. Phys. Chem. **87**, 4406 (1983).
23. J. HAGER and S. C. WALLACE. Unpublished results.
24. C. T. CHANG, C. Y. WU, A. R. MUIRHEAD, and J. R. LOMBARDI. Photochem. Photobiol. **19**, 347 (1974).
25. A. LAUTIÉ, M. F. LAUTIÉ, A. GRUGER, and S. F. FAKKRI. Spectrochim. Acta, **36**A, 85 (1979).
26. P. M. FELKER and A. H. ZEWAIL. Chem. Phys. Lett. **94**, 454 (1983).
27. S. R. MEECH, D. PHILLIPS, and A. G. LEE. Chem. Phys. **80**, 317 (1983).

Low-temperature Raman and Fourier transform infrared spectra of dodecacarbonyldirhenium(0), $Re_2(CO)_{10}$

PIERRE D. HARVEY AND IAN S. BUTLER
Department of Chemistry, Otto Maass Building, McGill University, 801 Sherbrooke St. West, Montreal, Que., Canada H3A 2K6

Received August 1, 1984

This paper is dedicated to Professor Camille Sandorfy on the occasion of his 65th birthday

PIERRE D. HARVEY and IAN S. BUTLER. Can. J. Chem. **63**, 1510 (1985).

The Raman spectrum of microcrystalline dodecacarbonyldirhenium(0), $Re_2(CO)_{10}$, has been reinvestigated at 67 K using one of the latest fully-computerized spectrometers available. Previously unobserved peaks have been detected mainly in the ^{13}CO-satellite (2150–1900 cm^{-1}), and overtone and combination regions (1300–700 and 4300–3800 cm^{-1}). This is the first time that Raman-active first CO overtones and combinations of a metal carbonyl complex have been reported. They were earlier thought to be too weak to be detected. Assignments are proposed for the majority of these new peaks together with those from a similar low-temperature (~70 K) FT-ir study. In general, the D_{4d} selection rules are obeyed, but the activity of some forbidden bands reveals that the molecule is slightly distorted in the solid state in agreement with its X-ray structure. The similarity of the low-temperature spectra to those obtained at room temperature indicates that no phase change occurs throughout the temperature range investigated.

PIERRE D. HARVEY et IAN S. BUTLER. Can. J. Chem. **63**, 1510 (1985).

Opérant à 67 K et utilisant un des plus récents spectromètres complètement informatisé, on a réétudié le spectre Raman du dodécacarbonyldirhenium(0), $Re_2(CO)_{10}$, microcristallin. On a pu détecter des bandes qui n'avaient pas été observées antérieurement, principalement dans les régions du satellite du ^{13}CO (2150–1900 cm^{-1}) et des harmoniques et des combinaisons (1300–700 et 4300–3800 cm^{-1}). Aucune publication antérieure n'avait fait rapport de l'observation, dans le spectre Raman, des premières bandes harmoniques et de combinaisons du CO d'un complexe de métal carbonyle. Il était antérieurement supposé que ces bandes étaient trop faibles pour être détectées. On propose des attributions pour la plupart de ces nouvelles bandes anisi que pour celles observées au cours d'une étude semblable effectuée à basse température et à l'aide d'un appareil de FT-ir. En général, les règles de sélection D_{4d} sont suivies; toutefois, l'activité de quelques bandes interdites révèle que, à l'état solide, la molécule est légèrement déformée comme le laissait supposer sa structure déterminée par diffraction des rayons-X. La similarité qui existe entre les spectres obtenus à basse température et ceux obtenus à la température ambiante suggère qu'il ne se produit pas de changement de phase sur la plage des températures étudiées.

[Traduit par le journal]

Introduction

The ir and Raman spectra of dodecacarbonyldirhenium(0), $Re_2(CO)_{10}$ have been investigated extensively since its discovery in 1941 (1). The molecule has a single Re—Re bond joining together two staggered square-pyramidal $Re(CO)_5$ fragments (2, 3) and is regarded as one of the important prototypes for metal–metal bonded cluster compounds. Despite the innumerable vibrational studies on $Re_2(CO)_{10}$ (4–18) from which the assignments of all the fundamentals are now well established, there are relatively few data for low intensity features such as naturally-occurring ^{13}CO-satellite peaks and overtone and combination modes. A few $\nu(^{13}CO)$ modes have been identified in the ir (4, 6, 9, 13, 14, 16) and Raman (13, 16) and some overtones and combinations in the ir (4, 8, 9, 13, 16) and near-ir (5, 9, 11, 14), but the analysis is still far from complete. In view of this and because the assignments for the fundamentals were so well known, we decided to reinvestigate the Raman spectra of $Re_2(CO)_{10}$ at 67 K and in CCl_4 solution using one of the latest computerized, high-resolution Raman spectrometers available. We are particularly interested in seeing whether or not we could observe any bands in the ν(CO) first overtone and combination region with this new type of instrumentation. All earlier attempts for metal carbonyls had failed in this regard. This region is especially important for determining the anharmonicities of the CO stretching vibrations. In this paper, we report the results of our new Raman study together with some FT-ir data for the solid (at ~70 K) and in CCl_4 solution at room temperature.

Experimental

Pure $Re_2(CO)_{10}$ from Strem Chemicals was used without further purification. The Raman spectra were recorded on an Instruments S.A. spectrometer equipped with a U-1000 Jobin-Yvon 1.0-m double monochromator coupled to a Columbia Data Products minicomputer using Instruments S.A. in-house software. The excitation source was the 514.5-nm green line of Spectra Physics model 164 argon-ion laser (~300 mW at the sample). The spectra were calibrated against the emission lines of a standard neon lamp and the peak positions are accurate to ±0.2 cm^{-1}. A Pyrex tube containing the white, microcrystalline solid was mounted on a Cryodyne Cyrocooler (Cryogenics Technology, Inc., model 21) for the variable-temperature measurements (±1 K). All FT-ir spectra were recorded on a Nicolet model 6000 spectrometer (accuracy ±0.2 cm^{-1}), the same cryostat described above being used for low-temperature (~70 K) measurements.

Results and discussion

The main investigations of the solid-state vibrational spectra of $Re_2(CO)_{10}$ have been by Adams *et al.* (17, 18) who have succeeded in assigning all the ir-active ($6b_2 + 8e_1$) and Raman-active ($7a_1 + 6e_2 + 8e_3$) fundamentals expected for D_{4d} molecular symmetry by very thorough ir reflectance and Raman measurements on single crystals. These assignments will be used extensively in our own work. The symmetry descriptions of the normal modes and their spectral activities for D_{4d} symmetry are given in Table 1, together with the selection rules for the first overtones and combinations.

The 200–10 cm^{-1} region

A typical Raman spectrum of solid $Re_2(CO)_{10}$ at 67 K is

TABLE 1. (*a*) Distribution and numbering of normal modes for D_{4d} symmetry $Re_2(CO)_{10}$

a_1 (Raman-active)	b_2 (Ir-active)	e_2 (Raman-active)
ν_1 ν(CO) equatorial	ν_{11} ν(CO) equatorial	ν_{25} ν(CO) equatorial
ν_2 ν(CO) axial	ν_{12} ν(CO) axial	ν_{26} δ(MCO)
ν_3 π(MCO)	ν_{13} π(MCO)	ν_{27} π(MCO)
ν_4 ν(M—CO)	ν_{14} ν(M—CO)	ν_{28} ν(M—CO) equatorial
ν_5 ν(M—CO)	ν_{15} ν(M—CO)	ν_{29} δ(CMC)
ν_6 π(CMC)	ν_{16} π(CMC)	ν_{30} π(CMC)
ν_7 ν(M—M)		
	e_1 (ir-active)	e_3 (Raman-active)
a_2 (inactive)	ν_{17} ν(CO) equatorial	ν_{31} ν(CO) equatorial
	ν_{18} δ(MCO)	ν_{32} δ(MCO)
ν_8 δ(MCO)	ν_{19} π(MCO)	ν_{33} π(MCO)
	ν_{20} ρ(MCO) axial	ν_{34} ρ(MCO) axial
b_1 (inactive)	ν_{21} ν(M—CO) equatorial	ν_{35} ν(M—CO) equatorial
	ν_{22} δ(CMC)	ν_{36} δ(CMC)
ν_9 δ(MCO)	ν_{23} π(CMC)	ν_{37} π(CMC)
ν_{10} Torsion	ν_{24} Δ	ν_{38} Δ

(*b*) The crystal selection rules

g × u = u	Ir-active
u × u = g	Raman-active
g × g = g	Raman-active

(*c*) Selection rules of overtones and combinations for $Re_2(CO)_{10}$ in D_{4d} symmetry*

	Overtones		
$(a_1)^2 = (b_1)^2 = (a_2)^2 = (b_2)^2 = A_1$	Raman	$(e_2)^2 = A_1 + B_1 + B_2$	Ir, Raman
$(e_1)^2 = A_1 + E_2$	Raman	$(e_3)^2 = A_1 + E_2$	Raman
	Combinations		
$a_1 \cdot b_1 = B_1$	Inactive	$b_1 \cdot e_1 = E_3$	Raman
$a_1 \cdot e_1 = E_1$	Ir	$b_1 \cdot e_2 = E_2$	Raman
$a_1 \cdot e_2 = E_2$	Raman	$b_1 \cdot e_3 = E_1$	Ir
$a_1 \cdot e_3 = E_3$	Raman	$b_2 \cdot e_1 = E_3$	Raman
$a_1 \cdot a_2 = A_2$	Inactive	$b_2 \cdot e_2 = E_2$	Raman
$a_1 \cdot b_2 = B_2$	Ir	$b_2 \cdot e_3 = E_1$	Ir
$a_2 \cdot b_1 = B_2$	Ir	$e_1 \cdot e_1 = A_1 + A_2 + E_2$	Raman
$a_2 \cdot b_2 = B_1$	Inactive	$e_1 \cdot e_2 = E_1 + E_3$	Ir, Raman
$a_2 \cdot e_1 = E_1$	Ir	$e_1 \cdot e_3 = B_1 + B_2 + E_2$	Ir, Raman
$a_2 \cdot e_2 = E_2$	Raman	$e_2 \cdot e_2 = A_1 + A_2 + B_1 + B_2$	Ir, Raman
$a_2 \cdot e_3 = E_3$	Raman	$e_2 \cdot e_3 = E_1 + E_3$	Ir, Raman
$b_1 \cdot b_2 = A_2$	Inactive	$e_3 \cdot e_3 = A_1 + A_2 + E_2$	Raman

*From ref. 22.

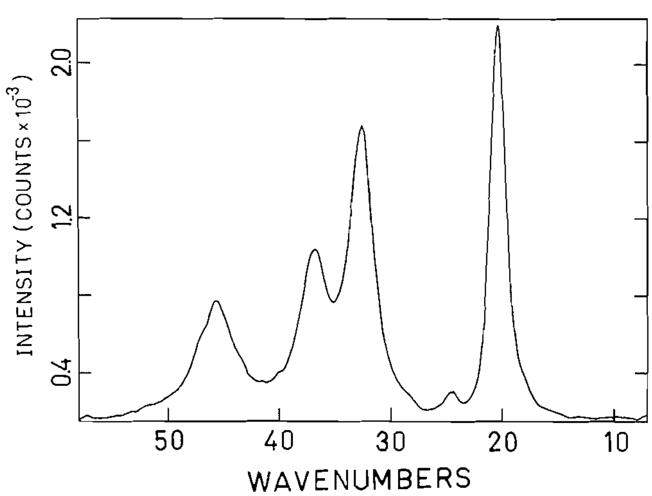

FIG. 1. Low-frequency Raman spectrum (60–7 cm^{-1}) of solid $Re_2(CO)_{10}$ at 67 K (excitation 514.5 nm, 300 mW, slit widths 30 μm, 1 scan, 1 s/data point, data point spacing 0.2 cm^{-1}, no smoothing).

shown in Fig. 1. We were able to approach to within 4 cm^{-1} of the Rayleigh line and in doing so we could resolve completely a feature at 24.5 cm^{-1}, unobserved in the low-temperature study of Adams *et al.* (11) and barely discernible in the spectrum published by Prasad (15). In their latest single crystal work, however, Adams and Hooper did manage to detect this lattice mode at room temperature (17). This peak has been assigned to a lattice translatory mode. While the overall quality of our data is clearly superior to those in the literature, we did not resolve the bands reported by Adams *et al.* (11) at 143 and 138 cm^{-1}, even using other laser excitation lines (e.g., 488.0 nm). The observed peaks are given in Table 2.

The 700–300 cm^{-1} region

The bands found in this region are given also in Table 2. In general, they correspond well with the literature values. A re-examination of the ir spectrum at ~70 K using superior quality FT-ir instrumentation did reveal some differences. The a_1, ν(Re—CO) mode was detected at 461.2 cm^{-1} (compared to 462.8 cm^{-1} in the Raman). Several of degenerate *e* modes are also split in the solid-state spectra.

TABLE 2. Raman- and ir-active frequencies for solid $Re_2(CO)_{10}$ at 67 K

Raman (cm^{-1})[a]	Infrared (cm^{-1})[b]	Assignments	Calculated frequencies (cm^{-1})	$\Delta\nu$[c]	Comments
	4210 sh	$\nu_1 + \nu_{11}$	4200	+10	?
4206		$\nu_1 + \nu_{11}$	4200	+6	?
	4196	$\nu_1 + \nu_{11}$	4197, 4200	−1,−4	
	4178	$\nu_1 + \nu_{11}$	4197	−21	?
	4158				?
	4149				?
	4143	$\nu_{11} \times 2$	4145	−2	Mol. forb.
	4127	$\nu_1 + \nu_{17}$	4132	−5	
	4101	$\nu_1 + \nu_{17}$	4129	−28	
4094		$\nu_{11} + \nu_{25}$	4100	−6	
		$\nu_1 + \nu_{31}$	4101	−7	
	4086	$\nu_1 + \nu_{12}$	4089, 4092	−3,−6	
4046 weak		$\nu_{25} \times 2$	4054, 4056	−8,−10	
	4067 weak sh	$\nu_1 + \nu_{12}$	4089	−22	
	4059	$\nu_{11} + \nu_{31}$	4062	−3	
		$\nu_{25} \times 2$	4055	−5	
		$\nu_{11} + \nu_2$	4049	−8	
	4050	$\nu_{25} \times 2$	4045	⋮	
	4041	$\nu_{11} + \nu_{31}$	4045	⋮	
	4031	$\nu_{17} + \nu_{25}$	4031	0	
	4005	$\nu_{25} + \nu_{31}$	4018	−13	
		$\nu_{17} + \nu_{25}$	4021	−16	
		$\nu_{25} + \nu_2$	4004, 3994	−14,−4	
3990 v. broad		$\nu_{25} + \nu_{31}$	4000	−10	
		$\nu_{17} + \nu_{31}$	3994	−4	Cryst. forb.
		$\nu_{25} + \nu_{12}$	3992	−2	
	3989	$\nu_{25} + \nu_{31}$	4001	−12	
		$\nu_{17} + \nu_{31}$	3994	−4	
3970		$\nu_{31} \times 2$	3980	−10	
	3969	$\nu_{17} + \nu_{31}$	3977	−8	
3962		$\nu_{17} + \nu_{12}$	3968	−6	
		$\nu_{31} + \nu_2$	3967	−5	
	3954 weak	$\nu_{17} + \nu_{31}$	3977	−23	
		$\nu_{31} + \nu_{12}$	3954	0	
3953		$\nu_{31} \times 2$	3963	−10	
	3939	$\nu_{31} + \nu_{12}$	3954	−15	
		$\nu_2 + \nu_{12}$	3941	−2	
3934		$\nu_{31} \times 2$	3956	−12	
	3920	$\nu_{31} + \nu_{12}$	3937	−17	
		$\nu_{12} \times 2$	3929	−9	Mol. forb.
3916		$\nu_2 \times 2$	3930, 3928	14,−12	
3880 weak					?
2128.5 (42.5) 2125.5 (13.7)		ν_1			a_1 (equatorial)
2073.5 (1.3)	2072	ν_{11}			b_2
2043.5 (1.0)	~2044	$\nu_{31} + \nu_L (R_z)$	2046.5	−3	
		$\nu_2 + \nu_{38}$	2046.4	−2.9	
2027.5 (66.0) 2017.5 (59.2)	2028	ν_{25}			e_2
~2011 sh (~3)		$\nu_{31} + \nu_L (R_{x,y})$	2011.8	~−1	
		$\nu_{31} + \nu_T$	2010.9	~0	
	2004 v. strong	ν_{17}			e_1
	~1998	$\nu_2 + \nu_T$	1998.4	~−0.4	
1990.0 (27.1) 1973.5 (13.4)		ν_{31}			e_3
1977.5 (12.5)		ν_2			a_1
1965.0 (1.3)	1964	ν_{12}			b_2
1945.0 (1.0)	1942	^{13}CO			a_1 axial
1932.0 (1.1)	1931	^{13}CO			
1231.5		$\nu_3 \times 2$	1232.8	−1.3	
1195.0		$\nu_3 + \nu_{18}$	1197.2	−2.2	
1185.0		$\nu_{32} + \nu_{18}$	1186.5	−1.5	Mol. forb.
		$\nu_{32} \times 2$	1185.2	−0.2	
	1157.9				?

TABLE 2. (*Continued*)

Raman (cm^{-1})[a]	Infrared (cm^{-1})[b]	Assignments	Calculated frequencies (cm^{-1})	$\Delta\nu$[c]	Comments
	1151.8	$\nu_3 + \nu_{19}$	1152.8	−1.0	
	1139.9 sh				?
1131 broad		$\nu_{32} + \nu_{33}$	1132.4, 1134.0	−1.4−3	
		$\nu_{32} + \nu_{19}$	1133.8	−2.8	Cryst. forb.
	1130.0	$\nu_{18} + \nu_{33}$	1130.5	−0.5	
	1124.4	$\nu_{18} + \nu_{33}$	1124.1	+0.4	
	1099.0 sh	$\nu_{18} + \nu_{19}$	1101.8	−2.8	
	1092.6	$\nu_{18} + \nu_{26}$	1094.3, 1095.2	−1.7, −2.6	
1083.5		$\nu_{18} + \nu_{26}$	1086.0	−2.5	
1070.5		$\nu_{19} \times 2$	1072.8	−2.3	
		$\nu_{19} + \nu_{33}$	1071.4	−0.9	Cryst. forb.
	1069.8	$\nu_3 + \nu_{15}$	1071.3	−1.5	
		$\nu_{19} + \nu_{33}$	1071.4	−1.6	
1056.5		$\nu_{18} + \nu_{14}$	1056.8	−0.2	
		$\nu_{32} + \nu_5$	1058.9	−2.4	Cryst. forb.
	1054.0 sh	$\nu_3 + \nu_{20}$	1054.1	−0.1	
		$\nu_{32} + \nu_5$	1054.1	−0.1	Mol. forb.
		$\nu_{33} + \nu_{28}$	1054.1	−0.1	
1051.5		$\nu_{32} + \nu_5$	1054.1	−2.6	Cryst. forb.
		$\nu_{33} + \nu_{26}$	1054.1	−2.6	Cryst. forb.
	1051.2	$\nu_3 + \nu_{20}$	1054.1	−2.9	
		$\nu_{32} + \nu_{15}$	1052.3	−1.1	
		$\nu_{32} + \nu_{27}$	1051.4	−0.2	Cryst. forb.
		$\nu_{32} + \nu_5$	1054.1	−2.9	Mol. forb.
		$\nu_{18} + \nu_5$	1051.9	−0.7	
		$\nu_{33} + \nu_{26}$	1054.1	−2.9	
	1038.8 sh	$\nu_3 + \nu_{28}$	1039.4	−0.6	Mol. forb.
		$\nu_{19} + \nu_{26}$	1041.6	−2.8	
		$\nu_{33} + \nu_{26}$	1039.8	−1.0	
1037.5		$\nu_3 + \nu_{28}$	1039.4	−1.9	
		$\nu_{33} + \nu_{26}$	1040.2	−2.7	
	1026.2	$\nu_{26} \times 2$	1027.1	−0.9	
1026.0		$\nu_{19} \times 2$	1028.8	−2.8	
		$\nu_{18} + \nu_{20}$	1026.8	−0.8	
		$\nu_{32} + \nu_{20}$	1026.1	−0.1	Cryst. forb.
~1010 sh		$\nu_{18} + \nu_{28}$	1012.1	−2.1	
		$\nu_{19} + \nu_{14}$	1012.4	−2.4	
		$\nu_{33} + \nu_4$	1012.8	−2.8	
		$\nu_{26} \times 2$	1010.4	−0.4	
	1006.2	$\nu_3 + \nu_{21}$	1007.0	−0.8	
	991.4 sh	$\nu_{32} + \nu_{21}$	991.6	−0.2	
977.0		$\nu_{18} + \nu_{21}$	979.7, 979.8	−2.7, −2.8	
		$\nu_{18} + \nu_{35}$	978.0	−1.0	Cryst. forb.
		$\nu_{33} + \nu_{20}$	979.1	−2.1	Cryst. forb.
		$\nu_{26} + \nu_5$	977.2	−0.2	
	972.1	$\nu_{18} + \nu_{35}$	972.4	−0.3	
		$\nu_{33} + \nu_{20}$	974.9, 972.7	−2.8, −0.6	
	968.2 sh	$\nu_{19} + \nu_{34}$	970.6	−2.4	
		$\nu_{33} + \nu_{20}$	968.5	−0.3	
		$\nu_{26} + \nu_{15}$	969.3	−1.1	Mol. forb.
	965.3	$\nu_{26} + \nu_{27}$	966.7	−1.4	
		$\nu_{26} + \nu_5$	967.6, 966.7	−2.3, −1.4	Mol. forb.
	957.6 sh	$\nu_{19} + \nu_{28}$	959.4	−1.8	
		$\nu_{33} + \nu_{28}$	958.0	−0.4	
		$\nu_{26} + \nu_{15}$	960.1	−2.5	Mol. forb.
		$\nu_{26} + \nu_{27}$	958.8	−1.2	
952.0		$\nu_{14} \times 2$	952.0	0	Cryst. forb.
		$\nu_{26} + \nu_{20}$	952.1	−0.1	
	951.6	$\nu_{26} + \nu_{20}$	952.1	−0.1	
		$\nu_4 + \nu_{14}$	953.8	−2.2	
	948.6	$\nu_{26} + \nu_{20}$	950.4	−1.8	Cryst. forb.
	935.8	$\nu_{33} + \nu_{23}$	938.6	−2.8	Cryst. forb.
		$\nu_{26} + \nu_{34}$	937.4	−1.6	Mol. forb.
		$\nu_{26} + \nu_{20}$	938.7	−2.9	

TABLE 2. (*Continued*)

Raman (cm^{-1})[a]	Infrared (cm^{-1})[b]	Assignments	Calculated frequencies (cm^{-1})	$\Delta\nu$[c]	Comments
935.0		$\nu_{19} + \nu_{28}$	935.4	−0.4	
		$\nu_{26} + \nu_{34}$	937.4, 935.7	−2.4, −0.7	
	917.5 sh	$\nu_5 + \nu_{15}$	917.7	−0.2	
	912.9	$\nu_{26} + \nu_{21}$	913.4	−0.5	
		$\nu_4 + \nu_{20}$	915.5	−2.6	
906.5		$\nu_{27} \times 2$	908.0	−1.5	
		$\nu_{14} + \nu_{20}$	909.5	−3.0	
	899.5	$\nu_{26} + \nu_{35}$	902.0	−2.5	
		$\nu_4 + \nu_{28}$	900.8	−1.3	Mol. forb.
		$\nu_5 + \nu_{20}$	900.5	−1.0	
894.0		$\nu_{26} + \nu_{35}$	896.8	−2.8	
		$\nu_{26} + \nu_{21}$	895.4	−1.4	
		$\nu_5 + \nu_{34}$	897.0	−3.0	
		$\nu_5 + \nu_{20}$	895.0	−1.0	Mol. forb.
	880.9				
877.0	877.0	$\nu_{15} + \nu_{28}$	877.9	−0.9	
		$\nu_{27} + \nu_{28}$	877.0	0	
871.0		$\nu_{20} \times 2$	871.2	−0.2	
	861.4	$\nu_5 + \nu_{21}$	861.8	−0.4	
	858.4	$\nu_5 + \nu_{35}$	860.0, 858.7	−1.6, −0.3	
		$\nu_5 + \nu_{21}$	860.5	−2.1	Mol. forb.
		$\nu_{20} + \nu_{28}$	860.7	−2.3	
	853.6	$\nu_{20} + \nu_{34}$	856.5	−2.9	
	851.3	$\nu_5 + \nu_{21}$	853.4	−2.1	
		$\nu_{15} + \nu_{35}$	852.1	−0.8	
		$\nu_{27} + \nu_{21}$	853.0	−1.7	
845.5		$\nu_{15} + \nu_{21}$	845.5	0	
		$\nu_{27} + \nu_{35}$	845.6	−0.1	
		$\nu_{34} \times 2$	846.0	−0.5	
	844.6	$\nu_{15} + \nu_{35}$	846.5	−1.9	
		$\nu_{27} + \nu_{35}$	845.6	−1.0	Cryst. forb.
		$\nu_{27} + \nu_{21}$	844.6	0	
		$\nu_{28} \times 2$	846.0	−1.4	
812.5		$\nu_{28} + \nu_{35}$	814.6	−2.1	
		$\nu_{28} + \nu_{21}$	813.6	−1.1	
~799 sh		$\nu_{21} \times 2$	798.0	~+1	
783.0		$\nu_{35} \times 2$	783.2	−0.2	
758.0		$\nu_3 + \nu_{29}$[d]	759.4	−1.4	
752.5		$\nu_3 + \nu_{29}$[d]	754.4	−1.9	
616.4 (4.4)		ν_3			a_1
597.4 (1.8), 592.6 (1.1)		ν_{32}			e_3
	589.1 (71), 580.8 (65)	ν_{18}			e_1
541.8 (2.2), 535.0 (3.8)		ν_{33}			e_3
	536.4 (23)	ν_{19}			e_1
514.4 (2.8)	512.7 (8), 504.8 (7)	ν_{26}			e_2
505.2 (2.2)					
477.8 (20.6)		ν_4			a_1
	476.0 (7)	ν_{14}			b_2
462.8 (48.4)	461.5 (4)	ν_5			a_1
	454.9 (3)	ν_{15}			b_2
454.0 (11.4)		ν_{27}			e_2
	437.7 (8), 433.5 (8)	ν_{20}			e_{21}
434.2 (1.3)		ν_{34}			e_3
423.0 (4.1)	423.0 (6)	ν_{28}			e_2
	399.0 (90), 390.6 (30)	ν_{21}			e_1
397.2 (16.8), 391.6 (16.8)		ν_{35}			e_3
138		ν_{29}			e_2
130		ν_6			a_1

TABLE 2. (*Concluded*)

Raman (cm^{-1})[a]	Infrared (cm^{-1})[b]	Assignments	Calculated frequencies (cm^{-1})	$\Delta\nu$[c]	Comments
124 }		ν_{36}			e_3
120 }					
110.7		ν_7			a_1
103.1 }		ν_{37}			e_3
97 }					
86.3 }		ν_{30}			e_2
81.5 }					
78					
73.0		ν_L			
68.9		ν_{38}			e_3
47.1		ν_L			
38.3		ν_L			
33.0 }		Translatory			
24.9 }		lattice modes			
20.9 }					

[a]The accuracy of Raman frequencies varies with the resolution, 4250–3850 cm^{-1}; ± 2 cm^{-1}, 2150–1900 cm^{-1}; ± 0.5 cm^{-1}, 1250–700 cm^{-1}; ± 0.5 cm^{-1}, 600–10 cm^{-1}; ± 0.2 cm^{-1}. The values in parentheses for selected frequencies represent relative intensities to 120 cm^{-1} peak taken to 100.

[b]The accuracy of ir frequencies is ± 0.1 cm^{-1}. In the 4250–3850 cm^{-1} and 2150–1900 cm^{-1} regions, the last significant figure is not considered. The values in parentheses for selected frequencies represent the relative intensity (in absorbance scale) to 2004 cm^{-1} peak taken to 100.

[c]$\Delta\nu$ = observed frequency − calculated frequency.

[d]According to ref. 11; sh, shoulder; v, very.

TABLE 3. Raman- and ir-active frequencies for $Re_2(CO)_{10}$ in CCl_4 solution in the 1950–2150 and 4200–3900 cm^{-1} regions

Raman (cm^{-1})	Infrared (cm^{-1})	Assignments	Calculated frequencies (cm^{-1})	$\Delta\nu$	Comments
	4195	$\nu_1 + \nu_{11}$	4199	−4	
	4133	$\nu_1 + \nu_{17}$	4140	−7	
	4120 weak sh	$\nu_1 + \nu_2$	4021	−1	Forbidden
	4097	$\nu_1 + \nu_{12}$	4101	−4	
	4079 v. weak sh	$\nu_{11} + \nu_{17}$	4083	−4	Forbidden
	4060 sh	$\nu_2 + \nu_{11}$	4064	−4	
	4049	$\nu_{25} \times 2$	4058	−9	
	4036	$\nu_{17} + \nu_{25}$	4041	−5	
	4003 sh	$\nu_{25} + \nu_{31}$	4009	−6	
	3998	$\nu_2 + \nu_{17}$	4005	−7	
	3980 sh	$\nu_{17} + \nu_{31}$	3992	−12	
	3946	$\nu_{12} + \nu_{31}$	3953	−7	
2128		ν_1			a_1
	2071	ν_{11}			b_2
2029		ν_{25}			e_2
	2012	ν_{17}			e_1
1993		ν_2			a_1
1980		ν_{31}			e_3
	1973	ν_{12}			b_2

Overtone and combination region (1300–700 cm^{-1})

Typical FT-ir and Raman spectra for this region are shown in Fig. 2. At the outset, it is apparent that there are not many coincidences between the two spectra, as would be expected for overtones and combinations of a D_{4d} symmetry molecule. The proposed assignments are given in Table 2. The calculated frequencies were generated by a computer program that matched all the allowed overtones and combinations from the accepted assignments of the fundamentals with the observed peaks assuming a variation of 0 to −3 cm^{-1}. Over 200 possibilities were initially generated and eventually 144 of these were selected to account for the 55 observed frequencies in accord with the D_{4d} molecular and C_{2h} crystal symmetry selection rules and bearing in mind the intensities of the original fundamentals. Many of the observed peaks could be assigned unambiguously, especially those appearing in the less complicated regions of the spectra.

CO stretching region (2150–1900 cm^{-1})

An example of the high-quality Raman spectrum obtained at 67 K is shown in Fig. 3 (the peak positions are given in Table 2). Two new peaks were detected for the first time: 2043.5 and 1965.0 cm^{-1}. These correspond to ir features, one of which was attributed to ν_{12} (b_2) by Adams and Taylor (18). There is most

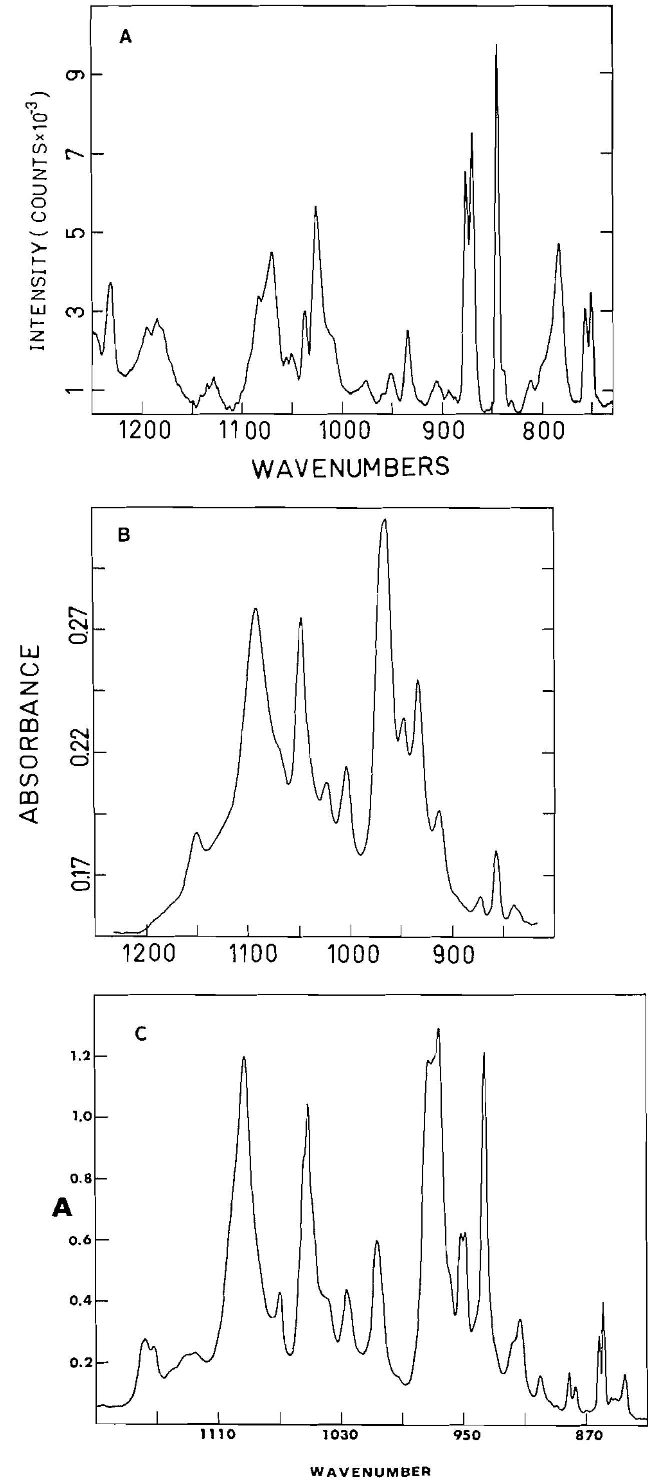

FIG. 2. (*A*) Raman spectrum (1250–700 cm^{-1}) of solid $Re_2(CO)_{10}$ at 67 K (excitation 514.5 nm, 350 mW, slit widths 150 μm, 5 scans, 1s/data point, data point spacing 0.5 cm^{-1}, 9-point smoothing). (*B*) FT-ir spectrum (same region) of $Re_2(CO)_{10}$ in CsI disk at 296 K (300 scans, 2 cm^{-1} resolution). (*C*) FT-ir spectrum (same region) of $Re_2(CO)_{10}$ in CsI disk at ~70 K (300 scans, 1 cm^{-1} resolution).

probably a combination mode in Fermi resonance with the 1980 cm^{-1} (ν_{31}, e_3) mode. Some additional data are available for the ^{13}CO-satellite peaks and the assignments for these are also listed in Table 2. These assignments are in part based on the calculated values from the work of Wozniak and Sheline (13).

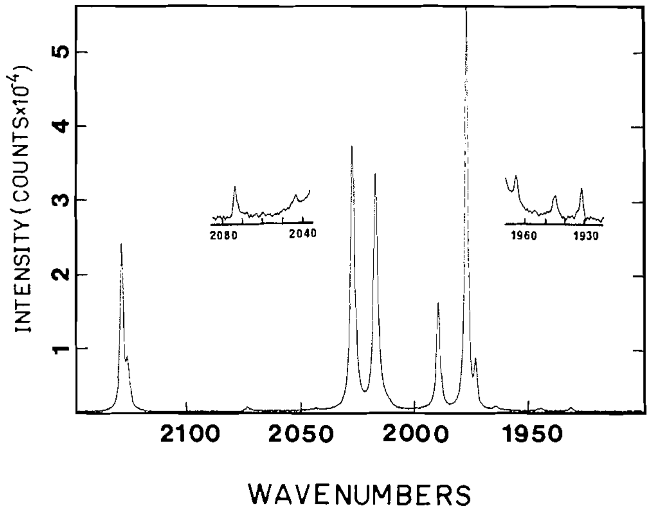

FIG. 3. Raman spectrum (2150–1900 cm^{-1}) of solid $Re_2(CO)_{10}$ at 67 K (excitation 514.5 nm, 300 mW, slit widths 50 μm, 1 scan, 1 s/data point, data point spacing, 0.2 cm^{-1}, no smoothing).

First CO stretching overtone and combination region (4300–3800 cm^{-1})

The FT-ir and Raman spectra of solid $Re_2(CO)_{10}$ in this region are presented in Fig. 4. Although there have been several detailed ir reports for various metal carbonyl complexes(19), Raman data have never been investigated previously in this region owing to the very low peak intensities anticipated and the lack of multiscanning and spectral enhancement capabilities in the earlier instrumentation. The poor response of the phototube removed from the exciting line was also a factor. However, it is now clear that with modern equipment, these problems are no longer insurmountable, at least for the solid. The proposed assignments are given in Table 2. Some CCl_4 solution ir data are also given (Table 3), but solution Raman data for this region still remain elusive. In general, the proposed assignments satisfy the D_{4d} selection rules, especially remembering that ν(CO) modes are highly anharmonic (19). The CCl_4 solution and solid-state ir spectra do exhibit some striking differences but it is possible to see that in the main there are some close similarities especially in terms of clusters of bands for the solid being associated with one or two bands for the solution. Two peaks do stand out in the comparison: the peaks at 4178 and 3920 cm^{-1} in the solid-state ir. The latter feature is by far the strongest band observed in the complete region. The assignment given for the peak necessitates a breakdown in the D_{4d} selection rules indicating a distortion of the $Re_2(CO)_{10}$ molecule in the solid state, as has been found in the two X-ray studies reported for the complex (2, 3).

In conclusion, it is clearly possible to use modern Raman spectrometers to obtain excellent spectra and to detect previously unobtainable features in the spectra of metal carbonyl complexes, especially in the ν(CO) first overtone and combination region. In addition, this particular region is strikingly sensitive to small distortions in the solid-state structures. Finally, although no room-temperature Raman spectra of solid $Re_2(CO)_{10}$ are presented here, the spectra are closely similar to the low-temperature data except for the poorer resolution indicating that there is no phase transition in the temperature range investigated. Adams and co-workers have reported a pressure-induced phase transition for this material, however (20, 21).

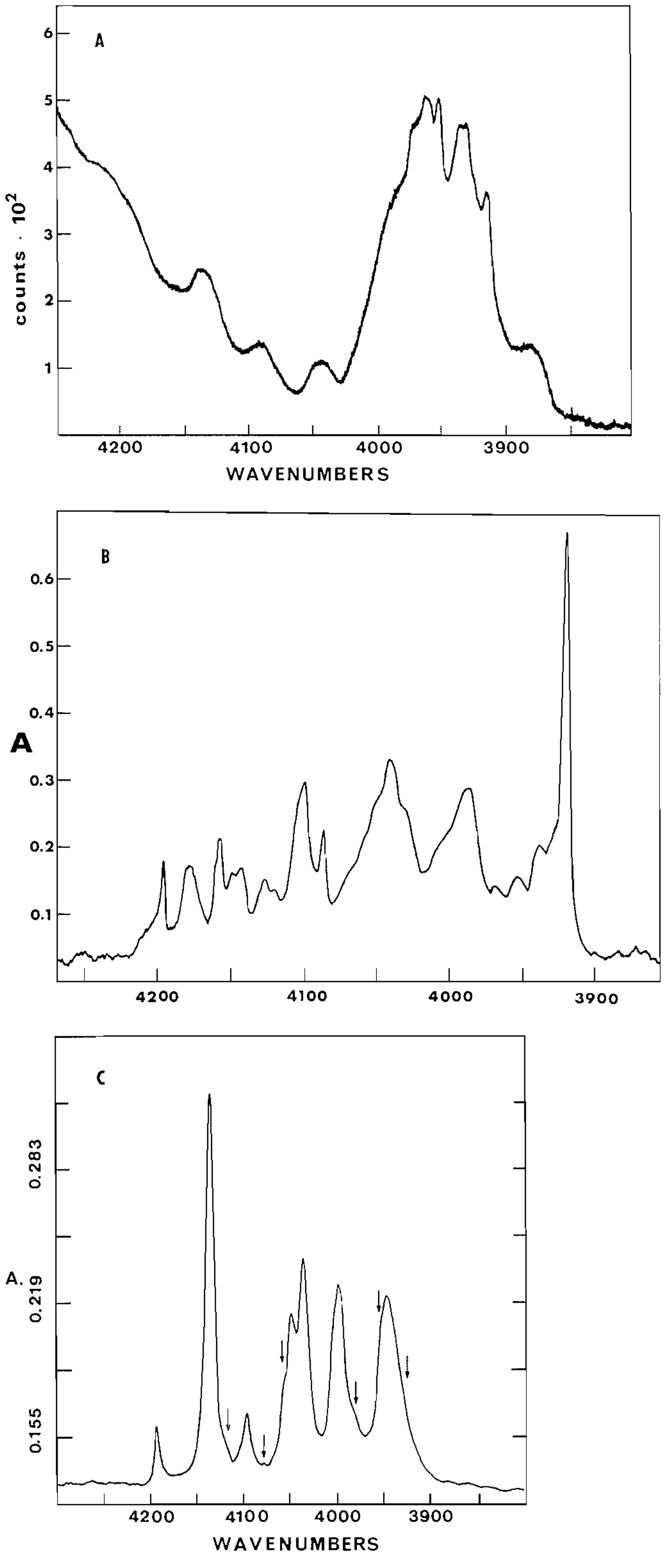

FIG. 4. (*A*) Raman spectrum (4250–3800 cm^{-1}) of solid $Re_2(CO)_{10}$ at 67 K (excitation 514.5 nm, 300 mW, slit widths 400 μm, 4 scans, 5 s/data point, data point spacing 1.0 cm^{-1}, baseline subtracted, 9-point smoothing). (*B*) FT-ir spectrum (same region) of $Re_2(CO)_{10}$ in CsI disk at ~70 K (300 scans, 2 cm^{-1} resolution). (*C*) FT-ir spectrum (same region) of $Re_2(CO)_{10}$ in CCl_4 solution at 296 K (300 scans, 1 cm^{-1} resolution).

Acknowledgments

This work was generously supported by operating grants from N.S.E.R.C. (Canada) and F.C.A.C. (Quebec). P.D.H. acknowledges McGill University Graduate Research Faculty and N.S.E.R.C. (Canada) for graduate assistantships. We would like to thank Professor Denis F. R. Gilson (McGill University) for having written and processed the computer program calculating the harmonics and combinations frequencies. One of us (I.S.B.) wishes to thank the C.N.R.S. Laboratoire de Chimie de Coordination, Toulouse, and the Laboratoire de Cristallochimie, Université de Rennes I, for their warm hospitality while on sabbatical leave in France during which period this manuscript was written.

1. W. HIEBER and H. FUCHS. Z. Anorg. Chem. **248**, 256 (1941).
2. L. F. DAHL, E. ISHISHI, and R. E. RUNDLE. J. Chem. Phys. **26**, 1750 (1957).
3. M. R. CHURCHILL, K. N. AMOH, and H. J. WASSERMAN. Inorg. Chem. **20**, 1609 (1981).
4. N. FLITCROFT, D. K. HUGGINS, and H. D. KAESZ. Inorg. Chem. **3**, 1123 (1964).
5. F. A. COTTON and R. M. WING. Inorg. Chem. **4**, 1328 (1965).
6. J. LEWIS, A. R. MANNING, J. R. MILLER, M. J. WARE, and F. NYMAN. Nature, **207**, 142 (1965).
7. R. W. HARRILL and H. D. KAESZ. Inorg. Nucl. Chem. Lett. **2**, 69 (1966).
8. A. DAVISON and J. W. FALLER. Inorg. Chem. **6**, 845 (1966).
9. I. J. HYAMS, D. JONES, and E. R. LIPPINCOTT. J. Chem. Soc. A, 1987 (1967).
10. R. J. H. CLARK and B. C. CROSSE. J. Chem. Soc. A, 224 (1969).
11. D. M. ADAMS, M. A. HOOPER, and A. SQUIRE. J. Chem. Soc. A, 71 (1971).
12. D. M. ADAMS, M. A. HOOPER, and A. SQUIRE. J. Chem. Soc. Chem. Commun. 1188 (1970).
13. W. T. WOZNIAK and R. K. SHELINE. J. Inorg. Nucl. Chem. **34**, 3765 (1972).
14. G. BOR and G. SBIGNADELLO. J. Chem. Soc. Dalton Trans. 440 (1974).
15. P. N. PRASAD. Specrochim. Acta, **33**, 335 (1977).
16. M. ARIF, A. M. CARTNER, D. N. KARIUKI, and S. F. A. KETTLE. J. Chem. Phys. **70**, 1031 (1979).
17. D. M. ADAMS and M. A. HOOPER. J. Organomet. Chem. **181**, 131 (1979).
18. D. M. ADAMS and I. D. TAYLOR. J. Chem. Soc. Faraday Trans. **78**, 1065 (1982).
19. P. S. BRATERMAN. Metal carbonyl spectra. Academic Press Inc., London Ltd. 1975. Chapt. 6.2, pp. 155–162 and references therein.
20. D. M. ADAMS, L. M. DAVEY, P. D. HALTON, and A. C. SHAW. J. Organomet. Chem. **184**, 415 (1982).
21. D. M. ADAMS, P. D. HALTON, A. C. SHAW, and T.-K. TAN. J. Chem. Soc. Chem. Commun. 226 (1981).
22. G. HERZBERG. Infrared and Raman spectra of molecules. Van Nostrand Reinhold Co., New York. 1945. pp. 126–129.

Germathione–silathione spectres photoélectroniques et structures électroniques par la méthode MS Xα[1]

JEAN-LUC GARCIA, DANIELLE GONBEAU ET GENEVIÈVE PFISTER-GUILLOUZO[2]
Laboratoire de Physico-Chimie Moléculaire, U.A. 474, Université de Pau et des Pays de l'Adour, Avenue de l'Université, 64000 Pau, France

ET

MICHEL ROCH ET JACQUES WEBER
Laboratoire de Chimie Théorique Appliquée, 30, Quai Ansermet, 1211 Genève 4, Suisse

Reçu le 1 août 1984

Cet article est dédié au Professeur Camille Sandorfy à l'occasion de son 65e anniversaire

JEAN-LUC GARCIA, DANIELLE GONBEAU, GENEVIÈVE PFISTER-GUILLOUZO, MICHEL ROCH et JACQUES WEBER. Can. J. Chem. **63**, 1518 (1985).

Une étude a été réalisée en MS Xα sur de nouvelles entités à courte durée de vie: la diméthyl germathione et la diméthyl silathione. La détection par spectroscopie photoélectronique de la diméthyl germathione a été confirmée sur la base de calculs effectués sur ce dérivé, le dimère et le trimère correspondants: potentiels d'ionisation et sections efficaces de photoionisation. L'examen comparatif des résultats obtenus pour la diméthyl germathione, la diméthyl silathione et leur homologue le thioformaldéhyde a permis de préciser certaines caractéristiques de leur structure électronique: forte polarité de la liaison, états de Rydberg de faible énergie.

JEAN-LUC GARCIA, DANIELLE GONBEAU, GENEVIÈVE PFISTER-GUILLOUZO, MICHEL ROCH, and JACQUES WEBER. Can. J. Chem. **63**, 1518 (1985).

A study was undertaken in MS Xα on new short-life species: dimethylgermathione and dimethylsilathione. The spectroscopic detection of dimethylgermathione was confirmed by calculations performed on this compound and the corresponding dimer and trimer: ionization potentials and photoionization cross sections. The analysis of results obtained for the dimethylgermathione, the dimethylsilathione and the parent compound, thioformaldehyde, has shown certain characteristics of their electronic structure: strong polarity of the bond, low-energy Rydberg states.

Introduction

Ces dernières années un intérêt croissant s'est manifesté pour les liaisons à caractère multiple mettant en jeu deux atomes de période différente et qualifiées habituellement de liaisons à caractère $p_\pi p_\pi$. C'est dans ce cadre que se situent les études entreprises pour générer des espèces organométalliques présentant une liaison double entre un atome de métal (Si, Ge) et un hétéroatome (2).

La difficulté d'accéder à de telles entités est liée à l'instabilité intrinsèque de ce type de liaison, leur très grande réactivité conduisant fréquemment à l'existence des seuls *n*-mères. Certaines de ces espèces à courte durée de vie ont toutefois pu être mises en évidence par voie spectroscopique. Ainsi, récemment la diméthyl germathione et la diméthyl silathione ont été détectées par dégradation thermique des trimères en spectroscopie photoélectronique (3).

Dans ce travail nous avons entrepris l'examen des caractéristiques électroniques de ces entités, en comparaison avec celles de leur homologue mieux connu le thioformaldéhyde. Cette étude a été effectuée sur la base d'une analyse précise de spectres photoélectroniques et de résultats de calculs réalisés dans le cadre de la méthode MS Xα (4).

Cette méthode qui a déjà conduit à des résultats satisfaisants pour les systèmes comportant des atomes de silicium ou de germanium (5), présente de plus des avantages certains de par son formalisme pour l'analyse des différentes grandeurs liées à l'ionisation (potentiels d'ionisation, sections efficaces de photoionisation).

Conditions de calcul

Nous avons travaillé à partir d'une version standard de la méthode MS Xα en utilisant le formalisme développé initialement par Dill et Dehmer (6) pour son extension à l'étude d'états du continu.

Suivant ce procédé, l'évaluation des sections efficaces de photoionisation nécessite la connaissance de deux fonctions monoélectroniques, l'une décrivant l'électron avant ionisation et l'autre après ionisation. La fonction d'état initial est une fonction normée obtenue par un calcul autocohérent MS Xα; la fonction d'état final est une fonction du continu parfaitement déterminée dès que l'on définit la valeur propre qui lui est associée. Compte tenu de l'utilisation de la méthode des perturbations dépendant du temps ces deux fonctions doivent être évaluées avec le même potentiel. Ceci nous a amené, contrairement à certains auteurs (7), mais en accord avec Dill et Dehmer et très récemment Grimm et coll. (8), à introduire la correction de Latter (9) pour le calcul de tous les états initiaux (états liés) en la prenant en compte à chaque itération de calcul MS Xα. Cette correction, qui nous a permis d'obtenir un potentiel strictement identique pour l'évaluation des fonctions d'états initial et final, s'est révélée indispensable pour obtenir une stabilisation des résultats de calculs de sections efficaces vis à vis d'une variation des différents paramètres de la méthode MS Xα (α, rayons des sphères, *l*).

Au niveau des atomes, les valeurs du paramètre α optimisées par Schwarz (10) ont été choisies, une moyenne pondérée des α atomiques ayant été utilisée pour les régions intersphère et outersphère. Les rayons des sphères atomiques ont été obtenus de façon non empirique (11), en réduisant de 12% les rayons obtenus à l'itération 0 pour des sphères englobant un nombre d'électrons égal au numéro atomique.

L'obtention de recouvrements trop importants (≃50%) dans

---

[1]Part XXIV de "Application of photoelectron spectroscopy to molecular properties." Part XXIII, voir la réf. 1.

[2]Auteur à qui adresser toute correspondance.

TABLEAU 1. $(Me_2GeS)_3$ (symétrie C_{3v}): niveaux d'énergie, distributions de charge et potentiels d'ionisation en MS Xα

Orbitale	Energie (eV)	Distributions de charge % S	Ge	C_4	C_5	H_6	H_7	H_8	H_9	Int	Out	PI (eV) théoriques	PI (eV) expérimentaux
$17e$	−7,905	73	2	1						24		9,95	8,45
$12a_1$	−8,225	60	4	8	1					27		10,22	8,77
$16e$	−9,124	63	16	4	1					16		11,16	9,88
$15e$	−10,145	16	27	2	37	1		1	2	13	1	11,99	10,3
$11a_1$	−10,335	35	20	20	3		1	1		20		12,24	10,7
$10a_1$	−10,680	15	24	6	30	2		2	1	19	1	12,53	
$5a_2$	−10,685	57	27	2	3		1		2	8		12,72	11,45
$14e$	−10,175	18	25	32	5	1	2	2		15		12,59	
$9a_1$	−12,532	1	3	1	47			13	9	26		14,22	

Paramètres géométriques: d_{Ge-S} = 2,22 Å, d_{Ge-C} = 1,95 Å, $\widehat{SGeS}$ = 115°, $\widehat{GeSGe}$ = 110°.

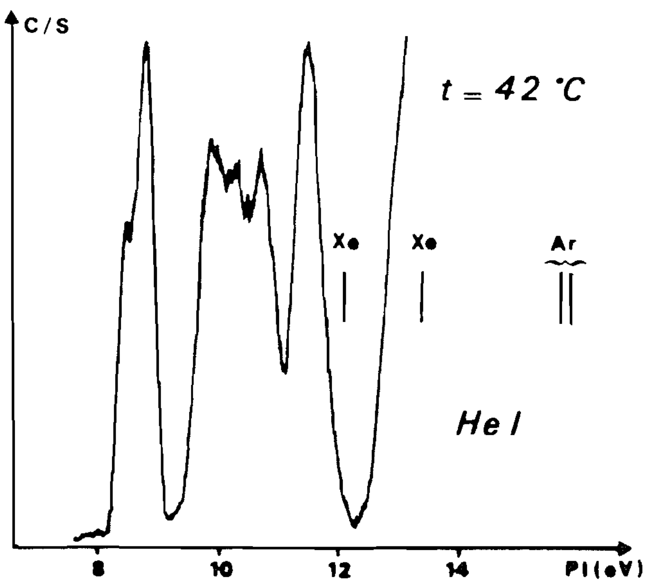

FIG. 1. Spectre photoélectronique (HeI) de $(Me_2GeS)_3$ à 42°C.

le cas de l'atome d'hydrogène nous a conduit à toujours faire choix, compte tenu de l'expérience acquise pour d'autres systèmes (12), de la valeur de 0,85 ua dans tous les cas.

Le calcul de la fonction d'état initial étant couplé à celui de la fonction d'état final pour l'évaluation des sections efficaces de photoionisation, nous avons adopté, pour chaque atome et pour le calcul de tous les états initiaux, en accord avec d'autres auteurs (13), une valeur de $l_{max} = l + 1$.

Pour les fonctions d'état final, les valeurs de l_{max} étant imposées par les règles de sélection au niveau des régions atomiques $l_{initial} = l_{final} + 1$, nous avons choisi $l_{max\,f} = l_{max\,i} + 1$, la valeur de l_{max} dans le cas de l'outersphère a été déterminée par l'examen de la convergence des résultats. ($l_{max\,f} = 7$ pour $Me_2Ge{=}S$, $l_{max\,f} = 10$ pour $(Me_2GeS)_2$.)

Spectres photoélectroniques de la diméthyl germathione, du tétraméthyl cyclodigermathione et de l'hexaméthyl cyclotrigermathione

Nous nous sommes attachés en un premier temps à préciser les potentiels d'ionisation caractéristiques de la diméthyl germathione, système pour lequel nous disposions d'un support expérimental important.

En effet, par pyrolyse à 273°C et 0,05 mbar, le spectre du trimère obtenu vers 42°C a été profondément modifié (figures 1 et 2), le nombre de bandes observées laissant présumer de la présence de deux entités. Si une conversion partielle trimère → monomère n'était pas envisageable étant donné les profondes modifications du spectre, une réaction de dimérisation ne pouvait être exclue. L'analyse du spectre du dimère stable de la n-butyl germathione a été réalisée et a permis de lever l'ambiguïté (fig. 3).

Afin de conforter les attributions antérieurement réalisées à l'aide de ces données expérimentales et d'un calcul pseudo-potentiel sur le monomère (3), nous avons abordé conjointement l'étude du trimère, du dimère et du monomère par la méthode MS Xα.

$(Me_2GeS)_3$

Sur la base des paramètres géométriques déterminés expérimentalement pour l'hexaméthyl cyclotrisilathione (14) nous avons réalisé un calcul MS Xα sur le trimère de la diméthyl germathione en symétrie C_{3v} (tableau 1), avec évaluation des potentiels d'ionisation selon le principe de l'état de transition.

Les valeurs ainsi calculées pour chaque potentiel d'ionisation ont été trouvées très voisines de celles des énergies monoélectroniques obtenues lors du calcul du potentiel d'ionisation associé au dernier niveau occupé. Ainsi, ce sont ces énergies monoélectroniques que nous avons retenues comme valeurs pour tous les potentiels d'ionisation dans le cas du trimère, ainsi que pour les systèmes examinés ultérieurement.

Le spectre obtenu pour le trimère à 42°C est caractérisé par une première bande aux environs de 9 eV avec un épaulement du côté des faibles énergies (fig. 1), attribué à des ionisations mettant en jeu les orbitales $17e$ et $12a_1$ caractéristiques des combinaisons de symétrie π des paires des atomes de soufre (tableau 1).

D'après l'allure du spectre on aurait attendu un ordre inverse $12a_1$, $17e$, il faut toutefois remarquer que les deux premiers potentiels d'ionisation sont obtenus voisins (9,95 et 10,22 eV).

Entre 10 et 11 eV, un massif intense apparaît avec trois potentiels d'ionisation distincts (9,88, 10,3 et 10,70 eV) correspondant à des ionisations faisant intervenir les paires libres de symétrie σ des atomes de soufre (orbitale $16e$) et les combinaisons des liaisons σ_{Ge-S} et σ_{Ge-C} (orbitales $15e$, $11a_1$). Les interactions notables observées entre ces liaisons sont imposées par la structure géométrique du cycle.

Enfin, à 11,45 eV on observe une bande intense liée à l'ioni-

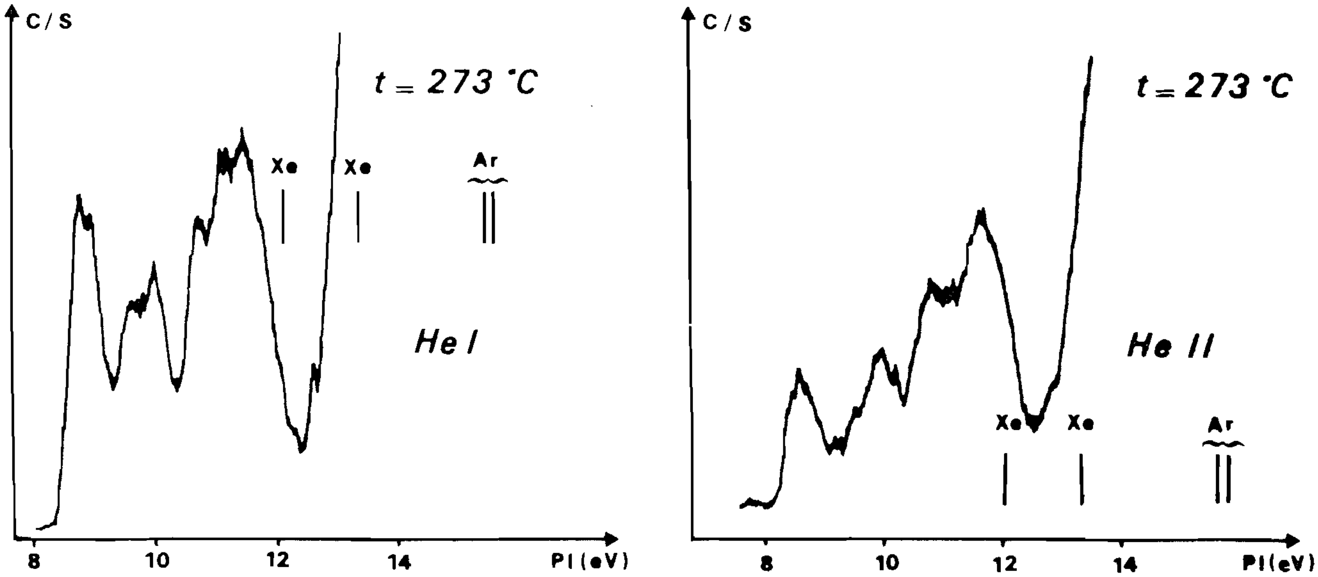

FIG. 2. Spectre photoélectronique (HeI, HeII) de $(Me_2GeS)_3$ à 273°C.

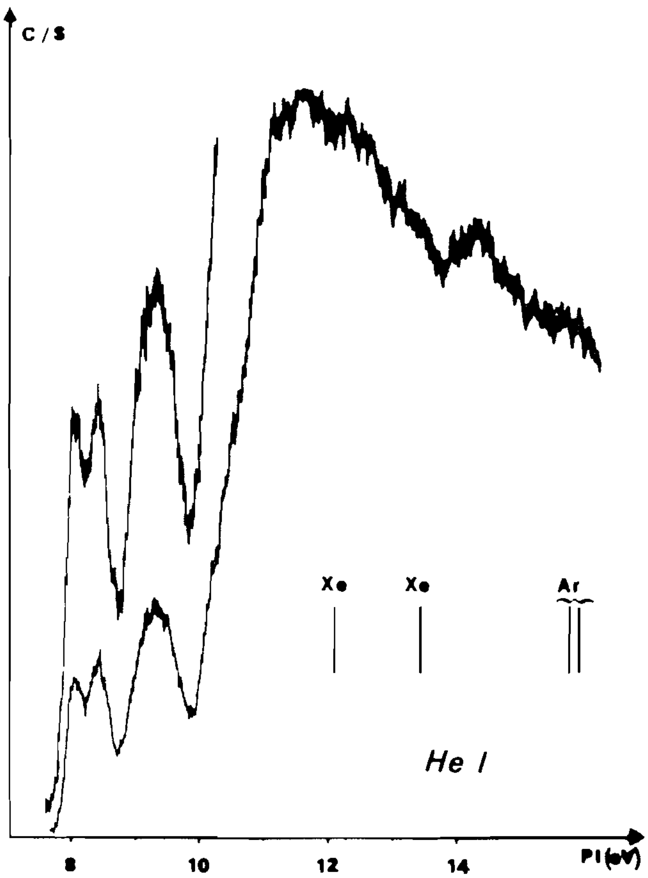

FIG. 3. Spectre photoélectronique (HeI) de $(nBu_2GeS)_2$.

sation des orbitales $10a_1$, $14e$ et $5a_2$ caractéristiques des liaisons σ_{Ge-C} et d'une combinaison des paires d'électrons libres de symétrie σ des atomes de soufre.

Me₂Ge=S, (Me₂GeS)₂

La complexité du spectre obtenu par pyrolyse du trimère à 272°C et certaines observations particulières concernant les variations d'intensité des bandes selon le rayonnement incident nous ont amenés à réaliser une étude complète des grandeurs liées à l'ionisation (potentiels d'ionisation, sections efficaces) pour le monomère et le dimère.

Potentiels d'ionisation

Les résultats présentés dans les tableaux 2 et 3 nous ont permis de proposer une attribution cohérente du spectre expérimental (tableau 4) qui s'interprète bien comme nous l'avions proposé par la présence du monomère et du dimère.

Le premier massif composé de deux bandes très proches à 8,6 eV et 8,85 eV (fig. 2) recouvre trois ionisations, celles mettant en jeu respectivement la paire non liante de l'atome de soufre de $Me_2Ge{=}S$ (orbitale $4b_1$) et les combinaisons liante et antiliante des paires π des atomes de soufre du dimère (orbitales $4b_{1u}$ et $2b_{3g}$).

Au niveau du deuxième massif, nous associons la bande à 9,55 eV à une ionisation faisant intervenir l'orbitale $2b_2$ ($\pi_{Ge=S}$) du monomère. La bande à 9,9 eV correspond au deuxième massif observé expérimentalement dans le cas de $(nBu_2GeS)_2$ (fig. 3); elle provient des états ioniques générés par éjection d'un électron des orbitales caractéristiques de la liaison σ_{Ge-S} et de la combinaison liante des paires σ des atomes de soufre (orbitales $4b_{3u}$ et $3b_{2u}$).

Pour le troisième massif, nous faisons correspondre à la bande à 10,75 eV une ionisation du monomère mettant en jeu l'orbitale $5a_1$ (σ_{Ge-S}). La bande observée à 11,15 eV est due à la présence du dimère et correspond à l'ionisation relative à l'orbitale $3b_{2g}$ associée aux liaisons σ_{Ge-C}. L'ionisation mettant en jeu l'orbitale $2b_{1g}$ du dimère intervient également vraisemblablement dans cette région. Pour les attributions respectives de ces bandes, il faut prendre en compte le fait qu'expérimentalement, sur une plage de température de 20°C autour de la température de décomposition du trimère, une diminution d'intensité du premier massif a été observée et conjointement, une légère augmentation des bandes à 9,9 eV et 11,15 eV.

Enfin, nous attribuons la bande à 11,47 eV à des ionisations du monomère et du dimère mettant en jeu les orbitales fortement localisées sur les σ_{Ge-C} dans le cas du monomère (orbitale $3b_1$) et sur les σ_{Ge-C} et σ_{Ge-S} dans le cas du dimère (orbitales $5a_g$ et $3b_{1u}$).

Sections efficaces de photoionisation

Comme le fait apparaître un examen de la fig. 2, le passage d'un rayonnement HeI à HeII a conduit à de très notables diminutions d'intensité au niveau des trois massifs. Si a priori de telles diminutions pouvaient être prévues pour les deux premiers massifs mettant en jeu essentiellement les atomes de soufre, celles concernant le troisième massif, et en particulier la diminution très nette observée pour la bande à 11,15 eV associée à une ionisation faisant intervenir les liaisons $\sigma_{Ge—C}$ du dimère, était difficilement explicable. Afin de compléter notre analyse et conforter les attributions précédentes nous avons donc réalisé pour les premiers états initiaux du monomère et du dimère le calcul des sections efficaces différentielles de photoionisation, grandeurs comparables aux intensité des bandes expérimentales.

Les résultats obtenus ont été visualisés sous forme de courbes (figures 4 et 5), un balayage en énergie cinétique par pas de 5 eV ayant été effectué dans un domaine compris entre 5 eV et 50 eV. Nous avons dans tous les cas matérialisé par des traits verticaux les énergies de photons correspondant aux deux sources de rayonnement utilisées HeI (21,22 eV) et HeII (40,81 eV).

Les données des figures 4 et 5 traduisent dans l'ensemble de façon satisfaisante les observations expérimentales: (*i*) pour une énergie de photons correspondant à un rayonnement HeI, nous observons aussi bien pour le monomère que pour le dimère des valeurs voisines et assez faibles de sections efficaces pour tous les états faisant intervenir les paires des atomes de soufre (aussi bien σ que π), les liaisons de type π comme σ du motif Ge═S. Par contre, des valeurs nettement plus élevées apparaissent lors d'ionisations mettant en jeu des orbitales caractéristiques des liaisons $\sigma_{Ge—C}$ (Me_2Ge═S: $3b_1$, $(Me_2GeS)_2$: $3b_{2g}$). De fait le spectre expérimental (fig. 2) présente bien deux premiers massifs d'intensité peu différenciée et au contraire un troisième massif nettement plus intense. (*ii*) En ce qui concerne les variations d'intensité en fonction du rayonnement incident, les sections efficaces calculées pour toutes les orbitales traduisent bien les diminutions observées expérimentalement pour l'ensemble du spectre lors du passage d'une énergie de photons de 21,22 eV à 40,81 eV (figures 4 et 5).

Compte tenu du recouvrement des différentes bandes il est difficile de discuter des importances respectives de ces diminutions; toutefois un certain nombre de remarques peuvent être faites.

Pour les deux bandes à 9,55 eV et 10,75 eV associées au monomère, le calcul conduit à des diminutions sensiblement du même ordre, légèrement plus importante pour l'état initial $2b_2$ que pour l'état $5a_1$, ce que l'on observe bien expérimentalement.

Un accord moins satisfaisant apparaît lorsque l'on compare les intensités respectives des bandes du monomère et du dimère, notamment de celles à 9,55 eV et 9,9 eV; d'après les résultats des calculs, les diminutions d'intensité sont attendues à peu près du même ordre pour ces deux bandes, ce qui n'est pas observé expérimentalement (diminution plus importante dans le cas du monomère). Notons toutefois que, lors de l'enregistrement des spectres HeI et HeII, la composition du mélange a pu être modifiée dans le sens d'un accroissement du dimère.

Le point le plus intéressant de cette analyse concerne la bande à 11,15 eV pour laquelle une diminution nette a été observée au niveau des spectres et que nous attribuons à une ionisation mettant en jeu l'orbitale $3b_{2g}$ du dimère caractéristique des liaisons Ge—C. Or précisément nous observons

TABLEAU 2. Me_2Ge═S (symétrie C_{2v}): niveaux d'énergie, distributions de charge et potentiels d'ionisation en MS Xα

		Distributions de charge %																										
		S					Ge					C				H₁			H₂				Out					
Orbitale	Énergie (eV)	Tot	*s*	*p*	*d*	*f*	Tot	*s*	*p*	*d*	*f*	Tot	*s*	*p*	*d*	Tot	*s*	*p*	Tot	*s*	*p*	Int	Tot	*s*	*p*	*d*	*f*	PI (eV) théoriques
$4b_2$	−1,921	1			86	14	9		100													8	82		99	1		
$7a_1$	−1,946	1	79	19	2							2	38	57	5							10	87		94	14	2	
$6a_1$	−3,073	2	60	31	8	1	2	9	1	68	22	4	69	30	1							35	57	92		8		
$3b_2$	−3,077	16		90	9	1	20		99	1		2		58	42				2	96	4	43	17		53	14	23	
$4b_1$	−6,185	61		100			3			87	13	6	13	86	1							23	7					8,84
$2b_2$	−6,771	54		99	1		9		86	11	3	1		68	32				1	98	2	30	5					9,42
$5a_1$	−8,416	50	5	89	4	1	26	1	88	10	2	16	3	95	2				2	95	5		6					11,09
$3b_1$	−8,965	4		88	9	3	27		92	6	2	47	2	97	1	3	95	5	2	87	13	13	4					11,36
$2b_1$	−11,717						1		67	11	22	49		95	5	16	97	3	10	96	4	19	5					13,99
$1a_2$	−11,792						1			73	27	50		95	5				27	97	3	17	5					14,05
$4a_1$	−11,824	3	56	39	4	1	2	43	33	23	1	47		95	5	16	97	3	9	96	4	19	4					14,12

Paramètres géométriques (15): $d_{Ge═S}$ = 2,02 Å, $d_{Ge—C}$ = 1,95 Å, $\widehat{CGeC}$ = 120°.

TABLEAU 3. $(Me_2GeS)_2$ (symétrie D_{2h}): niveaux d'énergie, distributions de charge et potentiels d'ionisation en MS Xα

		Distributions de charge %																						
		S					Ge					C				H₁			H₂			Int	Out	
Orbitale	Energie (eV)	Tot	*s*	*p*	*d*	*f*	Tot	*s*	*p*	*d*	*f*	Tot	*s*	*p*	*d*	Tot	*s*	*p*	Tot	*s*	*p*	Tot	Tot	PI (eV) théor.
$4b_{1u}$	−6,762	61		100			4		14	73	13	9	12	87	1				1	94	6	23	2	8,96
$2b_{3g}$	−6,779	71		100			2			74	26											26	1	9,02
$4b_{3u}$	−7,545	49		97	2	1	20	3	71	22	4	19	6	91	2				1	94	6	9	2	9,74
$3b_{2u}$	−7,715	69	1	98	1		17		84	14	3	1		65	35							12	1	9,99
$2b_{1g}$	−8,233	60		98	2		20		94	5	1	3		79	21				2	97	3	15		10,48
$3b_{2g}$	−8,991						31		86	12	2	52	2	96	2	3	95	5	2	87	13	9	3	11,00
$5a_g$	−9,122	36	4	93	3		27		92	7	1	21	1	96	3				3	95	5	11	2	11,27
$3b_{1u}$	−9,290	6		94	5	1	29		92	7	2	44	1	97	3	5	95	5	1	82	18	13	2	11,33
$2b_{2g}$	−11,402						2		77	1	22	51		95	5	16	96	4	11	96	4	17	3	13,32
$2b_{1u}$	−11,484						2		85	2	13	50		95	5	15	96	4	11	96	4	19	3	13,40
$3b_{3u}$	−11,533						2	3	61	35	1	50		95	5	18	96	4	8	95	5	20	2	13,51
$1b_{3g}$	−11,615						1			71	29	51		95	5				28	96	4	17	3	13,50

Paramètres géométriques (14): $d_{Ge—S}$ = 2,35 Å, $d_{Ge—C}$ = 1,95 Å, $\widehat{SGeS}$ = 105°, $\widehat{GeSGe}$ = 75°, $\widehat{CGeC}$ = 111,6°.
PI expérimentaux: $(nBu_2GeS)_2$: 8,00 eV − 8,45 eV − 9,45 eV − 11 eV.

TABLEAU 4. Attributions proposées pour le spectre obtenu par dégradation thermique du trimère à 272°C

	Me₂Ge═S		(Me₂GeS)₂	
PI exp. (eV)	PI théor. (eV)	États	PI théor. (eV)	États
8,6	8,84	$^2B_1$	8,96	$^2B_{1u}$
8,85			9,02	$^2B_{3g}$
9,55	9,42	$^2B_2$		
9,9			9,74	$^2B_{3u}$
			9,99	$^2B_{2u}$
10,75	11,09	$^2A_1$	(10,48)	$^2B_{1g}$
11,15			11,00	$^2B_{2g}$
11,47	11,36	$^2B_1$	11,27	^2A_g
			11,33	$^2B_{1u}$

(fig. 5) une allure de résonance aux environs de 22 eV et donc pour cet état initial une forte diminution de section efficace en passant de $h\nu$ = 21,22 eV à $h\nu$ = 40,81 eV. Les observations expérimentales et les résultats déduits des calculs de sections efficaces forment donc un ensemble tout à fait cohérent.

Ainsi, l'utilisation conjointe de calculs de potentiels d'ionisation et de sections efficaces en MS Xα nous a permis de réaliser une attribution précise des différentes bandes du spectre observé par dégradation thermique du trimère de la diméthyl germathione et donc d'interpréter sans ambiguïté les ionisations caractéristiques du monomère.

Caractéristiques électroniques de la diméthyl germathione et de la diméthyl silathione

La méthode MS Xα se révélant bien adaptée à l'étude de ces molécules thioorganométalliques, nous avons étendu notre approche à la silathione (3) et réalisé parallèlement un calcul sur le thioformaldéhyde (15).

État fondamental

Pour les trois dérivés $H_2C═S$, $Me_2Si═S$ et $Me_2Ge═S$ (tableau 2) nous notons une séquence analogue des dernières orbitales occupées:

X = C : $2b_1$ (−7,02 eV), $1b_2$ (−9,09 eV), $3a_1$ (−11,19 eV)
X = Si : $4b_1$ (−6,52 eV), $2b_2$ (−7,13 eV), $5a_1$ (−8,91 eV)
X = Ge: $4b_1$ (−6,18 eV), $2b_2$ (−6,77 eV), $5a_1$ (−8,42 eV).

La dernière orbitale occupée est associée à la paire libre non liante de l'atome de soufre. Les orbitales moléculaires suivantes correspondent respectivement aux liaisons $\pi_{X═S}$ et $\sigma_{X—S}$ (X = C, Si, Ge). La quatrième orbitale moléculaire met en jeu les liaisons $\sigma_{C—H}$ et les liaisons $\sigma_{X—C}$ (X = Si, Ge).

Les distributions de charge font apparaître des localisations voisines pour ces trois dérivés en ce qui concerne les orbitales caractéristiques de la paire libre de l'atome de soufre ($4b_1$ et $2b_1$) et celles associées aux liaisons $\sigma_{X—S}$ ($5a_1$ et $3a_1$); ces dernières presentent dans les trois cas une localisation importante sur l'atome de soufre.

Par contre, les orbitales $2b_2$ et $1b_2$ se différencient plus nettement. Dans le cas du thioformaldéhyde, nous observons une liaison π assez bien répartie sur les deux atomes (fig. 6). Pour la diméthyl silathione et la diméthyl germathione, les contours présentent une nette dissymétrie avec une forte densité autour de l'atome de soufre (fig. 6); cette dissymétrie a déjà été observée lors d'une étude réalisée sur $H_2Ge═S$ en PSHONDO (16).

Des conclusions similaires peuvent être déduites de l'analyse des distributions électroniques π pour les trois systèmes.

Un caractère polaire nettement plus marqué pour >Si═S et >Ge═S que pour >C═S apparaît, réflétant les électronégativités respectives des atomes, Si, Ge, C et S (en charges nettes q_{Si} = +0,69, q_S = −0,65; q_{Ge} = +0,71, q_S = −0,69; q_C = +0,23, q_S = −0,21).[3]

Cette très forte polarisation du système π dans la diméthyl silathione et la diméthyl germathione permet de prévoir a priori une grande réactivité de ces systèmes.

De fait, expérimentalement, il n'a pas été possible d'isoler ces entités; par contre différents *n*-mères ont pu être caractérisés. Dans le cas du thioformaldéhyde, seuls des polymères insolubles ont été obtenus alors que pour la diméthyl silathione et la diméthyl germathione, des dimères ont pu être isolés (2), la structure du tétraméthylcyclodisilathiane ayant d'ailleurs été déterminée par diffraction électronique (14).

L'analyse simultanée des contours tracés pour les $\pi_{X═S}$ et $\pi^*_{X═S}$ (X = C, Si, Ge) (fig. 6) nous a permis de mieux appré-

[3]La charge de l'intersphère a été répartie sur les atomes proportionnellement à leur participation à l'orbitale moléculaire.

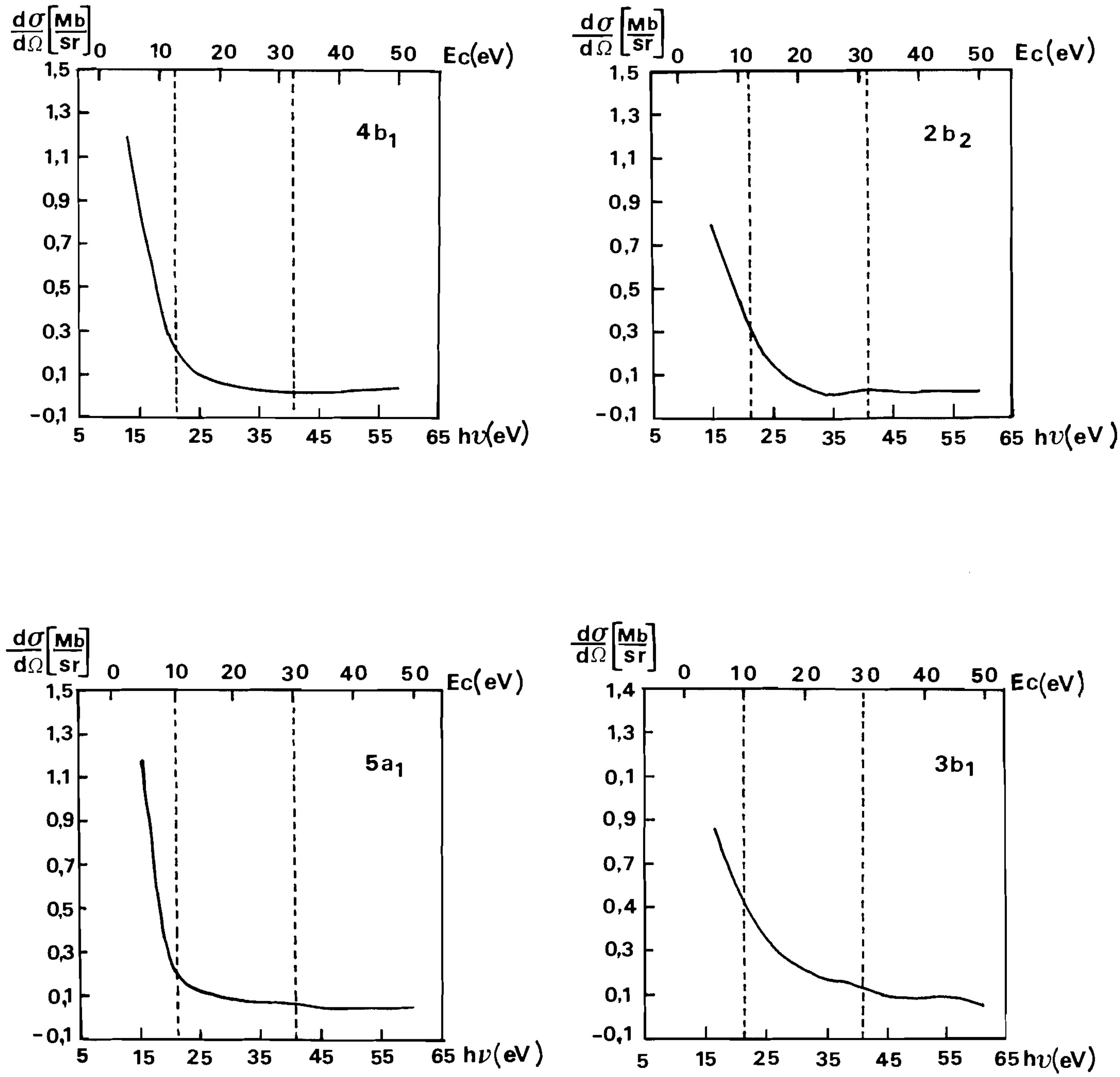

FIG. 4. dσ/dΩ pour les orbitales $4b_1$, $2b_2$, $5a_1$ et $3b_1$ de $Me_2Ge{=}S$.

hender ces différences de comportement.

Pour la diméthyl silathione et la diméthyl germathione, la dissymétrie des contours permet de lever la restriction bien connue de symétrie pour de telles dimérisations (17) (fig. 6). On conçoit alors que l'étape déterminante correspondra à la formation d'une liaison X—S puisqu'elle conduit à un recouvrement maximal entre les contours obtenus pour les orbitales occupées (autour de S) et les orbitales virtuelles (autour de Ge ou Si).

Ces caractéristiques déjà observées pour de nombreux dérivés $Me_2Si{=}CH_2$ (18), HP=NH (19) permettent d'expliquer la formation aisée de dimères tête-bêche.

Il n'en est pas de même en ce qui concerne le thioformaldéhyde où des contours symétriques sont observés pour les orbitales $\pi_{C=S}$ et $\pi^*_{C=S}$ (fig. 6). Ceci est en accord avec le fait qu'expérimentalement aucune formation de dimère n'a été observée dans ce cas.

États de Rydberg

Sans entreprendre une étude théorique complète des états excités des trois systèmes examinés, nous avons procédé à la caractérisation de leurs premières orbitales virtuelles, le formalisme de la méthode MS Xα étant particulièrement bien adaptée pour la description de ces orbitales vis à vis d'approches plus traditionnelles.

Compte tenu des valeurs relatives des charges partielles sur les sphères atomiques et sur l'outersphère, les différentes orbitales sont distinguées comme étant à caractère multicentrique (orbitale de valence) ou monocentrique (orbitale de Rydberg).

Dans le cas de $H_2C{=}S$, nous observons une première or-

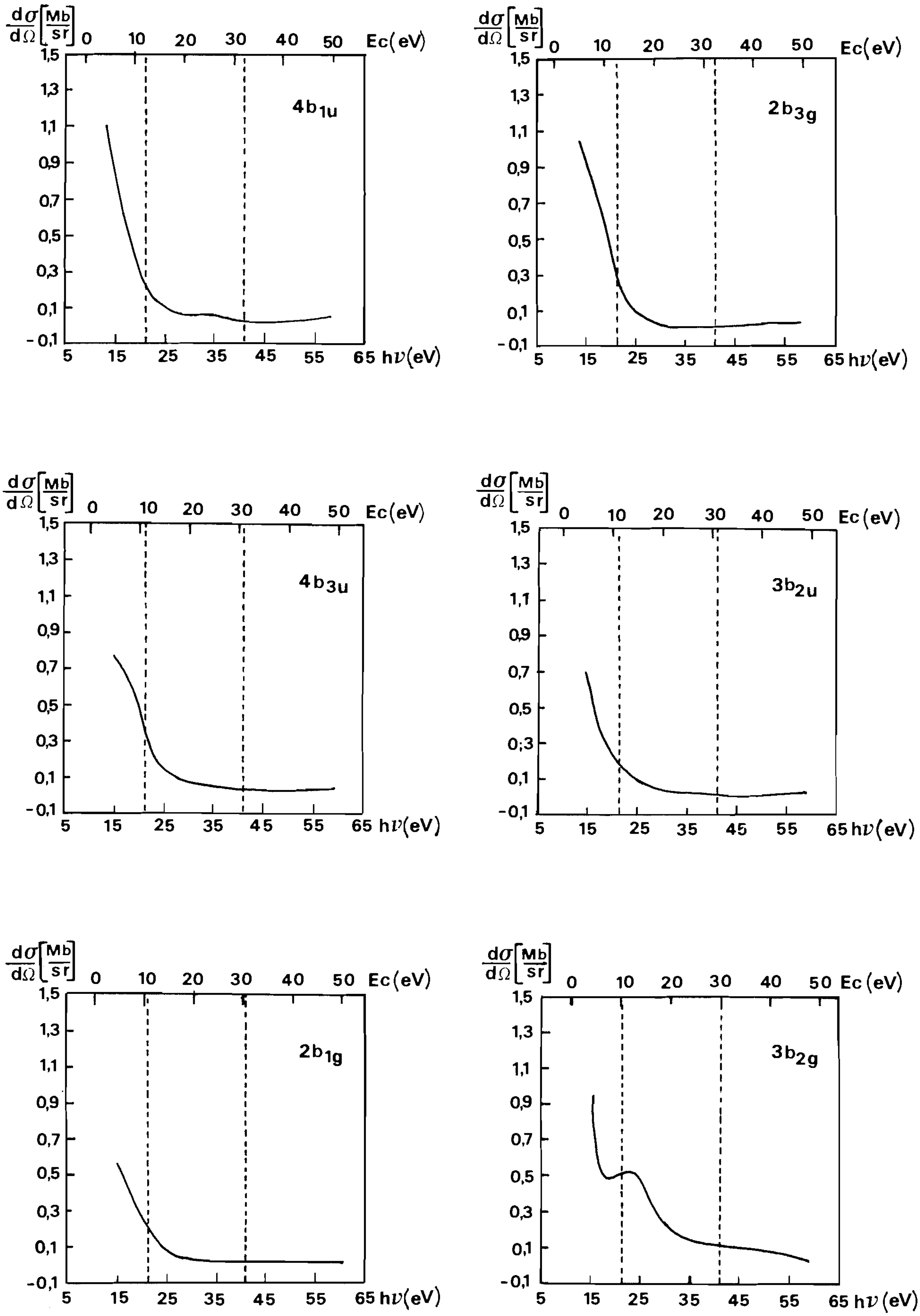

FIG. 5. $d\sigma/d\Omega$ pour les orbitales $4b_{1u}$, $2b_{3g}$, $4b_{3u}$, $3b_{2u}$, $2b_{1g}$ et $3b_{2g}$.

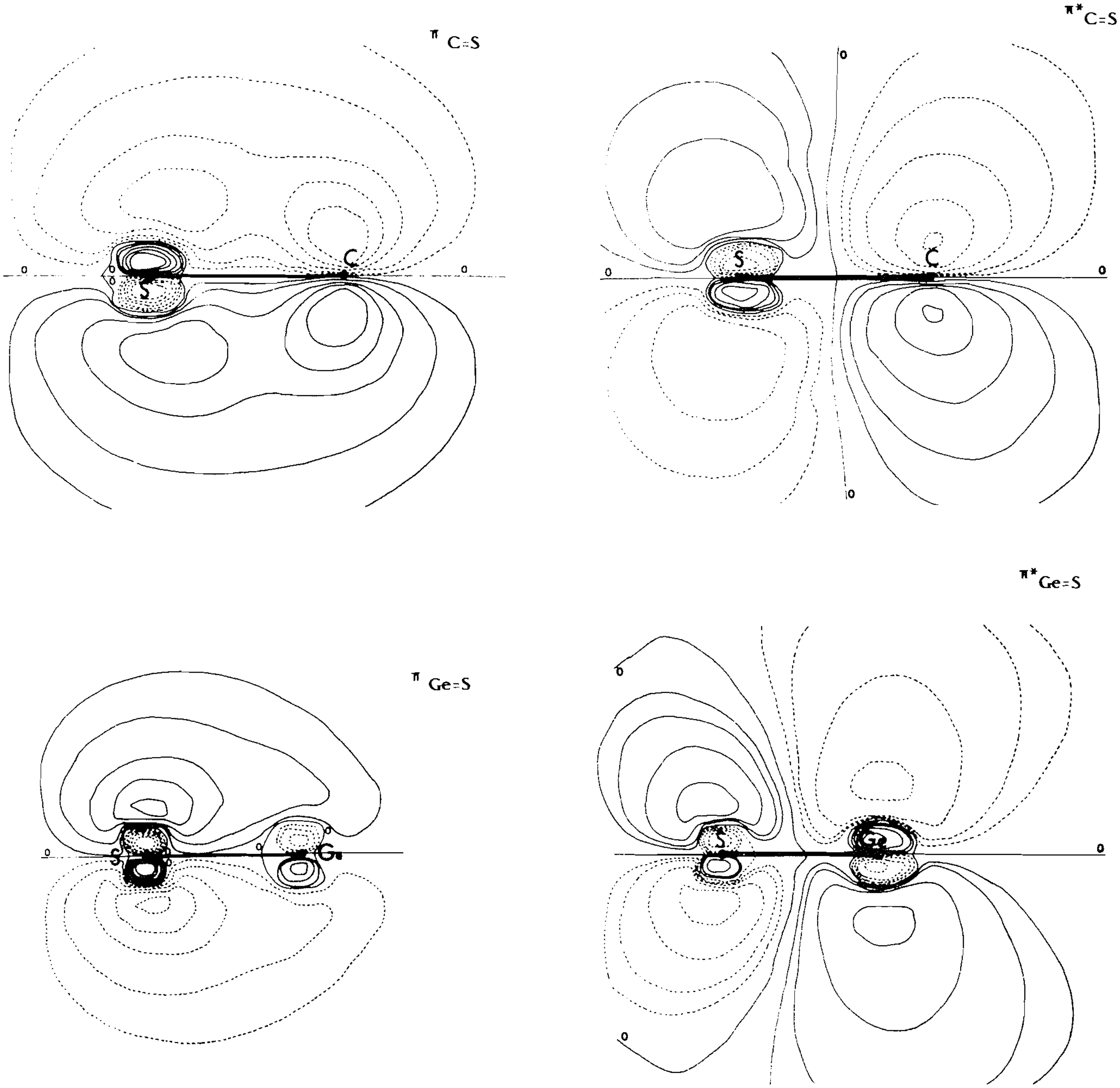

FIG. 6. Courbes de niveau pour les orbitales $\pi_{C=S}, \pi^*_{C=S}$ de $H_2C{=}S$ et $\pi_{Ge=S}, \pi^*_{Ge=S}$ de $Me_2Ge{=}S$ pour les valeurs suivantes de ψ:
$1b_2(\pi_{C=S})$: 0, ± 0,025, ± 0,05, ± 0,1, ± 0,15, ± 0,2 $(e/ua^3)^{1/2}$
$3b_2(\pi^*_{C=S})$: 0, ± 0,025, ± 0,05, ± 0,1, ± 0,2, ± 0,3 $(e/ua^3)^{1/2}$
$2b_2(\pi_{Ge=S})$: 0, ± 0,025, ± 0,05, ± 0,1, ± 0,15, ± 0,2 $(e/ua^3)^{1/2}$
$3b_2(\pi^*_{Ge=S})$: 0, ± 0,015, ± 0,025, ± 0,05, ± 0,1, ±0,2 $(e/ua^3)^{1/2}$.

bitale virtuelle de valence $2b_2$ (−4,80 eV) avec un relativement faible pourcentage d'outersphère (de l'ordre de 17%) et correspondant à la $\pi^*_{C=S}$.

Les orbitales suivantes $4a_1$ (−3,12 eV), $3b_1$ (−2,24 eV), $3b_2$ (−2,22 eV) et $5a_1$ (−2,16 eV) présentent des pourcentages de charge dans la région extramoléculaire de plus de 85% et sont donc à prédominance Rydberg, de type *s* pour l'orbitale $4a_1$ et de type *p* pour les orbitales $3b_1$, $3b_2$ et $5a_1$.

Les tracés reportés dans la fig. 7 font apparaître le caractère diffus de ces orbitales dans des régions loin des noyaux, de symétrie sphérique pour l'orbitale $4a_1$ et de type *p* pour l'orbitale $3b_1$.

Des tracés réalisés à une autre échelle ont permis de constater une intervention non négligeable des atomes dans les régions proches des noyaux. Ceci met bien en évidence, comme l'avaient déjà noté Roberge et Salahub (20) lors de calculs sur H_2S, les difficultés à établir une distinction nette entre orbitale de valence et orbitale de Rydberg.

Nos résultats, caractérisés par la présence d'orbitales Rydberg assez basses à caractère *s* et *p*, rejoignent ceux obtenus antérieurement par Bruna *et al.* (21) pour $H_2C{=}S$ lors d'un calcul Hartree Fock *ab initio* avec interaction de configuration.

Par ailleurs, étant donné les récents travaux spectroscopiques réalisés sur le thioformaldéhyde (22), nous avons procédé au

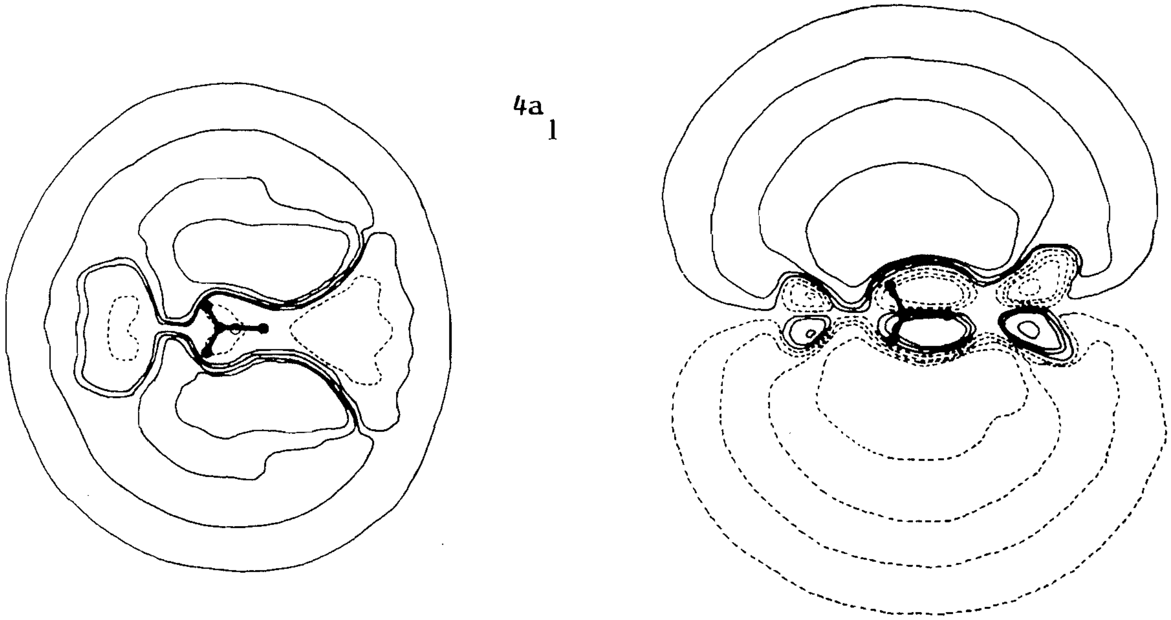

FIG. 7. Courbes de niveau pour les orbitales $4a_1$, $3b_1$ de $H_2C{=}S$ pour les valeurs suivantes de ψ:
$4a_1$: + 0,0003, + 0,001, + 0,003, ± 0,01 $(e/ua^3)^{1/2}$
$3b_1$: ± 0,0003, ± 0,001, ± 0,003, ± 0,01 $(e/ua^3)^{1/2}$.

calcul des premières transitions électroniques, en utilisant en version sans polarisation des spins la méthode de l'état de transition. Il faut cependant remarquer que les calculs ainsi réalisés ne permettent d'atteindre qu'une moyenne des énergies associées aux états singulet et triplet (23).

Expérimentalement, les états excités les plus hauts en énergie ont pu être caractérisés par analyse des structures fines rotationnelles; les bandes à 5,8, 6,6 et 6,82 eV ont été attribuées à des transitions 0—0 respectivement de type $n \rightarrow 3sa_1$ $(^1B_1)$, $n \rightarrow 3pb_1$ $(^1A_1)$, $n \rightarrow 3pa_1$ $(^1B_1)$, la faible bande à 5,6 eV correspondant à une transition $\pi \rightarrow \pi^*$ $(^1A_1)$.

Les résultats des calculs effectués confortent ces attributions expérimentales puisque nous obtenons par ordre d'énergie croissante pour les transitions permises $\pi \rightarrow \pi^*$ ($1b_2 \rightarrow 2b_2$: 4,33 eV), $n \rightarrow 3sa_1$ ($2b_1 \rightarrow 4a_1$: 4,91 eV), $n \rightarrow 3pb_1$ ($2b_1 \rightarrow 3b_1$: 6,30 eV), $n \rightarrow 3pa_1$ ($2b_1 \rightarrow 5a_1$: 6,45 eV).

Dans le cas de $Me_2Ge{=}S$ (tableau 2), nous observons une première orbitale virtuelle $3b_2$ essentiellement de valence (17% dans l'outersphère) caractéristique de la $\pi^*_{Ge=S}$.

L'orbitale suivante $6a_1$ apparaît à la fois à caractère Rydberg et de valence avec un pourcentage de 57% dans la région extramoléculaire (tableau 2). Les tracés réalisés mettent en évidence dans des régions éloignées des noyaux son caractère diffus d'orbitale *s* de Rydberg mais également près des noyaux les caractères antiliants Ge—S et Ge—C de cette orbitale.

Les deux autres orbitales $7a_1$ et $4b_2$ sont comme dans $H_2C{=}S$ à caractère Rydberg de symétrie *p*.

Les résultats obtenus pour $Me_2Si{=}S$ sont très voisins de ceux de $Me_2Ge{=}S$ quant aux distributions de charge, tant sur les atomes que sur l'outersphère. On remarque seulement une inversion des deux premières virtuelles $6a_1$ et $3b_2$ ainsi que de $4b_2$ et $7a_1$ vis à vis de $Me_2Ge{=}S$.

Nous n'avons pas entrepris de calculs de transitions électroniques pour la diméthyl germathione et la diméthyl silathione puisque nous ne disposions d'aucun support expérimental.

Il semblerait toutefois, compte tenu des résultats obtenus, que l'on puisse attendre pour ces deux systèmes des transitions de Rydberg dans la même région ou précédant les transitions de valence.

Conclusion

Cette étude menée par MS Xα nous a conduit à préciser certaines caractéristiques de nouvelles entités à courte durée de vie récemment mises en évidence la diméthyl silathione et la diméthyl germathione.

Nous avons en premier lieu confirmé la détection en spectroscopie photoélectronique de la diméthyl germathione par la détermination des diverses grandeurs liées à l'ionisation de ce système.

Par ailleurs, l'analyse comparative des résultats obtenus pour la diméthyl silathione, la diméthyl germathione et leur homologue le thioformaldéhyde nous a permis de mieux percevoir les modifications induites au niveau de la structure électronique (caractéristiques de l'état fondamental et des états Rydberg) lors du remplacement d'un atome de carbone par un atome de silicium ou de germanium.

Remerciements

Deux des auteurs (G.P. et D.G.) remercient le Professeur Salahub pour leur avoir communiqué le programme de calcul des sections efficaces et le Dr M. Roche pour de fructueuses discussions.

Une partie de ce travail a été accomplie dans le cadre d'une recherche subventionnée par le Fonds National Suisse de la Recherche Scientifique (projet 2.615-0.82). Les calculs ont été partiellement effectués sur un ordinateur aimablement mis à notre disposition par le Centre de Calcul de l'Université de Genève.

1. C. GUIMON, G. PFISTER-GUILLOUZO, G. RIMA, M. EL AMINE et J. BARRAU. Spectrosc. Lett. Sous presse.
2. J. SATGE. Adv. Organomet. Chem. 21 (1982), et références incluses.
3. C. GUIMON, G. PFISTER-GUILLOUZO, H. LAVAYSSIERE, G.

DOUSSE, J. BARRAU et J. SATGE. J. Organomet. Chem. **249**, C17 (1982).
4. (*a*) K. H. JOHNSON. Adv. Quantum Chem. **7**, 143 (1973); (*b*) J. C. SLATER. Quantum theory of molecules and solids. McGraw Hill, New York. 1974.
5. B. D. EL ESSA et A. HINCHLIFFE. J. Chem. Soc. Faraday Trans. 2, **76**, 1375 (1980); L. SCHEIRE, R. ROTTHIER et P. PHARISEAU. Int. J. Quant. Chem. **XX**, 879 (1981).
6. D. DILL et J. L. DEHMER. J. Chem. Phys. **61**, 692 (1974).
7. (*a*) J. W. DAVENPORT. Phys. Rev. Lett. **36**, 945 (1976); (*b*) F. A. GRIMM, T. A. CARLSON, W. B. DRESS, P. AGRON, J. O. THOMSON et J. W. DAVENPORT. J. Chem. Phys. **72**, 3041 (1980); (*c*) F. A. GRIMM, J. D. ALLEN, JR., T. A. CARLSON, M. O. KRAUSE, D. MEHAFFY, P. R. KELLER et J. W. TAYLOR. J. Chem. Phys. **75**, 92 (1981); (*d*) H. J. LEVINSON, T. GUSTAFSSON et P. SOVEN. Phys. Rev. (A), **19**, 1089 (1979).
8. T. A. CARLSON, M. O. KRAUSE, A. FAHLMAN, P. R. KELLER, J. W. TAYLOR, T. WHITLEY et F. A. GRIMM. J. Chem. Phys. **79**, 2157 (1983).
9. R. LATTER. Phys. Rev. **81**, 385 (1955).
10. K. SCHWARZ. Phys. Rev. Sect. B, **5**, 2466 (1972).
11. J. G. NORMAN JR. J. Chem. Phys. **61**, 4630 (1974).
12. C. GUIMON, D. GONBEAU, G. PFISTER-GUILLOUZO, G. DE LAUZON et F. MATHEY. Chem. Phys. Lett. **104**, 560 (1984).
13. (*a*) M. ROCHE, D. R. SALAHUB et R. P. MESSMER. J. Electron. Spectrosc. **19**, 273 (1980); (*b*) D. J. BRISTOW, G. M. BANCROFT et J. S. TSE. Chem. Phys. **75**, 263 (1983).
14. M. YOKOI, T. NOMURA et K. YAMASAKI. J. Am. Chem. Soc. **77**, 4484 (1955).
15. (*a*) D. R. JOHNSON et F. X. POWELL. Science, **169**, 679 (1970); (*b*) D. R. JOHNSON, F. X. POWELL et W. H. KIRCHHOFF. J. Mol. Spectrosc. **39**, 136 (1971).
16. G. TRINQUIER. Thèse de Doctorat d'Etat (1981), Université Paul Sabatier, Toulouse.
17. R. G. PEARSON. Acc. Chem. Res. **4**, 152 (1971).
18. M. D. CURTIS. J. Organomet. Chem. **60**, 63 (1973).
19. D. GONBEAU, G. PFISTER-GUILLOUZO et J. BARRANS. Can. J. Chem. **61**, 1371 (1983).
20. R. ROBERGE et D. R. SALAHUB. J. Chem. Phys. **70**, 1177 (1979).
21. P. J. BRUNA, S. D. PEYERIMHOFF et R. J. BUENKER. Chem. Phys. **3**, 35 (1974).
22. (*a*) D. J. CLOUTHIER et D. A. RAMSAY. Ann. Rev. Phys. Chem. **34**, 31 (1983); (*b*) C. R. DRURY et D. C. MOULE. J. Mol. Spectrosc. **92**, 469 (1982).
23. P. S. BAGUS et B. I. BENNETT. Int. J. Quantum Chem. **9**, 143 (1975).

Ab-initio calculations on the retinal Schiff base – formic acid and allylimine – formic acid hydrogen bonds

MILAN HODOŠČEK AND DUŠAN HADŽI
Boris Kidrič Institute of Chemistry and Lek-Pharmaceutical and Chemical Works, Ljubljana, Yugoslavia

Received August 1, 1984

This paper is dedicated to Professor Camille Sandorfy on the occasion of his 65th birthday

MILAN HODOŠČEK and DUŠAN HADŽI. Can. J. Chem. **63**, 1528 (1985).

The proton potential functions of Schiff base – formic acid complexes were calculated in the *ab-initio* scheme with STO-3G and 4-31G basis sets without and with the inclusion of a perturbing charge. The comparison of the curves with the retinal Schiff base and allylimine obtained by using the short base encouraged further calculations with the longer base on the truncated system only. The curve obtained with the 4-31G set on the allylimine – formic acid complex is of a double minimum type with the deeper well still at the formyl oxygen. Inclusion of a perturbing negative charge near the hydrogen bond reverses the depth of the wells making the N-protonated form more stable.

MILAN HODOŠČEK et DUŠAN HADŽI. Can. J. Chem. **63**, 1528 (1985).

Faisant appel à des schémas *ab-initio* et utilisant des bases STO-3G et 4-31G avec ou sans l'inclusion d'une charge perturbante, on a calculé les fonctions de potentiel des protons de complexes entre l'acide formique et des bases de Schiff. Une comparaison des courbes relatives à la base de Schiff du rétinal et de l'allylamine, obtenues à l'aide de la base la plus courte, nous a encouragé à procéder à des calculs plus approfondis que nous avons effectués uniquement sur le système tronqué en utilisant un base de calcul élargie. La courbe que nous avons obtenue pour le complexe de l'acide formique et de l'allylimine, en utilisant une base de calcul 4-31G, comporte un double minimum et le puit le plus profond est encore fixé à l'oxygène. L'inclusion, près de la liaison hydrogène, d'une charge perturbante négative renverse la profondeur des puits et rend ainsi la forme N-protonée plus stable.

[Traduit par le journal]

Introduction

In the series of hydrogen bonds involved in the light transduction mechanisms of both rhodopsin and bacteriorhodopsin (1, 2), the bond between the retinal Schiff base nitrogen (N_{16}) and a proton offering group in the opsin deserves particular attention. In explaining the bathochochromic shift that occurs upon bonding of retinal to the apoprotein it was necessary to invoke both a positive charge on N_{16} of the retinal Schiff base and a negative charge in the vicinity of C_{14} of retinal (refs. 3, 4 and references therein). Although the electronic absorption of the retinylic chromophore in the ground state could be explained equally well by assuming covalent N^+—H bonding or by a strong hydrogen bond between N_{16} and a proton donor belonging to the apoprotein (5), it was the interpretation of the resonance Raman spectra of rhodopsin that led to the prevalent opinion in favour of protonated N_{16} (6, 7). However, the ^{13}C nmr spectra of rhodopsin appeared to oppose this view (8) and also the results of differential kinetic infrared spectroscopy were interpreted in terms of the initially unprotonated N_{16} (9). Sandorfy and co-workers have elaborated a scheme (10–15) reconciling both extreme views, i.e. the protonated and unprotonated Schiff base. The essence of this scheme is a strong hydrogen bond with a double minimum type of the proton potential function with the deeper well away from N_{16} in the ground state and a reversal occurring upon excitation. A single minimum type, nearly symmetric hydrogen bond was also considered. By this assumption, substantiated with semi-empirical calculations of the electronic energies as well as by infrared spectroscopic investigations of model Schiff bases interacting with various proton donors, it was possible to explain the resonance Raman spectroscopic results. The latest infrared work (16, 17) is indicative of the ground state protonation the main argument being deuterium mass effect on the C=N stretching mode that was observed previously in the resonance Raman spectra.

Until now, there is no experimental evidence of the nature of the group donating a proton to N_{16} either in full protonation or by hydrogen bonding. In the theoretical calculations of the electronic spectra both a carboxylate and an ammonium group were considered to be potential proton donors to N_{16} (5, 18, 19). Recent *ab-initio* calculations of the proton potential function of the retinal chromophore modelling systems: (*i*) allylimine – formic acid and (*ii*) allylimine – ammonium ion have shown that in model (*i*) the proton is located nearer to the formyl oxygen whereas in (*ii*) a nearly symmetrical double minimum type curve resulted (18). The curve shapes were not essentially altered by the inclusion of an extraneous charge and of the reaction field. Thus this work appears to exclude the possibility of the protonation of N_{16} by a carboxylic group. From the point of view of the reprotonation of the Schiff base after the completion of the photochemical cycle a negative counterion appears to be more likely. Thus the theoretical work (18) just mentioned requires some qualification since the calculation was done using a short basis (STO-3G). The deficiencies of such basis sets in calculating the relative energies of neutral and charged species are well known (20, 21). Thus the use of a more flexible basis set is indicated for the treatment of systems such as are the present ones. The application of larger basis sets requires for reasons of economy a truncation of the retinal moiety which poses, however, the question of the effect of truncation on the resulting proton potential function. This question is certainly important for a conjugated system. Therefore, we performed the calculations first on the retinal (without methyl groups) Schiff base – formic acid system using the STO-3G basis and then, using the same base, on the allylimine – formic acid complex. Since there was no dramatic difference between the shapes of both curves, we have carried out subsequent calculations on the truncated system, but using the 4-31G basis. This resulted in a qualitatively different curve which can be considered to be more realistic.

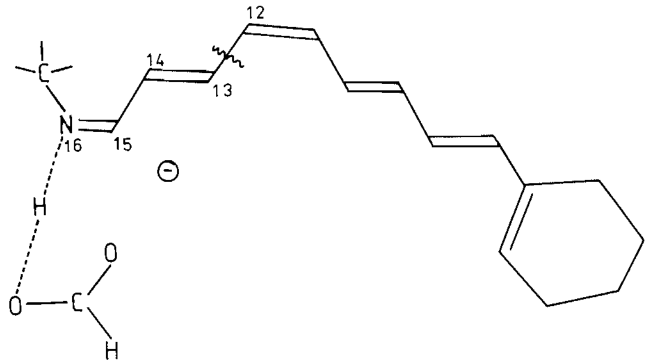

FIG. 1. Schematic representation of the (desmethyl) retinal Schiff base — formic acid system. ∿ indicates truncation and ⊖ the position of the negative charge.

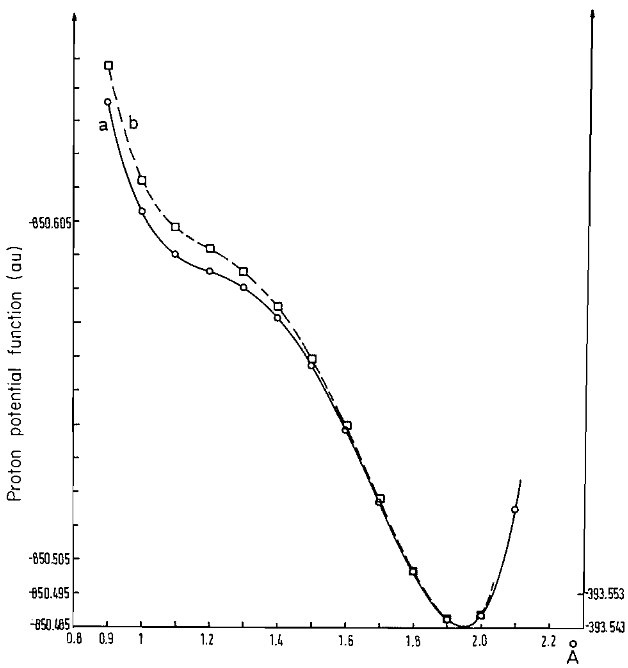

FIG. 2. Proton potential function (STO-3G basis) of (*a*) desmethyl retinal Schiff base — formic acid, and (*b*) allylimine — formic acid systems. Note the different energy scales. The horizontal scale in this and the following figures refers to the distance of the proton from the nitrogen.

Computational

Geometrical parameters

The parameters for the polyene Schiff base were taken from ref. 22 and those for the cyclohexene ring from available molecular mechanics calculations (D. Kocjan, private communication). The average plane of the ring and of the polyene chain were taken to be parallel. The geometric parameters for the amine — formic acid part (Fig. 1) were taken from ref. 22. The perturbing negative charge was placed (4) either in the N, O, C, O plane (distance from C_{13} = 3.0 Å and from N_{16} = 3.776 Å) or above the plane (distance from C_{14} = 3.030 Å, from C_{15} = 2.834 Å, and from N_{16} = 3.444 Å). The perturbing charge was introduced in the Fock Hamiltonian as an electrostatic perturbation of the form:

$$[1] \quad V' = q\int \frac{\rho^0}{|r - r'|} d^3r' + \sum_i \frac{Z_i q}{|r - r_i|}$$

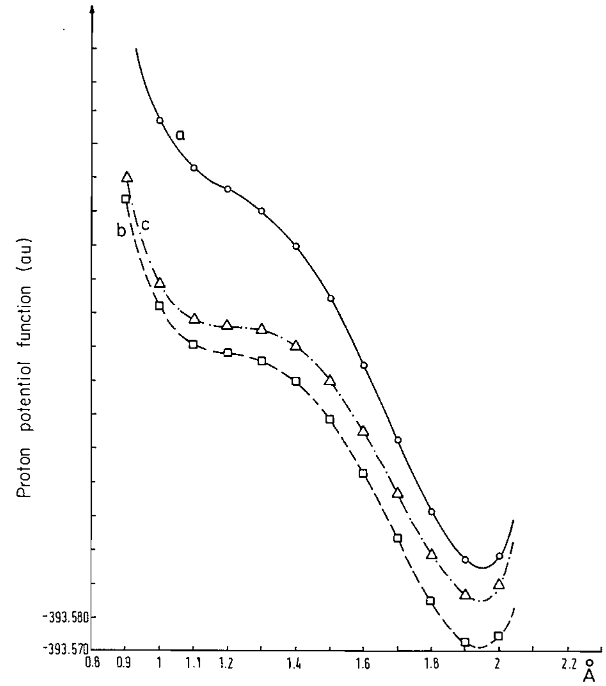

FIG. 3. Proton potential functions (STO-3G basis) of (*a*) allylimine — formic acid (no extra charge), (*b*) with unit negative charge in the plane, and (*c*) with charge above the plane (see Computational section).

where q is the value of the perturbing charge (equal to -1 au), ρ^0 is the unperturbed electron density of the respective molecule, r' is the position of the charge, and Z_i are the nuclear charges. The integral in [1] was solved using the *ab-initio* method described in ref. 23. The electrostatic potential V' was included in the Hamiltonian and the SCF procedure was switched on. The new energy was then obtained. For calculations the GAUSSIAN 80 program package (24) was used. The programs were implemented on a VAX 11/780 computer.

Results and discussion

Figures 2 and 3 show the proton potential curves for the retinylidene Schiff base — formic acid and allylimine — formic acid complexes computed using the STO-3G basis. The characteristic data are given in Table 1. The truncation of the conjugated chain has obviously a minor effect only on the depth of the inflection. This is considered to justify further calculations on the truncated system. The inclusion of a unit negative charge causes a flattening of the inflection which is more pronounced if the charge is placed above the plane. The results of the calculation with the 4-31G basis (Fig. 4) are more significant. The curve has now two minima separated by a low barrier. Without charge, the deeper well is still closer to the formyl oxygen whereas the inclusion of a charge in the plane makes the potential lower at the nitrogen site. For the charge placed above the plane we have calculated the energy in three points only (Table 1). The minimum nearer to the nitrogen is now deeper relatively to the one nearer to the oxygen, but the overall energy is less negative than with the charge in the plane. The results are qualitatively similar to those obtained previously on the methylamine — formic acid complex (21) except that in the latter the difference in energies of the two minima is larger. This corresponds well to the experimental estimate of the proton accepting propensities of alkylamines and aliphatic Schiff

TABLE 1. Calculated energies (in au) of the retinal Schiff base − formic acid (R) and allylimine − formic acid (A) systems at relevant distances v of the proton from nitrogen

	Energy					
	STO-3G			4-31G		
System	v = 1.9 Å	v = 1.5 Å	v = 1.1 Å	v = 2.0 Å	v = 1.5 Å	v = 1.1 Å
R	−850.4822	−850.4073	−850.3748	—	—	—
A	−393.5413	−393.4643	−393.4258	−398.1066	−398.0711	−398.0889
A	−393.5661	−393.500	−393.4780	−398.1426	−398.1193	−398.1473
A	−393.5517	−393.4886	−393.4708	−398.1168	−398.0968	−398.1279

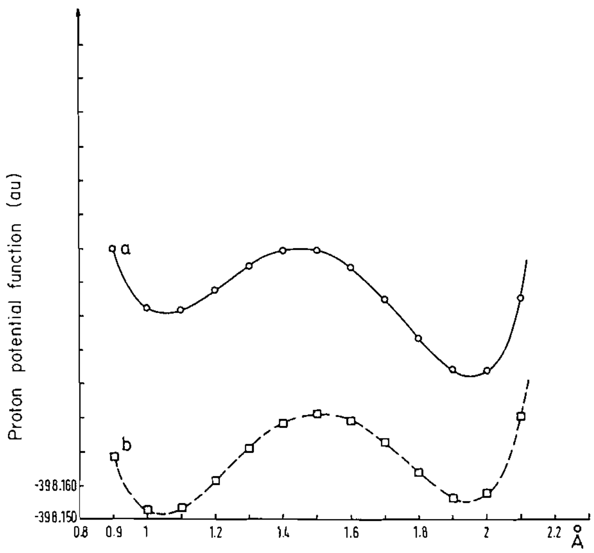

FIG. 4. Proton potential functions (4-31G basis) of allylimine − formic acid (a) without charge and (b) with a unit charge in the plane.

bases on the ground of infrared spectra of acid−base complexes carried out by Sandorfy and co-workers (5) by which it was shown that the Schiff bases are weaker proton acceptors than the amines. The results of our calculation indicate the tautomeric form $N^+H\ldots{}^-OCO$ to be the dominant one provided that a negative charge is present near the hydrogen bond. The analogous calculation on the full retinylidene system is expected to make the minimum nearer to N_{16} even deeper because the positive charge would be more dispersed. Higher levels of calculation should not radically change the picture. More extended basis sets including polarization functions are expected to lower somewhat the energy of the ionic form (20) whereas the electron correlation would lower the energy of the transition state that is anyway rather low (25, 26). Probably more important would be a full geometry optimization. Thus the results of the *ab-initio* calculation of the retinal Schiff base − formic acid are on the line considered by Sandorfy and co-workers (11−15), but give some more weight to the protonated form. We are continuing our *ab-initio* calculations in the direction of modelling possible groups that may subtend protons to the Schiff base − anion switch, and accept it from, after the photocycle had been completed.

NOTE ADDED IN PROOF: Recent uv and nmr investigations of hydrogen bonding between a dienylidene Schiff base and different halogeno acids indicate a rapid, dynamic equilibrium between the protomeric forms (27). Resonance Raman studies of hydrated and dried purple membrane of Halobacterium halobium lead to the conclusion that the protonated retinylidine Schiff base reverts to the unprotonated state in the absence of water (28). These results are in a good agreement with the theoretically predicted type of proton potential function.

Acknowledgements

This work was inspired by the discussions at the NATO Advanced Study Institute (Maratea, Italy, 1983) organized by Professors Camille Sandorfy and Theo Theophanides. It was financially supported by the Research Community of Slovenia. The generous allotment of computer time by IMP, Ljubljana, is gratefully acknowledged.

1. A. WARSHELL. Photochem. Photobiol. **30**, 285 (1979).
2. B. HONIG, T. EBREY, R. H. CALLENDER, U. DINUR, and M. OTTOLENGHI. Proc. Natl. Acad. Sci. **76**, 2503 (1979).
3. A. RAUDINO, F. ZUCCARELLO, and G. BUEMI. J. Chem. Soc. Faraday Trans. 2, **79**, 1750 (1983).
4. B. HONIG, U. DINUR, K. NAKANISHI, V. BALOGH-NAIR, M.-A. GAWINOWICZ, A. ARNABOLDI, and M. G. MOTTO. J. Am. Chem. Soc. **101**, 7084 (1979).
5. J. FAVROT, J. M. LECLERCQ, R. ROBERGE, C. SANDORFY, and D. VOCELLE. Photochem. Photobiol. **29**, 99 (1979).
6. R. MATHIES, A. R. OSEROFF, and I. STRYER. Proc. Natl. Acad. Sci. USA, **73**, 1 (1976).
7. B. ATON, A. G. DOUKAS, R. H. CALLENDER, B. BECHER, and T. G. EBREY. Biochemistry, **16**, 2995 (1977).
8. G. MASSIG, M. STOCKBURGER, W. GÄRTNER, D. OESTERHELD, and P. TOWNER. J. Raman Spectrosc. **12**, 287 (1982).
9. J. SHRIVER, G. MATEESCU, R. FAGER, D. TORCHIA, and E. W. ABRAHAMSON. Nature, **270**, 271 (1977).
10. F. SIEBERT and W. MÄNTELE. Biophys. Struct. Mech. **6**, 147 (1980).
11. F. I. HAROSI, J. FAVROT, J. M. LECLERCQ, D. VOCELLE, and C. SANDORFY. Rev. Can. Biol. **37**, 257 (1978).
12. P. DUPUIS, F. I. HAROSI, C. SANDORFY, J. M. LECLERCQ, and D. VOCELLE. Rev. Can. Biol. **39**, 247 (1980).
13. J. M. LECLERCQ and C. SANDORFY. Photochem. Photobiol. **33**, 361 (1981).
14. J. M. LECLERCQ, D. DUPUIS, and C. SANDORFY. Croat. Chem. Acta, **55**, 105 (1982).
15. J. M. LECLERCQ. Spectrosc. Int. J. **2**, 151 (1983).
16. K. J. ROTSCHILD and H. MARRERO. Proc. Natl. Acad. Sci. USA, **79**, 4045 (1982).
17. F. SIEBERT, W. MÄNTELE, and K. GERVERT. Eur. J. Biochem. **136**, 119 (1983).
18. F. ZUCCARELLO, A. RAUDINO, and G. BUEMI. J. Mol. Struct. **107** (Theochem.), 215 (1984).
19. A. RAUDINO, F. ZUCCARELLO, and G. BUEMI. J. Chem. Soc. Faraday Trans. 2, **79**, 1759 (1983).
20. J. VOOGD, L. DERISSEN, and F. B. VAN DUIJNEVELDT. J. Am. Chem. Soc. **103**, 7701 (1981).
21. J. KOLLER, M. HODOŠČEK, and D. HADŽI. J. Mol. Struct. **106**

(Theochem.), 301 (1984).
22. J. LECLERCQ, J. M. LECLERCQ, and C. SANDORFY. Chem. Phys. Lett. **91**, 246 (1982).
23. T. ŠOLMAJER, M. HODOŠČEK, and D. HADŽI. Int. J. Quant. Chem. **23**, 945 (1983).
24. D. HADŽI, M. HODOŠČEK, D. KOCJAN, T. ŠOLMAJER, and F. AVBELJ. Croat. Chem. Acta, **57**, 1065 (1984).
25. J. S. BINKLEY, R. A. WHITESIDE, R. KRISHNAN, R. SEEGER, D. J. DEFREES, H. B. SCHLEGEL, S. TOPIOL, L. R. KAHN, and J. A. POPLE. GAUSSIAN 80, QCPE No. 406, Indiana University, Bloomington, IN.
26. J. DEL BENE, M. J. FRISCH, K. RAGHAVACHARI, and J. A. POPLE. J. Phys. Chem. **86**, 1529 (1982).
27. M. BIZONETTE, H. L. THANK, and D. VOCELLE. Can. J. Chem. **62**, 1459 (1984).
28. P. HILDEBRANDT and M. STOCKBURGER. Biochemistry, **23**, 5539 (1984).

Reaction ergodography for dehydrogenation reaction of methanethiol

TOKIO YAMABE

Department of Hydrocarbon Chemistry, Faculty of Engineering and Division of Molecular Engineering, Graduate School of Engineering, Kyoto University, Kyoto 606, Japan

CHENG-DA ZHAO

Chemistry Department, North Eastern Normal University, People's Republic of China

MASAHIKO KOIZUMI

Department of Hydrocarbon Chemistry, Faculty of Engineering, Kyoto University, Kyoto 606, Japan

AKITOMO TACHIBANA

Department of Hydrocarbon Chemistry, Faculty of Engineering and Division of Molecular Engineering, Graduate School of Engineering, Kyoto University, Kyoto 606, Japan

AND

KENICHI FUKUI

Kyoto Institute of Technology, Kyoto 606, Japan

Received August 5, 1984

This paper is dedicated to Professor Camille Sandorfy on the occasion of his 65th birthday

TOKIO YAMABE, CHENG-DA ZHAO, MASAHIKO KOIZUMI, AKITOMO TACHIBANA, and KENICHI FUKUI. Can. J. Chem. **63**, 1532 (1985).

The dehydrogenation reaction paths of methanethiol CH_3SH were analyzed by *ab initio* MO calculations. The geometries and energies of the reactants, transition states, and products have been determined on the singlet potential energy surface of the ground state. We also analyze the similar dehydrogenation reactions of methanol (CH_3OH) and ethanol (CH_3CH_2OH) for the purpose of comparison. The activation energy and the heat of reaction calculated by incorporating the effect of electronic correlation shows that the product $H_2C{=}S$ is chemically more unstable than the product $H_2C{=}O$. "Reaction ergodography" along the intrinsic reaction coordinate (IRC) for these dehydrogenation paths clarifies the distinct differences in atomic movement. The path of methanethiol has two characteristic steps before the transition state, while neither paths of the two carbinols have such multisteps. The electronic intramolecular interaction between subsystems of the reactant molecule is investigated in terms of Interaction Hybrid Molecular Orbital (IHMO).

TOKIO YAMABE, CHENG-DA ZHAO, MASAHIKO KOIZUMI, AKITOMO TACHIBANA et KENICHI FUKUI. Can. J. Chem. **63**, 1532 (1985).

Utilisant des calculs d'OM *ab initio*, on a analysé les voies réactionnelles associées à la déshydrogénation du méthanethiol (CH_3SH). On a déterminé les géométries et les énergies des réactifs, des états de transition et des produits sur la surface d'énergie potentielle singulet de l'état fondamental. Pour fins de comparaisons, on a aussi analysé les réactions de déshydrogénation semblables du méthanol (CH_3OH) et de l'éthanol (CH_3CH_2OH). Les énergies d'activation et les chaleurs des réactions, calculées en incorporant l'effet de la corrélation électronique, montrent que le produit $H_2C{=}S$ est chimiquement plus instable que le produit $H_2C{=}O$. L'application de l'"ergodographie réactionnelle" aux coordonnées réactionnelles intrinsèques (CRI) de ces voies de déshydrogénation permet de clarifier les différences qui les distinguent au niveau du mouvement atomique. La voie du méthanethiol possède deux étapes caractéristiques avant son état de transition; par ailleurs, ni l'un ni l'autre des voies des carbinols ne possède de telles étapes multiples. Utilisant la notion d'interaction entre orbitales moléculaires hybrides, on a étudié l'interaction intramoléculaire électronique entre les sous-systèmes des molécules qui réagissent.

[Traduit par le journal]

1. Introduction

The dynamic analysis of elementary reaction is developed as part of a recent big stream of the theoretical study of chemical reactions. The selection of the reaction coordinate which shows the nature of structural change of reactant molecules during the reaction process is an important key, particularly for reactions in which polyatomic molecules participate. The reaction coordinate is hence considered to be an essential concept for constructing the theory of chemical reaction based on the chemical reaction pathway. There are many theories of chemical reaction in which the concept of the reaction coordinate plays an important role (1). The absolute rate theory of Eyring which first clarified the usefulness of the concept of the reaction coordinate is particularly well-known (2*a*). This is a representative theory of the so-called transition state theory and predicts the reaction rate based on the statistical treatment of molecules assuming the equilibrium between the reactants and the transition state (TS). As one focusses on the dynamical aspects, the unimolecular reaction rate theory of RRKM and its basic concept are developed to predict the reaction energy distribution of products and the effect of vibrational excitation (2*b*). The natural collision coordinate was introduced by Marcus to describe the statistical or dynamical aspects of chemical reaction using reaction coordinate and to treat the reactive scattering between an atom and a diatomic molecule (2*c*).

We have analyzed the dynamical aspects of various elementary reaction processes of polyatomic molecules in terms of the Intrinsic Reaction Coordinate (IRC) proposed by Fukui in 1970 (3), and investigated the topological structure of potential energy surface. The analysis of the dynamic aspects of some physical properties along IRC is called "reaction ergodography" (4). IRC is a solution of simultaneous first-order differential equations including the effect of mass of the nuclei which constitute the reactant molecules, and is useful to analyze the promoting mode of structural transformation, the quantum-mechanical tunneling effect, or the isotope effect of the reaction dynamics.

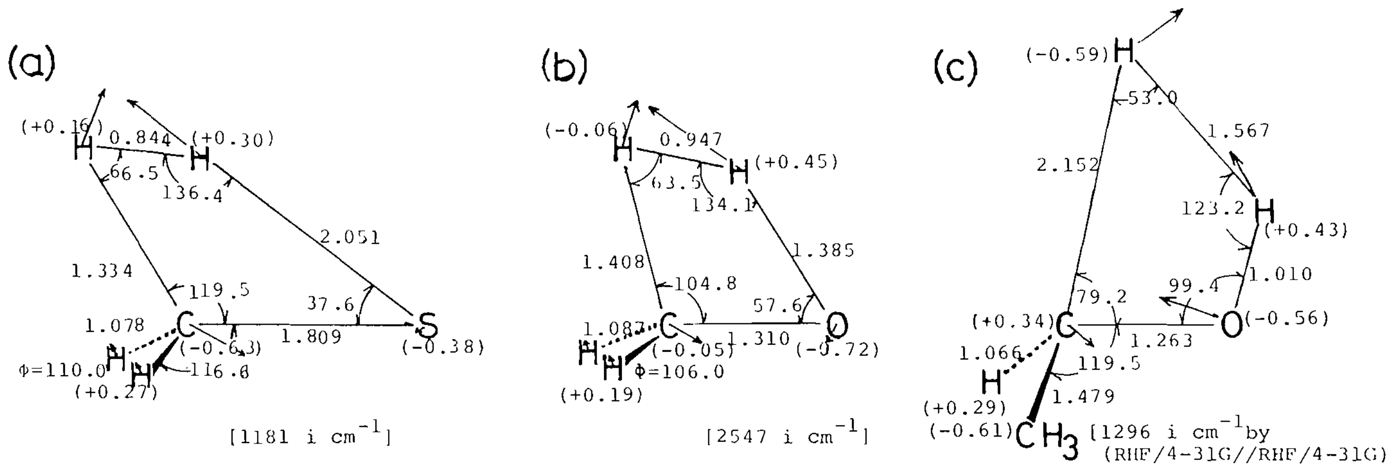

FIG. 1. RHF/6-31G fully-optimized geometries and displacement vectors of normal mode with imaginary frequency of transition states (TS's) for (*a*) methanethiol, (*b*) methanol, and (*c*) ethanol.

Thus reaction ergodography gives a clear definition of the concept of reaction coordinate which was previously used qualitatively and can present a dynamic picture of chemical reaction. Owing to the recent progress of large computers and software, it is now much easier to calculate the potential surface precisely by non-empirical method. The extent of reaction ergodography based on IRC is therefore more broadly applicable (5). The theoretical development to a special-functional molecule or to a dynamical analysis of reaction of the biochemically important molecules can be anticipated. Sulfur-containing organic compounds are of biochemical interest and little attention has been paid to their dynamical process, and their physical property and reactivity (6).

This article reports the reaction ergodography for the unimolecular reaction process of methanethiol which is a basic sulfur-containing compound. We analyzed the dehydrogenation path as the simplest example: $CH_3SH \rightarrow H_2C{=}S + H_2$. In order to investigate the electronic process of this reaction, we analyze the electronic interaction between intramolecular subsystems along the IRC using the Interaction Hybrid Molecular Orbital (IHMO) method (7). We also compare this reaction path with the similar dehydrogenation reaction paths of analogous compounds, methanol and ethanol:

$$CH_3OH \rightarrow H_2C{=}O + H_2$$

$$CH_3CH_2OH \rightarrow CH_3CH{=}O + H_2$$

2. Method of calculation

We used GAUSSIAN 80 (8) program package for the following *ab initio* MO calculations. The optimization of geometries of equilibrium points and the calculation of IRC were performed by the energy gradient method (9), with the 6-31G* basis set (10).

We performed the Møller-Plesset calculations (11) and configuration interaction (CI) calculations (12) with the 6-31G** basis set (10) in order to obtain more reliable energy estimates considering the effect of the electronic correlation at the 6-31G* optimized geometry. All the doubly excitations from the HF reference configuration were included in the CI wave functions with the 1*s* orbitals of carbon and oxygen and the 1*s*, 2*s* orbitals of sulfur kept fully occupied. In addition, the contribution of unlinked quadruple excitations (QC) was estimated (13).

The vibrational analysis and the tracing of IRC were carried out using the HONDO (14) program with the 6-31G* basis set. For ethanol, the vibrational and IRC analyses were carried out with the 4-31G basis set (15). The second derivatives of the potential energy surface required for the vibrational analysis at some optimized geometries were obtained by numerical differentiation of the analytically calculated energy gradient (9). The contribution of zero-point energy (ZC) was also used for more accurate total energy estimate.

The statistical *A* factors were estimated by the simplified transition state (TS) theory (2) expression

$$A_\infty = \frac{\nu_1 \nu_2 \ldots \nu_n}{\nu_1^\ddagger \nu_2^\ddagger \ldots \nu_{n-1}^\ddagger}$$

$$(n = 3N - 6; \quad N = \text{the number of atoms})$$

where ν_i and $\nu_i^\ddagger$ are the reactant and the TS vibrational frequencies, respectively.

3. Results and discussion

(1) Structures and vibrational modes of the transition states

The fully-optimized geometries of the TS's and the displacement vectors of normal modes with imaginary frequency are shown in Fig. 1. These vectors provide the initial direction of IRC leading to the products. The net charges on each atom are in parentheses. The TS of methanol (*b*) is optimized in Pople's early work (16). For TS of ethanol, we used the 4-31G geometry in our previous work (17). The first two TS (*a*), (*b*) have C_s symmetry of which symmetry planes are square C—X—H—H (X = S or O) plane, while the TS of ethanol (*c*) does not have C_s symmetry.

Let us compare the TS of methanethiol with that of methanol. The S—H bond length at the TS of CH_3SH (2.051 Å) is longer than the O—H bond length at the TS of CH_3OH (1.385 Å). This reflects the weakness of the S—H bond as compared with the strength of the O—H bond. Moreover, ∠CSH (37.6°) is lesser than ∠COH (57.6°). On the contrary, the breaking C—H bond of CH_3SH (1.334 Å) is shorter than that in CH_3OH (1.408 Å). These features show that the hydrogen atom separating from the heavy atoms are bound more strongly to the O atom than to the C atom in the CH_3OH molecule, to the C atom than to the S atom in the CH_3SH molecule.

Interestingly, in the TS of methanethiol, the H—H bond

TABLE 1. Calculated values for the activation energies and the heats of reactions in kcal/mol

Geometry (RHF/)	[4-31G]	[		6-31G*				]
Method	[	RHF	]	[RMP2]	[RMP3]	[CID[c] + QC[d]]	[CID + QC + ZC[e]]	[RMP4(SDQ)]
Basis Set	[4-31G]	[6-31G*]	[		6-31G**			]
$E_a(CH_3SH \rightarrow TS)$	100.1	103.7	99.2	96.8	98.2	98.5	95.6	
$\Delta E(\rightarrow CH_2S + H_2)$	40.3	42.0	42.5	37.3	39.5	38.5	30.8	
$E_a(CH_3OH \rightarrow TS)$	126.4	115.4[a]	111.4[a]	101.2[a]	105.2[a]	104.8	98.8	103.0[a]
$\Delta E(\rightarrow CH_2O + H_2)$	32.7	26.5[a]	28.7[a]	26.7[a]	29.6[a]	28.0	18.2	26.9[a]
E_a $(CH_3CH_2OH \rightarrow TS)$	118.3[b]							
ΔE $(\rightarrow CH_3CHO + H_2)$	26.4[b]							

[a]Results from ref. 16.
[b]Results from ref. 17.
[c]Configuration ineraction calculation of all the double excitations.
[d]Quadruple corrections.
[e]Zero-point energy corrections.

TABLE 2. RHF/6-31G* vibrational frequencies (cm^{-1}) and zero-point energies (kcal/mol)

Molecule	Frequencies						Zero-point energies
H_2[a]	4643 (σ_g)						6.6
CS[b]	1471 (σ)						2.1
H_2CS[c]	3393 (b_2),	3303 (a_1),	1658 (a_1),	1180 (a_1),	1158 (b_2),	1097 (b_1)	16.9
CH_3SH (reactant)[c]	3325 (a''),	3322 (a'),	3236 (a'),	2908 (a'),	1655 (a'),	1623 (a''),	31.2
	1521 (a'),	1220 (a'),	1080 (a''),	873 (a'),	776 (a'),	265 (a'')	
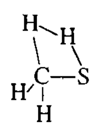 (TS)	3395 (a''),	3298 (a'),	3042 (a'),	2070 (a'),	1624 (a'),	1504 (a'),	28.3
	1471 (a''),	1037 (a''),	874 (a'),	773 (a''),	686 (a'),	1181i (a')	
CO[a]	2439 (σ)						3.5
H_2CO[a]	3233 (b_2),	3161 (a_1),	2030 (a_1),	1680 (a_1),	1383 (b_2),	1336 (b_1)	18.3
CH_3OH (reactant)[a]	4118 (a'),	3305 (a'),	3232 (a''),	3186 (a'),	1664 (a'),	1652 (a''),	34.7
	1637 (a'),	1508 (a'),	1289 (a''),	1188 (a'),	1164 (a'),	348 (a'')	
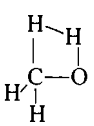 (TS)[a]	3278 (a''),	3209 (a'),	2320 (a'),	2053 (a'),	1657 (a'),	1626 (a'),	28.7
	1361 (a'),	1350 (a''),	1280 (a''),	1048 (a''),	886 (a'),	2554i (a')	

[a]Reference 16(a).
[b]Reference 10(b).
[c]Results from ref. 21.

length (0.844 Å) is rather close to the H—H bond length (0.730 Å) in the product, while the H—H bond length in the TS of methanol (a) (0.932 Å) is much longer (about 28%). It should also be noted that the C—S bond length in the TS of methanethiol (1.809 Å) does not change very much from the C—S bond length (1.817 Å) in the reactant, compared with the C—O bond length in the TS of methanol (1.310 Å) which is shorter (about 7%) than that in the reactant.

The C—O bond length (1.263 Å) in the TS of ethanol is also closer to that in the reactant ethanol than to the carbonyl bond length of the product acetaldehyde. The decomposing C—H bondlength is twice as long as that in the reactant and the Mulliken overlap population (0.041) between these two atoms shows that this bond is almost cleaved. In contrast, the decomposing O—H bond length (1.010 Å) stretches by only 5%. It should be noted that the H atom leaving the C atom is anionic while the other H atom leaving the O atom is cationic. The net charges of these atoms are −0.56 on the O atom, −0.59 on the H atom leaving the C atom, and +0.43 on the H atom leaving the O atom, respectively. This localization may be attributed to the long C—H bond length at TS, which is allowed by the electron-donating character of the substituted CH_3— group on the C atom of ethanol.

(2) Activation energies and frequency factors

Table 1 shows the various levels of calculated values for the activation energy and the heats of reaction and Table 2 lists the complete set of calculated harmonic frequencies (RHF/

TABLE 3. *A* factor for the three reactions

Reaction	(10^{-13}) *A* factor, s^{-1}
$CH_3OH \rightarrow H_2C{=}O + H_2$	6.000[a]
$CH_3SH \rightarrow H_2C{=}S + H_2$	2.473[b]
$CH_3CH_2OH \rightarrow CH_3CH{=}O + H_2$	30.85[c]

[a]RHF/6-31G* results from ref. 16(*b*).
[b]RHF/6-31G* results.
[c]RHF/4-31G results from ref. 17.

6-31G*). It shows the activation energy of CH_3SH to be 95.6 kcal/mol and the heat of reaction to be 30.8 kcal/mol, based on the CID + QC + ZC/6-31G**//RHF/6-31G* calculation. The activation energy and the heat of reaction for similar dehydrogenation of CH_3OH are 98.8 and 18.2 kcal/mol, respectively (16). These results indicate that the reactivity of CH_3SH is higher and the product $H_2C{=}S$ is more unstable chemically. These results agree with the experimental results (6).

The effect of electron correlation is estimated to be greater for CH_3OH than for CH_3SH with respect to all reactants, TS's, and products.

The second factor to be considered is the frequency factor (the *A* factor) for each process. The values calculated are given in Table 3 and show that the *A* factor of the methanol dehydrogenation is two times larger than that of the methanethiol. The former reaction is therefore considered more favorable than the latter in terms of the entropy factor. However, in this temperature region under moderate experimental conditions, this entropy factor may not be so important.

(3) Analysis of Intrinsic Reaction Coordinate (IRC)

Here we show the analysis for the reaction path of the dehydrogenation process of methanethiol. In Fig. 2(*a*), (*b*), (*c*), and (*d*) we show the change of potential energy, norm of energy gradient, bond length, and bond angles along the IRC of the reaction of methanethiol, respectively. For the reaction coordinate, s is the length measured along IRC on the potential energy surface and the unit of s is (atomic mass unit)$^{1/2}$ (bohr). The TS is located at $s = 0.0$ and the positive s values indicate the product region of the reaction. The reaction is thus considered to proceed as s value increases and by passing through the TS at $s = 0.0$.

Since the TS of this process has C_s symmetry, we assume that the IRC conserves this symmetry. It is interesting to note that the norm of the energy gradient has two local maxima before reaching the TS. This reaction thus proceeds through two characteristic stages. We can see from Fig. 2 (*c*) that the main process at the vicinity of the first local maximum $s = -3.0$ is the stretching of C—S bond length. On the other hand, we can read from Fig. 2 (*c*) and (*d*) that the main process at the vicinity of the second local maximum $s = -1.5$ is a decrease in the bond angle ∠CSHb, and an increase in the bond angles ∠SCHa accompanied by an increase in the S—Hb bond length.

Moreover, at the TS $s = 0.0$, both the C—Ha and the S—Hb bonds are weakened and the formation of the H_2 molecule has been accomplished.

Figure 3 shows the results from the analysis along the IRC of the similar dehydrogenation reaction of methanol.

In contrast to the case of CH_3SH, the potential barrier has a very sharp peak, corresponding to the large imaginary frequency of normal mode at TS, and the norm of the potential energy is bigger and has only a single local maximum before the TS.

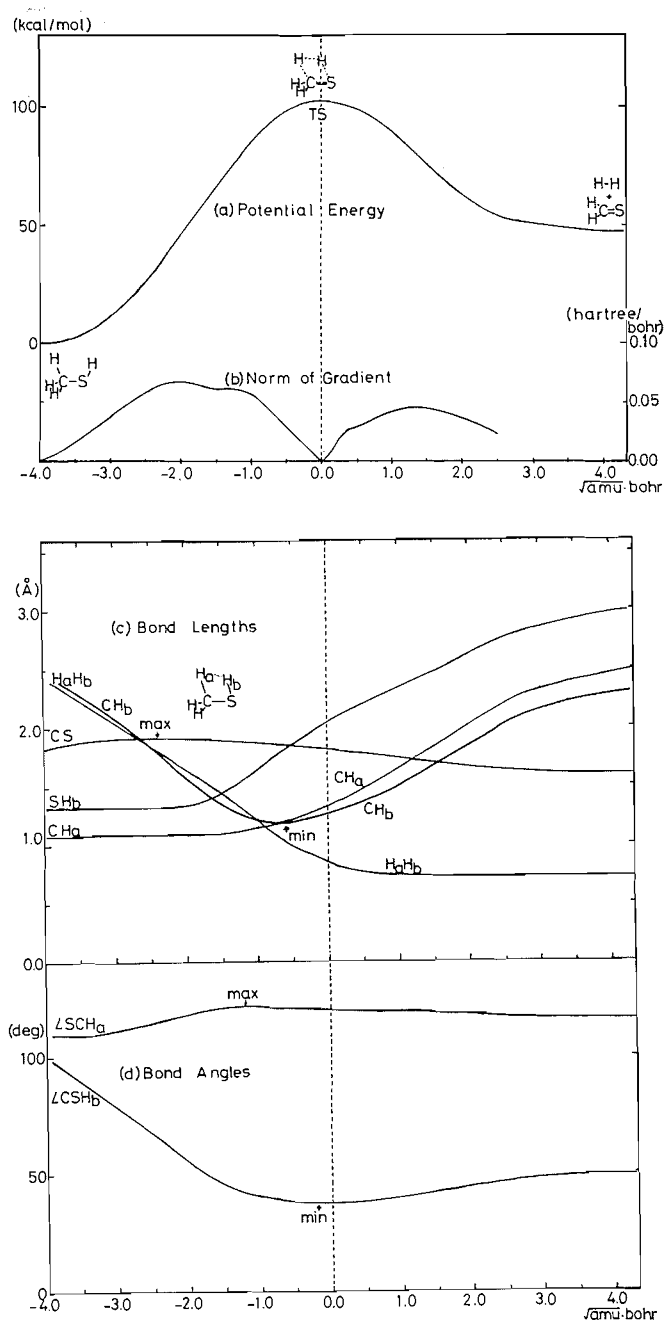

FIG. 2. Analysis for the reaction path of the dehydrogenation process of methanethiol. Change of (*a*) potential energy, (*b*) norm of gradient, (*c*) bond lengths, and (*d*) bond angles.

Parallelling the above statements, the geometry change along the IRC in Fig. 3 (*c*) and (*d*) does not have a two-step movement before reaching the TS as opposed to CH_3SH. For example, the bond length of CO is decreasing monotonically and does not have a local maximum as the CS bond length.

These observations can be explained by the different feature of MO's of each reactant. In the case of CH_3SH, the LUMO+1 of the reactant is antibonding CS—σ*. This will facilitate the electronic process of the C—S bond elongation. In contrast to this, the LUMO of CH_3OH does not have such character, but the LUMO+2 has the character of an antibonding CO—σ*.

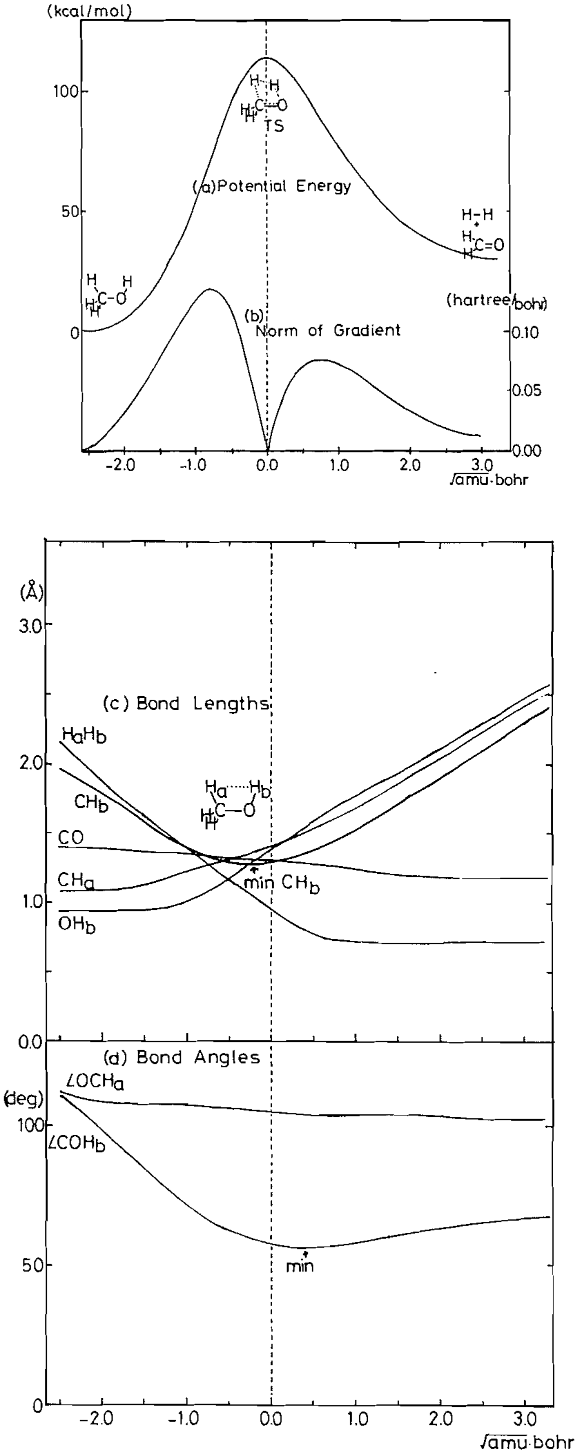

FIG. 3. Analysis for the reaction path of the dehydrogenation process of methanol. (*a*), (*b*), (*c*), and (*d*) are similar to Fig. 2.

The CS bond takes better advantage of the feasible electronic process for molecular deformation than does the CO bond, when the reaction proceeds. This contribution of antibonding CX bond (X = S or C) can be seen in the large difference of frequencies for each CX stretching mode (see Table 2) (9).

The atomic movement in similar dehydrogenation reaction of ethanol has appeared in our early study (17). Figure 4 shows the analysis of the IRC for this reaction. The substituted CH_3— group for one of the H's of CH_3OH brings about the large difference of the atomic movements. In the CH_3CH_2OH reac-

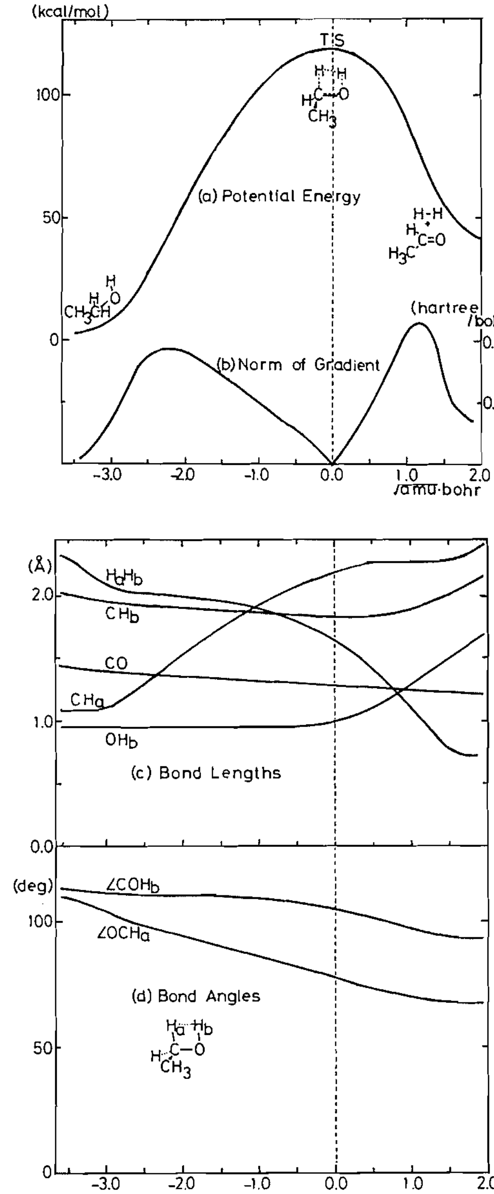

FIG. 4. Analysis for the reaction path of the dehydrogenation process of ethanol. (*a*), (*b*), (*c*), and (*d*) are similar to Fig. 2.

tion, the C—Ha bond stretches vigorously and almost breaks in the vicinity of the TS, the change of ∠OCHa is also very large. The H—H bond length is yet far from that of the product H_2 molecule in the vicinity of TS. Corresponding to these atomic movements, Ha becomes anionic and the reaction center C becomes cationic. This localized nature of charges is stabilized by the electron donation of the substituted CH_3— group, as mentioned before (17).

We try to explain the role of the vibrational modes of the reactant in the reaction selectivity of the experiment by using laser (18, 19). What kind of vibrational mode of a reactant molecule is excited initially and how does the reaction pathway interact with the excited vibrational mode?

Our previous work (5(*a*), 17) and others (20) have clarified the relationship between the vibrational modes and IRC in the asymptotic region of the reactant and the role of the vibrational modes are summarized below.

The dynamic aspects of a reacting system are well described by the coupling between IRC and the vibrational modes perpen-

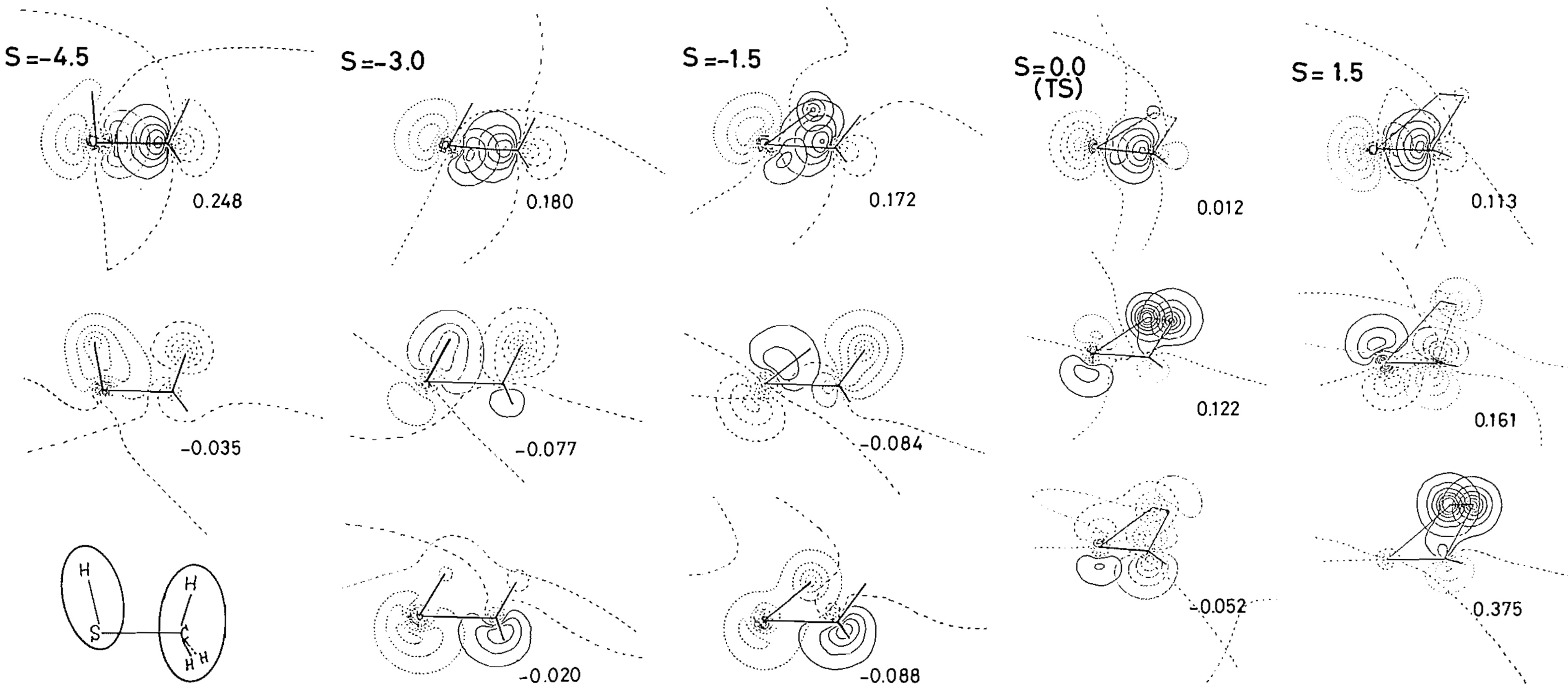

FIG. 5. Change of IHMO along the IRC for $s = -4.5$ to 1.5. Subsystems are CH_3 and SH.

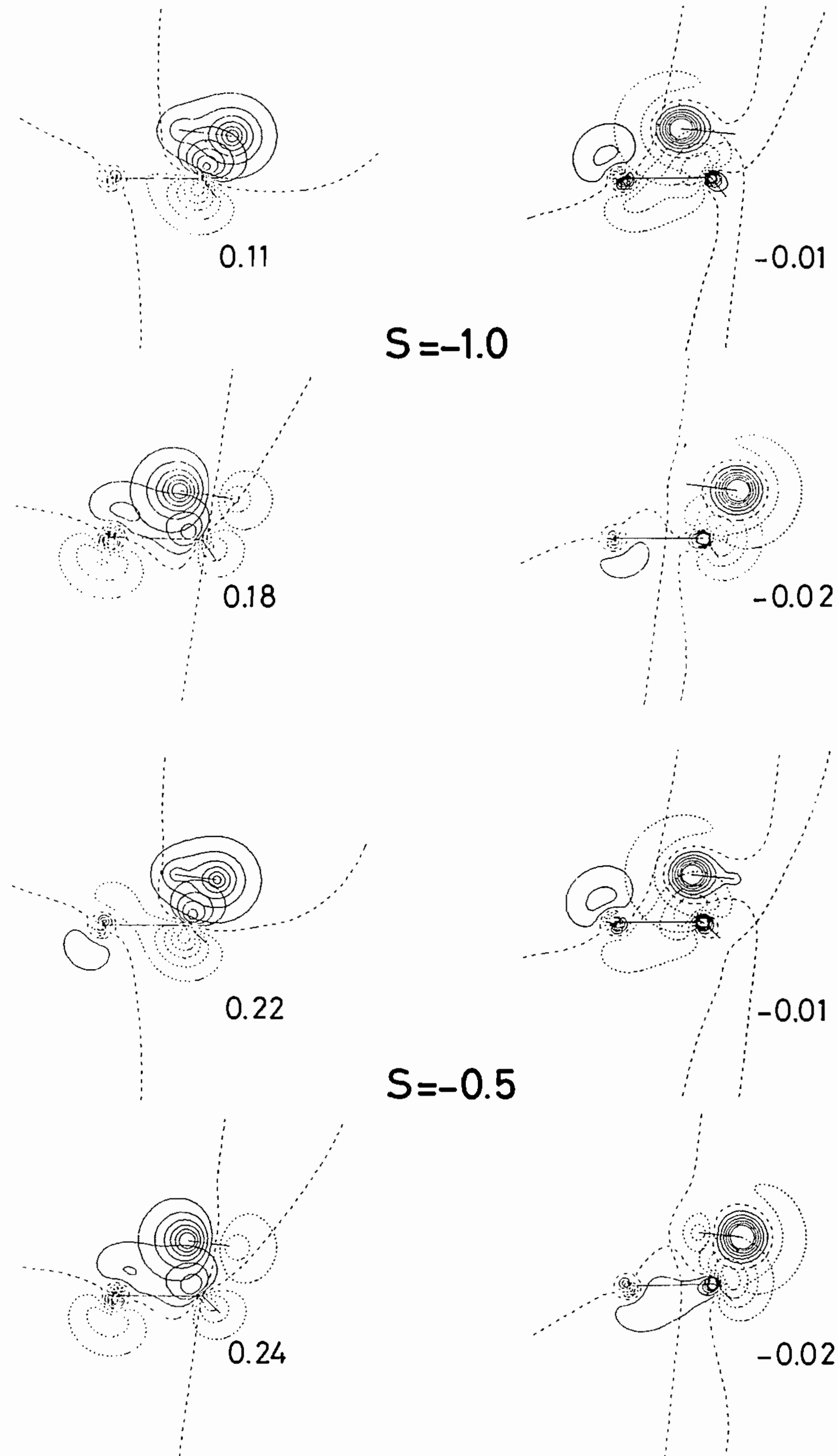

FIG. 6. Change of IHMO along the IRC for s = −1.0 to 1.5. Subsystems are $H_2C{=}S$ and H_2.

dicular to IRC. Some vibrational modes are strongly coupled with IRC and these strongly coupled modes twist IRC in the configuration space. Between the twisting of IRC and the location of the barrier, (*1*) the excitation of the vibrational mode to which IRC converged at the reactant is most effective for a channel where IRC twists after the TS (the late twisting IRC), (*2*) the excitation of a strongly coupled mode is most effective for a channel where IRC twists before the TS (the early twisting IRC). Another type of vibrational mode plays a part of energy supply mode. The vibrational energy pumped in this mode by laser is transferred to the particular mode mentioned above. A mechanism of this intramolecular vibrational energy transfer is determined by the mode coupling between the vibrational modes along IRC.

Table 2 shows the main normal vibrational modes of the methanethiol (reactant). It is well accepted that the ordering of vibrational frequencies are well reproduced in our level of calculations and that the experimental frequencies would be

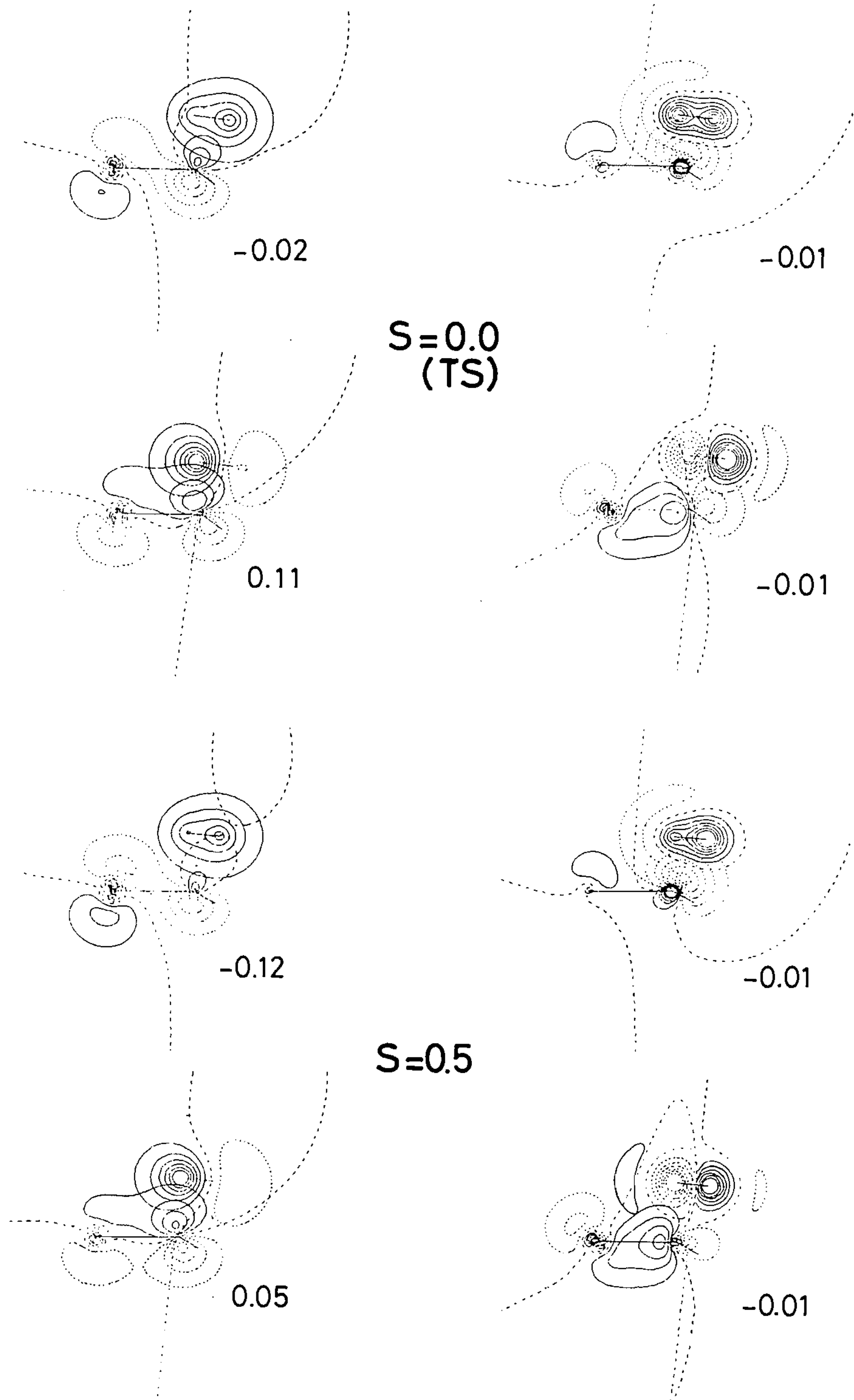

FIG. 6. (*Continued*)

obtained by a reduction of 10–15% from the calculated ones (9). Among these modes, the mode with an imaginary frequency 1181i cm^{-1} (RHF/6-31G*) corresponds to the displacement vector of IRC and this represents well the elimination of H_2 from the thiocarbonyl part $H_2C{=}S$. Reactant CH_3SH has a C—S stretching mode of 776 cm^{-1} and an asymmetric (A'') CSH bending mode of 874 cm^{-1}. These vibrational modes are considered to interact easily with the motion of nuclei along IRC at the early stage of the reaction process. Therefore, it can be predicted that the dehydrogenation of CH_3SH is directly promoted if either of the two modes is excited by a laser with an appropriate wave length.

(4) The electronic process on the reaction

Figure 5 shows the result obtained from the analysis of the electronic process following the reaction of CH_3SH along IRC from the viewpoint of IHMO.

Here the reactant molecule is separated into two subsystems CH_3 and SH based on the aspect of the weakened C—S bond and the newly forming H—H bond in the reactant region. Also

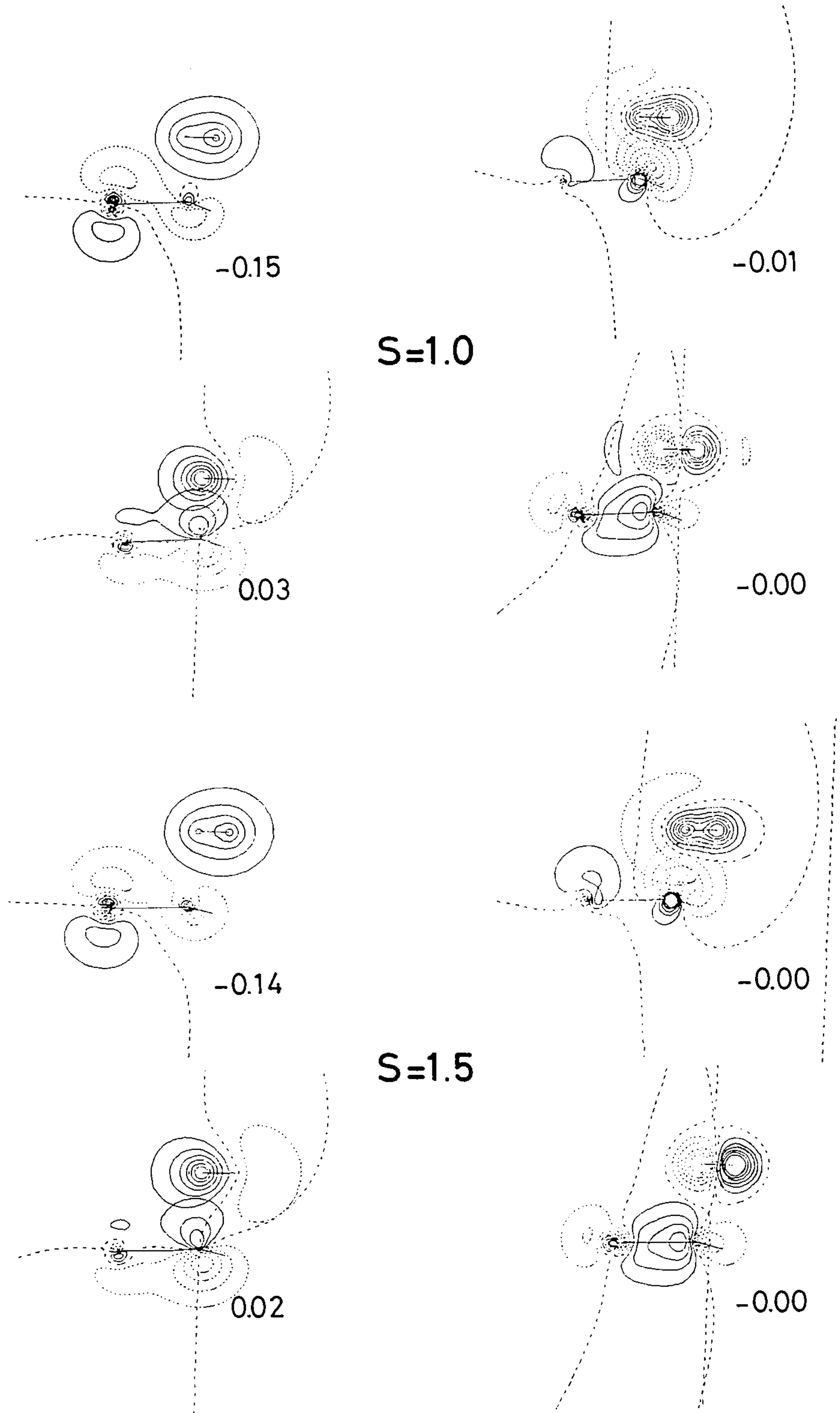

FIG. 6. (*Concluded*)

drawn are the IHMO's which diagonalize the overlap population matrix between these subsystems. Each number in this figure is the diagonalized value of the overlap population, so a larger positive value means a stronger interaction between these subsystems. At the early stage of the reaction $s = -3.0$, a σ-type IHMO is localized in the weakened C—S bond. Secondly, an IHMO representing the weakened S—H bond appears at $s = -1.5$. At the TS, the H—H σ bond which is near the value in the product H_2 molecule appears and it well represents the interaction between these two subsystems. At the product region $s = 1.5$ a new IHMO of C=S π bond appears clearly.

Now these subsystems are allocated to the product molecules H_2 and $H_2C{=}S$. The IHMO corresponding to these subsystems are shown in Fig. 6. If we obtain the IHMO whose interaction is that between H_2 and $H_2C{=}S$, we can easily describe the electronic process of the formation of H—H σ bond and C=S π bond and the elimination of S—H σ bond and C—H σ bond.

Among the four IHMO's at each s value, the first one is the charge transfer (CT) interaction from H—H σ bond to C═S π^* bond, and the second one is that from the C═S π bond to the H—H σ^* bond. These two HOMO–LUMO interactions are very important in the vicinity of the TS. Both of them have maximum values of overlap population at $s = -0.5$, and these values are decreasing, as the reaction proceeds through TS. The value of $\sigma \rightarrow \pi^*$ CT has already changed the sign at TS. It then decreased significantly, resulting in this interaction becoming unimportant. Compared with this, only the value of $\pi \rightarrow \sigma^*$ CT maintains a positive sign through $s = -1.0 \sim 1.5$, and this interaction is the most important of the four. It contributes to the formation of C—Hb bond, which corresponds to the fact that the C—Ha bond length is larger than the C—Hb bond length and the Hb atom is bound more strongly to the C atom than the Ha atom is bound to the C atom at the TS. The electronic processes along IRC are therefore remarkably described by the IHMO method as shown above.

4. Conclusion

In this study we investigated the reaction paths of the unimolecular decomposition of methanethiol.

The dehydrogenation path is analyzed by *ab initio* MO calculations. The geometries and energies of the reactants, TS's, reaction intermediates, and products have been determined on the singlet potential energy surface. We find that even similar dehydrogenation reactions of CH_3SH, CH_3OH, and CH_3CH_2OH have large differences in atomic movement. The dehydrogenation mechanism of CH_3SH is divided into two stages including the earlier stretching of the C—S bond and the reducing of the ∠CSHb angle as the first and the subsequent formation of the two stable molecules H_2 + H_2C═S as the second. The earlier activation energy of the reaction is attributed to the stretching of the C—S bond and the reducing of ∠CSHb, so if energy transfer to these modes can be possible, for example by laser, it is predicted that the reaction can proceed. The IRC analysis for the chemical reaction path is useful in laser chemistry. This theory is expected to apply to broader areas of chemistry in future.

Acknowledgements

This work was supported by a Grant-in-Aid for Scientific Research from the Ministry of Education of Japan, for which the authors are grateful. The numerical calculations were carried out at the Data Processing Center of Kyoto University and the Computer Center of Institute for Molecular Science (IMS). We also appreciate Mr. N. Koga of IMS for his assistance in calculating the IHMO's.

1. (*a*) R. B. WOODWARD and R. HOFFMANN. Angew. Chem. Intern. Ed. **8**, 781 (1969); (*b*) J. C. POLANYI. Acc. Chem. Res. **5**, 161 (1972).
2. (*a*) S. GLASSTONE, K. J. LAIDLER, and H. EYRING. Theory of rate processes. McGraw-Hill, New York. 1941; (*b*) P. J. ROBINSON and K. A. HOLBROOK. Unimolecular reactions. John Wiley and Sons, New York. 1972. (*c*) R. A. MARCUS. J. Chem. Phys. **45**, 2138 (1966); **45**, 2637 (1966); **45**, 4493 (1966); **45**, 4500 (1966); **49**, 2610 (1968); **49**, 2617 (1968).
3. (*a*) K. FUKUI. J. Phys. Chem. **74**, 4161 (1970); (*b*) K. FUKUI, S. KATO, and H. FUJIMOTO. J. Am. Chem. Soc. **97**, 1 (1975); (*c*) K. ISHIDA, K. MOROKUMA, and A. KOMORNICKI. J. Chem. Phys. **66**, 2153 (1977).
4. (*a*) K. FUKUI. *In* The world of quantum chemistry. *Edited by* R. Daudel and B. Pullman. D. Reidel Publishing Co., Dordrecht, Holland. 1974. p. 113; (*b*) S. KATO and K. FUKUI. J. Am. Chem. Soc. **98**, 6395 (1976).
5. (*a*) K. YAMASHITA, T. YAMABE, and K. FUKUI. Chem. Phys. Lett. **84**, 123 (1981); (*b*) S. KATO and K. MOROKUMA. J. Chem. Phys. **74**, 6268 (1981); (*c*) K. YAMASHITA, M. KAMINOYAMA, T. YAMABE, and K. FUKUI. Chem. Phys. Lett. **83**, 78 (1981); (*d*) K. YAMASHITA, M. KAMINOYAMA, T. YAMABE, and K. FUKUI. Theoret. Chim. Acta, **60**, 303 (1981); (*e*) K. YAMASHITA, T. YAMABE, and K. FUKUI. Theoret. Chim. Acta, **60**, 523 (1982); (*f*) T. YAMABE, K. YAMASHITA, M. KAMINOYAMA, M. KOIZUMI, A. TACHIBANA, and K. FUKUI. J. Phys. Chem. **88**, 1459 (1984).
6. (*a*) R. E. KUNITA, A. K. EDWARDS, G. L. GOOD, and J. BERKOWITZ. J. Chem. Phys. **77**, 5508 (1982); (*b*) D. J. MITCHELL, S. WOLFE, and H. B. SCHLEGEL. Can. J. Chem. **59**, 3280 (1981).
7. (*a*) K. FUKUI, N. KOGA, and H. FUJIMOTO. J. Am. Chem. Soc. **103**, 196 (1981); (*b*) H. FUJIMOTO, N. KOGA, and K. FUKUI. J. Am. Chem. Soc. **103**, 7452 (1981).
8. J. S. BINKLEY, R. A. WHITESIDE, R. KRISHNAN, R. SEEGER, D. J. DEFREES, H. B. SCHLEGEL, S. TOPIOL, L. R. KAHN, and J. A. POPLE. Quantum Chemistry Program Exchange. **13**, No. 406 (1981).
9. P. PULAY. *In* Modern theoretical chemistry. Vol. 4. *Edited by* H. F. Schaefer. Plenum, New York. 1977.
10. (*a*) D. J. DEFREES, B. A. LAVI, S. K. POLLACK, W. J. HEHRE, J. S. BINKLEY, and J. A. POPLE. J. Am. Chem. Soc. **101**, 4085 (1979); (*b*) M. M. FRANCL, W. J. PIETRO, W. J. HEHRE, J. S. BINKLEY, M. S. GORDON, D. J. DEFREES, and J. A. POPLE. J. Chem. Phys. **77**, 3654 (1982).
11. J. A. POPLE, J. S. BINKLEY, and R. SEEGER. Int. J. Quantum Chem. S**10**, 1 (1976).
12. J. A. POPLE, R. SEEGER, and R. KRISHNAN. Int. J. Quantum Chem. S**11**, 149 (1977).
13. E. R. DAVIDSON and D. W. SILVER. Chem. Phys. Lett. **52**, 403 (1977).
14. M. DUPUIS and H. F. KING. J. Chem. Phys. **68**, 3998 (1978).
15. R. DITCHFIELD, W. J. HEHRE, and J. A. POPLE. J. Chem. Phys. **54**, 724 (1971).
16. (*a*) L. B. HARDING, H. B. SCHLEGEL, R. KRISHNAN, and J. A. POPLE. J. Phys. Chem. **84**, 3394 (1980); (*b*) J. A. POPLE *et al.* *In* Potential energy surfaces and dynamics calculations. *Edited by* D. G. Truhlar. Plenum, New York. 1981.
17. T. YAMABE, M. KOIZUMI, K. YAMASHITA, and A. TACHIBANA. J. Am. Chem. Soc. **106**, 2255 (1984).
18. R. N. ZARE and R. B. BERNSTEIN. Phys. Today. Nov. 1980, p. 43.
19. (*a*) N. BLOEMBERGEN and E. YABLONOVITCH. Phys. Today. Nov. 1980. p. 83; (*b*) A. H. ZEWEIL (*Editor*). Advances in Laser Chemistry. Springer, New York. 1978; (*c*) K. L. KOMPA and S. D. SMITH (*Editors*). Laser-induced process in molecules. Springer. 1979.
20. W. H. MILLER, N. C. HANDY, and J. E. ADAMS. J. Chem. Phys. **72**, 99 (1980).
21. W. J. PIETRO, M. M. FRANCL, W. J. HEHRE, D. J. DEFREES, J. A. POPLE, and J. S. BINKLEY. J. Am. Chem. Soc. **104**, 5039 (1982).

Ab initio MRD-CI study of NO_2. 1. Multi-dimensional potential surfaces for the two lowest $^2A'$ states

GERHARD HIRSCH AND ROBERT J. BUENKER
Bergische Universität GH Wuppertal, FB 9 – Theoretische Chemie, Gaußstr. 20, D-5600 Wuppertal 1, West Germany

Received August 6, 1984

This paper is dedicated to Professor Camille Sandorfy on the occasion of his 65th birthday

GERHARD HIRSCH and ROBERT J. BUENKER. Can. J. Chem. **63**, 1542 (1985).

For a detailed theoretical *ab initio* study of the X^2A_1/A^2B_2 system of the NO_2 molecule, three-dimensional potential energy surfaces have been calculated with the MRD-CI method for both symmetric and asymmetric NO bond distances. The calculated data are given here together with the technical parameters of the respective treatment, and the main features of the surfaces are discussed. The geometrical locations and depths of the computed energy minima as well as the $A-X$ vertical transition energy are found to be in good agreement with all known experimental data and allow for a good qualitative understanding of the overall appearance of the observed spectrum. The wavefunctions and potential energy surfaces will be used in subsequent investigations for the study of various molecular properties and coupling elements involved in the X^2A_1/A^2B_2 system of NO_2.

GERHARD HIRSCH et ROBERT J. BUENKER. Can. J. Chem. **63**, 1542 (1985).

Dans le but d'effectuer une étude théorique *ab initio* très détaillée du système X^2A_1/A^2B_2 de la molécule de NO_2, on a calculé les surfaces d'énergie potentielle tri-dimensionnelles par la méthode de MRD-CI tant pour les longueurs des liaisons symétriques et non symétriques. On présente les données calculées ainsi que les paramètres techniques de chacune des études respectives et on discute des caractéristiques principales de ces surfaces. On a trouvé que les positions géométriques et les profondeurs calculées des puits d'énergie ainsi que l'énergie de transition verticale $A-X$ s'accordent très bien avec toutes les données expérimentales connues et permettent de bien comprendre qualitativement l'allure générale du spectre observé. Au cours de recherches subséquentes, on se servira des fonctions d'onde et des surfaces d'énergie potentielle dans le but d'étudier les diverses propriétés moléculaires et les éléments de couplage impliqués dans le système X^2A_1/A^2B_2 du NO_2.

[Traduit par le journal]

1. Introduction

The NO_2 molecule continues to attract a great deal of interest because it is not only an important element in the discussion of environmental pollution, but also a system possessing a very complex spectrum in the visible and near-infrared regions. In the last decade there has been progress in unravelling the details of the NO_2 spectrum, both by means of a variety of experimental methods (1) and also by various *ab initio* calculations (2–5). Jackels and Davidson (3) pointed out that a curve crossing between the $^2A_1$ ground and the $^2B_2$ excited states, with its associated Herzberg–Teller interaction, is mainly responsible for the almost chaotic appearence of the NO_2 spectrum in the visible and near-infrared regions. In more recent times more detailed experimental studies (6, 7) have concentrated on the $A^2B_2-X^2A_1$ transition, which is known to be responsible for the brown color of gaseous NO_2.

In surveying the latest experimental data on this problem it has become apparent that a quantitative theoretical treatment of the vibronic motion of the NO_2 molecule in its X and A electronic states would be extremely useful in helping to understand the complex nature of this spectrum. For this purpose it is first necessary that (three-dimensional) NO_2 potential surfaces be generated by employing large-scale CI calculations and a high-quality AO basis, along with the associated electronic wavefunctions. Beyond this task it is required that non-adiabatic effects associated with the Herzberg–Teller $X-A$ interaction be computed explicitly and that the vibronic functions associated with either the adiabatic (CI) or diabatic electronic states be allowed to mix to form the best possible approximations to the true solutions of the global Schrödinger equation for this system. The goal of the present study is to significantly improve upon the quality and scope of NO_2 potential surfaces available in the literature, which have thus far been limited in the main to a 2×2 non-orthogonal CI employing only a double-ζ AO basis (3) in addition to a small number of points obtained with order-100 orthogonal CI's in a basis containing some polarization functions (2). Problems arising during the course of the present calculations will be considered in some detail, and comparison with known details of the experimental spectral data will be given. Explicit treatment of the vibronic wavefunctions based on these potential surfaces, including computation of the key non-adiabatic coupling matrix elements, will then be the subject of a succeeding paper (8).

2. Technical details of the theoretical treatment

In the present work an AO basis proposed by Huzinaga (9) and Dunning (10) is employed. It consists of nine s and five p functions (9) in a $[5s\,3p]$ contraction (10) for both nitrogen and oxygen. In addition, a set of cartesian d polarization functions has been placed at each atom with exponents $\alpha(d) = 0.80$ for the nitrogen and $\alpha(d) = 0.85$ for the oxygen atoms having been chosen. This choice leads to a total number of 60 atomic orbitals, with 20 functions located at each atom.

The earlier study of Jackels and Davidson (3) employed a lobe-function variant of the double-ζ (DZ) contraction of Huzinaga's ($9s\,5p$) but did not add any polarization functions. A similar (DZ) basis augmented by Rydberg-type s and p functions (39 AO's in all) was used in the computation of the NO_2 vertical spectrum by Shih *et al.* (5). Finally the basis set of Gillispie *et al.* (2) did include d polarization functions, but employed a $[4s\,3p]$ contraction, i.e., one less s function per atom than in the present basis.

All calculations for the various conformations of the NO_2 system have been carried out in C_s symmetry. It is known (3, 11, 12) that imposition of symmetry constraints on SCF wavefunctions can result in an energy increase and cause potential surfaces to be discontinuous at conformations of higher symmetry if the highest-order pointgroup is always employed. Hence even in the case of equal bond lengths no C_{2v} symmetry constraints have been imposed on the wavefunction, since the results should describe the characteristics of the potential surfaces of the two lowest doublet states consistently over the whole range of geometrical conformations. All nuclear arrangements of the NO_2 molecule are expressed in terms of the three coordinates $r_1 = R_{NO1}$, $r_2 = R_{NO2}$ and the ONO bond angle θ. Such a procedure nevertheless gives rise to additional problems connected with the symmetry breaking which appear as instabilities in the electronic wavefunctions and energies (13, 14). Details concerning this point will be discussed in the following section.

The SCF calculations for this study have been carried out for the lowest $^2A'$ state corresponding to the configuration $9a'^2 2a''^2$ $10a'^1$. This occupation corresponds to a $^2A_1$ state in symmetric (C_{2v}) conformations for larger bond angles, but to the $^2B_2$ state for smaller bond angles. The configuration interaction treatment is of the standard MRD-CI type with configuration selection and energy extrapolation (15, 16) using Table CI algorithms (17–19). A core of six molecular orbitals of the a' irreducible representation corresponding to the $1s$ and $2s$ shells of nitrogen and the two oxygen atoms has been kept doubly occupied in all calculations, while the corresponding six complementary MO's with highest orbital energies in the a' representation have been excluded from consideration entirely; the eleven remaining valence electrons of NO_2 are then distributed among the remaining 48 MO's through single and double excitations relative to a given set of reference configurations. These have been chosen so as to give a final contribution of more than 90% to the CI wavefunctions for both the first and the second roots of $^2A'$ symmetry. The total number of symmetry-adapted functions (SAFT) generated by single and double excitations from this set of reference configurations varies from about 350 000 to 550 000. This dimension is reduced by employing an energy selection criterion (20) with a threshold of 10 μh with respect to the two lowest roots of the matrix for all calculations presented here. The number of reference configurations (reference), of generated SAF's (SAFT) and of selected SAF's (SAF) for each nuclear conformation treated can be found in the various tables to be discussed in the next section.

The lowest two eigenvalues have been calculated in each case by diagonalizing the matrix corresponding to the 10 μh threshold (dimension generally on the order of 10 000) as well as a smaller matrix (of order 7 000) corresponding to a 15 μh threshold throughout. The eigenvalues together with the summed perturbative energy lowerings of the non-selected configurations in the total MRD-CI space have then been employed in the usual way (21) to determine an extrapolated zero-threshold value designated as E_{CI} in the tables. Finally energy contributions of higher than double-excitation configurations are estimated in analogy to the formula $\Delta E = (1 - c_0^2)(E_{SCF} - E_{CI})$ of Langhoff and Davidson (22), i.e., by replacing E_{SCF} with the eigenvalues of a small-matrix corresponding only to the reference set, and substituting Σc_i^2 for c_0^2, where the latter sum runs over all contributions from the reference configurations which appear in the final (T = 10 μh) wavefunction. The resulting total energy is referred to as the full CI limit (E_{FCI}) in the ensuing discussion.

The level of CI undertaken thus goes far beyond that employed in the only previous comprehensive calculation of the lowest two $^2A'$ potential surfaces of NO_2 (3). In the latter study Jackels and Davidson employed a 2 × 2 non-orthogonal CI based on separately optimized SCF functions, leading to total energies which are on the average some 0.45 hartree (12.2 eV) higher than in the present study. The same authors reported larger (orthogonal) CI computations for several key geometries, but even in these cases the dimensions of the secular equations did not exceed on order of 3600 SAF's. Otherwise the work of Gillispie *et al.* (2), also dealing with these $^2A'$ states at a small series of geometries employs MC-SCF wavefunctions corresponding to only about 100 configurations. Finally, the earlier study of Shih *et al.* (5) does report large CI wavefunctions, of roughly half the order described in this work, but no geometries were considered other than that of the ground state at equilibrium in this instance.

3. Results of the calculations

SCF and CI calculations have been performed for a variety of nuclear conformations of NO_2 with both equal and unequal bond lengths r_1 and r_2. The results given here are restricted to the first two states of $^2A'$ symmetry. Table 1 contains the data calculated for a symmetric arrangement of NO_2 with r_1 and r_2 fixed at 2.32 bohr. This value has been chosen on the basis of the results by Jackels and Davidson (4) giving 2.32 bohr for the equilibrium bond distance and 132.7° for the equilibrium bond angle of the X^2A_1 ground state based on their *ab initio* study. The range of bond angles covered in the present calculation is from 90° up to the linear arrangement of 180°. It can be seen from Table 1 that a much closer grid of calculated points has been chosen from 95° to 120°, the interval containing the (non-) crossing of the two $^2A'$ states. Figure 1 gives the resulting potential curves for the X^2A_1 and A^2B_2 states, and also indicates the angular region near the crossing point which will be analyzed in greater detail in what follows (Fig. 2).

Three different bond lengths have been considered in this study, namely the value of 2.32 bohr already mentioned, along with 2.20 bohr and 2.50 bohr. Combination of these bond lengths yields six different cuts through the multidimensional potential surfaces.

Tables 2 and 3 contain information about the other symmetric combinations of bond distances: 2.20/2.20 and 2.50/2.50, respectively, with their respective graphical display shown in the Figs. 3 and 4. Problems arise in connecting the various calculated points in the crossing region (105°–110°) and interpolating them to give smooth $^2A_1$ and $^2B_2$ potential curves, as must be expected for such symmetric conformations. This situation can be seen clearly in the figures: the dots represent the actual calculated values for the extrapolated energy E_{CI} and the estimated full CI limit E_{FCI} with dashed lines for the E_{CI} and solid lines for the E_{FCI}. The lack of smoothness in the computed curves in this region is a consequence of the fact that all calculations are carried out in formal C_s symmetry, even when the bond lengths are equal; as a result symmetry-breaking artifacts in the SCF calculations still lead to instabilities at the large-scale CI level. The general features of symmetry breaking have been recently summarized by Davidson and Borden, including a discussion of the NO_2 example (13). Specifically the near degeneracy of the $9a'$ and $10a'$ MO's ($6a_1$ and $4b_2$ in C_{2v} notation) leads to apparent discontinuities in the Born–Oppenheimer SCF wavefunctions. These circumstances lead to special problems in the computation of non-adiabatic coupling matrix elements between the two $^2A'$ electronic states as well as other properties, as will be discussed in a subsequent paper (8) dealing explicitly with vibronic effects associated with the Herzberg–Teller interaction associated with the A and X states of NO_2. In principle the problem can be overcome by resorting to a full CI treatment, in which case the results are

TABLE 1. MRD-CI and estimated full CI results for the first two $^2A'$ states of NO_2, $r_1 = r_2 = 2.32$ bohr[a]

					$1^2A'$			$2^2A'$		
θ	E_{SCF}	Reference[b]	SAFT / SAF[c]		E_{CI}[d]	E_{FCI}[e]	Σc^2[f]	E_{CI}[d]	E_{FCI}[e]	Σc^2[f]
90°	−4.0130	15	472833 /	9243	−4.3306	−4.3536	0.917	−4.2455	−4.2711	0.913
95°	−4.0319	15	514978 /	8842	−4.3451	−4.3660	0.924	−4.2838	−4.3066	0.921
100°	−4.0452	15	514978 /	8944	−4.3497	−4.3701	0.925	−4.3173	−4.3408	0.918
105°	−4.0515	15	514978 /	9605	−4.3499	−4.3694	0.927	−4.3413	−4.3639	0.921
107°	−4.0572	15	514978 /	9848	−4.3514	−4.3713	0.926	−4.3498	−4.3726	0.921
110°	−4.0586	15	514978 /	9403	−4.3588	−4.3787	0.926	−4.3485	−4.3708	0.922
115°	−4.0630	15	514978 /	8410	−4.3726	−4.3930	0.925	−4.3389	−4.3608	0.922
120°	−4.0632	15	514978 /	8321	−4.3813	−4.4019	0.925	−4.3261	−4.3498	0.918
132.7°	−4.0627	16	474223 /	9963	−4.3907	−4.4109	0.926	−4.2789	−4.3037	0.916
140°	−4.0616	16	474223 /	9684	−4.3876	−4.4077	0.926	−4.2485	−4.2736	0.916
150°	−4.0522	15	466930 /	9926	−4.3738	−4.3939	0.926	−4.2071	−4.2321	0.913
180°	−4.0091	13	388609 /	8441	−4.3235	−4.3409	0.932	−4.1124	−4.1356	0.916

[a] All energies are given in hartree units with respect to −200.0 hartrees.
[b] Number of reference configurations.
[c] Number of generated (SAFT) and selected (SAF) symmetry adapted functions.
[d] MRD-CI energy, extrapolated to zero threshold.
[e] Estimated full CI energy.
[f] Sum of squares of the coefficients of the reference configurations.

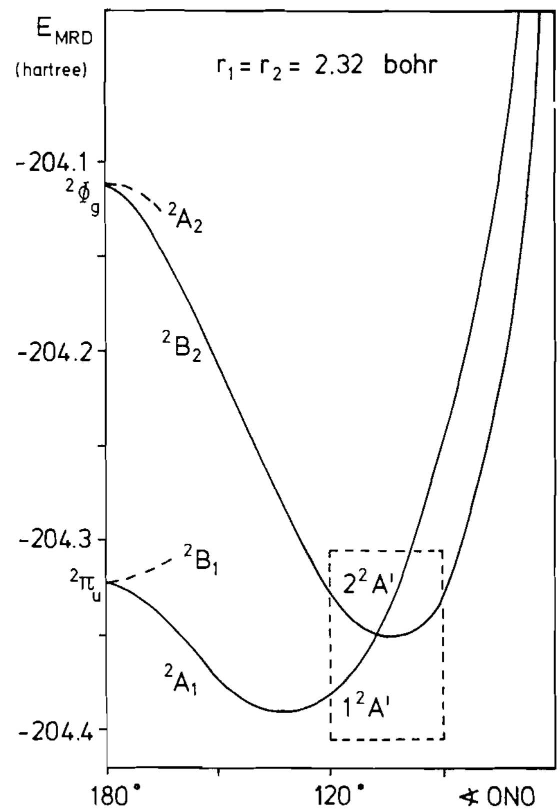

FIG. 1. Potential energy curves for NO_2 (X^2A_1 and A^2B_2) upon variation of the bond angle ($r_1 = r_2 = 2.32$ bohr).

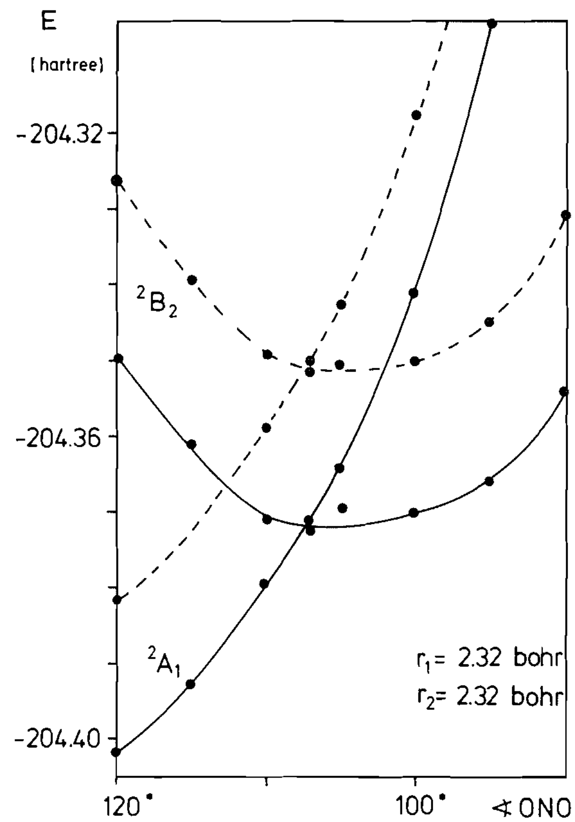

FIG. 2. Potential energy curves in the crossing region of the $^2A_1$ and $^2B_2$ states of NO_2 as a function of bond angle ($r_1 = r_2 = 2.32$ bohr). Solid lines correspond to the E_{FCI}, dashed lines to the E_{CI} values given in Table 1.

independent of the choice of one-electron transformation, but the MRD-CI results E_{CI}, in which only single and double excitations with respect to a limited series of reference configurations are treated, do not fulfill the same conditions. Instead the resulting potential curves tend to exhibit an avoided crossing similar to those which occur in true C_s geometries for which the NO bond lengths are unequal.

The higher-excitation corrections contained in the corresponding E_{FCI} data can only approximate the full CI limit and hence do not succeed completely in removing the above discontinuities, but the corresponding plots (E_{FCI}) in Figs. 2–4 show that at all three bond lengths a smaller energy gap separates the $^2A_1$ and $^2B_2$ states than is the case for the E_{CI} data. Since the dimensions of secular equations solved are already in the order of 10 000 it seems unlikely that the situation would be greatly improved by carrying out larger diagonalizations of still man-

TABLE 2. MRD-CI and estimated full CI results for the first two $^2A'$ states of NO_2, $r_1 = r_2 = 2.20$ bohr[a]

				$1^2A'$			$2^2A'$		
θ	E_{SCF}	Reference[b]	SAFT / SAF[c]	E_{CI}[d]	E_{FCI}[e]	Σc^2[f]	E_{CI}[d]	E_{FCI}[e]	Σc^2[f]
90°	−3.9852	15	472833 / 9460	−4.2960	−4.3169	0.924	−4.1895	−4.2128	0.920
95°	−4.0083	15	514978 / 9003	−4.3135	−4.3332	0.927	−4.2369	−4.2629	0.911
100°	−4.0256	15	514978 / 8863	−4.3220	−4.3408	0.929	−4.2811	−4.3037	0.920
105°	−4.0391	15	514978 / 9557	−4.3266	−4.3450	0.930	−4.3155	−4.3377	0.922
107°	−4.0430	15	514978 / 9712	−4.3302	−4.3486	0.930	−4.3214	−4.3433	0.923
110°	−4.0485	15	514978 / 9278	−4.3391	−4.3577	0.929	−4.3243	−4.3458	0.924
115°	−4.0470	15	514978 / 9978	−4.3601	−4.3789	0.930	−4.3104	−4.3370	0.910
120°	−4.0583	15	514978 / 10388	−4.3746	−4.3930	0.931	−4.2938	−4.3229	0.903
132.7°	−4.0771	11	346860 / 9935	−4.3889	−4.4083	0.928	−4.2533	−4.2790	0.913
140°	−4.0773	11	346860 / 9894	−4.3876	−4.4069	0.928	−4.2223	−4.2485	0.912
150°	−4.0679	16	480453 / 10011	−4.3769	−4.3957	0.930	−4.1771	−4.2006	0.917
180°	−4.0190	13	388609 / 8598	−4.3198	−4.3380	0.930	−4.0737	−4.0955	0.920

[a] All energies are given in hartree units with respect to −200.0 hartrees.
[b] Number of reference configurations.
[c] Number of generated (SAFT) and selected (SAF) symmetry adapted functions.
[d] MRD-CI energy, extrapolated to zero threshold.
[e] Estimated full CI energy.
[f] Sum of squares of the coefficients of the reference configurations.

TABLE 3. MRD-CI and estimated full CI results for the first two $^2A'$ states of NO_2, $r_1 = r_2 = 2.50$ bohr[a]

				$1^2A'$			$2^2A'$		
θ	E_{SCF}	Reference[b]	SAFT / SAF[c]	E_{CI}[d]	E_{FCI}[e]	Σc^2[f]	E_{CI}[d]	E_{FCI}[e]	Σc^2[f]
90°	−4.0052	15	472833 / 9103	−4.3375	−4.3644	0.906	−4.2695	−4.2993	0.901
95°	−4.0186	15	514978 / 8563	−4.3453	−4.3699	0.915	−4.2944	−4.3220	0.906
100°	−4.0268	15	514978 / 8849	−4.3467	−4.3704	0.917	−4.3202	−4.3459	0.913
105°	−4.0321	15	514978 / 9606	−4.3435	−4.3666	0.917	−4.3365	−4.3618	0.914
107°	−4.0333	15	514978 / 9648	−4.3438	−4.3668	0.918	−4.3396	−4.3648	0.914
110°	−4.0344	15	514978 / 9089	−4.3467	−4.3697	0.918	−4.3389	−4.3640	0.914
115°	−4.0290	15	514978 / 8402	−4.3542	−4.3776	0.918	−4.3331	−4.3594	0.912
120°	−4.0306	15	514978 / 7843	−4.3580	−4.3816	0.917	−4.3203	−4.3461	0.912
132.7°	−4.0047	15	466774 / 9477	−4.3597	−4.3848	0.911	−4.2733	−4.3056	0.899
140°	−4.0025	11	346860 / 9552	−4.3518	−4.3802	0.904	−4.2474	−4.2819	0.895
150°	−3.9941	16	480453 / 9745	−4.3396	−4.3640	0.915	−4.2107	−4.2410	0.900
180°	−3.9611	13	388609 / 7970	−4.2922	−4.3132	0.922	−4.1228	−4.1510	0.903

[a] All energies are given in hartree units with respect to −200.0 hartrees.
[b] Number of reference configurations.
[c] Number of generated (SAFT) and selected (SAF) symmetry adapted functions.
[d] MRD-CI energy, extrapolated to zero threshold.
[e] Estimated full CI energy.
[f] Sum of squares of the coefficients of the reference configurations.

ageable proportions. Furthermore the choice of another MO basis (e.g. $^4B_2$ or $^4A'$) does not remove the asymmetries in the molecular orbitals and there remain the consequences that individual configurations do not transform according to C_{2v} representations (4). On the other hand, a calculation in which C_{2v} symmetry is imposed for $r_1 = r_2$ gives rise to discontinuity problems, as already mentioned in the previous section and also as encountered by Gillispie *et al.* in their NO_2 study (2). The problem of the variation of CI results on the choice of the one-electron basis for close-lying electronic states has been previously discussed in a CI study of the sudden polarization effect (23, 24).

Figures 2–4 show that the crossing seam in the $^2A'$ surfaces is located near 107° for all chosen distances, but that the energy of the crossing goes up considerably when going to smaller bond distances. Essentially the same result is obtained for both the E_{CI} and the E_{FCI} curves. The data for the three pairs of unequal NO bond lengths are given in Tables 4–6 and the corresponding angular potential curves are plotted in Figs. 5–7. In these cases there is no reason to avoid the highest-order point group (C_s) in the SCF calculations and the calculated energy results do not show any discontinuities of the type noted for the more symmetric geometries.

The energy gaps between the two $^2A'$ states are found to be slightly increased in going from the MRD-CI to the estimated full-CI level of treatment, even though for the symmetric conformations discussed earlier it was noted that the full CI correction tends to reduce the magnitude of the artificial splitting which occurs in the region where the $^2A_1$ and $^2B_2$ potential curves should cross. The lowest-lying $^2A'$ state exhibits a double minimum for $r_1 = 2.32$ and $r_2 = 2.50$ bohr (Fig. 6), but at the (2.20, 2.50) bond-distance pair it is found that a very shallow E_{CI} minimum at small bond angles is not present in the E_{FCI} data. Finally it should be pointed out that all of the calculations in the 95°–120° range of bond angle have been carried out with the same set of 15 reference configurations, giving rise

TABLE 4. MRD-CI and estimated full CI results for the first two $^2A'$ states of NO_2, r_1 = 2.32, r_2 = 2.20 bohr[a]

				$1^2A'$			$2^2A'$		
θ	E_{SCF}	Reference[b]	SAFT / SAF[c]	E_{CI}[d]	E_{FCI}[e]	Σc^2[f]	E_{CI}[d]	E_{FCI}[e]	Σc^2[f]
90°	−4.0075	15	461262 / 9093	−4.3194	−4.3394	0.927	−4.2148	−4.2372	0.922
95°	−4.0290	15	514978 / 9087	−4.3322	−4.3523	0.925	−4.2598	−4.2858	0.910
100°	−4.0448	15	514978 / 9205	−4.3383	−4.3575	0.927	−4.2995	−4.3228	0.918
105°	−4.0548	15	514978 / 9660	−4.3422	−4.3606	0.930	−4.3303	−4.3527	0.922
107°	−4.0588	15	514978 / 9806	−4.3439	−4.3623	0.930	−4.3354	−4.3575	0.922
110°	−4.0627	15	514978 / 9440	−4.3506	−4.3693	0.929	−4.3383	−4.3598	0.924
115°	−4.0666	15	514978 / 8440	−4.3664	−4.3858	0.928	−4.3304	−4.3514	0.924
120°	−4.0685	15	514978 / 9013	−4.3767	−4.3966	0.926	−4.3170	−4.3410	0.916
132.7°	−4.0715	11	346860 / 9908	−4.3906	−4.4113	0.924	−4.2695	−4.2962	0.912
140°	−4.0709	11	346860 / 10170	−4.3869	−4.4071	0.925	−4.2367	−4.2630	0.912
150°	−4.0614	16	480453 / 9968	−4.3772	−4.3958	0.930	−4.1926	−4.2178	0.912
180°	−4.0154	13	388609 / 8437	−4.3230	−4.3427	0.926	−4.0927	−4.1157	0.917

[a] All energies are given in hartree units with respect to −200.0 hartrees.
[b] Number of reference configurations.
[c] Number of generated (SAFT) and selected (SAF) symmetry adapted functions.
[d] MRD-CI energy, extrapolated to zero threshold.
[e] Estimated full CI energy.
[f] Sum of squares of the coefficients of the reference configurations.

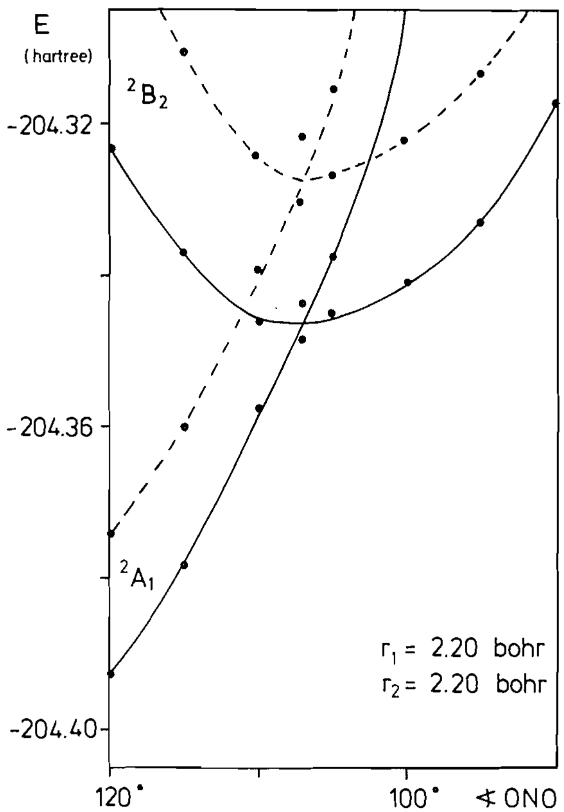

FIG. 3. Potential energy curves in the crossing region of the $^2A_1$ and $^2B_2$ states of NO_2 as a function of bond angle ($r_1 = r_2 = 2.20$ bohr). Solid lines correspond to the E_{FCI}, dashed lines to the E_{CI} values given in Table 2.

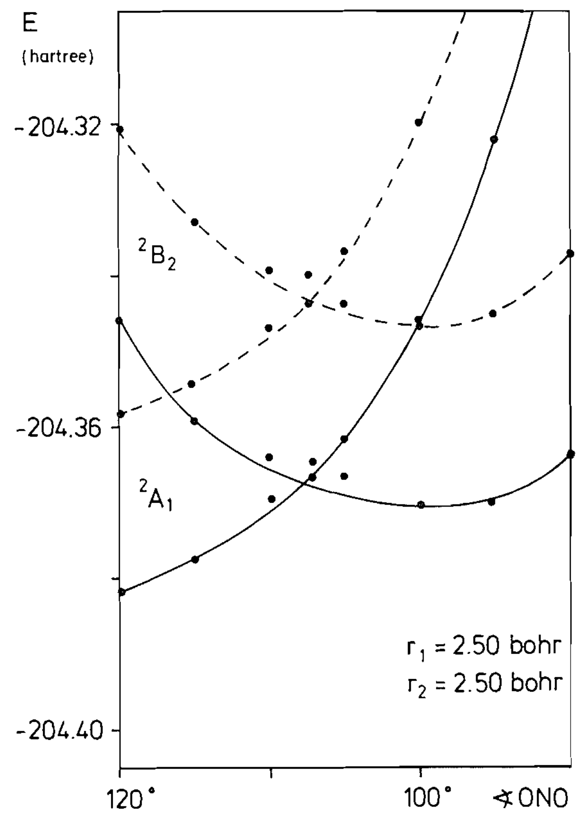

FIG. 4. Potential energy curves in the crossing region of the $^2A_1$ and $^2B_2$ states of NO_2 as a function of bond angle ($r_1 = r_2 = 2.50$ bohr). Solid lines correspond to the E_{FCI}, dashed lines to the E_{CI} values given in Table 3.

to an MRD-CI space of dimension 514978 (SAFT), from which from 8 000 to 10 000 functions are actually employed to construct the secular equations explicitly solved in the theoretical treatment. The high quality of the resulting calculations is indicated by the fact that these reference states comprise from 90 to 92% of the final CI wavefunctions on a Σc_i^2 basis for the entire geometrical region considered.

4. Comparison with experiment

There are four key geometrical conformations to be considered in the foregoing results for equal NO bond lengths and the corresponding internuclear distances, bond angles, and relative energies are given in Table 7. The X^2A_1 ground state equilibrium geometry is seen to be in good agreement with that deduced from experiment (θ = 134.07° and $r = r_1 = r_2 =$

TABLE 5. MRD-CI and estimated full CI results for the first two $^2A'$ states of NO_2, r_1 =2.32, r_2 = 2.50 bohr[a]

				$1^2A'$			$2^2A'$		
θ	E_{SCF}	Reference[b]	SAFT / SAF[c]	E_{CI}[d]	E_{FCI}[e]	Σc^2[f]	E_{CI}[d]	E_{FCI}[e]	Σc^2[f]
90°	−4.0035	15	461262 / 8384	−4.3406	−4.3647	0.916	−4.2602	−4.2835	0.920
95°	−4.0182	15	514978 / 8202	−4.3483	−4.3720	0.917	−4.2914	−4.3183	0.908
100°	−4.0286	15	514978 / 8305	−4.3503	−4.3735	0.918	−4.3235	−4.3483	0.915
105°	−4.0356	15	514978 / 9177	−4.3469	−4.3722	0.918	−4.3443	−4.3684	0.917
107°	−4.0368	15	514978 / 9471	−4.3496	−4.3737	0.917	−4.3473	−4.3700	0.919
110°	−4.0395	15	514978 / 8144	−4.3549	−4.3775	0.919	−4.3445	−4.3680	0.918
115°	−4.0409	15	514978 / 7495	−4.3655	−4.3881	0.920	−4.3332	−4.3567	0.918
120°	−4.0390	15	514978 / 7986	−4.3731	−4.3959	0.920	−4.3231	−4.3485	0.913
132.7°	−4.0372	15	466774 / 9718	−4.3776	−4.3999	0.919	−4.2814	−4.3095	0.907
140°	−4.0351	11	346860 / 9388	−4.3724	−4.3979	0.911	−4.2552	−4.2864	0.901
150°	−4.0285	16	480453 / 9624	−4.3590	−4.3811	0.921	−4.2113	−4.2396	0.905
180°	−3.9884	13	388609 / 8338	−4.3111	−4.3303	0.927	−4.1181	−4.1444	0.908

[a] All energies are given in hartree units with respect to −200.0 hartrees.
[b] Number of reference configurations.
[c] Number of generated (SAFT) and selected (SAF) symmetry adapted functions.
[d] MRD-CI energy, extrapolated to zero threshold.
[e] Estimated full CI energy.
[f] Sum of squares of the coefficients of the reference configurations.

TABLE 6. MRD-CI and estimated full CI results for the first two $^2A'$ states of NO_2, r_1 = 2.20, r_2 = 2.50 bohr[a]

				$1^2A'$			$2^2A'$		
θ	E_{SCF}	Reference[b]	SAFT / SAF[c]	E_{CI}[d]	E_{FCI}[e]	Σc^2[f]	E_{CI}[d]	E_{FCI}[e]	Σc^2[f]
90°	−3.9948	15	461262 / 8486	−4.3304	−4.3539	0.918	−4.2408	−4.2631	0.922
95°	−4.0095	15	461262 / 8133	−4.3386	−4.3619	0.918	−4.2810	−4.3039	0.920
100°	−4.0209	15	514978 / 7714	−4.3430	−4.3660	0.919	−4.3084	−4.3320	0.917
105°	−4.0280	15	461262 / 9053	−4.3420	−4.3675	0.915	−4.3400	−4.3626	0.919
107°	−4.0315	15	514978 / 9118	−4.3451	−4.3702	0.919	−4.3422	−4.3649	0.918
110°	−4.0220	15	461262 / 8754	−4.3534	−4.3754	0.922	−4.3414	−4.3662	0.916
115°	−4.0406	15	514978 / 7544	−4.3657	−4.3882	0.920	−4.3335	−4.3570	0.918
120°	−4.0400	15	461262 / 9497	−4.3754	−4.3977	0.921	−4.3221	−4.3473	0.915
132.7°	−4.0505	11	346860 / 9890	−4.3808	−4.4044	0.916	−4.2808	−4.3086	0.909
140°	−4.0487	11	346860 / 9806	−4.3767	−4.4006	0.915	−4.2521	−4.2813	0.905
150°	−4.0392	16	480453 / 9725	−4.3645	−4.3860	0.922	−4.2125	−4.2410	0.906
180°	−3.9986	13	388609 / 8582	−4.3113	−4.3339	0.918	−4.0996	−4.1275	0.905

[a] All energies are given in hartree units with respect to −200.0 hartrees.
[b] Number of reference configurations.
[c] Number of generated (SAFT) and selected (SAF) symmetry adapted functions.
[d] MRD-CI energy, extrapolated to zero threshold.
[e] Estimated full CI energy.
[f] Sum of squares of the coefficients of the reference configurations.

2.2552 bohr) (25). Since the latter state becomes degenerate with the $^2B_1$ at the linear nuclear arrangement, which in turn is known to be most stable in this geometry, it is also possible to extract the T_e value for the corresponding transition between $^2B_1$ and X^2A_1. This result is found to be 1.905 eV, which also compares favorably with that inferred experimentally of 1.83 eV (26). The calculated bond distance of both states are found to be equal, however, although the experimental data suggest that the $^2B_1$ value is 0.04 bohr larger. A Renner–Teller effect is expected and observed near the onset of this transition.

The A^2B_2 state is found to have a smaller bond angle than the ground state (102.4°), as is expected from Walsh's rules and the fact that the two states differ by a replacement of the $4b_2$ linear MO of $^2A_1$ by the strongly bent $6a_1$ species in $^2B_2$. The $^2B_2$ bond length is calculated to be 0.12 bohr greater than of X^2A_1. As the NO distances are reduced below 2.40 bohr the angular potential minimum of the X^2A_1 state is lowered relative to that of $^2B_2$ and the expected double minimum character of the lowest $^2A'$ adiabatic surface is gradually negated (see Fig. 1). The reverse is true for larger bond lengths but at the minimal energy of the C_{2v} $^2B_2$ state, there is only a slight well separating it from the X^2A_1 crossing point; this energy is only 0.917 eV above the ground state minimum. By comparison the lowest crossing energy (cusp) for the two states occurs at 0.955 eV, only 0.038 eV higher, and this for nearly the identical NO bond length of 2.395 bohr (Table 7).

These results mesh very well with the known facts about the key A–X transition in the NO_2 spectrum. The above T_e value does not take into account the influence of the antisymmetric stretch vibration but it at least suggests that the assumption of Douglas and Huber (27) that this spectrum extends beyond the last observed feature at 1.20 eV (10 300 Å) is correct. On the other hand, allowing the NO bond lengths to be unequal does not produce any significant energy lowering relative to the $^2B_2$

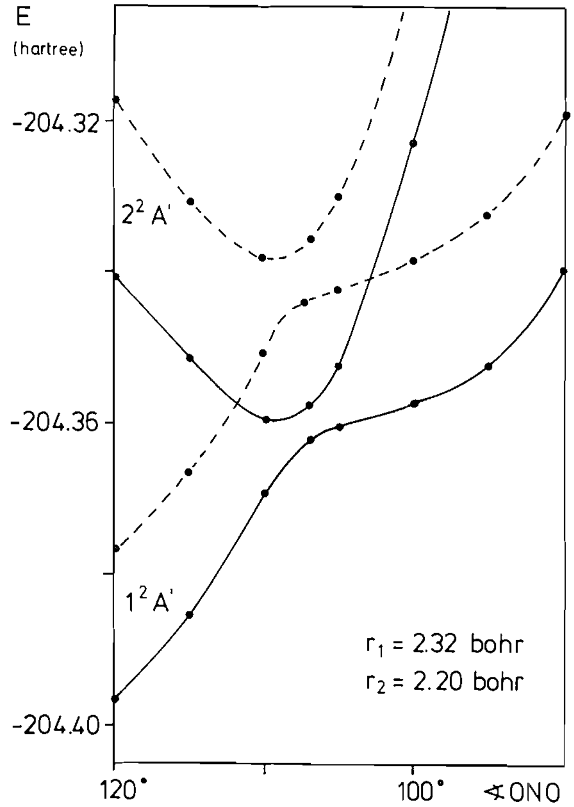

FIG. 5. Potential energy curves of the $1^2A'$ and $2^2A'$ states of NO_2 as a function of bond angle (r_1 = 2.32 bohr, r_2 = 2.20 bohr). Solid lines correspond to the E_{FCI}, dashed lines to the E_{CI} values given in Table 4.

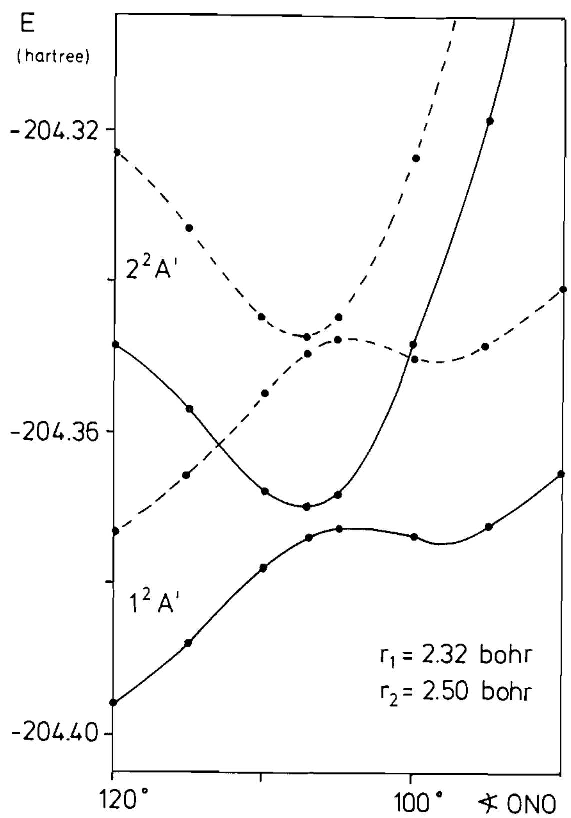

FIG. 6. Potential energy curves of the $1^2A'$ and $2^2A'$ states of NO_2 as a function of bond angle (r_1 = 2.32 bohr, r_2 = 2.50 bohr). Solid lines correspond to the E_{FCI}, dashed lines to the E_{CI} values given in Table 5.

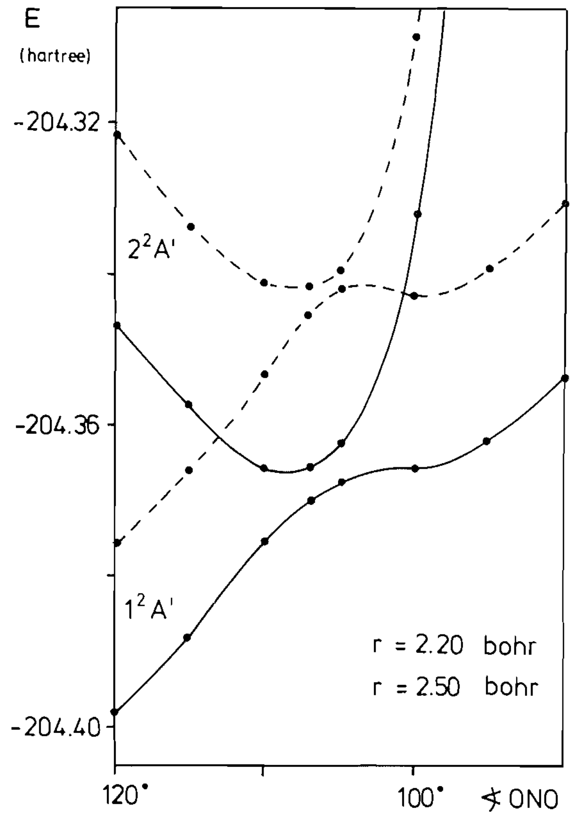

FIG. 7. Potential energy curves of the $1^2A'$ and $2^2A'$ states of NO_2 as a function of bond angle (r_1 = 2.20 bohr, r_2 = 2.50 bohr). Solid lines correspond to the E_{FCI}, dashed lines to the E_{CI} values given in Table 6.

TABLE 7. Calculated key geometrical conformations and corresponding energies

	r (bohr)	θ	E_{FCI} (hartree)	E_{rel} (eV)
X^2A_1 minimum	2.28	133.4°	−204.4118	0.0
A^2B_2 minimum	2.40	102.4°	−204.3781	0.917
$^2B_1$ minimum ($^2\Pi_u$)	2.28	180.0°	−204.3418	1.905
cusp $^2A_1/^2B_2$	2.395	107.8°	−204.3767	0.955

C_{2v} minimum shown in Table 7, as can be judged by the results of Tables 4–6, especially for r_1 = 2.32 and r_2 = 2.50 bohr. If the $^2B_2$ had a protracted potential well it could be expected that several progressions could be perceived in the experimental data, corresponding to transitions involving the NO symmetric stretching and bending vibrations for two well-defined adiabatic states. The lack of such a minimum in the calculations, however, indicates that even the lowest Born–Oppenheimer vibrational states of the A^2B_2 electronic state are strongly mixed with relatively high-lying X^2A_1 levels, making a conventional vibrational analysis very difficult. Furthermore, since the optimum bond angle and NO bond distance for the A^2B_2 state and those describing the cusp location for the $^2A_1$–$^2B_2$ surface crossing are so close to one another (differing by only about 5° and less than 0.01 bohr, Table 7), it follows that for higher vibrational quantum numbers similar mixing between Born–Oppenheimer vibronic levels should occur giving the spectrum a uniformally chaotic appearance up to the energy of the absorption maximum and beyond. The vertical transition energy relative to the X^2A_1 equilibrium geometry is computed to be 2.92 eV, which is also in good agreement with the finding that maximum absorption occurs in the 2.9–3.0 eV region of the NO_2 spectrum (28). The indication is therefore that the $^2B_2$ state can lower its energy by 2.0 eV through increasing its NO bond distance and decreasing its bond angle relative to the equilibrium values of the ground state, a circumstance which also contributes to the very broad appearance of the NO_2 spectrum in the 3 000 – 10 000 Å region.

Acknowledgements

The authors are grateful to Professor W. Demtröder for suggesting the present study and for valuable discussions. They also wish to thank Dr. H. Köppel for several discussions during the course of this work. The Deutsche Forschungsgemeinschaft is gratefully acknowledged for financial support given to this work in the form of the Sonderforschungsbereich 42. All calculations were carried out on the Perkin-Elmer 3242 minicomputer of the SFB 42.

1. D. K. Hsu, D. L. Monts, and R. N. Zare. Spectral atlas of nitrogen dioxide 5530 Å to 6480 Å. Academic Press, New York. 1978.
2. G. D. Gillispie, A. U. Khan, A. C. Wahl, R. P. Hosteny, and M. Krauss. J. Chem. Phys. **63**, 3425 (1975).
3. C. F Jackels and E. R. Davidson. J. Chem. Phys. **64**, 2908 (1976).
4. C. F Jackels and E. R. Davidson. J. Chem. Phys. **65**, 2941 (1976).
5. S. K. Shih, S. D. Peyerimhoff, and R. J. Buenker. Chem. Phys. Lett. **46**, 201 (1977).
6. J. C. D. Brand, K. J. Cross, and A. R. Hoy. Can. J. Chem. **60**, 1081 (1982).
7. H. J. Foth, H. J. Vedder, and W. Demtröder. J. Mol. Spectrosc. **88**, 109 (1981); H. J. Vedder, M. Schwarz, H. J. Foth, and W. Demtröder. J. Mol. Spectrosc. **97**, 92 (1983).
8. G. Hirsch and R. J. Buenker. To be published.
9. S. Huzinaga. J. Chem. Phys. **42**, 1293 (1965).
10. T. H. Dunning, Jr. J. Chem. Phys. **53**, 2823 (1970).
11. R. Manne. Mol. Phys. **24**, 935 (1972).
12. R. N. Dixon. Mol. Phys. **20**, 113 (1970).
13. E. R. Davidson and W. T. Borden. J. Phys. Chem. **87**, 4783 (1983).
14. L. Engelbrecht and B. Liu. *In* Energy storage and redistribution in molecules. *Edited by* J. Hinze. Plenum Press, New York and London. 1983. pp. 219–240.
15. R. J. Buenker and S. D. Peyerimhoff. *In* New horizons of quantum chemistry. *Edited by* P. O. Löwdin and B. Pullmann. Reidel Publ. Co., Dordrecht, Holland. 1983. pp. 183–219.
16. R. J. Buenker, S. D. Peyerimhoff, and W. Butscher. Mol. Phys. **35**, 771 (1978).
17. R. J. Buenker. *In* Proceedings of Workshop on Quantum Chemistry and Molecular Physics in Wollongong, Australia. February 1980.
18. R. J. Buenker. *In* Studies in physical and theoretical chemistry. Vol. 21. Current Aspects of Quantum Chemistry 1981. *Edited by* R. Carbó. Elsevier Scientific Publ. Co., Amsterdam. 1982. pp. 17–34.
19. R. J. Buenker and R. A. Phillips. J. Mol. Struct. Theochem. To be published.
20. R. J. Buenker and S. D. Peyerimhoff. Theor. Chim. Acta, **35**, 33 (1974).
21. R. J. Buenker and S. D. Peyerimhoff. Theor. Chim. Acta, **39**, 217 (1975).
22. S. R. Langhoff and E. R. Davidson. Int. J. Quantum Chem. **8**, 61 (1974).
23. R. J. Buenker, V. Bonacic-Koutecky, and L. Pogliani. J. Chem. Phys. **73**, 1836 (1980).
24. R. J. Buenker and V. Bonacic-Koutecky. *In* Energy storage and redistribution in molecules. *Edited by* J. Hinze. Plenum Press, New York and London. 1983. pp. 241–260.
25. G. R. Bird, J. C. Baird, A. W. Jache, J. A. Hodgeson, R. F. Curl, Jr., A. C. Kunkle, J. W. Bransford, J. Rastrup-Andersen, and J. Rosenthal. J. Chem. Phys. **40**, 3378 (1964).
26. J. L. Hardwick and J. C. D. Brand. Chem. Phys. Lett. **21**, 458 (1973).
27. A. E. Douglas and K. P. Huber. Can. J. Phys. **43**, 74 (1975).
28. M. Krauss, R. J. Celotta, S. R. Mielczarek, and C. W. Kuyatt. Chem. Phys. Lett. **27**, 285 (1974).

Relativistic Hartree–Fock–Roothaan wavefunctions for atoms

TAKASHI KAGAWA[1] AND GULZARI MALLI

Department of Chemistry, Simon Fraser University, Burnaby, B.C., Canada V5A 1S6

Received July 29, 1984

This paper is dedicated to Professor Camille Sandorfy on the occasion of his 65th birthday

TAKASHI KAGAWA and GULZARI MALLI. Can. J. Chem. **63**, 1550 (1985).

Relativistic Hartree–Fock–Roothaan (RHFR) wavefunctions have been calculated for a large number of atoms up to radon ($Z = 86$) under the point nucleus approximation using STO's as basis functions. The calculated total as well as orbital energies are in very good agreement with the corresponding results obtained by the numerical integration method.

TAKASHI KAGAWA et GULZARI MALLI. Can. J. Chem. **63**, 1550 (1985).

Utilisant des orbitales du type de Slater (STO) comme fonctions de base et travaillant dans l'approximation ponctuelle, on a calculé les fonctions d'onde relativistes de Hartree–Fock–Roothaan (RHFR) pour un grand nombre d'atomes allant jusqu'au radon ($Z = 86$). Les énergies totales ainsi qu'orbitales obtenues par ces calculs sont en très bon accord avec les résultats correspondants obtenus par la méthode d'intégration numérique.

[Traduit par le journal]

Introduction

The relativistic self-consistent-field (RSCF) Scheme (1) has been used to calculate the wavefunctions and energy levels of the ground states of atoms (2–5) using the numerical integration method.

Alternatively, Kim (6) developed a relativistic Hartree–Fock–Roothaan (RHFR) formalism for closed-shell atoms and reported the results for He, Be, and Ne atoms.

Kagawa (7) extended the RHFR (also called Dirac–Hartree–Fock–Roothaan (DHFR)) formalism of Kim (6) to a large class of open shells and he reported results for the ground as well as excited states for Sc through Cu atoms.

Theory and computations

We refer the reader to Kim (6) and Kagawa (7) for the details of the formalism for closed- and open-shell atoms, respectively. Kagawa's computer program, however, was severely limited because it was unable to calculate heavy atoms involving f-orbitals and because it could not handle a large enough number of basis sets necessary to represent the large number of occupied orbitals.

A computer program based upon his formalism has been developed in double-precision which at present can handle seven symmetries (s, $p_\pm$, $d_\pm$, and $f_\pm$) and for each symmetry up to a maximum of twenty Slater-type orbital (STO) basic functions can be used. The same set of non-integer STO (NISTO) basis set was used for the large and small components of the relativistic radial function where the STO (with non-integer principal quantum number) $f_{\kappa p}$ have the following form:

$$[1] \quad f_{\kappa p} = (2\zeta_{\kappa p})^{n'_{\kappa p}+1/2}\,[\Gamma(2n'_{\kappa p}+1)]^{-1/2}\, r^{n'_{\kappa p}} \times e^{-\zeta_{\kappa p} r}$$

where $\zeta_{\kappa p}$ is the orbital exponent, $\Gamma(X)$ is a gamma function, and

$$[2] \quad n'_{\kappa p} = n_{\kappa p} + (\kappa^2 - Z^2\alpha^2)^{1/2},\; n_{\kappa p} = 0, 1, 2, \ldots$$

In eq. [2], α is the fine-structure constant and κ, the relativistic quantum number, is given by the relation:

$$[3] \quad \kappa = \pm\,(j + 1/2) \text{ for } l = j \pm 1/2 \text{ and } \bar{l} = j \mp 1/2$$

where l and $\bar{l}$ denote the orbital angular momentum quantum numbers of the large $P(r)$ and small $Q(r)$ components of the radial wavefunction.

The pseudo-eigenvalue relativistic Hartree–Fock–Roothaan (RHFR) equations were solved for closed- and open-shell vectors of the expansion coefficients of the large and small components by an iterative procedure unti the self-consistency is obtained.

It should be pointed out that, in the relativistic Hartree–Fock calculations, the ground state energy is obtained as the lowest stationary value amongst the positive energy states because there are negative energy states below the state under consideration. The relativistic virial theorem for a system with a Coulomb force is given by

$$[4] \quad \langle T\rangle = -\langle V\rangle$$

which is different from the non-relativistic virial theorem. In all cases, the ratio of $\langle T\rangle/\langle V\rangle$ was found to be in excellent agreement with eq. [4], and so its tabulation is omitted. The maximum deviation was found to be ± 1 in the fifth figure. One should, however, be reminded that satisfying the relativistic virial theorem is not a sufficient condition for the energy obtained to be the lowest stationary value.

The number of STO basis functions used for radon were 12 for s_+, 11 for p_-, 10 for p_+, 7 for d_-, 6 for d_+, 5 for f_-, and 4 for f_+ symmetries, respectively; i.e., a total of 55 basis functions for a system of 86 electrons with 24 occupied orbitals. It should be mentioned that, although there is only one occupied orbital for f_- and f_+ symmetries, five f_- and four f_+ STO's were used, while for other symmetries it turns out that on the average about two STO's are needed for each occupied orbital.

The CPU time of 189.2 s was required for the radon calculation (the heaviest atom reported here), using the abovementioned set of 55 basis functions, while the numerical multiconfiguration Dirac–Fock (MCDF) programs of Grant (8) and Desclaux (9), for the identical calculation, took 179.5 and 153.8 s, respectively, on the IBM 3033 computer at SFU, operating under MTS. Furthermore, in all other cases, the CPU time was roughly the same for all the three computer programs. Unfortunately, the computer program used by Maly and Houssonnois (4) is not available to us and, thus, no statements about the CPU can be made regarding their calculation on radon.

[1] Permanent address: Department of Physics, Nara Women's University, Nara, Japan.

TABLE 1. Total relativistic energies (−E) in au for various atoms with closed-shell configurations

Atom	Z	Configuration[a]	$-E$ (present work)	$-E^b$ (numerical DF)
Kr	36	$(4p_-)^2(4p_+)^4$	2788.7640	2788.8842[b]
				2788.8845[c]
				2788.8961[d]
Xe	54	$(5p_-)^2(5p_+)^4$	7445.9738	7447.1586[b]
				7447.1605[c]
				7447.2186[d]
Hg	80	$(6s)^2$	19652.037	19653.622[b]
				19653.636[c]
				19653.870[d]
Rn	86	$(6p_-)^2(6p_+)^4$	23609.823	23611.151[b]
				23611.183[c]
				23611.517[d]

[a] Only the outermost shell occupation numbers are given here. All the inner shells are fully occupied.
[b] Calculated by the MCDF program of Grant (8).
[c] Calculated by the MCDF program of Desclaux (9).
[d] Reported by Maly and Houssonnois (4).

TABLE 2. Orbital energies ($-\epsilon$) in atomic units (au) for the ground state of radon atom (point nucleus)

Orbital	$-\epsilon$ (numerical DHF[a])	$-\epsilon$ (this work)
$1s$	3644.7959	3644.9210
$2s$	669.3840	669.4429
$3s$	166.9667	167.0889
$4s$	41.3483	41.4229
$5s$	8.4166	8.4340
$6s$	1.0727	1.0472
$2p_-$	642.3528	642.4252
$3p_-$	154.9004	155.0378
$4p_-$	36.0205	36.1327
$5p_-$	6.4089	6.3462
$6p_-$	0.5403	0.5692
$2p_+$	541.0817	541.1493
$3p_+$	131.7248	131.8749
$4p_+$	30.1187	30.2178
$5p_+$	5.1752	5.1210
$6p_+$	0.3839	0.3592
$3d_-$	112.5613	112.6625
$4d_-$	21.5464	21.6333
$5d_-$	2.1892	2.2203
$3d_+$	107.7539	107.8070
$4d_+$	20.4374	20.5237
$5d_+$	2.0162	2.0158
$4f_-$	9.1929	9.3235
$4f_+$	8.9272	9.0548

[a] Calculated by the MCDF program of Grant (8).

Results and discussion

In order to check the correctness of the computer program and the results reported here, we repeated the calculations reported by Kagawa (7) in double-precision and in *all* cases an excellent agreement was found. A large number of closed- as well as open-shell atoms have been calculated and a few representative results are presented in Tables 1 and 2.

The limitations of the RHFR wavefunction calculations and the details of the method of calculation, choice of basis set, etc., have been delineated in detail elsewhere (6, 7). However, we would like to make the following remarks. These calculations were performed under a point nucleus approximation which is not strictly valid for very heavy atoms (e.g., Hg and Rn); however, the effect of finite nucleus can be treated via a perturbation theory along with the Breit interaction, which we have also neglected in these calculations. One should bear in mind, however, that the effect of finite nucleus is especially important for the orbital energies of the inner shells $1s$ and $2p_-$, although its contribution to the total energy of the heavy systems is quite small.

Furthermore, the use of point-nucleus necessitates the use of non-integer "n quantum number" STO basis functions (6) in order to satisfy the relativistic wave equation at the origin. In addition, it is necessary to include in the basis set for the lower components of p_-, d_-, and f_- shells at least one basis function with (integer) $n = l$; i.e., $1p_-$, $2d_-$, and $3f_-$, respectively.

The orbital exponent (ζ) optimization at present was limited by *trial and error* which is quite time-consuming. The desirability of ζ optimization cannot be overstressed. We also use the relativistic virial (6) for ascertaining the "goodness" of the wavefunctions.

In Table 1, we present the total relativistic energies ($-E$) in atomic units (au) for the ground states of the various atoms with closed shell configurations (using the relativistic shell notation (1)). The corresponding results, calculated using the MCDF programs (8, 9) based on the numerical integration method, are given for comparison in Table 1 under the heading "Numerical DF", i.e. numerical Dirac–Fock, where the results reported by Maly and Houssonnois (4) are also included.

It can be seen that there is an excellent agreement between the results reported by the two methods, however, in some cases, our results differ by about 1.5 au from the more accurate results (4, 8, 9).

The orbital energies for radon (the heaviest atom reported by us) are collected in Table 2, which also contains the orbital energies calculated by the numerical integration method for radon (8). It is admitted that for some orbitals there are discrepancies of the order of 0.1 au; however, it is gratifying that the orbital energies of the inner shells as well as the outer shells can be calculated by the RHFR method with a fairly good accuracy so as to be comparable with the numerical Dirac–Fock (DF) method.

In conclusion, a lot of effort and time has been spent in developing this basis set and, although we can by no means claim the results as "final", we hope that further efforts will be directed to reveal the "deficiencies" so as to goad us and others to improve upon the present results.

Acknowledgements

This work was supported through grant No. A3598 by the Natural Sciences and Engineering Research Council of Canada (NSERC), which is gratefully acknowledged. We appreciate very much the continuous help, co-operation, and patience of the staff of our Computing Centre, without which these calculations could not be performed. Finally, we thank an anonymous referee for very constructive remarks which have helped to improve the manuscript.

1. I. P. GRANT. Proc. R. Soc. London, A**262**, 555 (1961).
2. J. B. MANN and W. R. JOHNSON. Phys. Rev. A**4**, 41 (1971).
3. J. P. DESCLAUX. At. Data Nucl. Data Tables, **12**, 311 (1973).
4. J. MALY and M. HOUSSONNOIS. Theor. Chim. Acta, **28**, 363 (1973).

5. I. P. GRANT. Adv. Phys. **19**, 747 (1970).
6. Y. K. KIM. Phys. Rev. **154**, 17 (1967).
7. T. KAGAWA. Phys. Rev. A**12**, 2245 (1975).
8. I. P. GRANT, B. J. MCKENZIE, P. H. NORRINGTON, D. F. MAYERS, and N. C. PYPER. Comput. Phys. Commun. **21**, 207 (1980).
9. J. P. DESCLAUX. Comput. Phys. Commun. **9**, 31 (1975).

Self-consistent-field calculations of the vibrational spectrum of undoped and doped transpolyacetylene

ANDREA PELUSO, MAX SEEL, and JANOS LADIK
Lehrstuhl für Theoretische Chemie, Friedrich-Alexander-Universität Erlangen-Nürnberg, Egerlandstrasse 3, D-8520 Erlangen, West Germany

Received August 7, 1984

This paper is dedicated to Professor Camille Sandorfy on the occasion of his 65th birthday

ANDREA PELUSO, MAX SEEL, and JANOS LADIK. Can. J. Chem. **63**, 1553 (1985).

Semiempirical self-consistent-field calculations are carried out to compute the force constants for various cluster models of periodic transpolyacetylene and of neutral and charged soliton and polaron defects. The phonon spectrum of undoped polyacetylene is analyzed and compared with the vibrational spectrum of various polyene chains in which soliton or polaron defects have been introduced in a random way. The results support the interpretation that the 1100 cm^{-1} Raman band of undoped polyacetylene should be ascribed to a C—C single bond stretching motion weakly coupled to a C—H in-plane bending vibration. The 1292 cm^{-1} infrared peak of pure transpolyacetylene is ascribed to the C—H in-plane deformation, the strong adsorption at 1015 cm^{-1} has to be assigned to an infrared-active out-of-plane C—H deformation. The new narrow band around 1300 cm^{-1} seen in the infrared spectrum of doped polyacetylene is ascribed to C—C bond stretching, the additional very broad band between 800 and 900 cm^{-1} results from in-plane C—C—H bending and C—H out-of-plane bending motions involving relaxed bond lengths of the defect sites. The interpretation is not uniquely in favor of the soliton picture, polaron defects can serve as alternative explanation.

ANDREA PELUSO, MAX SEEL et JANOS LADIK. Can. J. Chem. **63**, 1553 (1985).

On a effectué des calculs semi-empiriques en champ autocohérent dans le but d'évaluer les constantes de force pour divers modèles d'aggrégats de polyacétylène-*trans* périodique avec des défauts de polaron et de soliton neutres ou chargés. On a analysé le spectre phononique du polyacétylène qui n'a pas été dopé et on l'a comparé avec le spectre vibrationnel de diverses chaînes de polyènes dans lesquels on a introduit au hasard des défauts de soliton ou de polaron. Les résultats sont en accord avec l'interprétation selon laquelle la bande observée à 1100 cm^{-1} du spectre Raman du polyacétylène non dopé doit être attribuée à un mouvement d'élongation de la liaison simple C—C qui serait couplé à une vibration de déformation dans le plan d'une liaison C—H. La bande observée à 1292 cm^{-1} du spectre infrarouge du polyacétylène-*trans* pur est attribuée à une déformation dans le plan d'une liaison C—H alors que la forte absorption observée à 1015 cm^{-1} serait attribuable à une déformation hors du plan d'une liaison C—H qui serait active dans l'infrarouge. La nouvelle bande étroite observée vers 1300 cm^{-1} dans le spectre infrarouge du polyacétylène dopé est attribué à une élongation de la liaison C—C alors que la bande très large supplémentaire qui est observée entre 800 et 900 cm^{-1} proviendrait d'une déformation dans le plan des atomes C—C—H et de mouvements hors-plan de la liaison C—H qui impliqueraient des longueurs de liaisons relaxées des sites des défauts. L'interprétation ne favorise pas uniquement la théorie du soliton; les défauts de polaron peuvent aussi servir d'explication.

[Traduit par le journal]

I. Introduction

Long conjugated polyene chains have attracted the attention of chemists for a long time (1). Polyacetylene (PA), the prototype of this class of organic compounds, has recently stimulated much interest also among solid-state researchers due to its large increase in electrical conductivity upon doping (2). Although many techniques have been used which could provide information on the electronic and structural properties of *trans*-PA, a complete understanding has not yet been achieved; the main difficulty in the interpretation of the experimental results lies in the uncertainty of the real chemical structure of both doped and undoped PA.

The question whether undoped PA exhibits an equidistant or alternant structure (Peierls distorted ground state) seems to have settled, at least from the theoretical point of view, in favor of the alternant ground state solution (3–10). The latest calculation by Suhai (10) shows that the inclusion of correlation effects reduces the bond length alternation compared to the restricted Hartree–Fock (RHF) solution. The lowest energy equidistant unrestricted Hartree–Fock (UHF) ground state solution for PA (11, 12) shows a gap due to a spin density wave which is much too large.

X-ray diffraction (13, 14) gives only limited information about the structure due to the fibric nature of PA. The small number of reflection data excludes a full refinement of the structure. Infrared and Raman spectra have been highly useful in the investigation of the chemical properties and structure of undoped and doped PA (15–18). However, they cannot provide a complete and conclusive answer to the question whether the ground-state structure is equidistant or alternant. The presence of two different absorption peaks, by the majority assigned to C—C double and single bond stretching, does not ensure the presence of two different bond lengths. Symmetry considerations cannot distinguish because group theory predicts for the equidistant chain, belonging to the D_{2h} point group, and for the alternant chain, belonging to the C_{2h} point group, the same number of absorption peaks in the Raman and infrared spectrum (19).

The vibrational spectrum of doped PA was first interpreted in terms of soliton formation (20, 21), i.e., a defect which switches the phase of bond alternation. Recently, Zannoni and Zerbi have suggested (22, 23) that the interpretation is not uniquely in favor of solitons, but a polaron-like structure, i.e., a local relaxation of the bond alternation without changing the phase, may be an alternative explanation. This was thought to be consistent with the bipolaron or soliton–antisoliton pair picture (24) since a (singly charged) polaron seemed to be incompatible with esr experiments (25). However, it could be shown (26) that it is not necessary to invoke bipolarons since a polaron defect leads to localized states which are spin paired and therefore not in contradiction to the esr experiments when electron–electron interactions is included self-consistently.

The previous work on the interpretation of the vibrational spectrum of doped PA (20, 22, 23) has been based on a simple adaption of Hückel theory. Since there is no explicit treatment of electron–electron interaction, it is not possible to distinguish between neutral and charged defects. This paper is the first to calculate more seriously the vibrational spectrum of PA with soliton and polaron defects by taking into account electron–electron interaction in a self-consistent way. This allows for changes in the force constants for bond stretching, bending, and out-of-plane motions if an extra electron is added. The calculations are carried out using the semiempirical MNDO (modified neglect of differential overlap) scheme of Dewar and Thiel (27) which includes all valence σ and π electron interactions self-consistently. While it is an approximate scheme with limitations it will show the trends in the changes in the vibrational spectrum when PA is doped.

We report the phonon dispersion curves and the corresponding density of states of undoped PA and compare with previous interpretations of the vibrational spectrum. Then we focus on the explanation of the two new bands around 800 cm^{-1} and 1300 cm^{-1} seen in the infrared spectrum of PA doped both with donor and acceptor species. Our calculations show that they can be related best either to neutral solitons (but not to charged solitons) or to singly charged polarons leaving the latter defects as the more likely structural changes which occur upon charge transfer doping.

The organization of the paper is as follows: in Section II the method of calculation of the force constants and of the density of states of undoped PA as well as of doped PA with a random distribution of defects is described. Section III gives a discussion of the resulting force constants for cluster models of undoped PA and of neutral and charged soliton and polaron defects. The phonon dispersion curves and density of states of undoped PA are analyzed in Section IV. In Section V, the vibrational spectrum of PA with soliton and polaron defects is compared with the experimental spectrum of doped PA.

II. Method of calculation

II. A. Force constant calculation

Today the calculation of force constants by theoretical methods is carried out routinely. It is found that *ab initio* and appropriate semiempirical calculations reproduce the vibrational spectrum of a molecule with errors generally not larger than 20% (28). The theoretical force constants calculated in the harmonic approximation, the second derivative of self-consistent field Hartree–Fock (SCF HF) total energies, are usually overestimated. The errors for the diagonal stretching and bending force constants are about 10–20% both for *ab initio* and semiempirical methods, while the off-diagonal semiempirical coupling constants are much more overestimated, sometimes by up to 50% as compared to experimental and *ab initio* ones. However, a constructive comparison especially between theoretical and experimental off-diagonal force constants is quite difficult: the experimental ones are often obtained by using assumptions which have no counterpart in the theoretical calculation. These assumptions become necessary to overcome the problem that the number of experimental frequencies is smaller than the number of force constants.

The calculations were carried out in the MNDO approximation (27) using the QCPE-program package by Dewar *et al.* (29). MNDO is parametrized to optimize molecular geometries and heats of formation. Since the parameters are fitted to experimental data an (unknown) part of the electron correlation is included (30). In open shell cases (soliton, singly charged polaron model) an UHF treatment was used instead of the modified "half-electron" RHF treatment (31) (placing 1/2 electron of each spin in the open shell) which was employed by Boudreaux *et al.* (24). It should be emphasized that MNDO has been tested less rigorously for radical and ion geometries and it is an open question whether the use of the modified RHF half-electron scheme is superior to the UHF treatment. For the calculation of force constants difficulties arise in the case of the half-electron procedure because the resulting wave function is not variationally optimized (with respect to the total electronic energy); consequently it is not invariant under small changes in the geometry and therefore not suitable for calculating the derivative of the energy analytically (32). The use of the UHF treatment leads to some overallowance for electron correlation which can be corrected with a scale factor (32).

Gradients have been calculated analytically, force constants have been obtained by a numerical differentiation procedure. For details of the analytical derivation we refer to the fundamental work of Pulay (33). The force constant matrix has been calculated in a cartesian coordinate system. This choice avoids the occurrence of redundant coordinates. Moreover, the first derivative is easily calculated analytically. To improve agreement with the experimental vibrational spectrum we have introduced scale factors as suggested by Blom *et al.* (34). These factors have been obtained by comparing the MNDO with the experimental results for 1,3-butadiene (51) and they have then been used in the calculation of the spectrum of doped and undoped polyacetylene. To compare with experimental force constants one has to transform the calculated values from the cartesian to the internal coordinate system. The internal coordinate system has to be chosen in such a way as to avoid the presence of redundant coordinates (force constants for a redundant coordinate system cannot be determined (35)) and to allow for maximum transferability between related molecules. We have used local symmetric coordinates, first introduced by Shimanouchi (36) and defined in such a way that angle redundancies are avoided but transferability is still conserved (37). Then the transformation matrix $\mathbf{B}$ between internal coordinates R and cartesian coordinates X

$$[1] \quad R = \mathbf{B}X$$

is not singular, and the internal force constant matrix $\mathbf{F}_R$ can be obtained by the relation

$$[2] \quad \mathbf{F}_R = (\mathbf{B}^{\mathrm{T}})^{-1}\,\mathbf{F}_X\,\mathbf{B}^{-1}$$

$\mathbf{B}$ is a rectangular matrix $(3N - 6) \times 3N$, therefore it is necessary to calculate a generalized inverse defined in the following way (38)

$$[3] \quad \mathbf{B}^{-1} = (\mathbf{B}^{\mathrm{T}}\mathbf{B})^{-1}\,\mathbf{B}^{\mathrm{T}}$$

We have used this procedure instead of introducing six additional translational and rotational coordinates (39) in order to generate a square matrix $\mathbf{B}$.

II. B. Calculation of dispersion curves and density of states of a periodic chain

The dispersion curves for transpolyacetylene have been calculated by Wilson's well known **GF**-method (40) generalized to crystal vibrations by Piseri and Zerbi (41). The dispersion curve of the polymer are obtained from the eigenvalue equation

$$[4] \quad [\mathbf{D}(k) - \omega^2\,\mathbf{1}]\,L(k) = 0$$

with

$$[5]\quad \mathbf{D}(k) = \mathbf{M}^{-1/2}\,\mathbf{F}_x(k)\,\mathbf{M}^{-1/2}$$

M is a diagonal matrix whose elements are the masses of the atoms contained in the unit cell and $\mathbf{F}_x(k)$ is the force constant matrix in cartesian coordinates which is obtained from the force constant matrix in internal coordinates $\mathbf{F}_R(k)$

$$[6]\quad \mathbf{F}_R(k) = \mathbf{F}^0 + \sum_s (\mathbf{F}^{sT}\mathrm{e}^{-iks} + \mathbf{F}^s\mathrm{e}^{iks})$$

by an appropriate transformation

$$[7]\quad \mathbf{F}_x(k) = \mathbf{B}(k)^+\,\mathbf{F}_R(k)\,\mathbf{B}(k)$$

The density of states $N(\omega)$ has been calculated by replacing the δ-function with a Lorentzian of half-width ϵ

$$[8]\quad \delta[\omega - \omega(k)] = \frac{1}{\pi}\frac{\epsilon}{\epsilon^2 + [\omega - \omega(k)]^2}$$

and numerical integration

$$[9]\quad N(\omega) = \sum_i \int \mathrm{d}k\,\frac{1}{\pi}\frac{\epsilon}{\epsilon^2 + [\omega - \omega_i(k)]^2}$$

A trigonometric interpolation of the calculated frequencies for different wave vector values was used to obtain at least 50 points for each dispersion curve $\omega_i(k)$.

II. C. Calculation of density of states and eigenvectors of chains with defects

The density of states and normal modes for polyacetylene chains containing various soliton and polaron defects have been calculated using Dean's negative factor counting technique (42) in which the distribution of eigenvalues of a finite (random) chain is calculated numerically by a fast recursion algorithm. This method has been successfully applied to study the electronic (23, 43) and vibrational (22, 42, 44) spectrum of disordered polymers. The calculations are performed for four different polyacetylene chains, each consisting of 25 C_2H_2 units, which contain neutral or charged soliton or polaron defects distributed randomly. The force constant matrix of such a finite chain is built up from small matrix blocks corresponding to different subunits with or without defects. A subunit containing the polaron defect, for example, contains six CH units. For such a cluster, a self-consistent MNDO calculation is performed and yields the force constant matrix elements for the defect site and its surrounding. Selected eigenvectors of the finite chain have been calculated by the inverse iteration method (45).

III. Results and discussion of force constants

In order to obtain a reasonable force field for *trans*-PA we have calculated the force constants for the *trans*-1,3,5-hexatriene molecule in a geometry shown in Fig. 1. The geometrical parameters used are slightly different from the experimental geometry but more appropriate to simulate a *trans*-PA chain. The C—C double bond and single bond lengths have been assumed to be 1.36 and 1.44 Å, respectively, with the alternation parameter $r = 0.08$ Å, as suggested by recent calculations (46). Our molecular model is therefore also slightly different from the one used by Zannoni and Zerbi (15) and Inagaki (16). The scale factors have been transferred from the *trans*-butadiene molecule which was calculated previously. Table 1 shows the most important force constant of butadiene and hexatriene. As mentioned before the errors with respect to the experimental values are between 10 and 20%, only the carbon–carbon double bond force constant is somewhat more overestimated. The changes in the force constants in going from butadiene to hexatriene show the expected trend: the double bond force constant decreases, while the single bond one increases. Both C—C and C=C stretching force constants are larger than the ones obtained by Gavin and Rice (47) using the relationships deduced by Coulson (1) and Longuet–Higgins (3) for the dependence of stretching force constants on π-electron bond order and self-polarizability.

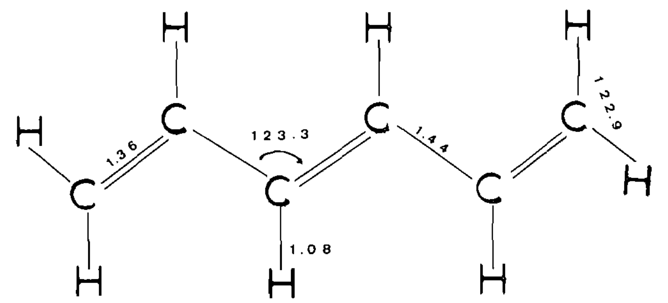

FIG. 1. Bond lengths and angles used for *trans*-1,3,5-hexatriene. The bond lengths are given in Å.

However, a direct comparison is not easy because quite different bond lengths have been used. For the same reason we find sensitive changes in C—C and C=C stretching force constants in going from butadiene to hexatriene that have no counterpart in the calculation of Gavin and Rice. On the other hand, the bending force constants and the C—H stretching force constants show only small changes. For the off-diagonal C=C/C—C stretching coupling the value of 0.84 mdyn/Å is in good agreement with 0.7 obtained by Gavin and Rice. The Kakitani sign rule (48) according to which the sign of the off-diagonal coupling force constant alternates (C=C/C—C is positive, C=C/C=C is negative etc.) is reflected in the MNDO results. Their absolute value is consistently smaller than the values of Gavin and Rice. This is very probably due to the short length of our cluster and therefore due to the unsufficient delocalization of the π-electrons.

On the basis of the considerations given above about theoretical and experimental force constants we introduce empirical scale factors. According to Török and Pulay (49), they can be obtained as the geometrical mean value of the corresponding diagonal force constants. The resulting force constants which are used for the calculation of the spectrum of PA and PA with defects are also given in Table 1.

The clusters used to calculate the force constants for solitonic and polaronic defects are shown in Fig. 2. The calculations have been carried out for neutral and singly charged clusters, assuming complete charge transfer of one electron from the donor dopant to the polymer backbone. For the open shell cases, the UHF treatment was used. As it was pointed out by Dewar (32) the overestimation of electron correlation can be reduced with a correction factor. In our case this was done by using a scale factor for the UHF–MNDO force constants which was the geometric mean of RHF scale factors for C=C and C—C stretching, or for the deformation and rocking-bending force constants, respectively.

The most important force constants are given in Table 2. As expected, important variations can be observed, especially when the defect creates an unpaired electron. The stretching force constant for the C=C double bond in the *neighborhood*

TABLE 1. The most important force constants for butadiene and hexatriene. For butadiene the MNDO and the experimental values are given, for the hexatriene the MNDO and the scaled MNDO force constants are shown. The force constants for stretching and stretching–stretching coupling are given in mdyn/Å, for bending in mdyn Å/rad² and for stretching–bending coupling in mdyn/rad; α denotes the deformation, β the rocking force constant

	1,3-Butadiene		1,3,5-Hexatriene	
Type	MNDO	Exp[a]	Unscaled	Scaled
$K_{C=C}$	11.9	8.15	11.083	7.53
$K_{C—C}$	7.4	6.07	8.46	6.94
$K_{C—H}$	6.3	5.07	6.48	5.18
H_α	0.828	0.61	0.80	0.60
H_β	0.574	0.53	0.60	0.55
$F_{C=C/C=C}$	0.0	0.0	0.073	−0.3[b]
$F_{C—C/C=C}$	0.778	0.58	0.837	0.63
$F_{C—C/C—C}$	—	—	0.027	−0.3[b]
$F_{C=C/CH}$	0.41	0.1	0.41	0.28
$F_{C—C/CH}$	0.36	—	0.37	0.29
$F_{\alpha/\alpha}$	0.03	—	0.12	0.10
$F_{\beta/\beta}$	0.035	—	0.038	0.0
$F_{C=C/\alpha}$	+0.33	—	+0.32	0.23
$F_{C—C/\alpha}$	+0.30	—	+0.33	+0.25
$F_{C—H/\alpha}$	−0.26	—	−0.26	−0.20
$F_{C=C/\beta}$	−0.31	—	−0.31	−0.25
$F_{C—C/\beta}$	−0.32	—	−0.32	−0.29
$F_{C—H/\beta}$	0.0	—	0.0	0.0

[a] From ref. 51.
[b] As suggested in ref. 47.

of the defect site decreases for the neutral soliton and charged polaron defects, while in the other cases the change is less pronounced. In all cases the force constants are lower with respect to the normal C=C bond. This leads to the conclusion that both the soliton and polaron defect are not localized in only two or three bonds. *On the defect site*, where the C—C bond length has been taken in our simple model as the average of the short and long bond, we found different behavior for the soliton and polaron cases. For the neutral soliton model the MNDO method predicts a very low force constant, comparable to the single bond case, while in the charged soliton as well as in both polaron models these force constants are close to the arithmetic mean of the single and double bond force constants.

In the neutral polaron defect the C—C stretching force constants decrease monotonously from the center of the defect on, while in the charged polaron case a small alternation is predicted. The general trend in the change of the bending force constant is the decrease of the deformation bending constant and the increase in the rocking force constant. It is also interesting to observe the increase of the coupling force constants between C—C bonds, especially in the neutral soliton cluster. A very large coupling is predicted for the double and intermediate bond and between the two intermediate C—C bonds. Long range coupling constants are increased.

Finally, we discuss briefly the out-of-plane force constants. Until now only one recent study (50) included also the out-of-plane motions of the hydrogen and the carbon atoms. We have included these motions because we believe they may be useful in the interpretation of the additional new bands in the infrared spectrum of doped PA. The scale factor for the out-of-plane C—H bending force constant has been obtained by comparing the MNDO results and experimental frequencies; the symmetry

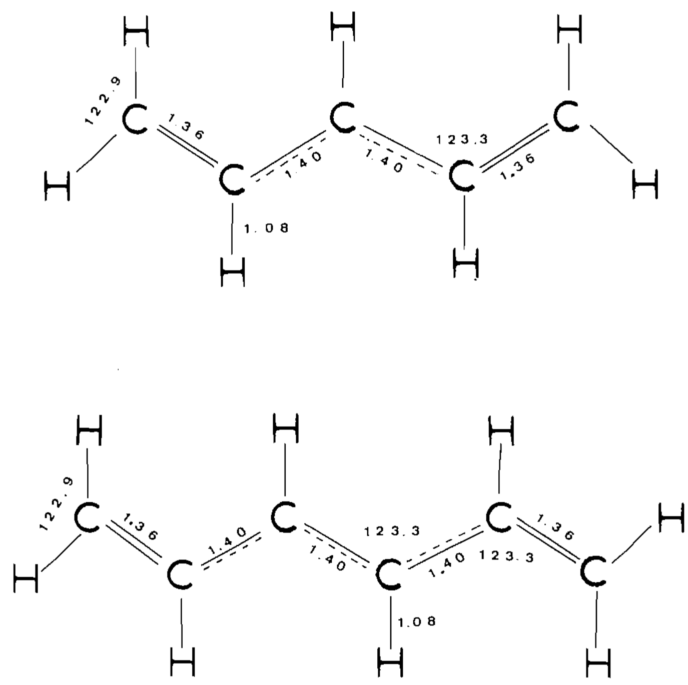

FIG. 2. Cluster model for a soliton (*a*) and a polaron (*b*) defect. The bond lengths are given in Å.

decoupling of these modes from the in-plane modes makes this procedure possible. The calculations confirmed our conjecture: a large lowering of out-of-plane force constants has been found for both soliton models and for the charged polaron cluster.

IV. Phonon dispersion curves for undoped polyacetylene

The force constant matrix $\mathbf{F}_R(k)$ for an infinite PA chain in internal coordinates has been constructed from the force constants from hexatriene discussed in the previous section. No changes of the long-range coupling force constants have been introduced in order to take into account electron–phonon coupling, as suggested by Mele and Rice (20) and Zannoni and Zerbi (15). We followed the suggestion of Gavin and Rice (47) according to which these interaction force constants do not decrease as the bond separation increases but retain a value between 30% and 50% of the nearest neighbor ones. The calculation has been carried out in the second neighbor interactions' approximation.

The phonon dispersion curves and the corresponding density of states are shown in Fig. 3, the atomic displacements of normal modes for $q = 0$ are sketched in Fig. 4. The Raman spectrum of all-*trans*-PA, measured by Shirakawa *et al.* (18), shows two strong bands at 1474 and 1080 cm^{-1} and a weak band at 1010 cm^{-1} (see Table 3). The last one has been ascribed to the C—H out-of-plane motion. The bands at 1474 and 1080 cm^{-1} were tentatively assigned to the C—C double and single bond stretching motions, respectively. However, this interpretation is still subject of discussions. Our results are in agreement with the ones of Zannoni and Zerbi (15) and Inagaki (16). The mode at 1100 cm^{-1} — our calculation gives 1142 cm^{-1} (all values are given, as usual, for $q = 0$) — should be ascribed mainly to the C—C stretching motion, coupled to C—H in-plane bending whereas Mele and Rice (20) and Schügerl and Kuzmany (52) find the single bond stretching mode at 1200 cm^{-1} and ascribe the 1100 cm^{-1} mode to C—H in-plane bending with some amount of C=C and C—C stretching mo-

TABLE 2. The unscaled and scaled MNDO force constants calculated for the soliton and polaron defect models. The units are the same as in Table 1. OOP stands for out-of-plane. $(\text{CH})_i$, i = 2, 3, denotes the ith C—H group in Fig. 2

	Soliton				Polaron			
	Charge = 0		Charge = −1		Charge = 0		Charge = −1	
Type	Unscaled	Scaled	Unscaled	Scaled	Unscaled	Scaled	Unscaled	Scaled
$K_{\text{C=C}}$	9.24	6.90	10.86	7.39	10.9	7.4	9.96	7.44
$K_{\text{=C}\cdots}$	8.75	6.56	9.51	7.13	9.96	7.44	9.46	7.01
H_{α_1}	0.68	0.56	0.833	0.62	0.92	0.69	0.68	0.58
H_{β_1}	0.57	0.47	0.576	0.53	0.58	0.53	0.57	0.44
H_{α_2}	0.62	0.51	0.727	0.55	0.60	0.50	0.60	0.50
H_{β_2}	0.60	0.50	0.615	0.56	0.62	0.55	0.60	0.51
$F_{\text{C=C/C=C}}$	0.27	0.20	0.11	0.075	0.008	0.0	0.16	0.12
$F_{\text{C=C/C}\cdots\text{C}}$	1.69	1.24	1.15	0.86	0.94	0.70	1.33	1.0
$F'_{\text{C=C/C}\cdots\text{C}}$	−0.17	−0.37[a]	−0.24	−0.25[a]	−0.045	−0.21[a]	−0.10	−0.3[a]
$F_{\text{C}\cdots\text{C/C}\cdots\text{C}}$	1.06	0.78	1.09	0.81	−0.09	−0.07	0.073	0.059
$F_{\text{C}\cdots\text{C/C—H}}$	0.41	0.29	0.41	0.29	0.38	0.27	0.40	0.28
F_{α_1/α_2}	0.075	0.06	0.019	−0.014	−0.14	0.11	0.11	0.09
F_{β_1/β_2}	0.040	0.033	0.023	−0.021	−0.019	0.017	−0.023	−0.021
$F_{\text{C=C}/\alpha_1}$	0.28	0.22	0.394	0.29	0.37	0.29	0.44	0.34
$F_{\text{C=C}/\beta_1}$	0.29	0.23	0.26	−0.21	0.27	0.22	0.273	0.22
$F_{\text{C}\cdots\text{C}/\alpha_1}$	0.32	0.26	0.35	0.27	0.39	0.31	0.30	0.24
$F_{\text{C}\cdots\text{C}/\alpha_2}$	0.36	0.29	0.36	0.28	0.20	0.16	0.41	0.32
$F_{\text{C}\cdots\text{C}/\beta_1}$	−0.35	−0.28	0.305	−0.26	−0.34	−0.27	−0.32	−0.26
$F_{\text{C}\cdots\text{C}/\beta_2}$	0.31	0.25	−0.33	−0.28	0.31	0.24	0.32	0.26
OOP(CH)_3	0.50	0.60	0.586	0.686	0.80	0.90	0.50	0.60
OOP(CH)_2	0.67	0.804	0.68	0.81	0.75	0.85	0.56	0.66
$K_{\text{=C—H}}$	6.28	5.0	6.25	5.0	6.51	5.20	6.46	5.17
$K_{\cdots\text{C—H}}$	6.48	5.18	6.44	5.15	6.48	5.18	6.44	5.15
$K_{\text{—C}\cdots\text{C}\cdots}$	—	—	—	—	9.38	7.26	9.75	7.40
$F_{\text{—C}\cdots\text{C}\cdots\text{/C}\cdots\text{C}}$	—	—	—	—	0.90	0.69	0.80	0.62
$F_{\text{C}\cdots\text{C/C=C}}$	—	—	—	—	−0.091	−0.21[a]	0.0073	0.3[a]

[a]As suggested in ref. 47.

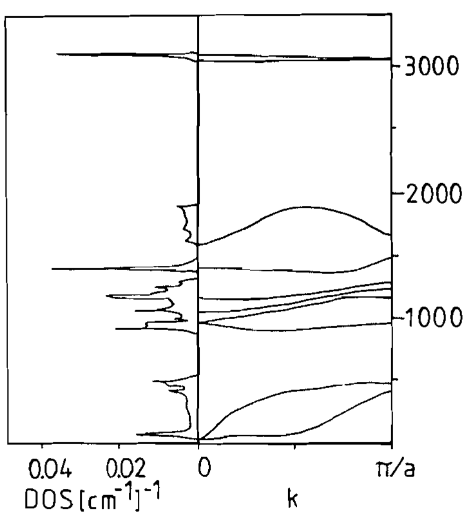

FIG. 3. Density of states (DOS) and phonon dispersion curves for *trans*-polyacetylene.

TABLE 3. Observed frequencies (in cm^{-1}) and tentative assignments in doped and undoped PA; s denotes strong, w weak, m medium, and v very

	Undoped tPA		Assignments
Raman[a]			
	1474	s	C=C stretching
	1291[c]	v v w	CCH in-plane bending
	1080	s	C—C stretching
	1016	w	C—H out-of-plane
Infrared[b]			
	1292	v w	CH in-plane deformation
	1015	v s	CH out-of-plane
	3013	m	CH stretching
	Doped tPA		**Assignments**
Infared[c]			
	888	(very broad) s	CH in-plane deformation
	1288	s	C⋯C stretching +
	1397	s	C⋯C—H deformation

[a]Reference 18*b*.
[b]Reference 18*a*.
[c]Reference 18*c*.

tions. We find a Raman-active C—H in-plane bending motion at a frequency of 1028 cm^{-1}, in very good agreement with the value of 1021 cm^{-1} calculated by Inagaki (16) while other authors (52) have found a value between 1200 and 1290 cm^{-1}. The band at 1474 cm^{-1} can be ascribed without doubt to the C=C stretching vibration weakly coupled with the C—H bending motion.

The infrared spectrum of polyacetylene shows three peaks at 3013, 1292, and 1015 cm^{-1} (18) (see Table 3). The peak at 3013 cm^{-1} is assigned to the C—H stretching vibration. Shirakawa and Ikeda assigned the mode at 1292 cm^{-1} to the *trans*-

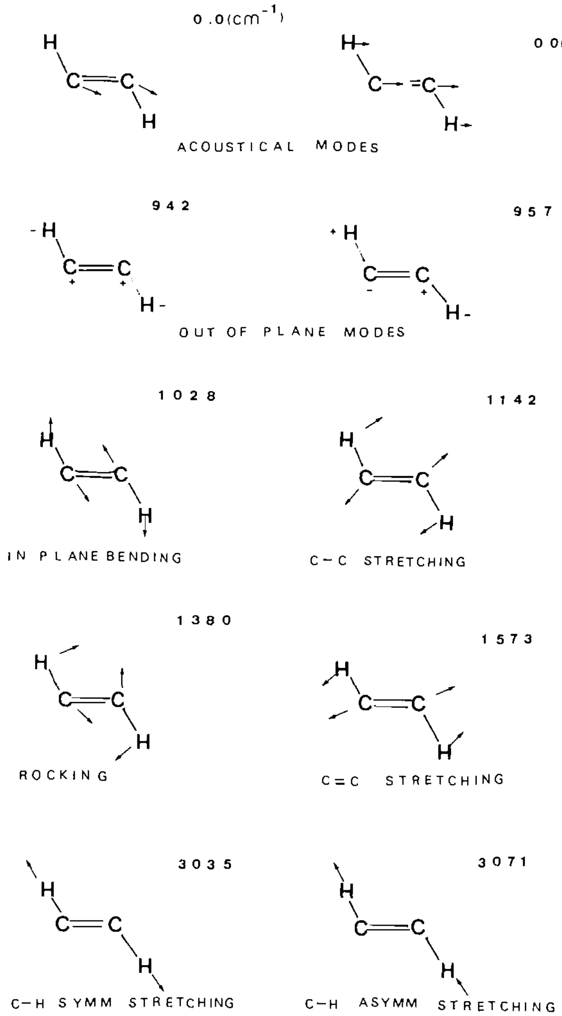

FIG. 4. Atomic displacements of normal modes for selected frequencies in periodic *trans*-polyacetylene. The numbers indicate the frequency and are given in cm^{-1}.

C—H in-plane deformation using previous results of Bellamy (53) and the band at 1015 cm^{-1} to the out-of-plane C—H deformation. Our results for these two bands are in good agreement with this interpretation.

For the out-of-plane motion we have found two bands between 950 cm^{-1} (infrared) and 1000 cm^{-1} (Raman), in good agreement with the experimental results obtained by Lunde and Zechmeister (54) for several conjugated systems.

V. Density of states of doped polyacetylene

The experimental spectra of PA doped both by donor and acceptor species show the following main features (see Table 3):

The Raman spectrum does not exhibit additional peaks compared with undoped PA. In the infrared spectrum, on the other hand, at least two additional bands have been detected. The first, very broad band falls between 800 and 900 cm^{-1}, the second, much narrower band lies around 1300 cm^{-1} (55). While there is agreement on the nature of the 1300 cm^{-1} band, the origin of the broad band starting at 800 cm^{-1} has been a matter of discussion for quite some time (20, 55, 56). Before introducing the soliton concept Heeger and co-workers (55) have suggested that this band is due to ionization of the dopant state in the semiconductor gap. Later on the isotopic shift of this band to lower frequencies found by Harada *et al.* (18*c*) demonstrated beyond doubt the vibrational origin of this band. These authors assigned the band to the in-plane C—C—H bending motion which is, in undoped PA, at 1010 cm^{-1}, but the reason of its large width could still not be explained.

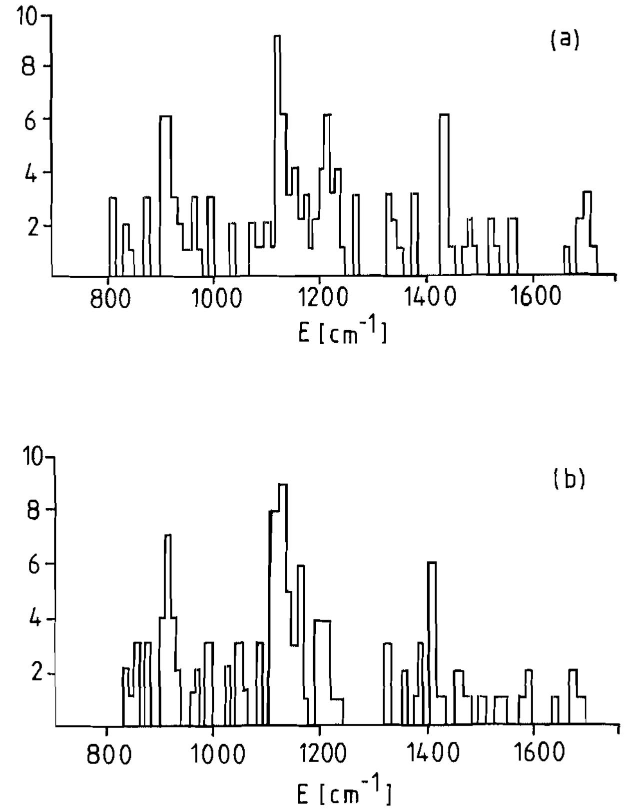

FIG. 5. Phonon density of state histogram of a $C_{50}H_{52}$ chain containing three neutral (*a*) or three negatively charged solitons (*b*).

The theoretical investigation of doped PA by Zannoni and Zerbi (44) has given a few peaks in this region. They ascribed the large band width to the overlap of several molecular-like absorptions caused by the large dimension of the defect or by the presence of a distribution of defects of the same type but with slightly different electronic and geometrical characteristics. In our opinion, however, it is difficult to understand the formation of defects with different characteristics in very lightly doped samples of PA which still show this very broad band.

In the band around 1300 cm^{-1} Harada *et al.* have found two peaks at 1288 cm^{-1} and 1397 cm^{-1}. The widths of these peaks is comparable to those of undoped PA. The band at 1397 cm^{-1} has been ascribed to the C—C stretching in the defect site. This assignment is in agreement both with the soliton and polaron model which predict bond relaxation in the middle of the defect and therefore a shift of the C=C double bond stretching vibration at 1474 cm^{-1} to lower frequencies. The other band near 1288 cm^{-1} has been ascribed to the C—H in-plane deformation which, in undoped PA, lies at 1290 cm^{-1}.

We have calculated the eigenvalue spectrum of four different finite PA chains. Each consists of 25 C_2H_2 units and contains three defects, either neutral (charged) solitons or neutral (charged) polarons, respectively, on positions 8, 18, and 23. These position numbers were generated by a random number generator. In Fig. 5, the densities of states for the chains containing neutral or charged solitons are shown, in Fig. 6 the

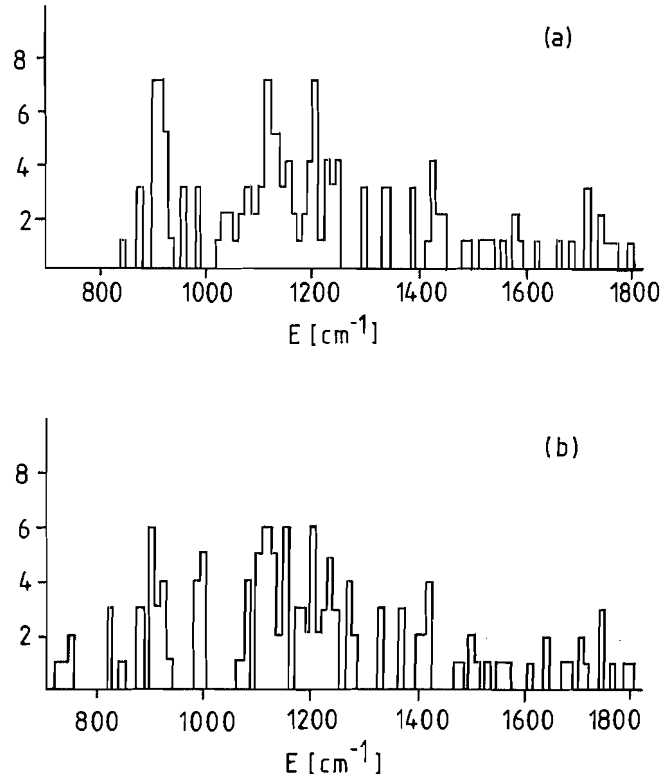

FIG. 6. Phonon density of state histogram of a $C_{50}H_{52}$ chain containing three neutral (a) or three negatively charged (b) polarons.

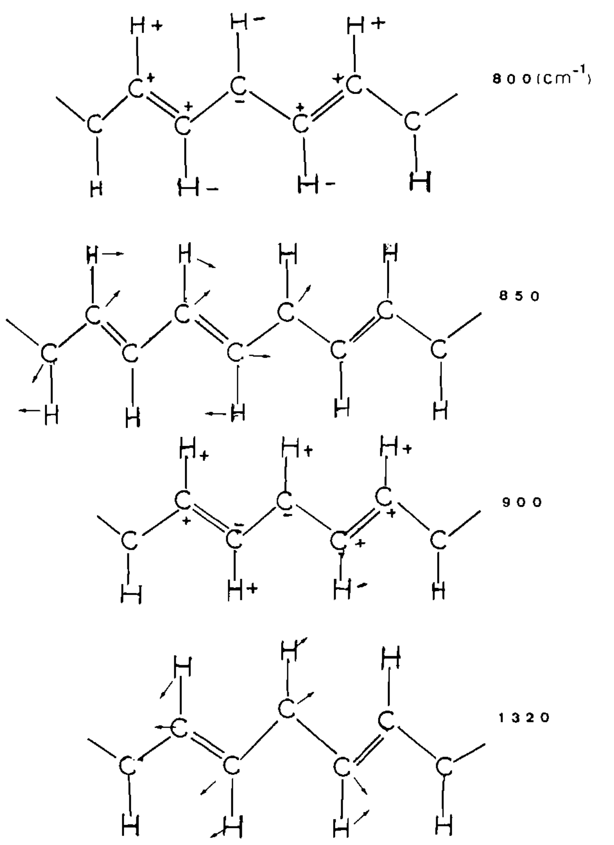

FIG. 7. Selected normal modes for the $C_{50}H_{52}$ chain with three neutral solitons. The numbers indicate the frequency and are given in cm^{-1}; +, indicates above-the-plane bending; −, below-the-plane bending.

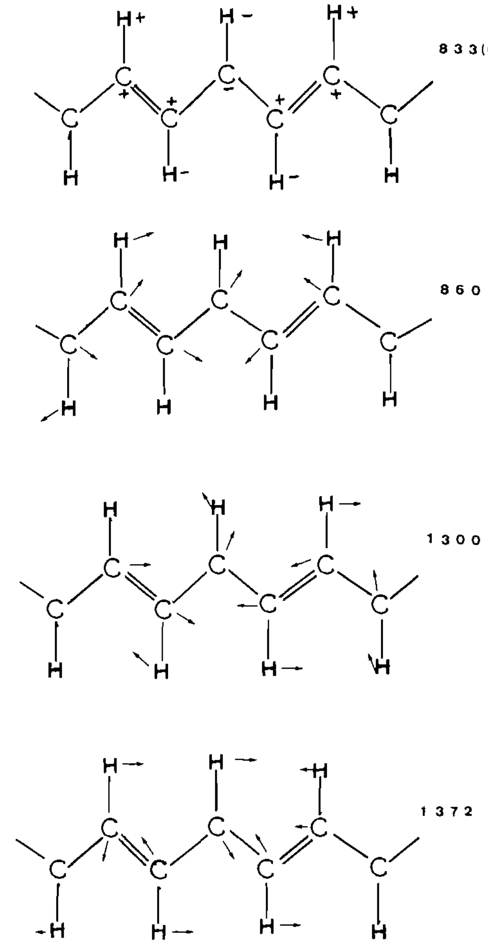

FIG. 8. Selected normal modes for the $C_{50}H_{52}$ chain with three negatively charged solitons.

densities of states for the corresponding polaron cases are plotted. Selected normal modes for the neutral and charged soliton cases are depicted in Fig. 7 and Fig. 8, respectively, and in Fig. 9 and 10 normal modes for the chains containing either three neutral or three charged polaron defects are shown.

First of all it has to be pointed out that no large differences between the four cases are found. The calculated spectra for the charged and neutral soliton as well as for the corresponding polaron defects are generally in agreement with the experimental trends and could at first sight explain the infrared spectrum of doped PA.

For the band approximately located around 1300 cm^{-1} our calculations yield the same assignment as the one given by Harada *et al.* Different behavior, however, has been found for the band at 800 cm^{-1}. In all four cases we have found in this range the presence of peaks which have to be assigned to out-of-plane C—H motions and to in-plane C—C—H bending motions. Harada *et al.* have discussed the possibility of assigning this band to C—H out-of-plane motions on the basis of deuteration and polarization experiments. In fact, the band at 888 cm^{-1} shifts to 790 cm^{-1} in the case of deuteration, while the C—D out-of-plane bending peak is located at 747 cm^{-1} in undoped PA. On the other hand, studies on the polarization dependence of these absorption bands have shown that the 800–900 cm^{-1} absorption are much more strongly polarized along the chain although a perpendicular polarization has also been observed. Therefore the possibility that the out-of-plane

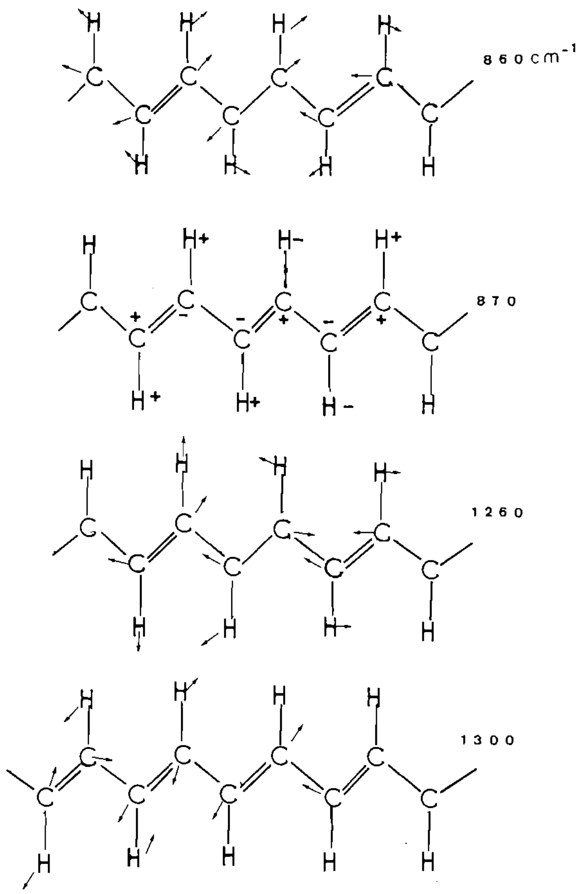

FIG. 9. Selected normal modes for the $C_{50}H_{52}$ chain with three neutral polarons.

C—H bending deformation lies in the same region as the in-plane C—C—H bending motions is, in our opinion, not ruled out by the experimental results. Our theoretical results strongly suggest that the broad band between 800 and 900 cm^{-1} is due to the presence of these two motions. This interpretation was also put forward by Zannoni and Zerbi (44) on the basis of preliminary calculations for the out-of-plane vibrations.

Finally, we discuss the differences in the spectra and normal modes of the four chains investigated in this study. In the case of the neutral polaron model we have found two peaks at 1290 and 1380 cm^{-1} which are in excellent agreement with experiment. In the range of 800–900 cm^{-1}, however, only a narrow band near 870 cm^{-1} (ascribed to the C—H out-of-plane bending) and one peak at 840 cm^{-1} (in-plane bending) are obtained. Therefore, the large width of the band is difficult to explain. In the case of charged soliton defects more peaks are found, but the majority of them has to be assigned to out-of-plane bending whereas the experiments show the dominant role of the in-plane motions. The spectrum most consistent with the experimental results is obtained for chains with either neutral solitons or charged polarons.

Our calculation of the vibrational spectrum of doped PA in which the electron–electron interaction is included for the first time in a self-consistent way shows that the infrared spectrum can be explained in terms of defects which invoke a local relaxation of the bond alternation. The interpretation is not uniquely in favor of the soliton picture. The polaron defect can serve as alternative explanation. The broad band between 800 and 900 cm^{-1} results from in-plane C—C—H bending and

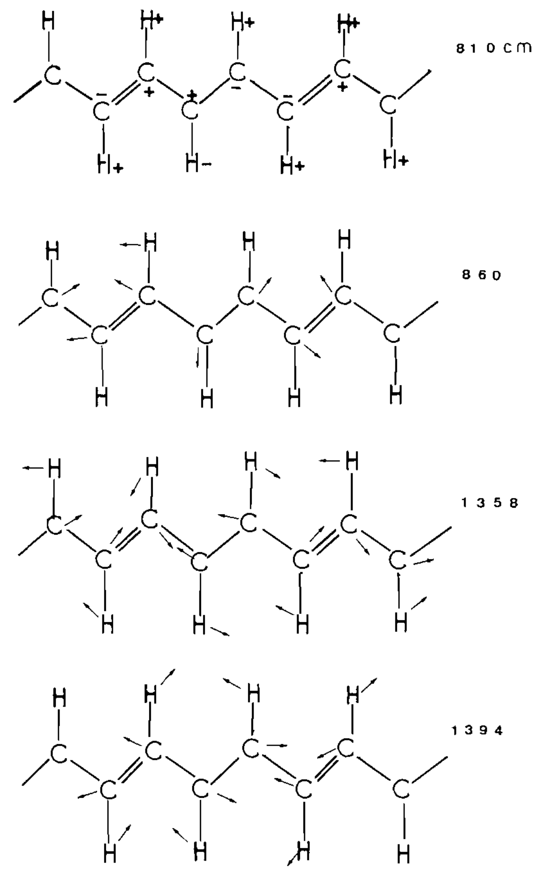

FIG. 10. Selected normal modes for the $C_{50}H_{52}$ chain with three negatively charged polarons.

C—H out-of-plane bending motions involving relaxed bond lengths of the defect site.

Acknowledgments

We would like to express our gratitude for the financial support of the "Deutsche Forschungsgemeinschaft" (Project No. La 371/14-4) and of the "Fond der Chemischen Industrie".

1. J. F. LENNARD-JONES. Proc. R. Soc. A**158**, 280 (1937); C. A. COULSON. Proc. R. Soc. A**169**, 413 (1939); M. J. S. DEWAR. J. Chem. Soc. 3546 (1952).
2. C. K. CHIANG, C. R. FINCHER, Y. W. PARK, A. S. HEEGER, H. SHIRAKAWA, E. J. LOUIS, S. C. GOU, and A. G. MACDIARMID. Phys. Rev. Lett. **39**, 1098 (1977).
3. H. C. LONGUET-HIGGINS and L. SALEM. Proc. R. Soc. London, A**251**, 172 (1959).
4. W. KUTZELNIGG. Theor. Chim. Acta, **4**, 417 (1966).
5. M. J. S. DEWAR and G. L. GLEICHER. J. Am. Chem. Soc. **87**, 692 (1965).
6. J.-M. ANDRÉ and G. LEROY. Int. J. Quant. Chem. **5**, 557 (1971).
7. M. KERTÉSZ, J. KOLLER, and A. AŽMAN. J. Chem. Phys. **67**, 1180 (1977).
8. A. KARPFEN and J. PETKOV. Solid State Commun. **29**, 251 (1979).
9. S. SUHAI. J. Chem. Phys. **73**, 3843 (1980).
10. S. SUHAI. Phys. Rev. B, **27**, 3506 (1983).
11. A. A. OVCHINNIKOV, I. I. UKRAINSKII, and G. F. KVENTSEL. Usp. Fiz. Nauk. **108**, 81 (1972); M. KERTÉSZ, J. KOLLER, and A. AŽMAN. Phys. Rev. B**19**, 2034 (1979).
12. M. KERTÉSZ. Adv. Quant. Chem. **15**, 161 (1982).
13. R. H. BAUGHMAN, S. L. HSU, G. P. PEZ, and A. J. SIGNORELLI. J. Chem. Phys. **68**, 5405 (1978); S. L. HSU, A. J. SIGNORELLI,

G. P. PEZ, AND R. H. BAUGHMAN. J. Chem. Phys. **69**, 106 (1978).
14. C. R. FINCHER, JR., D. MOSES, A. S. HEEGER, and A. G. MACDIARMID. Synth. Met. **6**, 243 (1983).
15. G. ZANNONI and G. ZERBI. Chem. Phys. Lett. **87**, 50 (1982); J. Mol. Struct. **100**, 485 (1983).
16. F. INAGAKI, M. TASUMI, and T. MIYAZAWA. J. Mol. Spectrosc. **50**, 286 (1974).
17. S. SUFRA, G. DELLEPIANE, G. MASETTI, and G. ZERBI. J. Raman Spectrosc. **6**, 267 (1977).
18. (*a*) J. SHIRAKAWA and S. IKEDA. Polym. J. **2**, 231 (1971); (*b*) J. SHIRAKAWA, T. ITO, and S. IKEDA. Polym. J. **4**, 460 (1973); (*c*) I. HARADA, Y. FURUKAWA, M. TASUMI, H. SHIRAKAWA, and S. IKEDA. J. Chem. Phys. **73**, 4746 (1980).
19. G. ZANNONI and G. ZERBI. Solid State Commun. **48**, 871 (1983).
20. E. J. MELE and M. J. RICE. Phys. Rev. Lett. **45**, 926 (1980).
21. S. ETEMAD, A. PRON, A. J. HEEGER, and A. G. MACDIARMID. Phys. Rev. B, **23**, 5137 (1981).
22. G. ZANNONI and G. ZERBI. Solid State Commun. **47**, 213 (1983).
23. G. ZANNONI and G. ZERBI. Solid State Commun. **50**, 55 (1984).
24. D. S. BOUDREAUX, R. R. CHANCE, J. L. BRÉDAS, and R. S. SILBEY. Phys. Rev. B, **28**, 6927 (1983).
25. B. R. WEINBERGER, J. KAUFER, A. PRON, A. J. HEEGER, and A. G. MACDIARMID. Phys. Rev. B, **20**, 223 (1979).
26. M. SEEL. Solid State Commun. In press.
27. M. J. S. DEWAR and W. THIEL. J. Am. Chem. Soc. **99**, 4899 (1977); **99**, 4907 (1977).
28. W. MEYER and P. PULAY. J. Chem. Phys. **56**, 2109 (1972); P. PULAY and F. TÖRÖK. Mol. Phys. **25**, 1153 (1973); A. ANNAMALAI and S. SINGH. J. Chem. Phys. **77**, 860 (1982).
29. (*a*) QCPE program number 353, Indiana University, Bloomington, Indiana; (*b*) M. J. S. DEWAR, G. P. FORD, M. L. MCKEE, H. S. RZEPA, W. THIEL, and Y. YAMAGUCHI. J. Mol. Struct. **43**, 135 (1978).
30. M. J. S. DEWAR and M. L. MCKEE. Pure Appl. Chem. **52**, 1431 (1980).
31. M. J. S. DEWAR, J. A. HASHMALL, and G. G. VERNIER. J. Am. Chem. Soc. **90**, 1952 (1968).
32. M. J. S. DEWAR and S. OLIVELLA. J. Am. Chem. Soc. **100**, 5290 (1978).
33. P. PULAY. *In* Applications of electronic structure theory. Modern Theoretical Chemistry. Vol. 4. *Edited by* H. F. Schaefer III. Plenum, New York. 1977. p. 153.
34. C. E. BLOM and C. ALTONA. Mol. Phys. **31**, 1377 (1976); C. E. BLOM, P. J. SLINGERLAND, and C. ALTONA. Mol. Phys. **31**, 1359 (1976); C. E. BLOM, L. P. OTTO, and C. ALTONA. Mol. Phys. **32**, 1137 (1976).
35. IUPAC. Appl. Spectrosc. **31**, 569 (1977).
36. T. SHIMANOUCHI. Phys. Chem. **4**, 233 (1970).
37. P. PULAY, G. FOGARASI, F. PANG, and J. E. BOGGS. J. Am. Chem. Soc. **101**, 2551 (1979).
38. B. RUST, W. R. BURRUS, and C. SCHNEEBERGER. Commun. ACM, **9**, 381 (1966).
39. S. CALIFANO. Vibrational states. Wiley, New York. 1976.
40. E. B. WILSON, J. C. DECIUS, and P. C. CROSS. Molecular vibrations. McGraw Hill, New York. 1955.
41. L. PISERI and G. ZERBI. J. Mol. Spectrosc. **26**, 254 (1968).
42. P. DEAN. Rev. Mod. Phys. **44**, 127 (1972).
43. D. PUMPERNIK, B. BORSTNIK, M. KERTÉSZ, and A. AŽMAN. Z. Naturforsch. **32**a, 295 (1977); M. SEEL. Chem. Phys. **43**, 103 (1979); M. KERTÉSZ and G. GÖNDÖR. J. Phys. C, **14**, L 851 (1981); R. S. DAY and F. MARTINO. Chem. Phys. Lett. **84**, 86 (1981); J. LADIK. Int. J. Quant. Chem. **23**, 1073 (1983).
44. G. ZANNONI and G. ZERBI. J. Mol. Struct. **100**, 505 (1983).
45. J. H. WILKINSON. The algebraic eigenvalue problem. Clarendon Press, Oxford. 1965. p. 633.
46. S. SUHAI. Chem. Phys. Lett. **96**, 619 (1983).
47. R. M. GAVIN, JR. and S. A. RICE. J. Chem. Phys. **55**, 2675 (1971).
48. T. KAKITANI. Prog. Theor. Phys. **51**, 656 (1979).
49. F. TÖRÖK. J. Mol. Struct. **32**, 93 (1970); K. KOZUMUTZA and P. PULAY. Theor. Chim. Acta, **37**, 67 (1975).
50. M. DAMNJANOVIC and M. VUJICIC. Phys. Rev. B, **28**, 1997 (1983).
51. K. K. VESETH, R. SEIP, and D. A. KOHL. Acta Chem. Scand. A, **34**, 3 (1980).
52. F. B. SCHÜGERL and H. KUZMANY. J. Chem. Phys. **74**, 953 (1981).
53. L. S. BELLAMY. The infrared spectra of complex molecules. Wiley, New York. 1954.
54. K. LUNDE and L. ZECHMEISTER. Acta Chim. Scand. **8**, 1421 (1954).
55. C. R. FINCHER, JR., M. OZAKI, A. J. HEEGER, and A. G. MACDIARMID. Phys. Rev. B, **19**, 4140 (1979).
56. B. HOROVITZ. Phys. Rev. Lett. **47**, 1491 (1981).

One-proton and multiproton hydrogen bonds between ammonium ions and hydrogen fluoride

HENRYK T. FLAKUS[1] AND RUSSELL J. BOYD[2]
Department of Chemistry, Dalhousie University, Halifax, N.S., Canada B3H 4J3

Received August 7, 1984

This paper is dedicated to Professor Camille Sandorfy on the occasion of his 65th birthday

HENRYK T. FLAKUS and RUSSELL J. BOYD. Can. J. Chem. **63**, 1562 (1985).

Extensive *ab initio* molecular orbital calculations are reported for the hydrogen bonded complexes of the formula $(CH_3)_mNH^+_{4-m}$---F—H and $(CH_3)_mNH_{3-m}$---H—F, where m = 0, 1, 2, and 3. The one-proton ("linear") hydrogen bonded complexes of the ammonium ions and hydrogen fluoride are predicted to be more stable by about 1 or 2 kcal/mol than the two- and three-proton ("bent") complexes. Several systematic trends and a number of differences between the neutral and protonated series of complexes are observed. The basis set dependence of the results, basis set superposition errors and electron correlation effects are discussed.

HENRYK T. FLAKUS et RUSSELL J. BOYD. Can. J. Chem. **63**, 1562 (1985).

On rapporte les résultats de calculs d'orbitales moléculaires *ab initio* étendus effectués sur des complexes de formules $(CH_3)_mNH^+_{4-m}$---F—H et $(CH_3)_mNH_{3-m}$---H—F, où m = 0, 1, 2 ou 3. Sur la base de ces calculs, on prédit que les complexes des ions ammonium et du fluorure d'hydrogène qui sont liés par des liaisons hydrogènes impliquant un seul proton ("linéaires") sont plus stables que ceux impliquant deux ou trois protons ("repliés") et que la différence d'énergie entre ces deux types de complexes est égale à environ 1 à 2 kcal/mol. On discute de la variation des résultats avec la nature des ensembles utilisés, de la superposition des erreurs avec la nature des ensembles utilisés et des effets de corrélation des électrons.

[Traduit par le journal]

Introduction

Very few studies of hydrogen bonds between positive ions and neutral molecules have been reported in comparison to the extensive literature on the theory of the normal (neutral) H-bond (1−25). The only major report with which we are familiar is the *ab initio* molecular orbital study of Desmeules and Allen (26) for the twenty-one binary complexes formed from the hydrides of N, O, F, P, S, and Cl. Their systematic investigation has shown that the 4-31G basis set is adequate for predicting the geometries of the strong hydrogen bonds formed between protonated complexes and that a linear relationship exists between the heavy atom separation and length of the hydrogen bond. The latter conclusion also applies to the corresponding negative ions and to the normal hydrogen bonds of second- and third-row hydrides (27). In four of the twenty-one complexes there is an unusual net gain of charge on the proton relative to the monomers at infinite separation.

In this paper we report a 4-31G study of the hydrogen bonded complexes of the general formula $(CH_3)_mNH^+_{4-m}$---F—H, where m = 0, 1, 2, and 3. Particular attention is paid to the strengths of the conventional one-proton hydrogen bonds relative to two- and three-proton hydrogen-bonded complexes,[3] as illustrated in Fig. 1 for the methylammonium complex, and to the effect of multiple substituents within the series of protonated complexes. For completeness we present a complementary study of the neutral H-bonds in the related $(CH_3)_mNH_{3-m}$---H—F complexes.

Method

The majority of the computations were performed on a Perkin-Elmer 3230 computer using the GAUSSIAN 80 series of programs (28). The structures of the monomers and complexes with m = 0 and 1 were optimized completely at the 4-31G level. For the monomers and complexes with m = 2 and 3, the following constraints were imposed on the optimizations: a model methyl group (r(C—H) = 1.080 Å and ∠(HCH) = 109.471°) was assumed, the CNC angles were fixed at 109.471°, and the C—N bond length was taken to be 1.472 Å. In every case the monomers and complex were treated at a uniform level of theory, i.e. the same geometrical parameters were optimized for both the monomers and complex. The N—F distance was optimized in all complexes.

Estimates of the basis set superposition errors were obtained by means of GAUSSIAN 76 calculations (29) on the Dalhousie University CYBER 170−730 computer.

Choice of the basis set

The neutral NH_3---H—F complex has been studied at a variety of theoretical levels (7, 11−20), while the corresponding protonated complex has only been treated at the 4-31G level (26). In order to provide some indication of the basis set error associated with our 4-31G calculations on the protonated complexes, we show in Table 1 the computed properties of the H-bond between NH_4^+ and HF at the STO-3G, 3-21G, 4-31G, and 6-31G* levels.

Our results for the one-proton H-bond indicate a strong basis set dependence with the length increasing and the strength decreasing as the flexibility of the basis set is improved. Adding another set of basis functions to the valence shell of each atom and polarization functions to the hydrogens (i.e. the 6-311G** basis set) lowers the H-bond energy to 13.3 kcal/mol at the 6-31G* geometry. Including the effects of electron correlation by means of Møller−Plesset perturbation theory (30−32) terminated at second (MP2) and third order (MP3) with the same triple-split valence, polarized basis set and 6-31G* geometry raises the H-bond energy to 14.2 and 13.9 kcal/mol, respectively.

Calculations on the two- and three-proton complexes be-

[1]On leave from Department of Chemistry, Silesian University, Katowice, Poland.

[2]To whom all correspondence should be addressed.

[3]This is a matter of continuing experimental interest both in the solid state (see, for example ref. 42) and in the gas phase (see, for example ref. 43). The problem has not been addressed previously by the methods of quantum chemistry.

TABLE 1. Computed properties of the H_3NH^+---F—H complex

Property	Basis set STO-3G	3-21G	4-31G	6-31G*
Total energy[a]	−154.47484	−155.72917	−156.37465	−156.55524
H-bond energy[b]	20.8	22.0	18.1	13.5
r(H—N)[c]	1.038	1.019	1.010	1.012
r(N—H)	1.082	1.035	1.021	1.018
r(N—F)	2.446	2.650	2.728	2.833
r(F—H)	0.946	0.942	0.928	0.919
∠HNH[d]	110.3	109.6	109.5	109.6

[a]In atomic units: 1 au = 27.2116 eV = 627.5095 kcal/mol.
[b]In kcal/mol.
[c]Bond lengths in Å and angles in deg. The bond lengths are given in the order in which they appear from left to right in the formula H_3NH^+---F—H.
[d]Angle formed by the proton of the hydrogen bond and the other protons.

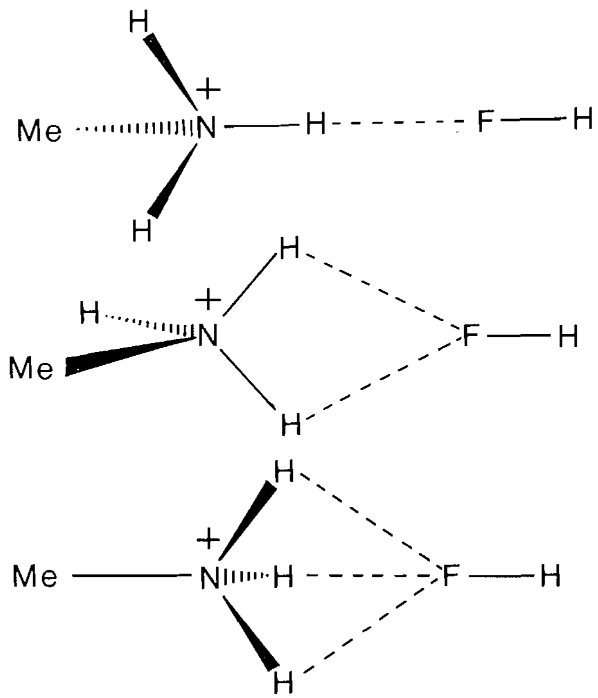

FIG. 1. One-, two- and three-proton hydrogen bonds for methylammonium ion − hydrogen fluoride complexes.

TABLE 2. 4-31G equilibrium N—H bond lengths[a] in the free amines and ammonium ions

m[b]	N—H bond length Amine	Ammonium ion
0	0.991	1.012
1	0.993	1.010
2	1.001	1.009
3	—	1.008

[a]In Å.
[b]The symbol "m" denotes the number of methyl groups.

tween NH_4^+ and HF show the same pattern: the H-bond energy decreases and the length of the H-bond increases as the flexibility of the basis set increases. The only exception occurs for the H-bond energy at the minimal basis set level. With basis sets of split-valence or better quality the trends are the same as those illustrated in Table 1.

On the basis of our calculations with extended basis sets and previous studies of the hydrogen bond (3−22, 24−27), we conclude that the 4-31G basis set represents a satisfactory compromise between computational convenience and reliability. We do not recommend the use of minimal basis sets for hydrogen bond studies and we do not think it is necessary to allow for electron correlation where the objective is to study chemical trends rather than to calculate accurate values of the H-bond energy.

Results and discussion

The 4-31G optimized N—H bond lengths of the free amines and ammonium ions are listed in Table 2. The 4-31G equilibrium geometries of the two series of complexes are listed in Table 3 and the corresponding total energies and hydrogen-bond energies are compiled in Table 4. For convenience we discuss first the neutral complexes and then the protonated complexes.

The 4-31G equilibrium geometries of the $(CH_3)_mNH_{3-m}$---H—F complexes show some very regular trends: the N—F and N—H distances of the hydrogen bond decrease with m, while the other bonds lengthen. The rate of change tends to diminish as m increases. Unfortunately there is insufficient experimental structural data for these complexes. As the length of the hydrogen bond decreases, the H-bond energy tends to increase. The one exception being the lower H-bond energy with m = 3. The somewhat lower H-bond energy for m = 3 may be a result of two opposing trends: the tendency of the H-bond to become shorter and stronger as a function of m and the increase in steric repulsion between the methyl groups and the H—F fragment of the complexes.[4] Although the H-bond energies of the complexes have not been measured, we note that the observed proton affinities of the methylamines also increase as a function of the number of methyl groups (33, 34). The difference between the 4-31G relative proton affinities (33) and the experimental values is remarkably constant: 14.5 ± 1.0 kcal/mol.

In accordance with the familiar correlation between the geometries of hydrogen-bonded complexes and their spectroscopic properties (1, 2) the H—F stretching frequencies of the

[4]A referee has suggested that a Morokuma energy component analysis (ref. 44), as reported by Kollman and Rothenberg (ref. 45), may provide an alternate explanation. We intend to investigate this suggestion in the future.

TABLE 3. Equilibrium geometries of complexes at 4-31G level

(*a*) Neutral H-bonds

Complex	r(H—N)	r(N—H)	r(H—F)	r(N—F)
m = 0 (C_{3v})[a]	0.998	1.734[d]	0.949	2.683
m = 1 (C_s)	0.999	1.691	0.954	2.645
m = 2 (C_s)	1.002	1.663	0.957	2.620
m = 3 (C_{3v})	—	1.648	0.959	2.607

(*b*) Ionic H-bonds

Complex	r(H—N)	r(N—H)	r(N—F)	r(F—H)
m = 0, p = 1 (C_{3v})[b]	1.010	1.021	2.728	0.928
p = 2 (C_{2v})	1.009	1.011	2.625	0.928
p = 3 (C_{3v})	1.008	1.009	2.549	0.928
m = 1, p = 1 (C_s)[c]	1.008	1.016	2.764	0.927
p = 2 (C_s)	1.008	1.009	2.660	0.927
p = 3 (C_{3v})	—	1.008	2.585	0.927
m = 2, p = 1 (C_s)	1.007	1.013	2.778	0.927
p = 2 (C_{2v})	—	1.008	2.676	0.927
m = 3, p = 1 (C_{3v})	—	1.011	2.796	0.927

[a]Point group of equilibrium conformation is indicated by the symbol in parentheses.
[b]The symbol "p" denotes the number of protons involved in the hydrogen bond and "m" is the number of methyl groups.
[c]The optimized C—N bond lengths are 1.517, 1.516, and 1.511 Å for p = 1, 2, and 3, respectively.
[d]An experimental value of 1.78 Å has been reported (see ref. 41).

TABLE 4. Computed properties of H-bonded complexes at 4-31G level

Complex	Total energy[a]	H-bond energy[b]	r(N—F)
Neutral H-bonds			
m = 0[c]	−156.01926	16.1	2.683
m = 1	−194.98441	16.7	2.645
m = 2	−233.95061	17.6	2.620
m = 3	−272.92058	17.3	2.607
Ionic H-bonds			
m = 0, p = 1[c]	−156.37465	18.1	2.728
p = 2	−156.37159	16.2	2.625
p = 3	−156.37107	15.9	2.549
m = 1, p = 1	−195.35384	16.5	2.764
p = 2	−195.35134	14.9	2.660
p = 3	−195.35077	14.6	2.585
m = 2, p = 1	−234.32920	15.5	2.778
p = 2	−234.32736	14.3	2.676
m = 3, p = 1	−273.30564	14.8	2.796

[a]In au.
[b]In kcal/mol.
[c]The symbol "m" denotes the number of methyl groups and "p" the number of protons involved in the hydrogen bond.

complexes are predicted to decrease relative to the isolated HF molecule, with the effect increasing with m. Furthermore the integral H—F stretching band intensities should increase as the number of methyl groups increases. On the other hand, the N—H bonds of the complexes are predicted to show very small differences (less than 0.007 Å versus up to 0.034 Å for the H—F bond) relative to the free amines and, therefore, hydrogen bonding is expected to have very little effect on the N—H stretching frequencies. The latter effects are likely to be more complex and of minor importance.

Ionic hydrogen-bonds in $(CH_3)_mNH^+_{4-m}$---F—H dimers

The 4-31G equilibrium structures suggest that the length of the one-proton hydrogen bond of the protonated complexes, as measured by the N—F distance, increases as a function of m, in contrast to the trend observed for the neutral complexes. Moreover, the length decreases in a regular fashion as the number of protons (denoted by the symbol "p") involved in hydrogen bonding increases: 0.103 ± 0.001 and 0.075 ± 0.001 Å for the first and second differences, respectively. As the N—F distance increases, a concomitant but smaller decrease of the N—H distance of the hydrogen bond is observed, in agreement with one of the observations of Desmeules and Allen (26). The other N—H bonds are relatively insensitive to the values of m and p, while the H—F bond remains almost constant (0.927 ± 0.001 Å) and close to the 4-31G value (0.925 Å) for the isolated molecule.

For a given type of hydrogen bond (that is fixed p), Table 4 reveals a strong correlation between the length and energy of the hydrogen bond: as the length increases the H-bond energy decreases monotonically. This observation may be contrasted with the situation in the complexes where the H-bond energy increases as a function of the number of methyl groups. Because the N—F distance of the ionic complexes increases as a function of m, repulsive interactions between methyl groups are expected to have less influence on the trends than in the neutral complexes where the H-bond energy of the m = 3 complex is an anomaly.

Hydrogen bonding is expected to decrease the N—H stretching frequencies relative to the isolated ammonium ion with the effect decreasing as m and p increase. The formation of a complex is predicted to have very little effect on the F—H frequencies and the N—H stretching frequencies of the N—H bonds not directly involved in hydrogen bonding.

The differences between the hydrogen bonds of the neutral and ionic complexes may be emphasized by considering the ratio between the N—F distance in the neutral and ionic complexes. The ratio decreases steadily from 0.98 for m = 0 to 0.93 for m = 3. Earlier work has shown that for a variety of complexes the ratio is close to 1.2 (26). The protonated complex between NH_4^+ and HF is an exception: our calculations and previous calculations (20, 26) yield 0.98, whereas the ratio has been incorrectly reported as 1.19 (26).

Linear (referred to herein as one-centre) hydrogen bonding lengthens the N—H bonds involved in hydrogen bonding more than bent (referred to herein as two- and three-centre) hydrogen bonding. The maximum lengthening is only 0.01 Å (compare Tables 2 and 3), while the shortening of the non-active N—H bonds is 0.003 Å or less. Within the two- and three-proton hydrogen bonded complexes, the N—H bond lengths remain within 0.004 Å of the free ion values.The small differences between the two- and three-proton complexes and the free ammonium ion suggest that the two forms would be indistinguishable by infrared spectroscopy, whereas the linear complex would show a larger shift of the N—H stretch to low frequency. The F—H bond length and, therefore, the F—H stretching frequency by inference is insensitive to the geometry of the complex, whereas the length of the C—N bond for m = 1 complexes diminishes from 1.517 to 1.511 Å as the number of protons in the hydrogen bond increases (see Table 3). For the m = 1 complexes the HNF angles of the multiproton hydrogen bonds vary by less than 0.5° as a function of the three basis sets listed in Table 5.

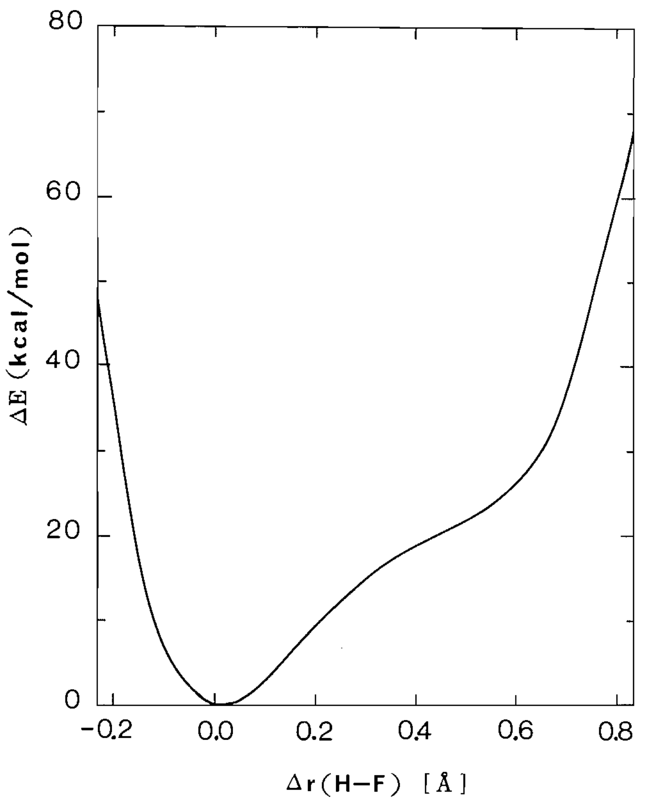

FIG. 2. 4-31G potential curve for stretching the H—F bond in the $(CH_3)_3N$---H—F complex.

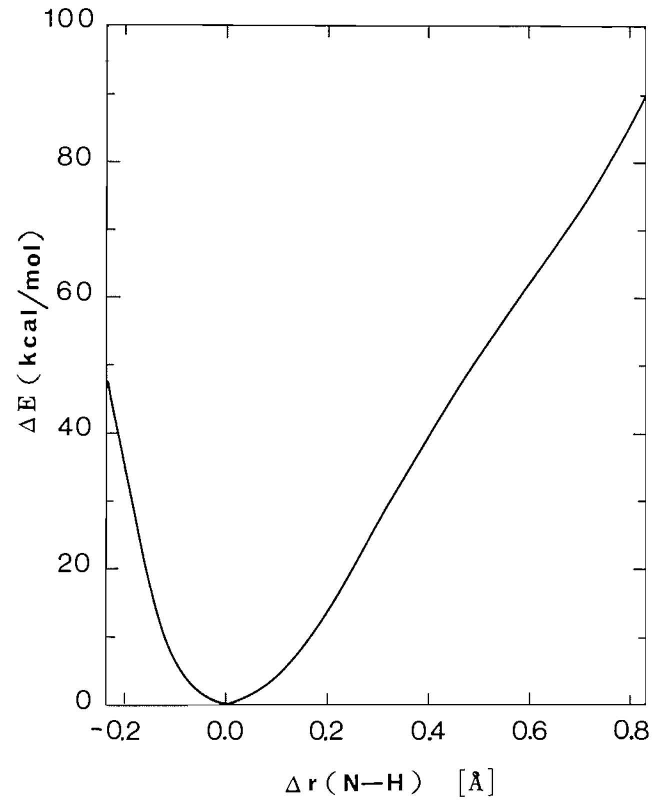

FIG. 3. 4-31G potential for N—H stretching motion in the $(CH_3)_3N^+$—H---F—H complex.

Proton motion in hydrogen-bonded complexes

Figure 2 illustrates the potential for the motion of the proton in the hydrogen bond of the trimethylamine – hydrogen fluoride complex, where the other nuclei are clamped in their equilibrium positions. Similar potentials have been calculated for the other complexes. Positive displacements of the proton correspond to stretching the H—F bond. The minimum represents the normal one-proton bond between $(CH_3)_3N$ and HF, while the shoulder associated with displacements of about 0.5 Å corresponds to a complex in which the proton has been totally transferred to the amine. The proton transfer may be represented schematically by

$$(CH_3)_3N\text{---}H\text{—}F \rightarrow (CH_3)_3N^+\text{—}H\text{---}F^-$$

With a stronger donor, i.e., weaker H—X bond we might expect a double minimum for the potential. In fact gas-phase studies of the trimethylamine – hydrogen bromide complex (3) indicate that the structure of the complex is $(CH_3)_3N^+$—H---Br^-, whereas the NH_3---HF and NH_3---HCl complexes do not exhibit proton transfer in the gas phase (7, 11, 22). Proton transfer also occurs in the gas phase complex of NH_3 and HI (22). Figure 2 implies that for a suitable choice of a donor and an acceptor the two minima would have equal stabilities and therefore a gas-phase complex would consist of a 1 : 1 ratio of the two types.

Figure 3 illustrates the analogous potential for the protonated complex in which the minimum is represented by $(CH_3)_3N^+$—H---F—H. The shoulder corresponding to transfer of the proton to HF is only slightly discernible. With a stronger donor and a stronger acceptor, proton transfer should occur. Where the protonated complex is formed by using the same compound for the donor and acceptor, e.g. HF or NH_3 (26), a double minimum will result:

$$H\text{—}F^+\text{—}H\text{---}F\text{—}H \leftrightarrow H\text{—}F\text{---}H\text{—}F^+\text{—}H$$

By suitable choice of the constituents, an unsymmetrical complex in which a double minimum exists for the motion of the proton could be formed.

Perturbations of the H-bonded complex by the environment, as for example in solution or in a crystal, can also change the donor and the acceptor properties of the dimer fragments. Previous theoretical work (35) has shown that the potential for H—F stretching in the NH_3---H—F complex exhibits a second minimum, corresponding to proton transfer, when the quantum chemical model is refined to allow for interactions between the dimer and a number of water molecules. Environmental effects are beyond the scope of the present study and are not considered further in this paper.

TABLE 5. Comparison of the H-bond energies of protonated complexes for different basis sets

	H-bond energy		
Complex	STO-3G	4-31G	6-31G*
$m = 0, p = 1$ (C_{3v})	20.8	18.1	13.5
$p = 2$ (C_{2v})	9.6	16.2	12.6
$p = 3$ (C_{3v})	8.2	15.9	12.8
$m = 1, p = 1$ (C_s)	18.0	16.5	12.3
$p = 2$ (C_s)	9.1	14.9	11.7
$p = 3$ (C_{3v})	8.0	14.6	11.7
$m = 2, p = 1$ (C_s)	16.4	15.5	—
$p = 2$ (C_{3v})	8.4	14.3	—

One-, two-, and three-proton ionic hydrogen bonds

Experimental data show that the majority of H-bonds involve the interaction of one proton with a single acceptor. There are, however, numerous examples of multicenter H-bonds in which one proton interacts with two or three proton acceptors (36). In this paper we consider yet another situation in which up to three protons interact with a single acceptor. A few *ab initio* studies of multiproton hydrogen bonds in neutral systems (7, 16, 19) have shown the one-proton ("linear") hydrogen bonds to be energetically favoured over the two- or three-proton ("bent") hydrogen bonds. For the protonated complexes we have reached the same conclusion. Table 5 lists the hydrogen-bond energies of the protonated complexes at three different theoretical levels. All calculations favour the one-proton hydrogen bonded complexes with the differences being greatest at the STO-3G level. With the larger basis sets the differences between the one-proton and multiproton hydrogen-bond energies are small.

The large differences at the STO-3G level require further comment. Our study of hydrogen bonding has been carried out within the supermolecule approximation and, therefore, the magnitude of the basis set superposition error (BSSE) should be assessed. By application of the counterpoise method (37–40) we have estimated the BSSE to be -9.2 kcal/mol for the one-proton complex and -1.4 kcal/mol for the three-proton complex of NH_4^+---F—H at the STO-3G level. The corresponding 4-31G values are -1.3 and -1.4 kcal/mol, respectively, which is comparable to the 4-31G BSSE in the neutral complexes of NH_3, H_2O, and HF (21). These results imply that the BSSE is fairly constant at the 4-31G level and not a serious source of error. At the STO-3G level the BSSE is a major source of error and in fact forms a large part of the hydrogen-bond energy of the one-proton hydrogen bonded ionic complexes.

Conclusions

On the basis of the calculations reported in this paper, the following conclusions regarding the hydrogen bonded complexes of ammonium ions and amines with hydrogen fluoride may be drawn.

(*1*) At the 4-31G level the one-proton hydrogen bonded complexes of the ammonium ions and hydrogen fluoride are predicted to be more stable by about 1 or 2 kcal/mol than the two- and three-proton complexes.

(*2*) The length (N—F distance) of the one-proton hydrogen bond of the protonated complexes increases systematically as a function of the number of methyl groups, whereas the same property decreases in neutral complexes.

(*3*) In agreement with earlier studies of hydrogen bonds between positive ions and neutral molecules (26), the N—H distance of the hydrogen bond of the protonated complexes decreases as the N—F distance increases.

(*4*) The ratio of the N—F distance in the neutral and ionic complexes decreases steadily from 0.98 to 0.93 as a function of the number of methyl groups. This may be contrasted with previous work (26) which has shown the ratio of heavy atom distances to be about 1.2 in a variety of complexes.

(*5*) The potentials for the motion of the proton in the hydrogen bond of the linear complexes of trimethylamine and the trimethylammonium ion with hydrogen fluoride have different shapes. For the neutral complex, a shoulder corresponding to transfer of the proton to the amine is clearly visible.

(*6*) Extensive calculations for the one-proton hydrogen bonded complex of NH_4^+ and HF exhibit a strong basis set dependence with the length increasing and the strength decreasing as the flexibility of the basis set improves. With a triple-split valence, polarized basis set (6-311G**) the MP2 and MP3 correlation corrections are only 0.9 and 0.6 kcal/mol, respectively.

(*7*) The basis set superposition error (BSSE) has been estimated by the counterpoise method to be -9.2 and -1.4 kcal/mol for the one-proton and three-proton complexes of NH_4^+---F—H at the STO-3G level. The corresponding 4-31G values are -1.3 and -1.4 kcal/mol.

(*8*) In every case the charge on the proton of the hydrogen bond decreases relative to the corresponding monomers at infinite separation. Earlier work (26) has shown that there are a few special cases where the charge increases.

(*9*) The 4-31G basis set represents a satisfactory compromise between computational convenience and reliability. Due to large variations in the BSSE the STO-3G basis set is not recommended for hydrogen bond studies. Electron correlation effects are of minor importance.

Acknowledgements

We would like to acknowledge Drs. L. C. Allen, M. Falk, and O. Knop for helpful discussion and the Natural Sciences and Engineering Research Council of Canada for financial support of this research.

1. P. SCHUSTER, G. ZUNDEL, and C. SANDORFY. (*Editors*). The hydrogen bond. Vols. I, II, and III. North Holland, Amsterdam. 1976.
2. H. RATAJCZAK and W. J. ORVILLE-THOMAS. (*Editors*). Molecular interactions. John Wiley and Sons Ltd., 1980.
3. A. BEYER, A. KARPFEN, and P. SCHUSTER. Top. Curr. Chem. **120**, 1 (1984).
4. P. A. KOLLMAN. *In* Modern theoretical chemistry. Vol. 4. *Edited by* H. F. Schaefer III. Plenum, New York. 1977. Chapt. 3.
5. G. H. F. DIERCKSEN. Theor. Chim. Acta, **21**, 335 (1971).
6. J. E. DEL BENE and J. A. POPLE. J. Chem. Phys. **52**, 4858 (1970).
7. P. A. KOLLMAN and L. C. ALLEN. J. Am. Chem. Soc. **93**, 4991 (1971).
8. P. A. KOLLMAN and L. C. ALLEN. Theor. Chim. Acta, **18**, 399 (1970).
9. P. A. KOLLMAN and L. C. ALLEN. Chem. Rev. **72**, 283 (1972).
10. P. A. KOLLMAN, A. JOHANSSON, and S. ROTHENBERG. Chem. Phys. Lett. **24**, 199 (1974).
11. P. A. KOLLMAN, J. MCKELVEY, A. JOHANSSON, and S. ROTHENBERG. J. Am. Chem. Soc. **97**, 955 (1975).
12. L. C. ALLEN. Proc. Natl. Acad. Sci. USA, **72**, 4701 (1975).
13. J. DILL, L. C. ALLEN, W. C. TOPP, and J. A. POPLE. J. Am. Chem. Soc. **97**, 7220 (1975).
14. L. C. ALLEN. J. Am. Chem. Soc. **97**, 6921 (1975).
15. H. UMEYAMA and K. MOROKUMA. J. Am. Chem. Soc. **98**, 7208 (1976).
16. H. UMEYAMA and K. MOROKUMA. J. Am. Chem. Soc. **99**, 1316 (1977).
17. H. UMEYAMA, K. MOROKUMA, and S. YAMABE. J. Am. Chem. Soc. **99**, 330 (1977).
18. S. YAMABE, S. KATO, H. FUJIMOTO, and K. FUKUI. Theor. Chim. Acta, **30**, 327 (1973).
19. R. C. KERNS and L. C. ALLEN. J. Am. Chem. Soc. **100**, 6587 (1978).
20. W. TOPP and L. C. ALLEN. J. Am. Chem. Soc. **96**, 5291 (1974).
21. G. LEROY, G. LOUTERMAN-LELOUP, and P. RUELLE. J. Chim. Phys. **76**, 113 (1979).
22. P. A. KOLLMAN, A. DEARING, and E. KOCHANSKI. J. Phys.

Chem. **86**, 1607 (1982).
23. M. M. SZCZESNIAK and S. SCHNEIDER. J. Chem. Phys. **80**, 1535 (1984)
24. V. C. SINGH and P. A. KOLLMAN. J. Chem. Phys. **80**, 353 (1984).
25. A. HINCHLIFFE. J. Mol. Struct. THEOCHEM. **15**, 361 (1984).
26. P. J. DESMEULES and L. C. ALLEN. J. Chem. Phys. **72**, 4731 (1980).
27. L. C. ALLEN. Private communication.
28. J. S. BINKLEY, R. A. WHITESIDE, R. KRISHNAN, R. SEEGER, D. J. DEFREES, H. B. SCHLEGEL, S. TOPIOL, L. R. KAHN, and J. A. POPLE. Department of Chemistry, Carnegie-Mellon University, Pittsburgh, PA 15213.
29. J. S. BINKLEY, R. A. WHITESIDE, P. C. HARIHARAN, R. SEEGER, J. A. POPLE, W. J. HEHRE, and M. D. NEWTON. QCPE, **11**, 368 (1978).
30. C. MØLLER and M. A. PLESSET. Phys. Rev. **46**, 618 (1934).
31. R. J. BARTLETT. Phys. Scr. **21**, 255 (1980).
32. J. A. POPLE, J. S. BINKLEY, and R. SEEGER. Int. J. Quantum Chem. **10**, 1 (1976).
33. D. H. AUE, H. M. WEBB, and M. T. BOWERS. J. Am. Chem. Soc. **98**, 311 (1976).
34. M. MEOT-NER (MAUTNER). J. Am. Chem. Soc. **106**, 1257 (1984).
35. P. SCHUSTER, W. JAKUBETZ, G. BEYER, W. MEYER, and B. M. RODE. Jerusalem Symposia on Quantum Chemistry and Biochemistry, VI, 257 (1974).
36. R. TAYLOR, O. KENNARD, and W. VERSICHEL. J. Am. Chem. Soc. **106**, 244 (1984).
37. S. F. BOYS and F. BERNARDI. Mol. Phys. **19**, 553 (1970).
38. M. BULSKI and G. CHALASINSKI. Theor. Chim. Acta, **44**, 399 (1977).
39. W. KOLOS. Theor. Chim. Acta, **51**, 219 (1979).
40. P. E. S. WORMER and A. VAN DER AVOIRD. J. Chem. Phys. **62**, 3326 (1975).
41. G. T. FRASER, K. R. LEOPOLD, and W. KLEMPERER. J. Chem. Phys. **80**, 1423 (1984).
42. (*a*) O. KNOP, I. A. OXTON, and M. FALK. Can. J. Chem. **57**, 404 (1979); (*b*) O. KNOP, T. S. CAMERON, M. A. JAMES, and M. FALK. Can. J. Chem. **61**, 1620 (1983); **62**, 1227 (1984). (*c*) T. S. CAMERON, M. A. JAMES, O. KNOP, and M. FALK. Can. J. Chem. **61**, 2192 (1983).
43. Y. K. LAU and P. KEBARLE. Can. J. Chem. **59**, 151 (1981).
44. S. IWATA and K. MOROKUMA. J. Am. Chem. Soc. **95**, 7563 (1973).
45. P. KOLLMAN and S. ROTHENBERG. J. Am. Chem. Soc. **99**, 1333 (1977).

Capacité calorifique de polyélectrolytes en solution

HUBERT DAOUST, HOA LE THANH,[1] PIERRE FERLAND[2] ET DANIEL ST-CYR[3]
Département de Chimie, Université de Montréal, Montréal (Qué.), Canada H3C 3V1

Reçu le 8 août 1984

Cet article est dédié au Professeur Camille Sandorfy à l'occasion de son 65e anniversaire

HUBERT DAOUST, HOA LE THANH, PIERRE FERLAND et DANIEL ST-CYR. Can. J. Chem. **63**, 1568 (1985).

Des mesures de capacité calorifique de polyélectrolytes en solution dans l'eau ont été réalisées à 25°C à l'aide d'un microcalorimètre dynamique du type Picker. Cet appareil est d'une précision telle que le calcul de capacité calorifique molaire apparente ($C_{p,\phi}$) du soluté devient possible même à haute dilution. Les polymères étudiés furent l'acide polyméthacrylique (HPMA) et l'acide polyacrylique (HPA) ainsi que son sel de sodium, de même que le polystyrènesulfonate de sodium. Les résultats montrent que pour les sels, la valeur de $C_{p,\phi}$ décroit rapidement avec la dilution à faible concentration en parfait accord avec une relation obtenue à partir de la théorie de Lifson et Katchalsky. Une étude de la variation de $C_{p,\phi}$, à concentration fixe, en fonction du degré de neutralisation de l'HPA et de l'HPMA a aussi été réalisée. Comme il a déjà été démontré par d'autres travaux, la chaîne de l'HPMA subit une transformation conformationnelle lorsque le degré de neutralisation atteint environ 25%. Cette transformation se réflète par une augmentation de $C_{p,\phi}$.

HUBERT DAOUST, HOA LE THANH, PIERRE FERLAND, and DANIEL ST-CYR. Can. J. Chem. **63**, 1568 (1985).

Heat capacities of polyelectrolytes in aqueous solutions have been measured at 25°C using a Picker-type dynamic microcalorimeter. The precision of the apparatus is such that it is possible to calculate the apparent molar heat capacity ($C_{p,\phi}$) of the solute, even at high dilution. The polymers that were studied include polymethacrylic acid (PMAH) and polyacrylic acid (PAH), as well as its sodium salt and the sodium salt of the polystyrenesulfonate. For the salts, the results show that the value of $C_{p,\phi}$ decreases rapidly with dilution to low concentrations; this result is in perfect concordance with a relation derived from the theory of Lifson and Katchalsky. A study of the variation of $C_{p,\phi}$, at a constant concentration, with the extent of the neutralization of the acids PMAH and PAH has also been conducted. As has been shown previously, the chain of the PMAH undergoes a conformational transformation when the level of neutralization gets close to 25%. This transformation implies an increase of the value of $C_{p,\phi}$.

[Journal translation]

Introduction

Les solutions de polyélectrolytes sans addition d'électrolyte neutre présentent un défi à tout traitement théorique global (1). Le comportement d'une chaîne polyélectrolytique change considérablement avec la dilution. En effet, cinq domaines de concentrations ont été décrits par Wolff (2) lors d'une étude sur la viscosité de solutions de polyélectrolytes et par Odijk (3) qui a appliqué la loi d'échelle aux solutions semi-diluées de polyélectrolytes. Trois concentrations critiques ont alors été définies: C_G^*, concentration à laquelle les chaînes de polyions fortement alongées ne peuvent plus s'orienter librement commencent à former un réseau tridimensionnel; C^*, concentration à laquelle les polyions interagissent assez fortement pour faire plier les chaînes; C^{**}, concentration à laquelle le réseau tridimensionnel est détruit. Contrairement à C_G^* et à C^*, C^{**} ne dépend pas de la longueur de la chaîne étalée. Les cinq domaines de concentrations sont alors (2, 3): (I) $C < C_G^*$, domaine très dilué où les chaînes sont étirées à leur longueur maximum et où les interactions entre polyions sont négligeables; (II) $C_G^* < C < C^*$, domaine dilué où les chaînes demeurent rigides mais interagissent fortement de façon à former un réseau tridimensionnel; (III) $C^* < C < C^{**}$, domaine semi-dilué où le réseau est toujours existant mais les dimensions de chaînes décroissent; (IV) $C > C^{**}$, domaine où le réseau tridimensionnel disparaît pour faire place à un système plus ou moins ordonnée de polyions de conformation sphérique en contact les uns avec les autres; (V), $C \gg C^{**}$, domaine où les polyions sont enchevêtrés et leur conformation est gaussienne tel un polymère neutre. Il serait très intéressant de pouvoir faire des études expérimentales couvrant tous les cinq domaines de concentrations. Cependant, les valeurs calculées pour C_G^* pour des chaînes vinyliques ayant des degrés de polymérisation de 10^4 et 10^5 sont $1,1 \times 10^{-6}$ et $1,1 \times 10^{-8}$ monomol L^{-1} respectivement (1). Les valeurs correspondantes pour C^* sont $7,6 \times 10^{-5}$ et $7,6 \times 10^{-6}$ monomol L^{-1}. Les domaines I et II ne sont donc pas accessibles à l'expérience, du moins pour des macromolécules ayant une masse molaire suffisamment élevée pour être considérées comme telles. D'autre part, le domaine III est accessible car la valeur de C^{**} est estimée à $4,3 \times 10^{-2}$ monomol L^{-1} (1). La loi d'échelle telle qu'appliquée par Odijk sous-évalue peut-être C^* et C^{**}. En effet, des résultats obtenus en diffusion quasi-élastique de la lumière par des solutions de polystyrènesulfonate de sodium indiquent que la dimension de la chaîne se rapproche de celle d'une chaîne complètement étendue (4). Les mêmes résultats indiquent aussi un comportement non-uniforme pour les chaînes dans le domaine de concentrations III; ceci est confirmé par des expériences en relaxation magnétique nucléaire dans le même domaine (5).

Les propriétés thermodynamiques de solutions de polyélectrolytes dépendent de plusieurs facteurs. Entre autres, les interactions électrostatiques sont très importantes. De fait, elles sont considérées comme étant l'unique facteur responsable de la valeur de la chaleur de dilution de solutions de polyélectrolytes dans le domaine de concentrations III (6). Parmi les fonctions thermodynamiques intéressantes, il y a la capacité calorifique.

Dans un article précédent (7), la capacité calorifique molaire apparente à pression constante, $C_{p,\phi}$, pour un polyélectrolyte a été définie par la somme de deux termes. Le premier, $C_{p,\phi n}$, est la contribution venant des effets non-électrostatiques et le second, $C_{p,\phi c}$, la contribution venant des interactions électros-

[1]Nouvelle adresse: Département de Chimie, Université du Québec à Montréal, Montréal (Qué.), Canada H3C 3P8.

[2]Nouvelle adresse: Alcan International Ltée, Laboratoire Arvida et Centre de Génie Expérimental, Jonquière (Qué.), Canada G7S 4K8.

[3]Nouvelle adresse: Du Pont Canada Inc., Research Centre, P.O. Box 5000, Kingston, Ont., Canada K7L 5A5.

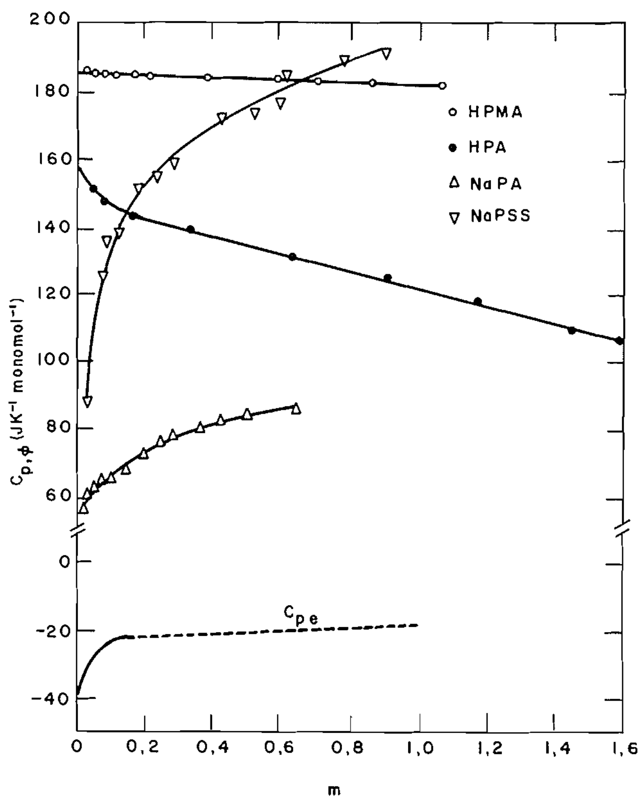

FIG. 1. Variation de la capacité calorifique molaire apparente en fonction de la molalité dans l'eau à 25°C.

tatiques. En posant $C_{p,\phi c} = C_{pc}$, il a été possible d'obtenir une relation pour C_{pc} à partir du modèle cellulaire de Lifson et Katchalsky (LK) pour un polyion en solution diluée (8):

$$[1] \quad C_{pc} = \frac{\alpha z_1 R}{z_2 \lambda}\left\{\mu\left(2 + 4\frac{\mathrm{d}\ln D}{\mathrm{d}\ln T} + \frac{T^2\mathrm{d}^2 D}{D\,\mathrm{d}T^2}\right) + \left(1 + \frac{\mathrm{d}\ln V}{\mathrm{d}\ln T}\right) \times \left[\frac{1+\beta^2}{2}\frac{\mathrm{d}\ln V}{\mathrm{d}\ln T} + \lambda\left(1 + \frac{\mathrm{d}\ln D}{\mathrm{d}\ln T}\right)\frac{1-\lambda^2+\beta^2}{(1-\lambda)^2-\beta^2}\right]\right\}$$

avec

$$[2] \quad \mu = (1+\beta^2)\gamma + \ln\{[(1-\lambda)^2 - \beta^2]/(1-\beta^2)\} + \lambda$$

où α est le degré d'ionisation du polyélectrolyte; z_1, le nombre de charges des groupements ionisés sur le polyion; z_2, le nombre de charges des contreions; λ, le paramètre de densité de charges; D, la constante diélectrique du solvant; V, le volume de la solution; β, une constante d'intégration et γ, un paramètre de la concentration. Il a été démontré que dans l'eau, C_{pc} est une quantité négative (7) et varie d'une façon logarithmique avec la concentration dans le domaine de concentrations où le modèle cellulaire le LK est applicable, soit dans les domaines I et II, et au début du domaine III. Des résultats expérimentaux obtenus autour de la concentration C^{**} semblent confirmer les prédictions théoriques (7). Tant qu'à $C_{p,\phi n}$, sa valeur est sûrement affectée par les forces électrostatiques qui ont une très grande influence sur les changements de conformation des chaînes et sur la mobilité des segments à l'intérieur des chaînes en fonction de la concentration. D'autres effets secondaires mais de très grande importance tels l'hydratation coulombique et les effets structuraux au niveau du solvant affectent la valeur de $C_{p,\phi n}$ (9). De plus, la solvatation hydrophobe affecte aussi cette quantité (9).

Dans le présent travail, une étude plus approfondie de la capacité calorifique des polyélectrolytes en solution sans addition d'électrolyte neutre est présentée. Les effets du degré d'ionisation sont discutés.

Partie expérimentale

Produits utilisés

Les différents polymères utilisés dans ce travail sont: un échantillon d'acide polyméthacrylique (HPMA) déjà décrit ailleurs (10) ayant un degré de polymérisation viscosimétrique moyen ($\overline{\mathrm{DP}}_v$) de 1920; un échantillon d'acide polyacrylique (HPA) provenant de chez Polysciences, Inc. et ayant un $\overline{\mathrm{DP}}_v$ de 2080; finalement, un échantillon de polystyrènesulfonate de sodium (NaPSS) provenant de chez Dow Chemical International (Sarnia, Ontario) et ayant un $\overline{\mathrm{DP}}_v$ de 2750. Le sel de sodium de HPA a été préparé selon une méthode décrite ailleurs (11). Tous les autres produits utilisés étaient des réactifs analytiques. Les solutions ont été préparées par voie gravimétrique, l'eau utilisée était distillée et déionisée.

Méthode expérimentale

Les capacités calorifiques volumiques (J mL^{-1}) des solutions ont été déterminées à l'aide d'un microcalorimètre différentiel dynamique Picker; elles ont été converties en capacités calorifiques massiques (J g^{-1}) en les divisant par les densités des solutions déterminées à l'aide d'un densimètre dynamique Picker. La technique expérimentale a déjà été décrite précédemment (12). L'erreur estimée sur le calcul de $C_{p,\phi}$ diminue sensiblement lorsque la concentration augmente. Par exemple, elle est moins de $\pm 10\%$ pour une molalité de 0,02 et moins de $\pm 2\%$ pour une molalité de 0,1. Tous les résultats sont exprimés pour une mole de motif de base.

Résultats et discussion

La variation de $C_{p,\phi}$ en fonction de la molalité est représentée sur la fig. 1 pour les différents polymères en solution dans l'eau à 25°C. Les données expérimentales sont disponibles sur demande.[4] Les résultats indiquent une diminution de $C_{p,\phi}$ lorsque la concentration augmente dans le cas des deux polyacides faibles. Des résultats similaires ont été obtenus pour le polyoxyéthylène dans l'eau (12). L'augmentation de la concentration intensifie l'enchevêtrement des chaînes, ce qui réduit leur mobilité ou leur mouvement de reptation et cela se reflète dans la valeur de $C_{p,\phi}$. Cependant, l'application de l'éq. [8] de la réf. 12 prévoit une augmentation de $C_{p,\phi}$ avec la concentration car le paramètre enthalpique d'interaction est positif et constant (0,48) à 25°C (13) et est positif mais plus petit et variable à 35°C.[5] Il semble bien que l'application seule de la thermodynamique des solutions de macromolécules ne suffit pas pour expliquer l'allure de la variation de $C_{p,\phi}$ avec la concentration.

Les résultats obtenus pour les deux polyélectrolytes forts sont aussi représentés sur la même figure. Pour NaPSS, la chute de $C_{p,\phi}$ lorsque la concentration diminue vers le domaine III est remarquable. Même lorsque la valeur de C_{pc}, indiquée au bas du graphique, est retranchée de celle de $C_{p,\phi}$, l'allure de $C_{p,\phi n}$ demeure très fortement affectée par la dilution. La dilution d'une solution aqueuse semi-diluée d'un polyélectrolyte fort est accompagnée par la rupture ou le relâchement de liaisons électrostatiques fortes entre les sites chargés sur les polyions et les contreions, ce qui donne lieu à l'augmentation du degré d'hydratation coulombique des espèces ioniques ainsi libérées. D'après la loi de Born, la

[4]Dépôt de données non publiées, ICIST, Conseil National de recherches du Canada, Ottawa, Ontario, Canada K1A 0S2.

[5]R. Darveau. Travaux non-publiés.

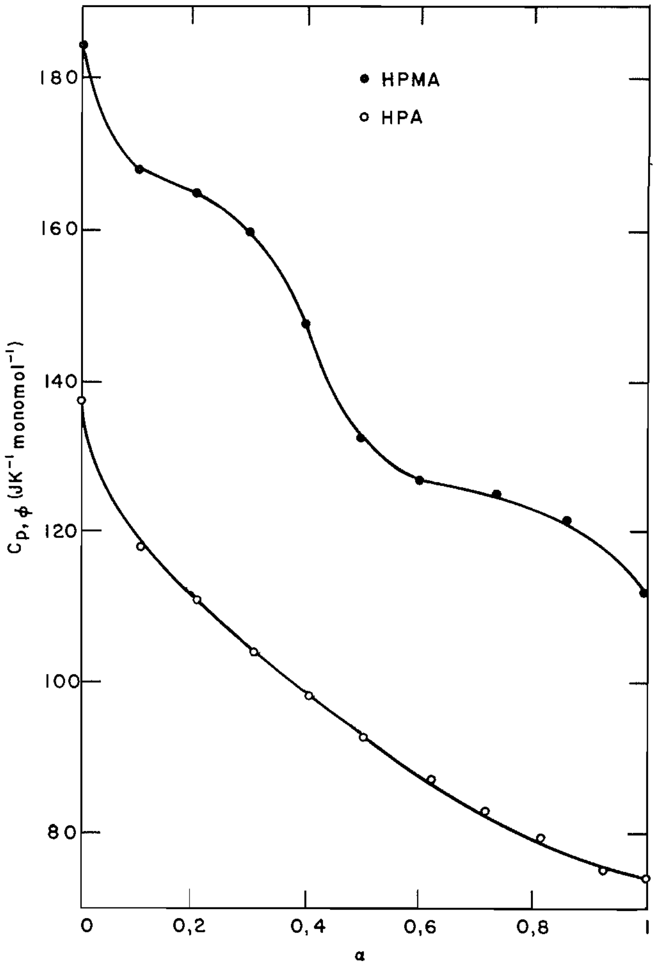

FIG. 2. Variation de la capacité calorifique molaire apparente moyenne en fonction du degré de neutralisation à 25°C (molalités: 0,32 pour HPA et 0,20 pour HPMA).

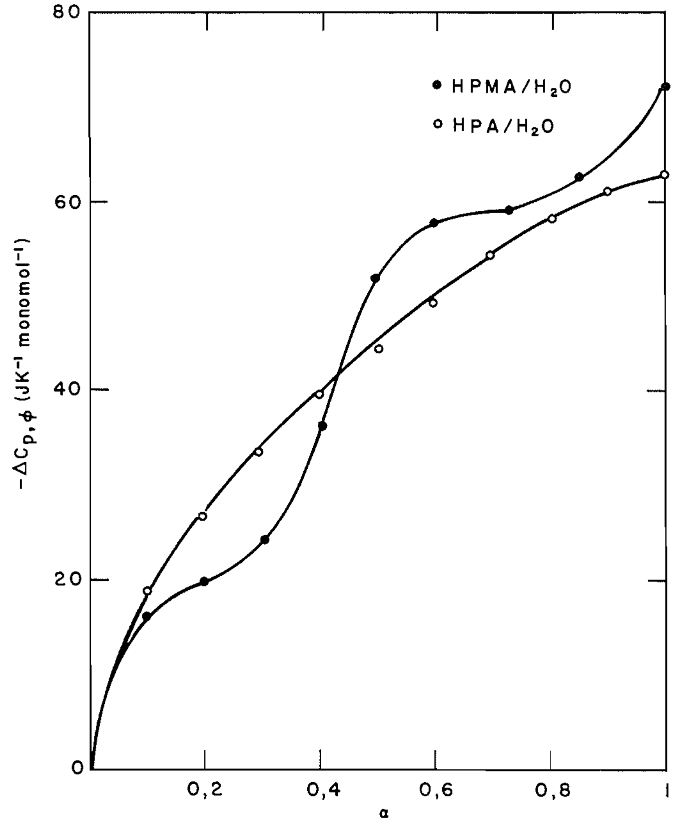

FIG. 3. Variation de l'incrément de la capacité calorifique molaire apparente moyenne en fonction du degré de neutralisation à 25°C (molalités: 0,32 pour HPA et 0,20 pour HPMA).

solvatation coulombique doit apporter une contribution négative à $C_{p,\phi}$ mais des résultats expérimentaux obtenus dans le cas de petits ions en solvants non-aqueux ont contredit cette prédiction théorique (9). La loi de Born serait peut-être applicable dans le cas de solutions aqueuses de polyélectrolytes. Par ailleurs, si la dilution doit conduire à un système tridimensionnel de polyions rigides (domaine II), en passant par un système plus ou moins ordonné de sphères rigides (domaine III), $C_{p,\phi}$ doit nécessairement chuter vers une valeur plus faible et ce passage devrait se faire graduellement. Dans le cas de NaPA, l'allure des résultats est semblable quoique moins prononcée. Cette différence pourrait être due au pourcentage élevé ($\approx$60%) d'ions sodium qui demeurent liés aux chaînes même à faible concentration de polymère (14).

La figure 2 représente la variation de la valeur moyenne de $C_{p,\phi}$ en fonction du degré de neutralisation, à concentration de polymère fixe, pour HPMA et pour HPA dans l'eau. Dans le cas présent, la masse molaire moyenne d'un motif de base est définie par $M_A + (1 - \alpha)M_H + \alpha\, M_{Na}$ où M_A est la masse molaire du motif acrylate ou méthacrylate selon le cas, M_H, celle de l'hydrogène et M_{Na}, celle du sodium. L'allure générale des résultats indique bien la diminution de $C_{p,\phi}$ avec l'augmentation de α en accord avec l'éq. [1], compte tenu du fait que la contribution de l'ion sodium à $C_{p,\phi}$ à dilution infinie est de 23 J K^{-1} mol^{-1} plus élevée que celle de l'ion hydrogène (15). (Cette contribution par rapport au proton hydrogène n'est pas connue.) Cette diminution de $C_{p,\phi}$ lorsque α augmente, se retrouve également lors de l'étude de la neutralisation de l'acide acétique (16, 17). Cependant, le grand écart entre la valeur de $C_{p,\phi}$ à $\alpha = 0$ et sa valeur à $\alpha = 1$ ne peut être expliqué seulement que par des interactions électrostatiques. Lors de l'ionisation, un effet destructeur de la structure de l'eau est produit par les ions formés et cet effet amène une contribution négative à $C_{p,\phi}$ (9, 17). La figure 3 permet une meilleure comparaison entre les résultats obtenus pour HPMA et HPA dans l'eau. La valeur de $\Delta C_{p,\phi}$ représente la différence entre celle de $C_{p,\phi}$ pour l'acide ($\alpha = 0$) et la valeur moyenne de $C_{p,\phi}$ pour la valeur de α correspondante. La valeur de $\Delta C_{p,\phi}$ diminue d'une façon monotone depuis l'acide jusqu'au sel dans le cas de HPA et cette courbe a la même allure que celle du pourcentage d'ions sodium fixés sur les polyions en fonction de α (14); ceci revient à dire que $\Delta C_{p,\phi}$ varie linéairement avec ce pourcentage d'ions liés. Dans le cas de HPMA, deux anomalies ressortent des résultats. La première anomalie apparaît autour d'une valeur d'environ 0,3 pour α. Cette anomalie doit correspondre à la transition bien connue pour la chaîne de HPMA qui passe d'une structure compacte globulaire où les groupements méthyles sont dirigés vers l'intérieur de la chaîne à une structure plus étendue où ces mêmes groupements deviennent accessibles aux molécules d'eau (18, 19). L'hydratation hydrophobe accompagnant cette transition expliquerait l'augmentation de $C_{p,\phi}$ (9) de HPMA partiellement neutralisé par rapport à HPA. Une augmentation de $C_{p,\phi}$ a aussi été observée lors de la dénaturation de plusieurs protéines gobulaires en solution dans l'eau par addition d'urée (16, 17). Cette dénaturation amène la protéine à se déplier en pelote statistique et l'aug-

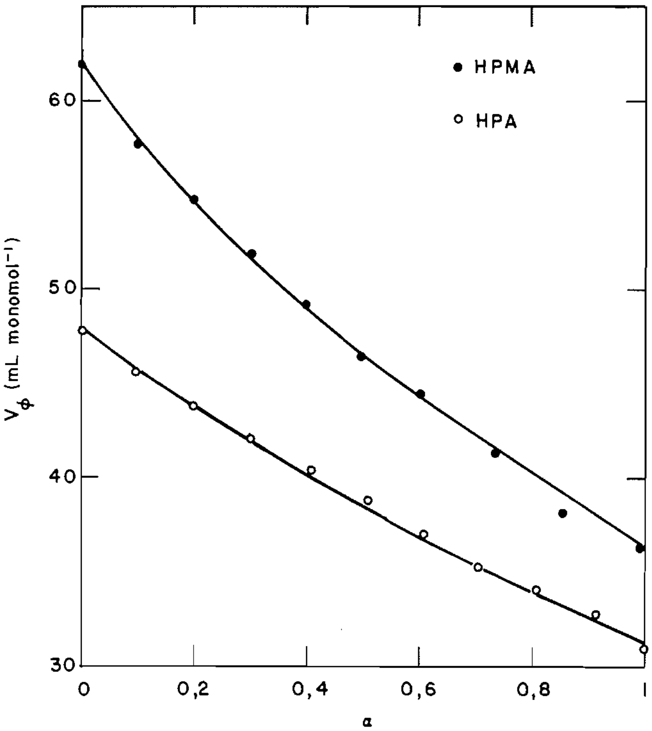

FIG. 4. Variation du volume molaire apparent moyen en fonction du degré de neutralisation à 25°C (molalités: 0,32 pour HPA et 0,20 pour HPMA).

mentation de $C_{p,\phi}$ est attribuée à l'hydratation hydrophobe qui accompagne la dénaturation. La courbe pour HPMA devrait demeurer sous celle de HPA au-delà de $\alpha = 0{,}3$ car seulement l'ionisation et l'hydratation coulombique devraient se poursuivre. Mais une deuxième anomalie se présente lorsque α augmente et cette fois $C_{p,\phi}$ diminue. La littérature ne rapporte pas de seconde transition lors de la neutralisation de HPMA. L'explication de cette deuxième anomalie pourrait se trouver dans une déshydratation partielle des groupements méthyles. Ce phénomène se passerait aussi dans le cas de solutions diluées d'espèces ioniques possédant des groupements hydrophobes (10, 20). Lors de l'ouverture de la chaîne polyméthacrylique, il est permis de présumer que presque tous les groupements méthyles s'hydratent. Mais à ce moment, la charge nette portée par la chaîne est faible. Au fur et à mesure que α augmente, cette charge nette augmente également et le champ électrostatique ainsi créé peut briser la structure pentagonale des molécules d'eau (21) autour de quelques groupements méthyles.

La figure 4 représente la variation du volume molaire apparent (V_ϕ) en fonction du degré de neutralisation pour les deux polyacides. L'allure des deux courbes est monotone et aucune anomalie ne ressort de la courbe relative à HPMA autour de $\alpha = 0{,}3$ et $\alpha = 0{,}6$. Cette absence de variation subite dans la valeur de V_ϕ lors de l'ouverture de la chaîne polyméthacrylique n'est pas unique au cas présent. Alors que la valeur de $C_{p,\phi}$ augmente appréciablement lors de la dénaturation des protéines globulaires, la valeur de V_ϕ varie peu ou ne varie pas lors de la transformation conformationnelle (16). Cependant, la chute de V_ϕ en fonction de α est initialement plus rapide lors de la neutralisation de HPMA comparativement à HPA. La présence du groupement méthyle sur le carbone porteur du groupement carboxylate et le changement conformationnel de HPMA ne sont sûrement pas étrangers à ce phénomène. En effet, l'hydratation hydrophobe, tout comme les interactions électrostatiques et l'effet destructeur de la structure de l'eau, apporte une contribution négative à V_ϕ (9).

Conclusions

Le modèle cellulaire de LK pour un polyion en solution très diluée et la structure d'une solution de polyélectrolyte évoluant avec la concentration tel que proposé par Wolff et Odijk semblent expliquer qualitativement l'allure des résultats obtenus à partir de mesures de capacités calorifiques. Par ailleurs, l'hydratation coulombique et l'hydratation hydrophobe jouent un rôle très important dans la valeur de cette quantité pour les polyélectrolytes.

Remerciements

L'aide financière fournie par le Conseil de Recherche en Sciences Naturelles et en Génie du Canada et par le Ministère de l'Education du Québec a rendu ce travail possible. Nous les en remercions.

1. M. MANDEL. Eur. Polym. J. **19**, 911 (1983).
2. C. WOLFF. J. Phys. (Paris), Colloq. **39**, C2-169 (1978).
3. J. ODIJK. Macromolecules, **12**, 688 (1979).
4. R. S. KOENE et M. MANDEL. Macromolecules, **16**, 973 (1983).
5. M. LEVIJ, J. DE BLEYSER et J. C. LEYTE. Chem. Phys. Lett. **83**, 183 (1981); **87**, 34 (1982).
6. D. DOLAR. *Dans* Polyelectrolytes. *Edité par* E. Sélégny. Reidel, Dordrecht. 1974.
7. H. DAOUST, P. FERLAND et D. ST-CYR. J. Polym. Sci. Polym. Phys. Ed. **21**, 1563 (1983).
8. S. LIFSON et A. KATCHALSKY. J. Polym. Sci. **13**, 43 (1954).
9. J. E. DESNOYERS et C. JOLICOEUR. *Dans* Treatise in electrochemistry. Vol. 5. *Edité par* J. O'M. Bockris, B. E. Conway, et E. Yeager. Plenum Press, New York. 1982. Chap. 1.
10. H. DAOUST et M.-A. CHABOT. Macromolecules, **13**, 616 (1980).
11. H. DAOUST et D. ST-CYR. Polym. J. **14**, 831 (1982).
12. H. DAOUST et D. ST-CYR. Macromolecules, **17**, 596 (1984).
13. J. P. CARTIER et H. DAOUST. Can. J. Chem. **49**, 3935 (1971).
14. M. NAGASAWA, I. NODA, T. TAKAHASHI et N. SHIMAMOTO. J. Phys. Chem. **76**, 2286 (1972).
15. J. E. DESNOYERS, C. DE VISSER, G. PERRON et P. PICKER. J. Solution Chem. **5**, 605 (1976).
16. B. RIEDL. Thèse de doctorat, Université de Sherbrooke, Sherbrooke, Québec, Canada. 1984.
17. B. RIEDL et C. JOLICOEUR. J. Phys. Chem. **88**, 3348 (1984).
18. V. CRESCENZI, F. QUADRIFOGLIO et F. DELBEN. J. Polym. Sci. C, **39**, 241 (1971).
19. F. DELBEN, V. CRESCENZI et F. QUADRIFOGLIO. Eur. Polym. J. **8**, 933 (1972).
20. N. ISE, K. MITA et F. OKUBO. J. Chem. Soc. Faraday Trans. 1, **69**, 106 (1973).
21. F. T. MARCHESE et D. L. BEVERIDGE. Chem. Phys. Lett. **105**, 431 (1984).

Violation of Hund's multiplicity rule in the electronically excited states of conjugated hydrocarbons

SHIRO KOSEKI AND TAKESHI NAKAJIMA[1]
Department of Chemistry, Faculty of Science, Tohoku University, Sendai 980, Japan

AND

AZUMAO TOYOTA
Department of Chemistry, Faculty of General Education, Yamagata University, Yamagata 990, Japan

Received August 10, 1984

This paper is dedicated to Professor Camille Sandorfy on the occasion of his 65th birthday

SHIRO KOSEKI, TAKESHI NAKAJIMA, and AZUMAO TOYOTA. Can. J. Chem. **63**, 1572 (1985).

Violation of Hund's multiplicity rule in the electronically excited states of conjugated hydrocarbons is studied by using the Pariser–Parr–Pople type SCF MO method and the *ab initio* MO method with STO-3G basis set, both methods being augmented by CI-type treatments. It is shown that for symmetrical structures (D_{2h}) of the nonalternant hydrocarbons, propalene, pentalene, and heptalene, the lowest excited singlet state is energetically lower than the corresponding triplet state. This is mainly due to the spin polarization (SP) effects. For D_{2h} structures of pentalene and heptalene the open-shell excited singlet state is predicted to be lower in energy than the closed-shell state, with the result that the former is really the ground state. Further, calculations made by including electron correlation effects reveal that in linear polyenes and polyacenes, the lowest excited singlet "minus" state (using Pariser's classification of the alternancy symmetry species) is lower in energy than the corresponding triplet state. The energy lowering of the singlet "minus" state in linear polyenes is due mostly to the mixing with the doubly excited configurations ($mm \rightarrow nn$), while the considerable part of it in polyacenes is due to the SP effects.

SHIRO KOSEKI, TAKESHI NAKAJIMA et AZUMAO TOYOTA. Can. J. Chem. **63**, 1572 (1985).

Utilisant la méthode des OM CAC du type de Pariser–Parr–Pople ainsi que la méthode des OM *ab initio* à l'aide d'un ensemble de base STO-3G alors que les deux méthodes ont été renforcées par des traitements de type IC, on a étudié la violation de la règle de multiplicité de Hund dans les états électroniques excités des hydrocarbures conjugués. On montre qu'au niveau des structures symétriques (D_{2h}) des hydrocarbures non alternants, comme le propalène, le pentalène et l'heptalène, le plus bas état singulet excité est énergiquement plus faible que l'état triplet correspondant. Ceci est dû principalement à des effets de polarisation de spin (PS). Dans les structures D_{2h} du pentalène et de l'heptalène, on prédit que l'état singulet excité à couche électronique incomplète est énergiquement plus faible que l'état à couche électronique complète; il en découle que le premier est réellement l'état fondamental. Des calculs plus poussés, incluant les effets de corrélation de l'électron, révèlent que dans les polyènes linéaires et les polyacènes, l'état singulet moins le moins excité (en utilisant la classification de Pariser des espèces de symétrie alternée) a une énergie inférieure à celle de l'état triplet correspondant. La baisse d'énergie de l'état singulet moins des polyènes linéaires est principalement due à un mélange avec des configurations doublement excitées ($mm \rightarrow nn$) tandis qu'une partie considérable de cette baisse d'énergie dans les polyacènes est due aux effets de PS.

[Traduit par le journal]

Introduction

The energetic order of the singlet–triplet pair arising from a given electronic configuration in atoms and molecules is determined by using Hund's multiplicity rule (1), and the utility of this rule has well been known. In certain cases (2–8), however, Hund's multiplicity rule breaks down. In molecular systems, of particular notice is the ground-state multiplicity of cyclobutadiene. Buenker and Peyerimhoff (3) have shown that in the square geometry (D_{4h}) of this molecule the B_{1g} singlet state is more stable than the A_{2g} triplet state by about 3.6 kcal mol^{-1}, both states arising from the same electronic configuration. The theoretical explanation of this unusual fact has firstly been given by Borden (4), followed by other authors (5–7). In connection with cyclobutadiene, the ground-state multiplicities in conjugated hydrocarbon diradicals have been examined by Borden and Davidson (6), and they have shown that the ground states of some diradicals are singlet. In these unusual molecules, the two Hueckel nonbonding molecular orbitals (NBMO's) are confined to disjoint sets of carbon atoms. In such a case, the exchange integral responsible for the energy separation of the singlet–triplet pair arising from the occupation of the NBMO's by a total of two electrons is negligibly small, and the spin polarization (SP) effects (5) can reverse the energy ordering such that the singlet state lies below the corresponding triplet state. On the other hand, if the NBMO's are not localized to disjoint sets of atoms, the triplet state lies well below the corresponding singlet state at the Hartree–Fock level, and it is less probable that the energy ordering is reversed by the SP effects.

Ruling out atomic systems, theoretical studies so far reported (3–7) have been limited to the ground-state multiplicities. In this paper, we are concerned with the possible violation of Hund's multiplicity rule for the singlet–triplet pair arising from the same singly excited electronic configuration in molecules, particularly conjugated hydrocarbons. In Section I, we give a brief account of the SP effect. In the first half of Section II, we study the energetic orders of the singlet–triplet pairs of the lowest excited states at the most symmetrical structures (D_{2h}) of the nonalternant hydrocarbons, propalene, pentalene and heptalene, which can be regarded as the weakly perturbed [4*n*]annulenes. In these antiaromatic annulenes, if they are assumed to have the most symmetrical structures, the doubly-degenerate NBMO's are confined to different sets of atoms. It follows then from the previous treatments of antiaromatic annulenes like cyclobutadiene that in the D_{2h} structures of propalene and its higher homologues Hund's multiplicity rule is most likely violated in the lowest excited states. It is shown by

[1]To whom all correspondence should be addressed.

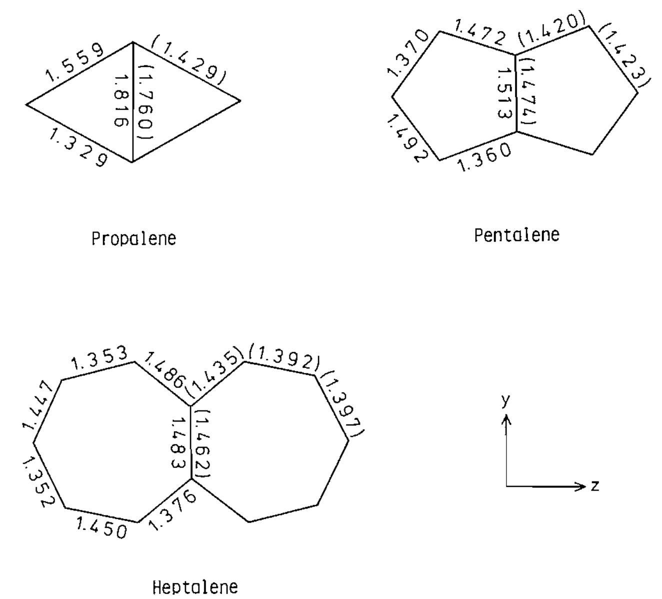

FIG. 1. Bond lengths (in Å) of the D_{2h} and C_{2h} structures of propalene, pentalene, and heptalene optimized by using the MNDO method and the choice of axes in the D_{2h} structures. The figures in parentheses are the bond lengths of the D_{2h} structures.

using the Pariser–Parr–Pople (PPP) type and *ab initio* MO methods, both the methods being augmented by the CI-type treatments, that in the D_{2h} structures of propalene, pentalene, and heptalene the lowest excited singlet state lies below the corresponding triplet state. Furthermore, in the D_{2h} structures of pentalene and heptalene, the lowest excited state ($^1B_{3g}$) is predicted to lie even below the closed-shell state (^1A_g), with the result that the open-shell singlet state is the true ground state. In the second half of Section II, we study the energetic orders of the singlet–triplet pairs of the low-lying excited "minus" and "plus" states (using Pariser's classification of the alternancy symmetry species) in linear polyenes and polyacenes.

I. Spin polarization (SP) effects

Here we give only a brief account of the SP effects on the lowest excited singlet–triplet pair, taking propalene (Fig. 1), the simplest molecule among those treated in this paper, as an example. Since propalene is formed by the introduction of a cross link to cyclobutadiene, we follow the treatment of the SP effects on the ground-state multiplicity of the square cyclobutadiene (3).

In propalene, there are four π orbitals, ϕ_1, ϕ_2, ϕ_3, and ϕ_4 in increasing order of energy. The lowest excited singlet state and the corresponding triplet state are represented by the two-determinantal wavefunctions:

$$[1a] \quad \Phi_{S,T} = \frac{1}{\sqrt{2}}(\Phi_A, \mp \Phi_B)$$

$$[1b] \quad \Phi_A = |\phi_1\, \bar{\phi}_1\, \phi_2\, \bar{\phi}_3|, \qquad \Phi_B = |\phi_1\, \bar{\phi}_1\, \bar{\phi}_2\, \phi_3|$$

where for the sake of simplicity only π orbitals were denoted. The SP effects for the singlet–triplet pair can be taken into account by including in a CI-type treatment the doubly excited configurations describing the further excitation of one electron from the doubly occupied orbital (ϕ_1) into the virtual orbital (ϕ_4), which have nonvanishing matrix elements with Φ_S and Φ_T, because ϕ_1 and ϕ_4 belong to the same irreducible representation (*vide infra*). The relevant doubly excited configurations are

$$[2a] \quad \Phi_S^1 = \frac{1}{2\sqrt{3}}\{2|\bar{\phi}_1\, \bar{\phi}_4\, \phi_2\, \phi_3| + 2|\phi_1\, \phi_4\, \bar{\phi}_2\, \bar{\phi}_3| - |\bar{\phi}_1\, \phi_4\, \bar{\phi}_2\, \phi_3| - |\phi_1\, \bar{\phi}_4\, \phi_2\, \bar{\phi}_3| - |\bar{\phi}_1\, \phi_4\, \phi_2\, \bar{\phi}_3| - |\phi_1\, \bar{\phi}_4\, \bar{\phi}_2\, \phi_3|\}$$

$$[2b] \quad \Phi_T^1 = \frac{1}{2}\{|\bar{\phi}_1\, \phi_4\, \bar{\phi}_2\, \phi_3| - |\phi_1\, \bar{\phi}_4\, \phi_2\, \bar{\phi}_3| + |\phi_1\, \bar{\phi}_4\, \bar{\phi}_2\, \phi_3| - |\bar{\phi}_1\, \phi_4\, \phi_2\, \bar{\phi}_3|\}$$

$$[2c] \quad \Phi_T^2 = \frac{1}{\sqrt{2}}\{|\bar{\phi}_1\, \bar{\phi}_4\, \phi_2\, \phi_3| - |\phi_1\, \phi_4\, \bar{\phi}_2\, \bar{\phi}_3|\}$$

It can be shown (4, 5) that the matrix element of Φ_S and Φ_S^1 is $\sqrt{3}$ times larger than that of Φ_T with Φ_T^1. On the basis of the second-order perturbation theory, it is shown that this leads to a stabilization which is three times larger for the singlet state than for the triplet state, provided that the energy denominators are equal. The matrix element of Φ_T with Φ_T^2 is negligibly small as compared with the above matrix elements: in the square cyclobutadiene in which ϕ_2 and ϕ_3 are the degenerate NBMO's, this matrix element is vanishing from the symmetry reasons. In addition, there are two more doubly excited configurations arising from the same electronic configuration, Φ_S^2 and Φ_T^3, which can mix with Φ_S and Φ_T respectively:

$$[3a] \quad \Phi_S^2 = \frac{1}{2}\{|\phi_1\, \bar{\phi}_4\, \phi_2\, \bar{\phi}_3| + |\bar{\phi}_1\, \phi_4\, \bar{\phi}_2\, \phi_3| - |\phi_1\, \bar{\phi}_4\, \bar{\phi}_2\, \phi_3| - |\bar{\phi}_1\, \phi_4\, \phi_2\, \bar{\phi}_3|\}$$

$$[3b] \quad \Phi_T^3 = \frac{1}{2}\{|\phi_1\, \bar{\phi}_4\, \phi_2\, \bar{\phi}_3| - |\bar{\phi}_1\, \phi_4\, \bar{\phi}_2\, \phi_3| + |\phi_1\, \bar{\phi}_4\, \bar{\phi}_2\, \phi_3| - |\bar{\phi}_1\, \phi_4\, \phi_2\, \bar{\phi}_3|\}$$

It can be shown, however, that the matrix element of Φ_S with Φ_S^2 and that of Φ_T with Φ_T^3 have the same value and that the energy gaps between Φ_S and Φ_S^2 and between Φ_T and Φ_T^3 are the same in general as far as Φ_S and Φ_T are written as eqs. [1*a*] and [1*b*]. Consequently, it is concluded that the energy separation between Φ_S and Φ_T is not affected by the inclusion of Φ_S^2 and Φ_T^3 in a CI-type treatment.

It is thus expected that in molecules in which the energy separation between Φ_S and Φ_T at the Hartree–Fock level is very small for certain reasons the SP effects which bring about the extra stabilization of Φ_S result in the violation of Hund's multiplicity rule such that Φ_S lies below Φ_T.

In larger molecules, there are in general many other doubly excited configurations like eqs. [2*a*]–[2*c*] responsible for the SP effects.

II. Results and discussion

1. Propalene

The ground state of propalene has two equilibrium structures with respect to C—C bond lengths, one being the delocalized structure with the D_{2h} symmetry corresponding to the saddle point of the potential energy surface, and the other the bond-alternating structure with the C_{2h} symmetry corresponding to the energy-minimum point (11). Geometrical structures of the two forms optimized by using the MNDO method (12, 13) by assuming the molecule to be planar are shown in Fig. 1, where only the C—C bond lengths are presented.

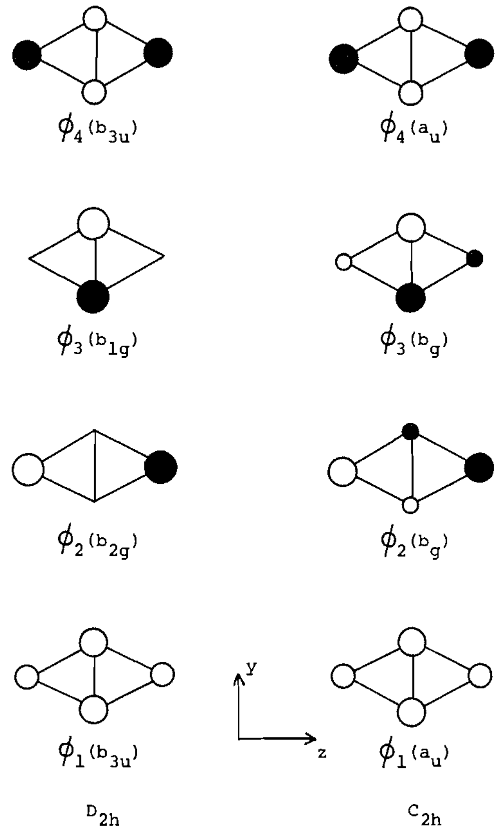

FIG. 2. The π molecular orbitals in the symmetrical (D_{2h}) and the distorted (C_{2h}) structure of propalene. White and black circles indicate the plus and minus signs of atomic-orbital coefficients, respectively.

In Fig. 2 are shown the schematic representations of π molecular orbitals for the two forms, together with orbital symmetries.

In the D_{2h} structure, the lowest excited singlet state (Φ_S) and the corresponding triplet state (Φ_T) arising from the electronic configuration $(b_{3u})^2(b_{2g})^1(b_{1g})^1$ belong to the B_{3g} irreducible representation. The singly occupied orbitals in the excited states, $\phi_2(b_{2g})$ and $\phi_3(b_{1g})$, are confined to the different carbon atoms from the symmetry reasons so that the exchange integral K_{23} responsible for the energy separation between Φ_S and Φ_T is expected to be very small: within the zero-differential overlap (ZDO) approximation the two states are degenerate (at the STO-3G level the energy separation is 0.124 eV). Thus, it is expected that $\Phi_S(B_{3g})$ lies well below $\Phi_T(B_{3g})$, provided that there exists a virtual orbital which can be used for constructing the doubly excited configuration relevant to the SP effects. Actually, $\phi_4(b_{3u})$ can be used as such a virtual orbital, and the resultant doubly excited configurations has the same symmetry (B_{3g}) as Φ_S and Φ_T.

On the other hand, in the C_{2h} structure, it is seen from the distributions of the atomic-orbital coefficients in ϕ_2 and ϕ_3 shown in Fig. 2 that the exchange integral K_{23} does not vanish even within the ZDO approximation. Actually, by using the PPP-type MO method, the energy difference between Φ_S and Φ_T is calculated to be 1.422 eV (3.934 eV at the STO-3G level). It is thus less possible that Hund's multiplicity rule can be violated in the C_{2h} structure.

In Table 1 are summarized the energy separations between Φ_S and Φ_T after the inclusion of electron correlation effects in both the structures calculated by using the second-order perturbation theory. The calculation methods used are (1) PPP+SP(RSPT), RSPT being the abbreviation of the Rayleigh–Schroedinger perturbation theory, (2) PPP+SDCI (RSPT) in which all the singly and doubly excited π configurations are included, and (3) STO-3G+CI(MR-BWPT) in which the singly and doubly excited configurations constructed from lower ten virtual orbitals (σ and π) and higher ten occupied ones and the main part of the triply and quadruply excited configurations are taken into account by using the multi-reference Brillouin–Wigner perturbation theory (MR-BWPT). For the PPP-type calculations, the geometrical structures optimized by using the PPP-type SCF MO method in conjunction with the variable bond-length technique (9–11, 15) are used, and for the *ab initio* MO calculations, those optimized by using the MNDO method (12, 13) are used.

TABLE 1. The calculated energy separations (in eV) of the lowest excited singlet–triplet pairs in nonalternant hydrocarbons[a]

Molecule	PPP	PPP+SP (RSPT)	PPP+SDCI (RSPT)	STO-3G+CI (MR-BWPT)
Propalene (D_{2h})	0	−0.366	−0.366	−0.248
Propalene (C_{2h})	1.422	1.155	0.223	1.974
Pentalene (D_{2h})	0.162	−0.400	−0.434	−0.534
Pentalene (C_{2h})	0.817	0.560	0.892	1.503
Heptalene (D_{2h})	0.140	−0.450	−0.471	
Heptalene (C_{2h})	0.661	0.394	0.905	

[a]The minus sign means that the singlet state is lower in energy than the triplet state.

As is expected, in the D_{2h} structure, the energy lowerings due to the inclusion of correlation effects turn out to be larger for $\Phi_S(B_{3g})$ than for $\Phi_T(B_{3g})$. On the other hand, in the C_{2h} structure, the PPP+SDCI and STO-3G+CI calculations indicate that the triplet state $\Phi_T(A_g)$ is lower in energy than the corresponding singlet state $\Phi_S(A_g)$, even though the lowering of $\Phi_S(A_g)$ (1.885 eV, PPP+SDCI; 9.03 eV, STO-3G+CI) is larger than that of $\Phi_T(A_g)$ (0.686 eV, PPP+SDCI; 7.04 eV, STO-3G+CI). This is due to the fact that $\Phi_T(A_g)$ is lower in energy than $\Phi_S(A_g)$ by a large amount before the inclusion of correlation effects.

It should be noted that the stabilization of $\Phi_S(B_{3g})$ in the D_{2h} structure (1.211 eV, PPP+SDCI) is due for the most part to the mixing with $\Phi_S^{\dagger}(B_{3g})$ (eq. [2*a*]) responsible for the SP effects, the stabilization energy due to this mixing being 0.974 eV, while that of $\Phi_S(A_g)$ in the C_{2h} structure (1.885 eV) is due substantially to the direct mixing with the doubly excited configurations (^1A_g), such as $(\phi_1)^2(\phi_3)^2$, which are not operative in lowering the energy of $\Phi_S(B_{3g})$ in the D_{2h} structure, the energy lowering of $\Phi_S(A_g)$ due to the mixing with $\Phi_S^{\dagger}(A_g)$ responsible for the SP effects being 0.518 eV.

It is added that the results obtained by using *ab initio* MO methods with extended basis sets are consistent at least qualitatively with the above results, though the energy separations, calculated by using 4-31G+CI(MR-BWPT) and 6-31G+CI (MR-BWPT), of the lowest excited singlet–triplet pair in the D_{2h} structure turn out to be considerably smaller (−0.038 eV and −0.055 eV, respectively).

The variations of the total energies of the various states of propalene with the nuclear distortion along the bond-alternating mode are shown in Fig. 3. The total energies taken to be the sum of the π-electron, σ-bond, and core-repulsion energies (10) were calculated at the PPP+SDCI(RSPT) level. It is seen that no molecular-symmetry reduction occurs in the excited

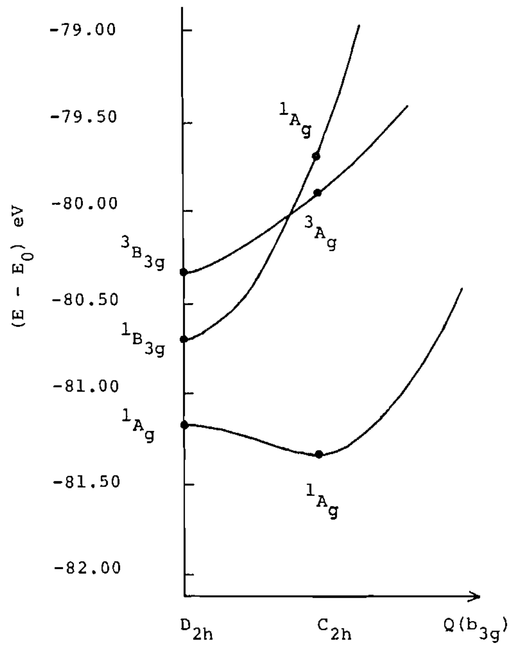

FIG. 3. The potential energy curves calculated by using the PPP+SDCI(RSPT) method of the ground state and the lowest $\pi \rightarrow \pi^*$ excited singlet and triplet states of propalene. E_0 is the sum of the σ-bond and core-repulsion energies at the D_{2h} structure (15).

states, Φ_S and Φ_T, and the potential energy curves for the two states intersect at a certain intermediate distorted nuclear arrangement.

2. Pentalene and heptalene

In these molecules, the HOMO and the LUMO originate from the doubly degenerate NBMO's of the corresponding $4n$ cyclic polyene, the HOMO's of propalene and heptalene and the LUMO of pentalene remaining still nonbonding. It is thus expected that in such molecules the exchange integral responsible for the energy separation between the excited singlet and triplet states originating from the electron jump HOMO $\rightarrow$ LUMO is rather small, and the SP effects lead to the violation of Hund's multiplicity rule.

Now it has well been known both theoretically (9–11, 14, 15) and experimentally (16–20) that the ground states of pentalene and heptalene undergo the molecular-symmetry reduction $D_{2h} \rightarrow C_{2h}$, as that of propalene does. The geometrical structures with respect to the C—C bond lengths of the symmetrical (D_{2h}) and distorted (C_{2h}) structures optimized by using the MNDO method are shown in Fig. 1.

The predicted energy lowerings of the lowest excited singlet–triplet pair due to the inclusion of correlation effects are listed in Table 1. In the D_{2h} structure of pentalene, the lowest excited triplet state $\Phi_T(B_{3g})$ is lower in energy than the corresponding singlet state $\Phi_S(B_{3g})$ by 0.162 eV (PPP) and 0.295 eV (STO-3G) before the inclusion of correlation effects, and the inclusion of correlation effects results in the violation of Hund's multiplicity rule such that $\Phi_S(B_{3g})$ is lower in energy than $\Phi_T(B_{3g})$ by 0.4–0.5 eV. In the D_{2h} structure of heptalene, the lowest triplet state $\Phi_T(B_{3g})$ is lower in energy than the corresponding singlet state $\Phi_S(B_{3g})$ only by 0.140 eV (PPP) before the inclusion of correlation effects. If we include these effects, it turns out that $\Phi_S(B_{3g})$ is lower than $\Phi_T(B_{3g})$ by ca. 0.5 eV.

By comparing the energy lowerings predicted by using the PPP+SP and PPP+SDCI methods, it is concluded that, as in the D_{2h} structure of propalene, the violation of Hund's multiplicity rule in the D_{2h} structures of pentalene and heptalene is due mainly to the SP effects. In the distorted structures (C_{2h}) of these molecules, Hund's multiplicity rule holds for the lowest excited singlet–triplet pair even after the inclusion of correlation effects.

It should be remarked that at the saddle points of the ground-state potential energy curves along the bond-alternating mode (the D_{2h} structures) of pentalene and heptalene, the energy lowering of the lowest excited singlet state ($^1B_{3g}$) is so large that this open-shell state lies most likely even below the closed-shell state (^1A_g) assumed to be the ground state before the inclusion of correlation effects. The *ab initio* MO calculations made by using the STO-3G+CI (MR-BWPT) method actually show that in pentalene the open-shell state ($^1B_{3g}$) is lower in energy than the closed-shell state (^1A_g) by 0.57 eV. Such a change of the nature of the ground state reduces considerably the energy difference between the energy-minimum state (C_{2h}) and the saddle point (D_{2h}) (21). In fact, all the energy differences so far calculated by assuming the ground state at the saddle point to be the closed-shell state (9–11, 14, 15) are too large to be comparable to the experimental activation energies for the isodynamic double-bond shift isomerization reaction in pentalene and heptalene (19, 20).

3. Alternant hydrocarbons

In alternant hydrocarbons, if the i-, j-, k-, and lth MO's are the next HOMO, the HOMO, the LUMO, and the next LUMO, respectively, the two singly excited configurations Φ_{ik} and Φ_{jl} are degenerate within the ZDO approximation owing to the pairing theorem.

$$[4a] \quad {}^{1,3}\Phi_{ik} = \frac{1}{\sqrt{2}}\{|\phi_i\,\bar{\phi}_k\,\phi_j\,\bar{\phi}_j| \mp |\bar{\phi}_i\,\phi_k\,\phi_j\,\bar{\phi}_j|\}$$

$$[4b] \quad {}^{1,3}\Phi_{jl} = \frac{1}{\sqrt{2}}\{|\phi_i\,\bar{\phi}_i\,\phi_j\,\bar{\phi}_l| \mp |\phi_i\,\bar{\phi}_i\,\bar{\phi}_j\,\phi_l|\}$$

The proper linear combinations of these degenerate configurations yield the two excited singlet and triplet states:

$$[5a] \quad {}^1\Phi^{\pm} = \frac{1}{\sqrt{2}}({}^1\Phi_{ik} \pm {}^1\Phi_{jl})$$

$$[5b] \quad {}^3\Phi^{\pm} = \frac{1}{\sqrt{2}}({}^3\Phi_{ik} \pm {}^3\Phi_{jl})$$

with the energies relative to the ground state given by

$$[6a] \quad {}^{1,3}E^{+} = \epsilon_k - \epsilon_i - J_{ik} + 2\,K_{ik} - K_{ij} \pm 2\,K_{ik}$$

$$[6b] \quad {}^{1,3}E^{-} = \epsilon_k - \epsilon_i - J_{ik} + K_{ij}$$

where ϵ_i is the orbital energy of the ith MO, and J_{ik} and K_{ik} are the Coulomb and exchange integrals between the ith and kth MO's, respectively.

In the lowest excited A_g states of linear polyenes and the lowest B_{2u} states of linear polyacenes treated in this paper, the relation that $2K_{ik} > K_{ij}$ holds (in larger linear polyacenes, the ith and lth MO's are not always the next HOMO and the next LUMO, respectively), and the energy ordering of the four excited states is such that ${}^3E^+ < {}^3E^- = {}^1E^- < {}^1E^+$ before the inclusion of correlation effects within the ZDO approximation. Since ${}^3\Phi^-$ and ${}^1\Phi^-$ are degenerate at this stage, it is expected that the inclusion of correlation effects lifts the degeneracy and leads to the energy ordering such that ${}^1\Phi^-$ lies below ${}^3\Phi^-$. Such

TABLE 2. The stabilization energies (in eV) calculated by using the various PPP type approximations of the singlet–triplet pairs of the lowest excited "minus" and "plus" states in linear polyenes and polyacenes[a]

Excited state	PPP[b]	PPP+SP (RSPT)	PPP+SDCI (RSPT)	PPP+SDCI (BWPT)	Singlet–triplet energy gap[c] (BWPT)
Butadiene					
${}^1A_g^-$	6.92	−0.62	−3.36	−1.78	−1.59
${}^3A_g^-$	6.92	−0.18	−0.19	−0.19	
${}^1A_g^+$	8.29	0	−0.31	−0.29	5.16
${}^3A_g^+$	3.00	−0.18	−0.17	−0.16	
Hexatriene					
${}^1A_g^-$	6.06	−0.45	−3.58	−1.75	−0.97
${}^3A_g^-$	6.06	−0.53	−0.98	−0.78	
${}^1A_g^+$	6.88	−0.02	−0.43	−0.40	4.20
${}^3A_g^+$	3.10	−0.11	−0.95	−0.82	
Octatetraene					
${}^1A_g^-$	5.46	−0.60	−3.39	−1.70	−0.67
${}^3A_g^-$	5.46	−0.68	−1.40	−1.03	
${}^1A_g^+$	5.98	−0.16	−0.51	−0.48	3.65
${}^3A_g^+$	2.82	−0.18	−1.13	−0.97	
Decapentaene					
${}^1A_g^-$	5.06	−0.62	−3.14	−1.65	−0.49
${}^3A_g^-$	5.06	−0.73	−1.62	−1.16	
${}^1A_g^+$	5.35	−0.18	−0.57	−0.53	3.24
${}^3A_g^+$	2.61	−0.20	−1.22	−1.03	
Dodecahexaene					
${}^1A_g^-$	4.79	−0.66	−2.90	−1.62	−0.35
${}^3A_g^-$	4.79	−0.77	−1.85	−1.27	
${}^1A_g^+$	4.89	−0.20	−0.63	−0.58	2.93
${}^3A_g^+$	2.47	−0.20	−1.31	−1.09	
Tetradecaheptaene					
${}^1A_g^-$	4.60		−2.71	−1.59	−0.25
${}^3A_g^-$	4.60		−2.04	−1.34	
${}^1A_g^+$	4.54		−0.68	−0.62	2.68
${}^3A_g^+$	2.39		−1.39	−1.15	
Benzene					
${}^1B_{2u}^-$ (${}^1L_b$)[d]	4.90	−1.18	−2.24	−1.88	−1.85
${}^3B_{2u}^-$ (${}^3L_b$)	4.90	−0.02	−0.03	−0.03	
${}^1E_{1u}^+$ (${}^1B_b$)	7.02	−0.24	−1.06	−0.94	3.03
${}^3E_{1u}^+$ (${}^3B_b$)	3.99	−0.87	−1.04	−0.94	
Naphthalene					
${}^1B_{2u}^-$ (${}^1L_b$)	4.31	−0.93	−1.98	−1.67	−1.14
${}^3B_{2u}^-$ (${}^3L_b$)	4.31	−0.24	−0.57	−0.53	
${}^1B_{2u}^+$ (${}^1B_b$)	5.83	−0.57	−1.22	−1.07	2.16
${}^3B_{2u}^+$ (${}^3B_b$)	3.80	−0.64	−1.39	−1.19	
Anthracene					
${}^1B_{2u}^-$ (${}^1L_b$)	3.91	−0.85	−1.98	−1.55	−0.89
${}^3B_{2u}^-$ (${}^3L_b$)	3.91	−0.27	−0.86	−0.76	
${}^1B_{2u}^+$ (${}^1B_b$)	5.14	−0.61	−1.33	−1.16	1.70
${}^3B_{12}^+$ (${}^3B_b$)	3.58	−0.62	−1.55	−1.30	
Naphthacene					
${}^1B_{2u}^-$ (${}^1L_b$)	3.70	−0.80	−2.01	−1.65	−0.72
${}^3B_{2u}^-$ (${}^3L_b$)	3.70	−0.27	−1.08	−0.93	
${}^1B_{2u}^+$ (${}^1B_b$)	4.70	−0.63	−1.43	−1.23	1.38
${}^3B_{2u}^+$ (${}^3B_b$)	3.47	−0.56	−1.67	−1.38	
Pentacene					
${}^1B_{2u}^-$ (${}^1L_b$)	3.59		−2.06	−1.67	−0.61
${}^3B_{2u}^-$ (${}^3L_b$)	3.59		−1.28	−1.06	
${}^1B_{2u}^+$ (${}^1B_b$)	4.41		−1.53	−1.30	1.13
${}^3B_{2u}^+$ (${}^3B_b$)	3.43		−1.79	−1.45	

TABLE 2. (*Concluded*)

Excited state	PPP[b]	PPP+SP (RSPT)	PPP+SDCI (RSPT)	PPP+SDCI (BWPT)	Singlet−triplet energy gap[c] (BWPT)
Phenanthrene (C_{2v})					
$^1A_1^-$ (^1L_b)	4.15	−0.58	−1.97	−1.61	−0.75
$^3A_1^-$ (^3L_b)	4.15	−0.23	−1.04	−0.86	
$^1A_1^+$ (^1B_b)	5.43	−0.43	−1.37	−1.15	1.88
$^3A_1^+$ (^3B_b)	3.68	−0.45	−1.55	−1.28	

[a]In linear polyacenes, the yz-plane is taken to be the molecular plane, the y axis being parallel to the molecular long axis.
[b]The state energies are given by eqs. [6*a*] and [6*b*].
[c]The minus sign means that the singlet state is lower in energy than the triplet state.
[d]The notations in parentheses are due to Platt (24).

an energy ordering is considered as forming an exception to Hund's multiplicity rule, though $^3\Phi^-$ and $^1\Phi^-$ are represented by the mixture of the two monoexcited configurations and the rule holds for the singlet-triplet pairs of the component monoexcited configurations ($E(^3\Phi_{ik}) < E(^1\Phi_{ik})$ and $E(^3\Phi_{jl}) < E(^1\Phi_{jl})$).

As for the energy lowering of low-lying excited states due to the inclusion of correlation effects in alternant hydrocarbons, Čížek *et al.* (22) have proposed the qualitative rule which states that it will be most pronounced for the singlet "minus" states as compared with the singlet "plus" and both "plus"and "minus" triplet states. They have demonstrated the validity of this rule for a number of actual molecules, but they have treated only the energy orderings of singlet states. Here, we discuss the energy orderings of the singlet−triplet pairs of the "minus" and "plus" states in linear polyenes and polyacenes by using the same methods as used above for the nonalternant hydrocarbons, paying special attention to the role of the SP effects. However, the SP effects on the singlet−triplet pairs of the "minus" and "plus" excited states in these molecules are not so simple as those described in Section I, because an excited state in this case is written by the linear combination of the degenerate monoexcited states, one corresponding to the HOMO → the next LUMO and the other to the next HOMO → LUMO, and there are, in general, four types of doubly excited configurations responsible for the SP effects on the singlet−triplet pairs of the excited state. It cannot be shown without numerical calculations how the SP effects affect the energy orderings of the singlet−triplet pairs of the "minus" and "plus" excited states.

(a) Linear polyenes

In Table 2 are presented the predicted stabilization energies of the lowest excited $A_g^\pm$ states due to the inclusion of correlation effects. The data obtained by using the PPP+SDCI approximations indicate that in all the molecules examined the stabilization energies of the $^1A_g^-$ states are distinctly larger than those of the $^3A_g^-$ states, though the energy differences between the two states tend to be less pronounced as the molecular size increases. On the other hand, the stabilization energies of the "plus" states are larger for the triplet states than for the singlet states (except for butadiene), and Hund's multiplicity rule holds for these singlet−triplet pairs even after the inclusion of correlation effects.

It is interesting to note that in linear polyenes the large energy intervals between the $^1A_g^-$ and $^3A_g^-$ states are not attributable even qualitatively to the SP effects apart from butadiene: the stabilization energies due to the SP effects are larger for the $^3A_g^-$ state than for the $^1A_g^-$ state (except for butadiene). The most important configurations contributory to the large stabilizations of the $^1A_g^-$ states are the doubly excited singlet configurations of A_g symmetry ($mm \rightarrow nn$), particularly that corresponding to the electron jump from the HOMO to the LUMO, and this is true for butadiene also. On the other hand, it can be shown that the contribution of such doubly excited configurations to the stabilization of the $^1A_g^+$ state is very small: the matrix elements of $^1A_g^+$ with the doubly excited configurations, $jj \rightarrow kk$ and $ii \rightarrow ll$, are vanishing within the ZDO approximation. More precisely, the matrix elements of the component singly excited configurations of ^1A_g, Φ_{ik}, and Φ_{jl}, with the above doubly excited configurations have the same absolute value but are opposite in sign.

In order to examine the contributions of the higher-order configuration interactions, the stabilization energies of the lowest excited $A_g^\pm$ states of butadiene and octatetraene are calculated by using the STO-3G+CI(MR-BWPT) approximation (Table 3). The results obtained indicate again that the large stabilizations of the $^1A_g^-$ state are little due to the SP effects. The energy differences between the $^1A_g^-$ and $^3A_g^-$ states presented in Table 3 are appreciably large as compared with those listed in Table 2, but if we use a more extended basis set and make a larger-scale CI calculation, considerably smaller values could be obtained (23).

(b) Polyacenes

The stabilization energies due to the inclusion of correlation effects of the singlet−triplet pairs of the lowest $B_{2u}^\pm$ states in linear polyacenes (the lowest B_{2u}^- and E_{1u}^+ states in benzene) calculated within the semiempirical approach (PPP) are shown in Table 2. In this table the data for the lowest excited $A_1^\pm$ states of phenanthrene are also included.

By comparing the energy differences between the singlet and triplet "minus" states in linear polyacenes calculated by using the PPP+SDCI(RSPT) method with those calculated by using the PPP+SP(RSPT) one, it is revealed that the considerable part (about one half) of the energy difference is due to the SP effects.

It should be remarked that the stabilization energies of the singlet "minus" states obtained by using the PPP+SDCI approximations are so large that these states become very near in energy to the triplet "plus" states. This is in qualitative agreement with the fact that the singlet "minus" states are experimentally estimated to be slightly lower in energy (by 0.1 − 0.3 eV) than the triplet "plus" states (24). The predicted energy

TABLE 3. The stabilization energies (in au) obtained by the *ab initio* calculations of the lowest "minus" and "plus" states in butadiene, octatetraene, benzene, and naphthalene

Excited state	SCF	STO-3G+SP (π)	STO-3G+CI (MR-BWPT)	Singlet−triplet energy gap[a] (in eV)
Butadiene				
$^1A_g^-$	−152.5843	−0.0342	−0.2961	−3.81
$^3A_g^-$	−152.5804	−0.0173	−0.1601	
$^1A_g^+$	−152.5016	−0.0020	−0.1959	7.01
$^3A_g^+$	−152.8522	−0.0096	−0.1028	
Octatetraene				
$^1A_g^-$	−304.5573	−0.0540	−0.2645	−3.78
$^3A_g^-$	−304.5552	−0.0480	−0.1275	
$^1A_g^+$	−304.5290	−0.0144	−0.1187	6.52
$^3A_g^+$	−304.7315	−0.0153	−0.1558	
Benzene				
$^1B_{2u}^-$ (^1L_b)[b]	−227.6109	−0.0799	−0.1959	−3.39
$^3B_{2u}^-$ (^3L_b)	−227.6175	0	−0.0648	
$^1E_{1u}^+$ (^1B_b)	−227.4557	−0.0210	−0.1719	4.68
$^3E_{1u}^+$ (^3B_b)	−227.6706	−0.0557	−0.1288	
Naphthalene				
$^1B_{2u}^-$ (^1L_b)	−378.4337	−0.0782	−0.1925	−2.26
$^3B_{2u}^-$ (^3L_b)	−378.4373	−0.0177	−0.1059	
$^1B_{2u}^+$ (^1B_b)	−378.3253	−0.0555	−0.1573	3.95
$^3B_{2u}^+$ (^3B_b)	−378.4690	−0.0555	−0.1587	

[a]The minus sign means that the singlet state is lower in energy than the triplet state.
[b]The notations in parentheses are due to Platt (24).

difference between the singlet and triplet "minus" states in linear polyacenes tends to decrease with the molecular size. This is not in agreement with Platt's assumption that in polyacenes this energy separation can be taken to be constant (4000 cm^{-1}) except for that in benzene (5600 cm^{-1}) (24), apart from the fact that the predicted energy separations are considerably large as compared with Platt's values.

The stabilization energies calculated by using the PPP+SDCI methods for the singlet "plus" state (B_{2u}^+) (the E_{1u}^+ state in benzene and the A_1^+ state in phenanthrene) are almost the same as those for the corresponding triplet states in all the polyacenes examined. This indicates that the energy separations of the singlet−triplet pairs of the "plus" states calculated at the naive PPP level are little affected by the inclusion of correlation effects. The predicted energy separations are rather large as compared with the experimentally estimated values (1.74 eV, benzene; 1.24 eV, naphthalene; 1.05 eV, anthracene and naphthacene; 1.08 eV, pentacene; 1.20 eV, phenanthrene), the agreement between the theoretical and experimentally estimated values in linear polyacenes becoming better as the molecular size increases.

The stabilization energies of the excited states under consideration due to the inclusion of correlation effects in benzene and naphthalene are calculated also by using the STO-3G+CI(MR-BWPT) approximation. The obtained results are consistent with those obtained above, though the calculated values (Table 3) are considerably larger than those presented in Table 2 because of the use of the minimal basis set and the inclusion of the limited configuration interactions (25).

Conclusion

Propalene and its higher homologues, pentalene and heptalene, are the pertinent molecules for understanding how the SP effects affect the energy ordering of the electronically excited singlet−triplet pair. It is revealed that in these molecules Hund's multiplicity rule breaks down for the lowest excited singlet−triplet pair at the saddle point of the ground-state energy surface. Further, at the saddle points of pentalene and heptalene, the lowest excited singlet state (B_{3g}) is predicted to lie even below the closed-shell state (^1A_g), with the result that the open-shell state ($^1B_{3g}$) is really the ground state.

Hund's multiplicity rule breaks down also for the singlet−triplet pairs of the lowest excited "minus" states in linear polyenes and polyacenes. The energy separations of the singlet−triplet pairs in linear polyenes are due mostly to the mixing of the singlet state with the doubly excited configurations ($mm \rightarrow nn$), while the considerable part of the energy separations of the singlet−triplet pairs in polyacenes are due to the SP effects.

Hund's multiplicity rule breaks down most likely for an excited singlet−triplet pair whose energy separation at the Hartree−Fock level is rather small because of the smallness of the exchange integral responsible for the energy separation. An example of such an excited singlet−triplet pair is given by the singlet−triplet pair of an n $\rightarrow \pi^*$ transition besides those of $\pi \rightarrow \pi^*$ transitions treated in this paper. In this connection, it is interesting to note that the INDO+CI calculations of the electronic spectra of benzoic acid made by Ridley and Zerner (26) show that the lowest $^1(n,\pi^*)$ is lower in energy than the corresponding triplet state by 0.56 eV.

In view of the present results it is perhaps useful to note that the descriptions of the electronically excited states in the framework of the naive PPP approximation do not yield the correct energy ordering in general, particularly for the accidentally degenerate states. In order to obtain the correct energy ordering within this semiempirical approximation, one has to employ the empirical parameters for use in evaluating the energies of excited triplet states which are different from those used in evaluating the energies of excited singlet states (27).

Hoping that the poor quality of the basis sets and the limited CI used in the present *ab initio* MO calculations do not impair the main conclusions obtained in this paper, we are now considering more accurate calculations particularly for pentalene and heptalene.

Acknowledgements

All *ab initio* MO calculations have been performed by using the GAUSSIAN 70 and EFCI programs at the Computer Center of Tohoku University. The authors thank Professors K. Morokuma and S. Iwata for providing these programs, and Dr. M. Hanamura for assistance in carrying out the *ab initio* MO calculations. We thank also Professors M. Ito and D. M. Silver for helpful discussions. This work was partially supported by the Ministry of Education, Japan, under grant-in-aid for the Scientific Research (No. 59540249).

1. F. HUND. Z. Phys. **33**, 345 (1925).
2. R. F. BACHER. Phys. Rev. **43**, 264 (1933).
3. R. J. BUENKER and S. D. PEYERIMHOFF. J. Chem. Phys. **48**, 354 (1968).
4. W. T. BORDEN. J. Am. Chem. Soc. **97**, 5968 (1975).
5. H. KOLLMAR and V. STAEMMLER. J. Am. Chem. Soc. **99**, 3583 (1977); H. KOLLMAR and V. STAEMMLER. Theor. Chim. Acta, Berlin, **48**, 223 (1978).
6. W. T. BORDEN and E. R. DAVIDSON. J. Am. Chem. Soc. **99**, 4587 (1977).
7. K. HASHIMOTO and H. FUKUTOME. Bull. Chem. Soc. Jpn. **54**, 3651 (1981).
8. J. W. WARNER, L. S. BARTELL, and S. M. BLINDER. Int. J. Quantum Chem. **18**, 921 (1980) and references cited therein.
9. H. YAMAGUCHI, T. NAKAJIMA, and T. L. KUNII. Theor. Chim. Acta, Berlin, **12**, 349 (1968).
10. A. TOYOTA, T. TANAKA, and T. NAKAJIMA. Int. J. Quantum Chem. **10**, 917 (1976).
11. A. TOYOTA and T. NAKAJIMA. Bull. Chem. Soc. Jpn. **46**, 3681 (1973); A. TOYOTA and T. NAKAJIMA. Theor. Chim. Acta, Berlin, **53**, 297 (1979).
12. M. J. S. DEWAR and W. THIEL. J. Am. Chem. Soc. **99**, 4899 4907 (1977).
13. M. J. S. DEWAR and G. P. FORD. J. Am. Chem. Soc. **101**, 5556 (1979).
14. A. TAJIRI, N. OHMICHI, and T. NAKAJIMA. Bull. Chem. Soc. Jpn. **44**, 2347 (1971).
15. Y. JEAN. Nouv. J. Chim. **4**, 11 (1980).
16. E. LE GOFF. J. Am. Chem. Soc. **84**, 3975 (1962).
17. B. KITSCHKE and H. J. LINDNER. Tetrahedron Lett. **29**, 2511 (1977); H. J. LINDNER and B. KITSCHKE. Angew. Chem. Int. Ed. Engl. **15**, 106 (1976); J. STEGEMANN and H. J. LINDNER. Tetrahedron Lett. **29**, 2515 (1977).
18. K. HAFNER and H. U. SUESS. Angew. Chem. **85**, 626 (1973).
19. E. VOGEL, H. KOENIGSHOFEN, J. WASSEN, K. MUELLEN and J. F. M. OTH. Angew. Chem. Int. Ed. Engl. **13**, 732 (1974).
20. K. HAFNER. Pure Appl. Chem. **54**, 939 (1982).
21. M. KATAOKA, S. KOSEKI, K. IIDA, and T. NAKAJIMA. Nouv. J. Chim. In press.
22. J. ČÍŽEK, J. PALDUS, and I. HUBAČ. Int. J. Quantum Chem. **8**, 951 (1974); J. PALDUS, J. ČÍŽEK, and I. HUBAČ. Int. J. Quantum Chem. Symp. **8**, 293 (1974).
23. R. P. HOSTENY, T. H. DUNNING JR., R. R. GILMAN, A. PIPANO, and I. SHAVITT. J. Chem. Phys. **62**, 4764 (1975).
24. H. B. KLEVENS and J. R. PLATT. J. Chem. Phys. **17**, 470 (1949); J. R PLATT. J. Chem. Phys. **18**, 1168 (1950); C. W. SCHERR. J. Chem. Phys. **21**, 1582 (1953); D. R. KEARNS. J. Chem. Phys. **36**, 1608 (1962); J. B. BIRKS, L. G. CHRISTOPHOROV, and R. H. HUEBNER. Nature, **217**, 809 (1968); J. P. DOERING. J. Chem. Phys. **51**, 2866 (1969).
25. P. J. HAY and I. SHAVITT. J. Chem. Phys. **60**, 2865 (1974); S. D. PEYERIMHOFF and R. J. BUENKER. Theor. Chim. Acta, Berlin, **19**, 1 (1970); R. J. BUENKER, J. L. WHITTEN, and J. D. PETKE. J. Chem. Phys. **49**, 2261 (1968).
26. J. E. RIDLEY and M. C. ZERNER. J. Mol. Spectrosc. **76**, 71 (1979).
27. J. N. MURRELL and K. L. MCEWEN. J. Chem. Phys. **25**, 1143 (1956); J. PANCÍŘ and R. ZAHRADNÍK. Theor. Chim. Acta, Berlin, **14**, 426 (1969).

Photoélectrochimie des phtalocyanines sans métal, de cuivre et de fer

BENOÎT MARSAN ET GUY BÉLANGER
Institut de Recherche d'Hydro-Québec, C.P. 1000, Varennes (Qué.), Canada J0L 2P0

ET

DOMINIQUE-LOUIS PIRON
Département de Génie Métallurgique, École Polytechnique, Université de Montréal, C.P. 6079, Succursale A, Montréal (Qué.), Canada H3C 3A7

Reçu le 16 août 1984

Cet article est dédié au Professeur Camille Sandorfy à l'occasion de son 65^e anniversaire

BENOÎT MARSAN, GUY BELANGER et DOMINIQUE-LOUIS PIRON. Can. J. Chem. **63**, 1580 (1985).

Le comportement cathodique et photocathodique d'électrodes de phtalocyanine sans métal, de cuivre et de fer (H_2Pc, CuPc et FePc) a été étudié en solutions acide, neutre et alcaline. Dans le noir, la courbe de polarisation de l'électrode de FePc présente deux pics de réduction qui n'ont pas été observés avec les autres phtalocyanines; ils sont associés à la réduction du cation central. L'illumination des électrodes semiconductrices n'a produit aucun effet sur la réaction du dégagement de l'hydrogène. L'analyse des courbes capacité–tension a révélé la présence de niveaux intermédiaires localisés à l'intérieur de la bande interdite des semiconducteurs et recouvrant environ 1% de leurs sites de surface. Les résultats sont expliqués en considérant les phtalocyanines comme des électrodes semiconductrices de type *p*. L'énergie des bandes et des états de surface a été illustrée dans un modèle d'interphase semiconducteur–électrolyte et la nature des transferts de charges inhibés par la présence de ces états interfaciaux a été discutée.

BENOÎT MARSAN, GUY BELANGER, and DOMINIQUE-LOUIS PIRON. Can. J. Chem. **63**, 1580 (1985).

The cathodic and photocathodic behavior of electrodes of phthalocyanines without metal or complexed to copper or iron (H_2Pc, CuPc, and FePc) has been studied in acidic, neutral, and alkaline media. In the dark, the polarization curve of the electrode of FePc shows two peaks of reduction which are not observed with the other phthalocyanines; these are associated with the reduction of the central cation. Lighting the semiconducting electrodes does not produce any effect on the reaction of production of hydrogen. An analysis of the curves of capacity vs. potential indicates the presence of intermediate levels localized within the forbidden band of the semiconductors and covering about 1% of their sites on the surface. The results can be explained if the phthalocyanines are considered to be semiconducting electrodes of type *p*. The energy of the bands and of the surface states can be depicted with a semiconductor–electrolyte interphase model and the nature of the charge transfers inhibited by the presence of these interfacial states is discussed.

[Journal translation]

1. Introduction

Les phtalocyanines ont récemment retenu beaucoup d'attention, en particulier sous forme de films minces. Leurs propriétés catalytiques, principalement vis-à-vis la réaction de réduction de l'oxygène (piles à combustible), ont été étudiées de façon approfondie (1–5). Les phtalocyanines sont des semiconducteurs organiques de type *p* (6) et leurs propriétés électriques ont été abondamment étudiées. La semiconductivité intrinsèque est associée aux électrons π mobiles des doubles liaisons conjuguées.

Le recouvrement important entre les orbitales π de la phtalocyanine et les orbitales *d* du métal suppose que ce dernier joue le rôle de pont lors d'un transfert électronique d'une molécule à une autre (7). Les impuretés ont également une influence sur la conductivité, en particulier l'oxygène qui diminue l'énergie d'activation de conduction des phtalocyanines (8). Ces dopants agissent comme pièges à électrons, entraînant la création d'un plus grand nombre de trous mobiles.

Étant donné que les phtalocyanines absorbent fortement dans la région visible du spectre solaire, avec une bande interdite de l'ordre de 1,8–2,1 eV (3), il a été suggéré de les utiliser dans des cellules photovoltaïques (9–16). Bien que le rendement de conversion de l'énergie solaire en énergie électrique soit très faible (<1%), à cause principalement du faible rendement quantique, certaines phtalocyanines (H_2Pc, CuPc, NiPc, MgPc) ont manifesté des activités intéressantes. Il a été observé que le rendement quantique peut être accru si les couches minces organiques sont exposées à l'air ambiant (11). Des études électrochimiques et photoélectrochimiques mettant en cause des électrodes de quelques phtalocyanines (H_2Pc, ZnPc, FePc, CuPc, NiPc) en couches minces ont également été rapportées (17, 18). De plus, des films de phtalocyanines ont été utilisés pour de la sensibilisation spectrale dans des cellules photoélectrochimiques (19–23).

Le présent travail se propose d'étudier le comportement électrochimique et photoélectrochimique des phtalocyanines sans métal, de cuivre et de fer évaporées en films minces dans des milieux acide, neutre et alcalin. Les résultats sont discutés en fonction des positions relatives des niveaux d'énergie des semiconducteurs, des couples $H^+(H_2O)/H_2$ et $O_2/H_2O(OH^-)$ en solution et des états de surface déterminés à partir des mesures de capacité différentielle.

2. Partie expérimentale

2.1 *Préparation des électrodes de phtalocyanine*

Une couche mince de H_2Pc, CuPc ou FePc provenant d'Eastman Kodak Co. et n'ayant été soumis à aucune autre purification ou autre traitement quelconque, d'une épaisseur approximative de 1000 Å, a été déposée par évaporation à 5×10^{-6} Torr (1 Torr = 133.3 Pa) sur un mince film d'or (~500 Å) préalablement formé sur une surface polie de cuivre dans une gaine de Kel-F (fig. 1). L'épaisseur des films a été évaluée par un contrôleur Varian modèle 980-6005. Les électrodes de phtalocyanine ont ensuite été chauffées dans une étuve à une température voisine de 100°C durant environ 2 h, puis exposées à l'air ambiant pendant 46 h avant leur immersion dans la solution, de manière à augmenter la conductivité des films semiconducteurs (17). Des évaporations successives d'or et de phtalocyanine (H_2Pc, CuPc ou FePc), formant des couches respectives d'une épaisseur voisine de 500 Å et 3000 Å, ont été effectuées sur une surface de graphite pour

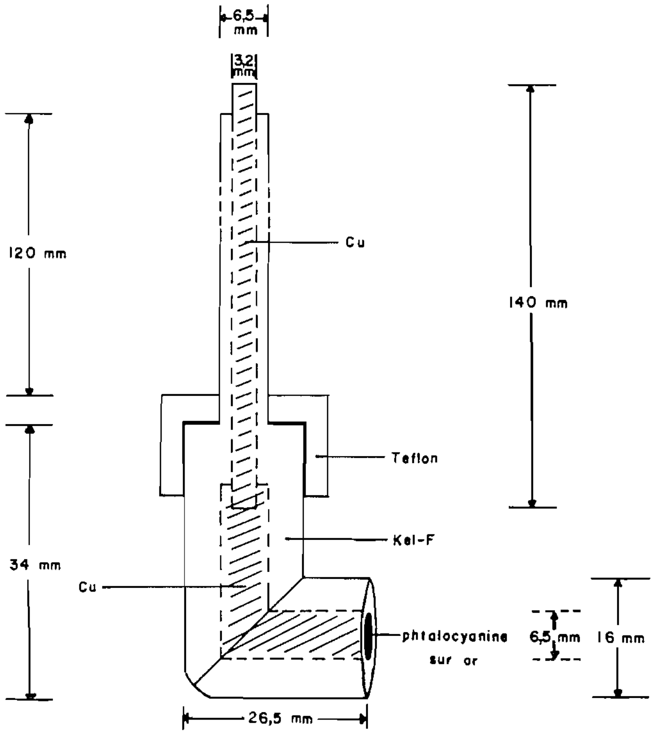

FIG. 1. Électrode de phtalocyanine utilisée pour les études photoélectrochimiques.

les mesures de capacité différentielle. Des traitements identiques à ceux subis par les électrodes employées pour les études potentiodynamiques ont par la suite été soumis aux électrodes avant leur immersion dans la solution.

Une cellule en Pyrex à trois compartiments séparés avec une électrode de travail (phtalocyanine), une électrode auxiliaire en platine et une électrode de référence réversible d'hydrogène, ERH, (électrode dans le même milieu que l'électrode de travail; milieux acide et neutre) ou Hg/HgO (milieu alcalin) a été utilisée pour les études photoélectrochimiques. La cellule est munie d'une fenêtre de quartz et une lampe au tungstène–halogène d'une puissance nominale de 650 W a été utilisée comme source lumineuse pour son spectre d'émission continu dans le proche ultraviolet et le visible.

2.2 *La préparation des essais*

Un barbotage d'hélium de 3 h a précédé l'immersion de l'électrode de phtalocyanine dans la solution appropriée, laquelle est demeurée sous atmosphère inerte pour toute la durée des essais. Les solutions préparées avec de l'eau triplement distillée possèdent les compositions suivantes: H_2SO_4 (Ultrex, J. T. Baker Chemical Co.) 0, 1 *N*; tampon KH_2PO_4 0,025 *M* – Na_2HPO_4 0,025 *M* (Fisher Scientific Co.); et KOH (Aristar, BDH Chemicals) 0,1 *N* dont le pH est de 1,4, 6,8 et 12,6 respectivement.

2.3 *Les techniques expérimentales utilisées*

Les courbes cyclovoltammétriques ont été obtenues par la méthode conventionnelle. Par ailleurs, la méthode utilisée pour les mesures de capacité différentielle est celle décrite par Morcos (24) et employant une perturbation à une fréquence de 200 Hz qui représente la fréquence optimale pour le système à l'étude.

3. Résultats expérimentaux et discussion

3.1 *Courbes capacité–tension*

Des films de H_2Pc, CuPc et FePc, polarisés anodiquement par intervalles d'environ 50 mV dans la région de potentiel correspondant à un courant résiduel négligeable, ont été soumis à des mesures d'impédance aux trois pH. Ainsi, les valeurs de capacité relevées représentent les capacités différentielles

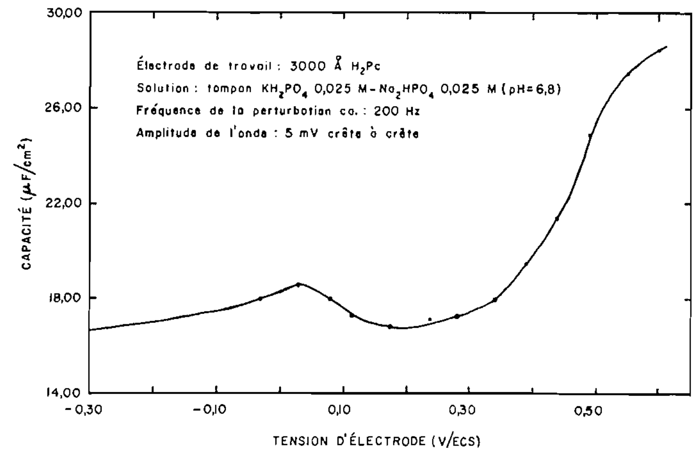

FIG. 2. Courbe capacité–tension pour la phtalocyanine sans métal (H_2Pc) en milieu neutre.

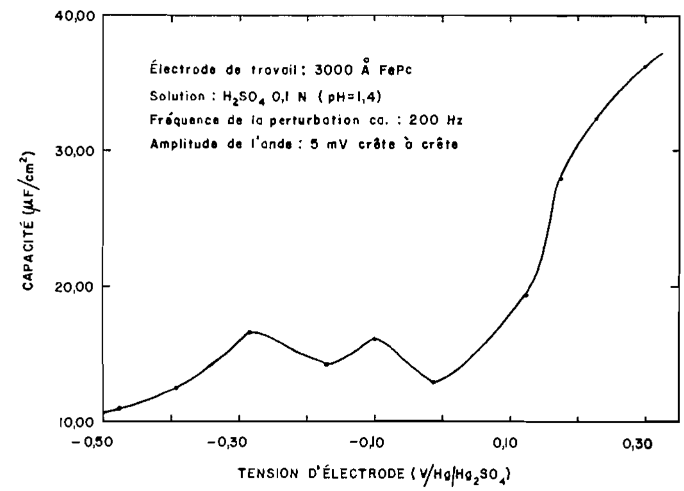

FIG. 3. Courbe capacité–tension pour la phtalocyanine de fer (FePc) en milieu acide.

de l'interface semiconducteur–électrolyte sans contribution faradique.

Comme l'illustre la fig. 2, la capacité différentielle de l'électrode de H_2Pc montre un maximum à 0,03 V/ECS. Cette caractéristique peut être expliquée en termes de niveaux intermédiaires situés à l'intérieur de la bande interdite du semiconducteur, lesquels augmentent la capacité différentielle en agissant comme réservoir de charges. Cela suggère donc une zone d'états de surface avec une densité maximale localisée à 0,27 V/ENH ou à une énergie de 4,77 eV sous le niveau du vide puisque l'énergie de Fermi standard du couple H^+/H_2 à l'équilibre (ENH) est approximativement de 4,5 eV sous le niveau du vide (25); cette valeur est comparable à celle obtenue par Fan et Faulkner (4,75 eV) (18). Une courbe similaire est obtenue avec l'électrode de CuPc et un second pic est observé dans le cas de la FePc (fig. 3).

L'analyse de ces courbes suggère une zone d'états de surface avec une densité maximale localisée à 0,40 V/ENH (−4,90 eV) pour la CuPc et deux zones d'états de surface dont la densité est maximale à 0,34 V/ENH (−4,84 eV) et à 0,52 V/ENH (−5,02 eV) pour la FePc; ces états de surface seront discutés plus loin. Il est à souligner qu'un changement de pH de la solution ne modifie pas l'allure des courbes capacité–tension.

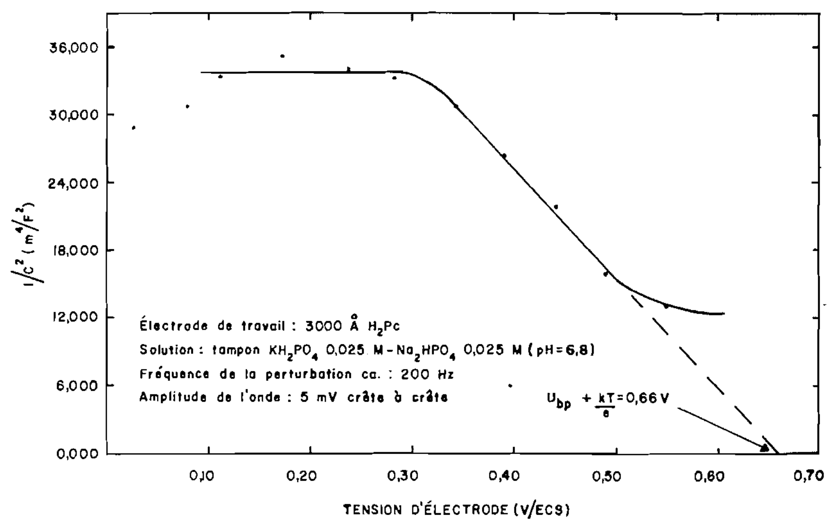

FIG. 4. Courbe Mott–Schottky pour la phtalocyanine sans métal (H_2Pc) en milieu neutre.

Une seconde évidence supportant l'idée de la présence d'états de surface est la valeur de la capacité différentielle qui est de l'ordre de 18 $\mu F/cm^2$ (H_2Pc), 20 $\mu F/cm^2$ (CuPc) et 13 $\mu F/cm^2$ (FePc) alors qu'elle est typiquement inférieure à 1 $\mu F/cm^2$ dans le cas d'une électrode semiconductrice (26). La densité maximale de ces états de surface (N_t) peut être estimée à partir de la hauteur de la capacité maximale des courbes capacité–tension (27):

$$[1] \quad C^0_{cs} \approx \left(\frac{e^2}{4kT}\right) N_t$$

où C^0_{cs} représente la capacité maximale à l'équilibre des états de surface; e, k et T correspondent respectivement à la charge de l'électron, la constante de Boltzmann et la température absolue. Les valeurs obtenues sont de l'ordre de $10^{13}/cm^2$, ce qui est équivalent à un recouvrement des sites de surface d'environ 1%.

3.2 *Courbes Mott–Schottky*

La connaissance du potentiel de bandes plates (U_{bp}) d'un semiconducteur nous indique si la photodécomposition de l'eau peut avoir lieu spontanément, c'est-à-dire sans l'application d'une tension à l'électrode semiconductrice en sus de l'illumination. Pour en déterminer la valeur, on applique en première approximation la relation de Mott–Schottky pour un semiconducteur non dégénéré, donnée par

$$[2] \quad \frac{1}{C_{sc}^2} = \frac{2}{e\epsilon\epsilon_0 N_A}\left(U_{appl} - U_{bp} - \frac{kT}{e}\right)$$

pour un semiconducteur du type p. Dans cette équation d'une droite, C_{sc} est la capacité de la région d'appauvrissement de charges à l'intérieur du semiconducteur, ϵ est la constante diélectrique du semiconducteur, ϵ_0 est la permitivité du vide, N_A est la concentration des accepteurs d'électrons et U_{appl} est la tension de l'électrode. La pente de la droite est proportionnelle à la concentration du dopant dans le semiconducteur et l'intersection avec l'axe des U_{appl} ($1/C_{sc}^2 = 0$) donne U_{bp} si le terme kT/e est négligé.

La courbe Mott–Schottky correspondant à une électrode de H_2Pc étudiée en milieu neutre est présentée dans la fig. 4, d'où l'on tire U_{bp} = 0,63 V/ECS (kT/e = 0,026 V à 24°C). Les valeurs obtenues pour les autres phtalocyanines sont données au tableau 1 qui indique également l'effet du pH sur ces valeurs. On remarque qu'une augmentation du pH de la solution tend à diminuer la valeur du potentiel de bandes plates, mais d'une façon très peu significative. Cette constatation suggère qu'aucune adsorption spécifique d'espèces ioniques ne se produit sur la surface des semiconducteurs qui permettrait de changer la chute de potentiel à travers la double couche d'Helmholtz lors d'une variation du pH de la solution, comme dans le cas de la plupart des semiconducteurs. Jaeger *et al.* (19) ont d'ailleurs observé que les niveaux d'énergie de H_2Pc demeuraient pratiquement inchangés lors d'une variation de pH.

TABLEAU 1. Variation de U_{bp} avec le pH et la phtalocyanine

pH (±0, 1)	U_{bp} (V/ENH) (±0,02 V)		
	H_2Pc	CuPc	FePc
1,4	0,92	0,87	0,84
6,8	0,88	0,83	0,80
12,6	0,85	0,81	*

*Instabilité de la FePc en milieu alcalin.

Le tableau met également en évidence l'effet de l'atome central de la molécule de phtalocyanine. On constate que la valeur du potentiel de bandes plates croît dans l'ordre FePc < CuPc < H_2Pc, bien que le changement soit à nouveau peu prononcé compte tenu de l'erreur expérimentale (±0,02 V). Dahlberg et Musser (12) ont mesuré les photovoltages à saturation dans des cellules photovoltaïques utilisant les mêmes électrodes de phtalocyanine et ils ont observé qu'ils croissaient suivant le même ordre. La valeur du photovoltage leur apparaît étroitement reliée à l'alignement de l'énergie des orbitales d du métal central avec la limite supérieure de la bande de valence de la phtalocyanine, déterminé à partir des spectres de photoémission de ces matériaux semiconducteurs. Ainsi, les orbitales $3d$ de symétrie e_g (d_{xz}, d_{yz}) de l'ion ferrique sont localisées au même niveau d'énergie que la plus haute orbitale occupée par des électrons π de la phtalocyanine et aucun photovoltage ne s'est manifesté avec la FePc. Par ailleurs, les orbitales $3d$ de l'ion cuivrique montrent une bonne séparation énergétique avec cette orbitale et un photovoltage légèrement

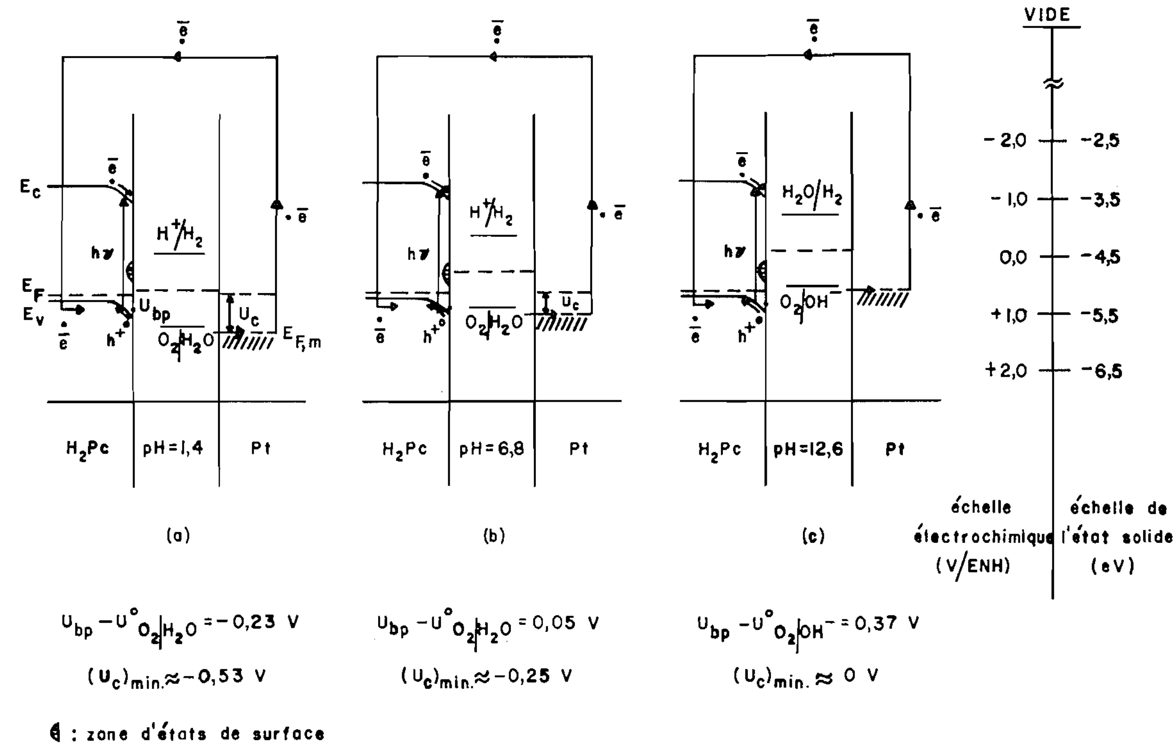

FIG. 5. Diagrammes de niveaux d'énergie pour la phtalocyanine sans métal (H_2Pc): (a) milieu acide; (b) milieu neutre; (c) milieu alcalin.

inférieur à celui présenté par la H_2Pc, ne possédant aucun électron *d*, a été observé avec la CuPc. Étant donné que la valeur du photovoltage à saturation correspond à la courbure des bandes du semiconducteur à l'équilibre (dans le noir), les raisons ci-haut mentionnées expliquent les différences obtenues dans les valeurs de potentiel de bandes plates.

La concentration des accepteurs d'électrons (N_A) déterminée à partir de la pente de l'équation Mott–Schottky est de l'ordre de $10^{21}/cm^3$ pour les trois phtalocyanines étudiées (ϵ mesurée = 3,8 ± 0,3); ceci représente une valeur très élevée, car les semiconducteurs hautement dopés possèdent des concentrations supérieures à $10^{18}/cm^3$. Ces résultats montrent le signe évident d'imperfections à la surface des phtalocyanines donnant lieu à des niveaux d'énergie discrets situés à l'intérieur de la bande interdite. Ces états de surface piègent les électrons provenant de la bande de valence en y créant un surplus de trous mobiles. Il est connu que les phtalocyanines sont activées lorsqu'elles absorbent l'oxygène, leur structure étant analogue à celle du groupe prosthétique de l'hémoglobine (28). De ce fait, l'oxygène doit être grandement responsable de la concentration élevée en porteurs majoritaires. Nos résultats sont en accord avec ceux obtenus précédemment par Crine[1] qui a utilisé la même méthode de mesure.

À la lumière des potentiels de bandes plates déduits des courbes Mott–Schottky, nous pouvons établir les diagrammes de niveaux d'énergie reliés aux cellules d'électrolyse photo-assistée de l'eau utilisant les électrodes de H_2Pc, CuPc et FePc, bien que l'on soit conscient des limitations de la mesure en raison de la présence des états de surface et de la seule fréquence utilisée (200 Hz). La figure 4 nous donne un potentiel de bandes plates de 0,63 V/ECS (−5,37 eV) pour H_2Pc étudiée en milieu neutre. Prenant une différence énergétique d'environ 0,1 eV entre la limite supérieure de la bande de valence et le niveau de Fermi (le semiconducteur est très dopé) et connaissant la valeur de la bande interdite des phtalocyanines (2,0 eV), on peut situer la limite inférieure de la bande de conduction à −3,47 eV (fig. 5(b)). Sur cette figure, la zone d'états de surface déduite de la courbe capacité–tension (fig. 2) possède une densité maximale localisée à −4,77 eV.

À pH 6,8, les couples H^+/H_2 et O_2/H_2O sont situés respectivement à 4,10 et 5,33 eV sous le niveau du vide. Étant donné que les concentrations d'hydrogène et d'oxygène dans la cellule sont nulles au début de l'électrolyse, le niveau de Fermi de l'électrolyte est fixé en plein centre des niveaux H^+/H_2 et O_2/H_2O, soit à −4,72 eV. Les potentiels de bandes plates déterminés en solutions acide et alcaline ont permis d'établir les diagrammes de niveaux d'énergie illustrés dans les figures 5(a) et 5(c). Des analyses similaires concernant les autres phtalocyanines (CuPc, FePc) ont mené aux diagrammes reproduits dans les figures 6 et 7.

3.3 *Courbes cyclovoltammétriques*

La voltamétrie cyclique a été utilisée pour caractériser le comportement électrochimique et photoélectrochimique des films de H_2Pc, CuPc et FePc vis-à-vis la réaction du dégagement de l'hydrogène. En l'absence de film phtalocyanine, l'électrode d'or montre une densité de courant beaucoup plus importante à partir de −0,40 V/ERH. Les courbes obtenues dans le noir révèlent un phénomène d'hystérésis entre les balayages d'aller et de retour, la densité de courant étant plus faible lors du balayage de retour (figures 8 et 9). L'irréversibilité du processus est attribuée à des espèces réductibles sur la surface du semiconducteur: au cours du balayage d'aller, la surface se nettoie par réduction irréversible des impuretés. Cet hystérésis diminue toutefois avec les cycles. La densité de courant correspondant à une tension d'électrode donnée diminue légèrement avec les cycles, ce qui peut être expliqué par la formation de bulles à la surface de l'électrode

[1]J. P. Crine. Communication privée. Varennes. 1979.

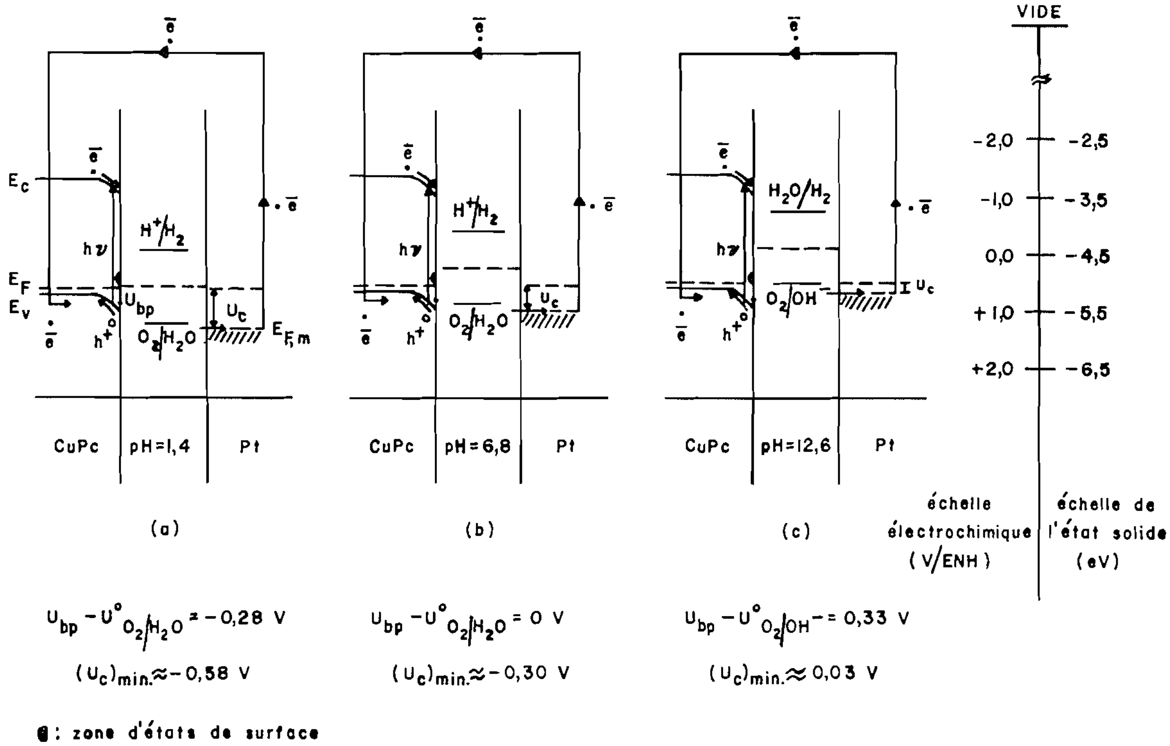

FIG. 6. Diagrammes de niveaux d'énergie pour la phtalocyanine de cuivre (CuPc): (a) milieu acide; (b) milieu neutre; (c) milieu alcalin.

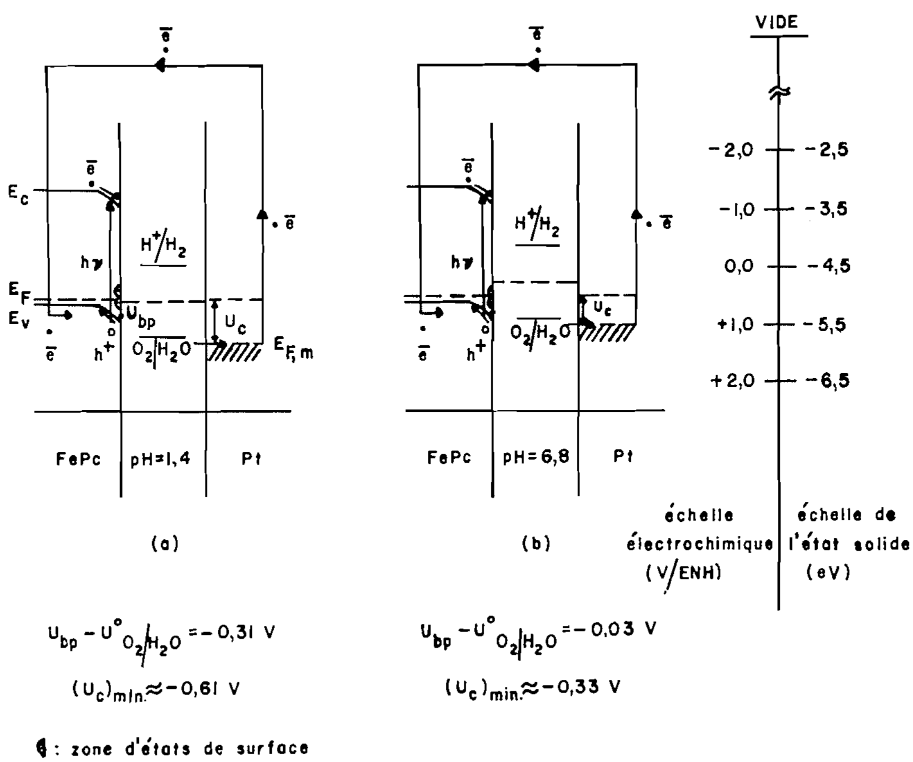

FIG. 7. Diagrammes de niveaux d'énergie pour la phtalocyanine de fer (FePc): (a) milieu acide; (b) milieu neutre.

lors du dégagement d'hydrogène, bloquant ainsi certains sites réactionnels. Notons que les électrodes de H_2Pc et CuPc présentent des courbes similaires.

La courbe de polarisation cathodique de l'électrode de FePc (fig. 9) présente deux pics de réduction, ce qui n'a pas été observé avec les autres phtalocyanines. Cela indique que ces pics ne sont pas associés à la réduction de la molécule organique de phtalocyanine, mais plutôt à celle du cation central. Compte tenu du traitement de l'électrode, le fer est probablement à l'état d'oxydation III donnant lieu au complexe à densité de spin élevé $Fe^{III}\ Pc^+\ O_2^-$. En effet, l'existence de Fe^{III} à l'état stable implique la présence d'un ligand supplémentaire

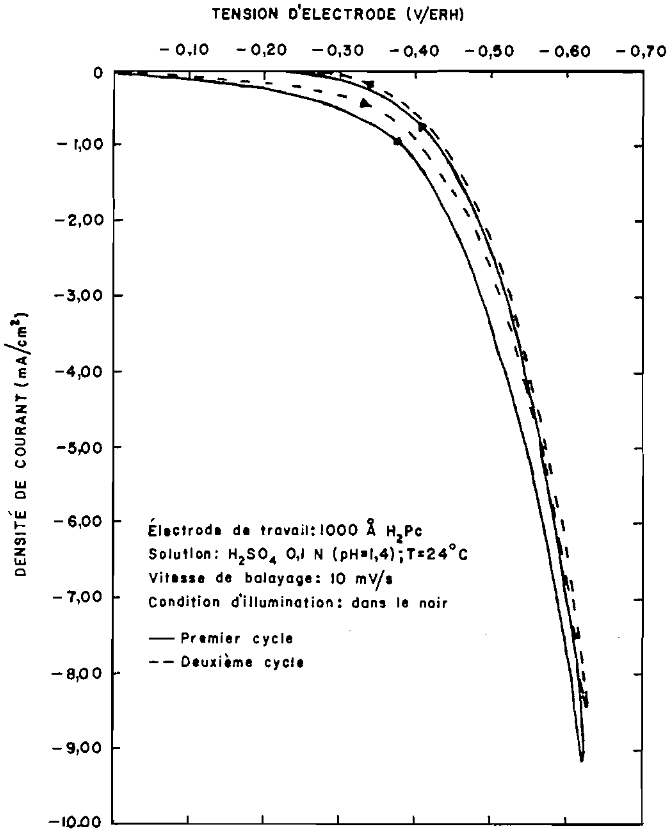

FIG. 8. Courbe de polarisation cyclovoltammétrique de la phtalocyanine sans métal (H_2Pc) en milieu acide.

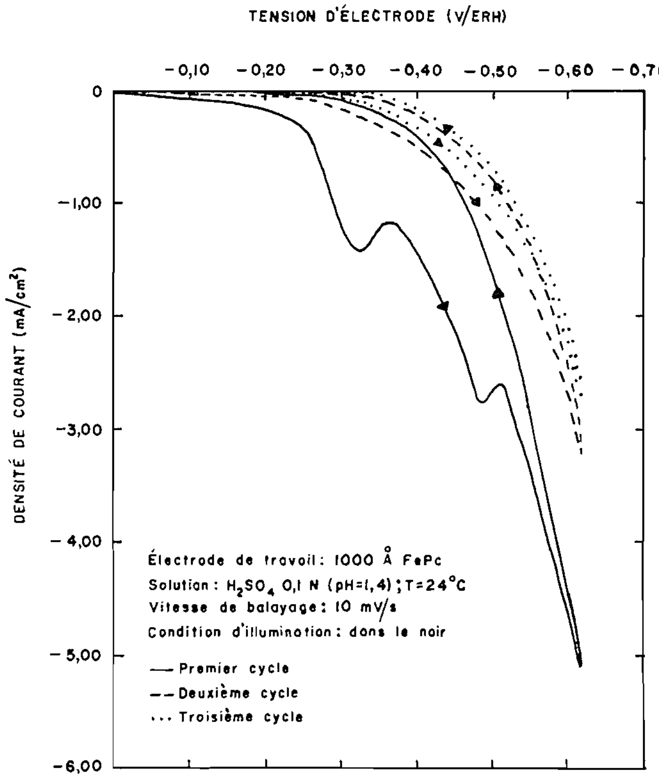

FIG. 9. Courbe de polarisation cyclovoltammétrique de la phtalocyanine de fer (FePc) en milieu acide.

accepteur (O_2) situé entre deux atomes de fer de deux molécules voisines pour des raisons de symétrie (29).

Les essais réalisés en solutions acide, neutre et alcaline ont permis d'étudier l'effet du pH de la solution: la densité de courant cathodique correspondant à une tension d'électrode donnée est réduite de façon appréciable en solution neutre (pH = 6,8), alors qu'elle varie peu lorsque le pH de la solution passe de 1,4 à 12,6. En solution neutre, la concentration ionique de l'électrolyte est plus faible et par conséquent la densité de courant cathodique mesurée est moins importante qu'en solutions acide et alcaline où les concentrations en ions H^+ et OH^- sont très élevées.

Lors de l'illumination des électrodes de phtalocyanine par une lampe au tungstène–halogène (150 mW/cm^2 *effectifs en surface de l'électrode*), aucun changement n'a été observé dans la variation de la densité de courant avec la tension imposée à l'électrode semiconductrice. Notre modèle d'interphase semiconducteur–électrolyte (figures 5–7) peut expliquer cette absence d'effet de la lumière sur le dégagement d'hydrogène.

Lorsqu'un photon est absorbé à l'électrode semiconductrice, une paire électron–trou est créée. Les paires photogénérées dans la région d'appauvrissement de charges sont immédiatement séparées par le champ électrique qui s'y trouve. Les électrons (porteurs minoritaires) sont dirigés vers la surface de l'électrode pour remplir des états interfaciaux qui agissent de médiateurs de transferts de charges à des accepteurs en solution (espèces oxydées) dont la densité des états d'énergie recouvre celle des états interfaciaux. Comme ces densités ne peuvent se recouvrir selon nos diagrammes de niveaux d'énergie (figures 5–7), les états de surface agissent plutôt comme centres de recombinaison, inhibant ainsi tout effet de lumière. Par ailleurs, la concentration très élevée en porteurs majoritaires confère aux phtalocyanines une région d'appauvrissement de charges relativement mince qui diminue de façon significative la quantité de photons absorbés.

En absence d'états de surface, le transfert d'électrons de la bande de conduction aux espèces oxydées H_3O^+ ou H_2O en solution serait facilité en milieu alcalin en raison du recouvrement plus important de la densité des états d'énergie de ces espèces (niveaux non occupés par des électrons) avec la bande de conduction; ce transfert devrait être plus appréciable dans le cas de l'électrode de H_2Pc en raison de la position moins élevée de ses bandes d'énergie. Par ailleurs, les diagrammes de niveaux d'énergie suggèrent un apport en énergie électrique moindre à pH alcalin pour initier la photodécomposition de l'eau, ce qui favorise un rendement de conversion de l'énergie optique en énergie chimique plus élevé. En effet, une tension cathodique (U_c) doit être appliquée à l'électrode de phtalocyanine en sus de l'illumination pour abaisser le niveau de Fermi de l'électrode auxiliaire métallique ($E_{F,m}$) au-dessous du niveau E_{O_2/H_2O} (E_{O_2/OH^-}) et ainsi assurer l'oxydation de l'eau. La tension minimale (théorique) requise pour mener cette réaction d'oxydation ($(U_c)_{min}$) diminue avec l'augmentation du pH de la solution, passant de 0,53 V (pH = 1,4) à 0,25 V (pH = 6,8) puis à 0 V (pH = 12,6) dans le cas de la cellule utilisant une électrode de H_2Pc (fig. 5). On peut remarquer qu'une courbure de bandes de l'ordre de 0,3 V, nécessaire à une séparation adéquate des paires électron–trou photogénérées par le champ électrique (30), a été respectée dans l'établissement des diagrammes de niveaux d'énergie.

En comparant les figures 5 à 7, on est en mesure de constater que l'apport en énergie électrique croîtrait dans l'ordre H_2Pc < CuPc < FePc, faisant état des différences dans les valeurs du potentiel de bandes plates. En effet, un potentiel plus négatif s'éloigne davantage de la tension U_{O_2/H_2O} (U_{O_2/OH^-}) exigeant par conséquent une tension supérieure pour amorcer l'oxydation de l'eau. Concernant l'électrode de FePc immergée en solution acide, la courbure de bandes résultant de la jonction semiconducteur–électrolyte est légèrement inférieure à 0,3 V, ce qui implique que l'illumination de cette électrode serait inefficace compte tenu du taux élevé de recombinaisons des paires électron–trou photogénérées.

4. Conclusion

L'illumination des électrodes de phtalocyanine n'a produit aucun effet sur la réaction du dégagement de l'hydrogène. Un modèle d'interphase semiconducteur–électrolyte établi à partir des mesures de capacité différentielle peut expliquer cette absence de photocourant. L'analyse des courbes capacité–tension a révélé la présence de niveaux intermédiaires localisés à l'intérieur de la bande interdite des semiconducteurs et recouvrant environ 1% de leurs sites de surface. Ces états interfaciaux qui piègent les électrons photogénérés dans la bande de conduction ne peuvent permettre leur transfert en solution en raison du non recouvrement de leur densité d'énergie avec la densité des états d'énergie des espèces oxydées H_3O^+ ou H_2O; ils agissent plutôt comme centres de recombinaison, empêchant la manifestation d'un photocourant. De plus, la concentration très élevée en porteurs majoritaires ($\sim 10^{21}/cm^3$) confère aux phtalocyanines une région d'appauvrissement de charges très mince qui diminue de façon significative la quantité de photons absorbés.

L'électrolyse photoassistée de l'eau deviendrait possible avec des électrodes de phtalocyanine qui absorbent fortement dans le visible par l'élimination des états de surface. Selon nos diagrammes de niveaux d'énergie, la réaction photocathodique du dégagement de l'hydrogène serait facilitée en milieu alcalin et avec une électrode semiconductrice de H_2Pc. Par ailleurs, l'apport en énergie électrique serait moins important dans ce même milieu et avec la même électrode de phtalocyanine pour initier la réaction anodique du dégagement de l'oxygène à l'électrode auxiliaire métallique, ce qui favoriserait également un rendement de conversion de l'énergie optique en énergie chimique supérieur; les rendements diminueraient dans l'ordre $H_2Pc > CuPc > FePc$. Une exposition moins prolongée des films de phtalocyanine à l'atmosphère atténuerait probablement la densité des états de surface, l'oxygène étant sans doute responsable de leur présence. Cependant, la grande résistivité des phtalocyanines (17) nécessite la présence d'une concentration suffisamment élevée d'oxygène jouant le rôle de dopant. En effet, il a été observé que le rendement quantique est accru lorsque les couches minces organiques sont exposées à l'air ambiant (11).

Remerciements

Les auteurs tiennent à remercier les Drs J. P. Crine, A. K. Vijh (IREQ) et A. Yelon (École Polytechnique) avec qui ils ont eu des discussions fructueuses.

1. G. SANSTEDE. From electrocatalysis to fuel cells. University of Washington Press, Seattle. 1972.
2. M. ICHIKAWA, M. SOMA, T. ONISHI et K. TAMARU. Trans. Faraday Soc. **63**, 1215 (1967).
3. F. H. MOSER et A. L. THOMAS. Phthalocyanine compounds. Reinhold, New York. 1963.
4. S. TANAKA, T. ONISHI et K. TAMARU. Bull. Chem. Soc. Jpn. **41**, 2557 (1968).
5. M. SUDO, M. ICHIKAWA, M. SOMA, T. ONISHI et K. TAMARU. J. Phys. Chem. **73**, 1174 (1969).
6. F. GUTMANN et P. E. LYONS. Organic semiconductors. Wiley, New York. 1967.
7. S. E. HARRISON et J. M. ASSOUR. J. Chem. Phys. **40**, 365 (1964).
8. G. H. HEILMEIER et S. E. HARRISON. Phys. Rev. **132**, 2010 (1963).
9. A. K. GHOSH, D. L. MOREL, T. FENG, R. F. SHAW et C. A. ROWE, JR. J. Appl. Phys. **45**, 230 (1974).
10. F. R. FAN et L. R. FAULKNER. J. Chem. Phys. **69**, 3341 (1978).
11. G. A. CHAMBERLAIN et P. J. COONEY. Chem. Phys. Lett. **66**, 88 (1979).
12. S. C. DAHLBERG et M. E. MUSSER. J. Chem. Phys. **70**, 5021 (1979).
13. R. O. LOUTFY et J. H. SHARP. J. Chem. Phys. **71**, 1211 (1979).
14. R. O. LOUTFY, J. H. SHARP, C. K. HSIAO et R. HO. J. Appl. Phys. **52**, 5218 (1981).
15. R. O. LOUTFY, Y. SHING et K. MURTI. Sol. Cells. **5**, 331 (1982).
16. M. SHIMURA et H. BABA. Denki Kagaku, **50**, 678 (1982).
17. H. TACHIKAWA et L. R. FAULKNER. J. Am. Chem. Soc. **100**, 4379 (1978).
18. F. R. FAN et L. R. FAULKNER. J. Am. Chem. Soc. **101**, 4779 (1979).
19. C. D. JAEGER, F. R. FAN et A. J. BARD. J. Am. Chem. Soc. **102**, 2592 (1980).
20. A. GIRAUDEAU, F. R. FAN et A. J. BARD. J. Am. Chem. Soc. **102**, 5137 (1980).
21. R. O. LOUTFY et L. F. MCINTYRE. Sol. Energy Mater. **6**, 467 (1982).
22. R. O. LOUTFY et L. F. MCINTYRE. Can. J. Chem. **61**, 72 (1983).
23. P. LEEMPOEL, F. R. FAN et A. J. BARD. J. Phys. Chem. **87**, 2948 (1983).
24. I. MORCOS. J. Electroanal. Chem. **72**, 389 (1976).
25. A. E. DIXON et J. D. LESLIE. Solar energy conversion, an introductory course. Pergamon Press, Toronto. 1979. p. 907.
26. A. K. VIJH. Electrochemistry of metals and semiconductors. Marcel Dekker, New York. 1973. p. 33.
27. H. EYRING, D. HENDERSON et W. JOST. Physical chemistry, an advanced treatise. Tome IXA. Academic Press, New York. 1970.
28. H. JAHNKE et M. SCHÖNBORN. 19th CITCE Meeting, Detroit. Septembre 1968.
29. M. SAVY, C. BERNARD et G. MAGNER. Electrochim. Acta, **20**, 383 (1975).
30. M. S. WRIGHTON. Acc. Chem. Res. **12**, 303 (1979).

Vibrational analysis of (*E*,*E*)-2,4-hexadienal, (*E*,*E*,*E*)-2,4,6-octatrienal, and (*E*,*E*,*E*)-3-methyl-2,4,6-octatrienal

M. M. ABO ALY,[1] M. H. BARON,[2] J. FAVROT, J. BELLOC, AND M. REVAULT
Laboratoire de Spectrochimie Infrarouge et Raman, C.N.R.S., 2 rue Henri Dunant, 94320 Thiais, France

Received August 16, 1984

This paper is dedicated to Professor Camille Sandorfy on the occasion of his 65th birthday

M. M. ABO ALY, M. H. BARON, J. FAVROT, J. BELLOC, and M. REVAULT. Can. J. Chem. **63**, 1587 (1985).

Attempted vibrational assignments of (*E*,*E*)-2,4-hexadienal, (*E*,*E*,*E*)-2,4,6-octatrienal, and (*E*,*E*,*E*)-3-methyl-2,4,6-octatrienal are given between 3100 and 50 cm^{-1}. We particularly discuss spectroscopic effects of the aldehydic group presence, enlargement of the polyenal chain length, and methyl lateral substitution.

M. M. ABO ALY, M. H. BARON, J. FAVROT, J. BELLOC et M. REVAULT. Can. J. Chem. **63**, 1587 (1985).

L'attribution d'ensemble des spectres ir et Raman de trois polyénals: (*E*,*E*)-hexadièn-2,4-al-1, (*E*,*E*,*E*)-octatrièn-2,4,6-al-1 et (*E*,*E*,*E*)-methyl-3-octatrièn-2,4,6-al-1 est proposée. Elle permet de discuter les effets spectroscopiques liés à l'introduction d'un groupement aldéhydique, à l'allongement des chaînes conjuguées et à leur substitution par un groupement méthyle.

1. Introduction

This work is included in the general frame of studies on polyenes, polyenals, and phototransformation of retinal and its imine derivatives (1–6). Progress in technology permits new very interesting vibrational studies on molecules of biological interest; however, complete vibrational analysis is not often possible and this limits the full significance of the results. In recent papers on retinal and imine derivatives, we have pointed out that deconjugated products can be obtained by irradiation with various laser lines (1–3, 5). Raman spectra of these new products show that the deconjugation may occur, according to the experimental conditions, on the eighth or on the tenth carbon of the polyenic chain. They also indicate that each of these new compounds may be present as various stereoisomers. An accurate analysis of these spectra would allow a better knowledge of the structure of these photoproducts. However, there are no vibrational assignments of stereochemically well-defined model polyenals with two or three successive conjugated double bonds.

We have already shown, from a detailed analysis of the ir and Raman spectra of the three stereoisomers of 2,4-hexadiene, that there are general spectroscopic trends characteristic of the configuration of the double bonds (4). Concerning aldehydic compounds, there is only a nmr study on 2,4-hexadienal stereoisomers (7). In this paper we propose the vibrational analysis of all *trans* polyenals with two or three conjugated C═C bonds, (*E*,*E*)-2,4-hexadienal (HAL) and (*E*,*E*,*E*)-2,4,6-octatrienal (OAL), respectively. Modifications on vibrational spectra introduced by lateral methyl substitution have also been interpreted from the study of (*E*,*E*,*E*)-3-methyl-2,4,6-octatrienal (MOAL).

2. Materials and methods

2,4-Hexadienal is commercially available from Aldrich Corp. as a mixture of stereoisomers. (*E*,*E*)-2,4-hexadienal (HAL) was purified following the method of Albriktsen and Harris (8). The raw product is cooled at −60°C and transferred to a precooled filter funnel at −40°C. The noncrystalline products are drawn out. The crystalline products are melted at −20°C, recooled to −60°C, and filtered at −20°C. A product, still crystalline at −20°C, is recovered at −12°C. The nmr and ir spectra indicate a purity of 99% for the (*E*,*E*) stereoisomer in this sample (one aldehydic doublet δ = 9.53 ppm in CD_3CN solvent (8), mp −18°C, λ in ethanol = 271 nm) (9).

(*E*,*E*,*E*)-2,4,6-octatrienal (OAL) was prepared by the method proposed by Blout and Fields (9). In the last step, OAL was purified by several sublimations, instead of distillation, followed by crystallization in hexane. A hplc qualitative analysis indicates the purity of the (*E*,*E*,*E*) stereoisomer: only one elution peak at 320 nm, (mp 56°C, λ in ethanol = 315 nm) (9).

(*E*,*E*,*E*)-3-methyl-2,4,6-octatrienal (MOAL) was obtained from 3,5-heptadiene-2-one prepared by the method of Attenburrow *et al.* (10). The following steps are described by Weedon and Woods (11). Activated MnO_2 is used for the oxidation of 3-Me-2,4,6-octatrienol to obtain the corresponding aldehyde. Finally, the all-*trans* stereoisomer is separated from the others by the same low temperature crystallization method used for HAL. The nmr spectrum of the purified sample indicates a purity of 95% for the (*E*,*E*,*E*) compound (aldehydic doublet δ = 10.08 ppm in CD_3CN solvent, mp 19°C, λ in ethanol = 322 nm).

The ir spectra between 4000 and 200 cm^{-1} were recorded on Perkin–Elmer spectrophotometers (PE 180 and PE 983), with spectral slits of 1 cm^{-1} above 600 cm^{-1} and about 4 cm^{-1} below 600 cm^{-1}. Below 200 cm^{-1} an evacuable Brucker spectrophotometer IFS-113 was used with a resolution of 4 cm^{-1}. Liquid samples were inserted between two CsI windows or in polyethylene cells. Spectra of solid OAL were obtained by introducing the sample directly, or as Nujol mulls, between CsI or polyethylene plates.

The Raman spectrophotometer was a model RT Dilor equipped with a Kr^+ (λ_{exc} = 6471 Å) Spectra-Physics laser. Solids, neat liquids, and solutions were inserted in 2-mm diameter tubes. For polarization measurements the spectrophotometer response was calibrated over the 0 to 4000 cm^{-1} range by using a white light lamp.

3. Results and discussion

The three all-*trans* compounds belong to the C_s point group. The 39 normal modes of HAL are represented by 26 A′ and 13 A″, the 51 normal modes of OAL by 34 A′ and 17 A″, and the 60 normal modes of MOAL by 39 A′ and 21 A″. Vibrational assignments for HAL, OAL, and MOAL will be successively proposed. In a fourth part, the attribution of the aldehydic modes will be confirmed by analysis of the ir and Raman spectra of these compounds in solution in CCl_4 or CS_2. Wavenumbers and descriptions of Raman and ir bands relative to HAL, OAL, and MOAL are listed in Tables 1, 2 and 3 respectively and the corresponding spectra are reported in Fig. 1.

---

[1] Permanent address: Ain Shams University, Faculty of Sciences, Chemistry Department, Cairo, Egypt.

[2] Author to whom correspondence should be addressed.

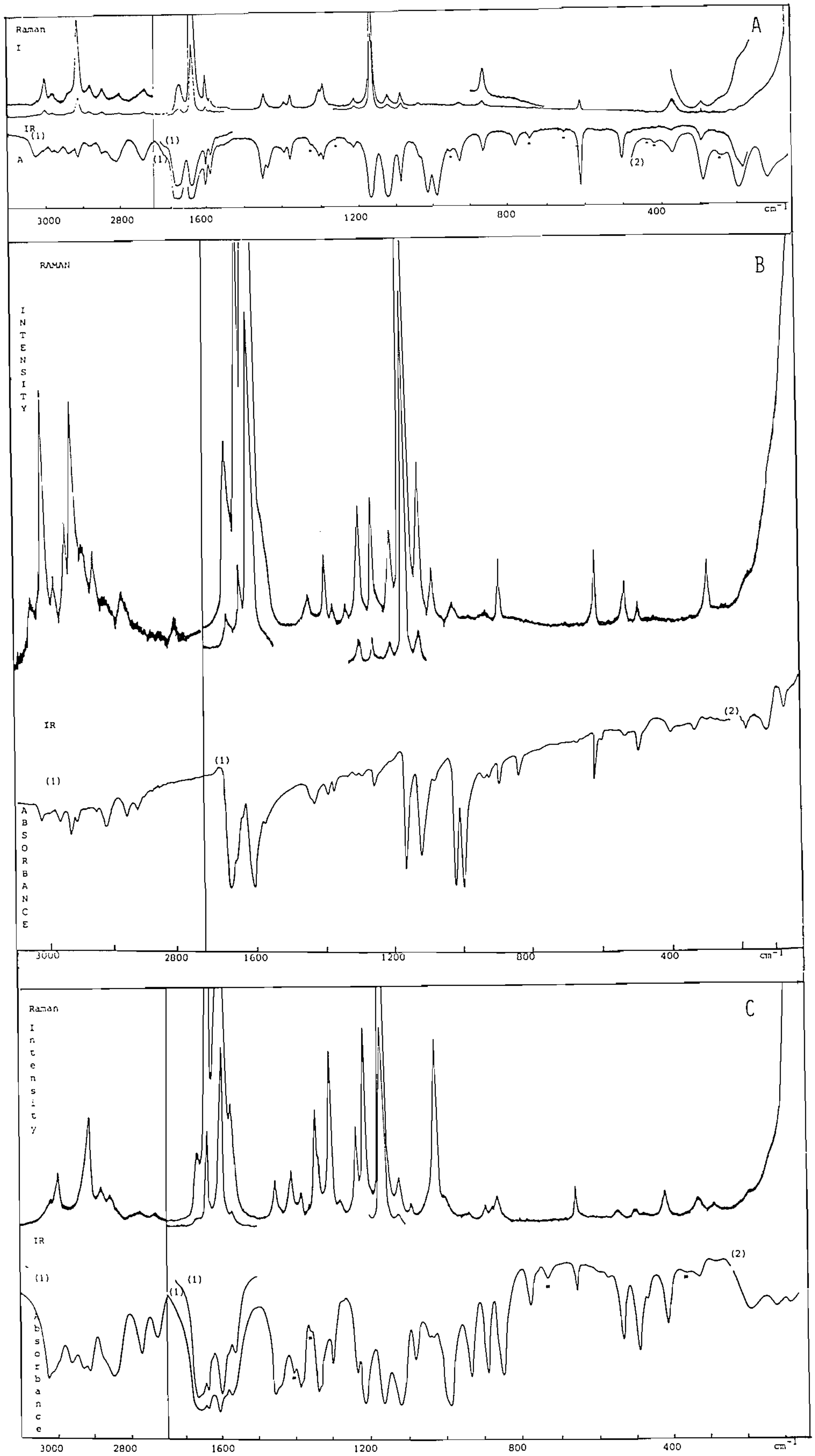

FIG. 1. (*E,E*)-2,4-hexadienal (A), (*E,E,E*)-2,4,6-octatrienal (B), (*E,E,E*)-3-methyl-2,4,6-octatrienal (C): ir and Raman spectra. A, C: neat liquid samples. (1) Film between CsI plates, (2) 100-μm polyethylene cell (A), film between TPX (poly-4-methyl-1-pentene) plates (C). Bands due to isomers are indicated by *. B: solid samples. (1) Solid film between CsI plates, (2) Nujol mull between TPX plates.

3-1. *(E,E)-2,4-hexadienal (HAL)* (Table 1, Fig. 1)

3-1-1. *Region 3100–2700 cm^{-1}*

Most assignments in this region are similar to those already given for (E,E)-2,4-hexadiene (4). However, a 2808-cm^{-1} band, which does not occur in (E,E)-2,4-hexadiene spectra, is assigned to the aldehydic CH stretching mode (ν CHa) (12–17). Another rather strong band at 2734 cm^{-1} corresponds to the overtone of the deformation mode of the same CH group (2 δ CHa), in Fermi resonance with the ν CHa (12–19).

3-1-2. *Region 1700–1000 cm^{-1}*

Classical assignments are given for the carbonyl stretching mode (ν CO) (20–22), the ethylenic modes (ν C=C), and methyl group CH deformations (δ_s', δ_a, and δ_s CH_3) (4, 23–25). For (E)-crotonaldehyde, δ_s CH_3 and δ CHa are assumed to be coupled (12). This may not be the case for HAL, where the CH_3 group is farther from the CHa group. We assign the weak ir and Raman line at 1394 cm^{-1} to δ CHa. Compared to (E,E)-2,4-hexadiene, the low frequency δ CHe at 1214 cm^{-1} may result from a coupling with an aldehydic motion, probably the δ CHa one The strong ir band and the Raman polarized line at 1166 cm^{-1} correspond to the central C—C stretching mode (ν C—C) (4). The stretching ν CCHO mode is observed at 1120 cm^{-1} as in acetaldehyde (15–17), slightly lower than for crotonaldehyde (12) and acrolein (26) and close to calculated and experimental frequencies obtained for retinal (27, 28).

Around 1000 cm^{-1}, the depolarized line at 1035 cm^{-1} is assigned to the A″ r CH_3 mode; both the r CH_3 and ν C—CH_3 are involved in the 1085 and 926-cm^{-1} A′ modes (polarized lines), as for other methylated products (12, 24, 25). We shall see, further, that this band also corresponds to a γ CHe mode, as in (E,E)-2,4-hexadiene (4). For crotonaldehyde, γ CHa has not been assigned (12). However, experimental results for this compound show that a band at 1011 cm^{-1} in the neat liquid moves to 1005 cm^{-1} in solution. With HAL, we observe the same experimental feature for a line at 1014 cm^{-1}, strong in the ir spectrum, weak and depolarized in the Raman one. We propose then to associate those bands with the γ CHa modes of the two enals.

3-1-3. *Region 1000–750 cm^{-1}*

Four bands in this range may be assigned to depolarized ethylenic out-of-plane CH motions (γ CHe). In the Raman spectrum, one has a medium intensity (863 cm^{-1}) and the three others are very weak (926 cm^{-1} (see above), 988, and 777 cm^{-1}). All of them have medium or strong intensity in the ir spectrum.

3-1-4. *Region 750–280 cm^{-1}*

Three kinds of carbon skeleton planar deformation modes are expected in this range: one δ CCO, one δ $CCCH_3$, and three δ CCC corresponding to central carbons. For crotonaldehyde, the deformation at higher frequency is the δ CCO mode (12). For (E,E)-2,4-hexadiene, among the four expected planar skeletal deformations, the two occurring at lower frequency correspond mainly to the δ $CCCH_3$ modes and the two at higher frequencies to the central δ CCC modes (4). For HAL, we clearly observe three polarized lines: one at 612 cm^{-1} is assigned to δ CCO, another at 298 cm^{-1} to δ $CCCH_3$, and the third one at 375 cm^{-1} to a central δ CCC. Two other ir bands (504 and 480 cm^{-1}), for which it was not possible to measure a depolarization ratio (not observed in Raman), are assigned to the two last δ CCC; those frequencies seem too high to correspond to out-of-plane torsion (t) modes (t C=C), the higher t C=C mode for (E,E)-2,4-hexadiene being proposed at 355 cm^{-1} (4).

3-1-5. *Region 300–50 cm^{-1}*

Although we have not been able to measure their depolarization ratio, all bands observed in this range should correspond to out-of-plane torsion modes for double and single bonds: two t C=C, one t C—C, one t CCH_3, and one t CCHO.

For (E)-2-butene (29) and (E)-crotonaldehyde (12), the t C=C, slightly coupled with a γ CHe, is observed at ca. 280 cm^{-1}. For (E)-1,3-pentadiene, it is given at 250 cm^{-1} (25). For (E,E)-2,4-hexadiene, one occurs at 355 cm^{-1}, the other at 235 cm^{-1} (4). For both dienes, the t C=C modes are configuration dependent, which suggests that t C=C motions are also coupled with out-of-plane motions. For HAL, the polarized 298 cm^{-1} line presents a shoulder which could correspond to the higher t C=C mode, the 242-cm^{-1} very weak ir and Raman band being an alternative assignment. The lower t C=C may account for the medium ir and very weak Raman peak at 200 cm^{-1}.

For propene (24, 30), pentadiene (25), (E)-2-butene (29, 31), and isoprene (32), t CCH_3 occurs also at ca. 200 cm^{-1}. Bands around 120 cm^{-1} are generally assigned to the t CCHO modes (12, 14, 26, 33) and the central t C—C modes are assumed to occur between 50 and 170 cm^{-1} (4, 25, 32–36). In our low frequency spectra, we clearly observe a medium ir line at 126 cm^{-1} and a shoulder at 145 cm^{-1}. As in (E,E)-2,4-hexadiene (4), t CCH_3 and t C—C may be coupled, and both contribute to these bands, however, the 126 cm^{-1} should also be assigned to t CCHO.

3-2. *(E,E,E)-2,4,6-octatrienal (OAL)* (Table 2, Fig. 1)

OAL is a solid at room temperature. Depolarization ratio measurements have been obtained from solution Raman spectra.

3-2-1. *Region 3100–2700 cm^{-1}*

Only four out of six expected ν CHe may be identified from the ir and Raman spectra. ν CHa and 2 δ CHa still in Fermi resonance are slightly higher than in HAL. An additional ir medium intensity band at 2716 cm^{-1} likely corresponds to a combination tone between ethylenic and aldehydic CH deformations; we shall see that a new δ CHe band occurs for OAL at 1334 cm^{-1}.

3-2-2. *Region 1700–1000 cm^{-1}*

The ν CO is assigned to the 1680-cm^{-1} Raman and 1670-cm^{-1} ir bands. The three ν C=C probably correspond to the 1638, 1604, and 1578 cm^{-1} bands (37, 38).

δ_s', δ_a, δ_s, r A′, r A″, δ CHa, ν CCHO, and γ CHa are observed at about the same frequencies for OAL and HAL. As expected, compared to HAL, there are two supplementary bands (1334 and 1256 cm^{-1}) in the δ CHe range. On the other hand, only one ν C—C is clearly observed at 1162 cm^{-1}, although two are expected as in hexatriene (37, 38). The second one may be assigned to a weak shoulder observed at ca. 1140 cm^{-1}. However, a slight amount of *cis* isomer would also give a band around this frequency (4).

3-2-3. *Region 1000–750 cm^{-1}*

For OAL, the ν CCH_3 is again assigned to a 929 cm^{-1} polarized line, but the close depolarized mode γ CHe at 938 cm^{-1} is well resolved in this case. The five other expected γ CHe observed in ir are very weak in Raman, except for the 892-cm^{-1} (dp) one, in analogy with the 863-cm^{-1} (dp) γ CHe of HAL.

TABLE 1. Experimental vibrational frequencies of (*E*,*E*)-2,4-hexadienal in neat liquid state (liq) and in carbon tetrachloride solution (sln) (c = 0.1 *M*)

Raman (liq)	ρ	Raman (sln)	Infrared (liq)	Infrared (sln)	Type	Assignment
3035 vw		3034 vw	3035 sh	3035 sh	A′	ν CHe
3026 vw		3021 vw	3026 m	3021 m	A′	ν CHe
			3010 sh		A′	ν CHe
3004 m	0.26	3005 m	3004 w	3004 sh	A′	ν CHe
2982 w	0.41	2982 w	2982 w	2982 w	A′	ν_s' CH_3
2968 vw		2968 vw	2968 m	2968 w	A′	ν C=C (1603) + δ_s CH_3
2938 w		2938 w	2938 m	2938 m	A″	ν_a CH_3
2914 s	0.24	2914 s	2914 m	2914 m	A′	ν_s CH_3
2882 m	0.2	2978 m	2882 w	2878 w	A′	2 δ_s' CH_3
2850 m	P	2850 m	2850 m	2850 m	A′	2 δ_a CH_3
2820 vw			2820 sh		A′	ν_s' CH_3 + δ CHa
2807 w		2807 m	2808 m	2807 m	A′	ν CHa
2734 m		2732 m	2734 m	2732 m	A′	2 δ CHa
1680 m	0.25	1685 m	1680 vs	1685 vs	A′	ν CO
1639 vs	0.19	1643 vs	1639 vs	1641 vs	A′	ν C=C
1603 m	0.17	1603 m	1603 m	1603 s	A′	ν C=C
1590 w	P	1590 w	1590 m	1590 m	A′	r CH_3 + δ CCC
1448 m	0.35	1447 m	1448 m	1447 m	A′	δ_s' CH_3
1435 sh	dp		1435 m	1432 m	A″	δ_a CH_3
1394 w	0.28	1390 w	1394 w	1390 sh	A′	δ CHa
1378 m	0.30	1377 m	1378 m	1377 m	A′	δ_s CH_3
1303 m	0.10	1300 m	1303 m	1300 m	A′	δ CHe
1292 m		1290 m	1292 m	1290 m	A′	δ CHe
1230 vw		1227 sh	1230 sh	1227 w	A′	δ CHe
1214 w	0.27	1211 w	1214 w	1211 w	A′	δ CHe
1166 vs	P	1163 vs	1166 vs	1163 vs	A′	ν C—C
1120 m	0.20	1116 m	1120 vs	1116 vs	A′	ν CCHO
1085 m	0.27	1083 m	1085 m	1083 m	A′	r CH_3
1035 w	0.75	1034 w	1035 sh	1035 sh	A″	r CH_3
1014 vw	dp		1014 s	1007 s	A″	γ CHa
988 vw	dp		988 s	986 s	A″	γ CHe
926 w	0.48	925 m	926 m	925 m	A′,A″	ν CCH_3, γ CHe
863	0.80	858 w	863 m	858 m	A″	γ CHe
777 vw			777 m		A″	γ CHe
612 m	0.32	609 m	612 s	609 s	A′	δ CCO
			504 m	503 m	A′	δ CCC
			480 sh		A′	δ CCC
375 m	0.29	376 m	375 w		A′	δ CCC
298 vw	0.43		298 m	298 w	A′	δ $CCCH_3$
			285 sh		A″	t C=C
242 vw			242 vw			
200 vw			200 m		A″	t C=C
			145 sh		A″	t CCH_3/t C—C
126 w			126 m		A″	t CCHO/t C—C

Abbreviations: P: $\rho < 0.7$; dp: $0.7 < \rho < 0.8$. Intensity: vw = very weak; w = weak; m = medium; s = strong; vs = very strong; sh = shoulder.

3-2-4. *Region 750–280 cm^{-1}*

Seven bands are observed in this range. Four are polarized. That at the highest frequency is assigned to δ CCO, the lowest one to δ $CCCH_3$, and the two in the middle to two out of the five expected δ CCC. The three other bands are weak and their depolarization ratios have not been obtained. Those at 410 and 475 cm^{-1} are also assigned to the δ CCC modes. The 343-cm^{-1} band may correspond to a t C=C mode.

3-2-5. *Region 280–50 cm^{-1}*

As for the assignment of the HAL low frequency spectra, we think that the two higher frequency bands (240 and 190 cm^{-1}) correspond to two t C=C modes, the 160-cm^{-1} shoulder to the t CCH_3 mode, and the 138-cm^{-1} band to the t CCHO mode. A supplementary absorption observed at 92 cm^{-1} is assigned to one of the two t C—C modes of OAL.

3-3. (E,E,E)*-3-methyl-2,4,6-octatrienal (MOAL)* (Table 3, Fig. 1)

3-3-1. *Region 3100–2700 cm^{-1}*

Four out of the five expected ν CHe are identified at about the same frequencies as for OAL. The wavenumbers of peaks corresponding to ν_s', ν_a, and ν_s CH_3 do not change, nor those assigned to δ CH_3 harmonic and combination tones, despite the presence of the lateral (lat) methyl group. On the other hand, the ir spectrum is significantly different in the 2850 to 2700 cm^{-1} range. Making the same assignments for OAL and MOAL, replacement of the 2816, 2750, and 2716-cm^{-1} bands of OAL by 2835, 2770, and 2725 cm^{-1}, respectively, for

TABLE 2. Experimental vibrational frequencies of (*E*,*E*,*E*)-2,4,6-octatrienal in solid state (sld) or in Nujol mull (a) and carbon tetrachloride or in carbon disulfide (b) solution (sln) ($0.3 > c > 0.1$ *M*)

Raman (sld)	Raman (sln)CCl_4	ρ	Infrared (sld)	Infrared (sln)CCl_4	Type	Assignment
3033 w	3036 w	P			A′	ν CHe
			3022 m	3022 m	A′	ν CHe
	3010 sh	P			A′	ν CHe
2994 m	2997 m	P	2992 w		A′	ν CHe
2966 w	2966 w		2966 m	2966 m	A′	ν'_s CH_3
2928 w	2930 w		2930 m	2930 m	A″	ν_a CH_3
2910 s	2915 s	P	2910 m	2915 m	A′	ν_s CH_3
2880 w	2884 w	P	2876 vw	2880 vw	A′	2 δ'_s CH_3
2848 w	2851 w	P	2848 w	2851 w	A′	2 δ_a CH_3
2815 vw	2805 vw	P	2816 m	2805 m	A′	ν CHa
2768 w						δ_s CH_3 + δ CHe (1334)
	2735 w		2750 m	2735 m	A′	2 × δ CHa
			2716 m	2710 m	A′	δ CHa + δ CHe (1334)
1680 m	1682 m	0.35	1670 s	1684 s	A′	ν CO
1638 s	1640 s	0.28	1638 sh	1640 w	A′	ν C═C
1617 sh	1616 vs	0.28		1616 s	A′	ν C═C
1604 vs	1600 w		1606 s	1600 w	A′	
1578 sh	1578 vw	P	1578 m	1578 m	A′	ν C═C
1447 w	1448 w	0.32	1447 sh	1448 m	A′	δ'_s CH_3
	1436 sh	dp	1435 m	1435 w	A″	δ_a CH_3
1394 m	1388 m	0.26	1394 w	1388 sh	A′	δ CHa
1376 w	1376 w	0.34	1376 w	1376 sh	A′	δ_s CH_3
1334 sh	1328 w	0.24	1334 w		A′	δ CHe
1310 w			1310 vw		A′	δ CHe
1292 m	1292 m	0.2	1292 vw	1292 vw	A′	δ CHe
1256 m	1252 m	0.3	1256 m	1252 m	A′	δ CHe
1238 sh	1238 vw		1235 sh		A′	δ CHe
1205 m	1202 m	0.32	1205 sh		A′	δ CHe
1162 vs	1162 vs	0.33	1162 s	1162 s	A′	ν C—C
	1140 sh		1140 sh		A′	ν C—C
1120 m	1112 m	0.3	1116 sh	1112 s	A′	ν CCHO
1080 w	1080 w	0.26	1080 w		A′	r CH_3
1030 w	1030 w	0.75	1030 sh		A″	r CH_3
1016 vw	1009 vw	dp	1016 s	1009 s	A″	γ CHa
			994 s	991 s	A″	γ CHe
975 vw	975 vw	0.52	975 sh	975 sh	A″	γ CHe
			938 w		A″	γ CHe
929 w	929 w	0.57	929 w	929 w	A′	ν CCH_3
892 m	882 m	0.75	892 m	882 m	A″	γ CHe
			836 m	825 w	A″	γ CHe
785 vw	785 vw(b)		785 vw		A″	γ CHe
620 m	618 m	0.30	620 m	618 m	A′	δ CCO
537 m	537 m	0.36	537 w	537 w	A′	δ CCC
497 vw	497 vw(b)	0.58	497 m	497 m	A′	δ CCC
			475 sh	470 sh	A′	δ CCC
			410 w	395 w	A′	δ CCC
343 vw	343 vw(b)		343 w	343 w	A″	t C═C
306 m	305 m(b)	P	306 vw	305 vw	A′	δ $CCCH_3$
240 vw			240 vw		A″	t C═C
190 w			190 w	190 w	A″	t C═C
			160 sh(a)		A″	t CCH_3
			138 m(a)		A″	t CCHO
			92 w(a)		A″	t C—C

See Table 1 for abbreviations.

MOAL may be due to increased frequencies of the ν CHa and δ CHa modes when the polyenal is 3-methyl substituted. We shall see that it is in agreement with the assignment of the 1402-cm^{-1} band to the δ CHa mode of MOAL. Furthermore, intensity enhancement of the 2 δ_a CH_3 harmonic (2850 cm^{-1}) may be due to its peculiar proximity to the ν CHa mode in MOAL.

3-3-2. *Region 1700–1020 cm^{-1}*

The ν CO mode and two of the three ν C═C modes occur, respectively, at lower frequency than for OAL. δ'_s and δ_a of the two methyl groups of MOAL are not resolved. Both the δ_s CH_3 differ by only 4 cm^{-1}. The δ CHa is assigned to the 1402 cm^{-1}; although the intensity of this peak decreases as the purity of the (*E*,*E*,*E*) stereoisomer increases, it stays relatively intense (me-

TABLE 3. Experimental vibrational frequencies of (*E,E,E*)-3-methyl-2,4,6-octatrienal in neat liquid state (liq) and in carbon disulfide solution (sln) ($0.3 > c > 0.1$ *M*)

Raman (liq)	ρ	Raman (sln)CS_2	Infrared (liq)	Infrared (sln)CS_2	Type	Assignment
3035 sh			3035 sh		A′	ν CHe
3024 vw	P		3024 m	3024 m	A′	ν CHe
			3010 sh	3010 sh	A′	ν CHe
2998 m	0.25		2998 sh		A′	ν CHe
2962 vw			2962 m	2962 m	A′	ν'_s CH_3
2930 sh			2930 m	2928 m	A″	ν_a CH_3
2912 m	0.22		2912 m	2910 sh	A′	ν_s CH_3
2878 w	0.30		2878 sh		A′	2 δ'_s CH_3
2851 w	0.30		2851 m	2851 sh	A′	2 δ_a CH_3
			2835 sh	2835 m	A′	ν CHa
2768 vw			2770 m	2763 m	A′	2 δ CHa
2730 vw			2725 m	2719 m	A′	δ CHa + δ CHe (1335)
1666 m	0.47	1670 m	1666 s	1670 s	A′	ν CO
1637 s	0.22	1642 s	1637 s	1638 s	A′	ν C=C
1600 vs	0.22	1604 vs	1600 s	1601 s	A′	ν C=C
1567 m	0.28	1570 m	1567 m		A′	ν C=C
1446 m	0.4	1446 m	1446 m		A′	δ'_s CH_3
1435 sh			1435 sh		A″	δ_a CH_3
1402 m	0.33	1402 m	1402 w	1402 w	A′	δ CHa
1384 sh	P		1384 m	1384 sh	A′	δ_s CH_3
1380 w	P	1378 w	1380 sh	1376 m	A′	δ_s CH_3
1335 m	0.35	1335 m	1335 m	1332 m	A′	δ CHe, ν C_3—C_4
1330 sh			1330 sh	1325 sh	A′	δ CHe
1297 m	0.24	1297 m	1297 m	1297 m	A′	δ CHe
1272 vw	P	1272 w	1272 w	1272 w	A′	δ CHe
1232 m	0.41	1232 m	1232 m	1230 m	A′	δ CHe
1210 m	0.38	1210 m	1210 s	1210 s	A′	ν C_3—C_4, δ C_2He
1164 vs	P	1164 s	1164 s	1164 s	A′	ν C—C
1117 m	0.44	1113 m	1120 s	1115 s	A′	ν C—CHO
1082 w	0.50		1082 m	1082 m	A′	r CH_3 (ter)
			1045 w	1041 w	A″	r CH_3 (lat)
			1032 w	1032 sh	A″	r CH_3 (ter)
1020 m	0.46	1016 m	1020 sh	1016 sh	A′	r CH_3 (lat)
996 sh			996 sh		A″	γ CHa
			987 s	984 s	A″	γ CHe
940 sh	dp		940 sh	942 w	A″	γ CHe
930 vw	0.62		930 m	928 m	A′	ν C—CH_3 (ter)
886 w	0.75		886 m	883 m	A″	γ CHe
855 w	0.57					ν C—CH_3 (lat)
			845 m		A″	γ CHe
775 vw	dp		775 m		A″	γ CHe
650 w	0.18		650 w		A′	δ CCO
575 vw			570 vw		A′	δ CCC
530 vw	0.36		532 m	528 m	A′	δ CCC
490 vw	0.32		490 m	490 m	A′	δ CCC
465 sh			465 w	465 sh	A″	t C=C
410 w	0.26		410 m		A′	δ CCC
325 w	0.28		325 w		A′	δ CCC
280 vw	0.48		280 vw		A′	δ $CCCH_3$ (ter), (lat)
			200 w		A″	t C=C
			190 sh		A″	t CCH_3 (lat)
			145 sh		A″	t CCH_3 (ter)
			131 w		A″	t CCHO
			87 w		A″	t C—C

See Table 1 for abbreviations.

dium in Raman) in the quasi pure product.

More important changes are expected below 1350 cm^{-1}. There must be: (*i*) one less δ CHe. As a matter of fact, a band at ca. 1310 cm^{-1} in the OAL spectra does not exist in the MOAL spectra; (*ii*) one more ν CCH_3. In isoprene (32) and 2-methylacrolein (12), where there is a lateral methyl group, ν C—C and ν C—CH_3 are coupled. According to retinal normal coordinates analysis (27, 28), δ C_{14}H also is coupled to ν C_{13}—CH_3 and ν C_{12}—C_{13}. In the MOAL spectra, new polarized bands appear at 1335 and 855 cm^{-1} and the intensity of the 1210 cm^{-1} is strongly enhanced relative to the 1205-cm^{-1} OAL band. These features resemble those for retinal (27, 28) and clearly point out the triple coupling among δ C_2H, ν C_3—C_4, and ν C_3CH_3 for this substituted octatrienal.

As for retinal (28), the r CH_3 modes of the lateral methyl group are assigned to the polarized line at 1020 cm^{-1} (A′) (medium in the Raman spectrum, very weak in the ir) and to the 1045-cm^{-1} peak (A″) (weak in ir). It should be noted that a band near 1020 cm^{-1} in the HAL and OAL spectra had to be assigned to the γ CHa mode, as it was depolarized. The γ CHa of MOAL may occur at lower frequency (27, 28).

Compared to OAL, other modes are not modified.

3-3-3. *Region 1000–700 cm^{-1}*

The ν CCH_3 mode of the lateral methyl group has already been assigned to the 855-cm^{-1} Raman polarized line, and the 930-cm^{-1} line corresponds, as for OAL, to ν CCH_3 of the terminal (ter) methyl group.

Compared to OAL, there is one less γ CHe mode. The γ CHa mode being assigned as for retinal (27, 28) to a shoulder at 996 cm^{-1}, the five observed depolarized bands have to be associated with the γ CHe modes.

3-3-4. *Region 750–280 cm^{-1}*

The polarized line at highest frequency (650 cm^{-1}) is assigned to δ CCO and the lowest one to both the δ $CCCH_3$ terminal and lateral modes. The four other polarized bands between these two correspond to four out of the five δ CCC expected. Among the two other weak bands for which depolarization ratios have not been obtained, the 570 cm^{-1} band has to be assigned to the fifth δ CCC. The other band at 465 cm^{-1} may be due to a t C═C mode, if we consider that the 3-methyl substituent of MOAL is in the *cis* position on the C_2═C_3 double bond relative to the C_1—C_2 bond (4).

3-3-5. *Region 280–50 cm^{-1}*

There are clearly not enough bands to assign all the expected out-of-plane torsional modes in this range. However, it seems relevant to assign one t C═C mode at ca. 200 cm^{-1}, one t C—C mode at 87 cm^{-1}, and the t CCHO mode at 131 cm^{-1}.

3-4. *Autoassociation effects on vibrational frequencies*

The differences in frequencies between spectra of solid and solution samples for OAL are more important than the observed differences between neat liquid and solution for HAL and MOAL. However, for the three products, the major shifts are obtained for bands associated with the vibrations of the aldehydic group: ν CO, δ CHa, ν CCHO, γ CHa, δ CCO. This confirms the assignment of these modes and proves that the aldehydic functions are more or less associated in the neat liquid and solid states. The γ CHe around 880–860 cm^{-1}, which is also dependent on the physical state of the sample, may be assigned to the C_2—H group in the three products.

Only for OAL one can observe a doublet at 1604 and 1617 cm^{-1} for the solid and neat liquid samples. The 1604-cm^{-1} band is the more intense in the solid state while the 1617-cm^{-1} band becomes the stronger in the neat liquid state spectra. To explain this effect, we propose a Fermi resonance between a ν C═C mode at ca. 1610 cm^{-1} and a combination tone whose frequency should depend on the physical state of OAL. The ν CCHO mode (1110 cm^{-1} in solution, 1120 cm^{-1} in the solid state) and the δ CCC mode (497 cm^{-1}) might give such a combination tone.

1. T. DELATOUR, J. FAVROT, M. H. BARON, J. BELLOC, and C. DE LOZE. Chem. Phys. Lett. **87**, 379 (1982).
2. T. DELATOUR, M. H. BARON, J. FAVROT, J. BELLOC, and C. DE LOZE. Proc. VIIIth International Conference on Raman Spectroscopy. *Edited by* J. Lascombe and P. V. Huong. John Wiley. 1982. p. 793.
3. T. DELATOUR, M. H. BARON, J. BELLOC, J. FAVROT and C. DE LOZE. J. Raman Spectrosc. **15**, 147 (1984).
4. M. M. ABO ALY, M. H. BARON, J. FAVROT, F. ROMAIN, and M. REVAULT. Spectrochim. Acta, Part A, **40**, 1037 (1984).
5. T. DELATOUR. Thèse 3ème cycle, Lille, France (1981).
6. M. M. ABO ALY, M. H. BARON, and J. FAVROT. Proc. IXth International Conference on Raman Spectroscopy. *Edited by* Org. Comm. Chem. Soc. Japan, Tokyo. 1984. p. 554.
7. J. P. CORSETTI. Ph.D. Thesis Harvard Univ. (1979), Uiv. Microfilms Inter. order no. 8011198, Ann Arbor, Michigan, U.S.A.
8. P. ALBRIKTSEN and R. K. HARRIS. Acta Chem. Scand. **27**, 3993 (1973).
9. E. R. BLOUT and M. FIELDS. J. Am. Chem. Soc. **70**, 189 (1948).
10. J. ATTENBURROW, A. F. B. CAMERON, J. H. CHAPMAN, R. M. EVANS, B. A. HEMS, A. B. A. JANSEN, and T. WALKER. J. Chem. Soc. 1094 (1952).
11. B. C. L. WEEDON and R. J. WOODS. J. Chem. Soc. 2687 (1951).
12. H. J. OELICHMANN, D. BOUGEARD, and B. SCHRADER. J. Mol. Struct. **77**, 179 (1981).
13. A. J. BOWLES, W. O. GEORGE, and W. F. MADDAMS. J. Chem. Soc. (B), 810 (1969).
14. J. R. DURIG, S. C. BROWN, V. F. KALASINSKY, and W. O. GEORGE. Spectrochim. Acta, Part A, **32**, 807 (1976).
15. J. C. EVANS and H. J. BERNSTEIN. Can. J. Chem. **34**, 1083 (1956).
16. P. COSSEE and J. H. SCHACHTSCHNEIDER. J. Chem. Phys. **44**, 97 (1966).
17. R. J. CAPWELL, JR. J. Chem. Phys. **49**, 1436 (1968).
18. D. F. EGGERS, JR. and W. E. LINDGREN. Anal. Chem. **28**, 1328 (1956).
19. E. L. SAIER, L. R. COUSINS, and M. R. BASILA. J. Phys. Chem. **66**, 232 (1962).
20. E. R. BLOUT, M. FIELDS, and R. KARPLUS. J. Am. Chem. Soc. **70**, 194 (1948).
21. Y. LERAUX and E. VAUTHIER. C. R. Acad. Sci. Paris, Série C, **271**, 1333 (1970).
22. G. V. KRYSHTAL, L. A. YANOVSKAYA, I. P. YAKOVLEV, and V. F. KUCHEROV. Izv. Akad. Nauk SSSR Ser. Khim. **1**, 172 (1973); Bull. Acad. Sci. USSR Ser. Chem. **22**, 177 (1973).
23. J. R. DURIG, C. K. TONG, C. W. HAWLEY, and J. BRAGIN. J. Phys. Chem. **75**, 44 (1971).
24. B. SILVI, P. LABARBE, and J. P. PERCHARD. Spectrochim. Acta, Part A, **29**, 263 (1973).
25. D. A. C. COMPTON, W. O. GEORGE, and W. F. MADDAMS. J. Chem. Soc. Perkin Trans. 2, 1311 (1977).
26. H. J. OELICHMANN, D. BOUGEARD, and B. SCHRADER. J. Mol. Struct. **77**, 149 (1981).
27. B. CURRY, A. BROEK, J. LUGTENBURG, and R. MATHIES. J. Am. Chem. Soc. **104**, 5274 (1982).
28. S. SAITO and M. TASUMI. J. Raman Spectrosc. **14**, 236 (1983).
29. I. W. LEVIN, R. A. R. PEARCE, and W. C. HARRIS. J. Chem. Phys. **59**, 3048 (1973).
30. W. G. FATELEY and F. A. MILLER. Spectrochim. Acta, **19**, 611 (1963).
31. J. R. DURIG, C. W. HAWLEY, and J. BRAGIN. J. Chem. Phys. **57**, 1426 (1972).
32. D. A. C. COMPTON, W. O. GEORGE, and W. F. MADDAMS. J. Chem. Soc. Perkin Trans. 2, 1666 (1976).
33. R. K. HARRIS. Spectrochim. Acta, **20**, 1129 (1964).
34. W. G. FATELEY, R. K. HARRIS, F. A. MILLER, and R. E. WITKOWSKI. Spectrochim. Acta, **21**, 231 (1965).
35. Y. N. PANCHENKO. Spectrochim. Acta, Part A, **31**, 1201 (1975).
36. Y. FURUKAWA, H. TAKEUCHI, I. HARADA, and M. TASUMI. Bull. Chem. Soc. Jpn. **56**, 392 (1983).
37. D. RAKOVIC, S. A. STEPANYAN, L. A. GRIBOV, and Y. N. PANCHENKO. J. Mol. Struct. Theochem. **90**, 363 (1982).
38. Y. N. PANCHENKO, P. CSASZAR, and F. TOROK. Acta Chim. Hung. **113**, 149 (1983).

Vertical electronic spectra of the isovalent molecules H_2CNH, H_2SiNH, H_2CPH, and H_2SiPH on the basis of MRD-CI calculations

PABLO J. BRUNA, VOLKER KRUMBACH, and SIGRID D. PEYERIMHOFF

Lehrstuhl für Theoretische Chemie, Universität Bonn, Wegelerstraße 12, D-5300 Bonn 1, West Germany

Received August 16, 1984

This paper is dedicated to Professor Camille Sandorfy on the occasion of his 65th birthday

PABLO J. BRUNA, VOLKER KRUMBACH, and SIGRID D. PEYERIMHOFF. Can. J. Chem. **63**, 1594 (1985).

Large-scale multi-reference single and double-excitation configuration interaction (MRD-CI) calculations are employed for the study of the isovalent compounds H_2CNH, H_2SiNH, H_2CPH, and H_2SiPH in their ground state equilibrium geometry. The dipole moments and charge distributions are given. The vertical excitation energies to the intra-valence states $^{3,1}(n,\pi^*)$ and $^{3,1}(\pi,\pi^*)$ and to the first members of the Rydberg series originating from n and π MO's respectively are predicted; the first two ionization potentials and the Rydberg term values are also calculated. In H_2CNH, mixing of Rydberg and valence-shell states with CN stretching is analyzed. The trends in relative stability of electronic and ionized states can be directly related to increased orbital stability of n relative to π as soon as a first-row constituent is replaced by a second-row atom. The calculations explain the diffuse character of the uv spectrum of imines; they treat the molecules H_2SiNH and H_2SiPH for the first time and present a large number of data for all four molecules which can serve as a basis for future experimental investigations on these and related compounds.

PABLO J. BRUNA, VOLKER KRUMBACH et SIGRID D. PEYERIMHOFF. Can. J. Chem. **63**, 1594 (1985).

On a utilisé des calculs d'interaction de configuration sur une grande échelle, à référence multiple et à excitation simple ou double pour étudier les composés isovalents H_2CNH, H_2SiNH, H_2CPH et H_2SiPH dans la géométrie d'équilibre de leur état fondamental. On rapporte les moments dipôlaires et les distributions de charges. On prédit les valeurs des énergies d'excitations verticales vers les états intra-valences $^{3,1}(n,\pi^*)$ et $^{3,1}(\pi,\pi^*)$ et vers les premiers termes des séries de Rydberg qui commencent respectivement aux OM n et π; on a aussi calculé les deux premiers potentiels d'ionisation et les valeurs des termes de Rydberg. Dans le cas du H_2CNH, on a analysé le mélange d'états de Rydberg et de couches valentielles avec l'élongation CN. Dès que l'on remplace un constituant de la première rangée par un atome de la deuxième rangée, on peut établir une relation directe entre les tendances dans les stabilités relatives des états électroniques et ionisés et l'augmentation de la stabilité des orbitales n par rapport aux orbitales π. Les calculs expliquent le caractère diffus des spectres uv des imines; on rapporte les résultats de la première étude traitant des entités H_2SiNH et H_2SiPH et, relativement aux quatre molécules, on présente un grand nombre de données qui peuvent servir de base pour de futures études expérimentales sur ces composés et sur d'autres qui leurs sont apparentés.

[Traduit par le journal]

I. Introduction

In recent years considerable interest has arisen for molecules which possess atoms from both the first and the second row of the periodic table. Numerous experimental (1, 2) and theoretical (3–5) studies have been undertaken in order to understand the electronic structure and properties, in particular for systems in which the first-row atoms C, N, and O are replaced by Si, P, and S respectively and which contain CP, SiN, and SiP bonds instead of the CN functional group.

For the simple diatomics C_2, CSi, and Si_2, for example, it has been found (6, 7) that the ground state electronic configuration is entirely different for the three isovalent systems: it is $X^1\Sigma_g^+$ for C_2, $X^3\Pi$ for CSi with constituents from the first and second row, and $X^3\Sigma_g^-$ for the second-row member Si_2. As a result, the reaction properties and the electronic spectra are quite different in these three compounds. In a similar manner, calculations for CN, CP, SiN, and SiP (4, 6, 8, 9) and the corresponding positive ions predict different electronic configurations for the lowest states ($X^2\Sigma^+$ for CN, for example, and $X^2\Pi_i$ for the isovalent SiP), and this pattern is also known for the simple hydrides CH_2 and SiH_2, whereby CH_2 possesses a X^3B_1 ground state while it is X^1A_1 in SiH_2 (5). These examples clearly point out that drastic changes in the electronic structure can take place in a family of given compounds upon substitution of one or two first-row atoms by their second-row analogues. Many of these systems containing one or two atoms from the second row are not yet known experimentally and hence *ab initio* calculations are presently the most powerful tool for the study of such compounds and for providing guidelines for further experimental work in this area.

In the present work we have selected the five-atom molecules H_2CNH, H_2SiNH, H_2CPH, and H_2SiPH for a theoretical investigation. Even though the two carbon-containing compounds have already been isolated experimentally, very little information is available on their electronic spectra. The two silicon-containing compounds are entirely unknown and are studied here for the first time.

The vertical spectrum of H_2CNH was studied theoretically by Macaulay, Burnelle, and Sandorfy (10) some time ago but these authors have already assumed that their results were of limited quality due to the restriction in the theoretical treatment. In further work Sandorfy has called attention to a better theoretical study of this molecule (11), in particular with respect to the relative position of the Rydberg states, which can be helpful for the classification and (or) understanding of the rather diffuse and quite complicated spectra of higher alkyl R^1R^2—C=N—R^3 imines.

The goal of the present study is to obtain a reliable description of the vertical position of the most important valence states (n,π^*) and (π,π^*) and the first (n,s_R) and (π,s_R) Rydberg members in the isovalent family H_2CNH, H_2CPH, H_2SiNH, and H_2SiPH. The additional determination of the lowest ionization potentials in these compounds allows the prediction of the corresponding term values, key information which can then easily be transfered to analyze the spectra of larger compounds containing similar >A=B-chromophore groups.

II. Technical details of the calculations

Two different AO basis sets have been employed for each compound, namely one of pure valence character (Basis A) and a second (Basis B), derived from the first Basis A by adding diffuse Rydberg-type functions. In general, both bases are of double-zeta quality augmented by *d*-polarization functions for all heavy atoms and by *p*-functions for the hydrogen atoms. The carbon and nitrogen atoms are described by the Huzinaga primitive set (12) in the $[4s2p]$ contraction according to Dunning and Hay (13). For silicon and phosphorus in the compounds H_2SiPH and H_2CPH, the primitive gaussians determined by Veillard (14) are chosen in contraction eight of that work. The Si basis in silylimine H_2SiNH stems from Huzinaga (15), again in the contraction scheme given by Dunning (13). The exponents for the *d*-polarization functions are: 0.70 (C), 0.95 (N), 0.30 (Si), and 0.43 (P), respectively, as recommended by Roos and Siegbahn (16). The hydrogen functions are those given by Huzinaga (12); the exponent for the *p*-polarization function is 0.75. This Basis A (pure valence character) contains in summary the following number of contracted functions: 47 (H_2CNH), 55 (H_2CPH and H_2SiNH), and 63 (H_2SiPH), respectively.

The vertical spectra were analyzed in a more expanded AO basis which includes Rydberg-type functions always placed in the center of the respective AB bonds of H_2ABH. This Basis B contains ten functions more than Basis A. The functions added are of *s*-, *p*-, and *d*-character. In the ordering H_2CNH, H_2CPH, H_2SiNH, and H_2SiPH, the exponents used are, respectively: α_s (0.025; 0.022; 0.021; 0.018), α_p (0.023; 0.019; 0.018; 0.015), and α_d = 0.015 (for all systems).

The MRD-CI method employed in all calculations is well documented in the literature (17–19). In contrast to the simple SD-CI method in which single and double excitations are generated only with respect to a single determinant, the multireference treatment employed in the present work accounts also for the most important higher-than-double excitations. Since the MRD-CI space consisting of all single and double excitations relative to a set of reference configurations is generally quite large, only a selected subset of configurations (all those which contribute more than a given threshold *T* to the CI energy) is treated directly in the secular equation, while the contribution of all others is accounted for in a perturbation-like treatment (18). Finally, the contribution of higher-than-double excitations is estimated in analogy to the Langhoff–Davidson formula (20) as

$$E_{\text{full CI}} = E_{\text{MRD-CI}} + \left(1 - \sum_{\text{ref}} c_0^2\right)(E_{\text{MRD-CI}} - E_{\text{ref}})$$

whereby the sum is taken over all reference configurations.

In all calculations a frozen core (always doubly occupied MO's) is employed in the CI procedure. It contains the inner-shell MO's of each molecule, namely two in H_2CNH, six in both H_2CPH and H_2SiNH, and ten orbitals in the heavier H_2SiPH molecule. In addition, the two highest MO's of a' symmetry are discarded in the calculations for the three lighter molecules, while in H_2SiPH the ten highest MO's (complementary to the frozen core) are omitted from the CI. Thus the MRD-CI calculations are carried out by correlating 12 valence electrons, while 53 MO's are available for partial occupation in the CI (Basis B) in H_2CNH and H_2SiPH and 57 in H_2CPH and H_2SiNH respectively. Further technical details of the MRD-CI calculations such as size of the reference set, selection threshold *T*, size of MRD-CI space, and contribution of the reference set to the total wavefunction are always listed with the respective results.

Various SCF MO's have been chosen for the study of the electronically excited states. In general, the parent SCF MO's are most appropriate in the sense that they require only a small number of reference configurations. Other MO's generally call for a larger reference set but then lead to essentially the same energy, as it should be when the CI is carried to the limit of a full CI. In some cases it seemed advantageous to employ the same set of MO's for various states, and this information is then always given together with the results. The $^1A'$ ground state MO's are also employed for the calculation of the ionic states. For H_2SiPH, not only the ground and $^3(n,\pi^*)$ MO's have been used but also natural orbitals obtained by direct diagonalization of the first-order density matrix of the preceding MRD-CI step.

III. Ground state properties

A. Molecular geometries

The ground state $^1A'$ geometry was optimized at the SCF level (with Basis A) using the gradient technique of the Gaussian 80 package. The resulting equilibrium structural parameters are contained in Table 1, together with experimental (21, 22) and other theoretical results (10, 23) for H_2CNH and H_2CPH. The equilibrium geometry of the isovalent H_2GeNH molecule as reported in recent theoretical work (24) is also given for purposes of comparison.

The optimization was also carried out for the two experimentally known species H_2CNH and H_2CPH in order to estimate the degree of reliability of the SCF gradient results. According to the data of Table 1 the discrepancies between SCF equilibrium geometries and their experimental counterpart are quite acceptable; they are on the order of 0.01 au for all hydrogenic bond lengths and deviations in the angles are less than 2° when compared with the experimental values. The largest disagreement is noted for the bond distances between the heavy atoms AB. This situation was easily expected on the basis of the double bond character and the failure of the SCF method to give a correct description of this portion of the molecule. The SCF method predicts R_e (AB) values which are invariably shorter than the actual bond lengths (the experimental CN and CP distances in H_2CNH and H_2CPH, respectively, are ca. 0.035 au greater than the values predicted at the SCF level). The inclusion of correlation effects automatically introduces antibonding character into the wavefunctions, primarily due to contributions of the $\pi^2 \rightarrow \pi^{*2}$ and $\pi \rightarrow \pi^*$ excitations relative to the ground state configuration, and hence remedies the situation.

According to the parameters contained in Table 1, the inclusion of correlation effects produces an elongation of 0.09 ± 0.01 au in R_e (AB) for both silicon compounds relative to the SCF value. A similar increment of +0.087 au has been reported for the GeN equilibrium distance in the isovalent H_2GeNH compound when correlation effects are explicitly considered (24).

The ground state geometries for the experimentally unknown species H_2SiNH and H_2SiPH have been partially reoptimized at the MRD-CI level with respect to the distance $>$A=B, always using the valence Basis A. All other geometrical parameters were kept constant and equal to the optimal values obtained at the SCF level. The angles H(1)AB (H(1) is the hydrogen in *cis* position) lie within 124–129° for all species given in Table 1,

TABLE 1. Equilibrium geometries for the various H_2ABH systems in their ground states obtained by the SCF gradient technique and comparison with corresponding data in the literature

	H_2CNH			H_2SiNH	H_2GeNH	H_2CPH			H_2SiPH
	This work	Expt. (ref. 21)	Theoretical (ref. 10)	This work	Theoretical (ref. 24)	This work	Expt. (ref. 22)	Theoretical (ref. 23)	This work
R_{AB} (au)	2.369 (2.40)[a]	2.406	2.375	2.997 (3.08)[a]	3.177 (3.264)[c]	3.128 (3.188)[a]	3.162 ±0.004	3.156	3.899 (3.997)[a]
$R_{AH(1)}$ (au)[b]	2.068	2.06	2.022	2.80	2.933	2.05	2.06 ±0.028	2.022	2.79
$R_{AH(2)}$ (au)	2.062	2.06	2.043	2.78	2.906	2.053	2.06 ±0.028	2.022	2.788
$R_{BH(3)}$ (au)	1.915	1.929	1.89	1.902	1.931	2.685	2.683 ±0.01	2.684	2.682
∠H(1)AB(°)[b]	124.6	125.1	120.0	128.6	128.8	125.1	124.4 ±0.8	124.7	126.5
∠H(2)AB(°)	119.1	117.9	123.5	119.5	118.1	119.3	118.4 ±1.2	119.5	122.2
∠H(3)BA(°)	111.4	110.4	114.5	122.4	122.8	98.9	97.4 ±0.4	100.0	92.0

[a] R_{AB} values are optimized in the MRD-CI treatment.
[b] H(1) labels the hydrogen atom in the *cis* position.
[c] CI value.

TABLE 2. Comparison of the equilibrium AB distances in related compounds. All values in atomic units. The references are given in parentheses

Molecule	State	CN	CP	SiN	SiP
AB:	$^2\Sigma^+$ $(\sigma\pi^4)$	2.214 (25,9)	2.952 (25)	2.970 (25,9)	3.83 (4,9)
	$^2\Pi_i$ $(\sigma^2\pi^3)$	2.330	3.156	3.09	3.98
HAB:	$^1\Sigma^+$ $(\sigma^2\pi^4)$	2.183 HCN (26) 2.213 HNC (26)	2.915 HCP (27)	2.97 HNSi (28)	3.78 HSiP (9) 3.81 HPSi (9)
H_2ABH:	$^1A'$ $(a'^2a''^2a'^2)$ $(a'^2\pi^2n^2)$[a]	2.406	3.162	3.08	3.997

[a] The a' orbital is either σ or in-plane π character depending on the molecule under consideration.

while the angle H(2)AB is invariably somewhat smaller and ranges from 118 to 112°. The angle ABH(3) is reduced by a larger amount when one substitutes the nitrogen by the phosphorus atom.

Finally it is of interest to compare the equilibrium distances of the A═B frame with the corresponding diatomic AB and triatomic HAB (or ABH) species. A summary of experimental and (or) theoretical predictions (4, 9, 25–28) is contained in Table 2. The 9-valence electron diatomics CN, CP, SiN, and SiP are characterized by the low-lying electronic states $^2\Sigma^+$ $(\sigma\pi^4)$ and $^2\Pi_i$ $(\sigma^2\pi^3)$, respectively (4). The ground state is $^2\Sigma^+$ for the first three species and $^2\Pi_i$ for SiP, as recently reported in MRD-CI calculations (9). Because the π MO's possess bonding character and the last σ MO is only slightly involved in the AB bonding, the $^2\Pi_i$ states have larger equilibrium distances than the $^2\Sigma^+$ states. A comparison between the R_e (AB) values for corresponding AB and HAB compounds (Table 2) reveals that the internuclear separation in the triatomic molecules resembles that of the $^2\Sigma^+$ state in the diatomic. These findings can be explained by the common π^4 occupation in both the $^2\Sigma^+$ (AB) and $^1\Sigma^+$ (HAB) states, respectively.

In going from HAB to H_2ABH one formally occupies the in-plane component of the π^* MO, which is generally characterized as n (non-bonding with respect to AB) MO. Hence this MO has very little influence on the AB bond. The original π^4 in the linear triatomic HAB decomposes in the planar H_2ABH molecules into a'^2 and a''^2, respectively. The double occupation of the lower-lying σ and the out-of-plane π (a'') species is also present in the $^2\Pi_i$ $(\sigma^2\pi^3)$ states of the diatomics AB and for this reason one observes that the internuclear distances in H_2ABH are approximately the same as reported for the $^2\Pi_i$ states. In the case of the H_2CNH one finds a slightly larger distance as in the corresponding CN radical, but for all other species this rule works quite well.

B. *Molecular orbitals*

The H_2ABH molecules under discussion possess 12 valence electrons, whereby only one occupied MO is of a'' (π) symmetry. The highest occupied MO of a' symmetry $(5a')$ is invariably associated with the lone-pair of the heavy B atom and characterized as n, while the $4a'$ is generally of σ or in-plane π type, in analogy with isovalent H_2AB molecules, as for example H_2CO, H_2CS, H_2SiO, H_2SiS, etc.. The most important canonical energies and the total SCF energies are summarized in Table 3, while the relative separations between the MO involved in the vertical excitation (of valence character only) are diagrammatically shown in Fig. 1.

It is seen (Table 3 and Fig. 1) that only in H_2CNH is the non-bonding $5a'$ (n) the highest occupied MO while in all other H_2ABH systems the a'' (π) is always less stable. The relative energetics between the highest occupied MO's are thereby quite similar in both mixed compounds H_2SiNH and H_2CPH. In

TABLE 3. Total SCF and canonical energies (in atomic units) obtained for the most important valence orbitals at the corresponding SCF equilibrium geometries (Basis A).[a] The calculated dipole moments (debye) are also given

ϵ_i[a]		H_2CNH	H_2SiNH	H_2CPH	H_2SiPH
E_{SCF}(GS): ($5a'^2 1a''^2$)		−94.04738	−345.06630	−380.30000	−631.34252
$3a'$		−0.6872	−0.5822	−0.6164	−0.5294
$4a'$ (σ)		−0.6058 (16.47)	−0.5159 (14.04)	−0.5272 (14.35)	−0.4751 (12.93)
$5a'$ (n)		−0.4268 (11.61)	−0.4033 (10.97)	−0.3967 (10.79)	−0.3925 (10.68)
$1a''$ (π)		−0.4535 (12.34)	−0.3768 (10.25)	−0.3649 (9.93)	−0.3233 (8.80)
$2a''$ (π^*)		0.1450	0.0708	0.0761	0.0400
$6a'$ (σ^*)		0.1900	0.1583	0.1711	0.1468
Dipole moment[b]	μ_x	1.544 (1.584)	2.310 (2.588)	0.909 (0.969)	1.745; 1.601 (1.998)
This	μ_y	1.550 (1.522)	1.261 (1.333)	0.601 (0.604)	0.633; 0.614 (0.638)
work	μ	2.188 (2.197)	2.632 (2.911)	1.090 (1.142)	1.856; 1.715 (2.098)
Literature	μ	2.024 (ref. 31) Expt. 2.44 (ref. 10) SCF	—	0.869 (ref. 22) Expt. 1.080 (ref. 29) SCF	— —

[a]The orbitals are labelled for the valence set only. Values in parentheses are $-\epsilon_i$ in eV.
[b]The molecular plane is (xy) and the AB bond collinear with the x-axis. The negative charge is concentrated around the atom B in all H_2ABH species. The first columns are MRD-CI (MO's) results at the corresponding equilibrium geometries, while the values in parentheses are SCF results (at the optimized SCF geometries). The data in the second column in H_2SiPH result from NO calculations.

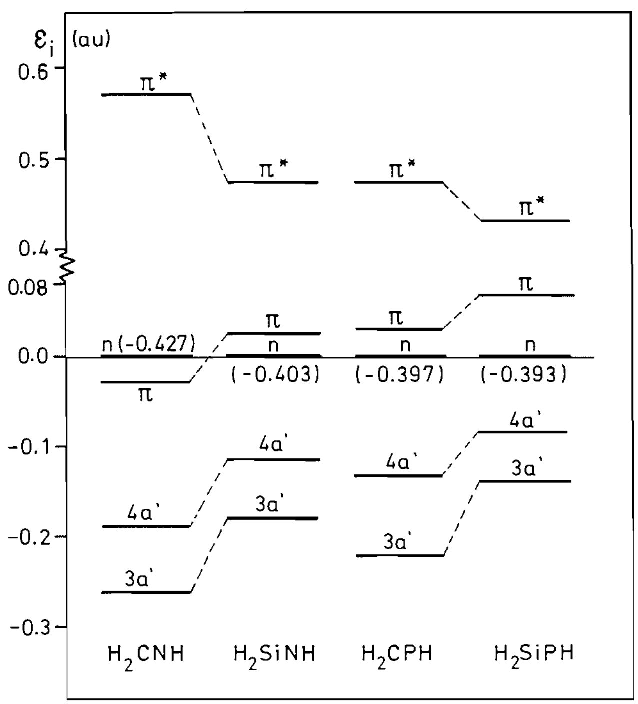

FIG. 1. Canonical orbital energies for the various species under consideration, obtained from the ground state SCF calculation.

H_2CNH one finds the situation familiar from H_2CO, while in H_2SiPH one observes a definite stabilization of the π^* (and n MO relative to the π MO's) and the opposite trend for the π MO which is shifted to higher canonical energies. Altogether the π^* becomes more stable upon substitution by a second-row atom relative to the original situation in H_2CNH (Fig. 1).

It should be pointed out that both the n and π^* orbitals correlate with the π^* (π_g-type) MO in the respective simple AB diatomics. Thus the in-plane n component achieves a considerably larger stabilization due to hydrogen admixture than its out-of-plane π^* counterpart, and this finally leads to a situation

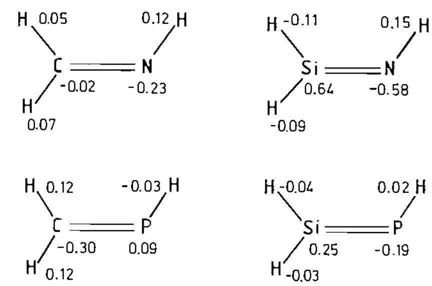

FIG. 2. Calculated net charge for the various compounds, obtained at the SCF level of treatment (Basis A).

in which the n orbital is placed even *below* the a'' MO which is originally associated with the π MO in the simple AB system. As a result one expects that the excitation energies for the $^{3,1}(n,\pi^*)$ and $^{3,1}(\pi,\pi^*)$ states are shifted to the red from H_2CNH to H_2SiPH, but that this effect is more pronounced for the $^{3,1}(\pi,\pi^*)$ multiplets.

C. *Charge distribution*

The Mulliken population analysis as well as the dipole moments give some insight into the charge distribution in the molecule. The population analysis has only been carried out at the SCF level of treatment (Basis A) and the results are indicated in Fig. 2. It is seen that the A atom is positive relative to B in the systems H_2CNH, H_2SiNH, and H_2SiPH, while in H_2CPH the situation is opposite and it is the phosphorus (atom B) which possesses the positive net charge in this analysis. In comparison with earlier results from the literature (29, 30), the charge separation is not as pronounced in the present work, however; Thomson (29) obtains a net charge of +0.38 for P and −0.35 for C in a STO-3G basis which changes to +0.31 (P) and −0.67 for C if the STO4-31G basis is employed (29, 30). Thus it is clear that the results are quite dependent on the quality of the AO basis.

The calculated dipole moments are also contained in Table 3. Generally the theoretical values are in relatively good agreement with the experimental data (22, 31) whereby the SCF value overestimates the dipole moment more than the MRD-CI result. All dipole moments indicate that the negative charge is concentrated in the BH region which is – with the exception of the H_2CPH system – in accordance with the Mulliken population analysis. The two spatial dipole moment components are almost equivalent in H_2CNH, while the direction is much closer to the Si=P bond in H_2SiPH ($\angle 18°$); the angles in the mixed compound (27° and 30°) lie, as expected, between the two extremes. The magnitude of μ is largest from H_2SiNH and almost the same as in the diatomic SiN radical (9).

IV. The Vertical Electronic Spectrum

One goal of the present work is to investigate the relative position of the valence $n \rightarrow \pi^*$ and $\pi \rightarrow \pi^*$ transitions in the various isovalent H_2ABH systems as well as that of the first $n \rightarrow s_R$ and $\pi \rightarrow s_R$ members of their Rydberg series. The calculation of the ionization potentials associated with $(n \rightarrow \infty)$ and $(\pi \rightarrow \infty)$ allows an estimate for the corresponding term values as well as for the respective quantum defects in the Rydberg series. The last point will be treated in Section V.

The H_2CNH molecule was analyzed in more detail than the other isovalent species. The potential energy curves for the lowest valence transitions are determined as a function of the CN internuclear separation in this case since it is well known from H_2CO or H_2CS that $n \rightarrow \pi^*$ and $\pi \rightarrow \pi^*$ excitations cause elongations of the AB bond. Additional Rydberg states are also treated for this molecule.

A. *Methylenimine H_2CNH*

There are earlier theoretical studies (10, 32–34) on the vertical spectrum of H_2CNH but all of them lack Rydberg-type AO as well as *d*-polarization functions on the heavy atoms. Another serious limitation of prior calculations is the inadequate treatment of the correlation energies, especially if one considers that only one reference configuration has been used in the older CI treatments.

We have studied this molecule in both Basis A and B. The study within the pure valence AO set could be considered as the *"diabatic valence"* portion of the potential curves (some of which possess valence-Rydberg character in the gas phase) or as the most likely potential curves of H_2CNH in condensed media. The valence transitions studied here are $^{3,1}(n,\pi^*)$, $^{3,1}(\pi,\pi^*)$, $^{3,1}(n,\sigma^*)$, $^{3,1}(\pi,\sigma^*)$, and $^{3,1}(\sigma,\pi^*)$, respectively. The first two multiplet pairs have also been studied in the more expanded Basis B, although it is to be expected that, with the exception of the high-lying $^1(\pi,\pi^*)$ state, both kinds of calculations give equivalent results.

The vertical transitions derived in the present work are contained in Tables 4 (Basis B) and 5 (Basis A), respectively, and in Fig. 3. In both cases a selection threshold of 5 μH (H, hartree) has been employed, leading to selected MRD-CI spaces ranging in order from 8000 to 12 000. The results for the MRD-CI and estimated full CI are given and show relatively little variance from one another; in the ensuing discussion the mean value of these will be used.

We analyse first the results obtained with the expanded AO basis. The lowest state in the vertical region is $^3(n,\pi^*)$, placed at 4.76 ± 0.03 eV, followed by the second triplet $^3(\pi,\pi^*)$ state, with an excitation energy of 5.10 ± 0.05 eV. The $^1(n,\pi^*)$ state is about 0.60–0.66 eV less stable than the corresponding triplet and located at ΔE = 5.42 ± 0.03 eV (Table 4).

According to Sandorfy and co-workers (10, 11, 36), the

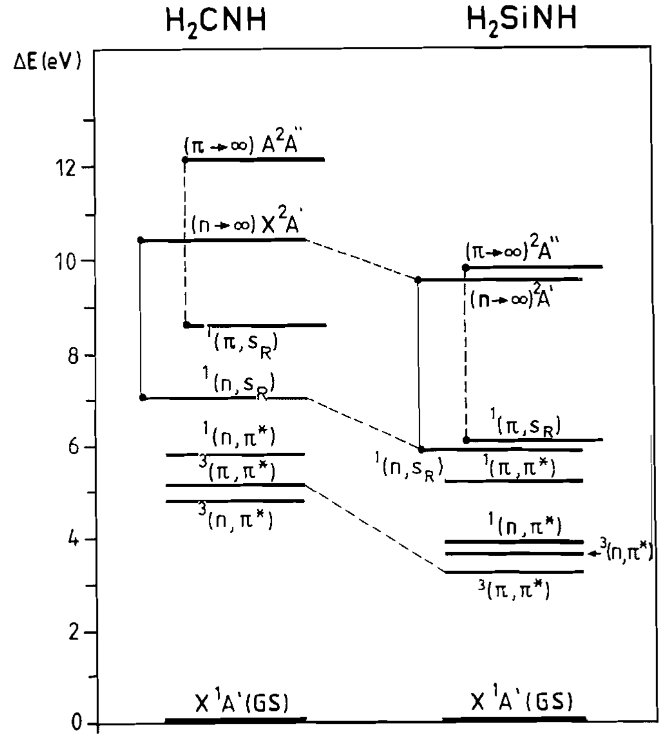

FIG. 3. Calculated vertical excitation energies (Basis B) in H_2CNH and H_2SiNH. Full CI results have been used.

$^1(n,\pi^*)$ transition is found between 41 000 and 43 000 cm^{-1} (i.e. 5.08–5.33 eV) for a series of azomethines. Our predicted value for the vertical excitation for the lowest singlet state in H_2CNH is in good agreement with this experimental finding since it is well known that the $^{3,1}(n,\pi^*)$ states acquire additional stabilization upon geometrical relaxation, i.e. elongation of the CN bond distance as well as loss of the C_s symmetry due to pyramidal-like structure in the excited states (10, 23). As discussed below, potential curves calculated at the MRD-CI level with respect to variations in the CN distance (and keeping all other geometrical parameters constant, however) find an extra stabilization of about 0.3–0.4 eV for the (n,π^*) multiplets, in comparison with the situation in the vertical region.

Although the earlier work of Macaulay *et al.* (10) has found a value for ΔE (ΔE = 4.68 eV) for the $^3(n,\pi^*)$ state quite comparable to the value reported in Table 4, by contrast the corresponding $^1(n,\pi^*)$ state was placed at an energy of 5.84 eV, i.e. ca. 0.40 eV higher than in the present study. Hence their predicted triplet–singlet splitting of 1.16 eV is too large when compared with our estimate of 0.66 ± 0.05 eV (see Table 4). Another theoretical study by Cimiraglia and Tomasi (32) locates the $^1(n,\pi^*)$ state slightly below the MRD-CI findings but places the $^3(n,\pi^*)$ state ca. 0.70 eV below the present value. This again leads to a splitting of 1.13 eV, quite similar to the value quoted in ref. 10. Other data for the $^1(n,\pi^*)$ states, also derived by theoretical methods, give 5.83 eV (34), while the excitation energy reported by Kitaura *et al.* (33) (i.e. 6.27 eV) seems to be definitely too high. The $^3(\pi,\pi^*)$ state is located vertically between the $^{3,1}(n,\pi^*)$ states around 5.10 ± 0.05 eV, i.e. ca. 4000 cm^{-1} above the prior estimate reported by Macaulay. The excitation energy of 3.93 eV cited in ref. 32 is apparently in error by more than 8000 cm^{-1}, however.

If one compares the $^{3,1}(n,\pi^*)$ states of H_2CNH with those of H_2CO one finds that the singlet–triplet splitting is comparable

TABLE 4. Calculated vertical excitation energies (in eV, Basis B) in H_2CNH and comparison with earlier work. Technical details of the MRD-CI treatment are also given

Transition	Treatment[a]	MRD-CI	Full CI estimate	Literature	Comparison with H_2CO (ref. 35)
$^1A'$ (GS)	5M1R,B1 144095/8146 (91.96%)	0.00 (−94.35288)[b]	0.00 (−94.37539)[b]		0.00
$^3A''$ $^3(n,\pi^*)$	2M1R,B2 127057/12656 (92.36%)	4.74	4.79	4.68 (10) 4.07 (32)	3.41
$^1A''$ $^1(n,\pi^*)$	2M1R,B2 76943/11550 (91.41%)	5.45	5.40	5.84 (10) 5.20 (32) 6.27 (33) 5.83 (34)	3.81
$^3A'$ $^3(\pi,\pi^*)$	1M1R,B3 82037/12099 (92.96%)	5.05	5.16	4.57 (10) 3.93 (32)	5.56 (5.69)
$^1A'$ Three roots selection[c]	19M3R,B3 616660/13659 (91.14%; 90.80%; 91.10%)	9.20 10.15 10.97	9.04 10.02 10.86	$^1(\pi,\pi^*)$ 10.33 (10) 10.18 (32)	12.13 (11.72)
Four roots selection[d]	23M4R,B1 673050/12387 (90.86%; 90.74%; 90.69%; 91.16%)	9.26 10.24 10.97 11.02	9.06 10.08 10.80 10.99		
$^1A'$ $^1(n,s_R)$	15M1R,B4 94041/10718 (92.44%)	6.99	7.07		7.38
$^1A'$ $^1(n,p_\sigma)$ $^1(n,p_\pi(a'))$	21M2R,B4 898835/9467 (92.42%; 92.49%)	7.38 7.92	7.45 7.89		
$^1A''$ $^1(n,p_\pi)$	15M1R,B4 534750/11933 (91.08%)	7.87	7.77		
$^1A''$ $^1(\pi,s_R)$	11M1R,B5 417398/10794 (92.39%)	8.54	8.61		
$^1A''$ $^1(\pi,p_\sigma)$	11M1R,B5 417398/10788 (92.29%)	9.31	9.37		
$^1A''$ $^1(\pi,p_\sigma)$	11M1R,B5 417398/12193 (92.66%)	9.54	9.61		

[a] The notation mMrR refers to m main or reference configurations while selection is carried out for r roots. The total MRD-CI space is of dimension DIM while the selected subspace treats only dim SAF's (indicated by DIM/dim in the column). The values in parentheses are the weight of the reference species ($\Sigma_{ref}\, c^2$) in percent. The MO basis employed is referred to as B1 to B5 corresponding to the SCF MO's of the ground state, $^3(n,\pi^*)$, $^3(\pi,\pi^*)$, $^3(n,s)$, and $^3(\pi,s)$ respectively.

[b] Total energies in hartree. T = 5 μH.

[c] Selection threshold used: T = 10 μH; E(GS) = −94.35319 au (MRD); −94.37490 au (full CI estimate). Using as nomenclature $A(\pi,p_\pi)$, $B(\pi,d_\pi)$, $C(\pi,d_\delta)$, and $D(\pi,\pi^*)$, the different roots have the composition:
(R1) 0.50 [A]; 0.25 [B]; 0.01 [C]; 0.13 [D]
(R2) 0.06 [A]; 0.13 [B]; 0.01 [C]; 0.65 [D]
(R3) 0.35 [A]; 0.54 [B]; 0.02 [D].

[d] Selection threshold used: T = 12.5 μH; E(GS) = −94.35131 au (MRD); −94.37280 au (full CI estimate). The composition of the different roots is:
(R1) 0.44 [A]; 0.11 [B]; 0.11 [C]; 0.13 [D]
(R2) 0.11 [A]; 0.29 [B]; 0.13 [C]; 0.36 [D]
(R3) 0.32 [A]; 0.50 [B]; 0.01 [C]; 0.07 [D]
(R4) 0.04 [A]; 0.02 [B]; 0.54 [C]; 0.31 [D].

(0.65 eV in H_2CNH and 0.40 eV in H_2CO) but that the absolute transition energies are shifted to higher values by 1.30–1.60 eV in H_2CNH. This behavior can be rationalized if one assumes that the hydrogen bound to the nitrogen atom stabilizes the n MO relative to the situation present in H_2CO.

There is no direct experimental information available about the location of the low-lying Rydberg states of H_2CNH. In the literature one can only find general trends on their relative

TABLE 5. Calculated vertical excitation energies for the valence-shell states of H_2CNH (in eV, Basis A)

Transition	Treatment[a]	MRD-CI	Full CI estimate	Literature
$^1A'$ (GS)	3M1R 53354/7756 (91.75%)	0.0 (−94.35223)[b]	0.0 (−94.37533)[b]	—
$^3(n,\pi^*)$	7M1R 318010/11274 (91.63%)	4.82	4.78	4.68 (10) 4.07 (32)
$^1(n,\pi^*)$	8M1R 194291/10131 (91.58%)	5.48	5.44	5.84 (10) 5.20 (32) 6.27 (33) 5.83 (34)
$^3(\pi,\pi^*)$	3M1R 139591/11406 (92.66%)	5.16	5.25	4.57 (10) 3.93 (32)
$^1(\pi,\pi^*)$	11M1R 221685/11218 (90.26%)	9.41	9.21	10.33 (10) 10.18 (32)
$^3(\pi,\sigma^*)$	12M1R 689156/10978 (90.45%)	8.13	7.99	8.59 (10) 8.17 (32)
$^1(n,\sigma^*)$	11M1R 346004/9961 (90.21%)	8.72	8.55	8.57 (32)
$^3(\pi,\sigma^*)$	12M1R 493654/11530 (90.54%)	9.88	9.73	9.10 (32)
$^1(\pi,\sigma^*)$	13M1R 263195/10111 (90.31%)	10.19	10.03	9.57 (32)
$^3(\sigma,\pi^*)$	7M1R 236748/11571 (91.26%)	9.71	9.65	—
$^1(\sigma,\pi^*)$	8M1R 145701/10325 (90.96%)	9.87	9.79	—

[a]The notation is the same as in Table 4. All calculations are undertaken with the SCF MO's of the ground state. The selection threshold was $T = 5$ μH.
[b]Total energies in atomic units.

excitation energies, which are based on observations for higher azomethine compounds. According to Sandorfy (11) the spectra of imines are diffuse in nature and this makes the Rydberg states difficult to locate. The $(n\rightarrow s_R)$ band is expected between 48 000 and 50 000 cm^{-1} (i.e. 5.95–6.20 eV). A comparison with the Rydberg transition energy predicted in the present work for the lowest state (see Table 4) shows that the theoretical values are ca. 8000 cm^{-1} higher than the experimental expectations. The transition $^1(n,p\pi)$ is located here at 7.82 ± 0.05 eV (i.e. 63 000 cm^{-1}), again in greater discrepancy with the predictions of Sandorfy, who assumes smaller values of 55 000 – 58 000 cm^{-1} (between 6.82 and 7.19 eV) for both the $(n\rightarrow 3p)$ and $(\pi\rightarrow 3s)$ transitions. We calculate the $^1(\pi,s_R)$ state at 8.58 ± 0.04 eV (69 000 cm^{-1}), that is, approximately 1.60 eV (≈13 000 cm^{-1}) higher than the absorption region expected from simple correlation with experimental results in related imine compounds.

A closer analysis of the basis for the various predictions removes the apparent discrepancies with the theoretical results. The estimates of Sandorfy have been based on general trends for term values and on the known first two ionization potentials of diverse azomethine compounds. In the meantime it is clear from experiments and our calculations (Section V) that the ionization processes in the simplest methylenimine need much more energy than the corresponding ionization in the higher compounds. For example, while the IP associated with $(n\rightarrow\infty)$ is placed around 9.44 eV in the heavier imine molecules, in H_2CNH it is shifted to higher values by 1.08 eV according to the experimental IP of 10.52 eV (37). If one considers the next ionization band associated with $\pi\rightarrow\infty$, the destabilization of the π MO in going from H_2CNH to larger azomethines is even more dramatic, as exemplified by an IP $(\pi\rightarrow\infty)$ of 12.43 eV (37) in methylenimine compared with 10.48 eV observed for various $R^1R^2C{=}NR^3$ systems (36). This difference of 1.95 eV between the second ionization potentials in the simplest and the largest species must also occur between the first members of the respective $(\pi\rightarrow s_R)$ Rydberg series. In other words, the values expected by Sandorfy and co-workers for the location of the $^1(n,s_R)$ and $^1(\pi,s_R)$ transitions in H_2CNH (11) must be adjusted upwards by ca. 8800 and 15 000 cm^{-1}, respectively.

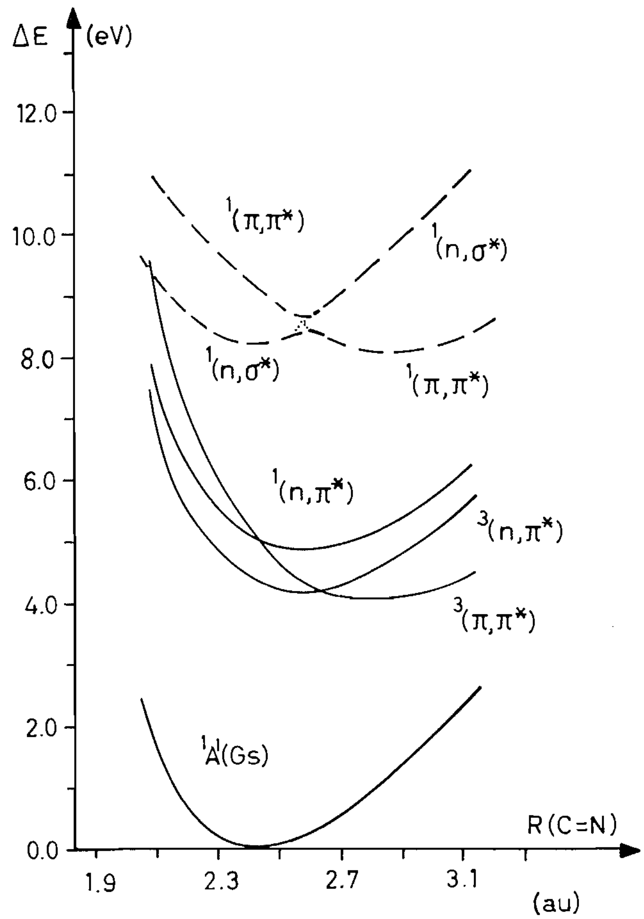

FIG. 4. Calculated potential energy curves as a function of C=N stretch for the lowest states of H_2CNH (Basis A). The $^1(\pi,\pi^*)$ and $^1(n,\pi^*)$ states are shown in dashed lines only because the actual behavior of potential energy curves is more complex as soon as Rydberg states are included (see Fig. 5).

After this shift, the experimental inferences and the present theoretical predictions are in good accord.

Before one analyzes the vertical transition energy for the $^1(\pi,\pi^*)$ state, the results obtained for variations in the CN distance in the lowest valence states $^{3,1}(n,\pi^*)$ and $^3(\pi,\pi^*)$, as well as in the ground state and the most important Rydberg states (Fig. 4), are of importance. All other internuclear geometrical parameters have been kept constant in these calculations.[1] The MO basis used in these CI investigations was obtained for the $^1A'$ ground state; the selection threshold was 12.5 μH, and leading to secular equations of the order 4000–6000. The results (Fig. 4) show that the $^3(\pi,\pi^*)$ state possesses the largest CN distance (about 2.8 au at equilibrium), while the other low-lying valence state curves for $^{3,1}(n,\pi^*)$ run parallel to each other and have a minimum at the somewhat shorter R(CN) ≈ 2.6 au. Similar results are reported by earlier SCF calculations (33). Both triplet states at their optimal geometries are in close energetic neighborhood and located around 4.0–4.2 eV above the ground state.

The $^1(\pi,\pi^*)$ state is placed within the restricted Basis A (of valence character only) at 9.30 ± 0.10 eV in the vertical region. A more refined treatment with the expanded Basis B leads to a more complicated picture: no unique state with predominant (π,π^*) composition is found any more. The lowest state of this symmetry is placed at 9.12 ± 0.08 eV and is fundamentally in nature 60% $\pi\rightarrow p\pi$ with ca. 20% contamination of the (π,π^*) configuration, while the next state contains more valence character, as given by the relative weights which are complementary to those in the lowest solution. The corresponding vertical excitation energy for the second state is 10.08 ± 0.08 eV. These results clearly demonstrate how the expansion of the AO basis by Rydberg functions splits the original "diabatic" eigenvalue of 9.30 eV into two states, one of them somewhat lowered with respect to it and with some degree of valence (π,π^*) character but essentially described by a Rydberg configuration, while the other component, placed around 81 000 cm^{-1}, contains the major portion of valence character.

The question of what happens with the $^1(\pi,\pi^*)$ state when the interatomic distance CN is increased has been investigated in two ways. First, only the valence-shell states are considered and the results are also contained in Fig. 4. The unperturbed $^1(\pi,\pi^*)$ configuration shows a similar CN stretch potential energy curve as the triplet counterpart with a minimum at relatively large CN separation (2.85 au). But in contrast to the situation for the $^3(\pi,\pi^*)$ state, which is located considerably *below* the $^3(n,\sigma^*)$ state according to Table 5, the singlet states show the reverse energetic ordering, leading to an interaction between both $^1(\pi,\pi^*)$ and $^1(n,\sigma^*)$ states as seen in Fig. 4. In other words, a stretching of the CN bond induces an avoided crossing between the (n,σ^*) and (π,π^*) configurations and will thus give rise to an irregular pattern in the vibrational structure of the ground state absorption.

The next step includes possible mixing of the $^1(\pi,\pi^*)$ state with Rydberg configurations. In this case only (π,π^*)-type configurations are considered which represent in the main the (π,π^*) valence-shell part and the $(\pi,p\pi_R)$ and $(\pi,d\pi_R)$ Rydberg states; since no $3d\pi$ functions are present in the AO basis, the higher π^*-type orbitals are only an approximation to such an MO. The results in Fig. 5 show a strong mixing among these configurations which is especially apparent at small CN separations. Generally the potential curves of the unperturbed Rydberg states should run essentially parallel to their ionic limit, also contained in Fig. 5. The strongly CN repulsive nature of the $^1(\pi,\pi^*)$ valence state perturbs this pattern; the $^1(\pi,\pi^*)$ valence potential energy curve crosses the $(\pi\rightarrow R)$ Rydberg manifold somewhat to the left of the Rydberg minima so that the valence character, present in the lowest $^1(\pi,\pi^*)$ state at large CN separation (for example 2.7 au), is gradually distributed among the $^1(\pi,\pi^*)$ states with decreasing CN values and is found in the third $^1(\pi,\pi^*)$ root at CN = 2.1 au. As a result, no single state with compact (π,π^*) character exists any more for CN values smaller than the equilibrium value of the X^1A' ground state, and considerable anomalies are expected in the energy levels and the intensity distribution of the absorption spectrum. To make the situation even more complicated, the $^1(\pi,\pi^*)$ state undergoes a further avoided crossing with the $^1(n,s_R)$ Rydberg state at CN values larger than 2.8 au. This behavior is also indicated in Fig. 5; the unperturbed $^1(n,s_R)$ potential energy curve would run strictly parallel to that of the $^2A'$ $(n\rightarrow\infty)$ molecular ion.

In summary, then, there is a manifold of states which couple with the $^1(\pi,\pi^*)$ whereby the interaction varies considerably

[1] The values reported by Macaulay *et al.* (10) for the internuclear angles and the hydrogenic bonds are taken for the calculation of the stretching potential curves; hence the starting geometry in the CN variations differs slightly from the best experimental data available (see Table 1).

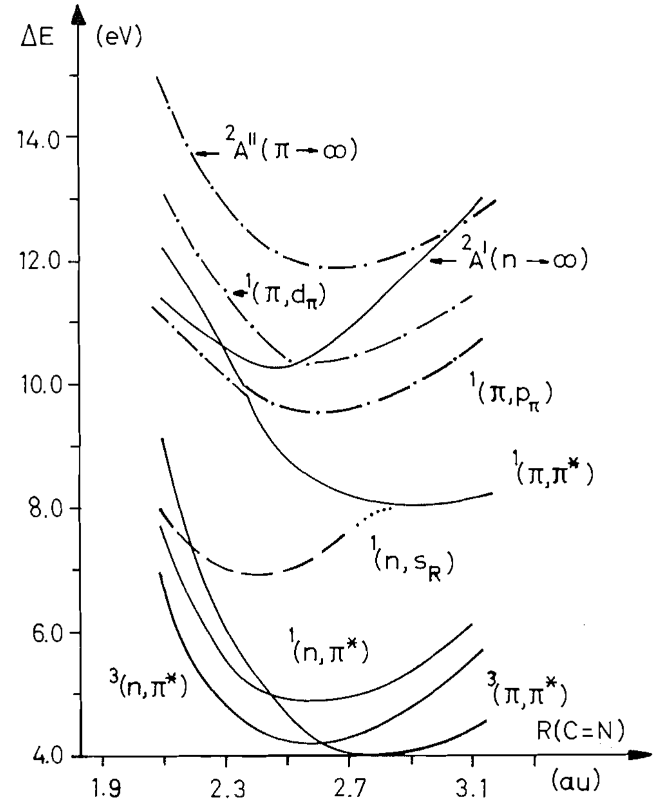

FIG. 5. Calculated mixing of Rydberg states of (π,π^*)-type symmetry as a function of CN stretch (Basis B).

with the change in CN bond length. It is thus not surprising that a quite diffuse and broad spectrum is obtained experimentally in this energy region.[2] This basic analysis can presumably be carried over to higher members in the $R^1R^2C{=}NR^3$ series and thus explains the complicated absorption and emission pattern in azomethines. The direct connection of the $^1(n,s_R)$ with $^1(\pi,\pi^*)$ potential curve shown in Fig. 5 is also in accordance with the observation by Sandorfy that the Rydberg states could be responsible for a part of the broad and highly asymmetrical low-wavenumber shoulder of the $^1(\pi,\pi^*)$ band in the spectra of imines.

Finally, if the results of the all-valence AO basis in Table 5 are compared with those obtained from the more flexible Basis B (Table 4) it is seen that the transition energies to the lowest $^{3,1}(n,\pi^*)$ and $^3(\pi,\pi^*)$ states are almost the same in both treatments, at least at the level of the estimated full CI. The $^{3,1}(n,\sigma^*)$ states are treated only in this basis (as are all other valence states) and are located at 8.06 ± 0.07 eV and 8.64 ± 0.08 eV (ca. 70 000 cm^{-1}) respectively. Even though the $^1(n,\sigma^*)$ is considerably above the first member of the Rydberg $^1(n,s_R)$ state at the ground state structure, this energy difference decreases with CN stretching until interaction of both states (Figs. 4, 5), as well as with the $^1(\pi,\pi^*)$ component, appears. Other valence states of interest are derived from the $\sigma\rightarrow\pi^*$ transition. They are characterized by the smallest singlet–triplet separation of the intravalence transitions studied so far. The highest states of (π,σ^*)-type are relatively close in energy to (σ,π^*) and show calculated excitation energies in the 10-eV region. Interactions of these states are also likely but have not been investigated in this work.

[2] Note that one can expect that the absorption maximum in this simplest H_2CNH imine is shifted to higher energies, when compared to the higher imines, for the same reason as discussed for the first members of the Rydberg series or the ionization potentials.

TABLE 6. Calculated relative energies for H_2SiNH (in eV)

Transition	Treatment[a]	MRD-CI	Full CI estimate
$^1A'$ (GS)	3M1R,B1 101363/7060 (90.55%)	0.0 (−345.34152)[b]	0.0 (−345.36677)[b]
$^3(n,\pi^*)$	3M1R,B2 265928/10473 (91.92%)	3.53	3.68
$^1(n,\pi^*)$	3M1R,B2 158762/9164 (91.45%)	3.82	3.93
$^3(\pi,\pi^*)$	3M1R,B2 404203/10719 (92.42%)	3.15	3.25
$^3(\pi,\pi^*)$	1M1R,B3 96916/10500 (92.12%)	3.04	3.21
$^1(\pi,\pi^*)$	19M1R,B3 708348/10136 (90.97%)	5.19	5.24
$^1(n,s_R)$	7M1R,B4 361633/9431 (91.39%)	5.79	5.90
$^1(\pi,s_R)$	15M1R,B5 655631/10755 (91.66%)	5.95	6.07

[a] The notation is the same as in Table 4; the selection threshold is $T = 5\ \mu$H.
[b] These values are absolute energies in au.

B. *Silylimine H_2SiNH*

The relative energies predicted for the excited states of H_2SiNH in the vertical region are displayed in Table 6 and Fig. 3. The lowest excited state is found to be the $^3A'$ (π,π^*), in contrast to the situation of the first-row analogue H_2CNH, in which this state is placed (vertically) between the $^{3,1}(n,\pi^*)$ multiplets. The state has been studied in two different MO basis sets (see Table 6). Using the parent SCF MO's and one reference configuration, one obtains relative energies comparable to working with three reference configurations in the $^3(n,\pi^*)$ MO basis; the respective full CI estimates differ by only 0.04 eV, while the difference in MRD-CI values is 0.11 eV. The corresponding contribution of the reference configurations to the total wavefunction as measured by Σc^2 is 92.12% if the parent SCF MO's and 91.42% if the $^3(n,\pi^*)$ MO's are employed, compared to 90.55% achieved in the ground state treatment. This in turn signals that the calculated MRD-CI excitation energy employing the parent MO's is somewhat too low (3.04 eV) simply because the excited state is described slightly better than the ground state. A somewhat more balanced description between ground and excited states is obtained in the $^3(n,\pi^*)$ MO basis. This balance in Σc^2 is quite important for a good description of the relative energies, as pointed out in the literature (17*b*, 38). The full CI level of treatment leads to more reliable results because the differences in Σc^2 are essentially removed. This observation is valid for all vertical transitions reported in this work.

The $^{3,1}(n,\pi^*)$ states located at 3.68 eV and 3.93 eV re-

TABLE 7. Calculated relative energies for H_2CPH (in ev)

Transition	Treatment[a]	MRD-CI	Full CI estimate
$^1A'$ (GS)	3M1R,B1 101303/7070 (90.26%)	0.0 $(-380.57110)^b$	0.0 $(-380.59586)^b$
$^3(n,\pi^*)$	2M1R,B2 313890/10872 (91.28%)	4.16	4.26
$^1(n,\pi^*)$	5M1R,B2 198738/9695 (90.06%)	4.96	4.94
$^3(\pi,\pi^*)$	1M1R,B3 96916/9836 (91.68%)	2.94	3.07
$^1(\pi,\pi^*)$	19M1R,B3 750500/8895 (89.72%)	6.51	6.44
$^1(n,s_R)$	16M1R,B4 822326/9378 (90.20%)	6.92	6.91
$^1(\pi,s_R)$	12M1R,B5 539510/9341 (90.56%)	6.67	6.71

[a]The notation is the same as in Table 4; the selection threshold is $T = 5$ μH.
[b]These values are absolute energies in au.

spectively are shifted to *lower* energies by about 9000–12 000 cm^{-1} when compared with the similar transitions in the H_2CNH compound. The $^3A'$ (π,π^*) state is stabilized by ca. 16 000 cm^{-1} in going from methylenimine to silylimine, but the most drastic stabilization is found for the $^1A'$ (π,π^*) state: taking as vertical excitation energy for the strongly perturbed singlet (π,π^*) state of H_2CNH an approximate value of 9.5–10.0 eV, this vertical absorption band is shifted in the silicon compound by about 36 000 cm^{-1} to longer wavelengths. As a result the $^1(\pi,\pi^*)$ state is placed *below* both Rydberg series, even in the vertical region of the spectrum. This finding suggests that the absorption band associated with this transition must be simpler than in H_2CNH: although a broad band is expected due to the difference in the equilibrium geometries of ground and excited states, the strong Rydberg-valence mixing observed for H_2CNH is absent in the silicon compound. If perturbations are present, they are probably due to valence transitions, for example A' $^1(n,\pi^*)$ or A'' $^1(\pi,\sigma^*)$.

The $^{3,1}(n,\pi^*)$ splitting is smaller than the corresponding triplet–singlet energy separation in the (π,π^*) states. These trends are in line with the spatial distribution of the corresponding MO's involved in the transitions. Both π and π^* species have their charge distribution maxima perpendicular to the molecular plane, while the n MO is more concentrated in the molecular plane. Hence the respective exchange integrals are larger for the (π,π^*) configuration than for (n,π^*) and the triplet–singlet splittings follow these trends. Comparing the $>$C=N- with the $>$Si=N-group, one notices that all key MO's are more extended in space in the molecule with a second-row constituent, and this results in a systematic reduction in the triplet–singlet separations as soon as second-row atoms are included.

The first members of both Rydberg series are placed close together. According to the full CI data, the $^1(n,4s_R)$ is found vertically at 5.90 eV while the $^1(\pi,4s_R)$ lies only 0.17 eV (1400 cm^{-1}) above. Due to the different properties of the n and π MO's with respect to elongation of the Si=N bond, one can assume that the $^1(\pi,4s_R)$ state at its equilibrium is possibly just below the $^1(n,4s_R)$ state. A comparison of the Rydberg states in both H_2CNH and H_2SiNH reveals a general lowering in the excitation energies, of the order of 9500 cm^{-1} for the (n,s_R) state and a much larger effect (about 20 500 cm^{-1}) for the π-Rydberg series. These findings indicate that the π MO is relatively more *destabilized* (by about 11 000 cm^{-1} = 1.40 eV) than the n species after substitution of a carbon by the silicon atom, as already seen in Fig. 1.

C. *Methylenephosphine H_2CPH*

The H_2CPH molecule is the simplest phosphane-alkene; it has recently been observed (22, 39, 40) in the laboratory and its microwave spectrum has been analyzed (22). The lowest ionization potentials have also been measured.[3] This molecule is rather unstable, with a tendency towards dimerization.

Some theoretical work on H_2CPH is reported in the literature but to the best of our knowledge none of its excited states have been studied so far. The first work of Thomson (29) was limited to an estimate of the ground state equilibrium geometry at the SCF level (without *d*-polarization functions) and the ordering of n below π MO (Fig. 1) was noted for the first time. In another SCF study (30) the charge distribution of the different MO's was discussed and the π-bond energy has been estimated. In more recent work carried out by Lohr *et al.* (41), the proton affinity of H_2CPH was studied with a more expanded AO basis, also including correlation effects according to the Møeller–Plesset (in 4th order) scheme. The SCF energy obtained in that work is −380.29294 au and is comparable with our result of −380.3000 au. The final energy derived with the perturbative method is −380.57549 au and lies in between the values −380.57110 au (MRD-CI) and −380.59586 au (full CI estimate) reported in the present study (Table 7). These authors have found that the P-site protonation is favored over the C-site protonation by about 50 kJ/mol, whereby the resulting $H_2CPH_2^+$ radical possesses a C_{2v} planar equilibrium geometry. As illustration it can be mentioned that a similar protonation on H_2CNH to $H_2CNH_2^+$ indicates a value larger by 150 kJ/mol for the N-site protonation than for the C-site (41). This behavior in turn strongly supports the charge distribution reflected by the dipole moment calculation (Section III), i.e. a negative site at phosphorus, in contrast to what can be derived on the basis of the Mulliken population analysis.

The predicted locations of the excited states in H_2CPH are given in Table 7 while the relative separation is shown in Fig. 6, together with the H_2SiPH homologue.

The valence states $^{3,1}(\pi,\pi^*)$ and $^{3,1}(n,\pi^*)$ follow in the vertical region the same pattern as discussed for the H_2SiNH compound containing a second-row atom. The $^3(\pi,\pi^*)$ state lies at ca. 24 000 cm^{-1}, i.e. about 2000 cm^{-1} below the excitation energy assigned to the equivalent state of H_2SiNH (see Table 6). The $^{3,1}(n,\pi^*)$ states are located at 4.26 eV and 4.94 eV, respectively. The transition energies for the last mentioned multiplets, when compared with H_2CNH, are found about 4000 cm^{-1} lower, but ca. 5600 cm^{-1} higher as predicted here for the H_2SiNH molecule. In other words, the (n,π^*) states of H_2CPH are characterized by excitation energies lying between the cor-

[3] H. W. Kroto, private communication.

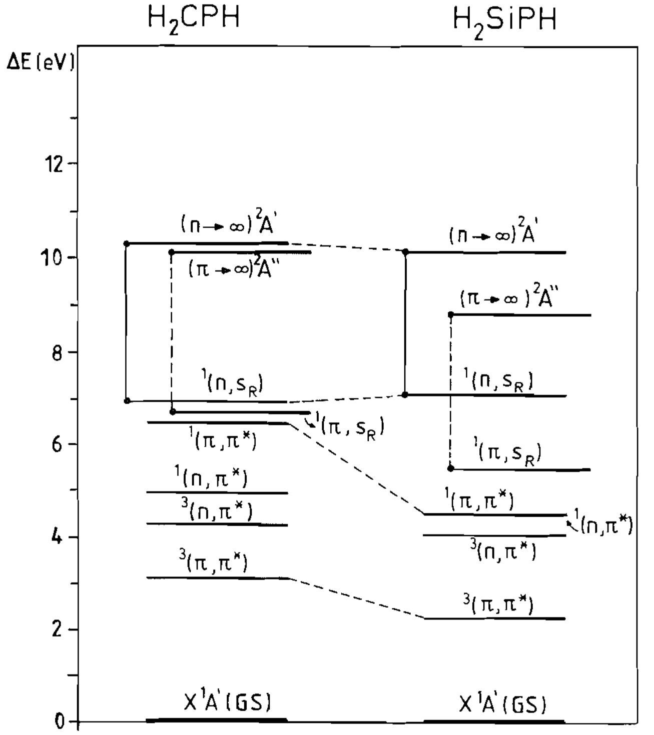

FIG. 6. Calculated vertical excitation energies (Basis B) in H_2CPH and H_2SiPH. Full CI results have been used.

TABLE 8. Calculated relative energies for H_2SiPH (in eV) using MO's

Transition	Treatment[a]	MRD-CI	Full CI estimate
$^1A'$ (GS)	4M1R,B1 104817/5073 (89.62%)	0.0 (−613.57902)[b]	0.0 (−631.60224)[b]
$^3A''$ $^3(n,\pi^*)$	1M1R,B2 77446/6740 (90.81%)	3.98	4.06
$^1A''$ $^1(n,\pi^*)$	3M1R,B2 120650/6448 (89.88%)	4.50	4.52
$^3A'$ $^3(\pi,\pi^*)$	5M1R,B2 549609/6281 (91.25%)	2.12	2.24
$^1A'$ $^1(\pi,\pi^*)$	14M1R,B2 574014/6142 (89.23%)	4.54	4.48
$^1A'$ $^1(n,s_R)$	21M1R,B1 941608/5926 (88.88%)	7.16	7.06
$^1A''$ $^1(\pi,s_R)$	14M1R,B1 527250/5830 (89.59%)	5.52	5.47

[a]The notation is the same as in Table 4; the selection threshold is $T = 7.5$ μH.
[b]These values are absolute energies in au.

responding values assigned to H_2CNH and H_2SiNH, respectively. The $^1(\pi,\pi^*)$ state lies 52 000 cm^{-1} above the ground state and this implies a singlet–triplet splitting of 3.37 eV (27 000 cm^{-1}), much larger than the 2.0 eV established for H_2SiNH. Generally the triplet–singlet separations predicted for H_2CPH are greater than in the two silicon compounds.

The results of Table 7 show that in H_2CPH the Rydberg states are also placed close together as observed in H_2SiNH, but by contrast the $^1(\pi,s_R)$ state is located below the $^1(n,s_R)$ already in the vertical region. Surprisingly both $^1(n,s_R)$ states in H_2CNH and H_2CPH are in approximately the same absorption region (i.e. 56 000 ± 1000 cm^{-1}) and this finding is confirmed by the similarity in the corresponding $n\rightarrow\infty$ ionization potentials. The Rydberg (π,s_R) series is stabilized by about 15 000 cm^{-1} upon formal substitution of the nitrogen atom in H_2CNH by phosphorus and this behavior runs parallel to the strong lowering in the ionization energy $(\pi\rightarrow\infty)$ leading to the ground state of H_2CPH^+.

D. *H_2SiPH*

There is practically no information available for small molecules containing the SiP bond. Recently the first *ab initio* studies on the experimentally unknown simple molecules SiP (4) and SiP^+ (8), as well as on the isomer pairs HSiP–HPSi (9), were carried out in this laboratory and thus the present report on H_2SiPH is an expansion of this work to improve our knowledge of the bonding properties of silicon–phosphorus compounds.

The excitation energies obtained from the MRD-CI calculations are summarized in Table 8 and Fig. 6. The technical treatment differs somewhat from the previous cases because the various electronic states have been studied by employing an MO as well as an NO basis. In the first run, the CI calculations were carried out using the ground state or the $^3(n,\pi^*)$ MO's; the corresponding wavefunctions were transformed to an NO basis and the CI calculations repeated with a selection threshold of 5 μH, i.e. 2.5 μH smaller than in the first run.

As discussed in Section III, this molecule is characterized by the largest relative stabilization of the n species in comparison with the π MO's, while on the other hand the energy difference between both π and π^* MO's is the smallest of the present family of molecules (Fig. 1). This must be reflected in the corresponding excitation energies, as well as the state ordering, when compared with related molecules.

The $^3A'$ (π,π^*) level lies only 18 000 cm^{-1} above the ground state, which means a stabilization of ca. 7000–8000 cm^{-1} if one takes the corresponding values of H_2CPH or H_2SiNH as reference. The $^1(\pi,\pi^*)$ state is located practically at the same excitation energy as the $^1(n,\pi^*)$ state (around 36 500 ± 1000 cm^{-1}) and this finding suggests a broad band in the corresponding absorption spectrum. Due to the aforementioned relative stabilization of the n MO, the (n,π^*) multiplets are shifted to somewhat higher energies than in H_2SiNH. The rather small excitation energies found for the (n,π^*) and (π,π^*) states are also in agreement with the low-transition energies previously predicted for the $^4\Pi$, $^4\Sigma^+$, $^4\Delta$, and $^4\Sigma^-$ states of the parent SiP diatomic molecule (9).

By the same token, the first Rydberg state is clearly the $^1(\pi,s_R)$, lying around 44 000 cm^{-1}. The other Rydberg transition $^1(n,s_R)$ lies about 13 000 cm^{-1} above the lowest $^1(\pi,s_R)$ and one can expect that other terms $(\pi,4p_R)$ and $(\pi,3d_R)$ are just below the first member of the Rydberg series starting with the second highest n-orbital.

The results obtained by employing natural orbitals are collected in Table 9. In general the results are quite similar to those obtained in the MRD-CI calculations based on the two different types of SCF-MO orbitals. The advantage can primarily be seen in a somewhat more contracted (fewer reference configurations) MRD-CI expansion.

TABLE 9. Calculated relative energies for H_2SiPH (in eV) using NO's

Transition	Treatment[a]	MRD-CI	Full CI estimate
$^1A'$ (GS)	5M1R 192670/5219 (90.72%)	0.0 (−631.58345)[b]	0.0 (−631.60280)[b]
$^3(n,\pi^*)$	3M1R 214320/7742 (89.72%)	4.07	3.97
$^1(n,\pi^*)^c$	3M1R 128836/6836 (89.41%)	4.55	4.44
$^3(\pi,\pi^*)$	2M1R 160712/7182 (90.78%)	2.22	2.21
$^1(\pi,\pi^*)^c$	12M1R 416534/6945 (88.94%)	4.73	4.55
$^1(n,s_R)$	6M1R 291629/6738 (89.44%)	7.45	7.37
$^1(\pi,s_R)$	7M1R 360759/6772 (90.57%)	6.07	6.07

[a] The notation is the same as in Table 4; the selection threshold is $T = 5$ μH.
[b] These values are absolute energies in au.
[c] The NO basis used stems from the corresponding triplets.

V. Ionization potentials and term values

The electronic states of the positive ions H_2ABH^+ studied here are $^2A'$ (n,∞) and $^2A''$ (π,∞), respectively. Technical details of the calculations are presented in Table 10, together with the corresponding numerical results. The relative positions with respect to the neutral ground states as well as to the related Rydberg series are contained in Figs. 3 and 6.

According to the bonding characteristics of the molecular orbitals from which the ionization takes place, one can expect that the $^2A''$ (π,∞) ionic states have larger equilibrium AB distances than the corresponding values in the neutral molecules. This feature leads to vibrational progressions in this portion of the photo-ionization spectrum. The other ionization process (n,∞), by contrast, probably does not alter the internuclear AB distance to a larger extent and by this reason the corresponding PES peaks should be relatively sharp without structure.

Inspection of Table 10 shows that the theoretical values for the two IP's of H_2CNH are in quite good agreement with the experimental findings (37). The underestimation error of 0.20 eV in the case of $^2A''$ can be considered as typical for this kind of calculation and is probably also valid for the ionization potentials of the other compounds. Both IP's are close together in the vertical region for the mixed compounds H_2CPH and H_2SiNH. The $^2A''$ state of H_2CPH^+ is already the lowest ionic state vertically, while in the case of H_2SiNH^+ it lies somewhat above the $^2A'$ state. The extra stabilization due to elongation of the SiN distance probably leads to a final situation in which the ground state of H_2SiNH^+ also corresponds to $^2A''$ (π,∞). It is thus suggested that the PES spectra of both H_2CPH and H_2SiNH are more complex than experimentally reported for H_2CNH, in which the two first ionization regions are well separated.

For H_2SiPH the calculations predict a more simple (or normal) PES, with two well-characterized ionization processes in which without doubt the ground state of H_2SiPH^+ is the $^2A''$ state. The $^2A'$ (n,∞) has been shifted to higher energies by ca. 1.40 eV, a pattern observed before in the respective Rydberg series of H_2SiPH. Finally, it is of interest that the IP (π,∞) calculated for H_2SiPH is comparable with the values of 9.07 ± 0.02 eV ($HSiP^+$) and 9.00 ± 0.03 eV ($HPSi^+$) recently reported in a MRD-CI study of the ionization of the isomer pairs HSiP–HPSi in their corresponding $^1\Sigma^+$ $(\sigma^2\pi^4)$ ground states and leading to the $^2\Pi$ ionic states (9).

Finally, the calculated term values and the quantum defects for the various Rydberg series in the molecules are collected in Table 11. The results obtained for H_2CNH are close to the experimental findings on the HCN molecule (42, 43). The transitions $(1\pi\rightarrow 3s_R)$ and $(5\sigma\rightarrow 3s_R)$ in HCN are characterized by term values of 27 260 ± 500 cm^{-1} and they are comparable with the values 27 830 cm^{-1} $(n\rightarrow s)$ and 29 520 cm^{-1} $(\pi\rightarrow s)$ derived here for H_2CNH. The term values associated with the $(n\rightarrow p\pi)$ or $(\pi\rightarrow p\pi)$ transitions, namely 21 450 cm^{-1} (Table 11) are about 1000–2000 cm^{-1} higher than the experimental data reported in the equivalent transitions of HCN.

In H_2CPH the energy differences between the $^1(n,s_R)$ and $^1(\pi,s_R)$ states with respect to the corresponding ionization limits are found to be quite similar for both series (≈27 000 cm^{-1}), in accordance with general qualitative rules. The H_2SiNH molecule is apparently characterized by somewhat larger term values than found for the other species. The quantum defect and term value predicted for the (π,s_R) transition of H_2SiPH are in accordance with general expectations, while the transition involving the n orbital has a term value ca. 2000 cm^{-1} smaller.

We hope that the term values reported here could help to locate the Rydberg states of future experimental uv absorption spectra, not only of higher $R^1R^2A{=}BR^3$ compounds related to the simple parent molecules studied in the present work, but also for the simple diatomics CN, CP, SiN, and SiP, as well as the corresponding stable HAB isomers of the three last-mentioned AB radicals. To the best of our knowledge, nothing has been experimentally reported on this topic.

VI. Summary and conclusion

The present investigation on selected low-lying electronic states of H_2CNH, H_2CPH, H_2SiNH, and H_2SiPH gives further examples of a general trend in the electronic structure, already observed in a series of simpler compounds, built up from atoms exclusively of the first or the second row and possessing at the same time atoms of both rows. This trend can be directly related to orbital stability.

For all the atoms of the first row one finds that $\langle r \rangle$ for both $2s$–$2p$ AO's are very similar, while the $3s$–$3p$ subshell of second-row atoms are well separated in their spatial extension. As discussed in more detail elsewhere (9, 44), the two bonding σ MO's derived from $2s$ and $2p$ avoid each other, so that the higher of them $(p\sigma+p\sigma)$ is placed above the π MO. When a second-row atom is involved in the AB bond the splitting between the two σ MO's is reduced somewhat, and the $\sigma(p\sigma+p\sigma)$ MO is even placed below the π MO if both atoms A and B are second-row elements. In effect, this amounts to a considerable stabilization of the σ MO relative to the π if second-row atoms are introduced into the AB bond. At the same time the antibonding π^* MO becomes stabilized upon such substitution, which can be rationalized by the more diffuse charge distribution or alternatively by the primarily symmetric

TABLE 10. Vertical ionization potentials (in eV). Values in parentheses are full CI estimate energies

	$^2A'$ (n,∞)		$^2A''$ (π,∞)	
	Treatment[a]	MRD-CI (Full CI)	Treatment	MRD-CI (Full CI)
H_2CNH^+	10M1R 607119/9465 (91.02%)	10.52 (10.44) 10.52, expt. (ref. 37)	6M1R 379170/9466 (91.21%)	12.26 (12.21) 12.43, expt. (ref. 37)
H_2SiNH^+	9M1R 685978/7697 (90.56%)	9.51 (9.54)	6M1R 392722/8134 (91.27%)	9.72 (9.80)
H_2CPH^+	11M1R 884038/8228 (89.96%)	10.30 (10.29)	9M1R 571840/8109 (90.09%)	10.09 (10.11)
H_2SiPH^+ (MO's)	9M1R 610775/5292 (89.36%)	10.16 (10.16)	4M1R 209505/5519 (89.51%)	8.79 (8.79)
H_2SiPH^+ (NO's)	4M1R 226016/6233 (90.65%)	10.09 (10.11)	5M1R 250482/5911 (91.31%)	8.80 (8.87)

[a]The notation is the same as in Table 4. The MO's of the neutral ground state are used in each case ($T = 5\mu H$, except for H_2SiPH^+ (MO's), with $T = 7.5\ \mu H$).

TABLE 11. Calculated term values and quantum defects (δ) for the lowest Rydberg series (values in cm^{-1})

	H_2CNH		H_2CPH		H_2SiNH		H_2SiPH	
	Term value	δ	Term value	δ	Term value	δ	Term value	δ
$n\rightarrow s$	27830	0.99	27260	1.99	29680	2.08	24600	1.89
$n\rightarrow p_\pi$	21450	0.73						
$\pi\rightarrow s$	29520	1.07	27500	·2.00	30330	2.09	26580	1.97
$\pi\rightarrow p_\sigma$	23300	0.83						
$\pi\rightarrow p_\pi$	21450	0.73						

$\pi-\pi^*$ splitting relative to the separated $3p\pi$ value.

In diatomics these trends cause, for example, a decrease in the energy separation between $X^2\Sigma^+$ $(\sigma\pi^4)$ and $^2\Pi$ $(\sigma^2\pi^3)$ states in the series of diatomics CN, CP, SiN, and SiP (9) which is around 9000 cm^{-1} to 7000 cm^{-1} for CN and CP respectively, 1000 cm^{-1} in SiN, and negative in SiP, i.e. $X^2\Pi_i$ is the ground state in SiP, and $A^2\Sigma^+$ the low-lying excited state. Similar behavior was earlier reported (6) for the series C_2, CSi, and Si_2 with the states corresponding to the electronic configurations π^4, $\sigma\pi^3$, $\sigma^2\pi^2$ or the corresponding negative ions C_2^- (45), CSi^- (4, 46), and Si_2^- (5). The increased π^* stability can be seen from the relative separation between $^4\Pi$ $(\sigma^2\pi^2\pi^*)$ and $^4\Sigma^+$, $^4\Delta$, $^4\Sigma^-$ $(\sigma\pi^3\pi^*)$, which is of the order of 4.5–4.6 eV in the light CN radical, compared to 2.0–3.0 eV predicted for the silicon compounds SiN and SiP (9).

In the H_2ABH systems treated in the present work these general trends can be seen in the relative position and ordering of low-energy excited states as well as in the ionization potentials (Figs. 1, 3, 6). The complementary behavior of π and π^* (decrease and increase in stability) by replacement of a first by a second-row atom is quite apparent from Fig. 1. The n orbital as the in-plane π^* component is lower than the out-of-plane π^* due to hydrogen admixture but otherwise shows a similar behavior relative to π, as does π^* with the exchange of first by second-row atoms, and as a result the n MO is below π in all the compounds with the exception of H_2CNH. These relative orbital stabilities explain the following various features:

1. The $^3(n,\pi^*)$ is the first excited state only in the first-row compound H_2CNH whereas it is the $^3(\pi,\pi^*)$ which is the lowest excited species in the mixed and second-row molecules; the relative separation between $^3(\pi,\pi^*)$ and $^3(n,\pi^*)$ increases from H_2SiNH to H_2SiPH. The singlet states follow in principle the equivalent pattern whereby singlet–triplet splittings are larger for (π,π^*) than for (n,π^*) states and decrease with increase in the number of second-row constituent atoms.

2. The order of n and π ionization potentials is different in the first-row (H_2CNH^+, X^2A' (n,∞)) and second-row ions (H_2SiPH^+, X^2A'' (π,∞)); both ionic states are well separated, while in the mixed compounds n and π ionization is close in energy.

3. The Rydberg states associated with the $n\rightarrow s_R$ and $\pi\rightarrow s_R$ transitions are shifted relative to one another in analogy to the shift in the corresponding ionization limits. Only for H_2CNH a large interaction between the $^1(\pi,\pi^*)$ valence and the low-lying Rydberg states is found.

Comparison of H_2CNH with H_2CO on the one hand and H_2SiPH and H_2CS on the other shows a relatively large similarity. In H_2CO the $^1(\pi,\pi^*)$ state is found quite close to the $n\rightarrow\infty$ ionization limit, while this state is definitely below ionization in H_2CS (47) and $(CH_3)_2$ CS (48). Both studies have found that semidiffuse $3d\pi$ functions are to some extent important for the description of the $^1(\pi,\pi^*)$ state in the vertical energy range;

since no such functions are included in the present treatment, there might be some doubt as to the reliability of the $^1(\pi,\pi^*)$ energies. On the other hand, all Rydberg states in H_2CPH, H_2SiNH, and H_2SiPH are found above the $^1(\pi,\pi^*)$ state in the vertical energy region so that it is expected that $3d\pi$ functions are less important than in the sulfur compounds.

Finally, it should be mentioned that the magnitude of the ionization potentials and, with it, the absolute location of the Rydberg states depends quite substantially on the character of the atomic species or radicals attached to the C=N group: in higher azomethines the alkyl groups influence the relative position of the n and π MO's considerably, as deduced from the lower values of the IP's compared to that of the simplest member H_2CNH. Furthermore, the present work has treated only the nuclear arrangement H_2ABH in the comparative study and has entirely neglected the possibility of $HABH_2$ or other structures. Calculations carried out on various germanium species (24, 49) have indicated that the isomers $HGeNH_2$ or HGeOH are more stable, by about 32 kcal/mol or 20 kcal/mol respectively, than their H_2GeNH or H_2GeO counterparts.

Acknowledgments

The present authors as well as other members of this laboratory wish to thank Prof. C. Sandorfy for many pleasant and fruitful discussions over the past ten years and for his continuous interest in our work. The computer time necessary for the present study was supplied by the University of Bonn Computer Center, and for H_2SiPH by the Perkin–Elmer 3242 at Wuppertal sponsored by the Deutsche Forschungsgemeinschaft in the framework of the Sonderforschungsbereich 42.

1. R. APPEL, F. KNOLL, and I. RUPPERT. Angew. Chem. **93**, 771 (1981).
2. L. E. GUSELNIKOV and N. S. NAMETKIN. Chem. Rev. **79**, 529 (1979).
3. P. J. BRUNA, G. HIRSCH, R. J. BUENKER, and S. D. PEYERIMHOFF. Molecular ions: geometric and electronic structures. NATO ASI Series B: Physics. Vol. 90. *Edited by* J. Berkowitz and K. O. Groeneveld. Plenum Publ. Co., New York. 1983. p. 309.
4. P. J. BRUNA, H. DOHMANN, J. ANGLADA, V. KRUMBACH, S. D. PEYERIMHOFF, and R. J. BUENKER. J. Mol. Struct. (Theochem), **93**, 309 (1983).
5. P. J. BRUNA and S. D. PEYERIMHOFF. Proc. 16th Intern. Symp. on Free Radicals, Belgium; Bull. Soc. Chim. Belg. **92**, 525 (1983).
6. P. J. BRUNA, S. D. PEYERIMHOFF, and R. J. BUENKER. J. Chem. Phys. **72**, 5437 (1980).
7. S. D. PEYERIMHOFF and R. J. BUENKER. Chem. Phys. **72**, 111 (1982).
8. H. DOHMANN, P. J. BRUNA, S. D. PEYERIMHOFF, and R. J. BUENKER. Mol. Phys. **51**, 1109 (1984).
9. P. J. BRUNA, H. DOHMANN, and S. D. PEYERIMHOFF. Can. J. Phys. **62**, 1508 (1984).
10. R. MACAULAY, L. A. BURNELLE, and C. SANDORFY. Theor. Chim. Acta, **29**, 1 (1973).
11. C. SANDORFY. *In* Topics in current chemistry. Vol. 86. Springer Verlag, Heidelberg. 1979. p. 91.
12. S. HUZINAGA. J. Chem. Phys. **42**, 1293 (1965).
13. T. H. DUNNING and P. J. HAY. *In* Methods of electronic structure theory. *Edited by* H. F. Schaefer. Plenum Press, New York. 1977. p. 1.
14. A. VEILLARD. Theor. Chim. Acta, **12**, 405 (1968).
15. S. HUZINAGA. J. Chem. Phys. **50**, 1371 (1969).
16. B. ROOS and P. SIEGBAHN. Theor. Chim. Acta **117**, 199 (1970).
17. (*a*) R. J. BUENKER, S. D. PEYERIMHOFF, and W. BUTSCHER. Mol. Phys. **35**, 771 (1978); (*b*) R. J. BUENKER and S. D. PEYERIMHOFF. New horizons of quantum chemistry. Proc. 4th Intern. Congress of Quantum Chemistry. *Edited by* P. O. Löwdin and B. Pullmann. Reidel Publ. Co., Dordrecht, Holland. 1983. p. 183.
18. R. J. BUENKER and S. D. PEYERIMHOFF. Theor. Chim. Acta, **35**, 33 (1974); **39**, 217 (1975).
19. (*a*) R. J. BUENKER. Proc. Workshop Mol. Phys. and Quant. Chem. into the 80's. *Edited by* P. Burton. Univ. of Wollongong, Australia. 1980. p. 1.5.1; (*b*) R. J. BUENKER. *In* Studies in physical and theoretical chemistry. Vol. 21. *Edited by* R. Carbó. Elsevier Publ. Co., New York. 1982. p. 17.
20. S. R. LANGHOFF and E. R. DAVIDSON. Int. J. Quant. Chem. **8**, 61 (1974).
21. R. PEARSON and F. J. LOVAS. J. Chem. Phys. **66**, 4149 (1977).
22. H. W. KROTO, J. F. NIXON, and K. OHNO. J. Mol. Spectrosc. **90**, 367 (1981).
23. W. J. PIETRO, M. M. FRANCL, W. J. HEHRE, D. J. DE FREES, J. A. POPLE, and J. S. BINKLEY. J. Am. Chem. Soc. **104**, 5039 (1982).
24. G. TRINQUIER, J. C. BARTHELAT, and J. SATGE. J. Am. Chem. Soc. **104**, 5931 (1982).
25. K. P. HUBER and G. HERZBERG. Molecular spectra and molecular structure. Vol. 4. Van Nostrand Reinhold Co., New York. 1979.
26. R. A. CREWELL, E. F. PEARSON, M. WINNEWISSER, and G. WINNEWISSER. Z. Naturforsch. Teil A, **31**, 221 (1976).
27. J. K. TYLER. J. Chem. Phys. **40**, 1170 (1964).
28. R. PREUSS, R. J. BUENKER, and S. D. PEYERIMHOFF. J. Mol. Struct. **49**, 171 (1978).
29. C. THOMSON. J. Chem. Soc. Chem. Commun. 322 (1977).
30. D. GONBEAU and G. PFISTER-GUILLOUZO. Can. J. Chem. **61**, 1371 (1983).
31. W. H. KIRCHHOFF, D. R. JOHNSON, and F. J. LOVAS. J. Phys. Chem. Ref. Data, **2**, 1 (1973).
32. R. CIMIRAGLIA and J. TOMASI. J. Am. Chem. Soc. **99**, 1135 (1977).
33. (*a*) K. KITAURA, Y. OSAMURA, and K. NISHIMOTO. Chem. Phys. Lett. **55**, 531 (1978); (*b*) Y. OSAMURA, K. KITAURA, K. NISHIMOTO, and S. YAMABE. Chem. Phys. Lett. **63**, 406 (1979).
34. R. DITCHFIELD, J. E. DEL BENE, and J. A. POPLE. J. Am. Chem. Soc. **94**, 703 (1972).
35. (*a*) R. J. BUENKER and S. D. PEYERIMHOFF. J. Chem. Phys. **53**, 1368 (1970); (*b*) S. D. PEYERIMHOFF, R. J. BUENKER, W. E. KAMMER, and H. HSU. Chem. Phys. Lett. **8**, 129 (1971).
36. D. VOCELLE, A. DARGELOS, R. POTTIER, and C. SANDORFY. J. Chem. Phys. **66**, 2860 (1977).
37. J. B. PEEL and G. D. WILLETT. J. Chem. Soc. Faraday Trans. 2, **77**(11), 1799 (1975).
38. (*a*) P. J. BRUNA, S. D. PEYERIMHOFF, and R. J. BUENKER. Chem. Phys. Lett. **72**, 278 (1980); (*b*) R. J. BUENKER, S. D. PEYERIMHOFF, and P. J. BRUNA. *In* Computational Theor. Organic Chem., NATO ASI. *Edited by* I. G. Csizmadia and R. Daudel. Reidel Publ. Co., Dordrecht, Holland. 1981. p. 35.
39. H. W. KROTO. Chem. Soc. Rev. **11**, 435 (1982).
40. H. W. KROTO and J. F. NIXON. *In* Phosphorus chemistry. *Edited by* L. D. Quin and J. Verkade. A.C.S. Symp. Series 171, Am. Chem. Soc. 1981. p. 283.
41. L. L. LOHR, H. B. SCHLEGEL, and K. MOROKUMA. J. Phys. Chem. **88**, 1981 (1984).
42. W. C. TAM and C. E. BRION. J. Electron Spectrosc. Relat. Phenom. **3**, 281 (1974).
43. C. FRIDH and L. ÅSBRINK. J. Electron Spectrosc. Relat. Phenom. **7**, 119 (1975).
44. W. KUTZELNIGG. Angew. Chem. **96**, 262 (1984).
45. M. ZEITZ, R. J. BUENKER, and S. D. PEYERIMHOFF. Chem. Phys. Lett. **64**, 243 (1979).
46. J. ANGLADA, P. J. BRUNA, S. D. PEYERIMHOFF, and R. J. BUENKER. J. Phys. B, **16**, 2469 (1983).
47. (*a*) P. J. BRUNA, S. D. PEYERIMHOFF, R. J. BUENKER, and P. ROSMUS. Chem. Phys. **3**, 35 (1974); (*b*) P. G. BURTON, S. D. PEYERIMHOFF, and R. J. BUENKER. Chem. Phys. **73**, 83 (1983).

48. (*a*) P. J. BRUNA, R. J. BUENKER, and S. D. PEYERIMHOFF. Chem. Phys. **22**, 375 (1977); (*b*) P. J. BRUNA. *In* Progress in Theor. Organic Chem. Vol. 2. *Edited by* I. G. Csizmadia. Elsevier Publ. Co., New York. 1977. p. 401.
49. G. TRINQUIER, M. PELISSIER, B. SAINT-ROCH, and H. LAVAYSSIERE. J. Organomet. Chem. **214**, 169 (1981).

Bonding in H_3AB compounds

MICHAEL W. SCHMIDT AND MARK S. GORDON
Department of Chemistry, North Dakota State University, Fargo, ND 58105, U.S.A.

Received August 16, 1984

This paper is dedicated to Professor Camille Sandorfy on the occasion of his 65th birthday

MICHAEL W. SCHMIDT and MARK S. GORDON. Can. J. Chem. **63**, 1609 (1985).

The nature of binding in the 14 valence electron H_3AB molecules is examined, where A and B are taken from the second and third rows. The AB bonding is inferred from the computed structures, *d* orbital populations, and localized orbitals. Near Hartree–Fock results are reported for the strongest bonding compounds, which are those with third row atoms A, and second row atoms B. Phosphine oxide, and to a lesser extent phosphine sulfide, are found to be effectively doubly bound. Amine oxide and sulfide are found to be ionic complexes. The thiazyl bond is confirmed as triple in nature. The exotic compound F_3IC is proposed as a synthetic target.

MICHAEL W. SCHMIDT et MARK S. GORDON. Can. J. Chem. **63**, 1609 (1985).

On a étudié le mode de liaison dans les molécules H_3AB à 14 électrons de valence dans lesquelles A et B sont des éléments des deuxième et troisième rangées. On déduit la nature de la liaison AB à partir des structures calculées, des populations des orbitales d et des orbitales localisées. On rapporte des résultats obtenus par une technique se rapprochant de celle de Hartree–Fock qui a été appliquée aux composés comportant les liaisons les plus fortes et qui sont ceux impliquant des atomes A de la troisième rangée et des atomes B de la deuxième rangée. On a trouvé que l'oxyde de phosphine et, à un degré moindre, le sulfure de phosphine comportent effectivement des doubles liaisons. On a trouvé que l'oxyde et le sulfure d'amine sont des complexes ioniques. On a confirmé que la liaison du thiazyle est triple. On suggère que le composé exotique F_3IC devrait s'avérer un but de synthèse intéressant.

[Traduit par le journal]

Introduction

Recent investigations in our group (1–3) dealing with the bonding in phosphoryl compounds have centered in part on the degree of multiple bonding present. For a compound such as H_3AB, with 14 valence electrons, the following bonding schemes may be considered (nominal bond orders are given under each structure):

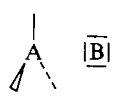

0

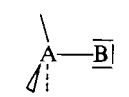

1

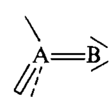

2

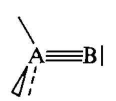

3

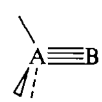

4

Structures **2**, **3**, and **4** contain hypervalent A atoms, which must use their *d* orbitals in binding in order to achieve the indicated expansion of their octets (4). The double and quadruple bonding structures shown above cannot be used in a description of binding, as the molecules to be considered here all possess three-fold rotational symmetry. Thus, any π binding present in addition to a σ bond is due to *e* symmetry orbitals, which of course come in pairs. Our findings for H_3PO (1, 3) and related substituted compounds (3) have shown that phosphine oxides are actually resonance hybrids between singly and triply bound structures. Thus, the effective (compromise) bond order in phosphine oxides was found to be somewhat less than two (3). In the present paper, we examine the bonding of phosphine oxide by comparison with a number of valence isoelectronic molecules.

Consider the following sequence of compounds: F_3SiF (tetrafluorosilane), F_3PO (trifluorophosphine oxide), and F_3SN (thiazyltrifluoride). The AB electronic structure in these molecules is usually depicted as single, double (5), or triple (6) bonding, respectively. These rather different bonding schemes are based on the normal valency of the atom B (F, O, or N), and on the experimental observation that the AB bond lengths decrease throughout this series. However, this sequence can be viewed in a more unified fashion, with each new member generated by transferring a proton from the nucleus of atom B to A. There are other similarities, as might be expected from their isoelectronic nature. All three compounds are gases at normal temperatures, and they possess quite strong AB bonds. The experimental SiF, PO, and SN bond strengths are 135 (7), 130 (7), and 93 (6) kcal/mol, respectively. (It is interesting that the bond strengths decrease in going from "single" to "double" to "triple".) The three compounds are also quite stable. For example, F_3SN will not react with metallic sodium below 300°C (6). In view of these similarities, and because of our finding (1, 3) that phosphine oxides possess bonding intermediate between single and triple bonding, one wonders whether or not the binding is similar in these compounds.

It is also obvious that the sequence F_3SiF, F_3PO, F_3SN of experimentally well characterized compounds may be extended in either direction, to hypothetical compounds. F_3AlNe contains a weak bond formed by donation of the rare gas lone pair to the σ accepting aluminum. An even more intriguing possibility is F_3ClC, an example of a "quadruply" bonded carbon at the exposed end of a molecule.

The atoms A and B in compounds such as these may also be chosen from different rows of the periodic table. For example phosphine sulfides and amine oxides are well known. We have considered most possible combinations of compounds with the atoms A and B chosen from the second and third rows of the periodic table. For simplicity the ligands to A have been chosen to be hydrogens, rather than fluorines.

Computational method

These compounds have been studied only at the Hartree–Fock level, and only the ground $^1A_1$ electronic states

TABLE 1. Structures and energies for H_3AB molecules[a]

	$q = -1$	$q = 0$	$q = 1$	$q = 2$	$q = 3$
	H_3BNe	H_3CF	H_3NO	H_3ON	H_3FC
Energy	−154.06048	−138.32226	−130.24849		
R(AB)	2.3751	1.3537	1.3876	no	
R(AH)	1.1885	1.0885	1.0229	minimum	
∠HAB	91.33	110.21	112.32		
AB stretch	170	1253	832		
	$q = -1$	$q = 0$	$q = 1$	$q = 2$	$q = 3$
	H_3AlNe	H_3SiF	H_3PO	H_3SN	H_3ClC
Energy	−370.12667	−388.16352	−415.23517	−451.25625	−496.10582
R(AB)	2.1597	1.5646	1.4587	1.4321	1.4842
R(AH)	1.5859	1.4696	1.3920	1.3597	1.4214
∠HAB	93.42	109.61	117.76	123.73	127.57
AB stretch	231	1025	1471	1437	1262
	$q = -1$	$q = 0$	$q = 1$	$q = 2$	$q = 3$
	H_3BAr	H_3CCl	H_3NS	H_3OP	H_3FCl
Energy	−550.59329	−496.72461	−451.46147		
R(AB)	3.1013	1.7844	1.8470	no	
R(AH)	1.1894	1.0820	1.0155	minimum	
∠HAB	90.31	108.23	110.68		
AB stretch	91	761	626		
	$q = -1$	$q = 0$	$q = 1$	$q = 2$	$q = 3$
	H_3AlAr	H_3SiCl	H_3PS	H_3SP	H_3ClSi[b]
Energy	−766.65534	−746.53344	−736.35299	−736.14350	−745.95226
R(AB)	3.3614	2.0512	1.9289	1.9053	1.9425
R(AH)	1.5844	1.4647	1.3895	1.3588	1.4638
∠HAB	90.41	108.38	117.31	124.00	128.58
AB stretch	55	573	683	653	604

[a] Distances in Å, angles in deg, energies in Hartrees, and vibrational frequencies in wavenumbers. All results are from basis I.

[b] This species is unstable with respect to a degenerate bend, as discussed in the text. All other species have positive definite force fields.

have been considered. The more exotic compounds, such as H_3ClC, have not been tested for the possibility of ground states of other space-spin symmetries. The stability of the singlet molecules was tested by calculation of the vibrational frequencies and normal coordinates.

Basis set I, used for structure determination, is the 3-21G basis (8), with polarization functions added to both atoms A and B. The d orbital exponents for second row atoms are taken from Hay and Dunning (9), and for the third row from Francl *et al.* (10). This basis, while it should give accurate structures, has three deficiencies: a relatively small sp basis on each atom, only one set of d orbitals on atom A to describe its possible hypervalent bonding, and no diffuse functions on atom B to describe its possible anionic character. These defects are ameliorated by basis II, which starts from the even-tempered bases of Schmidt and Ruedenberg (11). The hydrogen basis is $(4s/2s)$, scaled by 1.2. First row atomic bases are $(12s,6p/3s,2p)$ and third row atomic bases are $(16s,11p/4s,3p)$. These bases approach the atomic Hartree–Fock limits to within 5 millihartree. The single d exponent at atom A in basis I is split by the factors 0.4 and 1.4 to give two sets of d primitives at A, while atom B receives only a single set of d orbitals. The single d exponents are chosen as for basis I. s and p primitives, with exponents equal to the even-tempered parameter α, are added to the atom B so that the diffuse nature of a negatively charged B will be better represented. This basis is chosen so as to give very accurate Hartree–Fock electron densities for the AB bond. It describes the AH bonds less well due to the omission of p orbitals on hydrogen. For both bases the $3s$ contaminant of the Cartesian d orbitals was discarded.

The nature of the AB bonding is determined by means of Mulliken population analysis (12), and the determination of energy localized orbitals (13). Geometry optimizations and harmonic vibrational analysis were carried out using the GAUSSIAN 80 (14) series of programs. The ALIS program system (15) was used for energy and localized orbital calculations with basis II.

Results and discussion

Structures

The equilibrium geometries computed with basis I are shown in Table 1. The HAH angles may be readily obtained from the data in Table 1 by the formula

$$\angle HAH = \cos^{-1}[1 - 1.5\sin^2(180 - \angle HAB)]$$

In Table 1, q is the formal charge on atom A in the singly bound resonance structure. The value of q is also related to the formal charges present in the zero or triply bound structures:

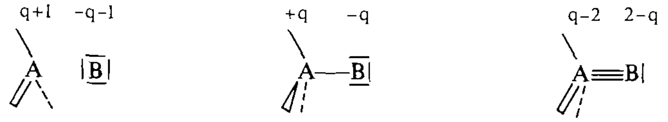

The structures in Table 1 were computed using basis I, which contains d orbitals on both atoms A and B, as both sets do affect the AB length. Bases without d orbitals at hypervalent centers give rather inaccurate bond lengths (16). Using d orbitals at atom B does have an effect on the AB distance, although much smaller than those at A. For example, the 3-21G* basis set (16*a*), containing d orbitals only on P, gives a PO bond length of 1.470 Å for H_3PO (2). This shrinks further to 1.459 upon adding d orbitals at oxygen.

Consider first columns of constant q within Table 1. For the rare gas to AlH_3 or BH_3 complexes ($q = -1$), the AB distances are quite long, and the HAB angles nearly 90°, indicating little binding interaction. The strongest interaction is in H_3AlNe, whose AB distance is actually less than that in H_3BNe, and whose HAB angle departs most from a right angle. The AB bond strength can be made more quantitative. Basis I gives bond lengths of 1.190 and 1.585 for BH_3 and AlH_3, with total energies -26.24886 and -242.30990, respectively. These results give the following AB bond energies: H_3BNe, 4.9 kcal/mol; H_3AlNe, 8.1; H_3BAr, 0.9; and H_3AlAr, 1.6. Neon is a better σ donor, aluminum a better acceptor.

There are no surprises in the $q = 0$ column, where HAB angles are nearly tetrahedral, and bond lengths are easily rationalized as sums of atomic radii.

Examination of the $q = 1$ column is more interesting. When A is phosphorus, the HAB angle increases from the tetrahedral values in the preceding column, and the AB distance contracts. This may be explained by the mixing in of a certain amount of triple bond character which should shorten the AB bond. Also, as atom A expands its octet the HAH angles must decrease. If, however, A is nitrogen, the HAB angle remains nearly tetrahedral and the AB distance increases slightly from the $q = 0$ column. Their structures indicate that the amine chalconides are singly bound ionic complexes, while the phosphine chalconides acquire at least some multiple bond character.

The discrepancy between second and third row central atoms becomes even more pronounced upon entering the $q = 2$ column. Here the compounds with central oxygen atoms do not exist as minima on the SCF potential energy surfaces. Instead geometry optimizations of trial structures revert to the amine or phosphine oxide. The failure to find stable compounds is somewhat surprising. H_3ON seems less exotic if thought of as a complex of hydronium ion with a nitrogen anion. The compounds with central sulfur atoms are a different matter, as they continue the trend of shortening AB distances and greater HAB angles as the AB bonding gains yet more triple character.

Finally, there are two compounds with $q = 3$. In light of the failure to find molecules with central oxygens, no attempt was made to find the two compounds with central fluorines. The molecules with central chlorines have slightly longer AB bonds than in the previous column, thus ending the trend to ever shorter bond lengths. However, the HAB angles continue their increase. Thus the structures indicate binding in the $q = 3$ column is similar to that in the previous column. Compared to methylchloride in column 0, the ClC bond is very short. The vibrational analyses described below indicate that H_3ClSi is unstable with respect to a degenerate e symmetry bend, while H_3ClC is indeed a stable molecule.

Vibrational analysis

A complete normal coordinate analysis in the harmonic approximation for all the molecules considered here was performed using basis I. All of the molecules save H_3ClSi were found to possess all real frequencies. Thus all but one of these molecules correspond to a relative minimum on their SCF potential energy surfaces. These are therefore at the least thermodynamically stable, no matter how exotic some may seem, and may perhaps be kinetically stable.

The computed AB stretching frequencies have also been included in Table 1. The differing effective masses in each mode make comparison of the stretching frequencies wihin a given column impossible. However, it should be possible to compare the values for a given row of this table, where at least the atoms A and B have similar masses. Such a comparison indicates that the amine chalconides have weaker AB bonds than the methyl halides, while the phosphine chalconides possess greater stretching frequencies than the silyl halides. Furthermore, the compounds H_3SN and H_3ClC possess stretching frequencies greater than silylfluoride. Bond strengths cannot be directly inferred from stretching frequncies (recall that the experimental bond strengths are in the order $F_3SiF > F_3PO > F_3SN$). However, the stretching frequency for H_3ClC indicates a considerable strength for this bond. It is interesting to note that H_3SN and H_3ClC have greater stretching frequencies than do H_3NS and H_3CCl, in spite of having considerably higher energies. This is an expression of the multiple character of these bonds.

H_3ClSi has an imaginary degenerate bending frequency of $893i$ cm^{-1}. This means this molecule is unstable with respect to such bending, and is therefore unisolable. The lowest normal mode in H_3ClC is also a degenerate bend, but with a real frequency 589 cm^{-1}. The stability of the carbide with respect to bending in contrast to the silicide's instability is a reflection of the reluctance of silicon to hold a negative charge.

Charge distributions

Further enlightenment into the AB bonding can be gleaned from the charge distributions found in Table 2. First consider the d orbital populations given in parentheses. The d orbital population of atom A is invariably greater than that of B. This is to be expected, as A forms more bonds than B and thus deforms its electron density more. Furthermore, A uses its d orbitals to participate in any hypervalent bonding. (Remember though that the seemingly less important d orbitals on B do affect the AB bond lengths.) The d orbital populations of A reveal much the same information on the AB binding as did the structures discussed above. When A is a third row atom, the d population of A increases steadily across the rows, tailing off only at H_3ClC and H_3ClSi. This shows the same increase in hypervalence, and hence multiple bond character already indicated by the decreasing AB bond lengths and increasing HAB angles. However, the molecules H_3NO and H_3NS show no increase in the N d population over their carbon neighbors. This reflects the not surprising fact that the d orbitals of nitrogen are energetically nearly inaccessible for binding, in spite of their shortening effect on the NO and NS bond lengths. Note, however, that amine oxide shows more multiple character than amine sulfide.

The total charges given in Table 2 are more difficult to interpret. The idealized charges shown in the resonance structures above are altered in reality by (*i*) mixing of the zero, singly, and triply bound structures, and (*ii*) polarization within the bonds. When the vagaries of the arbitrary Mulliken par-

TABLE 2. Charge distribution in H_3AB molecules[a]

	$q = -1$ H_3BNe	$q = 0$ H_3CF	$q = 1$ H_3NO	$q = 2$ H_3ON	$q = 3$ H_3FC
A	0.01(0.036)	−0.14(0.076)	−0.48(0.080)		
B	0.05(0.000)	−0.43(0.020)	−0.63(0.028)	no	
H	−0.02	0.19	0.37	minimum	
	$q = -1$ H_3AlNe	$q = 0$ H_3SiF	$q = 1$ H_3PO	$q = 2$ H_3SN	$q = 3$ H_3ClC
A	0.49(0.165)	1.01(0.263)	0.95(0.384)	0.62(0.461)	0.44(0.407)
B	0.09(0.001)	−0.48(0.012)	−0.74(0.029)	−0.70(0.048)	−0.52(0.062)
H	−0.19	−0.18	−0.07	0.03	0.03
	$q = -1$ H_3BAr	$q = 0$ H_3CCl	$q = 1$ H_3NS	$q = 2$ H_3OP	$q = 3$ H_3FCl
A	0.02(0.035)	−0.75(0.060)	−0.90(0.047)		
B	0.01(0.000)	−0.07(0.028)	−0.36(0.029)	no	
H	−0.01	0.27	0.42	minimum	
	$q = -1$ H_3AlAr	$q = 0$ H_3SiCl	$q = 1$ H_3PS	$q = 2$ H_3SP	$q = 3$ H_3ClSi[b]
A	0.50(0.140)	0.77(0.231)	0.40(0.271)	0.00(0.309)	−0.04(0.272)
B	0.01(0.000)	−0.42(0.018)	−0.46(0.045)	−0.35(0.072)	−0.03(0.095)
H	−0.17	−0.12	0.02	0.12	0.02

[a] Gross Mulliken charges on atoms A, B, or H. Total Mulliken *d* orbital populations are in parentheses. All results from basis I.
[b] See note *b* of Table 1.

titioning of the overlap populations is added, especially in the AH bonds, the total Mulliken charges are indeed difficult to interpret. The charge on atom B is a much better indicator of the AB charge separation than the charge on A, since the latter is also related to the AH charge separation.

In the $q = -1$ column, the charge on atom B is nearly zero rather than the +1 expected for a single bond. Thus, the bond order must be nearly zero. This is in keeping with the structural data and chemical intuition. Note that the most positive B occurs in H_3AlNe, which as already noted, does contain the strongest AB interaction.

The negative charges on B in the $q = 0$ column of Table 2 are more reasonably explained as a result of polarization of the single bonds in these compounds rather than admixture of the formally −2 B atoms in the triply bound resonance structure.

In the $q = 1$ column, atom B should possess a charge somewhere between the −1 value in the singly bound structure and the +1 value in the triply bound structure. As B possesses a substantial negative charge in all the compounds in this column, the singly bound contributor seems to dominate the position of the compromise between these resonance structures. Since these formal charges ignore the polarization of the bonds that certainly occurs, the charge populations reveal less about the bonding than do the structures and *d* orbital occupancies. The latter clearly indicate no appreciable multiple character for A = N, with at least some multiple bonding for A taken as phosphorus.

Were the bonding in the $q = 2$ column pure triple bonding, atom B would have zero charge. In fact the polarization of the SN bonds leads to a rather negative nitrogen, but less so than for oxygen in the previous column. Perhaps a fairer test is afforded by H_3SP, where the AB electronegativity difference is less than that for H_3SN. Phosphorus is indeed less negative here.

Although carbon and silicon should bear a unit of negative charge in the $q = 3$ column for triple AB binding, polarization of these bonds leads to considerably smaller negative charges. Note that silicon is able to carry only a very small negative charge in H_3ClSi, which no doubt contributes to the bending instability of this species.

Localized orbitals

A useful way of determining the nature of binding is the localization of the orbitals forming the SCF wavefunction. The concentration, or localization, of each electron pair into a particular spatial region of the molecule facilitates the interpretation of these pairs as bonds, nonbonding lone pairs, and so forth, while leaving the total many electron wavefunction unchanged. Since the bonding apparently changes dramatically from column to column, changes in the localized orbitals should reveal pictorially the changing nature of the AB bond. The molecules in the second row of Tables 1 and 2 contain the greatest potential for strong AB bonds. They have third row atoms A, possessing accessible *d* orbitals. They also have the more electronegative second row atoms B, favorable since the majority of these molecules have negatively charged atoms B. Thus, localized orbitals have been generated only for molecules in this row.

Calculations were carried out on these molecules with basis II and should represent near Hartree–Fock basis set limits for the electron densities. Hypervalent character in the AB bond should be well represented, as the atoms A possess twin *d* orbitals. Energies and Mulliken populations are shown in Table 3. Note that this basis gives *d* orbital populations approaching a full electron for the hypervalent H_3SN and H_3ClC. The *d* population of phosphorus in phosphine oxide is increased 54%

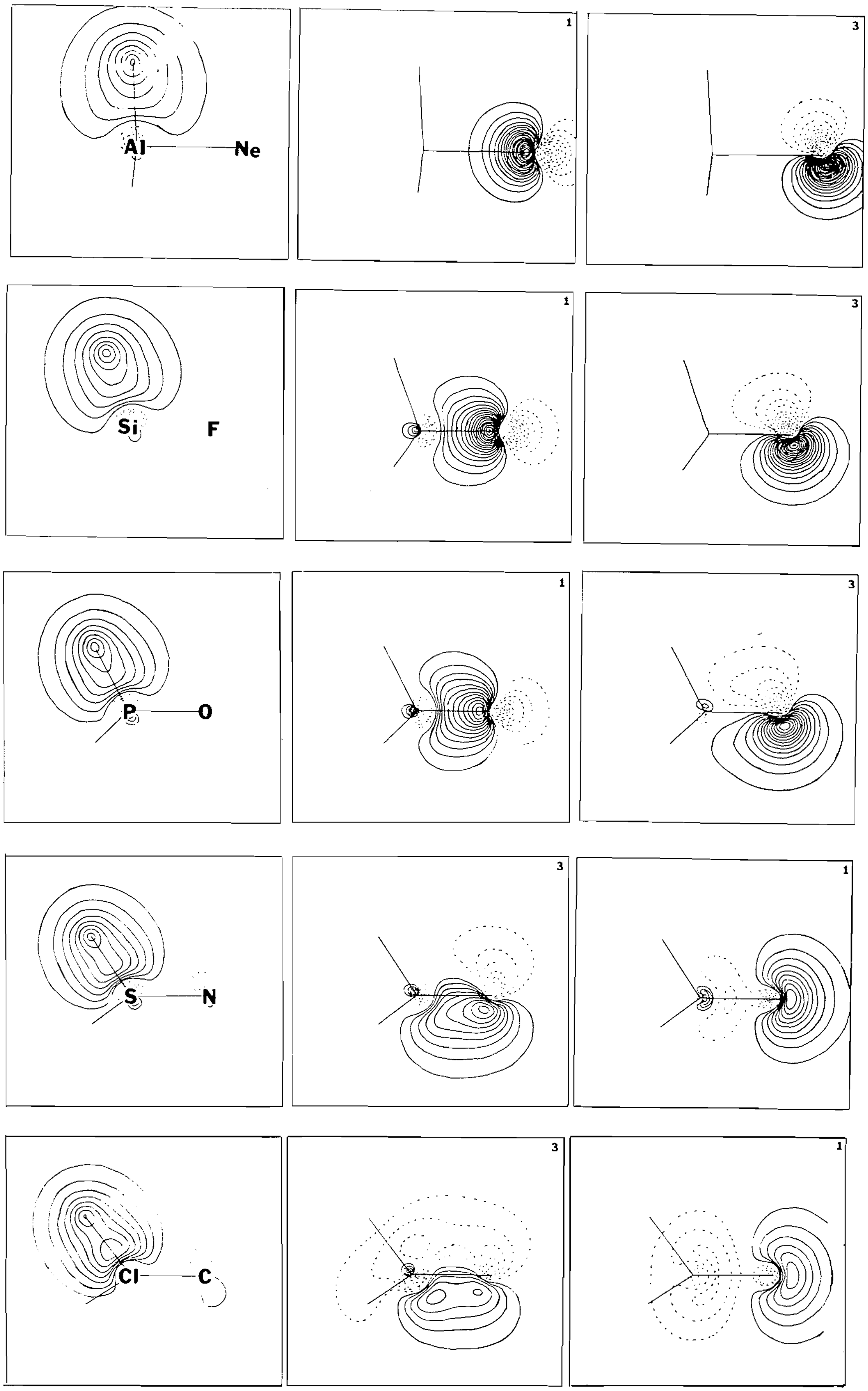

FIG. 1. Contour plots for energy localized orbitals, expanded in basis II. The increment between contours is 0.05 bohr$^{-3/2}$. The numerals indicate how many equivalent orbitals there are of each type.

TABLE 3. Results for selected H_3AB molecules[a]

Molecule	Energy	A[b]	B[b]	H
H_3AlNe	−372.16139	−0.194(0.307)	0.088(0.001)	0.035
H_3SiF	−390.21129	0.245(0.455)	−0.407(0.011)	0.054
H_3PO	−417.37157	0.196(0.719)	−0.563(0.029)	0.122
H_3SN	−453.52480	−0.010(0.943)	−0.529(0.049)	0.179
H_3ClC	−498.54330	0.017(0.952)	−0.431(0.061)	0.138

[a] All results taken from basis II. Energies are in hartrees.
[b] Gross Mulliken atomic charge, with *d* orbital population in parentheses.

of the way from singly bound H_3SiF towards triply bound H_3SN.

The localized orbitals themselves are shown in Fig. 1. Care has been taken in these plots to use identical distance scales, with atom A centered. The contour increments are the same in all plots, to facilitate comparison. Positive amplitudes are shown as solid curves, and negative amplitudes as dashed lines. Nodes, or regions of zero amplitude, are shown as dotted lines. Electron densities are, of course, given by the square of the amplitudes.

The first column shows one of the three equivalent AH bonds. The increase in the HAB angles as A becomes more hypervalent is quite apparent. One can also see the polarization of the AH bond change as A becomes more electronegative.

The second column in the figure shows the orbitals responsible for the AB bonding. For H_3AlNe the orbital is completely polarized to neon. This is not really a bond at all, but rather a lone pair on neon donating a nearly invisible amount of electron density to the accepting *p* orbital of AlH_3. The σ bond in silyl fluoride is quite polarized. The σ bond in phosphine oxide is less polarized. Upon reaching H_3SN, the bonding changes in an apparently dramatic fashion, with three equivalent bond pairs, arranged staggered with respect to the three SH bonds. Thus the bonding in this molecule has become triple. H_3ClC closely resembles H_3SN, except that the bonds are more polarized to the central atom. Thus, the bonding in this molecule is also triple.

The final column of the figure shows the nonbonding orbitals on B. There are three on neon and fluorine, and one on nitrogen and carbon. It is not entirely accurate to describe the three lone pairs on oxygen in H_3PO as nonbonding for they clearly show some donation of electron density to phosphorus. This $p_\pi - d_\pi$ backdonation to the phosphorus is responsible for the great strength of the PO bond, and is discussed in detail elsewhere (3). The PO bond is clearly more than a single bond while not yet the triple bond found in H_3SN.

The transition from single to triple bonding begins to appear in H_3PO. If the three lone pairs on oxygen were to be tipped in towards P, so that they might share their electron density more effectively with P, one would arrive at orbitals much like the three bonding orbitals in H_3SN. If at the same time the positive bulk of the PO σ bond were diminished, while the negative lobe beyond the oxygen increased, this orbital would become the unique lone pair in H_3SN. In fact, we have shown (3) that the $p_\pi - d_\pi$ interaction increases as more electronegative ligands are attached at phosphorus. As a result of this increased backbonding for F_3PO the localized orbitals yield three bonding orbitals between P and O, and a single nonbonding orbital on oxygen. Thus the phosphine oxides appear intermediate between single and triple binding. Less electronegative ligands (H, CH_3, SiH_3) give localized orbitals resembling single bonds with some π interaction, while more electronegative ligands (OH, F) give just enough additional bonding to give orbitals resembling the triply bound H_3SN (3).

The geometry, *d* orbital populations, and localized orbitals presented here indicate phosphine oxide and sulfide are poised on the edge dividing singly and triply bound compounds such as H_3SiF and H_3SN. An appropriate way to view their bonding is as effectively double bonding, that is possessing roughly equal contributions from the two group theoretically allowed bonding schemes, single or triple. Phosphine sulfide has somewhat less hypervalent character than phosphine oxide.

The sequence of compounds whose localized orbitals were presented can be thought of as arising from the sequence AlF_3, SiF_4, PF_5, SF_6, and ClF_7, all of which exist save the last. The compounds we have considered can be formed by replacing 0, 1, 2, 3, or 4 fluorines with Ne, F, O, N, or C, and replacing the remaining fluorines with the less stabilizing ligand hydrogen. As shown in Table 1, H_3ClC is very much less stable than the conventional isomer H_3CCl. However, this does not preclude the existence of such carbides, as H_3ClC was shown here to be a relative energy minimum, with a strong ClC bond. After all, F_3SN exists and is quite stable, even though H_3SN is less stable than H_3NS. If a synthesis of a molecule in the H_3ClC family were attempted, efforts should be directed at F_3IC, whose parent interhalogen IF_7 is already known. Such a carbide would likely be very reactive, and might well demonstrate a unique chemistry.

Acknowledgements

Computer time for this work was provided by the North Dakota State University Computer Center. This work was supported by AFOSR grant 82-0190.

1. M. W. SCHMIDT, S. YABUSHITA, and M. S. GORDON. J. Phys. Chem. **88**, 382 (1984).
2. M. S. GORDON, J. A. BOATZ, and M. W. SCHMIDT. J. Phys. Chem. **88**, 2998 (1984).
3. M. W. SCHMIDT and M. S. GORDON. J. Am. Chem. Soc. In press.
4. (*a*) D. W. J. CRUICKSHANK. J. Chem. Soc. 5486 (1961); (*b*) K. A. R. MITCHELL. Chem. Rev. **69**, 157 (1969); (*c*) H. KWART and K. G. KING. *d*-Orbitals in the chemistry of silicon, phosphorus, and sulfur. Springer-Verlag, Berlin. 1977.
5. R. F. HUDSON. Structure and mechanism in organophosphorus chemistry. Academic Press, New York. 1965. Chapt. 3.
6. O. GLEMSER and R. MEWS. *In* Advances in inorganic chemistry and radiochemistry. Vol 14. *Edited by* H. J. Emeleus and H. G. Sharpe. Academic Press, New York. 1972. p. 333.
7. J. E. HUHEEY. Inorganic chemistry. Harper and Row, New York. 1978. Appendix F.
8. (*a*) J. S. BINKLEY, J. A. POPLE, and W. J. HEHRE. J. Am. Chem. Soc. **102**, 939 (1980); (*b*) M. S. GORDON, J. S. BINKLEY, J. A. POPLE, W. J. PIETRO, and W. J. HEHRE. J. Am. Chem. Soc. **104**, 2797 (1982).
9. P. J. HAY and T. H. DUNNING. *In* Methods of electronic structure theory. *Edited by* H. F. Schaefer III. Plenum Press, New York. 1977. p. 1.
10. M. M. FRANCL, W. J. PIETRO, W. J. HEHRE, J. S. BINKLEY, M. S. GORDON, D. J. DEFREES, and J. A. POPLE. J. Chem. Phys. **77**, 3654 (1982).
11. M. W. SCHMIDT and K. RUEDENBERG. J. Chem. Phys. **71**, 3951 (1977).
12. R. S. MULLIKEN. J. Chem. Phys. **23**, 1833 (1955).
13. C. EDMISTON and K. RUEDENBERG. Rev. Mod. Phys. **35**, 457 (1963).

14. J. S. BINKLEY, R. A. WHITESIDE, R. KRISHNAN, R. SEEGER, D. J. DEFREES, H. B. SCHLEGEL, S. TOPIOL, L. R. KAHN, and J. A. POPLE. QCPE Catalog 13, Program 406. Indiana University, Bloomington, IN. 1981.
15. S. T. ELBERT, L. M. CHEUNG, and K. RUEDENBERG. NRCC Software Catalog. Program QM01. University of California, Berkeley, CA. 1980.
16. (*a*) J. B. COLLINS, P. VON R. SCHLEYER, J. S. BINKLEY, and J. A. POPLE. J. Chem. Phys. **64**, 5142 (1976); (*b*) H. WALLMEIER and W. KUTZELNIGG. J. Am. Chem. Soc. **101**, 2804 (1979).

Integrated dipole oscillator strengths and dipole properties for Ne, Ar, Kr, Xe, HF, HCl, and HBr

ASHOK KUMAR[1,2] AND WILLIAM J. MEATH[2]
Department of Chemistry, University of Western Ontario, London, Ont., Canada N6A 3B7

Received August 16, 1984

This paper is dedicated to Professor Camille Sandorfy on the occasion of his 65th birthday

ASHOK KUMAR and WILLIAM J. MEATH. Can. J. Chem. **63**, 1616 (1985).

Dipole oscillator strength distributions have been constructed, and used to evaluate integrated dipole oscillator strengths and a variety of dipole oscillator strength properties, for ground state Ne, Ar, Kr, Xe, HF, HCl, and HBr. Each distribution has been constructed by using experimental and theoretical photoabsorption cross sections and by subjecting the resulting dipole oscillator strength data to constraints provided by the Thomas–Reiche–Kuhn sum rule and molar refractivity or related data for the relevant dilute gases. The resulting dipole properties are generally the most or only reliable values available for the hydrogen halides, for the rare gases they largely augment reliable results for most of the properties already available in the literature. The results for HCl are used to discuss an interesting molecular effect in the photoabsorption spectrum of this molecule betwen ~200 eV and ~205 eV.

ASHOK KUMAR et WILLIAM J. MEATH. Can. J. Chem. **63**, 1616 (1985).

On a établi les distributions des forces d'oscillateurs dipolaires et on les a utilisé pour évaluer, pour les états fondamentaux de Ne, Ar, Kr, Xe, HF, HCl et HBr, les forces intégrées d'oscillateurs dipolaires ainsi qu'une variété de propriétés associées avec la force d'oscillateurs dipolaires. On a établi chaque distribution en faisant appel aux valeurs expérimentales et théoriques des sections droites de photoabsorption et en soumettant les données relatives aux forces d'oscillateurs dipolaires qui en résultent aux contraintes qui sont fournies par la règle des sommes de Thomas–Reiche–Kuhn et aux réfractivités molaires ou aux données apparentés pour les gaz dilués appropriés. Dans le cas des halogénures d'hydrogène, les propriétés dipolaires qui en résultent sont généralement les seules valeurs disponibles ou les plus fiables; pour les gaz rares, les résultats fiables sont grandement augmentés pour la plupart des propriétés qui sont déjà disponibles dans la littérature. On a utilisé les résultats obtenus avec le HCl pour discuter d'un effet moléculaire intéressant dans le spectre de photoabsorption de cette molécule entre environ 200 et 205 eV.

[Traduit par le journal]

1. Introduction

The accurate *ab initio* or direct experimental evaluation of many of the dipole properties for most atoms and molecules is a very difficult problem (1–7). On the other hand, a combination of experimental information and theoretical techniques can be used to evaluate many important dipole properties in a reliable way through the construction of globally reliable dipole oscillator strength distributions (1, 7–14). The main purpose of this paper is to present integrated dipole oscillator strengths and reliable values for the dipole oscillator strength sums S_k, $k = -10(1)-4, -3(\frac{1}{2})0$, 1, and 2, and the logarithmic dipole sums L_k, $k = -2(1)2$ for HF, HCl, HBr, Ne, Ar, Kr, and Xe.

The relationship between the dipole oscillator strength distribution (DOSD) and the dipole properties for a particular atom or molecule, and the method used to construct the DOSD are discussed in Section 2. The discussion includes a brief summary of various uses of the dipole properties and an outline of how experimental and theoretical dipole oscillator strength data, coupled with quantum mechanical constraint procedures using the Thomas–Reiche–Kuhn sum rule and molar refractivity or related data as constraints, can be used to evaluate reliable values for the dipole properties. The experimental and theoretical input data used to construct the DOSDs for the hydrogen halides, and the integrated oscillator strengths and the dipole properties for these molecules, are discussed and given in Section 3; the values for most of the dipole properties are the most reliable available. The results are used to augment and assess the molar refractivity data for these molecules as a function of wavelength λ and to discuss the oscillator strength data for HCl and HBr; of particular interest is a molecular effect occurring between ~200 eV and ~205 eV in the photoabsorption spectra of HCl. The adopted integrated DOSDs and dipole properties of the four rare gases studied here are given in Section 4. For common values of $k \le 0$ our results are usually in very good agreement with those of Leonard and Barker (11) and Leonard (15). Generally, significant improvements relative to their work is obtained only for $k > 0$. A discussion of our adopted results for the dipole properties of HF, HCl, HBr, Ne, Ar, Kr, and Xe, including a comparison with typical literature values, is given in Section 5. Literature results used explicitly to construct the DOSDs are discussed in Sections 3 and 4.

2. Relationship between DOSDs and the dipole properties

Properties

Knowledge of the dipole oscillator strength distribution (DOSD) for a molecule permits the evaluation of a variety of dipole properties for the molecule. Those of interest for this paper are the dipole sums S_k, the logarithmic dipole sums L_k, and the mean excitation energies I_k, defined by

$$[1]\quad S_k = \int_{E_0}^{\infty} \left(\frac{E}{2R}\right)^k \left(\frac{\mathrm{d}f}{\mathrm{d}E}\right) \mathrm{d}E$$

$$[2]\quad L_k = \int_{E_0}^{\infty} \left(\frac{E}{2R}\right)^k \left(\frac{\mathrm{d}f}{\mathrm{d}E}\right) \ln(E)\, \mathrm{d}E$$

$$[3]\quad I_k = 2R \exp\,[L_k/S_k]$$

where E_0 is taken to be the electronic absorption threshold, R

[1]On leave from the Department of Physics, Meerut University, Meerut, India.

[2]Associated with the Centre for Interdisciplinary Studies in Chemical Physics, University of Western Ontario, London, Ont., Canada N6A 3K7.

is the Rydberg constant of energy, (df/dE) is the differential dipole oscillator strength of the molecule for excitation energy E, and k can take on many different values (1, 7–14, 16, 17). Equations [1]–[3] are written for a continuous distribution of oscillator strengths. If the DOSD is made up of discrete and continuous parts these results should be modified such that, for example,

$$[4] \quad S_k = \sum_i \left(\frac{E_i}{2R}\right)^k f_i + \int_{E_0}^{\infty} \left(\frac{E}{2R}\right)^k \left(\frac{df}{dE}\right) dE$$

with a similar equation applying for L_k. In [4] the sum is over the discrete transitions for the molecule and E_0 is the absorption threshold for the continuum part of the DOSD. Usually the DOSD for a molecule is continuous in nature while that for an atom also contains a discrete part. The dipole properties defined by [1]–[4] are important in a variety of fields (1, 16, 17). For example, (a) the straggling (I_1, S_1), and the stopping (I_0), and the total (I_{-1}, S_{-1}) inelastic scattering cross sections, of fast charged particles in matter; (b) dipole polarizabilities $\alpha_d = a_0^3 S_{-2}$, where a_0 is the Bohr radius; (c) charge densities at nuclei (S_2); (d) Lamb shifts (I_2); (e) moments of the DOSD (S_{-2}, S_{-4}, S_{-6}, ...) occur in the Cauchy expansion of the frequency dependent polarizability or the molar refractivity (see below) of atoms or molecules; (f) S_{-1}, S_{-3}, $S_{-3/2}$, and L_{-2} can be used to obtain estimates for the dipole–dipole dispersion energies between atoms and molecules (12); and (g) the relevance of accurate results for the dipole properties in testing *ab initio*, non-empirical or other methods for evaluating the properties is well established (1, 5, 6, 12, 18), see also what follows.

Construction of DOSDs

The evaluation of the dipole properties is straightforward if reliable values for the dipole oscillator strengths (DOSs) are available from the absorption threshold to very large values of the excitation energy; for a discussion of the dependence of the dipole properties on the various spectral regions of the DOSD, see refs. 1, and 19 to 21. Unfortunately, there is often a lack of accurate DOS data over important photon energy regions for many interesting atoms and molecules. Also typical errors in DOS data ranges between 5–20% even for good oscillator strength data.

The procedure used to construct a dipole oscillator strength distribution for a given molecule from an initial data base of (df/dE) versus E values has been discussed in detail previously (13, 14), see also the discussion in ref. 22. The excitation energies for a given molecule are divided into N regions from the absorption threshold E_0 to very large values of E. The initial dipole oscillator strength data for the jth spectral region is modified according to

$$[5] \quad (df/dE)^j_{\text{mod}} = (1 + a_j)(df/dE)^j_{\text{initial}}, \qquad j = 1, 2, \ldots, N$$

so that the complete modified DOSD satisfies certain constraints through the choice of the a_j. If the input data contains discrete transitions, a parameter a_j is associated with each such transition.

The constraints used are furnished by the Thomas–Reiche–Kuhn sum rule (for a review of oscillator strength sum rules, see ref. 16), $S_0 = Z$ where Z is the number of electrons in the molecule, and preferably by two values of the molar refractivity R_λ of the relevant dilute gas corresponding to well separated wave lengths λ_1 and λ_2. If λ_2 and λ_1 are too close, $\Delta R_\lambda = R_{\lambda_2} - R_{\lambda_1}$ can become on the order of the experimental error in the refractivity data and the constrained least squares procedure used to determine the a_j cannot be carried out (19, 22). In such cases one value of R_λ, or the value of α_d or R_∞, can be used as a constraint with little loss in the reliability of many of the properties determined from the DOSD (22). The molar refractivity is related to the refractive index of the gas $n(\lambda)$, and to the frequency dependent or dynamic dipole polarizability $\alpha_d(\lambda)$ of the molecules making up the gas, by

$$[6] \quad R_\lambda = \frac{1}{\rho}\left[\frac{n^2(\lambda) - 1}{n^2(\lambda) + 2}\right] = \frac{4\pi}{3} N_A \alpha_d(\lambda)$$
$$= \frac{4\pi}{3} N_A (2R)^2 a_0^3 \int_{E_0}^{\infty} \frac{(df/dE)}{E^2 - (hc/\lambda)^2} dE$$

where ρ is the molar density of the gas, N_A is Avogadro's number, h is Planck's constant, and c is the speed of light. If the DOSD contains discrete transitions, [6] involves a sum over these as well as an integral over the continuum part of the DOSD, see, for example [4].

The constraints S_0 and R_λ are written as a sum of N terms (corresponding to discrete contributions from the discrete transitions and integrals for the continuum part of the DOSD), one for each a_j occurring in [5], and the parameters are determined for each initial DOSD by using the methods discussed in detail in ref. 13.

A DOSD can be constructed for each given initial data base for a given molecule. The total number of DOSDs constructed for a given molecule is given by

$$\prod_{k=1}^{N_{\text{input}}} N_k$$

where N_{input} is the number of input spectral regions and N_k is the number of independent sources of dipole oscillator strength data used for the kth input spectral region. If the N_k are large, choosing $N_{\text{input}} = N$ can lead to a very large number of distributions. In what follows this is reduced to manageable numbers by choosing N_{input} to be considerably less than N.

Each adopted DOSD is represented by a set of data points, E_l and $(df/dE)_l$, for $l = 1,\ldots,N_p \gg N$, and a set of interpolating functions to connect the points. For very high photon energies the differential dipole oscillator strengths are represented by the Born dipole formula (23), $AE^{-3.5}$. The dipole properties are readily evaluated using this representation of the DOSD.

3. DOSDs and dipole properties for HF, HCl, and HBr

The following photoabsorption and fast electron energy loss cross sections σ (proportional to (df/dE)) and dipole oscillator strength data were considered in the construction of the DOSDs:

HF: 8.0–150.0 eV (Carnovale and Brion (24)), 8.0–45.58 eV (Hitchcock and Brion (25)), 11.14–15.96 eV (Salama and Hasted (26)).

HCl: 5.64–11.82 eV (Myer and Samson (27)); 8.0–50 eV (Daviel *et al.* (28)), 200–280 eV (Ninomiya *et al.* (29)), 200–208.7 eV (Hayes and Brown (30)).

HBr: 5.39–7.0 eV (Huebert and Martin (31)), 7.0–100 eV (Brion and Thomson (32)).

For HF the energy loss cross sections (25, 26) have been normalized to the integrated oscillator strength obtained from Carnovale *et al.* (24) for common photon energy regions.

This experimental molecular data was augmented by employing the following mixture rules for relatively high photon energies:

$$[7] \quad \sigma(\text{HX}) = \tfrac{1}{2}\sigma(\text{H}_2) + \sigma(\text{X})$$

TABLE 1. Integrated dipole oscillator strengths for HF*, the absorption edge for HF occur at 684.7 eV [F_K] (34)

	Integrated dipole oscillator strengths		Integrated DOSs for original experimental and/or mixture rule data		
Energy range (eV)	Adopted DOSD	DOSD constrained to $\alpha_d = 5.330a_0^3$			
8.0–9.0	9.409(−3)(24)	9.403(−3)(24)	9.450(−3)(24)	3.677(−4)(25)	
9.0–11.14	7.859(−2)(24)	7.830(−2)(24)	8.100(−2)(24)	2.369(−2)(25)	
11.14–12.8	6.571(−2)(24)	6.562(−2)(24)	6.703(−2)(24)	1.033(−2)(25)	1.874(−1)(26)
12.8–13.52	6.485(−2)(24)	2.449(−2)(25)	6.599(−2)(24)	2.466(−2)(25)	1.146(−1)(26)
13.52–14.09	4.506(−2)(26)	2.059(−2)(25)	7.671(−2)(24)	2.070(−2)(25)	4.558(−1)(26)
14.09–15.96	1.295(−1)(26)	1.251(−1)(26)	2.669(−1)(24)	1.337(−1)(25)	1.290(−1)(26)
15.96–20.0	3.246(−1)(25)	3.248(−1)(25)	5.506(−1)(24)	3.300(−1)(25)	
20.0–25.0	6.010(−1)(25)	6.021(−1)(25)	7.414(−1)(24)	6.137(−1)(25)	
25.0–30.0	6.299(−1)(24)	6.316(−1)(24)	6.471(−1)(24)	6.683(−1)(25)	
30.0–35.0	5.597(−1)(24)	5.613(−1)(24)	5.695(−1)(24)	7.106(−1)(25)	
35.0–40.0	5.041(−1)(24)	5.054(−1)(24)	5.113(−1)(24)	7.223(−1)(25)	
40.0–45.58	5.067(−1)(24)	5.082(−1)(24)	5.139(−1)(24)	8.426(−1)(25)	
45.58–50.0	3.722(−1)(24)	3.732(−1)(24)	3.769(−1)(24)		
50.0–60.0	7.643(−1)(24)	7.660(−1)(24)	7.719(−1)(24)		
60.0–70.0	6.072(−1)(24)	6.197(−1)(24)	6.615(−1)(24)		
70.0–80.0	5.099(−1)(24)	5.185(−1)(24)	5.465(−1)(24)		
80.0–90.0	4.169(−1)(24)	4.169(−1)(24)	4.405(−1)(24)		
90.0–100.0	3.283(−1)(24)	3.283(−1)(24)	3.425(−1)(24)		
100.0–150.0	7.670(−1)(24)	7.670(−1)(24)	8.119(−1)(24)	8.114(−1)(M)	
150.0–684.7	9.507(−1)(M)	9.507(−1)(M)		9.980(−1)(M)	
684.7–1000	7.898(−1)(M)	7.898(−1)(M)		8.051(−1)(M)	
1000–10^5	9.745(−1)(M)	9.745(−1)(M)		9.834(−1)(M)	
10^5–∞	5.565(−5)(M)	5.565(−5)(M)		5.565(−5)(M)	

*This table contains the oscillator strengths for the adopted DOSD, constrained to $\alpha_d = 5.601a_0^3$ and $S_0 = 10$, constructed by consideration of the initial unmodified experimental or mixture rule DOS data for HF. The references associated with the adopted DOSD indicates the source of the DOS data for the indicated spectral region. Also included are the integrated DOSs corresponding to the DOSD constrained to $\alpha_d = 5.330a_0^3$ and $S_0 = 10$.

where X = F, Cl, or Br. The cross sections for H_2 are taken from the recommended DOSD of Zeiss *et al.* (13) while those for the halides X are from Henke *et al.* (33) for 50–100 eV and Veigele (34) for 100 eV – 100 keV. Because of the structure (29, 30) in the experimental photoabsorption results for HCl for 200–208.7 eV, only the experimental input data is subjected to the constraint procedure for these photon energies. In all cases the Stobbe formula (35) is used to generate the oscillator strength data for $E > 100$ keV. The mixture rule is used explicitly to construct the DOSDs for $E > 150$ eV for HF and for $E > 50$ eV for HCl and HBr.

The number of input spectral regions is chosen to be $N_{\text{input}} \sim 20$. To provide flexibility in applying the constraint procedure discussed in Section 2 the number of parameters a_j was chosen to be ~60, that is $N \approx 60$ in [5]. For each molecule all possible initial DOSDs are employed in the constraint procedure based on the input data associated with $N_{\text{input}} \sim 20$; the total number of initial DOSDs considered varies from ~5200 for HF to 1024 for HCl and HBr. The adopted DOSD for each molecule is that corresponding to the least overall adjustment of the initial DOS input data considered in the constraint procedure as judged by the value of

$$(\text{STD}) = \left[\sum_{j=1}^{N} (a_j - \bar{a})^2/N\right]^{1/2}$$

It is important to emphasize that given DOS input can lead to DOSDs that differ considerably as a function of E while agreeing well globally in that they yield very similar results for a variety of dipole properties (13, 18, 36). The integrated dipole oscillator strengths for each molecule are provided for the input spectral regions.

DOSD and properties for HF

Although there is some refractivity data available for HF, see below, it is rather uncertain and therefore not well suited for providing constraints for the construction of the DOSD for this molecule. Rather, we use as a constraint the value of the static dipole polarizability or S_{-2} determined as described below.

Werner and Meyer (2, 37) have calculated the static dipole polarizabilities α_d for the isoelectronic series Ne, HF, H_2O, NH_3, and CH_4 using both the coupled electron pair approximation (CEPA) and the pseudo natural orbital configuration interaction (PNO-CI) method. Accurate values (Section 4 and refs. 13, 38, 39) of α_d for Ne, H_2O, NH_3, and CH_4 lie between the CEPA and PNO-CI results suggesting that α_d for HF should be between $5.500a_0^3$ (PNO-CI) and $5.670a_0^3$. A plot of the percentage deviation of the accurate values from the mean of the PNO-CI and CEPA results is a straight line for Ne, H_2O, and NH_3 and interpolation yields a result of $5.601a_0^3$ which we use as a constraint for constructing the DOSD for HF. This value agrees with that obtained by interpolation of a plot of the accurate values of α_d, for Ne, H_2O, NH_3, and CH_4, versus the number of protons in the molecule, see also Klein *et al.* (40), and used recently by Brobjer and Murrell (41).

As a check we have estimated S_{-1} for HF from a plot of reliable values (Section 4 and refs. (13, 39)) of S_{-1} for Ne, H_2O, NH_3, and CH_4 versus the number of protons in the molecules. Interpolation of this (essentially) straight line plot yields $S_{-1} = 5.50$ for HF which is in good agreement with the value evaluated from our adopted DOSD for HF, see Table 2.

Integrated dipole oscillator strengths for the adopted DOSD corresponding to the constraints $\alpha_d = 5.601a_0^3$, or $S_{-2} = 5.601$, and $S_0 = 10$ are given in Table 1 and the corresponding

TABLE 2. Some dipole properties S_k and L_k for HF, HBr, and HCl evaluated using the adopted DOSDs for the molecules, also included are the results corresponding to the DOSD for HF that is constrained to $\alpha_d = 5.330a_0^3$

Property	Value			
	HF			
	Adopted	$\alpha_d=5.330a_0^3$	HCl	HBr
S_2	1.722(4)	1.724(4)	2.278(5)	4.154(6)
S_1	1.217(2)	1.222(2)	5.120(2)	2.584(3)
S_0	1.000(1)	1.000(1)	1.800(1)	3.600(1)
$S_{-1/2}$	6.501	6.440	1.126(1)	1.651(1)
S_{-1}	5.441	5.324	1.127(1)	1.468(1)
$S_{-3/2}$	5.248	5.064	1.351(1)	1.762(1)
S_{-2}	5.601	5.330	1.739(1)	2.374(1)
$S_{-5/2}$	6.486	6.093	2.332(1)	3.379(1)
S_{-3}	8.033	7.469	3.227(1)	4.978(1)
S_{-4}	1.440(1)	1.325(1)	6.712(1)	1.169(2)
S_{-5}	2.998(1)	2.762(1)	1.545(2)	2.996(2)
S_{-6}	6.896(1)	6.414(1)	3.893(2)	8.279(2)
S_{-7}	1.697(2)	1.598(2)	1.062(3)	2.446(3)
S_{-8}	4.379(2)	4.175(2)	3.102(3)	7.674(3)
S_{-9}	1.169(3)	1.127(3)	9.598(3)	2.541(4)
S_{-10}	3.205(3)	3.116(3)	3.119(4)	8.831(4)
L_2	1.162(5)	1.163(5)	1.806(6)	3.862(7)
L_1	4.569(2)	4.585(2)	2.459(3)	1.532(4)
L_0	1.257(1)	1.272(1)	3.020(1)	8.832(1)
L_{-1}	1.057	1.175	−2.719	−2.328
L_{-2}	−1.217	−1.012	−9.581	−1.570(1)

dipole properties are given in Table 2.

The experimental situation regarding the refractive index of gaseous HF is summarized in Table 3, which contains results for the molar refractivity obtained from the work of Penning *et al.* (42) and Drummond (43). The few available experimental results are considerably lower than those evaluated from our adopted DOSD, see Table 3; the disagreement is well outside the estimated experimental errors of ~2% for Penning *et al.* (42) and ~5% for Drummond (43). The difficulties in obtaining reliable results for the refractive index of HF have been discussed by these authors and of particular importance is the elimination of dimerization effects.

If anything our adopted value of

$$\alpha_d = \left(\frac{3}{4\pi N_A}\right) R_\infty = 5.601 a_0^3$$

is too high. To illustrate the effect of a lower value of α_d on the results obtained from our constraint procedure we have repeated the calculation associated with our adopted DOSD using $\alpha_d = 5.330a_0^3$ obtained by increasing the value of R_λ obtained from Drummond's result by 5% and by assuming λ = 28 000 Å = ∞. This value of α_d is in reasonable agreement with an additivity estimate of $5.40a_0^3$ obtained by Clark (46) and referred to in Landolt-Bornstein (47).

The integrated DOSs, dipole properties, and R_λ values for the DOSD constrained to $\alpha_d = 5.330a_0^3$ are included in Tables 1–3, respectively. The DOS is affected markedly only for 12.8 eV < E < 16.0 eV and, as expected, this influences the results for the S_k and L_k significantly only for negative values of k. The results for the dipole properties corresponding to the DOSD constrained to $\alpha_d = 5.330a_0^3$ are lower than the adopted results corresponding to $\alpha_d = 5.601a_0^3$; the discrepancies are ~1% for $k = -1/2$, ~4.8% for $k = -2$, ~8% for $k = -4$ and they decrease as k decreases further since the differences between the two DOSDs decreases for E < 13 eV. We prefer the adopted results for the DOSD and the dipole properties for the reasons given previously. The other results for the properties can be regarded as an extreme possibility for lower bounds to our recommended results. A reasonable error estimate, ~±1%, for our adopted value for α_d(HF) is furnished by comparison of the PNO-CI and CEPA results of Werner and Meyer (37).

TABLE 3. Comparison of the values of R_λ, in cm³ mol⁻¹, for HF evaluated using the adopted DOSD with the experimental values obtained from Penning *et al.* (42). The result R (λ = 28 000 Å) = 1.898 cm³ mol⁻¹ has been obtained from Drummond *et al.* (43);[a] the corresponding result for our adopted DOSD is 2.0951 cm³ mol⁻¹; also included in the table are values of R_λ evaluated from the DOSD that is constrained to $\alpha_d = 5.330a_0^3$, see text for details

λ (Å)	R_λ adopted DOSD	R_λ $\alpha_d=5.330a_0^3$	R_λ(PWR)[a]
6564	2.1202	2.0168	
5893	2.1268	2.0229	
5790	2.1281	2.0240	1.987
5462.25	2.1324	2.0281	
5460	2.1325	2.0281	2.002
4801	2.1444	2.0390	
4360	2.1558	2.0495	2.062
4109.25	2.1641	2.0572	
2926.25	2.2422	2.1293	
2577.07	2.2937	2.1769	

[a]The experimental refractivity results have been presented for 0°C and 1 atm assuming ideal behaviour. More complete corrections for non-ideal behaviour would probably lead to a reduction of the R_λ values obtained from the data in refs. 42 and 43; the article by Bosanac *et al.* (ref. 44, see also Redington (45)) contains a summary of available second virial coefficient data for HF.

DOSD and properties for HCl

There are apparently three sources of refractive index measurements for HCl, Cuthbertson and Cuthbertson (48) between 6707.9 Å and 4799.9 Å, Frivold (49) for 6564 Å to 4359 Å, and Larsen (50) between 5677.4 Å and 2302.8 Å. All are in very good agreement (within 0.2%) at the (essentially) common wavelength of 5462.25 Å. The Frivold data are used to generate molar refractivity constraints at 6564 Å and 4359 Å.

The integrated dipole oscillator strengths for the adopted DOSD are given in Table 4 and the properties evaluated from it are included in Table 2; our value of S_{-2} is identical to that obtained from the value of R_∞ given in Londolt-Bornstein (47). The values of R_λ calculated from the DOSD are in excellent agreement with the experimental values, see Table 5.

DOSD and properties for HBr

Refractive index data is available between 6707.9 Å and 2447.7 Å, see Cuthbertson and Cuthbertson (48) and Larsen (50). The results at λ = 6707.9 Å and 2675.8 Å were selected to provide the molar refractivity constraints for the construction of the DOSD for HBr. The integrated dipole oscillator strengths for the adopted DOSD are given in Table 6, the associated dipole properties in Table 2. Our result for S_{-2} is in excellent agreement with the value of 23.54 obtained from R_∞ given in ref. 47.

The molar refractivities evaluated from the adopted DOSD are compared with experiment in Table 7 and the agreement is excellent except in the case of R_λ values obtained from Larsen (50) for λ = 2464.8 Å and 2447.7 Å. Varying the molar

TABLE 4. Integrated dipole oscillator strengths for HCl (see also footnote for Table 1); the absorption edges occur at 208.7 eV (Cl_{L_2}) and 2822 eV (Cl_K) (34)

Energy range (eV)	Integrated dipole oscillator strengths	Integrated DOSs for original experimental and/or mixture rule data		
5.64–8.0	2.499(−2)(27)	2.443(−2)(27)		
8.0–9.0	7.918(−2)(28)	2.454(−2)(27)	7.650(−2)(28)	
9.0–11.82	2.226(−1)(27)	2.194(−1)(27)	7.520(−1)(28)	
11.82–14.0	9.466(−1)(28)		1.013 (28)	
14.0–17.0	1.164 (28)		1.436 (28)	
17.0–20.0	1.277 (28)		1.342 (28)	
20.0–30.0	2.504 (28)		2.555 (28)	
30.0–40.0	5.406(−1)(28)		5.415(−1)(28)	
40.0–50.0	1.650(−1)(28)		1.650(−1)(28)	1.629(−1)(M)
50.0–60.0	1.346(−1)(M)			1.344(−1)(M)
60.0–70.0	1.308(−1)(M)			1.306(−1)(M)
70.0–80.0	1.248(−1)(M)			1.245(−1)(M)
80.0–90.0	1.135(−1)(M)			1.133(−1)(M)
90.0–100.0	1.027(−1)(M)			1.025(−1)(M)
100.0–200.0	6.224(−1)(M)			6.137(−1)(M)
200.0–204.59	4.724(−2)(30)	3.749(−2)(29)	4.721(−2)(30)	9.097(−2)(M)
204.59–205.33	8.205(−3)(29)	8.204(−3)(29)	7.233(−3)(30)	1.810(−2)(M)
205.33–208.7	7.085(−2)(30)	5.217(−2)(29)	7.080(−2)(30)	8.664(−2)(M)
208.7–280.0	2.080 (M)	1.449 (29)		2.028 (M)
280.0–1000	5.268 (M)			5.175 (M)
1000–2822	7.661(−1)(M)			7.623(−1)(M)
2822–5000	1.037 (M)			1.030 (M)
5000–25000	5.458(−1)(M)			5.450(−1)(M)
25000–10^5	2.198(−2)(M)			2.198(−2)(M)
10^5–∞	1.089(−3)(M)			1.089(−3)(M)

refractivity constraints had little influence on the calculated values of R_λ unless Larsen's (50) data for $\lambda \leq 2464.8$ Å were used; it appears that the experimental data for these values of λ are significantly too high, see Table 7.

Further discussion of the properties of the hydrogen halides is reserved for Section 5. However, comments on the DOSDs are relevant here, particularly concerning HCl and HBr.

The HCl experimental integrated oscillator strengths obtained from Hayes and Brown (30) and Ninomiya *et al.* (29) agree reasonably well for 200–205.3 eV, within the experimental error given in ref. 30, while the mixture rule result is some 50% higher. As E increases, between 205.3 and 208.7 eV, the integrated oscillator strengths obtained from ref. 30 and the mixture rule agree within the estimated experimental error whereas the results due to Ninomiya *et al.* (29) apparently become too low and this trend continues between 208.7 and 280 eV. It seems that the disagreement between the mixture rule and the experimental data between 200–205.3 eV, within ~3 eV of the Chlorine L_2 edge, is a nice example of a molecular photoabsorption effect occurring at high photon energies, see also ref. 52. Unfortunately this (possible) effect cannot be investigated at the K edge of HCl, or the absorption edges for HF and HBr, because of an apparent lack of molecular photoabsorption cross sections for these photon energies.

For $7 \leq E \leq 50$ eV the adopted integrated dipole oscillator strengths for HBr, see Table 6, agree with the input DOS results obtained by Brion and Thomson (32) within the estimated experimental error of ~25%. As E increases, however, the experimental results seem too low with respect to the mixture rule data which should become reliable for these values of the photon energies (except possibly near the absorption edges, see above). Further evidence of the reliability of the mixture rule can be found in Table 1 for HF between 100 and 150 eV, in Table 4 for HCl between 40 and 50 eV, and through the agreement of the mixture rule integrated oscillator strength for HCl between 5000 and 25000 eV with the molecular result of 5.440 (−1) obtained from Millar and Greening (53).

4. DOSDs and dipole properties for Ne, Ar, Kr, and Xe

Dipole oscillator strength distributions for the rare gases have been developed, in the context of evaluating reliable results for the dipole properties of these atoms, by several authors. Probably the most extensive treatment is due to Leonard and Barker (11), see also Barker and Leonard (54) and Leonard (15), and of course the pioneering work of Dalgarno and co-workers (9, 10, 55, 56) and Margenau (8) should also be mentioned. For a more complete discussion see refs. 11, 12, and 55.

Much more recently Berkowitz (57) has discussed the oscillator strength data for the rare gases and has used the Thomas–Reiche–Kuhn sum rule, experimental values of $\alpha_d = S_{-2}a_0^3$, and calculated or experimental values of S_{-1}, to help test and discriminate between the experimental DOS data considered.

The review of the experimental DOS data for the rare gases by Leonard and Barker (11), see also Leonard (15), was very extensive up to the time of the original work (~1967). Since then many new papers on the rare gas DOSs have appeared, many of which have been considered in ref. 57. It seems reasonable then to reconsider the rare gases in the light of the constrained least squares procedure discussed in Section 2 and to obtain a data base for these atoms analogous to our work on a variety of other atoms and molecules (13, 14, 18–20, 36, 39), including the hydrogen halides discussed in Section 3. We consider only the rare gases Ne, Ar, Kr, and Xe; effective dipole oscillator strength distributions for He are readily available in the literature (9, 11, 58). However, since most of the dipole properties obtained from our adopted DOSDs agree very

TABLE 5. Comparison of the values of R_λ, in $cm^3\ mol^{-1}$, for HCl evaluated using the adopted DOSD with the experimental values obtained from Frivold (49), Cuthbertson and Cuthbertson (48), and Larsen (50)

λ (Å)	R_λ (DOSD)	R_λ (F)[a]	R_λ (CC)[b]	R_λ (L)[a]
6707.85	6.6197		6.6345	
6564	6.6251	6.625[c]		
6438.5	6.6302		6.6448	
5895	6.6560	6.6580		
5790.5	6.6619		6.6765	
5769.5	6.6631		6.6780	
5677.40	6.6687			6.6775
5462.25	6.6827	6.6849		6.6926
5460.7	6.6829		6.6980	
5209.1	6.7017		6.7174	
5085.8	6.7121		6.7289	
4917.41	6.7276	6.7267		6.7377
4799.9	6.7395		6.7558	
4359	6.7939	6.7939[c]		
4109.25	6.8336			6.8443
3802.72	6.8949			6.9070
3342.44	7.0264			7.0388
2926.25	7.2169			7.2291
2894.45	7.2358			7.2470
2760.54	7.3255			7.3366
2753.60	7.3307			7.3416
2675.78	7.3920			7.4014
2577.07	7.4815			7.4890
2464.81	7.6037			7.6060
2447.65	7.6247			7.6263
2380.74	7.7143			7.7113
2346.17	7.7661			7.7588
2302.83	7.8377			7.8222

[a]The data has been corrected to ideal gas conditions in refs. 49 and 50.
[b]The results are obtained by converting the data ($n_d - 1$) given in (48) to ideal gas conditions by using ($n^0_{1.760} - 1$) = 1.00063($n_d - 1$) (see ref. 51).
[c]Used as constraints in the construction of the DOSD.

well with those of Leonard and Barker (11, 15), the details of the analysis will be suppressed substantially.

The initial or unmodified integrated oscillator strengths used explicitly in our analysis are given in Tables 8−11 for Ne, Ar, Kr, and Xe, respectively; all the appropriate references for the data are included in these tables. Molar refractivity data and $S_0 = Z$ are used as constraints for the construction of the DOSDs. The molar refractivity constraints are chosen to be: Ne − λ = 5462.25 Å and 2894.4 Å from Cuthbertson and Cuthbertson (108) correcting for non-ideal behaviour by using the second virial coefficient of Michels *et al.* (109); Ar − λ = 6329.9 Å and 4766.2 Å from Coulon *et al.* (110); Kr − λ = 2632.1 Å and 1770.9 Å from Smith *et al.* (111); Xe − λ = 2537.0 Å and 1702.0 Å from Bideau-Mehu *et al.* (112). A very useful review and critique of the refractive index data for the rare gases up to ~1970 can be found in Leonard (113); ref. 108 occurs in this review while refs. 110−112 are considerably more recent. In all cases the molar refractivity values calculated from our adopted DOSDs are in excellent agreement with the experimental values obtained from refs. 108−112 for all relevant values of λ; the agreement with other comparable experimental data is generally also very satisfactory.

Compared to the molecules considered in Section 3, the sources of DOS input data for the rare gases are immense. Potentially this data gives rise to millions of DOSDs if the approach used for the hydrogen halides is used here. To simplify matters we first used the oscillator strengths suggested by Berkowitz's (57) analysis of the DOS data for the rare gases, or by well intentioned interpretations or modifications of this data, to construct the DOSDs for Ne, Ar, Kr, and Xe. For example, we augmented the data considered by Berkowitz by recent DOS results for the auto-ionization region, by high energy DOS data generated by the Stobbe formula and by employing Henke's (33) more recent compilation of rare gas photoabsorption cross sections. In addition we have also constructed many additional DOSDs by making selective adjustments in the DOS input data, using the initial calculations as a guide, by employing other DOS data sources in order to attempt to minimize (STD). The adopted DOSD corresponds to the minimum value of (STD) obtained although we emphasize that not all possible combinations of DOS input data has been considered for this purpose. In all cases the STD fell from ~2−5 to ~0.5.

The integrated dipole oscillator strengths for the adopted DOSDs are given in Tables 8−11 for Ne, Ar, Kr, and Xe, respectively. While the corresponding results obtained from our initial calculations based on Berkowitz's analysis can differ locally, they usually agree with our adopted results globally in the sense of yielding very similar results for many of the dipole properties of the rare gases (some exceptions are discussed briefly in Section 5). The dipole properties S_k and L_k evaluated from our adopted DOSDs are given in Table 12. The values of S_{-2} resulting from our adopted DOSDs are in excellent agreement with the recommended values given in the review by Teachout and Pack (38) and Leonard (113).

5. Discussion

Some of the experimental and literature results for the dipole properties of the molecules and atoms considered in this paper have been compared with our adopted results in Sections 3 and 4 in the context of the evaluation of the properties. Also, very recently, a refined quantitative study of valence shell absolute photoabsorption cross sections for HF, including a discussion of experimental difficulties associated with this molecule, has been carried out by Hitchcock *et al.* (114). We begin this section with a comparison and brief discussion of other literature results, many of which are *ab initio* calculations for the hydrogen halides, for some of the dipole properties of HF, HCl, HBr, Ne, Ar, Kr, and Xe.

Hydrogen halides

The most studied dipole property of this group of molecules is the static dipole polarizability of HF. A recent discussion of correlation corrections to coupled Hartree−Fock calculations of the dipole polarizability of HF, together with an excellent calculation of α_d and a summary of previous work at the SCF and higher levels, can be found in Mukherjee *et al.* (4). All of the results at the SCF level quoted, except those of O'Hare and Hurst (115) which are ~4% higher than our recommended result, are substantially too low (by ≤12%). The addition of correlation effects generally increases the value of α_d but only a few calculations (116), including some of those of Mukherjee (4) aided by Padé approximant techniques, lead to results comparable in reliability to those of Werner and Meyer (37) used to construct the DOSD for HF in Section 3. Reference 4 contains excellent discussions and examples of the difficulties involved in obtaining reliable *ab initio* results for the polarizabilities of even moderately small species. Other recent work, not included in ref. 4, includes a recent study by

TABLE 6. Integrated dipole oscillator strengths for HBr (see also footnote for Table 1); the absorption edges occur at 1550 eV [Br_{L_3}], 1596 [Br_{L_2}], 1782 eV [Br_{L_1}] and 13 470 eV [Br_K] (34)

Energy range (eV)	Integrated dipole oscillator strengths	Integrated DOSs for original experimental and/or mixture rule data	
5.39–7.0	1.722(−2)(31)	1.918(−2)(31)	
7.0–9.5	2.921(−1)(32)		4.360(−1)(32)
9.5–13.0	1.386 (32)		1.149 (32)
13.0–17.0	1.963 (32)		1.758 (32)
17.0–20.0	1.064 (32)		1.040 (32)
20.0–30.0	1.898 (32)		1.879 (32)
30.0–40.0	5.960(−1)(32)		5.950(−1)(32)
40.0–50.0	2.272(−1)(32)		2.270(−1)(32)
50.0–60.0	2.480(−1)(M)	2.478(−1)(M)	1.165(−1)(32)
60.0–70.0	2.208(−1)(M)	2.207(−1)(M)	7.502(−2)(32)
70.0–80.0	2.174(−1)(M)	2.174(−1)(M)	1.415(−1)(32)
80.0–90.0	2.589(−1)(M)	2.589(−1)(M)	6.675(−2)(32)
90.0–100.0	3.051(−1)(M)	3.052(−1)(M)	7.749(−2)(32)
100.0–183.4	3.884 (M)	3.935 (M)	
183.4–255.8	3.414 (M)	3.465 (M)	
255.8–500.0	6.114 (M)	6.166 (M)	
500.0–1000	3.478 (M)	3.485 (M)	
1000–1550	1.212 (M)	1.214 (M)	
1550–1596	2.449(−1)(M)	2.450(−1)(M)	
1596–1782	1.147 (M)	1.149 (M)	
1782–5000	5.477 (M)	5.498 (M)	
5000–13470	9.250(−1)(M)	9.254(−1)(M)	
13470–10^5	1.381 (M)	1.382 (M)	
10^5–∞	2.636(−2)(M)	2.636(−2)(M)	

TABLE 7. Comparison of R_λ, in $cm^3\ mol^{-1}$, for HBr evaluated using the adopted DOSD with the experimental values obtained from Cuthbertson and Cuthbertson (48) and Larson (50)

λ (Å)	R_λ (DOSD)	R_λ (CC)[a]	R_λ (L)[b]
6707.85	9.0827	9.0827[c]	
6438.5	9.1012	9.1015	
5790.5	9.1574	9.1565	
5769.5	9.1595	9.1582	
5677.4	9.1693		9.1822
5462.25	9.1943		9.2097
5460.7	9.1945	9.1931	
5209.1	9.2281	9.2251	
5085.8	9.2465	9.2430	
4917.41	9.2742		9.2884
4799.9	9.2955	9.2932	
4109.25	9.4645		9.4782
3802.72	9.5756		9.5920
3342.44	9.8169		9.8299
2926.25	10.1742		10.1820
2894.45	10.2104		10.2168
2760.54	10.3830		10.3795
2753.60	10.3930		10.3950
2675.78	10.5129		10.5129[c]
2577.07	10.6908		10.6978
2464.81	10.9408		11.3849
2447.65	10.9850		11.5641

[a]The results are obtained by converting the data ($n_d - 1$) given in ref. 48 to ideal conditions by using ($n^0_{1.760} - 1$) = 1.00063 ($n_d - 1$) (see ref. 51).
[b]The data have been corrected to ideal gas conditions in ref. 50.
[c]Used as constraints in the construction of the DOSD.

Jorgensen *et al.* (117) using the coupled Hartree–Fock (CHF) or time dependent Hartree–Fock (TDHF) methods and the second order polarization propagator approximation (SOPPA) in length, mixed, and velocity forms. The TDHF results are significantly low (≲18%) while the SOPPA results in the length, mixed, and velocity representations are ~15%, 11%, and 4% lower, respectively, than the adopted result. Also relevant is a recent study (118) of the problem by an equation of motion approach involving the random phase, the Tamm–Danoff and the single-transition approximations using length, velocity, acceleration, and various mixed representations. The RPA results are of similar reliability to the TDHF calculations discussed previously while the theoretically poorer TDA and STA calculations can yield values for α_d(HF) that are in closer agreement with the recommended value of $5.60a_0^3$. An interesting recent discussion of the dependence of coupled Hartree–Fock results for α_d on the nature of the gaussian basis set used in the calculation can be found in ref. 119.

There are apparently few *ab initio* calculations for the other dipole properties considered in this paper for HF or for the dipole properties of HCl or HBr. The most recent *ab initio* study of the polarizability of HCl is apparently that due to Oddershede and Svendsen (120) who obtain a TDHF result of 17.14 a_0^3 and a SOPPA value of $18.06a_0^3$ compared to our adopted result of $17.39a_0^3$. The older SCF (finite field) and SCF-CI results of Williams and Amos (121) lie ~12% and 10% lower than the recommended value. The coupled Hartree–Fock result of Gianturco and Guidotti (122) agrees well (within ~1%) with that of ref. 120. The CNDO/2 finite perturbation plus polarization orbitals calculations of Rhee *et al.* (123) yield α_d = 5.39, 16.1, and $22.9a_0^3$ for HF, HCl, and HBr, respectively, which are ~3.8%, 7%, and 3.5% lower than our adopted results of Section 3.

The dipole properties S_k, for k = 2, 1, and −1, can be evaluated rigorously by taking an expectation value of an appropriate quantum mechanical operator with respect to the exact ground state wave function for the relevant atom or mole-

TABLE 8. Integrated dipole oscillator strengths for Ne (see also footnote for Table 1) for the adopted DOSD and for the initial DOS input data; the absorption edges occur at 48.5 eV (L_1) and 866.9 eV (K). The molar refractivity constraints used to construct the adopted DOSD are $R(\lambda = 5462.25$ Å$) = 1.00537$ and $R(\lambda = 2894.44$ Å$) = 1.02573$ cm^3 mol^{-1}

Energy range (eV)	Adopted DOSD	Integrated dipole oscillator strengths for initial experimental or Stobbe dipole oscillator strength data						
Discrete[a]								
(16.67−21.48)	2.875(−1)	2.866(−1)[b]						
21.47−21.57	1.528(−3)(66)				1.528(−3)(66)			
21.57−21.67	5.593(−3)(66)			4.480(−3)(69)	5.592(−3)(66)			
21.67−22.20	3.172(−2)(67)	3.169(−2)(67)		2.562(−2)(69)				2.428(−2)(72)
22.20−30.0	5.815(−1)(67)	5.813(−1)(67)		5.159(−1)(69)	6.245(−1)(70)			5.287(−1)(72)
30.0−36.47	5.176(−1)(67)	5.207(−1)(67)		4.373(−1)(69)	5.737(−1)(70)	5.225(−1)(33)	5.038(−1)(71)	4.700(−1)(72)
36.47−48.48	8.864(−1)(67)	8.937(−1)(67)	9.265(−1)(68)	5.632(−1)(69)	9.487(−1)(70)	9.056(−1)(33)	8.983(−1)(71)	7.491(−1)(72)
48.48−63.1	1.050 (70)	9.322(−1)(67)	9.703(−1)(68)		1.056 (70)	9.629(−1)(33)	9.403(−1)(71)	
63.1−100.0	1.893 (70)	1.696 (67)	1.782 (68)	1.726 (73)	1.906 (70)	1.699 (33)	1.668 (71)	
100.0−150.0	1.403 (70)	1.254 (67)	1.366 (68)	1.198 (73)	1.453 (70)	1.212 (33)	1.153 (71)	1.259 (34)
150.0−230.0	8.284(−1)(33)	8.741(−1)(67)	9.313(−1)(68)	8.081(−1)(73)		8.389(−1)(33)	7.632(−1)(71)	8.244(−1)(34)
230.0−250.0	1.168(−1)(33)	1.191(−1)(67)	1.232(−1)(68)			1.172(−1)(33)	9.851(−2)(71)	1.140(−1)(34)
250.0−277.99	1.304(−1)(33)	1.326(−1)(67)	1.351(−1)(68)			1.308(−1)(33)		1.271(−1)(34)
277.99−309.96	1.144(−1)(33)		1.168(−1)(68)			1.147(−1)(33)		1.115(−1)(34)
309.96−866.2	4.862(−1)(33)					4.879(−1)(33)		4.886(−1)(34)
866.2−866.9	3.798(−4)(33)					3.798(−4)(33)		5.965(−4)(34)
866.9−1000	2.911(−1)(33)					2.918(−1)(33)		3.640(−1)(34)
1000−5000	1.307 (33)					1.321 (33)		1.345 (34)
5000−10 000	5.156(−2)(33)					5.159(−2)(33)		5.247(−2)(34)
10 000−25 000	1.403(−2)(34)							1.403(−2)(34)
25 000−100 000	2.131(−3)(34)							2.131(−3)(34)
100 000−∞	9.184(−5)(STOBBE)							9.184(−5)(STOBBE)

[a]The energy levels given in ref. 59 and a variety of DOS data sources were used to construct the discrete part of the DOSD; the sources of DOS data for the adopted results are refs. 60−65.
[b]Corresponds to the initial DOS data giving rise to the adopted result.

TABLE 9. Integrated dipole oscillator strengths for Ar (see also footnote for Table 1) for the adopted DOSD and for the initial DOS input data; the absorption edges occur at 245.2 eV (L_3), 247.3 eV (L_2), 320.0 eV (L_1), and 3202.9 eV (K). The molar refractivity constraints used to construct the adopted DOSD are $R(\lambda = 6329.9\ \text{Å}) = 4.1973$ and $R(\lambda = 4766.2\ \text{Å}) = 4.2407\ \text{cm}^3\ \text{mol}^{-1}$

Energy range (eV)	Adopted DOSD	Integrated dipole oscillator strengths for initial experimental or Stobbe dipole oscillator strength data								
Discrete[a] (11.62−15.60)	7.462(−1)	7.521(−1)[b]								
15.76−15.94	4.899(−2)(74)			4.901(−2)(74)		4.472(−2)(75)			4.188(−2)(76)	
15.94−17.70	5.939(−1)(74)	5.464(−1)(77)	5.311(−1)(67)	5.943(−1)(74)	5.344(−1)(78)	4.334(−1)(75)		5.302(−1)(79)	5.251(−1)(76)	
17.70−21.0	1.108 (80)	9.383(−1)(77)	1.081 (67)	1.234 (74)	1.044 (78)	8.662(−1)(75)	1.108 (80)	1.089 (79)	9.582(−1)(76)	
21.0−26.0	1.617 (80)	1.671 (81)	1.620 (67)	1.560 (82)	1.588 (78)	1.478 (83)	1.614 (80)	1.575 (79)	1.408 (76)	1.485 (84)
26.0−30.0	9.545(−1)(80)	1.085 (81)	1.043 (67)	1.022 (82)	9.714(−1)(78)	1.001 (83)	9.500(−1)(80)			9.188(−1)(84)
30.0−35.0	6.558(−1)(80)	7.374 (81)	6.613(−1)(67)	8.082(−1)(82)	7.988(−1)(78)	9.059(−1)(83)	6.539(−1)(80)		1.132 (33)	6.557(−1)(84)
35.0−40.0	2.594(−1)(80)		2.572(−1)(67)	3.416(−1)(82)	2.983(−1)(78)	4.176(−1)(83)	2.592(−1)(80)		8.053(−1)(33)	4.228(−1)(84)
40.0−49.30	1.315(−1)(68)		1.111(−1)(67)		1.411(−1)(78)	2.142(−1)(83)	1.900(−1)(80)	1.317(−1)(68)	6.284(−1)(33)	
49.30−59.24	1.039(−1)(68)		8.244(−2)(67)	1.190(−1)(85)	5.545(−2)(78)	1.030(−1)(83)	1.618(−1)(80)	1.039(−1)(68)	7.968(−2)(33)	
59.24−63.10	4.932(−2)(68)			5.059(−2)(85)	1.428(−2)(78)	4.407(−2)(83)	6.882(−2)(80)	4.932(−2)(68)	3.765(−2)(33)	
63.10−70.81	1.027(−1)(68)		9.329((−2)(73)	1.052(−1)(85)		9.557(−2)(83)		1.027(−1)(68)	8.640(−2)(33)	
70.81−100.0	3.779(−1)(68)		3.663(−1)(73)	3.872(−1)(85)		3.582(−1)(83)		3.779(−1)(68)	3.562(−1)(33)	
100.0−150.0	4.722(−1)(86)	4.721(−1)(86)	4.700(−1)(73)	4.643(−1)(85)	4.768(−1)(34)	4.509(−1)(83)		4.996(−1)(68)	4.805(−1)(33)	
150.0−217.2	3.788(−1)(86)	3.788(−1)(86)	3.585(−1)(73)	3.322(−1)(85)	3.783(−1)(34)	3.302(−1)(83)	3.647(−1)(87)	4.151(−1)(68)	3.882(−1)(33)	
217.2−245.2	1.049(−1)(86)	1.049(−1)(86)		1.266(−1)(85)	1.051(−1)(34)	1.186(−1)(83)	1.052(−1)(87)	3.650(−1)(68)	2.330(−1)(33)	
245.2−247.3	1.734(−2)(86)	1.734(−2)(86)		2.539(−2)(85)	2.743(−2)(34)	3.566(−2)(83)	1.170(−2)(87)	9.037(−2)(68)	2.591(−2)(33)	
247.3−275.52	1.046 (86)	1.046 (86)		7.526(−1)(85)	1.084 (34)	1.140 (83)	1.500 (87)	1.063 (68)	5.337(−1)(33)	
275.52−320.0	1.136 (86)	1.137 (86)		1.071 (85)	1.213 (34)	1.496 (83)	1.462 (87)		1.121(−1)(33)	
320.0−400.0	1.707 (86)	1.707 (86)		1.637 (85)	1.710 (34)	2.174 (83)	1.249 (87)		1.596 (33)	
400.0−500.0	1.366 (86)	1.367 (86)		1.250 (85)	1.348 (34)				1.372 (33)	
500.0−3000.0	3.432 (86)	3.433 (86)		3.101 (85)	3.318 (34)				3.477 (33)	
3000.0−3202.9	1.884(−2)(86)	1.888(−2)(86)			1.934(−2)(34)				2.971(−2)(33)	
3202.9−5000	8.555(−1)(86)	8.556(−1)(86)			8.964(−1)(34)				6.960(−1)(33)	
5000−10000	5.241(−1)(86)	5.241(−1)(86)			5.288(−1)(34)	5.221(−1)(88)			5.290(−1)(33)	
10000−25000	1.618(−1)(86)	1.618(−1)(86)			1.601(−1)(34)	1.621(−1)(88)				
25000−10^5	2.837(−2)(86)	2.837(−2)(86)			2.804(−2)(34)					
10^5−∞	1.413(−3)	1.413(−3)(STOBBE)								

[a]The energy levels given in ref. 59 and a variety of DOS data sources were used to construct the discrete part of the DOSD. The sources of DOS data for the adopted results are refs. 11, 60, and 62.
[b]Corresponds to the initial DOS data giving rise to the adopted result.

TABLE 10. Integrated dipole oscillator strengths for Kr (see also footnote for Table 1) for the adopted DOSD and for the initial DOS input data; the absorption edges occur at 1675 eV (L_3), 1727 eV (L_2), 1921 eV (L_1), and 14330 eV (K). The molar refractivity constraints used to construct the adopted DOSD are $R(\lambda = 2632.1$ Å$) = 7.0106$ and $R(\lambda = 1770.9$ Å$) = 8.3522$ cm^3 mol^{-1}

Energy range (eV)	Adopted DOSD	Integrated dipole oscillator strengths for initial experimental or Stobbe dipole oscillator strength data						
Discrete[a] (10.03–13.85)	1.073	1.069[b]						
14.0–14.67	2.529(−1)(91)	2.487(−1)(91)		2.892(−1)(74)		2.017(−1)(67)		
14.67–20.66	2.509 (92)	2.009 (76)	2.456 (92)	2.230 (93)		2.261 (67)		
20.66–24.78	1.319 (92)	1.180 (76)	1.310 (92)			1.231 (67)		
24.78–36.47	1.740 (92)		1.733 (92)			1.685 (67)		
36.47–49.49	4.517(−1)(68)	4.518(−1)(68)	4.729(−1)(92)	4.809(−1)(94)	7.846(−1)(33)	4.271(−1)(67)		
49.49–59.24	1.016(−1)(68)	1.016(−1)(68)		1.343(−1)(94)	1.095(−1)(33)	9.264(−2)(67)	1.735(−1)(95)	
59.24–62.49	2.395(−2)(68)	2.395(−2)(68)		3.072(−2)(94)	2.900(−2)(33)		4.211(−2)(95)	
62.49–90.0	1.679(−1)(68)	1.679(−1)(68)		2.249(−1)(94)	1.570(−1)(33)	1.475(−1)(96)	2.744(−1)(95)	
90.0–100.0	1.013(−1)(68)	1.013(−1)(68)		1.288(−1)(94)	7.792(−2)(33)	1.021(−1)(96)	1.393(−1)(95)	1.200(−1)(97)
100.0–120.0	3.544(−1)(68)	3.543(−1)(68)	3.608(−1)(34)	4.117(−1)(94)	3.253(−1)(33)	3.441(−1)(96)	4.144(−1)(95)	3.509(−1)(97)
120.0–250.0	5.614 (68)	5.600 (68)	6.052 (34)	5.405 (94)	5.954 (33)	5.870 (96)	3.976 (95)	
250.0–289.7	1.706 (34)	1.471 (68)	1.701 (34)	1.577 (94)	1.692 (33)		1.168 (95)	
289.7–500.0	5.595 (34)		5.567 (34)		5.545 (33)		3.967 (95)	
500.0–824.9	3.176 (34)		3.159 (34)		3.221 (33)			
824.9–1486.7	2.036 (34)		2.029 (34)	1.936 (98)	1.932 (33)			
1486.7–1675	2.218(−1)(34)		2.217(−1)(34)	2.229(−1)(98)	5.123(−1)(33)			
1675–1727	2.485(−1)(34)		2.485(−1)(34)	2.118(−1)(98)	2.543(−1)(33)			
1727–1921	1.090 (34)		1.089 (34)	9.739(−1)(98)	9.756(−1)(33)			
1921–8000	6.463 (34)		6.499 (34)	5.856 (98)	5.460 (33)			
8000–10000	1.811(−1)(34)		1.811(−1)(34)		1.638(−1)(33)			
10000–14330	1.792(−1)(34)		1.792(−1)(34)					
14330–80000	1.345 (34)		1.345 (34)					
80000–∞	4.837(−2)(STOBBE)	4.837(−2)(STOBBE)						

[a]The energy levels given in ref. 59 and a variety of DOS data sources were used to construct the discrete part of the DOSD. The sources of DOS data for the adopted results are refs. 60, 89, and 90.

[b]Corresponds to the initial DOS data giving rise to the adopted result.

TABLE 11. Integrated dipole oscillator strengths for Xe (see also footnote for Table 1) for the adopted DOSD and for the initial DOS input data; the absorption edges occur at 4782 eV (L_3), 5104 eV (L_2), 5453 eV (L_1), and 34560 eV (K). The molar refractivity constraints used to construct the adopted DOSD are $R(\lambda = 2537.0\ \text{Å}) = 12.1423$ and $R(\lambda = 1702.0\ \text{Å}) = 17.7290\ \text{cm}^3\ \text{mol}^{-1}$

Energy range (eV)	Adopted DOSD	Integrated dipole oscillator strengths for initial experimental or Stobbe dipole oscillator strength data							
Discrete[a]									
(8.44−11.99)	1.578	1.578[b]							
12.13−13.44	7.114(−1)(99)	7.184(−1)(99)	6.550(−1)(67)		8.932(−1)(74)				
13.44−14.42	6.157(−1)(99)	6.203(−1)(99)	5.494(−1)(67)	5.417(−1)(93)	6.692(−1)(74)	6.327(−1)(92)	5.472(−1)(76)		
14.42−20.66	2.809 (92)		2.551 (67)	2.351 (93)	3.157 (74)	2.885 (92)	2.715 (76)		
20.66−26.74	1.267 (92)		1.064 (67)			1.276 (92)	1.386 (76)		
26.74−28.22	1.704(−1)(92)		1.352(−1)(67)			1.706(−1)(92)			
28.22−36.47	4.371(−1)(92)		4.085(−1)(67)		3.473(−1)(100)	4.379(−1)(92)			
36.47−49.50	1.893(−1)(92)	2.361(−1)(101)	2.169(−1)(67)	4.058(−1)(33)	2.636(−1)(100)	1.893(−1)(92)	2.013(−1)(94)		
49.50−59.24	1.189(−1)(100)	1.383(−1)(101)	1.094(−1)(67)	2.189(−1)(33)	1.189(−1)(100)		1.217(−1)(102)		2.366(−1)(95)
59.24−64.39	6.092(−2)(100)	9.367(−2)(101)		1.782(−1)(33)	6.094(−2)(100)	1.028(−1)(103)	5.943(−2)(102)		1.423(−1)(95)
64.39−80.0	7.941(−1)(96)	8.705(−1)(101)	7.946(−1)(96)	7.125(−1)(33)	1.009 (100)	9.418(−1)(103)	7.352(−1)(102)	8.333(−1)(104)	1.179 (95)
80.0−100.0	3.699 (96)	3.992 (101)	3.711 (96)	3.408 (33)		4.114 (103)	4.258 (94)	4.112 (104)	4.484 (95)
100.0−150.0	5.484 (96)	5.795 (101)	5.508 (96)	5.807 (33)	7.423(−1)(34)	6.269 (103)	6.971 (94)	5.952 (104)	8.281 (95)
150.0−250.0	1.092 (96)	1.074 (101)	1.093 (96)	1.085 (33)	1.264 (34)		1.192 (94)		1.064 (95)
250.0−300.0	6.254(−1)(95)	6.644(−1)(101)		6.506(−1)(33)	7.209(−1)(34)				6.257(−1)(95)
300.0−500.0	2.287 (105)			2.247 (33)	2.283 (34)				2.291 (105)
500.0−676.7	1.274 (105)			2.212 (33)	1.239 (34)				1.275 (105)
676.7−790.0	3.054 (105)	3.708 (106)		4.252 (33)	3.349 (34)				3.061 (105)
790.0−824.9	8.230(−1)(34)			8.471(−1)(33)	8.240(−1)(34)				7.345(−1)(105)
824.9−1450	1.159(1)(34)	5.354 (98)		9.272 (33)	1.178(1) (34)				8.442 (105)
1450−4782	7.838 (34)	6.651 (98)		7.644 (33)	7.924 (34)				
4782−5104	4.285(−1)(34)	3.973(−1)(98)		4.114 (33)	4.286 (34)				
5104−5453	5.451(−1)(34)	5.163(−1)(98)		4.990(−1)(33)	5.453(−1)(34)				
5453−8000	2.617 (34)	2.524 (98)	2.404 (107)	2.561 (33)	2.622 (34)				
8000−10000	8.957(−1)(34)		8.967(−1)(107)	9.119(−1)(33)	8.962(−1)(34)				
10000−34560	1.691 (34)		1.726 (107)		1.691 (34)				
34560−10^5	1.137 (34)		9.262(−1)(107)		1.137 (34)				
10^5−∞	1.651(−1)(STOBBE)	1.651(−1)(STOBBE)							

[a]The energy levels given in ref. 59 and a variety of DOS data sources were used to construct the discrete part of the DOSD. The sources of DOS data for the adopted results are refs. 60, and 89.
[b]Corresponds to the initial DOS data giving rise to the adopted result.

TABLE 12. Adopted dipole properties S_k and L_k for Ne, Ar, Kr, and Xe; the relevant results due to Leonard and Barker (11) and Leonard (15) are included for comparison

	Neon		Argon		Krypton		Xenon	
Property	Adopted	Leonard and Barker	Adopted	Leonard and Barker	Adopted	Leonard and Barker	Adopted	Leonard and Barker
$S_2{}^a$	2.628(4)	2.319(4)	2.881(5)	2.572(5)	4.647(6)	4.290(6)	2.450(7)	2.119(7)
$S_1{}^b$	1.520(2)	1.460(2)	5.879(2)	5.625(2)	2.790(3)	2.691(3)	6.792(3)	6.642(3)
S_0	1.000(1)	1.000(1)	1.800(1)	1.800(1)	3.600(1)	3.600(1)	5.400(1)	5.400(1)
$S_{-1/2}$	5.467	—	9.861	—	1.512(1)	—	2.072(1)	—
$S_{-1}{}^c$	3.801	3.830	8.768	8.766	1.233(1)	1.213(1)	1.731(1)	1.805(1)
$S_{-3/2}$	3.035	—	9.490	—	1.360(1)	—	2.033(1)	—
S_{-2}	2.669	2.670	1.108(1)	1.108(1)	1.679(1)	1.678(1)	2.716(1)	2.711(1)
$S_{-5/2}$	2.526	—	1.345(1)	—	2.181(1)	—	3.847(1)	—
S_{-3}	2.533	2.527	1.678(1)	1.681(1)	2.923(1)	2.944(1)	5.639(1)	5.580(1)
S_{-4}	2.886	2.884	2.791(1)	2.798(1)	5.632(1)	5.665	1.296(2)	1.283(2)
S_{-5}	3.686	3.692	4.999(1)	5.001(1)	1.168(2)	1.164(2)	3.184(2)	3.160(2)
S_{-6}	5.063	5.081	9.506(1)	9.456(1)	2.567(2)	2.515(2)	8.247(2)	8.166(2)
S_{-7}	7.296	7.328	1.895(2)	1.869(2)	5.900(2)	5.661(2)	2.228(3)	2.221(3)
S_{-8}	1.086(1)	1.090(1)	3.915(2)	3.821(2)	1.404(3)	1.317(3)	6.227(3)	6.219(3)
S_{-9}	1.652(1)	—	8.314(2)	—	3.432(3)	—	1.789(4)	—
S_{-10}	2.553(1)	—	1.802(3)	—	8.558(3)	—	5.251(4)	—
L_2	1.829(5)	1.584(5)	2.314(6)	2.054(6)	4.345(7)	4.015(7)	2.499(8)	2.232(8)
L_1	5.970(2)	5.661(2)	2.873(3)	2.704(3)	1.661(4)	1.576(4)	4.482(4)	4.329(4)
L_0	1.573(1)	1.544(1)	3.462(1)	3.449(1)	9.400(1)	9.574(1)	1.586(2)	1.533(2)
L_{-1}	2.160	—	−2.285(−1)	—	1.169(−1)	—	−1.588	—
L_{-2}	4.735(−1)	—	−3.932	—	−8.099	—	−1.766(1)	—

[a] Hartree–Fock (128): S_2(Ne) = 2.596(4), S_2(Ar) = 2.984(5), S_2(Kr) = 4.857(6); CI (129): S_2(Ne) = 2.599.
[b] Hartree–Fock (128): S_1(Ne) = 1.514(3), S_1(Ar) = 5.742(2), S_1(Kr) = 2.670(3); CI (129): S_1(Ne) = 1.544(2).
[c] Hartree–Fock (128): S_{-1}(Ne) = 4.055, S_{-1}(Ar) = 1.095(1), S_{-1}(Kr) = 1.575(1); CI: S_{-1}(Ne) = 3.761, ref. 129; S_{-1}(Ar) = 8.53, ref. 130.

cule (16, 17); estimates can be obtained by using approximate ground state wave functions (6, 124). *Ab initio* double-ζ SCF results (6) for HF are given by S_2 = 16050, S_1 = 119.8, and S_{-1} = 5.886 and are in reasonable agreement with our adopted values given in Table 2. S_2 is determined by the charge densities at the nuclei of the molecule of interest and the higher quality SCF values for these for HF obtained by Ransil and Sinai (125) leads to a result of S_2 = 16880 which is only 2% lower than our recommended value of 17220.

The value of the mean excitation energy I_0 for HF obtained by Wilson *et al.* (126) in the local plasma approximation (γ parameter chosen to be 1.2) is only 0.8% higher than our recommended result of I_0 = 95.6 eV obtained from [3] and the results for S_0 and L_0 given in Table 2. A discussion of the local plasma approximation, and its limitations, can be found in Johnson and Inokuti (127).

Rare gases

We begin with a comparison of our adopted results for the dipole properties of Ne, Ar, Kr, and Xe with those of Leonard and Barker (11) which are also listed in Table 12. The agreement between the two sets of values is very good in all cases for $-6 \lesssim k \lesssim -1$, especially for $-5 \lesssim k \lesssim -2$, and it should be noted in both sets of calculations $S_0 = Z$ by construction. The dipole properties S_k for large negative values of k, which are not of much direct physical significance, are dominated by the very low photon energy part of the DOSD and are largely unaffected by the constraints used in the calculations (1, 13, 19, 20).

The dipole properties S_2 and S_1, especially S_2, are dominated by the high photon energy part of the DOSD and S_2 is not very sensitive to the constraints used to construct the DOSD (1, 13, 19, 20). The differences between the results for these properties obtained here and in ref. 11 result from the different high energy DOS input used in the calculations. In Leonard and Barker (11) the Stobbe formula was used to provide the DOS data for $E > E_K$ whereas in the present work the more reliable photoelectric results of Veigele (34), obtained from mass attenuation coefficients by subtraction of scattering contributions as needed, are used between the K edge E_K and 100 keV (80 keV for Xe); Veigele's results were not available at the time the work in ref. 11 was completed. In all cases Leonard and Barker's results for S_2 and S_1 are lower than our recommended results, by ~8–11% for S_2 and ~2–4% for S_1. Similar, but slightly larger, discrepancies can be seen in Table 12 for L_2 and L_1 as well. The results for L_0 disagree by a smaller amount, from 2–4%, and it should be noted that L_0 is more sensitive to the high energy part of the DOSD than is S_0.

In some cases, namely Kr and Xe, our adopted results for S_{-1} differ appreciably (by ≳2%) with those obtained from ref. 11; S_{-1} is sensitive to the constraints used to construct the DOSD. These discrepancies, and other less significant differences in some of the results for the other dipole sums, are due to differences in DOS input data; often we have used more recent sources of data not available to ref. 11.

Prior to the present study the results for the dipole properties for Ne, Ar, Kr, and Xe obtained by Leonard and Barker (11) were probably the most generally reliable. It is clear our results for the S_k essentially augment their work for $k \leq 0$ and represent an improvement generally only for $k > 0$ (except for S_{-1} for Kr and Xe). Many workers have investigated the dipole properties of the rare gases and it is not possible to list or discuss all the results here. The results for the static dipole polarizabilities have been surveyed through ~1970 by Teachout and Pack (38), including both experimental and theoretical results. Barker and Leonard (11) compare their results with a variety of literature values through ~1971. More recently literature results for some of the dipole properties of Ne, Ar, and Kr have been summarized in the work of Dehmer *et al.* (21) and Cummings (128). Mention has already been made of the pioneering work of Dalgarno and his colleagues in this field.

It is known that Hartree–Fock or near Hartree–Fock quality ground state wave functions can give very reasonable results for S_2 and S_1, the corresponding calculation for S_{-1} is generally not nearly as reliable (6, 128). Hartree–Fock results (128) for S_2, S_1, and S_{-1} for Ne, Ar, and Kr are included as footnotes to Table 12; in all cases agreement with our adopted values for S_2 and S_1 is superior to that for Leonard and Barker's results. Fifty term CI wave function results (129) for these dipole sums are also included in Table 12 for Ne. The effect of CI on S_2 is very small and the agreement with our adopted result for S_{-1} is improved relative to the Hartree–Fock results. A CI result (130) for S_{-1}(Ar) is included in a footnote to Table 12 and is in considerably closer agreement with the recommended value than the Hartree–Fock value.

The dipole properties S_k obtained from the DOSDs based on Berkowitz's (57) analysis of the rare gas spectra, see Section 4, generally agree with our adopted results to within their estimated uncertainties (see later). Exceptions are $S_{-1/2}$ and S_{-1} for Xe where the discrepancies amount to 5% and 3% respectively. The (STD) corresponding to the DOSD for Xe based on Berkowitz's analysis is 5.0 and the DOS input data requires large modifications (between 10 to 24%) in the 80–150 eV, 300–790 eV, and 825–4800 eV energy regions which contribute significantly to $S_{-1/2}$ and to a lesser extent to S_{-1}; a discrepancy of ~5% also occurs for L_0 for the same reason. Large differences also arise when the L_k are small, that is ~3% for L_{-2}(Ne), ~13% for L_{-1}(Ar), ~49% for L_{-1}(Kr) and ~62% for L_{-1}(Xe). This is caused by a cancellation effect discussed by Kumar and Meath (22) and depends on the energy unit used in the definition of the L_k, see also ref. 131. Following (22) one can write

$$[8]\quad L_k(E/(1\text{ eV})) = (2R)^k[L_k(E/(2R)) + \ln(2R)S_k(E/(2R))]$$

It is clear that for $L_k(E/(2R))$ small, the error in $L_k(E/(1\text{ eV})$ is controlled by the error in $\ln(2R)S_k(E/(2R))$. Using the data given in Table 12, it can be seen that the discrepancies between the relevant L_k, with an energy unit of 1 eV, is reduced markedly (<1% in all cases) relative to those corresponding to an energy unit of $2R$.

Fewer results are available for the dipole properties L_k. Our values are in reasonable agreement with the higher quality results given in (15, 21, 56, 128, 129) for Ne, Ar, Kr, and Xe. Results obtained by differentiation of the S_k with respect to k can be unreliable if the input S_k are inaccurate or if the representation used for S_k as a function of k is poor, see also ref. 131.

In general reliable *ab initio* calculations of the dipole properties S_k, for $k \leq -1$, or for the L_k are very difficult to carry out. The difficulties in this type of calculation have been discussed in the context of the hydrogen halides earlier. In general, uncoupled and coupled Hartree–Fock calculations are not sufficient, see for example refs. 4, 37 and the discussion and results given in Werner and Meyer (2) for Ne.

The errors in our adopted results for the dipole properties of the hydrogen halides and the rare gases considered here have been estimated following the methods used previously, namely, by comparison with values obtained from DOSDs constructed from a variety of (reasonable) input DOS data. In all cases the S_k and L_k for $k \geq 1$, and particularly for $k = 2$, can have uncertainties of ~3% which are related to the errors in the high energy input DOS data used in the calculations.

For the hydrogen halides the uncertainty in the S_k is $\lesssim$1% for $-3 \lesssim k \lesssim 0$ and increases gradually as k decreases; it is ~2% for L_0, S_1, and S_{-4} and about the same as in the corresponding S_k values for L_{-1} and L_{-2} except in the cases of HF where L_{-1} and L_{-2} are fairly small. On a 1 eV energy scale L_{-1}(HF) and L_{-2}(HF) have uncertainties of $\lesssim$1%. For the rare gases the estimated errors in the S_k, for $-6 \lesssim k \lesssim 0$, are $\lesssim$1%. L_0 and S_1 are uncertain by ~2% and the errors in the other L_k are ~1% except where they are small. Recasting the results for these L_k on a 1 eV energy unit yields results reliable to $\lesssim$1%. The error estimates for the S_k and L_k for $k < 0$ are made under the assumption that the values of the molar refractivity constraints (the value of α_d for HF) used in the construction of the DOSDs are reliable (errors $\lesssim$0.5%).

An important use of globally reliable DOSDs lies in the evaluation of the dipole–dipole and the triple–dipole dispersion energies between atoms and molecules. These energies involve double or triple integrals over the DOSDs for the molecules involved in the interaction and can be evaluated directly by using the relevant distributions. A more efficient method for doing this is to use pseudo-DOSD techniques (132, 133) which require accurate results for the S_k as a function of k. The pseudo-DOSDs for the hydrogen halides and the rare gases will be presented elsewhere together with a variety of important dispersion energy constants.

The approach used in this work is a practical and reliable method for evaluating a wide variety of rotationally averaged or isotropic dipole molecular properties. The extension to anisotropic dipole properties or higher multipole properties is non-trivial due to a lack of the required oscillator strength data and/or reliable constraints for most species (1, 6). The extension to anisotropic properties is currently under investigation.

Acknowledgements

The authors wish to thank Professor C. E. Brion for making recent (28, 32) dipole oscillator strength data for HCl and HBr available to us before publication. This research was supported by a grant from the Natural Sciences and Engineering Research Council of Canada.

1. W. J. MEATH, D. J. MARGOLIASH, B. L. JHANWAR, A. KOIDE, and G. D. ZEISS. *In* Intermolecular forces. *Edited by* B. Pullman. Reidel, Dordrecht. 1981, pp. 101–115.
2. H. J. WERNER and W. MEYER. Phys. Rev. A**13**, 13 (1976).
3. G. D. ZEISS, W. R. SCOTT, N. SUZUKI, D. P. CHONG, and S. R. LANGHOFF. Mol. Phys. **37**, 1543 (1979).
4. P. MUKHERJEE, T. MINATO, and D. P. CHONG. Int. J. Quant. Chem. **23**, 447 (1983).
5. F. MULDER, G. F. THOMAS, and W. J. MEATH. Mol. Phys. **41**, 249 (1980).
6. F. MULDER and W. J. MEATH. Mol. Phys. **42**, 629 (1981).
7. G. D. ZEISS, W. J. MEATH, J. C. F. MACDONALD, and D. J. DAWSON. Radiat. Res. **70**, 284 (1977); **63**, 64 (1975).
8. H. MARGENAU. Phys. Rev. **37**, 1425 (1931); **56**, 1000 (1939).
9. A. DALGARNO and N. LYNN. Proc. Phys. Soc. A**70**, 802 (1957).
10. A. DALGARNO and A. E. KINGSTON. Proc. Phys. Soc. **72**, 1053 (1958); **73**, 455 (1959); **78**, 607 (1961).
11. P. J. LEONARD and J. A. BARKER. *In* theoretical chemistry, advances and perspectives. Vol. 1. 1975. p. 117.
12. G. D. ZEISS and W. J. MEATH. Mol. Phys. **33**, 1155 (1976), and

the discussion and references therein.
13. G. D. ZEISS, W. J. MEATH, J. C. F. MACDONALD, and D. J. DAWSON. Can. J. Phys. **55**, 2080 (1977).
14. B. L. JHANWAR and W. J. MEATH. Can. J. Chem. **62**, 373 (1984) and some of the references therein.
15. P. J. LEONARD. M.Sc. Thesis. Melbourne, Australia, 1968.
16. J. O. HIRSCHFELDER, W. BYERS BROWN, and S. T. EPSTEIN. Adv. Quantum Chem. **1**, 255 (1964).
17. U. FANO and J. W. COOPER. Rev. Mod. Phys. **40**, 441 (1968); **41**, 724 (1969).
18. B. L. JHANWAR and W. J. MEATH. Chem. Phys. **67**, 185 (1982).
19. B. L. JHANWAR, W. J. MEATH, and J. C. F. MACDONALD. Can. J. Phys. **59**, 185 (1981).
20. G. D. ZEISS, W. J. MEATH, J. C. F. MACDONALD, and D. J. DAWSON. Mol. Phys. **39**, 1055 (1980).
21. J. L. DEHMER, M. INOKUTI, and R. P. SAXON. Phys. Rev. A**12**, 102 (1975).
22. A. KUMAR and W. J. MEATH. Can. J. Phys. In press.
23. H. A. BETHE and E. E. SALPETER. Quantum mechanics of one- and two-electron atoms. Academic Press, New York. 1957.
24. F. CARNOVALE and C. E. BRION. Chem. Phys. **74**, 253 (1983).
25. A. P. HITCHCOCK and C. E. BRION. Chem. Phys. **61**, 281 (1981).
26. A. SALAMA and J. B. HASTED. J. Phys. B**9**, L333 (1976).
27. J. A. MYER and J. A. R. SAMSON. J. Chem. Phys. **52**, 266 (1970).
28. S. DAVIEL, Y. ILDA, F. CARNOVALE, and C. E. BRION. Chem. Phys. **83**, 319 (1984).
29. K. NINOMIYA, E. ISHIGURO, S. IWATA, A. MIKUNI, and T. SASAKI. J. Phys. B**14**, 1777 (1981).
30. W. HAYES and F. C. BROWN. Phys. Rev. A**6**, 21 (1972).
31. B. J. HUEBERT and R. M. MARTIN. J. Phys. Chem. **72**, 3046 (1968).
32. C. E. BRION and J. P. THOMSON. J. Electron. Spectrosc. In press.
33. B. L. HENKE, P. LEE, T. S. TANAKA, R. L. SHIMABUKURO, and B. K. FUJIKAWA. At. Data, **27**, 1 (1982).
34. W. J. VEIGELE. At. Data, **5**, 51 (1973).
35. M. STOBBE. Ann. Phys. Leipzig, **69**, 81 (1930).
36. B. L. JHANWAR, W. J. MEATH, and J. C. F. MACDONALD. Can. J. Phys. **61**, 1027 (1983).
37. H. J. WERNER and W. MEYER. Mol. Phys. **31**, 855 (1976).
38. R. R. TEACHOUT and R. T. PACK. At. Data, **3**, 195 (1971).
39. G. F. THOMAS and W. J. MEATH. Mol. Phys. **34**, 113 (1977).
40. M. L. KLEIN, I. R. MCDONALD, and S. F. O'SHEA. J. Chem. Phys. **69**, 63 (1978).
41. J. T. BROBJER and J. N. MURRELL. Mol. Phys. **50**, 885 (1983).
42. D. F. PENNING, D. WEIMER, and W. J. RUMPEL. J. Chem. Phys. **59**, 2496 (1973).
43. D. L. DRUMMOND. Appl. Opt. **21**, 4331 (1982).
44. S. BOSANAC, J. T. BROBJER, and J. N. MURRELL. Mol. Phys. **51**, 313 (1984).
45. R. L. REDINGTON. J. Phys. Chem. **86**, 552 (1982).
46. C. H. D. CLARK. Trans. Faraday Soc. **31**, 585 (1935).
47. LANDOLT-BORNSTEIN. Zahlenwert und Funktionen. Vol 2. Part 8. Springer-Verlag, Berlin. 1963.
48. C. CUTHBERTSON and M. CUTHBERTSON. Phil. Trans. R. Soc. A**113**, 1 (1913).
49. O. E. FRIVOLD, O. HASSEL, and U. S. RUSTAD. Phys. Z. **38**, 191 (1937).
50. T. LARSEN. Z. Phys. **111**, 391 (1938).
51. LANDOLT-BORNSTEIN. Zahlenwert und Funktionen. Vol. 2. Part 6. Springer-Verlag, Berlin. 1962.
52. W. EBERHARDT, T. K. SHAM, R. CARR, S. KRUMMACHER, M. STRONGIN, S. L. WENG, and D. WESNER. Phys. Rev. Lett. **50**, 1038 (1983).
53. R. H. MILLAR and J. R. GREENING. J. Phys. B**7**, 2332 (1974).
54. J. A. BARKER and P. J. LEONARD. Phys. Lett. **13**, 127 (1964).
55. A. DALGARNO and W. D. DAVISON. Adv. At. Mol. Phys. **2**, 1 (1966); A. DALGARNO. Adv. Chem. Phys. **12**, 143 (1967) and references therein.
56. R. J. BELL and A. DALGARNO. Proc. Phys. Soc. **86**, 375 (1965); **89**, 55 (1966).
57. J. BERKOWITZ. Photoabsorption, photoionization, and photoelectron spectroscopy. Academic Press, New York. 1979. In particular pp. 73–90.
58. R. E. JOHNSON, S. T. EPSTEIN, and W. J. MEATH. J. Chem. Phys. **47**, 1271 (1967).
59. C. E. MOORE. Atomic energy levels. NSRDS-NBS35, 1971.
60. S. NATALI, C. E. KUYATT, and S. R. MIELCZAREK. Reported in ref. 57.
61. H. G. KUHN and E. L. LEWIS. Proc. R. Soc. A**299**, 423 (1967).
62. W. B. WESTERVELD, TH. F. A. MULDER, and J. VAN ECK. J. Quant. Spectrosc. Radiat. Transfer, **21**, 533 (1979).
63. P. F. GRUZDEV and A. V. LOGINOV. Opt. Spektrosk. **35**, 1 (1973).
64. P. S. GANAS. J. Quant. Spectrosc. Radiat. Transfer, **20**, 461 (1978).
65. G. M. LAWRENCE and H. S. LISZT. Phys. Rev. **178**, 122 (1969).
66. K. RADLER and J. BERKOWITZ. J. Chem. Phys. **70**, 216 (1979).
67. J. A. R. SAMSON. Adv. At. Mol. Phys. **2**, 177 (1966).
68. J. B. WEST and G. V. MARR. Proc. R. Soc. A**349**, 397 (1976).
69. P. O. LEE and G. L. WEISSLER. Proc. R. Soc. **220**, 71 (1953).
70. D. L. EDERER and D. H. TOMBOULIAN. Phys. Rev. A**133**, 1525 (1964).
71. M. J. VAN DER WIEL and G. WIEBES. Physica, **54**, 411 (1971).
72. R. N. DITCHBURN. Proc. Phys. Soc. **75**, 461 (1960).
73. W. S. WATSON. J. Phys. B**5**, 2292 (1972).
74. R. E. HUFFMAN, Y. TANAKA, and J. C. LARRABEE. J. Chem. Phys. **39**, 902 (1963).
75. M. YOSHINO, A. IDA, K. WAKIYA, and H. SUZUKI. J. Phys. Soc. Jpn. **27**, 978 (1969).
76. H. E. BLACKWELL, G. S. BAJWA, G. S. SHIPP, and G. L. WEISSLER. J. Quant. Spectrosc. Radiat. Transfer, **4**, 249 (1964).
77. P. O. LEE and G. L. WEISSLER. Phys. Rev. **99**, 540 (1955).
78. O. P. RUSTGI. J. Opt. Soc. Am. **54**, 464 (1964).
79. J. E. G. WHEATON. Appl. Opt. **3**, 1247 (1964).
80. R. W. CARLSON, D. L. JUDGE, M. OGAWA, and L. C. LEE. Appl. Opt. **12**, 409 (1973).
81. R. P. MADDEN, D. L. EDERER, and K. CODLING. Phys. Rev. **177**, 136 (1969).
82. F. J. COMES and A. ELZER. Z. Naturforch. **19**A, 721 (1964).
83. M. J. VAN DER WIEL and G. WIEBES. Physica, **53**, 225 (1971).
84. M. E. LEVY and R. E. HUFFMAN. J. Quant. Spectrosc. Radiat. Transfer, **9**, 1349 (1969).
85. A. P. LUKIRSKII and T. M. ZIMKINA. Bull. Acad. Sci. USSR, Phys. Ser. **27**, 808 (1963).
86. J. H. HUBBELL. Radiat. Res. **70**, 58 (1977).
87. D. R. DENNE. J. Phys. D**3**, 1392 (1970).
88. R. H. MILLAR. J. Phys. B**8**, 2015 (1975).
89. J. GEIGER. Z. Phys. A**282**, 129 (1977).
90. E. MATTHIAS, R. A. ROSENBERG, E. D. POLIAKOFF, M. G. WHITE, S. T. LEE, and D. A. SHIRLEY. Chem. Phys. Lett. **52**, 239 (1977).
91. V. L. CARTER and R. D. HUDSON. J. Opt. Soc. Am. **63**, 733 (1973).
92. O. P. RUSTGI, E. I. FISHER, and C. H. FULLER. J. Opt. Soc. Am. **54**, 745 (1964).
93. P. H. METZGER and G. R. COOK. J. Opt. Soc. Am. **55**, 516 (1965).
94. M. J. VAN DER WIEL and G. R. WIGHT. Phys. Lett. **54**A, 83 (1975); TH. M. EL-SHERBINI and M. J. VAN DER WIEL. Physica, **62**, 119 (1972).
95. A. P. LUKIRSKII, I. A. BRYTOV, and T. M. ZIMKINA. Opt. Spectrosc. USSR, **17**, 234 (1964).
96. J. LANG and W. S. WATSON. J. Phys. B**8**, L339 (1975).
97. R. HAENSEL, G. KEITEL, P. SCHREIBER, and C. KUNZ. Phys. Rev. **188**, 1375 (1969).

98. F. WUILLEUMIER. Phys. Rev. A**6**, 2067 (1972).
99. F. M. MATSUNAGA, R. S. JACKSON, and K. WATANABE. J. Quant. Spectrosc. Radiat. Transfer, **5**, 329 (1965).
100. R. B. CAIRNS, H. HARRISON, and R. I. SCHOEN. Phys. Rev. **813**, 52 (1969).
101. J. B. WEST and J. MORTON. At. Data, **22**, 104 (1978).
102. G. R. WIGHT and M. J. VAN DER WIEL. J. Phys. B**10**, 601, (1977).
103. D. L. EDERER and D. H. TOMBOULIAN. Reported in ref. 67.
104. R. HAENSEL, G. KEITEL, and P. SCHREIBER. Phys. Rev. Lett. **22**, 398 (1969).
105. P. P. LUKIRSKII, I. A. BRYTOV, and S. A. GIRIBOVSKII. Opt. Spectrosc. USSR, **20**, 203 (1966).
106. R. D. DESLATTES. Phys. Rev. Lett. **20**, 483 (1968).
107. J. H. MCCRARY, L. D. LOONEY, and C. P. CONSTANTEN. Phys. Rev. A**2**, 2489 (1970).
108. C. CUTHBERTSON and M. CUTHBERTSON. Proc. R. Soc. **135**A, 40 (1932).
109. A. MICHELS, T. WASSENAAR, and P. LOUWERSE. Physica, **26**, 539 (1960).
110. R. COULON, G. MONTIXI, and R. OCCELLI. Can. J. Phys. **59**, 1555 (1981).
111. P. L. SMITH, M. C. F. HUBER, and W. H. PARKINSON. Phys. Rev. A**13**, 1422 (1976).
112. A. BIDEAU-MEHU, Y. GUERN, R. ABJEAN, and A. JOHANNIN-GILLES. J. Quant. Spectrosc. Radiat. Transfer, **25**, 395 (1981).
113. P. J. LEONARD. At. Data, **14**, 21 (1974).
114. A. P. HITCHCOCK, G. R. J. WILLIAMS, C. E. BRION, and P. W. LANGHOFF. Chem. Phys. **88**, 65 (1984).
115. J. M. O'HARE and R. P. HURST. J. Chem. Phys. **46**, 2356 (1967).
116. (*a*) H. LISCHKA. J. Am. Chem. Soc. **96**, 4761 (1974); (*b*) R. J. BARTLETT and G. D. PURVIS III. Phys. Rev. A**20**, 1313 (1979).
117. P. JORGENSEN, J. ODDERSCHEDE, P. ALBERTSEN, and N. H. F. BEEBE. J. Chem. Phys. **68**, 2533 (1978).
118. P. LAZZERETTI, E. ROSSI, and R. ZANASI. Phys. Rev. A**27**, 1301 (1983).
119. J. G. C. M. VAN DUIJNEVELDT-VAN DE RIJDT and F. B. VAN DUIJNEVELDT. J. Mol. Struct. **89**, 185 (1982).
120. J. ODDERSHEDE and E. N. SVENDSEN. Chem. Phys. **64**, 359 (1982).
121. J. H. WILLIAMS and R. D. AMOS. Chem. Phys. Lett. **70**, 162 (1980).
122. F. A. GIANTURCO and C. GUIDOTTI. J. Phys. B, **11**, L385 (1978).
123. C. H. RHEE, R. M. METZGER, and F. M. WUJGUL. J. Chem. Phys. **77**, 899 (1982).
124. D. M. CHIPMAN, B. KIRTMAN, and W. E. PALKE. J. Chem. Phys. **67**, 2236 (1977).
125. B. J. RANSIL and J. J. SINAI. J. Chem. Phys. **46**, 4050 (1967).
126. J. W. WILSON, C. K. CHANG, Y. J. XU, and E. KAMARATOS. J. Appl. Phys. **53**, 828 (1982).
127. R. E. JOHNSON and M. INOKUTI. Comments At. Mol. Phys. **14**, 19 (1983).
128. F. E. CUMMINGS. J. Chem. Phys. **63**, 1960 (1975).
129. R. P. SAXON. Phys. Rev. A**8**, 839 (1973).
130. M. NAON, M. CORNILLE, and Y.-K. KIM. J. Phys. B**8**, 864 (1975).
131. B. L. JHANWAR and W. J. MEATH. To be published.
132. D. J. MARGOLIASH and W. J. MEATH. J. Chem. Phys. **68**, 1426 (1978).
133. D. J. MARGOLIASH, T. R. PROCTOR, G. D. ZEISS, and W. J. MEATH. Mol. Phys. **35**, 747 (1978).

Prediction of longitudinal electric polarizabilities of conjugated chain molecules by scaling of *ab initio* calculations

V. P. BODART, J. DELHALLE, AND J. M. ANDRÉ

Laboratoire de Chimie Théorique Appliquée Facultés, Universitaires Notre-Dame de la Paix, Rue de Bruxelles, 61 B-5000 Namur, Belgium

AND

J. ZYSS

Centre National d'Etudes de Télécommunications 196, rue de Paris F-92220 Bagneux, France

Received August 16, 1984

This paper is dedicated to Professor Camille Sandorfy on the occasion of his 65th birthday

V. P. BODART, J. DELHALLE, J. M. ANDRÉ, and J. ZYSS. Can. J. Chem. **63**, 1631 (1985).

The predictive use of scaled minimal basis sets calculations of electric polarizabilities for large hydrocarbons, proposed by Chablo and Hinchliffe, is further assessed by considering two series of oligomers, H—(CH═CH)$_n$—H and H—(C≡C)$_n$—H where n = 1, 2, 3, and 4. It is then applied to the yet experimentally untested vinylacetylene, 1,5-hexadiene-3-yne, and 1,5,9-decatriene-3,7-diyne for their polarizability.

V. P. BODART, J. DELHALLE, J. M. ANDRÉ et J. ZYSS. Can. J. Chem. **63**, 1631 (1985).

Utilisant deux séries d'oligomères, H—(CH═CH)$_n$—H et H—(C≡C)$_n$—H dans lesquels n = 1, 2, 3 et 4, on a réévalué l'utilité, comme méthode permettant de prédire correctement les polarisabilités électriques de grosses molécules, de la méthode proposée par Chablo et Hinchliffe et impliquant des calculs faisant appel à des ensembles de base restreints mais proportionnés. On a ensuite appliqué la méthode à la polarisabilité du vinylacétylène, de l'hexadiène-1,5 yne-3 et du décatriène-1,5,9 diyne-3,7 qui n'ont pas encore été testés expérimentalement.

[Traduit par le journal]

1. Introduction

Organic electrooptic and nonlinear optical materials are expected to be increasingly used in integrated optics and in optical communications. Though not being a sufficient condition, high values of α, β, and γ, respectively the electric polarizability, hyperpolarizability, and second order hyperpolarizability tensors of the constituting species (molecules, oligomers, chains), are essential for a given material to become a potential candidate for practical applications. Accordingly there is an obvious interest in prospective model calculations that could predict modified or novel organic structures having these desirable features. Among other factors, the existence and size of a delocalized π-system, the nature and position of substituents on the molecular framework are determining the numerical value of the components of α-, β-, and γ-tensors (1).

Simple theories such as the free-electron model and the Hückel method predict the π-electron polarizability, α, of a long chain molecule to be proportional to the cube of the molecular length (2, 3). Similarly, in a study of a family of donor–acceptor disubstituted phenyl polyene, the marked chain length influence on hyperpolarizability values has been pointed out (4). Thus chain length appears as a potentially useful parameter to consider in generating high values of α, β, and γ. However, both free-electron model and the simple Hückel method do not take into account Coulombic interactions explicitly, for example such as mediated by self-consistent field methods, a contribution which is likely to affect the above mentioned asymptotic relation. Additional investigations of the rate of increase of α with the size of chain molecules when interelectronic interactions are more explicitly included should be useful. Our preference is to perform *ab initio* calculations since other relevant properties such as equilibrium geometries can be consistenty evaluated within the limits of a chosen basis set. Unfortunately, to obtain quantitatively the polarizabilities from *ab initio* calculations substantially extended basis sets are needed. In spite of these dissuading results Chablo and Hinchliffe have reported on the feasibility of using predictively scaled minimal basis set results for large hydrocarbons (5).

The first aim of the present paper is to further test the validity of such a scaling procedure by comparing the longitudinal electric polarizability α_{zz}, calculated using STO-3G and 4-31G basis sets for two relevant series of oligomers, i.e. H—(CH═CH)$_n$—H and H—(C≡C)$_n$—H where n = 1, 2, 3, and 4. The second purpose is to use this procedure to predict the longitudinal polarizability of small molecules resulting from the combination of two reference moieties, —CH═CH— and —C≡C—.

2. Methodology

All the calculations reported in this work were done on a DEC 20-60 using a modified version of the GAUSSIAN 80 series of program (6). Standard STO-3G minimal (7*a*) and 4-31G split-valence (7*b*) basis sets were considered. Polarizabilities were calculated by the finite-field SCF method of Cohen and Roothaan (8) which is virtually equivalent to the analytic Coupled Hartree–Fock scheme. A term, $\mu \cdot E$, describing the interaction between the electric field, E, and the molecule is added to the unperturbed molecular Hamiltonian, H_0; μ is the total dipole moment of the molecule. At the Hartree–Fock level, the electric field appears explicitly in the one-electron part of the modified Fock operator, F(r),

$$[1] \quad F(r) = F_0(r) + e(r \cdot E)$$

where $F_0(r)$ is the molecular Fock operator in absence of electric field.

The numerical approach to the calculation of electric polarizabilities requires much higher accuracy of the total SCF energy than in standard applications. The convergence threshold on the density matrix elements was set up as 10^{-5}–10^{-6}. In this work we are only interested in the longitudinal component, α_{zz}, of the polarizability tensor α, the z-axis being directed along

TABLE 1. Theoretical and experimental longitudinal electric polarizabilities, α_{zz}, of acetylene and ethylene; the C—C bonds are directed along the z-axis

α_{zz} (au)	STO-3G	4-31G	Double-ζ	Exp.
Acetylene	18.1793[a]	27.9280[a]	—	30.6[b]
Ethylene	19.5983[a]	32.4075[a]	34.1882[c]	36.4[d]

[a]This work.
[b]Reference 11.
[c]Reference 5.
[d]Reference 12.

the chain. The value of α_{zz} is obtained from the first derivative of the field-dependent dipole moment, $\mu(E)$, with respect to E_z in the limit of zero-field. In practice this is done numerically using

$$[2] \quad \alpha_{zz} = [\mu_z(E_z) - \mu_z(-E_z)]/2E_z$$

Polarizability calculations were carried out using eq. [2] with four values of the external field, −0.002, −0.001, +0.001, and +0.002 au. The Richardson extrapolation procedure (9) was applied to check the numerical stability of the results, a point which remains difficult in the finite field approach.

Ideally this investigation on the ability of minimal basis set calculations of polarizabilities should help compare the theoretical polarizabilities with experimental values, unfortunately these are missing except for the first terms of the series, acetylene and ethylene. Chablo and Hinchliffe have shown that double-ζ basis set used in Snyder and Basch book (10) yields calculated values in reasonably good agreement with experiment. We have repeated these calculations using the standard 4-31G basis and reached similar agreement, Table 1. Therefore we decided to use the 4-31G results as a reference to which STO-3G could be compared to assess the validity of a scaling procedure in the first part and then to predict "experimental" values for three molecules assembled from —CH=CH— and —C≡C—. It is worth pointing out that as found by Chablo and Hinchliffe, this procedure works only for the longitudinal component of the polarizability likely because of the lack of flexibility in the basis sets in the other two directions. As far as we are concerned, this is not a limitation since, for practical applications, the longitudinal component is the most interesting part. Molecular geometries are taken or adjusted from experiment as indicated at the bottom of the tables.

3. Scaling procedure

Longitudinal electric polarizability, α_{zz}, calculated with minimal STO-3G and split-valence 4-31G bases for both series of oligomers are listed in Table 2. The evolution of these data is graphically depicted in Fig. 1. It is to be pointed out that the difference between α_{zz} values for ethylene reported in Tables 1 and 2, respectively, stems from the fact that in the former the C=C bond is exactly set parallel to z-axis while in Table 2 this C=C bond has been oriented with respect to the z-axis (ca. 30 deg) as are the C=C bonds of the other terms in the H—(CH=CH)$_n$—H series.

The first observation is certainly that, in both series of compounds, α_{zz} is not yet stabilized after $n = 4$ since the increment from one term to the next is still increasing. Consequently future investigations of larger oligomers will be soon beyond normal computational possibilities if doublble-ζ basis sets are to be used. This fact motivates for substitutes like a scaling procedure. A more comprehensive analysis, including data from free-electron and Hückel methods, of the way α_{zz} increases with the size for a larger set of H—(CH=CH)$_n$—H oligomers is in progress.

As previously pointed out it is however gratifying to find the ratios $R_n = \alpha_{zz}(\text{STO-3G})/\alpha_{zz}(\text{4-31G})$ for $n = 1$ to 4 being roughly constant and similar in both series of compounds. The interval of variation of R_n for > 1 is typically 0.65 to 0.70, with R_n being close to 0.70 as the length of the oligomer increases. Therefore, when using the minimal STO-3G basis, a value of $R_n = 0.70$ can reasonably be chosen in studies related to unsaturated hydrocarbon chains.

Assuming that the ratio of $\alpha_{zz}(\text{4-31G})/\alpha_{zz}(\text{exp.}) = 0.9$ for acetylene and ethylene calculated from data in Table 1 will stay reasonably constant for other unsaturated hydrocarbon molecules, it is then possible to predict data at the scale of experimental observations by applying the multiplicative constant $1.57(1/(0.9 \times 0.7))$ to the corresponding STO-3G values. In the next section we apply these rules to predict α_{zz} of three molecules yet untested for their polarizabilities.

4. Longitudinal polarizabilities of small molecules assembled from —C≡C— and —CH=CH— fragments

Polydiacetylenes have received considerable attention lately owing to their linear and nonlinear optical properties (1). These are associated with the conjugated nature of their backbone which, in a way, can be considered as being built out of —(CH=CH)— and —(C≡C)— fragments. Like in the field of mechanical properties, where to a copolymer do not generally correspond values that are the weighted sum of their homopolymer contributions, it is likely that patterns of nonadditivity will similarly be observed for polarizabilities.

It is beyond the aim of this paper to investigate effects of various distributions of the units in increasing size oligomers, H—(CH=CH—C≡C)$_m$—R (R = H or —CH=CH$_2$), but, considering the availability of the scaling factors obtained in Section 3, it is nonetheless attractive to make preliminary attempts on three precursors. From Table 2 it can be observed that if α_{zz}(STO-3G) of ethylene, 17.47 au, is nearly equal to that of acetylene, 18.18 au, the rate of increase when regular oligomers are growing is in favour of the former as can be seen from the value of 1,3,5,7-*trans*-octatetraene, 174.56 au, compared to 145.47 au for 1,3,5,7-octatetrayne. How will the polarizability of mixed compounds compare with molecules in H—(CH=CH)$_n$—H and H—(C≡C)$_n$—H series and including the same number of carbon atoms? Vinylacetylene (**A**), 1,5-hexadiene-3-yne (**B**), and 1,5,9-decatriene-3,7-diyne (**C**) have been selected for this preliminary study. Their polarizability values are listed in Table 3. The right-hand side column provides figures obtained after multiplication of the STO-3G values by 1.57, they should be close to the experimental measures if these were available.

It is interesting to notice that vinylacetylene, **A**, has its longitudinal polarizability larger than the sum of acetylene and ethylene contributions. It is, however, slightly smaller than either 1,3-*trans*-butadiene or 1,3-butadiyne. The difference is more important in the next term (**B**), whose α_{zz}, 85.30 au, is substantially smaller than 1,3,5-*trans*-hexatriene or 1,3,5-hexatriyne, see Table 2. The last compound **C**, displays also a small value of α_{zz}, 183.69 au, which comes quite close to the one of 1,3,5,7-*trans*-octatetraene, 174.56 au, this compound having two carbon atoms less than in **C**. From these simple

TABLE 2. Comparison of STO-3G and 4-31G calculated longitudinal electric polarizabilities of two series of oligomers, H—(CH═CH)$_n$—H and H—(C≡C)$_n$—H; n = 1, 2, 3, and 4

	α_{zz} (au) STO-3G	α_{zz} (au) 4-31G	α_{zz} (STO-3G)/ α_{zz} (4-31G)
Ethylene[a]	17.4773	29.1906	0.60
1,3-*trans*-Butadiene[b]	47.8512	73.3961	0.65
1,3,5-*trans*-Hexatriene[c]	104.1258	152.6748	0.68
1,3,5,7-*trans*-Octatetraene[d]	174.5574	246.1033	0.71
Acetylene[e]	18.1793	27.9280	0.65
1,3-Butadiyne[f]	50.6834	73.9655	0.69
1,3,5-Hexatriyne[g]	91.1179	131.3900	0.69
1,3,5,7-Octatetrayne[g]	145.4749	207.5293	0.70

[a]Experimental geometry, ref. 13.
[b]Experimental geometry, ref. 14.
[c]Experimental geometry, ref. 15.
[d]Geometry extrapolated from *c*.
[e]Experimental geometry, ref. 16.
[f]Experimental geometry, ref. 17.
[g]Optimized geometry with STO-3G basis set.

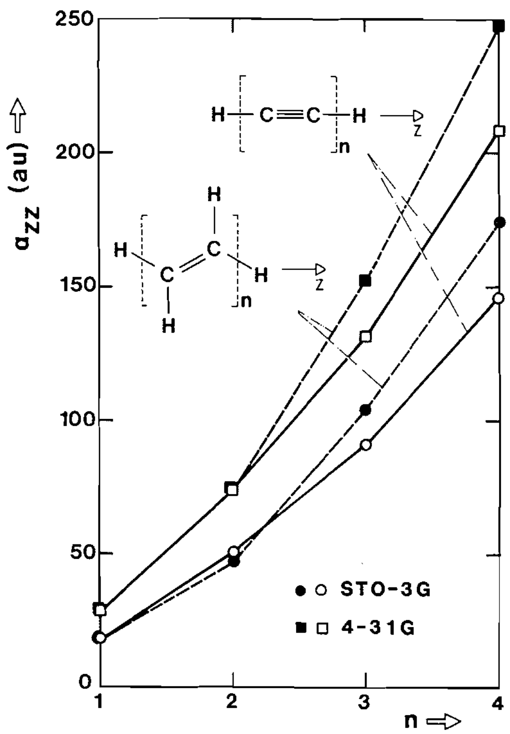

FIG. 1. Longitudinal polarizability of —(CH═CH)$_n$— and —(C≡C)$_n$— oligomers; n = 1, 2, 3, and 4.

TABLE 3. STO-3G longitudinal electric polarizabilities of vinylacetylene, 1,5-hexadiene-3-yne, and 1,5,9-decatriene-3,7-diyne and anticipated experimental value according to the scaling procedure

α_{zz} (au)	STO-3G	Anticipated experimental value
Vinylacetylene[a] (**A**)	44.6472	70.1
1,5-Hexadiene-3-yne[b] (**B**)	85.3020	133.9
1,5,9-Decatriene-3,7-diyne[c] (**C**)	183.69	288.4

[a]Experimental geometry (ref. 18).
[b]Geometry extrapolated from *a*.
[c]From the optimized geometry of the infinite chain (ref. 19).

TABLE 4. Longitudinal electric polarizabilities (α_{zz}) rescaled from STO-3G values

Compound	α_{zz}: anticipated experimental values (au)
Vinylacetylene	70.1
1,3-Butadiyne	79.6
1,3-*trans*-Butadiene	75.1
1,5-Hexadiene-3-yne	133.9
1,3,5-Hexatriyne	143.1
1,3,5-*trans*-Hexatriene	163.5
1,5,9-Decatriene-3,7-diyne	288.4
1,3,5,7,9-Decapentyne	324.5
1,3,5,7,9-Decapentene	341.1

manipulations it turns out that, in the idealized context of regular geometries, oligomeric structures H—(CH═CH—C≡C)$_n$—R (R = H or —CH═CH$_2$), H—(C≡C)$_{2n}$—H, and H—(CH═CH)$_{2n}$—H should be classified in that order of increasing longitudinal polarizability with the length of chains (Table 4).

5. Concluding remarks

From the present work it seems that a linear scaling procedure applied to minimal basis calculations is applicable to unsaturated hydrocarbon chains. This conclusion was drawn from the preassumed capability of double-ζ basis sets, to which the split-valence 4-31G basis belongs, to yield reasonably good values of the electric polarizabilities. It remains, however, that the field of electric polarizabilities and hyperpolarizabilities is badly missing the experimental data from which such a simple approach could and should be more appropriately tested.

In the course of testing we have experienced an extreme sensitivity of calculated polarizabilities to geometry changes and any attempt at using a scaling should be made consistently.

Finally, the results of Section 4 raise two questions for those who are attracted by prospective calculations with molecular engineering purposes: will mixed compounds inexorably lead to depleted polarizabilities? If this is not the case, then what are the type of moieties to be combined to enhance the resulting polarizability?

Acknowledgments

The authors are indebted to Dr. J. G. Fripiat for the implementation of the finite field method in the GAUSSIAN 80 series of programs and to Professor G. Berthier (ENSJF — Paris) and Mr. G. Baudoux for useful discussions. They acknowledge with appreciation the support of their collaboration under NATO grant #130.83. One of us (V.P.B.) is grateful to the Institut pour l'Encouragement de la Recherche Scientifique dans l'Industrie et l'Agriculture (IRSIA, Belgium) for financial support.

1. D. J. WILLIAMS (*Editor*). Nonlinear optical properties of organic and polymeric materials. Am. Chem. Soc. Symp. Ser. Washington. 1983.
2. P. L. DAVIES. Trans. Faraday Soc. **48**, 789 (1952).
3. (*a*) K. C. RUSTAGI and J. DUCUING. Opt. Commun. **10**, 258 (1974); (*b*) H. F. HAMEKA. J. Chem. Phys. **67**, 2935 (1977).
4. J. ZYSS. J. Chem. Phys. **71**, 909 (1979).
5. A. CHABLO and A. HINCHLIFFE. Chem. Phys. Lett. **72**, 149 (1980).
6. J. S. BINKLEY, R. A. WHITESIDE, R. KRISHNAN, R. SEEGER, D. J. DEFREES, H. B. SCHLEGEL, S. TOPIOL, L. R. KAHN, and J. A. POPLE. QCPE, **13**, 406 (1981).
7. (*a*) W. J. HEHRE, R. F. STEWART, and J. A. POPLE. J. Chem. Phys. **51**, 2657 (1969); (*b*) R. DITCHFIELD, W. J. HEHRE, and J. A. POPLE. J. Chem. Phys. **54**, 724 (1971).
8. H. D. COHEN and C. C. J. ROOTHAAN. J. Chem. Phys. **43**, 534 (1965).
9. H. RUTISHAUSER. Num. Math. **5**, 48 (1963).
10. L. C. SNYDER and H. BASCH. Molecular wavefunctions and properties. Wiley—Interscience, New York. 1972.
11. G. R. ALMS, A. K. BURNHAM, and W. H. FLYGARE. J. Chem. Phys. **63**, 3321 (1975).
12. G. W. HILLS and W. J. JONES. Faraday Trans. II, **71**, 812 (1975).
13. H. C. ALLEN and E. K. PHYLER. J. Am. Chem. Soc. **80**, 2673 (1958).
14. A. ALMENNINGEN, O. BASTIANSEN, and M. TRAETTENBERG. Acta Chem. Scand. **12**, 1221 (1958).
15. M. TRAETTENBERG. Acta Chem. Scand. **22**, 628 (1968).
16. J. L. DUNCAN, I. J. WRIGHT, and D. VAN LERBERKE. J. Mol. Spectrosc. **42**, 463 (1972).
17. J. H. CALLOMON, B. P. STOICHAFF. Can. J. Phys. **35**, 373 (1957).
18. T. FUKUY, K. KUCHITSU, and Y. MONNO. Bull. Chem. Soc. Jpn. **44**, 386 (1971).
19. A. KARPFEN. J. Phys. C, 5673 (1980).

Réflexions multiples et prédissociations moléculaires

R. LEFEBVRE

Laboratoire de Photophysique Moléculaire,[1] Campus d'Orsay, 91405 Orsay, France

Reçu le 31 août 1984

Cet article est dédié au Professeur Camille Sandorfy à l'occasion de son 65^e anniversaire

R. LEFEBVRE. Can. J. Chem. **63**, 1635 (1985).

La méthode semi-classique met l'accent sur les réflexions multiples des ondes et les interférences qui en découlent. On utilise cette approche pour étudier un cas à deux canaux avec compétition entre résonance de forme et résonance de Feshbach. Dans la limite des faibles taux de prédissociation il y a additivité des deux effets.

R. LEFEBVRE. Can. J. Chem. **63**, 1635 (1985).

The semi-classical theory of molecular predissociation puts emphasis on the multiple reflections of waves and the resulting interferences. This approach is used to examine a case with two channels including a competition between a shape resonance and a Fesbach resonance. In the limit of low predissociation rates there is additivity of the two effects.

I. Introduction

La méthode semi-classique (voir par exemple la réf. 1) possède le mérite de donner une interprétation simple de nombreux problèmes de physique moléculaire. Un stade préalable est la définition des canaux décrivant l'interaction de deux entités moléculaires dans des états internes donnés. La fonction d'onde associée à chaque canal reçoit la forme JWKB. Il faut ensuite envisager l'effet sur les ondes de certains points ou régions critiques. Un point tournant produit une réflexion totale avec changement de phase approprié. Un croisement entre les potentiels de deux canaux produit un effet comparable à celui de la lame semi-transparente d'un interféromètre pour une onde lumineuse: il y a partition d'une onde incidente appartenant à un canal donné en deux termes associés aux deux canaux. Une barrière de potentiel produit une réflexion et une transmission partielles. Le système quantique se comporte de même manière qu'un système optique: une onde incidente subit des réflexions, des partitions et des transmissions successives. Les amplitudes des ondes émergentes permettent de définir la matrice **S** du problème. Les pôles de cette matrice donnent les états résonnants. Pour les énergies (complexes) de ces pôles, la fonction d'onde ne présente que des termes émergents.

Cet article examine un cas à deux canaux avec présence simultanée des deux mécanismes de prédissociation appelés types I et III par Herzberg (2). Un état quasilié se décompose soit par suite du croisement de son potentiel avec celui d'un état répulsif, soit par franchissement d'une barrière de potentiel. On parle aussi de résonance soit de Feshbach soit de forme. Cette situation a été envisagée dans le cas de l'ion O_2^+ par Helm *et al.* (3). Ces auteurs ont attribué à la présence simultanée des deux effets le fait que les largeurs observées pour les niveaux $v = 3$ de faible J de l'état $f^4\Pi_g$ ne peuvent s'expliquer par la seule interaction avec l'état $d^4\Sigma_g^+$. L'hypothèse d'une additivité des effets est implicitement admise.

La méthode semi-classique permet d'aboutir à une condition de quantification définissant les énergies des états résonnants. Dans la limite des faibles taux de dissociation (faible couplage intercanal, barrière de potentiel difficile à franchir) on peut démontrer l'additivité des deux mécanismes. Hors ce cas particulier (mais important), l'approche semi-classique montre qu'il y a des effets d'interférence. Une situation semblable a été étudiée par Sink et Bandrauk (4) dans le cas d'un potentiel attractif intersecté par plusieurs potentiels répulsifs. Là aussi la non-additivité est la règle et l'additivité n'est obtenue que comme cas limite.

A titre d'illustration de l'effet des réflexions multiples qui sont à l'origine du phénomène de résonance, nous examinons au préalable le problème classique du puits rectangulaire.

II. Réflexions multiples et résonances

Considérons une particule de masse μ astreinte à se mouvoir sur le demi-axe $0 < r \leq \infty$ et dont l'énergie potentielle possède la forme (puits rectangulaire):

[1] $$V(r) = -V_0(0 < r < r_0,\ V_0 > 0);\ V(r) = 0(r_0 < r)$$

L'espace autorisé pour la particule est ainsi divisée en une région interne et une région externe. Pour une énergie E, on peut définir les nombres d'onde correspondants par les relations:

[2] $$k_i^2 = 2\mu\hbar^{-2}(E + V_0);\ k_e^2 = 2\mu\hbar^{-2}E$$

Il est bien connu (5, 6) que la solution de l'équation d'onde s'obtient en imposant à la fonction d'onde d'avoir la forme:

[3a] $A \sin\ k_i r$ dans la région interne

[3b] $-e^{-ik_e r} + Se^{ik_e r}$ dans la région externe

On trouve ainsi pour l'amplitude de diffusion S l'expression:

[4] $$S = \frac{k_i \cos k_i r_0 + ik_e \sin k_i r_0}{k_i \cos k_i r_0 - ik_e \sin k_i r_0}\, e^{-2ik_e r_0}$$

Si l'énergie E est choisie à partir de la condition,

[5] $$\mathrm{tg}\ k_i r_0 = -ik_i/k_e$$

qui correspond à l'annulation du dénominateur de S, la fonction d'onde dans la région externe (eq. [3b]) est dominée par le terme émergent. Ceci peut se produire pour des énergies réelles négatives (états liés) mais aussi pour des énergies complexes de la forme $E = E_r - i\Gamma$. Ces énergies correspondent à des états résonnants qui sont autant de modes de fragmentation du système.

Il est intéressant de remarquer que l'amplitude de diffusion S (éq. [4]) peut aussi s'écrire identiquement:

[1] Laboratoire du CNRS associé à l'Université Paris-Sud.

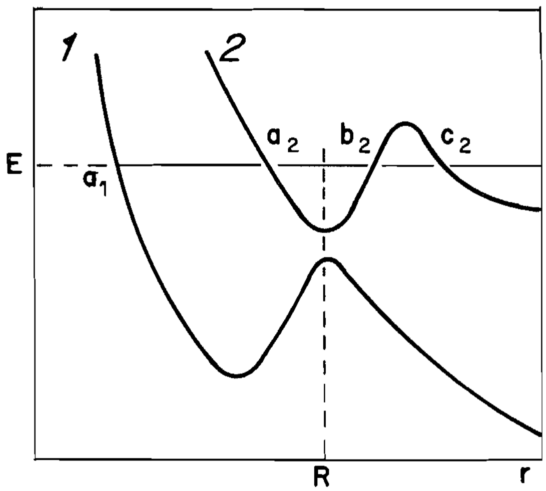

FIG. 1. Potentiels adiabatiques d'une situation comportant des prédissociations par franchissement d'une barrière de potentiel et par croisement de potentiels.

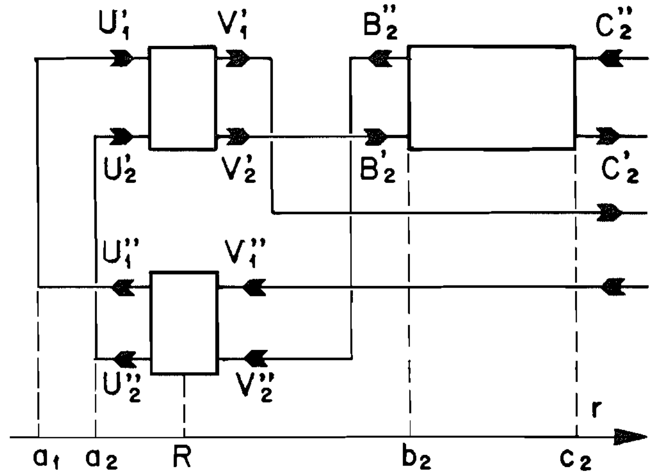

FIG. 2. Diagrammes des amplitudes JWKB entrantes et sortantes dans les régions classiquement accessibles. Les rectangles symbolisent l'effet du décroisement et de la barrière de potentiel sur les amplitudes.

[6] $$S = \left[\frac{k_i - k_e}{k_i + k_e}\,\mathrm{e}^{-2ik_e r_0}\right] + \left[\frac{2k_e}{k_i + k_e}\,\mathrm{e}^{i(k_i-k_e)r_0}\right] \times \left[\frac{2k_i}{k_i + k_e}\,\mathrm{e}^{i(k_i-k_e)r_0}\right] - \left[\frac{2k_e}{k_i + k_e}\,\mathrm{e}^{i(k_i-k_e)r_0}\right] \times \left[\frac{k_i - k_e}{k_i + k_e}\,\mathrm{e}^{2ik_i r_0}\right]\left[\frac{2k_i}{k_i + k_e}\,\mathrm{e}^{i(k_i-k_e)r_0}\right] + \left[\frac{2k_e}{k_i + k_e}\,\mathrm{e}^{i(k_i-k_e)r_0}\right]\left[\frac{k_i - k_e}{k_i + k_e}\,\mathrm{e}^{2ik_i r_0}\right]^2 \times \left[\frac{2k_i}{k_i + k_e}\,\mathrm{e}^{i(k_i-k_e)r_0}\right] - \ldots$$

expression que nous pouvons condenser en

[7] $$S = R + TT' - TR'T' + TR'^2T' - \ldots$$

Les amplitudes R, T, T' et R' sont définies par la comparaison des termes successifs de l'éq. [7] avec les quantités entre crochets du développement (éq. [6]). La signification de ces amplitudes est la suivante: R et T sont les amplitudes réfléchie et transmise correspondant à une onde d'amplitude unité incidente sur la discontinuité du potentiel en r_0, alors que R' et T' sont les amplitudes réfléchie et transmise correspondant à une onde émergente parvenant à cette discontinuité. Les termes successifs de l'éq. [7] correspondent aux évènements qui se produisent quand une onde incidente rencontre la région interne: (1) réflexion en r_0 (R); (2) transmission en r_0 (T), réflexion à l'origine et transmission en r_0 (T'); (3) transmission en r_0 (T), réflexion à l'origine, réflexion en r_0 (R'), réflexion à l'origine, transmission en r_0 (T'); etc.... La série figurant dans l'éq. [7] peut se sommer en

$$S = R + T\frac{1}{1 + R'}T'$$

et la condition $1 + R' = 0$ (pôles de S) redonne l'éq. [5]. On voit ainsi que ce sont les réflexions successives de l'onde dans la région interne qui sont à l'origine du phénomène de résonance.

La méthode semi-classique traite les problèmes moléculaires conduisant à des résonances de façon semblable. Ce sont les croisements et les barrières de potentiel qui jouent le rôle de la discontinuité de potentiel de l'exemple du puits rectangulaire. En dehors de ces régions les ondes se propagent librement sans réflexion, ainsi que l'admet l'approximation JWKB (7).

III. Condition de quantification semi-classique

Nous considérons maintenant la situation représentée sur la fig. 1. Les potentiels adiabatiques proviennent du décroisement par interaction de deux potentiels dont l'un présente une barrière de potentiel et l'autre est purement répulsif. Une méthode très efficace de traitement de ce type de problème a été donnée par Child (8). Les amplitudes JWKB sont définies dans chaque région classiquement accessible et loin des points tournants ou du point de décroisement R. Un diagramme tel que celui de la fig. 2 résume les "évènements" remarquables se produisant en raison des points tournants, du décroisement et de la barrière de potentiel. Les amplitudes U'_2 et U''_2 par exemple signifient que pour $r \ll R$ (mais $a_2 \ll r$) la fonction d'onde dans le canal 2 s'écrit:

[8] $$\psi_2(r) \sim [k_2(r)]^{-1/2}\left\{U'_2 \exp\left[i\int_R^r k_2(r')\,\mathrm{d}r'\right] + U''_2 \exp\left[-i\int_R^r k_2(r')\,\mathrm{d}r'\right]\right\}$$

Les rectangles figurant sur le diagramme symbolisent des transformations matricielles:

[9a] $$U'' = \mathbf{R}''V''$$

[9b] $$V' = \mathbf{R}'U'$$

[9c] $$C' = \mathbf{M}B''$$

Les points tournants à gauche a_1 et a_2 imposent en outre les relations:

[10] $$U'_1 = -i\mathrm{e}^{2i\alpha_1}U''_1; \qquad U'_2 = -i\mathrm{e}^{2i\alpha_2}U''_2$$

avec

$$\alpha_i = \int_{a_i}^{R} k_i(r)\,\mathrm{d}r$$

À noter qu'à la différence de Child (8) les notations 1 et 2 sont utilisées ici pour les potentiels adiabatiques, ce qui paraît préférable puisque la théorie semi-classique se formule entièrement à l'aide de ces potentiels (9). Une dernière information utile est le changement de phase subis dans le canal 2 entre R et b_2 soit:

[11] $V''_2 = B''_2 e^{i\beta_2}; \qquad B'_2 = V'_2 e^{i\beta_2}$

avec

[12] $\beta_2 = \int_R^{b_2} k_2(r)\, \mathrm{d}r$

Pour établir une condition de quantification, nous mettrons à profit le fait qu'il suffit de chercher les pôles d'un élément quelconque de la matrice **S** qui est ici une matrice 2 × 2, puisqu'avec le choix de l'énergie indiqué sur la fig. 1 il s'agit d'un problème à deux canaux ouverts.

La première étape du calcul est la prise en compte du décroisement et des points tournants de gauche. On peut, en utilisant successivement [9a], [11] et [9b] obtenir les amplitudes à la sortie du décroisement en fonction de celles imposées à l'entrée grâce à des relations linéaires dont la forme explicite n'est pas utile à ce stade:

[13a] $V'_1 = \mathcal{A}_{11} V''_1 + \mathcal{A}_{12} V''_2$

[13b] $V'_2 = \mathcal{A}_{12} V''_1 + \mathcal{A}_{22} V''_2$

Un choix possible pour les amplitudes des ondes incidentes est:

[14a] $V''_1 = -1$

[14b] $C''_2 = 0$

ce qui, compte tenu de [13b] et de [9c], conduit à

[15a] $V'_2 = -\mathcal{A}_{21} + \mathcal{A}_{22} V''_2$

[15b] $M_{21} B'_2 + M_{22} B''_2 = 0$

La condition [15b] est aussi, grâce à [11]:

[16] $M_{21} V'_2 e^{i\beta_2} + M_{22} V''_2 e^{-i\beta_2} = 0$

Les équations [15a] et [16] déterminent V'_2 et V''_2, donnant pour V''_2:

[17] $V''_2 = \dfrac{\mathcal{A}_{21}}{\mathcal{A}_{22} + M_{22} M_{21}^{-1} e^{-2i\beta_2}}$

V'_2 peut ensuite être écrit à l'aide de [16] en faisant apparaître le même dénominateur. Les éléments de la première colonne de la matrice de diffusion à courte portée $\mathbf{S}^{(s)}$ (réf 10) sont $S_{11}^{(s)} = V'_1$ et $S_{21}^{(s)} = C'_2$. Puisque

[18] $V'_1 = -\mathcal{A}_{11} + \mathcal{A}_{12} V''_2$

$C'_2 = M_{11} V'_2 e^{i\beta_2} + M_{12} V''_2 e^{-i\beta_2}$

le dénominateur résonant des éléments de la matrice **S** est identifiable à

[19] $\mathcal{A}_{22} + M_{22} M_{21}^{-1} e^{-2i\beta_2}$

Nous procèdons à un léger changement d'écriture pour formuler la condition de quantification semi-classique de ce problème

[20] $\boxed{1 + M_{21} M_{22}^{-1} \mathcal{A}_{22} e^{2i\beta_2} = 0}$

On a par ailleurs (conséquence de [9a], [11] et [9b]):

[21] $\mathcal{A}_{22} = -i e^{2i\alpha_1} R'_{21} R''_{12} - i e^{2i\alpha_2} R'_{22} R''_{22}$

la condition [20] et les formes données aux éléments des matrices **M**, **R**′ et **R**″ donnent en principe la solution de ce problème. Il est à remarquer que si l'on ne procède à aucune approximation justifiée par les conditions particulières d'un problème, il n'est guère possible d'aller au delà, sauf à utiliser des méthodes purement numériques. La section suivante examine le cas limite menant à une additivité des effets de barrière et de croisement de potentiel.

IV. Le cas limite des faibles taux de prédissociation

Les éléments des matrices **R**′, **R**″ et **M** dans la limite du faible couplage intercanal et d'une barrière difficilement franchissable peuvent être obtenus à partir d'expressions générales données par Child (8) (voir aussi Korsch (11)). On a ainsi:

[22] $R'_{22} = R''_{22} \rightarrow \sqrt{U} \exp\left[-i\dfrac{\pi}{4}\right]$

$R'_{21} = R''_{12} \rightarrow 1 - \dfrac{U}{2}$ et $R'_{21} R''_{12} \rightarrow 1 - U$

avec pour U (paramètre de Landau–Zener) l'expression:

[23] $U = \dfrac{2\pi\beta^2}{\hbar v \Delta F}$

β étant le couplage intercanal, v la vitesse classique et ΔF la différence des pentes des potentiels diabatiques, toutes ces quantités étant calculées au point de croisement diabatique. Par ailleurs:

[24] $M_{21} \rightarrow iK; \qquad M_{22} \rightarrow (1 + K^2)^{1/2}$

avec

[25] $K = \exp\left[\displaystyle\int_{b_2}^{c_2} |k_2(r')|\, \mathrm{d}r'\right]$

En conséquence:

[26] $M_{21} M_{22}^{-1} \rightarrow i(1 - 2^{-1} K^{-2})$

puisque dans ces hypothèses $K \gg 1$.

Définissons les deux angles:

[27] $\theta_d = \alpha_1 + \beta_2$ et $\theta'_a = \alpha_2 + \beta_2 - \dfrac{\pi}{4}$

Après multiplication de [20] par $\exp(-i\theta_d)$ et prise en compte de l'ensemble des relations [22]–[27], on obtient pour la condition de résonance:

[28] $$2 \cos \theta_d + 2U \exp[i(\theta'_a - \theta_d)] \cos \theta'_a - 2^{-1} K^{-2} \{U \exp[i(2\theta'_a - \theta_d)] + (1 - U) \exp[i\theta_d]\} = 0$$

Lorsque l'énergie est proche de celle d'un niveau d'énergie E_v du potentiel diabatique possèdant la barrière de potentiel, on a:

[29] $\theta_d \simeq \left(v + \dfrac{1}{2}\right)\pi$

ce qui permet d'utiliser les relations:

[30] $\cos \theta_d = (-1)^{v+1} \dfrac{\pi}{\hbar\omega_d}(E - E_v)$ et

$\exp[\pm i\theta_d] = \pm(-1)^v i$

En omettant le terme proportionnel à UK^{-2} on obtient comme solution de [28]:

$$[31] \quad E = E_v - i\frac{\hbar\omega_d}{\pi} U \cos\theta'_a \exp[i\theta'_a] - i\frac{\hbar\omega_d}{4\pi} K^{-2}$$

Le premier terme correctif à E_v se décompose en un déplacement et un élargissement qui sont ceux (8) de la limite diabatique du problème de prédissociation de type I. Le deuxième terme correctif représente l'élargissement dû à la barrière de potentiel. On a bien dans cette limite, comme attendu, une additivité des deux types d'effet.

Le terme proportionnel à UK^{-2} représente un effet d'interférence entre les deux types de prédissociations. Il contribue à l'énergie un terme correctif ΔE qui s'écrit:

$$[32] \quad \Delta E = i\frac{\hbar\omega_d}{2\pi} UK^{-2} e^{i\theta'_a} \cos\theta'_a$$

Ce terme contribue donc à la fois au déplacement et à l'élargissement. On constate en particulier que l'interférence joue dans le sens d'une diminution de l'élargissement. Ceci peut être attribué au fait qu'une ondelette parvenant soit au point de croisement, soit sur la barrière de potentiel a son amplitude affectée (diminuée) par le mécanisme de perte antérieur à celui considéré.

Signalons enfin comment le cas habituel de la prédissociation par croisement de potentiels se trouve inclus dans la situation examinée ici. La condition [16] peut aussi s'écrire:

$$[33] \quad V''_2 = -M_{21}M_{22}^{-1} e^{2i\beta_2} V'_2$$

Quand la barrière est infranchissable, $K \rightarrow +\infty$ et $M_{21}M_{22}^{-1} \rightarrow i$. La condition [33] devient celle imposée par un point tournant à droite.

V. Conclusion

L'exemple traité dans cet article vient s'ajouter à d'autres présentés dans la littérature pour illustrer la grande commodité de l'approche semi-classique. La fiabilité sur le plan numérique a été également maintes fois démontrée. L'aspect ondulatoire de la mécanique quantique se trouve mis à profit d'une manière particulièrement convaincante.

1. M. S. CHILD (*Éditeur*). Semi-classical methods in molecular scattering and spectroscopy. Reidel, Dordrecht. 1980.
2. G. HERZBERG. Spectra of diatomic molecules. van Nostrand, New York. 1950. Chap. VII.
3. H. HELM, P. C. COSBY et D. L. HUESTIS. J. Chem. Phys. **73**, 2629 (1980).
4. M. L. SINK et A. D. BANDRAUK. J. Chem. Phys. **66**, 5313 (1977).
5. H. M. NUSSENZWEIG. Nucl. Phys. **11**, 499 (1959).
6. D. L. HUESTIS. J. Math. Phys. **16**, 2148 (1975).
7. H. BREMMER. Comm. Pure Appl. Math. **4**, 105 (1951).
8. M. S. CHILD. J. Mol. Spectrosc. **53**, 280 (1974).
9. W. H. MILLER et T. F. GEORGES. J. Chem. Phys. **56**, 5637 (1972).
10. R. COLLE. J. Chem. Phys. **74**, 2910 (1981).
11. H. J. KORSCH. *Dans* Resonances – models and phenomena. Springer Lecture Notes in Physics. 1985.

Discriminative interactions between chiral molecules: internal discrimination in 1,2-difluorohydrazine

RUDOLF ZAHRADNÍK AND BOHDAN SCHNEIDER
J. Heyrovský Institute of Physical Chemistry and Electrochemistry, Czechoslovak Academy of Sciences, 121 38 Prague 2, Czechoslovakia

PAVEL HOBZA
Institute of Hygiene and Epidemiology, Centre of Industrial Hygiene and Occupational Diseases, 100 42 Prague 10, Czechoslovakia

ZDENĚK HAVLAS
Institute of Organic Chemistry and Biochemistry, Czechoslovak Academy of Sciences, 166 10 Prague 6, Czechoslovakia

AND

HANSPETER HUBER
Institute of Physical Chemistry, University of Basle, 4056, Switzerland

Received August 31, 1984

This paper is dedicated to Professor Camille Sandorfy on the occasion of his 65th birthday

RUDOLF ZAHRADNÍK, BOHDAN SCHNEIDER, PAVEL HOBZA, ZDENĚK HAVLAS, and HANSPETER HUBER. Can. J. Chem. **63**, 1639 (1985).

1,2-Difluorohydrazine represents a model for studying short-range discriminative interactions between two chiral radicals. Possible diastereomeric structures of the system were theoretically investigated by means of nonempirical SCF quantum chemical calculations. Four minima and six saddle points separating them were found on the potential energy surface. All the stable structures and one transition complex were completely optimized. Thermodynamic properties for the equilibrium between the two most stable conformers (*meso* and chiral) of difluorohydrazine are as follows (in kJ/mol): $\Delta H^0_{298.2} = -17.0$, $T\Delta S^0_{298.2} = -0.4$ (standard state: ideal gas at 101.325 kPa, 298 K).

RUDOLF ZAHRADNÍK, BOHDAN SCHNEIDER, PAVEL HOBZA, ZDENĚK HAVLAS et HANSPETER HUBER. Can. J. Chem. **63**, 1639 (1985).

La difluoro-1,2 hydrazine représente un bon modèle pour étudier les interactions discriminatoires à courte distance entre deux radicaux chiraux. Utilisant des calculs non-empiriques de chimie quantique en champ auto-cohérent, on a étudié sur une base théorique les structures diastéréomères possibles du système. Sur la surface d'énergie, on peut déceler quatre minima et six points maxima. On a complètement optimisé toutes les structures stables et un complexe de transition. Les propriétés thermodynamiques de l'équilibre entre les deux conformères les plus stables (*méso* et chiral) de la difluorohydrazine sont les suivantes (en kJ/mol): $\Delta H^0_{298.2} = -17.0$, $T\Delta S^0_{298.2} = -0{,}4$ (état standard: gaz idéal à 101,325 kPa, 298 K).

[Traduit par le journal]

The majority of important interactions in biological systems are highly selective or specific. Biological receptors do recognize absolutely a particular optical antipode derived from a certain chiral system. The discriminative nature of some terms of the perturbation interaction energy has been extensively and systematically studied by Craig and Mellor (1, 2). Mason has also published a review on this subject (3). It is now known that the discriminative power of chiral components was relatively small and that the enormous discriminative power of biological receptors is due to a different mechanism (4). In spite of this, it seems desirable to know more about the discriminative nature of weak intermolecular interactions because they occur in most important biological processes.

Systems derived formally by the combination of two chiral radicals represent useful models for studying short-range discriminative interactions. *Dextro* and *levo* methylcyanomethyl radicals, which can give *meso* and chiral isomers of 2,3-dicyanobutane, have been investigated theoretically by Craig, Radom, and Stiles (5). Isomers of 1,2-dimethylhydrazine, which is also a system with intramolecular discriminative interaction, have been studied extensively from both the theoretical and experimental point of view. Attention was paid to the abundance of conformers. Vibrational (6) and photoelectron (7) spectra, gas electron diffraction (8, 9), and microwave spectra (10) were studied and a nonempirical quantum chemical study was performed (9). However, chiral properties were not mentioned in the papers cited (6–10).

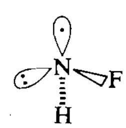

1

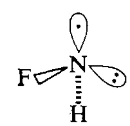

2

In this work, 1,2-difluorohydrazine (a formal product of interaction between *R*- and *S*-fluoroamidogens, **1**, **2**) is studied theoretically. The combination of **1** and **2** can yield a *meso* form **3** and chiral active forms **4** and **5**; **5** is a mirror image of **4**.

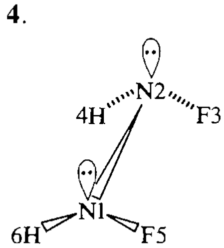

3

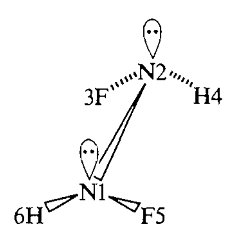

4

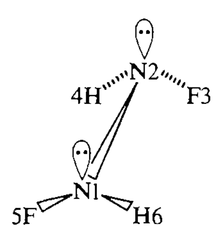

5

TABLE 1. Optimized bond lengths, and valence and dihedral angles[a] (in pm and degrees)

Bonds and angles	*meso* M1[b] 3-21G	*meso* M1[b] FOGO	Saddle point S5 3-21G	Saddle point S5 FOGO[c]	Chiral M3 3-21G	Chiral M3 FOGO	Chiral M4 3-21G
N1N2	142.3	141.5	133.5	133.0	141.0	139.9	142.7
N2F3	144.2	140.5	141.2	138.7	144.1	141.8	143.0
N2H4	100.4	101.1	98.6	99.3	100.8	100.9	100.4
N1F5	142.9	142.2	144.7	143.3	144.1	141.8	143.0
N1H6	100.7	101.0	100.2	100.5	100.8	100.9	100.4
N1N2F3	106.7	105.9	119.4	118.2	107.8	107.7	105.2
N1N2H4	106.6	107.6	125.3	126.5	107.6	106.0	110.5
N2N1F5	105.5	107.7	110.3	110.0	107.8	107.7	105.2
N2N1H6	108.8	104.7	112.9	110.4	107.6	106.0	110.5
F3N2H4	102.4	101.2	114.8	115.3	102.9	101.9	101.2
F5N2H6	102.2	101.7	102.2	100.2	102.9	101.9	101.2
F3N2N1F5	91.4	86.3	69.9	63.0	53.2	53.2	234.6
H4N2N1H6	91.4	86.5	128.1	133.4	167.6	163.7	16.8

[a] For the sake of convenience, one additional geometric parameter is used.
[b] The same parameters are obtained for enantiomer M2 except the dihedral angles, which have opposite signs.
[c] The inversion group was assumed to be planar.

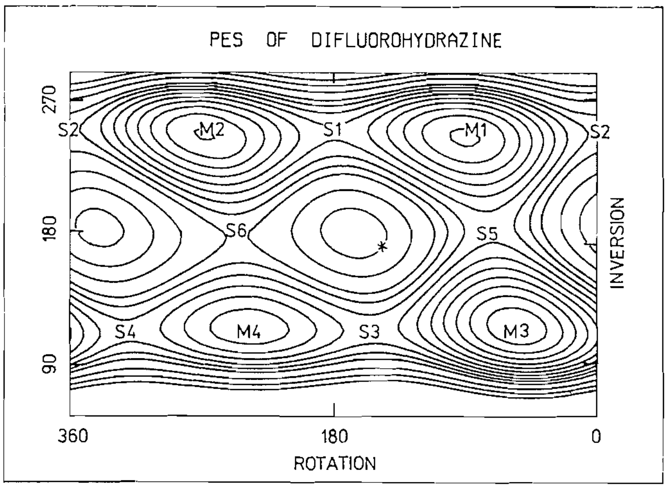

FIG. 1. Energy contour of PES cut for internal rotation around the N—N bond (torsion angle denoted as F3N2N1F5) and inversion of one of the NHF groups (angle F3N2N1H4). Absolute energy of the labeled contour line (*) is −307.000 au. The energy differences of the contour lines in the downhill direction are: 0.01, 0.01 au and then 0.005 au.

In a broader sense, the purpose of this study is to investigate the potential energy surface (PES) of the $N_2H_2F_2$ system. Particular attention has been paid to a special cut through the surface which contains the deepest minimum and its inversion product, including the respective saddle point.

Results and discussion

In order to get an idea about the internal rotation and inversion processes in 1,2-difluorohydrazine, a cut through the potential energy surface was studied. Calculations were performed by the Hartree–Fock SCF method with 3-21G basis set (11). A potential energy contour map constructed from 280 points is plotted in Fig. 1. On this cut of the PES, four minima (M) and six saddle points (S) are indicated. The minima M1 and M2 represent enantiomeric conformations of the *meso* form; they are asymmetric mirror images. These two minima are separated by saddle points possessing either symmetry plane (S1) or center of inversion (S2). The rotational barriers taken from the contour map are relatively high (65 and 95 kJ/mol); however, they do not guarantee the separability of the enantiomers at room temperature. The other two minima (M3 and M4) represent the chiral form, M4 being energetically significantly higher. These two minima are related by two rotational saddle points, S3 and S4, of a comparable height to those for the *meso* forms. It is worth mentioning that the inversional processes have almost the same barriers as the rotational ones. It seems that at room temperature there is no chance to isolate diastereomeric iosomers.

The energy profile of inversion M1 → S5 → M3 was studied in more detail, as well as minima M2 and M4. Geometry optimization of the stationary points with respect to all internal degrees of freedom was done by Hartree–Fock SCF calculations, using the Pople 3-21G basis set (11) and the FOGO method (12), with approximately DZ+P quality basis set.

Optimized bond lengths, and valence and dihedral angles obtained by *ab initio* SCF calculations (3-21G) and the FOGO method are summarized in Table 1. The nature of the located stationary points M1, M3, and S5 was ascertained by the number of negative eigenvalues of the Hessian. As expected, bond lengths and valence angles of the *meso* and chiral forms are very similar. The structure of the activated complex S5 fits the intuitive picture; the inversion group (N2F3H4) is almost planar (the deviation from planarity is about 10°) and all its bonds are shorter, in comparison with the bonds in either minima.

Energy characteristics are presented in Table 2 and Fig. 2. The inversion barrier for the process is found to be significantly higher than for the inversion of ammonia (about 28 kJ/mol) but much smaller than that for trifluoroammonia (328 kJ/mol; *ab initio* SCF with DZ+P basis set, ref. 13).

The thermodynamic calculation for the inversion process M1 ⇌ M3 is based on the rigid rotor – harmonic oscillator – ideal gas approximation (for details see, e.g., ref. 14). Vibrational frequencies of the systems were calculated by means of Wilson FG analysis (15) on the basis of 3-21G force constants. The thermodynamic characteristics for the equilibrium between the *meso* M1 and chiral M3 forms of difluorohydrazine (standard state: ideal gas at 101.325 kPa, 298 K) are (in kJ/mol) as follows: $\Delta H_0^0 = -16.9$, $\Delta H_{298.2}^0 = -17.0$, $T\Delta S_{298.2}^0 = -0.4$,

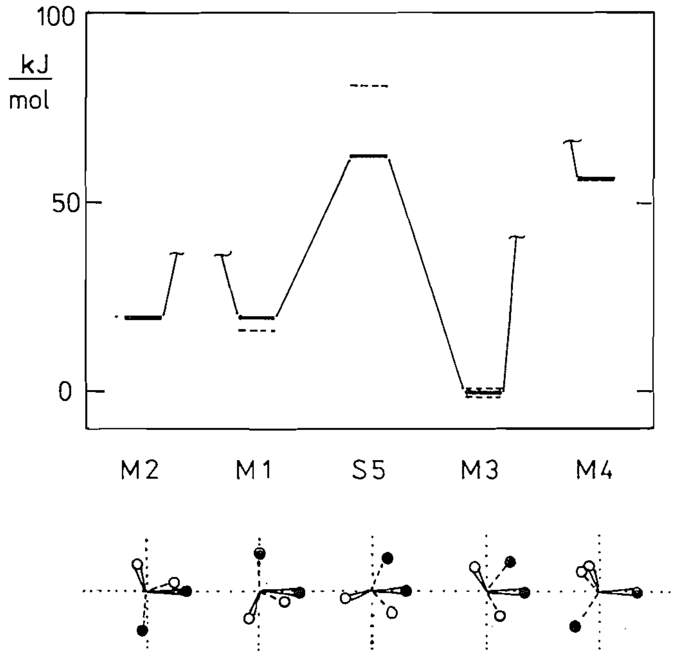

FIG. 2. Partial energy profile of the 1,2-difluorohydrazine system. Symbols: — 3-21G, ---- FOGO, ○ hydrogen atom, ● fluorine atom.

TABLE 2. Relative energies of the systems studied (kJ/mol)

System	3-21G	FOGO
meso M2	19.5	—
meso M1	19.5	16.0
Saddle point S5	62.6	80.1
Chiral M3	0.0[a]	0.0[b]
Chiral M4	50.6	—

[a] E(3-21G) = −307.07082 au.
[b] E(FOGO) = −308.3209 au.

$\Delta G^0_{298.2} = -16.6$. Equilibrium is controlled by the energy difference; the change in zero-point energy is small and the entropy change is negligible.

In conclusion, our calculations indicate that for the case of *intra*molecular discriminative interactions, the discriminative effects are small and not influenced by the entropy change: $\Delta E = -19.5$ kJ/mol; $\Delta H^0_{298.2} = -17.0$ kJ/mol; $\Delta G^0_{298.2} = -16.6$ kJ/mol. As a point of reference, the energy of thermal motion at 198.2 K is about 2.5 kJ/mol. Clearly, discriminative effects associated with *inter*molecular interactions are even smaller.

Acknowledgement

Thanks are due to Professor K. Bláha, Prague, for most valuable discussion.

1. D. P. CRAIG. *In* Optical activity and chiral discrimination. *Edited by* S. F. Mason. D. Reidel Publishing Co., Dordrecht. 1979, p. 293.
2. D. P. CRAIG and D. P. MELLOR. Top. Curr. Chem. **63**, 1 (1976).
3. S. F. MASON. Ann. Rep. **73**, 53 (1976).
4. A. FEHRST. Enzymes, structure and mechanism. W. H. Freeman and Co., Reading and San Francisco. 1977.
5. D. P. CRAIG, L. RADOM, and P. J. STILES. Proc. R. Soc. London Ser. A, **343**, 11 (1975).
6. J. R. DURIG and W. C. HARRIS. J. Chem. Phys. **55**, 1735 (1971).
7. K. KIMURA and K. OSAFUNE. Bull. Chem. Soc. Jpn. **4**, 2421 (1975).
8. K. KOHATA, T. FUKUYAMA, and K. KUCHITSU. Chem. Lett. **25**, 7 (1979).
9. N. S. CHIU, H. L. SELLERS, L. SCHÄFER, and K. KOHATA. J. Am. Chem. Soc. **101**, 5883 (1979).
10. M. NAKATA, H. TAKEO, CH. MATSUMURA, K. YAMANOUCHI, K. KUCHITSU, and T. FUKUYAMA. Chem. Phys. Lett. **83**, 246 (1981).
11. J. S. BINKLEY, J. A. POPLE, and W. J. HEHRE. J. Am. Chem. Soc. **102**, 939 (1980).
12. H. HUBER. Theor. Chim. Acta (Berlin), **55**, 117 (1980).
13. D. S. MARYNICK. J. Chem. Phys. **73**, 3939 (1980).
14. P. ČÁRSKY, R. ZAHRADNÍK, and V. KELLÖ. Collect. Czech. Chem. Commun. **43**, 1965 (1978).
15. E. B. WILSON, J. C. DECIUS, and P. C. CROSS. Molecular vibrations. McGraw–Hill, New York. 1955.

Relationships between geometries and energies of identity S_N2 transition states: the dominant role of the distortion energy and its origin

DAVID JOHN MITCHELL
DuPont Canada Research Centre, P.O. Box 5000, Kingston, Ont., Canada K7L 5A5

H. BERNHARD SCHLEGEL
Department of Chemistry, Wayne State University, Detroit, MI 48202, U.S.A.

SASON S. SHAIK[1]
Laboratoire de Chimie Théorique, Bâtiment 490, Université de Paris-Sud, 91405, Orsay, France

AND

SAUL WOLFE[2]
Department of Chemistry, Queen's University, Kingston, Ont., Canada K7L 3N6

Received September 13, 1984

This paper is dedicated to Professor Camille Sandorfy on the occasion of his 65th birthday

DAVID JOHN MITCHELL, H. BERNHARD SCHLEGEL, SASON S. SHAIK, and SAUL WOLFE. Can. J. Chem. **63**, 1642 (1985).

At the 4-31G computational level, the intrinsic barriers of eight identity S_N2 reactions $X^- + CH_3X \rightarrow XCH_3 + X^-$ are less than the energies required to distort CH_3X from its ground state geometry to its transition state geometry by a constant 25 kcal/mol. The distortion energy and its C—X stretching and H—C—X bending components can be calculated directly, or, alternatively, estimated from the force constants and bond dissociation energies of CH_3X. Regardless of the mode of computation, the distortion energies are found to be dominated by the C—X stretching deformations, and these are linearly correlated with the intrinsic barriers. The total deformation energies are also linearly correlated with the intrinsic barriers. The transition vectors of the eight identity reactions have been calculated; each is dominated by the C—X stretch. The percentage of C—X stretching at the transition state, here termed the Distortion Index (DI), reflects the "tightness" or "looseness" of this structure. The intrinsic barrier increases as the DI increases, i.e., as the transition state becomes more "exploded". This result does not agree with the predictions of a More O'Ferrall – Jencks potential energy surface diagram. However, as shown in some detail, all of the computational results of the present work are in harmony with the surface crossing diagram model of the barrier. The essential feature of this model is the notion that the activation process in an identity S_N2 reaction is a result of the distortion that is required to transfer one electron from X^- to CH_3X.

DAVID JOHN MITCHELL, H. BERNHARD SCHLEGEL, SASON S. SHAIK et SAUL WOLFE. Can. J. Chem. **63**, 1642 (1985).

Des calculs au niveau 4-31G indiquent que les énergies des barrières intrinsèques de 8 réactions S_N2 d'identité: $X^- + CH_3X \rightarrow XCH_3 + X^-$ sont systématiquement 25 kcal/mol de moins que celles requises pour déformer le CH_3X de sa géométrie de l'état fondamental jusqu'à celle de l'état de transition. L'énergie de déformation, ainsi que ses composantes d'élongation C—X et de déformation H—C—X peuvent être calculées directement, ou évaluées, à partir des constantes de force et des énergies de dissociation des liaisons du CH_3X. Peu importe le mode de calcul, on a trouvé que les énergies de dissociation sont dominées par les déformations de l'élongation du C—X et celles-ci peuvent être reliées linéairement aux barrières intrinsèques. Les énergies de déformation totale sont également reliées linéairement aux barrières intrinsèques. On a calculé les vecteurs de transition des 8 réactions d'identité; chacune est dominée par l'élongation de C—X. Le pourcentage d'élongation de C—X au niveau de l'état de transition, que l'on appelle ici l'indice de distortion (ID), reflète la nature compacte ou lâche de cette structure. La barrière intrinsèque augmente avec l'ID, c'est-à-dire au fur et à mesure que l'on s'éloigne de l'état de transition. Ce résultat ne s'accorde pas avec les prédictions d'un diagramme de surface d'énergie potentielle de More O'Ferrall – Jencks. Cependant, tel que montré avec certains détails, tous les résultats obtenus par le calcul sont en accord avec le modèle de diagramme de croisement de surface de la barrière. La caractéristique essentielle de ce modèle réside dans le fait que le processus d'activation dans une réaction S_N2 est un résultat de la distorsion qui est requise pour transférer un électron de X^- à CH_3X.

[Traduit par le journal]

Introduction

The course of an S_N2 reaction $Y^- + CH_3X \rightarrow YCH_3 + X^-$ is attended by a number of changes in molecular geometry. A deformation of the H—C—H angles occurs as the configuration about the carbon atom is inverted, the C—X bond stretches and is broken, and the C—Y bond shortens and is formed. The changes in geometry are accompanied by changes in the total energy of the system. For a gas phase reaction, the nature of the latter has been discussed extensively (1, 2), and the reaction coordinate has been found to have the form shown in Fig. 1. In Fig. 1, $Y^- \ldots CH_3X$ and $YCH_3 \ldots X^-$ are reactant and product ion–molecule complexes (clusters), and $(Y—CH_3—X)^-$ is the S_N2 transition structure.

In an earlier communication (3), it was observed that linear relationships exist between stretching and bending geometrical parameters of $(Y—CH_3—X)^-$ transition structures and the thermochemistry of non-identity S_N2 reactions. One objective of the present work is to study the relationships between calculated geometrical parameters of identity S_N2 transition structures $(Y = X)$ and the calculated barriers $(\Delta E_0^{\neq})$ associated with such reactions (see Fig. 2). A second objective is to demonstrate that the Surface Crossing Diagram (SCD) model (4–6), which ascribes the origin of the S_N2 barrier to the energy required to transfer *one* electron from X^- to CH_3X, accounts for

[1] Permanent address: Department of Chemistry, Ben Gurion University, Beer Sheva 84105, Israel.

[2] Author to whom correspondence may be addressed.

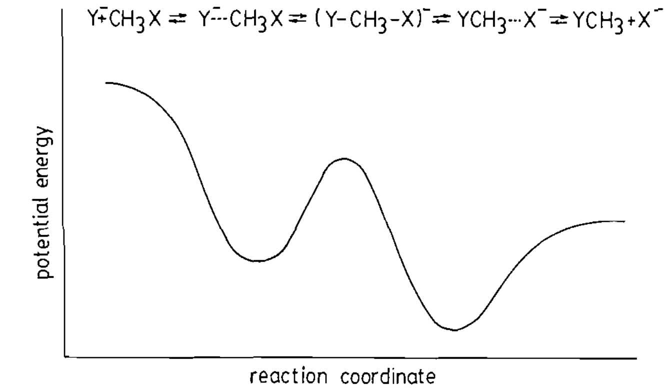

FIG. 1. Reaction coordinate for a non-identity S_N2 reaction $Y^- + CH_3X \rightarrow YCH_3 + X^-$.

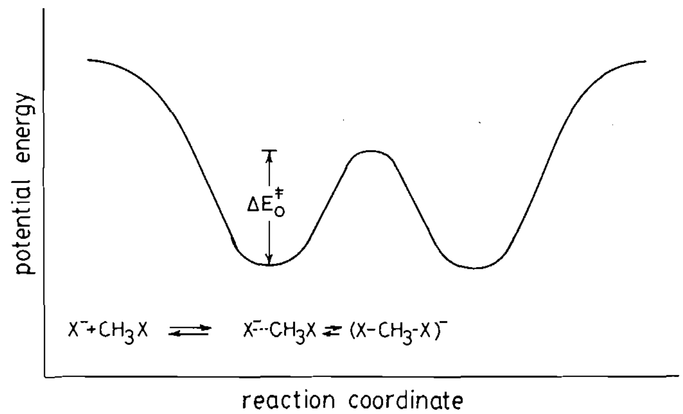

FIG. 2. Reaction coordinate for an identity S_N2 reaction $X^- + CH_3X \rightarrow XCH_3 + X^-$. The intrinsic barrier $\Delta E_0^{\ddagger}$ is given by the energy difference between the ion–molecule cluster $X^- \ldots CH_3X$ and the transition structure $(X—CH_3—X)^-$.

TABLE 1. Calculated intrinsic barriers, force constants, and C—X bond lengths for gas phase S_N2 reactions[a]

X	$\Delta E_0^{\ddagger}$ [b]	R_1 (Å)[c]	R_2 (Å)[d]	f_R (au)[e]	f_θ (au)[f]	$f_{R\theta}$ (au)[g]
H	52.0	1.089	1.730	0.378	0.926	0.068
CCH	50.4	1.465	2.124	0.387	1.059	0.144
*C*N	43.8	1.459	2.112	0.380	1.062	0.148
*N*C	28.5	1.441	2.013	0.407	1.133	0.207
OH	21.2	1.463	1.908	0.367	1.009	0.199
SH	15.6	1.914	2.459	0.195	0.846	0.138
F	11.7	1.462	1.828	0.450	1.142	0.213
Cl	5.5	1.965	2.382	0.285	1.033	0.192

[a] HF/4-31G calculations.
[b] In kcal/mol.
[c] Refers to C—X bond length in CH_3X having the geometry of the cluster.
[d] Refers to C—X bond length in CH_3X having the geometry of the transition state.
[e] Units are hartree $bohr^{-2}$; 1 hartree = 627.51 kcal/mol; 1 bohr = 0.529 Å.
[f] Units are hartree rad^{-2}.
[g] Units are hartree rad^{-1} $bohr^{-1}$.

TABLE 2. Intrinsic barriers, approximate deformation energies, and the components of these deformation energies,[a] for reactions $X^- + CH_3X \rightarrow XCH_3 + X^-$

X	$D_{C—X}$	ΔE_R^{approx}	ΔE_θ^{approx}	$\Delta E_{R\theta}^{approx}$	ΔE_{def}^{approx}	$\Delta E_0^{\ddagger}$
H	104	55.0	33.6	−17.7	70.9	52.0
CCH	117	60.5	44.2	−41.1	63.6	50.4
*C*N	114	58.6	41.8	−40.6	59.8	43.8
*N*C	90[b]	47.2	42.8	−48.8	41.2	28.5
OH	91	34.1	34.8	−34.8	34.1	21.2
SH	73	27.2	28.3	−29.1	26.4	15.6
F	108	32.3	36.6	−29.5	39.4	11.7
Cl	84	26.0	28.5	−28.5	26.3	5.5

[a] All energies are in kcal/mol.
[b] Estimated from $D_{CH_3—CN}$ (114 kcal/mol) and $-\Delta H$ for the isomerization of CH_3NC to CH_3CN (23.7 kcal/mol) (12).

all of the results.

For the reaction coordinate of Fig. 2, the region from cluster to cluster is of greatest interest, since it encompasses most of the geometrical changes. Because the fully optimized geometries and energies of $X^- \ldots CH_3X$ clusters and $(X—CH_3—X)^-$ transition structures were already available from HF/4-31G computations for X = H, HCC, NC, CN, HO, HS, F, Cl (2, 3, 7), a detailed examination of the relationships between these quantities was performed at this level. Additional computations were performed, as needed, using the 4-31G basis set and the GAUSSIAN 80 (8) or GAUSSIAN 82 (9) programmes.

Computational results

Table 1 summarizes the primary data: $\Delta E_0^{\ddagger}$ is the intrinsic barrier, R_1 is the C—X bond length of CH_3X in the cluster, R_2 is the C—X bond length in the transition structure, f_R is the calculated CH_3—X stretching force constant, f_θ is the calculated bending force constant for the umbrella deformation of the methyl group, and $f_{R\theta}$ is the stretch–bend interaction force constant.

The intrinsic barrier can be partitioned (10) into the energy required to deform the CH_3X moiety, and the interaction energy between X^- and the deformed CH_3X. An approximate estimate of the deformation energy can be obtained from the calculated force constants of CH_3X. To change CH_3X from its geometry in the cluster to its geometry in the transition state requires a stretch of the C—X bond by ΔR, and a bend of the H—C—X angle by $\Delta\theta$, as well as smaller changes in the rest of the molecule. Since stretching potentials are very anharmonic, it is not possible to estimate the energy associated with a C—X stretch from harmonic force constants alone. Therefore, to approximate the stretching anharmonicity, a Morse curve (11) was fitted to the calculated harmonic stretching force constant, f_R, and the experimental C—X bond dissociation energies, D, using eq. [1], where $\Delta R = R_2 - R_1$.

$$[1] \quad \Delta E_R^{approx} = D[1 - \exp(-\beta\Delta R)]^2; \quad \beta = (f_R/2D)^{1/2}$$

The data are shown in Table 2, and Fig. 3 is a plot of ΔE_R^{approx} versus $\Delta E_0^{\ddagger}$. The two quantities are linearly related (r = 0.975).

The energy required to bend an H—C—X angle can be estimated directly from the calculated harmonic force constant f_θ (eq. [2]), because the bond anharmonicity is small.

$$[2] \quad \Delta E_\theta^{approx} = \tfrac{1}{2} f_\theta(\Delta\theta)^2$$

The stretch–bend interaction must also be taken into account, because bending of the H—C—X angles is greatly facilitated by the stretch of the C—X bond. In the harmonic approximation, the stretch–bend interaction is given by eq. [3].

$$[3] \quad \Delta E_{R\theta}^{approx} = f_{R\theta}(\Delta R)(\Delta\theta)$$

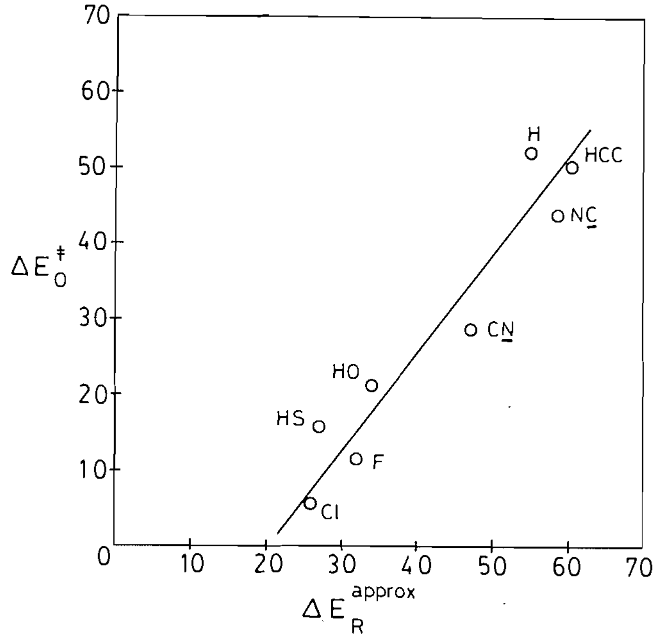

FIG. 3. A plot of $\Delta E_R^{\text{approx}}$ versus $\Delta E_0^{\ne}$ for eight identity S_N2 reactions. Energies are in kcal/mol.

In terms of the approximations of eqs. [1]–[3], the total deformation energy is given by eq. [4]. All of these quantities are included in Table 2.

$$[4] \quad \Delta E_{\text{def}}^{\text{approx}} = \Delta E_R^{\text{approx}} + \Delta E_\theta^{\text{approx}} + \Delta E_{R\theta}^{\text{approx}}$$

The deformation energies just described are approximations, because they are based on the calculated force constants and experimental dissociation energies of CH_3X. The actual deformation energies, ΔE_{def}, and their components can be calculated directly, as shown in Scheme 1. The stretching deformation energy, ΔE_R, is obtained from the energy difference between **3** and **1**, where **1** refers to CH_3X in the geometry of the cluster, and **3** is derived from **1** by a stretch of the C—X bond to its value in the transition structure **2**. The bending deformation energy, ΔE_θ, is obtained analogously from the energy difference between **1** and **4**, where **4** refers to bending of **1** to the bond angles of the transition structure. The total deformation energy is the energy difference between **1** and **2**. The quantities ΔE_{def}, ΔE_R, and ΔE_θ are collected in Table 3.[3]

Figures 4, 5, and 6 show, respectively, plots of ΔE_R, ΔE_θ, and ΔE_{def} versus $\Delta E_0^{\ne}$. The relationship between ΔE_R and $\Delta E_0^{\ne}$ is linear ($r = 0.954$), as is the relationship between ΔE_{def} and $\Delta E_0^{\ne}$ ($r = 0.979$), but ΔE_θ is poorly correlated with $\Delta E_0^{\ne}$. In addition, inspection of the data of Table 3 reveals that ΔE_{def} is dominated by the stretching deformation.

The most interesting observation is that the quantity ($\Delta E_{\text{def}} - \Delta E_0^{\ne}$) is constant. For this series of eight X's, at the HF/4-31G level, the difference is 25.1 ± 3.3 kcal/mol. *This is an important result. It implies that the differences in the intrinsic barriers result from the differences in* ΔE_{def}*; the effect of the anion* X^- *is approximately constant.* As will be discussed below, this finding, especially, constitutes strong support for the State Correlation Diagram (SCD) model of the S_N2 barrier.

[3] For X = F, the ΔE_{def} calculated from the energy difference between **1** and **2** is the same as the deformation energy obtained from a Morokuma analysis (10). The authors thank Dr. J. M. Lefour (Orsay) for checking this point.

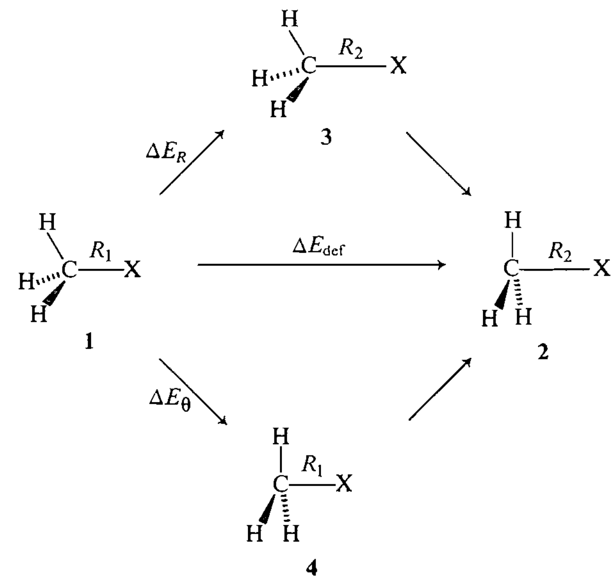

SCHEME 1

TABLE 3. Calculated deformation energies and the components of these deformation energies[a] for reactions $X^- + CH_3X \rightarrow XCH_3 + X^-$

X	ΔE_R	ΔE_θ	ΔE_{def}	$\Delta E_0^{\ne}$	$(\Delta E_{\text{def}} - \Delta E_0^{\ne})$
H	67.4	28.6	71.7	52.0	19.7
CCH	74.7	39.5	73.5	50.4	23.1
CN	68.7	36.0	67.0	43.8	23.2
*N*C	63.1	38.3	57.0	28.5	28.5
OH	45.7	45.9	52.1	21.2	30.9
SH	37.2	28.7	38.8	15.6	23.2
F	38.8	30.4	40.8	11.7	29.1
Cl	27.6	18.5	28.9	5.5	23.4

[a] In kcal/mol.

As an additional probe of the identity S_N2 surface near the top of the barrier, vibrational frequency calculations were carried out for the eight transition states. Each structure has one imaginary frequency whose magnitude depends on the mass of X and on the curvature of the surface. The normal coordinate that corresponds to the imaginary frequency is the transition vector, which points along the intrinsic reaction path linking reactants and products. The transition vectors for the eight identity reactions are summarized in Table 4. To facilitate comparisons, in Fig. 7 the vectors have been shifted by an overall translation, to allow the central carbon atoms to remain stationary.

All of the transition vectors are very similar, despite the differences in the intrinsic barriers, and are dominated in each case by a C—X stretch. There is also a component of bend. Analysis of the force constants of the transition structures reveals that the bending potential has a positive curvature, and the stretching potential has a small positive or negative curvature; the stretch–bend interaction is always negative, and accounts for a sizeable fraction of the negative curvature. This analysis therefore indicates that the C—X stretch dominates the energetics associated with the barrier process, but the intrinsic reaction path requires the concerted action of stretching and bending at the transition state.

The foregoing computational results may be summarized as follows.

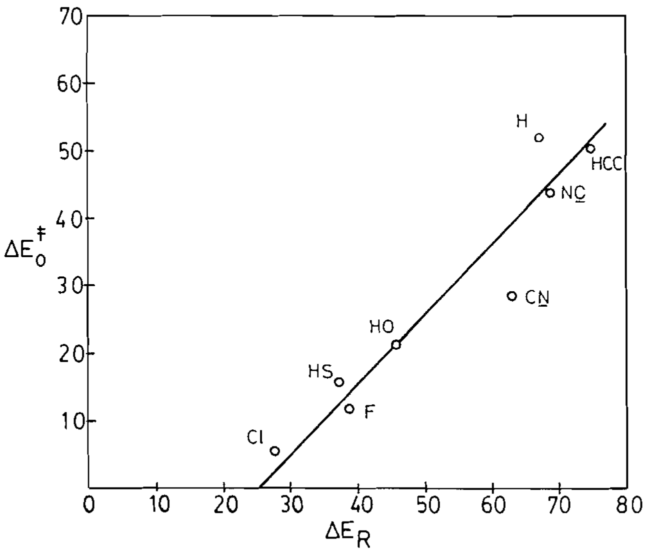

FIG. 4. A plot of ΔE_R versus $\Delta E_0^{\neq}$ for eight identity S_N2 reactions. Energies are in kcal/mol.

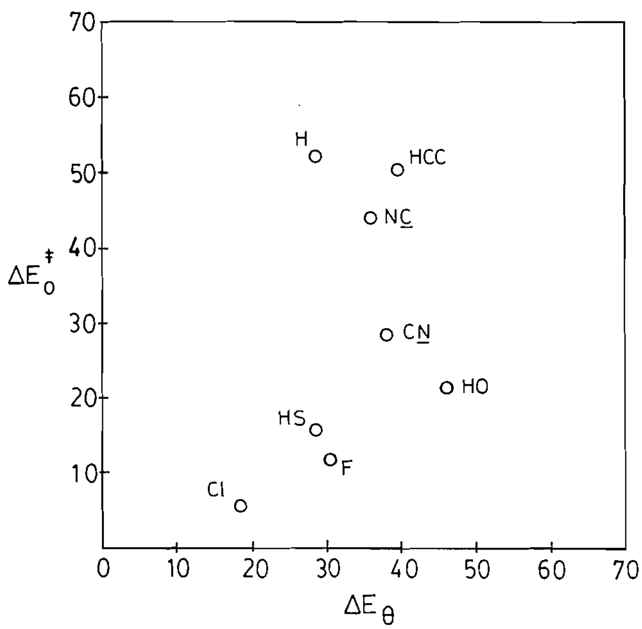

FIG. 5. A plot of ΔE_θ versus $\Delta E_0^{\neq}$ for eight identity S_N2 reactions. Energies are in kcal/mol

(a) The activation process of an identity S_N2 reaction is dominated by the deformation energy required to bring CH_3X from its geometry in the cluster to its geometry in the transition state.

(b) The deformation energy depends on the nature of X, and follows the order H ≃ HCC ≃ *C*N > *N*C > HO > HS > F > Cl.

(c) The C—X stretch is the distinguished deformation leading to the transition state.

(d) The C—X stretch required to achieve the transition state is linearly correlated with the intrinsic barrier.

Interpretation of the results in terms of the SCD model of the S_N2 barrier

An understanding of the activation process in the S_N2 reac-

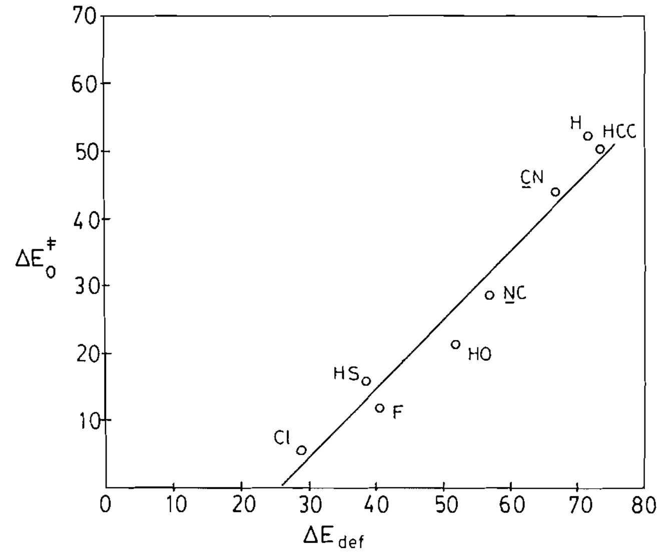

FIG. 6. A plot of ΔE_{def} versus $\Delta E_0^{\neq}$ for eight identity S_N2 reactions. Energies are in kcal/mol.

TABLE 4. X—CH_3—X transition vectors in internal coordinates

X	ΔR (C—X)[a]	$\Delta\theta$ (CH—C—X)[b]
H	0.797	0.206
HCC	1.012	0.506
*C*N	1.115	0.481
*N*C	1.125	0.461
HO	1.014	0.480
HS	1.122	0.492
F	1.120	0.531
Cl	1.128	0.439

[a] In atomic units.
[b] In radians.

tion requires an understanding of the results just described. In the SCD model, the correlation diagram appropriate to an identity S_N2 reaction is shown in Fig. 8 (5*a*, *b*), whose anchor points are the two ground states and the two charge transfer states of the clusters. The transition state results from an avoided crossing of the two curves, and its geometry coincides with the crossing point.

At this point, the ground state $X\!:^-$R—X and the charge transfer state X·(R$\dot{—}$X)$^-$ have the same energy. Because of the energy gap that separates the two states at the beginning of the reaction, the crossing that achieves the transition state must be driven by molecular distortions (5, 13). The effects of these distortions are a destabilization of the ground state, and a concomitant stabilization of the charge transfer state.

That the ground state should be destabilized by the distortions depicted in **5** is self-evident. The charge transfer state is stabilized by the transformation of the (R$\dot{—}$X)$^-$ radical anion bond into a covalent X—R bond on the opposite side of R.

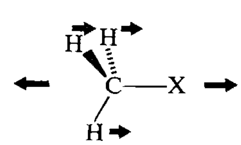

5

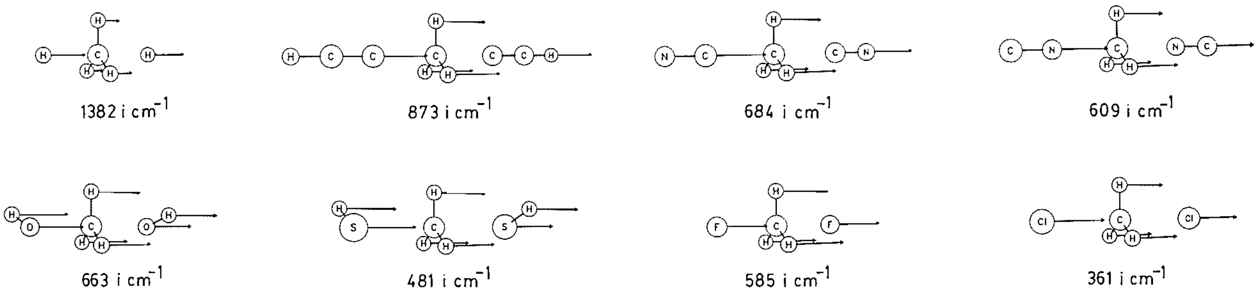

FIG. 7. Transition vectors for eight identity S_N2 transition structures. Calculations performed at the HF/4-31G level using GAUSSIAN 82.

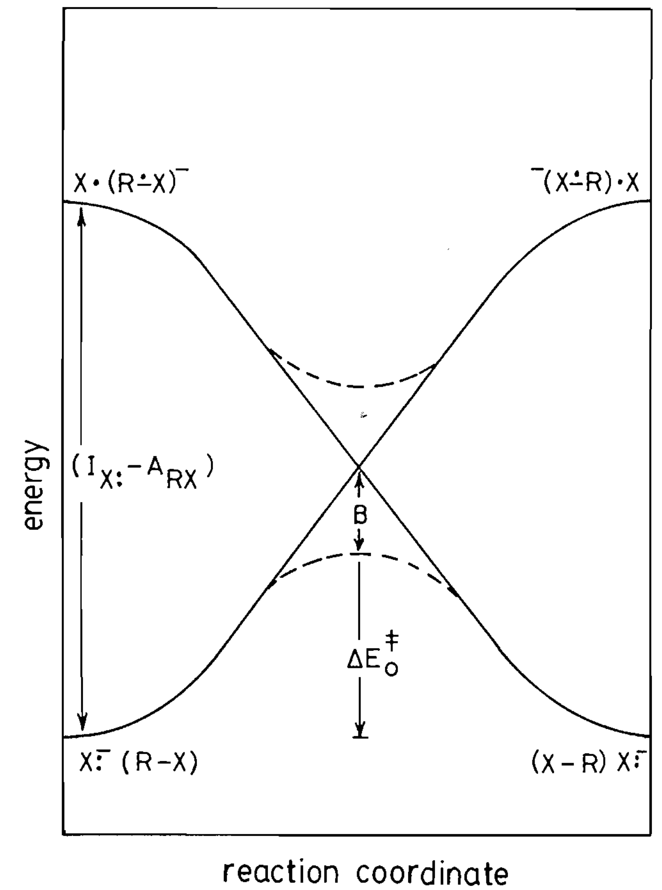

FIG. 8. State correlation diagram for the identity S_N2 reaction. The minima along the reaction coordinate refer to the ion–molecule clusters, and the maxima refer to the charge transfer states. The avoided crossing is given by B, $\Delta E_0^{\neq}$ is the central barrier, and $(I_X - A_{RX})$ is the electron transfer energy gap. The reaction coordinate can be defined as the difference between the X . . . R and R . . . X distances.

The conclusion that the S_N2 barrier results from the distortion required to reach the crossing point of the ground and charge transfer states provides a physical model for the correlation between $\Delta E_0^{\neq}$ and ΔE_{def}. In addition, two features of Fig. 8 allow the magnitudes of $\Delta E_0^{\neq}$ and ΔE_{def} to be estimated. One is the electron transfer energy gap (eq. [5]) that has to be overcome by the molecular distortions, where $I_{X:}$ is the ioniza-

$$[5] \quad \text{gap} = I_{X:} - A_{RX}$$

tion potential of X^- and A_{RX} is the electron affinity of RX. The second is the curvature of the functions that connect the ground and charge transfer states. When the distortion is inefficient, a shallow descent of the charge transfer state will be observed, as

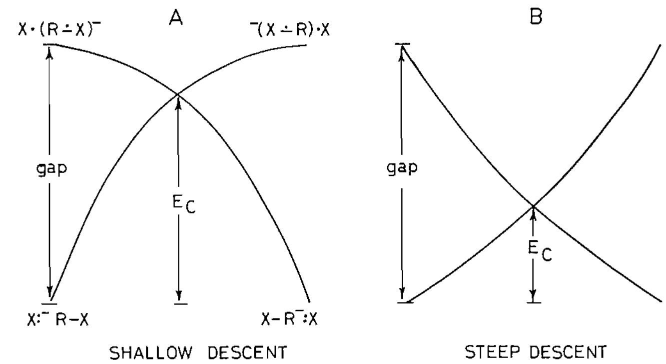

FIG. 9. (A) Shallow descent from the charge transfer state, a property of delocalized radical anions $(R\dot{-}X)^-$. (B) Steep descent from the charge transfer state, corresponding to efficient distortion of the charge transfer state.

shown in Fig. 9A. An efficient distortion will lead to a steep descent from the charge transfer state, as shown in Fig. 9B. For X's characterized by the same gap, the S_N2 barrier will decrease as the distortion becomes more efficient. As discussed elsewhere (5*a*, *b*, *d*, 6), the steepness or shallowness of descent in such cases is determined by the degree of delocalization of the odd electron in the radical anion $(R\dot{-}X)^-$. For example, delocalization in the radical anion results in a shallow descent for two reasons: (1) the distortion must overcome the delocalization energy; (2) the delocalization inhibits bond coupling between X· and $(R\dot{-}X)^-$.

A radical anion may possess two modes of delocalization, termed intralinkage and interlinkage. The intralinkage mode is defined by eq. [6], where $W_{R:}$ and $W_{X:}$ refer to the weights (i.e., the squares of the coefficients) of the resonance forms $R{:}^-{\cdot}X$ and $R{\cdot}{:}X^-$, respectively.

$$[6] \quad (R\dot{-}X)^- = W_{R:}(R{:}^-{\cdot}X) + W_{X:}(R{\cdot}{:}X^-); \quad W_{R:} + W_{X:} = 1$$

In a delocalized radical anion, $W_{R:}$ is large. This delocalizes the odd electron on X of $(R\dot{-}X)^-$ and leads to the inhibition of bond coupling noted above.

The interlinkage mode occurs whenever R bears two or more identical leaving groups X, as in CH_2Cl_2 or CH_4. In such cases the odd electron will be delocalized over all identical linkages (5*d*) as depicted in eq. [7] for $(CH_4)^{\dot{-}}$, where N is the normalization constant.

$$[7] \quad (CH_4)^{\dot{-}} = N[\text{H}\dot{-}\underset{\text{H}}{\overset{\text{H}}{\text{C}}}\text{—H} + \text{H—}\underset{\text{H}}{\overset{\text{H}}{\text{C}}}\dot{-}\text{H} + \ldots\ldots]$$

Since the odd electron may also exhibit intralinkage delocalization in the sense of eq. [6], such radical anions will be strongly delocalized; S_N2 reactions in these cases will be characterized by the shallow descent depicted in Fig. 9A.

The total index of delocalization $\bar{W}_{R:}$ can be taken as the product of the intralinkage index $W_{R:}$ and the interlinkage index. The latter is given by the inverse of the normalization constant of eq. [7], which takes into account the number of bonds that participate in delocalization. For example, in $(CH_4)^{\overset{\bullet}{-}}$ the interlinkage index is $(4)^{-1/2}$.

[8] $\bar{W}_{R:} = W_{R:}/N$

The deformation energy required to reach the transition state can be set approximately equal to the height of the crossing point E_C (Figs. 9A, 9B) above the cluster. As is evident from Figs. 8, 9A, and 9B, E_C is a fraction, f, of the energy gap ($I_{X:} - A_{RX}$), and this fraction is proportional to $\bar{W}_{R:}$, leading to eq. [9]. A similar expression holds for the barrier itself, with the modification that the avoided crossing B (Fig. 8) must be subtracted from E_C. This leads to eq. [10].

[9] $\Delta E_{def} \sim E_C = f(I_{X:} - A_{RX});\quad f \propto \bar{W}_{R:}$

[10] $\Delta E_0^{\neq} = f(I_{X:} - A_{RX}) - B;\quad f \propto \bar{W}_{R:}$

As discussed elsewhere (5, 6, 13), the avoided crossing is approximately constant for the identity reactions (B = 14 kcal/mol) (5*a*, *b*, *d*). This result is thus consistent with the HF/4-31G computational finding that ΔE_{def} differs from $\Delta E_0^{\neq}$ by a constant 25 kcal/mol. Equation [10] can be simplified further and given quantitative predictive ability by setting the proportionality constant between f and $\bar{W}_{R:}$ equal to unity (5) (eq. [11]).

[11] $\Delta E_0^{\neq}$ (kcal/mol) $= \bar{W}_{R:}(I_{X:} - A_{RX}) - 14$

Equations [9] and [11] reveal that trends in $\Delta E_0^{\neq}$ and in ΔE_{def} will be determined by the interplay between $\bar{W}_{R:}$ and ($I_{X:} - A_{RX}$). This point is illustrated by the data collected in Table 5, viz., the reactivity indices ($I_{X:} - A_{RX}$) and $\bar{W}_{R:}$, the calculated ΔE_{def}, the calculated $\Delta E_0^{\neq}$, and the $\Delta E_0^{\neq}$ given by eq. [11]. The deformation energy is large and the barrier is large when the electron transfer energy gap ($I_{X:} - A_{RX}$) is large, or when the shallowness index ($\bar{W}_{R:}$) is large. For example, in entries 1 and 2, $\bar{W}_{R:}$ is approximately constant; and the reaction $F^- + CH_3F$ has a higher $\Delta E_0^{\neq}$ and a higher ΔE_{def} than the reaction $Cl^- + CH_3Cl$ because the electron transfer energy is larger in the former case. Similarly, in entries 3, 4, and 5, $\bar{W}_{R:}$ is again approximately constant; in these cases as well, $\Delta E_0^{\neq}$ and ΔE_{def} increase as the electron transfer energy gap increases.

On the other hand, comparison of entries 1 and 4, for which the energy gap is approximately constant, shows that $HO^- + CH_3OH$, the reaction having the larger $\bar{W}_{R:}$, has the larger $\Delta E_0^{\neq}$ and the larger ΔE_{def}.

In summary, the Surface Crossing Diagram model (Fig. 8) and its quantitative representation (eq. [11]) reproduce the calculated trends in $\Delta E_0^{\neq}$ and ΔE_{def}. It follows that the activation process in an identity S_N2 reaction is a result of the distortion that is required to transfer one electron from $X:^-$ to CH_3X.

The availability of a physical model of the activation process allows the trends in the transition state geometries to be interpreted. In an identity S_N2 reaction, the distortion that distinguishes one X from another is $\Delta R = (R_2 - R_1)$, the change in the C—X bond length from the cluster to the transition state. The percentage of C—X lengthening at the transition state may be defined as the Distortion Index, DI (eq. [12]). This reflects the "tightness" or "looseness" of the transition state. A large DI corresponds to a looser or "exploded" (14) transition state.

TABLE 5. Reactivity indices, ΔE_{def}, $\Delta E_0^{\neq}$, and $\Delta E_0^{\neq}$ (eq. [11]), for $X^- + CH_3X \rightarrow XCH_3 + X^-$ reactions[a]

Entry	X	$I_{X:} - A_{RX}$[b]	$\bar{W}_{R:}$[b]	ΔE_{def}[c]	$\Delta E_0^{\neq}$	$\Delta E_0^{\neq}$ (eq. [11])[c]
1	Cl	113	0.251	28.9	5.5	14.4
2	F	135	0.242	40.8	11.7	18.7
3	HS	95	0.340	38.8	15.6	18.1
4	HO	109	0.357	52.1	21.2	24.9
5	HCC	145	0.362	73.5	50.4	38.5
6	NC	159	0.309	67.0	43.8	34.5
7	H	84	0.720	71.7	52.0	46.5

[a] In kcal/mol.
[b] See refs. 5*a*, *b*, *d*, and 6.
[c] Present work.

[12] $DI = 100\Delta R/R_1$

The factors that control the DI are, again ($I_{X:} - A_{RX}$) and $\bar{W}_{R:}$. The first defines the energy gap that must be overcome by the distortion. The second reflects the ability of the distortion to decrease the energy of the charge transfer state. The following trends are predicted.

(a) For a series of reactions $X^- + CH_3X$ in which the degree of radical anion delocalization ($\bar{W}_{R:}$) remains constant, DI will increase as the energy gap increases, i.e., the transition state will become looser.

(b) For a series of $X^- + CH_3X$ reactions in which the energy gap remains constant, DI will increase as $\bar{W}_{R:}$ increases.

The data of Table 6 illustrate these points. From entries 1 and 2, which have the same $\bar{W}_{R:}$, it is seen that the looser transition state (larger DI) is obtained for $F^- + CH_3F$, which has the larger charge transfer energy gap. Similarly, in entries 3, 4, and 5, the looseness of the transition state again increases as the energy gap increases. On the other hand, entries 1 and 4 demonstrate that, for a constant gap, the transition state becomes looser as $\bar{W}_{R:}$ increases. Clearly, delocalization of the radical anion (larger $\bar{W}_{R:}$) leads to a loosening of the transition structure. The loosest transition state is thus observed for $H^- + CH_4$, because this leads to the most delocalized radical anion.

Table 6 also illustrates an additional correlation, between $\Delta E_0^{\neq}$ and the Distortion Index. The tightest transition state ($Cl^- + CH_3Cl$) has the lowest barrier, and the loosest transition state ($H^- + CH_4$) has the highest barrier.

What has thus emerged is a direct link between deformation energies, barriers, and transition state geometries, each of which is a consequence of the activation process in an S_N2 reaction. This unified insight has resulted from the notion that the activation process is itself a result of the distortion required to transfer a single electron from $X:^-$ to X across the CH_3 moiety of CH_3X.

The foregoing analysis of the trends in transition state geometries should be contrasted with the predictions of potential energy surface diagrams (PESD) (cf. Fig. 10) (15). For an identity S_N2 reaction the four corners of the PESD model represent reactants, products, the triple ion configuration ($X^- + CH_3^+ + X^-$), and the high energy hypervalent structure $(XCH_3X)^-$. The transition state lies at the midpoint between reactants and products, and changes in X can make the transi-

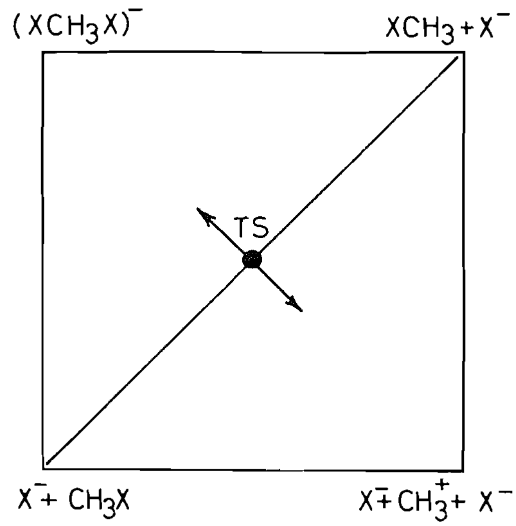

FIG. 10. Potential energy surface diagram for the identity S_N2 reaction.

TABLE 6. Electron transfer energies, radical anion delocalization indices, distortion indices, and intrinsic barriers for $X^- + CH_3X \rightarrow XCH_3 + X^-$ reactions

Entry	X	$I_{X:} - A_{RX}$ [a]	$\bar{W}_{R:}$	DI [b]	$\Delta E_0^{\neq a,b}$
1	Cl	113	0.251	21.1	5.5
2	F	135	0.242	25.0	11.7
3	HS	95	0.340	28.0	15.6
4	HO	109	0.357	30.4	24.9
5	HCC	145	0.362	45.0	50.4
6	NC	159	0.309	44.8	43.8
7	H	84	0.720	58.0	52.0

[a] In kcal/mol.
[b] 4-31G calculations.

tion state tighter or looser, as indicated by the arrows in Fig. 10. Ignoring the effect of the high energy $(XCH_3X)^-$ corner, as is customary, leads to the following conclusion: if a change in X decreases the energy of the triple ion corner, the transition state will shift towards this corner, *and become looser*. For example, replacement of X = H by X = Cl should lead to a looser transition state, because $(Cl^- + CH_3^+ + Cl^-)$ is at least 40 kcal/mol more stable than $(H^- + CH_3^+ + H^-)$.

The trends of Table 5 are just the opposite of this important prediction of the PESD model. It is, therefore, not clear how the PESD model can be employed to rationalize the computational results of the present work.

Acknowledgements

This work was supported by the Natural Sciences and Engineering Research Council of Canada and the National Science Foundation (U.S.A.). One of the authors (S.S.S.) thanks the Laboratoire de Chimie Théorique (Orsay) for support during his sabbatical leave.

1. M. J. PELLERITE and J. I. BRAUMAN. J. Am. Chem. Soc. **105**, 2672 (1983), and references cited therein.
2. D. J. MITCHELL. Ph.D. Thesis. Queen's University, 1981, and references cited therein.
3. S. WOLFE, D. J. MITCHELL, and H. B. SCHLEGEL. J. Am. Chem. Soc. **103**, 7692 (1981).
4. S. S. SHAIK. J. Am. Chem. Soc. **103**, 3692 (1981).
5. (*a*) S. S. SHAIK. Nouv. J. Chim. **6**, 159 (1982); (*b*) S. S. SHAIK and A. PROSS. J. Am. Chem. Soc. **104**, 2708 (1982); (*c*) S. S. SHAIK and A. PROSS. Bull. Soc. Chim. Belg. **91**, 355 (1982); (*d*) S. S. SHAIK. J. Am. Chem. Soc. **105**, 4359 (1983); (*e*) S. S. SHAIK. Nouv. J. Chim. **7**, 201 (1983); (*f*) A. PROSS and S. S. SHAIK. Acc. Chem. Res. **16**, 363 (1983); (*g*) S. S. SHAIK. J. Am. Chem. Soc. **106**, 1227 (1984).
6. S. S. SHAIK. Prog. Phys. Org. Chem. In press.
7. S. WOLFE, D. J. MITCHELL, and H. B. SCHLEGEL. J. Am. Chem. Soc. **103**, 7694 (1981).
8. J. S. BINKLEY, R. A. WHITESIDE, R. KRISHNAN, R. SEEGER, D. J. DEFREES, H. B. SCHLEGEL, S. TOPIOL, L. R. KAHN, and J. A. POPLE. QCPE, **13**, 406 (1981).
9. J. S. BINKLEY, M. J. FRISCH, D. J. DEFREES, K. RAGHAVACHARI, R. A. WHITESIDE, R. SEEGER, H. B. SCHLEGEL, and J. A. POPLE. To be published.
10. S. NAGASE and K. MOROKUMA. J. Am. Chem. Soc. **100**, 1666 (1978).
11. P. M. MORSE. Phys. Rev. **34**, 210 (1932).
12. M. H. BAGHAL-VAYJOODEE, J. L. COLLISTER, and H. O. PRITCHARD. Can. J. Chem. **55**, 2634 (1977).
13. S. S. SHAIK. Isr. J. Chem. In press.
14. B. L. KNIER and W. P. JENCKS. J. Am. Chem. Soc. **102**, 6789 (1980).
15. E. R. THORNTON. J. Am. Chem. Soc. **89**, 2915 (1967); R. A. MORE O'FERRALL. J. Chem. Soc. B, 274 (1970); W. P. JENCKS. Chem. Rev. **72**, 705 (1972); J. C. HARRIS and J. L. KURZ. J. Am. Chem. Soc. **92**, 349 (1970); J. E. CRITCHLOW. J. Chem. Soc. Faraday Trans. **68**, 1774 (1972); D. A. JENCKS and W. P. JENCKS. J. Am. Chem. Soc. **99**, 7948 (1977); A. J. KRESGE. Acc. Chem. Res. **8**, 354 (1975).

Intramolecular fluorescence quenching in aminocoumarines. Identification of an excited state with full charge separation

WOLFGANG RETTIG AND ANDRÉ KLOCK
Iwan-N.-Stranski-Institute, Technical University of Berlin, Straße des 17. Juni 112, D-1000 Berlin 12, Federal Republic of Germany

Received September 15, 1984

This paper is dedicated to Professor Camille Sandorfy on the occasion of his 65th birthday

WOLFGAND RETTIG and ANDRÉ KLOCK. Can. J. Chem. **63**, 1649 (1985).

The fluorescence of 6-aminocoumarine (A6C) is very weak and anomalously redshifted as compared to its 7-substituted analogues 4-methyl-7-aminocoumarine (A7C) and 4-methyl-7-diethylaminocoumarine (DEA7C). The solvatochromic redshift in homologous alcohols is much stronger for A6C, pointing to an increased dipole moment of the emitting state. A twisted intramolecular charge transfer (TICT) state with full charge separation is made responsible for this emission. This is rationalized by molecules-in-molecules calculations. The strong Stokes shift in n-hexane and in ethanol glass at 77 K suggests that A6C emits from a TICT state even under these conditions.

WOLFGAND RETTIG et ANDRÉ KLOCK. Can. J. Chem. **63**, 1649 (1985).

La fluorescence de l'amino-6 coumarine (A6C) est très faible et elle glisse de façon anormale vers le rouge si on fait une comparaison avec des composés analogues substitués en position-7 comme la méthyl-4 amino-7 coumarine (A7C) et la méthyl-4 diéthylamino-7 coumarine (DEA7C). Le glissement solvatochrome vers le rouge provoqué par les alcools homologues est plus prononcé avec le A6C et ceci suggère qu'il y a une augmentation du moment dipolaire de l'état qui émet. On attribue cette émission à un état de transfert de charge intramoléculaire croisé (TC1C) avec une séparation complète de charges. On rationalise ce fait en fonction des calculs sur des molécules dans des molécules. Le fort glissement de Stokes dans le n-hexane et dans l'éthanol à 77 K suggère que, même dans ces conditions, le A6C émet à partir de l'état TCIC.

[Traduit par le journal]

Introduction

Lippert and co-workers (1–5) observed several types of adiabatic and diabatic photoreactions in dilute solutions of 7-hydroxycoumarine and related compounds as revealed from multiple fluorescence spectra.

Only those coumarine dyes which possess an electron donor substituent in the 7 position showed a rather high and tunable LASER efficiency, whereas donor substitution in the 6 position strongly reduces the fluorescence quantum yield. Even some 7-dialkylamino coumarines are prone to undergo fluorescence quenching in polar solvents. This has been traced back by Jones, Halpern *et al.* (6, 7) to an adiabatic photoreaction towards a nonemissive state.

From the substituent and solvent dependence, this state was shown to be connected with the donor and acceptor properties of amine and coumarine moieties, and was assigned as a Twisted Intramolecular Charge Transfer (TICT) state (8) with the dialkylamino group twisted perpendicularly to the plane of the coumarine skeleton. By making this twisting motion unavailable through ring closure to the "rigidized structure" of Coumarine 102 or 153, the fluorescence quenching is suppressed (7). For the same reason, "rigidized" rhodamines show an enhanced fluorescence quantum yield at room temperature as compared to the nonrigidized strctures (rhodamine B vs. rhodamine 101 (9–11). Similarly, it has been shown that the extremely low fluorescence quantum yield of triphenyl methane dyes can be traced back to the formation of a charge-localized TICT state of very short lifetime (12), and that the comparatively low fluorescence quantum yield of 6-hydroxy-9-phenyl-fluoron (13), a close relative to fluorescein, can be understood on the same basis (rotation of the phenyl group).

In all of the above cases, the TICT state is found to be nonfluorescent. Emission from a TICT state seems to be more the exception than the rule. In the favourable cases of observable TICT emission, however, which often goes along with dual fluorescence (8, 14–19), this emission can yield important information on the properties of this state. Solvatochromic measurements show that the TICT state involves a complete charge separation even for symmetric compounds (18). Its photophysical properties are consistent with a forbidden radiative transition to the ground state (8, 20, 21).

Here, we report on the fluorescence of 6-aminocoumarine (A6C), which is weak (22) and strongly redshifted. The photophysical data are consistent with the emission from a TICT state.

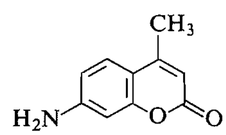

A7C

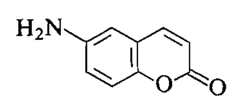

A6C

Experimental

6-Aminocoumarine (A6C) was a gift from Bayer/Leverkusen and showed, after purification, a mp 162.5–163.0°C (lit. (22) mp 162.6–163.4°C). 4-Methyl-7-aminocoumarine (A7C) and 4-methyl-7-diethylaminocoumarine (DEA7C) were purchased from Eastman (Coumarin 120 and 1, respectively). All compounds were purified by repeated recrystallization and subsequent vacuum sublimation. The solvents used were of Merck Uvasol quality or Fluka puriss. and showed no impurity emission at the sensitivity levels used.

Absorption spectra were taken on a Cary 17 spectrometer, and corrected fluorescence and fluorescence excitation spectra on a FICA 55 MK II or a Perkin Elmer 650-60 spectrofluorimeter. Fluorescence quantum yields (optical densities < 0.15) were determined for aerated solutions relative to DEA7C in ethanol (ϕ_f = 0.59 (6)) and are corrected for refractive index changes of the solvent. Decay time measurements were made on aerated solutions using an Edinburgh instruments single photon counting device. Decays were found to be monoexponential over 3 decades.

Molecules-in-molecules (MIM) calculations were performed using a program written by P. Straub and described in ref. 23. Details were kept as described in ref. 24. Ideal geometries (all angles 120°, $r_{C—C}$

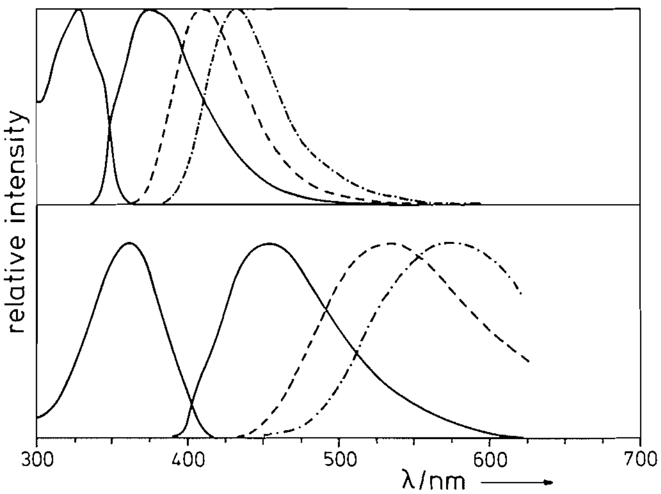

FIG. 1. Normalized fluorescence excitation and emission spectra (corrected for lamp profile and spectral sensitivity distribution) of A6C (lower part) and A7C (upper part) in n-hexane (—), and emission spectra in acetonitrile (- - -) and ethanol (-·-·-), at room temperature.

$= r_{C—O} = 1.40$, $r_{C—N} = 1.46$ Å) were assumed. The ionization potential of the dimethylamino group was taken to be 8.24 eV, the electron affinity of coumarine 0.482 eV. Nine locally excited coumarine states (each represented by linear combination of up to 3 configurations from a standard PPP-SCF-CI calculation) and 2 amino-to-coumarine charge transfer states were taken into consideration. For coumarine, Hückel MO's (heteroparameters taken from ref. 25) were used. A-factors for solvatochromic measurements were calculated using a program developed for the microstructural solvent interaction (MSI) model (16), with all bond lengths equal to 1.4 Å.

Results

Figure 1 shows the fluorescence excitation and emission spectra of A6C and A7C in hexane and the redshifted emission in ethanol and acetonitrile. Contrary to the excitation spectra, which do not differ strongly for the two compounds and which are identical to the absorption spectra, the emission spectra strongly differ but are independent of excitation wavelength and concentration. The Stokes shift $\Delta\tilde{\nu}_{St}$ (in cm^{-1}) is nearly doubled for A6C as compared to A7C, and the solvent polarity has much stronger effect in the case of A6C. This is shown more precisely by the fluorescence maxima in a series of homologous n-alcohols (Table 1).

The data of Table 1 can be converted into a solvatochromic plot (Fig. 2) using Lippert's equation [1] (26, 27).

$$[1] \quad \tilde{\nu}_a - \tilde{\nu}_e = \Delta\tilde{\nu}_{St} = \frac{2}{hc}\frac{(\mu_e - \mu_g)^2}{a^3} \cdot \Delta f + \text{const.}$$

where μ_g and μ_e are ground and excited state dipole moments, respectively, a is the Onsager radius, h and c are fundamental constants, and Δf is a solvent polarity function depending on dielectric constant ϵ and refractive index n (see Fig. 2). Although the Lippert equation does not take into account polarizability effects and the deviation from colinearity of $\boldsymbol{\mu}_g$ and μ_e, eq. [1] is used here, because the MIM calculations indicate the angle between μ_e and μ_g to be small.

The slopes and intercepts thus determined are collected in Table 2. For extracting $\Delta\mu = \mu_e - \mu_g$, the Onsager parameter a was taken as approximately 40% of the long axis of the molecules, a value suggested by Lippert for elongated nonspherical molecules (27). A more precise comparison of relative $\Delta\mu$ values can be obtained by using the microstructural solvent interaction (MSI) model (16) which takes into account the actual nonspherical shape of the molecule and its charge distribution differing from that of a point dipole. The resulting equation [2] closely resembles eq. [1] with the simple substitution of A_{MSI} for $1/a^3$.

$$[2] \quad \Delta\tilde{\nu}_{St} = k\, A_{MSI}\, (\mu_e - \mu_g)^2 \cdot \Delta f + \text{const.}$$

The values for $\Delta\mu$ determined by these two methods are also contained in Table 2.

Figure 3 shows the dependence of the fluorescence quantum yields ϕ_f on solvent polarity. For A6C, ϕ_f values are reduced by a factor of ~10 as compared to the other compounds and depend very strongly on solvent polarity. This dependence is

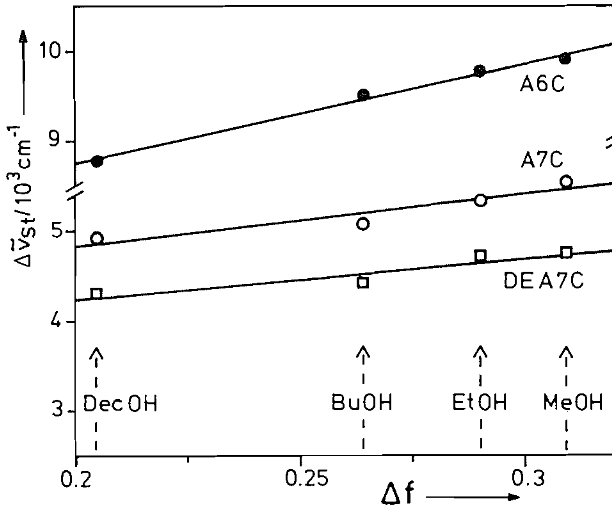

FIG. 2. Fluorescence solvatochromic plot for A6C, A7C, and DEA7C in homologous n-alcohols, $\Delta f = (\epsilon - 1)/(2\epsilon + 1) - (n^2 - 1)/(2n^2 + 1)$.

TABLE 1. Absorption and fluorescence maxima (nm) of A6C, A7C, and DEA7C in homologous alcohols

	A6C		A7C		DEA7C	
Solvent	abs	fluo	abs	fluo	abs	fluo
Methanol	368.5	580.0	350.5	435.0	374.0	454.5
Ethanol	370.5	580.5	352.0	433.0	372.0	451.0
n-Butanol	370.0	570.5	355.0	433.0	373.5	447.0
n-Decanol	375.0	559.0	355.0	430.0	371.5	442.0

TABLE 2. Solvatochromic slopes m ($cm^{-1}/\Delta f$) and interecepts b (cm^{-1}), Onsager radius a (pm) and MSI cavity factors (A^{rel}_{MSI}), and derived dipole moment differences $\Delta\mu = \mu_e - \mu_g$

Parameters	A6C	A7C	DEA7C
m	11000	5720	4530
b	6550	3680	3330
a[a]	4.35	4.35	5.23
$\Delta\mu^{Lip}$ (Debye units)	9.51	6.84	8.02
A^{rel}_{MSI}	"1.0"	1.07	0.71
$\Delta\mu^{rel}_{MSI}$	"1.0"	0.70	0.76

[a] 80% of the long half-axis of an ellipsoid surrounding the molecular skeleton including the van der Waals radii (from standard tables).

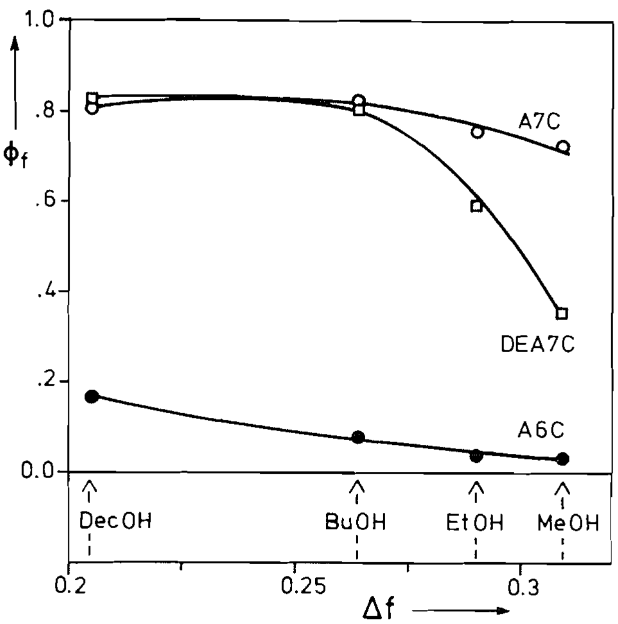

FIG. 3. The dependence of fluorescence quantum yields (±15%) of A6C, A7C, and DEA7C in homologous alcohols on the solvent polarity function Δf. The lines are for clarity only and emphasize the decrease of fluorescence quantum yield with increasing solvent polarity for all of the investigated compounds.

TABLE 3. Fluorescence decay times (ns) for A6C and A7C in different solvents

	Solvent		
	n-Hexane	Acetonitrile	Ethanol
A6C	3.5	9.4	2.3
A7C	3.9	3.3	4.3[a]

[a]In 50% ethanol from ref. 9, corrected for oxygen quenching.

much weaker for DEA7C and nearly absent for A7C. Table 3 contains the observed decay times which, together with ϕ_f, yield values for the radiative rate constant k_f. k_f is strongly reduced for A6C ($\approx 1.6 \times 10^8\ s^{-1}$ for A7C and $\approx 1.7 \times 10^7\ s^{-1}$ for A6C in ethanol).

Figure 4 shows the fluorescence spectra of A6C in ethanol at different temperatures down to 77 K.

Discussion

Both A7C and DEA7C show high solvatochromic slopes indicative of a large excited state dipole moment (Table 2). The wave functions of the excited state are thus of intramolecular charge transfer (ICT) character, i.e. contain the coumarine locally excited (LE) state (C*) with a high weight of the charge transfer configuration $|N^+C^-\rangle$, where N stands for the amino group and C for the coumarine moiety (6, 7). Solvatochromic slope and excited state dipole moment μ_e are even larger for A6C.

A further prominent difference of A6C from A7C and DEA7C is the large Stokes shift $\Delta\tilde{\nu}_{St}$, which for A7C in methanol amounts to ~5500 cm^{-1} and increases to ~9900 cm^{-1} for A6C. This Stokes shift is comparable to that of TICT fluorescence bands (~13 400 cm^{-1} for *N,N*-dimethylaminobenzonitrile (DMABN) in methanol (14) or 9800 cm^{-1} for

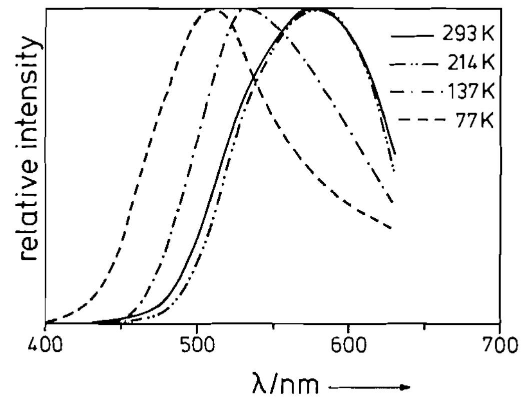

FIG. 4. Fluorescence spectra of A6C in ethanol at different temperatures.

bis(*N,N*-dimethylaminophenyl)-sulfone in methanol). Even in hexane, the strong difference from A7C in $\Delta\tilde{\nu}_{St}$ remains (see Fig. 1), consistent with the high intercept for A6C from the solvatochromic plot (Table 2). Thus, an excited state proton transfer mechaism can be excluded. Moreover, the halfwidth $\Delta\tilde{\nu}_{1/2}$ for the emission of A6C in methanol (3950 cm^{-1}) is much larger than that of A7C (2870 cm^{-1}).

We tentatively assign the emission of A6C as arising from a state with pure CT character, i.e. where the excited state wavefunction is represented by $\psi_e \approx |N^+C^-\rangle$ without admixture of $|C^*\rangle$. This is possible if $|C^*\rangle$ and $|N^+C^-\rangle$ belong to different irreducible symmetry representations and cannot interact in a configuration interaction sense. A way to achieve this is to twist the amino lone-pair axis into the plane of the coumarine skeleton, i.e. perpendicular to the coumarine p_z π-orbitals. This situation corresponds to what is known in the literature as the "Twisted Intramolecular Charge Transfer" (TICT) state (8) and is governed by the "minimum overlap rule" (8, 18): the increasing dipole moment for increasingly twisted geometries provides the driving force for the twist towards the TICT (90°) conformation with maximum charge separation via the polar solvent induced energetic stabilization (ΔE_{solv} in eq. [3] below).

By this same electrostatic interaction, the molecule is locked more or less flexibly in the perpendicular conformation.

The very low fluorescence quantum yield and its strong solvent polarity dependence for A6C (Fig. 4) can be interpreted using the above model. From a theoretical viewpoint, emission from a perpendicularly twisted TICT conformation is forbidden by symmetry. Moreover, nonradiative processes ("photochemical funneling") are enhanced for TICT-like structures because ground and excited states can come very closely together (28). The TICT emission thus has to derive from vibrationally excited levels of the S_1 (TICT) state (8), i.e. it corresponds to a hot fluorescence: vibronic coupling via the twisting motion around the perpendicular minimum can couple higher-lying allowed states to the transition moment. In the case of larger aromatics (anthracene, carbazole), a TICT fluorescence quantum yield of up to ~0.4 can thus be obtained (18, 29). The stronger the solvent interaction (more polar solvent), the more the molecule will be confined to a small angular range around ψ = 90° and, for solvent independent nonradiative TICT decay rates k_{nr}, reduced TICT fluorescence quantum yields are expected. For a more quantitative treatment, the solvent dependence of k_{nr} also has to be taken into account.

The very weak solvent dependence of ϕ_f (A7C), on the other

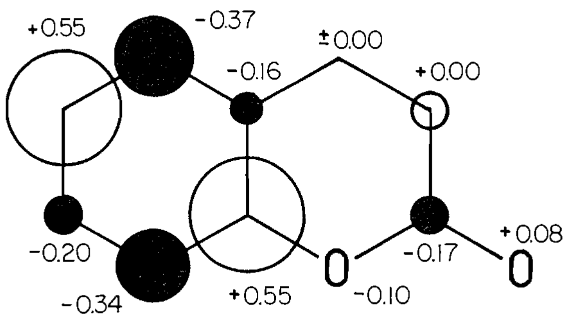

FIG. 5. Lowest unoccupied molecular orbital of coumarine according to the HMO calculation. The surface area of the circles is proportional to the square of the HMO coefficients.

TABLE 4. Coulomb integrals and TICT state energies of substitutional isomers of dimethylamino coumarines:

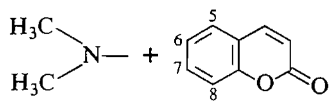

Position of substitution	C^a (eV)	$E(\text{TICT})^b$ (eV)	ΔE^c (eV)
5	−5.02	3.11	−0.37
6	−5.74	2.53	−0.95
7	−4.77	3.58	+0.10
8	−5.11	3.33	−0.15

[a] CT to the lowest unoccupied MO of coumarine, r_{C-N} = 1.46 Å.
[b] MIM calculation, ΔE_{solv} = 0 (gas phase).
[c] $\Delta E = E(\text{TICT}) - E(\text{LE})$, with E(LE) of coumarine = 3.48 eV.

hand, points to essentially solvent polarity independent k_f and k_{nr} rate constants of the ICT state. ϕ_f (DEA7C) is quenched by a factor of 2.3 in going from decanol to methanol. This may be due to the beginning formation of a nonradiative TICT state in this case, in accordance with results of G. Jones *et al.* (7) who find a very strong TICT participation in polar solvents (i.e. fluorescnce quenching) when the acceptor strength of the coumarine is increased by a CF_3 group.

Although fluorescence quantum yields are low for A6C, the decay times are long, characteristic for a forbidden transition. The resultant radiative rate constant k_f is lower than that for A7C by a factor of ≈10.

The question arises as to why the substitutional isomers A6C and A7C behave so differently. This can be rationalized by a consideration of the changes of the TICT energy, which is given by eq. [3].

$$[3] \quad E(\text{TICT}) = \text{IP(D)} - \text{EA(A)} + C + \Delta E_{solv}$$

IP(D) is the ionization potential of the donor (amino group in this case), EA(A) is the electron affinity of the acceptor (coumarine in this case), C is the Coulomb stabilization due to the attraction of radical cation (ionized amino group) and radical anion (reduced coumarine), and ΔE_{solv} is the energy gained by solvating the TICT dipole. For positional isomers, only C and ΔE_{solv} change. As the theoretical TICT dipole moment is quite similar for both A6C and A7C, ΔE_{solv} will also be similar in a given solvent. The main changes are thus due to the Coulomb interaction term C. Table 4 contains the C values calculated for several substitutional isomers of dimethylaminocoumarine, the calculated TICT state energies for the gas phase, and the energy difference ΔE between lowest LE and TICT state. Negative ΔE values indicate that the TICT state is situated below the LE state. The 6-isomer has the lowest-, the 7-isomer the highest-lying TICT state. This is readily visualized by inspecting the lowest unoccupied molecular orbital of coumarine (Fig. 5), which shows a large coefficient at the 6 position and a small one at the 7 position.

A6C is a very unusual TICT state forming molecule insofar as it involves the unsubstituted amino group as a donor. The only other example known to date is 9-aminofluorene, which emits dual fluorescence (19), whereas neither 4-aminobenzonitrile nor *N*-methyl-4-aminobenzonitrile populate a TICT state. Thus, the relatively weak donor character of the NH_2 group is compensated by EA(A) and C in the case of the coumarines (eq. [3]). Judging from the fluorescence spectrum in n-hexane, part of the emission may be due to a TICT state even in this nonpolar solvent. Some other compounds are known to emit TICT fluorescence in alkanes (30, 31).

The low temperature fluorescence spectra of A6C in ethanol (Fig. 4) are virtually insensitive to temperature down to ≈200 K. On further lowering of the temperature, a blue shift is observed which can be ascribed to the incomplete relaxation of the solvent during the excited state lifetime (26). But even at 77 K an anomalously large Stokes redshift (6950 cm^{-1}) is retained. This may be ascribed to the small size of the amino group which even in this rigid matrix can relax to the TICT geometry, possibly by taking advantage of the free volume (32).

Acknowledgements

The authors wish to thank Bayer AG, Leverkusen, for the generous gift of a research sample of A6C, PD Dr. O. S. Wolfbeis, Graz, and Prof. E. Lippert for fruitful discussions, Prof. G. Jones for providing preprints, and Prof. W. Schnabel and Dr. R. Frings, Hahn-Meitner-Institute, Berlin, for making possible the decay time measurements. The financial support by the Bundesministerium für Forschung und Technologie (project 05 286 LI I) and by the Fonds der Chemischen Industrie is gratefully acknowledged.

1. E. LIPPERT. *In* Organic molecular photophysics. Vol. 2. *Edited by* J. B. Birks. J. Wiley & Sons, New York. 1975. pp. 1–31.
2. T. KINDT and E. LIPPERT. *In* Excited states in organic chemistry and biochemistry. *Edited by* B. Pullmann and N. Goldblum. D. Reidel Publishing Company, Dordrecht. 1977. pp. 221–231.
3. O. S. WOLFBEIS, W. RAPP, and E. LIPPERT. Monatsh. Chem. **109**, 899 (1978).
4. O. S. WOLFBEIS and E. LIPPERT. Z. Naturforsch. Teil A, **33**, 238 (1978).
5. O. S. WOLFBEIS, E. LIPPERT, and H. SCHWARZ. Ber. Bunsenges. Phys. Chem. **84**, 1115 (1980).
6. G. JONES II, W. R. JACKSON, and A. M. HALPERN. Chem. Phys. Lett. **72**, 391 (1980).
7. G. JONES II, W. R. JACKSON, CH. CHOI, and W. R. BERGMARK. In press.
8. Z. R. GRABOWSKI, K. ROTKIEWICZ, A. SIEMIARCZUK, D. J. COWLEY, and W. BAUMANN. Nouv. J. Chim. **3**, 443 (1979); Z. R. GRABOWSKI and J. DOBKOWSKI. Pure Appl. Chem. **55**, 245 (1983).
9. T. KARSTENS and K. KOBS. J. Phys. Chem. **84**, 1871 (1980).
10. R. E. SCHWERZEL and N. E. KLOSTERMAN. NBS Spec. Publ. **526**, 3 (1978).
11. K. H. DREXHAGE. Structure and properties of laser dyes. *In* Topics in applied physics. Vol. 1. *Edited by* F. P. Schäfer. Springer, Berlin. 1973.
12. M. VOGEL and W. RETTIG. Proceedings of the Xth IUPAC Sym-

posium on Photochemistry, Interlaken, Switzerland. July 22–27, 1984. p. 579.
13. M. MARTIN. Chem. Phys. Lett. **35**, 105 (1975).
14. E. LIPPERT, W. LÜDER, and H. BOOS. *In* Advances in molecular spectroscopy. *Edited by* A. Mangini. Pergamon, Oxford. 1962. p. 443.
15. W. RETTIG, G. WERMUTH, and E. LIPPERT. Ber. Bunsenges. Phys. Chem. **83**, 692 (1979).
16. W. RETTIG. J. Mol. Struct. **84**, 303 (1982).
17. W. RETTIG and F. MARSCHNER. Nouv. J. Chem. **7**, 425 (1983).
18. W. RETTIG and M. ZANDER. Ber. Bunsenges. Phys. Chem. **87**, 1143 (1983).
19. B. S. VOGT and S. G. SCHULMAN. Chem. Phys. Lett. **89**, 320 (1982).
20. Z. R. GRABOWSKI, K. ROTKIEWICZ, W. RUBASZEWSKA, and E. KIRKOR-KAMIŃSKA. Acta Phys. Pol. A, **54**, 373 (1978).
21. W. RETTIG. J. Lumin. **26**, 21 (1981).
22. CH. A. WHEELOCK. J. Am. Chem. Soc. **81**, 1348 (1959).
23. G. HOHLNEICHER, R. KIESSLING, H. C. JUTZ, and P. A. STRAUB. Ber. Bunsenges. Phys. Chem. **70**, 60 (1966).
24. W. RETTIG, K. ROTKIEWICZ, and W. RUBASZEWSKA. Spectrochim. Acta, Part A, **40**, 241 (1984).
25. E. HEILBRONNER and H. BOCK. Das HMO-Modell und seine Anwendung, Grundlagen und Handhabung. Verlag Chemie, Weinheim. 1968. Part 1. p. 155.
26. E. LIPPERT, W. LÜDER, F. MOLL, W. NÄGELE, H. BOOS, H. PRIGGE, and I. SEIBOLD-BLANKENSTEIN. Angew. Chem. **73**, 695 (1961).
27. E. LIPPERT. Z. Naturforsch. Teil A, **10**, 541 (1955).
28. V. BONAČIĆ-KOUTECKÝ, J. KÖHLER, and J. MICHL. Chem. Phys. Lett. **104**, 440 (1984).
29. W. RETTIG and M. ZANDER. Chem. Phys. Lett. **87**, 229 (1982).
30. G. WERMUTH, W. RETTIG, and E. LIPPERT. Ber. Bunsenges. Phys. Chem. **85**, 64 (1981).
31. W. RETTIG. EPA newsletters, July 1984, p. 25.
32. W. RETTIG. J. Phys. Chem. **86**, 1970 (1982).

One-electron photooxidation of *N*-ethylcarbazole in the presence of carbon tetrachloride. Products and mechanism of the photochemical reaction

BOGUMIL ZELENT AND GILLES DUROCHER[1]

Département de Chimie, Université de Montréal, C.P. 6210, Succ. A, Montréal (Qué.), Canada H3C 3V1

Received September 25, 1984

This paper is dedicated to Professor Camille Sandorfy on the occasion of his 65th birthday

BOGUMIL ZELENT and GILLES DUROCHER. Can. J. Chem. **63**, 1654 (1985).

The mechanism of the photodecomposition of *N*-ethylcarbazole (NEC) in the presence of carbon tetrachloride has been discussed on the basis of the photoproducts identified. The photodissociation of the *N*-ethyl bond and the electron transfer in the transiently formed ex-CT complex, $^1(\mathrm{NEC}^{\delta+}\cdots\mathrm{CCl_4}^{\delta-})^*$, have been proposed as the primary photochemical processes involved in the singlet excited NEC molecule. The latter, treated as the main process, leads to the radical cation of NEC, chloride ion, and trichloromethyl radical in the solvent cage, $[\mathrm{NEC}^{+\cdot}\mathrm{Cl}^-\dot{\mathrm{C}}\mathrm{Cl_3}]$. The other reactions in the system studied are analysed following the decomposition of $\mathrm{NEC}^{+\cdot}$ in the presence of Cl^- and $\dot{\mathrm{C}}\mathrm{Cl_3}$, which can occur by the *N*-ethyl group and (or) by the aromatic ring. The formation of intermediate products such as

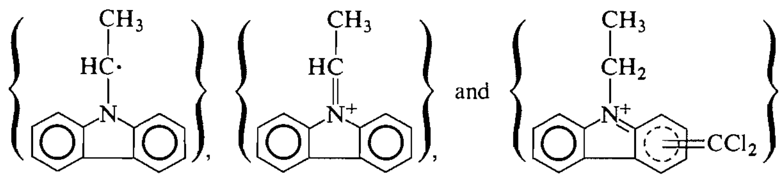

α_r α_k $\gamma_i'(i = 1, 2, 3, \text{or } 4)$

in the solvent cage gives rise to secondary photochemical reactions in the system studied. The polarity and chemical activity of the reaction media used strongly influence the nature of the secondary photochemical transformations both in and outside the solvent cage. The formation mechanism of the photochemical reaction products in CCl_4 when ammonia was used, after and during irradiation, has been explained mainly by the transformations of the radical α_r and cation α_k as well as by the carbazyl radical β, which is also formed in the reaction medium. On the other hand, reaction of the cation γ_i' explains the formation of the photoproducts in the irradiated solution of NEC with CCl_4 in ethanol. These photochemical results have been compared to the photochemical reactions involved in the carbazole–CCl_4 system.

BOGUMIL ZELENT et GILLES DUROCHER. Can. J. Chem. **63**, 1654 (1985).

Le mécanisme de la photodécomposition du éthyl-*N*-carbazole (NEC) en présence de tétrachlorure de carbone (CCl_4) est analysé suite à l'identification des photoproduits obtenus. La photodissociation du lien *N*-éthyl ainsi que le transfert électronique dans le complexe excité de transfer de charge $^1(\mathrm{NEC}^{\delta+}\cdots\mathrm{CCl_4}^{\delta-})^*$ peuvent être la cause de l'acte photochimique primaire suite à l'excitation du NEC dans son état premier singulet. Le phototransfert électronique conduit à l'apparition du radical cation du NEC, à l'anion chlorure et au radical trichlorométhyl dans la cage du solvant, $[\mathrm{NEC}^{+\cdot}\mathrm{Cl}^-\dot{\mathrm{C}}\mathrm{Cl_3}]$. La décomposition du radical cation en présence de Cl^- et de $\dot{\mathrm{C}}\mathrm{Cl_3}$ s'effectue par l'attaque du groupe *N*-éthyl ou par le noyau aromatique. Les produits intermédiaires suivants:

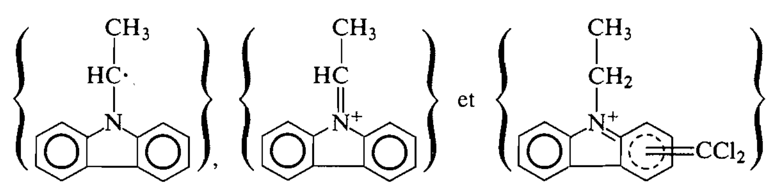

α_r α_k $\gamma_i'(i = 1, 2, 3, \text{ou } 4)$

dans la cage du solvant donnent lieu à l'ensemble des réactions photochimiques secondaires. La polarité ainsi que l'activité chimique du milieu réactionnel influencent fortement la nature des transformations photochimiques secondaires dans la cage du solvant et en dehors de celle-ci. Le mécanisme de formation des produits photochimiques dans le CCl_4 lorsque l'ammoniaque est ajouté au cours et après l'irradiation s'explique principalement par la transformation du radical α_r, du cation α_k et du radical carbazyl β qui est également présent dans le milieu réactionnel. Par ailleurs, la présence des cations γ_i' explique la formation des photoproduits du NEC dans les solutions d'éthanols auxquelles est ajouté du CCl_4. Ces résultats photochimiques ont été comparés à ceux obtenus pour le système carbazole–CCl_4.

Introduction

The photophysical properties of carbazole and its *N*-substituted derivatives (1–5) along with the photochemical reactions (6–8) have been the object of extensive studies in recent years. On the other hand, the electronic spectroscopic properties of carbazoles have also been thoroughly studied (9–12). Most of these investigations were correlated with the theoretical calculations which have been carried out in order to describe the ground and excited electronic states of carbazole (9, 13–15) and *N*-alkyl derivatives of carbazole (11, 16).

[1]Author to whom correspondence may be addressed.

TABLE 1. Photochemical reaction products of *N*-ethylcarbazole in the presence of carbon tetrachloride

		Reaction medium†		
No.	Compound	$CCl_4(NH_3)$	CCl_4-NH_3	CCl_4 in C_2H_5OH
NEC	*N*-Ethylcarbazole	s	s	s
C	Carbazole	a	a	b
1	Hexachloroethane	a	a	b
2	*N*-(Trichlorovinyl)carbazole	b	b	
3	*N*-(β-Dichlorovinyl)carbazole*	a		
4	*N*-(α-Methyl-β-dichlorovinyl)carbazole*	b		
5	*N*-(2-Trichloromethylpropenyl)carbazole*			b
6	1,1-Di(*N*-carbazyl)ethane*	b	a	
7	*N*-(α-Trichloromethylvinyl)carbazole*	a		
8	*N*-Cyanocarbazole	a	a	
9	1-Cyanocarbazole	b		
10	3-Cyanocarbazole	b	b	
11	3-Cyano-*N*-ethylcarbazole		b	
12	3-(Carboethoxy)carbazole			b
13	1-(Carboethoxy)-*N*-ethylcarbazole			b
14	3-(Carboethoxy)-*N*-ethylcarbazole			a
15	4-(Carboethoxy)-*N*-ethylcarbazole*			b
16	1,6-Di(carboethoxy)-*N*-ethylcarbazole*			b
17	2,6-Di(carboethoxy)-*N*-ethylcarbazole*			b
18	3,5-Di(carboethoxy)-*N*-ethylcarbazole*			b
19	3,6-Di(carboethoxy)-*N*-ethylcarbazole			a
20	1,5-Di(carboethoxy)-*N*-ethylcarbazole*			b

*New compound.
†Abbreviations: a, main product of the reaction studied (chemical yields between 5 and 20%); b, minor product of the reaction studied (chemical yields below 5%); s, remaining substrate.

Carbazole and its derivatives, like other aromatic amines in the presence of strong organic electron acceptors such as tetracyanoethylene, tetracyanoquinodimethane, 2,3-dichloro-5,6-dicyano-*p*-benzoquinone, trinitro and tetranitrofluorenones, *p*-chloranil, etc., form charge transfer (CT) complexes (17−22) with new asymmetric absorption bands in the visible region of the spectrum. The asymmetry of these new CT bands was interpreted (18, 19, 22) as being associated with the existence of two closely lying higher occupied molecular π-orbitals of carbazoles (12). The possibility of distinguishing two maxima in asymmetric absorption spectra of the complexes is due to the two CT transitions from the higher occupied molecular orbitals of carbazoles to the lowest vacant orbital of the acceptors. In these ground state CT interaction studies, much attention has been devoted to *N*-ethylcarbazole. The ionization potential of *N*-ethylcarbazole (21) obtained from CT complexes as well as the thermodynamic parameters of the formation of its CT complexes (18, 20) have also been presented and discussed. On the other hand, a singlet excited *N*-ethylcarbazole molecule in the presence of electron acceptor molecules is easily involved in electron transfer reaction, transforming itself to a radical cation (23, 24). The radical cation of *N*-ethylcarbazole in acetonitrile is well characterized by the absorption band at 780 nm (23, 24), which in nitrobenzene is at 800 nm (25).

Carbon tetrachloride is well known to be an efficient fluorescence quencher of a large variety of organic molecules (1, 2, 26−32). The fluorescence quenching process has usually been explained by the exciplex formation between the singlet excited molecule and the CCl_4 molecule. Such transient excited state interaction becomes an important step of photochemical reactions. The electronic excitation of donor molecules like aromatic amines, which possess comparatively low ionization potential in the presence of CCl_4, leads to electron transfer in the transiently formed exciplex (7, 33−35). This is accompanied by the heterolytic dissociation of a C—Cl bond in CCl_4. Such chemical activity in CCl_4 is connected not only with its significant electron affinity (2.12 eV) (28) but also with its comparatively low C—Cl bonding energy (231.2 kJ mol^{-1}) (36) and the low (~0) activation energy of the dissociative process for the electron attachment (37). Because of its properties, CCl_4 is frequently used as an active component in photochemical reactions.

The mechanism of photooxidation of carbazole in the presence of CCl_4 has been studied in our laboratory (7). The ethyl substitution in the carbazole molecule modifies the electronic structure of the aromatic ring system and the possibilities of the photochemical transformations of the molecule. This study proposes a mechanism which explains the photodecomposition of *N*-ethylcarbazole in the presence of CCl_4, based on the photoproducts identified. The mechanism presented will be compared to the photochemical reactions in the carbazole−CCl_4 system. These photochemical results along with the fluorescence spectra of the photoproducts also support the electron transfer mechanism proposed to explain the fluorescence quenching of carbazole and *N*-ethylcarbazole by halocarbons (1).

Results and discussion

In the *N*-ethylcarbazole (NEC) − carbon tetrachloride system the uv radiation absorbed in the ^1L_b band of NEC initiates a complex chemical reaction which leads to a large number of derivatives of carbazole. Table 1 shows the photoproducts obtained from the photodecomposition of NEC in the presence of CCl_4 when the photolyte was neutralized by ammonia gas after irradiation (first column) and during irradiation (second column) as well as when ethanol was used as a photochemical reaction medium (third column). Such products as carbazole (C), *N*-(trichlorovinyl)carbazole (**2**), *N*-(β-dichlorovinyl)-

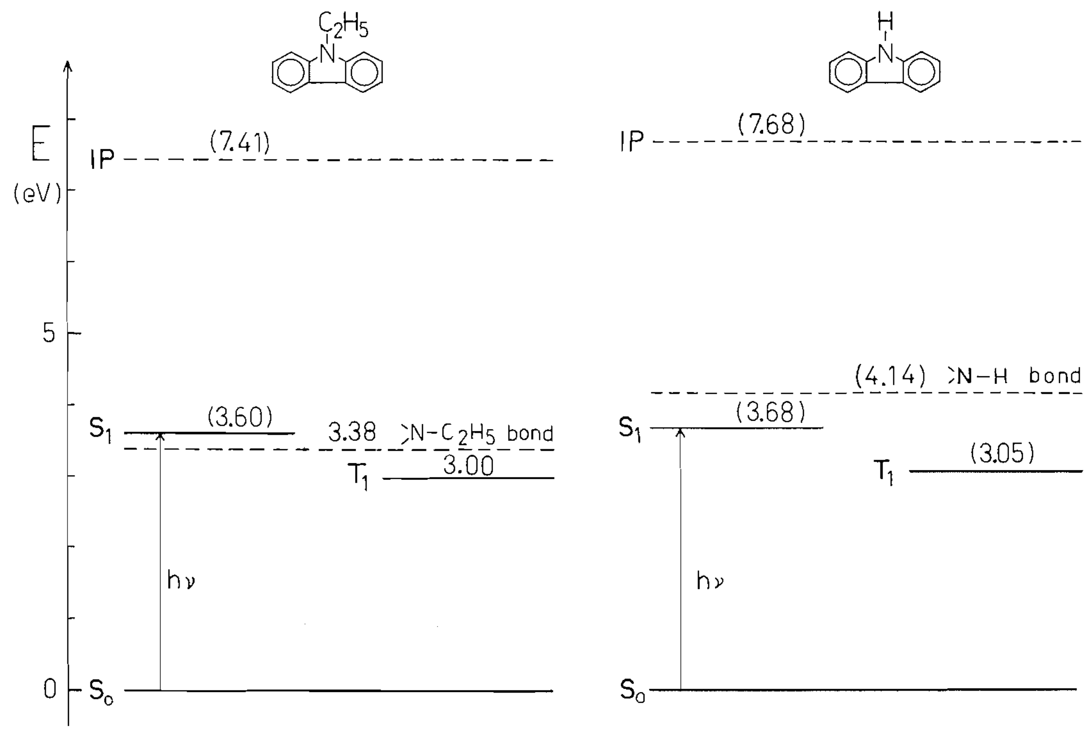

FIG. 1. Energy level diagram for *N*-ethylcarbazole and carbazole.

carbazole (**3**), *N*-(α-methyl-β-dichlorovinyl)carbazole (**4**), *N*-(2-trichloromethylpropenyl)carbazole (**5**), 1,1-di(*N*-carbazyl)-ethane (**6**), *N*-(α-trichloromethylvinyl)carbazole (**7**), and *N*-cyanocarbazole (**8**), as well as 1-cyanocarbazole (**9**) and 3-cyanocarbazole (**10**), indicate the possibilities of the photochemical transformations of NEC by the *N*-ethyl part of the molecule. On the other hand, the compounds **9**, **10**, and 3-cyano-*N*-ethylcarbazole (**11**), in addition to 3-(carboethoxy)-carbazole (**12**) and carboethoxy derivatives of NEC such as 1-(carboethoxy)-*N*-ethylcarbazole (**13**), 3-(carboethoxy)-*N*-ethylcarbazole (**14**), 4-(carboethoxy)-*N*-ethylcarbazole (**15**), 1,6-di(carboethoxy)-*N*-ethylcarbazole (**16**), 2,6-di(carboethoxy)-*N*-ethylcarbazole (**17**), 3,5-di(carboethoxy)-*N*-ethylcarbazole (**18**), 3,6-di(carboethoxy)-*N*-ethylcarbazole (**19**), and 1,5-di-(carboethoxy)-*N*-ethylcarbazole (**20**), which form in ethanol as a solvent, indicate also the participation of the aromatic ring of the NEC molecule in secondary reactions.

Figure 1 shows an energy level diagram for NEC and carbazole based on experimental data (6, 12, 38, 39). This simple energy level diagram indicates that the *N*-ethyl substituent decreases the ionization potential (IP) of the carbazole molecule, and the difference between the ionization potential and the energy of the first singlet state for the NEC molecule is lower than that of carbazole, $[\mathrm{IP(NEC)} - E_{S_1}(\mathrm{NEC})] < [\mathrm{IP(C)} - E_{S_1}(\mathrm{C})]$. Such a relation suggests that the formation of the excited CT complex between the singlet excited NEC molecule and CCl_4 is energetically more probable than it is in the case of carbazole. We also see in the diagram that the energy of the *N*-ethyl bond is lower than the energy of the first singlet state of NEC molecule. This energy diagram also indicates that there exists a certain probability for the photodissociation of the *N*-ethyl bond of the NEC molecule in its singlet excited state. In the case of carbazole, the energy of the first excited singlet state is lower than that of the N—H bond.

The photochemical reaction products obtained (Table 1) and the energy level diagram discussed (Fig. 1), along with the well-known photophysical (1, 26−30) and photochemical (7, 33−35) results in the aromatic electron donor − CCl_4 system, strongly suggest the following primary photophysical and photochemical processes of the NEC molecule in the presence of CCl_4:

$$\text{[1]}\quad \mathrm{NEC} + h\nu \longrightarrow {}^1\mathrm{NEC}^*$$

$$\text{[2]}\quad {}^1\mathrm{NEC}^* \longrightarrow \mathrm{NEC} + h\nu_F$$

$$\text{[3]}\quad {}^1\mathrm{NEC}^* + \mathrm{CCl_4} \rightsquigarrow \begin{cases} {}^3\mathrm{NEC}^* + \mathrm{CCl_4} \\ \mathrm{NEC} + \mathrm{CCl_4} \end{cases}$$

$$\text{[4]}\quad {}^1\mathrm{NEC}^* \rightsquigarrow$$

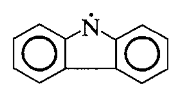

$$+ \dot{\mathrm{C}}_2\mathrm{H}_5$$

β

$$\text{[5]}\quad {}^1\mathrm{NEC}^* + \mathrm{CCl_4} \rightsquigarrow {}^1(\mathrm{NEC}^{\delta+}\cdots\mathrm{CCl_4}^{\delta-})^*_{\mathrm{solv}}$$

$$\text{[6]}\quad {}^1(\mathrm{NEC}^{\delta+}\cdots\mathrm{CCl_4}^{\delta-})^*_{\mathrm{solv}} \rightsquigarrow \begin{cases} {}^3\mathrm{NEC}^* + \mathrm{CCl_4} \\ {}^1\mathrm{NEC}^* + \mathrm{CCl_4} \\ \mathrm{NEC} + \mathrm{CCl_4} \end{cases}$$

$$\text{[7]}\quad {}^1(\mathrm{NEC}^{\delta+}\cdots\mathrm{CCl_4}^{\delta-})^*_{\mathrm{solv}} \rightsquigarrow \{\mathrm{NEC}^{+\cdot}\mathrm{Cl}^-\dot{\mathrm{C}}\mathrm{Cl}_3\}_{\mathrm{solv}}$$

The radiationless processes in the dissipation of the singlet excitation energy of the NEC molecule compete with fluorescence (eq. [2]). The photophysical processes can occur via the external spin orbital coupling with the CCl_4 molecule (eq. [3]) or via complexation (eqs. [5] and [6]). On the other hand, the photodissociation of the *N*-ethyl bond (eq. [4]) and the electron transfer in the excited CT complex (eq. [7]) are the photochemical processes.

We propose that the electron transfer from singlet excited NEC molecule to CCl_4 molecule in the transient excited CT complex, ${}^1(\mathrm{NEC}^{\delta+}\cdots\mathrm{CCl_4}^{\delta-})^*$, is the main primary photochemical process which initiates a complex chemical reaction.

It leads to the radical cation of NEC, chloride ion, and trichloromethyl radical in the solvent cage. Similarly to the radical cation of carbazole (7), the further transformations of the radical cation of NEC are conditioned by the presence of Cl^- and $\dot{C}Cl_3$ in the solvent cage. These transformations result in other active species according to the following:

[8]

[9]

[10]

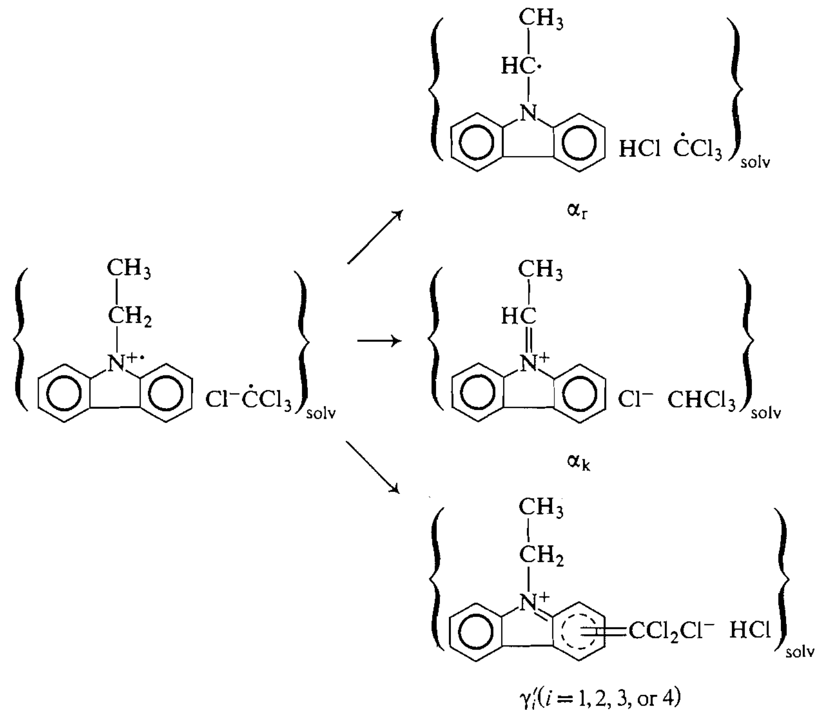

The formation of the α_r radical from the radical cation of NEC (eq. [8]) is promoted by the formation of thermodynamically stable hydrogen chloride. The reactions of the radical cation of NEC with the CCl_3 radical can lead to cation α_k and chloroform (eq. [9]) or cation γ_i' (eq. [10]).

The formation of radicals by abstraction of an α-proton from the radical cation of amine molecules has been postulated in reactions of chemical oxidation of *N*,*N*-dialkylanilines by benzoyl peroxide (40) and in photochemical oxidation of tertiary amines in the presence of halomethanes (41). On the other hand, in the reactions of benzoyl peroxide with *N*,*N*-dialkyl aromatic amine, the formation of the corresponding cations by the abstraction of a hydrogen atom from the radical cation of the amine molecule has also been postulated (42, 43). The proposed mechanism of the transformation of the radical cation of NEC in the solvent cage is consistent with earlier studies on the mechanism of the photochemical reactions in the aromatic amine – polychloromethane system (33, 34).

The formation of γ_i' (mainly with i = 1 or 3) is accompanied by the formation of hydrogen chloride. This reaction occurs with the participation of the aromatic ring system in the radical cation of NEC favoring the 1, 3, 6, and 8 positions. It is in good agreement with the charge density redistribution in the aromatic system. Indeed, theoretical calculations of the π electronic charge density in the carbazole molecule (8, 13, 14) show that the 1, 3, 6, 8, and 9 (N) positions are most favored. There exists a good correlation between the charge redistribution and the chemical properties of the carbazole radical cation and carbazyl radical. Such correlation has been confirmed by the products obtained from chemical (44, 45), electrochemical (14), and photochemical (7) reactions involving carbazole and carbazyl radical as well as by the products of the photochemical rearrangements of *N*-acetylcarbazole (8). On the other hand, it has also been exemplified in the literature that the alkyl substituent at nitrogen in carbazole influences the π electronic charge redistribution (11, 15, 16). The alkyl substituent increases the charge density in the ring system and decreases the electron density at the nitrogen atom in all electronic states of the molecule. There is an accompanying additional effect of polarization of the ring system, enhancing the electron density at the 1, 3, 6, and 8 positions and decreasing the electron density at the other positions.

The products presented in Table 1 show that the probability of transformations of the radical cation of NEC and further reactions of the intermediate species formed in the solvent cage strongly depends on the polarity and chemical activity of the reaction media used. The formation mechanism of the photochemical reaction products in nonpolar reaction medium like CCl_4 can be explained mainly by the secondary reactions of the radicals α_r, β, and $\dot{C}Cl_3$. On the other hand, intermediates γ_i' can explain the formation mechanism of the products in polar reaction medium like ethanol.

Reactions of cation α_k

Because of its electron acceptor properties, cation α_k can transform into the radical α_r in the presence of excited NEC molecule, such transformation resulting from the electron transfer in the excited charge transfer complex according to reaction (11):

[11] $^1NEC^* + \alpha_k \rightarrow {}^1(NEC^{\delta+} \cdots \alpha_k^{\delta-})^* \rightarrow NEC^{+\cdot} + \alpha_r$

In the presence of ammonia α_k cn also easily form the proper ammonium salt and decompose subsequently to give carbazole (eq. [12]).

[12] $Cl^{-}\alpha_k + NH_3 \rightarrow$ 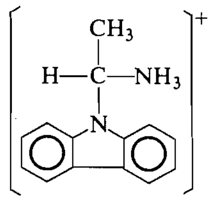 Cl^{-}

$\rightarrow C + CH_3CH{=}NH_2^{+}Cl^{-}$

The proposed mechanism of the formation and decomposition of the cation α_k in the reaction media studied here seems highly probable. Nevertheless this will obviously require further study.

Reactions of radical α_r

Apart from reactions [8] and [11] the radical α_r can also be formed by abstraction of α-hydrogen from the NEC molecule in the radical reaction medium. The interaction between radicals α_r and $\dot{C}Cl_3$ might be responsible for the appearance of such compounds as **3** and **4**, as well as radical β, by the decomposition of the intermediate product, *N*-(α-trichloromethylethyl)carbazole, unstable in the reaction medium (see eqs. [13]–[16]). Radical α_r in the presence of $\dot{C}Cl_3$ can transform to *N*-vinylcarbazole (eq. [16]). Similar reaction in the trialkylamine–polyhalomethane system (14) has been thoroughly studied. Nevertheless, *N*-vinylcarbazole in the photochemical reaction medium is highly unstable and will easily be

[13]

[14]

[15]

[16]

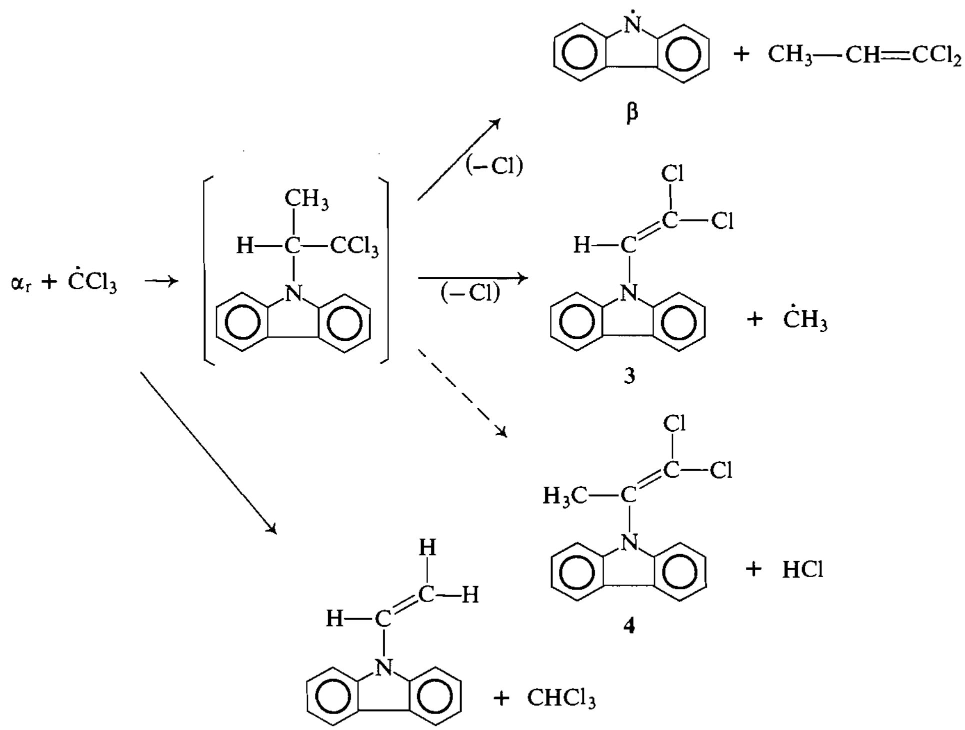

undergoing further transformation (17, 46–48). In the presence of CCl_4 and CCl_3 radicals the transiently formed *N*-vinylcarbazole probably becomes the precursor of **7** according to reaction [17]. In pure CCl_4 as the photochemical reaction medium, hexachloroethane (**1**), **3**, and **7** appear, among others, as the main products.

[17] 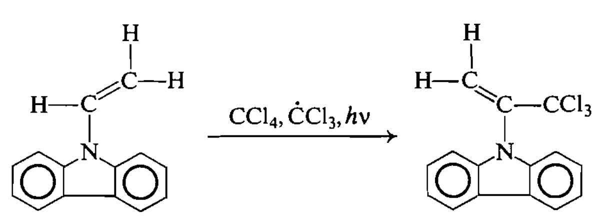

7

When ethanol was used as a solvent, we identified **5**. The formation of **5**, along with the low chemical yield of **1** (see Table 1), indicates the active role played by ethanol. The participation of ethanol in the reactions of CCl_3 radicals suggests the complex formation mechanism of **5** (eq. [18]).

[18] α_r 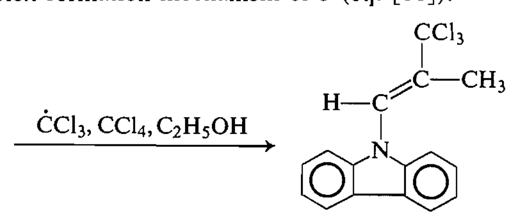

5

The reactions of CCl_3 radicals generated from CCl_4 with the primary alcohols are well known in the literature, where both α-hydrogen abstraction and chain reaction mechanism have been postulated (49, 50).

Reactions of radical β

The formation of carbazole and **6** as main products in CCl_4 when ammonia was used after and during irradiation (Table 1) (eqs. [19] and [20]) proves the existence of radicals β.

[19] 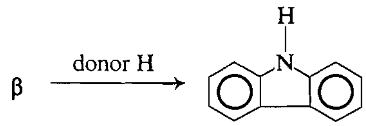

[20] 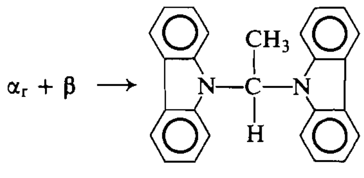

6

In an acid reaction medium, reaction [13] seems to be the main source of radical β. Comparatively low yield of carbazole when ethanol was used as a solvent and trace amount of carbazole obtained during irradiation of NEC in pure ethanol or in pure 3-methylpentane indicate that reaction [4] is not highly efficient. During irradiation of NEC in CCl_4 in the presence of ammonia gas the formation of radical β can be explained by the interaction of the radical cation of NEC with ammonia (eq. [21]). It has been found that interaction between the radical

[21] 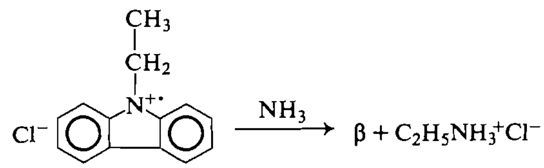

cation of an aromatic amine and ammonia results in the corresponding radicals (7*c*, 33). The comparatively low yield of **6** in the acid reaction medium as compared to the yield of **6** in the ammonia reaction medium can be explained by the competing influence of reactions [13]–[16] in which radicals α_r are involved.

Such compounds as **2**, **8**, **9**, and **10** that are found in the photolyte after irradiation of NEC in CCl_4 strongly suggest the formation of the intermediate species δ, α and γ_i. These intermediates can be formed by the reaction of radical β with the CCl_3 radical (eqs. [22]–[24]).

[22]

[23]

[24]

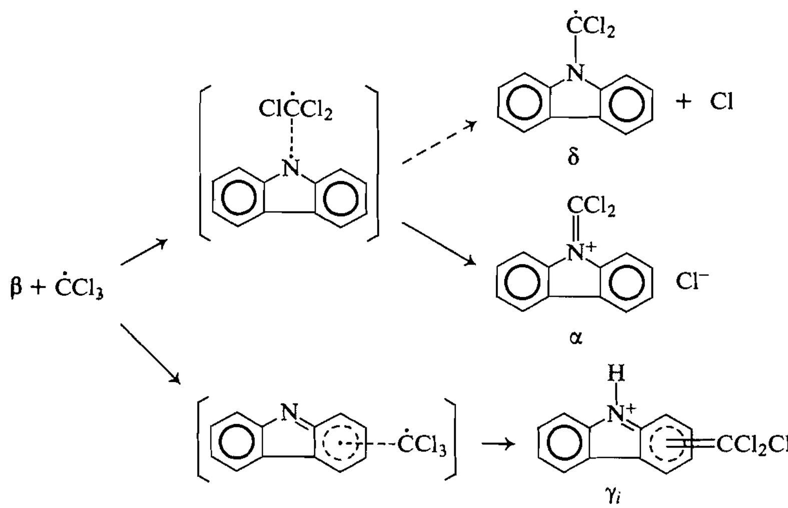

In an acid reaction medium, reaction [13] seems to be the main source of radical β. Comparatively low yield of carbazole reaction medium, intermediates α and γ_i can also be formed by reactions [26] and [27].

[25] 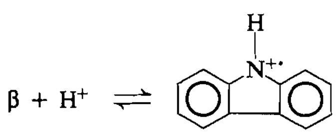

[26]

[27]

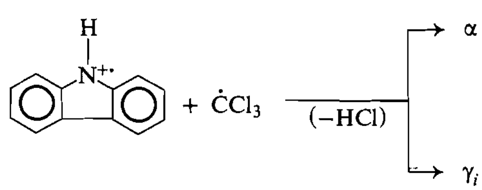

The intermediates δ, α, and γ_i convincingly explain the formation mechanism of the products **2**, **8**, **9**, and **10** (8) as follows:

[28] 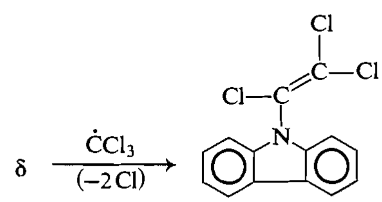

2

[29] 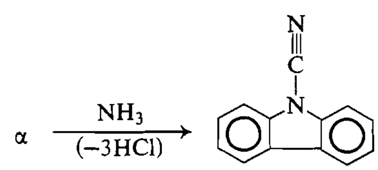

8

[30] 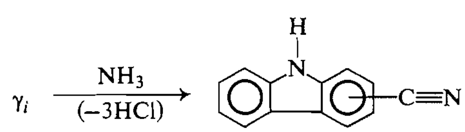

9,10

Among the identified products, the **8** forms as the main compound.

Comment on the reactions of radical CCl_3

Apart from the reaction of radical–radical type in the system studied, the trichloromethyl radicals can also react with carbazole or NEC molecules through the aromatic ring, resulting in the corresponding γ_i and γ_i' intermediates (eq. [31]). Ionic

R = H or C_2H_5

[31] 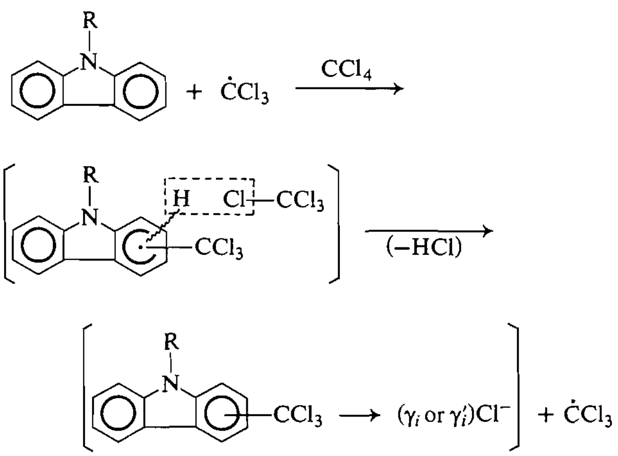

products γ_3 and γ_3' form mainly in the ammonia reaction medium by reaction [31]. This explains the formation mechanism of **10** and **11** according to reaction [30].

The relatively low bond energy of C—Cl in the CCl_4 molecule and the possibility of the formation of the stable hydrogen chloride molecule in the presence of CCl_4 and hydrogen donor molecules facilitate the chain reaction mechanism in CCl_4. Reaction [31] can constitute one of the links of the chain reaction in the NEC–CCl_4 system, such reaction being initiated by the CCl_3 radicals in the presence of CCl_4 as a good hydrogen acceptor.

TABLE 2. Fluorescence maxima of a series of (carboethoxy)-*N*-ethylcarbazole molecules in ethanol at room temperature excited at 340 nm

Molecule	λ_{max} (F) (nm)
N-Ethylcarbazole	365
Carbazole	357 (λ_{exc} = 320)
3-(Carboethoxy)carbazole	380
1-(Carboethoxy)-*N*-ethylcarbazole	410
3-(Carboethoxy)-*N*-ethylcarbazole	365
4-(Carboethoxy)-*N*-ethylcarbazole	437
1,6-Di(carboethoxy)-*N*-ethylcarbazole	395
2,6-Di(carboethoxy)-*N*-ethylcarbazole	405
3,5-Di(carboethoxy)-*N*-ethylcarbazole	412
3,6-Di(carboethoxy)-*N*-ethylcarbazole	361
1,5-Di(carboethoxy)-*N*-ethylcarbazole	430

Reactions of cation γ_i'

(Carboethoxy)-*N*-ethylcarbazoles are formed as the main photoproducts in the system NEC–CCl_4 when ethanol is used as a solvent (see Table 1). The formation mechanism of mono(carboethoxy)-*N*-ethylcarbazoles can only be explained by the reaction of ionic form γ_i' with ethanol (eq. [32]). In the photochemical reaction medium studied γ_i' can be formed in the solvent cage (eq. [10]) and out of it (eq. [31]).

[32] 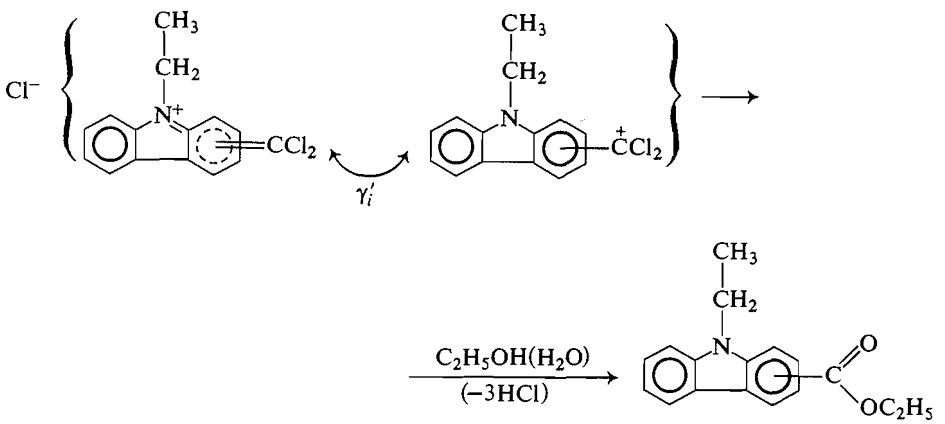

Mono(carboethoxy)-*N*-ethylcarbazoles formed during irradiation can also undergo photochemical reactions in the presence of CCl_4. This leads to di(carboethoxy)-*N*-ethylcarbazoles as follows:

[33] 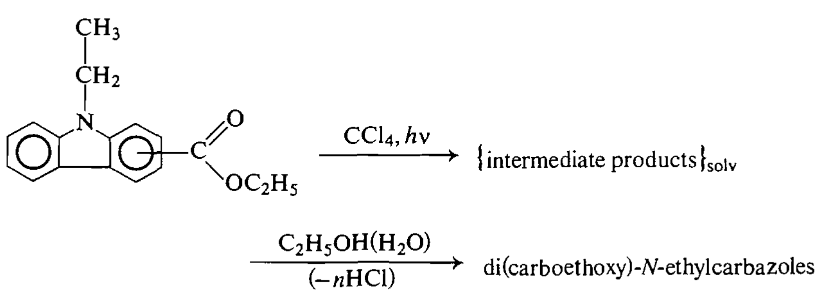

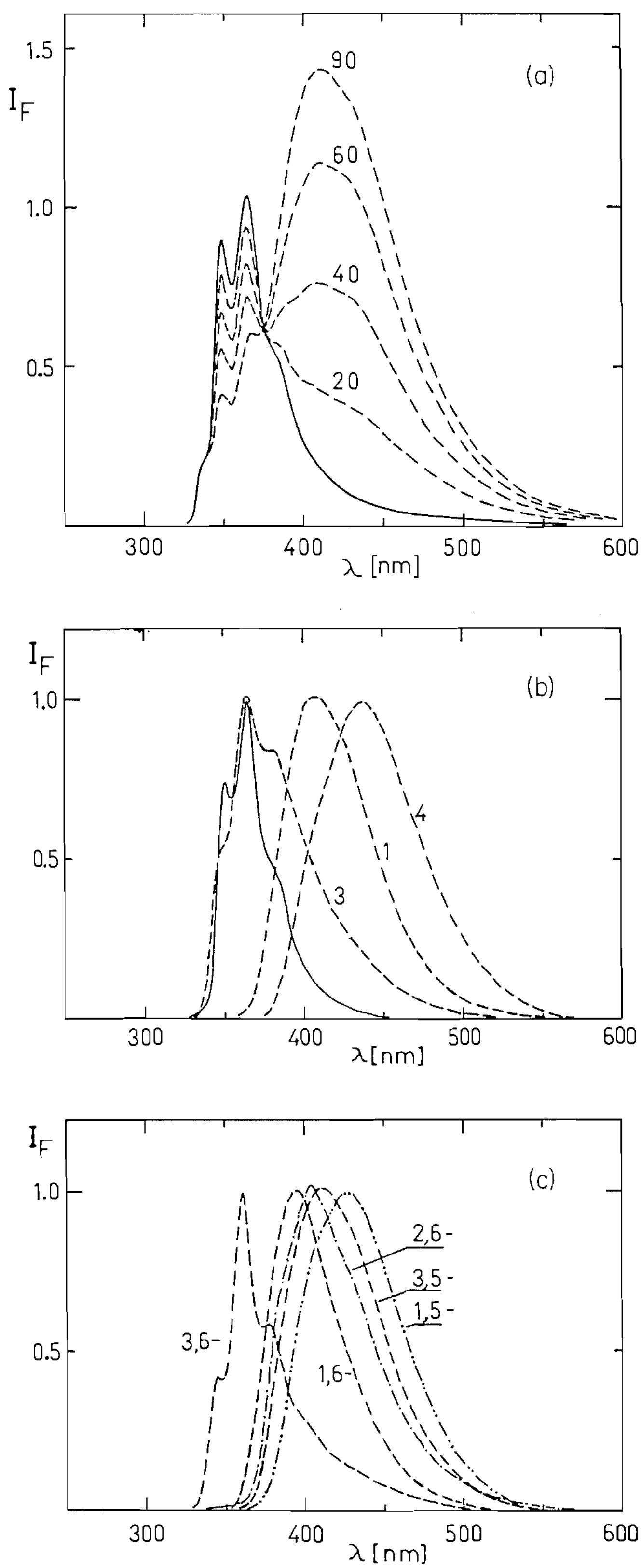

FIG. 2. Fluorescence spectra of an ethanol solution of (a) *N*-ethylcarbazole (1×10^{-4} *M*) in the presence of CCl_4 (0.1 *M*) before irradiation (_______), and after specified time of irradiation in seconds (– – –). The excitation wavelength was fixed at 340 nm; (b) *N*-ethylcarbazole (_______), and mono(carboethoxy)-*N*-ethylcarbazoles ($\sim 1 \times 10^{-4}$ *M*); (c) di(carboethoxy)-*N*-ethylcarbazoles ($\sim 1 \times 10^{-4}$ *M*).

The comparison between NEC and carbazole photochemistry

As shown in Fig. 1, the electron transfer from singlet excited NEC molecule to CCl_4 molecule in the ex-CT complex should be energetically more probable than that for cabazole, and from the same figure we can see that the photodissociation of the *N*-ethyl bond in the NEC molecule, as a primary photochemical process, is also possible.

The secondary photochemical reactions of NEC in CCl_4 which occur with the participation of cation α_k and radical α_r are peculiar only to NEC. On the other hand, the photochemical decomposition of the NEC molecule in the presence of CCl_4 in ethanol as a solvent is very similar to that of the carbazole molecule under the same conditions (7*b*). This has been well exemplified by the photoproducts identified, such as (carboethoxy)-*N*-ethylcarbazoles (see Table 1), which are formed in the same way as (carboethoxy)carbazoles from carbazole, as well as by the fluorescence spectra shown in Fig. 2. During irradiation of an ethanol solution of NEC in the presence of CCl_4 (Fig. 2a) the typical fluorescence of NEC decreases in intensity, while new fluorescences appear in the range 380–550 nm and increase in intensity. We have shown in Figs. 2b, 2c and Table 2 that mono and di(carboethoxy)-*N*-ethylcarbazoles in ethanol might all be responsible for the new fluorescence observed.

The observed changes in the fluorescence spectra of an ethanol solution of NEC in the presence of CCl_4 are similar to that of carbazole, and the maxima of the fluorescence bands are shifted to lower energy by about 8 nm. This is in good agreement with the substituent effect of the *N*-ethyl group.

The photodecomposition of NEC in CCl_4, can also lead to radical β, which in the presence of CCl_3 radical can transform to the same products as these observed in the photodecomposition of carbazole. This is indicated by the *N*- 1-, and 3-cyanocarbazoles as products, when ammonia was used as a scavenger of HCl. Radical β is one of the transient amine products that easily forms both in the photochemical reaction of carbazole and NEC in CCl_4. In the carbazole–CCl_4 system, radical β can only be formed from the radical cation of carbazole in the presence of chloride ion or ammonia (7). However, the photodecomposition of NEC in CCl_4 to radical β can occur by radical α_r in the presence of CCl_3 radical, the radical cation of NEC in the presence of ammonia, or by the photodissociation of the *N*-ethyl bond in the molecule. The formation mechanism of radical β from NEC molecule promoted by CCl_4 requires further study.

Experimental

Apparatus

The ^1H nmr spectra were determined with a Bruker WH-90 spectrometer operating at 90 MHz or a Bruker WP-80 spectrometer operating at 80 MHz. Chemical shift values are given in a δ scale with respect to TMS as an internal standard. Infrared spectra were recorded on a Perkin–Elmer 710B infrared spectrophotometer and mass spectra were taken with a VG Micromass 1212 mass spectrometer or a Kratos MS-9 mass spectrometer.

The absorption spectra were recorded on a Cary 17 spectrophotometer using 10-mm optical path cells. The emission spectra were recorded on a fluorescence spectrophotometer Model SF-1 "Fluorispec" (Baird-Atomic, Inc. Cambridge, MA). All solution examined in fluorescence were first deoxygenated with oxygen-free argon.

General procedure

N-Ethylcarbazole solutions (0.004 *M*) in pure carbon tetrachloride or 0.1 *M* carbon tetrachloride in ethanol were deoxygenated with

TABLE 3. R_f values of the photoproducts in the *N*-ethylcarbazole – carbon tetrachloride system

	Developing system† (v/v)					
		PE–EE				
No*	PE	100:1	10:1	5:1	2:1	B
NEC	0.40	0.62	0.78	0.80		0.84
C	0.03	0.05	0.23	0.36	0.59	0.78
2	0.71	0.76	0.83	0.86		0.90
3	0.59	0.75	0.82			
4	0.55	0.73	0.80			
5	0.58	0.74				
6	0.44	0.58				
7	0.42	0.56				
8	0.09	0.26	0.62	0.70		0.76
9			0.08	0.20	0.50	0.27
10			0.02	0.05	0.14	0.25
11		0.03	0.18	0.27	0.50	0.59
12			0.04	0.10	0.23	0.27
13	0.02	0.18	0.60	0.71	0.79	0.75
14		0.05	0.31	0.43	0.65	0.54
15	0.02	0.13	0.48	0.64	0.73	0.71
16			0.16	0.33	0.58	0.32
17			0.08	0.18	0.41	0.25
18			0.05	0.13	0.36	0.14
19			0.06	0.14	0.34	0.16
20			0.03	0.09	0.29	0.09

*Abbreviation and notation of compounds is the same as in Table 1.
†PE: petroleum ether; EE: ethyl ether; B: benzene.

oxygen-free argon and irradiated in a Pyrex Hanovia immersion-well reactor for 30 min with an Hanovia 679A36 450-W medium-pressure mercury lamp. Hydrogen chloride generated during these reactions was neutralized. The irradiated solution of *N*-ethylcarbazole in pure carbon tetrachloride was saturated with ammonia gas. But only sodium carbonate was added to the irradiated *N*-ethylcarbazole solution with carbon tetrchloride in ethanol. The solution was mixed and then the sediment was separated by decantation. Following that, the solutions of photolytes were concentrated. *N*-Ethylcarbazole solution (0.004 *M*) in carbon tetrachloride was also irradiated (30 min) in the presence of ammonia. A slow stream of ammonia gas was bubbled through the solution before and during irradiation. Hydrogen chloride generated during the photochemical reaction was thus removed from the reaction medium. After irradiation, the solution of photolyte was concentrated.

The photochemical reaction products were then analysed by tlc detected by uv (using Eastman-Kodak tlc plates, silica gel 13181 with fluorescent indicator No 6060) and separated by column chromatography. The columns were packed with silica gel (Kieselgel 60, Merck, particle size 0.040–0.063 mm). Developing systems consisted of petroleum ether (low boiling fraction) and ethyl ether or benzene. The developed distance on the tlc plates was kept at 10 cm. Identified products, on the basis of their ^{1}H nmr, ir, and mass spectra, have been listed in Table 1 and their R_f values on tlc plates with silica gel are listed in Table 3.

Materials

N-Ethylcarbazole 99% was obtained from Aldrich Chemical Co. and was further twice recrystallized in pure ethanol and then purified by column chromatography with silica gel using a petroleum ether – ethyl ether mixture (1000:1 v/v) as a developing system. Carbazole (zone refined 99.999%) was obtained from James Hinton Co. and was used without any further purification. 1-Cyano-*N*-ethylcarbazole, 3-cyano-*N*-ethylcarbazole, 1-(carboethoxy)-*N*-ethylcarbazole, and 3-(carboethoxy)-*N*-ethylcarbazole were synthesized by *N*-ethylation of the corresponding N—H derivatives with ethyl bromide in the presence of caustic solution and benzyltriethylammonium chloride as a phase-transfer catalyst, as described in ref. 51. The compounds were purified by column chromatography with silica gel, using a petroleum ether – ethyl ether mixture as a developing system. The purity of these compounds was checked by tlc.

1-Cyano-N-ethylcarbazole: crystalline solid (R_f 0.55, petroleum ether – ethyl ether, 10:1). Infrared (film) $\tilde{\nu}_{max}$: 3050 (vw), 2960 (w), 2910 (vw), 2200 (s, C≡N), 1620 (vw), 1590 (w), 1575 (w), 1485 (s), 1470 (m), 1455 (m), 1440 (w), 1375 (vw), 1340 (w), 1315 (s), 1260 (vw), 1230 (w), 1215 (vs), 1160 (vw), 1125 (s), 1100 (vw), 1070 (w), 1040 (w), 1015 (vw), 930 (vw), 900 (vw), 850 (vw), 790 (s), 770 (w), 740 (vs) cm^{-1}; ^{1}H nmr ($CDCl_3$) δ: 1.55 (t, J = 8 Hz, 3H, methyl), 4.75 (q, J = 8 Hz, 2H, methylene), 7.16–7.80 (m, 5H, arom), 8.05–8.34 (m, 2H, arom). Mass spectrum (70 eV) (mol. wt. for $C_{15}H_{12}N_2$: 220.28), m/e: 220 (M^+, 41), 205(100), 192(8), 191(8), 178(5), 177(7), 165(10), 164(13), 151(13), 138(7).

3-Cyano-N-ethylcarbazole: crystalline solid (R_f 0.18, petroleum ether – ethyl ether, 10:1). Infrared (film) $\tilde{\nu}_{max}$: 3050 (vw), 2970 (w), 2920 (vw), 2200 (vs, C≡N), 1630 (m), 1595 (vs), 1495 (s), 1475 (vs), 1460 (m), 1385 (m), 1350 (s), 1330 (m), 1320 (m), 1290 (w), 1235 (vs), 1165 (vw), 1150 (m), 1125 (w), 1085 (w), 1060 (vw), 1020 (vw), 940 (vw), 885 (w), 845 (w), 800 (m), 775 (vw), 765 (vw), 740 (s), 720 (m) cm^{-1}; ^{1}H nmr ($CDCl_3$) δ: 1.47 (t, J = 8 Hz, 3H, methyl), 4.41 (q, J = 8 Hz, 2H, methylene), 7.22–7.80 (m, 5H, arom), 8.06–8.09, 8.15–8.18 (2m, 1H, arom), 8.39–8.41 (m, 1H, arom). Mass spectrum (70 eV) (mol. wt. for $C_{15}H_{12}N_2$: 220.28), m/e: 220 (M^+, 34), 205(100), 191(6), 177(6), 165(5), 164(7), 151(9).

1-(Carboethoxy)-N-*ethylcarbazole*: oil (R_f 0.60, petroleum ether – ethyl ether, 10:1). Infrared (film) $\tilde{\nu}_{max}$: 3050 (vw), 2970 (m), 2920 (w), 2900 (vw), 1715 (vs, C=O), 1610 (vw), 1590 (w), 1575 (m), 1490 (m), 1475 (s), 1450 (s), 1415 (s), 1380 (w), 1360 (w), 1330 (m), 1320 (m), 1310 (m), 1260 (vs), 1215 (m), 1195 (vs), 1155 (vw), 1135 (vs), 1090 (s), 1065 (vs) 1035 (vw), 1010 (w), 940 (vw), 910 (vw), 850 (vw), 780 (vw), 745 (vs), 720 (m) cm^{-1}; ^{1}H nmr ($CDCl_3$) δ: 1.17 and 1.27 (2t, J = 8 Hz, 6H, methyl), 4.29 and 4.36 (2q, J = 8 Hz, 4H, methylene), 6.94–7.35 (m, 4H, arom), 7.60–8.10, (m, 3H, arom). Mass spectrum (70 eV) (mol. wt. for $C_{17}H_{17}NO_2$: 267.33), m/e: 267 (M^+, 100), 252(69), 238(7), 224(48), 222(11), 220(23), 208(13), 206(23), 204(18), 196(14), 194(11), 193(23), 192(9), 168(55), 167(30), 166(30), 165(25), 164(23), 152(8), 140(16), 139(21), 138(9).

3-(Carboethoxy)-N-*ethylcarbazole*: oil (R_f 0.31, petroleum ether – ethyl ether, 10:1). Infrared (film) $\tilde{\nu}_{max}$: 3050 (vw), 2970 (m), 2925 (w), 2890 (vw), 1705 (vs, C=O), 1625 (m), 1595 (s), 1490 (m), 1470 (s), 1460 (m), 1445 (m), 1385 (m), 1365 (s), 1345 (m), 1335 (s), 1325 (s), 1300 (s), 1280 (s), 1245 (vs), 1220 (s), 1170 (vw), 1140 (m), 1130 (m), 1120 (w), 1095 (s), 1080 (s), 1050 (w), 1020 (m), 940 (vw), 905 (w), 880 (w), 850 (vw), 820 (w), 765 (s), 755 (m), 740 (m), 715 (s) cm^{-1}; ^{1}H nmr ($CDCl_3$) δ: 1.27 and 1.30 (2t, J = 8 Hz, 6H, methyl), 4.20 and 4.29 (2q, J = 8 Hz, 4H, methylene), 7.03–7.40 (m, 4H, arom), 6.95–8.10, (m, 2H, arom), 8.67, 8.68 (d, 1H, arom). Mass spectrum (70 eV) (mol. wt. for $C_{17}H_{17}NO_2$: 267.33), m/e: 267 (M^+, 100), 252(85), 239(7), 224(53), 222(50), 194(15), 179(31), 178(14), 165(10), 164(11), 152(13), 139(7), 138(5).

N-Vinylcarbazole was prepared from carbazole following the method described in the literature (52). The compound was purified by column chromatography with silica gel, using a low boiling fraction of petroleum ether as a developing system. The purity of this compound was checked by tlc (R_f 0.55, petroleum ether). The ^{1}H nmr ($CDCl_3$) spectrum of the synthesized compound was the same as described in ref. 53.

Carbon tetrachloride from American Chemicals was a Spectrograde quality solvent and it was first washed with a saturated sodium carbonate solution and then repeatedly with water, dried with calcium chloride and phosphorus pentoxide, and redistilled.

Ethanol was purified by refluxing with concentrated sulfuric acid for 24 h and then was fractionally distilled. Petroleum ether and benzene were distilled before use.

Spectral characteristics of the photochemical products

Carbazole (C): this compound was identified by comparison with an authentic sample (R_f, ^{1}H nmr and ir spectra). *Hexachloroethane* (**1**): single crystals and N-*(trichlorovinyl)carbazole* (**2**): crystalline solid were identified as described previously (7*ab*). N-*(β-Dichlorovinyl)carbazole* (**3**): crystalline solid: infrared (film) $\tilde{\nu}_{max}$: 3060 (m), 1620 (w), 1600 (m), 1485 (s), 1480 (s), 1455 (vs), 1445 (vs), 1420 (w), 1335 (vs), 1310 (s), 1225 (vs), 1155 (s), 1140 (m), 1115 (vw), 1080 (m), 1065 (vw), 1025 (vw), 995 (vw), 920 (m), 875 (m), 880 (s), 745 (vs), 715 (vs) cm^{-1}. ^{1}H nmr ($CDCl_3$) δ: 6.87 (s, 1H, C—H), 7.20–7.58 (m, 6H, arom), 7.94–8.18 (m, 2H, arom). Mass spectrum (70 eV) (mol. wt. for $C_{14}H_9NCl_2$: 262.14), *m/e*: 263 (M^+, 32.2), 261 (M^+, 46.3), 228(13.4), 226(36.6), 191(100), 190(66.6), 166(5.2), 165(8.8), 164(16.2), 163(14.2), 140(12.9), 139(10.6).

N-*(α-Methyl-β-dichlorovinyl)carbazole* (**4**): crystalline solid; ^{1}H nmr ($CDCl_3$) δ: 1.56 (s, 3H, methyl), 7.20–7.60 (m, 6H, arom), 7.98–8.20 (m, 2H, arom). Mass spectrum (70 eV) (mol. wt. for $C_{15}H_{11}NCl_2$: 276.17), *m/e*: 277 (M^+, 42), 275 (M^+, 73), 260(14), 242(10), 240(38), 227(36), 225(100), 205(87), 204(79), 190(10), 164(3).

N-*(2-Trichloromethylpropenyl)carbazole* (**5**): crystalline solid: infrared (film) $\tilde{\nu}_{max}$: 3050 (w), 2970 (m), 2920 (m), 1620 (w), 1590 (m), 1570 (w), 1490 (w), 1480 (m), 1470 (m), 1450 (s), 1420 (s), 1380 (w), 1335 (m), 1310 (m), 1260 (w), 1215 (vs), 1175 (w), 1155 (w), 1125 (m), 1110 (vw), 1075 (w), 1070 (w), 1040 (w), 1015 (w), 1000 (vw), 970 (w), 930 (w), 915 (s), 900 (w), 885 (vw), 870 (vw), 860 (m), 810 (m), 780 (m), 775 (w), 740 (vs), 720 (w) cm^{-1}. ^{1}H nmr ($CDCl_3$) δ: 1.27 (s, 3H, methyl), 7.10–7.45 (m, 6H, arom and 1H, C—H), 8.0–8.20 (m, 2H, arom). Mass spectrum (70 eV) (mol. wt. for $C_{16}H_{12}NCl_3$: 324.64), *m/e*: 328 (M^+, 2.3), 327 (M^+, 14.8), 325 (M^+, 47.5), 323 (M^+, 41.3), 312(5.9), 310(19.0), 308(18.9), 292(1.1), 290(5.6), 288(10.1), 277(5.0), 276(14.2), 275(30.1), 274(60.4), 273(51.5), 272(92.8), 241(5.4), 240(31.9), 239(17.5), 238(100).

*1,1-Di(*N*-carbazyl)ethane* (**6**): crystalline solid; infrared (film) ν_{max}: 3040 (m), 2920 (m), 2840 (m), 1620 (w), 1600 (m), 1560 (w), 1480 (m), 1450 (vs), 1420 (w), 1380 (w), 1325 (s), 1310 (m), 1240 (m), 1225 (m), 1215 (m), 1205 (m), 1190 (w), 1160 (m), 1135 (w), 1120 (w), 1100 (vw), 1065 (w), 1025 (w), 1000 (vw), 965 (vw), 910 (m), 885 (w), 800 (s), 780 (s), 745 (vs), 715 (s) cm^{-1}. ^{1}H nmr ($CDCl_3$) δ: 2.21 (d, J = 7 Hz, 3H, methyl), 5.53 (q, J = 7 Hz, 1H, C—H), 7.20–7.60 (m, 12H, arom), 7.85–8.18 (m, 4H, arom). Mass spectrum (70 eV) (mol. wt. for $C_{26}H_{20}N_2$: 360.46), *m/e*: 360 (M^+, non-observed), 194(100), 167(62.5), 166(31.8), 140(19.4), 139 (16.3).

N-*(α-Trichloromethylvinyl)carbazole* (**7**): crystalline solid; infrared (film) $\tilde{\nu}_{max}$: 3050 (w), 2920 (w), 2850 (vw), 1615 (w), 1600 (m), 1580 (vw), 1480 (m), 1450 (vs), 1365 (m), 1335 (m), 1310 (m), 1270 (w), 1230 (s), 1195 (vw), 1165 (vw), 1150 (vw), 1120 (vw), 1105 (vw), 1070 (vw), 1030 (vw), 1005 (m), 955 (w), 915 (m), 900 (w), 850 (vw), 805 (w), 780 (w), 750 (vs), 720 (s) cm^{-1}. ^{1}H nmr ($CDCl_3$) δ: 4.72 (s, 2H, ethene), 7.20–7.60 (m, 6H, arom), 8.07–8.20 (m, 2H, arom). Mass spectrum (70 eV) (mol. wt. for $C_{15}H_{10}NCl_3$: 310.61), *m/e*: 315 (M^+, 2.5), 313 (M^+, 34), 311 (M^+, 85), 309 (M^+, 83.5), 278(63), 241(5.5), 240(19.5), 239(19), 238(50), 204(39.5), 167(50), 166(17), 140(27), 139(32), 87(19), 85(92), 83(100).

N-*Cyanocarbazole* (**8**): crystalline solid, 1-*cyanocarbazole* (**9**): crystalline solid; and 3-*cyanocarbazole* (**10**): crystalline solid were identified as described previously (7*c*).

*3-Cyano-*N*-ethylcarbazole* (**11**): this compound was identified by comparison with an authentic sample (R_f, ^{1}H nmr and ir spectra).

3-(Carboethoxy)carbazole (**12**): crystalline solid. The compound was identified as described previously (7*a*, *b*).

*1-(Carboethoxy)-*N*-ethylcarbazole* (**13**) and *3-(carboethoxy)-*N*-ethylcarbazole* (**14**) were identified by comparison with authentic samples (R_f, ^{1}H nmr and ir spectra).

*4-(Carboethoxy-*N*-ethylcarbazole* (**15**): oil; infrared (film) $\tilde{\nu}_{max}$: 3040 (vw), 2960 (m), 2910 (w), 1710 (vs, C=O), 1615 (w), 1590 (m), 1570 (w), 1490 (m), 1470 (m), 1460 (s), 1430 (s), 1380 (w), 1360 (vw), 1345 (vw), 1320 (s), 1295 (m), 1270 (vs), 1255 (vs), 1220 (w), 1185 (m), 1150 (m), 1130 (s), 1095 (vs), 1070 (m), 1020 (m), 990 (w), 960 (vw), 920 (vw), 845 (vw), 790 (vw), 745 (vs), 710 (m) cm^{-1}. ^{1}H nmr ($CDCl_3$) δ: 1.44 and 1.51 (2t, J = 8 Hz, 6H, methyl), 4.43 and 4.56 (2q, J = 8 Hz, 4H, methylene), 7.25–7.92 (m, 6H, arom), 8.84 and 8.93 (2s, 1H, arom). Mass spectrum (70 eV) (mol. wt. for $C_{17}H_{17}NO_2$: 267.33), *m/e*: 267 (M^+, 100) 252(61.2), 224(22.3), 222(9.5), 194(5.5), 179(6.8), 165(2.6).

*1,6-Di(carboethoxy)-*N*-ethylcarbazole* (**16**): crystalline solid; infrared (film) $\tilde{\nu}_{max}$: 3050 (vw), 2970 (m), 2920 (w), 2890 (w), 2860 (vw), 1710 (vs, C=O), 1620 (m), 1590 (m), 1580 (m), 1490 (m), 1470 (m), 1450 (m), 1410 (m), 1380 (w), 1365 (m), 1335 (m), 1315 (w), 1300 (m), 1270 (s), 1260 (vs), 1250 (vs), 1245 (vs), 1215 (m), 1195 (s), 1170 (w), 1140 (s), 1095 (vs), 1060 (s), 1015 (m), 945 (vw), 925 (vw), 900 (vw), 875 (vw), 850 (vw), 810 (vw), 765 (m), 740 (m), 725 (w) cm^{-1}. ^{1}H nmr ($CDCl_3$) δ: 1.27–1.68 (m, 9H, methyl), 4.32–4.73 (m, 6H, methylene), 7.15–8.37 (complex m, 5H, arom), 8.83 (s, 1H, arom). Mass spectrum (70 eV) (mol. wt. for $C_{20}H_{21}NO_4$: 339.45), *m/e*: 339 (M^+, 100), 324(47), 311(28), 296(29), 294(26), 278(40), 268(7), 266(12), 264(15), 237(41), 222(18), 220(14), 194(6), 193(9), 192(10), 191(10), 168(16), 167(19), 166(21), 165(25), 164(29), 139(12), 138(8).

*2,6-Di(carboethoxy)-*N*-ethylcarbazole* (**17**): crystalline solid; infrared (film) $\tilde{\nu}_{max}$: 3040 (vw), 2970 (m), 2920 (m), 2890 (m), 2840 (w), 1710 (vs, C=O), 1625 (m), 1600 (w), 1570 (w), 1495 (w), 1470 (m), 1455 (m), 1440 (m), 1430 (m), 1390 (w), 1375 (m), 1365 (m), 1340 (m), 1310 (m), 1300 (m), 1280 (m) 1245 (vs), 1225 (s), 1170 (vw), 1140 (w), 1100 (s), 1080 (m), 1050 (vw), 1015 (m), 950 (vw), 925 (vw), 900 (vw), 875 (vw), 820 (vw), 770 (w), 755 (w), 740 (m), 715 (vw) cm^{-1}. ^{1}H nmr ($CDCl_3$) δ: 1.48 (t, J = 8 Hz, 9H, methyl), 4.43 (q, J = 8 Hz, 2H, methylene), 4.47 (q, J = 8 Hz, 4H, methylene), 7.15–7.50 and 7.80–8.30 (2m, 5H, arom), 8.87 (s, 1H, arom). Mass spectrum (70 eV) (mol. wt. for $C_{20}H_{21}NO_4$: 339.45), *m/e*: 339 (M^+, 72), 324(70), 311(8), 296(40), 294(44), 268(38), 266(40), 251(15), 238(22), 224(19), 223(63), 222(22), 221(24), 194(21), 193(35), 192(56), 191(35), 180(20), 178(74), 166(19), 165(42), 164(100).

*3,5-Di(carboethoxy)-*N*-ethylcarbazole* (**18**): crystalline solid; infrared (film) $\tilde{\nu}_{max}$: 3050 (vw), 2970 (s), 2920 (m), 2840 (w), 1710 (vs, C=O), 1615 (m), 1590 (s), 1570 (w), 1495 (w), 1460 (s), 1420 (m), 1385 (m), 1365 (s), 1335 (s), 1320 (vs), 1295 (s), 1290 (s), 1275 (vs), 1260 (vs), 1240 (vs), 1235 (vs), 1225 (s), 1180 (s), 1135 (s), 1095 (vs), 1070 (s), 1020 (s), 960 (vw), 925 (vw), 880 (vw), 860 (vw), 845 (vw), 810 (w), 795 (w), 765 (s), 745 (m), 715 (m) cm^{-1}. ^{1}H nmr ($CDCl_3$) δ: 1.27–1.66 (m, 9H, methyl), 4.33–4.68 (m, 6H, methylene), 7.26–8.32 (complex m, 5H, arom), 9.55 (s, 1H, arom). Mass spectrum (70 eV) (mol. wt. for $C_{20}H_{21}NO_4$: 339.45), *m/e*: 339 (M^+, 100), 324(63), 311(12), 296(33), 294(86), 268(30) 266(40), 251(8), 238(9), 221(26), 193(20), 191(10), 178(14), 165(13).

*3,6-Di(carboethoxy)-*N*-ethylcarbazole* (**19**): crystalline solid; infrared (film) $\tilde{\nu}_{max}$: 3050 (vw), 2970 (s), 2920 (m), 1705 (vs, C=O), 1625 (w), 1595 (s), 1575 (w), 1490 (m), 1480 (m), 1465 (m), 1450 (m), 1425 (w), 1385 (m), 1370 (s), 1335 (m), 1305 (s), 1285 (s), 1255 (vs), 1245 (vs), 1215 (s), 1180 (vw), 1145 (m), 1130 (w), 1100 (s), 1080 (m), 1050 (w), 1025 (s), 965 (vw), 945 (vw), 910 (vw), 895 (w), 870 (vw), 850 (vw), 835 (vw), 820 (w), 765 (s), 745 (w), 720 (m) cm^{-1}. ^{1}H nmr ($CDCl_3$) δ: 1.48 (t, J = 8 Hz, 9H, methyl), 4.42 (q, J = 8 Hz, 2H, methylene), 4.46 (q, J = 8 Hz, 4H, methylene), 7.40 and 7.49 (2s, 2H, arom), 8.19 and 8.29 (2d, J = 1.8 Hz, 2H, arom), 8.88–8.90 (m, 2H, arom). Mass spectrum (70 eV) (mol. wt. for $C_{20}H_{21}NO_4$: 339.45), *m/e*: 339 (M^+, 100), 324(35), 311(8), 296(12), 295(8), 294(41), 268(10), 266(17), 251(4), 223(8), 221(5), 193(3), 192(3), 178(5), 165(3), 164(5).

*1,5-Di(carboethoxy)-*N*-ethylcarbazole* (**20**): crystalline solid; infrared (film) $\tilde{\nu}_{max}$: 3045 (vw), 2970 (s), 2920 (s), 2845 (m), 1715 (vs, C=O), 1625 (m), 1600 (s), 1585 (m), 1560 (w), 1495 (m), 1470 (s), 1445 (m), 1390 (m), 1375 (s), 1335 (m), 1265 (vs), 1235 (vs), 1170 (vw), 1150 (vw), 1130 (m), 1105 (s), 1090 (m), 1070 (m), 1045 (m), 1015 (s), 955 (vw), 900 (vw), 850 (vw), 775 (m), 760 (m), 740 (s), 715 (m) cm^{-1}. ^1H nmr ($CDCl_3$) δ: 1.27−1.57 (m, 9H, methyl), 4.29 −4.70 (m, 6H, methylene), 7.10−7.70 and 8.05−8.22 (2m, 5H, arom), 8.60 (s, 1H, arom). Mass spectrum (70 eV) (mol. wt. for $C_{20}H_{21}NO_4$: 339.45), *m/e*: 339 (M^+, 100), 324(63), 311(11), 296(13), 294(36), 266(92), 250(8), 222(11), 194(11), 179(15), 178(17), 164(5).

Conclusions

The irreversible electron transfer from singlet excited NEC molecule to CCl_4 molecule in the transient ex-CT complex, $^1(NEC^{\delta+}\cdots CCl_4^{\delta-})^*$, along with the photodissociation of the *N*-ethyl bond in the NEC molecule, have been proposed as the primary photochemical processes initiating the complex mechanism of secondary reactions in the system studied. Such intermediates as α_r, α_k, and γ'_i, formed by the transformation of the radical cation of NEC in the solvent cage, $[NEC^{+\cdot}Cl^-\dot{C}Cl_3]$, as well as carbazyl radical β, explain the formation mechanism of the photochemical reaction products depending on the reaction media used. The decomposition of $NEC^{+\cdot}$ in the presence of Cl^- and $\dot{C}Cl_3$ can occur by the *N*-ethyl group in a nonpolar solvent like CCl_4 or by the aromatic ring in a polar solvent like ethanol. This has been well exemplified by the photoproducts presented in Table 1.

When ethanol is used as a solvent, the photodecomposition of the NEC molecule in the presence of CCl_4 is similar to that already described for the carbazole molecule. Nevertheless, the secondary reactions in the system NEC−CCl_4, which occur with the participation of cation α_k and radical α_r, are characteristic of the NEC molecule only.

The scheme described for the transformation of $NEC^{+\cdot}$ in the solvent cage serves as a key for the explanation of the formation mechanism of all the photochemical reaction products in the NEC−CCl_4 system, depending on the reaction media used. On the contrary, these products, closely connected with the reactions of intermediates α_r, β, $\dot{C}Cl_3$, and γ'_i, strongly support the formation of the radical cation of NEC in the system studied.

All the results presented, along with our earlier studies on photochemical reactions in the carbazole−CCl_4 system, serves as chemical proof of the electron transfer mechanism used to explain the fluorescence quenching of carbazole and *N*-ethylcarbazole by halocarbons (1).

Acknowledgements

The authors would like to thank the Natural Sciences and Engineering Research Council of Canada and the "Ministère de l'Éducation du Québec" for financial assistance. The authors are also grateful to Professor Denis Gravel from this department for many valuable discussions concerning this work.

1. A. Ahmad and G. Durocher. Can. J. Spectrosc., **26**, 19 (1981); Photochem. Photobiol. **34**, 573 (1981).
2. G. E. Johnson. J. Phys. Chem. **84**, 2940 (1980).
3. M. Skrilec and L. J. C. Love. J. Phys. Chem. **85**, 2047 (1981).
4. H. Masuhara, Y. Tohgo, and N. Mataga. Chem. Lett. 59 (1975).
5. M. M. Martin and E. Bréhéret. J. Phys. Chem. **86**, 107 (1982).
6. U. Schmitt and D. M. Burland. J. Phys. Chem. **87**, 720 (1983), and references cited therein; D. M. Burland. Acc. Chem. Res. **16**, 218 (1983).
7. B. Zelent and G. Durocher. (*a*) J. Org. Chem. **46**, 1496 (1981); (*b*) Can. J. Chem. **60**, 945 (1982); (*c*) Can. J. Chem. **60**, 2442 (1982).
8. H. Shizuka, M. Kato, T. Ochiai, K. Matsui, and T. Morita. Bull. Chem. Soc. Jpn. **43**, 67 (1970).
9. R. W. Bigelow and G. E. Johnson. J. Chem. Phys. **66**, 4861 (1977).
10. G. E. Johnson. J. Phys. Chem. **78**, 1512 (1974).
11. R. W. Bigelow and G. P. Ceasar. J. Phys. Chem. **83**, 1790 (1979).
12. P. D. Harvey, B. Zelent, and G. Durocher. Spectrosc. Int. J. **2**, 128 (1983), and references cited therein.
13. I. Fischer-Hjalmars and M. Sundborn. Acta Chem. Scand. **22**, 607 (1968).
14. J. F. Ambrose and R. F. Nelson. J. Electrochem. Soc. **115**, 1159 (1968); J. F. Ambrose, L. L. Carpenter, and R. F. Nelson. J. Electrochem. Soc. **122**, 876 (1975).
15. L. E. Nitzsche, C. Chabalowski, and R. E. Christoffersen. J. Am. Chem. Soc. **98**, 4794 1976).
16. D. Murk, L. E. Nitzsche, and R. E. Christoffersen. J. Am. Chem. Soc. **100**, 1371 (1978).
17. L. P. Ellinger. *In* Advances in macromolecular chemistry. Vol. 1. *Edited by* W. M. Pasika. Academic Press, New York, 1968. p. 169.
18. K. Okamoto, M. Ozeki, A. Itaya, S. Kusabayashi, and H. Mikawa. Bull. Chem. Soc. Jpn. **48**, 1362 (1975).
19. U. Landman, A. Ledwith, D. G. Marsh, and D. J. Williams. Macromolecules, **9**, 833 (1976); R. Solaro, E. Chiellini, and A. Ledwith. J. Chem. Soc. Chem. Commun. 580 (1980); 583 (1980).
20. S. Iwatsuki and K. Arai. Makromol. Chem. **178**, 2307 (1977).
21. Cr. I. Simionescu and V. Percec. Rev. Roum. Chim. **24**, 171 (1979), and references cited therein.
22. E. E. Sirotkina, I. L. Gaibel', V. I. Malkova, and V. D. Filimonov. Zh. Obshch. Khim. **50**, 1589 (1980).
23. Y. Taniguchi, Y. Nishina, and N. Mataga. Bull. Chem. Soc. Jpn. **46**, 1646 (1973).
24. Y. Yamaguchi, T. Miyashita, and M. Matsuda. J. Phys. Chem. **85**, 1369 (1981).
25. S. Tagawa and Y. Tabata. Chem. Phys. Lett. **64**: 255 (1979); M. Washio, S. Tagawa, and Y. Tabata. J. Phys. Chem. **84**, 2876 (1980).
26. A. Namiki, N. Nakashima, and K. Yoshihara. J. Chem. Phys. **71**, 925 (1979).
27. P. C. Alford, C. G. Cureton, R. A. Lampert and D. Phillips. Chem. Phys. **76**, 103 (1983).
28. D. Saperstein and E. Levin. J. Chem. Phys. **62**, 3560 (1975).
29. H. A. Kwaja, G. P. Semeluk, and I. Unger. Can. J. Chem. **60**, 1767 (1982); **61**, 1952 (1983); **62**, 1487 (1984).
30. M. V. Encinas, M. A. Rubio, and E. A. Lissi. J. Photochem. **18**, 137 (1982); Photochem. Photobiol. **37**, 125 (1983).
31. R. O. Loufty and A. C. Somersall. Can. J. Chem. **54**, 760 (1976).
32. T. Takahashi, K. Kikuchi, and H. Kokubun. J. Photochem. **14**, 67 (1980).
33. T. Latowski and B. Zelent. Rocz. Chem. **48**, 831 (1974); J. Org. Chem. **44**, 3559 (1979).
34. K. Wyrzykowska, M. Grodowski, K. Weiss, and T. Latowski. Photochem. Photobiol. **28**, 311 (1978).
35. T. Iwasaki, T. Sawada, M. Okuyama, and H. Kamada. J. Phys. Chem. **82**, 371 (1978); Photogr. Sci. Eng. **22**, 312 (1978).
36. J. R. Bews and Ch. Glidewell. J. Mol. Struct. **71**, 287 (1981).
37. J. A. Ayola, W. E. Wentworth, and E. C. M. Chen. J. Phys. Chem. **85**, 3989 (1981); H.-U. Scheunemann, E. Illenberger, and H. Baumgärtel. Ber. Bunsenges. Phys. Chem. **84**, 580 (1980).
38. V. A. Borovkowa, Kh. S. Bagdasar'yan, V. K. Pikel'ni, V. A. Kolosov, and Yu. I. Kiryukhin. Dokl. Akad. Nauk SSSR, **224**, 616 (1975).
39. S. L. Murov. Handbook of photochemistry. Marcel Dekker Inc.,

New York. 1973.
40. F. HRABÁK and M. VACEK. Collect. Czech. Chem. Commun. **30**, 573 (1965).
41. S. A. MARKARIAN and H. FISCHER. J. Chem. Soc. Chem. Commun. 1055 (1979); S. A. MARKARIAN. Zh. Org. Khim. **18**, 252 (1982); Arm. Khim. Zh. **35**, 281 (1982).
42. J. M. FAYADH, D. W. JESSOP and G. A. SWAN. J. Chem. Soc. (C), 1605 (1966).
43. R. B. ROY and G. A. SWAN. J. Chem. Soc. Chem. Commun. 427 (1966); G. A. SWAN. J. Chem. Soc. Chem. Commun. 1376 (1968); R. B. ROY and G. A. SWAN. J. Chem. Soc. (C), 1886 (1969); G. A. SWAN. J. Chem. Soc. (C), 2880 (1971).
44. W. A. WATERS and J. E. WHITE. J. Chem. Soc. (C), 740 (1968).
45. J. SUGITA. Nippon Kagaku Zasshi, **88**, 659 (1967); Chem. Abstr. **69**, 10319z (1968).
46. L. P. ELLINGER. Polymer, **5**, 559 (1964).
47. S. TAZUKE. J. Phys. Chem. **74**, 2390 (1970).
48. K. HAMANOUE, H. TERANISHI, M. OKAMATO, Y. FUROKAWA, S. TAGAWA, and Y. TABATA. J. Polym. Sci. Polym. Chem. Ed., **18**, 91 (1980).
49. G. SCHLICHT and D. SCHULTE-FROHLINDE. Photochem. Photobiol. **16**, 183 (1972).
50. L. FELDMAN and Z. B. ALFASSI. Int. J. Chem. Kinet. **14**, 659 (1982).
51. H. NISHI, H. KOHNO, and T. KANO. Bull. Chem. Soc. Jpn. **54**, 1897 (1981).
52. V. D. FILIMOMOV, E. E. SIROTKINA, and N. A. TSEKHANOVSKAYA. Zh. Org. Khim. **15**, 174 (1979).
53. J. PIELICHOWSKI and Z. KOWALCZYK. Tetrahedron, **37** 1403 (1981).

Deep levels in semiconductors

B. A. Lombos

Department of Electrical Engineering, Concordia University, Montreal, Que., Canada H3G 1M8

Received September 26, 1984

This paper is dedicated to Professor Camille Sandorfy on the occasion of his 65th birthday

B. A. Lombos. Can. J. Chem. **63**, 1666 (1985).

The role of deep-lying trapping centers in semi-insulating GaAs, polysilicon and polycrystalline tin oxide transparent electrode has been systematically investigated. It was demonstrated that some of the peculiar transport properties of these semiconductors can be elucidated by deep level compensation. A multilevel model is presented to determine the position of the Fermi level as a function of impurity concentrations. These include, quantitatively, the deep-lying levels which have been introduced by doping in the case of GaAs and by grain boundaries in the case of polycrystalline films. In the latter cases the dangling bonds, associated to lattice defects, are characterized by energy levels which are localized in the energy gap. These dangling bonds can act as electron traps when empty and hole traps when occupied. These are the deep levels.

In each of the investigated three cases, this concept permitted the elucidation of some of the transport properties of these semiconductors.

B. A. Lombos. Can. J. Chem. **63**, 1666 (1985).

On a étudié d'une façon systématique le rôle des centres profonds de piègeage dans le GaAs semi-isolant, dans le polysilicium et dans une électrode transparente d'oxyde d'étain polycristallin. On démontre que l'on peut élucider quelques unes des propriétés particulières de transport de ces semi-conducteurs en faisant appel à une compensation par des niveaux profonds. On présente un modèle à plusieurs niveaux pour déterminer la position du niveau de Fermi en fonction des concentrations des impuretés. Ceux-ci comprennent quantitativement les niveaux profonds que l'on a introduit par dopage dans le cas du GaAs et par les joints des grains dans le cas des films polycristallins. Dans ces derniers cas, les liaisons pendantes associées aux défauts du réseau sont associées à des niveaux d'énergie qui sont localisés dans la bande interdite. Ces liaisons pendantes peuvent agir comme piège d'électrons quand elles sont vides et comme piège de trous lorsqu'elles sont occupées. Ce sont les niveaux profonds.

Dans chacun des trois cas étudiés, ce concept permet d'élucider certaines propriétés de transport de ces semi-conducteurs.

[Traduit par le journal]

Introduction

The role of deep-lying impurity levels in semiconductors became important with the discovery of semi-insulating GaAs (SI GaAs) (1). This modification of the normally semiconducting GaAs resulted in the possibility of the realization of a number of solid state devices and integrated circuits by epitaxial technology. Due to the inherent electrical properties of GaAs, superior to those of silicon and germanium, the well-known classical active materials for the microelectronic industry, GaAs components have improved properties. These include their high frequency response, high temperature or power handling capacity, radiation hardness for satellite electronics, and the possibility for optoelectronic applications, such as solid state lasers. Some of these, naturally, could not have been realized with either silicon or germanium, since they are lower and indirect gap materials (2, 3). The extensive investigations of deep-lying levels, relative to room temperature thermal excitations, responsible for SI GaAs resistivities larger than 10^8 (ohm cm), were reviewed by Lin and co-workers (4, 5). Different compensation mechanisms were developed in the analyses of the experimental data. It was, however, *a priori* assumed that the material is semi-insulating in the calculations of the Fermi level (6, 7). Recently, a multilevel model without any *a priori* assumptions was employed, by considering the effect of all electrically active impurities in a quantitative explanation of the conditions required to realize semi-insulating GaAs (8).

This multilevel model was successfully used to analyze the transport properties of some polycrystalline thin film semiconductors as well.

Shockley (9) first recognized the importance of the dangling bonds associated with lattice defects and their acceptor behavior in the diamond structure. The theory has been worked out by Read (10), treating this dangling bond as having an unpaired electron. Then an electron in the conduction band of a semiconductor could diminish its energy by being paired to it. Consequently, an energy level, localized in the energy gap, can be expected to be associated with it (11). In the case of polysilicon, extensively used in the thin film form for microelectronics, this concept was used in the elucidation of its peculiar transport properties (12, 13). Here, the grain boundaries were the crystal defects, introducing deep levels. Then a compensation mechanism could account for the large change in room temperature resistivities, by a factor of 10^9 (ohm cm), of polysilicon films. In addition, the deep level concept could be extended to the formation of impurity bands elucidating the experimentally observed mobility minima in polysilicon (14). Following Mott's discussion of the Anderson transition (15), in the case of overlapping wave functions of the ionized impurities, a metallic impurity band can be formed in the band gap of the semiconductor. Then, when the Fermi level is in this impurity band, the propagation of the charge carriers is regarded as a diffusion process in a random system. As a result, the periodicity of the host lattice loses its role in the conduction process. This results in the replacement of the effective mass with the rest mass of the charge carriers, giving rise to characteristic low mobilities (16). Consequently, the observed mobility minima in polysilicon films can be quantitatively associated with the crossing of the Fermi level through the above mentioned metallic impurity band which has been created by the grain boundaries introduced deep-lying trapping centers (17).

Using the same model of deep levels, the measured transport properties of polycrystalline thin film of tin oxide could also be partially elucidated (18).

In this work the role of the deep-lying impurities will be treated with the analysis of some new results obtained in the case of chemical vapor deposited tin oxide films.

TABLE 1. Spark source mass spectrographic analyses of GaAs samples 1 to 5*

	Sample *1* SC Fused silica†		Sample *2* SI Fused silica†		Sample *3* SC Boron nitride †		Sample *4* SI Fused silica†		Sample *5* SC Fused silica†	
Impurity	ppm atomic	at. cm^{-3} $\times 10^{6}$	ppm atomic	at. cm^{-3} $\times 10^{16}$	ppm atomic	at. cm^{-3} $\times 10^{16}$	ppm atomic	at. cm^{-3} $\times 10^{16}$	ppm atomic	at. cm^{-3} $\times 10^{16}$
C	1.0	4.0	0.3	1.3	0.4	1.8	0.6	2.6	0.6	2.6
N_2	0.3	1.0			0.3	1.3	0.1	0.4	0.02	0.09
O_2	4.0	17.0	0.2	0.9	0.4	1.8	0.4	1.8	1.0	4.0
Na	Intf.	Intf.	Intf.	Intf.	Intf.	Intf.	Intf.	Intf.	Intf.	Intf.
Mg	0.01	0.4								
Al	0.1	0.4	0.1	0.4	0.2	0.9	0.02	0.09	0.2	0.9
Si	1.0	4.4	0.1	0.44	1.0	4.4	0.2	0.9	0.2	0.9
S	0.08	0.4	0.06	0.3	0.06	0.3	0.1	0.4	0.04	0.18
K	0.01	0.04	0.05	0.2	0.03	0.1	0.03	0.1	0.01	0.04
Ca			0.005	0.02			0.005	0.02	0.003	0.01
Cr	0.3	1.3	0.7	3.1			1.0	4.4		
Fe	0.03	0.1								
Sb						0.03	0.1			

*SC = semiconductor; SI = semi-insulator; Intf. = triply ionized Ga interference with sodium prevents Na measurements.
†Boat material.

Multilevel model

The determination of the position of the Fermi level is of fundamental importance in solid state electronics for the characterization of the transport properties of semiconductors and devices. Following an elegant graphical method developed by Shockley (19) the Fermi energy E_f at any temperature, T; donor and acceptor concentrations, N_{dj} and N_{ai}; the impurity ionization energies, E_{dj} and E_{ai}; and band gap, E_g can be determined from the neutrality condition:

$$[1] \quad n + \sum_{i=1}^{l} N_{ai}^{-} = p + \sum_{j=1}^{m} N_{dj}^{+}$$

In large gap semiconductors the Fermi level is within the band gap several kT units away from the band edges, especially in the case of SI GaAs. Therefore Maxwellian statistics can be used. In this case the free electron concentration, n, is given by the well-known expression

$$[2] \quad n = 2(2\pi m_e k T/h^2)^{3/2} \exp\left(-\frac{E_g - E_f}{kT}\right)$$

here k is the Boltzmann constant, h is the Planck constant, and in the case of GaAs, $m_e = 0.069\, m_0$ (20) is the density of state effective mass of the electrons and the band gap is given by (20)

$$[3] \quad E_g(T) = 1.522 - \frac{5.8 \times 10^{-4}\, T^2}{T + 300}$$

The ionized acceptor concentration as the function of energy, E, can be determined by:

$$[4] \quad N_{ai}^{-} = N_{ai}\left(1 + 1/g \exp\frac{E_{ai} - E_f}{kT}\right)^{-1}$$

The expression describing the ionized donors' concentration is given by:

$$[5] \quad N_{dj}^{+} = N_{dj}\left(1 + g \exp\frac{E_{dj} + E_f - E_g}{kT}\right)^{-1}$$

The degeneracy factor, g, was taken to be 4 for the shallow acceptors, however, in the case of deep-lying acceptors a value of 2 was used as in the case of the donors. The hole concentration, p, is given by the equivalent expression to the one for the free electrons (2) by:

$$[6] \quad p = 2(2\pi m_h kT/h^2)^{3/2} \exp\left(-\frac{E_f}{kT}\right)$$

where in the case of GaAs,

$$m_p = 0.58\, m_0$$

The Fermi level can now be determined by plotting the terms in expression [1] as a function of energy, E, using the above given expressions in eqs. [2] to [6]. The running index, E, will be equal to the Fermi energy, E_f if the neutrality condition expressed in eq. [1] is satisfied. The position of the Fermi level, in turn, gives the corresponding free electron and hole concentrations of the material, then with the appropriate mobilities, the resistivity and the Hall coefficient can be computed and correlated to the experimentally measured ones.

The case of GaAs

In Table 1 the results of semiquantitative mass spectrographic analyses are collected for five GaAs single crystals, grown by a heat pipe assisted zone refiner using fused silica and boron nitride boats (21). The electrically active impurities in the case of GaAs are carbon shallow acceptor with $E_{ai} = 0.019$ eV, oxygen deep-lying donor, with $E_{dj} = 0.68$ eV, silicon shallow donor with $E_{dj} = 0.002$ eV, sulphur shallow donor with $E_{dj} = 0.006$ eV, and finally chromium deep-lying acceptor with $E_{ai} = 0.9$ eV, respectively. The ionization energies of the shallow impurities were taken from Sze's work (20) while the ones for the deep-lying levels were obtained from Lin's data (4, 5). To demonstrate the above described graphical method for the determination of the Fermi level and the corresponding free carrier concentrations, in Fig. 1 the calculated Shockley curves are given using the mass spectrographic data of sample 1 collected in Table 1. The limits of accuracy of the semi-quantitative spark source mass spectrographic analyses have been discussed in a previous publication (8). Figure 2 depicts the curves obtained using the results of sample 2 collected in the same table. It can clearly be seen that sample **1** is

TABLE 2. The measured (obsd.) and calculated (calcd.) Hall coefficients (R_H), electron (n), hole (p) concentrations, mobilities (μ (H)), and resistivities (ρ) of samples 1 to 5

Parameter	Value				
	Sample *1* E_f = 1.39 eV	Sample *2* E_f = 0.71 eV	Sample *3* E_f = 1.39 eV	Sample *4* E_f = 0.72 eV	Sample *5* E_f = 1.35 eV
R_H ($cm^3\ C^{-1}$) (calcd.)	-7.8×10^1	-6.4×10^{12}	-7.8×10^1	-7.8×10^{12}	-3.7×10^2
R_H ($cm^3\ C^{-1}$) (obsd.)	-2.0×10^1	-1.0×10^{12}	—	—	-1.1×10^2
n (cm^{-3}) (calcd.)	9.5×10^{16}	3.5×10^5	9.5×10^{16}	5.2×10^5	2.0×10^{16}
n (cm^{-3}) (obsd.)	3.1×10^{17}	6.2×10^6	—	—	5.7×10^{16}
p (cm^{-3}) (calcd.)	0.0	1.2×10^8	—	3.5×10^6	—
μ_{Hn} ($cm^2\ V^{-1}\ s^{-1}$) (calcd., ref. 20)	4800	6000	4800	6000	6000
μ_{Hn} ($cm^2\ V^{-1}\ s^{-1}$) (obsd.)	3600	2267	—	—	4728
μ_{Hp} ($cm^2\ V^{-1}\ s^{-1}$) (calcd., ref. 20)	260	320	260	320	320
ρ (ohm cm) (calcd.)	1.4×10^{-2}	1.7×10^9	1.4×10^{-2}	1.5×10^9	5.2×10^{-2}
ρ (ohm cm) (obsd.)	5.8×10^{-3}	4.4×10^8	1×10^{-3}	—	2.4×10^{-2}

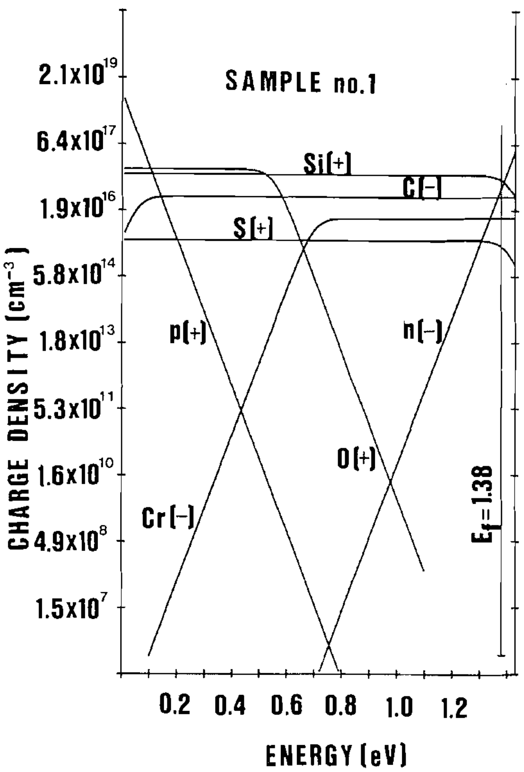

FIG. 1. Calculated Shockley curves for semiconducting GaAs, based on the mass spectrographic analyses, collected in Table 1, sample *1*.

a semiconductor having the Fermi level close to the conduction band, E_f = 1.38 eV above the valence band. This is to be compared with the room temperature band gap of GaAs E_g = 1.435 eV, according to the Varshany equation (3). In Fig. 2 the Fermi energy is close to the band gap center, E_g = 0.65 eV, resulting in a practically intrinsic material, due to the deep level compensation, characterized by a very low carrier concentration. The calculated and measured electron concentrations of this sample are 3.5×10^4 and 6.2×10^6 (cm^{-3}), respectively. These are to be compared to the ones of the semiconducting sample 1, characterized by calculated and measured electron concentrations of 6.4×10^{16} and 3.1×10^{17} (cm^{-3}), respectively. The ratio of the carrier concentrations of these two samples are in the range of 10^{11}, correctly reflecting a semiconducting and a semi-insulating GaAs crystal. The corresponding calculated and measured resistivities are in the range of 10^{-2}, 10^{-3} for the semiconductor and 10^8 (ohm cm) for the semi-insulator, respectively. For comparison purposes the measured and calculated data for the five crystals are collected in Table 2. It can clearly be seen that the calculations, in each of these cases, yield the proper semiconductor or semi-insulator character of the crystals. It is to be mentioned that even in relatively recent publications the role of deep-lying levels in the compensation mechanisms for semi-insulating GaAs results in some "intriguing" aspects related to semi-insulating and semi-intrinsic materials (22, 23). To clarify these problems, based on the results of the above described multilevel model, using Shockley's graphical method, the simple conditions for semiconducting and semi-insulating behavior can be given as follows. Assuming for simplicity, that the sum of the shallow-ionized donor and acceptor concentrations are N_D and N_A, while the deep-lying total donor and acceptor concentrations are N_{Dd} and N_{Ad}, respectively, the following four cases can be distinguished; based on the systematic comparison of the calculated (calcd.) and measured (obsd.) transport properties of five crystals, collected in Table 2:

(*I*) The material is n-type if

[7] $N_D - N_A > 0$

it is semi-insulating if

[8] $N_D - N_A < N_{Ad}$

it is semiconducting if

[9] $N_D - N_A > N_{Ad}$

In the case of n-type materials the deep-lying donors have negligible influence on the electrical properties of the crystal, as it can clearly be seen by examining the curves of Figs. 1 and 2.

(*II*) The material is p-type if

[10] $N_D - N_A < 0$

it is semi-insulating if

[11] $N_A - N_D < N_{Dd}$

it is semiconducting if

[12] $N_A - N_D > N_{Dd}$

In the case of p-type material the deep-lying acceptors have a

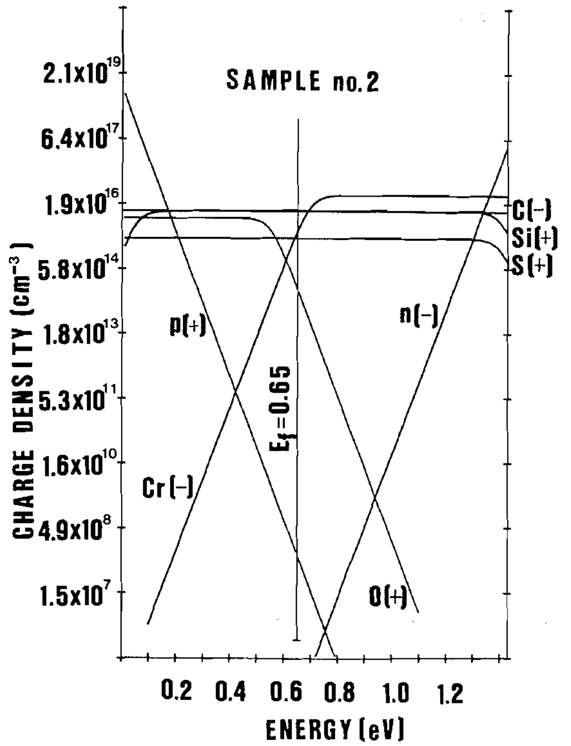

FIG. 2. Calculated Shockley curves for semi-insulating GaAs, based on the mass spectrographic analyses, collected in Table 1, sample 2.

correspondingly negligible influence on the electrical properties of the crystals. These conditions are in complete agreement with the results presented in Figs. 1 and 2 based on the measured mass spectrographic analyses collected in Table 1. The calculated and measured data are summarized in Table 2. The free carrier concentrations are determined by the position of the Fermi level, which is given by the corresponding impurity concentrations, introduced intentionally or unintentionally. The clarification and the understanding of the mechanisms for semi-insulating properties is necessary in order to determine the conditions for reproducible growth of SI GaAs. These crystals have a great potential as a substrate material for epitaxial GaAs integrated circuit and other solid state devices.

The case of polysilicon

This form, of the well-known semiconductor, has an increasing application in solid state electronics (24). A polycrystalline material is composed of small crystallites joined together by grain boundaries. The electrical properties of this type of system were first discussed by Shockley (9) and were treated theoretically by Read (10). Some recent experimental investigations, using Deep Level Transient Spectroscopy (DLTS), established the fact that crystal defects introduce deep-lying donor and acceptor states (25). Their electrical behaviours are similar to the ones introduced by impurities, discussed above in the case of GaAs.

Grain boundaries, characteristic of polycrystals, are complex structures. They are considered to consist of a few atomic layers of disordered surface atoms. These create a transition region between the different orientations of the neighboring crystallites. Inside each grain, the atoms are arranged in a periodic manner. A grain can therefore be considered as a small single crystal. The grain boundaries are characterized by incomplete atomic bonds. These result in hybridized surface dangling bonds, which are randomly distributed, characterizing a polycrystal. They can act as electron traps when empty and hole traps when occupied. Some direct evidence for carrier recombination at a tilt boundary in n-type germanium was presented by Vogel *et al.* (29). Following Shockley and Pearson (30), measurements have confirmed that the density of these surface states is in the order of the density of the surface atoms (31).

This dangling bond model permits the evaluation of the concentrations of the deep-lying levels. These can be computed by considering the average surface area of the grains, knowing their average sizes and assuming that one dangling bond exists per surface atom (12, 13, 17, 26). Then, considering the compensation effect of the deep-lying trapping centers, the position of the Fermi level can be determined, using the above described multilevel model.

In the case of polysilicon the position of acceptor traps was taken to be 0.37 eV below the conduction band, according to Seto (27). The position of the deep-lying donors has been valued at 0.37 eV above the valence band (28). Then, for example, if the average grain size, determined by scanning electron microscopy (13), is 3 μm and the characteristics dangling bond density in silicon (111) surface is 7.8×10^{14} cm^{-2}, the corresponding trapping center concentration, deep-lying donor in this case, can be calculated to be $N_{Dd} = 1.56 \times 10^{19}$ cm^{-3}. Now, if the position of the Fermi level is determined as a function of the doping shallow acceptor density N_A, it is found (12) that the Fermi energy will cross the deep-lying donor level at a characteristic acceptor concentration. It is of interest to note, that at this acceptor density a mobility minimum has been observed (17, 27). This can be interpreted by the concept of metallic impurity band conduction. According to Mott and co-workers (15, 16), if the average ionized impurity separation is commensurable with the Bohr radius then the wave functions of these impurities can overlap, forming an impurity band. This band is separated from the corresponding conduction or valence band edges by many kT's, especially in the case of deep-lying levels. In this case, if the Fermi level is in this impurity band then the conduction processes will be guided by its random system properties. Consequently, the effect of lattice periodicity looses its role in the transport properties of the solid. This results in the replacement of the effective mass of the free carriers in the impurity band, by the rest mass of the electron. Since the carrier mobilities are related to the effective mass, this phenomenon is characterized by low mobilities. These can be estimated by an expression given by Mott (16):

$$[13] \quad \mu_{min} < \frac{2\pi e R^2}{6h}$$

where R is the average impurity separation and e is the electronic charge.

The calculated value in the above mentioned case is 32 (cm^2 V^{-1} s^{-1}), which is of the same order of magnitude as the measured ones at the experimental mobility minima (12).

Finally, the position of the Fermi level determines the free carrier concentration, as it has been demonstrated in the case of GaAs (see Figs. 1 and 2). Thus knowing the carrier mobilities one can calculate the resistivity of polysilicon films as a function of the doping concentration. The results are collected in Fig. 3. Here, curves 1 and 2 depict the experimental and calculated values of Seto (27), curve 3 shows the calculated values

TABLE 3. Tin oxide film thicknesses, d (μm); grain sizes l (μm); fractions of (100), (200), (211), (301), and (400) crystallites with the total trapping centers density, $N(t)$ and charge carrier densities, n

d (μm)	l (μm)	F(110)	F(200)	F(211)	F(310)	F(400)	$N(t)$ (cm^{-3}) × (10^{20})	n(cm^{-3}) × (10^{20})
0.14	0.03	0.45	0.32	0.23	0.0	0.0	3.92	0.64
0.39	0.07	0.53	0.33	0.09	0.03	0.02	1.75	0.86
0.76	0.13	0.14	0.74	0.05	0.02	0.05	0.29	1.97
1.65	0.27	0.04	0.76	0.06	0.01	0.13	0.06	1.99
2.9	0.46	0.02	0.72	0.02	0.02	0.22	0.02	1.99
3.0	0.48	0.02	0.59	0.17	0.10	0.12	0.08	1.98
3.7	0.59	0.004	0.65	0.01	0.03	0.31	0.01	2.00
4.5	0.71	0.007	0.51	0.06	0.20	0.22	0.06	1.98
5.3	0.83	0.12	0.43	0.28	0.12	0.05	0.09	1.95

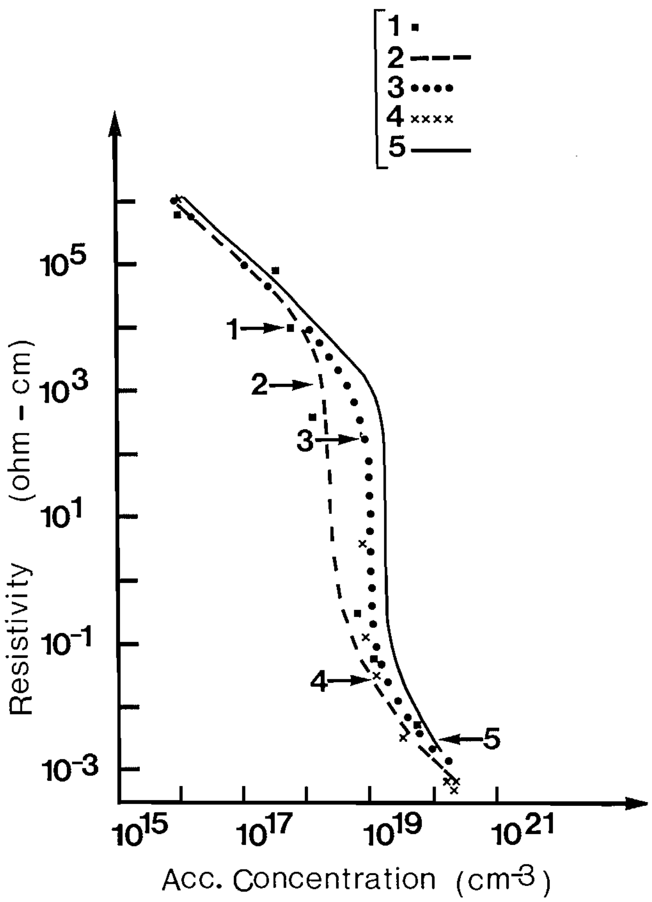

FIG. 3. Resistivities (ohm cm) as a function of doping concentration for *1*, experimental data of ref. 27; *2*, theoretical curve of ref. 27; *3*, calculated curve for p-type film; *4*, experimental points of p-type film; *5*, calculated curve of n-type film.

of p-type polysilicon using the multilevel model discussed above, curve 4 represents the experimental data of this investigation (12, 13) and curve 5 has been calculated in the case of an n-type film. In all cases good agreements can be seen between the experimental and calculated results. They represent, correctly, the characteristic large variation of the resistivities of polysilicon films. These are in the range of 10^9 (ohm cm) which were never observed in the case of single crystal silicons. It can be pointed out, that the existence of quasi semi-insulating polysilicon, in analogy to SI GaAs, is due to grain-boundaries-introduced deep-lying trapping centers compensation.

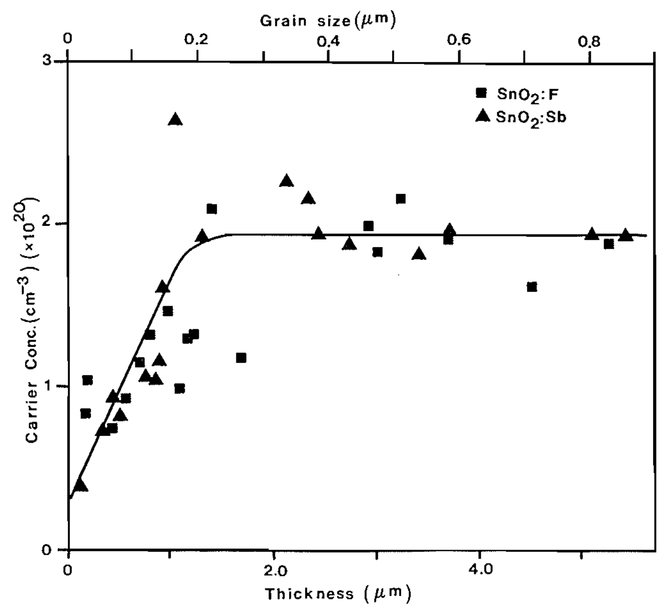

FIG. 4. Carrier concentration as a function of film thickness of CVD deposited tin oxide. Calculated curve, full line; experimental data of fluorine doped tin oxide, full squares; experimental data of antimony doped tin oxide, full triangles.

The case of tin oxide

These polycrystalline films are of interest as transparent electrodes for photovoltaic and photoelectrochemical solar energy converters. They combine high electrical conductivity with low optical absorption in the visible part of the spectrum (32). The films were grown by the technique of Chemical Vapor Deposition (CVD) (32). The transport properties of the transparent electrodes were determined by Hall effect measurements described previously (21). It was found that films doped for a free carrier density of 2×10^{20} (cm^{-3}) have thickness-dependent transport properties, below a layer thickness of 1 μm. Above this value, the carrier concentration, mobility, and consequently the film resistivity become layer thickness independent. The measured values of resistivities are shown in Fig. 4, where the triangles represent the data obtained in the case of antimony doping, while the squares are the ones for fluorine doping. It can be seen that the measured resistivities are also independent of the doping species. The obtained X-ray diffraction spectra suggest again the existence of grain boundaries introduced deep-lying trapping centers. In Table 3 the measured film thicknesses, d(μm); average grain sizes

l(μm); and the fraction of crystallites having different orientations, $F(110)$, $F(200)$, $F(211)$, $F(301)$, and $F(400)$, respectively, are collected based on previous works (18). This table includes the calculated trapping centers concentrations, $N(t)$ (cm^{-3}), and the resulting free carrier concentrations, at constant doping, using the above discussed deep-lying compensating impurity model. In this case, however, some characteristic properties of the grain boundaries in tin oxide have been taken into account. Following the results obtained by X-ray Photoconduction Spectroscopy (XPS) and Ultraviolet Photoconduction Spectroscopy (UPS) (32) it can be argued that grains of (200) (in the second order (400)) orientations do not participate in the trapping mechanisms (33). This was taken into account in the calculation of the trapping centers density, $N(t)$, using the fractions of the occurrence of different orientations, collected in Table 3, obtained from the X-ray diffraction spectra. Taking the measured average charge carriers mobility of tin oxide films to be 18 ($cm^2\ V^{-1}\ s^{-1}$), the resistivity as a function of the layer thickness, can be calculated. The results are shown in Fig. 4 by the curve drawn in full line. It can be seen that the calculated curve and the measured data are in good agreement. This indicates once more the validity of the deep-levels compensation model in the case of tin oxide as well.

Conclusions

The compensation mechanisms, due to deep-lying trapping centres, having been examined to elucidate some of the particular transport properties characteristic of semi-insulating GaAs, polysilicon, and polycrystalline tin oxide transparent electrodes. In the first case the deep-lying levels can be introduced by chromium or oxygen doping. In the case of polycrystals their origin could be related to dangling bonds created by the grain boundaries.

The determination of the Fermi level, based on complete mass spectrographic analyses, led to the establishment of the quantitative conditions required for deep levels compensation in the case of single crystal GaAs. Polysilicon films are characterized by peculiar mobility minima as a function of carrier concentrations and by a very large resistivity range compared to single crystals. The deep level compensation mechanisms, combined with metallic impurity conduction, have been used to analyze these phenomena. In the case of polycrystalline tin oxide films the measured thickness dependence of resistivities could be elucidated by this model applied with some relevant modifications.

Acknowledgments

The author is grateful to the members of the collaborating group: Dr. J. P. Dodelet, Mr. D. Belanger, and Miss. D. Cote of the INRS-Energie (Varennes, Que.); Dr. M. A. Bartkowski of the Chemistry Division, National Research Council of Canada (Ottawa, Ont.), Dr. I. Dickson of Ecole Polytechnique (Montreal, Que.), and Mr. G. McLaughlin of Concordia University (Montreal, Que.) for their valuable contributions in different parts of this investigation; and to Drs. D. S. Russel, A. Mykytiuk, and D. Williams of the Chemistry Division, National Research Council (Ottawa, Ont.), for the spark source mass spectrographic analyses.

1. G. R. CRONIN and R. W. HAISTY. J. Electrochem. Soc. 874 (1964).
2. R. ZUCCA. *In* Semi-insulating III-V Materials Conference. Publishing Institute of Physics, London SW1X8QX, University of Nottingham. 1980. p. 105.
3. R. N. HALL, G. E. FENNER, J. D. KINGSLEY, T. J. SOLTYS, and R. O. CARLSON. Phys. Rev. Lett. **9**, 366 (1962).
4. A. L. LIN and R. H. BUBE. J. Appl. Phys. **47**, 1859 (1976).
5. A. L. LIN, E. OMELIANOVSKI, and R. H. BUBE. J. Appl. Phys. **47**, 1852 (1976).
6. R. ZUCCA. J. Appl. Phys. **48**, 1987 (1977).
7. G. M. MARTIN, J. R. FARGES, G. JACOB, and J. P. HALLAIS. J. Appl. Phys. **51**, 2840 (1980).
8. B. A. LOMBOS, N. YEMENIDJIAN, and M. AVEROUS. Can. J. Phys. **60**, 35 (1982).
9. W. SHOCKLEY. Phys. Rev. **91**, 228 (1953).
10. W. T. READ JR. Phil. Mag. **45**, 775 (1955); **46**, 111 (1955).
11. W. SHOCKLEY and W. T. READ. Phys. Rev. **87**, 835 (1952).
12. B. A. LOMBOS, S. YEE, M. PIETRANTONIO, and M. AVEROUS. J. Phys. **43**, C1-199 (1982).
13. B. A. LOMBOS, S. YEE, M. BARTKOWSKI, and M. PIETRANTONIO. Proc. 33-rd Electronic Component Conference, Orlando, FL. 1983 p. 29.
14. M. E. COWHER and T. O. SEDQUICK. J. Electrochem. Soc. **119**, 1565 (1972).
15. N. F. MOTT. *In* Electronic and structural properties of amorphous semiconductors. *Edited by* P. G. Comber and J. Marts. Academic Press, New York, NY. 1973 p. 1.
16. N. F. MOTT and W. D. TWOSE. Adv. Phys. **10**, 107 (1961).
17. B. A. LOMBOS and M. PIETRANTONIO. J. Can. Cer. Soc. **51**, 6 (1982).
18. D. BELANGER, M. BARTKOWSKI, J. P. DODELET, B. A. LOMBOS, I. DICKSON, and L. DAO. J. Can. Cer. Soc. **52**, 28 (1983).
19. W. SHOCKLEY. Electrons and holes in semiconductors. D. Van Nostrand, Prinston, NJ. 1950.
20. S. M. SZE. Physics of semiconductor devices. J. Wiley, New York, NY. 1981. p. 21.
21. N. YEMENIDJIAN and B. A. LOMBOS. J. Cryst. Growth. **56**, 163 (1982).
22. E. J. JONSON, J. A. KAFALAS, and R. W. DAVIES. J. Appl. Phys. **54**, 204 (1983).
23. T. KIKUTA and K. ISHIDA. 11-th Intern. Symp. on GaAs and related Comp. C2, Sept. 26–28, 1984. Biarritz, France.
24. T. YOSHIKARA, A. YOSUKA, and H. ABE. J. Electrochem. Soc. **127**, 1603 (1980).
25. C. MERLET. Etudes Spectroscopique des Niveaux Profonds dans les Matériaux à Haute Resistivité Si et GaAs. Thèse 3-me cycle. Académie de Montpellier, 10, July, 1979. France.
26. T. I. KAMINS. J. Appl. Phys. **42**, 4357 (1971).
27. J. Y. W. SETO. J. de Phys. **46**, 5247 (1975).
28. A. J. MILNES. *In* Deep impurities in semiconductors. J. Wiley, New York, NY. 1973.
29. F. L. VOGEL, W. T. READ JR., and L. C. LOVEL. Phys. Rev. **94**, 1791 (1954).
30. W. SHOCKLEY and G. L. PEARSON. Phys. Rev. **74**, 2321 (1948).
31. F. C. ALLEN and G. W. GABELI. Phys. Rev. **127**, 150 (1962).
32. K. H. COX, R. G. EGDELL, C. HARDING, W. R. PATTERSON, and P. J. TAVENER. Surf. Sci. **123**, 179 (1982).
33. D. BELANGER, J. P. DODELET, B. A. LOMBOS, and J. I. DICKSON. J. Electrochemical Soc. In press.

Ab initio study of rotational isomerism in acrolein[1]

GEORGE R. DE MARÉ
Laboratoire de Chimie Physique Moléculaire, Faculté des Sciences, CP. 160, Ave. F. D. Roosevelt, 50 B. 1050 Brussels, Belgium

Received August 31, 1984

This paper is dedicated to Professor Camille Sandorfy on the occasion of his 65th birthday

GEORGE R. DE MARÉ. Can. J. Chem. **63**, 1672 (1985).

Analytic gradient (force) methods at the STO-3G, 3-21G, and 6-31G* basis set levels have been used to optimize the geometry of acrolein completely at each critical point (minima, maximum) in the torsional potential energy curves for rotation about the single C—C bond (dihedral angle θ). The STO-3G and 6-31G* optimizations predict the planar *trans* conformation (θ = 180°) to be more stable than the *cis* conformation (θ = 0°) by 1.87 and 6.97 kJ/mol, respectively. The 3-21G optimizations, in disagreement with experiment, place the planar *cis* structure below the *trans* by 4.5 J/mol. The predicted relative energy (Δ*E*) and position for the transition state (*TS*) for rotation from the *trans* conformer are Δ*E* = 22.35, 37.14, and 34.41 kJ/mol and θ = 91.8, 91.6, and 91.0° for the STO-3G, 3-21G, and 6-31G* optimizations, respectively. The computed and experimental geometries, relative energies, dipole moments, and coefficients for the torsional potential expansion are compared.

GEORGE R. DE MARÉ. Can. J. Chem. **63**, 1672 (1985).

La géométrie de l'acroléine a été optimisée complètement par la méthode force (gradients analytiques) avec les bases STO-3G, 3-21G et 6-31G* à chaque point critique (minima, maximum) de la courbe d'énergie potentielle pour la rotation autour de la liaison C—C simple (angle dièdre θ). Les optimisations avec les bases STO-3G et 6-31G* situent la forme plane *trans* (θ = 180°) à 1,87 et 6,97 kJ/mol, respectivement, en dessous de la forme plane *cis* (θ = 0°). Par contre les optimisations avec la base 3-21G placent le rotamère *trans* 4,5 J/mol au dessus du *cis*, en désaccord avec les données spectroscopiques. L'énergie (Δ*E*) et la position de l'état de transition (*TS*) pour la rotation *trans* → *cis* sont Δ*E* = 22,35, 37,14 et 34,41 kJ/mol et θ = 91,8, 91,6 et 91,0° pour les optimisations avec les bases STO-3G, 3-21G et 6-31G*, respectivement. Les géométries, énergies relatives, moments dipolaires, et coefficients de l'expansion en série du potentiel de torsion, obtenus dans ce travail, sont comparés avec les données expérimentales.

Introduction

Ab initio torsional potential energy curves for rotation about the C—C bond adjacent to the CH═X group in a number of R—CH═X compounds (where R = cyclopropyl, CH═CH_2 or CH═O and X = CH_2 or O) have been generated recently by De Maré and co-workers (1−4) using various basis sets and complete geometry optimization by analytic gradient methods. For 1,3-butadiene (3, 4) and vinylcyclopropane (1), optimization along the torsional potential energy curve with a larger than minimal basis set reveals a *gauche*/s-*trans*[2] conformer equilibrium in agreement with experiment (5, 6). In contrast, only the *cis* and *trans* positions represent minima in the torsional potential energy curves for the oxygen-containing compounds, regardless of the basis set used (2, 3). For these compounds, however, the predicted relative energies of the *cis*, *TS*, and *trans* structures are very basis set dependent (2, 3). For cyclopropanecarboxaldehyde (*CPCA*) (2), the predicted relative energies have been shown to depend more on the basis set used for the computations than on the basis set used for the geometry optimizations. The same conclusion applies to glyoxal (7) for which certain discrepancies between experimental and *ab initio* optimized geometrical parameters persist (8). Although good experimental estimates of the energy difference between the most stable acrolein conformer (*trans*) and a higher energy rotamer have been available for more than 10 years (9), the complete structure of the latter has been only just reported (10).

This paper presents a detailed study of the geometries and relative energies of the *trans*, *TS*, and *cis* acrolein structures (see Fig. 1) obtained with the minimal STO-3G, split-valence 3-21G, and 6-31G* basis sets.

Computational method

The references for the basis sets used in the present study are STO-3G (11), 3-21G (12), 3-21G** (13), 4-31G (14), 6-31G* (15), and 6-31G** (15). For the optimizations, non-planar acrolein structures (dihedral angles of 5°) with initial values of θ = 5, 90, or 175° (see Fig. 1) were constructed using bond lengths and valence angles deduced from the corresponding STO-3G, 3-21G, or 6-31G* optimized parameters in *CPCA* (2) and 1,3-butadiene (4). The optimizations were carried out within the Hartree−Fock formalism (16), using the analytic gradient (13) of the SCF energy with respect to the internal geometrical parameters (bond lengths, valence, and dihedral angles). The Optimally Conditioned (OC) minimization technique (17*a*)[3] was used to determine the optimal geometry at each minimum. The VA05AD sum of squares technique (18) was used for the *TS* optimizations and to confirm the order[4] of the stationary points revealed by the OC method.

All computations were performed with the MONSTERGAUSS *ab initio* program (19) on the CYBER 170/750 computer system at the University of Brussels.

[1]Presented in part at the 14ème Congrès des Chimistes Théoriciens d'Expression Latine, Louvain-la-Neuve, 1983 and 29th IUPAC Congress, Cologne, 1983.

[2]With the STO-3G basis set, complete optimization of the vinylcylopropane and 1,3-butadiene geometries along the torsional potential energy curves reveals only s-*cis* and s-*trans* minima (see refs. 1, 4). In the remainder of the text s-*cis* and s-*trans* will be denoted by *cis* and *trans*, respectively.

[3]The routine is described in ref. 17(*b*).

[4]The order of a critical point is equal to the number of negative eigenvalues of the Hessian or force constant matrix (second derivatives of the energy with respect to the internal geometrical parameters). The order of a minimum, maximum, second order, saddle point, … is 0, 1, 2, … .

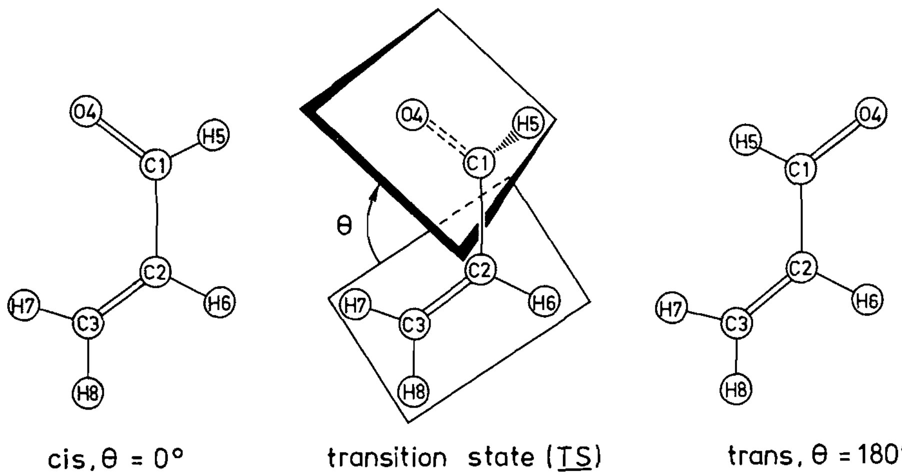

FIG. 1. Nomenclature and atom numbering used throughout the text. The atom numbering is the same as that used by Blom, Grassi, and Bauder (10).

Results and discussion

Critical point structures and potential energy curves

The optimized geometrical parameters, energy, dipole moment, and order obtained with the STO-3G, 3-21G, and 6-31G* basis sets for acrolein at each critical point in the torsional potential energy curves (see Fig. 2) are listed in Table 1.

Stable acrolein rotamers

The OC optimizations with all three basis sets and starting values of $\theta = 5$ and 175° lead to completely planar *cis* and *trans* structures, respectively. In each case the order of the Hessian is zero, as is required for an energy minimum.[4] The predicted positions of the minima are thus in agreement with experiment: the planar *trans* conformer has long been known to be the most stable (20) while the structure of the higher energy rotamer, first detected in 1971 (9) has recently been shown to be definitely *cis* planar (10, 21).

Although Devaquet, Townshend, and Hehre (22) used the STO-3G basis to optimize the geometries of *cis* and *trans* acrolein in 1976, they did not report the optimized geometrical parameters. They found energies of −188.30219 and −188.30284 hartree for the completely optimized *cis* and *trans* structures, respectively. These values are significantly higher than those found in this work (see Table 1). The discrepancies are probably the result of different cut-off criteria[5] since the relative energies of the rotamers differ by about 10% (1.87 (this work) compared to 1.71 (22) kJ/mol).

Whereas the STO-3G optimizations correctly predict the *trans* acrolein structure to be most stable, the above energy difference appears to be too small. (George, Bock, and Trachtman (23) have optimized the geometries of *cis* and *trans* acrolein completely with the 4-31G basis set and found an energy difference of −0.0013 au or 3.4 kJ/mol, which is also apparently too small. It is less than that obtained in 4-31G//BASIS1 computations in this study (see Table 2). Indeed,

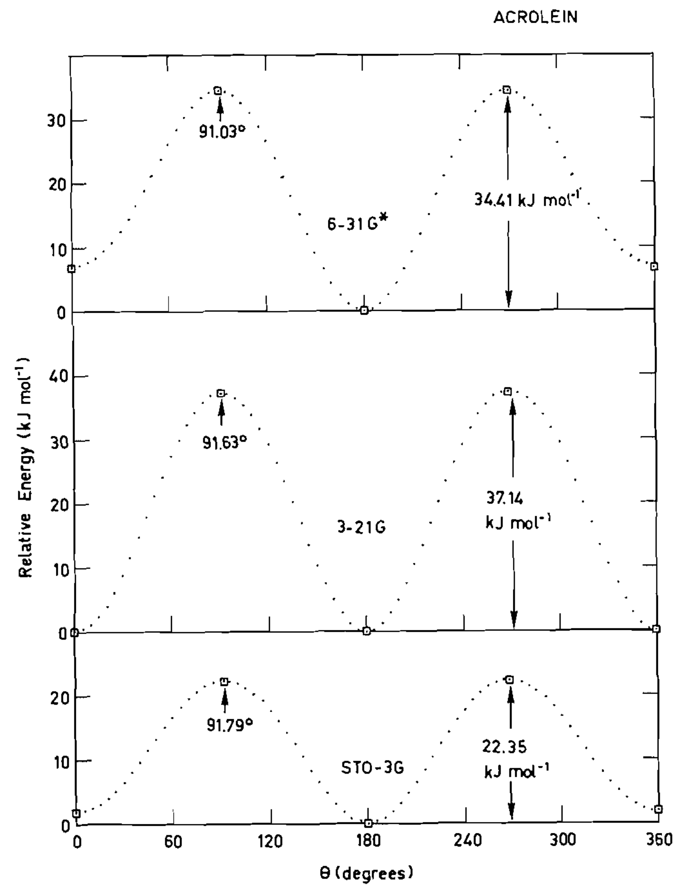

FIG. 2. Relative energies for rotation around the C—C single bond in acrolein. The *cis* conformation corresponds to dihedral angles of 0 and 360°, the *trans* conformation to 180°.

estimates obtained from gas-phase near ultraviolet (9) and Raman (24) spectroscopy lie in the range 570−700 cm^{-1} or 6.8−8.4 kJ/mol.[6] Thus only the 6-31G* optimizations yield a "reasonable" energy difference between the *cis* and *trans* acrolein conformers. *The 3-21G basis actually predicts the* cis *structure to be more stable than the* trans, even if only by

[5]In this work the optimizations were terminated when the gradient length, $|g| = \left[\sum_{i}^{n} (\delta E/\delta q_i)^2/n\right]^{1/2}$, was reduced below 5×10^{-4} mdyn. The q_i are the internal coordinates (bond lengths, bond angles and dihedral angles) and the sum is over the n optimized coordinates (25). The cut-off criterion generally yields energies stable below the μhartree level (25).

[6]The experimental error limits extend this range somewhat, but not enough to include the STO-3G or 4-31G predictions.

TABLE 1. STO-3G, 3-21G, and 6-31G* optimized parameters for acrolein (see Fig. 1 for atom numbering; bond lengths are in pm and angles in deg)

Parameters	*trans* (θ = 180°)			TS			*cis* (θ = 0°)		
	STO-3G	3-21G	6-31G*	STO-3G θ = 91.79°	3-21G θ = 91.63°	6-31G* θ = 91.03°	STO-3G	3-21G	6-31G*
C—C	151.00	147.36	147.84	152.72	149.47	149.84	151.17	147.82	148.59
C═C	131.17	131.74	132.11	130.85	131.46	131.66	131.24	131.82	132.12
C═O	122.06	121.01	118.98	121.87	120.92	118.76	122.13	121.23	119.08
C1—H5	110.37	108.76	109.48	110.56	108.57	109.40	110.32	108.45	109.36
C2—H6	108.38	107.20	107.55	108.52	107.56	107.82	108.29	107.22	107.65
C3—H7	108.32	107.53	107.69	108.25	107.41	107.63	108.35	107.34	107.45
C3—H8	108.23	107.18	107.45	108.21	107.26	107.49	108.26	107.20	107.47
∠C2C1O4	124.03	124.31	123.85	124.23	125.07	123.83	123.84	124.13	124.37
∠C2C1H5	114.21	114.22	115.27	114.69	114.29	115.85	114.70	114.80	115.35
∠O4C1H5	121.76	121.47	120.88	121.08	120.64	120.32	121.46	121.07	120.28
∠C1C2C3	122.39	121.06	121.24	123.61	123.21	123.43	122.39	120.52	121.47
∠C3C2H6	121.67	122.35	122.36	120.87	120.96	120.96	121.60	122.29	121.53
∠C1C2H6	115.94	116.59	116.40	115.52	115.83	115.61	116.01	117.19	117.00
∠H7C3C2	121.74	121.54	121.51	122.33	122.06	122.02	121.16	120.17	120.67
∠H8C3C2	122.36	122.21	122.09	121.92	121.60	121.44	122.48	122.46	121.83
∠H7C3H8	115.90	116.25	116.40	115.75	116.34	116.54	116.36	117.37	117.50
μ(D)	1.94	3.47	3.51	1.70	2.99	2.95	1.68	2.88	2.92
E (hartree)	−188.303526	−189.689882	−190.762426	−188.295013	−189.675738	−190.749318	−188.302813	−189.689883	−190.759771
ΔE (kJ mol^{-1})	0.00	0.0045	0.00	22.35	37.14	34.41	1.87	0.00	6.97
Order	0	0	0	1	1	1	0	0	0

TABLE 2. BASIS2//BASIS1 computations for acrolein: BASIS2 was used to compute the SCF energy for the BASIS1 optimized geometry, *trans* conformer, SCF energies (hartree); other structures, energies (kJ/mol) relative to the same BASIS2//BASIS1 computation for the *trans* conformer

		BASIS2					
Conformer (θ°)	BASIS1	STO-3G	3-21G	3-21G**	4-31G	6-31G*	6-31G**
trans (180)	STO-3G	−188.303526	−189.688373	[a]	−190.477667	−190.759475	−190.766501
	3-21G	−188.301624	−189.689882	−189.801179	−190.479639	−190.761540	−190.768519
	6-31G*	−188.300059	−189.689010	[a]	−190.478859	−190.762426	−190.769409
TS (91.8)	STO-3G	22.35	36.47	[a]	34.97	33.96	33.72
(91.6)	3-21G	21.64	37.13[b]	36.83	35.73	34.94	34.73
(91.0)	6-31G*	21.90	37.63	[a]	35.70	34.41	34.17
cis (0)	STO-3G	1.87	0.11	[a]	3.68	6.13	6.03
	3-21G	1.78	−0.004	2.72	4.58	7.32	7.21
	6-31G*	0.87	0.37	[a]	4.70	6.97	6.89

[a]Not computed.
[b]Barrier height from the *cis* structure = 37.14 kJ/mol.

4.5 J/mol. This failure of the 3-21G basis was unexpected since it has yielded apparently reliable relative energies, not only for optimized hydrocarbon structures (1, 4), but also for oxygen-containing species (i.e. CH_3CHO ground, triplet n → π* and n → 3*s* electronic states (25)).

In view of the present results, it is likely that the *cis−trans* energy difference in *CPCA* is nearer to 1.2 than to 7.0 kJ/mol (6-31G* and STO-3G optimized values, respectively (2)). Note that only the STO-3G basis computations (even with optimized geometries from the larger basis sets) gave a higher energy for *cis* than for *trans* CPCA (2).

Position and height of the TS

As previously observed for *CPCA* (2), the predicted position of the *TS* is remarkably basis set independent for acrolein. In going from the minimal STO-3G to the extended 6-31G* basis, the predicted location of the *TS* only ranges from 91.79 to 91.03°. The *TS* structure is thus very close to that with the double bonds perpendicular to one another. The situation in acrolein is therefore, as might have been expected, intermediate to those in 1,3-butadiene and glyoxal where the 6-31G* basis predicts the *TS* to be at θ = 101.5 (4) and 73.0° (3), respectively. For the latter two molecules, the minimal basis set optimizations predict the *TS* to lie closer to the perpendicular structure than does the 6-31G* basis (3, 4).

The barrier heights to rotation from the predicted most stable rotamer, obtained by the 3-21G, 6-31G*, and STO-3G optimizations, are 37.1, 34.4, and 22.3 kJ/mol, respectively. Thus although the trend is the same as that revealed in the *CPCA* study, the variation in the values (31.7, 24.3, and 13.8 kJ/mol, respectively) was much more pronounced for *CPCA* (2).

The experimentally determined values for the rotational *trans* → *cis* barrier in acrolein lie between those predicted by the STO-3G and 6-31G* optimizations. Carreira (24) found 2236 ± 135 cm^{-1} (26.76 ± 1.62 kJ/mol) by fitting the torsional overtones in the low frequency gas phase Raman spectrum of acrolein to a potential function of the form

$$[1]\quad V(\phi) = \sum_i (0.5V_i(1 - \cos i\phi))$$

where φ = 0 corresponds to the stable *trans* configuration. (The *cis−trans* energy difference derived from the same analysis is 584 ± 180 cm^{-1} (6.99 ± 2.15 kJ/mol) (24).) A slightly higher value, 2460 cm^{-1} (29.4 kJ/mol), for the barrier was deduced by De Groot and Lamb (26) from ultrasonic measurements on acrolein in the liquid phase.[7]

Dependence of the geometrical parameters on the basis set and on the dihedral angle θ; comparison of experimental and theoretical geometries

As mentioned above, George, Bock, and Trachtman (23) have optimized the geometries of *cis* and *trans* acrolein completely using gradient methods with the unscaled 4-31G basis set (14). For the optimization on *trans* acrolein, they report a total energy of −190.4693 hartree, a value much higher than that (−190.4798 hartree) obtained in an optimization with the 4-31G basis set or in 4-31G//BASIS1 computations reported in Table 2. The C—H bond lengths they obtain are longer than those obtained here (7). The comparison of their results and ours thus falls outside the scope of the present work.

Although comparison of theoretical and experimental parameters below the 1 pm/1° level may be dubious (27), it is nevertheless interesting to see if the observed trends in the data are consistent. Such a comparison is made in Table 3 where the experimental and predicted (6-31G*) differences in the parameters in *cis* and *trans* acrolein are given. The variation in the parameters will now be discussed in some detail.

∠H7C3C2, ∠H8C3C2, and ∠H7C3H8

The experimental trend for ∠H7C3C2 (*trans* > *cis* value by 1.2°) is reproduced and the computed differences (0.58 (STO-3G), 1.37 (3-21G), and 0.84° (6-31G* optimized values)) are reasonable. Both the STO-3G and 3-21G basis sets predict a small *increase* in ∠H8C3C2 in the *cis* compared to the *trans* conformer. Only the 6-31G* basis reproduces the experimental trend, predicting ∠H8C3C2 to be 0.26° smaller in *cis* acrolein (compared to an experimental Δ*ct* of 0.7° (Table 3)). The optimized values of ∠H7C3H8 change very little on going from the *trans* to the *TS* structure, then increase by 0.6 to 1.1° in the *cis* conformation. The *ab initio* and experimental results are again in agreement on the direction, but not on the magnitude, of the change in this angle.

∠C1C2C3

The contrast in the predicted behaviour of the CCC bond

[7]Although the *ab initio* values are comparable to the gas phase, note that De Groot and Lamb (26) obtained a *cis−trans* energy difference of 8.6 kJ/mol, within experimental error of the gas phase values.

TABLE 3. Experimental geometries for *trans* and *cis* acrolein; bond lengths and angles in pm and deg, respectively; the error limits are those given in the original references

Parameter	*trans*[a]	*trans*[b]	*trans*[c]	*cis*[c]	$(\Delta ct)_{exp.}$[d]	$(\Delta ct)_{theor.}$[d]
C—C	147.0±0.3	148.23±0.4	146.8±0.4	147.8±0.6	+1.0	+0.75
C=C	134.5±0.3	134.09±0.3	134.0±0.4	134.0±0.4	0.0	+0.01
C=O	121.9±0.5	121.25±0.3	121.4±0.4	121.5±0.6	+0.1	+0.10
C1—H5	110.8±0.3	111.2 ±3.0	111.3±0.6	110.6±0.3	−0.7	−0.12
C2—H6	108.4±0.3	108.3 ±1.0	108.4±0.5	108.8±0.4	+0.4	+0.10
C3—H7	108.6±0.5	—	109.0±0.4	109.8±0.5	+0.8	−0.24
C3—H8	108.6±0.5	—	108.0±0.3	108.1±0.3	+0.1	+0.02
∠C2C1O4	123.3±0.3	123.27±0.7	124.0±0.6	124.2±0.4	+0.2	+0.52
∠C2C1H5	115.1±0.2	114.4 ±2.7	114.7±0.5	115.8±0.4	+1.1	+0.08
∠O4C1H5	—	—	121.3±0.6	120.1±0.4	−1.2	−0.60
∠C1C2C3	119.8±0.2	120.30±0.7	120.4±0.5	121.5±0.4	+1.1	+0.23
∠C3C2H6	122.8±0.2	122.9 ±1.8	122.4±0.5	121.1±0.4	−1.3	−0.83
∠C1C2H6	—	—	117.2±0.5	117.4±0.4	+0.2	+0.60
∠H7C3C2	120.0±0.2	119.6±1.1	119.7±0.3	118.5±0.3	−1.2	−0.84
∠H8C3C2	121.4±0.2	121.5±1.1	122.2±0.5	121.5±0.6	−0.7	−0.26
∠H7C3H8	—	—	118.1±0.6	120.0±0.5	+1.9	+1.10

[a] r_s structure determined from the microwave spectra of eleven isotopic acrolein species with C3—H7 assumed equal to C3—H8 (28).
[b] Average structure in the ground vibrational state determined by the combined use of the electron diffraction intensities and rotational constants (20).
[c] r_s structures determined by Blom, Grassi, and Bauder (10) from the microwave spectra of normal and highly enriched, singly D, ^{13}C, and ^{18}O substituted acrolein species. The error limits given are equal to three times the standard deviation from the least squares treatment (10).
[d] $(\Delta ct)_{exp.}$ and $(\Delta ct)_{theor.}$ are the differences between the values for the parameters in the *cis* and *trans* acrolein structures from ref. 10 and from the 6-31G* optimizations (Table 1), respectively.

angles in acrolein and 1,3-butadiene is striking. Whereas the ∠CCC's in *trans*-1,3-butadiene are found to be almost basis set independent (4), the ∠C1C2C3 obtained for *trans* acrolein with the STO-3G basis is more than 1° larger than the 3-21G or 6-31G* optimized values. Whereas the optimized CCC bond angles in 1,3-butadiene are predicted to be largest (by about 3°) for a near *cis*-structure (4), the optimized ∠C1C2C3 values for acrolein are largest in the *TS* structure. The differences in the values for this angle in the *cis* and *trans* conformers of acrolein are small and erratic. The 6-31G* optimizations reproduce the experimental trend but the predicted change is only about 20% of the experimental one.

C—H bond lengths

As is generally observed (see ref. 2), each C—H bond length for a given critical point structure varies according to STO-3G > 6-31G* > 3-21G optimized value. Also, as observed for *CPCA* (2), the STO-3G optimizations predict the aldehydic C—H bond to be longest in the *TS* whereas both the 3-21G and 6-31G* optimizations predict it to be longest in the *trans* conformer. The shorter C1—H5 optimized bond length in the *cis* compared to that in the *trans* acrolein rotamer reproduces the experimental trend. Note that the combined uncertainties in the experimental bond lengths are fairly large.

Excluding the C1—H5 bond length discussed above, all the optimized C—H bond lengths fall in the range 107.18−108.52 pm. For a given basis set and a given environment (see below), the variation in the C—H bond length is much smaller. The optimized values can therefore be used without optimization (or as excellent starting values for optimizations) in larger molecules.

In agreement with the small difference in the experimental values of the C3—H8 bond length in the *cis* and *trans* conformers (108.1 and 108.0 pm, respectively), all three basis sets give a C3—H8 bond length which is relatively independent of θ. The STO-3G values for C3—H7 vary according to *cis* > *trans* > *TS* value whereas for both the 3-21G and 6-31G* basis sets, the *trans* > *TS* > *cis* optimized values. This is sharp contradiction with the experimental finding that C3—H7 is 0.8 pm longer in the *cis* structure (10). One might expect that non-bonding interactions between H7 and the O-atom in the *cis* configuration would lead to a lengthening of the C3—H7 bond. Note also that the behaviour of the optimized values for C3—H7 with the larger basis sets parallels that predicted by the same basis sets for the corresponding C—H bonds in 1,3-butadiene where a repulsive interaction between the H-atoms destabilizes the *cis* structure (3, 4).

C=O and C=C bond lengths

As, expected, the optimized C=O and C=C bonds for a given basis set are predicted to be shortest in the *TS* structure. These bonds are predicted to be slightly shorter in the *trans* than in the *cis* conformer. This behaviour is similar to that found for the double bonds in 1,3-butadiene (+0.2 pm in the *cis* rotamer compared to the *trans* 6-31G* optimized value) (4). In *CPCA* the 6-31G* C=O optimized bond lengths are 118.88 and 119.14 pm in the *trans* and *cis* conformations, compared to 118.98 and 119.08 pm for acrolein. These theoretical results support the experimental findings that the C2=C3 bond is the same length in *trans* and *cis* acrolein while the C1=O4 bond is slightly longer in the *cis* structure ((10); see Table 3).

C1—C2 bond length

The results are very similar to those obtained for the bond joining the ring and CHO group in *CPCA* (2). The difference between the *cis* and *trans* optimized C1—C2 bond lengths increases with basis set size to 0.75 pm for the 6-31G* basis. These findings are in agreement with the microwave results of Blom *et al.* (10) which give 146.8 and 147.8 pm for the C1—C2 bond length in *trans* and *cis* acrolein, respectively.

TABLE 4. Computed net charges on the H5—C1—O4, H6—C2, and H7—C3—H8 groups (δ^1, δ^2, and δ^3, respectively) in the *trans*, *TS*, and *cis* acrolein structures; see Fig. 1 for the atom numbering

	trans			*TS*			*cis*		
Basis set	δ^1	δ^2	δ^3	δ^1	δ^2	δ^3	δ^1	δ^2	δ^3
STO-3G[a]	−0.020	−0.007	+0.027	−0.008	−0.006	+0.014	−0.023	−0.019	+0.042
3-21G[a]	+0.011	−0.102	+0.091	+0.017	−0.093	+0.075	+0.011	−0.167	+0.156
3-21G**[b]	+0.044	−0.138	+0.093	+0.050	−0.113	+0.063	+0.044	−0.203	+0.159
4-31G[a]	−0.048	−0.018	+0.067	—	—	—	—	—	—
(7, 3)[d]	−0.003	−0.090	+0.093	—	—	—	+0.002	−0.169	+0.167
6-31G*[a]	−0.024	−0.008	+0.032	−0.003	−0.018	+0.021	−0.022	−0.074	+0.096
6-31G**[c]	−0.023	−0.020	+0.043	−0.003	−0.027	+0.030	−0.021	−0.088	+0.109

[a]From the final computation in the geometry optimization.
[b]From the 3-21G**//3-21G computation.
[c]From the 6-31G**//6-31G* computation.
[d]Calculated from the values given in ref. 23 for computations without dipole moment optimization.

The agreement between the theoretical and experimental trends in the C1—C2 bond on going from the *trans* to the *cis* acrolein conformers is in sharp contrast with the present situation for glyoxal (7, 8, 29).

Relative energies of acrolein structures computed using the optimized geometry from another basis set

The complete geometry optimization of the *trans*, *TS*, and *cis* acrolein structures with the 6-31G** basis set would be fairly costly in terms of computer time. Nevertheless, it would be interesting to investigate the effect of adding polarization functions on the H-atoms. Also, why are the relative energies obtained for *trans* and *cis* acrolein with the 3-21G basis set so different from those expected? For both *CPCA* (2) and 1,3-butadiene (4) BASIS2//BASIS1 computations (where BASIS2 is used for the computation with the BASIS1 optimized geometry) showed that the trends in the relative rotamer energies obtained by BASIS2 optimizations were satisfactorily reproduced. A series of BASIS2//BASIS1 computations is reported in Table 2.

For a given BASIS1, the relative energies of the *TS* or *cis* acrolein structures obtained with the 6-31G**//BASIS1 computations are slightly lower than (but well within 2% of) the relative energy obtained with the 6-31G*//BASIS1 computations. It is thus very unlikely that geometry optimization with the 6-31G** basis set would lead to relative energies or conformer stabilities which are meaningfully different from those obtained with the 6-31G** basis set in the present study.

For a given BASIS2, each set of BASIS2//BASIS1 computations gives relative energies for the *trans*, *TS*, and *cis* acrolein structures which are quite consistent, showing that the differences depend on the basis sets and not on the optimized geometry. It is apparent that complete optimization of the bond lengths and bond angles, even with the minimal STO-3G basis, leads to geometries which can be used with other basis sets to obtain reasonable relative energies (for the other basis sets and not necessarily compared to the real relative energies!).

With the 3-21G** basis set, the relative energies for the optimized *TS* and *cis* structures are closer than the 3-21G ones to those predicted by the 6-31G* computations. The relative energy for the *cis* conformer is still unsatisfactory, however. It is clear that, for oxygen-containing species, geometry optimization with the 3-21G basis set on several isomers should be followed by 6-31G* computations to check the 3-21G basis predictions for the relative energies.

Basis set dependence of the computed net charges from Mulliken population analysis

The computed net charges on the H5—C1—O4, C2—H6, and H7—C3—H8 groups (δ^1, δ^2, and δ^3, respectively) derived from the Mulliken population analysis (30) are given in Table 4.

The δ^1 values predicted by the 3-21G and 3-21G** basis sets are *positive*, just as the net charges on the CHO group in *CPCA* predicted by the 3-21G and 6-21G basis sets are positive. With the STO-3G, 4-31G, 6-31G*, and 6-31G** basis sets, *negative* δ^1 values are predicted for all the acrolein structures. With all the basis sets used in this study, the δ^1 values for the *TS* are less negative (thus more positive for the 3-21G and 3-21G** basis sets) than in the *trans* and *cis* conformers. The positive values of δ^1 obtained with the 3-21G and 3-21G** basis sets are apparently the result of a larger computed positive charge on the aldehydic H-atom with these basis sets. From the (7, 3) basis set results reported by Bock, George, and Trachtman (23), one obtains $\delta^1 = -0.003$ for the *trans* and +0.002 for the *cis* acrolein structures.[8] This variation may simply reflect the near balance of the sum of the charges on the atoms in the CHO group with the (7, 3) basis. Indeed, this type of behaviour has already been noted for the net charges computed for the CHO group in various *CPCA* rotamers with the 6-31G and 6-31G* basis sets (2). There the net charges are near zero and oscillate between negative and positive values.

With all the basis sets used in this study δ^2 is negative and δ^3 is positive for all the acrolein structures. This is in sharp contrast to the results obtained for 1,3-butadiene where the 3-21G and 6-21G basis sets consistently predicted a net positive charge on the CH_2 groups, while the 6-31G, 6-31G*, and 6-31G** basis sets predicted net negative charges on the CH_2 groups.

Whether hydrogen bonding or an electrostatic interaction in *cis* acrolein causes this rotamer to be relatively more stable than the *cis* rotamer or glyoxal (see below) has been discussed in detail by Bock, George, and Trachtman (23). For acrolein, 1,3-butadiene, and glyoxal, the *trans* conformer is the most stable and it is in equilibrium with a higher energy rotamer (the *cis*, except for 1,3-butadiene where a cisoid *gauche* rotamer lies about 3 kJ/mol below the *cis* (3, 4)). The energies of the

[8]Without dipole moment optimization; with dipole moment optimization δ^1 = +0.008 for both *cis* and *trans* acrolein (23).

TABLE 5. Comparison of the net charges in the CH_2 groups of acrolein (**A**) and 1,3-butadiene (**B**) as obtained in the Mulliken population analysis of 6-31G**//6-31G* computations. For simplicity the numbering of the H-atoms is the same as that of the vinyl group of acrolein (Fig. 1)

	cis		*TS*		*trans*	
Atom	**A**	**B**	**A**	**B**	**A**	**B**
H7	+0.17567	+0.12482	+0.14243	+0.12873	+0.14573	+0.12586
C3	−0.21464	−0.27979	−0.25768	−0.26361	−0.25843	−0.29541
H8	+0.14763	+0.13123	+0.14517	+0.12756	+0.15607	+0.13172
O5	−0.49781	—	−0.45329	—	−0.49788	—

TABLE 6. Coefficients (kJ/mol) for the torsional potential energy curves for rotation about the single C—C bond in acrolein, determined by a six-term least-squares expansion of eq. [1]

Source	V_1	V_2	V_3	V_4	V_5	V_6	V^*
STO-3G[a]	0.302	21.422	1.336	0.237	0.231	−0.028	106.6
3-21G[a]	1.538	37.179	−1.265	0.290	−0.268	−0.072	134.2
6-31G*[a]	3.991	31.035	2.663	−0.428	0.317	−0.118	148.9
Carreira[b]	3.66	22.96	4.04	−1.15	−0.68	—	96.5
Fateley *et al.*[c]	12.4	28.2	−3.8	—	—	—	88.7
Cole and Green[d]	—	—	—	—	—	—	90.8

[a]Calculated using the energies of the fully optimized *cis*, *TS*, and *trans* structures and at least 21 additional data points.
[b]Reference 24.
[c]Reference 32; tentative values for V_1, V_2, and V_3.
[d]Reference 33.

6-31G* optimized *TS* structures, relative to the *trans* conformer, are quite similar (34.4, 25.4, and 30.0 kJ/mol, respectively (Table 1; (3))). In contrast, one finds relative energies for the optimized *cis* structures of 7.0, 16.0, and 23.5 kJ/mol with the same basis set, compared to experimental values of 6.8−8.6, about 16, and 13.5 kJ/mol, respectively, for the higher energy rotamer. (The "low" relative energy for *cis* glyoxal (13.5 kJ/mol from spectroscopic measurements) compared to those obtained with double ζ or double ζ + polarization basis sets has been discussed by Osamura and Schaefer (8).) In spite of the discrepancy between the theoretical and experimental energy differences for *cis* and *trans* glyoxal, it is quite apparent that some additional stabilization process is present in *cis* acrolein.

If one compares only the charge distributions on the CH_2 group and the O-atom in *cis* and *trans* acrolein, there is little evidence for hydrogen bonding in the *cis* structure. (In contrast to the findings of Bock, George, and Trachtman (23) with a (7, 3) basis set, the charges on the O-atom in *cis* and *trans* acrolein are found to be equal in 6-31G**//6-31G* computations (Table 5).) A more detailed examination of the data is possible. In Table 5, the net charges on the atoms of the CH_2 groups in the *cis*, *TS*, and *trans* acrolein and 1,3-butadiene structures are given for comparison. The net charge on the C-atom is smallest in the *TS* for 1,3-butadiene and smallest in the *cis* rotamer of acrolein, respectively. The net "electron loss" on this atom on going from the *trans* to the *cis* acrolein structure was taken as direct evidence against hydrogen bonding in acrolein (23). The behaviour of the net charges on the hydrogen atoms, when compared to that in 1,3-butadiene, is probably more in favour of hydrogen bonding than previously supposed. Indeed, in the *TS* structure of each molecule the net charges on H8 and H7 are almost equal. Further, in 1,3-butadiene the net charges on H8 (and on H7) are almost equal in the *cis* and *trans* conformers with the net charge on H8 greater than that on H7. For acrolein, whereas the net charge on H8 is about 7% larger than that on H7 in the *trans* conformation, the situation is completely reversed in the *cis* rotamer with the net charge on H7 about 19% larger than that on H8. It would be very interesting to have detailed density plots in these molecules.

Fourier expansion of the torsional potential

The torsional potential energy curves obtained for acrolein have been simulated by a least-squares procedure using eq. [1]. The relationship between ϕ and θ is $\phi = 180 - \theta$, since V must be zero for $\phi = 0$ (this relationship was also used for the 3-21G torsional potential, neglecting the small energy difference between the *cis* and *trans* conformations). At least 21 additional data points (7 near each critical point) were computed for use in the least-squares simulation to ensure that the resulting torsional curves were "smooth". The coefficients are given in Table 6.

Although the coefficients for the 3-21G torsional potential curve simulation are given, they are probably only useful for reproducing the computed data since they reflect the unrealistic *cis−trans* energy difference (nearly zero) predicted by the basis. Also, because of this near zero energy difference, with the maximum very near the perpendicular position, a second solution with negative V_1 and positive V_3 and V_5 (but nearly identical absolute values of the V_i) exists. The first three terms of the expansion are the most important, as has been observed previously by Carreira (24) for the series derived to fit the Raman torsional overtone spectrum of acrolein. The V_1 term in the STO-3G series is very small compared to that in the 6-31G* series. Except for the high V_2 value in the 6-31G* simulation (which essentially reflects the *trans−cis* barrier) there is fairly good agreement between the V_i from the simulation of the 6-31G* optimal curve and the values obtained by Carreira.

TABLE 7. Dipole moments for acrolein structures (D)

Source	$\mu(cis)$	$\mu(TS)$	$\mu(trans)$
STO-3G[a]	1.68	1.70	1.94
3-21G[a]	2.88	2.99	3.47
3-21G**[b]	2.58	2.65	3.13
6-31G*[a]	2.92	2.95	3.51
6-31G**[c]	2.92	2.95	3.51
Microwave[d]	2.552	—	3.117
Microwave[e]	—	—	3.11

[a]Computed with the optimized geometry with the same basis set.
[b]From the 3-21G**//3-21G computation.
[c]From the 6-31G**//6-31G* computation.
[d]From ref. 10.
[e]From ref. 34, calculated from $\mu_a = 3.06 \pm 0.04$ and $\mu_b = 0.54 \pm 0.14$ D.

The values of V^*, which is given by eq. [2] (see ref. 32),

$$[2] \quad V^* = \sum_{i=1}^{n} i^2 V_i$$

are also given in Table 6. Those derived from the *ab initio* torsional potential curves are higher than the "experimental" ones. Once again the largest deviations are observed where the barrier to rotation was predicted to be the highest.

Dipole moments

The dipole moments computed in the present study are given in Table 7 for comparison with those available in the literature.

For all of the basis sets used in this study, the dipole moment of *cis* acrolein is computed to be smaller than that for the *trans* conformation. The STO-3G values are too small, being 62 and 66% of the experimental values of the dipole moments for the *trans* ($\mu(trans)$) and *cis* ($\mu(cis)$) acrolein rotamers. This is very similar to the results obtained with the STO-3G basis set for the optimized *CPCA* structures where the computed $\mu(trans)$ and $\mu(cis)$ values are 60 and 64%, respectively, of the experimental values. The 3-21G**//3-21G computations give dipole moments which are very close to the experimental ones. For the 3-21G, 6-31G*, and 6-31G**//6-31G* computations, remarkably constant values of $\mu(trans)$ and $\mu(cis)$ are obtained. Whereas the 3-21G and 6-31G* computed values of the dipole moments for *trans* and *cis CPCA* were about 6−8% larger than the experimental ones (2), the differences observed for acrolein are slightly larger, being from 11 to 15%. This agreement is still quite satisfactory.

Conclusions

The geometry optimizations at the STO-3G, 3-21G, and 6-31G* basis set levels all predict a two-well torsional potential for acrolein with stable *cis* and *trans* rotamers, in agreement with experiment. Only the computations with the extended 6-31G* and 6-31G** basis sets yield satisfactory relative energies for these stable structures, however. The smaller basis sets used (STO-3G, 3-21G, 3-21G**, and 4-31G) all lead to *cis−trans* energy differences which are too small. As observed previously for *CPCA* (2) and 1,3-butadiene (4), the relative energies of the acrolein structures depend more on the basis set used for the computations than on that used for the optimizations.

The STO-3G optimized single and double bond lengths are all longer and shorter, respectively, than those obtained with the 3-21G and 6-31G* optimizations. The optimized values for ∠H7C3C2 are smaller in *cis-* than in *trans*-acrolein, in agreement with experiment. This decrease in ∠H7C3C2, as well as an observed increase in the C3—H7 bond length, in *cis-* compared to *trans*-acrolein, have been interpreted as reflecting an attraction between H7 and the oxygen atom in the *cis*-conformer (10). The 3-21G and 6-31G* optimizations predict the C3—H7 bond to be *shorter* in the *cis*-acrolein conformer, however, in apparent disagreement with experiment. Hydrogen bonding in the *cis* conformer may nevertheless be reflected by the computed net charges (31): the computed net charge on H7 is lower and higher than that on H8 in *trans-* and *cis*-acrolein, respectively.

As previously observed for *CPCA* (2), STO-3G values for the dipole moments of the acrolein rotamers are too small (about 65% of the observed ones). Those computed with the larger basis sets are quite satisfactory, however, all being within 15% of the experimental ones.

Acknowledgements

Dr. C. E. Blom (Justus-Liebig-Universität Giessen) is thanked for supplying a copy of the manuscript on the structure of *cis-* and *trans*-acrolein prior to its publication. It is also a pleasure to acknowledge the assistance of the staff of the Computing Center at the University of Brussels.

1. G. R. DE MARÉ and M. R. PETERSON. J. Mol. Struct. Theochem. **89**, 213 (1982).
2. G. R. DE MARÉ and M. R. PETERSON. J. Mol. Struct. Theochem. **104**, 115 (1983).
3. G. R. DE MARÉ. J. Mol. Struct. Theochem. **107**, 127 (1984).
4. (*a*) G. R. DE MARÉ and D. NEISIUS. J. Mol. Struct. Theochem. **109**, 103 (1984); (*b*) G. R. DE MARÉ. *In* Computational organic chemistry. *Edited by* I. G. Csizmadia and R. Daudel. NATO ASI Series C, **67**, 371 (1981).
5. (*a*) G. R. DE MARÉ and J. S. MARTIN. J. Am. Chem. Soc. **88**, 5033 (1966); (*b*) A. DE MEIJERE and W. LÜTTKE. Tetrahedron, **25**, 2047 (1969).
6. Y. FURUKAWA, H. TAKEUCHI, I. HARADA, and M. TASUMI. Bull. Chem. Soc. Jpn. **56**, 392 (1983).
7. G. R. DE MARÉ. Unpublished results.
8. Y. OSAMURA and H. F. SCHAEFER, III. J. Chem. Phys. **74**, 4576 (1981).
9. (*a*) A. C. P. ALVES, J. CHRISTOFFERSEN, and J. M. HOLLAS. Mol. Phys. **20**, 625 (1971); **21**, 384 (1971); (*b*) G. A. OSBORNE and D. A. RAMSAY. Can. J. Phys. **51**, 1170 (1973); E. J. BLAIR, W. GOETZ, and D. A. RAMSAY. Can. J. Phys. **49**, 2710 (1971).
10. C. E. BLOM, G. GRASSI, and A. BAUDER. J. Am. Chem. Soc. In press.
11. W. J. HEHRE, R. F. STEWART, and J. A. POPLE. J. Chem. Phys. **51**, 2657 (1969).
12. J. S. BINKLEY, J. A. POPLE, and W. J. HEHRE. J. Am. Chem. Soc. **102**, 939 (1980).
13. J. S. BINKLEY, R. A. WHITESIDE, R. KRISHNAN, R. SEEGER, D. J. DEFREES, H. B. SLEGEL, S. TOPIOL, L. R. KAHN, and J. A. POPLE. GAUSSIAN 80. Dept. of Chemistry, Carnegie-Mellon University, Pittsburgh, PA.
14. R. DITCHFIELD, W. J. HEHRE, and J. A. POPLE. J. Chem. Phys. **54**, 724 (1971).
15. P. C. HARIHARAN and J. A. POPLE. Chem. Phys. Lett. **16**, 217 (1972); Theor. Chim. Acta, **28**, 213 (1973).
16. C. C. J. ROOTHAAN. Rev. Mod. Phys. **23**, 69 (1951).
17. (*a*) W. C. DAVIDON. Mathematical Programming, **9**, 1 (1975); (*b*) W. C. DAVIDON and L. NAZARETH. Technical Memos. 303 and 306. Applied Mathematics Division, Argonne National Laboratories, Argonne IL.

18. M. J. D. POWELL. Program VA05AD, AERE Subroutine Library, Harwell, Gt. Britain.
19. M. R. PETERSON and R. A. POIRIER. Program MONSTERGAUSS, University of Toronto, Ont., Canada, 1981.
20. K. KUTCHITSU, T. FUKUYAMA, and Y. MORINO. J. Mol. Struct. **4**, 41 (1969), and references therein.
21. C. E. BLOM and A. BAUDER. Chem. Phys. Lett. **88**, 55 (1982).
22. A. J. P. DEVAQUET, R. E. TOWNSHEND, and W. J. HEHRE. J. Am. Chem. Soc. **98**, 4068 (1976).
23. P. GEORGE, C. W. BOCK, and M. TRACHTMAN. J. Mol. Struct. **69**, 183 (1980).
24. L. A. CARREIRA. J. Phys. Chem. **80**, 1149 (1976).
25. M. R. PETERSON, G. R. DE MARÉ, I. G. CSIZMADIA, and O. P. STRAUSZ. J. Mol. Struct. Theochem. **92**, 239 (1983).
26. M. S. DE GROOT and J. LAMB. Proc. R. Soc. London, A**242**, 36 (1957).
27. J. A. POPLE. Modern Theor. Chem. **4**, 1 (1977).
28. E. A. CHERNIAK and C. C. COSTAIN. J. Chem. Phys. **45**, 104 (1966).
29. C. W. BOCK, P. GEORGE, G. J. MAINS, and M. TRACHTMAN. J. Mol. Struct. **49**, 211 (1978).
30. R. S. MULLIKEN. J. Chem. Phys. **23**, 1833 (1955).
31. P. A. KOLLMAN and L. C. ALLEN. Chem. Rev. **72**, 283 (1972).
32. W. G. FATELY, R. K. HARRIS, F. A. MILLER, and R. E. WITKOWSKI. Spectrochim. Acta, **21**, 231 (1965).
33. A. R. H. COLE and A. A. GREEN. J. Mol. Spectrosc. **48**, 232 (1973).
34. R. WAGNER, J. FINE, J. W. SIMMONS, and J. H. GOLDSTEIN. J. Chem. Phys. **26**, 634 (1957).

Un problème toujours d'actualité: trois électrons – trois centres

G. BERTHIER

Laboratoire de Biochimie Théorique, (L.A. n° 77), Institut de Biologie Physico-Chimique,
13, rue Pierre et Marie Curie, F-75005 Paris, France

Reçu le 6 août 1984

Cet article est dédié au Professeur Camille Sandorfy à l'occasion de son 65e anniversaire

G. BERTHIER. Can. J. Chem. **63**, 1681 (1985).

On discute l'état présent des calculs théoriques sur les radicaux libres en prenant l'allyle comme point de repère. La nature des produits atomiques de dissociation contenus dans une fonction d'onde en forme de déterminant adaptée à la symétrie fournit un critère heuristique utile en cas de brisure de symétrie.

G. BERTHIER. Can. J. Chem. **63**, 1681 (1985).

The present status of theoretical calculations on free radicals is discussed, taking allyl as a benchmark. The nature of the atomic dissociation products included in a symmetry-adapted determinantal wave function gives a useful, heuristic criterion for symmetry-breaking cases.

Depuis quarante ans environ, l'étude de la répartition de trois électrons entre trois atomes munis chacun d'une orbitale (au moins) est un thème récurrent en chimie théorique. Le radical allyle CH_2CHCH_2, avec ses trois carbones porteurs d'électrons π, constitue l'archétype des systèmes de ce genre, aussi bien dans les applications classiques de la théorie de Hückel ou celle de la mésomérie aux hydrocarbures conjugués (voir p. ex. 1–6) que dans le développement ultérieur de méthodes de calcul plus explicites.

L'allyle a servi d'exemple lors de la mise au point de traitements théoriques pour les systèmes à couches électroniques incomplètes comme les radicaux libres ou les biradicaux. Il en a été ainsi pour les deux variantes possibles de la méthode du champ self-consistant dans l'approximation LCAO-MO, celle dite "UHF, sans contrainte de spin S^2 (7–9), et celle dite "RHF", qui conserve la notion intuitive d'orbitales moléculaires dioccupées, puis mono-occupées pour les électrons non appariés (10, 11). Il en est de même de la méthode d'interaction de configuration, soit sous sa forme initiale (12), soit dans la version "atomes dans les molécules" (13). La méthode des orbitales moléculaires alternantes, où l'on réalise une interaction de configuration de forme prédeterminée à partir de spinorbitales de type UHF(14) a été aussi éprouvée sur l'exemple du système π de l'allyle (15).

Les travaux précédents ont eu, dans le domaine des structures moléculaires, des conséquences qui dépassent l'intérêt chimique d'un tel système: ils ont servi à illustrer la notion de densité de spin négative, dont la présence sur certains atomes joue un grand rôle en résonance paramagnétique électronique (16–18) et en diffraction des neutrons polarisés (19). Enfin, les configurations excitées dues au saut d'un électron π vers l'orbitale moléculaire non-liante ou vers l'orbitale anti-liante du système allyle (20, 21) forment la base de l'interprétation des transitions doublet–doublet caractéristiques des radicaux libres non-saturés (voir 22–25 et références jointes).

Au cours de la dernière décennie, le système à trois électrons réapparaît comme exemple-type, en théorie du champ self-consistant de difficultés dues à d'éventuelles brisures de symétrie durant la résolution des équations de Hartree–Fock (26). En général, celles-ci sont dues au fait que les contraintes de symétrie d'espace et de spin imposées aux fonctions d'onde, solutions du problème RHF à une particule ne sont – selon la reformulation du théorème de Delbrück (27) donnée par Ripka (28) – que des propriétés de self-consistance; cela n'exclut nullement la possibilité de solutions moins restrictives dans certains cas, mais qu'il convient de purifier de leurs composantes d'espace ou de spin indésirables, d'où le dilemne de symétrie de Löwdin (29). Parmi toutes les formes d'extremums locaux possibles (pour un exemple simple, voir la réf. 30), on dit, selon Thouless (31) qu'une fonction Hartree–Fock est instable si la dérivée seconde de l'énergie totale E par rapport à certaines orbitales est négative au lieu d'être définie, positive. Ces caractéristiques de la théorie du champ self-consistant, d'abord reconnues en physique des noyaux (32), sont maintenant bien comprises en physique atomique (33, 34) et moléculaire (35–40 et références jointes).

TABLEAU 1. Exemples de fonctions d'onde à symétrie brisée dans des systèmes de formule générale A_3 ou ABA (calculs *ab initio*)

	Etat spectroscopique	Nature	Références
H_3	Voir texte	σ	52, 53
LiO_2	$^2A_2$	π	54, 56
NO_2	$^2A_1$, $^2B_2$	σ	55
CO_2	$^3A_2$, $^3B_2$		60
HCO_2	$^2A_2$	π	*
NCN	$^3\Sigma_g^-$	$\pi_x\ \pi_y$	*
Allyle	$^2A_1$	π	45–48
Na_3	$^2A_1$, $^2B_2$	σ	57
Cu_3	$^2A_1$	σ	*
Ag_3	$^2A_1$	σ	*

* Calculs inédits: HCO_2 (Y. Ellinger et A. D. McLean); NCN (G. Berthier et L. Kurdi); Cu_3 et Ag_3 (G. Berthier, I. Dangeard et Tao Yuan Qi).

Un examen des fonctions d'onde moléculaires non-Delbrück qui ont été signalées dans la littérature (voir la réf. 41) montre que beaucoup des composés répertoriés peuvent être assimilés à des systèmes à trois électrons – trois centres. La liste de résultats présentée dans le tableau 1 comporte des types chimiques variés dans des états doublets et triplets, fondamentaux ou excités. Selon la terminologie usitée en chimie organique (42–44), il s'agit aussi bien de radicaux σ que π, l'électron non-apparié occupant dans la configuration de référence soit une orbitale de composantes atomiques s ou σ symétriques, soit une orbitale de composantes π antisymétriques par rapport au plan des trois centres.

Les propriétés d'instabilité des orbitales moléculaires de type Hückel trouvées par Paldus et Čižek (37) dans l'allyle subsistent quel que soit le niveau de l'approximation LCAO-MO utilisée, et pour une gamme très étendue de longueurs et angles de liaison: calculs avec davantage d'électrons de valence ou calculs complets en base minimale (45, 46), calculs en base étendue allant de distances internucléaires très grandes à la conformation d'équilibre (47, 48). Par rapport à un système d'orbitales adapté à la symétrie C_{2v} d'un squelette nucléaire à liaisons CC égales, on y constate que la perte de l'opération σ_v' (plan perpendiculaire au motif $C_1C_2C_3$) dans la fonction d'onde électronique entraîne un abaissement d'énergie qui s'amplifie quand on permet aux noyaux de suivre la brisure de symétrie du nuage électronique. Il s'agit en quelque sorte de "suivisme nucléaire",[1] qu'on peut interpréter comme une pseudo-distorsion de Jahn–Teller (49), aboutissant à la formation d'une structure de Lewis localisée, avec une double liaison entre les deux carbones de gauche et un électron non-apparié à droite, ou vice-versa. La tendance générale des systèmes d'électrons π à se localiser sous l'effet des brisures de symétrie (50) est tout à fait vérifiée par l'allyle. Il en résulte aussi que la surface d'énergie obtenue à partir d'orbitales moléculaires correspondant à des solutions instables qui restent adaptées à la symétrie nucléaire présente une discontinuité au passage du groupe ponctuel C_{2v} (liaisons CC égales) au groupe C_s (liaisons CC différentes), et que celle obtenue avec les solutions stables à symétrie brisée a un caractère non-analytique dans la même région (38). D'autres causes d'instabilité que la contrainte de symétrie σ_v' peuvent être étudiées concurremment ou indépendamment, telle l'hypothèse de la double occupation des orbitales moléculaires, dont la levée conduit à une fonction d'onde UHF non-exactement doublet, ou la symétrie d'alternance PPP des hydrocarbures conjugués (40, 51).

Les brisures de symétrie signalées pour les autres radicaux à trois centres proviennent généralement aussi d'une perte de symétrie gauche–droite, qu'il reste à concilier avec les résultats expérimentaux. Le cas du trihydrogène H_3, où l'on peut dire que la perte de symétrie obtenue dans les calculs Hartree–Fock préfigure l'état normal du système: une molécule H_2 liée à un atome H par interaction de van der Waals (52, 53) est particulier. Une solution souvent adoptée (54–57) consiste à effectuer une interaction de configuration avec les orbitales moléculaires de la symétrie la plus basse; mais en raison de possibles défauts d'analyticité on devrait, pour tenir compte correctement de la corrélation électronique, éliminer les composantes de symétrie indésirables des solutions sans contraintes des équations de Hartree–Fock avant le calcul variationnel lui-même, ce qui revient à un traitement de champ self-consistant multi-configurationnel (38). Dans le cas du radical allyle, il s'avère qu'un calcul MC-SCF direct à l'intérieur du sous-système π, suivi d'une interaction de configuration mettant en jeu les mono- et diexcitations, reproduit correctement les propriétés de symétrie C_{2v} des données expérimentales (58). Une autre ressource est l'interaction de "résonance" entre structures déformées gauche–droite et droite–gauche équivalentes (55, 59; voir aussi la réf. 60).

De tous les travaux précédents se dégage la nécessité d'avoir clairement notion des brisures de symétrie susceptibles de se manifester dans les calculs de surfaces d'énergie. Une étude rigoureuse du problème, basée par exemple sur le signe des valeurs propres des matrices d'instabilité (35–39) est souvent longue et coûteuse, et l'analyse de la fragmentation de la molécule considérée en fragments plus petits peut donner certains renseignements (48). Heureusement, une comparaison des produits de dissociation *atomiques* contenus dans les configurations avec différents types d'orbitales quand les distances internucléaires deviennent infiniment grandes, fournit rapidement une idée de la situation. Le critère proposé ici étend aux composés à trois électrons et plus l'explication bien connue selon laquelle un déterminant construit à partir d'une orbitale moléculaire doublement occupée de symétrie σ_g^+ ne représente pas correctement la molécule H_2 parce qu'il contient une contribution trop forte de structures ioniques, tandis qu'un déterminant formé de deux spinorbitales purement atomiques a un bon comportement asymptotique; cette situation demeure pour des molécules diatomiques plus compliquées (61, 62).

TABLEAU 2. Poids en % des structures ioniques et covalentes du système à trois électrons – trois centres

$\psi_{sym.ad.}$ (RHF)*		$\psi_{sym.ad.}$ (UHF)†		$\psi_{sym.br.}$	
$C^-A^\cdot - A^-C^\cdot$	25	$C^-A^\alpha - A^-C^\alpha$	16,66	$A^-C^\cdot$	25
$B^-A^\cdot - B^-C^\cdot$	25	$B^-A^\alpha - B^-C^\alpha$	33,33	$B^-C^\cdot$	25
$A^-B^\cdot - C^-B^\cdot$	12,5	$A^-B^\alpha - C^-B^\alpha$	8,33	$(A - B)\,C^\cdot$	50
$A^\cdot B^\cdot C^\cdot$	37,5	$A^\beta B^\alpha C^\alpha - A^\alpha B^\alpha C^\beta$	8,33		
		$A^\alpha B^\beta C^\alpha$	33,33		

*Orbitales de Hückel. L'expression détaillée des structures indiquées se trouve dans la réf. 13; $A^\cdot B^\cdot C^\cdot$ est l'une des fonctions doublets possibles pour le problème à trois spins (ici $A^\alpha B^\alpha C^\beta - 2A^\alpha B^\beta C^\alpha + A^\beta B^\alpha C^\alpha$).

†Orbitales de Hückel avec $\lambda = \sqrt{2}$ et $\mu = 1$.

Le tableau 2 donne pour trois centres A, B, C le résultat d'un développement tout à fait analogue au calcul classique mentionné plus haut pour le système AB avec deux fonctions de base χ_a et χ_b. Dans la première colonne sont indiqués les poids des formules ioniques et covalente contenues dans déterminant de la forme $\psi_{sym.ad.} = |\phi_1\alpha\phi_1\beta\phi_2\alpha|$, où ϕ_1 et ϕ_2 sont des orbitales moléculaires de type Hückel adaptées à la symétrie C_{2v} (ϕ_1: $\chi_a + \sqrt{2}\,\chi_b + \chi_c$; ϕ_2: $\chi_a - \chi_c$). Les coefficients de ces fonctions se trouvent dans des publications antérieures (13, 40). La troisième colonne contient les résultats correspondants pour le déterminant $\psi_{sym.br.}$, où ϕ_1 et ϕ_2 sont des orbitales de symétrie C_s, localisées l'une entre A et B, l'autre sur C ($\phi_1 = \chi_a + \chi_b$; $\phi_2 = \chi_c$). On voit immédiatement que pour des distances internucléaires très grandes le déterminant à symétrie brisée $\psi_{sym.br.}$ doit fournir une énergie plus basse, puisque le poids des structures ioniques y est moins fort (50% au lieu de 62,5% dans $\psi_{sym.ad.}$). Le même état de choses subsiste quand on passe d'une description RHF à symétrie d'espace et de spin adaptée à une description UHF à symétrie d'espace seulement, c'est à dire si l'on prend $\psi_{sym.ad.}$ (UHF) $= |\phi_1\alpha\phi_2\beta\phi_3\alpha|$ où ϕ_1 et ϕ_2 sont des orbitales de Hückel différentes (17, 63) selon le spin de l'électron considéré (ϕ_1: $\chi_a + \lambda\chi_b + \chi_c$; ϕ_2: $\chi_a + \mu\chi_b + \chi_c$; ϕ_3: $\chi_a - \chi_c$ avec $\lambda > \mu \simeq 1$). On trouve encore que le poids des structures ioniques dans le déterminant UHF reste prépondérant: 58,33% dans le cas $\mu = 1$. Il apparaît très nettement ici l'importance de l'opération σ_v' du groupe C_{2v} comme contrainte d'espace effective pour les systèmes à trois électrons – trois centres. On notera que le caractère σ ou π éventuel des orbitales atomiques χ n'intervient pas dans ce résultat; en outre, on constate que les systèmes à trois centres avec deux ou quatre électrons ne donnent aucun signe de brisure de symétrie dans leurs produits de dissociation atomiques.

[1] L'expression "suivisme nucléaire" est une transposition pour le cas des noyaux du terme "orbital following". Dans le cas des molécules A_3 ayant la forme d'un triangle équilatéral et où il existe un niveau monoélectronique doublement dégénéré, occupé par un seul électron, la distorsion $D_{3h} \rightarrow C_{2v}$ est un véritable effet Jahn–Teller.

L'examen des produits de dissociation ne saurait pourtant remplacer une analyse détaillée de l'origine des brisures de symétrie, comme l'indique le cas de la molécule H_2 elle-même où un déterminant RHF donne une description acceptable quand on se rapproche de la distance internucléaire d'équilibre. C'est seulement un critère heuristique commode qu'on peut sans doute généraliser à davantage d'électrons. Ainsi, si l'on prend comme modèle d'un biradical triplet dans l'état fondamental le système d'électrons π du triméthylèneméthane $(CH_2)_3$ C (64), on trouve que le déterminant construit à l'aide d'orbitales de Hückel adaptées à la symétrie D_{3h} avec deux électrons sur la première et un électron sur la seconde et la troisième contient 66,66% de structures ioniques, contre 50% dans le cas d'une description localisée de symétrie C_{2v} avec deux électrons formant liaison avec l'atome central A et un atome terminal B et deux électrons non appariés sur les deux autres atomes C, D. On pourrait traiter des systèmes plus compliqués en utilisant un algorithme de calcul sur ordinateur qui a été récemment developpé pour extraire les formules de valence contenues dans un déterminant de Slater (65, 66), et même étudier des situations multi-configurationnelles en profitant du fait que les programmes du genre ZDO avec interaction de configuration conviennent très bien pour les grandes distances interatomiques.

Remerciements

L'auteur dédie cet article au professeur Camille Sandorfy pour son soixante-cinquième anniversaire; il remercie ses collègues parisiens et grenoblois qui lui ont communiqué des résultats encore inédits.

1. E. HÜCKEL. Z. Phys. **83**, 632 (1933); Z. Elektrochem. **43**, 752 (1937).
2. C. A. COULSON. Proc. R. Soc. A, **164**, 383 (1938); Trans. Faraday Soc. **22**, 106 (1946); **22**, 265 (1946).
3. J. SYRKIN et M. DIATKINA. Acta Phys. Chem. URSS, **21**, 641 (1946).
4. A. PULLMAN. Faraday Soc. Disc. n° 2, 26 (1947).
5. W. E. MOFFITT et C. A. COULSON. Trans. Faraday Soc. **44**, 81 (1948).
6. A. PULLMAN et G. BERTHIER. Bull. Soc. Chim. Fr. **15**, 1056 (1948).
7. G. BERTHIER. C.R. Acad. Sci. **238**, 91 (1954).
8. G. BERTHIER. J. Chim. phys. **51**, 363 (1954); **52**, 141 (1955).
9. J. A. POPLE et R. K. NESBET. J. Chem. Phys. **22**, 571 (1954).
10. J. HIGUCHI. J. Chem. Phys. **26**, 151 (1957).
11. C. C. J. ROOTHAAN. Rev. Mod. Phys. **32**, 179 (1960).
12. O. CHALVET. C. R. Acad. Sci. **234**, 2369 (1952).
13. W. MOFFITT. Proc. R. Soc. **218**, 486 (1953).
14. P. O. LÖWDIN. Phys. Rev. **97**, 1509 (1955).
15. H. H. DEARMAN et R. LEFEBVRE. J. Chem. Phys. **34**, 72 (1961).
16. H. M. MCCONNELL. J. Chem. Soc. **28**, 1188 (1958); **29**, 244 (1958).
17. A. D. MCLACHLAN. Mol. Phys. **3**, 233 1960).
18. R. LEFEBVRE, H. H. DEARMAN et H. M. MCCONNELL. J. Chem. Phys. **32**, 176 (1960).
19. J. X. BOUCHERLE, B. GILLON, J. MARUANI et J. SCHWEIZER. J. Phys. **C7**, 227 (1982).
20. M. J. S. DEWAR et H. C. LONGUET-HIGGINS. Proc. Phys. Soc. (London), Sect. A, **68**, 795 (1954).
21. G. BERTHIER. *Dans* Molecular orbitals in chemistry, physics and biology. *Édité par* P. O. Löwdin et B. Pullman. Academic Press, New York. 1976. p. 57.
22. L. GRAJCAR et S. LEACH. J. Chim. Phys. **61**, 1523 (1964).
23. M. SUARD et J. BAUDET. J. Chim. Phys. **67**, 1088 (1970).
24. C. BRANCIARD-LARCHER, E. MIGIRDICYAN et J. BAUDET. Chem. Phys. **2**, 95 (1973).
25. C. COSSART-MAGOS et S. LEACH. J. Chem. Phys. **64**, 4006 (1976).
26. E. R. DAVIDSON. Int. J. Quantum Chem. Symp. **15**, 65 (1981).
27. M. DELBRÜCK. Proc. R. Soc. A, **129**, 686 (1930).
28. G. RIPKA. Adv. Nucl. Phys. **1**, 183 (1968).
29. P. O. LÖWDIN. Proceedings of the Nikko Symposium, Japan (1953).
30. M. HARVEY et A. S. JENSEN. Nucl. Phys. A, **164**, 641 (1971).
31. D. J. THOULESS. The quantum mechanics of many-body systems. Academic Press, New York. 1961. Chapt. 3.
32. R. E. PEIERLS et J. YOCCOZ. Proc. Phys. Soc. (London), Sect. A, **70**, 381 (1957).
33. R. F. PRAT. Phys. Rev. A, **6**, 1735 (1972).
34. G. DELGADO-BARRIO et R. F. PRAT. Phys. Rev. A, **12**, 2288 (1975).
35. J. ČIŽEK et J. PALDUS. J. Chem. Phys. **47**, 3976 (1967); **53**, 821 (1970).
36. J. PALDUS et J. ČIŽEK. J. Chem. Phys. **52**, 2919 (1970); **54**, 2293 (1971).
37. J. PALDUS et J. ČIŽEK. J. Polym. Sci. **C29**, 199 (1970).
38. J. ČIŽEK et J. PALDUS. Phys. Rev. A, **3**, 525 (1971).
39. J. PALDUS et J. ČIŽEK. Phys. Rev. A, **2**, 2268 (1970).
40. A. LAFORGUE, J. ČIŽEK et J. PALDUS. J. Chem. Phys. **59**, 2560 (1973).
41. G. BERTHIER. Stud. phys. theor. chem. **21**, 145 (1982).
42. M. R. C. SYMONS. J. Chem. Soc. 2276 (1964).
43. M. BETHOUX, H. LEMAIRE et A. RASSAT. Bull. Soc. Chim. Fr. **31**, 1985 (1964).
44. G. BERTHIER, H. LEMAIRE, A. RASSAT et A. VEILLARD. Theoret. Chim. Acta, **3**, 213 (1965).
45. J. MCKELVEY et W. J. HEHRE. Mol. Phys. **25**, 983 (1973).
46. J. M. MCKELVEY et G. BERTHIER. Chem. Phys. Lett. **41**, 476 (1976).
47. J. PALDUS et A. VEILLARD. Chem. Phys. Lett. **50**, 6 (1977).
48. J. PALDUS et A. VEILLARD. Mol. Phys. **35**, 445 (1978).
49. K. DEGUCHI, K. NISHIKAWA et S. AONO. J. Chem. Phys. **75**, 4165 (1981).
50. R. PRAT. *Dans* Localization and delocalization in quantum chemistry. Vol. 1, *Édité par* O. Chalvet, R. Daudel, S. Diner et J. P. Malrieu. D. Reidel Publishing Co., Dordrecht. 1975. p. 131.
51. J. PALDUS, J. ČIŽEK et A. LAFORGUE. Int. J. Quantum Chem. **13**, 41 (1978).
52. B. LIU. J. Chem. Phys. **68**, 1925 (1973).
53. P. SIEGBAHN et B. LIU. J. Chem. Phys. **68**, 2457 (1978).
54. S. V. O'NEIL, H. F. SCHAEFER III et C. F. BENDER. J. Chem. Phys. **59**, 3608 (1973).
55. C. F. JACKELS et E. R. DAVIDSON. J. Chem. Phys. **64**, 2908 (1976).
56. D. T. GROW et R. M. PITZER. J. Chem. Phys. **67**, 4019 (1977).
57. R. L. MARTIN et E. R. DAVIDSON. Mol. Phys. **35**, 1713 (1978).
58. T. TAKADA et M. DUPUIS. J. Am. Chem. Soc. **105**, 1713 (1983).
59. A. F. VOTER et W. A. GODDARD III. J. Chem. Phys. **75**, 3638 (1981); Chem. Phys. **57**, 253 (1981).
60. L. ENGELBRECHT et B. LIU. J. Chem. Phys. **78**, 3097 (1983).
61. V. KLIMO et J. TIÑO. Mol. Phys. **41**, 477 (1980); **41**, 483 (1980).
62. A. BRUCEÑA, P. VERMEULIN, P. ARCHIREL et G. BERTHIER. Int. J. Quantum Chem. **20**, 1285 (1981).
63. A. JULG et O. JULG. Croat. Chem. Acta, **54**, 335 (1981).
64. D. FELLER, W. T. BORDEN et E. R. DAVIDSON. J. Chem. Phys. **74**, 2256 (1981).
65. P. C. HIBERTY et C. LEFORESTIER. J. Am. Chem. Soc. **100**, 2012 (1978).
66. J. LIEVIN, J. BREULET, PH. CLERCQ et J. Y. METZ. Theor. Chim. Acta, **61**, 513 (1982).

La mécanique de la liaison hydrogène: résultats de spectroscopie infrarouge

Y. MARÉCHAL[1]

Centre d'Etudes Nucléaires de Grenoble, Département de Recherches Fondamentales, 85X, F 38041 Grenoble Cedex, France

Reçu le 6 août 1984

Cet article est dédié au Professeur Camille Sandorfy à l'occasion de son 65e anniversaire

Y. MARÉCHAL. Can. J. Chem. **63**, 1684 (1985).

Nous passons en revue la mécanique de la liaison hydrogène telle que nous la connaissons par la spectroscopie ir. Nous montrons comment traiter les différents couplages anharmoniques des vibrations ν_s (X—$\vec{H}$ . . . Y) de façon à éliminer les éléments parasites des spectres ir et de façon à ne garder que les éléments susceptibles de donner des informations sur la dynamique de la liaison hydrogène, telle que sa capacité de transférer des protons ou son mécanisme de rupture, qui sont des processus encore très mal connus. Nous décrivons aussi les possibilités de la spectroscopie vibrationnelle pour acquérir des informations sur ces mécanismes, qui peuvent avoir un rôle important en biologie.

Y. MARÉCHAL. Can. J. Chem. **63**, 1684 (1985).

We review the mechanics of H-bonds as revealed by ir spectroscopy and show how the various (strong) anharmonic couplings of the ν_s vibrations (X—$\vec{H}$ . . . Y) of H-bonds may be treated so as to eliminate the irrelevant features of the spectra and keep only those features which may give information on the still unknown dynamical quantities of the H-bonds, such as the transfer of protons through H-bonds or the mechanism of rupture of H-bonds. We also describe the possibilities offered by vibrational spectroscopy for studying these dynamical quantities, which may be important in biology.

La spectroscopie ir de la liaison hydrogène (LH) est un domaine de recherche où le Professeur C. Sandorfy a eu une contribution des plus éminentes. Il s'agit d'un domaine qui a connu pendant plus de deux décades un développement important, qui semble avoir cumulé vers les années 1980, et qui apparaît, en 1985, comme un sujet en plein mutation. Il peut donc être judicieux de saisir cette occasion du 65e anniversaire du Pr. C. Sandorfy pour faire le point de nos connaissances sur la mécanique de la LH telle que la spectroscopie ir nous l'a révélée, et pour préciser les perspectives de recherche dans ce domaine, telles qu'elles apparaissent aujourd'hui. Mais tout d'abord nous allons rapidement évoquer comment ce sujet s'est révélé dans les années 1955–1960.

Ce domaine de recherche sur la LH est apparu, il y a quelques 25 années (1) comme un domaine d'importance fondamentale pour comprendre la physique de nombreux mécanismes moléculaires. La LH est en effet une liaison dont l'énergie de formation est de quelques kT à l'ambiante, ce qui la distingue d'une liaison de valence ou d'une liaison de van der Waals. Cela lui donne une importance particulière dans les innombrables réactions se passant à la température ambiante, et en particulier les réactions aqueuses. Elle intervient aussi bien dans les domaines de la science des matériaux (les polymères en particulier) qu'en biologie où elle est vraiment la liaison-reine. C'est elle qui donne à un liquide aussi courant et répandu que l'eau ses propriétés physiques, chimiques et biologiques exceptionnelles.

On peut détecter et étudier cette LH essentiellement par des méthodes de spectroscopie vibrationnelle (ir, ir lointain, Raman, neutrons inélastiques . . .) et de rmn. Cependant, parmi ces méthodes, l'ir tient une place à part car elle présente une propriété frappante (2) que l'on retrouve dans toutes les LH X—H . . Y: la bande d'élongation de l'hydrogène ν_s (X—$\vec{H}$ . . . Y) a une intensité particulièrement grande (1 à 2 ordres de grandeur plus intense que la raie ν_{X-H} (X—$\vec{H}$) correspondante du composé X—H sans LH); de plus elle est large, structurée et décalée vers les basses fréquences. Un exemple en est donné dans le spectre de l'acide acétique en phase vapeur de la

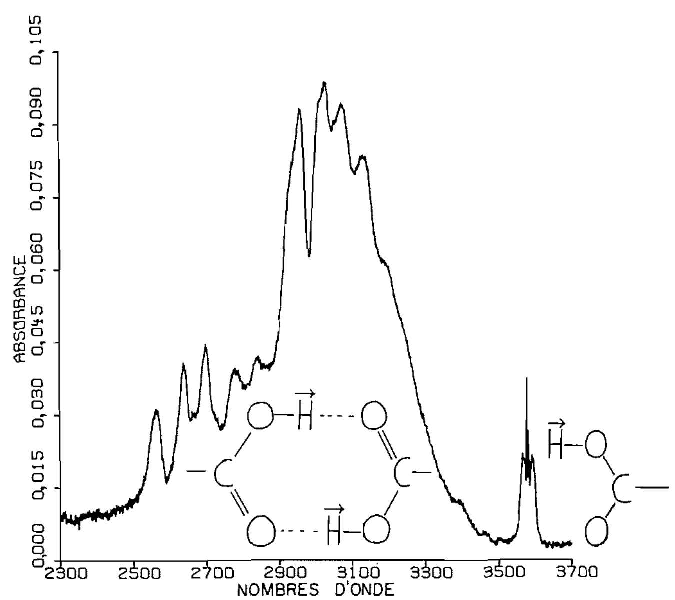

FIG. 1. Spectre ir de l'acide acétique en phase gazeuse à 300 K. La quantité de monomères et de dimères est équivalente.

fig. 1 où les quantités de monomères sans LH, CH_3COOH et de dimères cycliques liés par LH, $(CH_3COOH)_2$ sont équivalentes. Ces traits particuliers que l'on retrouve dans la fig. 1 sont caractéristiques de la LH.

Il est très vite apparu qu'il serait très utile de connaître l'origine de ces traits caractéristiques pour pouvoir tirer du spectre ir de la liaison hydrogène des informations précises sur la nature de cette liaison. Au congrès de Ljubljana (1957), une première réponse était donnée à ce problème,[2] avec la suggestion que la largeur et la structure particulières de ν_s étaient dues à deux forts couplages anharmoniques: le premier couple ν_3 avec les vibrations basse fréquence (50–200 cm^{-1}) de la LH (du type $\overleftrightarrow{X}$—$\vec{H}$ . . . $\overleftrightarrow{Y}$ ou X$\overset{H\cdot}{\uparrow}$·Y) et le second couple ν_s

[1]CNRS.

[2]S. Bratos et D. Hadzi, dans la réf. 1; N. Sheppard, aussi dans la réf. 1.

avec des niveaux de vibrations non accessibles optiquement et tombant en quasi-résonance avec ν_s. Ce dernier type de couplage de résonance est connu sous la dénomination de "résonances de Fermi". La responsabilité relative de ces deux couplages dans la forme, l'intensité et la position (en fréquence) de ν_s a été très longue à déterminer et a suscité de très nombreuses controverses. Celles-ci n'ont réellement pris fin qu'avec l'apparition de méthodes quantitatives permettant de séparer ces deux effets d'une manière précise. La mise au point de ces méthodes a en fait exigé de nombreuses expériences et analyses théoriques qui se sont poursuivies jusque vers les années 1980. Si cela a pris tant de temps, c'est parce que ces deux couplages anharmoniques sont en général tous les deux importants et de grandeur comparable (3–5) ce qui n'est apparu que lorsqu'on a pu les mesurer.

Nous allons décrire dans le prochain paragraphe le principe de ces approches quantitatives qui permettent de séparer ces deux effets, de les mesurer, et finalement d'éliminer du spectre ir de la LH les effets parasites, ce qui permet de ne garder que les informations susceptibles d'être utilisées pour comprendre le rôle que joue la LH à la température ambiante. Avant d'aborder ce paragraphe, notons cependant, que la spectroscopie ir de la LH, avec la puissance potentielle qui est la sienne, n'a pas attendu l'apparition de ces méthodes pour fournir de précieux renseignements sur la LH. C'est ainsi que des corrélations entre le centre de gravité de la bande ν_s et la distance X . . . Y dans la liaison X—H . . . Y ont été publiées (2). Elles permettent, après une simple mesure ir, d'estimer la longueur d'une LH, évitant ainsi tout le lourd travail d'analyse d'une structure par rayons X ou neutrons. Ce type de corrélation a été fortement développé et raffiné par A. Novak (6). De même, le Pr. C. Sandorfy et sa collaboratrice di Paolo (7) ont t-ils pu utiliser avec succès la présence de cette bande intense pour corréler la force anesthésiante des fluorocarbones à leur pouvoir de casser les LH, ce qui donne un point du vue intéressant sur le mécanisme de l'anesthésie.

Analyse de la bande ν_s

La première des caractéristiques frappantes de ν_s est sa très forte intensité, qui rend la spectroscopie ir si sensible à la LH. Cette intensité est due au déplacement des électrons nettement différent dans X—H . . . Y que dans X—H lorsqu'on allonge la distance X—H. L'origine physique de cette propriété n'est pas encore complètement claire, bien que des explications aient été avancées (8). Il faut dire que peu de résultats expérimentaux concernant les intensités des bandes ν_s ont été publiés. Ceci tient à la difficulté rencontrée pour mesurer des valeurs absolues d'intensités spectrales. Parmi les rares résultats expérimentaux, signalons cependant ceux concernant les intensités relatives $P_{\nu_s^H}/P_{\nu_s^D}$ des bandes ν_s pour les liaisons X—H . . . Y et X—D . . . Y correspondantes. Dans les dimères cycliques liés par LH, ce rapport prend une valeur anormalement grande (9), qui a été expliquée par la présence d'une forte anharmonicité électrique. Ce type d'anharmonicité semble être lui aussi général dans les LH (10), mais cela n'explique pas pourquoi cette valeur anormalement grande n'a été trouvée que dans les dimères cycliques (11).

Parmi les autres effets marquants caractérisant ν_s, le déplacement important de son centre de gravité vers les basses fréquences demande certainement aussi la connaissance précise de la structure électronique de la LH, bien qu'une théorie purement vibrationnelle (12) ait aussi permis d'en donner une explication satisfaisante. Les autres propriétés marquantes de ν_s peuvent s'expliquer par la présence des deux couplages anharmoniques dont nous avons parlé précédemment. Nous allons décrire leurs effets plus en détail.

Couplage ν_s – vibrations basse fréquence de la LH

Il s'agit, comme nous allons le voir, du couplage le plus intéressant en soi. Il a pu être étudié sur de (rares) systèmes où il est le seul couplage existant (13). On peut représenter très simplement ce type de couplage en supposant que le potentiel correspondant à ν_s est un potentiel harmonique dont la fréquence ω est modulée par l'une des vibrations basse fréquence de la LH ($\vec{\mathrm{X}}$—$\vec{\mathrm{H}}$ . . . $\overleftarrow{\mathrm{Y}}$ ou $\mathrm{X}\diagup\overset{\mathrm{H}\cdot}{\uparrow}\,\cdot\cdot\mathrm{Y}$) (9, 14, 16). Cette supposition est la plus simple et semble réaliste quand l'on sait que si la transition $0 \rightarrow 1$ en ν_s est très intense, les transitions $0 \rightarrow n$, elles, sont très faibles.[3] Dans le cas des LH fortes, cependant, cette supposition est moins exacte, et il peut être nécessaire (17) de considérer un potentiel anharmonique pour ν_s, dont les constantes sont modulées par ces vibrations basse fréquence. Pour une liaison faible ou intermédiaire, si l'on désigne par q la coordonnée représentant la vibration ν_s et par Q un des modes basse fréquence de la LH, le potentiel $V(q, Q)$ pour ces deux oscillateurs sera donc de la forme:

$$[1] \quad V(q, Q) = \frac{1}{2}m\omega^2(Q)q^2 + \frac{1}{2}M\Omega^2Q^2$$

m = masse du proton et M = masse réduite de l'oscillateur Q. Les fonctions d'onde $\psi(q, Q)$ correspondant à un tel potentiel seront très bien approchées par les fonctions d'onde adiabatique du type (14, 18):

$$[2] \quad \Psi(q, Q) = \phi_n(q, Q)\alpha_n^l(Q)$$

ou $\phi_n(q, Q)$ est la n-ème fonction d'onde ($n = 0, 1$) décrivant la vibration ν_s et $\alpha_n^l(Q)$ une fonction d'onde du vibrateur Q. Cette approximation se justifie par le fait que la fréquence ω est de l'ordre de 3000 cm^{-1} alors que Ω est de l'ordre de 150 cm^{-1}. On a donc un rapport entre ces fréquences aussi favorable que dans la séparation électrons–noyaux où cette approximation est une approximation de base. Elle revient à considérer que la vibration de l'hydrogène est suffisamment rapide pour pouvoir s'adapter immédiatement à toute nouvelle valeur de Q. L'oscillateur Q de son côté, est suffisamment lent pour ne voir que l'effet moyen de la vibration ν_s, si bien que son potentiel effectif $W_n(Q)$, qui dépend du degré d'excitation n de ν_s est:

$$[3] \quad W_n(Q) = \left\langle \phi_n(q, Q) \left| \frac{p^2}{2m} + V(q, Q) \right| \phi_n(q, Q) \right\rangle_q$$

$$= \frac{1}{2}M\Omega^2Q^2 + \left(n + \frac{1}{2}\right)\hbar\omega(Q)$$

$$p = -i\hbar\frac{\mathrm{d}}{\mathrm{d}q}$$

Dans le case du couplage électrons–noyaux, une telle situation donne lieu à des spectres du type "Franck–Condon", et c'est effectivement ce qu'il advient dans notre cas, lorsque ce couplage est le seul en jeu (19).

Avec un tel potentiel, on peut facilement montrer que le centre de gravité $\bar{\omega}$ de la bande ν_s ainsi que sa largeur quadratique moyenne σ s'écrivent:

---

[3]C. Sandorfy dans la réf. 15, chap. 13.

$$[4] \quad \bar{\omega} = \langle \omega(Q) \rangle_Q = \omega(\langle Q \rangle_Q) + \frac{1}{2}\frac{d^2\omega}{dQ^2} \times \langle (Q - \langle Q \rangle_Q)^2 \rangle_Q + \ldots$$

$$[5] \quad \sigma^2 = \left(\frac{d\omega}{dQ}\right)^2_{\langle Q \rangle} \langle (Q - \langle Q \rangle_Q)^2 \rangle_Q + \ldots$$

où $\langle\,\rangle_Q$ signifie que l'on prend la moyenne sur tous les états Q dont la population dépend de la température (selon une loi de Boltzmann par exemple) et que la dépendance de ω en Q est approchée par un développement en puissances de Q.

L'équation [4] est intéressante, car elle est valable même en présence de résonances de Fermi, et elle permet de comprendre la dérive de $\bar{\omega}$ avec la température. Celle-ci est très générale pour la LH et, à notre connaissance, toujours dans le même sens: lorsque la température augmente, $\bar{\omega}$ augmente. Deux types d'explications en ont été donnés: la première (20) fait jouer un rôle particulier à la quantité $\langle Q \rangle_Q$, qui représente alors la valeur moyenne de la longueur X . . . Y, quantité qui croît certainement avec la température (dilatation thermique). Q est donc la coordonnée de la vibration ν_σ ($\overleftarrow{\mathrm{X}}$—$\overrightarrow{\mathrm{H}}$ . . . $\overleftarrow{\mathrm{Y}}$). . Dans ce cas, on s'attend à ce que $d\bar{\omega}/dT$ soit positif, car $d\omega(Q)/dQ$ l'est certainement (plus la longueur moyenne X . . . Y est grande, plus $\bar{\omega}$ est grand (6)). La deuxième explication (21) suppose que l'effet de température sur $\bar{\omega}$ vient du dernier membre de l'éq. [4]. La quantité $\langle (Q - \langle Q \rangle_Q)^2 \rangle_Q$ représente le carré de l'amplitude de vibration de la vibration Q qui augmente avec la température (comme $1/\tanh \hbar\Omega/2kT$) pour un potentiel harmonique). Pour que $d\bar{\omega}/dT$ soit positif, il faut donc que $d^2\omega/dQ^2$ soit aussi positif, ce qui oblige à considérer que Q est alors la coordonnée de la vibration de torsion

(X╱H·↑·Y). En effet, d'après les courbes de Novak (6), un $d^2\omega(Q)/dQ^2$ positif est très improbable pour la vibration ν_σ. Nous avons testé ces deux hypothèses quantitativement (3, 4) pour les cristaux d'imidazole et d'acide adipique et en avons déduit que seule la deuxième explication est réaliste dans ces cas là: entre 77 K et 300 K la dilatation $\langle Q \rangle_Q$ de la distance X . . . Y telle qu'elle est mesurée aux neutrons ou rayons X n'est pas du tout suffisante pour expliquer cette dérive $d\bar{\omega}/dT$ (4, 22). C'est un résultat intéressant, car il permet de décrire avec précision la sensibilité thermique de certaines propriétés de la LH, ce qui peut avoir un impact non négligeable en biologie. De plus il met en lumière le rôle des vibrations basse

fréquence de torsion (X╱H··Y) de la LH. Ces vibrations ont peut-être un rôle plus important qu'on ne le croit d'ordinaire, en particulier dans le processus de rupture de la LH, qui peut être lui aussi très important en biologie.

L'équation [5] traduit le fait que la largeur σ de la bande ν_s pour ce processus dépend fortement de la température. Elle permet aussi d'expliquer pourquoi la bande ν_s de la liaison X—D . . . Y est plus étroite que celle de la liaison X—H . . . Y.

Résonances de Fermi

Il s'agit d'un processus d'intéraction entre le premier niveau excité de ν_s et un niveau non accessible optiquement, qui sera en pratique une combinaison binaire de premiers niveaux excités d'autres vibrations (q_δ) de la molécule X—H. Le potentiel V_F représentant une telle intéraction sera de la forme:

$$[6] \quad V_F = q \sum_{\delta,\delta'} F_{\delta,\delta'} q_\delta q_{\delta'}$$

Un potentiel décrivant un couplage anharmonique de cette forme a, en général, peu d'effet sur le spectre, sauf près de la résonance, c'est à dire lorsque l'énergie $\omega_\delta + \omega_{\delta'}$ du premier niveau excité en δ et δ' est de l'ordre de grandeur de ω. Dans ce cas le potentiel de ν_s sera $1/2\, m\omega^2 q^2$, avec ω indépendant de Q (résonances de Fermi pures). Si $V_F = 0$, le spectre consistera en une seule raie d'intensité I, de fréquence ω et de largeur nulle. Si V_F est différent de 0 le spectre se partagera alors en N raies (N = nombre de termes effectifs dans le $\sum_{\delta,\delta'}$ de l'éq. [6]) dont l'intensité totale sera encore I, le centre de gravité ω et la largeur quadratique moyenne égale à σ_F tel que:

$$[7] \quad \sigma_F^2 = \frac{\hbar}{8} \sum_{\delta,\delta'} F^2_{\delta,\delta'} \frac{1}{m_\delta \omega_\delta} \cdot \frac{1}{m_{\delta'} \omega_{\delta'}} \cdot \frac{1}{m\omega}$$

ou m_δ et ω_δ sont la masse effective et la fréquence de vibration du mode δ.

On voit donc que les résonances de Fermi n'ont aucun effet sur l'intensité et le centre de gravité de la bande ν_s. Ils ont un effet sur la largeur de ν_s mais cette largeur σ_F a la propriété d'être indépendante de la température. Ceci est dû à ce que ces résonances n'affectent pas l'état fondamental de ν_s, mais seulement son premier niveau excité qui est thermiquement inaccessible (3000 cm^{-1} = 4500 K).

Effet de ces deux couplages simultanés

Lorsque ces deux couplages anharmoniques sont présents, le potentiel correspondant est la somme $V(q, Q) + V_F$ (équations [1] et [6]). Il est alors aisé de montrer que le centre de gravité $\bar{\omega}$ de ν_s est toujours donné par l'éq. [4] (les résonances de Fermi n'ont aucune influence sur le centre de gravité) et que la largeur quadratique moyenne μ de ν_s est telle que (3, 4, 23):

$$[8] \quad \mu^2 = \sigma^2 + \sigma_F^2$$

où σ^2 et σ_F^2 sont donnés par les équations [5] et [7]. Dans cette équation la variation de μ avec la température vient uniquement de celle de σ (σ_F est indépendant de T). Les variations thermiques du centre de gravité $\bar{\omega}$ de ν_s et de sa largeur μ ne proviennent donc que du couplage de ν_s avec les vibrations basse fréquence de la LH. Cette propriété a permis de mesurer les grandeurs relatives de ces deux couplages par une analyse des variations des spectres de certains corps à LH entre 10 K et 300 K (3, 4). Cette analyse a alors montré que à température ambiante ces deux couplages étaient de grandeur comparable, alors qu'à 10 K, les résonances de Fermi étaient prédominantes.

On peut en fait pousser plus loin l'analyse de la forme de raie pour la transition $0 \rightarrow 1$ en ν_s lorsque le potentiel de ν_s est $V(q, Q) + V_F$. Une première approche à ce problème avait été décrite dans le cas particulier où la vibration basse fréquence Q n'est pas décrite quantiquement mais peut être traitée dans sa limite classique. C'est le cas, par exemple, d'une LH diluée dans un liquide sans LH, où une solution qualitativement satisfaisante pour la forme de raie a alors été obtenue (24). Le cas où la vibration Q ne peut être considérée dans sa limite classique est plus complexe. C'est celui très général des gaz ou des cristaux à LH. La transition $0 \rightarrow 1$ en ν_s pour une telle LH isolée est schématisée fig. 2: la transition ir s'effectue à partir d'un niveau du potentiel $W_0(Q)$ (eq. [3]) vers un niveau du potentiel $W_1(Q)$. Les niveaux de ce dernier ne sont cependant pas des niveaux propres du système de vibrations de la LH car ils sont en intéraction avec des niveaux (de résonance) définis par les potentiels $W_0(Q) + \hbar(\omega_\delta + \omega_{\delta'})$. Sur la fig. 2 nous n'avons dessiné, pour plus de commodité, que l'une de ces résonances δ, δ'. Ces niveaux de résonance ne peuvent pas être

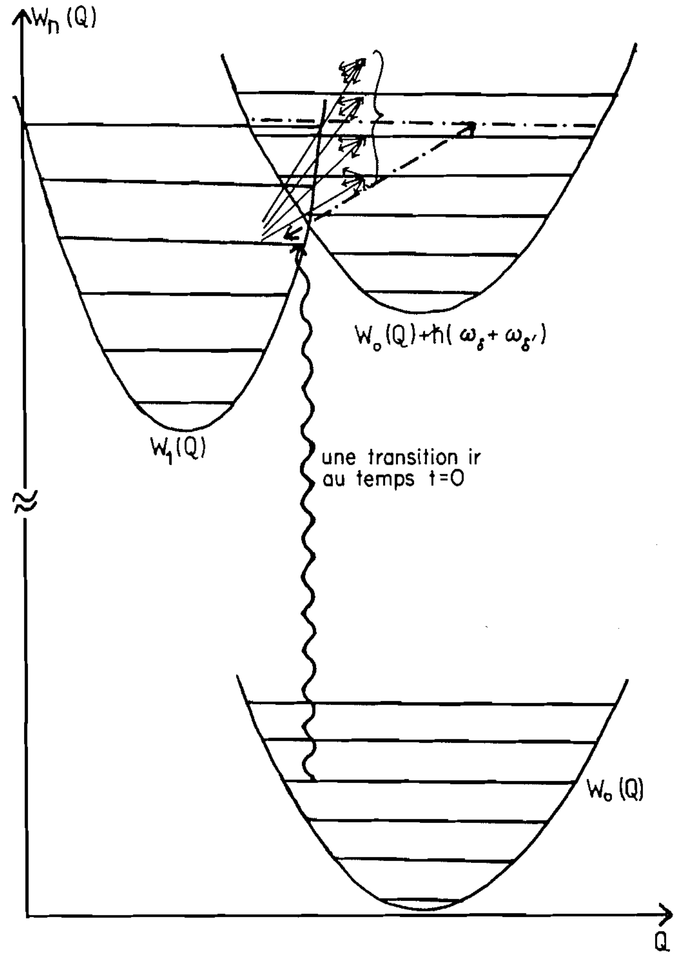

FIG. 2. Schéma de la transition $0 \rightarrow 1$ en ν_s.

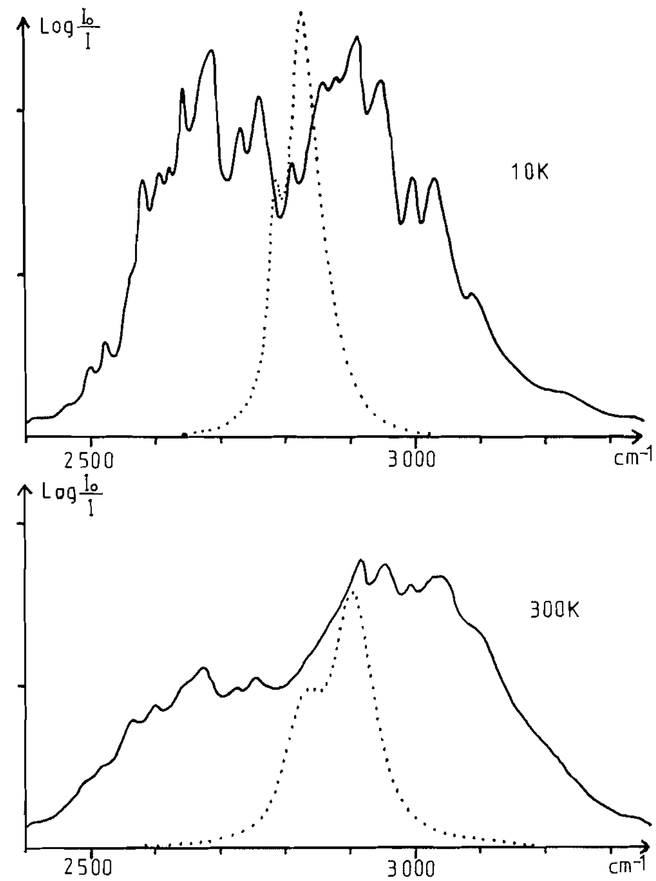

FIG. 3. Bande ν_s de monocristaux d'acide adipique H à 10 K et 300 K: spectre expérimental $\omega \cdot s(\omega)$ (en traits pleins —) et spectre calculé $\omega \cdot g(\omega)$ en pointillé . . .) après élimination des résonances de Fermi. Les échelles pour ces deux spectres sont différentes.

atteints directement par la transition ir. Cependant l'excitation créée par cette transition ir au temps $t = 0$ en $W_1(Q)$ passera, au bout d'un certain temps t sur des niveaux de $W_0(Q) + \hbar(\omega_\delta + \omega_{\delta'})$, puis reviendra sur des niveaux de $W_1(Q)$, etc. . . On peut simplifier considérablement le problème si on remplace l'ensemble des niveaux de Fermi $W_0(Q) + \hbar(\omega_\delta + \omega_{\delta'})$ atteints au bout du temps t par un niveau virtuel d'énergie égale à la moyenne des énergies des niveaux atteints (niveau ---- dans la fig. 2). Cette moyenne est indépendante du temps t. Pour tout niveau de Fermi défini par le couple δ, δ', on définit une telle moyenne. Le prix à payer pour une telle simplification se retrouve dans une perte de résolution, qui interdit de pouvoir inclure des éléments très fins du spectre. Cela revient à considérer que l'approximation faite en introduisant cette simplification est une approximation de temps court.

On peut alors définir (23), à partir de la forme $s(\omega)$ expérimentale de la bande ν_s (le spectre expérimental étant proportionnel à $\omega s(\omega)$), une forme $g(\omega)$, qui est la forme "épluchée" de ν_s, c'est-à-dire la forme qu'aurait ν_s si les résonances de Fermi étaient égales à zéro. Une relation simple, qui se prête particulièrement bien à une computation existe alors entre s et g. Nous montrons dans les figures 3 et 4 la forme $\omega g(\omega)$ du spectre pour les acides adipiques H et D à différentes températures, ainsi que le spectre expérimentale $\omega s(\omega)$ (les deux courbes $\omega s(\omega)$ et $\omega g(\omega)$ sont dessinées, pour des raisons de présentation à deux échelles différentes; elles ont même intensité intégrée). Les spectres $\omega g(\omega)$ pour l'imidazole et les acides carboxyliques en phase vapeur seront publiés prochainement. Nous voyons que l'élimination des résonances de Fermi simplifie considérablement les spectres, et qu'il est alors beaucoup plus facile d'en tirer des informations sur les couplages de ν_s avec les vibrations basse fréquence de la LH. Ces couplages sont, comme nous l'avons déjà mentionné, très intéressants à connaître en eux-mêmes, car ils sont à l'origine de la sensibilité de ν_s à la température, et peuvent aussi donner des indications sur les processus de rupture de la LH. Par contre les résonances de Fermi, que nous avons éliminées, apparaissent comme des effets parasites dans la bande ν_s: ce sont des effets qui ne se retrouvent que dans les niveaux excités de ν_s, qui sont thermiquement inaccessibles, et ne peuvent donc pas se manifester dans les propriétés de la LH à température ambiante. Ce sont en fait de purs artifices de la spectroscopie vibrationnelle.

Perspective de recherches

La spectroscopie ir est une technique puissante pour étudier la LH. Elle a cependant longtemps trainé ce problème de résonances de Fermi, qui ont empêché de l'utiliser à sa pleine puissance. Maintenant que l'interprétation des spectres peut être grandement simplifiée par l'élimination de ces résonances, les perspectives de la spectroscopie ir sont très intéressantes, en particulier pour étudier les propriétés dynamiques de la LH, telles que son mécanisme de rupture, sa capacité de transférer des protons, etc. . . De ces mécanismes nous ne connaissons que très peu de choses. Pourtant la rupture d'une LH dans l'eau constitue une source d'énergie de quelques kT à l'ambiante, qui

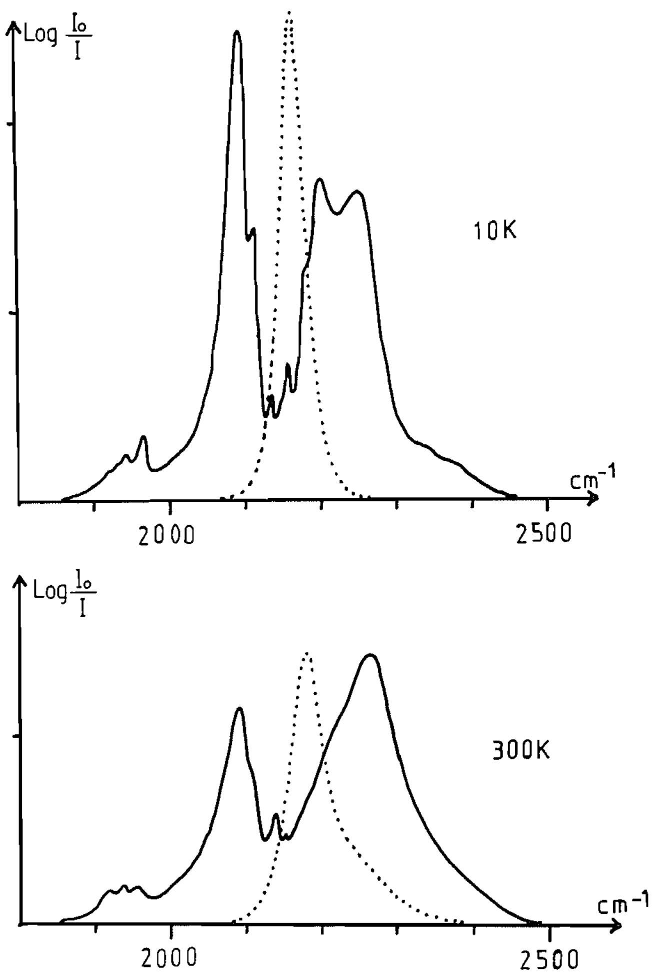

FIG. 4. Bande ν_s de monocristaux d'acide adipique D à 10 K et 300 K: spectre expérimental $\omega \cdot s(\omega)$ (en traits pleins —) et spectre calculé $\omega \cdot g(\omega)$ (en pointillé . . .) après élimination des résonances de Fermi. Les échelles pour ces deux spectres sont différentes.

semble capable de se déplacer très rapidement dans l'eau (25). Elle a une énergie très comparable à l'énergie d'une réaction ATP $\rightleftarrows$ ADP. Il n'est donc pas impossible qu'elle ait de ce fait un rôle important dans les mécanismes bio-énergétiques. Il semble donc extrêmement utile de connaître en détail les mécanismes de rupture de la LH, leur mode de propagation (exciton, soliton, . . ?) et bien sûr l'effet de la température sur ces mécanismes. De même le transfert des protons est certainement un mécanisme essentiel dans toutes les réactions aqueuses. L'eau est en effet un liquide présentant une densité de LH exceptionnelle (presque un ordre de grandeur plus élevée que pour les autres liquides à LH tels que méthanol, éthanol, etc . . .) où ce transfert peut être particulièrement efficace. On peut penser que c'est leur différence de capacité à transférer les protons ou deutérons qui donne à l'eau et à l'eau lourde leur si grande différence de propriétés biologiques.

Par sa grande densité de LH, l'eau est cependant un corps compliqué à étudier. De plus elle est pratiquement opaque en ir. C'est donc par d'autres techniques spectroscopiques (Raman, diffusion Rayleigh (25) ou de neutrons essentiellement) qu'elle pourra être abordée. Cependant l'ir sera une technique très précieuse si l'on veut aborder l'étude de ces mécanismes dynamiques dans la LH sur des corps plus simples que l'eau qui pourront alors servir de modèles de base pour l'eau. Nous pensons en particulier aux dimères cycliques des acides carboxyliques en phase vapeur ou des diacides carboxyliques en cristaux. Ces systèmes sont d'excellents modèles de LH simples, relativement faciles à manipuler, et une approche théorique des mécanismes de transferts de protons dans ces cycles dimériques a déjà été proposée (26).

Par ailleurs une extension de la spectroscopie ir vers l'ir lointain semble aussi actuellement pleine d'avenir. Ce type de spectroscopie a récemment accompli des progrès marquants avec l'apparition de nouveaux détecteurs plus sensibles et plus rapides. Nous avons vu le rôle qui jouent dans le spectre de ν_s les vibrations basse fréquence de la LH. La mécanique de ces vibrations basse fréquence, et en particulier leurs couplages anharmoniques sont encore très mal connus. Leur connaissance précise peut cependant être très utile pour connaître le rôle exact de la température dans tous les systèmes à LH, biologiques en particulier.

Nous voyons ainsi que la spectroscopie ir de la LH, qui a constitué un domaine important de recherche jusque vers les années 1980, a encore de nombreux sujets à étudier, qui concernent essentiellement la dynamique de la LH. On peut penser qu'il s'agit en fait d'un domaine nouveau très riche, qui est susceptible de fournir des constantes fondamentales pour la biologie ou la science des matériaux.

1. D. HADZI (*Éditeur*). Hydrogen bonding. Pergamon Press, New York. 1959.
2. G. C. PIMENTEL et A. L. MCCLELLAN. The hydrogen bond. Freeman, San Francisco. 1960.
3. G. AUVERT et Y. MARÉCHAL. J. Phys. (Paris), **40**, 735 (1979).
4. P. EXCOFFON et Y. MARÉCHAL. Chem. Phys. **52**, 237 (1980); **52**, 245 (1980).
5. J. BOURNAY et G. N. ROBERTSON. Chem. Phys. Lett. **60**, 286 (1979).
6. A. NOVAK. *Dans* Structure and bonding. Vol. 18. *Edité par* J. D. Dunitz. Springer, Berlin. 1974. p. 177.
7. T. DI PAOLO et C. SANDORFY. Chem. Phys. Lett. **26**, 466 (1974).
8. H. RATAJCZAK, W. J. ORVILLE-THOMAS et C. N. R. RAO. Chem. Phys. **17**, 197 (1976).
9. Y. MARÉCHAL. *Dans* Molecular interactions. *Edité par* H. Ratajczak et W. J. Orville-Thomas. Wiley, New York. 1980.
10. F. FILLAUX. Chem. Phys. **74**, 395 (1983); **74**, 405 (1983).
11. Y. MARÉCHAL. Croat. Chem. Acta, **55**, 129 (1982).
12. N. D. SOKOLOV et V. A. SAVEL'EV. Chem. Phys. **22**, 383 (1977).
13. D. J. MILLEN. J. Mol. Struct. **100**, 351 (1983).
14. Y. MARÉCHAL et A. WITKOWSKI. J. Chem. Phys. **48**, 3697 (1968).
15. P. SCHUSTER, G. ZUNDEL et C. SANDORFY (*Éditeurs*). The hydrogen bond – recent developments in theory and experiments. North-Holland, Amsterdam. 1976.
16. G. L. HOFACKER, Y. MARÉCHAL et M. A. RATNER. *Dans* The hydrogen bond – recent developments in theory and experiments. *Edité par* P. Schuster, G. Zundel et C. Sandorfy. North-Holland, Amsterdam. 1976. Chap. 6.
17. S. BRATOS et H. RATAJCZAK. J. Chem. Phys. **76**, 77 (1982).
18. H. ROMANOVSKI et J. M. BOWMAN. Chem. Phys. Lett. **110**, 235 (1984).
19. Y. BOUTEILLER et E. MARÉCHAL. Mol. Phys. **32**, 277 (1976).
20. H. ROMANOWSKI et L. SOBCZYK. Chem. Phys. Lett. **58**, 73 (1978).
21. J. BOURNAY et G. N. ROBERTSON. Mol. Phys. **39**, 163 (1980).
22. J. L. LEVIEL, G. AUVERT et J. M. SAVARIAULT. Acta Crystallogr. Sect. B, **37**, 2185 (1981).
23. Y. MARÉCHAL. Chem. Phys. **79**, 69 (1983); **79**, 85 (1983).
24. S. BRATOS. J. Chem. Phys. **63**, 3499 (1975).
25. O. CONDE et J. TEIXEIRA. J. Phys. (Paris), **44**, 525 (1983).
26. G. N. ROBERTSON et M. C. LAWRENCE. Chem. Phys. **62**, 131 (1981).

Molecular orbital studies of carbyne reactions: addition and insertion reaction paths for the $CH(\tilde{X}^2\Pi) + C_2H_4(\tilde{X}^1A_g)$ reaction

RATNAKAR K. GOSAVI, IMRE SAFARIK, AND OTTO P. STRAUSZ
Department of Chemistry, University of Alberta, Edmonton, Alta., Canada T6G 2G2

Received August 1, 1984

This paper is dedicated to Professor Camille Sandorfy on the occasion of his 65th birthday

RATNAKAR K. GOSAVI, IMRE SAFARIK, and OTTO P. STRAUSZ. Can. J. Chem. **63**, 1689 (1985).

Potential energy hypersurfaces have been studied for the $CH(\tilde{X}^2\Pi) + C_2H_4(\tilde{X}^1A_g)$ addition and insertion reactions by *ab initio* molecular orbital theory. 6-31G basis set was used for complete geometry optimization of CH, C_2H_4, the cyclopropyl and allyl radicals as well as the reaction intermediates involved, with the RHF open shell SCF method. CI calculations were then performed at the SCF level optimized geometry. Analysis of the potential energy hypersurfaces predicts, in agreement with reported experimental data, a zero activation energy for the addition reaction via a non least motion, asymmetric reaction path, while the insertion reaction features a computed activation energy of 15 kcal mol^{-1}.

RATNAKAR K. GOSAVI, IMRE SAFARIK et OTTO P. STRAUSZ. Can. J. Chem. **63**, 1689 (1985).

Utilisant la théorie des orbitales moléculaires *ab initio*, on a étudié les hypersurfaces d'énergie potentielle pour les réactions d'addition et d'insertion $CH(\tilde{X}^2\Pi) + C_2H_4(\tilde{X}^1A_g)$. On a utilisé un ensemble de base 6-31G pour effectuer une optimisation des radicaux CH, C_2H_4, cyclopropyle et allyle; on a aussi effectué une optimisation des intermédiaires réactionnels en faisant appel à la méthode des couches ouvertes de RHF en champ auto-cohérent. On a alors effectué des calculs IC au niveau de la géométrie optimisée en champ auto-cohérent. Pour la réaction d'addition, une analyse des hypersurfaces d'énergie potentielle permet de prédire que l'énergie d'activation est égale à zéro et que la réaction se produit par le biais d'une réaction asymétrique ne procédant pas par une voie de moindre déplacement; ces prédictions sont en accord avec les données expérimentales existantes. Pour la réaction d'insertion, la même analyse permet de prédire que l'énergie d'activation est égale à 15 kcal/mol.

[Traduit par le journal]

Introduction

The chemistry of carbynes, the family of monovalent carbon radicals has been explored experimentally for the past quarter century (1) and in recent years, comparative rate data have become available for the reactions of ground $^2\Pi$ state diatomic methylidynes, CH (2, 3), CF, CCl, and CBr with C_2H_4 and alkanes (1, 4–6). Quantitative kinetic studies with the direct spectroscopic observation of the transient methylidyne species lead to the determination of absolute rate constant values and in some cases, the Arrhenius parameters. The mechanistic aspects of these reactions, however, have remained largely obscure owing to the complexity of the carbyne generating reactions, which in all cases, produce a variety of other reactive intermediates as well. Detailed mechanistic studies of a carbyne species have only been carried out on the solution phase reactions of carbethoxymethylidyne, C—COOEt (7) where it was shown that the doublet ground state methylidyne undergoes concerted stereospecific cycloaddition to olefins and regio selective insertion into the C—H bonds of paraffins and olefins. Hydrogen abstraction by the carbyne was not observed in these studies. On the basis of these results it can be assumed with reasonable confidence that all four diatomic carbynes studied to date, CH, CF, CCl, and CBr exhibit analogous reactivity in their doublet ground state with olefins and paraffins.

Theoretical studies of the ground and excited states of diatomic carbynes, CH (8, 9), CF (10, 11), and CCl (12, 13) have concordantly shown that in agreement with experiment they all have a $^2\Pi$ ground state with a low lying $^4\Sigma^-$ state as the lowest excited state. In contrast, a recent *ab initio* study of CLi (14) predicts the inversion of energy levels in this species with the lowest excited $^2\Pi$ state to lie ~34 kcal mol^{-1} above the $^4\Sigma^-$ ground state. Kim, So, and Schaefer (15) investigated the equilibrium geometries and relative energies of the low-lying electronic states of carbohydroxymethylidyne, HOC(=O)—C, — the parent species of carbethoxymethylidyne which had been studied experimentally — and its isomeric formoxymethylidyne, HC(=O)O—C, with the SCF and CI methods using double ζ and double ζ plus *d* basis sets. The results predict the *cis* $^2A''$ state to be the ground state for carbohydroxymethylidyne, closely followed by a $^2A'$ (10 kcal mol^{-1}) and a $^4A''$ (17 kcal mol^{-1}) states. The formoxymethylidyne, on the other hand, has a *trans* $^2A'$ ground state with the *cis* $^2A''$ and the $^4A''$ states lying at 12 and 70 kcal mol^{-1}, respectively, higher than the $^2A'$ ground state.

The first molecular orbital study of a methylidyne reaction was reported by Brooks and Schaefer (16). They investigated the potential energy surfaces for the insertion of doublet methylidyne into molecular hydrogen and abstraction of hydrogen by the quartet methylidyne. *Ab initio* molecular orbital studies with configuration interaction with double ζ and double ζ + polarization functions gave an energy barrier of ~75 kcal mol^{-1} for the least motion insertion reaction path, where the CH approach is perpendicular to the H—H bond at the center of the bond. In the non least motion insertion path, where the C—H axis is parallel with the H—H axis and the carbon atom approaches the center of the H—H bond, the energy barrier was only 4 kcal mol^{-1}. For H abstraction by the quartet methylidyne the computed barrier was ~11 kcal mol^{-1}.

In our previous molecular orbital studies on the reaction path of doublet methylidyne addition to ethylene (17), we calculated the potential energy surface at the SCF level with the Unrestricted Hartree Fock (UHF) method using the minimal STO-4G basis set. We had considered two reaction paths for the addition reaction; in one C—H is approaching at the center of the C=C bond from above the ethylene plane. This symmetric addition path has a small activation energy of ~7.7 kcal mol^{-1}. The other reaction surface studied was for the asymmetric approach where the C—H approaches off center again from above the ethylene plane. The potential energy surface for this asymmetric reaction path showed no activation energy and it was concluded that the addition of $CH(\tilde{X}^2\Pi)$ to ethylene ($\tilde{X}^1A_g$)

proceeds without any activation energy along the asymmetric path.

Here we report the results of another, higher quality *ab initio* molecular orbital study with limited configuration interaction on the potential energy surfaces of both the addition and insertion reactions of ($\tilde{X}^2\Pi$) ground state methylidyne to ethylene ($\tilde{X}^1A_g$).

Method

All the molecular geometrical parameters of ground state ethylene (^1A_g), CH($^2\Pi$), doublet cyclopropyl and allyl radicals, and the reaction intermediates involved were optimized at the SCF level by the energy gradient method (18, 19) with 6-31G basis set (for C, see ref. 20*a*; for H, see ref. 20*b*). The Restricted Hartree Fock (RHF) open shell SCF method was used for the doublet state radicals. Configuration interaction (CI) calculations include all singly and doubly excited configurations (CISD) with respect to the SCF configuration, and were done using the direct CI method (21) at the SCF level optimized geometry. Davidson's formula (22) was applied to the CI results to estimate the correction for the quadruple excitations (CISDQ). The lowest three orbitals corresponding to the core orbitals of carbon 1*s* were kept doubly occupied and frozen, and the top ten virtual orbitals were also kept frozen in the CI calculations. All the computations were performed with the "MONSTERGAUSS" Program (23) on an AMDAHL 5860 computer at the University of Alberta.

Results

The optimized C—H bond distance of 1.117 Å calculated for the $^2\Pi$ ground state of methylidyne is in good agreement with the experimental value of 1.120 Å (24). The optimized molecular parameters for ethylene (^1A_g) are summarized in Table 1 and the double ground state optimized geometry for the cyclopropyl radical, the product of the addition reaction is shown in Fig. 1. These values are in close agreement with the earlier optimized geometry with minimal (17, 26) and extended (4-31G) (27) basis sets. The radical center in the cyclopropyl radical is non planar with an out-of-plane angle between C_1H_{10} and the CCC ring, of 40.86°. The corresponding planar (C_{2v}) structure has the optimized geometry of $R(C_1—C_2) = 1.467$ Å, $R(C_2—C_3) = 1.539$ Å, $R(C_1—H_{10}) = 1.060$ Å, $R(C_2—H_6) = 1.076$ Å, $\angle H_6C_2H_7 = 113.36°$, $\angle C_3C_2H_6 = 117.86°$, and $H_6C_2C_3C_1$ out-of-plane $\angle = 109.06°$, with total energies: $E_{SCF} = -116.354881$ au, $E_{CISDQ} = -116.502782$ au. This transition state structure for the inversion motion of the radical center is 4.3 kcal mol^{-1} at the SCF and 9.0 kcal mol^{-1} at the CISDQ level higher in energy than the C_s symmetry lowest energy structure. The CH insertion into the ethylene C—H bond yields an allyl radical. The SCF optimized geometries of both C_s and C_{2v} structures are depicted in Fig. 2. Electron spin resonance studies (28) have shown that the allyl radical has a C_{2v} symmetry. Several theoretical studies on electronic structure (29, 30), doublet instability (31–34), and symmetry dilemma (35, 36) have been reported for the allyl radical. The RHF SCF geometry optimization for three center, three π electron systems usually overestimates the stability of structures containing one short and one long bond (C_s) (Fig. 2*a*) relative to the one with intermediate equal bond lengths (C_{2v}) (Fig. 2*b*). This problem has been solved by inclusion of the correlation energy (32, 33). The optimized geometry of the symmetric allyl radical is similar to the one obtained from 4-31G basis set

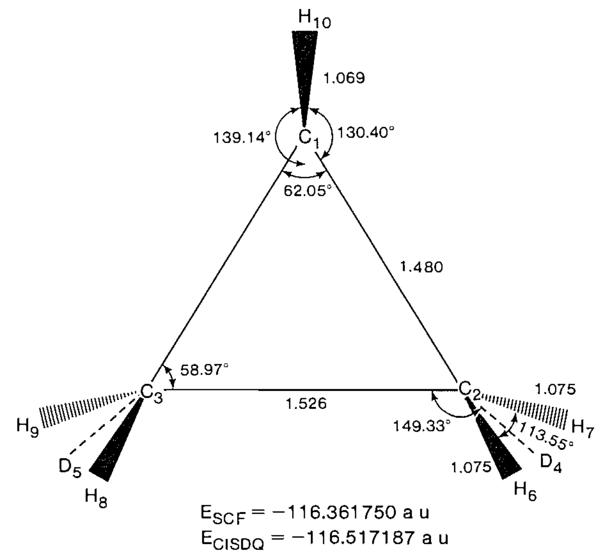

FIG. 1. Doublet ground state, RHF-SCF optimized geometry of the cyclopropyl radical. Bond distances are in Å and bond angles in degree.

TABLE 1. SCF-optimized molecular parameters of ethylene ($\tilde{X}^1A_g$) with 6-31G basis set

Molecular parameters	Calculated	Experimental[a]
R(C—C) (Å)	1.322	1.330
R(C—H) (Å)	1.074	1.076
∠HCH (deg)	116.14	116.6

[a]Reference 25.

calculations (29). As expected, at the SCF level the C_s symmetry radical is more stable — by 1.8 kcal mol^{-1} — than the C_{2v} structure but the inclusion of the correlation energy has the effect of lowering the energy of the C_{2v} structure below the C_s symmetry structure by 1.2 kcal mol^{-1}.

The addition reaction path

Two reaction paths for the addition of CH($^2\Pi$) to ethylene (^1A_g) have been studied; in both cases CH is approaching at the center of the C=C bond, from the plane perpendicular to the ethylene, Fig. 3. Total energies as a function of the $X_1—C_4$ distance (d, Fig. 3) have been calculated for the SCF level optimized geometry and CI calculations were then done on the SCF optimized geometry. In the first reaction path, C_4H_9 and X_1 are in the plane perpendicular to the $C_2C_3C_4$ plane .The single electron on the C_4 atom remains in the p_x orbital until the $X_1—C_4$ distance reaches 1.85 Å, and Localized Molecular Orbital (LMO) analysis shows ethylene and methylidyne as separate entities. At 1.85 Å distance partial bond formation between $C_4—C_2$ and $C_4—C_3$ takes place. Below this distance the single electron moves from the p_x orbital to the p_y orbital on C_4. This transition complex has a small energy barrier of 3 kcal mol^{-1} at the SCF level, Fig. 4, which disappears in the CISDQ potential energy surface, Fig. 5.

In the second reaction path, where the CH approach is in the plane of $C_2C_3C_4H_9$, the single electron remains always in the p_y orbital of C_4. LMO analysis of the reaction intermediates shows that CH and ethylene remain as separate entities until the $X_1—C_4$ distance again reaches 1.85 Å, at which point partial bond formation between $C_4—C_2$ and $C_4—C_3$ takes place. The

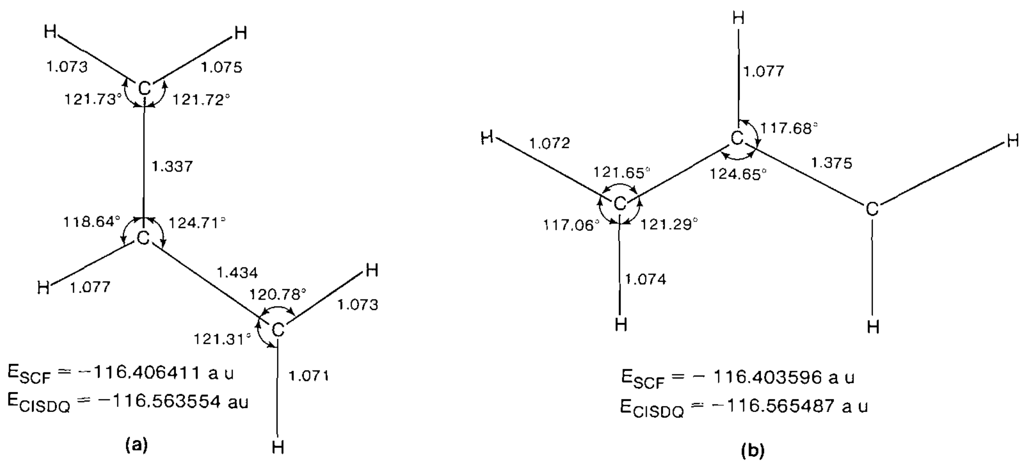

FIG. 2. Doublet ground state, RHF-SCF optimized geometry of the allyl radical. (*a*) C_s symmetry ($^2A''$); (*b*) C_{2v} symmetry ($^2A_2$). Bond distances are in Å and bond angles in degree.

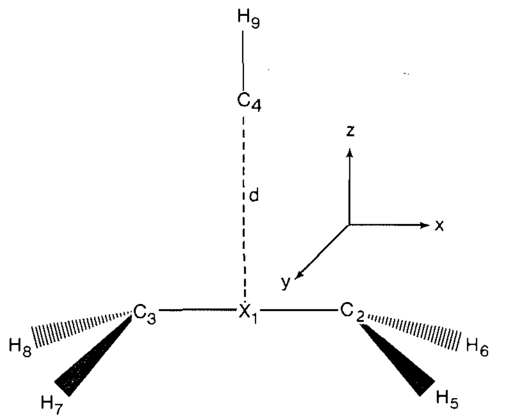

FIG. 3. Addition and insertion reaction path.

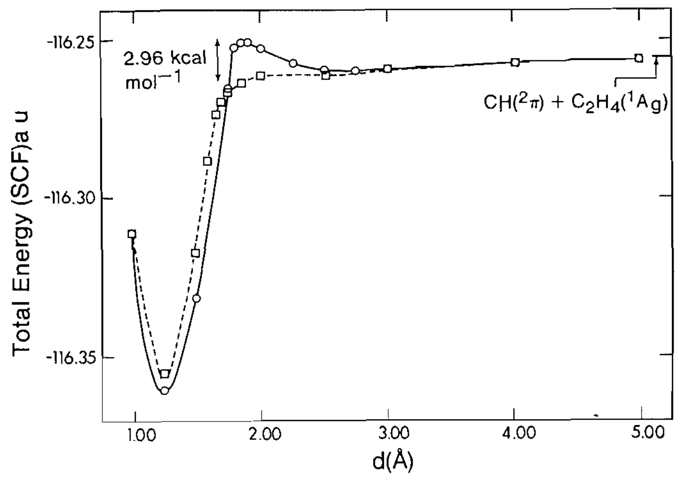

FIG. 4. Potential energy surface of lowest doublet state addition of CH + C_2H_4 reaction path at the SCF level. ○, perpendicular approach; □, planar approach of CH.

$C_2X_1C_4$ angle at this distance is 104.5° and the $X_1C_4H_9$ angle is 95.2°. The $C_2X_1C_4$ angle in the first reaction path remains at 90°, whereas in the second reaction path this angle is greater than 100° until the X_1—C_4 distance reaches a value of 1.60 Å. For this in-plane approach both the SCF and CI calculations predict no activation energy (Figs. 4 and 5).

The insertion reaction path

In the insertion reaction path CH is approaching in the plane of the ethylene molecule. The total energy of the $^2A''$ state as a function of the X_1—C_4 distance (*d*) has been calculated with optimizing all the rest of the molecular parameters, Fig. 6. The $C_2X_1C_4$ angle at large distances is small (e.g. at d = 5 Å, $\angle C_2X_1C_4$ = 42.6°) and increases as the distance decreases reaching a maximum of 99° at 2.5 Å. Then again it starts decreasing as *d* decreases to the final product of the allyl radical. LMO analysis shows that methylidyne and ethylene remain as separate entities until *d* reaches a value of 2.325 Å corresponding to the transition complex, Fig. 7, where C_2—C_4 bond formation starts to take place. At this transition state the C_4 atom is right above the C_2 carbon, i.e. $\angle C_3C_2C_4 \simeq 93°$ and H_6 is still bound to the C_2 atom. Below d = 2.325 Å the H_6 migrates from C_2 to C_4. The energy barrier at the SCF level is 29 kcal mol^{-1}. The configuration interaction studies on the potential energy surface with the SCF optimized geometries, Fig. 6, for the insertion reaction predicts an activation energy of ~15 kcal mol^{-1}.

Discussion

The first addition reaction path studied, where the CH is approaching in the plane perpendicular to the CCC plane is similar to the symmetric path we reported earlier (17). At the RHF open shell SCF level with 6-31G basis set, the energy barrier, 3 kcal mol^{-1}, is smaller than the minimal STO-4G UHF value of 7.7 kcal mol^{-1}. On inclusion of the correlation energy by configuration interaction computation, the energy barrier disappears completely (Fig. 5). The second reaction path, the in-plane approach, where C—H is approaching in the CCC plane, is close to the asymmetric approach reported earlier (17) where the reaction coordinate was the $C_2X_1C_4$ angle while in the present study we choose the X_1—C_4 distance as the reaction coordinate. This asymmetric approach, both at minimal STO-4G basis (UHF-SCF) and 6-31G basis (with RHF-SCF), predicts no energy barrier for the addition reaction even at the SCF level. On inclusion of correlation energy by the CI calculations, the energy along the addition reaction path decreases monotonically and again without any energy barrier (Fig. 5).

The LMO analysis at the critical level of 0.07 for bond identification shows partial bond formation between C_4—C_2 and C_4—C_3 at an X_1—C_4 distance of 1.85 Å in both reaction paths. Bond formation probably takes place by the p_z electrons

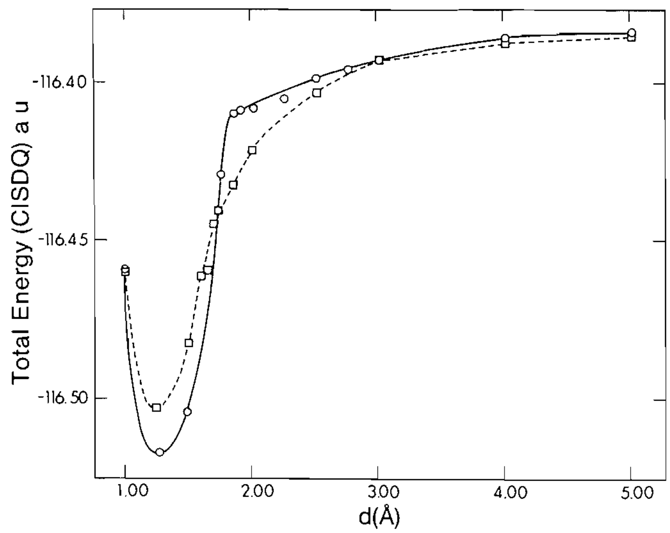

FIG. 5. Potential energy surface of lowest doublet state addition of CH + C_2H_4 reaction path at CISDQ level. ○, perpendicular approach; □, planar approach of CH.

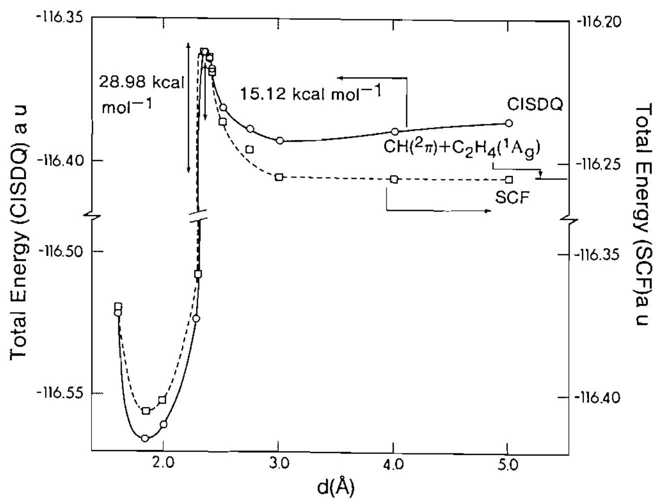

FIG. 6. Potential energy surface for CH insertion into ethylene. --- SCF; —— CISDQ level.

of the ethylene (C_2C_3) moving to the p_z in-plane empty orbital of methylidyne C_4 in both cases but back donation occurs from the lone pair of the p_x orbital of C_4 in path two and in path one the single p_x electron forms a partial bond with a carbon atom of ethylene. In the latter case, below d = 1.85 Å, one electron from the lone pair in the p_y orbital of methylidyne moves to the in-plane p_x orbital to complete the bond formation with ethylene. This electron rearrangement could perhaps be the reason why the asymmetric approach, reaction path two initially has a lower energy until d reaches a value of ~1.75 Å below which the symmetric path lies lower in energy leading to the cyclopropyl radical structure (Figs. 4 and 5). In either case the addition appears to be a one-step, concerted process, in agreement with the experimental stereospecific addition results obtained for the carbethoxymethylidyne. These potential energy surface calculations suggest that the addition of ($\tilde{X}^2\Pi$) ground state methylidyne to ethylene (^1A_g) follows the asymmetric path two in the early stages of the reactions until d = 1.75 Å, then crosses over to the symmetric path one, without any energy barrier. This asymmetric approach is in line with the predic-

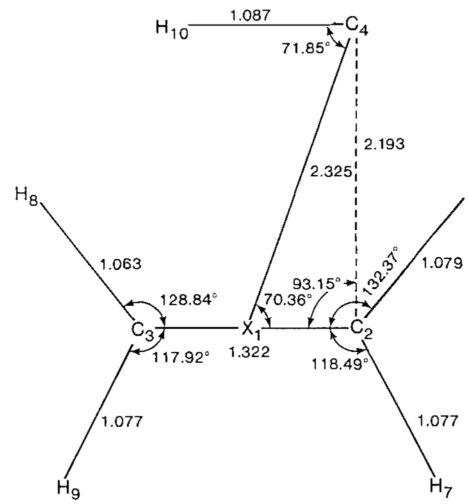

$E_{SCF} = -116.209395$ a u
$E_{CISDQ} = -116.361519$ a u

FIG. 7. RHF-SCF optimized geometry of the transition complex of CH insertion into ethylene. Bond distance in Å and bond angles in degree.

tions of the molecular orbital studies of the reaction path for the addition of singlet ($^1A_1$) methylene to ethylene (37, 38) favoring the asymmetric approach without any activation energy. Asymmetric reaction paths were also predicted for several singlet ($^1A_1$) substituted carbene cycloaddition reactions with some activation energy (37, 39).

The present computational results' prediction of a zero activation energy for the addition reaction of CH($\tilde{X}^2\Pi$) to $C_2H_4(\tilde{X}^1A_g)$ compares well with the experimental value of −0.35 kcal mol^{-1} recently reported by Berman, Fleming, Harvey, and Lin (2).

The knowledge of the geometry of the activated complex makes it also possible to estimate a value for the preexponential factor of the reaction on the basis of transition state theory.

The preexponential factor of the reaction has been reported to be $1.34 \times 10^{11}\ M^{-1}\ s^{-1}$ (2). Assuming that the preexponential factor for the insertion reaction into the C—H bonds of ethylene is the same as the one measured for methane (3), $0.30 \times 10^{11}\ M^{-1}\ s^{-1}$, we correct the experimental value for the ethylene reaction by subtracting the experimental value for methane $1.34 \times 10^{11} - 0.30 \times 10^{11} = 1.04 \times 10^{11}\ M^{-1}\ s^{1}$.

From the above experimental A factor the entropy of activation at 300 K

$$\Delta S_c^{\ddagger} = R \ln\left(\frac{hA}{e^2kT}\right) = -12.11 \text{ eu}$$

and

$$\Delta S_p^{\ddagger} = \Delta S_c^{\ddagger} - \Delta n\, R \ln (RT) = -18.47 \text{ eu}$$

The standard entropy for the activated complex is obtained from the equation

$$\Delta S_p^{\ddagger} = S_p^0(\mathrm{AC}) - S_p^0(\mathrm{CH}) - S_p^0(\mathrm{C_2H_4})$$

Taking $S_p^0(\mathrm{CH})$ = 43.7 eu and $S_p^0(\mathrm{C_2H_4})$ = 52.4 eu (40) the entropy of activation calculated from the experimental A factor yields the value $S_p^0(\mathrm{AC})$ = 77.63 eu for the standard entropy of the activated complex.

Based on the similarity between the cyclopropyl radical and the optimized structure computed for the activated complex of the CH + C_2H_4 addition, the standard entropy for the activated complex, S_p^0(AC), can be estimated using Benson's method (40). Starting out with the standard entropy for the cyclopropyl radical, $S_p^0 = 60.4$ eu (40), the longer C(H)—C(H_2) bonds will give 1 eu additional rotational and 3−4 eu additional vibrational contributions for the entropy of the activated complex. The vibrational contribution is compensated somewhat by the increased frquencies of the CH_2 groups due to the shorter H_2C—CH_2 bond. Thus, the standard entropy for the activated complex is estimated to be about $S_p^0(AC) \simeq 65 \pm 2$ eu, in serious disagreement with the value derived from the experimental A factor. The A factor derived from the estimated S_p^0(AC) value lies in the range of $6.5 \times 10^7 - 4.9 \times 10^8\ M^{-1}\ s^{-1}$ which is over two orders of magnitude lower than the reported experimental value.

We are not able at present to rationalize this discrepancy.

Turning to the insertion reaction, the transition state complex at d = 2.325 Å still resembles the reactant state (Fig 7), with the methylidyne carbon C_4 being close to C_2 at an angle $C_3C_2C_4$ = 93°, and the C_2—C_3 distance being similar to ethylene. At d = 2.30 Å the H_6 hydrogen migrates from C_2 to C_4 and C_2—C_4 bond formation begins to take place with C_2—C_4 distance of 1.735 Å. The energy barrier is 15 kcal mol^{-1} which is higher than the measured activation energies for insertion into the C—H bonds which are all negative and have values in the order of 0.4−0.06 kcal mol^{-1} (3). The computed energy barrier is sensitive to the correlation energy and geometry optimization at the CI level would very likely have a significant decreasing effect on it. The computed energy barrier, 4 kcal mol^{-1}, for the insertion of CH($\tilde{X}^2\Pi$) into the hydrogen molecule (16) is also probably somewhat larger than the experimental value.

Acknowledgment

The authors thank the Natural Sciences and Engineering Research Council of Canada for continuing financial support.

1. F. C. James, H. K. J. Choi, B. Ruzsicska, O. P. Strausz, and T. N. Bell. Frontiers of free radical chemistry. *Edited by* W. A. Pryor. Academic Press, New York. 1980. p. 139.
2. M. R. Berman, J. W. Fleming, A. B. Harvey, and M. C. Lin. Chem. Phys. **73**, 27 (1982).
3. M. R. Berman and M. C. Lin. Chem. Phys. **82**, 435 (1983).
4. B. P. Ruzsicska, A. Jodhan, H. K. J. Choi, O. P. Strausz, and T. N. Bell. J. Am. Chem. Soc. **105**, 2489 (1983).
5. W. J. R. Tyerman. J. Chem. Soc. A, 2483 (1969).
6. J. J. Tiee, F. B. Wampler, and W. W. Rice. Chem. Phys. Lett. **73**, 519 (1980).
7. O. P. Strausz, G. J. A. Kennepohl, F. X. Garneau, T. DoMinh, B. Kim, S. Valenty, and P. S. Skell. J. Am. Chem. Soc. **96**, 5723 (1974).
8. G. C. Lie, J. Hinze, and B. Liu. J. Chem. Phys **57**, 625 (1972); **59**, 1872 (1973); **59**, 1887 (1973).
9. H. Sun and K. F. Freed. Chem. Phys. Lett. **78**, 53 (1981).
10. J. A. Hall and W. G. Richards. Mol. Phys. **23**, 331 (1972).
11. T. H. Dunning, Jr., W. P. White, R. M. Pitzer, and C. W. Mathews. J. Mol. Spectrosc. **75**, 297 (1979); **75**, 318 (1979).
12. M. Bialski and F. Green. J. Mol. Spectrosc. **61**, 321 (1976).
13. M. Larsson, M. R. A. Blomberg, and P. E. M. Siegbahn. Mol. Phys. **46**, 365 (1982).
14. A. Mavridis and J. F. Harrison. J. Am. Chem. Soc. **104**, 3827 (1982).
15. K. S. Kim, S. P. So, and H. F. Schaefer. J. Am. Chem. Soc. **104**, 1457 (1982).
16. B. R. Brooks and H. F. Schaefer. J. Chem. Phys. **67**, 5146 (1977).
17. R. K. Gosavi, O. P. Strausz, and H. E. Gunning. Chem. Phys. Lett. **76**, 159 (1980).
18. P. Pulay. Mol. Phys. **17**, 197 (1969); **18**, 473 (1970); *In* Modern theoretical chemistry. Vol. 4. *Edited by* H. F. Schaefer. Plenum Press, New York. 1977. p. 153.
19. (*a*) H. B. Schlegel. Ph.D. Thesis, Queen's University, Kingston, Ont. 1975; (*b*) H. B. Schlegel, S. Wolfe, and F. Bernardi. J. Chem. Phys. **63**, 3632 (1975).
20. (*a*) W. J. Hehre, R. Ditchfield, and J. A. Pople. J. Chem. Phys. **56**, 2257 (1972); (*b*) R. Ditchfield, W. J. Hehre, and J. A. Pople. J. Chem. Phys. **54**, 724 (1971).
21. N. C. Handy, J. D. Goddard, and H. F. Schaefer. J. Chem. Phys. **71**, 426 (1979).
22. S. R. Langhoff and E. R. Davidson. Int. J. Quantum Chem. **8**, 61 (1974).
23. M. R. Peterson and R. A. Poirier. MONSTERGAUSS 81, Department of Chemistry, University of Toronto, Toronto, Ont., Canada 1981.
24. G. Herzberg and J. W. C. Johns. Astrophys. J. **158**, 399 (1969).
25. K. Kuchitsu. J. Chem. Phys. **44**, 906 (1966).
26. N. C. Baird. J. Org. Chem. **40**, 624 (1975).
27. M. Dupuis and J. Pacansky. J. Chem. Phys. **76**, 2511 (1982).
28. R. W. Fessenden and R. H. Schuler. J. Chem. Phys. **39**, 2147 (1963).
29. T. Takada and M. Dupuis. J. Am .Chem. Soc. **105**, 1713 (1983).
30. N. C. Baird, R. R. Gupta, and K. F. Taylor. J. Am. Chem. Soc. **101**, 4531 (1979).
31. J. McKelvey and G. Berthier. Chem. Phys. Lett. **41**, 476 (1976).
32. J. Paldus and A. Veillard. Chem. Phys. Lett. **50**, 6 (1977); Mol. Phys. **35**, 445 (1978).
33. O. Kikuchi. Chem. Phys. Lett. **72**, 487 (1980).
34. A. F. Voter and W. A. Goddard III. Chem. Phys. **57**, 253 (1981); J. Chem. Phys. **75**, 3638 (1981).
35. T. McKelvey and W. J. Hehre. Mol. Phys. **25**, 983 (1973).
36. P. O. Löwdin. Rev. Mod. Phys. **35**, 496 (1963); Adv. Chem. Phys. **14**, 283 (1969).
37. B. Zurawski and W. Kutzelnigg. J. Am. Chem. Soc. **100**, 2654 (1978).
38. R. Hoffman, D. M. Hayes, and P. S. Skell. J. Phys. Chem. **76**, 664 (1972).
39. N. G. Rondan, K. N. Houk, and R. A. Moss. J. Am. Chem. Soc. **102**, 1770 (1980).
40. S. W. Benson. Thermochemical kinetics. 2nd ed. John Wiley and Sons, New York, NY. 1976.

Electrostatic lock-and-key model for the analysis of inhibitor recognition by dihydrofolate reductase

PÉTER NAGY
Gedeon Richter Ltd., H-1475 Budapest, P.O.B. 27, Hungary

AND

GÁBOR NÁRAY-SZABÓ
CHINOIN Pharmaceutical and Chemical Works, H-1325 Budapest, P.O.B. 110, Hungary

Received August 3, 1984

This paper is dedicated to Professor Camille Sandorfy on the occasion of his 65th birthday

PÉTER NAGY and GÁBOR NÁRAY-SZABÓ. Can. J. Chem. **63**, 1694 (1985).

We propose a simple electrostatic model for the analysis of ligand binding to proteins. Besides a geometric fit electrostatic complementarity is also needed to allow favourable hydrogen bonding and ion-pair interactions. Nonpolar regions of the ligand and the biomacromolecule active site should match to reduce unfavourable hydrophobic effects, i.e., to lower the Gibbs free energy of the complex in aqueous solution. These principles are applied to the inhibition of dihydrofolate reductase by methotrexate. The enzyme active site is represented by an electrostatic lock which is derived from the macromolecular electrostatic potential and field at certain reference points. The key, defined similarly for the ligand, should fit into the lock to ensure complementarity, i.e., recognition. Hydrogen bonding and ion-pair interactions can be studied by the "potential key" while the "field key" accounts for hydrophobic complementarity. Analyzing the dihydrofolate reductase–methotrexate interaction in the light of the above principles the relative importance of various molecular fragments in binding can be determined.

PÉTER NAGY et GÁBOR NÁRAY-SZABÓ. Can. J. Chem. **63**, 1694 (1985).

Nous proposons un modèle électrostatique simple pour analyser les propriétés de liaison des ligands à des protéines. En plus d'un accord géométrique, une complémentarité électrostatique est nécessaire pour permettre l'existence de liaisons hydrogènes et d'interactions ion-paire favorables. Les régions non polaires du ligand et le site actif de la biomacromolécule doivent correspondre pour réduire les effets hydrophobes défavorables, c'est à dire pour diminuer l'énergie libre de Gibbs du complexe en solution aqueuse. On a appliqué ces principes à l'étude de l'inhibiteur de la réductase dihydrofolate par le méthotréxate. On représente le site actif de l'enzyme par un verrou électrostatique qui découle du potentiel et du champs électrostatique macromoléculaire, à certain points de référence. La clé, définie d'une façon analogue pour le ligand, doit s'adapter au verrou pour assurer la complémentarité, c'est à dire la reconnaissance. On peut étudier les liaison hydrogènes et les interactions ion-paire pour une "clé du potentiel" tandis que la "clé du champ" s'utilise pour la complémentarité hydrophobe. Une analyse de l'interaction réductase dihydrofolate–méthotréxate, à la lumière de ces principes, permet de déterminer l'importance relative des divers fragments moléculaires dans les liaisons.

[Traduit par le journal]

Introduction

The molecular basis of biological specificity is recognition of certain systems or parts of them by others. This process is pictorially modeled by the lock-and-key concept: locks (mostly crevices in proteins, nucleic acids, or other biomacromolecules) accommodate keys (inhibitors, substrates, or other ligands). Biological response is achieved if keys "fit" into the lock, a concept widely used but, in general, not unequivocally defined. The lock-and-key model is elegantly exploited in modern computer graphics (1–4) which, however, account only for close contacts between nonbonded atoms, i.e. excluded molecular configurations. There are at least two further requirements to be met: electrostatic complementarity and matching of nonpolar (hydrophobic) regions (5–7). In order to be recognized the ligand has to interact favourably with the active site and in biochemical systems interactions are mainly determined by electrostatic forces. Thus an electrostatic complementarity between the biopolymer and the ligand is also necessary to ensure binding. Finally, matching of nonpolar regions is required; this is a manifestation of the hydrophobic effect.

In this paper we propose a simple model which accounts for geometric, electrostatic, as well as hydrophobic complementarity. While the geometric requirement is considered conventionally, electrostatic and hydrophobic matching is studied in terms of the molecular electrostatic potential and field, respectively. The model is qualitative and certainly does not compete with up-to-date sophisticated numerical calculations which should, in principle, substitute experimental data. Rather, it is developed to analyze ligand binding in general, e.g., to recognize those fragments of the interacting molecules which are necessary for binding. Since numerical calculations yield figures which are often difficult to use for such analyses important trends may be overlooked. Ideally, the two types of approaches should complement each other: working hypotheses offered by the qualitative model could be checked numerically. In the next section we describe the model and later we illustrate its use on the inhibition of dihydrofolate reductase (DHFR) by methotrexate (MTX **1**).

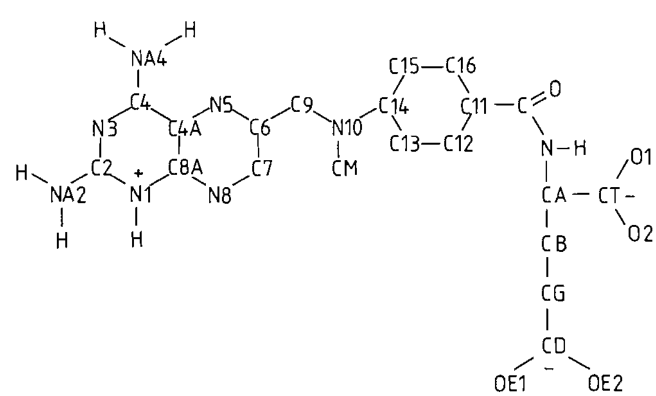

1

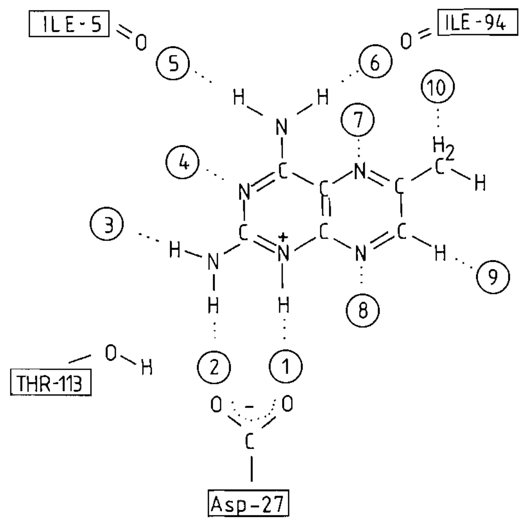

FIG. 1. Fragment A of MTX for calculation of atomic charges. Reference points, as defined in the text, are indicated by numbers in circles.

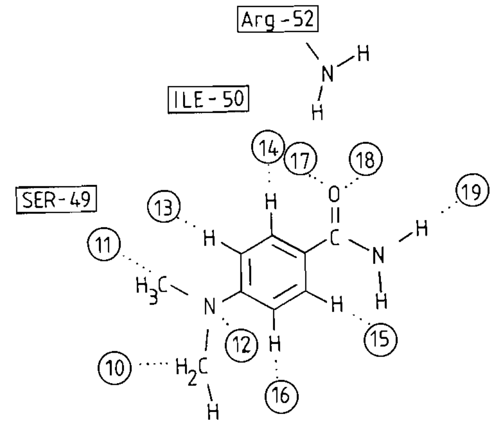

FIG. 2. The same as in Fig. 1 for fragment B of MTX.

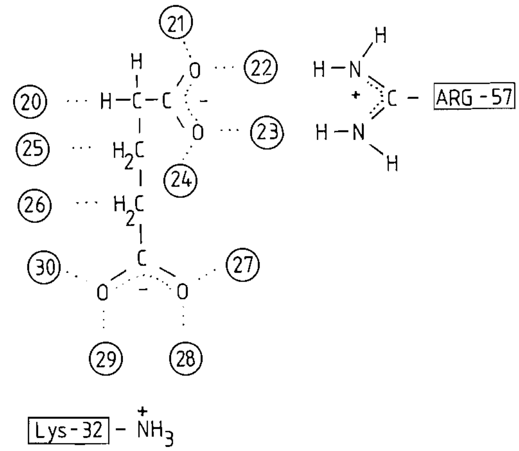

FIG. 3. The same as in Fig. 1 for fragment C of MTX.

Model and method

In this paper we model keys in two different ways. The "charge key" is simply the atomic charge pattern of the molecule which can be obtained from some quantum chemical, e.g. CNDO/2, calculations. A complementarity between the electrostatic lock and the charge key means that the approximate value of the interaction energy,

$$[1] \quad E_{\text{int}} = \sum_a V(\boldsymbol{r}_a)q_a$$

where $V_m(\boldsymbol{r}_a)$ is the electrostatic potential of the biomacromolecule at atom a bearing a net charge of q_a, is negative indicating binding (5). On the other hand, the definition of the "potential key" is based on a model by Douglas and Kollman (8) where the electrostatic potentials of the interacting systems at given reference points are used to estimate binding energies.

To study the matching of hydrophobic regions we use the "field lock" determined by the electrostatic field map of the enzyme. At a given site the molecular electrostatic field orients and interacts with point dipoles, modeling water molecules. The stronger the interaction the larger is the absolute value of the electrostatic field (9); thus hydrophobic regions around a molecule are indicated by small fields. Hydrophobic complementarity means matching of small field regions.

To determine the electrostatic lock of DHFR from *Escherichia coli* we considered all enzyme atoms. Coordinates were taken from the Protein Data Bank (10, 11). Because of the shielding effect of counter ions (12) we considered all surface side chains unionized. On the other hand, side chains of Asp-27, Lys-32, and Arg-57, located in the vicinity of the ionized inhibitor, were treated as charged (see, e.g., ref. 13).

We calculated the electrostatic potential of DHFR and MTX from bond contributions (14). This allows us to treat very large molecules with several thousands of atoms since, due to the approximate transferability of bond orbitals and neglect of non-orthogonality terms the computational work increases only linearly with the number of bonds. This is an advantage over empirical force field methods which are restricted to systems with at most 500 atoms (15). Further details of the calculation are given elsewhere (5, 12). Atomic point charges were calculated by the CNDO/2 method (16). Schematic arrangement of reference points for the potential key is depicted in Figs. 1−3. The distance of the reference points from the neighbouring atoms is 100 pm and the orientation is trigonal or tetrahedral, corresponding to hybridization. For C—H bonds chemically plausible orientations are considered and reference points lie 150 pm or 180 pm from the hydrogen or carbon atom, respectively. In some cases reference points may get too close to a neighbouring enzyme atom, thus a slight correction was necessary (cf. Table 1).

Results and discussion

The electrostatic potential lock for DHFR from *Escherichia coli* and the fit with the charge key of MTX is illustrated in Figs. 4−6. Fitting the potential lock with the potential key is seen in Figs. 7 and 8. Inspection of Figs. 4 and 7 indicates that most atoms of the pyrazine part in MTX (C6, C7, and N8 in Fig. 4, reference points 8 and 9 in Fig. 7) fit badly in the DHFR lock. This is in accord with the experience that the principal structural characteristics necessary for binding to DHFR is a 2,4-diaminopyrimidine or an *s*-triazine structure (3, 4, 13, 17−19). The unfavourable binding of the pyrazine moiety is also seen from the electrostatic interaction energies calculated from eq. [1]. E_{int} is −117 kJ/mol and +23 kJ/mol for the 2,4-diaminopyrimidine and pyrazine fragments, respectively. Another strongly binding region of MTX is the α-carboxyl group of glutamate (CT, O1, and O2 in Fig. 6, reference points

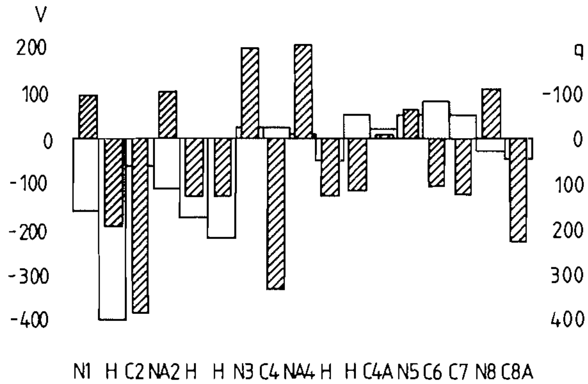

FIG. 4. Electrostatic potential lock of DHFR (open bars) and charge key of the MTX A fragment, Fig. 1 (hatched bars). Hydrogen atoms of C—H bonds are omitted. The V electrostatic potential is given in kJ/mol the q charge in millielectrons.

TABLE 1. Cartesian coordinates (in pm) of reference points given in Figs. 1–3; enzyme atoms involved in hydrogen (or ion-pair) bonding with the inhibitor are indicated in the footnote

No.	x	y	z	No.	x	y	z
1[a]	2436	5914	2578	17[e]	1705	6579	2674
2[b]	2570	5745	2510	18[e]	1806	6705	2610
3	2545	5601	2217	19	2052	6431	2381
4	2354	5698	2141	20	1800	6852	2582
5[c]	2191	5557	2022	21[f]	2068	6560	2278
6[d]	1914	5670	2159	22[f]	2043	6674	2150
7	1916	5816	2236	22A[f]	2083	6635	2201
8	2185	5973	2603	23[g]	1964	6878	2196
9	1885	6078	2719	23A[g]	2088	6860	2262
10	1650	5878	2309	24[g]	1930	6921	2360
11	1757	5830	2808	25	2241	6596	2554
12	1589	6023	2488	26	2092	7006	2536
13	1599	6078	2845	27[h]	1963	6845	2818
14	1669	6466	2857	28[h]	2081	6825	2943
15	2000	6422	2252	29[h]	2294	6808	2898
16	1928	6038	2242	30[h]	2350	6814	2734

[a]Asp-27 OD1.
[b]Asp-27 OD2 and Thr-113 OG1.
[c]Ile-5 O.
[d]Ile-94 O.
[e]Arg-52 NH1.
[f]Arg-57 NH1.
[g]Arg-57 NH2.
[h]Lys-32 NZ.

21, 22, 23, and 24 in Fig. 8). Ion-pair interaction (and hydrogen bonding) with the side chain of Arg-57 is very strong here. On the other hand, the terminal carboxyl of glutamate (CD, OE1, and OE2 in Fig. 6 and reference points 27, 28, 29, and 30 in Fig. 8) feels a much weaker attraction by the charged Lys-32 side chain. The OE1 . . . NZ(Lys-32) distance is as large as 627 pm. Elongation of the glutamate side chain by one or two methylene units should improve the fit between the lock and the key, thus enhancing the interaction between the enzyme and its inhibitor.

Figures 4–6 and 7 and 8 allow one to compare predictive (and illustrative) powers of the charge key and potential key concepts outlined in the Model and method section. The potential key is more illustrative. In fact, charge alternation (e.g. for atoms of a N—H bond) renders difficult to recognize good fits between the potential lock and its charge key. On the other hand, the possibility to estimate binding energy increments of certain molecular fragments is an attractive feature of the charge key concept.

Field locks are depicted in Figs. 9 and 10. Good fits are observed for the 2,4-diaminopyrimidine region (reference points 1–6) and for the α-carboxylate group (reference points 22 and 23). Here the strong field of the inhibitor finds its counterpart in the enzyme active site. This is completed by matching the potential lock and its key, with the formation of ion pairs or hydrogen bonds (cf. Figs. 1–3 and footnotes to Table 1). The complementarity of strong field regions indicate that favourable hydration has to be overbalanced by the attractive interaction between matching groups. This is indeed the

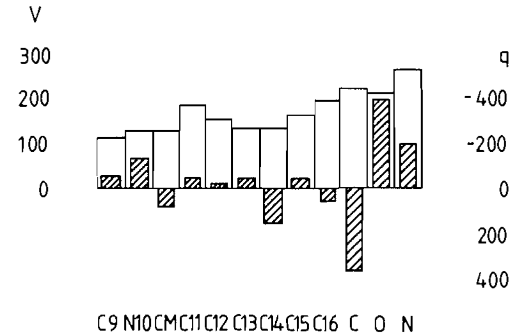

FIG. 5. The same as in Fig. 4 for the MTX B fragment (Fig. 2).

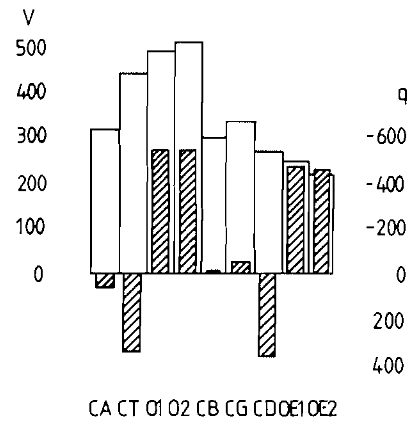

FIG. 6. The same as in Fig. 4 for the MTX C fragment (Fig. 3).

FIG. 7. Electrostatic potential lock of DHFR (open bars) and potential key of MTX (hatched bars) for reference points 1–19 (Figs. 1, 2). The V electrostatic potential is given in kJ/mol.

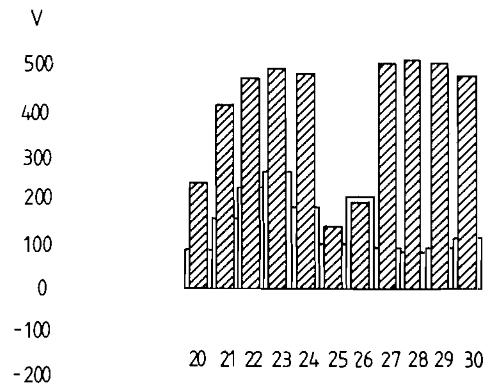

FIG. 8. The same as in Fig. 7 for reference points 20−30 (Fig. 3).

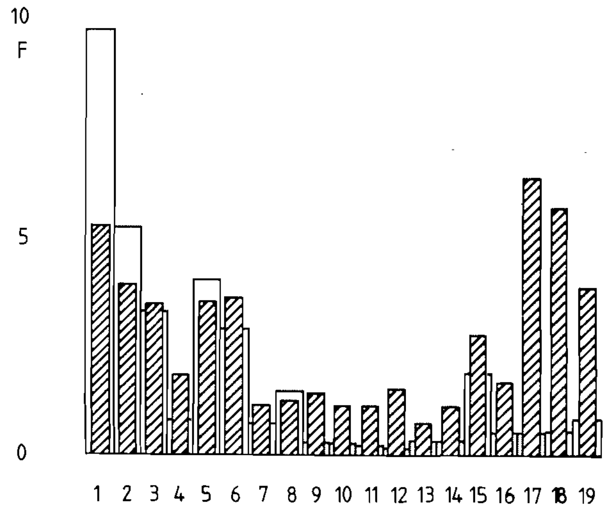

FIG. 9. Electrostatic field lock of DHFR (open bars) and field key of MTX (hatched bars) for reference points 1−19 (Figs. 1, 2). The F electrostatic field is given in V/nm.

case as indicated by the good fit of the potential key into its lock (Figs. 7 and 8).

Weak field regions ($F < 1.5$ V/nm) around the alkyl groups and the phenyl ring (reference points 9−11, 13, 14, 16, 20, and 25) match with the enzyme field lock, indicating that hydrophobic regions of the inhibitor are recognized by DHFR. The fit is bad for the amide region (reference points 17−19) and for the terminal carboxylate group of glutamate (reference points 28 and 29) where a small enzyme field finds a strong inhibitor field as counterpart. In both cases the bad fit is due to unfavourably large distances between atoms of a hydrogen (or ion-pair) bond. For the amide group the NH1(Arg-52) . . . O distance (356 pm) is large compared to the typical value (280 pm). As we have mentioned above the NZ(Lys-32) . . . OG1 distance is too large even for an ion-pair bond. Though both amide and terminal carboxylate groups contribute to the bonding of the inhibitor (cf. Figs 7 and 8) their favourable hydration is not balanced by the attraction between potentially matching regions of MTX and DHFR.

It is a bit astonishing that for reference point 15 of MTX both potential and field values are larger than expected for a hydrophobic group (cf. Figs. 7 and 9). This is due to the through-space electrostatic effect of the distant carboxylate group (cf. ref. 20). The same effect enhances the field in reference point 16. Interestingly, in spite of large distances from enzyme

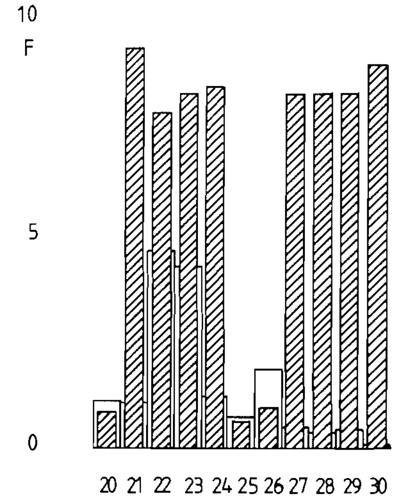

FIG. 10. The same as in Fig. 9 for reference points 20−30 (Fig. 3).

groups capable to form ion-pair or hydrogen bonds, the DHFR lock potential and field is relatively large at reference point 15, thus ensuring a good fit.

Conclusions

(*1*) Recognition of a ligand (key) by a biomacromolecule (lock) requires geometric fit and a complementarity between electrostatic potential and field patterns of the lock and its key. Matching potential patterns corresponds to optimal electrostatic interaction while an optimal field pattern fit should minimize unfavourable hydrophobic effects upon association of the biomacromolecule with the ligand.

(*2*) A simple way to define the electrostatic lock and its key is to calculate the potential and field at some characteristic reference points around the biomacromolecule and its ligand. In our case the quoted electrostatic potentials were calculated by an additive scheme using bond fragments.

(*3*) Applying the above principles to the dihydrofolate reductase−methotrexate complex it was found that the 2,4-diaminopyrimidine and α-carboxylate parts of the inhibitor are mainly responsible for binding to the enzyme. Furthermore, elongation of the glutamate side chain by one or two methylene units would improve the electrostatic fit, i.e. make binding stronger.

1. R. LANGRIDGE, T. E. FERRIN, I. D. KUNTZ, and M. L. CONNOLLY. Science, **211**, 661 (1981).
2. J. M. BLANEY, E. C. JORGENSEN, M. L. CONNOLLY, T. E. FERRIN, R. LANGRIDGE, S. J. OATLEY, J. M. BURRIDGE, and C. C. F. BLAKE. J. Med. Chem. **25**, 785 (1982).
3. V. CODY and S. F. ZAKRZEWSKI. J. Med. Chem. **25**, 427 (1982).
4. C. HANSCH, B. HATHAWAY, Z. GUO, C. DIAS SELASSIE, S. W. DIETRICH, J. M. BLANEY, R. LANGRIDGE, K. W. VOLZ, and B. T. KAUFMAN. J. Med. Chem. **27**, 129 (1984).
5. G. NÁRAY-SZABÓ. J. Am. Chem. Soc. **106**, 4584 (1984); Erratum: J. Am. Chem. Soc. **106**, 7296 (1984).
6. J. AVERY. Int. J. Quant. Chem. **26**, 843 (1984).
7. G. NÁRAY-SZABÓ and P. NAGY. *In* Proceeding of Symposium on Molecular Basis of Cancer. *Edited by* R. Rein. Alan Liss, New York. 1984.
8. J. E. DOUGLAS and P. A. KOLLMAN. J. Am. Chem. Soc. **102**, 4295 (1980).
9. G. PEINEL, H. FRISCHLEDER, and F. BIRNSTOCK. Theor. Chim. Acta, **57**, 245 (1980).
10. F. C. BERNSTEIN, T. F. KOETZLE, G. T. B. WILLIAMS, E. F.

MAYER, JR., M. D. BRICE, J. R. ROGERS, O. KENNARD, T. SHIMANOUCHI, and M. TASUMI. J. Mol. Biol. **112**, 535 (1977).
11. J. T. BOLIN, A. MATTHEWS, and J. KRAUT. Protein Data Bank File **68SB13**, 119 (1980).
12. J. ÁNGYÁN and G. NÁRAY-SZABÓ. J. Theor. Biol. **103**, 349 (1983).
13. C. R. BEDDELL. *In* X-ray crystallography and drug action. *Edited by* A. S. Horn and C. J. De Ranter. Clarendon, Oxford. 1984. p. 169.
14. G. NÁRAY-SZABÓ. Int. J. Quant. Chem. **16**, 265 (1979).
15. G. WIPFF, A. DEARING, P. WEINER, J. BLANEY, and P. KOLLMAN. J. Am. Chem. Soc. **105**, 997 (1983).
16. J. A. POPLE and D. L. BEVERIDGE. Approximate molecular orbital theory. McGraw Hill, New York. 1970.
17. B. R. BAKER. Cancer Chemother. Rep. **4**, 1 (1959).
18. J. J. BURCHALL and G. H. HITCHINGS. Mol. Pharmacol. **1**, 126 (1965).
19. S. F. ZAKRZEWSKI. J. Biol. Chem. **238**, 1485 (1963); **238**, 4002 (1963).
20. K. ŐSAPAY and G. NÁRAY-SZABÓ. J. Mol. Struct. THEOCHEM. **92**, 57 (1983).

Effect of salt on the tyrosine and protonated Schiff base deprotonation kinetics in bacteriorhodopsin

PAUL DUPUIS AND M. A. EL-SAYED[1]

Department of Chemistry and Biochemistry, University of California at Los Angeles, 405 Hilgard Ave., Los Angeles, CA, U.S.A. 90024

Received July 30, 1984

This paper is dedicated to Professor Camille Sandorfy on the occasion of his 65th birthday

PAUL DUPUIS and M. A. EL-SAYED. Can. J. Chem. **63**, 1699 (1985).

It is observed that the number of protons pumped per M_{412} formed in the bacteriorhodopsin photocycle almost doubles at high salt concentrations. In this paper, we studied the rates of deprotonation of tyrosine and of the two components of the protonated Schiff base at high salt concentrations, and at different pHs and temperatures. It is found that at pH = 7, increasing the salt concentration decreases the rates of deprotonation of the protonated Schiff base and tyrosine. This strongly suggests that the observed gain in the quantum yield of proton release per M_{412} formed when the salt concentration is increased is not a result of an increase in these rates. However, at high pH, e.g. 9.6, increasing the salt concentration increases the rate of deprotonation of the Schiff base by about 50%. Under all conditions, the slow component of the Schiff base is found to lose its proton prior to tyrosine.

PAUL DUPUIS et M. A. EL-SAYED. Can. J. Chem. **63**, 1699 (1985).

À de fortes concentrations en sel, le nombre de protons pompés pour chaque M_{412} formé au cours du photocycle de la bactériorhodopsine est pratiquement doublé. Dans cette publication, nous rapportons les résultats d'une étude, à des fortes concentrations en sel, à divers pH et à diverses températures, sur les vitesses de déprotonation de la tyrosine et des deux composantes de la base de Schiff protonée. On a trouvé qu'à un pH de 7 l'augmentation de la concentration en sel diminue les vitesses de déprotonation de la base de Schiff protonée et de la tyrosine. Ceci suggère fortement que l'augmentation observée du rendement quantique des protons libérés pour chaque M_{412} formé lorsqu'on augmente la concentration du sel n'est pas dû à une augmentation de ces vitesses. Cependant, si on opère à un pH d'environ 9,6 et que l'on augmente la concentration du sel, on provoque aussi une augmentation de la vitesse de déprotonation de la base de Schiff de l'ordre de 50%. On a trouvé que, quelles que soient les conditions, la composante lente de la base de Schiff perd son proton avant la tyrosine.

[Traduit par le journal]

Introduction

Bacteriorhodopsin (bR), the only protein in the purple membrane of *Halobacterium Halobium*, contains one molecule of retinal covalently bound to the ϵ-amino group of a lysine residue via a protonated Schiff base (1, 2). When it absorbs light, it undergoes a photochemical cycle (3) with at least four intermediates appearing and decaying in a time scale that varies from picoseconds to milliseconds:

$$bR_{570} \rightarrow K_{610} \rightarrow L_{550} \rightarrow M_{412} \rightarrow O_{640} \rightarrow bR_{570}$$

During this cycle, protons are pumped from the inside to the outside of the cell, resulting in a pH gradient across the cell membrane. This proton gradient drives some metabolic processes such as ATP synthesis (4–9). The exact mechanism of the proton pump remains unclear. However, protons are ejected from the cell on a time scale comparable to the L_{550} to M_{412} transformation (10, 11). A good correlation has been found between the number of protons pumped by the purple membrane and the amount of the slow decaying form of M_{412} (12).

M_{412} is unique, as it is the only intermediate whose Schiff base is unprotonated, while the parent pigment and all the other intermediates are protonated (4, 13–17). Some studies have inferred that the Schiff base deprotonation is closely associated with the proton pump mechanism (18, 19) and the effect of chemically modified tyrosines on the rate of decay of M_{412} suggests a coupling between some tyrosines and M_{412} (20–24).

Recently, the kinetics of formation of both the tyrosinate ion absorption at 296 nm and the deprotonated Schiff base (M_{412}) absorption were studied simultaneously as a function of pH and temperature (25). The results show two formation rates for M_{412}, in agreement with previous observations (11, 18). The slow one is dominant under physiological conditions and is found to be slightly faster than that for the tyrosinate formation (25). This is in disagreement with the proposal that the tyrosinate formation is a prerequisite to the deprotonation of the Schiff base (18, 19). Furthermore, the ratio of the amplitudes of the fast and slow components of the M_{412} formation is found to be very sensitive to pH and, at any pH, can be used (25) to calculate a pK_A value of about 9.6. This is explained by having two different sites for the protonated Schiff base within the protein. In one site, the Schiff base is near an amino acid with a pK_A of 9.6, e.g. tyrosine, but lysine is also a possibility. This gives rise to the slow M_{412} component. In the second site, the Schiff base is near the conjugate base of the amino acid. This gives rise to the fast M_{412} component. The formations of the slow and fast components of M_{412} as well as that of the tyrosinate ion all have activation energies that are comparable to H-bond energies (25). These studies were performed on suspensions of bR in water; the pH was adjusted with phosphate buffers.

According to experiments on purple membrane sheets, the quantum yield of proton release depends on the medium. As salt concentrations increase, the quantum yield of M_{412} remains the same but the H^+/M_{412} ratio goes from 1 to >2 (26, 27). The purpose of this work is to carry out experiments similar to those of ref. 25, this time varying the salt concentration of the external medium to see how the formation rates and the relative amplitudes of the two M_{412} components, as well as those for the tyrosinate ion, are affected. We want to determine if the variation in any of these parameters can account for the change in the quantum yield of proton release.

At pH = 7.0, in a 0.5 *M* KCl solution, the rate constants and the relative amplitudes of the two M_{412} components are found

---

[1] Author to whom correspondence may be addressed.

to be the same as in a low salt solution. In a basal salt solution, the rate constants are smaller than in a low salt medium at pH = 7. The same observations are made for the tyrosine deprotonation. These results strongly indicate that the doubling of proton release per M_{412} formed is not a consequence of the change in the kinetics of deprotonation of the Schiff base or tyrosine at physiological pH. In salt solutions, however, as the pH increases, the sum of the weighted average values of the rate constants for the two M_{412} components increases. This is a result of a more rapid increase in the relative amplitude of the fast component, with pH, in the presence of high salt concentrations.

Experimental

Master slants of the ET1-001 strain of H. Halobium were provided by Dr. R. A. Bogomolni and Dr. W. Stoeckenius. The procedure for the growth and purification of the purple membrane was a combination of those outlined by Oesterhelt and Stoeckenius (28) and Becher and Cassim (29).

The experimental setup used to monitor the uv and visible absorption changes in bR is the same as the one used in ref. 25. Briefly, the monitoring wavelengths of 297 nm (for the tyrosinate ion) and 405 nmr (for M_{412}) were provided by the collimated output of a 1000-W Xe/Hg lamp (Canrad Hanovia, Newark, NJ) which was passed through a 5-cm water filter and focused onto the entrance slit of a 0.25-m monochromator (Jarrell–Ash, Waltham, MA) by a quartz lens. The light from the exit slit was passed through a 0.3 optical neutral density filter acting as a beam splitter, allowing 30% of the light to enter a reference RCA 1P28A photomultiplier tube while the remaining light was focused onto a 0.5 × 1.0 cm jacketed water-cooled quartz cell (Precision Cells, Hicksville, NY). The transmitted light was passed through a Corning 7-54 or 7-59 visible cutoff filter (Corning Glassworks, Corning, NY) and collected by the photocathode of the sampling RCA 1P28A phototube. The output of a differential oscilloscope displaying the transient absorbance was connected to a Biomation 805 Waveform Recorder which was interfaced to an Apple II computer. This computer was used to signal average the data and store it on magnetic floppy discs. For the tyrosinate signal, 512 scans were averaged while the M_{412} signal required only 128 scans. The data was then sent to a VAX computer and analysed and plotted via a special computer program.

Photolysis of the sample was accomplished with a focused 6-ns, 532-nm beam obtained from the frequency doubled output of a Nd:YAG laser (Quanta-Ray, Mountainview, CA), at a repetition rate of 10 Hz. Care was taken to insure that the photolysis beam overlapped with the probe beam so that the whole volume would be photolysed. Photolysis powers were kept at 50 mW by attentuating the laser beam with a 045 Corning filter.

For both the temperature and pH studies, the concentration of bR was approximately 1.6×10^{-5} M, assuming an extinction coefficient of 63000 M^{-1} cm^{-1} at 570 nm. The temperature was kept constant by using a temperature controlled cell connected to a water bath circulator and was monitored using a Markson pH/Temp meter. The bR was susepended in water containing 0.5 M KCl or in water containing most of the salts present when the bacteria are grown (NaCl, 4.3 M; KCl, 2.7×10^{-2} M; $CaCl_2$, 1.8×10^{-3} M). In addition, for the pH studies, the suspensions contained 0.1 M KH_2PO_4 buffers which were adjusted to the desired pH by addition of 0.2 M NaOH. The pHs of all suspensions were checked prior to the experiment.

Laser photolysis experiments were carried out for bR_{570} suspensions over the range $7.0 \leq pH \leq 10.0$ at 22°C. The temperature studies were conducted in the range 5.0–25°C by 5° increments. In all cases, identical conditions were maintained with respect to the bR concentration and laser pulse intensity.

Results and discussion

The present studies were done on bR suspensions in two different media: a medium containing KCl, 0.5 M, and a medium similar to the "basal salt" solution in which the bacterium grows: NaCl, 4.3 M; KCl, 2.7×10^{-2} M; $CaCl_2$, 1.8×10^{-3} M. $MgSO_4$ was not used because of the precipitate formed upon the addition of NaOH to change the pHs. In both of these solutions the quantum yield of proton release per M_{412} formed is approximately twice what it is in a medium having a very low salt concentration (26, 27). All the results will be discussed in comparison to the data obtained for bR suspensions in water, without any salt added besides the buffers (25).

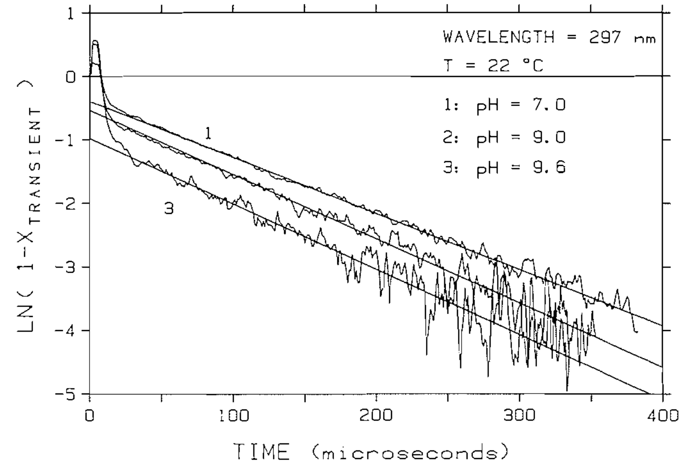

FIG. 1. A plot of ln $(1 - X_t)$ versus time for the absorbance change at 297 nm at pH = 7.0, 9.0, and 9.6 (bR suspensions in 0.5 M KCl). The fast component corresponds to changes in absorption of the retinal chromophore. The positive spike at $t = 0$ is caused by the scattering of the incident laser beam which was not totally filtered out.

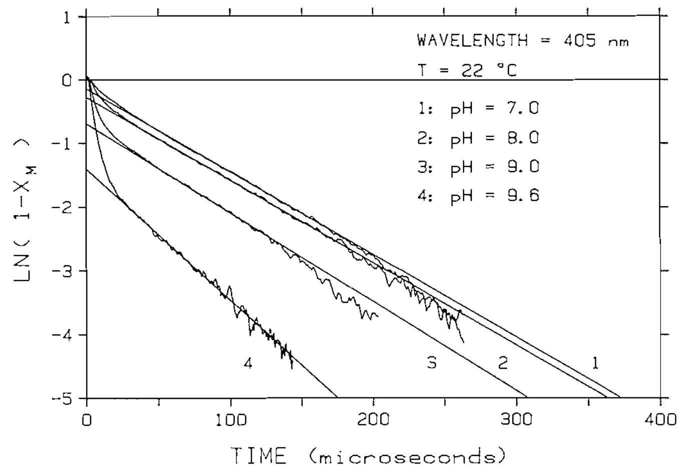

FIG. 2. A plot of ln $(1 - X_M)$ versus time for M_{412} at pH = 7.0, 8.0, 9.0, and 9.6 (bR suspensions in 0.5 M KCl). Note that the amplitude of the fast component becomes more important as the pH increases.

A. *Deprotonation kinetics of the Schiff base and tyrosine*

1. *In a 0.5* M *KCl solution*

Both the M_{412} and tyrosinate absorptions were normalized to the maximum absorbance change observed at 405 and 297 nm respectively. The normalized absorption of the transient is assumed to be proportional to its mole fraction, X_t, at time t, and $1 - X_t$ is the mole fraction of the precursor (L_{550} for M_{412} and tyrosine for tyrosinate).

Figures 1 and 2 show semilogarithmic plots (ln $(1 - X_t)$ vs. time) for the tyrosinate and M_{412} formations, respectively, at

TABLE 1. The values of $k_{M\,fast}$ and $k_{M\,slow}$ for M_{412} formation and k_{tyr} for tyrosinate formation obtained at each pH for bR suspended in a medium containing 0.5 *M* KCl. Relative amplitudes for the two M_{412} components are given in parentheses. The pK_A for tyrosine are those calculated from eq. [2]. T = 22°C

pH	$k_{M\,fast}$ (10^4 s^{-1})	$k_{M\,slow}$ (10^4 s^{-1})	k_{tyr} (10^4 s^{-1})	pK_A
7.0	12 ± 2 (0.12)	1.31 ± 0.02 (0.88)	0.85 ± 0.03	7.9
8.0	18 ± 3 (0.23)	1.32 ± 0.02 (0.77)	0.92 ± 0.04	8.5
8.2	18 ± 5 (0.27)	1.36 ± 0.05 (0.73)	0.93 ± 0.01	8.6
8.4	20 ± 6 (0.31)	1.36 ± 0.04 (0.69)	0.94 ± 0.02	8.7
8.5	23 ± 6 (0.30)	1.44 ± 0.04 (0.70)	0.95 ± 0.05	8.9
8.6	21 ± 5 (0.38)	1.40 ± 0.03 (0.62)	0.99 ± 0.07	8.8
8.8	18 ± 3 (0.47)	1.44 ± 0.06 (0.53)	0.99 ± 0.02	8.9
9.0	19 ± 3 (0.51)	1.47 ± 0.07 (0.49)	0.97 ± 0.05	9.0
9.2	18 ± 4 (0.60)	1.52 ± 0.06 (0.40)	1.05 ± 0.07	9.0
9.4	18 ± 3 (0.71)	1.8 ± 0.2 (0.29)	1.1 ± 0.1	9.0
9.6	19 ± 3 (0.78)	2.08 ± 0.03 (0.22)	1.08 ± 0.08	9.1
9.8	24 ± 3 (0.79)	3.3 ± 0.2 (0.21)	1.04 ± 0.03	9.2

TABLE 2. The values of $k_{M\,fast}$ and $k_{M\,slow}$ for M_{412} formation and k_{tyr} for tyrosinate formation obtained at each pH for bR suspended in a 0.1 *M* phosphate buffer (25). T = 22°C

pH	$k_{M\,fast}$ (10^4 s^{-1})	$k_{M\,slow}$ (10^4 s^{-1})	k_{tyr} (10^4 s^{-1})	pK_A
7.0	15 ± 3 (0.12)	1.3 ± 0.1 (0.88)	0.92 ± 0.04	—
9.0	16 ± 4 (0.40)	1.4 ± 0.1 (0.60)	0.97 ± 0.04	9.2
9.2	15 ± 3 (0.44)	1.4 ± 0.1 (0.56)	0.98 ± 0.04	9.3
9.4	18 ± 3 (0.45)	1.5 ± 0.1 (0.55)	1.0 ± 0.1	9.5
9.6	18 ± 2 (0.55)	1.6 ± 0.1 (0.45)	0.99 ± 0.04	9.5
9.8	17 ± 3 (0.58)	1.7 ± 0.1 (0.42)	1.1 ± 0.1	9.7
10.0	18 ± 2 (0.70)	1.8 ± 0.2 (0.30)	1.1 ± 0.1	9.6
10.2	17 ± 3 (0.77)	2.1 ± 0.2 (0.23)	1.2 ± 0.2	9.7
10.4	22 ± 3 (0.83)	3.4 ± 0.4 (0.17)	1.2 ± 0.1	9.7

different pHs. These plots, as expected, are very similar to those for bR suspensions in water without KCl (25). Both figures show the presence of two components.

In the case of the absorbance change monitored at 297 nm (Fig. 1), the very fast component corresponds to changes in the retinal absorption, which is also observed at this wavelength (30). The positive spike at $t = 0$ is caused by scattering from the laser beam which could not be completely filtered out. The slower component corresponds to the tyrosinate absorbance (30, 31). M_{412} shows a biphasic formation and the intensities of the slow and fast components depend on the pH of the external medium (Fig. 2). The corresponding change in the tyrosinate plot can be attributed to the fact that, as the pH increases, equilibrium favors the tyrosinate form, and there are fewer tyrosines that can deprotonate during the photocycle.

Table 1 shows the rate constant values for the formation of M_{412} ($k_{M\,fast}$ and $k_{M\,slow}$) and of the tyrosinate ion (k_{tyr}). For the sake of comparison, Table 2 shows the same rate constants for the experiment performed on suspensions of bR in low salt solutions (buffers present) (25).

In both sets of experiments, the pH was increased up to the point where we were unable to accurately determine the slow M_{412} component or the tyrosinate formation. In 0.5 *M* KCl, at pH > 9.8, the amplitude of the slow M_{412} component was too small to determine its rate constant, and for the tyrosinate ion, at pH > 9.8, most of the absorbance change at 297 nm was caused by the retinal absorption. In the low salt solutions, the experiment could be done up to pH = 10.6.

The first observation that can be made is that whether KCl is present or not, both components of the M_{412} generation process are still faster than the tyrosinate formation. Secondly, at the same pH, the amplitude of the fast M_{412} component increases as the KCl concentration increases. Finally, at pH < 9.4, all rate constants are about the same in both sets of experiments but, at pH ≥ 9.4, the rate constants for the slow M_{412} component are larger when KCl is present in the external medium. However, at pH ≥ 9.4, the amplitude of the fast component becomes more and more important and it is more and more difficult to resolve the pure slow component. This apparent increase in the rate constant of the slow component should be taken as an indication of the importance of the fast component rather than as representative of a major change in the real value of the constant itself.

We have previously discussed the Schiff base deprotonation in the following manner (25). It is proposed that two sites for the protonated Schiff base exist within the protein. In one site, the Schiff base is located near an amino acid (AH) with a pK_A of 9.6 and, in the other, it is located near the conjugate base (A^-). This describes the two different rise times for M_{412} as follows:

a. $L_{550}\,[=\overset{+}{N}H,\ AH] \rightarrow M_{412}$ slow

b. $L_{550}\,[=\overset{+}{N}H,\ A^-] \rightarrow M_{412}$ fast

One would then expect the time dependence of the M_{412} absorption to be given by:

$$[1]\quad \ln\,(1 - X_M) = \ln\,[C_1 \exp\,(-k_A t) + C_2 \exp\,(-k_{AH} t)]$$

This assumes: (a) two different independent chromophore populations, (b) the rate of $AH \rightleftharpoons A^- + H^+$ equilibration is slow compared to the rate of formation of L_{550} and M_{412}, and (c) M_{412} has the same absorption coefficient in the two sites. Obviously, the relative amplitudes (C_1, C_2) of the two components will depend on the pH. In Fig. 2, one observes that the contribution of the amplitude of the fast component of the generation process becomes greater as the pH of the external medium increases.

If this idea is valid, then the dissociation constant of the amino acid group could be determined from the rise curve of M_{412} (25).

The dissociation constant for the amino acid side chain is given by:

$$K_A = [H^+]\,[A^-]/[AH]$$

This results in the following equations (25):

$$[2]\quad pK_A = pH - \log\,[A^-]/[AH] = pH - \log C_1/C_2$$

where C_1 and C_2 are the constants given in eq. [1] corresponding to the concentrations or mole fractions of the chromophore near the deprotonated form (A^-) and the protonated form (AH) of the amino acid group. If tyrosine is assumed to be that titratable amino acid group, then C_1 and C_2 are the concentrations of the chromophore near the tyrosinate ion and tyrosine respectively. C_1 and C_2 can be determined from extrapolation at time $t = 0$ of the semilogarithmic plots of Fig. 2.

For the experiments performed in water without addition of salt, such a calculation yielded a value of about 9.6 (25) for the

pK_A of the amino acid controlling the formation of M_{412} (Table 2). This value is not very different from the pK_A of tyrosine.

For the medium containing KCl, at any given pH, the amplitude of the fast M_{412} component is more important than in a low salt solution. We expect the pK_A value calculated from eq. [2] to be smaller than those of Table 2. Indeed, Table 1 shows that eq. [2] yields a pK_A value around 8.9.

This is an unexpected result. It could be interpreted in two different ways: either another amino acid is controlling the appearance of M_{412} or something happened to tyrosine (or lysine) so that its pK_A is much lower in presence of KCl. The former possibility should be eliminated because the only amino acid with a pK_A remotely close to 8.9 is cysteine ($pK_A = 8.33$) and there is no cysteine in bacteriorhodopsin (32). Then how do we explain the decrease in pK_A of tyrosine? When the concentration of salt gets to be as high as 0.5 *M*, the ionic strength is not negligible and we have to take it into consideration when we calculate the pK_A of tyrosine. In eq. [2], we have used the absorbance change at 405 nm to estimate the concentrations of the fast and slow M_{412} components. Absorbance under these conditions of bR concentrations follows closely the Beer–Lambert equation and is directly proportional to the concentrations of M_{412}. But in our calculation for the pK_A of tyrosine we should use activities instead of concentrations. By using a pH meter for our pH measurements, we immediately get the activity of H^+. The activity coefficient of tyrosine should be close to 1 since it is a neutral species, but the activity coefficient of the tyrosinate ion depends on the ionic strength. For KCl, 0.5 *M*, the activity coefficient is 0.649 (33). The use of the Davies equation, as an alternate method to evaluate $\gamma_\pm$, yields a value of 0.750 when we take into account the ionic strength caused by KCl and the buffers.

We rewrite eq. [2] with the activity coefficient of the tyrosinate ion:

$$[3] \quad pK_A = pH - \log (C_1/C_2) - \log \gamma_{tyr^-}$$

We should subtract the value of $\log \gamma_{tyr^-}$ from the values calculated by eq. [2] to correct for the ionic strength of the solution. But, with the value of $\gamma_\pm$ found above (0.649), we can only increase the pK_A value to 9.0. In order to raise the pK_A value from 8.9 to 9.6, the activity coefficient of the tyrosinate ion should be around 0.2. Of course one has to be careful when using equilibrium constants and activity coefficients for a system such as bR, but it seems that we still need another explanation to account for the change in the pK_A of tyrosine.

This explanation is possibly found from the studies on deionized bR (34, 35). When the purple membrane is deionized on a cation exchange column or when it is washed first with >2 *N* NaCl followed by deionized water, its absorption maximum changes from 568 nm to about 600 nm. Elemental analysis shows that it contains no Ca^{2+} or Mg^{2+} ions while the native bR contains about 1 Ca^{2+} and 3 Mg^{2+} (35). Addition of salt to a suspension of the blue (deionized) membrane restores the 568 nm absorption maximum. What controls the change in absorption seems to be the cation, and any cation is capable of regenerating the purple color (34). However, when monovalent cations (e.g. K^+, Na^+, . . .) are used, subsequent dilution with deionized water reverses the effect, while Ca^{2+} or Mg^{2+}-restored purple membrane is not affected by dilution. Furthermore, a much higher concentration of K^+ or Na^+ is needed to obtain the purple color. This seems to indicate that Ca^{2+} or Mg^{2+} are tightly bound to the protein while monovalent cations are not. To change the absorption maximum of the retinal chromophore, the cations have to be in close proximity to it. These cations close to the chromophore may also be close to the tyrosine controlling the appearance of M_{412}. At low salt concentration (e.g. for bR suspensions in deionized water), the only cations close to the chromophore should be the tightly bound Ca^{2+} and Mg^{2+} ions. But in KCl, 0.5 *M* (or in a basal salt solution), some monovalent cations should also be near the chromophore and the presence of these additional positive charges might account for the lower pK_A calculated for tyrosine under these conditions.

TABLE 3. The values of $k_{M\,fast}$ and $k_{M\,slow}$ for M_{412} formation and k_{tyr} for tyrosinate formation obtained at each pH for bR suspended in a basal salt solution. $T = 22°C$

pH	$k_{M\,fast}$ ($10^4\ s^{-1}$)	$k_{M\,slow}$ ($10^4\ s^{-1}$)	k_{tyr} ($10^4\ s^{-1}$)	pK_A
7.0	6 ± 1 (0.19)	1.00 ± 0.03 (0.81)	0.70 ± 0.03	7.6
8.0	8 ± 3 (0.27)	1.05 ± 0.05 (0.73)	0.69 ± 0.02	8.4
8.2	9 ± 3 (0.33)	1.07 ± 0.05 (0.67)	0.70 ± 0.03	8.5
8.4	9 ± 3 (0.43)	1.12 ± 0.03 (0.57)	0.70 ± 0.05	8.5
8.5	9 ± 2 (0.46)	1.14 ± 0.06 (0.54)	0.77 ± 0.05	8.6
8.6	9 ± 1 (0.52)	1.14 ± 0.03 (0.48)	0.76 ± 0.01	8.6
8.8	14 ± 2 (0.60)	1.28 ± 0.07 (0.40)	0.78 ± 0.03	8.6
9.0	16 ± 5 (0.67)	1.34 ± 0.07 (0.33)	0.77 ± 0.05	8.7
9.2	17 ± 3 (0.71)	1.45 ± 0.05 (0.29)	0.8 ± 0.1	8.8
9.4	16 ± 2 (0.78)	1.56 ± 0.06 (0.22)	0.86 ± 0.09	8.8
9.6	18 ± 3 (0.85)	1.8 ± 0.2 (0.15)	0.82 ± 0.09	8.8

2. *In basal salt solution*

Table 3 shows the rate constants for the formation of M_{412} and the tyrosinate ion for the bR suspensions in a basal salt solution. When compared to the values of Table 1, all rate constants are smaller. It is clear that the rate constants are affected by the basal salt medium, but still the tyrosinate formation is slower than both components of the M_{412} appearance. There is no easy explanation for the slowing down of the rate constants, but it is interesting to note that vesicles loaded with and suspended in NaCl develop approximately twice the transmembrane electric potential found if KCl is present (36). So this change in the rate constants may have to do with the nature of the salts themselves.

The pK_A value of tyrosine calculated from eq. [2] is around 8.6. This value is lower than that determined in low salt or KCl solutions. This might be due to the presence of a much higher concentration of cations in the solution.

B. *Temperature studies*

1. *In KCl, 0.5* M

Table 4 shows the values for the different rate constants as a function of temperature. It also gives the corresponding activation energies. For the same experiment done in deionized water, the values were the following (25):

$$E_A(M_{412\,fast}) = 42 \pm 3 \text{ kJ/mol}$$

$$E_A(M_{412\,slow}) = 47 \pm 3 \text{ kJ/mol}$$

$$E_A(tyr^-) = 39 \pm \text{ kJ/mol}$$

Within experimental error, all these activation energies are the same whether KCl is present in the solution or not. In light of this fact, the difference in quantum yield of proton release in both mediums does not seem to have anything to do with the activation energy for the formation of M_{412}, in agreement with the small sensitivity of the rate constants to the presence of

TABLE 4. The values of $k_{M\,fast}$ and $k_{M\,slow}$ for M_{412} formation and k_{tyr} for tyrosinate formation obtained at each temperature for a bR suspension in a medium containing 0.5 *M* KCl. The activation energy of each transient at different pHs is also given

T (°C)	$k_{M\,fast}$ (10^4 s^{-1})	$k_{M\,slow}$ (10^4 s^{-1})	k_{tyr} (10^4 s^{-1})
25	15 ± 5	1.69 ± 0.04	0.91 ± 0.01
20	9 ± 2	1.17 ± 0.02	0.67 ± 0.02
15	12 ± 7	0.83 ± 0.02	0.51 ± 0.03
10	5 ± 1	0.58 ± 0.02	0.47 ± 0.07
5	3.7 ± 0.4	0.40 ± 0.02	0.32 ± 0.03
Activation energy (kJ/mol)			
No buffer	43 ± 9	50 ± 2	40 ± 2
pH = 8.5	44 ± 8	50 ± 1	44 ± 2
pH = 9.0	47 ± 7	51 ± 1	47 ± 2
pH = 9.6	53 ± 6	63 ± 2	51 ± 4

TABLE 5. The values of $k_{M\,fast}$ and $k_{M\,slow}$ for M_{412} formation and k_{tyr} for tyrosinate formation obtained at each temperature for a bR suspension in a basal salt solution. The activation energy of each transient at different pHs is also given

T (°C)	$k_{M\,fast}$ (10^4 s^{-1})	$k_{M\,slow}$ (10^4 s^{-1})	k_{tyr} (10^4 s^{-1})
25	6.5 ± 0.7	1.37 ± 0.06	0.71 ± 0.04
20	4.4 ± 0.4	0.96 ± 0.03	0.56 ± 0.07
15	3.8 ± 0.8	0.67 ± 0.02	0.42 ± 0.03
10	2.6 ± 0.4	0.45 ± 0.01	0.31 ± 0.03
5	2.1 ± 0.1	0.31 ± 0.01	0.24 ± 0.02
Activation energy (kJ/mol)			
No buffer	34 ± 3	51 ± 1	39 ± 3
pH = 7.0	38 ± 5	52 ± 1	42 ± 1
pH = 8.5	47 ± 6	53 ± 1	44 ± 2
pH = 9.0	38 ± 2	58 ± 1	45 ± 1

KCl.

We checked if increasing the pH has any effect on the activation energies. As can be seen in Table 4, all activation energies increase with increasing pH.

2. *In basal salt solution*

Table 5 gives the same information as Table 4, but for the basal salt medium. The activation energies for the slow M_{412} component and the tyrosinate ion are about the same as before. On the other hand, the fast M_{412} component has a lower activation energy than in the previous experiments. This decrease in activation energy is surprising. However, the rate constant of the fast M_{412} is the most affected by the basal salt solution; then it is not unexpected that the resulting activation energy will be more affected than the others. Since the quantum yield of proton release is the same in KCl, 0.5 *M*, and in a basal salt solution (27), once again the major change in activation energy of the fast M_{412} component does not appear to be directly correlated to the proton pumping mechanism.

A study of the variation of the activation energy as a function of pH shows that the activation energies increase with increasing pH, as was the case for the KCl solution.

Conclusions

Bacteriorhodopsin suspensions in three different media were studied. Two media contained the high salt concentration for which it is reported that 2 protons are pumped per M_{412} formed. When compared to the results for a lower salt concentration, some differences are observed, but nothing that really seems to account for the differences in the quantum yield of proton release. The following are the important observations.

1. In all solutions studied, the M_{412} formation is faster than the tyrosinate ion formation; also, the rate of deprotonation for tyrosine is found to be the same or slightly smaller in the presence of salts. Therefore, the change in the quantum yield of proton release cannot be correlated to changes in the rate of deprotonation of tyrosine.

2. At pH = 7.0, the total rate of deprotonation from the slow and the fast components is 2.6×10^4 s^{-1}, 2.0×10^4 s^{-1}, and 2.9×10^4 s^{-1} in KCl, basal salt, and low salt solutions respectively. It shows that the salt does not increase the overall rate of deprotonation for the protonated Schiff base at physiological pH.

3. The total rate of deprotonation for the protonated Schiff base can be calculated from Table 2 for low salt solutions. At pH = 7.0, this rate is 2.9×10^4 s^{-1} while at pH = 9.6, it is 10.5×10^4 s^{-1}. This shows that the rate increases as the pH increases. This behavior is opposite to the observed efficiency of proton pumping, which is better at lower pH (12, 37). Again, this argues against any correlation between the quantum efficiency of pumping and the kinetics of deprotonation of the protonated Schiff base.

4. At pH = 9.6, the total rate of deprotonation is *larger* in a salty solution than in a low salt solution. This rate is 15.3×10^4 s^{-1}, 15.6×10^4 s^{-1}, and 10.6×10^4 s^{-1} in KCl, basal salt, and low salt solutions respectively. This shows that the addition of salt increases the rate of deprotonation by about 50% at pH = 9.6, while it decreases at pH = 7.0.

5. At pH = 7.0, the relative amplitudes of the slow M_{412} component are 0.88, 0.81, and 0.88 in KCl, basal salt, and low salt solutions respectively. The rate constants for this component are 1.3×10^4 s^{-1}, 1.0×10^4 s^{-1}, and 1.3×10^4 s^{-1} in the same solutions. These results show that the slow component does not change in kinetic behavior, again suggesting that these rate parameters do not account for the increase in the proton pumping yield.

6. The pK_A value for the amino acid which is proposed to be responsible for the two M_{412} components (25) is found to have a much lower value in salty solutions than in low salt solutions. This is explained in part by the effect of the ionic strength of the solutions, but mostly by the probable presence of some cations near the retinal chromophore.

7. The relative amplitude of the fast component increases in the presence of salt. Since the proton pump is more efficient at low pHs (12, 37) and since the slow forming M_{412} is dominant at low pH, the increase in the fast M_{412} component observed as the salt concentration increases can hardly account for the change in the number of protons pumped per M_{412} formed.

8. In the absence of buffers, all activation energies in the three media seem to be about the same except for the fast M_{412} component in the basal salt solution. In this case the activation energy decreased significantly. Once again, this does not seem to greatly affect the proton pumping efficiency.

9. The fact that the salt does not increase the rate of deprotonation of the protonated Schiff base and tyrosine at pH = 7, but increases the yield of proton pumping, might lead to one or both of the following conclusions: (a) a fraction of the protons pumped out of the cell comes from acids that are not being monitored by our probes, or (b) the salt affects the rate of proton transport *after* the deprotonation of the protonated Schiff base and tyrosine. The latter could result from a change in the electrochemical potential or the structure of the part of the membrane involved in the proton pumping process.

10. The activation energies increase as a function of pH. This might account for part of the decrease in proton pumping efficiency as the pH increases.

11. A comparison is now made between the results we obtained for the M_{412} formation in a basal salt solution with the results for its decay in a similar medium (12). For both the decay and the rise of M_{412}, the amplitudes of the slow and fast components are equal at a pH of about 8.5, but at pH = 7.0 the fast component of the decay is more important than the fast component of the formation. Also, at constant pH, for the formation of M_{412}, we do not observe a radical change in the amplitudes of both components as a function of temperature. In the decay, at temperatures higher than 25°C, the fast component becomes more important than the slow component. There is no clear correlation between the two components of each process. However, one should remember that the amplitudes of the two components determined from the rise time give the relative amount of the L_{550} intermediate in the two sites. In the decay, the amplitudes of the fast and slow decaying components give the relative amounts of the M_{412} intermediates in the two sites. During the L_{550} to M_{412} transformation, other processes (25), e.g. $AH \rightleftharpoons A^- + H^+$ equilibration, salt movements, and protein conformational changes, could have taken place to change both the nature and the relative concentrations of the two sites.

Acknowledgements

This work was supported by the Department of Energy, Office of Basic Sciences. P. D. would like to thank the Natural Sciences and Engineering Research Council of Canada for a postdoctoral fellowship.

1. D. OESTERHELT and W. STOECKENIUS. Nature (London), New Biol. **233**, 149 (1971).
2. J. BRIDGEN and I. D. WALTER. Biochemistry, **15**, 792 (1976).
3. R. LOZIER, R. A. BOGOMOLNI, and W. STOECKENIUS. Biophys. J. **15**, 955 (1975).
4. W. STOECKENIUS, R. LOZIER, and R. A. BOGOMOLNI. Biochim. Biophys. Acta, **505**, 215 (1979).
5. R. HENDERSON. Ann. Rev. Biophys. Bioeng. **6**, 87 (1977).
6. B. HONIG. Ann. Rev. Phys. Chem. **29**, 31 (1978).
7. N. DENCHER and M. WILMS. Biophys. Struct. Mech. **1**, 259 (1975).
8. J. W. BELLIVEAU and J. K. LANYI. Arch. Biochem. Biophys. **178**, 308 (1977).
9. W. STOECKENIUS and R. A. BOGOMOLNI. Ann. Rev. Biochem. **51**, 587 (1982).
10. R. H. LOZIER, W. NIEDERBERGER, R. A. BOGOMOLNI, S.-B. HWANG, and W. STOECKENIUS. Biochem. Biophys. Acta, **440**, 545 (1976).
11. D. R. ORT and W. W. PARSON. J. Biol. Chem. **253**, 6158 (1978).
12. Q.-q. LI, R. GOVINDJEE, and T. G. EBREY. Proc. Natl. Acad. Sci. U.S.A. **81**, 7079 (1984).
13. A. LEWIS, J. SPOONHOWER, R. A. BOGOMOLNI, R. H. LOZIER, and W. STOECKENIUS. Proc. Natl. Acad. Sci. U.S.A. **71**, 4462 (1974).
14. M. MARCUS and A. LEWIS. Science, **195**, 1328 (1977).
15. B. ATON, A. DOUKAS, R. H. CALLENDER, B. BECHER, and T. G. EBREY. Biochemistry, **16**, 2995 (1977).
16. M. BRAIMAN and R. MATHIES. Biochemistry, **19**, 5421 (1980).
17. K. BAGLEY, G. DOLLINGER, L. EISENSTEIN, K. SINGH, and L. ZIMANYI. Proc. Natl. Acad. Sci. U.S.A. **79**, 4972 (1982).
18. O. KALISKY, M. OTTOLENGHI, B. HONIG, and R. KORENSTEIN. Biochemistry, **20**, 649 (1981).
19. V. ROSENBACH, R. GOLDBERG, C. GILON, and M. OTTOLENGHI. Photochem. Photobiol. **36**, 197 (1982).
20. T. KONISHI and L. PACKER. FEBS Lett. **92**, 1 (1978).
21. P. SCHERRER, L. PACKER, and S. SELTZER. Arch. Biochem. Biophys. **212**, 589 (1981).
22. H.-D. LEMKE and D. OESTERHELT. Eur. J. Biochem. **115**, 595 (1981).
23. E. LAM, S. SELTZER, T. KATSURA, and L. PACKER. Arch. Biochem. Biophys. **227**, 321 (1983).
24. P. SCHERRER and W. STOECKENIUS. Biochemistry. In press.
25. J. H. HANAMOTO, P. DUPUIS, and M. A. EL-SAYED. Proc. Natl. Acad. Sci. U.S.A. **81**, 7083 (1984).
26. D. R. ORT and W. W. PARSON. Biophys. J. **25**, 341 (1979).
27. R. GOVINDJEE, T. G. EBREY, and A. R. CROFTS. Biophys. J. **30**, 231 (1980).
28. D. OESTERHELT and W. STOECKENIUS. Methods Enzymol. **31** 667 (1974).
29. B. BECHER and J. Y. CASSIM. Prep. Biochem. **5**, 161 (1975).
30. D. KUSCHMITZ and B. HESS. FEBS Lett. **138**, 137 (1982).
31. B. HESS and D. KUSCHMITZ. FEBS Lett. **100**, 334 (1979).
32. H. G. KHORANA, G. E. GERBER, W. C. HERLIHY, C. P. GRAY, R. J. ANDEREGG, K. NIHEI, and K. BIEMANN. Proc. Natl. Acad. Sci. U.S.A. **76**, 5046 (1979).
33. R. C. WEAST (*Editor*). Handbook of chemistry and physics, 60th ed. CRC Press, Inc., Boca Raton. 1979–1980. p. D-169.
34. Y. KIMURA, A. IKEGAMI, and W. STOECKENIUS. Photochem. Photobiol. **40**, 641 (1984).
35. J. G. CHEN, C.-H. CHANG, R. GOVINDJEE, and T. EBREY. Biophys. J. **45**, 214a (1984).
36. J. K. LANYI, S. L. HELGERSON, and M. P. SILVERMAN. Arch. Biochem. Biophys. **193**, 329 (1979).
37. M. RENARD and M. DELMELLE. Biophys. J. **32**, 993 (1980).

Hydrogen sulphide – halogen complexes studied by matrix isolation vibrational spectroscopy

U. P. AGARWAL,[1] A. J. BARNES, AND W. J. ORVILLE-THOMAS
Department of Chemistry and Applied Chemistry, University of Salford, Salford M5 4WT, U.K.

Received July 27, 1984

This paper is dedicated to Professor Camille Sandorfy on the occasion of his 65th birthday

U. P. AGARWAL, A. J. BARNES, and W. J. ORVILLE-THOMAS. Can. J. Chem. **63**, 1705 (1985).

Infrared spectra are reported of mixtures of hydrogen sulphide with chlorine or bromine in low-temperature argon or nitrogen matrices. The $H_2S \ldots Cl_2$ and $H_2S \ldots Br_2$ complexes were identified from the perturbed halogen stretching vibration. Absorptions due to the corresponding hydrogen halides provided evidence that reaction was occurring between the hydrogen sulphide and halogen (despite the use of a twin-jet deposition), and other reaction products were tentatively identified from the observed absorptions.

U. P. AGARWAL, A. J. BARNES et W. J. ORVILLE-THOMAS. Can. J. Chem. **63**, 1705 (1985).

Opérant à basses températures et dans des matrices d'argon ou d'azote, on a déterminé les spectres infrarouges de mélanges de sulfure d'hydrogène avec du chlore ou du brome. On a identifié les complexes $H_2S \ldots Cl_2$ et $H_2S \ldots Br_2$ en se basant sur la perturbation de la vibration d'élongation de l'halogène. Des absorptions dues aux halogénures d'hydrogène correspondants suggèrent qu'il se produit une réaction entre le sulfure d'hydrogène et les halogènes (en dépit du fait que les produits ont été déposés à l'aide de deux jets séparés); en se basant sur les absorptions observées, on a pu identifier d'autres produits de réactions sur une base préliminaire.

[Traduit par le journal]

Introduction

Charge transfer complexes have been extensively studied in liquid solutions using a variety of techniques. However, vibrational spectra obtained from such solutions may be due to 1:2, 2:1, or even larger complexes, rather than the simple 1:1 complex. Matrix isolation spectroscopy provides a method of studying 1:1 complexes free from interactions with other donor or acceptor molecules (1). The technique also enables the study of interactions between molecules which react together under normal conditions, providing information about the structure of the reaction intermediate.

A number of halogen complexes have been studied in low-temperature matrices by infrared and uv/visible absorption spectroscopies (2–9) and also by Raman spectroscopy (10). The systems studied include the water–halogen complexes (2, 4) but the corresponding hydrogen sulphide complexes have not previously been reported. Hydrogen sulphide is known to react with chlorine or bromine, leading to the formation of a number of products (11). It was thus of interest to investigate the interaction between hydrogen sulphide and halogens using matrix isolation spectroscopy. Mixtures of hydrogen sulphide with chlorine or bromine in matrices were found to exhibit similar behaviour, whereas mixtures of hydrogen sulphide with iodine gave complicated spectra arising from a variety of reaction products (with no evidence for the presence of an $H_2S \ldots I_2$ complex). The present paper is thus confined to the interaction of hydrogen sulphide with chlorine and bromine.

Experimental

Since chlorine or bromine reacts rapidly with hydrogen sulphide at room temperature in the gas phase, matrix samples were prepared by simultaneous deposition of twin jets of hydrogen sulphide/matrix gas and halogen/matrix gas mixtures onto a cold caesium iodide window. The window was maintained at ca. 15 K using an Air Products Displex closed-cycle refrigerator. Infrared spectra (3000–200 cm^{-1}) were recorded using a Perkin-Elmer 225 spectrophotometer.

Hydrogen sulphide (Matheson) was dried over P_2O_5 before use. Chlorine and bromine were each degassed under vacuum. The matrix gases used were high purity argon and nitrogen, which were further dried by being passed through a liquid nitrogen cold trap. The matrix and solute gases were mixed in the desired proportions using standard manometric techniques.

Results

A number of spectra were recorded of mixtures of hydrogen sulphide with chlorine or bromine in argon or nitrogen matrices with an overall matrix:solute ratio of ca. 100 and an hydrogen sulphide:halogen ratio of ca. 1:1 or 1:2. Typical spectra are illustrated in Figs. 1 and 2, and the absorptions observed are listed in Tables 1 and 2. Little variation was found between the various spectra recorded, with the exception of changes in the relative intensities of the hydrogen sulphide monomer, dimer, and multimer bands. These were readily identified by comparison with previous studies of hydrogen sulphide in argon and nitrogen matrices (12–14).

As an aid to identification of the hydrogen sulphide – halogen complex absorptions, spectra were also recorded of water–chlorine and dimethyl sulphide – chlorine mixtures in argon matrices. The water–chlorine complex gave an absorption at 535 and 525 cm^{-1} (with the intensity ratio, 3:2, expected for $^{35}Cl_2$:$^{35}Cl^{37}Cl$ isotopic splitting) in good agreement with the previously reported value of 535.5 and 528.2 cm^{-1} in a nitrogen matrix (4). Dimethyl sulphide – chlorine mixtures were studied since, unlike hydrogen sulphide – chlorine mixtures, reaction cannot occur. An absorption due to the dimethyl sulphide – chlorine complex was observed at ca. 525 cm^{-1}.

Discussion

Hydrogen sulphide – halogen complexes

For hydrogen sulphide – chlorine mixtures, the strong bands at 518 and 510 cm^{-1} in an argon matrix and at 507 cm^{-1} in a nitrogen matrix are readily assigned to the chlorine stretching vibration of the hydrogen sulphide – chlorine complex. The doublet in the argon matrix is clearly due to isotopic splitting, which is only partially resolved in the nitrogen matrix. The

[1] Present address: The Institute of Paper Chemistry, Appleton, WI 54912, U.S.A.

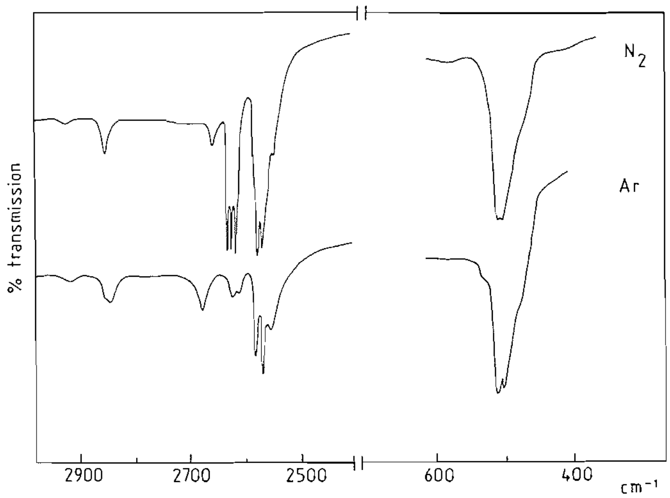

FIG. 1. Infrared spectra of hydrogen sulphide – chlorine mixtures in argon and nitrogen matrices.

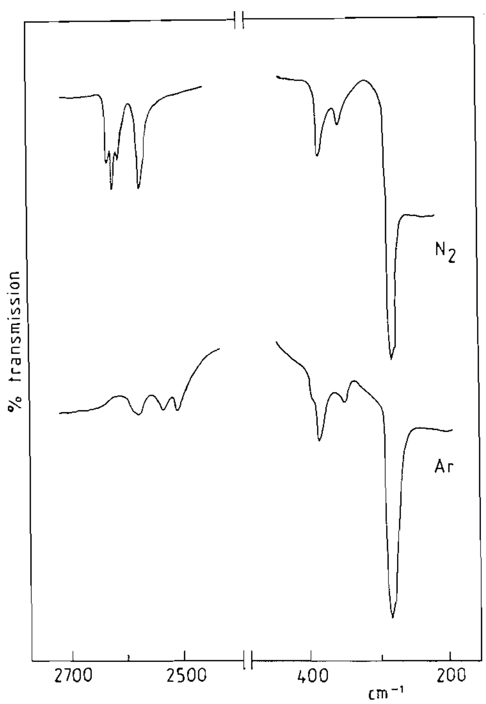

FIG. 2. Infrared spectra of hydrogen sulphide – bromine mixtures in argon and nitrogen matrices.

wavenumber of the chlorine stretching vibration is similar to that in the dimethyl sulphide – chlorine complex and in line with the general trend of other chlorine complexes (Table 3). The strength of the complex is rather greater than that with water, but much lower than that with ammonia. There were no additional bands in the hydrogen sulphide stretching region which could be attributed to the complexed hydrogen sulphide molecule.

Hydrogen sulphide – bromine mixtures exhibit a prominent band at 285 cm^{-1} in argon matrices and at 280 cm^{-1} in nitrogen matrices. This is clearly due to the bromine stretching mode of the hydrogen sulphide – bromine complex, and is again in line with the bromine stretching frequencies of related complexes (Table 3). As for the corresponding chlorine complex, no

TABLE 1. Bands observed (cm^{-1}) for hydrogen sulphide – chlorine mixtures trapped in low-temperature matrices

Ar matrix	N_2 matrix	Assignment
2920	2925	(?)
	2854	HCl monomer
2845		HCl
2674	2660	H_2S . . . HCl complex
	2632	H_2S monomer ν_3
2625	2625	H_2S dimer ν_{3a}
	2619	H_2S monomer ν_1
2616		H_2S dimer ν_{1a}
2583	2580	H_2S dimer ν_{1d}
2569	2572	H_2S multimer
2555	2560	H_2S multimer
518	507	H_2S . . . $^{35}Cl_2$ complex
510		H_2S . . . $^{35}Cl^{37}Cl$ complex
485 (sh)	470 (sh)	HSCl(?)

TABLE 2. Bands observed (cm^{-1}) for hydrogen sulphide – bromine mixtures trapped in low-temperature matrices

Ar matrix	N_2 matrix	Assignment
	2630	H_2S monomer ν_3
	2618	H_2S monomer ν_1
2583		H_2S dimer
	2570	H_2S multimer
2532		HBr
2508		HBr
400 (sh)		
385	385	HSBr(?)
355	355	BrSSBr ν_{as} (S—Br)
285	280	H_2S . . . Br_2 complex

perturbed hydrogen sulphide stretching vibrations could be identified.

Reaction products

Although a twin-jet deposition technique was used to obtain the hydrogen sulphide – halogen matrices, a number of other absorptions were apparent in the spectra which must be due to reaction products. Mixtures of hydrogen sulphide and chlorine in the gas or liquid phase react to give sulphur or sulphur chlorides (11):

$$Cl_2 + H_2S \rightarrow 2HCl + S$$

$$2Cl_2 + H_2S \rightarrow 2HCl + SCl_2$$

$$3Cl_2 + 2H_2S \rightarrow 4HCl + S_2Cl_2$$

Thiohypochlorous acid is proposed as an intermediate in the production of polysulphide species:

$$Cl_2 + H_2S \rightarrow HCl + HSCl$$

$$HSCl + H_2S \rightarrow HCl + H_2S_2$$

$$HSCl + H_2S_2 \rightarrow HCl + H_2S_3$$

etc.

Thiohypohalous acid species have not been isolated, although the hypohalous acids have been identified in low-temperature matrices (15).

The hydrogen sulphide – chlorine mixtures exhibited absorptions in the HCl stretching region, in particular a band at 2674

TABLE 3. Comparison of X—X stretching frequencies (cm^{-1}) of various electron donor – halogen complexes in argon matrices

Complex	$^{35}Cl_2$	Br_2	Reference
X_2	549	318	10
$H_2C{=}O \ldots X_2$	542		8
$H_2O \ldots X_2$	535		*a*
$C_6H_6 \ldots X_2$	532[b]	306[b]	6
$C_2H_4 \ldots X_2$	526	307	10
$Me_2S \ldots X_2$	525		*a*
$H_2S \ldots X_2$	518	285	*a*
$C_2Me_4 \ldots X_2$	464	263	10
$H_3N \ldots X_2$	460[b]		7

[a]This work.
[b]N_2 matrix.

cm^{-1} in argon matrices and 2660 cm^{-1} in nitrogen matrices which can be identified as the hydrogen sulphide – hydrogen chloride complex (16). Other weak bands in the region are probably due to isolated HCl or the chlorine – hydrogen chloride complex. Hydrogen sulphide – bromine mixtures in argon matrices exhibited weak absorptions in the HBr stretching region, although these did not correspond with previously reported HBr monomer or aggregate band positions (17). Possibly they are due to the bromine – hydrogen bromide complex. The hydrogen sulphide – hydrogen bromide complex (16) was not observed in these mixtures.

The presence of hydrogen halides in the matrices implies that other reaction products must also be present. In the hydrogen sulphide – chlorine mixtures, the only evidence of such species was a shoulder, at ca. 485 cm^{-1} (argon) or 470 cm^{-1} (nitrogen), on the low frequency side of the $H_2S \ldots Cl_2$ complex absorption. This does not correspond to the S—Cl stretching vibration of any reported sulphur–chlorine species. In particular, SCl_2 absorbs at ca. 520 cm^{-1} (18) and S_2Cl_2 at ca. 450 cm^{-1} (19). We attribute it tentatively to the S—Cl stretching mode of thiohypochlorous acid.

In the hydrogen sulphide – bromine mixtures, well-defined bands were observed in the S—Br stretching region at 385 and 355 cm^{-1}. The latter absorption corresponds approximately with the reported position of the SBr stretching modes of the S_2Br_2 molecule (19). We tentatively attribute the 385 cm^{-1} absorption to the S—Br stretching mode of thiohypobromous acid. However, the vibrational spectrum of SBr_2 has not been reported; conceivably the 385 cm^{-1} band could be due to this species.

Conclusions

Infrared spectra of mixtures of hydrogen sulphide and chlorine or bromine trapped in low-temperature matrices have shown that the hydrogen sulphide and halogen molecules interact to form a molecular complex $H_2S \ldots X_2$. This is presumably an intermediate in the reaction

$$H_2S + X_2 \rightarrow HX + HSX$$

Stable products can then be formed by reactions such as

$$HSX + X_2 \rightarrow HX + SX_2$$

$$HSX + SX_2 \rightarrow HX + S_2X_2$$

etc.

Acknowledgements

One of us (U.P.A.) wishes to thank the Leverhulme Trust for the award of a Leverhulme Visiting Fellowship. P. J. Walkden is thanked for technical assistance.

1. A. J. BARNES. *In* Molecular interactions. Vol. 1. *Edited by* H. Ratajczak and W. J. Orville-Thomas. Wiley. 1980. Chapt. 9, p. 273.
2. L. FREDIN. Chem. Script. **4**, 97 (1973).
3. L. FREDIN and B. NELANDER. J. Mol. Struct. **16**, 205 (1973).
4. L. FREDIN and B. NELANDER. J. Mol. Struct. **16**, 217 (1973).
5. L. FREDIN and B. NELANDER. J. Am. Chem. Soc. **96**, 1672 (1974).
6. L. FREDIN and B. NELANDER. Mol. Phys. **27**, 885 (1974).
7. G. RIBBEGARD. Chem. Phys. Lett. **25**, 333 (1974).
8. B. NELANDER. J. Mol. Struct. **69**, 59 (1980).
9. H. FREI, L. FREDIN, and G. C. PIMENTEL. J. Chem. Phys. **74**, 397 (1981).
10. S. HOLROYD, A. J. BARNES, S. SUZUKI, and W. J. ORVILLE-THOMAS. J. Raman Spectrosc. **12**, 162 (1982).
11. M. SCHMIDT and W. SIEBERT. *In* Comprehensive inorganic chemistry. Vol. 2. *Edited by* J. C. Bailar, H. J. Emeleus, R. Nyholm, and A. F. Trotman-Dickenson. Pergamon. 1973. p. 830 and references therein.
12. A. J. TURSI and E. R. NIXON. J. Chem. Phys. **53**, 518 (1970).
13. A. J. BARNES, H. E. HALLAM, and J. D. R. HOWELLS. J. Chem. Soc. Faraday Trans. 2, **68**, 737 (1972).
14. S.-Y. TANG and C. W. BROWN. J. Raman Spectrosc. **2**, 209 (1974).
15. I. SCHWAGER and A. ARKELL. J. Am. Chem. Soc. **89**, 6006 (1967).
16. A. J. BARNES and M. P. WRIGHT. To be published.
17. A. J. BARNES, H. E. HALLAM, and G. F. SCRIMSHAW. Trans. Faraday Soc. **65**, 3150 (1969); **65**, 3159 (1969).
18. D. BIELEFELDT and H. WILLNER. Spectrochim. Acta, Part A, **36**, 989 (1980).
19. M. FEUERHAHN and G. VAHL. Chem. Phys. Lett. **65**, 322 (1979).

Vibrational spectra and rotational isomerism of ethanethiol and ethanethiol-D_1

HANS WOLFF AND JERZY SZYDLOWSKI[1]

Physikalisch-chemisches Institut, Universität Heidelberg, D-69 Heidelberg, Federal Republic of Germany

Received August 6, 1984

This paper is dedicated to Professor Camille Sandorfy on the occasion of his 65th birthday

HANS WOLFF and JERZY SZYDLOWSKI. Can. J. Chem. **63**, 1708 (1985).

The infrared spectra of gaseous, liquid, and solid C_2H_5SD, and the Raman spectrum of the liquid compound are analyzed and the corresponding spectra of C_2H_5SH were reinvestigated under improved conditions. In the deuterated compound the CH_2 rocking vibration does not interact with the SD bending vibration and therefore does not split into vibrations of the conformers. The measurements suggest for gaseous and liquid C_2H_5SH and C_2H_5SD the simultaneous presence of the *trans* and *gauche* conformers, appearing at room temperature in the ratio of the order of 1:3. In analogy to solid C_2H_5SH, the exclusive presence of the *gauche* conformers can be inferred for solid C_2H_5SD. The spectra reported in the literature for the C_2H_5SH molecules embedded in matrices at low temperatures permit a similar interpretation. The doublet structure observed for the vibrational bands, not only of pure solid C_2H_5SH and C_2H_5SD but also of their solid mixtures, may be due to non-equivalent sites of the unit cell.

HANS WOLFF et JERZY SZYDLOWSKI. Can. J. Chem. **63**, 1708 (1985).

On a analysé les spectres infrarouges du C_2H_5SD dans les états gazeux, liquide et solide, le spectre Raman du composé liquide ainsi que les spectres correspondants du C_2H_5SH qui ont été réexaminés dans des conditions améliorées. Dans le composé deutéré, la vibration de rocking du CH_2 n'interfère pas avec la vibration de déformation du SD; elle ne se sépare donc pas en vibrations des conformères. Dans les composés C_2H_5SH et C_2H_5SD gazeux ou liquides, les mesures à la température ambiante suggèrent que les conformères gauche et trans existent simultanément dans des rapports de 1:3. Par analogie avec les résultats obtenus avec la C_2H_5SH, on peut suggérer que le C_2H_5SD à l'état solide existe exclusivement sous la conformation gauche. Sur la base des spectres rapportés dans la littérature pour des molécules de C_2H_5SH imbriquées dans des matrices à basses températures, on peut proposer une interprétation semblable. La présence de doublets qui ont été observés dans les bandes vibrationnelles, non seulement du C_2H_5SH et du C_2H_5SD purs à l'état solide mais aussi dans leurs mélanges solides, pourrait être due à des sites qui ne sont pas équivalents dans la maille unitaire.

[Traduit par le journal]

A. Introduction and measurements

For ethanethiol one *trans* form and two equivalent *gauche* forms are to be considered. The manifestation of these forms in the vibrational spectra has been studied in low temperature infrared spectra including those of matrices and especially in infrared and Raman spectra in the range of torsional transitions (1−7). Some of these investigations have also been performed for C_2H_5SD. However, there has been no systematic infrared study of the deuterated compound. To fill in the blanks and to expand the investigations on rotational isomerism of ethanethiol, the infrared spectra of gaseous, liquid, and solid C_2H_5SD were measured. In addition, the Raman gas spectra known from the measurements of Durig *et al.* (7) were supplemented by determining the Raman liquid spectra. Further, the infrared spectra of crystallized mixtures of C_2H_5SH and C_2H_5SD were recorded. They were analyzed together with those of C_2H_5SH which in part were reinvestigated under improved conditions.

The infrared measurements were carried out with the Perkin-Elmer 225 spectrometer by using conventional methods for obtaining the gas and liquid spectra, and the method of Wagner and Hornig (8) for the solid phase spectra. The Raman liquid spectra were recorded with the Coderg PH 1 spectrometer with excitation with the 6328 Å line of the helium−neon laser. C_2H_5SH and C_2H_5SD were the highly purified products which had been utilized for the determination of the vapour pressure isotope effect of the two compounds (9).

B. Results and discussion

1. Gaseous compounds

Considering the relevant features of the spectra in Fig. 1, the infrared spectra of gaseous C_2H_5SD in the range of the SD stretching and bending vibrations are compared with the corresponding spectra of C_2H_5SH (measured wave numbers in Table 1). The spectra of C_2H_5SD show similar splittings as those of C_2H_5SH, as do in part the Raman spectra of the gaseous compounds (7). From the intensities of the Q-branches the high-frequency component of the doublets of the stretching vibrations is estimated to be markedly weaker than the low-frequency component. Relating the splitting to the presence of the conformers and considering the explanation which states the *gauche* forms are the dominant conformers in the gaseous state (2, 5, 7) (see below), it can be supposed that the high-frequency component belongs to the *trans* form. The low-frequency component, which is separated from the high-frequency satellite by 9 cm^{-1} for C_2H_5SH and by 6 cm^{-1} for C_2H_5SD, corresponds to the *gauche* forms.

For the purpose of comparison with C_2H_5SD, Fig. 2*a* represents the infrared spectrum obtained in the range of the CH_2 rocking vibration for gaseous C_2H_5SH. The spectrum shows in addition to the more intense band at 735 cm^{-1}, a less intense one at about 780 cm^{-1}. Smith, Devlin, and Scott (2) observed this splitting for liquid and glassy C_2H_5SH, and explained it by the assumption that the rocking vibration of the *gauche* forms is shifted to the wave number of 735 cm^{-1} owing to interaction with the SH bending vibration appearing at 875 cm^{-1}. The interaction does not occur with the rocking vibration of the *trans* form at 780 cm^{-1}, as that conformer belongs to the point group C_s and its rocking and bending vibrations are of different symmetry. With this in mind, the higher intensity of the band at 735 cm^{-1} confirms that the *gauche* forms are the dominant conformers in the gaseous state at room temperature. The missing of the band at 780 cm^{-1} in the Raman gas spectra (7) suggests an insufficient Raman activity.

[1]Permanent address: Department of Chemistry, University of Warsaw, Warsaw, Poland.

TABLE 1. Infrared (IR) and Raman (R) frequencies observed for the fundamentals of gaseous ethanethiol and of gaseous, liquid, and solid ethanethiol-D_1 (cm^{-1})[a]

C_2H_5SH	C_2H_5SD				
IR gas	IR gas	IR liquid	R liquid	IR solid	Approximate assignment
2989 vs, gt	2989 vs, gt	2978 vs, gt		2981 2975 vs, g	CH_3, CH_2 stretching vibrations
2972 vs, gt	2972 vs, gt	2966 vs, gt	2966 sh, gt	2963 2959 vs, g	
2942 vs, gt	2941 vs, gt	2930 vs, gt	2931 vs, gt	2932 2927 vs, g	
2887 vs, gt	2884 s, gt	2871 s, gt	2874 m, gt	2866 m, g	
2600 m, t? 2591 m, g?	1889 w, t? 1883 w, g?	1860 w, gt?	1872 vs, gt?	1849 1836 vs, g[b]	SH (SD) stretching vibration
1457 vs, gt	1456 s, gt	1452 s, gt	1449 s, gt	1464 1460 1455 1452 m, g	CH_3, CH_2 bending vibrations
	1451 s, gt	1444 s, gt		1444 1442 vs, g	
				1430 1425 m, g	
1382 s, gt	1382 m, gt	1377 s, gt	1387 w, gt	1374 w, g 1371 s, g	
1277 vs, gt	1275 vs, gt	1268 vs, gt	1277 m, gt	1287 vw, g 1280 w, g 1271 s, g	CH_2 wagging
1255 ?, gt	1253 ?, gt		1254 w, gt	1252 s, g 1248 m, g	CH_2 twisting
1101 m, gt	1072 w, gt	1066 m, gt	1073 vs, gt	1069 1065 m, g	CH_3 rocking
	1048 w, gt		1060 m, gt	1051 m, g	CH_3 rocking
969 m, gt	974 m, gt	972 s, gt	981 m, gt	970 s, g	CC stretching
879 w 874 w g[c] 871 m	625 vw 619 vw gt 614 vw	614 w, gt	633 m, gt	619 613 m, g	SH (SD) bending
782 w, t 735 w, g	785 m, gt	783 s, gt	786 vw, g	789 780 s, g	CH_2 rocking
663 m, gt	677 m, gt	670 m, gt	660 vs, gt	672 670 m, g	CS stretching
317 vw, gt	327 vw, gt	327 vw, gt	335 s, gt	333 m, g	CCS bending
				254 m, g[d]	CH_3 torsion
				237 m, g	SD torsion
				203 s, g	

[a]Abbreviations: w weak, m middle, s strong, sh shoulder, v very, g *gauche*, t *trans*; gt indicates that presumably both conformers contribute to the measured frequency; however, the *gauche* forms contribute more.

[b]The SH stretching vibrations measured for crystallized C_2H_5SH are 2544 and 2527 cm^{-1} (vs).

[c]SH bending vibration of the *trans* form of gaseous C_2H_5SH, being expected at 830–835 cm^{-1} (see text), may be unobserved not only because of the presence of this conformer in the ratio of merely 1:3, but also because of lower activity.

[d]CH_3 torsion of crystallized C_2H_5SH is found at 261 cm^{-1} (m).

Figure 3*a*, representing the infrared spectrum of gaseous C_2H_5SD, shows no band at 735 cm^{-1}, but one at the wave number 780 cm^{-1} at which in the infrared spectrum of C_2H_5SH the rocking vibration of the *trans* form is found. This wave number is therefore chosen for the rocking vibration of the *trans* form of C_2H_5SD and, as to be seen in the following, also for the vibration of the *gauche* forms.

The rocking vibration of the *gauche* forms of C_2H_5SH is observed on the low-frequency side of the vibration of the *trans* form. The rocking vibration of the *gauche* forms of C_2H_5SD should occur on the high-frequency side, if it would interact with the bending vibration of the sulfhydryl group appearing for the deuterated compound at 620 cm^{-1}. However, such a satellite is not observed. Assuming the rocking vibration of the *gauche* forms to occur near that of the *trans* form, the frequency distance from the bending vibration with 160 cm^{-1} is obviously too large. The corresponding distance for C_2H_5SH is only 40–50 cm^{-1} with the calculation based on the values of 780–785 and 830–835 cm^{-1} for the unperturbed vibrations.

2. *Liquids*

In the Raman gas spectra where the band at 780 cm^{-1} was not observed, a band at 696 cm^{-1} had been assigned to the rocking vibration of the *gauche* forms of C_2H_5SD. However, as stated in the preceding paragraph, the approximate coincidence of the rocking vibrations of the different conformers of C_2H_5SD near 780 cm^{-1} is suggested by observation of a weak band in the Raman spectrum of the liquid compound at 786 cm^{-1}. Because of the inactivity of the rocking vibration of the *trans* form, this band can only be assigned to the *gauche* forms. This assign-

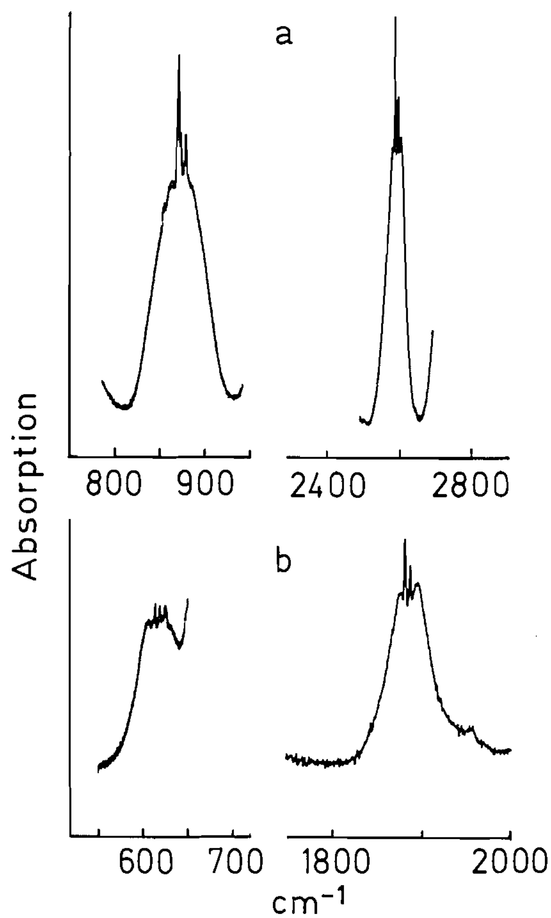

FIG. 1. (a) Splitting of the SH stretching and bending vibrations in the infrared spectrum of gaseous C_2H_5SH; (b) splitting of the SD stretching and bending vibrations in the infrared spectrum of gaseous C_2H_5SD.

ment is supported by the observation that the corresponding band of C_2H_5SH appears at 740 cm^{-1} (2) and, in agreement with the interpretation of the infrared spectra, belongs to the *gauche* forms vibration, which is shifted due to the interaction.

From the infrared spectrum of liquid C_2H_5SH reproduced in Fig. 2b, I_{trans}/I_{gauche}, the ratio of the integrated intensities of the two rocking bands, is determined to be about 1:3.2. Excluding a greater intensity change of the rocking vibration due to the interaction with the bending vibration, the ratio of the quantities of the *trans* and the *gauche* conformers present in the liquid at room temperature is therefore of the order of 1:3.

Under these circumstances the enthalpy difference between the two conformers of C_2H_5SH is obtained from

$$[1]\quad \Delta H = R\frac{T_1T_2}{T_2 - T_1}\ln\left[(I_{gauche}/I_{trans})_{T_1}/(I_{gauche}/I_{trans})_{T_2}\right]$$

where $(I_{trans}/I_{gauche})_{T_1}$ and $(I_{trans}/I_{gauche})_{T_2}$ are the ratios of the integrated intensities at the temperatures T_1 and T_2, and R is the universal gas constant. In addition to the value for I_{trans}/I_{gauche} from the spectrum of the liquid at the measuring temperature of 300–320 K, the value from the spectrum of the glass at liquid nitrogen temperature (Fig. 2c) is used for the calculation, considering the latter spectrum as that of the liquid at liquid nitrogen temperature. The average result for ΔH of somewhat more than 1400 J mol^{-1} is in the order of that of 1300 J mol^{-1} derived from thermodynamic measurements and agrees with the assumption of the gauche forms as the more stable conformers (2, 7).

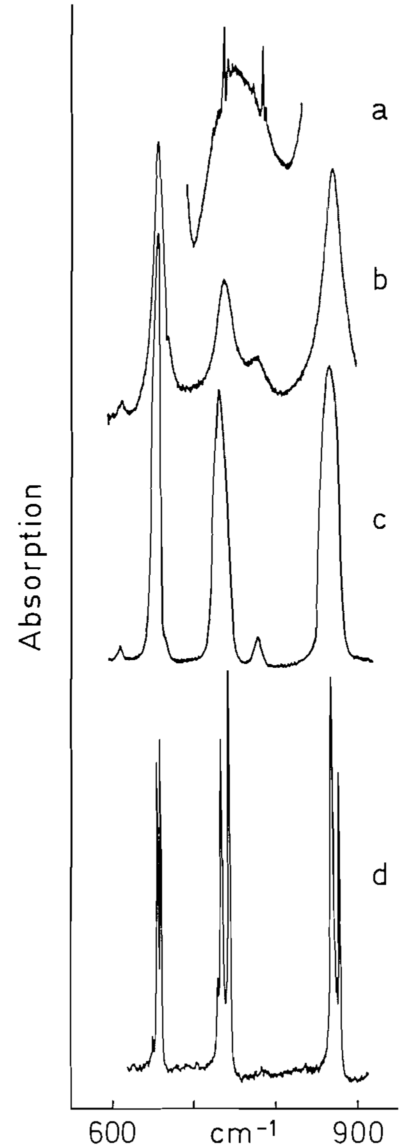

FIG. 2. Infrared absorption in the region of the CH_2 rocking vibration of (a) gaseous C_2H_5SH (350 Torr), (b) liquid C_2H_5SH (path length 0.025 mm), (c) and (d) glassy and solid C_2H_5SH at liquid nitrogen temperature.

The ratio I_{trans}/I_{gauche} for the gas at room temperature is similar to that of the liquid, and there is probably no large difference between the rotational isomerism of C_2H_5SH and C_2H_5SD. The above results for the liquid are therefore approximately valid also for the gas, and the results for C_2H_5SH also nearly for C_2H_5SD.

3. *Solids*

Like gaseous and liquid C_2H_5SD, the solid compound shows for the CH_2 rocking vibration merely the absorption at 780 cm^{-1} (Fig. 3c), while the band of solid C_2H_5SH appears at 735 cm^{-1} (2) (Fig. 2d). Assuming similar behaviour of C_2H_5SH and C_2H_5SD with regard to the rotational isomerism, however, unlike gaseous and liquid C_2H_5SD, the absorption of the solid compound can be solely assigned to the *gauche* conformers. In solid C_2H_5SH only these forms remain from the different conformers of the gaseous and of the liquid compound

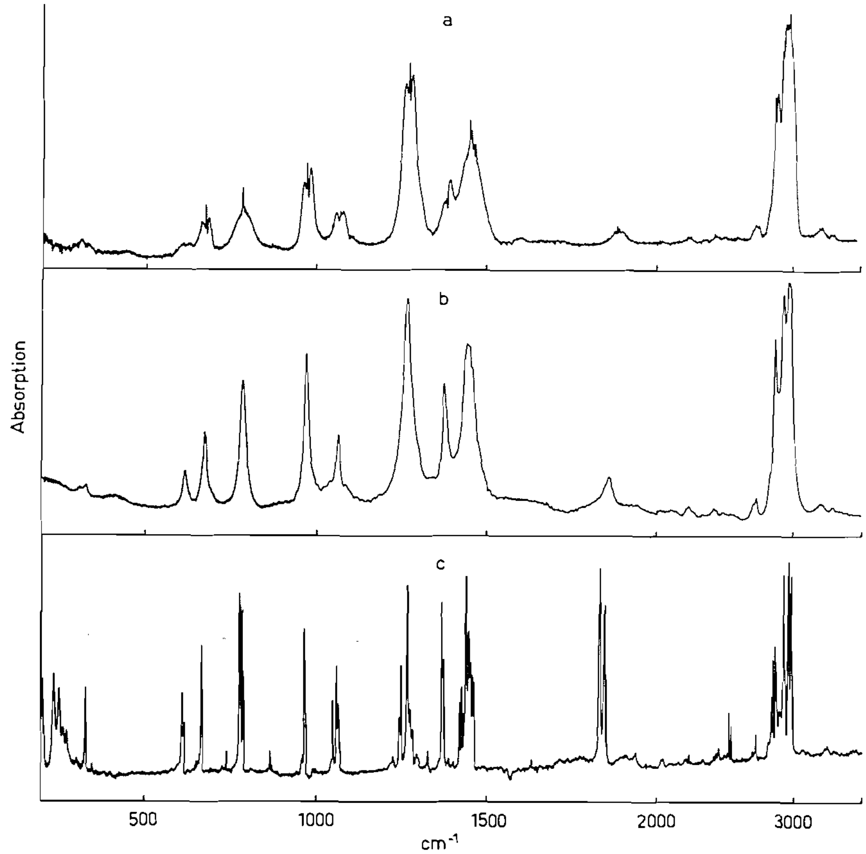

FIG. 3. Infrared spectra of (*a*) gaseous, (*b*) liquid, (*c*) solid C_2H_5SD.

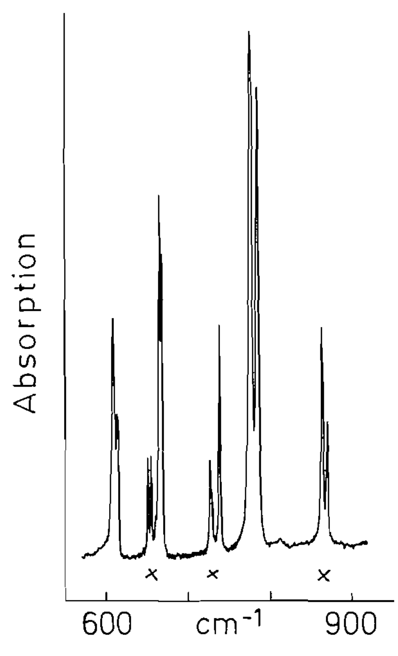

FIG. 4. Infrared bands of CS stretching, CH_2 rocking, and SH bending vibrations of C_2H_5SH in a solid mixture with C_2H_5SD (1:10). The doublets appearing for the vibrations of C_2H_5SH are indicated by crosses.

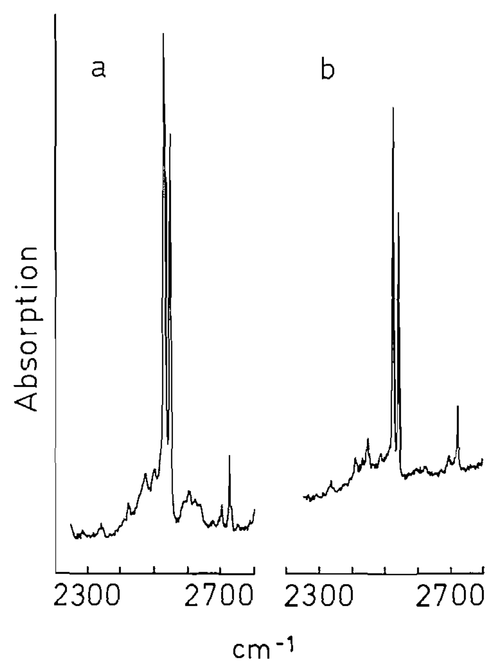

FIG. 5. Infrared band of the SH stretching vibration in (*a*) pure solid C_2H_5SH, (*b*) a solid mixture of C_2H_5SH with C_2H_5SD (1:10).

(2) (Fig. 2*a*–*d*).

Also, like the bands of solid C_2H_5SH (2), the band at 780 cm^{-1} and most other vibration bands of solid C_2H_5SD are split into mainly two components. In the spectra of the solid mixtures of C_2H_5SH and C_2H_5SD the doublets remain nearly uninfluenced by the isotopic dilution. This is shown in Fig. 4 in comparison with Fig. 2*d* for the CS stretching, for the CH_2 rocking, and for the SH bending vibration bands and in Fig. 5 for the SH stretching vibration band of C_2H_5SH. The intensity ratios of the doublet components are only insignificantly changed with the isotopic dilution, and the wave numbers of the doublets of the pure solid and of the solid mixture are nearly the same; they are in the sequence of the listed vibrations 659/656 and 658/654 cm^{-1}, 743/733 and 742/731 cm^{-1}, 877/868 and 874/868 cm^{-1}, and 2544/2527 and 2546/2530 cm^{-1}. The splittings may therefore arise from non-equivalent sites of the unit cell. Then separate frequencies corresponding to the different sites can be expected on isotopic dilution even for non-degenerate vibrations (10, 11).

In the infrared spectra obtained from C_2H_5SH on high dilution in an argon matrix, and analogously in other matrices, Barnes, Hallam, and Howells (4) found a doublet at 731.0 and 732.8 cm^{-1}, but no absorption at 780 cm^{-1}. Considering the intensity ratio of the doublet components and assuming that the equilibrium at room temperature is frozen out in the matrix, the authors assigned only the low-frequency component to the rocking vibration of the *gauche* conformers, but the high-frequency component to that of the *trans* conformer. One would, however, expect that with transition to 20 K merely the association equilibrium at room temperature freezes out and the equilibrium of rotational isomers at the low temperature is largely adjusted. Therefore, both doublet components may be assigned to the *gauche* conformers in agreement with the preceding explanations, the splitting of only 1.8 cm^{-1} (compared to 10 cm^{-1} in the pure solid) being due to matrix or other effects. The CH_2 rocking vibration of matrix-isolated C_2H_5SD has not been measured. Unlike the matrix isolation value of C_2H_5SH, but similar to the vibration of gaseous, liquid, and solid C_2H_5SD, it can however be expected to appear near 780 cm^{-1}.

The frequency shifts in the solids relative to the gases amount to 60−75 cm^{-1} for the SH and to 40−50 cm^{-1} for the SD stretching vibrations. The shift in the liquid compounds are not much greater than half of the values for the solids. The low magnitude of these shifts corresponds to the results of investigations on hydrogen bonding of other thiols and indicates the weakness of the H or D bonds of these compounds (4, 12). It is further to be noticed that in reasonable relation to the frequencies measured for the methyl torsion vibrations of gaseous C_2H_5SH and C_2H_5SD (7) the values of 261 and 254 cm^{-1} are found for the crystallized compounds. All other assignments can be taken from Table 1, or from the former investigations (2, 4, 7).

C. Conclusions

It is evident from the infrared investigation of C_2H_5SD that the conditions for interaction of the CH_2 rocking vibration with the bending vibration of the sulfhydryl group are satisfied for the *gauche* conformers of C_2H_5SH but not of C_2H_5SD. The observation of a single band for the rocking vibration of gaseous and liquid C_2H_5SD therefore supports the explanation for the splitting of C_2H_5SH through the interaction to which only the vibrations of the *gauche* conformers are subjected. The rocking vibration of the *trans* form is Raman-inactive, but the different wave numbers for the vibration of the *gauche* forms in the Raman spectra of C_2H_5SH and C_2H_5SD agree with the interpretation. The infrared intensities of the components of the rocking vibration of C_2H_5SH reveal for the gaseous and the liquid compounds at room temperature the appearance of the *trans* form and of the *gauche* forms in the ratio of about 1:3. In reasonable relation to other measurements and calculations a value of the order of 1400 J mol^{-1} results from the intensities of the rocking bands of C_2H_5SH for the enthalpy difference of the two forms. Analogously to C_2H_5SH, the exclusive appearance of the *gauche* conformers can be inferred for solid C_2H_5SD. The spectra reported in literature for the ethanethiol molecules embedded in matrices at low temperatures permit a similar interpretation. The doublet structure of the vibrational bands of the solids even on isotopic dilution most likely arises from non-equivalent sites of the unit cell.

Acknowledgements

We gratefully acknowledge support of this work by the Deutsche Forschungsgemeinschaft, Bad Godesberg, by the Fonds der Chemie, Frankfurt, and by BASF, Ludwigshafen. J. S. expresses his gratitude to Deutscher Akademischer Austauschdienst for financial support.

1. N. SHEPPARD. J. Chem. Phys. **17**, 79 (1949).
2. D. SMITH, J. P. DEVLIN, and D. W. SCOTT. J. Mol. Spectrosc. **25**, 174 (1968).
3. D. W. SCOTT and G. A. CROWDER. J. Mol. Spectrosc. **26**, 477 (1968).
4. A. J. BARNES, H. E. HALLAM, and J. D. R. HOWELLS. J. Chem. Soc. Faraday Trans. II, **68**, 736 (1972).
5. F. INAGAKI, I. HARADA, and T. SHIMANOUCHI. J. Mol. Spectrosc. **46**, 381 (1973).
6. A. S. MANOCHI, W. G. FATELEY, and T. SHIMANOUCHI. J. Phys. Chem. **77**, 1977 (1973).
7. J. R. DURIG, E. BUCY, C. J. WURREY, and L. A. CARREIRA. J. Phys. Chem. **79**, 988 (1975).
8. E. L. WAGNER and D. F. HORNIG. J. Chem. Phys. **18**, 296 (1950).
9. J. SZYDLOWSKI and H. WOLFF. Can. J. Chem. **57**, 1350 (1979).
10. S. KRIMM. Infrared spectroscopy and molecular structure. *Edited by* M. Davies. Elsevier Publishing Company, London. 1963. p. 270.
11. J. C. DECIUS and R. M. HEXTER. Molecular vibrations in crystals. McGraw-Hill Inc., New York. 1977. Chapt. 7.
12. R. BICCA DE ALENCASTRO and C. SANDORFY. Can. J. Chem. **50**, 3594 (1972) and references therein.

Fourier transform infrared study on black soap films

JUNZO UMEMURA, MUTSUO MATSUMOTO, TAKESHI KAWAI, AND TOHRU TAKENAKA
Institute for Chemical Research, Kyoto University, Uji, Kyoto-fu 611, Japan

Received August 10, 1984

This paper is dedicated to Professor Camille Sandorfy on the occasion of his 65th birthday

JUNZO UMEMURA, MUTSUO MATSUMOTO, TAKESHI KAWAI, and TOHRU TAKENAKA. Can. J. Chem. **63**, 1713 (1985).

Fourier transform infrared (FT-IR) spectra in the range 3800–2800 cm^{-1} have been recorded of the first and second black films in air prepared from aqueous solutions of sodium dodecylsulfate (SDS) without and with the addition of sodium chloride, respectively. It is found that in both films the methylene chains of SDS, which are located outside the aqueous core of the sandwich structure, are in an oriented liquid crystalline state. In a first black film, the thickness of the aqueous core is determined to be 9.6 nm, by recording polarized infrared spectra with various angles of incidence to the film surface, and by analyzing them with the aid of thin layer optics. It is found that this value varies in the range 5 ~ 10 nm from film to film. The extinction coefficients of the aqueous core are also examined. In the second black film, the thickness of the aqueous core is found to be about 1 nm. The OH stretching band of water in the second black film appears at appreciably higher wavenumbers (by 60 cm^{-1}) than those of the first black film, indicating a high ionic strength in the aqueous core. In both black films, there is no sign of molecular orientation or rigidified structure of water.

JUNZO UMEMURA, MUTSUO MATSUMOTO, TAKESHI KAWAI et TOHRU TAKENAKA. Can. J. Chem. **63**, 1713 (1985).

On a enregistré les spectres infrarouges par transformation de Fourier dans la région de 3800 à 2800 cm^{-1} des premier et deuxième films noirs dans l'air préparés à partir de solutions aqueuses de dodécylsulfate de sodium (DSS) respectivement avec et sans chlorure de sodium. On a trouvé que dans chacun de ces films, les chaînes méthylènes du DSS, qui sont situées à l'extérieur du noyeau aqueux de la structure en sandwiche, sont dans un état cristallin liquide orienté. En enregistrant les spectres infrarouges polarisés sous divers angles d'incidence par rapport à la surface du film et en les analysant à l'aide de principes d'optique pour les couches minces, on a évalué que l'épaisseur du noyeau aqueux du premier film noir est égale à 9,6 nm. On a trouvé que cette valeur varie de 5 à 10 nm suivant le film. On a aussi examiné les coefficients d'extinction des noyeaux aqueux. Dans le deuxième film noir, on a trouvé que l'épaisseur du noyeau aqueux est égale à 1 nm. Par rapport au premier film noir, la bande de vibration OH de l'eau du deuxième film noir se trouve à des nombres d'onde beaucoup plus élevés (environ 60 cm^{-1}); ce résultat indiquerait la présence d'une force ionique élevée dans le noyeau aqueux. Dans les deux films noirs, il n'existe aucun signe d'orientation moléculaire ou de structure rigidifiée de l'eau.

[Traduit par le journal]

Introduction

By withdrawing a metal frame from soap solution to air through the interface, a single planar foam film can be easily prepared. At equilibrium, such a film is sufficiently thin (4–50 nm) to appear black by reflected light. Thus, the film is called "black soap film" or "black foam film" (1). The black soap film takes the sandwich structure consisting of a thin sheet of aqueous solution (aqueous core) enclosed by two surface monolayers of soap molecules. Such black films in air have been of great interest for centuries (1), because they provide easily formed, geometrically well-defined model systems for investigating the stability of foams. The black film is also a good model to study surface forces of the London-dispersion type (2) or of electrical double layers (3). Besides, black soap films in air have striking similarities, in various aspects, with bimolecular (black) lipid membranes in aqueous solution (4). Thus, the investigation of black soap films is closely related to the understanding of biological membranes.

Hitherto, the experimental methods used for studying the black soap films are limited to radioactive-tracer (5, 6), optical reflectance (7, 8), light scattering (9), X-ray diffraction (10, 11) techniques, and so on. Modern spectroscopic techniques such as infrared or nuclear magnetic resonance spectroscopy are principally expected to provide valuable structural informations on these films. In reality, however, these techniques have suffered from their poor detection limits, because of the minute amount of constituents in thin soap films. For example, the infrared spectra of multiple sheets of black soap films obtained by using a dispersion type instrument with a PbS detector (7) could only give a very rough estimate of the thickness of the aqueous core, whose accuracy is crucial to the theoretical investigation of the surface forces.

On the other hand, the innovation of the Fourier transform infrared (FT-IR) technique has enormously improved the detection limit of infrared measurements, and has made it possible to investigate the systems interesting to colloid and interface scientists, such as aqueous micellar solutions (12, 13), multibilayer lipid membranes in aqueous media (14, 15), Langmuir-Blodgett monomolecular film (16), and trace amounts of oriented water in a liquid crystalline matrix (17).

In the present work, the FT-IR technique has been applied to the study of black films in air prepared from aqueous solutions of sodium *n*-dodecylsulfate (SDS). Without the addition of inorganic electrolyte, the SDS solution at room temperature provides the "first black" film, whose equilibrium thickness is believed to be performed by a balance between van der Waals attraction and electrostatic double-layer repulsion (1). By adding a sufficient amount of inorganic electrolyte like NaCl, the SDS solution provides the "second black" film of about 4.4 nm (18). Both first and second black films have been investigated here with polarized infrared radiation to see the state and orientation of the surfactant and water molecules in the films.

Experimental

SDS (purity >99%) and NaCl (purity >99.9%) were purcased from Nakarai Cemicals, Ltd., Kyoto, Japan. Doubly distilled water was used for the preparation of aqueous solutions. The sample cell adopted in this experiment is illustrated in Fig. 1. The main cell body (75 mm internal diameter and 100 mm high) is made of polymethylmethacrylate. The rectangular frame of 51 mm wide and 38 mm high, which is made of a 1.2 mm ϕ platinum wire, was used to support soap films. In order to prepare the soap film, the frame was once dipped

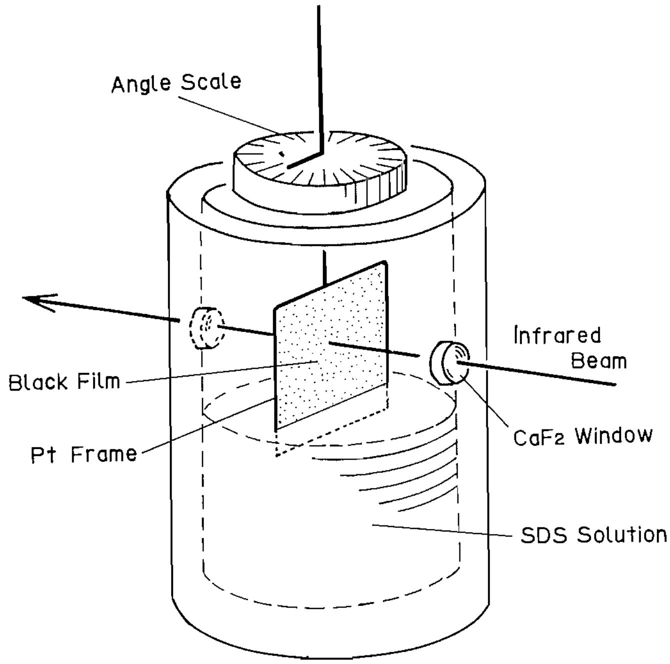

FIG. 1. Sample cell for FT-IR measurements of black films.

into the aqueous solution with SDS concentration larger than the critical micellization concentration (80 mM, ref. 19), and then it was slowly lifted up to air. The frame can be rotated around its center axis so that the angle of incidence of infrared radiation can be changed freely. The infrared radiation passed through the soap film and two CaF_2 windows (8 mm diameter) on the cell wall. In the case of normal incidence to the film surface, the spot of the infrared beam on the film was as small as about 0.5 mm ϕ. To achieve the equilibrium of temperature and vapor pressure inside the cell, prior to the withdrawal of the film, the cell was placed overnight in the sample compartment of the FT-IR spectrophotometer set in a temperature-controlled room, with a continuous supply of infrared radiation. Under these conditions, the temperature inside the cell was 29°C. Then the film was lifted up from the solution and was subjected to infrared measurements.

Infrared spectra were recorded on a Nicolet 6000 FT-IR spectrophotometer equipped with an InSb detector. Typically, 500 to 2000 interferograms collected with the maximum optical retardation of 0.25 cm were coadded, apodized with a Happ-Genzel function, and Fourier transformed with one-level of zero-filling to yield spectra of high S/N ratio with a resolution of 4 cm^{-1}. Polarization measurements were performed by using a wire-grid polarizer with AgBr substrate. Special attention was paid to the cancellation of the infrared bands due to atmospheric water and a slight amount of frost formed upon the detector surface. The latter is inevitable to commercial detectors cooled by liquid nitrogen. Since the amount of frost changes with time, the back ground spectra were recorded before and after a series of measurements for one film. Then, the background spectrum corresponding to each sample spectrum was obtained by a time-weighted average of the above two spectra.

For numerical calculations and graphical plottings of the results, a Facom M-180 II AD computer of this institute was utilized.

Results and discussion

1. *First black film*

When the film is drawn from the aqueous SDS solution, or more precisely from the surface of the solution, its initial thickness is fairly large. However, the aqueous core of the film immediately starts to thin by drainage, and the black film is first formed at the top of the film. The area of the black part

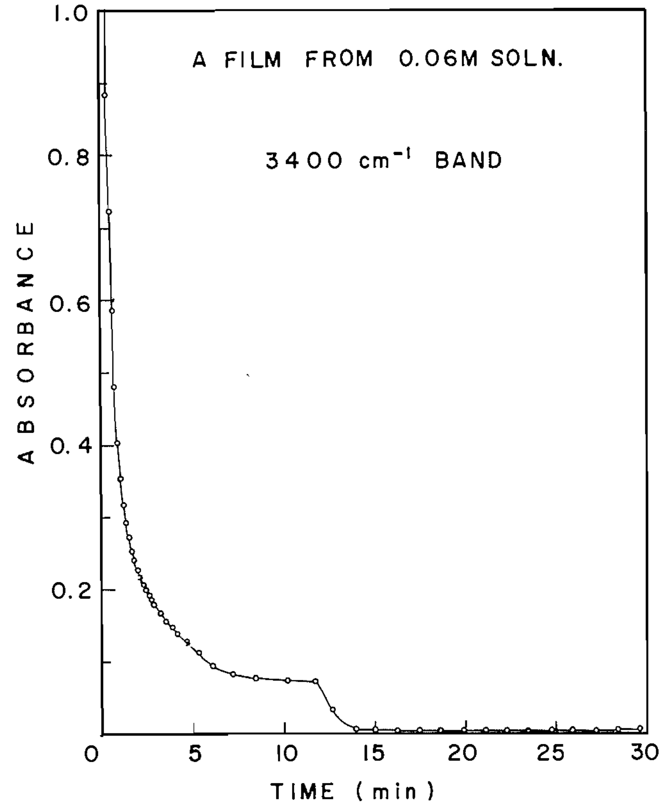

FIG. 2. Change in absorbance of water at 3400 cm^{-1} with time for a film drawn from 0.06 M aqueous solution of SDS.

gradually increases, the horizontal border between the black part and thicker part descending downwards. The feature of the thinning can be monitored by measuring the absorbance of the OH stretching band of water (3400 cm^{-1}) at a fixed position in the film. The typical result for the film drawn from the 0.06 M SDS solution is shown in Fig. 2, where each point represents the result of an accumulation of 10 scans. Within about 7 min, the absorbance becomes nearly constant at 0.075 which corresponds to a 88 nm thick aqueous core (see below for the evaluation of the thickness). At this stage, the film appears silvery. In 12 to 14 min, the part of the spot of the infrared beam becomes black, giving an absorbance of 0.0085. All of the film becomes black after 30 min. The infrared spectrum of this equilibrated black film is shown in Fig. 3*A*. The broad OH stretching band of water peaked at ~3400 cm^{-1} and weaker CH stretching bands of the methylene chain of SDS at 2960–2850 cm^{-1} are observed. The features of the 3400 cm^{-1} band (peak wavenumber, bandwidth, and contour) are very similar to those of bulk liquid water (20).

In Fig. 3*B* and *C*, the spectra of equilibrated black films obtained by different withdrawals from the same 0.06 M SDS solutions were also displayed. It is found from the absorbance of each film in Fig. 3*A–C* that the thickness of the outer SDS monolayers (monitored by the CH bands) are invariant in all the films, but the thickness of aqueous core (monitored by the water band) varies in each film. It is usually believed that the equilibrium thickness of the first black film is determined by the ionic strength in the aqueous core (18). However, the result in Fig. 3 indicates that the actual equilibrium thickness is also affected by the delicate difference in each experimental condition, such as that in minute quantities of surface-active impurities (1) which can be introduced by the dehydration of SDS

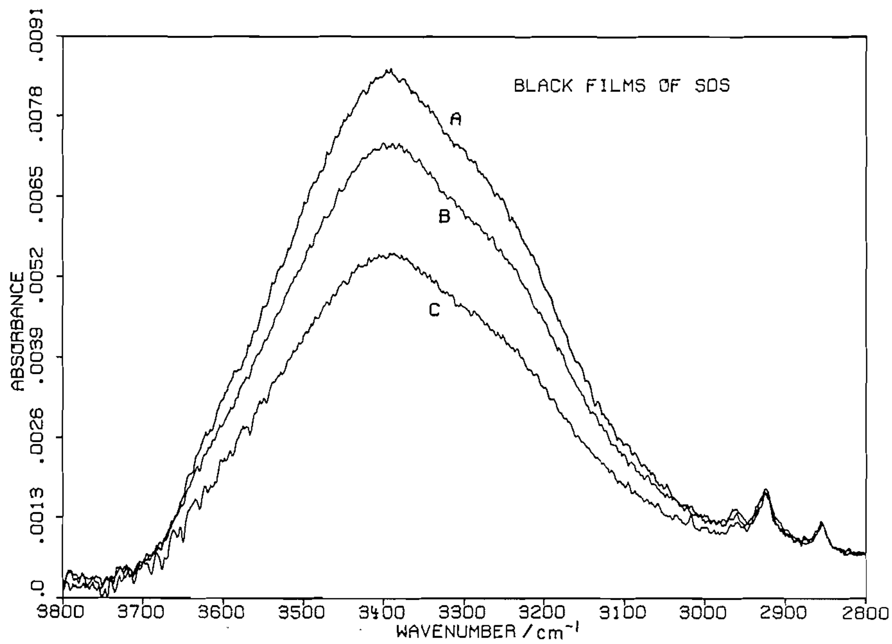

FIG. 3. Infrared spectra in the 3800–2800 cm^{-1} region of three different first black films drawn from 0.06 *M* aqueous solutions of SDS.

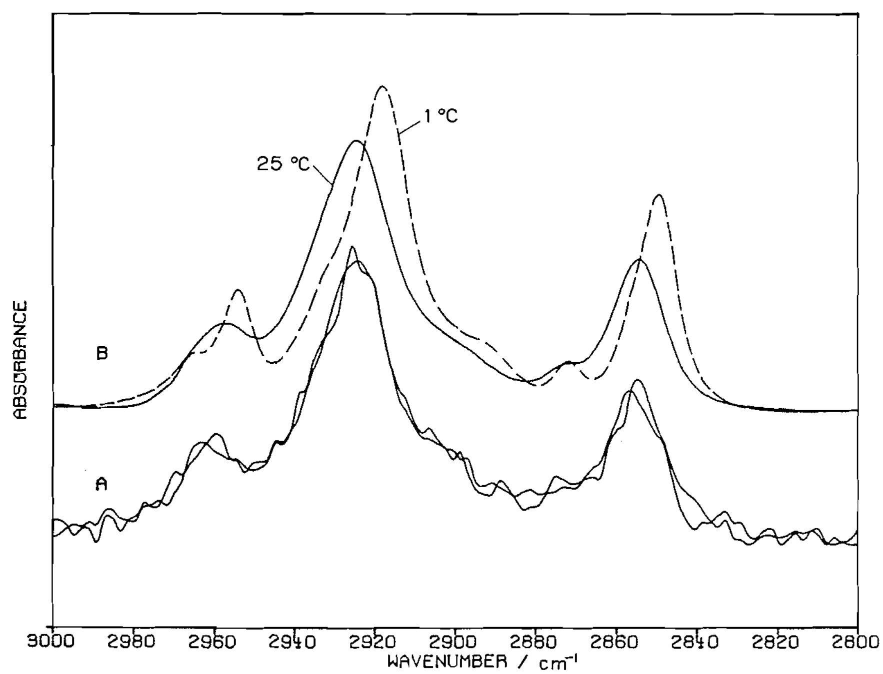

FIG. 4. Infrared spectra in the CH stretching region of SDS. *A*; Two different first black films drawn from 0.06 *M* aqueous solution. *B*; 1.5 *M* aqueous solution at 25°C (—, liquid crystalline phase) and at 1°C (- - -, coagel II phase). Ordinate scale has been normalized so that the intensities of corresponding bands are nearly the same in *A* and *B*.

(21). In the following sections, the state and orientation of the methylene chain in SDS and water will be examined mainly using the spectral data for the first black film of Fig. 3*A*, unless otherwise stated.

2. The CH stretching bands of SDS in first black films

Figure 4*A* shows two spectra in the CH stretching region recorded for different films. The reproducibility and noise level of spectra are apparent in this figure. Figure 4*B* reproduces spectra of 1.5 *M* aqueous solutions of SDS at 1 and 25°C, which are in the coagel II (hydrated crystalline) and liquid crystalline phases, respectively (22). By comparison of Fig. 4*A* and *B*, the methylene chain of SDS in the black film is easily identified as being in liquid crystalline state. This is rationalized by the following consideration. The occupied area per molecule in the SDS black film is thought to be about 0.52 nm^2/molecule (8, 23). This value is in good agreement with the reported value of 0.57 nm^2/molecule (24) for the SDS molecule in a liquid crystalline phase, and is much larger than the molecular cross section of 0.21 nm^2/molecule of a hydrated SDS crystal (25).

To investigate the orientation of the methylene chain of SDS,

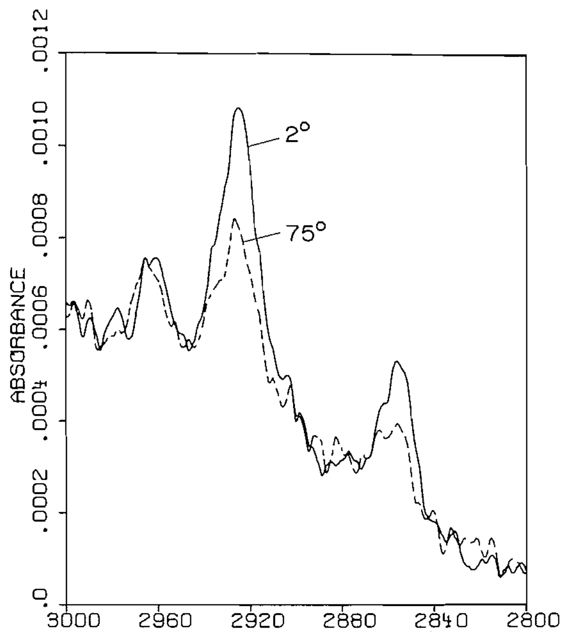

FIG. 5. Polarized infrared spectra in the CH stretching region of a first black film of SDS drawn from 0.06 *M* aqueous solution. Angles of incidence are 2° (—) and 75° (- - -) with electric vector parallel to the plane of incidence. Path lengths have been corrected for the oblique incidence.

the polarized infrared spectra of the film were recorded. First, it was ascertained by normal incidence of the polarized beam that there was no dichroism within the film surface. Then, the film was tilted around the center axis of the platinum frame, and the polarized beam with electric vector parallel to the plane of incidence was irradiated. To evaluate the angle of incidence, the infrared measurements were performed at various angles between −80° and +80°, and the angle 0° was obtained from the center of the symmetrical plot of various spectral parameters, such as peak wavenumber or intensity. This procedure made us read "normal" in the scale as 2°. The spectra at the angle of incidence of 2° and 75° are shown in Fig. 5. Here, the difference in path length has been corrected for the oblique incidence, by assuming the refractive index of SDS layer to be 1.4. Although the noise level is not small, the presence of the dichroism in the antisymmetric (2925 cm^{-1}) and symmetric (2854 cm^{-1}) CH_2 stretching bands is evident. The larger intensity in the 2° incidence reveals that the director of the methylene chains as an average tends to orient normal to the film surface. The dichroism for the asymmetric CH_3 stretching band at 2963 cm^{-1} does not seem to exist. This is reasonable if we consider that the methylene chain is in a liquid crystalline state.

3. Water bands in the first black film

To examine the orientation of water molecules in the film, the tilting method was also applied by using polarized infrared radiations with electric vector parallel to the plane of incidence. The result is given in Fig. 6. In this case, no correction has been made for the difference in path length. With increasing angle of incidence, the peak maximum shifts to higher wavenumbers. The peak intensity, on the other hand, first decreases and then increases. These results are not normally encountered for the well-resolved infrared band with a small absorptivity. Since the OH stretching band of water is believed to consist of many components (26, 27), the complexity in Fig. 6 seemed, at first, to be due to the presence of various dichroism depending on the components. However, for very intense bands as in this case, we have to be careful about distortions of band shapes due to reflection and interference effects at interfaces (28). Therefore, we tried to estimate these effects numerically. For thin layered films, Hansen has derived explicit formulas for the transmittance and reflectance (29). In this case, we consider a symmetric plane bounded system of five layers, that is, air/SDS/aqueous solution/SDS/air. For the *j*th layer, let us suppose that $\hat{n}_j$ is the complex refractive index, *i.e.*, $\hat{n}_j \equiv n_j + ik_j$, θ_j the

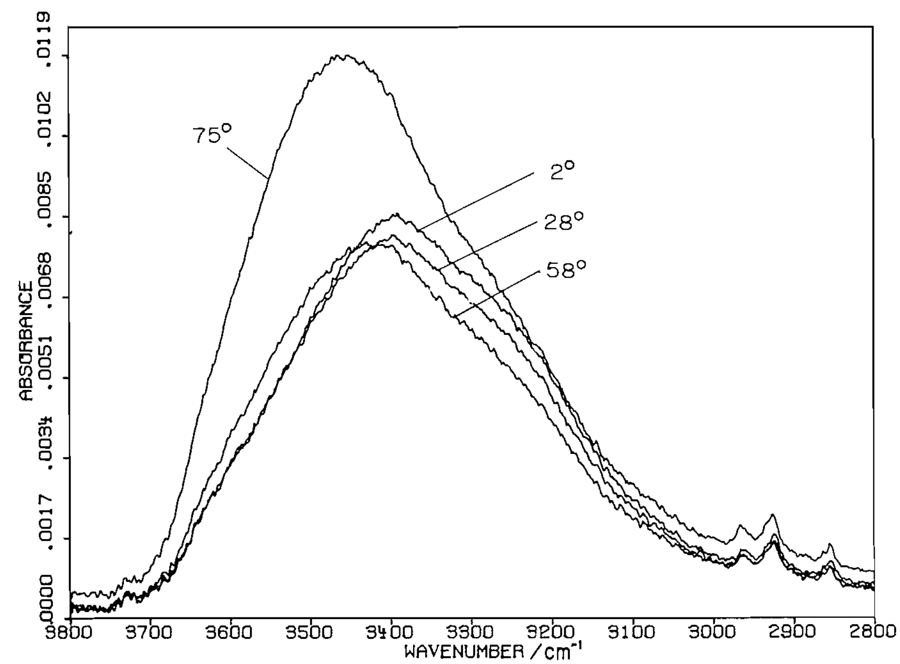

FIG. 6. Polarized infrared spectra of a first black film of SDS drawn from 0.06 *M* aqueous solution. The angles of incidence of polarized radiations with electric vector parallel to the plane of incidence are shown.

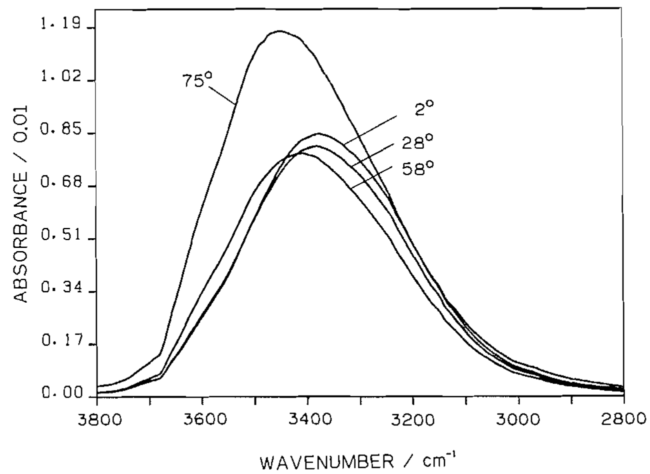

FIG. 7. Calculated absorbance curves in the OH stretching region of a first black film of SDS. The data correspond to the observed results shown in Fig. 6. In this calculation, $h_2 = h_4 = 1.1$ nm, $h_3 = 9.6$ nm, $\hat{n}_1 = \hat{n}_5 = 1$, $\hat{n}_2 = \hat{n}_4 = 1.4$, and $k(3400\ \text{cm}^{-1}) = 0.36$ are used.

angle of incidence or refraction, h_j the thickness, $q_j = \cos\theta_j/n_j$, ν the wavenumber of infrared radiation, and that $\beta_j = 2\pi\nu h_j\hat{n}_j \times \cos\theta_j$. If we make the usual assumption that the magnetic permeabilities of all the layers are unity, the transmittance of the system for the parallel polarization is expressed by (29)

$$[1]\quad T_p = \frac{Re(\cos\theta_5/\hat{n}_5)}{\cos\theta_1/n_1}\left|\frac{2q_1}{(m_{11}+m_{12})q_1+m_{21}+m_{22}q_5}\right|^2$$

where m_{kl} is the klth element of the matrix M characteristic of the total plane bounded system:

$$[2]\quad M = M_2M_3M_4$$

with

$$[3]\quad M_j = \begin{bmatrix} \cos\beta_j & -(i/q_j)\sin\beta_j \\ -iq_j\sin\beta_j & \cos\beta_j \end{bmatrix}$$

For the calculation, we assumed $\hat{n}_1 = \hat{n}_5 = 1$, $\hat{n}_2 = \hat{n}_4 = 1.4$, and $h_2 = h_4 = 1.1$ nm (estimated from the data in refs. 23 and 30). For the complex refractive index $\hat{n}_3(\nu)$ of water in the infrared region, we first adopted the data reported by Downing and Williams (31). However, it was not fully successful to reproduce the data in Fig. 6. The literature survey (32) shows that the values of the imaginary part k_3 (3400 cm^{-1}) of $\hat{n}_3$, *i.e.*, extinction coefficient of water at the 3400 cm^{-1} peak are widely distributed from 0.17 (33) to 0.92 (7), though the newly reported values converge into the range between 0.28 and 0.31 (20, 31, 34). Further, when ions are dissolved in water, the value is expected to change (35). Thus, in this calculation, we tried to calculate absorbance curves which give rise to the best fit to the experimental curves of Fig. 6, by changing both the $k_3(\nu)$ values of Downing and Williams by a constant factor and the thickness of the aqueous core, h_3. For the real part $n_3(\nu)$ of $\hat{n}_3$, we used the data of Downing and Williams (31). The final calculated results are demonstrated in Fig. 7. The experimental curves are surprisingly well reproduced for all angles of incidence examined. Thus, we have $h_3 = 9.6$ nm and k_3 (3400 cm^{-1}) = 0.36 as the converged values. The latter value means that the constant factor is 1.28. From the inspection of calculated data, the accuracy of these values is estimated to be better than a few percent. The change in the $\hat{n}_2$ value between 1.35 and 1.45 and that in the h_2 value between 0.85 (8) and 1.7 nm (24) had little effect on the calculated absorbances.

In this calculation, we used the optical parameters of unoriented bulk water. Thus it can be said that the water in the aqueous core between the two SDS monolayers does not show any specific orientation or structure formation.

4. *Second black films*

The second black film was produced by adding 0.35 M NaCl to the 0.01 M aqueous solution of SDS. The spectrum of the equilibrated second black film is illustrated in Fig. 8*A*, being

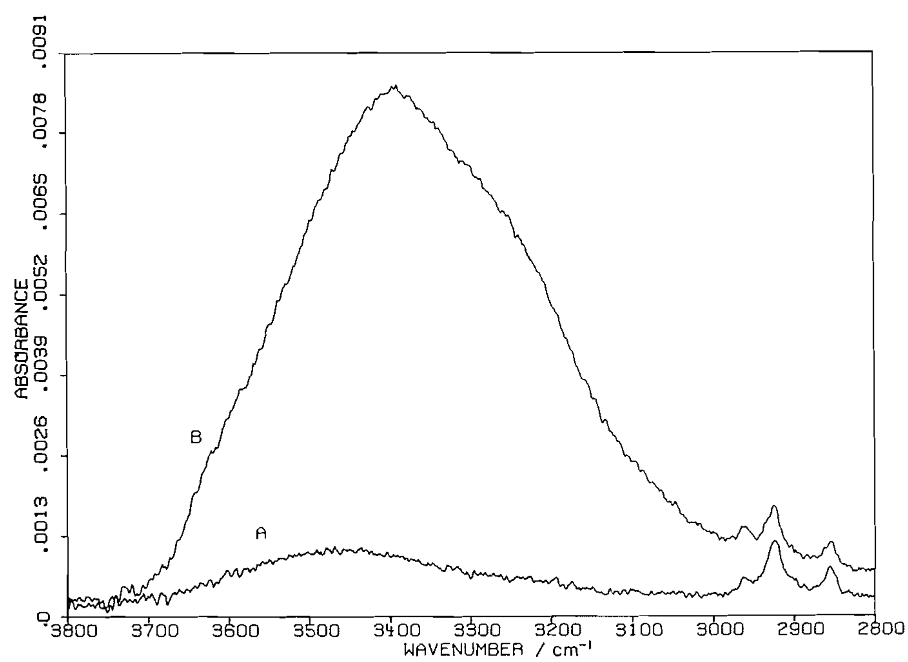

FIG. 8. Infrared spectra of a second black film (A) drawn from 0.01 M SDS solution + 0.35 M NaCl, compared with that of the first black film (B) drawn from 0.06 M SDS solution.

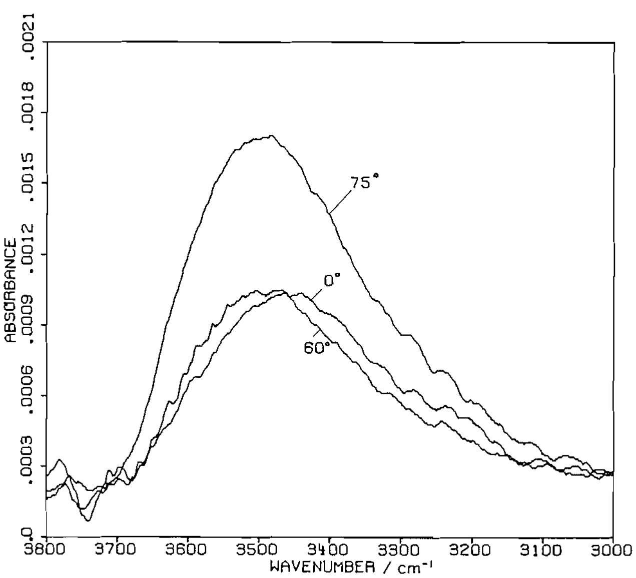

FIG. 9. Polarized infrared spectra of a second black film drawn from 0.01 M SDS solution + 0.35 M NaCl. The angles of incidence for polarized radiations with electric vector parallel to the plane of incidence are shown.

compared with that of the first black film from 0.06 M SDS solution (Fig. 8*B*). The intensity of the CH stretching bands in the second black film is almost the same as that of the first black film, suggesting that the thickness of the SDS layers are identical in both cases. However, the intensity of the water band in the second black film is about one-tenth of that of the first black film. This leads us to a conclusion that the thickness of the aqueous core is about 1 nm, considering that the absorptivities of both films are nearly the same (35). Adding this value to the SDS bilayer thickness of 2.2 nm (see above), we have the total film thickness of 3.2 nm. This is a little less than the reported value of 4.4 nm (18).

Furthermore, the peak wavenumber of the second black film is about 60 cm^{-1} higher than that of the first black film. Addition of 0.35 M NaCl to the bulk aqueous solution of SDS may result in a small wavenumber shift of a few cm^{-1} (35, 36). Thus, the large higher wavenumber shift of the second black film in Fig. 8*A* indicates that the aqueous core is in a highly ionic atomosphere. This is reasonable if we consider the presence of double layers of concentrated ions in the very thin aqueous core mentioned above.

The polarization measurements were also carried out for this second black film. The results are shown in Fig. 9 for three incident angles, 0°, 60°, and 75°. The trends of the wavenumber shift and intensity change are the same as in the case of the first black films shown in Fig. 6. Since the optical constants are thought to be different from those of pure water, we have not tried to reproduce the experimental absorbance curves in Fig. 9. However, it seems likely that there is no specific orientation or rigidified structure of water even in this thin second black film, as has been speculated by Lyklema *et al.* (8) who have characterized the SDS black films as "mobile" ones. A similarity between the bulk water and the water layers thicker than a few angstroms has been also pointed out by Clliford (37).

Acknowledgements

We are grateful to Professor Teruko Yamanaka of Chiba University for her helpful advices. Thanks are also due to Professor Masao Kimura of Hokkaido University for valuable information on the infrared intensities of water.

1. J. S. CLUNIE, J. F. GOODMAN, and B. T. INGRAM. *In* Surface and colloid science. Vol. 3. *Edited by* E. Matijevic. Wiley-Interscience, New York. 1971. p. 167.
2. A. SCHELUDKO. Adv. Colloid Interf. Sci. **1**, 391 (1967).
3. K. J. MYSELS and M. N. JONES. Discuss. Faraday Soc. **42**, 42 (1966).
4. H. TI TIEN. Bilayer lipid membranes (BLM). Theory and practice. Marcel Dekker, New York. 1974.
5. J. M. CORKILL, J. F. GOODMAN, D. R. HAISMAN, and S. P. HARROLD. Trans. Faraday Soc. **57**, 821 (1961).
6. J. S. CLUNIE, J. F. GOODMAN, and J. R. TATE. Trans. Faraday Soc. **64**, 1965 (1968).
7. J. M. CORKILL, J. F. GOODMAN, C. P. OGDEN, and J. R. TATE. Proc. R. Soc. London, A**273**, 84 (1963).
8. J. LYKLEMA, P. C. SCHOLTEN, and K. J. MYSELS. J. Phys. Chem. **69**, 116 (1965).
9. A. VRIJ. Adv. Colloid Interf. Sci. **2**, 40 (1968).
10. J. S. CLUNIE, J. M. CORKILL, and J. F. GOODMAN. Discuss. Faraday Soc. **42**, 34 (1966).
11. G. F. DASHER and A. J. MABIS. J. Phys. Chem. **64**, 77 (1960).
12. J. UMEMURA, H. H. MANTSCH, and D. G. CAMERON. J. Colloid Interf. Sci. **83**, 558 (1981).
13. T. KAWAI, J. UMEMURA, and T. TAKENAKA. Colloid Polym. Sci. **262**, 61 (1984).
14. D. G. CAMERON, A. MARTIN, and H. H. MANTSCH. Science, **219**, 180 (1983).
15. H. H. MANTSCH, S. C. HSI, K. W. BUTLER, and D. G. CAMERON. Biochim. Biophys. Acta, **728**, 325 (1983).
16. J. F. RABOLT, F. C. BURNS, N. E. SCHLOTTER, and J. D. SWALEN. J. Chem. Phys. **78**, 946 (1983).
17. N. KIMURA, J. UMEMURA, S. HAYASHI, and T. TAKENAKA. J. Mol. Struct. **116**, 153 (1984).
18. M. N. JONES, K. J. MYSELS, and P. C. SCHOLTEN. Trans. Faraday Soc. **62**, 1336 (1966).
19. P. MUKERJEE and K. J. MYSELS. Critical micelle concentrations of aqueous surfactant systems. NSRDS-NBS 36. US Government Printing Office, Washington, DC. 1971.
20. T. MOTOJIMA, S. IKAWA, and M. KIMURA. J. Quant. Spectrosc. Radiat. Transfer, **25**, 29 (1981).
21. M. P. MCDONALD and W. E. PEEL. J. Chem. Soc. Faraday Trans. I, **72**, 2274 (1976).
22. T. KAWAI, J. UMEMURA, and T. TAKENAKA. Bull. Inst. Chem. Res. Kyoto Univ. **61**, 314 (1983).
23. F. VAN VOORST VADER. Trans Faraday Soc. **56**, 1067 (1960).
24. V. LUZZATI and F. HUSSON. J. Cell Biol. **12**, 207 (1962).
25. S. SUNDEL. Acta Chem. Scand. A**31**, 799 (1977).
26. W. F. MURPHY and H. J. BERNSTEIN. J. Phys. Chem. **76**, 1147 (1972).
27. M. FALK. *In* Chemistry and physics of aqueous gas solutions. The Electrochemical Society, New York. 1975. p. 19.
28. T. FUJIYAMA, J. PERRIN, and B. L. CRAWFORD, JR. Appl. Spectrosc. **24**, 9 (1970).
29. W. N. HANSEN. J. Opt. Soc. Am. **58**, 380 (1968).
30. F. REISS-HUSSON and V. LUZZATI. J. Phys. Chem. **68**, 3504 (1964).
31. H. D. DOWNING and D. WILLIAMS. J. Geophys. Res. **80**, 1656 (1975).
32. W. M. IRVINE and J. B. POLLACK. Icarus, **8**, 324 (1968).
33. J. F. FOX and A. E. MARTIN. Proc. R. Soc. A**174**, 234 (1940).
34. V. M. ZOLOTAREV, B. A. MIKHAILOV, L. I. ALPEROVICH, and S. I. POPOV. Opt. Spektrosk. **27**, 790 (1969).
35. T. MOTOJIMA, S. IKAWA, and M. KIMURA. J. Quant. Spectrosc. Radiat. Transfer, **26**, 177 (1981).
36. K. A. HARTMAN, JR. J. Phys. Chem. **70**, 270 (1966).
37. J. CLLIFORD. *In* Water – a comprehensive treatise. Vol. 5. *Edited by* F. Franks, Plenum Press, New York. 1975. Chapt. 2.

Orbital angular momentum eigenfunctions for many-particle systems

JOHN AVERY
Department of Physical Chemistry, H.C. Ørsted Institute, University of Copenhagen, DK-2100 Denmark

Received September 6, 1984

This paper is dedicated to Professor Camille Sandorfy on the occasion of his 65th birthday

JOHN AVERY. Can. J. Chem. **63**, 1719 (1985).

Methods are presented for constructing eigenfunctions of the total orbital angular momentum operator of a many-particle system without the use of the Clebsch–Gordan coefficients. One of the equations derived in this paper is analogous to Dirac's identity for total spin; and through this equation, a connection is established between eigenfunctions of L^2 and irreducible representations of the symmetric group S_n.

JOHN AVERY. Can. J. Chem. **63**, 1719 (1985).

On présente des méthodes qui permettent d'établir, sans faire appel aux coefficients de Clebsch–Gordan, les fonctions de eigen de l'opérateur total du moment angulaire de l'orbitale d'un système à plusieurs particules. L'une des équations ainsi obtenue dans ce travail est analogue à celle d'identité de Dirac relative au spin total; au moyen de cette équation, on a établi une corrélation entre les fonctions de eigen de L^2 et les représentations irréductibles du groupe de symétrie S_n.

[Traduit par le journal]

Introduction

In the quantum mechanical treatment of many-particle systems, one is often faced with the problem of constructing eigenfunctions of the total angular momentum operator

$$[1] \quad L^2 = \boldsymbol{L} \cdot \boldsymbol{L}$$

where

$$[2] \quad \boldsymbol{L} = \sum_{a=1}^{N} \boldsymbol{\ell}_a$$

and where

$$[3] \quad \begin{aligned} \ell_{ax} &= \frac{1}{i}\left(y_a \frac{\partial}{\partial z_a} - z_a \frac{\partial}{\partial y_a}\right) \\ \ell_{ay} &= \frac{1}{i}\left(z_a \frac{\partial}{\partial x_a} - x_a \frac{\partial}{\partial z_a}\right) \\ \ell_{az} &= \frac{1}{i}\left(x_a \frac{\partial}{\partial y_a} - y_a \frac{\partial}{\partial x_a}\right) \end{aligned}$$

Often the Clebsch–Gordan coefficients are used to construct eigenfunctions of L^2 and L_z. In this paper, we shall discuss an alternative method which avoids the use of Clebsch–Gordan coefficients.

An identity for L^2 analogous to Dirac's identity for S^2

From eqs. [1]–[3] it follows that

$$[4] \quad \begin{aligned} \boldsymbol{L}x_a &= (0, -iz_a, iy_a) \\ \boldsymbol{L}y_a &= (iz_a, 0, -ix_a) \\ \boldsymbol{L}z_a &= (-iy_a, ix_a, 0) \end{aligned}$$

so that

$$[5] \quad \begin{aligned} (\boldsymbol{L}x_a)\cdot(\boldsymbol{L}x_b) &= x_b x_a - (ab) \\ (\boldsymbol{L}y_a)\cdot(\boldsymbol{L}y_b) &= y_b y_a - (ab) \\ (\boldsymbol{L}z_a)\cdot(\boldsymbol{L}z_b) &= z_b z_a - (ab) \\ (\boldsymbol{L}x_a)\cdot(\boldsymbol{L}y_b) &= x_b y_a \\ (\boldsymbol{L}x_a)\cdot(\boldsymbol{L}z_b) &= x_b z_a \\ (\boldsymbol{L}y_a)\cdot(\boldsymbol{L}z_b) &= y_b z_a \qquad a, b = 1, 2, \ldots, N \end{aligned}$$

where, for the sake of brevity, we have introduced the notation

$$[6] \quad (ab) \equiv x_a x_b + y_a y_b + z_a z_b$$

Now let us suppose that L^2 acts on a product of the particle coordinates of the form

$$[7] \quad f = \underbrace{x_a x_b x_c \ldots y_d y_e y_g \ldots z_h z_i z_j \ldots}_{n \text{ factors}}$$

Since

$$[8] \quad L^2 f = \boldsymbol{L}\cdot(\boldsymbol{L}f) = \boldsymbol{L}\cdot[(\boldsymbol{L}x_a)x_b x_c \ldots + x_a(\boldsymbol{L}x_b)x_c \ldots + \ldots]$$

we have

$$[9] \quad L^2 f = \left[2n + 2\frac{(\boldsymbol{L}x_a)\cdot(\boldsymbol{L}x_b)}{x_a x_b} + 2\frac{(\boldsymbol{L}x_a)\cdot(\boldsymbol{L}x_c)}{x_a x_c} + \ldots \text{ (all possible pairs)}\right] f$$

Making use of eq. [5], we can rewrite [9] in the form

$$[10] \quad L^2 f = 2(n + Q - C) f$$

where Q is a sum of permutation operators

$$[11] \quad Q \equiv \underbrace{P_{ab} + P_{ac} + P_{bc} + \ldots}_{\frac{n(n-1)}{2} \text{ terms}}$$

and where C is a "contraction operator" defined by the relation

$$[12] \quad Cf \equiv \left[\frac{(ab)}{x_a x_b} + \ldots \text{ (all possible pairs of } x\text{'s)} + \frac{(de)}{y_d y_e} + \ldots \text{ (all possible pairs of } y\text{'s)} + \frac{(hi)}{z_h z_i} + \ldots \text{ (all possible pairs of } z\text{'s)}\right] f$$

It is understood that if C acts more than once on f, then the only pairs formed are between coordinates not already contracted. Thus, for example, if $f = x_a x_b x_c y_d y_e$, then

$$Cf = (ab)x_c y_d y_e + (ac)x_b y_d y_e + (bc)x_a y_d y_e + x_a x_b x_c (de)$$

[13] $$C^2 f = 2(de)\,[(ab)x_c + (ac)x_b + (bc)x_a]$$
$$C^3 f = 0$$

Equation [10] is analogous to Dirac's identity for the total spin operator. However, it should be noticed that the operator Q is a class-invariant of the symmetric group S_n, not of S_N, where n is the degree of the mononomial f, while N is the number of particles in the system (1–4).

Construction of symmetric eigenfunctions of L^2 and L_z with $M = 0$

We now let (5–8)

[14] $$F \equiv \underbrace{z_a z_b z_c z_d \ldots}_{n \text{ factors}}$$

Since F contains only z's, with no x's or y's, it is completely symmetric with respect to the interchanges P_{ab}, P_{ac}, ... etc. Therefore

[15] $$QF = \frac{n(n-1)}{2} F$$

and

[16] $$L^2 F = [n(n+1) - 2C]F$$

Furthermore, since

[17] $$L^2(ab)f = (ab)L^2 f$$

it follows that

[18] $$L^2 C^t F = [(n-2t)(n-2t+1) - 2C]C^t F$$

We would now like to show that, for $L = n, n-2, \ldots,$ the function

[19] $$F_L \equiv \frac{2L+1}{\left(\frac{n-L}{2}\right)!\,(n+L+1)!!} \times \sum_{s=0}^{[\frac{1}{2}L]} \frac{(-1)^s}{s!}(2L-2s-1)!!\,C^{s+(1/2)(n-L)} F$$

is an eigenfunction of L^2 corresponding to the eigenvalue $L(L+1)$. In other words, we would like to show that

[20] $$L^2 F_L = L(L+1)F_L \qquad L = n, n-2, n-4, \ldots$$

Letting L^2 act on the sum in eq. [19] and making use of [18], we obtain

$$L^2 \sum_{s=0}^{[\frac{1}{2}L]} \frac{(-1)^s}{s!}(2L-2s-1)!!\,C^{s+(1/2)(n-L)}F$$

[21] $$= \sum_{s=0}^{[\frac{1}{2}L]} \frac{(-1)^s}{s!}(2L-2s-1)!!\,[(L-2s)(L-2s+1) - 2C]C^{s+(1/2)(n-L)}F$$

$$= L(L+1)\sum_{s=0}^{[\frac{1}{2}L]} \frac{(-1)^s}{s!}(2L-2s-1)!!\,C^{s+(1/2)(n-L)}F$$

so that eq. [20] is established.

As an example, let us consider the case where $n = 2$. Then

[22] $$F = z_a z_b$$

and

[23] $$F_2 = F - \frac{1}{3}CF = z_a z_b - \frac{1}{3}(ab)$$
$$F_0 = \frac{1}{3}(ab) \qquad a, b = 1, 2, \ldots, N$$

It is easy to verify that F_2 is an eigenfunction of L^2 corresponding to the quantum number $L = 2$, while F_0 is an eigenfunction corresponding to $L = 0$; and this is true for all possible values of the particle indices a and b. If $a = b$, then F_2 has the angular dependence of a d-orbital, while if $a \neq b$, F_2 represents two p-orbitals coupled together.

As a second example, let us consider the case where $n = 3$, so that

[24] $$F = z_a z_b z_c$$

Then

[25] $$F_3 = F - \frac{1}{5}CF = z_a z_b z_c - \frac{1}{5}[(ab)z_c + (ac)z_b + (bc)z_a]$$
$$F_1 = \frac{1}{5}CF = \frac{1}{5}[(ab)z_c + (ac)z_b + (bc)z_a]$$

As in our previous example, no matter what values the particle indices take on, the functions F_L will still be eigenfunctions of L^2. If $a = b = c$, then F_3 corresponds to an f-orbital; if $a = b \neq c$, it corresponds to a d-orbital coupled to a p-orbital; and if $a \neq b$, $b \neq c$, and $c \neq a$, F_3 corresponds to three p-orbitals coupled together.

For $n = 4$, we have

[26] $$F_4 = F - \frac{1}{7}CF + \frac{1}{70}C^2F$$
$$F_2 = \frac{1}{7}CF - \frac{1}{21}C^2F$$
$$F_0 = \frac{1}{30}C^2F$$

Notice that

[27] $$F_0 + F_2 + F_4 = F$$

and in general,

[28] $$\sum_{L=0,2,\ldots}^{n} F_L = F$$

so that F_L corresponds to a projection of F onto that part of Hilbert space spanned by eigenfunctions of L^2 belonging to the quantum number L. Other examples, corresponding to higher values of n, are shown in Table 1.

Eigenfunctions of L^2 and L_z with $M = L$

The symmetric eigenfunctions of L^2 and L_z generated means of eq. [19] correspond to $M = 0$. Eigenfunctions corresponding to other values of M can of course be obtained from them by use of the raising and lowering operators

[29] $$L_\pm = L_x \pm iL_y$$

However, this procedure is somewhat laborious, and therefore it is interesting to see that eigenfunctions of L^2 with $M = L$ can be written down directly. To see this, we make use of the identity

TABLE 1. Totally symmetric eigenfunctions of L^2 and L_z with $M = 0$; $F \equiv z_a z_b z_c \ldots$, $a, b, c, \ldots = 1, 2, \ldots, N$; the "contraction operator" C is defined by eq. [12]

n	L	Eigenfunctions of L^2 and L_z
1	1	$F = z_a$
2	2	$F - \frac{1}{3}CF = z_a z_b - \frac{1}{3}(ab)$
	0	$\frac{1}{3}CF = \frac{1}{3}(ab)$
3	3	$F - \frac{1}{5}CF$
	0	$\frac{1}{5}CF$
4	4	$F - \frac{1}{7}CF + \frac{1}{70}C^2F$
	2	$\frac{1}{7}CF - \frac{1}{21}C^2F$
	0	$\frac{1}{30}C^2F$
5	5	$F - \frac{1}{9}CF + \frac{1}{126}C^2F$
	3	$\frac{1}{9}CF - \frac{1}{45}C^2F$
	1	$\frac{1}{70}C^2F$
6	6	$F - \frac{1}{11}CF + \frac{1}{198}C^2F - \frac{1}{4158}C^3F$
	4	$\frac{1}{11}CF - \frac{1}{77}C^2F + \frac{1}{770}C^3F$
	2	$\frac{1}{126}C^2F - \frac{1}{378}C^3F$
	0	$\frac{1}{630}C^3F$

[30] $L^2 = L_z(L_z + 1) + L_-L_+$

and we introduce the notation

[31] $a_+ \equiv x_a + iy_a$

Next we notice that

$$L_+a_+ = 0$$

[32] $$L_+a_+b_+ = 0$$

$$L_+a_+b_+c_+ = 0$$

etc. $\qquad a, b, c, \ldots = 1, 2, \ldots, N$

and that

$$L_za_+ = a_+$$

[33] $$L_za_+b_+ = 2a_+b_+$$

$$L_za_+b_+c_+ = 3a_+b_+c_+$$

etc. $\qquad a, b, c, \ldots = 1, 2, \ldots, N$

so that

TABLE 2. Eigenfunctions of L^2 and L_z with $M = L$; $a_+ \equiv x_a + iy_a$; (ab), $(a \times b)_+$, and $|abc|$ are defined respectively by eqs. [6], [31], and [38]; $a, b, c, \ldots = 1, 2, 3, \ldots, N$

n	L	
1	1	a_+
2	2	a_+b_+
	1	$(a \times b)_+$
	0	(ab)
3	3	$a_+b_+c_+$
	2	$(a \times b)_+c_+$
	1	$(ab)c_+$
	0	$\|abc\|$
4	4	$a_+b_+c_+d_+$
	3	$(a \times b)_+c_+d_+$
	2	$(a \times b)_+(c \times d)_+$
		$(ab)c_+d_+$
	1	$(ab)(c \times d)_+$
		$\|abc\|d_+$
	0	$(ab)(cd)$

[34]
$$L^2 \underbrace{a_+b_+c_+}_{n \text{ factors}} \ldots = n(n+1)a_+b_+c_+ \ldots$$

$$L_za_+b_+c_+ \ldots = na_+b_+c_+ \ldots$$

We then introduce the notation

[35] $(a \times b)_+ \equiv y_az_b - z_ay_b + i(z_ax_b - x_az_b)$

From [29], [2], and [3] it follows that

[36]
$$L_+(a \times b)_+ = 0$$

$$L_z(a \times b)_+ = (a \times b)_+$$

so that

[37]
$$[L^2 - n(n-1)]\underbrace{a_+b_+c_+ \ldots}_{n-2 \text{ factors}}(d \times e)_+ = 0$$

$$[L_z - (n-1)]a_+b_+c_+ \ldots (d \times e)_+ = 0$$

Finally we introduce the notation

[38] $|abc| \equiv \det \begin{vmatrix} x_a & y_a & z_a \\ x_b & y_b & z_b \\ x_c & y_c & z_c \end{vmatrix}$

and notice that

[39] $\mathbf{L}|abc| = 0$

so that

$$[40]\quad \begin{aligned} &[L^2 - (n-3)(n-2)]\,|abc|\underbrace{d_+e_+f_+\ldots}_{n-3\text{ factors}} = 0 \\ &[L_z - (n-3)]\,|abc|d_+e_+f_+\ldots = 0 \end{aligned}$$

Proceeding in this way, we can construct simultaneous eigenfunctions of L^2 and L_z corresponding to the quantum numbers L and $M = L$ as shown in Table 2.

If we compare Table 1 with Table 2, we notice immediately that the functions corresponding to odd values of $n - L$ are missing from Table 1. This is because the functions in Table 1 are required to be completely symmetric with respect to interchanges of the particle indices $a, b, c, \ldots$, while the functions corresponding to odd values of $n - L$ correspond to other irreducible representations of S_n. By allowing other symmetries, it is possible to use eq. [19] and Table 1 to generate eigenfunctions of L^2 and L_z with $M = 0$ also for odd values of $n - L$. For example, if we replace z_b in eq. [22] by $(b \times c)_z = x_b y_c - y_b x_c$, eqs. [22] and [23] take on the modified form

$$[41]\quad F' = z_a(x_b y_c - y_b x_c)$$

and

$$[42]\quad \begin{aligned} F_2' &= z_a(x_b y_c - y_b x_c) - \frac{1}{3}|abc| \\ F_0' &= \frac{1}{3}|abc| \end{aligned}$$

It is easy to verify that F_2' and F_0' are eigenfunctions of L^2 corresponding respectively to the quantum numbers $L = 2$ and $L = 0$.

Discussion

The fact that the functions in Tables 1 and 2 are eigenfunctions of L^2 and L_z regardless of the values taken on by the particle indices $a, b, c, \ldots$ can be understood as a consequence of the fact that the transformation properties of these functions under rotations of the system as a whole are independent of the particle indices. The method for constructing eigenfunctions of total orbital angular momentum discussed here is closely related to the method for generating hyperspherical harmonics by harmonic projection which we treated in our previous papers (5–7). It is also closely related to the irreducible tensor formalism, a discussion of which can be found, for example, in Hamermesh (9).

To see the relationship between the methods presented here and the usual methods for coupling angular momenta, we can compare the functions shown in eq. [23] with functions obtained using Clebsch–Gordan coefficients. Let us consider the case where $a \neq b$. Then

$$[43]\quad F_2 = z_a z_b - \frac{1}{3}(x_a x_b + y_a y_b + z_a z_b)$$

represents a d-orbital obtained by coupling two p-orbitals. If we instead used Clebsch–Gordan coefficients, we would find:

$$[44]\quad |L = 2, M = 0\rangle = \frac{1}{\sqrt{6}}|1, -1\rangle + \sqrt{\frac{2}{3}}|0, 0\rangle + \frac{1}{\sqrt{6}}|-1, 1\rangle$$

where

$$[45]\quad \begin{aligned} |1, -1\rangle &= -\frac{1}{2}(x_a + iy_a)(x_b - iy_b) \\ |0, 0\rangle &= z_a z_b \\ |-1, 1\rangle &= -\frac{1}{2}(x_a - iy_a)(x_b + iy_b) \end{aligned}$$

If we substitute [45] into [44] we obtain

$$[46]\quad |L = 2, M = 0\rangle = \frac{3}{\sqrt{6}}\left[z_a z_b - \frac{1}{3}(x_a x_b + y_a y_b + z_a z_b)\right]$$

which is proportional to the function shown in eq. [43].

When several angular momenta are coupled, there may be several different functions all of which correspond to the same values of L and M. These functions can be classified by Young operators, a situation which is analogous to the coupling of spins in the Yamanouchi–Kotani branching diagram. For this reason, the connection between angular momentum and the permutation group is an interesting one.

Acknowledgements

I would like to thank Stud. Scient. Peter Sommer Larsen, Lektor Sten Rettrup, Dr. Birte L. Christensen–Dalsgaard and Stud. Scient. Shen Hengyi for helpful conversations. I would also like to express my gratitude to Professors Jens Peder Dahl, Hendrik J. Monkhorst, Roy McWeeny, Jan Linderberg, and Yngve Öhrn for their interest and encouragement.

1. P. A. M. DIRAC. Proc. R. Soc. London, **A123**, 714 (1929).
2. P.-O. LÖWDIN and O. GOSCINSKI. Int. J. Quantum Chem. **3**, 533 (1970).
3. S. RETTRUP. Ph.D. Dissertation, Danmarks tekniske Højskole, Lyngby, Denmark. 1978.
4. S. RETTRUP. To be published.
5. J. AVERY and Z. Y. WEN. Int. J. Quantum Chem. **25**, 1069 (1984).
6. Z. Y. WEN and J. AVERY. J. Math. Phys. In press.
7. J. AVERY, B. CHRISTENSEN-DALSGAARD, P. SOMMER LARSEN, and H. SHEN. Int. J. Quantum Chem. Symposium **18**, (1984).
8. J. AVERY and P. SOMMER LARSEN. To be published.
9. M. HAMERMESH. Group theory and its application to physical problems. Addison-Wesley. 1962.

Rôle de la liaison hydrogène intra et intermoléculaire dans l'étude des propriétés spectroscopiques et photophysiques. Cas types: dérivés du carbazole

PIERRE D. HARVEY[1] ET GILLES DUROCHER[2]

Département de Chimie, Université de Montréal, C.P. 6210, Succ. A, Montréal (Qué.), Canada H3C 3V1

Reçu le 10 octobre 1984

Cet article est dédié au Professeur Camille Sandorfy à l'occasion de son 65^e^ anniversaire

PIERRE D. HARVEY et GILLES DUROCHER. Can. J. Chem. **63**, 1723 (1985).

Nous avons étudié les spectres d'absorption et de fluorescence de même que les rendements quantiques et les durées de vie de fluorescence des dérivés cyanurés et carboéthoxylés du carbazole en position 1 en phase gazeuse, dans les solutions fluides polaire et non-polaire de même que dans des matrices rigides à 77 K. Nous avons montré que le cyano-1 carbazole forme un dimère cyclique dans le méthyl-3 pentane avec une enthalpie de complexation de -39 kJ mol^{-1} et une entropie de complexation de -78 J mol^{-1} K^{-1}. Par ailleurs, aucun tautomère formé suite à l'excitation du dimère n'a pu être mis en évidence. Par ailleurs, la liaison hydrogène intramoléculaire prime chez le carboéthoxy-1 carbazole en phase gazeuse ou dissous dans les solvants non-polaires à l'état électronique fondamental de la molécule (système lié). Le rendement quantique de fluorescence de ce système lié à 23°C est par ailleurs très faible de sorte que seul le système libre émet à température ambiante. Par contre à 77 K en matrice rigide de 3MP, le système lié émet fortement en fluorescence. Cette liaison hydrogène intramoléculaire est par ailleurs rompue pour faire place à une liaison hydrogène intermoléculaire dans l'éthanol. Il en est ainsi pour le cyano-1 carbazole. Nous montrons que tous ces dérivés substitués en position 1 du carbazole forment des exciplexes lorsque dissous dans l'éthanol à 23°C. On explique la formation de ces exciplexes par le caractère transfert de charge élevé de l'état ^1L_b de ces molécules.

PIERRE D. HARVEY and GILLES DUROCHER. Can. J. Chem. **63**, 1723 (1985).

The absorption and fluorescence spectra along with the fluorescence quantum yields and lifetimes of the 1-cyano and 1-carboethoxy derivatives of carbazole in polar and non-polar fluids and in rigid solutions at 77 K have been investigated. The existence of the cyclic dimer has been confirmed for 1-cyanocarbazole in 3-methylpentane. The enthalpy and entropy of complexation are evaluated to be -39 kJ mol^{-1} and -78 J mol^{-1} K^{-1} respectively. No tautomeric species has been observed following excitation of the dimer. On the other hand, the intramolecular hydrogen bonding system always predominates in the gas phase and in non-polar solvents in the ground electronic state. This intramolecular hydrogen bonding has been shown to be broken in ethanol, where intermolecular hydrogen bonding to the solvent takes place. 1-Cyano carbazole follows the same behaviour in ethanol. All the 1-substituted derivatives of carbazole show exciplex fluorescence in ethanol and the formation of these exciplexes has been explained by the strong charge transfer character involved in the excited ^1L_b states of these molecules.

Introduction

Le Professeur Camille Sandorfy a tracé la voie depuis de nombreuses années à tous les chercheurs impliqués dans l'étude des effets de la liaison hydrogène dans les états électroniques fondamentaux des molécules en phase gazeuse (1) et en solutions (2). Nous avons voulu dans cet article, par quelques exemples choisis de dérivés substitués du carbazole, montrer comment la liaison hydrogène aussi bien intra qu'intermoléculaire influence les propriétés spectroscopiques et photophysiques de certaines molécules organiques.

La spectroscopie de même que la photophysique moléculaire des premiers états singulet et triplet excités du carbazole dans différents milieux ont fait l'objet de plusieurs études fondamentales au cours des années 1970 à 1980 (voir références dans l'article de G. E. Johnson (3)). Le carbazole est impliqué dans des autoassociations moléculaires (4) (dimères ou aggrégats) où encore il est lié par liaison hydrogène avec les solvants et cela dans son état électronique fondamental (5–7) ou dans ses états électroniques excités (8, 9). Par ailleurs contrairement à l'indole (10–13) ou au 3-H indole (14, 15) et à leurs dérivés, le carbazole en présence d'éthanol ou de solvants polaires ne forme pas de complexes excités (exciplexe) en solution fluide. Nous avons par ailleurs montré que le carbazole formait des exciplexes avec des molécules reconnus pour leur grande affinité électronique (les halocarbures aliphatiques) (16). Cependant, la constante de vitesse de second ordre pour la désactivation bimoléculaire s'est avérée plus faible pour le carbazole que pour l'indole et cela quel que soit l'halocarbure utilisé (17). Ce comportement s'explique par la théorie de Weller et Rehm qui tient compte de la différence d'énergie libre entre les états relaxés de la paire non-ionisée ($^1A_1 \ldots Q$) et de la paire d'ions ($^2A_0^+ \ldots {}^2Q^-$) (18).

Par ailleurs, outre les potentiels d'ionisation différents, les composés de l'indole possèdent une première bande électronique dans laquelle les transitions $^1L_b \leftarrow {}^1A$ et $^1L_a \leftarrow {}^1A$ sont très rapprochées en énergie ce qui confère à cette bande un caractère transfert de charge très important (à cause de l'intervention de l'état ^1L_a) qui est en fait absent dans la première transition ($^1L_b \leftarrow {}^1A$) du carbazole (19). Sachant que la substitution sur le noyau carbazole d'un groupement électroattracteur avait comme conséquence de réduire l'écart énergétique entre les transitions $^1L_b \leftarrow {}^1A$ et $^1L_a \leftarrow {}^1A$ du carbazole, nous avons procédé à la photosynthèse de plusieurs dérivés du carbazole substitués aux positions N, 1 et 3 du noyau (20) ainsi qu'à l'étude de la nature des différentes transitions électroniques chez ces mêmes composés (21–23). Les propriétés spectrales et photophysiques varient beaucoup d'un dérivé du carbazole à un autre. C'est ainsi qu'aucun transfert de charge intramoléculaire de torsion (TCIT) n'a pu être mis en évidence à l'état singulet excité dans le bichromophore du carbazole: le *N,N'*-di-carbazole (NNDC). La géométrie perpendiculaire du NNDC dans son état électronique fondamental est transformée en géométrie oblique dans l'état premier singulet relaxé sans intervention aucune de la polarité du solvant (24). D'autre part il a été

[1] Adresse actuelle: Département de Chimie, Université McGill, Montréal.

[2] Auteur à qui adresser la correspondance.

démontré récemment que les dérivés substitués aux positions de l'azote (N) et en position 3 du carbazole par des groupements électroattracteurs tels —CN et —COOEt sont très sensibles à la polarité du milieu. Les dérivés substitués en position 3 forment des exciplexes avec l'éthanol en solution fluide confirmant l'hypothèse de départ que plus l'écart énergétique entre les transitions $^1L_b\ (S_1) \leftarrow {}^1A$ et $^1L_a\ (S_2) \leftarrow {}^1A$ diminue plus la probabilité de formation d'exciplexes avec les solvants polaires augmente (25).

Les dérivés substitués en position 1 sont peut-être les plus intéressants à étudier en photophysique moléculaire puisque l'écart S_2-S_1 chez ces dérivés est approximativement identiques à celui du carbazole, et que d'autre part, d'autres possibilités d'interaction à l'état électronique fondamental s'offrent à ces molécules. En effet, la substitution d'un groupement carboethoxylé engendre une liaison hydrogène intramoléculaire (22). Par ailleurs, la substitution d'un groupement cyanuré provoque une dimérisation immédiate en solvant non-polaire, le dimère cyclique (double liaison hydrogène intermoléculaire) est stabilisé, comme nous l'avons confirmé récemment par une étude quantitative en infrarouge de transformée de Fourier (26). Il est aussi connu que d'autres dérivés du carbazole substitués en position 1 comme l'aza-1 carbazole (27) ainsi que l'aza-7 indole (28) se dimérisent à l'état électronique fondamental et que ce dimère lorsque photoexcité se tautomérise dans les solvants non-polaires produisant des fluorescences fortement déplacées vers le rouge suite à ces transferts de protons.

Le but de ce travail est donc de caractériser les diverses interactions intra et intermoléculaires de plusieurs dérivés substitués par des groupes électroattracteurs en position 1 du carbazole dans différents solvants et à diverses températures et cela dans leurs états électroniques fondamentaux et premiers singulets excités. Nous montrerons que ces divers types de liaison hydrogène affectent beaucoup les propriétés des états électroniques fondamentaux et excités de ces dérivés en plus de modifier en profondeur toute la dynamique des états excités de ces molécules.

Partie expérimentale

(a) *Produits*

Le carboethoxy-1 carbazole (1-COOEC) ainsi que le cyano-1 carbazole (1-CNC) ont été obtenus par photolyse du carbazole en présence de CCl_4 et ces produits ont été purifiés tel que décrit antérieurement (20). Le (carboethoxy)-1 éthyl-*N* carbazole (1-COOENEC) et le cyano-1 éthyl-*N* carbazole (1-CNNEC) ont été synthétisés par éthylation des dérivés N—H correspondant en utilisant la réaction catalytique de transfert de phase (29). Ces composés ont été purifiés par chromatographie sur colonne de gel de silice en utilisant un mélange d'éther de pétrole et d'éther éthylique (1:1) comme éluant. La pureté a été vérifiée par chromatographie sur couche mince et les produits ont été caractérisés par les spectroscopies de masse, ^{1}H rmn et infrarouge. Le méthyl-3 pentane (3MP) "pure grade" provenait de la compagnie Phillips Petroleum et il a été purifié tel que décrit antérieurement (16, 17). L'isopentane "pure grade" provenant de Phillips Petroleum et l'éther éthylique "analysed reagent" de la compagnie Baker ont été reflués sur H_2SO_4 concentré (4 mL/L) pendant 24 h et lavés plusieurs fois avec de l'eau bidistillé avant d'être distillé par fractionnement sur sodium. L'éthanol (EtOH) a été reflué sur H_2SO_4 (4 mL/L) pendant 24 h et distillé par fractionnement.

(b) *Instrumentation*

Les spectres d'absorption électronique ont été enregistré sur un spectrophotomètre Cary modèle 17. Une cellule métallique construite à nos ateliers, nous a permis d'enregistrer les spectres d'absorption aux diverses températures entre la température ambiante et celle de l'azote liquide (30). Les spectres de fluorescence ainsi que les spectres d'excitation corrigés de fluorescence ont été enregistrés à l'aide d'un spectrofluorimètre Spex Fluorolog modèle 1902 (14). Cet appareil est équipé d'un bain thermostaté fonctionnant entre 100 et −20°C. Aux températures inférieures, un montage à débit d'azote refroidi a été mis au point qui permet de stabiliser les températures à un degré près jusqu'à 77 K. Les spectres d'émission à l'état gazeux ont été obtenus à l'aide d'une cellule de quartz scellée sous un vide de 10^{-3} Torr (1 Torr = 133.3 Pa), puis placée dans un bain d'éthylène glycol chauffé à 160°C.

Les durées de vie de fluorescence ont été mesurées à l'aide d'un fluochronomètre construit dans nos laboratoires et qui utilise la technique de comptage de photon unique. Cet appareil de comptage comportant plusieurs modules de la compagnie Ortec Inc. a été décrit antérieurement (31). La méthode de convolution réitérative a été utilisée ainsi que la méthode statistique du χ^2 pour juger de la monoexponentialité des décroissances observées.

(c) *Procédure expérimentale*

Les solutions sans oxygène ont été obtenues par barbottage d'argon dans la solution. Le taux et le temps de barbottage ont été ajustés de façon à bien reproduire la durée de vie de fluorescence du carbazole obtenue par la méthode du gel–dégel. Les rendements quantiques de fluorescence ont été déterminés en utilisant le carbazole préalablement calibré par le diphényl-9,10 anthracène comme standard primaire (32). Les rendements quantiques de fluorescence ont tous été mesurés à des concentrations telles que l'autoabsorption ne puisse jouer aucun rôle. Les constantes théoriques de désactivation radiative ($k_F^{(t)}$) ont été calculées par l'équation de Birks et Dyson (33). Cette équation implique la connaissance de la variation de l'indice de réfraction du milieu en fonction de la longueur d'onde. Pour les solvants EtOH et 3MP à 23°C et pour l'EPA (éthanol, éther éthylique et isopentane 2:5:5) à 77 K, une expression pour la variation de l'indice de réfraction en fonction de la longueur d'onde a été décrite (24). Pour le 3MP à 77 K, la relation approximative suivante a été obtenue à partir des données de la littérature (34, 35):

$$n_{3MP}^{77\ K} \cong \left(2.2193 + \frac{7.450 \times 10^5}{\lambda^2}\right)^{1/2}$$

où λ est exprimée en angstrom (Å).

Les constantes radiatives (k_F) et non-radiatives (k_{nr}) de désactivation de la fluorescence ont été déterminées de façon usuelle par:

$$k_F = \phi_F/\tau_F$$

et

$$k_{nr} = (1 - \phi_F)/\tau_F$$

où ϕ_F et τ_F sont respectivement le rendement quantique et la durée de vie mesurée de la fluorescence de l'échantillon.

Résultats et discussion

I. *Cyano-1 carbazole: thermodynamique de formation du dimère à l'état électronique fondamental*

La figure 1 montre bien l'équilibre qui existe entre le monomère et une autre espèce lorsque l'on fait varier la température d'une solution 5×10^{-5} *M* (à 23°C) de 1-CNC dans le 3MP. Deux nouvelles bandes à 360 nm et à 342 nm apparaissent dans le spectre d'absorption et augmentent en intensité avec l'abaissement de la température alors que les bandes (0,0) et (0,1) de la première transition électronique $^1L_b \leftarrow {}^1A$ du 1-CNC respectivement situées à 347 et 333 nm diminuent avec l'abaissement de la température. Plusieurs points isobestiques apparaissent dans les spectres.

Un effet similaire sur le spectre est également observé lorsqu'à température fixe la concentration du 1-CNC est variée entre $3,3 \times 10^{-6}$ *M* et $2,3 \times 10^{-4}$ *M* dans le méthyl-3 pentane.

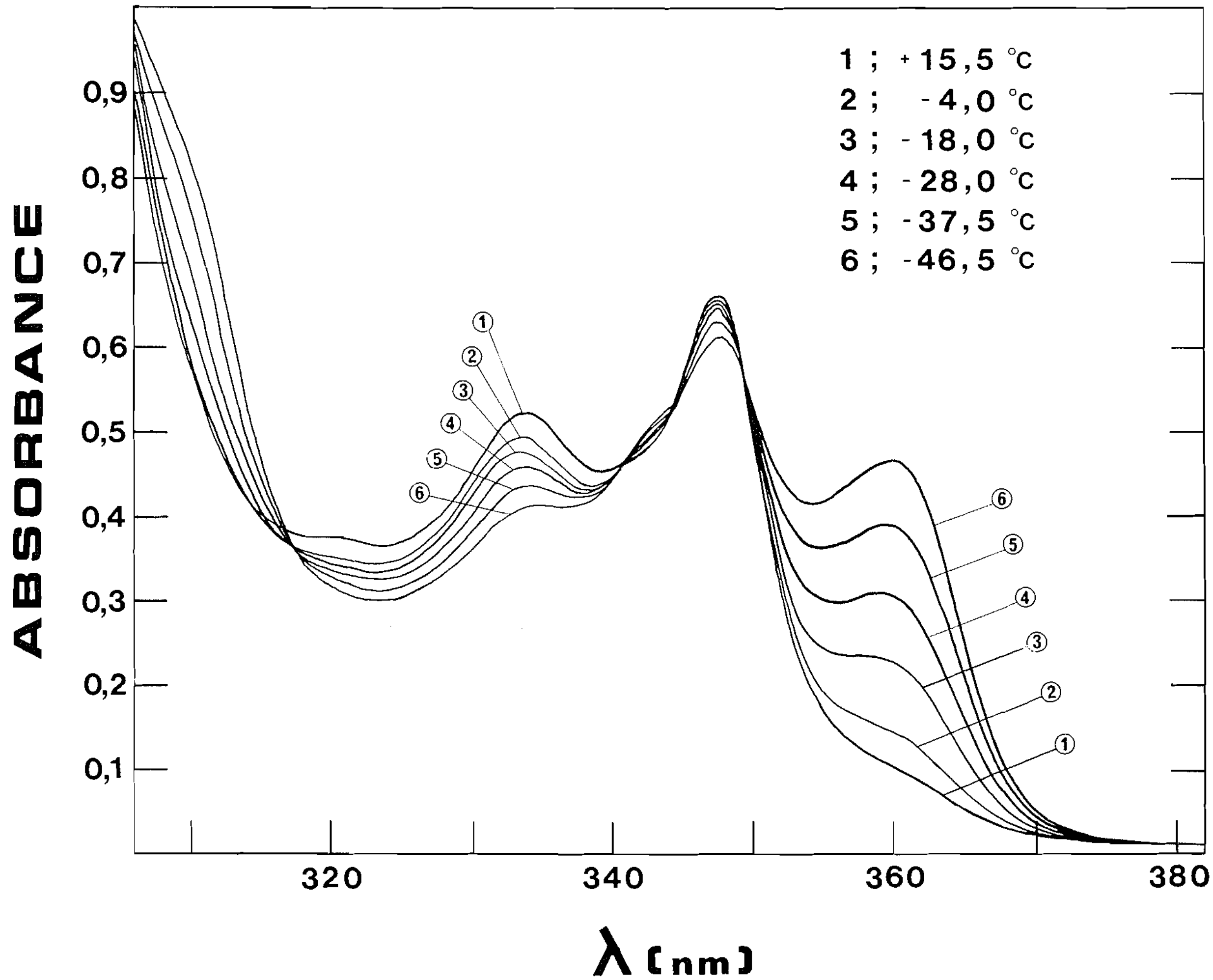

FIG. 1. Spectre d'absorption électronique du 1-CNC dans le 3MP à différentes températures. Concentration: $5{,}0 \times 10^{-5}$ M à 23°C.

Or nous avons montré récemment par spectroscopies ^{1}H rmn et infrarouge que le 1-CNC formait un dimère cyclique en solution dans le tétrachlorure de carbone (26).

Considérons un équilibre général entre n molécules de monomère (M) et un agrégat (P)

$$[1] \quad n\,\mathrm{M} \rightleftharpoons \mathrm{P}$$

La constante d'équilibre (K) à une température donnée est définie par:

$$[2] \quad K = \frac{[\mathrm{P}]}{[\mathrm{M}]^n} = \frac{[\mathrm{P}]}{(C_0 - n[\mathrm{P}])^n}$$

puisque la concentration totale C_0 qui est constante est toujours égale à $[\mathrm{M}] + n[\mathrm{P}]$. À condition qu'il n'y ait aucun recouvrement entre l'absorption de l'agrégat considéré et l'absorption du monomère à 360 nm, la concentration de l'agrégat peut être mesurée par son absorbance A:

$$[3] \quad [\mathrm{P}] = \frac{A}{\epsilon_{\mathrm{P}} l}$$

où ϵ_{P} devient le coefficient d'absorptivité molaire de l'agrégat considéré. Remplaçant [P] dans l'équation [2] par sa valeur en [3] on obtient la relation suivante:

$$[4] \quad \frac{C_0}{A} = \frac{n}{\epsilon_{\mathrm{P}}^{2/n} l^{2/n}} + \left(\frac{1}{\epsilon_{\mathrm{P}} l K}\right)^{1/n} \left(\frac{1}{A}\right)^{1-1/n}$$

Cette relation doit être linéaire pour la bonne valeur de n puisque C_0/A n'est pas une variable indépendante de $A^{(1/n-1)}$. Nous avons montré sur la fig. 2 qu'à toutes les températures utilisées dans cette étude, la variation de (C_0/A) en fonction de $(A)^{(1/n-1)}$ était linéaire lorsque $n = 2$ montrant clairement que l'agrégat considéré ici correspond à un dimère. Les résultats de la fig. 2 nous ont par la suite permis d'obtenir à chacune des températures la constante d'équilibre ainsi que le coefficient d'absorptivité molaire du dimère à 360 nm. La variation d'enthalpie et d'entropie de complexation a par la suite été calculée en utilisant l'équation de Van't Hoff (26). Ces résultats sont tous rassemblés au tableau 1. Les valeurs de ΔH et ΔS de complexation du 1-CNC dans le méthyl-3 pentane sont pratiquement identiques à celles obtenues dans le CCl_4 par infrarouge de transformée de Fourier compte-tenu des erreurs expérimentales inhérentes aux deux méthodes spectrales utilisées (26). Ceci implique donc que le dimère cyclique est également la structure la plus plausible dans les solvants hydrocarbonés étant donné la valeur très élevée obtenue pour le ΔH de complexation. On peut également souligner que l'ordre de grandeur des constantes d'équilibres obtenues se compare bien avec celui des constantes d'équilibre publiées pour les dimères cycliques de l'aza-1 carbazole (27) et de l'aza-7 indole (28) dans le même solvant.

Par ailleurs, le coefficient d'absorptivité molaire de la bande (0,0) du dimère semble augmenter régulièrement avec la dimi-

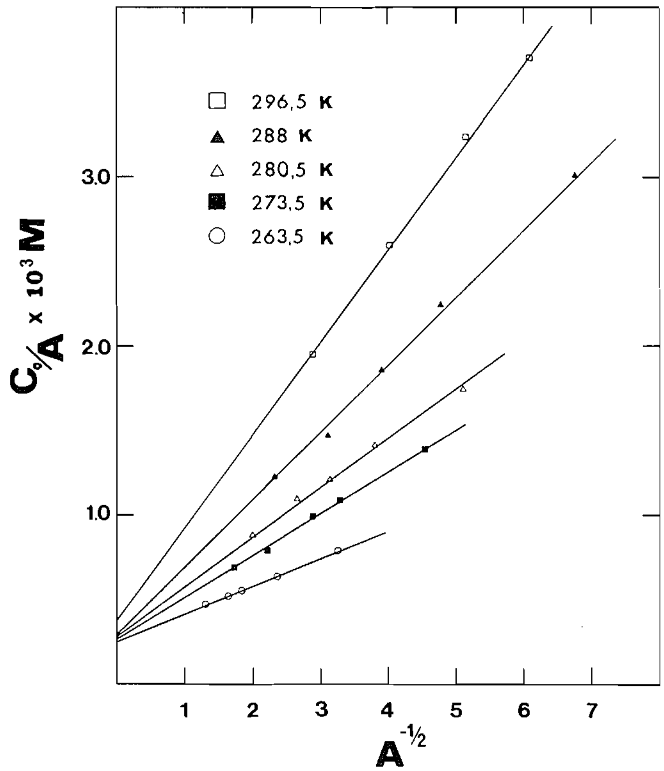

FIG. 2. Graphique de $[C_0]/A$ en fonction de $(A)^{-1/2}$ pour le système monomère–dimère (n = 2) du 1-CNC dans le 3MP où l'absorbance est mesurée à 360 nm et C_0 varient entre $6{,}0 \times 10^{-5}$ et $3{,}0 \times 10^{-4}$ M.

nution de la température du milieu comme le démontre la fig. 3. Ce coefficient atteint la valeur de 12×10^4 dm^2 mol^{-1} à 77 K toujours mesuré à 360 nm. Nous avons tracé sur la même figure la variation de la fréquence infrarouge du vibrateur NH lié dans ce même dimère en fonction de la température, données tirées d'un article récent (26). Il semble que plus la force de la liaison hydrogène augmente, plus grande est la probabilité de la première transition électronique dans le dimère cyclique du 1-CNC. Ceci va cependant à l'encontre d'un recouvrement entre les systèmes électronique-π des deux noyaux carbazoles par l'intermédiaire des atomes d'azote des deux groupements nitriles. En effet, si ce recouvrement existait, à cause de la symétrie C_{2h} du dimère, la première transition électronique serait permise en ordre zéro et la seconde interdite ce qui, suite à un calcul d'interaction de configurations, conduirait à prédire une diminution de l'intensité de cette première transition électronique comparativement à celle du monomère. Cette constatation ne favorise certainement pas le transfert des protons et la tautomérisation dans ce dimère (27, 28).

II. *Fluorescence du dimère du cyano-1 carbazole*

Sur la figure 4 apparaissent les spectres de fluorescence du 1-CNC dans le 3MP (c = $2{,}0 \times 10^{-5}$ M) à diverses températures. Le point isobestique à 368 nm montre bien qu'un équilibre existe entre le monomère et une autre entité. Le spectre de fluorescence du dimère pur est obtenu en matrice rigide de 3MP à 77 K et reproduit à la fig. 5. On peut voir la ressemblance qui existe entre le spectre de fluorescence du dimère à 77 K et le spectre 5 de la fig. 4. De plus une excellente image-miroir existe entre les spectres d'absorption et de fluorescence du dimère à 77 K. Peu importe la température de la

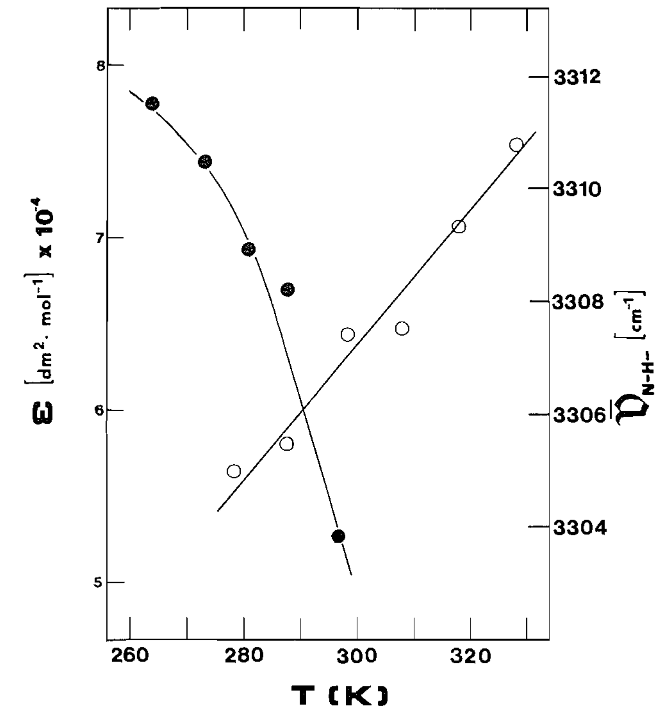

FIG. 3. Graphique du coefficient d'absorptivité molaire à 360 nm du dimère dans le 3MP (-•-•-•-) et de la fréquence de la vibration d'élongation du N—H associé du dimère dans le CCl_4 (o-o-o) en fonction de la température.

TABLEAU 1. Données spectrales et thermodynamiques de la formation du dimère du cyano-1 carbazole dans le méthyl-3 pentane mesurées à 360 nm

T (K)	$\epsilon_P \times 10^{-2}$ (dm^2 mol^{-1})	K (dm^3 mol^{-1})	ΔH^0 (kJ mol^{-1})	ΔS^0 (J mol^{-1} K^{-1})
296,5	525 ± 12	630 ± 20		
288,0	670 ± 26	910 ± 40		
280,5	693 ± 22	2050 ± 90	−39 ± 6	−78 ± 6
273,5	744 ± 23	2730 ± 120		
263,5	776 ± 22	4740 ± 130		

verses longueurs d'onde de fluorescence correspondent à une superposition des spectres d'absorption du monomère et du dimère. Une variation de la concentration du 1-CNC entre 1×10^{-6} M et 4×10^{-4} M n'a montré aucune différence dans les spectres de fluorescence et d'excitation de fluorescence enregistrés à 77 K dans le 3MP. Contrairement à l'aza-7 indole, aucun oligomère n'a pu être mis en évidence (28*c*). Par ailleurs, aucune phosphorescence n'a pu être détectée pour le dimère en matrice rigide de 3MP à 77 K. Il est en effet connu que les dimères de ce type n'émettent que très faiblement en phosphorescence (28*c*).

Aucun excimère ou tautomère n'a pu être détecté en fluorescence. Ceci montre que le tautomère ne peut se former à partir du dimère excité à cause d'une part, du peu de recouvrement entre les systèmes-π des deux chromophores du carbazole comme discuté antérieurement et en conséquence de la distance trop importante qui doit exister entre les protons et les atomes d'azote des groupements nitriles.

III. *Carboéthoxy-1 carbazole: liaison hydrogène intramoléculaire*

La géométrie du 1-COOEC favorise la formation d'une liai-

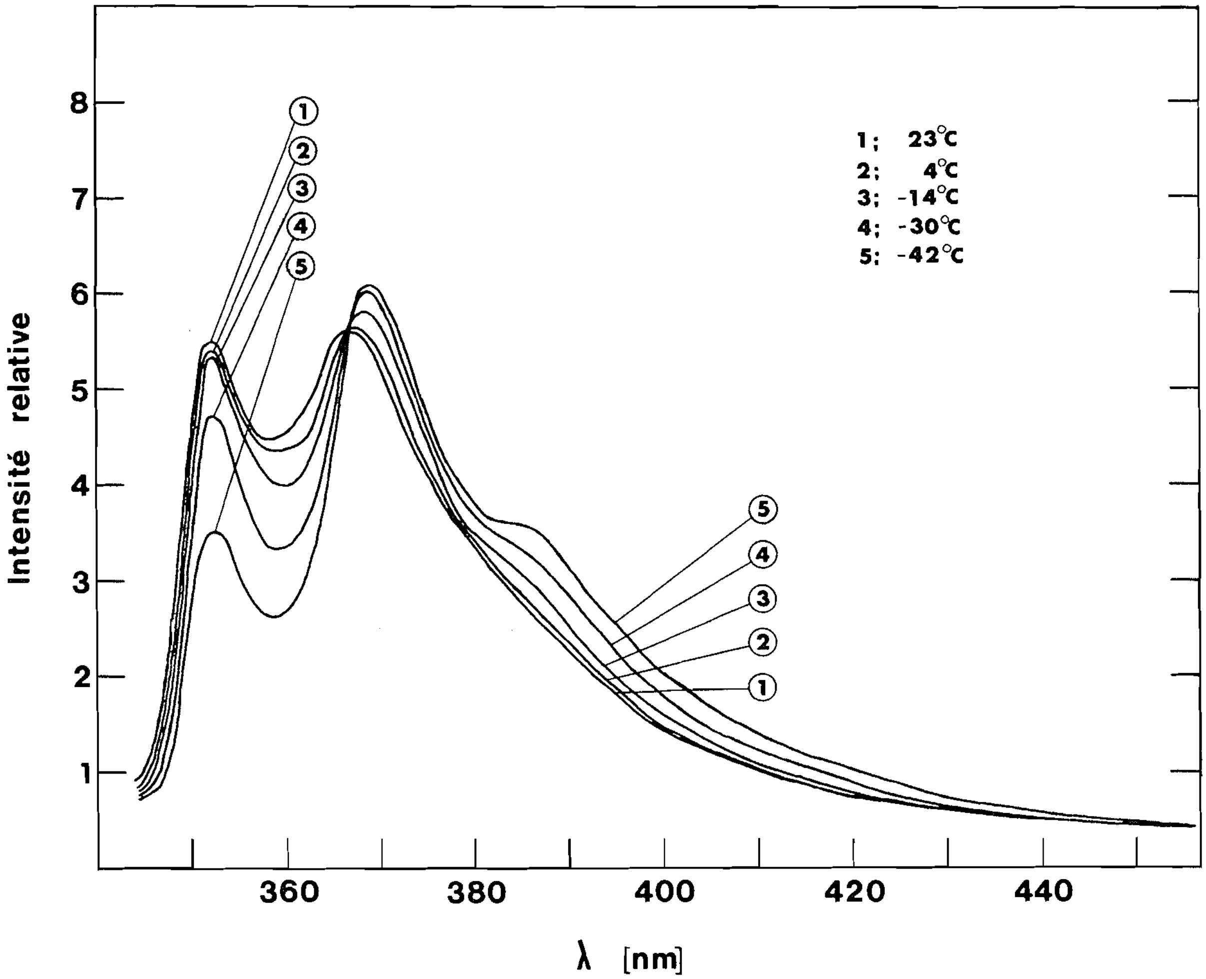

FIG. 4. Spectre de fluorescence du système monomère–dimère du 1-CNC dans le 3MP à différentes températures. Concentration: 2,0 × 10^{-5} *M* (23°C); λ (exc) = 340 nm.

son hydrogène intramoléculaire entre le groupement NH et une paire électronique du groupement carbonyle:

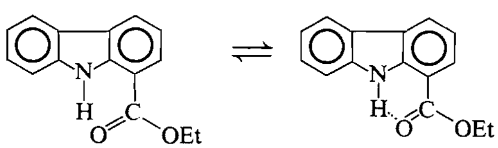

Cependant, une telle interaction ne peut se produire que lorsque le lien C═O du groupement carboéthoxylé est dans le plan moléculaire. Nous avons montré récemment par infrarouge de transformée de Fourier qu'un équilibre existait entre une conformation planaire (système lié) et une autre non-planaire (système libre) (26). La constante d'équilibre obtenue entre les deux systèmes dans le tétrachlorure de carbone comme solvant est de 1,7 à 0°C et de 1,0 à 55°C montrant bien que l'équilibre se déplace que très lentement vers la forme libre en fonction de l'augmentation de la température.

Les spectres d'absorption électronique du 1-COOEC dans l'éthanol et le 3MP sont reproduits à la fig. 6. Les nombres d'onde de la transition ${}^1L_b \leftarrow {}^1A$ du 1-COOEC dans différents milieux sont donnés au tableau 2. Le 1-COOEC ainsi que le 1-CNC dans l'éthanol forment une liaison hydrogène intermoléculaire avec le solvant comme l'indique leurs nombres d'onde respectif de 27 860 et 28 090 cm^{-1}, ce qui correspond à un déplacement bathochrome d'environ 700 cm^{-1} pour le 1-CNC en passant du 3MP à l'éthanol, déplacement conventionnel pour ce type d'interaction dans le carbazole (22). Contrairement au 1-CNC dans le 3MP, le 1-COOEC dans le 3MP montre un spectre d'absorption quasi identique à celui dans l'éthanol à 23°C. Nous attribuons ce spectre surtout au conformère planaire liée de façon intramoléculaire. Dans le but de vérifier l'équilibre entre les conformères liée et libre, nous avons enregistré les spectres d'absorption du 1-COOEC dans l'hexadécane normal à plusieurs températures entre 23°C et 125°C et aucune modification visible n'est apparue dans le spectre d'absorption montrant par le fait même que dans les hydrocarbures aliphatiques l'équilibre est fortement déplacé vers la forme associée qui est surtout responsable de l'absorption. Même à l'état gazeux (160°C; 10^{-3} Torr) le système lié semble être la forme prédominante dans le spectre d'absorption électronique comme le démontre la fig. 7. La bande (0,0) de la première transition ${}^1L_b \leftarrow {}^1A$ apparaît à 28 200 cm^{-1} ce qui représente un déplacement hypsochrome par rapport au 3MP d'environ 400 cm^{-1}, valeur généralement obtenue entre un hydrocarbure aliphatique comme solvant et la phase gazeuse (voir données sur le carbazole (24, 36)).

Le spectre de fluorescence du 1-COOEC en phase gazeuse est reproduit sur la figure 7. Le spectre d'excitation corrigé de cette fluorescence se superpose relativement bien au spectre d'absorption ce qui indique que le système lié est à l'origine de l'espèce qui émet la fluorescence. Cependant, il est évident que

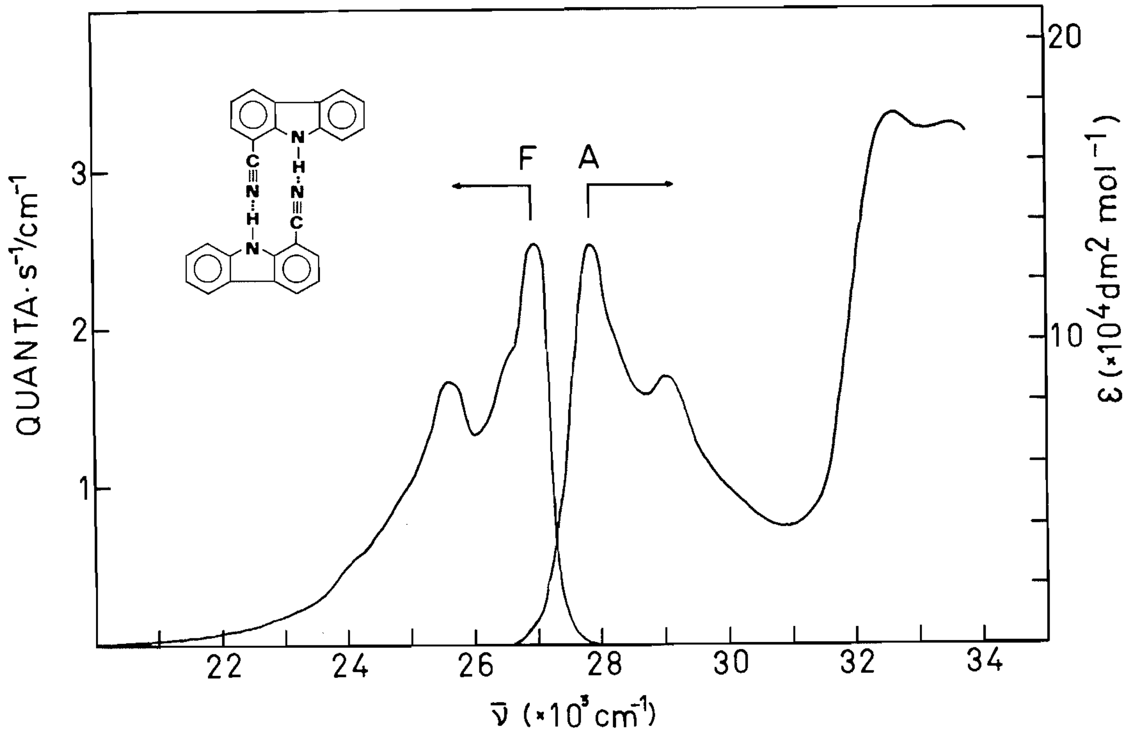

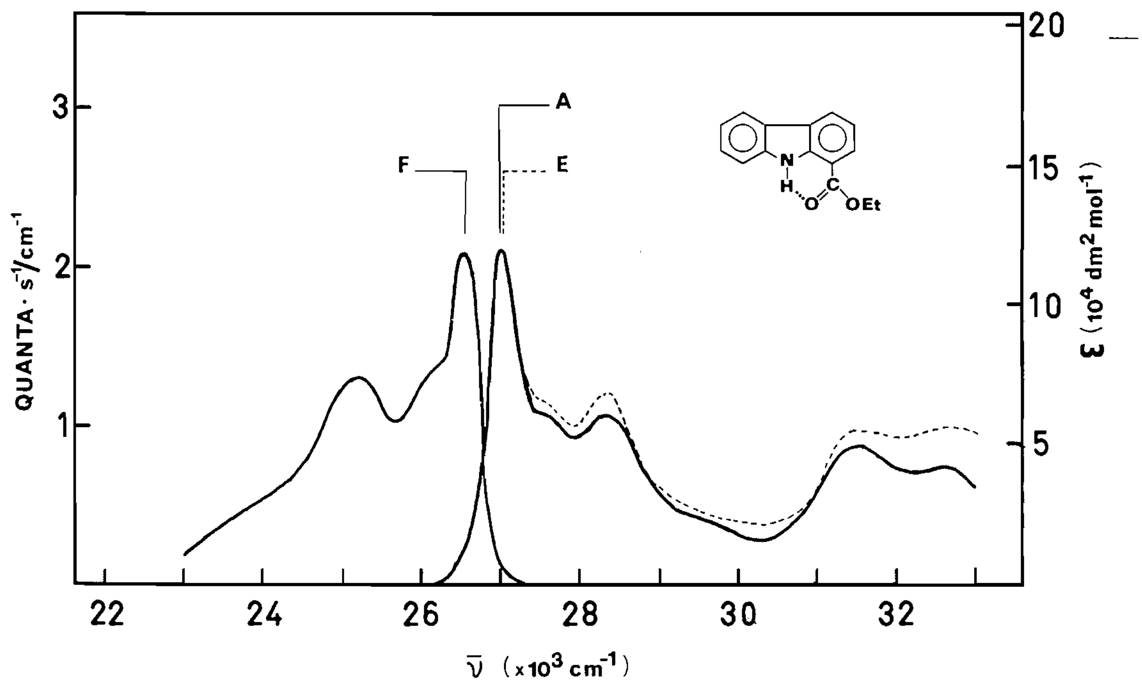

FIG. 5. Haut: spectre d'absorption et de fluorescence du dimère du 1-CNC dans le 3MP à 77 K. Concentration: (23°C) pour l'absorption: 2,0 $\times 10^{-5}$ *M*; pour le fluorescence: 3,0 $\times 10^{-6}$ *M*. Bas: spectres d'absorption, de fluorescence et d'excitation de la fluorescence du 1-COOEC dans le 3MP à 77 K.

l'image-miroir n'existe pas entre l'absorption et la fluorescence. De plus un déplacement Stokes de 2200 cm^{-1} existe entre les deux spectres. La largeur à la demi-hauteur du spectre de fluorescence est de 4000 cm^{-1}. Ce sont autant de caractéristiques qui semblent démontrer qu'une autre espèce que les systèmes lié ou libre est à l'origine de cette fluorescence en phase gazeuse à 160°C. Un transfert de proton à l'état excité de la forme associée et donc la formation d'une espèce tautomérique pourrait expliquer les caractéristiques observées. Une étude dynamique de la fluorescence picoseconde pourrait confirmer ou infirmer cette hypothèse.

Les spectres de fluorescence du cyano-1 carbazole protoné et *N*-éthylé de même que ceux du carboéthoxy carbazole protoné et *N*-éthylé dans le 3MP et dans l'éthanol sont présentés à la fig. 8 et les données spectroscopiques se retrouvent au tableau 2. Les spectres d'excitation de ces émissions correspondent tous

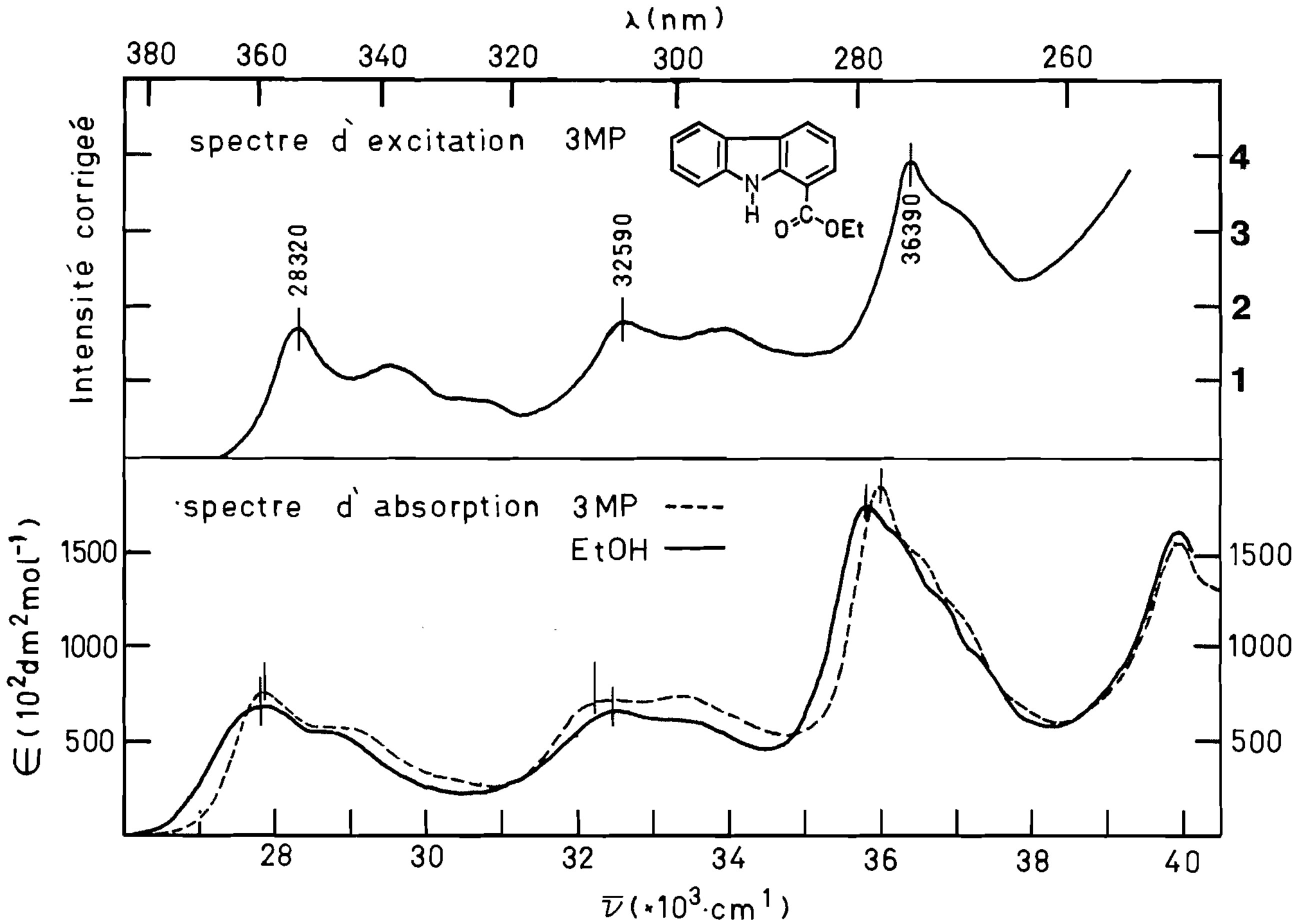

FIG. 6. Haut: spectre d'excitation de la fluorescence du 1-COOEC dans le 3MP à la température ambiante (peu importe la longueur d'onde de fluorescence observée). Bas: spectre d'absorption électronique du 1-COOEC dans le 3MP (---) et l'EtOH (—) à la température ambiante.

aux spectres d'absorption correspondant à la transition $^1L_b \leftarrow {}^1A$ de la molécule considérée sauf pour celui du 1-COOEC dans le 3MP que l'on peut voir sur la fig. 6. Un déplacement de 480 cm^{-1} vers le bleu est observé dans le spectre d'absorption dans le 3MP. Les bandes (0,0) des transitions $^1L_a \leftarrow {}^1A$ (32 590 cm^{-1}) et $^1B_b \leftarrow {}^1A$ (36 390 cm^{-1} (22)) subissent également un déplacement hypsochrome dans le spectre d'excitation de la fluorescence. D'autre part l'espèce responsable de l'émission ne peut être identique à celle qui absorbe puisque la bande (0,0) en absorption recouvre passablement la bande (0,0) de l'espèce émettrice et qu'il est connu pour les systèmes liés (EPA à 77 K dans le tableau 2) que les déplacements Stokes sont de l'ordre de 700 cm^{-1}. Nous attribuons donc la fluorescence observée à 23°C pour le 1-COOEC dans le 3MP au système libre.

Le système lié possède donc un rendement quantique pratiquement nul à la température ambiante. Cette attribution est aussi corroborée, en plus des deux points cités plus haut, par le fait que le rendement quantique apparent de cette émission est très faible (ϕ_F = 0,020; tableau 3). Puisque c'est le système lié qui est surtout responsable de l'absorption, ce rendement faible n'est donc pas le rendement réel du système libre. Cette attribution au système libre est de plus corroborée par le déplacement bathochrome de 1040 cm^{-1} observée pour la fluorescence dans le 3MP entre le 1-COOEC et le 1-COOENEC. Ce déplacement est identique à celui obtenu entre le carbazole et le *N*-éthyl carbazole dans le même solvant (17, 24, 26) pour lequel le groupement N—H du carbazole était libre. Il faut par surcroît noter que ce déplacement de 1040 cm^{-1} est en réalité plus élevé puisque la bande (0,0) du système libre subit un effet d'autoabsorption important à cause du recouvrement avec l'absorption du système lié. Le déplacement Stokes de 760 cm^{-1} dans le tableau 2 est assurément trop élevé pour le système libre à cause de cet effet.

Par abaissement de la température du 3MP, la fluorescence se déplace vers le rouge pour atteindre 26 560 cm^{-1} à 77 K. Son intensité augmente considérablement, le rendement quantique de fluorescence atteignant la valeur de 0,64 à 77 K. Par ailleurs, le spectre d'excitation de la fluorescence à 77 K se superpose parfaitement au spectre d'absorption du système lié à cette température comme le démontre la fig. 5. Ces résultats montrent clairement que la fluorescence observée en phase gazeuse ne peut provenir ni des systèmes lié ou libre. D'autre part, il semble que l'intensité de fluorescence du système lié soit très sensible à la température ou à la viscosité du milieu. A 77 K, cette fluorescence est également très sensible aux traces d'eau dans le 3MP produisant un élargissement du spectre, un déplacement vers le rouge, une diminution de l'intensité et une quasi extinction de la phosphorescence. Le spectre obtenu à la fig. 5 l'a été suite à des mesures extrêmes de protection du solvant contre l'eau atmosphérique.

IV. *Effet de l'éthanol sur les propriétés spectroscopiques des dérivés substitués en position 1 du carbazole*

Les spectres de quelques dérivés substitués du carbazole en position 1 dissous dans le 3MP et dans l'éthanol à 23°C sont rassemblés à la fig. 8. Une structure vibrationnelle bien déve-

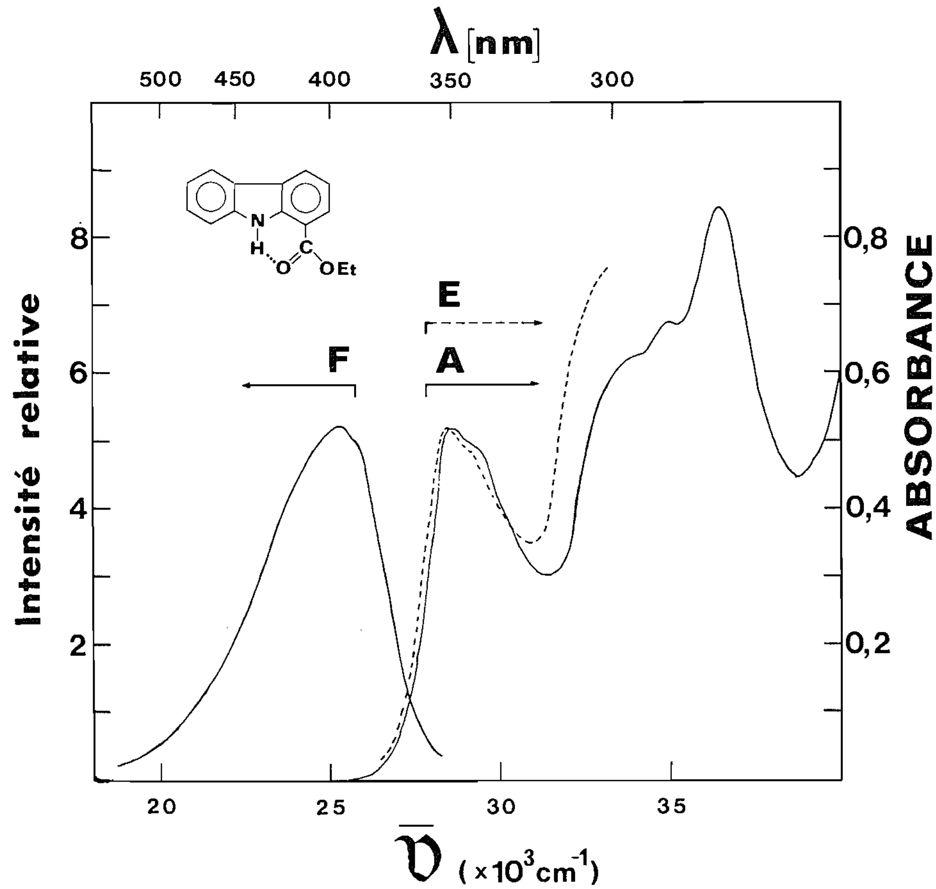

FIG. 7. Spectres d'absorption, de fluorescence et d'excitation de la fluorescence du 1-COOEC à l'état vapeur à 160°C et 10^{-3} Torr.

TABLEAU 2. Propriétés spectrales de quelques dérivés substitués en position 1 du carbazole dans divers milieux

Molécules	Conditions expérimentales	$\bar{\nu}_A$ (0,0) $^1L_b \leftarrow {}^1A$ (cm^{-1})	$\bar{\nu}_F$ (0,0) (cm^{-1})	Δ^a (cm^{-1})	$\Delta\bar{\nu}_{F_{1/2}}{}^b$ (cm^{-1})	$\Delta\bar{\nu}_A{}^c$ (cm^{-1})	$\Delta\bar{\nu}_F{}^d$ (cm^{-1})
1-COOEC	3MP, 23°C	27 840 ± 40(1)	—	—	—	—	—
	3MP, 77 K	27 060	26 560 ± 40	500	1960	1260	1000
	3MP, 23°C	28 320(2)	(27 560)	(760)	2280	—	—
	EtOH, 23°C	27 860	E	—	3040	460	—
	EPA, 77 K	27 400	26 760	740	2220	920	800
1-CNC	3MP, 23°C	28 800	28 490	310	2500	—	—
	EtOH, 23°C	28 090	E	—	3040	710	—
	EPA, 77 K	27 930	27 200	730	2300	870	1290
$(1\text{-CNC})_2$	3MP, 77 K	27 800	26 920	980	1980	—	—
1-COOENEC	3MP, 23°C	~(28 250)	26 520	?	2800	—	—
	EtOH, 23°C	~(28 250)	E		3280	~0	—
1-CNNEC	3MP, 23°C	27 600	27 350	250	1960	—	—
	EtOH, 23°C	27 560	E	—	2920	40	—

E: Exciplexe. (1) Bande due à la molécule liée de manière intramoléculaire et observée dans le spectre d'absorption; (2) bande attribuée à la molécule libre et observée dans le spectre d'excitation de la fluorescence.
[a] Déplacement Stokes défini par $\bar{\nu}_A$ (0,0) − $\bar{\nu}_F$ (0,0).
[b] Largeur à la mi-hauteur de la bande de fluorescence.
[c] Déplacement bathochrome de la bande (0,0) en absorption entre le 3MP et l'éthanol.
[d] Déplacement bathochrome de la bande (0,0) en fluorescence entre le 3MP et l'éthanol.

loppée existe dans les spectres où le 3MP sert de solvant. Par contre tous les spectres enregistrés pour les solutions d'éthanol à 23°C montrent une perte de structure fine vibrationnelle, une augmentation considérable de la largeur à la demi-hauteur, une augmentation du déplacement Stokes entre l'absorption et la fluorescence et une perte de l'image-miroir entre l'absorption et la fluorescence (voir tableau 3). Les spectres d'excitation de fluorescence correspondent bien aux spectres d'absorption cor-

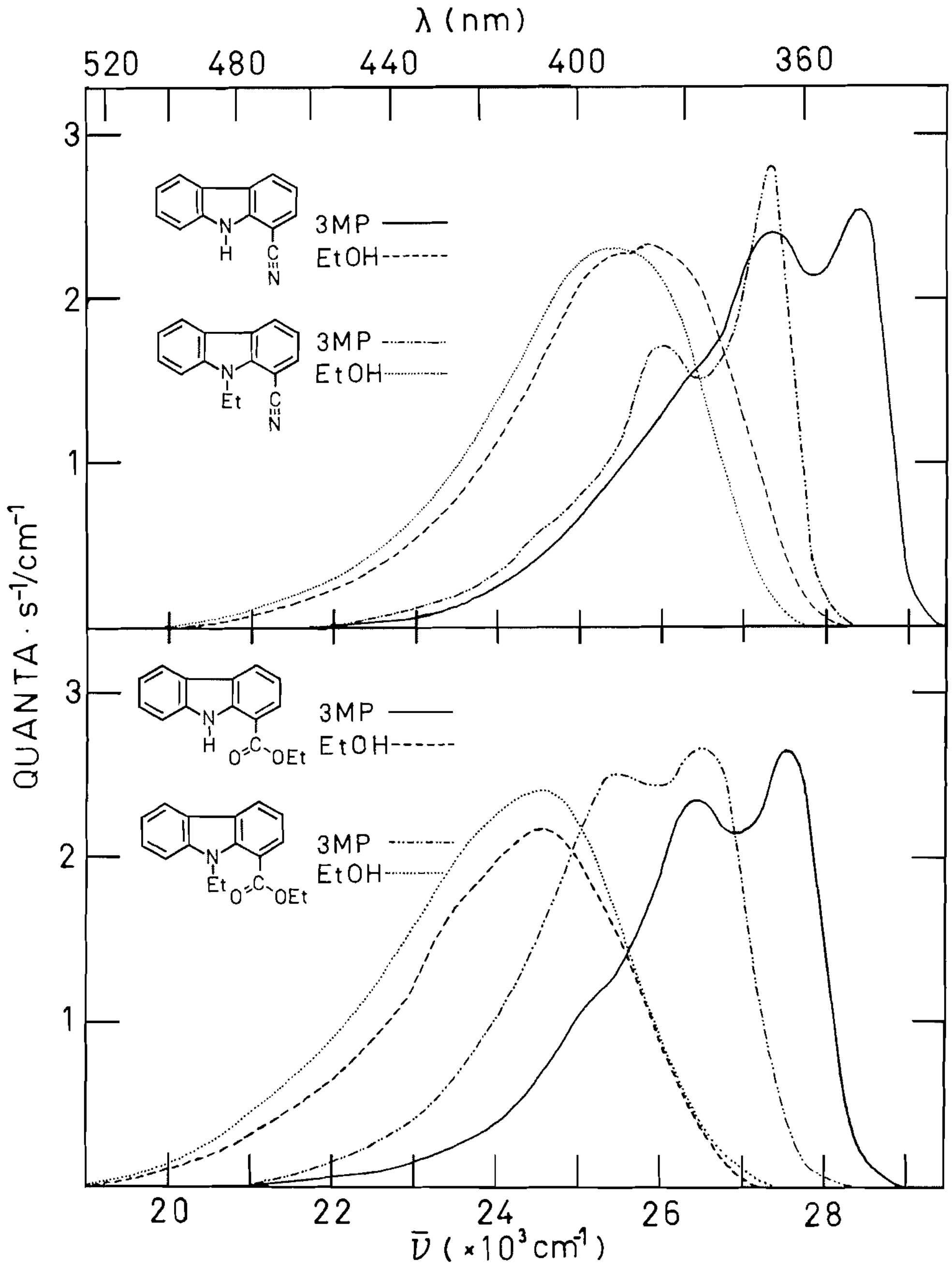

FIG. 8. Spectres de fluorescence du 1-CNC, 1-CNNEC, 1-COOEC et 1-COOENEC dissous dans le 3MP et l'éthanol à 23°C. Les concentrations étaient de 2,0 × 10^{-6} M pour le 1-CNC et de 1,0 × 10^{-5} M pour les autres dérivés étudiés.

respondant.

Le 1-CNC et le 1-COOEC forment avec l'éthanol un complexe par liaison hydrogène intermoléculaire à l'état électronique fondamental à 23°C et ce complexe existe également dans l'EPA comme le démontrent les valeurs de $\Delta\bar{\nu}_A$ dans le tableau 2. Rien de tel n'existe pour le 1-CNNEC et pour le 1-COOENEC puisque le groupement NH est remplacé par un groupement N—Et.

Une nouvelle espèce est donc responsable de la fluorescence de tous ces dérivés dans l'éthanol à 23°C. Le fait qu'un spectre bien structuré réapparaisse dans l'EPA ou l'éthanol à 77 K avec une largeur de bande de l'ordre de 2200 cm^{-1} ajouté aux autres caractéristiques déjà décrites enrichi l'hypothèse de l'exciplexe comme entité responsable de l'émission de fluorescence dans ces molécules dissoutes dans l'éthanol. Un exciplexe de stoïchiométrie 1 : 1 pourrait être responsable de la fluorescence du 1-CNNEC et du 1-COOENEC alors qu'un exciplexe de stoïchiométrie supérieure serait responsable de la fluorescence du 1-COOEC et 1-CNC dans l'éthanol puisque ces deux dernières molécules existent déjà sous forme complexée à l'état électronique fondamental (37). Une étude plus approfondie de chacune de ces molécules dans le 3MP avec ajout d'éthanol et d'eau est actuellement en cours de manière à définir la stoïchiométrie de ces exciplexes.

Par ailleurs, on sait que le carbazole et l'éthyl-*N* carbazole ne forment aucun exciplexe avec les alcools aliphatiques. Une explication possible pouvait être le fait que l'écart énergétique S_1-S_2 est relativement élevé (~4500 cm^{-1}) dans ces molécules alors que l'on sait que c'est la transition $^1L_a \leftarrow {}^1A$ chez les amines aromatiques qui confère le caractère transfert de charge

TABLEAU 3. Propriétés photophysiques de quelques dérivés substitués en position 1 du carbazole

Molécules	Conditions expérimentales	ϕ_F[a]	τ_F[b] (ns)	$k_F \times 10^{-6}$ (s^{-1})	$k_{nr} \times 10^{-6}$ (s^{-1})	$k_F^{(t)} \times 10^{-6}$ (s^{-1})	Image miroir
1-COOEC	3MP, 23°C	(0,020)	6,2	(3,2 ± 0,4)	(160 ± 10)	(68 ± 3)	—
	3MP, 77 K	0,64	8,1	79 ± 6	44 ± 3	68 ± 3	Oui
	EtOH, 23°C	(0,17)	8,4	(20 ± 2)	(100 ± 2)	(47 ± 2)	Non
	EPA, 77 K	0,32	7,5	43 ± 7	90 ± 10	39 ± 3	Oui
1-CNC	3MP, 23°C	0,57	11,8	48 ± 4	37 ± 4	46 ± 2	Oui
	EtOH, 23°C	(0,64)	14,0	(46 ± 2)	(26 ± 1)	(36 ± 2)	Non
	EPA, 77 K	0,75	9,8	76 ± 8	25 ± 3	64 ± 3	Oui
$(1\text{-CNC})_2$	3MP, 77 K	0,61	10,3	59 ± 5	38 ± 4	100 ± 6	Oui
1-COOENEC	3MP, 23°C	0,22	5,0	44 ± 6	160 ± 20	44 ± 6	Oui
	EtOH, 23°C	(0,14)	6,9	(20 ± 3)	(130 ± 20)	(36 ± 2)	Non
1-CNNEC	3MP, 23°C	0,49	10,7	46 ± 3	50 ± 3	53 ± 3	Oui
	EtOH, 23°C	(0,49)	12,1	(40 ± 4)	(42 ± 4)	(40 ± 2)	Non

[a] Ces rendements quantiques sont la moyenne de trois mesures individuelles qui se retrouvent toujours à l'intérieur d'une marge d'erreur de ± 0,02.

[b] Ces durées de vie proviennent de la moyenne de deux mesures expérimentales dont la marge d'erreur est de ± 0,25 ns. Ces décroissances sont toutes monoexponentielles.

nécessaire à la stabilisation de l'exciplexe (28*b*). Une étude récente des dérivés substitués en position 3 du carbazole semblait confirmer l'hypothèse de l'écart énergétique puisqu'il était réduit à 3000 cm^{-1} environ et que ces dérivés formaient des exciplexes avec l'éthanol (25). Cette hypothèse ne peut assurément pas expliquer la formation d'exciplexes entre les dérivés du carbazole substitués en position 1 et l'éthanol puisque les écarts S_1–S_2 pour l'ensemble des molécules étudiées varient entre 4350 cm^{-1} et 5040 cm^{-1} (22). La substitution d'un groupement électro-attracteur en position 1 du noyau doit donc être responsable du caractère transfert de charge nécessaire dans la fonction d'onde excitée ($^1L_b \leftarrow {}^1A$) pour permettre la stabilisation de l'exciplexe avec l'éthanol. Ceci est corroboré par le rapport des coefficients d'absorptivité molaire des bandes (0,0) des transitions $^1L_b \leftarrow {}^1A$ et $^1L_a \leftarrow {}^1A$ qui sont les suivants: 1-COOEC (1,1); 1-COOENEC (0,9); 1-CNC (0,6); 1-CNNEC (0,7) comparativement au carbazole (0,2) et à l'éthyl-*N* carbazole (0,2) (22). Chez les mêmes dérivés substitués en position de l'azote, ces rapports varient entre 0,3 et 0,4 (21) alors que chez les dérivés substitués en position 3, ils varient entre 0,2 et 0,4 (23). Nous croyons donc que l'écart énergétique ($^1L_b - {}^1L_a$) joue un rôle important dans la formation des exciplexes entre les dérivés substitués aux positions N et 3 du carbazole et l'éthanol, alors que c'est plutôt le caractère transfert de charge important de la transition $^1L_b \leftarrow {}^1A$ des dérivés substitués en position 1 du carbazole qui est responsable de la formation des exciplexes avec l'éthanol.

V. *Propriétés photophysiques de l'ensemble de ces systèmes*

Nous avons regroupé au tableau 3 l'ensemble des propriétés photophysiques des dérivés substitués en position 1 du carbazole. Nous remarquons un effet notable et du substituant et du milieu sur ces propriétés. Tout comme chez les dérivés substitués en position 3 (25) les dérivés cyanurés possèdent un rendement quantique de fluorescence plus élevé que celui des dérivés carboéthoxylés peu importe le milieu. Ceci peut être attribué à la rotation gênée du groupe carboéthoxylé comparativement au groupe cyanuré dans l'état S_1 relaxé puisque les durées de vie de fluorescence sont toujours plus élevées pour ces derniers dérivés dans le 3MP. Pour le 1-COOEC, le rendement quantique n'est pas significatif puisque l'absorption se fait par les deux systèmes libre et lié (mais surtout par ce dernier). Cependant, le système libre, seul responsable de l'émission possède une durée de vie de 6,2 ns, la plus faible valeur obtenue pour ces systèmes avec celle du 1-COOENEC dans le 3MP (5,0 ns) et ceci peut s'expliquer par la rotation gênée des groupements d'atomes en position 1 dans l'état premier singulet excité. La liaison hydrogène, qu'elle soit intramoléculaire (1-COOEC dans le 3MP à 77 K) ou intermoléculaire (1-COOEC dans l'EPA à 77 K), augmente la durée de vie des molécules à l'état S_1 d'environ 2 ns. Lorsque la rotation du groupement carboéthoxylé est complètement annihilée (1-COOEC dans le 3MP à 77 K) par la liaison hydrogène intramoléculaire, d'une part la probabilité radiative de transition $k_F^{(t)}$ ou k_F augmente considérablement (par un facteur 2 environ) par rapport à celle du carbazole (25) alors que la constante non-radiative n'augmente que très légèrement, ces deux facteurs conjugués sont responsables du rendement quantique relativement élevé du 1-COOEC dans le 3MP à 77 K.

Les paramètres photophysiques de tous ces dérivés dans l'éthanol à 23°C ne sont pas nécessairement significatifs sauf pour les durées de vie de fluorescence. Quant aux rendements quantiques, il se peut dans certains cas que la fluorescence observée soit un mélange d'exciplexe et de molécule non-complexée bien que les décroissances soient monoexponentielles peu importe la région du spectre de fluorescence observée. Une étude dynamique de la formation de ces exciplexes devrait être faite par ajout d'éthanol au 3MP pour mieux comprendre ces résultats globaux dans l'éthanol comme solvant. On remarque cependant que de façon très systématique, la durée de vie de fluorescence de toutes ces molécules dans l'éthanol est de 2 ns plus élevée que celle dans le 3MP. Enfin, le dimère du cyano-1 carbazole possède des propriétés photophysiques très semblables à celles du 1-COOEC liée de manière intramoléculaire en ce sens que dans ces deux structures rigides, la constante de désactivation non-radiative s'apparente à celle du carbazole et les probabilités de transitions radiatives sont beaucoup plus élevées.

Conclusion

Dans cet article, nous avons voulu montrer l'importance de la liaison hydrogène, qu'elle soit intermoléculaire ou intramoléculaire, sur la perturbation des propriétés spectroscopiques et photophysiques de certains dérivés substitués en position 1 du carbazole.

Le cyano-1 carbazole forme un dimère cyclique dans le 3MP avec une enthalpie et une entropie de complexation identiques à celles obtenues antérieurement pour la même molécule dans le tétrachlorure de carbone. Plus la force de la liaison hydrogène augmente dans le dimère, plus l'intensité de la première transition électronique du dimère augmente. Dû au peu de recouvrement des systèmes π des deux chromophores du carbazole, aucun tautomère n'a pu être détecté en fluorescence.

Le carboéthoxy-1 carbazole existe surtout sous forme liée de façon intramoléculaire dans les solvants non-polaires et en phase gazeuse dans son état électronique fondamental. Cette liaison hydrogène intramoléculaire est par ailleurs rompue pour faire place à une liaison hydrogène intermoléculaire dans l'éthanol. Le rendement quantique de fluorescence du système lié (intramoléculaire) est par ailleurs très faible en solution fluide de 3MP si bien qu'à température ambiante, seul le système libre émet. Ce phénomène a été confirmé par l'étude du spectre d'excitation de la fluorescence ainsi que par la valeur des durées de vie de fluorescence comparées. Par ailleurs, à 77 K en matrice rigide de 3MP, le système lié émet fortement comme le confirme le rendement quantique de 0,64. Le système libre du 1-COOEC possède une durée de vie de fluorescence plus courte que les systèmes liés de forme intermoléculaire ou intramoléculaire et ceci est surtout attribué à la rotation du groupement carboéthoxylé à l'état excité S_1. Par ailleurs, nous attribuons surtout à l'augmentation de la constante radiative (probabilité de transition $^1L_b \leftarrow {}^1A$), le fait que le rendement quantique de fluorescence du système lié dans le 3MP soit si élevé.

Nous avons également montré que tous les dérivés substitués du carbazole en position 1 forment des exciplexes avec l'éthanol. Les spectres d'excitation de la fluorescence de ces exciplexes démontrent que c'est la molécule libre qui est à l'origine de la formation des exciplexes pour le 1-CNNEC et le 1-COOENEC alors que ce sont les complexes 1-COOEC – EtOH et 1-CNC – EtOH (par liaison hydrogène intermoléculaire) qui sont à l'origine de la formation des exciplexes chez les molécules possédant un groupement NH. Par ailleurs, l'argument de l'écart énergétique réduit entre les états S_1 et S_2 invoqué pour expliquer la stabilisation des exciplexes entre les dérivés substitués du carbazole aux positions N et 3 et l'éthanol ne peut être utilisé pour les dérivés substitués en position 1 du noyau. Par contre, l'état ^1L_b de ces dérivés possède déjà un caractère transfert de charge important si l'on en juge par les rapports des coefficients d'absorptivité des deux premières transitions électroniques dans ces molécules.

Remerciements

Les auteurs remercient le Conseil de Recherches en sciences naturelles et en génie du Canada ainsi que le Ministère de l'Education du Québec pour leur assistance financière. Nous désirons aussi remercier le Dr. Bogumil Zelent de notre laboratoire pour les nombreuses discussions que nous avons eu concernant ce travail.

1. C. SANDORFY. *Dans* Vibrational spectra of hydrogen bonded systems in the gas phase. Topics in current chemistry. Vol. 120. *Edité par* F. L. Boschke. Springer, Berlin, Heidelberg. 1984. pp. 42–88.
2. C. SANDORFY. *Dans* Overtones and combination tones: application to the study of molecular associations. Infrared and Raman spectroscopy of biological molecules. *Edité par* T. M. Theophanides. D. Reidel Publishing Co., Dordrecht, Holland. 1979. pp. 305–318.
3. G. E. JOHNSON. J. Phys. Chem. **84**, 2940 (1980).
4. M. MARTINAUD. Thèse d'Etat, Université de Bordeaux (1975).
5. A. CAMPILLO et M. MARTINAUD. Chem. Phys. Lett. **33**, 126 (1975).
6. M. MARTINAUD et A. KADIRI. Chem. Phys. **28**, 473 (1978).
7. R. W. BIGELOW et G. P. CEASAR. J. Phys. Chem. **83**, 1790 (1979).
8. T. S. SPENCER et C. M. O'DONNELL. J. Am. Chem. Soc. **94**, 4846 (1972).
9. M. MARTIN et W. R. WARE. J. Phys. Chem. **82**, 2770 (1978).
10. G. WEBER. Biochemistry, **75**, 335 (1960).
11. S. V. KONEV. Fluorescence and phosphorescence of proteins and nucleic acids. Plenum Press, New York. 1967.
12. M. S. WALKER, T. W. BEDNAR et R. LUMRY. J. Chem. Phys. **47**, 1020 (1967).
13. S. T. COLLINS. J. Phys. Chem. **87**, 3202 (1983).
14. M. BELLETÊTE et G. DUROCHER. Can. J. Spectrosc. **24**, 87 (1979); Can. J. Chem. **57**, 2539 (1979); Can. J. Chem. **60**, 2332 (1982); J. Photochem. **21**, 251 (1983).
15. M. BELLETÊTE. Thèse de doctorat (Ph.D), Université de Montréal (1982).
16. A. AHMAD et G. DUROCHER. Can. J. Spectrosc. **26**, 19 (1981).
17. A. AHMAD et G. DUROCHER. Photochem. Photobiol. **34**, 573 (1981).
18. A. WELLER et D. REHM. Ber. Bunsenges Phys. Chem. **73**, 834 (1969); Isr. J. Chem. **8**, 259 (1970).
19. G. WEBER. *Dans* Light and life. *Edité par* McElroy et Glass. John Hopkins University Press, Baltimore, MD. 1970. p. 82.
20. B. ZELENT et G. DUROCHER. J. Org. Chem. **46**, 1496 (1981); Can. J. Chem. **60**, 945 (1982); Can. J. Chem. **60**, 2442 (1982); Can. J. Chem. **63**, 1654 (1985).
21. P. D. HARVEY, B. ZELENT et G. DUROCHER. Spectrosc. Int. J. **2**, 128 (1983).
22. B. ZELENT, P. D. HARVEY et G. DUROCHER. Can. J. Spectrosc. **28**, 188 (1983).
23. B. ZELENT, P. D. HARVEY et G. DUROCHER. Can. J. Spectrosc. **29**, 23 (1984).
24. P. D. HARVEY et G. DUROCHER. Can. J. Spectrosc. **29**, 84 (1984); J. Photochem. **27**, 29 (1984).
25. P. D. HARVEY et G. DUROCHER. J. Lumin. Sous presse.
26. B. ZELENT et G. DUROCHER. J. Phys. Chem. **88**, 5430 (1984).
27. (*a*) C. CHANG, N. SHABESTARY ET M. A. EL-BAYOUMI. Chem. Phys. Lett. **75**, 107 (1980); (*b*) J. WALUK, A. GRABOWSKA, B. PAKULA et J. SEPIOL. J. Phys. Chem. **88**, 1160 (1984).
28. (*a*) K. C. INGHAM et M. A. EL-BAYOUMI. J. Am. Chem. Soc. **96**, 1674 (1974); (*b*) S. T. COLLINS. J. Phys. Chem. **87**, 3202 (1983); (*c*) H. BULSKA, A. GRABOWSKA, B. PAKULA, J. SEPIOL, J. WALUK et U. P. WILD. J. Lumin. **29**, 65 (1984).
29. M. NISKI, K. HISAO et T. KANO. Bull. Chem. Soc. Jpn. **54**, 1897 (1981).
30. P. D. HARVEY. Thèse de maîtrise, Université de Montréal (1983).
31. D. RIVEST-FILION, K. THAMMAVONG et G. DUROCHER. Spectrochim. Acta Part A, **37**, 627 (1981).
32. E. C. LIM, J. D. LAPOSA et J. M. H. YU. J. Mol. Spectrosc. **19**, 412 (1966).
33. J. B. BIRKS et D. J. DYSON. Proc. R. Soc. London, Ser. A, **275**, 135 (1963).
34. C. CHENEVEAU. International critical tables. Vol. VII. p. 12.
35. J. TIMMERMANS. Physico-chemical constants of pure organic compounds. Elsevier Publishing Co. Inc., New York. 1950.
36. C. A. PINKHAM et S. C. WAIT, JR. J. Mol. Spectrosc. **27**, 326 (1968).
37. G. E. JOHNSON et W. W. LIMBURG. J. Phys. Chem. **88**, 2211 (1984).

The electronic structures of bis(η^6-benzene)- and bis(η^6-naphthalene)chromium(0)

JACQUES WEBER[1] AND E. PETER KUNDIG
Section de Chimie, Université de Genève, 30 quai Ernest Ansermet CH-1211 Genève 4, Switzerland

AND

ANNICK GOURSOT AND EDOUARD PENIGAULT
Laboratoire de Photochimie Générale, ERA au CNRS n° 386, Ecole Nationale Supérieure de Chimie, 3 rue Alfred Werner, F-68093 Mulhouse Cedex, France

Received July 27, 1984

This paper is dedicated to Professor Camille Sandorfy on the occasion of his 65th birthday

JACQUES WEBER, E. PETER KUNDIG, ANNICK GOURSOT, and EDOUARD PENIGAULT. Can. J. Chem. **63**, 1734 (1985).

SCF MS Xα molecular orbital calculations are reported for the bis(η^6-benzene)- and bis(η^6-naphthalene)chromium(0) complexes. The bonding may be essentially discussed in terms of the covalent interactions between the metal 3*d* and ligand π and π^* orbitals. The different charges on chromium atom in the two systems are explained by the different balances between ligand-to-metal (bonding) and metal-to-ligand (back-bonding) electron donations. Some resemblances are found between the electronic structures of the two compounds and it is possible to correlate to a large extent the energy levels of their molecular orbitals. However, a shift towards lower values is predicted for the energy levels of the naphthalene complex, together with a large disruption of all the virtual π^* and $3d^*$ levels. This would undoubtedly favor nucleophilic attack followed by metal–ring or carbon–carbon bond cleavage, in agreement with the extreme lability of the coordinated arene rings observed in this complex.

JACQUES WEBER, E. PETER KUNDIG, ANNICK GOURSOT et EDOUARD PENIGAULT. Can. J. Chem. **63**, 1734 (1985).

On a effectué des calculs d'orbitales moléculaires MS Xα en champ autocohérent pour les complexes bis(η^6-benzène)- et bis(η^6-naphtalène)chrome(0). On peut decrire la liaison dans le complex presque essentiellement à l'aide des interactions covalentes entre les orbitales 3*d* du métal et les orbitales π et π^* du ligand. On explique les différentes charges sur l'atome de chrome dans les deux systèmes par des bilans differents entre la donation directe d'électrons ligand–métal et la rétro-donation métal–ligand. Toutefois, on prédit un déplacement vers des valeurs plus basses pour les niveaux énergétiques du complexe de naphtalène ainsi qu'un mélange important de tous les niveaux virtuels π^* et $3d^*$. Ceci devrait de toute évidence favoriser une attaque nucléophile, suivie d'une rupture de la liaison métal–cycle ou carbone–carbone, en accord avec la labilité extrême observée dans ces complexes pour les cycles aréniques coordonnés.

[Traduit par le journal]

Introduction

Whereas bis(η^6-benzene)chromium(0), **1**, has been known for thirty years (1), it is only recently that the preparation of bis(η^6-naphthalene)chromium(0), **2**, the parent compound with fused six-membered ring ligands, has been reported (2, 3).

One of the chief differences between **1** and **2** concerns the lability of the coordinated arene rings: whereas **1** is inert to arene displacement reactions, the naphthalene ligands of **2** are known to easily undergo substitution reactions. A similar situation exists in the $Cr(CO)_3$ complexes of the two arenes. The lability of the naphthalene—Cr bond is certainly at the origin of the catalytic properties of the naphthalene–$Cr(CO)_3$ complex (4, 5). This somewhat unexpected difference in reactivity between **1** and **2** may probably be related to differences in electronic structure and metal–ligand interactions in complexes with condensed aromatic ligands as compared with arene–metal complexes. It was therefore of interest to perform a comparative theoretical study of the electronic structure of **1** and **2** in an attempt to understand the different properties of these compounds. To this end, the multiple scattering (MS) Xα molecular orbital (MO) model was chosen since it has been previously shown to give reliable predictions of the electronic structure and related properties of organometallic compounds such as **1** (6) or several members of the metallocene series (7–11).

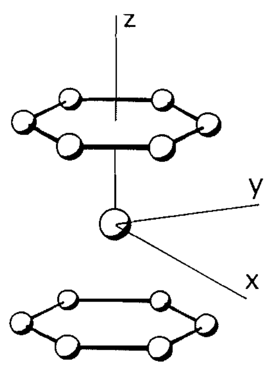

1

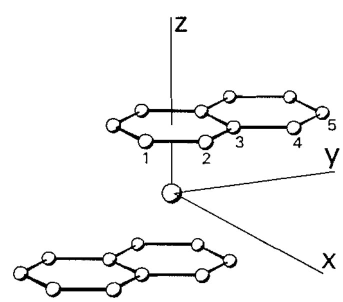

2

Method

The standard version of the SCF MS Xα method was used

[1] To whom all correspondence should be addressed.

TABLE 1. Calculation parameters

	Compound **1**		Compound **2**	
	α	Sphere radii (au)	α	Sphere radii (au)
Cr atom	0.71352	2.38411	0.71352	2.38237
C atom	0.75928	1.68070	0.75928	1.64763
H atom	0.77725	0.89409	0.77725	0.91535
Empty sphere	0.76608	1.34456	0.76581	1.31810
Outer sphere	0.76608	6.53712	0.76581	10.35810
Intersphere	0.76608	—	0.76581	—

(12). For the geometry of $(\eta^6\text{-}C_6H_6)_2Cr$, the electron diffraction data of Haaland (13) are used, i.e., an eclipsed structure of D_{6h} symmetry with planar ligands, the bond lengths being C—C 1.423 Å, C—H 1.090 Å, and the vertical metal-to-ring distance 1.613 Å.

For the bisnaphthalene complex, a standard C_{2h} symmetry is assumed, with *anti*-oriented naphthalene rings. This is at variance with a recent X-ray crystal structure determination of **2** which concluded to *syn*-oriented ligands (14). However, most of the observations involving this compound being performed in vapor or liquid phase, the barrier to internal rotation is low enough to permit large amplitude torsional motion. In addition, the nature of ligand–metal interactions is very similar in both *anti*- and *syn*-forms. In order to make the comparison of electronic structures easier, the same metal-to-ring distance as for **1** (1.613 Å) has been chosen for **2**. Actually, this distance is only 0.05 Å smaller than the value deduced from the X-ray measurements performed for **2** (14). Similarly, a standard geometry has been adopted for the planar naphthalene rings, with C—C bond lengths and C—C—C bond angles assumed to be all equal to 1.395 Å and 120°, respectively. Actually, these data are the average values of the corresponding parameters obtained from the X-ray study of **2**. Finally, the C—H bond lengths of **2** have all been chosen as 1.085 Å.

Table 1 presents the MS Xα calculation parameters used. The values of atomic exchange parameters α are those optimized by Schwarz (15), except for hydrogen where we have chosen the spin-polarized value (16). A weighted average of the atomic values is chosen for the α value in interatomic, extramolecular (outer sphere), and intersphere regions.

Appropriate values for the radii of atomic spheres have been chosen according to the procedure previously described for the metallocenes (7, 9): the carbon and hydrogen touching sphere radii (i.e. of tangential atomic spheres) are first determined by the C—C and C—H bond distances, and then increased by 25%, leading thus to overlapping atomic spheres. The radius of chromium sphere is chosen to be tangent to the enlarged carbon sphere. Additional "empty" spheres are located in the center of all the phenyl rings. An externally tangent outer sphere is used in all the calculations. Partial waves up to $l = 2$ are included in the multiple scattering expansions in chromium sphere and extramolecular region, up to $l = 1$ in carbon and empty spheres, and for $l = 0$ in hydrogen spheres.

Results and discussion

The ground-state electronic structures of $(\eta^6\text{-}C_6H_6)_2Cr$ and $(\eta^6\text{-}C_{10}H_8)_2Cr$ are presented in Tables 2 and 3 and compared graphically in Fig. 1.

One should note that the results obtained for **1** differ slightly from those we have previously reported (6), since the radius of

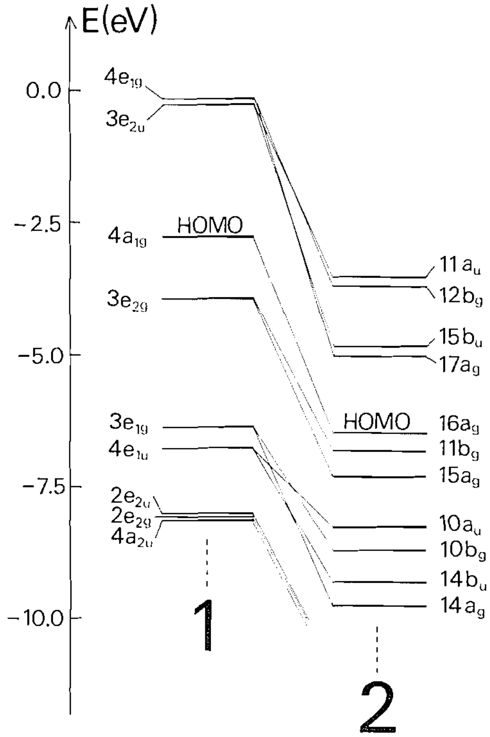

FIG. 1. Upper valence ground-state energy levels for compounds **1** and **2**.

metal sphere has been modified so as to be the same as that used for compound **2**, which actually leads to a more realistic value for this parameter.

The ground-state configuration of **1** is ${}^1A_{1g}\,(3e_{2g})^4\,(4a_{1g})^2$, the sequence of predominantly metal 3d orbitals being $3e_{2g}(3d\delta) \leq 4a_{1g}(3d\sigma) \leq 4e_{1g}(3d\pi)$,[2] in agreement with the general ligand field theory of such metal sandwich complexes (17).

It is seen from both Table 2 and Fig. 2 that these orbitals have different bonding characters: whereas the $3e_{2g}$ MO is strongly bonding through an in-phase combination of metal $3d\delta$ and ligand π orbitals, the $4a_{1g}$ MO, which is the highest occupied MO (HOMO), has a much larger metal character and it is essentially nonbonding. As to the virtual $4e_{1g}$ MO, it is strongly antibonding through an out-of-phase combination of metal $3d\pi$ and ligand π orbitals. It is seen from Table 2 that $4e_{1g}$ is not the lowest unoccupied MO (LUMO) of system **1**, as there is a pure ligand π^* orbital, namely $3e_{2u}$, which lies imme-

[2] According to pseudoaxial ligand field theory, the d-orbital set in D_{6h} symmetry is split into three irreducible representations: $a_{1g}(\sigma\text{: } d_{z^2})$, $e_{1g}(\pi\text{: } d_{xz}, d_{yz})$, $e_{2g}(\delta\text{: } d_{x^2-y^2}, d_{xy})$, where z is the sixfold rotational axis.

TABLE 2. Upper valence ground-state energy levels (eV) and charge distribution of bis(η^6-benzene)-chromium

			Charge distribution (%)[a]									
			Cr			C[b]			H	Empty	Inter	Outer
Orbital	Occ.	Energy	*s*	*p*	*d*	*s*	*p*σ	*p*π	*s*	sphere	sphere	sphere
$4e_{1g}$	0	−0.16			73	2	2	10			5	8
$3e_{2u}$	0	−0.27						73			27	
$4a_{1g}$	2	−2.85	1		82		1	1	1	4	9	1
$3e_{2g}$	4	−4.01			50		2	21			27	
$3e_{1g}$	4	−6.53			16		1	52			30	1
$4e_{1u}$	4	−6.90		4				49			47	
$2e_{2u}$	4	−8.19					60		17		23	
$2e_{2g}$	4	−8.21			1		60		18		19	2
$4a_{2u}$	2	−8.26		4				61		1	31	3
$3a_{1g}$	2	−9.56	8					53		1	35	3

[a]The C, H, and empty sphere charge distributions refer to the charge contained in all the respective spheres of the same type.
[b]The notations *p*σ and *p*π refer to planar benzene rings (σ: $2p_x$ and $2p_y$; π: $2p_z$).

TABLE 3. Upper valence ground-state energy levels (eV) and charge distribution of bis(η^6-naphthalene)-chromium

			Charge distribution (%)[a]									
			Cr			C[b]			H	Empty	Inter	Outer
Orbital	Occ.	Energy	*s*	*p*	*d*	*s*	*p*σ	*p*π	*s*	sphere	sphere	sphere
$14b_g$	0	−3.04			33			48			18	1
$19a_g$	0	−3.09			25		3	13			51	8
$13b_g$	0	−3.32			16		3	12			60	9
$18a_g$	0	−3.36			28	1		16			48	7
$11a_u$	0	−3.63						69			31	
$12b_g$	0	−3.79			48	1	1	9			37	4
$15b_u$	0	−4.85		1				66			33	
$17a_g$	0	−5.08	1		27		1	43			28	
$16a_g$	2	−6.59	1		83		4			4	8	
$11b_g$	2	−6.89			60		1	22			17	
$15a_g$	2	−7.41			58		2	21			19	
$10a_u$	2	−8.41		1				66			33	
$10b_g$	2	−8.94			13			56			31	
$14b_u$	2	−9.53		3				64			33	
$14a_g$	2	−9.89			13			59			28	
$9a_u$	2	−10.52		3				62			35	
$9b_g$	2	−10.59			13		2	58			27	
$13b_u$	2	−11.27		3				62		1	34	
$13a_g$	2	−11.41	2		4		1	61		1	31	
$12b_u$	2	−12.46					63		20		17	
$12a_g$	2	−12.52			1		63		19		17	
$11b_u$	2	−12.74		3				65		1	31	

[a]For the sake of conciseness, all the C and H charge distributions, though arising from five non-equivalent atoms, have been summed up and are presented as single entries. The same procedure applies to empty sphere contributions.
[b]The notations *p*σ and *p*π refer to planar naphthalene rings (σ: $2p_x$ and $2p_y$; π: $2p_z$).

diately below it. This result is at variance with our previous calculation (6) which concluded to the opposite ordering for the $4e_{1g}$ and $3e_{2u}$ MOs, and therefore to a LUMO with predominant metal character. The result $3e_{2u} \leq 4e_{1g}$ is, however, that deduced for the anion $\mathbf{1}^-$ from both a detailed analysis of the esr spectrum and SCF MS Xα calculations (18). For the neutral system **1** this question is of minor importance since: (*i*) the energy difference between $3e_{2u}$ and $4e_{1g}$ is very small and (*ii*) there is no experimental evidence as to the nature of the LUMO level.

In the ground-state electronic structure of **1**, one finds at lower energies the ligand-based levels, which may be classified into pairs of π-type orbitals ($3e_{1g}$, $4e_{1u}$), σ-type ones ($2e_{2u}$, $2e_{2g}$) and again π-type ones ($4a_{2u}$ and $3a_{1g}$). Among them, $3e_{1g}$ has appreciable (16%) metal *d* character and, together with $3e_{2g}$, these levels are responsible for most of the metal–ligand bonding interactions in $(\eta^6\text{-}C_6H_6)_2Cr$. Let us turn now to **2** in order to see to which extent the electronic structure of this system resembles that of **1**.

It is immediately seen from Fig. 1 that despite a stabilizing

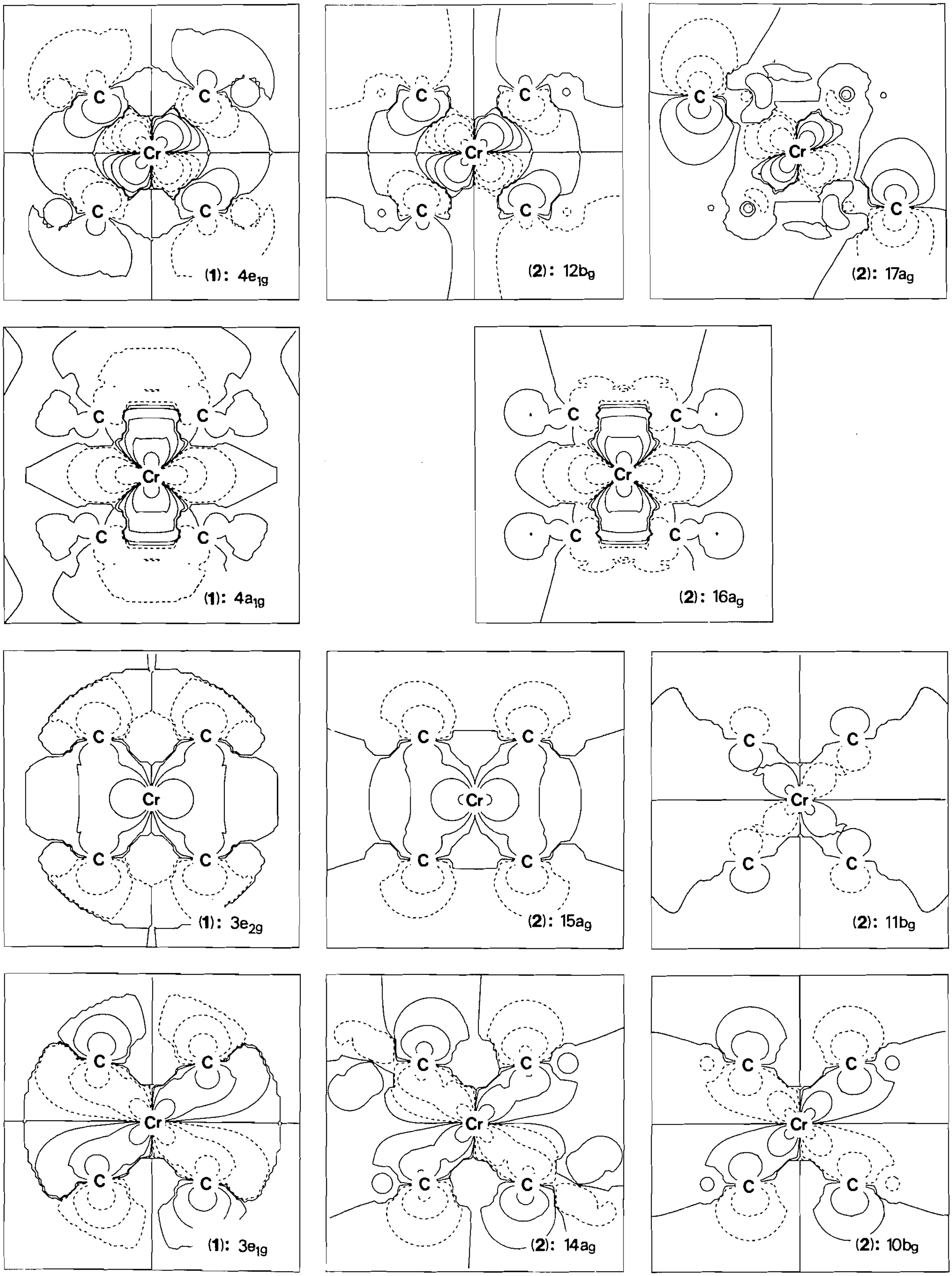

FIG. 2. Wave function contours of selected MOs of systems **1** and **2**. Except for the $17a_g$ level of **2**, which is plotted in a vertical plane containing the Cr and C_4 atoms, all the MOs are represented in the XOZ plane. Positive wave function contours are indicated by a solid line while negative contours are represented by a dashed line.

TABLE 4. Correlation table for D_{6h} to C_{2h} descent in symmetry

D_{6h}	C_{2h}
A_{1g}, A_{1u}	A_g, A_u
A_{2g}, A_{2u}	B_g, B_u
B_{1g}, B_{1u}	B_g, B_u
B_{2g}, B_{2u}	A_g, A_u
E_{1g}, E_{1u}	$A_g + B_g$, $A_u + B_u$
E_{2g}, E_{2u}	$A_g + B_g$, $A_u + B_u$

energy shift of 3–4 eV, the orbital pattern of **2** is to a large extent similar to that of **1**, the correlation for D_{6h} to C_{2h} descent in symmetry presented in Table 4 enabling a better comparison between the two systems.

The ground-state configuration of **2** is ^1A_g $(15a_g)^2$ $(11b_g)^2$ $(16a_g)^2$, with the sequence of predominantly metal 3d orbitals $15a_g(3d_{x^2-y^2}) \leq 11b_g(3d_{xy}) \leq 16a_g(3d_{z^2}) \leq 17a_g(3d_{yz}) \leq 12b_g(3d_{xz})$. This ordering is in perfect agreement with the result obtained for system **1**, since the $3e_{2g}(3d\delta)$ MO of **1** correlates with the $15a_g$ and $11b_g$ MOs of **2**, $4a_{1g}(3d\sigma)$ of **1** with $16a_g$ of **2** and $4e_{1g}(3d\pi)$ of **1** with $17a_g$ and $12b_g$ of **2**. The $16a_g$ MO of **2** is thus the HOMO and $17a_g$ the LUMO. However, the HOMO–LUMO energy gap is significantly smaller (by 1.07 eV) in **2** than in **1**. Inspection of Table 3 and Fig. 2 reveals a striking resemblance between $3e_{2g}$ (**1**) and $15a_g$ (**2**), $4a_{1g}$ (**1**) and $16a_g$ (**2**), $4e_{1g}$ (**1**) and $12b_g$ (**2**): $15a_g$, and to a lesser extent $11b_g$, are strongly bonding through in-phase combinations of 3$d\delta$ with ligand π orbitals and these two MOs play for system **2** the same role as $3e_{2g}$ for **1**, with a metal character larger by about 10%, however. The relative stability of $15a_g$ with respect to $11b_g$ is due to the different types of carbon atoms involved in metal–ligand bonding: in $15a_g$ the largest ligand contribution arises from the nearest C_2 atom whereas in $11b_g$ the farther C_4 and C_5 atoms contribute the most, which explains its slightly minor bonding character. Whereas the $16a_g$ HOMO of **2** has exactly the same nonbonding character as the $4a_{1g}$ HOMO of **1**, it is interesting to examine in detail the nature of the antibonding $17a_g$ and $12b_g$ MOs, which correlate with the $4e_{1g}$ level of system **1**. As a general result, we see that, the ligand π^* $15b_u$ and $11a_u$ MOs excepted, the low-lying virtual orbitals of **2** are considerably delocalized over the whole molecule and exhibit some antibonding character. Taking indeed the $17a_g$ and $12b_g$ MOs as examples, their metal character is only 27% and 48%, respectively, as compared with 73% in their $4e_{1g}$ counterpart in **1**. Moreover, the antibonding characters of these two MOs are very different as shown in Fig. 2: whereas $12b_g$ is metal–C_2 antibonding, $17a_g$ is mainly metal–(C_5,C_6) antibonding, with the result that $12b_g$ is much more antibonding than $17a_g$. This leads to a large destabilization of $12b_g$ with respect to $17a_g$ (1.29 eV), the energy difference between these MOs being much larger than that between the bonding MOs $15a_g$ and $11b_g$. When comparing systems **1** and **2**, and this point will be discussed in some detail further on, we may already point out that their different chemical properties are probably related to: (*i*) the important shift towards lower energies observed for all the MO levels of **2**; (*ii*) the significantly smaller HOMO-LUMO energy difference in **2**; and (*iii*) the larger delocalization of the LUMO and low-lying virtual levels of **2** over the whole compound.

At lower energies, i.e. below the predominantly metal 3d MOs, one finds the ligand-based levels which can be easily correlated with the corresponding levels of **1**: $14a_g$ and $10b_g$ correlate with $3e_{1g}$ as may be seen from Fig. 2, and their metal character is nearly the same as that of their congener in **1**. The $14b_u$ and $10a_u$ MOs are almost pure ligand π levels and correspond to $4e_{1u}$ in **1**, whereas $9a_u$ correlates with $4a_{2u}$. However, as there are 8 additional ligand π electrons and 28 additional ligand σ electrons in $(\eta^6\text{-}C_{10}H_8)_2Cr$ as compared with $(\eta^6\text{-}C_6H_6)_2Cr$, the orbital pattern of the former system is characterized by the presence of additional MOs. This is typically the case for $9b_g$ which has no counterpart in **1**. Finally, looking at the low-lying valence levels of **2**, it is seen that, as for system **1**, there is no clear-cut separation between predominantly π and σ ligand levels, but the highest σ levels intermingle with the lowest π orbitals. As for system **1**, the σ framework of ligands in **2** contributes very little to the bonding in the complex and most of the covalent metal–ligand interactions involve Cr 3d and ligand π orbitals.

Concerning the origin of the stabilizing shift in orbital energies between compounds **1** and **2**, one might conceivably attribute it to muffin-tin effects: due to the large intersphere volume in **2**, as compared with **1**, the volume averaging in this region tends to significantly delocalize the charge density over the whole molecule, which in turn leads to a stabilization of the levels. However, according to our experience and to some test calculations we have recently performed for the anion $\mathbf{1}^-$, this spurious effect is likely not to exceed 1–2 eV in our case, which suggests that on a qualitative basis the stabilization of the energy levels of **2** with respect to **1** is a real effect which is due to the different nature of the ligands in both complexes.

Table 5 presents the electronic configuration of the metal in the two complexes. The problem of charge partitioning has been solved by attributing both intersphere and outer sphere charges fully to the ligands. This procedure has been previously found to be adequate in the case of metallocenes (7, 9–11) as it leads to (*i*) a reasonable charge of the order of +0.5 on metal; (*ii*) a total metal 3d participation of nearly 100% in each pair of bonding–antibonding MOs of the same symmetry, which is a good criterion for the orthogonality of the wavefunctions. However, this scheme could be not very well suited to compound **2**, which exhibits a large intersphere volume, and we decided to use also for both compounds another charge partitioning procedure attributing to metal a large part of the interatomic charge. The results obtained using this alternative scheme do not change the main conclusions to be drawn from Table 5 and they will be summarized later on in this section. It is seen from Table 5 that 4s and 4p populations do not undergo great changes when going from system **1** to **2** and remain rather small, which indicates that the role of these orbitals in the bonding of the complexes is not important. However, substantial differences appear when comparing the populations of metal 3d orbitals: the partial populations of all the 3d components are larger in **2**, with the result that the total metal 3d population in **2** is larger by 0.62e than the corresponding value in **1**. A detailed analysis performed for all the occupied levels of the valence shell shows that: (*i*) the predominantly metal 3d MOs (i.e. $4a_{1g}$ and $3e_{2g}$ in **1**, and their counterparts in **2**) accommodate 0.36 additional 3d electrons in **2**, with respect to **1**; (*ii*) the ligand based MOs (i.e. all the occupied levels lying below $3e_{2g}$ in **1**, and their counterparts in **2**) contribute to the overall metal 3d population by 0.26 additional electrons in **2**, with respect to **1**. The increase in metal 3d population observed in **2** is therefore due to a larger metal 3d character exhibited by all the MOs of proper symmetry, the predominantly metal 3d levels con-

TABLE 5. Metal configuration in the complexes

	Electron population on chromium[a]									
			$3d^b$							
Complex	$4s$	$4p$	z^2	x^2-y^2	xy	xz	yz	Total	Metal charge
1	0.28	0.42	1.70	1.04	1.04	0.46	0.46	4.70	+0.60
2	0.28	0.44	1.76	1.20	1.36	0.54	0.46	5.32	−0.04

[a]The electron population of chromium atomic orbitals has been obtained by summing up over all the occupied MOs of the valence shell, with the intersphere, and outer sphere charge fully attributed to ligands.
[b]The x, y, and z axes are defined in structures **1** and **2**.

tributing the most. This leads ultimately to an almost neutral chromium atom in **2**, whereas the charge on this atom is +0.60 in **1**. Actually, starting from a Cr free atom configuration $3d^6$, the chromium charge of +0.60 in **1** (resp. −0.04 in **2**) results from: (*i*) a ligand-to-metal donation of 0.92e (resp. 1.00e) from the $2p\pi$ orbitals of ligand rings to metal $3d_{xz}$ and $3d_{yz}$ orbitals; (*ii*) a transfer of 0.70e (resp. 0.72e) from the $2p$ orbitals of the ligand rings to metal $4s$ and $4p$ orbitals; (*iii*) a back-bonding transfer of 2.22e (resp. 1.68e) from metal $3d_{z^2}$, $3d_{x^2-y^2}$, and $3d_{xy}$ orbitals to ligand $2p$ levels. We see thus that it is through the different balances between ligand-to-metal and metal-to-ligand donations that the effective charge on chromium is so different in both systems. As this feature is probably related to the different chemical properties of both systems, it is interesting to examine their ground-state electronic structures in more detail in order to seek an explanation for this difference in metal configurations.

As the formal oxidation state of metal in both systems is 0, one may reasonably expect that the calculations will lead to a small effective charge on metal atom. This means that both ligand-to-metal and metal-to-ligand donations should roughly compensate, which is the case for system **2**. When comparing the results obtained for systems **1** and **2**, we see that the total ligand-to-metal charge donation is smaller in **1** by 0.24e. This is undoubtedly due to the fact that the highest occupied MOs of π type lie at higher energies in naphthalene than in benzene, as exemplified by the first ionization energy of the two compounds: 8.15 eV for naphthalene (19) and 9.25 eV for benzene (20). This should lead for system **1** to a smaller admixture of metal $3d_{xz}$ and $3d_{yz}$ orbitals into the π MOs of ligands and, ultimately, to a smaller ligand-to-metal donation. The larger back-bonding metal-to-ligand donation in **1** as compared with **2** (0.40e) is slightly more difficult to explain. Indeed, according to the optical and uv absorption spectra of benzene and naphthalene (21), the energy gap between the π HOMO and the π^* LUMO is larger in benzene by approximately 1.0–1.5 eV, i.e. the same amount as the difference in ionization energies, which means that on an absolute scale and ignoring their interaction with the metal, the lowest virtual π^* levels of both systems should have roughly the same energy. According to this crude argument, they should thus mix equally with the metal $3d_{z^2}$, $3d_{x^2-y^2}$, and $3d_{xy}$ orbitals and lead to the same amount of back-bonding transfer, which is obviously not the case. Instead, we suggest that the solution to our problem has to be found in the D_{6h} to C_{2h} descent in symmetry when going from **1** to **2**: the virtual, predominantly ligand π^* MO of e_{2g} symmetry which is the main source of back-bonding in **1** through its significant metal $3d_{x^2-y^2}$, $3d_{xy}$ character, correlates in system **2** with a pair of MOs $a_g + b_g$. Because they are allowed to interact with several other low-lying virtual MOs of the same symmetry, these MOs are found in system **2** at much higher energies than their counterpart in **1**, which results in a significantly lower admixture of metal $3d_{x^2-y^2}$, $3d_{xy}$ orbitals, and therefore to a smaller back-bonding donation in **2**.

As there is no unique way to distribute the intersphere charge among the muffin-tin spheres, we decided to check the above conclusions by using another charge partition scheme. In view of the large difference in intersphere volumes in both compounds, one may indeed ask whether the attribution of the whole intersphere charge to the ligands is a realistic procedure and, consequently, whether the different charges on metal obtained for **1** and **2** are not an artifact of the calculation. As another, significantly different, charge partition scheme, we decided to use the alternative of distributing for each MO the interatomic charge among all atoms in the molecule proportionally to the amount of orbital charge (originating from this orbital) included in each sphere (6). This procedure leads to the following metal configurations: $3d^{5.66}\,4s^{0.34}\,4p^{0.52}$, i.e. $Cr^{-0.52}$ for **1**; $3d^{6.14}\,4s^{0.36}\,4p^{0.54}$, i.e. $Cr^{-1.04}$ for **2**. Though, as expected, the metal atom bears now a negative charge in both compounds, the same conclusions as before may be drawn: the $3d$ shell is significantly more populated in **2** than in **1** (+0.48e), which leads to a larger electronic charge on metal in **2**, the difference being −0.52e. In view of the drastic differences in the partition schemes used, one may expect that any other procedure would probably lead to metal populations and charges lying in between those obtained in our two calculations. Therefore, one may safely conclude that the differences in metal configurations obtained for the two compounds is a real trend which can be probably related to their different reactivity.

Finally, we would like to make a few comments on the possible correlation between the differences in reactivity exhibited by compounds **1** and **2** and the main features of their electronic structures. As we have pointed out above, all the valence levels of **2** undergo a negative energy shift with respect to **1**, with the result that the energy of the LUMO is lowered by almost 5 eV. Obviously, the system **2** presents an appreciable electrophilic character. Furthermore, the coordinated arene rings in **2** are almost neutral, whereas each of the arene rings in **1** bears a charge of −0.3, and the low-lying virtual orbitals of **2** show appreciable C_4—C_5 π antibonding character on the uncomplexed ring, as revealed by a detailed analysis of the distribution of charge of the $17a_g$ and $15b_u$ MOs. These features would favor reactions involving nucleophilic attack on the ligand rings, followed by cleavage of the C_4—C_5 bond, or on the metal, contributing thus to the remarkable lability of **2** towards naphthalene displacements by two-electron donor ligands (22).

Coming back to system **1**, the main difference is that it presents a significantly less electrophilic character because of its LUMO lying at a higher energy. It is therefore less reactive towards nucleophilic attack. However, to our knowledge, no reaction of nucleophilic addition to the arene rings in **1** or **2** has been reported.

Among the other electronic factors susceptible to shed some light on the reactivity of the compounds, the electron density on metal should not be underestimated since it is known to possibly affect arene reactivity in metal complexes (23). The substantial differences in metal charges between **1** and **2** (0.64e) indicates that the girdle of electron density around the Cr atom is larger in **2** than in **1**, resulting in different conditions for direct electrophilic and nucleophilic attacks at the metal and probably also at the ligand sites. Finally, both a large disruption of ligand π and π^* levels and a shift towards lower energies of all the valence levels have been recently found in a series of tetraperoxo metal complexes to be possible indicators as to an enhanced reactivity of the system (24). The present results suggest that this statement could also apply to organometallic complexes with arene or condensed arene ligands.

Acknowledgments

This work is part of Project 2.615-0.82 of the Swiss National Science Foundation. The Computer Center of the University of Geneva is gratefully acknowledged for a grant of computer time.

1. E. O. Fischer and W. Hafner. Z. Naturforsch. B**10**, 665 (1955).
2. E. P. Kundig and P. L. Timms. J. Chem. Soc. Chem. Commun. 912 (1977).
3. C. Elschenbroich and R. Mockel. Angew. Chem. Int. Ed. Engl. **16**, 870 (1977).
4. M. Cais, D. Fraenkel, and K. Weidenbaum. Coord. Chem. Rev. **16**, 27 (1975).
5. O. Gandolfi and M. Cais. J. Organomet. Chem. **125**, 141 (1977).
6. J. Weber, M. Geoffroy, A. Goursot, and E. Penigault. J. Am. Chem. Soc. **100**, 3995 (1978).
7. A. Goursot, E. Penigault, and J. Weber. Nouv. J. Chim. **3**, 675 (1979).
8. J. Weber. *In* Current aspects of quantum chemistry 1981. *Edited by* R. Carbo. Elsevier, Amsterdam. 1982, p. 437.
9. J. Weber, A. Goursot, E. Penigault, J. H. Ammeter, and J. Bachmann. J. Am. Chem. Soc. **104**, 1491 (1982).
10. J. C. Giordan, J. H. Moore, J. A. Tossell, and J. Weber. J. Am. Chem. Soc. **105**, 3431 (1983).
11. M. V. Rajasekharan, R. Bucher, E. Deiss, L. Zoller, A. K. Salzer, E. Moser, J. Weber, and J. H. Ammeter. J. Am. Chem. Soc. **105**, 7516 (1983).
12. K. H. Johnson. Adv. Quantum Chem. **7**, 143 (1973).
13. A. Haaland. Acta Chem. Scand. **19**, 41 (1965).
14. C. Elschenbroich, R. Mockel, W. Massa, M. Birkhahn, and U. Zenneck. Chem. Ber. **115**, 334 (1982).
15. K. Schwarz. Phys. Rev. B**5**, 2466 (1972).
16. J. C. Slater. Intern. J. Quantum Chem. **7S**, 533 (1973).
17. K. D. Warren. Struct. Bonding, **27**, 45 (1966).
18. C. Elschenbroich, E. Bilger, J. Koch, and J. Weber. J. Am. Chem. Soc. **106**, 4297 (1984).
19. F. Brogli, E. Heilbronner, and T. Kabayashi. Helv. Chim. Acta, **55**, 274 (1972).
20. E. E. Koch and A. Otto. Chem. Phys. Lett. **12**, 476 (1972).
21. H. B. Klevens and J. R. Platt. J. Chem. Phys. **17**, 470 (1949).
22. E. P. Kundig and P. L. Timms. J. Chem. Soc. Dalton, 991 (1980).
23. V. Desobry and E. P. Kundig. Helv. Chim. Acta, **64**, 1288 (1981).
24. M. Roch, J. Weber, and A. F. Williams. Inorg. Chem. **23**, 4571 (1984).

Charge distributions and chemical effects. XXXVI. Charge analysis involving configuration interaction: application to alkanes

C. MIJOULE,[1] J.-M. LECLERCQ,[1] S. ODIOT,[2] AND S. FLISZÁR

Département de Chimie, Université de Montréal, C.P. 6210, Succ. A, Montréal (Qué.), Canada H3C 3V1

Received July 27, 1984

This paper is dedicated to Professor Camille Sandorfy on the occasion of his 65th birthday

C. MIJOULE, J.-M. LECLERCQ, S. ODIOT, and S. FLISZÁR. Can. J. Chem. **63**, 1741 (1985).

An analysis of atomic charges is presented for simple alkanes. Basically, Mulliken's scheme is followed, except for the partitioning of CH overlap populations. This achieves a relative ordering of atomic charges which is independent of the basis sets used in *ab initio* calculations. The absolute magnitude of atomic charges, however, is basis set dependent. Extensive geometry and scale factor optimizations yield the following results (in 10^{-3} e units) for the carbon net charge in ethane: 69.4 (STO-3G), 55.1 (STO-3G + CI), 42.8 (4-31G), and 37.8 (4-31G + CI). It appears that charge analyses converge toward the empirical result, 35.1×10^{-3} e, provided they are carried out after configuration interaction involving reasonably large optimized basis sets.

C. MIJOULE, J.-M. LECLERCQ, S. ODIOT et S. FLISZÁR. Can. J. Chem. **63**, 1741 (1985).

On rapporte une analyse des charges atomiques d'alcanes simples. On utilise principalement le schéma de Mulliken, excepté pour la répartition des recouvrements des populations de CH. Ceci permet d'établir un ordre relatif des charges atomiques qui est indépendant des ensembles de base utilisés dans les calculs *ab initio*. Toutefois, la valeur absolue des charges atomiques dépend de l'ensemble de base utilisé. A la suite d'optimisations importantes des géométries et des facteurs d'échelle, on a pu obtenir les résultats suivants (en unités 10^{-3} e) pour la charge nette du carbone de l'éthane: 69,4 (STO-3G), 55,1 (STO-3G + CI), 42,8 (4-31G) et 37,8 (4-31G + CI). Si les analyses sont effectuées après des interactions de configurations impliquant des ensembles de bases optimisés relativement étendus, les analyses convergent vers le résultat empirique de $35,1 \times 10^{-3}$ e.

[Traduit par le journal]

Introduction

The concept of atomic charge is popular in chemistry. The quantity which is referred to in most cases is the net charge $q_k = Z_k - N(k)$, where Z_k is the nuclear charge of center k and $N(k)$ the number of electrons assigned to it. Numerous studies have dealt with the problem of charge partitioning, which are well reviewed (1): the disturbing fact is that charge results vary widely, depending on the methods involved in their calculation.

The question asked here is one concerning a realistic, physically meaningful partitioning which will not defeat itself in applications and comparisons involving experimental results. Though limited in scope (as we are primarily discussing saturated hydrocarbons), this work attempts to show what level of calculation fulfills the requirements for achieving this goal, a task involving some kind of experimental assessment of the theoretical results.

With this in mind, advantage is taken from earlier studies (2, 3) indicating that the individual bond energies of ground-state molecules are (to a good approximation) linearly dependent on the charges of the bond-forming atoms,[3] i.e.,

$$[1] \qquad \epsilon_{ij} = \epsilon_{ij}^0 + a_{ij}\Delta q_i + a_{ji}\Delta q_j$$

The sum of the ϵ_{ij}'s plus a small nonbonded contribution, $\Delta E_{\mathrm{nb}} = -E_{\mathrm{nb}}$, yields the atomization energy of the molecule in its hypothetical vibrationless state at 0 K,

$$[2] \qquad \Delta E_{\mathrm{a}}^* = \Sigma\epsilon_{ij}^0 + \Sigma_i\Sigma_j a_{ij}\Delta q_i - E_{\mathrm{nb}}^*$$

This expression, and comparison with experimental ΔE_{a}^* values, has the merit of permitting evaluations regarding the validity of calculated charges because, evidently, the use of "wrong" charges in eq. [2] leads to incorrect estimates of ΔE_{a}^* energies.

As concerns the charges, two basic aspects need to be considered, namely, (*i*) their *relative ordering* with respect to some arbitrarily selected reference and (*ii*) their *absolute magnitude*. Net charges deduced from Mulliken's analysis (4) do not satisfy eq. [2]. Indeed, when deduced from SCF (Hartree Fock) wave functions, this analysis yields charge results which are strongly basis set dependent (3, 5), both as regards their relative ordering and their magnitude.

The relative ordering, however, is easily acted upon with the use of a generalized Mulliken scheme (6), i.e., in conventional notation,

$$[3] \qquad N(k) = 2\sum_i\sum_r\left(c_{r_k i}^2 + \sum_{l \neq k} c_{r_k i}c_{s_l i}S_{r_k s_l}\lambda_{r_k s_l}\right)$$

where $\lambda_{r_k s_l}$ lifts the constraint of halving overlap populations between dissimilar atoms ($\lambda = 1$ in Mulliken's scheme). In terms of the difference between Mulliken charges and those given by eq. [3], it follows that

$$[4] \qquad q_k = q_k^{\mathrm{M}} + \sum_{l \neq k} p_{kl}$$

where charge normalization is ensured by the condition $p_{lk} = -p_{kl}$. For the saturated hydrocarbons under study, we approximate $\Sigma p_{\mathrm{CH}} = N_{\mathrm{CH}}p$ where p is the departure from the usual halving of the CH overlap population for one CH bond and N_{CH} is the number of hydrogen atoms bonded to a given carbon atom: eq. [4] simplifies to (6)

[1] Visiting scientists, on leave from the Centre de Mécanique Ondulatoire Appliquée, Paris, France.

[2] Visiting scientist, on leave from the Université P. et M. Curie (Paris VI), Paris, France.

[3] That bond energies should depend on the charges of the bond-forming atoms comes as no surprise. Equation [1] features the effects due to changes in net atomic charges (Δq_i and Δq_j) with respect to the charges q_i^0 and q_j^0 of the same atom pair in a reference bond with energy ϵ_{ij}^0. The a_{ij} and a_{ji} parameters, which are deduced from theory (2, 3), measure the effect of unitary charge variations at atoms i (bonded to j) and j (bonded to i), respectively. These parameters can safely be treated as constants in the case of alkanes, namely, $a_{\mathrm{CC}} = -0.777$, $a_{\mathrm{CH}} = -0.394$, and $a_{\mathrm{HC}} = -1.007$ au (2, 3).

[5] $q_H = q_H^M - p$

[6] $q_C = q_C^M + N_{CH}p$

In this manner, with the use of an empirically determined p, we may well achieve a correct ordering of charges in a relative scale but not necessarily converge toward good absolute values: in fact, the latter turn out to be basis set dependent, which is precisely the point investigated here. This point matters because if all the charges (now supposed to be correctly ordered) were in error by a certain multiplying factor, so would be the $\Sigma_i\Sigma_j a_{ij}\Delta q_i$ term of eq. [2] calculated for each individual molecule, thus revealing the extent of the discrepancy between theoretical charges and those satisfying eq. [2].[4]

The present work concludes eventually that eqs. [5] and [6] are, indeed, satisfactory in conjunction with eq. [2] provided that charge analyses are carried out after configuration interaction involving sufficiently large optimized basis sets.

Relative ordering of net charges

This problem is most conveniently discussed with the aid of general formulas (2, 5, 6) expressing the net charges of selected alkanes in a relative scale. This scale is defined here with reference to the net charge of the ethane carbon atom, taken at 1 arbitrary charge unit. Multiplication of these relative charges by the "true" value (in charge units) of the ethane carbon atom, q_C^0, yields the corresponding results in charge units. The relative ordering is defined by n; q_C^0 determines the absolute magnitude. The important point is that Mulliken charges derived from any basis set satisfy these formulas[5] (2, 5, 6), with n and q_C^0 values differing from one basis set to another. Moreover, the general formulas of Table 1 apply equally well to results deduced from eqs. [5] and [6].

For a given basis set SCF calculation, Let n^M and q_C^{0M} represent the appropriate parameters corresponding to a Mulliken population analysis and let n and q_C^0 represent their counterparts for the more general solutions indicated in eqs. [5] and [6]. It has been shown (2, 6) that the following relationship holds:

[7] $$\frac{q_C^0}{n} = \frac{q_C^{0M}}{n^M}$$

Accordingly, the connection with eqs. [5] and [6] is established by

[8] $p = q_C^{0M}(n - n^M)/3n^M$

thus showing that the evaluation of the "true" n leads to p, and vice versa.

Let us examine an application involving STO-3G Mulliken charges corresponding to $q_C^{0M} = -20.96$ me ($= 10^{-3}$ electron units) and $n^M = 1.3325$ (Table 1). These charges enter eqs. [5] and [6] which, in turn, are introduced into eq. [2] with an undetermined multiplier intended to correct for a possible error in the absolute charge values used as input. A least-squares analysis involving experimental ΔE_a^*'s leads to $p = 30.3 \pm 0.3$ me (2). On the other hand, the same set of charges correlate with ^{13}C nmr shifts with $p = 30.12$ me (6): the corresponding n is -4.4122. The n value deduced from these analyses holds independently of the LCAO-MO method selected for calculating Mulliken charges because, evidently, the "physically true" relative ordering of charges is unique. Briefly, $n \approx -4.41$ satisfies energy calculations, eq. [2], correlations with ^{13}C nmr shifts, and ionization potentials of alkanes (7). This n value also follows from SCF-Xα-SW charge analyses (8) and, quite significantly, from Bader's virial partitioning method (9, 10). Moreover, this result is appealing because $n \simeq -4.41$ describes a situation in which all changes in electron populations occur "most reluctantly", thus keeping them as small as possible (2,6). On these grounds, it seems reasonable to consider that the problem regarding the "relative ordering" of charges is adequately taken care of for the alkane molecules under scrutiny.

TABLE 1. Net charges of selected atoms: general formulas and comparison with STO-3G results from Mulliken's analysis (5)

Molecule	Atom	Formula	Net charge (me) From formula[a]	Net charge (me) STO-3G
Methane	C	$4(n + 1)/3n$	−48.92	−48.92
Ethane	C	1	−20.96	−20.96
Propane	C_{prim}	$(3n + 0.55)/3n$	−23.84	−23.81
	C_{sec}	$(2n - 3.8)/3n$	5.95	5.94

[a]Calculated with $n = 1.3325$, $q_C^0 = -20.96$ me. For additional examples see ref. 5.

The real problem which now remains to be solved is that of the physically correct magnitude of net charges, i.e., that of the ethane carbon atom, q_C^0, which serves as reference. From regression analyses involving experimental ΔE_a^*'s one finds $q_C^0 \simeq 35.1$ me[4] (2). The disturbing circumstance is that present SCF charge analyses do not agree with this empirical result. For example, assuming now $n = -4.4122$ as a correct description of the relative ordering, eq. [7] predicts $q_C^0 = -4.4122 \times (-20.96)/1.3325 = 69.40$ me on the basis of fully optimized STO-3G calculations. Similarly, the q_C^0's corresponding to $7s3p|3s$ and 6-31G calculations are 60 and 58 me, respectively (3). Clearly, it is now time to examine results derived from improved wave functions.

Outline of calculations

SCF calculations, as well as the computation of the bielectronic integrals $\langle\phi_i\phi_j|\phi_k\phi_l\rangle$ used in the CI part, were carried out by means of the MONSTERGAUSS *ab initio* program (11). Molecular geometries and scale factor exponents were optimized with a split valence 4-31G basis, using the Davidson optimally conditioned minimization technique (12), until the gradient length

$$|g| = \left[\sum_{i=1}^{n} \frac{1}{n}(\partial E/\partial q_i)^2\right]^{1/2}$$

fell below 5×10^{-4} mdyn. Optimization results are indicated in Appendix I.

The configuration interaction following the optimized SCF calculation includes ~250 configurations, i.e., mono- ($k \rightarrow v$) and diexcited ($k, k \rightarrow v, v$; $k, k \rightarrow v, t$; $k, l \rightarrow v, v$; $k, l \rightarrow v, t$) states representing five excitation classes, where k and l refer

[4]Using the carbon net charge of ethane ($q_C^0 = 35.1$ me) as reference in the evaluation of the Δq_i's, $\Sigma_i\Sigma_j a_{ij}\Delta q_i$ is 20.82 for butane and 60.60 kcal mol^{-1} for cyclohexane (2, 3). If the assumed reference charge q_C^0 and, hence, all Δq_i's were in error by 10%, the resulting errors would be, in these examples, 2.08 and 6.06 kcal mol^{-1}, respectively. The validity of the estimated ethane C net charge (35.1 me) is best illustrated by the small average deviation, ~0.2 kcal mol^{-1}, between calculated and experimental ΔE_a^* energies, covering a body of ~150 molecules.

[5]This holds also true in semiempirical MO calculations, e.g., the extended Hückel method (2, 5).

TABLE 2. Mulliken net charges from 4-31G and 4-31G + CI calculations, compared with those deduced from the formulas indicated in Table 1

		Mulliken net charge (me)			
Molecule	Atom	4-31G	n = 39.45	4-31G + CI	n = 44.1
Methane	C	−523.2	−523.2	−515.7	−515.7
Ethane	C	−382.7	−382.7	−378.2	−378.2
Propane	C_{prim}	−384.0	−384.5	−380.8	−379.8
	C_{sec}	−244.9	−242.8	−243.4	−241.3

to fundamental closed shells, and v, t refer to virtual orbitals. Details regarding the calculation of the CI matrix using $\hat{S}^2$ eigenfunctions rather than single determinants are described elsewhere (13). The selection of monoexcited configurations, $\psi^{(i)}$, was made on the basis of $\Delta E = \langle\psi^{(i)}|H|\psi^{(i)}\rangle$ values and that of diexcited configurations also considered the value of the correlation at the second-order perturbation, $\Delta = -\langle\psi^{(i)}|H|\psi^{(0)}\rangle^2/(E_i - E_0)$.

As regards the charge analysis, we proceed as follows. For a wave function represented by a single determinant, $\psi = \psi^{(0)}$, the matrix element of the monoelectronic density operator $\hat{D}$, is defined as follows

$$[9] \quad D^{(0)}_{\mu\nu} = \langle\chi_\mu|\hat{D}|\chi_\nu\rangle = \sum_{i=1} n_i c_{i\mu} c_{i\nu}$$

where χ_μ and χ_ν are atomic basis functions, and $c_{i\mu}$, $c_{i\nu}$ are the expansion coefficients for χ_μ, χ_ν of the molecular orbital ψ_i. The occupation number of ψ_i is n_i (0, 1, 2), and the summation is over all molecular orbitals. Mulliken's population matrix elements are then

$$P^{(0)}_{\mu\nu} = D^{(0)}_{\mu\nu} S_{\mu\nu}$$

in which $S_{\mu\nu}$ is an element of the overlap matrix **S**. More generally, for a wave function developed over several determinants (a CI function), it is

$$\psi = \sum_{k=1} \alpha_k \psi^{(k)}$$

$$P_{\mu\nu} = D_{\mu\nu} S_{\mu\nu}$$

In this case, the density matrix element, $D_{\mu\nu}$, of the operator $\hat{D}$ must be redefined because $\hat{D}$ depends on the form of the wave function ψ. The overlap matrix **S**, however, remains unchanged because it depends only on the atomic basis functions χ. Finally, $D_{\mu\nu}$ is defined as follows

$$[10] \quad D_{\mu\nu} = \sum_{k=1} \sum_{l\neq 1} \alpha_k \alpha_l D^{kl}_{\mu\nu}$$

where $D^{kl}_{\mu\nu}$ is the matrix element associated with the determinants $\psi^{(k)}$ and $\psi^{(l)}$ of the density operator $\hat{D}$. For $k = l$, $D^{kl}_{\mu\nu}$ is simply as indicated in eq. [9]. For $k \neq l$, $D^{kl}_{\mu\nu}$ defines an element of a transition density matrix, $\mathbf{D}^{kl}$, constructed from determinants k and l (14). This $\mathbf{D}^{kl}$ matrix has nonzero elements only when $\psi^{(k)}$ and $\psi^{(l)}$ differ from one another by not more than one spin orbital. Equation [10] expresses the idea that the density matrix for a many-determinant wave function is simply a weighted sum of "transition density matrices" connecting all different pairs of determinants in the expansion. It is formulated as

$$D^{kl}_{\mu\nu} = a(c_{n\mu} c_{m\nu} + c_{n\nu} c_{m\mu})$$

when the determinants $\psi^{(k)}$ and $\psi^{(l)}$ differ from one another in their spin orbitals ψ_n and ψ_m; a is a coefficient given by Slater's rules.

Results

The charge results deduced from 4-31G and 4-31G + CI calculations are indicated in Table 2, together with their counterparts corresponding to the formulas given in Table 1. Geometry and scale factor optimizations were carried out automatically, with reference to the gradient of the total energy. For propane, a slight but non negligible oscillation in the charge values was noted toward the end of the optimization, particularly for the secondary carbon and hydrogen atoms. The latter results are thus not as accurate as those deduced for methane and ethane. A similar behavior was also observed earlier in STO-3G calculations of propane (15). Indeed, significantly more refined optimizations of the ζ's turned out to be necessary for the secondary C and H atoms (as compared with what is usually required) in order to ensure stabilization of the charge results for these atoms. In the present case, all ζ optimizations were uniformly carried out to the 4th significant figure. Additional optimization cycles were not performed for propane because, in spite of the minor uncertainties affecting its theoretical charges, the results are sufficiently clear to serve as an illustration for the general validity of the arguments leading to the formulas given in Table 1.

For comparison, we have also studied the effect of introducing configuration interaction at the level of optimized STO-3G calculations. The results are included in the following discussion.

Discussion

We now come to the main topic of this work, i.e., the value of the ethane carbon net atomic charge, q^0_C, corresponding to the assumed correct ordering defined by $n = -4.4122$. This value is easily deduced from eq. [7] using the Mulliken net charges of methane and ethane carbons for calculating n^M (see Table 1).

From the optimized STO-3G results ($n^M = 1.3325$ and $q^{0M}_C = -20.96$ me), it follows that $q^0_C = 69.40$ me. An optimized STO-3G calculation + CI gives $q^M_C = -46.37$ and -22.28 me for methane and ethane, respectively, leading to $n^M = 1.7828$ and $q^0_C = 55.1$ me, which is already significantly better than the value, 69.40 me, obtained without CI. At the 4.31G level ($n^M = 39.45$), it follows from eq. [7] that $q^0_C = 42.8$ me. The improvement over the STO-3G result is noticeable. Finally, applying now CI to the 4-31G calculations, it is found from $n^M = 44.1$ that $q^0_C = 37.8$ me.

It is clear that improvements in the basis set descriptions, and the final touch provided by CI, yield charge results for the ethane carbon atom converging toward its empirical counter-

TABLE 3. Geometries obtained from optimizations at the 4-31G level

Molecule	Parameter	Calculated[a]
Methane	r_{CH}	1.082
Ethane	r_{CC}	1.528
	r_{CH}	1.084
	$\angle$HCH	107.67
Propane	r_{CC}	1.528
	r_{CH} (sec–sec)	1.086
	r_{CH} (prim–prim a)	1.084
	r_{CH} (prim–prim s)	1.083
	$\angle$CCC	112.63
	$\angle H_{sec}C_{sec}H_{sec}$	105.81
	$\angle C_{sec}C_{prim}H_{prim\,s}$	111.34
	$\angle C_{sec}C_{prim}H_{prim\,a}$	110.93
	$\angle H_{prim\,s}C_{prim}H_{prim\,a}$	107.91

[a] Distances in Å, angles in deg.

TABLE 4. Optimization results for ζ

Molecule	Method	Parameter	ζ Standard	ζ Optimized
Methane	STO-3G	$\zeta_C(s_K)$	5.67	5.70605
		$\zeta_c(s_L, p)$	1.72	1.76536
		$\zeta_H(s)$	1.24	1.17195
Ethane	STO-3G	$\zeta_C(s_K)$	5.67	5.70529
		$\zeta_C(s_L, p)$	1.72	1.75919
		$\zeta_H(s)$	1.24	1.17599
Methane	4-31G	$\zeta_C(s_K)$	1.0	0.99902
		$\zeta(s'_L, p')$	1.0	0.99372
		$\zeta_C(s''_L, p'')$	1.04	1.07236
		$\zeta_H(s')$	1.20	1.19972
		$\zeta_H(s'')$	1.15	1.10369
Ethane	4-31G	$\zeta_C(s_K)$	1.0	0.99906
		$\zeta_C(s'_L, p')$	1.0	0.99340
		$\zeta_C(s''_L, p'')$	1.04	1.06907
		$\zeta_H(s')$	1.20	1.19922
		$\zeta_H(s'')$	1.15	1.11127
Propane	4-31G	$\zeta_{Cprim}(s_K)$	1.00	0.99904
		$\zeta_{Cprim}(s'_L, p)$	1.00	0.99276
		$\zeta_{Cprim}(s''_L, p)$	1.04	1.07024
		$\zeta_{Csec}(s_K)$	1.00	0.99891
		$\zeta_{Csec}(s'_L, p')$	1.00	0.99059
		$\zeta_{Csec}(s''_L, p'')$	1.04	1.06018
		$\zeta_{Hprim\,s}(s')$	1.20	1.19857
		$\zeta_{Hprim\,s}(s'')$	1.15	1.11186
		$\zeta_{Hprim\,a}(s')$	1.20	1.19664
		$\zeta_{Hprim\,a}(s'')$	1.15	1.10600
		$\zeta_{Hsec}(s')$	1.20	1.19992
		$\zeta_{Hsec}(s'')$	1.15	1.12029

part, 35.1 me, deduced with the help of the energy expression, eq. [2]. It is also clear that carbon atoms in saturated hydrocarbons are unmistakably slightly electron deficient (2, 3, 6) (a fact which is often forgotten or occasionally rediscovered in recent literature) and that the proposed value of 35.1 me for the ethane carbon presently represents the estimate which is best supported by theoretical and empirical arguments: this result is pivotal in numerous appplications of the energy expression, eq. [2], whose accuracy is abundantly illustrated by comparisons with experimental data (2).

Finally, it seems important to have gained knowledge about *realistic* atomic charges and the inclusion of correlation effects therein because of relevant implications in the interpretation of eqs. [1] and [2], namely, as regards correlations between tetrahedrally localized orbitals. The familiar approximate empirical bond additivity of thermochemistry could lead us to expect that the valence shell correlation energies of molecules like CH_4, C_2H_6, . . . would consist mainly of bond correlations. In contrast, the elegant analysis offered by Sinanoğlu and Skutnik (15) reveals that correlations between neighboring tetrahedral orbitals contribute about twice as much to the valence shell correlation energy of methane as the correlation within the four doubly occupied ("bonds") tetrahedral pairs. "Nonbonded interactions" are thus not negligible but may be an important part of the correlation energies of saturated molecules. (A more approximate semiempirical version of the theory for molecular correlation energies was also given and tested for π-electron systems (16).) While these studies analyze all-important theoretical aspects related to the origin of correlation energies, the present use of eqs. [1] and [2] involving charges obtained after configuration interaction implies that all contributions to correlation, including those due to nonbonded interactions, are already reflected in the Δq_i charges. Consequently, a specific correlation energy contribution arising from nonbonded terms is not part of the E_{nb} energy appearing in eq. [2]. Estimates of E_{nb}, using Del Re's approximation (17), reveal that (in the sense of eq. [2]) nonbonded Coulomb interactions are minor, indeed, about 0.02–0.05% of ΔE^*_a, whereas the true correlation energy, i.e., the difference between exact and Hartree–Fock energies, contains important contributions originating in terms other than those associated with chemical bonds.

TABLE 5. Calculated energies (au) from optimized bases

Method	Energy calculated for Methane	Ethane	Propane
STO-3G	−39.73164	−78.31493	−116.89899
STO-3G + CI	−39.81000	−78.42583	
4-31G	−40.14037	−79.11709	−118.09556
4-31G + CI	−40.21340	−79.17426	−118.12426

Acknowledgements

The supports of the National Research Council of Canada and the "France-Québec" Exchange Program are gratefully acknowledged.

Appendix

The geometries obtained from an optimization at the 4-31G level are reported in Table 3. The corresponding optimized ζ's are indicated in Table 4. Finally, we indicate the calculated energies in Table 5.

1. V. H. SMITH. Phys. Script. **15**, 147 (1977); A. JULG. Top. Curr. Chem. **58**, 1 (1975).
2. S. FLISZÁR. Charge distributions and chemical effects. Springer-Verlag, New York. 1983.
3. S. FLISZÁR. J. Am. Chem. Soc. **102**, 6946 (1980).
4. R. S. MULLIKEN. J. Chem. Phys. **23**, 1833 (1955); **23**, 1841 (1955); **23**, 2338 (1955); **23**, 2343 (1955).
5. S. FLISZÁR, G. KEAN, and R. MACAULAY. J. Am. Chem. Soc. **96**, 4353 (1974).
6. S. FLISZÁR, A. GOURSOT, and H. DUGAS. J. Am. Chem. Soc. **96**, 4358 (1974).

7. H. HENRY and S. FLISZÁR. Can. J. Chem. **52**, 3799 (1974).
8. A. E. FOTI, V. H. Smith, and S. FLISZÁR. J. Mol. Struct. **68**, 227 (1980).
9. R. F. W. BADER. Acc. Chem. Res. **8**, 34 (1975); G. R. RUNTZ and R. F. W. BADER. Mol. Phys. **30**, 129 (1975); R. F. W. BADER and G. R. RUNTZ. Mol. Phys. **30**, 117 (1975); R. F. W. BADER and R. R. MESSER. Can. J. Chem. **52**, 2268 (1974); S. SREBRENIK and R. F. W. BADER. J. Chem. Phys. **63**, 3945 (1975).
10. M. COMEAU, G. CARDINAL, and S. FLISZÁR. To be published.
11. M. R. PETERSON and R. A. POIRIER. University of Toronto, Ont., Canada. 1981.
12. W. C. DAVIDSON. Math. Prog. **9**, 1 (1975).
13. J. LECLERCQ and J.-M. LECLERCQ. Chem. Phys. **22**, 221 (1977).
14. R. MCWEENY and B. T. SUTCLIFFE. Methods of molecular quantum mechanics. Academic Press, London. 1969.
15. O. SINANOĞLU and B. SKUTNIK. Chem. Phys. Lett. **1**, 699 (1968).
16. O. SINANOĞLU and H. Ö. PAMUK. Theoret. Chim. Acta, **27**, 289 (1972); O. SINANOĞLU and H. Ö. PAMUK. J. Am. Chem. Soc. **95**, 5435 (1973).
17. G. DEL RE. Gazz. Chim. Ital. **102**, 929 (1972).

Quantum mechanical calculation of thermodynamic functions of solvation of ammonium ions in water

RENATO CONTRERAS AND GILLES KLOPMAN[1]
Department of Chemistry, Case Western Reserve University, Cleveland, OH 44106, U.S.A.

Received August 14, 1984

This paper is dedicated to Professor Camille Sandorfy on the occasion of his 65th birthday

RENATO CONTRERAS and GILLES KLOPMAN. Can. J. Chem. **63**, 1746 (1985).

The application of an extended version of the generalized Born formula including dielectric saturation effects, implemented within the SCF-CNDO/2 approximation, provides a complete set of data concerning the thermodynamics of solvation of some ammonium ions in water. The calculated free energies of solvation are in good agreement with experimental data. An estimation of the entropy and enthalpy of solvation is also given and satisfactory qualitative trends are obtained.

RENATO CONTRERAS et GILLES KLOPMAN. Can. J. Chem. **63**, 1746 (1985).

L'application d'une version étendue de la formule de Born généralisée incluant des effets de saturation diélectrique permet, dans le cadre de l'approximation SCF-CNDO/2, l'obtention des fonctions thermodynamiques de solvatation d'un nombre d'ions ammoniums dans l'eau. Les valeurs d'énergie libre de solvatation obtenues par cette méthode sont en bon accord avec l'expérience. Une estimation de l'entropie et de l'enthalpie de solvatation est faite et les résultats montrent une tendence qualitative satisfaisante.

1. Introduction

With the recently introduced ion cyclotron resonance technique, measurement of gas-phase basicities of amines combined with heats of hydration and heats of protonation of these compounds in water have provided, for the first time, reliable thermochemical data concerning solvation of a large number of ammonium ions (1). Thermodynamics of ion solvation within this series has been found to play a key role in the "anomalous order" of amine basicities in aqueous solutions (2–4). Up to now, quantum mechanical calculations of solvation energies, including a wide variety of molecules and molecular ions, have been performed following three different general approaches: (*a*) the well known supermolecule technique, suitable for the study of relatively small molecular system with a number of solvent molecules explicitly taken into account (5–7); (*b*) continuum models based mainly on the generalized Born formula (8–11), and (*c*) mixed continuum-supermolecule models (5, 12).

In the supermolecule approach, the solvation energy is calculated as the solute–solvent interaction energy, which corresponds essentially to an enthalpy of solvation (13). A complete thermodynamic picture of the solvation process may be achieved only, within this approach, by including Monte Carlo simulation techniques in order to account for the temperature averaging effects (14).

The second approach is based on the well-known Born equation (15), which gives the change in electrostatic free energy that takes place when a charge Q_0 is transferred from a conducting sphere of radius a, in vaccuum, to a sphere of equal radius in a polarizable medium characterized by its temperature-dependent bulk dielectric constant ϵ_B. It is written as

$$[1] \quad \Delta G_S(\epsilon_B) = -(1/2)\,(1 - 1/\epsilon_B)\,Q^2/a$$

Although in principle this model allows a complete thermodynamic picture of ion solvation (16, 17), it is well established that for monoatomic ions in water at 25°C, the values of the free energy, enthalpy, and entropy of solvation predicted by this model are too high (17, 18). The overestimation of these quantities is related mainly to two problems: (*a*) the increase in the crystallographic radii due to solvation and (*b*) the dielectric saturation in the vicinity of the solvated ions, reducing the effective dielectric constant of the medium.

Equation [1] has been generalized in order to allow the calculation of solvation energies (and other physico-chemical properties) in a wide variety of molecules and molecular ions within a quantum mechanical framework (8–11). In this approach, the solute–solvent interactions are treated within the framework of the reaction field (RF) theory and the solvation energies are expressed as a sum of Born-like terms, each one corresponding to the partially charged atomic centers of the solute molecule. For instance, within a CNDO/2 type approximation, we write:

$$[2] \quad \Delta E_S(\epsilon_B, P) = -(1/2)\,(1 - 1/\epsilon_B) \sum_A \sum_B Q_A(P)\,Q_B(P)\,\gamma_{AB}$$

which is the well-known Generalized Born Formula (GBF). It is expressed as a function of the net charges $Q_A(P)$ associated with the atomic A-center of the solute, the two electron Coulomb integrals γ_{AB}, representing the solute–solvent interaction, and the bulk dielectric constant of the solvent ϵ_B. Although some confusion concerning the physical meaning of this energy has been made in the literature (19, 20), it has been emphasized recently (21, 22) that the quantity ΔE_S represents the free energy variation of the solute–solvent system, maintained at a given temperature, when the polarized solute is transferred from the gas phase to the solvent.

As in the case of eq. [1], the application of the GBF yields free energies of solvation that are considerably overestimated when compared with experimental data. In a previous publication (18), we have discussed this problem in detail, and we have proposed an extension of the GBF, within the SCF-CNDO/2 approximation, in order to account for local dielectric effects (LRF model hereafter). This approach allows simulation, within a continuum framework, of the mixed continuum-supermolecule model of solvent effects where at least the first solvation layer is explicitly taken into account.

In this work, we present further development of this model that allows a complete thermodynamic picture of ion solvation to be obtained. As an illustration of the reliability of this extended formalism, calculations of thermodynamic functions of

[1] To whom all correspondence should be addressed.

solvation of a number of ammonium ions in water were performed.

2. Theory

(a) The modified GBF expression

The LRF theory is based upon the classical model proposed by Beveridge and Schnuelle (23). In this approach, a general expression was deduced for the free energy of a charge distribution imbedded in a spherical cavity $S(0,a)$, surrounded by a local concentric region of thickness R_S where a local dielectric value, $\epsilon_L < \epsilon_B$, was defined. This system is supposed to be immersed in the bulk solvent of dielectric constant ϵ_B. From this formalism, we have deduced the reaction field potential acting back on the charge distribution whose net charge is Q_0 (18). In the framework of the effective charge approximation, it is written as a function of the local and bulk dielectric constant as follows,

$$[3]\quad V_R(\epsilon_L, \epsilon_B) = -(1 - 1/\epsilon_L)Q_0/a - (1/\epsilon_L - 1/\epsilon_B)Q_0/(a + R_S)$$

which represents the reaction potential created by the polarization charges induced at the surfaces $S(0,a)$ and $S(0,a+R_S)$. These polarization charges are redefined here, without changing the results of the previous formulation (18), as:

$$[4]\quad Q_i^{\mathrm{pol}}(\epsilon_L, Q_0) = -(1 - 1/\epsilon_L)Q_0$$

and

$$[5]\quad Q_e^{\mathrm{pol}}(\epsilon_L, \epsilon_B, Q_0) = -(1/\epsilon_L - 1/\epsilon_B)Q_0$$

respectively. In this way, the reaction field potential may be conveniently divided into two contributions: one coming from the internal polarization charge distribution, Q_i^{pol}, induced in the local region, and the other coming from the external polarization charge distribution, Q_e^{pol}, induced in the bulk region. The solvation free energy $\Delta G_S(\epsilon_L, \epsilon_B)$ is then given by:

$$[6]\quad \Delta G_S(\epsilon_L, \epsilon_B) = (1/2)\, \Sigma_k Q_k[V_R^{\mathrm{i}}(\epsilon_L, a) + V_R^{\mathrm{e}}(\epsilon_L, \epsilon_B, a+R_S)]_k$$

Based on eq. [6], the modified GBF may be written as a function of the density matrix P as:

$$[7]\quad \Delta G_S(\epsilon_L, \epsilon_B, P) = (1/2) \sum_A Q_A(P)[V_R^{\mathrm{i}}(\epsilon_L, P) + V_R^{\mathrm{e}}(\epsilon_L, \epsilon_B, P)]_A$$
$$= -(1/2)(1 - 1/\epsilon_L) \sum_A \sum_B Q_A(P)Q_B(P)\gamma_{AB}^{\mathrm{i}}$$
$$-(1/2)(1/\epsilon_L - 1/\epsilon_B) \sum_A \sum_B Q_A(P)Q_B(P)\Gamma_{AB}^{\mathrm{e}}(R_S)$$

In this expression, γ_{AB}^{i} and $\Gamma_{AB}^{\mathrm{e}}(R_S)$ are the internal and external polarization charge–electron interaction integrals, respectively. Details about the calculation of these quantities are given in the next section of this paper.

(b) Estimation of the entropy of solvation

As was proposed recently (22), the total free energy of the solute–solvent system is obtained by adding to the total energy of the isolated solute, the electrostatic solvation energy $\Delta G_S(\epsilon_L, \epsilon_B, P)$ which corresponds to the free energy variation of the solute–solvent system, when the polarized solute is inserted isothermically into the solvent. This solvation term may be partitioned according to (21, 22):

$$[8]\quad \Delta G_S(\epsilon_L, \epsilon_B, P) = E_{s-\Sigma}(\epsilon_L, \epsilon_B, P) + E_\Sigma^{\mathrm{pol}}(\epsilon_L, \epsilon_B, P)$$

$$[9]\quad E_{s-\Sigma}(\epsilon_L, \epsilon_B, P) = -(1 - 1/\epsilon_L) \sum_A \sum_B Q_A(P)Q_B(P)\gamma_{AB}^{\mathrm{i}}$$
$$-(1/\epsilon_L - 1/\epsilon_B) \sum_A \sum_B Q_A(P)Q_B(P)\Gamma_{AB}^{\mathrm{e}}(R_S)$$

where $E_{s-\Sigma}(\epsilon_L, \epsilon_B, P)$ (eq. [9]), is the electrostatic solute–solvent interaction energy and $\Delta E_\Sigma^{\mathrm{pol}}(\epsilon_L, \epsilon_B, P)$ is the solvent polarization energy. This last term represents the orientational entropy change induced by the opposite effects of the orienting electric field arising from the ionic charge and the averaging temperature effects. These two quantities are related by the expression:

$$[10]\quad \Delta E_\Sigma^{\mathrm{pol}}(\epsilon_L, \epsilon_B, P) = -(1/2)E_{s-\Sigma}(\epsilon_L, \epsilon_B, P)$$

Within the RF model neglecting dielectric saturation, the solvent polarization is assumed to be entirely orientational and for a given temperature T, the following "incorrect" relation is then obtained:

$$[11]\quad T\Delta S_S(\epsilon_B, P) = \Delta E_\Sigma^{\mathrm{pol}}(\epsilon_B, P)$$
$$= (1/2)(1 - 1/\epsilon_B) \sum_A \sum_B Q_A(P)Q_B(P)\gamma_{AB}$$
$$= -\Delta G_S(\epsilon_B, P)$$

As a result, largely overestimated values of the term $-T\Delta S_S(\epsilon_L, \epsilon_B, P)$ are to be expected with this model.

The consideration of local dielectric effects allows a more realistic evaluation of the entropic contribution to ion solvation. Indeed, starting from eq. [7] and using eqs. [8] and [10], the solvent polarization energy may be expressed as:

$$[12]\quad \Delta E_\Sigma^{\mathrm{pol}}(\epsilon_L, \epsilon_B, P) = (1/2)(1 - 1/\epsilon_B) \sum_A \sum_B Q_A(P)Q_B(P)\gamma_{AB}^{\mathrm{i}}$$
$$+ (1/2)(1/\epsilon_L - 1/\epsilon_B) \sum_A \sum_B Q_A(P)Q_B(P)\Gamma_{AB}^{\mathrm{e}}(R_S)$$

The resulting eq. [12] is consistent with the classical theory of dielectric polarization. In fact, as was proposed by Marcus (24), the polarization of any dielectric medium may be regarded as consisting of electronic, atomic, and orientation contributions. Furthermore, if, as a first approximation, the atomic contribution is neglected, we may write the total polarization vector $\boldsymbol{P}_t(\boldsymbol{r})$ as:

$$[13]\quad \boldsymbol{P}_t(\boldsymbol{r}) = \boldsymbol{P}_{el}(\boldsymbol{r}) + \boldsymbol{P}_{or}(\boldsymbol{r})$$

where the first term in eq. [13] represents the electronic polarization associated with the electronic motion of the solvent molecules. It is interesting to note that, following a quite different procedure, the module of this electronic term has been found by Jortner (25) to be identical to our "internal polarization charge" defined in eq. [4]. In the same way, the module of the second term in eq. [13] representing the orientational polarization, is formally identical with our "external polarization charge" defined in eq. [5]. The temperature-dependent orientation polarization given by the second term of eq. [12] may be assimilated, in the framework of the LRF theory, to the orientational entropy change which, added to the solute–solvent interaction energy defined in eq. [9], gives the expression of the solvation free energy (eq. [7]).

Based on the above consideration we may write:

$$[14] \quad -T\Delta S_S(\epsilon_L, \epsilon_B, P) = (1/2)\,(1/\epsilon_L - 1/\epsilon_B) \sum_A \sum_B Q_A(P) Q_B(P) \Gamma_{AB}{}^{c}(R_S)$$

Finally, combining eqs. [7] and [14], the following expression for the enthalpy of solvation is obtained:

$$[15] \quad \Delta H_S(\epsilon_L, \epsilon_B, P) = -(1/2)\,(1 - 1/\epsilon_L) \sum_A \sum_B Q_A(P) Q_B(P) \gamma_{AB}{}^{i} - (1/\epsilon_L - 1/\epsilon_B) \sum_A \sum_B Q_A(P) Q_B(P) \Gamma_{AB}{}^{c}(R_S)$$

3. Results and discussion

The LRF model of solvent effects discussed in the previous section, was applied to the calculation of the thermodynamic functions of solvation of some ammonium ions in water. All bond angles were taken as 109.47. The following bond lengths were used: C—C = 1.53 Å , C—N = 1.47 Å, C—H = 1.09 Å, and N—H = 1.00 Å.

The internal polarization charge–electron interation integrals $\gamma_{AB}{}^{i}$ were calculated according to the parametrization suggested by Miertus and Kysel (19): that is, for AO's associated with the same atomic center as the polarization charge Q_A, $\gamma_{AA}{}^{i}$ is given by $1/r_A$, where r_A is the Pauling's Van der Waals radius of the particular atom (26). When the AO's and the internal polarization charges are associated with different atomic centers, A and B, the internal solute–solvent interaction integrals were calculated as:

$$[16] \quad \gamma_{AB}{}^{i} = 1/(R_{AB} + r_B)$$

where R_{AB} is the interatomic distance calculated, as in our previous work in terms of the $\gamma_{AB}{}^{i}$ integrals, as (18):

$$[17] \quad \Gamma_{AA}{}^{c}(R_S) = \gamma_{AA}{}^{i}/(1 + R_S\gamma_{AA}{}^{i})$$

and

$$[18] \quad \Gamma_{AB}{}^{c}(R_S) = 1/[R_{AB} + (1/2)(1/\Gamma_{AA}{}^{c}(R_S) + 1/\Gamma_{BB}{}^{c}(R_S)]$$

respectively.

The parameter R_S, measuring the extent of the local dielectric region, was taken as $R_S = n\, d_{H_2O}$ (n = 1,2), with d_{H_2O} equal to the diameter of a water molecule (i.e., 2.80 Å). Finally, as suggested in ref. 27 and based on previous calculations (18), we used the values ϵ_L = 5.0 and ϵ_B = 78.5.

The results of the calculations of free energies, enthalpies and entropies of solvation for a number of ammonium ions in water are shown in Table 1. Examination of the calculated free energies of solvation reveals a significant agreement with experimental data: within the primary ammonium ions series, alkylation of the NH_4^+ ion results in a decrease of ΔG_S in the order $NH_4^+ > MeNH_3^+ > EtNH_3^+ > n\text{-}PrNH_3^+ > n\text{-}BuNH_3^+$. With the only exception of Et_3NH^+, the same trend observed within the secondary and tertiary series are also satisfactorily accounted for by the LRF model. Methylation of the ion pyrrolidinium resulted in a decrease of ΔG_S of about 5.6 kcal/mol (for n = 1), compared with an experimental value of 6.6 kcal/mol.

TABLE 1. Thermodynamic functions of solvation of some selected ammonium ions in water[a]

Solute	Experimental[b] ΔG	ΔH	$-T\Delta S$	Calculated[c] ΔG	ΔH	$-T\Delta S$
NH_4^+	78.0	84.6	6.6	71.9	82.9	11.0
				69.6	76.6	7.0
$MeNH_3^+$	67.7	75.4	7.7	61.8	71.8	10.0
				59.9	66.5	6.6
$EtNH_3^+$	64.7	75.2	10.5	60.5	74.8	14.3
				58.4	67.9	9.5
n-$PrNH_3^+$	63.0	74.2	11.2	58.8	74.0	15.2
				56.8	67.2	10.4
n-$BuNH_3^+$	62.5	74.6	12.1	58.4	75.9	17.5
				56.3	68.4	12.1
$Me_2NH_2^+$	61.0	69.7	8.8	54.6	63.1	8.5
				52.8	58.4	5.6
$Et_2NH_2^+$	56.5	68.4	12.0	53.3	69.9	16.6
				51.5	62.7	11.2
n-$Pr_2NH_2^+$	54.1	68.8	14.8	50.6	67.0	16.4
				48.7	60.1	11.4
n-$Bu_2NH_2^+$	52.9	69.9	17.0	49.9	69.8	19.9
				48.0	62.0	14.0
Me_3NH^+	54.4	63.3	8.9	49.5	56.5	7.0
				47.7	52.5	4.8
Et_3NH^+	48.6	61.4	12.9	50.1	75.6	25.5
				48.2	65.7	17.5
n-Pr_3NH^+	45.9	—	—	48.2	87.7	39.5
				46.1	74.0	27.9
Pyrrolidinium	56.7	69.2	12.5	52.4	65.0	12.6
				50.5	59.0	8.5
N-Methyl pyrrolidinium	50.1	61.8	11.8	46.8	57.3	10.5
				45.1	52.3	7.2

[a] All values in kcal/mol.
[b] From ref. 1.
[c] First value corresponds to RS = 2.80 Å and the second one to RS = 5.60 Å.

It is interesting to notice that the best description of the ΔG_S values are obtained with n = 1, which corresponds to R_S = 2.80. This is approximately the value found by Laidler (28) and Conway (29) to be the critical distance from the ion where the dielectric saturation effects manifests itself. Furthermore, in a recent paper Kebarle *et al.* (30) concluded, from ion–solvent molecule equilibria studies, that relative solvation energies for ammonium ions can be obtained by considering the interaction of the ion and a few solvent molecules only. These results are consistent with our "one solvation layer" continuum model with n = 1. Recently, Kebarle's conclusions have been confirmed by *ab-initio* calculations reported by Ikuta (31).

Estimation of entropies of solvation using eq. [14] are also summarized in Table 1. For NH_4^+, a calculated value of 11.0 kcal/mol is obtained compared with an experimental value of 6.6 kcal/mol reported by Aue *et al.* (1). Although this property is not satisfactorily accounted for in quantitative terms, it may be seen that the general trends observed within the family of substituted ammonium ions is quite reasonable: within the primary amine series, alkylation of the ammonium ions results in an increase of the $-T\Delta S_S$ contribution in the order $MeNH_3^+ < EtNH_3^+ < n\text{-}PrNH_3^+ < n\text{-}BuNH_3^+$, in agreement with the observed data. In the same way, the variation of the entropy of solvation in the secondary amine series follows the order $Me_2NH_2^+ < Et_2NH_2^+$, $n\text{-}Pr_2NH_2^+ < n\text{-}Bu_2NH_2^+$, compared with the observed sequence $Me_2NH_2^+ < Et_2NH_2^+ < n\text{-}Pr_2NH_2^+ < n\text{-}Bu_2NH_2^+$. For the tertiary ammonium ions, although the order $Me_3NH^+ < Et_3NH^+$ is qualitatively reproduced (there is no experimental data available concerning $n\text{-}Pr_3NH^+$), the LRF model predicts a largely overestimated value of the entropy of solvation, and this, for both the Et_3NH^+ and $n\text{-}Pr_3NH^+$ ions. Finally, the decrease of $-T\Delta S_S$ by methylation of the pyrrolidinium ion is also qualitatively accounted for by the LRF model.

The overestimation of the entropy of solvation for the tertiary amine series could be related to the fact that the solvent–solvent polarization energy has been represented, within this model, by the interaction of hard spheres of radius $(r_A + R_S)$. As a result, two (or more) atoms in the molecule are close enough so that their cosphere overlap. In such a case, one would want some of the overlapping cosphere material to be displaced in a process in which the local dielectric material relaxes to the state of the normal bulk solvent (32). This effect which is expected to be even more pronounced when bulky substituents are incorporated into the molecule, is not accounted for in the present approach. Further developments of the present model, allowing for this steric hindrance effect to solvation to be included, is expected to improve the description of the entropy of solvation of sterically hindered molecular ions.

Finally, taking into account the correct trends predicted for the $-\Delta G_S$ contributions, it may be concluded that the somewhat irregular order of the enthalpy of solvation predicted by eq. [15] arises mainly from the overestimated $-T\Delta S_S$ contributions. This fact, as was discussed above, dramatically manifests itself in the tertiary ammonium ions.

Concluding remarks

The main conclusions that may be drawn from this work are the following: (*a*) The quantum mechanical extension of the Born formalism including dielectric saturation effects appears to work reasonably well, at least qualitatively, in accounting for the variations of the thermodynamic functions of solvation associated with changes in size of ions and substituent effects. This has been shown for ammonium ions and may hopefully be applied to other molecular systems as well. (*b*) Since the method necessarily involves a semi-empirical choice of ϵ_L and R_S, as well as a semi-empirical adjustment of the solute–solvent interaction integrals, we cannot consider the results obtained as quantitatively significant.

In spite of the above considerations, the present approach represents a considerable progress with respect to the current quantum mechanical approaches based on the Born formula. For the first time, to our knowledge, a complete thermodynamic picture of solvation for molecular ions has been obtained. This could be particularly useful in connection with the theoretical study of acid–base equilibria in solution involving a wide variety of systems.

Acknowledgement

Acknowledgement is made to the donors of the Petroleum Research Fund, administered by the American Chemical Society, for the support of this research (PRF 14100-AC4).

1. D. H. Aue, H. M. Webb, and M. T. Bowers. J. Am. Chem. Soc. **98**, 318 (1976).
2. E. M. Arnett, F. M. Jones, M. Taagepera, W. G. Henderson, J. L. Beauchamp, D. Holtz, and R. W. Taft. J. Am. Chem. Soc. **94**, 4724 (1972).
3. D. H. Aue, H. M. Webb, and M. T. Bowers. J. Am. Chem. Soc. **94**, 4726 (1972).
4. J. I. Brauman and L. K. Blair. J. Am. Chem. Soc. **90**, 6561 (1968).
5. P. Claverie, J. P. Daudey, J. Langlet, B. Pullman, D. Piazzola, and M. J. Huron. J. Phys. Chem. **82**, 405 (1978).
6. P. Cremaschi, A. Gamba, and M. Simonetta. J. Chem. Soc. Perkin II, 162 (1977).
7. J. D. Dill, L. C. Allen, W. C. Topp, and J. A. Pople. J. Am. Chem. Soc. **97**, 7220 (1975).
8. G. Klopman. Chem. Phys. Lett. **1**, 200 (1967).
9. R. Constanciel and O. Tapia. Theoret. Chim. Acta, **48**, 75 (1978).
10. H. A. Germer. Theoret. Chim. Acta, **34**, 145 (1978).
11. R. Contreras and J. S. Gomez-Jeria. J. Phys. Chem. **88**, 1905 (1984).
12. G. W. Schnuelle and D. L. Beveridge. J. Phys. Chem. **79**, 2566 (1975).
13. M. D. Newton and S. Ehrenson. J. Am. Chem. Soc. **93**, 4971 (1971).
14. G. W. Schnuelle, S. Swaminathan, and D. L. Beveridge. Theoret. Chim. Acta, **48**, 17 (1978).
15. M. Born. Z. Phys. **1**, 45 (1920).
16. M. Salomon. J. Phys. Chem. **74**, 2519 (1970).
17. W. A. Millen and D. W. Watts. J. Am. Chem. Soc. **89**, 6051 (1967).
18. R. Contreras and A. Aizman. Int. J. Quantum Chem. In press.
19. S. Miertus and O. Kysel. Chem. Phys. Lett. **65**, 395 (1979).
20. D. A. MacDonaill and D. A. Morton. Theoret. Chim. Acta, **65**, 13 (1984).
21. R. Constanciel and R. Contreras. C. R. Acad. Sci. Paris, **296**, 333 (1983).
22. R. Constanciel and R. Contreras. Theoret. Chim. Acta, **65**, 1 (1984).
23. D. L. Beveridge and G. W. Schnuelle. J. Phys. Chem. **79**, 2562 (1975).
24. R. A. Marcus. J. Chem. Phys. **24**, 966 (1956).
25. J. Jortner. J. Chem. Phys. **30**, 839 (1959).
26. L. Pauling. The nature of the chemical bond. Cornell University Press, New York. 1960. p. 260.
27. R. H. Stokes. J. Am. Chem. Soc. **84**, 513 (1962).
28. K. J. Laidler. Can. J. Chem. **37**, 138 (1959).
29. B. E. Conway. Ann. Rev. Phys. Chem. **17**, 481 (1966).
30. P. Kebarle, W. R. Davidson, J. Sunner, and S. Meza-Hojer. Pure Appl. Chem. **51**, 63 (1979).
31. S. Ikuta. Chem. Phys. Lett. **95**, 604 (1983).
32. H. L. Friedman and C. V. Krishnan. *In* Water a comprehensive treatise. Vol. 3. *Edited by* F. Franks. Plenum Press, New York. 1973. p. 1.

Triethylammonium halides, Et_3NHX (X = Cl, Br, I): simple structure, complex spectrum[1]

MARGARET ANN JAMES, T. STANLEY CAMERON, AND OSVALD KNOP
Department of Chemistry, Dalhousie University, Halifax, N.S., Canada B3H 4J3

AND

MURRAY NEUMAN AND MICHAEL FALK
Atlantic Research Laboratory, National Research Council of Canada, Halifax, N.S., Canada B3H 3Z1

Received August 22, 1984

This paper is dedicated to Professor Camille Sandorfy on the occasion of his 65th birthday

MARGARET ANN JAMES, T. STANLEY CAMERON, OSVALD KNOP, MURRAY NEUMAN, and MICHAEL FALK. Can. J. Chem. **63**, 1750 (1985).

A crystal structure determination has shown that the ethyl groups in the three isostructural ($P6_3mc$, Z = 2) triethylammonium halides, Et_3NHX (X = Cl, Br, I), at room temperature are orientationally disordered and the N—H···X groups are linear by symmetry. The unusual extent and complexity of the NH and ND stretching absorptions in the ir spectra of all three compounds between 10 and 293 K are discussed in terms of Fermi resonance interactions. The centroid ν(NH) and ν(ND) frequencies extracted from the spectra correlate with the $H_N \cdots X$ distances. It is shown that if Fermi resonance is the sole cause of the complexity of the stretching absorptions, then these centroids represent the ν(NH) and ν(ND) frequencies unperturbed by Fermi resonance. The centroid frequencies in the three halides are unusually low, pointing to strong N—H···X hydrogen bonding.

MARGARET ANN JAMES, T. STANLEY CAMERON, OSVALD KNOP, MURRAY NEUMAN et MICHAEL FALK. Can. J. Chem. **63**, 1750 (1985).

Une détermination de structure cristalline a permis de montrer que, à la température ambiante, les groupements éthyles des trois halogénures de triéthylammonium, Et_3NHX (X = Cl, Br, I), isostructuraux ($P6_3mc$, Z = 2) ne sont pas ordonnés du point du vue de l'orientation et que les groupements N—H···X ont une symétrie linéaire. Opérant à des températures allant de 10 à 293 K, on a mesuré les spectres infrarouges des trois composés qui présentent des absorptions d'élongation NH et ND dont l'importance et la complexité sont inhabituelles; on en discute en fonction d'interactions de résonance de Fermi. On peut établir une corrélation entre les fréquences centroïdes ν(NH) et ν(ND) que l'on peut extraire des spectres et les distances $H_N \cdots X$. On démontre que, si la résonance de Fermi est la seule cause de la complexité des absorptions d'élongation, ces centroïdes représentent les fréquences ν(NH) et ν(ND) qui ne sont pas perturbées par la résonance de Fermi. Les fréquences centroïdes des trois halogénures sont particulièrement basses et ce résultat suggère qu'il existe une liaison hydrogène N—H···X importante.

[Traduit par le journal]

The N—H···X bond in the three hexagonal Et_3NHX halides is known (1, 2) to be on a threefold axis and fairly short; in the chloride d(N···X) ~ 3.11 Å (2). The NH groups are all crystallographically equivalent and well separated (d(N···N) ~ 6 Å or longer). A single NH stretching absorption free from complications would thus be expected in the ir spectrum, and since the N—H···X bond is linear by symmetry, the three halides would seem to offer an excellent opportunity for correlating the N···X and H···X distances with the NH stretching frequency. However, the results of a number of ir studies of these compounds (3–7) are completely at variance with the expectation. The observed ν(NH) absorption is not a single peak but a complex multicomponent absorption extending over at least 400 cm^{-1} of the spectrum; the full extent and complexity of this absorption, and of the corresponding ν(ND) absorption in deuterated material, become evident at low temperatures (3, 6, 7). Similar observations have been made with other alkylammonium salts (8–14). While general explanations of this complexity have been advanced (4, 5, 8) (see below), the frequency–distance correlation was not pursued in any detail, both because of lack of accurate structural information on the three halides at the time and because of the uncertainty as to how to extract from each spectrum a single ν(NH) or ν(ND) frequency value to be used in such a correlation.

In the present investigation we have attempted to contribute toward a resolution of these problems in two ways. We have redetermined the crystal structure of the chloride and determined the structures of the bromide and iodide. We have also obtained high-quality ir spectra, between 10 and 293 K, of the undeuterated and partially deuterated halides, from which we have derived frequency centroids of the NH and ND stretching absorptions to be used in the frequency–distance correlation. It is shown that if Fermi resonance is the sole cause of the complexity of the stretching absorption, then on certain assumptions these centroids represent the ν(NH) and ν(ND) frequencies unperturbed by Fermi resonance.

Experimental

The title compounds were prepared by neutralizing Et_3N in aqueous solution with the appropriate aqueous HX. They were recrystallized from 50% EtOH. The crystal data of the three halides are listed in Table 1.

Space group

The lattice parameters are in reasonable agreement with those determined previously (1, 2). In each case there are two formula units in the hexagonal unit cell, which requires the N atoms to be situated in special positions but not at centres of symmetry, as the cation is not centrosymmetric. The systematic absence of $hkil$ reflections with $l = 2n + 1$ is consistent with the space groups $P31c \subset (P6_3mc, P\bar{6}2c, P\bar{3}1c) \subset P6_3/mmc$. Unless it is assumed from the outset that the cations are orientationally disordered, $P6_3/mmc$, $P\bar{6}2c$, and $P\bar{3}1c$ can be ruled out, as none of these contains twofold equipoints compatible in symmetry with the stereochemistry of the cation. In the two remain-

[1] NRCC No. 24020.

TABLE 1. Crystal data of Et_3NHX (X = Cl, Br, I)*

	X = Cl†	X = Br	X = I
Formula	$C_6H_{16}ClN$	$C_6H_{16}BrN$	$C_6H_{16}IN$
fw	137.65	182.11	229.11
a, Å	8.329(1)	8.449(3)	8.700(3)
c, Å	7.058(2)	7.373(2)	7.883(2)
c/a	0.847	0.873	0.906
V, Å^3	424.0(2)	455.8(5)	516.7(5)
ρ_o, g/cm^3 (1)	1.07	1.32	1.51
ρ_c, g/cm^3	1.078(1)	1.327(2)	1.472(1)
μ_{Mo}, cm^{-1}	3.24	43.30	28.25
$F(000)$, e	152	188	224
Reflections:			
Total measured	1333	746	1664
Unique total	265	145	322
Unique used‡	179	125	132
100R; 100R_w	4.73; 4.33	3.01; 3.00	5.04; 5.78§

*Mo $K\alpha_1$, λ = 0.70926 Å (graphite monochromator); θ-range, 2–23°. Space group, $P6_3mc$ (no. 186); Z = 2.
†Reference 2: a = 8.38(2) Å, c = 7.07(2) Å, c/a = 0.84, V = 429 Å^3, ρ_o = 1.01 g/cm^3.
‡$I > 1\sigma(I)$.
§Reflections 002 and 004 omitted from refinement.

ing groups the N and X atoms would be situated on threefold axes, in $P6_3mc$ with site symmetry $3m$ and in $P31c$ with site symmetry 3. Since for structures containing atoms in general positions the equalities $|F(\bar{h}kl)| = |F(h\bar{k}l)|$ and $|F(hkl)| = |F(hk\bar{l})|$ hold in $P6_3mc$ but not in $P31c$, the space-group ambiguity can, in principle, be resolved by comparing the appropriate $|F_o|$ values. Under this scrutiny the space group $P6_3mc$ adopted by both Hendricks (1) and Genet (2) has been confirmed.

Structure determination

A CAD-4 four-circle diffractometer was used in the determination of the unit-cell dimensions and in the intensity collection. The intensities were reduced by routine procedures (15). Lorentz and polarization corrections were applied but not absorption or extinction corrections. The scattering factors for neutral atoms were taken from ref. 16. The structures were solved by Patterson and Fourier methods using the SHELX system (17). To ensure proper convergence, the C—H bond lengths were constrained in the refinement to 1.08 Å and the N—H to 1.03 Å in the chloride, 1.025 Å in the bromide, and 1.02 Å in the iodide. The CH_2 and CH_3 groups were refined as rigid bodies.

The positional parameters are listed in Table 2, the thermal parameters in Table 3,[2] structure factors in Tables 4–6,[2] and interatomic distances and bond angles in Table 7.

Infrared spectra

For the survey spectra, the finely ground sample powders were mulled in hydrocarbon or fluorocarbon oil and the mulls were held between CaF_2 windows. The spectra were recorded on a Perkin-Elmer model 180 grating spectrometer or a Bomem DA3.02 Fourier-transform ir spectrometer fitted with a closed-cycle He refrigerator (Displex model 202, Air Products and Chemicals Co.). For the more detailed study of the ND stretching band at isotopic dilution the salts were deposited as solid films on CaF_2 plates by forced evaporation of C_2H_5OH or 5:95 C_2H_5OD–C_2H_5OH solutions. The films were prepared in 0% D|5% D pairs matched in thickness. Their spectra at room temperature were recorded on the Bomem spectrometer and the spectral profiles of the ND absorptions were obtained by digital subtraction of the spectra of the matched pairs. The centres of gravity were determined by integrating the digital spectra.

[2]These tables have been deposited. Copies are available, at a nominal charge, from the Depository of Unpublished Data, CISTI, National Research Council of Canada, Ottawa, Ont., Canada K1A 0S2.

TABLE 2. Positional parameters (×10^4) of Et_3NX*

Atom	X = Cl† x, y, z	X = Br x, y, z	X = I x, y, z
N	1/3	1/3	1/3
	2/3	2/3	2/3
	4402(8)	4423(20)	4561(27)
H(1)	1/3	1/3	1/3
	2/3	2/3	2/3
	2942(8)	3032(20)	3267(27)
C(1)	1781(8)	1805(17)	1825(44)
	6951(8)	6933(18)	6861(46)
	4983(15)	4915(41)	4857(97)
H(11)	0608(8)	0547(17)	0675(44)
	5604(8)	5723(18)	5764(46)
	5223(15)	4535(41)	4276(97)
H(12)	2373(8)	1854(17)	1664(44)
	7646(8)	7092(18)	6786(46)
	6282(15)	6371(41)	6218(97)
C(2)	1854(11)	1834(30)	1730(101)
	8634(10)	8583(30)	8366(99)
	4056(9)	4148(21)	4335(54)
H(21)	0578(11)	0671(30)	0527(101)
	8618(10)	8679(30)	8360(99)
	4373(9)	4606(21)	4686(54)
H(22)	1986(11)	1782(30)	1884(101)
	8581(10)	8435(30)	8475(99)
	2539(9)	2691(21)	2973(54)
H(23)	3009(11)	3078(30)	2854(101)
	9894(10)	9808(30)	9482(99)
	4604(9)	4529(21)	4926(54)

*The X atom is in $2(b)$ – $\frac{1}{3}, \frac{2}{3}$, 0 etc. of $P6_3mc$. The C and H atoms are in $12(d)$ – xyz etc. with an occupancy factor of $\frac{1}{2}$ (see text).
†Reference 2: N, z = 0.440; C(1), x = 0.180, y = 0.695, z = 0.488; C(2), x = 0.165, y = 0.865, z = 0.401.

TABLE 7. Et_3NHX: uncorrected interatomic distances (Å) and bond angles (deg)

	X = Cl	X = Br	X = I
Distances:			
N···X	3.107(6)	3.261(14)	3.595(21)
H(1)···X*	2.08(2)	2.24(3)	2.58(3)
N—C(1)	1.484(7)	1.463(16)	1.424(37)
C(1)—C(2)	1.520(10)	1.493(23)	1.414(62)
Angles:			
C(1)—N—H(1)	106.1(5)	104.4(13)	99.4(31)
N—C(1)—C(2)	113.1(6)	116.5(16)	123.1(43)
C(1)—N—C(1)	112.7(4)	114.1(10)	117.4(17)

*To allow for the uncertainty introduced by constraining the N—H bond length (see Experimental), 0.01 Å has been added to the esd's from the refinement.

Results and discussion

Crystal structures

To be compatible with the crystal data (Table 1), the N and X atoms must be located in equipoint $2(b)$ – $\frac{1}{3}, \frac{2}{3}, z$ etc. Hendricks (1) in 1928 placed both carbons of the C_2H_5 group in $6(c)$ – $x, \bar{x}, z$ etc., i.e. on the mirror plane. Genet (2) placed both carbons in the chloride in $12(d)$ – x, y, z etc., i.e. off the

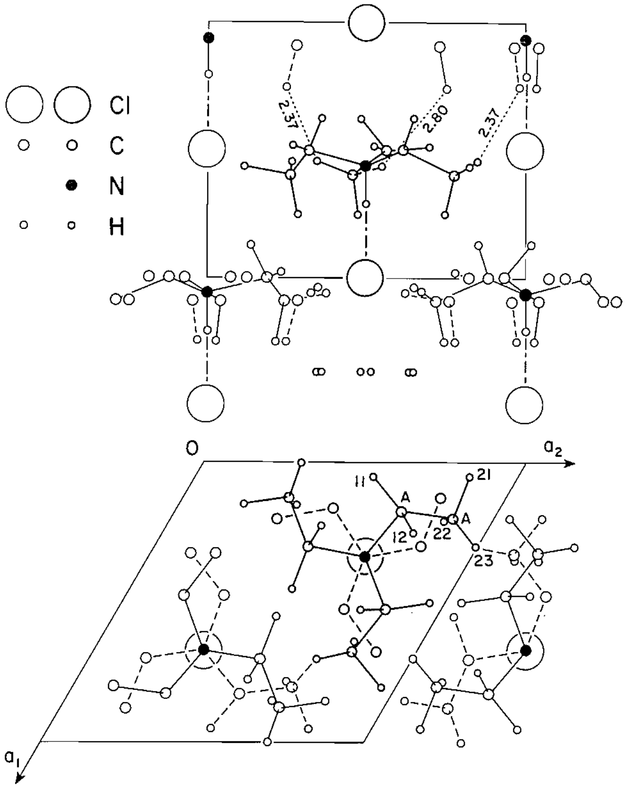

FIG. 1. $Et_3NH\underline{C}l$: projections of a portion of the structure on (0001) (*bottom*) and (10$\bar{1}$0) (*top*). The two possible orientations of a C_2H_5 group are distinguished by solid and broken lines, respectively. The N—H bonds are drawn as dash–dot lines, the shortest intermolecular $H_C \cdots H_C$ distances as dotted lines. The top projection shows the environment of a Et_3NHCl unit oriented as per Table 2.

mirror planes, which introduces twofold orientational disorder with respect to the mirrors; the final R was 0.10.

In our refinements both models were tried as well as a third model, with C(1) in 12(d) with half occupancy and C(2) in 6(c). The lowest R values (anisotropic temperature factors, hydrogens not yet included) for all three halides were obtained with C(1) and C(2) both disordered. This establishes that the three compounds are isostructural and the structure proposed for the chloride by Genet is correct. Inclusion of the H atoms lowered the R to 4.73% for the chloride, 3.01% for the bromide, and 5.04% for the iodide.

Unlike the structures of some alkylammonium salts (13), in which the "ionic" (i.e. —NH^+/anion containing) layers alternate with layers of the "fatty" alkyl residues, the Et_3NHX structures consist of identically populated staggered layers ‖(0001) stacked in an ABAB. . . sequence (Fig. 1). Each layer contains both the —NEt_3 groups (in a nearly flat conformation) and the X^- ions. The vertical separation of these layers, $c/2$, is almost equal to the N$\cdots$X distance; the N—H$\cdots$X bonds are parallel to c and thus perpendicular to the layers.

The Et groups, relative to the N—H bonds, are arranged indifferently in left-handed and right-handed Et_3NH units of C_3 symmetry. The structure may thus be regarded as a racemic crystal with a random distribution of the two chiralities. Genet (2) observed that, in the chloride, the minimum distances between atoms of neighbouring cations are too large for an effective interaction capable of giving rise to orientational ordering, at least at room temperature. Indeed, in Et_3NHCl the shortest intermolecular distance between two ethyl hydrogens is

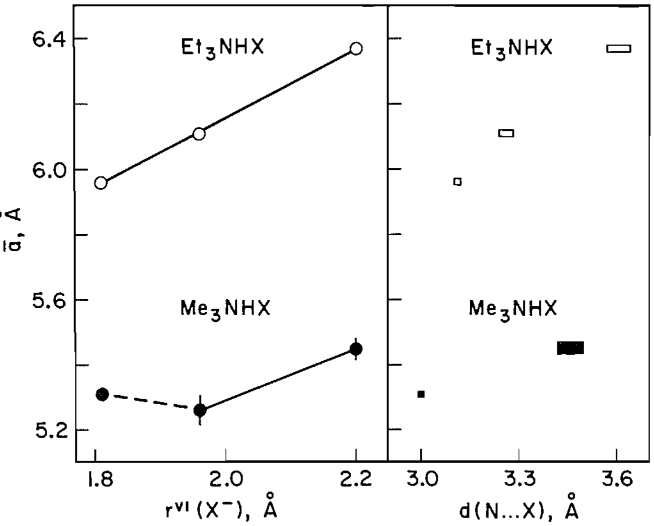

FIG. 2. Variation of the mean linear unit-cell dimension $\bar{a} = (V/Z)^{1/3}$ of Et_3NHX and Me_3NHX with the effective ionic radius of X^- (*left*) and d(N$\cdots$X) (*right*).

H(23A)$\cdots$H(22M) ~ 2.37 Å, followed by H(21C)$\cdots$H(22G) ~ 2.79 Å and H(21C)$\cdots$H(22K) ~ 2.96 Å; all the other $H_C \cdots H_C$ distances are greater than 3.5 Å.[3] In the bromide and iodide the corresponding distances are at least 2.7 Å. The structure thus has a considerable flexibility which increases from the chloride to the iodide. This is reflected in the esd's of the positional parameters (Table 2) and in the unusually large values of the thermal parameters in the iodide (Table 3[2]).

Comparison with Me_3NHX

Unlike the three Et_3NHX halides, the three Me_3NHX halides are not isostructural among themselves, even though they all have the same space-group symmetry, $P2_1/m$ (18–20), and they differ in important respects from the Et_3NHX in the organization of their structures. For Et_3NHX the variation of the mean linear unit-cell dimension $\bar{a} = (V/Z)^{1/3}$ with the effective ionic radius r^{vi} (X^-) (Fig. 2) is linear (r^2 = 0.999, σ = 0.009 Å), as would be expected for an isostructural salt series. In contrast, in the corresponding plot for Me_3NHX the points for X = Br and X = I define a straight line almost parallel to that for Et_3NHX, but the Cl point is significantly above this line. This is not unexpected: the structures of the chloride (19) and the iodide (20) are different, and while the structure of the bromide does not appear to have been determined, the unit-cell dimensions of that compound are similar to those of the iodide (18).

The d(N$\cdots$X) in Et_3NHX range from 3.11 to 3.60 Å (Table 7). These values are about 3% larger than the corresponding values for Me_3NHCl and Me_3NHI. The N$\cdots$Cl distance in Me_3NHCl is exceptionally small, about 10% smaller than the d(N$\cdots$Cl) in simple cubic NH_4Cl, so that in ref. 19 the structure of Me_3NHCl is regarded as consisting of neutral [$Me_3NH^+Cl^-$] ion pairs.

In the two trimethyl structures the N$\cdots$X (and by implication the N—H) vectors are arranged in parallel layers (Fig. 3), within which they are antiferro-ordered. The minimum perpendicular separation of these vectors is 4.3 Å in the chloride and ~4.5 Å in the iodide. In the polar Et_3NHX structures,

[3] Symmetry code: A, x, y, z; C, $y - x, 1 - x, z$; G, $1 - x, 1 - y, \frac{3}{2} + z$; K, $y, x, \frac{3}{2} + z$; M, $1 + x - y, 1 - y, \frac{3}{2} + z$.

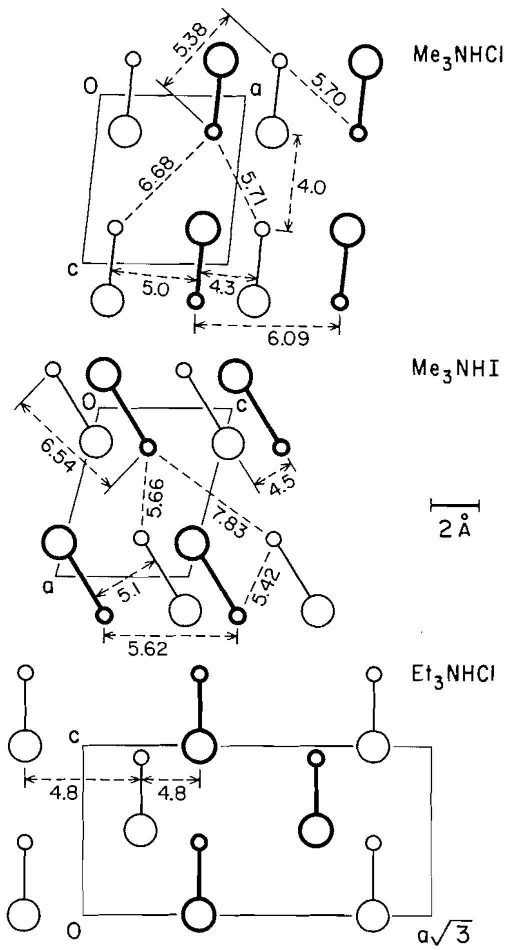

FIG. 3. Orientation and minimum perpendicular separation of the N—X vectors in the structures of Me_3NHCl, Me_3NHI, and Et_3NHCl. The large circles represent Cl or I, the small circles represent N.

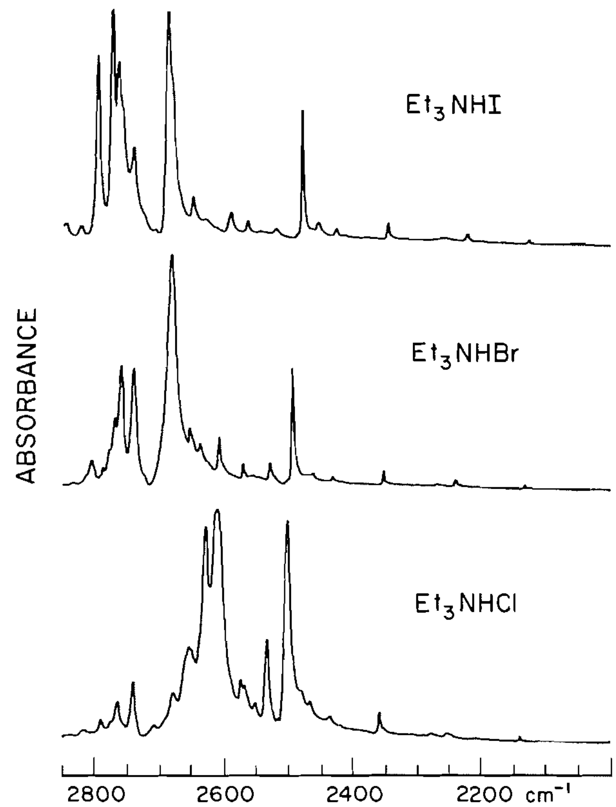

FIG. 4. NH stretching absorption in the ir spectrum of the three Et_3NHX halides at 10 K (0% D, fluorocarbon mulls). The absorbance was arbitrarily scaled to the same maximum peak height.

on the other hand, the packing is such that the N—H vectors are all *ferro*-ordered within staggered layers parallel to (0001); the minimum perpendicular separation of the threefold axes on which the N—H vectors are located is ≥4.8 Å, while the minimum $H_N \cdots H_N$ = N···N distance is ~6 Å or more. The considerably larger separation of the NH groups in Et_3NHX has important implications for vibrational coupling (see below).

Infrared spectra: previous studies

In the ir spectra of trialkylammonium halides, absorptions due to the NH and ND stretching fundamentals can extend over several hundreds of cm^{-1} and contain many sharp components. Sandorfy *et al.* (4, 5) and Lord and McDowell (3, 6, 7) made this observation with Et_3NHX, and Ebsworth and Sheppard (8) with Me_3NDI, some 25 years ago. The studies that have been published since, both on triethylammonium (10, 11, 14, 21, 22), trimethylammonium (9, 23–25), and higher trialkylammonium (21) halides bear witness to the continued interest in this phenomenon, and are not confined to the simple halides but include other alkylammonium salts as well (12, 13). The complex NH and ND stretching absorptions persist, with band sharpening and increased detail, down to liquid-helium temperature (3, 6) and are observed also in solution spectra of these salts (9–11, 14, 21, 22).

Sandorfy *et al.* (4, 5) interpreted the complexity of the NH stretching absorption in Et_3NHX in terms of combination bands involving mainly deformation vibrations, the ir intensity of which derives from electrical anharmonicities induced by the strong hydrogen bonds; Ebsworth and Sheppard (8) regarded the numerous strong absorption bands near the ND stretching fundamental of Me_3ND^+ as overtone and combination bands interacting with the ND stretching fundamental through Fermi resonance. That Fermi resonance perturbations are responsible for the complexity has been concluded also from the observation that the NH stretching absorption in the solution spectra of Et_3NH^+ salts is independent of the solvent (11, 14) and from the study of the ir spectra of the trimethylammonium–pyridine and triethylammonium–pyridine complex cations (9, 10). On this view the complexity of the NH and ND stretching absorptions in Et_3NHX arises from overtones and binary combinations of fundamental vibrations of the cations in the 1000–1500 cm^{-1} region, enhanced by extensive Fermi resonance with the NH or ND stretching fundamental.

Infrared spectra: present work

Such spectral changes as occur in the NH and ND stretching regions of the spectra of the three halides between 10 and 293 K are gradual and do not point to the existence of phase transitions in this temperature interval.

NH stretching absorption (Fig. 4). In undeuterated Et_3NHCl the complex absorption extends from above 2800 cm^{-1}, where it merges with the CH stretching fundamentals, to about 2100 cm^{-1}, where absorption peaks become sparse and gradually vanish into the background. The spectra agree very well with those recorded by McDowell (7) at the two temperatures studied, 80 and 300 K, except for the somewhat better resolution of our spectrometers.

TABLE 8. Et_3NHX: fine structure of the NH stretching fundamental (cm^{-1})*

X = Cl		X = Br		X = I	
10 K	293 K	10 K	293 K	10 K	293 K
2837 vw	a	2833 vw	a	2822 w	2818
2816 vw	2810	2805 w	2802	2796 s	2793
2790 vw	~2786	2787 vw	a		
		2776 vw	a	2774 vs	2767
2774 vw	a	2768 w	a	2763 s	2761
2763 w	a	2759 m	2756	2758 w	a
2740 m	2739	2740 m	2738	2741 m	a
2708 vw	a			2708 vw	a
		2695 w	a	2689 vs	2681
		2683 vs	2677	~2682 w	a
2679 m	~2666				
~2660 w	a				
2655 s	~2648	2654 w	2653	2649 w	2651
~2651 m	a	~2650 w	a		
		2638 w	a	~2631 vw	a
2629 vs	2622	~2626 vw	a	~2612 vw	a
2612 vs	2604	2608 m	2600	2591 w	2584
2575 m	2576	2571 w	2570	2565 w	2566
2568 m	a	2557 vw	a	2547 vw	a
2553 w	a	2546 vw	a	~2539 vw	a
2534 s	2531	2530 w	2527	2521 w	~2525
2502 vs	2498	2495 s	2491	2481 s	2478
2482 vw	a			2477 vw	a
2467 vw	~2463	2463 vw	a	2456 w	a
2436 vw	2436	2433 vw	2431	2428 w	2428
2359 w	2359	2354 w	2353	2347 w	2347
2354 vw	a			~2341 vw	a
2280 vw	2275	2271 vw	a	2264 vw	a
2254 vw	2251	2241 w	2236	2224 vw	2222
2140 vw	2139	2133 vw	2132	2126 vw	2126

*a, broadened and merged with other bands; vw, very weak; w, weak; m, medium; s, strong; vs, very strong; ~, broader peaks or shoulders, position uncertain by more than 1 cm^{-1}.

More than 20 absorption peaks are clearly resolved at 10 K; with increasing temperature they gradually broaden and coalesce. The NH stretching absorptions of the undeuterated bromide and iodide yield complex patterns of peaks similar to those of Et_3NHCl: sharp spectral features in the absorptions of the three compounds appear to correspond in relative intensity and temperature shift (Table 8). The positions of corresponding peaks tend to shift by a few cm^{-1} to lower wavenumbers going from the chloride to the iodide. The correspondence is most obvious in the low-frequency wing and disappears toward the band centre.

Assuming that the NH stretching absorption ends and the CH stretching absorption begins at 2850 cm^{-1}, the frequency centroids of the NH stretching absorption are computed as

Temperature	Frequency centroid (cm^{-1}) Cl	Br	I
10 K	2611(2)	2685(2)	2740(2)
293 K	2598(2)	2676(2)	2727(2)

Examination of the effect of N-deuteration indicates that in fact the NH absorption extends somewhat beyond 2850 cm^{-1} and allowance must be made for the NH/CH overlap, which increases from Cl to I. The true positions of the centroids are estimated to be ~5 cm^{-1} (Cl), ~10 cm^{-1} (Br), and ~30 cm^{-1} (I) higher than the respective above values.

Two trends are clearly demonstrated in spite of our uncertainty about the absolute positions of the NH centroids:

(*i*) The centroids shift to lower wavenumbers with increasing temperature. This agrees with the independent observation that most of the *individual* component peaks also shift in this direction (Table 8).

(*ii*) The centroid frequencies increase from Cl to I; the shifts are much larger than the experimental uncertainty.

ND stretching absorption (Figs. 5 and 6). As illustrated in Fig. 5 for the chloride, the ND absorption too extends over a wide range. The positions of the component peaks were found to be independent of the degree of deuteration. The ND spectra of the bromide and iodide resemble those of the chloride; their behaviour with temperature (Fig. 5) shows a close similarity to the NH spectra.

Unlike for $(C_2H_5)_3NH^+$, in $(C_2H_5)_3ND^+$ there is no interference from the CH stretching absorptions. The positions of the frequency centroids of the ND absorption can therefore be determined with considerable accuracy, as the subtraction procedure for the 0% D| 5% D matched spectra cancels, to a good approximation, all spectral features except those due to the ND stretching. At room temperature the centres of gravity were 2007(2) cm^{-1} for the chloride, 2062(2) cm^{-1} for the bromide, and 2135(2) cm^{-1} for the iodide. The above anion dependence of the NH centroids is thus confirmed beyond doubt.[4]

Infrared spectra: discussion

Vibrational coupling. The positions (and to a large extent the widths) of the component NH and ND stretching absorptions are independent of the degree of deuteration. This points to the absence of any appreciable dynamic coupling of vibrations of neighbouring NH or ND groups in the $Et_3N(H, D)X$ crystals. Such coupling thus does not contribute to the spectral complexity of the NH and ND stretching absorptions. A similar observation has been made with $(Et_3NH)_2SnCl_6$ (12) and $(Me_3NH)_2SnCl_6$ and $(Me_3NH)_2SnBr_6$ (13). However, evidence of vibrational coupling has been reported for Me_3NHCl (24).

The absence of vibrational coupling may be accounted for by the large separation of neighbouring NH groups in the crystal. In Me_3NHCl, where coupling appears to exist, the minimum N···N distance is 5.38 Å, and in Me_3NHI it is 5.42 Å. In comparison, in Et_3NHX it is at least ~6 Å, and in $(Me_3NH)_2SnCl_6$ (13) and $(Me_3NH)_2TeCl_6$ (26) it is >6.2 Å.

The configuration of the N—X vectors (the direction of which in Me_3NHX and Et_3NHX coincides more or less with that of the N—H vectors) may also be a factor. The nearest-neighbour N—X vectors in all three structures, Me_3NHCl, Me_3NHI, and Et_3NHX, are related by the operation of a two-fold screw axis. However, in the trimethyl compounds these vectors are in mirror planes perpendicular to the screw axis, whereas in Et_3NHX they are parallel to it (Fig. 3). The layers containing the N—X vectors are parallel to (001) in Me_3NHCl, to (100) in Me_3NHI, and to (0001) in Et_3NHX. The arrangement of the vectors in these layers is antiparallel in the trimethyl compounds, but in Et_3NHX the vectors are parallel and offset by the $c/2$ screw translation. In the triethyl compounds the N—X vectors are perpendicular to the layers, whereas they

[4]If this were desired, the NH/CH overlap problem in the NH centroid determination could be resolved by working from $(C_2D_5)_3NHX$ instead of $(C_2H_5)_3NHX$ spectra.

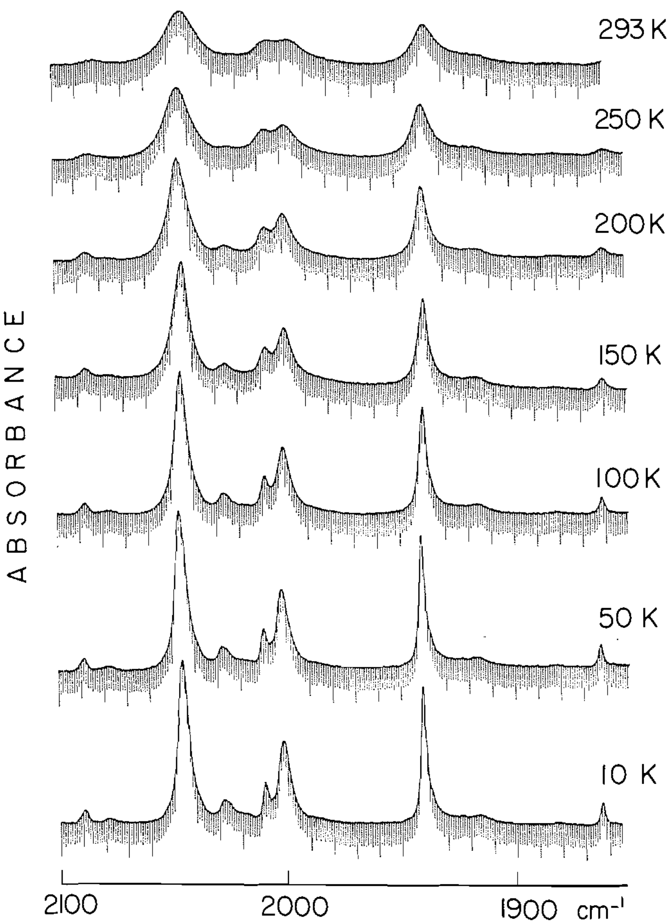

FIG. 5. The central part of the ND stretching absorption in the ir spectrum of Et_3NHCl (5% D) (fluorocarbon mull) at different temperatures.

are canted in the trimethyl compounds, ~85° relative to the layer in the chloride and ~60° in the iodide.

Frequency centroids. While the centres of gravity of the absorptions in the NH and ND stretching regions of Et_3NHX can be determined with considerable confidence, the question remains as to how the frequency values so obtained are related to the single frequencies that would be observed in the absence of spectral complications and thus measure, unambiguously, the relative strength of the hydrogen bonding in Et_3NHX.

The subtraction procedure using matched 0% D|5% D pairs practically eliminates spurious peaks, so that each peak in the ND stretching region of the difference spectrum (Fig. 6) can be considered as involving the ND stretching fundamental. The stretching absorptions are insensitive to the degree of deuteration, and the arbitrary choice of the cut-off limits of the integration interval cannot have a serious effect, as the peak intensities of the complex absorption fall off rapidly toward the limits of the interval. The centroid frequencies may thus be regarded as authentic spectral parameters of the three halides.

What do the centroids represent? The answer depends on what is taken to be the cause of the spectral complexity. If it is assumed, with the majority of authors (8, 9, 11–14, 24, 27), that the complex fine structure of the extensive stretching absorption results *entirely* from Fermi resonance and that the participating combination and overtone levels have no inherent intensity, then it can be shown (see Appendix) that the centroid frequency represents the ν(NH), or ν(ND), frequency *un-*

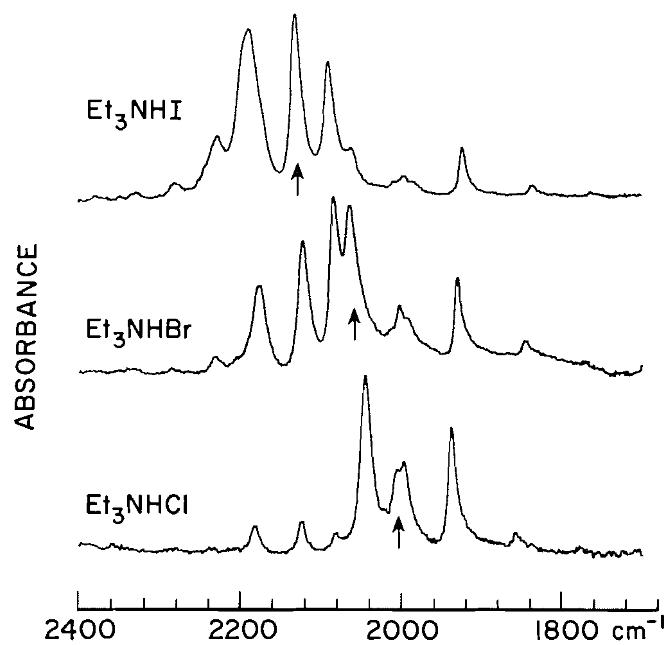

FIG. 6. Difference spectra of matched 0% D|5% D films of Et_3NHX at room temperature (solid films on CaF_2 plates). Absorbance scaled as in Fig. 4. Arrows represent centroids of the ND stretching absorptions.

perturbed by Fermi resonance and hence measures the relative strength of the N—H···X hydrogen bond in this isostructural series.

Sandorfy *et al.* (4, 5) consider Fermi resonance involving a single NH (or ND) fundamental as unlikely to give rise, alone, to an absorption as extensive as observed in the Et_3NHX spectra, although it may be operative close to the fundamental. However, the following observations support the view that Fermi resonance *is* the main cause of the complexity.

In the spectra of $(Me_3NH)_2SnX_6$ (X = Cl, Br) the fine structure of the absorption in the region of the NH and ND stretching fundamentals undergoes changes that may be described as temperature and anion tuning: when the fundamental moves away, as a result of change of temperature or change of the anion, from the nearby overtone and combination levels, the intensity of these levels decreases drastically (13). This is typical of Fermi resonance. In $(Me_3NH)_2SnX_6$ the hydrogen bonding is weak and the fine structure extends over only about 100 cm^{-1}. With increasing strength of the N—H···X bond the ir absorptions in the ν(NH) and ν(ND) regions become more intense and the extent of the fine structure increases (13). In Et_3NHX, where the hydrogen bonding is strong (see below), the fine structure extends over some 600 cm^{-1}. Temperature shifts are small compared with this wavenumber interval and temperature tuning is not appreciable, but anion shifts are large and anion tuning is clearly observed: as the centroid of the ν(NH) or ν(ND) absorption moves to higher frequencies in the series Cl—Br—I, the "corresponding" peaks in the low-frequency wing decrease in intensity, while those in the high-frequency wing increase in intensity (Figs. 4 and 6). These intensity changes are consistent with the participating overtone and combination levels borrowing much of their intensity from the fundamental by Fermi resonance, although it is not clear whether they also possess some inherent intensity independent of the resonance.

Hydrogen bonding and the frequency-distance correlation.

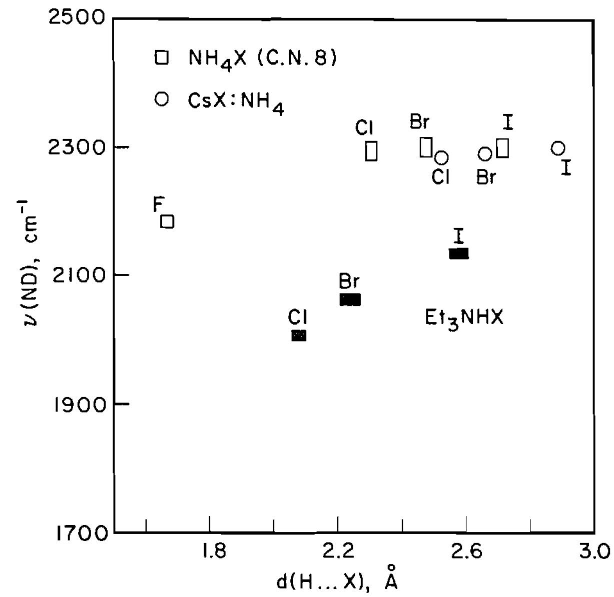

FIG. 7. Plot of the centroid frequency of the ND stretching absorption vs. $d(H\cdots X)$ in Et_3NHX at room temperature. NH_4X (X = F, Cl, Br, I) and $CsX:NH_4$ (X = Cl, Br, I) are included for comparison.

The quasi-normal distribution of intensity in the NH and ND stretching regions (Fig. 6) would seem to suggest that the effect of the perturbing factors will be the greatest near the unperturbed ν(NH) and ν(ND) frequencies. Hence whatever the real reasons for the complexity, the centroid cannot be far from the unperturbed frequency, and if Fermi resonance is *mainly* responsible, then the centroid is a sufficient approximation to the unperturbed ν(NH) and ν(ND).

The three points in the centroid frequency vs. $d(H\cdots X)$ plot (Fig. 7) lie on a curve of the expected curvature, viz. the frequency tends to level off with increasing $d(H\cdots X)$. Compared with the NH_4X halides and with NH_4^+ dispersed at low concentration in CsX matrices, the centroid ν(ND) frequencies are very low, in fact the lowest found for N—H···X (X = F, Cl, Br, I) to date. The centroid ν(ND) frequency in Et_3NHI is lower than the isotopically isolated ν(ND) frequency in NH_4F, which is the lowest such frequency in ammonium halides, simple or complex; the N—H···F bond in NH_4F is effectively linear and considered as strong. In contrast, in weakly deuterated $(Et_3NH)_2SnCl_6$ (12) the complex ν(ND) absorption centres at ~2320 cm^{-1}, and similar high values are observed in $(Et_3NH)PF_6$ and $(Et_3NH)BPh_4$ (unpublished results). An uncertainty of say 50 cm^{-1} in the Et_3NHX centroid ν(ND) frequency would not significantly affect the relative position of Et_3NHX in this set of compounds. It must be concluded that the N—H···X bonds in Et_3NHX are the strongest on record. If Et_3NHF isostructural with Et_3NHCl could be prepared, extrapolation in Fig. 7 would suggest that its unperturbed ν(ND) frequency would fall below 1900 cm^{-1}.

The absolute intensities of the ν(NH) absorptions could not be determined because of uncertain film thickness. However, the *ratios* of the integrated intensities of the NH and CH stretching absorptions in the 10 K spectra (computed on the not completely valid assumption that the 2850 cm^{-1} split corresponds to a clean separation of the two absorptions, see above) were found to increase from I to Cl. Since the intensity of the CH stretching absorption is not likely to change much from one halide to another, it is concluded that the NH absorption itself increases in this direction, consistent with the observed shifts to lower wavenumbers and with a strengthening of the hydrogen bond. The NH intensity changes from halide to halide are quite large and the trend is not affected by the uncertainties due to the NH/CH overlap.

Comparison of the NH absorptions of Et_3NHX in crystal and in solution

Odinokov *et al.* (28) in a recently published paper report the ir spectra of solutions of triethylammonium salts in $CHCl_3$.[5] These spectra, which presumably correspond to $Et_3NH^+|X^-$ ion pairs well separated by solvent molecules, invite comparison of the NH stretching fundamental in the solution spectra of the three halides (Fig. 1 and Table I of ref. 28) with that in the spectra of the corresponding crystals.

(*i*) The absorption in the NH stretching region in the solution spectra consists of broad and complex bands extending over the same spectral region as in the spectra of the corresponding crystals. This confirms that the absorbing entities in both cases are the same, viz. strongly hydrogen-bonded $Et_3NH^+|X^-$ ion pairs.

(*ii*) The component peaks in the solution spectra are broader and far less well resolved than in the crystal spectra. Such broadening is characteristic of the spectra of liquids compared with those of crystals.

(*iii*) The trends are the same for the solution spectra as for the crystal spectra: the centroids move to lower wavenumbers and relative intensities increase from I to Cl. This is consistent with the H···X bonds becoming stronger, in that order, in solution as well as in the crystal.

(*iv*) The NH stretching frequency centroids in the solution spectra are lower, relative to the crystal, by about 100 cm^{-1} for the chloride, ~75 cm^{-1} for the bromide, and ~40 cm^{-1} for the iodide. This implies that the hydrogen bonding in the $CHCl_3$ solution is considerably stronger. Presumably the ideal hydrogen-bonding situation is more nearly achieved in solution that in the crystal, where the dominant factor determining the shortest cation–anion distances (i.e. $N^+\cdots X^-$) is the electrostatic lattice energy rather than the hydrogen-bonding energy.

Acknowledgments

We thank Professor R. C. Lord for bringing to our attention his early results on Et_3NHX and for providing us with a copy of ref. 7. This work was supported by research grants from the Natural Sciences and Engineering Research Council of Canada to T.S.C. and O.K.

1. S. B. HENDRICKS. Z. Kristallogr. **67**, 472 (1928).
2. F. GENET. Bull. Soc. Fr. Min. Crist. **88**, 463 (1965).
3. R. C. LORD. Techniques of infrared spectroscopy. Final Technical Report, Engineering Research and Development Laboratory, Ft. Belvoir. 1955. pp. 121ff (cited in ref. 7).
4. B. CHENON and C. SANDORFY. Can. J. Chem. **36**, 1181 (1958).
5. C. BRISSETTE and C. SANDORFY. Can. J. Chem. **38**, 34 (1960).
6. G. C. PIMENTEL and A. L. MCCLELLAN. The hydrogen bond. W.H. Freeman and Co., San Francisco. 1960. Fig. 3–21, p. 107.
7. R. S. MCDOWELL. Doctoral thesis. Massachusetts Institute of Technology, Cambridge, MA. 1960.
8. E. A. V. EBSWORTH and N. SHEPPARD. Spectrochim. Acta, **13**, 261 (1959).
9. F. N. MASRI and J. L. WOOD. J. Mol. Struct. **14**, 201 (1972).

[5] We are indebted to the referee for bringing this paper to our attention.

10. B. BORAH and J. L. WOOD. J. Mol. Struct. **22**, 237 (1974).
11. V. P. GLAZUNOV, A. A. MASHKOVSKY, and S. E. ODINOKOV. J. Chem. Soc. Faraday 2, **75**, 629 (1979).
12. O. KNOP, T. S. CAMERON, M. A. JAMES, and M. FALK. Can. J. Chem. **59**, 2550 (1981).
13. O. KNOP, T. S. CAMERON, M. A. JAMES, and M. FALK. Can. J. Chem. **61**, 1620 (1983); (errata) **62**, 1227 (1984).
14. A. A. MASHKOVSKY, A. A. NABIULLIN, and S. E. ODINOKOV. J. Chem. Soc. Faraday 2, **79**, 951 (1983).
15. T. S. CAMERON and R. E. CORDES. Acta Crystallogr. B, **35**, 748 (1979).
16. International tables for X-ray crystallography. Vol. IV. The Kynoch Press, Birmingham, England. 1974.
17. G. M. SHELDRICK. SHELX system report. University Chemical Laboratories, Lensfield Road, Cambridge, England. 1976.
18. F. MUSSGNUG. Naturwiss. **29**, 256 (1941).
19. J. LINDGREN and I. OLOVSSON. Acta Crystallogr. B, **24**, 554 (1968).
20. G. M. SHELDRICK and W. S. SHELDRICK. Acta Crystallogr. B, **26**, 1334 (1970).
21. E. MORENO-GONZALEZ, M. MARAUD, and J. NEEL. J. Chim. Phys. **74**, 563 (1977).
22. J. B. RULINDA and TH. ZEEGERS-HUYSKENS. Bull. Soc. Chim. Belg. **87**, 329 (1978).
23. M. SCHLAAK, M. COUZI, and P. V. HUONG. Ber. Bunsenges. **80**, 881 (1976).
24. P. V. HUONG and M. SCHLAAK. Chem. Phys. Lett. **27**, 111 (1974).
25. J. BELLANATO. Spectrochim. Acta, **16**, 1344 (1960).
26. M. H. BEN GHOZLEN and J. W. BATS. Acta Crystallogr. B, **38**, 1308 (1982).
27. S. E. ODINOKOV, A. A. MASHKOVSKY, V. P. GLAZUNOV, A. V. IOGANSEN, and B. V. RASSADIN. Spectrochim. Acta, **32A**, 1355 (1976).
28. S. E. ODINOKOV, V. P. GLAZUNOV, and A. A. NABIULLIN. J. Chem. Soc. Faraday 2, **80**, 899 (1984).
29. J. OVEREND. *In* Infrared spectroscopy and molecular structure. *Edited by* M. Davies. Elsevier, Amsterdam. 1963. pp. 351–352.
30. G. BAYM. Lectures on quantum mechanics. W. A. Benjamin, Reading, MA. 1969. pp. 237ff.
31. G. HERZBERG. Infrared and Raman spectra of polyatomic molecules. Van Nostrand, Princeton, NJ. 1945. p. 216.
32. J. KILLINGBECK and G. H. A. COLE. Mathematical techniques and physical applications. Academic Press, New York. 1971. p. 79.
33. G. KABISCH and G. MÖBIUS. Spectrochim. Acta, **38A**, 1195 (1982).

Appendix

Compensation for effect of Fermi resonance on observed vibrational frequencies

Often, as in the present work, it is useful to correct measured ir frequencies for the effects of Fermi resonance. In the following we prove a simple rule that is helpful for that purpose.

Fermi resonance causes important intensity transfers, as well as large frequency perturbations, among the transitions it affects. In the usual case, a single ir-active transition (commonly a fundamental) donates intensity, through the resonance interaction, to one or more nearby transitions (commonly overtones or combinations) that would otherwise be essentially forbidden. In this single-donor case the intensity transfer and the frequency perturbations turn out to be simply related, and it has been shown (29) how the unperturbed frequencies may be recovered from the observed frequencies and intensity ratio of a Fermi doublet. This rule has been expressed (13) in an especially convenient form: the observed centroid of the Fermi doublet coincides with the unperturbed frequency of the donor transition. *Ad hoc* extensions of the centroid rule to Fermi multiplets of order greater than two are found in numerous practical attempts (9–11, 27) to deduce an unperturbed donor frequency. To furnish a theoretical footing for these generalizations, we undertake to prove that, for a Fermi multiplet of *any* order, the centroid of the observed multiplet coincides with the unperturbed donor frequency. We retain the assumption of a single donor transition; indeed, the theorem fails otherwise.

According to "near-degenerate" perturbation theory (30) the perturbed wave functions and energy levels in an Nth-order resonance multiplet are governed (cf. ref. 31) by

$$[1] \qquad \begin{pmatrix} E_1^{(0)} & V_{12}\cdots V_{1N} \\ V_{21} & E_2^{(0)} \\ \cdot & \cdot \\ \cdot & \quad\cdot \\ \cdot & \qquad\cdot \\ V_{N1} & \qquad E_N^{(0)} \end{pmatrix} \begin{pmatrix} c_1^k \\ \cdot \\ \cdot \\ \cdot \\ \cdot \\ c_N^k \end{pmatrix} = E_k \begin{pmatrix} c_1^k \\ \cdot \\ \cdot \\ \cdot \\ \cdot \\ c_N^k \end{pmatrix}$$

$k = 1, \ldots, N$. Here $E_j^{(0)}$ is the energy of the jth unperturbed state $|j^{(0)}\rangle$; V_{ij} is the matrix element of the (anharmonic) perturbation V mixing $|i^{(0)}\rangle$ and $|j^{(0)}\rangle$; the eigenvalue E_k is the energy of the kth perturbed state $|k\rangle$; the c_i^k forming the kth eigencolumn represent the projections of $|k\rangle$ on the various $|i^{(0)}\rangle$, with the understanding that the c_i^k are normalized in the usual way so that

$$\sum_{i=1}^{N} c_i^{k*} c_i^k = 1$$

for each k. For brevity we rewrite eq. [1] as

$$[1'] \qquad \mathbf{H}\cdot\mathbf{c}^k = E_k\mathbf{c}^k$$

with the obvious definition of the variables. **H** is an Hermitian matrix if V is an Hermitian operator.

We suppose that $|m^{(0)}\rangle$ is the donor level. The matrix elements for the actual transitions may be written

$$\langle 0|\mathbf{p}|k\rangle = \sum_{i=1}^{N} c_i^k \langle 0|\mathbf{p}|i^{(0)}\rangle$$

where $\mathbf{p}$ is the dipole moment operator and $|0\rangle$ the ground state from which all the transitions are supposed to arise. Since it was assumed that, among the various transitions $0 \rightarrow i^{(0)}$ conceivable in the absence of resonance, only $0 \rightarrow m^{(0)}$ has intrinsic intensity, we have $\langle 0|\mathbf{p}|i^{(0)}\rangle = 0$ for $i \neq m$. Hence

$$\langle 0|\mathbf{p}|k\rangle = c_m^k \langle 0|\mathbf{p}|m^{(0)}\rangle$$

The observed intensities of the several $0 \rightarrow k$ are therefore, within a common multiple, just the respective values of $|c_m^k|^2$.

The centroid of the observed multiplet is given by the intensity-weighted average of the various transition energies $E_k - E_0$ from the ground state, namely

$$[2] \qquad \overline{\Delta E} = \sum_{k=1}^{N} |c_m^k|^2 (E_k - E_0) / \sum_{k=1}^{N} |c_m^k|^2$$

Since **H** is Hermitian it may be written in a "spectral representation" (32):

$$\mathbf{H} = \mathbf{U}\boldsymbol{\Lambda}\mathbf{U}^\dagger$$

where $\boldsymbol{\Lambda}$ is a diagonal matrix with the eigenvalues of **H** as diagonal elements, i.e. $\Lambda_{ij} = E_i\delta_{ij}$; **U** is the unitary matrix formed by the orthonormal eigencolumns of **H**, i.e. $U_{ij} = c_i^j$. Now

$$H_{ij} = \sum_k U_{ik}(\mathbf{\Lambda U}\dagger)_{kj} = \sum_k U_{ik} \sum_l \Lambda_{kl} U_{lj}\dagger$$
$$= \sum_k c_i^k \sum_l E_k \delta_{kl} c_j^{l*} = \sum_k E_k c_i^k c_j^{k*}$$

Since $H_{mm} = E_m^{(0)}$ by definition, it follows that

[3] $$E_m^{(0)} = \sum_k |c_m^k|^2 E_k$$

Further, since **U** is unitary, its rows as well as its columns are orthonormal:

$$(\mathbf{UU}\dagger)_{ij} = (\mathbf{UU}^{-1})_{ij} = \delta_{ij}$$

or $\sum_k c_i^k c_j^{k*} = \delta_{ij}$. For $i = j = m$ this gives

[4] $$\sum_k |c_m^k|^2 = 1$$

This incidentally shows that Fermi resonance preserves the original intrinsic intensity, merely redistributing it among the several $0 \rightarrow k$. Using eqs. [3] and [4] in eq. [2], we find $\overline{\Delta E} = E_m^{(0)} - E_0$. This establishes what we set out to prove, namely that the observed centroid of the multiplet coincides with the unperturbed frequency of $0 \rightarrow m^{(0)}$. A similar result has been derived previously (33) for Raman spectra perturbed by Fermi resonance.

Metal oxide coated p–n junction silicon electrodes for photoelectrochemical solar energy conversion

HIROSHI TSUBOMURA, YOSHIHIRO NAKATO, MASAHIRO HIRAMOTO, AND HIROYUKI YANO

Laboratory for Chemical Conversion of Solar Energy and Department of Chemistry, Faculty of Engineering Science, Osaka University, Toyonaka, Osaka, 560 Japan

Received August 6, 1984

This paper is dedicated to Professor Camille Sandorfy on the occasion of his 65th birthday

HIROSHI TSUBOMURA, YOSHIHIRO NAKATO, MASAHIRO HIRAMOTO, and HIROYUKI YANO. Can. J. Chem. **63**, 1759 (1985).

Photoelectrochemical properties of p^+–n junction silicon electrodes, abbreviated as p^+n–Si, coated with thin oxide films of titanium, tungsten, or iron have been investigated in aqueous solutions of hydrogen iodide and iodine. The films were deposited by electron-beam evaporation of the metal oxide sinters. The photocurrent in a p^+n–Si electrode coated with TiO_2 increased dramatically when it was heated at temperatures higher than 500°C, though the O/Ti atomic ratio as determined by ESCA analysis was unchanged. The fill factor of the photovoltaic cell composed of this electrode, a platinum counter electrode and an aqueous solution of 7.6 *M* HI and 0.03 *M* I_2 was improved by coating with ruthenium or its oxide. The photovoltaic cell attained a high solar to electrical energy conversion efficiency of 9.3% (AM1), with an open circuit photovoltage of 0.58 V, a short circuit photocurrent of 26.6 mA cm^{-2} and a fill factor of 0.61. The photocurrent was stable for 350 h. For the cases of electrodes coated with a Fe_2O_3 or WO_3 film, high fill factors were obtained even without ruthenium coating. The effect of the nature of Si – metal oxide junctions, the donor density in the oxide, the relations between the flat band potential of the oxide and the redox potential of the solution, etc., on the conversion efficiency was discussed.

HIROSHI TSUBOMURA, YOSHIHIRO NAKATO, MASAHIRO HIRAMOTO et HIROYUKI YANO. Can. J. Chem. **63**, 1759 (1985).

Opérant dans des solutions aqueuses d'iodure d'hydrogène et d'iode, on a étudié les propriétés photoélectrochimiques d'électrodes de silicium, à jonction p^+–n représentées par p^+n–Si, recouvertes de minces couches d'oxydes de titane, de tungstène ou de fer. On a déposé les films en faisant appel à l'évaporation par faisceaux d'électrons de frittages d'oxydes de métaux. Le courant photoélectrique de l'électrode p^+n–Si sur laquelle on a déposé du TiO_2 augmente d'une façon dramatique lorsqu'on la chauffe à des températures supérieures à 500°C; on obtient ce résultat même si le rapport atomique de O/Ti, tel que déterminé par une analyse ESCA, demeure inchangé. Le facteur de remplissage de la cellule photovoltaïque composée de cette électrode, d'une contre-électrode de platine et d'une solution aqueuse 7,6 *M* en HI et 0,03 *M* en I_2 augmente si l'on y dépose du ruthénium ou son oxyde. On peut atteindre un haut degré (9,3% AM1) d'efficacité pour la conversion de l'énergie solaire en énergie électrique si l'on opère avec un photovoltage en circuit ouvert de 0,58 V, un photocourant de court circuit de 26,6 $mAcm^{-2}$ et un facteur de remplissage de 0,61. Le photocourant s'est avéré stable pour 350 h. Dans les cas des électrodes sur lesquelles on a déposé des films de Fe_2O_3 ou de WO_3, on a pu obtenir des facteurs de remplissage élevés sans même déposer du ruthénium. On discute de l'effet de la nature des jonctions Si – oxydes métalliques, de la densité des donneurs dans l'oxyde, des relations entre la bande de potentiel plane de l'oxyde et le potentiel redox de la solution, etc sur l'efficacité de la conversion.

[Traduit par le journal]

Introduction

Photoelectrochemical cells provided with semiconductor electrodes are the most promising tools for direct conversion of solar energy into chemical energy. For practical purposes, however, we must solve the problem of how to prevent the corrosion of semiconductor electrodes. We reported many years ago that semiconductor electrodes such as Si and GaP could be stabilized by coating with noble metals (1). The noble metal coating also displayed catalytic activity to enhance electrode reactions (2). Later, the stabilization effect by surface layers of noble metals (3, 4), metal oxides (5–15), metal silicides (16, 17), and organic materials (18–25) has been studied.

Recently, we reported that the decomposition of hydrogen iodide into hydrogen and iodine was achieved using a silicon single crystal electrode with a p^+–n junction inside (abbreviated as p^+n–Si) coated with platinum or its silicide, achieving an approximately 8% conversion efficiency and 4500 h stability (26–28). A similar efficiency has been obtained for hydrogen iodide decomposition using Pt-coated n^+p–Si electrodes (29).

Although these results are very encouraging, further improvements are desirable, because certain loss of the incident light energy is unavoidable by use of metal coatings. In this respect, we took up an approach to apply transparent metal oxide coatings. Although metal oxide coatings were studied by some workers, it appears that in many cases the mismatch in the electronic bands between the semiconductor and the oxide is troublesome. Bard and co-workers (6) studied the oxygen evolution reactions on Si, CdS, InP, etc., coated with TiO_2, and reported that the photocurrents arose only by the direct excitation of TiO_2. Tomkiewicz and Woodall (7) reported the similar results. Morisaki *et al.* (5) studied the oxygen evolving reaction on a pn–silicon electrode coated with TiO_2, and reported that the photocurrent was observed only when both Si and TiO_2 were simultaneously excited. Morisaki *et al.* (8, 9) and Nogami *et al.* (10) reported that the Si electrodes coated with iron oxide caused photocurrent by excitation of Si only. But the onset potential for it was close to that for the oxygen evolution on a platinum electrode. More recently, reports have been made for silicon electrodes with thin SiO_2 layers coated with conductive tin oxide or indium – tin oxide films (12–15), which gave fairly high photovoltages due to the MIS type junctions.

In this paper, we will report on the p^+n–Si electrodes coated with metal oxide films in aqueous solutions of hydrogen iodide and iodine. It has been found that these electrodes successfully undergo photoelectrolysis with the excitation of silicon.

Experimental

The p^+n–Si wafers prepared by ion implantation of boron on the (100) surface of n-type Si wafers were provided by Mitsubishi Electric Corp. The p-layer is ca. 0.9 μm thick, with a high boron concentration of 2×10^{20} cm^{-3}, and has a metallic conductivity.

The p^+n–Si wafers were etched in 46% hydrogen fluoride solutions for 2 min, promptly evacuated and metal oxide films were deposited on the p^+ surface by electron beam evaporation of sintered discs of TiO_2, or TiO_2 containing 6 wt.% Nb_2O_5, or pressed discs of iron oxide or tungsten oxide. The average thicknesses of the metal oxide films, monitored with a quartz vibrator, were from 3 to 20 nm, the deposition speed being 0.01, 0.05, and 0.003 nm s^{-1}, respectively, for TiO_2, WO_3, and Fe_2O_3. The temperature of the substrate, monitored with a chromel–alumel thermocouple, reached 80°C during the deposition. In some cases, the substrate was heated to a temperature of 350 to 450°C during the deposition. After the deposition, the wafers were in most cases heated at 400 to 600°C for 1 h under vacuum using a radiation heater, and were left in the vacuum till they cooled down to 100°C. Ruthenium oxide or ruthenium was attached either by electron beam evaporation of ruthenium dioxide, or by spraying a 2-propanol solution of ruthenium trichloride on the sample placed on a hot plate of 100°C, followed by heating under vacuum.

ESCA analysis (Electron Spectroscopy for Chemical Analysis) was performed using a Shimadzu ESCA 750 instrument. The surface atomic composition was determined from the area under the ESCA peaks, corrected for the ionization cross sections. The depth profiles of the atomic compositions were obtained by combining the ESCA analysis with 2 keV argon ion beam sputtering, the rate of sputter being estimated to be 0.04 nm s^{-1} for Si and 0.03 nm s^{-1} for TiO_2.

The electrodes were prepared by applying indium–gallium alloy on the back side of the wafer for ohmic contact. In some cases, the potentials of the p^+–Si surface and the TiO_2 layer were measured, by making ohmic contact with indium–gallium alloy for the former, and with a vacuum evaporated indium for the latter. A tungsten–halogen lamp or a Wacom solar simulater (AM1, 100 mW cm^{-2}) was used as the light source. The long term stability tests were carried out by cooling the electrochemical cells with circulating water. A saturated calomel electrode (SCE) was used as the reference electrode.

Results

Typical current density (j) – potential (U) curves for the p^+n–Si photoanodes coated with 20 nm thick TiO_2 in a solution of HI/I_2 are shown in Fig. 1. The TiO_2 film contains a small amount of Nb oxide. Only weak photocurrent flowed even under strongly positive potential region in the electrode coated with TiO_2 under 1×10^{-6} Torr (curve a), and the coated film peeled off partly during the measurement. When the TiO_2 coated electrode was heat-treated under 1.0×10^{-6} Torr at 500°C for 1 h, the photocurrent dramatically increased as shown by curve b. The onset potential also shifted extensively, to 0.45 V more negative than the redox potential of the I_3^-/I^- couple, $E(I_3^-/I^-)$. The heat treatment at 500 and 600°C was effective, but ineffective at 400°C. Curve c is for the case where TiO_2 was deposited under 1.0×10^{-6} Torr with the silicon substrate heated at 350°C, followed by the same heat treatment as for curve b. The onset potential of the photocurrent in this case was shifted more to the negative. When the electrode, prepared in the same way as for the case of curve a, was coated with ruthenium by applying a 2-propanol solution of $RuCl_3$ and heating at 500°C under 1.0×10^{-6} Torr for 1 h, the fill factor was further improved (curve d). The similar result was obtained when RuO_2 was electron beam evaporated.

The similar results as mentioned above were obtained for TiO_2 films without containing Nb oxide, though the fill factor was a little smaller. Little photocurrent was obtained for electrodes coated with TiO_2 thinner than 5 nm.

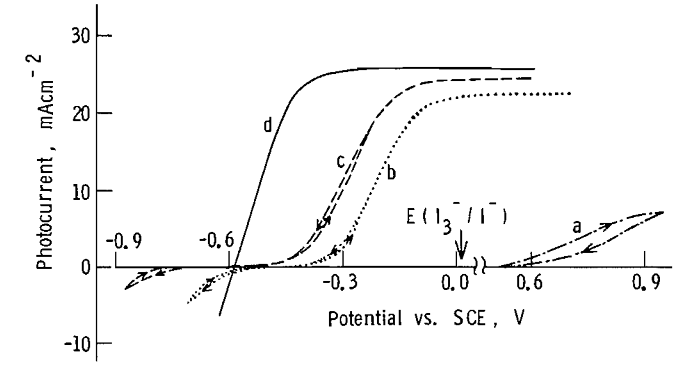

FIG. 1. Photocurrent (j) – potential (U) curves of TiO_2-coated p^+n–Si electrodes in a stirred solution of 7.6 M HI and 0.03 M I_2, illuminated with a Wacom solar simulator.

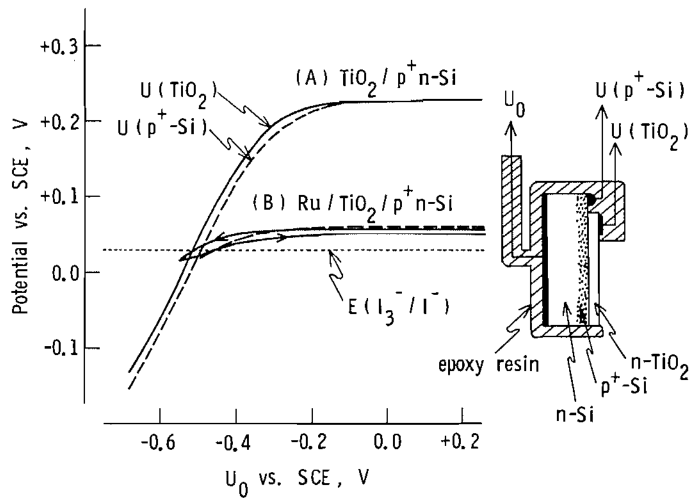

FIG. 2. Potential of the p^+–Si layer, $U(p^+{-}Si)$, and that of the TiO_2 film, $U(TiO_2)$, against the potential of the silicon electrode, U_0, controlled by a potentiostat in a stirred solution of 7.6 M HI and 0.05 M I_2. (A) is for a TiO_2-covered electrode and (B) is for a Ru-TiO_2-covered electrode. They are prepared in the same way as for the electrodes used for measurements of curves c and d in Fig. 1.

The result that the fill factor of the electrode coated with TiO_2 was greatly improved by a small amount of RuO_2 or Ru (Fig. 1, b and d) means that there is a high resistance at the interface between the TiO_2 film and the solution. The electrode coated with TiO_2 and RuO_2 (or Ru) gave a j–U curve nearly as good as that for a Pt coated p^+n–Si electrode (27). This implies that the p^+–Si layer and the TiO_2 film are in ohmic contact. These were confirmed by the measurements of the potential of the p^+–Si layer, that of the TiO_2 layer, and that of the electrode (Fig. 2). As shown in the figure, $U(TiO_2)$ and $U(p^+{-}Si)$ are close to each other at any of the U_0 value, irrespective of whether the electrode has Ru or not. The difference between $U(TiO_2)$ and $E(I_3^-/I^-)$ corresponds to an overvoltage at the working state of the electrode. It is very small (ca. 0.02 V) in the case where ruthenium is applied on the surface of the electrode. Without ruthenium, it increases with U_0 and reaches a constant value of 0.2 V, where the photocurrent becomes light intensity limited.

Figure 3 shows a result of ESCA analysis of a p^+n–Si surface covered with 20 nm TiO_2 and a small amount of RuO_2 and vacuum heated at 500°C for 1 h. The ratio of oxygen vs. titanium is a little higher than two in the region of the Ar^+ ion

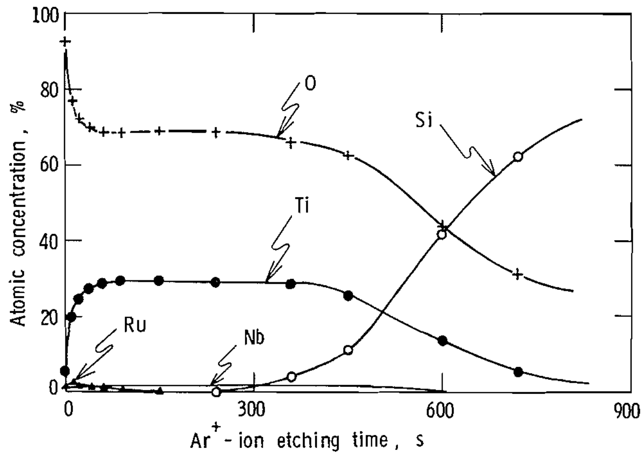

FIG. 3. Relative atomic concentrations as a function of Ar ion etching time, i.e., depth profile, of the $p^{+}n-Si$ surface covered with 20 nm TiO_2 and RuO_2, and heated at 500°C for 1 h under vacuum.

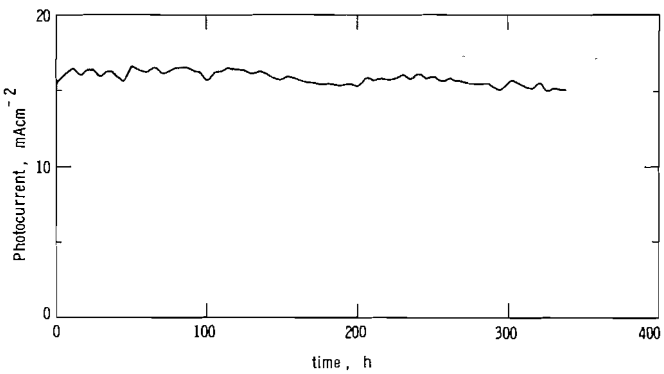

FIG. 4. A stability test for a $p^{+}n-Si$ electrode coated with TiO_2 and Ru, illuminated with a tungsten–halogen lamp. The small oscillatory change is probably due to light intensity fluctuation.

etching time from 60 to 400 s. This is considered to indicate that TiO_2 was formed by the electron beam evaporation of TiO_2, if the unavoidable oxygen contamination is taken into account. The atomic profile was almost unchanged by the heat treatment. In the case where $RuCl_3$ solution was applied and the wafer vacuum heated, the Ru concentration at the surface was almost equal to that of Ti and decreased toward the interior. The oxygen concentration at the surface was much lower than that expected from RuO_2 formed on TiO_2, suggesting that Ru is present almost in the form of metal in this case.

The best data were obtained from an electrode which was covered with a TiO_2 layer 20 nm thick treated with a $RuCl_3$ solution and heated at 500°C under 1.0×10^{-6} Torr for 1 h. The photocell composed of this electrode, a platinum counter-electrode and a solution of 7.6 *M* HI and 0.03 *M* I_2 showed an open circuit photovoltage of 0.58 V, a short-circuit photocurrent of 26.6 mA cm^{-2}, a fill factor of 0.61, and an energy conversion efficiency of 9.3% under AM1 radiation. This is nearly the same as the best value obtained by us with a platinum-covered $p^{+}n-Si$ electrode (27).

The long-term stability of the above cell was tested with the Si and Pt electrodes connected through a 200Ω resistance. This load resistance was used because it gave a potential difference of the maximum power point. The photocurrent, 16 mA cm^{-2}, was quite stable for 350 h (Fig. 4). The $j-U$ curve measured after the test agreed completely with that of the initial. The depth profile of the electrode did not change either.

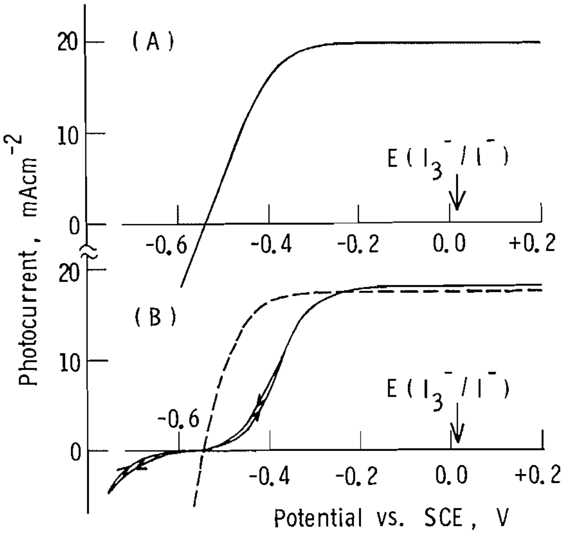

FIG. 5. Photocurrent–potential curves of $p^{+}n-Si$ electrodes under illumination with a Wacom solar simulator in a stirred solution of 7.6 *M* HI and 0.03 *M* I_2. (*A*) is for an electrode coated with iron oxide and (*B*) is for an electrode coated with tungsten oxide. For details see text.

In Fig. 5 are given the results for coatings of diiron trioxide and tungsten trioxide. The solid line in Fig. 5*A* shows the $j-U$ curve for an electrode on which iron oxide, 20 nm thick, was evaporated under 1.0×10^{-5} Torr and vacuum heated at 500°C under 1.0×10^{-6} Torr for 1 h. The solid lines in Fig. 5*B* are for the electrode on which 20 nm tungsten oxide was deposited under 1.0×10^{-4} Torr while the Si substrate was heated at 450°C, and heat-treated under 1.5×10^{-4} Torr at 450°C for 1 h. For these cases also, the heat treatment after the vacuum deposition was effective for obtaining good electrode characteristics. In the case of tungsten oxide, the fill factor was much improved when the electrode was kept under −5.0 V vs. SCE for 10 min in an HI/I_2 solution (broken lines in Fig. 5*B*). In both cases of iron and tungsten oxides, the onset potentials are deeply negative and the fill factors are pretty high, comparable to those for electrodes coated with TiO_2 and Ru (Fig. 1, curve *d*). It is worthwhile to note that high fill factors are obtained in these cases even without Ru coatings.

Discussion

As described in the previous section, the $p^{+}n-Si$ electrode coated with TiO_2 and not heat-treated causes weak photocurrent, and the TiO_2 film is liable to be removed. But the photocurrent is very much enhanced and the film becomes stable by heating under vacuum. Kaito *et al.* (30) reported on the basis of transmission electron microscopy that the TiO_2 film formed by deposition at room temperature was amorphous and it became crystalline by heating in air at 450 to 500°C for several hours. Their results seem to explain the stabilization in our case. In addition, as we heated the sample under vacuum, the film might have been reduced to some extent, yielding oxygen vacancies which make the film conductive, though this was not confirmed by our ESCA analysis because the change in the oxygen concentration was too small.

The overall process of the photoreactions in the electrode is explained by the energy diagram shown in Fig. 6. From the known band positions of TiO_2 and Si, the conduction band of the former is estimated to be considerably higher than the valence band of the latter. Therefore, when the two are in contact, an energy barrier should be formed at the interface.

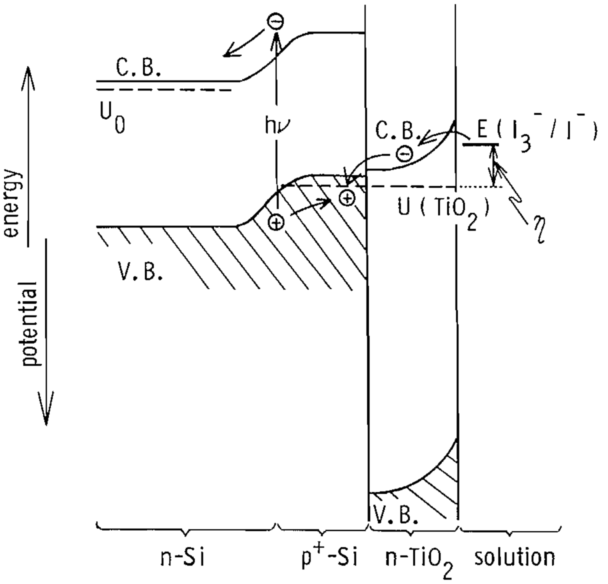

FIG. 6. An energy level diagram for the p^+n–Si electrode coated with TiO_2 in a HI/I_2 solution under illumination. η denotes the overpotential, C.B. the conduction band, and V.B. the valence band.

The results in Figs. 1 and 2 show, however, that the contact is ohmic. This can be explained by assuming that a reaction of the type, $TiO_2 + Si \rightarrow TiO_{2-x} + SiO_x$, occurs during the TiO_2 deposition and the heat treatment after that, forming interfacial TiO_2 having many O vacancies which warrants an ohmic contact between the TiO_2 film and the highly doped silicon. This assumption is supported by our ESCA analysis, which showed that a weak Si2*p* peak corresponding to Si oxide is present at the TiO_2–Si interface after the TiO_2 deposition, slightly growing by the heat treatment.

As the flat-band potential of *n*-TiO_2 is ca. 0.3 V more negative than the redox potential of the I_3^-/I^- couple, a Schottky barrier should be formed at the interface between TiO_2 and the solution, as shown in Fig. 6. Without RuO_2 or Ru, the fill factor of the j–U curve was small (Fig. 1), indicating that the electron transfer reaction from iodide in the solution to TiO_2 is slow, in harmony with the above supposition. The great decrease of the overpotential caused by applying RuO_2 or Ru can be explained by the disappearance of the barrier probably because the metallic RuO_2 or Ru makes ohmic contact with TiO_2. Another factor is that the Ru species works as a good catalyst for the electron transfer reaction.

It was reported in the previous section that a high fill factor was obtained for the case where Fe_2O_3 or WO_3 was coated. The flat band potentials of these oxides are either nearly the same as or more positive than the redox potential of the I_3^-/I^- couple, and hence no barrier should be formed at the interface between the oxides and the solution. In these cases an ohmic contact is expected to form, in agreement with the experimental results. That the short circuit photocurrents for these oxides were somewhat smaller than those for TiO_2 can be explained by assuming that these oxide films are more liable to be reduced and the reduced films absorb near-infrared part of the radiation. It was confirmed that these oxides absorb in the near-infrared region when they are reduced.

In conclusion, the silicon electrodes coated with metal oxides show high efficiencies and are promising for the chemical conversion of solar energy, in that they have high transparency and stability. It has been clarified in the present paper that the degree of crystallinity, that of reduction of the oxide, i.e., the donor density, and the relationship between the flat band potential of the oxide and the redox potential of the solution are the important factors in determining the performance of the photoelectrochemical cells.

1. Y. NAKATO, T. OHNISHI, and H. TSUBOMURA. Chem. Lett. 883 (1975); Y. NAKATO, K. ABE, and H. TSUBOMURA. Ber. Bunsenges. Phys. Chem. **80**, 1002 (1976).
2. Y. NAKATO, S. TONOMURA, and H. TSUBOMURA. Ber. Bunsenges. Phys. Chem. **80**, 1289 (1976).
3. S. MENEZES, A. HELLER, and B. MILLER. J. Electrochem. Soc. **127**, 1268 (1980).
4. K. W. FRESE, JR., M. J. MADOU, and S. R. MORRISON. J. Electrochem. Soc. **128**, 1939 (1981).
5. H. MORISAKI, T. WATANABE, M. IWASE, and K. YAZAWA. Appl. Phys. Lett. **29**, 338 (1976).
6. P. A. KOHL, S. N. FRANCK, and A. J. BARD. J. Electrochem. Soc. **124**, 225 (1977).
7. M. TOMKIEWICZ and J. M. WOODALL. J. Electrochem. Soc. **124**, 1436 (1977).
8. H. MORISAKI, H. ONO, H. DOHKOSHI, and K. YAZAWA. Jpn. J. Appl. Phys. **19**, L148 (1980).
9. H. ONO, H. MORISAKI, and K. YAZAWA. Jpn. J. Appl. Phys. **21**, 1075 (1982).
10. G. NOGAMI, H. YAMAGUCHI, G. MAEDA, K. BEPPU, Y. UEDA, and T. NAKAMURA. J. Appl. Phys. **54**, 1605 (1983).
11. H. KITAYAMA, K. EJIRI, N. HIROTA, and T. OSAKA. Denki Kagaku, **51**, 408 (1983).
12. F. DECKER, J. MELSHEIMER, and H. GERISCHER. Israel J. Chem. **22**, 195 (1982).
13. F. DECKER, M. FRACASTRO-DECKER, W. BADAWY, K. DOBLHOFER, and H. GERISCHER. J. Electrochem. Soc. **130**, 2173 (1983).
14. L. THOMPSON, J. DUBOW, and K. RAJESHWAR. J. Electrochem. Soc. **129**, 1934 (1982).
15. G. HODES, L. THOMPSON, J. DUBOW, and K. RAJESHWAR. J. Am. Chem. Soc. **105**, 324 (1983).
16. F.-R. F. FAN, G. A. HOPE, and A. J. BARD. J. Electrochem. Soc. **129**, 1647 (1982).
17. F.-R. F. FAN, R. G. KEIL, and A. J. BARD. J. Am. Chem. Soc. **105**, 220 (1983).
18. J. M. BOLTS, A. B. BOCARSLY, M. C. PALASSOTTO, E. G. WALTON, N. S. LEWIS, and M. S. WRIGHTON. J. Am. Chem. Soc. **101**, 1378 (1979).
19. A. B. BOCARSLY, E. G. WALTON, N. S. LEWIS, and M. S. WRIGHTON. J. Am. Chem. Soc. **102**, 3390 (1980).
20. Y. NAKATO, M. SHIOJI, and H. TSUBOMURA. J. Phys. Chem. **85**, 1670 (1981).
21. P. LEEMPOEL, M. CASTRO-ACUNA, F.-R. F. FAN, and A. J. BARD. J. Phys. Chem. **86**, 1396 (1982).
22. R. NOUFI, A. J. FRANK, and A. J. NOZIK. J. Am. Chem. Soc. **103**, 1849 (1981).
23. T. SKOTHEIM, I. LUNDSTRÖM, and J. PREJZA. J. Electrochem. Soc. **128**, 1625 (1981).
24. F.-R. F. FAN, B. L. WHEELER, and A. J. BARD. J. Electrochem. Soc. **128**, 2042 (1981).
25. A. J. FRANK and K. HONDA. J. Phys. Chem. **86**, 1933 (1982).
26. Y. NAKATO, A. TSUMURA, and H. TSUBOMURA. Chem. Lett. 1071 (1982).
27. Y. NAKATO, M. YOSHIMURA, M. HIRAMOTO, A. TSUMURA, T. MURAHASHI, and H. TSUBOMURA. Bull. Chem. Soc. Jpn. **57**, 355 (1984).
28. Y. NAKATO, M. HIRAMOTO, Y. IWAKABE, and H. TSUBOMURA. J. Electrochem. Soc. **132**, 330 (1985).
29. Y. NAKATO, Y. EGI, M. HIRAMOTO, and H. TSUBOMURA. J. Phys. Chem. **88**, 4218 (1984).
30. M. SHIOJIRI, T. MIYANO, and C. KAITO. Jpn. J. Appl. Phys. **18**, 1937 (1979).

A theoretical study of the electronic structure and spectra of metalloporphine cations

W. DANIEL EDWARDS AND MICHAEL C. ZERNER
Quantum Theory Project, University of Florida, Gainesville, FL 32611, U.S.A.
and
Guelph Waterloo Center for Graduate Work in Chemistry, University of Guelph, Guelph, Ont., Canada N1G 2W1

Received August 13, 1983

This paper is dedicated to Professor Camille Sandorfy on the occasion of his 65th birthday

W. DANIEL EDWARDS, and MICHAEL C. ZERNER. Can. J. Chem. **63**, 1763 (1985).

A theoretical study is made of the electronic spectra of Mg(II), Zn(II), and Co(III) porphine and their π cations using the INDO/S-CI spectroscopic model. The calculated electronic spectra for the neutral compounds compare well with experiment. The two low-lying π cations, one of $^2A_{1u}$ and one of $^2A_{2u}$ symmetry are both examined for each of these systems. The $^2A_{1u}$ cations are calculated to lie lower in energy than the $^2A_{2u}$ cations by only 4 kcal/mol, consistent with the findings that both ions are found depending on substituents and solvent.

The visible region of the spectrum of the $^2A_{1u}$ species is predicted to consist of three separate bands decreasing in intensity with increasing energy, while that of the $^2A_{2u}$ species is calculated to consist of three allowed transitions of near equal intensity, in agreement with experimental findings. In general the Soret region of the $^2A_{1u}$ ions is dominated by one transition, while at least three strong bands are calculated in the Soret region for the $^2A_{2u}$ ions, again in reasonable accord with experiment. Charges, ionization energies, and spin densities are reported and discussed for all compounds.

W. DANIEL EDWARDS et MICHAEL C. ZERNER. Can. J. Chem. **63**, 1763 (1985).

Faisant appel au modèle spectroscopique INDO/S-IC, on a effectué une étude théorique des spectres électroniques des sels de Mg(II), de Zn(II) et de Co(III) des porphines et de leurs cations pi. Les spectres électroniques calculés pour les composés neutres se comparent bien avec les résultats expérimentaux. Pour chacun de ces systèmes, on a examiné les deux cations pi de faible valence: l'un de symétrie $^2A_{1u}$ et l'autre de symétrie $^2A_{2u}$. On a calculé que l'énergie des cations $^2A_{1u}$ est plus faible que celle des cations $^2A_{2u}$, que la différence entre les deux états n'est que 4 kcal/mol et que ceci est en accord avec le fait observé que les deux ions dépendent des substituants et du solvant.

On prédit que la région visible du spectre des espèces $^2A_{1u}$ consistera en trois bandes séparées dont l'intensité décroît lorsque l'énergie croît; par ailleurs, on calcule que le spectre des espèces $^2A_{2u}$ consistera en trois transitions permises d'intensités à peu près égale et ceci est en accord avec les faits expérimentaux. En général, une transition domine la région Soret des ions $^2A_{1u}$; par ailleurs, on calcule qu'il existera au moins trois bandes fortes dans la région Soret des ions $^2A_{2u}$ et encore une fois ces prédictions sont en accord avec les faits expérimentaux. Pour chacun des composés, on rapporte les charges, les énergies d'ionisation et les densités de spin pour tous les composés et on en discute.

[Traduit par le journal]

I. Introduction

Based on the calculated electronic structure of magnesium porphine, we have proposed a possible mechanism for the initial photochemical event occurring in photosynthesis. This mechanism is outlined in Paper I (1). In a subsequent paper (2) we calculated the electronic structure of magnesium pheoporphine — a closer analogue of chlorophyll — and found qualitatively the same features.

However, independent of the exact nature of the initial photochemical event, all photosynthesis models predict the formation of reduced acceptor molecules and oxidized chlorophyll molecules. It is therefore clear that the nature of chlorophyll cations will play an important role in understanding photosynthesis. In this paper we present some preliminary work on the electronic structure of Co(III), Zn(II), and Mg(II) porphine, Fig. 1.

One of the earliest and most successful models for explaining the electronic spectra of metallo porphines is the 4-orbital model proposed by Gouterman (3). In this picture, only the two highest occupied and two lowest unoccupied orbitals are considered, Fig. 2. In D_{4h} symmetry, the Lowest Unoccupied Molecular Orbitals (LUMOs) are degenerate and of $e_g(\pi)$ symmetry. The Highest Occupied Molecular Orbitals (HOMOs) are of $a_{1u}(\pi)$ and $a_{2u}(\pi)$ symmetry, respectively. Since the a_{1u} and a_{2u} orbitals lie near in energy, electronic transitions from HOMOs to LUMOs would also lie very close in energy and would be expected to interact strongly. This configuration interaction would raise the energy of one transition and lower the energy of the other. The oscillator strengths for these two transitions should reinforce each other for the higher energy transition and cancel each other for the lower. This would give rise to a weakly allowed transition in the visible and an intense transition in the uv. This is the pattern seen in nearly all metalloporphyrins and is verified in nearly all calculations.

It is clear from this picture that there should be two low energy cations of metalloporphines, one of $^2A_{1u}$ symmetry and one of $^2A_{2u}$ symmetry. (In certain metalloporphine systems, removal of an electron from a transition metal d orbital is also low lying.) The nature of these π cations in chlorophyll and in many related systems has been widely studied and characterized through their optical spectra (4−11) and magnetic resonance spectra (5, 6, 11−19).

It is the purpose of this paper to examine the electronic properties of metalloporphine cations. The Co(III) system is included since two different, well-characterized spectra exist for the cation that correspond to the $^2A_{1u}$ and $^2A_{2u}$ π cations (21−23). Zn porphine is examined as a simple, relatively stable system (experimentally) with an obvious relationship to Mg porphine. Finally Mg porphine is examined. All of these systems have at least C_{4v} symmetry, and this high symmetry is used to aid in these calculations. Closer analogues of chlorophyll such as the Mg pheoporphine of our earlier studies (1, 2) are considerably more difficult to calculate accurately due to their lack of symmetry and will be considered in a subsequent

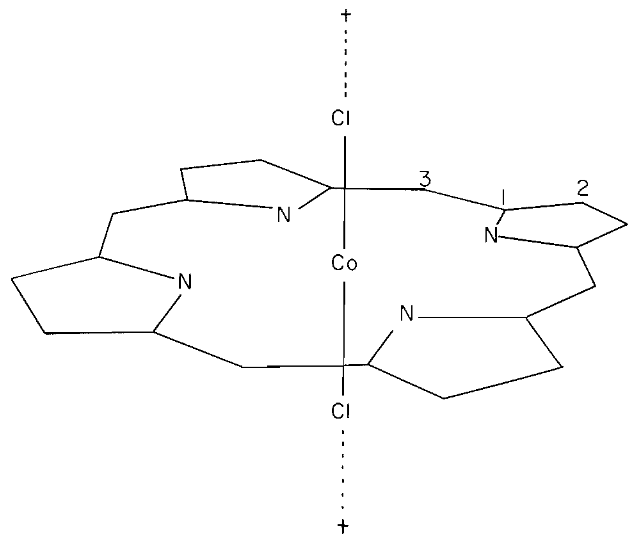

FIG. 1. The model and numbering for the compounds of this study. Shown is the $[Co(III)\ porphine]^{2+}$ π cation with 2 chlorine atoms 2.25 Å above and below the porphine plane and two positive point charges 2.25 Å from the chlorine atoms. For MgP and MgP^+ π cations the Mg is 0.40 Å above the porphin plane.

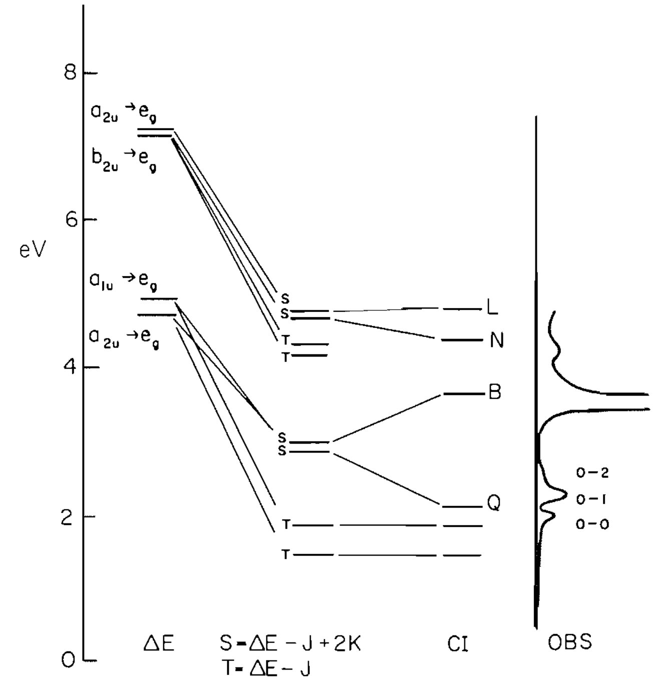

FIG. 2. The "four orbital model" consists of the configurational mixing of the two lowest singlet(s) states giving rise to the weakly allowed Q band and the strongly allowed B (Soret) band. As indicated in the synthesized spectrum, vibrational structure is often observed for the Q band.

work.

Previous calculations of the cation radicals of ethylchlorophyllide a and ethyl bacteriochlorophyllide a have been performed by Petke, Maggiora, Shipman, and Christoffersen (20) using an *ab initio* technique and, where appropriate, we will compare their results with those reported here. Earlier calculations of the Pariser–Parr–Pople π electron type were performed on "metal-like" porphine cations by Fajer, Borg, Forman, Dolphin, and Felton in which the potential importance of these π radical species in photosynthesis was stressed (24).

II. Methods

The calculations performed are of the INDO/S type, followed by configuration interaction (CI) (25, 26). The open shell systems are calculated using a restricted Hartree–Fock method (27), followed by a CI generated using Rumer diagram techniques (28, 29). Transition moments are calculated using the dipole length operator and keeping all one center terms.

The molecules of this study have either C_{2v} or D_{2h} Abelian subgroup symmetry, and this information is used to ease the CI calculation. After initial investigation with larger CI expansions, it was found that the calculated transitions in the visible and near uv region are reproduced with only about 400 configurations (100 for each of the four irreducible representations in C_{2v}) and about 200 for the open shell calculation. In both sets of calculations only single excitations are included in the CI. Higher excitations do affect the Soret region by depressing the calculated energies, bringing the predicted transitions in closer accord to that observed, but the general features of the Soret region are not changed. In these calculations, the higher energy transitions (N, L, M) do require the higher excitations in the CI for a good description of the transition energies and a more proper description of the states involved.

With these simplifications each of the closed shell calculations take about 18 min and each of the open shell calculations 90 min on the VAX 11/780 computer.

Geometries were based on symmetrized X-ray structures (30). For Co(III)P the Co—N bond length was set to 1.976 Å (31). For Zn(II)P the Zn—N bond length was fixed at 2.042 Å and both a planar structure (32) and a non-planar structure with the Zn atom placed 0.37 Å above the porphine plane (33, 34) were examined. For the Mg(II)P calculations the symmetrized structure with a Mg—N bond length of 2.092 Å was used (35); the Mg atom was placed 0.40 Å out of the porphine plane as suggested by the crystal structure of chlorophyll a (38).

III. Spectrum of closed shell metalloporphines

The electronic spectra of Zn(II), Mg(II), and Co(III) porphine have been calculated and are compared to experimental spectra in Tables 1, 2, and 3. It is clear from these tables that the Spectroscopic INDO method used is capable of accurately predicting transitions in the visible. For all three molecules, the lowest allowed transition is calculated within a few hundred wavenumbers of the experimentally observed band. Transitions which fall in the uv are not calculated as well and the average error for the Soret band is of the order of 5 000 cm^{-1}. In these calculations the four orbital model is an accurate description for these compounds since in the CI wavefunction, greater than 97% of the visible band and 91% of the Soret (B) band are constructed from these four excitations. The inclusion of higher excitations in the CI as mentioned in Section II has been shown to affect the Soret prediction (37–41) and is the principle reason for the high energy prediction of bands in the uv using the truncated CI of this study. These results are similar in accuracy to those we obtained in the study of Mg pheoporphine (2) where the energies and relative intensities of the Q_x and Q_y bands are accurately reproduced and the Soret band is calculated some 5000 cm^{-1} higher than their observed values.

Table 1 compares the calculated spectrum of both planar and non-planar Zn(II)P structures with those observed for Zn(II) octaethyl porphyrin (ZnOEP) (41). Very little difference is

TABLE 1. Calculated versus experimental spectrum of Zn porphine (1 000 cm^{-1})

Transition	Calcd[a] In plane	Calcd[a] Out-of-plane[b]	Observed[c]	Comments[d]
$^1E_u(\pi-\pi^*)$	17.2 (0.05)	17.1 (0.05)	Q_{00} 17.5	$0.4[a_{2u}(\pi)-e_g(\pi^*)]$ $0.6[a_{1u}(\pi)-e_g(\pi^*)]$
			Q_{01} 18.3	
$^1E_u(\pi-\pi^*)$	30.7 (5.83)	30.3 (5.66)	B 25.7	$0.4[a_{2u}(\pi)-e_g(\pi^*)]$ $0.6[a_{1u}(\pi)-e_g(\pi^*)]$
$^1A_{1u}(\pi-\mathrm{Zn})$[e]	36.3 f	31.6 f		$a_{1u}(\pi)-\mathrm{Zn}$
$^1B_{1g}$	32.0 f	31.8 f		$0.8[a_{1u}(\pi)-b_{1u}(\pi^*)]$
$^1A_{2u}(\pi-\mathrm{Zn})$[e]	36.8 (0.00)	33.0 (0.01)		$a_{2u}(\pi)-\mathrm{Zn}$
$^1A_{2g}(\pi-\pi^*)$	34.5 f	34.3 f		$0.9[e_g(\pi)-e_g(\pi^*)]$
$^1B_{2g}(\pi-\pi^*)$[f]	34.7 f	34.6 f		$0.7[e_g(\pi)-e_g(\pi^*)]$ $0.2[a_{2u}(\pi)-b_{1u}(\pi^*)]$
$^1E_u(\pi-\pi^*)$	36.4 (0.54)	36.01 (30.7)	N 30.7	$0.8[b_{2u}(\pi)-e_g(\pi^*)]$
$^1E_g(\sigma-\pi^*)$	38.9 f	39.5 (0.17)		$b_{1g}(\sigma)-e_g(\pi^*)$
$^1E_u(\pi-\pi^*)$	41.5 (0.90)	41.2 (1.02)	L(?) 34.1	$0.7[a_{2u}'(\pi)\rightarrow e_g(\pi^*)]$ $0.1[b_{2u}(\pi)\rightarrow e_g(\pi^*)]$

[a]Numbers in parentheses are calculated oscillator strengths.
[b]The Zn atom is placed 0.37 Å above the porphine plane.
[c]For Zn OEP, ref. 42. See also ref. 21.
[d]For the in-plane calculation. The numbers are the percentages of the indicated configuration.
[e]Charge transfer from porphine to Zn. The D_{4h} symmetry designation is not meaningful for the out-of-plane case in which the Zn "4s" orbital has considerable $4p_z$ character.

TABLE 2. Calculated versus experimental spectrum of Mg porphine (1 000 cm^{-1})

Transition	Calcd[a]	Observed[b]
$^1E_u(\pi-\pi^*)$	17.4 (0.06)	Q_{00} 17.2
		Q_{01} 18.5
$^1A_{1u}(a_{1u}\rightarrow \mathrm{Mg})$[c]	29.5	
$^1E_u(\pi-\pi^*)$	30.4 (5.53)	B 25.8
$^1A_{2u}(a_{2u}\rightarrow \mathrm{Mg})$[c,d]	31.5 (0.03)	
$^1E_u(\pi-\pi^*)$	36.3 (0.24)	
$^1E_u(\pi-\pi^*)$	38.9 (0.10)	N 30.8
$^1E_u(\pi-\pi^*)$	41.8 (0.81)	
$^1E_u(\pi-\pi^*)$	47.0 (0.12)	L(?) 42.2
$^1E_u(\pi-\pi^*)$	48.1 (0.05)	
$^1E_u(\pi-\pi^*)$	49.9 (1.49)	M 47.2

[a]Numbers in parentheses are oscillator strengths. Symmetry labels given are for D_{4h} even though molecule is C_{4v}.
[b]For vapor phase Mg Etio I, ref. 42.
[c]Charge transfer from $\pi\rightarrow$Mg(54% $3p_z$, 28% 3s).
[d]Only transitions with sizable oscillator strength are reported at higher energies.

TABLE 3. Calculated versus experimental spectrum of Co(III) porphine

Transition	Calcd[a]	Observed[b] ClO_4^-	Observed[b] Br^-
$^1E_g(d_\pi\rightarrow d_{z^2})$	12.4		
$^1A_{1u}(a_{1u}\rightarrow d_{z^2})$	14.4		
$^1A_{2u}(a_{2u}\rightarrow d_{z^2})$	16.1 (0.02)		
$^1E_u(\pi-\pi^*)$	17.3 (0.12)	Q_{00} 18.0	18.2 m
		Q_{01} 19.4	20.0 wk
$^1B_{1u}(a_{1u}\rightarrow d_{x^2-y^2})$	21.2		
$^1B_{2u}(a_{2u}-d_{x^2-y^2})$	23.0	24.7 (sh)	25 ?
$^1B_{2g}(d_{xy}\rightarrow d_{z^2})$	23.9		
$^1E_g(d_\pi\rightarrow d_{x^2-y^2})$	29.4		
$^1E_u(\pi-\pi^*)$	29.5 (4.14)	B 27.0	27.0 st
$^1A_{2g}(d_{xy}\rightarrow d_{x^2-y^2})$	31.3[c]		
$^1E_u(\pi-\pi^*)$	37.8 (0.76)		
$^1A_{2u}$ $(a_{2u}-d_{z^2})$	37.8 (0.07)		
$^1E_u(\pi-\pi^*)$	40.4 (1.28)		
$^1E_u(\pi-\pi^*)$	44.8 (0.36)		

[a]On dichloro Co(III) porphine, RCo—Cl = 2.25 Å, numbers in parentheses are oscillator strengths.
[b]From ref. 21, Co(III)OEP^{2+}.
[c]Only those transitions with calculated oscillator strengths are reported for transition above 31 300 cm^{-1}.

noted in the predicted Q or B bands. The porphine to Zn charge transfer bonds, designated $^1A_{1u}(\pi\rightarrow s)$ and $^1A_{2u}(\pi\rightarrow s)$ in D_{4h}, in contrast, are sensitive to this out-of-plane coordinate; these transitions decrease in energy with increasing Zn to porphine-plane distance (2). Above 35 000 cm^{-1} there are a great many transitions calculated and only the more intense are reported in the table. The N and L bands, both of ^1E_u symmetry, receive most of their intensity from a mixing between $b_{2u}(\pi)\rightarrow e_g(\pi^*)$ and $a_{2u}'(\pi)\rightarrow e_g(\pi^*)$, where the $a_{2u}'(\pi)$ is the second MO of that symmetry down in energy from the HOMO, see Fig. 1. As with the Soret band these states are also predicted to mix with double excitations not included here. The calculated energy is depressed to a value in better accord with experiment. The total oscillator strengths in the N and L region remain much the same after this mixing, but the intensity is spread over several near lying states. Of some interest is the $^1E_g(\sigma-\pi^*)$ excitation predicted at about 39 000 cm^{-1} in both calculations that arises from the promotion of an electron in an MO of $b_{1g}(\sigma)$ symmetry (71% nitrogen lone pair) to the LUMO $e_g(\pi^*)$. Although forbidden in the planar structure, in the non-planar structure, this excitation is of the same symmetry as the near-lying N and L (^1E) and picks up considerable intensity from them.

TABLE 4. The calculated spectra of the $^2A_{1u}$ and $^2A_{2u}$ Zn porphine cations, in 1 000 cm^{-1}; the $^1A_{1g}$ geometry of the neutral species is used for both cations

	$^2A_{1u}$			$^2A_{2u}$		
Species	In plane	Out-of-Plane	Species	In plane	Out-of-plane	Experiment[b]
$^2A_{2u}$	4.1	4.1	$^2A_{1u}$	1.2	1.3	
^2E_g[a]	15.0 (0.04)	14.9 (0.02)	^2E_g[a]	15.5 (0.01)	15.3 (0.00)	14.7 (broad)
^2E_g	17.4 (0.00)	17.4 (0.01)	^2E_g	16.9 (0.00)	16.7 (0.02)	16.7
^2E_g	18.6 (0.01)	18.5 (0.00)	^2E_g	19.8 (0.01)	18.8 (0.07)	17.7
			$^2A_{1g}$	21.3 (0.01)		19.6
^2E_g	30.6 (0.02)	30.5 (0.00)	^2E_g	30.0 (0.01)	29.6 (0.24)	22.9 (sh)
^2E_g	32.5 (3.85)	32.1 (4.40)	^2E_g	32.9 (4.42)	32.3 (5.12)	24.4 (st)
^2E_g	37.0 (1.37)	36.6 (1.23)	^2E_g	36.6 (0.00)	36.1 (0.08)	27.2
^2E_g	40.5 (0.47)	40.1 (0.65)	^2E_g	42.2 (0.21)	42.5 (0.43)	32.2
			^2E_g	43.5 (0.39)	42.7 (0.57)	

[a]Only states with calculated oscillators strength of greater than 0.01 are given if they lie above 15 000 cm^{-1}.
[b]From ref. 21, ZnTPP$^+$ClO$_4^-$: see also ref. 18.

Although INDO calculations have known deficiencies in the calculation of molecular geometries, a fully optimized calculation on Zn(II)P places the Zn atom 0.13 Å above the mean porphine plane and suggests a very flat potential around this minimum for Zn out-of-plane motion.

The calculated spectrum of Mg(II)P is reported in Table 2 and has much the same appearance as that of the non-planar Zn(II)P of Table 1. The $^1A_{1u}(a_{1u} \rightarrow \mathrm{M})$ is calculated to lie below the Soret band in the Mg complex, which may have significance in photosynthesis (2). We assign three separate allowed transitions to the N band region as suggested in Table 2 (but only two for the ZnP case, Table 1). The calculations of Christoffersen (39) find two states of ^1E symmetry with a very similar intensity pattern in this region.

In the Co(III) porphine calculation, the position of two Cl atoms 2.25 Å above and below the porphine plane, Fig. 1, determine the position of the $d_\pi \rightarrow d_{z^2}$ and $d_{xy} \rightarrow d_{z^2}$ Laporte transitions. The lowest of these is predicted at 12 400 cm^{-1}. The same is true of the two low-lying charge transfer excitations predicted at 14 400 cm^{-1} and 16 100 cm^{-1}. The position of the metal $d_{x^2-y^2}$ orbital, however, is less sensitive to those fifth and sixth position ligands, providing the metal atom remains in the mean plane of the four nitrogen atoms, and should be calculated reasonably well for an aqueous environment. The charge transfer excitations $^1B_{1u}(a_{1u}(\pi) \rightarrow d_{x^2-y^2})$ and $^1B_{2u}(a_{2u}(\pi) \rightarrow d_{x^2-y^2})$, however, have no intensity of their own and are calculated to lie near the intense Soret band. Similarly the $^1E_g(d_\pi \rightarrow d_{x^2-y^2})$ and $^1A_{2g}(d_{xy} \rightarrow d_{x^2-y^2})$ Laporte transitions are calculated to lie in a region of allowed $\pi-\pi^*$ transitions and therefore might not be observed.

IV. Spectrum of Zn porphine cations

The calculation of the spectrum of doublet ions is a more difficult task. For such molecules, an open shell ground state SCF calculation is performed and an open shell CI done on these states. Since there are two near-lying doublet states, both states must be calculated and comparable CI calculations done on each. The results for $^2A_{1u}$ and $^2A_{2u}$ Zn(II)P$^+$ are presented in Table 4 as are the results from experiment (21). Again a planar and a non-planar structure are reported. Due to the large number of calculated lines, it is difficult to decide on the basis of transition energies alone which species is experimentally found. However, by examining the oscillator strengths, it is possible to deduce that the experimentally observed spectrum comes from the $^2A_{2u}$ ground state. (Note that above 15 000 cm^{-1}, only those bands with non-zero oscillator strengths are reported.) This supports the conclusions reached by Browett and Stillman on the basis of MCD experiments (21) and Dolphin *et al.* on the basis of the uv and esr spectra (23).

It should be noted that these calculations predict the $^2A_{1u}$ state to be lower in energy, both at the SCF and at the CI level and both for the planar and non-planar structures. From the spectra of the Co(III) porphine cations discussed below, it is known that the two states must lie so close in energy that very weak perturbations and even solvent affects can reverse them.

V. The spectrum of cobalt (III) porphine cations

The electronic spectra of Co(III) porphine and Co(III) porphine cations have been experimentally measured (21–23) and are reproduced in Fig. 3 (43). Based on features in the spectrum and on the MCD results, it is concluded that the spectra of most metalloporphine cations arise from excitations from the $^2A_{2u}$ ground state. However, for the Co(III) OEP porphine cations, the ground state symmetry apparently depends on the nature of the counter ion. If the counter ions are perchlorate, the spectrum shows a typical $^2A_{2u}$ absorption spectrum. If the perchlorate ions are replaced by bromide ions, the spectrum changes dramatically and is best rationalized by assuming that the spectrum arises from an $^2A_{1u}$ ground state cation.

The results of our calculations on Co(III) porphine ions are presented in Table 5. For these calculations (as well as for the closed shell Co(III) porphine) the fifth and sixth position ligands were replaced by chloride ions at a distance of 2.25 Å. In order to maintain an appropriate charge on these chloride ions, positive point charges were also added at a distance of 2.25 Å from each of the chloride ions. These point charges also served to improve the self consistent field convergence properties of the calculations. The results in Table 5 are similar to those obtained for the Zn(II)P$^+$ cases. The $^2A_{1u}$ calculated spectrum shows a single strong peak at 15 000 cm^{-1} followed by a few weaker peaks at higher energy. The $^2A_{2u}$ calculated spectrum shows a series of peaks starting at 15 000 cm^{-1} and increasing in intensity through the visible. The experimental spectra show similar trends. The bromide shows a moderately strong peak at 15 000 cm^{-1}, followed by two weaker peaks at higher energy. These form a broad envelope of decreasing intensity. The perchlorate on the other hand shows a broad envelope of increasing intensity starting at 15 000 cm^{-1}. At higher energy, the bromide shows three intense peaks between 24 000 and 35 000 cm^{-1}, while the perchlorate shows one

TABLE 5. The calculated spectra of the $^2A_{1u}$ and $^2A_{2u}$ [Co(III) porphine]$^{2+}$ complex in 1 000 cm^{-1}; the neutral $^1A_{1g}$ geometry is assumed for both calculations; the oscillator strengths are given in parentheses

$^2A_{1u}$			$^2A_{2u}$		
Species	Calcd	Obsd(2Br$^-$)[a]	Species	Calcd	Obsd(2ClO$_4^-$)[a]
$^2A_{2u}$	5.8		$^2A_{1u}$	−1.4	
^2E_g	15.1[b] (0.095)	15.0 (m)	^2E_g	14.7[b] (0.006)	15.7 (w)
$^2A_{2g}$	17.3 (0.001)	16.6 (w)	^2E_g	15.5 (0.001)	
^2E_g	18.1 (0.041)		$^2A_{1g}$	18.7 (0.009)	19.4 (m)
$^2A_{2g}$	18.3 (0.015)	18.3 (w)	^2E_g	19.5 (0.003)	
^2E_g	19.5 (0.000)		^2E_g	28.1 (0.165)	
^2E_g	31.3 (1.908)	24.4 (s)	^2E_g	31.8 (3.252)	25.3 (s)
^2E_g	33.2 (0.209)		$^2A_{1g}$	34.9 (0.029)	26.7 (sh)
$^2A_{2g}$	37.6 (0.016)		^2E_g	36.1 (0.021)	
^2E_g	37.7 (1.234)	29.4 (s)	^2E_g	37.2 (0.075)	30.8 (w)
$^2A_{2g}$	38.9 (0.042)		$^2A_{1g}$	39.6 (0.009)	
^2E_g	39.2 (0.805)	35.1 (s)	^2E_g	40.8 (0.118)	
^2E_g	41.8 (0.021)				

[a]From ref. 43.
[b]Only allowed bands above this value are given.

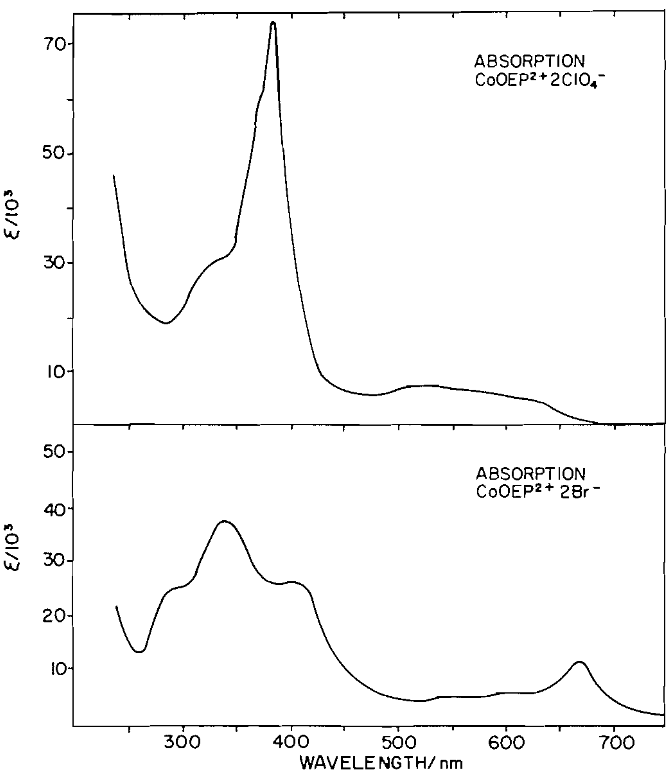

FIG. 3. The observed spectra of two Co(III)$^{2+}$ octaethylporphyin π cations, ref. 43. The only chemical difference is the counterion.

intense peak at 25 000 cm^{-1} and two weaker shoulders at higher energy. The calculated spectra reproduce these features. The $^2A_{1u}$ spectrum is calculated to have three intense peaks, but suggests the first of these is the most intense. Experimentally, the second peak appears most intense, but the experimental asymmetry of the first peak makes this uncertain. The transition energies for the Soret region bands are again calculated to be too high by approximately 6 000 cm^{-1}.

Figure 4 shows pictorially the molecular orbital energies that we obtain for $^1A_{1g}$ — Co(III)P$^+$, $^2A_{1u}$ — Co(III)P^{2+}, and $^2A_{2u}$ — Co(III)P^{2+}. There appears to be very little reorganization among the orbitals upon the loss of an electron from either an a_{1u} or a_{2u} orbital. These two MOs stay rather isolated from the next occupied MO of $e_g(\pi)$ symmetry and dominate the spectra of these species.

There is an apparent failure of the aufbau principal demonstrated here (and also for the Zn(II)P$^+$ and Mg(II)P$^+$ cases) for the $^2A_{2u}$ state, with a "hole" in the second highest occupied MO. Although relaxation in the SCF procedure is usually sufficient to reorder the orbital energies (especially among the highest lying occupied MOs when the orbitals involved contain no metal *d* character), this does not appear to be the case here. Since, however, the open shell orbital and the closed shell orbitals do not "see" quite the same (Fock) potential (27, 44, 45) and orbital energies approximate ionization potentials via Koopmans' approximation only for our closed shell operator (the open shell orbital energy needs a small exchange correction) we do not think there is any special significance in the observation of the single occupied a_{2u} MO "below" the doubly occupied a_{1u}. Promotion of an electron from the $a_{1u}(\pi)$ MO to the $a_{2u}(\pi)$ MO in the $^2A_{2u}$ state, Fig. 4, leads to the $^2A_{1u}$ state estimated to lie 1 400 cm^{-1} (0.17 eV) *below* the $^2A_{2u}$ references, Table 5. This difference in energy is less than the 5 800 cm^{-1} value (Table 5) calculated when starting from the $^2A_{1u}$ state and generating the orbital excitation $a_{2u}(\pi) \rightarrow a_{1u}(\pi)$. This difference reflects the energy advantage the self consistent field calculation affords the reference state and would disappear with a large enough CI.

Table 6 summarizes the nature of the excited states generated from the $^2A_{1u}$ and $^2A_{2u}$ cations of [Co(III)P]$^{2+}$, and they differ only in detail from the ZnP$^+$ and MgP$^+$ cases. In the neutral species the visible and near-uv spectrum (Q and B bands) are dominated by $a_{1u}(\pi) \rightarrow e_g(\pi^*)$ and $a_{2u}(\pi) \rightarrow e_g(\pi^*)$ transitions (Fig. 2). The positive ion spectra is much more complicated, the more intense bands involving not only those transitions, but also transitions from the doubly occupied πMOs to the singly occupied $a_{1u}(\pi)$ or $a_{2u}(\pi)$ orbitals (Fig. 4). Note also the Rydberg-like transitions calculated at 17 300 cm^{-1} for the $^2A_{1u}$ ion and 18 700 cm^{-1} for the $^2A_{2u}$ ion. The apparent similarity of the single intense peak in the Soret region calculated at 31 800 cm^{-1} for the $^2A_{2u}$ ion to that of the neutral species is misleading in the sense that the former has a considerable $e_g(\pi) \rightarrow a_{2u}(\pi)$ component.

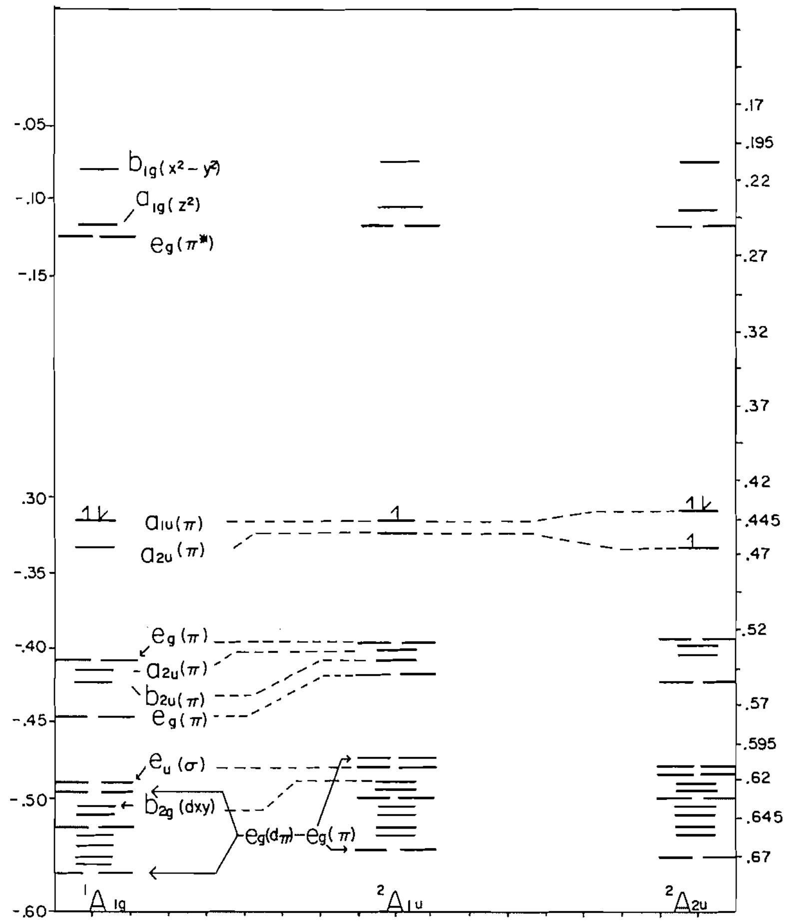

FIG. 4. The calculated molecular orbital energies of the $^2A_{1g}$ state of $[Co(III)P]^+Cl_2$ and the $^2A_{1u}$ and $^2A_{2u}$ states of $[Co(III)P]^{2+}Cl_2$, see Fig. 1.

VI. The spectrum of magnesium porphine cations

The calculated spectra of $^2A_{1u}$ and $^2A_{2u}$ $Mg(II)P^+$ are presented in Table 7, where they are compared with the experimental results on $Mg(II)OEP^+$ and $Mg(II)TPP^+$ (45). The geometry was optimized for the $^2A_{1u}$ state and compared with a similar optimization for the $^1A_{1g}$ state of Mg(II)P. The largest coordinate change was of the order of 0.006 Å, and the total energy lowering amounted to only 6.7 kJ/mol relative to the closed-shell optimized geometry. For a molecule of this size, this implies that the $^2A_{1u}$ geometry is nearly identical to the $^1A_{1g}$ geometry. A similar conclusion is deduced from the X-ray crystallographic study of the $Mg(II)TPP^+ClO_4^-$ cation by Barkigia, Spaulding, and Fajer (35).

$Mg(II)OEP^+$ is believed to be a $^2A_{1u}$ π cation. Three separate peaks are observed in the visible with decreasing intensity upon increasing transition energy, in good agreement with these calculated results. In contrast the spectrum of $Mg(II)TPP^+$ shows at least four less well-defined peaks in the visible. The apparent peak at 17 900 cm^{-1} may correspond to the Q_{10} peak of non-oxidized Mg(II)TPP. The position of the peak at 16 400 cm^{-1} may similarly be influenced by the weaker Q_{00} band of Mg(II)TPP. With these provisos, the calculated energies and their intensities are in excellent accord with the observed $Mg(II)TPP^+$ spectrum.

The $^2A_{1u}$ and $^2A_{2u}$ ions have predicted charge transfer excitations $^2A_{2g}$(TX) and $^2A_{1g}$(TX) calculated at 25 200 cm^{-1} and 25 500 cm^{-1}, respectively. The experimental spectra both show bands at about 22 000 cm^{-1} of the appropriate relative intensities to be assigned to these predicted transitions. States of this nature are not predicted to be present this low in energy in the $Zn(II)P^+$ spectra and, if the assignment of these bands could be verified, would provide a check of the relative position of the calculated charge transfer bands in these systems. These predictions require not only the correct positioning of the macrocycle π orbitals, but also of the Mg orbitals relative to these π orbitals. In the neutral Mg(II)P case, the charge transfer bands are predicted to lie under the Soret and no anomalous band is, in fact, seen. Confirmation of the assignment of the charge transfer assignment of the band observed at about 22 000 cm^{-1} makes the calculated position in the Mg(II)P case firmer and the possible importance of this state in photosynthesis more plausible (2).

The Soret region for $Mg(II)OEP^+$ has two intense peaks separated by about 1 100 cm^{-1}, in reasonable accord with the calculated values at 29 700 cm^{-1} and 30 700 cm^{-1}. Although these peaks are overlapping, the experiment indicates that the first of these should be more intense than the second, in contradiction to the calculated prediction. $Mg(II)TPP^+$ has one dominant peak at 24 400 cm^{-1} which we assign to the calculated ^1E_g state at 30 400 cm^{-1}. Another broad strong peak is observed at 26 700 cm^{-1}, which we assign to the ^1E_g state calculated at 33 400 cm^{-1}. The calculated spread of these two peaks of 3 000 cm^{-1} is in reasonable accord with that observed of 2 300 cm^{-1}. The Soret region of the $Co(III)OEP^{2+}$ $^2A_{1u}$ cation spectrum is characterized by three distinct peaks, Fig. 3, some 11 000 cm^{-1} from peak-to-peak. This region for the $MgOEP^+$ $^2A_{1u}$ cation spectrum is not as well resolved and perhaps contains four peaks, as suggested in Table 7. Assigned

TABLE 6. The nature of the low-lying states of $[Co(III)\ porphine]^{2+}$ complexes

$^2A_{1u}$			$^2A_{2u}$		
Energy[a]		Description[b]	Energy[a]		Description[b]
5.8	$^2A_{2u}$	$0.9[a_{2u}(\pi)\rightarrow a_{1u}(\pi)]$	−1.4	$^2A_{1u}$	$0.9[a_{1u}(\pi)\rightarrow a_{2u}(\pi)]$
15.1	^2E_g	$0.8[a_{1u}(\pi)\rightarrow e_g(\pi^*)]$	14.7	^2E_g	$0.7[e_g(\pi)\rightarrow a_{2u}(\pi)]$
					$0.2[a_{2u}(\pi)\rightarrow e_g(\pi^*)]$
17.3	$^2A_{2g}$	$0.9[a_{2u}(\pi)\rightarrow a_{1g}(4s)]$	15.5	^2E_g	$0.8[a_{1u}(\pi)\rightarrow e_g(\pi^*)]$
18.1	^2E_g	$0.8[e_g(\pi)\rightarrow a_{1u}(\pi)]$	18.7	$^2A_{1g}$	$0.9[a_{2u}(\pi)\rightarrow a_{1g}(4s)]$
18.3	$^2A_{2g}$	$0.9[a_{2u}(\pi)\rightarrow a_{1g}(4s)]$	19.5	^2E_g	$0.5[a_{2u}(\pi)\rightarrow e_g(\pi^*)]$
					$0.4[e_g(\pi)\rightarrow a_{2u}(\pi)]$
19.5	^2E_g	$0.5[e_g(\pi)\rightarrow a_{1u}(\pi)]$	28.1	^2E_g	$0.8[a_{1u}(\pi)\rightarrow e_g(\pi^*)]$
					$0.1[e_g(\pi)\rightarrow a_{2u}(\pi)]$
31.3[c]	^2E_g	$0.7[a_{2u}(\pi)\rightarrow e_g(\pi^*)]$	31.8[c]	^2E_g	$0.4[e_g(\pi)\rightarrow a_{2u}(\pi)]$
		$0.1[e_g(\pi)\rightarrow a_{1u}(\pi)]$			$0.3[a_{2u}(\pi)\rightarrow e_g(\pi^*)]$
					$0.2[a_{1u}(\pi)\rightarrow e_g(\pi^*)]$
33.2	^2E_g	$0.5[a_{2u}(\pi)\rightarrow e_g(\pi^*)]$			
		$0.4[e_g(\pi)\rightarrow a_{1u}(\pi)]$			
37.7	^2E_g	$0.4[b_{2u}(\pi)\rightarrow e_g(\pi^*)]$			
		$0.2[a_{2u}(\pi)\rightarrow e_g(\pi^*)]$			
		$0.1[e_g(\pi)\rightarrow a_{1u}(\pi)]$			
39.2	^2E_g	$0.5[a_{2u}(\pi)\rightarrow e_g(\pi^*)]$			
		$0.4[b_{2u}(\pi)\rightarrow e_g(\pi^*)]$			

[a] 1 000 cm^{-1}.
[b] X[ ] represents X% of the transition designated in the brackets.
[c] Beyond 30 000 cm^{-1} only the more intense transitions are given.

TABLE 7. The calculated spectra of the $^2A_{1u}$ and $^2A_{2u}$ $[Mg\ porphine]^+$ cations, in 1 000 cm^{-1}

	$^2A_{1u}$	$MgOEP^{+b}$		$^2A_{2u}$	$MgTPP^{+b}$
$^2A_{2u}$	3.8		$^2A_{1u}$	0.8	
$^2E_g{}^a$	13.9 (0.077)	15.0	$^2E_g{}^a$	14.7 (0.016)	14.8
^2E_g	16.1 (0.013)	17.0	^2E_g	15.6 (0.006)	16.4
					17.9 (?)
^2E_g	17.9 (0.002)	18.2	^2E_g	19.6 (0.011)	19.5
$^2A_{2g}$ (TX)	25.2 (0.032)	22.2	$^2A_{1g}$ (TX)	25.5 (0.017)	22.5
^2E_g	29.7 (0.502)	25.6 st	^2E_g	28.2 (0.268)	23.5 sh?
^2E_g	30.7 (2.434)	26.7 st	^2E_g	30.4 (2.954)	24.4 st
^2E_g	34.2 (0.405)	28.6 ?	^2E_g	33.4 (0.412)	26.7
^2E_g	38.4 (0.850)	30.8 st	^2E_g	38.1 (0.062)	
^2E_g (TX)	41.2 (0.264)		^2E_g	40.3 (0.595)	
			^2E_g (TX)	41.6 (0.818)	

[a] Only allowed bands above this energy are given. TX is charge transfer.
[b] From ref. 46, in CH_2Cl_2.

to this region in the $Mg(II)OEP^+$ $^2A_{1u}$ case are four strong transitions.

In the above discussions we have used the traditional D_{4h} symmetry labels even though the non-planar cases possess only C_{4v} symmetry. This labelling seems appropriate except for the virtual molecular orbital localized to the Mg or Zn atom and which is responsible for the porphyrin to metal charge transfer bands. In the planar Zn(II)P cases, this orbital is a_{1g} with about 65% 4s character. In the non-planar Zn(II)P case, this orbital is a_1 with 56% 4s and 14% $4p_z$. In the non-planar Mg(II)P case this a_1 orbital is calculated to be even more p_z-like: 28% 3s and 54% $3p_z$. The association between D_{4h} and C_{4v} for the two low-lying π cations are $^2A_{2u} \leftrightarrow {}^2A_1$ and $^2A_{1u} \leftrightarrow {}^2A_2$.

VII. Ionization potentials

The calculated ionization potentials for all systems studied are summarized in Table 8. For comparison, ionization potentials for similar systems are reported at 6.25 to 6.80 eV (47) in very good agreement with the calculated values. For some systems a shoulder is reported about 0.13 eV higher in energy, which may correspond to the second ionization process (47). It is interesting to further note that the ionization potentials calculated for our model $Co(III)P^+$ are slightly lower than those of Zn(II)P and Mg(II)P, even though the former complex is locally positive. Experimentally Mn(II) *trans*-octaethylchlorin has an ionization potential about 0.27 eV less than that of free base octaethylchlorin (47). Non-planarity has very little effect on the calculated ionization potentials of ZnP.

VIII. Charge and spin densities

A summary of the charge and spin density obtained through a Mulliken population analysis is presented for $[Co(III)P]^+$ and its two low-lying cations in Table 9. Spin density results for Zn(II)P and Mg(II)P and their cations are given in Table 10.

TABLE 8. Calculated ionization potentials for some metalloporphines in eV

		ZnP			
		Planar	Non-planar	MgP	[Co(III)P][a]
Neutral	$^1A_{1g}$	0	0	0	0
Koopmans	$^2A_{2u}$	6.68	6.67	6.56	6.55
	$^2A_{1u}$	6.42	6.40	6.29	6.11
SCF	$^2A_{2u}$	6.55	6.48	6.36	6.33
	$^2A_{1u}$	6.30	6.23	6.10	5.92
SCF-CI	$^2A_{2u}$	6.21	6.14	6.10 (6.20)[b]	6.12 (5.93)[b]
	$^2A_{1u}$	6.06	5.98	5.85 (6.38)[c]	5.72 (6.44)[c]

[a]On $\{[Co(III)P]^+Cl_2\}^-$ plus two axial points 2 Å above and below the Cl atoms of +0.5 charge.
[b]Calculated for the $^2A_{1u}$ state using the SCF of the $^2A_{2u}$ state as reference.
[c]Calculated for the $^2A_{2u}$ state using the SCF of the $^2A_{1u}$ state as reference.

TABLE 9. The Mulliken charge (and spin) distribution calculated for the ground state of $[Co(III)P]^+$, and its two low-lying cations

	$^1A_{1g}$	$^2A_{1u}$	$^2A_{2u}$
Co total	7.407	7.463	7.461
$d_{x^2-y^2}$	0.514	0.566	0.569
d_{z^2}	0.625	0.749	0.753
d_{xy}	1.993	1.994	1.994
d_{xz} and d_{yz}	1.984	1.990	1.990
N total	5.392	5.411	5.376
π	1.525	1.568	1.488 (0.069)
C_1 total	3.871	3.827	3.875
π	0.955	0.848 (0.102)	0.969 (0.005)
C_2 total	4.084	4.045	4.051
π	1.017	0.970 (0.023)	0.976 (0.014)
C_3 total	4.050	4.042	3.982
π	1.031	1.043	0.878 (0.135)
H_1 total	0.933	0.888	0.893
H_2 total	0.946	0.912	0.897
C_1 total	7.968	7.997	7.982
Net charge	1+	2+	2+

The results for these three complexes are reasonably similar, except for the total charges on the metal atom, as noted in Table 9. The net charge on the Co atom is about +1.5 and is similar for all three states of the Co complex. The metal atoms in the $^2A_{2u}$ cases have the greatest net charges, the neutral $^1A_{1g}$ cases the least, in keeping with intuition that all the atoms in the molecule share in the loss of this electron. Since the a_{2u} MO has some metal p_z character, loss of an electron from this orbital removes more electrons from the central metal than loss of an electron from an a_{1u} MO with two nodes through the metal.

As noted in Tables 9 and 10, the $^2A_{1u}$ and $^2A_{2u}$ states have quite different spin densities, and these have been used traditionally to help characterize the nature of the ground states of these ions through EPR and ENDOR measurements (48). Most often for this purpose the hyperfine constants for protons are approximated through the McConnell relation (49)

$$a_{Hi} = Q\rho_i^\pi$$

where ρ_i^π is the π spin density on the neighboring atom, and Q is a constant characteristic of that neighbor. Table 10 contains a comparison of the spin densities obtained by Fujita, Hanson, Walker, and Fajer (18) using the interative extended Hückel (IEH) method for a $Zn(II)P^+$ pyridine complex. The spin densities obtained from both methods for the $^2A_{1u}$ state are very similar; those obtained for the $^2A_{2u}$ state are somewhat different. For the $^2A_{2u}$ state, the INDO/S method used here places far more unpaired spin density on the methine bridge carbon atom C_3 than it does on the chelating nitrogen atom.

Table 10 also contains spin densities obtained from Pariser–Parr–Pople (PPP) π electron calculations (24) for comparison. The $^2A_{1u}$ state results are again very similar to those we obtain here. The $^2A_{2u}$ results are essentially the same for the spin density on the nitrogen atom and for C_1 and C_2. The accumulated small differences are noted, however, on the methine bridge carbon, C_3, with the INDO/S results of this study nearly the average of the PPP and IEH results. The small negative spin density of the PPP computation for C_1 are the result of an analysis of a CI wave function. The INDO/S results reported in this study are from restricted calculations (all closed shell "electrons" are in spacially paired orbitals), and negative values cannot be obtained at the level of theory (Hartree–Fock) reported in this table.

For further comparison, Petke, Maggiora, Shipman, and Christoffersen (20) obtain a ground state of the ethyl chlorophyllide a and ethyl bacteriochlorophyllide a cations with an average spin density of 0.109 electrons on each of the 8 C_1 atoms (these atoms are not equivalent in the chlorophyll analogues calculated by Petke *et al.*), clearly corresponding to the $^2A_{1u}$ π cation of this study. Although not definitive, the experimental spin densities obtained through McConnell's relation (16) seem in reasonable accord (20). The calculations of Petke *et al.* also suggest a low-lying singlet state (~5 000 cm^{-1} for Et-chl-a$^+$ and ~7 000 cm^{-1} for Et-Bchl-a$^+$) with an average of 0.17 electrons on each of the four methine bridge C_3 atoms and 0.09 electrons on each of the chelating nitrogen atoms, corresponding to the $^2A_{2u}$ states of this study. The INDO/S calculations suggest a greater spin delocalization in the $^2A_{2u}$ state (0.017e on each of 8 C_2 atoms) than either the *ab initio* calculations of Petke, Maggiora, Shipman, and Christoffersen (20) or the extended Hückel calculations of Fujita *et al.* (18).

Before concluding this section, we note (Table 10) that in the $^2A_{2u}$ state there is a net spin density on the metal atom that is not present in the $^2A_{1u}$ ions, as expected from the model structure of the half-filled MO that gives rise to the symmetries of these states.

IX. Conclusions

We report here the calculated spectra of the $^2A_{1u}$ and $^2A_{2u}$ π cations of Mg(II), Zn(II), and Co(III) porphine, and the electron spin properties of these two near lying states.

The $^2A_{2u}$ spectrum is calculated to have three allowed bands in the visible region of near equal intensity and a Soret region of at least three allowed bands, but the intensity of this region is dominated by but one of them. This seems to be in accord with experimental observations. In contrast, the $^2A_{1u}$ spectrum is calculated to have again three allowed transitions in the visible but with decreasing intensity with increasing transition energy, again in agreement with experiment. The Soret region is calculated to be characterized by at least four allowed bands spread some 10 000 cm^{-1}. In the $Co(III)P^{2+}$ and $Zn(II)P^+$ cases, three bands well separated are calculated to carry the intensity. The $Co(III)TPP^{2+}$ experimental spectrum shows three well separated band peaks in the Soret region. We do not have access to experimental $Zn(II)P^+$ $^2A_{1u}$ spectra. In the $Mg(II)P^+$ $^2A_{1u}$ calculation, four transitions are calculated to carry the intensity. Experimentally four transitions can be dis-

TABLE 10. Mulliken π spin densities for the cations of ZnP^+ and MgP^+

	ZnP^+		MgP^+		MP^{+c}	
	$^2A_{2u}$	$^2A_{1u}$	$^2A_{2u}$	$^2A_{1u}$	$^2A_{2u}$	$^2A_{1u}$
M	0.016 (0.003)[a]	0.000 (0.000)[a]	0.009[b]	0.000		
N	0.048 (0.113)	0.000 (0.000)	0.043	0.000	0.049	0.000
C_1=C_α	0.005 (0.000)	0.100 (0.095)	0.005	0.098	−0.009	0.098
C_2=C_β	0.017 (0.001)	0.025 (0.030)	0.019	0.027	0.013	0.026
C_3=C_m	0.154 (0.102)	0.000 (0.00)	0.151	0.000	0.000	0.001

[a]For ZnP^+ with a pyridine molecule in the fifth position. The values in parentheses have been symmetrized from ref. 18, and are obtained from an iterative extended Hückel calculation. The net spin density on the pyridine is 0.11 electrons.
[b]For this calculation the Mg atom is out of plane. Even so, very little spin density is found in the σ system except for a net 0.019 e in the Mg(3s).
[c]For "metal" porphine from Pariser–Parr–Pople π electron calculations, ref. 24.

TABLE 11. Net metal populations in the $^1A_{1g}$ stage of MgP, ZnP, and $[Co(III)P]^+$ and their $^2A_{2u}$ and $^2A_{1u}$ cations

Species	$^1A_{1g}$	$^2A_{2u}$	$^2A_{1u}$
MgP	+0.62	+0.73	+0.70
ZnP	+0.90	+0.94	+0.93
$[Co(III)P]^+$	+1.52	+1.54	+1.54

tinguished, but only the lower energy two are truly resolved.

The spin properties of the $^2A_{2u}$ and $^2A_{1u}$ π cations of these systems are dominated by the nodal structure of the corresponding molecular orbitals, are relatively insensitive to central atom displacement and remain very diagnostic of these two possible ground states.

Finally, our calculations suggest that at the optimized $^1A_{1g}$ geometry the $^2A_{1u}$ cation is lower in energy than the $^2A_{2u}$. This does not appear to be in accord with the more common situation for metal porphines, but is often observed, as discussed, for some $[Co(III)P]^{2+}$, ZnP^+, MgP^+, and RuP^+ complexes. Preliminary studies show that while geometry optimization of the doublet ions lowers their energy by only a few kcal/mol it is not sufficient to reverse the $^2A_{1u}$, $^2A_{2u}$, but only brings them closer in energy. The ground state observed for Et-chl-a$^+$ and Et-Bchl-a$^+$ (of considerably lower symmetry) probably also corresponds to the $^2A_{1u}$ states calculated here, and calculations on these more complex systems are currently underway.

Acknowledgements

This work was sponsored in part through a grant from the Natural Sciences and Engineering Council of Canada and from the Division of Sponsored Research at the University of Florida. We are very grateful for discussions and suggestions made by Dr. Louise Hanson and Dr. Jack Fajer of the Brookhaven National Laboratories.

1. W. D. EDWARDS, J. D. HEAD, and M. C. ZERNER. J. Am. Chem. Soc. **104**, 5833 (1982).
2. W. D. EDWARDS and M. C. ZERNER. Int. J. Quantum Chem. **23**, 1407 (1983).
3. M. P. GOUTERMAN. J. Mol. Spectrosc. **6**, 138 (1961).
4. D. DOLPHIN and R. H. FELTON. Acc. Chem. Res. **7**, 26 (1974).
5. J. FAJER, D. C. BORG, A. FORMAN, R. H. FELTON, D. DOLPHIN, and L. VEGH. Proc. Natl. Acad. Sci. U.S.A. **71**, 994 (1974).
6. D. C. BORG, J. FAJER, R. H. FELTON, and D. DOLPHIN. Proc. Natl. Acad. Sci. U.S.A. **67**, 813 (1970).
7. J. H. FUHRHOP and D. MAUZERALL. J. Am. Chem. Soc. **91**, 4174 (1969).
8. P. A. LOACH, R. A. BOMBARA, and F. J. RYAN. Photochem. Photobiol. **13**, 247 (1971).
9. R. H. FELTON, D. DOLPHIN, D. C. BORG, and J. FAJER. J. Am. Chem. Soc. **91**, 196 (1969).
10. H. S. SEKI, S. ARAI, T. SHIDA, and M. IMAMURA. J. Am. Chem. Soc. **95**, 3404 (1973).
11. C. K. CHANG, L. K. HANSON, P. F. RICHARDSON, R. YOUNG, and J. FAJER. Proc. Natl. Acad. Sci. U.S.A. **78**, 2652 (1981).
12. A. J. HOFF and K. MOBIUS. Proc. Natl. Acad. Sci. U.S.A. **75**, 2296 (1978).
13. J. D. MCELROY, G. FEHER, and D. C. MAUZERALL. Biochem. Biophys. Acta, **267**, 363 (1972).
14. M. E. DRUYAN, J. R. NORRIS, and J. J. KATZ. J. Am. Chem. Soc. **95**, 1682 (1973).
15. J. R. NORRIS, M. E. DRUYAN, and J. J. KATZ. J. Am. Chem. Soc. **95**, 1680 (1973).
16. H. SCHEER, J. J. KATZ, and J. R. NORRIS. J. Am. Chem. Soc. **99**, 1372 (1977).
17. J. R. BOLTON and J. T. WARDEN. Ann. Rev. Plant Physiol. **27**, 375 (1976).
18. I. FUJITA, L. K. HANSON, F. A. WALKER, and J. FAJER. J. Am. Chem. Soc. **105**, 3296 (1983).
19. J. FAJER, I. FUJITA, M. S. DAVIS, A. FORMAN, L. K. HANSON, and K. M. SMITH. *In* Advances in Chemical Series No. 201, Electrochemical and Spectrochemical Studies of Biological Redox Components. *Edited by* K. M. Kadish. 1982.
20. J. D. PETKE, G. M. MAGGIORA, L. L. SHIPMAN, and R. E. CHRISTOFFERSEN. Photochem. Photobiol. **31**, 243 (1980).
21. W. R. BROWETT and M. J. STILLMAN. Inorg. Chem. Acta, **49**, 69 (1981).
22. R. H. FELTON, G. S. OWEN, D. DOLPHIN, A. FORMAN, D. C. BORG, and J. FAJER. Ann. N.Y. Acad. Sci. **206**, 504 (1973).
23. D. DOLPHIN, A. FORMAN, D. C. BORG, J. FAJER, and R. H. FELTON. Proc. Natl. Acad. Sci. U.S.A. **68**, 614 (1971).
24. J. FAJER, D. C. BORG, A. FORMAN, D. DOLPHIN, and R. H. FELTON. J. Am. Chem. Soc. **92**, 3451 (1970).
25. J. RIDLEY and M. C. ZERNER. Theor. Chim. Acta, **32**, 111 (1973); **42**, 223 (1976).
26. M. C. ZERNER, G. H. LOEW, R. F. KIRCHNER, and U. T. MUELLER-WESTERHOFF. J. Am. Chem. Soc. **102**, 589 (1980).
27. W. D. EDWARDS and M. C. ZERNER. To be published.
28. R. PAUNCZ. Spin eigenfunctions. Plenum, New York. 1979.
29. W. D. EDWARDS, J. MCKELVEY, and M. C. ZERNER. To be published.
30. M. C. ZERNER and M. GOUTERMAN. Theor. Chim. Acta, **4**, 44 (1966).
31. T. SAKURAI, K. YAMAMOTO, N. SEINO, and M. KATSUTA. Acta

Crystallogr. **31**, 2514 (1975).
32. E. B. FLEISCHER, C. K. MILLER, and L. E. WEBB. J. Am. Chem. Soc. **86**, 2342 (1964).
33. M. A. BOBRIK and F. A. WALKER. Inorg. Chem. **19**, 3383 (1980).
34. L. D. SPAULDING, P. G. ELLER, J. A. BERTRAND, and R. H. FELTON. J. Am. Chem. Soc. **96**, 982 (1974).
35. K. M. BARKIGIA, L. D. SPAULDING, and J. FAJER. Inorg. Chem. **22**, 349 (1983).
36. C. KRATKY and J. D. DUNITZ. Acta. Crystallogr. B31, 1586 (1975).
37. J. D. PETKE, G. MAGGIORA, L. L. SHIPMAN, and R. E. CHRISTOFFERSEN. J. Mol. Spectrosc. **73**, 311 (1978).
38. D. SPANGLER, G. MAGGIORA, L. L. SHIPMAN, and R. E. CHRISTOFFERSEN. J. Am. Chem. Soc. **99**, 7470 (1977).
39. R. CHRISTOFFERSEN. Int. J. Quantum Chem. **16**, 573 (1979).
40. G. H. LOEW, Z. S. HERMAN, and M. C. ZERNER. Int. J. Quantum Chem. **18**, 481 (1980).
41. D. C. RAULINGS, E. R. DAVIDSON, and M. GOUTERMAN. Int. J. Quantum Chem.
42. L. EDWARDS, D. H. DOLPHIN, and M. GOUTERMAN. J. Mol. Spectrosc. **35**, 90 (1970).
43. These spectra have been courteously supplied by Dr. Martin Stillman, Univ. of Western Ontario, London, Ontario, Canada.
44. C. C. J. ROOTHAAN. Rev. Mod. Phys. **32**, 179 (1960).
45. K. HIRAO. J. Chem. Phys. **60**, 3215 (1974).
46. D. DOLPHIN, Z. MULJIANI, K. ROSSEAUX, D. C. BORG, J. FAJER, and R. H. FELTON. Ann. N.Y. Acad. Sci. **206**, 177 (1973).
47. P. DUPUIS, R. ROBERGE, and C. SANDORFY. Chem. Phys. Lett. **75**, 434 (1980).
48. F. FAJER and M. S. DAVIS. *In* The prophyrins. Vol. IV. *Edited by* D. Dolphin. Academic Press, New York. 1979.
49. H. M. MCCONNELL. J. Chem. Phys. **24**, 764 (1956).

The adiabatic approximation in the ground-state manifold

D. P. CRAIG

Research School of Chemistry, Australian National University, GPO Box 4, Canberra, ACT 2601, Australia

AND

T. THIRUNAMACHANDRAN

Department of Chemistry, University College London, 20 Gordon Street, London WC1H 0AJ, U.K.

Received August 18, 1984

This paper is dedicated to Professor Camille Sandorfy on the occasion of his 65th birthday

D. P. CRAIG and T. THIRUNAMACHANDRAN. Can. J. Chem. **63**, 1773 (1985).

The adiabatic approximation to vibronic interactions, and its relation to the crude adiabatic and other methods, need careful scrutiny when applied to processes where both participating states belong to the same electronic manifold. The processes include vibrational transitions by both electronic and magnetic mechanisms, and the property of vibrational circular dichroism in chiral systems. When moments and properties are calculated, general questions of dependence on the chosen origin of coordinates have to be resolved. These problems are examined.

D. P. CRAIG and T. THIRUNAMACHANDRAN. Can. J. Chem. **63**, 1773 (1985).

L'approximation adiabatique aux interactions vibroniques ainsi que sa relation à la méthode adiabatique grossière et autres ne doivent être appliquer qu'avec circonspection aux processus dans lesquels les deux états participants appartiennent au même niveau électronique. Ces processes comprennent les transitions vibrationnelles tant par des mécanismes électronique que magnétique ainsi que la propriété du dichroïsme circulaire vibrationnel dans des systèmes chiraux. Quand on calcule les moments et les propriétés, on doit résoudre les questions générales de la dépendance des coordonnées sur l'origine choisie. On examine ces problèmes.

[Traduit par le journal]

Introduction

In the early postwar years, when Camille Sandorfy was at the start of his career, the urgent problem in theoretical chemistry seemed to many of us to be how the principles of the theory of valency, enshrined for brevity in HLSP (Heitler–London–Slater–Pauling) and HMH (Hund–Mulliken–Hückel), were to be applied to complex aromatic molecules. In the years since new challenges have appeared. In a surprising number, not least in Professor Sandorfy's notable contributions to spectroscopy, interaction of nuclear and electronic motions is a central theme. His recent review (1) on vibrational spectra of hydrogen-bonded systems illustrates the point in transitions within the ground state manifold.

The present paper is on this interaction, which is germane also to theories of chemical kinetics and molecular dynamics. In the study of the coupling between electronic and nuclear motions the adiabatic approximation has been the basis of almost all work on vibronic interactions since its publication by Born and Oppenheimer (2). Very small molecules, H_2^+ and H_2, can be treated exactly (Kolos and Wolniewicz, ref. 3; Bishop and Cheung, ref. 4) and an interesting new approach has been suggested by Lathouwers and van Leuven (5) but for larger molecules no alternative method has been found suitable for general use.

The term adiabatic is used variously, and the adiabatic approximation applied at different levels. We begin by outlining the main models, and then apply them to infrared absorption and to rotational strength in chiral molecules. Finally, noting that results of calculations made in this approximation may be dependent on the choice of coordinate origin, we analyse the problem of origin-dependence, and give the conditions necessary for origin-independent results.

We have not given any discussion of the diabatic approximation (see e.g. Smith (6)), which is unlikely to be useful in the lower vibronic levels of the ground electronic state.

The adiabatic approximation

The Hamiltonian for a molecule can be partitioned as

$$[1] \quad H = T_N + T_e + U(q, Q)$$

where T_N and T_e are the nuclear and electronic kinetic energy operators and $U(q, Q)$ is the potential energy; q and Q are the electronic and nuclear coordinates. To solve the full Schrödinger equation [2]

$$[2] \quad H\Psi(q, Q) = E\Psi(q, Q)$$

we assume, in the adiabatic approximation, that the solutions of the electronic wave equation [3]

$$[3] \quad H_e\phi_n(q, Q) = E_n(Q)\phi_n(q, Q)$$

with

$$[4] \quad H_e = T_e + U(q, Q)$$

are known for sets of fixed values of Q, each set specifying a molecular configuration. With $\{\phi_n(q, Q)\}$ as a basis set, we expand the total wavefunction $\Psi(q, Q)$ according to [5] (7, 8),

$$[5] \quad \Psi(q, Q) = \sum_m \chi_m(Q)\phi_m(q, Q)$$

where the expansion coefficients are clearly functions of Q. Substituting in [2], multiplying both sides by $\bar{\phi}_n(q, Q)$, and integrating over the electronic coordinates, we get

$$[6] \quad \sum_m \int \bar{\phi}_n(q, Q)(T_N + H_e)\phi_m(q, Q)\mathrm{d}q\chi_m(Q) = E\sum_m \int \bar{\phi}_n(q, Q)\phi_m(q, Q)\mathrm{d}q\chi_m(Q)$$

so that, with [3], and the orthonormality of the electronic eigenfunctions $\{\phi_n(q, Q)\}$,

$$[7]\quad \left(T_N + E_n(Q)\right)\chi_n(Q) - \frac{\hbar^2}{2}\sum_m\left(\int\bar{\phi}_n(q, Q)\frac{\partial^2}{\partial Q^2}\phi_m(q, Q)\mathrm{d}q\right)\chi_m(Q) - \hbar^2\sum_m\int\left(\bar{\phi}_n(q, Q)\frac{\partial}{\partial Q}\phi_m(q, Q)\mathrm{d}q\right)\frac{\partial}{\partial Q}\chi_m(Q) = E\chi_n(Q)$$

Separating the diagonal terms from the sums and rearranging we find [8]

$$[8]\quad \left(T_N + E_n(Q) - \frac{\hbar^2}{2}\int\bar{\phi}_n(q, Q)\frac{\partial^2}{\partial Q^2}\phi_n(q, Q)\mathrm{d}q - E\right) \times \chi_n(Q) = \frac{\hbar^2}{2}\sum_{m\neq n}\left(\int\bar{\phi}_n(q, Q)\frac{\partial^2}{\partial Q^2}\phi_m(q, Q)\mathrm{d}q\right)\chi_m(Q) + \hbar^2\sum_{m\neq n}\left(\int\bar{\phi}_n(q, Q)\frac{\partial}{\partial Q}\phi_m(q, Q)\mathrm{d}q\right)\frac{\partial}{\partial Q}\chi_m(Q)$$

Equations [8] are a set of coupled differential equations with n taking different values according to [3]. The terms on the right hand side of [8] represent the coupling between the electronic functions through nuclear motion. If these terms are set equal to zero, the equations become uncoupled, giving [9]

$$[9]\quad \left(T_N + E_n(Q) - \frac{\hbar^2}{2}\int\bar{\phi}_n(q, Q)\frac{\partial^2}{\partial Q^2}\phi_n(q, Q)\mathrm{d}q - E\right) \times \chi_n(Q) = 0$$

which can be written as

$$[10]\quad (T_N + U_n(Q))\chi_{nv}(Q) = E_{nv}\chi_{nv}(Q)$$

where

$$[11]\quad U_n(Q) = E_n(Q) - \frac{\hbar^2}{2}\int\bar{\phi}_n(q, Q)\frac{\partial^2}{\partial Q^2}\phi_n(q, Q)\mathrm{d}q$$

In eq. [10], a further subscript v has been added to distinguish the different eigenvalues and eigenfunctions for a given n. The neglect of the terms on the right hand side of [8] is the basis of the *adiabatic approximation*. In adiabatic motion, electrons do not make transitions from one state to another. Instead, the electron distribution adapts itself by following the nuclear displacements. The potential energy $U_n(Q)$, given by [11], serves as the potential for nuclear motion in [10].

The adiabatic approximation may be distinguished from the original Born–Oppenheimer approximation (2) because the potential $U_n(Q)$ for the latter is simply $E_n(Q)$; that is, the expectation value of the nuclear kinetic energy over the electronic wavefunction $\phi_n(q, Q)$, given as the second term of [11], is neglected. This is a good approximation for many problems because of the small electron to nuclear mass ratio. In the Born–Oppenheimer approximation the potential is independent of the nuclear masses, and identical for different isotopes.

Higher order corrections can be made in the adiabatic model by including the coupling between different electronic functions, which was neglected in the derivation of the wave equation [10] for nuclear motion. Thus with the adiabatic products as basis functions, the off-diagonal elements of the total Hamiltonian are

$$[12]\quad \int\bar{\chi}_{n'v'}(Q)\bar{\phi}_{n'}(q, Q)H\phi_n(q, Q)\chi_{nv}(Q)\mathrm{d}q\mathrm{d}Q = -\frac{\hbar^2}{2}\int\bar{\chi}_{n'v'}(Q)\left(\int\bar{\phi}_{n'}(q, Q)\frac{\partial^2}{\partial Q^2}\phi_n(q, Q)\mathrm{d}q\right)\chi_{nv}(Q)\mathrm{d}Q - \hbar^2\int\bar{\chi}_{n'v'}(Q)\left(\int\bar{\phi}_{n'}(q, Q)\frac{\partial}{\partial Q}\phi_n(q, Q)\mathrm{d}q\right)\frac{\partial}{\partial Q}\chi_{nv}(Q)\mathrm{d}Q$$

The second term of [12] gives the coupling of electronic to nuclear motion caused by the nuclear momentum. It is usually larger than the first, which is often neglected. In the simplest case of the same vibrational force system in the coupled levels n and n', and unchanged molecular structure, the first term couples the states with the same vibrational quantum number. The second term couples states with $v' = v \pm 1$.

The crude adiabatic approximation

In the crude adiabatic model, the electronic factors $\phi_n^0 \equiv \phi_n(q, Q_0)$ are not functions of Q but apply to the equilibrium nuclear configuration for state n. The partitioning of the total Hamiltonian is now given by

$$[13]\quad H = T_N + T_e + U(q, Q_0) + U(q, Q) - U(q, Q_0) = T_N + H_e^0 + \Delta U$$

where

$$[14]\quad H_e^0 = T_e + U(q, Q_0)$$

and

$$[15]\quad \Delta U = U(q, Q) - U(q, Q_0)$$

The electronic eigenfunctions $\phi_n(q, Q_0)$ of H_e^0 are now used as the basis set for expanding the complete wavefunction $\Psi(q, Q)$:

$$[16]\quad (T_N + H_e^0 + \Delta U)\sum_m\chi_m(Q)\phi_m(q, Q_0) = E\sum_m\chi_m(Q)\phi_m(q, Q_0)$$

After multiplying both sides of [16] by $\bar{\phi}_n(q, Q_0)$, integrating over the electron coordinates, and rearranging

$$[17]\quad \left(T_N + E_n(Q_0) + \int\bar{\phi}_n(q, Q_0)\Delta U\phi_n(q, Q_0)\mathrm{d}q - E\right)\chi_n(Q) = -\sum_{m\neq n}\int\bar{\phi}_n(q, Q_0)\Delta U\phi_m(q, Q_0)\mathrm{d}q\chi_m(Q)$$

The crude adiabatic approximation involves setting the sum on the right hand side of [17] equal to zero. Thus the equation for nuclear motion is

$$[18]\quad \left(T_N + E_n(Q_0) + \int\bar{\phi}_n(q, Q_0)\Delta U\phi_n(q, Q_0)\mathrm{d}q\right)\chi_{nv}(Q) = E_{nv}\chi_{nv}(Q)$$

so that the potential for nuclear motion is

$$[19]\quad U_n(Q) = E_n(Q_0) + \int\bar{\phi}_n(q, Q_0)\Delta U\phi_n(q, Q_0)\mathrm{d}q = \int\bar{\phi}_n(q, Q_0)H_e\phi_n(q, Q_0)\mathrm{d}q$$

The vibrational wave functions found in the crude adiabatic method are not the same as in the adiabatic approximation, where they belong to the potential function [11].

Herzberg–Teller coupling and adiabatic motion

In the Herzberg–Teller model (12), the electronic wavefunctions are the same as those used in the crude adiabatic model. They are the eigenfunctions of H_e^0. With ΔU given by [15] as the perturbation, the electronic wavefunction for state n, correct to first order, is

$$[20] \quad \phi_n^{\mathrm{HT}}(q, Q) = \phi_n(q, Q_0) - \sum_{m \neq n} \frac{\int \bar{\phi}_m(q, Q_0)\Delta U \phi_n(q, Q_0)\mathrm{d}q}{E_m^0 - E_n^0} \phi_m(q, Q_0)$$

and the electronic energy is

$$[21] \quad E_n^{\mathrm{HT}}(Q) = E_n(Q_0) + \int \bar{\phi}_n(q, Q_0)\Delta U \phi_n(q, Q_0)\mathrm{d}q - \sum_{m \neq n} \frac{\left| \int \bar{\phi}_m(q, Q_0)\Delta U \phi_n(q, Q_0)\mathrm{d}q \right|^2}{E_m^0 - E_n^0}$$

Since $H_e = H_e^0 + \Delta U$, the wavefunction [20] can be regarded as the adiabatic electronic wavefunction, correct to first order in ΔU. It is of interest to note that if a product of the form $\phi_n^{\mathrm{HT}}(q, Q)\chi_{nv}^{\mathrm{HT}}(Q)$ is chosen to describe the vibronic state $|n,v\rangle$, then $\chi_{nv}(Q)$ satisfies eq. [22]

$$[22] \quad (T_{\mathrm{N}} + E_n^{\mathrm{HT}}(Q))\chi_{nv}^{\mathrm{HT}}(Q) = E_{nv}\chi_{nv}^{\mathrm{HT}}(Q)$$

where $E_n^{\mathrm{HT}}(Q)$ of eq. [21] serves as the potential for nuclear motion. In obtaining [22], the effect of T_{N} on $\phi_n^{\mathrm{HT}}(q, Q)$ has been ignored, as in the Born–Oppenheimer approximation. In contrast to the crude adiabatic potential [19] for nuclear motion, $E_n^{\mathrm{HT}}(Q)$ includes the second order contribution (third term of [21]). Hence $\phi_n^{\mathrm{HT}}(q, Q)\chi_{nv}^{\mathrm{HT}}(Q)$ may be considered to be a better approximation than $\phi_n(q, Q_0)\chi_{nv}(Q)$.

Off-diagonal terms in the adiabatic and crude adiabatic schemes

A useful insight into the relation of the two approximations comes from considering the Taylor expansion of the adiabatic electronic wave function $\phi_n(q, Q)$ in terms of crude adiabatic functions,

$$[23a] \quad \phi_n(q, Q) = \phi_n(q, Q_0) + (Q - Q_0)\left\{\frac{\partial}{\partial Q}\phi_n(q, Q)\right\}_0 + \ldots\ldots$$

$$[23b] \quad = \phi_n(q, Q_0) - (Q - Q_0)\sum_{m \neq n} \frac{\int \left\{\phi_m \frac{\partial U}{\partial Q}\phi_n\right\}_0 \mathrm{d}q}{E_m^0 - E_n^0} \phi_m(q, Q_0)$$

where the second form (9) follows using

$$[24] \quad \left(\frac{\partial}{\partial Q}\phi_0(q, Q)\right)_0 = -\sum_{m \neq 0} \frac{\left(\int \phi_m(q, Q)\frac{\partial U}{\partial Q}\phi_0(q, Q)\mathrm{d}q\right)_0}{E_m^0 - E_0^0} \phi_m(q, Q_0)$$

so that, up to the term linear in Q, the adiabatic vibronic wave function for the state $|n, v\rangle$ can be written as

$$[25] \quad |n, v\rangle = \phi_n^0\chi_{nv} + \sum_{m \neq n} \frac{\int \left\{\phi_m \frac{\partial U}{\partial Q}\phi_n\right\}_0 \mathrm{d}q}{E_m^0 - E_n^0} \phi_m^0 Q \chi_{nv}$$

showing that the adiabatic wave function already includes corrections of a type which in the crude adiabatic have to be brought in as off-diagonal terms by use of first-order pertubation theory. Also, terms [12] which are off-diagonal in the adiabatic method do not appear at all in the crude adiabatic method, in which coupling by nuclear motion is not taken account of.

In summary, the off-diagonal coupling between crude adiabatic vibronic states is included in zero-order adiabatic states. Off-diagonal matrix elements between the latter states are typically small.

Transitions within the ground state vibrational manifold

When the adiabatic approximation is applied to electric or magnetic transitions involving different electronic levels as in $\langle m, v'| \leftarrow \langle n, v|$, the nuclear part of the transition moment operator does not contribute. This is because adiabatic electronic wave functions belonging to different electronic energies are orthogonal for each set of values of the nuclear coordinates Q. However, infrared and vibrational Raman transitions, and transitions showing vibrational circular dichroism in chiral molecules, take place between different levels of the same (ground) electronic state. Both nuclear and electronic parts of the transition moment operator may contribute, and some interesting new problems have to dealt with.

Let us consider the transition $|0,1\rangle \leftarrow |0,0\rangle$ and suppose that only one mode is active and that the levels are non-degenerate. The wavefunctions can then be chosen to be real. With the adiabatic products $\phi_0(q, Q)\chi_{00}(Q)$ and $\phi_0(q, Q)\chi_{01}(Q)$ representing the molecular states, the electric and magnetic dipole transition moments are

$$[26] \quad \langle 1,0|\boldsymbol{\mu}|0,0\rangle = \int \chi_{01}(Q)\phi_0(q, Q)\boldsymbol{\mu}\phi_0(q, Q)\chi_{00}(Q)\mathrm{d}q\mathrm{d}Q$$

$$[27] \quad \langle 1,0|\boldsymbol{m}|0,0\rangle = \int \chi_{01}(Q)\phi_0(q, Q)\boldsymbol{m}\phi_0(q, Q)\chi_{00}(Q)\mathrm{d}q\mathrm{d}Q$$

where $\boldsymbol{\mu}$ and $\boldsymbol{m}$ are sums of nuclear and electronic terms. It is easily shown by integrating over electronic coordinates that the electronic contribution to the magnetic dipole transition moment is zero. For the electric dipole transition moment both electronic and nuclear terms contribute. The electric dipole moment operator is given by

$$[28] \quad \mu_i = -e \sum_{\alpha,\zeta} r_i(\alpha, \zeta) + e \sum_{\alpha} Z_\alpha R_i(\alpha)$$

where $Z_\alpha e$ is the charge on nucleus α and $\boldsymbol{R}(\alpha)$ is the position vector: $\boldsymbol{r}(\alpha, \zeta)$ is the position vector of electron ζ associated with nucleus α. In the case that the solutions to the electronic equation [3] are found in an all-electron *ab initio* framework the charges $Z_\alpha e$ are bare nuclear charges. In that case the large terms in the dipole moment [26] from the second term of [28] are at least partially cancelled by those from the first term, which is a sum over all electrons. In many calculations it is a good approximation to restrict the sum over electrons to valence electrons, and then the $Z_\alpha e$ must be treated as effective charges, with allowance for the screening by core electrons. In that case the reduced nuclear contribution to [26] is set against a matching reduction in the electronic contribution. Thus in different models that may be set up for calculating the adiabatic wave functions, defined by a range of Hamiltonians at different levels of approximation, there are different partitions of the electric moment. We note later the special importance of model dependence in the treatment of the magnetic moment.

In order to be able to use the electric moment operator [28] in [26], we need to express $R_i(\alpha)$ in terms of normal coordinates Q_k, and $r_i(\alpha, \zeta)$ in terms of relative coordinates $q_i(\alpha, \zeta)$. If $\boldsymbol{R}^0(\alpha)$ is the equilibrium position of nucleus α, then

$$[29] \quad R_i(\alpha) = R_i^0(\alpha) + M_\alpha^{-1/2} \sum_{k=1}^{3N-6} l_{ik}(\alpha) Q_k$$

where $k = 1, 2, \ldots, (3N-6)$, after elimination of translational and rotational degrees of freedom. The coefficients l_{ik} satisfy the orthonormality conditions

$$\sum_i l_{ki}(\alpha) l_{il}(\alpha) = \delta_{kl}$$

The coordinates $\boldsymbol{q}(\alpha, \zeta)$ are defined by [30]

$$[30] \quad \boldsymbol{q}(\alpha, \zeta) = \boldsymbol{r}(\alpha, \zeta) - \boldsymbol{R}^0(\alpha)$$

With the use of [29] in [26] the nuclear contribution to the electric dipole transition moment follows immediately. To calculate the electronic contribution, a convenient starting point is the expansion of the electronic wavefunction about the equilibrium position in the active normal coordinate as in [23a]. Using [23a] in [26] the leading term of $\boldsymbol{\mu}$ is found to be

$$[31] \quad 2\int \chi_{01}(Q)\phi_0(q, Q_0) Q \boldsymbol{\mu}^{\mathrm{elec}} \left(\frac{\partial}{\partial Q}\phi_0(q, Q)\right)_0 \chi_{00}(Q)\mathrm{d}q\mathrm{d}Q = 2\int \phi_0(q, Q_0)\boldsymbol{\mu}^{\mathrm{elec}} \left(\frac{\partial}{\partial Q}\phi_0(q, Q)\right)_0 \mathrm{d}q \int \chi_{01}(Q) Q \chi_{00}(Q)\mathrm{d}Q$$

The electronic integral depends on the ground state electronic wavefunction and its derivative evaluated at Q_0. This form of the integrand, depending solely on the ground state wave function and its Q derivative, may be convenient from a computational point of view. An alternative form (9) involving the electronic excited states can be obtained using [24]. The same result [31] can be obtained from the crude adiabatic approach. In this formalism, the wave function for the ground state $|0,0\rangle$, correct to first order, is

$$[32] \quad |0,0\rangle = \phi_0(q, Q_0)\chi_{00}(Q) - \sum_{mv} \int \frac{\chi_{mv}(Q)\phi_m(q, Q_0)\Delta U \phi_0(q, Q_0)\chi_{00}(Q)}{E_{mv} - E_{00}} \mathrm{d}q\mathrm{d}Q \times \phi_m(q, Q)\chi_{00}(Q)$$

A similar wavefunction holds for $|0,1\rangle$. The electric dipole transition moment is then found to be

$$[33] \quad -\sum_{mv} \int \chi_{01}(Q)\phi_0(q, Q_0)\boldsymbol{\mu}^{\mathrm{elec}}\phi_m(q, Q_0)\chi_{mv}(Q)\mathrm{d}q\mathrm{d}Q \times \frac{\int \chi_{mv}(Q)\phi_m(q, Q_0)\Delta U \phi_0(q, Q_0)\chi_{00}(Q)\mathrm{d}q\mathrm{d}Q}{E_{mv} - E_{00}}$$
$$- \sum_{mv} \frac{\int \chi_{01}(Q)\phi_0(q, Q_0)\Delta U \phi_m(q, Q_0)\chi_{mv}(Q)\mathrm{d}q\mathrm{d}Q}{E_{mv} - E_{01}} \times \int \chi_{mv}(Q)\,\phi_m(q, Q_0)\boldsymbol{\mu}^{\mathrm{elec}}\phi_0(q, Q_0)\mathrm{d}q\mathrm{d}Q$$

Expanding ΔU about Q_0 and retaining the leading terms, namely, $(Q - Q_0)\,(\partial U/\partial Q)_0$, expression [33] simplifies to

$$[34] \quad -2\sum_m \int \phi_0(q, Q_0)\boldsymbol{\mu}^{\mathrm{elec}}\phi_m(q, Q_0)\mathrm{d}q \times \frac{\int \phi_m(q, Q_0) Q (\partial U/\partial Q)_0 \phi_0(q, Q_0)\mathrm{d}q \int \chi_{01}(Q) Q \chi_{00}(Q)\mathrm{d}Q}{E_m^0 - E_0^0}$$

where the vibrational energy differences in the denominators have been neglected. Consequently, it has been possible to effect closure over the vibrational states associated with the intermediate state $\phi_m(q, Q_0)$. The use of the relationship [24] in [34] leads to the result [31] obtained from the adiabatic approach. It must be noted that, in making this identification, it has been tacitly assumed that the vibrational wavefunctions in the adiabatic and the crude adiabatic formalisms are essentially the same.

We now turn to the evaluation of the magnetic dipole transition moment. The electronic and nuclear parts of the magnetic dipole moment operator are given by

$$[35] \quad \boldsymbol{m} = \frac{e}{2m}\sum_{\alpha,\zeta}\{\boldsymbol{r}(\alpha, \zeta) \times \boldsymbol{p}(\alpha, \zeta)\} + \frac{e}{2}\sum_\alpha \frac{Z_\alpha}{M_\alpha}\{\boldsymbol{R}(\alpha) \times \tilde{\boldsymbol{P}}(\alpha)\}$$

where $\boldsymbol{p}$ and $\tilde{\boldsymbol{P}}$ are the electronic and nuclear momenta. The moments are taken about the centre of mass. In terms of $\boldsymbol{q}$ and $\boldsymbol{Q}$, we have for the ith component

$$[36] \quad m_i = -\frac{e}{2m}\sum_{\alpha,\zeta}\{\boldsymbol{R}^0(\alpha) \times \boldsymbol{p}(\alpha, \zeta)\}_i - \frac{e}{2m}\sum_{\alpha,\zeta}\{\boldsymbol{q}(\alpha, \zeta) \times \boldsymbol{p}(\alpha, \zeta)\}_i + \frac{e}{2}\sum_\alpha \frac{Z_\alpha}{M_\alpha}\{\boldsymbol{R}^0(\alpha) \times \tilde{\boldsymbol{P}}(\alpha)\}_i$$
$$+ \frac{e}{2}\epsilon_{ijl}\sum_\alpha \frac{Z_\alpha}{M_\alpha^{1/2}} \sum_{k=1}^{3N-6} l_{jk}(\alpha) Q_k \tilde{P}_l(\alpha)$$

In [36] the $\tilde{P}_l(\alpha)$ are not canonically conjugate to $Q_l(\alpha)$. They can be transformed according to

$$[37] \quad \tilde{P}_l(\alpha) = \sum M_\alpha^{1/2}\, l_{lk}(\alpha) P_k$$

where P_k are the canonical conjugates of Q_k. For the case where one mode only is active, the situation which we consider in this paper, the last term of [36] does not contribute. With zeroth-order adiabatic functions, the magnetic dipole transition is entirely made up of the nuclear contribution and is given by

$$[38]\quad \langle\chi_{01}(Q)|\langle\phi_0(q,Q)|m_i|\phi_0(q,Q)\rangle|\chi_{00}(Q)\rangle = \frac{e}{2}\epsilon_{ijl}\sum_\alpha M_\alpha^{-1/2}Z_\alpha R_j^0(\alpha)l_{lk}(\alpha)\int \chi_{01}(Q)P_k\chi_{00}(Q)\mathrm{d}Q$$

In contrast, as seen earlier, the electric dipole transition moment has both electronic and nuclear contributions with zeroth-order adiabatic functions.

Higher order contributions to transition moments

In the adiabatic model, the wavefunctions corrected to first order are obtained using the coupling [12]. For $|0,0\rangle$ we get

$$[39]\quad |0,0\rangle = \phi_0(q,Q)\chi_{00}(Q) + \hbar^2\sum_{mv}\int \chi_{mv}(Q)\int \phi_m(q,Q)\frac{\partial}{\partial Q}\phi_0(q,Q)\mathrm{d}q\frac{\partial}{\partial Q}\chi_{00}(Q)\mathrm{d}Q\phi_m(q,Q)\chi_{mv}(Q)$$
$$+\frac{\hbar^2}{2}\sum_{mv}\int \chi_{mv}(Q)\int \phi_m(q,Q)\frac{\partial^2}{\partial Q^2}\phi_0(q,Q)\mathrm{d}q\chi_{00}(Q)\mathrm{d}Q\phi_m(q,Q)\chi_{mv}(Q)$$

and a similar wavefunction for $|0,1\rangle$. With these wavefunctions, the corrections to the electric dipole transition moment are given by

$$[40]\quad \hbar^2\sum_{mv}\int \chi_{01}(Q)\boldsymbol{\mu}^{0m}(Q)\chi_{mv}(Q)\mathrm{d}Q\,\frac{\int\chi_{mv}(Q)\int \phi_m(q,Q)\frac{\partial}{\partial Q}\phi_0(q,Q)\mathrm{d}q\frac{\partial}{\partial Q}\chi_{00}(Q)\mathrm{d}Q}{E_{mv}-E_{00}}$$
$$+\hbar^2\sum_{mv}\int \chi_{00}(Q)\boldsymbol{\mu}^{0m}(Q)\chi_{mv}(Q)\mathrm{d}Q\,\frac{\int\chi_{mv}(Q)\int \phi_m(q,Q)\frac{\partial}{\partial Q}\phi_0(q,Q)\mathrm{d}q\frac{\partial}{\partial Q}\chi_{01}(Q)\mathrm{d}Q}{E_{mv}-E_{01}}$$
$$+\frac{\hbar^2}{2}\sum_{mv}\int \chi_{01}(Q)\boldsymbol{\mu}^{0m}(Q)\chi_{mv}(Q)\mathrm{d}Q\,\frac{\int\chi_{mv}(Q)\int \phi_m(q,Q)\frac{\partial^2}{\partial Q^2}\phi_0(q,Q)\mathrm{d}q\chi_{00}(Q)\mathrm{d}Q}{E_{mv}-E_{00}}$$
$$+\frac{\hbar^2}{2}\sum_{mv}\int \chi_{00}(Q)\boldsymbol{\mu}^{0m}(Q)\chi_{mv}(Q)\mathrm{d}Q\,\frac{\int\chi_{mv}(Q)\int \phi_m(q,Q)\frac{\partial^2}{\partial Q^2}\phi_0(q,Q)\mathrm{d}q\chi_{01}(Q)\mathrm{d}Q}{E_{mv}-E_{01}}$$

where

$$[41]\quad \boldsymbol{\mu}^{0m}(Q) = \int \phi_0(q,Q)\boldsymbol{\mu}^{\mathrm{elec}}\phi_m(q,Q)\mathrm{d}q$$

To find the leading contribution from the first two terms, we approximate the electronic integral

$$\int \phi_m(q,Q)\frac{\partial}{\partial Q}\phi_0(q,Q)\mathrm{d}q$$

by the value at Q_0, and also put $\boldsymbol{\mu}^{0m}(Q) = \boldsymbol{\mu}^{0m}(Q_0)$. We then get

$$[42]\quad \hbar^2\sum \boldsymbol{\mu}^{0m}(Q_0)\left(\int \phi_m(q,Q)\frac{\partial}{\partial Q}(q,Q)\mathrm{d}q\right)_0\left\{\frac{1}{E_{mv}-E_{00}}\int \chi_{01}(Q)\chi_{mv}(Q)\mathrm{d}Q\int \chi_{mv}(Q)\frac{\partial}{\partial Q}\chi_{00}(Q)\mathrm{d}Q\right.$$
$$\left.+\frac{1}{E_{mv}-E_{01}}\int \chi_{00}(Q)\chi_{mv}(Q)\mathrm{d}Q\int \chi_{mv}(Q)\frac{\partial}{\partial Q}\chi_{01}(Q)\mathrm{d}Q\right\}$$

If the vibrational energy differences in the denominators are neglected, then closure over the intermediate state vibrational wavefunctions may be effected to give

$$[43]\quad \hbar^2\sum \frac{\boldsymbol{\mu}^{0m}(Q_0)}{E_m^0-E_0^0}\left(\int \phi_m(q,Q)\frac{\partial}{\partial Q}\phi_0(q,Q)\mathrm{d}q\right)_0\left\{\int \chi_{01}(Q)\frac{\partial}{\partial Q}\chi_{00}(Q)\mathrm{d}Q + \int \chi_{00}(Q)\frac{\partial}{\partial Q}\chi_{01}(Q)\mathrm{d}Q\right\}$$

The vibrational integrals within the braces are equal and opposite, so that the correction to this order is zero. However, if the vibrational energy differences are retained then there is a small residual term from [42].

The contribution from the last two terms of [40] is found in a similar manner. It is given by

$$[44]\quad \hbar^2\sum \frac{\boldsymbol{\mu}^{0m}(Q_0)}{E_m^0-E_0^0}\left(\int \phi_m(q,Q)\frac{\partial^2}{\partial Q^2}\phi_0(q,Q)\mathrm{d}q\right)_0\int \chi_{01}(Q)\chi_{00}(Q)\mathrm{d}Q$$

which is zero because of the orthogonality of the vibrational wavefunctions.

The calculations for the magnetic dipole transition moment follow similar lines, with the important difference that $\boldsymbol{m}^{0m} = -\boldsymbol{m}^{m0}$. The leading contribution from the analogues of the first two terms of [40] is

$$[45]\quad -2\hbar^2 \sum \frac{m^{m0}(Q_0)}{E_m^0 - E_0^0}\left(\int \phi_m(q,Q)\frac{\partial}{\partial Q}\phi_0(q,Q)\mathrm{d}q\right)_0 \int \chi_{01}(Q)\frac{\partial}{\partial Q}\chi_{00}(Q)\mathrm{d}Q$$

The analogues of the last two terms are zero as in the electric dipole case because of the orthogonality of vibrational wavefunctions.

The question of model dependence is here of special importance. Different model Hamiltonians involve values of nuclear charge Z_α chosen to accord with assumptions about which electrons are to be treated as part of a nuclear core. The nuclear contribution to the magnetic transition moment [38] is proportional to the Z_α, and if the total moment is to be independent of model, there must be compensation by the electronic contribution. Since there is no electronic contribution in the same (zeroth) order, as in the electric moment, we look for compensation from the higher order terms [45]. It is essential to keep these perturbation corrections as small as possible, especially if only first order corrections are taken, and therefore essential to choose a model with the lowest realistic values of effective nuclear charge.

Circular dichroism can appear in vibrational transitions of optically active molecules. The total transition rate for such a transition $|0,1\rangle \leftarrow |0,0\rangle$ is

$$[46]\quad \Gamma^{(R/L)} = \frac{2\pi}{3\hbar}\left(\frac{n\hbar ck}{2\epsilon_0 V}\right)|\langle 1,0|\boldsymbol{\mu} \pm i\boldsymbol{m}|0,1\rangle|^2\rho$$

the plus and minus signs holding for right- and left-circularly polarized light, respectively. Circular dichroism is given by the difference in absorption rates:

$$[47]\quad \langle\Gamma^{(L)}_{01,00}\rangle - \langle\Gamma^{(R)}_{01,00}\rangle = \frac{2I}{3\hbar^2 c\epsilon_0}R^{01,00}$$

where I is energy density per unit frequency and

$$[48]\quad R^{01,00} = \langle 0,0|\boldsymbol{\mu}|0,1\rangle\cdot\langle 1,0|\boldsymbol{m}|0,0\rangle$$

Using the expressions for the electric and magnetic transition moments calculated in the previous sections, the expression for $R^{01,00}$ follows directly.

Origin-dependence of transition moments and rotatory strength

It is well known that the matrix elements of the electric dipole moment are origin-independent in neutral molecules. Writing the electric dipole moment operator as

$$[49]\quad \boldsymbol{\mu} = \sum_\alpha e_\alpha \boldsymbol{r}_\alpha$$

where the sum is over all the charged particles, and displacing the origin of the vectors $\boldsymbol{r}_\alpha$ by $\boldsymbol{\rho}$, we find the change in dipole moment, $\Delta\boldsymbol{\mu}$ to be

$$[50]\quad \Delta\boldsymbol{\mu} = -\boldsymbol{\rho}\sum e_\alpha$$

which vanishes if the net charge on the molecule is zero. Since the result applies to the dipole operator it holds for the matrix elements of the dipole moment in any basis, exact or approximate.

The matrix elements of the magnetic dipole moment are, however, origin-dependent, even in an exact basis. Writing the magnetic dipole moment operator as

$$[51]\quad \boldsymbol{m} = \frac{1}{2}\sum_\alpha\left(\frac{e_\alpha}{m_\alpha}\right)\boldsymbol{r}_\alpha \times \boldsymbol{p}_\alpha$$

the change caused in the matrix elements of $\boldsymbol{m}$ by an origin displacement by $\boldsymbol{\rho}$ is

$$[52]\quad \Delta\boldsymbol{m}^{n0} = -\frac{1}{2}\sum_\alpha\left(\frac{e_\alpha}{m_\alpha}\right)\boldsymbol{\rho}\times\boldsymbol{p}_\alpha^{n0}$$

If $|0\rangle$ and $|n\rangle$ are exact eigenstates of the molecular Hamiltonian, we can replace the matrix elements of $\boldsymbol{p}_\alpha$ by those of $\boldsymbol{r}_\alpha$,

$$[53]\quad \boldsymbol{p}_\alpha^{n0} = -\left(\frac{m_\alpha}{i\hbar}\right)E_{n0}\boldsymbol{r}_\alpha^{n0}$$

where E_{n0} is the transition energy. Substitution in [52] gives

$$[54]\quad \Delta\boldsymbol{m}^{n0} = \left(\frac{E_{n0}}{2i\hbar}\right)\sum_\alpha e_\alpha\boldsymbol{\rho}\times\boldsymbol{r}_\alpha^{n0} = \left(\frac{E_{n0}}{2i\hbar}\right)\boldsymbol{\rho}\times\boldsymbol{\mu}^{n0}$$

where $\boldsymbol{\mu}^{n0}$ is the matrix element of the electric dipole transition moment. Thus $\boldsymbol{m}$ is origin-dependent since [54] is not, in general, zero. However, if the electric dipole transition moment is zero, then [54] vanishes and the magnetic dipole transition moment is origin-independent. Similarly, the electric quadrupole transition moment, which is of the same order as the magnetic moment, can be shown to be origin-independent when the electric moment is zero.

We next show that matrix elements for circular dichroism are origin-independent in an exact basis, but not generally. The optical rotatory strength for a transition $n \leftarrow 0$ is given by [55].

$$[55]\quad R^{n0} = \mathrm{Im}\,\boldsymbol{\mu}^{0n}\cdot\boldsymbol{m}^{n0}$$

If the origin is displaced by $\boldsymbol{\rho}$ the change in the rotatory strength is given by [56], taking account of the origin-independence of $\boldsymbol{\mu}$

$$[56]\quad \Delta R^{n0} = \epsilon_{ijk}\mathrm{Im}\,\mu_i^{0n}\rho_j\sum_\alpha\left(\frac{e_\alpha}{2m_\alpha}\right)p_{k(\alpha)}^{n0}$$

where the states are eigenstates of the molecular Hamiltonian [1], we use the result [54] for the change in the magnetic moment and find for the change in the optical rotatory strength

$$[57]\quad \Delta R^{n0} = \left(\frac{E_{n0}}{2i\hbar}\right)\epsilon_{ijk}\mathrm{Im}(\mu_i^{0n}\rho_j\mu_k^{n0}) = 0$$

the zero coming from the symmetry of the dipole moment product to i, j interchange coupled with the antisymmetry of ϵ_{ijk}. Thus for exact eigenfunctions, the pseudoscalar rotatory strength R^{n0} is independent of choice of origin. However, if approximate wavefunctions are used to describe the states, then the relation [53] between $\boldsymbol{p}$ and $\boldsymbol{r}$ does not hold, and the calculated circular dichroism depends on the origin chosen.

For many calculations the origin is mostly conveniently chosen at the centre of mass. Translational motion is then uncoupled, and rotational averages of transition rates for randomly oriented molecules, calculated for this origin, can be compared with experimental values.

The minimal coupling Hamiltonian and origin dependence

The problem of origin-dependence in calculated quantities may be analysed within a broader frame, including the radiation field as well as the molecule. Origin-dependence is then a property of observables such as transition rate, instead of molecular properties such as multipole moments. In the minimal coupling formalism, the total Hamiltonian may be partitioned as

$$[58] \quad H = H_{\mathrm{mol}} + H_{\mathrm{rad}} + H_{\mathrm{int}}$$

where H_{mol} and H_{rad} are the molecule and radiation Hamiltonians and the radiation-molecule coupling H_{int}, correct to order e, is

$$[59] \quad H_{\mathrm{int}} = \sum_{\alpha} (e_\alpha/m_\alpha)\boldsymbol{p}_\alpha \cdot \boldsymbol{a}(\boldsymbol{q}_\alpha)$$

In [59] $\boldsymbol{p}_\alpha$ is the momentum of the αth particle with charge e_α, and $\boldsymbol{a}(\boldsymbol{q}_\alpha)$ is the vector potential at the particle position $\boldsymbol{q}_\alpha$. The matrix element for the transition $n \leftarrow 0$ is found, by the standard procedure (10, 11)

$$[60] \quad M_{n0} = (\hbar/2\epsilon_0 ckV)^{1/2} \sum_{\alpha} (e_\alpha/m_\alpha)\boldsymbol{e}\cdot\langle n|\boldsymbol{p}_\alpha \exp(i\boldsymbol{k}\cdot\boldsymbol{q}_\alpha)|0\rangle$$

where $\boldsymbol{k}$ is the wavevector of the incident photon resonant with the transition frequency,

$$[61] \quad \omega = ck = (E_n - E_0)/\hbar$$

and $\boldsymbol{e}$ is the photon polarization vector.

For many calculations it is sufficient to retain the leading term of [60] found by expanding the exponential term. Retention of this term only corresponds to treating the vector potential as uniform over the molecule; it is the electric dipole term and evidently origin-independent. However, for calculation of quantities such as the differential absorption rates, it is necessary to retain the following term containing the first derivative of the vector potential. This adds the electric quadrupole and the magnetic dipole terms in the multipolar formalism. The matrix element to this order is

$$[62] \quad M_{n0} = (\hbar/2\epsilon_0 ckV)^{1/2} \sum_{\alpha} (e_\alpha/m_\alpha)e_i\{p^{n0}_{i(\alpha)} + ik_j(p_{i(\alpha)}q_{j(\alpha)})^{n0}\}$$

From the Fermi rule, it follows that the absorption rate Γ is proportional to the modulus square of the matrix element, so that the correction to the pure electric dipole contribution is

$$[63] \quad \Delta\Gamma \propto \bar{e}_i e_j \bar{p}^{n0}_i (p_j q_k)^{n0} k_k - e_i \bar{e}_j p^{n0}_i \overline{(p_j q_k)}^{n0} k_k$$

In [63] the summation over the charges is implicit. The correction term arises from the interference between the pure electric dipole term and the electric quadrupole and the magnetic dipole terms. Suppose we displace the origin by $-\boldsymbol{\rho}$ so that $\boldsymbol{q} \rightarrow \boldsymbol{q} + \boldsymbol{\rho}$. Then the change ΔΓ is proportional to

$$[64] \quad \bar{e}_i e_j \bar{p}^{n0}_i p^{n0}_j \rho_k k_k - e_i \bar{e}_j p^{n0}_i \bar{p}^{n0}_j \rho_k k_k$$

which is clearly zero, as may be seen by interchanging the indices i and j in one of the terms. Thus the transition rate to this order is origin-independent and the result holds for any basis functions, exact or approximate.

A similar analysis within the multipolar framework leads to the result that observables such as absorption rates are, in general, origin-dependent if approximate wavefunctions are used for the calculations. With exact wavefunctions the rates are origin-independent. To illustrate the origin-dependence with approximate wavefunctions, we consider circular dichroism which is proportional to the rotational strength R^{n0} for a randomly oriented system. Recalling that

$$[65] \quad R^{n0} = \mathrm{Im}\, \boldsymbol{\mu}^{0n}\cdot\boldsymbol{m}^{n0} = \frac{e^2}{2m}\,\mathrm{Im}\,\langle 0|\boldsymbol{r}|n\rangle\cdot\langle n|\boldsymbol{r}\times\boldsymbol{p}|0\rangle$$

a change of origin by $\boldsymbol{\rho}$ gives rise to the additional term

$$[66] \quad \frac{e^2}{2m}\,\mathrm{Im}\,\langle 0|\boldsymbol{r}|n\rangle\cdot\langle n|\boldsymbol{\rho}\times\boldsymbol{p}|0\rangle$$

To keep the arguments simple, it is assumed that the wavefunction for the ground state is exact and that for the excited state is approximate. The excited state wavefunction can be expanded according to [67]

$$[67] \quad |\phi_n\rangle = \sum_m c_m|m\rangle$$

where $|m\rangle$ are the eigenfunctions of H_{mol}. Then the ρ-dependent term [66] becomes

$$[68] \quad \frac{e^2}{2m}\,\mathrm{Im} \sum_{m,m'} c_m c_{m'} \boldsymbol{r}^{0m}\cdot(\boldsymbol{\rho}\times\boldsymbol{p}^{m'0})$$

using the identity [53], the above term can be re-written as

$$[69] \quad \frac{e^2}{2\hbar}\boldsymbol{\rho}\cdot\sum_{m,m'} c_m c_{m'} E_{m'0}\boldsymbol{r}^{0m}\times\boldsymbol{r}^{m'0} = -\frac{e^2}{4\hbar}\boldsymbol{\rho}\cdot\sum_{m,m'} c_m c_{m'}(E_{m'0} - E_{m0})\boldsymbol{r}^{0m}\times\boldsymbol{r}^{m'0}$$

which is not necessarily zero, thus demonstrating the origin dependence of rotational strength calculated using approximate wavefunctions.

1. C. SANDORFY. Top. Current Chem. **120**, 42 (1984).
2. M. BORN and J. R. OPPENHEIMER. Ann. Phys. **84**, 457 (1927).
3. W. KOLOS and L. WOLNIEWICZ. J. Chem. Phys. **49**, 404 (1968).
4. D. M. BISHOP and L. M. CHEUNG. Adv. Quantum Chem. **12**, 1 (1980).
5. L. LATHOUWERS and P. VAN LEUVEN. Chem. Phys. Lett. **67**, 436 (1979).
6. F. T. SMITH. Phys. Rev. **179**, 111 (1969).
7. M. BORN. Gott. Nachr. Math. Phys. Kl, 1 (1951).
8. M. BORN and K. HUANG. Dynamical theory of crystal lattices. Oxford University Press. 1954.
9. D. P. CRAIG. and T. THIRUNAMACHANDRAN. Mol. Phys. **35**, 825 (1978).
10. D. P. CRAIG and T. THIRUNAMACHANDRAN. Adv. Quantum Chem. **16**, 97 (1982).
11. D. P. CRAIG and T. THIRUNAMACHANDRAN. Molecular quantum electrodynamics. Academic Press. 1984.
12. G. HERZBERG and E. TELLER. Z. Phys. Chem. **21**, 410 (1933).

Adsorption of carbon monoxide on the surfaces of polycrystalline transition metals and alloys: electron energy loss and ultraviolet photoelectron spectral studies[1]

C. N. R. RAO,[2] P. VISHNU KAMATH, K. PRABHAKARAN, AND M. S. HEGDE

Solid State and Structural Chemistry Unit, Indian Institute of Science, Bangalore – 560012, India

Received August 24, 1984

This paper is dedicated to Professor Camille Sandorfy on the occasion of his 65th birthday

C. N. R. RAO, P. VISHNU KAMATH, K. PRABHAKARAN, and M. S. HEGDE. Can. J. Chem. **63**, 1780 (1985).

Adsorption of CO has been investigated on the surfaces of polycrystalline transition metals as well as alloys by employing electron energy loss spectroscopy (eels) and ultraviolet photoelectron spectroscopy (ups). CO adsorbs on polycrystalline transition metal surfaces with a multiplicity of sites, each being associated with a characteristic CO stretching frequency; the relative intensities vary with temperature as well as coverage. Whilst at low temperatures (80–120 K), low coordination sites are stabilized, the higher coordination sites are stabilized at higher temperatures (270–300 K). Adsorption on surfaces of polycrystalline alloys gives characteristic stretching frequencies due to the constituent metal sites. Alloying, however, causes a shift in the stretching frequencies, indicating the effect of the band structure on the nature of adsorption. The up spectra provide confirmatory evidence for the existence of separate metal sites in the alloys as well as for the high-temperature and low-temperature phases of adsorbed CO.

C. N. R. RAO, P. VISHNU KAMATH, K. PRABHAKARAN et M. S. HEGDE. Can. J. Chem. **63**, 1780 (1985).

Faisant appel à la spectroscopie par perte d'énergie électronique (spee) et à la spectroscopie photoélectronique ultraviolette (spu), on a étudié l'adsorption du CO sur des surfaces de métaux de transition polycristallins ainsi que sur des alliages. Le CO s'adsorbe sur les surfaces polycristallines des métaux de transition avec une multiplicité de sites et chacun est associé à une fréquence d'élongation du CO qui est caractéristique; les intensités relatives varient avec la température ainsi qu'avec le niveau de couverture. Alors qu'à basse température (80–120 K) les sites de basse coordination sont stabilisés, les sites de coordination plus élevée sont stabilisés à des températures plus élevées (270–300 K). L'adsorption sur des surfaces d'alliages polycristallins fournit des fréquences d'élongation caractéristiques qui sont dues aux sites métalliques qui les constituent. La formation d'alliages provoque toutefois un déplacement dans les fréquences d'élongation et la SPU fournit des données qui confirment l'existence de sites métalliques séparés dans les alliages ainsi que la présence de phases de haute ainsi que de basse températures pour l'adsorption du CO.

[Traduit par le journal]

Introduction

Adsorption of carbon monoxide on single crystal surfaces of transition metals has been investigated extensively by employing ultraviolet photoelectron spectroscopy (ups) and electron energy loss spectroscopy (eels) (1–5). We considered it most valuable to investigate the adsorption of CO on polycrystalline metal surfaces by employing eels and ups because of the similarity between polycrystalline surfaces and catalyst surfaces, and to compare the results with those obtained on single crystal surfaces. Since eels is especially sensitive to the geometry of the adsorption site, the study was expected to throw light on the available sites on polycrystalline surfaces. We have carried out studies on several transition metals including Mn, Fe, Co, Ni, Cu, Pd, Pt, and Ag in order to compare the reactivity of the metals with respect to CO. After having obtained the information on the multiplicity of sites on polycrystalline metal surfaces, we have examined the adsorption of CO on the surfaces of polycrystalline binary alloys of copper (Cu–Mn, Cu–Ni, and Cu–Pd) in order to compare the behaviour with that on pure metal surfaces. The study of adsorption on binary alloys is expected to be of relevance to the behaviour of bimetallic catalysts.

Band structure of alloys is a subject of great interest and has been investigated widely by employing photoelectron spectroscopy (6–8). These studies have shown that while the d-bands essentially behave as predicted by the coherent potential model, the s-bands mix and fall into a rigid band (9). The rigid band model has interesting consequences for the adsorption of molecules such as CO on alloy surfaces. Alloys composed of metals varying widely in their reactivities would be expected to show intermediate reactivities. The phenomenon of chemisorption can thus be a potential tool for understanding the electron states of alloys. It was our interest to explore whether the reactivities of alloy surfaces could be designed to lie in between those of the constituent metal surfaces, and also to determine in what way the alloy reactivity depends on the alloy composition.

Experimental

All electron spectroscopic measurements were performed on the ESCA III Mark 2 and VG ESCALAB - EELS spectrometers of V.G. Scientific Ltd., England. Both the spectrometers are fitted with sample preparation chambers and independent gas handling systems for carrying out adsorption studies. The spectrometers have been described elsewhere (10, 11).

Polycrystalline foils of metals and their alloys were mounted on special temperature-variable probes and cleaned by etching with argon ions. At no time was the temperature of the sample allowed to go beyond 500 K. The X-ray photoelectron signals of the various impurity levels were monitored using AlKα radiation ($h\nu$ = 1486.6 eV) to ensure sample purity.

High purity CO gas was introduced into the chamber using precision leak valves and exposures were measured in Langmuirs (L) (1 Langmuir = 10^6 Torr-s; 1 Torr = 133.3 Pa).

It is well known that the surface composition of alloys varies greatly from the bulk composition due to surface segregation on annealing at high temperatures. The sample temperature was therefore not allowed to go beyond 500 K. The metal core levels in the alloys were carefully

[1] Contribution No. 268 from the Solid State and Structural Chemistry Unit.

[2] Author to whom all correspondence should be addressed.

TABLE 1. Bulk and surface composition of the alloys[a]

Alloy	Nominal (bulk) composition atom percentage	Surface composition atom percentage
Cu–Pd	8.9 Pd	9 Pd
Cu–Pd	24.6 Pd	25 Pd
Cu–Pd	50 Pd	49 Pd
Cu–Mn	25 Mn	11.3 Mn
Cu–Ni	80 Ni	75 Ni
Cu–Ni	40 Ni	42 Ni

[a]Sample temperatures were generally below 500 K and no alloy was annealed at higher temperatures.

monitored in the XPS, throughout the experiment, to characterize the surface composition. The surface compositions were calculated by employing the method described in the literature (12, 13) and, in Table 1, we show the nominal (bulk) and surface compositions of the alloys studied by us. It was found that etching did not alter the surface composition significantly. Throughout the text, we have shown only the nominal compositions.

The loss peak arising from the CO stretching vibration was decomposed into component peaks, each having a line shape identical to the shape of the elastic peak, by using a least-squares fit. The component spectra were shifted with respect to one another until the best fit between the recorded spectrum and the constructed spectrum was obtained. We have found loss peaks as narrow as the elastic peaks on some metal surfaces, where invariably a single species is present. We have illustrated one such instance in Fig. 1.

A similar treatment of the peak arising from the metal–C stretching vibration could not be carried out, due to its close proximity to the elastic peak.

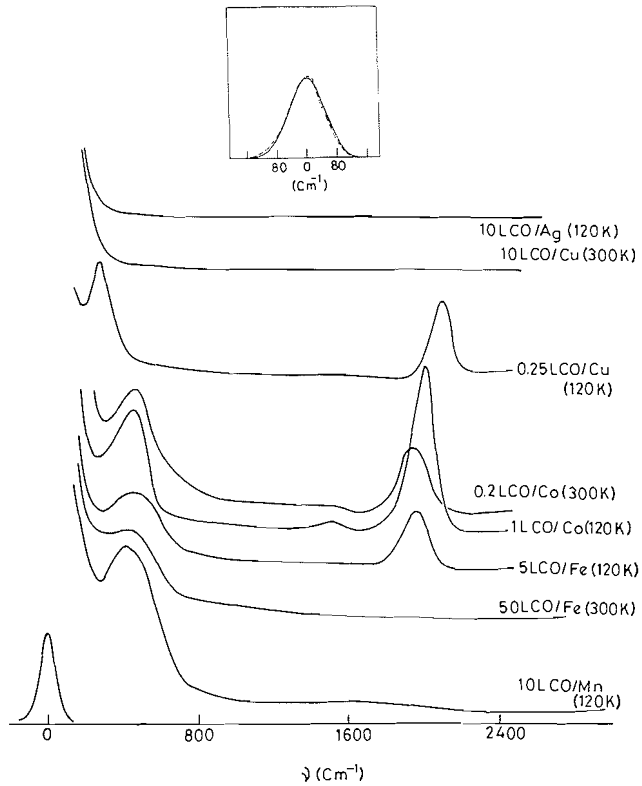

FIG. 1. Typical eel spectra of CO adsorbed on a series of first row transition metal surfaces. In the inset is shown a comparison of the elastic peak (full line) and the loss peak (dashed line) in the case of CO adsorbed on Cu (50 L) to illustrate that the two have an identical line shape.

Results and discussion

Adsorption of CO on polycrystalline metal surfaces by electron energy loss spectroscopy

Adsorption of CO on single crystal transition metal surfaces has been studied extensively and these results have been reviewed in the literature (14). The eels of chemisorbed CO shows two characteristic vibration frequencies due to the metal–carbon and the carbon–oxygen bond stretching modes. The appearance of the latter in eels suggests that the CO axis may be nearly perpendicular to the metal surface (15) as indeed established by LEED and other studies (16, 17).

CO binds to the metal site through its 5σ non-bonding orbital, while at the same time the metal back-donates substantial electron density into the 2π* level (18). This back-donation lowers the bond order in adsorbed CO, leading to a decreased stretching frequency. Depending on the strength of the metal–CO interaction, the CO stretching frequency lies in the ranges 1992–2110 cm^{-1}, 1850–1970 cm^{-1}, 1650–1850 cm^{-1}. Sheppard and Nguyen (19) have assigned these frequencies to CO in the linear, B_2 bridged, and B_4 bridged species. At step and kink sites, values of CO stretching frequencies as low as 1530 cm^{-1} are found (20). These values correspond well with those of the analogous transition metal complexes.

While the CO bond stretching frequency is known to vary with the change in the adsorption site, variation between the different single crystal surfaces is rather small for the same given site. Thus, while the B_2 bridged site and the linear on-top site show CO stretching frequencies of 1927 and 2064 cm^{-1} respectively on a Ni(100) surface (15), the B_2 bridged site on a Ni(111) surface shows a frequency of 1911 cm^{-1} (21). This shows that the effect of the surface structure of the adsorbent is secondary in nature. Similar conclusions have been derived by Broden *et al.* (23) in their systematic studies of the heats of adsorption of CO on transition metals.

In Fig. 1 we show typical eel spectra of CO adsorbed on a series of polycrystalline transition metal surfaces. The loss peaks are generally much broader than the elastic peaks in all cases, suggesting the existence of a multiplicity of adsorbed CO species on the polycrystalline metal surfaces. We have therefore decomposed the loss peak due to the CO stretch into several components in each case and the results of these analyses are summarized in Table 2. The loss peaks shift on increasing exposure, indicating the existence of strong lateral interactions in the adsorbate layer.

Polycrystalline Mn surfaces are extremely reactive to the adsorption of CO, on account of the very high enthalpy of formation of MnO and MnC (22). Accordingly, CO undergoes dissociative chemisorption on Mn at all temperatures ranging from 120–300 K and eel spectra show only a single loss peak in the low-energy range, corresponding to the Mn—O and Mn—C stretching frequencies.

Iron lies close to the border line (in the periodic table) separating metals which exhibit molecular adsorption of CO from those that exhibit dissociative adsorption (23). Consequently the behaviour of Fe is ambivalent and it adsorbs CO dissociatively at 300 K and molecularly at 120 K. In the low-temperature phase, the peak due to CO stretch is 60% broader than the elastic peak over the entire range of exposures, with a pronounced asymmetry on the lower-energy side. Decomposition of this peak into three distinct components yields the

TABLE 2. Stretching frequencies of CO adsorbed on polycrystalline transition metal surfaces[a]

Metal	Temp (K)	ν(M—C) (cm^{-1})	ν(CO) (cm^{-1})
Mn	120	419	—
	300	419	—
Fe	120	483	1790; 1895; 1967(1846,1935,2008)
	300	387	
Co	120	483(451)	1895; 1967; 2024(1863,1967,2040)
	300	451(387)	1846; 1951; 2016(1871,1975,2072)
Ni	120	354(370)	1790; 1927; 2092
	300	451(322)	1887; 2024(1967)
Cu	120	274(258)	2056; 2096(2096)
	300	—	—
Pd	120	322	1846; 1943; 2000; 2080
	300	290	1838; 1935; 2000
Pt	120	435	2080(1887,2096)
	300	451(419)	2064(1871,2080)
Ag	120	—	—
	300	—	—

[a]Values in parentheses are at high exposures.

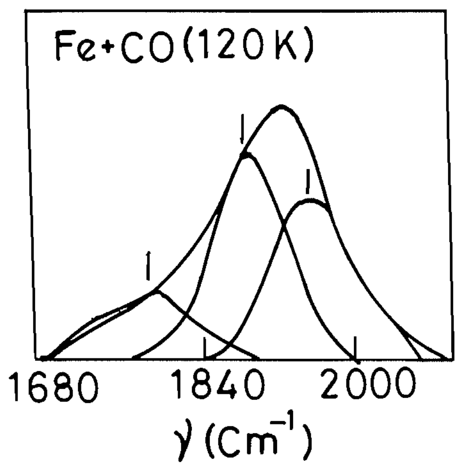

FIG. 2. CO stretching bands in eels of CO adsorbed on Fe along with the component peaks.

best fit between the recorded and the constructed spectra (Fig. 2); the three stretching frequencies at 1790, 1895, and 1967 cm^{-1} can be assigned to the B_4, B_2, and on-top linear species respectively. These frequencies progressively shift to 1846, 1935, and 2008 cm^{-1}, with increasing exposure (up to 60 L). These shifts could be due to adsorbate–adsorbate interaction. The nature of the species essentially remains unchanged. The 1895 cm^{-1} peak is about 47% in intensity over the whole range of exposures. The on-top linear species gains marginally in intensity at the expense of the B_4 species on increasing the exposure.

Cobalt exhibits molecular chemisorption of CO over the entire range of temperatures from 120–300 K. The nature of the species and their relative intensities, however, are different at 120 K and 300 K. At 120 K, we can discern three species with CO stretching frequencies at 1863, 1967, and 2040 cm^{-1}; the last of these, corresponding to the on-top linearly adsorbed species, grows rapidly with exposure to become the predominant species. At 300 K, the three peaks appear at 1822–1887, 1951, and 2016 cm^{-1}; with increasing exposure, the species at 1951 cm^{-1} grows in intensity at the expense of the species at 2016 cm^{-1}. The former is clearly due to the B_2 bridged CO while the latter is due to the linear on-top CO. While the on-top linear CO is the stable species at low temperatures (up to 120 K), the B_2 site appears to be the preferred site at 300 K.

CO adsorption on polycrystalline Ni shows characteristics identical to those on single crystal Ni surfaces (15). At low temperature (120 K), we see two stretching frequencies at 1927 and 2092 cm^{-1}, respectively, due to the B_2 bridged and linear on-top adsorption sites. In addition, a peak of low intensity is seen at 1790 cm^{-1}, which can be assigned to a CO bound to a higher coordination site. However, at 273 K, we do not see any CO stretch below 1800 cm^{-1}. At very low exposures (<1 L), we see two distinct peaks at 1887 and 2024 cm^{-1}. These two, however, merge at higher exposures to give a single broad peak with its maximum centred at 1967 cm^{-1}. This change has been attributed to a surface phase transition in adsorbed CO, in which a compression of the adsorbed layer lattice occurs (15).

Copper exhibits molecular chemisorption of CO at low temperatures (120–200 K) while at 300 K, even after prolonged exposure, no ad-layer pick-up is seen (Fig. 1). In the low-temperature phase, the peak due to the CO stretch is 20% broader than the elastic peak below 10 L exposure. The peak, however, gets progressively narrower and becomes as narrow as the elastic peak beyond 50 L; there is, however, no significant change in the peak position. We therefore sought to decompose the peaks at low exposures into two component peaks (see Fig. 3a); the decomposition yields two peaks at 2056 cm^{-1} and 2096 cm^{-1}, the intensity of the former progressively decreasing with increasing exposure. Clearly, at low exposures the presence of a large number of vacant sites permits the adsorption of CO in more than one geometry. On increasing the exposure, however, one of the species grows at the expense of the other (Fig. 3b).

CO adsorbs molecularly on Pd over the 120–300 K range forming a number of species. While the spectra at 300 K can be decomposed into three component peaks, spectra at 120 K show the existence of four peaks. The predominant peak at 300 K appears at 1935 cm^{-1}, having 50–60% of the total intensity, while the predominant peak at 120 K appears at 2000 cm^{-1}. The 1935 cm^{-1} peak is due to bridged B_2 CO, while the 2000 cm^{-1} peak is due to on-top linear CO. The low-temperature phase shows the existence of yet another weakly bound termi-

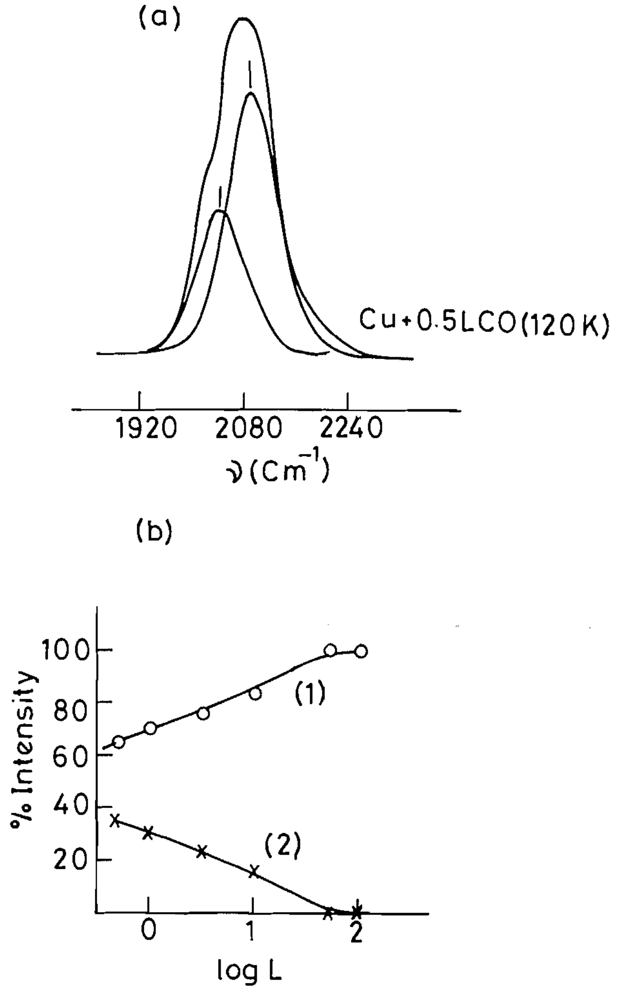

FIG. 3. (a) The eels of CO adsorbed on Cu showing the two-component peaks. (b) Variation of the intensity of the two-component peaks (expressed as a percentage of the total intensity) with exposure (in Langmuirs). Curve (1) is for the 2096 cm^{-1} peak and curve (2) is for the 2056 cm^{-1} peak.

nal CO at 2080 cm^{-1}, which is absent in the spectra recorded at 300 K. The predominant species in the 300 K spectra appears as the second most intense peak in the low-temperature spectra. The B_3 bridged CO at 1838 cm^{-1} appears with 11–25% intensity in the 300 K spectra, while at low temperature its intensity is ~10% of the total intensity. These observations indicate that at low temperatures the lower-coordination species are preferred, while at higher temperatures the higher-coordination species are preferred.

Pt also adsorbs CO molecularly at all temperatures from 120–300 K. At low exposures (<0.1 L at 300 K and <0.5 L at 150 K), we see a single sharp peak at 2064 cm^{-1}. On going to higher exposures, a second CO stretching peak at 1870 cm^{-1} appears. But the relative proportions of the two peaks remain unchanged on further exposure up to 1000 L. These two peaks can be readily assigned to the on-top linear (2064 cm^{-1}) and the B_2 bridge site (1871 cm^{-1}) adsorption respectively (Fig. 4). The proportion of the bridged site species is approximately 10% at 300 K and 16% at 150 K over a wide range of exposures.

Ag does not show any ad-layer pick-up, even on prolonged exposure to CO over the entire temperature range of 80–300 K. However, physisorption of CO seems to occur on Ag at temperatures below 50 K (24).

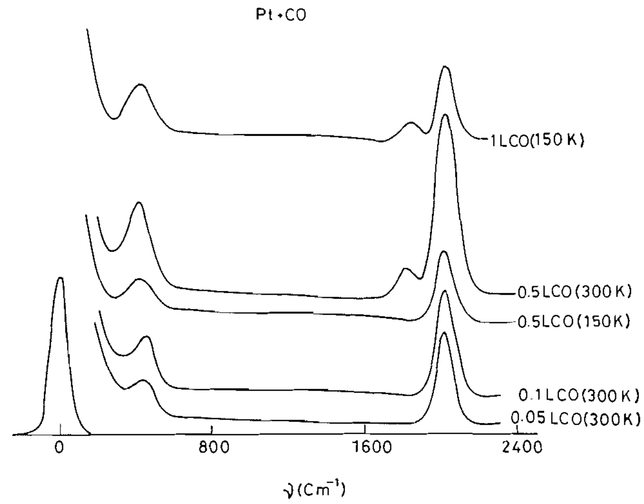

FIG. 4. The eel spectrum of CO adsorbed on polycrystalline Pt.

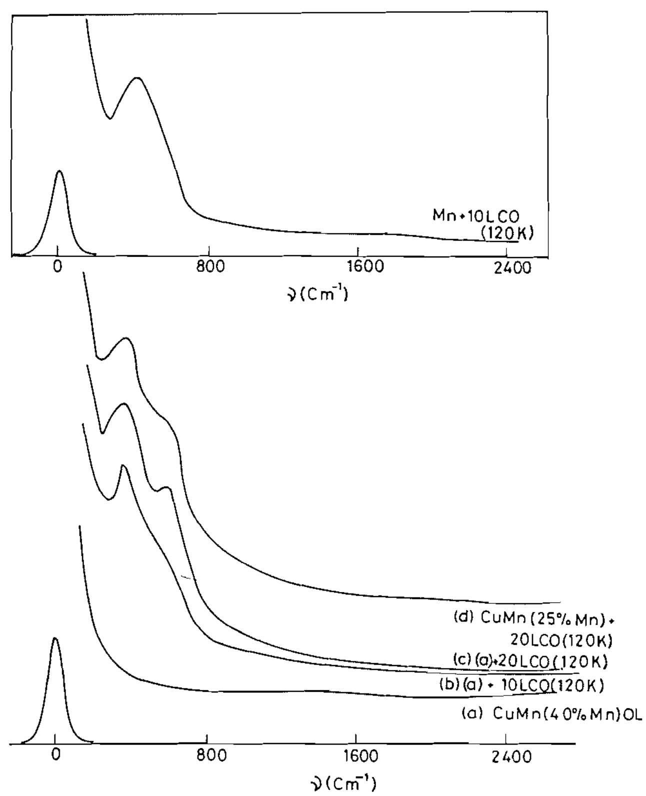

FIG. 5. The eel spectra of CO adsorbed on CuMn alloy surfaces. Inset shows the eel spectrum of CO adsorbed on polycrystalline Mn.

These studies of the adsorption of CO on polycrystalline metal surfaces suggest that the metal reactivity with respect to adsorption of CO varies in the order Mn ≈ Fe (300 K) > Fe (120 K) ≈ Co ≈ Ni ≈ Cu (120 K) > Cu (300 K) ≈ Ag. At one end we see dissociative chemisorption, while at the other end we see no chemisorption. We therefore thought it instructive to study the adsorption of CO on binary alloys of metals widely varying in their reactivities and also in the nature of adsorbed species they stabilize.

Adsorption of CO on polycrystalline alloy surfaces by electron energy loss spectroscopy

The eel spectrum of CO adsorbed on Cu–Mn alloys with

TABLE 3. Stretching frequencies for CO adsorbed on copper alloys

Alloy	Temp (K)	ν(M—C) (cm^{-1})	ν(CO) (cm^{-1})
CuMn(25% Mn)	120	371; 596	—
CuMn(40% Mn)	120	371; 596	—
CuPd(9% Pd)	120	435	2032(1887,2056)[a]
	300	—	—
CuPd(49% Pd)	120	306	1927; 2096
	300	338	1911; 2056
CuNi(80% Ni)	300	322	1854; 2032(1814,1935,2088)

[a] Values in parentheses are peak positions observed at high exposures.

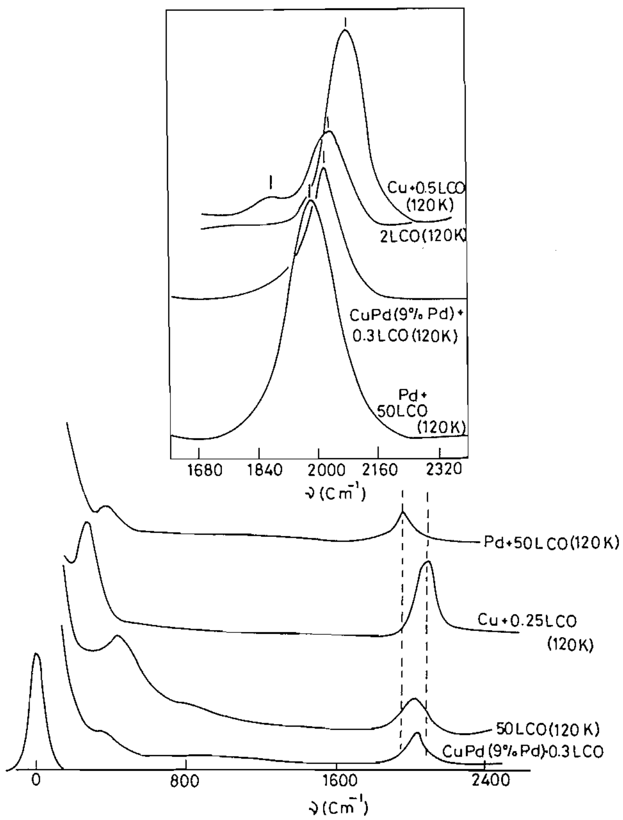

FIG. 6. The eel spectra of CO adsorbed on polycrystalline CuPd (9% Pd). Inset shows the peak due to the CO stretch. Vertical lines mark the peak positions.

25% Mn and 40% Mn are shown in Fig. 5. Two peaks at 371 cm^{-1} and 596 cm^{-1} can be seen and there are no peaks in the energy range 1700–2100 cm^{-1}. These two can be assigned to the metal–C and metal–O stretches of the mixed carbide–oxide layer arising from the dissociative chemisorption of CO on the alloy.

CO adsorbed on Cu–Ni alloys shows peaks at 1814, 1935, and 2088 cm^{-1} (Table 3), similar to those seen on Ni at low temperature (120 K). However, unlike those on pure Ni, the peaks do not merge at high exposures to give a single broad peak. It appears as though the Ni sites in Cu–Ni alloys are considerably different from those on pure Ni surface. Thus they exhibit features which are essentially those of Ni at low temperatures even at 273 K. It is, however, not clear if the Cu sites show adsorption at 273 K, for any such adsorption would lead to a peak at 2096 cm^{-1} (which cannot be explicitly resolved). The peak at 2088 cm^{-1}, however, has a much higher relative intensity in Cu–Ni alloys than in pure Ni, suggesting that the extra intensity could arise from the species adsorbed on the Cu sites of the alloy. We believe that the substantial changes found with the Cu–Ni alloys (compared to the parent metals) cannot be brought about by one of the metals merely acting as a spacer; this is particularly so in the Ni-rich alloys.

$Cu_{0.91}Pd_{0.09}$ does not show any ad-layer even after prolonged exposure to CO at 273 K. However, at lower temperatures (120 K), it shows a single peak at 2030 cm^{-1} at low exposures and two peaks at 1887 and 2056 cm^{-1} at higher exposures (Fig. 6). These two peaks can be attributed to CO stretching vibrations arising from the CO bonded to the Pd and the Cu sites respectively. As mentioned earlier, we observe two kinds of linearly adsorbed CO species on the surface of pure Cu, with stretching frequencies of 2056 and 2096 cm^{-1}. In $Cu_{0.91}Pd_{0.09}$ alloy, although the Cu and Pd sites remain distinct, it is the 2056 cm^{-1} species that is stabilized. This is indicative of a certain degree of mixing of the Cu and Pd bands on alloying. The Pd site shows a peak at 1887 cm^{-1}, which is different from those seen on pure Pd (Table 3).

In $Cu_{0.51}Pd_{0.49}$, low-temperature (120 K) adsorption gives rise to peaks at 1927 and 2096 cm^{-1}, probably due to CO adsorbed on Pd and Cu sites, respectively. At 273 K, there is a shift of the 2096 cm^{-1} peak to 2056 cm^{-1}, the latter corresponding to the peak found on Cu at low exposures (Fig. 7). It is noteworthy that on pure Cu there is no adsorption at 273 K.

Ultraviolet photoelectron spectra of CO adsorbed on polycrystalline metals and alloys

The up spectra of adsorbed CO generally consist of two peaks arising from the ($5\sigma + 1\pi$) and 4σ levels. This has been described in detail elsewhere (25). While CO adsorbed on Pd and Ni exhibits the characteristic two-peak spectrum in ups, CO adsorbed on Cu shows a complicated structure (Fig. 8) similar to that described by other workers (26). This distinct difference in the up spectra of CO adsorbed on Cu and other transition metals makes the study of CO adsorption on alloys feasible (Table 4).

The up spectrum of CO adsorbed on Cu–Mn alloys shows only one prominent peak at 6 eV below the Fermi level. Such a spectrum is characteristic of photoionization from the O(2p) level of atomic oxygen. This clearly shows that CO adsorbs dissociatively on the CuMn alloy surfaces (as also shown by eels); Cu–Mn alloys behave essentially like pure Mn, even in Cu-rich compositions.

The case of Cu–Pd alloys is more interesting. In Fig. 9 we show the up spectra of CO adsorbed on $Cu_{0.91}Pd_{0.09}$. At low exposures at 100 K we see the two-peak structure characteristic of CO adsorbed on Pd sites, although the peaks are substantially broader than on pure Pd (27). On increasing the exposure, the spectrum becomes more complicated, like that of Cu. This is understandable from the point of view of metal reactivity to

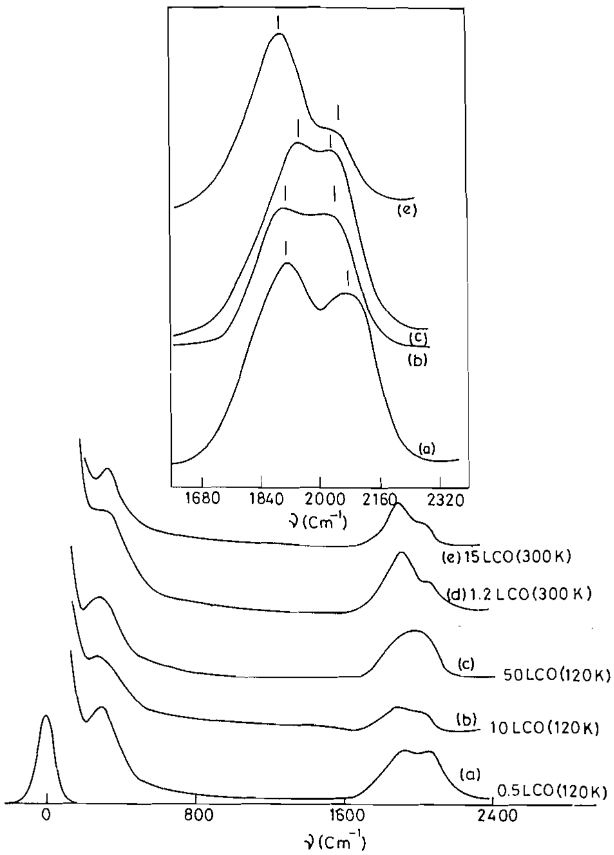

FIG. 7. The eel spectra of CO adsorbed on polycrystalline CuPd (49% Pd). Inset shows the peak due to CO stretch. Vertical lines mark the peak positions.

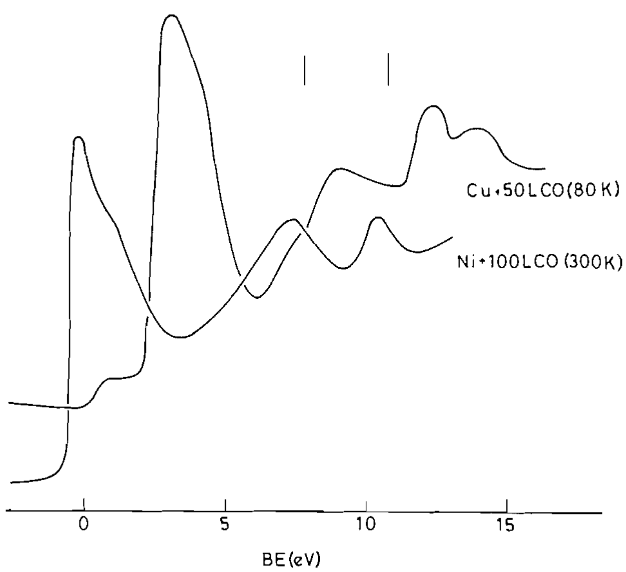

FIG. 8. Typical HeII spectra of CO adsorbed on polycrystalline Cu and Ni. Vertical lines in the figure mark the peak positions of CO adsorbed on polycrystalline Pd (ref. 27).

CO. Pd, being more reactive, gets covered first, the Cu sites being occupied only at higher exposures. On heating the alloy surface to 200 K, the spectral features revert to those found on the Pd surface. The high-temperature spectrum is much narrower and is shifted to lower energies. Such differences in the high-temperature and low-temperature phases have been observed earlier on $Cu_{0.08}Ni_{0.92}$ alloy (28) and can be attributed to adsorbate–adsorbate interactions. At 300 K, $Cu_{0.91}Pd_{0.09}$ does not show any CO pick-up, like Cu, while pure Pd metal adsorbs CO at room temperature.

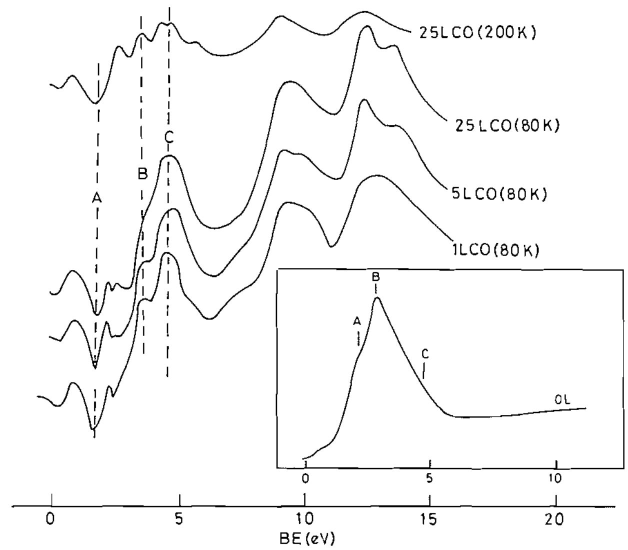

FIG. 9. Typical difference spectra for CO adsorbed on CuPd (9% Pd). For a description of the features marked A, B, and C, see the text.

TABLE 4. Electron states (in eV) of CO adsorbed on alloys[a]

Alloy			$(5\sigma + 1\pi)$	4σ
CuPd(9% Pd)	(80 K)	4.7(4.7)	9.5(9.5)	13(12.5; 13.9)
	(200 K)	—	9.2	12.5
CuPd(25% Pd)	(80 K)	5.0	9.5	12.6
	(272 K)	5.1	8.9	11.8
CuNi(40% Ni)	(80 K)	4.7(4.7)	9.4(9.4)	12.6(12.2; 14.4)
	(200 K)	—	8.6	11.8
CuNi(80% Ni)	(80 K)	4.6	9.2	12.6
	(300 K)	—	8.6	11.7
CuMn(25% Mn)	(80 K)	—	8.5	—

[a]The features around 5 eV may be due to a level derived from the 5σ (CO) or a metal d $\pm$ $2\pi^*$ (CO) level.

The region of the spectrum in the energy range 0–5 eV is extremely interesting. The valence band of clean $Cu_{0.91}Pd_{0.09}$ alloy shows a new feature A, in addition to the s-band and d-band of pure Cu; the latter is marked B in Fig. 9. Feature A is clearly the contribution of Pd to the alloy valence band. On exposing the clean surface to CO, an additional feature marked C grows on the higher binding energy side of the alloy valence band. These peak shape changes are exemplified in the difference spectra shown in Fig. 9. The region A, where Pd contributes to the alloy valence band, clearly shows a depletion in electron density, while the region B clearly shows substantial remnant d-band electron density. The feature C appearing at ~4.8 eV is intense. We can conclude from these changes that the Pd sites are mainly responsible for electron transfer from the alloy to the adsorbed CO molecule. While it is possible that the feature C could be due to a 5σ-metal (d) derived level, we cannot preclude the possibility of its arising rom $\psi_{metal} \pm \psi_{2\pi^*(CO)}$ type of levels, which are expected to lie close to the Fermi level (29, 30). The nature of the spectrum remains essentially unchanged in the high-temperature phases of adsorbed

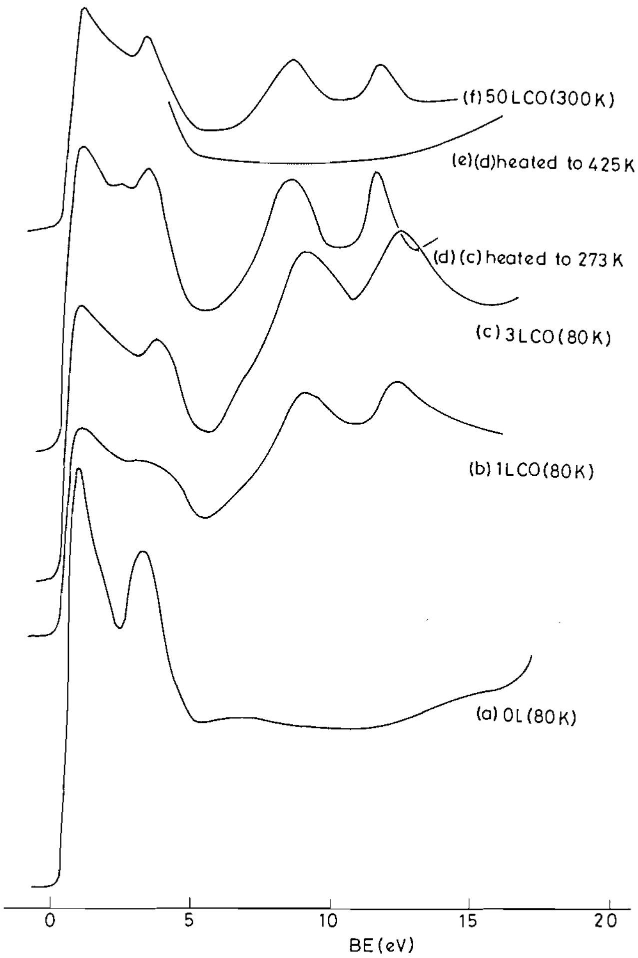

FIG. 10. Typical HeII spectra of CO adsorbed on polycrystalline CuNi (80% Ni) alloy.

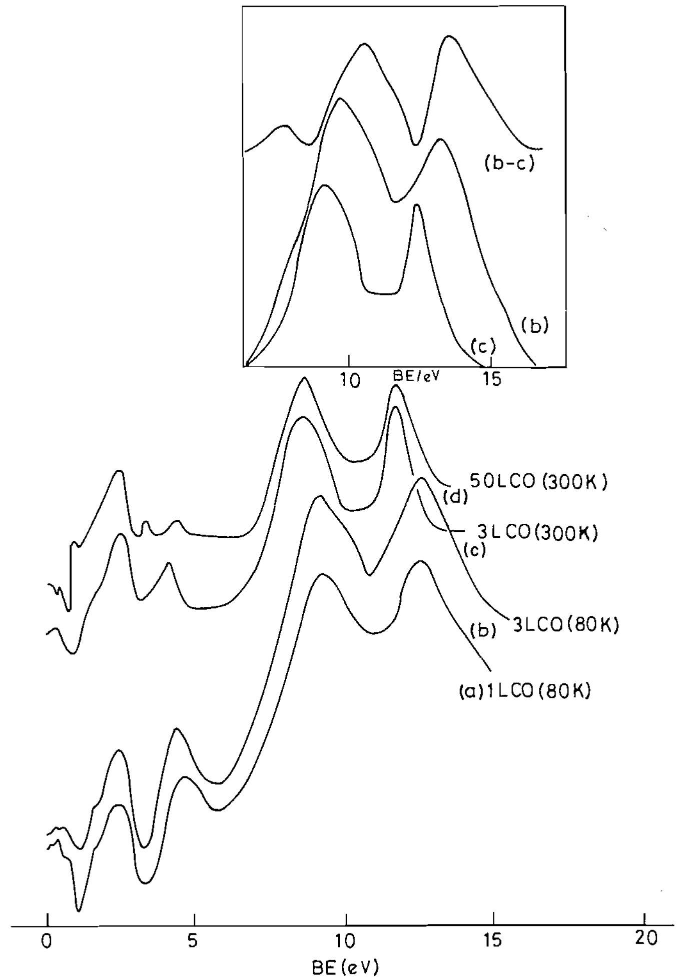

FIG. 11. Typical difference spectra for CO adsorbed on polycrystalline CuNi (80% Ni) alloy. Inset shows the spectra of low and high temperature phases of adsorbed CO.

CO, thus indicating that the nature of alloy–CO bonding also remains essentially unchanged.

In $Cu_{0.75}Pd_{0.25}$, adsorption characteristics of CO are identical to those seen in the case of pure Pd. There is, however, a small shift towards lower binding energy in the room temperature adsorbed phase compared to the low-temperature (80 K) adsorbed phase. The features in the 0–5 eV region remain similar to those observed in the case of $Cu_{0.91}Pd_{0.09}$ alloy.

$Cu_{0.60}Ni_{0.40}$ behaves similar to the $Cu_{0.91}Pd_{0.09}$ in that it shows a two-peak spectrum characteristic of CO adsorbed on the Ni sites at low exposures, while at higher exposures a complex spectrum similar to that found on Cu surface is seen. Warming the surface gives back the two-peak (Ni-like) spectrum, which is shifted to lower energies by nearly 1 eV.

$Cu_{0.20}Ni_{0.80}$ shows the two-peak spectrum characteristic of CO adsorbed on Ni at all exposures and over the entire 80–300 K range (see Fig. 10). There is, however, a 1-eV shift in the binding energies of the low- and high-temperature adsorbed phases, as in the case of the other alloys (see Fig. 11). The difference spectra with the Cu–Ni alloys show the existence of a third peak in the low-energy (0–5 eV) region similar to the one seen in the case of $Cu_{0.91}Pd_{0.09}$. The Ni d-band shows considerable depletion in electron density on adsorption of CO, showing thereby that Ni plays a role analogous to that of Pd in CuPd alloys.

Although eels shows the existence of several species in metals and alloys, ups seems to more clearly distinguish the different metal sites in alloys. The eels also provides information about the stereochemistry of the various adsorbed species.

Acknowledgement

The authors thank the Department of Science and Technology, Government of India, for support of this research.

1. A. M. BRADSHAW. Surf. Sci. **80**, 215 (1979).
2. T. E. MADEY, J. T. YATES, A. M. BRADSHAW, and F. M. HOFFMANN. Surf. Sci. **89**, 370 (1979).
3. K. KISHI and M. W. ROBERTS. J. Chem. Soc. Faraday Trans. 1, **71**, 1715 (1975).
4. G. ERTL, M. NEUMANN, and K. M. STREIT. Surf. Sci. **64**, 393 (1977).
5. H. CONRAD, G. ERTL, J. KOCH, and E. A. LATTA. Surf. Sci. **43**, 462 (1974).
6. J. C. FUGGLE, F. U. HILLEBRECHT, R. ZELLER, Z. ZOLNIEREK, P. A. BENNET, and CH. FREIBURG. Phys. Rev. B, **27**, 2145 (1982); **27**, 2179 (1982); **27**, 2194 (1982).
7. P. WEIGHTMAN and P. T. ANDREWS. J. Phys. C, **13**, L821 (1980).
8. P. WEIGHTMAN, P. T. ANDREWS, G. M. STOCKS, and H. WINTER. J. Phys. C, **16**, L81 (1983).
9. P. SEN, D. D. SARMA, and C. N. R. RAO. Pramana, **23**, 815 (1984).
10. C. N. R. RAO, D. D. SARMA, and M. S. HEGDE. Proc. R. Soc.

London Ser. A, **370**, 269 (1980).
11. D. D. SARMA and C. N. R. RAO. J. Electron Spectrosc. Rel. Phenom. **20**, 25 (1980).
12. C. J. POWELL and P. E. LARSON. Appl. Surf. Sci. **1**, 186 (1978).
13. M. S. HEGDE, T. S. SAMPATHKUMARAN, and R. M. MALLYA. Appl. Surf. Sci. **17**, 97 (1983).
14. C. N. R. RAO, A. SRINIVASAN, and K. JAGANNATHAN. Int. Rev. Phys. Chem. **1**, 45 (1981); N. SHEPPARD and J. ERKELENS. Appl. Spectrosc. **38**, 471 (1984).
15. S. ANDERSSON. Solid State Commun. **21**, 75 (1977).
16. S. ANDERSSON and J. B. PENDRY. Phys. Rev. Lett. **43**, 363 (1979).
17. C. L. ALLYN, T. GUSTAFSSON, and E. W. PLUMMER. Chem. Phys. Lett. **47**, 127 (1979); Solid State Commun. **28**, 85 (1978).
18. G. BLYHOLDER. J. Phys. Chem. **68**, 2772 (1964).
19. N. SHEPPARD and T. T. NGUYEN. Adv. Infrared Raman Spectrosc. **5**, 67 (1978).
20. W. ERLEY, H. IBACH, S. LEHWALD, and H. WAGNER. Surf. Sci. **83**, 585 (1979).
21. W. ERLEY, H. WAGNER, and H. IBACH. Surf. Sci. **80**, 612 (1979).
22. J. B. BENZIGER. Appl. Surf. Sci. **6**, 105 (1980).
23. G. BRODEN, T. N. RHODIN, C. BRUCKER, R. BENBOW, and Z. HURYCH. Surf. Sci. **59**, 593 (1976).
24. S. KRAUSE, C. MARIANI, K. C. PRINCE, and K. HORN. Surf. Sci. **138**, 305 (1984).
25. P. M. WILLIAMS, P. BUTCHER, J. WOOD, and K. JACOBI. Phys. Rev. B, **14**, 3215 (1976); R. MIRANDA, K. WANDELT, D. RIEGAR, and R. D. SCHNELL. Surf. Sci. **139**, 430 (1984); D. RIEGAR, R. D. SCHNELL, and W. STEINMANN. Surf. Sci. **143**, 157 (1984).
26. C. MARIANI, H. V. MIDDELMANN, M. IWAN, and K. HORN. Chem. Phys. Lett. **93**, 308 (1982).
27. H. LUTH, G. W. RUBLOFF, and W. D. GRORBMAN. Surf. Sci. **63**, 325 (1977).
28. D. T. LING and W. E. SPICER. Surf. Sci. **94**, 403 (1980).
29. P. V. KAMATH, D. D. SARMA, and C. N. R. RAO. Proc. Ind. Acad. Sci. **93**, 335 (1984).
30. S. ISHI and Y. ONO. Surf. Sci. **139**, L219 (1984).

Potentiel d'erreur et seconde quantification: application à la corrélation

ALEXANDRE LAFORGUE

Laboratoire de Mécanique Ondulatoire Appliquée, B.P. 347, Université de Reims, 51062 Reims Cedex, France

Reçu le 20 août 1984

Cet article est dédié au Professeur Camille Sandorfy à l'occasion de son 65[e] anniversaire

ALEXANDRE LAFORGUE. Can. J. Chem. **63**, 1788 (1985).

On soumet à un nouvel examen une méthode reposant sur le concept de potentiel d'erreur. La correction perturbative de l'erreur est analysée sur l'exemple de la corrélation. On peut substituer à un ensemble d'opérations dont le résultat ne peut être linéaire un opérateur de "perturbation corrective de l'erreur" indicé d'une configuration qui, lui, est linéaire dans tout l'espace des interactions. Sommant sur toutes les configurations, on parvient à un opérateur de correction linéarisée de l'erreur (Cle) indicé du rang de la correction et dont l'itération indéfinie réalise l'interaction de configuration complète, sans processus de diagonalisation. Une récurrence rapidement convergente permet la détermination de cet opérateur et son itération réalise un opérateur de corrélation adapté à toutes les configurations de la base. La seconde quantification permet de développer en polynomes de création–destruction tant la correction linéarisée de l'erreur que la corrélation globale. L'une et l'autre peuvent faire l'objet d'un développement en grappes. La matrice d'excitation apparait alors comme la somme d'une série de matrices calculables par perturbation.

ALEXANDRE LAFORGUE. Can. J. Chem. **63**, 1788 (1985).

We reexamine an error potential method. The so-called "perturbative error correction" is analysed on the pattern of the correlation problem. In the whole C.I. space the idea of a perturbation correction of each w.f., cannot lead to a linear operator. But a restriction of this process to the uncorrelated q-configurations only permits proposing a q-operator which is of linear form in the whole C.I. space. Summing over q we obtain a Cle$_r$ operator adapted to an r-repetitive method which performs the whole C.I. without diagonalization. On the other hand Cle$_r$ is determined by a rapidly convergent, recurrent process. Its r-times product has as a limit a correlation operator adapted to all the electronic configurations. Now, the second quantization formalism expands under a polynomial form both the cle$_r$ and the correlation operator. Both these operators can be expanded in clusters. Then the excitation matrix appears to be a sum of an infinite set of r-matrices which can be determined by an ordinary perturbation.

I. Introduction

I-1. *Historique*

J'ai rencontré Camille Sandorfy à Paris dès 1949 et il a guidé mes premiers pas dans les calculs de la chimie quantique. C'est pourquoi je voudrais consacrer cet article à un nouvel examen d'un sujet que j'ai développé à cette époque.

La théorie la plus séduisante était alors celle des chaînes organiques conjuguées (1) et des cycles aromatiques, où les approximations de Hückel en méthode des orbitales moléculaires donnent un accord étonnant avec l'expérience. Mais l'introduction des hétéroatomes étant un problème mal résolu, je tentais, comme beaucoup (2), de développer une extension cohérente (3–6). Dans notre cas, le concept d'approximations physiques successives corrigeant les contradictions du modèle (par exemple, modèration des moments polaires (7), ou, au contraire, apparition de moments polaires négligés en première approximation (8)) s'exprimait par l'emploi systèmatique de l'effet de charge (3), de l'effet de valence libre (4). Il conduisait à la recherche de l'erreur (9).

L'interaction de configuration (10–12) fournissait d'autre part un modèle intéressant de représentation de l'erreur (12–14). L'une des configurations en effet, largement dominante en général, peut être dite l'approximation non correllé et chacune des autres, si nombreuses soient-elles, n'est que l'une des composantes de l'erreur sur la fonction d'onde. Elle invite plus généralement encore à comparer toute approximation proposée à la solution rigoureuse (15).

I-2. *Potentiel d'erreur*

La notion introduite à cette fin est très simple et très générale (16–20). C'est le potentiel d'erreur que l'on doit ajouter au potentiel d'un système pour retrouver comme solution telle fonction approchée que l'on désire. Il est défini dans l'espace de configuration mais reçoit parfois une signification physique directe.

Ce potentiel permet soit l'analyse de l'erreur, soit sa correction (soit sur les structures, soit sur l'énergie) par des méthodes soit variationnelles soit perturbatives.

Une correction perturbative par le potentiel d'erreur attache à toute fonction d'onde une autre "meilleure", cette qualité étant précisée par le calcul de l'erreur à craindre sur les diverses grandeurs physiques. On est donc conduit à une correction indéfinie de l'erreur. Par exemple on résoud le problème de l'interaction de configuration, ce processus ayant pour effet de diagonaliser la matrice Hamiltonienne.

On imagine enfin des algorithmes élargissant le domaine de recherche au fur et à mesure que l'on progresse vers la solution optimale (21).

Les possibilités d'applications ne semblent pas limitées à un type étroit de problèmes. Le potentiel d'erreur intervient dans la compréhension des forces quantiques (20), dans la discussion de l'équation d'onde (21, 22), dans chacun des modes de construction des fonctions d'onde moléculaires.

Ainsi, les effets de charge et de valence libre étaient expliqués, les conséquences de l'interaction de configurations étaient interprétées, mais surtout on pouvait conclure qu'un problème essentiel de la chimie quantique était résolu: construire par des algorithmes répétitifs des fonctions d'onde s'approchant, autant qu'il est requis, de la solution exacte avec une incertitude calculable à l'avance sur une grandeur physique donnée.

I-3. *Discussion du potentiel d'erreur*

Or, trente ans plus tard, on constate que cette voie qui a pu séduire n'a pas été généralement suivie. Pourtant des formes particulières du potentiel d'erreur ont été retrouvées indépendamment par différents auteurs de 1960 à 1980: potentiel de fluctuation de Sinanoglu (23*a*); développements de Nesbet

(23b); méthodes d'interaction de configuration basées sur la théorie, telle M R D C I (23c) ou C I P S I (23d); théorie des paires d'electrons couplés de Cizek et Paldus (24a). D'autre part on assiste, dans la même période, au développement de la littérature sur le calcul d'erreur (voir par exemple la réf. 24b).

Enfin on peut citer, à l'actif de la théorie, des filiations avec les pseudo-potentiels (voir la réf. 24c), et plus généralement avec les Hamiltoniens effectifs, avec les techniques itératives de détermination des structures moléculaires, avec l'analyse d'une fonction d'onde en orbitales de recouvrement maximum (24d), sans parler de l'épistémologie de la chimie quantique.

Certes en 1954, le calcul électronique (sous une forme qui nous semble très archaïque) commençait tout juste à être mis en oeuvre en chimie quantique (3).

Mais je ne vois qu'une seule raison intrinsèque à la rareté d'utilisation de la théorie initiale: si nous envisageons, sous sa forme la plus directe, la perturbation corrigeant le potentiel d'erreur, *l'opérateur qui la représente globalement ne peut être linéaire*. Cette non-linéarité contrarie les formalismes mathématiques usuels, les habitudes de pensée, entraîne des difficultés pratiques.

I-4. *Objet de cet article*

Dans ce travail, nous essayons d'une part de surmonter cet obstacle, d'autre part de rattacher l'idée d'une correction perturbative de l'erreur au développement des méthodes de seconde quantification (24a, 25–27). Notre fil directeur sera la linéarisation de cet opérateur. Notre exemple privilégié sera celui de la corrélation.

On parvient d'abord à une formulation précise de cet opérateur implicite en se restreignant aux configurations pures, non correllées. Sommant sur ces configurations, on parviendra à un opérateur de "correction linéaire de l'erreur" (Cle). Une récurrence rapidement convergente détermine ces opérateurs.

Cet opérateur linéarisé s'exprime très directement dans les termes de la seconde quantification. Il en est de même du résultat d'une infinité d'itérations qui est un opérateur de corrélation adapté à toutes les configurations. L'un et l'autre pourront être développés en grappes (expanded in clusters). La matrice d'excitation apparaitra alors comme la somme d'une série de matrices attachées aux corrections successives. Ce nouvel accès aux méthodes de seconde quantification éclaire leur signification physique, semble permettre une nouvelle analyse de leurs résultats et de leurs extensions possibles, suggère une méthode alternative de calcul de la matrice d'excitation et donc des abaissements d'énergie.

II. Correction répétée du défaut de corrélation par perturbation

II-1. *Principe*

La chimie quantique construit fréquemment des fonctions non correllées. Il en résulte (17) un potentiel d'erreur. La correction perturbative de l'erreur représentée par ce potentiel, puis par les potentiels d'erreur successifs attachés aux fonctions de plus en plus correllées, constitue une méthode de correction indéfinie du défaut de corrélation.

Plus précisément, considérons un ensemble **U** d'orbitales moléculaires orthonormées l'ensemble $\{j\}$ des spinorbitales j correspondantes, l'ensemble $\{\phi\}$ des fonctions déterminants ϕ construites sur ces spinorbitales, l'ensemble des fonctions de configuration Γ construites sur ces déterminants et sous-tendant un espace $\mathscr{E}$. On peut indicer les Γ de $q = 0$ à $Q - 1$, selon les valeurs croissantes de l'intégrale

$$E_q = \langle \Gamma_q | \hat{H} | \Gamma_q \rangle$$

déduite de l'Hamiltonien $\hat{H}$. À chaque valeur de q correspond, souvent sans ambiguïté, un état propre $|\Lambda, q\rangle$ de $\hat{H}$ appartenant à une énergie propre W_q. La représentation $(\hat{H})$ de $\hat{H}$ dans $\mathscr{E}$ définit $|\Lambda^{\mathrm{IC}}, q\rangle$ et W_q^{IC} par interaction de configuration (IC) dite complète. La suite $|\Gamma, q\rangle$, E_q est l'approximation non correllée de la suite $|\Lambda^{\mathrm{IC}}, q\rangle$, W_q^{IC}, elle-même approximation de la suite $|\Lambda, q\rangle$, W_q. Il lui correspond la suite des potentiels d'erreur

$$[1] \qquad \mathscr{V}_q = (\Gamma, q)^{-1} (E_q - \hat{H}) (\Gamma, q)$$

(Nous ecrivons ici (Γ, q) parce qu'il s'agit de la forme analytique de la fonction et non du vecteur d'état.)

Nous avons proposé de représenter un opérateur de corrélation convenant à un état q par le produit d'une suite infinie de corrections approchées. Dans $\mathscr{E}$ ces divers opérateurs sont représentés par des matrices $(\hat{\mathbf{C}}_q)$ de telle sorte que

$$[2] \qquad |\Lambda^{\mathrm{IC}}, q\rangle = (\hat{\mathbf{C}}_q)\, |\Gamma, q\rangle$$

Ces corrections successives font intervenir une chaîne de fonctions approchées $|\psi, r\rangle$ depuis $|\Gamma, q\rangle$ jusqu'à $|\Lambda^{\mathrm{IC}}, q\rangle$:

$$[3] \qquad |\psi_0, q\rangle \equiv |\Gamma, q\rangle$$

$$[4] \qquad |\psi_\infty, q\rangle \equiv |\Lambda^{\mathrm{IC}}, q\rangle$$

Par définition la "correction perturbative de l'erreur, pour le niveau q approché", est *la perturbation par un potentiel* $-\mathscr{V}_q$ *– opposé du potentiel d'erreur*. Nous admettons ici que $|\psi_r, q\rangle$ ne peut être une moins bonne approximation que $|\psi_{r-1}, q\rangle$. Dans une discussion plus complète, on introduit un coefficient modulant ce potentiel (17), et on démontre la proposition précédente.

Le modèle d'un espace des interactions de configuration ainsi construit va nous servir dans les chapitres II et III, à développer la théorie selon des formules indépendantes de l'idée physique de corrélation. La corrélation proprement dite sera introduite au chapitre IV avec le formalisme de la seconde quantification.

II-2. *Réalisation de la perturbation corrective de l'erreur pour le niveau* q

Pour effectuer la correction perturbative, nous avons suggèré (17) d'utiliser formellement l'expression de Schrödinger en remplaçant la suite des états propres de $\hat{H} + \mathscr{V}_r$ par l'ensemble fini des $|\psi_r, q\rangle$ obtenus pour les divers niveaux q. Cette base est donc variable avec le rang r de l'itération.

Or la base obtenue par le perturbation seule, nécessairement tronquée à un ordre fini, n'est pas orthogonale. Nous pouvons soit adapter la formule des perturbations à une base oblique (17, Note 50, paragraphe XIII, 4), soit construire une base orthogonale $|\psi_r', q\rangle$ à partir d'une base oblique $|\theta_r, q\rangle$ selon un processus connu:

$$[5a] \qquad |\psi_r', q\rangle = |\theta_r, q\rangle + \sum_{r=0}^{q-1} \mu_p^{(r)}\, |\theta_r, p\rangle\, \langle \psi_r', p | \psi_r, q\rangle$$

$$[5b] \qquad p = 0, \ldots q - 1$$

Normalisons:

$$[6a] \qquad |\psi_r, q\rangle = \nu_r^q |\psi_r', q\rangle$$

$$[6b] \qquad (\nu_r^q)^2 \cdot \langle \psi_r', q | \psi_r', q\rangle = 1$$

Les Q equations [5] définissent les coefficients $\mu_p^q(r)$. La base construite $|\psi_r, q\rangle$ est la même pour l'étude de chaque niveau q, bien que ne contenant généralement pas $|\theta_r, q\rangle$ si $q \neq 0$.

On peut alors effectuer la perturbation par l'opposé du potentiel d'erreur sur $|\psi_r, q\rangle$:

$$[7a] \quad |\theta_{r+1}, q\rangle = |\psi_r, q\rangle + \sum_{p \neq q} \left[\rho_{pq}^{(r)} + \sum_{p \neq m \neq q} \rho_{pm}^{(r)} \rho_{mq}^{(r)} + \ldots \right] |\psi_r, p\rangle$$

$$[7b] \quad \delta_{r+1} E_q = \sum_{p \neq q} \rho_{pq}^{(r)} H_{pq}^{(r)} + \ldots.$$

$$[7c] \quad H_{pq}^{(r)} = \langle \psi_r, p|\hat{H}|\psi_r, q\rangle \quad \text{etc.} \ldots$$

$$\rho_{pq}^{0}(r) = \frac{H_{pq}^{(r)}}{H_{qq}^{(r)} - H_{pp}^{(r)}} \quad \text{etc.} \ldots$$

base orthogonale $\mathcal{A}$:

$$[8a] \quad \rho_{pq}^{(r)} = \rho_{pq}^{0}(r) \qquad \mu_p^q(r) \text{ selon } [5a,b]$$

base oblique $\mathcal{B}$:

$$[8b] \quad \mu_p^q(r) = 0 \qquad \rho_{pq}^{(r)} = \rho_{pq}^{0}(r) \left[1 - \frac{H_{pp}^{(r)}}{H_{pq}^{(r)}} \langle \psi_r, p|\psi_r, q\rangle \right]$$

Le potentiel d'erreur n'a ainsi servi que d'intermédiaire de calcul (17). On vérifie que dans le développement $\delta_r E_q$ de l'énergie de perturbation, la perturbation première est nulle.

Les vecteurs $|\psi_r, q\rangle$ constituent les approximations successives du vecteur $|\Lambda^{IC}, q\rangle$. Il résulte de la discussion (17, 19) que le processus [7a], [5] diminue l'erreur à craindre sur l'énergie. D'autre part il ne se ramène à l'opérateur identité que si

$$H_{pq}^{(r)} = 0 \quad \forall p$$

c'est-à-dire si l'on est parvenu à un vecteur propre de $\hat{H}$.

L'application de [7a], [6] aux divers niveaux résoud le problème de l'interaction de configuration complète en évitant la résolution des systèmes d'équations linéaires correspondantes mais avec l'obligation de redéfinir une base $\mathcal{A}$ ou $\mathcal{B}$ de $\mathcal{E}$ selon les équations [5], [6]... à chaque élévation de rang r.

Nous allons vérifier ces propriétés sur le modèle à deux niveaux et déterminer dans ce cas la vitesse de convergence.

II-3. *Modèle à deux niveaux*

Soit la matrice Hamiltonienne réelle

$$(\hat{H}) = \begin{pmatrix} E_0 & E_{01} \\ E_{01} & E_1 \end{pmatrix}$$

représentant $\hat{H}$ dans $\mathcal{E} = |\Gamma, 0\rangle \otimes |\Gamma, 1\rangle$. Ses valeurs propres sont

$$[9a] \quad \begin{aligned} W_0^{IC} &= \frac{E_0 + E_1}{2} - \frac{E_0 - E_1}{2 \cos \omega} \\ W_1^{IC} &= \frac{E_0 + E_1}{2} + \frac{E_0 - E_1}{2 \cos \omega} \end{aligned}$$

ses vecteurs propres sont

$$[9b] \quad \begin{aligned} |\Lambda^{IC}, 0\rangle &= \cos \omega\, |\Gamma, 0\rangle + \sin \omega\, |\Gamma, 1\rangle \\ |\Lambda^{IC}, 1\rangle &= \sin \omega\, |\Gamma, 0\rangle + \cos \omega\, |\Gamma, 1\rangle \end{aligned}$$

en posant

$$[9c] \quad \text{tg } 2\,\omega = \frac{2E_{10}}{E_1 - E_0} = 2\rho_{01}^{0}(0)$$

Retrouvons ces résultats par la correction indéfinie de potentiel d'erreur selon les formules [5], [6] et [7a,c]. Pour cela, utilisons le référentiel orthogonal mobile. L'itération de rang r s'écrit, après re-normalisation:

$$[10a] \quad |\psi_r, 0\rangle = \cos \gamma_r\, |\psi_r, 0\rangle + \sin \gamma_r\, |\psi_r, 1\rangle$$

$$[10b] \quad |\psi_r, 1\rangle = \sin \gamma_r\, |\psi_r, 0\rangle + \cos \gamma_r\, |\psi_r, 1\rangle$$

en posant

$$[10c] \quad \text{tg } \gamma_r = \rho_{01}^{0}(r)$$

On observe que [10a] est entièrement déterminé par la perturbation [7a] alors que [10b] est déterminé par l'orthogonalisation [6a,b]. On remarque la différence entre la formule [9c] qui détermine l'interaction de configuration et [10c] qui détermine la correction perturbative de l'erreur. À la première itération

$$[10d] \quad \text{tg } \gamma_0 = \tfrac{1}{2} \text{ tg } 2\omega$$

Lorsque l'erreur est petite,

$$\omega \simeq \frac{E_{10}}{E_1 - E_0} \simeq \gamma_0$$

la première correction conduit très près de l'interaction de configuration complète, l'erreur étant donnée par

$$[10e] \quad \gamma_0 - \omega = -\frac{1}{2} \left(\frac{E_{01}}{E_1 - E_0} \right)^3$$

Revenant au réferentiel fixe $|\Gamma, 0\rangle$, $|\Gamma, 1\rangle$.

$$[11a] \quad \begin{aligned} |\psi_r, 0\rangle &= |\Gamma, 0\rangle \cos \alpha_r + |\Gamma, 1\rangle \sin \alpha_r \\ |\psi_r, 1\rangle &= -|\Gamma, 0\rangle \sin \alpha_r + |\Gamma, 1\rangle \cos \alpha_r \end{aligned}$$

Nous avons (17, Note 51 du paragraphe XVI, 5) la relation de récurrence, équivalente à [10d] à la rotation près du réferentiel:

$$[11b] \quad \text{tg } (\alpha_r - \alpha_{r-1}) = \tfrac{1}{2} \text{ tg } 2(\omega - \alpha_{r-1})$$

La récurrence [11b] entraîne

$$[11c] \quad |\alpha_r - \alpha_{r-1}| \langle |\omega - \alpha_r|$$

et la suite α_r ne peut diverger.

Lorsque l'itération se poursuit

$$[11d] \quad \omega = \lim_{r \to \infty} \alpha_r = \sum_{r=0}^{\infty} \gamma_r$$

$$\lim_{r \to \infty} |\psi_r, 0\rangle = |\Lambda^{IC}, 0\rangle \qquad \lim_{r \to \infty} |\psi_r, 1\rangle = |\Lambda^{IC}, 1\rangle$$

Posant $\alpha_r - \omega = \epsilon_r$, on trouve par un développement limité de [11b], lorsque ϵ_r est suffisement petit (ou par usage du résultat [10e])

$$[11e] \quad \epsilon_r \simeq -\tfrac{1}{2} \epsilon_{r-1}^3$$

qui assure une convergence vers 0 par valeurs alternées. Plus précisément, cette convergence est analogue à celle de la suite

$$[11f] \quad \epsilon_r \approx (-1)^r \sqrt{2} \exp{(-3^r)} \text{ radian}$$

L'erreur correspondante sur l'énergie est:

$$\Delta E \simeq \epsilon_r^2 (E_0 + E_1)$$

À la quatrième itération

$\epsilon_r \approx 10^{-37}$ radian

$$\frac{\Delta E}{0{,}5\,(E_0 + E_1)} \approx 10^{-74}$$

Si nous désignons un opérateur de rotation dans le plan $\mathscr{C}$ par l'angle de rotation surmonté du symbole opérateur, les équations [10*a*,*b*], [11*a*] et [9*b*] s'écrivent encore pour $p = 1{,}2$

[12*a*] $|\psi_r, p\rangle = (\hat{\gamma}_r)\,|\psi_r, p\rangle$

[12*b*] $|\Gamma, p\rangle = (\hat{\alpha}_r)\,|\Gamma, p\rangle$

[12*c*] $|\Gamma, p\rangle = (\hat{\omega})\,|\Gamma, p\rangle$

Les angles γ_r, α_r, ω sont définis respectivement par [10*c*], [11*b*] et [9*c*] et vérifient [11*d*].

Nous allons généraliser les transformations [12*a*,*b*,*c*].

II-4. *Modèle à plusieurs niveaux*

Compte tenu de la discussion du paragraphe II-2 on peut dans les deux options représenter la perturbation par l'expression déduite de [7*a*], [7*c*]:

[12*d*] $$|\psi'_{r+1}, q\rangle = |\psi_r, q\rangle + \sum_{p \neq q} F_{pq}^{(r)}\,|\psi_r, p\rangle$$

normalisée selon [6*a*,*b*].

$\mathscr{A}$: Si le réferentiel mobile est orthogonalisé, selon [8*a*]

$$\rho_{pq}^{(r)} = \rho_{pq}^{0}(r)$$

$\mu_{p<q}^{q}(r)$ résulte de [5*a*,*b*] et on pose en outre

[13] $$\mu_{p>q}^{q}(r) = 0$$

$\mathscr{B}$: Si le réferentiel mobile n'est pas orthogonalisé, $\rho_{pq}^{(r)}$ résulte de [8*b*]; par construction

$$\mu_{pq}(r) \equiv 0$$

Dans les deux bases on peut écrire:

[14] $$F_{pq}^{(r)} = \mu_p^q(r) + \sum_m (\delta_{mq} + \mu_m^q(r)) \left[\rho_{pm} + \sum_{p \neq o \neq m} \rho_{po}^{(r)}\rho_{om}^{(r)} + \ldots\right]$$

δ_{mq} étant le symbole de Kronecker.

Passant du réferentiel mobile $|\psi_r, q\rangle$ au référentiel fixe $|\Gamma, q\rangle$,

[15*a*] $$|\psi_r, q\rangle = \sum_q x_q^m(r)\,|\Gamma, m\rangle$$

$F_{pq}^{(r)}$ étant défini par [14], $\rho_{pq}^{(r)}$ prend la valeur [8*a*] ou [8*b*], l'expression [7*c*] devenant

[15*b*] $$\rho_{pq}^{0}(r) = \frac{\sum_l \sum_m x_{pm}^{(r)} x_{ql}^{(r)} E_{lm}}{\sum_l \sum_m [x_q^l(r)\,x_q^m(r) - x_p^l(r)\,x_p^m(r)]E_{lm}}$$

et la correction [8*b*] s'écrivant

[15*c*] $$\rho_{pq}^{(r)} = \rho_{pq}^{0}(r) + \left(\sum_l \sum_m x_p^m x_q^l\right)\left(1 - \sum_l \sum_m x_p^m x_q^l E_{lm}\right)^{-1}$$

la matrice (E_{lm}) étant $(\hat{H})$ sur la base $|\Gamma, q\rangle$: $E_{lm} \equiv H_{lm}^{(o)}$.

Les coordonnées sont initialisées selon [3] par

[15*d*₁] $$x_q^m(o) = \delta_{qm}$$

La relation qui définit la normalisation [6*a*] est

[15*d*₂] $$x_q^m(r) = \nu_r^q\, x_q^{\prime m}(r)$$

La relation de récurrence est alors

[15*d*₃] $$x_q^m(r) = x_q^m(r-1) + \sum_{p \neq q} x_p^m(r-1)\,F_{pq}^{(r-1)}$$

ν_r^q étant défini par [6*b*]

[15*d*₄] $$(\nu_r^q)^2 \cdot \Sigma\,[x_q^{\prime m}(r)]^2 = 1$$

Si le processus est convergent,

[16*a*] $$\lim_{r \to \infty} x_q^m(r) = x_q^m(\mathrm{IC})$$

[16*b*] $$|\Lambda^{\mathrm{IC}}, q\rangle = \sum_m x_q^m(\mathrm{IC})\,|\Gamma, m\rangle$$

$$\nu_q^{\mathrm{IC}} = 1$$

Pour étudier la convergence, posons

$$\xi_q^m(r) = x_q^m(r) - x_q^m(\mathrm{IC}),$$

$$\xi_q^m(r) \to 0 \quad |r \to \infty, \forall\, q$$

La relation [15*d*] de récurrence devient [16*c*]:

[16*c*] $$\xi_q^m(r) - \xi_q^m(r-1) = \sum_{p \neq q} \xi_p^m(r-1)\,F_{pq}^{(r-1)}$$

où $F_{pq}^{(r-1)}$ est défini par [14*b*] avec l'expression [15*c*] qui devient pour $r \to \infty$:

$$\rho_{pq}^{0}(r) \simeq \frac{-\sum_l \sum_m [x_p^m(\mathrm{IC})\,\xi_q^l(r) + x_q^m(\mathrm{IC})\,\xi_p^l(r)]E_{lm}}{\sum_l \sum_m [x_q^l(\mathrm{IC})\,x_q^m(\mathrm{IC}) - x_p^l(\mathrm{IC})\,x_p^m(\mathrm{IC})]E_{lm}}$$

et [8*a*] ou [8*b*], alors

$$F_{pq}^{(r)} \sim \rho_{pq}^{(r)}$$

La discussion des signes montre, comme dans le cas des deux niveaux, une correction alternée de l'erreur. La relation [16*c*] s'écrit, en module:

$$|\xi_q^m(r)| + |\xi_q^m(r-1)| = \sum_{p \neq q} |\xi_p^m(r-1)|\,F_{pq}^{(r-1)}$$

Soit

$$\xi_{r-1} = \sup|\xi_q^m(r-1)|$$

$$E = \sup|E_{lm}|$$

$$W = \inf|W_q^{\mathrm{IC}} - W_p^{\mathrm{IC}}|$$

On trouve

$$\xi_r \gtrsim B\,\xi_{r-1}^2 \qquad B = \frac{2(Q-1)^2 E}{W}$$

Une suite majorante en module à partir d'un certain rang est

$$B^{-1}\exp(-2^r)$$

Puisque selon [11*f*] la convergence peut être plus rapide, disons que la convergence est analogue à celle d'une suite proportionnelle à

[16*d*] $$\exp(-K^r) \quad 2 \leq K \leq 3$$

II-5. *Discussion de la correction répètée*

Selon l'eq. [4], la suite des fonctions $|\psi_r, q\rangle$ converge vers la fonction propre $|\Lambda^{IC}, q\rangle$ et les énergies $H_{qq}^{(r)} = \langle\psi_r, q|\hat{H}|\psi_r, q\rangle$ convergent vers W_q^{IC}, valeur propre de la matrice $(\hat{H})$. En outre la formule [7*b*] donne en même temps que $|\psi_r,q\rangle$ une approximation de rang plus élevé de l'énergie. Les coordonnées $x_q^m(r)$ sont initialisées par [15d_1] et calculées par [15d_2] et [15d_3], le coefficient de normalisation ν_r^q etant déterminé par [15d_4]. On utilise pour celà les coefficients de perturbation $F_{pq}^{(r)}$ calculés selon [14] avec deux options. Dans l'option $\mathcal{B}$, non orthogonalisée, les μ_p^q sont nuls et les $\rho_{pq}^{(r)}$ calculés selon [15*b*] et [15*c*] à partir de la matrice (E_{lm}).

Cette technique est alternative de la diagonalisation purement mathématique de la matrice Hamiltonienne. Les intermédiaires de calcul ont un sens physique. Chaque approximation apporte la partie principale de l'erreur sur le résultat.

Mais elle n'est pas limitée à l'objectif d'une diagonalisation de matrice dans un espace donné. On peut se proposer la modification des spinorbitales *j* pour des arguments qui n'ont pas nécessairement le caractère d'un calcul variationnel. Nous avons discuté en particulier (17) de l'amélioration du potentiel d'erreur par des conditions locales. Cette modification des spinorbitales revient à considèrer un espace $\mathcal{E}$ mobile à l'intérieur d'un espace de Hilbert. On peut alterner les deux types de correction, donc utiliser à l'iteration *r* une matrice $(E_{lm}^{(r)})$ qui a été légèrement modifiée par rapport à $(E_{lm}^{(r-1)})$. Celà ne semble pas entraver la procédure indiquée ici.

III. Correction linearisée de l'erreur

III-1. *Correction de l'erreur par un operateur non linéaire*

Nous avons formulé la dite "correction perturbative de l'erreur pour le niveau *q*" selon [12*d*] pour les seules approximations successives du niveau *q* initié par la configuration pure $|\Gamma, q\rangle$.

Pour tenter d'effectuer cette correction pour d'autres vecteurs de $\mathcal{E}$ on pourrait se reporter à la définition, spécialement celle ($\mathcal{B}$), qui indique la perturbation par l'opposé du potentiel d'erreur, non suivie d'une orthogonalisation. Certains résultats semblent évidents (correction nulle pour les $|\Lambda^{IC}, q\rangle$).

Si l'on procède à une telle généralisation on constate que la correction nulle sur les $|\Lambda^{IC}, p\rangle$ définis par [9*b*] ne peut être mise sous la forme de la somme pondérée des corrections sur $|\Gamma, 0\rangle$ et sur $|\Gamma, 1\rangle$. L'opérateur ainsi généralisé ne serait pas linéaire.

Pour intéressante que soit cette idée, les formalismes disponibles ne se prêtent guère à en tirer les conséquences.

III-2. *Correction de l'erreur par un opérateur linéaire*

La correction que nous avons calculée au chapitre II s'exprime par la transformation [12*d*] éventuellement suivie de [6*a*]. Elle est donc effectuée par l'action de l'opérateur $|\psi_r^q, q\rangle\langle\psi_{r-1}, q|$ ou de l'opérateur $|\psi_r, q\rangle\langle\psi_{r-1}, q|$. Ces deux opérateurs sont définis dans $\mathcal{E}$ et linéaires. Ils sont physiquement équivalents, mais le premier est idempotent, c'est un opérateur de projection; le second conserve la norme. Nous consacrerons le chapitre III au second, le chapitre IV au premier.

La mise en oeuvre de cet opérateur pour le niveau *q* ne peut pas se séparer de la construction du référentiel mobile; nous sommes amenés à introduire un opérateur de "correction linéaire de l'erreur à l'ordre *r*" (cle_r)

$$[17] \quad \text{cle}_r = \sum_q |\psi_r, q\rangle\langle\psi_{r-1}, q|$$

L'expression [17] traduit l'évolution du référentiel mobile. Plus explicitement,

$$[18] \quad \text{cle}_r = \sum_q \nu_r^q |\psi_r, q\rangle\langle\psi_r, q| + \sum_q \sum_{p \neq q} \nu_r^q F_{pq}^{(r)} |\psi_r, p\rangle\langle\psi_r, q|$$

($F_{pq}^{(r)}$ étant défini par [14]). Tenant compte de [15*a*],

$$[19] \quad \text{cle}_r = \sum_p \sum_q \nu_r^q [\delta_{pq} + F_{pq}^{(r)}] \sum_l \sum_m x_p^m(r)\, x_l^q(r)\; |\Gamma, m\rangle\langle\Gamma, l|$$

L'itération de cet opérateur est représentée par l'equation

$$[20] \quad \text{cle}_r \cdot \text{cle}_{r+1} = \sum_q |\psi_{r+1}, q\rangle\, \langle\psi_{r-1}, q|$$

On obtient donc

$$[21] \quad \prod_{s=0}^{r} \text{cle}_s = \sum_q |\psi_s, q\rangle\, \langle\Gamma, q| = \sum_q \sum_m x_q^m(r)\, |\Gamma, m\rangle\, \langle\Gamma, q|$$

$x_q^m(r)$ dans [19], [21] et les équations suivantes, défini par [15*a*], se calcule selon [15$d_{1,2,3}$].

L'aboutissement du calcul est selon [16*a*]

$$[22] \quad \prod_{s=0}^{\infty} \text{cle}_s = \sum_q |\Lambda^{IC}, q\rangle\, \langle\Gamma, q| = \sum_q \sum_m x_q^m(\text{IC})\, |\Gamma, m\rangle\, \langle\Gamma, q|$$

$\prod_{s=0}^{\infty} \text{cle}_s$ est un opérateur de corrélation valable pour n'importe lequel des niveaux *q* et dont nous déclarons qu'il opère la corrélation dans l'espace $\mathcal{E}$: à un mélange de configurations pures, il fait correspondre le mélange statistique d'états de même pondération

$$\text{cle}_r \sum_q x_q\, |\Gamma, q\rangle = \sum_q x_q\, |\Lambda^{IC}, q\rangle$$

III-3. *Modèle à deux niveaux*

Dans l'exemple (paragraphe II-3) du modèle à deux niveaux, les opérateurs [18], [21] et [22] prennent tous la même forme, selon [12a, b, c]:

$$[23] \quad (\hat{\theta}) = \hat{I} \cos\theta + (|\Gamma, 1\rangle\, \langle\Gamma, 0| - |\Gamma, 0\rangle\, \langle\Gamma, 1|) \sin\theta$$

avec

$$[24] \quad \text{cle}_r = (\hat{\gamma}_r), \quad \prod_{s=0}^{\infty} \text{cle}_s = (\hat{\alpha}_r), \quad \prod_{s=0}^{\infty} \text{cle}_s = (\hat{\omega})$$

III-4. *Discussion de la correction linéaire*

En conclusion, les opérateurs cle_r, $\prod_{s=0}^{r} \text{cle}_s$, $\prod_{s=0}^{\infty} \text{cle}_s$ ne modifient pas la suite des calculs indiqués au paragraphe II-5. Leur intérêt est de parvenir à un opérateur de corrélation $\prod_{s=0}^{\infty} \text{cle}_s$ valable pour toute configuration, et de le construire sous forme d'un produit infini d'opérateurs partiels dont chacun cle_r corrige la partie principale de l'erreur et possède la signification très intuitive de perturbation corrective de l'erreur appliquée simultanément à l'ensemble du référentiel $|\psi_r, q\rangle$.

La forme générale des opérateurs de corrélation a par ailleurs été discutée. Pour que la condition [2] soit réalisée par

TABLEAU 1. Expression des opérateurs d'excitation B_p^q de H_3^+

	q			
p	0	1	2	3
0	$\hat{I}$	$\frac{1}{\sqrt{2}}(X_{\bar{u}}^+ X_{\bar{v}} + X_u^+ X_v)$	$X_{\bar{w}}^+ X_w^+ X_u X_{\bar{u}}$	$X_{\bar{u}} X_u X_v X_{\bar{v}}$
1	$\frac{1}{\sqrt{2}}(X_v^+ X_u + X_{\bar{v}}^+ X_{\bar{u}})$	$\hat{I}$	$\frac{1}{\sqrt{2}} X_{\bar{w}}^+ X_w^+ (X_u X_{\bar{v}} + X_v X_{\bar{u}})$	$\frac{1}{\sqrt{2}}(X_v^+ X_u + X_{\bar{v}}^+ X_{\bar{u}})$
2	$X_{\bar{u}}^+ X_u^+ X_w X_{\bar{w}}$	$\frac{1}{\sqrt{2}}(X_{\bar{v}}^+ X_u^+ + X_{\bar{u}}^+ X_v^+) X_w X_{\bar{w}}$	$\hat{I}$	$X_{\bar{v}} X_v X_w X_{\bar{w}}$
3	$X_{\bar{v}}^+ X_v^+ X_u X_{\bar{u}}$	$\frac{1}{\sqrt{2}}(X_v^+ X_u + X_{\bar{v}}^+ X_{\bar{u}})$	$X_{\bar{w}}^+ X_w^+ X_v X_{\bar{v}}$	$\hat{I}$

l'expression générale (réf. 25, éq. 2*a*)

$$\hat{C} = \Sigma\, c_{pg}\, |\Lambda^{\mathrm{IC}}, p\rangle \langle \Gamma, q|$$

il faut et il suffit que

$$c_{pq} = \delta_{pq}$$

L'expression [22] est donc bien la seule correllant selon [2] toutes les configurations $|\Gamma, q\rangle$.

Les opérateurs $\prod_{s=0}^{\infty} \mathrm{cle}_s$ sous forme matricielle ($\mathbf{x}_q^m$(IC)) seront utiles pour construire les opérateurs de décorrelation et par suite d'ionisation et d'attachement (25).

IV. Développement en grappes de la correction linearisée de l'erreur de corrélation

IV-1. *Utilisation des opérateurs de seconde quantification*

Les opérateurs de corrélation ont essentiellement été développés dans l'application des concepts de la seconde quantification à la chimie. Il y a donc lieu de comparer l'opérateur $\prod_{s=0}^{\infty} \mathrm{cle}_s$ aux opérateurs de corrélation auxquels conduit ce point de vue.

A. *Modèle à deux niveaux. Molécule H_2 en base minimale*

Les orbitales moléculaires de symètrie $1\sigma_g$ (respectivement $1\sigma_u$) étant désignées par i (resp. j), les deux configurations pures s'écrivent avec des notations évidentes:

$$|\Gamma, 0\rangle = |i\bar{i}| \quad |\Gamma, 1\rangle = |j\bar{j}\rangle$$

Appelons X (resp. X^+) les opérateurs de destruction (resp. création) indicés des spinorbitales. L'expression [23] s'écrit

$$[25a] \quad \hat{\theta} = \hat{I} \cos\theta + (X_j^+ X_{\bar{j}}^+ X_i X_{\bar{i}} - X_{\bar{i}}^+ X_i^+ X_j X_{\bar{j}}) \sin\theta$$

Sont de cette forme les opérateurs

$$[25b] \quad \mathrm{cle}_r = \hat{\gamma}_r \quad \prod_{s=0}^{r} = \hat{\alpha}_r \quad \prod_{s=0}^{\infty} \mathrm{cle}_s = \hat{\omega}_r$$

Ils admettent donc la relation générale

$$[25c] \quad \hat{\sigma} = \hat{\theta}_1 \cdot \hat{\theta}_2 \quad |\sigma = \theta_1 + \theta_2$$

Nous généraliserons cette relation au modèle à plusieurs niveaux par le concept de développement en grappes.

B. *Modèle à quatre niveaux. H_3^+ linéaire symètrique en base minimale*

Les orbitales moléculaires de symètrie $1\sigma_g$, $2\sigma_g$, $1\sigma_u$ désignées par u, v, w dépendent d'un paramètre (coefficient de l'orbitale atomique médiane dans u) dont les valeurs remarquables correspondent successivement aux orbitales de Hückel, orbitales de recouvrement maximum, orbitales naturelles, orbitales de pseudo-symètrie, orbitales de champ autocohérent (17, 21, 25, 28, 37). Les 4 configurations pures sont avec des notations évidentes (17, 25):

$$|\Gamma, 0\rangle = |u\bar{u}\rangle \quad |\Gamma, 1\rangle = \frac{1}{\sqrt{i}}(u\bar{v} + v\bar{u})$$

$$|\Gamma, 2\rangle = |w\bar{w}\rangle; \, |\Gamma, 3\rangle = |v\bar{v}\rangle$$

Les opérateurs d'excitation satisfaisant l'équation

$$[26a] \quad B_q^p\, |\Gamma, q\rangle = |\Gamma, p\rangle$$

sont indiqués par le tableau 1.

Voici (cf. la réf. 25) l'expression de ces mêmes opérateurs en fonction des ketbras de configuration: si

$$[26b] \quad p = q \quad \hat{B}_q^q = \hat{I} + \sum_{q=0}^{3} |\Gamma, q\rangle \langle \Gamma, q|$$

si

$$[26c] \quad p = 0,\, q = 1 \text{ ou } p = 1,\, q = 3$$

$$\hat{B} \uparrow\; = \hat{B}_0^1 = \hat{B}_1^3 = |\Gamma, 1\rangle \langle \Gamma, 0| + |\Gamma, 3\rangle \langle \Gamma, 1|$$

si

$$[26d] \quad p = 1,\, q = 0 \text{ ou } p = 3,\, q = 1$$

$$\hat{B} \downarrow\; = \hat{B}_1^0 = \hat{B}_3^1 = |\Gamma, 0\rangle \langle \Gamma, 1| + |\Gamma, 1\rangle \langle \Gamma, 3|$$

si non

$$[26e] \quad \hat{B}_p^q = |\Gamma, q\rangle \langle \Gamma, p|$$

Après avoir fait le calcul de l'interaction de configuration directement (31) ou indirectement selon [16*b*]

$$[26f] \quad |\Lambda^{\mathrm{IC}}, q\rangle = \sum_{p=0}^{3} x_q^p(\mathrm{IC})\, |\Gamma, p\rangle$$

on connait bien évidemment un opérateur de corrélation adapté à la configuration $|\Gamma, q\rangle$

$$[26g] \quad \hat{C}_q = \sum_{p=0}^{3} x_q^p(\mathrm{IC})\, B_p^q$$

Voici l'expression de cet opérateur en fonction linéaire des ketbras de configuration (compte tenu de [26*f*])

$$[26h] \quad \hat{C}_q = |\Lambda^{\mathrm{IC}}, q\rangle \langle \Gamma, q| + \sum_{p \neq q} x_p^r(\mathrm{IC})\, |\Gamma, p\rangle \langle \Gamma, p|$$

$$+ \delta_{q0}\, \delta_{p1}\, x_0^1(\mathrm{IC})\, |\Gamma, 3\rangle \langle \Gamma, 1| + \delta_{q1}\, \delta_{p3}\, x_1^3(\mathrm{IC})\, |\Gamma, 1\rangle \langle \Gamma, 0|$$

$$+ \delta_{q1}\, \delta_{p0}\, x_1^0(\mathrm{IC})\, |\Gamma, 1\rangle \langle \Gamma, 3| + \delta_{q3}\, \delta_{p1}\, x_3^1(\mathrm{IC})\, |\Gamma, 0\rangle \langle \Gamma, 1|$$

Cet opérateur est sensiblement différent de l'opérateur [22] adapté aux 4 configurations soit encore

$$[26i] \quad \prod_{s=0}^{\infty} \text{cle}_s = \sum_{q=0}^{3} |\Lambda_q^{\text{IC}}\rangle \langle \Gamma_q|$$

C. *Discussion de l'utilisation de l'algèbre de seconde quantification*

On peut donc se proposer de remplacer l'ensemble des $\hat{C}_q$ de configuration particulière par $\prod_{s=0}^{\infty}$ cle$_s$ valable pour toutes.

On peut d'autre part chercher à construire cet opérateur global de corrélation par multiplication des opérateurs de correction successifs. Cela nous a conduit dans le cas du modèle à deux niveaux (paragraphe IV-1A) à l'addition des angles γ_r successifs pour donner ω.

Or l'idée du développement en grappes (24*a*, 29, 37) est la recherche d'un polynome des excitations T tel que e^T soit l'opérateur de correlation. On pourrait donc se proposer de chercher un développement en grappe de même forme pour les opérateurs de correction de manière que le produit des opérateurs de correction soit exprimé par l'addition d'un polynome partiel d'excitation attaché à cette correction, de sorte que la matrice des excitations soit la somme de ces matrices successives attachées à la correction.

Toutefois l'opérateur cle$_s$ que nous avons défini [17] n'a pas une forme identifiable à un développement en série entière. Par exemple son terme inexcité est

$$[27] \quad \hat{K} = \sum_q \nu_r^q |\psi_{r-1}, q\rangle \langle \psi_{r-1}, q|$$

D. *Nouvelle forme de la correction linéarisée de l'erreur*

Si au contraire nous partons de l'opérateur idempotent défini au chapitre III-2, nous introduisons le nouvel opérateur Cle$_r$:

$$[28a] \quad \text{Cle}_r = \sum_q |\psi'_r, q\rangle \langle \psi_{r-1}, q|$$

Cet opérateur ne satisfait pas l'éq. [2]. Mais pour toute configuration $|\Gamma, p\rangle$ il existe un opérateur proportionnel à Cle$_r$ qui la satisfait

$$[28b] \quad \nu_r^p \, \text{Cle}_r = |\psi_r, p\rangle \langle \psi_{r-1}, p| + \sum_{q \neq p} \frac{\nu_r^q}{\nu_r^q} |\psi_r, q\rangle \langle \psi_{r-1}, q|$$

D'autre part cet opérateur est relié à celui étudié jusqu'à présent

$$[28c] \quad \text{cle}_r = \text{Cle}_r \cdot \hat{K}$$

Son développement fait apparaitre l'opérateur unité

$$[28d] \quad \text{Cle}_r = \hat{I} + \sum_q \sum_{p \neq q} F_{pq}^{(r)} |\psi_r, p\rangle \langle \psi_r, q|$$

$$[28e] \quad \text{Cle}_r = \hat{I} + \sum_q \sum_{p \neq q} F_{pq}^{(r)} x_q^m x_p^l |\Gamma, l\rangle \langle \Gamma, m|$$

Le résultat de deux opérations successives de correction sera

$$[29a] \quad \text{Cle}_r \cdot \text{Cle}_{r+1} = \sum_q \frac{1}{\nu_r^q} |\psi'_{r+1}, q\rangle \langle \psi_{r-1}, q|$$

On calculera donc de proche en proche

$$[29b] \quad \prod_{s=0}^{r} \text{Cle}_s = \sum_q \left(\prod_{s=0}^{r} \frac{1}{\nu_r^s}\right) |\psi_s, q\rangle \langle \Gamma, q|$$

$$[29c] \quad \prod_{s=0}^{\infty} \text{Cle}_s = \sum_q \left(\prod_{s=0}^{\infty} \frac{1}{\nu_r^s}\right) |\Lambda^{\text{IC}}, q\rangle \langle \Gamma, q|$$

$$[29d] \quad \prod_{s=0}^{\infty} \text{Cle}_s = \sum_q \left(\prod_{s=0}^{\infty} \frac{1}{\nu_r^s}\right) \sum_m x_q^m(\text{IC}) |\Gamma, m\rangle \langle \Gamma, q|$$

Pour calculer ces diverses expressions, la suite des matrices $(\mathbf{x}_q^m(r))$ et des coefficients de normalisation ν_r^q ainsi que leurs limites $((\mathbf{x}_q^m(\text{IC}))$ et 1) résultent des équations [15d_{1-4}] compte tenu de [14] et [15*b*, *c*] comme il a été indiqué au paragraphe II-5.

Voici l'exemple du modèle à 4 niveaux de H_3^+ linéaire, symétrique: selon le tableau 1, le polynome Cle$_r$ ordonné selon le nombre Z d'excitations se déduit de [28*e*]

$$[30] \quad \text{Cle}_r = \hat{I} + \text{Cle}_r^{[1]} + \text{Cle}_r^{[2]}$$

$$\text{Cle}_r^{[1]} = \sum_{q=0}^{3} \sum_{p \neq q} F_{pq}^{(r)} [(\delta_{m0}\, \delta_{l1}\, x_q^0(r)\, x_p^1(r) + \delta_{m1}\, \delta_{l3}\, x_q^1(r)\, x_p^3(r))\, \hat{B} \uparrow \; + (\delta_{m1}\, \delta_{l0}\, x_q^1(r)\, x_p^0(r) + \delta_{m3}\, \delta_{l1}\, x_q^3(r)\, x_p^1(r))\, \hat{B} \downarrow]$$

$$\text{Cle}_r^{[2]} = \sum_{q=0}^{3} \sum_{p \neq q} F_{pq}^{(r)} \sum\sum_{(m \neq l) \neq \begin{cases}(0,1)\\(1,3)\\(1,0)\\(3,1)\end{cases}} x_q^m(r)\, x_p^l(r)\, \hat{B}_m^l$$

les x étant donnés par solution des équations de récurrence.

Plus généralement chaque couple de configurations permet de définir un nombre d'excitations

$$[31a] \quad [p, q] = Z$$

On propose alors un développement, ordonné sur les couples *lm* et tronqué sur les couples *pq*.

$$[31b] \quad \text{Cle}_r = \hat{I} + \sum_Z \text{Cle}_r^{[Z]}$$

$$\text{Cle}_r\,[Z] = \sum\sum_{[P,Q] \leq Z} F_{pq}^{(r)} \sum\sum_{[m,l]=Z} \eta(m, l)\; x_q^m(r; Z)\, x_p^m(r; Z)\, \hat{B}_l^m$$

Les équations définissant $x_q^m(r; Z)$ sont déduites de [15$d_{1,3}$], la normalisation [15$d_{2,4}$] restant la même.

Les valeurs seront initialisées par

$$[32a] \quad x_q^m(0; Z \leq 2) = \delta_{qm}\; x_q^m(0; Z > 2) = x_q^m(\infty; Z - 1)$$

La relation de récurrence sera tronquée:

$$[32b] \quad x_q^{'m}(r; Z) = x_q^m(r - 1; Z) + \sum\sum_{[p,q] \leq Z} x_p^m(r - 1; Z)\, F_{pq}^{(r-1)}$$

IV-2. *Utilisation du développement en grappes*

Dans le cas général $\prod_{s=0}^{\infty}$ Cle$_s$ est un opérateur de corrélation pouvant en particulier prendre la forme [31*b*] d'un polynome de création–destruction. On peut donc le comparer aux opérateurs écrits dans les méthodes de seconde quantification (24*a*, 25, 27–34).

On sait que ces opérateurs sont "développés en grappes". Convenons d'utiliser ce terme chaque fois qu'un opérateur $\mathbb{O}$ résulte de l'exponentiation d'un polynôme T de création–destruction défini à partir de ses éléments matriciels $\langle \mathbf{t} \rangle$ selon les équations:

$$[33a] \quad \mathbb{O} = e^T = \sum_{k=0}^{\infty} \frac{1}{k!} T^k$$

$$[33b]\quad T = \sum_{z=0}^{N} T_z$$

$$[33c]\quad T_z = \sum \langle j_1'' \ldots j_3'' | t | j_1' \ldots j_3' \rangle X_{j_1''}^{+} \ldots X_{j_3''}^{+} X_{j_1'} \ldots X_{j_3'}$$

Nous pouvons développer en grappes, soit les opérateurs de corrélation, soit les opérateurs de correction linéarisée ordonnés,

$$[34]\quad \mathrm{Cle}_r = e^{G,r}$$

$$[35]\quad \prod_{s=0}^{\infty} \mathrm{Cle}_r = e^{T}$$

L'opérateur T généralise l'opérateur d'excitation dans la méthode de Cizek (24a, 25).

Les relations [34] et [35] entrainent:

$$[36]\quad T = \sum_{r=0}^{\infty} G, r$$

$$[37]\quad T_z = \sum_{r=0}^{\infty} G_z, r$$

D'autre part l'opérateur G, r peut être déterminé par l'éq. [34] en identifiant le développement de Cle_r ordonné en Z, avec un développement de la forme [33a,b,c] appliqué à G, r:

$$[38]\quad \begin{aligned} \mathrm{Cle}_r^{[1]} &= G_1, r \\ \mathrm{Cle}_r^{[2]} &= G_2, r + \frac{1}{2}(G_1, r)^2 \\ \mathrm{Cle}_r^{[3]} &= G_3, r + G_2, r \cdot G_1, r + \frac{1}{6}(G_1, r)^3 \\ \mathrm{Cle}_r^{[4]} &= G_4, r + G_3, r \cdot G_1, r + \frac{1}{2}(G_2, r)^2 \\ &\quad + \frac{1}{2} G_2, r \cdot (G_1, r)^2 + \frac{1}{24}(G_1, r)^4 \text{ etc.}\ldots \end{aligned}$$

$$[39]\quad \begin{aligned} G_1, r &= \mathrm{Cle}_r^{[1]} \\ G_2, r &= \mathrm{Cle}_r^{[2]} - \frac{1}{2}(\mathrm{Cle}_r^{[1]})^2 \\ G_3, r &= \mathrm{Cle}_r^{[3]} - \mathrm{Cle}_r^{[2]}\,\mathrm{Cle}_r^{[1]} + \frac{1}{3}(\mathrm{Cle}_r^{[1]})^3 \\ G_4, r &= \mathrm{Cle}_r^{[4]} - \mathrm{Cle}_r^{[3]}\,\mathrm{Cle}_r^{[1]} - \frac{1}{2}(\mathrm{Cle}_r^{[2]})^2 \\ &\quad + \mathrm{Cle}_r^{[2]}(\mathrm{Cle}_r^{[1]})^2 - \frac{3}{3}(\mathrm{Cle}_r^{[4]})^4 \end{aligned}$$

On en déduit selon [37], [39]

$$[40]\quad \begin{aligned} \langle j_1'' | t | j_1' \rangle &= \sum_{r=0}^{\infty} \langle j_1'' | g,r | j_1' \rangle = \sum_{r=0}^{\infty} \langle j_1'' | \mathrm{Cle}_r^{[1]} | j_1' \rangle \\ \langle j_1'' j_2'' | t | j_1' j_2' \rangle &= \sum_{r=0}^{\infty} \langle j_1'' j_2'' | g,r | j_1' j_2' \rangle \\ &= \sum_{r=0}^{\infty} \Big[\langle j_1'' j_2'' | \mathrm{Cle}_r^{[2]} | j_1' j_2' \rangle \\ &\quad - \frac{1}{2} \langle j_1'' | \mathrm{Cle}_r^{[1]} | j_1' \rangle \langle j_2'' | \mathrm{Cle}_r^{[1]} | j_2' \rangle \Big] \\ \langle j_1'' j_2'' j_3'' | t | j_1' j_2' j_3' \rangle &= \sum_{r=0}^{\infty} \langle j_1'' j_2'' j_3'' | g,r | j_1' j_2' j_3' \rangle \\ &= \sum_{r=0}^{\infty} [\langle j_1'' j_2'' j_3'' | \mathrm{Cle}_r^{[3]} | j_1' j_2' j_3' \rangle \\ &\quad - \langle j_1'' j_2'' | \mathrm{Cle}_r^{[2]} | j_1' j_2' \rangle \langle j_3'' | \mathrm{Cle}_r^{[1]} | j_3' \rangle \\ &\quad + \frac{1}{3} \langle j_1'' | \mathrm{Cle}_r^{[1]} | j_1' \rangle \langle j_2'' | \mathrm{Cle}_r^{[1]} | j_2' \rangle\, \mathrm{Cle}_r^{[1]} j_3' \rangle] \text{ etc.}\ldots \end{aligned}$$

Ce sont les éléments matriciels $\langle \mathbf{t} \rangle$ et $(\mathbf{g}, \mathbf{r})$ qui définissent les opérateurs T et G, r; ce sont les opérateurs $\mathrm{Cle}_r^{[Z]}$ qui définissent les élements $\langle \mathrm{Cle}_r^{[Z]} \rangle$.

Les équations [40] signifient que les éléments matriciels de G_Z, r forment des séries convergentes lorsque $r \rightarrow \infty$ dont la somme est l'élément matriciel, de même forme, de l'opérateur T. Le terme général de chacune de ces séries reçoit une expression utilisant les termes du développement ordonné de Cle_r.

IV-3. *Utilisation de l'Hamiltonien normal*

La forme "normale" de l'Hamiltonien est (24a, 31):

$$\hat{H} - \langle \Omega | \hat{H} | \Omega \rangle = \sum_{12} \langle 1 | \hat{f} | 2 \rangle \,\mathrm{N}\,[X_1^{+} X_2] + \frac{1}{2} \sum_{1234} \langle 12 | \hat{y} | 34 \rangle \,\mathrm{N}\,[X_1^{+} X_2^{+} X_3 X_4]$$

1,2,3,4 désignant les spinorbitales, N le produit normal, $\hat{f}$ contenant une partie de la répulsion interelectronique $\hat{y}$ selon une transformation citée en référence (méthode de Cizek).

On en déduit selon [7c] la matrice que l'on tronquera en fonction de Z

$$E_{[p,q] \leq Z} = \langle \Gamma_q | \hat{H} \hat{B}_p^q | \Gamma_q \rangle$$

le calcul des éléments matriciels de $\hat{H}\hat{B}_p^q$ renvoie à la méthode diagrammatique (23, 24, 31, 33). On déduit $\rho_{pq}^{(r)}[Z]$ selon [15b] et [15c], $F_{pq}^{(r)}[Z]$ selon [14]. Ils sont également tronqués en fonction de $[p, q] \leq Z$. Cle_r selon [28b] ordonné en création–destruction selon [31b], contient les $\hat{B}_l^m$ définis par [26a], les coordonnées $x_q^m(r; Z)$ solutions des équations [32a], [32b] et [15$d_{2,4}$]. La construction des $\mathrm{Cle}_r^{[Z]}$ de création–destruction permettra d'obtenir les $\langle y_Z, r \rangle$, d'où les $\langle T \rangle$.

Il faut souligner que l'expression [42] des éléments matriciels d'énergie d'excitation permet l'usage des diagrammes (24a) ou des tables qui les compilent (33). La différence essentielle avec la méthode utilisée jusqu'à présent est que la résolution de systèmes d'équations non linéaires à multiples inconnues disparait. On remarquera aussi que les concepts d'énergie asymètrique et de prénormalisation ne sont pas utilisés ici. Enfin on n'a pas particularisé la configuration fondamentale.

V. Conclusion

V-1. *Généralisations possibles*

Nous nous bornerons à signaler une perspective, la transcription des calculs indiqués sur les fonctions d'onde en calculs sur les matrices densités qui les traduisent, puis sur la généralisation de ces matrices en "diagrammes moléculaires" (35) précisés par les "opérateurs symètriques fondamentaux" (36). Mais surtout la théorie précédente n'est pas limitée au problème de la corrélation.

V-2. *Résultats acquis*

Parmi les diverses méthodes ouvertes par le concept de potentiel d'erreur, la plus facile à exprimer semble la correction perturbative de l'erreur par l'opposé de ce potentiel et sa correction indéfinie. Remarquant que les états à corriger sont un mélange d'états propres (ou vice versa) l'opérateur qui exprimerait cette correction dans tout l'espace des états ne pourrait être linéaire.

Mais d'autre part pour mettre en oeuvre une méthode de perturbation s'inspirant de la formulation de Schrödinger, il faut associer l'état erroné à un ensemble d'autres considérés comme conséquence d'une même erreur physique. Dès lors on ne peut corriger de cette erreur que les états de la base. Mais on peut construire, sur l'ensemble des corrections ainsi définies, un opérateur de correction, linéaire dans tout l'espace de la base

$$\sum_{\text{base}} |\text{corrigé}\rangle\langle\text{erroné}|$$

il peut être appliqué autant de fois qu'il sera requis. Il se ramène à l'opérateur identique à mesure que la correction devient négligeable, les états corrigés étant devenus les états propres. La discussion montre que la convergence est rapide, chaque correction correspondant à la partie principale de l'erreur restant à corriger.

L'espace des interactions de configuration à l'intérieur duquel ce processus est convergent pourrait être rendu mobile par rapport à l'espace des états, à chaque correction partielle, permettant ainsi d'explorer ce dernier à la recherche de l'état propre.

L'itération de l'opérateur de correction linéarisée du défaut de corrélation conduit à un opérateur de corrélation commun à toutes les configurations. De même que l'opérateur de corrélation, l'opérateur de correction linéarisé peut être écrit comme un polynôme de création–destruction. L'un et l'autre peuvent se développer en grappes, c'est-à-dire qu'on peut en déterminer un transformé par inversion de l'exponentielle. On considère ici le transformé de la correction linéarisée de l'erreur. Ses éléments matriciels successifs ont pour somme les éléments de la matrice d'excitation. Ils sont calculables par perturbation en utilisant l'Hamiltonien normal et l'analyse diagrammatique. On dispose ainsi d'un calcul d'erreur des methodes de seconde quantification qui doit permettre entre autres de discuter les extensions récemment proposées (31, 32) et apparemment aussi d'une méthode alternative pour la pratique.

1. C. A. COULSON et H. C. LONGUET-HIGGINS. Rev. Sci. **85**, 929 (1947); J. LENNARD-JONES *et al.* Proc. R. Soc. Ser. A, **198**, 1 (1949); **198**, 14 (1949); **202**, 155 (1950); **202**, 166 (1950); **202**, 323 (1950); **202**, 336 (1950); **205**, 357 (1951); 541 (1951); etc...; H. C. LONGUET-HIGGINS. Proc. Phys. Soc. **60**, 270 (1948); O. CHALVET, R. DAUDEL, M. ROUX et C. VROELANT. C. R. Acad. Sci. **233**, 1277 (1951); B. H. CHIRGWIN et C. A. COULSON. Proc. R. Soc. **201**, 316 (1950); C. A. COULSON et G. S. RUSHBROOKE. Proc. Cambridge Philos. Soc. **36**, 193 (1940).
2. M. J. S. DEWAR. J. Chem. Soc. 463 (1949); G. W. WHELAND et D. A. MANN. J. Chem. Phys. **17**, 264 (1949); R. S. MULLIKEN. J. Chim. Phys. **46**, 497 (1949); **46**, 675 (1949); W. MOFFITT. Proc. R. Soc. Ser. A, **196**, 510 (1949).
3. A. LAFORGUE. C. R. Acad. Sci. **228**, 1430 (1949); **231**, 439 (1950); J. Chim. Phys. **46**, 568 (1949).
4. A. LAFORGUE. C. R. Acad. Sci. **229**, 1234 (1949).
5. A. LAFORGUE et D. LAFORGUE-KANTZER. C. R. Acad. Sci. **228**, 1935 (1949).
6. O. CHALVET, R. DAUDEL, A. LAFORGUE et C. VROELANT. J. Phys. Chem. **56**, 365 (1952).
7. A. LAFORGUE. Cah. Phys. **42**, 1 (1953).
8. A. LAFORGUE. J. Chim. Phys. **48**, 17 (1951).
9. A. LAFORGUE. C. R. Acad. Sci. **236**, 202 (1953).
10. C. A. COULSON et I. FISCHER. Phil. Mag. **40**, 386 (1949).
11. C. SANDORFY. C. R. Acad. Sci. **232**, 2449 (1949).
12. R. DAUDEL, A. LAFORGUE et C. SANDORFY. Conference on quantum mechanical method in valence theory. 1951.
13. R. DAUDEL et A. LAFORGUE. C. R. Acad. Sci. **233**, 1608 (1951).
14. A. LAFORGUE et C. VROELANT. C. R. Acad. Sci. **234**, 2198 (1952); R. DAUDEL, A. LAFORGUE et C. VROELANT. J. Chim. Phys. **49**, 545 (1952).
15. A. LAFORGUE. C. R. Acad. Sci. **236**, 1356 (1953).
16. A. LAFORGUE. C. R. Acad. Sci. **238**, 1933 (1954).
17. A. LAFORGUE. Thèse Paris (1954); Cah. Phys. **57–58**, 23; **63**, 18; **64**, 11; **59**, 16 (1954).
18. A. LAFORGUE. Sven. Kem. Tidskr. **67**, 383 (1954).
19. A. LAFORGUE. C. R. Acad. Sci. **240**, 2112 (1955).
20. A. LAFORGUE. Actes du Congrès de Caen. 1955. Association française pour l'avancement des Sciences, Paris, p. 127.
21. A. LAFORGUE. Cah. Phys. **112**, 495 (1959).
22. A. LAFORGUE. Colloque sur le calcul des fonctions d'onde moléculaires. *Edité par* C.N.R.S., Paris. 1958. p. 157.
23. (*a*) O. SINANOGLU. Proc. R. Soc. A, **260**, 379 (1961); (*b*) R. K. NESBET. Phys. Rev. **122**, 1497 (1961); O. SINANOGLU. Adv. Chem. Phys. **6**, 315 (1963); **9**, 321 (1965); (*c*) R. J. BUENKER et S. D. PEYERIMHOFF. Theoret. Chim. Acta, **35**, 33 (1974). (*d*) B. HURON, J. P. MALRIEU et P. RANCUREL. J. Chem. Phys. **58**, 5745 (1973).
24. (*a*) J. CIZEK et J. PALDUS. J. Chem. Phys. **45**, 4526 (1966); Adv. Chem. Phys. **14**, 35 (1969); Adv. Quantum Chem. **9**, 105 (1975); (*b*) M. H. ALEXANDER. J. Chem. Phys. **51**, 5650 (1969); (*c*) H. PREUSS. Acta Phys. Acad. Sci. Hung. **27**, 191 (1969).
25. M. SAUTE et A. LAFORGUE. J. Chim. Phys. **75**, 679 (1978).
26. J. A. POPLE, J. S. BINKLEY et R. SEEGES. Int. J. Quantum Chem. **10**, 1 (1976); R. J. BARTLETT. Ann. Rev. Phys. Chem. **32**, 359 (1981).
27. A. LAFORGUE et S. ROSZAK. C. R. Acad. Sci. **297**, 459 (1983).
28. M. SAUTE et A. LAFORGUE. Int. J. Quantum Chem. **16**, 501 (1979).
29. H. P. KELLY. Adv. Chem. Phys. **14**, 35 (1969).
30. O. SINANOGLU. J. Chem. Phys. **36**, 706 (1962).
31. M. SAUTE. Thèse Phys. Theor., Lyon (1972); Thèse Dr. Sci., Reims (1976).
32. J. PALDUS, J. CIZEK, M. SAUTE et A. LAFORGUE. Phys. Rev. A, **17**, 805 (1978).
33. A. LAFORGUE, M. SAUTE et S. ROSZAK. À paraitre.
34. A. LAFORGUE, S. ROSZAK et M. SAUTE. C. R. Acad. Sci. II **299**, 229 (1984).
35. A. LAFORGUE. Cah. Phys. **53**, 9 (1955).
36. J. KOUTECKY et A. LAFORGUE. Int. J. Quantum Chem. **11**, 505 (1977).
37. H. PRIMAS. Modern Quantum Chemistry Istanbul Lectures. Part II. 1965. *Edité par* O. Sinanoglu. Academic Press, New York. 1965. p. 45.

Hartree–Fock instabilities in the trisulphur–trinitride anion

M. BÉNARD
Laboratoire de Chimie Quantique, Université Louis Pasteur, 4 rue Blaise Pascal, 6700 Strasbourg, France

W. G. LAIDLAW[1]
Department of Chemistry, University of Calgary, Calgary, Alta., Canada T2N 1N4

AND

J. PALDUS
Department of Applied Mathematics, University of Waterloo, Waterloo, Ont., Canada N2L 3G1

Received September 10, 1984

This paper is dedicated to Professor Camille Sandorfy on the occasion of his 65th birthday

M. BÉNARD, W. G. LAIDLAW, and J. PALDUS. Can. J. Chem. **63**, 1797 (1985).

Crystallographic evidence indicates that the structure of the trisulfur trinitride anion, $S_3N_3^-$, is planar with equal SN bond lengths. Although the recent literature contains a number of molecular orbital calculations of D_{3h} symmetry there are also calculations which indicate inequivalent nitrogens, suggesting broken symmetry. The results of an investigation of Hartree–Fock instabilities of the *ab initio* molecular orbital description of this system are reported. The D_{3h} solution is indeed singlet stable but there are relatively close-lying C_{2v} broken-symmetry solutions. In the broken-symmetry solutions the π electron network encompasses only five centres; the sixth centre, essentially free of π charge, may be either a sulphur or a nitrogen, thus yielding two distinct broken-symmetry solutions.

M. BÉNARD, W. G. LAIDLAW et J. PALDUS. Can. J. Chem. **63**, 1797 (1985).

Les données cristallographiques indiquent que l'anion trinitrure de soufre, $S_3N_3^-$, a une structure plane avec des longueurs de liaisons SN qui sont égales. Quoique l'on retrouve dans la littérature récente un certain nombre de calculs d'orbitales moléculaires de symétrie D_{3h}, on y trouve également des calculs qui indiquent des azotes non équivalents et ceci suggère une rupture de la symétrie. On rapporte les résultats d'une étude des instabilités de Hartree–Fock pour la description ab initio de l'orbitale moléculaire de ce système. La solution D_{3h} est effectivement stable pour le singulet mais il y a des solutions de symétrie rompue C_{2v} qui y sont assez étroitement associées. Dans les solutions de symétrie rompue, le réseau d'électrons π entoure seulement cinq centres; le sixième centre qui est essentiellement dépourvue de charges π pourrait être soit le soufre soit l'azote et ceci conduit donc à deux solutions distinctes de symétrie rompue.

[Traduit par le journal]

I. Introduction

There has been considerable interest in unsaturated SN compounds as the recent reviews by Roesky (1), Chivers and Oakley (2), and Gleiter (3) attest. There are rings, cages, chains, cations, anions, and neutral species; many of these were made in the last 10 years. The particular focus of this work is the planar $S_3N_3^-$ anion first prepared by Bojes and Chivers in 1977 (4). The tetrabutylammonium salt yields stable yellow crystals which have been analyzed structurally by X-ray diffraction to yield the results depicted in Fig. 1. The bond lengths are 1.60 ± 0.02 Å and the system is planar to within 1°. A similar structure has been reported for this anion in $(Tl^+)_2$ $(S_3N_3^-)$ $(S_4N_5^-)$ (5). Consequently a reasonable representation of the molecular framework is a "hexagon" with bond lengths of 1.60 Å and internal angles of 120°, i.e., the symmetry point group of the nuclei is D_{3h}. The $S_3N_3^-$ anion has 34 valence electrons and, using a Hartree–Fock–Slater (HFS) single determinant wavefunction, Bojes *et al.* reported (6) that 10 of these were π electrons. Thus, the $S_3N_3^-$ anion is a π "electron-rich" system (7). The essential features of the eigenvalue manifold are given in Fig. 2 where it is to be noted that, in addition to the π "bonding orbitals", the degenerate antibonding π^* orbitals $2e''$ are also fully occupied. Bojes *et al.* (6) further characterized this anion in terms of bond orders and charge densities and all six SN bonds were found to be the same, all three nitrogens were equivalent, and all three sulphurs were equivalent.

[1] To whom all correspondence should be addressed.

Following the appearance of the first analysis of $S_3N_3^-$ (6), Bhattacharya and Turner reported CNDO/2 calculations (8) in which all three nitrogens were not equivalent, suggesting that $S_3N_3^-$ could be represented with a localized NSN π bond and a unique charged nitrogen. As such their calculation "broke symmetry" from D_{3h} to C_{2v}. The *ab initio* HFS calculations (7, 9) had, of course, shown no such tendency! Indeed a rather extensive investigation by Smith and co-workers (10) utilizing both a HFS scattered-wave procedure and the CNDO/2 method gave results indicating D_{3h} symmetry. Further a Hartree–Fock calculation by Nguyen and Ha (11), using an extended basis set, also gave a solution with D_{3h} symmetry. Other workers also reported only D_{3h} solutions to the SCF equations for a variety of calculational procedures (12). However, the question remained as to whether the Hartree–Fock results were stable to C_{2v} perturbations, i.e., under what circumstances was symmetry breaking possible.

The past two decades have seen considerable interest in symmetry breaking (cf. the reviews by Fukutome (13*a*) and by Löwdin *et al.* (13*b*)) and the problem has received steady attention since Löwdin formulated his "symmetry dilemma" (14) for the approximate variational wavefunctions in 1963. The response of the system to different variational parameters can provide a useful insight into the sources and mechanism of the Hartree–Fock instabilities. In earlier semiempirical work (15, 16) the ratio of the two- and one-electron interactions (i.e., the ratio γ_{ij}/β_{ij} of the Coulomb and resonance integrals of the Pariser–Parr–Pople π-electron Hamiltonian), representing the coupling constant for these models, was used to drive a given

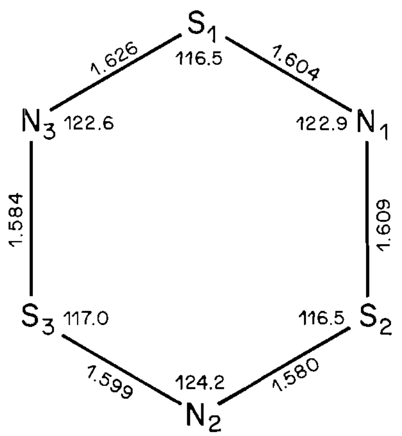

FIG. 1. Structure of the $S_3N_3^-$ anion (bond length in Å).

system to the instability, if present. Since the occurrence of broken-symmetry solutions is a direct consequence of the incorrect description of co-valent bond dissociation provided by the restricted Hartree–Fock method, the internuclear separation(s) can also serve in lieu of the coupling constant, particularly when one employs an *ab initio* Hamiltonian approach (17). Clearly, a large value of the coupling constant enhances the importance of the long range Coulomb interaction relative to the short range chemical forces which are responsible for the chemical bond formation. Such an enhancement will occur automatically in electron-rich or electron-crowded π-electron systems. Consequently, the 10π electron $S_3N_3^-$ anion seems to be a good candidate for the occurrence of the Hartree–Fock instability, at least for the coupling constants (i.e., the SN bond length) which are in the vicinity of their proper equilibrium values.

II. Broken symmetry

In order to establish notation we will review briefly some of the notions associated with symmetry breaking of self-consistent Hartree–Fock wave functions. In the Born–Openheimer approximation, the symmetry operators which leave the nuclear framework invariant commute with the exact Hamiltonian, so that solutions of the Schroedinger equation form a basis for the irreducible representations of the symmetry group, i.e., they are symmetry adapted. Thus,

[1] $H\Psi = E\Psi$ and $[H, R] = 0$ imply that $R\Psi = \lambda\Psi$

where R is a symmetry operator.

However, the Hartree–Fock operator, H_{SCF}, is defined in terms of the self-consistent field given by a density distribution of electrons. It is a non local opeator and in principle need not commute with the point group operators of the nuclear framework. In turn, the calculated Hartree–Fock wave function need not be an eigenfunction of the symmetry operators. As a result the Hartree–Fock wavefunction may exhibit "broken symmetry" — a lower symmetry than that of the nuclear framework. We should emphasize that this is not a Jahn–Teller symmetry distortion insofar as the HOMO-LUMO gap is nonzero; this is a symmetry breaking of the wavefunction, not of the nuclear framework.

To see how this symmetry breaking arises recall that the variational procedure ensures that the solution is a stationary point of the energy, i.e.,

[2] $\delta^{(1)}E = 0$

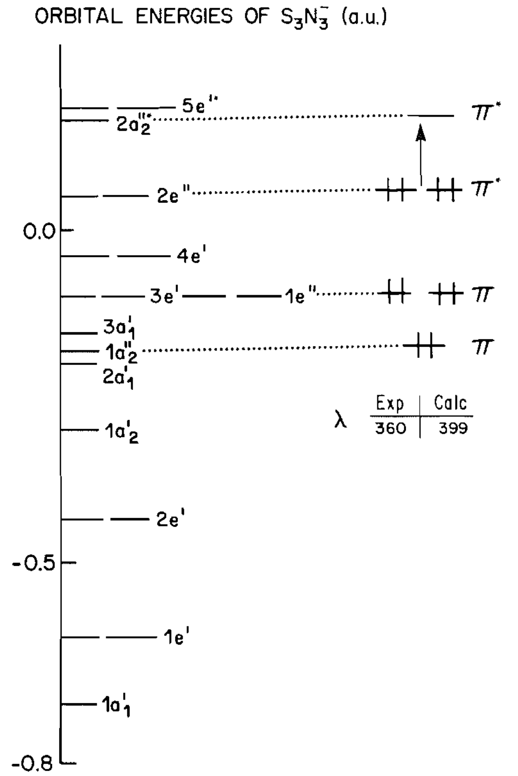

FIG. 2. Orbital energies of $S_3N_3^-$ (au).

where

[3] $E = \langle\Psi|H|\Psi\rangle/\langle\Psi|\Psi\rangle$

However, this stationary point can have complex character, as, for example, pointed out in Fig. 3, the stationary point can be a maximum or a saddle point with reference to a wider class of variations. In this figure we depict an energy surface as a function of bond length and symmetry type. Imagine that this is the SN bond length R in $S_3N_3^-$ and as the figure indicates the surface has a local minimum at R_a with respect to variations which break symmetry to C_{2v}. However, at R_b, a calculation in D_{3h} symmetry is in fact a saddle point and would break symmetry to a lower C_{2v} solution if permitted. The HF solution could break symmetry at the point R_b!

To determine whether a solution would break symmetry one needs to calculate δ^2E in the neighbourhood of the stationary point without imposing any symmetry restriction. If $\delta^2E > 0$ then the system is stable to the variation considered whereas if $\delta^2E < 0$ the system is unstable; hence we need only the sign of δ^2E.

The appropriate formulation of the problem dates back to the work of Thouless in 1961 (18) and a tractable method for spin-independent Hamiltonians was developed by Cizek and Paldus (15) in the late sixties.

One constructs a variational function, Ψ_{BS} for the potentially broken-symmetry solution using, as a basis, the symmetry-adapted solutions obtained at the stationary point of interest. It is worth pointing out that a combination of symmetry-adapted orbitals, belonging to two different irreducible representations, really does allow symmetry breaking. Consider the combination, depicted in Fig. 4, of two symmetry-adapted orbitals π and π^* of a homonuclear diatomic. The combinations $\pi' = \pi \pm \pi^*$ generate an orbital with density around one nucleus only; thus π' is certainly a broken-symmetry orbital. At the N-

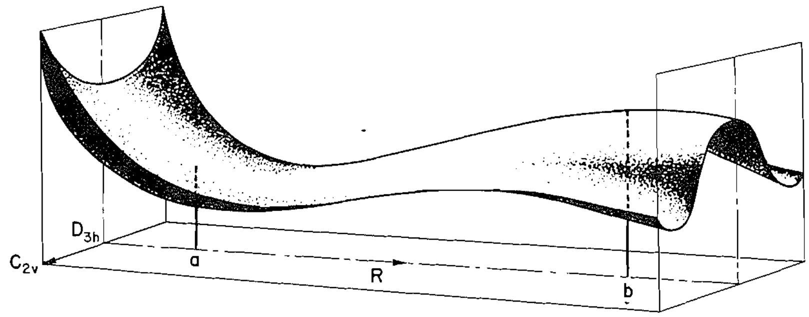

FIG. 3. A complex energy surface with potential for symmetry breaking.

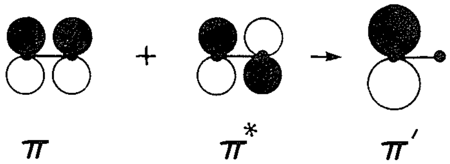

FIG. 4. Formation of a broken symmetry orbital.

electron level such an orbital implies that a general broken-symmetry wavefunction, Ψ_{BS}, can be expressed as a sum of the symmetry-adapted function, Ψ_{SA}, and the functions Ψ_1 and Ψ_2 generated by single and double excitations $\Psi_{SA}(i \to j)$ and $\Psi_{SA}\binom{i\to j}{k \to l}$. Thus

[5] $\Psi_{BS} = \Psi_{SA} + \Psi_1 + \Psi_2$

where

[6] $\Psi_1 = \Sigma d_{ij} \Psi_{SA}(i \to j)$

and

[7] $\Psi_2 = \Sigma d_{ij} d_{kl} \Psi_{SA}\binom{i\to j}{k \to l}$

The second variation, $\delta^2 E$, can be written as a quadratic form in d_{ij}

[8] $\delta^2 E = \Sigma\{d_{ij} d_{kl} A_{ijkl} + (1/2) d_{ij} d_{kl} B_{ijkl} + (1/2) d_{ij} d_{kl} \bar{B}_{ijkl}\}$

where the matrix elements A_{ijkl} and B_{ijkl} are defined by

[9] $A_{ijkl} = \langle i \to j | H - E_{SA} | k \to l \rangle$, $B_{ijkl} = \langle \binom{i\to j}{k \to l} | H - E_{SA} | \rangle$

where H is the Hamiltonian and E_{SA} is the energy of the symmetry-adapted solution at the stationary point of interest.

The sign of $\delta^2 E$ can be determined by calculating the eigenvalues λ_i of the characteristic matrix of the quadratic form given in eq. [8]. As shown by Cizek and Paldus (15) this problem can be broken into a number of subproblems depending on the constraints placed on the broken-symmetry solution. We require that the broken-symmetry solution be a singlet and write the singlet stability problem as

[10] $\begin{pmatrix} \mathbf{A} & \mathbf{B} \\ \bar{\mathbf{B}} & \bar{\mathbf{A}} \end{pmatrix} \begin{pmatrix} \mathbf{D} \\ \bar{\mathbf{D}} \end{pmatrix} = \lambda \begin{pmatrix} \mathbf{D} \\ \bar{\mathbf{D}} \end{pmatrix}$

where the elements of **A** and **B** are defined by eq. [9] and D_i are vectors giving the mixing coefficients d_{ij} corresponding to the broken-symmetry solution $\Psi_{BS,i}$. A positive value of λ_i indicates stability of the symmetry-adapted solution whereas a negative λ_i indicates the existence of a broken-symmetry solution of lower energy.

II. Calculations

For our stability calculations we have utilized a Hartree–Fock procedure with a minimal basis for the internal shells and a double ζ basis set for the valence shell. The basis sets used were those of Huzinaga (20); an 11.7 contracted to 5.3 for sulphur and a 9.5 contracted to 4.2 for nitrogen. The symmetry-adapted D_{3h} solution gave a minimum in energy at the SN bond length of 1.72 Å. The charges on sulphur and nitrogen were calculated to be $q_S = 0.6$ and $q_N = -0.9$ which are somewhat larger than expected but our orbital eigenvalue ordering is similar to that of Nguyen and Ha (11) and of Chivers *et al.* (7). Inclusion of a d orbital basis function (cf. Nguyen and Ha (11)) can lower the distance for minimum HF energy to 1.64 Å so that our basis could certainly be improved; however, for purposes of probing stability it should suffice. In fact, Hartree–Fock instability is induced by the large correlation effects associated with the dissociation of covalent bonds. These effects are not expected to be significantly basis-dependent. For instance, calculations carried out for the hexagonal H_6 model system (21) and for the allyl ion did not produce significant changes as the basis sets were extended. For our stability calculations we employed the "Asterix routine" (22) and we considered excitations involving orbitals between $2E'$ (cf. Fig. 2) and $11E'$ (a total of 41 MO's).

We have calculated the D_{3h} solution at a number of bond lengths R_{SN} from 1.6 to 2.4 Å. In each calculation, all bond lengths R_{SN} are the same, i.e., we consider a uniform expansion of all bonds and we always retain a D_{3h} nuclear framework. From the molecular orbitals in each case we generate the matrix elements A,B for the singlet stability problem outlined earlier. We then solved for the stability eigenvalues λ_i and eigenvectors D_i. If negative λ_i are found we solved the HF equations for the broken-symmetry solutions, using the D_i as a guide to construct the starting vector.

The dependence of the lowest stability eigenvalues, on the internuclear separation R_{SN}, is plotted in Fig. 5. All eigenvalues remain positive up to about 2.0 Å. Thus the symmetry-adapted D_{3h} solution remains stable to all singlet symmetry-breaking variations up to this point. In fact the first negative eigenvalue arises in a subproblem leading to C_{2v} symmetry breaking rather than a C_{3h} symmetry even though C_{3h} is the next lowest symmetry to the D_{3h} starting point. At about 2.0 Å one of the roots has crossed the zero axis, indicating that the stationary D_{3h} solution is no longer stable with reference to a C_{2v} broken-symmetry solution. The critical value of $R_{SN}^{crit} = 1.95$ Å is relatively close to the equilibrium bond distance of 1.60 Å — certainly much closer than is the critical value of $R_{CC}^{crit} \simeq 2.20$ Å in benzene (19) to the equilibrium bond distance of 1.4 Å, or of $R_{HH}^{crit} = 5.8$ Å to the equilibrium value of $R_{HH} = 1.92$ Å in H_6 (17).

In order to analyze the "driving force" for this instability we considered the stability of the π system separately, i.e., we

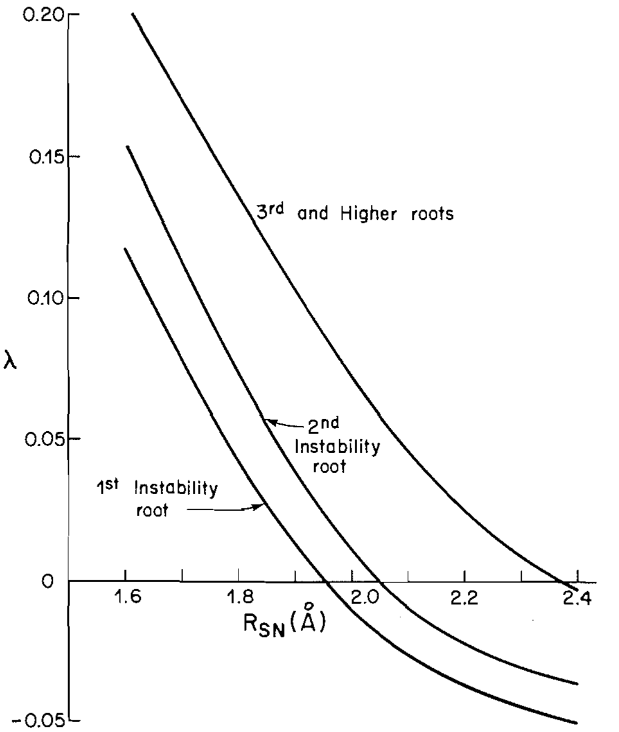

FIG. 5. Dependence of broken symmetry eigenvalues on internuclear distance R_{SN} in $S_3N_3^-$.

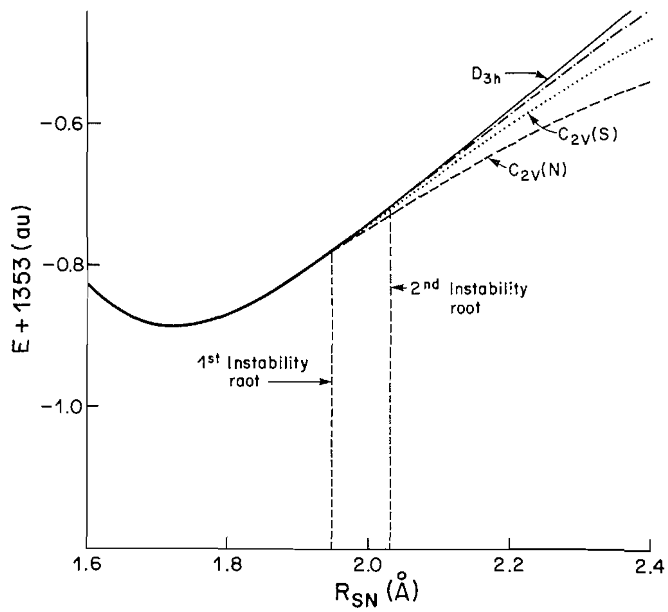

FIG. 6. Dependence of energy of symmetry adapted and broken symmetry HF solutions on internuclear distance R_{SN} in $S_3N_3^-$. Both the C_{2v}(N), - - -, and C_{2v}(S), ·····, solutions arise from the first instability root. The solution denoted by -·-·-· is of C_s symmetry and arises from the second instability root.

considered only excitations of π orbitals. In this case the eigenvalues of the stability problem are much higher, i.e., the system is more stable. For example at R_{SN} = 1.60 Å the stability eigenvalue was 0.28 but *with* $\sigma-\pi$ interaction it was less than half this at 0.12 so that σ-electron rearrangement helps to drive the stability eigenvalue towards its critical value of zero. Clearly both the σ and π interactions are responsible for the relative

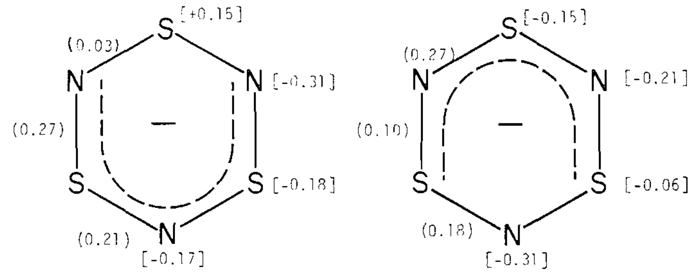

FIG. 7. Charges [ ] and bond overlap population ( ) in the C_{2v} broken symmetry HF solution at R_{SN} = 2.40 Å. (*a*) The C_{2v}(S) or sulphur π-hole solution; (*b*) the C_{2v}(N) or nitrogen π-hole solution.

TABLE 1. Charges, q_i, and bond overlap populations, p_{ij}, at R_{SN} = 2.40 Å*

	Value		
Parameter	D_{3h}	C_{2v} N "π-hole"	C_{2v} S "π-hole"
q_{S_1}	−0.17	−0.15	+0.15
$q_{S_2} = q_{S_3}$	−0.17	−0.06	−0.18
q_{N_4}	−0.17	−0.31	−0.17
$q_{N_5} = q_{N_6}$	−0.17	−0.21	−0.31
$q^{\pi}_{S_1}$	1.44	1.98	0.20
$q^{\pi}_{S_2} = q^{\pi}_{S_3}$	1.44	1.96	2.00
$q^{\pi}_{N_4}$	1.90	0.10	2.00
$q^{\pi}_{N_5} = q^{\pi}_{N_6}$	1.90	2.00	1.9
$p_{S_1N_5}$	0.26	0.28	0.03
$p_{S_2N_5}$	0.26	0.10	0.27
$p_{S_2N_4}$	0.26	0.18	0.21
Energy (au)	−1353.4188	−1353.5407	−1353.4809

*For designation of S_1, N_1, etc., see Fig. 1.

ease of symmetry breaking here.

Perhaps more interesting is that the single C_{2v} root leads to two different broken-symmetry solutions. We find that both C_{2v} broken-symmetry solutions are 10π-electron systems and, as Fig. 6 shows, in the range 2.0 to 2.4 Å they are lower in energy than the D_{3h} symmetry-adapted solution, by as much as 35 and 70 kcal/mol at R_{SN} = 2.4 Å. The difference between the two C_{2v} solutions is intriguing also. Analysis of the orbital overlap populations given in Table 1, shows that in the lower of the C_{2v} broken-symmetry solutions, C_{2v}(N), the 10π-electrons are largely confined to the five atom SNSNS system and the unique nitrogen does not participate in the π system — it is an N π-hole as depicted in Fig. 7(*b*). The other C_{2v} solution, C_{2v}(S), has the 10π-electron system confined to the five atom NSNSN chain and the unique sulphur does not participate in the π system, it is an S π-hole as depicted in Fig. 7(*a*). Further the overlap populations (cf. Table 1) in the two are quite different. For example, at 2.40 Å the N π-hole system has a weak bond between the NSN and SNS fragments whereas the S π-hole has very weak bond (see Fig. 7) between the unique sulphur and the rest of the system.

III. Discussion

The appearance of C_{2v} as the lowest broken-symmetry solution for $S_3N_3^-$ is, at first glance, unexpected. One might have expected that the scheme would follow the D_{3h} subgroup chain, namely:

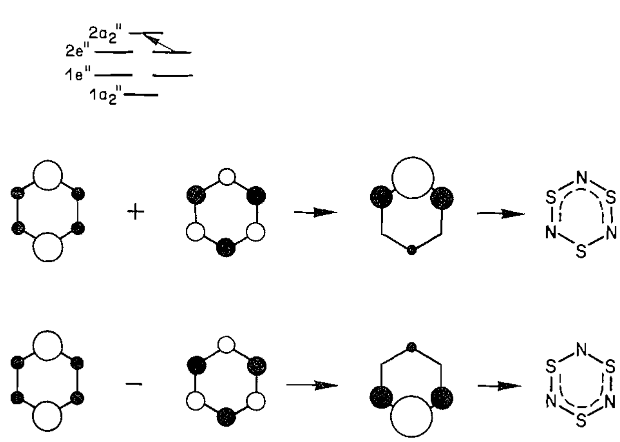

FIG. 8. Excitations generating C_{2v} symmetry.

D_{3h} (symmetry adapted with six equivalent SN bonds)
$\rightarrow C_{3h}$ (with 3 "double" and 3 "single" SN bonds)
$\rightarrow C_{2v}$ (with a unique nitrogen or sulphur)
$\rightarrow C_s$, etc.

For example, the symmetry-breaking route in cyclic polyenes, such as benzene, is first to the next lowest symmetry, i.e., for benzene the symmetry adapted D_{6h} breaks to D_{3h} (Kekulé structures). One can, however, explain this difference by recalling that $S_3N_3^-$ is a π "electron-rich" system where both $1e''$ and $2e''$ (cf. Fig. 2) are doubly occupied. Consequently the first low-lying available excitation is from $2e'' \rightarrow 2a_2''$. As Fig. 8 indicates mixing a $2e''$ orbital with $2a_2''$ leads to broken-symmetry orbitals of C_{2v} type. The mixing of $1e''$ and $2e''$ would, as Fig. 9 indicates, certainly result in C_{3h} type broken-symmetry solutions. However, since these orbitals are fully occupied in the 10π $S_3N_3^-$ system these excitations do not occur! This is of course not the case in the 6π system of benzene where they would be available and where, as mentioned above, one does indeed go to the nearest symmetry type, D_{3h}.

The lifting of the degeneracy for the C_{2v} problem is also different than the usual situation in cyclic polyenes where the plus and minus combination of symmetry-adapted orbitals remain degenerate. As the illustrations in Fig. 8 indicate, the excitation $2e_a'' \rightarrow 2a_2''$ giving either $2e_a'' + c2a_2''$ or $2e_a'' - c2a_2''$ yield different solutions due to the nonequivalence of the S and N sites and it is just these excitations which generate the broken-symmetry C_{2v}(N) and C_{2v}(S) solutions in $S_3N_3^-$. The $1e'' \rightarrow 2e''$ excitations yielding $1e'' \pm c2e''$ would, as Fig. 9 shows, remain degenerate and this is what one sees in benzene and what one would see in $S_3N_3^-$ except that they are not available for symmetry breaking.

The lower energy of the N π-hole broken-symmetry solution compared to the S π-hole can be explained by consideration of the σ and π electron system. An analysis of Table 1 and Fig. 7(*b*) would show that N_4 loses 1.8 π-electrons on going from D_{3h} to C_{2v}(N), (the π population changes from 1.9 to 0.1). However, the total charge on N_4 increases by 0.14 (i.e. -0.17 to -0.31) indicating a gain of about 1.9 σ electrons. Thus the σ electrons "move" in the opposite direction to the π electrons on breaking symmetry from D_{3h} to C_{2v}(N). A similar comparison of D_{3h} and C_{2v}(S) will show that the unique sulphur, S_1, loses about 1.2 π electrons but gains about 0.9 σ electrons so that here too the reorganization of σ and π electrons is in "opposite directions". It is well known (23) that the σ electronegativity of nitrogen is greater than that of sulphur; consequently nitrogen is better able to accept the rather massive σ charge required on the unique atom in the C_{2v} symmetry.

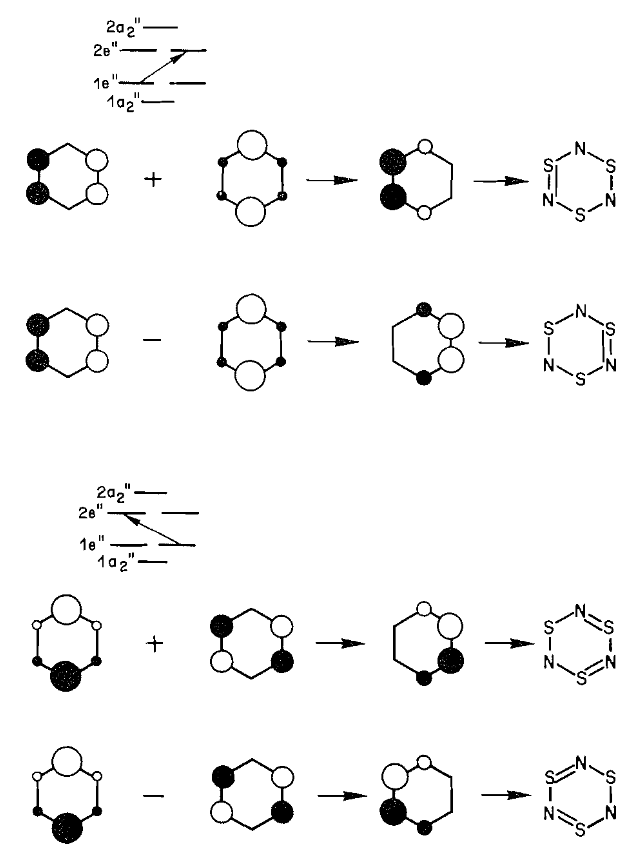

FIG. 9. Excitations generating C_{3h} symmetry.

Further investigation of the role of electronegativity differences in controlling HF instabilities is underway.

IV. Implications

The first and most obvious implication is that the Hartree–Fock D_{3h} solution is stable in the region of $R_{SN} = 1.6-1.8$ Å i.e., in the neighbourhood of the experimental bond length. This supports the contention of Smith and co-workers (10) and our own remarks (9) that the solution obtained by Bhattacharya and Turner (8) is spurious and is not a reflection of symmetry breaking. On a more positive note our investigations allow us to sketch the HF energy surface as in Fig. 10. As this figure shows the HF energy surface becomes more complex as the nuclear framework is uniformly stretched. At 2.0 Å the D_{3h} solution is unstable and at 2.4 Å there are three close-lying 10π electron systems indicating the inadequacy of the HF representation. However, broken-symmetry solutions can, in such a case, give an indication of the preferred distortions and or dissociations. In the lowest of the broken-symmetry solutions, the C_{2v} (N), one of the nitrogens does not even participate in the 10π system and the SN bond between the NSN and SNS fragments is markedly weaker. These are indeed the fragments which have been proposed (24) in the thermal degradation of this system as

[12] 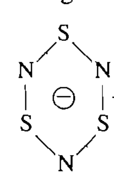

$\rightarrow S_2N^- + N_2S$

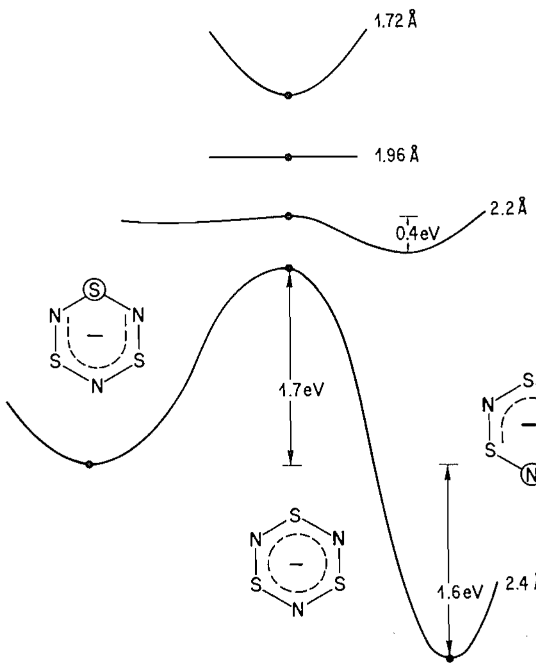

FIG. 10. Essential features of the HF energy surface in $S_3N_3^-$.

Acknowledgements

The authors acknowledge support of a C.N.R.S. (France) grant for MB and NSERC (Canada) grants for WGL and for JP. It is also a pleasure to acknowledge stimulating conversations on this problem with Tris Chivers, Tom Ziegler, and Vedene Smith.

1. H. W. ROESKY. Angew. Chem. Intl. Ed. **18**, 91 (1979).
2. T. CHIVERS and R. T. OAKLEY. Top. Curr. Chem. **102**, 117 (1982).
3. R. GLEITER. Angew Chem. Int. Ed. **20**, 444 (1981).
4. J. BOJES and T. CHIVERS. J. Chem. Soc. Chem. Commun. 953 (1977).
5. H. MARTIN and J. WEISS. Acta Crystallogr. **C39**, 959 (1983).
6. J. BOJES, T. CHIVERS, W. G. LAIDLAW, and M. TRSIC. J. Am. Chem. Soc. **101**, 4517 (1979).
7. T. CHIVERS. Acc. Chem. Res. **17**, 166 (1984).
8. A. A. R. BATTACHARYA, A. BHATTACHARYA, and A. G. TURNER. Inorg. Chim. Acta, **45**, L13 (1980).
9. T. CHIVERS, W. G. LAIDLAW, R. T. OAKLEY, and M. TRSIC. Inorg. Chim. Acta, **53**, L189 (1981).
10. V. H. SMITH, J. R. SABIN, E. BROCLAWIK, and J. MROZEK. Inorg. Chim. Acta, **77**, L101 (1983).
11. M. T. NGUYEN and T-K. HA. J. Mol. Struct. **105**, 129 (1983).
12. (*a*) B. M. GIMARC and N. TRINAJSTIC. Pure Appl. Chem. **52**, 1443 (1980); (*b*) J. GODDARD. University of Guelph, Presentation, CIC Symposium, Montreal, June 1984.
13. (*a*) H. FUKOTOME. Int. J. Quantum Chem. **20**, 955 (1981); (*b*) P. O. LÖWDIN, J.-L. CALAIS, and J. M. CALAZANS. Int. J. Quantum Chem. **20**, 1201 (1981).
14. P. O. LÖWDIN. Rev. Modern Phys. **35**, 496 (1963).
15. J. CIZEK and J. PALDUS. J. Chem. Phys. **47**, 3976 (1967); **53**, 821 (1970); J. PALDUS and J. CIZEK. J. Chem. Phys. **52**, 2919 (1970); **54**, 2293 (1971); Phys. Rev. A, 2268 (1970).
16. W. G. LAIDLAW. Int. J. Quantum Chem. VIII, 87 (1973).
17. M. BÉNARD and J. PALDUS. J. Chem. Phys. **72**, 6546 (1980).
18. D. J. THOULESS. The quantum mechanics of many body systems. Academic Press. 1961.
19. M. BÉNARD. Unpublished.
20. S. HUZINAGA. J. Chem. Phys. **42**, 1293 (1965).
21. J. PALDUS and A. VEILLARD. Chem. Phys. Lett. **50**, 6 (1977); Mol. Phys. **35**, 445 (1978).
22. M. BÉNARD, A. DEDIEU, J. DEMUYMCK, M. M. ROHMER, A. STUCH, R. WIESK, and A. VEILLARD. "Asterix", a system of programs for the Univac 1110, unpublished; M. BÉNARD and M. BARRY. Comp. Chem. **3**, 121 (1979).
23. K. F. PURCELL and J. C. KOTZ. Inorganic chemistry. W.B. Saunder and Co. 1977. pp. 54 to 61.
24. T. CHIVERS, W. G. LAIDLAW, R. T. OAKLEY, and M. TRSIC. J. Am. Chem. Soc. **102**, 5773 (1980).

Hartree–Fock stability and symmetry breaking: oxygen doubly negative ion

JOSEF PALDUS AND JIŘÍ ČÍŽEK

Quantum Theory Group, Department of Applied Mathematics, and Department of Chemistry and (GWC)[2], Waterloo Campus, University of Waterloo, Waterloo, Ontario, Canada N2L 3G1

Received September 10, 1984

This paper is dedicated to Professor Camille Sandorfy on the occasion of his 65th birthday

JOSEF PALDUS and JIŘÍ ČÍŽEK. Can. J. Chem. **63**, 1803 (1985).

The Hartree–Fock stability problem, its relationship to the broken symmetry solutions, and the implications for a molecular nuclear framework distortion are briefly reviewed. The case where no nuclear framework distortion is possible is studied for the oxygen doubly negative ion, using an *ab initio* Slater-type orbital analytical approach, in order to illustrate other possible implications of the symmetry breaking in the independent particle models. It is shown that the existing pure singlet broken symmetry solutions for this ten electron ion, which were obtained earlier by *ad hoc* procedures, follows systematically and straightforwardly from the HF stability problem for the corresponding symmetry adapted solution which shows a strong singlet instability. The chemical and physical implications of this type of symmetry breaking are briefly discussed.

JOSEF PALDUS et JIŘÍ ČÍŽEK. Can. J. Chem. **63**, 1803 (1985).

On passe brièvement en revue le problème de la stabilité des solutions des équations de Hartree–Fock. On a mis en évidence le rôle des solutions de symétrie brisée et les implications par rapport à une distorsion du squelette nucléaire moléculaire. Dans le but d'illustrer d'autres implications possibles du bris de symétrie dans le modèle à particules indépendantes, on a utilisé une approche analytique *ab initio* avec des orbitales du type de Slater pour étudier l'ion doublement négatif de l'oxygène, un cas où il n'y a pas de possibilité de distorsion du squelette nucléaire. On démontre que, pour cet ion à dix électrons, les solutions de symétrie brisée correspondant à des singulets purs, qui ont été obtenues antérieurement par des procédures *ad hoc*, découlent systématiquement et d'une façon directe du problème de la stabilité HF. La solution correspondante adaptée pour la symétrie possède une instabilité forte du type singulet. On discute brièvement des implications chimiques et physiques de ce type de bris de symétrie.

[Traduit par le journal]

Introduction

About 15 years ago we introduced the concepts of singlet, non-singlet (triplet), and doublet stabilities (1, 2) for solutions to the restricted Hartree–Fock (RHF) equations, following the general stability criteria given by Thouless (3). This was just at the time when we had been privileged to establish personal contacts with Professor Camille Sandorfy, shortly after joining the University of Waterloo in 1968. Although we have been very fortunate to work at Waterloo, the time following our exodus from Czechoslovakia was rather difficult for us. Professor Sandorfy, who himself went through a similar ordeal earlier, took a deep interest in both our personal and professional problems, and we shall be forever grateful to him for his continued encouragement and friendship. We thus wish to dedicate this paper to him on the occasion of his 65th birthday as a small token of our respect and gratitude. We chose this topic both for personal reasons and also because the topic is still very much alive today as we shall explain.

It is well known that the exact wavefunction Ψ represents a simultaneous eigenstate of the (Born–Oppenheimer) Hamiltonian H of an atomic or molecular system, and all of its constants of motion (we assume for simplicity that Ψ is nondegenerate). In other words, the exact wavefunction is automatically symmetry-adapted with respect to all symmetry operations which leave H invariant. In contrast, for an approximate variational wavefunction Φ, the requirement of symmetry adaptation represents an additional constraint on the variational problem which can only raise the energy. Thus, one often finds a broken symmetry wavefunction Φ' to yield a lower energy than the symmetry-adapted one. This fact was first clearly stated by Löwdin and is known as the symmetry dilemma (4). A physical or chemical interpretation of the symmetry breaking is far from being straightforward: it may indeed imply a distortion of the molecular framework, or the chemical reaction to proceed in certain ways, but it can also be only a signal of the inadequacy of the given approximation. To give general global criteria for a variational wavefunction to correspond to the absolute minimum of the energy hypersurface is extremely difficult (cf. e.g. ref. 5). We thus restrict ourselves to the requirement that at least locally a given variational solution corresponds to a minimum on the energy hypersurface. Such a solution is referred to as *stable*, while in the opposite case, when the solution is *unstable*, we know that another solution with lower energy must exist. The mathematical formulation of the corresponding stability conditions is achieved in terms of the second variation, or in the usual finite dimensional case in terms of the corresponding Hessian. For the HF wavefunctions this was first done by Thouless (3) and for the Brueckner (maximum overlap) wavefunctions by Paldus, Čížek, and Keating (6).

The Hamiltonians encountered in the molecular electronic structure determination are generally spin-independent, so that both $\hat{S}_z$ and $\hat{S}^2$ operators represent an integral of motion. Using this fact we have formulated the multiplicity-preserving stability conditions. Thus, in the one-determinantal closed shell singlet case we distinguish the *singlet* and the *nonsinglet (triplet) stability conditions* (1): the former preserve the singlet character while the latter do not. Consequently, in case of instability, the former lead to pure singlet single-determinantal broken symmetry solutions (usually it is the space symmetry which gets broken) while the latter lead to the DODS (different orbitals for different spins)-type UHF (unrestricted Hartree–Fock) solutions. Similarly, we define *doublet* and *non-doublet instabilities* (2) in a simple open-shell case, etc. The stability is simply characterized by the vanishing index (the number of negative eigenvalues) of the pertinent Hessian. The eigenvector associated with the lowest negative eigenvalue, in case of an instability, can be shown to define the direction of the steepest descent on the energy hypersurface. (A similar interpretation can be made for higher eigenvalues and corresponding eigenvectors.) Following this direction one finds the wavefunction with lower energy which can be expected to be in the neighborhood of the corresponding broken-symmetry solution (similar to the "catchment regions" of Mezey (7)) and thus can conveniently be used as the starting approximation in iterating the HF equations. More general classification of the HF instabilities, in which not only the spin operators are considered but also the time-reversal (and spatial) symmetry, was given later by Fukutome (8). Stability conditions for RHF triplet states were also formulated (9). More recently, generalizations of projected HF schemes (10, 11), the formulations in terms of gap equations (12) as well as several other developments (13) have appeared. Presently, several excellent reviews are also available (10, 14, 15). We must also mention a close relationship of the HF stability criteria with other methodological developments, particularly with the RPA (random phase approximation) or TDHF (time-dependent Hartree–Fock) approaches (16, 17), and the polarization propagator and Green function approaches (18), but also with the MCSCF (multiconfiguration self-consistent-field) method (19) and the convergence problem for various SCF schemes (20), as well as with other approaches such as the generator coordinate method (21), complex molecular orbital approach (22), cluster expansion method (23), and sudden polarization (24).

For a large number of closed shell systems the symmetry-adapted RHF solutions are singlet-stable. However, for certain systems, particularly the so-called electron-rich systems, the symmetry-adapted RHF solution is singlet-unstable (the non-singlet instability is rather common and the UHF solutions for closed shell systems, which have a lower energy than the corresponding RHF solution, have been known (25) before the non-singlet stability conditions were formulated). Often the pertinent Hessian has more than one negative eigenvalue so that several broken symmetry solutions with lower than RHF energy can be found. The first systems for which the RHF ground state was found to be singlet unstable were cyclic polyene models C_NH_N, $N = 4\nu + 2$, $(\nu = 1, 2, \ldots)$ described by the semiempirical PPP (Pariser–Parr–Pople)-type Hamiltonians (1, 26). Later, a number of other π-systems have been examined and various instabilities found (27–29). Similar instabilities were also found at the *ab initio* level for the H_N systems, modelling a linear hydrogen metal (30), as well as for a number of other systems (31–37), even though the broken-symmetry solutions are often obtained without a prior examination of the character of the symmetry-adapted RHF solution (38–40). The singlet instabilities proved to be particularly important for transition metal complexes and systems containing multiple metal–metal bonds (34, 35, 41, 42), where one often finds the index of the pertinent Hessian, associated with the ground state symmetry-adapted RHF solution, to have very high values (~5). Thus, the stability conditions mentioned above have often been applied to various HF solutions (43–46), and broken-symmetry solutions are today known for many systems, both small and large, treated either at the *ab initio* or semiempirical levels (47).

When an instability of a given HF solution is found, it implies the existence of a broken symmetry solution with lower energy (1, 2), as schematically indicated in Fig. 1*a*. Though the converse does not hold, and a broken symmetry solution with lower energy can exist even when the RHF solution is stable (cf. Fig. 1*b*), no such case is actually known except for

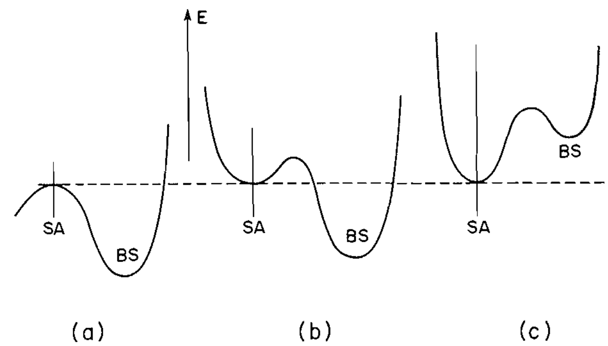

FIG. 1. A schematic representation of the variational energy hypersurface as a function of the variational parameters, indicating the basic possibilities for the relationship between the symmetry-adapted (SA) and broken-symmetry (BS) Hartree–Fock solutions.

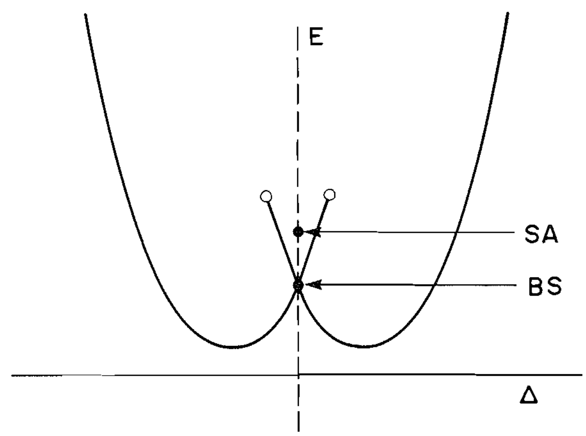

FIG. 2. A schematic representation of the HF potential energy surface as a function of the symmetry-breaking nuclear framework distortion (or vibrational coordinate) Δ. The symmetry adapted solution (SA) can only be obtained for the undistorted structure characterized by $\Delta = 0$. The broken symmetry (BS) solutions for $\Delta = 0$ are degenerate and each can be smoothly continued to $\Delta \neq 0$. The energy of each solution decreases when the nuclear framework is distorted as suggested by the charge density wave of the BS solution (in-phase distortion), both potential energy curves intersecting at the finite angle for undistorted ($\Delta = 0$) structure. When out of phase distortion is made, the energy rises but the solution usually disappears for larger distortions as indicated by open circles.

a simple one-electron model system studied by Katriel and Kventzel (48). The possible types of unstable (*a*) and stable (*b*, *c*) RHF solutions with related broken-symmetry solutions are schematically illustrated in Fig. 1. Clearly, the possibility represented by Fig. 1*b* cannot be *a priori* excluded. We must also stress that Fig. 1 depicts schematically the HF energy hypersurface as a function of variational parameters and *not* the potential energy surface of a given molecule. The latter may in fact possess a highly non-analytic character (as well as the former one, of course, see e.g. ref. 49) if the CDW (charge density wave) associated with the broken symmetry solution implies an actual distortion of the nuclear framework: designating by Δ the parameter (or vibrational coordinate) which characterizes this distortion (e.g., bond length alternation in long polyenes, asymmetric stretch in AB_2 type systems, etc.), the behavior of the potential energy surface as a function of Δ is schematically shown in Fig. 2 (30, 31, 50). (For a general bifurcation structure of the potential energy surface see the last entry in ref. 8.)

The problem of a possible physical significance of various broken symmetry solutions has often been addressed but there is still no simple and universal answer available. Undoubtedly, the instability is often only an indication of the inadequacy of the IPM (independent particle model) picture and of the necessity to use more sophisticated, multi-reference, approaches. This seems particularly to be the case for most small molecular species, although even here the instability can persist to the MC SCF or even CI (configuration interaction) levels (40), and can in fact imply a distorted geometry for certain states or, at least, the existence of vibrational modes with a very flat potential (39), as it does for large and extended systems (see below). A general argument for the possibility of broken symmetry solutions to describe physical phenomena, based on the ideas of Peierls and Yoccoz (51) and BCS theory of superconductivity (52), was extensively discussed by Fukutome (14). A very interesting link between the singlet instabilities (or near-instabilities) and the existence of negative force constant for a normal coordinate along which the pseudo Jahn–Teller distortion or the symmetry reduction may occur was recently established by Deguchi *et al.* (53). In the case of the energetically more efficient spin-symmetry breaking there is also significant evidence for possible chemical or physical implications, as was shown for example by Yamaguchi, Fueno, and collaborators (43, 54) in their classification of organic reaction mechanisms into the bi-radicaloid and non-radicaloid types. Finally, the symmetry breaking is of great importance for the electronic structure of extended systems, particularly for the organic polymers with conjugated double bonds. It is closely related with the so-called dimerization or Peierls' distortion found in linear chains (50, 55–57). These problems received a new impetus with the synthesis of polyacetylene films which show the most remarkable and promising electric, magnetic, optical, and other properties (58). Many important studies, both with semiempirical and *ab initio* Hamiltonians have been carried out in this direction (55–57, 59–66).

We can thus conclude that the existence of a singlet instability for closed shell ground states clearly indicates the need to investigate the studied system in higher approximation than the IPM. Even though the broken-symmetry solution, which inherently accounts for some part of the correlation error, will generally provide a better description of various properties than the RHF solution, great care must be exercised as far as actual distortion of the nuclear framework is concerned. Conversely, the instability may be present even when no space symmetry can be broken, say for the ABC-type triatomics and analogous polyatomic systems (e.g. CH_2CHO, CH_2CN etc.). In this case one can talk about the breaking of an *approximate symmetry* when the system is related with isoelectronic (AB_2 type) system. In a number of cases, however, there is no natural vibrational coordinate which can be related with the appearance of the instability, which thus must have other implications than the nuclear framework distortion. In such cases the instability is solely associated with the structure of the electronic cloud, as for example in the case of core-hole or valence-hole ionized diatomic species. Obviously, one should also have this possibility in mind even when considering polyatomic systems. The clearest form of this type of instability will be found in atomic systems, where no nuclear framework distortion is possible. We thus investigate such a case in this paper, considering the singlet instability of the oxygen doubly negative ion, O^{2-}, and the broken-symmetry solutions associated with it. One such broken-symmetry solution was found empirically by Prat (67). An exploitation of singlet instability conditions helped not only to recover this same solution, and to show that the situation characterized by Fig. 1*a* rather than Fig. 1*b* takes place, but also to find yet another pure singlet broken-symmetry solution with even lower energy (68). We shall also see what physical implications, if any, have the instabilities involving solely the electronic cloud.

Singlet and non-singlet stability conditions

We first briefly recall the explicit form of stability conditions for the closed shell systems. Consider the spin-independent Hamiltonian H,

$$[1] \quad H = Z + V = \sum_i z_i + \sum_{i<j} v_{ij}$$

and a single determinantal closed-shell RHF wavefunction Φ_0,

$$[2] \quad \Phi_0 = \det \|\phi_1\alpha\ \phi_1\beta\ \phi_2\alpha \ldots\ \phi_n\alpha\ \phi_n\beta\|,$$

where α and β are spin up and spin down functions, respectively, and ϕ_i ($i = 1, \ldots, n$) are occupied RHF MO's. Designating the virtual MO's by primed indices, ϕ_i', and labeling the monoexcitations $i \rightarrow j'$, arranged in some arbitrary but fixed order, by the single index u, $u \equiv u(i \rightarrow j')$, we can state the stability conditions as follows (1, 2). The HF solution [2] is singlet (x = s) or non-singlet (triplet) (x = t) stable, if the Hessian

$$[3] \quad \begin{vmatrix} \mathbf{A}^x & \mathbf{B}^x \\ \bar{\mathbf{B}}^x & \bar{\mathbf{A}}^x \end{vmatrix}$$

has only positive eigenvalues. The square matrices $\mathbf{A}^x$, $\mathbf{B}^x$ (x = s, t), whose rows and columns are labeled with all possible monoexcitations u, have the form

$$[4] \quad \begin{aligned} A^t_{uv} &\equiv \langle i \rightarrow j' | A^t | k \rightarrow l' \rangle \\ &= \epsilon_{j'}\delta_{j'l'} - \epsilon_i\delta_{ik} - \langle kj' | \hat{v} | il' \rangle \\ B^t_{uv} &= -\langle j'l' | \hat{v} | ki \rangle \\ A^s_{uv} &= A^t_{uv} + 2\langle kj' | \hat{v} | l'i \rangle \\ B^s_{uv} &= B^t_{uv} + 2\langle j'l' | \hat{v} | ik \rangle \end{aligned}$$

where ϵ_i designate HF canonical orbital energies, $\langle ij | \hat{v} | kl \rangle$ are the two-electron interaction matrix elements in the MO basis $\langle \phi_i\phi_j | \hat{v} | \phi_k\phi_l \rangle$, and $\bar{\mathbf{X}}$ designates the complex conjugate of $\mathbf{X}$.

When $\mathbf{A}^x$ and $\mathbf{B}^x$ (x = s, t) are real, we can further factorize the Hessian [3] and instead consider the matrices (1, 2)

$$[5] \quad (\mathbf{A}^x \pm \mathbf{B}^x)$$

The relationship between the eigenvectors of [3] and [5] is easily found (1, 2, 28). Finally, designating the eigenvector of [3] associated with the lowest eigenvalue λ_0 by $\boldsymbol{d} = \|d_{i\rightarrow j'}\|$, the trial wavefunction $\Phi(\kappa)$,

$$[6] \quad \Phi(\kappa) = \det \|\psi_1\alpha\ \psi_1\beta\ \psi_2\alpha \ldots \psi_n\alpha\ \psi_n\beta\|$$

with

$$[7] \quad \psi_i = \phi_i + \kappa \sum_{j'} d_{i\rightarrow j'}\phi_{j'}$$

gives the direction of the steepest descent ($\lambda_0 < 0$) or the slowest ascent ($\lambda_0 > 0$) on the mean-energy hypersurface, given by

$$[8] \quad E(\kappa) = \langle \Phi(\kappa) | \hat{H} | \Phi(\kappa) \rangle / \langle \Phi(\kappa) | \Phi(\kappa) \rangle$$

TABLE 1. Symmetry adapted and two broken symmetry pure singlet single determinantal analytic HF solutions for O^{2-} using C STO basis (69)

	ζ	Symmetry adapted		Broken symmetry D-type		Broken symmetry P-type	
		C_1	C_2	C_{1s}	C_{2s}	C_{1s}	C_{2s}
1s	7.6169	0.89703329	−0.20152875	0.89672766	−0.19498540	0.89659302	−0.19272560
1s	12.2200	0.06382970	−0.01235049	0.06394390	−0.01765727	0.06399675	−0.01955873
2s	2.7615	0.00416833	0.70968220	0.00424202	0.74660245	0.00426314	0.76053416
2s	7.0898	0.05143088	−0.08240032	0.05165880	−0.09393527	0.05175945	−0.09812775
2s	1.4861	−0.00059170	0.40237427	−0.00071195	0.36807258	−0.00075519	0.35498446

	ζ	Symmetry adapted C_{2p}	Broken symmetry D-type		Broken symmetry P-type		
			$C_{2p}(m = \pm 1)$	$C_{2p}(m = 0)$	$C_{2p}(m = -1)$	$C_{2p}(m = 0)$	$C_{2p}(m = 1)$
2p	1.5566	0.59510037	0.66669126	0.44348729	0.37929611	0.67921088	0.68635610
2p	3.4300	0.29158910	0.35914358	0.10909184	0.06600694	0.36604473	0.37475190
2p	0.4302	0.51518380	−0.07801201	2.2322808	2.5123643	−0.04423676	−0.00544717
2p	0.5501	−0.13409263	0.15881511	−1.5655839	−1.8186695	0.09637648	0.03722407
2p	8.1268	0.01046048	0.01059886	0.01006973	0.00930318	0.01059185	0.01011568

TABLE 2. Symmetry adapted and two broken symmetry pure singlet single determinantal analytic HF solutions for O^{2-} using H basis (70)

	ζ	Symmetry adapted		Broken symmetry D-type		Broken symmetry P-type	
		C_{1s}	C_{2s}	C_{1s}	C_{2s}	C_{1s}	C_{2s}
1s	12.7577210	0.07790863	0.00417542	0.07793731	0.00318141	0.07794958	0.00296282
1s	7.0933082	0.95484232	−0.26350014	0.95469559	−0.26740582	0.95464118	−0.26806414
3s	8.9708141	−0.03357747	−0.02650787	−0.03344653	−0.03335632	−0.03340379	−0.03475910
2s	2.7536019	0.00280790	0.69343133	0.00295507	0.74107646	0.00301103	0.75017136
2s	1.5266549	−0.00010910	0.40903619	−0.00030061	0.36378359	−0.00035315	0.35509378

	ζ	Symmetry adapted C_{2p}	Broken symmetry D-type		Broken symmetry P-type		
			$C_{2p}(m = \pm 1)$	$C_{2p}(m = 0)$	$C_{2p}(m = -1)$	$C_{2p}(m = 0)$	$C_{2p}(m = 1)$
2p	4.9957954	0.08475623	0.09234045	0.02798305	0.01600424	0.09156060	0.09069900
2p	2.4493782	0.48127389	0.63711724	0.18093053	0.11497113	0.65067164	0.67290908
2p	1.0421145	0.46702474	0.39749172	0.18069158	0.09877251	0.38237784	0.35675130
2p	0.1651966	0.34191712	−0.01331587	0.90688484	0.96093625	−0.01429082	−0.01455778

as a function of the mixing parameter κ. In other words, the eigenvector components $d_{i \rightarrow j'} \equiv d_u$ give the ratios in which the virtual orbitals must be admixed to the occupied orbitals in order to obtain a trial function corresponding to the direction of the steepest descent (slowest ascent) at the studied point represented by Φ_0 (1, 2, 28). We shall exploit this procedure to find the starting point for the usual SCF iterative method, which will converge to the broken-symmetry solution associated with a given negative root of the singlet stability problem.

Symmetry-adapted RHF solutions for O^{2-}

We shall use analytic HF solutions with the orbitals (i.e., "molecular" orbitals) expressed as linear combinations of Slater-type orbitals (STO's). The Hartree–Fock–Roothaan equations are then used to determine the linear coefficients in this expansion. We shall exploit two different bases in order to be able to discern the basis dependence of our considerations as much as possible. The first basis is taken from an early study of Clementi and McLean (69) and will be designated as the C-basis for short. The second basis, referred to as the H-basis, is that of Huzinaga and collaborators (70).

The HF problem for doubly negative ions has been often plagued with convergency problems, particularly when the usual SCF iterative procedure for solving of Hartree–Fock–Roothaan equations is employed (69, 71–73). These problems are further amplified in the numerical integration schemes (74), where it is generally impossible to obtain a converged HF solution (75).

We have encountered no difficulty in solving the pertinent Hartree–Fock–Roothaan SCF equations when we proceeded as follows. We have first increased the nuclear charge in order to obtain a neutral system and subsequently lowered the nuclear charge, in sufficiently small steps when necessary, always using the converged solution for higher nuclear charge as the initial approximation. In the studied case we started with the Ne atom ($Z = 10$), proceeding via F^- ($Z = 9$) and, after several steps, reaching O^{2-} ($Z = 8$). The converged solutions, given in Tables 1–3, are practically identical with those obtained earlier (70).

Stability calculation and broken-symmetry solutions

We have next applied the singlet and non-singlet stability conditions (see above) to the symmetry-adapted RHF solutions obtained for the O^{2-} ion. The Hessians [5] can be further factorized using the spatial symmetry of the problem and the relevant subproblems can be conveniently labeled by the change in the magnetic quantum number m. Rather than to restrict ourselves to the ion O^{2-}, it is instructive to follow a few

TABLE 3. Total HF energy (E), one- and two-particle HF energies (E_1 and E_2) and orbital energies ϵ_i (all in au's) for the symmetry-adapted and broken-symmetry HF solutions for the O^{2-} ion with both C and H STO bases (69, 70)

	Value					
	C			H		
Parameter	SA	D-type	P-type	SA	D-type	P-type
E	−74.48442081	−74.52342673	−74.55067490	−74.50712723	−74.60124816	−74.63511929
E_1	−108.36912568	−106.69988996	−106.09343605	−107.74699828	−105.26882899	−104.75186577
E_2	33.88470486	32.17646323	31.54276115	33.23987105	30.66758082	30.11674648
ϵ_{1s}	−20.04764922	−20.243963	−20.315934	−20.12626670	−20.426798	−20.486311
ϵ_{2s}	−0.62861241	−0.81983662	−0.88915855	−0.70445197	−0.99674781	−1.0574566
$\epsilon_{2p}(m = -1)$		−0.13189108	0.14959442		−0.31015432	0.07362854
$\epsilon_{2p}(m = 0)$	0.12546792	0.15409991	−0.20575861	0.06569686	0.07702090	−0.37332864
$\epsilon_{2p}(m = 1)$		−0.1318910	−0.24270050		−0.31015432	−0.41571933

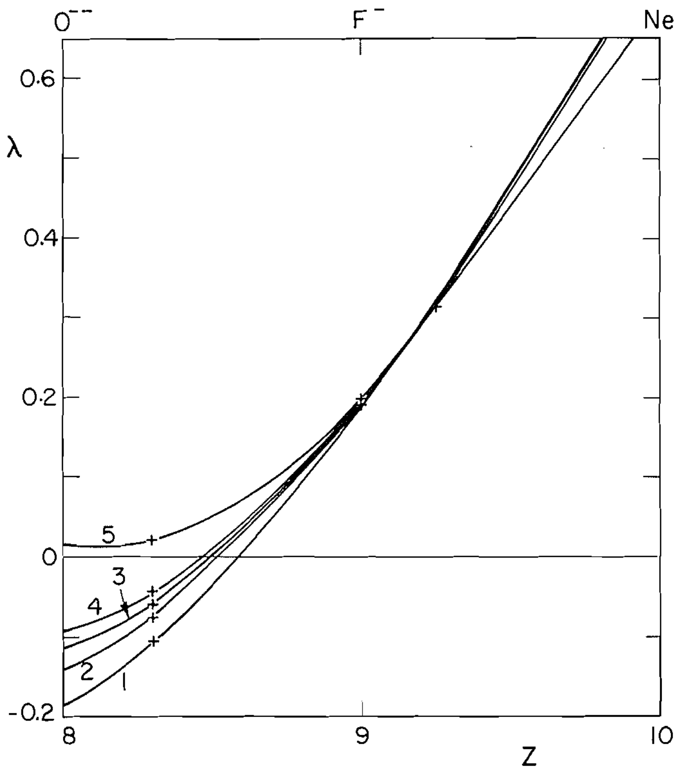

FIG. 3. The dependence of the first three triplet (*1–3*) and singlet (*3–5*) stability roots λ as a function of the nuclear charge Z for the 10-electron atomic system. The points Z = 8, 9, and 10 correspond to O^{2-}, F^-, and Ne atoms, respectively, as indicated at the top of the figure. Note that the third triplet stability root ($\mathbf{A}^t + \mathbf{B}^t$) is identical to the lowest singlet stability root ($\mathbf{A}^s + \mathbf{B}^s$), both represented by the curve *3*. The lowest singlet stability root (*3*) is triply degenerate and the second one (*4*) is quintuply degenerate.

lowest roots of the stability problem as a function of the nuclear charge Z, $8 \leq Z \leq 10$. While no negative roots are found for either the Ne or F^- cases, the three lowest triplet instability roots cross zero and become negative at about $Z \sim 8.6$. These are immediately followed by the two lowest singlet instability roots. In fact, the lowest singlet instability root, arising from the ($\mathbf{A}^s + \mathbf{B}^s$) subproblem, is identical to the third ($\mathbf{A}^t + \mathbf{B}^t$) root (see Fig. 3). The lowest singlet instability root is triply degenerate and occurs in the $\Delta m = 0$ and $\Delta m = \pm 1$ subproblems, while the second lowest root is quintuply degenerate, occurring in all Δm = 0, ±1, and ±2 subproblems. Consequently, we

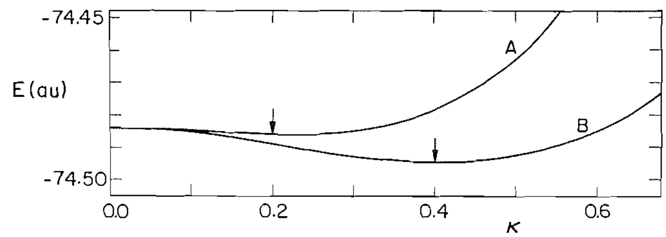

FIG. 4. Dependence of the mean energy value E (in au) on the mixing parameter κ, eqs. [6], [7], for O^{2-} with the C STO basis (69), for the singlet stability roots *3* and *4* of Fig. 3.

refer to these roots, and to the corresponding broken-symmetry solutions, as being of the P and D type, respectively.

In order to find the corresponding broken-symmetry solutions we first optimize the energy [8] as a function of the mixing parameter κ, eqs. [6], [7]. This energy mean-value dependence is shown in Figs. 4 and 5 for the cases of C and H bases, respectively. The Hartree–Fock solution corresponding to the minimum energy is then used as the starting point in solving iteratively the Hartree–Fock–Roothaan equations (without any constraints placed on the individual orbitals). The convergence is often rather slow and over 100 iterations may be required to achieve the desired accuracy. The resulting broken symmetry solutions of both P and D types are given in Tables 1–3.

The D-type solution, associated with the second lowest root of the stability problem, is identical to the solution found earlier by Prat (67). In this solution, the $m = +1$ and $m = -1$ $2p$ orbitals are still identical while the $m = 0$ $2p$ orbital is distinct. It is this unique orbital, whose orbital energy remains to be positive (note that all three (identical) $2p$ orbitals in the symmetry-adapted case have positive orbital energies).

The lowest root of the Hessian [3] yields another broken symmetry solution, which is referred to as the P-type solution (see Tables 1–3). In this case all three $2p$ orbitals are distinct, even though there is a great similarity between the $m = 0$ and $m = +1$ orbitals, while the $m = -1$ orbital, which has again positive orbital energy, is unique. Clearly, using the eigenvectors associated with other degenerate roots of the stability problem we could obtain analogous solutions characterized by other distribution of magnetic quantum numbers.

Discussion

We first briefly examine the character of obtained broken symmetry solutions. To get a better idea of the type and extent

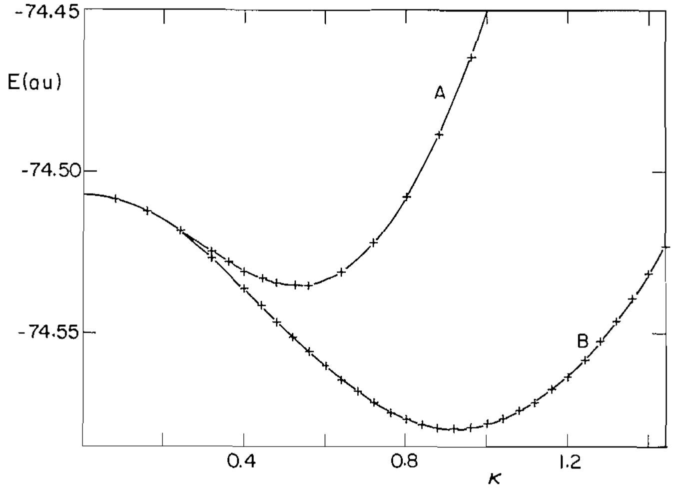

FIG. 5. Same as Fig. 4 for the H STO basis (70).

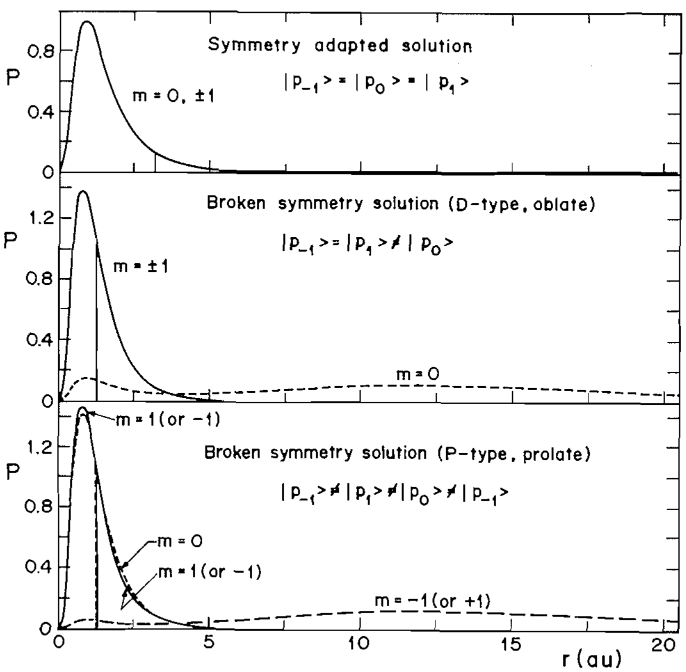

FIG. 6. The radial charge distribution P, eq. [10], as a function of the radial distance r (in au) for the symmetry-adapted and broken-symmetry solutions of the prolate and oblate types (see the text for details).

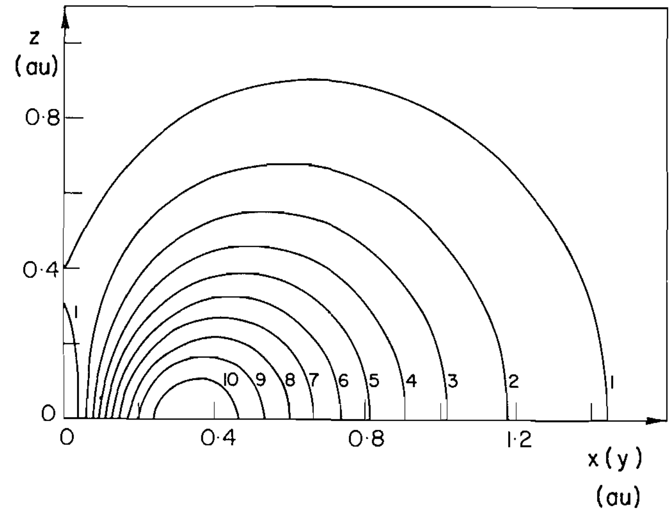

FIG. 7. Angular distribution of the electron density for the oblate D-type broken symmetry solution of the O^{2-} ion (with the H basis).

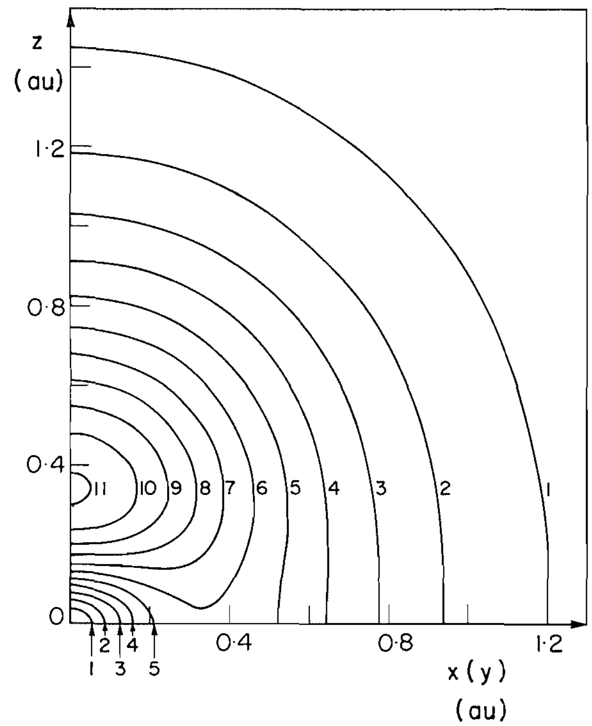

FIG. 8. Same as Fig. 7 for the prolate P-type broken-symmetry solution.

of the symmetry breaking involved, we first examine the radial density distribution for the p-orbitals in both symmetry-adapted and broken-symmetry cases (we present only the results obtained with the H basis, since the C basis results are very similar). Designating by $\gamma_m^{\mathrm{rad}}(r)$ the radial component of the one-density matrix $\gamma(1|1)$,

$$[9] \quad \gamma_m^{\mathrm{rad}}(r) = \frac{2}{\pi} \sum_{\mu,\nu} C_\mu^{(m)} C_\nu^{(m)} (\zeta_\mu \zeta_\nu)^{5/2} r^2 \exp\left[-(\zeta_\mu + \zeta_\nu) r\right]$$

where $C_\mu^{(m)}$ are pertinent expansion coefficients given in Table 2, we have plotted the radial charge distribution P,

$$[10] \quad P(r) = \frac{4\pi}{3} r^3 \gamma_m^{\mathrm{rad}}(r)$$

as a function of the radial distance r, in Fig. 6. We thus find that compared to the symmetry-adapted solution, two $2p$ orbitals for each broken symmetry solution contract while the third one becomes very diffuse. Depending on whether the diffuse orbital is associated with $m = 0$ or $m \neq 0$ $2p$ orbital, we get two distinct types of the symmetry breaking, the latter one being slightly more efficient in the energy lowering.

The angular distribution of the electron density for the two broken symmetry solutions is shown in Figs. 7 and 8. We see that the D-type broken-symmetry solution gives the electron distribution of the oblate-top type, while that of the lowest energy P-type solution can be characterized as being of the prolate-top type. In each case we see a clear tendency of electrons to "escape", and thus to lower the ionicity. Qualitatively, this escape would be expected to be more efficient energy-wise for the prolate-top deformation as is indeed the case (note,

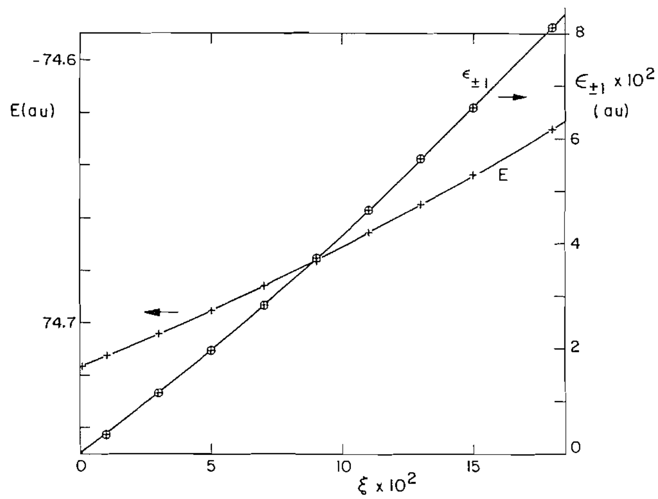

FIG. 9. Dependence of the total HF energy E (in au) and of the highest occupied HF orbital energy $\epsilon_{\pm}$ (in au) on the orbital exponent ζ of the most diffuse STO in the basis, for the lowest energy broken symmetry solution of O^{2-} and the H basis (70) (for which $\zeta = 0.1651966$).

however, that only the D-type solution possesses the exact rotational symmetry about the z axis). These broken symmetry solutions can thus be regarded as a clear indication of the physical instability of the O^{2-} ion, at least at the HF level of approximation. This is also the reason why no convergence was achieved with the numerical HF programs (74, 75), even when the nuclear charge was slowly decreased as explained above for the analytic-type solutions used here. While the F^- solution could be obtained without any difficulty, no converged solution was obtained for $Z < 8.5$, while the orbitals were showing a tendency to become plane waves (75). This tendency is clearly restricted by using a finite STO basis of the analytic approach, which confines the electrons to a more or less limited part of the space. A very similar effect could be achieved by placing the ion into a spherical cavity in an infinite dielectric medium.

In order to clearly demonstrate the tendency of electrons to "escape", we have performed a series of calculations with varying orbital exponents. In particular, varying the orbital exponent of the most diffuse orbital ($\zeta = 0.1651966$ in the H basis), we observe that the electron pair occupying this orbital has a tendency to ionize. As Fig. 9 shows, the total energy decreases with increasing diffuse character of the highest orbital, and its (positive) orbital energy gradually approaches zero as ζ does. We see already from Tables 2 and 3 that it is this most diffuse STO which is by far the highest lying orbital with positive energy in both broken-symmetry solutions. This is a clear indication that O^{2-} wants to rid itself of both excess electrons, since we are within the closed shell formalism. Should the spin-symmetry breaking be allowed, only one electron would leave leaving the stable O^- ion (68).

We thus see that in this particular case the space symmetry breaking, as implied by the singlet instability (triplet instability implying a similar result, see e.g. ref. 68) is indicative of the physical instability of the system considered. The broken symmetry solutions clearly show the tendency of the excess electrons to occupy free-electron, continuum states (73, 75). It would of course be interesting to study the HF solutions of the O^{2-} ion placed in the center of a spherical cavity in an infinite dielectric medium. In this way, the situation encountered in actual systems, be it a crystal lattice or a liquid, could be modelled. The dielectric surrounding would have a similar effect as the truncation of the AO basis, since it would represent a barrier for the electronic cloud, thus effectively stabilizing the symmetry-adapted O^{2-} solutions.

In concluding we would like to stress that the example studied in this paper amply illustrates the usefulness of the HF stability criteria, which are easy to apply, and which can provide useful information about the possible broken-symmetry solutions as well as to facilitate their systematic determination.

Acknowledgements

This research has been supported by an NSERC Grant-in-Aid of Research which is hereby gratefully acknowledged. We also wish to thank Dr. Chin Wong for helping with numerical computations and to Dr. R. F. Prat for stimulating discussions.

1. J. ČÍŽEK AND J. PALDUS. J. Chem. Phys. **47**, 3976 (1967).
2. J. PALDUS and J. ČÍŽEK. Chem. Phys. Lett. **3**, 1 (1969); J. Chem. Phys. **52**, 2919 (1970).
3. D. J. THOULESS. The quantum mechanics of many body systems. Academic, New York. 1961.
4. P.-O. LÖWDIN. Rev. Mod. Phys. **35**, 496 (1963).
5. N. MOISEYEV and J. KATRIEL. Intern. J. Quantum Chem. **10**, 1011 (1976).
6. J. PALDUS, J. ČÍŽEK, and B. KEATING. Phys. Rev. **A8**, 640 (1973).
7. P. G. MEZEY. Theor. Chim. Acta, **58**, 309 (1981).
8. H. FUKUTOME. Prog. Theor. Phys. **52**, 115 (1974); **52**, 1766 (1974); **53**, 1320 (1975).
9. Y. YOSHIOKA, K. YAMAGUCHI, and T. FUENO. Mol. Phys. **35**, 33 (1978).
10. P.-O. LÖWDIN, J.-L. CALAIS, and J.-M. CALAZANS. Intern. J. Quantum Chem. **20**, 1201 (1981).
11. P. KARADAKOV and O. CASTAÑO. Intern. J. Quantum Chem. **22**, 1033 (1982); **24**, 453 (1983).
12. J.-L. CALAIS. Theor. Chim. Acta, **61**, 135 (1982); B. SYKJA and J.-L. CALAIS. Intern. J. Quantum Chem. **25**, 331 (1984).
13. V. R. BLOK. Zh. Fiz. Khim. **52**, 1117 (1978); M. MESTECHKIN. Intern. J. Quantum Chem. **13**, 469 (1978); **15**, 601 (1979); F. A. MATSEN and C. J. NELIN. Intern. J. Quantum Chem. **15**, 751 (1979); R. M. ABBASOV, V. I. PUPYSHEV, and N. F. STEPANOV. Vestnik Moskov. Univ. Ser. Khim. **22**, 351 (1981).
14. H. FUKUTOME. Intern. J. Quantum Chem. **20**, 955 (1981).
15. A. B. SANNIGRAHI and B. GUHA NIYOGI. J. Sci. Ind. Res. **40**, 502 (1981).
16. N. S. OSTLUND. J. Chem. Phys. **57**, 2994 (1972); K. D. JORDAN. Intern. J. Quantum Chem. Symp. **7**, 491 (1973); O. MATSUOKA and H. ITO. Theor. Chim. Acta, **39**, 111 (1975); J. O. ZWICKER and R. YARIS. J. Chem. Phys. **62**, 1276 (1975).
17. P. JØRGENSEN. Ann. Rev. Phys. Chem. **26**, 539 (1975); J. ODDERSHEDE, P. JØRGENSEN, and N. H. F. BEEBE. J. Chem. Phys. **63**, 2996 (1975); P. JØRGENSEN, J. ODDERSHEDE, and M. RATNER. J. Chem. Phys. **61**, 710 (1974); Y. ÖHRN and J. LINDERBERG. Intern. J. Quantum Chem. **15**, 343 (1979).
18. J. ODDERSHEDE, P. JØRGENSEN, and N. H. F. BEEBE. Chem. Phys. **25**, 451 (1977); G. H. F. DIERCKSEN, N. E. GRUNER, and J. ODDERSHEDE. Comp. Phys. Commun. **30**, 349 (1983); K. TOYODA, T. IWAI, and O. TANIMOTO. Prog. Theor. Phys. **54**, 333 (1975); K. TOYODA and O. TANIMOTO. Prog. Theor. Phys. **57**, 1178 (1977); L. S. CEDERBAUM and W. DOMCKE. J. Chem. Phys. **66**, 5084 (1977).
19. J. W. DOWNING, J. MICHL, P. JØRGENSEN, and E. W. THULSTRUP. Theor. Chim. Acta, **32**, 203 (1974); E. DALGAARD and P. JØRGENSEN. J. Chem. Phys. **69**, 3833 (1978); E. DALGAARD. Chem. Phys. Lett. **65**, 559 (1979); W. H. FINK, A. BANERJEE, and J. SIMONS. J. Chem. Phys. **79**, 6104 (1983).
20. D. H. PHILLIPS and J. C. SCHUG. J. Chem. Phys. **61**, 1031

(1974); J. DANCZ and K. D. JORDAN. J. Chem. Phys. **61**, 2977 (1974); B. H. LENGSFIELD and J. C. SCHUG. Chem. Phys. Lett. **57**, 442 (1978); J. DOUADY, Y. ELLINGER, R. SUBRA, and B. LEVY. Comp. Phys. Commun. **17**, 23 (1979); J. Chem. Phys. **72**, 1452 (1980); A. BRUCENA, P. VERMEULIN, P. ARCHIREL, and G. BERTHIER. Intern. J. Quantum Chem. **20**, 1285 (1981); R. CARBO, L. DOMINGO, and J. J. PERIS. Adv. Quantum Chem. **15**, 215 (1982); J. C. FACELLI and R. H. CONTRERAS. J. Chem. Phys. **77**, 1076 (1982); **79**, 3421 (1983); F. MOSCARDO and J. R. ALVAREZ COLLADO. Phys. Rev. A**19**, 463 (1979); R. SEEGER and J. A. POPLE. J. Chem. Phys. **66**, 3045 (1977); P. G. MEZEY, O. P. STRAUSZ, and R. K. GOSAVI. J. Comput. Chem. **1**, 178 (1980).
21. B. LASKOWSKI, J. DIAMOND, A. WALEH, and B. HUDSON. J. Chem. Phys. **69**, 5222 (1978).
22. J. HENDEKOVIC. Chem. Phys. **9**, 105 (1975); Theor. Chim. Acta, **41**, 79 (1976), Intern. J. Quantum Chem. **10**, 1025 (1976).
23. K. HIRAO and H. NAKATSUJI. J. Chem. Phys. **69**, 4535 (1978); **69**, 4548 (1978).
24. V. BONAČIĆ-KOUTECKÝ and SHINGO-SHIMARU. J. Am. Chem. Soc. **99**, 8134 (1977); G. BERTHIER, B. LEVY, and L. PRAUD. Gaz. Chim. Ital. **108**, 377 (1978); J.-P. MALRIEU and G. TRINQUIER. Theor. Chim. Acta, **54**, 59 (1979); M. PERSICO and V. BONAČIĆ-KOUTECKÝ. J. Chem. Phys. **76**, 6018 (1982); V. BONAČIĆ-KOUTECKÝ, L. POGLIANI, M. PERSICO, and J. KOUTECKÝ. Tetrahedron, **38**, 741 (1982).
25. J. KOUTECKÝ. J. Chem. Phys. **46**, 2443 (1967).
26. J. PALDUS and J. ČÍŽEK. Phys. Rev. A**2**, 2268 (1970).
27. J. ČÍŽEK and J. PALDUS. J. Chem. Phys. **53**, 821 (1970).
28. J. PALDUS and J. ČÍŽEK. J. Chem. Phys. **54**, 2293 (1971), J. Polym. Sci. Pt.C 29, 199 (1970).
29. W. G. LAIDLAW. Intern. J. Quantum Chem. **7**, 87 (1973); W. G. LAIDLAW and K. VASUDEWAN. Theor. Chim. Acta, **26**, 387 (1972).
30. M. BENARD and J. PALDUS. J. Chem. Phys. **72**, 6546 (1980).
31. J. PALDUS and A. VEILLARD. Chem. Phys. Lett. **50**, 6 (1977); Mol. Phys. **35**, 445 (1978).
32. J. M. MCKELVEY and G. BERTHIER. Chem. Phys. Lett. **41**, 476 (1976).
33. G. CHAMBAUD, B. LEVY, and P. MILLIE. Theor. Chim. Acta, **48**, 103 (1978).
34. M. BÉNARD. J. Chem. Phys. **71**, 2546 (1979); M. BÉNARD and A. VEILLARD. Chem. Phys. Lett. **90**, 160 (1982).
35. M. BÉNARD. Theor. Chim. Acta, **61**, 379 (1982); Chem. Phys. Lett. **96**, 183 (1983).
36. R. BROER and W. C. NIEUWPOORT. Chem. Phys. **54**, 291 (1981); H. B. BROER-BRAAM. Ph.D. Thesis. University of Groningen, The Netherlands. 1981.
37. A. P. KLYAGINA and A. A. LEVIN. Koord. Khim. **10**, 579 (1984).
38. N. C. BAIRD, R. R. GUPTA, and K. F. TAYLOR. J. Am. Chem. Soc. **101**, 4531 (1979); L. FARNELL, J. A. POPLE, and L. RADOM. J. Phys. Chem. **87**, 79 (1983); T. FICKER. Theor. Chim. Acta, **65**, 127 (1984); K. VANDERMEER and J. J. C. MULDER. Chem. Phys. Lett. **34**, 189 (1975); O. KIKUCHI. Chem. Phys. Lett. **72**, 487 (1980); Bull. Chem. Soc. Jpn. **53**, 3149 (1980); L. ENGELBRECHT and B. LIU. J. Chem. Phys. **78**, 3097 (1983); W. J. BOUMA, D. POPPINGER, S. SAEBØ, J. K. MACLEOD, and L. RADOM. Chem. Phys. Lett. **104**, 198 (1984).
39. D. A. KLEIER, R. L. MARTIN, W. R. WADT, and W. R. MOOMAW. J. Am. Chem. Soc. **104**, 60 (1982).
40. E. R. DAVIDSON and W. T. BORDEN. J. Phys. Chem. **87**, 4783 (1983).
41. L. NOODLEMAN and J. G. NORMAN. J. Chem. Phys. **70**, 4903 (1979); Y. YAMAGUCHI. Chem. Phys. Lett. **68**, 477 (1979).
42. M. C. BOHM. Chem. Phys. Lett. **81**, 284 (1981); **83**, 533 (1981); Chem. Phys. **60**, 277 (1981); Z. f. Naturforsch. A**37**, 241 (1982); Ber. Buns. Gesellsch. Phys. Chem. **85**, 755 (1981), **86**, 56 (1982); Mol. Phys. **64**, 683 (1982); Theor. Chim. Acta, **60**, 233 (1981); Intern. J. Quantum Chem. **24**, 185 (1983); J. Phys. B, **16**, L 397 (1983).
43. K. YAMAGUCHI. Chem. Phys. Lett. **35**, 230 (1975); K. YAMAGUCHI, K. OHTA, S. YABUSHITA, and T. FUENO. J. Chem. Phys. **68**, 4323 (1978); T. TATSUMI, K. YAMAGUCHI, and T. FUENO. J. Mol. Catal. **2**, 437 (1977) and references therein; K. YAMAGUCHI and T. FUENO. Chem. Phys. Lett. **38**, 47 (1976); T. OKADA, K. YAMAGUCHI, and T. FUENO. Tetrahedron, **30**, 2293 (1974); K. YAMAGUCHI. Intern. J. Quantum Chem. **18**, 101 (1980); Chem. Phys. **29**, 117 (1978); K. YAMAGUCHI, S. YABUSHITA, and T. FUENO. J. Chem. Phys. **71**, 2321 (1979).
44. B. Y. SIMKIN, M. N. GLUKHOVTSEV, and V. I. MINKIN. Chem. Phys. Lett. **71**, 284 (1980); Zh. Org. Khim. **18**, 1337 (1982); **18**, 1345 (1982); Dokl. Akad. Nauk. **250**, 142 (1980); M. N. GLUKHOVTSEV, B. A. SIMKIN, V. I. MINKIN, and I. A. YUDILEVICH. J. Struct. Chem. **23**, 184 (1982); M. N. GLUKHOVTSEV, B. Y. SIMKIN, and V. I. MINKIN. J. Struct. Chem. **21**, 413 (1980); M. N. GLUKHOVTSEV, M. M. MESTECHKIN, V. I. MINKIN, and B. Y. SIMKIN. J. Struct. Chem. **23**, 176 (1982).
45. A. TOYOTA, T. TANAKA, and T. NAKAJIMA. Intern. J. Quantum Chem. **10**, 917 (1976); A. TOYOTA and T. NAKAJIMA. Theor. Chim. Acta, **53**, 297 (1979); **61**, 505 (1982); Tetrahedron Lett. **24**, 1179 (1983); Bull. Chem. Soc. Jpn. **57**, 151 (1984); A. TOYOTA, M. SAITO, and T. NAKAJIMA. Theor. Chim. Acta, **56**, 231 (1980).
46. M. C. BOHM. J. Chem. Phys. **80**, 2704 (1984); M. C. BOHM, P. BICKERT, K. HAFNER, and V. BOEKELHEIDE. Proc. Natl. Acad. Sci. USA, **81**, 2589 (1984); M. C. BOHM, R. GLEITER, F. DELGADOPENA, and D. O. COWAN. J. Chem. Phys. **79**, 1154 (1983); H. VOGLER and M. C. BOHM. Mol. Phys. **49**, 945 (1983).
47. A. AIZMAN and D. A. CASE. J. Am. Chem. Soc. **104**, 3269 (1982); C. P. KEIJZERS, P. S. BAGUS, and J. P. WORTH. J. Chem. Phys. **69**, 4032 (1978); L. E. NITZSCHE and E. R. DAVIDSON. Chem. Phys. Lett. **58**, 171 (1978); C. F. JACKELS and E. R. DAVIDSON. J. Chem. Phys. **64**, 2908 (1976); D. FELLER, E. S. HUYSER, W. T. BORDEN, and E. R. DAVIDSON. J. Am. Chem. Soc. **105**, 1459 (1983); W. T. BORDEN, E. R. DAVIDSON, and D. FELLER. Tetrahedron, **38**, 737 (1982); E. R. DAVIDSON. Intern. J. Quantum Chem. Symp. **15**, 65 (1981); D. FELLER, E. R. DAVIDSON, and W. T. BORDEN. J. Am. Chem. Soc. **106**, 2513 (1984); S. KATO, K. MOROKUMA, D. FELLER, E. R. DAVIDSON, and W. T. BORDEN. J. Am. Chem. Soc. **105**, 1791 (1983); E. S. HUYSER, D. FELLER, W. T. BORDEN, and E. R. DAVIDSON. J. Am. Chem. Soc. **104**, 2956 (1982); J. C. SCHUG, B. H. LENGSFIELD, and D. A. BREWER. J. Phys. Chem. **82**, 1436 (1978); R. L. MARTIN. J. Chem. Phys. **74**, 1852 (1981); R. L. MARTIN and W. R. WADT. J. Phys. Chem. **86**, 2382 (1982); S. CANUTO, O. GOSCINSKI, and M. ZERNER. Chem. Phys. Lett. **68**, 232 (1979); H. BAUMANN. J. Am. Chem. Soc. **100**, 7196 (1978); J. LANGLET and J.-P. MALRIEU. Theor. Chim. Acta, **33**, 307 (1974); G. E. SCUSERIA and R. H. CONTRERAS. Theor. Chim. Acta, **59**, 437 (1981); L. R. LOZES, O. GOSCINSKI, and U. I. WAHLGREN. Chem. Phys. Lett. **63**, 77 (1979); W. S. LEE and J. M. SCHULMAN. J. Am. Chem. Soc. **102**, 5184 (1980); S. NAGASE and K. MOROKUMA. J. Am. Chem. Soc. **100**, 1661 (1978); Y. G. SMEYERS and G. DELGADO BARRIO. Phys. Rev. A**15**, 1359 (1977); D. A. KLEIER and W. N. LIPSCOMB. Inorg. Chem. **18**, 1312 (1979); R. F. FENSKE and J. R. JENSEN. J. Chem. Phys. **71**, 3374 (1979); J. MÜLLER, E. POULAIN, O. GOSCINSKI, and L. KARLSSON. J. Chem. Phys. **72**, 2587 (1980).
48. N. MOISEYEV, J. KATRIEL, and C. TRINDLE. Intern. J. Quantum Chem. **12**, 759 (1977).
49. J. ČÍŽEK and J. PALDUS. Phys. Rev. A**3**, 525 (1971); J. KATRIEL and E. DOMANY. Intern. J. Quantum Chem. **8**, 559 (1974).
50. J. PALDUS and E. CHIN. Intern. J. Quantum Chem. **24**, 373 (1983).
51. R. E. PEIERLS, and J. YOCCOZ. Proc. Phys. Soc. London, A**70**, 381 (1957).
52. J. BARDEEN, L. N. COOPER, and J. R. SCHRIEFFER. Phys. Rev. **108**, 1175 (1957).

53. K. DEGUCHI, K. NISHIKAWA, and S. AONO. J. Chem. Phys. **75**, 4165 (1981).
54. K. YAMAGUCHI, Y. YOSHIOKA, T. TAKATSUKA, and T. FUENO. Theor. Chim. Acta, **48**, 185 (1978).
55. J. PALDUS, E. CHIN, and M. G. GREY. Intern. J. Quantum Chem. **24**, 395 (1983); R. PAUNCZ and J. PALDUS. Intern. J. Quantum Chem. **24**, 411 (1983); J. PALDUS and M. TAKAHASHI. Intern. J. Quantum Chem. **25**, 423 (1984); M. TAKAHASHI and J. PALDUS. Intern. J. Quantum Chem. **26**, 349 (1984).
56. M. TAKAHASHI, J. PALDUS, and J. ČÍŽEK. Intern. J. Quantum Chem. **24**, 707 (1983).
57. H. FUKUTOME and M. SASAI. Prog. Theor. Phys. **67**, 41 (1982); **69**, 1 (1983).
58. H. SHIRAKAWA and S. IKEDA. Polym. J. **2**, 231 (1971); H. SHIRAKAWA, T. ITO, and S. IKEDA. Polym. J. **4**, 460 (1973); T. ITO, H. SHIRAKAWA, and S. IKEDA. J. Polym. Sci. Polym. Chem. Ed. **12**, 11 (1974); **13**, 1943 (1975); H. SHIRAKAWA, E. J. LOUIS, A. G. MACDIARMID, C. K. CHIANG, and A. J. HEEGER. J. Chem. Soc. Chem. Commun. **14**, 578 (1977); C. K. CHIANG, C. R. FINCHER, JR., Y. W. PARK, A. J. HEEGER, H. SHIRAKAWA, E. J. LOUIS, S. C. GAU, and A. G. MACDIARMID. Phys. Rev. Lett. **39**, 1098 (1977); A. J. HEEGER and A. G. MACDIARMID. *In* Physics and chemistry of low dimensional solids. *Edited by* L. Alcacer. Reidel, Dordrecht, The Netherlands. 1980. p. 353; Y. W. PARK, M. A. DRUY, C. K. CHIANG, A. J. HEEGER, A. G. MACDIARMID, H. SHIRAKAWA, and S. IKEDA. J. Polym. Sci. B, Polym. Lett. **17**, 195 (1979); C. R. FINCHER, JR., D. L. PEEBLES, A. J. HEEGER, M. A. DRUY, Y. MATSUMURA, A. G. MACDIARMID, H. SHIRAKAWA, and S. IKEDA. Solid State Commun. **27**, 489 (1978); B. R. WEINBERGER, M. AKHTAR, and S. C. GAU. Synth. Met. **4**, 187 (1982); B. R. WEINBERGER, E. EHRENFREUND, A. PRON, A. J. HEEGER, and A. G. MACDIARMID. J. Chem. Phys. **72**, 4749 (1980); S. IKEHATA, J. KAUFER, T. WOERNER, A. PRON, M. A. DRUY, A. SIVAK, A. J. HEEGER, and A. G. MACDIARMID. Phys. Rev. Lett. **45**, 1123 (1980); M. NECHTSHEIN, F. DEVREUX, R. L. GREENE, T. C. CLARKE, and G. B. STREET. Phys. Rev. Lett. **44**, 556 (1980); C. B. DUKE and H. W. GIBSON. *In* Kirk-Othmer encyclopedia of chemical technology. Vol. 18. 3rd ed. Wiley, New York. 1982; p. 755 and references therein.
59. J.-L. CALAIS. Intern. J. Quantum Chem. Symp. **11**, 547 (1977); Ann. Soc. Sci. Bruxelles, Ser. 1, **93**, 91 (1979); J.-L. CALAIS and B. SYKJA. J. Phys. C, **15**, 3093 (1982).
60. M. KERTESZ, J. KOLLER, and A. AZMAN. Kem. Kozl. **52**, 369 (1979); Intern. J. Quantum Chem. **18**, 645 (1980); M. KERTESZ. Adv. Quantum Chem. **15**, 161 (1982).
61. S. SUHAI. J. Chem. Phys. **73**, 3843 (1980); Chem. Phys. Lett. **96**, 619 (1983); J. Pol. Sci. Pol. Phys. **21**, 1341 (1983); Phys. Rev. B, **27**, 3506 (1983); S. SUHAI and J. LADIK. J. Phys. C, **15**, 4327 (1982); Mol. Cryst. Liq. Cryst. **83**, 1231 (1982); R. S. DAY and E. MARTINO. Chem. Phys. Lett. **84**, 86 (1981); R. DAY, J. LADIK, and F. MARTINO. Chem. Phys. Lett. **81**, 494 (1981); M. SEEL, P. S. BAGUS, and J. LADIK. J. Chem. Phys. **77**, 3123 (1982).
62. O. CASTAÑO and P. KARADAKOV. Intern. J. Quantum Chem. **22**, 367 (1982); P. KARADAKOV and O. CASTAÑO. Intern. J. Quantum Chem. **22**, 351 (1982); Chem. Phys. Lett. **106**, 280 (1984).
63. L. BRÉDAS. Ann. Soc. Sci. Bruxelles, Ser. 1, **94**, 83 (1981); J.-M. ANDRÉ, J.-L. BRÉDAS, J. DELHALLE, Y. KALENOV, L. PIELA, and J.-L. CALAIS. Intern. J. Quantum Chem. Symp. **14**, 419 (1980); J.-M. ANDRÉ, J. DELHALLE, and C. LAMOTTE. Bull. Soc. Chim. Belg. **89**, 691 (1980); J. G. FRIPIAT, J. DELHALLE, and J.-M. ANDRÉ. Intern. J. Quantum Chem. **23**, 1179 (1983).
64. S. F. OSHEA and D. P. SANTRY. Chem. Phys. Lett. **25**, 164 (1974); F. E. WANG and Y. N. CHIU. Chem. Phys. **12**, 225 (1976); A. A. BERLIN, G. A. VINOGRADOV and A. A. OVCHINNIKOV. J. Macromol. Sci.-Chem. A**11**, 1701 (1977); G. F. KVENTSEL. Intern. J. Quantum Chem. **22**, 825 (1982); K. HASHIMOTO. Intern. J. Quantum Chem. **22**, 397 (1982).
65. M. H. WHANGBO. J. Chem. Phys. **75**, 4983 (1981); Acc. Chem. Res. **16**, 95 (1983); M. BALDO, G. PICCITTO, R. PUCCI, and P. TOMASELLO. Phys. Lett. A**95**, 201 (1983); S. N. DIXIT and S. MAZUMDAR. Phys. Rev. B, **29**, 1824 (1984).
66. N. N. TYUTYULKOV. Intern. J. Quantum Chem. **9**, 683 (1975); N. TYUTYULKOV, J. PETKOV, O. E. POLANSKY, and J. FABIAN. Theor. Chim. Acta, **38**, 1 (1975); N. N. TYUTYULKOV and O. E. POLANSKY and J. FABIAN. Z.f. Naturforsch. A**30**, 1308 (1975); N. N. TYUTYULKOV and O. E. POLANSKY. A**32**, 490 (1977); N. N. TYUTYULKOV, J. I. PETKOV, and I. N. KANEV. Z. Phys. Chem. Leipzig, **257**, 409 (1976); N. TYUTYULKOV, I. KANEV, O. POLANSKY, and J. FABIAN. Theor. Chim. Acta, **46**, 191 (1977); N. N. TYUTYULKOV, J. I. PETKOV, and P. SCHUSTER. Phys. Stat. Solid. B, **86**, 385 (1978); N. TYUTYULKOV, I. KANEV, O. CASTAÑO, O. POLANSKY, and H. BARENTZEN. Theor. Chim. Acta, **55**, 207 (1980); N. TYUTYULKOV, F. DIETZ, J. FABIAN, A. MELHORN, and A. TADJER. Theor. Chim. Acta, **60**, 185 (1981).
67. R. F. PRAT. Phys. Rev. A**6**, 1735 (1972).
68. G. DELGADO-BARRIO and R. F. PRAT. Phys. Rev. A**12**, 2288 (1975).
69. E. CLEMENTI and A. D. MCLEAN. Phys. Rev. **133**, A419 (1964).
70. S. HUZINAGA and A. HART-DAVIS. Phys. Rev. A**8**, 1734 (1973).
71. J. KOUTECKÝ and V. BONAČIĆ. J. Chem. Phys. **55**, 2408 (1971); J. KOUTECKÝ and V. BONAČIĆ-KOUTECKY. Chem. Phys. Lett. **15**, 558 (1972).
72. T. A. KAPLAN and W. H. KLEINER. Phys. Rev. **156**, 1 (1967).
73. R. AHLRICHS. Chem. Phys. Lett. **34**, 570 (1975).
74. C. FROESE-FISCHER. The Hartree–Fock method for atoms: a numerical approach. Wiley, New York. 1977.
75. C. FROESE-FISCHER. Private communication.

The well-tempered GTF basis sets and their applications in the SCF calculations on N_2, CO, Na_2, and P_2

S. HUZINAGA AND M. KLOBUKOWSKI

Department of Chemistry, The University of Alberta, Edmonton, Alta., Canada T6G 2G2

AND

H. TATEWAKI

Research Institute for Catalysis, Hokkaido University, Sapporo, Japan

Received August 6, 1984

This paper is dedicated to Professor Camille Sandorfy on the occasion of his 65th birthday

S. HUZINAGA, M. KLOBUKOWSKI, and H. TATEWAKI. Can. J. Chem. **63**, 1812 (1985).

We have started to prepare a new family of high-quality Gaussian-type function basis sets capable of producing near Hartree–Fock atomic and molecular wave functions. A conspicuous feature of the family of basis sets is that many of the exponent parameters are shared among *s*-, *p*-, *d*-, and *f*-basis functions. In the present paper we report the first phase of the work covering atoms from Li to Ar, together with near Hartree–Fock calculations on N_2, CO, Na_2, and P_2 as the applications. A modified form of Raffenetti's contraction scheme is used.

S. HUZINAGA, M. KLOBUKOWSKI et H. TATEWAKI. Can. J. Chem. **63**, 1812 (1985).

Nous avons commencé à préparer une nouvelle famille d'ensembles de base, de haute qualité et du type de fonction gaussienne qui nous permettent de produire des fonctions d'onde moléculaires et atomiques qui se rapprochent de celles de Hartree–Fock. Une caractéristique évidente de cette famille d'ensembles de base réside dans le fait que plusieurs paramètres exponentiels sont répartis entre des fonctions de base *s*, *p*, *d* et *f*. Dans le présent travail, nous rapportons la première phase du travail couvrant les atomes allant du Li à l'argon ainsi que des calculs de Hartree–Fock sur le N_2, le CO, le Na_2 et le P_2, comme applications. On a utilisé une forme modifiée du schéma de contraction de Raffenetti.

[Traduit par le journal]

1. Introduction

The Hartree–Fock approximation gives the lowest energy of a many-electron system within the framework of independent electron (orbital) model. Remaining errors in the energy and other properties are attributed to electron correlation. This conceptual picture has attractive clarity. If we obtain the Hartree–Fock wave functions for a molecule and for the constituent atoms, we may talk about changes from atoms to molecules in the language of polarization, configurational change, electron transfer, etc.

Unfortunately, the majority of *ab initio* calculations of molecular electronic wave functions have been conducted using unsaturated Gaussian-type function (GTF) basis sets which do not produce near Hartree–Fock results. The economics of computation prevails; the clear-cut conceptual picture is blurred and the language of theoretical interpretation becomes ambiguous.

We are preparing a family of high-quality GTF basis sets capable of producing near Hartree–Fock atomic and molecular wave functions. In the present paper we report the first phase of the work covering atoms from Li to Ar, together with near Hartree–Fock calculations on N_2, CO, Na_2, and P_2 as the applications.

The basis set is termed as well-tempered (wohltemperierte). To illustrate the essential feature, the (16*s*13*p*8*d*) set for Kr is shown in Table 1. There are 16 distinct exponent parameters in the set. For the *s* functions all sixteen of them are used. For the *p* functions thirteen of them (numbered as 4, 5, 6, 7, . . . , 16) and for the *d* function eight of them (numbered as 7, 8, 9, . . . , 14) are used. These eight exponent parameters are shared among the *s*, *p*, and *d* functions.

2. Well-tempered GTF basis sets

The "even-tempered" basis set was proposed by Raffenetti and Ruedenberg (1) in 1973. A set of even-tempered atomic basis functions is defined by

$$[2.1] \quad N_l(\zeta_{lk}) \exp(-\zeta_{lk} r^p)\, r^n S_{lm}(\theta, \phi),\ k = 1, 2, \ldots, K_l$$

where $S_{lm}(\theta, \phi)$ are normalized real spherical harmonics, $p = 1$ for STF and $p = 2$ for GTF. $N_l(\zeta_{lk})$ are normalization factors for the radial functions. The name "even-tempered" comes from the constraint imposed on the choice of the exponent parameters

$$\{\zeta_{l_1}, \zeta_{l_2}, \ldots, \zeta_{lK_l}\}$$

$$[2.2] \quad \zeta_{lk} = \alpha_l \beta_l^{k-1},\ \alpha_l,\ \beta_l > 0,\ \beta_l \neq 1$$

$$k = 1, 2, \ldots, K_l$$

That is to say, they form a geometric sequence, α_l, $\alpha_l\beta_l$, $\alpha_l\beta_l^2$, ... There are only two parameters, α_l and β_l, to be optimized per group of atomic functions belonging to the same symmetry species. For example, for the ground states of *B* ($1s^22s^22p^1$, ^2P) through Ca ($1s^22s^22p^63s^23p^64s^2$, ^1S) only four parameters α_0, β_0, α_1, and β_1 are to be determined. For the first transition metal atoms there are six parameters α_0, β_0, α_1, β_1, α_2, and β_2 to be optimized.

Bardo and Ruedenberg (2) explored the possibility of using a common set of α and β for all *l*;

$$[2.3] \quad \zeta_k = \alpha\beta^{k-1},\ k = 1, 2, \ldots, K$$

Clementi and Corongiu (3) combined this restricted form of even-temperedness with the idea of the universal basis set (4) and managed to cover all the way from H to Sr by using the following two geometric sequences:

$$[\mathrm{I}] \quad \alpha = 0.016, \quad \beta = 3.0, \quad K = 20$$

$$[\mathrm{II}] \quad \alpha = 0.012, \quad \beta = 3.0, \quad K = 20$$

From the sequence [I], the small and the medium size sets were

Table 1. Kr 1S (16s,13p,8d)

Total energy	Virial (-Pot/Kin)
-2752.040259	2.000009017

Orb. symmetry		1s	2s	3s	4s
Orb. energy		-520.16188	-69.901928	-10.848439	-1.1522443
Orb.	**exponent**	**Expansion coefficients**			
1s	826606.45	-0.14898807E-03	-0.46862149E-04	0.18811967E-04	0.59944596E-05
1s	131163.09	-0.11190805E-02	-0.35282882E-03	0.14147779E-03	0.45038284E-04
1s	29210.966	-0.60923405E-02	-0.19244994E-02	0.77342548E-03	0.24657519E-03
1s	8156.7678	-0.25256754E-01	-0.81040898E-02	0.32547532E-02	0.10359938E-02
1s	2649.7239	-0.84442732E-01	-0.28015528E-01	0.11340374E-01	0.36212157E-02
1s	960.44868	-0.22061177	-0.80744070E-01	0.32949132E-01	0.10506912E-01
1s	372.57014	-0.40175395	-0.18222724	0.77095793E-01	0.24815029E-01
1s	150.82764	-0.34391834	-0.24139262	0.10786618	0.34780037E-01
1s	62.134097	-0.65070050E-01	0.10342193	-0.51944518E-01	-0.16605489E-01
1s	26.566302	-0.51345194E-03	0.68947060	-0.51535085	-0.18283457
1s	11.486045	0.36637649E-03	0.36192367	-0.36386857	-0.13268328
1s	4.9941865	-0.39049755E-03	0.79360314E-02	0.66492706	0.29589970
1s	2.1668098	0.30542594E-03	0.80959037E-02	0.65049127	0.55645570
1s	0.85482273	-0.15304814E-03	-0.33378029E-02	0.45146739E-01	-0.21449214
1s	0.33896199	0.65569159E-04	0.13651936E-02	0.24053413E-02	-0.84407611
1s	0.12277414	-0.17744859E-04	-0.37630318E-03	-0.37189846E-03	-0.22420495

Orb. symmetry		2p	3p	4p
Orb. energy		-63.008909	-8.3305503	-0.52363188
Orb.	**exponent**	**Expansion coefficients**		
2p	8156.7678	0.44293786E-03	-0.18032917E-03	0.48889638E-04
2p	2649.7239	0.22277237E-02	-0.90912597E-03	0.24802020E-03
2p	960.44868	0.11921895E-01	-0.49062439E-02	0.13323820E-02
2p	372.57014	0.49358113E-01	-0.20696135E-01	0.56607847E-02
2p	150.82764	0.16867918	-0.73664772E-01	0.20176356E-01
2p	62.134097	0.38271595	-0.17877778	0.49679261E-01
2p	26.566302	0.42196381	-0.19835141	0.54541056E-01
2p	11.486045	0.14260193	0.15588044	-0.55838767E-01
2p	4.9941865	0.49430598E-02	0.57167277	-0.20676061
2p	2.1668098	0.23037445E-02	0.38468424	-0.15242208
2p	0.85482273	-0.78273232E-03	0.39628000E-01	0.28884843
2p	0.33896199	0.34866925E-03	-0.20639877E-03	0.58184910
2p	0.12277414	-0.10320221E-03	0.16659019E-03	0.31780143

Orb. symmetry		3d
Orb. energy		-3.8243211
Orb.	**exponent**	**Expansion coefficients**
3d	372.57014	-0.15696804E-02
3d	150.82764	-0.81624561E-02
3d	62.134097	-0.40081499E-01
3d	26.566302	-0.13717399
3d	11.486045	-0.30910849
3d	4.9941865	-0.40522282
3d	2.1668098	-0.30163835
3d	0.85482273	-0.83520988E-01

developed. In the small set ($9s5p$) is chosen for Ne and ($18s11p5d$) for Sr. In the medium set ($10s6p$) for Ne and ($18s12p7d$) for Sr. From the sequence [II] the large set ($13s8p$) for Ne is constructed. For Sr the largest set is ($20s13p8d$) which gives -3131.4824 au as the ground state energy. The Hartree–Fock value is -3131.5379 au.

In 1982, apparently unaware of either Bardo-Ruedenberg's work or Clementi-Corongiu's, Kosugi (5) conceived a similar idea and started coding a molecular integral program based on the assumed availability of such basis sets that the GTF exponents are shared among *s, p, d*, and *f* functions. In response to Kosugi's request, we initiated a compilation of a new family of GTF basis sets, less ambitious than Clementi's and with different emphases.

In order to attain high accuracy with smaller basis size, the universal character is not sought and in place of the even-tempered formula [2.3] a generalized formula,

$$[2.4] \quad \zeta_k = \alpha\beta^{k-1}[1 + \gamma(k/K)^{\delta}], \quad k = 1, 2, \ldots, K$$

is used for generation of exponents which are then shared among radial functions with different l. Here α, β, γ, and δ are the four parameters to be optimized through the energy calculation of an individual atom. The generalized formula [2.4] shares with the even-tempered formula the ease of opti-

Table 2. The total and orbital energies (a.u.) of atoms from Li to Ar.

		-T.E.	-ε(1s)	-ε(2s)	-ε(2p)	-ε(3s)	-ε(3p)
Li(^{2}S)	WT[a]	7.4327216	2.4777352	0.1963224			
	HF[b]	7.4327257	2.47773	0.19632			
Be(^{1}S)	WT	14.573010	4.7326604	0.3092658			
	HF	14.573021	4.73267	0.30927			
B(^{2}P)	WT	24.529029	7.6953065	0.4946875	0.3098560		
	HF	24.529057	7.69533	0.49469	0.30986		
C(^{3}P)	WT	37.688524	11.325485	0.7056054	0.4333252		
	HF	37.688612	11.32554	0.70563	0.43335		
N(^{4}S)	WT	54.400842	15.629017	0.9452942	0.5675622		
	HF	54.400924	15.62909	0.94531	0.56758		
O(^{3}P)	WT	74.809243	20.668605	1.2442799	0.6318669		
	HF	74.809370	20.66866	1.24433	0.63192		
F(^{2}P)	WT	99.409111	26.382702	1.5724961	0.7299702		
	HF	99.409300	26.38273	1.57254	0.73001		
Ne(^{1}S)	WT	128.54671	32.772411	1.9303713	0.8503745		
	HF	128.54705	32.77248	1.93043	0.85044		
Na(^{2}S)	WT	161.85853	40.478300	2.7968709	1.5179746	0.1820635	
	HF	161.85890	40.47850	2.79702	1.51814	0.18210	
Mg(^{1}S)	WT	199.61402	49.031697	3.7676880	2.2821608	0.2530253	
	HF	199.61461	49.03160	3.76760	2.28211	0.25300	
Al(^{2}P)	WT	241.87572	58.501044	4.9106472	3.2182142	0.3933549	0.2099523
	HF	241.87668	58.50105	4.91069	3.21834	0.39340	0.21002
Si(^{3}P)	WT	288.85330	68.812300	6.1563909	4.2558235	0.5396957	0.2970592
	HF	288.85431	68.81239	6.15647	4.25598	0.53978	0.29703
P(^{4}S)	WT	340.71773	79.969522	7.5109365	5.4007530	0.6962659	0.3916204
	HF	340.71869	79.96965	7.51102	5.40038	0.69636	0.39161
S(^{3}P)	WT	397.503695	92.004224	9.0041224	6.6822887	0.8793601	0.4372420
	HF	397.50485	92.00447	9.00431	6.68253	0.87955	0.43739
Cl(^{2}P)	WT	459.48062	104.88417	10.607297	8.0719804	1.0727376	0.5062522
	HF	459.48187	104.88469	10.60777	8.07252	1.07311	0.50652
Ar(^{1}S)	WT	526.81590	118.61003	12.321929	9.5711752	1.2771523	0.5908398
	HF	526.81739	118.61039	12.32219	9.57150	1.27735	0.59102

a) WT Energy values calculated using the well-tempered basis set.

b) HF Near Hartree-Fock energy values given by Clementi and Roetti. (Atomic Data and Nuclear Data Tables, 14, 177 (1974)).

mization. The (16s13p8d) set optimized through these four parameters gives −2752.0324 au as the ground state energy of Kr, while the largest (18s13p8d) set of Clementi and Corongiu gives −2752.0026 au. The $\{\zeta_k\}$ obtained through [2.4] were further individually optimized with the only constraint that they are still to be shared among s, p, and d radial functions. The resulting (16s13p8d) set is shown in Table 1 and it gives −2752.0403 au which is fairly close to the Hartree–Fock value −2752.0546 au.

On account of the parent well-tempered formula [2.4], the newly prepared basis sets may be called well-tempered because they are no longer "even-tempered" but still maintain averaged-out, well-spaced exponent values common for s, p, d, and f radial functions.

Table 2 shows the total and orbital energies of the ground states of Li through Ar obtained by our well-tempered basis sets. Their basis set parameters are given in Tables 3–18.

3. SCF calculations on N_2, CO, Na_2, and P_2

The well-tempered GTF basis sets reported in the present

Table 3. Li 2S (14s)

Total energy		Virial (-Pot/Kin)	
-7.432721641		2.000000680	
Orb.	symmetry	1s	2s
Orb.	energy	-2.4777352	-0.19632241
Orb.	exponent	Expansion coefficients	
1s	22419.736	-0.25371339E-04	-0.39623900E-05
1s	3411.9206	-0.19229319E-03	-0.30068882E-04
1s	791.56798	-0.98006999E-03	-0.15308551E-03
1s	230.19930	-0.39389822E-02	-0.61767564E-03
1s	77.244972	-0.13645109E-01	-0.21437396E-02
1s	28.215353	-0.42188668E-01	-0.67309902E-02
1s	10.945320	-0.11102421	-0.18126512E-01
1s	4.4555099	-0.23195752	-0.40329152E-01
1s	1.8912349	-0.34855593	-0.69110668E-01
1s	0.84168088	-0.30735813	-0.97953426E-01
1s	0.38245884	-0.10060880	-0.90997614E-01
1s	0.10712717	-0.26489712E-02	0.23770429
1s	0.49489457E-01	0.29608485E-03	0.59988601
1s	0.22097232E-01	-0.31428571E-03	0.27875265

Table 4. Be 1S (14s)

Total energy		Virial (-Pot/Kin)	
-14.57301049		2.000000930	
Orb.	symmetry	1s	2s
Orb.	energy	-4.7326604	-0.30926579
Orb.	exponent	Expansion coefficients	
1s	39869.444	0.26638308E-04	0.48501555E-05
1s	5843.7849	0.20894521E-03	0.38143032E-04
1s	1353.8748	0.10578159E-02	0.19253071E-03
1s	390.76208	0.43527501E-02	0.79782278E-03
1s	128.91355	0.15368737E-01	0.28166043E-02
1s	46.835765	0.47076888E-01	0.88292658E-02
1s	18.238445	0.12247206	0.23561038E-01
1s	7.4653007	0.25244318	0.53117503E-01
1s	3.1885072	0.36569645	0.91465582E-01
1s	1.4242168	0.28114261	0.12552466
1s	0.65378289	0.67230540E-01	0.41748955E-01
1s	0.23546536	0.98297194E-03	-0.30974101
1s	0.96077389E-01	-0.55594615E-04	-0.57572520
1s	0.39979165E-01	0.84452237E-05	-0.24565321

paper are of near Hartree–Fock quality for atoms as seen in Table 2. We have tested their effectiveness as basis sets for molecular calculations by performing carefully controlled SCF calculations on N_2, CO, Na_2, and P_2.

Raffenetti's general contraction scheme (6) is used throughout the work with a slight modification. Since we regard Raffenetti's contraction scheme as an integral part of our well-tempered basis sets, we shall explain the scheme using the (14*s*9*p*) set for N given in Table 7.

The minimal basis set obtained from the set by Raffenetti's scheme is composed of three distinct atomic radial functions,

$$[2.5] \quad s_1(r) = \sum_{k=1}^{14} a_{1s,k}\, g_s(\zeta_k; r)$$
$$s_2(r) = \sum_{k=1}^{14} a_{2s,k}\, g_s(\zeta_k; r)$$
$$p_1(r) = \sum_{k=6}^{14} a_{2p,k}\, g_p(\zeta_k; r)$$

where g_s and g_p are normalized radial functions,

$$[2.6] \quad g_s(\zeta; r) = N_s(\zeta) \exp(-\zeta r^2)$$
$$g_p(\zeta; r) = N_p(\zeta) r^1 \exp(-\zeta r^2)$$

and the expansion coefficients and the well-tempered exponents are given in Table 7. This minimal set may be denoted as (14, 14/9).

More flexible contracted basis sets can be generated by adding some primitive functions chosen from the original (14*s*9*p*) set to the above minimal set (14,14/9). For example, the following four functions,

$$[2.7] \quad s_3(r) = g_s(\zeta_{13}; r)$$
$$s_4(r) = g_s(\zeta_{14}; r)$$
$$p_2(r) = g_p(\zeta_{13}; r)$$
$$p_3(r) = g_p(\zeta_{14}; r)$$

Table 5. B 2P (14s,9p)

Total energy		Virial (-Pot/Kin)	
-24.52902873		2.000000857	
Orb. symmetry		1s	2s
Orb. energy		-7.6953065	-0.49468754
Orb.	exponent	Expansion coefficients	
1s	52671.047	0.32735824E-04	0.66063425E-05
1s	7957.4520	0.25228261E-03	0.50998123E-04
1s	1821.4858	0.13064668E-02	0.26375724E-03
1s	525.02748	0.52996202E-02	0.10759756E-02
1s	174.90474	0.18404924E-01	0.37513456E-02
1s	63.720725	0.56343646E-01	0.11762648E-01
1s	24.672197	0.14562714	0.31622340E-01
1s	10.018008	0.29130576	0.70537469E-01
1s	4.2343440	0.38466094	0.12038262
1s	1.8442068	0.22725114	0.13406155
1s	0.76474042	0.25938077E-01	-0.63734504E-01
1s	0.31422572	-0.34308932E-03	-0.44712397
1s	0.12844228	0.30563356E-03	-0.51494368
1s	0.52561458E-01	-0.35836045E-05	-0.11586248
Orb. symmetry		2p	
Orb. energy		-0.30985597	
Orb.	exponent	Expansion coefficients	
2p	63.720725	0.71072216E-03	
2p	24.672197	0.20461652E-02	
2p	10.018008	0.91844969E-02	
2p	4.2343440	0.25636121E-01	
2p	1.8442068	0.78346519E-01	
2p	0.76474042	0.20568589	
2p	0.31422572	0.36777335	
2p	0.12844228	0.38864350	
2p	0.52561458E-01	0.15640522	

Table 6. C 3P (14s,9p)

Total energy		Virial (-Pot/Kin)	
-37.68856236		2.000001012	
Orb. symmetry		1s	2s
Orb. energy		-11.325485	-0.70560544
Orb.	exponent	Expansion coefficients	
1s	84441.826	-0.28825455E-04	0.61397905E-05
1s	12759.357	-0.22450664E-03	0.47873222E-04
1s	2871.2562	-0.11957958E-02	0.25486463E-03
1s	812.70822	-0.49685619E-02	0.10637218E-02
1s	267.55420	-0.17400959E-01	0.37455199E-02
1s	97.036042	-0.53815033E-01	0.11845527E-01
1s	37.285626	-0.14272335	0.32797210E-01
1s	14.969245	-0.29394449	0.75464641E-01
1s	6.2484109	-0.39211622	0.13164013
1s	2.6917790	-0.22435639	0.13497769
1s	1.1193666	-0.23937518E-01	-0.92735498E-01
1s	0.46209858	-0.66813449E-03	-0.46204834
1s	0.18941458	-0.13256753E-03	-0.49116196
1s	0.76703306E-01	-0.79383046E-04	-0.10633647
Orb. symmetry		2p	
Orb. energy		-0.43332521	
Orb.	exponent	Expansion coefficients	
2p	97.036042	0.76001697E-03	
2p	37.285626	0.23010141E-02	
2p	14.969245	0.10569369E-01	
2p	6.2484109	0.31447856E-01	
2p	2.6917790	0.95168715E-01	
2p	1.1193666	0.23260290	
2p	0.46209858	0.37607727	
2p	0.18941458	0.36078491	
2p	0.76703306E-01	0.13297418	

Table 7. N 4S (14s,9p)

Total energy		Virial (-Pot/Kin)	
-54.40084206		2.000001166	
Orb. symmetry		1s	2s
Orb. energy		-15.629017	-0.94529417
Orb.	exponent	Expansion coefficients	
1s	119657.57	0.27858954E-04	0.61379195E-05
1s	17980.371	0.21410780E-03	0.47214543E-04
1s	4150.4007	0.10990962E-02	0.24232205E-03
1s	1189.9422	0.45599198E-02	0.10093066E-02
1s	389.70172	0.16345839E-01	0.36391458E-02
1s	139.00490	0.52136306E-01	0.11860218E-01
1s	52.598303	0.14104941	0.33569603E-01
1s	20.965405	0.29349457	0.78180076E-01
1s	8.7294161	0.39440376	0.13760720
1s	3.7476394	0.22605492	0.13554657
1s	1.5622986	0.24306392E-01	-0.10625996
1s	0.64519308	0.12462144E-02	-0.46703613
1s	0.26362662	0.84751683E-04	-0.48094001
1s	0.10550470	0.11806700E-03	-0.10331640
Orb. symmetry		2p	
Orb. energy		-0.56756217	
Orb.	exponent	Expansion coefficients	
2p	139.00490	-0.77232046E-03	
2p	52.598303	-0.24783868E-02	
2p	20.965405	-0.11388147E-01	
2p	8.7294161	-0.35025934E-01	
2p	3.7476394	-0.10500653	
2p	1.5622986	-0.24622673	
2p	0.64519308	-0.37810219	
2p	0.26362662	-0.34572765	
2p	0.10550470	-0.12357070	

Table 8. O 3P (14s,9p)

Total energy		Virial (-Pot/Kin)	
-74.80924315		2.000002168	
Orb. symmetry		1s	2s
Orb. energy		-20.668605	-1.2442799
Orb.	exponent	Expansion coefficients	
1s	164589.30	0.26373491E-04	0.59844887E-05
1s	24444.592	0.20614961E-03	0.46767577E-04
1s	5588.4836	0.10701415E-02	0.24312289E-03
1s	1591.3453	0.44814417E-02	0.10199691E-02
1s	514.83307	0.16477605E-01	0.37828195E-02
1s	180.11709	0.53990529E-01	0.12638070E-01
1s	66.904230	0.14879509	0.36705391E-01
1s	26.223953	0.31029576	0.86189289E-01
1s	10.771973	0.40001119	0.15029433
1s	4.5545639	0.20195207	0.12500603
1s	1.8923962	0.15160616E-01	-0.15951911
1s	0.77844111	0.24575049E-02	-0.50334543
1s	0.31526075	-0.38918050E-03	-0.43545737
1s	0.12339884	0.24096779E-03	-0.68375909E-01
Orb. symmetry		2p	
Orb. energy		-0.63186693	
Orb.	exponent	Expansion coefficients	
2p	180.11709	0.82940955E-03	
2p	66.904230	0.28590932E-02	
2p	26.223953	0.13155974E-01	
2p	10.771973	0.42222342E-01	
2p	4.5545639	0.12395351	
2p	1.8923962	0.26676617	
2p	0.77844111	0.37213773	
2p	0.31526075	0.32427572	
2p	0.12339884	0.11651812	

Table 9. F 2P (14s,9p)

Total energy		Virial (-Pot/Kin)	
-99.40911077		2.000003127	
Orb. symmetry		1s	2s
Orb. energy		-26.382702	-1.5724961
Orb.	exponent	Expansion coefficients	
1s	210965.41	-0.25861368E-04	-0.59877856E-05
1s	31872.592	-0.19814938E-03	-0.45845448E-04
1s	7315.8374	-0.10314189E-02	-0.23914553E-03
1s	2077.2153	-0.43410166E-02	-0.10073949E-02
1s	669.99910	-0.16073698E-01	-0.37664276E-02
1s	232.13639	-0.53856655E-01	-0.12854890E-01
1s	84.995730	-0.15132439	-0.38179798E-01
1s	32.901241	-0.31855804	-0.90860171E-01
1s	13.363318	-0.40407031	-0.15805949
1s	5.5881415	-0.19063532	-0.11767404
1s	2.3190587	-0.11728993E-01	0.18996711
1s	0.95009281	-0.29540465E-02	0.51821053
1s	0.38254192	0.53609828E-03	0.40742845
1s	0.14784040	-0.27847409E-03	0.54563563E-01
Orb. symmetry		2p	
Orb. energy		-0.72997019	
Orb.	exponent	Expansion coefficients	
2p	232.13639	-0.84283443E-03	
2p	84.995730	-0.30733041E-02	
2p	32.901241	-0.14215767E-01	
2p	13.363318	-0.47300065E-01	
2p	5.5881415	-0.13609919	
2p	2.3190587	-0.27835526	
2p	0.95009281	-0.36924168	
2p	0.38254192	-0.31049830	
2p	0.14784040	-0.11084351	

Table 10. Ne 1S (14s,9p)

Total energy		Virial (-Pot/Kin)	
-128.5467125		2.000006178	
Orb. symmetry		1s	2s
Orb. energy		-32.772411	-1.9303713
Orb.	exponent	Expansion coefficients	
1s	224935.42	0.31385902E-04	-0.73764240E-05
1s	34295.050	0.22902943E-03	-0.53729030E-04
1s	8406.8016	0.10767981E-02	-0.25362105E-03
1s	2499.4775	0.43997968E-02	-0.10348784E-02
1s	813.77043	0.16512481E-01	-0.39323323E-02
1s	278.11584	0.57116299E-01	-0.13836316E-01
1s	99.577882	0.16367253	-0.42220052E-01
1s	37.850674	0.34053218	-0.10033812
1s	15.161831	0.40363912	-0.16911573
1s	6.2058473	0.15960706	-0.93068268E-01
1s	2.5433614	0.44399807E-02	0.25758027
1s	1.0377188	0.36906084E-02	0.53240416
1s	0.42170694	-0.92742147E-03	0.34367685
1s	0.16646318	0.36334927E-03	0.35318368E-01
Orb. symmetry		2p	
Orb. energy		-0.85037453	
Orb.	exponent	Expansion coefficients	
2p	278.11584	-0.92224622E-03	
2p	99.577882	-0.36223315E-02	
2p	37.850674	-0.16691212E-01	
2p	15.161831	-0.57199336E-01	
2p	6.2058473	-0.16088080	
2p	2.5433614	-0.30276992	
2p	1.0377188	-0.36520034	
2p	0.42170694	-0.27769431	
2p	0.16646318	-0.90193871E-01	

Table 11. Na 2S (16s,9p)

Total energy	Virial (-Pot/Kin)
-161.8585255	2.000001959

Orb.		1s	2s	3s
Orb. symmetry		1s	2s	3s
Orb. energy		-40.478300	-2.7968709	-0.18206350
Orb.	exponent	Expansion coefficients		
1s	415780.43	-0.18211947E-04	0.44482994E-05	0.66792657E-06
1s	62811.131	-0.14383747E-03	0.35114292E-04	0.52880933E-05
1s	14035.585	-0.76356666E-03	0.18670773E-03	0.28000330E-04
1s	3975.6979	-0.32332156E-02	0.79125548E-03	0.11932988E-03
1s	1265.4338	-0.12308099E-01	0.30356427E-02	0.45501855E-03
1s	431.89542	-0.42705574E-01	0.10701748E-01	0.16173427E-02
1s	155.14008	-0.12723098	0.33447901E-01	0.50276462E-02
1s	58.742794	-0.29200747	0.85698088E-01	0.13098632E-01
1s	23.336142	-0.41583913	0.16132142	0.24700969E-01
1s	9.6640214	-0.23426266	0.14365139	0.23596264E-01
1s	4.0174167	-0.22707887E-01	-0.14832316	-0.27399891E-01
1s	1.6698317	-0.29632159E-02	-0.51549215	-0.92118175E-01
1s	0.69327959	0.55525517E-03	-0.43828661	-0.14805683
1s	0.27766610	-0.43985092E-03	-0.64288864E-01	-0.97444869E-01
1s	0.69040233E-01	0.13793391E-03	0.15824423E-02	0.53756357
1s	0.26517216E-01	-0.52767264E-04	-0.75502468E-03	0.58783865

Orb.		2p
Orb. symmetry		2p
Orb. energy		-1.5179746
Orb.	exponent	Expansion coefficients
2p	431.89542	-0.66461762E-03
2p	155.14008	-0.26039608E-02
2p	58.742794	-0.12888261E-01
2p	23.336142	-0.45831505E-01
2p	9.6640214	-0.13582627
2p	4.0174167	-0.28283400
2p	1.6698317	-0.37701244
2p	0.69327959	-0.30354040
2p	0.27766610	-0.91606394E-01

Table 12. Mg 1S (16s,9p)

Total energy	Virial (-Pot/Kin)
-199.6140189	2.000006773

Orb.		1s	2s	3s
Orb. symmetry		1s	2s	3s
Orb. energy		-49.031697	-3.7676880	-0.25302530
Orb.	exponent	Expansion coefficients		
1s	392037.18	-0.23802204E-04	-0.60191268E-05	0.11591980E-05
1s	62898.863	-0.17420377E-03	-0.43971816E-04	0.84786810E-05
1s	14238.305	-0.94455991E-03	-0.23927714E-03	0.46062970E-04
1s	3965.5048	-0.40602307E-02	-0.10275205E-02	0.19826139E-03
1s	1264.0415	-0.15216330E-01	-0.38967774E-02	0.75036425E-03
1s	433.01931	-0.52183101E-01	-0.13583424E-01	0.26268645E-02
1s	155.73137	-0.15198912	-0.42033142E-01	0.81327533E-02
1s	58.934046	-0.33017145	-0.10388502	0.20373740E-01
1s	23.394191	-0.41321502	-0.18227273	0.36368428E-01
1s	9.5299750	-0.17632515	-0.10948110	0.23207480E-01
1s	3.9208593	-0.59743652E-02	0.26839663	-0.62300162E-01
1s	1.6325316	-0.43647079E-02	0.57718244	-0.15573180
1s	0.69204306	0.16951350E-02	0.30856902	-0.21031429
1s	0.27101061	-0.91078468E-03	0.12770615E-01	0.56936010E-01
1s	0.99092006E-01	0.38460504E-03	0.12223915E-02	0.64160037
1s	0.37251448E-01	-0.11376962E-03	-0.47341217E-03	0.44625772

Orb.		2p
Orb. symmetry		2p
Orb. energy		-2.2821608
Orb.	exponent	Expansion coefficients
2p	433.01931	-0.95240341E-03
2p	155.73137	-0.37610524E-02
2p	58.934046	-0.17971622E-01
2p	23.394191	-0.63939086E-01
2p	9.5299750	-0.18160842
2p	3.9208593	-0.33785996
2p	1.6325316	-0.38407943
2p	0.69204306	-0.21866928
2p	0.27101061	-0.31293264E-01

Table 13. Al 2P (16s,11p)

Total energy		Virial (-Pot/Kin)		
-241.8757152		2.000011983		
Orb.	symmetry	1s	2s	3s
Orb.	energy	-58.501044	-4.9106472	-0.39335485
Orb.	exponent	Expansion coefficients		
1s	440776.56	-0.26216901E-04	0.68201337E-05	-0.15755990E-05
1s	65831.353	-0.20447041E-03	0.53092904E-04	-0.12246634E-04
1s	14631.361	-0.11405421E-02	0.29727835E-03	-0.68725937E-04
1s	3973.7002	-0.49953179E-02	0.13012042E-02	-0.30004544E-03
1s	1265.9148	-0.18454917E-01	0.48729337E-02	-0.11282788E-02
1s	433.24269	-0.63066758E-01	0.16987282E-01	-0.39252321E-02
1s	155.60934	-0.17837366	0.51596905E-01	-0.12035865E-01
1s	59.121707	-0.36206887	0.12212410	-0.28678531E-01
1s	23.585787	-0.39397086	0.19531392	-0.47748386E-01
1s	9.5268459	-0.12788357	0.60826660E-01	-0.14395168E-01
1s	3.8981602	-0.26529679E-03	-0.38193851	0.10583556
1s	1.6375444	-0.37207830E-02	-0.58066025	0.24109211
1s	0.70342483	0.13997265E-02	-0.18908996	0.18589675
1s	0.24683657	-0.66591787E-03	0.34708151E-03	-0.39257972
1s	0.97079720E-01	0.33251333E-03	-0.17196128E-02	-0.67062944
1s	0.37687043E-01	-0.96711832E-04	0.46053428E-03	-0.14149550
Orb.	symmetry	2p	3p	
Orb.	energy	-3.2182142	-0.20995227	
Orb.	exponent	Expansion coefficients		
2p	433.24269	-0.13251696E-02	-0.24126152E-03	
2p	155.60934	-0.52383956E-02	-0.93013541E-03	
2p	59.121707	-0.24048459E-01	-0.44168044E-02	
2p	23.585787	-0.84186851E-01	-0.15290406E-01	
2p	9.5268459	-0.22692091	-0.43158541E-01	
2p	3.8981602	-0.37986591	-0.70989507E-01	
2p	1.6375444	-0.36100270	-0.81411141E-01	
2p	0.70342483	-0.13835395	0.87724895E-02	
2p	0.24683657	-0.92229114E-02	0.29744016	
2p	0.97079720E-01	0.29327195E-03	0.52023347	
2p	0.37687043E-01	-0.25752884E-03	0.30871981	

may be added to the basis functions in [2.5] and the resulting contracted basis set may be denoted as (14,14,1,1/9,1,1). Both sets, (14,14/9) and (14,14,1,1/9,1,1), reproduce exactly the same total and orbital energies of the atom given in Table 2. There is no need of recalculating the atomic energies when a contracted basis set is generated from the original primitive ($14s9p$) set by Raffenetti's scheme.

It is possible to make Raffenetti's basis set less bulky while retaining the same accuracy and convenience. By combining the following three contracted basis functions,

$$[2.8]\qquad \begin{aligned} s_1'(r) &= \sum_{k=1}^{12} a_{1s,k}\, g_s(\zeta_k;\, r) \\ s_2'(r) &= \sum_{k=1}^{12} a_{2s,k}\, g_s(\zeta_k;\, r) \\ p_1'(r) &= \sum_{k=6}^{12} a_{2p,k}\, g_p(\zeta_k;\, r) \end{aligned}$$

with the four primitive functions in [2.7], we obtain a contracted basis set, (12,12,1,1/7,1,1). This modified contraction offers the same accuracy and flexibility as the original form (14,14,1,1/9,1,1) for atomic and molecular calculations.

3.1. N_2

We have performed a series of SCF calculations on N_2, first without, then with polarization functions. Table 19 shows the total energy and orbital energies at the internuclear distance of 2.068 au. The abbreviated designation of basis sets used in Table 19 corresponds to the one used in the previous section as follows,

(14,14/9)	[2/1]
(13,13,1/8,1)	[3/2]
(12,12,1,1/7,1,1)	[4/3]
(11,11,1,1,1/6,1,1,1)	[5/4]
(10,10,1,1,1,1/5,1,1,1,1)	[6/5]
.	.
.	.
.	.
.	.

The basis set denoted as [5/4/3*] in Table 19 is the (11,11,1,1,1/6,1,1,1) set supplemented by the following three primitve d radial functions

$$[2.9]\qquad \begin{aligned} d_1(r) &= g_d(\zeta_{11};\, r) \\ d_2(r) &= g_d(\zeta_{12};\, r) \\ d_3(r) &= g_d(\zeta_{13};\, r) \end{aligned}$$

where

$$[2.10]\qquad g_d(\zeta;\, r) = N_d(\zeta) r^2 \exp\,(-\zeta r^2)$$

Table 14. Si 3P (16s,11p)

Total energy	Virial (-Pot/Kin)		
-288.8533043	2.000009410		
Orb. symmetry	1s	2s	3s
Orb. energy	-68.812300	-6.1563909	-0.53969571

Orb. exponent — Expansion coefficients

Total energy	Potential energy	Kinetic energy	2-electron energy	Virial (-Pot/Kin)
-397.5036947	-795.0050891	397.5013944	151.8855842	2.000005787

Orbital symmetry		1s	2s	3s
Energy		-92.004223	-9.0041224	-0.87936006
Exponent				
1s	855633.84	0.19100262E-04	-0.52781147E-05	-0.15327931E-05
1s	129252.19	0.14938338E-03	-0.41241787E-04	-0.11963304E-04
1s	29011.892	0.79651668E-03	-0.22040581E-03	-0.64043610E-04
1s	8192.5384	0.33629179E-02	-0.93081242E-03	-0.26995071E-03
1s	2610.5195	0.12900000E-01	-0.36038189E-02	-0.10484154E-02
1s	877.87116	0.46061860E-01	-0.13090757E-01	-0.38049145E-02
1s	309.90741	0.13886125	-0.41730668E-01	-0.12224802E-01
1s	116.30399	0.31266013	-0.10671869	-0.31526449E-01
1s	46.201024	0.41710662	-0.19456423	-0.59592883E-01
1s	19.065330	0.20504110	-0.14041368	-0.44485728E-01
1s	8.0369385	0.12274160E-01	0.25380160	0.88538671E-01
1s	3.4830361	0.41582792E-02	0.61718338	0.30708316
1s	1.5449017	-0.17754164E-02	0.29334198	0.27489477
1s	0.60342137	0.87621687E-03	0.10319550E-01	-0.40145368
1s	0.23776272	-0.41397392E-03	0.20589616E-02	-0.70241558
1s	0.89861851E-01	0.10981748E-03	-0.28926774E-03	-0.15445302

Orbital symmetry		2p	3p
Energy		-6.6822887	-0.43724204
Exponent			
2p	877.87116	-0.92237059E-03	-0.23748862E-03
2p	309.90741	-0.38533368E-02	-0.97264979E-03
2p	116.30399	-0.18841648E-01	-0.48954513E-02
2p	46.201024	-0.68527869E-01	-0.17736809E-01
2p	19.065330	-0.19481599	-0.52877627E-01
2p	8.0369385	-0.36310851	-0.99104995E-01
2p	3.4830361	-0.38577110	-0.12056579
2p	1.5449017	-0.16298845	0.17774277E-01
2p	0.60342137	-0.13224922E-01	0.36718972
2p	0.23776272	-0.24368386E-03	0.51596542
2p	0.89861851E-01	-0.34716927E-03	0.24481584

and ζ_{11}, ζ_{12}, ζ_{13} are given in Table 7. The polarization functions used in [6/5/3*] and [7/6/3*] are the same as above. (In all calculations the 3s component of d orbitals is excluded.)

As is shown in Table 7, the 2s and 2p atomic orbitals are mainly composed of the four outermost primitive GTFs. Therefore the set [6/5] gives a limit of splitting of the valence shell. Proceeding from [2/1] to [14/9], we find that all the quantities listed in Table 19 change considerably from [2/1] to [4/3], but moderately from [4/3] to [6/5] and they are almost constant from [6/5] to [14/9]. The change in the total energies from [6/5] to [14/9] is only 0.00008 au ~ 0.05 kcal/mol. Contribution to the chemical bonding from the core electrons is negligibly small. The results of [5/4/3*], [6/5/3*], and [7/6/3*] show the importance of the polarization functions.

In this paragraph, the total energies and orbital energies given by the present work are compared with those of Cade, Sales, and Wahl (CSW) (7) who performed STF SCF calculations of N_2. Their basis set is basically composed of five s- and three p-type orbitals; they have, however, dropped one $p\sigma_u$ orbital and have employed eight σ_g, seven σ_u, and three π_u orbitals when the polarization functions are disregarded. The abbreviation for this set is (8 × 7 × 3) and the results are also shown in Table 19. The total energy by (8 × 7 × 3) at R = 2.068 au is between [3/2] and [4/3], although the atomic total energy given by them is slightly lower than the present one. The disregard of one of the $p\sigma_u$ orbitals results in the rather shallow total energy of (8 × 7 × 3). Adding the $3d\sigma_g$, $3d\sigma_g'$, $3d\sigma_g''$, $4f\sigma_g$, $3d\sigma_u$, $3d\pi_u'$, and $4f\pi_u$ to (8 × 7 × 3), they have constructed the set of (12 × 8 × 6). The total energy calculated is −108.9897 au which is only 0.0002 au lower than that by [6/5/3*]. The small difference between the two calculations may again be attributed to disregarding of one of the $2p\sigma_u$ orbitals. These days, only very rarely are the exponential parameters optimized in molecular calculations. In 1966 CSW performed careful exponent optimization which led to the substantial energy lowering of 0.0031 au (see the final row in Table 19).

The spectroscopic constants are summarized in Table 20. The sets [2/1] and [3/2] give the repulsive potential for the internuclear distance (r) ≤ 2.15 au, while others yield attractive ones. All the constants calculated with the full valence shell splitting set [6/5] are close to those of [14/9]. This is in

Table 15. P 4S (16s,11p)

Total energy	Virial (-Pot/Kin)		
-340.7177301	2.000005486		

Orb. symmetry	1s	2s	3s
Orb. energy	-79.969522	-7.5109365	-0.69626586
Orb. exponent	Expansion coefficients		
1s 863942.88	0.15275580E-04	-0.41502460E-05	-0.11406198E-05
1s 134721.08	0.12657501E-03	-0.34343930E-04	-0.94281103E-05
1s 27439.348	0.76452917E-03	-0.20798280E-03	-0.57185302E-04
1s 7356.7386	0.33880945E-02	-0.92150129E-03	-0.25292344E-03
1s 2256.0614	0.13488302E-01	-0.37056786E-02	-0.10201105E-02
1s 750.26785	0.47245985E-01	-0.13198979E-01	-0.36299624E-02
1s 268.98537	0.13765861	-0.40697682E-01	-0.11279904E-01
1s 102.51380	0.30825615	-0.10300426	-0.28756205E-01
1s 40.789588	0.41937652	-0.19130012	-0.55278402E-01
1s 16.642091	0.20812139	-0.13990076	-0.41720226E-01
1s 6.8934248	0.10644807E-01	0.25746427	0.84395075E-01
1s 2.9419921	0.48891606E-02	0.61318791	0.28098046
1s 1.2949344	-0.22155563E-02	0.29246645	0.26833837
1s 0.50197017	0.11423092E-02	0.10160943E-01	-0.33957542
1s 0.20100313	-0.54447804E-03	0.17101969E-02	-0.70694859
1s 0.77549886E-01	0.14837943E-03	-0.27848204E-03	-0.19550724

Orb. symmetry	2p	3p
Orb. energy	-5.4007530	-0.39162039
Orb. exponent	Expansion coefficients	
2p 750.26785	-0.93316270E-03	-0.22400433E-03
2p 268.98537	-0.37010462E-02	-0.87267776E-03
2p 102.51380	-0.17899453E-01	-0.43322484E-02
2p 40.789588	-0.65690932E-01	-0.15850252E-01
2p 16.642091	-0.19196263	-0.48327551E-01
2p 6.8934248	-0.36259892	-0.91866926E-01
2p 2.9419921	-0.38803164	-0.11127635
2p 1.2949344	-0.17092869	-0.24019021E-02
2p 0.50197017	-0.15030430E-01	0.32931823
2p 0.20100313	0.40708036E-03	0.53266180
2p 0.77549886E-01	-0.25191639E-03	0.26880104

line with the cases of the total energies and orbital energies shown in Table 19. The spectroscopic constants given by the sets augmented with the polarization functions are quite similar to those of (12 × 8 × 6) except for $w_c\chi_c$ and D_c. In this work, the spectroscopic constants have been calculated with the third degree polynomials (8), which might be too crude to evaluate $w_c\chi_c$. The difference of ~0.08 eV in D_c arises from disregarding the *f* function in the present calculations.

3.2. CO

Total energies and orbital energies for CO calculated in this work are compared in Table 21 with those of McLean and Yoshimine (MY) (9) who employed five *s*-, four *p*-, one *d*-, and one *f*-type STFs. The values of the spectroscopic constants are collected in Table 22. The results of fully split valence shell set [6/5] in the two tables well simulate those of fully split set [14/9] as in the case of N_2, although the effect of splitting the orbital of the 1*s* core is larger than the case of N_2. The difference in the total energy and dissociation energy between [6/5] and [14/9] is ~0.36 kcal/mol, but it still remains in the acceptable error of 1 ~ 2 kcal/mol. The sets augmented with polarization functions give almost the same results as those of McLean and Yoshimine. The larger differences between the two calculations are in the total energies and dissociation energies (0.0024 au ~ 1.51 kcal/mol). The sum of the atomic total energies of carbon and oxygen by (5*s*4*p*) of STF is 0.0002 au lower than that by the present set and exponent optimization performed by MY brings extra energy lowering of 0.0005 au; the main reason for the difference between the two calculations rests in disregarding the *f*-type polarization functions in the present work.

Values of dipole moment as well as those of quadrupole moments at $R = 2.132$ au are presented in Table 23. They show the same tendency as the total energies, the orbital energies, and the spectroscopic constants.

The set [7/6/3*] gives the dipole moment of −0.104 au (C^+O^-) which has the opposite sign to that of experiment. Table 24 shows the dipole moment at different values of the internuclear distance. The moment calculated is parallel to that of Huo (10). It is to be noted that the sign of the moment changes around $R = 2.015$ au (C^-O^+), but according to the Mulliken population analysis (11) the molecule is still C^+O^-, indicating that the population analysis is not adequate to analyze the charge distribution of the CO molecule.

3.3. Na_2

Table 25 presents total energies and orbital energies obtained in the SCF calculations at R(Na—Na) = 6 au using the basis set from Table 11. Basis set [3/1] (16,16,16/9) is the minimal basis set corresponding to (16*s*9*p*) basis of the sodium atom in its ground state. The basis sets [4/1] and [5/1] have been obtained by consecutively releasing the primitives ζ_{16} and ζ_{15}.

Table 16. S 3P (16s,11p)

Total energy		Virial (-Pot/Kin)		
-397.5036947		2.000005787		
Orb.	symmetry	1s	2s	3s
Orb.	energy	-92.004223	-9.0041224	-0.87936006
Orb.	exponent	Expansion coefficients		
1s	855633.84	0.19100262E-04	-0.52781147E-05	-0.15327931E-05
1s	129252.19	0.14938338E-03	-0.41241787E-04	-0.11963304E-04
1s	29011.892	0.79651668E-03	-0.22040581E-03	-0.64043610E-04
1s	8192.5384	0.33629179E-02	-0.93081242E-03	-0.26995071E-03
1s	2610.5195	0.12900000E-01	-0.36038189E-02	-0.10484154E-02
1s	877.87116	0.46061860E-01	-0.13090757E-01	-0.38049145E-02
1s	309.90741	0.13886125	-0.41730668E-01	-0.12224802E-01
1s	116.30399	0.31266013	-0.10671869	-0.31526449E-01
1s	46.201024	0.41710662	-0.19456423	-0.59592883E-01
1s	19.065330	0.20504110	-0.14041368	-0.44485728E-01
1s	8.0369385	0.12274160E-01	0.25380160	0.88538671E-01
1s	3.4830361	0.41582792E-02	0.61718338	0.30708316
1s	1.5449017	-0.17754164E-02	0.29334198	0.27489477
1s	0.60342137	0.87621687E-03	0.10319550E-01	-0.40145368
1s	0.23776272	-0.41397392E-03	0.20589616E-02	-0.70241558
1s	0.89861851E-01	0.10981748E-03	-0.28926774E-03	-0.15445302
Orb.	symmetry	2p	3p	
Orb.	energy	-6.6822887	-0.43724204	
Orb.	exponent	Expansion coefficients		
2p	877.87116	-0.92237059E-03	-0.23748862E-03	
2p	309.90741	-0.38533368E-02	-0.97264979E-03	
2p	116.30399	-0.18841648E-01	-0.48954513E-02	
2p	46.201024	-0.68527869E-01	-0.17736809E-01	
2p	19.065330	-0.19481599	-0.52877627E-01	
2p	8.0369385	-0.36310851	-0.99104995E-01	
2p	3.4830361	-0.38577110	-0.12056579	
2p	1.5449017	-0.16298845	0.17774277E-01	
2p	0.60342137	-0.13224922E-01	0.36718972	
2p	0.23776272	-0.24368386E-03	0.51596542	
2p	0.89861851E-01	-0.34716927E-03	0.24481584	

Table 17. Cl 2P (16s,11p)

Total energy		Virial (-Pot/Kin)		
-459.4806271		2.000005631		
Orb.	symmetry	1s	2s	3s
Orb.	energy	-104.88417	-10.607297	-1.0727376
Orb.	exponent	Expansion coefficients		
1s	1165033.4	-0.15699898E-04	0.44027159E-05	-0.13327186E-05
1s	163171.39	-0.13345009E-03	0.37391250E-04	-0.11302145E-04
1s	35736.875	-0.72480080E-03	0.20351278E-03	-0.61648237E-04
1s	9801.0566	-0.32428787E-02	0.91088594E-03	-0.27524862E-03
1s	3002.2425	-0.12945699E-01	0.36695619E-02	-0.11130301E-02
1s	999.95105	-0.45386562E-01	0.13091032E-01	-0.39641875E-02
1s	356.86262	-0.13488702	0.41107368E-01	-0.12561165E-01
1s	134.62024	-0.30797801	0.10637998	-0.32747059E-01
1s	53.270671	-0.42078064	0.19798608	-0.63361458E-01
1s	21.824847	-0.21068641	0.14609928	-0.48295131E-01
1s	9.1232245	-0.12104860E-01	-0.26686288	0.97669100E-01
1s	3.9413793	-0.44273626E-02	-0.63125299	0.34254938
1s	1.7427191	0.21078734E-02	-0.27092488	0.25966766
1s	0.70774319	-0.10475491E-02	-0.74838705E-02	-0.45095411
1s	0.27994321	0.48166233E-03	-0.28345439E-02	-0.68411493
1s	0.10563808	-0.12539788E-03	0.38059318E-03	-0.13623021
Orb.	symmetry	2p	3p	
Orb.	energy	-8.0719804	-0.50625224	
Orb.	exponent	Expansion coefficients		
2p	999.95105	-0.93454880E-03	-0.25379837E-03	
2p	356.86262	-0.37919629E-02	-0.10155453E-02	
2p	134.62024	-0.18770584E-01	-0.51455765E-02	
2p	53.270671	-0.69422520E-01	-0.19082947E-01	
2p	21.824847	-0.20088248	-0.57677166E-01	
2p	9.1232245	-0.37543447	-0.10983800	
2p	3.9413793	-0.38404423	-0.12624270	
2p	1.7427191	-0.14485597	0.42811923E-01	
2p	0.70774319	-0.97801932E-02	0.39165311	
2p	0.27994321	-0.12690389E-02	0.50052334	
2p	0.10563808	-0.29956347E-03	0.22378063	

Table 18. Ar 1S (16s,11p)

Total energy		Virial (-Pot/Kin)		
-526.8158975		2.000005163		
Orb.	symmetry	1s	2s	3s
Orb.	energy	-118.61003	-12.321929	-1.2771523
Orb.	exponent	Expansion coefficients		
1s	1192038.6	0.17305586E-04	-0.49147845E-05	0.15369211E-05
1s	176715.15	0.13435386E-03	-0.38137958E-04	0.11906033E-04
1s	40309.619	0.71440268E-03	-0.20311205E-03	0.63567096E-04
1s	11089.577	0.31863191E-02	-0.90687329E-03	0.28301770E-03
1s	3461.2322	0.12289484E-01	-0.35262185E-02	0.11051141E-02
1s	1163.6413	0.43710502E-01	-0.12766044E-01	0.39925857E-02
1s	409.93944	0.13373761	-0.41205929E-01	0.13010322E-01
1s	153.08437	0.30677257	-0.10732601	0.34139752E-01
1s	60.637511	0.41903258	-0.19872606	0.65823715E-01
1s	25.040039	0.21491507	-0.15147321	0.51809790E-01
1s	10.550746	0.14438353E-01	0.25902250	-0.98047675E-01
1s	4.5717265	0.39559770E-02	0.63983386	-0.36427178
1s	2.0156106	-0.19000793E-02	0.27208357	-0.25947516
1s	0.83635000	0.94975494E-03	0.68703571E-02	0.47007306
1s	0.33252985	-0.44076827E-03	0.35278189E-02	0.67734807
1s	0.12551473	0.11184878E-03	-0.46924385E-03	0.13254477
Orb.	symmetry	2p	3p	
Orb.	energy	-9.5711752	-0.59083979	
Orb.	exponent	Expansion coefficients		
2p	1163.6413	-0.90221931E-03	-0.25363546E-03	
2p	409.93944	-0.38132488E-02	-0.10617606E-02	
2p	153.08437	-0.18982288E-01	-0.53895467E-02	
2p	60.637511	-0.69788676E-01	-0.19954009E-01	
2p	25.040039	-0.20027829	-0.59717025E-01	
2p	10.550746	-0.37701830	-0.11546895	
2p	4.5717265	-0.38637685	-0.13082636	
2p	2.0156106	-0.13946518	0.56539880E-01	
2p	0.83635000	-0.78005469E-02	0.40415945	
2p	0.33252985	-0.75104684E-03	0.49164663	
2p	0.12551473	0.13000542E-03	0.21222626	
2p	1.9877938	-0.13523594	0.61405327E-01	
2p	0.82539259	-0.73273324E-02	0.40851642	
2p	0.32763250	-0.72778290E-03	0.48975697	
2p	0.12386124	0.12504363E-03	0.20638305	

TABLE 19. Comparison of the total and orbital energies (au) of N_2 molecule at R = 2.068 au[a]

Basis	T.E.	$1\sigma_g$	$1\sigma_u$	$2\sigma_g$	$2\sigma_u$	$3\sigma_g$	$1\pi_u$
[2/1]	−108.74330	−15.9033	−15.9001	−1.5860	−0.8372	−0.6677	−0.6999
[3/2]	−108.85973	−15.7657	−15.7623	−1.5386	−0.7853	−0.6302	−0.6459
(8 × 7 × 3)[b]	−108.8967	−15.7169	−15.7133	−1.5381	−0.7823	−0.6374	−0.6311
[4/3]	−108.90624	−15.7122	−15.7086	−1.5312	−0.7761	−0.6328	−0.6278
[5/4]	−108.90800	−15.7124	−15.7088	−1.5289	−0.7770	−0.6329	−0.6267
[6/5]	−108.90913	−15.7134	−15.7098	−1.5279	−0.7771	−0.6332	−0.6263
[7/6]	−108.90939	−15.7133	−15.7097	−1.5279	−0.7771	−0.6332	−0.6263
[8/7]	−108.90944	−15.7132	−15.7096	−1.5279	−0.7771	−0.6332	−0.6263
[14/9]	−108.90947	−15.7132	−15.7096	−1.5278	−0.7771	−0.6332	−0.6263
[5/4/3*]	−108.98928	−15.6832	−15.6796	−1.4761	−0.7783	−0.6359	−0.6155
[6/5/3*]	−108.98946	−15.6836	−15.6800	−1.4760	−0.7783	−0.6360	−0.6154
[7/6/3*]	−108.98963	−15.6836	−15.6800	−1.4759	−0.7784	−0.6360	−0.6154
(12 × 8 × 6)[c]	−108.9897	−15.6791	−15.6755	−1.4723	−0.7761	−0.6339	−0.6126
(12 × 8 × 6)[d]	−108.9928	−15.6820	−15.6783	−1.4736	−0.7780	−0.6350	−0.6154

[a] Atomic total energy by present basis set = −54.40084 au.
[b] The STF basis set without the polarization function; the numbers of STFs for σ_g, σ_u, and π_u are 8, 7, and 3, respectively. See ref. 7.
[c] The STF basis set with the d and f polarization functions; the number of STFs for σ_g, σ_u, and π_u are 12, 8, and 6. See ref. 7.
[d] The same basis set as the case c, but with all the exponents optimized.

TABLE 20. Comparison of spectroscopic constants of N_2

Basis	D_e (eV)	R_e (au)	ω_e (cm^{-1})	$\omega_e\chi_e$ (cm^{-1})	B (cm^{-1})	α (cm^{-1})	κ (dyn/cm × 10^{-6})
[2/1]	Repulsive for $R \leq 2.15$ au						
[3/2]							
[4/3]	2.852	2.051	2619	24	2.044	0.014	2.830
[5/4]	2.901	2.050	2578	21	2.045	0.013	2.742
[6/5]	2.931	2.050	2563	20	2.045	0.013	2.709
[7/6]	2.939	2.049	2559	21	2.047	0.013	2.702
[8/7]	2.941	2.049	2559	20	2.047	0.013	2.702
[14/9]	2.941	2.049	2559	21	2.047	0.013	2.701
[5/4/3*]	5.174	2.015	2732	23	2.116	0.014	3.078
[6/5/3*]	5.180	2.015	2729	22	2.117	0.013	3.073
[7/6/3*]	5.185	2.015	2731	22	2.117	0.013	3.076
(12 × 8 × 6)[a]	5.27	2.013	2730	8.4	2.121	0.014	3.073
Exptl.[a]	9.90	2.074	2358	14.2	1.999	0.018	2.291

[a] From ref. 7.

TABLE 21. Comparison of total and orbital energies (au) of CO at R = 2.132 au

Basis	T.E.	1σ	2σ	3σ	4σ	5σ	1π
[2/1]	−112.56616	−20.7822	−11.5893	−1.6171	−0.8389	−0.5960	−0.7017
[3/2]	−112.68062	−20.7001	−11.4424	−1.5748	−0.8044	−0.5583	−0.6603
[4/3]	−112.71164	−20.6808	−11.3984	−1.5669	−0.8012	−0.5584	−0.6495
[5/4]	−112.71478	−20.6846	−11.3944	−1.5651	−0.8006	−0.5594	−0.6480
[6/5]	−112.71647	−20.6853	−11.3951	−1.5642	−0.8007	−0.5598	−0.6476
[7/6]	−112.71690	−20.6849	−11.3952	−1.5641	−0.8007	−0.5598	−0.6475
[8/7]	−112.71700	−20.6849	−11.3950	−1.5641	−0.8007	−0.5598	−0.6475
[14/9]	−112.71704	−20.6851	−11.3950	−1.5641	−0.8007	−0.5598	−0.6475
[5/4/3*]	−112.78620	−20.6660	−11.3618	−1.5240	−0.8059	−0.5554	−0.6403
[6/5/3*]	−112.78655	−20.6660	−11.3621	−1.5236	−0.8058	−0.5554	−0.6401
[7/6/3*]	−112.78671	−20.6658	−11.3622	−1.5235	−0.8057	−0.5555	−0.6401
MCL-YOSH[a]	−112.78911	−20.6643	−11.3597	−1.5210	−0.8038	−0.5544	−0.6395

[a] See ref. 9.

TABLE 22. Comparison of spectroscopic constants of CO

Basis	D_e (eV)	R_e (au)	ω_e (cm^{-1})	$\omega_e\chi_e$ (cm^{-1})	B (cm^{-1})	α (cm^{-1})	κ (dyn/cm × 10^{-6})
[2/1]	Repulsive for $R \leq 2.366$ au						
[3/2]	5.049	2.194	2272	23	1.823	0.014	2.086
[4/3]	5.819	2.129	2290	17	1.935	0.012	2.119
[5/4]	5.905	2.124	2276	16	1.944	0.011	2.093
[6/5]	5.952	2.122	2275	16	1.948	0.011	2.092
[7/6]	5.964	2.121	2278	16	1.950	0.011	2.097
[8/7]	5.967	2.121	2279	16	1.950	0.011	2.099
[14/9]	5.968	2.121	2279	16	1.950	0.011	2.100
[5/4/3*]	7.892	2.085	2463	25	2.018	0.015	2.451
[6/5/3*]	7.902	2.085	2463	25	2.019	0.015	2.451
[7/6/3*]	7.907	2.085	2463	24	2.019	0.015	2.452
MCL-YOSH[a]	7.971	2.083	2478	24	2.022	0.015	2.483
Exptl[b]	11.242[b]	2.132[c]	2170[c]	13[c]	1.931[c]	0.018[c]	1.902[c]

[a] STF SCF calculation by McLean and Yoshimine: spectroscopic constants are calculated by the use of their energies. See ref. 9.
[b] Reference 20.
[c] Reference 21.

The basis set [5/11*] has been obtained by adding one p-type GTF with ζ_{15} to improve the description of the p-space; similarly, the [5/12*] basis contains both ζ_{15} and ζ_{16} functions in the p-space. (Addition of these two functions is important due to the $3s$–$3p$ near-degeneracy.) Atomic calculations in the extended ($16s9p2p^*$) basis set give $E(^2P) - E(^2S) = 1.99$ eV, quite close to the experimental value of 2.10 eV (12). In the [6/22*] basis the s- and p-type GTFs with ζ_{13} are uncontracted to improve flexibility of the basis functions in the $2s$ and $2p$ regions. Finally, the [5/12*/3*] basis set is obtained by adding three sets of $3d$ GTFs with exponents ζ_{13}, ζ_{14}, and ζ_{15}.

The largest decrease of the total energy is obtained upon

TABLE 23. Dipole and quadruple moments of CO by various basis sets at R = 2.132 au

Basis	Dipole (au)	Quadrupole (au)	Population	
			C	O
[2/1]	−0.0838	−2.5044	+0.38	−0.38
[3/2]	−0.1169	−2.4302	+0.12	−0.12
[4/3]	−0.2001	−2.2278	+0.34	−0.34
[5/4]	−0.2086	−2.2209	+0.32	−0.32
[6/5]	−0.2104	−2.2198	+0.32	−0.32
[7/6]	−0.2105	−2.2195	+0.31	−0.31
[8/7]	−0.2104	−2.2194	+0.31	−0.31
[14/9]	−0.2100	−2.2193	+0.31	−0.31
[5/4/3*]	−0.1025	−1.5246	+0.28	−0.28
[6/5/3*]	−0.1039	−1.5193	+0.29	−0.29
[7/6/3*]	−0.1039	−1.5174	+0.34	−0.34
Huo[a]	−0.108	−1.59	—	—
Exptl[b]	0.0441 ±0.0020	—	—	—

[a] See ref. 10. The basis set is (4/3/1) for the σ and π orbitals of the oxygen atom while they are (4/2/1) and (4/2/1/1) for the σ and π orbitals of the carbon atom.
[b] Reference 22.

TABLE 24. Dipole moment (au) of CO at different values of R (au) by Huo and [6/5/3*]

R	Huo[a]	[6/5/3*]	Population	
			C	O
1.898	+0.119	+0.125	0.24	−0.24
2.015	—	+0.014	0.27	−0.27
2.132	−0.114	−0.104	0.29	−0.29
2.249	—	−0.226	0.32	−0.32
2.366	−0.366	−0.352	0.34	−0.34

[a] See ref. 10.

inclusion of the first p-polarization function (0.004 au or 2.7 kcal/mol). Polarization of 2s and 2p AOs due to the chemical bonding seems to be negligible. The role of the d polarization functions seems to be negligible on the SCF level. However, they have been included in view of the later MCSCF calculations (*vide infra*).

Table 26 presents the potential curve parameters calculated with various basis sets and compared with other available all-electron SCF results. Again, addition of the polarization functions is required to secure convergence of the calculated properties. The Na_2 molecule is unbound with respect to the limit of two isolated Na(^2S) atoms. It seems that the bonding of 0.038 eV calculated by Martin and Davidson (14) at 5.82 au probably results from the basis set superposition error (cf. the review article by Tatewaki in ref. 15). Our [5/12*/3*] values of both D_e and R_e are very close to the results of Partridge *et al.* (13). It should be noted (Table 25) that their SCF total energy at the internuclear distance of 6 au is about 0.025 au above the [5/12*/3*] total energy.

For the sodium dimer we have also performed preliminary MC SCF calculations using the ALIS system of programs (16) to optimize a wave function which had the same structure as the N9XC function of Konowalow *et al.* (17). The calculations have been done using the [5/12*/3*] basis set at the internuclear distance of 6 au (close to the N9XC equilibrium distance). The MC SCF procedure gave in eight iterations the total energy of −323.742941 au (stable to $<10^{-6}$ au) which is only 0.06 kcal/mol above the value of −323.743039 au obtained by Konowalow *et al.* using a large STF basis set (17). (No f functions were included in either calculation.)

It is worth mentioning that calculation of integrals takes about 70% of the CPU time spent in the complete SCF calculation; this, however, is reduced to less than 10% of the CPU time needed for complete MCSCF calculation. (The ALIS sys-

TABLE 25. Comparison of the total and orbital energies (au) of Na_2 at R = 6.0 au

Basis	T.E.	$1\sigma_g$	$1\sigma_u$	$2\sigma_g$	$2\sigma_u$	$3\sigma_g$	$1\pi_u$	$1\pi_g$	$3\sigma_u$	$4\sigma_g$
[3/1]	−323.711386	−40.4738	−40.4738	−2.7942	−2.7941	−1.5161	−1.5149	−1.5147	−1.5147	−0.1677
[4/1]	−323.711432	−40.4714	−40.4714	−2.7918	−2.7918	−1.5138	−1.5126	−1.5123	−1.5124	−0.1671
[5/1]	−323.711652	−40.4755	−40.4755	−2.7939	−2.7949	−1.5170	−1.5158	−1.5156	−1.5156	−0.1677
[5/11*]	−323.715966	−40.4676	−40.4676	−2.7862	−2.7861	−1.5081	−1.5071	−1.5069	−1.5067	−0.1644
[5/12*]	−323.715998	−40.4673	−40.4673	−2.7860	−2.7860	−1.5079	−1.5069	−1.5067	−1.5065	−0.1643
[6/22*]	−323.716024	−40.4659	−40.4659	−2.7854	−2.7853	−1.5073	−1.5064	−1.5062	−1.5059	−0.1643
[5/12*/3*]	−323.716317	−40.4668	−40.4668	−2.7857	−2.7856	−1.5075	−1.5067	−1.5065	−1.5061	−0.1646
[a]	−323.69129									

[a] Reference 13.

TABLE 26. Comparison of spectroscopic constants of Na_2

Basis	D_e (eV)	R_e (au)	ω_e (cm^{-1})	$\omega_e\chi_e$ (cm^{-1})	B (cm^{-1})	α (cm^{-1})	κ (mdyn/Å)
[3/1]	−0.154	6.042	156.3	0.53	0.1434	0.00032	0.16
[4/1]	−0.153	6.018	151.5	0.62	0.1446	0.00043	0.15
[5/1]	−0.146	6.027	150.5	0.63	0.1442	0.00043	0.15
[5/11*]	−0.029	6.036	156.9	0.60	0.1437	0.00038	0.17
[5/12*]	−0.028	6.039	156.5	0.61	0.1436	0.00040	0.17
[6/22*]	−0.028	6.039	156.3	0.60	0.1436	0.00039	0.16
[5/12*/3*]	−0.020	6.043	156.7	0.61	0.1434	0.00039	0.17
[a]	−0.01	6.047					
[b]	0.038						

[a] Reference 13.
[b] Reference 14. The value has been obtained at the experimental bond length of 5.82 au.

tem uses Raffenetti's BIGGMOLI integral program tailored for the general contraction scheme (6).)

3.4. P_2

Table 27 shows the behaviour of the total energy and the orbital energies of P_2 at the internuclear distance of 3.4974 au. For comparison, the corresponding values from a large STF calculation by Mulliken and Liu (18) are also given. Complete releasing of the valence GTFs (ζ_{14}, ζ_{15}, and ζ_{16}) is needed to obtain convergence of the total energy to $<10^{-3}$ au. Further releasing of ζ_{13} in [7/6] basis set lowers the total energy by only 0.0002 au. The [6/5] total energy is slightly lower (by about 0.0004 au or 0.26 kcal/mol) than the value obtained with the corresponding (no polarization functions) STF basis set (see row *a* in Table 27).

Inclusion of the *d* polarization functions brings about good agreement between the present orbital energies and the ones reported by Mulliken and Liu for STF basis with both *d* and *f* polarization functions. The relative ordering of the outer $1\pi_g$ and $3\sigma_u$ orbitals of the almost degenerate set derived from the atomic $2p$ orbitals would probably require releasing of more GTFs.

Convergence of the potential curve parameters is shown in Table 28. The [6/5] basis predicts that the P_2 molecule is unbound by 0.60 eV, quite close to the value of 0.66 eV obtained in STF calculations. Addition of the *d* polarization functions makes the P_2 molecule bound with respect to two isolated $P(^4S)$ atoms by 1.58 eV. Slightly larger bonding (1.71 eV) obtained by Mulliken and Liu is partly due to the presence of the *f* polarization functions in their basis set. Presence of the *d* polarization functions influences significantly the remaining parameters as well. The trends in the values as found using the STF basis set (without and with the polarization functions) are the same as found with the present GTF sets.

4. Concluding remarks

A quarter century ago, at the very beginning of the era of *ab initio* molecular calculations, the Chicago group produced the near Hartree–Fock wave functions for a number of basic diatomic molecules using STF basis sets. It is truly remarkable that they conducted such careful numerical studies with computer resources which were extremely limited by today's standard.

The present authors feel strongly that the use of GTF basis sets should have been administered as carefully and critically as the Chicago group did with the use of STF.

In the present paper we have shown that the high-quality well-tempered GTF basis sets can produce near Hartree–Fock wave functions for N_2, CO, Na_2, and P_2 *without* reoptimizing exponential parameters in molecules. These basis sets are expensive to use on currently available computers and programs because the number of primitive functions is large. However, the number of distinct exponent values of a well-tempered GTF basis set is far smaller than that of conventional GTF basis set of comparable quality.

This feature holds a great future potential for economizing the integral computations over the well-tempered GTF basis set especially when a molecular calculation involves the calculation of gradient of the energy expression. We anticipate that a properly designed algorithm which takes advantage of the shared exponent parameters among symmetry species and the program implementation on next-generation computers (large and small) will make high-quality molecular calculations fea-

TABLE 27. Comparison of the total and orbital energies (au) of P_2 at 3.4974 au

Basis	T.E.	$1\sigma_g$	$1\sigma_u$	$2\sigma_g$	$2\sigma_u$	$3\sigma_g$	$1\pi_u$	$1\pi_g$	$3\sigma_u$	$4\sigma_g$	$4\sigma_u$	$5\sigma_g$	$2\pi_u$
[3/2]	−681.350666	−80.0689	−80.0689	−7.6099	−7.6091	−5.5041	−5.4975	−5.4971	−5.5013	−0.9896	−0.6338	−0.4133	−0.4178
[4/3]	−681.402671	−79.9998	−79.9998	−7.5496	−7.5488	−5.4432	−5.4378	−5.4375	−5.4404	−0.9682	−0.6087	−0.4068	−0.3925
[5/4]	−681.406778	−79.9932	−79.9932	−7.5445	−7.5437	−5.4383	−5.4326	−5.4322	−5.4354	−0.9670	−0.6082	−0.4073	−0.3913
[6/5]	−681.407846	−79.9957	−79.9958	−7.5457	−7.5448	−5.4397	−5.4340	−5.4337	−5.4369	−0.9665	−0.6083	−0.4076	−0.3910
[7/6]	−681.408050	−79.9973	−79.9973	−7.5460	−7.5451	−5.4401	−5.4343	−5.4340	−5.4373	−0.9664	−0.6083	−0.4076	−0.3909
[6/5/3*]	−681.493620	−79.9681	−79.9681	−7.5134	−7.5126	−5.4067	−5.4041	−5.4038	−5.4037	−0.9135	−0.6019	−0.4102	−0.3770
[7/6/3*]	−681.493688	−79.9690	−79.9690	−7.5137	−7.5128	−5.4071	−5.4042	−5.4039	−5.4041	−0.9135	−0.6019	−0.4102	−0.3770
[a]	−681.40743												
[b]	−681.50039	−79.968	−79.968	−7.512	−7.511	−5.405	−5.403	−5.403	−5.402	−0.911	−0.602	−0.409	−0.377

[a] STF calculation, no polarization functions, ref. 18.
[b] STF calculation, *d* and *f* polarization functions included, ref. 18.

TABLE 28. Comparison of spectroscopic constants of P_2

Basis	D_e (eV)	R_e (au)	ω_e (cm^{-1})	$\omega_e\chi_e$ (cm^{-1})	B (cm^{-1})	α (cm^{-1})	κ (mdyn/Å)
[3/2]		No minimum for $r \leq 3.88$ au					
[4/3]	−0.67	3.689	815.0	4.15	0.2855	0.00107	6.06
[5/4]	−0.61	3.670	796.4	3.61	0.2886	0.00099	5.79
[6/5]	−0.60	3.667	796.5	3.66	0.2891	0.00101	5.79
[a]	−0.66	3.663	799.2	3.97	0.2896	0.00107	5.83
[6/5/3*]	1.58	3.505	914.6	4.04	0.3163	0.00106	7.63
[b]	1.71	3.497	919.7	3.89	0.3178	0.00102	7.72

[a] STF calculation, no polarization functions, ref. 18.
[b] STF calculation, *d* and *f* polarization functions included, ref. 18. (Both *a* and *b* values were obtained by the third-degree polynomial fitting using points given in ref. 18, Table III.)

sible for a variety of chemically interesting molecules.

Furthermore, in calculations which include electron correlation beyond the Hartree–Fock level the integral evaluation step takes only a minor part of the total computer time but the quality of the one-electron basis functions is of great importance. To quote I. Shavitt: "No amount of configuration interaction can remedy defects due to basis-set inadequacies in the underlying SCF calculation" (19).

1. R. C. RAFFENETTI and K. RUEDENBERG. Even-tempered representations of atomic self-consistent-field wave functions. Ames Laboratory. 1973.
2. R. D. BARDO and K. RUEDENBERG. J. Chem. Phys. **60**, 918 (1974).
3. E. CLEMENTI and G. CORONGIU. Geometrical basis set for molecular computations. IBM, Poughkeepsie. 1982.
4. D. M. SILVER and W. C. NIEUWPOORT. Chem. Phys. Lett. **57**, 421 (1978).
5. N. KOSUGI. Private communication. 1982; Supercomputer Workshop, Report 1, 85. Institute for Molecular Science, Okazaki, Japan. 1983.
6. R. C. RAFFENETTI. J. Chem. Phys. **58**, 4452 (1973).
7. P. E. CADE, K. D. SALES, and A. C. WAHL. J. Chem. Phys. **44**, 1973 (1966).
8. G. HERZBERG. Spectra of diatomic molecules. Van Nostrand, New York. 1967.
9. A. D. MCLEAN and M. YOSHIMINE. Tables of linear molecular wave functions. IBM, San Jose. 1967.
10. W. M. HUO. J. Chem. Phys. **43**, 624 (1965).
11. R. S. MULLIKEN. J. Chem. Phys. **23**, 1833 (1955).
12. W. J. STEVENS, M. M. HESSEL, P. J. BERTONCINI, and A. C. WAHL. J. Chem. Phys. **66**, 1477 (1977).
13. H. PARTRIDGE, CH. W. BAUSCHLICHER, JR., S. P. WALCH, and B. LIU. J. Chem. Phys. **79**, 1866 (1983).
14. R. L. MARTIN and E. R. DAVIDSON. Mol. Phys. **38**, 1713 (1978).
15. J. HIGUCHI (*Editor*). The basic theories in quantum chemistry. Kyoritsu Shuppan, Tokyo. 1985. In press.
16. S. T. ELBERT, L. M. CHEUNG, and K. RUEDENBERG. "ALIS", Nat. Resour. Comput. Chem. Software Cat., Program No. QH01, Vol. 1, 1980.
17. D. D. KONOWALOW, M. E. ROSENKRANTZ, and M. L. OLSON. J. Chem. Phys. **72**, 2612 (1980).
18. R. S. MULLIKEN and B. LIU. J. Am. Chem. Soc. **93**, 6738 (1971).
19. I. SHAVITT. *In* Methods of electronic structure theory. *Edited by* H. F. Schaefer III. Plenum. 1977. p. 243.
20. A. G. GAYDON. Dissociation energies and spectra of diatomic molecules. Chapman and Hall Ltd., London. 1953.
21. D. H. RANK, A. H. GUENTHER, G. D. SAKENA, J. N. SHEARER, and T. A. WIGGINS. J. Opt. Soc. Am. **47**, 686 (1957).
22. B. ROSENBLUM, A. H. NETHERCOT, JR., and C. H. TOWNES. Phys. Rev. **109**, 400 (1958); C. A. BURRUS. J. Chem. Phys. **28**, 427 (1958).

Photoreluctant azoalkanes: 185-nm photolysis of *E*- and *Z*-diazacyclooct-2-ene

WALDEMAR ADAM[1] AND THOMAS OPPENLÄNDER[2]
Institut für Organische Chemie, Universität Würzburg, Am Hubland, D-8700 Würzburg, West Germany

Received July 30, 1984

This paper is dedicated to Professor Camille Sandorfy on the occasion of his 65th birthday

WALDEMAR ADAM and THOMAS OPPENLÄNDER. Can. J. Chem. **63**, 1829 (1985).

The 185-nm photolyses of *E*- and *Z*-1,2-diazacyclooct-1-enes (**1**) result mainly in denitrogenation, affording 1-hexene and cyclohexane in a 2:1 ratio. In comparison to the direct 350-nm photolyses the denitrogenation efficiencies are enhanced by 42- and 26-fold for the *E*- and *Z*-isomers, respectively. It is proposed that the photoisomerization (350 nm) takes place from the $S_1(n_-,\pi^*)$-state and the photodenitrogenation (185 nm) out of the S_2-state.

WALDEMAR ADAM et THOMAS OPPENLÄNDER. Can. J. Chem. **63**, 1829 (1985).

Les photolyses à 185 nm des diaza-1,2 cyclooctènes-*E* et -*Z* (**1**) provoquent principalement des déazotations qui conduisent à l'hexène-1 et au cyclohexane dans un rapport de 2/1. Par comparaison avec les photolyses directes à 350 nm, les efficacités des déazotations sont augmentées respectivement par des rapports de 42 et 26 pour les isomères -*E* et -*Z*. On suggère que la photoisomérisation (350 nm) se produit à partir de l'état $S_1(n_-,\pi^*)$ alors que la photodéazotation (185 nm) se produit à partir de l'état S_2.

[Traduit par le journal]

The importance of azoalkanes in the mechanistic studies of radicals and diradicals (1) and in synthetic applications (2) has been amply demonstrated over a number of decades. Through these studies, however, a group of azoalkanes, namely the structure types shown, have become recognized to be reluctant in eliminating molecular nitrogen on thermal as well as photochemical activation. Those in the fourth category include bridgehead-centered (3) and cyclopropyl (4) groups. Reasons for photoreluctance include deactivation of the n,π*-excited states via fluorescence, radiationless decay, intramolecular cyclization, hydrogen abstraction, phototautomerism and/or *cis–trans* isomerization (5). By means of photolysis in the gas phase or at elevated temperatures and introduction of radical-stabilizing substituents at the nitrogen-bearing carbons photoreluctance can be in part counteracted (6). More effective for this purpose is photolysis at 185 nm in solution, as demonstrated for all the structure types above but the 1,2-diazocyclooctene (3, 7).

For the latter, so far (8) only the direct and triplet-sensitized photolyses above 300 nm have been investigated, resulting in efficient *cis–trans* isomerization with merely <3% denitrogenation. It was, therefore, the purpose of this study to examine the 185-nm photochemistry of the reluctant *Z*- and *E*-1,2-diazacyclooct-1-enes (**1**) and compare it with the established behavior at long wavelengths (λ > 300 nm). While in the latter irradiations usually only n_-,π^*- excited states are involved (1), during excitation in the vacuum ultraviolet region (λ < 200 nm) higher excited states such as n_+,π^{*-}, π,π^{*-}, n_+,σ^{*-} and also molecular Rydberg states are feasible (Fig. 1) (9). In view of the distinct molecular symmetry of the *Z*- and *E*-isomers of **1**, the various possible excitations are of different probability and thus these isomers might show distinct photochemical behavior on 185-nm irradiation. For example, while for both isomers the π,π^{*-} transitions are allowed and thus intensive, for the *E*-isomer also the n_+,π^{*-} excitation and the $n_-,3p$-Rydberg transitions are symmetry-allowed, but for the *Z*-isomer additionally only the $n_-,3s$-Rydberg excitation (Fig. 1). Nevertheless, at least a greater efficiency of denitrogenation compared to *cis–trans* isomerization is expected (3, 7) at 185 nm compared to >300 nm for the azoalkane **1**. Herein we report the results of this study.

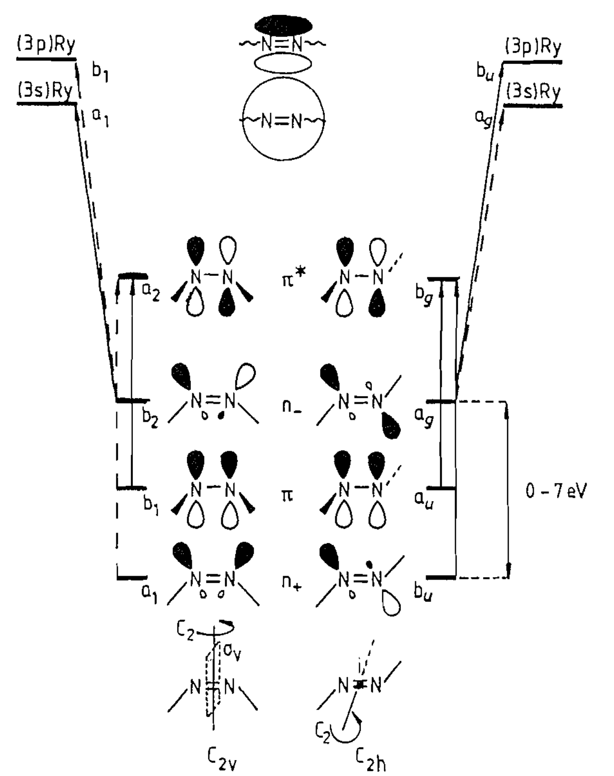

FIG. 1. Allowed (→) and forbidden (-→) electronic transitions for *cis*- and *trans*-azoalkanes.

Results

The synthesis of *Z*-**1** could be significantly improved (8) by employing the copper complex method (reaction [1]) for generating the azoalkane from its hydrazo derivative.

[1] To whom all correspondence should be addressed.

[2] Doctoral Fellow (1982–1984) of the Fonds der Chemischen Industrie. This paper is part of the Doctoral Dissertation, University of Würzburg, July 1984.

TABLE 1. Quantum yields for the 185-nm and the 350-nm photolyses of *Z*- and *E*-diazacyclooct-1-ene

				Photoproducts, ϕ_p[d]		
Substrate	Photolysis conditions[a]	ϕ_S[b]	ϕ_{iso}[c]	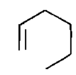	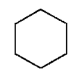	$\Sigma\phi_p + \phi_{iso}$
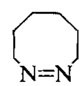 [e,f]	350 nm, 25°C[g]	0.78	0.77	0.008	0.004	0.78
	185 nm, 25°C[h]	0.44	0.14	0.20	0.11	0.45
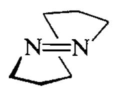 [e,i]	350 nm, 25°C[g]	0.61	0.60	0.006	0.003	0.61
	185 nm, 25°C[h]	0.48	0.03	0.25	0.13	0.41

[a] All photolyses were performed in *n*-pentane.
[b] ϕ_S = quantum yield of consumption of azoalkanes *Z*-**1** and *E*-**1**, respectively.
[c] ϕ_{iso} = quantum yield of the formation of isomerized azoalkane.
[d] The experimental error corresponds to ca. 10–15% of the stated values.
[e] The benzophenone-sensitized photolyses ($\lambda > 300$ nm) led after 20 h irradiation to photostationary state of 55% *E*-**1** and 15% *Z*-**1**.
[f] [*Z*-**1**] = 0.0177 *M*.
[g] Aktinochrome R was used as actinometer (ref. 12).
[h] *cis–trans* isomerization of cyclooctene was used as actinometer (ref. 11).
[i] [*E*-**1**] = 0.0110 *M*.

[1] 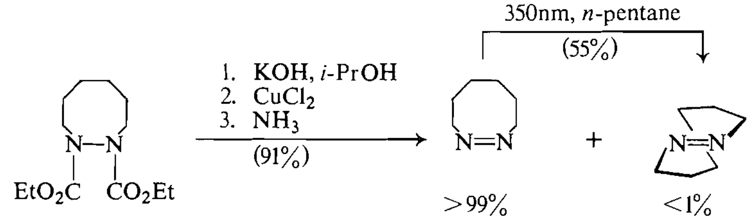

With the copper complex method (10) higher yields and stereoisomerically pure *Z*-**1** were obtained. Photoisomerization at 350 nm afforded the *E*-**1** isomer (reaction [1]). Both isomers are stable at room temperature (ca. 20–25°C), but quite photolabile even on exposure to daylight leading to photoisomerization.

Photolysis at 185 nm in *n*-pentane (cf. Experimental Section for details) led also to significant *cis–trans* isomerization, together with the denitrogenation products cyclohexane and 1-hexene. Concentration–time profiles of a typical 185-nm photolysis for each isomer are given in Fig. 2. During the first 20 min of photolysis the mass balance (Σ%) for both isomers was exceptionally high. The denitrogenation products cyclohexane and 1-hexene were, as expected, stable under the applied 185-nm photolysis conditions and were formed in a relative ratio of 2:1, as in the long wavelength ($\lambda > 300$ nm) irradiations.

The quantitative analyses were conducted by capillary gc using standardization plots and are summarized in Table 1. To assess the quantum yields for the 185-nm photolyses, the previously established (11) actinometry (*cis–trans* cyclooctene isomerization) was employed. For comparison the 350-nm photolyses were also performed. For this purpose the recently published (12) Aktinochrome R actinometer proved especially advantageous for the determination of the quantum yields in the long wavelength irradiations. The determination of quantum yields at 350 nm was based on the quantitative description of the *cis–trans* isomerization process (11) and corrected for back-reaction according to [2].

$$[2]\quad \frac{dy}{dt} = \frac{I_0 l}{VF}\left[\phi_{E\to Z}\epsilon_E(1-y) - \phi_{Z\to E}\epsilon_Z y\right]$$

where $y = [Z]/[Z]_0$, fraction of *Z*-isomer; I_0 = absolute light intensity, determined by using Aktinochrome R (248/334) (12); l = pathlength (cm); V = sample volume (l); $F = D/(1 - e^{-D})$ = fraction of incident light absorbed, in which the optical density $D = \ln I_0/I = C_0 l[\epsilon_E + (\epsilon_Z - \epsilon_E)y]$; $C_0 = [Z] + [E]$ = total concentration; ϵ = molar absorption coefficient at 350 nm (M^{-1} cm^{-1}); and ϕ_E = quantum yield of *E*-isomer formation and ϕ_Z = quantum yield of *Z*-isomer formation. Applying the steady-state conditions ($dy/dt = 0$, $t = \infty$) and integration of eq. [2] leads to eq. [3].

$$[3]\quad -f([Z]) = ([Z_0] + B[Z]_\infty)\ln A + B([Z] - [Z]_0) = mt + \text{constant}$$

where $A = ([Z] - [Z]_\infty)/([Z]_0 - [Z]_\infty)$, $B = (\epsilon_Z - \epsilon_E)/\epsilon_E$, $m = (I_0\phi_{E\to Z})/Vy_\infty$, and $\phi_{E\to Z} = my_\infty N_L/1000I_0$. The subscript indicates the photostationary state at infinite time and $N_L = 6.023 \times 10^{23}$ mol^{-1}.

To establish that $I_0 = I_{abs} = (3.66 \pm 0.14) \times 10^{16}$ quanta min^{-1} cm^{-3}, the photolysis of *Z*-**1** was performed at high concentrations ([*Z*-**1**] = 0.229 *M*) in the region of total absorption. Using the slope $m = (9.96 \pm 0.32) \times 10^{-5}$ *M* min^{-1} of the plot of $-f([Z])$ versus t and $y_\infty = 0.363$, the quantum yield of *Z*-isomer formation was determined to be $\phi_{E\to Z} = 0.60$. From eq. [4],

$$[4]\quad \phi_{Z\to E}\epsilon_Z[Z_\infty] = \phi_{E\to Z}\epsilon_E[E_\infty]$$

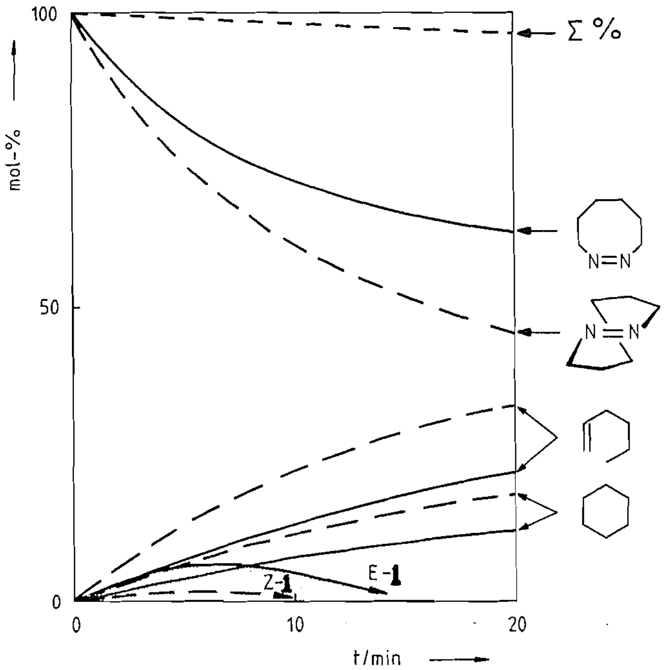

FIG. 2. Concentration–time profile of the 185-nm photolyses of Z- and E-1,2-diazacyclooct-1-ene in n-pentane.

it was possible to calculate $\phi_{Z\to E} = 0.77$ with $\epsilon_Z^{350} = 44.6$, $\epsilon_E^{350} = 37.4$, $[Z]_\infty = 0.0831$ M, and $[E]_\infty = 0.128$ M.

The results in Table 1 reveal that on 350-nm irradiation the main photo-reaction by far is *cis–trans* isomerization ($\phi_{Z\to E} + \phi_{E\to Z} = 1.37$). However, at 185 nm this isomerization is substantially reduced ($\phi_{Z\to E} + \phi_{E\to E} = 0.17$) compared to denitrogenation ($\phi_{N_2} = 0.31$ and 0.38, respectively, for Z- and E-isomers). Thus, photodenitrogenation at 185 nm was ca. 26-fold more efficient than at 350 nm for the Z-isomer and ca. 42-fold for the E-isomer. Formation of the E-isomer was more efficient than of the Z-isomer at both wavelengths.

Discussion

The mechanistic interpretation of the photochemical results in Table 1 are presented in eq. [5]. The percentages in parentheses are for the 350-nm photolyses, the others at 185 nm. As

[5]

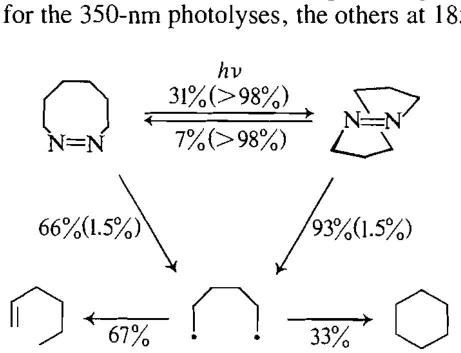

already stated, at the short wavelengths the main photoprocess is denitrogenation, while at the long wavelengths it is *cis–trans* isomerization. Furthermore, photodenitrogenation at 185 nm is considerably more efficient for the E-isomer, i.e. 93% versus 69%. Whether this enhanced photodenitrogenation of the E-isomer reflects the fact that for this isomer both the π,π^{*-} and n_+,π^{*-} excitations are symmetry-allowed (Fig. 1), is at this point difficult to know with certainty because the vacuum ultra-

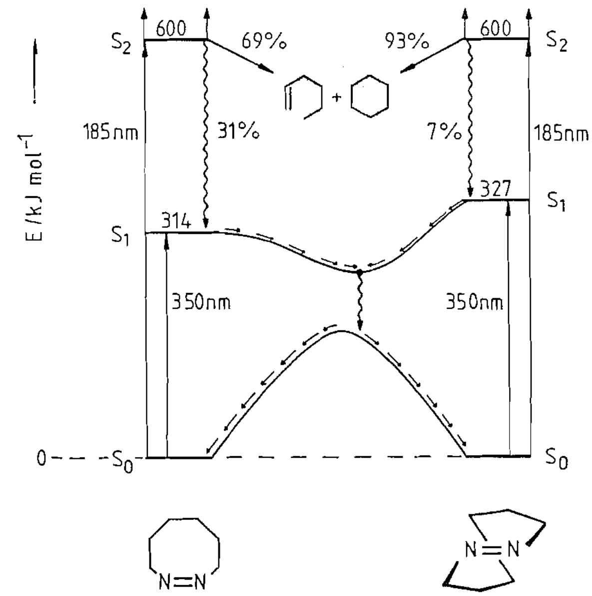

FIG. 3. Qualitative state diagram for the photolysis of E- and Z-1,2-diazacyclooct-2-ene.

violet spectroscopy of this system is still lacking. Besides, both isomers possess symmetry-allowed but distinct Rydberg transitions, namely $(n_-,3p)$Ry and $(n_-,3s)$Ry, respectively, for E-**1** and Z-**1**, so that a rigorous spectroscopic analysis would be complicated. Nevertheless, the greater efficiency of photodenitrogenation at 185 nm for the E-isomer is at least consistent with symmetry-allowed n_+,π^* excitation.

Irradiation at 350 nm leads to a photostationary state consisting of 60% E-isomer and 40% Z-isomer. This implies that for the potential energy surface that connects the S_1-states of the excited E- and Z-isomers, the energy minimum is displaced in favor of the E-isomer (Fig. 3). We postulate that *cis–trans* isomerization of the azoalkane **1** occurs from the $S_1(n_-,\pi^*)$-state, while the S_2-state is responsible for denitrogenation. The latter is reached on 185-nm excitation. Since radiationless deactivation ($S_2 \to S_1$) is expected to compete with denitrogenation, the observed *cis–trans* isomerization in the 185-nm photolyses can be rationalized by population of the $S_1(n_-,\pi^*)$-state via this pathway. However, a photostationary state in the 185-nm irradiations cannot be attained in view of competitive photodenitrogenation from the S_2-state. As already stated, at this point it is not possible to define the electronic configuration of the S_2-state that is generated in the 185-nm photolyses.

An additional point of photomechanistic interest is the fact that the sum of the quantum yields for *cis–trans* isomerization at 350 nm does not correspond to unity, i.e., $\phi_{Z\to E} + \phi_{E\to Z} = 1.37$. According to Hammond (13) this suggests that this photoisomerization does not involve a common intermediate. This feature supports the hypothesis made by Weiss and Warshel (14) concerning the dynamics of photoisomerization.

Experimental section

General aspects

All photolyses were performed in spectrograde n-pentane (11) under nitrogen atmosphere at room temperature (25°C). Before photolysis, the solutions were deoxygenated by bubbling through a slow stream of purified nitrogen. During photolysis the mixture was stirred effectively by means of a magnetic stirring bar.

Light sources and quantum yields

Photolyses above 300 nm were carried out on semi-preparative scale (150 mL) using a Rayonet Photochemical Reactor with the appropriate light sources (RPR-350-nm lamps) and a quartz tube. Quantum yields at this wavelength were determined on an optical bench, equipped with a xenon high pressure lamp (XBO-1600W, Osram) connected to a monochromator (Schoeffel Instrument GmbH, Kratos, f/36) using a quartz cuvette (QS, Hellma, 2.5 mL). For chemical actinometry the Aktinochrome R (248/334)-system (Amko company) was used, following the detailed literature procedure (12). The light intensity of the xenon lamp at 334 nm was determined by this method to be $I_0 = (3.66 \pm 0.14) \times 10^{16}$ quanta min^{-1} cm^{-3}.

Photolyses (185 nm) on preparative scale were carried out in a reaction vessel equipped with nitrogen inlet and a Suprasil tube, containing a low pressure mercury arc (HNS 10W/UoZ-Osram). During photolysis the 185-nm lamp was cooled by a slow stream of nitrogen. Quantitative 185-nm photolyses were performed by using a Suprasil cuvette (4 mL) with the nitrogen inlet placed directly in front of a sigmoidal low pressure mercury arc (15) (capillary lamp No. 4, Gräntzel Co., Karlsruhe). Photoreactivity at 254 nm (the main output of the 185-nm light sources) was established by selecting the 254-nm line (and higher wavelength) by means of a Vycor filter (M 235, Heraeus, Hanau).

Quantum yields at 185 nm were determined as described previously (11) using the *cis–trans* isomerization of cyclooctene as actinometer. The light intensity of the capillary lamp was $(6.56 \pm 0.19) \times 10^{17}$ quanta min^{-1} cm^{-3}.

Product analysis

All photoproducts were identified by ^{1}H-nmr (60 MHz) spectroscopy photolyzing 0.05 *M* solutions of the azoalkanes in C_6F_{14} directly in a quartz nmr tube at 185 nm or 350 nm. In addition the photoproducts were characterized by cgc coinjection with authentic samples on two different capillary columns (50 m × 0.8 mm Carbowax 20 M and 50 m × 0.8 mm Apiezon L). Quantitative product analyses were performed using a Carlo Erba Model 2900 capillary gas chromatograph (FID) and a 50 m × 0.8 mm glass capillary column with nitrogen carrier gas flow = 0.6 mL/min, column, injector, and detector temperatures of 30, 150, and 175°C, respectively. After 12 min, the column temperature was raised from 30°C up to 120°C (39°C/min). Calibration curves were constructed for the *Z*-**1** and *E*-**1** azoalkanes and for the denitrogenation products 1-hexene and cyclohexane affording calibration factors $f_i = 1.99 \pm 0.07$, $f_i = 1.75 \pm 0.02$, $f_i = 2.01 \pm 0.04$, and $f_i = 1.72 \pm 0.04$, respectively, against nonane as cgc standard.

Materials

Nonane (cgc standard), 1-hexene, and cyclohexane were commercially available in purities better than 99%.

(Z)-1,2-Diazacyclooct-1-ene. (**1**) (8*b*) was synthesized in 99% purity (cgc) by refluxing a solution of 0.50 g (1.9 mmol) 1,2-bis-(ethoxycarbonyl)-1,2-diazacyclooctane (8*b*) and 0.50 g (8.9 mmol) potassium hydroxide in 2 mL of isopropanol under nitrogen atmosphere for 5 h. After cooling the reaction mixture to room temperature (ca. 20°C), 10 mL of distilled water were added, and the solution was neutralized using concentrated HCl. Then 10 mL of a saturated copper(II) chloride solution were added and the reaction mixture was stirred for 6 h at ca. 20°C. The dark red precipitate was recovered by means of filtration and washed once with 10 mL of distilled water and with 10 mL of absolute ether. After drying over silica gel at 15 Torr, the copper complex was stirred with 5 mL of concentrated ammonia. Extraction of the blue solution with methylene chloride (4 × 10 mL) and washing the organic layer once with 10 mL saturated NaCl solution and with 10 mL distilled water yielded after drying over $MgSO_4$ a yellow solution. Evaporating the solvent in the dark at 0°C/18 Torr afforded a yellow oil which was distilled at 42°C/0.1 Torr to yield 0.20 g (91%) of a slight yellow oil. The infrared and ^{1}H-nmr (90 MHz) data were in agreement with published data (8). Ultraviolet (*n*-pentane): λ_{max} (ϵ) = 185 (2970), 254 (<5), 382 nm (158).

(E)-1,2-Diazacyclooct-1-ene. (**1**) was synthesized according to the known procedure (8) by photoisomerization of a 0.05 *M* solution of azoalkane *Z*-**1** in *n*-pentane at 350 nm. Isolation and purification of the *E*-isomer was achieved by preparative gc, using a Carlo Erba 4200 gas chromatograph equipped with glass column (1.5 m × 8 mm) packed with 10% Apiezon L on Chromosorb WHP (60/80 mesh) and a nitrogen carrier gas flow of 25 mL/min, column, injector, and detector temperatures of 80, 150, and 180°C, respectively. The azoalkane was obtained as a pale yellow oil in 99% purity (cgc). Infrared and ^{1}H-nmr (90 MHz) data were in agreement with the published data (8). Ultraviolet (*n*-pentane): λ_{max} (ϵ) = 185 (7880), 254 (<5), 366 nm (48).

254-nm corrections

Control experiments at 254 nm (and higher wavelength) were performed using the capillary lamp directly connected to a Vycor filter by photolyzing 0.01 *M* solutions of the azoalkanes at this wavelength and analyzing at distinct time intervals by means of cgc. The optical density of the Vycor filter at 254 nm was greater than 90%. The same experiment was repeated without Vycor filter under the same conditions and concentrations were corrected according to eq. [6].

$$[6] \quad [C]_{185} = [C]_{185+254} - [C]_{254}$$

Acknowledgements

Generous financial support by the Deutsche Forschungsgemeinschaft and the Fonds der Chemischen Industrie is gratefully appreciated. We thank Professor H.-D. Brauer, Universität Frankfurt, for supplying us a sample of Aktinochrome R.

1. P. S. ENGEL. Chem. Rev. **80**, 99 (1980).
2. W. ADAM and O. DE LUCCHI. Angew. Chem. Int. Ed. Engl. **19**, 762 (1980).
3. W. ADAM, F. MAZENOD, Y. NISHIZAWA, P. S. ENGEL, S. A. BAUGHMAN, W.-K. CHAE, D. W. HORSEY, H. QUAST, and B. SEIFERLING. J. Am. Chem. Soc. **105**, 6141 (1983).
4. P. S. ENGEL, C. J. NALEPA, R. A. LECKONBY, and W. K. CHAE. J. Am. Chem. Soc. **101**, 6435 (1979).
5. P. S. ENGEL and C. STEEL. Acc. Chem. Res. **6**, 275 (1973).
6. P. S. ENGEL, D. W. HORSEY, D. E. KEYS, C. J. NALEPA, and L. R. SOLTERO. J. Am. Chem. Soc. **105**, 7108 (1983).
7. (*a*) W. ADAM and F. P. MAZENOD. J. Am. Chem. Soc. **102**, 7131 (1980); (*b*) W. ADAM, A. FUSS, F. P. MAZENOD, and H. QUAST. J. Am. Chem. Soc. **103**, 998 (1981).
8. (*a*) C. G. OVERBERGER, M.-S. CHI, D. G. PUCCI, and J. A. BARRY. Tetrahedron Lett. 4565 (1972); (*b*) C. G. OVERBERGER and J. W. STODDARD. J. Am. Chem. Soc. **92**, 4922 (1970); (*c*) G. VITT, E. HÄDICKE, and G. QUINKERT. Chem. Ber. **109**, 518 (1976); (*d*) C. G. OVERBERGER and T. F. MERKEL. J. Org. Chem. **46**, 442 (1981).
9. (*a*) M. B. ROBIN. *In* The chemistry of the hydrazo, azo and azoxy groups. Vol. 1. *Edited by* S. Patai. John Wiley and Sons, New York. 1975. p. 1; (*b*) C. SANDORFY. *In* Chemical spectroscopy and photochemistry in the vacuum-ultraviolet. *Edited by* C. Sandorfy, P. J. Ausloos, and M. B. Robin. D. Reidel Publishing Company: Dordrecht, Holland/Boston, USA. 1975. pp. 149–175.
10. M. HEYMAN, V. T. BANDURCO, and J. P. SNYDER. J. Chem. Soc. Chem. Commun. 297 (1971).
11. W. ADAM and T. OPPENLÄNDER. Photochem. Photobiol. **39**, 719 (1984).
12. H.-D. BRAUER and R. SCHMIDT. Photochem. Photobiol. **37**, 587 (1983).
13. D. O. COWAN and R. L. DRISKO. Elements of organic photochemistry. Plenum Press, New York. 1976. Chapt. 9.
14. R. M. WEISS and A. WARSHEL. J. Am. Chem. Soc. **101**, 6131 (1979).
15. D. SÄNGER and C. VON SONNTAG. Tetrahedron **26**, 5489 (1970).

Vacuum–ultraviolet photolysis (185 nm) of liquid 1,3-dioxan

HEINZ-PETER SCHUCHMANN AND CLEMENS VON SONNTAG
Max-Planck-Institut für Strahlenchemie, Stiftstr. 34-36, D-4330 Mülheim a.d. Ruhr, W.-Germany

Received September 26, 1984

This paper is dedicated to Professor Camille Sandorfy on the occasion of his 65th birthday

HEINZ-PETER SCHUCHMANN and CLEMENS VON SONNTAG. Can. J. Chem. **63**, 1833 (1985).

1,3-Dioxan photolytic destruction at 185 nm occurs with a quantum yield of about 0.3 in the liquid phase. Of the 22 products determined, the major ones are *n*-propylformate (ϕ = 0.10), formaldehyde (0.075), 1,3-diox-4-en (0.06), hydrogen (0.05), ethylene (0.04), and 3-methoxypropionaldehyde (0.04). A number of the minor products are of the general type **B**,

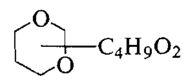

B

some of which bear a hydroxyl function at the end of the side chain. N_2O interacts with excited 1,3-dioxan, leading to the production of N_2.

Some experiments have been carried out in the vapour phase, the results of which indicate that considerable fragmentation of hot primary intermediates and products into low-molecular-weight products occurs. The nature of these products cannot be linked directly to the primary photolytic processes inferred from the liquid-phase studies.

Certain contrasts in the photolytic behaviour of 1,3-dioxan and 1,4-dioxan are discussed.

HEINZ-PETER SCHUCHMANN et CLEMENS VON SONNTAG. Can. J. Chem. **63**, 1833 (1985).

La destruction du dioxanne-1,3 lors de sa photolyse à 185 nm se produit avec un rendement quantique près de 0,3 dans la phase liquide. Parmi les 22 produits mesurés, le formiate de propyl (ϕ = 0,16), le formaldéhyde (0.075), le diox-1,3-ène-4 (0,06), l'hydrogène (0,05), l'éthylène (0,04) et le méthoxy-3-propionaldéhyde (0,04) sont les majeurs. Divers produits, mineurs, dont quelques-uns portent une fonction hydroxyl au bout de la chaîne latérale, revêtent la structure générale **B**.

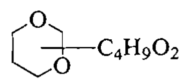

B

Le N_2O interagit avec le dioxanne-1,3 excité, ce qui mène à la production de N_2.

Quelques expériences ont été faites en phase vapeur, dont les résultats indiquent une fragmentation considérable des intermédiaires et produits primaires, chauds. La nature des produits finaux ainsi formés ne peut pas être associée directement aux processus photolytiques primaires que l'on saurait reconnaître moyennant les études faites en phase liquide.

Certaines différences entre le dioxanne-1,3 et le dioxanne-1,4, en ce qui concerne leur comportement photolytique, sont discutées.

Introduction

Sandorfy (1) has shown that the first absorption band of saturated alcohols and ethers is due to an essentially $3s \leftarrow n$ transition. Its band maximum is around 185 nm where the low-pressure Hg arc has a strong emission line. Studies on the liquid-phase 185 nm photolysis of open-chain ethers have shown that the predominant process is the scission of a C—O linkage, a reaction the quantum yield of which can approach unity (2, 3). In cyclic ethers the same process also occurs, but the quantum yields are often considerably lower due to reclosure of the intermediate (singlet) diradical. A similar situation prevails in the series of open-chain acetals (4–6) and cyclic acetals (7, 8). Another member of this group is 1,3-dioxan, whose photochemistry was of special interest to us because it is an isomer of 1,4-dioxan whose photochemistry (9–13) and photophysics (13–15) have so far been receiving more attention.

Experimental

1,3-Dioxan was prepared from 1,3-propanediol and paraformaldehyde (16). The fractionated product showed a gas chromatographic purity of 99.97% by flame ionization detection.

Samples (2 mL) of the neat liquid contained in a suprasil cell (a photograph of the setup is shown and its use described in ref. 17) were deaerated by purging with argon for 30 min and irradiated with the unfiltered light of a low-pressure mercury lamp at a dose rate, determined by means of the Farkas actinometer (2), of 4.0×10^{17} quanta (185 nm) per min received by the sample. The 254 nm light is inactive in this system. 1,3-Dioxan begins to absorb near 200 nm. From its spectrum, measured on a Cary model 14 spectrophotometer, molar extinction coefficients of 9 and 0.6 M^{-1} cm^{-1} were calculated at 185 and 193 nm, respectively. (A small shoulder was observed at the onset of the absorption, near 220 nm, when the absorbance of the material was measured in a 1 cm cell.) Some samples containing N_2O at different concentrations were also photolyzed to investigate the influence of this additive. Since photoexcited 1,4-dioxan shows a fluorescence in the condensed phase (10, 13–15), it was decided to look for a similar fluorescence in liquid 1,3-dioxan also. This was done by exciting the compound with the 193 nm line of an ArF excimer laser (Spectra Physics).

The products except formaldehyde were analyzed by gc and identified by the use of reference material and/or their mass spectra obtained through gc–ms. Glass capillary columns were employed, the carrier gas being hydrogen. Non-derivatized, acetylated and benzoylated samples were analyzed on CW-20M, silylated ones on SE-30. Non-derivatized samples were also analyzed on PC-240 for better resolution of the more volatile products such as *n*-propanol, propyl formate, and 1,3-diox-4-en. Quantitative time-course studies were done only with non-derivatized samples. A levelling-off of the dose–yield curves of the products, in particular that of 1,3-diox-4-en, which is thought to have the highest extinction coefficient of all the products at 185 nm, was not observed even at maximum conversion which was of the order of 10^{-3}. Thus, photolysis of products is not expected to have been significant. The internal standard (18) was $C_{14}H_{30}$. The derivatized samples were prepared and analyzed in order to better recognize the nature of some of the photolysis products.

The following derivatizations were carried out: (*a*) treatment of irradiated 1,3-dioxan with bis(trimethylsilyl)trifluoroacetamide in order to trimethylsilylate those products that contain a hydroxyl function; (*b*) treatment of the photolysis products, after evaporation of the 1,3-dioxan, with acetic anhydride/sodium acetate to acetylate products with a hydroxyl function; (*c*) esterification with benzoic anhydride/sodium benzoate; and (*d*) hydrolysis of the photolysis products that contain an acetalic function, after evaporation of the remaining 1,3-dioxan, with hydrochloric acid at pH ~ 0.5 for two days at 60°C, neutralization and reduction of the hydrolysate with sodium borodeuteride overnight, removal of the boric acid after acidification by repeated evaporation with methanol, and trimethylsilylation of the evaporation residue.

The volatile products such as hydrogen, nitrogen (from N_2O-containing samples), ethylene, and carbon oxides were analyzed after purging them from the irradiated liquid with a carrier gas, to be collected into a flask for aliquots to be taken (ethylene), or to be swept directly into the gas chromatograph (hydrogen and nitrogen). Hydrogen and nitrogen were determined by thermal conductivity detection, ethylene, and carbon oxides (the latter after on-line catalytic reduction to methane) by flame ionisation detection. Formaldehyde was determined photometrically using acetylacetone/ ammonium acetate reagent (19). This procedure could be applied even though large amounts of 1,3-dioxan are present because 1,3-dioxan does not liberate formaldehyde under these conditions. For vapour phase photolysis experiments, liquid 1,3-dioxan was purged with argon, then kept at 10°C and the vapour transferred with a slow argon stream into a suprasil cell such as the above. After photolysis, the sample was expanded into a flask from which aliquots were taken and analyzed on an OV-225-coated capillary column, or alternatively on a column packed with activated alumina.

Results

In the photolysis of liquid 1,3-dioxan the major products are propyl formate, formaldehyde, ethylene, 3-methoxypropanal, 1,3-diox-4-en, and hydrogen. Furthermore, there is a considerable number of higher-molecular-weight products. Table 1 includes the most prominent ones. These are all formed in low yields, and structural determination has been carried only so far as to be able to identify their essential features. The yield of the products increased linearly with irradiation time, hence quantum yields could be calculated. They are based on $\phi(H_2) = 0.4$ for the Farkas actionometer (5 *M* ethanol in water) (2).

The determination of the low-molecular-weight products was straightforward since reference material was available, while the assignment of the products of higher molecular weight deserves some comment. In cases where reference material was not readily synthesized or mass spectra were not interpretable unambiguously, derivatives were prepared and their mass spectra recorded. Thus, the mass spectra obtained from derivatized samples suggest the presence of the compounds referred to in Table 2. Derivatives were generated by trimethylsilylation, acetylation, and benzoylation, as well as hydrolysis/reduction/trimethylsilylation. Beside the derivatives obtained by the latter procedure, listed in Table 3, there appears a number of lesser gc peaks at higher retention times whose mass spectra are suggestive of higher polyol trimethylsilyl ethers, among the precursors of which one might expect compounds such as **I–III**.

The derivative TMSO—CHD—CH_2—O—CH_2—CH_2—

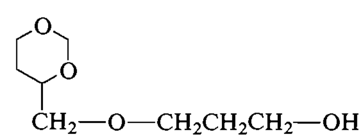

I

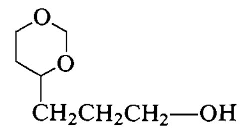

II

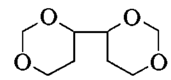

III

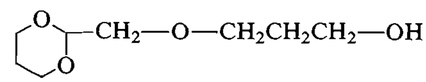

IV

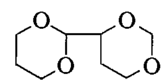

V

CH_2—OTMS has not been seen, which seems to suggest that compound **IV** is not produced in the photolysis. There is also no hint of the deuterated derivative which would be formed on hydrolysis of compound **V** and reduction.

Some experiments have been carried out in the gas phase. Only gaseous products have been measured. They are listed in Table 4. Values are normalized to the ethylene yield since quantum yields have not been determined.

In our attempt to draw a comparison between 1,3-dioxan and 1,4-dioxan, we decided to look for fluorescence in 1,3-dioxan, and found an emission ($\lambda_{max} \approx 285$ nm) on laser excitation at 193 nm. Although the experiments did not permit an accurate measurement of the fluorescence lifetime, a rough estimate of $t_{1/2} = 20$ ns could be extracted by comparing the half-width of the signal to that of the laser pulse. This fluorescence is strongly quenched on saturation with O_2, but hardly if at all affected by N_2O (which is known to quench the fluorescence in 1,4-dioxan) even at saturation where $[N_2O] \approx 0.29$ *M*. Ausloos *et al.* (13) did not detect direct fluorescence upon radiolysis of 1,3-dioxan but found that methylnaphthalene was excited to fluoresce in that solvent. In view of these results we consider it not unlikely that the fluorescence seen in the present experiments could have been due to the intervention of an impurity whose signature might be the small shoulder which had been observed at the onset of the 1,3-dioxan absorption band. Moreover, in a further experiment, the intensity of this fluorescence was measured as a function of the excitation wavelength (using a Xenon lamp), and it was found that the intensity began to increase strongly as the excitation wavelength went below 250 nm, still far above the onset of absorption of the 1,3-dioxan proper.

Even though it does not quench the fluorescence, it is clear that in the 185 nm photolysis N_2O does indeed interact with an excited, 1,3-dioxan-derived species under formation of N_2. The nitrogen quantum yields obtained at different N_2O concentrations are given in Table 5 and are corrected for a contribution from the direct N_2O photolysis, assuming a quantum yield of

TABLE 1. Products[a] and quantum yields of the photolysis of liquid deaerated 1,3-dioxan (185 nm)

	Product	Quantum yield
1	H_2	0.05
2	CO	0.006
3	CO_2	≤0.01
4	CH_2O	0.075
5	C_2H_4	0.04
6	$CH_2{=}CH—CH_2—OH$	0.01
7	n-C_3H_7OH	0.01
8	$C_3H_7OCH{=}O$[b]	0.10
9	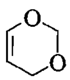 [c]	0.06
10	$CH_3OCH_2CH_2CH{=}O$[d]	0.04
11	$CH_3O—CH_2—CH_2—CH_2—OH$[e]	0.005
12	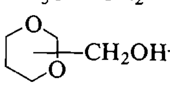 [f]	0.003
13	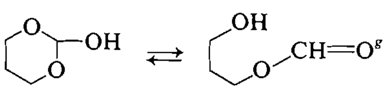 [g]	0.004
14	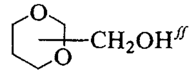 [ff]	2×10^{-4}
15	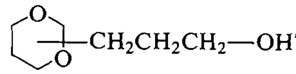 [h]	0.004
16	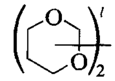 [l]	0.001
17	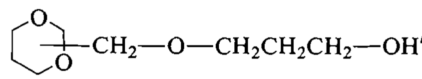 [ii]	0.002
18	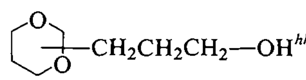 [hh]	0.001
19	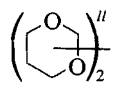 [ll]	5×10^{-4}
20	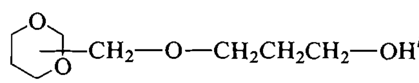 [i]	0.01
21	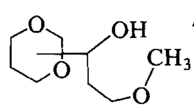 [k]	0.003
22	$(HO—CH_2CH_2CH_2—O—CH_2)_2$[j]	Absent ($< 3 \times 10^{-4}$)

[a] A combined gc–ms analysis was carried out to aid in the identification. (Products **10–22** are listed in the order of increasing gc elution times.)
[b] Reference material was synthesized from propanol and formic acid.
[c] Reference material was synthesized (20).
[d] Reference material was synthesized (21).
[e] Reference material was obtained through reduction of 3-methoxypropanal with sodium boranate in aqueous solution, or from sodium 3-hydroxypropylate and methyl iodide.
[f] Characteristic ms features: m/e (%) 31 (100), 87 (70), 59 (20), 41 (15), 117 = M − 1 (1).
[ff] Characteristic ms features: m/e (%) 31 (100), 87 (65), 28 (60), 45 (40), 57 (40), 29 (25), 117 = M − 1 (1).
[g] Reference material was synthesized from 1,3-propanediol and formic acid.
[h] Characteristic ms features: m/e (%) 87 (100), 31 (55), 59 (20), 41 (20), 40 (20), 145 = M − 1 (6), 102 (2), 103 (2), 116 (2).
[hh] Characteristic ms features: m/e (%) 31 (100), 87 (95), 42 (70), 45 (60), 57 (60), 71 (55), 41 (45), 29 (40), 43 (35), 44 (30), 55 (25), 58 (25), 60 (25), 115 (20), 116 (10), 128 (2), 145 = M − 1 (1).
[i] Characteristic ms features: m/e (%) 87 (100), 31 (40), 59 (25), 45 (22), 41 (15), 118 (10), 175 (0.5), 176 = M (0.3).
[ii] Characteristic ms features: m/e (%) 87 (100), 31 (45), 59 (15), 41 (10), 43 (6), 45 (3), 100 (1), 101 (1), 175 = M − 1 (0.5).
[j] Reference material prepared by heating a mixture of ethylene glycol and 1,3-propanediol with a trace of iodine whereupon the various lower polyglycol ethers are formed (22). Gas chromatographic analysis of this mixture and comparison with the 1,3-dioxan photolysis products indicate that this compound is not formed.
[k] Characteristic ms features m/e (%) 31 (100), 87 (60), 45 (60), 59 (40), 57 (35), 41 (30), 43 (27), 29 (55), 89 (15), 58 (15), 27 (15), 61 (10), 100 (6), 101 (5), 102 (5).
[l, ll] Gas chromatograhic retention time and mass spectra of l and ll are identical to those of reference material obtained in the Hg-sensitized photolysis of 1,3-dioxan, where dehydrodimers are expected as the main products. Characteristic ms features of l: m/e (%) 87 (100), 31 (55), 59 (15), 41 (10), 29 (10), 45 (5), 57 (5), 173 = M − 1 (1), 113 (0.5), 115 (0.5), 127 (0.5), 128 (0.5). Characteristic ms features of ll: m/e (%) 87 (100), 31 (45), 59 (15), 41 (10), 115 (1), 173 = M − 1 (1).

TABLE 2. 1,3-Dioxan photolysis. gc–ms analysis of derivatized samples with respect to derivatives[a] of photoproducts[b]

Precursor	Products: TMS-ether	Acetate	Benzoate
11	−	+	−
12, 14	−	+	++
13	−	−	−
15, 18	+	+	++
17, 20	++	++	++
22	−	−	−

[a] − = none detected, + = one detected, ++ = both detected.
[b] Numbering as in Table 1.

unity for N_2 formation through the latter process, and bearing in mind that for N_2O, $\epsilon(185) = 36\ M^{-1}\ cm^{-1}$ (23). As to its influence on the formation of the other products, it is noteworthy that the quantum yield of formaldehyde is doubled to 0.15 and that of ethylene slightly lowered to 0.03 on saturation with N_2O. The effect regarding the remaining products (Table 1) appears to be small and has not been followed quantitatively.

Discussion

With $\epsilon(185\ nm) = 9\ M^{-1}\ cm^{-1}$, 1,3-dioxan is a liquid of a relatively low extinction coefficient, in line with other acetals (4, 5). Ethers tend to have a much higher extinction coefficient at this wavelength: cf. $\epsilon(185\ nm)$ (1,4-dioxan) = $2 \times 10^3\ M^{-1}$ cm^{-1}. Also, the ionisation potentials of acetals tend to be higher

TABLE 3. Compounds identified by gc–ms of 1,3-dioxan photolysis products (after hydrolysis, reduction with $NaBD_4$ and trimethylsilylation), and their probable precursors

Derivative	Precursor
CHD(OTMS)—CH_2OTMS	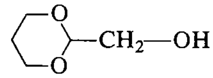
CH_2(OTMS)—CH_2OTMS	$CH_2OH—CH_2OH$
CH_2(OTMS)—CH_2—CH_2OTMS	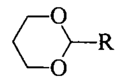
CHD(OTMS)—CH_2—CH_2—CH_2OTMS	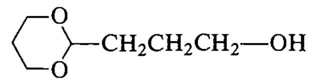
CH_2(OTMS)—CD(OTMS)—CH_2OTMS	Dihydroxyacetone (from trimerization of formaldehyde?)
CH_2(OTMS)—CH(OTMS)—CH_2—CH_2OTMS	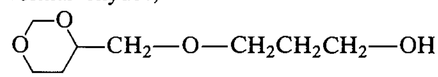

TABLE 4. Some products and their relative yields (ethylene yield ≡ 1) in the gas phase photolysis (at 185 nm) of 1,3-dioxan: total pressure 1 atm, room temperature

Product	Relative yield	Product	Relative yield
H_2	0.33	C_2H_6	0.67
CH_4	0.44	C_3H_6	0.12
C_2H_2	0.55	C_3H_8	1.22
C_2H_4	1.0	n-C_4H_{10}	0.44

TABLE 5. N_2 quantum yields from the 185 nm photolysis of liquid 1,3-dioxan at different N_2O concentrations

$[N_2O]$ (mol/L)	ϕ_{N_2}	$\phi_{N_2,\mathrm{corr}}$[a]
0.29	0.31	0.24_3
0.087	0.11	0.08_4
0.029	0.03_9	0.03_0
0.0087	0.01_3	0.01_0

[a] N_2 quantum yields corrected for the nitrogen formed through direct photolysis of N_2O, assuming a quantum yield of unity for the latter process: $\phi_{N_2,\mathrm{corr}} = \phi_{N_2}(\epsilon_{\mathrm{diox}} \times [\mathrm{diox}] + \epsilon_{N_2O}[N_2O])/\epsilon_{\mathrm{diox}}[\mathrm{diox}] - \epsilon_{N_2O}[N_2O]/\epsilon_{\mathrm{diox}}[\mathrm{diox}]$.

than those of ethers: 10.15 eV for 1,3-dioxan vs. 9.47 eV for 1,4-dioxan (24). It has been shown (13) that 185 nm light does not lead to ionization in the neat liquid dioxans: for 1,4-dioxan the threshold is at about 7.6 eV (165 nm); for 1,3-dioxan it must be higher still as the gas phase ionization potential of the latter compound lies above that of the former.

In order to rationalize the major products propyl formate, formaldehyde, ethylene, 3-methoxypropanal, 1,3-dioxen, and hydrogen (cf. Table 1), reactions [1]–[11] are postulated (Scheme 1). Based on the results of the photolysis of other cyclic acetals (8) one assumes that the scission of the C—O bonds as exemplified by reactions [2] and [4] will play a major role. The resulting diradicals may disproportionate (reactions [8], [8*a*], and [11]), thereby leading to products whose formation could also be envisioned through a rearrangement in the excited state (reactions [1] and [5]). A decision between these two types of processes cannot be made at present. Diradicals also undergo reclosure (reactions [−2] and [−4]). In the present system such processes cannot be monitored because they lead back to the starting material, but with suitably substituted cyclic acetals this type of reaction has been shown to occur (8). Although oxyl radicals are known to undergo β-fragmentation, reactions [9] and [10] are not likely to occur in the liquid phase because the excess energy remaining in the diradical after ring-opening (ca. 60 kcal mol^{-1}) is rapidly degraded at liquid densities, as has been inferred from results obtained on other cyclic systems (25), especially also from 1,4-dioxan (see below). It is in fact likely that the fragment products result from a breakdown of the molecule in the excited state (cf. ref. 25). Besides, there is formation of some hydrogen and 1,3-dioxen, either concomitantly as written (reaction [6]), or in reactions involving H atoms and other radicals with subsequent disproportionation of the resulting 1,3-dioxanyl radicals. That some 1,3-dioxen is formed in processes other than reaction [6] is suggested by the fact that its quantum yield is somewhat higher than that of hydrogen.

In the gas phase, fragmentation is more pronounced, and owing to a lack of easy deactivation a variety of secondary fragments arise (Table 5). We do not propose to explore the relationship between these fragments here. We do think that these phenomena in the gas phase are interesting in their own right, and that this liquid-phase study might serve as a starting point for such investigation.

The ring-opened and fragmentation products found in the present system are reminiscent of those that occur in the photolysis of liquid 1,4-dioxan (10) (cf. Table 6), but in contrast to the latter, the photolysis of liquid 1,3-dioxan is further characterized by the formation of a relatively large number of products with their molecular weight in the dimer range (Table 1). Their combined quantum yield does not approach that of the products in the monomer range. The complete identification of these products proves to be elusive, and insofar as their nature is uncertain the photolysis mechanism remains tentative. However, the identification of these products is put on firmer ground by the additional information obtained through gc–ms analysis of their derivatives. It appears that the products in the dimer range fall into two categories (**A** and **B**). The products

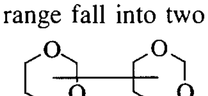
A

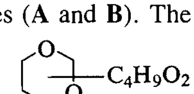
B

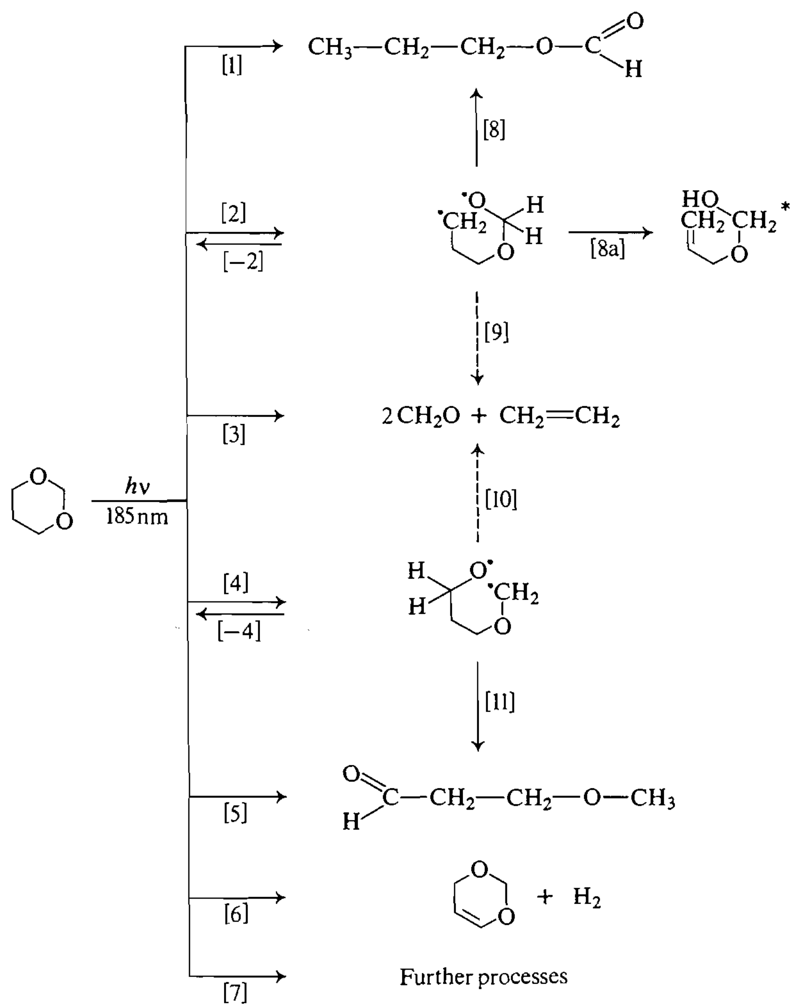

SCHEME 1. Asterisk denotes decomposition into allyl alcohol and formaldehyde under the conditions of analysis.

belonging to **A** might be formed via reactions [12]–[14]

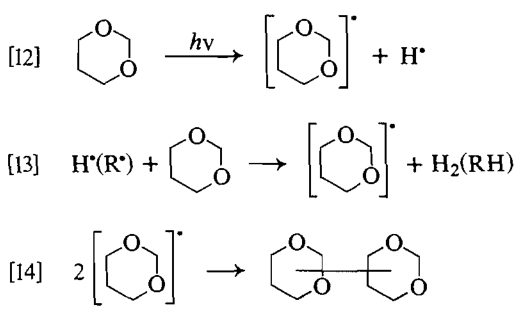

These products (dehydro-dimers) are relatively unimportant and present no interesting aspect compared to the 185 nm photolysis of other ethers carried out in the liquid phase (cf. ref. 3 and references therein).

The products of category **B** may be distinguished further (**B**1, **B**2, **B**3, **B**4) whereby the experimental results (see tables) suggest that only those compounds that can be thought of formally as resulting from the insertion of an alkyl oxyl diradical into a 1,3-dioxan C—H bond should be considered.

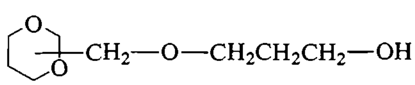

B1

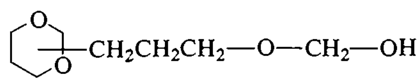

B2

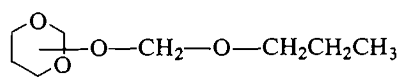

B3

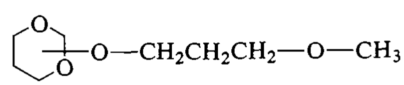

B4

Compounds of category **B**1 are observed, namely **17** and **20**. Compounds of category **B**2, which are hemiacetals, should easily lose formaldehyde and yield products such as **15** and **18**.

The formation of *n*-propanol **7** and 3-hydroxypropylformate **13** hints at the existence of at least one class **B**3 compound, **VI**,

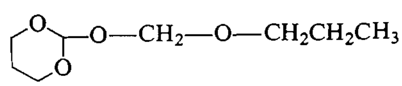

VI

which is presumed to be particularly sensitive towards adventitious moisture. It is not clear whether any compound of class **B**4 is formed.

TABLE 6. Comparison of the photolytic behaviour of deaerated neat liquid 1,3-dioxan and 1,4-dioxan when illuminated with 185 nm light in the liquid phase

	1,3-dioxan		1,4-dioxan	
Reaction	Products	Yield	Products	Yield
Ring fragmentation	$2\ CH_2O + CH_2{=}CH_2$	0.04	$2\ CH_2O + CH_2{=}CH_2$	0.15
			CH_2O + 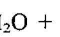	0.04
Disproportionation products	$CH_3-CH_2-CH_2-O-CHO$	0.10	$HO-CH_2CH_2-O-CH{=}CH_2$	0.17
	$CH_2{=}CH-CH_2-OCH_2OH$	0.01		
	$CH_3O-CH_2-CH_2CHO$	0.04		
$H^\bullet$ and H_2 elimination	H_2	0.05	H_2	0.04
Further processes		~0.05		
Total		~0.3		~0.4

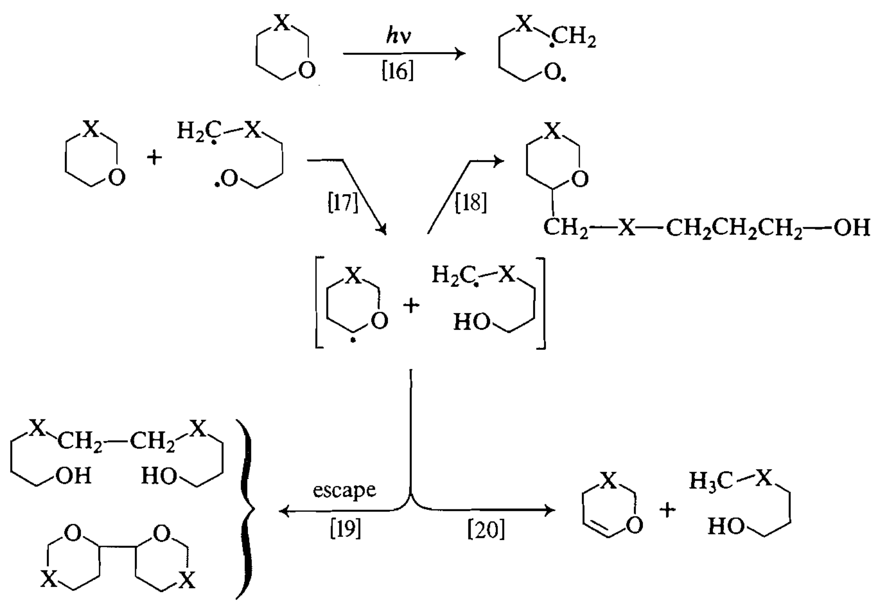

SCHEME 2

The formation of such dimers recalls analogous compounds from the photolysis of tetrahydropyran (26) and oxepan (27). Particularly in the case of tetrahydropyran, the quantum yield of that product was so high (0.21) compared to that of the escape products that it appeared necessary to postulate (26, 27) a reaction such as [15] ($X = CH_2$) rather than a reaction sequence (such as [16]–[18]; $X = CH_2$) involving a diradical; see Scheme 2.

[15] 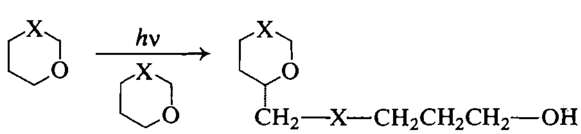

In the present case the situation seems less clearcut. The total dimer quantum yield is quite small, in absolute as well as in relative terms. The quantum yield of the dehydrodimers found, **16** and **19**, is not a lot smaller than that of the total dimers, and the glycol **22** is difficult to measure if present in only small amounts. Moreover, swift combination of the initial radical pair is favoured compared to the diffusion encounter pair case, since if the diradical is in the singlet state the ensuing radical pair would also be singlet, whereas an encounter pair would only have a 25% probability to be in this state. In fact, the product 3-methoxypropanol **11** might be most easily explained by a diradical mechanism ([16], [17], [20] X = O; see Scheme 2) where one must, however, assume that the radical pair is created by the hot alkyl oxyl diradical. Thermalized alkoxyl radicals are expected to react by hydrogen abstraction, in this and in similar systems, with a rate constant of between 10^5 and $10^6\ M^{-1}\ s^{-1}$, cf. ref. 28. On the other hand, self-termination of singlet diradicals is supposed to be fast, with rate constants ranging from 10^9 to $10^{12}\ s^{-1}$ (29–31). Bearing in mind that in the present case the available hydrogen donor concentration (the substrate itself) is about 10 M one realizes that self-termination must predominate for the thermalized diradical.

The comparison of the photobehaviour of 1,3-dioxan with that of 1,4-dioxan is phenomenological and therefore somewhat unsatisfying. It is felt that a deeper penetration necessitates the application of quantum-chemical calculations to their photochemistry. Simpler heterosystems such as methanol and methylamine are already being tackled with some success (32, 33). For the time being, such comparison reveals that fragmentation processes (see Table 6) occur about three times more readily in 1,4-dioxan; products ascribable to direct ring cleavage are formed on comparable scale. It has been suggested that the formation of small unsaturated product compounds, such as ethylene and formaldehyde in the photolysis of the dioxans, is due to the "unzipping" of initial diradical species (34). We prefer the concept of molecular fragmentation, avoiding the diradical intermediate in these processes. Arguments in favour of this supposition have been presented elsewhere (25). We consider the fact that the quantum yields of such fragmentation products contrast so strongly in the two dioxans (Table 6), culminating, in particular, in the absence of oxetane from 1,3-dioxan, also supportive of our concept. Dimer formation, not shown by 1,4-dioxan, results in a variety of products from 1,3-dioxan.

In 1,4-dioxan, fluorescence is observed at 250 nm (half-life about 2 ns (15)). Due to its large Stokes shift this fluorescence has been attributed to an eximer. This fluorescence is quenched by N_2O; and N_2, as well as oxygen atoms which insert into C—H bonds (10), are formed. N_2O also interferes with an excited state of 1,3-dioxan, thereby producing N_2. The yield of ethylene is also reduced, but that of formaldehyde is increased. This observation can be rationalized by the hypothesis that oxygen atoms insert into the C—H bonds at position 4. The resulting hemiacetal is expected to be unstable and to release formaldehyde under the conditions of the assay.

The data shown in Table 5 indicate that the N_2O-quenchable state might have a lifetime as short as 1 ns if one assumes that the reaction producing N_2 in competition against the unimolecular decay of the N_2O-quenchable state, has a second-order rate constant of 10^9 M^{-1} s^{-1}. This estimate drops to 0.1 ns if a rate constant of 10^{10} M^{-1} s^{-1} is assumed.

Acknowledgement

We thank Dr. Görner for carrying out the laser experiments.

1. C. SANDORFY. Top. Current Chem. **86**, 91 (1979).
2. C. VON SONNTAG and H.-P. SCHUCHMANN. Adv. Photochem. **10**, 59 (1977).
3. C. VON SONNTAG and H.-P. SCHUCHMANN. *In* Ethers, crown ethers, hydroxy groups and their sulfur analogues. Part 2. The chemistry of functional groups. *Edited by* S. Patai. Wiley, New York. 1980. Suppl. E. p. 903.
4. H.-P. SCHUCHMANN and C. VON SONNTAG. J. Chem. Soc. Perkin Trans. II, 1408 (1976).
5. H.-P. SCHUCHMANN and C. VON SONNTAG. Z. Naturforsch. **32**b, 205 (1977).
6. P. NADERWITZ, H.-P. SCHUCHMANN, and C. VON SONNTAG. Z. Naturforsch. **32**b, 209 (1977).
7. E. CETINKAYA, H.-P. SCHUCHMANN, and C. VON SONNTAG. J. Chem. Soc. Perkin Trans. II, 985 (1978).
8. H.-P. SCHUCHMANN and C. VON SONNTAG. J. Photochem. **21**, 213 (1983).
9. R. R. HENTZ and C. F. PARRISH. J. Phys. Chem. **75**, 3899 (1971).
10. H.-P. SCHUCHMANN, H. BANDMANN, and C. VON SONNTAG. Z. Naturforsch. **34**b, 327 (1979).
11. C. VON SONNTAG and H. BANDMANN. J. Phys. Chem. **78**, 2181 (1974).
12. J. KIWI. J. Photochem. **7**, 237 (1977).
13. P. AUSLOOS, C. LUTZ, F. SCHWARZ, and S. G. LIAS. Radiat. Phys. Chem. **23**, 97 (1984).
14. F. HIRAYAMA, C. W. LAWSON, and S. LIPSKY. J. Phys. Chem. **74**, 2411 (1970).
15. A. M. HALPERN and W. R. WARE. J. Phys. Chem. **74**, 2413 (1970).
16. P. A. LAURENT, P. TARTE, and B. RODRIGUES. Bull. Soc. Chim. Fr. 946 (1959).
17. F. WEEKE, E. BASTIAN, and G. SCHOMBURG. Chromatographia, **7**, 163 (1974).
18. R. KAISER. Chromatographie in der Gasphase. Vol. IV. Bibliographisches Institut, Mannheim. 1965.
19. B. KAKAĆ and Z. J. VEJDELEK. Handbuch der photometrischen Analyse organischer Verbindungen. Vol. 1. Verlag Chemie, Weinheim. 1974. p. 257.
20. R. CAMERLYNCK and M. ANTEUNIS. Tetrahedron, **31**, 1837 (1975).
21. K. F. BEAL and C. J. B. THOR. J. Polymer Sci. **1**, 543 (1946).
22. S. Z. PERRY and H. HILBERT. Can. J. Res. B, **14**, 77 (1936).
23. M. ZELIKOFF, K. WATANABE, and E. C. Y. INN. J. Chem. Phys. **21**, 1643 (1953).
24. G. J. HERNANDEZ and A. B. F. DUNCAN. J. Chem. Phys. **36**, 1504 (1962).
25. N. KIZILKILIĆ, H.-P. SCHUCHMANN, and C. VON SONNTAG. Can. J. Chem. **58**, 2819 (1980).
26. H.-P. SCHUCHMANN, P. NADERWITZ, and C. VON SONNTAG. Z. Naturforsch. **33**b, 942 (1978).
27. H.-P. SCHUCHMANN and C. VON SONNTAG. J. Photochem. **13**, 347 (1980).
28. D. H. ELLISON, G. A. SALMON, and F. WILKINSON. Proc. R. Soc. London, A**328**, 23 (1972).
29. F. J. J. DE KANTER and R. KAPTEIN. J. Am. Chem. Soc. **104**, 4759 (1982).
30. J. C. SCAIANO. Tetrahedron, **38**, 819 (1982).
31. L. WOJNÁROVITS, L. KOZÁRI, CS. KESZEI, and G. FÖLDIÁK. J. Photochem. **19**, 79 (1982).
32. E. KASSAB, J. T. GLEGHORN, and E. M. EVLETH. J. Am. Chem. Soc. **105**, 1746 (1983).
33. R. J. BUENKER, G. OLBRICH, H.-P. SCHUCHMANN, B. L. SCHÜRMANN, and C. VON SONNTAG. J. Am. Chem. Soc. **106**, 4362 (1984).
34. A. A. SCALA, I. COLON, and W. ROURKE. J. Phys. Chem. **85**, 3603 (1981).

Resonance Raman study of phenylhydrazonopropanedinitriles

JEAN CLAUDE MERLIN
Laboratoire de Spectrochimie Infrarouge et Raman (CNRS), Université de Lille I, Bât. C.5, 59655 Villeneuve d'Ascq Cedex, France

EMRYS W. THOMAS
Department of Biological Sciences, Salford University, Salford M54WT, United Kingdom

AND

GUISLAINE PETIT
Laboratoire de Spectrochimie Infrarouge et Raman (CNRS), Université de Lille I, Bât. C.5, 59655 Villeneuve d'Ascq Cedex, France

Received August 6, 1984

This paper is dedicated to Professor Camille Sandorfy on the occasion of his 65th birthday

JEAN CLAUDE MERLIN, EMRYS W. THOMAS, and GUISLAINE PETIT. Can. J. Chem. **63**, 1840 (1985).

Resonance Raman spectra and band assignments of some phenylhydrazonopropanedinitriles, including the 3-chloro and the 2-carboxy derivatives, in the 900–2300 cm^{-1} spectral range are presented and discussed. ^{15}N and ^{2}H isotopic shifts have been used to clarify the assignments, which have been made for both protonated and deprotonated forms of the compounds. The resonance Raman spectra of the protonated forms show strong coupling between NH deformation and hydrazone vibrations. This coupling is lost in the anionic forms, which are considered to have considerable carbanion character. By using the drastic changes between the resonance Raman spectra of protonated and deprotonated forms, the pK_a value of the 2-carboxy derivative has been determined.

JEAN CLAUDE MERLIN, EMRYS W. THOMAS et GUISLAINE PETIT. Can. J. Chem. **63**, 1840 (1985).

Les spectres Raman de résonance et l'attribution de leurs raies pour certains dérivés du phénylhydrazonopropanedinitrile comprenant les dérivés 3-chloro et 2-carboxy, dans la région spectrale 900–2300 cm^{-1} sont présentés et discutés. Les déplacements isotopiques obtenus en utilisant ^{15}N et ^{2}H ont permis de justifier l'attribution proposée à la fois pour les formes protonées et déprotonées des composés. Le spectre Raman de résonance de la forme protonée indique qu'un fort couplage existe entre la déformation du groupe NH et les vibrations du groupe hydrazone. Ce couplage disparaît dans la forme anionique qui présente alors une structure avec un caractère carbanion très marqué. Les profondes modifications observées dans les spectres Raman de résonance lors de la formation des formes protonées ou déprotonées ont permis de déterminer la valeur du pK_a du dérivé *méta*-carboxylé.

Introduction

Substituted phenylhydrazonopropanedinitriles (also known as carbonylcyanide phenylhydrazones) display a range of biological activities; they act as uncouplers of biological energy transducing systems (1), have bacteriostatic and fungistatic properties (2), and react rapidly with thiols in aqueous solution (3). In view of the usefulness of resonance Raman spectroscopy in studying biomolecular interactions at high dilution, we have obtained resonance Raman spectra of a number of the title compounds, including phenylhydrazonopropanedinitrile, 3-chloro-phenylhydrazonopropanedinitrile, and 2-carboxy-phenylhydrazonopropanedinitrile (abbreviated as PHPD, (3-Cl)-PHPD and (2-carboxy)-PHPD, respectively), together with selected ^{15}N and ^{2}H labelled analogues. The band assignments obtained lead to a clearer understanding of the protonic equilibria displayed by these compounds, and also provide a firm basis for resonance Raman studies on their interactions in biological systems.

Experimental

Preparation of compounds

All analogues were prepared by coupling the appropriate diazotized aromatic amine with malononitrile as described (4), and isolated by acidification of the reaction mixtures to pH 1, filtering, and washing with excess H_2O. Samples were then recrystallized from either chloroform or ethyl alcohol to constant melting point.

A ring deuterated analogue of PHPD, designated PHPD-d_5, was prepared using aniline-2,3,4,5,6-d_5 (Aldrich Chemical Co.).

A ^{15}N-labelled analogue of PHPD, incorporating ^{15}N in the nitrogen atom proximal to the aromatic ring, and designated PHPD-α ^{15}N, was prepared using aniline-^{15}N (95 atom%, BOC Limited, London, U.K.).

A ^{15}N-labelled analogue of (3-Cl)-PHPD, incorporating ^{15}N in the nitrogen atom proximal to the propanedinitrile group, and designated (3-Cl)-PHPD-β ^{15}N, were prepared by diazotization of 3-chloroaniline using $NaNO_2$-^{15}N (99 atom%, BOC Limited).

All compounds proved homogeneous by tlc, and had melting points agreeing with literature values (2). Mass spectral characterization of the ^{15}N-labelled analogues confirmed substitution by ^{15}N:PHPD; M^+ 170; PHPD-α ^{15}N:M^+ 171; (3-Cl)-PHPD:M^+ 204; (3-Cl)-PHPD-β ^{15}N:M^+ 205.

Spectral measurements

Resonance Raman spectra were obtained using a DILOR RT.30 spectrometer and an argon laser (Spectra Physics 164 AC) for excitation at 488 nm. Line frequencies were quoted to an accuracy of ±2 cm^{-1} by using plasma lines for calibration. Techniques and precautions used in the acquisition of resonance Raman spectra were fully described in previous publications (5, 6). The pK_a determination for (2-carboxy)-PHPD involved plotting the ratio of the intensities of the 1368 cm^{-1} and 1250 cm^{-1} lines (characteristic of the acid and basic forms of the molecule) against pH. When pH = pK_a, the corresponding intensity ratio equaled the Raman cross-section ratio for the two lines. This latter value was obtained from spectra measured at pH 5.7 and 12.0, using the 982 cm^{-1} line of Na_2SO_4 as an internal standard. Visible absorption spectra were recorded using a Pye-Unicam SP 1800 Spectrophotometer.

Results and discussion

In aqueous solution at pH 12, most of the compounds examined show intense ($\epsilon \simeq 2 \times 10^4 M^{-1} cm^{-1}$) absorption bands

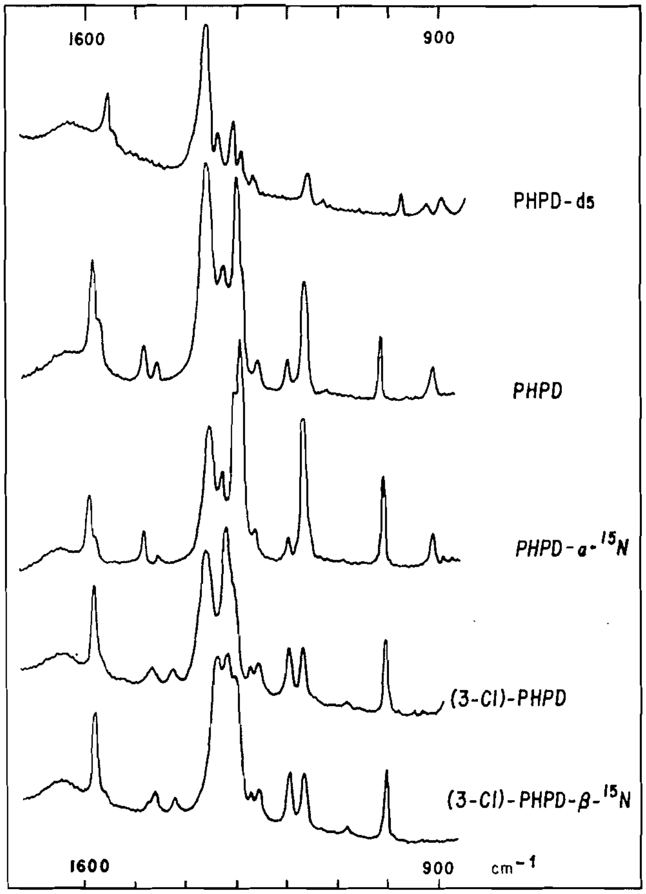

FIG. 1. Resonance Raman spectra of PHPD derivatives at alkaline pH (approximately 3×10^{-4} *M* in 0.01 *M* NaOH solution). Excitation wavelength at 488 nm (100 mW) and 6 cm^{-1} spectral slit width.

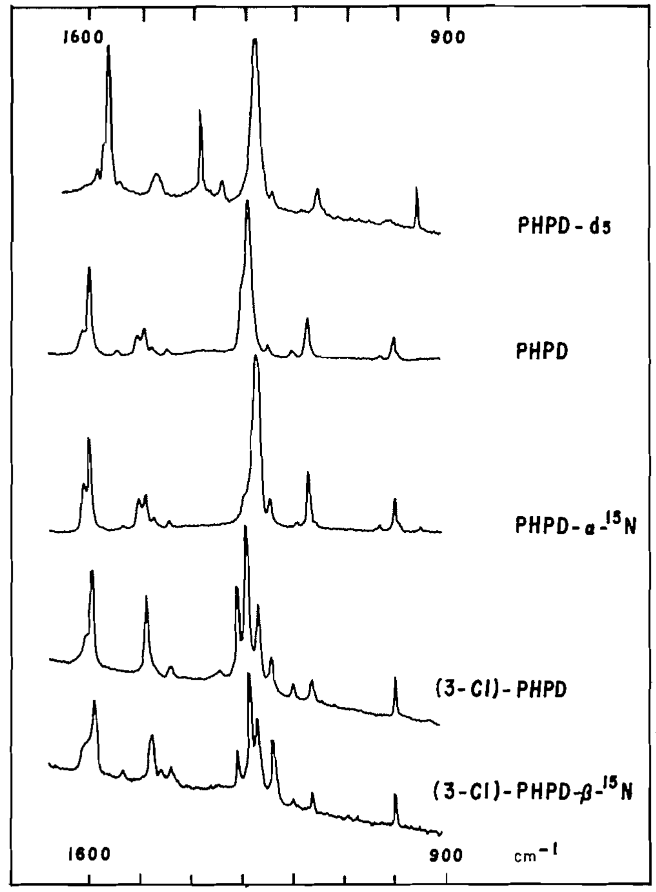

FIG. 2. Resonance Raman spectra of PHPD derivatives in the solid state. Excitation wavelength at 488 nm (50 mW) and 5 cm^{-1} spectral slit width.

at about 390 nm originating from the anionic form of the compound in question. Thus PHPD had λ_{max} 380 nm, $\epsilon = 1.97 \times 10^4\ M^{-1}\ cm^{-1}$; (3-Cl)-PHPD had λ_{max} 378 nm, $\epsilon = 2.37 \times 10^4\ M^{-1}\ cm^{-1}$; (2-carboxy)-PHPD had λ_{max} 376 nm, $\epsilon = 2.31 \times 10^4\ M^{-1}\ cm^{-1}$. In acidic media, protonated forms exist with bands near 360 nm: PHPD had λ_{max} 358 nm, $\epsilon = 1.77 \times 10^4\ M^{-1}\ cm^{-1}$; (3-Cl)-PHPD had λ_{max} 357 nm, $\epsilon = 2.10 \times 10^4\ M^{-1}\ cm^{-1}$; (2-carboxy)-PHPD had λ_{max} 365 nm, $\epsilon = 2.05 \times 10^4\ M^{-1}\ cm^{-1}$. Spectrophotometric titrations in all cases (data not shown) indicated participation of just two ionic species in the studied pH range, with the equilibrium described by pK_a value of $\simeq 6$ (7). (2-carboxy)-PHPD proved anomalous in this regard, displaying only a small (~ 10 nm) spectral shift on ionization with an approximate pK_a value of 9. Titration (results not shown) of (2-carboxy)-PHPD (in methanol/water, 2:1 v/v) clearly indicated two separate ionizations: one, governed by a pK_a values of about 3.75, is presumably due to the carboxyl group, while another ionization with $pK_a \sim 11$, is ascribed to the NH ionization (perturbed from the spectrophotometric pK_a due to the high methanol concentration in the titration medium).

With 488 nm excitation (in the pre-resonance region) good quality resonance-enhanced spectra were observed from low concentration solutions. Intense resonance Raman bands in the 900–1700 cm^{-1} spectral range were observed from basic solutions of all compounds (Fig. 1), with two additional lines in the 2200 cm^{-1} region (data not shown). These spectra originated from the anionic forms. Resonance Raman spectra of solid samples (Fig. 2) were typical of the neutral protonated forms; good quality spectra were not easy to obtain from acidic solutions due to poor solubility, but we included representative spectra obtained at pH 5.7 for comparison purposes (Fig. 3).

In the spectral range investigated, the following modes would be expected to be resonance Raman enhanced. (*1*) benzene ring modes: C—C stretching vibrations and C—H in-plane bending vibrations; (*2*) stretching modes of the ring substituents coupled with benzenoid ring modes; (*3*) hydrazonopropane group vibrations, strongly perturbed by protonation equilibria; and (*4*) nitrile function vibrations.

Tentative assignments for characteristic lines of the protonated and deprotonated forms are shown in Table 1, and merit discussion.

Deprotonated forms

(*i*) Two vibrations, involving a symmetric and antisymmetric stretching of the nitrile groups, are observable in the 2150–2200 cm^{-1} region.

(*ii*) Benzene ring vibrational modes, using standard assignments (10, 11), are easily distinguishable on the basis of spectral shifts observed on ring deuteration or substitution.

(*iii*) The Ph—N^- stretching, coupled with phenyl ring vibrations, and called "*e*" mode, should give an intense Raman band in the 1290–1370 cm^{-1} region (12, 13); this mode should be sensitive to both ring deuteration and α ^{15}N labelling. The 1303 cm^{-1} line in PHPD is accordingly assigned to the "*e*" (Ph—N^-) mode; it shifts to lower frequencies on α ^{15}N

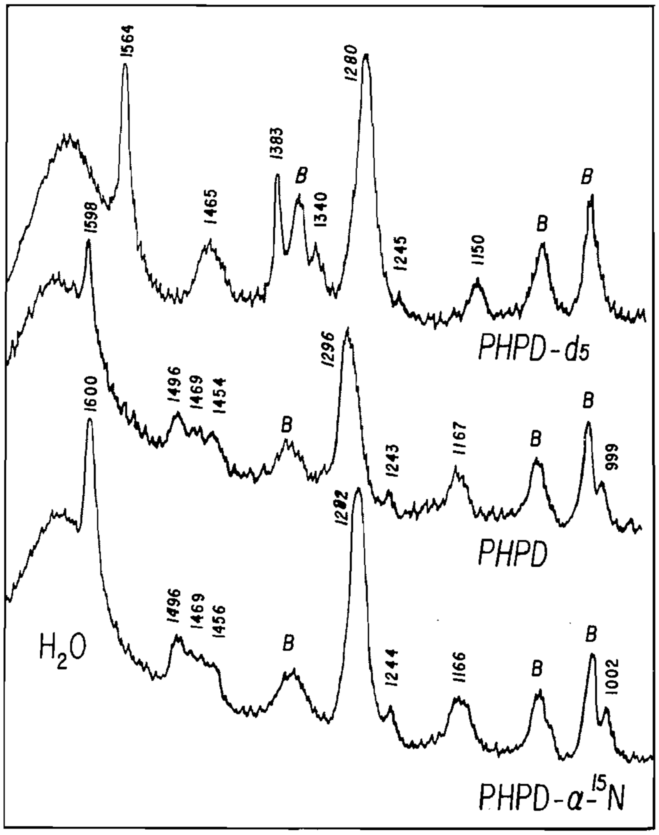

FIG. 3. Resonance Raman spectra of some PHPD derivatives in phosphate buffer solution (pH 5.7). The saturated solutions used are approximately 10^{-5} *M*. Excitation wavelength at 488 nm (350 mW) and 8 cm^{-1} spectral slit width. B indicates the buffer lines.

substitution, and disappears on ring deuteration.

The ring modes perturbed by deuteration are not strongly coupled to the Ph—N$^-$ stretching mode, and the wavenumber of the "*e*" (Ph—N$^-$) mode (now better described as a Ph—N$^-$ stretching) is expected to shift to higher values on ring deuteration. This shifted line in the PHPD-d_5 spectrum is presumably overlapped by other spectral features (perhaps the 1362 cm^{-1} line) which are not perturbed by ring deuteration.

(*iv*) The N—N stretching mode has been previously observed at 1202 cm^{-1} for diazoaminobenzene (11) and in the 1160–1200 cm^{-1} spectral range for other azobenzene derivatives in acid solution where hydrazone forms appear (6, 14, 15), so it is expected between 1150 and 1210 cm^{-1}. However, α and β ^{15}N labelling unambiguously assigns the 1363 cm^{-1} line in the PHPD spectrum as the N—N stretching; its relatively high frequency in this case would indicate a correspondingly high N—N bond order. If the anionic forms are described by three hybrid structures (Scheme 1) in which form **III** predominates, the relatively high stretching frequency can be rationalized.

(*v*) When comparing the resonance Raman spectra of (3-Cl)-PHPD and (3-Cl)-PHPD-β ^{15}N, no other frequency shifts distinct from that noted in (*iv*) are observed, and accordingly the C=N stretching mode cannot be assigned. If, however, as shown in Scheme 1, the bond orders and the force constants for the N⋯N and C⋯N bonds are of the same magnitude, a characteristic vibration for each bond would not be expected.

(*vi*) Two lines (1300 cm^{-1}; and 1250 cm^{-1} in PHPD spec-

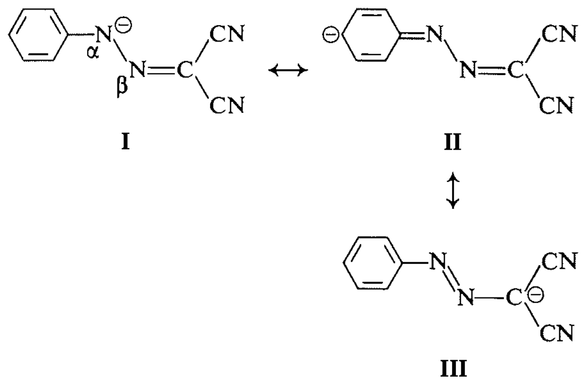

SCHEME 1

trum), insensitive to ring deuteration and both α and β ^{15}N substitution, are assigned to symmetric and antisymmetric C—C stretching modes of the propanoid group.

Protonated forms

(*i*) Resonance Raman spectra of both solid samples and aqueous solutions at pH 5.7 are dominated by a strong band in the 1270–1300 cm^{-1} spectral range, assigned to the "*e*" (Ph—NH) mode. As this mode results from a coupling between a ring mode and the Ph—NH stretching, ^2H and α ^{15}N isotope shifts are of the same magnitude. The β ^{15}N shift of this band seen in the (3-Cl)-PHPD-β ^{15}N spectrum shows that this line is rather representative of an "*e*" (Ph—NH—N) mode; the force constants for the Ph—NH and N—N bonds should be of the same magnitude in this conjugated system.

(*ii*) The significant shift (19 cm^{-1}) of the above discussed line on ionization is explicable by participation of the N—H deformation mode: strong coupling between N—H bending and Ph—NH stretching can be invoked. A similar coupling perturbed by deuterium exchange of a N—H group in an analogous system has been previously observed (6).

(*iii*) Spectral shifts resulting from ring deuteration are different for the protonated and deprotonated forms. For protonated PHPD, deuterium substitution results in a shift of the "*e*" (Ph—NH—N) mode to lower frequency (1286 $cm^{-1} \rightarrow$ 1273 cm^{-1}). For the deprotonated form, the corresponding shift of the "*e*" (Ph—N$^-$) mode is to higher frequency (1303 $cm^{-1} \rightarrow$ 1362 cm^{-1}). Again, changes in coupling of "*e*" modes with N—H deformation mode explain these shifts. Analogous results have been previously obtained for phenylhydrazone functions developed when dimethylaminoazobenzene derivatives are examined in acid solution (15).

(*iv*) The symmetrical and antisymmetrical nitrile stretching modes are affected by the pH change. The increase in wavenumber (40 cm^{-1}) for the protonated forms is consistent with a decrease in conjugation within the protonated molecule (11) also manifested as a blue shift in the visible absorption band.

(*v*) Phenyl ring vibrational modes are easily assigned on the basis of deuterium shift, except for the 1400–1550 cm^{-1} spectral range where C=N stretching and N—H deformation modes must be considered (13). It is difficult to precisely locate the bands in this region, but the N—H deformation mode can be attributed to the weak 1543 cm^{-1} line in the PHPD spectrum, which shifts to 1532 cm^{-1} in the PHPD-α ^{15}N spectrum; these two lines are only observed for the solid state, probably being too weak to be seen in the solution spectra. The C=N stretching vibration can be located at lower wavenumbers (16); for both solution and solid state, the single line at 1465 cm^{-1},

TABLE 1. Line position (cm^{-1}) and tentative assignments of Raman bands of PHPD derivatives in the protonated (solid state) and deprotonated (alkaline solution) forms

Basic form — aqueous solution						Neutral form — solid state				
PHPD-d_5	PHPD	(3-Cl)-PHPD α-^{15}N	(3-Cl)-PHPD	PHPD β-^{15}N	Tentative assignments	(3-Cl)-PHPD β-^{15}N	(3-Cl)-PHPD	PHPD α-^{15}N	PHPD	PHPD-d_5
2196 (m)	2203 (m)	2202 (m)	2196 (m)	2194 (m)	C≡N stretching	2230 (m)	2230 (m)	2232 (m)	2232 (m)	2233 (m)
2174 (m)	2185 (m)	2184 (m)	2175 (m)	2174 (m)		2220 (m)	2220 (m)	2215 (m)	2215 (m)	2216 (m)
1560 (m)	1593 (s)	1594 (m)	1590 (s)	1588 (s)	8a,b ring modes	1604 (sh)	1604 (sh)	1607 (m)	1608 (sh)	1571 (sh)
1549 (sh)	1580 (sh)	1578 (sh)	1576 (sh)	1576 (sh)		1589 (s)	1591 (s)	1599 (s)	1598 (s)	1563 (vs)
										1584 (w)
					NH deformation	1536 (w)		1532 (vw)	1543 (vw)	1540 (vw)
								1501 (m)	1501 (m)	
1380 (sh)	1483 (w)	1483 (w)	1460 (w)	1465 (w)	19a,b ring modes	1475 (m)	1487 (s)	1487 (m)	1488 (m)	1380 (s)
1333 (m)	1457 (w)	1457 (vw)	1427 (w)	1425 (w)	C=N stretching	1456 (w)	1475 (sh)	1473 (w)	1474 (w)	1338 (w)
						1437 (w)	1440 (w)	1443 (w)	1443 (w)	1468 (w)
1364 (vs)	1363 (vs)	1350 (s)	1358 (vs)	1333 (vs)	N—N stretching					
1286 (m)	1328 (s)	1322 (m)			14 ring mode	1340 (vw)	1342 (w)			
(1364) (vs)	1303 (vs)	1289 (vs)	1317 (vs)	1312 (vs)	*e*(Ph—N$^-$) mode					
1302 (m)	1295 (sh)	1297 (sh)	1300 (sh)	1300 (sh)	C—CN stretching (as)	1307 (m)	1308 (s)	1296 (sh)	1299 (sh)	—
					e(Ph—NH—N) mode	1284 (vs)	1292 (vs)	1270 (vs)	1286 (vs)	1273 (vs)
			1268 (w)	1267 (w)	*e*(Ph—Cl) mode	1268 (s)	1269 (s)			
1256 (w)	1258 (w)	1258 (w)	1252 (w)	1250 (w)	C—CN stretching (s)	1237 (s)	1242 (m)	1243 (m)	1245 (w)	1242 (w)
1147 (m)	1193 (w)	1190 (w)	1189 (m)	1188 (m)	9a,b ring modes	1198 (w)	1199 (w)	1193 (vw)	1197 (w)	1151 (w)
876 (w)	1163 (s)	1162 (s)	1160 (m)	1160 (m)		1162 (w)	1161 (w)	1168 (m)	1170 (m)	825 (w)
			1070 (vw)	1071 (w)	ring mode			1026 (vw)	1027 (vw)	
960 (w)	998 (m)	998 (m)	998 (s)	997 (m)	12 ring mode	994 (m)	996 (m)	997 (m)	997 (m)	955 (m)

*sh = shoulder, vw = very weak, w = weak, m = medium, s = strong, vs = very strong. The Wilson (8) and Kohlrausch (9) notations are used to describe the vibrational modes.

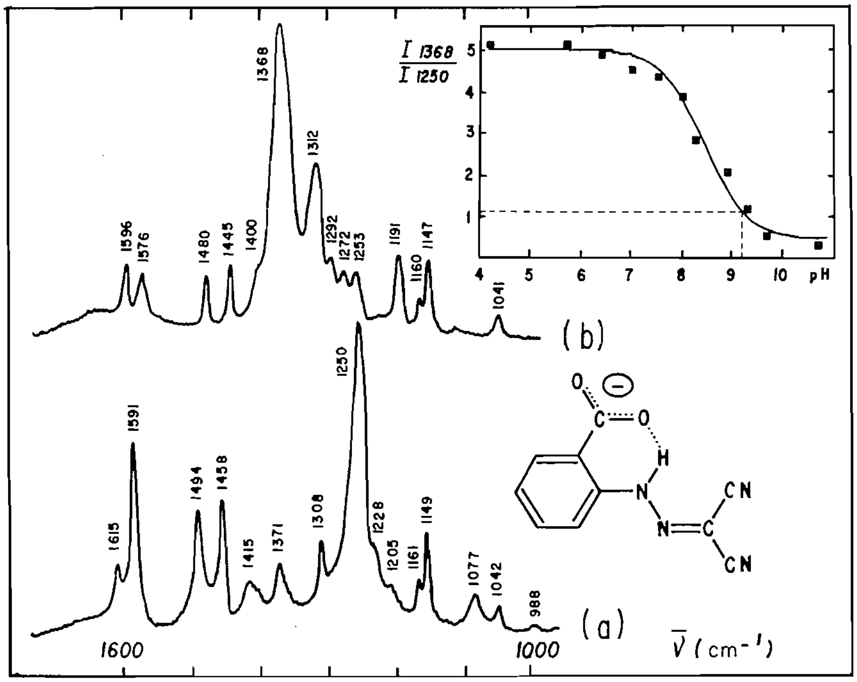

FIG. 4. Resonance Raman spectra of (2-carboxy)-PHPD in aqueous solution. Excitation wavelength at 488 nm (100 mW) and 6 cm^{-1} spectral slit width. The solution are approximately 3×10^{-4} *M*: (*a*) in phosphate buffer (pH 5.7), (*b*) in 0.01 *M* NaOH (pH 12.0). Insert: The titration curve obtained by non-linear least squares analysis and the structure of (2-carboxy)-PHPD at pH 5.7.

observed in the PHPD-d_5 spectrum, is assigned to this mode, being also consistent with the β ^{15}N shift observed in this region for (3-Cl)-PHPD-β ^{15}N.

*p*K$_a$ *value determination*

The dramatic differences in the resonance Raman spectra of the protonated and deprotonated forms, particularly for the "*e*" (Ph—NH) mode, allows a convenient assessment of pK_a values in those cases where spectrophotometric titration is not accurate (due to small spectral shifts). (2-carboxy)-PHPD is such a case; the relevant resonance Raman spectra shown in Fig. 4 are very similar to those of PHPD derivatives above discussed and indicate that the observed changes can be related to the deprotonation of the NH group. A fitted plot of the relative intensities of the two strong lines (I_{1368}/I_{1250}) vs. pH allows the pK_a determination. The relatively high pK_a value (9.2) is obviously a consequence of an intramolecular interaction between the carboxyl and NH groups (Fig. 4).

Conclusion

The resonance Raman data, together with the ^2H and ^{15}N isotope shifts, allow assignment of most of the observed bands, and also allow the protonated and deprotonated forms to be clearly distinguished. A strong line attributed to an "*e*" (Ph—NH—N) mode disappears at high pH due to ionization at N—H; the consequent increase in N—N bond order leads to a splitting whereby both "*e*" (Ph—N^-) and N—N stretching modes are observable in the spectra of the anionic form. This form is best defined by a resonance hybrid with strong carbanion character stabilized by the two electron-withdrawing nitrile groups. Such a structure explains well the chemical unreactivity of PHPD derivatives towards thiols at high pH (3) and also the instability of tetrahedral adducts of PHPD with thiols at high pH (3). The extensive charge delocalization within the anion is also relevant to its ability to diffuse across lipid bilayers, and thereby act as an uncoupling agent.

1. P. G. HEYTLER. Methods in enzymology LV, Academic Press, New York. 1979. pp. 469–470.
2. T. ZSOLNAI. Biochem. Pharmacol. **13**, 285 (1964).
3. L. DROBNICA and E. STURDIK. Biochim. Biophys. Acta, **585**, 462 (1979).
4. P. M. BARNA. Biochem. Prep. **13**, 82 (1971).
5. E. W. THOMAS, J. C. MERLIN, and J. L. LORRIAUX. Biochim. Biophys. Acta, **708**, 68 (1982).
6. J. C. MERLIN, J. L. LORRIAUX, A. DUPAIX, and E. W. THOMAS. J. Raman Spectrosc. **11**, 131 (1981).
7. V. H. PARKER. Biochem. J. **97**, 658 (1965).
8. E. B. WILSON. Phys. Rev. **45**, 706 (1934).
9. K. W. F. KOHLRAUSCH. Der Smekal Raman Effekt Ergazungsband, J. Springer, Berlin. 1938.
10. G. VARSANYI. Assignments for vibrational spectra of 700 benzene derivatives. A. Hilger, London. 1974.
11. N. B. COLTHUP, C. H. DALY, and S. E. WIBERLEY. Introduction to infrared and Raman spectroscopy. 2nd ed. Academic Press, New York. 1975.
12. F. MATHIS. Structure et propriétés moléculaires. Vol. VII. Masson et Cie, Paris. 1970.
13. A. PERRIER-DATIN and J. M. LEBAS. J. Chim. Phys. **69**, 591 (1972).
14. R. KUBLER, W. LÜTTKE, and S. WECKHERLIN. Z. Elektrochem. **64**, 650 (1960).
15. J. C. MERLIN and E. W. THOMAS. Spectrochim. Acta, **35A**, 1243 (1979).
16. J. W. LEWIS and C. SANDORFY. Can. J. Chem. **61**, 809 (1983).

Photochemistry of alkenes. 9. Medium-sized cycloalkenes[1]

PAUL J. KROPP,[2] J. DEREK MASON, AND GARDINER F. H. SMITH
Department of Chemistry, University of North Carolina, Chapel Hill, NC 27514, U.S.A.

Received August 31, 1984

This paper is dedicated to Professor Camille Sandorfy on the occasion of his 65th birthday

PAUL J. KROPP, J. DEREK MASON, and GARDINER F. H. SMITH. Can. J. Chem. **63**, 1845 (1985).

The behavior of the three medium-sized cycloalkenes cyclooctene (**10**), cyclodecene (**17**), and cyclododecene (**21**) on direct irradiation in pentane and methanol solution has been studied. The results are summarized in Tables 1–3. Irradiation of medium-sized cycloalkenes is a convenient procedure for the preparation of bicyclic products (cf. **13**, **14**, **19**, **20**, and **23**) through transannular insertion reactions of carbene intermediates (cf. **11**, **18**, and **22**) thought to arise from rearrangement of the $^1[\pi,R(3s)]$ state via a 1,2-hydrogen shift. The formation of *trans*-decalin (**20**) is in contrast to the reported formation of the *cis* isomer on base-initiated decomposition of the corresponding tosylhydrazone. None of the three cycloalkenes **10**, **17**, or **21** underwent competing nucleophilic trapping of the $^1[\pi,R(3s)]$ state in methanol, in contrast with other alkenes previously studied. However, cyclododecene (**21**) afforded the methyl ether **25**, which apparently resulted from protonation of the $^1(\pi,\pi^*)$ state, and the epoxide **26**, which is thought to arise from electron transfer to oxygen by the $^1[\pi,R(3s)]$ state followed by protonation of the resulting superoxide ion and oxidation of unreacted cyclododecene (**21**).

PAUL J. KROPP, J. DEREK MASON et GARDINER F. H. SMITH. Can. J. Chem. **63**, 1845 (1985).

Opérant dans des solutions dans le pentane ainsi que dans le méthanol, on a étudié le comportement, vis-à-vis de l'irradiation directe, des trois cycloalkènes à cycles moyens suivants: cyclooctène (**10**), cyclodécène (**17**) et cyclododécène (**21**). On rapporte les résultats dans les tableaux 1–3. L'irradiation des cycloalkènes à cycles moyens est une méthode appropriée de préparer des produits bicycliques (comme **13**, **14**, **19**, **20** et **23**) par le biais de réactions intramoléculaires d'insertions transannulaires des carbènes intermédiaires (comme **11**, **18** et **22**) qui proviendraient d'une transposition de l'état $^1[\pi,R(3s)]$ via un déplacement-1,2 d'hydrogène. La formation de la décaline-*trans* (**20**) est en opposition avec le fait que des auteurs ont rapporté la formation de l'isomère *cis* lors de la décomposition, initée par les bases, de la tosylhydrazone correspondante. Par opposition avec les résultats obtenus avec les autres alkènes étudiés antérieurement, aucun des trois cycloalkènes **10**, **17** ou **21** ne subit de trappage nucléophile de l'état $^1[\pi,R(3s)]$ par le méthanol. Toutefois, le cyclododécène (**21**) conduit au méthyl éther **25**, qui proviendrait de la protonation de l'état $^1(\pi,\pi^*)$, ainsi qu'à l'époxyde **26** qui proviendrait dans une première étape d'un transfert électronique par l'état $^1[\pi,R(3s)]$ qui serait suivi d'une protonation de l'ion superoxyde qui en résulte et de l'oxydation du cyclododécène (**21**) qui n'a pas réagi.

[Traduit par le journal]

Introduction

Although theoretical and spectroscopic aspects of the Rydberg excited states of various organic chromophores have long been studied, little attention has been given to the chemical properties of these species.[3] This is particularly surprising in the case of a chromophore such as the carbon–carbon double bond, in which a Rydberg excited state is either the lowest lying or close in energy to the lowest lying singlet excited state.[4] As depicted in Scheme 1 for the case of 2,3-dimethyl-2-butene (**1**), studies in these laboratories directed toward elucidating the chemical properties of the $^1[\pi,R(3s)]$ state of alkenes have shown that irradiation of alkenes in hydroxylic media results in the formation of a mixture of saturated and unsaturated ethers (**6** and **7**), which appear to arise via nucleophilic trapping of the $^1[\pi,R(3s)]$ state (**2**) followed by disproportionation of the resulting alkoxy radical (**3**) (4).

In the absence of nucleophilic trapping the $^1[\pi,R(3s)]$ intermediate undergoes, instead, rearrangement via a carbene intermediate. Thus irradiation of **1** in non-hydroxylic media results in a mixture of the rearranged alkene **8** and the cyclopropane **9**, the expected 1,2- and 1,3-insertion products from the carbene intermediate **5** (5). These two reactions, nucleophilic trapping in hydroxylic media and rearrangement via a carbene intermediate in non-nucleophilic media, are apparently the first two observations of the chemical properties of the $^1[\pi,R(3s)]$ state. They have since been observed for a number of alkenes (for a review of the photobehavior of alkenes in solution see ref. 6).

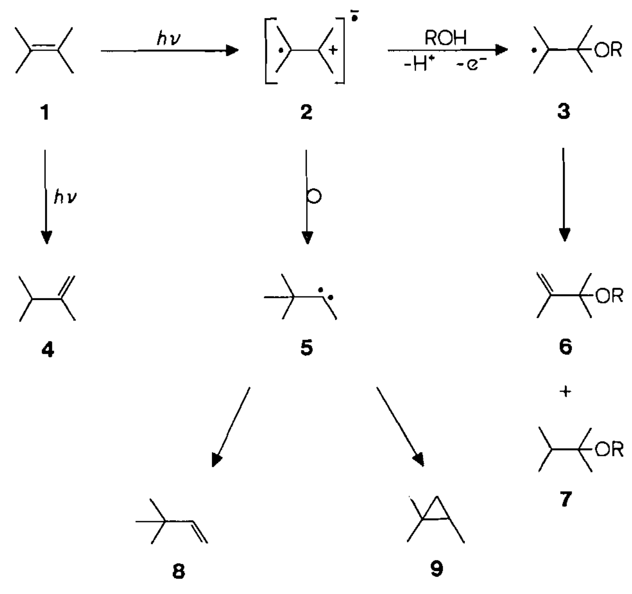

SCHEME 1

These processes occur in competition with $E \rightleftharpoons Z$ isomerization of the alkene, which is not observable in the case of **1** and probably involves the π,π^* excited state (6), and with double bond migration, which gives rise to isomer **4** in the case

[1] For Part 8, see ref. 1.
[2] Author to whom correspondence may be addressed.
[3] Professor Sandorfy has been a leader in calling attention to the probable involvement of Rydberg intermediates in photochemical reactions. See, for example, ref. 2.
[4] For discussion of the excited states of alkenes see ref. 3.

of **1** and apparently involves yet a third excited intermediate (7, 8). In some cases reduction of the double bond is also observed, but it is not clear which excited state is involved in this process.

Photorearrangement of alkenes via carbene intermediates has the potential of useful synthetic applications but has the drawback of competing double bond migration. One way of eliminating the loss of material due to this competing isomerization is to incorporate the double bond in a cyclic environment such as that of cyclooctene (**10**), cyclodecene (**17**), or cyclododecene (**21**), in which double bond migration is an identity process. Such medium-sized cycloalkenes offer a further potential for synthetic interest arising from their propensity for undergoing transannular reactions. We report here the photobehavior of cycloalkenes **10**, **17**, and **21** induced by direct irradiation in solution.

Results

The results from irradiation of cycloalkenes **10**, **17**, and **21** are summarized in Tables 1–3, respectively. In addition to undergoing $E \rightleftharpoons Z$ isomerization, each alkene afforded one or more bicyclic products (**13**, **14**, **19**, **20**, and **23**).[5] The product

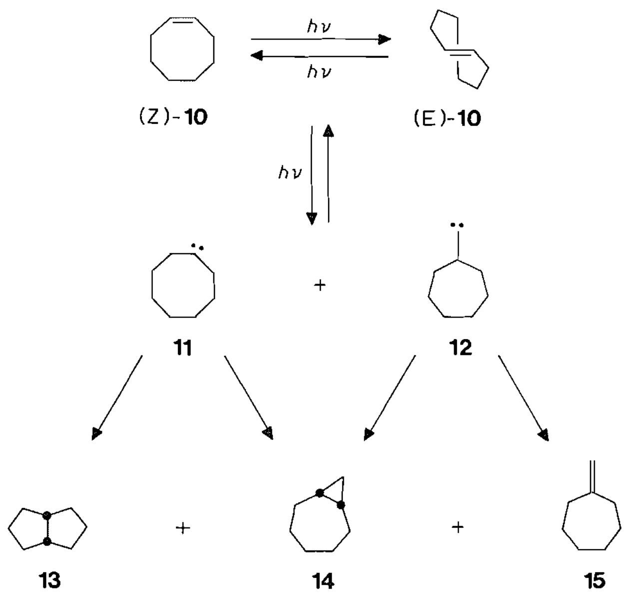

from cyclododecene (**21**) is assigned the novel bicyclo[7.3.0]-dodecane structure **23** on the basis of its ^{13}C nmr spectrum, as described in the experimental section, but the stereochemistry at the ring fusion is uncertain. Cyclooctene (**10**) afforded, in addition, the ring-contracted isomer **15**. In several cases acyclic cleavage products were observed: 1-octene (**16**) from **10** and 1-dodecene (**29**) and 1-dodecyne (**30**) from **21**. Since these products underwent competing destruction under the irradiation conditions, their yields decreased on extended irradiation. Cyclododecene (**21**) also afforded the reduction product **24**, the methyl ether **25**, and, in some runs, the oxide **26**. This latter product apparently arose from residual dissolved oxygen since its formation ceased after a short time.

Discussion

As predicted, irradiation of medium-sized cycloalkenes is a convenient method for preparing bicylic isomers. The products **13** and **14** from cyclooctene (**10**) are those expected for the carbene intermediate **11**, which is reported to undergo competing 1,5-, 1,3-, and 1,2-insertion when generated by base-initiated decomposition of the corresponding tosylhydrazone to afford a mixture of **13**, **14**, and cyclooctene (**10**) (10). In the present case any cyclooctene (**10**) formed would, of course, simply have been recycled. The accompanying formation of methylenecycloheptane (**15**) implies that the carbene intermediate **12**, which has previously been found to undergo competing 1,2- and 1,3-insertion to afford a mixture of **14** and **15** (11), is also formed. Thus the $^1[\pi,R(3s)]$ state of **10** apparently undergoes competing rearrangement via a 1,2-hydrogen shift to afford the carbene intermediate **11** and a 1,2-alkyl shift to afford **12**. By contrast, only products arising from the carbene intermediates **18** and **22**, formed via a 1,2-hydrogen shift, were observed for the larger-ring homologs **17** and **21**.

[5] Originally **14** and **15**, but not **13**, were reported as products from irradiation of cyclooctene (**10**) at 185 nm (9*a*). Since the initiation of our studies, **13** has also been reported (9*b*).

TABLE 1. Irradiation of cyclooctene (**10**)[a]

		Yield, %[b]					
Solvent	Time, h	(*Z*)-**10**	(*E*)-**10**	**13**	**14**	**15**	**16**
C_5H_{12}	60	1	2	20	6	3	2
CH_3OH	40	1	5	5		1	

[a] Irradiations were conducted as described in the experimental section using 100-mL solutions 0.05 *M* in alkene (*Z*)-**10**.
[b] Determined by gas chromatographic analysis relative to an internal hydrocarbon standard.

TABLE 2. Irradiation of cyclodecene (**17**)[a]

		Yield, %[b]			
Solvent	Time, h	(*Z*)-**17**	(*E*)-**17**	**19**	**20**
C_5H_{12}	60	4	[c]	43	7
CH_3OH	40	9	[c]	34	6

[a] Irradiations were conducted as described in the experimental section using 100-mL solutions 0.05 *M* in **17** that had an initial *Z*/*E* ratio of 5:1.
[b] Determined by gas chromatographic analysis relative to an internal hydrocarbon standard.
[c] Trace.

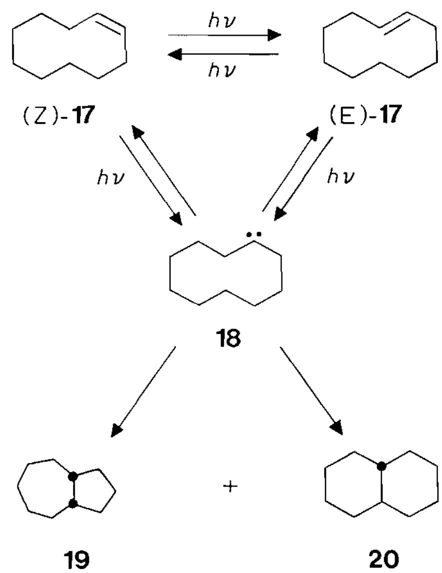

TABLE 3. Irradiation of cyclododecene (**21**)[a]

		Yield, %[b]							
Solvent	Time, h	(*Z*)-**21**	(*E*)-**21**	**23**	**24**	**25**	**26**	**29**	**30**
C_5H_{12}	60	48	10	8	[d]			3	6
CH_3OH	20	28	11	11	[c]	5	[d]	3	5
	60	9	7	15	[c]	11	[d]	2	4
CH_3OD	20	34	13	11	1	5	4	4	8
	100	7	6	14[e]	2	9[f]	4	1	4

[a]Irradiations were conducted as described in the experimental section using 100-mL solutions 0.05 *M* in **21** that had an initial *Z*/*E* ratio of 1 : 1.5.
[b]Determined by gas chromatographic analysis relative to an internal hydrocarbon standard.
[c]Trace.
[d]None detected.
[e]100% d_0.
[f]23% d_0, 70% d_1, 7% d_2.

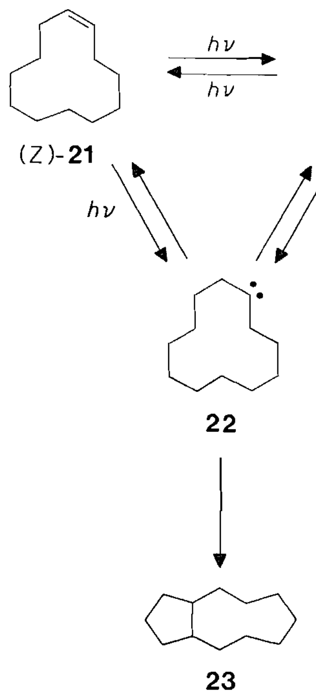

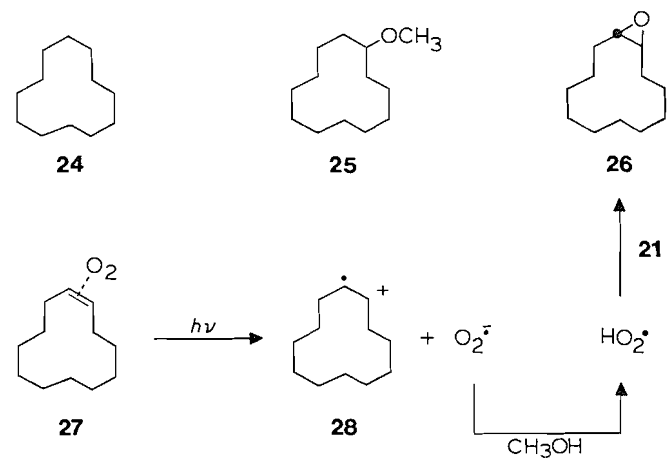

Generation of the C_{10} carbene intermediate **18** by base-initiated decomposition of the corresponding tosylhydrazone in aprotic media is reported to afford principally *cis*-bicyclo[5.3.0]decane (**19**), accompanied by (*Z*)- and (*E*)-cyclodecene (**17**) and *cis*-decalin (10). Medium-sized cyclic carbenes formed in this fashion generally afford *cis*-fused transannular cyclization products, presumably because they are formed in their singlet state and undergo concerted insertion into a transannular axial C—H bond (10). By contrast, irradiation of cyclodecene (**17**) afforded only the *trans* isomer **20**. This might suggest that the carbene intermediate **18** is formed photochemically in its triplet state, which undergoes a two-step insertion process via a radical intermediate that selectively closes to the thermodynamically more stable *trans* isomer **20**.[6] However, such a process should similarly afford the thermodynamically more stable *trans* isomer of **19**.[7] Perhaps the difference simply lies in the carbene intermediate being generated in a different geometry or with a different amount of residual energy from the two routes.

Generation of the C_{12} carbene intermediate **22** by base-initiated decomposition of the corresponding tosylhydrazone in aprotic media is reported to afford a mixture of (*Z*)- and (*E*)-cyclododecene (**21**) (14, 15) accompanied by a small amount of a bicyclic product, presumably **23**, which was formed in insufficient quantity to be characterized (15). In the present case any cyclododecene (**21**) arising from reversion of the carbene intermediate **22** would have been recycled, thus permitting substantially greater accumulation of the bicyclic product **23**. Quite surprisingly, irradiation of cyclododecene (**21**) in methanol afforded the two oxygen-containing products **25** and **26**.[8] When the irradiation was conducted in methanol-*d*, ether **25** was formed with substantial incorporation of deuterium, which was shown by ^{2}H nmr spectroscopy not to be located α to the methoxyl group. The incorporation of deuterium, along with the absence of any accompanying unsaturated ether, indicate that ether **25** does not arise via nucleophilic trapping of the ^{1}[π,R(3*s*)] state **27** in analogy with the formation of ethers **6** and **7** from alkene **1**. Indeed, it is noteworthy that none of the three cycloalkenes **10**, **17**, or **21** afforded products from nucleophilic trapping of the ^{1}[π,R(3*s*)] state. It has previously been found that disubstituted derivatives of ethene undergo nucleophilic trapping very inefficiently rela-

[6]For the relative stabilities of *cis*- and *trans*-decalin see ref. 12.
[7]The *trans* isomer of bicyclo[5.3.0]decane has been found to predominate at equilibrium, but only slightly; see ref. 13.

[8]Products having retention times corresponding to those of the C_{10} homologs of **25** and **26** were obtained on irradiation of cyclodecene (**17**), but in quantities insufficient for complete identification.

tive to rearrangement (6, 16). This behavior may be enhanced in medium-sized cycloalkene systems by steric encumbrance about the double bond, as previously observed with *tert*-butyl-substituted alkenes (1).

The lack of any detectable incorporation of deuterium in the α position also indicates that ether **25** does not arise via trapping of the carbene intermediate **22**. This is not surprising since alkyl carbenes generally undergo intramolecular insertion more rapidly than intermolecular trapping.

There remains a third alternative, which is consistent with the available data, that ether **25** arises via protonation of the $^1(\pi,\pi^*)$ state, which is thought to have dipolar character once it has relaxed to an orthogonal geometry (17). Protonation of this state does not normally occur because internal conversion to the ground state and relaxation to the *E* or *Z* isomer is generally more rapid than intermolecular trapping. However, an orthogonal species might have a lifetime longer than usual in the case of cyclododecene (**21**), simply because of the inability of this medium-ring system to relax to either the *E* or *Z* geometry without passing through large conformational barriers. Similar behavior was recently observed for *tert*-butyl-substituted alkenes (1).

The formation of oxides such as **26** on direct irradiation of alkenes has been observed previously (4), but no mechanism has been established. An attractive possibility involves initial reduction of oxygen to superoxide by electron transfer from the $^1[\pi,R(3s)]$ state (**27**) followed by attack on an unreacted molecule of cyclododecene (**21**). In methanol, protonation (18) and subsequent attack by the resulting hydroperoxy radical may be involved (19).

Conclusions

It is thus clear that irradiation of medium-sized cycloalkenes is a convenient method for the formation of bicyclic isomers. The photocyclization process is stereospecific and, in some cases, yields stereoisomers not afforded by the corresponding carbene intermediate when generated by conventional methods. The photochemical approach has the further advantage that competing reversion of the carbene intermediate to cycloalkene simply regenerates starting material, which is recycled. This is thus a useful illustration of the importance of Rydberg excited states in determining the photobehavior of an organic chromophore.

Experimental

General procedures

Infrared spectra were obtained in carbon tetrachloride solution with a Beckman 4250 spectrophotometer. Gas chromatographic analyses were performed on a Hewlett–Packard 5750 instrument with 10 ft × 0.125 in. stainless steel columns packed with either 20% (A) Carbowax 20M, (B) SF-96, or (C) β,β'-oxydipropionitrile on 60–80 mesh Chromosorb W. Preparative gas chromatographic separations were effected on a Varian Aerograph 90-P instrument with 10 ft × 0.25 in. stainless steel columns packed as described above. Melting points were determined on a Thomas–Hoover instrument and are uncorrected and uncalibrated. Nuclear magnetic resonance spectra were obtained in chloroform-*d* solution with a Varian XL-100 or Brucker WM-250 spectrometer. Isotopic compositions were calculated from mass spectra obtained on a VG Micromass 7070F spectrometer.

Irradiations

Irradiations were conducted under an atmosphere of nitrogen on 0.05 *M* solutions with the broad spectrum of a Hanovia 450-W medium-pressure mercury arc and either a water-cooled quartz immersion well or an Ace 7883 reflector and a quartz tube suspended in a water-cooled quartz immersion well. Before irradiation and after each aliquot was taken for analysis, nitrogen was bubbled through the solution for 10 min. After irradiation the solvent was removed by distillation through a Vigreux column.

*Irradiation of (*Z*)-cyclooctene ((*Z*)-**10**)*

A commercial specimen was redistilled at 45–46°C (17 Torr; 1 Torr = 133.3 Pa)) prior to use. From the irradiations described in Table 1 the following products were isolated by preparative gas chromatography.

cis-*Bicyclo[3.3.0]octane (**13**)* was isolated as a colorless liquid; ν_{max}: 2955, 2870, 1455 cm^{-1}; ^{1}H nmr δ: 2.6 (br m, 2, CH-1 and -5), 1.66 (m, 4), 1.5 (m, 2), 1.19 (m, 4) (lit. (20) ^{1}H nmr δ: 2.4, 1.7–1.1).

cis-*Bicyclo[5.1.0]octane (**14**)* was isolated as a colorless liquid; ^{1}H nmr δ: 2.11 (br m, 2, CH-1 and -7), 1.74 (br, 2), 1.32 (br q, 4), 0.02 (q, 1, axial cyclopropyl H) (lit. (21) ^{1}H nmr δ: −0.06 (1)).

*Methylenecycloheptane (**15**)* and *1-octene (**16**)* were isolated as colorless liquids having infrared and nmr spectra similar to those of commercial specimens.

*(*E*)- and (*Z*)-cyclodecene ((*E*)- and (*Z*)-**10**)*

A. *Preparation*

In a modification of the procedure of Brown and Ham (22), 2.83 g (18.1 mmol) of cyclodecanol in 25 mL of dry pyridine was added with cooling to a solution of 3.79 g (19.9 mmol) of *p*-toluenesulfonyl chloride in 25 mL of dry pyridine. The mixture was stirred until homogeneous, cooled for 24 h, diluted with 75 mL of distilled water, and extracted with 2 × 50 mL of diethyl ether. The ether extracts were combined, washed with 5 × 25 mL of cold 5% HCl and 2 × 30 mL each of saturated sodium bicarbonate and saturated sodium chloride solutions, and then dried over anhydrous sodium sulfate. The ether was partially removed by rotary evaporation, and the remaining ether was allowed to evaporate overnight. The resulting liquid was placed in a vacuum desiccator at room temperature for 48 h, then dissolved in pentane, extracted with 2 × 25 mL each of saturated sodium bicarbonate solution and saturated sodium chloride solution, and dried over anhydrous sodium sulfate. Evaporation of the pentane and distillation on a spinning band column gave 2.10 g (84% yield) of a 1:5 mixture of (*E*)- and (*Z*)-**17** as a colorless liquid; bp 52–53°C (13 Torr); ν_{max}: 3010, 2920, 2860, 2680, 1650, 1481, 1452 cm^{-1}; ^{1}H nmr δ: 5.37 (t, 2, CH=CH), 2.23 (m, 4, C=C—CH$_2$), 1.53 (s, 14)[9] (lit. (23) ν_{max}: 2915, 2680, 1456 cm^{-1}; ^{1}H nmr δ: 5.36 (2, CH=CH), 1.5 (14)).

B. *Irradiation*

From the irradiations described in Table 2 the following products were isolated by preparative gas chromatography.

cis-*Bicyclo[5.3.0]decane (**19**)* was isolated as a colorless liquid; ν_{max}: 2925, 2860, 1455 cm^{-1}; ^{1}H nmr δ: 1.98 (br m, 2, CH-1 and -7), 1.78 (br m, 4), 1.60 (br m, 4), 1.20 (m, 8); ^{13}C nmr δ: 43.5 (C-1 and -7), 35.8 (C-2 and -6), 33.0 (C-8 and -10), 31.7 (C-4), 29.7 (C-3 and -5), 26.4 (C-9) (lit. (24) ^{13}C nmr δ: 43.6, 35.9, 33.1, 31.8, 29.8, 26.1).

trans-*Decalin (**20**)* was isolated as a colorless liquid; ^{1}H nmr δ: 1.66 (br d, 4), 1.53 (br t, 4), 1.22 (br m, 4), 0.89 (br m, 6) (lit. (25) ^{1}H nmr δ: 1.66 (4), 1.53 (4), 1.23 (4), 0.93 (4), 0.84 (2)).

*Irradiation of (*E*)- and (*Z*)-cyclododecene ((*E*)- and (*Z*)-**21**)*

A commercial specimen which had an *E*/*Z* ratio of 1.5:1 was employed. From the irradiations described in Table 3 the following products were isolated.

*Bicyclo[7.3.0]dodecane (**23**)* was isolated as a colorless liquid; ν_{max}: 2920, 2866, 1441 cm^{-1}; ^{1}H nmr δ: 1.85 (br m, 2, CH-1 and -9), 1.45 (br m, 20); ^{13}C nmr δ: 43.2 (C-1 and -9), 34.4 (C-2 and -8), 28.9 (C-10 and -12), 27.9 (C-3 and -7), 26.2 (C-11), 25.3 (C-4 and -6), and 21.5 (C-5); mass spectrum, *m*/*e*: 166.1720 (calcd. for $C_{12}H_{22}$, 166.1721), 166 (41), 110 (28), 109 (35), 97 (31), 96 (88), 95 (57),

[9] Absorptions at δ 2.05 and 1.40 corresponding to (*E*)-**10** were also observed.

83 (43), 82 (100), 81 (72), 69 (40), 70 (46), 67 (90), 55 (77).

Cyclododecane (24) and methoxycyclododecane (25) were isolated as colorless liquids which exhibited spectral properties in agreement with those of specimens prepared independently as described below.

13-Oxabicyclo[10.1.0]tridecane (26) was isolated as a colorless liquid that was characterized by comparison of its spectral properties with those of a commercial specimen.

1-Dodecene (27) was isolated as a colorless liquid; ^{1}H nmr δ: 5.82 (m, 1, C=CH—C), 4.96 (br t, 2, C=CH_2), 2.05 (m, 2, C=CH_2), 1.28 (m, 16), 0.88 (t, 3, CH_3) (lit. (26) ^{1}H nmr δ: 5.75 (m, 1), 4.96 (br t, 2), 2.00 (m, 2), 1.3 (s, 16), 0.88 (t, 3)).

1-Dodecyne (28) was isolated as a colorless liquid; ν_{max}: 3335, 2130 cm^{-1}; ^{1}H nmr δ: 2.18 (t of d, J = 3.7 and 7.5, —CH_2—C≡C), 1.93 (t, 1, J = 3.7, —C≡CH), 1.28 (br s, 16, —CH_2—), 0.88 (t, 3, J = 7.5, —CH_3) (lit. (27) ν_{max}: 2120 cm^{-1}; ^{1}H nmr δ: 2.0–2.2 (m, CH_2—C≡C), 1.7 (t, —C≡CH), 0.9 (t, —CH_3)).

From the irradiation conducted in methanol-*d* the specimen of ether **25** which was isolated was found by mass spectral analysis to be 23% d_0, 70% d_1, 7% d_2; ^{2}H nmr δ: 1.58, 1.45. The specimen of bicyclo[7.3.0]dodecane (**23**) isolated showed no incorporation of deuterium.

Independent preparation of cyclododecane (24)

A solution of 260 mg of a commercial mixture of (E)- and (Z)-cyclododecene ((E)- and (Z)-**21**) in 30 mL of methanol was stirred with 21 mg of 10% palladium-on-charcoal under an atmosphere of hydrogen. Absorption ceased after the consumption of 1.1 molar equiv. of hydrogen. Removal of the catalyst by filtration and of the solvent by distillation afforded a colorless oil which crystallized slowly on standing; mp 58–60°C; ν_{max}: 1463, 1441, 1340, 714 cm^{-1}; ^{1}H nmr δ: 1.34 (s) (lit. (28) mp 61°C; lit. (29) ν_{max}: 1343 (s), 714 (s)).

Independent preparation of methoxycyclododecane (25)

A solution of 1.84 g (10.0 mmol) of cyclododecanol in 30 mL of ether was treated with 480 mg (20 mmol) of sodium hydride, and the resulting mixture was stirred under an atmosphere of nitrogen for 16 h. A solution of 7.10 g (50 mmol) of iodomethane in 30 mL of ether was then added and the reaction mixture was heated under reflux for 50 h. The excess sodium hydride was quenched by the careful addition of 5 mL of water and the resulting mixture was transferred to a separatory funnel. The ether layer was dried over 5 mL of saturated sodium chloride solution followed by anhydrous sodium sulfate and the solvent was removed by distillation through a Vigreux column. Gas chromatographic analysis of the residue revealed the formation of a single product in 69% yield and the continued presence of 30% of the starting alcohol. Isolation by preparative gas chromatography afforded ether **25** as a colorless liquid; ν_{max}: 1471, 1447, 1094 cm^{-1}; ^{1}H nmr δ: 3.33 (s, 4, CH-1 and —OCH_3), 1.35 (br s, 22) (lit. (30) ^{1}H nmr δ: 3.2 (?), 3.23).

Acknowledgements

Financial assistance from the Donors of the Petroleum Research Fund, administered by the American Chemical Society, and the University Research Council is gratefully acknowledged. We are indebted to F. P. Tise for some initial experiments with cyclododecene.

1. P. J. KROPP and F. P. TISE. J. Am. Chem. Soc. **103**, 7293 (1981).
2. C. SANDORFY. Int. J. Quantum Chem. **19**, 1147 (1981) and references cited therein.
3. A. J. MERER and R. S. MULLIKEN. Chem. Rev. **69** 639 (1969); F. H. WATSON, JR., A. T. ARMSTRONG, and S. P. MCGLYNN. Theor. Chim. Acta, **16**, 75 (1970); F. H. WATSON, JR. and S. P. MCGLYNN. Theor. Chim. Acta, **21**, 309 (1971).
4. P. J. KROPP, E. J. REARDON, JR., Z. L. F. GAIBEL, K. F. WILLARD, and J. H. HATHAWAY, JR. J. Am. Chem. Soc. **95**, 7058 (1973); H. G. FRAVEL, JR. and P. J. KROPP. J. Org. Chem. **40**, 2434 (1975).
5. T. R. FIELDS and P. J. KROPP. J. Am. Chem. Soc. **96**, 7559 (1974).
6. P. J. KROPP. Org. Photochem. **4**, 1 (1979).
7. P. J. KROPP, H. G. FRAVEL, JR., and T. R. FIELDS. J. Am. Chem. Soc. **98**, 840 (1976).
8. Y. INOUE, T. MUKAI, and T. HAKUSHI. Chem. Lett. 1665 (1983).
9. (*a*) Y. IONOUE, S. TAKAMUKU, and H. SAKURAI. J. Phys. Chem. **81**, 7 (1977); Synthesis, 111 (1977); (*b*) H.-P. SCHUCHMANN, C. VON SONNTAG, and R. SRINIVASAN. J. Photochem. **15**, 159 (1981).
10. L. FRIEDMAN and H. SHECHTER. J. Am. Chem. Soc. **83**, 3159 (1961); A. C. COPE, M. BROWN, and G. L. WOO. J. Am. Chem. Soc. **87**, 3107 (1965).
11. W. KIRMSE and CH. HASE. Angew. Chem. Int. Ed. Engl. **7**, 891 (1968).
12. N. L. ALLINGER and J. L. COKE. J. Am. Chem. Soc. **81**, 4080 (1959).
13. N. L. ALLINGER and V. B. ZALKOV. J. Am. Chem. Soc. **83**, 1144 (1961).
14. A. P. KRAPCHO and J. DIAMANTI. Chem. Ind. (London), 847 (1965).
15. J. CASANOVA and B. WAEGELL. Bull. Soc. Chim. Fr. 1289 (1971).
16. C. R. Jones and P. B. DERVAN. J. Am. Chem. Soc. **99**, 6772 (1977), and private communication.
17. V. BONACIC-KOUTECKY, P. BRUCKMANN, P. HILBERTY, J. KOUTECKY, C. LEFORESTIER, and L. SALEM. Angew. Chem. Int. Ed. Engl. **101**, 307 (1975).
18. D. BEHAR, G. CZAPSKI, J. RABANI, L. M. DORFMAN, and H. A. SCHWARZ. J. Phys. Chem. **74**, 3209 (1970); D.-H. CHIN, G. CHIERICATO, JR., E. J. NANNI, JR., and D. T. SAWYER. J. Am. Chem. Soc. **104**, 1296 (1982).
19. D. G. HENDRY and D. SCHUETLE. J. Org. Chem. **41**, 3179 (1976).
20. W. B. MONIZ and J. A. DIXON. J. Am. Chem. Soc. **83**, 1671 (1961).
21. K. B. WIBERG and A. DE MEIZERE. Tetrahedron Lett. 519 (1969).
22. H. C. BROWN and G. HAM. J. Am. Chem. Soc. **78**, 2735 (1956).
23. V. PRELOG, K. SCHENKER, and H. H. GUNTHARD. Helv. Chim. Acta, **35**, 1598 (1953).
24. K. B. BECKER. Helv. Chim. Acta, **60**, 68 (1977).
25. API ^{1}H nmr spectral data, 12X (1982).
26. API ^{1}H nmr spectral data, 2636 (1982).
27. A. MEDLIK-BALAN and J. KLEIN. Tetrahedron, **36**, 299 (1980).
28. L. RUZICKA, PL. A. PLATTNER, and A. WILD. Helv. Chim. Acta, **29**, 1611 (1946).
29. E. BILLETER and HS. H. GUNTHARD. Helv. Chim. Acta, **43**, 338 (1958).
30. H.-J. SCHNEIDER and F. THOMAS. Tetrahedron, **22**, 2005 (1976).

Hydrogen bridges and electron transfer in biomolecules. Study of a possible mechanism on a model charge–recombination system

GIUSEPPE DEL RE, ANDREA PELUSO, AND CAMILLA MINICHINO
Cattedra di Chimica Teorica, Università di Napoli, Via Mezzocannone 4, I-80134 Napoli, Italy

Received August 16, 1984

This paper is dedicated to Professor Camille Sandorfy on the occasion of his 65th birthday

GIUSEPPE DEL RE, ANDREA PELUSO, and CAMILLA MINICHINO. Can. J. Chem. **63**, 1850 (1985).

It is suggested that internal electron transfer in biomolecules such as multiheme proteins can take place along H-bridge/peptide-link chains by a proton-relay process followed by radicalic return to the initial condition. The plausibility of such a process is assessed by (a) reference to published suggestions and evidence; (b) estimates of vibrational characteristics and of the free energies of the various states of a model system consisting of three H-bridges and one peptide group. It appears that the proposed mechanism is highly efficient and very fast, at least if the H-bonds formed by a peptide group evolve in a concerted manner.

GIUSEPPE DEL RE, ANDREA PELUSO et CAMILLA MINICHINO. Can. J. Chem. **63**, 1850 (1985).

On suggère que le transfert électronique interne dans des biomolécules, comme les protéines de multihème, peut se produire le long des chaînes ponts-H/liaisons-peptidiques par un processus de relais de protons qui serait suivi d'un retour radicalique à la condition initiale. On essaye de déterminer si un tel processus est plausible en faisant appel à (a) des références à des suggestions et à des données expérimentales publiées; (b) des évaluations des caractéristiques vibrationnelles et des énergies libres des divers états d'un système modèle comportant les trois ponts-H et un groupement peptidique. Il semble que le mécanisme proposé soit très efficace et très rapide, au moins si les liaisons H formées par un groupement peptidique évoluent d'une manière concertée.

[Traduit par le journal]

1. "Assisted through-bond" ET mechanism

1a. When biomolecules containing several hemes participate in a redox process, intramolecular electron transfer (ET) between hemes is likely to be a feature of the overall phenomenon. The problem then arises of establishing the mechanism by which that interheme ET takes place (1). In general, the interheme distances and orbital overlaps have values such that direct electron jumps from one macrocycle to another require resonance conditions, even if they proceed through bridge molecules (1). Therefore, alternative mechanisms are worth investigating. In this paper an "assisted through-bond" ET mechanism is proposed and discussed. An example of molecules to which it applies are the multiheme cytochromes. In molecules of that class it is possible that internal ET takes place along a continuous H-bond/peptide-link chain, involving a few peptide links and possibly a water molecule, and connecting the imidazole rings of two hemes: although structural details are still unreliable, published work indicates that the chain in question could start with a bridge between an imidazole and the oxygen of a peptide link and terminate with the same type of H-bridge in the opposite order (2).

The ET mechanism to be associated with such a chain would consist in a proton-relay process followed by a radicalic rearrangement:

$$a:\quad e^- + \mathrm{A}\ldots\mathrm{H{-}B}\ldots\mathrm{H{-}C} \rightarrow \mathrm{A}^-\ldots\mathrm{H{-}B}\ldots\mathrm{H{-}C} \rightarrow \dot{\mathrm{A}}\mathrm{{-}H}\ldots\mathrm{B}^-\ldots\mathrm{H{-}C} \rightarrow \dot{\mathrm{A}}\mathrm{{-}H}\ldots\mathrm{B{-}H}\ldots\mathrm{C}^- \rightarrow \dot{\mathrm{A}}\mathrm{{-}H}\ldots\mathrm{B{-}H}\ldots\mathring{\mathrm{C}} + e^-$$

(I*a*)

where the dot denotes an electron and the small circle a hole; and

$$b:\quad \dot{\mathrm{A}}\mathrm{{-}H}\ldots\mathrm{B{-}H}\ldots\mathring{\mathrm{C}} \xrightarrow[\text{one or more steps}]{} \mathrm{A}\ldots\mathrm{H{-}B}\ldots\mathrm{H{-}C}$$

(I*b*)

In stage **I***b* actual ET takes place, because the hole on C attracts a proton *plus one electron*, and so on until the initial situation is restored.

1b. In order to assess the plausibility of mechanism **I**, two major questions must be answered. First: are such chains of H-bonds actually present in multiheme proteins? Second: is the proposed mechanism sufficiently fast and efficient?

The first question requires consideration of the specific protein structure (cf. section 2). In this paper we focus on the second question, by presenting a study of a model system which contains the most relevant features of a possible real system. A major drawback remains, in that highly reliable potential energy (PE) surfaces are difficult to obtain even for such a simplified system. Even *ab initio* computations, due to basis effects and correlation errors, do not yield uniformly reliable barrier heights and vibrational frequencies (3, 4). Fortunately, fair estimates of free-energy profiles are sufficient for our purposes: what may be very important is that temperature dependent effects should be taken into account.

2. A specific example: heme–heme ET

2a. Consider, as a concrete example, the hemes of a multiheme cytochrome in their oxidized state. They may be represented by the abbreviated formulas

$$\mathrm{H{-}Im} \rightarrow \mathrm{Fe(M_1){-}Im}, \qquad \mathrm{H{-}Im} \rightarrow \mathrm{Fe(M_2){-}Im}$$

II

where Im stands for imidazolyl, M_1 and M_2 for the porphyrin macrocycles; the arrows denote dative N—Fe bonds, the dashes ordinary (covalent) N—Fe bonds resulting from substitution of a hydrogen atom by iron. Consider now the H-bond/peptide-bond chain:

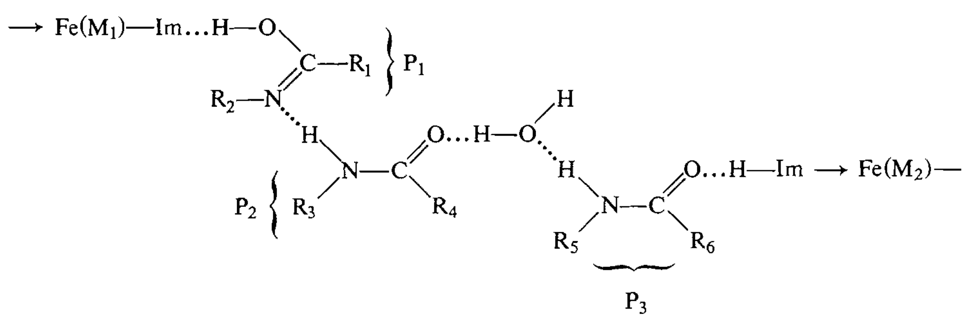

III

Note: the *cis* and *trans* positions are not realistic

An electron-relay process of the type summarized by scheme **I** could take place (with M_1 acting as the electron acceptor and M_2 as the electron donor) along the chain of scheme **III** according to the following sequence of events.

A: An electron received by M_1 is transferred to the right-hand Im ligand, which becomes negative.

B: The resulting Im^- ring attracts the proton of the neighboring peptide group, P_1, which is initially in the enol form.

C: The negative charge now appearing on the end nitrogen of P_1 attracts the proton of P_2, which then goes over to the enol form.

D, E: Similar events take place at the water molecule and at P_3.

F: The second heme has now lost a proton, and has an imidazolate ion on its left-hand side. The negative charge is transferred to M_2, so that a hole is localized on Im.

G: M_2^- releases an electron to the external acceptor (or to another heme).

H: The electron-deficient left-hand imidazole of M_2 recalls the lost proton together with an electron.

I, J, K: The lost protons are taken back (with one electron) by P_3, the water molecule, P_2, and P_1 in succession. The left-hand heme thus loses the excess electron received at step A.

The whole mechanism just described is set "in motion", of course, when there are both a source of electrons acting on the left and an electron acceptor which creates the "driving force" on the right. If the latter were missing, reduction of the first heme would cause protons to shift so as to create a negatively charged deprotonated peptide group P_2^-; there would be no further motion because the high proton affinity of the OH^- makes the water molecule a very effective barrier.

2b. Aside from considerations specific to given protein structures, the following general questions must now be dealt with.

1. Is the oxidized-heme form **II** a reasonable assumption as compared with $[\text{H-Im—Fe(M)—Im-H}]^+$?

2. Is the assumption of a stable peptide bond in the enol form chemically plausible and consistent with available information?

3. Are the free-energy barriers involved in the charge-relay events A to G low enough?

The first point is easily disposed of, since the essential difference between the two cases is a normal covalent bond replacing a dative bond to iron, a proton being involved in any case in an H-bond connected to the imidazole, and one cannot see what should make that kind of bond less probable. In fact, the "deprotonated" oxidized form has been considered in several papers as a possible important feature of biological processes: "hydrogen bonding or actual deprotonation of imidazole ligands provides a means whereby the tertiary structure of the protein could moderate the reactivity or redox potential of the iron center" (5).

The second question requires a more detailed study. The enol form of the peptide bond is consistent with the rules of valency, but has never been observed. A theoretical study of the reaction formamide + water ⇄ formamidic acid + water suggests that the keto form has an energy ca. 60 kJ/mol lower than the enol form; the activation energy when a single water molecule plays the donor–acceptor role is ca. 100 kJ/mol. These results indicate that the energy changes involved in the keto–enol isomerization of the peptide bond are high enough to control the kinetics, but not so high that the process should be forbidden. Moreover, the above results apply to the gas phase; the presence of a special environment such as certainly exists close to a heme group may well bring about energy changes of the order of ca. 100 kJ/mol. The objection that peptide bonds permanently in the enol form would be detected by nmr does not apply to a typical protein of more than 100 aminoacid residues, since then only less than 4% of the peptide groups would be in the enol form.

As concerns energy barriers or, more generally, energy profiles, it might seem that, at least for simple models, straightforward *ab initio* calculations followed by evaluation of vibrational contributions is a safe procedure. Quite instructive papers (dealing, however, with energy differences between minima) have in fact been published according to this philosophy (6). Nevertheless, as has been mentioned, two orders of difficulties remain. First, without a fairly accurate study of the whole PE hypersurface the results lose much of their significance. Secondly, as has been extensively shown, in particular by Scheiner (7), the results for barriers are dramatically basis dependent. Scheiner has suggested that the 4.31 G basis should provide fairly reliable estimates, but he bases this conclusion on a few comparisons with $6.311\ G^{++}$ results corrected for correlation according to a special formula. Thus, for systems involving more than one hydrogen bond and a comparatively large number of atoms (as is the case with the model discussed below), a rigorous quantitative study of energy profiles is a

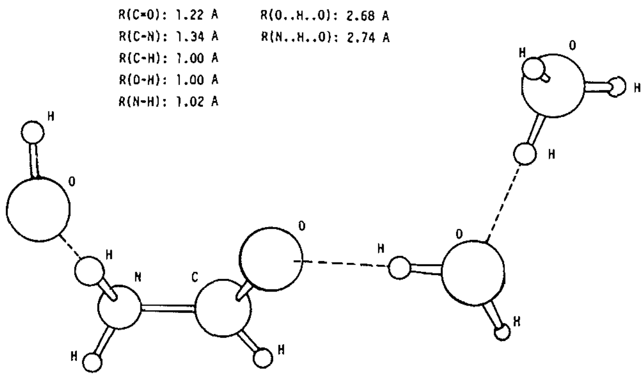

FIG. 1. Geometrical representation of model peptide residue.

problem for the future. Less ambitious semiempirical calculations are certainly open to many reservations. In the present context they are the most reasonable choice because of the above considerations, because, as will be seen, they give acceptable results, and, most important, because all we really need is a semiquantitative description of the whole process under study. Moreover, as will be illustrated below, electronic calculations are in general just starting points for the evaluation of force constants, which require some kind of interpolation technique and the introduction of correction factors in all cases.

With the above premises, we intend to suggest that the answer to question 3 above is positive; indeed, we proceed to introduce our simplified model and to discuss the various aspects of the mechanism under study starting precisely with consideration of PE profiles.

3. The model system

3a. A system which appears to us to incorporate the critical features of **III** is the triple-bridge system

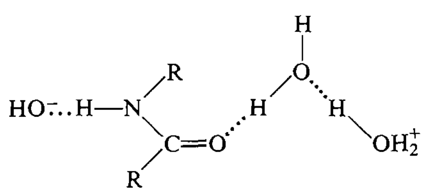

$(R = H, CH_3)$

(**IV***a*)

which undergoes charge recombination by proton shifts from right to left. The two terminal ions simulate the left-hand heme + P_i system (after it has received an electron) and the right-hand heme, together with the virtual acceptor which creates the "driving force". Another feature characteristic of chain **III** is present, inasmuch as the recombined form contains a peptide group in the enol form:

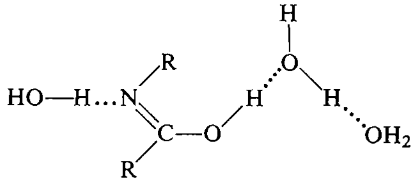

(**IV***b*)

As the model peptide unit we have chosen *N*-methylacetamide, in agreement with Del Bene (8), but for the geometry (cf. Fig. 1) we have used the standard data for a peptide residue (9). The valency angle for the C═O . . . H—O bridge has been taken to be 120°, in agreement with current estimates (10). For the H-bond distances we have taken 2.68 Å and 2.72 Å for O . . . O and N . . . O respectively.

Semiempirical (MNDO, ref. 15) computations yield the expected results for the Born–Oppenheimer (B.O.) potential energy profile along the H-bond line. No barrier is found for the end N . . . O and O . . . O bonds.

The absence of a barrier for the transition

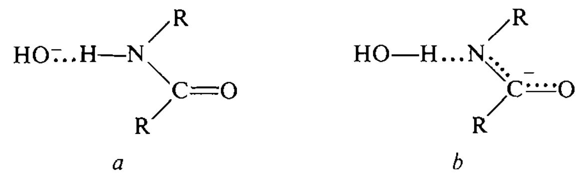

a *b*

(**V**)

may appear somewhat surprising, the more so as the B.O. energy difference between **V***a* and **V***b* of system **III** is predicted to be 249 kJ/mol (ca. 60 kcal/mol) in favor of **V***b*. In fact, neither STO 3G nor 4.31 G calculations predict a barrier at 2.8 Å (11, 12), and the greater stability of **V***b* is obviously related to the fact that the proton affinity of OH^- is particularly high (13).

The barrier to proton shift for the C═O . . . H—O bond is 82 kJ/mol in the right-to-left hand direction. This barrier includes electron rearrangement in the peptide group, because it corresponds to the process

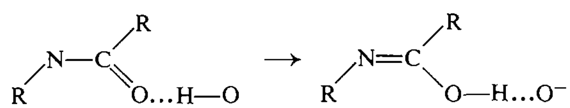

a *b*

(**VI**)

System **IV** at stage **VI** is predicted to be less stable by only ca. 27 kJ/mol than the preceding stages; this is probably a result of the stabilization of OH^- by H_3O^+, viz., a consequence of the "driving force" produced by the terminal ions.

The absence of a barrier for the third bridge is in full agreement with the best *ab initio* results (14), which predict only ca. 11 kJ/mol at 2.75 Å for $H_3O_2^-$. This last step is characterized by the expected very large drop in energy, ca. 320 kJ/mol.

In short, the B.O. energies obtained by the MNDO (15) calculations are entirely reasonable and sufficient for our purposes. Their physical significance, however, is worth a more detailed discussion in connection with mechanism **I**.

What is somewhat puzzling is the physical meaning of having placed the two terminal ions so close to the central part of system **IV**. Had we selected distances 20% longer, at least the N . . . O bond would have shown a large B.O. barrier – as 4.31 G calculations go. Of course, a more complete study of **IV** as such should include consideration of this possibility, since one could imagine that the OH^- ion, for instance, slowly approaches the rest of the system, in which case the proton could be exchanged already at distances larger than 2.68 Å. (Although it may be noted that work by Brickmann (16), together with the results of ref. 7, predicts that the proton transfer times become exceedingly long already at 2.95 Å.)

Our problem here, however, is related to a given rigid structure, which relaxes very little upon reduction or oxidation (17). Therefore, it is correct to ignore relaxation and, especially, situations where the terminal ions are initially far from their "equilibrium" positions. Indeed, we have to think that at least the left-hand one is formed in place, as happens to Im in mechanism **III**.

Thus, we must accept as a possibility the absence of barriers at the terminal H-bonds. The question then arises: how will the process take place in time?

At first sight, one could expect that step **V** will take place upon formation of OH^-, followed by step **VI**, which must be preliminary to the last one. If this were so, we should think of a stepwise mechanism as most probable. However, this picture ignores the possibility that step **VI** may be immediately switched on as the removal of the NH proton from N begins. This is revealed in a PE surface by the fact that a path where the protons move concertedly (cf. below) involves a lower barrier (MNDO: 31 kJ/mol).

All this can be made somewhat more quantitative by consideration of thermodynamic characteristics of the process. As has been mentioned, the latter are the really significant quantities, not the Born–Oppenheimer potential energy in any degree of approximation.

4. Vibrational analysis

4a. As has been mentioned, the importance of vibrational contributions to physically significant quantities associated with the processes under consideration may be very large. This applies in particular to both terms of the free energy expression

$$[1] \quad \Delta G = \Delta H - T\,\Delta S$$

which must be estimated for the initial, activated, and final states of each reaction step. This can be done theoretically using the well-known rigid-rotator, harmonic-oscillator, and ideal-gas approximations, whereby eq. [1] can be cast into the form

$$[2] \quad \Delta G = \Delta E + \Delta G^{\mathrm{transl}} + \Delta G^{\mathrm{rot}} + \Delta G^{\mathrm{vib}} + \Delta E^{zp}$$

ΔE standing for the difference in interaction energies, ΔE^{zp} standing for the corresponding zero-point vibrational energy, and other symbols having the standard meanings (18). The terms corresponding to rotations and translations could be easily evaluated, if needed. In our case they play no role. On the other hand, evaluation of vibrational contributions is quite difficult, especially if an activated state is also to be studied. Theoretical estimates of vibrational frequencies are necessary because of the lack of experimental data for transition and activated states. Calculation of a complete force field is then necessary for the equilibrium states as well, lest inconsistencies be introduced.

For the reasons explained above, we have started from current semiempirical (MNDO) calculations, carried out for those equilibrium and activated states of the model system **IV** which correspond to (a) a stepwise mechanism where the protons move in succession along the H-bond lines; (b) a concerted mechanism where the protons also move along the H-bond lines, but cover simultaneously the same fraction of the distance between their initial and final positions. In agreement with the scope of this study, the part of the computations devoted to vibrations has been carried out by treating as hydrogens the methyl groups used for estimates of the PE profiles. This further simplification is justified because, whereas the methyl groups serve to fix the C—N and C=O equilibrium lengths at more realistic values, they have no important effect on the vibrational properties of H-bonds.

The errors of "theoretical" force constants arise mainly from the basis set choice and lack of correlation in *ab initio* calculations, and from the well-known drawbacks of the formulae in semiempirical calculations. Those errors can be eliminated to a large extent by transforming the Cartesian force constants to those associated with internal coordinates and applying suitable correction factors (19). Such correction factors can be determined from equilibrium states, where also experimental values are known. For activated states the assumption that the same correction factors apply is obviously a daring one, but there seems to be no other way out. Very important support for this assumption comes from the fact that with the correction factors obtained below the activated states do show one negative eigenvalue of the frequency matrix: this feature proves that the values used for the force constants are physically consistent. The six frequencies associated with rotations and translations are not exactly zero because (again to avoid not indispensable complications) we have not carried out a point-by-point optimization along the chosen reaction path.

4b. The most important results (Table 1) of force constant calculations can be summarized as follows. The force constants associated with the intermolecular NH . . . O and C—O—H . . . O stretching modes are both negative (−0.05 and −0.16 mdyn/Å, respectively), no barrier being predicted in these cases (4.31 G calculations confirm this for the NH . . . O bond (12)). The force constant of the CO bond appears to increase when the proton comes closer to the oxygen atom, while the CN force constant behaves normally. This surprising result may be due to the fact that we have not allowed for relaxation of the heavy nuclei during proton motion, but further *ad hoc* studies are perhaps necessary.

In agreement with experimental and theoretical results (26), our computations yield a comparatively high value of the force constant corresponding to the interaction between CN and CO stretching (2.2 mdyn/Å). This is in line with the expectation that the nitrogen lone pair is involved in the amide π-system.

The *intramolecular* stretching force constants of NH . . . O, CO . . . HO, and OH . . . O in the activated state for the concerted mechanism are all found to be ~1.9 mdyn/Å. The NH . . . O *intermolecular* force constant is negative (−0.33 mdyn/Å), while the other two are positive (CO . . . HO: 0.29 mdyn/Å; OH . . . O: 0.45 mdyn/Å). Of course, in the three activated states of the stepwise mechanism, the three intermolecular force constants are all negative.

4c. The corrected force constants have been used to compute the vibrational frequencies. The well-known **GF** method (20) has been used, the only variant being that, instead of computing the kinetic energy matrix **G** we have obtained the dynamical matrix by the expression

$$\mathbf{D} = \mathbf{M}^{-1/2}\,\tilde{\mathbf{B}}\mathbf{F}_{\mathrm{R}}\,\mathbf{B}\,\mathbf{M}^{-1/2}$$

where **M** is the (diagonal) matrix of the atomic masses, $\mathbf{F}_{\mathrm{R}}$ is the force constant matrix in the internal coordinates, and **B** is the matrix representing the transformation from the internal to the Cartesian coordinate system.

Table 1 contains the results, including mode assignments. The modes indicated correspond to the initial geometry. We have also tried to refer to the same geometry the modes of the activated and final states, so as to facilitate interpretation of frequency shifts. Of course, this means that the description given is not as detailed as it could be without this restriction.

The symbols used in the assignment of the intermolecular modes are in line with current literature (21). The inter-

TABLE 1. Vibrational frequencies (cm^{-1}) and normal modes of model system IVa (see Fig. 1)

Initial state*	Initial state**	Activated state*	Activated state**	Final state	
90	90	128[a]	93	887	ν_t C=O..HO + ν_t O..HO
188	191	—	238[b]	93	ν_σ CO..H—O
252	252	395[a]	253	204	ν_σ H_2O..H—OH_2
405	651	1253	622	251	ν_b HO—H..O=C
486	405[c]	797	440[c]	1119	ν_t N—H..O
496	500	1772	451	125	ν_b H_2O..H—OH_2
603	520	1511[d]	1733[b]	386	ν_b N—H..O
649	1417	543	1417	620	N—C=O skeletal motions
818	813	379	950	869	ν_t C=O..H—O
956	955	930	969	1015	Out-of-plane C=O
1129	995	700	982	995	Out-of-plane N—H
1192	1216	301[a]	1219	1198	Bending N—C=O
1381	1681	1206	1674	1408	Bending H—N—C
1417	1415[e]	1381	1428[e]	2261	Out-of-plane H_2O..H—OH_2 + N—H..O
1479	1558[f]	1977	1549[f]	1560	N—C(H)=O skeletal motions
1888	1852[g]	1721	1893[g]	1909	Stretch. C=O + C—N
1929	1961[h]	2362	2211[h]	1679	Bending NH
1963	2263	1960	1062	1432	Bending H_2O
1983	2006[i]	1931	2011[i]	1814	Bending H_3O^+
1994	2020[j]	2076	2030[j]	2194	Bending ..H$\overset{+}{O}$(H)H
2895	2896	2897	2904	2911	Stretch. C—H
3043	3123[k]	913	3129[k]	3125	Stretch. N—H..
3347	3352	856	—	2903	Stretch. ..H—OH
3391	3361	3373	3359	3362	Stretch. N—H
3520	3506	1405	3621	3475	Stretch. H—$\overset{+}{O}H_2$
3622	3631	3613	3630	3619	Sym. stretch. ..H$\overset{+}{O}$(H)H
3659	3659	3644	3642	3666	Stretch. ..HO—H
3702	3697	3689	3693	3708	Asym. stretch. ...H$\overset{+}{O}$(H)H
3810	3862	3829	3862	3862	Asym. stretch. H—O..

*Concerted mechanism. **Stepwise mechanism.
[a] Intermolecular modes (see text).
[b] Not assignable.
[c] ν_σ N—H..O.
[d] Intermolecular H—O..HN + O...H—N.
[e] ν_t O...H—$\overset{+}{O}$(H)H.
[f] N—C=O skeletal motion.
[g] + bending.
[h] Bending H—O..HN.
[i] Asymmetric bending H_3O^+.
[j] Symmetric bending H_3O^+.
[k] Stretching OH^-.

molecular wagging and torsional modes, which depend very weakly on the position of the proton in the bridge, have not been included in the table.

Table 1 falls into two parts. The intermolecular modes range from 100 to 800 cm^{-1}. The intramolecular modes range from 1200 cm^{-1} to 3800 cm^{-1}. The intermolecular O—H..O modes at 252 and 405 cm^{-1} are in satisfactory agreement with the values found on the water dimer (272 and 483 cm^{-1} respectively) (22) by a much more sophisticated method.

In the range 1200–1800 cm^{-1} we have found the intramolecular modes of the amide system, as expected. The bending modes of the H_2O and H_3O^+ groups fall in the range 1800–2000 cm^{-1}, and are thus overestimated by ~300 cm^{-1} (22, 23, 25). The OH and NH stretching modes fall between 3000 and 3800 cm^{-1}. The predicted shifts for the intramolecular OH and NH stretching modes are of ca. 350 cm^{-1}, in agreement with the experimental value of ca. 300 cm^{-1} (24). Certain *ab initio* investigations (23) predict much lower intramolecular frequency shifts, e.g. 53 cm^{-1} for the stretching frequency of OH in an OH...O bridge.

We emphasize that, given the scope of our calculations, even refinements such as allowance for anharmonic corrections have

TABLE 2. Thermodynamic functions for concerted and stepwise mechanism at 300 K for recombination of system IVa

Parameters		States					
		a	b	c	b′	a′	a
Partition function		11.25	4.82	18.65	8.19	10.37	11.25
Vibrational ΔG		−6	−4	−7	−5	−6	−6
$E^{zp} + \Delta E$		0	2	−551	−174	−240	0
ΔG total		−6	−2	−559	−179	−246	−6
ΔG (a → c)	−553						
ΔG (a → b: barrier)	6						
ΔG (e → b′: barrier)	67						

Notes. Energies in kJ/mol; a: initial state IVa; b, b′: transition states for concerted and stepwise mechanisms, resp.; c: final state IVb. E^{zp} is the zero-point vibrational energy, ΔE the computed B. O. energy (cf. text); e: initial state . . . HOH . . . NR=CR—O$^-$. . . of the first barrier crossing (scheme V).

been excluded. Suffice here to recall that they may be comparatively important in connection with intermolecular modes. Failure to take them into account might explain the grossly underestimated values obtained in *ab initio* calculations (22, 23). As concerns semiempirical calculations, we have not found examples of anharmonic corrections in the literature; it is possible that the predicted values would be further increased, and thus become overestimated.

4d. In the activated state, one vibrational degree of freedom becomes a dissociative one. For the concerted mechanism our calculations suggest that the major contribution to that dissociative mode comes from the CO . . . H . . . O stretching motion. There are still two frequencies (~300 and ~900 cm^{-1}) which correspond *grosso modo* to the proton motions along the O . . . H . . . O and N . . . H . . . O bridges, respectively.

In the stepwise mechanism the situation is more clearcut, and the dissociative mode appears to be exclusively the stretching one associated with the proton of the C=O . . . H—O bridge.

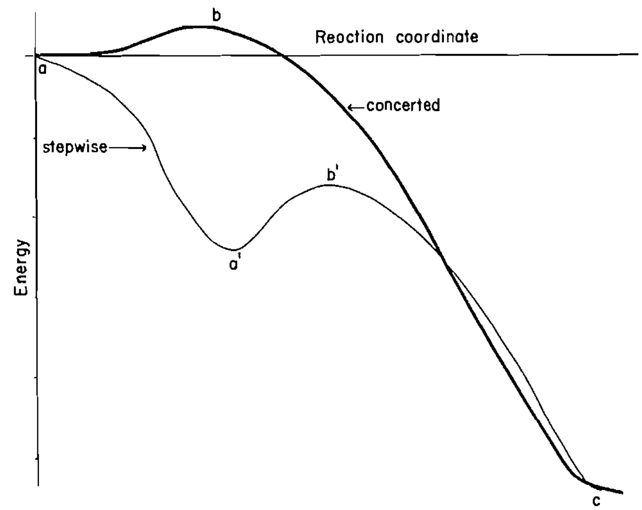

FIG. 2. Calculated energy profiles for proton motion in chain IV.

5. Discussion and conclusion

We are now in a position to go back to system **IV** and obtain some feeling for the thermodynamical quantities relevant to its evolution from **IV**a to **IV**b. Under the assumption that relaxation plays no decisive role, the relevant quantities have the values shown in Table 2. As expected, the concerted mechanism appears to be highly favored: the barrier is extremely low. Therefore the overall crossing time should be of the order of a vibration, i.e. very short as compared with diffusion times. The "yield" – which is the same in the stepwise mechanism, since it is measured by the equilibrium concentrations – is very large, due to the overall ΔG of more than 132 kcal/mol. Thus, at least in the concerted case, mechanism **I**a (with a "driving force" comparable to that of system **IV**) is physically plausible. It stands to reason that relaxation could only make it more efficient; at any rate, the estimated switching time is so short that, in fact, the assumption that relaxation is not important can be accepted.

The crucial question regarding the enol form of the peptide bond is also answered: the keto–enol transition is very easy if it is synchronous to the motions of all the H-bridge protons.

Of course, many points remain open. Here we shall only comment on one of them: the alternative between the concerted and the stepwise mechanisms.

The energy profiles obtained in our calculations are shown in Fig. 2, where the various states are labelled as in Table 2. Note first of all that the initial state *a* lies at the bottom of a well only in the profile associated with the concerted mechanism (thick line): this means that in a suitable multidimensional potential-energy map *a* would lie at a saddle point. This is not surprising if the system is assumed to originate from loss of a proton by the water molecule parent of the leftmost hydroxyl ion of **IV***a*, since then it is clear that formation of OH$^-$ corresponds to an energy maximum as far as the first H-bridge is concerned. Indeed, the preference for the concerted mechanism might be just a consequence of having adopted the point of view of transition state theory. According to that theory, the stepwise mechanism must be decomposed into three steps (a–a', a'–b', b'–c), and the rate-determining step a'–b' has the characteristics shown in Table 2. Now, this separation into three steps, each associated with a specific equilibrium, is not fully convincing in our case. The initial state is essentially a highly energetic transition state itself; therefore, it would appear more reasonable to treat the energy profile for the stepwise mechanism as if the first minimum at a' did not exist. In fact, the kinetic energy of the system after descent to a' cannot be ignored, at variance with what would happen if a were in turn at equilibrium with some previous stable species.

In short, if we assume that the minimum at a' is occupied by vibrationally highly excited molecules, whatever the temperature, just because of energy transfer from potential energy of a to vibrational energy of a', we have to assign to a' a vibrational contribution much larger than the zero-point one. Then the stepwise mechanism may become a greatly favored one. This conclusion may be important, because in large biomolecules the perturbations produced by the tertiary structure and the solvent could make a concerted mechanism more unlikely.

Acknowledgements

This paper is dedicated by Giuseppe Del Re to Camille Sandorfy as a token of friendship and scientific exchange extending over more than fifteen years. Support of the Italian CNR and Ministry of Education is acknowledged. Thanks are expressed to Dr. R. Haser (CRMCC, Marseille) for having pointed out the importance of the biochemical problem to which this paper refers and for many discussions and bibliographical indications.

1. S. LARSSON. J. Chem. Soc. Faraday Trans. 2, **79**, 1375 (1983).
2. M. PIERROT, R. HASER, M. FREY, F. PAYAN, and J. P. ASTIER. J. Biol. Chem. **257**, 14341 (1982).
3. G. KARLSTROM, B. JONSSON, B. ROOS, and H. WENNERSTRÖM. J. Am. Chem. Soc. **98**, 6850 (1976).
4. P. PULAY, G. FOGARASI, F. PANG, and J. E. BOGGS. J. Am. Chem. Soc. **101**, 2550 (1979).
5. M. NAPPA, J. S. VALENTINE, and P. A. SNYDER. J. Am. Chem. Soc. **99**, 5799 (1977).
6. P. HOBZA, F. MULDER, and C. SANDORFY. J. Am. Chem. Soc. **103**, 1360 (1981).
7. S. SCHEINER. Int. J. Quantum Chem. **23**, 753 (1983).
8. J. DEL BENE. J. Am. Chem. Soc. **100**, 1387 (1978).
9. L. PAULING. The nature of the chemical bond. 3rd ed. Cornell Univ. Press, Ithaca, NY. 1960. p. 282.
10. S. SCHEINER and C. W. KERN. J. Am. Chem. Soc. **99**, 7042 (1977).
11. F. ZUCCARELLO, A. RAUDINO, and G. BUEMI. J. Mol. Struct. (Theochem) **107**, 215 (1984).
12. S. SCHEINER and L. B. HARDING. Chem. Phys. Lett. **79**, 39 (1981).
13. P. SCHUSTER. *In* Hydrogen bond – recent developments in theory and experiments. *Edited by* P. Schuster, G. Zundel, and C. Sandorfy. North Holland Publ. Co., Amsterdam. 1976. p. 27.
14. S. SCHEINER, M. M. SZCZESNIAK, and L. D. BIGHAM. Int. J. Quantum Chem. **23**, 739 (1983).
15. M. J. S. DEWAR and W. THIEL. J. Am. Chem. Soc. **99**, 4899 (1977).
16. J. BRICKMANN. *In* Hydrogen bond – recent developments in theory and experiments. *Edited by* P. Schuster, G. Zundel, and C. Sandorfy. North Holland Publ. Co., Amsterdam. 1976. p. 217.
17. A. WARSHEL. J. Phys. Chem. **86**, 2218 (1982).
18. M. M. SZCZESNISAK and P. HOBZA. J. Phys. Chem. **87**, 2608 (1983).
19. C. E. BLOM and C. ALTONA. Mol. Phys. **31**, 1377 (1976).
20. E. B. WILSON, J. C. DECIUS, and P. C. CROSS. Molecular vibration. McGraw–Hill, New York. 1955.
21. J. BERTIE and M. V. FALK. Can. J. Chem. **51**, 1713 (1973).
22. J. R. REIMERS and R. O. WATTS. Chem. Phys. **85**, 83 (1984).
23. L. A. CURTISS and J. A. POPLE. J. Mol. Spectrosc. **55**, 1 (1975).
24. J. N. VINOGRADOV and R. H. LINNELL. Hydrogen bonding. Van Nostrand, New York. 1971.
25. A. J. TURSI and E. R. NIXON. J. Chem. Phys. **52**, 1521 (1970).
26. T. MIYAZAWA, T. SHIMANOUCHI, and S. MIZUSHIMA. J. Chem. Phys. **29**, 611 (1958).

Cluster expansion of the wavefunction. Potential energy curves of the ground, excited, and ionized states of Li_2

H. NAKATSUJI,[1] J. USHIO, AND T. YONEZAWA
Division of Molecular Engineering, Graduated School of Engineering, Kyoto University, Kyoto 606, Japan

Received August 6, 1984

This paper is dedicated to Professor Camille Sandorfy on the occasion of his 65th birthday

H. NAKATSUJI, J. USHIO, and T. YONEZAWA. Can. J. Chem. **63**, 1857 (1985).

The SAC (symmetry-adapted-cluster) and SAC-CI theories based on the cluster expansion of the wavefunction have been applied to the calculations of the potential energy curves of the ground, excited, and ionized states of the Li_2 molecule. The potential energy curves and the spectroscopic properties calculated agree well with the available experimental data and the previous theoretical results of Olson and Konowalow. For the $2^1\Sigma_g^+$ state, our calculation is the first and predicts a bound state whose minimum is at R_e = 6.8 bohr and 2.5 eV above the ground state. This state dissociates into ^2P and ^2S states of the Li atoms and has a hump which is higher than and outside of the hump of the $B^1\Pi_u$ state. The long-range behavior of the states which dissociate into ^2P and ^2S states of the Li atom is well predicted by the resonance interaction theory.

H. NAKATSUJI, J. USHIO et T. YONEZAWA. Can. J. Chem. **63**, 1857 (1985).

On a appliqué les théories SAC et SAC-CI, qui sont basées sur une expansion de l'agglomération de la fonction d'onde, au calcul des courbes d'énergie potentielle des états fondamental, excité et ionisé de la molécule Li_2. Les courbes d'énergie potentielle et les propriétés spectroscopiques calculées sont en bon accord avec les données expérimentales disponibles ainsi qu'avec les résultats théoriques antérieurs de Olson et Konowalow. Dans le cas de l'état $2^1\Sigma_g^+$, nos calculs correspondent à une première et ils prédisent un état lié dont le minimun se trouverait à R_e = 6,8 bohr et à 2,5 eV au-dessus de l'état fondamental. Cet état se dissocie dans les états ^2P et ^2S de l'atome de Li et il présente un maximum qui est plus élevé que et en dehors du maximum de l'état $B^1\Pi_u$. On peut facilement prédire le comportement à long terme des états qui se dissocient dans les états ^2P et ^2S de l'atome de Li en faisant appel à la théorie de l'interaction de résonance.

[Traduit par le journal]

Introduction

Accurate information on the potential energy hypersurfaces and the electronic structures of molecules, especially those of excited states, are very important for the study of chemical reactions and the dynamic behavior of molecules in excited states. Professor Sandorfy, who has developed various aspects of chemical spectroscopy (1, 2), has accumulated detailed knowledge on excited states, especially those of Rydberg type (3). These activities have, at the same time, increased the need for accurate theoretical data on electronic structures and potential energy hypersurfaces for excited-state molecules.

So far, a practical method of calculating accurate wavefunctions for molecules in excited states in a wide range of molecular configurations has been the CI method applied very carefully by experts. Buenker, Peyerimhoff, and their coworkers (4), for example, have been active in this field. The MC-SCF method has also been applied frequently, though the applicability is rather limited for higher excited states.

Cluster expansions of the wavefunction give another efficient way of calculating accurate correlated wavefunctions for the ground state and the various excited states of molecules (5, 6). We are currently using the Symmetry-Adapted Cluster (SAC) theory (7, 8) for calculations of the lowest closed-shell states, and the SAC-CI theory (8, 9) for calculations of the excited and ionized states generated therefrom. These theories have been successfully applied to the studies of molecular spectroscopy of valence and Rydberg excitations (10, 11) and ionizations of outer and inner valence electrons (11–13). The theory has also been applied to the study of the hyperfine splitting constants of doublet radicals in order to investigate the coupling of spin and electron correlations (14).

For the closed-shell ground state, Bartlett, Purvis, and coworkers (15–17) studied the applicability of the coupled-cluster theory (18) to the potential curves of N_2, Be + $H_2 \rightarrow BeH_2$, and the H_2O molecule with the elongated OH distance. They showed the superiority of the coupled-cluster theory in comparison with the CI theory including only single and double excitations from the Hartree–Fock configuration. Their conclusion applies also to the present SAC theory because of the similarity of the two methods. For molecules including multiple bonds, however, an ordinary single-reference coupled-cluster theory fails when the bond length is considerably elongated. There, the multi-reference version of the theory becomes necessary (19–21). Recently, we have developed multi-reference (MR) SAC theory (22). It is exact and unique without imposing completeness on the multi-reference space. It gives accurate descriptions of not only ordinary ground states but also quasi-degenerate states and excited states. This was confirmed from the calculations of the potential energy curves of the ground and excited states of the CO molecule (23).

In this paper, we consider applications of the SAC and SAC-CI theories to calculations of the potential energy curves of the Li_2 molecules in ground, excited, and ionized states. For the Li_2 molecule, the theory is capable of describing the proper dissociation of the ground and lower excited states.

The potential energy curves of the ground state and the lower excited states of Li_2 have been studied extensively by Olson and Konowalow (24) by the MC-SCF method. They studied all the states leading to the lower two separated atom limits, i.e., ^2S + ^2S and ^2S + ^2P, except for the $2^1\Sigma_g^+$ and $2^3\Sigma_u^+$ states. Kutzelnigg *et al.* (25) studied the potential curves of the ground and lowest $^3\Sigma_u^+$ states. Kahn *et al.* (26) studied the $B^1\Pi_u$ potential energy curve. Davies and Jones (27) and Takada *et al.* (28) calculated the lower potential curves by the quasi-degenerate many body perturbation method. Uzer and co-workers (29) analyzed the photodissociation of Li_2 based on the theoretical potential energy curve. Konowalow and Fish (30) recently studied the potential energy curve of the $3^1\Sigma_g^+$ state. We will calculate here the

[1] To whom all correspondence should be addressed.

potential energy curves and the spectroscopic constants of all the states which dissociate into the lower two separated atom limits, $^2S + ^2S$ and $^2P + ^2S$, except for the $2^3\Sigma_u^+$ state. This is the first paper which clarifies the bound nature and the existence of a hump in the $2^1\Sigma_g^+$ state.

For the cation of Li_2, Henderson *et al.* (31) reported the potential curves of low-lying states at the Hartree–Fock SCF level. Bottcher and Dalgarno (32) reported accurate model potential calculation. Müller and Jungen (33) reported extensive calculations of the potential energy curves. We will study the potential curve of the lowest $^2\Sigma_g^+$ state.

Method of selecting linked and unlinked operators

The method of calculations in the SAC and SAC-CI theories has already been described in detail (9, 11). The dimension of the matrices to be diagonalized is the same as the number of the linked operators. In the present application, the linked operator includes the identity operator and the single and double excitation operators from the closed-shell Hartree–Fock configurations. The triple and quadruple excitations are considered in the unlinked term. Even in this approximation, the number of linked operators easily becomes large even for moderate basis sets, so that we have adopted a systematic method of selection of linked operators (11). Further, since the calculation of the integrals for the unlinked terms is a time-consuming part, we have also adopted an appropriate method of selecting unlinked terms (11). However, in the calculations of the potential surface, an independent selection of operators for independent geometries may lead to a discontinuity of the potential curve and the properties. Therefore, we have adopted the following method of selections which we call the GSUM method.

An essential point of the GSUM method is to take the group sum of the operators (linked and unlinked) selected for all the representative points in the nuclear configuration space. We first select several representative points in the nuclear configuration space which cover the reaction under consideration. The Hartree–Fock MO's of each geometry are rearranged so as to have the same ordering as the MO's of the adjacent geometries. The linked and unlinked operators are selected for each geometry by the method described in ref. 11. We then take the group sum of these operators and the calculations are carried out at each geometry using the same set of this group sum of operators. This method is appropriate to study continuous changes in the potential energy curves and the properties along the change in nuclear configuration.

Calculational details

The molecular orbitals of Li_2 were calculated by the closed-shell Hartree–Fock–Roothaan method (34), using a slightly modified version of the HONDOG program (35). The HF MO's of the ground state were used as reference MO's for all the ground and excited states studied here. The basis set is $(9s5p)$ GTO's of Huzinaga (36) contracted to $(4s2p)$ set by Dunning (37) augmented with their derivative bases and one s-type GTO ($\zeta = 0.01$) as a Rydberg AO. This basis set consists of 74 CGTO's. The derivative bases, which are p and d GTO's for the s and p GTO's, respectively, are best suited for describing the polarization of the electron cloud in the course of the reaction as studied previously (38, 39). In the Appendix, we have shown some important effects of these derivative bases on the spectroscopic properties of the ground and lower excited states of Li_2.

TABLE 1. Dimensions of the linked operators in the SAC and SAC-CI calculations of Li_2

State	Space[a] symmetry	SE[b]	DE[b]	Total
Ground	s	77	234	312
Singlet excited	s	77	579	656
	a	76	562	638
Triplet excited	s	77	627	704
	a	76	707	783
Ionized	s	2	86	88
	a	1	77	78

[a] s and a denote symmetric and antisymmetric, respectively, with respect to the reflection plane perpendicular to the molecular axis.
[b] SE: single excitation, DE: double excitation.

The SAC and SAC-CI calculations were carried out with the program coded by Nakatsuji. As active MO's, we have taken the energetically lowest 54 MO's at the experimental internuclear distance and the corresponding MO's at any internuclear distances. The excitation operators were selected by the method described in ref. 11. The values of the thresholds λ_g and λ_e are 1×10^{-5} au. In the unlinked term, we have included all the double excitation operators whose coefficients are larger than 1×10^{-5} in the SDCI of the ground state. We selected five representative points at 4.0, 5.051, 6.5, 8.0, and 12.0 bohr in the internuclear distances. We have selected the excitation operators at the individual geometries and took the group sum of them by the GSUM method to cover all the reaction path. The dimension of the calculation after the GSUM method is shown in Table 1. They are relatively small by virtue of the cluster expansion theory. The ground state was calculated by the SAC theory and the excited and ionized states were calculated by the SAC-CI theory.

Results

The potential energy curves of the ground and lower excited states of Li_2 are displayed in Fig. 1. We have calculated all the singlet and triplet states of Li_2 which dissociate into the lowest two separated atom limits, $^2S + ^2S$ and $^2P + ^2S$, except for the $2^3\Sigma_u^+$ state. Figure 2 shows the potential energy curves for the lowest ionized states. Table 2 is a summary of the energies of these Li_2 system at various internuclear distances.

We show in Table 3 the spectroscopic constants of all the bound states of Li_2 studied here. The present theoretical values were calculated by the method of Dunham (40) from the potential curves displayed in Fig. 1. The experimental values were cited from Huber and Herzberg (41), Kusch and Hessel (42), and others (43, 44). In cases where the experimental values are not available, we have cited the theoretical values from Olson and Konowalow (24) for Li_2, and from Müller and Jungen (33) and Henderson *et al.* (31) for Li_2^+.

For the ground and lower excited states of Li_2, the general trends and the shapes of the potential energy curves shown in Fig. 1 are very similar to the results of the extensive MC-SCF calculations due to Olson and Konowalow (24). For the $2^1\Sigma_g^+$ state, the present result appears to be the first one reported. It shows an interesting potential curve which will be discussed in more detail later. The quality of the calculated potential curves is judged in detail by a comparison of the spectroscopic constants between theory and experiment (Table 3). For the $X^1\Sigma_g^+$, $A^1\Sigma_u^+$, and $B^1\Pi_u$ states, the adiabatic excitation energy T_e, equi-

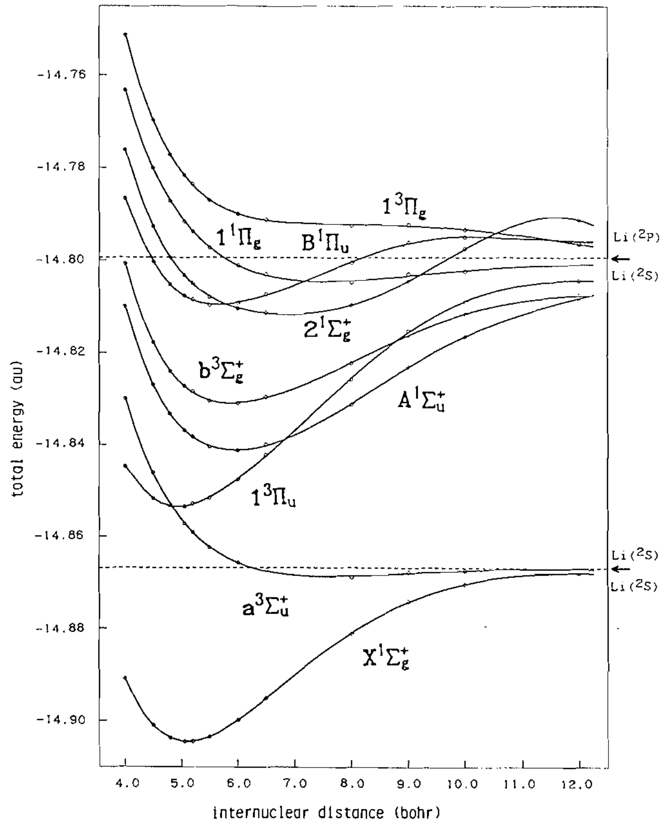

FIG. 1. Potential energy curves of the ground and lower excited states of Li_2.

librium length R_e, and the vibrational frequency ω_e show excellent agreement between theory and experiment. For other states where experimental values are not available, the present results show very good agreement with the results of Olson and Konowalow, except for the $a^3\Sigma_u^+$ state. This agreement is particularly excellent for the excitation energy, which is most reliable from the viewpoint of the data analysis.

The long range behavior of the potential energy curve of the state which dissociates into the ^2P and ^2S states of the Li atom is predicted from the resonance interaction theory for differently excited like atoms (45–47). Between the ^2P and ^2S states of Li atoms, the excitation energy is transferred in a resonant fashion and it gives rise to a first-order interaction which is written as

$$[1] \quad \Delta E = C_a/R^3 + \ldots$$

where the coefficient C_a depends on the specific state under consideration. From the sign of the coefficient C_a determined by Mulliken (47), we can predict the nature of the long-range interaction as follows.

$$[2] \quad \begin{array}{l} \text{Attractive: } {}^1\Sigma_u^+,\ {}^3\Sigma_g^+,\ {}^1\Pi_g,\ {}^3\Pi_u \\ \text{Repulsive: } {}^1\Sigma_g^+,\ {}^3\Sigma_u^+,\ {}^1\Pi_u,\ {}^3\Pi_g \end{array}$$

Here we assumed for the Σ states that the resonance interaction predominates the valence-type interaction.

Referring to Fig. 1, we see that all the states calculated here follow the prediction given in eq. [2]. The states $1^3\Pi_u$, $A^1\Sigma_u^+$, $b^3\Sigma_g^+$, and $1^1\Pi_g$ approach the dissociation limit from below, but the states $2^1\Sigma_g^+$, $B^1\Pi_u$, and $1^3\Pi_g$ approach it from above. Further, since the $2^1\Sigma_g^+$ and $B^1\Pi_u$ states have a minimum in the

TABLE 2. Calculated energy of the Li_2 system with the SAC and SAC-CI methods (au)

Internuclear distance	Singlet state				Triplet state				Cation
	$X^1\Sigma_g^+$	$A^1\Sigma_u^+$	$2^1\Sigma_g^+$	$B^1\Pi_u$	$1^1\Pi_g$	$a^3\Sigma_u^+$	$1^3\Pi_u$	$b^3\Sigma_g^+$	$1^3\Pi_g$	$^2\Sigma_g^+$
4.0	−14.89079	−14.81001	−14.77611	−14.78661	−14.76321	−14.82991	−14.84470	−14.80081	−14.75118	−14.68500
4.5	−14.90092	−14.82689	−14.79272	−14.80036	−14.78002	−14.84613	−14.85173	−14.81780	−14.76971	−14.70275
4.8	−14.90368	−14.83330	−14.79939	−14.80528	−14.78715	−14.85297	−14.85337	−14.82399	−14.77720	−14.70944
5.05106	−14.90442	−14.83688	−14.80337	−14.80778	−14.79167	−14.85721	−14.85346	−14.82733	−14.78173	−14.71317
5.2	−14.90435	−14.83823	−14.80503	−14.80855	−14.79371	−14.85903	−14.85289	−14.82850	−14.78364	−14.71457
5.5	−14.90330	−14.84037	−14.80792	−14.80968	−14.79734	−14.86239	−14.85159	−14.83041	−14.78700	−14.71679
6.0	−14.89976	−14.84119	−14.81042	−14.80924	−14.80108	−14.86568	−14.84748	−14.83094	−14.78999	−14.71764
6.5	−14.89504	−14.83998	−14.81137	−14.80739	−14.80311	−14.86738	−14.84223	−14.82967	−14.79124	−14.71637
8.0	−14.88103	−14.83115	−14.80960	−14.80049	−14.80471	−14.86879	−14.82576	−14.82228	−14.79233	−14.70725
9.0	−14.87412	−14.82311	−14.80454	−14.79617	−14.80301	−14.86776	−14.81537	−14.81615	−14.79234	−14.69906
10.0	−14.87031	−14.81651	−14.79750	−14.79499	−14.80235	−14.86737	−14.80894	−14.81162	−14.79343	−14.69222
12.0	−14.86785	−14.80817	−14.79121	−14.79606	—	—	−14.80438	−14.80759	−14.79647	−14.68169
∞	−14.86678	−14.79946	−14.79946	−14.79946	−14.79946	−14.86678	−14.79946	−14.79946	−14.79946	−14.67050

TABLE 3. Spectroscopic constants for the ground, excited, and ionized states of Li_2

State	Source	T_e (eV)	R_e (Bohr)	D_e (cm^{-1})	ω_e (cm^{-1})	$\omega_e x_e$ (cm^{-1})	B_e (cm^{-1})	α_e (10^{-3} cm^{-1})	$\tilde{D}_e$ (10^{-6} cm^{-1})[j]
$X^1\Sigma_g^+$	Present calc.	0.0	5.097	8258[h]	343	2.533	0.6605	6.010	9.811
	Exptl.[b]	0.0	5.051	8436[d]	351	2.610	0.6726	7.04	9.87
$A^1\Sigma_u^+$	Present calc.	1.72	5.938	9161[h]	250	1.113	0.4868	4.449	7.355
	Exptl.[b]	1.74	5.873	8940[d]	255	1.58	0.4975	5.40	7.54
$B^1\Pi_u$	Present calc.	2.58	5.630	2241[h] (3302)[i]	259	4.468	0.5415	11.15	9.470
	Exptl.[b]	2.53	5.546	3102[e]	270	2.673	0.5577	8.5	9.45
$2^1\Sigma_g^+$	Present calc.	2.52	6.940	2682[h] (~4708)[i]	164	4.482	0.3564	−9.9785	6.733
$1^1\Pi_g$	Present calc.	2.71	7.504	1184[g]	139	2.366	0.3047	2.945	5.856
	Previous calc.[a,c]	(2.71)	(7.863)	(1297)	(83)	(1.3)			
$a^3\Sigma_u^+$	Present calc.	0.973	7.565	409[h]	96	3.211	0.2998	11.84	11.62
	Previous calc.[a,c]	(0.99)	(8.001)	(292)	(61)	(3.2)			
$1^3\Pi_u^+$	Present calc.	1.39	4.948	11861[h]	342	2.773	0.7009	4.258	11.78
	Previous calc.[a,c]	(1.44)	(4.974)	(11483)	(339)	(2.5)			
$b^3\Sigma_g^+$	Present calc.	2.00	5.862	6913[h]	244	2.591	0.4994	8.951	8.381
	Previous calc.[a,c]	(2.03)	(5.851)	(6811)	(245)	(2.2)			
$^2\Sigma_g^+$ (Li_2^+)	Present calc.	5.08	5.918	10341[h]	255	1.733	0.4900	6.333	7.247
	Previous calc.[a]	5.00	(5.98)[f]	(10160)[f]	(255)[g]	(1.5)[e]			

[a] Values in the parentheses are the previous calculated results.
[b] Reference 41.
[c] Reference 24.
[d] Reference 42.
[e] Reference 43.
[f] Reference 33.
[g] Reference 31.
[h] Relative to the dissociation limit.
[i] Relative to the top of the hump.
[j] $\tilde{D}_e$ denotes the centrifugal distortion constant, which is entirely different from the binding energy (D_e).

TABLE 4. The hump of the $B^1\Pi_u$ and $2^1\Sigma_g^+$ states of Li_2

Property	$B^1\Pi_u$ state: Theoretical: Present	Theoretical: Olson–Konowalow[a]	Exptl.	$2^1\Sigma_g^+$ state, this work
Height (cm^{-1})	1056	656	523[b], 928[c]	~2030
Position (bohr)	9.73	10.43	—	~11.6

[a] Reference 24.
[b] Reference 43.
[c] Reference 44.

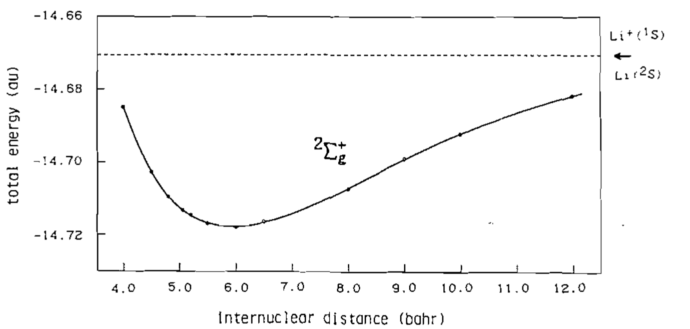

FIG. 2. Potential energy curves of the lowest ionized states.

shorter bond length region, the potential curves of these states should have a hump somewhere between the valence-type and resonance-type regions. For the $B^1\Pi_u$ state, the hump is at 10.1 bohr and for the $2^1\Sigma_g^+$ state it is at about 11.7 bohr. In Table 4 we have summarized the constants of these humps. Further from this consideration we expect that the shape of the hump is not symmetric with respect to the top position because the nature of the interaction is drastically different between shorter and longer regions. For the $1^3\Pi_g$ state our calculation didn't show any minimum. It is repulsive throughout.

We now discuss each state separately. The ground state, $X^1\Sigma_g^+$ was calculated by the SAC theory. It gives excellent results for the spectroscopic constants and shows a reasonable asymptotic behavior. In the calculation of the excited and ionized states, the electron correlation in this ground state was used as a starting point in the SAC-CI formalism (8, 9).

The $a^3\Sigma_u^+$ state is only very weakly bound, as pointed out by Kutzelnigg *et al.* (25). The calculated equilibrium length is longer than those of Olson and Konowalow. Our potential is more attractive than theirs. However, since the number of sampling points is not enough in the region near the potential minimum, we are not definitive on this conclusion.

The $1^3\Pi_u$ state was interesting due to its relation to the possibility of an alkali-dimer laser. Figure 1 shows that the $1^3\Pi_u$ state potential curve is crossed by the $a^3\Sigma_u^+$ potential curve at its repulsive limb. Therefore the present calculation supports the conclusion of Olson and Konowalow that the Li_2 laser is impossible (24).

The $B^1\Pi_u$ state is an interesting state which has a hump. It is attractive at shorter range because of the valence-type force but repulsive at long range because of the resonance force as shown by eq. [2]. This is the origin of the hump, which is therefore strongly unsymmetric with respect to the position of the hump maximum. From Table 4, the position of the hump maximum is at about 10.1 au. The hump height was calculated to be 981 cm^{-1}, which is closer to the experimental value of Velasco *et al.* (44). For the valence minimum, both the adiabatic excitation energy T_e and the equilibrium length R_e agree well with experiment (Table 3). The dissociation energy D_e is 2263 cm^{-1}, if it is relative to the dissociation limit. The value in parentheses, 3244 cm^{-1}, is measured relative to the hump maximum. The latter one is closer to the experimental value (43).

The $2^1\Sigma_g^+$ state is reported for the first time in this paper. It is a very interesting state which has a deeper valence-type minimum and higher hump than the $B^1\Pi_u$ state. The origin of the hump is the same as for the $B^1\Pi_u$ state. The maximum position and the height of the hump were analyzed to be 11.7 bohr and 1900 cm^{-1}, respectively, as shown in Table 4. However, since the number of calculated points near the hump is small, these values should be considered to be only semi-quantitative. Near the valence minimum the potential is rather deep but flat. The dissociation energy is 2794 cm^{-1}, if it is measured relative to the dissociation limit, but is about 5300 cm^{-1} relative to the maximum of the hump.

The $^3\Pi_g$ state is calculated to be repulsive throughout the internuclear distance but has a shoulder between 7.0 and 9.0 bohr as seen from Fig. 1. This feature also corresponds well to the result of Olson and Konowalow. Further, they suggested that an addition of the $\pi-\delta$ configurations to their calculations would lower the potential curve of this state at smaller internuclear distances to produce a local minimum. However, despite the inclusion of the $\pi-\delta$ configurations in our calculation, the present potential curve does not have any local minimum throughout the calculated range.

Lastly, we discuss the $^2\Sigma_g^+$ state of the Li_2 cation. The calculated potential curve is shown in Fig. 2 and the spectroscopic constants are given at the bottom of Table 3. Because of a loss of an electron from the bonding σ_g orbital, the equilibrium bond length is elongated by about 0.8 au. The potential also becomes flatter near the equilibrium length. However, since the ionization energy of the Li atom, (5.39 eV (48)) is larger than that of the $X^1\Sigma_g^+$ state of Li_2, (5.00 eV (41)), the dissociation energy of Li_2^+ is larger than that of Li_2.

Conclusion

The SAC and SAC-CI theories based on the cluster expansion of the wavefunction have been applied to studies of the potential energy curves of the ground, excited, and ionized states of the Li_2 molecule. The calculated potential energy curves and spectroscopic properties agree well with available experimental data and with the previous theoretical results of Olson and Konowalow (24). For the $2^1\Sigma_g^+$ state, the present result is the first calculation. It is an interesting state which has a deep valence minimum at 6.8 bohr and 2.5 eV above the ground state. It also has a hump of about 1900 cm^{-1} high at about 11.7 bohr. The long-range behavior of the potential curves of the states which dissociate into the $^2P + {}^2S$ states of the Li atom are well predicted from the first-order resonance interaction theory (45–47).

For the bond involved in the ground state of the Li_2 molecule, the SAC theory is shown to give an excellent potential curve up to the dissociation limit. The SAC-CI theory is essentially a multi-reference type theory (9) so that it gives a reasonable description of the excited and ionized states. Based on this research, the usefulness of the SAC and SAC-CI theory in the study of molecular excited states and molecular spectroscopy is extended.

TABLE 5. Comparison of the spectroscopic constants of the ground and lower excited states of Li_2 calculated with and without including the derivative bases

State	Source	T_e (eV)	R_e (au)	D_e (cm^{-1})	ω_e (cm^{-1})
$X^1\Sigma_g^+$	Basis I	0.0	5.165	7682	324
	Basis II	0.0	5.097	8258[d]	343
	Exptl.	0.0	5.051[b]	8436[c]	351[b]
$A^1\Sigma_u^+$	Basis I	1.62	5.980	9364	258
	Basis II	1.72	5.938	9161[d]	250
	Exptl.	1.74	5.873[b]	8940[c]	255[b]
$B^1\Pi_u$	Basis I	2.66	5.877	932[d] (1089)[e]	241
	Basis II	2.58	5.630	2246[d] (3302)[e]	259
	Exptl.	2.53	5.546[b]	3102[f]	270[b]

[a] Basis II includes the derivative basis but Basis I does not.
[b] Reference 41.
[c] Reference 42.
[d] Relative to the dissociation limit.
[e] Relative to the top of the hump.
[f] Reference 43.

Acknowledgements

We acknowledge Messrs. O. Kitao, M. Okumura, and M. Nishimura for their active collaboration. The calculations were carried out with HITAC M-200H computer at the Institute for Molecular Science and with FACOM M-382 computer at the Data Processing Center of Kyoto University. Part of this study was supported by the Japan Society for the Promotion of Science.

1. C. SANDORFY. *In* Chemical spectroscopy and photochemistry in the vacuum-ultraviolet. *Edited by* C. Sandorfy, P. J. Ausloos, and M. B. Robin. D. Reidel Pub. Co., Canada. 1973. pp. 149, 177.
2. C. SANDORFY. *In* Topics in current chemistry. Vol. 86. Springer, Heidelberg. 1979.
3. C. SANDORFY. Int. J. Quantum. Chem. **19**, 1147 (1981).
4. R. J. BUENKER and S. D. PEYERIMHOFF. *In* New horizons of quantum chemistry. *Edited by* P.-O. Löwdin and B. Pullman. D. Reidel Pub. Co. 1983. p. 183.
5. R. J. BARTLETT. Ann. Rev. Phys. Chem. **32**, 359 (1981), and references therein.
6. J. PALDUS. *In* New horizons of quantum chemistry. *Edited by* P.-O. Löwdin and B. Pullman. D. Reidel Pub. Co. 1983. p. 31 and references therein.
7. H. NAKATSUJI and K. HIRAO. J. Chem. Phys. **68**, 2053 (1978).
8. H. NAKATSUJI. Chem. Phys. Lett. **59**, 362 (1978).
9. H. NAKATSUJI. Chem. Phys. Lett. **67**, 329 (1979); **67**, 334 (1979).
10. H. NAKATSUJI, K. OHTA, and K. HIRAO. J. Chem. Phys. **75**, 2952 (1981); H. NAKATSUJI. J. Chem. Phys. **80**, 3703 (1984).
11. H. NAKATSUJI. Chem. Phys. **75**, 425 (1983).
12. H. NAKATSUJI and T. YONEZAWA. Chem. Phys. Lett. **87**, 426 (1982); H. NAKATSUJI. Chem. Phys. **76**, 283 (1983).
13. H. NAKATSUJI. Intern. J. Quantum Chem. Symposium, **17**, 241 (1983).
14. H. NAKATSUJI, K. OHTA, and T. YONEZAWA. J. Phys. Chem. **87**, 3068 (1983).
15. R. J. BARTLETT and G. D. PURVIS III. Phys. Script. **21**, 255 (1980).
16. (*a*) G. D. PURVIS III, R. SHEPARD, F. B. BROWN, and R. J. BARTLETT. Intern. J. Quantum Chem. **23**, 835 (1983); (*b*) Y. S. LEE and R. J. BARTLETT. Intern. J. Quantum Chem. Symposium, **17**, 347 (1983).
17. R. J. BARTLETT, H. SEKINO, and G. D. PURVIS III. Chem. Phys. Lett. **98**, 66 (1983).
18. G. D. PURVIS III and R. J. BARTLETT. J. Chem. Phys. **76**, 1910 (1982).
19. D. MUKHERJEE, R. K. MOITRA, and A. MUKHOPADHYAY. Mol. Phys. **30**, 1861 (1975); **33**, 955 (1977).
20. B. JEZIORSKI and H. MONKHORST. Phys. Rev. A**24**, 1668 (1981).
21. W. D. LAIDIG and R. J. BARTLETT. Chem. Phys. Lett. **104**, 424 (1984).
22. H. NAKATSUJI. J. Chem. Phys. In press.
23. H. NAKATSUJI. To be published.
24. M. L. OLSON and D. D. KONOWALOW. Chem. Phys. Lett. **39**, 281 (1976); Chem. Phys. Lett. **21**, 393 (1977); Chem. Phys. Lett. **22**, 29 (1977); D. D. KONOWALOW and M. L. OLSON. J. Chem. Phys. **71**, 450 (1979).
25. W. KUTZELNIGG and M. GELUS. Chem. Phys. Lett. **7**, 296 (1970); W. KUTZELNIGG, V. STAEMMLER, and M. GELUS. Chem. Phys. Lett. **13**, 496 (1972).
26. L. R. KAHN, T. H. DUNNING, JR., N. W. WINTER, and W. A. GODDARD III. J. Chem. Phys. **66**, 1135 (1977).
27. D. W. DAVIES and G. J. R. JONES. Chem. Phys. Lett. **81**, 279 (1981).
28. T. TAKADA, M. G. SHEPPARD, and K. F. FREED. J. Chem. Phys. **79**, 325 (1983).
29. (*a*) T. UZER and A. DALGARNO. Chem. Phys. Lett. **65**, 1 (1979); (*b*) D. L. COOPER, J. M. HUTSON, and T. UZER. Chem. Phys. Lett. **86**, 472 (1982).
30. D. D. KONOWALOW and J. L. FISH. J. Chem. Phys. **76**, 4571 (1982).
31. G. A. HENDERSON, W. T. ZEMKE, and A. C. WAHL. J. Chem. Phys. **58**, 2654 (1973).
32. C. BOTTCHER and A. DALGARNO. Chem. Phys. Lett. **36**, 137 (1975).
33. W. MÜLLER and M. JUNGEN. Chem. Phys. Lett. **40**, 199 (1976).
34. C. C. J. ROOTHAAN. Rev. Mod. Phys. **23**, 69 (1951).
35. H. F. KING, M. DUPUIS, and J. RYS. Program Library HONDOG (No. 343) of the Computer Center of the Institute for Molecular Science. 1979.
36. S. HUZINAGA. J. Chem. Phys. **42**, 1293 (1963).
37. T. H. DUNNING, JR. J. Chem. Phys. **55**, 716 (1971).
38. H. NAKATSUJI, K. KANDA, and T. YONEZAWA. Chem. Phys. Lett. **75**, 340 (1980).
39. H. NAKATSUJI, K. KANDA, M. HADA, and T. YONEZAWA. J. Chem. Phys. **77**, 1961 (1982); **77**, 3109 (1982); **79**, 2493 (1983).
40. J. L. DUNHAM. Phys. Rev. **41**, 713 (1932); **41**, 721 (1932).
41. K. P. HUBER and G. HERZBERG. Molecular spectra and molecular structure. IV. Constants of diatomic molecules. Van Nostrand, Princeton. 1979.
42. P. KUSCH and M. M. HESSEL. J. Chem. Phys. **67**, 586 (1977).
43. M. M. HESSEL and C. R. VIDAL. Cited in M. L. Olson and D. D.

Konowalow, Chem. Phys. **22**, 29 (1977).
44. R. VELASCO, C. OTTINGER, and R. N. ZARE. J. Chem. Phys. **51**, 5522 (1969).
45. R. EISENSCHITZ and F. LONDON. Z. Phys. **60**, 491 (1930).
46. G. W. KING and J. H. VAN VLECK. Phys. Rev. **55**, 1165 (1939).
47. R. S. MULLIKEN. Phys. Rev. **120**, 1674 (1960).
48. C. E. MOORE. Atomic energy levels. Vol. 1. National Bureau of Standard, Washington. 1971.
49. T. H. DUNNING, JR. and P. J. HAY. *In* Modern theoretical chemistry. Vol. 3. *Edited by* H. F. Schaefer III. Plenum, New York. 1977. p. 1.

Appendix

In Table 5 we have shown some spectroscopic properties of the ground and lower excited states of Li_2 calculated with and without including the derivative bases. Basis I is $(3s2p)$ set (49) and Basis II is the basis set used in the text which includes the derivative bases. From Table 5, it is seen that the results calculated with Basis II are consistently superior to those calculated with Basis I. This implies that the role of the derivative functions is important for the calculations of the potential curve.

The effects of selected gases upon ethanol: hydrogen bond breaking by O_2 and N_2

T. L. MATHERS, G. SCHOEFFLER, AND S. P. MCGLYNN
Chemistry Department, The Louisiana State University, Baton Rouge, LA 70803, USA

Received September 14, 1984

This paper is dedicated to Professor Camille Sandorfy on the occasion of his 65th birthday

T. L. MATHERS, G. SCHOEFFLER, and S. P. MCGLYNN. Can. J. Chem. **63**, 1864 (1985).

The temperature dependency of the phosphorescence properties of aromatic hydrocarbons in alcoholic glasses exhibits a number of phenomena that have not been described previously. Chief among these are the effects of added gases (O_2, N_2, C_2H_6, Ar), some of which produce major changes in the luminescence characteristics. These are discussed, and rationalized in terms of a model which presumes that O_2 and N_2 can disrupt the normal hydrogen bonding process between alcohol molecules.

T. L. MATHERS, G. SCHOEFFLER et S. P. MCGLYNN. Can. J. Chem. **63**, 1864 (1985).

L'effet de la température sur les propriétés de phosphorescence des hydrocarbures aromatiques dans des verres d'alcools présente un certain nombre de phénomènes inconnus jusqu'à maintenant. On peut souligner notamment l'effet des gaz ajoutés (O_2, N_2, C_2H_6, Ar) dont certains provoquent des changements importants au niveau des caractéristiques de la luminescence. On discute de ces changements et on les rationalise en fonction d'un modèle qui présume que le O_2 et le N_2 peuvent rompre les liaisons hydrogènes normales entre les molécules d'alcool.

[Traduit par le journal]

Introduction

The use of a luminescent probe to study a host system (i.e., crystal, glass, DNA, etc.) is well known (1). We have used this technique to study the effects of added gases on low-temperature ethanol matrices. Ethanol exhibits a well-known glass transition temperature and a well-defined crystalline form, and its properties are sensitively dependent (2−4) upon a strong hydrogen-bonding tendency that leads to dimers, trimers, and even polymeric chains at low temperatures. The present study indicates (5, 6) that certain nonpolar gases possess a heretofore unnoted quality, namely the ability to interfere with the hydrogen bonds in low-temperature ethanol matrices and, therefore, with the onsets of the glassy and crystalline phases.

In this work, the host was ethanol and the luminescent probe was phenanthrene. The two gases found to be especially effective in disrupting normal behavior of the ethanol matrix were oxygen and nitrogen. These gases, as well as all others, were individually added to a degassed ethanolic solution of phenanthrene which was then cooled to 77 K. In all cases, the onset of luminescence loss in both the glassy and crystalline regions of O_2-doped and N_2-doped ethanol initiated at significantly lower temperatures than normal. Conversely, the onset of the same luminescence losses in degassed ethanol occurred at higher temperatures than normal, normalcy in all instances being defined as the behavior of an ethanol system which had been equilibrated, prior to freezing, with ambient air at ~1 atm. Such large shifts were not observed upon the addition or removal of any other nonpolar gases.

The signal used to define normalcy or abnormalcy was the phosphorescence of the phenanthrene guest. The intent of the work was to address three questions: (*i*) why degassing produces such an unusual effect upon these systems; (*ii*) whether the well-known quenching ability of molecular oxygen can explain (*i*); and (*iii*) what is the nature of N_2-quenching? Other workers have studied similar systems (7, 8) and have assumed that the answer to question (*ii*) was "yes"; however, our work leads to different conclusions, the salient finding being that nitrogen affects both phases, glass and crystal, almost as much as does oxygen. Thus, the imputation that the quenching effect of O_2 is the pertinent (or dominant) characteristic is called into question.

The present work reveals certain difficulties in some prior interpretations (e.g. that of ref. 8 where certain suppositions may require alteration). The work of Lesikar (2−4), however, remains inviolate and relevant: Lesikar's study of binary alcoholic mixtures clearly delineates the effects of the hydrogen bonding of ethanol on its glass-formation temperature.

The relevance of this work to that of the Sandorfy school is tangential, yet pertinent. The Montreal investigations (9−12) have uncovered a relationship between the hydrogen bond breaking (HBB) ability of fluorocarbons and their anaesthetic potency. This connectedness, if it continues to be significant, will undoubtedly beget new advances in anaesthesiology. The relevance of the present work lies in the finding that oxygen and nitrogen also disrupt hydrogen bonds in ethanol and that this HBB ability manifests itself in readily demonstrable luminescence phenomena. Thus, in a most direct sense, we have shown, in conformity with Sandorfy, that rather subtle hydrogen bonding effects can produce major consequences. While it is not inappropriate to point out the anaesthetic-like properties (13, 14) of N_2 and the known toxicity of O_2, both at high pressures, it certainly is premature to associate these latter properties with the HBB abilities of N_2 and O_2. Such an extension of the Sandorfy correlation is not warranted by our findings. Nonetheless, it is proper to stress the *in vivo* ubiquity of hydrogen bonding of oxygen and of nitrogen and to suggest that their interplay will be of some biological importance (15).

Experimental

All sample tubes were equipped with vacuum stopcocks and could sustain pressures of approximately 2 atm. All samples were degassed by a minimum of 10 freeze−evacuate−thaw cycles, the maximum pressure in the evacuation stage being 1 mTorr.

The refrigeration apparatus consisted of a large-volume dewar, for better temperature stability, through which flowed chilled nitrogen vapors obtained by passing tank nitrogen through a copper coil immersed in liquid N_2. Since the rate of cooling is an important parameter in determining glass quality, average cooling rates of approximately 20 K/min were maintained down to the glass temperature of ethanol (~100 K), whereupon the rate was slowed to less than 5 K/min. These rates were sufficiently slow to produce uniform glasses and to minimize many of the effects noted by the French workers (8).

Temperature measurements were made by taping a copper−constantan thermocouple onto the outside of the sample tube. The flow of nitrogen refrigerant was adjusted until a stable temperature was

TABLE 1. The temperatures observed for sudden phosphorescence increase (T_i) and loss (T_l) in the glassy domain; the temperature observed for phosphorescence onset (T_o), phosphorescence maximum (T_m), and phosphorescence disappearance (T_d) in the crystalline domain

(*a*) Ethanol

	T_i (K)	T_l (K)	T_o (K)	T_m (K)	T_d (K)
Degassed	106–109	108–117	133	144	154
1000 Torr Ar	101–103	104–111	135	140	152
500 Torr Ethane	93–95	96–109	135	144	156
Nondegassed	86–90	90–100	124	129	145
O_2-saturated	—	83–93	113	130	139
500 Torr O_2	90–92	94–105	129	140	150
500 mTorr O_2	97–99	102–115	133	139	153
N_2-saturated	—	90–95	127	135	147
1000 Torr N_2	92	93–98	128	134	143

(*b*) 2,3-Dimethylpentane

	T_i (K)	T_l (K)
Nondegassed	89–91	91–100
Degassed	89–91	102–122
1026 Torr N_2	89–91	102–120

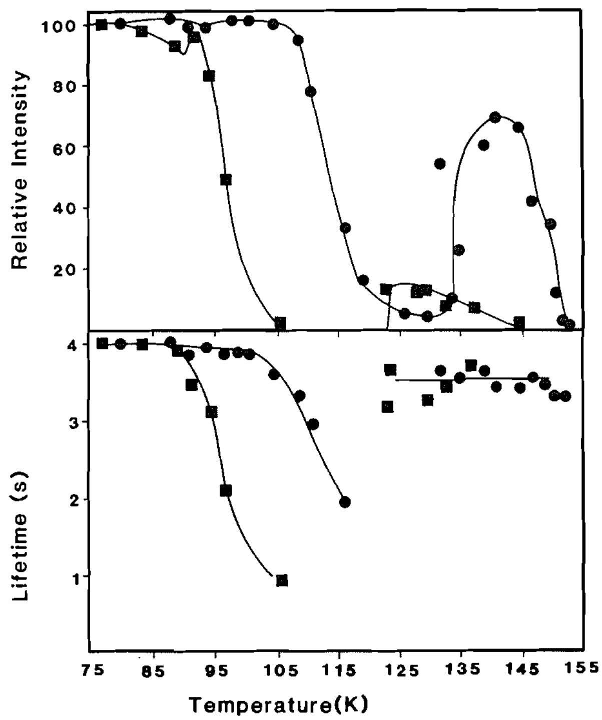

FIG. 1. Relative intensities and absolute lifetimes for the phosphorescence of phenanthrene in ethanol as a function of temperature: nondegassed sample (squares) and degassed sample (circles).

achieved and, after a wait of 5 min to permit thermal equilibration, observations proceeded. The average rate of warming during the course of a given set of measurements was approximately 1 K/min. The accuracy of the temperature measurement was ±2 K.

Most of the phosphorescence work was performed on an Amino-Keirs Spectrophosphorimeter with excitation at 285 nm and emission at 500 nm. Phosphorescent lifetimes were obtained by shuttering the excitation source and monitoring the emission decay on an electrometer–recorder system of 0.75 s inherent decay time. Polarization studies and fluorescence measurements were performed on an SLM Spectrofluorimeter (Model 4800).

Results and discussion

Glassy systems are notoriously difficult to control and their literature is beset with problems that originate in defects whose types and numbers are either irreproducible or reproducible only with utmost difficulty. Thus, one must exercise care in attempting to separate the real from the artifact, and one must be resigned to an almost endless repetition of experiment. By the same token, one must always remain wary of the urge to interpret. We believe we have satisfied both of these imperatives. We also believe that many of our results are novel and that they can be interpreted in a self-consistent way. However, we also admit that certain of our observations do not yield to any conclusive interpretation and that a great deal more work will be required in order to unravel their complexity. For that reason, and in order to stress the empirical nature of the work, a rather unorthodox mode of presentation is adopted in this paper. Six sets of data, each pointing up a new class of observation, have been chosen and each data set is discussed under the figure number that synopsizes that data set. Finally, parameters pertinent to all six data sets are collected in Table 1.

The temperature range of most figures, 75–160 K, covers two distinct ethanolic domains: (*i*) the glass domain which exhibits a normal transition range (3, 16) of 90–100 K and (*ii*) the crystal domain which consists of crystalline ethanol, possibly containing entrapped islets of phenanthrene, extending from 125 to 155 K with a maximum at some intermediate temperature.

Figure 1. The phosphorescence intensities and lifetimes of nondegassed and degassed samples are compared in Fig. 1. The onset of the low-temperature luminescence-loss for the non-degassed sample occurs in the region 90–100 K and corresponds well to the accepted values (3, 16) for the glass transition of ethanol. The primary observation is that the low-temperature onset in the degassed ethanol solution shifts upwards by +15 to +20 K. However, it is not clear at this point (i.e., from Fig. 1) whether this shift arises solely from diminution of oxygen quenching or from other unknown effects of air on the nature of the ethanol glass.

The crystalline ethanol region (i.e., the high-temperature luminescence domain) also shifts to higher temperatures upon degassing. Since the diffusion of quenchers such as O_2 is inhibited in the crystalline ethanol matrix, it is not possible to explain this luminescence behavior by invoking an oxygen diffusion and quenching mechanism. The lifetime data of Fig. 1 reinforce this surmise. In the low-temperature glassy domain, the phosphorescence lifetime curves are excellent mimics of the intensity curves whereas, in the high-temperature crystalline domain, this mimicry is absent. Indeed, apart from some scatter that might be associable with the coupling of phonon modes, the lifetimes in this latter domain remain essentially constant and independent of both temperature and the degassed/nondegassed character of the ethanol.

The interpretation is relatively straightforward:

(*i*) In the nondegassed sample, the quenching that occurs in the 95–115 K region is attributable, in part at least, to both oxygen and triplet–triplet annihilation. In the same region of the degassed sample, the quenching is attributable, in large part, to triplet–triplet annihilation, a supposition bolstered by the increase of delayed fluorescence observed (8) as

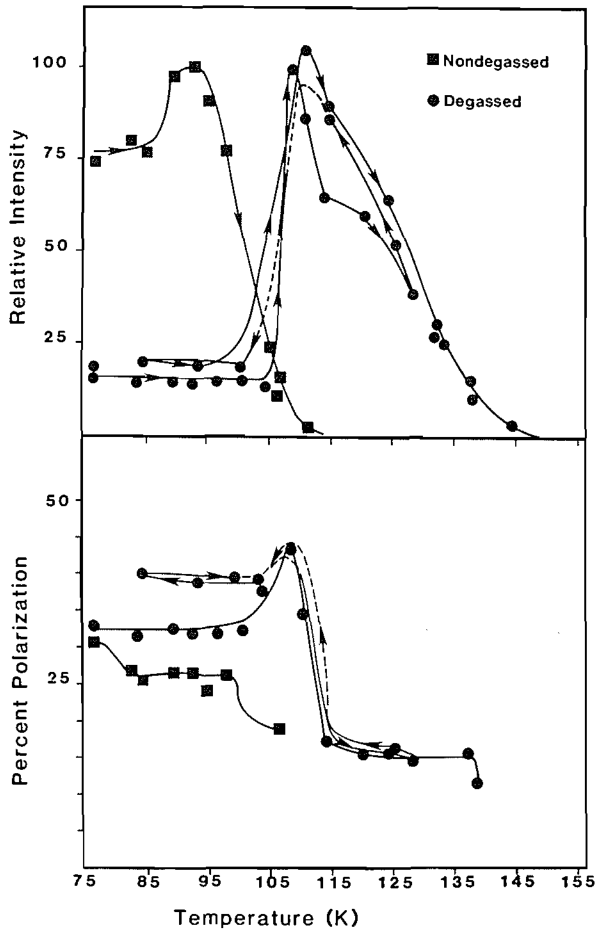

FIG. 2. Phosphorescence intensities and polarization for phenanthrene in ethanol: nondegassed samples (squares) and degassed sample (circles). The degassed sample was recooled and then rewarmed to check the reproducibility of results. The direction of the arrow indicates heating or cooling.

phosphorescence diminishes.

(*ii*) The intensity maximum observed in the region 125–155 K is associated with the formation of ethanol microcrystallites containing entrapped phenanthrene islets and their disappearance at higher temperatures. Indeed, the point of complete phosphorescence loss in the degassed sample (154 K) is quite consonant with the accepted melting point (17) of crystalline ethanol, namely 155 K. Thus, as the microcrystals grow, the intensity increases and, as they disappear, the intensity wanes. The lifetime, on the other hand, being characteristic of the crystal and independent of crystallite size or number remains unchanged throughout this region.

(*iii*) The absence of any effect of degassing on the lifetime in the crystalline region implies immobilization of O_2 in, or exclusion of O_2 from this environment. Thus, the shift of the intensity curves in the crystalline region is taken to imply an inhibition of crystal growth in the nondegassed sample, a supposition that will be discussed in some detail later.

Figure 2. A new set of phenomena is shown in Fig. 2. These phenomena occur at random in various sample preparations. In the present instance, they have been purposely maximized and made non-random by directing the excitation beam through the vicinity of the meniscus, where stresses and void concentrations are highest.

The low-temperature domain now splits into two subregions such that the constancy of intensity and polarization in the hard-glass, lower-temperature subregion is followed by a sudden increase of both the intensity and polarization in the soft-glass, higher temperature subregion. The onset of this sudden increase is clearly connected to the glass transition temperature and is, we believe, caused by the "annealing-out" of scattering centers such as cracks and inhomogeneities and the "filling-in" of voids both internal to the glassy matrix and at the interface between the matrix and the sample tube surface.

The absence of a crystalline region in Fig. 2 is noteworthy. The presence of a crystalline region is not always observed and its occurrence is in some way determined by the presence of appropriate seeding centers, whether in bulk or at the sample tube surface. In the present instance, both the ethanol and phenanthrene were highly-purified, fresh materials and it is probable that the absence of the crystalline region is associated with the purity and freshness of these materials.

Despite all of these oddities (i.e., the splitting of the glassy domain into two subregions and the absence of a crystalline phase), the +15 to +20 K differential of the quenching temperatures of the degassed and non-degassed samples is maintained, demonstrating the validity of this particular observation for samples that exhibit very different behavior.

Hysteresis of the degassed samples was also studied, one example being shown in Fig. 2, and was found to be surprisingly small. The reproducibility is taken to be indicative of a high degree of fidelity in reforming the meniscus region of the glass. The increase of polarization is taken to be supportive of an annealing mechanism that becomes operative prior to melting or hardening of the glass.

The point of Fig. 2 is to emphasize a behavior that, because of its lack of hysteresis, might be thought to be real but which, in reality, is almost certainly artifact. By the word "artifact" we mean, in this case, that the observed effect is a function of both sample preparation and the part of the glass that is sampled by the excitation beam.

Figure 3. The behavior of samples to which argon and ethane were added is shown in Fig. 3. In the low-temperature domain, the luminescence loss-mechanism for the degassed sample appears to lie ~4 K to higher temperatures. However, since this increment lies within the experimental error range, it is difficult to confirm it experimentally. Consequently, we assert that, within the limits of error, all three samples exhibit similar glass behavior.

The high temperature ranges for all three samples are also essentially identical. It seems that the crystal region, when observed, is fairly reproducible, the onset and the disappearance temperatures being especially so.

The salient point is that all three samples, apart from certain, presumedly-artifactual details, behave identically, at least within experimental error, in both the glassy and crystalline domains. We conclude that argon and ethane have little or no effect on the luminophore or the glass/crystallite characteristics.

We conclude from this behavior that, contrary to the effects of N_2 and O_2, both Ar and C_2H_6 produce only minor disruptive effects on the intermolecular H-bonding between the ethanol solvent molecules.

Figure 4. The results for several oxygenated samples are presented in Fig. 4. The O_2 "saturated" sample exhibits an extremely abrupt quenching in low-temperature domain, one whose onset lies well below the accepted glass transition temperature. In this same domain, the 500 Torr oxygen sample,

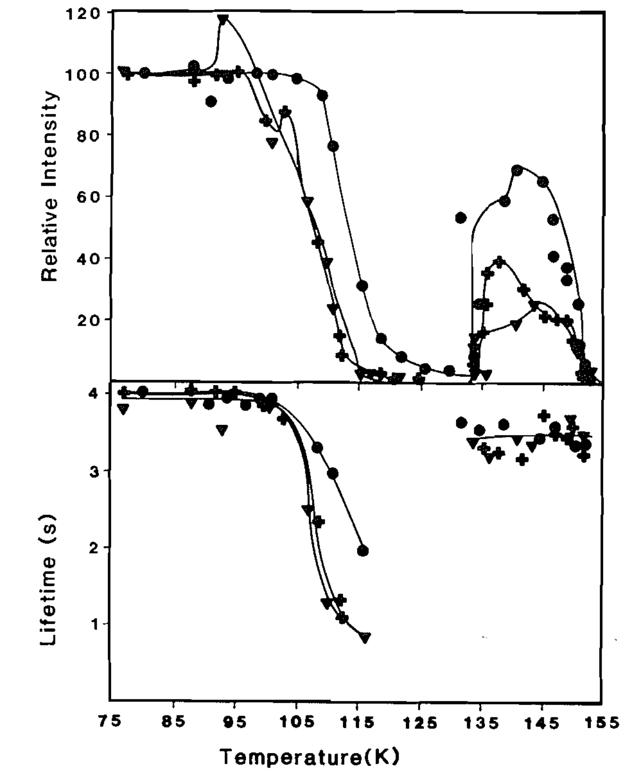

FIG. 3. Phosphorescence intensities and lifetimes for phenanthrene in ethanol: degassed samples (circles), degassed sample + 1000 Torr Ar (crosses) and degassed sample + 500 Torr ethane (triangles).

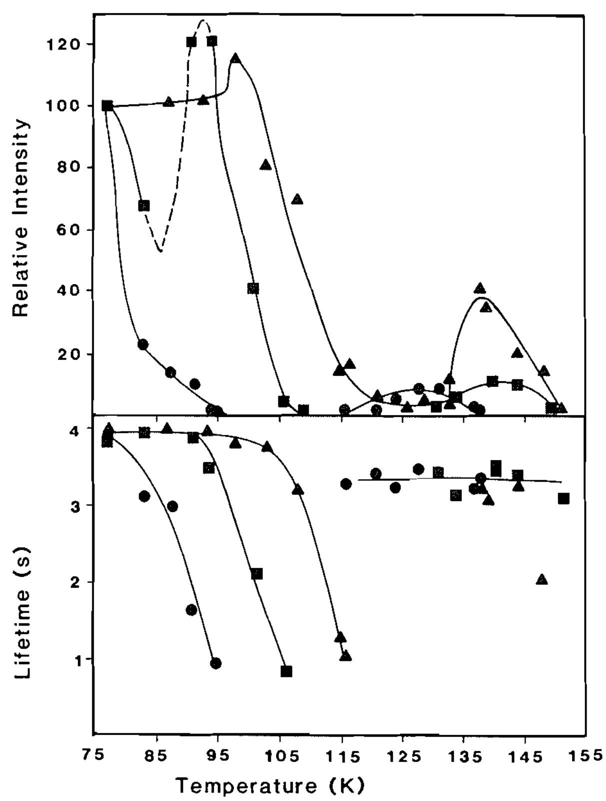

FIG. 4. Phosphorescence intensities and lifetimes for phenanthrene in ethanol: degassed sample + 500 mTorr O_2 (triangles), degassed sample + 500 Torr O_2 (squares), and O_2 "saturated" sample (circles). The O_2 "saturated" sample refers to a nondegassed solution which had been bubbled with pure O_2 until equilibrated at room temperature.

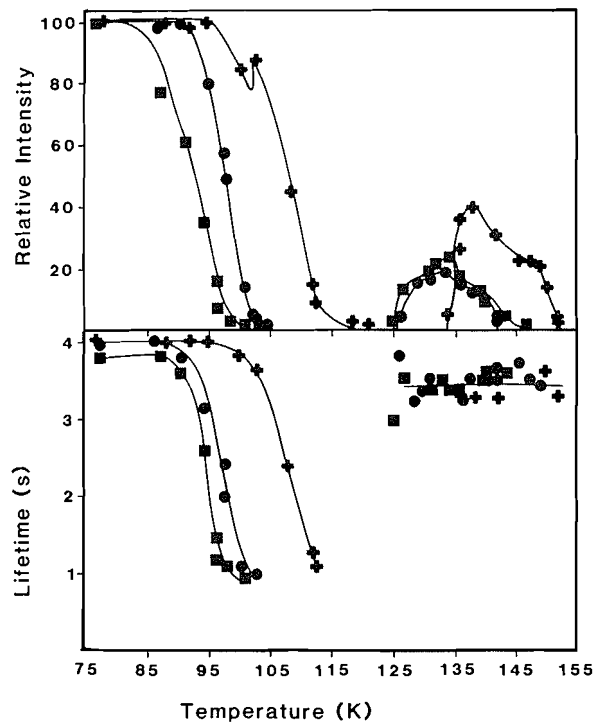

FIG. 5. Phosphorescence intensities and lifetimes of phenanthrene in ethanol: degassed sample + 1000 Torr Ar (crosses), degassed sample + 1000 Torr N_2 (circles), and N_2 "saturated" sample (squares).

apart from the presence of a strong Fig. 2-like characteristic, exhibits behavior intermediate between that of non-degassed and degassed samples. Finally, the 500 mTorr oxygen sample exhibits thermal characteristics which, within experimental error, are identical to those of the degassed sample. In the crystal domain, the O_2 "saturated" sample exhibits a 15 K decrement of onset, maximum, and disappearance relative to the degassed sample. Again, the 500 Torr sample exhibits intermediate behavior between the saturated and 500 mTorr specimens.

The interpretation of these data discords with current ideas (8). Firstly, in the O_2-saturated sample, quenching does occur at temperatures below the normally-accepted rigid glass point, suggesting that O_2 is mobile in ethanol glass even at temperatures below 80 K. Secondly, this sample also exhibits a shift of the crystal region to lower temperatures, suggesting both a decrease of the barrier to crystallite formation and a thermal destabilization of the crystalline region. It seems to us that the only reasonable interpretation of these data is that O_2 interferes with intermolecular H-bonding between the ethanol molecules.

Figure 5. Figure 5 shows two samples with nitrogen added and, for comparison, an Ar-added sample. In the low-temperature domain, both nitrogen samples exhibit large shifts relative to the argon sample. In the high-temperature domain, a remarkable similarity of the two nitrogen samples is evident and a consistent shift of -10 K relative to the Ar-added sample is observed. Thus, regardless of certain small peculiarities, there is no doubt that the addition of nitrogen produces significant differences relative to either Ar-added or degassed samples.

This figure demonstrates the distinctiveness of the N_2-effect relative to the null behavior of argon.

Figure 6. Finally, we investigated a glass-forming solvent,

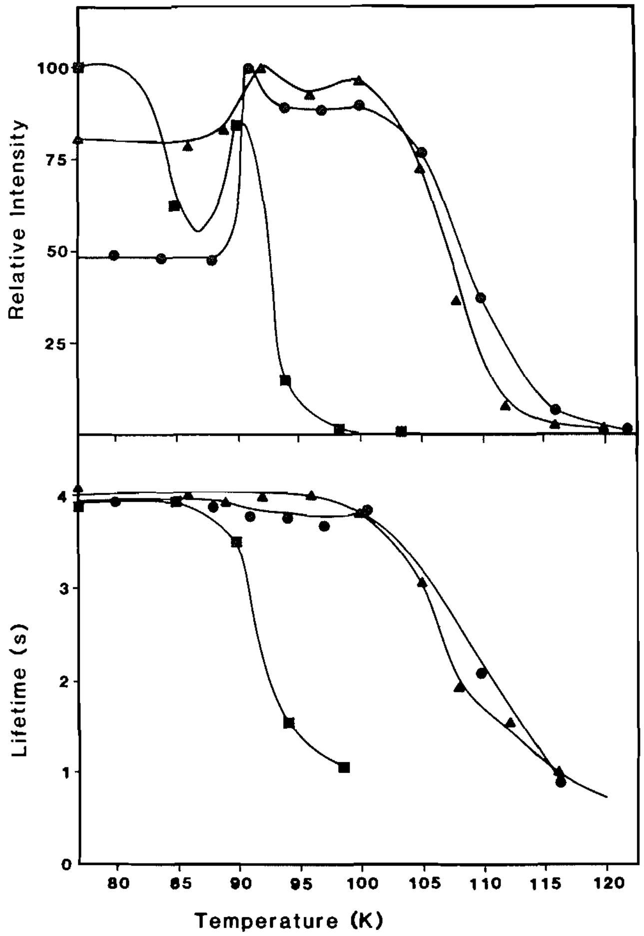

FIG. 6. Phosphorescence intensities and lifetimes for phenanthrene in 2,3-dimethylpentane: nondegassed sample (squares), degassed sample (circles), and degassed sample + 1026 Torr nitrogen (triangles).

2,3-dimethylpentane, that does not contain hydrogen bonds. Unfortunately, this solvent does not exhibit a crystal region. Regardless, we compare nondegassed, degassed, and degassed plus 1026 Torr N_2 samples in Fig. 6. The most interesting point is that the nitrogen-added and degassed samples are identical within experimental error. Furthermore, the point at which the sudden increase of intensity is observed (i.e., ~90 K) is the same within experimental error for all three samples.

We interpret these data in the following manner:

(*i*) Since the solvent does not hydrogen bond, the dissolved air and nitrogen gases are not expected to affect the glass transition point other than indirectly through dilution effects. Such effects, because of the low concentrations of the dissolved gases, are expected to be small.

(*ii*) The shift of the nondegassed sample relative to the nitrogen-added and the degassed samples is attributable to the dominance of oxygen quenching in the former sample and the imposed preference for T−T quenching in the latter samples.

(*iii*) The point of intensity increase (~90 K) in the glassy region is common to all three samples, suggesting an association between this point and the true glass transition temperature (reportedly (16) 80−85 K). As with the interpretation under the discussion of Fig. 2, we believe that this increase is associated with extensive miniscus formation and severe volume contraction exhibited by this solvent at its glass transition point. These effects, as well as the extensive strains, cracks and inhomogeneities that they impose are thought to be responsible for this behavior in the glass region.

Conclusion

The original question that motivated this work has been answered. The shift of the phosphorescence intensity or phosphorescence lifetime curves to higher temperatures caused by degassing is attributable to the removal of O_2 quenchers *and* to an elevation of both glass transition and crystal region temperatures. The importance of the latter mechanism is predicated upon the results obtained in the N_2-added systems as well as upon all data obtained for the crystalline regions. These results, in turn, are caused, we believe, by an interference of O_2 and N_2 with the dominant intermolecular interaction of ethanol, namely hydrogen bonding — oxygen being slightly more effective than nitrogen in this regard.

The characteristics observed here may prove useful for the general study of glasses. In particular, while we have demonstrated the incorrectness of the Martinez (8) assumption that these phenomena are predicated solely on oxygen quenching, there remains little doubt that the work of these authors (8) is an invaluable addition to the study of heating and cooling rates on glasses. Indeed, their results, in conjunction with ours, point to the probability of multiple "glass" points. That is, while one degree of freedom may dominate the transition of liquid to glass, the possibility that other degrees of freedom, ones frozen into non-equilibrium configurations by rapid cooling, may become extremely important may not be disregarded.

The only other glass-forming solvent investigated here (18), namely, isopropyl alcohol, exhibited little or no difference between degassed, nondegassed, and oxygen-saturated samples. This result may be understood in light of Lesikar's finding that hydrogen bonding is much more important in normal alcohols than in branched alcohols, at least insofar as the determination of glass transition temperatures is concerned.

The subsplitting of the glassy domain, attributed here to voids and other imperfections, requires elaboration. In particular, alternative techniques (e.g., DTA; molecular beam studies of complexes between H-bonding and HBB molecules; theoretical calculations of alcohol clusters (19) with a single added molecule of an HBB entity, etc.) could provide considerable elaboration of the theses presented in this work.

1. S. P. McGlynn, T. Azumi, and M. Kinoshita. Molecular spectroscopy of the triplet state. Prentice Hall Inc., Englewood Cliffs, NJ. 1969.
2. A. V. Lesikar. J. Chem. Phys. **63**, 2297 (1975).
3. A. V. Lesikar. Phys. Chem. Glass. **16**, 83 (1975).
4. A. V. Lesikar. J. Chem. Phys. **66**, 4263 (1977).
5. T. L. Mathers. Ph.D. Dissertation, The Louisiana State University, Baton Rouge, LA. 1982.
6. T. L. Mathers, G. Schoeffler, and S. P. McGlynn. J. Phys. Chem. **87**, 4355 (1983).
7. A. Schmillen and A. Tschampa. Z. Naturforsch. **19**a, 190 (1964).
8. A. Martinez, A. Garcia, G. Scarsi, and A. Rousset. J. Chim. Phys. **72**, 366 (1975).
9. T. diPaolo and C. Sandorfy. Nature, **252**, 471 (1974); J. Med. Chem. **17**, 809 (1974); Can. J. Chem. **52**, 3612 (1974).
10. A. Nagyrevi and C. Sandorfy. Can. J. Chem. **55**, 1593 (1977).
11. R. Massada and C. Sandorfy. Can. J. Chem. **55**, 3211 (1977).
12. G. Trudeau, K. C. Cole, R. Massada, and C. Sandorfy. Can. J. Chem. **56**, 1681 (1978).
13. R. D. Jennings and B. Breck. Aviat. Space Envir. Med. **46**, 922 (1975).

14. B. FOWLER and K. N. ACKLES. Aero. Med. **43**, 1219 (1972).
15. S. E. V. PHILLIPS and B. P. SCHOENBORN. Nature, **292**, 81 (1981).
16. W. KAUZMANN. Chem. Rev. **43**, 219 (1948).
17. CRC Handbook. 53rd ed. CRC Press, OH. 1973.
18. K. G. STOLZLE. Ph.D. Dissertation. The Louisiana State University, Baton Rouge, LA. 1968.
19. L. A. CURTISS and C. L. EISGRUBER. J. Chem. Phys. **80**, 2022 (1984).

Broadband ν_3 sub-Doppler spectrum of HCN: application of a color center laser optothermal molecular beam spectrometer

E. K. KYRÖ, P. SHOJA-CHAGHERVAND, M. ELIADES, D. DANZEISER, S. G. LIEB, AND J. W. BEVAN
Chemistry Department, Texas A&M University, College Station, Texas 77843, USA

Received March 7, 1985

This paper is dedicated to Professor Camille Sandorfy on the occasion of his 65th birthday

E. K. KYRÖ, P. SHOJA-CHAGHERVAND, M. ELIADES, D. DANZEISER, S. G. LIEB, and J. W. BEVAN. Can. J. Chem. **63**, 1870 (1985).

A broadband ν_3 sub-Doppler spectrum of HCN has been recorded in the range 3340–3280 cm^{-1} using a single frequency continuously scanable computer-controlled color center laser optothermal molecular beam spectrometer. Absolute frequencies for rovibrational transitions R(9) through P(9) have been determined to an accuracy $\leq$ 20 MHz or 2 parts in 10^7. An unconstrained five-parameter fit to this datum results in molecular constants: $B'' = 1.47822146(182)$, $D'' = 2.881(23) \times 10^{-6}$, $B' = 1.46779974(154)$, $D' = 2.863(18) \times 10^{-6}$, and $\nu_0 = 3311.47758(2)$ cm^{-1}, respectively.

E. K. KYRÖ, P. SHOJA-CHAGHERVAND, M. ELIADES, D. DANZEISER, S. G. LIEB et J. W. BEVAN. Can. J. Chem. **63**, 1870 (1985).

Faisant appel à un spectromètre à faisceau moléculaire optothermique utilisant un laser dont le centre lumineux est contrôlé par ordinateur et dont les fréquences individuelles sont balayées d'une façon continue, on a enregistré le spectre sous-Doppler ν_3 à bande large de la molécule de HCN. On a déterminé les fréquences absolues des transitions rovibrationnelles de R(9) à P(9) avec une précision $\leq$ 20 MHz, soit 2 parties dans 10^7. Utilisant un ajustement sans contraintes à cinq paramètres de ces données, on a pu obtenir les constantes moléculaires suivantes: $B'' = 1{,}47822146(182)$, $D'' = 2{,}881(23) \times 10^{-6}$, $B' = 1{,}46779974(154)$, $D' = 2{,}863(18) \times 10^{-6}$ et $\nu_0 = 3311{,}47758(2)$ cm^{-1}.

[Traduit par le journal]

Introduction

The rovibrational ν_3 spectrum of HCN is an important secondary frequency standard (1) in the 3 μm region and for this reason has been the subject of numerous rovibrational analyses using both classical and laser spectroscopic methods (2–4). Although high resolution spectra do exist for isolated transitions in this band (5, 6), most previous studies have, however, been carried out in the gas phase under situations in which Doppler and pressure broadening often result in transition overlap and consequently inaccuracies in frequency determination. Although very accurate ground and excited state microwave rotational spectra (7) are available for J $0 \rightarrow 1$; $1 \rightarrow 2$, $2 \rightarrow 3$, $00^0 0$ and J $0 \rightarrow 1$, $1 \rightarrow 2$, $2 \rightarrow 3$ and $3 \rightarrow 4$, $00^0 1$, states absolute rovibrational transition frequencies accurate to $\leq$ 30 MHz have not been determined for frequency calibration purposes.

The advent of broadly tunable single frequency color center laser optothermal molecular beam spectrometers (8) offer the opportunity of recording the broadband rovibrational spectrum of ν_3 HCN at sub-Doppler resolution in the cold collisionless situation of seeded molecular beams. In this paper, we report the broadband sub-Doppler spectrum of ν_3 HCN for rovibrational transitions R(9) through P(9). The absolute order and free spectral range of a highly stabilized Fabry-Perot etalon have been determined and used to calibrate the absolute frequencies of these transitions with an estimated accuracy of $\leq$ 20 MHz. Rotational constants B'', B'; distortional constants D'', D' and band origin frequency, ν_0, have also been determined from this data and are compared with the precisely determined parameters evaluated from other spectroscopic studies.

Experimental

Spectra have been recorded using a simple computer-controlled continuously tunable single frequency color center laser optothermal molecular beam spectrometer assembled in our laboratory (8). A schematic of the components necessary to control and monitor continuous single frequency scanning of the laser spectrometer are shown in Fig. 1. The system consists of a Kr^+ laser pumped Burleigh FCL-20 color center laser, diagnostic box, bolometric molecular beam detector (9), and a Micromation Z-64 microcomputer used to synchronously scan[1] the three tuning elements, (grating, 21.6 GHz internal etalon and folding mirror) of the color center laser necessary to provide broadband single frequency scanning of the spectrometer. For these experiments, 0.9 W of 6471 Å Kr^+ laser output was used to pump a RbCl:Li color center crystal producing 0.17–0.85 mW of continuously tunable single frequency laser output power from 3338–3284 cm^{-1} which could be tuned over segments of $\geq$ 30 cm^{-1} at a time. Although higher output power could have been obtained for continuous single frequency scans of shorter segments (approximately 2–3 cm^{-1}), it ultimately led to mode instability and was not used. 3 GHz and 150 MHz FSR etalons were used to calibrate the transition frequency separations. The spectrometer utilized a 50 μm cw stainless steel nozzle with a 250 μm skimmer at approximately 0.8 cm distance and a 1.7 K, 4 mm Ge:Ga bolometer (NEP 4.7×10^{-14} $W\sqrt{Hz^{-1}}$) at 60 cm. For the ν_3 HCN transitions, scans of 30 cm^{-1} took approximately 10 to 12 h which corresponded to the hold time in the helium Dewar of the bolometer. The sub-Doppler ν_3 spectrum was thus recorded in two segments with sufficient common transitions in each segment to ensure accurate frequency determination. Seeded mixtures of HCN/He varying from 1:15 to 0.5:100 were used with nozzle backing pressures of 0.4–7.7 atm. HCN was obtained from Fumico Inc., Amarillo, TX, and used without further purification. The laser output beam crossed the molecular beam orthogonally and was focussed by a CaF_2 F100 lens to produce FWHM linewidths of $\leq$ 5.8 MHz in ν_3 transitions of HCN (Fig. 2). The geometry of the spectrometer is expected to contribute $\leq$ 1.2 MHz of this linewidth. The remainder reflects transit time broadening but is primarily contributed by instabilities in the free running color center laser system. The incident infrared laser beam was modulated at 40 Hz, the bolometer signal amplified $\times$ 200 and then detected using a HR-8 lock-in amplifier. A Doppler-limited ν_3 HCN gas phase spectrum was simultaneously recorded to facilitate assignment and calibration of the spectrum.

Our current laser system has no Michaelson interferometer to enable accurate absolute frequency determination of any of the transitions to $\leq$ 30 MHz and no reference spectra exist within the continuous tuning

[1] J. W. Bevan *et al.* Unpublished results.

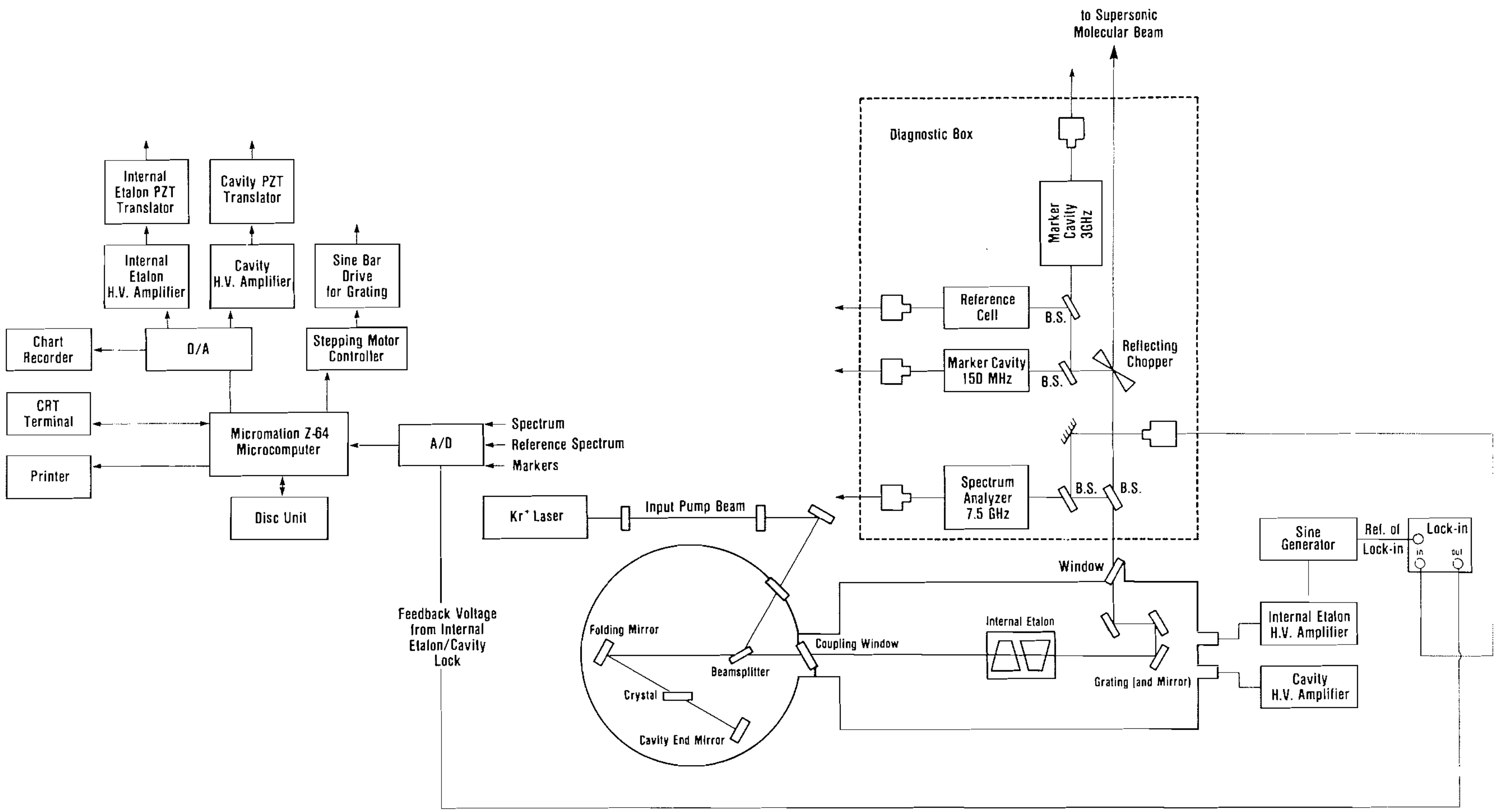

FIG. 1. Schematic diagram of computer-controlled color center laser optothermal molecular beam spectrometer.

TABLE 1. Absolute frequencies of HCN ν_3

Transition	Obs.* freq/cm^{-1}	Obs. − calcd/ cm^{-1} × 10^{-5}	Transition obs. freq/cm^{-1}	Obs.* freq/cm^{-1}	Obs. − calcd/ cm^{-1} × 10^{-5}
R(9)	3339.88429	−0.55	P(9)	3284.12773	+1.41
R(8)	3337.13936	+1.22	P(8)	3287.24835	−2.02
R(7)	3334.37293	−1.88	P(7)	3290.34874	−0.25
R(6)	3331.58516	+0.30	P(6)	3293.42878	−0.49
R(5)	3328.77609	+2.97	P(5)	3296.48838	−0.08
R(4)	3325.94572	+0.30	P(4)	3299.52748	−0.57
R(3)	3323.09415	−1.37	P(3)	3302.54604	−0.63
R(2)	3320.22152	−2.06	P(2)	3305.54395	+0.69
R(1)	3317.32783	−1.50	P(1)	3308.52115	+0.13
R(0)	3314.41318	+1.98			

*Estimated absolute accuracy 6.7 × 10^{-4} cm^{-1}.

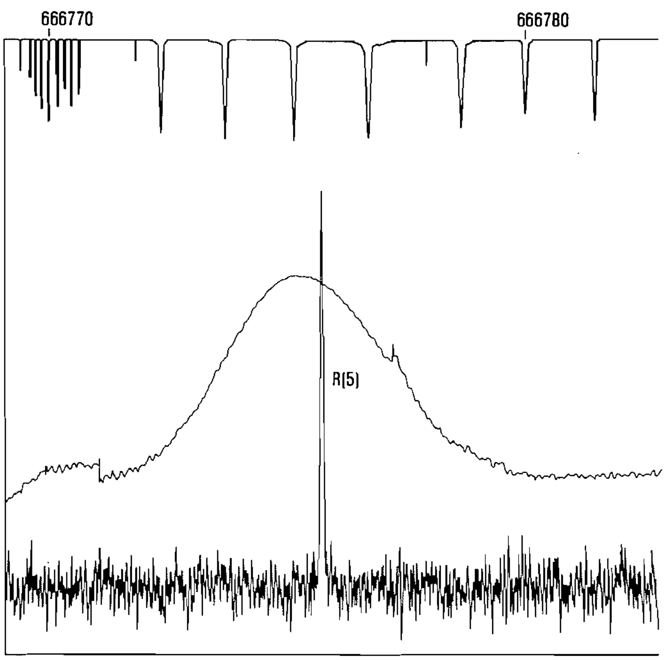

FIG. 2. A sub-Doppler spectrum of the R(5) ν_3 HCN transition. The 5.8 MHz sub-Doppler FWHM can be compared with a profile corresponding to the Doppler-limited transition. The etalon markers are separated by 149.666456(30) MHz; the glitch after every four etalon markers indicates the cavity reset. The etalon markers on the left of the spectrum have been compressed but are included to illustrate single mode scan over a larger range. The two spectra are not coincidental due to displaced recorder pen positions.

range of the spectrometer with that accuracy. The problem was overcome by calibrating the absolute order number of the 150 MHz confocal etalon and determining its free spectral range precisely using differences between rotational transition frequencies. The temperature of the etalon was stabilized to ±0.01°C using a Burleigh TC-10 temperature controller and the system evacuated with a small diffusion pump. The residual absolute pressure in the etalon was carefully monitored with a 220 BHS MKS Baratron gauge and the free spectral range (FSR) determined using the expression:

$$F = \frac{\Delta\nu n_a n_b}{(\Delta m + \Delta n_b m_a - \Delta n_a m_b)}$$

where

$$\frac{\nu_a}{F_a} = m_a = \frac{\nu_1 - \delta_1 F_1}{F_a}, \frac{\nu_b}{F_b} = m_b = \frac{\nu_2 + \delta_2 F_2}{F_b} \text{ and } F = \frac{c}{4n_{\text{vac}}d}$$

for a confocal etalon. $\Delta\nu$ is the frequency separation between specific rovibrational transitions determined from highly accurate microwave rotational transition frequencies; $n_a - n_b$, $\Delta n_a = (n_a - n_{\text{vac}})$, $\Delta n_b = (n_b - n_{\text{vac}})$ refer to refractive indices of dry air at etalon order numbers m_a and m_b occurring at frequencies ν_a, ν_b, respectively. The absolute order number of the etalon was readily determined from available rovibrational spectroscopic data (4) using the above expressions. Δm is the corresponding separation $\nu_1 - \nu_2$ of the transition pair and $\delta_1 = m_1 - m_a$, $\delta_2 = m_b - m_2$ in FSR's. A weighted average of transition separations was used to improve the estimated accuracy of the FSR permitting frequency determination to ≤ 20 MHz. Corrections were applied to take into account non-linearities in laser scanning and the effects of ^{14}N quadrupole coupling in HCN (6).

Results

The molecular beam sub-Doppler spectra of 19 P(J) and R(J) ν_3 HCN rovibrational transitions have been recorded in the frequency range 3340–3284 cm^{-1}. The observed linewidths are ≤ 5.8 MHz and we are able to determine absolute transition frequencies to within 20 MHz. A partial scan of the R(5) transition between absolute order numbers 666770 and 666780 in Fig. 1 corresponds to a FSR = 149.666456(30) MHz. The absolute transition frequencies for all measured transitions are given in Table 1. Also included in Table 2 are the results of a least-squares fit to the expression

$$\nu_m = \nu_0 + (B' + B'')m + (B' - B'' - D' + D'')m^2 - 2(D' + D'')m^3 - (D' - D'')m^4$$

where $m = -J$ for P branch lines and $J + 1$ for R branch lines. The data were not considered sufficiently accurate for inclusion of H′, H″ constants in the fit. The results of the unconstrained five parameter fit are given in Table 2 and can be compared with molecular constants evaluated in previous spectroscopic studies (4, 7). The standard deviation in the frequency fit is 1.56 × 10^{-5} cm^{-1} or 0.47 MHz for the 19 transitions considered and reflects the influence of a number of instrumental factors. The reset of the color center laser cavity and instabilities associated with the scanning of the free running laser are considered primary contributors. Molecular constants determined from this restricted data set compare favorably with the most accurate currently available (4, 7) (Table 2).

Conclusions

In this investigation we were extremely fortunate that very precise rotational spectra were available in both 00^00 and 00^01 states of HCN. This permitted us not only to determine the absolute order number of the confocal etalon but also enabled

TABLE 2. Molecular constants from least-squares-fit

Constants*/cm^{-1}	Value		
	This work	Reference 4	Reference 7
B''	1.47822146(182)	1.478221825(40)	1.47822183(13)
D''	$2.881(23) \times 10^{-6}$	$2.90851(530) \times 10^{-6}$	$2.9100(20) \times 10^{-6}$
B'	1.46779974(154)	1.4677979(3)	1.4677989(5)
D'	$2.863(18) \times 10^{-6}$	$2.8835(3) \times 10^{-6}$	$2.907(20) \times 10^{-6}$
ν_0	3311.47758(2)	3311.4775(15)	—

*Estimated errors 2 standard deviations to our fit.

us to calibrate its FSR and consequently rovibrational transition frequencies to ≤ 2 parts in 10^7 without utilizing a Michaelson interferometer or a frequency standard of corresponding accuracy. This method of determining absolute rovibrational transition frequencies will become increasingly feasible in other molecules as more rotational transitions are investigated in vibrationally excited states by microwave infrared double resonance techniques. This approach does, however, place stringent instrumental requirements on broadband laser tunability and can only produce absolute transition frequencies of intermediate accuracy for spectral calibration. It appears, however, that this is the first time that the ν_3 HCN rovibrational transition frequencies have been determined with an absolute accuracy of ≤ 20 MHz. These ν_3 HCN rovibrational transitions are very convenient secondary frequency standards for high resolution laser spectroscopy in the 3.0 μm region. We have recently used them to absolutely calibrate Doppler-limited and sub-Doppler transition frequencies in ν_1 $CH_3C{\equiv}CH$, ν_1 H—C≡CH, ν_2 HCN---HF, and ν_2 HCN---HCl.[1]

Acknowledgements

This research was supported by NSF grant number CHE-8300592. CEMR, TAMU and The Shell Development Company are thanked for support contributing to the development of the laser spectrometer. P. S-C. and S.G.L. thank the Robert A. Welch Foundation (Grant #A-747) for Post-Doctoral Research Fellowships. We express our sincerest thanks to Professors T. E. Gough and G. Scoles, University of Waterloo and E. S. Fry (TAMU), for their advice and encouragement in construction of the optothermal molecular beam spectrometer.

1. K. N. RAO, C. J. HUMPHREYS, and D. H. RANK. Wavelength standards in the infrared. Academic Press, London. 1966.
2. (*a*) D. H. RANK, G. SKORINKO, D. P. EASTMAN, and T. A. WIGGINS. J. Opt. Soc. Am. **50**, 421 (1960); (*b*) D. H. RANK, A. M. GUENTHER, G. D. SAKSENA, J. N. SHEARER, and T. A. WIGGINS. J. Opt. Soc. Am. **47**, 686 (1957).
3. K. R. GERMAN and W. S. GORNALL. J. Opt. Soc. Am. **71**, 1452 (1981).
4. A. G. MAKI. J. Mol. Spectrosc. **58**, 308 (1975).
5. T. E. GOUGH, R. E. MILLER, and G. SCOLES. Discuss. Faraday Soc. **71**, 77 (1981).
6. W. L. EBENSTEIN and J. S. MUENTER. J. Chem. Phys. **80**, 3989 (1984).
7. F. C. DE LUCIA and P. A. HELMINGER. J. Chem. Phys. **67**, 4262 (1977).
8. E. K. KYRÖ, P. SHOJA-CHAGHERVAND, M. ELIADES, D. DANZEISER, J. W. BEVAN. To be published.
9. T. E. GOUGH, R. E. MILLER, and G. SCOLES. Appl. Phys. Lett. **30**, 338 (1977).

The γ-alkylation of cyclic β-ketoesters via their enamine derivatives

Denis Gravel[1] and Marc Labelle[2]

Département de Chimie, Université de Montréal, C.P. 6210, Montréal (Qué.), Canada H3C 3V1

Received August 16, 1984

This paper is dedicated to Professor Camille Sandorfy on the occasion of his 65th birthday

Denis Gravel and Marc Labelle. Can. J. Chem. **63**, 1874 (1985).

The γ-alkylation – functionalization of cyclic β-ketoesters via their enamine derivatives is discussed with particular emphasis on their preparation from β-ketoesters and their reaction with various electrophiles such as electrophilic olefins, halogenoïds, and allylic and benzylic halides. Although the amine ring size does not appear to affect reactivity to a great extent, the reaction is very sensitive to β-ketoester ring size, with six-membered rings giving the best results. In the latter case the alkylation–functionalization is general and specific to the γ-position and therefore provides an important complement to the dianion and related methodologies.

Denis Gravel et Marc Labelle. Can. J. Chem. **63**, 1874 (1985).

L'alkylation–fonctionnalisation en γ des β-cétoesters cycliques à partir de leurs dérivés énamines est discutée en regard de leur préparation à partir de β-cétoesters et leur réaction avec divers électrophiles tels que: les oléfines électrophiliques, les halogénoïdes et les halogénures allyliques et benzyliques. Quoique la grandeur de cycle de l'amine ne semble pas influencer la réactivité de façon importante, celle-ci est très sensible à la grandeur de cycle du β-cétoester où le cycle à six chaînons donne les meilleurs résultats. Dans ce dernier cas, la réaction d'alkylation–fonctionnalisation est générale et spécifique à la position-γ et donc constitue de toute évidence un complément important à la méthode des dianions et les autres méthodologies reliées.

Introduction

During the course of a synthetic investigation, we were confronted with the problem of gaining access to compounds of the 1-carbalkoxy-3-methyl-9-oxobicyclo[3.3.1]non-2-ene (**1**) type. One of the original plans envisaged called for the specific alkylation at the γ-position of a β-ketoester such as **2**, using methacrolein or an equivalent as the electrophile. From a

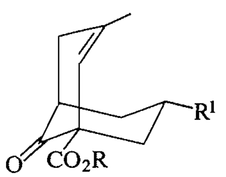

1

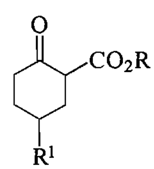

2

formal point of view, the problem reduces to finding ways of making the γ-position more reactive than the α-position. Examination of the literature revealed that this has been achieved in various ways and a number of methods of varying degrees of generality have become available.

The first such method which showed some generality is that of the dianions (1). This procedure has allowed chemospecific γ-alkylation with a number of different electrophiles such as: alkyl halides (2), α-chloroethers (3), esters (4), aldehydes and ketones (5), nitroolefins (6), and α,ω-dihaloalkanes (7). Further illustration of the efficiency of the method is provided in various multistep syntheses (8, 9) and an elegant solution (10) to the problem of regio-controlled access to the bicyclic alkene **1** with R = Me and R^1 = H, using a sulfur based equivalent of methacrolein (11) as alkylating agent. The same sequence was later applied in our own laboratory to test a selenium based equivalent of methacrolein which we developed (12) for this purpose.

An alternative method to that of the dianions was developed later and involves the reaction of the corresponding neutral bis-trimethylsilylenolethers (13, 14) or enamino trimethylsilylenolether (15) with various electrophiles such as: bromine, acid chlorides, aldehydes, ketones, acetals, α,β-unsaturated esters, and protected β-ketoaldehydes.

A third method of directing electrophilic reactions at the γ-position is based on the corresponding vinylogous carbamate anion which may be alkylated with various electrophiles (16, 17). The method, however, appears to be much less satisfactory with cyclic β-ketoesters (18), which are of prime importance in the present context.

Aside from the above methods of controlled γ-alkylation of β-ketoesters there are also other reported procedures which are of either limited applicability or which were isolated observations. These include the sequence: α-alkylation, retro-Dieckmann, Dieckmann cyclization to the γ-alkyl derivative (19), or many cases of α-functionalization followed by rearrangement to the γ-position. Some reactions which follow this pattern are: phenylselenenylation (20), bromination (21), dialkylaminomethylation (22), and phenylsulfoxyethylation (23). Finally, other cases of γ-functionalization have been observed and involve enamino derivatives of β-dicarbonyl compounds or equivalents thereof; these are the γ-trimethylenedithiolation of the vinylogous carbamate of ethyl acetoacetate (24) and many cases of enamine acylations that were found to yield the 1,3-diacyl derivative with reagents such as ethyl chloroformate (25), phenylisocyanate (26), phosgene (27), and methanesulfonyl chloride (28), which can be included in this category.

A last interesting case is that reported by Colonna *et al.* (29), who, while searching for a chemical method to evaluate the relative amounts of conjugated versus non-conjugated forms of various enamino derivatives of β-ketoesters at equilibrium, found important proportions of γ-functionalization using phenylisocyanate and diethyl azodicarboxylate, due to the displacement of the equilibrium as a result of the greater reactivity of the enamino form **3*a*** over the vinylogous carbamate form **3*b***.

[1] Author to whom correspondence should be addressed.

[2] Predoctoral fellow, Ministère de l'Education du Québec and Natural Sciences and Engineering Research Council of Canada: 1978–1982.

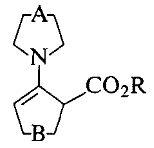

3*a*

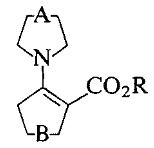

3*b*

In conclusion, it appeared that although the dianion method had allowed the synthesis of models (10, 12) of compound **1**, neither this nor the other *direct alkylation* methods reviewed above were appropriate to the synthetic plan which involved the use of an intermediate sensitive to strong bases. Therefore, the problem at hand did not appear to have a ready solution and it seemed worthwhile to investigate the possibility of developing a *mild method* of γ-alkylation of β-ketoesters, based on the reported observations of γ-reactivity in their enamino derivatives (24–29).

Results and discussion

Preparation of the enamino derivatives of the cyclic β-ketoesters

The most frequently used method is the acylation of the enamine derivative of the chosen ketone. However, this procedure, although used throughout Colonna's work (29), was not retained for our experiments for various reasons: (*i*) widely varying yields (30), (*ii*) frequent formation of 1,3-diacylated products (25–28), and (*iii*) this method, starting from the enamine derivative at equilibrium, should not offer good prospects of regio-control in the case of 3-substituted ketone enamines.

In the hope of having access to a more appropriate method to obtain these compounds we turned to the reverse sequence, which consists of first preparing the β-ketoester from the ketone and then generating the corresponding enamine derivative. Thus, the cyclic β-ketoesters (31) were treated under the usual enamination conditions (32) developed for cyclic ketones (33) and used generally for aliphatic β-ketoesters (34), but with some slight modification. Indeed, due to the extreme slowness of the reaction with our substrates, conditions had to be optimized for reaction temperature, amount of amine, and amount of *p*-toluenesulfonic acid using the piperidino enamine of 2-carbomethoxycyclohexanone as model (see Experimental).

γ-Alkylation – functionalization of enamine derivatives of cyclic β-ketoesters

Since it was well established following the definitive paper by Stork *et al.* (33) in 1963 that saturated alkyl halides do not give good yields in the alkylation of enamines, the present investigation was therefore restricted to some representative electrophilic olefins and allylic (and benzylic) halides which are efficient with enamines and offer the possibility of further functional elaboration; the same reason also applies to the bromination and phenylselenenylation reactions which were also examined in passing. Finally, acylation was not included in the study because a number of examples were already known in the literature through the acylation of enamine studies (25–29, *vide supra*).

The results obtained in the γ-alkylation – functionalization of enamine derivatives of cyclic β-ketoesters are presented in Table 1. It should also be noted that the amine used, i.e. piperidine or pyrrolidine, is adjusted to the electrophilic reagent based on known enamine reactivity (32).

The first and most important observation to be made upon

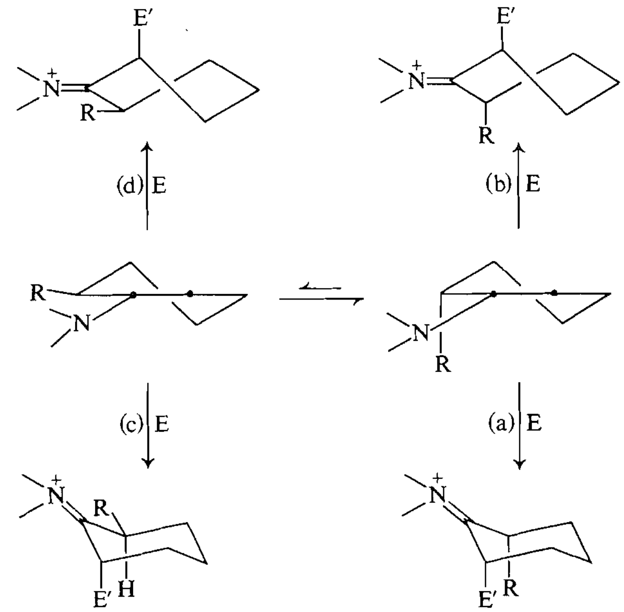

R = Me or COOEt
E = R′—X, E′ = R′
or E = $\diagup\!\!\diagdown$ Z, E′ = $\diagup\!\!\diagdown$ Z; Z
= electron withdrawing group, -M type.

SCHEME 1

inspection of Table 1 is that electrophiles react with enamine derivatives of *six-membered ring β-ketoesters to give only the γ-functionalized product* in fair to quite good yields (cf. entries 1 to 9), thus providing a *useful complement to the dianion and related methodologies* which require the use of strong bases. A second observation for the same entries, except 2 and 3, is that the contact times involved are generally long compared to the corresponding unsubstituted enamine alkylations. The reason here must be very similar to that which explains the relative slowness of reaction in the case of enamines of 2-methylcyclohexanone (38) (see Scheme 1). Indeed it is known (39, 40) that these, which exist under acid catalyzed equilibrium between the trisubstituted and the disfavored ($A^{1,3}$ strain) (41) tetrasubstituted forms, bear the methyl group in a quasi-axial position in the former in order to minimize $A^{1,2}$ strain (41); this then causes electrophilic reaction to take place at a reduced rate because of developing 1,3 diaxial interactions in an axial attack (a) or of increasing steric interactions due to the intermediacy of a twist-boat conformation in an equatorial attack (b).

On the other hand, axial attack (c) on the quasi-equatorial conformer should require a higher energy of activation than axial attack (a) on the quasi-axial conformer because of developing $A^{1,3}$ interactions.[3] Finally, there is evidence which indicates that equatorial attack (d) is also less favored on the quasi-equatorial conformer than on the quasi-axial one (42). In the case of reaction with electrophilic olefins, however (see Scheme 1), the reason for slowness of reaction is most probably (38) the involvement of the high energy intermediate (because of developing $A^{1,3}$ interactions) resulting from axial attack (c) on the enamine having a quasi-equatorial substituent, which in

[3] In the case of allyl halides, the reaction should proceed via N-alkylation followed by aza-Claisen rearrangement, and axial attack (a) for C—C bond formation should also be favored, see ref. 38, pp. 2018–2020.

TABLE 1. γ-Alkylation – functionalization of enamine derivatives of cyclic β-ketoesters

Entry	Enamine derivative	Electrophilic reagent	Contact time and T (°C)	γ-Reaction product[a]	% Yield[a]
1	**3** A = CH_2 B = CH_2 R = Me	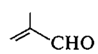	9 days 70°C	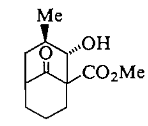 **4**	48[b]
2	**3** A = CH_2 B = CH_2 R = Et	Br_2	2 h −95°C	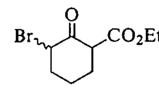 **5**	64[c]
3	**3** A = CH_2 B = CH_2 R = Et	PhSeCl	25 min −110, −80°C	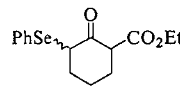 **6**	93[d]
4	**3** A = CH_2 B = CH_2 R = Et	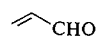	9 h 101°C	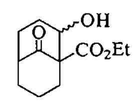 **7** + 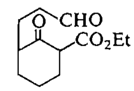 **8**	51[e]
5	**3** A = CH_2 B = CH_2 R = Et	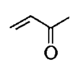	66 h 101°C	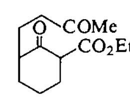 9	72[f]
6	**3** A = — B = CH_2 R = Et	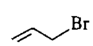	11 h 101°C	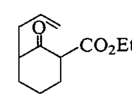 **10**	75[g]
7	**3** A = — B = CH_2 R = Et	$PhCH_2X$	97 h 95°C	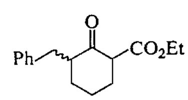 **11**	64[h] (X = Br) ~0 (X = Cl)
8	**3** A = — B = CHOAc R = Et	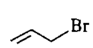	48 h 101°C	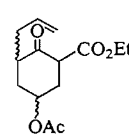 **12**	67[i]
9	**3** A = CH_2 B = CHOAc R = Et	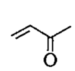	36 h 101°C	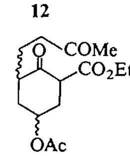 **13**	77
10	**3** A = — B = — R = Et	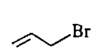	5 days 101°C	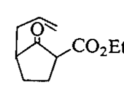 **14** 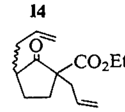 **15**	13[j] + 14[j]

TABLE 1. (*Continued*)

Entry	Enamine derivative	Electrophilic reagent	Contact time and T (°C)	γ-Reaction product[a]	% Yield[a]
11	**3** A = CH_2 B = — R = Et	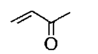	30 h 23°C	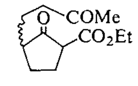 **16**	60
12	**3** A = — B = $(CH_2)_2$ R = Et	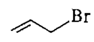	19 h 101°C	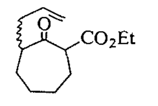 **17** 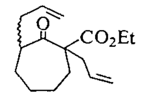 **18**	27[k] + 2[k]
13	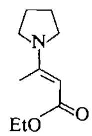 **19**	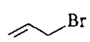	17 h 101°C	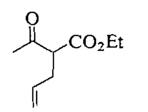 **20**	90[l]
14	**19**			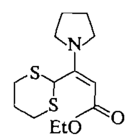	21[m] (ref. 24)

[a] Structures and regiochemistry follow mainly from spectroscopic data, see Experimental. Isolated after hydrolysis of the resulting vinylogous carbamate; it should be noted here that such hydrolyses are relatively difficult (35) compared to that of simple enamines and thus often require prolonged heating under acidic conditions.

[b] Low yield is due mostly to the difficulty in separating the product from the methacrolein polymer. The structure and regiochemistry of alkylation follow, aside from nmr analysis and fragmentation in mass spectrometry, from conversion to the known bicyclo[3.3.1] derivative **1**.

[c] The ir spectrum corresponds with that reported in the literature (21*a*) for the same compound obtained by an alternate route.

[d] The nmr spectrum observed is similar to that reported (20) for the carbomethoxy analog.

[e] The product is isolated as a mixture of stereoisomers and tautomers after hydrolysis and no attempt was made to convert it quantitatively to the bicyclic aldol.

[f] The electrophilic olefin is added in small portions throughout the reaction.

[g] Higher yields upon prolonged heating are probably due to N-alkylation of the amine followed by a thermal [3.3] sigmatropic shift of the chain to the γ-position in analogy to the case of simple enamines (36).

[h] Filtration of the benzyl bromide over basic alumina gives a reaction which is very slow to begin but gradually accelerates; this indicates the beneficial influence of a trace of acid in probably catalyzing the enamine – vinylogous carbamate equilibrium. This was supported by observing the positive influence of a trace of *p*-toluenesulfonic acid in a reaction mixture where the benzyl bromide was filtered over basic alumina.

[i] Obtained by integration of appropriate signals in the nmr spectrum of the hydrolyzed mixture because of difficulty of separation; the isolated yield was only 16%; see, however, entry 9.

[j] From the outset, the reaction gives a mixture of numerous products.

[k] Monitoring by vpc shows a simple chromatogram with disappearance of the starting material and appearance of a major product; hydrolysis, however, proved difficult (36 h, 10% HCl, 63°C) and yielded only 50% of the crude neutral fraction expected, from which only 27% of **17** and 2% of **18** were obtained. Attempts to prepare the piperidino enamine of the starting β-ketoester in order to examine its reactivity with methyl vinyl ketone failed.

[l] This reaction which, contrary to the cyclic analogs, gives α-alkylation was already reported in 1916 by Robinson (37) under slightly different conditions. Attempted reaction of the piperidino derivative of the same β-ketoester with methyl vinyl ketone gave a complex mixture of products.

[m] This case, reported by Woodward *et al.* (24), to our knowledge represents the only example of the γ-functionalization of an enamine derivative of an aliphatic β-ketoester.

an efficient and stereoelectronically controlled intramolecular axial proton transfer would go to product; on the other hand, equatorial attack (d) on the same form or axial (a) or equatorial (b) attack on the form having a quasi-axial substituent would yield intermediate zwitterions which would most often revert to starting enamine because of the unavailability of an axial intramolecular proton for charge neutralization. Intermolecular proton transfer, although available, should not be efficient under the normal dilution conditions generally used.

A third observation which can be made upon inspection of Table 1 is that the enamine derivatives of five- and seven-membered ring β-ketoesters (entries 10, 11, 12) are not as uniformly reactive as their six-membered ring analogs. However, a trend favoring γ-reactivity is apparent in those cases and the selective development of specific reaction conditions might be necessary in each case. Finally, it appears that the enamine derivatives of aliphatic β-ketoesters (entries 13, 14) also do not form a uniformly reactive series, as γ and α selectivity are both apparent depending on the electrophile and conditions.

Preparation of 1-carbomethoxy-3-methyl-9-oxobicyclo-[3.3.1]non-2-ene (**1**, R = Me, R[1] = H)

Attempted tosylation of **4** (Table 1, entry 1) under standard conditions (43) for 15 days failed to give the desired product; mesylation (44), however, yielded up to a maximum of 40% of the corresponding mesylate **21**. This suggested that the pyridine used in the reaction was causing a displacement of the

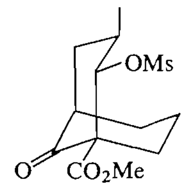

21

aldol equilibrium to the open form, thus slowing down the mesylation reaction considerably and allowing side reactions to compete. The same reaction was then tried in acid medium using methanesulfonyl anhydride (45) but to no avail. Fortunately, however, we observed that the only way the acetate of ketol **4** could be prepared was by using pyridine in acetyl chloride, which are known ketene generating conditions (46). Also, we observed that the corresponding phenylcarbamate could easily be prepared from phenylisocyanate in acidic medium. These observations strongly suggested that the solution to the problem lay in using the corresponding sulfene as mesylating agent rather than methanesulfonyl chloride. Indeed, the reagent is linear, as are ketene and phenylisocyanate, as well as being very reactive. Therefore, by using a set of conditions inspired from the literature (47), we could obtain the desired mesylate **22** in the crystalline form and in a 70% yield. Various fruitless attempts were made to shorten the reaction time; for example, use of *N,N,N*-diethylmethyl methanesulfonyl ammonium ("Easy Mesyl"), recognized as a potent sulfene generator (48), failed to give the desired product (**21**) in good yield. It appears that use of these conditions with ketol **4** generates the sulfene too rapidly for uptake by the substrate, causing it to polymerize (49) and thus complicating isolation of the desired product (**21**).

The last step, i.e. the *cis* elimination, in the projected sequence was achieved in a 70% yield by heating the mesylate **21** in collidine (160°C) for 29 h. The 1-carbomethoxy-3-methyl-9-oxobicyclo[3.3.1]non-2-ene (**1**) thus obtained shows in the nmr a vinyl proton in the form of a broadened singlet at 5.38 ppm, a sharp singlet at 3.78 ppm for the carbomethoxy group, and a broadened singlet at 1.82 ppm for the allylic methyl protons. These values are in accord with those reported in the literature (10) as well as those observed in our own laboratory (12)[4] for the same compound prepared by two additional different methods.

Conclusion

Although the present study is based on a limited number of enamine derivatives, electrophiles, and reaction conditions, it nevertheless provides a good cross section of the possibilities of γ-alkylation(−functionalization) of enamine derivatives of cyclic β-ketoesters. Thus, the method is very good for the γ-alkylation or functionalization of β-ketoesters in the cyclohexane series but its prospects appear much more limited in the cyclopentane and cycloheptane series as well as the aliphatic series. The method is also applicable to substrates bearing base sensitive functionality, thus making it an important complement to the dianion and related methodologies which are usually not applicable in these cases.

From the point of view of electrophiles, electrophilic olefins provide the best results, as is usually the case with simple ketone enamines (32, 34, 38, 50); the generality of halogenation and phenylselenenylation, although assured in the six-membered ring series, remains to be tested in the other series.

Finally, this study has been first and foremost an exploration into the possibilities of the enamine reaction (32, 33, 38, 50) for the γ-alkylation (−functionalization) of β-ketoesters, with the aim of bringing out similarities and distinctions between β-ketoesters and simple ketones. As a result, a certain number of fundamental observations stand out from the preceding experiments. Thus, the chemoselectivity of alkylation in the six-membered ring series is noteworthy; the inertia of the vinylogous carbamate form (**3***b*) towards α-alkylation is most probably due to a weakness of conjugation or overlap of the amine lone pair with the double bond because of strong $A^{1,3}$ interactions. This is supported by the fact that aliphatic vinylogous carbamates, where the amine and carbalkoxy groups are *trans*, show good reactivity in the α-position at least with alkyl halides (see entry 13, Table 1). Also, the observed selectivity for monoalkylation is most important from a synthetic methodology point of view and is probably due to the fact that the monoalkylated or functionalized product exists solely (29) in the now more stable and less reactive vinylogous carbamate form.

A study of factors affecting the enamino versus the vinylogous carbamate forms in enamine derivatives of β-ketoesters has been carried out and is reported in the accompanying paper.

Experimental

Melting points were taken on a Büchi apparatus and are uncorrected. The ^{1}H nmr spectra were recorded, unless otherwise stated, in $CDCl_3$ using either a Bruker WH90 (90 MHz) or a Bruker WH400 (400 MHz). Chemical shifts (δ) are expressed in ppm with respect to tetramethylsilane (TMS) used as internal standard and multiplicities are expressed as "s" for singlet, "d" for doublet, "t" for triplet, "q" for quartet, "h" for heptuplet, and "m" for multiplet. Coupling constants are reported in Hz.

Infrared spectra were recorded on a Perkin Elmer, model 710B, apparatus either in $CDCl_3$, as pure liquid films, or in KBr pellets. High resolution mass spectra (EI) were taken on a AEI MS-902 apparatus and low resolution (EI or CI) were taken on a V.G. Micromass, model 12-12, apparatus. Homogeneity of all compounds prepared was ascertained by tlc or vpc, and ^{1}H nmr. In many cases, ^{13}C nmr spectra were recorded and are available in M. Labelle's Ph.D. thesis and partly in the following paper.

The vpc analyses were done under the following conditions; injection of 1 μL of solution in a Varian model 1200 chromatograph with a flame ionization detector. The column used was 3.5 m × 3 mm and packed with 3% OV-1 on 60–80 mesh Chromosorb W AW-DMCS and helium was used as carrier gas at a rate of 25 mL/min. Injector temperature was maintained at 230°C and the detector at 300°C. Finally, relative peak areas were taken as relative product composition and the results obtained were sufficiently accurate for the present purpose.

Thin-layer chromatography (tlc) was done on Merck Kieselgel 60

[4] Also, D. Gravel and D. Thoroval, unpublished results.

F_{254} using aluminium support and visualization was done by means of either uv light, iodine vapour, or sulfomolybdic mixture (51). Flash chromatography was done following the Still method (52) using Merck 40- to 63-μ mesh silica gel.

Purification of solvents and reagents used in this study was done according to the methods described below and is specified in the Experimental with the appropriate letter, (A) to (E). A: product distilled under inert atmosphere. B: product distilled over a sodium–potassium (1:1 w/w) liquid alloy and a little benzophenone under inert atmosphere. C: product distilled over calcium hydride under inert atmosphere. D: product filtered over basic alumina, activity I, under inert atmosphere. E: product distilled over calcium hydride under inert atmosphere and received in a flask containing (approx. 1% w/w) hydroquinone.

Preparation of enamine derivatives of β-ketoesters

General procedure

In a dry apparatus fitted with a Dean–Stark separator are introduced 1 equiv. of the β-ketoester (prepared by the slightly modified procedure of Ruest, Blouin, Deslongchamps (31)), 5 equiv. of the amine, and 0.05 equiv. of *p*-toluenesulfonic acid monohydrate. The mixture is then diluted with benzene, 20 mL per gram of β-ketoester, and the solution heated to reflux, using an oil bath at a temperature below 100°C since *higher temperatures often cause formation of the corresponding β-ketoamide*. The reaction is monitored by vpc and considered complete when the β-ketoester and β-ketoamide (formed on the column) peaks have disappeared and when the stoichiometric amount of water has been formed. Isolation of the product is carried out by evaporation at 45°C under 15 Torr (1 Torr = 133.3 Pa), by coevaporation with toluene at 45°C under 15 Torr, and by fractional distillation. The products may then be kept frozen under a pressure of approximately 25–50 psi of argon.

Methyl-2-(1-piperidinyl)-2 (and -1) -cyclohexenecarboxylate (**3***a* and **3***b*, A = CH_2, B = CH_2, R = Me)

The reaction was carried out according to the general procedure. Reagents: methyl-2-oxo-cyclohexanecarboxylate (31) (3.0 g, 19.2 mmol) and piperidine. The reaction was complete after about 3 days of light reflux. Distillation: yellowish liquid, 2.73 g (64%) (79–86% with lower bath temperature), bp 78–79°C/8.4 × 10^{-4} Torr; ir (film) ν_{max}: 1730, 1680, 1640, and 1550 cm^{-1}; ^1H nmr (90 MHz) δ: 4.89 (t, J = 4 Hz, 0.66H), 3.69 (s, 3H), and 3.33 (t broadened, 0.66H). Mass spectrum (CI, CH_4) m/e: 224 MH^+, 208 M − CH_3, 164 (100%) M − COOMe. *Exact Mass* calcd. for $C_{13}H_{21}NO_2$: 223.1572; found: 223.1569.

Ethyl-2-(1-piperidinyl)-2 (and -1) -cyclohexenecarboxylate (**3***a* and **3***b*, A = CH_2, B = CH_2, R = Et)

The reaction was carried out according to the general procedure. Reagents: ethyl-2-oxo-cyclohexanecarboxylate (31, 53) (10.0 g, 59 mmol) and piperidine. The reaction was complete after about 5 days of light reflux. Distillation: yellowish liquid, 9.68 g (70%), bp 73–86°C/3.6 × 10^{-4} Torr; ir ($CHCl_3$) ν_{max}: 1720, and 1630 cm^{-1}; ^1H nmr (90 MHz) δ: 4.88 (t, J = 5 Hz, 0.85H), 4.15 (q, J = 7 Hz, 2H), 3.30 (t broadened, 0.85H), and 1.26 (t, J = 7 Hz, 3H). Mass spectrum (EI, 70 eV) m/e: 237 $M^{+\cdot}$, 222 M − Me, 208 M − Et, 192 M − OEt, 164 (100%) M − COOEt. *Exact Mass* calcd. for $C_{14}H_{23}NO_2$: 237.1728; found: 237.1732. These data are in good accord with those reported (29, 54) for the same product.

Ethyl-2-(1-pyrrolidinyl)-2 (and -1) -cyclohexenecarboxylate (**3***a* and **3***b*, A = —, B = CH_2, R = Et)

The reaction was carried out according to the general procedure. Reagents: ethyl-2-oxo-cyclohexanecarboxylate (31, 53) (3.0 g, 17.7 mmol) and pyrrolidine. The reaction was complete after 4.5 h of light reflux. Distillation (Vigreux column): yellowish liquid, 2.04 g (52%). When the reaction was performed on a 6.0-g scale and omitting the Vigreux column for the distillation, the yield was raised to 85%, bp 84–90°C/3.4 × 10^{-4} Torr; ir (film) ν_{max}: 1730, 1670, and 1550 cm^{-1}; ^1H nmr (90 MHz) δ: 4.49 (t broadened, 0.12H), 4.12 (q, J = 7 Hz, 2H), 3.25 (t broadened, ~4H), 2.96 (t broadened, 0.12H), 4.12 (q, J = 7 Hz, 2H), 3.25 (t broadened, ~4H), 2.96 (t broadened, 0.48H), 2.41 (s, broad, ~4H), and 1.26 (t, J = 7 Hz, 3H). Mass spectrum (EI, 70 eV) m/e: 223 $M^{+\cdot}$, 208 (M − Me, 194 M − Et, 150 M − COOEt. *Exact Mass* calcd. for $C_{13}H_{21}NO_2$: 223.1572; found: 223.1576. These data are in good accord with those reported (29, 55) for the same product.

Ethyl-5-acetoxy-2-(1-pyrrolidinyl)-1-cyclohexenecarboxylate (**3***b*, A = —, B = CHOAc, R = Et)

The reaction was carried out according to the general procedure. Reagents: ethyl-5-acetoxy-2-oxo-cyclohexanecarboxylate (30) (2.12 g, 9.3 mmol) and pyrrolidine. The reaction was complete after 1.5 h of light reflux. Distillation: very viscous greenish liquid, 2.13 g (81%), bp 123–130°C/5.5 × 10^{-4} Torr; ir (film) ν_{max}: 1720, 1660, and 1550 cm^{-1}; ^1H nmr (90 MHz) δ: 4.96 (m, 1H), 4.11 (q, J = 7 Hz, 2H), 2.05 (s, 3H), and 1.25 (t, J = 7 Hz, 3H). Mass spectrum (CI, CH_4) m/e: 282 MH^+, 236 M − OEt, 221 M − CH_3COOH.

Ethyl-5-acetoxy-2-(1-piperidinyl)-2 (and -1) -cyclohexenecarboxylate (**3***a* and **3***b*, A = CH_2, B = CHOAc, R = Et)

The reaction was carried out according to the general procedure. Reagents: ethyl-5-acetoxy-2-oxo-cyclohexanecarboxylate (30) (4.0 g, 17.6 mmol) and piperidine. The reaction was complete after about 4 days of light reflux. Distillation: yellowish liquid, 2.6 g (50%), bp 105–136°C/3.2 × 10^{-4} Torr; ir (film) ν_{max}: 1730, 1680, 1640, and 1550 cm^{-1}; ^1H nmr (90 MHz) δ: 5.0 (m, 1.82H), 4.17 and 4.13 (2q, J = 7 Hz, 2H), 3.47 (t broadened, 0.82H), 2.04 and 2.03 (2s, 3H), and 1.26 (t, J = 7 Hz, 3H). Mass spectrum (EI, 70 eV) m/e: 295 $M^{+\cdot}$, 235 M − CH_3COOH, 162 (100%) M − CH_3COOH − COOEt.

Ethyl-2-(1-pyrrolidinyl)-1-cyclopentenecarboxylate (**3***b*, A = —, B = —, R = Et)

The reaction was carried out according to the general procedure. Reagents: ethyl-2-oxo-cyclopentanecarboxylate (31, 53) (2.76 g, 17.7 mmol) and pyrrolidine. The reaction was complete after 2 h of light reflux. Distillation: yellowish liquid, 2.08 g (57%); an experiment where the temperature of the oil bath did not exceed 98°C gave a 72% yield, bp 94–98°C/6.2 × 10^{-4} Torr; ir (film) ν_{max}: 1670 and 1560 cm^{-1}; ^1H nmr (90 MHz) δ: 4.11 (q, J = 7 Hz, 2H), 3.44 (t broadened, 4H), 2.62 and 2.61 (2t, J = 7 Hz, 4H), 1.86 and 1.74 (t, J = 7 Hz and q, J = 7 Hz, 6H), and 1.26 (t, J = 7 Hz, 3H). Mass spectrum (EI, 70 eV) m/e: 209 $M^{+\cdot}$, 180 M − Et, 164 M − OEt, 136 M − COOEt. These data are in accord with those reported in the literature (54) for the same product.

Ethyl-2-(1-piperidinyl)-1-cyclopentenecarboxylate (**3***b*, A = CH_2, B = —, R = Et)

The reaction was carried out according to the general procedure. Reagents: ethyl-2-oxo-cyclopentanecarboxylate (53) (2.76 g, 17.7 mmol) and piperidine. The reaction was complete after 16 h of light reflux. Distillation: yellowish liquid, 2.67 g (68%), bp 55–67°C/6.2 × 10^{-4} Torr; ir (film) ν_{max}: 1670 and 1560 cm^{-1}; ^1H nmr (90 MHz) δ: 4.12 (q, J = 7 Hz, 2H), 3.34 (s broadened, 4H), 2.63 and 2.56 (2t, J = 7 Hz, 4H), 1.83 (t, J = 7 Hz, 2H), 1.61 (s broadened, 6H), and 1.26 (t, J = 7 Hz, 3H). Mass spectrum (EI, 70 eV) m/e: 223 $M^{+\cdot}$, 194 M − Et, 178 M − OEt, 150 (100%) M − COOEt. *Exact Mass* calcd. for $C_{13}H_{21}NO_2$: 223.1572; found: 223.1525.

Ethyl-2-(1-pyrrolidinyl)-1-cycloheptenecarboxylate (**3***b*, A = —, B = $(CH_2)_2$, R = Et)

The reaction was carried out according to the general procedure. Reagents: ethyl-2-oxo-cycloheptanecarboxylate (31, 53) (3.0 g, 16.3 mmol) and pyrrolidine. The reaction was complete after 27 h of light reflux. Distillation: yellowish liquid, 3.14 g (81%), bp 88–98°C/5.5 × 10^{-4} Torr. At −15°C, this liquid solidifies to a white product which melts at 57–63°C; ir (film) ν_{max}: 1650 and 1530 cm^{-1}; ^1H nmr (90 MHz) δ: 4.11 (q, J = 7 Hz, 2H), 3.30 (t broadened, 4H), 2.6 (m, 4H), 1.85 (t broadened, 4H), 1.62 (m, 6H), and 1.25 (t, J = 7 Hz, 3H). Mass spectrum (CI, CH_4) m/e: 238 MH^+, 237 (100%) M^+, 222 M − CH_3, 208 M − Et, 192 M − OEt, 164 M − COOEt. *Exact Mass* calcd. for $C_{14}H_{23}NO_2$: 237.1728; found: 237.1700.

Ethyl-3-(1-pyrrolidinyl)-2-butanoate (**19**)

The reaction was carried out according to the general procedure. Reagents: ethyl-3-oxo-butanoate (6.5 g, 50 mmol) and pyrrolidine. The reaction was complete after 8 h of light reflux. Distillation: yellowish liquid, 6.83 g (75%), bp 105–110°C/1 × 10^{-3} Torr; ir (film) ν_{max}: 1670 and 1570 cm^{-1}; ^1H nmr (90 MHz) δ: 4.44 (s, 1H), 4.08 (q, J = 7 Hz, 2H), 3.29 (s broadened, 4H), 2.45 (s, 3H), 1.93 (m, 4H), and 1.24 (t, J = 7 Hz, 3H). *Exact Mass* calcd. for $C_{10}H_{17}NO_2$: 183.1259; found: 183.1239. These data are identical to those reported in the literature (33).

Methyl-2-hydroxy-3-methyl-bicyclo[3.3.1]nonan-9-one-1-carboxylate (**4**)

Under dry and inert atmosphere, a solution of enamino derivative **3**, A = CH_2, B = CH_2, R = Me (6.1 g, 27.3 mmol) in dioxane (B) (100 mL) was heated with an oil bath at 70°C and treated with freshly distilled methacrolein (E) (8.5 g, 121 mmol). After 9 days of heating, the solvent was evaporated under vacuum at 50°C and the residue stirred with 10% HCl (50 mL) during 90 min. Extraction with ether and treatment under the usual conditions gave a semi-solid which was distilled at 125°C/4 × 10^{-3} Torr in a Kugelrohr apparatus to yield a yellowish solid (2.94 g, 48%), mp 88–120°C. Recrystallization from CCl_4 gave a white solid, mp 122–123°C; ^1H nmr (90 MHz) δ: 3.98 (d, J = 10 Hz, 1H), 3.79 (s, 3H), and 1.09 (d, J = 6 Hz, 3H). *Exact Mass* calcd. for $C_{12}H_{18}O_4$: 226.1205; found: 226.1212.

Ethyl-3-bromo-2-oxo-cyclohexanecarboxylate (**5**)

Under dry and inert atmosphere, a solution (prepared at −20°C) of enamino derivative **3**, A = CH_2, B = CH_2, R = Et (500 mg, 2.11 mmol) in CH_2Cl_2 (A) (20 mL) was treated at −20°C with triethylamine (1.16 mL, 8.44 mmol) and the temperature lowered to −95°C. There was then added, over a 5-min period, a solution of bromine (338 mg, 2.11 mmol) in CH_2Cl_2 (10 mL). The yellow solution was maintained at −95°C for 2 h after which the reaction was quenched with 5% HCl (6 mL). The mixture was left overnight under strong stirring and the organic phase decanted, dried, and evaporated under vacuum (40°C) to give an oil (656 mg) which distilled at 95°C/6 × 10^{-4} Torr in a Kugelrohr apparatus to yield a colorless liquid (338 mg, 64%); ir ($CDCl_3$) ν_{max}: 1730, 1710, 1650, and 1610 cm^{-1}; ^1H nmr (90 MHz) δ: 12.10 (s, 0.6H), 4.69 (t, broadened, 0.6H), 4.55 (t, broadened, 0.4H), 4.24 (q, J = 7 Hz, 2H), 3.4 (m, 0.4H), and 1.31 and 1.29 (2t, J = 7 Hz, 3H). *Exact Mass* calcd. for $C_9H_{13}BrO_3$: 250.0028; found: 250.0039.

Ethyl-3-phenylselenenyl-2-oxo-cyclohexanecarboxylate (**6**)

Under dry and inert atmosphere a solution of enamino derivative **3**, A = CH_2, B = CH_2, R = Et (430 mg, 1.81 mmol) in THF (B) (10 mL) was cooled to about −110°C and treated, under stirring and over a 5-min period, with a solution of phenylselenenyl chloride (356 mg, 1.86 mmol) in THF (5 mL). The temperature was allowed to rise to −80°C (20 min) and the mixture quenched with water (8 mL) and ether (10 mL). Gradual warming of the mixture to room temperature (3 h) was then followed by the addition of 5% HCl (1 mL) to complete the hydrolysis during 12 h. The aqueous phase was decanted and extracted with ether (10 mL). Treatment of the organic phases in the usual manner gave a yellow oil (640 mg) which contained some diphenyldiselenide. Flash chromatography (ether–hexane, 3:97) purification of a small portion gave a colorless liquid, relatively unstable in air; ir (film) ν_{max}: 3025, 1730, 1700, 1640, and 1600 cm^{-1}; ^1H nmr (90 MHz) δ: 12.32 (s, ~1H), 7.65 and 7.29 (2m, 5H), 4.21 (q, J = 7 Hz, 2H), 4.10 (t, broadened, 1H), and 1.29 (t, J = 7 Hz, 3H). This spectrum corresponds very well with that of the methyl ester reported in the literature (20). Mass spectrum (EI, 70 eV) m/e: 226, 224, 222 and 220 M − CH_2CH_2 − COOEt, 168 M − PhSeH, 159, 157, 155 and 153 $PhSe^{+\cdot}$, 123 (100%) M − PhSeH − OEt.

Ethyl-2-hydroxy-bicyclo[3.3.1]nonan-9-one-1-carboxylate (**7**) *and ethyl-3-(3-oxo-propyl)-2-oxo-cyclohexanecarboxylate* (**8**)

Under dry and inert atmosphere, a solution of the enamino derivative **3**, A = CH_2, B = CH_2, R = Et (2.29 g, 9.6 mmol) and hydroquinone (100 mg) in dioxane (B) (50 mL) was heated to reflux (bath temp. 115°C) and treated with freshly distilled acrolein (E) (1.77 g, 28.8 mmol). The reaction was monitored by vpc and, after 3.5 h, an additional amount of acrolein (E) (0.88 g, 14.4 mmol) was added and the reflux prolonged for an additional 5.5 h. At the end of the reaction period, the excess acrolein was drawn away by a stream of argon during reflux. The dioxane was evaporated under vacuum (40°C) and the residue taken up in ether (50 mL). The organic phase was washed with 5% Na_2CO_3 (20 mL) and stirred vigorously with 5% HCl (10 mL) during 8.5 h at room temperature. The organic phase was decanted and the aqueous phase diluted with brine (10 mL) and extracted twice with ether (2 × 25 mL). The organic phases were treated in the usual way to yield an oil (1.58 g) which was distilled: bp 97–98°C/6 × 10^{-4} Torr to give a yellowish liquid (1.12 g, 51%) composed of a mixture of tautomers and isomers of the expected product; ir (film) ν_{max}: 3400, 2830, 1730, 1720, 1710, 1670, and 1630 cm^{-1}; ^1H nmr (90 MHz) δ: 12.44 (s, 0.17H), 9.77 (m, 0.5H), 4.5 (m, 0.5H), 4.25 and 4.21 (q, J = 7 Hz, 2H), 3.4 (m, 0.33H), 3.05 (s, broad, 0.5H) shifts with change in concentration, and 1.32, 1.30, 1.28 and 1.26 (4t, J = 7 Hz, 3H). Mass spectrum (EI, 70 eV) m/e: 208 M − H_2O, 180 M − H_2O − EtOH, 170 M − CH_2=CHCHO.

Ethyl-2-oxo-3-(3-oxo-butyl)-cyclohexanecarboxylate (**9**)

Under dry and inert atmosphere, a solution of the enamino derivative **3**, A = CH_2, B = CH_2, R = Et (320 mg, 1.36 mmol) in dioxane (B) (3 mL) was treated with freshly distilled methylvinylketone (E) (114 mg, 1.63 mmol) and the mixture heated to reflux on an oil bath at 120°C. The reaction was monitored by vpc and in the present case required the addition of further methylvinyl ketone (E) (20 mg, 0.33 mmol per addition) after 19, 43, and 54 h in order to bring the reaction to completion after 66 h. Evaporation of the solvent and unreacted methylvinylketone under vacuum at 45°C gave a residue which was taken up in $CHCl_3$ (10 mL) and the resulting solution stirred vigorously for 90 min with 10% HCl (4 mL). After separation, the aqueous phase was reextracted with $CHCl_3$ (15 mL) and the organic phases treated in the usual manner to yield a residue (320 mg) which was distilled in a Kugelrohr apparatus at 85°C under 3.3 × 10^{-4} Torr to give a slightly yellowish liquid (230 mg, 72%); ir (film) ν_{max}: 1730, 1710, 1630, and 1600 cm^{-1}; ^1H nmr (90 MHz) δ: 12.43 (s, 0.33H), exchangeable with D_2O, 4.21 (q, J = 7 Hz, 2H), 3.38 (m, 0.67 H), 2.16 and 2.13 (2s, 3H), and 1.30, 1.28, and 1.27 (3t, J = 7 Hz, 3H). Mass spectrum (EI, 70 eV) m/e: 222 M − H_2O, 195 M − OEt, 182 M − CH_3COCH_3, 168 M − $CH_3CH_2COCH_3$, 137 M − OEt − CH_3COCH_3.

Ethyl-3-(2-propenyl)-2-oxo-cyclohexanecarboxylate (**10**)

Under dry and inert atmosphere, a solution of the enamino derivative **3**, A = —, B = CH_2, R = Et (850 mg, 3.81 mmol) in dioxane (B) (10 mL) was heated to reflux in an oil bath at 125°C and treated with 3-bromopropene (1.40 g, 11.4 mmol). Monitoring by vpc showed that the reaction was complete after 11 h of reflux. The mixture was evaporated under vacuum (45°C), diluted with $CHCl_3$ (10 mL), and stirred vigorously with 5% HCl (5 mL) at 60°C; vpc monitoring showed the hydrolysis to be complete after 5 h. The organic phase was decanted and treated in the usual way to give a yellow oil (600 mg, 75%) of approximately 90% purity (vpc). A pure sample was prepared by flash chromatography (hexane–$CHCl_3$, 6:4); ir (film) ν_{max}: 3040, 1735, 1710, 1640, and 1600 cm^{-1}; ^1H nmr (90 MHz) δ: 12.44 (s, 0.55H), exchangeable with D_2O, 5.8 (m, broad, 1H), 5.10 and 4.97 (2m, 2H), 4.21 (q, J = 7 Hz, 2H), 3.6 (m, 0.45H), exchangeable with D_2O, K_2CO_3, 63°C, 15 min, and 1.30, 1.28, and 1.27 (3t, J = 7 Hz, 3H). Mass spectrum (EI, 70 eV) m/e: 210 $M^{+\cdot}$, 181 M − Et, 168 M − CH_2=$CHCH_3$, 164 M − CH_3CH_2OH, 137 M − COOEt. These data are in accord with those reported in the literature (2) for the corresponding methyl ester.

Ethyl-3-benzyl-2-oxo-cyclohexanecarboxylate (**11**)

Under dry and inert atmosphere, a solution of the enamino derivative **3**, A = —, B = CH_2, R = Et (530 mg, 2.37 mmol) in dioxane (B) (10 mL) was treated with benzyl bromide (721 mg, 4.22 mmol) and then heated to 95°C. Monitoring by vpc showed the disappearance of the enamino derivative after 97 h. The violet mixture was evaporated under vacuum (40°C) and the residue diluted with $CHCl_3$ (15 mL) and stirred under reflux with 10% HCl (5 mL). Hydrolysis was complete (vpc) after 2.25 h. The aqueous phase was decanted, extracted with $CHCl_3$ (15 mL), and the organic phases treated in the usual way to give a red oil. Distillation in a Kugelrohr apparatus at 110°C/5.8 × 10^{-4} Torr gave a colorless oil (385 mg, 64%); ir (film) ν_{max}: 3040, 1740, 1710, 1640, and 1610 cm^{-1}; ^1H nmr (90 MHz) δ: 12.54 (s, 0.4H), 7.22 and 7.18 (2s, 5H), 4.22 (q, J = 7 Hz, 2H), 3.30 (m, 1.6H), and 1.29 (t, J = 7 Hz, 3H). Mass spectrum (EI, 70 eV) m/e: 260 $M^{+\cdot}$, 242 M − H_2O, 214 M − CH_3CH_2OH, 187 M − COOEt, 169 M − CH_2Ph.

Ethyl-5-acetoxy-3-(2-propenyl)-2-oxo-cyclohexanecarboxylate (12)

Under dry and inert atmosphere, a solution of enamino derivative **3**, A = —, B = CHOAc, R = Et (420 mg, 1.5 mmol) and *p*-toluenesulfonic acid monohydrate (6 mg, 0.03 mmol) in dioxane (B) (10 mL) was heated to reflux on an oil bath at 115°C and treated with allyl bromide (C) (1.09 g, 90 mmol). Monitoring (vpc) showed the reaction to be complete after 48 h of reflux. The mixture was evaporated under vacuum (45°C), and the residue dissolved in $CHCl_3$ (10 mL). The resulting solution was stirred vigorously at 63°C with 5% HCl (7 mL). After 2 h, the aqueous layer was decanted and extracted with $CHCl_3$; the organic phases were treated in the usual manner to give an oil (301 mg) which was shown by nmr to contain 81% of alkylated product, giving thus a yield of 67% for the reaction. Due to the similar chromatographic properties of the alkylated and non-alkylated products, purification was done by medium pressure liquid chromatography (1 m × 1 cm column, ether–hexane 2:8) and, despite those efforts, yielded only 49 mg (16%) of the pure product; ir (film) ν_{max}: 3050, 1730, 1640, and 1600 cm^{-1}; ^1H nmr (90 MHz) δ: 12.53 and 12.49 (2s, 1H), 6.0–4.7 (m, 4H), 4.21 (q, J = 7 Hz, 2H), 2.06 and 2.05 (2s, 3H), and 1.30 (t, J = 7 Hz, 3H). Mass spectrum (CI, CH_4) m/e: 269 MH^+, 223 M − OEt, 209 (100%) M − $OCOCH_3$.

Ethyl-5-acetoxy-2-oxo-3-(3-oxo-butyl)-cyclohexanecarboxylate (13)

Under dry and inert atmosphere, a solution of enamino derivative **3**, A = CH_2, B = CHOAc, R = Et (1.0 g, 3.05 mmol) in dioxane (B) (10 mL) was heated to reflux on an oil bath at 115°C and then treated with methylvinylketone (E) (425 mg, 6.1 mmol). Monitoring by vpc showed that after 36 h of reflux the reaction appeared about complete. The solvent was evaporated under vacuum (45°C) and the residue taken up in $CHCl_3$ (15 mL); hydrolysis took place by stirring vigorously with 5% HCl (10 mL) for 10 h. The organic phase was decanted and treated in the usual manner to give a yellow oil (900 mg). Flash chromatography (ether–hexane, 1:1) gave a colorless oil (651 mg, 77%); ir (film) ν_{max}: 1735, 1710, 1650, and 1610 cm^{-1}; ^1H nmr (90 MHz) δ: 12.52 and 12.47 (2s, 1H), exchangeable with D_2O, 5.07 (m, broad, 1H), 4.21 (q, J = 7 Hz, 2H), 2.16 (s, 3H), 2.05 (s, 3H), and 1.30 (t, J = 7 Hz, 3H). Mass spectrum (EI, 70 eV) m/e: 280 M − H_2O, 238 M − CH_3COOH, 220 M − CH_3COOH − H_2O.

Ethyl-3-(2-propenyl)-2-oxo-cyclopentanecarboxylate (14) and ethyl-bis-1,3-(2-propenyl)-2-oxo-cyclopentanecarboxylate (15)

Under dry and inert atmosphere, a solution of enamino derivative **3**, A = —, B = —, R = Et (560 mg, 2.68 mmol) and *p*-toluenesulfonic acid monohydrate (25 mg, 0.13 mmol) in dioxane (B) (10 mL) was heated to reflux using an oil bath at 105°C and treated with allyl bromide (C) (3.24 g, 26.8 mmol). Monitoring (vpc) showed that the reaction ceased progressing after 5 days. The reaction mixture, evaporated under vacuum (45°C) and co-evaporated with toluene under the same conditions, was taken up in $CHCl_3$ (12 mL) and hydrolyzed by vigorous stirring with 10% HCl (3 mL) during 16 h. The aqueous phase was decanted and extracted twice with $CHCl_3$ (3 mL); the organic phases were treated in the usual manner to yield an oily residue (450 mg). Flash chromatography (ether–hexane, 1:9) gave the dialkylated product **15** as a yellowish oil (88 mg, 14%), the monoalkylated product **14** (70 mg, 13%), and some 2-carbethoxycyclopentanone (29 mg, 5%).

Compound 14: ir (film) ν_{max}: 3060, 1745, 1720, and 1630 cm^{-1}; ^1H nmr (90 MHz) δ: 5.7 (m, 1H), 5.1 (m, 2H), 4.70 and 4.16 (2 q, J = 7 Hz, 2H), and 1.28 and 1.25 (2t, J = 7 Hz, 3H). Mass spectrum (CI, CH_4) m/e: 197 MH^+, 168 M − $CH_2{=}CH_2$, 151 M − OEt, 150 M − CH_3CH_2OH.

Compound 15: ir (film) ν_{max}: 3060, 1745, 1715, and 1630 cm^{-1}; ^1H nmr (90 MHz) δ: 5.7 (m, 2H), 5.1 (m, 4H), 4.15 (q, J = 7 Hz, 2H), and 1.25 (t, J = 7 Hz, 3H). Mass spectrum (CI, CH_4) m/e: 237 (100%) MH^+, 208 M − $CH_2{=}CH_2$, 195 M − $CH_2CH{=}CH_2$, 191 M − OEt, 163 M − COOEt.

Ethyl-2-oxo-3-(3-oxo-butyl)cyclopentanecarboxylate (16)

Under dry and inert atmosphere, a solution of enamino derivative **3**, A = CH_2, B = —, R = Et (520 mg, 2.33 mmol) and *p*-toluenesulfonic acid monohydrate (4 mg, 0.02 mmol) in dioxane (B) (5 mL) was treated with methylvinylketone (E) (326 mg, 4.66 mmol) at room temperature. Monitoring by vpc showed the reaction to be complete after 30 h. Evaporation of the mixture under vacuum (40°C) and co-evaporation with toluene under the same conditions gave a residue which was taken up with $CHCl_3$ (10 mL) and stirred vigorously with 5% HCl (2 mL) for 18 h (vpc monitoring). The aqueous phase was decanted, extracted twice with $CHCl_3$ (4 mL), and the organic phases treated in the usual manner to give a residue which was separated by flash chromatography; elution with ether–hexane (20:80) gave in the first fractions 2-carbethoxycyclopentanone (72 mg); elution with ether–hexane (40:60) gave a yellowish liquid (300 mg, 60%) which is the monoalkylated product; ir (film) ν_{max}: 1740 and 1710 cm^{-1}; ^1H nmr (90 MHz) δ: 4.19 and 4.18 (2q, J = 7 Hz, 2H), 3.14 (m, 1H), 2.60 and 2.57 (2t, J = 7 Hz, 2H), 2.15 (s, 3H), and 1.28 (t, J = 7 Hz, 3H). Mass spectrum (EI, 70 eV) m/e: 208 M − H_2O, 181 M − OEt, 180 M − CH_3CH_2OH, 169 M − CH_2COCH_3, 156 M − $CH_2{=}CHCOCH_3$.

Ethyl-3-(2-propenyl)-2-oxo-cycloheptanecarboxylate (17) and ethyl-bis-1,3-(2-propenyl)-2-oxo-cycloheptanecarboxylate (18)

Under dry and inert atmosphere, a solution of enamino derivative **3**, A = —, B = $(CH_2)_2$, R = Et (480 mg, 2.02 mmol) and *p*-toluenesulfonic acid monohydrate (22 mg, 0.1 mmol) in dioxane (B) (10 mL) was heated to 100°C and treated with allyl bromide (C) (2.78 g, 20.2 mmol). Monitoring by vpc showed that the reaction ceased progressing after 19 h. Evaporation of the solvent under vacuum (40°C) led to a residue which was taken up in $CHCl_3$ (10 mL) and hydrolyzed by vigorously stirring at 63°C for 3 h with 10% HCl (3 mL). The aqueous phase was then decanted and reextracted with $CHCl_3$ (4 mL). The organic phases were treated in the usual manner to yield a brown liquid (246 mg). Flash chromatography (ether–hexane, 5:95) gave in the first fractions the dialkylated product **18** (9 mg, 2%) and in later fractions the monoalkylated product (**17**) (100 mg, 27%) as a mixture of 2 stereoisomers.

Compound 17: ir (film) ν_{max}: 3050, 1730, 1700, and 1630 cm^{-1}; ^1H nmr (90 MHz) δ: 5.7 (m, 1H), 5.0 (m, 2H), 4.19 and 4.15 (2q, J = 7 Hz, 2H), 3.52 (m, 1H), and 1.27 and 1.25 (2t, J = 7 Hz, 3H). Mass spectrum (CI, CH_4) m/e: 225 (100%) MH^+, 185 M − $CH_2CH{=}CH_2$, 179 M − OEt, 178 M − CH_3CH_2OH, 151 M − COOEt.

Compound 18: ir (film) ν_{max}: 3050, 1725, 1700, and 1630 cm^{-1}; ^1H nmr (90 MHz) δ: 5.7 (m, 2H), 5.1 (m, 4H), 4.21 (q, J = 7 Hz, 2H), and 1.28 (t, J = 7 Hz, 3H). Mass spectrum (CI, CH_4) m/e: 265 (100%) MH^+, 219 M − OEt.

Ethyl-2-acetyl-4-pentenoate (20)

Under dry and inert atmosphere, a solution of enamino derivative **19** (670 mg, 3.66 mmol) and *p*-toluenesulfonic acid monohydrate (26 mg, 0.18 mmol) in dioxane (B) (10 mL) was heated to 100°C and treated with allyl bromide (C) (3.3 g, 36.6 mmol). Monitoring by vpc showed the reaction to be complete after 17 h. The reaction mixture was evaporated under vacuum (40°C), the residue taken up in $CHCl_3$ (10 mL), and the solution stirred for 11 h with 5% HCl (vpc monitoring). The aqueous phase was decanted and extracted twice with $CHCl_3$ (4 mL); the organic phases were treated in the usual manner to yield a pale yellow liquid (560 mg, 90%) which showed only one peak by vpc; ir (film) ν_{max}: 3050, 1730, 1710, and 1630 cm^{-1}; ^1H nmr (90

MHz) δ: 5.7 (m, 1H), 5.11 (m, 2H), 4.20 (q, J = 7 Hz, 2H), 3.53 (t, J = 7 Hz, 1H), 2.60 (t, broadened, 2H), 2.24 (s, 3H), and 1.27 (t, J = 7 Hz, 3H). These data are in accord with those reported in the literature (56).

Methyl-2-methanesulfonyloxy-3-methyl-9-oxo-bicyclo[3.3.1]nonane-carboxylate (21)

Under dry and inert atmosphere, a solution of ketol ester **4** (20 mg, 88 μmol) in 400 μL of $CDCl_3$ (Merck) was treated with methanesulfonyl chloride (A) (41 mg, 350 μmol) and pyridine (C) (16 mg, 200 μmol) and progress of the reaction was monitored by nmr. After 5 days at room temperature, the reaction mixture was extracted with water (0.1 mL) and the aqueous phase reextracted with $CHCl_3$ (0.5 mL). The organic phases were combined and treated in the usual manner. The residue obtained was distilled in a Kugelrohr apparatus at 120°C/3.7 × 10^{-4} Torr to give a yellowish liquid (19 mg, 70%). In an alternate experiment, a crystalline product was obtained (mp 127–128°C ($CHCl_3$)) in a lower yield but showing the same spectroscopic characteristics as the former; ir ($CDCl_3$) ν_{max}: 1740, 1720, 1340, and 1170 cm^{-1}; ^1H nmr (90 MHz) δ: 5.25 (d, J = 10 Hz, 1H), 3.80 (s, 3H), 2.99 (s, 3H), and 1.19 (d, J = 6 Hz, 3H). Mass spectrum (CI, CH_4) m/e: 209 M − OSO_2CH_3, 208 M − CH_3SO_3H, 177 M − CH_3SO_3H − OCH_3, 149 M − CH_3SO_3H − $COOCH_3$.

Methyl-3-methyl-9-oxobicyclo[3.3.1]non-2-enecarboxylate (2)

Under inert atmosphere, a solution of ketomesylate **21** (266 mg, 0.87 mmol) in collidine (2 mL) was heated to 160°C for 29 h. The solution was cooled and the solvent evaporated at room temperature (0.5 Torr) to give a black residue. The latter was taken up in ether (3 mL) and 10% HCl (1 mL). The aqueous phase was decanted and extracted 3 times with ether (3 mL). The organic phases were treated in the usual manner to give a yellow oil (153 mg). Distillation in a Kugelrohr apparatus (75°C/4 × 10^{-4} Torr) gave a colorless liquid (129 mg, 71%); ir (film) ν_{max}: 1735 and 1710 cm^{-1}; ^1H nmr (400 MHz) δ: 5.38 (s, broadened, 1H), 3.78 (s, 3H), and 1.82 (s, 3H). Mass spectrum (CI, CH_4) m/e: 209 MH^+. *Exact Mass* calcd. for $C_{12}H_{16}O_3$: 208.1100; found: 208.1101. These data correspond to those reported in the literature (10, 12) for the same compound.

Acknowledgements

Financial support from the Natural Sciences and Engineering Research Council of Canada and the Ministère de L'Education du Québec, in the form of grants to D.G. and scholarships to M.L., is gratefully acknowledged.

1. E. M. KAISER, J. D. PETTY, and P. L. A. KNUTSON. Synthesis, 509 (1977).
2. S. N. HUCKIN and L. WEILER. J. Am. Chem. Soc. **96**, 1082 (1974).
3. P. E. SUM and L. WEILER. J. Chem. Soc. Chem. Commun. 91 (1977).
4. S. N. HUCKIN and L. WEILER. Can. J. Chem. **52**, 1343 (1974).
5. S. N. HUCKIN and L. WEILER. Can. J. Chem. **52**, 2157 (1974).
6. V. EHRIG and D. SEEBACH. Chem. Ber. **108**, 1961 (1975).
7. P. E. SUM and L. WEILER. Can. J. Chem. **55**, 996 (1977).
8. P. E. SUM and L. WEILER. Can. J. Chem. **57**, 1475 (1979).
9. D. H. R. BARTON, G. DRESSAIRE, B. J. WILLIS, A. G. M. BARRETT, and M. PFEFFER. J. Chem. Soc. Perkin Trans. 1, 665 (1982).
10. A. S. KENDE and J. A. SCHNEIDER. Synth. Commun. **9**, 419 (1979).
11. A. J. MURA, D. A. BENNETT, and T. COHEN. Tetrahedron Lett. 4433 (1975).
12. D. GRAVEL, R. DÉZIEL, and L. BORDELEAU. Tetrahedron Lett. **24**, 699 (1983).
13. T. H. CHAN and P. BROWNBRIDGE. J. Chem. Soc. Chem. Commun. 578 (1979).
14. P. BROWNBRIDGE and T. H. CHAN. Tetrahedron Lett. 4437 (1979).
15. T. H. CHAN and G. J. KANG. Tetrahedron Lett. **23**, 3011 (1982).
16. M. YOSHIMOTO, N. ISHIDA, and T. HIRAOKA. Tetrahedron Lett. 39 (1973).
17. (*a*) R. B. GAMMILL and T. A. BRYSON. Synthesis, 401 (1976); (*b*) T. A. BRYSON and R. B. GAMMILL. Tetrahedron Lett. 3963 (1974).
18. (*a*) J. FROBORG, C. MAGNUSSON, and S. THORÉN. Tetrahedron Lett. 1621 (1975); (*b*) G. C. GERRANS, A. S. HOWARD, and B. S. ORLEK. Tetrahedron Lett. 4171 (1975).
19. (*a*) H. J. LIU and E. N. C. BROWNE. Can. J. Chem. **59**, 601 (1981); (*b*) H. BOHME and K. KREITZ. Arch. Pharm. **291**, 566 (1958); (*c*) N. S. VUL'FSON, V. B. BERZIN, M. N. SIZOI, and L. G. ISAEVA. J. Org. Chem. USSR, **10**, 230 (1974); T. M. JACOBS, P. A. VATAKENCHERRY, and S. DEV. Tetrahedron, **20**, 2821 (1964).
20. S. J. FALCONE and M. E. MUNK. Synth. Commun. **9**, 719 (1979).
21. (*a*) J. E. BRENNER. J. Org. Chem. **26**, 22 (1961); (*b*) H. GAULT and L. KLESS. Bull. Soc. Chim. **39**, 883 (1926); (*c*) P. G. GASSMAN, T. J. VAN BERGEN, D. P. GILBERT, and B. W. CUE, JR. J. Am. Chem. Soc. **96**, 5496 (1974); (*d*) M. JULIA and J. LENZI. Bull. Soc. Chim. Fr. 2262 (1962).
22. R. B. MILLER and B. F. SMITH. Synth. Commun. **3**, 129 (1973).
23. J. BRUHN, H. HEIMGARTNER, and H. SCHMID. Helv. Chim. Acta, **62**, 2630 (1979).
24. R. B. WOODWARD, I. J. PACHTER, and M. L. SCHEINBAUM. J. Org. Chem. **36**, 1137 (1971).
25. E. W. COLVIN, J. MARTIN, and B. SHROOT. Chem. Ind. (London), 2130 (1966).
26. (*a*) S. HÜNIG, K. HÜBNER, and E. BENZING. Chem. Ber. **95**, 926 (1962); (*b*) G. A. BERCHTOLD. J. Org. Chem. **26**, 3043 (1961).
27. I. BELSKY. Tetrahedron, **28**, 771 (1972).
28. B. LAMM. Acta Chem. Scand. Ser. B, **29**, 332 (1975).
29. F. P. COLONNA, G. PITACCO, and E. VALENTIN. Tetrahedron, **27**, 5481 (1971).
30. C. GAGNON. Mémoire de maîtrise, Université de Montréal (1975).
31. L. RUEST, G. BLOUIN, and P. DESLONGCHAMPS. Synth. Commun. **6**, 169 (1976).
32. A. G. COOK. Enamines: synthesis, structure and reactions. Marcel Dekker, New York. 1969.
33. G. STORK, A. BRIZZOLARA, H. LANDESMAN, J. SZMUSZKOVICZ, and R. TERRELL. J. Am. Chem. Soc. **85**, 207 (1963).
34. A. G. SANCHEZ and J. BELLANATO. J. Chem. Soc. Perkin Trans. 2, 1561 (1975).
35. E. E. VAN TAMELEN and S. ROSENBERG BOCH. J. Am. Chem. Soc. **81**, 2907 (1958).
36. V. B. PISKOV. J. Org. Chem. USSR, **1**, 1254 (1965).
37. R. ROBINSON. J. Chem. Soc. **109**, 1038 (1916).
38. P. W. HICKMOTT. Tetrahedron, **38**, 1975 (1982), and references cited therein.
39. F. JOHNSON and A. WHITEHEAD. Tetrahedron Lett. 3825 (1964).
40. H. J. SCHAEFFER and V. K. JAIN. J. Org. Chem. **29**, 2595 (1964).
41. F. JOHNSON. Chem. Rev. **68**, 375 (1968).
42. P. HICKMOTT, P. J. COX, and G. A. SIM. J. Chem. Soc. Perkin Trans. 1, 2544 (1974).
43. E. W. COLVIN, J. MARTIN, W. PARKER, R. A. RAPHAEL, B. SHROOT, and M. DOYLE. J. Chem. Soc. Perkin Trans. 1, 860 (1972).
44. Z. HORRI, T. IMANISHI, S. KIM, and I. NINOMIYA. Chem. Pharm. Bull. **16**, 1918 (1968).
45. R. P. LINSTEAD, L. N. OWEN, and R. F. NEBB. J. Chem. Soc. 1225 (1953).
46. W. E. HANFORD and J. C. SAUER. Org. React. **3**, 108 (1946).
47. (*a*) J. F. KING and D. R. K. HARDING. Can. J. Chem. **54**, 2652 (1976); see also (*b*) J. F. KING. Acc. Chem. Res. **8**, 10 (1975).
48. J. F. KING and J. R. DU MANOIR. J. Am. Chem. Soc. **97**, 2566 (1975).
49. J. S. GROSSERT and M. M. BHARADWAJ. J. Chem. Soc. Chem. Commun. 144 (1974).

50. M. E. KUEHNE. Synthesis, 510 (1970).
51. H. EL KHADIM and S. HANESSIAN. Anal. Chem. **30**, 1965 (1958).
52. W. C. STILL, M. KAHN, and A. MITRA. J. Org. Chem. **43**, 2923 (1978).
53. S. J. RHOADS and C. PRYDE. J. Org. Chem. **30**, 3212 (1965).
54. S. CARLSSON and S. O. LAWESSON. Tetrahedron, **38**, 413 (1982).
55. S. A. G. DE GRAAF and U. K. PANDIT. Tetrahedron, **29**, 2141 (1973).
56. Y. GAONI. J. Chem. Soc. (C), 2925 (1968).

Tautomeric equilibrium of cyclic β-ketoester enamines

MARC LABELLE[1] AND DENIS GRAVEL[2]
Département de chimie, Université de Montréal, C.P. 6210, Succ. A, Montreal (Qué.), Canada H3C 3V1

Received August 22, 1984

This paper is dedicated to Professor Camille Sandorfy on the occasion of his 65th birthday

MARC LABELLE and DENIS GRAVEL. Can. J. Chem. **63**, 1884 (1985).

The conjugated–unconjugated tautomerism of β-ketoester enamines has been investigated. Enamines with different amine ring size, ketone ring size, and ester alkyl group have been prepared. Equilibrium ratios of the conjugated and unconjugated forms have been determined. A three-point rationalization is presented: (1) the relative instability of the conjugated form is due to a large steric interaction; (2) the ring size combination largely determines the equilibrium ratio because of energy differences between the resonance hybrid structures of the conjugated forms; (3) the ester alkyl group slightly affects the equilibrium ratio, through a difference in rotational freedom in the conjugated form. The degree of instability of double bonds exocyclic to 5-, and 6-, and 7-membered rings is discussed.

MARC LABELLE et DENIS GRAVEL. Can. J. Chem. **63**, 1884 (1985).

L'équilibre tautomérique des formes conjuguées et déconjuguées des énamines de β-cétoesters a été étudiée. Plusieurs énamines de diverses grandeurs de cycle à l'amine et au cétoester et divers groupes alkyles à l'ester ont été préparées. Les proportions de formes conjuguées et déconjuguées à l'équilibre sont rapportées. Les résultats sont expliqués à partir de trois effets: (1) l'instabilité relative des formes conjuguées est due à une importante interaction stérique; (2) les proportions des deux formes sont surtout controlées par la grandeur des cycles impliqués, en raison de différences d'énergie entre les structures hybrides de résonance; (3) la nature du groupe alkyle de l'ester influence le rapport des deux formes à cause d'une différence de liberté de rotation dans la forme conjuguée. Le degré d'instabilité des doubles liens exocycliques à des cycles à 5, 6 et 7 chaînons est discuté.

In the course of our study on the scope and limitations of β-ketoester enamines in organic synthesis (1), we became interested in investigating the factors which control the equilibrium between the conjugated and unconjugated forms in β-ketoester enamines (Scheme 1). An examination of the literature revealed that the presence, at equilibrium, of significant amounts of the unconjugated form is not a phenomenon limited to β-ketoester enamines (2–4) but has also been observed with β-ketoamide enamines (5–7), β-diketone enamines (4, 8, 9), β-ketosulfone enamines (10), and β-ketothioamide enamines (7). The presence of this equilibrium has also been frequently noted in the results of enamine acylations (3, 5, 8, 10, 11) which often give some 1,3-diacylated product, resulting from acylation of the unconjugated form of the monoacylated product.

The only systematic study dealing with the equilibrium between the conjugated and unconjugated forms in β-dicarbonyl enamines has been published by Colonna *et al.* (3). In this paper, the authors report the observed equilibrium proportions of conjugated and unconjugated forms for a number of β-dicarbonyl enamines, as well as the results of the reaction of these compounds with two electrophiles, namely phenylisocyanate and diethyl azodicarboxylate. A rationale for the equilibrium ratios, based on steric arguments (as in the case of 2-methylcyclohexanone enamines (12)), inductive and resonance effects, and differences in the conjugating ability of the amine moiety, is proposed by the authors (3).

In the present paper, we wish to report the results of a study focused on the case of β-ketoester enamines. The effect of both the ketone and the amine ring size, as well as that of the ester alkyl group have been examined. These new parameters should give a better characterization of the phenomenon and should allow a more accurate formulation of the factors responsible for the proportions of conjugated and unconjugated forms in β-ketoester enamines.

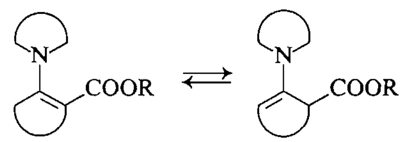

SCHEME 1

Synthesis of the enamine derivatives

The enamines were synthesized as previously described (1), using a β-ketoester,[3] 5 equivalents of the amine, and 0.05 equivalent of *p*-toluenesulfonic acid in gently refluxing benzene. The reactions are monitored by vpc, where disappearance of the β-ketoester and β-ketoamide[4] peaks, and appearance of the enamine peak could be observed. Interestingly, both the conjugated and unconjugated forms elute together in all the enamines studied, which indicates a rapid rate of equilibration between the two forms under the vpc conditions.

The enamine purification involves a distillation under high vacuum. In a few cases, the distillate solidified to a waxy solid on standing. This phenomenon was observed only with enamines where the conjugated form largely dominates the equilibrium. In order to confirm that the solid product is the conjugated form alone, the oily solid ethyl 2-(1-pyrrolidinyl) 1-(and 2-)cyclohexenecarboxylate (**1**), which is an 88 : 12 mixture of the conjugated and unconjugated forms at the equilibrium ($CDCl_3$, 23°C), was dissolved in hexane and cooled to −78°C to precipitate a white powder. This treatment, repeated once

[1] Holder of Natural Sciences and Engineering Research Council of Canada and FCAC (Québec) fellowships, 1978–1982.

[2] Author to whom correspondence should be addressed.

[3] This approach to β-ketoester enamines required the preparation of several β-ketoesters as starting materials. For this purpose, a published preparation of methyl 2-oxocyclohexenecarboxylate (13) was used, which, with slight modifications, was extended into a fairly general method for generating β-ketoesters from cyclic ketones (see Experimental).

[4] The β-ketoamide is formed on the vpc column from the β-ketoester and the amine (see ref. 27).

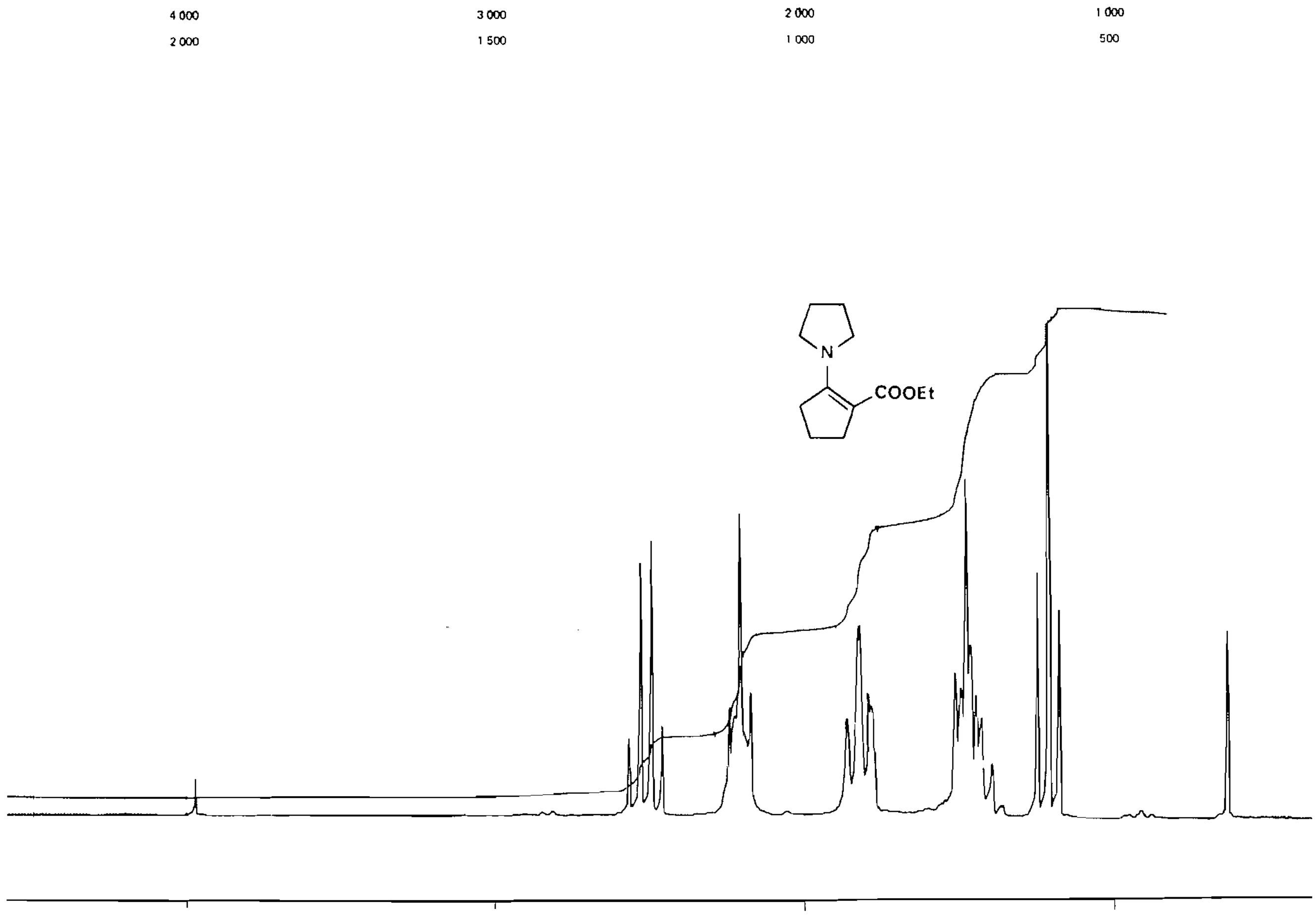

FIG. 1. ^{1}H nuclear magnetic resonance spectrum of compound **9**.

more, yielded a dry powder which, in a KBr emulsion at room temperature, showed only one set of ir bands, at 1670 and 1550 cm^{-1}, corresponding to vinylogous carbamate absorptions (14). This demonstrates that the solid form of the compound is indeed the vinylogous carbamate.

Interestingly, when this same powder was melted (40°C) between NaCl plates, the 1730 cm^{-1} enamine ir band appeared immediately, indicating that the compound had returned to the equilibrium mixture containing some unconjugated form. On cooling to room temperature, the compound did not solidify, and the ir spectrum was unchanged. This experiment shows that a rapid equilibration in the neat liquid phase is occurring for this particular enamine. As we shall see below, however, not all enamines equilibrate so rapidly at or around room temperature.

Results

The ratios of unconjugated to conjugated forms for the various enamines were determined by nmr. Typical spectra are shown in Figs. 1 and 2. The unconjugated form olefinic proton, when well separated (see Fig. 2), is a reliable source of quantitative information. However, in the case of the pyrrolidinoenamines ethyl and isopropyl 2-(1-pyrrolidinyl) 2- (and 1-)cyclohexenecarboxylate, **1** and **2**, this olefinic proton signal was masked by another band, and the desired unconjugated–conjugated ratio was obtained through the relative integration of the protons on the carbon attached to the nitrogen in the amine ring. This signal displays a considerable difference in chemical shift depending on whether the enamine double bond is conjugated to the ester or not.

Semi-quantitative support for the proton nmr derived ratios is obtained from the ^{13}C nmr and ir spectra. The carbon nmr shows several signals attributable to either the unconjugated or conjugated form. Their relative intensity, or the absence of one of the sets of signals, is an indication of the equilibrium ratio. The ir spectra provide the same kind of support to the proton nmr integration, especially through the relative intensity of the carbonyl band (unconjugated around 1730 cm^{-1}, conjugated around 1680 cm^{-1}) and the olefin band (unconjugated around 1640 cm^{-1}, conjugated around 1550 cm^{-1}).

A crucial aspect of these measurements is to make sure that the state of equilibrium has been reached when the ratio is measured. In some instances, especially for piperidinoenamines, the complete equilibration was rather slow. This was noticed when a careful fractional distillation of the enamine **3** was done, leading to a significant enrichment in the more volatile unconjugated form. In such cases, an nmr spectrum recorded 10 min after distillation has given ratios up to 92:8 in favor of the unconjugated form. The ratio of this solution, however, reached the equilibrium value of 75:25 within 3 days. This control of the equilibration has been performed on several other enamines but the equilibration of enamines with ring size combinations other than 6,6 appears to be much faster.

Table 1 represents the proportion of unconjugated form obtained for various enamines. Some of these compounds were already reported in the literature, as shown in Table 2. Part of the discrepancies observed may be due to different equi-

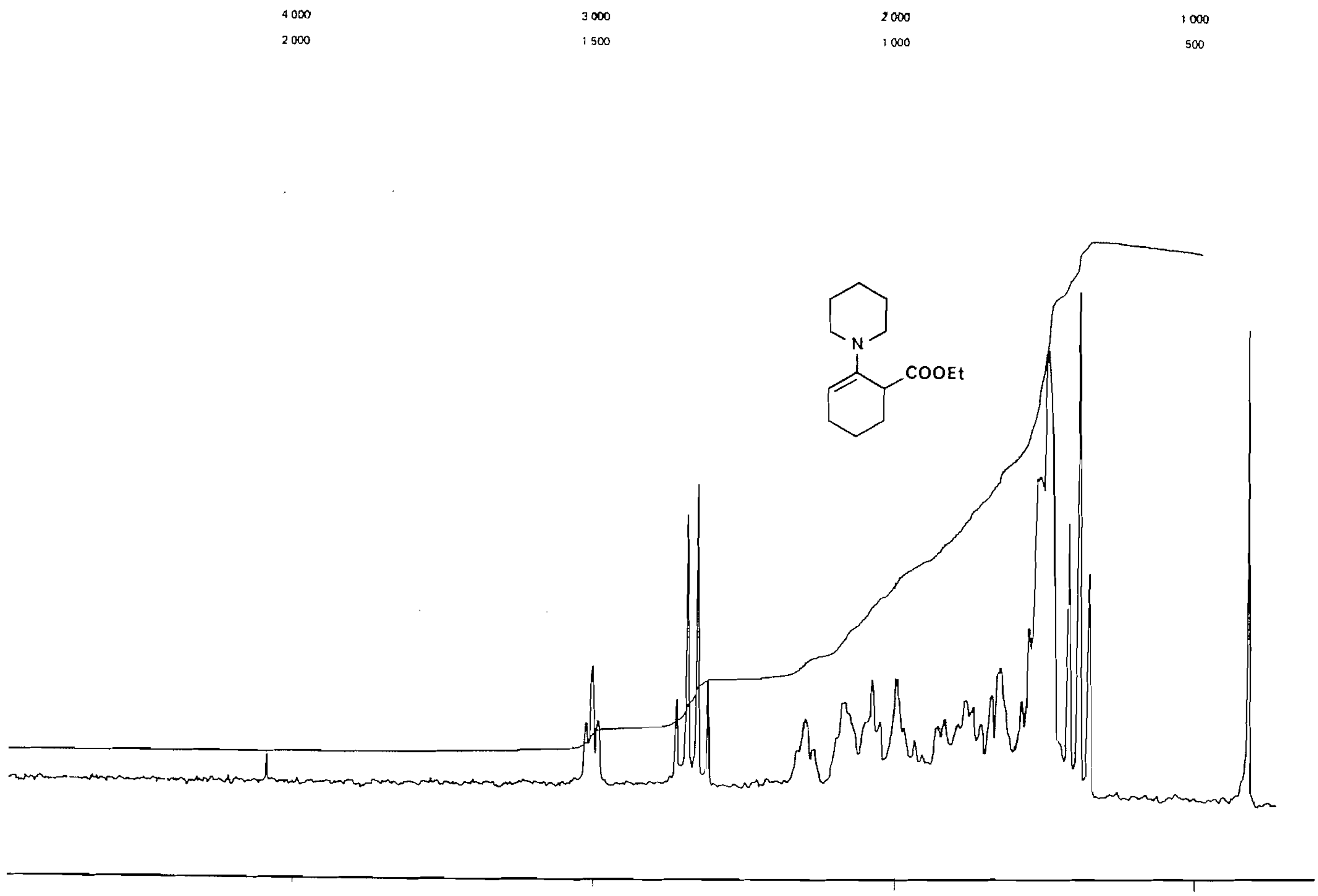

FIG. 2. [1]H nuclear magnetic resonance spectrum of compound **3**.

TABLE 1. Percentage of unconjugated form in β-ketoester enamines

β-Ketoester	Amine 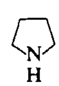	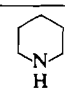	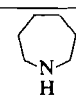
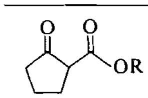	**4** R = Me: <1% **9** R = Et: <1%	(**5**) R = Me: <5% (**6**) R = Et: <5%	(**7**) R = Et: <5%
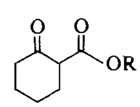	**8** R = Me: 5% **1** R = Et: 12% **2** R = iPr: 15%	(**10**) R = Me: 66% (**3**) R = Et: 75% (**11**) R = iPr: 75%	(**12**) R = Me: 25% (**13**) R = Et: 36% (**14**) R = iPr: 36%
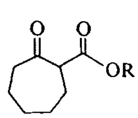	**15** R = Et: <5%		

libration conditions, since these conditions were not always specified in the literature.

In Table 1, one observes in the horizontal direction that the proportion of unconjugated form is smaller for a pyrrolidino-enamine than for a hexahydroazepino-enamine, which is smaller than that for a piperidino-enamine. The amine ring size therefore shows a 6 > 7 > 5 order for the tendency to unconjugation.

In the vertical direction, the effect of the β-ketoester ring size on the tendency towards unconjugation seems to be the same as that for the amine, the cyclopentanone showing less unconjugated form than the cyclohexanone, and the cycloheptanone being somewhere in between (only one example, however).

Within each ring size combination, the effect observed in varying the ester alkyl group is that a methyl ester shows less unconjugated form than the corresponding ethyl or isopropyl esters, which are about equal.

TABLE 2. β-Ketoester enamines reported in the literature

Enamine	% of unconjugated form (this work)	% of unconjugated form (literature)	Reference
1	12	0	25
		15	3
		30	2
3	75	73	3
		0[a]	25
8	5	10	3
9	<1	0	25
10	66	51	3

[a]The work reporting 0% of unconjugated form is based on ^{13}C nmr as only purity criterion, and the chemical shifts reported do not match ours.

TABLE 3. Time required for the formation of ethyl β-ketoester enamines (hours)

β-Ketoester ring	Amine ring 5	Amine ring 6	Amine ring 7
5	2	16	4
6	4.5	125	47
7	27	Very long[a]	Very long[a]

[a]Very slow reaction; only the competing β-ketoamide formation is observed.

TABLE 4. Distance between O and H in the model and percentage of unconjugated form

Amine/β-ketoester ring sizes	O—H distance (Å)	% of unconjugated form
5/5	1.4	<1
5/6	1.4	12
6/5	0.4	<5
6/6	0.4	75

Discussion

In order to carry out a more systematic study of the effect of both ring sizes on the conjugated–unconjugated ratios, the preparation of all 9 possible ring size combinations using the most common 5-, 6-, and 7-membered rings was attempted. Unfortunately, the piperidino and hexahydroazepino enamines of ethyl 2-oxo cycloheptanecarboxylate (**16**) resisted all attempts of preparation by our method (1). Only starting material was recovered under normal conditions, and a higher reaction temperature resulted in the formation of β-ketoamide. Another method (15), using $TiCl_4$ as the dehydrating agent, also failed, although it has been used successfully for difficult cases with normal ketones. These results suggest that these two enamines probably cannot be prepared by a simple β-ketoester and amine dehydrative condensation, and that some more indirect route will be necessary.

This relative slowness of the 7-membered ring ketoesters to form the enamine is consistent with data from cycloheptanone enamines (16) as well as with the rest of our data. The time needed for the formation of the various enamines is shown in Table 3. As seen from the first column, the β-ketoester ring size affects the rate of reaction in the order 5 faster than 6, faster than 7. On the other hand, the first two rows show that the 5-membered ring amine gives faster reactions than the 7-membered ring analog, which is, this time, faster than the

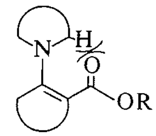

SCHEME 2

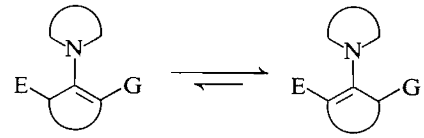

E = COOEt G = N—NH—COOEt ref. 3
COOEt
E = CN G = CH_3 ref. 16
E = CONHPh G = CH_3 ref. 5*b*

SCHEME 3

6-membered ring analog. From these trends, the two slowest reactions expected are precisely the two that did not work. The exact reason for this phenomenon is not known but one can safely speculate that it must be a combination of the difference in immonium ion energy and the rates of formation of the carbinolamines. Stork *et al.* (17) have observed that both steps are important in determining the rate of formation of simple ketone enamines, and our results clearly cannot be rationalized in terms of a single common rate-limiting step.

The equilibrium ratios of unconjugated and conjugated forms presented in Table 1 are rationalized by invoking three distinct factors.

(1) The first factor, which explains the unexpected presence of the unconjugated form, is present in the conjugated form of all enamines. It is the high energy steric interaction ($A^{1,3}$ strain) that would be present in the planar form required for optimal conjugation. The energy forcing this molecule out of the perfect π-plane can be appreciated from Drieding models (Table 4), which show very large van der Waals interactions between the carbonyl O and the amine H's (Scheme 2). This strain forces at least one of the conjugating groups out of plane, making the resonance stabilization of the conjugated form so weak that its energy is of the same order of magnitude as that of the unconjugated form, thus making the relative abundances of the two forms about equal.

The steric, as opposed to electronic, nature of this interaction is supported by the very normal conjugation behavior of the closely related 6-alkyl systems (Scheme 3), which have a conjugating and a non-conjugating substituent in both α-positions of the enamine. In this case, where the enamine can experience steric hindrance in or out of conjugation, the conjugated form is the only one detected.

One could suggest that the magnitude of the steric interaction that would be encountered in the planar form could be related to the equilibrium ratio observed for the two forms. However, the O-to-H distances in Drieding models (Scheme 2, Table 4) and the unconjugated vs. conjugated form ratios do not correlate for all enamines, even when only the stereochemically well-defined 5- and 6-membered rings are considered. The problem arises when the 6/5 combination, expected to show mostly the unconjugated form from the short O-to-H distance in the model, actually exists in >95% in the conjugated form. The large equilibrium displacement from the expected "all

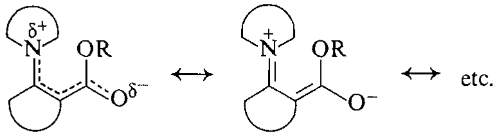

SCHEME 4

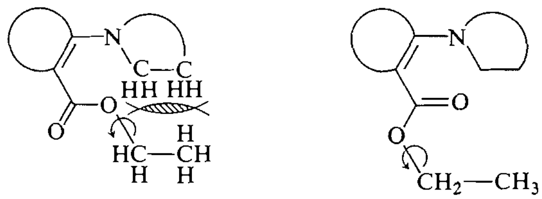

SCHEME 5

conjugated" situation brought about by steric interactions may still depend to a certain extent on the magnitude of that interaction. However, the strain is certainly avoided by an out-of-plane rotation of the amine ring[5] or of the carboxylate, and this type of strain relief is much less senstive to the exact size of the interacting groups, therefore contributing very little to the difference in energy among the various enamines.

(2) Since the first factor seems to affect all ring size combinations to a comparable extent, a second factor must be invoked to explain the differences observed upon ring size variation. It seems very plausible that the relative stability of the resonance hybrid (Scheme 4) is at the origin of the observed trends.[6] In fact, it is known (18) that the energy difference between exocyclic and endocyclic double bonds varies with the ring size. Thus, the number of double bonds exocyclic to unfavorable rings (6-membered, and 7-membered to a lesser extent) in the conjugated form (Scheme 4) could very well be related to the instability of that tautomer and therefore to its abundance at equilibrium. Table 5 illustrates this relationship. Assuming that an exocyclic double bond to a 7-membered ring is less stable than that to a 5-membered ring, but more than that to a 6-membered one, our results show an interesting correlation between the number of double bonds exocyclic to unfavorable rings and the position of the equilibrium between the two forms.

This order of exocyclic double bond "instability" with the 7-membered ring about halfway between the 5- and the 6-membered ones is not a very well established concept, and will be further discussed below.

(3) Finally, a third factor slightly alters the relative stabilities of the various alkyl esters. Our results indicate that the methyl esters have less tendency to unconjugation than the ethyl and isopropyl esters. The equivalence of the latter two alkyl groups suggests that the inductive effect of the alkyl group (3) cannot be the only cause of the greater instability of the ethyl and isopropyl conjugated forms. We therefore propose that the ethyl and isopropyl ester enamines, having the alkoxy chain one atom longer than the methyl ester, suffer a loss of rotational freedom (Scheme 5) in the electronically more stable *cis-s-trans* configuration (14) of the conjugated form, therefore slightly increasing the energy of that tautomer and thereby displacing the equilibrium towards the unconjugated form.

TABLE 5. Relation between the number of exocyclic double bonds and the percentage of unconjugated form in ethyl esters

Amine/β-ketoester ring sizes	% of unconjugated form	Number of exocyclic double bonds to various rings		
		5	7	6
5/5	<1	3		
6/5	<5	2		1
7/5	<5	2	1	
5/7	<5	1	2	
5/6	12	1		2
7/6	36		1	2
6/6	75			3

Stability of double bonds exocyclic to 7-membered rings

The Brown generalization (18), despite early criticism, has been used successfully to explain many phenomena in organic chemistry. It specifies that exocyclic double bonds to 5-membered rings (5mr) are less unstable than double bonds to 6-membered rings (6mr). In the original paper, no mention of 7-membered rings (7mr) was made. Shortly thereafter, Brown and Ichikawa (19) published kinetic data of the borohydride reduction of many cycloalkanones, as well as kinetics for solvolysis of cycloalkyl chlorides and tosylates. The results, that 7mr and 5mr are solvolysed more rapidly or reduced more slowly than 6mr, were interpreted in terms of *I*-strain differences between the starting materials and the intermediates or the products. These results cannot, however, be considered as definitive concerning the position of 7mr relative to 6mr and 5mr in the relative exocyclic double bond instability, since other kinetic experiments have come to different conclusions. Thus, the exocyclic double bond instability order $6 \gg 7 > 5$ was obtained from the solvolysis of 1-alkyl cycloalkyl chlorides (20) and from the hydrolysis of lactams (21), whereas the oxygen exchange of cycloalkanones (22) gave an order of instability of $6 > 7 > 5$ in acid and $6 > 5 = 7$ in base.

Another way of evaluating the relative instability of the various exocyclic double bonds is based on measurements of the equilibrium ratio for compounds which can exist with a double bond exo- or endocyclic to the ring, as a function of the ring size. To our knowledge, there are two such cases reported in the literature, where the 7 mr are described. They are presented in eqs. [1] (ref. 23) and [2] (ref. 24).

[1] 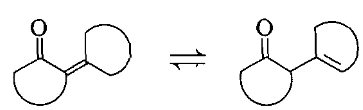

[2] 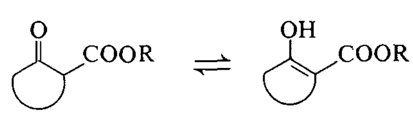

In both cases, the exocyclic/endocyclic ratio follows the order $5 > 7 > 6$. This order of ratio is also the one given by our data, and we believe that it represents the relative tendency of the various rings to bear an exocyclic double bond. Since our

[5] Rotation about the N—C bond of the less hindered *trans* aliphatic vinylogous carbamates have $\Delta G^{\ddagger}$ of the order of 10–15 kcal/mol in refs. 14 and 26.

[6] The stability of the unconjugated forms should also be considered in determing the expected ratio of the two forms, but since the conjugation energy involved in the conjugated form is much larger, the energy difference can be assumed to be mostly dependent on the energy of the conjugated forms.

TABLE 6. ^{13}C nuclear magnetic resonance chemical shifts for β-ketoester enamines

Compound	1U	1C	3C	3U	4U	2C	5C	5U
1	174.70	166.86	155.17	140.23	97.13	93.99	51.04	47.62
2	173.94	167.50	154.62	140.14	97.05	94.34	50.91	47.52
3	174.86	169.10	156.78	144.97	104.86	102.67	51.41	50.24
6		165.95	162.17			95.60	51.77	
7		166.43	160.48			94.96	52.88	
8	174.95	168.08	155.61		96.98	93.41	51.04	47.54
9		165.97	158.96			93.85	51.63	
10	175.23	169.17	157.29	144.89	104.86	101.94	51.55	50.24
11	174.78	168.66	155.68	145.04	104.79	104.26	51.26	50.24
12	175.23	168.88	158.75	141.76	98.15	97.49	52.07	50.53
13	174.57	168.52	158.31	141.61	97.93	97.79	51.99	50.02
14	174.13	168.30	157.65	141.92	98.66	98.15	51.99	50.10
15		167.50	162.25			98.37	51.70	

[a]The carbon numbering system refers to Scheme 6. Chemical shifts labeled C are those attributed to the conjugated form, the ones labeled U belong to the unconjugated form.

data on 7mr consist mainly of hexahydroazepine enamines, however, it is not absolutely certain that a cyclopentanone–cyclohexanone–cycloheptanone enamine series would yield the same result. The only case we have seems, however, to indicate that, at least, no major change in the expected trend has occurred.

Conclusion

This study has shed some light on the somewhat unusual tendency towards unconjugation observed in certain β-ketoester enamines. Although the rationale of the phenomenon proposed by Colonna *et al.* (3) was basically correct, the present broader study has served to define more clearly the factors determining the proportions of the two tautomers of β-ketoester enamines at equilibrium. Three factors have been identified as influencing the position of this equilibrium. Firstly, all β-ketoester enamine conjugated forms suffer a large $A^{1,3}$ strain in their planar conformation, which reduces the conjugative stabilization and makes both tautomers of roughly equal energies. Secondly, the stabilization energy of the resonance hybrid has partial double bonds exocyclic to the rings, and the stability of exocyclic double bonds varies with the ring size. Finally, a hindered O-alkyl bond rotation in the conjugated form of esters larger than methyl slightly destabilizes them, thus increasing the amount of unconjugated form at the equilibrium.

Experimental

Melting points were recorded on a Büchi oil bath apparatus and are not corrected. Proton nmr spectra were recorded as $CDCl_3$ solutions from a Bruker WH90 or Bruker WP80, and ^{13}C nmr spectra were recorded on the Bruker WP80. A Perkin–Elmer 710B was used to obtain ir spectra. Low resolution mass spectra were recorded on a V.G. Micromass 12-12, and mass analyses were performed on an AEI MS-902 updated with a V.G. console and a V.G. System 2000 computer. A Varian model 1200 vapor phase chromatograph with a 3 mm × 3.5 m glass 3% OV-1/Chromosorb W AW-DMCS column and flame ionization detector was used for vpc analyses.

Synthesis of the starting β-ketoesters

Ethyl 2-oxo cyclopentanecarboxylate (**16**) is available from Aldrich. Methyl 2-oxo cyclohexanecarboxylate (**17**) was prepared in 92% yield as described by Ruest *et al.* (13). The other starting β-ketoesters were obtained following Ruest's procedure, but the ketone addition time and the reflux time were changed as described below.

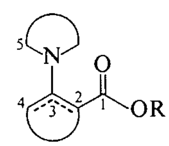

SCHEME 6

Methyl 2-oxo cyclopentanecarboxylate (**18**) was obtained in 72% yield when the ketone was added over 60 min and the mixture refluxed for 30 min after the addition. Spectroscopic data match those reported in the literature (13).

Ethyl 2-oxo cyclohexanecarboxylate (**19**) was obtained in 88% yield. The ketone addition time was 75 min and the reflux time 30 min. Spectroscopic data are as described in the literature (26).

Isopropyl 2-oxo cyclohexanecarboxylate (**20**) was obtained in 78% yield. The ketone addition time was 210 min and the reflux time 90 min. Colorless liquid, bp 63–65°C under 0.55 Torr (1 Torr = 133.3 Pa); ir: 1730, 1710, 1640, 1600 cm^{-1}; nmr: 12.36 (s, 0.88H), 5.09 (septet, J = 6 Hz, 1H), 3.34 (t, 0.12H), 1.28 (d, J = 6 Hz, 6H); ms: 185, 143, 125.

Ethyl 2-oxo cycloheptanecarboxylate (**21**) was prepared in 90% yield with a ketone addition time of 60 min and a reflux time of 30 min. Spectroscopic data match those described in the literature (26).

Synthesis of the enamines

The following enamines were prepared as previously described (1): ethyl 2-(1-pyrrolidinyl) 1-cyclopentenecarboxylate (**9**), ethyl 2-(1-piperidinyl) 1-cyclopentenecarboxylate (**6**), ethyl 2-(1-pyrrolidinyl) 1-cyclohexenecarboxylate (**1**), ethyl 2-(1-piperidinyl) 1-cyclohexenecarboxylate (**3**), ethyl 2-(1-pyrrolidinyl) 1-cycloheptenecarboxylate (**15**), and methyl 2-(1-piperidinyl) 1- (and 2-)cyclohexenecarboxylate (**10**). The ^{13}C nmr data for the enamines are reported in Table 6, with the numbering system of Scheme 6.

Methyl 2-(1-pyrrolidinyl) 1-cyclopentenecarboxylate (**4**) was prepared by the method previously described (1), using 21 mmol of methyl 2-oxo cyclopentanecarboxylate (**18**) and pyrrolidine. A 1.85-g (45%) fraction distilled between 86 and 89°C under 3.3 × 10^{-4} Torr. On cooling to −15°C, this yellow oil solidified to a yellowish solid, mp 57–61°C (sealed tube); ir: 1670, 1560 cm^{-1}; nmr: 3.64 (s, 3H), 3.44 (t, 4H), 2.61 (t, J = 7 Hz, 4H); ms (EI): 195, 180, 164, 136.

Methyl 2-(1-piperidinyl) 1-cyclopentenecarboxylate (**5**) was prepared by the method previously described (1), using 19 mmol of methyl 2-oxo cyclopentanecarboxylate (**18**) and piperidine. A 2.21-g (56%) fraction of colorless liquid distilled between 76 and 80°C under 3.3 × 10^{-4} Torr; ir: 1660, 1550 cm^{-1}; nmr: 3.64 (s, 3H), 3.34 (s, 4H), 2.62 (t, J = 7 Hz) and 2.54 (t, J = 7 Hz, 4H), 1.74 (q, J = 7 Hz), and 1.61 (s, 8H); ms (EI): 209, 194, 178, 166, 150.

Ethyl 2-(1-hexahydroazepinyl) 1-cyclopentenecarboxylate (**7**) was prepared by the method previously described (1), using 17.7 mmol of ethyl 2-oxo cyclopentanecarboxylate (**16**) and hexahydroazepine. A 3.10-g (74%) fraction of yellowish liquid distilled between 101 and 110°C under 2×10^{-2} Torr; ir: 1728, 1675, 1560 cm^{-1}; nmr: 4.99 (t, <0.05H), 4.10 (q, J = 7 Hz, 2H), 3.48 (t, 4H), 2.63 (m, 4H), 1.74 (m, 6H), 1.57 (s, 4H), 1.26 (t, J = 7 Hz, 3H).

Methyl 2-(1-pyrrolidinyl) 1- (and 2-)cyclohexenecarboxylate (**8**) was prepared by the method previously described (1), using 19.2 mmol of methyl 2-oxo cyclohexanecarboxylate (**17**) and pyrrolidine. A 2.81-g (70%) fraction of colorless liquid distilled between 90 and 97°C under 8×10^{-4} Torr. On standing, this liquid solidified to a white solid, mp 69–79°C (sealed tube). ir: 1720, 1660, 1610, 1540 cm^{-1}; nmr: 4.50 (t, J = 3 Hz, 0.05H), 3.67 (s, 3H), 3.26 (t, 4H), 2.41 (t, 4H), 1.84 (m, 4H), 1.56 (m, 4H); ms (CI, CH_4): 210, 194, 178, 150. *Exact Mass* calcd.: 209.1415; found: 209.1401.

Isopropyl 2-(1-pyrrolidinyl) 1- (and 2-)cyclohexenecarboxylate (**2**) was prepared by the method previously described (1), using 16.3 mmol of isopropyl 2-oxo cyclohexanecarboxylate (**20**) and pyrrolidine. A 3.08-g (80%) fraction of colorless liquid distilled between 80 and 85°C under 9×10^{-4} Torr. On standing, this liquid solidified to a white solid, mp 51–57°C (sealed tube). ir: 1720, 1680, 1630, 1540 cm^{-1}; nmr:[7] 4.99 (septet, J = 6 Hz, 1H), 4.49 (t, J = 4 Hz, 0.17H), 3.24 (t, 3.3H), 2.96 (t, 0.7H), 2.40 (s, 4H), 1.23 (d, J = 6 Hz, 6H); ms (CI, CH_4): 238, 178, 150. *Exact Mass* calcd.: 237.1728; found: 237.1735.

Isopropyl 2-(1-piperidinyl) 1- (and 2-)cyclohexenecarboxylate (**11**) was prepared by the method previously described (1), using 16.3 mmol of isopropyl 2-oxo cyclohexanecarboxylate (**20**) and piperidine. A 2.68-g (72%) fraction of colorless liquid distilled between 75 and 77°C under 4.7×10^{-4} Torr; ir: 1720, 1640 cm^{-1}; nmr:[7] 5.02 (septet, J = 6 Hz, 1H), 4.88 (t, J = 4 Hz, 0.79H), 3.25 (t, 0.79H), 1.26 (d, J = 6 Hz), and 1.23 (d, J = 6 Hz, 6H); ms (CI, CH_4): 252, 192, 164. *Exact Mass* calcd.: 251.1848; found: 251.1885.

Methyl 2-(1-hexahydroazepinyl) 1- (and 2-)cyclohexenecarboxylate (**12**) was prepared by the method previously described (1), using 19.7 mmol of methyl 2-oxo cyclohexanecarboxylate (**17**) and hexahydroazepine. A 2.48-g (53%) fraction of colorless liquid distilled between 88 and 89°C under 8×10^{-4} Torr; ir: 1725, 1670, 1630, 1540 cm^{-1}; nmr:[7] 4.64 (t, J = 4 Hz, 0.32H), 3.70 (s) and 3.67 (s, 3H), 3.2 (m, 4H); ms (CI, CH_4): 238, 222, 206, 178. *Exact Mass* calcd.: 237.1728; found: 237.1711.

Ethyl 2-(1-hexahydroazepinyl) 1- (and 2-)cyclohexenecarboxylate (**13**) was prepared by the method previously described (1), using 17.7 mmol of ethyl 2-oxo cyclohexanecarboxylate (**19**) and hexahydroazepine. A 2.59-g (58%) fraction of yellowish liquid distilled between 76 and 80°C under 6×10^{-4} Torr; ir: 1720, 1660, 1620, 1540 cm^{-1}; nmr:[7] 4.63 (t, J = 4 Hz, 0.35H), 4.16 (q, J = 7 Hz) and 4.13 (q, J = 7 Hz, 2H), 3.17 (m, 4H), 1.26 (t, J = 7 Hz, 3H); ms (EI): 251, 236, 222, 207, 178. *Exact Mass* calcd.: 251.1885; found: 251.1908.

Isopropyl 2-(1-hexahydroazepinyl) 1- (and 2-)cyclohexenecarboxylate (**14**) was prepared by the method previously described (1), using 16.3 mmol of isopropyl 2-oxo cyclohexanecarboxylate (**20**) and hexahydroazepine. A 2.30-g (53%) fraction of yellowish liquid distilled between 82 and 90°C under 4.8×10^{-4} Torr; ir: 1720, 1670, 1630, 1550 cm^{-1}; nmr: 5.03 (septet, J = 6 Hz) and 4.99 (septet, J = 6 Hz, 1H), 4.63 (t, J = 4 Hz, 0.36H), 3.1 (m, 4.4H), 1.23 (d, J = 6 Hz, 6H); ms (CI, CH_4): 266, 206, 178. *Exact Mass* calcd.: 265.2041; found: 265.2046.

Proportions of enamine and vinylogous carbamate

The equilibrium proportions of unconjugated and conjugated forms in Table 1 were obtained from proton nmr spectra of $CDCl_3$ solutions at 23°C. The ir and ^{13}C nmr spectra used to secure the value obtained from this integration were also obtained from $CDCl_3$ at 23°C.

In order to make sure that the ratios observed are really representative of the equilibria under these conditions, random controls were performed in which an nmr tube containing the enamine solution under examination was sealed under vacuum and allowed to stand for several days at room temperature, in the dark. Under these conditions, constant ratios were obtained for all enamines tested. All equilibrations proved to be fast, except for that of alkyl 2-(1-piperidinyl) 1- (and 2-)cyclohexenecarboxylates **3**, **10**, and **11**, which were complete within 3 days.

[7] The conjugated–unconjugated ratio discrepancy between Table 1 and this spectrum is due to the fact that this sample was not allowed to equilibrate fully before recording the spectrum.

Acknowledgments

We wish to thank the Fonds FCAC (Québec) and the Natural Sciences and Engineering Research Council of Canada for financial support through grants and fellowships, and Samuel H. Gellman for useful comments.

1. D. Gravel and M. Labelle. Can. J. Chem. **63**, 1874 (1985).
2. S. A. G. De Graff and U. K. Pandit. Tetrahedron, **29**, 2141 (1973).
3. F. P. Colonna, G. Pittaco, and E. Valentin. Tetrahedron, **27**, 5481 (1971).
4. H. W. Durbeck and L. L. Duttka. Tetrahedron, **29**, 4285 (1973).
5. (*a*) S. Hunig, K. Hubner, and E. Benzing. Chem. Ber. **95**, 926 (1962); (*b*) G. A. Berchtold. J. Org. Chem. **26**, 3043 (1961).
6. R. H. Rynbrandt and F. L. Schmidt. J. Med. Chem. **14**, 54 (1971).
7. H. Mazargil and A. Lattes. Bull. Soc. Chim. Fr. 3874 (1972).
8. I. Belsky. Tetrahedron, **28**, 771 (1972).
9. R. Jacquier, C. Petrus, F. Petrus, and M. Valentin. Bull. Soc. Chim. Fr. 2629 (1970); H. Hoch and S. Hunig. Chem. Ber. **105**, 2660 (1960).
10. B. Lamm. Acta Chem. Scand. Ser. B, **29**, 332 (1975).
11. R. B. Woodward, I. J. Pachter, and M. L. Scheinbaum. J. Org. Chem. **36**, 1137 (1971); E. W. Colvin, J. Martin, and B. Shroot. Chem. Ind. (London), 2130 (1966).
12. W. D. Gurowitz and M. A. Joseph. J. Org. Chem. **32**, 3289 (1967).
13. L. Ruest, G. Blouin, and P. Deslongchamps. Synth. Commun. **6**, 169 (1976).
14. A. G. Sanchez and J. Bellanato. J. Chem. Soc. Perkin Trans. 2, 1561 (1975).
15. W. A. White and H. Weingarten. J. Org. Chem. **32**, 213 (1967); R. Carlson, R. Phan-Tan-Luu, D. Mathieu, F. S. Ahouande, A. Babadjamian, and J. Metzger. Acta Chem. Scand. B, **32**, 335 (1978).
16. M. E. Kuehne. J. Am. Chem. Soc. **81**, 5400 (1959).
17. G. Stork, A. Brizzolara, H. Landesman, J. Szmuszkovicz, and R. Terrell. J. Am. Chem. Soc. **85**, 207 (1963).
18. H. C. Brown, J. H. Brewster, and H. Shechter. J. Am. Chem. Soc. **76**, 467 (1954); H. C. Brown. J. Org. Chem. **22**, 439 (1957).
19. H. C. Brown and K. Ichikawa. Tetrahedron, **1**, 221 (1957).
20. K. Ranganayakulu, M. Vasumathi Devi, R. Balaji Rao, and K. Rajeswari. Can. J. Chem. **58**, 1484 (1980).
21. P. Wan, T. A. Modro, and K. Yates. Can. J. Chem. **58**, 2423 (1980).
22. P. Greenzaid, Z. Luz, and D. Samuel. Trans. Faraday Soc. **64**, 2787 (1968).
23. S. J. Rhoads. J. Org. Chem. **31**, 171 (1966).
24. R. C. Cookson and N. R. Rogers. J. Chem. Soc. Perkin Trans. 1, 1037 (1974).
25. S. Carlsson and S. O. Lawesson. Tetrahedron, **38**, 413 (1982).
26. S. J. Rhoads and C. Pryde. J. Org. Chem. **30**, 3212 (1965).
27. M. Labelle and D. Gravel. J. Chem. Soc. Chem. Commun. 105 (1985).

Photochemical reactions of bacteriorhodopsin in Triton X-100 solution studied by low temperature spectrophotometry[1]

TATSUO IWASA AND FUMIO TOKUNAGA
Department of Physics, Faculty of Science, Tohoku University, Sendai 980, Japan

AND

TÔRU YOSHIZAWA[2]
Department of Biophysics, Faculty of Science, Kyoto University, Kyoto 606, Japan

Received August 16, 1984

This paper is dedicated to Professor Camille Sandorfy on the occasion of his 65th birthday

TATSUO IWASA, FUMIO TOKUNAGA, and TÔRU YOSHIZAWA. Can. J. Chem. **63**, 1891 (1985).

The photochemical reaction of purple membrane solubilized with Triton X-100 (T-BR) was investigated by low temperature spectrophotometry. The batho- and meta-intermediates of T-BR were observed to resemble bacteriorhodopsin in native purple membrane. Two photoproducts characteristic of the T-BR system were found, which were named the "490-nm complex" and the "380-nm complex". The 490-nm complex was in thermal equilibrium with T-BR in the dark. Cooling T-BR to low temperature favoured the 490-nm complex, which was photoinsensitive. On the other hand, the 380-nm complex was produced by warming the batho-intermediate and reverted to the original T-BR. The meta-intermediate of T-BR may possibly be in thermal equilibrium with the 380-nm complex. On the basis of the above results, the possible role of the membrane structure was discussed.

TATSUO IWASA, FUMIO TOKUNAGA et TÔRU YOSHIZAWA. Can. J. Chem. **63**, 1891 (1985).

Faisant appel à la spectrophotométrie à basse température, on a étudié la réaction photochimique de la membrane pourpre en solution dans le Triton X-100 (T-BR). Par example, on a observé les intermédiaires batho et méta du T-BR, comme la bactériorhodospine dans la membrane pourpre naturelle. On a trouvé deux produits photochimiques qui sont caractéristiques du système T-BR; on leur a donné les noms de "complexe 490 nm" et "complexe 380 nm". Dans l'obscurité, le complexe 490 nm est en équilibre thermique avec T-BR. Le refroidissement du T-BR favorise le complexe 490 nm qui est photosensible. Par ailleurs, le complexe 380 nm est obtenu en chauffant l'intermédiaire batho et il se retransforme en T-BR original. Il est possible que l'intermédiaire méta du T-BR soit en équilibre thermique avec le complexe 380 nm. À partir de ces résultats, on discute du rôle possible de la structure de la membrane.

[Traduit par le journal]

Introduction

Bacteriorhodopsin (BR) is the sole protein in the purple membrane of *Halobacterium halobium* (1). Like animal rhodopsin, BR has a retinal as its chromophore which binds to the ϵ-amino group of lysine residue of the protein moiety through a Schiff base linkage (2, 3). The retinylidene chromophore of light-adapted BR (BR^L) is in an all-*trans* form. On absorption of light, BR^L (*trans*-bR) converts to several intermediates such as batho- (K), lumi- (L), and meta-*trans*-BR (M) and eventually reverts to the original pigment (4, 5). This photochemical cycle forms an electrochemical gradient of protons across the membrane (1).

According to an electron diffraction analysis, BR molecules form a trimer structure aligned in a hexagonal lattice with the lattice distance of about 62 Å (6). The retinylidene chromophores of BR in the trimer exhibit a typical circular dichroic (cd) band owing to an exciton coupling. The purple membrane solubilized with Triton X-100 (T-BR), however, displays no exciton cd band because of dissociation of the trimer structure, though it has a small positive cd band due to an intrinsic one (7, 8). This indicates that T-BR should be in monomeric form (9).

Now the question is whether or not such a lattice structure has any physiological meaning. To answer this question, we have tried to investigate the photoreaction of T-BR. Irradiation of T-BR produced photointermediates, similar to the batho- and meta-intermediates in purple membrane, but the meta-intermediate of T-BR was more stable than that in purple membrane. We also found two new molecular species named the "490-nm complex" and the "380-nm complex", which are characteristic of the T-BR system.

Materials and methods

The purple membrane was prepared from *Halobacterium halobium* R_1 by a slight modification (5) of the method described by Oesterhelt and Stoeckenius (10), and suspended in 10 m*M* phosphate buffer (pH 6.8). To solubilize the membrane, a Triton X-100 solution (10% v/v) was mixed with the membrane suspension to give a final concentration of 1% (v/v) (about 10^3 moles/mole BR). The mixture (16 μ*M* BR) was used for spectroscopic and cd measurements at room temperature. The cd spectra were measured with a recording spectropolarimeter (Jasco J-20). An optical cell containing the sample (10-mm light path; 1 OD) was placed close to the window of the detector to reduce the scattering of the measuring light.

For low temperature spectrophotometry, glycerol in a final concentration of 75% (v/v) was added to the mixture (160 μ*M* BR, 50−100 moles of Trixon X-100/mole BR) and a recording spectrophotometer (Hitachi 323, 320 or Shimadzu MPS 5000) was equipped with a cryostat described by Yoshizawa (11). The sample was placed in an optical cell composed of two quartz plates and a rubber ring (1- or 2-mm light path; 1 OD) under dim red light and incubated in the dark at least for 8 h to be fully dark-adapted. The temperature of the sample was monitored continuously with a copper vs. constantan thermocouple attached to the sample holder made of copper.

A 500-W xenon lamp (Ushio) was used as a light source for irradiation of the sample. The wavelength of the actinic light was selected by a combination of interference and (or) cut-off filters (Toshiba).

[1]A part of this work was presented at the U.S.−Japan Cooperative Seminar on "The purple membrane of Halobacteria" held in May 1980 in Japan.

[2]Author to whom all correspondence should be addressed.

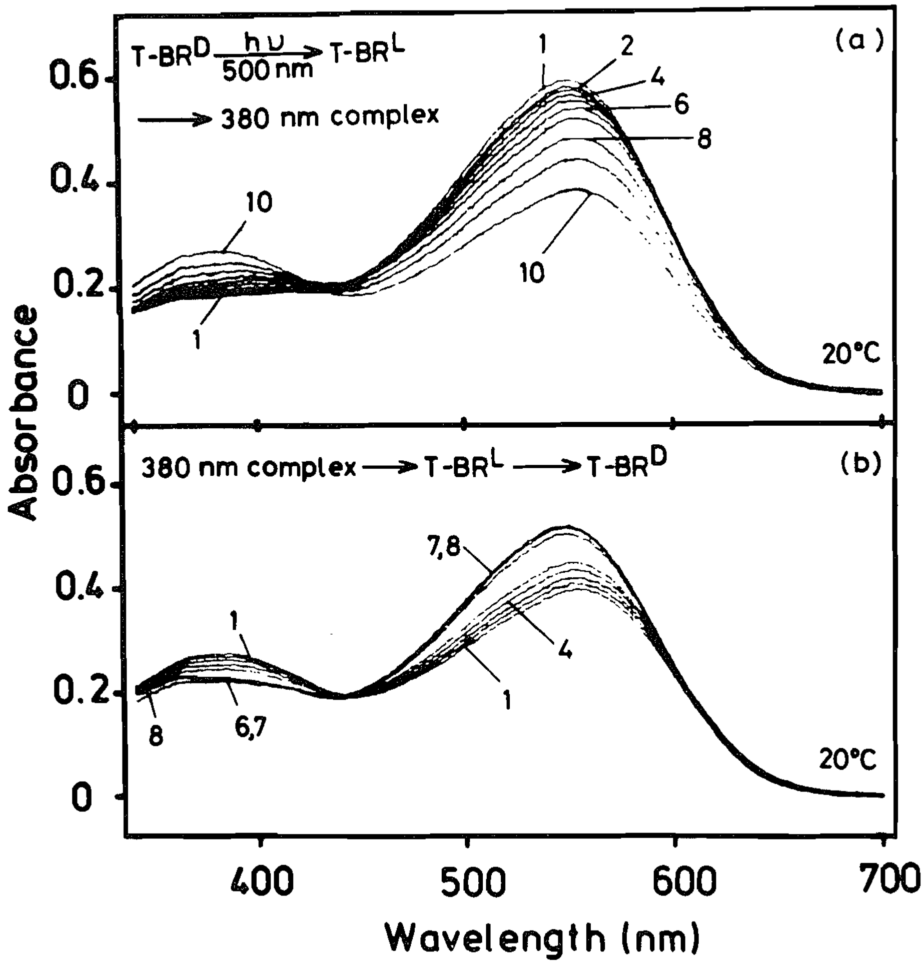

FIG. 1. (a) Photoreaction of T-BR^D at 20°C. Curve 1: T-BR^D (~10^3 moles of Triton X-100/mole BR). Curves 2–10: products of the successive irradiation of T-BR^D at 500 nm for 10, 10, 20, 40, 80, 160, 320, 640, and 1280 s, respectively. Curve 10 is a mixture of T-BR^L and the 380-nm complex. (b) Dark-reversion at 20°C. Curve 1: the mixture redrawn from curve 10 in (a). Curves 2–7: products of the successive dark incubation of the mixture. The spectra were measured at 5, 15, 40, 90, 585, and 955 min from the beginning of the dark incubation, respectively. Curve 8: a product of the dark incubation for more than 30 h.

The extraction of the chromophoric retinal from BR or T-BR was performed according to Tsuda *et al.*, (12). The sample (nearly 1 OD) was mixed with an equivolume of CH_2Cl_2 and the mixture was sonicated for a total of 5 min in an ice bath. After addition of 3 volumes of petroleum ether, 10–20 μL of the upper phase was injected to the hplc system (Jasco Tri-Rotar II with porous silica gel SS-05 column). All procedures were carried out at 0°C under dim red light and repeated 3 times.

Results

Photoreaction of dark-adapted T-BR and its thermal reversion; appearance of the "380-nm complex"

Upon addition of Triton X-100 to dark-adapted BR (BR^D, λ_{max}: 560 nm) the scattering of the measuring light decreased within 1 min, and the λ_{max} shifted to shorter wavelength (about 10 nm) within 7 min (data not shown), probably owing to some destruction of the membrane structure. The time course of these changes depends on the molecular ratio of Triton X-100 to BR molecules (13).

The dark-adapted T-BR (T-BR^D) thus obtained is shown in Fig. 1a as curve 1. An irradiation of T-BR^D with 500-nm light for 40 s at 20°C caused a bathochromic shift of the λ_{max} from 550 nm to 560 nm with a small decrease of absorbance at the λ_{max} (curves 2–4 in Fig. 1a). Since this spectral change can be regarded as that corresponding to the light-adaptation of the native BR, the product was designated as T-BR^L. Further irradiation with the same light caused a decrease of the absorbance around the λ_{max} and an increase in the wavelength region shorter than 440 nm, resulting in formation of a photoproduct having λ_{max} at 380 nm. Since the λ_{max} is located at a wavelength about 10 nm longer than that of free all-*trans* retinal, the chromophore seems to attach to the protein moiety. It is plausible that the chromophore may be located in the binding site, because the subsequent dark incubation slowly recovered the absorbance at 570 nm, with disappearance of the peak at 380 nm (Fig. 1b). Therefore, we designated the product as the "380-nm complex".

This slow "dark-reversion" is composed of two sequential reaction processes; one is the reversion from the 380-nm complex to T-BR^L and the other is the dark-adaptation of T-BR^L to T-BR^D. The reason is that the spectrum of the early stage in the spectral change (curve 3 – curve 1 in Fig. 1b) was similar in shape to that between the 380-nm complex and T-BR^L (curve 10 – curve 7 in Fig. 1a), indicating that the 380-nm complex reverted to T-BR^L. Also, the difference spectrum of the later stage (curve 7 – curve 4 in Fig. 1b) displayed a different shape from that of the early stage; the former showed the maximum in the shorter wavelength region and a smaller ratio of absorb-

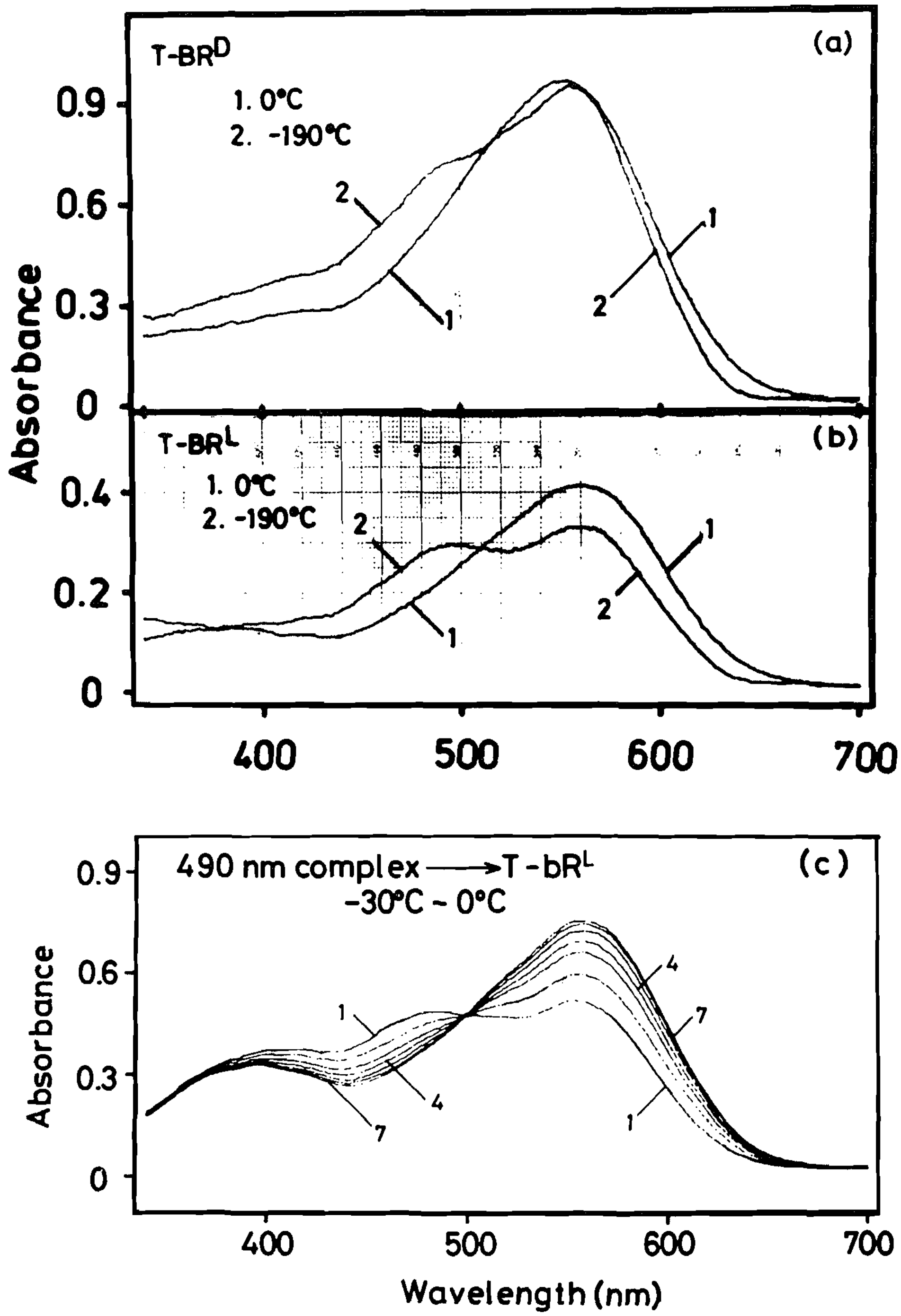

FIG. 2. Cooling effect on spectra of T-BR^D and T-BR^L. (a) T-BR^D (~10^3 moles of Triton X-100/mole BR). Curve 1: 0°C. Curve 2: −190°C. (b) T-BR^L (~10^3 moles of Triton X-100/mole BR). Curve 1: 0°C. Curve 2: −190°C. (c) Spectral change of T-BR^L on warming from −190°C to 0°C. Curves 1−7 were measured at −30, −25, −20, −15, −10, −5, and 0°C, respectively.

ance between the maximum and minimum than the latter. In addition, the semi-log plot of the absorbance change at 550 nm against the incubation time did not display a single exponential curve but, rather, the kinetics composed of two sequential thermal reactions, i.e. dark-reversion of the 380-nm complex to T-BR^L and dark-adaptation of T-BR^L to T-BR^D. The absorption spectrum of the final product of the dark-reversion (curve 8 in Fig. 1b) was smaller in absorbance than that of the initial one (curve 1 in Fig. 1a), presumably due to the destruction of the pigment during the slow dark-reversion.

Cooling effects on spectra of T-BR^D and T-BR^L; appearance of the "490-nm complex"

On cooling T-BR^D to −190°C, a shoulder around 490 nm appeared in the absorption spectrum (Fig. 2a). Upon warming to 0°C in the dark, the spectrum recovered its original shape. This spectral change was perfectly reversible. A similar experiment was performed on T-BR^L which had been prepared by irradiating T-BR^D with 500-nm light for 5 min at 0°C (Fig. 2b). It should be noted that the shoulder of T-BR^L at −190°C was more prominent than that of T-BR^D (Figs. 2a and b). On

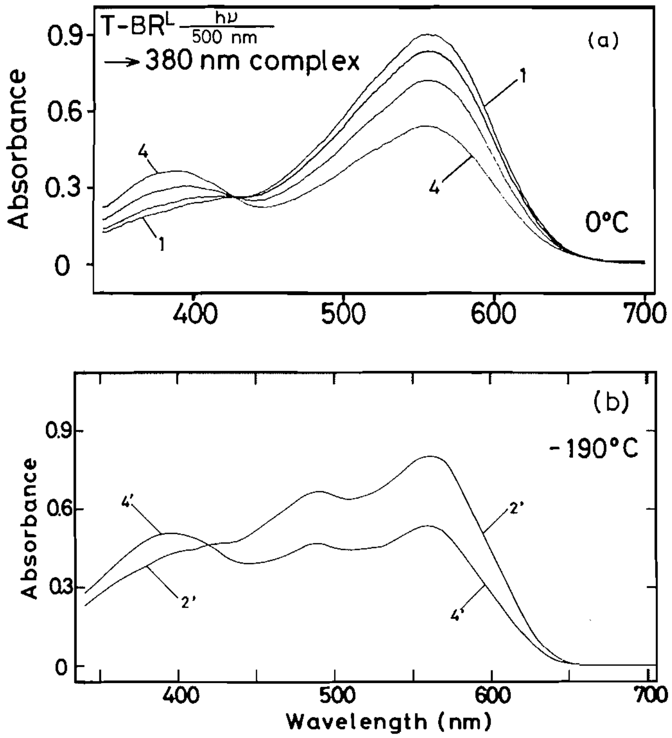

FIG. 3. Absorption spectra of mixtures composed of T-BR^L, 380-nm complex, and 490-nm complex. (a) Formation of the 380-nm complex by irradiation of T-BR^L ($\sim 10^3$ moles of Triton X-100/mole BR) (curve 1) with 500-nm light for 17, 40, and 70 min (curves 2−4), respectively. (b) Low temperature spectra of the products. Each product was cooled to −190°C and then spectra were measured. Curves 2′ and 4′ show low temperature spectra of the products designated as curves 2 and 4 in (a), respectively.

warming T-BR^L above −30°C, the absorbance at the shoulder decreased, with formation of an isosbestic point at 505 nm (Fig. 2c). This result indicates the presence of a thermal equilibrium between T-BR^L and a molecular species named the "490-nm complex"; low temperatures favoured the 490-nm complex. A similar spectral change was observed in warming T-BR^D from −190°C. The amount of 490-nm complex in the light-adapted sample was more than in dark-adapted one. The amount of 490-nm complex on cooling depends on the molar ratio of Triton X-100 to BR; the larger the ratio, the more 490-nm complex is formed.

A possibility that the 380-nm complex might convert to the 490-nm complex on cooling was excluded by the following experiment: T-BR^L was irradiated at 0°C for given periods in order to prepare the sample containing different amounts of 380-nm complex (Fig. 3a), and then their spectra were measured at −190°C. As shown in Fig. 3b, the absorption band characteristic of the 380-nm complex shifted to around 400 nm at −190°C. Thus it is clear that the 380-nm complex can not convert to the 490-nm complex on cooling.

Photoreactions at −190°C; formation of batho-intermediates

The photoreaction of T-BR was first examined by use of the sample shown in Figs. 2 and 3. The spectral changes of T-BR^L in the sample at −190°C were very small because of the large amount of 490-nm complex, which was photo-insensitive or less photosensitive (see below), present in the sample. In order to reduce the amount of 490-nm complex in the sample, a lesser amount of Triton X-100 was added to the purple membrane suspension (about 50 moles of Triton X-100/mole BR). As shown in Figs. 4 and 5, the amount of 490-nm complex in the sample was about 1/4 of that in Figs. 2 and 3. The shoulder around 520 nm seen in Figs. 4 and 5 was due to non-flatness of the baseline. It was confirmed that the shape of spectral change of photoreactions of T-BR at −190°C was independent of the molar ratio of Triton X-100 to BR, except for the amount of the spectral change.

Now the sample containing T-BR^D was irradiated at −190°C with light at 500 nm (curve 1 in Fig. 4a). The spectrum shifted to longer wavelengths. The absorbances in the range between 410 nm and 563 nm decreased and simultaneously those at longer wavelengths than 563 nm increased (curves 2−8 in Fig. 4a), indicating formation of a bathochromic intermediate (T-batho-BR^D). A prolonged irradiation yielded a photosteady-state mixture (curves 7 and 8 in Fig. 4a) designated as T-state^D. Then, another irradiation of T-state^D with red light at 718 nm, which was absorbed by mainly T-batho-BR^D, caused it to revert to T-BR^D (Fig. 4b). During the irradiation, the curve-intersection point of the spectra shifted from 585 nm to 550 nm (curves 1−10). On further irradiation with light of wavelengths longer than 640 nm (>640 nm), all the T-batho-BR^D reverted to the original T-BR^D (curve 11).

In the case of irradiation of BR^D in purple membrane at −190°C, two kinds of batho-intermediates, namely batho-*trans*-BR and batho-13-*cis*-BR, were formed (14), because BR^D in purple membrane is an equimolar mixture of *trans*-BR and 13-*cis*-BR (15, 16). The same was true in the T-BR^D system, because the hplc analysis of retinal isomers extracted from T-BR^D revealed that T-BR^D was a mixture of T-BR^t (51.3 ± 3%) and T-BR^{13} (48.7 ± 3%), though the spectral change did not display a clear distinction between the photoreaction due to *trans*-pigment (T-BR^t) and that due to 13-*cis*-pigment (T-BR^{13}).

In order to prepare T-BR^L, the T-BR^D (curve 11 in Fig. 4b) was warmed to 0°C and then irradiated with 500-nm light for 5 min. After cooling it to −190°C, the absorption spectrum was measured, which displayed λ_{max} at 568 nm and a shoulder due to the 490-nm complex (curve 1 in Fig. 5a). Irradiation of the preparation with 500-nm light caused a bathochromic shift with an isosbestic point at 584 nm (curves 2−7 in Fig. 5a), and finally reached a photosteady state, designated as T-state^L (curves 6 and 7 in Fig. 5a). Irradiation of T-state^L (curve 1 in Fig. 5b) with light at 718 nm caused a photoreversion to T-BR^L (curves 2−7 in Fig. 5b). For the complete reversion of the batho products, another irradiation with light of shorter wavelengths (>640 nm) was required. The spectrum of the final photoproduct of the irradiation (curve 8 in Fig. 5b) was in good agreement with the original T-BR^L (curve 1 in Fig. 5a). Thus, T-BR^L showed a photoreversible change at −190°C, like BR^L in purple membrane. The curve-intersection points among a series of spectra, however, shifted from 590 nm to 570 nm (Fig. 5b), suggesting that T-BR^L would be a mixture of T-BR^t and T-BR^{13}. In fact, the hplc analysis of retinal isomers extracted from T-BR^L demonstrated that the amount of 13-*cis* retinal (13.0 ± 2% of total amount) in T-BR^L was pretty large in comparison with that in BR^L (8.9 ± 2% of the total amount).

A question whether or not the 490-nm complex might be photosensitive was examined. The preparations containing the 490-nm complex ($\sim 10^3$ or ~ 50 moles of Triton X-100/mole BR) were irradiated at −190°C with various lights of wavelengths shorter than 500 nm. Their spectral changes due to the photoreactions were calculated, and were similar to

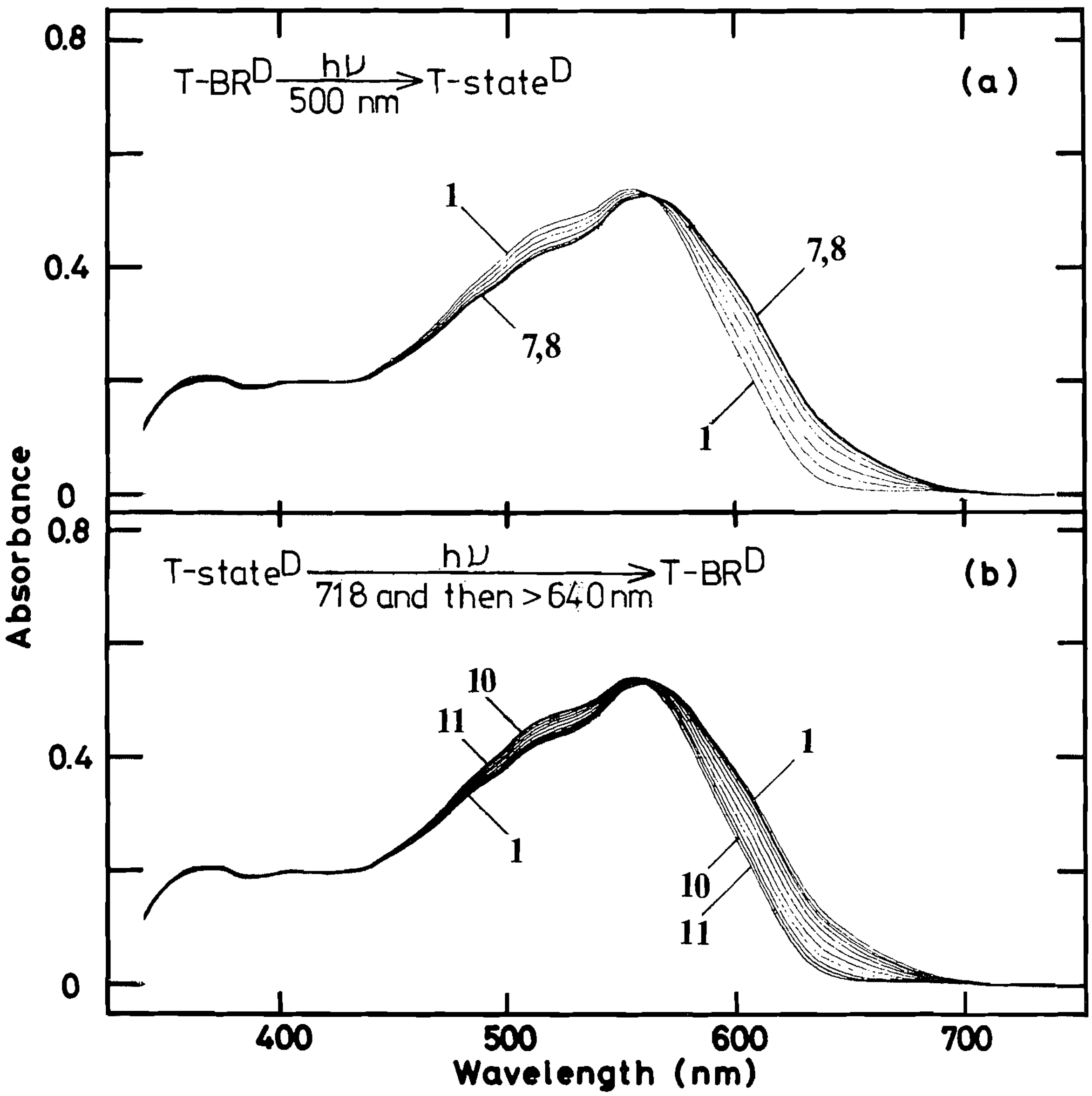

FIG. 4. Photoreaction of T-BR^D at −190°C. (a) Curve 1: T-BR^D (~50 moles of Triton X-100/mole BR) at −190°C. Curves 2−8: products of the successive irradiations of T-BR^D with 500-nm light for 5, 5, 10, 20, 40, 80, and 160 s, respectively. Curves 7 and 8 correspond to photosteady-state mixture designated as T-state^D. (b) Curve 1: T-state^D redrawn from curve 8 in (a). Curves 2−10: products of the successive irradiations of T-state^D with light at 718 nm for 10, 10, 20, 40, 80, 160, 320, 640, and 1280 s, respectively. Curve 11 was a product of further irradiation with red light (>640 nm) for 5 min, and in good agreement with curve 1 in (a).

those shown in Fig. 5. This fact indicates that the 490-nm complex at −190°C is photo-insensitive or has very low photosensitivity.

Photoreaction at −50°C; formation of the meta-intermediate

Irradiation of T-BR^L at −50°C with orange light (>580 nm) yielded a meta-like intermediate designated as T-meta-BR^i, which was stable at −50°C in the dark; a prolonged irradiation converted all the T-BR^L into T-meta-BR^i (curve 1 in Fig. 6a). The formation of T-meta-BR^i is composed of fast and slow phases. These results indicate that at −50°C the 490-nm complex slowly converted to T-BR^L in the dark. It should be noted that meta-BR^i (λ_{max}: 418 nm) in the purple membrane is not stable at −50°C under the same conditions (10 m*M* phosphate buffer, pH 6.8) (5).

The thermal conversion of T-meta-BR^i consisted of three elementary steps (Fig. 6). Warming from −50°C to −45°C decreased the absorbances around 410 nm and simultaneously increased those around 565 nm, forming an isosbestic point at 458 nm (curves 1−3 in Fig. 6a and circles in Fig. 6b). The difference spectrum between curves 3 and 1 is similar to that between meta-BR^i and BR^i (5) except for the fact that the wavelengths of the maximum and minimum in the difference spectrum and the isosbestic point are shorter by about 10 nm than those in the BR^i system. This shift is comparable to the shift of λ_{max} on addition of Triton X-100. Therefore, this spectral change should be regarded as a decay of T-meta-BR^i to T-BR^i.

On warming from −45°C to −35°C the absorbance around 380 nm decreased and that around 565 nm increased (curves 3−5 in Fig. 6a and triangles in Fig. 6b). The difference spectrum of this spectral change was similar in shape to that between the 380-nm complex and T-BR^L shown in Fig. 1b. In both spectra the isosbestic points were located at about 445 nm,

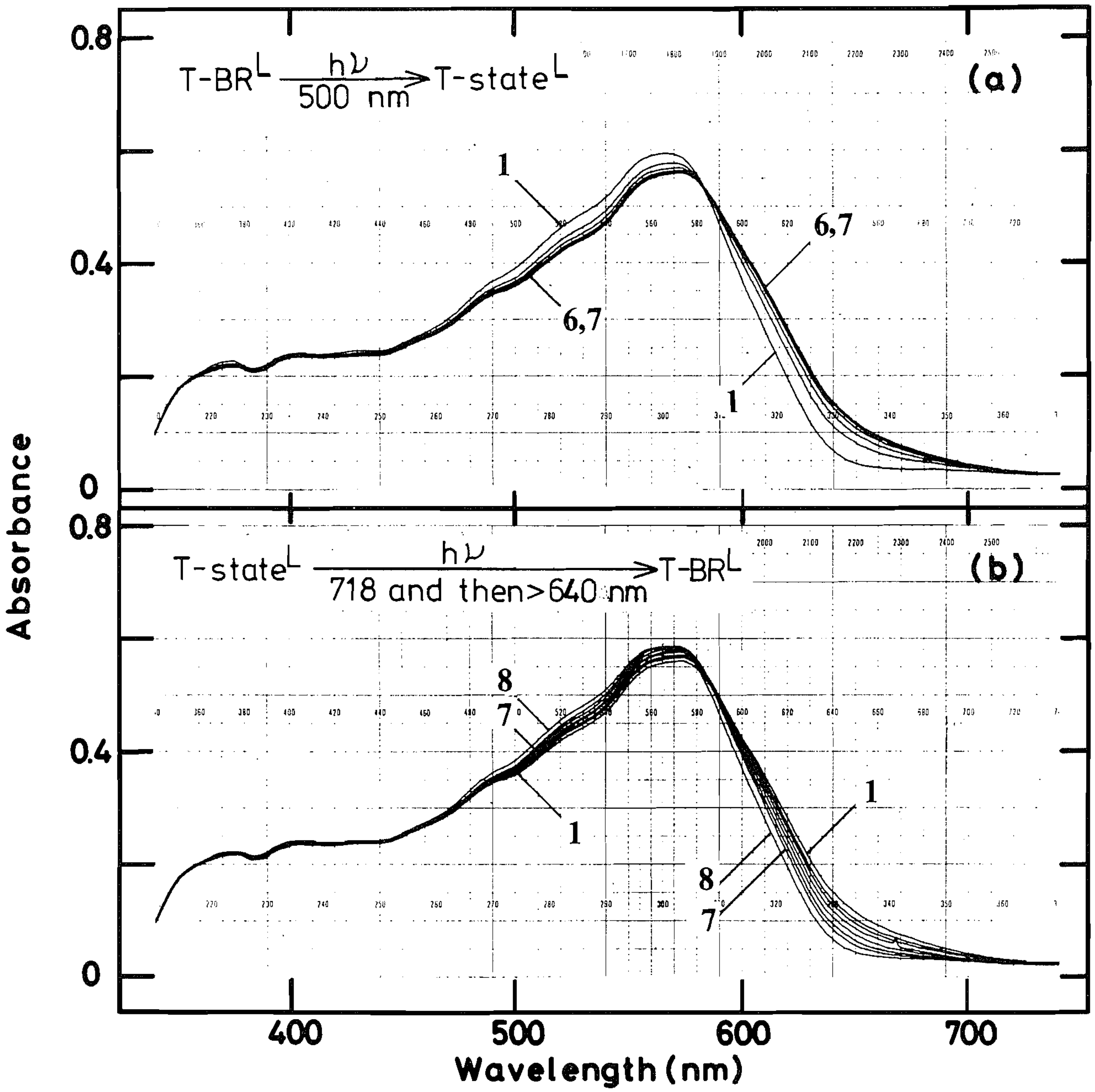

FIG. 5. The photoreaction of T-BR^L at −190°C. (a) Curve 1: T-BR^L (~50 moles of Triton X-100/mole BR) at −190°C. Curves 2−7: products of the successive irradiations of T-BR^L with 500-nm light for 10, 10, 15, 20, 40, and 80 s, respectively. Curves 6 and 7 represent a photosteady-state mixture designated as T-state^L. (b) Curve 1: T-state^L redrawn from curve 7 in (a). Curves 2−7: products of the successive irradiations of T-state^L (curve 1) with 718-nm light for 10, 10, 20, 40, 80, and 160 s, respectively. Curve 8: a product of the further irradiation with red light (>640 nm) for 5 min. Curve 8 is in good agreement with curve 1 in (a).

and the ratios in absorbance between the difference maximum and minimum were 0.37. These facts indicate that the spectral change may correspond to a conversion of the 380-nm complex to T-BR^L. It is not clear yet whether the 380-nm complex may be formed from T-meta-BR^l or from other earlier intermediates.

Above −25°C, the absorbance around 460 nm decreased and that around 565 nm increased (curves 7−12 in Fig. 6a and squares in Fig. 6b). This spectral change should be due to the decay of the 490-nm complex, because both the shape of the spectral change and the temperature range in which it was observed were in good agreement with those of the change of 490-nm complx to T-BR^L (Fig. 2c).

Discussion

We have described several properties of the T-BR system different from the BR system: the formation of the 490-nm and 380-nm complexes, and the stabilization of meta-intermediates. Needless to say, these differences can be attributed to the difference in the environment around the BR molecule. BR molecules in the purple membrane are in the lattice structure and form a "trimer" structure. The molecules in the trimer interact with each other as demonstrated in the energy transfer (17), the exciton cd band (7, 8), and the rate of dark-adaptation (18). According to the cd measurements, the solubilization of purple membrane with a detergent causes the lattice structure to dissociate, resulting in loss of the interaction among the mole-

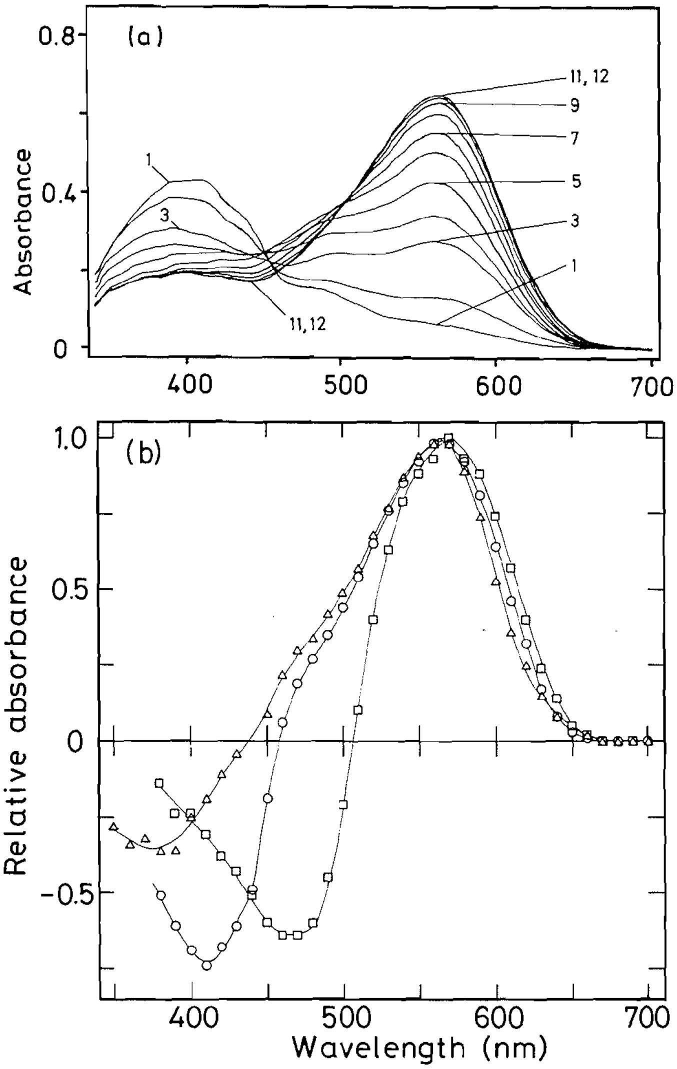

FIG. 6. (a) The thermal decay of T-meta-BR^t obtained by irradiation of T-BR^L at −50°C for 70 min with orange light (>580 nm). T-meta-BR^t was gradually warmed in the dark. The spectra were measured at −50, −48, −45°C (curves 1, 2, and 3) and then at intervals of 5°C (curves 4−12). (b) Circles (○—○): the difference spectrum between the spectra measured at −45 and −50°C (3 − 1). Triangles (▲—▲): the difference spectrum between −35 and −45°C (5 − 3). Squares (■—■): the difference spectrum between 0 and −25°C (12 − 7).

cules. An ultra-centrifugation experiment (9) showed that BR molecules in 2% Triton X-100 solution, probably in a micelle composed of Triton X-100 and several lipids, were in a monomeric form. Thus, the properties of T-BR different from the BR system mentioned above (see Fig. 7) should be attributed to some differences in lipid−protein, protein−protein, and detergent−protein interactions.

The 380-nm complex

The irradiation of T-BR brought an increase of absorbance at 380 nm (refs. 18, 19, and the present work). If the formation of the 380-nm complex was an indication of destruction of the Schiff base linkage between retinal and the ε-amino group of the lysine residue, the dark recovery would be a regeneration of T-BR from all-*trans* retinal and bacterioopsin. In order to test this possibility, all-*trans* retinal was mixed with bacterioopsin in 1% Triton X-100 solution. No pigment formation was observed. Thus, the 380-nm complex is a product formed not

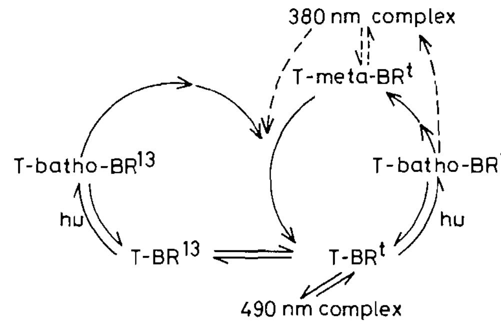

FIG. 7. A reaction cycle of T-BR. *Trans*-BR and 13-*cis*-BR in Triton X-100 solution, designated as T-BR^t and T-BR^{13}, respectively, formed batho-intermediates, i.e., T-batho-BR^t and T-batho-BR^{13}. The *meta*-intermediate was formed only from T-BR^t. Whether or not a lumi-like intermediate was formed has not yet been clarified, because the spectral complexity due to formation of the 490-nm complex. The 490-nm and 380-nm complexes are both characteristic of the T-BR photocycle.

by destruction of the Schiff base linkage, but by deprotonation of the Schiff base by some change of the microenvironment around the chromophore.

The 490-nm complex

The 490-nm complex was formed only by cooling to a temperature lower than 0°C. Its amount increased with decrease of temperature and reached a steady level at −40°C. The spectral change on cooling may possibly be due to change of pK value of a certain charged group or the phase transition of the glycerol−Triton−lipid micelle containing BR molecules.

We did not observe a molecular species similar to the 490-nm complex at 25°C in the pH range between 2.96 and 10.65. Below pH 4 a decrease of absorbance at λ_{max}, an increase at longer wavelengths (~650 nm), and an increase at shorter wavelengths (~360 nm) were observed. At pH higher than 9, a decrease of the absorbance at λ_{max} and an increase of that around 365 nm were observed. In the case of BR in purple membrane, an increase of absorbance around 470 nm can be observed in the pH region higher than 11, due to deprotonation of the Schiff base (20). However, such a molecular species having λ_{max} around 470 nm has never been observed in pH titration experiments of Triton-treated BR. According to Lozier *et al.* (21), BR in a phospholipid vesicle at pH 8.6 displays the λ_{max} at 480 nm. Such a blue shift of the λ_{max} has never been observed in any cell envelope vesicles. BR molecules in a phospholipid vesicle do not exhibit the exciton cd band, because BR molecules become monomeric in a phospholipid vesicle under these conditions. Because of similarities between the 480-nm absorbing species and the 490-nm complex, in conditions for their formation and their absorption maxima, it is indicated that both pigments may have a retinylidene chromophore in a similar microenvironment.

A few years ago, we reported the formation of a molecular species absorbing around 500 nm which was produced from acid-induced species with orange light irradiation (22). The isomeric form of the retinal extracted from this product was 9-*cis* retinal. When 9-*cis* retinal was mixed with bacterioopsin under neutral pH conditions, no formation of the pigment was observed, as reported by Oesterhelt and Schuhmann (23). It is not plausible that the 490-nm complex has 9-*cis* retinal as its chromophore. Further information about the structure of these molecular species would give some clue to explaining the coloration of BR.

Another noteworthy point is that the amount of the 490-nm complex formed from T-BR^{L} was larger than that from T-BR^{D} (Fig. 2). In the case of BR in the purple membrane, BR^{L} has only all-*trans* retinal as its chromophore but BR^{D} has both all-*trans* and 13-*cis* retinals in equimolar amount (15, 16). The present experiment showed that the ratios of 13-*cis* to all-*trans* retinals in T-BR^{L} and T-BR^{D} were 13.0 ± 2/87.0 ± 2 and 51.3 ± 3/48.7 ± 3, respectively. It should be noted that a part of T-BR^{L} has 13-*cis* retinal as its chromophore. The existence of 13-*cis* retinal in T-BR^{L} has already been reported by Casadio and Stoeckenius (18), but their result (38 ± 2% of the total amount) is much larger than ours. It is not yet clear why they are so different from each other. In any case, the species having all-*trans* retinal (T-BR^{t}) is more abundant in T-BR^{L} than in T-BR^{D}. Thus it may be safe to say that the 490-nm complex comes from T-BR^{t} rather than T-BR^{13}.

Stabilization of the meta-intermediate

The meta-intermediate was stabilized under several conditions: Oesterhelt and Hess (24) found that the 412-nm complex was easily formed by irradiating BR suspended in about 3.6 *M* NaCl solution saturated with ether, and mentioned that the ether could stabilize the 412-nm complex. Becher and Ebrey (25) reported that the high salt and high pH conditions (1 *M* NaCl, pH 10) could stabilize the meta-intermediate. Yoshida *et al.* (26) showed that guanidine hydrochloride prolonged the decay time of the meta-intermediate, and this effect depended on the concentration of guanidine hydrochloride. Even 8 *M* solution did not saturate this effect. Recently we investigated the photoreaction of tyrosine-iodinated BR at low temperature, and found meta-intermediates of tyrosine-iodinated BR stable at −65°C (27). As shown in the present paper and by Lam and Packer (28), the meta-intermediate also is more stable in Triton X-100 solution than under native conditions. The stabilization effects of guanidine hydrochloride, high salt − high pH conditions, and iodination of tyrosine on the meta-intermediate were probably due to change in the interaction between the retinylidene chromophore and charges on the bacterioopsin. This idea may be supported by the fact that the stabilization effect was also observed in replacement of guanidine hydrochloride by arginine hydrochloride. The effect resulting from ether or Triton X-100, however, was not explained clearly, because structural information about BR in both solutions is limited. The tertiary structure of the protein was changed with Triton X-100, as shown in the cd spectrum, and probably the secondary structure would be changed. These structural changes would result in charge replacement which might stabilize the meta-intermediate. Whether or not such an explanation can be applied to the effect needs further investigation, in order to obtain detailed information on the structure of the meta-intermediate and the protein moiety in such a micelle structure or organic solvent.

The investigation of solubilized BR revealed that the destruction of the lattice structure resulted in formation of by-products of the photoreaction cycle of BR, such as the 490-nm and 380-nm complexes; the former is probably formed from T-BR^{t}, and the latter slowly reverts to the original pigment. It seems probable that the lattice structure can stabilize the BR^{t} by preventing it from formation of by-products and can play a role in rapid rotation of the photoreaction cycle. Of course the possibility that the results mentioned above may be due to direct interaction between Triton X-100 molecule and BR rather than destruction of the lattice structure can not be excluded. Further investigation of the structure of BR in the micelle must be made. Such investigation may provide important information regarding structure and function of membrane proteins extracted with the aid of detergents.

Acknowledgements

This work was supported in part by Grants-in-Aid for the Special Research Project on Photosynthesis and Photoconversion of Solar Energy to F.T. (59045016) and for Scientific Research to T.Y. (59440003) from the Japanese Ministry of Education, Science and Culture.

1. W. STOECKENIUS, R. H. LOZIER, and R. A. BOGOMOLNI. Biochim. Biophys. Acta, **505**, 215 (1979).
2. N. V. KATRE, P. K. WOLBER, W. STOECKENIUS, and R. M. STROUD. Proc. Natl. Acad. Sci. U.S.A. **78**, 4068 (1981).
3. H. BAYLEY, K.-S. HUANG, R. RADHAKRISHNAN, A. H. ROSS, Y. TAKAGI, and H. G. KHORANA. Proc. Natl. Acad. Sci. U.S.A. **78**, 2225 (1981).
4. R. H. LOZIER, R. A. BOGOMOLNI, and W. STOECKENIUS. Biophys. J. **15**, 955 (1975).
5. T. IWASA, F. TOKUNAGA, and T. YOSHIZAWA. Biophys. Struct. Mech. **6**, 253 (1980).
6. P. N. T. UNWIN and R. HENDERSON. J. Mol. Biol. **94**, 425 (1975).
7. M. P. HEYN, P. J. BAUER, and N. A. DENCHER. Biochem. Biophys. Res. Commun. **67**, 897 (1975).
8. B. BECHER and T. G. EBREY. Biochem. Biophys. Res. Commun. **69**, 1 (1976).
9. J. A. REYNOLDS and W. STOECKENIUS. Proc. Natl. Acad. Sci. U.S.A. **74**, 2804 (1977).
10. D. OESTERHELT and W. STOECKENIUS. *In* Methods in enzymology. Vol. 31. Biomembranes Part A. *Edited by* S. Fleisher and L. Packer. Academic Press, New York. 1974. pp. 668−678.
11. T. YOSHIZAWA. *In* Handbook of sensory physiology. Vol. VII/1. *Edited by* H. J. A. Dartnall. Springer Verlag, Berlin. 1972. pp. 146−179.
12. M. TSUDA, M. GLACCUM, B. NELSON, and T. G. EBREY. Nature (London), **287**, 351 (1980).
13. N. A. DENCHER and M. P. HEYN. FEBS Lett. **96**, 322 (1978).
14. F. TOKUNAGA, T. IWASA, and T. YOSHIZAWA. FEBS Lett. **72**, 33 (1976).
15. A. MAEDA, T. IWASA, and T. YOSHIZAWA. J. Biochem. (Tokyo), **82**, 1599 (1977).
16. M. J. PETTEI, A. P. YUDD, K. NAKANISHI, R. HENSELMAN, and W. STOECKENIUS. Biochemistry, **16**, 1955 (1977).
17. J. B. HURLEY and T. G. EBREY. Biophys. J. **22**, 49 (1978).
18. R. CASADIO and W. STOECKENIUS. Biochemistry, **19**, 3374 (1980).
19. T. YOSHIZAWA. Biochemical and chemical use of solar energy (in Japanese). *Edited by* K. Shibata. Gakkai Shuppan Center, Tokyo. 1978. pp. 113−120.
20. S. DRUCKMANN, M. OTTOLENGHI, A. PANDE, J. PANDE, and R. H. CALLENDER. Biochemistry, **21**, 4953 (1982).
21. R. H. LOZIER, W. NIEDERBERGER, R. A. BOGOMOLNI, S.-B. HWANG, and W. STOECKENIUS. Biochim. Biophys. Acta, **440**, 545 (1976).
22. A. MAEDA, T. IWASA, and T. YOSHIZAWA. Biochemistry, **19**, 3825 (1980).
23. D. OESTERHELT and L. SCHUHMANN. FEBS Lett. **44**, 262 (1974).
24. D. OESTERHELT and B. HESS. Eur. J. Biochem. **37**, 316 (1973).
25. B. BECHER and T. EBREY. Biophys. J. **17**, 185 (1977).
26. M. YOSHIDA, K. OHNO, and Y. TAKEUCHI. J. Biochem. (Tokyo), **87**, 491 (1980).
27. T. IWASA, K. TAKEDA, F. TOKUNAGA, P. SCHERRER, and L. PACKER. Biosci. Rep. **2**, 949 (1982).
28. E. LAM and L. PACKER. Arch. Biochem. Biophys. **221**, 557 (1983).

Electron states and electron transport in quasi-one-dimensional molecular systems

ALEXANDR S. DAVYDOV AND IVAN I. UKRAINSKII
Institute for Theoretical Physics, Academy of Sciences of the Ukrainian S.S.R., 252130 Kiev, Metrologicheskaya Street, 14-b, U.S.S.R.

Received September 5, 1984[1]

This paper is dedicated to Professor Camille Sandorfy on the occasion of his 65th birthday

ALEXANDR S. DAVYDOV and IVAN I. UKRAINSKII. Can. J. Chem. **63**, 1899 (1985).

It is shown that the concept of electron pairs may be introduced in conducting quasi-one-dimensional systems with electron delocalization such as $(CH)_x$ and the stacks of molecule-donors and acceptors of electrons TMTSF, TTT, TCNQ, etc. The introduction of pairing proves to be useful and electronic structure and electronic processes can be easily visualized. The two causative factors in the appearance of pairs in a many-electron system with repulsion are pointed out. The first one is the electron Fermi-statistics that does not allow a spatial region to be occupied by more than two electrons. The second one is the interaction of electrons with a soft lattice. The first of these factors is important at large and intermediate electron densities $\rho \gtrsim 1$, the second one dominates at $\rho \ll 1$. The kink-type excitation parameters in $(CH)_x$ are considered with a non-linear potential obtained in an electron-pair approach for the many-electron wave function of $(CH)_x$.

ALEXANDR S. DAVYDOV et IVAN I. UKRAINSKII. Can. J. Chem. **63**, 1899 (1985).

On démontre que le concept des paires d'électrons peut être introduit dans les systèmes conducteurs quasi-unidimensionnels avec une délocalisation électronique, comme $(CH)_x$, ou avec des empilements des molécules donneurs et accepteurs d'électrons, comme TMTSF, TTT, TCNQ, etc. L'introduction de pairages s'avère utile et les structures électroniques ainsi que les processus électroniques peuvent facilement être visualisés. On a mis en évidence les deux facteurs qui provoquent l'apparition de paires dans les systèmes à plusieurs électrons avec répulsion. Le premier est relié aux statistiques de Fermi de l'électron qui font qu'une région de l'espace ne peut être occupée par plus de deux électrons. Le deuxième est l'interaction des électrons avec un réseau douce. A des densités électroniques élevées ou moyennes, $\rho \gtrsim 1$, le premier de ces facteurs est important alors que le second domine lorsque $\rho \ll 1$. On considère les paramètres d'excitation du type "kink" dans les groupes $(CH)_x$ de concert avec un potentiel non-linéaire qui est obtenu dans une approche par paire d'électrons pour les fonctions d'onde à plusieurs électrons de $(CH)_x$.

[Traduit par le journal]

1. Introduction

The recent decade has witnessed considerable progress in the physics and physical chemistry of quasi-one-dimensional systems. The model of quasi-one-dimensional crystals that allows one to use the methods of solid-state theory seems to be the most suitable one for carrying out theoretical investigations of such systems. The most interesting for experimentalists and theorists are the properties inherent to quasi-one-dimensional crystals whose number of electrons per unit cell is odd. Therefore they have a metallic band structure. As examples of such quasi-one-dimensional systems we may cite the stacks of donor molecules or acceptor molecules in donor–acceptor molecular crystals, for example, crystals based on TCNQ, TTF, TTT molecules as well as their selenium and methyl derivatives, TMTTF, TST, etc.

Another class of quasi-one-dimensional systems with a metal-like structure of the one-particle spectrum is represented by polymer chain molecules with conjugate bonds such as sulphur nitride $(SN)_x$, polyacetylenes $(CH)_x$, and polydiacetylenes $({=}CR{-}C{\equiv}C{-}CR{=})_x$.

Of these polymers polyacetylenes $(CH)_x$ have assumed ever increasing importance. Owing to their electronic structure both polyacetylenes and molecular stacks in donor–acceptor crystals are many-particle systems where electron delocalization is important. This makes the correct description of these systems complicated, since it requires an account of delocalization and correlation of electrons and also their interaction with the lattice.

In molecules with saturated bonds the many-electron problem is easier to solve since all the electrons are pairwise localized in bonds and correlation is essential only in the electron pairs (1, 2).

Here we would like to show that the concept of electron pairs may also be introduced in quasi-one-dimensional systems with delocalization such as $(CH)_x$ and the stacks of donors and acceptors TMTSF, TTT etc. The electron pairs in this case are partially localized. However, the introduction of pairing proves to be useful and the electronic structure and electronic processes can be easily visualized.

We can point out two causative factors in the appearance of pairs in a many-electron system with repulsion. The first one is the electron Fermi-statistics that does not allow a spatial region to be occupied by more than two electrons. The second one is the interaction of electrons with a soft lattice. The first of these factors is important at large and average densities of electrons $\rho \lesssim 1$, the second one dominates at $\rho \ll 1$. For a quantitative description, we introduce the Hamiltonian of our quasi-one-dimensional system. Using second quantization we write the Hamiltonian as

$$[1.1] \quad \hat{H} = \hat{H}_{\text{el}} + \hat{H}_{\text{el-ph}} + \hat{H}_{\text{ph}}$$
$$= \sum_{m,\sigma} (-\beta)\left(\hat{C}^+_{m\sigma}\hat{C}_{m+1,\sigma} + \hat{C}^+_{m+1,\sigma}\hat{C}_{m\sigma}\right)$$
$$+ \frac{1}{2}\sum_{m,\sigma}\left(\gamma\hat{C}^+_{m\sigma}\hat{C}_{m\sigma}\hat{C}^+_{m,-\sigma}\hat{C}_{m,-\sigma}\right.$$
$$\left. + \sum_{\sigma'}\gamma_1\hat{C}^+_{m\sigma}\hat{C}_{m\sigma}\hat{C}^+_{m+1,\sigma'}\hat{C}_{m+1,\sigma'}\right)$$
$$+ \sum_{m,\sigma}\beta'\left(\hat{C}^+_{m\sigma}\hat{C}_{m+1,\sigma} + \hat{C}^+_{m+1,\sigma}\hat{C}_{m\sigma}\right)(x_{m+1} - x_m)$$
$$+ \frac{1}{2}\sum_{m}\left(K_0(x_m - x_{m+1})^2 + M\dot{x}^2_m\right)$$

[1]Revision received March 12, 1985.

where $\hat{C}^{+}_{m\sigma}$ is the operator for electron creation at point m with spin σ; β, β', γ, $\gamma_1 > 0$, M is the molecular mass, x_m is the displacement of the mth molecule from its equilibrium position.

In [1.1] the first term describes the resonance jump of an electron between the molecular chain centers, the second and the third terms deal with the interaction of electrons and the last two correspond to the molecular vibrations in the chain. A Hamiltonian of type [1.1] whose parameters have been properly chosen (3–5), describes well the properties of conjugate polymers and small molecules. It is also valid in studying donor–acceptor molecular crystals (6, 7).

In quantum chemistry the Pople Hamiltonian is widely used (3). The electron part of the expression [1.1] is just the cut Pople Hamiltonian. The important parameter for one-dimensional systems with the Hamiltonian [1.1] is the density of electrons:

[1.2] $$\rho = N_e/N$$

where N_e is the total number of electrons in the chain of $N \to \infty$ centers.

We consider two cases $\rho \approx 1$ and $\rho \ll 1$. The first case corresponds to such systems as $(CH)_x$, polyacetylene while the second corresponds to stack molecular chains with $\rho \ll 1$ (for example, crystal $(TMTSF)_2\ ClO_4$).

The case $\rho \ll 1$ is described in Section 2, and that of $\rho = 1$ in Section 3.

Notice that, in general, to the Hamiltonian [1.1] there corresponds the dispersion law of one-particle states. However, in the limit of small density $\rho \ll 1$, we can use the effective mass approximation, i.e., $\epsilon_k \sim k^2$.

2. Electron pairing and the mass of current carriers at $\rho \ll 1$

Let us consider small densities of the conduction electrons $\rho \ll 1$.

In this limit the Hamiltonian [1.1] can be replaced by its continuous analogue (see, for example, refs. 8–15).

We first examine one electron. The total Hamiltonian of the system as in [1.1] constitutes the sum of three terms, namely, the electron Hamiltonian, the phonon Hamiltonian, and the operator for their interaction:

[2.1] $$\hat{H} = \hat{H}_{el} + \hat{H}_{ph} + \hat{H}_{el-ph}$$

where

[2.2] $$\hat{H}_{el} = -\int \frac{dx}{a}\left[\frac{\hbar^2}{2m}\left(\frac{d\psi}{dx}\right)^2\right]$$

[2.3] $$\hat{H}_{ph} = \frac{M}{2}\int \frac{dx}{a}\left[\left(\frac{dR}{dt}\right)^2 + \left(\frac{dR}{dx}\right)^2 \frac{V_0^2}{a^2}\right]$$

[2.4] $$\hat{H}_{el\text{-}ph} = \chi \int \frac{dx}{a}\,|\psi|^2\,\frac{dR}{dx}$$

$R(x, t)$ is the phonon variable, a continuous analogue of points x_m displacements in [1.1], $\psi(x, t)$ is the normalized electron wave function

$$\int_{-\infty}^{\infty} dx\,|\psi(x, t)|^2 = 1$$

The equations of motion are in the form of (8–11)

[2.5]
$$\left[i\hbar\frac{d}{dt} + \frac{\hbar^2}{2m}\frac{d^2}{dx^2} + \chi\frac{dR}{dx}\right]\psi(x, t) = 0$$
$$\left[\frac{d^2}{dt^2} - V_0^2\frac{d^2}{dx^2}\right]\rho + \frac{a^2}{M}\chi|\psi(x, t)|^2 = 0$$
$$\rho(x, t) = dR(x, t)/dx$$

Let us introduce the wave variable

[2.6] $$\xi = x - Vt$$

and assume $\rho = \rho(\xi)$ (11) and

[2.7]
$$\psi(x, t) = \phi(\xi)\exp\{i(mVx - (\epsilon + mV^2/2)t]/\hbar\}$$
$$\rho(x, t) = \rho(\xi)$$

Then the system [2.5] reduces to a nonlinear Schrödinger equation for ϕ (8–11) which has the soliton-type solutions

[2.8] $$\phi(\xi) \sim 1/\cosh(\xi/l)$$

The soliton energy at sufficiently small velocities $V \ll V_0$ is always less than that of zone electrons by the value

[2.9] $$E_{sol} = g^2/4$$

where

$$g = ma^4\chi^2/[V_0^2 M(1 - V^2/V_0^2)\hbar]$$

The effective size of a soliton (in the constant lattice units a) l and its effective mass M_{sol} depend on the parameters m, M, V_0, χ, β, K_0 in [2.5] (8, 9, 11)

[2.10] $$l = 3K_0\beta/\chi^2 = 3K_0\hbar^2/(\chi^2 ma^2)$$

[2.11] $$M_{sol} = m_{el} + 4\chi^4 M/(27K_0^2 V_0^2\beta)$$

An account must be taken of the fact that there is an infinitely large number of electrons in our molecular chain, however, their density (see [1.2]) is small

$$\rho \ll 1$$

We choose the wave function of the many electron system as an antisymmetrized product of the functions of electron pairs (geminals)

[2.12] $$\Psi(1, 2, \ldots, 2M - 1, 2M) = \hat{A}\prod_{i=1}^{M} G_i(2i - 1, 2i)$$

where $\hat{A}$ is the antisymmetrization operator. Geminals have been introduced by Fock and his disciples in refs. 16 and 17.

In the simplest case each geminal in [2.12] can be chosen in the form of a Slater determinant corresponding to the singlet state of the pair

[2.13] $$G_i = \|\phi_i(x_{2i-1})\phi_i(x_{2i})\alpha(2i - 1)\beta(2i)\|$$

As it is seen from [2.13], the spatial functions (orbitals) of electrons of every pair coincide. The condition of orthonormalization

[2.14] $$\int dx\,\phi_i^*(x)\phi_j(x) = \delta_{ij}$$

is identical to that of a strong orthogonality of geminals G_i and G_j which greatly simplifies the calculations (18). The relation [2.14] can also be satisfied with good accuracy for the case of [2.8] type soliton states. Let

[2.15] $$\phi_n(x) = \cosh^{-1}[(\xi - nR_0)/l]$$

Then the relation is strictly satisfied if the distance between solitons $R_0 \gg l$, the soliton size, i.e. in the limit of small density

[2.16] $\rho = N_c/N = 2/R_0 \ll 1$

However, the expression [2.14] will be also fulfilled sufficiently accurately if $R_0 \gtrsim 4l$, i.e.

[2.17] $\rho = 2/R_0 \leqq 1/2l = \chi^2 Mma^2/(V_0^2\hbar^2)$

In this case the wave function [2.12] corresponds to a one-dimensional lattice with a period R_0.

A similar soliton lattice was first introduced in ref. 10. Our concept is most unique in that it allows electron–electron interaction and that our soliton lattice can move as a whole with velocity $V < V_0$, transferring the charge eN_c. Then the effective mass reads $N_c M_{sol}$ where M_{sol} corresponds to expression [2.11]. The binding energy of electron pairs in soliton states ϕ_n geminals G_n, exceeds the double value of the energy [2.9] since in the equation for ρ in [2.5] one should take into account the density of both electrons (19) which corresponds to the increase in the electron–phonon interaction constant χ by a factor of $\sqrt{2}$. In this case the binding energy increases by a factor of 4. In our opinion, this is just the effect of electron pairing through the lattice.

In order to determine the advantage attained by this pairing, we compare the energy gain $g^2/2$ with the repulsion of electrons in the pair $\tilde{K}$. To calculate $\tilde{K}$, we restrict ourselves to the consideration of the first term in the interaction operator in [1.1], i.e. the Hubbard approximation:

$$\hat{H}_{el-el} = \frac{1}{2}\sum_{m\sigma} \gamma \hat{C}^{+}_{m\sigma}\hat{C}_{m\sigma}\hat{C}^{+}_{m,-\sigma}\hat{C}_{m,-\sigma}$$

or within a continuum model

[2.18] $$H_{el-el} = \iint dx_1 dx_2\, |\psi_1(x_1)|^2|\psi_2(x_2)|^2\delta(x_1 - x_2)\cdot\gamma = \gamma\int dx\phi_1(x)^2\phi_2(x)^2 = \tilde{K}$$

Taking into account that for the pair

$$\phi_1(x) = \phi_2(x) = \cosh^{-1}(x/l)/\sqrt{2l}$$

we find

[2.19] $$K = \frac{\gamma}{4l^2}\int dx \cosh^{-4}(x/l) = \gamma/3l$$

So, the electron pairing is advantageous if

[2.20] $g^2/2 > \gamma/(3l)$

3. Electron pairs and the properties of carriers at $\rho = 1$

To describe the ground state of a cyclic chain of $N = 2M$ centers possessing $N_c = N$ electrons, we choose a variational function as (20)

[3.1] $$\psi_{VLG} = \prod_{m=1}^{M}(\cos\varphi \hat{f}^{+}_{m\uparrow}\hat{f}^{+}_{m\downarrow} + \sin\varphi \hat{\hat{f}}^{+}_{m\uparrow}\hat{\hat{f}}^{+}_{m\downarrow})|0\rangle$$

where the Fermi-operators $\hat{f}^{+}_{m\sigma}$ and $\hat{\hat{f}}^{+}_{m\sigma}$ correspond to the Wannier-type states

$$\hat{f}_{m\sigma} = \frac{1}{\sqrt{M}}\sum_{|k|<k_F} e^{-ikR_m}(\cos\theta_k\hat{a}_{k\sigma} + i\sin\theta_k\hat{a}_{\bar{k}\sigma})$$

[3.2] $$\hat{\hat{f}}_{m\sigma} = \frac{1}{\sqrt{M}}\sum_{|k|<k_F} e^{-ikR_m}(i\sin\theta_k\hat{a}_{k\sigma} + \cos\theta_k\hat{a}_{\bar{k}\sigma})$$

$$(\bar{k} = k + 2k_F, \qquad k_F = \pi/2a)$$

where k is the wave number, φ and θ_k are variational parameters and the operators $\hat{a}_{k\sigma}$ diagonalize the first term of the Hamiltonian [1.1] at $x_m = 0$,

[3.3] $$\hat{a}_{k\sigma} = N^{-1/2}\sum_n \hat{C}_{n\sigma}e^{ikn}$$

$$2\theta_k = 2k$$

[3.4] $R_m/a = 2m + \delta$

At $\varphi = 0$ and $\theta_k = 0$ the function [3.1] transforms into the Slater determinant (20)

[3.5] $$\psi_{VLG}(\varphi = 0, \theta_k = 0) = \prod_{|k|<k_F} a^{+}_{k\uparrow}a^{+}_{k\downarrow}|0\rangle$$

Hence, varying φ and θ_k we obtain the corrections to the energy.

The wave function [3.1] refers to the type of antisymmetrized product of strongly orthogonal geminals (APSG). The geminals or two electron functions have been introduced into the theory by V. A. Fock and his disciples (16, 17). The APSG approximation was proposed in ref. 18. One of the authors has introduced the approximation [3.1]–[3.4] to calculate correlation effects in quasi-one-dimensional systems (20–22). We call this approximation the varied localized geminals (VLG) approximation since the geminals

[3.6] $$\hat{G}^{+}_m = (\cos\varphi\hat{f}^{+}_{m\uparrow}\hat{f}^{+}_{m\downarrow} + \sin\varphi\hat{\hat{f}}^{+}_{m\uparrow}\hat{\hat{f}}^{+}_{m\downarrow})|0\rangle$$

are partially localized.

The VLG ground state [3.1] is doubly degenerate in the parameter δ when $x_m = 0$ in [1.1] (see ref. 20). When $\delta = +1/2$ and the value of λ in expression [3.4] tends to $+0.5$ the orbitals [3.2] become

$$f_{m\sigma} = (1/2)^{1/2}(C_{2m\sigma} + C_{2m+1,\sigma})$$

When $\delta = -1/2$ and $\lambda = -0.5$ we must replace the operator $C_{2m+1,\sigma}$ in this expression by $C_{2m-1,\sigma}$. So, the parameter δ determines the localization of orbitals [3.2]. At $\delta = 1/2$ they are localized on even C—C bonds and at $\delta = -1/2$ on the odd ones.

Thus, the functions $\psi_{VLG}(\delta = 0.5)$ and $\psi_{VLG}(\delta = -0.5)$ can be compared with the two resonant structures of polyacetylene ...—C=C—C=... and ...=C—C=C—...

When all the displacements of atoms in [1.1] $x_m = 0$, the VLG function has the form (22)

[3.7] $\psi_{VLG} = a\psi_{VLG}(+) + b\psi_{VLG}(-)$

and $|a| = |b|$, $\psi_{VLG}(\pm) = \psi_{VLG}(\delta = \pm 1/2)$.

If we introduce the periodic Peierls-type deformation

[3.8] $x_m = x\cos(Qma + \varphi_0)$

where $Q = 2k_F$ then the weight of one of the structures in [3.7] goes to zero, and the total energy takes the form

[3.9] $E_{VLG}(x) = (C_1x^2 + W^2)^{1/2}$

where

[3.10] $W = \langle\psi^{(+)}_{VLG}|\hat{H}|\psi^{(-)}_{VLG}\rangle \sim e^{-rN}$

$r > 0$ depends on the system parameters (21). From [3.9] it follows that for large systems ($N \rightarrow \infty$)

[3.11] $E_{VLG}(x) = (C_1)^{1/2}|x|$

Minimizing the total energy [1.1] in the adiabatic approximation $\dot{x}_m = 0$ we find the equilibrium amplitude of the Peierls deformation

$$[3.12] \quad x_0 = \sqrt{(C_1)}/K_0$$

where the two signs correspond to two resonant structures.

Attention should be called to the analogy with the above consideration of solitons at $\rho \ll 1$. Each pair of electrons occupies geminal [3.6] and is localized on one of the bonds. In addition, this bond is reduced by $2x_0$.

Besides purely qualitative analogy there is a formal one (see [2.5]), since the orbitals f_m satisfy the variational equation

$$\beta(f_{m+1} - f_{m-1}) - \tilde{K}|f_m|^2 f_m = \epsilon_m f_m$$

The ground state of the system is degenerate in the sign of the deformation amplitude [3.12]. The dependence of the potential energy on x is of a characteristic form with two minima. In such a system soliton excitations of a specific nature, kinks, are possible (23–25). These states can be described in the VLG method. To do this, the structure of the function [3.1] near a kink is changed as follows

$$[3.13] \quad \psi_{\mathrm{VLG}}^{(\mathrm{kink})} = \prod_{m<0} \tilde{G}_m^+(+) C_{0\sigma} \prod_{m>0} \tilde{G}_m^+(-)$$

The sign of the operators $\hat{G}_m$ [3.6] denotes their slight modification in order to satisfy the strong orthogonality condition. The modification affects, actually, the state with ± 1, ± 2 and reduces to changing

$$[3.14] \quad f_1 \rightarrow f_1 - (S_{11}/2)f_{-1} - S_{10}C_0$$

$$(S_{ij} = \langle f_i | f_j \rangle)$$

etc.

Qualitatively the properties of the soliton described by [3.13] at $\gamma > 0$ differ somewhat from those of the soliton in the approximation of noninteracting electrons (23–25): (*1*) the soliton is localized on 2–3 bonds with the parameters of the Hamiltonian [1.1] characteristic for $(CH)_x$ (6) $\beta = 2.5$ eV, $\beta' = 4$ eV/Å, $K_0 = 47$ eV/Å^2, $M = M_{CH}$; and (*2*) the energy of the electron transfer from the soliton level into the conduction band is inside the forbidden zone of polyacetylene.

The difference between our picture and the model of noninteracting electrons is that in our model the formation of neutral kinks is energetically advantageous compared with that of charged ones. This is supposed to be the unique fact able to explain the low conductivity of pure $(CH)_x$ films PA $\sigma < 10^{-9}$ (ohm cm)$^{-1}$ in the presence of paramagnetism χ_p.

In the model of noninteracting electrons the number of charged kinks should approximately coincide with that of neutral kinks.

Now some words about the mass of the kink-type soliton in $(CH)_x$. Up to now, there have been no rigorous calculations of this value in $(CH)_x$. Therefore we present the results of the model calculation. The model calculation of the kink dynamics consists in that a certain velocity V is given to a stationary kink without changing its form (23–25).

One may also consider a model elastic chain with energy

$$[3.15] \quad V = \sum_m \left[\frac{M}{2}\dot{y}_m^2 + K_1(y_m - y_{m+1})^2 + U(y_m)\right]$$

The potential $U(y)$ must have at least two minima. Using the expression [3.11] we obtain

$$[3.16] \quad U(y) = -A|y| + \tfrac{1}{2}K_0 y^2$$

The parameters A and K_0 in this expression are calculated in ref. 5 for $(CH)_x$: $A = 1.8$ eV/Å and $K_0 = 44$ eV/Å^2.

Within a continuous approach we can obtain from [3.15] and [3.16] the equation of motion

$$[3.17] \quad My_{tt} - K_1 a^2 y_{xx} + K_0 y - A \text{ sign }(y) = 0$$

This equation has a kink solution

$$[3.18] \quad y = y_0(1 - \exp(-\alpha|\xi|)) \text{ sign }(\xi)$$

where $y_0 = \pm A/K_0$ and

$$[3.19] \quad \xi = x - Vt, \qquad \alpha^2 = K_0/(2K_1a^2 - MV^2)$$

V is the kink velocity which should be less than $a\sqrt{2K_1/M} = V_0$.

Using eqs. [3.17]–[3.19] we can obtain the effective mass of kinks

$$[3.20] \quad M_{\mathrm{sol}} = M_{\mathrm{CH}}(y_0/a)^2(2K_0/K_1)^{1/2}$$

Since $K_1 \approx K_0$ (5) and the experimental estimates (26, 27) yield $2x_0 = 2y_0 = 0.035$Å, $a = 1.4$Å we find that $M_{\mathrm{sol}} \ll M_{\mathrm{CH}}$.

Note that using the sine-Gordon form of the potential [3.16]

$$U_{\mathrm{SG}}(y) = \tilde{A}\left(1 - \cos\frac{2\pi}{x_0}y\right)$$

we obtain nearly the same value of the kink mass

$$[3.21] \quad M_{\mathrm{sol}} = \frac{3}{2\pi}(K_0/K_1)^{1/2}(y_0/a)^2 M_{\mathrm{CH}}$$

Thus, solitons in $(CH)_x$ are rather mobile.

1. C. SANDORFY. Can. J. Chem. **33**, 1337 (1955).
2. C. SANDORFY. Acta Phys. Hungarica, **27**, 191 (1969).
3. M. DEWAR. The molecular orbital theory of organic chemistry. McGraw-Hill, New York. 1963.
4. I. A. MISURKIN and A. A. OVCHINNIKOV. Usp. Khim. **46**, 1835 (1977).
5. I. A. MISURKIN, I. E. BELINSKII, A. A. OVCHINNIKOV, and I. I. UKRAINSKII. Intern. J. Quantum Chem. **22**, 761 (1982).
6. A. A. OVCHINNIKOV and I. I. UKRAINSKII. Fiz. Tverd. Tela, **16**, 3239 (1974).
7. V. E. KLYMENKO, V. YA. KRIVNOV, A. A. OVCHINNIKOV, I. I. UKRAINSKII, and A. F. SHVETS. Zh. Eksp. Teor. Fiz. **69**, 240 (1975).
8. A. S. DAVYDOV. Zh. Eksp. Teor. Fiz. **78**, 789 (1980).
9. A. S. DAVYDOV. Usp. Fiz. Nauk. **138**, 603 (1982).
10. V. YA. KRIVNOV and A. A. OVCHINNIKOV. Zh. Eksp. Teor. Fiz. **72**, 1559 (1977).
11. A. S. DAVYDOV and A. A. EREMKO. Ukrain. Fiz. Zh. **22**, 881 (1977).
12. A. S. DAVYDOV and V. Z. ENOLSKII. Zh. Eksp. Teor. Fiz. **79**, 1888 (1980).
13. E. I. RASHBA. Opt. Spectrosc. **2**, 88 (1957).
14. T. HOLSTEIN. Ann. Phys. **8**, 343 (1959).
15. A. A. OVCHINNIKOV. Zh. Struct. Khim. **6**, 291 (1965).
16. V. A. FOCK, M. G. VESELOV, and M. I. PETRASHENI. Zh. Eksp. Teor. Fiz. **10**, 723 (1940).
17. V. A. FOCK. Dokl. Acad. Sci. USSR, **73**, 735 (1950).
18. A. C. HURLEY, J. LENNARD-JONES, and J. A. POPLE. Proc. R. Soc. A**235**, 124 (1956).
19. L. S. BRIZHIK and A. S. DAVYDOV. Preprint ITP-83-57E, Kiev, 1983.
20. I. I. UKRAINSKII. Teor. Matemat. Fiz. **32**, 392 (1977).
21. I. I. UKRAINSKII. Zh. Eksp. Teor. Fiz. **76**, 760 (1979).
22. I. I. UKRAINSKII. Phys. Status Solidi, (b), **106**, 55 (1981).

23. W. P. SU, J. R. SCHRIEFFER, and A. J. HEEGER. Phys. Rev. Lett. **42**, 1698 (1979).
24. M. J. RICE. Phys. Lett. **71**A, 152 (1979).
25. W. P. SU, S. KIVELSON, and J. R. SCHRIEFFER. *In* Physics in one dimension. Springer, Berlin – Heidelberg – New York. 1981. p. 201.
26. C. S. YANNONI and T. C. CLARKE. Phys. Rev. Lett. **51**, 1191 (1983).
27. C. R. FINCHER, JR., C.-E. CHEN, A. J. HEEGER, A. G. MACDIARMID, and J. B. HASTINGS. Phys. Rev. Lett. **48**, 100 (1982).

Characterization of DNA structures by infrared spectroscopy: double helical forms of poly(dG-dC)·poly(dG-dC), poly(dD^{8}G-dC)·poly(dD^{8}G-dC), and poly(dG-dm^{5}C)·poly(dG-dm^{5}C)

J. A. TABOURY, J. LIQUIER, AND E. TAILLANDIER

Laboratoire de Spectroscopie Biomoléculaire, Université Paris Nord, 74 rue Marcel Cachin, F93012 Bobigny Cedex, France

Received July 17, 1984

This paper is dedicated to Professor Camille Sandorfy on the occasion of his 65th birthday

J. A. TABOURY, J. LIQUIER, and E. TAILLANDIER. Can. J. Chem. **63**, 1904 (1985).

Infrared spectroscopy in the 1750–700 cm^{-1} region is used to characterize the right- and left-handed helices of poly(dG-dC)·poly(dG-dC) with sodium counterions. The use of polymers selectively deuterated on the C8 of guanines and methylated on the C5 of cytosines allows us to propose explanations for several spectroscopic modifications which occur under the $B \rightarrow Z$ transition. Similar substitutions on nucleosides and nucleotides are used so as to assign base absorptions in poly(dG-dC)·poly(dG-dC). A set of ir bands characteristic of DNA conformations, which can be used in studies of interactions with this polynucleotide and to identify the left handed Z conformation in more complex systems, is proposed.

J. A. TABOURY, J. LIQUIER, et E. TAILLANDIER. Can. J. Chem. **63**, 1904 (1985).

La spectroscopie infrarouge dans la région 1750–700 cm^{-1} permet de caractériser la forme droite et la forme gauche de la double hélice de poly(dG-dC)·poly(dG-dC). L'étude de dérivés du poly(dG-dC)·poly(dG-dC) deutériés sélectivement sur le C8 de la guanine ou méthylés sur le C5 de la cytosine permet d'expliquer différentes modifications du spectre de ce polynucléotide au cours de la transition $B \rightarrow Z$. Des modifications similaires sur des nucléotides ou nucléosides apportent également des informations pour l'attribution des bandes d'absorption des bases du poly(dG-dC)·poly(dG-dC). Nous proposons un ensemble de bandes d'absorption caractéristiques des conformations de l'ADN, qui pourra être utilisé pour l'étude d'interactions avec ce polynucléotide ou pour la mise en évidence de la conformation en double hélice gauche dans des systèmes plus complexes.

Introduction

The DNA molecule, which for a long time had been considered a rather rigid entity, is now known to be extremely flexible and capable of adopting a great variety of secondary structures. The study of purine–pyrimidine alternating copolymers has, moreover, shown that classical right-handed A and B helices can be turned into left-handed forms belonging to the so-called Z family. These novel structures were first characterized in the case of poly(dG-dC)·poly(dG-dC) by the modification of the uv absorbance spectrum and by the inversion of the cd (circular dichroism) signal (1). Their existence has been definitively proved by X-ray diffraction studies on d(C-G)$_3$ crystals (2). Nuclear magnetic resonance (nmr) (3, 4) and Raman spectroscopy (5–9) have also been used to investigate Z DNA. Thamann *et al.* (6) showed that the Raman spectrum of the Z DNA d(C-G)$_3$ crystal is essentially identical to the high salt solution spectrum of poly(dG-dC)·poly(dG-dC). Secondary structures of native or synthetic DNAs can be successfully studied by ir spectroscopy. A and B geometries and the $B \rightarrow A$ conformational transition of DNA, alone or in the presence of polypeptides, proteins, or drugs, in highly concentrated conditions (hydrated films), have been characterized and followed by this technique (10–12). The left-handed Z structure of poly(dG-dC)·poly(dG-dC) has also been investigated by ir spectroscopy (13–17), and we have previously shown that, in films, the reversible $B \rightarrow Z$ transition can be induced by varying the relative humidity (18). This conformational transition has been identified by correlating the ir and uv absorbance spectroscopy results obtained on the same films, in the same salt and hydration conditions. In this work we present a detailed study of the ir spectra of both B and Z conformations of poly(dG-dC)·poly(dG-dC) and two polynucleotides obtained by either selective deuteration of the C8 site of guanines or by methylation of the C5 site of cytosines. (The latter modification of cytosines is often encountered in native systems and may play an important role in transcription.) The simultaneous study of these three DNAs allows us to assign many of the absorption bands in the ir spectrum. This work was undertaken to identify the ir wavenumbers and intensities characteristic of the B and Z conformations of poly(dG-dC)·poly(dG-dC) in the vibrational region between 1750 and 700 cm^{-1}, both for deuterated and nondeuterated samples, for use as a basis for further studies of interactions of these synthetic polynucleotides with drugs, metal ions, and proteins.

Material and methods

All the ir spectra, which will be discussed below were obtained using DNA films. The counterion content and the water content were rigorously controlled as these two parameters are essential to stabilize a given secondary structure of the polynucleotide.

Poly(dG-dC)·poly(dG-dC) and poly(dG-dm^{5}C)·poly(dG-dm^{5}C) were obtained from P. L. Biochemicals, dissolved in 0.1 M NaCl pH 7, ethanol precipitated, washed so as to eliminate excess NaCl, deposited on the infrared plate (ZnSe), and gently dried so as to obtain homogeneous films. Known amounts of Na^+ (usually 1 Na^+ in excess per nucleotide) were added as a droplet allowed to diffuse in the film and then slowly dried. The films were then sealed in cells with controlled relative humidity (100–32% r.h.). The desired hydration was obtained by the introduction of small vessels containing saturated solutions of different salts. The exact amount of water contained in the film was determined directly on the ir spectrum by recording the water absorption bands around 3400 cm^{-1} and 700 cm^{-1}. The films were also exposed to saturated D_2O solutions of previously dehydrated salts. The corresponding spectra, which in the text will be referred to as "in D_2O", allow the infrared regions obscured by the intense H_2O absorptions (especially the 1650 cm^{-1} and 800 cm^{-1} regions) to be investigated. Selective deuteration of the C8 of guanines has been obtained by incubation of the poly(dG-dC)·poly(dG-dC) in 0.1 M NaCl D_2O at 80°C for 3 h.

The ir spectra were recorded with a Perkin Elmer 180 double-beam ratio recorder spectrophotometer coupled to a Hewlett–Packard 9825 A calculator. The stored data were treated in several ways: (1) the

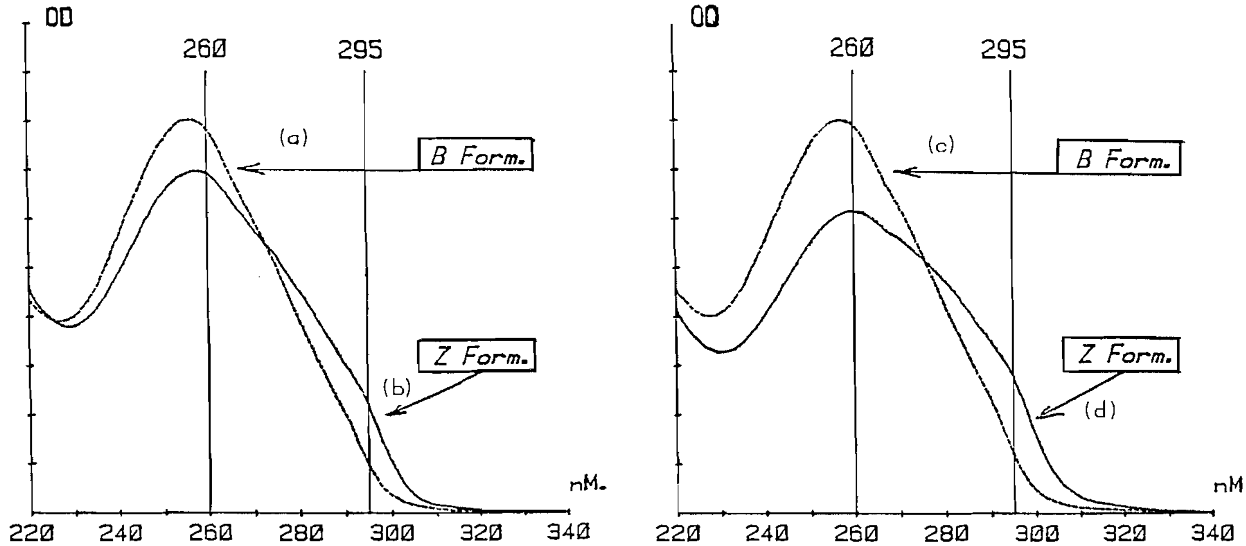

FIG. 1. Ultraviolet absorption spectra of poly(dG-dC)·poly(dG-dC)-Na^+. (a) Solution (0.1 *M* NaCl, 5 m*M* phosphate pH 7); (b) solution (4 *M* NaCl, 5 m*M* phosphate pH 7); (c) film 98% r.h. H_2O; (d) film 86% r.h. H_2O.

baseline was corrected using previously recorded spectra of the sample cells, so as to eliminate any possible difference between sample and reference cells; (2) the polynucleotide spectrum was corrected for the water contribution by subtracting a previously stored water spectrum; (3) the spectra were smoothed using 3 or 5 points and drawn using a Hewlett–Packard 7825 A digital plotter.

In the case of poly(dG-dC)·poly(dG-dC), we controlled the induction of the $B \rightarrow Z$ transition in the films by recording the corresponding uv absorption spectra. The uv absorption spectrum of a highly hydrated (98% r.h.) film (Fig. 1c) is the same as that of a low salt solution (0.1 *M* NaCl) (Fig. 1a) reflecting a *B*-type conformation. If the relative humidity is decreased to 86% r.h., a slight redshift and a weak hypochromicity of the 260-nm band are detected, along with an important hyperchromicity effect in the 295-nm region (Fig. 1d). This new spectrum is similar to that observed for the high salt solution (4 *M* NaCl) (Fig. 1b) and correlated with the *Z* conformation.

Results and discussion

The $B \rightarrow Z$ conformational transition of poly(dG-dC)·poly(dG-dC) is induced in films by a decrease of the hydration, as shown by the parallel study performed on the same samples in the same relative humidity conditions by ir and uv absorption spectroscopy. Above 93% r.h., poly(dG-dC)·poly(dG-dC) and poly(dD^{8}G-dC)·poly(dD^{8}G-dC) adopt a *B* conformation. Below 93% r.h., the secondary structure belongs to the *Z*-helical form. As regards the methylated polynucleotide, poly(dG-dm^{5}C)·poly(dG-dm^{5}C), it is well known that C5-methylation of cytosines greatly favours the *Z* conformation (19, 20). Therefore, in condensed phase, the ir spectrum of the *B* form is not obtained, even by exposing the film to 100% relative humidity. The *B* form spectrum of poly(dG-dC)·poly(dG-dC) and the *Z* form spectra of poly(dG-dC)·poly(dG-dC), poly(dD^{8}G-dC)·poly(dD^{8}G-dC), and poly(dG-dm^{5}C)·poly(dG- dm^{5}C) are presented in Fig. 2 between 1750 cm^{-1} and 700 cm^{-1}. The wavenumbers of the main absorptions as well as their assignments are summarized in Table 1. We shall discuss in detail the different spectral regions using expanded figures corresponding mainly to the deoxyribose vibrations coupled to the *G* or *C* motions and involving the C—N glycosidic linkage (Fig. 3) and to the phosphodiester chain and out-of-plane base vibrations (Fig. 4). Below 1550 cm^{-1}, many of the base absorptions of the polymer have been assigned by comparison with the spectra of 2′-deoxycytidine and 2′-deoxyguanosine-5′-phosphate (12, 21). Moreover, the effects of C5-methylation of cytosines and C8-deuteration of guanines on poly(dG-dC)·poly(dG-dC) spectra have been correlated with similar effects on cytidine and 5′-dGMP spectra respectively. Contributions of the two bases can be distinguished in the ir spectrum of the polymer. Thus the 1294 cm^{-1} and 1498 cm^{-1} bands of poly(dG-dC)·poly(dG-dC) are due to cytosine vibrations, while only a weak contribution of guanine is expected at 1482 cm^{-1}. Both bases are involved in the absorptions located at 1527 cm^{-1}, 1420–1409 cm^{-1}, and at 778 cm^{-1}.

1. *In-plane double bond stretching vibrations of bases*

In H_2O, after subtraction of the water contribution, the $B \rightarrow Z$ transition is detected by the shift of the 1710 cm^{-1} band (*B* form) to 1692 cm^{-1} (*Z* form) and by the presence of an absorption at 1630 cm^{-1} (Fig. 2*a*). The 1692 cm^{-1} band may be assigned to a guanine double-bond in-plane stretching vibration involving mainly the C6=O6 carbonyl group, as in the *Z* form spectrum of d(C-Br^{8}G-C-G-C-Br^{8}G), this band is split into two components located at 1697 cm^{-1} and 1680 cm^{-1}, reflecting the bromination effect on the initial and terminal guanines (22).

In D_2O, the two main absorptions of poly(dG-dC)·poly(dG-dC) are shifted from 1681–1649 cm^{-1} in the *B* form to 1666–1635 cm^{-1} in the *Z* form (Table 1). In the spectrum of the C5-methylated polymer in the *Z* form, these bands are found at higher wavenumbers, 1674–1643 cm^{-1}. Upon C5-methylation, a similar high wavenumber shift is also observed with 2′-deoxycytidine: the 1650 cm^{-1} band in the 2′-deoxycytidine spectrum is detected at 1666 cm^{-1} for the methylated nucleoside. This suggests that cytosine double-bond vibrations are involved in the two 1666–1635 cm^{-1} bands in the spectrum of poly(dG-dC)·poly(dG-dC) in heavy water. The in-plane double bond vibration region had also been studied by Raman spectroscopy. In the case of the unmethylated polymer, the $B \rightarrow Z$ transition is detected by shifts of the Raman lines from 1688 cm^{-1} and 1635 cm^{-1} to 1662 cm^{-1} and 1634 cm^{-1} (D_2O solutions) and from 1715 cm^{-1} to 1695 cm^{-1} (H_2O solutions) (8).

The 1750–1550 cm^{-1} spectral region is considered as being

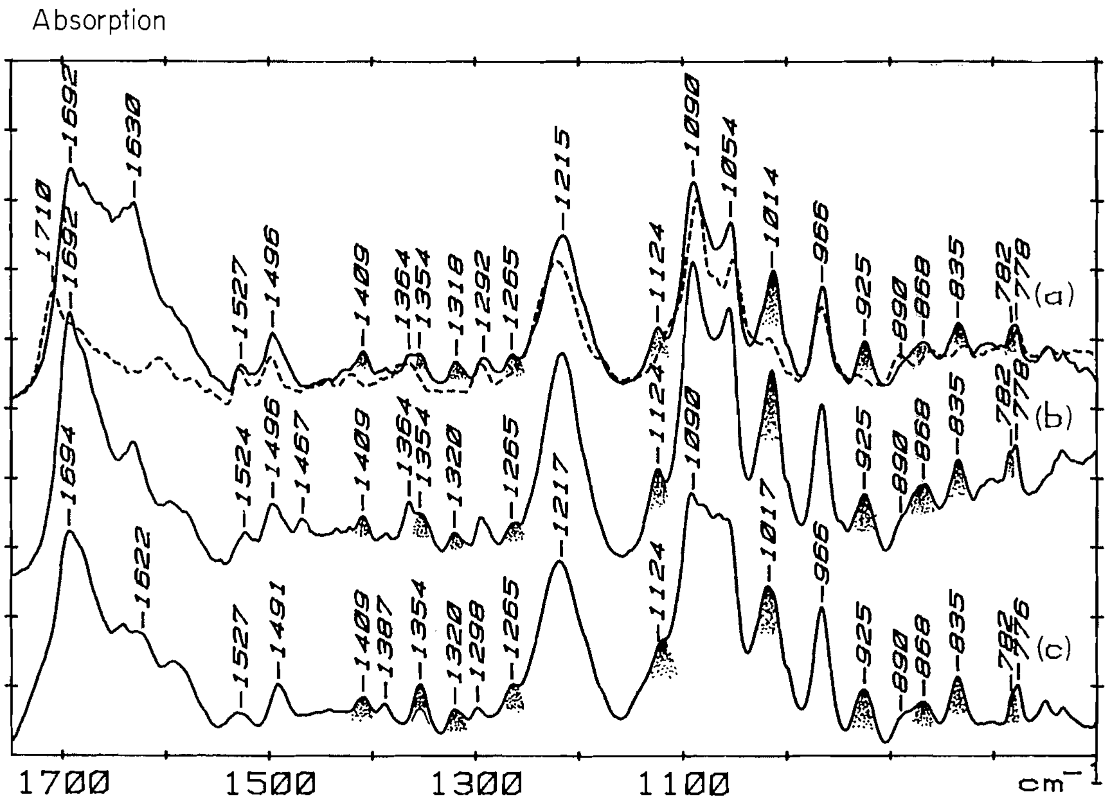

FIG. 2. Infrared absorption spectra of: (a) poly(dG-dC)·poly(dG-dC)-Na^+; —— *Z* form (86% r.h. H_2O); --- *B* form (98% r.h. H_2O). The ir spectrum of the water present in the film has been subtracted; (b) poly(dD^8G-dC)·poly(dD^8G-dC)-Na^+ at 86% r.h. (H_2O), *Z* form; (c) poly(dG-dm^5C)·poly(dG-dm^5C)-Na^+ at 86% r.h. (H_2O), *Z* form. The main bands assigned to the *Z* form have been shadowed.

sensitive to base pairing and to base stacking (23, 24). It has been shown by X-Ray diffraction that the *Z* form is a double helix structure with Watson–Crick base pairing. The *Z* configuration differs from the *B* one as cytosine bases are stacked on each other, while guanine bases are no longer stacked but in contact with the O1′-oxygen atoms of the adjacent deoxyribose residues (2). In polynucleotides, the existence of transition dipole coupling for C=O stretching vibrations was first pointed out by Tsuboi *et al.* (23). As the base pair stacking is changed under the $B \rightarrow Z$ transition, the dipole interaction is modified, as can be detected by shifts of the ir absorption bands.

2. *dG, dC, and C—N glycosidic linkage vibrations*

The spectral region between 1550 and 1250 cm^{-1} is useful to characterize the *B* and *Z* geometries of poly(dG-dC)·poly(dG-dC), as can be clearly observed in Fig. 3. The existence of the *Z* conformation of this polymer is reflected by the presence of two new absorptions at 1265 cm^{-1} and 1318 cm^{-1}, by shifts of the 1374–1364 cm^{-1} doublet to 1364–1354 cm^{-1}, and of the 1420 cm^{-1} band to 1409 cm^{-1}. Similar modifications are observed in the case of poly(dD^8G-dC)·poly(dD^8G-dC) upon the $B \rightarrow Z$ transition (Fig. 3c). The *Z* form spectrum of the methylated derivative (Fig. 3d) shows only one intense band at 1354 cm^{-1}, which may be interpreted as the sum of the shifted 1364 cm^{-1} band and of the 1354 cm^{-1} band. The low wavenumber shift of the 1364 cm^{-1} band is due to C5-methylation of cytosines as, in a similar way, the corresponding band at 1364 cm^{-1} in 2′-deoxycytidine is shifted to 1356 cm^{-1} upon C5-methylation (12). Therefore the 1364 cm^{-1} absorption in the ir spectrum of poly(dG-dC)·poly(dG-dC) reflects a vibrational mode of cytosine. The 1354 cm^{-1} band of *Z* form poly(dG-dC)·poly(dG-dC) may be assigned to a guanine vibration, as selective bromination of this base in the case of the d-(C-Br^8G-C-G-C-Br^8G) hexamer in the *Z* form reveals a low frequency shift of the 1354 cm^{-1} band to 1340 cm^{-1} (22). The dG residue which is in an *anti* conformation in the *B* form adopts a *syn* conformation in the *Z* form. This geometry modification may be reflected by the 1374–1354 cm^{-1} band shift in poly(dG-dC)·poly(dG-dC) and poly(dD^8G-dC)·poly(dD^8G-dC). This assignment is in agreement with the result of a theoretical calculation based on the GF-Wilson method performed on CpG and GpC sequences in *B* and *Z* geometries. The calculated results show that upon the $B \rightarrow Z$ transition, the important shifts from 1374 cm^{-1} to 1354 cm^{-1} (infrared bands) and from 685 cm^{-1} to 625 cm^{-1} (Raman lines) are essentially due to the *anti* → *syn* and C2′-*endo* → C3′-*endo* conformational modifications of the guanine residue and its associated sugar (16).

The band located at 1498 cm^{-1} in the *B* form poly(dG-dC)·poly(dG-dC) spectrum (1496 cm^{-1} in the *Z* form) (Fig. 3a, b) involves mainly cytosines with a weak contribution of guanines as previously mentioned. This can be deduced from the ir study of the methylation effect on cytosines: the shift of the 1496 cm^{-1} absorption (Fig. 3b) to 1491 cm^{-1} in the methylated polymer (Fig. 3d) is quite comparable to the displacement of the 1490 cm^{-1} band in 2′-deoxycytidine to 1485 cm^{-1} in 5-methylated 2′-deoxycytidine. The contribution of guanines to the absorption at 1498 cm^{-1} can be evidenced in the following way. Deuteration of the C8 site of 5′-dGMP shifts the 1482 cm^{-1} band to 1460 cm^{-1}. Similarly, selective deuteration of the C8 site of guanines in poly(dG-dC)·poly(dG-dC) shifts the

TABLE 1. Infrared wavenumbers and assignments of poly(dG-dC)·poly(dG-dC) infrared bands

poly(dG-dC)·poly(dG-dC) poly(dD^8G-dC)·poly(dD^8G-dC)						poly(dG-dm^5C)·poly(dG-dm^5C)		
B form			*Z* form			*Z* form		
Wavenumber cm^{-1}	Intensity	Assignment	Wavenumber cm^{-1}	Intensity	Assignment	Wavenumber cm^{-1}	Intensity	Assignment
1710	S	G	1692	S	G	1694	S	G
1681*	S	C	1666*	S	C	1674*	S	m^5C
1649*	S	C	1635*	S	C	1643*	S	m^5C
			1630	S		1622	S	
1582*	m		1582*	m		1580*	m	
1564*	m		1564*	m		1564*	m	
1528	w	G, C	1527	w	G, C	1527	w	G, m^5C
			1524**	w	D^8G			
1504*	m	C	1500*	m	C	1502*	m	m^5C
1498	m	C, G[a]	1496	m	C, G[a]	1491	m	m^5C, G(1)
1467**	w	D^8G	1467**	w	D^8G			
1420	w		1409	w		1409	w	
1387	w		1387	w		1387	w	
1374	w	d G						
1364	w	d C	1364	w	d C			
			1354	w	d G	1354	m	d G, dm^5 C
			1318	w	d G	1320	w	d G
1294	w	C	1292	w	C	1298	w	m^5C
			1265	w		1265	w	
1220	S	$\nu_{as}PO_2^-$	1215	S	$\nu_{as}PO_2^-$	1217	S	$\nu_{as}PO_2^-$
			1124	m	d	1124	m	d
1115	sh							
1086	S	$\nu_sPO_2^-$	1090	S	$\nu_sPO_2^-$	1090	S	$\nu_sPO_2^-$
1050	S	d	1054	S	d	1054	S	d
1020	sh		1014	S	d	1017	S	d
966	m		966	m		966	m	
930	w		925	m	d	925	m	d
893	m	[b]	890	sh	[b]	890	sh	[b]
860–853*	w		868	w		868–865*	w	
830–828*	w		835	w		835–837*	w	
800*	w		802*	w		802*	w	
			782–784*	w	G	782–784*	w	G
778	w	G, C	778	w	C	776–768*	w	m^5C
740*	w		745*	w		745*	w	
730*	w		735–730*	w		730*	w	
703*	w		710*	w		710*	w	

Abbreviations: S: strong, m: medium, w: weak, sh: shoulder, d: deoxyribose, G: guanine, C: cytosine, ν: stretching vibration, m^5C: 5-methylcytosine; *: in D_2O; **poly(dD^8G-dC)·poly(dD^8G-dC).

[a]Mainly cytosine, weak contribution of guanine.

[b]Deoxyribose and phosphodiester backbone.

guanine band, hidden by the presence of the strong cytosine component at 1498 cm^{-1}, to 1467 cm^{-1} (Fig. 3c). The 1467 cm^{-1} band, which is well isolated and not modified by the $B \rightarrow Z$ transition, involves the motion of the N7 atom of guanines. Modifications of the intensity or shifts of this band will be extremely useful to evidence any interaction with this site of the polynucleotide (17).

3. *Phosphodiester chain and out-of-plane base vibrations*

The spectral region below 1030 cm^{-1} has been studied in D_2O so as to avoid the important water contribution. In Fig. 4 are presented the spectra of poly(dG-dC)·poly(dG-dC) (*B* and *Z* forms) and of poly(dG-dm^5C)·poly(dG-dm^5C) (*Z* form) recorded in D_2O.

Important modifications can be detected due to the $B \rightarrow Z$ transition. The intensity of the 893 cm^{-1} band is drastically decreased, whereas two absorptions at 925 cm^{-1} and 1014 cm^{-1} (1017 cm^{-1} for the methylated polynucleotide) are now observed. These bands can be associated with deoxyribose vibrations coupled to backbone vibrations, their strong hyperchromicity possibly reflecting the effect of the electronic polarization of the C—O—C deoxyribose atoms close to the guanine ring in the *Z* structure (2). The phosphodiester chain vibrations observed in D_2O at 828 cm^{-1} and 853 cm^{-1} in the *B*

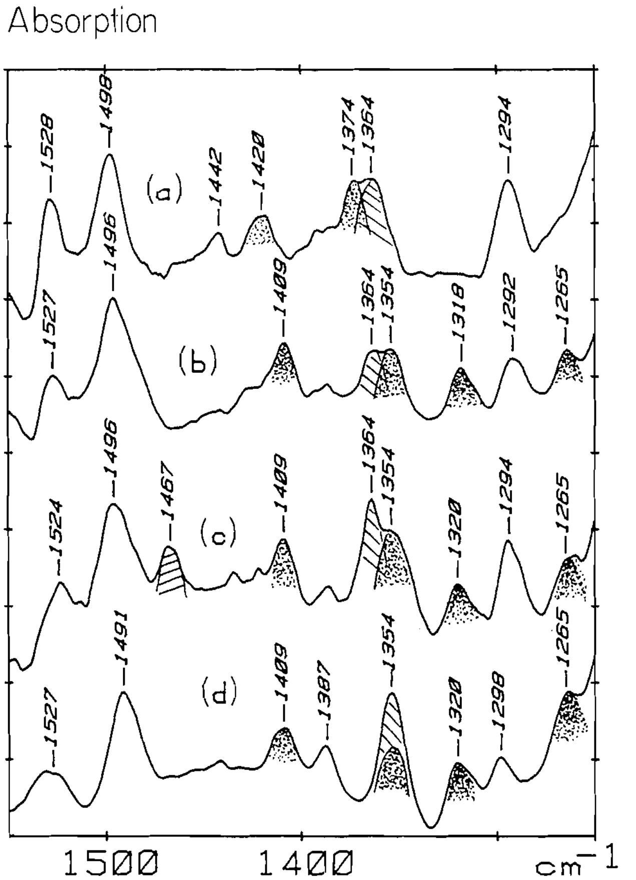

FIG. 3. Spectral region of base and deoxyribose–base vibration modes. Effect of the $B \rightarrow Z$ transition on the ir spectrum of poly(dG-dC)·poly(dG-dC)-Na^+; (a) B form (98% r.h. H_2O); (b) Z form (86% r.h. H_2O); Effect of specific substitutions. (c) At the C8 position of guanine in poly(dD^{8}G-dC)·poly(dD^{8}G-dC)-Na^+; Z form (86% r.h. H_2O); (d) At the C5 position of cytosine in poly(dG-dm^{5}C)·poly-(dG-dm^{5}C)-Na^+; Z form (86% r.h. H_2O).

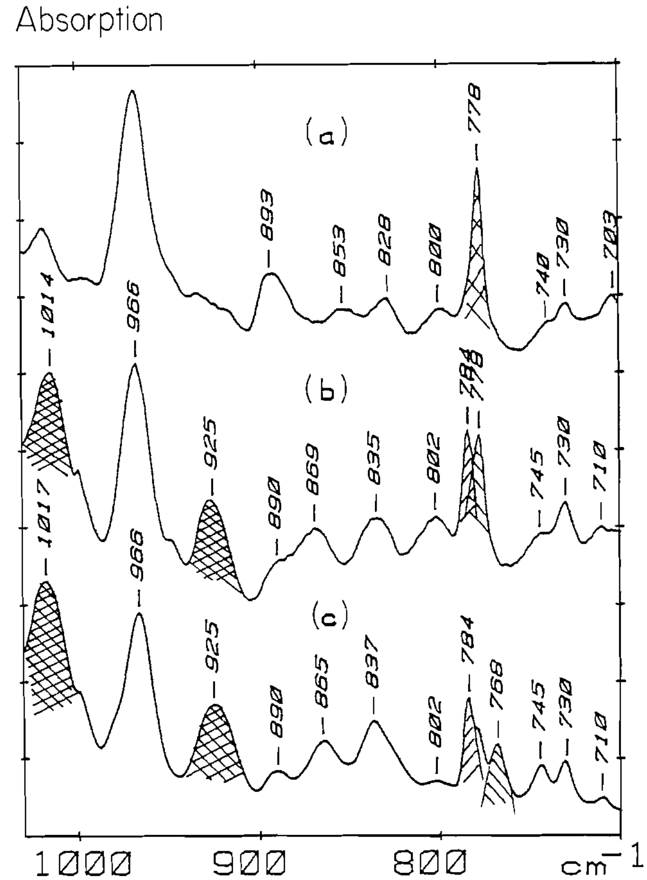

FIG. 4. Phosphodiester chain and out-of-plane base vibrations; (a) poly(dG-dC)·poly(dG-dC)-Na^+ B form (98% r.h. D_2O); (b) poly(dG-dC)·poly(dG-dC)-Na^+ Z form (86% r.h. D_2O); (c) poly(dG-dm^{5}C)·poly(dG-dm^{5}C)-Na^+ Z form (86% r.h. D_2O).

form are shifted to 835 cm^{-1} and 868 cm^{-1} in the Z form (837 cm^{-1} and 865 cm^{-1} for poly(dG-dm^{5}C)·poly(dG-dm^{5}C)). Finally, the sharp band at 778 cm^{-1} in the B form (Fig. 4a) is split into two components well separated in D_2O, at 784 cm^{-1} and 778 cm^{-1}, for Z form poly(dG-dC)·poly(dG-dC) (Fig. 4b). Methylation of cytosines in Z form poly(dG-dm^{5}C)·poly-(dG-dm^{5}C) induces a shift of the cytosine component from 778 cm^{-1} to 768 cm^{-1} (Fig. 4c) (776 cm^{-1} in H_2O, Fig. 2c). In a similar way bromination of the guanines shifts the absorption located at 784 cm^{-1} (22).

Thus in the poly(dG-dC)·poly(dG-dC) Z form spectrum the 784 cm^{-1} band is due to a guanine vibration while the 778 cm^{-1} band is due to a cytosine vibration. These two absorptions are assigned to out-of-plane ring vibrations, possibly coupled to the glycosidic torsion and carbonyl out-of-plane motions; as on the polarized ir spectra of oriented samples, these two absorptions remain parallelly polarized, whatever the DNA conformation (18). The corresponding transition dipole moments are thus oriented parallelly to the helix axis. The Raman spectrum in this region is also extremely sensitive to the $B \rightarrow Z$ conformational transition. The different Raman lines have been discussed either in terms of vibrations of the phosphate groups and of the cytosines (8) or in terms of base vibrations (7). The infrared spectrum presents two sharp bands at 784–778 cm^{-1} (bandwidth 8 cm^{-1}) assigned to base vibrations. However, deconvolution of this spectral region shows that a broad band located at 802 cm^{-1} (40 cm^{-1} bandwidth), probably due to a phosphate chain vibration mode, should be taken into account (12).

In summary, our study allows us to propose a set of characteristic features of the Z conformation spectrum of poly-(dG-dC)·poly(dG-dC) and to assign a number of absorptions by comparison with nucleosides, nucleotides, and modified polynucleotides (C8-deuteration of guanines and C5-methylation of cytosines): the $B \rightarrow Z$ transition is reflected by: (*i*) new or enhanced absorptions: 1630 cm^{-1}, 1318 cm^{-1}, 1265 cm^{-1}, 1124 cm^{-1}, 1014 cm^{-1}, 925 cm^{-1}; (*ii*) band shifts (in parentheses are wavenumbers of the corresponding absorptions in the B form): 1409 cm^{-1} (1420 cm^{-1}), 1354 cm^{-1} (1374 cm^{-1}). In H_2O: 1692 cm^{-1} (1710 cm^{-1}). In D_2O: 1666 cm^{-1} (1681 cm^{-1}), 1635 cm^{-1} (1649 cm^{-1}); (*iii*) band splitting: 784–778 cm^{-1} (778 cm^{-1}); (*iv*) decrease of the intensity of the absorption located at 893 cm^{-1}.

Besides, selective deuteration of C8 of guanines shifts the guanine contribution, overlapped by a cytosine band at 1496 cm^{-1}, to 1467 cm^{-1}, allowing evidence of interactions on the N7 site of the base.

These characteristic features of the ir spectrum of the Z conformation determined in the case of poly(dG-dC)·poly-(dG-dC) will be useful to help the detection of left-handed structures in other polynucleotides which have been theoretically predicted as able to adopt such conformations: regularly alternating purine–pyrimidine polymers such as poly(dA-dC)·poly(dG-dT) and poly(dA-dT)·poly(dA-dT). The absorptions which could therefore be used are those involving the deoxyribose phosphate backbone and, possibly, also bands common to the purine bases. In the high wavenumber range (double-bond stretching vibrations in the base plane), shifts to lower wavenumbers are expected, due to changes in base stacking during the $B \rightarrow Z$ transition. The displacement of the bands cannot be exactly predicted as it must depend both on nature of base and primary sequence of the alternating purine–pyrimidine DNA. The *anti* $\rightarrow$ *syn* transition of the purines should be reflected by a shift of the purine absorption coupled to the glycosyl linkage from 1374 cm^{-1} to 1354 cm^{-1}.

Below 1000 cm^{-1} native and synthetic DNA conformations may be distinguished by distinct sets of ir absorption bands. The right-handed geometries of the B family with a C2′-*endo anti* conformation of the nucleosides have been characterized by ir absorptions around 890 cm^{-1} and 835 cm^{-1}, whereas the right-handed A family helices with a C3′-*endo anti* conformation of nucleosides are detected by ir absorptions at about 890 cm^{-1}, 878 cm^{-1}, 860 cm^{-1}, and 805 cm^{-1} (11, 25). The left-handed helices with C2′-*endo anti* and C3′-*endo syn* alternating geometries may be identified, as in the case of poly(dG-dC)·poly(dG-dC), by ir bands occurring around 925 cm^{-1}, 868 cm^{-1}, 835 cm^{-1}, and 802 cm^{-1}.

1. F. M. POHL, and T. M. JOVIN. J. Mol. Biol. **67**, 375 (1972).
2. A. H-J. WANG, G. J. QUIGLEY, F. J. KOLPAK, J. L. CRAWFORD, J. H. VAN BOOM, G. VAN DER MAREL, and A. RICH. Nature, **282**, 680 (1979).
3. D. J. PATEL, L. L. CANUEL, and F. M. POHL. Proc. Natl. Acad. Sci. U.S.A. **76**, 2508 (1979).
4. S. TRAN-DINH, J. TABOURY, J. M. NEUMANN, T. HUYNH-DINH, B. GENISSEL, B. LANGLOIS D'ESTAINTOT, and J. IGOLEN. Biochemistry, **23**, 1362 (1984).
5. F. M. POHL, A. RANADE, and M. STOCKBURGER. Biochem. Biophys. Acta, **335** 85 (1973).
6. T. J. THAMANN, R. C. LORD, A. H-J. WANG, and A. RICH. Nucleic Acids Res. **9**, 5443 (1981).
7. Y. NISHIMURA, M. TSUBOI, T. NAKANO, S. HIGUCHI, T. SATO, T. SHIDA, S. UESUGI, E. OHTSUKA, and M. IKEHARA. Nucleic Acids Res. **11**, 1579 (1983).
8. J. M. BENEVIDES and G. J. THOMAS, R. Nucleic Acids Res. **11**, 5747 (1983).
9. R. M. WARTELL, J. T. HARRELL, W. ZACHARIAS, R. D. WELLS. J. Biomol. Struct. Dyn. **1**, 83 (1983).
10. J. PILET and J. BRAHMS. Nature (London) New Biol. **236**, 99 (1972).
11. J. LIQUIER, J. TABOURY, E. TAILLANDIER, and J. BRAHMS. Biochemistry, **16**, 3262 (1977).
12. E. TAILLANDIER, J. LIQUIER, and J. A. TABOURY. Advances in infrared and Raman spectroscopy. Vol. 12. *Edited by* R. J. H. Clark and R. E. Hester. Heyden Publ. Co., Holland. 1985. pp. 65–114.
13. E. TAILLANDIER, J. TABOURY, J. LIQUIER, P. SAUTIERE, and M. COUPPEZ. Biochimie, **63**, 895 (1981).
14. J. A. TABOURY and E. TAILLANDER. Magnesium, **3**, 152 (1984).
15. J. PILET and M. LENG. Proc. Natl. Acad. Sci. U.S.A. **79**, 26 (1982).
16. M. GHOMI, J. A. TABOURY, and E. TAILLANDIER. Biochimie, **66**, 43 (1984).
17. J. A. TABOURY, P. BOURTAYRE, J. LIQUIER, and E. TAILLANDIER. Nucleic Acids Res. **12**, 4247 (1984).
18. L. CHINSKY, B. JOLLES, A. LAIGLE, P. Y. TURPIN, J. TABOURY, and E. TAILLANDIER. Biopolymers, **23**, 1931 (1984).
19. M. BEHE, and G. FELSENFELD. Proc. Natl. Acad. Sci. U.S.A. **73**, 1619 (1981).
20. S. FUJII, A. H-J. WANG, G. VAN DER MAREL, J. H. VAN BOOM, and A. RICH. Nucleic Acids Res. **10**, 7879 (1982).
21. M. TSUBOI, Y. KYOGOKU, and T. SHIMANOUSHI. Biochem. Biophys. Acta, **55**, 1 (1962).
22. J. A. TABOURY, E. TAILLANDIER, P. LOMBROSO, J. M. NEUMANN, S. TRAN DINH, B. LANGLOIS D'ESTAINTOT, T. HUYNH DINH, and J. IGOLEN. J. Biomol. Struct. Dyn. Submitted.
23. M. TSUBOI, S. TAKAHASHI, and I. HARADA. *In* Physico-chemical properties of nucleic acids. Vol. 2. *Edited by* J. Duchesne. Academic Press, New York. pp. 91–145.
24. M. TSUBOI and Y. NISHIMURA. *In* Raman spectroscopy linear and non linear. *Edited by* J. Lascombe and P. V. Huong. John Wiley & Sons, New York. 1982. pp. 683–702.
25. S. BRAHMS, J. BRAHMS, and J. PILET. Israel J. Chem. **12**, 153 (1974).

Features of the thioformaldehyde potential energy surfaces

JOHN D. GODDARD
Guelph–Waterloo Centre for Graduate Work in Chemistry, Department of Chemistry and Biochemistry, University of Guelph, Guelph, Ont., Canada N1G 2W1

Received August 16, 1984

This paper is dedicated to Professor Camille Sandorfy on the occasion of his 65th birthday

JOHN D. GODDARD. Can. J. Chem. **63**, 1910 (1985).

The structures of seven minima and five transition states of the S_0 and T_1 potential energy surfaces of thioformaldehyde have been located at the 3-21G* SCF level. Further calculations have been carried out to determine harmonic vibrational frequencies and to examine the effects of larger basis sets and of configuration interaction on energy differences. The molecular dissociation limit of H_2 and CS is thermodynamically accessible at the energy of the lowest n,π^* excited states and the singlet thiohydroxymethylenes lie only slightly too high. However, there are large barriers of ~85 to 90 kcal mol^{-1} to the molecular dissociation or to the 1,2-hydrogen shifts from thioformaldehyde to the thiohydroxymethylenes. The dissociation to H and HCS requires ~85.4 kcal mol^{-1} on the ground singlet and faces a barrier of several kcal mol^{-1} relative to products on the triplet surface. Any unimolecular photochemistry of thioformaldehyde is likely to require excitation to higher excited states than the lowest n,π^* states.

JOHN D. GODDARD. Can. J. Chem. **63**, 1910 (1985).

Les structures de sept minima et de cinq états de transition des surfaces d'énergie potentielle S_0 et T_1 du thioformaldéhyde ont été localisées au niveau autocohérent 3-21G*. On a effectué d'autres calculs pour déterminer les fréquences vibrationnelles harmoniques et pour examiner les effets d'ensembles de base plus larges et d'interactions de configuration sur les différences d'énergie. La limite de dissociation moléculaire en H_2 et CS est thermodynamiquement accessible au niveau d'énergie des états excités n,π^* les plus bas et les thiohydroxyméthylènes singulets sont situés à un niveau légèrement trop élevé. Toutefois, les barrières à la dissociation moléculaire ou aux transpositions-1,2 d'hydrogènes du thioformaldéhyde au thiohydroxyméthylènes sont très élevées, ~85 à 90 kcal mol^{-1}. La dissociation en H et HCS nécessite ~85.4 kcal mol^{-1} au niveau fondamental alors qu'au niveau de l'état triplet il existe une barrière de plusieurs kcal mol^{-1} par rapport aux produits. Toute photochimie unimoléculaire du thioformaldéhyde demandera probablement une excitation à des états excités supérieurs en énergie aux états n,π^* les plus bas.

[Traduit par le journal]

Introduction

The spectroscopy and photophysics of the thioformaldehyde molecule, H_2CS, have recently been extensively studied by experimentalists and to a somewhat lesser degree by quantum chemists (1–9). Much of the work on the electronic and vibrational spectroscopies of thioformaldehyde in its ground and lowest-lying excited states has recently been reviewed (1). Spectroscopic studies aimed at determining the molecular constants of the $\tilde{a}\,^3A_2$ state have appeared (2) and are complemented to an extent by a DZ** SCF quantum chemical study (8). The photophysics of H_2CS in its lowest excited states has attracted recent attention (3–6) and there have been some speculations on the question of thioformaldehyde photochemistry (3, 5, 6). Some controversy exists as to whether thioformaldehyde may dissociate into the molecular products, H_2 + CS, on the S_0 surface reached by internal conversion from an initially excited $\tilde{A}(^1A_2)$ state (5, 6). Such a process is well known in the oxygen analogue, formaldehyde, (10) and has been examined in detail by computational studies (e.g. refs. 12, 13). Kawasaki *et al.* (5) raise the possibility of the nonradiative decay of H_2CS ($\tilde{A}\,^1A_2$) to H_2 and CS but this channel is dismissed by Bruno and Steer (6). The molecular products are probably thermodynamically accessible relative to the low-lying n,π^* states but there may be a large barrier to this dissociation (3, 6) if the formaldehyde molecule may serve as a guide (12, 13). The fact that the $^{3,1}n,\pi^*$ origins of thioformaldehyde are at 14 614 cm^{-1} or 41.8 kcal mol^{-1} and 16 395 cm^{-1} or 46.9 kcal mol^{-1}, as compared to 25 194 cm^{-1} or 72.0 kcal mol^{-1} and 28 188 cm^{-1} or 80.6 kcal mol^{-1} for formaldehyde (1), means that considerably less energy will be available for any unimolecular photochemical reactions of H_2CS after excitation into its lowest excited electronic states.

There has been a recent DZ** SCF and CI study (11) on the thioformyl radical, HCS, which is one probable product of any thioformaldehyde photochemistry. Most of the quantum chemical studies on H_2CS have focussed on the molecular structures and vibrational frequencies of the lowest triplet state (7, 8) or the vertical electronic excitation energies (9). There have been no quantum chemical studies on thioformaldehyde, investigating many features of the S_0 and T_1 potential energy surfaces, as there have been, for example, for formaldehyde (12, 13). In particular, the isomerization of thioformaldehyde to thiohydroxymethylenes may be thermodynamically feasible out of the lowest excited states (although the barrier height is unknown). In the case of formaldehyde, the hydroxymethylene isomer has received considerable attention from computationalists (e.g. refs. 12, 14, 15) and has been invoked in the interpretation of certain experiments (16).

The present study examines a number of minimum energy and transition state structures on the ground state, (S_0), and lowest triplet state, (T_1), surfaces of H_2CS. All geometries were optimized using SCF gradient methods and the 3-21G* basis set which includes 6-*d* type Gaussians on S. The natures of all stationary structures (i.e. minima, transition states) were verified by calculating the harmonic vibrational frequencies using analytic second derivatives. Higher level calculations both in terms of basis sets (6-31G*, 6-31G**) and electron correlation (3-21G* CISD) were carried out at the 3-21G* geometries. Potential energy surface features examined include: H_2CS (S_0 and T_1), *cis*- and *trans*-HCSH (thiohydroxymethylenes S_0), the transition state for the internal rotation interconverting the singlet thiohydroxymethylenes, the rearrangement barrier from H_2CS to *trans*-HCSH, the molecular dissociation limit of H_2 and CS and the transition state for this pathway, the radical dissociation products of H + HCS, triplet thiohydroxymethylene, the transition structure for triplet H_2CS rearranging to triplet HCSH, and the barrier for the dissociation of H_2CS (T_1) to H + HCS.

Computational methods

All computations were performed with the GAUSSIAN 82 program system (17). Geometries were optimized at the SCF level using analytic gradient methods and the 3-21G* basis set (18, 19). Note that the 3-21G* basis set includes a set of 6 *d*-type Gaussian functions only on S. Harmonic vibrational frequencies were calculated for all stationary point structures using analytic second derivatives (20) at the 3-21G* SCF level. Basis set extension effects on energy differences at the SCF level were examined at the 3-21G* geometries with single point 6-31G* (19, 21) and 6-31G** (21) computations. Recall that the 6-31G* basis involves sets of *d*-functions on C and S and that the 6-31G** augments the 6-31G* by adding *p*-functions on the hydrogens. Effects of electron correlation on energy differences were accounted for by singles and doubles configuration interaction (3-21G* CISD) relative to the SCF reference configuration with six frozen core MO (approximately the C $1s$ and S $1s2s$ $2p_x2p_y2p_z$ AO) excluded and all virtuals included. The effects of higher excitations were estimated by a size consistency correction (22). In the cases of the molecular (H_2 + CS) and radical (H + HCS) limits, computations were done in the "supermolecule approximation" with the fragments separated by a large distance. Changes in thermal energies were calculated as in GAUSSIAN 82 with a rigid rotator/harmonic oscillator model (e.g. ref. 19) but using the calculated 3-21G* SCF harmonic frequencies to determine zero point energy differences. Best estimates of energy differences were obtained by including the thermal corrections and assuming the additivity of polarization and correlation effects as has been shown to be approximately valid (23).

Results and discussion

The total energies as well as the energy differences relative to ground state thioformaldehyde at five levels of computation are presented in Table 1 for all twelve stationary points. Table 2 collects the 3-21G* SCF optimized geometries (r_e structures) for the seven minimum energy and five transition state structures. Table 3 displays the 3-21G* SCF harmonic vibrational frequencies in cm^{-1} along with these values scaled by 0.9 (see below) and the symmetry label where appropriate. Note that all transition state structures have exactly one imaginary frequency as required for a true transition state. Table 4 presents an analysis of the results in Tables 1 and 3 to yield the best estimates of this study for the thermochemical energy changes or barrier heights to reaction.

Energies

Comparisons of the calculated energy differences with experiment are in order where spectroscopic or thermochemical data exist. Spectroscopy places the T_1 origin in thioformaldehyde at 14 614 cm^{-1} or 41.8 kcal mol^{-1} (1), which is in quite good agreement with the computed value of 42.3 kcal mol^{-1} (3-21G* CISD + size consistency correction (SCC)) or the estimate of 40.9 kcal mol^{-1} (Table 4). The enthalpy difference between ground state H_2CS and the hydrogen molecule plus carbon monosulphide may be computed from thermochemical data (3, 24, 25) to be 31 ± 7.6 kcal mol^{-1} (a value of ~40 kcal mol^{-1} is used in Figs. 1 and 3 of refs. 3 and 6 respectively), which agrees reasonably well with the result of this study, 34.9 kcal mol^{-1}. As a partial test of the effects of using geometries optimized with correlated methods on the predicted energy differences, the H_2 + CS and H_2CS (S_0) structures were redetermined at the 3-21G* CISD level. At these CI geometries (and employing the thermal and basis set extension effects in Table 4), the energy change between ground state thioformaldehyde and the molecular dissociation limit is 36.5 kcal mol^{-1} and thus differs from the prediction at the SCF optimized geometries by only 1.6 kcal mol^{-1}. The enthalpy difference between S_0 thioformaldehyde and a hydrogen atom plus a thioformyl radical, HCS, is given as 90 ± 24 kcal mol^{-1} from experiment (3, 25, 26), with the large uncertainty due to the heat of formation of HCS of 63 ± 19 kcal mol^{-1} (26). The calculated value, in this work, of 85.4 kcal mol^{-1} for $H_2CS \rightarrow H + HCS$ is certainly reasonable.

As the 3-21G* basis set is relatively small, it is quite possible that the SCF energy differences are slightly too large due to basis set superposition errors (BSSE). However, as only the H_2CS minimum and the radical and molecular limits are of interest relative to experiment, it is unlikely that BSSE would be of very great significance on a scale of 34.9 or 85.4 kcal mol^{-1}, the computed dissociation energies. Corrections for such errors could become highly important in an accurate treatment of all regions of the potential surface, including very weak interactions.

For the other minimum energy species, the singlet and triplet thiohydroxymethylenes, no comparisons with experiment are possible. Some obvious and interesting comparisons with each other and with formaldehyde suggest themselves. Thiohydroxymethylene is a singlet stable carbene as is expected for a methylene with a hydrogen replaced by a somewhat electronegative substituent bearing lone pair electrons (27). The values in Table 4 place triplet HCSH ~9.1 kcal mol^{-1} higher in energy than singlet *trans*-HCSH. The comparable energy gap between *trans*-HCOH (S_0) and *gauche*-HCOH (T_1) has been computed to be ~25 kcal mol^{-1} (14). For the singlet thiohydroxymethylenes the *trans* isomer is slightly (2 kcal mol^{-1}) more stable than the *cis* form. In hydroxymethylene, HCOH, this difference is somewhat larger at 5.5 kcal mol^{-1} (12, 15). Relative to the oxygen analogues, there appears to be a "leveling effect" in the sulphur case with smaller energy gaps between the various thiohydroxymethylenes.

Two final comparisons of energy differences between minima, namely, H_2CS (S_0) vs. *trans*-HCSH (S_0) and H_2CS (T_1) vs. *gauche*-HCSH (T_1) should be made. *trans*-Thiohydroxymethylene singlet is predicted to be 52.3 kcal mol^{-1} higher in energy than ground state thioformaldehyde. In the case of H_2CO, the best calculated energy differences for the comparable quantity are in the range 52.6 to 55.4 kcal mol^{-1} (12, 15). *gauche*-Triplet thiohydroxymethylene lies ~19.2 kcal mol^{-1} above triplet thioformaldehyde while for the oxygen analogue this difference was calculated to be ~14 kcal mol^{-1} (14*b*). The relative energies of H_2CX and HCXH, singlet or triplet, are thus similar for X = O and S.

Certain qualitative features regarding the heights of reaction barriers should first be noted. Considerations of orbital or state correlation diagrams (28) suggest that the dissociation of H_2CS to H and HCS radicals on the S_0 surface should face no barrier beyond the reaction endothermicity. A barrier to the dissociation of triplet thioformaldehyde to the same radicals is predicted (28) and such a feature was approximately located in SCF computations on H_2CO (T_1) (29). A symmetry analysis of

TABLE 1. Total energies in hartree and energy differences relative to ground state thioformaldehyde in kcal mol^{-1}. All calculations were carried out at the 3-21G* SCF optimized geometries

	3-21G* SCF		6-31G* SCF		6-31G** SCF		3-21G* CISD		3-21G* CISD + SCC	
S_0	$E(+434)$	ΔE	$E(+436)$	ΔE	$E(+436)$	ΔE	$E(+434)$	ΔE	$E(+434)$	ΔE
H_2CS	−0.446459	0.0	−0.506439	0.0	−0.509930	0.0	−0.666496	0.0	−0.687657	0.0
trans-HCSH	−0.363564	52.0	−0.429539	48.3	−0.435189	46.9	−0.572708	58.9	−0.592658	59.6
cis-HCSH	−0.361032	53.6	−0.425701	50.7	−0.431338	49.3	−0.570248	60.4	−0.590240	61.1
HC(H)S rearrangement	−0.280108	104.4	−0.344294	101.7	−0.354265	97.7	−0.506302	100.5	−0.531384	98.1
HCSH internal rotation t.s.	−0.312028	84.4	−0.376798	81.4	−0.382831	79.8	−0.516152	94.3	−0.535660	95.4
H_2 + CS Molecular limit	−0.369035	48.6	−0.431110	47.3	−0.435629	46.6	−0.593975	45.5	−0.617637	43.9
Molecular dissociation t.s.	−0.261109	116.3	−0.323737	114.6	−0.334939	109.8	−0.498223	105.6	−0.527604	100.4
T_1										
H_2CS	−0.415546	19.4	−0.474316	20.2	−0.478190	19.9	−0.605476	38.3	−0.620324	42.3
gauche-HCSH	−0.382102	40.4	−0.439709	41.9	−0.445557	40.4	−0.569957	60.6	−0.584723	64.6
HC(H)S rearrangement	−0.314674	82.7	−0.376983	81.2	−0.385473	78.1	−0.514397	95.4	−0.532934	97.1
H + HCS Radical limit	−0.322848	77.6	−0.381163	78.6	−0.383203	79.5	−0.517869	93.3	−0.540821	92.1
Radical dissociation t.s.	−0.310084	85.6	−0.369216	86.1	−0.371486	86.9	−0.513638	95.9	−0.534968	95.8

the dissociation of formaldehyde to the molecular products, H_2 and CO, (e.g. ref. 30) suggests a high barrier and a transition state structure which may remain planar but is distorted from C_{2v} symmetry. Similar results may hold for thioformaldehyde. Consideration of the highest occupied molecular orbital (HOMO) in the case of the 1,2-hydrogen shift from singlet H_2CO to singlet *trans*-HCOH (31) suggests a large barrier to such a rearrangement as H_2CS (S_0) → *trans*-HCSH (S_0).

Turning to the computational results in Tables 1 and 4, the 3-21G* SCF barrier to the molecular dissociation is very large at 116.3 kcal mol^{-1}, relative to ground state thioformaldehyde. All the more elaborate calculations and the thermal correction act to decrease this barrier but it is still large at 87.1 kcal mol^{-1} for a best estimate. The energy requirement is some 46.2 kcal mol^{-1} above the calculated energy of the lowest excited n,π^* triplet state or ~40 kcal mol^{-1} above the experimental energy of the $^1n,\pi^*$ excited state. Relative to the molecular products of hydrogen molecule and carbon monosulphide the energy barrier is 52.2 kcal mol^{-1} as the reaction H_2CS (S_0) → H_2 + CS is overall endothermic by 34.9 kcal mol^{-1}. By way of comparison, the barrier in formaldehyde to dissociation to H_2 and CO is calculated to be 80.6 ± 3 kcal mol^{-1} (13*b*). There has been a detailed discussion regarding the adequacy of a single reference configuration for this transition state in H_2CO (13*b*). It is probable that for H_2CS a multi-reference CISD or MCSCF + CI calculation would predict a lower barrier by perhaps 5 to 10 kcal mol^{-1}. However, the barrier is certain to remain considerably greater than the energy available in the lowest n,π^* excited states of thioformaldehyde.

The barrier to the 1,2-hydrogen shift linking singlet thioformaldehyde to *trans*-thiohydroxymethylene is predicted to be 85.9 kcal mol^{-1} in Table 4. Thus, the reverse barrier from the *trans*-methylene to the aldehyde isomer is 33.6 kcal mol^{-1}. These barriers are quite reminiscent of those in formaldehyde whose analogous rearrangements require 84.4 to 85.9 and 29.0 to 30.0 kcal mol^{-1} (12, 15). Once again, the effects considered beyond the 3-21G* SCF calculation (barrier 104.4 kcal mol^{-1}) all lowered the energy for rearrangement. This energy requirement of 85.9 kcal mol^{-1} for the hydrogen shift is very similar to that for the molecular dissociation of 87.1 kcal mol^{-1} and to the dissociation energy to radicals on the S_0 surfaces at 85.4 kcal mol^{-1}.

The transition state for the triplet rearrangement from H_2CS to *gauche*-HCSH requires 46 kcal mol^{-1} relative to the aldehyde isomer. The reverse reaction faces a barrier of 26 kcal mol^{-1}. The analogous rearrangement of triplet formaldehyde has not been investigated. The 1,2-hydrogen shift from triplet vinylidene to triplet acetylene (32) has a large classical barrier of ~55 kcal mol^{-1} and proceeds through a decidedly nonplanar transition structure.

The energy required for the internal rotation from *trans*- to *cis*-thiohydroxymethylene is calculated to be 33.6 kcal mol^{-1} relative to *trans* or 31.6 kcal mol^{-1} relative to *cis*. Such a barrier is, of course, large for an internal rotation about a single bond. However, the CS bond acquires considerable double bond character through donation of the lone pairs on S into the formally vacant carbene C $p\pi$ type orbital (12). This favourable interaction is essentially lost at the transition state where the dihedral angle is nearly 90°. In formaldehyde the comparable barrier has been calculated to be ~29 kcal mol^{-1} (12, 15).

The dissociation of triplet state thioformaldehyde to the ground states of H and HCS has been calculated to have a thermodynamic energy requirement of 43.2 kcal mol^{-1}. However, as anticipated from symmetry arguments (28), there is an additional small barrier of ~5 kcal mol^{-1} relative to the dissociated radicals at infinite separation. The lowest triplet state of H_2CO also has a similar small hump in the potential for the cleavage to radicals of ~9 kcal mol^{-1} at the small basis set SCF level (29).

Structures

The 3-21G* SCF r_e geometries for S_0 and T_1 thioformaldehyde and for the molecular dissociation products, H_2 and CS,

TABLE 2. 3-31G* SCF optimized geometries for stationary points on the S_0 and T_1 surfaces of H_2CS; bond lengths (r) in angstrom and angles (α) in degrees. The H_2 + CS molecular and H + HCS radical limit structures were determined in supermolecule calculations with the fragments separated by a large distance

Species	S_0		Species	T_1	
H_2CS	r(CS)	1.594	H_2CS	r(CS)	1.720
	r(CH)	1.076		r(CH)	1.072
	α(SCH)	122.34		α(SCH)	119.66
	α(HCH)	115.32		α(oop)	1.00
				α(HCH)	120.68
trans-HCSH	r(CS)	1.677	*gauche*-HCSH	r(CS)	1.723
	r(CH)	1.095		r(CH)	1.073
	r(SH)	1.328		r(SH)	1.332
	α(SCH)	107.08		α(SCH)	130.46
	α(CSH)	99.90		α(CSH)	98.79
				τ(HCSH)	92.29
cis-HCSH	r(CS)	1.657			
	r(CH)	1.089			
	r(SH)	1.344			
	α(SCH)	114.26			
	α(CSH)	107.81			
HC(H)S rearrangement t.s.	r(CS)	1.693	HC(H)S rearrangement t.s.	r(CS)	1.733
	r(CH)	1.086		r(CH)	1.072
	$r(CH_r)$	1.403		$r(H_rS)$	1.494
	$\alpha(SCH_r)$	55.96		$\alpha(SCH_r)$	55.30
	α(SCH)	119.60		α(SCH)	130.59
	$\tau(HCSH_r)$	180.0		$\tau(HCSH_r)$	96.21
HCSH internal rotation t.s.	r(CS)	1.858			
	r(CH)	1.099			
	r(SH)	1.333			
	α(SCH)	105.01			
	α(CSH)	90.79			
	τ(HCSH)	89.00			
H_2 + CS molecular limit	r(CS)	1.523	H + HCS radical limit	r(CS)	1.588
	r(HH)	0.735		r(CH)	1.072
				α(SCH)	135.62
Molecular dissociation t.s.	r(CS)	1.565	Radical dissociation t.s.	r(CS)	1.573
	$r(CH_1)$	1.588		$r(CH_1)$	1.073
	$r(CH_2)$	1.156		$r(CH_2)$	2.032
	$r(H_1H_2)$	1.036		$\alpha(SCH_1)$	136.06
	$\alpha(SCH_2)$	148.91		$\alpha(SCH_2)$	105.02
	$\alpha(SCH_1)$	108.24		$\alpha(H_2CH_1)$	85.04

may be compared with experimental results. The 3-21G* SCF predictions for the structures of these species as well as for that of the thioformyl radical, HCS, may also be examined relative to earlier SCF calculations employing somewhat larger Gaussian basis sets. The experimental results for r_e(CS) and r_e(CH) in $\tilde{X}A_1$ H_2CS are 1.6110 Å and 1.0856 Å (33), in very reasonable agreement with the 3-21G* SCF predictions from Table 2 of 1.594 Å and 1.076 Å. The α_z(HCH) angle from the microwave spectrum is 116.2° (34) and is only 0.9° larger than the 3-21G* SCF value of 115.32°. The predicted CS bond length of 1.720 Å for $\tilde{a}\,^3A''$ thioformaldehyde is 0.037 Å longer than the experimental r_e value of 1.683 (8) Å (35). Difficulties in predicting an acceptable SCF bond length in the lowest triplet state of H_2CS have been discussed previously (7, 8). A similar problem may be noted in the SCF level CO bond length in the $^3n,\pi^*$ state of formaldehyde (36). The values of r_e(CH) = 1.072 Å and α_e (HCH) = 120.68° for the 3-21G* SCF geometry of T_1 thioformaldehyde are in reasonable agreement with experiment, 1.082 Å and 119.3° (35). Triplet H_2CS is not calculated to be pyramidal enough with the 3-21G* SCF method as the experimental out-of-plane angle is ~12° (35). However, motion out-of-plane in the n,π^* triplet state of thioformaldehyde is along an exceedingly soft potential with an inversion barrier estimated to be 4.1 cm^{-1} (35). Considerable sensitivity of the out-of-plane angle to basis set effects is understandable (7, 8). r_e(CS) in carbon monosulphide is calculated to be 1.523 Å (in a supermolecule along with H_2), which is slightly shorter than the experimental result of 1.534941 Å (37) and nearly identical to a DZ* SCF result (11). The hydrogen molecule bond length is predicted to be 0.735 Å whilst the experimental result is 0.74144 Å (37). The 3-21G* SCF clearly provides very reasonable representations relative to experiment of the molecular structures of a number of the species of interest in this study.

Although the 3-21G* SCF geometries appear reasonable and adequate for present purposes, the geometries of ground state thioformaldehyde and of the H_2 + CS system were reoptimized at the 3-21G* CISD level. The predicted CISD bond lengths

TABLE 3. 3-21G* SCF harmonic vibrational frequencies in cm^{-1}. Frequencies for the molecular and radical limits were calculated in the supermolecule approximation. Symmetry designations are in parentheses along with the value of the frequency scaled by 0.9 to allow for anharmonicity and the SCF approximation

S_0						
H_2CS	3356 (3026, b_2)	3274 (2947, a_1)	1666 (1499, a_1)	1190 (1071, a_1)	1172 (1055, b_1)	1112 (1001, b_2)
trans-HCSH	3129 (2816, a')	2871 (2584, a')	1273 (1146, a')	1033 (930, a')	1000 (900, a'')	870 (783, a')
cis-HCSH	3186 (2867, a')	2728 (2455, a')	1239 (1115, a')	1019 (917, a')	973 (876, a'')	836 (752, a')
HC(H)S rearrangement t.s.	3189 (2870, a')	2167 (1950, a')	1176 (1058, a')	913 (822, a')	347 (312, a'')	2433i (2190i, a')
HCSH internal rotation t.s.	3063 (2757, a)	2839 (2555, a)	1234 (1111, a)	792 (713, a)	645 (581, a)	1097i (987i, a)
H_2 + CS molecular limit	4657 (4191, HH)	1419 (1277, CS)				
Molecular dissociation t.s.	2690 (2421, a')	1528 (1375, a')	1147 (1032, a')	964 (868, a'')	587 (528, a')	2069i (1862i, a')
T_1						
H_2CS	3436 (3092)	3312 (2981)	1520 (1368)	901 (811)	840 (756)	134 (121)
gauche-HCSH	3355 (3020, a)	2827 (2544, a)	1038 (934, a)	974 (877, a)	855 (770, a)	361 (325, a)
HC(H)S rearrangement t.s.	3370 (3033, a)	1867 (1680, a)	954 (859, a)	862 (776, a)	681 (613, a)	2045i (1841i, a)
H + HCS radical limit	3357 (3021, a)	1032 (929, a)	947 (852, a)			
Radical dissociation t.s.	3347 (3012, a)	1150 (1035, a)	894 (805, a)	729 (656, a)	392 (353, a)	851i (766i, a)

TABLE 4. Energy differences relative to ground state H_2CS in kcal mol^{-1} at the 3-21G* SCF level; changes in these differences with corrections for (a) translation, rotation, and zero point vibration, (b) basis set extension (6-31G** basis), and (c) correlation (3-21G* CISD + SCC); estimated energy difference assuming additivity of the effects

		$\Delta(\Delta E)$			
S_0	ΔE 3-21G* SCF	Thermal	6-31G** SCF	3-21G* CISD + SCC	ΔE (Additivity)
H_2CS	0.0	0.0	0.0	0.0	0.0
trans-HCSH	52.0	−2.2	−5.1	+7.6	52.3
cis-HCSH	53.6	−2.5	−4.3	+7.5	54.3
HC(H)S rearrangement t.s.	104.4	−5.5	−6.7	−6.3	85.9
HCSH internal rotation t.s.	84.4	−4.5	−4.6	+11.0	86.3
H_2 + CS Molecular limit	48.6	−7.0	−2.0	−4.7	34.9
Molecular dissociation t.s.	116.3	−6.8	−6.5	−15.9	87.1
T_1					
H_2CS	19.4	−1.9	+0.5	+22.9	40.9
gauche-HCSH	40.4	−3.2	0.0	+24.2	61.4
HC(H)S rearrangement t.s.	82.7	−5.7	−4.1	+14.4	87.3
H + HCS radical limit	77.6	−8.6	+1.9	+14.5	85.4
Radical dissociation t.s.	85.6	−7.3	+1.3	+10.2	89.8

in H_2 and CS (experimental values in parentheses) were: $r_e(HH) = 0.744$ Å (0.741 Å (37)) and $r_e(CS) = 1.543$ Å (1.535 Å (37)). In thioformaldehyde, the CISD parameters were $r_e(CS) = 1.614$ Å (1.611 Å (33)) and $r_e(CH) = 1.088$ Å (1.0856 Å (33)) and $\alpha_e(HCH) = 116.4°$ (116.2° (34)). The CISD bond lengths have all increased relative to the optimum SCF values and are now in better agreement with experimental results, although all are slightly (0.003 to 0.007 Å) too long. In light of recent studies on SO_2 and SO_3^{2-} (40), it is possible that a more appropriate choice of d-function exponent (in the 3-21G* basis) might yield yet shorter SCF bond lengths and thus even better agreement with experiment when correlation is included. However, such effects on CS bonds do not appear to be as large as those found in the case of the SO bonds (40).

The 3-21G* basis set with 6 d-functions on S only is a fairly compact basis set that may prove useful in studies of larger thioketones. Therefore, comparison of the 3-21G* SCF geometries with those from 6-31G* calculations where 6 d-functions are also included on carbon (19) is of value. The 6-31G* SCF r_e(CS) in carbon monosulphide is 1.520 Å (19) within 0.003 Å of the 3-21G* result in this work of 1.523 Å. For $\tilde{X}\,^1A_1$ H_2CS, the 6-31G* SCF geometry (19) is r_e(CS) = 1.597 Å, r_e(CH) = 1.078 Å, and α_e(HCH) = 115.5°, which is quite close to the 3-21G* SCF result of 1.594 Å, 1.076 Å, and 115.32°. In the case of the $\tilde{a}\,^3A_2$ state of thioformaldehyde, the 3-21G* SCF results of r_e(CS) = 1.720 Å and r(CH) = 1.072 Å compare favourably with the DZ** SCF values of 1.732 Å and 1.075 Å (7). The geometry for the ground state of the thioformyl radical is (in the supermolecule with H) r_e(CS) = 1.588 Å, r_e(CH) = 1.072 Å, and α_e(SHC) = 135.62° while the DZ** SCF parameters are 1.559 Å, 1.080 Å, and 134.8° (11). For those stationary point structures for which comparisons with experiment or earlier calculations or both are possible, the 3-21G* SCF geometries are quite adequate.

The other minimum energy structures, namely the *trans*- and *cis*-thiohydroxymethylene singlets and the *gauche*-thiohydroxymethylene triplet, should be compared one with another as well as with the hydroxymethylenes (12, 14, 15). The most noteworthy structural features of the singlet thiohydroxymethylenes are the relatively short CS bond lengths of 1.677 Å (*trans*) or 1.657 Å (*cis*). These short bond lengths are strong evidence of the partial double bond character created by the donation of the sulphur lone pair electrons into the formally vacant carbene carbon $p\pi$ orbital. Recall that a typical CS single bond distance in methanethiol is 1.819 Å, or 0.13 to 0.17 Å greater than the CS distances in the singlet thiohydroxymethylenes. The CS distances are 0.063 to 0.083 Å greater in the methylene isomer than for the double bond in ground state thioformaldehyde. The shorter CX distance in the *cis* rather than the *trans* form has also been noted in singlet HCOH (12, 14, 15). The CH distances in the thiohydroxymethylenes are 1.095 or 1.089 Å, which are longer than in H_2CS but fairly typical of CH lengths in singlet methylenes (e.g. in $^1A_1$ CH_2, r(CH), is 1.11 Å (38)). The r_e(SH) of 1.328 Å *trans* and 1.344 Å *cis* may be compared to the r_0 value of 1.328 Å in H_2S (38a). The SH bond distance in the *cis*-isomer is lengthened somewhat, presumably due to some steric crowding. The bond angles in the *trans*-isomer of SCH, 107.08°, and CSH, 99.90°, are ~5° and 8° larger than comparable angles in singlet CH_2 of 102.4° (38) and H_2S of 92.2° (38a). In the *cis* species, these angles open up considerably to α_e(SCH) = 114.26° and α_e(CSH) = 107.81°. A note of caution regarding the optimized geometries for the singlet thiohydroxymethylenes should be struck. It has often been seen (e.g. ref. 39) that an improved description of the electronic structures and geometries of species such as methylenes or silylenes is given by a two-configuration SCF calculation rather than the usual single-configuration SCF employed here. This point is currently under investigation for the singlet thiohydroxymethylenes.

Triplet thiohydroxymethylene adopts a *gauche* conformation with τ(HCSH) = 92.29° since, with the carbene C$p\pi$ orbital singly occupied, any donation of the S lone pair electron density into this orbital is inhibited. For a similar reason the CS distance in triplet-HCSH increases to 1.723 Å, a value markedly longer than in the singlet-thiohydroxymethylenes and very similar to the *calculated* distance in H_2CS (T_1). The r_e(SH) at 1.332 Å is similar to the value in *trans*-HCSH (S_0) or in H_2S (38). The r_e(CH) distance of 1.073 Å is close to the experimental value of 1.078 Å in $^3B_1$ methylene (38). The SCH angle of 130.46° is typical of a triplet carbene (e.g. $^3B_1$ CH_2 136° (38)) while the CSH angle of 98.79° is close to that in the *trans*-thiohydroxymethylene singlet.

The structures of the thioformaldehyde transition states may be referenced to the reactants and products of the process concerned, as well as to the calculations on formaldehyde (12, 13). The transition state structure for the internal rotation connecting the *trans*- and *cis*-HCSH singlet species occurs, as might be expected, at a dihedral angle close to 90° (89.00°) and with a significantly larger CS distance of 1.858 Å. The CH distance of 1.099 Å and the SH distance of 1.333 Å are close to their values in *trans*-HCSH. With the much longer CS distance the SCH angle closes down by ~2° relative to the *trans*-isomer to a value of 105.01° and the CSH angle decreases by ~9°, relative to *trans*, to 90.79°.

The transition state structures for the rearrangements of H_2CS (S_0) to *trans*-HCSH (S_0) and for H_2CS (T_1) to *gauche*-HCSH (T_1) make an interesting comparison. The hydrogen that is migrating is labelled H_r in Table 2. The singlet rearrangement proceeds through a planar transition state (τ(HCSH$_r$) = 180°), while in the triplet case this dihedral angle is 96.21°. The r(CS) of the singlet transition state is 1.693 Å, or 0.016 Å greater than the product value of 1.677 Å in *trans*-HCSH. The shifting hydrogen is 1.403 Å from the C it is leaving and 1.475 Å from the S to which it will become bonded in the singlet transition state. The SCH$_r$ angle is 55.96°. For the triplet hydrogen shift, the CS distance in the transition structure is only slightly longer than in triplet thioformaldehyde or thiohydroxymethylene. The hydrogen which migrates is 1.436 Å from C, 1.494 Å from S, and forms an SCH$_r$ angle of 55.30° in the triplet transition structure. The triplet transition state is thus slightly "looser" than the singlet one. The triplet torsional angle of 96.21° in the transition state will become 92.29° in the product, *gauche*-thiohydroxymethylene. For the structural features less directly involved in the rearrangement, in the singlet case r(CH) of 1.086 Å is nearly exactly midway between the distance in H_2CS (S_0) of 1.076 Å and that in *trans*-HCSH (S_0) of 1.095 Å. The SCH angle of 119.60° in the singlet transition state is ~2.7° less than in thioformaldehyde, but ~12.5° greater than in *trans*-HCSH. The triplet rearrangement transition structure has an SCH angle of 130.59°, which is essentially the final value in *gauche*-HCSH of 130.46°. The r_e(CH) of 1.072 Å in the triplet transition geometry is nearly equal to that in either the aldehyde or methylene triplet isomers.

The transition state for the dissociation to molecular products is reminiscent of the formaldehyde case (12, 13). It is planar but highly distorted with both hydrogens on the same side of the CS axis. One hydrogen (H_1 in Table 2) is at a very large distance from the carbon, namely 1.588 Å, while the other (H_2) is more modestly lengthened to $r_e(CH_2)$ = 1.156 Å. The H_1H_2 distance in the transition state structure is 1.036 Å, much greater than its calculated value in the final product H_2 of 0.735 Å. The CS distance in the molecular dissociation transition state is 1.565 Å, which is modestly greater than the calculated value in the product, carbon monosulphide, of 1.523 Å. On the basis of this transition state structure alone, strongly vibrationally excited H_2 but only modest vibrational excitation in CS could be predicted for the molecular dissociation products.

On the T_1 potential energy surface, the transition structure for the dissociation to radicals is noteworthy. The departing hydrogen atom is quite far removed from the thioformyl radical at the transition state with $r_e(CH_2) = 2.032$ Å. The dissociating H is nearly perpendicular to the HCS fragment as $\alpha_e(H_2CH_1) = 85.04°$ and $\alpha_e(SCH_2) = 105.02°$. In the thioformyl group, the H_1CS angle of 136.06° is less than 0.5° from its final calculated value of 135.62°. $r_e(CH_1)$ at 1.073 Å in the transition state is essentially equal to the value in the product HCS. $r_e(CS)$ equals 1.573 Å in the radical dissociation transition state, which is 0.015 Å shorter than in the product. A qualitatively similar transition state (particularly with regards to the near "perpendicularity" of the departing hydrogen atom) has been approximately located in the triplet radical dissociation of H_2CO (29).

Vibrational frequencies

The harmonic vibrational frequencies calculated at the 3-21G* SCF level and collected in Table 3 verify the nature (minimum, transition state) of the stationary point structures found in the geometry optimizations. For the minima, these frequencies may be scaled (in parentheses in Table 3) to allow both for anharmonic effects and the SCF approximation (e.g. ref. 41) and then compared with experimental results for H_2CS (S_0 and T_1), H_2, and CS. The scaled frequencies for the singlet and triplet thiohydroxymethylenes are first predictions of the vibrational spectra of these species. Inspection of the imaginary frequency for the different transition state structures provides additional information as to the nature of the reaction coordinate.

The optimum value of a scaling factor for calculated 3-21G* SCF harmonic frequencies is not known precisely but is likely to be ~0.90, on the basis of 3-21G SCF results on a number of molecules containing only first row atoms (41) and of DZ** SCF frequencies for $\tilde{X}\,^1A_1$ H_2CS and $^1\Sigma$ CS (8, 11). Using a scale factor of 0.90 to give the frequencies in brackets in Table 3 and the experimental frequencies of ground state H_2CS from ref. 1, the comparison is (scaled 3-21G* SCF/experiment): 3020/3024.6 b_2, 2947/2971 a_1, 1499/1457.3 a_1, 1071/1059.2 a_1, 1055/990.2 b_1, and 1001/991.0 b_2. The agreement is to within 65 cm^{-1} in the worst case and averages 28 cm^{-1} in magnitude. In the lowest triplet state, with experimental frequencies from refs. 1 and 2 or calculated and scaled DZ** SCF frequencies (8), if no experimental result is available after the slash the comparisons are (symmetry labels as in C_{2v}): 3092/3078 b_2, 2981/2962 a_1, 1368/1320 a_1, 810/861.6 a_1, 756/762.3 b_2, and 121/356 b_1. Except for the out-of-plane b_1 mode, which is at any rate poorly described in any harmonic approximation (8), the agreement is satisfactory. The 3-21G* scaled frequency for CS is 1277 cm^{-1} (in the supermolecule with H_2) which compares nicely with the experimental ω_e of 1285.08 cm^{-1} (37). The scaled frequency for the hydrogen molecule (21G description) is 4191 cm^{-1}, which is not in quite so good agreement with experiment (4401.21, ref. 37).

The predicted vibrational frequencies for the singlet and triplet thiohydroxymethylenes may aid in the identification of these species. In *trans*-HCSH (S_0), the modes which are predominantly the CH and SH stretches are at 2816 cm^{-1} and 2854 cm^{-1} respectively. The CH stretch shifts to slightly higher, 2867 cm^{-1}, and the SH stretch to slightly lower, 2455 cm^{-1}, frequency in the *cis*-isomer, nicely reflective of the CH and SH bond length changes (Table 2). The CH stretches may be compared to the best calculated values in the oxycarbenes of 3002 cm^{-1} and 2912 cm^{-1} (12). The SH stretches are at frequencies quite similar to that of the SH stretch in methanethiol of 2605 cm^{-1} (42). The out-of-plane modes (a'') in the thiohydroxymethylenes of 900 cm^{-1} *trans* or 876 cm^{-1} *cis* indicate clearly the stability of the planar forms. The modes which are largely CS stretches in the thiohydroxymethylenes have frequencies of 783 cm^{-1} (*trans*) or 752 cm^{-1} (*cis*), which are 27 to 30% less than the CS double bond stretch calculated for H_2CS (S_0) at 1071 cm^{-1} but greater than the observed CS single bond stretch in CH_3SH of 710 cm^{-1} (42).

The CH stretch in triplet thiohydroxymethylene is predicted at 3020 cm^{-1}, nearly 200 cm^{-1} higher than in the singlets. The SH stretch at 2584 cm^{-1} in the triplet is, however, quite similar to that in the singlets, especially the *cis*-isomer. The torsional mode for the triplet thiohydroxymethylene is fairly low at 325 cm^{-1} (although the harmonic approximation may not be a particularly good one for this mode). A mode dominated by the CS stretching is at 770 cm^{-1} in the triplet thiohydroxymethylene.

The imaginary frequency for the transition state structures corresponding to motion along the reaction coordinate at that point is of particular interest, but so also are the values of certain other frequencies relative to reactants or products. In the singlet rearrangement transition state from H_2CS (S_0) to *trans*-HCSH (S_0), the out-of-plane mode of 312 cm^{-1} verifies the planarity of the transition state but is considerably softer than the comparable vibrations in thioformaldehyde, 1055 cm^{-1}, or *trans*-thiohydroxymethylene, 900 cm^{-1}. The CH stretch, which is not involved in the shift, is at 2870 cm^{-1} or very nearly at the thiohydroxymethylene value of 2816 cm^{-1} and well below the CH stretches in thioformaldehyde at 3020 and 2947 cm^{-1}. The imaginary frequency of 2190i cm^{-1} is rather high as it involves principally motion of a hydrogen. The imaginary frequency for the 1,2-hydrogen shift transition state in the triplet case is 1841i cm^{-1}. The CH stretch for the hydrogen not rearranging is 3033 cm^{-1} and nearly equal to the value of 3020 cm^{-1} in *gauche*-HCSH. The mode at 613 cm^{-1} is chiefly the torsion and is ~160 cm^{-1} less than in the product thiohydroxymethylene.

The distorted transition state for the dissociation to molecular products is planar with an out-of-plane frequency (a'') of 868 cm^{-1}, only some 200 cm^{-1} less than the value in H_2CS (S_0). The mode which is principally a CS stretch occurs at 1032 cm^{-1} in this transition state, 1071 cm^{-1} in the reactant thioformaldehyde, and 1277 cm^{-1} in the product carbon monosulphide. The imaginary frequency of 1826i cm^{-1} is associated with the motions of the two hydrogens swinging across the CS axis and coming together in an incipient formation of the H_2 product.

The transition structure for the dissociation to radicals on the T_1 surface has an interesting pattern of vibrational frequencies. The CH stretch at 3012 cm^{-1} is within 10 cm^{-1} of its value in the thioformyl radical product, while the CS stretch at 1035 cm^{-1} and the bend at 805 cm^{-1} are slightly further from their values in HCS of 929 cm^{-1} and 852 cm^{-1}. The imaginary frequency of 766i cm^{-1} is almost totally involved with the $r(CH_2)$ distance, with a small component of the angular variables characterizing the near-dissociation hydrogen atom.

Concluding remarks

This fairly detailed examination of features on the S_0 and T_1

potential energy surfaces of thioformaldehyde has revealed many similarities to earlier results on the oxygen analogue, formaldehyde. Although still larger computations may change some of the energy differences of Table 4 by perhaps 5 kcal mol^{-1}, nevertheless much has been learned of the energetics of reaction of thioformaldehyde. Notably, the rearrangement barriers from singlet or triplet thioformaldehyde to the respective thiohydroxymethylenes, the internal rotation interconverting *trans*- and *cis*-HCSH (S_0), the molecular dissociation transition state, and the radical dissociations on either the S_0 or T_1 surfaces all require ~85 to 90 kcal mol^{-1} of energy relative to ground state H_2CS. Thus, with respect to the first excited n,π^* triplet state the excess energy requirement is ~40 to 45 kcal mol^{-1}. Clearly, if thioformaldehyde is to react photochemically and unimolecularly, involvement of higher excited electronic states (e.g. experimentally the origin of the S_2 state is at ~132 kcal mol^{-1} (3)) will be required.

As the calculations reported herein were nearing completion, Pope *et al.* published a communication (43) dealing with the rearrangement and fragmentation of H_2CS (S_0). The geometries determined at the triple-ζ plus C and S *d* function SCF level are similar to the comparable 3-21G* SCF structures in this work. Their triple-ζ plus two sets of *d* functions on C and S and *p* on H multireference CI yielded energy differences generally slightly smaller than the best estimates of Table 4. Their communication does *not* deal with *cis*-HCSH, the internal rotation transition state connecting *trans*- and *cis*-HCSH, or any of the triplet state species.

Acknowledgements

It is a pleasure to thank Professor Sandorfy for his assistance at several times during the author's graduate student days. The author's interest in thioformaldehyde was initiated through numerous discussions with Dr. D. J. Clouthier. Financial support of this work by the University of Guelph Research Board in the form of a start-up grant and by an operating grant from the Natural Sciences and Engineering Research Council of Canada is gratefully acknowledged.

1. D. J. CLOUTHIER and D. A. RAMSAY. Ann. Rev. Phys. Chem. **34**, 31 (1983).
2. T. SUZUKI, S. SAITO, and E. HIROTA. J. Chem. Phys. **79**, 1641 (1983).
3. D. J. CLOUTHIER, P. A. HACKETT, A. R. KNIGHT, and R. P. STEER. J. Photochem. **17**, 319 (1981).
4. D. J. CLOUTHIER and C. M. L. KERR. Chem. Phys. **70**, 55 (1982).
5. M. KAWASAKI, K. KASATANI, Y. OGAWA, and H. SATO. Chem. Phys. **74**, 83 (1983).
6. A. E. BRUNO and R. P. STEER. J. Chem. Phys. **78**, 6660 (1983).
7. J. D. GODDARD. Can. J. Chem. **59**, 3200 (1981).
8. J. D. GODDARD and D. J. CLOUTHIER. J. Chem. Phys. **76**, 5039 (1982).
9. P. G. BURTON, S. D. PEYERIMHOFF, and R. J. BUENKER. Chem. Phys. **73**, 83 (1982).
10. C. B. MOORE and J. C. WEISSHAAR. Ann. Rev. Phys. Chem. **34**, 525 (1983).
11. J. D. GODDARD. Chem. Phys. Lett. **102**, 224 (1983).
12. (*a*) J. D. GODDARD and H. F. SCHAEFER III. J. Chem. Phys. **70**, 5117 (1979); (*b*) J. D. GODDARD, Y. YAMAGUCHI, and H. F. SCHAEFER III. J. Chem. Phys. **75**, 3459 (1981).
13. (*a*) M. J. FRISCH, R. KRISHNAN, and J. A. POPLE. J. Phys. Chem. **85**, 1467 (1981); (*b*) M. DUPUIS, W. A. LESTER, JR., B. H. LENGSFIELD, and B. LIU. J. Chem. Phys. **79**, 6167 (1983).
14. (*a*) M. R. HOFFMANN and H. F. SCHAEFER III. Astrophys. J. **249**, 563 (1981); (*b*) R. R. LUCCHESE and H. F. SCHAEFER III. J. Am. Chem. Soc. **100**, 298 (1978).
15. J. A. POPLE, K. RAGHAVACHARI, M. J. FRISCH, J. S. BINKLEY, and P. V. R. SCHLEYER. J. Am. Chem. Soc. **105**, 6389 (1983).
16. (*a*) J. R. SODEAU and E. K. C. LEE. Chem. Phys. Lett. **57**, 71 (1978); (*b*) J. W. HEPBURN, R. J. BUSS, L. J. BUTLER, and Y. T. LEE. J. Phys. Chem. **87**, 3638 (1983).
17. J. S. BINKLEY, M. FRISCH, K. RAGHAVACHARI, D. DEFREES, H. B. SCHLEGEL, R. WHITESIDE, E. FLUDER, R. SEEGER, and J. A. POPLE. GAUSSIAN 82 RELEASE A. Department of Chemistry, Carnegie–Mellon University, Pittsburgh, PA. 1983.
18. (*a*) J. S. BINKLEY, J. A. POPLE, and W. J. HEHRE. J. Am. Chem. Soc. **102**, 939 (1980); (*b*) M. S. GORDON, J. S. BINKLEY, J. A. POPLE, W. J. PIETRO, and W. J. HEHRE. J. Am. Chem. Soc. **104**, 2797 (1982).
19. M. M. FRANCL, W. J. PIETRO, W. J. HEHRE, J. S. BINKLEY, M. S. GORDON, D. J. DEFREES, and J. A. POPLE. J. Chem. Phys. **77**, 3654 (1982).
20. J. A. POPLE, R. KRISHNAN, H. B. SCHLEGEL, and J. S. BINKLEY. Int. J. Quantum Chem. **13S**, 225 (1979).
21. P. C. HARIHARAN and J. A. POPLE. Theor. Chim. Acta, **28**, 213 (1973).
22. J. A. POPLE, R. SEEGER, and R. KRISHNAN. Int. J. Quantum Chem. **11S**, 149 (1977).
23. (*a*) M. L. MCKEE and W. N. LIPSCOMB. J. Am. Chem. Soc. **103**, 4673 (1981); (*b*) R. H. NOBES, W. J. BOUMA, and L. RADOM. Chem. Phys. Lett. **89**, 497 (1982).
24. S. W. BENSON. Thermochemical kinetics, 2nd ed. Wiley, New York. 1976.
25. A. JONES and F. P. LOSSING. J. Phys. Chem. **71**, 4111 (1967).
26. G. CONDE-CAPRACE and J. E. COLLIN. Org. Mass. Spectrom. **6**, 415 (1972).
27. (*a*) N. C. BAIRD and K. F. TAYLOR. J. Am. Chem. Soc. **100**, 1333 (1978); (*b*) D. FELLER, W. T. BORDEN, and E. R. DAVIDSON. Chem. Phys. Lett. **71**, 22 (1980).
28. L. SALEM. J. Am. Chem. Soc. **96**, 3486 (1974).
29. D. M. HAYES and K. MOROKUMA. Chem. Phys. Lett. **12**, 539 (1972).
30. V. BACHLER and E. A. HALEVI. Theoret. Chim. Acta, **59**, 595 (1981).
31. Y. OSAMURA, J. D. GODDARD, H. F. SCHAEFER III, and K. S. KIM. J. Chem. Phys. **74**, 617 (1981).
32. M. P. CONRAD and H. F. SCHAEFER III. J. Am. Chem. Soc. **100**, 7820 (1978).
33. P. H. TURNER, L. HALONEN, and I. M. MILLS. J. Mol. Spectrosc. **88**, 402 (1981).
34. A. P. COX, S. D. HUBBARD, and H. KATO. J. Mol. Spectrosc. **93**, 196 (1982).
35. P. JENSEN and P. R. BUNKER. J. Mol. Spectrosc. **95**, 92 (1982).
36. G. F. ADAMS, G. D. BENT, R. J. BARTLETT, and G. D. PURVIS. J. Chem. Phys. **75**, 834 (1981).
37. K. P. HUBER and G. HERZBERG. Constants of diatomic molecules. Van Nostrand, Princeton. 1979.
38. (*a*) G. HERZBERG. Electronic spectra of polyatomic molecules. Van Nostrand, Princeton. 1966; (*b*) G. HERZBERG and J. W. C. JOHNS. Proc. R. Soc. London, Ser. A, **295**, 107 (1966); (*c*) J. Chem. Phys. **54**, 2276 (1971).
39. J. D. GODDARD, Y. YOSHIOKA, and H. F. SCHAEFER III. J. Am. Chem. Soc. **102**, 7644 (1980).
40. A. STROMBERG, U. WAHLGREN, L. PETTERSSON, and P. E. M. SIEGBAHN. Chem. Phys. **89**, 323 (1984).
41. J. A. POPLE, H. B. SCHLEGEL, R. KRISHNAN, D. J. DEFREES, J. S. BINKLEY, M. J. FRISCH, R. A. WHITESIDE, R. F. HOUT, and W. J. HEHRE. Int. J. Quantum Chem. **15S**, 269 (1981).
42. I. W. MAY and E. L. PACE. Spectrochim. Acta, Part A, **24**, 1605 (1968).
43. S. A. POPE, I. H. HILLIER, and M. F. GUEST. J. Chem. Soc. Chem. Commun. 623 (1984).

Magnetic circular dichroism spectra of cobalt(III) amine complexes of photochemical importance

BRYAN R. HOLLEBONE
Department of Chemistry, Carleton University, Ottawa, Ont., Canada K1S 5B6

AND

COOPER H. LANGFORD[1] AND ARAMICE Y. S. MALKHASIAN
Department of Chemistry, Concordia University, Montreal (Que.), Canada H3G 1M8

Received August 6, 1984

This paper is dedicated to Professor Camille Sandorfy on the occasion of his 65th birthday

BRYAN R. HOLLEBONE, COOPER H. LANGFORD, and ARAMICE Y. S. MALKHASIAN. Can. J. Chem. **63**, 1918 (1985).

Magnetic circular dichroism spectra of several acidoamine cobalt(III) complexes are reported which reveal *B* terms for the spin allowed bands and *A* terms for the spin forbidden bands. It is shown that ligand field parameters derived from fitting of a full set of spin forbidden bands, including the quintet, gives Racah *B* and *C* electron repulsion parameters closer to those anticipated from theory than has been common using mainly the singlets and a single weak low energy absorption feature assigned to a triplet. The spectra indicate that the quintet which has figured in numerous photochemical speculations lies at relatively high energy. This conclusion is a consequence of both the recognition of an *A* term assignable to the quintet and the best fit ligand field parameters for all bands.

BRYAN R. HOLLEBONE, COOPER H. LANGFORD, et ARAMICE Y. S. MALKHASIAN. Can. J. Chem. **63**, 1918 (1985).

On a déterminé les spectres mcd de plusieurs complexes d'acidoamine de cobalt(III) qui mettent en évidence les termes *B* des bandes permises de spin et les termes *A* des bandes interdites de spin. On montre que les paramètres de champs de ligand que l'on peut obtenir en ajustant un ensemble complet de bandes interdites de spin, y compris le quintuplet, donne des paramètres de répulsion électronique du type Racah *B* et *C* qui se rapprochent d'avantage de ceux que l'on a généralement obtenus en faisant principalement appel aux singulets et à une caractéristique unique et faible d'absorption de basse énergie qui était attribuée à un triplet. Les spectres indiquent que l'énergie du quintuplet que l'on invoque dans plusieurs spéculations photochimiques se situe à un niveau relativement élevé. Cette conclusion résulte à la fois de la reconnaissance du terme *A* attribuable au quintuplet ainsi qu'à un meilleur ajustement des paramètres de champ du ligand pour toutes les bandes.

[Traduit par le journal]

Introduction

The assignment of the ligand field states and appropriate ligand field parameters to complexes of the d^6 Co(III) acido amine complexes is a classic problem in ligand field theory (1). Yet it remains incomplete in the sense that empirical information on the spin forbidden states is sparse.

This report concerns the gains in information which result from the use of magnetic circular dichroism (mcd) spectra. These are mainly a result of the very much greater relative intensities of the spin forbidden bands as compared to spin allowed bands in mcd (2). It proves possible to assign transitions to both of the triplet bands that are expected in octahedral d^6 complexes and as well to assign the position of the previously unreported quintet. These accomplishments in cobalt spectroscopy are not without precedent. In earlier work, it has proven possible to use mcd to resolve a spin forbidden ligand field band from under the tail of an allowed charge transfer transition (3) and to assign a doublet band which occurs between the two spin allowed bands in the spectrum of an octahedral d^3 Cr(III) complex (4).

The bands are interpreted in terms of octahedral local splittings. Reductions in symmetry are not large enough to be well defined. With some misgiving, we retain O_h labels, but this should be understood as a way of emphasizing the limit on resolution in these spectra!

It is perhaps useful to note that there is a current reason for renewed interest in this spectral problem. In the course of photochemical studies of chloroamine cobalt(III) complexes, we have found a complex pattern of wavelength dependence which requires consideration of intersystem crossing between singlet, triplet, and perhaps quintet excited states.

[1]Author to whom correspondence should be addressed.

Experimental

The complexes were chloropentaminecobalt(III) chloride, *cis* and *trans* dichloro-bis(ethylenediamine)cobalt(III) chloride, and *cis* chloroisothiocyanatobis(ethylenediamine)cobalt(III) chloride. These were all prepared by well-established methods (5−8). Solutions were prepared by weighing into small beakers (to the nearest 0.01 mg) an amount of the solid salt about three to four times the quantity needed to prepare solutions for conventional absorption spectroscopy. A few milliliters of ultrapure water (Millipore system) were added and the beakers warmed gently until all the salt was dissolved. The mcd spectra were recorded immediately. Conventional absorption spectroscopy was carried out using a Perkin−Elmer 557.

The mcd spectra were recorded on a custom-built spectrometer using in sequence a xenon 150-W lamp, Cary 14 monochromator, Glan−Taylor polarizer, Hind's International Piezooptical polarizer, Walker Engineering 2.2 T electromagnet, and Hamamatsu 955 photomultiplier detector. The phototube DC current is kept constant by a feed-back circuit controlling a Hamamatsu power supply. The AC signal representing the 50-kHz mcd differential absorption is decoupled at the preamplifier mounted in the phototube socket, filtered, and amplified in a PAR Model 124 lock-in amplifier. The output is digitized by a 12-bit A/D converter linked to a Motorola Exorcisor II which automatically scans the spectrometer through the desired wavelength range under the desired signal-to-noise quality conditions. Baseline and spectrum data files are subsequently merged digitally and the resulting spectra plotted on a digital X−Y recorder.

The final aspect of the assignment of mcd spectra is the location of the zero, since the experiment is inherently single beam. This requires the choice of "lock" frequencies where the signal is taken to be zero. The locks in these spectra are set at the long wavelength end where absorption spectra show features have been exhausted. The other lock

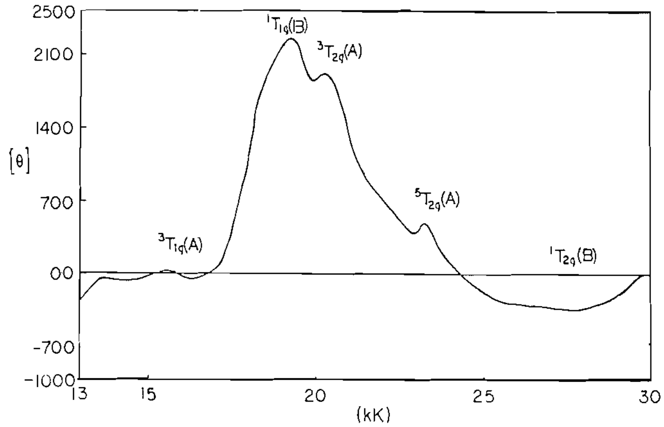

FIG. 1. The mcd spectrum of $Co(NH_3)_5Cl^{2+}$. Concentration 0.0521 *M*. Lock points at 13 kK and 24 kK.

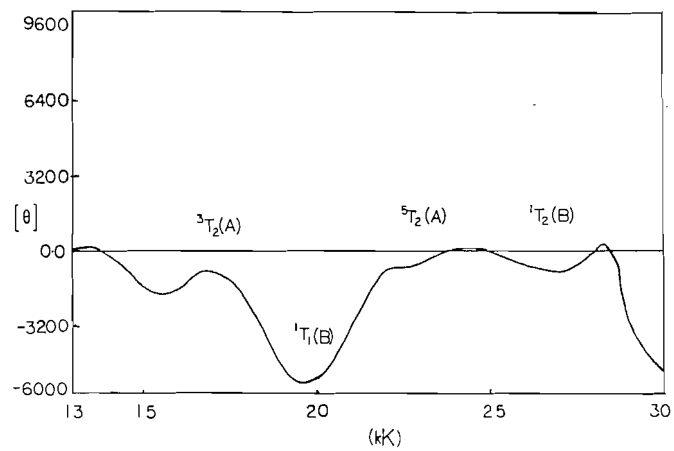

FIG. 2. The mcd spectrum of *trans*-$Coen_2Cl^+$. Concentration 0.0371 *M*. Lock points at 14 kK and 28 kK.

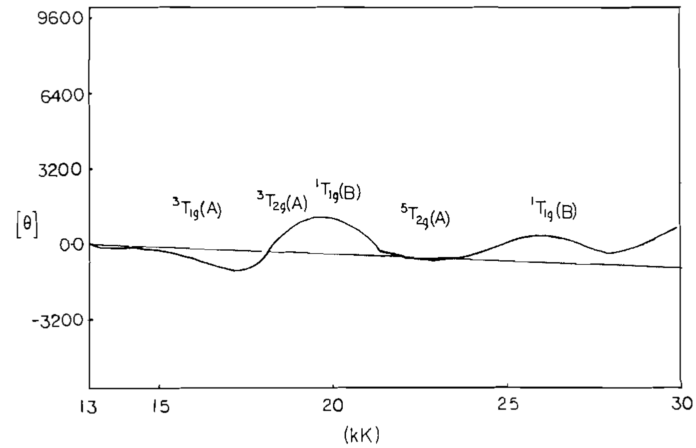

FIG. 3. The mcd spectrum of *cis*-$Coen_2Cl^+$. Concentration 0.0285 *M*. Lock points at 14 kK and 27 kK.

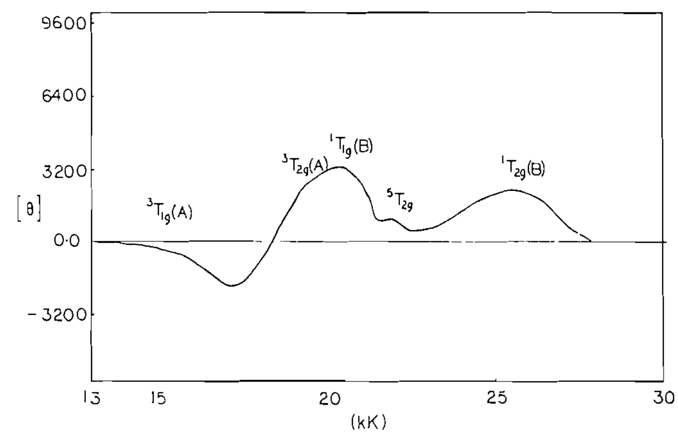

FIG. 4. The mcd spectrum of *cis*-$Coen_2(NCS)Cl^+$. Concentration 0.018 *M*. Lock points at 14 kK and 28 kK.

wavelength is set at the minimum point in the conventional absorption spectrum between the "*B*" terms associated with the singlets. This is a "debatable" choice and will involve some approximation in all cases. In consequence of the lack of a second lock point which is well defined, there will inevitably be some error in assignment of band centres. The sometimes poor agreement of "observed" with "calculated" values in Table 1 is in part a result. The essential correctness of the choice of lock points is indicated by the agreement of the peak frequencies of the *B* terms which are assigned to the singlets with the frequencies assigned to the same singlets in the ordinary absorption spectra.

Results

The four spectra are presented in Figs. 1 through 4 and Table 1. Assignments are indicated on the figures. The signal-to-noise ratio in these spectra is only slightly lower than the pen width indicates. Thus, the inflections indicating the presence of *A* terms are readily identified. However, this *qualitative* good resolution does not carry over into definition of band centres. The bands are broad, as expected, and it is difficult to identify peaks. The uncertainty in energies assigned is *rather large*! In addition to the lock point problems we call special attention to the width of the *B* terms. Precision in centre location is not much better than ± 1.0 kK. These spectra are to be compared with early mcd spectra reported by McCaffry, Stephens, and Schatz in 1967 (9). The error bars shown in ref. 9 indicated that, as expected, developments in signal recording and processing have allowed for much improved signal-to-noise in the current spectra. Thus, the spectra of ref. 9 do not reveal the *A* terms assigned in the figures. This lack of "resolution" also causes two problems. In the spectra of the *cis* dichloro ion, the "lock" point implied by the published spectrum (it is not explicitly stated) does not correspond to the minimum in the absorption spectrum. This leads to the assignment of two negative *B* terms which do not match peaks of the absorption spectrum. If the "lock" is placed at the minimum, the result is a single positive *B* term which does match the peak in the absorption spectrum. The negative features are revealed here to be a part of *A* terms. Similarly, there is a lock problem in the spectrum of the chloropentaamine complex shown in ref. 9. At the low energy end, the spectrum is brought to zero at too long a wavelength. The rough constancy of the spectrum from about 16.5 kK to 13 kK shows that the last "peak" shown in ref. 9 is an artifact. The modification of the point has the consequence of changing the first *B* term to a positive term. The resulting peaks agree with the absorption maxima from the conventional absorption spectra within the uncertainty.

Conventional absorption spectra determined with the present samples were in excellent agreement with earlier reports. These spectra are only summarized in the table, not plotted.

The treatment of the specta is conventional first order (10). All parameter assignments are derived using the mcd spectra as input data. Values of the Racah *B* parameters are derived from

TABLE 1. Spectra of Co(III) d^6 complexes in approximate octahedral symmetry

Complex	Transition	Absorption (kK)	Magnetic circular dichroism (kK ± 1)	Calculated [a] (kK)
$Co(NH_3)_5Cl^{2+}$	$^1T_{1g}$ $^1A_{1g}$	18.7	18.8(B)	18.8
	$^1T_{2g}$	27.5	27.5(B)	27.4
	$^3T_{1g}$	—	15.0(A)	15.0
	$^3T_{2g}$	—	18.3(A)	19.3
	$^5T_{2g}$	—	23.2(A)	23.5
trans-$Coen_2Cl_2^+$	$^1T_{1g}$ $^1A_{1g}$	19.2[b]	18.8(B)	18.3
	$^1T_{2g}$	25.0	26.8(B)	26.3
	$^3T_{1g}$	—	[d]	13.9
	$^3T_{2g}$	—	16.2(A)	17.9
	$^5T_{2g}$	—	22.9(A)	20.9
cis-$Coen_2Cl_2^+$	$^1T_{1g}$ $^1A_{1g}$	19.9	20.5(B)	18.9
	$^1T_{2g}$	25.0	26.8(B)	27.3
	$^3T_{1g}$	—	15.5(A)	14.9
	$^3T_{2g}$	—	18.5(A)	18.9
	$^5T_{2g}$	—	22.0(A)	23.3
cis-$Coen_2NCSCl^+$	$^1T_{1g}$ $^1A_{1g}$	19.9	20.5(B)	19.8
	$^1T_{2g}$	[c]	25.5(B)	24.6
	$^3T_{1g}$	—	15.5(A)	14.8
	$^3T_{2g}$	—	18.5(A)	17.6
	$^5T_{2g}$	—	22.0(A)	23.7

[a]Calculated from LF parameters in Table 2.
[b]Average of the two lower symmetry components.
[c]Band hidden under the CT tail.
[d]There is some indication of this band in the spectrum but the centre cannot be placed.

TABLE 2. State energies and ligand field parameters

Transition energies (ref. 10)

$$E(^1T_{1g}) - E(^1A_{1g}) = \Delta - C$$
$$E(^1T_{2g}) - \quad = \Delta + 16B - C$$
$$E(^3T_{1g}) - \quad = \Delta - 3C$$
$$E(^3T_{2g}) - \quad = \Delta + 8B - 3C$$
$$E(^5T_{1g}) - \quad = 2\Delta - 5B - 8C$$

Complex	Parameters (kK)			
		B	C	C/B
$Co(NH_3)_5Cl^{2+}$	20.7	0.54	1.9	3.5
trans-$Co(en)_2Cl_2$	20.5	0.50	2.2	4.4
cis-$Co(en)_2Cl_2^+$	20.9	0.50	2.0	4.0
cis-$Co(en)_2NCSCl^+$	21.1	0.35	2.1	6.0

the singlet–singlet splittings. Values of C are determined from the average of values from two singlet–triplet splittings using the B previously obtained. The octahedral splitting parameter is then fit. Only in the case of the *trans* dichloro complex where one triplet is missing was a general iteration used. Better agreement of calculated spectra could be obtained using general interation in all cases, but our purpose is to demonstrate the qualitative success of the fit with *minimal* adjustment. The spectral precision does not warrant quantitative interpretation of A, B, and C.

Discussion

In the figures, the mcd bands are assigned as either A or B terms. A terms arise (9) from a transition between a nondegenerate ground state and a degenerate excited state. Thus, it is expected that all of the singlet to triplet or quintet transitions in Co(III) ligand field spectra should correspond to A terms. B terms do not require a degeneracy. They involve the coupling of the states in the transition to all other states of the molecule in consequence of the perturbation produced by the magnetic field. It is therefore not surprising, and indeed consistent with results of ref. 9, that all singlet–singlet bands are B terms. In ref. 9, it was suggested that some of the splitting corresponding to the C_{4v}, C_{2v}, and D_{4h} symmetries of the mixed ligand complexes studied here could be resolved in mcd. Especially, two B terms are reported for the T_{1g} octahedral state of the *cis* dichloro ion. In point of fact, the resolution of these B terms exceeded the splittings that are seen in ordinary absorption spectra! This is not expected. The "derivative" shape of an A term or a C term can aid in spectral resolution of overlapping bands. However, there is no inherent reason why B terms of the same sign should show improved resolution. As was noted above, the resolution reported in ref. 9 appears to have been an artifact of poorer signal/noise and a slightly unfortunate choice of a lock point. We assign one band as B and a lower energy band as an A term. With this change, all singlets are poorly resolved and there is no basis for treatment of the spectra in an effective symmetry lower than octahedral. Therefore, we have attached O_h symmetry labels to all transitions as a reminder of this failure.

In octahedral symmetry, the strong field treatment of the state energies yields the energies of the transitions collected in Table 2 (10). Using these expressions for the energies, the octahedral ligand field splitting parameter, Δ, and the Racah electron repulsion parameters, B and C, are calculated and collected in Table 2. Table 1 shows the calculated spectra using these parameters.

The first point to note is that the A terms assigned to the lower triplets in these spectra are near the region of the spectrum where the well-characterized triplet of the hexaamine-cobalt(III) ion which has been extensively discussed recently by Wilson and Solomon (11) is found. However, the small peaks at about 10.5 kK which have been recorded several times for halopentaaminecobalt(III) ions are at much lower energy. Unfortunately, this region is not accessible to us. These low energy peaks have been assigned as ${}^3T_{1g}$ by several authors (10). This cannot be valid if the LF (ligand field) parameters calculated here are correct. That there is a problem is hinted by the fact that these bands appear at an energy more than 2 kK below the triplet of the hexaamine but *do not* vary with the ligand field strength of the halide ligand. If the triplets are lower, contribution by the halide to Δ would be the cause. Such a contribution has never been reported for the singlets (10), nor is it seen for singlets found in mcd. The origin of the 10.5-kK feature may be the overtone of an —NH_2 vibration which was identified at this energy by Wilson and Solomon from the comparison of Co and Cr amine complexes and by deuteration. (The other possibility is that the band is a "hot" band of the hypersensitive type since the singlet–triplet transition is associated with a $\Delta J = 2$ (12).)

An interesting specific feature of the —NCS complex is the reversal of the sign of the second B term compared to all the others. This may be a reminder of the charge transfer mixing into this band.

We now turn our attention to the parameters in Table 2. The values of the orbital splitting parameter, Δ, are slightly smaller than those reported earlier (10). They are similarly (10) insensitive to the ligand field strength of the halide. This may simply reflect low resolution. However, it does seem that insensitivity to reduced symmetry is typical for Co(III). The value of the mcd spectra is in the opportunity to observe spin forbidden bands. Earlier efforts to fit LF parameters to spin forbidden bands in acidoamine complexes (e.g. ref. 13) have produced rather odd values of the Racah parameters. The ratio C/B is expected to be 4 (10). Values calculated were nearer 8. This is now seen to be the consequence of the assignment of the lowest triplet at approximately 10.5 kK. With the triplet as seen here, the expected ratio is, in fact, obtained. Thus, although the mcd spectra may involve unusually weak bands for spin allowed transitions with consequent large error in the location of band centres, they appear to give us qualitatively correct LF spectra and parameters.

This leads to the point of photochemical significance (11, 14). The quintet appears to be located between the two singlet bands. This conclusion is established by two distinct arguments: first, and most directly, by the assignment of the A terms in this region; second, by the fitted position using the qualitatively correct LF parameters. The photochemical discussion has centered on the possibility that the quintet might be the lowest excited state. For this to be the case in the vertical excitation of absorption spectroscopy would require a value of the Racah parameter C much too large to match expectations from the simple theory which appears to be quite adequate.

Acknowledgements

We acknowledge the financial support of operating grants from NSERC. A.Y.S.M. is grateful for fellowships from the Government of Iraq.

1. C. J. BALLHAUSEN. Introduction to ligand field theory. McGraw–Hill, New York. 1962.
2. P. N. SCHATZ and A. J. MCCAFFRY. Q. Rev. **23**, 552 (1969).
3. C. H. LANGFORD and C. HOLUBOV. Inorg. Chim. Acta Letts. **53**, 159 (1981).
4. B. R. HOLLEBONE. Theor. Chim. Acta, **56**, 45 (1980).
5. G. S. SCHLESSINGER. Inorg. Synth. **9**, 160 (1967).
6. M. KRISHNAMURTHY. J. Inorg. Nucl. Chem. **34**, 3915 (1972).
7. J. C. BLAIR. Inorg. Synth. **2**, 222 (1946).
8. A. WERNER. Ann. **1**, 386 (1912).
9. A. J. MCCAFFRY, P. J. STEPHENS, and P. N. SCHATZ. Inorg. Chem. **6**, 1614 (1967).
10. C. K. JORGENSEN. Absorption spectra and chemical bonding in complexes. Addison–Wesley, Reading, MA. 1962. Chapt. 5.
11. R. B. WILSON and E. I. SOLOMON. J. Am. Chem. Soc. **102**, 4085 (1980).
12. B. R. HOLLEBONE and M. STILLMAN. Chem. Phys. Letts. **66**, 248 (1979).
13. V. S. SASTRI and C. H. LANGFORD. Can. J. Chem. **47**, 4237 (1969).
14. C. H. LANGFORD and A. Y. S. MALKHASIAN. J. Chem. Soc. Chem. Commun. 1210 (1982).

Pseudopotentials for second row atoms. *Ab initio* molecular calculations on PH_3, H_2S, and HCl

REZSŐ GÁSPÁR
Institute of Theoretical Physics, Kossuth Lajos University, H-4010 Debrecen, Hungary

AND

REZSŐ GÁSPÁR, JR.
Department of Biophysics, Medical University of Debrecen, H-4012 Debrecen, Hungary

Received July 16, 1984

This paper is dedicated to Professor Camille Sandorfy on the occasion of his 65th birthday

REZSŐ GÁSPÁR and REZSŐ GÁSPÁR, JR. Can. J. Chem. **63**, 1922 (1985).

Gaussian nonlocal pseudopotentials are introduced for the simplification of the description of second row elements. Pseudopotential parameters for P, S, and Cl are presented. The pseudopotential method is applied to HCl, H_2S, and PH_3. Substantial reduction in the dimension of the orbital basis set is achieved. Results on total valence energies, binding energies, ionization potentials, force constants, equilibrium bond angles, bond lengths, and dipole moments are presented and compared to experiment as well as to the results of calculations with other methods.

REZSŐ GÁSPÁR et REZSŐ GÁSPÁR, JR. Can. J. Chem. **63**, 1922 (1985).

Dans le but de simplifier la description des éléments de la deuxième rangée, on introduit des pseudopotentiels gaussiens qui ne sont pas localisés. On présente les paramètres de pseudopotentiel pour le P, le S et le Cl. On applique la méthode du pseudopotentiel au HCl, au H_2S et au PH_3. On réduit ainsi considérablement la dimension des ensembles de base des orbitales. On rapporte les résultats obtenus pour les énergies de valence totale, les énergies de fixation, les potentiels d'ionisation, les constantes de force, les angles d'équilibre des liaisons, les longueurs des liaisons et les moments dipolaires et on les compare avec les résultats expérimentaux ainsi qu'avec les résultats obtenus par calculs à l'aide d'autres méthodes.

[Traduit par le journal]

Introduction

A recently described pseudopotential method suitable for the treatment of molecules containing first row elements (Gáspár (1)) has been extended to second row elements and applied to molecular calculations. Pseudo- and model-potential approaches for second row elements of the periodic table have been published by Bonifacic and Huzinaga and by Topiol, Moskowitz, Melius, Newton, and Jafri (2). The perspective of the present method with respect to the general tendencies of the pseudopotential approach has been outlined in detail by Gáspár (1). The primary purpose of this article is to test the usefulness of the newly introduced pseudopotential parameters in molecular calculations. The molecules that have been investigated are HCl, H_2S, and PH_3.

The overall performance of the method in the molecular applications is satisfactory. Reasonable agreements have been obtained between bond lengths, bond angles, total valence energies, binding energies, and dipole moment values obtained by the pseudopotential calculations and by experiment. Results of calculations with other methods are also included for comparison.

The reduction in computing requirements is substantial for second row elements, for there is no reference in the present scheme to basis functions representing the core states. Basis sets and computing times are reduced substantially. Mini-, micro-, and even well equipped professional personal computers may be used to get results on molecules with second row elements. Due to the special parametrization of the pseudopotential, the core-valence electron correlation and relativistic effects are also taken into account implicitly by the present approach.

The computations have been performed by the program PSEUSMALLOBE, a modified version of Shillady's SMALLOBE (3).

All quantities in this paper are given in atomic units except when otherwise stated.

Method and basis set

For the pseudopotential treatment of second row elements the following form of the model pseudopotential has been chosen

$$[1]\quad V(r) = -\sum_{\alpha} \frac{Z^{\alpha} - N_c^{\alpha}}{r_{\alpha}} + \sum_{\alpha} \sum_{l=0}^{l_c+1} V_l(r_{\alpha})P_l$$

In formula [1] Z^{α} is the atomic number of the nucleus α at the position R_{α}, N_c^{α} is the number of electrons in the core α, and $Z^{\alpha} - N_c^{\alpha}$ is the reduced atomic number. P_l^{α} are the angular momentum projection operators with the center at R_{α}, and $r_{\alpha} = |r - R_{\alpha}|$. The radial factor in eq. [1] has been selected to be

$$[2]\quad V_l(r) = \sum_{i=1}^{m} A_l^i \exp(-a_l^i r^2)$$

The above form of the potential has been successfully employed in the pseudopotential description of first row elements (Gáspár (1)). For first row elements only one term in eq. [2] has been retained. For second row elements the summation has been extended, $m = 2$ has been selected for $l = 0$, and $m = 1$ for $l = 1$ and $l = 2$. In eq. [1] all terms with $l > l_c + 1$, where l_c is the greatest of the l quantum numbers of the core electrons, have been dropped, the corresponding ionic terms being hydrogenic to the desired accuracy.

For the determination of the pseudopotential parameters in eq. [2] a procedure, based on the numerical integration of the Schrödinger equation, has been described by Gáspár (1). Pseudopotential parameters for the Li isoelectronic series and extrapolation formulae of the A_0 and a_0 pseudopotential parameters have been published (Gáspár (1)). In the present calculations the extrapolation formulae of A_0 and a_0 have been used

TABLE 1. Parameters of the pseudopotential $V_l(r) = \sum_i A_l^i \exp(-a_l^i r^2)$ for $l = 0$ ($m = 2$); $l = 1$ and $l = 2$ ($m = 1$)[a]

Element	Reduced atomic no.	A_0^1	a_0^1	A_0^2	a_0^2
P	5	299.88839	49.62646	34.65294	3.40000
S	6	344.73943	56.83387	42.62604	4.03812
Cl	7	392.72626	64.45309	49.53048	4.66780
		A_1^1	a_1^1	A_2^1	a_2^1
P	5	18.26902	2.87256	−4.57366	2.85388
S	6	23.70853	3.54252	−5.84997	3.75059
Cl	7	28.11780	4.17165	−9.15531	5.38553

[a]For the determination of the A_0^1, a_0^1 parameters the extrapolation formulae published in Gáspár (1) have been used.

TABLE 2. Basis set generating *Znl* parameters of PSEUSMALLOBE and radii ρ_i of the primitive Gaussians – centered on the nuclei – for the *s* states

Element	Reduced atomic no.	$Z3p$	$Z4s$	$Z4p$	$HZ1s$	ρ_1	ρ_2
P	5	0.9	1.7	1.4	1.2	0.9	1.5
S	6	1.0	1.85	1.4	1.2	0.8	1.4
Cl	7	1.1	2.0	1.4	1.2	0.7	1.3

to determine the A_0^1 and a_0^1 pseudopotential parameters of second row elements. The rest of the A_l^i and a_l^i parameters have been determined by the numerical procedure referred to above, and their values are displayed in Table 1 for P, S, and Cl.

The form of the pseudopotential outlined above has been introduced into molecular calculations and the PSEUSMALLOBE procedure has been established (Gáspár (1)). Spherical Gaussian orbitals (SGO) and linear combinations of SGOs are employed by the PSEUSMALLOBE method and, depending on the values of the *Znl* parameters, contracted basis sets are generated for the description of the atomic orbitals. Individually positioned primitive Gaussians with radii ρ_i may also be included in the orbital basis set of the molecule under investigation. In the present calculations the representation of the *s* functions has been mainly solved by this latter option. Further details of the method are described by Shillady (3). In Table 2 values of the *Znl* parameters together with the radii of two primitive Gaussians, centered on the nuclei for the description of the *s* functions, may be found for P, S, and Cl. The primitive Gaussian generated through $Z4s$ is also included in the *s* function description. Throughout the molecular calculations presented in this paper the pseudopotential LCAO-MO-SCF procedure PSEUSMALLOBE with the parametrization represented by Tables 1 and 2 has been used.

Results and discussion

In Tables 3 and 4 results of pseudopotential LCAO-MO-SCF calculations using the proposed form of the pseudopotential with the numerical parameters of Table 1 are displayed for PH_3, H_2S, and HCl. For each molecule an orbital basis set, characteristic of the PSEUSMALLOBE procedure, has been generated according to the *Znl* parameters of Table 2.

At the beginning, a few calculations with preguessed basis sets were performed for orientation. Former calculations and experience on analogous molecules with heavier elements from

TABLE 3. Calculated and experimental valence-only total energies E_T^V, bond lengths r_e, and bond angles ϕ_e of PH_3, H_2S, and HCl

	Molecule	E_T^V	r_e	ϕ_e (deg)
PH_3	Present work	−7.97789	2.68	95.8
	Expt.	−8.01245[a,b]	2.68[b]	93.3[c]
H_2S	Present work	−11.09671	2.58	96.5
	MP(411/311)[d]	—	2.54	95.9
	MP(411/311)[d]	—	2.53	94.0
	Expt.	−11.41900[a,b]	2.52[b]	92.1[c]
HCl	Present work	−15.41042	2.44	—
	MP(411/311)[d]	—	2.44	—
	MP 411/311[d]	—	2.41	—
	VE[e]	—	2.40	—
	Expt.	−15.69730[a,b]	2.40[b]	—

[a]Estimated value of total valence energy using experimental ionization potentials and bond energies.
[b]See Sutton, Landolt-Börstein, and Vedeneyev *et al.* (4).
[c]See Gordon *et al.* (6).
[d]See Sakai and Huzinaga (16).
[e]See Pelissier and Durand (15).

the first row of the periodic table have helped also substantially in the selection of the appropriate basis set. For H the standard basis set with $HZ1s = 1.2$ was used. It was observed also that the internuclear distances of the hydrides of P, S, and Cl are substantially larger than those of the corresponding molecules in the first row, and this made the basis set less sensitive to the central atom in the outer region.

Many basis sets have been suggested for the elements in the second row of the periodic table (Pietro *et al.* (5), Gordon *et al.* (6), Gianolio and Clementi (12), McLean and Chandler (13)). The most detailed study on basis sets of H_2S is given by Poirier *et al.* (14) and we select their Uniform Quality Basis Set UQ-5G $s \neq p$ for discussion. This basis set contains 15 spherical Gaussians for the description of *s* states partitioning into 11 Gaussians describing the $(1s)^2$ $(2s)^2$ core states and the inner part of the 3*s* valence state. For the outer part of 3*s* and for the virtual excited orbitals only 4 Gaussians are left. We use only 3 Gaussians for the description of the outer part of 3*s*. For the *p* states there are 3 × 10 Cartesian Gaussians, namely (7 and 3) × 3 for the inner and outer regions respectively, and we use 3 × 3 mimics for the *p* states in S. The pseudopotential is a one-electron operator and its effect on the computations with respect to time and storage is negligible. Its introduction permits a substantial reduction in the size of the orbital basis set and a great reduction in the number of two-electron integrals, together with a corresponding reduction in computer time and storage.

Calculated and experimental values of interatomic distances, bond angles, valence-only total energies, and electric dipole moments, belonging to the minimum-energy geometry of the molecules, are presented in the tables. Table 4 also contains dipole moment values for PH_3, H_2S, and HCl obtained by other calculational methods for comparison.

Tables 5 and 6 present a comparison of the calculated and experimental binding energy spectra of PH_3 and H_2S. For H_2S the results of single-zeta *ab initio* calculations using STOs, and calculations involving GTOs with the incorporation of diffuse low-exponent functions, are also available. In Table 5 the results of these calculations have also been included.

Recently the results of valence energy calculations involving the use of *ab initio* effective core potentials have been pub-

TABLE 4. Calculated and experimental electric dipole moments (Debyes)[a]

Molecule	Expt.[b]	Present work	STO-3G//STO-3G[c]	4-31G//4-31G[c]	3-21G//3-21G[b]	VE[d]
PH_3	0.58	1.25	0.65	1.07	1.24	—
H_2S	0.97	1.60	1.03	1.78	1.83	—
HCl	1.08	1.77	1.76	1.87	1.86	1.26

[a]Nomenclature A//B indicates a calculation of a property at level A performed by using geometry which is optimum for level B.
[b]Experimental, 3-21G results have been obtained from Pietro *et al.* (5).
[c]See Gordon *et al.* (6).
[d]Effective potential III, basis set 5*s* 5*p* 1*d* for chlorine. See Pelissier and Durand (15).

TABLE 5. Calculated and experimental binding energy spectrum for PH_3

Orbital	Expt.[a]	Present work
$5a_1$	0.3896	0.4241
$2e$	0.4925	0.5696
$4a_1$	0.8085[b]	0.9651

[a]See Cook *et al.* (7).
[b]The centroid of all MFS (multiple final state).

TABLE 6. Calculated and experimental binding energy spectrum for H_2S

Orbital	Expt.[a]	Present work	DG[a,c]	SZ[a,b]
$2b_1$	0.3859	0.4248	0.4631	0.3796
$5a_1$	0.4961	0.5314	0.5557	0.4730
$2b_2$	0.5623	0.6248	0.6457	0.5785
$4a_1$	0.9923	1.0698	1.1146	0.9816

[a]See Cook *et al.* (7).
[b]Single-zeta *ab initio* calculation using STOs with the exponents of Clementi and Raimondi (8).
[c]Calculation involving GTOs with the incorporation of diffuse low-exponent functions.

lished for HCl by Hay *et al.* (9). The results of the above calculations, -15.82516 and -15.66918, are compared to the valence-only total energy of HCl, -15.41042, provided by the pseudopotential approach of the present article. For HCl, ionization potential and force constant values have been derived from the results of the pseudopotential calculations. The calculated value of 0.48509 compares favourably with the experimental value of 0.46844 for the ionization potential of HCl (see Huber and Herzberg (10), p. 284). Similar good agreement has been found for the HCl force constant, the calculated value being 0.479 dyn/cm $\times$ 10^6 while the experimental value is 0.516 dyn/cm $\times$ 10^6. Unrestricted RHF calculations with different basis sets resulted in force constant values in the range of 0.470–0.614 dyn/cm $\times$ 10^6 (Sakai *et al.* (11)) and the model potential calculations of Sakai and Huzinaga (16) in the range of 0.497–0.563 dyn/cm $\times$ 10^6.

1. R. GÁSPÁR. Int. J. Quantum Chem. **23**, 1017 (1983).
2. V. BONIFACIC and S. HUZINAGA. J. Chem. Phys. **62**, 1507 (1975); S. TOPIOL, J. W. MOSKOWITZ, C. F. MELIUS, M. D. NEWTON, and J. JAFRI. Erda Energy Res. Abstr. 1(8)Abstr. No. 14822, 105 (1976).
3. D. D. SHILLADY. Quantum Chem. Program Exchange **11**, 239 (1974).
4. L. E. SUTTON. Tables of interatomic distances and configurations in molecules and ions. Spec. Publ. 11, The Chemical Society, London. 1958; LANDOLT-BÖRNSTEIN. Atom- und Molecularphysik 1. Teil Atome und lonen, Springer-Verlag, Berlin. 1950. p. 211; V. I. VEDENEYEV, L. V. GURVICH, V. N. KONDRATYEV, V. A. MEDVEDEV, and YE. L. FRANKEVICH. Bond energies ionization potentials and electron affinities. Edward Arnold Publ. Ltd., London. 1966.
5. W. J. PIETRO, M. M. FRANCL, W. J. HEHRE, D. J. DEFREES, J. A. POPLE, and J. S. BINKLEY. J. Am. Chem. Soc. **104**, 5039 (1982).
6. M. S. GORDON, J. S. BINKLEY, J. A. POPLE, W. J. PIETRO, and W. J. HEHRE. J. Am. Chem. Soc. **104**, 2797 (1982).
7. J. P. D. COOK, C. E. BRION, and A. HAMNETT. Chem. Phys. **45**, 1 (1980).
8. J. E. CLEMENTI and D. L. RAIMONDI. J. Chem. Phys. **38**, 2686 (1963).
9. P. J. HAY, W. R. WADT, and L. R. KAHN. J. Chem. Phys. **68**, 3059 (1978); L. R. KAHN, P. BAYBUTT, and D. G. TRUHLAR. J. Chem. Phys. **65**, 3826 (1976).
10. K. P. HUBER and G. HERZBERG. Molecular spectra and molecular structure. Constants of diatomic molecules. Van Nostrand Reinhold Company, New York. 1979.
11. Y. SAKAI, H. TATEWAKI, and S. HUZINAGA. J. Comput. Chem. **2**, 108 (1981).
12. L. GIANOLIO and E. CLEMENTI. Gazz. Chim. Ital. **110**, 179 (1980).
13. A. D. MCLEAN and G. S. CHANDLER. Contracted Gaussian basis sets for molecular calculations, second row atoms, $z = 11-18$. Research Report, IBM, Yorktown Heights, New York.
14. R. A. POIRIER, R. DAUDEL, P. G. MEZEY, and I. G. CSIZMADIA. Int. J. Quantum Chem. **21**, 799 (1982).
15. M. PELISSIER and PH. DURAND. Theor. Chim. Acta, **55**, 43 (1980).
16. Y. SAKAI and S. HUZINAGA. J. Chem. Phys. **76**, 2552 (1982).

Characterization of cooperative conformational transitions by Fourier transform infrared spectroscopy: application to phospholipid binary mixtures[1]

R. A. DLUHY, D. MOFFATT, AND D. G. CAMERON
Division of Chemistry, National Research Council of Canada, Ottawa, Ont., Canada K1A 0R6

R. MENDELSOHN
Department of Chemistry, Rutgers University, 73 Warren Street, Newark, NJ 07102, U.S.A.

AND

H. H. MANTSCH
Division of Chemistry, National Research Council of Canada, Ottawa, Ont., Canada K1A 0R6

Received September 15, 1984

This paper is dedicated to Professor Camille Sandorfy on the occasion of his 65th birthday

R. A. DLUHY, D. MOFFATT, D. G. CAMERON, R. MENDELSOHN, and H. H. MANTSCH. Can. J. Chem. **63**, 1925 (1985).

Temperature-induced cooperative conformational transitions in biopolymers may be examined in aqueous solution by the use of Fourier transform infrared spectroscopy. The transition is described in terms of a two-state model with a fractional population parameter (which describes the degree of transition at various values intermediate between the two limiting cases) that can be generated by a least-squares technique. This procedure allows for calculation of a conformational index without assuming a linear dependence of the infrared parameter on the extent of transition. Calculations based on the Zimm–Bragg theory of cooperative conformational transitions allow thermodynamic quantities to be derived using the conformational index in conjunction with calorimetric measurements.

The method is illustrated with data from the gel/liquid-crystalline phase transitions of binary phospholipid vesicles where the use of isotopic substitution allows the conformation of each component of the binary mixture to be independently monitored. The data suggest the coexistence of well-defined structural domains of phospholipid as well as the preferential clustering of one of the lipid components at the interface between the two phases.

R. A. DLUHY, D. MOFFATT, D. G. CAMERON, R. MENDELSOHN et H. H. MANTSCH. Can. J. Chem. **63**, 1925 (1985).

On peut étudier les transitions conformationnelles coopératives induites par la température des biopolymères en solution aqueuse en faisant appel à la spectroscopie infrarouge par transformation de Fourier. On peut décrire la transition en fonction d'un modèle à deux états avec un paramètre de population fractionnaire (qui décrit le degré de transition des diverses valeurs intermédiaires entre les deux cas limites) que l'on peut généré par la technique des moindres carrés. Ce procédé permet de calculer un indice conformationnel sans faire l'hypothèse qu'il existe une relation linéaire entre le paramètre infrarouge et le degré de transition. Des calculs basés sur la théorie de Zimm–Bragg des transitions conformationnelles coopératives permettent d'évaluer des quantités thermodynamiques à l'aide de l'indice conformationnel couplé à des mesures calorimétriques.

On illustre la méthode avec des données provenant de transitions de phases gel/liquide cristallin de vésicules de phospholipides binaires où l'utilisation de la substitution isotopique permet de déterminer d'une manière indépendante la conformation de chacun des composants du mélange binaire. Les données suggèrent qu'il y a une coexistence de domaines structuraux de phospholipides bien définis ainsi qu'une aggrégation préférentielle de l'un des lipides composants à l'interface entre les deux phases.

[Traduit par le journal]

Introduction

Recently, there have been numerous attempts to describe in detail the molecular events that occur during the cooperative conformational transitions of biopolymers. Such models generally rely on a statistical mechanical approach to characterize the phase transition. Thus, the contribution to the total energy of the molecule from various internal forces can be estimated (1–4).

An alternative approach to describing the individual, microscopic molecular events of a conformational phase transition is to consider the biopolymer on a macroscopic phenomenological level. In this approach, the phase transition is described as a simple order–disorder transition in which the two phases have considerably different thermodynamic parameters (5, 6).

Spectroscopic methods have had considerable success in elucidating the conformational behavior of biomolecules. Techniques such as nmr, esr, fluorescence, infrared and Raman spectroscopy have provided detailed information about the molecular events that occur within biomolecules during conformational transitions (7). Infrared spectroscopy, in particular, offers several advantages for the study of conformational transitions. Infrared spectra are sensitive to displacements of the dipole moment during vibrations which in turn depend upon changes in conformation and configuration of the bonds making up the normal mode of vibration (8). Identification of a group frequency characteristic of a certain aspect of molecular conformation allows the observation of changes in conformation as environmental conditions are varied without the use of perturbing probe molecules. The application of infrared techniques to the study of aqueous biophysical systems has been hindered mainly by the strong infrared absorptions of water. To this end, several techniques have been developed which partially overcome this handicap. Examples include solvent substitution (i.e., D_2O) and spectral data processing techniques (9, 10).

The current study describes the use of FT-IR spectroscopy to monitor cooperative conformational phase transitions of biopolymers. A simple two-state model is introduced in which

[1]NRCC No. 23642.

changes in a conformation-sensitive infrared spectral feature are related to a fractional conformation parameter. The use of a least-squares optimization procedure to generate this parameter removes the assumption that the observed infrared spectral changes are linear functions of the extent of the conformational transition. Such a refinement allows a more accurate calculation of the degree of transition at intermediate values. Finally, the use of the two-state model in conjunction with calorimetric measurements allows calculation of thermodynamic parameters based on the Zimm–Bragg theory of cooperative conformational transitions.

The method described here is illustrated using data from the temperature-induced gel/liquid-crystalline phase transition of binary phospholipid mixtures. The deuteration of one component of the mixture shifts its conformation-sensitive spectral features to a region of the spectrum free from interfering absorptions. Consequently, the conformation of each component of the binary mixture may be monitored separately throughout the conformational transition.

Materials and methods

Materials

DPPC and perdeuterated DMPC (DMPC-d_{54}) were purchased from Avanti Biochemicals (Birmingham, AL). Lipids were stored in chloroform under nitrogen at −40°C. Lipid concentrations were determined by phosphorous assay. Each lipid gave a single spot on TLC plates.

Sample preparation

Multilamellar lipid vesicles were prepared as follows: aliquots of the lipid chloroform solution containing the desired amounts of lipid (either pure or binary mixtures) were placed in a test tube and incubated at 50°C for 10 min. Solvent was removed with a stream of dry nitrogen followed by overnight evacuation. The lipid film was rehydrated in 50 m*M* Tris, pH 7.4 by vortexing. The lipid multilayers were heated above the phase transition and cooled to insure complete hydration and mixing. This cycle was repeated several times. The composition of the binary lipid vesicles was checked by gas chromatography of the methyl esters of the lipid acyl chains.

Fourier transform infrared spectroscopy

Samples were prepared for infrared analysis in 25 μm thick cells with CaF_2 windows. Spectra were recorded on a Digilab FTS-15 Fourier transform infrared spectrometer equipped with a HgCdTe detector. Two hundred and fifty interferograms, collected with an optical velocity of 1.26 cm s^{-1} and a maximum optical retardation of 0.25 cm, were coadded, apodized with a triangular function, and Fourier transformed with one level of zero filling to yield spectra with a resolution of 4 cm^{-1} and data encoded every 2 cm^{-1}.

Temperatures were controlled by a thermostatted EtOH–H_2O mixture flowing through a hollow cell mount and monitored by a copper–constantan thermocouple placed against the edge of the cell window (11). Frequencies were determined by computing the center of gravity of the C—H or C—D stretching bands from the topmost five data points; to remove baseline fluctuations due to the absorption of liquid water, all calculations were performed on derivative spectra (10). The use of special algorithms described elsewhere (12) permits the determination of the band maxima in a series of homologous infrared spectra with an uncertainty of less than 0.02 cm^{-1}.

Differential scanning calorimetry

Calorimetry measurements were made on a Micro-cal MC1 calorimeter. Sample volumes of 0.70 mL containing 1.4–2.0 mg of the appropriate lipid mixture were injected into the calorimeter sample cell with the same volume of H_2O used as a reference. Samples were scanned at ca. 24° h^{-1} starting at 4°C after a minimum of 2 h equilibration. Onset and completion data were determined as described. Duplicate runs of the same sample gave onset and completion temperatures reproducible to ±0.2°C. Independent samples gave data reproducible to 0.5°C. Excess heat capacity data were calibrated with a standard electronic pulse. Typically, the value of the enthalpy for a multilamellar suspension of DPPC was $\Delta H = 7.1 \pm 0.5$ kcal mol^{-1}.

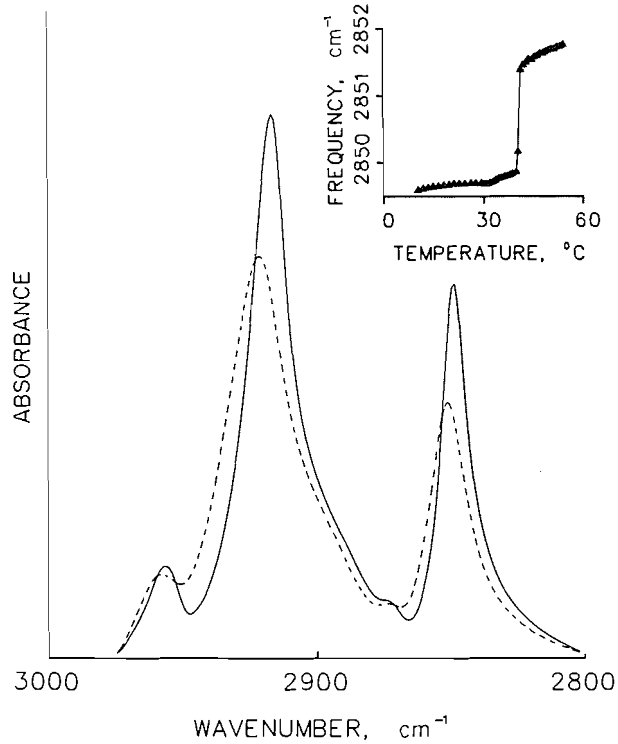

FIG. 1. Temperature dependence of the infrared spectra of 1,2-dipalmitoyl-*sn*-glycero-3-phosphocholine (DPPC) in the region of the C—H stretching bands. The upper spectrum (solid line) represents DPPC in the gel phase at 10°C. The lower spectrum (dashed line) represents DPPC in the liquid-crystalline phase at 50°C. *Inset*: The relationship between frequency and temperature for the CH_2 symmetric stretching band of DPPC.

Results

Part A. Generation of an infrared fractional conformational parameter

The procedure described here is developed for the case of a two-state transition where the molecule can exist only in the initial state, A, and the final state, B, with no thermodynamically stable intermediates present. Many biophysically relevant transitions have been described as cooperative two-state processes. Examples include: (*i*) helix–coil transitions in polypeptides (5, 13), (*ii*) double helix–coil transitions of nucleic acids (14), (*iii*) thermal denaturation of proteins (6), and (*iv*) phospholipid gel to liquid-crystalline phase transitions (15–17).

In the case of phospholipids, the infrared spectroscopic parameters used to identify phase changes include band frequency, bandwidth, peak height, and integrated intensity (18). Figure 1 illustrates the temperature dependence of the infrared spectra of the conformation-sensitive C—H stretching region for 1,2-dipalmitoyl-*sn*-glycero-3-phosphocholine (DPPC). The spectral features arise from the asymmetric and symmetric CH_3 stretching modes near 2956 and 2872 cm^{-1} (weak infrared bands), while the antisymmetric and symmetric CH_2 stretching modes (strong infrared bands) are observed at 2920 and 2850 cm^{-1} (19). An increase in temperature results in reductions of peak height and integrated intensity, an increase in bandwidth

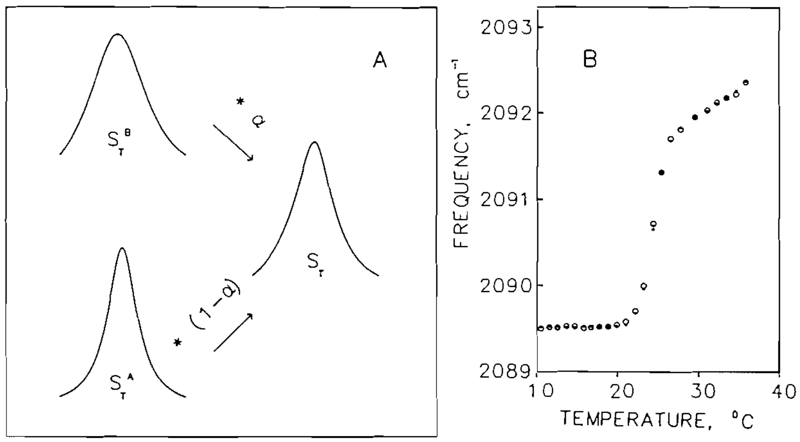

FIG. 2. Part *A*: Generation of a calculated spectrum S_T, from a linear combination of S_T^A and S_T^B. Part *B*: Temperature-dependence of the CD_2 frequency of experimental (open symbols) and calculated (closed symbols) spectra (S_T) of a binary lipid mixture.

and a shift in frequency to higher wavenumbers, with all the parameters showing discontinuities at the transition temperature. The temperature dependence of the band frequencies can be attributed on a molecular level to variations in the conformation of the mostly all-*trans* phospholipid acyl chains in the gel phase, with the introduction of *gauche* conformers at the characteristic phase transition temperature (20). As has been previously demonstrated (21) and illustrated in the inset in Fig. 1, the frequencies of the CH_2 stretching bands are sensitive indicators of the phospholipid gel to liquid-crystalline phase transition. The sensitivity of the C—H frequency to phase changes for various hydrocarbon systems has been attributed to changes in the interaction constants between adjacent CH_2 groups as the relative orientation of these groups changes with the introduction of *gauche* conformers (19).

A two-state transition model rests on the assumption that the initial and final states have measurably different thermodynamic properties (22). To unambiguously characterize these states via infrared spectroscopy, they must also have measurably different spectral characteristics. As seen above for the case of a phospholipid two-state phase transition, measurable changes occur in frequency, bandwidth and/or intensity. Computer simulations have shown that when two Lorentzian lineshapes with differing bandwidths and frequencies (corresponding to the bandshape of a pure initial and pure final state) are summed in varying proportions, the resulting changes in frequency and bandwidth are not linearly correlated with the proportion of either component (21, 23). This implies that changes in the commonly measured spectral parameters (e.g. frequency, bandwidth, etc.) are not linear indicators of the extent of transition due to the inherent spectral characteristics of overlapping band contours.

Efforts to quantitatively describe the extent of transition using observable experimental parameters generally have assumed the following relation between the degree of transition, α, and the observable parameter, r

$$\alpha = (r_A - r)/(r_A - r_B)$$

where r_A and r_B are the values of the experimental parameter in states A and B, respectively (24). The disadvantage of this method is that it assumes a linear dependence of r on α. Since this is not a reasonable assumption for a two-state cooperative transition characterized via infrared parameters (21), we have taken the following approach. For any two-state process, the infrared spectrum at a particular temperature, S_T, is a superposition of two bandshapes that correspond to the initial state A, S_T^A, and final state B, S_T^B. The proportion by which the two limiting-case bandshapes are added to generate the observed spectrum depends on α, the degree of transition. That is

$$[1] \quad S_T = (1 - \alpha)S_T^A + \alpha S_T^B$$

In order to generate bandshapes corresponding to the initial and final states at a particular temperature (i.e., S_T^A and S_T^B), the following procedure is employed. First, a conformation-sensitive vibrational feature is identified (e.g., the frequency of a C—H stretching band). Then, at each frequency, regression coefficients are generated by a linear least-squares fit of absorbance versus temperature. The resulting coefficients are used to calculate the pure component spectra S_T^A and S_T^B in the region of the transition. At any particular temperature within the two-phase region, S_T is estimated by a linear combination of S_T^A and S_T^B (Fig. 2*A*) and the value of α is calculated to minimize the squared residual between the band contour of S_T and the band contour of the experimental spectrum. Figure 2*B* compares the temperature dependence of the symmetric CD_2 stretching frequency of experimental versus calculated spectra (S_T) when the above procedure is applied to the infrared spectra of a binary mixture of DPPC : DMPC-d_{54}. The advantage of this procedure is that it removes the necessity for assuming a linear dependence of α on the experimental parameters and therefore gives a more accurate estimate of the degree of transition.

Part B. Description of the cooperative transition

In this section, the fractional degree of transition derived from the infrared measurements in the previous section is used in conjunction with the theory of cooperative transitions developed originally by Zimm and Bragg (13, 25) and widely applied to biomolecules (13–17). As the theory has been extensively discussed (26), only the results relevant to the present discussion will be described.

This type of approach to conformational transitions assumes that the initial and final states exist in discrete temperature-dependent clusters or domains that coexist in dynamic equilibrium during the cooperative transition (15). The thermodynamic properties of the transition can be characterized by two parameters, a cooperativity parameter, σ, and a partition function, s (26). Since the cooperativity parameter is related to the interfacial free energy between the two domains, it is also possible to describe the fraction of molecules at the interfacial region between the two domains (16).

If a transition of the form

$$A \rightleftharpoons B$$

is assumed and a degree of transition, α, defined as in Part A, then the apparent equilibrium constant for the transition is

$$K = \frac{\alpha}{1 - \alpha}$$

The temperature dependence of K is described by the van't Hoff equation:

$$\frac{\mathrm{d} \ln K}{\mathrm{d}T} = \frac{\Delta H_{\mathrm{vh}}}{RT^2} = \frac{1}{\alpha(1 - \alpha)} \frac{\mathrm{d}\alpha}{\mathrm{d}T}$$

At the transition midpoint (T_{m}), $\alpha = \frac{1}{2}$ and

$$[2] \quad \Delta H_{\mathrm{vh}} = 4RT_{\mathrm{m}}^{2} \left(\frac{\mathrm{d}\alpha}{\mathrm{d}T}\right)_{T_{\mathrm{m}}}$$

where ΔH_{vh} is the van't Hoff enthalpy which corresponds to the enthalpy of transition of the cooperative unit. If the $A \rightleftharpoons B$ interconversion is represented as an equilibrium with an equilibrium constant K, then a partition function, s, can be defined as

$$s = z_{\mathrm{b}}/z_{\mathrm{a}}$$

where z_a and z_b are the molecular partition functions for molecules in states A and B, respectively (26), and s is equal to the partition function for a unit in state B relative to state A. Also, thermodynamically,

$$[3] \quad s = \exp\,(\Delta G^{0}_{\mathrm{A \to B}}/RT)$$

where $\Delta G^{0}_{\mathrm{A \to B}}$ is the free energy change per molecule for the conversion of state A to state B. At the midpoint of the transition,

$$\Delta G^{0}_{\mathrm{A \to B}} = 0 \text{ and } s = 1$$

From the relationship between the calorimetric enthalpy and the van't Hoff enthalpy, a cooperativity parameter, σ, can be defined which essentially describes the steepness of the transition:

$$[4] \quad \sigma = (\Delta H_{\mathrm{cal}}/\Delta H_{\mathrm{vh}})^2$$

Also, σ is defined as the factor by which the partition function is diminished by the addition of a unit of B; $-RT \ln \sigma$ then corresponds to the interfacial free energy between the microscopic domains (16, 26). Therefore:

$$\sigma = \exp\,(\Delta G^{0}_{\mathrm{I \to B}}/RT)$$

and $\Delta G^{0}_{\mathrm{I \to B}}$ is defined as above.

The total molecular partition function can be described (26) as

$$Z = \sum_{n_b, n_a, n_i} (z_b^{n_b} z_a^{n_a} \sigma^{n_i})$$

where z_a, z_b, and σ are as defined, and n_a, n_b, and n_i correspond to the number of molecules in state A, B, and at the interface, respectively.

It has been shown (16, 26) that the mean fraction of molecules in state B can be expressed as

$$\theta = \frac{\langle n_b \rangle}{n} = \frac{1}{n} \frac{\partial \ln z}{\partial \ln s}$$

which reduces to

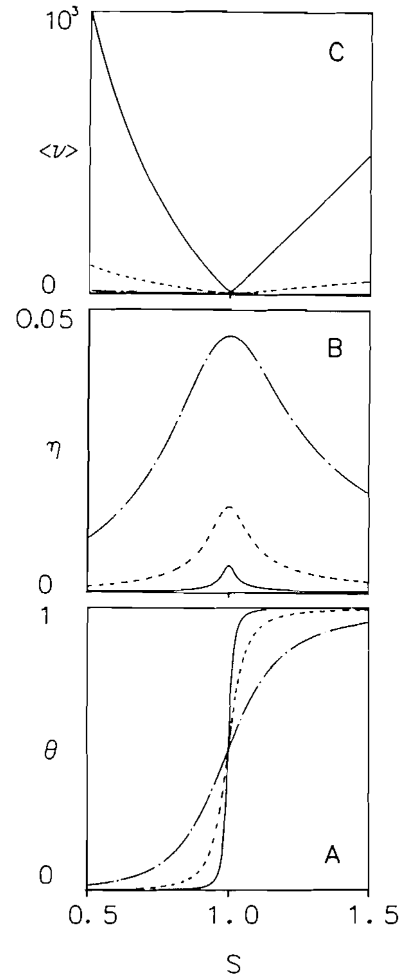

FIG. 3. Calculated values for the derived parameters of the Zimm–Bragg cooperative transition model. *A*: Fraction of molecules in the final phase (i.e., degree of transition). *B*: Fraction of molecules at the interfacial region between the phase boundaries. *C*: Mean size of the initial and final phases. All three parameters are plotted against the normalized temperature parameter, s, for three different values of the cooperativity parmeter σ, i.e., $\sigma = 10^{-4}$ (—), $\sigma = 10^{-3}$ (- - -) and σ 10^{-2} (-·-·-·-).

$$[5] \quad \theta = \frac{1}{2}\left[1 + \frac{s - 1}{\sqrt{(s-1)^2 + 4\sigma s}}\right]$$

Similarly, the mean fraction of molecules at the interfacial region between the two macroscopic domains, η, is expressed as

$$\eta = \frac{1}{n} \frac{\partial \ln z}{\partial \ln \sigma}$$

and, by substitution

$$[6] \quad \eta = \frac{2\sigma s}{(1+s)[(1-s)^2 + 4\sigma s]^{1/2} + (1-s)^2 + 4\sigma s}$$

The analytical expressions for θ and η thus depend upon σ, a cooperativity parameter, and s, a partition function. σ can be experimentally determined by use of eq. [4]. Equation [3] shows that s is dependent on the free energy difference between the two macroscopic states. To calculate s, it is known that at T_{m}, $\Delta G^{0}_{\mathrm{A \to B}} = 0$ and $s = 1$. For small deviations of s and T_{m}, a linear dependence of s with temperature is assumed (26) and a Taylor series expansion is performed about the midpoint T_{m}. Therefore,

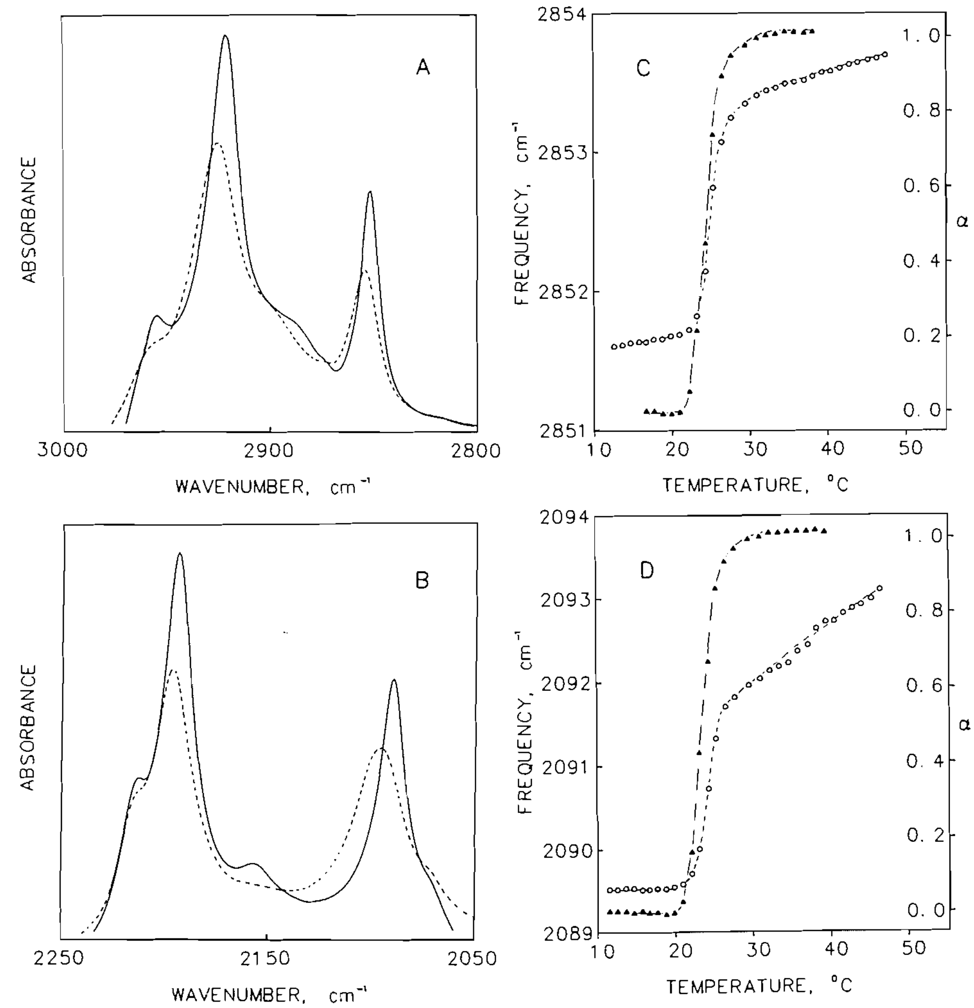

FIG. 4. *A*: Temperature dependence of the C—H stretching region in the infrared spectra of the DPPC component of a 75:25 binary mixture of DPPC:DMPC-d_{54}. *B*: The C—D stretching region of the DMPC-d_{54} component of the same binary mixture as in *A*. For the purposes of display, linear baselines extending from 3000 to 2800 cm^{-1} (in *A*) and 2300 to 2000 cm^{-1} (in *B*) have been subtracted. Solid lines indicate low temperature (15°C) spectra while dashed lines indicate high temperature (45°C) spectra. *C*: Temperature induced variation in the frequency of the CH_2 symmetric stretching band of DPPC (open symbols), along with the α values (closed symbols) calculated according to the procedure described in the text. *D*: Temperature induced variation in the frequency of the CD_2 symmetric stretching band of DMPC-d_{54} (open symbols) along with the calculated α values (closed symbols).

TABLE 1. Calorimetric data for DPPC:DMPC-d_{54} mixtures[a]

Mole ratio DPPC:DMPC-d_{54}	T_{onset}	T_m	T_{compl}	ΔH_{cal}[b]	σ[c]
0.85:0.15	35.2	39.0	40.4	7.04	4.96×10^{-4}
0.67:0.33	29.7	36.0	37.4	6.46	1.36×10^{-3}
0.50:0.50	26.0	32.3	34.6	5.89	3.03×10^{-3}
0.33:0.67	22.6	25.3	29.8	5.37	2.22×10^{-3}
0.15:0.85	20.1	21.6	24.4	4.52	2.89×10^{-3}

[a]Onset, midpoint, and completion temperatures in °C.
[b]In kcal mol^{-1}.
[c]σ was calculated by (1) first calculating ΔH_{vh} by the equation $\Delta H_{vh} = 6.9 \times (T_m^2/\Delta T_{1/2})$ (38), (2) $\sigma = (\Delta H_{cal}/\Delta H_{vh})^2$.

$$[7] \quad s = \frac{\Delta H_{cal}}{R T_m^2}(T - T_m) + 1$$

where ΔH_{cal} equals the calorimetrically determined enthalpy change of the transition.

Given the mean fraction of molecules in state B and the mean fraction of molecules in the interfacial region (eqs. [5] and [6] above), it is possible to express the relative size of the regions of state A and state B as the mean number of molecules in that state per interfacial molecule (17). That is, for state B

$$[8] \quad \langle \nu_b \rangle = \frac{\theta}{\eta}$$

and for state A

$$[9] \quad \langle \nu_a \rangle = \frac{1 - \theta}{\eta}$$

In this fashion, the changes in the relative size of the two domains throughout the transition may be monitored.

Figure 3 illustrates the application of the above parameters for calculated transition curves and various quantities of the cooperativity parameter, σ. Plotting these parameters versus s in effect normalizes the transition temperature for the various parameters since at T_m, $s = 1$ (26). Figure 3*A* shows that for very non-cooperative transitions ($\sigma = 10^{-2}$) the fraction of molecules in state B increases very slowly and allows for the coexistence of the two phases over the transition range (Fig.

TABLE 2. Spectroscopic data for DPPC:DMPC-d_{54} mixtures[a]

Mole ratio DPPC:DMPC-d_{54}	DPPC				DMPC-d_{54}			
	T_{onset}	T_m	$T_{completion}$	σ^b	T_{onset}	T_m	$T_{completion}$	σ^b
0.81:0.19	32.9	36.1	39.5	9.39×10^{-4}	29.3	34.6	37.6	1.39×10^{-4}
0.62:0.38	28.5	33.0	38.0	1.21×10^{-3}	26.7	31.6	34.8	3.13×10^{-4}
0.48:0.52	26.5	30.8	35.0	4.21×10^{-4}	25.2	29.4	32.6	4.78×10^{-4}
0.37:0.63	23.8	27.4	31.6	1.96×10^{-4}	23.0	26.1	30.3	8.20×10^{-4}
0.25:0.75	22.1	24.6	28.6	3.11×10^{-5}	21.2	23.6	27.4	5.76×10^{-4}
0.14:0.86	20.9	23.0	26.3	7.7×10^{-6}	20.7	22.7	25.7	2.3×10^{-4}

[a] Onset, midpoint, and completion temperatures in °C.
[b] σ was calculated by (1) first calculating ΔH_{vh} according to eq. [2], (2) assuming $\Delta H_{cal(1)} = \Delta H_{cal} \cdot X_1$, (3) $\sigma = (\Delta H_{cal(1)}/\Delta H_{vh})^2$.

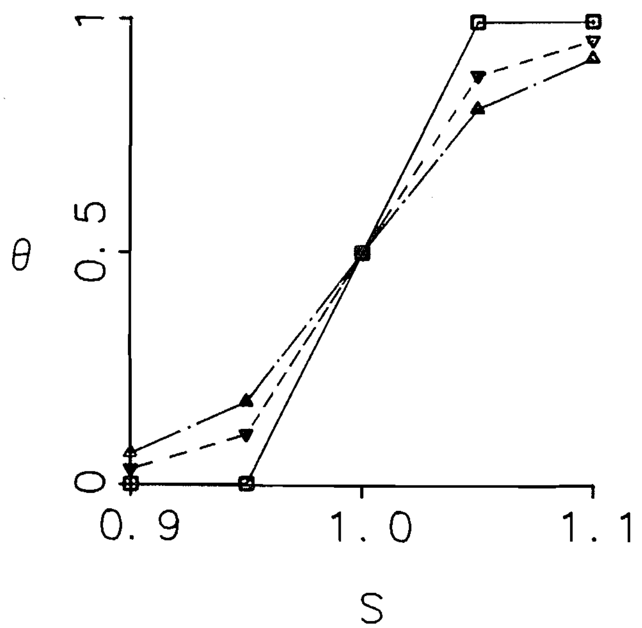

FIG. 5. Fraction of molecules in the fluid phase (i.e., degree of transition) plotted against the normalized transition temperature, s, for various mole fractions of DPPC in DPPC:DMPC-d_{54} binary mixtures. Mole fraction DPPC, 0.142 (—); 0.479 (- - -); and 0.808 (-·-·-·-).

3*C*). In addition, a low cooperativity transition has a high fraction of molecules at the phase boundaries between the two states (Fig. 3*B*).

Part C. Application of the model to phospholipid binary mixtures

The importance of the phospholipid phase transition to the structure and function of biological membranes has been extensively investigated in recent years (27); such processes as enzyme activity, active transport, and ion permeability have been shown to be dependent on the lipid phase state (28). In addition, in complex mixtures of lipids, the coexistence of laterally segregated domains of lipids differing in their physical structure may provide a particular chemical environment conducive to functional properties (29–31). Since the majority of biophysical membrane studies have focused on single lipid species, less information is available on the physical and chemical structure of binary lipid mixtures. Especially lacking is information concerning the cooperative nature of the transition for each component of the mixture and how that relates to the overall thermodynamic properties of the membrane.

Infrared spectroscopy offers certain advantages for the study of binary mixtures. In particular, if one component of the mixture is isotopically labelled in its conformation-sensitive region, the conformation of each component may be monitored simultaneously. Such an approach has been applied to phospholipids (32), where the synthetic incorporation of perdeuterated acyl chains allows the monitoring of the conformation-sensitive C—D stretching modes in a manner analogous to that of non-labelled acyl chains (Part A). In addition, for phospholipid mixtures, the C—D stretching modes of the deuterated chains occur in a spectral region free of interference from other lipid vibrational bands and are easily monitored (21). The data presented here illustrate the application of the two-state cooperative transition model described above to binary mixtures of 1,2-dipalmitoyl-*sn*-glycero-3-phosphocholine (DPPC) and acyl chain perdeuterated 1,2-dimyristoyl-*sn*-glycero-3-phosphocholine (DMPC-d_{54}). These phospholipids differ only by two carbons in the length of their acyl chains and have been shown to form nearly ideal mixtures (33). As a consequence of the perdeuteration of the DMPC acyl chains, the conformation of both components of the mixture may be monitored.

Figures 4*A* and 4*B* give the temperature dependence of the C—H and C—D stretching bands for a binary mixture of DPPC and DMPC-d_{54} (DPPC:DMPC-d_{54} mole ratio, 0.75:0.25). In the C—D stretching region (Fig. 4*A*), the CD_3 groups give rise to the weaker bands at 2212 (asymmetric stretch) and 2070 and 2156 cm^{-1} (symmetric stretch) while the strong bands at 2194 and 2089 cm^{-1} are the CD_2 antisymmetric and symmetric stretching bands, respectively (21, 34–37). The spectral assignments for the features in the C—H region of the non-deuterated acyl chain DPPC are given in Part A.

Figures 4*C* and 4*D* show the temperature-induced variation in the symmetric CD_2 and CH_2 frequencies for both components of the binary mixture. As expected for a binary system displaying miscibility (33), the frequency changes for the mixtures occur over a wider temperature interval than that of a pure lipid (compare Fig. 4 and Fig. 1). A further confirmation of a broadened transition in the binary mixtures comes from the calorimetric data for various mole ratios of DPPC and DMPC-d_{54} (Table 1).

Table 2 describes the six binary mixtures of DPPC and DMPC-d_{54} that were used in the spectroscopic experiments. For each mixture, temperature-induced changes in the frequency of the C—H or C—D stretching bands were documented as in Fig. 4. Then, in order to quantitate the degree of transition throughout the phase transition region for both components of the mixture, the melting profiles were analyzed according to eq. [1] and the procedure described in Part B.

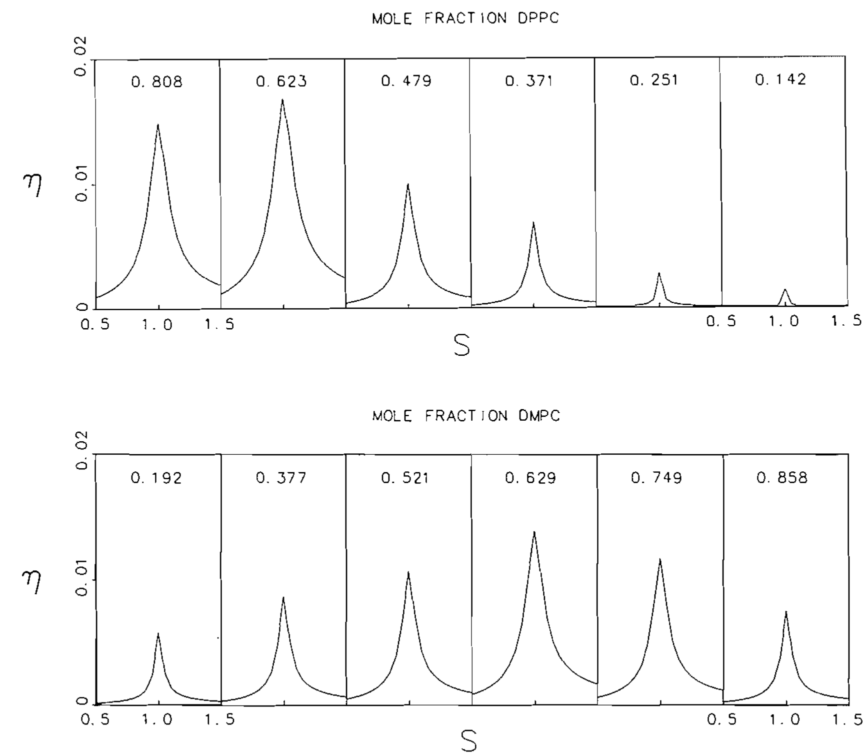

FIG. 6. Calculated values for the fraction of interfacial lipid, η, for each component of the six binary mixtures described in Table 2, plotted against the normalized transition temperature, s. η was calculated from eq. [6] and σ from eq. [4]; the values of σ are listed in Table 2.

Representative results for the DPPC component of three binary mixtures are shown in Fig. 5 and may be compared with the calculated curves of Fig. 3. The data in Fig. 5 indicate that at a low mole fraction (0.142), DPPC acts in a highly cooperative manner while a high mole fraction (0.808) has a much more broadened transition. Equimolar DPPC acts in an intermediate fashion. The diagrammatic results of Fig. 5 are summarized in Table 2 by the cooperativity parameter σ which was calculated using eq. [4]. Low mole fractions of DPPC result in the smallest values of σ and hence melt more cooperatively. The trend is to increasing values of σ with increasing mole fraction of DPPC. While not as great in magnitude, the same trend is observed for the σ values of the DMPC-d_{54} component.

The changes in the cooperative properties of the components of the binary lipid mixture with changes in their respective mole fractions has implications for the physical structure of the membrane. High cooperativity implies that one component has segregated into domains and that a lateral phase separation of the two components has occurred. Defects in crystal packing are likely to occur at the phase boundaries between the two domains and therefore, one of the components of the mixture might congregate specifically at the phase boundary.

Evidence for the specific clustering of one of the lipid components at the phase boundary between segregated domains is presented in Fig. 6. These curves were generated using eq. [6] and correspond to the mean fraction of molecules of each component at the interface between the two macroscopic domains. At equimolar values of DPPC and DMPC-d_{54} (0.521:0.479), both components are present at the interfacial regions in roughly equal amounts. Perturbing this equilibrium by increasing the mole fraction of one component causes the component in the minority to melt more cooperatively (compare the σ values in Table 2) implying the beginning of a lateral phase separation process. The molecules of the component in excess then begin to populate the interfacial regions to a greater extent (Fig. 6).

It should be emphasized that the process described above as lateral phase separation does not imply the existence of gel phase immiscibility in the two components. Calorimetric studies have shown DPPC and DMPC-d_{54} form nearly ideal mixtures (33). Rather, it suggests that ordered and fluid regions of lipid coexist in a dynamic equilibrium mediated by temperature and/or mole fraction.

Using eqs. [8] and [9] from Part B, it is possible to calculate the relative sizes of the gel and liquid crystalline domains compared to the amount of interfacial lipid for each component of the mixture. This is plotted in Fig. 7. The curves in Fig. 7 demonstrate that at low mole fraction, DPPC or DMPC-d_{54} tend to form clusters or domains, as suggested by Fig. 6. This tendency decreases at higher mole fractions, where the gel and liquid crystalline domains decrease in size relative to the amount of interfacial lipid, indicating a more monodisperse and homogeneous system, that coexists throughout the center of the transition.

Summary

The results from the previous sections have shown that monitoring a conformation-sensitive infrared band during a cooperative phase transition allows the calculation of a fractional conformation parameter that describes the degree of transition. The use of this parameter in conjunction with calorimetric measurements leads to calculations that describe the detailed thermodynamic behaviour of the system.

The application of this model to DPPC:DMPC-d_{54} phospholipid binary mixtures provides evidence for lateral phase separation and the coexistence of well-defined structural domains of phospholipid. In addition, the data suggest preferential clustering of one of the lipid components at the interface

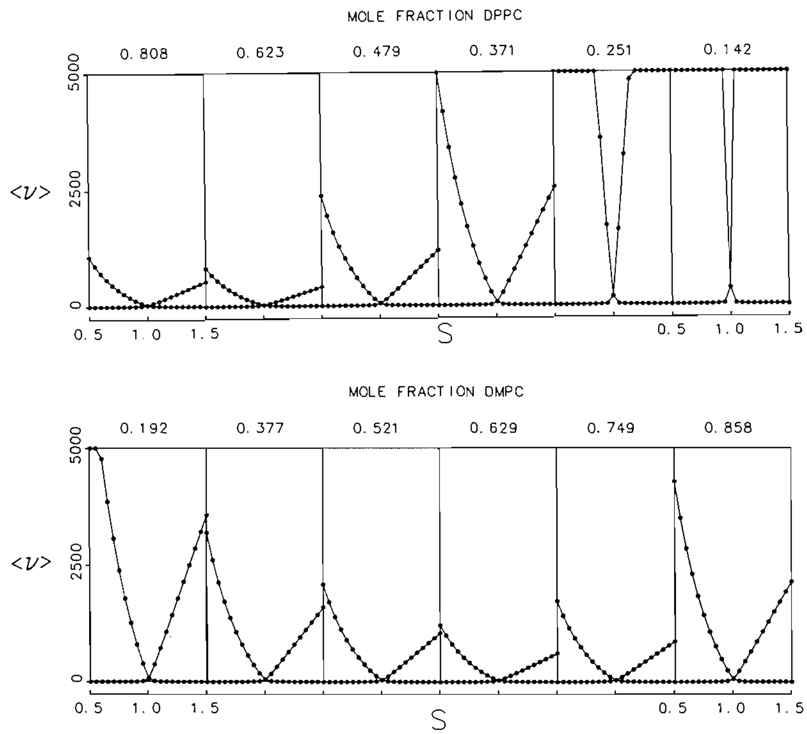

FIG. 7. Calculated values for the mean size of the gel and liquid crystalline domains for each component of the six binary mixtures described in Table 2, plotted against the normalized transition temperature, s. $\langle\nu_a\rangle$ (closed symbols) and $\langle\nu_b\rangle$ (open symbols), were calculated for each component using eq. [8] or [9], respectively. σ was calculated using eq. [4] and is listed in Table 2.

between the two phases. These results agree with recent experimental results which suggest that the compositional segregation of lipids at phase boundaries of binary lipid vesicles is responsible for permeability phenomena (29, 31).

1. K. A. DILL and P. J. FLORY. Proc. Natl. Acad. Sci. USA, **77**, 3115 (1980).
2. D. GRUEN. Biochim. Biophys. Acta, **595**, 161 (1980).
3. F. JAHNIG. Proc. Natl. Acad. Sci. USA, **80**, 3691 (1983).
4. J. NAGLE. Ann. Rev. Phys. Chem. **31**, 157 (1980).
5. J. ENGEL and G. SCHWARZ. Angew. Chem. Int. Ed. **9**, 389 (1970).
6. E. FREIRE and R. BILTONEN. Biopolymers, **17**, 463 (1978).
7. E. GRELL (*Editor*). Membrane spectroscopy. Springer-Verlag, Berlin. 1981.
8. E. B. WILSON, J. C. DECIUS, and P. C. CROSS. Molecular vibrations. McGraw-Hill, New York. 1955.
9. D. G. CAMERON, H. L. CASAL, and H. H. MANTSCH. J. Biochem. Biophys. Methods, **1**, 21 (1979).
10. D. G. CAMERON and D. J. MOFFATT. J. Test. Eval. **12**, 78 (1984).
11. D. G. CAMERON and R. N. JONES. Appl. Spectrosc. **35**, 448 (1981).
12. D. G. CAMERON, J. K. KAUPPINEN, D. J. MOFFATT, and H. H. MANTSCH. Appl. Spectrosc. **36**, 245 (1982).
13. B. H. ZIMM and J. K. BRAGG. J. Chem. Phys. **31**, 526 (1959).
14. J. APPLEQUIST. J. Chem. Phys. **50**, 600 (1969).
15. E. FREIRE and R. BILTONEN. Biochim. Biophys. Acta, **514**, 54 (1978).
16. D. MARSH, A. WATTS, and P. KNOWLES. Biochemistry, **15**, 3570 (1976).
17. D. MARSH, A. WATTS, and P. KNOWLES. Biochim. Biophys. Acta, **465**, 500 (1977).
18. H. H. MANTSCH. J. Mol. Struct. **113**, 201 (1984).
19. R. G. SNYDER, H. L. STRAUSS, and C. A. ELLIGER. J. Phys. Chem. **86**, 5145 (1982).
20. D. G. CAMERON, H. L. CASAL, and H. H. MANTSCH. Biochemistry, **19**, 3665 (1980).
21. R. A. DLUHY, R. MENDELSOHN, H. L. CASAL, and H. H. MANTSCH. Biochemistry, **22**, 1170 (1983).
22. R. A. KLEIN. Q. Rev. Biophys. **15**, 667 (1982).
23. J. UMEMURA, H. H. MANTSCH, and D. G. CAMERON. J. Coll. Interf. Sci. **83**, 558 (1981).
24. M. P. HEYN, A. BLUME, M. REHOREK, and N. A. DENCHER. Biochemistry, **20**, 7109 (1981).
25. B. H. ZIMM and J. K. BRAGG. J. Chem. Phys. **28**, 1246 (1958).
26. P. FLORY. Statistical mechanics of chain molecules. Interscience. New York. 1969.
27. R. C. ALOIA (*Editor*). Membrane fluidity in biology. Vol. 2. Academic Press, New York. 1983.
28. A. PARSEGIAN (*Editor*). Biophysical discussions; protein-lipid interactions in membranes. Rockefeller University Press, New York. 1982.
29. R. D. KLAUSNER, A. M. KLEINFELD, R. L. HOOVER, and M. J. KARNOVSKY. J. Biol. Chem. **255**, 1286 (1980).
30. M. SINGER. Chem. Phys. Lipids, **31**, 145 (1982).
31. M. Y. TSE and M. SINGER. Can. J. Biochem. **62**, 72 (1984).
32. R. MENDELSOHN and C. KOCH. Biochim. Biophys. Acta, **598**, 260 (1980).
33. H. KLUMP, B. GABER, W. PETICOLAS, and P. YAGER. Thermochim. Acta, **48**, 361 (1981).
34. S. SUNDER, D. G. CAMERON, H. L. CASAL, Y. BOULANGER, and H. H. MANTSCH. Chem. Phys. Lipids, **28**, 137 (1981).
35. D. G. CAMERON, H. L. CASAL, H. H. MANTSCH, Y. BOULANGER, and I. SMITH. Biophysical J. **35**, 1 (1981).
36. H. L. CASAL, D. G. CAMERON, H. C. JARRELL, I. C. P. SMITH, and H. H. MANTSCH. Chem. Phys. Lipids, **30**, 17 (1982).
37. S. C. HSI, A. P. TULLOCH, H. H. MANTSCH, and D. G. CAMERON. Chem. Phys. Lipids, **31**, 97 (1982).
38. S. MABREY and J. STURTEVANT. *In* Methods in membrane biology. *Edited by* E. Korn. Plenum, New York. 1978.

A study of the molecular–cellular interface in visual photoreceptors by light scattering photometry

T. BORYS, S. DESHPANDE, R. JONES, AND E. W. ABRAHAMSON
Department of Chemistry and Biochemistry, University of Guelph, Guelph, Ont., Canada N1G 2W1

Received September 26, 1984

This paper is dedicated to Professor Camille Sandorfy on the occasion of his 65th birthday

T. BORYS, S. DESHPANDE, R. JONES, and E. W. ABRAHAMSON. Can. J. Chem. **63**, 1933 (1985).

The correlation of molecular events with structural changes within the cell requires a non-destructive relaxation technique that can be adapted to measure such cellular changes in a time range of milliseconds to minutes. Light scattering relaxation techniques have proved useful for such studies as they can often be measured simultaneously or in parallel with absorption or fluorescence spectral changes characterizing molecular or macromolecular processes. Such techniques are proving useful in the study of photobiological processes such as visual photoreception where specific cytological changes produced photochemically can be effected by alternate controlled perturbations such as osmotic shrinking or swelling of cell organelles and (or) whole cells. This paper illustrates how light scattering relaxation spectrophotometry can be applied to the correlation of molecular and cellular events in visual photoreceptors.

T. BORYS, S. DESHPANDE, R. JONES et E. W. ABRAHAMSON. Can. J. Chem. **63**, 1933 (1985).

Pour étudier des corrélations d'évènements se produisant au niveau moléculaire avec des changements de structure à l'intérieur de la ceullule, il faut disposer d'une technique de relaxation non destructive que l'on peut modifier pour mesurer de tels changements cellulaires à des temps allant des millisecondes à des minutes. Les techniques de relaxation de la lumière diffusée se révèlent pratiques dans de telles études puisqu'on peut souvent les mesurer soit simultanément soit en parallèle avec des changements dans les spectres d'absorption ou de fluorescence qui caractérisent les processus moléculaires ou macromoléculaires. De telles techniques se révèlent utiles dans l'étude des processus photobiologiques comme la photoréception visuelle au cours desquels des changements cytologiques spécifiques produits photochimiquement peuvent être affectés par des perturbations alternées et contrôlées, comme la contraction ou l'expansion osmotique d'organelles de cellules et/ou de cellules complètes. Cette communication démontre que l'on peut utiliser la spectrophotométrie de relaxation par dispersion de la lumière pour établir une corrélation entre des comportements moléculaires et cellulaires dans les photorécepteurs visuels.

[Traduit par le journal]

Introduction

The interface of two organizational domains is a classic problem in the sciences and particularly in the biological sciences. Generally the study of such an interface presents problems which are not easily anticipated and only appreciated as the study progresses. The study of visual transduction, i.e. the process beginning with the absorption of a photon of light by a visual pigment molecule and terminating with a hyperpolarization of the rod and (or) cone cell, in vertebrate photoreceptors is such a process. Since the mid 1950's the photochemistry of the macromolecular visual pigment, rhodopsin, has been studied (1, 2) by the flash photolysis technique, and the details of the primary photochemical process and the subsequent rapid dark reactions are gradually emerging through the study of rapid absorption spectral changes. These rapid spectral changes which monitor molecular chromophoric and macromolecular changes in rhodopsin, however, give us no clue as to what is occurring at the cellular level. Electrophysiological studies can monitor the rapid electrical changes within the photoreceptor rod cell and show that the cell is rapidly "hyperpolarized" within milliseconds after the absorption of a photon by the visual pigment rhodopsin, but so far such studies have given only minor clues as to the sequence of processes that mediates light absorption and receptor potential generation. One looks for other cytological parameters such as size, shape, and electrical changes within the cell and its organelles, i.e. the pigment containing thylakoid disks, and the rod outer segment, to reveal the coupling details of the pigment molecule–cell interface.

For the study of the broad time range of intracellular changes, light-scattering techniques are coming into prominent use. In the present paper, by way of illustrating the potential of the method, we present an overview of the technique and a summary of the studies which our own laboratory has made to date using this technique to study "structural" changes in suspensions of vertebrate rod outer segments preceding and following their flash illumination with actinic light. One will note a formal resemblance of this technique of "light scattering photometry" to the conventional flash photolysis technique wherein rapid changes in absorption and (or) fluorescence spectra of molecules are studied.

Theory of light scattering

The light scattering properties of molecules and particles fall into three size domains: (*i*) Rayleigh scattering in which the molecule or particle is less than $\lambda/20$, where λ is the wavelength of the scattered light, (*ii*) Rayleigh–Gans–Debye scattering where the size of the particle is in the range $\lambda/20$ to $\lambda/2$, and (*iii*) Mie – van de Hulst scattering for particles with at least one dimension larger than $\lambda/2$. Einstein (3) and Debye (4) developed eq. [1] for application to particles of size less than $\lambda/20$ where I_θ is the intensity of light of wavelength scattered at angle θ and I_0 is the incident intensity of the unpolarized light. The parameters r, M, c, and N are, respectively, the distance between the scattering particle and the detector, the molecular weight of the particle, the concentration of particles, and Avagadro's number. The derivative $\mathrm{d}n/\mathrm{d}c$ is the differential increase in refractive index, n, with particle (solute) concentration. It is evident from eq. [1] that I_θ will depend on the size of the particle as measured by M, the concentration of the particles, c, and the refractive index, n (real part).

$$[1] \quad I_\theta = I_0 \frac{2\pi^2(\mathrm{d}n/\mathrm{d}c)^2 Mc(1+\cos^2\theta)}{N\lambda^4 r^4}$$

If the particle absorbs in addition to scattering radiation, this will have a pronounced effect on the scattering properties; the closer an absorption band is to the wavelength of the scattered light, the larger will be the refractive index n. Thus if a change in the light absorption of a particle occurs during a light scattering measurement there is a corresponding shift in the profile of the anomalous dispersion spectrum which markedly changes n and dn/dc. A hypsochromic (blue) shift in the absorption spectrum will produce a corresponding hypsochromic shift in the anomalous dispersion spectrum, resulting in a decrease in n and dn/dc at wavelengths bathochromic (red) to the absorption band.

Most solutions of macromolecules and small particles have at least one dimension which is larger than $\lambda/20$ and so fall in the Rayleigh–Gans region. This situation gives rise to the phenomenon of destructive interference of the scattered light arising from different regions of the particle. Complete destructive interference can set in when the particles approach $\lambda/2$ in size. The angular dependence $P(\theta)$ in this case is much more complex than the simple $(1 + \cos^2 \theta)$ of Rayleigh scattering and is given by eq. [2]:

$$[2] \quad P(\theta) = \frac{2}{W^2}(e^{-W} + W^{-1})$$

where $W = (4\pi/\lambda)(\sin^2 \theta/2) R_G$, where R_G is the radius of gyration of the particle, which varies markedly with shape. For example, in the case of a particle with a molecular weight of 5×10^5 g, R_G is calculated to be 45 Å for a sphere and 2500 Å for a rod 10 Å in diameter (5).

Hofmann *et al.* (6) have used the Rayleigh–Gans treatment to interpret their light scattering data from disk preparations. Our own studies of suspensions of rod outer segments (ROS) which, though not strictly homogeneous in size, are, for the most part, whole ROS with perforated membranes, fall in the Mie – van de Hulst scattering range (7, 8). For particle suspensions in this size range (length of rod $> \lambda/2$), I_0 is dependent on size, shape, and internal structure of the rod and becomes a complicated function of λ, θ, and $m = n_{\text{particle}}/n_{\text{medium}}$ (9).

Although the scattering and transmission of light by solutions or suspensions of biological particles are sensitive and convenient indicators of a variety of physiological processes, the complications described above have made it difficult to relate, theoretically, changes in light scattering intensity as a function of λ and θ to a particular physical or conformational change of (or within) the particle, e.g. a volume change (8). To identify the conformational change giving rise to any given change in the scattered light intensity therefore requires alternate experimental methods that clearly produce the same scattered light λ and θ intensity patterns.

Osmotically induced volume changes in rod-like bacteria have been made by Bateman (10). He has measured scattered light intensity changes I_0 at 90° but his results, when fitted to Mie theory, gave only partial agreement with van de Hulst's treatment, as the optical changes proved to be very sensitive to particle size and suspension concentration. The latter parameter is particularly important as "multiple particle" scattering can occur and the onset of this complicating situation is a function not only of particle concentration but also of the shape and volume of the containing vessel. Reliable, interpretable data require that "single particle" scattering conditions be maintained. A further complication arises if the particles are not "mono-dispersed", i.e. if they are not homogenous in size, shape, and internal structure. Thus meaningful light scattering measurements, from which interpretations of qualitative and quantitative structural changes in a particle can be made, depend on how carefully the conditions described above are met.

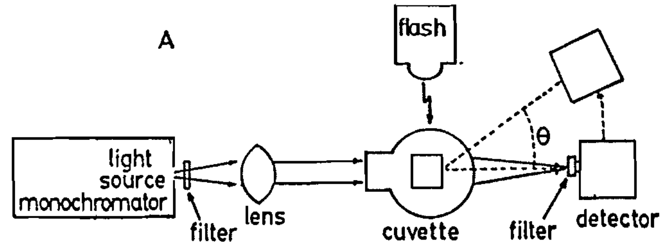

FIG. 1. Schematic representation of the light scattering apparatus.

Light scattering relaxation photometry

For the measurement of light scattering transients an apparatus similar to a conventional flash photolysis unit can be used. In fact, such a unit can be constructed so as to measure absorption and scattering changes simultaneously. Shown in Fig. 1 is a schematic of the unit we orginally used in our laboratory, which was designed to measure scattering changes only.

A commercial PRA xenon flash unit provided pulsed flashes of actinic light (450–550 nm) of controlled intensity and duration (50 μs). A tungsten lamp focused on the slit of a Bausch and Lomb monochromator (grating blased at 750 nm) served as a source of near infra-red radiation. The emergent parallel light was directed through a water (or occasionally air) thermostated cuvette containing an aqueous ROS suspension. The scattered light detector was an EG&G photodiode (UV 44B) mounted on an adjustable protractor which could be set at the desired angle.

A 1-cm square quartz cuvette with four transparent optically clear faces served as the light scattering cell. This was mounted in a spherical transparent water thermostat. An air thermostat, which used a Cambion model 801-2001-01 thermoelectric module for temperature regulation, was occasionally employed. The square cuvette limited the practical angular range of measurement from 0 to 30°. For larger angles a cylindrical cuvette was employed.

Measurements were routinely made at $\theta = 10°$ and at $\lambda = 810$ nm. Scattered light intensity voltage signals from the photodiode detector were passed through a preamplifier and compensated to zero voltage and then collected and displayed on a Nicolet Explorer III digital storage oscilloscope; the signals were stored on floppy disks for visual comparison or printing on an Omnigraph XY recorder.

Photoreceptor cell structure

There are two morphologically and functionally distinct regions in the vertebrate rod photoreceptor cell (Fig. 2): (*1*) the inner segment (RIS) containing organelles concerned with metabolic functions, such as the nucleus and the energy producing mitochondria, and (*2*) the outer segment (ROS), containing the visual pigment rhodopsin, which is connected to the RIS by a tubular ciliary process. The ROS consists of a stack of 500 to 2000 disks (depending on the species) enveloped by a plasma membrane (11). In bovine cells the ROS are quite small; they are 1 μm in diameter and up to 10 μm in length. The disks are flat saccules with a phospholipid bilayer membrane 60–70 Å thick enclosing an aqueous space (lumen) from 10 to 30 Å in depth (12). A cytoplasmic region of about 150 Å in thickness apparently containing a negatively charged gel-like polysaccharide matrix (13) separates the disks one from another. Recent electron microscopic evidence points to the existence of filamentary connections between adjacent disks[1] and there is

[1] M. L. Applebury, private communication.

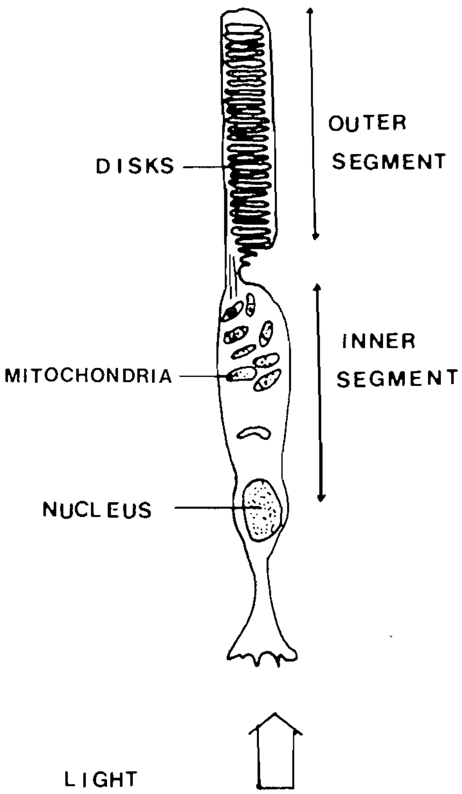

FIG. 2. Vertebrate rod outer segment (ROS), not drawn to scale. The arrow represents the direction of incident light.

the further suggestion that direct connections exist between the disk rims and the region exterior to the plasma membrane (14).

Rhodopsin and its photochemistry

Vertebrate rhodopsin is a hydrophobic glycoprotein with a molecular weight of about 39 000 daltons. Its amino acid sequence has recently been determined by two groups (15, 16). Hargrave (15) finds seven hydrophobic helical regions ranging from 21 to 28 amino acids which are oriented asymmetrically in serpentine transmembrane fashion in the disk membrane surface, the carboxyl terminal group at the cytoplasmic surface, and the amino terminus and carbohydrate moiety at the inner lumen surface. The retinylidene chromophore is attached to the ϵ-amino group of a lysine residue in the interior of the membrane on helix number 7. There are approximately 200 000 rhodopsin molecules in each bovine disk.

The 11-*cis* retinylidene chromophore is joined to the ϵ-amino group of lysine via a protonated Schiff base linkage (Fig. 3). Assuming the 7 helices are arranged in a cylindrical tertiary structure, the estimated diameter of the rhodopsin molecule is about 900 Å.

The absorption spectrum of rhodopsin (Fig. 3) has three characteristic regions: a principal long wavelength chromophoric band with a maximum in the vicinity of 500 nm, a weaker chromophoric (*cis*) band with a maximum near 350 nm, and a third apoprotein band whose maximum lies at 280 nm.

The absorption of a photon in the chromophoric regions of the spectrum of the rhodopsin molecule initiates a series of intermediate processes characterized by spectral changes occurring over several time ranges varying from picoseconds to minutes (Fig. 4). The times shown in Fig. 4 are the approximate transition times at 37°C. The initial very rapid primary

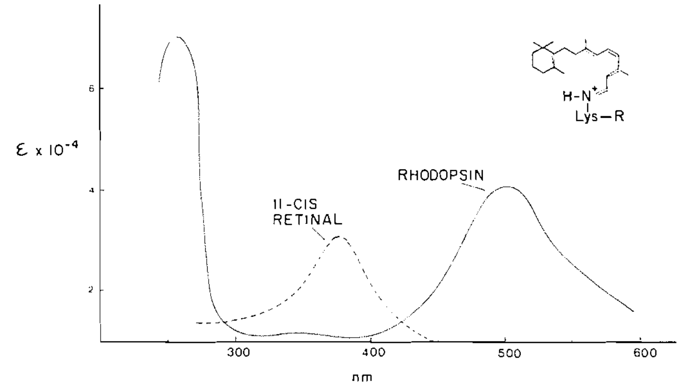

FIG. 3. The absorption spectrum of rhodopsin. The spectroscopy was carried out in 3% Ammonyx in 150 m*M* Pipes and 10 m*M* hydroxylamine.

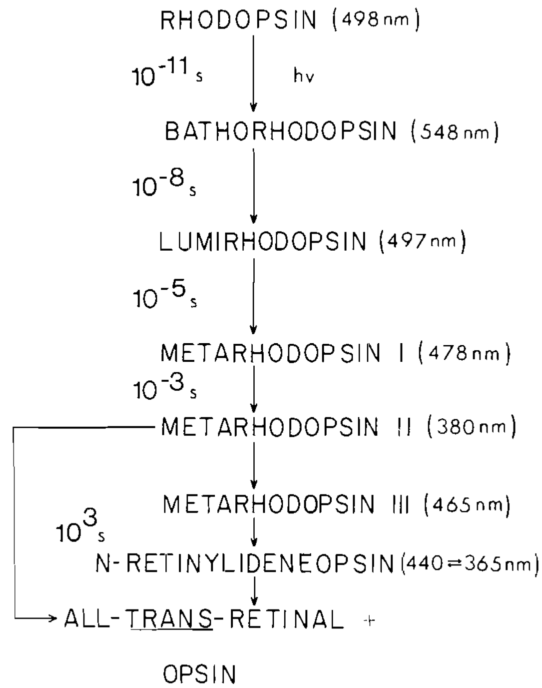

FIG. 4. The bleaching sequence of rhodopsin at 37°C.

photochemical process involves a partial photoisomerization of the chromophore to its all-*trans* isomeric form, possibly linked to a displacement of a hydrogen bond at the Schiff base nitrogen of the chromophore–protein linkage. Since visual transduction occurs in times of the order of 10 milliseconds, the latest process in the sequence shown in Fig. 4 that can be involved directly in this process is the metarhodopsin I → metarhodopsin II process. Significantly, this process is the first in the sequence that involves reaction with the environment, i.e. hydrogen ion uptake, and for this reason it is the process most likely to couple molecular with cellular domains.

The bulk of our studies have been performed on Bovine (heifer) rod outer segments (ROS). The eyes were excised within a few minutes of the animal's death and stored on ice in the dark. The retina were harvested and the ROS were prepared by a sucrose density gradient technique (17). Following this the ROS suspensions were passed through a syringe needle packed with glass wool. This operation served to perforate the plasma membrane as indicated by electron micrographs. The prepara-

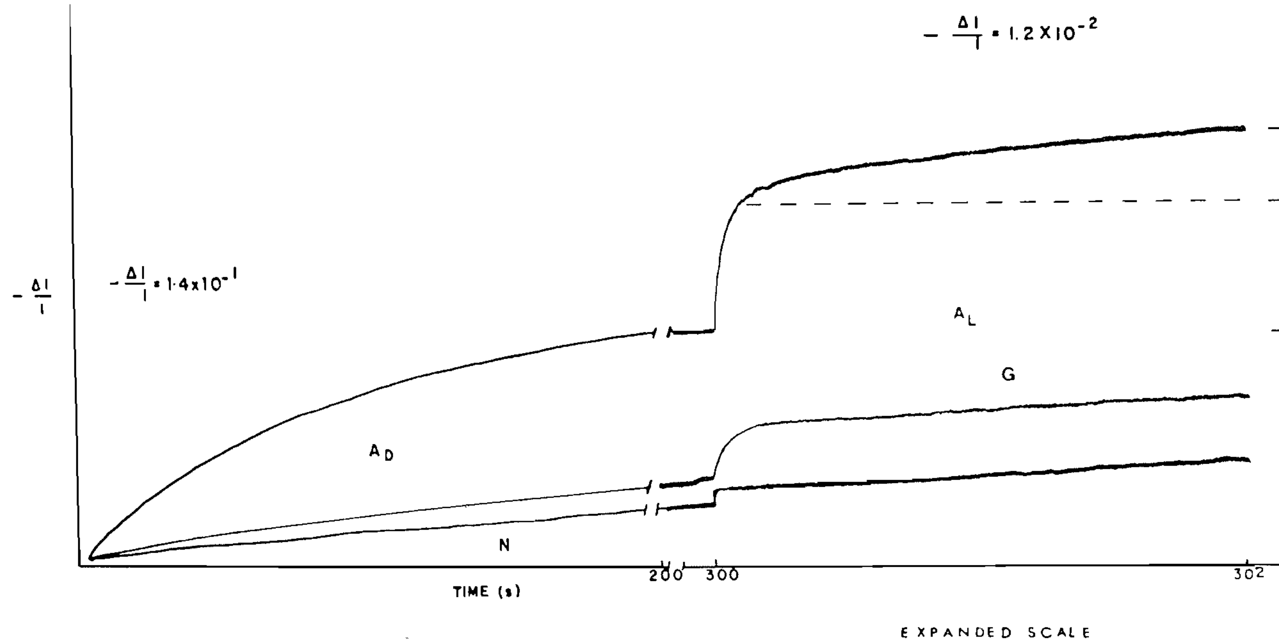

FIG. 5. The A, G, and N signals as observed from our scattering apparatus. Note the expanded scale at the point of actinic illumination.

tions were stored in plastic vials under liquid nitrogen until ready for use. This treatment had only a minimal effect on the scattering properties after several months of storage as compared to fresh preparations.

To ensure that measurements would be made in the single particle scattering range, the density of the ROS suspension was maintained at less than 2 μM rhodopsin. For the bulk of the studies flash intensities were such that less than 25% of the rhodopsin molecules were photobleached by a single flash.

A number of distinct types of light scattering signals were observed in ROS suspensions under a variety of conditions. The ones investigated in our laboratory are described below.

The N signal

The N signal (Fig. 5) describes the behavior of the relative scattered light intensity ($-\Delta I/I$) at a given λ and θ as a function of time. It is a simple "step" function in which a sudden increase in ($-\Delta I/I$) occurs contemporal with the light flash. It can be described as a summation of two processes: (*1*) internal, structural and electrical changes accompanying the metarhodopsin I $\rightarrow$ metarhodopsin II (MI/MII) process and (*2*) a hypsochromic shift of the anomalous dispersion spectral profile following the partial photobleaching of rhodopsin. These effects produce substantial changes in the refractive index n and dn/dc, which result in marked light scattering changes in the Mie scattering region.

The A signal

The A signal (Fig. 5) arises when Mg-ATP is added to a buffered suspension of ROS. It is unique in that it shows both a dark-A_D, and a light-stimulated component, A_L (18).

The dark A_D signal is produced when varying amounts of Mg-ATP are added to an ROS suspension buffered at pH = 7.3 with Tris-HCl. One observes a relative decrease in scattered light intensity ($-\Delta I/I$) which reaches near saturation at room temperature in approximately 10 min. This decrease, plotted as an increase in $-\Delta I/I$, accompanies an increase in inorganic phosphate (19), suggesting that ATP has been hydrolyzed via a Mg-ATPase contained in the disk membranes (18, 20). The fact that the A signal is insensitive to ouabain, and succinate dehydrogenase activity is negligible, indicates that the ATPase cannot be a Na^+/K^+ dependent arising from inner segment or mitochondrial contamination.

Summarizing our studies, we have found that the dark A_D light scattering signal has the following properties (17–20). (*i*) It is substantially inhibited by the non-hydrolyzable ATP analogue AMP-PNP at concentrations comparable to ATP. Furthermore, GMP-PNP has no effect on A_D. This suggests that the A_D signal arises from a process mediated by a disk membrane bound ATPase. Furthermore, the ATPase appears to have multi-subunits as indicated by the sigmoid character of a plot of the maximum $\Delta I/I$ amplitude versus ATP concentration.

(*ii*) Calcium and vanadate ions at concentrations 1/10 that of Mg^{2+} exhibited substantial inhibitory effects on the A_D.

(*iii*) The nucleotide cGMP when present at 1/10th the concentration of ATP shows a substantial enhancement of A_D.

(*iv*) The A_D signal is independent of the presence of "G" protein which has been identified as a disk associated GTPase; a low ionic strength extraction which removes "G" protein from the disks (4 mM Tris at 4°C) has no effect on A_D.

(*v*)The kinetics of A_D is essentially first order in the presence of excess Mg-ATP. Its activation energy, E_a, is estimated at 24 kcal/mol in the temperature range 15–37°C.

(*vi*) Comparison of the θ dependency of the A_D signal with that obtained from the controlled osmotic swelling of ROS suspension showed near identity of these patterns. It appears, therefore, that the A_D signal arises from the swelling of the disk matrix of the ROS.

(*vii*) The A_D signal is sensitive to the ROS particle concentration. In our apparatus, the single particle scattering range was between 0 and 2 μM rhodopsin. Most of our experiments were performed at concentrations of rhodopsin of 1 μM or less. There is essentially a linear increase in ($-\Delta I/I$) with rhodopsin concentration at constant flash intensity and at 10 $\pm$ 1° of scattering angle. Measurements performed on ROS suspensions having rhodopsin concentration greater than 2 μM showed erratic behavior; there was an actual decrease in the amplitude $-\Delta I/I$ versus particle concentration. The angular resolution is very important, particularly in the range 0–10°, as the variation of $-\Delta I/I$ versus θ varies sharply and shows biphasic behavior in this angular range.

The light stimulated A_L signal

If, after allowing the development of the dark A_D signal over a period of several minutes, the ROS suspension is flash illuminated with actinic light (500–550 nm) there is an instantaneous increase in the amplitude of $(-\Delta I/I)$ similiar to that occurring in the N signal, save that it is much larger in amplitude. The initial portion (50 ms) is termed A_{LF}. A_{LF} is followed by a much slower increase in amplitude over a period of several seconds. This slower portion of the signal is designated as A_{LS}.

Kinetically, the A_{LS} process, like A_D is first order but with a much faster rate than A_D which increases with the extent of photobleaching. At very low levels of photolysis the rate of A_{LS} approaches that of A_D.

A_{LS} in all its properties studied so far, save rate, duplicates those of A_D (17). λ and θ dependencies of A_L are the same as A_D. The rate of inorganic phosphate appearance is enhanced over that of A_D in the initial period following flash illumination consistent with the increased rate of A_{LS} over A_D (19). As in the case of A_D, A_{LS} is inhibited by calcium ions and enhanced by cGMP (17–20). Also similiar to A_D is the variation in scattering signal time profile of A_{LS} at particle densities greater than the single particle range.

The fast component of the A_L signal, A_{LF}, has much the same characteristics as that of the N signal with regard to λ and θ dependencies, suggesting that the structural and the electrical changes in the ROS were essentially those occurring as a direct consequence of the photolysis of rhodopsin to metarhodopsin II. The properties of A_D and A_{LS} can be logically interpreted as a "swelling" of the ROS disks in consequence of the ATPase mediated pumping of ions into the disk lumen. Our studies of the ions being pumped are described below.

Ion pumping accompanying the A signal

Cation pumping

In the dark, the disk membranes in the absence of nucleotides are impermeable to most anions (21). However, as a consequence of the ATPase activity one might expect cation pumping to accompany the A signal. In order to ascertain whether such cation pumping did in fact occur, the effects of various ionophores on the A_D and A_L signals were investigated. Proton ionophores were unique in their behavior; the powerful mitochondrial ATPase uncoupler, SF6847, at a concentration of 9 μM completely abolished the A_{LS} signal and substantially reduced A_D (17). Tributyl tin, an ionophore which exchanges OH^- and Cl^- across membranes, gave A signals identical to N signals when present at a concentration of 9 μM (17). Ionophores specific for cations other than protons did not show this behavior.

The most direct confirmation of proton pumping activity associated with the ATPase-induced A signal, A_D and A_{LS}, is shown by the following experiment. When the ROS suspension, after incubation with Mg-ATP for several minutes, was sonicated to rupture the disks, protons were released into the aqueous media as indicated by a decrease in pH. No such decrease in pH was observed on sonicating a control sample in which no Mg-ATP was added. Therefore, pumping of protons into the disk lumen appears to be the primary activity of the ATPase-driven A signal.

Anionic symport

Anion symport generally accompanies ATPase cation pumping to maintain electrical neutrality. Usually the symported

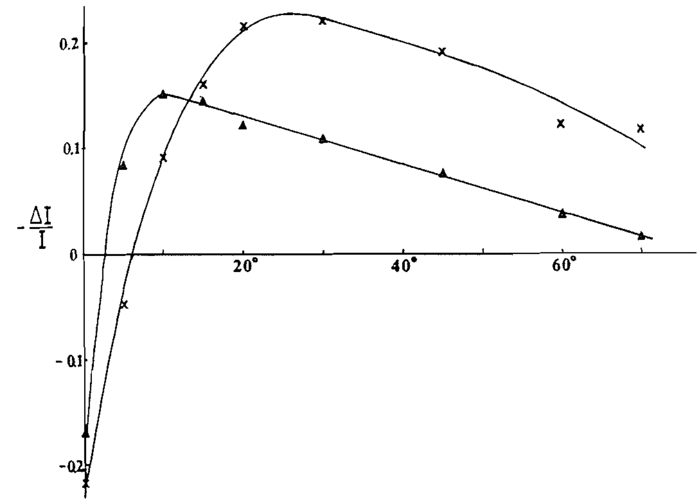

FIG. 6. Comparison of A_D and A_L versus the scattering angle. The (X) represents the A_L, and the (▲) represents the A_D.

anion is an impermeable one which requires a protein carrier closely coupled to the cation ATPase pump. A known blocking agent for such anion carriers is diisothiocyanostilbene sulfonic acid (DIDS). We found that DIDS substantially reduced the amplitude of the A signal. In the case of normally permeant anions such as SCN^-, no protein carrier is required and we observed that when this anion, SCN, was present, the rates of both A_D and A_{LS} were enhanced relative to their rates when Cl^- was present alone. Of the normally impermeant anions, Cl^- appears to be the most effective. Bicarbonate anion, although it can replace Cl^-, yields an A signal whose amplitude is considerably reduced over the Cl^-, suggesting a buffering action of bicarbonate ion within the disk lumen that alters the MI/MII ratio in favour of MI.

A physiological basis for the A signal

The A signal can also be observed in ROS preparations where the plasma membrane is intact. In such cases no exogenous Mg-ATP is needed to produce either A_D or A_L. Apparently, what happens in such cases is that endogenous Mg-ATP is present in the ROS and begins to act as soon as the frozen ROS preparation is brought to room temperature by the addition of the Tris buffer solution. Significantly, the A_D and A_L signals seen under these conditions are comparable to those observed in the presence of Cl^- ions rather than bicarbonate ions. These observations point to the A signal as having a physiological basis and that the active anion in the rods in this case is the Cl^-.

A molecular basis for the A signal

It is clear from Fig. 6 that both A_D and A_L can be interpreted as disk swelling processes. Furthermore, their first-order kinetics and the dependence of the rate constants on the concentration of ATP, together with the proton ionophore experiments, point to the principal molecular process involved as an ATPase mediated pumping of protons into the disk lumen. This suggests that the physiological role of the A_D and A_L signals is to insure protonation of rhodopsin in preparation for the metarhodopsin I $\rightarrow$ metarhodopsin II process, i.e. to maintain a high ratio of MII/MI according to eq. [3].

$$[3] \quad MI + H^+ \rightleftarrows MII$$

It is not possible from the kinetic studies made so far to determine the nature of the "saturation" of A_D or A_L; simple reversal of the pumping process and (or) mechanical limitations on the swelling could account for saturation.

We have mentioned that the A_L signal probably involves two processes: the hypsochromic shift in the anomalous dispersion spectrum and what can be interpreted as a rapid (20 ms) "shrinkage" of the disks. This shrinkage may possibly be accounted for by the rapid expulsion of cations from the disk lumen. The aforementioned proton ionophore experiments suggest that protons may be rapidly ejected from the lumen. But atomic absorption and specific ion electrode studies made in our laboratory indicate that Na and Ca ions are also ejected by light after dark incubation in the presence of ATP, suggesting that ATPases other than the proton ATPase are present in the disk (22). At the present time we have no data on the time course of the appearance of any of these cations.

The G signal

If one replaces exogenous Mg-ATP in a suspension of ROS with GTP along with a divalent cation (Mg^{2+}, Ca^{2+}, Mn^{2+}) one observes on flash illumination a scattering signal ($-\Delta I/I$) which increases with time, approaching near saturation in about 30 sec. This is termed the G signal. Unlike the A signal, there is no dark signal associated with the G signal comparable to A_D. Furthermore, the G signal is studied at levels of rhodopsin bleaching less than 10%, compared to levels approaching 25% usually used in the case of the A signal. There is no pronounced initial sharp amplitude increase in the G signal comparable to the N signal associated with A. Kuhn *et al.* (23) have studied the G signal under conditions of high multiple scattering concentrations and very low total levels of rhodopsin photobleaching (0.08%). At such high particle densities, the photobleaching will be highly inhomogenous and the scattering, as well as the photobleaching, should be limited to the outer layers of the suspension. Their scattering profiles are very much different than our G signals taken under conditions of single particle scattering (19).

In addition to those differences mentioned above, the G signal differs from the A signal in the following respects.

(*i*) The G signal is inhibited by the non-hydrolyzable analogue GMP-PNP but not by AMP-PNP. This is in contrast to the A signal, which is inhibited by AMP-PNP but not GMP-PNP. The two signals, A and G, therefore appear to be completely independent, the A signal arising from an ATPase activity and the G signal arising from a GTPase activity.

(*ii*) The G signal requires the presence of a multi-subunit "G protein" associated with a GTPase as shown by Kuhn *et al.* (23). The A signal, on the other hand, as mentioned previously is independent of the presence of the "G protein".

(*iii*) The G signal does not show Ca^{2+} ion inhibition as does the A signal.

(*iv*) cGMP, when present in concentrations less than that of the GTP, inhibits the G signal. The A signal is enhanced by the presence of cGMP in comparable concentration ratios.

(*v*) The G signal increases in amplitude with the extent of photobleaching, reaching saturation at about 10% photobleaching. The A signal does not show this saturation in amplitude.

A molecular basis for the G signal

The experimental evidence gathered in our laboratory indicates that the G signal is very complex; it cannot be interpreted in terms of simple molecular processes as is the case for the A signal. Differences in kinetic reaction order as well as thermal and pH dependency are observed in different temporal regions of the overall signal. In addition, changes in θ and λ dependencies which suggest different structural changes appear in different regions of the overall signal. GTP hydrolysis does not occur until the latter stage of the process, as is indicated by the inhibition of this portion by GMP-PNP. At the present time we offer a provisional molecular mechanism underlying this complex molecular–cellular process (Fig. 7) based on our own studies, which is similar although not identical to that presented by others (23).

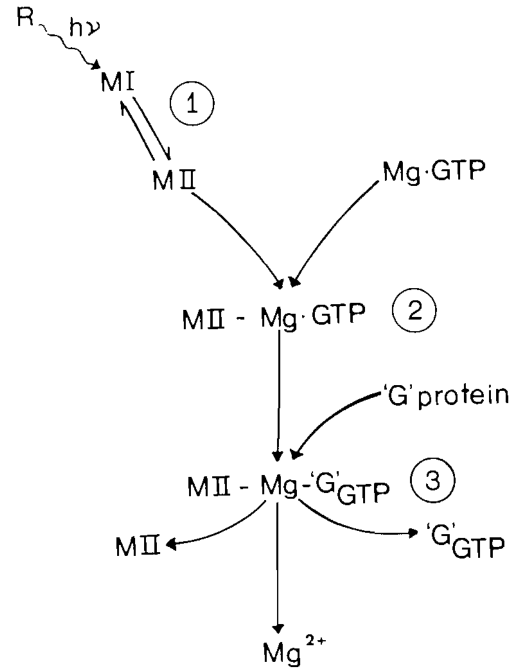

FIG. 7. A simple molecular mechanism for the G signal.

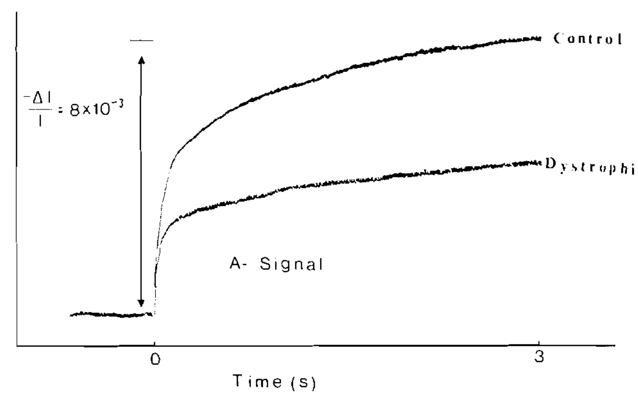

FIG. 8. A comparison of the A signals in control and dystrophic Royal College of Surgeons (RCS) rats.

The A and G signals in rat rod outer segments

The A and G scattering signals reflect complex physiological processes within the disk matrix in vertebrate ROS. They therefore serve to monitor key facets of the vertebrate visual photoreception process. With this thought in mind, we have been exploring the use of these signals in characterizing retinal dystrophies in laboratory animals. Our studies so far have focused on a colony of RCS (Royal College of Surgeons) rats which

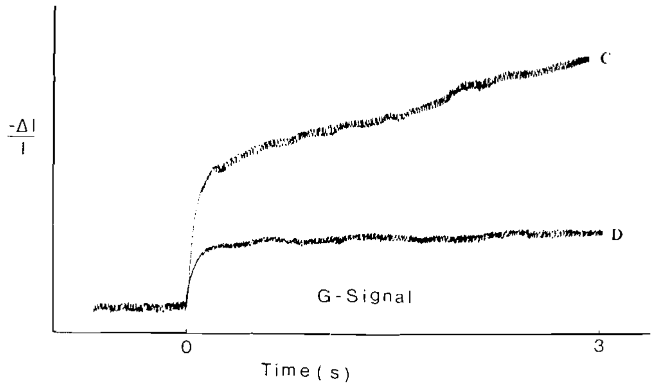

FIG. 9. A comparison of the G signals in control (C) and dystrophic (D) Royal College of Surgeons (RCS) rats.

have retinal dystrophy, mimicking in some respects the human disease retinitis pigmentosa. In our studies so far, we have found that A and G signals can be elicited from ROS preparations of both normal and dystrophic rats. In the dystrophic rat ROS, however, the progression of the disease is accompanied by the decrease in the amplitude of the A signal and the complete disappearance of the G signal (Figs. 8, 9). These processes are currently being studied in more detail (24).

Acknowledgements

This work was supported by an NSERC Grant to E. W. Abrahamson. The aid of Jenny Harold in the preparation of the manuscript is gratefully acknowledged.

1. K. P. HOFMANN, R. UHL, W. HOFFMANN, and W. KREUTZ. Biophys. Struct. Mech. **2**, 61 (1976).
2. R. UHL, K. P. HOFMANN, and W. KREUTZ. Biochemistry, **17**, 5347 (1978).
3. A. EINSTEIN. Ann. Phys. **25**, 205 (1908).
4. P. DEBYE. J. Appl. Phys. **15**, 338 (1944).
5. C. TANFORD. Physical chemistry of macromolecules. John Wiley and Sons, New York, London. 1963.
6. K. P. HOFMANN, A. SCHLEICHER, D. EMEIS, and J. REICHERT. Biophys. Struct. Mech. **8**, 67 (1981).
7. G. MIE. Ann. Phys. **25**, 377 (1908).
8. H. C. VAN DE HULST. Light scattering by small molecules. John Wiley and Sons, New York, London. 1957.
9. P. LATIMER, D. MOORE, and F. BRYANT. J. Theor. Biol. **21**, 348 (1968).
10. J. BATEMAN. J. Colloid Interface Sci. **27**, 458 (1968).
11. R. UHL and E. W. ABRAHAMSON. Chem. Rev. **81**, 291 (1981).
12. C. R. WORTHINGTON. Ann. Rev. Biophys. Bioeng. **3**, 53 (1974).
13. D. CORLISS. Ph.D. Thesis, University of Albama at Birmingham (1979).
14. P. SCHNETKAMP. Biochim. Biophys. Acta, **598**, 66 (1980).
15. P. A. HARGRAVE, J. H. MCDOWELL, D. R. CURTIS, J. WANG, E. JUSZCZAK, S. L. FONG, J. K. MOHANNA-RAV, and P. ARGOS. Biophys. Struct. Mech. **9**, 235 (1983).
16. Y. A. OVCHINNIKOV, N. G. ABDULAEV, M. Y. FEIGINA, I. D. ARTAMOV, A. S. ZOLATAREV, A. S. BOGACHUK, A. I. MIROSHNIKOV, V. I. MARTINOV, and A. B. KUDELIN. Bioorg. Khim. **8**, 1011 (1982).
17. T. J. BORYS. Ph.D. Thesis, University of Guelph (1981).
18. R. UHL, T. J. BORYS, and E. W. ABRAHAMSON. Photochem. Photobiol. **29**, 703 (1979).
19. T. J. BORYS, R. UHL, and E. W. ABRAHAMSON. Nature, **304**, 733 (1983).
20. R. UHL, T. J. BORYS, and E. W. ABRAHAMSON. FEBS Lett. **107**, 317 (1979).
21. R. UHL, P. KURAS, K. ANDERSON, and E. W. ABRAHAMSON. Biochim. Biophys. Acta, **601**, 462 (1980).
22. S. DESHPANDE, T. BORYS, and E. W. ABRAHAMSON. ARVO Abstr. 538 (1985).
23. H. KUHN, N. BENNETT, M. MICHEL-VILLAZ, and M. CHABRE. Proc. Natl. Acad. Sci. U.S.A. **78**, 6873 (1981).
24. T. BORYS, J. PARKER, S. DESHPANDE, and E. W. ABRAHAMSON. ARVO Abstr. 59 (1984).

Study of the reorientational motions of NH_3 groups in crystalline sulphamic acid by quasi-elastic neutron scattering and heat capacity measurements

J. F. BOCQUET,[1] K. CHHOR,[1] AND G. LUCAZEAU
Université Paris-Nord, Laboratoire de Chimie Physique du Solide, Avenue J. B. Clément 93430 Villetaneuse, France
AND
A. J. DIANOUX
Institut Laue-Langevin, 156X, 38042 Grenoble Cedex, France

Received July 24, 1984

This paper is dedicated to Professor Camille Sandorfy on the occasion of his 65th birthday

J. F. BOCQUET, K. CHHOR, G. LUCAZEAU, and A. J. DIANOUX. Can. J. Chem. **63**, 1940 (1985).

Incoherent quasi-elastic neutron scattering experiments between 250–400 K and heat capacity measurements between 10–310 K have been performed on polycrystalline samples of NH_3SO_3. It is concluded that NH_3 groups undergo jumps of $2\pi/3$ and that the associated residence time is of 2×10^{-11} s at 300 K, while the activation energy is equal to 12 kJ mol^{-1}. These results are compared with those in the literature, in particular, we point out that the frequency derived from the Arrhenius relation is in fair agreement with the torsional frequency measured in Raman spectroscopy (247 cm^{-1}) while the activation energy is similar to that found by nmr. Finally the relative magnitude of potential barriers deriving from intra- and intermolecular interactions is estimated from potential calculation based on atom–atom potentials, the dominant terms are due to hydrogen bondings.

J. F. BOCQUET, K. CHHOR, G. LUCAZEAU et A. J. DIANOUX. Can. J. Chem. **63**, 1940 (1985).

Un échantillon polycristallin d'acide sulphamique, NH_3SO_3, a été étudié entre 250 et 450 K par diffusion quasi-élastique de neutrons. La courbe de capacité calorifique entre 10 et 310 K a également été obtenue. Les paramètres déterminant la dynamique des groupements NH_3 ont été déterminés: les protons effectuent des sauts de $2\pi/3$ avec des temps de résidence de 2×10^{-11} s à 300 K; l'énergie d'activation correspondante est égale à 12 kJ mol^{-1}. Ces résultats sont comparés avec ceux de la littérature; la fréquence d'attaque déduite de la relation d'Arrhénius est en bon accord avec la fréquence de torsion mesurée en Raman (247 cm^{-1}). L'énergie d'activation est très proche de celle trouvée en rmn. La barrière de potentiel s'opposant à la rotation des NH_3 a également été calculée à partir de potentiels atome–atome; les termes dominants sont dûs aux liaisons hydrogène.

I. Introduction

This work is a part of a general study about reorientational processes which take place in inorganic molecular crystals. We have systematically shown how the combination of neutron and Raman scattering and of heat capacity measurements can pinpoint the mechanism of reorientational motions which take place in molecular crystals such as metallocenes (1–3), arene metal carbonyls (4–8) or $NH_3(CH_2)_3NH_3MnCl_4$ (9,10) and to what extent they are responsible for phase transitions. The temperature dependence of the quasi-elastic neutron scattering function allows the determination of the activation energy which can generally be identified with the potential barrier hindering the reorientational motion, while the geometry of the motion can be derived from the Q dependence of the scattering function; for these reasons and because of the various resolutions available at ILL (Grenoble) the incoherent quasi-elastic neutron scattering (IQENS) can be considered the soundest technique of determining the parameters which characterize the hydrogen motions in a solid, specifically when several reorientational motions take place.

In this article, we shall first present and interpret our neutron results. We shall then discuss and compare our results with those of the literature: Raman (11, 12), nmr (13), particularly in terms of potential barriers originating from intra- and intermolecular interactions. Finally, we shall present some results of potential barrier calculations performed with the WMIN Busing's program (14) by using coulombian, Van der Waals, and hydrogen bonding atom–atom potentials.[2] A forthcoming paper, devoted to the discussion of the factors responsible for the Raman band broadening (reorientational motion, vibrational dephasing, anharmonicity) of the NH_3 torsion in sulphamic acid will be based on the conclusions of the present paper and on the neutron diffraction results recently recorded for ten temperatures between 4 and 300 K (15).

II. Experimental conditions

Sample

Sulphamic acid NH_3SO_3 was commercially obtained. The sample was purified by repeated recrystallizations from water–methanol mixture and dried in high vacuum. For heat capacity experiments, 13.99 g of the sample was used and loaded in the calorimetric vessel in which air was replaced with a few kPa of helium gas at 300 K. For IQENS experiments, powder samples were contained in circular thin-walled aluminum cans (5 cm in diameter). The thickness of the sample was adjusted to ensure a transmission of about 90%. Samples were examined by infrared analysis before and after experiments in order to check that no decomposition process had taken place.

Neutron scattering

Neutron experiments were performed at the Institut Laue-Langevin (I.L.L. Grenoble) with the time of flight (TOF) IN6 instrument. The angle between the sample plane and the incident neutron beam was taken equal to 135° for incident wavelength λ_0 = 5.1 Å and equal to 45° for λ_0 = 5.9 Å.

Ten temperatures ranging from 250 to 443 K were investigated. We used a heating and cooling loop device which operates between 77 and 700 K. However, due to a bad thermal contact between the sample holder and the loop, some of our measured temperatures may be in error by as much as 10 K. The average resolution for λ = 5.1 and 5.9 Å are 109 and 53 μeV, respectively, while the Q range investigated at 5.1 Å is between 0.25 and 2.21 Å^{-1}.

Angles that were contaminated by Bragg reflections were eliminated from the data. The spectra were corrected by standard ILL

[1]Unité Associée au C.N.R.S. N° 453.
[2]The computer program WMIN is capable of manipulating static and dynamic models of crystal or isolated molecules and calculating their energies from interatomic potential functions.

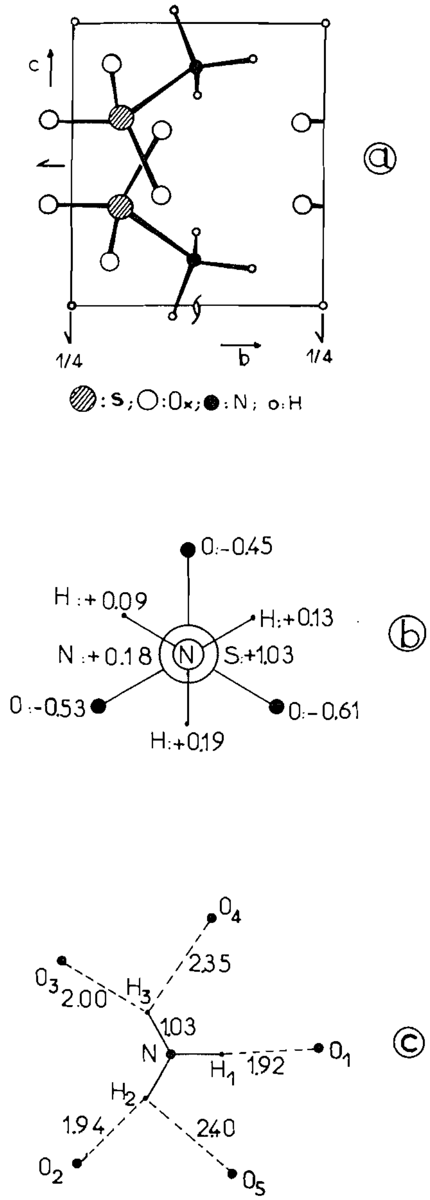

FIG. 1. Structural data on sulphamic acid: (*a*), projection of the crystal structure on (100) plane, 1/4 of the unit cell is represented; (*b*), view along N—S axis of an NH_3SO_3 molecule. Net atomic charges from ref. 18 are given in parentheses; (*c*), view along N—S axis of the nearest neighbouring atoms of an NH_3 group. The interatomic distances from refs. 18 and 13 are given in parentheses.

programs for detector efficiency, sample container efficiency, scattering absorption and self-shielding. All the TOF spectra were normalized to the elastic scattering from vanadium.

Calorimetric procedure

Heat capacity measurements were performed on an automatic adiabatic calorimeter from 10 to 310 K. Thermodynamic functions and C_p values will be reported in a separate paper.

The calorimeter and computer-operated adiabatic assembly is described elsewhere (16). Temperatures were determined by a germanium or a platinum thermometer in the ranges 10−30 K and 30−310 K, respectively.

The thermal analysis between 300−450 K was performed on a differential scanning calorimeter (M.C.B. Arion Grenoble, France) the heating and cooling rates were 0.5 K $\min^{-1}$ and the sample used was about 400 mg.

III. Structural data

The crystal structure is described by the *Pbca* space group with eight molecules per unit cell (Fig. 1*a*). The atomic positions have been reported at 300 K and 78 K from X-ray (17) and neutron (18) diffraction measurements. The intra- and intermolecular bond distances are reported on Fig. 1*b* and 1*c*, respectively. The three H atoms of a given NH_3 group are involved in three short NH---O hydrogen bonds and two long NH---O bonds. The atomic positions of ref. 18 were used in our potential calculations. The electron density has been determined from X—N maps (18). The S—N and S—O bonds have been found to be similar to bonds between first row atoms. The S—O double bond character has been deduced from its shortening (1.44 Å) with respect to the S—O single bond (1.69 Å). The net atomic charges reported in ref. 18 are given in Fig. 1*b*.

IV. Heat capacity results

Neither the heat capacity curve (Fig. 2) (10−310 K) nor the DTA curve (300−450 K) exhibit any anomaly which could indicate the presence of static disorder. In other words, the protons do not occupy distinguishable sites which could create an entropy increment: $\Delta S = R \ln N$ observable on the C_p curve. Thus, we can ignore the presence of subminima (for instance at $2\pi/6$) and safely assume that the approximate local threefold symmetry of a molecule as found by neutron diffraction (18) at 78 K is preserved at higher temperature. In this case we must consider that the potential function governing the NH_3 motion around the N—S bond has three deep minima which are essentially occupied between 10 and 310 K and that no drastic potential modification occurs in this temperature range.

V. Neutron scattering

V.1. Theoretical background

The neutron incoherent scattering law for a random motion of a uniaxial rotator in an *N*-fold cosine potential has been derived by Dianoux and Volino (19). They have shown that when the relative barrier height

$$\gamma = \frac{1}{2}\frac{V_0}{kT}$$

is large (in practice > 1.2) the scattering function $S(Q,\omega)$ can be written as in the case of instantaneous jumps between definite sites (20). In the present case, the experiments have been performed at about 300 K and we expect that the potential barrier is larger or equal to 12 kJ mol^{-1}, thus γ is larger or equal to 2.5 and the above condition is fulfilled.

The scattering law $S(Q,\omega)$ is obtained from the time Fourier transform of the intermediate scattering function $I_s(Q,t)$, for one mobile particule:

$$[1] \quad I_s(Q,t) = b_{\mathrm{inc}}^2 \iint g(\boldsymbol{r}_0)\, \mathrm{d}\boldsymbol{r}_0\, e^{iQ(r-r_0)}\, G_S(\boldsymbol{r}, \boldsymbol{r}_0, t)\, \mathrm{d}\boldsymbol{r}$$

in which $G_S(\boldsymbol{r}, \boldsymbol{r}_0, t)$ is the probability function to find the particle at $\boldsymbol{r}$ at time t if it was at $\boldsymbol{r}_0$ at time zero, with the probability distribution $g(\boldsymbol{r}_0)$ of initial position $\boldsymbol{r}_0$ as a weighting factor. In the rotational jump model the integral over initial positions ($\mathrm{d}\boldsymbol{r}_0$) is replaced by a summation over the three positions that a given proton can occupy; the integral over instantaneous positions is replaced by a summation over equilibrium positions of the proton. The G_S function writes $\sum_j \delta(\boldsymbol{r} - \boldsymbol{r}_{ij})P_j(t)$ in which $P_j(t)$ measures the time dependent

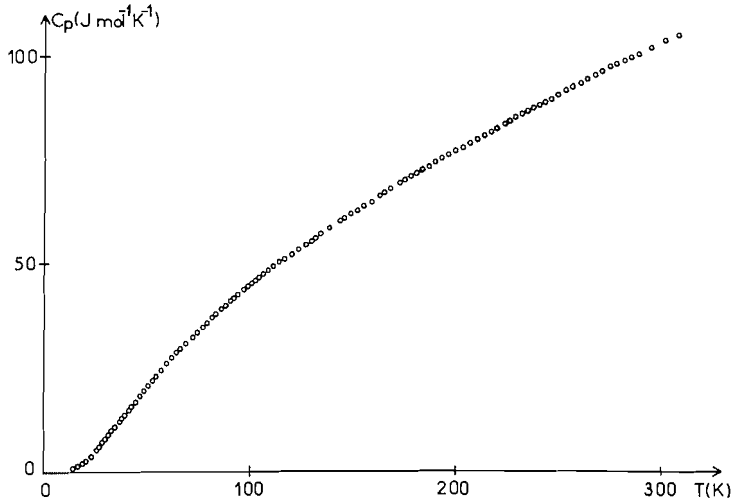

FIG. 2. Heat capacity curve of crystalline sulphamic acid.

probability of finding the proton at the site r_j if it was at r_i at $t = 0$, the jump distance r_{ij} being equal to $r_j - r_i$. Moreover, for NH_3SO_3 the three sites have an equal population and the jump rate from i to j is equal to that from j to i. Under these conditions, for an uniaxial rotation on a circle of radius R, and for a sample in a powdered form, the rotational scattering law takes the form:

$$[2] \quad s_{\text{inc}}^{\text{rot}}(Q,\omega) = A_0(Q)\delta(\omega) + \frac{1}{\pi}\sum_{l=1}^{N-1} A_l(Q)\, L\,(\tau_l^{-1})$$

where

$$[3] \quad A_l\,(Q) = \frac{1}{N}\sum_{j=1}^{N} j_0\,(2\,QR\,\sin\,(\pi j/N))\,\cos\,(2\pi lj/N)$$

l refers to the different jumps, j refers to the N-allowed sites. j_0 is the spherical Bessel function of the first kind of order zero ($j_0\,(x) = \sin x/x$) and $L(\tau_l^{-1})$ is the Lorentzian function,

$$[4] \quad L(\tau_l^{-1}) = \tau_l/(1 + \omega^2\tau_l^2)$$

in which τ_l^{-1} is the half-width at half-maximum (hwhm) and the characteristic times are given by

$$[5] \quad \tau_l = \tau_c/2\,\sin^2\,(\pi l/N)$$

where τ_c is the correlation time (residence time) between two successive jumps of a proton. It has been shown that the first broadened term in the summation over all the possible jumps gives the largest contribution and, therefore, the experimental hwhm of the quasi-elastic peak may be sometimes approximated by $1/\tau_1$; moreover in the limit $N \rightarrow \infty$, the jump probability $1/\tau_1$ can be identified with the rotational diffusion coefficient D_r. The term $A_0\,(Q)$ in eq. [2] represents the elastic incoherent structure factor (EISF): it is the fraction of the intensity due to mobile protons, that is contained in the purely elastic peak. The EISF is directly related to the geometry of the molecular motion. It is thus useful to measure the EISF as a function of Q and compare it with the calculated one for different models. In the present case a jump angle of $2\pi/3$ is the most probable for uniaxial rotational motion and we have considered that in the average each proton describes a circle of radius $R \simeq 0.97$ Å around the SN axis.

The quasi-elastic peak intensity increases with the $Q \cdot R$ product. Figure 3 shows this enhancement while conversely one observes the decrease of the pure elastic peak.

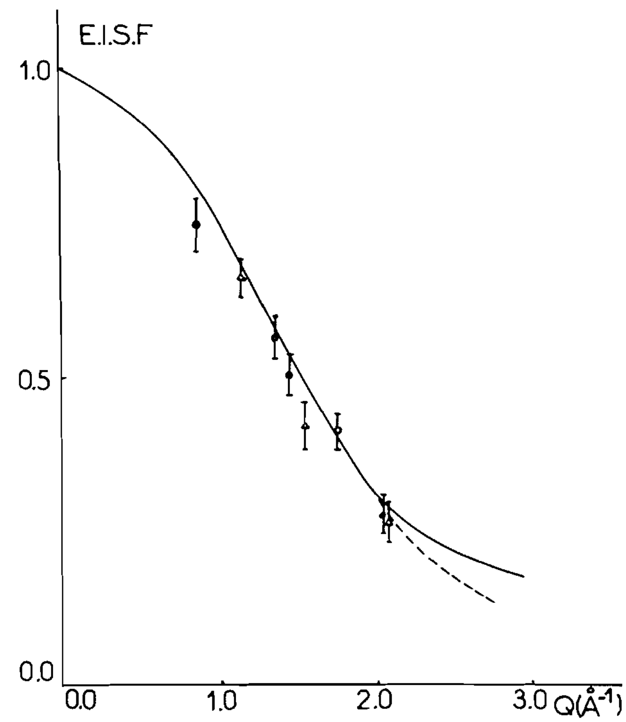

FIG. 3. Elastic incoherent structure factor: solid line, theoretical curve for the $2\pi/3$ jump model; dotted line, theoretical curve for the $2\pi/6$ jump model. Some experimental points ($I_{\text{elastic}}/I_{\text{total}}$) are reported: ●, 400 K, 5.1 Å; △, 333 K, 5.1 Å; ○, 403 K, 5.9 Å.

V.2. Results

Figures 4, 5 and 6 show some typical corrected spectra of NH_3SO_3 obtained on the time of flight IN6 spectrometer. The Q dependence of the relative fraction of elastic to the total elastic + quasi-elastic intensity (EISF) is represented and compared to the theoretical curves in Fig. 3. Figure 7 shows the variation of the mean residence time on a site against reciprocal temperature.

The EISF values reported in Fig. 3 have been extracted by fitting the corrected spectra in the 250–400 K temperature range to a single Lorentzian plus an elastic peak folded with the instrumental resolution. One cannot choose between the models corresponding to reorientational jumps of $2\pi/3$ or

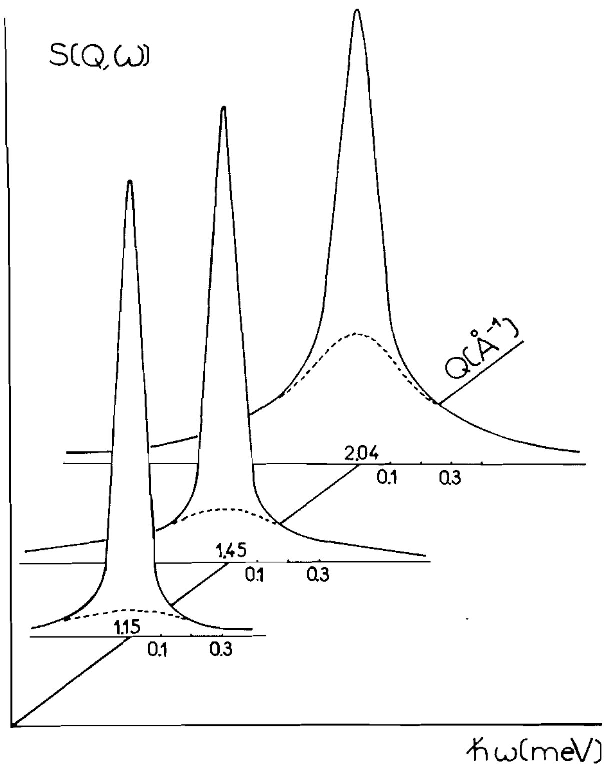

FIG. 4. Corrected quasi-elastic neutron scattering spectra for polycrystalline sample of NH_3SO_3 at 400 K for an incident wavelength $\lambda_0 = 5.1$ Å. The quasi-elastic contribution is represented by a dotted line in order to show its Q dependence.

$2\pi/6$. A broader Q range should be necessary, this would imply smaller incident wavelength. As a consequence the resolution would be smaller and the precision on the EISF determination would be very poor. Note that the $2\pi/6$ jump model almost corresponds to the diffusive case (21) in the observed Q range.

V.2.1. Determination of the residence times and of the activation energy

We have fitted the corrected spectra with those calculated by folding the scattering law for uniaxial rotational motions of protons with the instrumental resolutions for each angle.

The parameters used in the fitting procedure have been described elsewhere (4). Among these is τ_1^{-1}, which governs the width of the Lorentzian function appearing in the scattering function (see eq. [2]). In the case of $2\pi/3$ jump model there is a single τ_1 value and thus from eq. [5] the correlation time τ_c is found equal to $1.5\tau_1$. The two other parameters of importance are the radius of gyration R, which was fixed to 0.94 Å and the proportion of the non mobile protons p found to tend towards zero whatever the $2\pi/3$ or $2\pi/6$ jump model is introduced to fit the data. The fitting procedure has been performed on 10 angles simultaneously. The result of these fittings are reproduced in Table 1. This shows that at 406 K the fwhm ($2\tau_1^{-1}$) is two to four times larger than the experimental resolutions and therefore in such a favorable situation the dispersion of the points in Fig. 7 can only be explained by bad temperature measurements as indicated in the Experimental section.

The slope of the straight line (Fig. 7) representing the Arrhenius variation of τ_c as function of temperature gives a measure of the activation energy of the jump process, and is found equal to $E_a = 12 \pm 2$ kJ mol^{-1}.

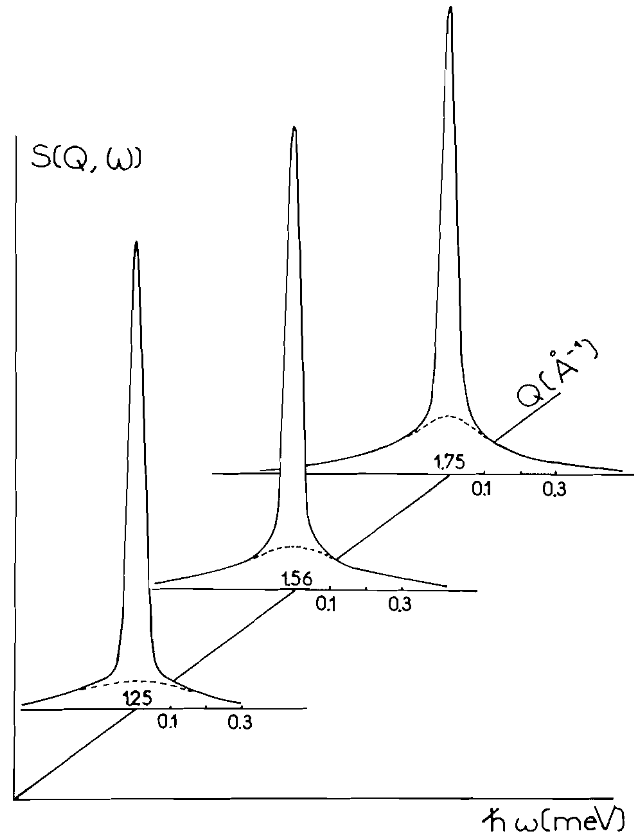

FIG. 5. Corrected quasi-elastic neutron scattering spectra of polycrystalline NH_3SO_3 at 400 K for an incident wavelength of 5.9 Å. The quasi-elastic contribution is represented by dotted line.

TABLE 1. Correlation times deduced from the different fits within the $2\pi/3$ jump model of NH_3 in sulphamic acid*

Configuration	Incident λ_c (Å)	T (K)	$1/\tau_1$ (μeV)	$\tau_c \times 10^{12}$ (s)
		250	26.7	36.96
		273	35.7	27.66
		293	47.4	20.82
135°	5.1	333	138	7.15
		374	203	4.86
		400	265	3.72
		443	410	2.41
		253	46.9	21.05
45°	5.9	323	104	9.48
		406	171	5.77

*$(\tau_1)^{-1}$ is a direct measure of the width of the Lorentzian function appearing in the quasi-elastic part of the spectra.

V.2.2. Conclusion relative to the neutron scattering experiments

The dynamics of the NH_3 groups is associated with $2\pi/3$ or $2\pi/6$ rotational jumps characterized by a residence time $\tau_c^{300\,K} = 2.1 \times 10^{-11}$ s at room temperature and an activation energy of 12 ± 2 kJ mol^{-1}.

VI. Discussion and comparison with literature results

– The Raman band observed at about 247 cm^{-1} at 300 K which shifts to 274 cm^{-1} at 30 K and which is characterized by an H/D isotopic ratio of 1.35 was assigned to an NH_3 torsional motion in which the SO_3 groups are weakly involved, the ratio

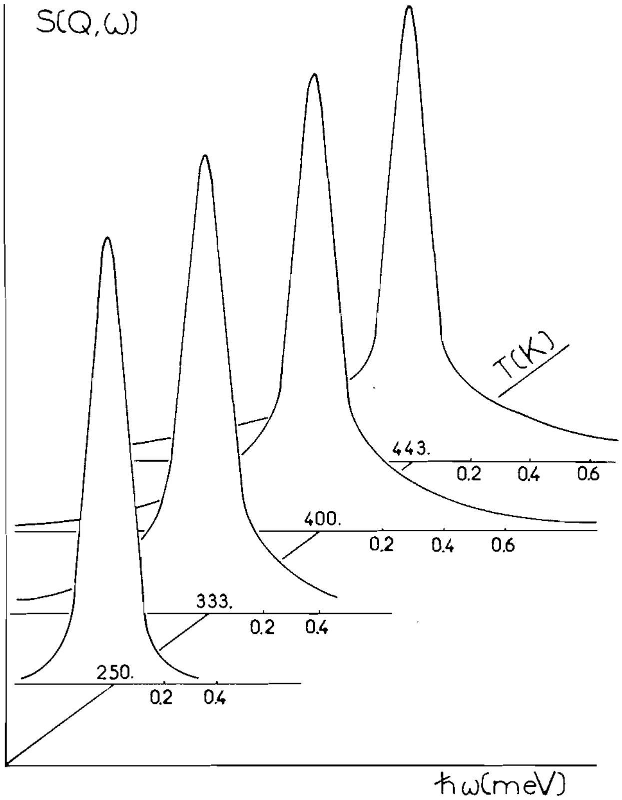

FIG. 6. Corrected quasi-elastic neutron scattering spectra of polycrystalline NH_3SO_3 for an incident wavelength of 5.1 Å at Q = 1.95 Å^{-1} for different temperatures.

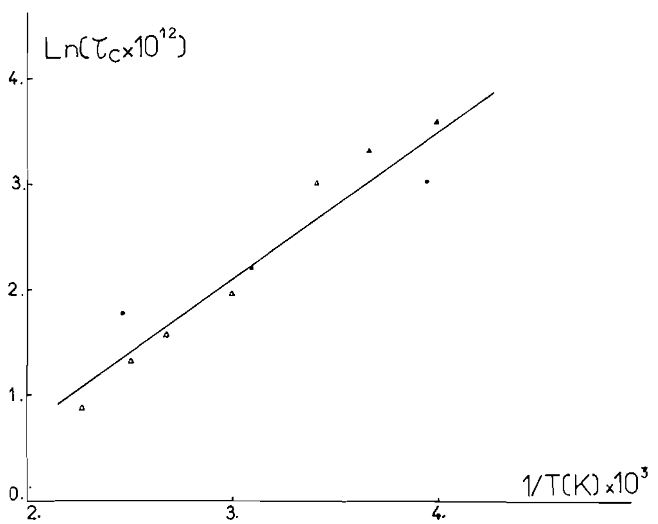

FIG. 7. Arrhenius plot of the mean residence time (τ_c) against reciprocal temperature; ●, 5.9 Å; △, 5.1 Å. The slope of the straight line gives an activation energy of 12 kJ mol^{-1}.

of square roots of reduced moment of inertia H/D (equal to 1.39, see Table V in ref. 11) being very near to the experimental frequency ratio. If the libration around S—N bond of the molecule as a whole was involved, the isotopic ratio would tend towards 1.02 (the corresponding libration band Ru was reported at about 90 cm^{-1}). Thus under these conditions where the SO_3 group libration amplitude is very small even at 300 K, a potential barrier V_3^0 of 14.6 kJ mol^{-1} at 300 K was derived through the assumption that the potential hindering the NH_3 rotation is of threefold order and that it can be written $V = (V_3^0/2)(1 - \cos 3\theta)$ where θ is the rotational coordinate of one proton. By subtracting the zero point energy, the rotational energy is equal to 11.9 kJ mol^{-1}. In the case where a sixfold potential V_6 is considered the barrier is four times lower. The perfect agreement of the V_3^0 barrier corrected from zero point energy with the neutron activation energy is thus in favor of the three-fold order as suggested by the heat capacity measurements.

Finally, the preexponential term of the Arrhenius relation can be derived from our neutron data; at 293 K it is equal to $\tau_c^0 = 1.55 \times 10^{-13}$ s, thus its inverse which represents the attempt frequency, $\nu_0 = 215$ cm^{-1}, is in fair agreement with the torsional frequency measured in Raman.

It is worthwhile to notice that the torsional motion in NH_3SO_3 in the above model is considered as an Einstein oscillator. Actually this is not a bad approximation. The coupling of this mode between the eight molecules in a unit cell gives rise to only four Raman frequencies spreading between 244 and 251 cm^{-1}. Moreover the density of states spectra deduced from inelastic neutron scattering (22) is sufficiently narrow (~30 cm^{-1}) to accept the above approximation. However, the dispersion of frequencies being smaller at $k = 0$ (~7 cm^{-1} for Raman modes) it appears preferable to consider correlated NH_3 in phase rotations for calculating potential barriers from atom–atom interactions (see last section). This remark allows us to account for a difference between the activation energy measured in neutron or nmr and the Raman potential barrier when the torsional mode is dispersive.

A second cause of discrepancy can also be due to the fact that the three-fold potential considered above is only an approximation. Strictly speaking, the NH_3 groups occupy general crystallographic positions and the general expression of the potential should be written:

$$V = \frac{V_1}{2}(1 - \cos\theta) + \frac{V_2}{2}(1 - \cos 2\theta) + \frac{V_3}{2}(1 - \cos 3\theta) + \text{---}.$$

The neglect of V_1 and V_2 terms is only based on qualitative local geometry considerations. In this respect Ratcliffe *et al.* (13) have underlined that the distribution of neighbouring oxygen atoms around NH_3 group is near a five-fold environment. If this were a perfect pentagon the first term to contribute would be $(V_{15}/2)(1 - \cos 15\,\theta)$, i.e., it would generate a quasi-free rotation at room temperature. Actually, the slight distortion is sufficient to avoid the cancellation of the V_3 terms. Ratcliffe *et al.*, assuming that the three-fold interaction potential between the three protons of one NH_3 group and a neighbouring oxygen atom is the same for the five oxygens and is equal to V_3'', have written that the total potential is

$$V = \frac{V_3''}{2}\left[5 - \sum_{i=1}^{5} \cos 3(\theta - \eta_i)\right]$$

where η_i are the angular positions of surrounding oxygens. The corresponding barrier height given by $V(\theta = 0) - V(\theta = 2\pi/6)$ is found equal to be 0.65 V_3''. If the η_i angles were multiples of $2\pi/5$ (instead of crystallographic values), this barrier would be zero, and it would be necessary to consider higher order terms such as V_{15}. One of the aims of the last section is thus to see to what extent similar conclusions can be obtained when the number of surrounding atoms is substantially increased. The second aim is to try to estimate the con-

TABLE 2. Comparison of activation energies, potential barriers, and correlation times for NH_3 reorientation in NH_3SO_3[g]

		IQENS ($2\pi/3$)			Nmr ($2\pi/3$)			Raman ($2\pi/3$)		
	T (K)	E_a (kJ mol^{-1})	τ_c[f] (s)	ν_0 (cm^{-1})	E_a (kJ mol^{-1})	τ_c[f] (s)	ν_0 (cm^{-1})	ν_0 (cm^{-1})	V_3° (kJ mol^{-1})	V_3° − ZPE (kJ mol^{-1})
	300−500	12[a]	2×10^{-11}	215				247[c]	12.9	11.7
NH_3SO_3	80−260				11.3[b]	6.2×10^{-10}	444			
	20−80							274	15.9	14.6
MnPDA	280−300	26.6[d]	1×10^{-11}	1.4×10^5				311[e]	20.1	19.4

[a]This work.
[b]From ref. 13.
[c]From ref. 11.
[d]From ref. 10.
[e]From ref. 9.
[f]Values obtained at 300 K.
[g]MnPDA: $NH_3(CH_2)_3NH_3MnCl_4$; ZPE: zero point energy $= \frac{1}{2} h\nu_0$; for IQENS, the attempt frequency in some cases (e.g., NH_3SO_3) compares well with vibrational frequency, however, it cannot be systematically identified with it (e.g. MnPDA). The activation energies deduced from nmr and IQENS are in a general agreement with the local barrier potential. In most cases these two quantities are in a close agreement.

tribution of intra- and intermolecular interactions to the total barrier or alternatively to analyse the relative weight of conformational isomerism and of matrix effects. In particular, if one assumes that the interaction potential between the NH_3 rotor with the three oxygens belonging to the same molecule is V_3' and that the intra term can be written $V = (3V_3'/2)(1 - \cos 3\theta)$, one finds a potential barrier equal to $3V_3'$. The relative magnitude of V_3' and V_3'' is difficult to estimate *a priori*, although Ratcliffe *et al.* consider that the total torsional barrier[3] can be decomposed as $V^0_{\rm intra} = 8.6$ kJ mol^{-1} and $V^0_{\rm inter} = 4.7$ kJ mol^{-1}, i.e. $V_3' = 7.2$ kJ mol^{-1} and $V_3'' = 2.9$ kJ mol^{-1}, in other terms, the intermolecular potential of the NH_3 group with surrounding atoms is larger than the intramolecular one.

Nuclear magnetic resonance spin lattice relaxation measurements in NH_3SO_3 (13) have been interpreted in terms of NH_3 reorientations. An activation energy E_a of 11.3 kJ mol^{-1} is reported while a preexponential factor $\tau_c^0 = 7.5 \times 10^{-11}$ s is given. Thus a nice agreement between the energetic parameters is found between neutron and nmr measurements. However, the preexponential factor when converted gives 400 cm^{-1}, i.e. a frequency far from the torsional one, and consequently the corresponding residence time at 300 K, $\tau_c = \tau_c^0 \exp(E_a/kT)$, is twice as large as that obtained in our neutron study. Because this correlation time is directly given by the fwhm of the quasielastic contribution we think that this value is more reliable. Table 2 illustrates this discussion; a comparison with NH_3 reorientation in $NH_3(CH_2)_3NH_3MnCl_4$ (10) is also given. In this last compound the NH_3 group is hydrogen bonded to only three chlorine atoms and as stated above, it is not surprising to find that the potential barrier is higher than for NH_3SO_3.

VII. Calculation of potential functions hindering the rotation of NH_3 group and NH_3SO_3 as a whole

The present calculation consists in computer simulating a postulated type of motion and evaluating the intermolecular interaction along the path of motion. Thus in the case of librational motion of NH_3 and SO_3 groups the pair wise interactions given by the expression

$$V(r) = V_c + V_{\rm vw} + V_R + V_{\rm HB}$$

[3]The intermolecular oxygen interactions are not taken into consideration due to the small amplitudes of SO_3 groups in the torsional mode.

which combines coulombian, Van der Waals, repulsion, and hydrogen bonding potentials, are added for each orientation of the groups of atoms and a curve referred to below as a torsional or librational potential is constructed. The WMIN Busing's program was used, as stated before it gives the advantage of considering correlated displacements and the main difference with similar approaches (e.g. Goldberg (23)) is that the neighbouring hydrogen atoms are not stationary. In other words, the potential curve reported in Fig. 8 corresponds to the relative variations of the potential energy when the eight NH_3 groups belonging to one unit cell are rotated in order to respect the cell symmetry and the NH_3 groups in neighbouring cells are rotated by the same angle that the congruent groups of the unit cell at the origin.

We are interested only in the relative variations of the torsional or librational potential energy and because no direct comparison with thermodynamic data such as lattice energy was possible (24), we have not attempted to adjust all the potential parameters by minimizing the energy, but we have only tried to adjust the most sensitive ones, in order to derive a potential curve compatible with the constraints listed below. The tests of convergence of Coulomb and Van der Waals energies in both direct and reciprocal spaces have shown that 7 Å and 0.4 Å^{-1} represent the corresponding limits for which no relative energy change larger than 10^{-4} was obtained. For 7 Å, 669 pair interactions were considered.

VII.1. Potentials used in the calculations

We have considered the same pair potentials for compounds in which NH---O (25), O---O, N---H, N---N, S---S interactions were reported (26) and which were fitted in a WMIN calculation without the addition of electrostatic terms such as those reported by Righini *et al.* for crystalline ammonia (27).

(*a*) For the coulombian interactions, the net charges deduced from X—N data (18) and reported in Fig. 1*b* were introduced in

$$V_c = -\frac{q_i q_{jj}}{r_{ij}}$$

(*b*) The Van der Waals attractive potential was written as

$$V_{\rm vw} = -\sum_{ij} \frac{C_{ij}}{r^6}$$

where the parameters C were taken from ref. 23. For S—H

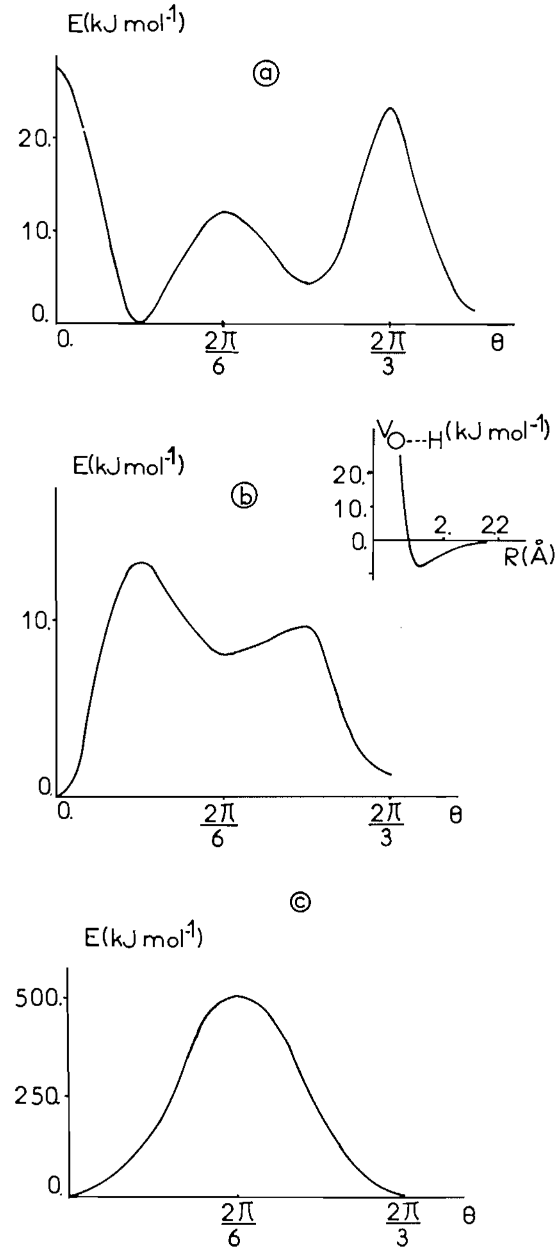

FIG. 8. Potential curves for the NH_3 rotation around the N—S axis in sulphamic acid. (*a*), calculated with coulombian interactions between net atomic charges and with Van der Waals and repulsion potentials; (*b*), calculated with the same parameters as in (*a*) plus a specific potential (represented on the right part) for the hydrogen bonds. Only the relative variations are reported; (*c*), potential curve for the rotation of the NH_3SO_3 molecule as a whole.

interactions we have considered the geometric average of SO and OH parameters.

(*c*) The repulsions were represented by the expression:

$$V_R = + \sum_{ij} \frac{a_{ij} \exp(-b_{ij} r_{ij})}{r_{ij}^d}$$

and the *a*, *b*, and *d* parameters were chosen in the same manner as *C* parameters.

(*d*) However, for hydrogen and oxygen atoms directly connected by a hydrogen bond, a specific Morse-like potential was introduced in such a way that it is zero for H---O distances larger than 2.2 Å and present a minimum at 1.92 Å (experimental average value). The depth of this minimum has been varied between 4 and 12.5 kJ mol^{-1}. The simple electrostatic H^+---O^- potential combined with a repulsive potential was not appropriate to generate a three fold order external potential (intermolecular) hindering the NH_3 rotation. In the literature, this difficulty has been overcome by using similar potentials (28). The Schroeder's model of a bent NH---O was not considered; the wide range of directions covered by the interatomic contacts giving an indirect account of the angle dependence. The expression given below gave satisfactory results; the repulsive part for $r < 1.85$ Å is not involved in the NH_3 rotation, the H---O contacts being all larger than this value.

$$V_{(r_{O\cdots H})} = D\left[1 - (1 - \exp(-\gamma(r - r_e))^2\right]$$

All H---O interactions are taken into account. This means that a given H can interact with several oxygens. However, the contributions of interactions for *r* larger than 2.5 Å are negligible and it is observed that for all configurations there are at maximum two H--O contacts for a given H which contribute to the energy.

(*e*) In order to examine the conformational isomerism of an isolated NH_3SO_3 molecule and to see at what extent the staggered conformation in the isolated molecule can be stabilized, we have also considered that the electrons of NH and SO bonds can interact with each other and with all the other charges. Their mutual interaction could be described by using a multipole expansion (28), but because of the lack of data on the local quadrupoles and octopoles of NH and SO bonds, the electrostatic interaction between two charge distributions were reduced to the Coulombian form given below:

$$V_{\alpha,\beta} = \sum_i \sum_j \frac{\alpha_i q_j}{r_{ij}} + \sum_j \sum_k \frac{\beta_k q_j}{r_{kj}} + \sum_i \sum_k \frac{\alpha_i \beta_k}{r_{ik}} + \sum_i \sum_{i'} \frac{\alpha_i \alpha_{i'}}{r_{ii'}}$$

The α_i and β_k parameters are for electronic charges of NH and SO bonds respectively, while q_j are for net atomic charges and r_{ij}, r_{kj}, r_{ik} are the inter-charge distances. The α, β parameters are introduced as formal charges located at the mid point of the NH and SO bonds. This potential was calculated for the isolated molecule and for the crystal. The polarization forces which are weaker than Van der Waals and electrostatic forces have been neglected, moreover, the induced dipole–dipole interactions being attractive, they cannot contribute to the stabilization of the staggered conformation, the existence of which is questioned here.

VII.2. Constraints

The different constraints that we introduced in our calculations are the following:

(*a*) The minima of the total potential function must be located at $\theta = 0$, $2\pi/3$, $4\pi/3$ where $\theta = 0$ corresponds to the crystallographic position of one proton. Subminima are allowed but their energy must be high enough for their occupation factor at 300 K is negligible.

(*b*) The maxima are also distant of $2\pi/3$ and the corresponding barrier is equal to 12 kJ mol^{-1}.

(*c*) The repulsive and attractive Van der Waals parameters for O---O, O---H, N---O, N---H interactions are fixed to the literature values derived for atoms involved in similar interactions. The other interactions are varied (the initial values are taken as geometric average).

(*d*) The coulombian charges on atoms are taken from X—N data (18).

(*e*) The potential barrier hindering the NH_3SO_3 rotation as a

TABLE 3. Van der Waals and repulsion potential constants (in kJ mol^{-1})

Interaction	a	b	c	d
N---N[a]	268 168.	3.64	1 685	0.
N---O[c]	538 802.	1.82	1 588	6.
H---H[a]	9 075.	3.74	101.9	0.
H---O[c]	99 095.	1.87	390.8	6.
H---N[c]	49 332.	3.69	414.2	0.
O---O[a]	1 082 620.	0.0	1 498.5	12.
S---S[b]	418 000.	3.5	4 427	0.
O---S[c]	672 708.	1.75	2 575	6.
S---N[c]	334 805.	3.57	2 729	0.
S---H[c]	61 588.	3.62	673	0.

[a]Reference 23.
[b]Reference 26.
[c]Obtained by taking the geometrical mean of the relevant homonuclear interaction parameters.

whole must be much larger than that associated to the torsion; it is expected to be larger than 50 kJ mol^{-1}.[4]

VII.3. Results

Four stages have been developpped in our calculation:

(a) The net atomic charges and the set of parameters given in Table 3 are entered in the calculation and a sixfold potential function is obtained (Fig. 8a). The coulombian terms in the energy and thus its relative variations are the leading terms. The O---H Van der Waals attractions or repulsions terms inside a given molecule playing a negligible role because of the long interatomic distances ($d_{\mathrm{H}\cdots\mathrm{O}} > 2.67$ Å), thus the intermolecular potential is mainly coulombian. The interactions between bonded atoms are entered but do not contribute to the relative variations of the potential.

(b) In order to satisfy the constraint mentionned in (a), a specific potential for hydrogen bonds (see VII-1-d) is added to the above set of parameters and a three-fold potential function is obtained. Its depth can be varied by adjusting the D parameters. For $D = -8.4$ kJ mol^{-1} and $\gamma = 15.35$ the potential barrier is found equal to 13.4 kJ mol^{-1} Fig. 8b. The minimum at $2\pi/3$ is slightly higher than that at 0°, but their energy difference is sufficiently small for their occupation being equal above 200 K. The subminimum at $2\pi/6$ is much higher in agreement with the constraint (a).

(c) The coulombian interactions involving the NH and SO electronic charges were introduced.

Arbitrary values of bond charges α_{NH} and β_{NH} were used. Figure 9 represents the variation of the intramolecular electrostatic energy : for $\alpha = 0.1$, $\beta = 0.1$ and for $\alpha = 0.1$, $\beta = 1$ in both cases the staggered conformation is favored and the energy variation is less than 1.7 kJ mol^{-1}. This is due to the fact that the sums $\Sigma\, 1/r_{ij}$, $\Sigma\, 1/r_{kj}$, $\Sigma\, 1/r_{ik}$ do not vary appreciably

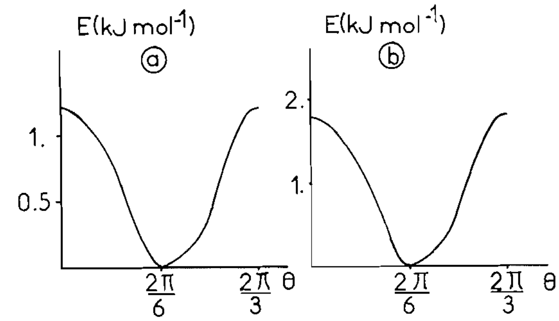

FIG. 9. Intramolecular potential curve for the torsion of NH_3 in an "isolated" molecule. The electrostatic interactions between net atomic charges q_i and charges α and β placed in the middle of the NH and SO bonds, respectively, are considered. (a), $\alpha = \beta = -0.1$; the total electrostatic energy varies between -1343.8 for $\theta = 0°$ and -1345 kJ mol^{-1} for $\theta = 60°$, i.e., $\Delta E = 1.2$; (b), $\alpha = -0.1$, $\beta = -1$; the total electrostatic energy varies between 1162.3 for $\theta = 0°$ and 1160.6 kJ mol^{-1} for $\theta = 60°$, i.e., $\Delta E = 1.7$ kJ mol^{-1}.

when NH_3 is rotated. One can conclude that the electrostatic interactions do not contribute significantly to the intramolecular torsional barrier. Moreover the overlap between S and O orbitals which could contribute to the torsional energy is expected weaker than in molecules such as ethane (the NH_3SO_3 molecule is not stable in the gas phase) and the intramolecular torsional potential barrier is likely much smaller than 4.2 kJ mol^{-1} and can be ignored.

(d) The NH_3SO_3 molecules were rotated as a whole. Figure 8c represents the variation of the energy calculated with the set of parameters of Table 3 plus the hydrogen-bond potential, the total potential function is of three-fold order the associated V_3 barrier is found equal to 500 kJ mol^{-1}, this value is mainly determined by the repulsive part of the hydrogen-bond potential, actually there are O---H distances of 1.78 Å for $\theta = 60°$, thus when varying the form of the potential we could decrease this barrier at a large extent. However, as already stated it must remain high enough for keeping the oxygen atoms fixed in the lattice and we think that the hydrogen-bond potential of Fig. 8b is not far from the actual situation.

VIII. Conclusions

The reorientation of the NH_3SO_3 molecules as a whole is strongly hindered by O---H and at a smaller extent by O---O repulsions; a potential barrier of 300 kJ mol^{-1} was derived.

The contributions of intermolecular H---H interactions to the relative variations of V' and V'' were found negligible and thus taking into account the correlated NH_3 motions does not change the potential results which could be obtained with a rigid lattice.

The staggered configuration is not generated by intramolecular interactions but rather by intermolecular O---H hydrogen bonding attractions.

The total potential function hindering the NH_3 reorientations has been derived, it presents minima separated by $2\pi/3$, the H---O interactions were chosen to give a potential barrier of 12 kJ mol^{-1}. The subminima found in the potential are not pronounced and can be considered as anharmonic contributions explaining the broadness of the Raman torsional band at 300 K. This point will be discussed in a forthcoming paper.

The coulombian and hydrogen bonding interactions dominate the relative potential variations and this can be related to the fact that the staggered form of NH_3SO_3 is only stabilized in

[4]The value 50 kJ mol^{-1} is obtained from the libration frequency observed at $R'_{\mathrm{u}} \simeq 80$ cm^{-1} (11). Assuming a threefold order sinusoidal potential, the relation:

$$V_3^0 = \frac{\nu^2 8\pi^2}{9h^2} I_{\mathrm{u}}$$

(where $I_{\mathrm{u}} = 97$ uma Å^2 is the inertia moment of the molecule around its long axis) gives a crude approximation of the barrier hindering the rotation of the molecule. This model considers that the bottom of the potential function can be osculated by a parabola. It is completely false for large angles for which strong repulsions can occur.

the crystal or solvents in which hydrogen bonds can be established (28).

Finally, this paper shows how the conjunction of heat capacity measurements, Raman and neutron scattering (29) delivers sufficiently sound experimental data which can be used as a basis before undertaking potential calculations. The calculations reported here are highly empirical, however they have the merit to show that the relative variations of the potential barrier are mainly determined by NH---O hydrogen bonds.

1. K. CHHOR. Thèse Doctorat d'État, Université Paris XIII. 1982.
2. K. CHHOR, C. SOURISSEAU, and G. LUCAZEAU. J. Raman Spectrosc. **11**, 183 (1981).
3. C. SOURISSEAU, G. LUCAZEAU, A. J. DIANOUX, and C. POINSIGNON. Mol. Phys. **48**, 367 (1983).
4. G. LUCAZEAU, K. CHHOR, C. SOURISSEAU, and A. J. DIANOUX. Chem. Phys. **76**, 307 (1983).
5. K. CHHOR and G. LUCAZEAU. Inorg. Chem. **23**, 462 (1984).
6. K. CHHOR, C. POMMIER, and M. DIOT. Mol. Cryst. Liq. Cryst. **100**, 193 (1983).
7. K. CHHOR and G. LUCAZEAU. J. Raman Spectrosc. **13**, 235 (1982).
8. K. CHHOR, J. F. BOCQUET, G. LUCAZEAU, and A. J. DIANOUX. Chem. Phys. **91**, 471 (1984).
9. C. SOURISSEAU and G. LUCAZEAU. J. Raman Spectrosc. **311**, 8 (1979).
10. C. SOURISSEAU, G. LUCAZEAU, and A. J. DIANOUX. J. Phys. **44**, 967 (1983).
11. G. LUCAZEAU, A. LAUTIE, and A. NOVAK. J. Raman Spectrosc. **3**, 161 (1975).
12. C. I. RATCLIFFE, W. F. SHERMAN, and G. R. WILKINSON. J. Raman Spectrosc. **14**, 246 (1983).
13. C. I. RATCLIFFE and B. A. DUNELL. J. Chem. Soc. Faraday Trans. **77**, 2169 (1981).
14. W. R. BUSING. ORNL report, n° 5747, Acta Crystallogr. A**28**, 5252 (1972).
15. A. W. HEWAT, J. R. GAVARRI, and G. LUCAZEAU. To be published.
16. K. CHHOR, J. F. BOCQUET, and C. POMMIER. J. Chem. Thermodyn. To be published.
17. F. A. KANDA and A. J. KING. J. Am. Chem. Soc. **73**, 2315 (1951).
18. J. W. BATS, P. COPPENS, and T. F. KOETZLE. Acta Crystallogr. B**33**, 37 (1977).
19. A. J. DIANOUX and F. VOLINO. Mol. Phys. **34**, 1263 (1977).
20. A. J. DIANOUX, F. VOLINO, and H. HERVET. Mol. Phys. **30**, 1181 (1975).
21. M. BEE, J. P. AMOUREUX, and A. J. DIANOUX. Mol. Phys. **41**, 325 (1980).
22. J. HOWARD, T. C. WADDINGTON, and E. NACHABAUR. J. Chem. Soc. Dalton Trans. 921 (1978).
23. U. SCHMUELI and J. GOLDBERG. Acta Crystallogr. B**29**, 2466 (1973).
24. G. A. BENSON and W. J. SPILLANE. Chem. Rev. **80**, 151 (1980).
25. A. T. HAGLER, E. E. HULER, and S. LIFSON. J. Am. Chem. Soc. **96**, 5319 (1974).
26. S. CERRINI and G. S. PAWLEY. Act. Crystallogr. A**29**, 660 (1973).
27. R. RIGHINI, N. NETO, and S. CALIFANO. Chem. Phys. **33**, 345 (1978).
28. R. SCHROEDER and E. R. LIPPINCOTT. J. Chem. Phys. **23**, 1099 (1955).
29. G. LUCAZEAU, K. CHHOR, and C. POMMIER. Spectrosc. Int. J. **2**, 79 (1983).

The photoabsorption of chlorodifluoroethenes in the vacuum ultraviolet

ECKART RÜHL, HANS-WERNER JOCHIMS, AND HELMUT BAUMGÄRTEL
Institut für Physikalische Chemie, Freie Universität Berlin, Takustr. 3, D-1000 Berlin 33

Received July 27, 1984

This paper is dedicated to Professor Camille Sandorfy on the occasion of his 65th birthday

ECKART RÜHL, HANS-WERNER JOCHIMS, and HELMUT BAUMGÄRTEL. Can. J. Chem. **63**, 1949 (1985).

The gas phase absorption spectra of 2-chloro-1,1-difluoroethene, *cis*- and *trans*-1-chloro-1,2-difluoroethene have been measured in the photon energy range from 6.5 to 25 eV. The $\pi \rightarrow \pi^*$ transition is assigned to bands centered around 7.17–7.20 eV for all three isomers. Four Rydberg series are observed in all the spectra, converging to the π ionization potential: two *np*-type Rydberg series, one *ns*, and one *nd* series are assigned. The convergence limits are: 9.84 eV (2-chloro-1,1-difluoroethene), 9.86 eV (*cis*-1-chloro-1,2-difluoroethene), and 9.85 eV (*trans*-1-chloro-1,2-difluoroethene). In the case of 2-chloro-1,1-difluoroethene four additional Rydberg series are found converging to the *n*Cl ionization potential. The convergence limit of these series is 12.15 eV.

Above 12 eV broad absorption bands dominate the spectra.

ECKART RÜHL, HANS-WERNER JOCHIMS et HELMUT BAUMGÄRTEL. Can. J. Chem. **63**, 1949 (1985).

Opérant à des énergies photoniques allant de 6,5 à 25 eV, on a mesuré les spectres d'absorption en phase gazeuse du chloro-2 difluoro-1,1 éthène et des chloro-1 difluoro-1,2 éthènes-*cis* et -*trans*. On attribue les bandes que l'on retrouve autour de 7,17 à 7,20 eV dans chacun de ces produits à la transition $\pi \rightarrow \pi^*$. Dans chacun des spectres, on a observé quatre séries de bandes de Rydberg; elles convergent vers le potentiel d'ionisation π: deux séries de bandes de Rydberg du type *np*, une série du type *ns* et une série du type *nd*. Les limites de convergence sont les suivantes: 9,84 eV (chloro-2 difluoro-1,1 éthène), 9,86 eV (chloro-1 difluoro-1,2 éthène-*cis*) et 9,85 eV (chloro-1 difluoro-1,2 éthène-*trans*).

Dans le cas dichloro-2 difluoro-1,1 éthène, on a trouvé quatre autres séries de bandes de Rydberg qui convergent vers le potentiel d'ionisation du *n*Cl. La limite de convergence de cette série est égale à 12,15 eV.

Au-dessus de 12 eV, les bandes d'absorption dominent le spectre.

[Traduit par le journal]

Introduction

The vacuum ultraviolet (vuv) absorption spectra of ethene and its halogen derivatives have long been of interest since a variety of excitations have been observed: e.g. Rydberg series, containing vibrational progressions, associated with the π-bond and halogen lone-pair excitations.

The vuv spectra of fluoroethenes, chloroethenes, and some chlorofluoroethenes have been studied between 6 eV and 12 eV (1). In particular, the influence of the substitution scheme on the vuv spectra was examined for dichloroethenes (1), difluoroethenes (2), and dibromoethenes (17). In these cases it was possible to apply the dipole selection rules to the observed electronic transitions. As the haloethenes studied in the present paper have C_s-symmetry no restrictions concerning dipole selection rules are expected (5).

Experimental

The experimental system consists of a 1 m normal incidence monochromator (McPherson 225) equipped with a single beam absorption cell behind the exit slit. Light detection was provided by a photomultiplier. Synchrotron radiation from the Berlin electron storage ring BESSY was used as a light source. In the 6.5 eV to 11 eV energy range the absorption cell was isolated from the monochromator by a lithium fluoride window, thus suppressing the higher order spectra and allowing exact pressure measurement by means of a capacitance manometer (Baratron 22). In the region above 9 eV the window was not used and the calibration of the absorption coefficient scale was provided by fitting the curves to the absolutely measured spectra in the overlapping region between 9 and 11 eV. This leads to an estimated overall uncertainty of about 15% in the absorption coefficient. All the spectra have been measured with about 0.1 nm wavelength resolution.

Syntheses

1,2-Difluoro-1,1,2-trichloroethane was prepared in 35% yield by reduction of 1,2-difluoro-1,1,2,2-tetrachloroethane with $LiAlH_4$ refluxing in absolute ether (18). The distilled product was dehalogenated with zinc dust in ethanol at 78°C yielding 75% of a mixture of *cis*- and *trans*-1-chloro-1,2-difluoroethene (15). The stereoisomers were separated by gas chromatography in two steps, in which the *trans* isomer was eluted first (11). (*1*) Preseparation: two columns packed with 15% squalane (length: 4 m each) at −6°C and 0°C, respectively; and (*2*) final separation: first column packed with KelF (length: 4 m) at 0°C, second column packed with 15% squalane (length: 4 m) at −10°C. After drying over Sicapent (Merck, Darmstadt) the *cis*- and *trans*-isomers were obtained in a purity exceeding 99.985%. The isomers were identified by means of their infrared spectra (11).

The 2-chloro-1,1-difluoroethene sample was purchased from PCR Inc., U.S.A. Gas chromatographic analysis showed no significant impurities.

Results and discussion

The spectra are presented in Figs. 1–7. Origins and vibrational excitations of Rydberg states are indicated by arrows. The corresponding numerical values are listed in Tables 1–4.

Many sharp bands appearing in the spectrum can be assigned according to the Rydberg formula:

$$[1] \quad E = \mathrm{IP}(n) - R/(n - \delta)^2$$

where E is the excitation energy of the observed transition, IP(n) is the corresponding ionization potential, δ is the quantum defect, and n is the principal quantum number. Several vibrational excitations have been observed which belong to Rydberg transitions with low principal quantum numbers. They have been assigned through comparison of vibrationally resolved photoelectron bands in 2-chloro-1,1-difluoroethene and with the aid of the fundamental vibrations (10, 11). Besides the sharp bands broader ones are observed and will be discussed below in connection with the Rydberg transitions belonging to higher ionization potentials. Reliable adiabatic ionization potentials are obtained from photoelectron spectra (PES) (*geminal* isomer (7)) or photoionization-mass-spectrometry (PIMS) (*vicinal* isomers (4)).

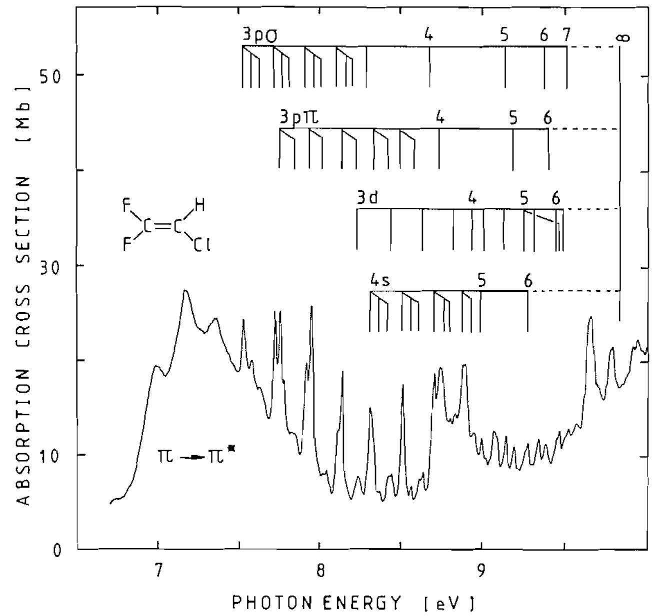

FIG. 1. Absorption spectrum of 2-chloro-1,1-difluoroethene in the energy range 6.5–10 eV.

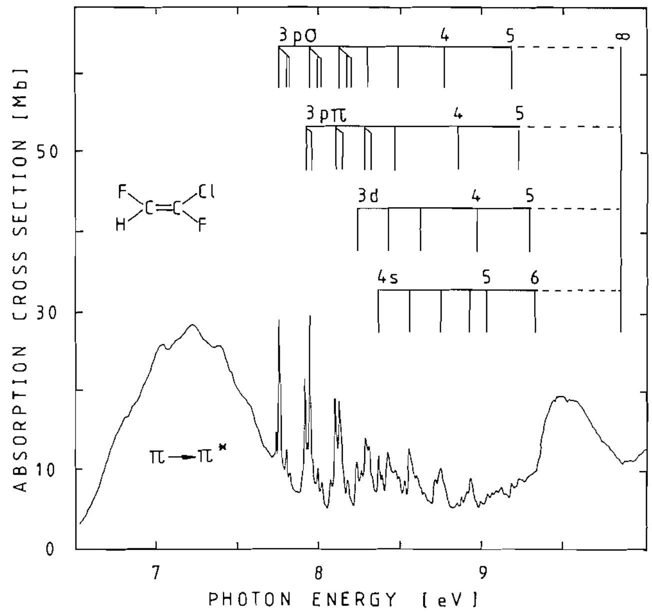

FIG. 3. Absorption spectrum of *trans*-1-chloro-1,2-difluoroethene in the energy range 6.5–10 eV.

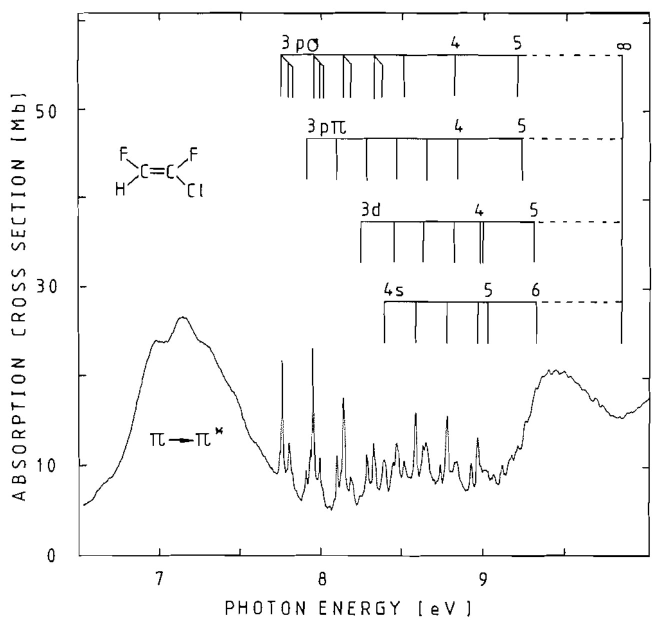

FIG. 2. Absorption spectrum of *cis*-1-chloro-1,2-difluoroethene in the energy range 6.5–10 eV.

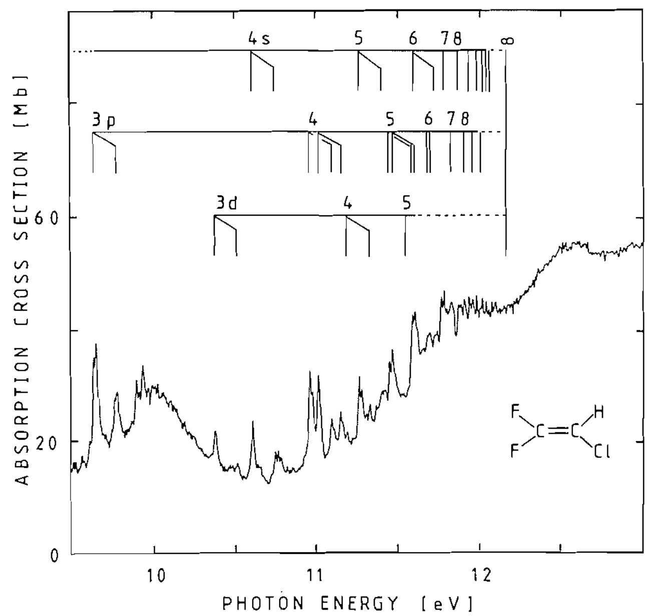

FIG. 4. Absorption spectrum of 2-chloro-1,1-difluoroethene in the energy range 9.5–13 eV.

1. The 6.5 – 10 eV region

A. 2-Chloro-1,1-difluoroethene

The first band which peaks at 7.17 eV is assigned to the $\pi \rightarrow \pi^*$ transition in agreement with the interpretation given by Scott and Russell (3). It shows the broad and intense structure typical for the $\pi \rightarrow \pi^*$ transition of all the haloethenes (1). Superimposed on this band are peaks resulting from vibrational excitations of the totally symmetric C=C stretching mode in the π^* state. The vibrational spacings (see Table 1) are significantly reduced compared to the ground state vibration (1745 cm^{-1}) (10). In the gas phase absorption spectrum in general no other valence transitions have been observed, but in fluoroethenes $\pi \rightarrow \sigma^*$ transitions have been identified by comparison with solid state and Kr matrix absorption spectra between 6.5 and 7.5 eV (6).

Four Rydberg series located in this energy region can be readily assigned to $\pi \rightarrow np$, nd, and ns transitions (Fig. 1). They all converge to 9.83 eV. Only the first members of each series reveal resolvable vibrational fine structure, with the exception of the $\pi \rightarrow nd$ transitions. Two p type Rydberg series (δ = 0.57 and δ = 0.44) can be clearly identified. In analogy to diatomic molecules the two p series may be related to $p\sigma$ and $p\pi$ subseries (13). The spectra of chloroethenes (1) and bromoethenes (16, 17) also show more than one electronic origin belonging to $\pi \rightarrow 3p$ Rydberg transitions. In fluoroethenes only one $\pi \rightarrow 3p$ transition is observed (1). Three fundamental vibrations belonging to the $\pi \rightarrow np$ transitions are observed (Table 1): (*i*) ν_2 = 1510–1560 cm^{-1} (C=C stretching, 1745

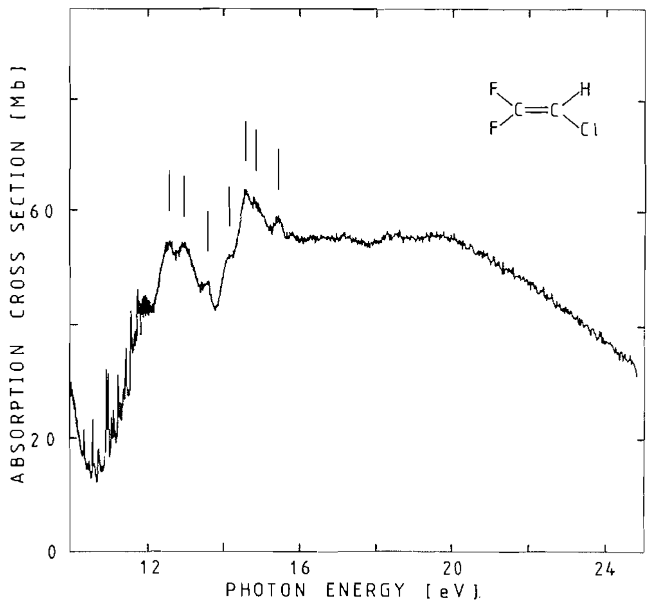

FIG. 5. Absorption spectrum of 2-chloro-1,1-difluoroethene in the energy range 10–25 eV.

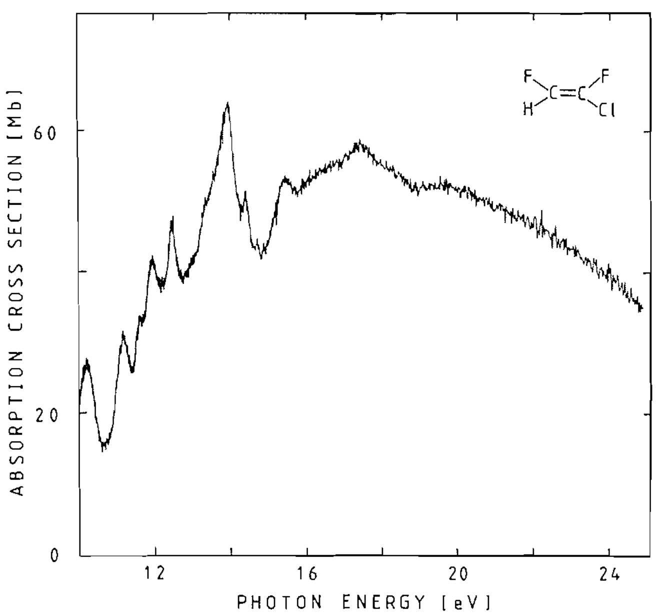

FIG. 6. Absorption spectrum of *cis*-1-chloro-1,2-difluoroethene in the energy range 10–25 eV.

$\mathrm{cm^{-1}}$ in the ground state), (*ii*) ν_6 = 815–860 $\mathrm{cm^{-1}}$ (C—Cl stretching, 845 $\mathrm{cm^{-1}}$ in the ground state), (*iii*) ν_8 = 420–460 $\mathrm{cm^{-1}}$ (C—Cl bending, 433 $\mathrm{cm^{-1}}$ in the ground state). The assignment of these vibrations is based on ir data (10); the description of the normal modes follows Craig *et al.* (11). Compared to the vibrations in the electronic ground state only the C—C stretching mode is red-shifted, which confirms the assignment of the Rydberg series. The vibrational spacings of the Rydberg transitions reported here correlate well with those of molecular ions observed in PES spectra, as was pointed out by Wittel *et al.* (9).

The $\pi \rightarrow nd$ Rydberg series begins with the weak $\pi \rightarrow 3d$ transition (δ = 0.08) at 8.225 eV (Table 1). A five membered progression in ν_2 belongs to the $\pi \rightarrow 3d$ Rydberg state. Vibrations are also observed in the $\pi \rightarrow 4d$ and $\pi \rightarrow 5d$ states.

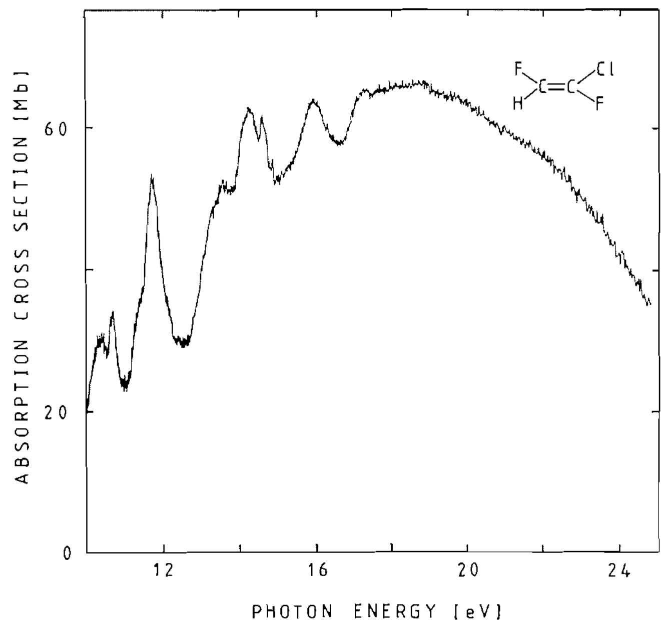

FIG. 7. Absorption spectrum of *trans*-1-chloro-1,2-difluoroethene in the energy range 10–25 eV.

The first member of the $\pi \rightarrow ns$ Rydberg series observed here is the $\pi \rightarrow 4s$ transition. Vibrational progressions in ν_2 belong to this transition are found. The $\pi \rightarrow 3s$ Rydberg state is not observed here, probably because of coupling with the π^* valence state.

There are two broad and intense pairs of structures at about 8.8 and 9.7 eV. The intense band at 8.8 eV was assigned to the $\pi \rightarrow 4s$ transition by Scott and Russell (3). Due to the high oscillator strength and the corresponding term value (27 600 $\mathrm{cm^{-1}}$) we believe this band has to be assigned instead to an excitation of the a' chlorine lone-pair electron. Therefore this transition is assigned to $n\mathrm{Cl} \rightarrow 3s$. The splitting of the absorption band is well correlated with that of the corresponding PES band. Following the arguments of Wittel and Bock (8) the PES band at 12.29 eV has to be interpreted as a vibrational excitation of the $\tilde{A}$-state of the molecular cation. A splitting of about 1100 $\mathrm{cm^{-1}}$ between these photoelectron peaks might be due to δ(C—H) excitation as observed in the PES spectrum of chloroethene (8). In 2-chloro-1,1-difluoroethene it cannot be decided whether the δ(C—H) vibration or the a(C—F) stretching causes this splitting (ground state vibrations: δ(C—H) = 1333 $\mathrm{cm^{-1}}$, a(C—F str.) = 1199 $\mathrm{cm^{-1}}$). Similarly the 9.7 eV absorption band also shows a splitting of 1100 $\mathrm{cm^{-1}}$ which results from vibrational excitation. The term value is 20 300 $\mathrm{cm^{-1}}$ which is typical for the so called D-bands (1). Therefore we assign this band to the $n\mathrm{Cl} \rightarrow 3p$ transition.

B. cis- *and* trans-*1-Chloro-1,2-difluoroethene*

Based on several similarities of the absorption spectra (Figs. 2, 3) a parallel treatment in interpretation is suggested.

In both isomers the $\pi \rightarrow \pi^*$ transition is located at nearly the same energy (Table 2). Compared to the geminal isomer no characteristic shift of this transition is observable. This indicates a negligible influence of substitution in contrast to the observation made in the case of difluoroethenes and dichloroethenes (1). Weak superimposed structures are assigned to the C=C— stretching mode of 1380–1480 $\mathrm{cm^{-1}}$, which may be compared with the molecular values of 1716 $\mathrm{cm^{-1}}$ (*cis*) and 1708 $\mathrm{cm^{-1}}$ (*trans*) (11), the decreased frequencies resulting

TABLE 1. Valence transitions and Rydberg progressions of 2-chloro-1,1-difluoroethene converging to the first IP at 9.84 eV

Energy (eV)	δ	Assignment	Δν (cm^{-1})
6.985		$\pi \rightarrow \pi^*$	Origin
7.174			1528
7.385			1481
7.528	0.57	$\pi \rightarrow 3p\sigma$	Origin
7.583			441
7.632			841
7.722			1560
7.766			439
7.828			860
7.914			1555
7.969			446
8.018			836
8.106			1550
8.159			430
8.211			839
8.296			1531
7.758	0.44	$\pi \rightarrow 3p\pi$	Origin
7.859			818
7.946			1519
8.051			843
8.133			1508
8.236			830
8.317			1486
8.419			825
8.495			1436
8.598			822
8.245	0.08	$\pi \rightarrow 3d$	Origin
8.434			1527
8.625			1538
8.816			1546
9.008			1550

Energy (eV)	δ	Assignment	Δν (cm^{-1})
8.310	1.02	$\pi \rightarrow 4s$	Origin
8.366			453
8.414			842
8.505			1563
8.561			457
8.609			852
8.696			1546
8.750			439
8.797			815
8.883			1514
8.935			420
8.677	0.57	$\pi \rightarrow 4p\sigma$	Origin
8.750	0.45	$\pi \rightarrow 4p\pi$	Origin
8.953	0.07	$\pi \rightarrow 3d$	Origin
9.142			1532
9.331			1525
9.519			1516
8.984	1.00	$\pi \rightarrow 5s$	Origin
9.137	0.58	$\pi \rightarrow 5p\sigma$	Origin
9.175	0.45	$\pi \rightarrow 5p\pi$	Origin
9.269	0.08	$\pi \rightarrow 5d$	Origin
9.459			1533
9.287	1.00	$\pi \rightarrow 6s$	Origin
9.373	0.56	$\pi \rightarrow 6p\sigma$	Origin
9.388	0.46	$\pi \rightarrow 6p\pi$	Origin
9.443	0.09	$\pi \rightarrow 6d$	Origin
9.505	0.56	$\pi \rightarrow 7p\sigma$	Origin

from the lowering of the C═C bond strength in the antibonding π^* state.

On the high energy side of the $\pi \rightarrow \pi^*$ band, two $\pi \rightarrow 3p$ Rydberg subseries can be discerned. However, the corresponding quantum defects are decreased with respect to the value for the geminal isomer, indicating a decreased perturbation of the π-system by the substituents. There are pronounced vibrational progressions ranging from 1450 to 1550 cm^{-1}. They are assigned to the symmetrical C═C stretching mode in analogy to the geminal isomer. In contrast to the $\pi \rightarrow \pi^*$ transition these stretching frequencies are less reduced in the Rydberg transitions, indicating a stronger C═C bond in the Rydberg state than in the antibonding π^* state. Weak vibrations of about 367−377 cm^{-1} (*cis*) and 364−417 cm^{-1} (*trans*) are observed. These intervals correspond to the C—Cl bending frequency in the Rydberg state. From ir spectra the ground state vibrations are 361 cm^{-1} (*cis*), 397 cm^{-1} (*trans*) (11). The C—Cl bending mode remains unchanged in both electronic states. Weak vibrations are found which correspond to the antisymmetric (C—F) bending mode: 490−492 cm^{-1} (*cis*), 565−584 cm^{-1} (*trans*). These vibrations also remain essentially unchanged (ground state: 480 cm^{-1} (*cis*), 578 cm^{-1} (*trans*), indicating that the excitation of the π electron does not seriously perturb the C—Cl and C—F bonds.

There are two weaker structures that are assigned to $\pi \rightarrow nd$ ($\delta = 0.1$) and $\pi \rightarrow ns$ ($\delta = 1.0$) transitions. Only the $\pi \rightarrow 3d$ and $\pi \rightarrow 4s$ transitions exhibit C═C stretching vibrations (1530−1550 cm^{-1}). Weaker vibrations are not revealed since several Rydberg transitions with vibrational excitations overlap in this energy region. Again, a $\pi \rightarrow 3s$ transition which is expected to be at 6.36 eV, is not observed. The ionization potentials obtained from series convergence are 9.86 eV (*cis*) and 9.85 eV (*trans*). These values agree well with those found by photoionization spectrometry (PI) (9.86 eV (*cis*), 9.84 eV (*trans*) (4).

Instead of the split band observed at 8.8 eV for 2-chloro-1,1-difluoroethene, a new band occurs centered around 9.4 eV (*cis*) and 9.5 eV (*trans*). As in the case of the *geminal* isomer these broad and structureless bands are assigned to nCl $\rightarrow 3s$ transitions. This predicts an $\tilde{A}$ photoelectron band which is blue-shifted relative to the PES band of the geminal isomer at 12.16 eV. The broad bands lying at 10.4 eV should be due to the nCl $\rightarrow 3p$ transition (D band) or a Rydberg transition belonging to a higher ionization potential. The band shapes suggest that the corresponding PES bands should be broad and structureless as well.

2. *The 10 eV − 25 eV region*

A. *2-Chloro-1,1-difluoroethene*

In the region between the first and the second ionization potentials (9.83−12.15 eV) there are pronounced structural features belonging to a set of Rydberg series converging to

TABLE 2. Valence transitions and Rydberg progressions of *cis*- and *trans*-1-chloro-1,2-difluoroethene converging to the first IP at 9.86 eV and 9.85 eV, respectively

cis-1-Chloro-1,2-difluoroethene				*trans*-1-Chloro-1,2-difluoroethene			
Energy (eV)	δ	Assignment	$\Delta\nu$ (cm^{-1})	Energy (eV)	δ	Assignment	$\Delta\nu$ (cm^{-1})
6.985		$\pi \rightarrow \pi^*$	Origin	7.025		$\pi \rightarrow \pi^*$	Origin
7.156			1382	7.208			1482
7.312			1255	7.377			1382
7.746	0.46	$\pi \rightarrow 3p\sigma$	Origin	7.743	0.45	$\pi \rightarrow 3p\sigma$	Origin
7.792			369	7.793			402
7.807			492	7.813			565
7.935			1525	7.933			1533
7.979			360	7.983			402
7.996			490	8.005			584
8.123			1520	8.117			1482
8.169			367	8.167			404
				8.189			584
8.312			1520	8.300			1479
8.357			366				
8.499			1512	8.481			1460
7.894	0.37	$\pi \rightarrow 3p\pi$	Origin	7.903	0.35	$\pi \rightarrow 3p\pi$	Origin
				7.953			409
8.084			1531	8.094			1534
				8.143			402
8.269			1495	8.276			1471
				8.325			392
8.452			1478	8.459			1480
8.632			1452				
8.235	0.11	$\pi \rightarrow 3d$	Origin	8.221	0.11	$\pi \rightarrow 3d$	Origin
8.420			1523	8.413			1547
8.612			1522	8.591			1440
8.801			1522				
8.988			1512				
8.377	0.97	$\pi \rightarrow 4s$	Origin	8.353	0.99	$\pi \rightarrow 4s$	Origin
8.569			1547	8.547			1567
8.758			1526	8.739			1549
8.948			1529	8.920			1458
8.785	0.44	$\pi \rightarrow 4p\sigma$	Origin	8.760	0.47	$\pi \rightarrow 4p\sigma$	Origin
8.817	0.39	$\pi \rightarrow 4p\pi$	Origin	8.840	0.33	$\pi \rightarrow 4p\pi$	Origin
8.968	0.09	$\pi \rightarrow 4d$	Origin	8.960	0.09	$\pi \rightarrow 4d$	Origin
9.000	1.00	$\pi \rightarrow 5s$	Origin	9.017	0.96	$\pi \rightarrow 5s$	Origin
9.192	0.48	$\pi \rightarrow 5p\sigma$	Origin	9.180	0.49	$\pi \rightarrow 5p\sigma$	Origin
9.218	0.40	$\pi \rightarrow 5p\pi$	Origin	9.218	0.36	$\pi \rightarrow 5p\pi$	Origin
9.293	0.10	$\pi \rightarrow 5d$	Origin	9.296	0.05	$\pi \rightarrow 5d$	Origin
9.305	1.05	$\pi \rightarrow 6s$	Origin	9.331	0.95	$\pi \rightarrow 6s$	Origin

the second IP (Fig. 4). As the $\tilde{A}$ photoelectron band is sharp and split, the Rydberg transitions also exhibit these features. As in the 6.5–10 eV region, four Rydberg series are assigned (Table 3): two slightly separated *np* series (δ = 0.56 and δ = 0.63), one *ns* series (δ = 1.03–1.10), and only one weak *nd* series (δ = 0.23). All series start with a principal quantum number of three if one includes the strong absorption bands at 8.8 eV and 9.8 eV. This agrees well with generalized term value rules (1, 12). The typical vibrational excitation in this energy range is 1100 cm^{-1} to 1140 cm^{-1} which is assigned to the C—H bending or antisymmetric C—F stretching modes. The convergence limit of all Rydberg series coincides at 12.16 eV in excellent agreement with the value 12.15 eV obtained from the photoelectron spectrum (7).

The absorption spectrum at energies exceeding the second IP shows only flat and broad structures superimposed on an intense ionization continuum (Fig. 5). We cannot give a straightforward interpretation of these weak structures. Some of these may be assigned to D bands associated with higher chlorine ionization potentials (1). A similar interpretation is given by Sandorfy and co-workers for chlorofluoromethanes (14). Due to the rapid decrease of intensity only the first or second Rydberg members remain observable. A tentative interpretation of these structures using the Rydberg formula is given in Table 4.

Above 16 eV no significant structure is observed. Beyond 20 eV the absorption coefficient decreases continuously. This is commonly observed in photoabsorption spectra when the

TABLE 3. Rydberg progressions of 2-chloro-1,1-difluoroethene converging to the second IP at 12.16 eV

Energy (eV)	δ	Assignment	Δν (cm^{-1})
8.743	1.01	nCl → 3s	Origin
8.884			1137
9.648	0.67	nCl → 3p	Origin
9.788			1127
10.393	0.23	nCl → 3d	Origin
10.523			1109
10.614	1.03	nCl → 4s	Origin
10.751			1108
10.963	0.63	nCl → 4$p\sigma$	Origin
11.100			1108
11.015	0.56	nCl → 4$p\pi$	Origin
11.153			1109
11.197	0.24	nCl → 4d	Origin
11.335			1109
11.268	1.10	nCl → 5s	Origin
11.408			1128
11.453	0.63	nCl → 5$p\sigma$	Origin
11.589			1099
11.473	0.56	nCl → 5$p\pi$	Origin
11.611			1119
11.568	0.22	nCl → 5d	Origin
11.597	1.10	nCl → 6s	Origin
11.836			1119
11.690	0.63	nCl → 6$p\sigma$	Origin
11.701	0.57	nCl → 6$p\pi$	Origin
11.773	1.09	nCl → 7s	Origin
11.831	0.60	nCl → 7p	Origin
11.877	1.10	nCl → 8s	Origin
11.913	0.63	nCl → 8p	Origin
11.945	1.10	nCl → 9s	Origin
11.968	0.64	nCl → 9p	Origin
11.991	1.09	nCl → 10s	Origin
12.006	0.67	nCl → 10p	Origin
12.025	1.06	nCl → 11s	Origin
12.047	1.13	nCl → 12s	Origin
12.065	1.19	nCl → 13s	Origin

ionization quantum efficiency approaches unity.

B. cis- *and* trans-*1-Chloro-1,2-difluoroethene*

Unlike the *geminal* isomer absorption spectrum, for the vicinal isomers there are no sharp structures that unambiguously correspond to Rydberg series (Figs. 6, 7). Obviously a geminal fluorine substitution distorts the non-bonding character of the a' chlorine lone-pair orbital.

The lack of PES data impedes a straightforward assignment of the absorption bands in this energy region. Comparison of photoionization mass spectra with vuv spectra may elucidate the influence of preionization as was pointed out by Momigny (4). Moreover, predissociation that leads to fragment ions is expected to correlate with the absorption bands found in the vuv spectra.

Conclusions

In this investigation on all the chlorodifluoroethenes a number of new Rydberg series and vibronic excitations have been assigned for the first time. The effect of substitution on electronic transitions has been discussed in connection with quantum defects and term value arguments. As there exist no experimental data for haloethenes in the energy range from 11 to 25 eV an assignment of these absorption bands remains somewhat tentative. Further theoretical studies and more experimental data may help to overcome this drawback.

TABLE 4. Rydberg states of 2-chloro-1,1-difluoroethene above 12.5 eV

Energy (eV)	δ	Assignment
12.60	0.98	IP=15.94 eV → 3s
13.02	0.53	IP=15.25 eV → 3p
	0.98	IP=16.38 eV → 3s
13.62	0.58	IP=15.94 eV → 3p
14.16	0.47	IP=15.25 eV → 4p
	0.52	IP=16.38 eV → 3p
14.61	1.05	IP=18.18 eV → 3s
	0.23	IP=16.38 eV → 3d
14.85	1.02	IP=16.38 eV → 4s
	0.98	IP=18.18 eV → 3s
15.50	1.06	IP=16.38 eV → 5s

Acknowledgments

Financial support by the Bundesministerium für Forschung und Technologie and by the Fonds der Chemischen Industrie is gratefully acknowledged.

1. M. B. ROBIN. The higher excited states of polyatomic molecules. Vols. 1 and 2. Academic Press, New York. 1974, 1975, and references cited there.
2. R. MCDIARMID. J. Chem. Phys. **69**, 2043 (1978).
3. J. D. SCOTT AND B. R. RUSSELL J. Am. Chem. Soc. **94**, 2634 (1972).
4. J. MOMIGNY. Nature, **99**, 1179 (1963).
5. G. HERZBERG. Molecular spectra and molecular structure. III. Electronic spectra and electronic structure of polyatomic molecules. Van Nostrand Reinhold, New York. 1966.
6. P. DAUBER and M. BIRTH. Chem. Phys. **11**, 143 (1975).
7. R. F. LAKE and H. THOMPSON. Proc. R. Soc. London, A**315**, 323 (1970).
8. K. WITTEL and H. BOCK. Chem. Ber. **107**, 317 (1974).
9. K. WITTEL, W. S. FELPS, L. KLASINC, and S. P. MCGLYNN. J. Chem. Phys. **65**, 3698 (1976).
10. J. R. NIELSEN, C. Y. LIANG, and D. C. SMITH. J. Chem. Phys. **20**, 1090 (1952).
11. N. C. CRAIG, D. A. EVANS, L. G. PIPER, and V. L. WHEELER. J. Phys. Chem. **74**, 4520 (1970).
12. G. SCHEIBE, D. BRÜCK, and F. DÖRR. Chem. Ber. **85**, 867 (1962).
13. E. LINDHOLM. Arkiv Fysik. **40**, 97 (1969).
14. R. GILBERT, P. SAUVAGEAU, and C. SANDORFY. J. Chem. Phys. **60**, 4820 (1974).
15. A. L. HENNE and E. C. LADD. J. Am. Chem. Soc. **58**, 402 (1936).
16. W. LOHR, H. W. JOCHIMS, and H. BAUMGÄRTEL. Ber. Bunsenges. Phys. Chem. **79**, 901 (1975).
17. J. SCHANDER and B. R. RUSSELL. J. Am. Chem. Soc. **98**, 6900 (1976).
18. R. F. NYSTROM and W. G. BROWN. J. Am. Chem. Soc. **70**, 3738 (1948).

Spherical box model and reduction of Coulomb interactions in the crystal field theory of $3d^n$ ions

ANDRÉ JULG AND ODETTE JULG
Laboratoire de Chimie Théorique, Université de Provence, Place Victor Hugo, 13331 Marseille 3, France

Received November 30, 1984

This paper is dedicated to Professor Camille Sandorfy on the occasion of his 65th birthday

ANDRÉ JULG and ODETTE JULG. Can. J. Chem. **63**, 1955 (1985).

With an accuracy of 0.1 eV, all the electron transitions in any $3d$ transition element and in the corresponding ions, isolated or inside a crystal, can be obtained with the Hartree–Fock model by using hydrogen d orbitals with suitable effective charges ζ. When the ion is embedded in a crystal, the value of ζ is generally weaker than that in the isolated state. For a given ion, the value of the reduction factor depends on the nature of the crystal. This phenomenon is explained by the boundaries imposed on the ion by the presence of the first neighboring ions (box effect). The application to some crystals (oxides and carbonates) corroborates this interpretation. An empirical relationship between the size of the ion and that of the cavity in which it is confined is proposed.

ANDRÉ JULG et ODETTE JULG. Can. J. Chem. **63**, 1955 (1985).

A la précision de 0.1 eV, toutes les énergies de transition des éléments de transition $3d$ et de leurs ions, à l'état isolé ou dans un cristal, peuvent être obtenues dans le cadre de Hartree–Fock en utilisant des orbitales hydrogénoïdes d de charge effective ζ convenable. La valeur de ζ pour un ion dans un cristal est en général plus petite que celle à l'état libre. Pour un ion donné, la valeur du facteur de réduction dépend de la nature du cristal. Le phénomène est expliqué par les limites imposées à l'ion par la présence des ions voisins (effet de boîte). L'application à divers cristaux (oxydes et carbonates) confirme cette interprétation. Une formule empirique est proposée pour calculer le facteur de réduction en fonction de la taille de l'ion et de celle de la cavité dans laquelle il est enfermé.

The interpretation of the spectra of atoms and ions, in the isolated state and inside a complex or a crystal, is often considered one of the greatest successes of quantum mechanics. In fact, the quantitative interpretation of these spectra necessitates the replacing of the exactly calculated values of the various terms which appear in the calculation of the transition energies, by values fitted to experiment (Slater–Condon integrals, Racah parameters) (1). Moreover, the Coulomb parameters corresponding to an ion in a complex or a crystal are, in general, weaker than those corresponding to the isolated state (1, 2). In order to explain this reduction, a partial covalency is often invoked (2, 3). Certain authors have also envisaged a modification in the form of the atomic orbitals (4, 5). We shall see that another factor, essentially geometric in origin, can also be invoked. Whatever that may be, it would be very helpful to the chemist (non specialist in sophisticated quantum calculations) to know the reduction factor directly. Indeed, the *a priori* knowledge of the absorption spectrum not only permits the identification of impurities inside the minerals, but also helps to lead the experimentalist in preparing inorganic compounds which possess well-determined optical properties (artificial gems (6), colored filters, and lasers).

Some results concerning atoms in the isolated state and within a crystal field

In order to simplify the discussion, we shall consider $3d^n$ ions only, the core-electrons being assumed to be completely localized around the nucleus. Since the reduction we propose to study brings modifications in energy for various levels much more important (ca. 100 times) than the splittings between the components of a given multiplet arising from the spin–orbit coupling, the latter will be neglected. The actual levels corresponding to a given ^{2S+1}X term (leaving J out of account) will be replaced by their center of gravity.

Using the Hartree–Fock model, the various states are described by linear combinations of Slater determinants, built up from the d-atomic orbitals. Their energies appear as follows

$$[1] \quad E = nI + \bar{C}$$

where I corresponds to the monoelectronic terms of the Hamiltonian (kinetic energy + core-attraction energy) and $\bar{C}$ is the total electron repulsion energy. The term I is the same for all d^n-states, so that it does not play any role in the d-transitions. The term $\bar{C}$ can be expressed as a linear function of the Coulomb and exchange integrals (in Slater's notation, F and G, respectively (7), or in SCF molecular methods (8), J and K). If we assume that all the d-orbitals possess the same radial function $f(r)$, these integrals can be expressed as linear functions of three of them, so that, in fact, $\bar{C}$ depends only on three parameters. For convenience, Racah proposed to replace the F and G Slater integrals by three linear combinations of these F and G: A, B, and C(9). In fact, the d-transition energies depend only on the B and C parameters, with the A parameters canceling out in the calculations.

The J and K, or F and G, or B and C parameters are calculable from the analytic expression for $f(r)$. Unfortunately, the exact expression for $f(r)$ is unknown. If we utilize hydrogenic functions with an effective charge ζ_m determined by the minimization of the ground state energy, or with charge ζ_{sl} given by Slater's rules (10) (both values are very close), the energies obtained for the transitions are too small (80% of the experimental values only), from which one concludes that the theoretical values have to be replaced by values fitted to experiment, without making the exact form of the orbitals precise. In the general case, two parameters (e.g. B and C) have to be determined. If we assume that $f(r)$ corresponds to a hydrogenic function, the ratio B/C is fixed (ca. 0.25), so that only one arbitrary parameter remains: B, for instance, or the single orbital Coulomb integral $J = \langle d^2|r^{-1}|d^2\rangle$ (the same for all the real d-orbitals). *A priori*, fitting by means of two parameters must lead to a better agreement with experiment than a one-parameter fit. In fact, if we are content with an accuracy of

TABLE 1. Values of J fitted to experiment (11) and values of the effective charge ζ, assuming the orbitals are hydrogenic ($J = 2.51\ \zeta$ eV)

M^{2+}	J (eV)	ζ	M^{3+}	J (eV)	ζ
Ni^{2+}	20.5	8.2			
Co^{2+}	19.6	7.8			
Fe^{2+}	18.5	7.4	Fe^{3+}	20.1	8.0
Mn^{2+}	16.8	6.7	Mn^{3+}	19.2	7.7
Cr^{2+}	16.0	6.4	Cr^{3+}	17.5	7.0
V^{2+}	14.4	5.8	V^{3+}	16.6	6.6
Ti^{2+}	13.4	5.3			

0.1 eV for all the energy levels of the transition elements and their ions, the use of one parameter (e.g. J) is sufficient. In Table 1, we have listed the smoothed values of J, and the values of ζ corresponding to the hydrogen d-orbitals, which are, of course, equivalent to Slater-type orbitals for the present case ($3d$).

The situation is the same when the atom is embedded inside a crystal. Within the same 0.1 eV accuracy, it is possible to reproduce the spectrum using, on the one hand, only one Coulomb parameter, J, and, on the other, parameters linked to the intensity and the symmetry of the crystal field. As an example, we show the case of the Ni^{2+} ion, in the isolated state, and inside a MgO matrix (Table 2).

The fact that it is possible to reproduce the spectra of an ion using the Hartree–Fock model, in the isolated state or inside a crystal, by means of a unique Coulomb parameter J, means that, with the accuracy of 0.1 eV for the energy, (i) explicit treatment of electron correlation can be neglected due to the parametric approach; and (ii) for the calculation of the Coulomb interaction, at least, it is possible to replace the actual orbitals by hydrogen-like functions with suitable effective charges.

With respect to the isolated state, the decrease in the Coulomb repulsion energy in a crystal can be interpreted as arising from a modification of the orbitals, which can be (formally at least) simulated by a simple ζ variation. We will completely neglect the question why, for the p-orbitals, Slater or optimum effective ζ's give larger J values than experiment (12, 13), whereas, for the d-orbitals, these same ζ's give smaller values. Our purpose, indeed, is only to study the difference in behavior of an ion in the isolated state and inside a crystal.

The reduction of the Coulomb interaction inside an ionic crystal

According to Table 2 concerning the Ni^{2+} ion in an MgO matrix, we see that it is necessary to reduce J by the factor $\lambda = 0.87$. In Table 3, the reader will find other examples for which we have calculated the reduction factor λ from experimental spectra published by various authors. Consequently, we find the same phenomenon as in the complex ions in solution. The interpretation of the spectra of these compounds, indeed, necessitates a reduction of Coulomb parameters (1, 20), adapted to the case under consideration.

In these ions, the reduction of the Coulomb interaction is usually explained by invoking a covalency effect (2, 3). Nevertheless, the question is far from being very clear, owing to the fact that in the molecular semiempirical π-methods — Parr–Pariser method (12) or the improved LCAO method (13) — the Coulomb parameters fitted to isolated atoms, lead to excellent values for the molecular transition energies. Given that, in this case, the bond-effect plays the main role, we are led to think that in crystals another factor must necessarily be introduced. As we have recalled in the Introduction, certain authors have envisaged a modification in the form of the atomic orbitals designed to take into account the boundary conditions assigned to the electron density by the surrounding ions.

The case of Cr^{3+} in MgO is very significant concerning the importance of the boundary conditions. The reduction indeed is greater than that for the other ions. The phenomenon is certainly connected with the small radius of Cr^{3+} (0.55 Å) which provokes a local relaxation of the lattice with a reduction of the R_{CrO} distance, whereas no relaxation appears for Ni^{2+} and Co^{2+} in MgO (3, 14), Ni^{2+} in NiO, and Mn^{2+} in MnO. We will come back to the case of Cr^{3+} in MgO later on. Moreover, in the planar π-systems, the electron density is essentially located above and below the plane of the molecule, i.e. within domains where no hindrance exists. All these remarks lead us to examine the eventual effect of the confinement of an atom inside a box.

The box effect

In order to study the problem in a detailed manner, we will consider the simple case of a helium atom located at the center of a spherical box of radius R. The case of a hydrogen atom (21) and that of various atoms belonging to the first row (31) in such a situation has been considered by many authors using various methods. The problem of the Coulomb repulsion does not seem to have been explicitly considered.

As for the case of ions in a crystal, we will remain within the Hartree–Fock framework. In order to simplify the calculations, we will consider the particular case for which the radius R is such that the product $R\zeta$ is equal to 2. The solution is then obvious.

$$\chi = \frac{\zeta^{3/2}}{\sqrt{32\pi}} (2 - r\zeta) \exp(-r\zeta/2) \qquad (0 < r \leq 2/\zeta)$$

The kinetic, nuclear repulsion, and Coulomb repulsion integrals are, respectively, equal to

$$\langle T \rangle = 1.410\zeta^2,\ \langle r^{-1} \rangle = 1.535\zeta \text{ and } \langle r_{\mu\nu}^{-1} \rangle = 1.046\zeta \text{ au}$$

If R is infinite (free atom), these integrals are respectively equal to $\zeta^2/2$, ζ, and $(5/8)\zeta$ au.

Inside the box, the energy of the atom is

$$E = 2.820\zeta^2 - 6.140\zeta + 1.046\zeta$$

The condition $\partial E/\partial \zeta = 0$ determines ζ (and consequently R), and the repulsion energy:

$$\zeta = 0.903; \qquad R = 2.215 \text{ au}; \qquad \bar{C} = 0.945 \text{ au}$$

If $R = \infty$, $\zeta = 1.698$ and $\bar{C} = 1.055$ au. Consequently within a box of a finite radius, the average electron repulsion is weaker than that for an isolated atom (the validity of this conclusion has been verified for various values of R). In the present case, where $R = 2.215$ au, $\lambda = 0.90$. More generally, for a He-like ion of a nuclear charge equal to Z, we have

$$\lambda = \frac{0.570Z - 0.195}{0.625Z - 0.195}$$

Practically, whatever Z may be, λ always remains very close to 0.9.

At first sight, this reduction can appear as surprising, given

TABLE 2. Absorption spectrum of Ni^{2+}, isolated and in MgO

(a) In the isolated state*

Transition	Exp. (13)	Calculated from ζ_m = 7.37,	J = 20.5 eV,	B = 1100, and C = 4120 cm^{-1}
$^3F \rightarrow {}^3D$	1.62 eV	1.54	1.70	1.70
^3P	1.96	1.78	1.97	2.04
^1G	2.74	2.37	2.63	2.66

*ζ_m corresponds to J = 18.5 eV.

(b) In MgO

Transition	Exp. (3)	Calculated from $\tilde{J}$ = 17.8 eV and Δ = 1.08 eV*
$^3A_2 \rightarrow {}^3T_{2g}$	1.07 eV	1.07
$^3T_{1g}$	1.78	1.78
$^3T_{1g}$	3.04	3.11
^1E_g	1.66	1.72
$^1T_{2g}$	2.67	2.68
$^1T_{1g}$	3.51	3.47
$^1T_{2g}$	4.28	4.29

*Δ = Crystal field parameter (O_h symmetry).

TABLE 3. Reduction factor $\lambda = \tilde{J}/J$ ($\tilde{J}$ corresponding to the crystal and J to the isolated ion); ionic radius, r_M; distance from the nearest-neighboring atoms without relaxation, R_{MO} (values in parentheses are those with relaxation)

M^{2+}	Crystal	λ	r_M (18)	R_{MO} (19)	λ_{calcd} from [2]
Ni^{2+}	MgO (3)	0.87	0.69 Å	2.11 Å	0.87
Co^{2+}	MgO (14)	0.85	0.72	2.11	0.85
Cr^{3+}	MgO (15)	0.80	0.55	2.11 (1.8)	0.93 (0.81)
Ni^{2+}	NiO (16)	0.86	0.69	2.08	0.86
Mn^{2+}	MnO (17)	0.86	0.80	2.22	0.86

that on the average the electrons are nearer to each other inside a box than in the free state. In fact, the decrease in the average distance enhances the mutual screening effects, so that ζ decreases.

This result can be applied qualitatively to our problem. We will remark, first, that if the sphere inside which the atom is confined, is uniformly charged, inside this sphere the potential is modified only by an additive constant, which does not change the result. Moreover, as a first approximation, we can approximate the field created by the atoms surrounding the central ion by that created by a continuous charge distribution.

Practically, we can say, of course, that the reduction of the Coulomb interaction arises from a modification in the radial function of the atomic orbitals, arising from boundary conditions. Nevertheless, the direction of the variation is not that which Sugano *et al.* have proposed (2). These authors, indeed, suggested that the radial functions are expanded towards the ligands. Our calculation can better be compared with attempts made by certain authors which take the presence of the neighboring atoms into account to evaluate the characteristics of the central ion. Kleiner, for instance, cuts the radial functions of the central atom at a certain distance from the nucleus (4). For his part, Watson, treating an Mn^{2+} ion surrounded by six point charges, obtains F and G terms slightly greater (by about 2%) than in the free ion (5).

Practical consequences

The previous calculation shows that, within the simple Hartree–Fock model, the confinement of an ion inside a crystal lattice provokes a reduction of the Coulomb interaction which can be simulated by a simple reduction of the effective nuclear charges ζ of the atomic orbitals. Independent of any eventual covalent effect, the box effect has to be taken into account.

In numerous cases, both of these effects can seem to be connected with each other, a large interionic distance corresponding to a weak bond-order, i.e. to a weak electron transfer from the anions to the cations. For instance, in cubic oxides (MgO, NiO, MnO): the net charges $Q \sim 1.6-1.8$ and $R_{MO} \sim 2.0 - 2.2$ Å, whereas in D_{3d} carbonates ($CaCO_3$, $FeCO_3$): $Q \sim 1.9$ and $R_{MO} \sim 3.2-3.5$ Å (22–23). In $MgCO_3$ and $MnCO_3$, however, Q is weaker (1.6 and 1.4 respectively) although $R > 3$ Å, so that the connection between the ionicity and the geometrical parameters is not obvious. In order to evaluate the relative contribution of both effects, we will consider various carbonates, pure or containing ionic impurities, namely: $CaCO_3$ with Fe^{2+}, Fe^{3+}, Ni^{2+}, $MgCO_3$ with Ni^{2+}, $FeCO_3$ and $MnCO_3$. This series corresponds to lattices in which the box effect should not interfere, owing to the large size of the cavity in which the chromophore ion is located. In other terms, $\lambda = 1$. In contrast, the degrees of covalency vary in a large range from 1.4 in $MnCO_3$ to 1.9 in $CaCO_3$.

In a first stage, we shall neglect any covalency effect, i.e. we will adopt the effective charges ζ which correspond to the isolated ions (Table 1).

Remark on the practical calculation of the crystal field potential

The calculation of the transition energies in a crystal requires not only the knowledge of the J integral corresponding to the

TABLE 4. Corrections to the orbital energies arising from the crystal field (net charges of crystal assumed equal to 2)*

Crystal	Symmetry	Corrections δe (in eV)	
MgO	O_h	δ: $538\zeta^{-4}+1852\zeta^{-6}$	
NiO	O_h	δ: $567\zeta^{-4}+1993\zeta^{-6}$	
MnO	O_h	δ: $412\zeta^{-4}+1273\zeta^{-6}$	
$CaCO_3$	D_{3d}	δe_1: $-52.10\zeta^{-2}+136.44\zeta^{-4}$	δe_2: $-26.05\zeta^{-2}-90.96\zeta^{-4}$
$MgCO_3$	D_{3d}	δe_1: $-50.9\zeta^{-2}+158.7\zeta^{-4}$	δe_2: $-25.5\zeta^{-2}-105.8\zeta^{-4}$
$FeCO_3$	D_{3d}	δe_1: $-50.9\zeta^{-2}+158.7\zeta^{-4}$	δe_2: $-25.5\zeta^{-2}-105.8\zeta^{-4}$
$MnCO_3$	D_{3d}	δe_1: $-66.6\zeta^{-2}+222.1\zeta^{-4}$	δe_2: $-33.3\zeta^{-2}-148.1\zeta^{-4}$

* $1 = d_{z^2}$; $2 = d_{xz}$; $3 = d_{yz}$; $4 = d_{xy}$; $5 = d_{x^2-y^2}$; for O_h symmetry; $\delta e_1 = \delta_{e5} = 3\delta$; $\delta e_2 = \delta e_3 = \delta e_4 = -2\delta$ ($5\delta = \Delta$); for D_{3d} symmetry; $\delta e_2 = \delta e_3$ and $\delta e_4 = \delta e_5$ ($\Sigma\delta e_i = 0$).

TABLE 5. Transition energies (in eV) for various ions in cubic oxides and rhombohedral carbonates; numbers in parentheses are wavelengths in nm, when the transition is located in the visible (400−780 nm); Q = net charge of the crystal (22)

				Energy	
Ion	Crystal	λ	Q	Calculated	Observed
Ni^{2+}	MgO	0.87	1.7	1.1/1.7(730)/1.8(600)/2.7(460)/ 3.1(410)/3.5/4.3	1.1/1.7/1.8/2.7/3.0/3.5/4.3 green (3)
Co^{2+}	MgO	0.85	1.7	1.1/2.3(540)/2.4(520)	1.1/2.3/2.5 light-pink (14)
Ni^{2+}	NiO	0.86	1.7	1.1/1.7(730)/1.8(690)/2.7(460) = yellow + green	Yellow−green* (16)
Mn^{2+}	MnO	0.86	1.6	2.1(590)/2.5(500)/2.8(440)/3.4	2.0/2.5/2.7/3.5 green* (16, 17)
Fe^{2+}	$CaCO_3$	1	1.9	1.8(690) = green−blue	Green−blue
Fe^{3+}	$CaCO_3$	1	1.9	2.3(540)/2.2(560)/3.2(390)	Brown
Fe^{2+}	$FeCO_3$	1	1.8	1.6(780) = practically colorless	Colorless (26)
Ni^{2+}	$CaCO_3$	1	1.9	1.9(650)/3.0(410) = yellow	Lemon−yellow (27)
Ni^{2+}	$MgCO_3$	1	1.6	1.7(720)/2.7(460) = green	Light−green (28)
Mn^{2+}	$MnCO_3$	1	1.4	2.2(560)/2.3(540)/3.2(390) = red−purple	ca. 2.3/3.1 (29) red−rose

*Color of crystals indicated in ref. 16.

central ion, but also that of the values of the crystal field parameters. Using a one-electron potential, these latter terms are easily calculable, on the one hand, from the analytical expression of the atomic orbitals, and, on the other, from the positions and the values of the charges which create the field. Although the charges carried by the first nearest-neighboring ions bring a contribution greater than 80% to the actual field (24), it is more advisable to utilize a multipole development. In this paper, we will utilize the method we have previously described (25).

Practically, the coefficients A_n of the multipoles P_n are obtained by writing that the potential $V = \Sigma A_n P_n$ is equal to the Madelung potential at the point where the chromophore ion is located, and that $V = 0$ for a certain number of points, determined by symmetry (e.g., in O_h symmetry: $a/2$, 0, 0; $a/2$, $a/2$, $a/2$; etc., a being the value of the distance between the nearest-neighboring ions). In order to obtain the coefficients of the N first multipoles, we must consider $(N - 1)$ points for which $V = 0$. It follows that the variation of the orbital energy e is equal to $\delta e = \Sigma A_n \langle d|P_n|d\rangle = \Sigma a_n \zeta^{-n}$. Table 4 gives the results corresponding to various crystals.

An important point is the following. According to the Slater rules (10), the electron transfer modifies the effective charges ζ. For instance, a transfer equal to 0.2 electron leads to a decrease of $0.2 \times 0.35 = 0.07$ which corresponds to a relative decrease in the transition energies of 1%, i.e. to 0.02−0.03 eV in the visible. Such a correction is much less than the accuracy (0.1 eV) of the model. For this reason, we will use the effective charges of the isolated ions to calculate the electronic Coulomb interactions. On the contrary, the electron transfers can play a non-negligible role in the evaluation of the crystal field. The electric potential, indeed, is proportional to the charges which create it. This effect has to be taken into account.

Results concerning O_h oxides and D_{3d} carbonates

In Table 4, we give the expressions of the terms arising from the crystal field, and in Table 5, the results corresponding to the spectra. When the spectrum is not determined experimentally, we indicate the color of the mineral.

Manifestly, the agreement with experiment is excellent. But the most remarkable point is that the spectra of carbonates can be interpreted from the effective charges ζ of the isolated ions ($\lambda = 1$) without introducing any covalent effect. The fact is all the more interesting since the degree of covalency varies in this series from 5 to 30%, whereas for oxides this degree varies from 15 to 20% only. In other terms, in the cases under consideration, the box effect does play a more important role than the covalency effect.

An empirical relationship between the reduction factor and the geometrical parameters

Independent of any theoretical consideration we can try to connect the reduction factor λ with the size of the cavity and the radius of the ion r. The following relationship

$$[2] \quad \lambda = 1 - 0.40 \left(\frac{r}{R_{MO} - 1.1}\right)^3 \qquad (r \text{ and } R_{MO} \text{ in Å})$$

leads to very satisfying results. The calculated values corresponding to oxides are listed in Table 3. For the carbonates, λ is practically equal to 1. Moreover, we have previously remarked that the reduction factor for Cr^{3+} in MgO is weaker (0.80) than the factors corresponding to the other cases (Table 3) and we have thought that the difference might arise from the small size of Cr^{3+} which would provoke a local relaxation. If we admit that Cr^{3+} is in contact with the oxygen ions ($R \sim 1.8$ Å), formula [2] gives $\lambda = 0.81$, i.e., a value very close to the actual value (0.80).

Another example which corroborates our interpretation is that of lizardite $(Mg, Ni)_3Si_2O_5(OH)_4$. In this mineral a certain proportion of Mg^{2+} ions is substituted by Ni^{2+} ions. The NiO distances are practically equal to 2.1 Å, i.e. to the value in an MgO matrix. The reduction factor is equal to 0.87−0.88, i.e. practically equal to that calculated for Ni^{2+} in MgO, even though lizardite presents a notable degree of covalency (30).

1. J. S. GRIFFITH. The theory of transition-metal ions, Cambridge Univ. Press. 1961.
2. S. SUGANO, Y. TANABE, and H. KAMIMURA. Multiplets of transition-metal ions in crystals, Academic Press, New York. 1970.
3. W. LOW. Phys. Rev. **109**, 247 (1958).
4. W. H. KLEINER. J. Chem. Phys. **20**, 1784 (1952).
5. R. E. WATSON. Phys. Rev. **117**, 742 (1960).
6. K. NASSAU. Gems made by man. Chilton Book Co., Radnor PA. 1980.
7. E. U. CONDON and G. H. SHORTLEY. Theory of atomic spectra. Cambridge University Press. 1935.
8. C. C. J. ROOTHAAN. Rev. Mod. Phys. **23**, 69 (1951).
9. G. RACAH. Phys. Rev. **61**, 186 (1942); **62**, 438 (1942).
10. J. C. SLATER. Phys. Rev. **36**, 57 (1930).
11. C. E. MOORE. Atomic energy levels. Natl. Bur. Std., Washington D.C. 1949.
12. R. PARISER and R. G. PARR. J. Chem. Phys. **21**, 466 (1953).
13. A. JULG. J. Chim. Phys. **57**, 19 (1960).
14. W. LOW. Phys. Rev. **109**, 256 (1958).
15. W. LOW. Phys. Rev. **105**, 801 (1957).
16. L. HACKSPILL, J. BESSON and A. HEROLD. Chimie Minérale, Presses Univ. France, Paris, 1958.
17. K. L. KEESTER and W. B. WHITE. Crystal field spectra and chemical bonding in Mn minerals. Papers and Proc. 5th Gen. Meet. Cambridge, Mineral Soc., London. 1968.
18. J. A. A. KETELAAR. Chemical constitution. Elsevier Publ. Co., Amsterdam. 1953.
19. R. W. G. WYCKOFF. Crystal structures. Wiley, New York. 1963.
20. C. K. JØRGENSEN. Discuss. Faraday Soc. **26**, 110 (1958).
21. F. V. LUDEÑA. J. Chem. Phys. **66**, 468 (1977); F. M. FERNANDEZ and E. A. CASTRO. J. Math. Phys. **23**, 1103 (1982) and the numerous references quoted in the latter article.
22. A. JULG. Crystals as giant molecules. Lecture notes in chemistry. vol. 9, Springer-Verlag, Berlin. 1978.
23. A. JULG. Phys. Chem. Miner. **3**, 45 (1978).
24. M. T. HUTCHINGS. *In* Solid state physics. Vol. 16 *Edited by* F. Seitz and D. Turnbull. Academic Press, New York, 1954. p. 227.
25. A. JULG and D. LETOQUART. Phil. Mag. **33**, 721 (1976).
26. A. S. MARFUNIN. Physics of minerals and inorganic materials. Springer-Verlag, Berlin. 1979.
27. J. M. NUSSIK. Izv. Akad. Nauk. SSR. Ser. Geol. **3**, 108 (1969).
28. D. L. WOOD and A. A. BALLMAN. Am. Min. **51**, 216 (1966).
29. R. STEVENSON. J. Appl. Phys. **39**, 1143 (1968).
30. B. D. CERVELLE and M. MAQUET. Clay Miner. **17**, 377 (1982); A. JULG and O. JULG. Clay Miner. **19**, 107 (1984).
31. E. V. LUDEÑA. J. Chem. Phys. **69**, 1770 (1978); **71**, 2235 (1979).

Investigations of the assignment of the 2190 cm^{-1} infrared band in polyfumaronitrile

KENNETH L. GALLAHER, DOROTHY LUKCO, AND JEANETTE G. GRASSELLI[1]

The Standard Oil Company (Ohio) Research and Development Center, 4440 Warrensville Center Road, Cleveland, OH 44128, U.S.A.

Received August 6, 1984

This paper is dedicated to Professor Camille Sandorfy on the occasion of his 65th birthday

KENNETH L. GALLAHER, DOROTHY LUKCO, and JEANETTE G. GRASSELLI. Can. J. Chem. **63**, 1960 (1985).

Polyfumaronitrile exhibits a band at 2190 cm^{-1} which has at various times been associated with a β-aminonitrile, an iminonitrile, or with C═N in an α-pyrrolenine ring. This band is of particular interest because it sometimes appears in degraded polyacrylonitrile and nitrile-containing resins. The previous conflicting assignments were made on the basis of ir, uv, ^{1}H nmr, and chemical results. This paper reports new infrared, esr, and solid-state carbon nmr results which indicate that the 2190 cm^{-1} band is most likely due to a β-aminonitrile functionality. The close spectral similarity with 3-amino crotonitrile is particularly noted. A mechanism is proposed which would explain the presence of such a nitrile in polyfumaronitrile.

KENNETH L. GALLAHER, DOROTHY LUKCO et JEANETTE G. GRASSELLI. Can. J. Chem. **63**, 1960 (1985).

Le spectre du polyfumaronitrile présente une bande à 2190 cm^{-1} qui a été attribué, par divers auteurs, soit à un β-aminonitrile, soit un iminonitrile ou à un C═N en α d'un cycle pyrrolénine. Cette bande présente un intérêt particulier à cause du fait qu'elle apparaît quelquefois dans les spectres de résines contenant des nitriles ou des polyacrylonitriles dégradés. Les attributions divergentes antérieures ont été faites sur la base de spectres ir, uv ou rmn du ^{1}H ainsi que sur des résultats chimiques. Dans le présent travail, on rapporte les résultats de nouvelles mesures en ir, en rpe et en rmn du ^{13}C à l'état solide; ces résultats indiquent que la bande à 2190 cm^{-1} est probablement due à un groupe β-aminonitrile. On note particulièrement la très grande ressemblance avec l'amino-3 crotonitrile. On propose un mécanisme qui pourrait expliquer la présence d'un tel nitrile dans le polyfumaronitrile.

[Traduit par le journal]

Introduction

Polyfumaronitrile (poly (*trans*-1,2-dicyanoethylene)), PFN, exhibits an absorbance at about 2190 cm^{-1} in its infrared spectrum. This band, which has at various times been associated with a β-aminonitrile, an iminonitrile, or with C═N in an α-pyrrolenine ring (Table 1), also sometimes appears in acrylonitrile-containing polymers as well as in degraded polyacrylonitrile. The most detailed study of PFN by Liepins *et al.* (1), using ir, uv, ^{1}H nmr, and a number of chemical tests, concluded that only the α-pyrrolenine structure was present and that a nitrile functionality was not present in the polymer.

Part of Liepins' argument was that 2190 cm^{-1} is low for a nitrile absorption and, indeed, Bellamy (2, 3) quotes the range in which nitriles absorb as between 2215 and 2260 cm^{-1}. However, there are a number of examples of nitrile-containing compounds which absorb considerably below 2200 cm^{-1} (4). This fact places some doubt on Liepins' interpretation, along with the fact that Liepins did not propose any alternative assignment except to state that the 2190 cm^{-1} band was "characteristic" of the structure he proposed. In order to better determine the true structure of polyfumaronitrile, further work was done using some new spectroscopic techniques such as carbon-13 nmr and carbon-13 solid-state nmr, which Liepins did not have readily available.

Experimental

Synthesis of the PFN was done according to Liepins' published method (1). Approximately 1 g of fumaronitrile was placed in a glass bottle with di-*tert*-butyl peroxide and reacted at 160°C in a metal bomb. It was determined that lower temperature and (or) shorter reaction time decreased molecular weight and increased solubility. Solubility was essential in order for any liquid phase nmr work to be done. But the reduced time and temperature also reduced the yield to as low as 1% in some cases. Residual fumaronitrile was removed by vacuum sublimation. This avoided the solvent contamination problems Liepins reported; however, it also reduced the yield of product since high speed gpc indicated that sublimation induced a nearly two-fold decrease in molecular weight and depolymerization back to the monomer in low molecular weight polymers. The polymer obtained ranged from a brown powder for lower molecular wieght material to a black shiny powder in the high molecular weight samples. Elemental analyses gave an empirical formula close to that of fumaronitrile with about 3% by weight oxygen. However, there was also as much as 10% "ash" which could either have been inorganic contaminants or graphite-type materials not fully consumed by the CHN analyzer.

All infrared spectra were obtained on a Nicolet 7199 FT-IR spectrometer. Sample spectra were obtained as KBr pellets. The KBr was not ground in order to minimize water contamination. The ^{1}H nmr spectra were obtained on a Varian EM-390 CW NMR with a Nicolet 1180 data system. Liquid ^{13}C nmr spectra were obtained on a Varian XL-100 with Nicolet multinuclear probe and data system. Solid state nmr spectra were obtained on a Nicolet S-100 instrument.

TABLE 1. Proposed assignment for 2190 cm^{-1} infrared band

$H_2N—\overset{\vert}{C}═\overset{\vert}{C}—C≡N$	β-Aminonitrile (enaminonitrile)
$HN═\overset{\vert}{C}—\overset{\vert}{C}H—C≡N$	Iminonitrile
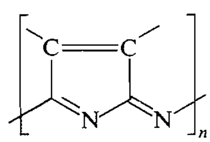	α-Pyrrolenine

Results and discussion

A. *Infrared*

The ir spectra contained a number of surprises. The high and low molecular weight polymers are clearly quite different (Fig. 1). The spectra show many differences in band intensities and

[1] Author to whom correspondence may be addressed.

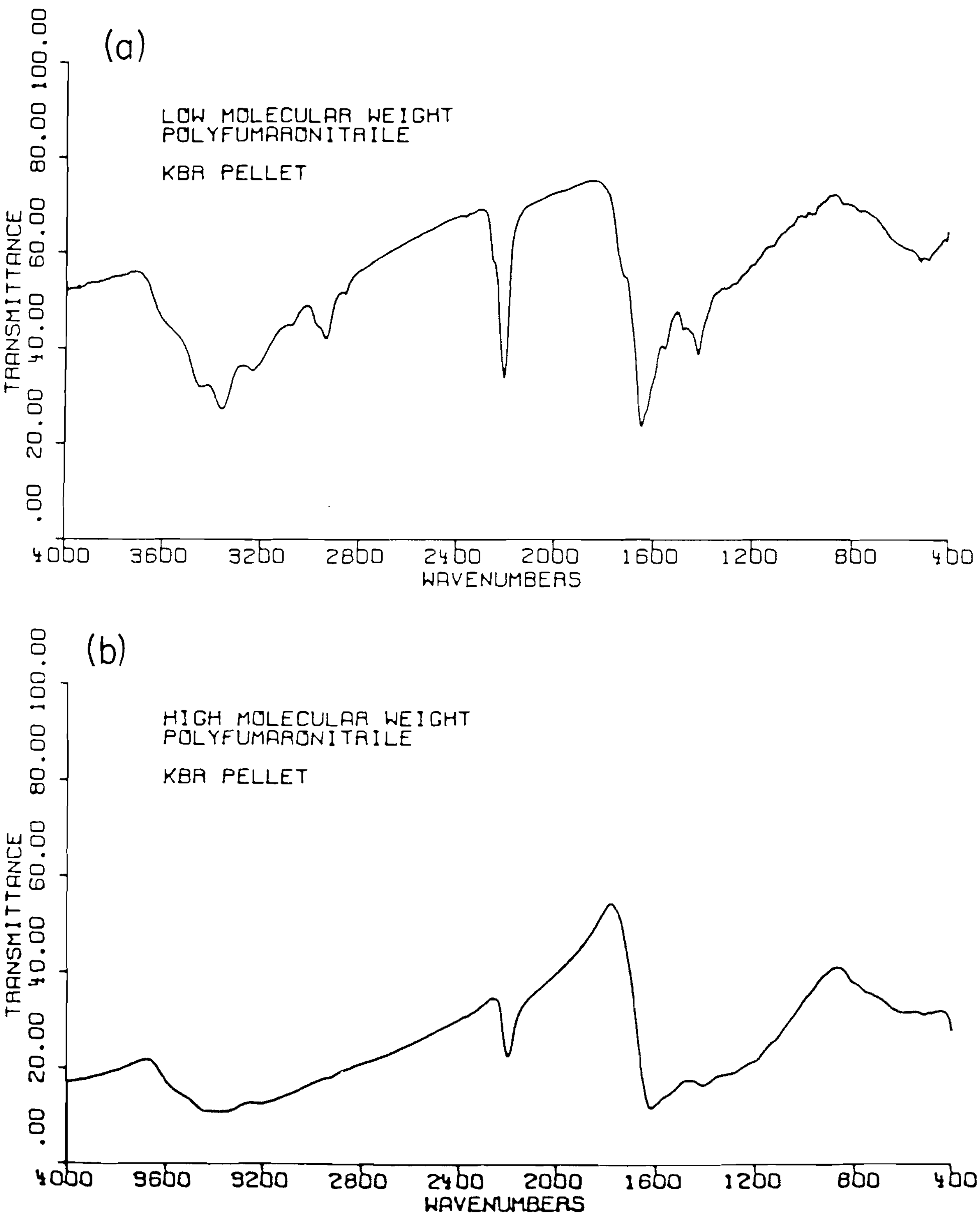

FIG. 1. Infrared spectra of polyfumaronitrile. (a) Low molecular weight; (b) High molecular weight.

position. The low molecular weight polymer in particular appears to contain primary amine. There are three fairly well resolved bands at 3442, 3359, and 3233 cm^{-1}, which are most likely due to N—H stretch. The strongest band in the spectrum has its maximum at 1648 cm^{-1} and could well be due to NH deformation in a primary amine. The sloping background between 900 and 500 cm^{-1} is also evidence for amine. This is, of course, completely contrary to the α-pyrrolenine structure, which contains only olefinic hydrogens. The high molecular weight polymer still shows absorption in the 3600–3000 region but it is less well resolved. The 1648 maximum has either disappeared or moved down to 1621 cm^{-1}. This shift could be due to increased conjugation, similar to that observed in azide- or aldehyde-substituted polyenes. Long chain polyenes all have a complex C═C absorption in the 1650–1600 cm^{-1} region with the strongest band always at 1650 cm^{-1}. However, when

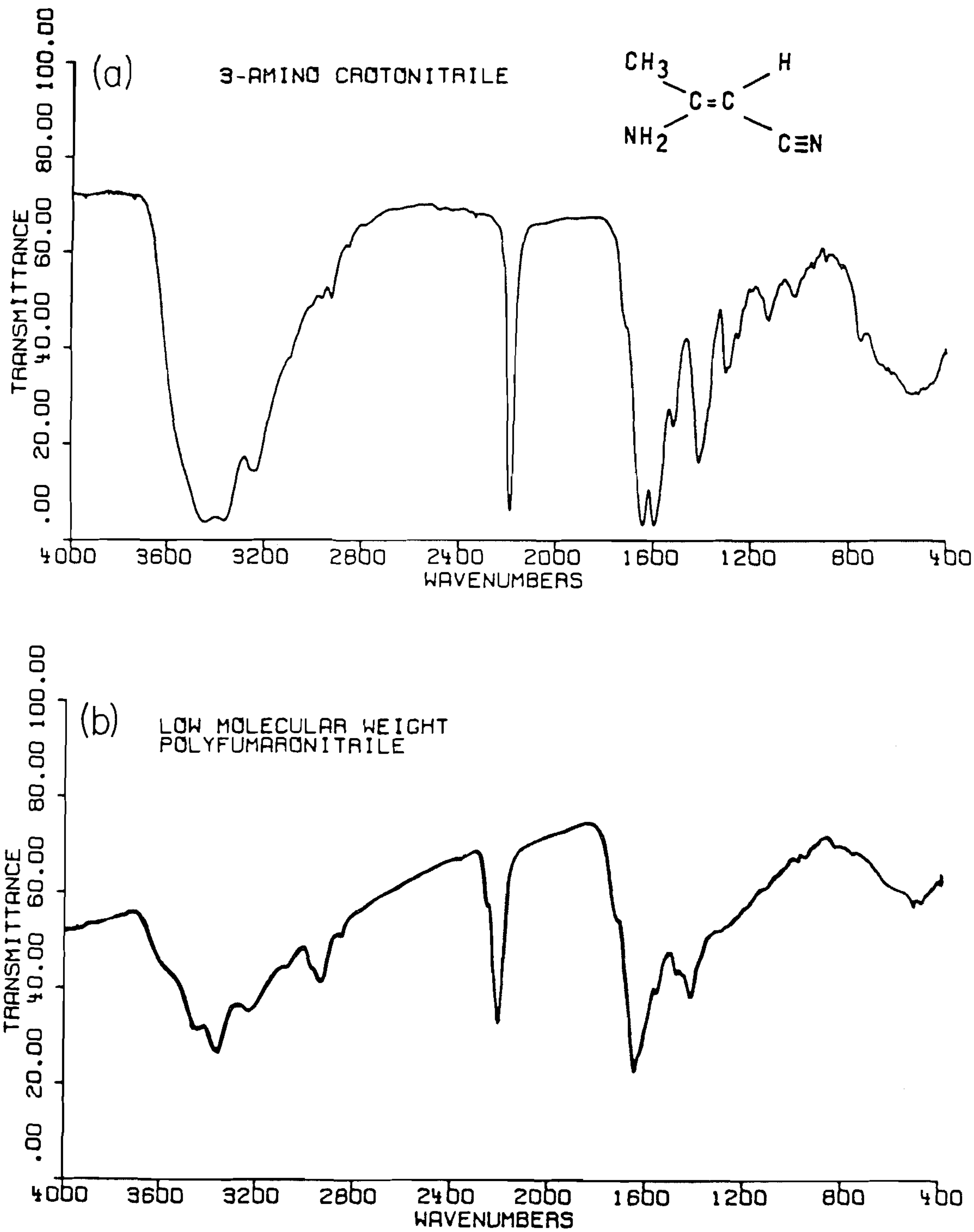

FIG. 2. (a) Infrared spectrum of 3-amino crotonitrile. (b) Infrared spectrum of low molecular weight polyfumaronitrile.

substituted with another kind of unsaturated functionality like an aldehyde or azide, the C═C vibration shifts to progressively lower frequency as the number of bonds in the conjugation increases (5). The "2190 cm^{-1}" band itself also moves. In the high molecular weight material the vibration is at 2195 cm^{-1}, while in the low molecular weight material it is at 2206 cm^{-1}.

Another piece of data which tends to support some of these interpretations is the ir spectrum of 3-amino crotonitrile (1-cyano 2-amino propylene) (Fig. 2). The overall resemblance to the low molecular weight PFN is striking. The N— H stretch bands are present, along with the 1650 cm^{-1} band and the weaker bands at 1415 and 1520 cm^{-1}. The nitrile peak position is 2185 cm^{-1}.

The spectral feature worthy of note in the low and high molecular weight polymers is the broadness of the 2190 cm^{-1} bands, which are nearly twice the width of the typically sharp nitrile vibration. There is also an upward sloping background in the high energy end of the ir spectra, especially in that of the high molecular weight polymer. Even extensively ground samples show this background, and so it is believed to be real, and not due to light scattering. A group of compounds which ex-

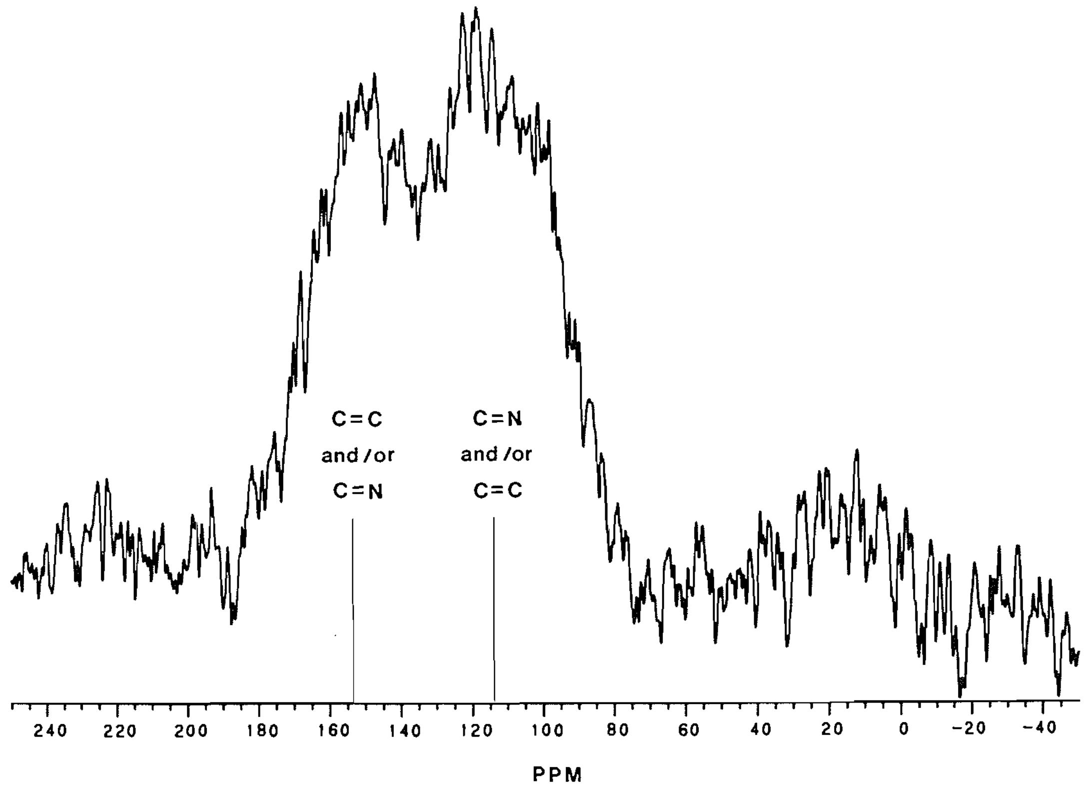

FIG. 3. Solid state ^{13}C nmr spectrum of high molecular weight polyfumaronitrile.

hibit similar spectral characteristics are 7,7,8,8-tetracyanoquinodimethane (TCNQ) and its salts (6). Most widely known for the high conductivity of its salts, TCNQ itself shows a narrow nitrile vibration at about 2220 cm^{-1}, while the corresponding band in the triethyl ammonium salt is considerably broadened and is between 2175 and 2198 cm^{-1}. Further, the salts show a broad near-ir band with a maximum at about 8000 cm^{-1} which is ascribed to electronic rather than vibrational absorption.

B. *^1H and ^{13}C nuclear magnetic resonance*

Efforts were also made to obtain good liquid nmr spectra. High molecular weight PFN is totally insoluble in a wide variety of solvents. Low molecular weight PFN appeared to dissolve in DMSO-d_6 to give a very dark, slightly viscous solution. However, the proton and carbon nmr spectra which were obtained were very weak and clearly not representative of the total material in the nmr tube. It is possible that the sample was not really as soluble as it appeared, or that free electrons might have seriously broadened the spectra.

The next step was to analyze the samples by esr (electron spin resonance), since if free electrons were present in large numbers they may well broaden an nmr spectrum; however, they will be observable by esr. There are a number of examples which suggest that the existence of free electrons in PFN is reasonable. For example, Rieger *et al.* (7) found that dissolving some polycyanocarbons in DMF was sufficient to produce anion radicals. Also tetracyanoethylene readily forms ion-radical salts with an esr spectrum that shows all of the 20 lines due to ^{13}C splitting as well as the nine lines expected from four equivalent nitrogens. Further, two nitrile bands are observed in these salts, one at 2210 and the other at 2180 cm^{-1}. Unlike TCNQ salts, these salts are not semiconductors. As one would expect, the high conductivity TCNQ salts do exhibit strong esr spectra.

Liepins himself reports that PFN has an esr spectrum and that its conductivity is in the semiconductor range. This implies extended conjugation in the polymer. However, no temperature study was done to determine if the polymer was truly a semiconductor. Liepins does not interpret this data, which makes the meaningfulness of his own (unpublished) ^1H nmr data questionable.

The esr spectra were obtained on both a low molecular weight PFN sample dissolved in DMSO-d_6 and also on a finely ground high molecular weight polymer. A large broad signal was obtained in both cases, indicating enough free electrons to possibly explain the lack of nmr signal if the unpaired electrons are widely diffused over the molecule. This is similar to what Liepins found. He apparently went to some lengths to observe coupling in the esr spectrum but, similar to our results, he found none.

C. *Solid state nuclear magnetic resonance*

In spite of the esr results, an attempt was made to obtain a solid state nmr spectrum. PFN is far from the ideal polymer to examine via solid state nmr. One can expect long relaxation times due to its rigid nature, and poor sensitivity because of the few hydrogens present, possibly none of which are on a carbon. There has also been discussion of broadening effects due to ^{14}N coupling. However, the spectrum shown in Fig. 3 was obtained for a high molecular weight PFN, although it required an unusually long (24 h) acquisition time.

In order to determine if this spectrum was reasonable, the proton and carbon nmr spectra of amino crotonitrile were closely examined. The ^1H nmr spectrum looks like a roughly 50:50 mixture of *cis* and *trans* compound (Fig. 4a). The ratio of the exchangeable protons to the olefin to the methyl is 2:1:3. There is no evidence for imine formation, although the strong upfield shift of the olefin certainly indicates a strong amine

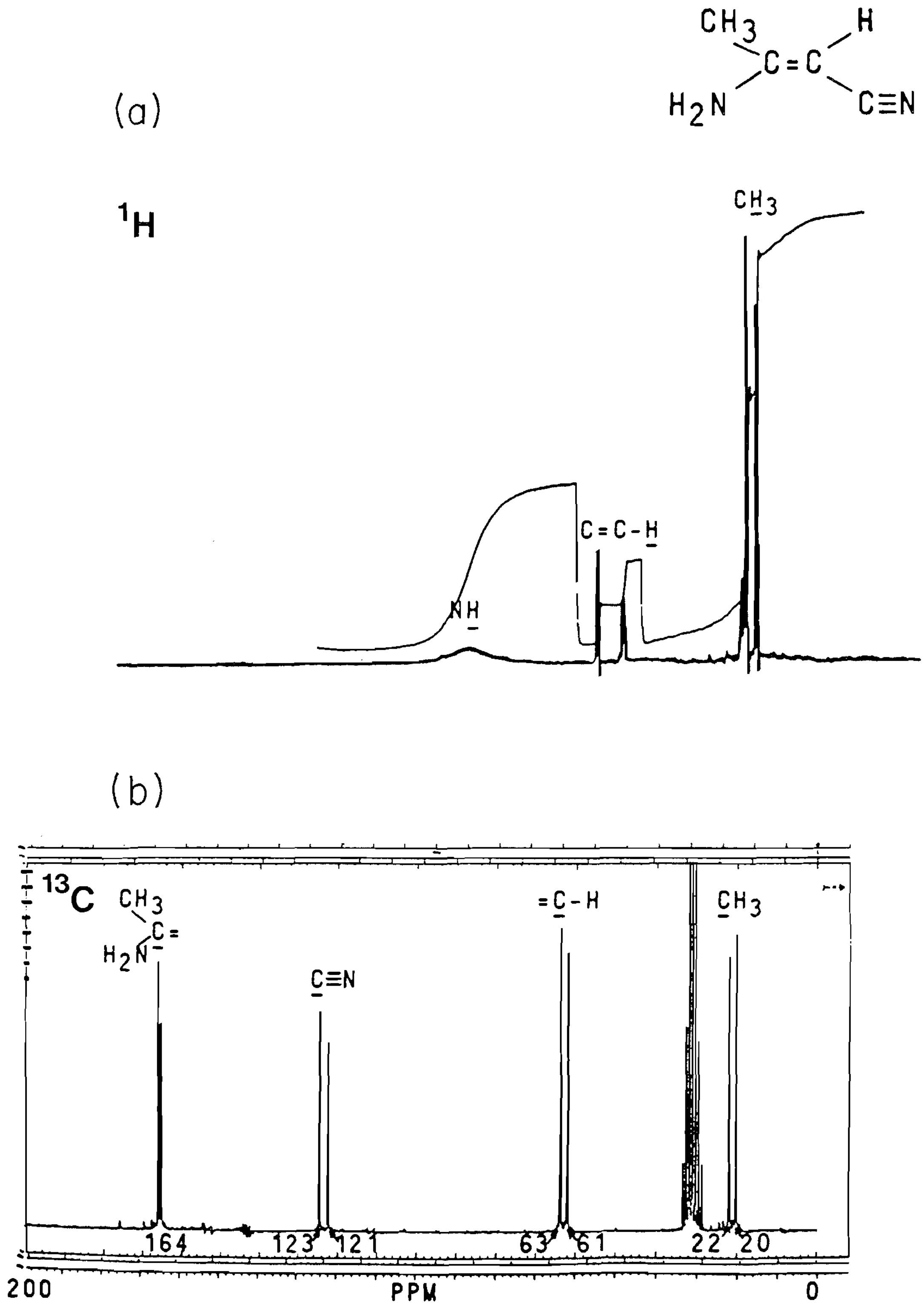

FIG. 4. Nuclear magnetic resonance spectra of 3-amino crotonitrile; (a) ^1H nmr; (b) ^{13}C nmr.

interaction. The higher field of the two olefin peaks no doubt corresponds to the isomer with the amino group *trans* to the olefinic hydrogen, both because one expects the *trans* interaction to be stronger and because the greater linewidth indicates coupling with the NH.

The ^{13}C spectrum can be interpreted similarly (Fig. 4b). The chemical shifts indicate a strong tendency towards the imine form, but no shift of hydrogen. The amine substituted carbon is pushed far downfield in the direction of the C=N bonded carbon, the nitrile and methyl carbons are in nearly normal positions, and the nitrile-substituted carbon is far upfield. Single frequency off-resonance decoupling experiments confirm no hydrogen transfer.

The PFN solid nmr resonance centered at 120 ppm could indeed be due in part to nitrile, while the resonance at 150 ppm could be due to olefin. There is little or no saturated carbon.

D. *Possible PFN mechanism*

How could a polyfumaronitrile that would contain enaminonitrile functionality form? The following mechanism has been postulated. In the initiation step, the fumaronitrile is attacked by a free radical, ·R (e.g. $\cdot CH_3$, $\cdot OC(CH_3)_3$):

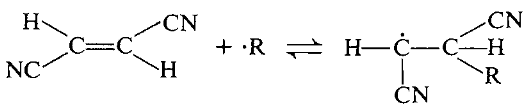

The ·N=C< then becomes the propagating radical, instead of ·R to give

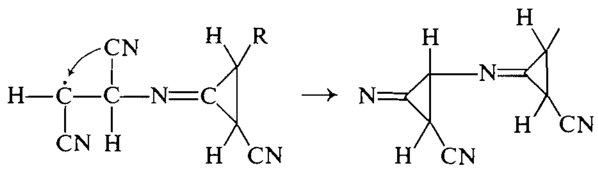

This intermediate could then rearrange to give more stable structures.

At low temperatures a simple proton shift could easily occur, so as to give a conjugated nitrile system:

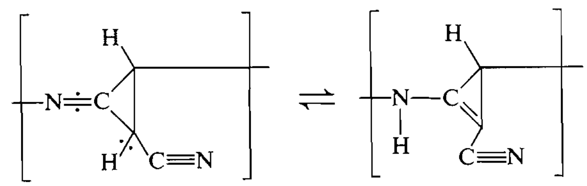

At higher temperatures, ring cleavage will occur. The probable product would be the highly stable ladder structure with six-membered rings. Following the formation of this ladder structure, the same proton shift would occur to give a conjugated nitrile system.

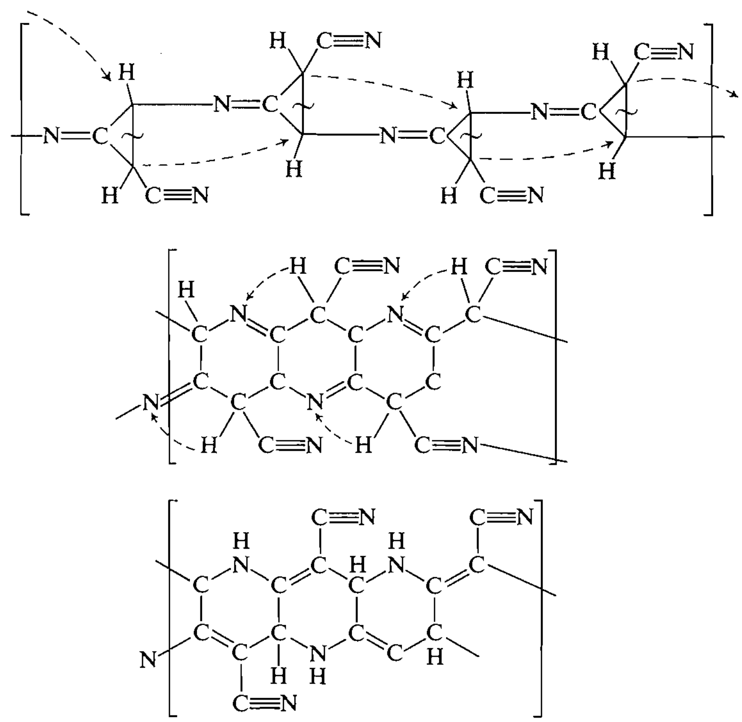

What is the assignment of the 2190 cm^{-1} band in PFN? The resemblance of the low molecular weight PFN ir spectrum to that of amino crotonitrile is so strong that it is hard to assign the 2205 cm^{-1} band to anything but the nitrile absorption in an enaminonitrile. The comparison with the ^{1}H and ^{13}C spectra of amino crotonitrile further confirms that it is an enaminonitrile rather than an iminonitrile.

The 2195 cm^{-1} band is harder to assign. There still appears to be NH present, and it is easy to believe that more extended conjugation lowers the nitrile band 10 cm^{-1}. There are known nitrile compounds with even lower nitrile vibrations. Further, there is solid state nmr evidence for a structure much like that of amino crotonitrile in the high molecular weight (2195 cm^{-1}) material as well. However, the structure shown above cannot be completely correct since the solid's nmr shows so little aliphatic carbon. Further aromatization must be occurring.

Several possible structures for polyfumaronitrile have been proposed, some more reasonable than others. The α-pyrrolenine structure cannot be eliminated as being one component of the polymer. PFN is not a single homogeneous material. An initial structure is formed which is high in enaminonitrile functionality. As is observed in many other cyano polymers, increased reaction time results in further cyclization and (or) conjugation with loss or change of nitrile and NH.

The proposed structure must allow for extended conjugation and free electrons to explain the observed esr spectra and the high conductivity. A ladder structure like that of the ideal black Orlon with a polyene backbone might explain the high thermal stability and insolubility. The proposed reaction mechanism given above for the formation of polyfumaronitrile also supports a ladder-like structure composed of conjugated nitrile rings.

Acknowledgements

The authors would like to thank Dr. Dave Compton from The Standard Oil Co. for his ideas on the proposed reaction mechanism. They are also grateful to T. E. Hammond for helping them obtain a good solid state nmr spectrum.

1. R. LIEPINS, D. CAMPBELL, and C. WALKER. J. Polym. Sci. Part A-1, **6**, 3059 (1968).
2. L. J. BELLAMY and L. BEECHER. J. Chem. Soc. 4487 (1954).
3. L. J. BELLAMY. The infrared spectra of complex molecules. 3rd ed. John Wiley and Sons, New York. 1975. p. 296.
4. S. BALDWIN. J. Org. Chem. **26**, 3288 (1961).
5. L. J. BELLAMY. J. Org. Chem. **26**, 45 (1961).
6. L. R. MELBY, R. J. HARDER, W. R. HERTLER, W. MAHLER, R. E. BENSON, and W. E. MOCHEL. J. Am. Chem. Soc. **84**, 3374 (1962).
7. P. H. RIEGER, I. BERNAL. W. H. REINMUTH, and G. K. FRAENKEL. J. Am. Chem. Soc. **85**, 683 (1963).

Two-photon spectroscopy of the Schiff base of all-*trans*-retinal. Nature of the low-lying $\pi\pi^*$ singlet states

LIONEL P. MURRAY AND ROBERT R. BIRGE[1]
Department of Chemistry, Carnegie-Mellon University, 4400 Fifth Avenue, Pittsburgh, PA 15213, U.S.A.

Received August 23, 1984

This paper is dedicated to Professor Camille Sandorfy on the occasion of his 65th birthday

LIONEL P. MURRAY and ROBERT R. BIRGE. Can. J. Chem. **63**, 1967 (1985).

The two-photon excitation spectrum of all-*trans*-N-retinylidene-*n*-butylamine (ATRSB) in EPA at 77 K is obtained over the wavelength region from 370 to 455 nm ($\lambda_{ex}/2$) using linearly polarized light. The two-photon excitation maximum is observed at ~422 nm ($\lambda_{ex}/2$) and is red shifted ~2800 cm^{-1} from the one-photon absorption maximum at ~377 nm. We assign the two-photon excitation spectrum to the "$^1A_g^{*-}$" $\leftarrow S_0$ transition which indicates that the "$^1A_g^{*-}$" $\pi\pi^*$ state lies below the "$^1B_u^{*+}$" $\pi\pi^*$ state in ATRSB. Comparisons of the one-photon absorption, two-photon excitation, and fluorescence spectra of ATRSB with the corresponding spectra of all-*trans*-retinal are presented. PPP-CISD calculations correctly predict the directions but not the magnitudes of the blue shifts of the $\pi\pi^*$ excited state transition energies in going from all-*trans*-retinal to ATRSB. We postulate that the "$^1A_g^{*-}$" $\pi\pi^*$ state is preferentially stabilized relative to both the ground state and the nearby "$^1B_u^{*+}$" state by hydrogen bonding to solvent molecules. Comparison of the spectra reported here with the two-photon spectra of rhodopsin provides further evidence that the chromophore in rhodopsin is protonated.

LIONEL P. MURRAY et ROBERT R. BIRGE. Can. J. Chem. **63**, 1967 (1985).

Faisant appel à de la lumière polarisée linéairement, opérant à des longueurs d'onde allant de 370 à 455 nm ($\lambda_{ex}/2$) et à une température de 77 K, on a mesuré le spectre d'excitation à deux photons de la *N*-rétinylidène *n*-butylamine complètement *trans* (ATRSB) dans l'EPA. L'absorption maximale pour l'excitation à deux photons se produit vers 422 nm ($\lambda_{ex}/2$) et est déplacée vers le rouge ~2800 cm^{-1} par comparaison avec l'absorption maximale à un photon qui est observée vers ~377 nm. On attribue le spectre d'excitation à deux photons à la transition "$^1A_g^{*-}$" $\leftarrow S_0$; ceci indique que, dans l'ATRSB, l'énergie de l'état "$^1A_g^{*-}$" $\pi\pi^*$ est plus faible que celle de l'état "$^1B_u^{*+}$" $\pi\pi^*$. On rapporte des comparaisons des spectres d'absorption à un photon, d'excitation à deux photons et de fluorescence de l'ATRSB avec les spectres correspondants du rétinal complètement *trans*. Des calculs PPP-CISD permettent de prédire correctement les directions, mais non les amplitudes, des déplacements vers le bleu des énergies de transition de l'état excité $\pi\pi^*$ lorsqu'on passe du rétinal complètement *trans* au ATRSB. Nous postulons que, par rapport tant à l'état fondamental qu'à l'état voisin "$^1B_u^{*+}$", l'état "$^1A_g^{*-}$" $\pi\pi^*$ est stabilisé d'une façon préférentielle par des liaisons hydrogènes avec des molécules de solvant. Une comparaison des spectres rapportés ici avec ceux des spectres à deux photons de la rhodopsine fournit des preuves supplémentaires que le chromophore de la rhodopsine est protoné.

[Traduit par le journal]

I. Introduction

The level ordering of the low-lying excited singlet states of the visual chromophores has been the subject of extensive theoretical and spectroscopic study (1–27).[2] It is now recognized that polyenes possess two low-lying excited singlet states, a strongly one-photon allowed excited state of $^1B_u^{*+}$ parentage and a canonically forbidden excited state of $^1A_g^{*-}$ parentage (1–7, 28–32). In long-chain linear polyenes, the forbidden $^1A_g^{*-}$ state is the lowest-lying excited state (1–7, 28–32). The presence of this lowest-lying forbidden state is responsible for many of the "anomalous" spectroscopic and photochemical properties that long-chain polyenes exhibit (1–7, 31). This level ordering, however, is not directly transferrable to the visual chromophores because the level ordering in these molecules is dependent upon molecular conformation, polarity, and solvent environment (1).

The location of the low-lying "forbidden" $^1A_g^{*-}$-like $\pi\pi^*$ state in the visual chromophores is now recognized to be of importance in defining the photochemical properties of these molecules (1, 2). This is particularly relevant in the case of rhodopsin where calculations indicate that the interaction of this state with a lowest-lying "$^1B_u^{*+}$" state may be directly responsible for producing a barrierless excited state potential energy surface for *cis–trans* isomerization (1, 6, 33). The extremely rapid formation of bathorhodopsin may therefore be a consequence of the photochemical lability of the "$^1A_g^{*-}$" state (1, 6). Excited state level ordering is also important in defining the photochemical properties of the visual chromophores in solution (1, 2, 18, 34, 35).

Previous two-photon investigations have shown that both all-*trans*-retinol (24) and all-*trans*-retinal (25) possess lowest lying $^1A_g^{*-}$-like states. More recent studies, however, indicate that this level-ordering may be reversed in the protonated Schiff bases and in the chromophore in rhodopsin (5). The present two-photon study of the *n*-butylamine Schiff base of all-*trans*-retinal was motivated by a desire to better understand how molecular and environmental perturbations influence the level ordering of these two states. A knowledge of the level ordering in the Schiff base of all-*trans*-retinal is important if we are to understand the electronic origin of the level ordering inversion observed for the chromophore in rhodopsin (5).

II. Experimental

All-*trans*-*N*-retinylidene-*n*-butylamine (ATRSB) was made by reacting all-*trans*-retinal (ATR) under nitrogen in freshly distilled *n*-butylamine in the presence of 3A molecular sieves at 0°C for 6 h following the procedures of Christensen *et al.* (12). The *n*-butylamine is added in molar excess (50:1) and then removed by rotary evaporation upon completion of the reaction.

Low temperature (77 K) absorption spectra were obtained using a Varian Cary 17D spectrophotometer using an optical Dewar assembly filled with liquid nitrogen. Uncorrected emission spectra were obtained using a Spex Fluorolog spectrofluorimeter also equipped with

[1]To whom all correspondence should be addressed.
[2]For relevant reviews, see refs. 1–5.

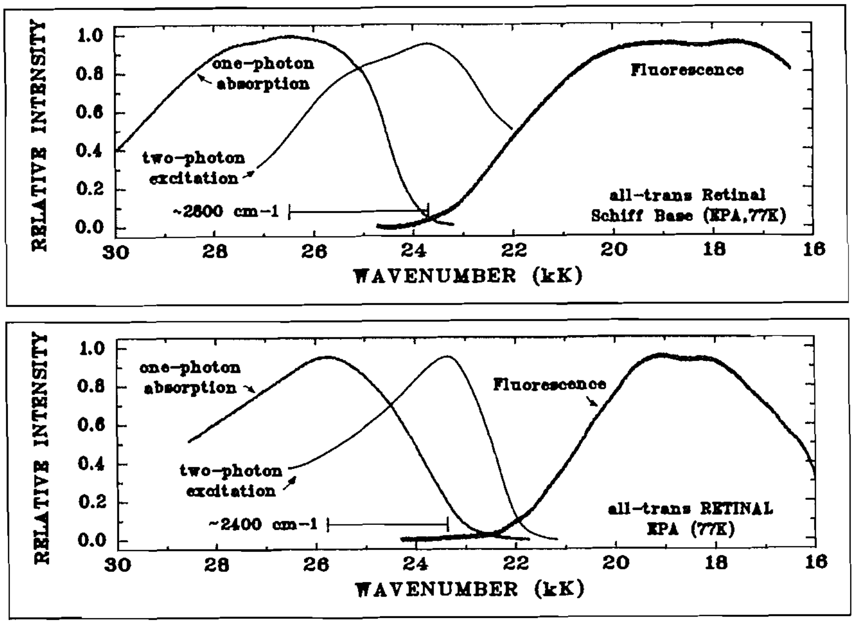

FIG. 1. Comparison of the two-photon excitation spectra with the one-photon absorption and fluorescence spectra of ATRSB (top) and ATR (bottom) in EPA solvent at 77 K. The two-photon data are plotted as a function of (laser excitation wavelength)/2.

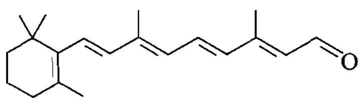

all-*trans*-Retinal (ATR)

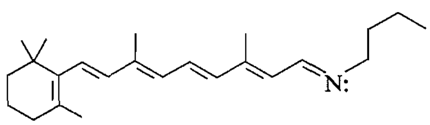

all-*trans*-*N*-Retinylidene-*n*-butylamine (ATRSB)

an optical Dewar assembly. Fluorescence was monitored perpendicular to the excitation beam.

The two-photon excitation spectrum was obtained using the apparatus described in ref. 25. Laser excitation from a nitrogen-pumped dye laser was focussed using an 85 mm achromatic lens into a cylindrical quartz cell containing ATRSB (1×10^{-3} *M*) in degassed EPA (diethyl ether – isopentane – ethyl alcohol, 5:5:2 v/v) immersed in liquid nitrogen (77 K). The two-photon induced fluorescence of ATRSB was monitored perpendicular to the laser excitation beam through a Corning 4-65 glass filter in series with a 5 cm cell containing a nearly saturated (1.1 *M*) solution of $CuSO_4$ (see Fig. 19 of ref. 36). Although the transmission maximum of this filter combination ($\lambda_{max} \sim 490$ nm) is to the blue of the emission maximum of ATRSB ($\lambda_{max} \sim 570$ nm), this filter combination is effective in blocking scattered laser light in the wavelength range 650–950 nm. The use of an RCA 1P28 photomultiplier to detect the fluorescence further improves discrimination of the scattered laser light because this photomultiplier exhibits a very low quantum efficiency above 700 nm.

The two-photon character of the observed fluorescence signal was verified by determining the slope of the log (I_f) vs. log (I_r) at selected wavelengths using neutral density filters to attenuate the laser excitation beam (see ref. 36, pp. 165–167). At the two-photon excitation maximum ($\lambda_{ex} \cong 843$ nm) the slope was observed to be 1.85 ± 0.36.

III. Theoretical

Wave functions for the ground and excited electronic states of ATRSB were calculated using PPP-CISD molecular orbital procedures (15). The restricted π-electron PPP-CISD procedures included all 36 single and all 666 double excitations in the CI Hamiltonian. Repulsion integrals were calculated using the Ohno formula (37). Resonance integrals were calculated using the Roos and Skancke relationship (38). The semiempirical parameters listed in refs. 15 and 39 were adopted.

The two-photon properties of the excited states were calculated using the procedures described by Birge and Pierce (15). The basis set of intermediate states contained the ten lowest electronic states ($N = 10$ in eqs. 1, 2, 4–7 of ref. 15). Although the initial and final states should be formally included in the summation over intermediate states (see ref. 40), they were not included in the calculations reported here. We neglected these contributions because they are proportional to the changes in the dipole moment upon excitation. The PPP-CISD calculations do not include the entire retinyl framework and usually underestimate the dipole moments in both the ground and excited states. We believe that the accuracy of two-photon absorptivity calculations is decreased by the inclusion of the initial and final states when PPP-CISD calculations are used to generate the dipole moments.

IV. Results and discussion

The two-photon excitation spectrum of ATRSB in EPA (77 K) is compared to the one-photon absorption spectrum and the uncorrected fluorescence spectrum in the upper portion of Fig. 1. The two-photon excitation spectrum was obtained using linearly polarized laser excitation and is plotted as a function of (laser excitation wavelength)/2 to facilitate comparison with the one-photon absorption spectrum. Analogous spectra of all-*trans*-retinal in the same solvent environment at 77 K are shown in the lower portion of Fig. 1 for comparison.

(A) Analysis of one-photon and two-photon spectra

Both the one-photon absorption spectrum and the two-photon excitation spectrum are broad and unstructured, a spectroscopic property associated with severe inhomogeneous

TABLE 1. Comparison of observed (EPA, 77 K) and calculated (PPP-CISD) one-photon and two-photon properties of the "$^1A_g^{*-}$" and "$^1B_u^{*+}$" $\pi\pi^*$ excited states of all-*trans*-retinal and its Schiff base

Property (Units)	all-*trans*-Retinal (ATR)[a]	all-*trans*-Retinal Schiff base (ATRSB)[b]	Δ(ATRSB − ATR)[c]
ΔE("$^1B_u^{*+}$" ← S_0) (eV) (obsd)[d]	3.20±0.01	3.29±0.02	0.09±0.02
ΔE("$^1B_u^{*+}$" ← S_0) (eV) (calcd)	3.411	3.507	0.096
ΔE("$^1A_g^{*-}$" ← S_0) (eV) (obsd)[d]	2.90±0.02	2.94±0.03	0.04±0.02
ΔE("$^1A_g^{*-}$" ← S_0) (eV) (calcd)	3.172	3.301	0.129
$\Delta\Delta E$("$^1B_u^{*+}$" − "$^1A_g^{*-}$") (cm^{-1}) (obsd)[d]	2400±300	2800±400	400±300
$\Delta\Delta E$("$^1B_u^{*+}$" − "$^1A_g^{*-}$") (cm^{-1}) (calcd)	1928	1661	−267
f("$^1B_u^{*+}$" ← S_0) (obsd)	1.18±0.05	1.21±0.05	0.03±0.02
f("$^1B_u^{*+}$" ← S_0) (calcd)	0.965	1.112	0.147
f("$^1A_g^{*-}$" ← S_0) (calcd)	0.251	0.070	−0.181
δ_{max}("("$^1B_u^{*+}$" ← S_0)") (Marias) (calcd)[e]	14.17	7.38	−6.79
δ_{max}("$^1A_g^{*-}$" ← S_0) (Marias) (calcd)[e]	29.93	65.84	35.91
$\mu(S_0)$ (D) (calcd)[f]	3.566	2.218	−1.348
μ("$^1B_u^{*+}$") (D) (calcd)[f]	4.955	3.075	−1.880
μ("$^1A_g^{*-}$") (D) (calcd)[f]	8.125	4.673	−3.452
$\Delta\mu$("$^1B_u^{*+}$" − S_0) (D) (calcd)[f]	1.389	0.857	−0.532
$\Delta\mu$("$^1A_g^{*-}$" − S_0) (D) (calcd)[f]	4.559	2.455	−2.104

[a]Experimental data for all-*trans*-retinal in EPA (77 K) from ref. 25.
[b]Experimental data for all-*trans*-*N*-retinylidene-*n*-butylamine (ATRSB) in EPA (77 K).
[c]Change in given property in going from all-*trans*-retinal (ATR) to its *n*-butylamine Schiff base (ATRSB).
[d]Observed transition energies (ΔE) and state separations ($\Delta\Delta E$) are assigned using the absorption and/or excitation (Franck–Condon) maxima.
[e]Two-photon absorptivity at maximum in Marias (1.0×10^{-50} cm^4 s $molecule^{-1}$ $photon^{-1}$) for two linearly polarized photons of equal polarization and energy.
[f]Ground and excited state dipole moments are for the π-system only and are predicted to underestimate the total molecular dipole moments.

broadening (27). This observation precludes accurate assignment of the system origins of the electronic states. The two-photon excitation maximum lies approximately 2800 cm^{-1} below the one-photon absorption maximum. We assign the two-photon excitation spectrum to the "$^1A_g{}^{*-}$" excited $\pi\pi^*$ state based on arguments analogous to those used to assign the two-photon spectrum of all-*trans*-retinal (25). Accordingly, ATRSB has a lowest-lying "$^1A_g{}^{*-}$" state. Our level ordering assignment agrees with that of Das *et al.* (17).

As noted by one of the referees of this paper, the two-photon excitation spectrum and the fluorescence spectrum display an anomalously large overlap in the region of the system origins. This prompted the referee to suggest the possibility that the fluorescence might originate from the higher energy $^1B_u{}^{*+}$-like excited state. The low symmetry of the molecule and the close proximity of the two low-lying excited states suggests that the vast majority of the emission is occurring from the lowest-lying $^1A_g{}^{*-}$-like state. The anomalous overlap is best explained as resulting from an inhomogeneous distribution of lowest-lying excited states involving varying degrees of hydrogen bonding between the solute and the solvent. In particular, we have noted that the shape of the fluorescence spectrum reversibly changes with temperature with the maximum shifting to lower energy with decreasing temperature. (An analogous study of the two-photon excitation spectrum was not possible, however, because the quantum yield of emission drops dramatically with increasing temperature preventing acquisition of a reliable two-photon excitation signal at temperatures above ~90 K.) The one-photon absorption spectrum does not show a large temperature effect suggesting that the one-photon absorbing state is not the state responsible for the emission spectrum. These observations coupled with the solvent effect studies described in ref. 17 suggest that the $^1A_g{}^{*-}$-like state is more energetically stabilized than the $^1B_u{}^{*+}$-like state by the hydrogen bonding solvent, a conclusion which is discussed in greater detail below.

A comparison of the observed and calculated one-photon and two-photon properties of the low-lying $\pi\pi^*$ excited states of all-*trans*-retinal and its Schiff base are presented in Table 1. The following observations can be made by reference to this table. Formation of the Schiff base linkage generates a blue shift in the Franck–Condon maxima of both the "$^1A_g{}^{*-}$" state and the "$^1B_u{}^{*+}$" state. The blue shift of the allowed state was predicted in earlier theoretical studies (see ref. 9). The present PPP-CISD calculations correctly predict the observed trends although the calculations significantly overestimate the observed blue shift in the "$^1A_g{}^{*-}$" state (see below). Accordingly, the observed increase in the separation of the two $\pi\pi^*$ low-lying states in going from retinal to its Schiff base is not accurately simulated in the PPP-CISD calculations. In particular, we observe an increase of approximately 400 cm^{-1} in the Franck–Condon separations, whereas the calculations predict that the Schiff base should actually have a smaller "$^1A_g{}^{*-}$"–"$^1B_u{}^{*+}$" separation. In analyzing this discrepancy, we must recognize that the calculations are for a molecule in a vacuum whereas our experimental observations are for polar molecules in a polar solvent environment. Given the small energy differences involved, a major portion of the discrepancy between experiment and theory may be due to solvent induced shifts rather than intrinsic electronic properties of the chromophore in vacuum. This possibility would appear to gain support from a casual inspection of the calculated dipole moments which are shown at the bottom of Table 1 for the ground and two lowest-lying $\pi\pi^*$ states. In particular, we note that the ground and excited state dipole moments of all-*trans*-retinal are larger than those of the corresponding states in the Schiff base.

Furthermore the change in dipole moments upon excitation, which will determine the magnitude of the solvent-induced red shift, are much larger in all-*trans*-retinal than in its Schiff base. The relative differences predicted by the PPP-CISD calculations agree with the experimental measurements of Corsetti and Kohler (41). These authors measured ground state dipole moments for ATR and ATRSB of 4.6 D and 2.1 D, respectively. The corresponding excited ("$^1B_u{}^{*+}$") state dipole moments were observed to fall in the ranges 7–10.3 D (ATR) and 4.7–6.4 D (ATRSB) (see Table VI of ref. 41). Accordingly, the PPP-CISD calculations appear to underestimate the dipole moments in both the ground and excited states, but correctly reproduce the observed trends in going from all-*trans*-retinal to its Schiff base. A closer examination of the calculated results, when analyzed in terms of the prevailing theories of electrostatic solvent shifts (see ref. 41 and references therein), suggest that the "$^1A_g{}^{*-}$" state in all-*trans*-retinal should be red-shifted by solvent polarity to a larger degree than the corresponding state in the Schiff base. Furthermore, analogous arguments can be used to predict that level separation should be enhanced in all-*trans*-retinal relative to its Schiff base based on electrostatic solvent shifts. (These arguments assume, of course, identical solvent environments.) We conclude that electrostatic solvent shifts do not explain the failure of the PPP-CISD calculations to accurately predict the observed increase in the level separation in going from all-*trans*-retinal to its Schiff base.

Dispersive solvent shift effects will also tend to increase the observed level separation in all-*trans*-retinal versus the Schiff base. This is due to the fact that the low-lying "$^1A_g{}^{*-}$" state has a larger calculated oscillator strength in all-*trans*-retinal than in its Schiff base (see Table 1). Accordingly the magnitude of the dispersive red shift for the "$^1A_g{}^{*-}$" state in all-*trans*-retinal will be greater than that for the corresponding state in the Schiff base and this will also enhance the level separation in all-*trans*-retinal relative to its Schiff base.

There are a number of possible explanations for the observed failure of the PPP-CISD calculations to properly reproduce the observed increase in the excited state level separation in going from ATR to ATRSB. We suggest the following as the most likely possibility based on an analysis of the data presented in Table I and inspection of the spectra shown in Fig. 1. We note first of all that the PPP-CISD calculations accurately reproduce the "$^1B_u{}^{*+}$" transition energies in going from all-*trans*-retinal to the Schiff base. In contrast the PPP-CISD calculations greatly overestimate the blue shift in the "$^1A_g{}^{*-}$" state. The solvent environment appears to be stabilizing the "$^1A_g{}^{*-}$" in the Schiff base by an anomalous amount. This observation is supported by the experimental work of Das and co-workers (17) who studied the all-*trans*-retinal Schiff base in both 3-methylpentane and EPA at 77 K. They noted that the emission maximum dramatically red-shifted in going from 3-methylpentane to EPA, whereas the absorption maximum red-shifted by a much smaller amount. A comparison of their results with our two-photon excitation data suggests that the Schiff base in EPA forms a hydrogen-bonded complex with the solvent and that this hydrogen-bonded complex is responsible for the anomalous red shift in both the "$^1A_g{}^{*-}$" excitation maximum as well as the fluorescence maximum. (Note that fluorescence originates from the "$^1A_g{}^{*-}$" state.) Analysis of Fig. 1 supports this conclusion in that the spectra of ATRSB are much broader than the spectra of ATR and suggest that the Schiff base in EPA is in a very inhomogeneous environment. We propose that the inhomogeneity, which induces an increased broadness in the absorption, excitation, and fluorescence spectra, is associated with hydrogen-bonding which tends to lower the energy of the excited state relative to the ground state. A range of species are therefore present in solution with varying degrees of hydrogen bonding and correspondingly different excitation energies.

The detailed calculations of Favrot *et al.* (20) and LeClercq and Sandorfy (42) demonstrate that hydrogen bonding to a Schiff base will red shift the absorption maximum of the "$^1B_u{}^{*+}$" state. Our experimental results suggest that the "$^1A_g{}^{*-}$" state experiences a similar but slightly larger red shift upon hydrogen-bonding. This experimental observation is indirectly supported by the PPP-CISD calculations which indicate that the "$^1A_g{}^{*-}$" state has a more negative nitrogen atom (−0.242) than the "$^1B_u{}^{*+}$" state (−0.233).

(B) Implications for the binding site of rhodopsin

Theoretical calculations suggest that protonation of the Schiff base will induce a level inversion and generate a lowest-lying "$^1B_u{}^{*+}$" state (1, 6, 15). Recent two-photon studies on the protonated Schiff base of all-*trans*-retinal support this conclusion (5) although it appears that the calculations overestimate the extent of the level reversal. A recent two-photon thermal lens study of rhodopsin indicates that the "$^1B_u{}^{*+}$" state lies approximately 2000 cm^{-1} below the "$^1A_g{}^{*-}$" state in the protein bound chromophore (5). The present work indicates that hydrogen-bonding tends to preferentially stabilize the "$^1A_g{}^{*-}$" state. If the chromophore in rhodopsin were a hydrogen-bonded Schiff base, rather than a protonated Schiff base, the "$^1A_g{}^{*-}$" state would lie below the "$^1B_u{}^{*+}$" state.

We are differentiating between two energetically possible situations. In one model, a neutral Schiff base chromophore is stabilized by hydrogen bonding to a residue with an "acidic" hydrogen near the Schiff base nitrogen atom. In the second model, a protonated Schiff base chromophore is stabilized by a negatively charged residue in the vicinity of the nitrogen atom. Based on these definitions, we can conclude from our present spectroscopic study that the chromophore in rhodopsin must be protonated.

Acknowledgments

This work was supported in part by grants to R.R.B. from the National Institutes of Health (EY-02202) and the National Science Foundation (CHE-7916336). R.R.B. thanks Professor C. Sandorfy for many interesting and helpful discussions on the nature of the binding site of rhodopsin and the effect of hydrogen bonding on the spectroscopic properties of Schiff bases.

1. R. R. BIRGE. Ann. Rev. Biophys. Bioeng. **10**, 315 (1981).
2. M. OTTOLENGHI. Adv. Photochem. **12**, 97 (1980).
3. B. S. HUDSON, B. E. KOHLER, and K. SCHULTEN. Excited States, **6**, 1 (1982).
4. H. SHICHI. Biochemistry of vision. Academic Press, Inc., New York. 1983.
5. R. R. BIRGE, L. P. MURRAY, B. M. PIERCE, H. AKITA, V. BALOGH-NAIR, L. A. FINDSEN, and K. NAKANISHI. Proc. Natl. Acad. Sci. USA, In press; R. R. BIRGE, B. M. PIERCE, and L. P. MURRAY. Two-photon spectroscopy of biological molecules. *In* The Proceedings of the NATO Advanced Studies Institute on the Spectroscopy of Biological Molecules. Maratea, Italy. July 4–15, 1984. *Edited by* C. Sandorfy and T. Theophanides. D. Reidel, Boston. pp. 473–486.
6. R. R. BIRGE and L. M. HUBBARD. J. Am. Chem. Soc. **102**, 2195 (1980).

7. K. L. D'AMICO, C. MANOS, and R. L. CHRISTENSEN. J. Am. Chem. Soc. **102**, 1777 (1980).
8. R. L. CHRISTENSEN and B. E. KOHLER. Photochem. Photobiol. **18**, 293 (1973).
9. A. M. SCHAFFER, W. H. WADDELL, and R. S. BECKER. J. Am. Chem. Soc. **96**, 2063 (1974).
10. W. H. WADDELL, A. M. SCHAFFER, and R. S. BECKER. J. Am. Chem. Soc. **95**, 8223 (1973).
11. R. S. BECKER, G. HUG, P. K. DAS, A. M. SCHAFFER, T. TAKEMURA, N. YAMAMOTO, and W. H. WADDELL. J. Phys. Chem. **80**, 2265 (1976).
12. B. PALMER, B. JUMPER, W. HAGAN, J. C. BAUM, and R. L. CHRISTENSEN. J. Am. Chem. Soc. **104**, 6907 (1982).
13. A. M. SCHAFFER, T. YAMAOKA, and R. S. BECKER. Photochem. Photobiol. **21**, 297 (1975).
14. C. S. IRVING and P. A. LEERMAKERS. Photochem. Photobiol. **7**, 665 (1968).
15. R. R. BIRGE and B. M. PIERCE. J. Chem. Phys. **70**, 165 (1979).
16. R. S. BECKER, P. K. DAS, and G. KOGAN. Chem. Phys. Lett. **67**, 463 (1979).
17. P. K. DAS, G. KOGAN, and R. S. BECKER. Photochem. Photobiol. **30**, 689 (1979).
18. T. TAKEMURA, P. K. DAS, G. HUG, and R. S. BECKER. J. Am. Chem. Soc. **100**, 2626 (1978).
19. P. DUPUIS, C. SANDORFY, and D. VOCELLE. Photochem. Photobiol. **39**, 391 (1984).
20. J. FAVROT, J.-M. LECLERCQ, R. ROBERGE, C. SANDORFY, and D. VOCELLE. Photochem. Photobiol. **29**, 99 (1979).
21. J.-M. LECLERCQ, P. DUPUIS, and C. SANDORFY. Croatica Chemica Acta CCACAA, **55**, 105 (1982).
22. P. DUPUIS, F. I. HAROSI, C. SANDORFY, J.-M. LECLERCQ, and D. VOCELLE. Rev. Can. Biol. **39**, 247 (1980).
23. R. R. BIRGE. Methods in enzymology. **88**, 522 (1982).
24. R. R. BIRGE, J. A. BENNETT, B. M. PIERCE, and T. H. THOMAS. J. Am. Chem. Soc. **100**, 1533 (1978).
25. R. R. BIRGE, J. A. BENNETT, L. M. HUBBARD, H. L. FANG, B. M. PIERCE, D. S. KLIGER, and G. E. LEROI. J. Am. Chem. Soc. **104**, 2519 (1982).
26. R. S. BECKER, G. HUG, P. K. DAS, A. M. SCHAFFER, T. TAKEMURA, N. YAMAMOTO, and W. WADDELL. J. Phys. Chem. **80**, 2265 (1976).
27. R. R. BIRGE, D. A. BOCIAN, and L. M. HUBBARD. J. Am. Chem. Soc. **104**, 1196 (1982).
28. J. A. BENNETT and R. R. BIRGE. J. Chem. Phys. **73**, 4234 (1980).
29. M. GIRARD, E. ARVIDSON, and R. L. CHRISTENSEN. J. Chem. Phys. **80**, 2265 (1984).
30. B. E. KOHLER and T. A. SPIGLANIN. J. Chem. Phys. **80**, 5465 (1984).
31. B. S. HUDSON and B. E. KOHLER. J. Chem. Phys. **59**, 4984 (1973); Ann. Rev. Phys. Chem. **25**, 437 (1974).
32. R. A. GOLDBECK, A. J. TWAROWSKI, E. L. RUSSELL, J. R. RICE, R. R. BIRGE, E. SWITKES, and D. S. KLIGER. J. Chem. Phys. **77**, 3319 (1982).
33. R. R. BIRGE and L. M. HUBBARD. Biophys. J. **34**, 517 (1981).
34. W. H. WADDELL and J. L. WEST. Chem. Phys. Lett. **62**, 431 (1979).
35. B. HONIG. Ann. Rev. Phys. Chem. **29**, 31 (1978).
36. R. R. BIRGE. *In* Ultrasensitive laser spectroscopy. *Edited by* D. S. Kliger. One-photon and two-photon excitation spectroscopy. Academic Press, Inc., New York. 1983. pp. 109–174.
37. K. OHNO. Theor. Chim. Acta. **2**, 219 (1964).
38. B. ROOS and P. N. SKANCKE. Acta Chem. Scand. **21**, 233 (1967).
39. K. SCHULTEN. Ph.D. Thesis, Harvard University, Cambridge, MA. 1975.
40. O. S. MORTENSEN and E. N. SVENDSEN. J. Chem. Phys. **74**, 3185 (1981).
41. J. P. CORSETTI and B. E. KOHLER. J. Chem. Phys. **67**, 5237 (1977).
42. J.-M. LECLERCQ and C. SANDORFY. Photochem. Photobiol. **33**, 361 (1981).

Group theory of constrained reaction mechanisms

PAUL G. MEZEY

Department of Chemistry, University of Saskatchewan, Saskatoon, Sask., Canada S7N 0W0

Received July 30, 1984

This paper is dedicated to Professor Camille Sandorfy on the occasion of his 65th birthday

PAUL G. MEZEY. Can. J. Chem. **63**, 1972 (1985).

It is shown that the family of all possible reaction mechanisms on a given potential energy hypersurface, which reaction mechanisms are constrained by a *local stability criterion*, has an algebraic structure. The fundamental relations among all such "λ-constrained" reaction mechanisms are described in terms of a group, the one dimensional *homotopy group* $\pi_1(Y)$. In contrast with the *energy-dependent group* $\pi_1(F)$ of *fundamental reaction mechanisms*, proposed earlier for the *low energy domains F* of potential energy hypersurfaces, the new group $\pi_1(Y)$ is fully determined by the *distribution of catchment regions, representing chemical species* on the potential energy hypersurface.

PAUL G. MEZEY. Can. J. Chem. **63**, 1972 (1985).

On démontre que l'ensemble de tous les mécanismes de réaction possibles apparaissant sur une hypersurface donnée d'énergie potentielle et circonscris par un *critère de stabilité locale* est régi par une structure algébrique. Les relations fondamentales entre tous ces mécanismes de réaction "λ-circonscris" peut être décrit en fonction d'un groupe, le *groupe homotopie unidimensionnel* $\pi_1(Y)$. Par opposition avec le *groupe dépendant de l'énergie* $\pi_1(F)$ des mécanismes de réactions fondamentales, proposé antérieurement pour les *domaines de basse énergie F* des hypersurfaces d'énergie potentielle, le nouveau groupe $\pi_1(Y)$ est complètement déterminé par la *distribution des régions d'attachement, qui représente les espèces chimiques* sur l'hypersurface d'énergie potentielle.

[Traduit par le journal]

Introduction

Theoretical models, suitable for the description of entire families of molecules within a single mathematical framework, are powerful tools for the study of general trends and fundamental relations among chemical species (1, 2). The most fundamental relations often take the form of an algebraic structure. This has been the case in reaction topology, suitable for the quantum chemical description of all interconversion reactions of all chemical species composed from a given set of nuclei and a given number k of electrons, confined to a given potential energy hypersurface. (For recent reviews of reaction topology see refs. 3 and 4.) As it has been shown (5), by identifying quantum chemical reaction mechanisms with *classes* of homotopically equivalent reaction paths (that is, by equivalence classes of paths where within each class the reaction paths are continuously deformable into one another, *below* some energy limit A), the family of all fundamental reaction mechanisms on the potential surface form a *group*, the *fundamental group of reaction mechanisms* (5). Whereas this terminology is in part inherited from the homotopy theoretical concept of *fundamental group* (one dimensional homotopy group) of the relevant topological space (6), it also expresses the chemical significance of this algebraic structure. This group is indeed of fundamental role in the chemistry along the given potential energy hypersurface, as it describes the relations among all reaction mechanisms which are distinguishable at some energy bound A (5).

The fundamental group of reaction mechanisms has been defined in terms of a *level set F* of the nuclear configuration space M, i.e. in terms of a collection of nuclear configurations where the energy does not exceed some fixed value A (5). By a suitable choice of A the analysis can be restricted to the chemically most important *low energy regions* of the hypersurface, however, the method is general and the analysis is applicable for any choice of A. Such level sets reflect a global energy criterion (7), relevant to the *global stability* of various chemical species on the hypersurface. However, *local stability* is also of chemical importance, that may also serve as a basis for an analysis of reaction paths and reaction mechanisms. Local stability (8, 9), in turn, has been shown to be related to index λ of *catchment regions* $C(\lambda, i)$ of the potential energy hypersurface $E(K)$ (10). Catchment regions with higher λ indices, $\lambda \geq 2$, are of little direct importance in chemistry, however, chemical species represented by catchment regions of lower indices ($\lambda = 0$, and $\lambda = 1$) are of major importance: these are the stable molecules and transition structures. Hence, it is of some importance to study reaction paths and reaction mechanisms which are *constrained* to a collection of $C(\lambda, i)$ catchment regions of *small* λ *indices*.

In this study we shall describe the algebraic structure (a *group*) of λ-*constrained reaction mechanisms*, reflecting the local stability properties of various domains of the potential energy hypersurface. Pictorially, two reaction paths having common origin (beginning) and common extremity (end) will be regarded to belong to the same λ-*constrained reaction mechanism*, if they can be continuously deformed into each other *without* involving any highly unstable formal species, represented by a $C(\lambda, i)$ of high index λ. Reaction paths fulfilling this condition are chemically equivalent in the following sense: they both lead from a given reactant to a given product, through the same "passes" or "bottlenecks" of the hypersurface, as defined by a local stability condition. Otherwise, the difference between the two reaction paths will be regarded as essential, and the two paths to belong to two different λ-constrained reaction mechanism. The precise definition of λ-constrained reaction mechanisms as homotopy equivalence classes of reaction paths will simplify the problem to a remarkable extent. The direct analysis of all possible trajectories is an intractable problem, however, each homotopy class contains infinitely many reaction paths, hence using these *classes* as fundamental entities, formally the problem becomes infinitely simpler. It will be shown that the family of these constrained reaction mechanisms has an algebraic structure: a groupoid, containing a group. Some relations to the "reaction polyhedron", generated by a mapping to a compact manifold (11), and to the relevant homology and cohomology groups will be pointed out.

λ-constrained reaction mechanisms

First we shall recall some of the basic concepts of reaction topology (3, 4), necessary for the introduction of λ-constrained reaction mechanisms. For a given collection of N atomic nuclei the $3N - 6$ dimensional reduced nuclear configuration space M is the *quotient space* (space of equivalence classes) obtained from the $3N$ dimensional euclidean nuclear configuration space spanned by the mass-weighted cartesian coordinates of the N nuclei (4). This quotient space is defined with respect to the laboratory-frame equivalence of nuclear configurations related by rigid translation and rigid rotation. M is a metric space with a well-defined metric d (4). The energy expectation value functional $E(K)$, $K \in M$, with respect to some specified electronic state, defines an energy hypersurface E over M. With respect to any given E the catchment regions $\boldsymbol{C}(\lambda, i)$ of M are given as the collections of all those points K from where a formal steepest descent path leads to a common extremity $K(\lambda, i)$, that extremity is, typically, a critical point of E. Index λ is the number of negative canonical curvatures of E at $K(\lambda, i)$, i is an index of ordering. A catchment region $\boldsymbol{C}(\lambda, i)$ represents a stable molecular species if $\lambda = 0$, a transition structure if $\lambda = 1$, and an unstable, formal "species" if $\lambda \geq 2$, which latter formal "species" must also be considered for a complete partitioning of the nuclear configuration space M. The family of these catchment regions and their closures in the metric d serves as the defining subbase for the unique *reaction topology* T_C on M, associated with the given energy hypersurface E.

In practice it is often sufficient to consider, instead of the full space M, only a suitable connected subset $X \subset M$, e.g. when disregarding the internal motions of nuclei within a methyl group. Catchment regions defined within X lead to an analogous topologization of X, that topology is in fact the relative topology (10) on $X \subset M$, defined by T_C of M. Hence, we shall use the same notations, $\boldsymbol{C}(\lambda, i)$ and T_C within X with the understanding that only a subset $X \subset M$ is considered throughout this study. However, in the special case of $X = M$, the original topological space (M, T_C) is obtained.

In order to give a precise definition and to establish the relations between various λ-constrained reaction mechanisms, we consider the following subset of X:

$$[1] \quad Y = \bigcup_{\lambda' \leq \lambda \leq \lambda''} \boldsymbol{C}(\lambda, i)$$

Whereas the case of $\lambda' = 0$, $\lambda'' = 1$ is the most relevant to the usual pictorial interpretation of semiclassical nuclear rearrangements (restricting the analysis to formal stable molecular species and transition structures), other index choices within the general model [1] are also of certain theoretical interest (e.g., in boundary-network relations (12)), hence we shall consider the above general case throughout. The chemically most important choices for X, λ', and λ'' are those which lead to a *connected* set Y. If, however, Y is disconnected, then the following analysis is applicable for each maximum connected component Y_k of Y separately. In the following Y will denote the union defined by eq. [1], if it is connected, or one of the Y_k components, if the union is disconnected.

Our next task is to define λ-constrained *configuration-to-configuration* reaction mechanisms within set Y. Evidently, any reaction path, hence also any reaction mechanism within Y is, by definition, λ-constrained: $\lambda' \leq \lambda \leq \lambda''$. Each path p in Y is parametrized by the unit interval $I = [0, 1]$, points $p(0)$ and $p(1)$ being the *origin* and *extremity* of p, respectively. It is convenient to regard each p as a mapping from I to Y

$$[2] \quad p: I \rightarrow Y$$

We denote the family of *all* paths within Y by $\boldsymbol{p}(Y)$ or in short, by $\boldsymbol{p}$. Any two paths $p, p' \in \boldsymbol{p}$ are *homotopically equivalent*, $p \sim p'$, if $p(0) = p'(0)$, $p(1) = p'(1)$ (that is, their endpoints coincide) and if they are continuously deformable into each other within Y. Due to the definition of set Y, this is precisely the condition used in the introduction for the classification of reaction paths in terms of local stability, since for $\lambda' = 0$ and $\lambda'' = 1$ $p \sim p'$ implies that there is no highly unstable $\boldsymbol{C}(\lambda, i)$, $(\lambda \geq 2)$ formal species separating reaction paths p and p'. Hence the $p \sim p'$ homotopy equivalence does, indeed, reflect a well-defined *chemical equivalence* of reaction paths p and p'.

The following step is a straightforward application of homotopy theory to set $\boldsymbol{p}$ of Y, that nonetheless, leads to a remarkable simplification of the chemical problem. We denote the *class* of all paths of $\boldsymbol{p}$ which are *homotopically equivalent* to p by $[p]$. All of the following relations and results are independent of which actual path p from class $[p]$ is used to represent this class in the $[p]$ notation. *Each* class $[p]$ can then be regarded to represent a *λ-constrained reaction mechanism leading from configuration* $p(0)$ to *configuration* $p(1)$. These endpoints themselves can be regarded as "single point" paths (or, as constant mappings):

$$[3] \quad L^*(p) \in \boldsymbol{p}, \qquad L^*(p): I \rightarrow Y,\ L^*(p)\ (I) = p(0)$$

$$[4] \quad R^*(p) \in \boldsymbol{p}, \qquad R^*(p): I \rightarrow Y,\ R^*(p)\ (I) = p(1)$$

where the *left unit* $L^*(p)$ [*right unit* $R^*(p)$] of path p is itself a path in Y, hence an element of $\boldsymbol{p}$, which path maps the entire unit interval I onto the single point $p(0)$ [$p(1)$, respectively]. Interpreting these left and right units as some "degenerate" paths, rather than simply points, is essential in the following algebraic constructions.

The fundamental group of λ-constrained reaction mechanisms

The *product* pq of any two paths p, $q \in \boldsymbol{p}$, for which the condition

$$[5] \quad R^*(p) = L^*(q)$$

holds, is defined as the unique path obtained by *joining* q to p (continuing p by q). In particular,

$$[6] \quad L^*(pq) = L^*(p)$$

$$[7] \quad R^*(pq) = R^*(q)$$

This product exists if and only if [5] is fulfilled, hence product exists only for some ordered pairs of paths. The *inverse* p^{-1} of path p runs through the same points of Y as does p, but in reversed order, in particular,

$$[8] \quad L^*(p^{-1}) = R^*(p)$$

$$[9] \quad R^*(p^{-1}) = L^*(p)$$

Using the above algebraic concepts for individual reaction paths, similar algebraic concepts can be defined for their equivalence classes, that is, for reaction mechanisms. The *product* of *λ-constrained reaction mechanisms* $[p]$ and $[q]$ is defined as the λ-constrained reaction mechanism $[pq]$,

$$[10] \quad [p][q] = [pq]$$

that is, the homotopy class containing the product path pq, that product exists if and only if pq exists (condition [5]). The product $[p][p'][p'']$ is evidently associative, whenever it exists, since for the product of reaction paths $(pp')p'' \sim p(p'p'')$. Left unit $L([p])$ and right unit $R([p])$ of reaction mechanism $[p]$ are defined similarly:

[11] $L([p]) = [L^*(p)]$

[12] $R([p]) = [R^*(p)]$

that is, as the homotopy classes of all paths which are homotopically equivalent to (in fact, contractible to) single point paths $L^*(p)$ and $R^*(p)$, respectively. The *inverse* of λ-constrained reaction mechanisms $[p]$ is defined as

[13] $[p]^{-1} = [p^{-1}]$

Whereas the product pp^{-1} is *not* in general a unit element $L^*(p)$, the homotopy equivalence within $[pp^{-1}]$ ensures that the product $[p]\,[p]^{-1}$ is *necessarily* a unit element

[14] $[p]\,[p]^{-1} = L([p]) = R([p]^{-1})$

This is the very reason why reaction mechanisms (equivalence classes) have superior algebraic properties, as compared to individual reaction paths.

As follows from a general result of homotopy theory (6) the above listed properties guarantee that the family

[15] $\pi(Y) = \{[p]\}$

of *all λ-constrained reaction mechanism* has an *algebraic structure:* $\pi(Y)$ is a *groupoid*, that is, an associative algebraic structure with inverse and unit elements, but not in general with the closure property. Hence $\pi(Y)$ is not in general a group.

Groupoid $\pi(Y)$ of λ-constrained configuration-to-configuration reaction mechanisms $[p]$ is *much simpler* than the set of all possible reaction paths $\boldsymbol{p}$, since each $[p]$ is a collection of *infinitely many* paths $p \in \boldsymbol{p}$ which paths occur in *none of the other* λ-constrained mechanisms, $p \notin [q]$ if $[q] \neq [p]$. Hence in a formal sense $\pi(Y)$ is infinitely simpler than set $\boldsymbol{p}$ of all reaction paths within Y. Furthermore, $\boldsymbol{p}$ has no useful algebraic structure of its own, whereas $\pi(Y)$ is a groupoid with the "usual" relations between units and inverses.

By its construction, $\pi(Y)$ is the *fundamental groupoid* of the topological space (Y, d). Hence, as every fundamental groupoid, it contains an important subgroupoid that is also a group (6): the *fundamental group* $\pi_1(Y)$. In the following we shall consider a chemical interpretation of the fundamental group $\pi_1(Y)$.

Consider a special subset $\pi_1(Y, K_0)$ of $\pi(Y)$:

[16] $$\pi_1(Y, K_0) = \{[p]\colon [p]\in\pi(Y),\quad L([p]) = R([p]) = [p_0],\ p_0(I) = K_0\}$$

which is the family of all λ-constrained circular (or "loop") reaction mechanisms having their left and right units identical and common, which unit $[p_0]$ contains the unique constant path (single point path) p_0 at point $K_0 \in Y$.

$\pi_1(Y, K_0)$ is also a groupoid, a *subgroupoid* of $\pi(Y)$, but much more is true. Evidently, within $\pi_1(Y, K_0)$ all left and right units are identical to $[p_0]$, hence there exists a *unique unit element* in $\pi_1(Y, K_0)$. Furthermore, the product exists for any two λ-constrained reaction mechanisms from $\pi_1(Y, K_0)$, since condition [5] is necessarily valid for all choices. This implies, that besides a unique unit element, $\pi_1(Y, K_0)$ also has the *closure property* with respect to product defined by [10]. Associativity and unique inverse for each element have been inherited from groupoid $\pi(Y)$, hence $\pi_1(Y, K_0)$ is a *group*, the *fundamental group* of topological space (Y, d).

This group, henceforth referred to as the *fundamental group of λ-constrained reaction mechanisms*, is of particular interest to us. Since *any* λ-constrained reaction mechanism $[q] \in \pi(Y)$ can be extended to a "loop" mechanism (a circular chemical process) $[p] \in \pi_1(Y, K_0)$, therefore segments of mechanisms from group $\pi_1(Y, K_0)$ represent *all possible λ-constrained mechanisms within* Y. Consequently, group $\pi_1(Y, K_0)$ (or the family of groups $\pi_1(Y_k, K_k)$ of the maximum connected components Y_k of a disconnected set Y) expresses the interrelations among all λ-constrained reaction mechanisms within set $X \subset M$. Similarly to the group $\pi_1(F)$ of fundamental reaction mechanisms on a connected level set F (5), a typical group $\pi_1(Y, K_0)$ of a potential surface is a *finitely generated free group*, where the finite set of group generators, the *generator mechanisms* for Y, *are sufficient to generate any λ-constrained reaction mechanism* in X.

There is one apparent property of group $\pi_1(Y, K_0)$ that seems to be contrary to the underlying feature of Reaction Topology, of replacing *individual nuclear configurations* by *open sets* of configurations. Group $\pi_1(Y, K_0)$ implies a direct reference to an individual *point* $K_0 \in Y$. However, this apparent inconsistency is precisely that: only an apparent one, and can be removed easily. As follows from a general invariance property of fundamental groups (6), within any connected set Y, i.e., in any connected union of λ-constrained catchment regions $\boldsymbol{C}(\lambda, i)$, the fundamental group of λ-constrained reaction mechanisms, as an abstract group, is *invariant* to the choice of reference point $K_0 \in Y$. Hence, as far as the general relations between reaction mechanisms are concerned, the specification of K_0 is unnecessary. K_0 can be replaced by a reference to a given chemical species (catchment region) $\boldsymbol{C}(\lambda, i)$, $\lambda' \le \lambda \le \lambda''$. The actual group $\pi_1(Y, \boldsymbol{C}(\lambda, i))$ then formally refers to all circular λ-constrained reaction mechanisms passing through chemical species $\boldsymbol{C}(\lambda, i)$. In the extreme case, all reference to individual points and individual chemical species can be omitted, since the *abstract* fundamental group of λ-constrained reaction mechanisms, $\pi_1(Y)$ is *isomorphic* to any concrete group given as $\pi_1(Y, K_0)$, $K_0 \in Y$ or $\pi_1(Y, \boldsymbol{C}(\lambda, i))$, $\boldsymbol{C}(\lambda, i) \subset Y$. In fact, $\pi_1(Y)$ is a *topological invariant,* being the same for any union Y of catchment regions on the same or *even on two different potential energy hypersurfaces*, as long as the two sets Y and Y' are *topologically equivalent,* that is, if there exists a homeomorphism (one-to-one and onto mapping with a continuous inverse) between Y and Y'. Hence, fundamental groups are convenient devices for a classification of large families of seemingly unrelated potential surfaces, as these groups reflect the fundamental similarities between systems of reaction mechanisms, even if they involve very different molecular species, of different stoichiometries. In this context we note that a more detailed classification of families of potential energy hypersurfaces is possible by their mappings to compact manifolds (11), e.g. to hyperspheres or to more complicated manifolds. Since the energy hypersurface is then defined on the manifold, the catchment region partitioning on the manifold can be represented by an abstract polyhedron. For example, in the simple case of a two dimensional sphere the energy functional is analogous to the geographical concept of elevation above the sea level on the globe. The partitioning of the surface of the globe by the actual geographical watersheds and catchment regions is topologically equivalent to the polyhedron, with faces, edges and vertices corresponding to geographical catchment regions, mountain ridges and hilltops, respectively. Such abstract *"reaction polyhedra"* in the general, multidimensional case, are useful to establish relations between the numbers of various stable molecular species and interconversion processes (11). Whereas the fundamental groups $\pi_1(F)$ (5) and $\pi_1(Y)$ of the present study lead to an intuitively straightforward classification of various potential energy hypersurfaces, a more detailed classification is possible using multidimensional reaction polyhedra. As any polyhedra, reaction polyhedra obtained by compactification of nuclear configuration spaces (11), can be characterized in terms of *homology groups* and *cohomology groups* (6) of homology theory. These groups are topological (and also homotopical) invariants. Some of the topological invariants of simple homology groups have already been used for the estimation of the number of different chemical species on a hypersurface (ref. 11 and references therein). The reaction polyhedron model and the relative merits on the relevant homology groups and cohomology groups, as compared to the $\pi_1(F)$ and $\pi_1(Y)$ homotopy groups of ref. 5 and of the present study, will be discussed elsewhere in more detail (13).

The chemical significance of groups $\pi_1(Y)$ of reaction mechanism is illustrated by the following two problems: (*i*) knowing the existence of some reaction mechanisms within some domain X of a potential surface, how can one predict the existence of further reaction mechanisms? (*ii*) How to obtain a concise representation of all the relations among all reaction mechanisms controlled by a given potential energy hypersurface, that representation is suitable for applications in computer-based synthesis design?

The algebraic relations among elements of group $\pi_1(Y)$ provide a convenient test for problem (*i*). Unless the known reaction mechanisms already form a set of loop mechanisms of a *subgroup* of $\pi_1(Y)$, the extension of the known mechanisms to loops and subsequent generation of group products does lead to new reaction mechanisms.

The group $\pi_1(Y)$ over a given X domain (where X can be M, the full nuclear configuration space) represents all the essential relations among all reaction mechanisms. These relations may appear rather simple for two and three dimensional problems, where one may rely on simple visualization of "mountain passes" and "bottlenecks". However, no such visualization is possible for higher dimensional potential energy hypersurfaces, and one must rely on formal mathematical relations. With the rapid progress in supercomputer technology, computer-based synthesis design (relying on multidimensional potential surfaces) is expected to become feasible in the near future. The groups $\pi_1(Y)$ of reaction mechanisms serve as an algebraic framework for the quantum chemical analysis of large families of reaction mechanisms. This algebraic framework has the potential to aid the discovery of new reaction mechanisms and the development of computer-based molecular design.

Acknowledgments

I have been privileged to benefit from many interesting conversations with Professor Camille Sandorfy. I am very grateful for his interest and encouragement which have been a continuous source of stimulation.

This work has been supported by a research grant from the Natural Sciences and Engineering Research Council of Canada.

1. G. G. HALL. Int. J. Quantum Chem. Q.C. Symp. **17**, 425 (1983).
2. R. G. PARR. Ann. Rev. Phys. Chem. **34**, 631 (1983).
3. P. G. MEZEY. J. Chem. Phys. **78**, 6182 (1983).
4. P. G. MEZEY. Reaction topology: manifold theory of potential surfaces and quantum chemical synthesis design. *In* Chemical applications of topology and graph theory. *Edited by* R. B. King. Elsevier, Amsterdam. 1983, pp. 75–98.
5. P. G. MEZEY. Int. J. Quantum Chem. Q.C. Symp. **18**, 77 (1984); Theor. Chim. Acta, **67**, 43 (1985); **67**, 91 (1985).
6. E. H. SPANIER. Algebraic topology. McGraw-Hill, New York. 1966. Chapts. 1–5.
7. P. G. MEZEY. Theor. Chim. Acta, **60**, 97 (1981).
8. J. N. MURRELL and K. J. LAIDLER. Trans. Faraday Soc. **64**, 371 (1968).
9. J. N. MURRELL and G. L. PRATT. Trans. Faraday Soc. **66**, 1680 (1974).
10. P. G. MEZEY. Theor. Chim. Acta, **58**, 309 (1981); **62**, 133 (1982); **63**, 9 (1983).
11. P. G. MEZEY. Int. J. Quantum Chem. Q.B. Symp. **10**, 153 (1983).
12. P. G. MEZEY. Int. J. Quantum Chem. Q.C. Symp. **18**, 675 (1984).
13. P. G. MEZEY. Int. J. Quantum Chem. Symp. In press.

Carbon-13 nuclear magnetic resonance study of potassium and thallium ion binding to the Gramicidin A transmembrane channel

D. W. URRY, T. L. TRAPANE, C. M. VENKATACHALAM, AND K. U. PRASAD
Laboratory of Molecular Biophysics, University of Alabama at Birmingham School of Medicine, Birmingham, AL 35294, U.S.A.

Received July 27, 1984

This paper is dedicated to Professor Camille Sandorfy on the occasion of his 65th birthday

D. W. URRY, T. L. TRAPANE, C. M. VENKATACHALAM, and K. U. PRASAD. Can. J. Chem. **63**, 1976 (1985).

By means of carbon-13 nuclear magnetic resonance, carbonyl carbon ion-induced chemical shifts of the Gramicidin A channel are determined at 70°C and analyzed as a function of potassium ion concentration and as a function of thallium ion concentration. In both cases two binding processes are observed. The estimated binding constants for potassium ion binding are $28/M$ and $2.4/M$ for the tight (single ion occupancy) and weak (double ion occupancy) sites, respectively, and for thallium ion binding are of the order of $10^3/M$ for the tight site and approximately $70/M$ for the weak site. These studies, which utilize a 90% enriched carbonyl carbon within the binding site of the channel to monitor ion interaction, argue for the presence of two ions in the channel for conditions under which planar bilayer transport studies are commonly carried out.

D. W. URRY, T. L. TRAPANE, C. M. VENKATACHALAM et K. U. PRASAD. Can. J. Chem. **63**, 1976 (1985).

Utilisant la résonance magnétique nucléaire du ^{13}C et opérant à 70°C, on a déterminé l'effet d'induction ionique sur les déplacements chimiques des carbones de la fonction carbonyle du canal de la Gramicidine A et on les a analysé en fonction de la concentration en ion potassium et aussi en fonction de la concentration en ion thallium. Dans chacun de ces cas, on a observé deux processus de fixation. On a évalué les constantes de fixation du potassium qui sont respectivement $28/M$ et $2{,}4/M$ pour les sites compacts (comportant un seul ion) et pour les sites faibles (comportant deux ions); celles du thallium sont de l'ordre de $10^3/M$ pour le site compact et environ $70/M$ pour le site faible. Ces études, qui utilisent des carbones enrichis à 90% à l'intérieur du site d'association du canal pour repérer les interactions ioniques, suggèrent la présence de deux ions dans le canal pour les conditions dans lesquelles les études de transport de doubles couches sont généralement effectuées.

[Traduit par le journal]

Introduction

It has been shown that heat incubation of Gramicidin A, HCO-L · Val^1-Gly^2-L · Ala^3-D · Leu^4-L · Ala^5-D · Val^6-L · Val^7-D · Val^8-L · Trp^9-D · Leu^{10}-L · Trp^{11}-D · Leu^{12}-L · Trp^{13}-D · Leu^{14}-L · Trp^{15}-$NHCH_2CH_2OH$ (1), with lysolecithin results in channel formation (2, 3). Sodium-23 (4, 5) and lithium-7 (6) nuclear magnetic resonance (nmr) and dielectric relaxation (7) studies have been carried out on this system to provide estimates of binding constants and rate constants, and these constants in the case of sodium ion have been shown to be capable of calculating single channel currents over wide ranges of ion activity and of applied potential when Eyring rate theory is utilized to introduce voltage dependence to the rate constants derived in the absence of an applied field (5, 8). It is useful, however, to have verification that the ion-nmr-derived binding constants are indeed due to ion binding within the channel and not due to interaction with lipid components.

As a series of Gramicidin A syntheses (in each of which a single carbonyl carbon has been 90% enriched) have been carried out to locate the ion binding sites within the channel (9), the ion-induced carbonyl carbon chemical shift of an enriched residue at a binding site may also be followed as a function of ion concentration to provide an estimate of binding constants. Such a study would be unequivocal with respect to ion interaction with the channel since a channel site is used for monitoring and as the magnitude of ion induced chemical shift indicates direct binding of ion with carbonyl oxygen.

In the present effort carbon-13 nmr of (1-^{13}C)Trp^{11}-Gramicidin A (GA) and (1-^{13}C) Trp^{13}-GA as a function of ion concentration is used to follow the binding of potassium ion and of thallium ion to the GA transmembrane channel. In both cases, and most dramatically and unambiguously with thallium ion, two binding processes are observed with binding constants which differ by more than an order of magnitude.

Experimental

Sample preparation and handling

The samples used to determine potassium and thallium ion binding by following the carbonyl carbon chemical shift were prepared from 1-^{13}C enriched Trp^{13}-GA and (1-^{13}C)Trp^{11}-GA which were synthesized and characterized in this laboratory (10). The conversion of (1-^{13}C)Trp^{11}-GA to the malonyl dimer was as previously described (5). Gramicidin channels were packaged into lysolecithin structures in ^2H_2O using the sonication and heat incubation procedure previously established (2). L-α-lysolecithin containing 75% palmitic and 25% stearic acids was purchased from Avanti Polar Lipids, Inc., Birmingham, AL. The purity of the lipid was confirmed by carbon-13 nmr and thin layer chromatography and was used without further purification. During sample preparation, the lipid to channel ratio was 30:1 and the ion concentration was 0.5 mM NaCl. This concentration of NaCl causes a negligible carbon-13 carbonyl chemical shift, but it is included to assess completion of channel formation as monitored by the sodium-23 chemical shift which is a sensitive indicator of channel concentration. After incubation, the samples were centrifuged to remove any peptide which had not been packaged into the lipid, and the supernatants were taken for the nmr studies. A small aliquot of each supernatant was lyophilized and resuspended in methanol in order to determine the concentration of channels associated with the lipid by observing the ultraviolet spectrum. Using an extinction coefficient in methanol of ϵ_{282} = 45 000 L/mol-cm for the Gramicidin dimer, channel concentrations in the 1-^{13}C enriched Gramicidin samples were found to be 2.9 mM for each of the samples used for the potassium ion and the thallium ion binding studies. Verification of the ion-interacting channel state was achieved by observing the circular dichroism spectrum and by determining the ion nmr chemical shift at 30°C. The CD spectra for both preparations are given in Fig. 1. For the (1-^{13}C)Trp^{13}-GA samples the chemical shift for 0.5 mM sodium ion in the presence of 2.9 mM channels was found to be −11.7 ppm (i.e. upfield) from the (10 mM NaCl in ^2H_2O) reference for the potassium ion titration and −12.2 ppm for the thallium ion binding study. These results indicate essentially complete channel formation (5, 8, 11). The potassium ion titrations were carried out by addition of dry

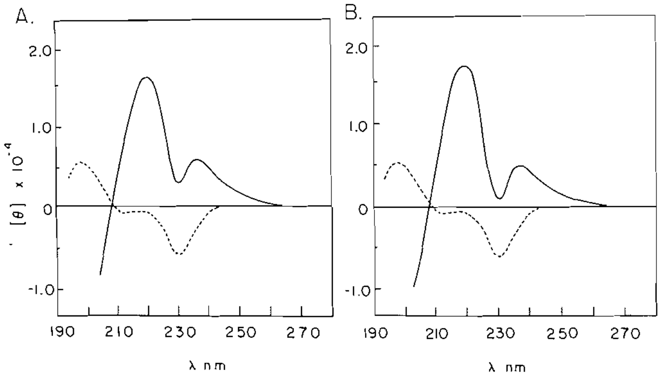

FIG. 1. Circular dichroism spectra in H_2O of 1-^{13}C enriched Trp^{13} Gramicidin A packaged into L-α-lysolecithin. These preparations were used for the potassium ion binding studies (*A*) and for the thallium ion binding studies (*B*). Both spectra indicate that the peptide has been properly incorporated as the channel state. When gramicidin has been completely packaged into the lipid in the proper ion-interacting conformation, a spectra, such as the one represented by the solid curve, is obtained. The dashed curves are due to a lysolecithin – Gramicidin A associated state which has insignificant interaction with cations. Conversion from the lipid-associated state to incorporation as the channel state is achieved by heating for 20 h at 70°C.

KCl (J. T. Baker Chemical Co., Phillipsburg, NJ, analytically certified ULTREX Lot 307081) to a fixed volume of sample in the nmr tube. Thallium acetate (Alfa Products, MA, Lot No. 031177) was added from a 200 m*M* stock solution up to 7 m*M* TlAc. Above this concentration the increments were greater and TlAc could be added dry.

Both heating of Gramicidin A with L-α-lysolecithin to form lipid bilayers (12, 13) and carbon-13 nmr observation of the enriched carbonyl carbon are carried out at 70°C. It is necessary, therefore, to be assured of sample stability during these extended periods of heating. Thin layer chromatography (tlc) using chloroform/methanol/water (65:25:4) and carbon-13 nmr were used to demonstrate the purity of the lipid after prolonged heating at 70°C. These methods, e.g., tlc, using chloroform/methanol/acetic acid (85:15:3), as well as circular dichroism, were utilized to demonstrate the absence of detectable Gramicidin A breakdown. In all, some nine samples have been successfully titrated at 70°C; a tenth effort using sodium ion was not successful due to growth of a thermophilic organism. Thallium ion, of course, is a toxic substance and care should be taken to avoid contact with the skin and to avoid inhalation of the dry powder.

Nuclear magnetic resonance

The (1-^{13}C)Trp^{13}-GA and the mal(1-^{13}C)Trp^{11}-GA carbonyl carbon chemical shifts were measured on a JEOL FX-100 nuclear magnetic resonance spectrometer equipped with a 10 mm multinuclear probe operating at 25 MHz under conditions of complete proton noise decoupling and internal deuterium lock. The spectra were accumulated at 70°C in order to facilitate observation of the broad signal of the enriched peptide carbonyl. Spectra of the lysolecithin packaged channel are given in Fig. 2 where the Trp^{13} carbonyl carbon is seen as the broad resonance just upfield from the sharp signal of the lysolecithin carbonyl carbon at 174 ppm.

When incorporated into lysolecithin–Gramicidin bilayers, the chemical shifts of the enriched Trp^{11} and Trp^{13} labels in the presence of negligible ion concentration (0.5 m*M* NaCl) at 70°C are 170.23 and 170.16 ppm, respectively, from external hexamethyldisiloxane. (In practice measurement is from the —$(CH_2)_n$— resonance of the fatty acid which is found to be 29.1 ppm from external hexamethyldisiloxane.) These values were obtained from the spectra of three different incorporations of the (1-^{13}C)Trp^{11}-Gramicidin and five incorporations with eight separate nmr samples of the (1-^{13}C)Trp^{13}-Gramicidin and are reported with a standard deviation of ±0.06 ppm. This provides a measure of the precision with which the enriched carbonyl

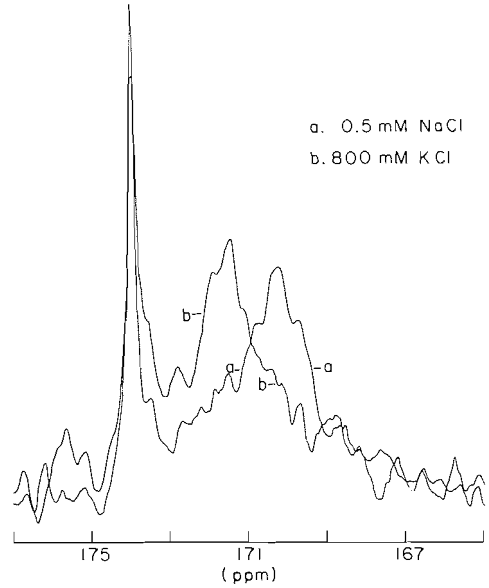

FIG. 2. Carbon-13 nuclear magnetic resonance spectra at 25 MHz and 70°C of the carbonyl region of lysolecithin packaged 1-^{13}C enriched Trp^{13} Gramicidin A. The broad upfield resonance is from the enriched peptide label and the sharp resonance at 174 ppm is from the lipid carbonyl. Two spectra are overlaid — one without (curve *a*) and one with (curve *b*) potassium ion present — showing the change in the chemical shift of the Trp^{13} carbonyl carbon upon addition of 800 m*M* KCl.

carbon chemical shift values may be determined in this system. Upon addition of ion, the change in chemical shift of the peptide carbonyl was determined by overlaying the lineshapes of the Trp^{13} or Trp^{11} signals in the presence of potassium or thallium ion with a reference spectrum taken without any potassium or thallium ion present. With this overlay the difference between the sharp lipid carbonyl signals (which did not exhibit a change in chemical shift upon addition of ion) becomes the ion-induced chemical shift.

Data analysis

From the dependence of the ^{13}C chemical shift on the KCl and TlAc concentrations, binding constants and the values of the chemical shifts due to site occupancy may be derived by fitting the titration curves according to the correct occupancy model. It has been demonstrated that there are two sites related by two-fold symmetry (refs. 9, 14 and see Discussion below). The method of analysis for studying ion nmr data has been already discussed in detail elsewhere (4–6, 8). Slight modification in procedure is required for analyzing the ^{13}C chemical shifts. The procedure is given for the two-site case. Taking δ_f to be the observed ^{13}C chemical shift in the absence of ion binding, δ_t to be the chemical shift when one ion is in the channel and exchanging rapidly between the two sites, and δ_w to be the chemical shift at the high ion concentration limit, i.e., the chemical shift when the second site is also occupied, the observed chemical shift, δ, will be given by

$$[1] \quad \delta = \frac{C_0}{C_T}\delta_f + \frac{C_1}{C_T}\delta_t + \frac{C_2}{C_T}\delta_w$$

where, C_0, C_1 and C_2 are, respectively, the concentrations of empty, singly occupied, and doubly occupied channel molecules. If only one site is occupied, the two carbons experience the same chemical shift due to rapid exchange (i.e. xo ⇄ ox). The concentration ratios appearing in this equation are dependent on the binding constants K_b^t and K_b^w (see eqs. A3, A4, A5, and A6 in ref. 4). Measuring only the *change* in the ^{13}C chemical shift on addition of ion gives a $\delta_f = 0$. Then, eq. [1] reduces to

$$[2] \quad \delta = \frac{C_1}{C_T}\delta_t + \frac{C_2}{C_T}\delta_w$$

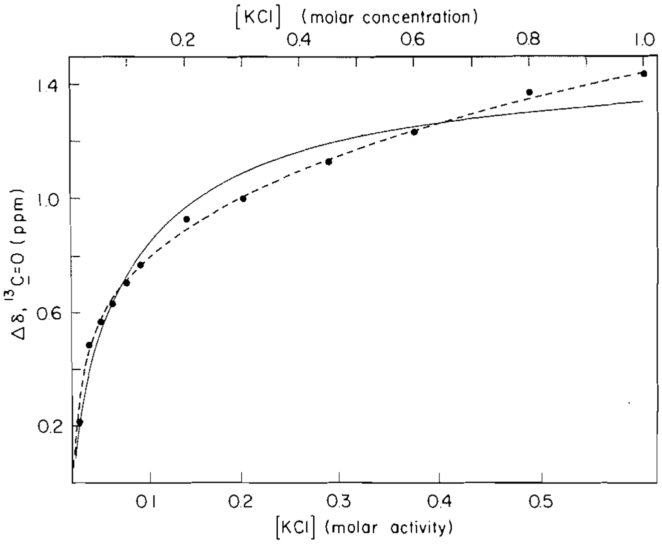

FIG. 3. Experimental data for the enriched carbonyl carbon chemical shift dependence on potassium ion concentration for the Trp[13] carbonyl carbon of the gramicidin channel. The dashed curve is calculated for a two site model which gives very good agreement to the observed shifts. The solid curve is the best fit which may be obtained assuming a single binding site in the channel which can be seen to correspond very poorly to the experimental data.

where C_T is the total channel concentration.

The activity coefficients were obtained for KCl at 70°C for the concentration range of 5 mM to 1 M by taking into account the experimental activities at 25°C for various concentrations (Table 12-2-2A of ref. 15), the temperature dependence of activity coefficient (eq. 12-4-3 of ref. 15) and the low concentration dependence (eq. 12-1-9 and Table 12-1-3A of ref. 15). The activity coefficients so obtained were found to be reproduced by the following equation:

$$[3] \quad \log (\text{activity coeff.}) = -\frac{0.57\sqrt{m}}{1 + 1.32\sqrt{m}} + 0.021\, m$$

where m is the molality.

The fitting procedure employed to obtain binding constants is as follows: the concentrations of the various species, such as ion-free channel, free ions, singly- and doubly-bound channel are dependent on the binding constants, K_b^t and K_b^w, and the total ion and channel concentrations. For the two-site model these dependences are given by eqs. A1 to A8 of ref. 4. An iterative procedure (4) is employed for solving these equations to obtain the complex concentrations from the binding constants and the total channel and ion concentrations. The curve fitting procedure consisted of adjusting the binding constants, K_b^t and K_b^w, and the chemical shifts, δ_t and δ_w of eq. [2], so as to minimize the sum of squares of differences between observed and calculated chemical shifts for various total ion concentrations. The binding constants were systematically varied in a step-wise manner; for a given pair of values of the binding constants, the chemical shifts, δ_t and δ_w, were optimized using a quasi-Newton algorithm to minimize the residual. This procedure was repeated for various values of K_b^t and K_b^w in a wide region in the K_b^t–K_b^w lattice until the lowest residual was obtained.

Results

Potassium ion binding

Non-linear least squares analysis of the observed variation of the ^{13}C chemical shift, δ, with KCl activity, using eq. [2], yielded the following values for the various constants: $K_b^t = 28/M$, $K_b^w = 2.4/M$, $\delta_t = 0.75$ ppm and $\delta_w = 2.48$ ppm. Figure 3 gives the experimental points and the theoretically calculated curve (dashed line). The agreement is very good.

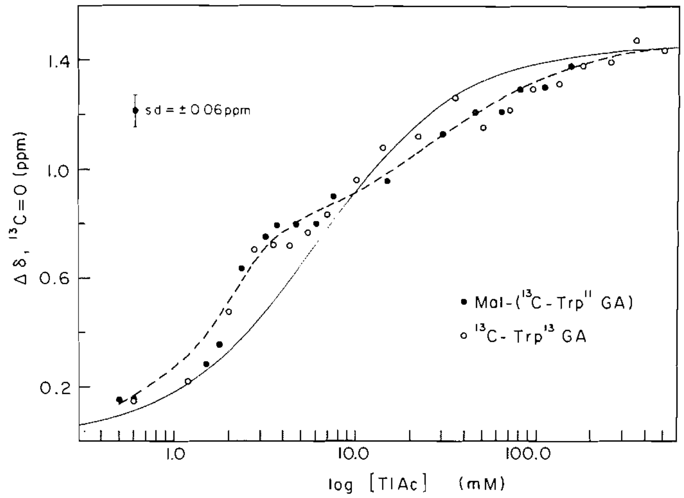

FIG. 4. Carbon-13 chemical shift dependence on thallium ion concentration for (1-^{13}C)Trp[11] mal-GA (●) and (1-^{13}C)Trp[13]-GA (○) carbonyl carbons of the gramicidin channel. The data are plotted as a function of log TlAc concentration so that the low concentration range and the two sigmoid curves — delineating the two channel binding sites — may be clearly seen. The standard deviation (sd) for determining chemical shift as discussed in the Experimental is given as a bar denoting ±0.06 ppm. The dashed curve represents a calculated fit to the data for a two site channel. The solid curve is that required for single site binding (K_b = 100/M) with a maximal chemical shift of about 1.5 ppm. For this curve to be reasonable the error near 3 mM TlAc would have to be as great as 0.3 ppm which is five times greater than the standard deviation for the measurements. The greater curvature of the experimental data at low ion concentration is considered in the Discussion.

That it is necessary to invoke multiple occupancy in the channel in order to successfully analyze these data, may best be demonstrated by a further fitting of the data assuming $K_b^w = 0$, i.e. by disallowing a second ion to bind a singly occupied channel. The best fit obtained holding $K_b^w = 0$, i.e. for single occupancy only, is shown in Fig. 3 as the solid curve. The optimum values for this fitting are $K_b^t = 6.6\ M^{-1}$ and $\delta_t = 1.51$ ppm. It is readily apparent that the agreement with experimental data is not satisfactory for a situation limited to single occupancy. The observed data, showing a steep rise at low ion concentration, i.e. up to 150 mM, and a slow increase continuing to 1000 mM, is inconsistent with a single occupancy model. This provides evidence for two binding sites in the channel with both of them being occupied to an appreciable fraction at high ion concentrations. The presence of two separate binding processes is even more apparent for thallium ion (see below).

Thallium ion binding

The thallium ion induced carbonyl carbon chemical shifts for (1-^{13}C)Trp[13]-GA and for mal(1-^{13}C)Trp[11]-GA are plotted in Fig. 4 as a function of log [TlAc]. The two sets of data are plotted together to show clearly the close similarity between data obtained on both GA and mal-GA and to show the extent of scatter within a given titration. Two sigmoid curves are clearly seen within the two sets of data and within the scatter for each. One sigmoid curve is centered between 1.5 mM and 2 mM TlAc and the second near 20 mM TlAc. While there is more scatter in these latter data, there could be a suggestion that the second binding process is slightly weaker for mal-GA than for GA as was found for sodium ion (5, 8). What is apparent when

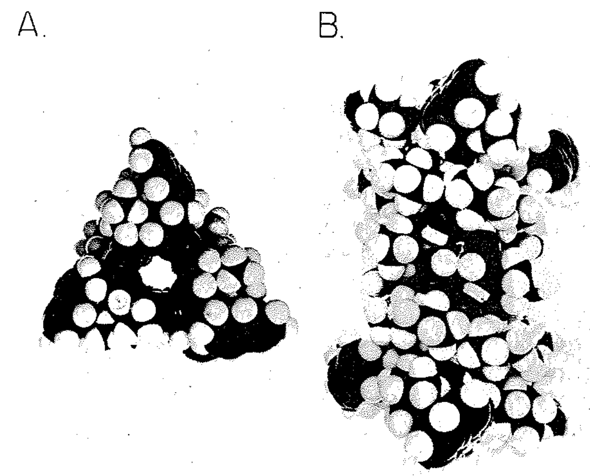

FIG. 5. Molecular structure of the Gramicidin A transmembrane channel. *A*. Space filling model in channel view showing peptide carbonyl oxygens of residues 15, 13, and 11 directed outward into solution. *B*. Channel side view showing two molecules associated head-to-head (formyl end to formyl end) with the formyl hydrogens in contact at center. Reproduced with permission from ref. 21.

WIRE MODEL AND ION BINDING SITES OF THE GRAMICIDIN A TRANSMEMBRANE CHANNEL

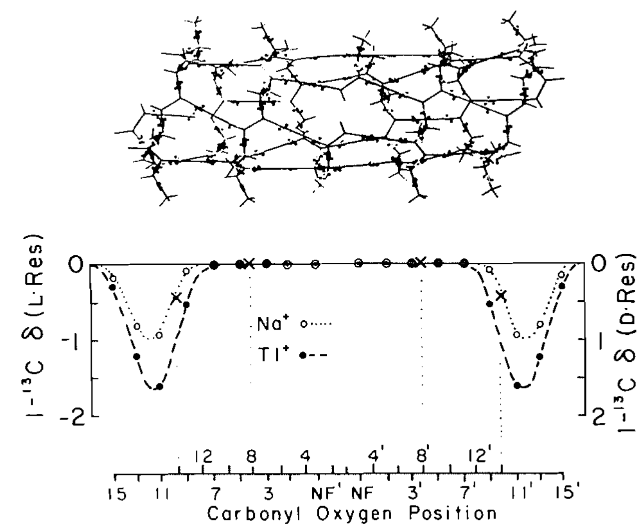

FIG. 6. Above: Wire model of the Gramicidin transmembrane channel displayed with the two formyl moieties at center as in Fig. 5*B*. Below: Plotted with respect to the carbonyls of the wire model above are the ion induced carbonyl carbon chemical shifts for thallium ion and for sodium ion. The observed chemical shift for Tl^+ is larger than for Na^+ because at the ion concentrations used there was greater occupancy for Tl^+ than Na^+. Plotted on the left hand ordinate are the downfield chemical shifts exhibited by the L·residue carbonyl carbons showing two well-defined and localized binding sites with two-fold symmetry. The chemical shifts due to the D·Val^8 and D·Leu^{14} residues (given as ×'s) are plotted on the right hand ordinate. The shift exhibited by the D·Leu^{14} residue but not by the D·Val^8 residue demonstrates that the structure is that of a left-handed helix. Reproduced with permission from ref. 3.

following the channel itself is that there are two binding processes, one with a binding constant of the order of $10^3/M$ or greater and a second which is weaker by an order of magnitude or more. The dashed curve in Fig. 4 was calculated using eq. [2] with $K_b^t = 5000/M$, $K_b^w = 70/M$, $\delta_t = 0.8$ ppm and $\delta_w = 1.4$ ppm. An intriguing feature of the data is the sharpness of curvature coming into the first sigmoid near 1 m*M* TlAc which cannot be fit even with a tight binding constant of $5000/M$. Additional experiments have been run to check this sharpness and indeed it is very reproducible. This feature is discussed below in terms of an ion induced disaggregation of channels giving rise to a positive cooperativity.

Discussion

While there have been a number of structural motifs suggested for the Gramicidin A channel (14–18), it is now well-established, both in planar bilayers (19) and in suspensions of channels (9, 20), that the structure is as proposed in 1971 (14) and as given in Fig. 5. This is a head-to-head (formyl end to formyl end) hydrogen bonded dimer of two left-handed, single stranded — $\beta_{3.3}^{6.3}$ — helices (21). Ion-induced carbonyl carbon chemical shifts observed in a set of single residue (1-^{13}C) enriched syntheses (10) are seen in Fig. 6. In the upper part of the figure is a wire model, including backbone atoms and β-carbons of the channel structure, and plotted below it are the ion-induced carbonyl carbon chemical shifts which demonstrate two ion binding sites related by a two-fold symmetry axis and separated by about 22 Å. This two-fold symmetry is responsible for the symmetric current/voltage curves exhibited by single channels (22) which requires that the free energy profile for ion movement through the channel be symmetric about the midpoint (3). Thus the activity of the malonyl dimer (14, 23) in which the formyl moiety is removed from each of two GA molecules and the two molecules are covalently bridged by the —CO—CH_2—CO— moiety in itself, is demonstration of the structure in Fig. 5. The issue is now one of ionic mechanism, and the already demonstrated location of ion binding sites is an important step in determining mechanism. As shown in this report, the ion-induced carbonyl carbon chemical shifts of a carbonyl at the binding site can also be used to estimate the magnitude of binding constants and to determine the conditions for single and double ion occupancy.

An estimate of the expected magnitude of carbonyl carbon chemical shift resulting from monovalent cation binding can be obtained from a carbon-13 nmr study of potassium ion binding to enniatin B (24). The crystal structure of the enniatin B–K^+ complex has been determined; the direct binding of carbonyls with K^+ has been demonstrated; and the relative orientation of K^+ and carbonyls is known (25). In analogy to Gramicidin A, enniatin B has an alternating L–D sequence; being a cyclic hexapeptide it has six residues in a cycle. This is analogous to the GA channel with 6.3 residues/turn. Accordingly monovalent cation binding would be very similar. The enniatin B–K^+ complex may be considered to be the cyclic conformational correlate of the cation containing Gramicidin A channel; and the chemical shifts exhibited by enniatin B carbonyls on binding K^+ of 1.5 to 2 ppm (24) can provide an estimate of the expected carbonyl carbon chemical shift on complete occupancy of a GA channel binding site. Since the magnitude of the observed carbonyl carbon chemical shift is proportional to the ion concentration and the resonance line width does not vary significantly through the titration, the sites are under conditions of rapid exchange. This being the case, one ion in the channel would be equivalent to half occupancy of the two structurally equivalent sites and the expected chemical shift for one ion in the channel would be 0.7 to 1 ppm. Two ions in the channel, one at each site, would be expected to result in a chemical shift of 1.5 to 2 ppm. As is apparent in the Results section (see Fig. 3 and the corresponding analysis), δ_t for potassium is 0.75 ppm. The chemical shift due to complete occupancy, δ_w, is 2.48 ppm, i.e. close to the maximum expected for the enniatin B–K^+ study (24). For the thallium ion binding study the two binding processes are easily resolved and the obvious break in the titration curve near 0.8 ppm on the chemical shift axis and 4 m*M* on the ion concentration axis defines completion of the titration for entry of the first ion in the channel. Above this concentration double occupancy is occurring. Thus it is clear that, at ion concentrations where single channel conductances are commonly measured in the planar bilayer studies, substantial double ion occupancy would be occurring at 70°C.

Since conductance studies are normally carried out at lower temperatures, it is useful to have some understanding as to the temperature dependence of the ion binding constants. This has been done by determining ion binding to the malonyl GA channel at 30°C, 45°C, 60°C, and 75°C by means of sodium-23 nmr longitudinal relaxation rate studies. Over this temperature range ΔH and ΔS are found to be quite small and the binding constant for the tight site (single ion occupancy) changes by less than a factor of three (Urry, Trapane, and Venkatachalam, to be published). It has also been found, using potassium-39 nmr longitudinal relaxation rate studies, that the binding constant for the weak site at 30°C is approximately $3.5/M$ which is essentially the same as obtained from analysis of the data in Fig. 3 (i.e. $2.4/M$). Thus it is not unreasonable to consider the data of Figs. 3 and 4 to be relevant to conductance by the Gramicidin transmembrane channel as measured by planar bilayer studies and to be similar to data obtained at 25 to 30°C.

Before considering estimates of binding constants from planar bilayer studies, it is useful to note an additional feature that is apparent in the Tl^+ titration of Fig. 4 when the tight binding constant is of the order of $10^3/M$. The sharpness of the curvature of the titration curve between 0.6 and 2 m*M* TlAc suggests a positive cooperativity, that is, a process whereby the binding constant increases with increasing concentration. Such an effect could result from an ion induced structural change from a low binding state to a higher binding state. It is relevant to note that the channels incorporated into lysolecithin bilayers, as described in the Experimental section, results in particles being seen in freeze fracture electron microscopy studies indicative of clusturing of channels, possibly up to a hexameric aggregate (26). Thus the early ion binding could be weak until sufficient binding occurs to result in disaggregation at which point the tight binding site is formed.

The working hypothesis is that ion binding is weak when the channel is aggregated, that initial ion binding causes disaggregation and that ion binding to the dispersed channel is stronger. Freeze fracture electron microscopy studies are underway to examine the incorporated state of the channel as a function of ion concentration. Preliminary results indicate an absence of observable aggregates when thallium ion concentration is 10% greater than the channel concentration (I. Pasquali-Ronchetti, L. Masotti, and D. W. Urry, unpublished data).

On the basis of the preceding several paragraphs, the binding constants obtained in this study may now be compared to previous studies of channels in suspensions and to studies involving fitting of conductances observed in planar bilayer studies. The estimates obtained here for the binding constants for potassium ion binding to the Gramicidin A channel are $28/M$ for the tight site (single ion occupancy) and $2.4/M$ for the weak site (double ion occupancy). These values may be compared with those obtained from conductance studies by Eisenman *et al.* (27) of $40/M$ and $1.5/M$ and by Urban *et al.* (28) of $410/M$ and $0.7/M$, respectively for the tight and weak sites. More recent values of Eisenman and Sandblom give $12/M$ for the tight site (29). The correspondence with the data of Eisenman *et al.* is quite satisfactory.

While for thallium ion the apparent positive cooperativity must yet be properly analyzed, it is reasonable to consider values of $\sim 1000/M$ for the tight site. For this site Veatch and Durkin (30) report values of 500 to $1000/M$ using equilibrium dialysis with dimyristoyl phosphatidylcholine vesicles, and Hinton *et al.* (31, 32) report a value of $900/M$ using the same system as studied here but following binding by thallium-205 nmr chemical shift. Values derived from planar bilayer conductance have ranged from $500/M$ to $3600/M$ due to studies of Eisenman *et al.* (29, 33) and $9000/M$ due to Hladky *et al.* (34). Part of this variation could be due to the need to consider properly the positive cooperativity apparent in Fig. 4.

Acknowledgement

This work was supported in part by the National Institutes of Health, Grant No. GM-26898.

1. R. SARGES and B. WITKOP. Biochemistry, **4**, 2491 (1965).
2. D. W. URRY, A. SPISNI, and M. A. KHALED. Biochem. Biophys. Res. Commun. **88**, 940 (1979).
3. D. W. URRY. *In* The enzymes of biological membranes. *Edited by* A. N. Martonosi. Plenum Publishing Corporation, New York, New York. 1985. pp. 229–257.
4. C. M. VENKATACHALAM and D. W. URRY. J. Magn. Reson. **41**, 313 (1980).
5. D. W. URRY, C. M. VENKATACHALAM, A. SPISNI, R. J. BRADLEY, T. L. TRAPANE, and K. U. PRASAD. J. Membr. Biol. **55**, 29 (1980).
6. D. W. URRY, T. L. TRAPANE, C. M. VENKATACHALAM, and K. U. PRASAD. J. Phys. Chem. **87**, 2918 (1983).
7. R. HENZE, E. NEHER, T. L. TRAPANE, and D. W. URRY. J. Membr. Biol. **64**, 233 (1982).
8. D. W. URRY, C. M. VENKATACHALAM, A. SPISNI, P. LÄUGER, and M. A. KHALED. Proc. Natl. Acad. Sci. USA, **77**, 2028 (1980).
9. D. W. URRY, T. L. TRAPANE, and K. U. PRASAD. Science, **221**, 1064 (1983).
10. D. W. URRY, T. L. TRAPANE, S. ROMANOWSKI, R. J. BRADLEY, and K. U. PRASAD. Int. J. Pept. Protein Res. **21**, 16 (1983).
11. L. MASOTTI, A. SPISNI, and D. W. URRY. Cell Biophys. **2**, 241 (1980).
12. A. SPISNI, I. PASQUALI-RONCHETTI, E. CASALI, L. LINDNER, P. CAVATORTA, L. MASOTTI, and D. W. URRY. Biochim. Biophys. Acta, **732**, 58 (1983).
13. J. A. KILLIAN, B. DE KRUIJFF, C. J. A. VAN ECHTELD, A. J. VERKLEIJ, J. LEUNISSEN-BIJVELT, and J. DE GIER. Biochim. Biophys. Acta, **728**, 141 (1983).
14. D. W. URRY, M. C. GOODALL, J. D. GLICKSON, and D. F. MAYERS. Proc. Natl. Acad. Sci. USA, **68**, 1907 (1971).
15. H. S. HARNED and B. B. OWEN. The physical chemistry of electrolyte solutions. 3rd ed. Reinhold Publishing Corp., New York, 1967.
16. W. R. VEATCH, E. T. FOSSEL, and E. R. BLOUT. Biochemistry, **13**, 5249 (1974).
17. YU. A. OVCHINNIKOV and V. T. IVANOV. *In* Conformation in biology. *Edited by* R. Srinivasan and R. H. Sarma. Adenine

Press, New York. 1982. pp. 155–174.
18. S. V. SYCHEV and V. T. IVANOV. *In* Membranes and transport. Vol. 2. *Edited by* A. N. Martonosi. Plenum Press, New York. 1982. pp. 301–307.
19. E. BAMBERG, H.-J. APELL, and H. ALPES. Proc. Natl. Acad. Sci. USA, **74**, 2402 (1977).
20. S. WEINSTEIN, B. A. WALLACE, E. R. BLOUT, J. S. MORROW, and W. VEATCH. Proc. Natl. Acad. Sci. USA, **76**, 4230 (1979).
21. D. W. URRY, M. M. LONG, M. JACOBS, and R. D. HARRIS. Ann. NY Acad. Sci. **264**, 203 (1975).
22. D. BUSATH and G. SZABO. Nature, **294**, 371 (1981).
23. E. BAMBERG and K. JANKO. Biochim. Biophys. Acta, **465**, 486 (1977).
24. D. W. URRY. *In* Enzymes of biological membranes. Vol. 1. *Edited by* A. Martonosi. Plenum Publishing Corp., New York. 1976. pp. 31–69.
25. M. DOBLER, J. D. DUNITZ, and J. KRAJEWSKI. J. Mol. Biol. **42**, 603 (1969).
26. A. SPISNI, I. PASQUALI-RONCHETTI, E. CASALI, L. LINDNER, P. CAVATORTA, L. MASOTTI, and D. W. URRY. Biochim. Biophys. Acta, **732**, 58 (1983).
27. G. EISENMAN, J. SANDBLOM, and E. NEHER. Biophys. J. **22**, 307 (1978).
28. B. W. URBAN, S. B. HLADKY, and D. A. HAYDON. Biochim. Biophys. Acta, **602**, 331 (1980).
29. G. EISENMAN and J. P. SANDBLOM. *In* Physical chemistry of transmembrane ion motions. *Edited by* G. Spach. Elsevier Science Publishers, B. V., Amsterdam. 1983. pp. 329–347.
30. W. R. VEATCH and J. T. DURKIN. J. Mol. Biol. **143**, 411 (1980).
31. J. F. HINTON, G. YOUNG, and F. S. MILLETT. Biochim. Biophys. Acta, **727**, 217 (1983).
32. J. F. HINTON, G. YOUNG, and F. S. MILLETT. Biochemistry, **21**, 651 (1982).
33. G. EISENMAN, J. SANDBLOM, and E. NEHER. *In* Metal–ligand interactions in organic chemistry and biochemistry. *Edited by* B. Pullman and N. Goldblum. D. Reidel, Dordrecht-Holland. Part 2, 1977. p. 1.
34. S. B. HLADKY, B. W. URBAN, and D. A. HAYDON. *In* Membrane transport processes. Vol. 3. *Edited by* C. F. Stevens and R. W. Tsien. Raven Press, New York. 1979. pp. 89–104.

Molecular and electronic structure of ozone and thiozone from LCAO local density calculations

MARIO MORIN, ANIKO E. FOTI, AND DENNIS R. SALAHUB

Département de Chimie, Université de Montréal, C.P. 6210, Succursale A, Montréal, (Qué.), Canada H3C 3V1

Received September 17, 1984

This paper is dedicated to Professor Camille Sandorfy on the occasion of his 65th birthday

MARIO MORIN, ANIKO E. FOTI, and DENNIS R. SALAHUB. Can. J. Chem. **63**, 1982 (1985).

LCAO local density calculations for ozone yield a ground state geometry in good agreement with experiment (R = 1.27 Å vs. 1.278 Å (exp.), θ = 117.5° vs. 116.8° (exp.)). A second local minimum is found about 45 kcal/mol higher for a cyclic geometry (R = 1.44 Å, θ = 60°). For S_3 the calculations predict a bent ground state (R = 2.00 Å, θ = 116°) with the cyclic geometry (R = 2.125 Å, θ = 58°) about 15 kcal/mol higher.

MARIO MORIN, ANIKO E. FOTI et DENNIS R. SALAHUB. Can. J. Chem. **63**, 1982 (1985).

Des résultats de calculs du type LCAO densité locale sont en bon accord avec l'expérience pour la géométrie de l'état fondamental de l'ozone (R = 1.27 Å vs. 1.278 Å (exp.); θ = 117.5° vs. 116.8° (exp.)). Un deuxième minimum local pour une géométrie cyclique (R = 1.44 Å, θ = 60°) est prédit à une énergie plus élevée d'environ 45 kcal/mol. Pour S_3 les calculs prédisent une géométrie ouverte (R = 2.00 Å, θ = 116°) pour l'état fondamental avec la forme cyclique (R = 2.125 Å, θ = 58°) à peu près 15 kcal/mol plus haute.

Introduction

The ozone molecule has been the object of numerous experimental (1–6) and theoretical (7–13) studies. Because of its high biradical character (7, 9, 11, 12) it has become a classic example of a case where single determinantal Hartree–Fock theory is inadequate. In the usual wave function theory at least two determinants must be mixed to achieve a reasonable qualitative description. On the other hand, Xα (14–16) calculations, which should be viewed as approximate applications of density functional theory (17, 18), have yielded the correct singlet ground state and accurate values for the ionization potentials and many low-lying excitation energies (8, 13). These Xα calculations were performed with either the scattered-wave (16) or LCAO (Gaussian) (19, 20) version of the method and only the equilibrium geometry was considered. A direct optimization of the geometry was carried out by Laidlaw and Trsic (10) using the discrete variational (21, 22) Xα (Hartree–Fock–Slater) method. Their results were discouraging in that a closed geometry having a bond angle near 60° and involving six π electrons was predicted to lie lower in energy than the experimentally observed open form (θ = 117°) which involves four π electrons.

Ozone's third row congener thiozone is less well characterized. Although S_3 has been observed in sulfur vapour and liquid and its ionization potential is known (23) its structure has not been experimentally determined. Only a few electronic structure calculations have been performed for S_3. The Xα-SW method was applied (24) to the study of structural changes accompanying oxidation or reduction. Examination of the orbital energies and wave functions led to the suggestion that an open form with an angle of about 120° would be a reasonable choice for the ground state. Hartree–Fock calculations (25) using a double ζ basis set predict the closed form as the lowest energy conformer although the authors point out, by analogy with more accurate calculations for ozone, that correlation and polarization effects would likely reverse the order and place the open form lower. The DVM-Xα (HFS) calculations of Laidlaw and Trsic (10) also predict the closed form as the more stable conformer. However, as mentioned above, similar calculations for ozone yield erroneous results.

In this paper results of LCAO local density calculations for O_3 and S_3 are reported. The study was undertaken: (i) to determine whether the false energetic ordering of the closed and open forms of O_3 (and perhaps S_3) found in the DVM study (10) represents an intrinsic failure of local density functional theory or rather is due to inaccuracies in the particular method chosen to solve the local density equations; (ii) to complement our previous Xα-SW (8) and LCAO-Xα (13) studies of O_3 by optimizing the geometries of both open and closed forms; (iii) to complement our previous Xα-SW study of S_3 (24) with total energy results; (iv) to provide a further comparison (26–29) of Xα results with those obtained using a more accurate treatment of correlation in the underlying calculations on the homogeneous electron gas (30); and (v) to check for the possibility of broken-symmetry (antiferromagnetic) solutions (29) which might be suspected for the case of a singlet biradical.

Our calculations indicate that: (i) for both O_3 and S_3 the open form is more stable. This is in contrast to the published DVM results but agrees with a more recent study (31) using a transition state approach to the binding energy. The latter approach is thought to be more accurate; (ii) the calculated geometry of ozone is in good agreement with experiment; (iii) the rough geometry prediction for S_3 based on Xα-SW calculations (24) is borne out by the LCAO-Xα total energy results; (iv) Xα and VWN (30) potentials yield very similar results for S_3; and (v) the symmetry-adapted (C_{2v}) solutions are stable with respect to broken-symmetry (C_s) configurations of biradical (antiferromagnetic) character.

Computational details

The calculations were performed with the LCAO-Xα code of Dunlap *et al.* (20) slightly modified to permit the use of different approximations for the exchange-correlation potential and energy. Those employed here are Xα with the value of α taken from Schwarz's compilation (32) and the correlated potential of Vosko, Wilk, and Nusair (30). The latter represents an accurate interpolation–extrapolation of Monte-Carlo calculations (33) on the correlated homogeneous electron gas which are thought to be nearly exact. Hence, if the local density equations are solved to high accuracy using the VWN potential, any remaining errors should be ascribed to non-local effects.

The ($9s/5p$) orbital basis set for O was taken from Huzinaga

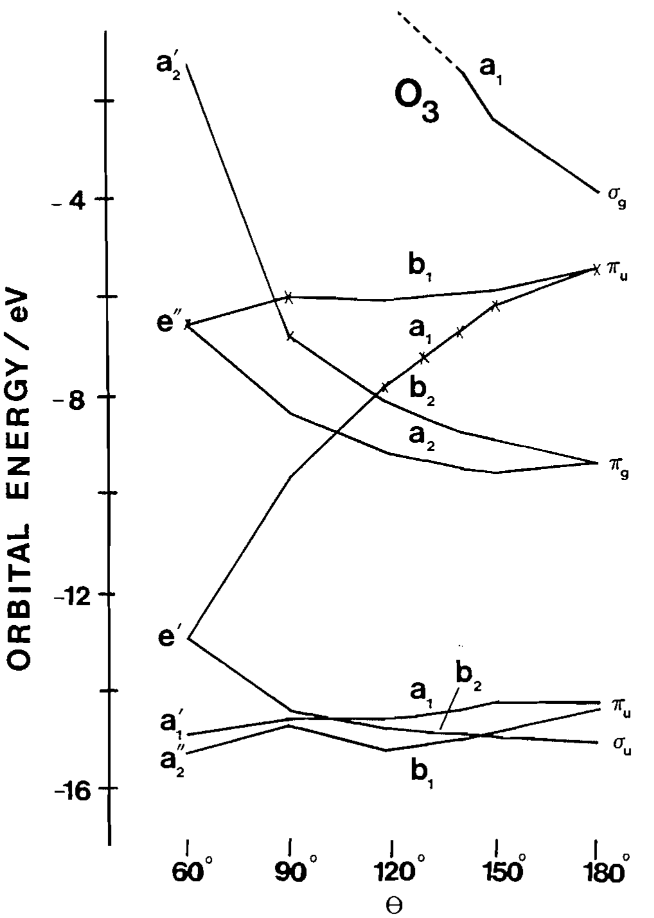

FIG. 1. LCAO-LD (VWN) Walsh Diagram (orbital energy vs. bond angle, θ) for R = 1.27 Å. The HOMO is marked by an ×. For θ = 90° double occupation of either the uppermost b_2 or b_1 level led to violation of Fermi statistics so the values shown are for single occupation of each of these levels. The slight lack of degeneracy for the lower π_u level at θ = 180° arises since the calculations were performed with C_{2v} symmetry constraints and the exchange fitting grid is not exactly cylindrically symmetric.

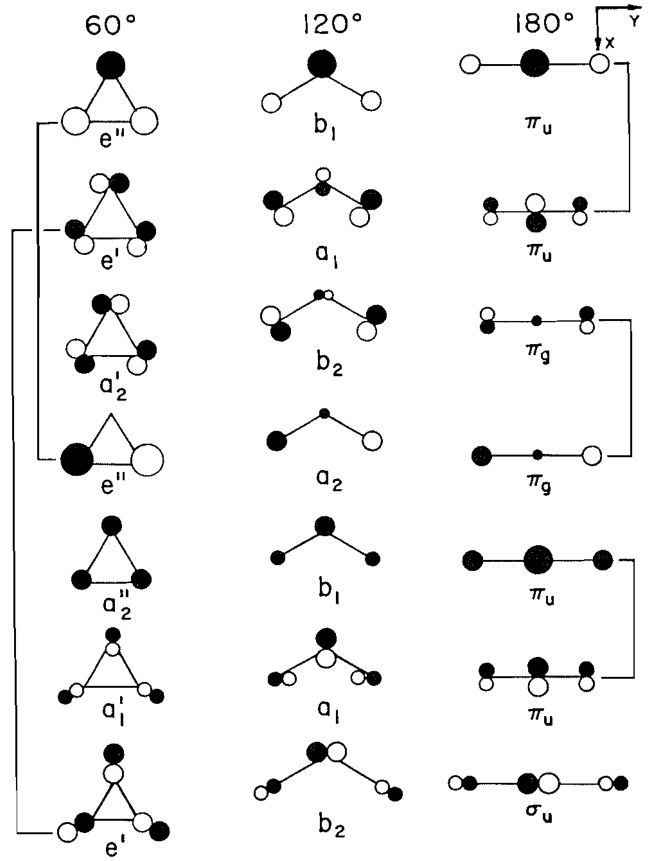

FIG. 2. Schematic diagram for the one-electron orbital wave functions of O_3 and S_3 for θ = 60, 120, and 180°. The orbitals are not shown in energetic order for the 60° column but rather are aligned with the C_{2v} orbital to which they correspond. The orbital energies may be found in Figs. 1 and 4. For degenerate orbitals both symmetry components of the orbital are given. The π orbitals are designated by circles. Black indicates positive and white negative values of wave function.

(34) and either augmented or not with a set of d functions of exponent 0.8. For S we have used the Veillard (35) ($12s/9p$) basis again either augmented or not with d polarization functions (exponent 0.8). Some tests were made for S with a slightly more diffuse d function (exponent 0.6). While this led to a slight lowering of the total energy (~6 kcal/mol for each point considered) the equilibrium geometry was negligibly affected. These basis sets, including the polarization functions, are very similar to those used by Huzinaga and Yoshimine (36) for calculations on SO_2. The significance of the d functions will be addressed later.

Auxiliary basis sets to fit the charge density and the exchange-correlation potential and energy were constructed as suggested by Dunlap *et al.* (20) including the use of bond-centered s functions (exponents 1.0 and 0.25). Tests for the cyclic form of ozone, in which zero, two or three bond-centered fitting functions were employed showed their effect to be negligible (<0.2 kcal/mol).

Results and discussion

Ozone

Two regions of the potential energy surface are of particular interest. The ground state equilibrium geometry has a bond length of 1.278 Å and an angle of 116.8° (1). The electronic configuration ($\ldots 1b_1^2\, 2b_2^2\, 3a_1^2\, 1a_2^2\, 3b_2^2\, 4a_1^2$) involves four π ($b_1$ and a_2) electrons. A second local minimum exists in the region of 60° and its configuration ($3a_1^2\, 1b_1^2\, 2b_2^2 4a_1^2\, 1a_2^2\, 2b_1^2$) has six π electrons. The rationale for the configuration change may be readily gleaned from the Walsh diagram shown in Fig. 1 and sketches of the MOs (Fig. 2). Briefly stated, if one starts with the equilateral form, then both the bonding (b_1 (a_2'' under D_{3h})) and antibonding (a_2 and b_1 (e'' under D_{3h})) π orbitals are occupied. The anti-bonding (b_2 (a_2' under D_{3h})) σ level is empty. Opening the angle stabilizes the σ level (relieving the 1–3 antibonding interaction) and destabilizes the b_1 component of the upper π level which is 1–3 bonding, leading to the configuration change. While this qualitative aspect of ozone's electronic structure seems straightforward enough, the question of the relative stabilities of the two forms is a quantitative one and rather delicate. It can serve as a stringent test of a quantum chemical method.

The salient results of our calculations using the VWN correlated potential are gathered in Table 1. We first note that with the polarized basis set agreement with the experimental geometry is excellent. The closed form is predicted to lie about 46 kcal/mol above the ground state. This may be compared with the value of 28 kcal/mol derived from the configuration interaction calculations of Hay and Dunning (9). After the

TABLE 1. Calculated LCAO-LD (VWN) and experimental geometries and energies for O_3

	Basis	R (Å)	θ (deg)	E (hartree)	ΔE^{a}_{pol} (kcal/mol)	ΔE^{b}_{o-c} (kcal/mol)
Exp.		1.278[c]	116.8[c]			
Open form	(9s/5p/1d)	1.27	117.5	−223.9459925	41.6	
	(9s/5p)	1.35	119	−223.8798338		
Closed form	(9s/5p/1d)	1.44	60	−223.8723637	40.9	46.3
	(9s/5p)	1.50	61	−223.8072955		45.6

[a]Effect of d polarization functions on energies.
[b]Energy difference between open and closed forms.
[c]Reference 1.

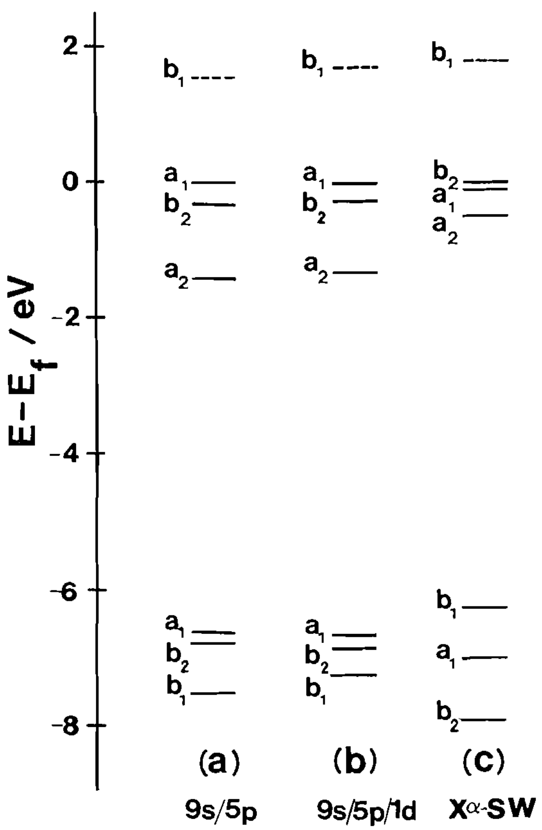

FIG. 3. Orbital energies for ozone relative to that of the HOMO (E_f) for: (a) the (9s/5p) basis, VWN potential, R = 1.27 Å, θ = 117.5°; (b) the (9s/5p/1d) basis, VWN potential, R = 1.27 Å, θ = 117.5°; (c) the Xα-SW results read from Fig. 1 of ref. 8. R = 1.278 Å, θ = 116.8°. The values of E_f are (a) −6.4 eV, (b) −6.1 eV, and (c) −8.1 eV.

original version of this paper was submitted, results were reported of an extensive CI study including ≈600 000 configurations by the Møller-Plesset barycenter method. Feng *et al.* (41) find the closed form 38 kcal/mol above the open form. In their transition state DVM calculations, Laidlaw and Trsic (31) find an open–closed separation of 21 kcal/mol, thus reversing their previous conclusion (10) about the energetic order of the two forms within the HFS(Xα) model. While the agreement between the two techniques (DVM and LCAO (Gaussian)) of solving the Xα equations is improved by the new calculations, there remains a discrepancy of about 25 kcal/mol. To our knowledge there is no experimental information on the energy position or the geometry of the closed form.

Consistent with the experience from *ab initio* calculations (9) we find that the (9s/5p) basis leads to significant errors in the bond lengths. The polarized basis yields shorter bonds by 0.08 Å and 0.06 Å for the open and closed geometries, respectively. The energy lowerings (including the effects of geometry relaxation) are nearly identical for the open and closed forms. Hence, the open–closed energy difference is correctly predicted by the *sp* basis even though the *sp* geometries are seriously in error. The effect of the *d* functions on the orbital energies at the equilibrium geometry is shown in Fig. 3. The HOMO's have been aligned, which involves a shift of 0.3 eV. Once this is done the positions of the levels with and without polarization functions agree to within 0.25 eV, an adequate precision for spectral assignments (13). However, for quantitative results, it is clear that the widely used (9s/5p) basis should be augmented with polarization functions.

We also show in Fig. 3 the orbital eigenvalues from Xα-SW calculations (8). Comparison of these results, which involve the muffin-tin approximation, with those of the LCAO method will serve to quantify the errors in the former. We note first, as has been previously pointed out (13) that the uppermost a_1 and b_2 levels are inverted, the LCAO results following the experimental order. However, since these levels lie very close to each other this should not be viewed as a serious condemnation of the SW results. In addition the a_2 π level is significantly more stable in the LCAO results. The same is true of the lower-lying b_1 π level, the differential shift being about 1 eV. The relative positions of the lower-lying a_1 and b_2 σ levels are also significantly different in the two methods. While the general features of the ozone electronic structure are reasonably given by the SW approach and the ionization potentials and several excitation energies involving the upper three occupied orbitals are of a useful accuracy (8), the comparison provided by Fig. 3 should make it clear that interpretations based on finer details of the SW results for a molecule such as this should be viewed with caution.

Thiozone

Not surprisingly the Walsh diagram for S_3 (Fig. 4) has a similar structure to that of O_3. There is some noticeable difference in the behaviour of the unoccupied a_1 level in the region near the linear geometry. For S_3 it proved impossible to satisfy the Fermi statistics for this geometry, the σ_g and π_u levels being nearly degenerate; whereas for O_3 the σ_g level is about 0.8 eV above π_u. Figure 4 is also quite similar to that previously generated by the Xα-SW method (Fig. 2 of ref. 24). Again the detailed behaviour of the unoccupied a_1 level differs between

TABLE 2. Calculated LCAO-LD (VWN and Xα) geometries and energies for S_3

	Basis	R (Å)	θ (deg)	E (hartree)	ΔE^{a}_{pol} (kcal/mol)	ΔE^{b}_{o-c} (kcal/mol)
				VWN		
Open form	(12s/9p/1d)	2.00	116	−1190.520476	40.5	
	(12s/9p)	2.11	116	−1190.456167		
Closed form	(12s/9p/1d)	2.125	58	−1190.498012	35.2	14.1
	(12s/9p)	2.27	61	−1190.442064		8.9
				Xα		
Open form	(12s/9p/1d)	1.99	116	−1192.809771	41.9	
	(12s/9p)	2.11	116	−1192.743089		
Closed form	(12s/9p/1d)	2.125	58	−1192.785316	36.2	15.4
	(12s/9p)	2.26	61	−1192.727739		9.7

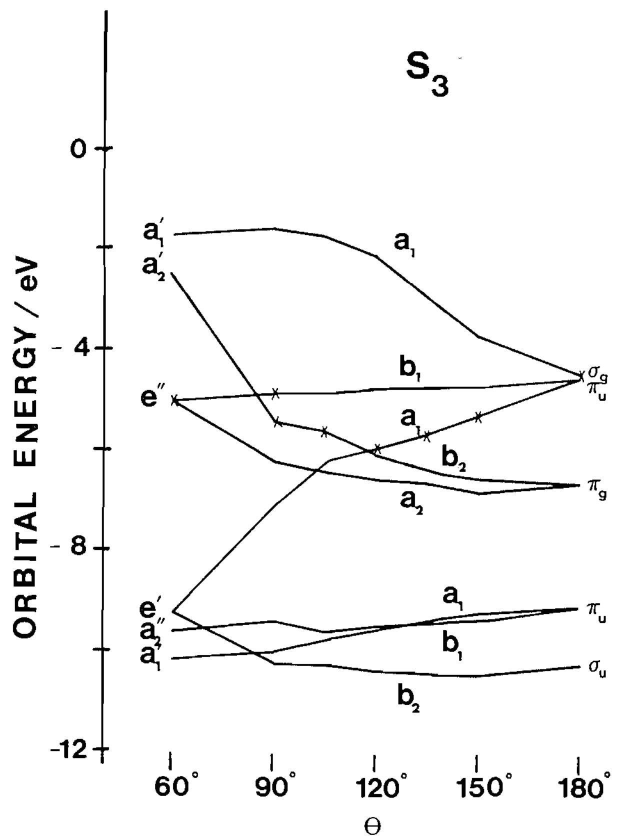

FIG. 4. LCAO-Xα Walsh diagram (orbital energy vs. bond angle, θ) for S_3 calculated for R = 1.99 Å. The HOMO is marked by an ×. For θ = 90° double occupation of either the uppermost b_2 or b_1 level led to violation of Fermi statistics so the values shown are for single occupation of each of these levels. For θ = 180° the Fermi statistics are not satisfied, π_u is empty — see text.

the two methods. This may be due to muffin-tin errors, the lack of d waves in the SW calculation and/or an inadequacy of the LCAO basis set for this higher-lying orbital. Since the orbital is empty for the physically interesting geometries we will not dwell on the matter.

The geometry and total energy results are summarized in Table 2. We first point out that the Xα and VWN potentials yield nearly identical geometries and energy differences. As was the case for ozone, the ground state of thiozone is found to be the open form, with a bond angle of 116°. The closed form lies about 15 kcal/mol higher. This may be compared with the value 17 kcal/mol from the very recent CI calculations of Feng *et al.* (41) and with the DVM transition state (31) value of 11 kcal/mol. Once again the d polarization functions have a large effect. They account for a shrinking of the bond length of about a tenth of an Ångstrom for all cases. The effect of polarization functions on the relative energies of the closed and open forms is considerably more marked for S_3 than was the case for O_3; the open–closed separation increases by about 5 kcal/mol when d functions are added to the basis.

The effect of the d functions and the choice of exchange-correlation potential on the orbital energies is shown in Fig. 5. After a uniform shift of 0.6 eV the (relative) Xα and VWN eigenvalues are practically identical. The differential shifts due to the d functions are again quite small, the largest being about 0.25 eV.

Comparison with the SW results follows similar lines as for ozone. The muffin-tin calculation correctly interprets the general features; however once again the π levels are destabilized relative to the LCAO results and there is a significant change in the spacing of the lower lying σ levels.

Symmetry breaking

Ab initio calculations (7, 9–12) have shown that ozone has a high biradical character. Within the Generalized Valence Bond (GVB) approach (7) this can be interpreted in terms of partially localized orbitals which result from strong "left–right" correlation. Proper space- and spin-symmetry adapted many electron wave functions are then constructed from these broken-symmetry orbitals. The simplest reasonable wave function consists of two determinants, the first having an up-spin π electron localized primarily on one terminal atom and a down-spin π electron localized on the other. The second determinant is the mirror image of the first. A somewhat analogous situation arises in the antiferromagnetic transition metal dimers (29) and here it has been found that localization of the Local Spin Density (LSD) orbitals is an important aspect of the calculations.

We have therefore examined the possibility of symmetry-breaking for O_3 and S_3. Spin-polarized calculations were started by arranging the exchange-correlation fitting coefficients to be fully polarized in an antiferromagnetic manner and imposing C_s symmetry constraints. For both molecules the

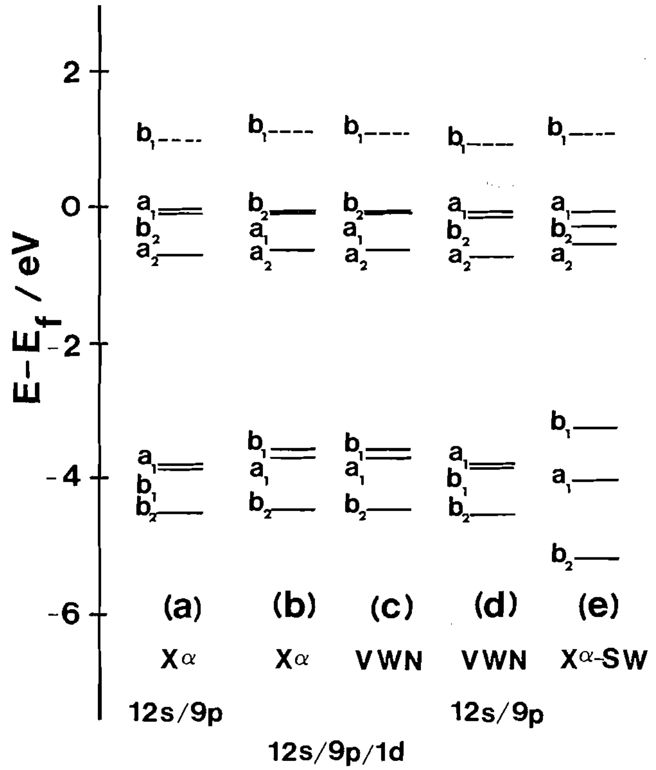

FIG. 5. Orbital energies for thiozone relative to that of the HOMO (E_F) for (*a*) the (12*s*/9*p*) basis, Xα potential, R = 2.11 Å, θ = 116°; (*b*) the (12*s*/9*p*/1*d*) basis, Xα potential, R = 1.99 Å, θ = 116°; (*c*) the (12*s*/9*p*/1*d*) basis, VWN potential, R = 2.11 Å, θ = 116°; (*d*) the (12*s*/9*p*) basis, VWN potential, R = 2.00 Å, θ = 116°; (*e*) the Xα-SW overlapping spheres results from ref. 24, R = 1.98 Å, θ = 120°. The values of E_f are (*a*) −6.0 eV, (*b*) −5.99 eV, (*c*) −6.60 eV, (*d*) −6.60 eV, (*e*) −6.60 eV.

calculations converged back to the fully symmetry-adapted (C_{2v}) situation. We also performed similar tests for bond angles increased to as much as 150° which should favour localization. In all cases fully delocalized orbitals resulted. The situation is somewhat analogous to that found for H_2 (37), Na_2 (38), or Cu_2 (39) where LSD calculations yield delocalized orbitals in the region of the equilibrium geometry. The orbital localization which is necessary for correct dissociation only occurs at much longer R. GVB orbitals for H_2 (40) are already partially localized at the equilibrium distance and the situation would undoubtedly be similar for Na_2 or Cu_2. In all of these cases the local density approach yields very satisfactory values of R_e and ω_e.[1]

Concluding remarks

Contrary to the impression which may have been created by ref. 10 the present results for ozone show that local density functional theory is capable of furnishing accurate geometrical information for molecules of this type. The ozone results also allow us to state with confidence that thiozone is bent with a bond angle of about 116° and an SS distance of about 2.00 Å.

Acknowledgements

We are grateful to Professor W. G. Laidlaw for several useful discussions and for communicating results prior to publication. Dr. N. A. Baykara's advice and help with the computations is most appreciated as is financial support from the Natural Sciences and Engineering Research Council of Canada and the Ministère de l'Education du Québec. Computing services were provided by the Centre de Calcul de l'Université de Montréal.

[1]NOTE ADDED IN PROOF: Jones (42) has recently reported Linear Muffin Tin Orbital LD calculations for ozone. He finds an open–closed separation of 32 kcal/mol.

1. G. HERZBERG. Molecular spectra and molecular structure. Vol. 3. Van Nostrand, Princeton, NJ. 1966 and references therein.
2. D. C. FROST, S. T. LEE, and C. A. MCDOWELL. Chem. Phys. Lett. **24**, 149 (1974).
3. C. R. BRUNDLE. Chem. Phys. Lett. **26**, 25 (1974).
4. J. M. DYKE, L. GOLOB, N. JONATHAN, A. MORRIS, and M. OKUDA. J. Chem. Soc. Faraday Trans. **2**, 1828 (1974).
5. R. J. CELOTTA, S. R. MIELCZAREK, and C. E. KUYATT. Chem. Phys. Lett. **24**, 428 (1974).
6. N. SWANSON and R. J. CELOTTA. Phys. Rev. Lett. **35**, 783 (1975).
7. P. J. HAY, T. H. DUNNING JR., and W. A. GODDARD III. J. Chem. Phys. **62**, 3912 (1975).
8. R. P. MESSMER and D. R. SALAHUB. J. Chem. Phys. **65**, 779 (1976).
9. P. J. HAY and T. H. DUNNING, JR. J. Chem. Phys. **67**, 2290 (1977).
10. W. G. LAIDLAW and M. TRSIC. Chem. Phys. **36**, 323 (1979).
11. C. W. WILSON, JR., and D. G. HOPPER. J. Chem. Phys. **74**, 595 (1981).
12. W. D. LAIDIG and H. F. SCHAEFER, III. J. Chem. Phys. **74**, 3411 (1981).
13. D. R. SALAHUB, S. H. LAMSON, and R. P. MESSMER. Chem. Phys. Lett. **85**, 430 (1982).
14. J. C. SLATER. The self-consistent field for molecules and solids. Vol. 4. McGraw-Hill, Kuala Lumpur. 1974 and references therein.
15. J. C. SLATER. Adv. Quantum Chem. **6**, 1 (1972).
16. K. H. JOHNSON. Adv. Quantum Chem. **7**, 143 (1973).
17. P. HOHENBERG and W. KOHN. Phys. Rev. **136**, B864 (1964).
18. W. KOHN and L. J. SHAM. Phys. Rev. **140**, A 1133 (1965).
19. H. SAMBE and R. H. FELTON. J. Chem. Phys. **62**, 1122 (1975).
20. B. I. DUNLAP, J. W. D. CONNOLLY, and J. R. SABIN. J. Chem. Phys. **71**, 3396 (1970); **71**, 4993 (1970).
21. G. S. PAINTER and D. E. ELLIS. Phys. Rev. B**1**, 4747 (1970).
22. D. E. ELLIS and G. S. PAINTER. Phys. Rev. B**2**, 2887 (1970).
23. J. BERKOWITZ and C. LIPSCHITZ. J. Chem. Phys. **48**, 4346 (1968).
24. D. R. SALAHUB, A. E. FOTI, and V. H. SMITH, JR. J. Am. Chem. Soc. **100**, 7847 (1978).
25. N. R. CARLSEN and H. F. SCHAEFER, III. Chem. Phys. Lett. **48**, 390 (1977).
26. K. SCHWARZ. J. Phys. B**11**, 1339 (1978).
27. G. S. PAINTER and F. W. AVERILL. Phys. Rev. B**26**, 1781 (1982).
28. A. PELLEGATTI, B. N. MCMASTER, and D. R. SALAHUB. Chem. Phys. **75**, 83 (1983).
29. N. A. BAYKARA, B. N. MCMASTER, and D. R. SALAHUB. Mol. Phys. **52**, 891 (1984).
30. S. H. VOSKO, L. WILK, and M. NUSAIR. Can. J. Phys. **58**, 1200 (1980).
31. W. G. LAIDLAW and M. TRSIC. Can. J. Chem. **63**, 2044 (1985).
32. K. SCHWARZ. Phys. Rev. B**5**, 2466 (1972).
33. D. M. CEPERLEY and B. J. ALDER. Phys. Rev. Lett. **45**, 566 (1980).
34. S. HUZINAGA. J. Chem. Phys. **42**, 1293 (1965).
35. A. VEILLARD. Theoret. Chim. Acta, **12**, 405 (1968).
36. S. HUZINAGA and M. YOSHIMINE. J. Chem. Phys. **68**, 4486 (1978).

37. O. GUNNARSSON and B. I. LUNDQVIST. Phys. Rev. B**13**, 4274 (1976).
38. R. CAR, R. A. MEULI, and J. BUTTET. J. Chem. Phys. **73**, 4511 (1980).
39. E. RADZIO, J. ANDZELM, and D. R. SALAHUB. Unpublished.
40. W. A. GODDARD, III, T. H. DUNNING, JR., W. J. HUNT, and P. J. HAY. Acc. Chem. Res. **6**, 368 (1973).
41. W. L. FENG, O. NOVARO, and J. GARCIA-PRIETO. Chem. Phys. Lett. **111**, 297 (1984).
42. R. O. JONES. J. Chem. Phys. **82**, 325 (1985).

Ab initio studies on structures and proton affinities of fluoromethanols

F. GREIN

Department of Chemistry, University of New Brunswick, Fredericton, N.B., Canada E3B 6E2

Received August 13, 1984

This paper is dedicated to Professor Camille Sandorfy on the occasion of his 65th birthday

F. GREIN. Can. J. Chem. **63**, 1988 (1985).

Using gradient optimization techniques with 4-31G basis sets, the geometries of methanol, the three fluoromethanols, and their protonated species were optimized. Protonation on oxygen and fluorine was considered. The calculated proton affinities (PA) in kcal/mol are 181.0/178.1 for CH_2FOH, 162.3/162.6 for CHF_2OH, and 148.0/142.5 for CF_3OH, the first number for O- and the second for F-protonation.

F. GREIN. Can. J. Chem. **63**, 1988 (1985).

Utilisant des techniques d'optimisation des gradients avec des ensembles de base 4-31G, on a optimisé les géométries du méthanol, les trois fluorométhanols ainsi que celles de leurs espèces protonées. On a considéré la protonation de l'oxygène ainsi que celle du fluor. Les affinités pour le proton (AP), calculées en kcal/mol, sont de 181,0/178,1 pour le CH_2FOH, de 162,3/162,6 pour le CHF_2OH et de 148,0/142,5 pour le CF_3OH. Les premières valeurs correspondent aux fluorométhanols non protonés sur le O tandis que les secondes correspondent aux protonations sur le fluor.

[Traduit par le journal]

Introduction

α-Fluoro alcohols are difficult to synthesize due to elimination of HF. Trifluoromethanol CF_3OH has recently been prepared by Klöter and Seppelt (1) at low temperature. It has a boiling point of −20°C, and decomposes to CF_2O and HF at room temperature. The protonated form of H_2FCOH has been reported by Olah and Mateescu (2). The structure was identified by nmr. Attempts to isolate the free alcohol failed due to the loss of HF. Protonated difluoromethanol, $HF_2COH—H^+$, has been identified by Clair and McMahon (3). It is known that the proton affinity (PA) of HF_2COH is smaller than that of water (4).

Preparations to obtain all protonated fluoromethanols and to measure their proton affinities by ion cyclotron resonance (ICR) spectroscopy techniques are under way (4), and some more information should be available soon.

In aiding the experimental work, the equilibrium structures of the three fluoromethanols and their protonated species have been calculated by quantum chemical *ab initio* methods, and their proton affinities predicted from the energy differences of the optimized structures.

Methods

All geometry optimizations (SCF gradient methods) were performed using the 4-31G basis set and modified versions of the HONDO5 (5) and an IBM version (6*a*) of the GAUSSIAN80 (6*b*) computer programs. Usually, geometries were first optimized by the STO-3G basis set, providing the starting geometry for the (more expensive) 4-31G optimizations. All geometry parameters, both distances and angles, were allowed to vary, although in some cases one angle had to be fixed, as will be outlined. Protonation both on oxygen and fluorine was considered.

Results

Methanol

The proton affinity of methanol was calculated by Del Bene *et al.* (7) to be 194.9 kcal/mol (185.8 kcal/mol if zero-point energy differences and perturbation estimates of the correlation energy are included), using a 6-31G** basis set for both the parent and the protonated species. The most recent experimental value of the PA is 182.2 ± 2 kcal/mol obtained by ICR spectroscopy (8). Del Bene *et al.* found a large increase of the C—O bond length upon protonation (from 1.400 to 1.511 Å), indicating a possible dissociation to $H_2O + CH_3^+$.

Although there is no need to repeat the geometry optimization of CH_3OH and its protonated species by the 4-31G basis set, it was found to be useful for comparisons. The optimized geometries are shown in structures **I** and **II**, and given in Tables 1 and 2. The energies including PA are found in Table 4. Comparison with the experimental geometry of methanol (9) shows bond distance deviations up to 0.02 Å which are considered to be acceptable. Due to the inclusion of polarization functions, the optimized CO distance of Del Bene *et al.* is too short. On the other hand, the CO length increases upon protonation by about the same amount (from 1.430 to 1.542 Å in this work). Our calculated proton affinity is 200.0 kcal/mol, about 5 kcal/mol higher than the 6-31G** value obtained by Del Bene *et al.* Therefore, 4-31G calculations on the more difficult fluoromethanols are considered to be a reasonable compromise between accuracy obtained and effort made. Due to the emphasis placed in this paper on proton affinities, other theoretical treatments of methanol only will be ignored.

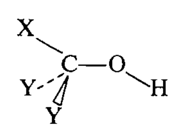

I

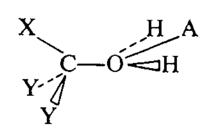

II

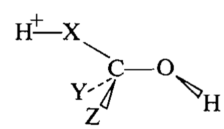

III

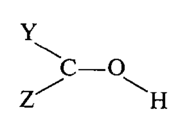

IV

Monofluoromethanol

For this molecule and the following members of the series, protonation on both oxygen and fluorine is possible, and it would be difficult from qualitative arguments to predict the preferred protonation site. Therefore, both types of protonation have been included in the calculations. The neutral species of

TABLE 1. Optimized 4-31G geometries of fluoromethanols, structure **I**,[a] distances in Å, angles in deg

	Distance				Angle		
XY_2COH	C—O	O—H	C—X	C—Y	C—O—H	X—C—O	Y—C—O
HH_2COH	1.430	0.951	1.080	1.083	113.2	109.0	111.7
expt, ref. 9	1.428	0.967	1.098	1.098	107.3		
FH_2COH[a]	1.384	0.952	1.407	1.070	114.5	110.7	107.3
HF_2COH	1.352	0.955	1.065	1.376	115.4	109.9	111.0
FF_2COH	1.338	0.954	1.357	1.346	115.9	112.1	110.7
ref. 11	1.346	0.947	1.347	1.347	115.6	110.9	110.9

[a]As described in the text, FH_2COH optimizes with OH staggered between CF and CH_a. The distance C—H_a is 1.070 Å, as given in the table, whereas C—H_b is 1.076 Å. The angle H_a—C—O is 107.3°, and H_b—C—O is 112.7°. The energy is 6.5 kcal lower than the energy of the optimized structure **I**.

TABLE 2. Optimized 4-31G geometries of fluoromethanols, protonated on O, structure **II**, distances in Å, angles in deg

	Distance				Angle				
$XY_2COH_2^+$	C—O	O—H	C—X	C—Y	C—O—H	X—C—O	Y—C—O	C—O—A[a]	H—O—H
$HH_2COH_2^+$	1.542	0.958	1.072	1.072	121.7	105.8	104.5	176.4	116.5
$FH_2COH_2^+$	1.547	0.963	1.347	1.069	121.2	106.0	104.5	166.3	115.6
$HF_2COH_2^+$	1.523	0.967	1.067	1.325	120.9	107.6	103.4	171.3	117.3
$FF_2COH_2^+$	1.487	0.971	1.314	1.314	121.1	107.2	104.9	178.9	117.8

[a]Point A in structure **II** is a reference point, lying in the X—C—O plane, such that OA bisects the HOH angle.

TABLE 3. Optimized 4-31G geometries of fluoromethanols protonated on F, structure **III**,[a] distances in Å, angles in deg

	Distance						Angle				
$(H^+X)YZCOH$	C—O	O—H	C—X	C—Y	C—Z	X—H^+	C—O—H	X—C—O	Y—C—O	Z—C—O	C—F—H^+
$(H^+F)H_2COH$	1.252	0.963	2.275	1.069		0.929	123.4	105.4	119.2		175.9
$(H^+F)FHCOH$	1.240	0.969	2.265	1.290	1.065	0.930	125.2	100.6	120.4	120.9	180.0[b]
$(H^+F)F_2COH$	1.235	0.969	2.223	1.277		0.930	125.3	96.3	121.5		180.0[b]

[a]The YZCOH fragments optimized to be nearly planar. Deviations from planarity are not given.
[b]Not allowed to optimize.

TABLE 4. Energies (in hartree) of fluoromethanols and their protonated species, structures **I** to **III**; predicted proton affinities (PA) in kcal/mol

Molecule	Neutral	O-protonated	F-protonated	PA-O	PA-F
H_3COH	−114.87150	−115.19017		200.0	
H_2FCOH	−213.61221	−213.90052	−213.89595	181.0	178.1
HF_2COH	−312.36022	−312.61877	−312.61933	162.3	162.6
F_3COH	−411.09844	−411.33418	−411.32552	148.0	142.5

fluoromethanol is described by structure **I**, the O-protonated species by structure **II**, and the F-protonated species by structure **III**. In structure **III**, YZCOH is nearly planar, with CZ and OH in *cis* positions. The optimized geometries are given in Tables 1 to 3, and the energies in Table 4.

One would assume neutral monofluoromethanol to have structure **I**, with O—H *trans* to C—F (C_s symmetry). However, it was found that a geometry with the dihedral angle of O—H 60.2° relative to C—F, starting from a *cis*-conformation, or O—H in staggered position between C—F and C—H, leads to a lower energy (−213.61221 vs. −213.60192 hartree), with an energy difference of 6.5 kcal/mol. This indicates less repulsion with (the more distant) fluorine than with a methyl hydrogen. An explanation based on the anomeric effect will be given later. The geometry parameters given in Table 1 are for the F/H staggered conformation. Optimization for structure **I**, imposing C_s symmetry, leads to slightly different bond lengths (R_{CO} = 1.398 Å, R_{OH} = 0.951 Å, R_{CF} = 1.386 Å, R_{CH} = 1.077 Å).

For O-protonation (Table 2), the C—O distance increases by 0.16 Å, whereas the C—F distance decreases by 0.06 Å. The C—H and O—H distances remain nearly unchanged. The F-protonated molecule is characterized by the very large C—F bond length of 2.275 Å, indicating the formation of the molecular complex $HF\cdots H_2COH^+$. Indeed, as will be shown later, the geometry of the complex is very close to the geometries of the individual components. The C—O distance shortens by 0.14 Å.

The calculated proton affinities are 181.0 and 178.1 kcal, for the O- and F-protonated species, respectively. They are remarkably close together. Protonation on oxygen is preferred, in agreement with the analysis of protonated monofluoromethanol

TABLE 5. Optimized 4-31G geometries and energies of (planar) $YZCOH^+$ cations, structure **IV**; distances in Å, angles in deg, energy E in hartree, ΔE in kcal/mol[a, b]

	Distance						
$YZCOH^+$	C—O	O—H	C—Y	C—Z	∠C—O—H	E	ΔE
H_2COH^+	1.246	0.967	1.072	1.075	124.6	−113.98129	17.2
$FHCOH^+$	1.235	0.973	1.289	1.071	126.6	−212.70217	18.8
F_2COH^+	1.232	0.973	1.270	1.282	127.2	−311.40526	20.7

[a] ΔE is the stabilization energy of the molecular complex $HF\cdots YZCOH^+$.
[b] HF has a 4-31G optimized distance of 0.922 Å with an energy of −99.88728 hartree.

done by Olah and Mateescu (2). These authors found a triplet pmr spectrum for OH_2, consistent with structure **II**, but not with structure **III**.

Difluoromethanol

The optimized geometry for the neutral molecule is given in Table 1, and for the O- and F-protonated species in Tables 2 and 3.

Protonation on O leads to an increase in the C—O bond length by 0.17 Å. The difference to monofluoromethanol arises mainly from the shorter C—O bond in HF_2COH, which understandably decreases with increasing fluorine substitution. The C—F bond length decreases by 0.05 Å.

In the case of F-protonation, the proton could be attached to either one fluorine, or to two, being then located on the axis bisecting the FCF angle. Optimization leads to attachment to one fluorine, again resulting in a molecular complex consisting of HF and $HFCOH^+$ (structure **III**). This geometry is energetically more favourable than that of the proton interacting with two fluorines, who could not both separate from the remainder of the molecule. A similar observation was made in the case of the protonation of F_2CS (10), where a molecular complex of the form $HF\cdots FCS^+$ is preferred to a symmetric interaction of the proton with both fluorine atoms.

The calculated proton affinities (162.3 vs. 162.6 kcal/mol) give a slight preference to the F-protonation site. However, such small energy differences are beyond the accuracy expected from Hartree–Fock calculations, and the only important conclusion to be drawn is that the proton affinities are very similar. McMahon (4) found the PA of HF_2COH to be smaller than that of water. Our result obtained for HF_2COH is about 8 kcal/mol lower than the experimental PA of H_2O (170.3 ± 2 kcal/mol) (8).

Trifluoromethanol

The optimized geometry of the neutral molecule is compared in Table 1 with that of Olsen and Howell (11). The slight differences, combined with the lower energy obtained here (the energy of ref. 11 is −411.0982), suggest that Olsen and Howell forced the oxygen to lie on the C_3 symmetry axis defined by the symmetric CF_3 group. In our case, structure **I** is allowed to be "nonaxial", as can be seen in Table 1. For methanol and its trifluoro derivative the distances C—X, C—Y and the angles X—C—O and Y—C—O are allowed to be unequal.

The O-protonated F_3COH is again characterized by an increase in the CO (by 0.15 Å) and a decrease in the CF distance (by 0.03 Å). When allowing for F-protonation, the complex $HF\cdots F_2COH^+$ has the lowest energy, rather than a cation where H^+ interacts with two or even three negatively charged fluorines. The complex has a slightly smaller PA than the O-protonated molecule (142.5 vs. 148 kcal/mol); however, the two numbers are still quite close.

Molecular complexes

In Table 5, the stabilization energies ΔE of the complexes $HF\cdots YZCOH^+$ are given. These are the energy differences between the F-protonated fluoromethanols, Tables 3 and 4, and the separate HF plus $YZCOH^+$ fragments. Positive values of ΔE indicate that the complex is more stable than the separate parts, in agreement with the automatic geometry optimization which settles on a definite CF distance rather than leading to dissociation.

The geometry of HF and the three $YZCOH^+$ cations were optimized separately. All cations (structure **IV**) are planar. The geometry parameters are included in Table 5.

The stabilization energies range from 17.2 to 20.2 kcal/mol, similar to those of the $HF\cdots YCS^+$ systems of ref. 10 (17.2 kcal/mol for $HF\cdots HCS^+$ and 14.9 kcal/mol for $HF\cdots FCS^+$).

The geometries of the $YZCOH^+$ cations (Table 5) are close to the geometries of the cations in the complex (Table 3). Differences in bond distances are 0.005 Å or less.

Discussion

For the three fluorides of methanol, protonation on oxygen leads to very similar proton affinities as protonation on F. These values decrease with increasing fluorination, and range from 181.0 to 148 kcal/mol for the (usually slightly more stable) protonation on oxygen. According to the analysis done by Del Bene *et al.* (7), the calculated PA of methanol is reduced both by the zero-point energy correction and by differences in correlation energy. For methanol, the zero-point energy correction is 8.3 and the correlation correction 0.8 kcal/mol, for a total correction of 9.1 kcal/mol. Corrections with a similar trend would have to be expected for the fluoromethanols, although no quantitative values are available. One could argue that the correlation correction should be larger for F-protonation than for O-protonation, due to the larger changes in the C—F distances. Indeed, examples can be found in ref. 7 to support this argument. On the other hand, larger distance changes result in smaller zero-point energy corrections (see ref. 7 again for examples), which will partly or fully compensate for the increased correlation corrections. Therefore, in the absence of detailed correction energies for the molecules studied here, no general arguments can be applied to support higher corrections to the PA values in the case of F-protonation.

Protonation on F always leads to a molecular complex consisting of HF and $YZCOH^+$, having a long CF bond of 2.2 to 2.3 Å. The complex stabilization energies are typically 20 kcal/mol, and dissociation with the elimination of HF should be easily possible. In all O-protonated fluorides, the C—O distance increases by 0.15 to 0.17 Å.

The optimized geometries contain no surprises except for the structure of neutral monofluoromethanol. Here, the O—H hydrogen optimizes in a staggered position between C—F and

C—H, and not between the two C—H bonds of the methyl group as one would expect. Apparently, the nonsymmetrical structure has a lower repulsion between the O—H hydrogen and the CH_2F group, and the larger number of electrons on fluorine is compensated for by the larger CF distance. Actually, the structure obtained is another example of the anomeric effect (12). If one considers oxygen to be sp^3 hybridized, then one of the oxygen lone pairs is antiperiplanar (*trans*) to the polar C—F bond. This model results in a dihedral angle of 60° for the O—H group relative to C—F, in agreement with the calculations.

A brief check on the stability of neutral fluoromethanols with regard to decomposition into HF and formaldehyde or its fluorides showed that electronically the fluoromethanols are more stable than their dissociation products by 17 to 20 kcal/mol. The observed dissociation at normal temperatures should therefore be an entropy effect, in qualitative agreement with the synthesis of CF_3OH at low temperature, and its observed dissociation at higher temperatures (1).

Conclusion

The proton affinities of the fluoromethanols were predicted using quantum chemical Hartree–Fock methods with the 4-31G basis set. The geometries of the neutral, as well as O- and F-protonated species were optimized. From the energy differences, proton affinities, uncorrected for both zero-point vibrational energy and correlation energy, were obtained. The PA's decrease with increasing fluorine substitution. Protonation on oxygen is slightly preferred, although the difference in energy is never more than 5.5 kcal/mol. Protonation on fluorine leads to molecular complexes where HF has a large distance from the remaining cation. Since zero-point energy corrections would give a slight preference to the more loosely bound F-protonated species, F-protonation is expected to be in strong competition with O-protonation. For neutral monofluoromethanol, a conformation where the OH hydrogen is staggered between CF and CH has been found to have the lowest energy, in agreement with the concept of the anomeric effect.

Acknowledgements

I am grateful to Dr. T. B. McMahon for suggesting this topic, and for his continued interest. Thanks to Uday Sishta, Chris Grein, and Neilan Mehta for performing most of the calculations. Financial support by NSERC, and a generous grant of computer time by the University of New Brunswick, are gratefully acknowledged. I would also like to thank Dr. P. Deslongchamps for providing an explanation to the optimized structure of fluoromethanol via the anomeric effect.

1. G. Klöter and K. Seppelt. J. Am. Chem. Soc. **101**, 347 (1979).
2. G. A. Olah and G. D. Mateescu. J. Am. Chem. Soc. **93**, 781 (1971).
3. R. L. Clair and T. B. McMahon. Can. J. Chem. **58**, 863 (1980).
4. T. B. McMahon. Private communication.
5. M. Dupuis, J. Rys, and H. King. QCPE, **11**, 338 (1977).
6. (*a*) P. N. van Kampen, F. A. A. M. de Leeuw, G. F. Smits, and C. Altona. QCPE, **14**, 437 (1982); (*b*) J. S. Binkley, R. A. Whiteside, R. Krishnan, R. Seeger, D. J. de Frees, H. B. Schlegel, S. Topiol, L. R. Kahn, and J. A. Pople. QCPE, **13**, 406 (1981).
7. J. E. Del Bene, M. J. Frisch, K. Raghavachari, and J. A. Pople. J. Phys. Chem. **86**, 1529 (1982).
8. J. F. Wolf, R. H. Staley, I. Koppel, M. Taagepera, R. T. McIver, Jr., J. L. Beauchamp, and R. W. Taft. J. Am. Chem. Soc. **99**, 5417 (1977).
9. J. D. Swalen. J. Chem. Phys. **23**, 1739 (1955).
10. F. Grein. Can. J. Chem. **62**, 253 (1984).
11. J. F. Olsen and J. M. Howell. Theoret. Chim. Acta, Frankfurt, **47**, 39 (1978).
12. P. Deslongchamps. Stereoelectronic effects in organic chemistry. Pergamon Press. 1983.

From crystal orbitals to strange electronic states. I. Crystal orbitals by direct recursion (transfer matrix) method (DRM)

GÉZA BICZÓ

Central Research Institute of Chemistry, Hungarian Academy of Sciences, H-1525 Budapest 114, P.O. Box 17, Hungary,[1] *and Division of Theoretical Chemistry, Friedrich-Alexander-Universität Erlangen-Nürnberg, Egerlandstrasse 3, D-8520 Erlangen, Federal Republic of Germany*

Received November 22, 1984

This paper is dedicated to Professor Camille Sandorfy on the occasion of his 65th birthday

GÉZA BICZÓ. Can. J. Chem. **63**, 1992 (1985).

The history of Bloch's and Tamm's states is sketched. The present stage in the theory of the bounded infinite polymers and crystals and strange electronic states is outlined. To lay the foundations of the SCF LCAO bounded crystal orbital (BCO) method applicable for surface electronic problems, the direct recursion (transfer matrix) method (DRM) is formulated for perfect cyclic polymers and crystals. A simple combination of block-decomposition and matrix transpositions is applied to calculate $\mathbf{U}^{-1}$ directly from the blocks of $\mathbf{U}$, the similarity transformation bringing the recursion matrix $\mathbf{T}$ into its normal form. Several forms are given for the auxiliary and fundamental equation of the DRM. The crystal orbitals are derived by the DRM. Full matrix expression is presented for the resolvent (Green) matrix of perfect cyclic polymers, the unperturbed system in the SCF local-density approach of Ladik and Seel. The formulae of the charge-bond order matrix are derived both by the DRM and the indirect (Green matrix) recursion method (IRM).

GÉZA BICZÓ. Can. J. Chem. **63**, 1992 (1985).

On présente une revue de l'histoire des états de Bloch et de Tamm. On présente l'état actuel de la théorie relative aux polymères infinis qui sont liés et aux cristaux ainsi qu'aux états électroniques particuliers. Dans le but d'établir les bases de la méthode LCAO-SCF des orbitales cristallines liées (BCO) pour des polymères et des cristaux parfaits, on a développé une méthode de récurrence directe (matrice de transfert) (DRM) qui serait applicable aux problèmes de la structure électronique des surfaces. On utilise une combinaison simple de décompositions en blocs et de transpositions de matrices pour calculer $\mathbf{U}^{-1}$ directement à partir des blocs de $\mathbf{U}$; la transformation de similarité transforme la matrice de récurrence $\mathbf{T}$ en sa forme normale. On présente plusieurs formes pour les équations auxiliaire et fondamentale de la DRM. Utilisant la DRM, on a déduit les orbitales du cristal. On présente une expression pour la matrice complète de Green de polymères cycliques parfaits, le système non perturbé dans l'approche à densité locale en champ auto-cohérent de Ladik et Seel. Utilisant la DRM et la méthode de récurrence indirecte (matrice de Green) (IRM), on a déduit les formules de la matrice des charges et des ordres de liaison.

[Traduit par le journal]

1. Introduction

The purpose of this series is threefold: (*i*) To demonstrate the power of the *direct recursion* (transfer matrix) *method* (DRM) for the solution of various problems, *from bulk to strange electronic states*. (*ii*) To present a novel full matrix *self-consistent field linear combination of atomic orbitals bounded crystal orbital* (SCF LCAO BCO) formalism for bounded crystals in the infinite size limit. (*iii*) To point out possible experimental indications for the existence of *intermediate* (electronic) *states* (IS).

The important ideas and interrelationships are introduced below in six points. Namely, the history of Bloch's and Tamm's states (I, II), the present stage in the theory of bounded infinite crystals (III), the physical significance (IV), and the history (V) of the IS are recapitulated and finally a futuristic question is posed (VI).

(I) Forty five years elapsed between the discovery of *Floquet's theorem* in 1883 (1) and its application to the bulk electronic states of crystalline solids by *Bloch* (2) and another period of 39 years until its *general full matrix ab initio SCF LCAO CO* (Hartree-Fock-Roothaan-type (3)) *formulation* in 1967 for 3-dimensional *perfect infinite crystals* (4, 5), although a 2-dimensional (not *ab initio*) version was applied to graphite 8 years earlier (6). Note that even today, 17 years later, no similar formulation exists to include electronic correlation.

(II) Bloch's theorem was immediately applied to interpret the observed properties of solids. On the contrary, only the very recent advent of high vacuum science has led to the experimental verification of *Tamm's* theoretical prediction of 1932 (7) concerning the existence of *surface states in half-infinite* crystalline solids. This happened more than three decades later!

(III) The theory of half-infinite crystals is not yet at the 1967 stage of Bloch's theory. To proceed towards that *general full matrix ab initio SCF LCAO BCO* level, first its key term, the *charge-bond order matrix* was derived *for bounded polymers and solids in the infinite size limit* by DRM. The main results were published in ref. 8 and detailed in an unpublished preprint (Preprint TCG-1-77, CRIC HAS, Budapest, March, 1977, available by direct request). This formulation has completely described the *bulk state distortion* (BSD), *the dominating SCF effect*. It was given, however, only for simple (non-overlapping) energy band systems. The next paper (9), written with the same aim, presented an indirect (exact) perturbational method (IPM), a full matrix Koster-Slater-type (10) resolvent (Green's function) approach. The BSD, however, was not taken into account there. Nevertheless, the more advanced versions (11–13) of the SCF local-impurity formalism (14) developed for linear polymers already include the BSD and show how to generalize them for surface problems. (For further details concerning the other, more approximate but also SCF IPM calculations, see the references in refs. 11–14.)

(IV) The possible *physical significance* of the *third notable electronic state of the finite crystalline solids*, besides the well understood delocalized (bulk) and localized (surface, impurity, etc.) states, was studied only very recently (8, 15–20). This state is neither localized, as the surface states are, nor is it

[1]Permanent address.

uniformly delocalized, as for the bulk states. Therefore, it may be called an intermediate state, IS. The IS is a one-electron state of zero probability as compared to the other two, the bulk and the localized states, at least at first sight (15). It may appear under the fulfilment of special boundary conditions with one-electron energies lying at the centers of resonance (Van Hove singularities) and band edges (15, 16). The existence of a critical energy interval around the sharp energy of the IS was proved where any one-electron state becomes very similar to the central IS (17, 18). These almost IS (AIS) already have non-zero probability of appearance which is very advantageous with respect to their observability. All these were reviewed in a symposium paper (18), together with other considerations such as the effect of vibrations, possible host systems for IS, etc. The above statements are merely theoretical predictions.

(V) The history of the above third kind of solutions concerning its mathematical treatment was recently reviewed (21). At least two authors, however, are omitted in this review. Fairbairn (22) has mentioned the appearance of the above solutions. Unfortunately, he relegated the problem to a footnote, saying that it is simpler to consider the new kind of solution as a limiting case of the others than to treat it separately. Most correctly, Cottey has always treated separately the band edge states (BES) (23–26) which are special cases of the IS. He studied almost exclusively symmetrical models, when he refined the theory of the quantum size effect (QSE) (25*a*–*f*, 26*a*, *b*), solving the one-dimensional Schrödinger equation for a periodic potential terminated by two infinite abrupt potential barriers. The symmetrical models, however, can produce only bulk-like, uniformly delocalized states. Only a brief section is given on unsymmetric layers and their equation (25*d*). In a detailed paper (24), he has observed the linear variation in the amplitude of the BES leading to the intermediate character of the IS. He has also concluded that a BES cannot be a real physical state in an infinite or even in a semi-infinite crystal but only that of a finite one (25*a*).

Cottey's considerations (26*a*) strongly support the contention that certain observed structures in the tunnelling current through an oxide layer into a thin metal layer are due to the one-electron QSE levels. Naturally, some of the QSE levels may be IS or, rather, AIS. Thus they must be observable from the structure of the above tunnelling current curve, from certain well observable shoulders in the absorption spectrum, and from the characteristic structures appearing in photoelectric yield spectra. Experiments focused on the observation of the IS were proposed (19, 20).

(VI) Finally, with special attention to point (II) above, one can ask the poetic question. How many years will elapse until the acceptable experimental verification or complete rejection of the very recent theoretical predictions concerning the existence of strange electronic states, say, IS? This period is significantly lengthened by the sensitivity and other exceptional properties (15, 18) of these states. Our intention is to decrease the length of the period in question by presenting this paper.

2. Crystal orbitals by DRM

This section is devoted to introducing some technical details of the DRM. For this reason, the simplest full matrix problem, that of a perfect cyclic polymer is treated in the first neighbour's interaction approximation. Recurrence relations and boundary conditions (I), fundamental equation (II), auxiliary equations (III), a novel easy calculation of the inverse matrix in the similarity transformation (IV), spectral resolution (V), other forms of the fundamental equation (VI), and charge-bond order matrix (VII) are given.

(I) The transfer matrix approach was originally formulated for vibrational problems (27–32). Its use was later extended to the treatment of, e.g., LEED experiments (33–36), bulk and surface electronic structures (8, 15–20, 37–47), disordered systems (1–5, 48–50), structure factor calculations (51), and even random resistor networks (52). (See also the references in the papers quoted above.)

According to the nomenclature introduced by Grimley (53), the transfer matrix method is a DRM since it solves the matrix representation of the Schrödinger equation directly, utilizing the translational symmetry shown by the blocks of the Hamiltonian hypermatrix from a certain block on (41*a*, 44, 47). The indirect methods determine first the resolvent (or Green) matrix and then use it as a basis for all further calculations. The oldest class of indirect methods is the IPM already mentioned in point 1.III. The IPM is an exact perturbational method because of the absence of the series expansion. Its advantage is the easy calculation of the resolvent for the perfect bulk polymer as an unperturbed system (refs. 9–14, 53–58, and references therein). The indirect recursion methods (IRM) represents the newer class (58–65) and are the realizations of an old idea (66). They utilize the recurrence relations valid for the matrix blocks of the total resolvent describing the whole (possibly perturbed) system. The connection of the IRM and the DRM was already clarified (41*a*). In an actual ZnO (1010) surface calculation, a special DRM was faster than a Koster-Slater-type IPM (10) by about a factor of 11 (42*a*).

Using the LCAO method[2] and the nearest neighbour approximation one can characterize intra- and inter-cell interactions by the matrices $\mathbf{A} = \mathbf{F}_{11} - \lambda\mathbf{S}_{11}$ and $\mathbf{B} = \mathbf{F}_{12} - \lambda\mathbf{S}_{12}$ of, say, order n. They contain the block of form $\mathbf{F}_{jk}$ for the Fock matrix elements of the electronic Hamiltonian between the atomic basis functions, $\mathbf{S}_{jk}$ for the overlap integrals and λ is the one-electron energy. $\mathbf{F} = \{\mathbf{F}_{jk}\}$, the Fock hypermatrix of the whole perfect cyclic polymer reflects the symmetry of the system: $\mathbf{F}_{jj} = \mathbf{F}_{11}$ and $\mathbf{F}_{jj+1} = \mathbf{F}_{12}$ for $j = 1, 2, \ldots, N$ (when $j = N$, the value 1 must be used for index $j + 1$ instead of $N + 1$), if it consists of N monomers ("cells"). The same is valid for the overlap hypermatrix $\mathbf{S} = \{\mathbf{S}_{jk}\}$. The eigenvalue problem of the whole system has the usual form

$$[1] \quad \mathbf{F}c = \lambda\mathbf{S}c$$

which can be rewritten in a more convenient way as

$$[2] \quad (\mathbf{F} - \lambda\mathbf{S})c = \begin{bmatrix} \mathbf{A} & \mathbf{B} & & & & \mathbf{B}' \\ \mathbf{B}' & \mathbf{A} & \mathbf{B} & & & \\ & \mathbf{B}' & \cdot & & & \\ & & & \cdot & & \\ & & & \cdot & \mathbf{B} & \\ & & & \mathbf{B}' & \mathbf{A} & \mathbf{B} \\ \mathbf{B} & & & & \mathbf{B}' & \mathbf{A} \end{bmatrix} \begin{bmatrix} c_1 \\ c_2 \\ c_3 \\ \vdots \\ c_{N-1} \\ c_N \end{bmatrix}.$$

The prime means transposition and the blank spaces are zero blocks. The jth block row of [2] reads as

$$[3] \quad \mathbf{B}'c_{j-1} + \mathbf{A}c_j + \mathbf{B}c_{j+1} = 0$$

This equation is valid for all $j = 1, \ldots, N$, if the cyclic boundary condition

$$[4] \quad c_0 = c_N \quad \text{and} \quad c_{N+1} = c_1$$

[2] A special version of, but sometimes the LCAO method itself is called the tight binding method in solid state physics.

is introduced. One can decide before executing the next step on the use of either the older Schmidt-Hori-Asahi-type DRM (8, 27–32, 37–43, 45–46) or the newer inversion free DRM (IF DRM, 44, 47, 71). The former is applicable only when $\mathbf{B}$ is nonsingular and the latter for arbitrary $\mathbf{B}$. Restricting the treatment here to the former case, one can premultiply [3] by $\mathbf{B}^{-1}$:

$$c_{j+1} = (\mathbf{D}\ \mathbf{G})\begin{pmatrix} c_{j-1} \\ c_j \end{pmatrix}$$

where $\mathbf{D} = -\mathbf{B}^{-1}\mathbf{B}'$ and $\mathbf{G} = -\mathbf{B}^{-1}\mathbf{A}$. Completing this equation with the identity

$$c_j = (\mathbf{0}\ \mathbf{I})\begin{pmatrix} c_{j-1} \\ c_j \end{pmatrix}$$

and defining the recursion (transfer) matrix (27, 28)

$$[5]\quad \mathbf{T} = \begin{pmatrix} \mathbf{0} & \mathbf{I} \\ \mathbf{D} & \mathbf{G} \end{pmatrix}$$

and the column vector of two consecutive column vector blocks c_{j-1} and c_j from the hyper-columnvector c of eq. [1], [2]

$$x_j = \begin{pmatrix} c_{j-1} \\ c_j \end{pmatrix}$$

one can write [3] and [4] as

$$[6]\quad x_{j+1} = \mathbf{T}x_j$$

and

$$[7]\quad x_{N+1} = x_1$$

The recurrence relation [6] will have this form for perturbed and non-perfect polymers, too, only $\mathbf{T}$ will depend also on the index of the actual cell, $\mathbf{T} = \mathbf{T}_j$ must be written in [6]. The boundary condition [7] will have various forms for different problems.

(II) Contracting eq. [6], [7] by successive substitutions one obtains the *fundamental equation*

$$[8]\quad x_1 = \mathbf{T}^N x_1$$

This is its first form. It is a homogeneous linear equation for matrix $\mathbf{T}^N - \mathbf{I}$ which is a function of λ. It has non-trivial solutions at and only at the eigenvalues of the original generalized eigenvalue problem [1], where its determinant vanishes:

$$[9]\quad |\mathbf{T}^N - \mathbf{I}| = 0.$$

This characteristic equation is of order $2n$. For its evaluation, however, some auxiliary equations or the spectral resolution of $\mathbf{T}$ must be used because of the appearance of a high or even infinite power of $\mathbf{T}$.

(III) The spectral properties of the recursion matrix $\mathbf{T}$ play a very important role in the determination of the characteristic properties of the eigensolutions of [1]. For example, the appearance of Jordan blocks in the normal form of $\mathbf{T}$ are responsible for the creation of certain strange electronic states (8, 15–20, 41b). In perfectly periodic systems, however, these are not allowed states (24, 25a). At this point, therefore, one can accept Fairbairn's strategy restricting the treatment to the principal case when $\mathbf{T}$ is semisimple. In this case both the left and the right eigenvalue problems of $\mathbf{T}$ have complete systems of eigenvectors which can be used to form the non-singular matrices $\mathbf{U}$ and $\mathbf{Q}$. These eigenvalue problems, which are our auxiliary equations, have the compact form

$$[10]\quad \mathbf{UT} = \boldsymbol{\tau}\mathbf{U}$$

and

$$[11]\quad \mathbf{TQ} = \mathbf{Q}\boldsymbol{\tau}$$

where the diagonal matrix $\boldsymbol{\tau}$ contains the eigenvalues of $\mathbf{T}$ in the order of their absolute values (8). Namely, for

$$|\mu_1| \leqq |\mu_2| \leqq \ldots \leqq |\mu_n| \leqq |\nu_n| \leqq \ldots \leqq |\nu_2| \leqq |\nu_1|$$

the following relationship holds

$$[12]\quad \boldsymbol{\mu\nu} = \mathbf{I}, \qquad \boldsymbol{\tau} = \begin{pmatrix} \boldsymbol{\mu} & \mathbf{0} \\ \mathbf{0} & \boldsymbol{\nu} \end{pmatrix}$$

$$[13]\quad \mathbf{UQ} = \mathbf{I}, \quad \mathbf{U} = \begin{pmatrix} \mathbf{X} & \mathbf{Y} \\ \mathbf{W} & \mathbf{Z} \end{pmatrix}, \quad \text{and} \quad \mathbf{Q} = \begin{pmatrix} \mathbf{J} & \mathbf{K} \\ \mathbf{L} & \mathbf{M} \end{pmatrix}$$

Equation [12] is a direct consequence of the fact that $\mathbf{T}$ and $\mathbf{T}^{-1}$ (compare [5] and [34] on the left side of [10] and the right side of [11] eigenvalue equations of $\mathbf{T}$) have the same characteristic equation (8, 41a). It has already been shown (41a) that the $\mathbf{B}^{-1}$-free reduced forms of auxiliary equations [10], [11] are related to the fundamental equation of the Fromm-Koutecký IRM by a similarity transformation.

(IV) It is well known that a Hermitian matrix $\mathbf{H}$ can be diagonalized by a unitary matrix $\mathbf{U}$ as $\mathbf{UHU}^+ = \boldsymbol{\chi}$, where $\boldsymbol{\chi}$ is diagonal, $^+$ means adjoint and $\mathbf{U}^{-1} = \mathbf{U}^+$ can be determined simply by forming the adjoint. One might think, at first sight, that such a computationally advantageous procedure is impossible for $\mathbf{T}$, owing to its non-symmetrical structure. The more symmetrical form of the reduced auxiliary equations (41a), however suggests that a more or less similar procedure must exist for the blocks of $\mathbf{U}$ and $\mathbf{Q}$. It will be shown here that this is the case.

Let $\mathbf{YB}^{-1} = \mathbf{E}$ and $\mathbf{ZB}^{-1} = \mathbf{H}$. Then the upper block components of [10] lead to

$$[14]\quad -\mathbf{EB}' = \boldsymbol{\mu}\mathbf{X}$$

or, by [12], $\mathbf{X} = -\boldsymbol{\nu}\mathbf{EB}'$ and $\mathbf{X} - \mathbf{EA} = \boldsymbol{\mu}\mathbf{Y}$ or, by eliminating $\mathbf{X}$ through [14],

$$[15]\quad \mathbf{EB}' + \boldsymbol{\mu}\mathbf{EA} + \boldsymbol{\mu}^2\mathbf{EB} = \mathbf{0}$$

By analogy ($\mathbf{X}$, $\mathbf{Y}$, $\boldsymbol{\mu}$ correspond to $\mathbf{W}$, $\mathbf{Z}$, and $\boldsymbol{\nu}$),

$$[16]\quad \mathbf{W} = -\boldsymbol{\mu}\mathbf{HB}'$$

and

$$[17]\quad \mathbf{HB}' + \boldsymbol{\nu}\mathbf{HA} + \boldsymbol{\nu}^2\mathbf{HB} = \mathbf{0}$$

One can similarly split eq. [11]

$$[18]\quad \mathbf{L} = \mathbf{J}\boldsymbol{\mu}$$

$$[19]\quad \mathbf{B}'\mathbf{J} + \mathbf{AJ}\boldsymbol{\mu} + \mathbf{BJ}\boldsymbol{\mu}^2 = \mathbf{0}$$

$$[20]\quad \mathbf{M} = \mathbf{K}\boldsymbol{\nu}$$

and

$$[21]\quad \mathbf{B}'\mathbf{K} + \mathbf{AK}\boldsymbol{\nu} + \mathbf{BK}\boldsymbol{\nu}^2 = \mathbf{0}$$

Transposing, rearranging and postmultiplying [15] by $\boldsymbol{\nu}^2 = \boldsymbol{\mu}^{-2}$ (see [12]), one obtains the same equation [21] for $\mathbf{E}'$ as was obtained for $\mathbf{K}$ above. In the above assumed principal case (semi-simple $\mathbf{T}$), however, the eigenvectors of [10], [11] are determined up to a free constant factor. Thus

$$[22]\quad \mathbf{K} = \mathbf{E}'\boldsymbol{\gamma}$$

where $\boldsymbol{\gamma}$ is a diagonal matrix of order n containing half the free factors above. The rest of these factors are collected in the diagonal matrix $\boldsymbol{\delta}$ which appears in the analogous equation

$$[23] \quad \mathbf{J} = \mathbf{H}'\boldsymbol{\delta}$$

Substituting [14], [16], [18], [20], [22], [23] into [13], its two diagonal blocks determine $\boldsymbol{\gamma}$ and $\boldsymbol{\delta}$ as

$$[24] \quad \boldsymbol{\delta} = (\mathbf{EBH}'\boldsymbol{\mu} - \boldsymbol{\nu}\mathbf{EB}'\mathbf{H}')^{-1}$$

and

$$[25] \quad \boldsymbol{\gamma} = (\mathbf{HBE}'\boldsymbol{\nu} - \boldsymbol{\mu}\mathbf{HB}'\mathbf{E}')^{-1} = \boldsymbol{\gamma}' = -\boldsymbol{\delta}$$

The two off-diagonal blocks yield interesting non-trivial relations

$$[26] \quad \boldsymbol{\nu}\mathbf{EB}'\mathbf{E}' = \mathbf{EBE}'\boldsymbol{\nu} = (\mathbf{EB}'\mathbf{H}')'\boldsymbol{\nu}$$

and

$$[27] \quad \boldsymbol{\mu}\mathbf{HB}'\mathbf{H}' = \mathbf{HBH}'\boldsymbol{\mu} = (\mathbf{HB}'\mathbf{H}')'\boldsymbol{\mu}$$

which are very useful in the simplification of various formulae. Other useful relationships

$$[28] \quad \mathbf{H}'\boldsymbol{\delta\mu}\mathbf{E} - \mathbf{E}'\boldsymbol{\delta\nu}\mathbf{H} = \mathbf{B}^{-1}$$

and

$$[29] \quad \mathbf{H}'\boldsymbol{\delta}\mathbf{E} = \mathbf{E}'\boldsymbol{\delta}\mathbf{H} = (\mathbf{H}'\boldsymbol{\delta}\mathbf{E})'$$

are obtained from $\mathbf{QU} = \mathbf{I}$. (The other two expressions are merely the transposes of [28] and [29].)

Summarising,

$$[30] \quad \mathbf{U} = \begin{pmatrix} -\boldsymbol{\nu}\mathbf{EB}' & \mathbf{EB} \\ -\boldsymbol{\mu}\mathbf{HB}' & \mathbf{HB} \end{pmatrix}$$

and

$$[31] \quad \mathbf{Q} = \mathbf{U}^{-1} = \begin{pmatrix} \mathbf{H}'\boldsymbol{\delta} & -\mathbf{E}'\boldsymbol{\delta} \\ \mathbf{H}'\boldsymbol{\delta\mu} & -\mathbf{E}'\boldsymbol{\delta\nu} \end{pmatrix}$$

where $\boldsymbol{\delta}$ is given by [24], $\mathbf{E} = \mathbf{YB}^{-1}$ and $\mathbf{H} = \mathbf{ZB}^{-1}$.

(V) In accordance with [10]–[13], [30], [31],

$$[32] \quad \mathbf{T}^{j} = \mathbf{U}^{-1}\boldsymbol{\tau}^{j}\mathbf{U} = \begin{pmatrix} -\mathbf{V}_{j-1}\mathbf{B}' & \mathbf{V}_j\mathbf{B} \\ -\mathbf{V}_j\mathbf{B}' & \mathbf{V}_{j+1}\mathbf{B} \end{pmatrix}$$

is the spectral resolution, where

$$[33] \quad \mathbf{V}_j = \mathbf{H}'\boldsymbol{\delta\mu}^{j}\mathbf{E} - \mathbf{E}'\boldsymbol{\delta\nu}^{j}\mathbf{H}$$

It is evident from [29] and [28] that $\mathbf{V}_0 = \mathbf{0}$ and $\mathbf{V}_1 = \mathbf{B}^{-1}$. The first form (with $\boldsymbol{\tau}^j$) in [32] is the usual, and the second is a block-wise spectral resolution which reflects the reciprocal character of the problem. This reciprocity is a direct consequence of the physical structure of the system studied, namely, that the forward and backward propagation of the electronic states follow the same rules. The latter is easily demonstrated by a reversed numbering of the monomers (cells) and also by the simple inversion rule of the recursion matrix:

$$[34] \quad \mathbf{T}^{-1} = \begin{pmatrix} -\mathbf{B}'^{-1}\mathbf{A} & -\mathbf{B}'^{-1}\mathbf{B} \\ \mathbf{I} & \mathbf{0} \end{pmatrix}$$

The use of the block-wise spectral resolution is especially advantageous when a standard computer routine is available for the solution of the generalized eigenvalue problems of monic matrix polynomials (matrix pencils) (67) such as [15] and [17], since their order is only n and not $2n$ as for the original auxiliary equation [10].

The difference between these two methods of calculation is even more pronounced when farther than the first, say, the kth neighbour's interaction approximation is applied. Then further off-diagonal block positions are occupied in [2]; the jth upper and $(N-j)$th lower by $\mathbf{B}_j$, the jth lower and $(N-j)$th upper off-diagonal positions by $\mathbf{B}_{-j} = \mathbf{B}_j'$. Now, following Matsuda [29], [30], one can define the recursion matrix as

$$[35] \quad \mathbf{T} = \begin{bmatrix} \mathbf{0} & \mathbf{I} & \dots & \mathbf{0} & \mathbf{0} & \mathbf{0} & \dots & \mathbf{0} \\ & & & \dots & & & & \\ \mathbf{0} & \mathbf{0} & \dots & \mathbf{I} & \mathbf{0} & \mathbf{0} & \dots & \mathbf{0} \\ \mathbf{0} & \mathbf{0} & \dots & \mathbf{0} & \mathbf{I} & \mathbf{0} & \dots & \mathbf{0} \\ \mathbf{0} & \mathbf{0} & \dots & \mathbf{0} & \mathbf{0} & \mathbf{I} & \dots & \mathbf{0} \\ & & & \dots & & & & \\ \mathbf{0} & \mathbf{0} & \dots & \mathbf{0} & \mathbf{0} & \mathbf{0} & \dots & \mathbf{I} \\ \mathbf{D}_{-k} & \mathbf{D}_{1-k} & \dots & \mathbf{D}_{-1} & \mathbf{G}_k & \mathbf{D}_1 & \dots & \mathbf{D}_{k-1} \end{bmatrix}$$

where $\mathbf{G}_k = -\mathbf{B}_k^{-1}$ and $\mathbf{D}_j = -\mathbf{B}_k^{-1}\mathbf{B}_j$ $(j = -k, \dots, -1, 1, \dots, k-1)$. Its eigenvalue problem [10] is of order $2kn$. At the same time, the polynomial equation

$$[36] \quad \mathbf{EB}_k' + \dots + \boldsymbol{\mu}^{k-1}\mathbf{EB}_1' + \boldsymbol{\mu}^{k}\mathbf{EA} + \boldsymbol{\mu}^{k+1}\mathbf{EB}_1 + \dots + \boldsymbol{\mu}^{2k}\mathbf{EB}_k = \mathbf{0}$$

analogous to [15], still remains of order n. Note that [35] is just the first companion operator associated with [36] having an important role in the spectral analysis of matrix polynomials (68).

(VI) The second form of the fundamental equation is obtained by premultiplying [8] with $\mathbf{U}$ and using [10]:

$$[37] \quad (\boldsymbol{\tau}^N - \mathbf{I})\mathbf{Ux}_1 = \mathbf{0}.$$

Evidently, a non-trivial solution exists only when at least one eigenvalue of $\mathbf{T}$ is a complex root of unity:

$$[38] \quad \mu_m = \mu_m(q) = \exp(2\pi i q/N), \qquad 1 \leqq m \leqq n$$

Here μ_m and $\nu_m = \mu_m^{-1} = \exp[2\pi i(N-q)/N]$ have similar roles, but one can distinguish them by definition, requiring $0 \leqq q \leqq N/2$. The well-known double degeneracy of the Bloch states is striking now from [37] and [38] for $0 < q < N/2$, since then $\mu_m \neq \nu_m$ warrants two independently non-zero components in the column vector $\mathbf{Ux}_1$. This double degeneracy disappears when $q = 0$ or $N/2$, because $\mathbf{T}$ becomes defective and $\mu_m = \nu_m = +1$ or -1 introduce a Jordan block

$$[39] \quad \boldsymbol{\eta} = \begin{pmatrix} \epsilon & 1 \\ 0 & \epsilon \end{pmatrix} = \epsilon\mathbf{I} + \boldsymbol{\zeta}$$

where $\epsilon = \pm 1$ and $\boldsymbol{\zeta} = \begin{pmatrix} 0 & 1 \\ 0 & 0 \end{pmatrix}$. Here $\boldsymbol{\zeta}^2 = 0$, thus the expansion of $\boldsymbol{\eta}^N$ by the binomial theorem contains only two non-zero terms:

$$[40] \quad \boldsymbol{\eta}^N = \epsilon^N\mathbf{I} + \binom{N}{1}\epsilon^{N-1}\boldsymbol{\zeta} = \epsilon^N\begin{pmatrix} 1 & \epsilon N \\ 0 & 1 \end{pmatrix}$$

When such a block appears in [37] only one non-zero component can correspond to it in $\mathbf{Ux}_1$ and the other component must be zero just to exclude the appearance of coefficient N which would lead to an asymmetric IS violating the cyclic symmetry of the system. This is the mathematical mechanism which permits the occurrence of only bulk-like, uniformly distributed IS in the cyclic systems. A more detailed treatment of the defective case, together with the IF DRM, will be given elsewhere (71).

The derivation of the third, block decomposed form of the fundamental equation is very convenient from the block-wise spectral resolution, the second expression in [32], when bounded polymers or crystals are studied with free boundary conditions, as will be seen later. However, its application here would unnecessarily complicate the problem. At the same time, the usual spectral resolution given in the first expression of [32] yields again [37]. Its decomposition is trivial in the semisimple case:

$$[41] \quad (\boldsymbol{\mu}^N - \mathbf{I})\boldsymbol{d}_N = 0 \quad \text{and} \quad (\boldsymbol{\nu}^N - \mathbf{I})\boldsymbol{d}_1 = 0$$

or, premultiplying the latter by $-\boldsymbol{\mu}^N$,

$$[42] \quad (\boldsymbol{\mu}^N - \mathbf{I})\boldsymbol{d}_1 = 0$$

where $\boldsymbol{d}_N$ and $\boldsymbol{d}_1$ mean the upper and the lower component of $\mathbf{Ux}_1$. One fact must be observed here that one can always reformulate the blocks of the block-decomposed fundamental equation so that they contain only $\boldsymbol{\mu}$, i.e., only those eigenvalues of the recursion matrix which have absolute value not greater than 1. This was already shown for the auxiliary equation after eq. [21] and this possibility leads to the IF DRM (41*a*, 44, 47, 71).

(VII) The charge-bond order matrix will be derived by two different approaches: a DRM (*i*) and an IRM (*ii*).

(*i*) In point (VI) above, μ_m and ν_m were distinguished by definition. This will be important later when bounded systems will be studied. Here, for the cyclic system, it is simpler to treat them on the same footing permitting q to run from 1 to N when eq. [38] is used as is common in band theories. Thus one can get all the linearly independent solutions to [1], if only one non-zero component is kept in $\mathbf{Ux}_1$, say, $(\mathbf{Ux}_1)_m$ or $(\mathbf{Ux}_1)_{m+n}$. In the latter case $J(q)$ is also used for the K of eq. [21] and $\tau_m = \tau_m(q) = e^{i\kappa}$ $(\kappa = 2\pi q/N)$ for μ_m or ν_m. Now the less compact but most common eigenvalue equation form of [19] and [21] will be applied as one single equation

$$[43] \quad (\mathbf{B}' + \mathbf{A}\tau_m + \mathbf{B}\tau_m^2)\,\mathbf{J}_{*m}(q) = 0$$

where $\mathbf{J}_{*m}$ means the mth column vector of the n by n matrix $\mathbf{J}$. Multiplying [43] with τ_m^{-1}, using κ as the variable instead of q $(0 < \kappa \leqq 2\pi)$ and the definitions of $\mathbf{A}$ and $\mathbf{B}$ one obtains

$$[44] \quad (\mathbf{F}'_{12}e^{-i\kappa} + \mathbf{F}_{11} + \mathbf{F}_{12}e^{i\kappa})\,\mathbf{J}_{*m}(\kappa) = \lambda(\mathbf{S}'_{12}e^{-i\kappa} + \mathbf{S}_{11} + \mathbf{S}_{12}e^{i\kappa})\,\mathbf{J}_{*m}(\kappa)$$

This is just the well-known LCAO CO equation of finite or even infinite one-dimensional crystals if κ is regarded as continuous (4–6).

Now [6] and [32] yield

$$[45] \quad \mathbf{x}_{j+1} = \mathbf{T}^j\mathbf{x}_1 = \mathbf{Q}\boldsymbol{\tau}^j\mathbf{Ux}_1$$

and, with the above modified notations,

$$[46] \quad \boldsymbol{c}_j = \mathbf{J}_{*m}(\kappa)\,e^{ij\kappa}\,d$$

follows from the upper component of [45], d being the actual non-zero component of $\mathbf{Ux}_1$. It is convenient to use the normalized eigenvector block

$$[47] \quad \mathbf{C}_{*m}(\kappa) = |\mathbf{J}_{*m}(\kappa)|^{-1}\,\mathbf{J}_{*m}(\kappa)$$

where $||$ denotes the absolute value of the vector in question defined through the metric matrix

$$\mathbf{S} = \mathbf{S}'_{12}e^{-ik} + \mathbf{S}_{11} + \mathbf{S}_{12}e^{ik}$$

as $|\boldsymbol{v}| = (\boldsymbol{v} + \mathbf{S}\boldsymbol{v})^{1/2}$ where $\boldsymbol{v}$ is a column vector. If the hypereigenvector $\boldsymbol{c}$ is normalized to 1 and [47] is substituted into [46], then

$$[48] \quad c_j = \frac{1}{\sqrt{N}}\,\mathbf{C}_{*m}(\kappa)\,e^{ij\kappa}$$

In the simplest closed shell case, the charge-bond order matrix has the blocks

$$[49] \quad \mathbf{P}_{jk} = \frac{2}{N}\sum_{q=1}^{N} e^{2\pi i(j-k)q/N} \sum_{m}^{\text{occ.}} \mathbf{C}_{*m}(2\pi q/N)\mathbf{C}_{*m}(2\pi q/N)$$

for finite N and

$$[50] \quad \mathbf{P}_{jk} = \frac{1}{\pi}\int_0^{2\pi} e^{i(j-k)\kappa} \sum_{m}^{\text{occ.}} \mathbf{C}_{*m}(\kappa)\mathbf{C}^{+}_{*m}(\kappa)\,d\kappa$$

in the infinite size limit $(N \to \infty)$. Here "occ." on the summation means that just the labels m of the occupied bands have to be included.

(*ii*) The relation (69)

$$[51] \quad \mathbf{P}_{jk} = -\frac{2}{\pi}\int_{-\infty}^{\lambda_F} \operatorname{Im}[\mathbf{R}^0_{jk}(x)]\,dx$$

will be used here to derive the charge-bond order matrix. The factor two is due to the double occupancy which is assumed here. The abbreviation Im means imaginary part, λ_F is the Fermi level, the resolvent (Green) hypermatrix $\mathbf{R}$ is defined as

$$[52] \quad (z\mathbf{S} - \mathbf{F})\mathbf{R} = \mathbf{I}$$

it has the blocks $\mathbf{R}_{jk}(z)$ $(z = x + iy)$ of order n, and the superscript 0 indicates that first Im $[\mathbf{R}_{jk}(x + iy)]$ must be integrated for a positive y which afterwards approaches zero.

Generalizing the idea of McIntosh *et al.* (32) for the full matrix case, just the DRM will be applied here to determine $\mathbf{R}$ from [52]. This is the precise meaning that an IRM is used to calculate $\mathbf{P}$. Note that such an approach was already used to study the Green function method (G. Biczó, preprint TCG-1-77 quoted in point 1.III and ref. 39) and will be published in detail elsewhere (72).

Now

$$[53] \quad -\mathbf{B}'\mathbf{R}_{j-1k} - \mathbf{A}\mathbf{R}_{jk} - \mathbf{B}\mathbf{R}_{j+1k} = \delta_{jk}\mathbf{I}$$

is the block-decomposed form of [52] for $j, k = 1, \ldots, N$ if $j, k = 0$ or $N + 1$ corresponds to N or 1, respectively, and $\lambda = z = x + iy$ is substituted in the definition of $\mathbf{A}$ and $\mathbf{B}$. Comparing [52], [53] with [2], [3], one can observe two essential differences. First, that matrix blocks now occupy the places of the column vectors $\boldsymbol{c}_j$ of [3] and second that, contrary to [2], [52] represents a set of inhomogeneous linear matrix equations and not a homogeneous equation. Accordingly,

$$\mathbf{r}_{j+1} = \begin{pmatrix} \mathbf{R}_{jk} \\ \mathbf{R}_{j+1k} \end{pmatrix}$$

replaces $\mathbf{x}_{j+1}$ and the boundary condition is similar to [7]:

$$[54] \quad \mathbf{r}_{N+1} = \mathbf{r}_1$$

Naturally, [6] will be somewhat modified:

$$[55] \quad \mathbf{r}_{j+1} = \mathbf{T}\mathbf{r}_j + \delta_{jk}\mathbf{b} \qquad \text{with} \quad -\mathbf{b} = \begin{pmatrix} 0 \\ \mathbf{B}^{-1} \end{pmatrix}$$

The fundamental equation comes from [54] and [55]:

$$\mathbf{r}_{k+1} = \mathbf{T}\mathbf{r}_k + \mathbf{b} = \mathbf{T}^k\mathbf{r}_1 + \mathbf{b} = \mathbf{T}^k\mathbf{r}_{N+1} = \mathbf{T}^N\mathbf{r}_{k+1} + \mathbf{b}$$

or in a more explicit form

[56] $\mathbf{r}_{k+1} = (\mathbf{I} - \mathbf{T}^N)^{-1}\mathbf{b}$

This is valid independent of the actual value of k. For example, if $k = N$, then

[57] $\begin{pmatrix} \mathbf{R}_{jN} \\ \mathbf{R}_{j+1N} \end{pmatrix} = \mathbf{r}_{j+1} = \mathbf{T}^j\mathbf{r}_1 = \mathbf{T}^j\mathbf{r}_{N+1} = \mathbf{T}^j(\mathbf{I} - \mathbf{T}^N)^{-1}\mathbf{b}$

holds for $j = 1, \ldots, N-1$ giving all blocks of $\mathbf{R}$ either directly or by transposition and cyclic permutation of the blocks.

The second, block-decomposed form follows from equations [22]–[25], [32], [55]–[57]:

[58] $\mathbf{R}_{jN} = \mathbf{R}'_{Nj} = \mathbf{H}'\boldsymbol{\delta}\boldsymbol{\mu}^j(\boldsymbol{\mu}^N - \mathbf{I})^{-1}\mathbf{E} - \mathbf{E}'\boldsymbol{\delta}\boldsymbol{\nu}^j(\boldsymbol{\nu}^N - \mathbf{I})^{-1}\mathbf{H}$

being valid for $j = 0, \ldots, N$.

It is evident that outside the allowed continuous spectrum belonging to [1], $\mathbf{T}$ cannot have eigenvalues of absolute value 1. This is the case for real $\lambda = z = x$ by definition. Otherwise, supposing $\lambda = z = x + iy$ and $y \neq 0$, the existence of at least one such eigenvalue, say $e^{i\kappa}$, would warrant [44] to be a Hermitian generalized eigenvalue problem with a pure real spectrum for λ. This contradicts with the supposition $y \neq 0$.

As a consequence of the above fact and the very definition of eigenvalues μ_m, their absolute values are all less than 1. Thus, in the infinite size limit $N \to \infty$, $\boldsymbol{\mu}^N$ approaches $\mathbf{0}$ and [58] will be largely simplified:

[59] $\mathbf{R}_{jk} = \begin{cases} -\mathbf{E}'\boldsymbol{\delta}\boldsymbol{\mu}^{k-j}\mathbf{H} & \text{for } j \leqq k \\ -\mathbf{H}'\boldsymbol{\delta}\boldsymbol{\mu}^{j-k}\mathbf{E} & \text{for } k \leqq j \end{cases}$

where $\boldsymbol{\delta}$ is given by [24], $\mathbf{E}$ and $\mathbf{H}$ satisfy [15] and [17], while [29] warrants the equality of the two different expressions in [59] for the case of $j = k$.

Both the conceptual and computational advantages of the purely algebraic expression [59] are striking when it is compared with the usual integral expression (69)

[60] $[\mathbf{R}_{jk}(z)]_{pq} = \dfrac{1}{2\pi} \sum_{m=1}^{n} \int_{-\pi}^{\pi} \dfrac{\mathbf{C}_{pm}(\kappa)\mathbf{C}^*_{qm}(\kappa)}{z - \lambda_m(\kappa)} e^{i(j-k)\kappa}\, d\kappa$

which is evaluated by the use of the Dirac identity for $1/z$ and other relations for the delta functions, by integral transformations and the Kramers-Kronig relation, and by numerical integration techniques with a particular approach near the band edge singularities (12). Here the superscript * means complex conjugation, [44] and [47] define the eigenvectors $\mathbf{C}_{*m}(\kappa)$ and the eigenvalues $\lambda_m(\kappa)$ belonging to the mth band and to κ, the latter being proportional to the wave vector.

To point out the differences between [59] and [60] more markedly, one can pose an exercise; namely, to prove the equality

[61] $\dfrac{1}{2\pi} \int_{-\pi}^{\pi} \dfrac{e^{i\kappa(k-j)}}{z - a - 2b\cos\kappa}\, d\kappa = \dfrac{\mu^{|k-j|}}{b(\nu - \mu)}$

where $z = x + iy$, a and b are constants, k and j are nonnegative integers, $\mu = \text{minabs}[w \pm (w^2 - 1)^{1/2}] = \nu^{-1}$, $w = (z - a)/2b$ and minabs means that one has to choose one which is smaller in absolute value. The whole arsenal of the theory of complex functions must be applied to evaluate the left side of eq. [61], arriving finally at the compact algebraic expression of the right side, if we do not know the background of the problem. A numerical test of [61] would also be more tedious for the left than for the right side, because of the possibly singular integrand. At the same time, it is now evident that [61] is nothing but $\mathbf{G}_{jk}(z)$ of the simplest one-atomic chain ($\mathbf{F}_{11} = a$, $\mathbf{S}_{11} = 1$, $\mathbf{A} = a - \lambda$, $\mathbf{S}_{12} = 0$, and $\mathbf{B} = \mathbf{F}_{12} = b$) written in two different forms [60] and [59].

It has to be pointed out that one can work with expression [59] purely on the real axis of the complex energy plane. Instead of executing a limiting process $y \to +0$, one can calculate everything listed after eq. [59] just for the real values of $z = \lambda$, i.e., by substituting $y = 0$. Expression [59] so-obtained correctly displays the well-known characteristics of the resolvent, producing imaginary contributions inside the bands and singularities at the band edges and at the other Van Hove sites, and remaining purely real outside the bands (69). (Singularities caused usually by the discrete spectrum are naturally absent here in the cyclic problem.)

To be more explicit, expression [59] for $\mathbf{R}_{jk}$ will be decomposed as

[59a] $\mathbf{R}_{jk} = \sum_{m=1}^{n} \mathbf{R}^m_{jk} = \mathbf{R}^{\text{band}}_{jk} + \mathbf{R}^{\text{exp}}_{jk}$

where

[59b] $\mathbf{R}^m_{jk} = -\delta_{mm}\mu_m^{|k-j|}\,\mathbf{R}^m$

[59c] $\mathbf{R}^m = \begin{cases} (\mathbf{E}_{m*})'\mathbf{H}_{m*} & \text{for } j \leqq k \\ (\mathbf{H}_{m*})'\mathbf{E}_{m*} & \text{for } k < j \end{cases}$

[59d] $\mathbf{R}^{\text{band}}_{jk} = \sum_{m}^{|\mu_m|=1} \mathbf{R}^m_{jk}$

and

[59e] $\mathbf{R}^{\text{exp}}_{jk} = \sum_{m}^{|\mu_m|\neq 1} \mathbf{R}^m_{jk}$

Now

[24a] $\delta_{mm} = [\mathbf{E}_{m*}(\mathbf{B}\mu_m - \nu_m\mathbf{B}')(\mathbf{H}_{m*})']^{-1}$

follows from [24]. The decomposed forms

[15a] $\mathbf{E}_{m*}(\mathbf{B}'\nu_m + \mathbf{A} + \mathbf{B}\mu_m) = 0$

and

[17a] $\mathbf{H}_{m*}(\mathbf{B}'\mu_m + \mathbf{A} + \mathbf{B}\nu_m) = 0$

of eqs. [15] and [17] (for the derivation, compare them with [44]) have the common characteristic equation $|\mathbf{B}'t^{-1} + \mathbf{A} + \mathbf{B}t| = 0$. This is equivalent to the characteristic equation of [10] and [11]. Its reciprocal character was already mentioned after [13]. In addition, it is a real algebraic equation of order $2n$ for the variable t. This means that a real algebraic equation of order n determines $t + t^{-1} = x$. One can distinguish three cases when its solutions are classified.

(i) $|t| = 1$ if and only if x is a real number and $|x| \leqq 2$, defining by this way the allowed energy bands. Then $t^{-1} = t^*$, or, for an actual eigenvalue: $\nu_m = \mu^*_m$.

(ii) $|t| \neq 1$ and t is real if and only if x is real and $|x| > 2$. Here $|\mu_m| < 1$, $|\nu_m| > 1$ and both are real.

(iii) $|t| \neq 1$ and t is not real if and only if x is not real. In this case, however, due to the fundamental theorem of algebra, x^* is also a root of the above real algebraic equation of order n. Evidently, if just $\mu_m + \nu_m = x$, then $x^* = \mu_{m'} + \nu_{m'}$, $m' \neq m$, $\mu_{m'} = \mu^*_m$, and $\nu_{m'} = \nu^*_m$. The latter two cases lead to exponentially varying quantities outside the allowed bands.

In case (i), the complex conjugated form of [15a] is just equivalent to [17a], therefore $\mathbf{H}_{m*} = \mathbf{E}^*_{m*}$. Then [24$a$] yields

$$[24b] \quad \delta_{mm} = [\mathbf{E}_{m*}(\mathbf{B}\mu_m - \nu_m\mathbf{B}')(\mathbf{E}_{m*})^+]^{-1}$$

which is now purely imaginary, because $\mathbf{B}\mu_m - \nu_m\mathbf{B}'$ is antihermitian. Consequently, [59d] represents the complex contributions of the bands having non-zero imaginary part, where the specific form

$$[59f] \quad \mathbf{R}^m = \begin{cases} (\mathbf{H}_{m*})^+\mathbf{H}_{m*} & \text{for } j \leqq k \\ (\mathbf{E}_{m*})^+\mathbf{E}_{m*} & \text{for } k < j \end{cases}$$

of eq. [59c] is valid. Strikingly, $\mathbf{R}^m$ defined by [59f] has real diagonal elements. Thus the diagonal elements in [59d] are purely imaginary for $j = k$ and are complex otherwise.

In case (ii), both [15a] and [17a] give real solutions warranting the reality of the other quantities concerned here.

In case (iii), eqs. [15a] and [17a] written for index m' are equivalent to their complex conjugated forms stated for m. Therefore, $\mathbf{E}_{m'*} = \mathbf{E}_{m*}^*$, $\mathbf{H}_{m'*} = \mathbf{H}_{m*}^*$, etc., for all the other appearing quantities in [59b], [59c], and [59e]. In this way the sum of the pairs' contributions is always real.

Consequently, $\mathbf{R}_{jk}^{\text{exp}}$ of [59e] is purely real, too.

The second form of the charge-bond matrix mentioned above follows from [51], [59], and [59a]–[59f].

$$[62a] \quad \mathbf{P}_{jk} = (\mathbf{P}_{kj})' = -\frac{2}{\pi}\int_{-\infty}^{\lambda_F} \text{Im}\,(\mathbf{R}_{jk}^{\text{band}}|_{y=0})\,dx$$
$$= \frac{2}{\pi}\int_{-\infty}^{\lambda_F} \sum_{m}^{|\mu_m|=1} \text{Im}\,[\delta_{mm}\mu_m^{|k-j|}(\mathbf{E}_{m*})'\mathbf{E}_{m*}^*\,dx$$

where δ_{mm} is given by [24b], $\mu_m = e^{i\kappa_m}$ and $\mathbf{E}_{m*}^+ = \mathbf{J}_{*m}(\kappa_m)$ is just the solution of the LCAO CO eq. [44].

Note that in actual calculations one can always choose the more convenient one from the two dual forms [19] (or particularly [43]) and [44] of the auxiliary equation (41a).

Namely, [19] is a generalized polynomial eigenvalue problem (68) with eigenvalues μ_m (τ_m) for any fixed value of λ. The use of a standard routine to its solution is very advantageous if the size of the elementary cell (n) is large. Otherwise one can obtain its solutions with a standard eigenvalue routine from the original auxiliary equation [11], too. The latter is, however, a real but essentially asymmetrical eigenvalue problem. At the same time, it contains the complete information on both "band"- and "exp"-like solutions.

The other "dual" form [44] is a generalized Hermitian eigenvalue problem with eigenvalue λ for any fixed value of κ taken from the interval $(0, \pi)$. Whenever a band structure calculation is given, in fact, one has its solutions. To have the "exp"-like solutions, however, one has to use the original τ_m of [43] in [44] instead of $e^{i\kappa}$, when [44] becomes a genuinely asymmetrical (real or complex) generalized eigenvalue problem.

It is quite evident that the DRM has led to the simpler expression of the charge-bond order matrix [50], although [62] is already much simpler than the "pure IPM" expression would be from the combination of eqs. [51] and [60]. One can expect, therefore, significant simplifications in the calculation of several other physical quantities when the DRM, or at least the IRM is applied instead of the IPM.

It is interesting to note finally that eq. [44] is just one component for the block-diagonalized form of the starting eigenvalue problem [1]. Namely, reverting from $\kappa = 2\pi q/N$ to the original integer variable q, collecting the column vectors [47] for $m = 1, \ldots, n$ in matrix $\mathbf{C}(q)$ and defining the hypermatrices $\mathbf{C} = \{\boldsymbol{\delta}_{jq}\mathbf{C}(q)\}$ and $\boldsymbol{\Omega} = \{\boldsymbol{\Omega}_{pj}\}$ of order N with blocks $\mathbf{C}(q)$ and $\boldsymbol{\Omega}_{pj} = \mathbf{N}^{-1/2}\,\mathbf{I}\exp(2\pi ipj/N)$ of order n, the unitary matrix $\boldsymbol{\Omega}$ just block diagonalizes [1] and the unitary matrices $\mathbf{C}(q)$ diagonalize the blocks, as is well-known (4–6, 70): $\mathbf{C}^+\boldsymbol{\Omega}^+\mathbf{F}\boldsymbol{\Omega}\mathbf{C} = \mathbf{C}^+\boldsymbol{\Omega}^+\mathbf{S}\boldsymbol{\Omega}\mathbf{C}\boldsymbol{\Lambda}$ is the completely diagonal form, $\boldsymbol{\Omega}^+\mathbf{F}\boldsymbol{\Omega}$ and $\boldsymbol{\Omega}^+\mathbf{S}\boldsymbol{\Omega}$ are block diagonal, $\boldsymbol{\Lambda} = \{\delta_{pq}\Lambda(q)\}$ $(p, q = 1, \ldots, N)$ and $\Lambda(q) = \{\boldsymbol{\delta}_{km}\boldsymbol{\lambda}_m(q)\}(k, m = 1, \ldots, n)$. Here the DRM has led to both forms in one step. The block-diagonalization technique was learned from a special evaluation method of cyclic determinants in ref. 4 although the use of group theory is the most common.

3. Summary

More and more new problems arise when the simplest perfect infinite periodic models of polymers and crystals are complicated by boundaries and various other perturbations step by step. To make their description and understanding simpler, these problems were treated (and will be studied in the forthcoming papers) immediately at that step in which these first appear.

Deriving several forms for the fundamental and the auxiliary equations of the DRM, a simple combination of block-decomposition and transpositions was applied to calculate $\mathbf{U}^{-1}$ directly from the blocks of $\mathbf{U}$, the similarity transformation bringing the recursion matrix $\mathbf{T}$ into its normal form $\boldsymbol{\tau}$. Full-matrix expressions were given for the blocks of the resolvent (Green) matrix of perfect cyclic systems which can largely simplify the SCF local-impurity approach (11–14), where these blocks play a central role. Expressions for the charge-bond order matrix were derived both by the DRM and the IRM, providing a deeper insight into the relation of these methods.

Acknowledgements

The author would like to express his gratitude to Professor J. Ladik for his invitation to Germany and his hospitality, and stimulating discussions while the author was working there. It is a pleasure to thank Mr. M. Gies, Professor P. Otto, and Dr. M. Seel for their continuous kind help and fruitful discussions. Miss S. Patzak is also thanked for her kind assistance.

1. G. FLOQUET. Ann. Sci. l'Ecole Norm. Super. Paris, Ser. 2, **12**, 47 (1883).
2. F. BLOCH. Z. Physik. **52**, 555 (1928).
3. C. C. J. ROOTHAAN. Rev. Mod. Phys. **23**, 69 (1951).
4. G. DEL RE, J. LADIK, and G. BICZÓ. Phys. Rev. **155**, 997 (1967).
5. J.-M. ANDRÉ, L. GOUVERNEUR, and G. LEROY. Int. J. Quantum Chem. **1**, 451 (1967).
6. T. E. PEACOCK and R. MCWEENY. Proc. Phys. Soc. London, **74**, 385 (1959).
7. I. TAMM. Phys. Z. Soviet Union. **1**, 733 (1932); Z. Physik. **76**, 849 (1932).
8. G. BICZÓ. *In* Proc. 7th Int. Vacuum Congr. and 3rd Int. Conf. Solid Surfaces. Vol. I. *Edited by* R. Dobrozemsky *et al.* F. Berger and Söhne, Vienna. 1977. pp. 407–410.
9. J. LADIK. Phys. Rev. B**17**, 1663 (1978).
10. G. F. KOSTER and J. C. SLATER. Phys. Rev. **95**, 1167 (1954).
11. G. DEL RE and J. LADIK. Chem. Phys. **49**, 321 (1980).
12. M. SEEL, G. DEL RE, and J. LADIK. J. Comput. Chem. **3**, 451 (1982).
13. M. SEEL. Int. J. Quantum Chem. In press.
14. J. LADIK and M. SEEL. Phys. Rev. B**13**, 5338 (1976).
15. G. BICZÓ and I. LUKOVITS. Int. J. Quantum Chem. **16**, 31 (1979).
16. G. BICZÓ. Tjd. Vacuumtechnol. **16**, 195 (1978).
17. G. BICZÓ. *In* Proc. 4th Int. Congr. Solid Surfaces and 3rd Eur. Conf. Solid Surfaces. Vol. II. *Edited by* D. A. Degras and M. Costa. SFV, Paris. 1980. pp. 910–913.
18. G. BICZÓ and I. LUKOVITS. Int. J. Quantum Chem. Quantum

Biol. Symp. **8**, 347 (1981).
19. G. BICZÓ. Acta Biochim. Biophys. Acad. Sci. Hung. (*a*) **18**, 17 (1983); (*b*) In press.
20. G. BICZÓ. Polymer Theory Abstracts. July, 1984, pp. 16–17.
21. M. W. P. STRANDBERG. Am. J. Phys. **51**, 60 (1983).
22. W. M. FAIRBAIRN. Surface Sci. **9**, 439 (1968).
23. A. A. COTTEY. J. Phys. C, **4**, 1734 (1971).
24. A. A. COTTEY. Am. J. Phys. **39**, 1235 (1971).
25. A. A. COTTEY. J. Phys. C, (*a*) **5**, 2583 (1972); (*b*) **5**, 2591 (1972); (*c*) **6**, L16 (1973); (*d*) **6**, 2446 (1973); (*e*) **8**, 4135 (1975); (*f*) **9**, 2365 (1976).
26. A. A. COTTEY. Phys. Stat. Sol. B, (*a*) **67**, 619 (1975); (*b*) **88**, 207 (1978).
27. H. SCHMIDT. Phys. Rev. **105**, 425 (1957).
28. J. HORI and T. ASAHI. Prog. Theor. Phys. Kyoto, **17**, 523 (1957).
29. H. MATSUDA. Prog. Theor. Phys. Kyoto Suppl. **23**, 22 (1962).
30. H. MATSUDA, K. OKADA, T. TAKASE, and T. YAMAMOTO. J. Chem. Phys. **41**, 1527 (1964).
31. J. HORI. Spectral properties of disordered chains and lattices. Pergamon, Oxford. 1968.
32. H. V. MCINTOSH, M. HEHENBERGER, and R. REYES-SANCHEZ. Intern. J. Quantum Chem. **10**, 191 (1976); **11**, 189 (1977).
33. E. G. MCRAE. Surface Sci. **11**, 479 (1968); **11**, 492 (1968).
34. D. W. JEPSEN and P. M. MARCUS. *In* Computational methods in band theory. *Edited by* P. M. Marcus, J. F. Janak, and A. R. Williams. Plenum, New York. 1971. pp. 416–443.
35. J. B. PENDRY. Low energy electron diffraction. Academic Press, New York. 1974.
36. D. W. JEPSEN. Phys. Rev. B, **22**, 5701 (1980).
37. Y. YIDO, T. INAGAKI, and H. FUKUTOME. Prog. Theor. Phys. Kyoto **48**, 808 (1972).
38. G. BICZÓ. Tjd. Vacuumtechnol. **16**, 236 (1978).
39. M. TOMÁŠEK and G. BICZÓ. Acta Phys. Hung. **44**, 357 (1978).
40. C. Y. FONG. *In* Electrons and phonons in layered crystal structures. *Edited by* T. J. Wieting and M. Schlüter. Reidel, Dordrecht–Boston–London. 1979. Chapt. B, pp. 59–144.
41. G. BICZÓ. *In* Recent developments in condensed matter physics. *Edited by* J. T. DeVreese, L. F. Lemmens, V. E. Van Doren, and J. Van Royen. Plenum, New York. 1981. (*a*) Vol. II. pp. 341–352; (*b*) Vol. IV, pp. 243–250.
42. D. H. LEE and J. D. JOANNOPOULOS. Phys. Rev. B, (*a*) **23**, 4988 (1981); (*b*) **23**, 4997 (1981); (*c*) **24**, 6899 (1981).
43. H. FUKUTOME and M. SASAI. Prog. Theor. Phys. Kyoto, (*a*) **67**, 41 (1982); (*b*) **69**, 1 (1983); (*c*) **69**, 373 (1983).
44. G. BICZÓ. Zh. Fiz. Khim. **57**, 1144 (1983).
45. J. N. SCHULMAN and Y. CHANG. Phys. Rev. B, **27**, 2346 (1983).
46. C. MAILHIOT, D. L. SMITH, and T. C. MCGILL. J. Vac. Sci. Technol. B, **1**, 637 (1983).
47. G. BICZÓ, J. KOUTECKÝ, and A. LEE. Polymer Theory Abstracts. March, 1984. pp. 16–17.
48. M. GODA. *In* Physics in one dimension. *Edited by* J. Bernasconi and T. Schneider. Springer-Verlag, Berlin – Heidelberg – New York. 1981. pp. 265–276.
49. D. J. THOULESS. *In* Physics in one dimension. *Edited by* J. Bernasconi and T. Schneider. Springer-Verlag, Berlin – Heidelberg – New York. 1981. pp. 306–309.
50. B. S. ANDERECK and E. ABRAHAMS. *In* Physics in one dimension. *Edited by* J. Bernasconi and T. Schneider. Springer-Verlag, Berlin – Heidelberg – New York. 1981. pp. 317–320.
51. M. DROZ and A. MALASPINAS. J. Phys. C, **16**, L231 (1983).
52. B. DERRIDA and J. VANNIMENUS. J. Phys. A, **15**, L557 (1982).
53. T. B. GRIMLEY. Adv. Catal. **12**, 1 (1960).
54. I. M. LIFSHITZ. Zh. Eksperim. Teor. Fiz. (*a*) **17**, 1017 (1947); (*b*) **17**, 1076 (1947).
55. G. R. BALDOCK. Proc. Cambridge Phil. Soc. **48**, 457 (1952).
56. J. KOUTECKÝ. Phys. Rev. **108**, 13 (1957).
57. T. B. GRIMLEY. CRC Solid State Sci. **6**, 238 (1976).
58. J. KOUTECKÝ. *In* Excited states in quantum chemistry. *Edited by* C. A. Nikolaides and D. R. Beck. Reidel, Dordrecht. 1978. pp. 531–556.
59. O. FROMM and J. KOUTECKÝ. *In* Catalysis in chemistry and biochemistry. Theory and experiment. *Edited by* B. Pullman. Reidel, Dordrecht. 1979. pp. 335–346.
60. R. HAYDOCK, V. HEINE, and M. J. KELLY. J. Phys. C, **5**, 2845 (1972).
61. E-NI FOO, M. F. THORPE, and D. WEAIRE. Surface Sci. **57**, 323 (1976).
62. K. S. DY, S.-Y. WU, and T. SPRATLIN. Phys. Rev. B, **20**, 4237 (1979).
63. J. D. BRASER and K. S. DY. Phys. Rev. B, **22**, 4868 (1980).
64. V. HEINE. Solid State Phys. **35**, 1 (1980).
65. M. J. KELLY. Solid State Phys. **35**, 295 (1980).
66. I. M. LIFSHITZ and L. N. ROSENZWEIG. Isz. Akad. Nauk USSR Ser. Fiz. **12**, 667 (1948).
67. B. KAGSTRÖM and A. RHUE (*Editors*). Matrix pencils. *In* Lecture notes in mathematics. Vol. 973. Springer-Verlag, Berlin. 1983.
68. I. GOHBERG, P. LANCASTER, and L. RODMAN. J. Lin. Alg. Appl. (*a*) **20**, 1 (1978); (*b*) **21**, 65 (1978).
69. E. N. ECONOMOU. Green's functions in quantum physics. Springer-Verlag, Berlin. 1979.
70. P.-O. LÖWDIN. J. Appl. Phys. **33**, 251 (1962).
71. G. BICZÓ and A. LEE. To be published.
72. G. BICZÓ and M. TOMÁŠEK. To be published.

Infrared spectra of some matrix isolated organoisothiocyanate molecules[1]

J. R. DURIG,[2] J. F. SULLIVAN, AND D. T. DURIG
Department of Chemistry, University of South Carolina, Columbia, SC 29208, U.S.A.

AND

STEPHEN CRADOCK
Department of Chemistry, University of Edinburgh, West Mains Road, Edinburgh, Scotland EH9 3JJ, UK

Received August 14, 1984

This paper is dedicated to Professor Camille Sandorfy on the occasion of his 65th birthday

J. R. DURIG, J. F. SULLIVAN, D. T. DURIG, and STEPHEN CRADOCK. Can. J. Chem. **63**, 2000 (1985).

The infrared (3500 to 300 cm^{-1}) spectra of methylisothiocyanate, ethylisothiocyanate, isopropylisothiocyanate, and cyclopropylisothiocyanate isolated in argon and nitrogen matrices have been recorded. In general, the spectra were more complex in the nitrogen matrices and, for ethylisothiocyanate, nearly all of the fundamentals appeared as doublets in the nitrogen matrix but for the most part as single bands in the argon matrix. No evidence could be found for a second conformer for either ethylisothiocyanate or isopropylisothiocyanate. Even though cyclopropylisothiocyanate has been shown to exist as the *cis* and *trans* conformers at ambient temperature, little conclusive evidence could be found for two isomers in the infrared matrix material. The complex spectra observed in the NCS antisymmetric stretching region as well as in the 520 cm^{-1} region appear to arise in part from combinations involving the low-frequency large amplitude CNC bend or asymmetric torsion of these organoisothiocyanate molecules. It appears that the vibrational spectra of these molecules are not sensitive to the orientation of the NCS moiety.

J. R. DURIG, J. F. SULLIVAN, D. T. DURIG et STEPHEN CRADOCK. Can. J. Chem. **63**, 2000 (1985).

On a enregistré les spectres infrarouges (3500 à 300 cm^{-1}) des isothiocyanates de méthyle, d'éthyle, d'isopropyle et de cyclopropyle isolés dans des matrices d'argon et d'azote. D'une façon générale, les spectres enregistrés dans des matrices d'azote sont plus complexes que ceux enregistrés dans des matrices d'argon; dans le cas de l'isothiocyanate d'éthyle, pratiquement toutes les fondamentales se présentent sous forme de doublets dans la matrice d'azote alors qu'elles se présentent généralement sous forme de singulets dans la matrice d'argon. On n'a pas pu mettre en évidence l'existence d'un deuxième conformère dans les isothiocyanates d'éthyle ou d'isopropyle. Même s'il est connu que l'isothiocyanate de cyclopropyle existe sous les conformations *cis* et *trans* à la température ambiante, on n'a pas obtenu de données fermes relativement à la présence de ces deux conformères dans les matrices examinées par infrarouge. Le spectre complexe que l'on observe dans la région de vibration de valence antisymétrique du NCS ainsi que dans la région de 520 cm^{-1} semble résulter en partie de combinaisons impliquant soit la vibration de déformation angulaire du CNC de basse fréquence et de forte amplitude soit la vibration de torsion asymétrique de ces molécules d'organoisothiocyanates. Il semble que les spectres vibrationnels de ces molécules ne soient pas sensibles à l'orientation de la portion NCS.

[Traduit par le journal]

Introduction

We recently reported (1) the mid-infrared spectra of matrix isolated ethylisothiocyanate in a nitrogen matrix and observed that several of the fundamentals appeared as doublets. Since only one matrix material was utilized it was not possible to ascertain whether these doublets were due to two different matrix sites or whether the molecule was being trapped in two different conformations. The other vibrational data could be readily explained on the basis of a single conformer with C_s symmetry (*cis* conformer) with the isothiocyanate group eclipsing the methyl group. The major lines in the microwave spectrum could be explained (2) on the basis of this single conformer although there were additional microwave lines which were not assigned. The earlier conclusions (3) that ethylisothiocyanate exists as two conformers at low temperature was based on the assignment of two bands at 2199 and 2154 cm^{-1} in the infrared spectrum of the solid as the NCS antisymmetric stretches of the *gauche* and *trans* conformers. The most interesting spectral region is the 2080 to 2250 cm^{-1} region where unusual intensity changes and frequency shifts have been previously observed with changes in physical state or solvents. Although Kniseley *et al.* (3) agreed that a portion of the complexity in the spectral region is due to the overtone of the NCS symmetric stretch being in Fermi resonance with the antisymmetric mode, the fact that they observed four strong bands in the infrared spectrum of the solid led them (3) to conclude that two conformers are present in the solid state. In order to provide additional data for this spectral region, we recorded (4) the vibrational spectra of methylisothiocyanate and methyl-d_3-isothiocyanate where no conformers can exist and found three infrared bands in this spectral region of the solid. Additionally, unusual intensity changes were found in going from the gas or liquid to the solid state, but the frequency shifts or intensity changes could be readily explained on the basis that the lower frequency band in the Fermi doublet in the gas phase has a significantly larger amount of the antisymmetric NCS stretch whereas in the solid state the higher frequency band has a predominance of this fundamental (4). The third band was assigned as a combination band of the methyl deformation with the C_α—N stretch.

In order to provide additional spectral data on the NCS

[1] Taken in part from the thesis of D. T. Durig which will be submitted to the Department of Chemistry in partial fulfillment of his Ph.D. degree requirement.

[2] I had the pleasure of serving with Camille Sandorfy for a number of years on the IUPAC Commission I.5 on Molecular Structure and Spectroscopy and Camille always did more than his share of the work. He was a delightful colleague and always contributed significantly to our biannual meetings. As Chairman of this Commission, I would like to indicate on behalf of all the members that we shall surely miss his guidance, counsel, and overall contributions at our next meeting in 1985.

TABLE 1. Observed[a] bands (cm^{-1}) in the infrared spectra of gaseous and matrix isolated methylisothiocyanate

Gas[b]	Rel. int.	Ar matrix	Rel. int.	N_2 matrix	Rel. int.	ν_i	Assignment[c]
2983	vw	2998	w	3000	w, bd	ν_6	CH_3 antisymmetric stretch
2953	w	2952	s	2955	s		
				2951	w, sh	ν_1	CH_3 symmetric stretch
2900	vw	2887	w				$2\nu_7 \cong 2910$
2823	vw	2818	vw				$2\nu_3 \cong 2842$
2789	vw	2791	m	2791	m		$\nu_2 + \nu_5 \cong 2787$
		2256	w	2242	w		
		2236	w	2235	w		$\nu_2 + \nu_{10} \cong 2232$
		2217	m, sh				
2224	s	2211	s	2209	s		$2\nu_4 = 2212$ (Fermi resonance with ν_2)
2111	vs						
		2126	vvs				
2089	vvs	2118	vvs	2135	vvs	ν_2	NCS antisymmetric stretch
		2085	m	2072	w		$\nu_3 + \nu_5 \cong 2084$ (argon)
		1459	m	1458	m, bd		
~1460	vw	1452	m	1453	m, bd	ν_7	CH_3 antisymmetric deformation
		1421	vvs	1422	vvs		
1424	ms	1420	sh	1418	vvs	ν_3	CH_3 symmetric deformation
~1142	vw					ν_8	CH_3 rock
		1109	w, sh				
1110	vw	1106	s	1103	s	ν_4	NCS symmetric stretch
676	vw	668	s	662	vw	ν_5	C—N stretch
		661	s	652	s, bd		
530	w						$\nu_9 + \nu_{10} \cong 521$
411	mw	459	m	451	m	ν_9	NCS bend
152 80	mw					ν_{10}	CNC bend

[a] Abbreviations used: s, strong; m, medium; w, weak; v, very; sh, shoulder; and bd, broad.
[b] Data for the gas taken from ref. 4.
[c] We have kept the numbering of the fundamentals the same as in ref. 4 which is for a molecule with a quasi-linear heavy atom skeleton with C_{3v} symmetry although ν_6 through ν_{10} should be doublets for a molecule with C_s symmetry.

antisymmetric stretching mode, we have recorded the infrared spectra of some matrix isolated organoisothiocyanates. For the ethylisothiocyanate molecule, we were interested in whether the previously observed doubling of the fundamentals in the nitrogen matrix is due to the presence of conformers or to matrix site effects. Additionally, we have investigated the cyclopropylisothiocyanate molecule in order to determine if conformers can be identified from the vibrational data of the isothiocyanate molecules since we have found two conformers for this molecule at ambient temperature from a microwave study (5). However, from the previous vibrational study (6) of this molecule the authors assigned the observed spectra on the basis of a single conformer. The results of the study of the infrared spectra of matrix isolated methylisothiocyanate, ethylisothiocyanate, isopropylisothiocyanate, and cyclopropylisothiocyanate are reported herein.

Experimental

All the compounds were obtained from commercial sources and purified by low-temperature fractionation on a vacuum sublimation column. The infrared spectra of the samples isolated in either an Ar or N_2 matrix at ratios varying from 400:1 to 1000:1 were recorded with a Perkin-Elmer model 225 grating spectrophotometer between 3500 and 300 cm^{-1}. The matrix samples were prepared by the "pulsed-deposition" method on a CsI window held at ~10 K by an Air Products model CS-202 microrefrigerator. Samples were annealed to 30–35 K, but no significant changes in the spectra were noted except for the appearance of greater amounts of aggregated molecules.

Results

In order to ascertain the matrix effect on the normal modes of these organoisothiocyanates, we recorded the infrared spectra in both argon and nitrogen matrices. For the most part the argon matrices gave sharper bands and there certainly was less doubling of the fundamentals, except in the case of cyclopropylisothiocyanate. Therefore, for each molecule, we shall discuss the results obtained in the argon matrix and then compare them to those obtained in the nitrogen matrix.

Methylisothiocyanate

In Table 1, we have listed the frequencies for the normal modes of methylisothiocyanate which had previously been obtained (4) for the gas along with the observed frequencies in the two different matrices. For the most part there is reasonable agreement between the gas phase frequencies and those obtained in the matrix except for a few gas phase bands where it was difficult to ascertain the band centers because of the breadth of the bands. For example, the CH_3 antisymmetric stretch is found at 2998 cm^{-1} in the spectra of the matrices which is probably more nearly the band center in the gas phase rather than the lower frequency of 2983 cm^{-1} which was reported earlier (4). However, there was no indication that this band is split as it should be if the molecule has effective C_s symmetry at this low temperature. There are three other bands in this same general region at 2887, 2818, and 2791 which are as strong as the ν_6 fundamental but are obviously due to two combination bands and an overtone band. These same three bands were observed in the spectrum of the gas although $2\nu_7$ appears to have a lower frequency in the matrix, but it could well be due to the breadth of this band in the gas phase and the difficulty in choosing the band center.

There are a few differences between the gas phase frequencies and those obtained in the matrices which should be noted. In particular the ν_9 fundamental, the NCS bend, is broad in the gas with the maximum occurring at about 411 cm^{-1} and certainly not higher than 418 cm^{-1} but, in the argon matrix, this fundamental appears at 459 cm^{-1}, and at 451 cm^{-1} in the nitrogen matrix. This significant shift to higher frequency is attributed to the added constraints placed on the molecule by the matrix. The C_α—N stretch, ν_5, has a shift in the opposite direction where it is found at 676 cm^{-1} in the gas, as a doublet at 668 and 661 cm^{-1} in the argon matrix, and 652 cm^{-1} in the nitrogen matrix. The third fundamental which is significantly affected is the NCS antisymmetric stretch which shifts from 2089 cm^{-1} in the gas to a doublet at 2126 and 2118 cm^{-1} in the argon matrix but a single band at 2135 cm^{-1} in the nitrogen matrix. Overall, it appears that the nitrogen matrix has a greater effect on the fundamentals than the argon matrix. For example the CH_3 symmetric deformation, ν_3, appears as an intense doublet at 1422 and 1418 cm^{-1} in the nitrogen matrix whereas the same mode in the argon matrix appears at 1421 cm^{-1} with a possible shoulder at 1420 cm^{-1}. Although the CH_3 antisymmetric deformation, ν_7, appears as a sharp doublet at 1459 and 1452 cm^{-1} in the argon matrix (Fig. 1) the two corresponding bands at 1458 and 1453 cm^{-1} in the nitrogen matrix are very broad and each appears to contain at least two or possibly more bands. This is really the only mode which would be expected to be degenerate for a quasi-linear heavy atom skeleton that shows doubling in the spectrum of the matrix isolated material.

The most interesting spectral region is the 2100 cm^{-1} region where the NCS antisymmetric stretch, ν_2, appears. In the spectrum of the argon matrix this fundamental can readily be assigned to the doublet at 2126 and 2118 cm^{-1}, and to the single band at 2135 cm^{-1} in the nitrogen matrix. The overtone of the NCS symmetric stretch is significantly weaker than the ν_2 fundamental but again it appears as a doublet at 2217 and 2211 cm^{-1} in the argon matrix and as a single band at 2209 cm^{-1} in the nitrogen matrix. A third set of bands appear as doublets at 2256/2236 cm^{-1} in argon and 2242/2235 cm^{-1} in nitrogen which have been assigned as the combination of $\nu_2 + \nu_{10}$. These bands were not previously observed in either the infrared spectrum of the gas or solid. For further support of this assignment we annealed both matrices to 35 K and the bands became quite broad. This behavior is exactly what would be expected for the combination of $\nu_2 + \nu_{10}$. It should also be noted that with annealing the NCS bend, ν_9, shifted to lower frequency, i.e., ~435 cm^{-1}, and it became quite broad. The remaining fundamentals showed little change upon annealing except for the NCS antisymmetric stretch which developed a number of bands on the high frequency side where there had been a shoulder, but these bands are undoubtedly due to aggregate bands. The remaining band in this region is at 2085 cm^{-1} in the argon matrix and 2072 cm^{-1} in the nitrogen matrix. We believe this band is due to a combination of $\nu_3 + \nu_5$ which would be predicted to be about 12 cm^{-1} lower in the nitrogen matrix since ν_5 is 12 cm^{-1} lower in this matrix compared to the value in argon. The higher intensity of this band in the argon matrix may be due to greater Fermi resonance with ν_2 since it has a value closer to this fundamental in the argon matrix. With these assignments for the bands in this spectral region for the methylisothiocyanate molecule, we believe that we can provide a better explanation for the bands observed in this spectral region for the other simple organoisothiocyanate molecules.

Based on these studies in both the argon and nitrogen matrices, it should be noted that great care needs to be exercised in attempting to identify conformers from infrared matrix studies of organoisothiocyanate molecules. It appears that the argon matrix is better for this purpose but, even for this matrix, the ν_2, ν_5, and ν_7 fundamentals of methylisothiocyanate appeared as doublets with nearly equal intensities whereas only ν_7 should be split if the effective symmetry is C_s rather than C_{3v}.

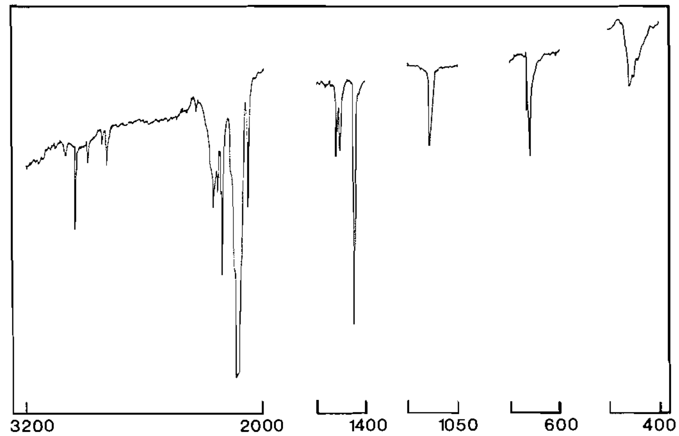

FIG. 1. Infrared spectrum of methylisothiocyanate isolated in an argon matrix. The indicated abscissa intervals below 1500 cm^{-1} are 100 cm^{-1}.

Ethylisothiocyanate

In the initial study (1) of matrix isolated ethylisothiocyanate, nitrogen was used as the host and practically all of the fundamentals were doublets and it was not possible to ascertain whether this doubling was due to matrix effects or the presence of a second conformer. Therefore we have recorded the infrared spectrum of this molecule in an argon matrix. There is a striking difference between the results for the two matrices for most of the fundamentals with the exception of the NCS antisymmetric stretch. In the nitrogen matrix most of the fundamentals appear as doublets whereas for the argon matrix most of the fundamentals are single bands. Therefore we have concluded that the doubling in the nitrogen matrix is due to matrix effects, i.e., the molecule is sitting on two different sites, or some other orientational effect relative to the matrix lattice is occurring. The absence of this doubling in argon is particularly noteworthy for the carbon–hydrogen bending modes.

For the most part there is reasonable agreement among the fundamental frequencies in the gas and the two matrices. Notable differences occur for the NCS bend(s), the NCS antisymmetric stretch, and the C—C stretch. The first two vibrations also showed significant differences in frequencies between the gas and matrices for the corresponding methyl compound. For example, the NCS bend in methylisothiocyanate is found at 411 cm^{-1} in the gas, but it is 40 cm^{-1} higher in the nitrogen matrix and 48 cm^{-1} higher in argon whereas for the ethyl compound these differences are 37 and 47 cm^{-1}, respectively. However, for the NCS antisymmetric stretch in methylisothiocyanate, the nitrogen matrix gives the highest frequency whereas for the ethyl compound it is the argon matrix. However, it should be noted that for the overtone of the symmetric NCS stretch as well as the two combination bands which appear in this region for CH_3NCS the highest frequencies appear in the argon matrix. One other similarity in this region should also be noted. In the argon matrix, both the overtone of the symmetric NCS stretch as well as the anti-

TABLE 2. Observed[a] bands (cm^{-1}) in the infrared spectra of gaseous and matrix isolated ethylisothiocyanate

Gas[b]	Rel. int.	Ar matrix	Rel. int.	N_2 matrix	Rel. int.	ν_i	Assignment
		3007	w				
2993	ms	2998	w	3003	w	ν_1, ν_{17}	CH_3 antisymmetric stretch
2961	m	2955	w	2957	w	ν_{16}	CH_2 antisymmetric stretch
(2940)		~2930	vvw			ν_2	CH_3 symmetric stretch
2908	w					ν_3	CH_2 symmetric stretch
2248	mw						
2102	s						
2082	vvs	2132	vs	2109	vs	ν_4	NCS antisymmetric stretch and
		2129	vs				$2\nu_2$ in Fermi resonance with ν_4
		2118	vs	2090	s		
		2109	vs	2080	s		$\nu_5 + \nu_{12} \cong 2105$
		2073	m				
		2063	m	2059	s		$\nu_9 + \nu_{11} \cong 2065$
		2052	m				
1475	w	1472	m	1471	vw	ν_5	CH_3 antisymmetric deformation
				1462	vw		
1462	mw	1454	m	1453	m	ν_{18}	CH_3 antisymmetric deformation
(1444)						ν_6	CH_2 deformation
1387	mw	1382	m	1389	m	ν_7	CH_3 symmetric deformation
				1384	m		
1350	s	1348	vs	1353	vs	ν_8	CH_2 wag
(1284)		1286	w	1290	w	ν_{19}	CH_2 twist
				1284	w		
1160	w	1141	vw	1149	w	ν_{20}	CH_3 rock
				1138	w		
1128	w	1118	w	1120	w	ν_9	CH_3 rock
		1115	vw, sh	1112	m		
		1073	w				
		1067	w, sh				
1070	mw	1065	s	1071	s	ν_{10}	NCS symmetric stretch
940	mw	939	m	953	m	ν_{11}	C—C stretch
		929	m	940	m		
(793)		795	m	803	w	ν_{21}	CH_2 rock
665	w	640	w, sh	659	w	ν_{12}	C—N stretch
		637	m	633	w		
528	m			505	m		$\nu_{13} + \nu_{15}$
430	w	477	w	467	m	ν_{13}, ν_{22}	NCS bends
379	w	385	w				
		379	w	380	w	ν_{14}	CCN bend
265	vvw					ν_{23}	CH_3 torsion
~120	mw					ν_{15}	CNC bend
~68	w						

[a]See Table 1 for an explanation for the abbreviations used.
[b]Data for gas and nitrogen matrix taken from ref. 1; bands in parentheses are taken from the spectrum of the solid.

symmetric NCS stretch show doubling in the argon matrix whereas these bands are single bands in the nitrogen matrix for both ethyl- and methylisothiocyanate. In general the argon matrix leads to a more complex pattern in this spectral region.

Since the symmetric NCS stretch is at a lower frequency (1065 cm^{-1}) in ethylisothiocyanate than in the methyl compound (1106 cm^{-1}) the overtone is nearly coincident with the NCS antisymmetric stretch so that the Fermi resonance gives two bands in the 2100 cm^{-1} region of equal intensity and it is not possible to identify a particular band as the ν_4 fundamental. Additionally, the C_α—N stretch with the CH_3 or CH_2 deformations give combination frequencies in this same general region and it is probable that one of these combinations is also in Fermi resonance with the NCS antisymmetric stretch which gives rise to the other very strong band in this region. There are numerous combination bands, including those with the CNC bend or the asymmetric torsion with ν_4, which fall slightly higher in frequency than the NCS antisymmetric stretch which can explain the other weaker bands in this spectral region. The spectral assignments are summarized in Table 2.

The greater complexity in this spectral region compared to the methyl compound is apparently part of the reason why in the earlier studies it was concluded that two conformers exist in the solid state (3). Since the antisymmetric NCS stretch shifts to higher frequency by more than 100 cm^{-1} with solidification, the relative amounts of Fermi interaction with specific combinations or overtones vary with physical state. Additionally it should be noted that the symmetric NCS stretch shifts only slightly to lower frequency with solidification so that the overtone of this mode is expected to be at nearly the same frequency in the various physical states. This gives rise to significant alterations in intensity depending on the degree of Fermi resonance with the NCS antisymmetric stretch.

Isopropylisothiocyanate

We (7) recently reported the rotational and vibrational spec-

TABLE 3. Observed[a] bands (cm^{-1}) in the infrared spectra of gaseous and matrix isolated isopropylisothiocyanate

Gas[b]	Rel. int.	Ar matrix	Rel. int.	N_2 matrix	Rel. int.	ν_i	Assignment
2991	vs	2992	m	2996	m	ν_{20}, ν_{21}	CH_3 antisymmetric stretches
2950	s	2946	m	2950	w	ν_1, ν_2	CH_3 antisymmetric stretch, CH stretch
2925	s			2924	w	ν_3, ν_{22}	CH_3 antisymmetric and symmetric stretch
2890	m			2883	w	ν_4	CH_3 symmetric stretch
				2199	m		
				2192	m		
2162	vs	2170	m	2167	s		$\nu_{11} + \nu_{12} = 2141$ (Fermi resonance with ν_5)
		2160	m	2153	w		or $\nu_5 + \nu_{33} = 2167$
		2132	m				
		2104	s	2122	vs		
2065	vs	2087	vs	2108	m	ν_5	NCS antisymmetric stretch
		2083	sh	2097	w		
		2074	sh	2078	m		
		2069	vs	2069	w		
2020	vs, sh	2039	w	2057	w		$2\nu_{12} = 2022$
		2014	m	2031	m		
1475	sh	1469	w	1474	w	ν_6	CH_3 antisymmetric deformation
1465	m	1460	m	1462	m	ν_7, ν_{23}	CH_3 antisymmetric deformation
1458	sh						
		1423	w	1424	w	ν_{24}	CH_3 antisymmetric deformation
1390	m	1389	m	1392	m	ν_{25}	CH_3 symmetric deformation
1370	m	1371	m	1374	m	ν_8	CH_3 symmetric deformation
		1346	w	1351	m		
1335	vs	1342	m	1346	m	ν_9	CH bend
		1339	m				
(1318)		1332	m, bd	1336	s	ν_{26}	CH bend
				1282	m		
[1295]		1271	m	1264	m	$2\nu_{14}$	
1170	s	1172	m	1173	m	ν_{10}	CH_3 rock
				1169	sh		
		1150	m				
1137	s	1143	w	1142	m	ν_{27}	C—C—C antisymmetric stretch
1129	sh	1130	m	1134	m	ν_{11}	CH_3 rock
1015	s	1011	m	1021	m	ν_{12}	NCS symmetric stretch
				1019	sh		
(950)						ν_{28}	CH_3 rock
(933)		930	vw			ν_{29}	CH_3 rock
865	m	861	m	863	m	ν_{13}	C—C—C symmetric stretch
650	w	655	w	634	m	ν_{14}	C—N stretch
		638	w				
530	s	520	m				$\nu_{16} + \nu_{19}$
		501	w				
[470]						ν_{15}	CC_2 deformation
				448	m		
439	w	437	m	435	m	ν_{16}, ν_{30}	NCS bend
388	w	391	m	395	m	ν_{31}	CC_2 twist
332	w			~330	m	ν_{17}	CC_2 wag
[285]						ν_{32}	CH_3 torsion
[250]						ν_{18}	CH_3 torsion
73						ν_{19}	CNC bend
45						ν_{33}	Asymmetric torsion

[a] See Table 1 for an explanation for the abbreviations used.
[b] Data for the gas taken from ref. 7; bands in parentheses are taken from the spectrum of the solid and the bands in brackets are from the Raman spectrum of the gas or solid.

tra of isopropylisothiocyanate and the microwave spectrum could be interpreted on the basis of a single conformer where the sum of the B and C rotational constants is consistent with the *skew* conformer with the NCS moiety eclipsing one of the methyl groups. Additionally, there was no evidence for a second conformer from the vibrational data. Similarly, for the spectrum of the matrix isolated material, there is no convincing evidence for the presence of a second conformer, since there is no consistent pattern of doubling in either the nitrogen or argon matrices. For example, the C_α—N stretch appears as a doublet in the argon matrix but a single band in the nitrogen matrix, whereas the CC_2 antisymmetric stretch appears as a doublet in the argon matrix but a single band in the nitrogen matrix. The CC_2 symmetric stretch shows no doubling in either spectrum.

The same complications observed in the NCS antisymmetric stretching region as observed for the methyl and ethyl compounds are also observed in the matrix isolated spectra of isopropylisothiocyanate. In these cases, ν_5 appears at 2065

TABLE 4. Observed[a] bands (cm^{-1}) in the infrared spectra of gaseous and matrix isolated cyclopropylisothiocyanate

Gas[b]	Rel. int.	Ar matrix	Rel. int.	N_2 matrix	Rel. int.	ν_i	Assignment
3107	w					ν_1	CH_2 antisymmetric stretch
(3078)						ν_{17}	CH_2 antisymmetric stretch
(3036)						ν_2	CH stretch
3036	w					ν_3, ν_{18}	CH_2 symmetric stretch
		2234	m				
2231	w, sh	2228	m	2234	m		
		2221	w				
		2207	br	2202	m		
2190	mw, sh	2192	s	2196	m		
		2185	m				
2146	m, sh	2162	vs	2153	s		$\nu_4 + \nu_{27} \cong 2150$?
		2124	m				
2076 Q	vvvs	2106	vvs	2125	vs	ν_4	NCS antisymmetric stretch
		2092	m	2097	sh		
		2081	br	2068	vw		
		2070	w				
		2062	w	2044	w		$2\nu_{10} = 2036$
		2040	m				
		2020	m				
1456 Q	vw	1457	m	1456	m	ν_5	CH_2 deformation
(1410)		1422	m	1423	w	ν_{19}	CH_2 deformation
		1359	s	1358	sh		
1359 ctr	m	1356	sh	1356	s	ν_6	CH bend
1211 ctr	w	1216	w	1211	m	ν_7	Ring breathing
				1169	m		
1169 Q	w	1163	w	1165	m	ν_{20}	CH_2 twist
(1081)						ν_8	CH_2 twist
		1051	m	1061	sh		
(1048)		1049	m	1055	bd	ν_{21}	CH_2 wag
		1032	m	1042	sh		
1031	sh	1024	m	1038	bd	ν_9	CH_2 wag
		1018	m	1025			
1018 ctr	mw	1013	m	1023	m	ν_{10}	NCS symmetric stretch
		970				ν_{22}	CH bend
918 Q	w, bd	916	m	919	m	ν_{23}	Ring deformation
		909	w				
		861	w	864	sh		
860 ctr	vw	851	m	860	br, w	ν_{11}	Ring deformation
(812)		808	m	818	m	ν_{24}	CH_2 rock
		790	vw				
773 Q	w					ν_{12}	CH_2 rock
749 Q	w	728	w				
		697	w				
640	w, bd	659	w	662	w	ν_{13}	C—N stretch
		621	w	636	br, w		
520	s	510	vw				$\nu_{14} + \nu_{16} \cong 550$
~470	m	473	m	469	w	ν_{25}	NCS bend
~450	w	446	m	446	w	ν_{14}	NCS bend
382	w	395	m				
		383	w	364	br, w	ν_{26}	CCN bend
374 Q	m	372	w				
		357	w	350	br, m	ν_{15}	CCN bend
337	w	340	w				
104	m					ν_{16}	CNC bend

[a] See Table 1 for an explanation for the abbreviations used.
[b] Data for the gas taken from ref. 6; bands in parentheses are from the solid. The CH_2 twist, ν_8, has not been observed or assigned.

cm^{-1} and shifts to 2087 cm^{-1} in argon and to 2122 cm^{-1} in the nitrogen matrix. However, for this molecule, one particular band appears to be stronger than the other ones and we have chosen it as the fundamental. Nevertheless, there are combination and overtone bands which also appear to be relatively strong in this spectral region.

There is a significant difference between the nitrogen and argon matrix spectra in the NCS bending region. For this molecule there does not appear to be any significant shift among the gas phase or matrix frequencies for this mode as was found for the methyl and ethyl compounds, but in the nitrogen matrix this mode appears as a doublet whereas in the argon matrix it is a single band but the combination band of this fundamental with the CNC bend is clearly observed in the argon matrix. We can not provide any reasonable explanation for these observations but it is quite evident that the different matrices have a profound effect on the frequency and number of bands for the motions associated with the NCS moiety for all of these organoisothiocyanate molecules.

The spectral data obtained from the matrices support, for the most part, the assignment previously given for isopropylisothiocyanate with the exception of two fundamentals. The matrix-isolated spectra indicate that one of the CH_3 antisymmetric deformations should be assigned at 1423 cm^{-1} and there is an indication that the 1271 cm^{-1} band could be assigned as a fundamental, possibly as one of the CH bending motions. However, this frequency fits that expected for $2\nu_{14}$ and we have tentatively assigned it as such. It should also be noted that the CC_2 deformation, which was previously observed only in the Raman spectrum, was not observed in the infrared matrix isolated spectra. The assignment is summarized in Table 3.

Cyclopropylisothiocyanate

We were particularly interested in the cyclopropylisothiocyanate molecule since in the initial investigation of the vibrational spectrum of this molecule the investigators (6) concluded that there is only one conformer present at ambient temperature but we (5) found both the *cis* and *trans* conformers present from a microwave study. Therefore we expected to find doublets for the CCN bends as well as the modes associated with the NCS moiety in the spectra of both matrices. An inspection of the data in Table 4 shows that most of these fundamentals are doublets in the spectrum of the argon matrix isolated material but in the nitrogen matrix many of these fundamentals appear as single bands, i.e., ν_{14}, ν_{15}, ν_{25}, and ν_{26}. Although many more of the fundamentals appear as doublets, particularly in the argon matrix, there really is no strong evidence for the presence of two conformers. The major difference in the spectrum of this molecule compared to the other three is the presence of two NCS bending modes and greater complexity in the NCS antisymmetric stretching region. It should also be noted that there appears to be little change in the frequencies of the NCS bends in the matrix material from those in the gas phase although it is much easier to obtain the band centers from the spectrum of the matrix compared to the broad nondescript bands found in the gas phase.

It is not possible to give very convincing assignments for the larger number of bands found in the NCS antisymmetric stretching region. Since the overtone of the NCS symmetric stretch falls at a lower frequency than in the methyl and ethyl compounds, it does not appear to be in Fermi resonance with the antisymmetric mode. It is possible that the band at 2162 cm^{-1} (argon matrix) is due to the combination of the NCS antisymmetric stretch with the asymmetric torsion. This portion of the spectrum appears to be very similar to that found in this region for the isopropylisothiocyanate molecule so that similar assignments should be appropriate for these two molecules. Thus, there is no reason to believe that the second strong band in this region is due to the second conformer.

We have made only two minor changes in the vibrational assignment (Table 4) from that previously proposed (6). The CH_2 twisting mode was not assigned earlier but it is very probable that this mode should be assigned to the 1081 cm^{-1} band and that the CH out-of-plane bend corresponds to the weak band observed at 970 cm^{-1} in the argon matrix. Finally, it should be noted that we followed the same assignment for the 520 cm^{-1} band as that given for the other isothiocyanate molecules where we believe this band arises from the combination of the NCS bend with the CNC bend. This particular band appears to be present in all of the organoisothiocyanate molecules where it is relatively strong in the gas but weak in the spectrum of the solid and usually not observed in the spectrum of the matrix isolated material.

Conclusions

The infrared spectra of the matrix isolated organoisothiocyanate molecules make it possible to obtain the band centers of the fundamentals, many of which are very broad and nondescript in the gas phase. The spectrum of the methylisothiocyanate molecule could be interpreted on the basis of a quasilinear molecule with effective C_{3v} symmetry. The previously reported (1) doubling of the fundamentals of ethylisothiocyanate in the nitrogen matrix is due to matrix effects and not due to the presence of a second conformer since comparable doubling was not found in the argon matrix. No evidence was found for a second conformer for isopropylisothiocyanate, and conclusive evidence for a second conformer of cyclopropylisothiocyanate could not be found even though this molecule has been found to exist at ambient temperature as the *cis* and *trans* conformers from a microwave study (5). Therefore it is concluded that the vibrational spectra of these molecules are not sensitive to the orientation of the NCS moiety and other techniques must be used to establish the presence of conformers in the organoisothiocyanate molecules. All these molecules give complex spectra in the NCS antisymmetric stretching region which is partly due to the overtone of the symmetric mode as well as possible combinations of the CNC bend or asymmetric torsion with this stretch. Certainly the large amplitude motions of the two low frequency fundamentals give rise to a complex band structure in the 570 cm^{-1} region which appears to be in combination with the NCS bend(s), and probably also contribute to the complex spectra in the NCS antisymmetric stretching region.

Acknowledgements

The authors gratefully acknowledge the financial support for this study by the National Science Foundation by Grant CHE-83-11279, and the NATO Scientific Affairs Division through the collaborative research program by Grant No. 140/82.

1. J. R. Durig, H. L. Heusel, J. F. Sullivan, and S. Cradock. Spectrochim. Acta. **40**A, 739 (1984).
2. T. Sakaizumi, O. Ohashi, and I. Yamaguchi. Bull. Chem. Soc. Jpn. **49**, 948 (1976).
3. R. N. Kniseley, R. P. Hirschmann, and V. A. Fassel. Spectrochim. Acta, **23**A, 109 (1967).
4. J. R. Durig, J. F. Sullivan, H. L. Heusel, and S. Cradock. J. Mol. Struct. **100**, 241 (1983).
5. J. R. Durig, A. B. Nease, J. F. Sullivan, Y. S. Li, and C. J. Wurrey. J. Chem. Phys. To be published.
6. C. J. Wurrey, R. Krishnamoorthi, and A. B. Nease. J. Raman Spectrosc. **9**, 334 (1980).
7. J. R. Durig, J. F. Sullivan, T. S. Little, and S. Cradock. J. Mol. Struct. **118**, 103 (1984).

Adaptation of the Gelius intensity model in semiempirical HAM/3 molecular orbital calculations of valence photoelectron spectra excited by X-ray radiation

DELANO P. CHONG

Department of Chemistry, University of British Columbia, 2036 Main Mall, Vancouver, B.C., Canada V6T 1Y6

Received August 15, 1984

This paper is dedicated to Professor Camille Sandorfy on the occasion of his 65th birthday

DELANO P. CHONG. Can. J. Chem. **63**, 2007 (1985).

The Gelius intensity model has been adapted in the semiempirical HAM/3 method to calculate the valence ionization energies and intensities in XPS. Both semiempirical and *ab initio* Hartree–Fock–Slater atomic photoionization cross-sections can be used. Results presented for C_2H_2, C_2H_4, N_2, H_2O, CH_3OH, and CH_2F_2 demonstrate that the present method can facilitate the interpretation of experimental XPS.

DELANO P. CHONG. Can. J. Chem. **63**, 2007 (1985).

On a adapté le modèle d'intensité de Gélius dans la méthode semi-empirique HAM/3 pour calculer les énergies d'ionisation et les intensités de XPS. On peut utiliser aussi bien des sections droites de photoionisation atomique semi-empirique que les valeurs *ab initio* de Hartree–Fock–Slater. Les résultats rapportés pour les molécules de C_2H_2, C_2H_4, N_2, H_2O, CH_3OH et CH_2F_2 démontrent que la présente méthode peut faciliter l'interprétation de XPS expérimentaux.

[Traduit par le journal]

The Gelius intensity model

A model for calculating relative intensities in the valence region of X-ray photoelectron spectra (XPS) was presented by Gelius (1) over ten years ago. According to this model, the relative intensity for ionization from molecular orbital j is given by

$$[1] \quad I_j^{\mathrm{MO}} = \left[2 + \frac{\beta}{2}\right] \sum_A \sum_\lambda P_{A\lambda j}\, \alpha_{A\lambda}^{\mathrm{AO}}$$

where β is the asymmetry parameter, $P_{A\lambda j}$ is the gross atomic population on atom A from atomic orbital λ in molecular orbital j, and $\sigma_{A\lambda}^{\mathrm{AO}}$ is the relative photoionization cross-section of atomic orbital $A\lambda$. The asymmetry parameter was set to 2 except for π orbitals of linear molecules, in which case $\beta = -1$ was used. For MgKα radiation, Gelius gave values of $\sigma_{A\lambda}^{\mathrm{AO}}$ for the $2s$ and $2p$ orbitals of C, N, O, F, and Ne, and for the $3s$ and $3p$ orbitals of S and Ar. The model was successfully applied to the XPS of C_6H_6, C_4H_4O, C_4H_4S, CF_4, SF_6, C_3O_2, and N_2, despite the preliminary nature of the cross-section ratios.

Several changes have been made since then. A few relative cross-sections $\sigma_{A\lambda}^{\mathrm{AO}}$ were changed (2, 3). The asymmetry parameter was altered to $\beta = 0$ for π orbitals of linear molecules (3). Finally, $P_{A\lambda j}$ was taken to mean the net atomic population (3).

Adaptation of the Gelius model to the semiempirical HAM/3 method

The net atomic population is simply $C_{A\lambda j}^2$. In the semiempirical HAM/3 computer program (4), an additional set of orbital coefficients $\bar{C}_{A\lambda j}$ is available and is associated with the basis set of Löwdin orthogonalized atomic orbitals. The relative intensities obtained by using $C_{A\lambda j}^2$ and $\bar{C}_{A\lambda j}^2$ are similar and only the results from $\bar{C}_{A\lambda j}^2$ will be presented below.

In addition to the semiempirical relative cross-sections of the Gelius model (1–3), we have also incorporated the *ab initio* relative cross-sections for both MgKα (1253.6 eV) and AlKα (1486.6 eV) radiation of Nefedov *et al.* (5) based on the Hartree–Fock–Slater method. A complete list of $\sigma_{A\lambda}^{\mathrm{AO}}$ values used in this work is given in Table 1. The results from semiempirical and *ab initio* cross-sections are similar and only the relative intensities from *ab initio* cross-sections are presented in the figures.

Finally, since our version of the HAM/3 program (6) has been extended to include configuration-interaction (CI) calculations for valence-electron shake-up (VESU) satellite bands, the XPS intensities have likewise been extended. It was demonstrated (6) that the VESU results from HAM/3 can compete with those from two-particle-hole Tamm–Dancoff approximation (2ph-TDA) within the Green's function (GF) approach, especially when a truncated set of molecular orbitals and/or a limited set of atomic orbitals are used.

Results and discussion

The new version of the HAM/3 program was used to calculate the XPS of C_2H_2, C_2H_4, N_2, H_2O, CH_3OH, and CH_2F_2. These molecules were chosen partly because their gas-phase XPS are available and partly because HAM/3 can only handle molecules containing those five elements. The experimental equilibrium geometries for these molecules (7, 8) were used.

In Tables 2 to 7, we summarize the results of the computations. The vertical ionization potentials listed under PES and under VESU come from the runs excluding and including shake-up satellites, respectively. The column heading $\sigma = 1$ refers to the uniform in-phase non-interfering cross-section approximation, which was used previously (6) and corresponds to the so-called spectroscopic factor (9). Finally, the calculated results using *ab initio* atomic cross-sections are compared with the experimental spectra (10–14) in Figs. 1 to 5. In Figs. 2 to 5, contamination by the MgK$\alpha_{3,4}$ satellite line(s) is present as discussed by the experimental workers.

In Fig. 1, the calculated intensity of the shake-up band at 28 eV appears to be too low. However, the correct interpretation of the observed XPS of acetylene is still unclear. Neither CI (10) nor GF (14) calculations produce the experimental pattern around 27 eV. The latest synchrotron results (15) reconfirmed the difficulties of the interpretation, suggesting two different origins of the borrowed intensities for the VESU bands at 26.5 eV and 28 eV, as well as a new peak at 31.0 eV (all in agreement with the present results).

In Fig. 2, the VESU peak at 27 eV is given a new interpretation. The presence of two VESU states in this energy region of the XPS of ethylene is supported by GF results (16). These two cases show that the present HAM/3 approach is

TABLE 1. Relative photoionization cross-sections (relative to C 2s) used in this work

Atomic orbital		Gelius MgKα	Nefedov *et al.*[d] MgKα	Nefedov *et al.*[d] AlKα
H	1s	0[a]	0.0102	0.0093
C	2s	1	1	1
	2p	0.045[c]	0.0389	0.0324
N	2s	1.2[a]	1.781	1.821
	2p	0.1091[a]	0.1048	0.0902
O	2s	1.3[b]	2.848	2.948
	2p	0.148[b]	0.2307	0.2029
F	2s	2.0[a]	4.229	4.429
	2p	0.2[a]	0.4505	0.4016

[a]Reference 1.
[b]Reference 2.
[c]Reference 3.
[d]Reference 5.

TABLE 2. Semiempirical HAM/3 results for the XPS of C_2H_2 excited by AlKα with and without VESU

State	PES (eV)	Rel. intensity Gelius	Rel. intensity Nefedov	VESU (eV)	$\sigma = 1$	Rel. intensity Gelius	Rel. intensity Nefedov
$^2\Pi_u$	11.59	0.060	0.043	11.57	1.999	0.060	0.043
$^2\Sigma_g$	17.18	0.036	0.030	16.94	0.982	0.036	0.030
$^2\Sigma_u$	19.70	0.322	0.323	19.12	0.946	0.305	0.305
$^2\Sigma_g$	24.12	0.766	0.767	23.59	0.886	0.677	0.678
$^2\Sigma_g$				26.91	0.082	0.063	0.063
$^2\Sigma_u$				28.53	0.036	0.012	0.012
$^2\Sigma_g$				30.96	0.050	0.027	0.027
$^2\Sigma_u$				33.01	0.012	0.004	0.004

TABLE 3. Semiempirical HAM/3 results for the XPS of C_2H_4 excited by MgKα with and without VESU

State	PES (eV)	Rel. intensity Gelius	Rel. intensity Nefedov	VESU (eV)	$\sigma = 1$	Rel. intensity Gelius	Rel. intensity Nefedov
$^2B_{1u}$	10.53	0.045	0.039	10.49	0.999	0.045	0.039
$^2B_{1g}$	13.20	0.025	0.026	12.95	0.978	0.024	0.025
^2A_g	14.84	0.053	0.050	14.74	0.993	0.052	0.050
$^2B_{2u}$	16.28	0.028	0.028	15.76	0.910	0.025	0.025
$^2B_{3u}$	19.84	0.341	0.345	19.35	0.908	0.310	0.313
^2A_g				23.36	0.075	0.026	0.026
^2A_g	24.29	0.630	0.633	23.66	0.807	0.508	0.510
^2A_g				25.55	0.100	0.063	0.063
				28.22	0.098	0.059	0.059

moderately successful. It is in the next example that the shortcoming of our limited configurational space is more evident.

In Fig. 3, the weak peak at 32 eV is missing in the calculated spectrum because it is due to 2-particle-3-hole contributions (9), which are completely absent in our VESU configuration interaction as well as in 2ph-TDA GF calculations (17, 18). The interpretation of the peak at 27 eV in the XPS of N_2 is also quite complicated (9, 19). In fact, there are many significant VESU satellites in the inner valence region of N_2, as shown by the work of Nyholm *et al.* (20) and the present HAM/3 picture is undoubtedly an oversimplification.

In the next three cases, the present method works very well, providing grounds for its use.

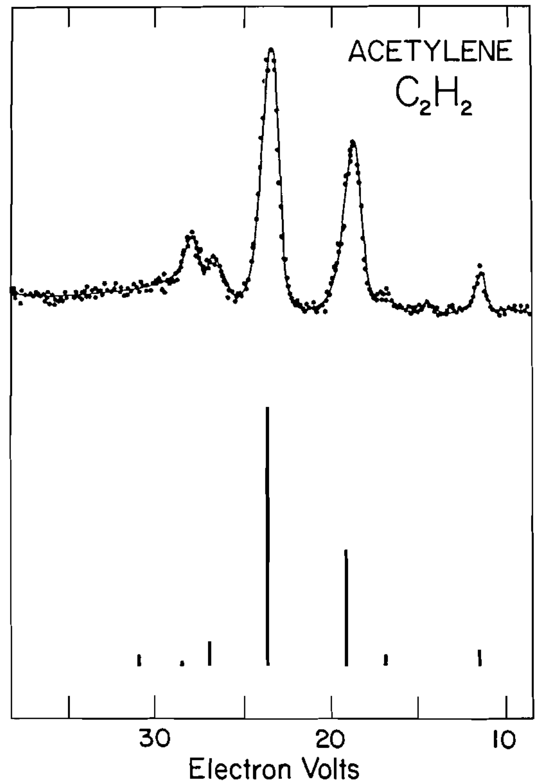

FIG. 1. Comparison of experimental (10) and calculated AlKα photoelectron spectrum of C_2H_2.

TABLE 4. Semiempirical HAM/3 results for the XPS of N_2 excited by AlKα with and without VESU

State	PES (eV)	Rel. intensity Gelius	Rel. intensity Nefedov	VESU (eV)	$\sigma = 1$	Rel. intensity Gelius	Rel. intensity Nefedov
$^2\Sigma_g$	15.43	0.304	0.404	15.23	0.985	0.299	0.393
$^2\Pi_u$	16.21	0.155	0.140	16.07	1.988	0.145	0.092
$^2\Sigma_u$	18.40	0.805	1.173	17.92	0.943	0.759	1.126
$^2\Sigma_u$				23.74	0.040	0.032	0.048
$^2\Sigma_u$				27.48	0.013	0.010	0.015
$^2\Sigma_g$				27.61	0.034	0.029	0.043
$^2\Sigma_g$				27.94	0.008	0.007	0.010
$^2\Sigma_g$	37.39	1.005	1.482	37.72	0.967	0.972	1.461

TABLE 5. Semiempirical HAM/3 results for the XPS of H_2O excited by MgKα with and without VESU

State	PES (eV)	Rel. intensity Gelius	Rel. intensity Nefedov	VESU (eV)	$\sigma = 1$	Rel. intensity Gelius	Rel. intensity Nefedov
$^2B_1$	12.93	0.148	0.231	12.87	0.997	0.148	0.230
$^2A_1$	15.39	0.234	0.438	15.35	0.999	0.234	0.437
$^2B_2$	18.28	0.107	0.170	18.24	0.998	0.107	0.169
$^2A_1$	32.88	0.872	1.913	31.30	0.521	0.455	0.997
$^2A_1$				34.01	0.435	0.379	0.833
$^2A_1$				37.98	0.015	0.013	0.028
$^2A_1$				40.93	0.025	0.022	0.048

The XPS of H_2O and CH_3OH are presented in Fig. 4. The HAM/3 results obtained in this work can reproduce the experimental spectra very well. More elaborate calculations have been performed on these molecules using the 2ph-TDA GF

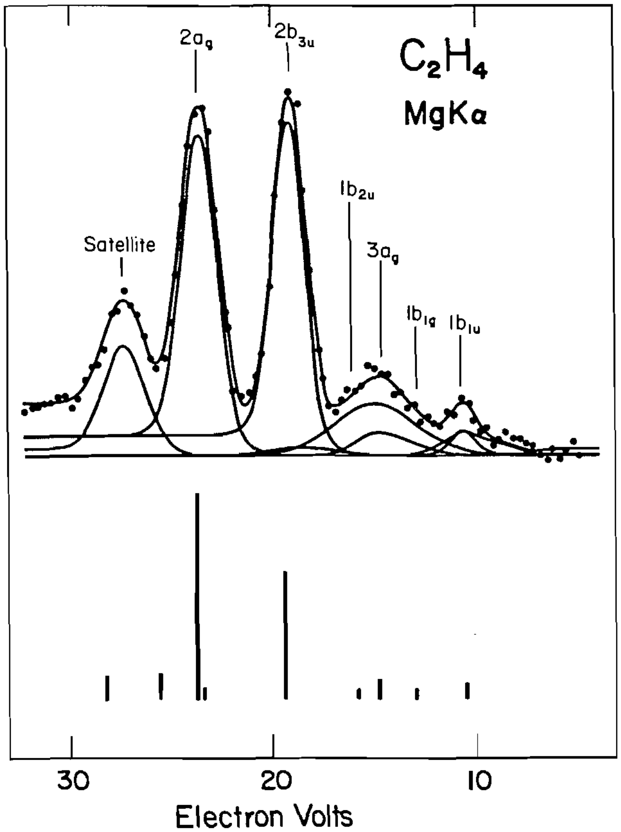

FIG. 2. Comparison of experimental (11) and calculated MgKα photoelectron spectrum of C_2H_4.

TABLE 6. Semiempirical HAM/3 results for the XPS of CH_3OH excited by MgKα with and without VESU

State	PES (eV)	Rel. intensity Gelius	Rel. intensity Nefedov	VESU (eV)	$\sigma = 1$	Rel. intensity Gelius	Rel. intensity Nefedov
$^2A''$	11.04	0.122	0.188	10.80	0.990	0.121	0.186
$^2A'$	12.65	0.125	0.216	12.52	0.994	0.124	0.214
$^2A'$	14.99	0.098	0.147	14.87	0.994	0.097	0.146
$^2A''$	15.77	0.053	0.070	15.59	0.990	0.052	0.069
$^2A'$	17.57	0.117	0.200	17.37	0.988	0.116	0.198
$^2A'$	22.31	0.437	0.525	22.20	0.987	0.431	0.518
$^2A'$				29.60	0.243	0.226	0.476
$^2A'$	31.93	0.931	1.965	31.35	0.340	0.316	0.667
$^2A'$				31.97	0.014	0.011	0.024
$^2A'$				32.28	0.121	0.111	0.234
$^2A'$				33.07	0.045	0.042	0.089
$^2A'$				33.45	0.019	0.017	0.036
$^2A'$				33.52	0.058	0.054	0.114
$^2A'$				34.28	0.093	0.086	0.182
$^2A'$				34.30	0.010	0.008	0.017
$^2A'$				37.45	0.024	0.021	0.045

method (21–23) but the relative intensities in those calculations are based on the $\sigma = 1$ model.

Finally, the HAM/3 results on CH_2F_2 are compared with the observed spectrum in Fig. 5. The outer-valence photoelectron spectrum of CH_2F_2 is well understood (24). The inner-valence region has been studied by the 2ph-TDA GF method (25) but the ionization energies and spectroscopic factors are inferior to the present results.

By relying heavily on Slater's screening concept, the semi-

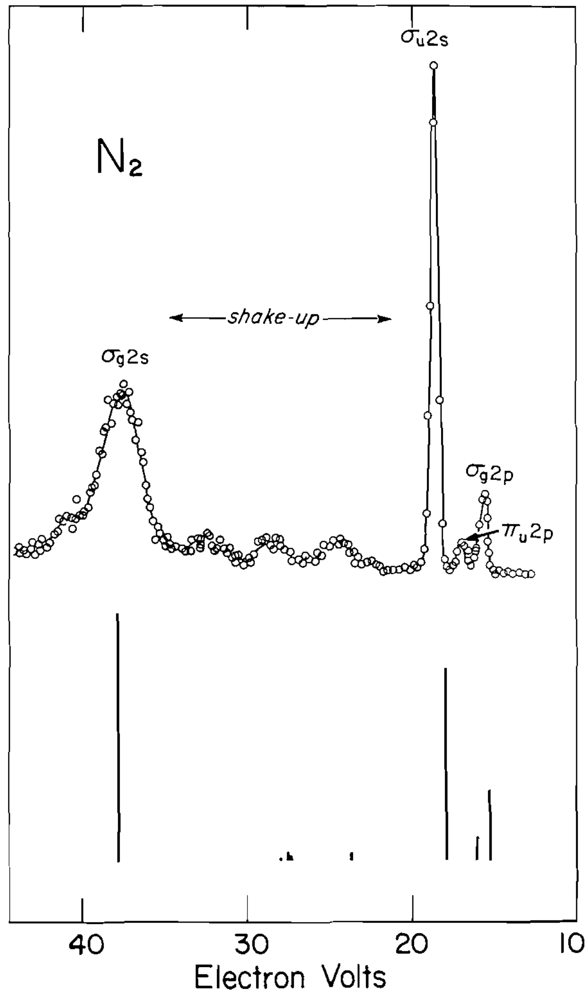

FIG. 3. Comparison of experimental (12) and calculated AlKα photoelectron spectrum of N_2.

TABLE 7. Semiempirical HAM/3 results for the XPS of CH_2F_2 excited by MgKα with and without VESU

State	PES (eV)	Rel. intensity Gelius	Rel. intensity Nefedov	VESU (eV)	$\sigma = 1$	Rel. intensity Gelius	Rel. intensity Nefedov
$^2B_2$	13.10	0.118	0.252	13.05	0.998	0.117	0.252
$^2B_1$	15.47	0.200	0.451	15.43	0.998	0.200	0.450
$^2A_1$	15.66	0.186	0.400	15.61	0.998	0.186	0.399
$^2A_2$	15.78	0.200	0.451	15.67	0.996	0.199	0.449
$^2B_1$	19.18	0.261	0.564	19.15	0.999	0.261	0.563
$^2B_2$	19.27	0.108	0.222	19.20	0.997	0.108	0.222
$^2A_1$	19.31	0.218	0.457	19.26	0.998	0.217	0.456
$^2A_1$	24.04	0.529	0.760	24.03	1.000	0.529	0.760
$^2B_1$				37.57	0.088	0.146	0.309
$^2B_1$	38.48	1.655	3.489	38.01	0.694	1.148	2.420
$^2B_1$				38.55	0.154	0.254	0.536
$^2A_1$	39.98	1.680	3.421	39.46	0.915	1.537	3.129
$^2B_1$				42.19	0.023	0.039	0.082
$^2B_1$				44.95	0.032	0.052	0.110
$^2A_1$				45.61	0.060	0.100	0.204

empirical HAM/3 method simplifies the true situation by using a minimal basis set. The present version of the program also limits the configurational space for cationic CI to determinants with either one or three singly occupied molecular orbitals.

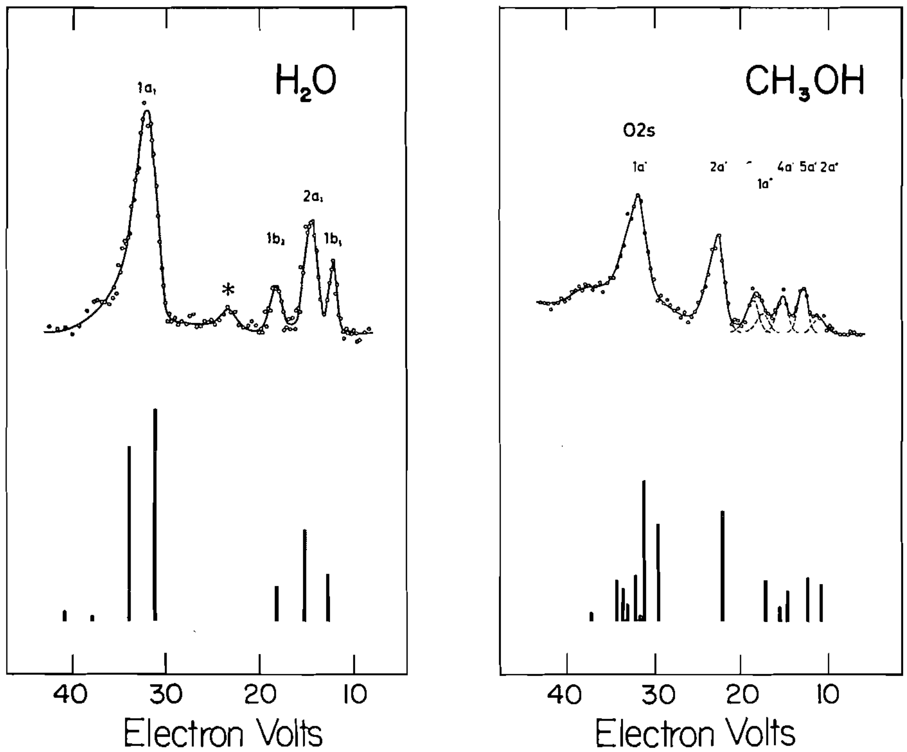

FIG. 4. Comparison of experimental (13) and calculated MgKα photoelectron spectra of H_2O and CH_3OH. The asterisk indicates contamination by MgK$\alpha_{3,4}$.

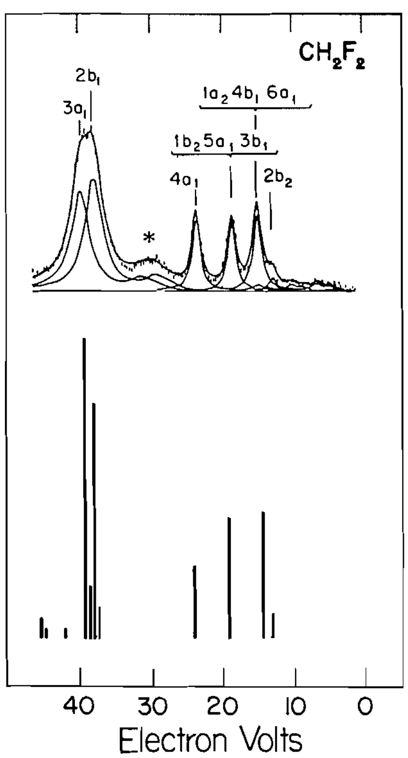

FIG. 5. Comparison of experimental (14) and calculated MgKα photoelectron spectrum of CH_2F_2. The asterisk indicates contamination by MgK$\alpha_{3,4}$.

Nevertheless, this version of the HAM/3 program performs remarkably well. The six molecules studied in this work required a total of 15 s of CPU time on an Amdahl V/8 computer.

In principle, the 2ph-TDA GF approach can be more reliable. In practice, however, severe truncation of the atomic orbital basis set and the molecular orbital space has led to considerable loss of accuracy. Moreover, most of the GF papers give spectroscopic factors rather than XPS intensities. Related to the present study is the work of Honjou *et al.* (26) who computed *ab initio* photoionization cross-sections with the plane-wave approximation, but their ionization energies tend to be less reliable because they use minimal Slater-type orbitals as basis set.

Other semiempirical approaches should be mentioned. Bigelow based his calculations on CNDO (27) and Schulz *et al.* (28) compared CNDO with MNDO and LNDO. In both cases, only the spectroscopic factors are obtained.

In summary, in spite of its simplicity, the present version of HAM/3 can provide useful calculated XPS to facilitate the interpretation of experimental spectra.

Acknowledgements

The author wishes to thank the Natural Sciences and Engineering Research Council of Canada for financial support, and Dr. N. P. C. Westwood for valuable discussions.

1. U. GELIUS. Electron spectroscopy. *Edited by* D. A. Shirley. North Holland, Amsterdam. 1972. p. 311.
2. U. GELIUS, C. J. ALLAN, D. A. ALLISON, H. SIEGBAHN, and K. SIEGBAHN. Chem. Phys. Lett. **11**, 224 (1971).
3. U. GELIUS. J. Electron Spectrosc. **5**, 985 (1974).
4. L. ÅSBRINK, C. FRIDH, and E. LINDHOLM. Quantum Chemistry Program Exchange **12**, No. 393 (1980).
5. V. I. NEFEDOV, N. P. SERGUSHIN, I. M. BAND, and M. B. TRZHASKOVSKAYA. J. Electron Spectrosc. **2**, 383 (1973).
6. D. P. CHONG. Can. J. Chem. **61**, 1 (1983).
7. K. H. HELLWEGE. Landolt-Börnstein numerical data and functional relationships in science and technology. New Series, Group II, Vol. 7. Springer, Berlin. 1976.

8. K. P. HUBER and G. HERZBERG. Molecular spectra and molecular structure. Vol. 4. Van Nostrand, Princeton. 1979.
9. P. W. LANGHOFF, S. R. LANGHOFF, T. N. RESCIGNO, J. SCHIRMER, L. S. CEDERBAUM, W. DOMCKE, and W. VON NIESSEN. Chem. Phys. **58**, 71 (1981).
10. J. MÜLLER, R. ARNEBERG, H. ÅGREN, R. MANNE, P-Å. MALMQUIST, S. SVENSSON, and U. GELIUS. J. Chem. Phys. **77**, 4895 (1982).
11. M. S. BANNA and D. A. SHIRLEY. J. Electron Spectrosc. **8**, 255 (1976).
12. U. GELIUS, E. BASILIER, S. SVENSSON, T. BERGMARK, and K. SIEGBAHN. J. Electron Spectrosc. **2**, 405 (1974).
13. K. SIEGBAHN, C. NORDLING, G. JOHANSSON, J. HEDMAN, P. F. HEDÉN, K. HAMRIN, U. GELIUS, T. BERGMARK, L. O. WERME, R. MANNE, and Y. BAER. ESCA applied to free molecules. North Holland, Amsterdam. 1969. pp. 83, 100.
14. M. S. BANNA, B. E. MILLS, D. W. DAVIS, and D. A. SHIRLEY. J. Chem. Phys. **61**, 4780 (1974).
15. S. SVENSSON, P-Å. MALMQUIST, M. Y. ADAM, P. LABLANQUIE, P. MORIN, and I. NENNER. Chem. Phys. Lett. **111**, 574 (1984).
16. L. S. CEDERBAUM, W. DOMCKE, J. SCHIRMER, W. VON NIESSEN, G. H. F. DIERCKSEN, and W. P. KRAEMER. J. Chem. Phys. **69**, 1591 (1978).
17. J. SCHIRMER, L. S. CEDERBAUM, W. DOMCKE, and W. VON NIESSEN. Chem. Phys. **26**, 149 (1977).
18. J. SCHIRMER and O. WALTER. Chem. Phys. **78**, 201 (1983).
19. L. S. CEDERBAUM and H. KÖPPEL. Chem. Phys. Lett. **87**, 14 (1982).
20. R. NYHOLM, A. BERNDTSSON, R. NILSSON, J. HEDMAN, and C. NORDLING. Phys. Script. **16**, 383 (1977).
21. L. S. CEDERBAUM. Mol. Phys. **28**, 479 (1974).
22. W. VON NIESSEN, L. S. CEDERBAUM, J. SCHIRMER, G. H. F. DIERCKSEN, and W. P. KRAEMER. J. Electron Spectrosc. **28**, 45 (1982).
23. W. VON NIESSEN, G. BIERI, and L. ÅSBRINK. J. Electron Spectrosc. **21**, 175 (1980).
24. S. R. LANGHOFF and D. P. CHONG. Chem. Phys. Lett. **86**, 487 (1982).
25. R. CAMBI, G. CIULLO, A. SGAMELLOTTI, F. TARANTELLI, R. FANTONI, A. GIARDINI-GUIDONI, and A. SERGIO. Chem. Phys. Lett. **80**, 295 (1981).
26. N. HONJOU, T. SASAJIMA, and F. SASAKI. Chem. Phys. **57**, 475 (1981).
27. R. W. BIGELOW. Chem. Phys. **80**, 45 (1983); Chem. Phys. Lett. **100**, 445 (1983).
28. R. SCHULZ, A. SCHWEIG, and W. ZITTLAU. J. Am. Chem. Soc. **105**, 2980 (1983).

Structure of bacteriorhodopsin in the acidified membrane and at high ionic strength: resonance Raman study

G. MASSIG, M. STOCKBURGER,[1] AND TH. ALSHUTH

Max-Planck-Institut für Biophysikalische Chemie, 3400 Göttingen-Nikolausberg, Federal Republic of Germany

Received November 27, 1984

This paper is dedicated to Professor Camille Sandorfy on the occasion of his 65th birthday

G. MASSIG, M. STOCKBURGER, and TH. ALSHUTH. Can. J. Chem. **63**, 2012 (1985).

Resonance Raman (RR) spectra of the retinylidene Schiff's base (SB) chromophore of bacteriorhodopsin (BR) were obtained from purple membrane (PM) suspensions of *Halobacterium halobium* in three different equilibrium states: (1) the native state at neutral pH; (2) BR-605, the acidified membrane at pH 2; (3) BR-565(Cl^-) or BR-545 (F^-), at low pH and high ionic strength. In the native state the retinyl chromophore is stabilized by an ion-pair complex of the protonated SB group with a negative carboxylate counterion (A^-) of the protein, giving SBH^+---A^-. In the acidic form, BR-605, it is inferred from the RR spectra that the chromophore is immobilized. This is ascribed to a breakdown of the ionic interaction by protonation of A^-. In the two (3) forms the RR spectra show that the original structure of the chromophore in the native state is reestablished, which is attributed to the formation of SBH^+---Cl^-(F^-) complexes with the anions. It thus turns out from RR spectroscopic evidence that the retinyl chromophore in BR is largely governed by the SBH^+---A^- ion-pair formation, which is stabilized by surrounding water molecules.

G. MASSIG, M. STOCKBURGER et TH. ALSHUTH. Can. J. Chem. **63**, 2012 (1985).

On a obtenu les spectres de résonance Raman (RR) du chromophore de la bactériorhodopsine (BR) de la base de Schiff (BS) du rétinylidène, à partir de suspensions de la membrane pourpre (MP) du *Halobacterium halobium* dans trois états d'équilibre différents: (1) l'état naturel à pH neutre; (2) BR-605, la membrane acidifiée à un pH de 2; (3) BR-565 (Cl^-) ou BR-545 (F^-) à des pH faibles et à une force ionique élevée. À l'état naturel, le chromophore rétinyle est stabilisé par un complexe formé d'une paire d'ions du groupe BS protoné par l'ion carboxylate (A^-) de la protéine en donnant le BSH^+---A^-. Sur la base du spectre RR de la forme acidifiée, BR-605, on déduit que le chromophore est immobilisé. On attribue ceci à une rupture de l'interaction ionique par suite de la protonation de A^-. Dans les deux formes (3), le spectre RR indique que la structure originale du chromophore à l'état naturel est rétablie. On attribue ceci à la formation de complexes SBH^+---Cl^- (F^-) avec les anions. Il ressort donc des données spectroscopiques que le chromophore rétinyle de la BR dépend fortement de la formation de la paire d'ions SBH^+---A^- qui est stabilisée par les molécules d'eau environnantes.

[Traduit par le journal]

Introduction

Bacteriorhodopsin (BR) is a retinal-binding protein in the cell membrane of *Halobacterium halobium.* In the so-called purple membrane (PM) fraction it forms two-dimensional regular arrays and acts as a light-driven proton pump (1). This function is controlled by a chromophoric center which contains retinal bound to the protein via a Schiff's base (SB) linkage (for a review, see ref. 2). In the dark BR exists in a nearly 1 : 1 ratio of two forms with retinal in the all-*trans* (BR-570) and 13-*cis* (BR-548) configuration, respectively (Fig. 1) (3, 4). In the light the equilibrium is shifted towards the all-*trans* component, BR-570, the initial state of a light-induced cyclic process which induces BR's function as a proton pump (Fig. 2) (2).

The colour of a BR chromophore is largely determined by the state of protonation of the SB group. Thus protonation at the SB nitrogen induces a big red-shift (5, 6). As will be outlined below, the positive charge at the SB group interacts strongly with a negative counterion in the side group of an amino acid residue. The absorption maximum (λ_{max}) of a BR chromophore largely depends on the strength of this ionic interaction (5).

It was reported that λ_{max} of the light-adapted PM shifts from 570 to 605 nm when the pH value is decreased from 7 to 2. In more systematic titration experiments with hydrochloric acid it was found by Mowery *et al.* (7) that this transition to a new state, BR-605, can be described by a pK value of 2.9. When the pH value is decreased below 2 by addition of hydrochloric

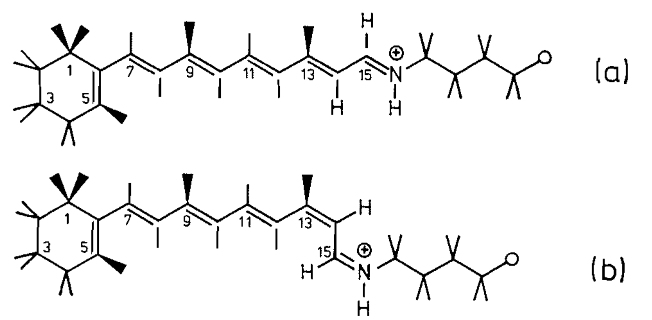

FIG. 1. In the BR chromophore retinal is bound to the ϵ-amino group of a lysine residue via a Schiff's base linkage; (a) native chromophore BR-570: all-*trans* retinal, 15-*anti* protonated SB group (21); (b) native chromophore BR-548: 13-*cis* retinal, 15-*syn* protonated SB group (21).

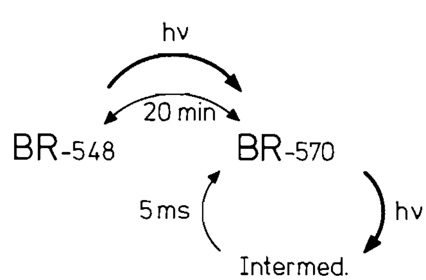

FIG. 2. Photoreactions of native bacteriorhodopsin. Light adaption shifts the equilibrium to BR-570, which runs through a photochemically induced cyclic process. The time constants refer to room temperature.

[1]Author to whom all correspondence should be addressed.

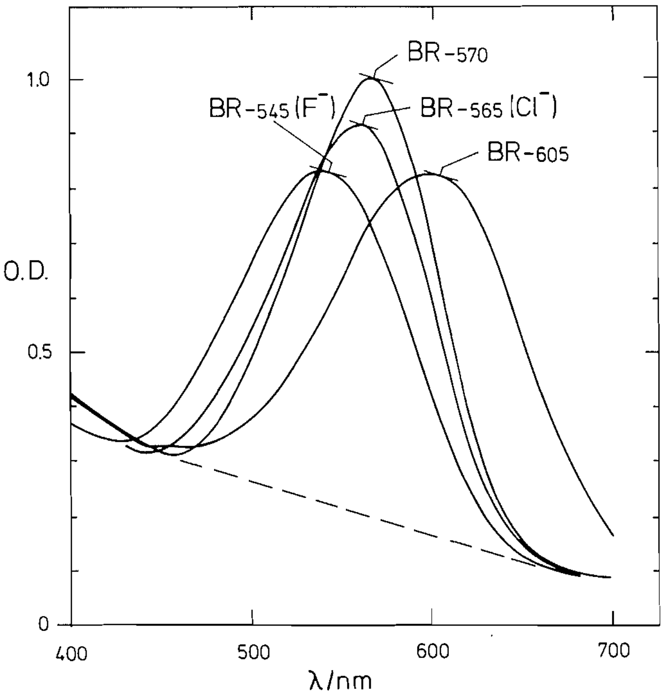

FIG. 3. Absorption spectra from purple membranes embedded in polyacrylamide gels. BR-570: neutral pH value. BR-605: equilibrated with HCl solution at pH 2. BR-565(Cl^-): equilibrated with HCl solution at pH 0. BR-545(F^-): equilibrated with solution of 0.67 *M* hydrofluoric acid and 0.33 *M* NaF, at pH 2.2. All absorption spectra refer to the same concentration of PM.

acid, a second equilibrium state with λ_{max} at 565 nm is established (Fig. 3). While the first transition to BR-605 obviously involves a proton transfer reaction, it could be demonstrated by Fischer and Oesterhelt (8) that the second transition is catalyzed by chloride or fluoride anions leading to final states with λ_{max}

$$[1]\quad \text{BR-570} \underset{\text{I}}{\overset{H^+}{\rightleftharpoons}} \text{BR-605} \underset{\text{II}}{\overset{Cl^-, F^-}{\rightleftharpoons}} \left\{ \begin{matrix} \text{BR-565}(Cl^-) \\ \text{BR-545}(F^-) \end{matrix} \right\}$$

at 565 and 545 nm, respectively (Fig. 3). Equilibrium constants of 1 $M[Cl^-]$ and 0.1 $M[F^-]$ were estimated for the anion-induced transitions (8).

The following view of the molecular mechanism of the reactions in eq. [1] was given by Fischer and Oesterhelt (8). In the parent chromophore, BR-570, the positively charged SB group interacts with a negative counterion giving SBH^+---A^-. When the environmental proton concentration is increased, A^- becomes protonated from the outside. The p*K* value of 2.9 for this reaction argues that A^- might be a carboxylate group of an aspartic or glutamic acid residue. Such a group presumably is located in close vicinity to the chromophore. This is supported by the observation that a carboxylate anion in the protein becomes protonated and deprotonated synchronously with intermediates of the photochemical cycle (9). Once the intrinsic anion is protonated, the original ion-pair interaction is interrupted giving (SBH^+, AH), which corresponds to the red-shifted species BR-605. When the ion strength is further increased, the role of the intrinsic anion can be taken over by extrinsically introduced anions like Cl^- or F^-, reestablishing ion-pair interaction of the form SBH^+---Cl^- (F^-) and shifting λ_{max} back to the blue.

In the present paper we have studied resonance Raman (RR) spectra of the acidified chromophore BR-605 and the two anion complexes BR-565(Cl^-) and BR-545(F^-). In an RR experiment the chromophoric site is selectively probed and one obtains from the vibrational spectra information on the configuration of the retinal chain or the state of protonation of the SB group. The analysis of the RR spectra therefore provides detailed information on the modified chromophoric species and consequently also on the structure of the native chromophore.

Experimental

In order to prevent aggregation of purple membranes arising at low pH values or at high ionic strength the PM patches were embedded into polyacrylamide gels. The gels were prepared as described in ref. 8 and PM was added to the gel at a concentration of 3×10^{-5} *M*. To adjust the pH value and (or) ionic strength and to exchange H_2O for D_2O the gel preparation was immersed in an aqueous reference solution and kept there several hours for equilibration. To record absorption spectra the gel was polymerized into a Plexiglass cuvette with apertures in the side walls to enable diffusional equilibration with the reference solution.

For resonance Raman measurements a demountable spinning cell of cylindrical shape made of Plexiglass was used (10). The cylinder had an inner diameter of 40 mm and a length of 5 mm. The cell was only half filled with liquid gel suspension and then rotated so that the liquid was pressed against the cylindrical wall. Rotation was continued until polymerization was complete, leaving behind a gel layer of a few millimeters in thickness. For equilibration with the reference solution the cell was demounted and the cylindrical wall with the gel layer was immersed in the solvent.

For excitation of Raman scattering the beam of a CW ion laser (argon or krypton) was aligned in the gel layer parallel to the cylindrical wall. The beam was focussed with a 200-mm lens into the middle of the cell, giving a focal diameter of 70 μm. The cell was rotated at a repetition rate of 50 s^{-1}. The conversion of a photolabile species is determined by the product $I_0 \Delta t$, where I_0 is the rate of the photoreaction which is proportional to the irradiation power and Δt is the transit time of a molecule across the focal area of the beam (11). This "photoconversion parameter" was kept below 0.2 for the native chromophore and for BR-605, which means that less than 10% of photoproducts are probed by the laser beam (11). For RR measurements with BR-565(Cl^-) and BR-545(F^-) this parameter was elevated by a factor of three, since up to this value no photointermediates were found.

Raman scattering was monitored perpendicular to the laser probe beam. The spectra were recorded by conventional equipment as described previously (12) using a spectral bandwidth of 3.7 cm^{-1}. The RR spectra of the unphotolyzed chromophores BR-570 and BR-548 were obtained from light- and dark-adapted PM in aqueous suspension as described previously (11–13). In all experiments the temperature was 25°C.

Purple membranes were isolated from *Halobacterium halobium* cells in the conventional way (14).

Results

At pH values between 5 and 7 the RR spectra obtained from gel-suspended PM were identical with the spectra from aqueous solution. In the following the solution spectra of the unphotolyzed species BR-570 and BR-548 will be taken as reference and therefore a brief account of the vibrational assignments will be given in advance. The characteristic bands of the terminal SB group can easily be inferred from a comparison of the spectra in H_2O and D_2O, since upon solvent exchange the proton at the nitrogen is replaced by a deuteron. From the spectra of BR-570 in Fig. 4, therefore, it follows that the band at 1641 cm^{-1} can be assigned to the C=N stretching motion of the $HC{=}NH^+$ group. This band shifts to 1624 cm^{-1} for the $HC{=}ND^+$ group. Similarly the bands at 1349 cm^{-1} in

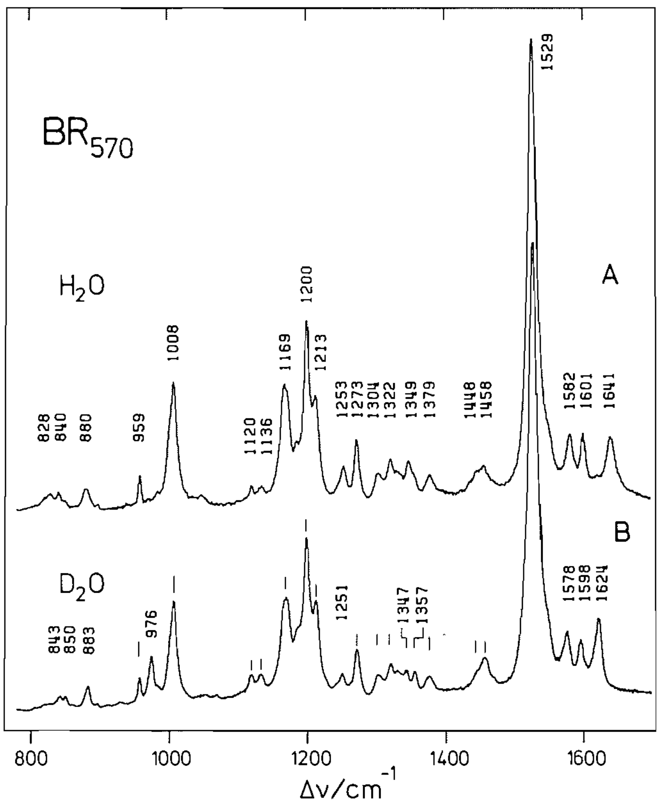

FIG. 4. Resonance Raman spectra of BR-570 from aqueous suspension of PM, excited at 514 nm.

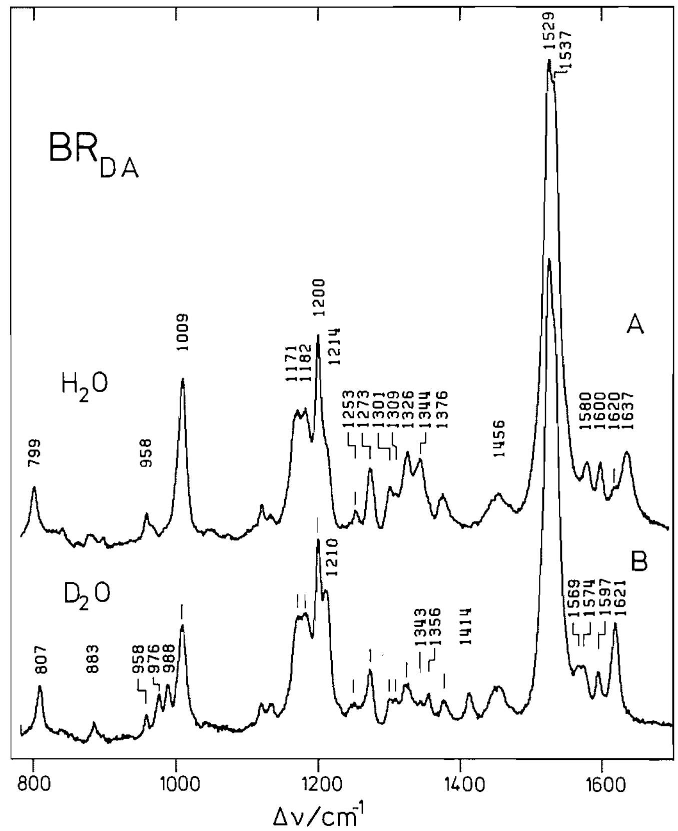

FIG. 5. Resonance Raman spectra from dark-adapted aqueous suspensions of PM, excited at 514 nm.

H_2O and at 976 cm^{-1} in D_2O can be assigned to a vibrational mode whose main component is the N—H or N—D in-plane bending motion. A qualitative assignment of the vibrational bands of the retinal moiety can be made on the basis of normal mode calculations of retinal (15–17). Thus the strongest band in the spectra at 1529 cm^{-1} refers to an "in-phase" stretching motion along the various C—C double bonds. The frequency of this "C═C stretch" varies as the inverse of λ_{max} of a chromophore and therefore is a measure of π-electron distribution along the retinal chain (11, 12, 18). The group of fairly strong bands between 1150 and 1220 cm^{-1} corresponds to vibrations which mainly involve a C—C single bond stretching component which, however, is strongly coupled with the C—H (N—H) in-plane (i.p.) bending motion. Such normal modes are fairly delocalized and therefore are sensitive to structural changes. The group of bands between 1150 and 1220 cm^{-1} thus constitutes a fingerprint for the configuration of the retinal moiety. Similarly the weaker bands between 1250 and 1400 cm^{-1}, which involve the C—H (N—H) in-plane bending motion as a principal component which is coupled to C—C single bond stretches, are also characteristic of the structure of retinal. C—H (N—H) out-of-plane modes lie between 800 and 1000 cm^{-1}. The appearance of intense RR bands in this region has been interpreted as a sign for considerable conformational distortion (13, 19, 20). In the spectra of BR-570 a few weak bands of this type are observed between 820 and 960 cm^{-1}. The fairly strong band at 1008 cm^{-1}, however, obtains its intensity mostly from the in-phase in-plane bending mode of the two methyl groups at the C(9) and C(13) position of the retinal chain (15).

The spectra of the dark-adapted PM in aqueous solution which consists of a 1:1 mixture of BR-570 and the 13-*cis* chromophore BR-548 are depicted in Fig. 5. The contribution of BR-548 is reflected by a number of new vibrational features. Thus a new C═C stretch appears at 1537 cm^{-1}, which corresponds to the shift of λ_{max} to 548 nm. In the fingerprint region a new band arises at 1182 cm^{-1} while in the H_2O spectrum intensity decreases at 1214 cm^{-1}. The fairly distinct feature at 800 cm^{-1} has been attributed to the C_{14}—H out-of-plane (o.p.) bending mode (16). The characteristic vibrations of the SB group can be inferred from isotope effects in Fig. 5. The rather strong band at 1344 cm^{-1} was assigned to a coupled i.p. bending mode of the two SB hydrogens from which the C_{15}—H component appears as a clear feature at 1414 cm^{-1} in the D_2O spectrum (13). The corresponding C_{15}—H o. p. bending mode was assigned to the 988 cm^{-1} band in the D_2O spectrum (13). It must be noted that the band at 1210 cm^{-1} in D_2O has been recently assigned to a C—C single bond stretch. In H_2O this is coupled to the N—H i. p. bend and therefore shifts down to 1160 cm^{-1} (20). It thus appears that the characteristic bands of the SB group are different for the two chromophores BR-570 and BR-548. This can be ascribed to the fact that the two SB hydrogens are in *anti* and *syn* position, respectively (Fig. 1) (21). A "pure" spectrum of BR-548 was obtained by subtracting the contribution of BR-570 (13).

The RR spectra obtained from a PM containing polyacrylamide gel at a pH value of 2 are shown in Fig. 6. Although the BR concentration was as low as 3×10^{-5} *M*, the resonantly enhanced scattering from the chromophore was about five times more intense than Raman scattering from the gel alone, whose contribution therefore could be easily subtracted. It is known that the chromophore established at pH 2, BR-605, is photolabile (22, 24). It also runs through a photochemical cycle

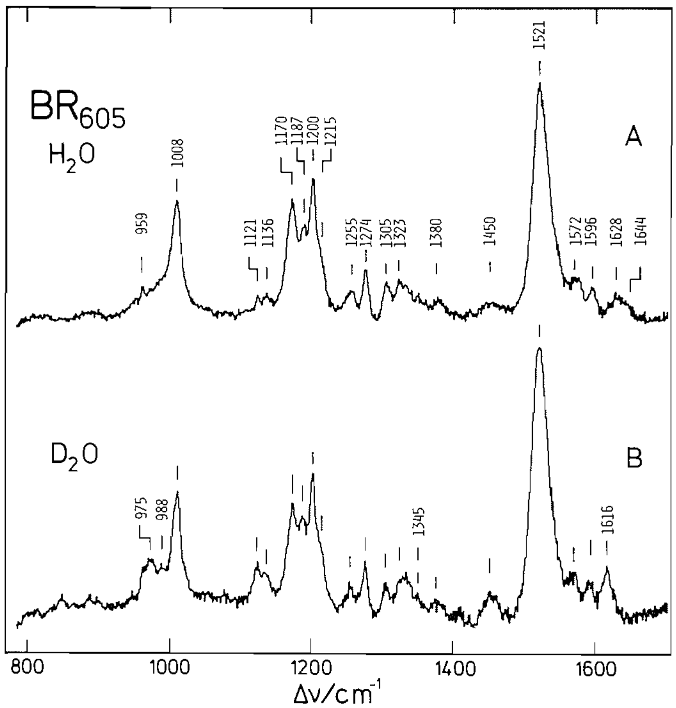

FIG. 6. Resonance Raman spectra of BR-605 excited at 568 nm. BR-605: PM in polyacrylamide gel equilibrated with HCl at pH 2.

with intermediates comparable to K-590 and L-550 of the native chromophore BR-570 (24). For the "L" intermediate a lifetime >700 μs is reported (24). In our RR experiments with a spinning cell it is estimated that less than 20% of photoproducts are formed during the transit of sample across the beam. However, since in the gel the BR molecules are in a fixed position, photointermediates or products whose lifetime is longer than the 20-ms cyclic period of the spinning cell might be accumulated. In the spectra of Fig. 6 the C=C stretch lies at 1521 cm^{-1}, which correlates with λ_{max} at 605 nm. This is strong evidence that in our RR experiment the unphotolyzed species BR-605 predominantly was probed. It is interesting to note that a second C=C stretch at 1533 cm^{-1} increases in intensity at the expense of the 1521 cm^{-1} line when the wavelengths of the Raman probe beam are tuned below 500 nm and therefore are out of resonance with BR-605. It may be that the 1533 cm^{-1} line belongs to the "L" intermediate of BR-605 whose RR scattering is resonantly enhanced in the blue-green region and therefore can be detected even at low concentration. Another possibility would be that the 1533 cm^{-1} line reflects the 9-*cis* photoproduct of BR-605, which also absorbs in the blue-green region (22, 23). Finally, it must be noted that after 10 min of irradiation under the conditions of our RR experiment a 3% bleaching of BR-605 and a concomitant decrease of its RR intensity are observed.

The spectra of BR-605 in Fig. 6 can now be compared with the spectra of the native membrane in Figs. 4 and 5. First of all, it can be concluded from isotopic shifts that the SB group in BR-605 is protonated. In the fingerprint region the intensity ratio of the two diagnostic bands at 1187 and 1215 cm^{-1} is similar to that in the dark-adapted membrane in H_2O suspension (Fig. 5A), suggesting that in BR-605 a mixture of all-*trans* and 13-*cis* retinal is established. This conclusion is in line with biochemical extraction experiments in which a nearly equal amount of the two isomers was found in the light- and dark-adapted state of the acidified membrane at pH 2 (7). On the other hand, the characteristic hydrogen bending modes of the SB group in the 13-*cis*/15-*syn* component of the dark-adapted membrane (799 and 1344 cm^{-1} in H_2O; 807, 988, and 1210 cm^{-1} in D_2O), giving rise to well-resolved vibrational features in the spectra of Fig. 5, cannot be identified in the spectra of BR-605. This implies that the SB group in the 13-*cis* component of BR-605 does not have the same structure as in the 13-*cis* component of the dark-adapted membrane. In this respect it is interesting to compare also other bands of the SB group of BR-605 with related bands of the dark-adapted membrane. Thus the band at 975 cm^{-1} in the spectrum of the acid membrane (Fig. 6B), which refers to the N—D i. p. bending mode of the all-*trans*/15-*anti* component, is much broader than the related band at 976 cm^{-1} in the spectra of the native membrane (Figs. 4B, 5B). This broadening obviously reflects an inhomogeneous structural distribution of the SB group. The C=N stretch in BR-605 is reflected by a fairly weak and broad feature at 1628 cm^{-1} (Fig. 6A) that in D_2O shifts to 1616 cm^{-1}. In the dark-adapted membrane this vibration gives rise to a much narrower band with higher peak intensity at 1637 cm^{-1}. Therefore the C=N stretch of BR-605 at 1628 cm^{-1} cannot be simply obtained by superposition of all-*trans*/15-*anti* and 13-*cis*/15-*syn* components as they occur in the native membrane, but rather reflects also a variety of different structures of the SB group.

Finally we consider the C=C stretch of the acidified membrane that peaks at 1621 cm^{-1} (Fig. 6). The width of this band is 27 cm^{-1} (FWHH) which is large compared with the width of the C=C stretch of the all-*trans* component in the native membrane, which is 15 cm^{-1} (Fig. 4). While in the spectra of the dark-adapted membrane the two components can be easily distinguished by two peaks at 1529 and 1537 cm^{-1}, only a single peak is observed in the spectra of BR-605. This is another clear indication that the BR-605 state is not a pure superposition of the two components of the native membrane.

On the basis of spectroscopic evidence the following picture is obtained. In the native membrane the chromophore is kept in a rather fixed position by interaction with the protein, giving rise to two stable components with all-*trans*/15-*anti* and 13-*cis*/15-*syn* configuration. In the acidified membrane at pH 2 the all-*trans* and 13-*cis* configuration of the retinal moiety is preserved while the fixed structure of the SB group is lost. In particular, the "15-*syn*" structure of this group as it is observed in the dark-adapted native membrane is no longer identified. It thus appears that in BR-605 the SB group obtains more structural mobility than in the native state.

Following the arguments of Fischer and Oesterhelt (8), the transition from BR-605 to a second equilibrium state is due to the increase of the ionic strength. In the present study RR spectra were obtained from two different samples. The first sample was equilibrated with 1 *M* HCl solution at a pH value of 0, the second sample with a solution of 0.67 *M* HF and 0.33 *M* NaF at a pH value of 2.2. The RR spectra in Fig. 7 from the two different samples are nearly identical, which implies that it is not the decrease in pH from 2 to 0 but the increase in ionic strength which is responsible for the transition II (eq. [1]). No indication was found for a long-lived photointermediate, so that the spectra in Fig. 7 represent the unphotolyzed species.

The spectra of the two species, BR-565(Cl^-) and BR-545(F^-), in Fig. 7 differ in many details from the spectrum of BR-605. Thus the C=C stretches at 1531 and 1536 cm^{-1} are narrow compared with BR-605. The C=NH stretch corre-

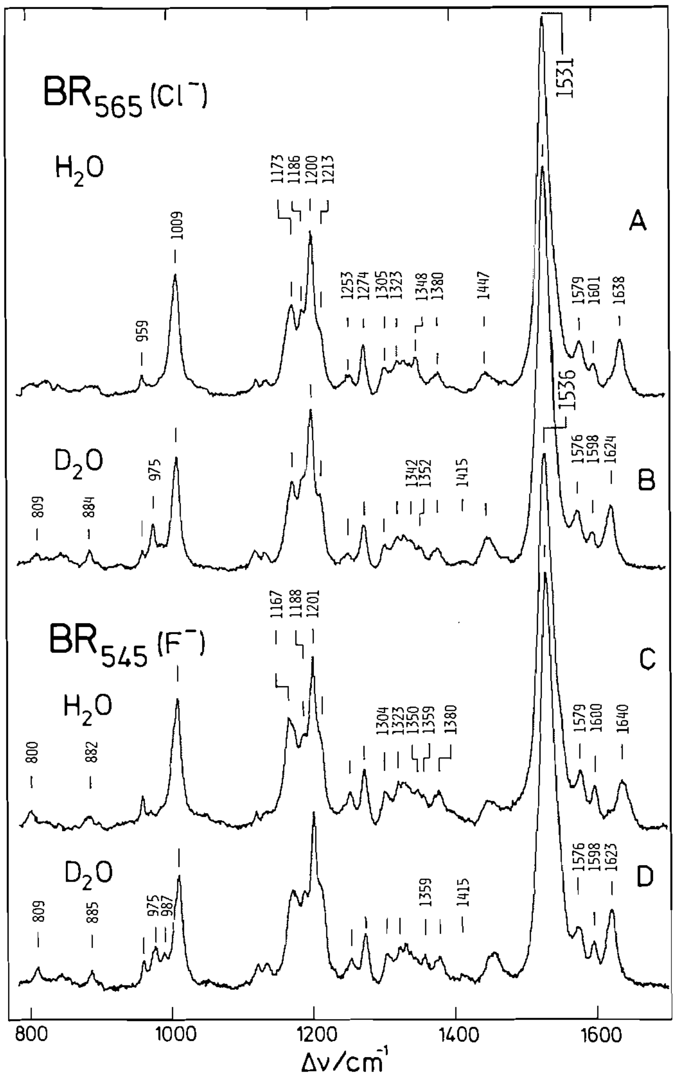

FIG. 7. Resonance Raman spectra from PM embedded in polyacrylamide gels, excited at 514 nm. BR-565(Cl^-): equilibrated with HCl solution at pH 0. BR-545(F^-): equilibrated with solution of 0.67 *M* HF and 0.33 *M* NaF at pH 2.2.

sponds now to bands at 1638 and 1640 cm^{-1}, which are narrower and higher in peak intensity than in the spectra of BR-605. Bands at 1348 and 1350 cm^{-1} can be clearly identified as N—H i. p. bending modes, which in D_2O move to 975 cm^{-1}. These bands correspond in all details to the SB group vibrations of the native chromophore BR-570. But, on the other hand, weak bands at 987, 1415, 800, and 809 cm^{-1} are found in Fig. 7, which correspond to SB group vibrations of BR-548. From spectroscopic evidence it is thus concluded that in BR-565(Cl^-) and BR-545(F^-) the all-*trans*/15-*anti* configuration dominates, while a minor fraction is in the 13-*cis*/15-*syn* form. On the basis of a 1:1 ratio of these two components in the spectra of the dark-adapted membrane (Fig. 5), a 85:15 ratio is estimated from the spectra of BR-545(F^-).

No evidence is obtained from absorption spectra at high ionic strength for a differentiation into light- and dark-adapted states as in the native chromophore (8). Obviously there is no preferential unidirectional phototransition which could establish a light-adapted state. The 85:15 ratio stated above therefore reflects the thermal equilibrium between the two components.

The spectra in Fig. 7 as a whole closely resemble the spectra of BR-570 in Fig. 4. This is in support of the above conclusion that at high ionic strength the all-*trans* (15-*anti*) component dominates. The similarity holds even for weak vibrational features like the two bands between 1570 and 1600 cm^{-1} in the C=C stretching region or the bands at 959 and 884 cm^{-1} in the o. p. bending region. This suggests that the structure of the relevant species is similar even with respect to conformational distortions of the retinal chain. It further appears that inhomogeneous broadening of the C=C and C=N stretching bands is much less pronounced in the spectra of Fig. 7 than was observed for BR-605. This suggests that in the states BR-565(Cl^-) and BR-545(F^-), at high ionic strength, the retinyl chromophore is immobilized in a similar way as in BR-570. It is important to note that analogous conclusions are suggested from circular dichroism studies (7).

Conclusions

It was proposed in a previous study that the interaction between the positively charged SB group and its negative counterion in native BR chromophores is stabilized by water molecules which are located in the immediate vicinity of the SB group (25). One important piece of evidence had been inferred from the fact that the width of the C=N stretch is narrowed when H_2O as a solvent is replaced by D_2O. This effect was ascribed to the strong interaction between the C=N stretch and the nearly degenerate bending mode of neighbouring H_2O molecules. This interaction contributes to the width of the C=N band at 1641 cm^{-1} in H_2O but vanishes for D_2O where the frequency match is no longer valid (see also Figs. 4 and 5).

From the spectra of Figs. 6 and 7 it is suggested that also at low pH and high ionic strength water molecules are closely attached to the SB group. Thus in the spectra of BR-605 the C=N stretch at 1616 cm^{-1} in D_2O is narrower and has a higher peak intensity than the corresponding band at 1628 cm^{-1} in H_2O. The same holds for the bands at 1640 and 1623 cm^{-1} in the spectra of BR-545(F^-). In the spectra of BR-565(Cl^-) this effect is less pronounced although a slight increase in peak intensity of the C=N stretch in D_2O (1624 cm^{-1}) is observed. For interpreting the results of the present study the influence of water molecules therefore has to be taken into account.

The most important phenomenon we observed is the formation of stable BR chromophores with the extrinsic anions Cl^- and F^- from the solution. It could be demonstrated that the structure of such complexes is very similar to that of the native species BR-570. It seems that the formation of BR-605 has to anticipate the formation of the Cl^-(F^-) complexes. In this respect a recent paper of Kimura *et al.* (26) is of interest, in which is demonstrated that BR-605 is also established by deionization of the membrane.

The fact that such different anions as the intrinsic carboxylate group and Cl^- or F^- from the solution form nearly identical chromophoric complexes can be better understood when water is considered as a common structural feature. It thus appears that the stability of SBH^+---A^- complexes is largely determined by the water molecules sitting between the ionic species. It is conceivable that a few water molecules in the electrostatic field of the two ions form microstructures which stabilize the ion-pair complex. Indeed, it could be concluded from RR spectra of dehydrated membranes that the influence of water is restricted to the terminal SB group and that the retinal chain is in a more hydrophobic environment (25).

In conclusion, the results of the present paper confirm that the terminal ion-pair complex is largely responsible for the structure and stability of the retinylidene chromophore in BR. This structure probably is important for BR's function as a light-driven proton pump.

Acknowledgements

We thank Prof. A. Weller for encouragement and support. Purple membrane was a gift from the laboratory of Prof. Dr. Oesterhelt which is gratefully acknowledged.

1. D. OESTERHELT and W. STOECKENIUS. Proc. Natl. Acad. Sci. U.S.A. **70**, 2853 (1973).
2. W. STOECKENIUS, R. H. LOZIER, and R. A. BOGOMOLNI. Biochim. Biophys. Acta, **505**, 215 (1979).
3. D. OESTERHELT, M. MEENTZEN, and L. SCHUHMANN. Eur. J. Biochem. **40**, 453 (1973).
4. W. SPERLING, P. CARL, D. N. RAFFERTY, and N. A. DENCHER. Biophys. Struct. Mech. **3**, 79 (1977).
5. B. HONIG, A. D. GREENBERG, U. DINUR, and T. G. EBREY. Biochemistry, **15**, 4593 (1976).
6. J. FAVROT, J. M. LECLERCQ, R. ROBERGE, C. SANDORFY, and D. VOCELLE. Photochem. Photobiol. **29**, 99 (1979).
7. P. C. MOWERY, R. H. LOZIER, Q. CHAE, Y. W. TSENG, M. TAYLOR, and W. STOECKENIUS. Biochemistry, **18**, 4100 (1979).
8. U. FISCHER and D. OESTERHELT. Biophys. J. **28**, 211 (1979).
9. F. SIEBERT, W. MÄNTELE, and W. KREUTZ. FEBS Lett. **141**, 82 (1982).
10. G. MASSIG. Ph.D. thesis, University of Göttingen (1982).
11. M. STOCKBURGER, W. KLUSMANN, H. GATTERMANN, G. MASSIG, and R. PETERS. Biochemistry, **18**, 4886 (1979).
12. G. MASSIG, M. STOCKBURGER, W. GÄRTNER, D. OESTERHELT, and P. TOWNER. J. Raman Spectrosc. **12**, 287 (1982).
13. TH. ALSHUTH and M. STOCKBURGER. Ber. Bunsenges. Phys. Chem. **85**, 484 (1981).
14. D. OESTERHELT and W. STOECKENIUS. Methods Enzymol. **31**, 667 (1974).
15. B. CURRY, A. BROEK, J. LUGTENBURG, and R. MATHIES. J. Am. Chem. Soc. **104**, 5274 (1982).
16. B. CURRY, I. PALINGS, A. BROEK, J. A. PARDOEN, P. P. J. MULDER, J. LUGTENBURG, and R. MATHIES. J. Phys. Chem. **88**, 688 (1984).
17. S. SAITO and M. TASUMI. J. Raman Spectrosc. **14**, 236 (1983).
18. M. E. HEYDE, D. GILL, R. G. KILPONEN, and L. RIMAI. J. Am. Chem. Soc. **93**, 6776 (1971).
19. G. EYRING, B. CURRY, A. BROEK, J. LUGTENBURG, and R. MATHIES. Biochemistry, **21**, 384 (1982).
20. A. WARSHEL and N. BARBOY. J. Am. Chem. Soc. **104**, 1469 (1982).
21. S. O. SMITH, A. B. MYERS, J. A. PARDOEN, C. WINKEL, P. J. MULDER, J. LUGTENBURG, and R. MATHIES. Proc. Natl. Acad. Sci. U.S.A. **81**, 2055 (1984).
22. A. MAEDA, T. IWASA, and T. YOSHIZAWA. Biochemistry, **19**, 3825 (1980).
23. U. FISCHER, P. TOWNER, and D. OESTERHELT. Photochem. Photobiol. **33**, 529 (1981).
24. T. KOBAYASHI, H. OHTANI, J. IWAI, A. IKEGAMI, and H. UCHIKI. FEBS Lett. **162**, 197 (1983).
25. P. HILDEBRANDT and M. STOCKBURGER. Biochemistry, **6**, 5539 (1984).
26. J. KIMURA, A. IKEGAMI, and W. STOECKENIUS. Photochem. Photobiol. **40**, 641 (1984).

A model for the geometries of Van der Waals complexes

A. D. BUCKINGHAM
Department of Theoretical Chemistry, University Chemical Laboratory, Lensfield Road, Cambridge CB2 1EW, U.K.

AND

P. W. FOWLER[1]
Department of Chemistry, University of Durham, South Road, Durham DH1 3LE, U.K.

Received August 6, 1984

This paper is dedicated to Professor Camille Sandorfy on the occasion of his 65th birthday

A. D. BUCKINGHAM and P. W. FOWLER. Can. J. Chem. **63**, 2018 (1985).

Structures of Van der Waals complexes are predicted by a simple model based on electrostatic interaction between the monomers. Point multipoles are assigned to the atoms and embedded in hard spheres to represent short-range repulsions. Structures deduced for some 29 complexes are in agreement with experiment, and numerous predictions are made.

A. D. BUCKINGHAM et P. W. FOWLER. Can. J. Chem. **63**, 2018 (1985).

On peut prédire les structures des complexes de Van der Waals à l'aide d'un modèle simple qui est basé sur les interactions électrostatiques entre les monomères. On attribue des multipôles ponctuels aux atomes que l'on inclut dans des sphères rigides pour représenter les répulsions de faible portée. Les structures prévues pour 29 complexes sont en accord avec les données expérimentales.

[Traduit par le journal]

Introduction

In recent years Van der Waals complexes have been at the focus of much experimental and theoretical effort. The structures of many complexes, particularly those of the H-bonded type, have been determined by high-resolution spectroscopy (1–3). *Ab initio* calculations have been used to predict or confirm structures of small complexes with some success, e.g., refs. 4–6. Although quantitative details of a Van der Waals complex may result from sophisticated and expensive supermolecule calculations, there is a need for simpler theoretical approaches which enable us to understand the complex in terms of the properties of the monomers and the long-range forces between them (7).

Of the various components of the long-range interaction energy, the electrostatic contribution is known to be important in hydrogen bonding (4, 8, 9) and in particular in the angle dependence of the H bond potential energy (4, 9–11). This suggests that it should be possible to construct a simple physical model, involving electrostatic interactions and short-range repulsions, to predict equilibrium geometries of H-bonded complexes from the charge distributions of the isolated molecules. Such a model has been proposed (12) and is discussed further in the present paper.

Having reduced the problem from the supermolecule to the monomers, we can find the charge density of any particular monomer from accurate *ab initio* calculations of manageable size. In order to keep the model computationally simple the continuous charge densities are replaced by point multipoles.

2. The model

Each monomer charge distribution is described by sets of point multipoles — charges, dipoles, and quadrupoles — with values determined by *distributed multipole analysis* (= DMA) (13) of an *ab initio* wavefunction. The multipoles are located on the atoms and, in some cases, additionally at bond midpoints. They describe departures from local spherical symmetry in the molecular charge distribution and are often easily interpreted in terms of familiar concepts from valence theory. Thus a bonding pair or single lone pair can give rise to an atomic dipole, whereas the lone pairs on O in H_2O or H_2CO give an atomic quadrupole. An anisotropic bonding density such as the π cloud in C_2H_4 is represented by a quadrupole moment at the bond centre.

As well as satisfying chemical intuition, this multicentre representation of the charge distribution shows superior convergence behaviour to the one-centre molecular multipoles in calculations of the electrostatic potential around a molecule (13, 14). A DMA with a sensible choice of multipole sites is a compact summary of the information contained in the electronic wavefunction or in an electrostatic potential map in a form suitable for calculation of electrostatic interaction energies.

The wavefunctions we use have generally been calculated at the SCF level with large basis sets. Inclusion of electron correlation is known to affect multipole moments, e.g., typically decreasing the dipole moment by 5–10% (15) but is not expected to cause qualitative changes in our predicted structures. One example where correlation might be expected to be important, the CO molecule, has been examined at both SCF and Møller–Plesset levels. Although second-order Møller–Plesset correlation corrections reverse the small SCF dipole moment, the predicted structures of complexes containing CO at SCF and MP levels agree with each other and with experiment, as we show later in this paper.

The second important ingredient of the model is the way it treats the shapes of the monomer molecules. When two closed-shell molecules are sufficiently close that their charge clouds have appreciable overlap they experience a short-range repulsive force, which effectively defines the size and shape of each molecule. In our present molecule hard spheres are placed on the atomic centres to simulate this effect.

For heavy atoms the Van der Waals radii are taken from Pauling (16) without modification. CH_2 and CH_3 groups are treated as spheres of radius 2 Å. Pauling assigns a radius of 1.2 Å to H but, while useful for hydrocarbons, this is not appropriate for hydrogen-bonded complexes. A study of the

[1]Present address: Department of Theoretical Chemistry, University Chemical Laboratory, Lensfield Road, Cambridge CB2 1EW, U.K.

TABLE 1. An approximation for hydrogen bond lengths; the experimental distance $R(X...H—Y)$ between the X and Y atoms is compared with the sum of the heavy-atom Van der Waals radii $\sigma(X) + \sigma(Y)$ for a number of H-bonded complexes

Complex	$R(X...H—Y)$ (Å)	$\sigma(X) + \sigma(Y)$	Reference
$H_2CO...HF$	2.66	2.75	41
$H_2O...HF$	2.66	2.75	3
OC...HF	3.05	3.05	60
OC...HCN	3.67	3.40	63
HCN...HF	2.80	2.85	57

distances $R(X...H—Y)$ in hydrogen-bonded Van der Waals complexes shows that the X...Y distance is usually approximated to within 0.1 Å by assuming that the heavy-atom spheres are in contact,

$$R(X...H—Y) \simeq \sigma(X) + \sigma(Y)$$

and that the proton is inside the Van der Waals sphere of its Y partner. Some examples are given in Table 1. When Y is electronegative we expect that withdrawal of electron density from around H in the H—Y bond leads to a smaller effective Van der Waals radius for H. The small size of H, lacking an inner core of electrons, has been noted as a distinguishing feature of the hydrogen bond (7). It is perhaps significant that the only example in Table 1 where $R(X...H—Y)$ is greater than the sum of the Van der Waals radii is for Y = C, i.e., when Y is not very electronegative.

The equilibrium structure of a complex A...B is predicted by a constrained minimization of the electrostatic interaction of two assemblies of point multipoles (7). The total energy is a sum of pair terms,

$$U = \sum_{a \in A} \sum_{b \in B} U_{ab}$$

where

$$(4\pi\epsilon_0)U_{ab} = q^a q^b/R - R_\alpha(\mu^b_\alpha q^a - \mu^a_\alpha q^b)/R^3 + (3R_\alpha R_\beta - R^2\delta_{\alpha\beta})(q^a\theta^b_{\alpha\beta} + q^b\theta^a_{\alpha\beta} - 3\mu^a_\alpha\mu^b_\beta)/3R^5 + \ldots$$

$\boldsymbol{R}$ is the vector from site a in monomer A to site b in monomer B and q, μ, θ are site charge, dipole and quadrupole moments, respectively. The minimization is subject to the condition that no atoms are allowed to be closer than the sum of their hard-sphere radii,

$$R \geqslant \sigma(a) + \sigma(b) \text{ for all } a \in A,\ b \in B$$

One simple procedure is to place the monomers in contact and allow one molecule to roll over the other until a minimum in U is found. This is repeated for all possible contacts to find the global minimum in U.

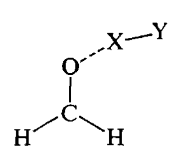

XY = HF, HCl, HCN, F_2, Cl_2; θ_1 = ∠COX; θ_2 = ∠OXY

1

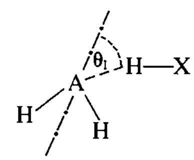

HX = HF, HCl, HCN; A = O, S; θ_2 = ∠AHX

2

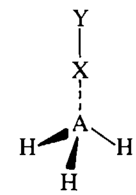

XY = HF, HCl, HCN, F_2, Cl_2, H—CCH, ClF; A = N, P

3

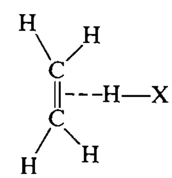

X = F, Cl, CN

4

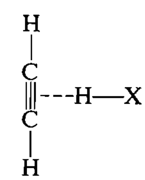

X = F, Cl, CN

5

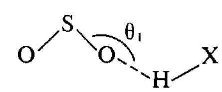

X = F, Cl, CN; θ_1 = ∠SOH; θ_2 = ∠OHX

6

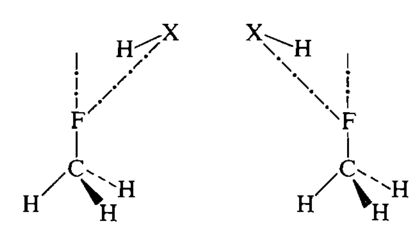

X = F, Cl, CN; θ_1 = ∠CFX; θ_2 = ∠FXH

7a 7b

N≡N- -H—X
H—C≡N- -H—X
O=C- -H—X

X = F, Cl, CN

8

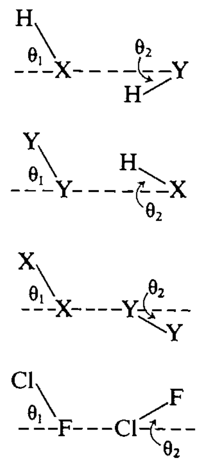

(X,Y) = (F,F), (F,Cl), (Cl,Cl)

9

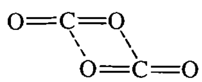

10

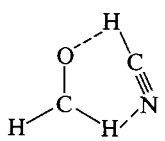

11

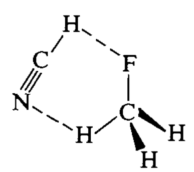

12

3. Predictions of complex geometries

In a previous paper (12) we reported distributed multipoles for seven small molecules. Tables 2 and 3 give results for an extended list of eighteen molecules obtained at the SCF level using the HONDO/CADPAC program (17). In all cases the basis set was of at least double-zeta-plus-polarization quality. Bond-centre functions were added for F_2, N_2, Cl_2, CO, and SO_2. The total SCF energy and molecular moments are generally close to the Hartree–Fock limit. For instance, the SCF energy of SO_2 of $-547.21081E_h$ is the lowest so far achieved (cf. ref. 18).

In Table 2 the value of μ(H) in HCN is -0.288 au, correcting a misprint in (12). For C_2H_4 the hydrogen multipoles were moved to the nearest carbon to give the more manageable three-centre DMA shown in Table 3.

A large number of Van der Waals complexes may be constructed by taking any pair of monomers from this list and Table 4 lists the minimum energy structures predicted for a selection of them. Many of these complexes have been observed and, in all cases but one, where an experimental structure is known for a complex in Table 4, the model reproduces it qualitatively and often quantitatively. Thus the model distinguishes correctly between alternative H-bonded structures, e.g. finding that H_2O...HF is more stable than HF...H_2O, and HF...HCl than HCl...HF. It predicts details of the molecular shape, e.g., that $(HF)_2$ is bent whereas OC...HF is linear, and that H_3N...HX and H_3P...HX complexes have C_{3v} symmetry. In many cases the angles predicted for complexes of lower symmetry are in quantitative agreement with experiment. The angles for H_2CO...HF and H_2S...HF are striking examples of this.

TABLE 2. Monomer geometries and multipole moments (in au) for linear molecules; * is a bond midpoint; the origin is taken as the centre-of-mass of the commonest isotopomer; the DMA point multipoles are origin independent

Molecule		z	q	μ_z	θ_{zz}	Reference
HF	F	0.087	−0.540	0.177	0.198	37
	H	−1.645	0.540	0.002	0.076	
HCl	Cl	0.068	0.324	−0.744	2.163	37
	*	−1.137	−0.537	0.309	0.261	
	H	−2.341	0.213	−0.169	−0.007	
HCN	N	1.125	−0.389	0.087	−0.283	38
	C	−1.055	0.322	−0.114	−0.162	
	H	−3.068	0.068	−0.288	−0.118	
CO	C	1.218	0.366	−0.398	−1.062	34
	*	0.152	−0.516	−0.161	0.585	
	O	−0.914	0.150	0.430	0.128	
N_2	N	1.037	0	0.271	−1.021	39
F_2	F	1.340	0	−0.077	0.466	39
Cl_2	Cl	1.878	0.259	−0.627	2.533	38
	*	0.0	−0.518	0	0.260	
ClF	Cl	1.407	0.158	−0.527	2.646	38
	*	−0.132	0.560	0.164	0.022	
	F	−1.670	−0.718	−0.538	−0.052	
CO_2	C	0.0	1.609	0	−0.244	38
	*	1.097	−0.454	0.021	0.532	
	O	2.194	−0.351	−0.075	0.233	
C_2H_2	*	0	−1.428	0	1.135	38
	C	1.137	0.809	−0.166	0.020	
	H	3.140	−0.095	0.418	−0.214	

Some of the results in Table 4 appeared in ref. 12. An error affecting H_2S complexes has been corrected, leading to small changes in the predicted angles for H_2S...HF and H_2S...HCl, but more importantly to a reversal of the relative stability of H_2S...HCN and HCN...H_2S. The H_2S...HX form is now predicted to be more stable for HX = HF, HCl, *and* HCN, in agreement with experimental results (19, 20). The structures of HX...H_2S and other secondary minima in the electrostatic energy surfaces are given in Table 5. Some of these less stable forms of Van der Waals complex have been observed when formed in inert gas matrices. For example, in an argon matrix at 12 K nonlinear HF...HCN is the preferred product but is converted to the more stable linear HCN...HF on warming above 20 K (21). Under similar conditions the antiparallel CH_3CN/HCN is formed but is converted on annealing to the C_{3v} CH_3CN...HCN (22).

The complexes SO_2...HX appear in both Tables 4 and 5 as HX may form a nearly linear H bond to O at two different angles, approximating to the directions of the two oxygen lone pairs, with HF and HCl preferring one direction, HCN the other. Although as mentioned above the DMA calculation on SO_2 is probably the best done so far, the details of the charge

TABLE 3. Monomer geometries and multipole moments (in au) for some nonlinear molecules; * is a bond midpoint

Molecule		x	z	q	μ_x	μ_z	θ_{xx}	θ_{zz}	θ_{xz}	Reference
H_2CO	O	0	1.135	−0.542	0	0.077	−0.339	0.148	0	40
	C	0	−1.138	0.679	0	0.115	−0.150	−0.216	0	
	H	1.766	−2.231	−0.068	0.182	−0.115	0.015	0.008	0.055	
H_2O	O	0	0.123	−0.802	0	0.093	0.364	0.022	0	37
	H	1.432	−0.986	0.401	0.031	0.007	0.618	0.028	−0.129	
H_2S	S	0	0.103	0.033	0	−0.204	1.423	0.407	0	39
	H	1.808	−1.637	−0.016	0.164	−0.139	0.028	0.060	−0.041	
NH_3	N	0	0	−0.160	0	−0.494	0.437	−0.875	0	38
	H	1.772	−0.721	0.534	0.163	−0.010	0.077	−0.047	−0.092	
SO_2	S	0	0	1.806	0	−1.628	1.328	−1.219	0	38
	*	1.169	−0.681	−0.323	−0.038	0.213	0.222	0.372	−0.417	
	O	2.338	−1.363	−0.580	−0.031	−0.011	0.273	−0.221	−0.384	
C_2H_4	C	0	1.265	0.539	0	−0.254	0.551	0.110	−0.254	38
	*	0	0	−1.077	0	0	0.419	0.872	0	
CH_3F	F	0	2.619	−0.430	0	−0.044	−0.193	0.386	0	38
	C	0	0	0.789	0	0.342	−0.359	0.718	0	
	H	1.961	−0.660	−0.120	0.245	−0.074	−0.011	0.019	0.023	
PH_3	P	0	0	0.412	0	−0.601	0.744	−1.488	0	38
	H	2.255	1.458	−0.137	0.159	−0.084	0.046	0.006	−0.100	

distribution may not be well enough known to decide if the apparent switch in structure is significant. A supermolecule calculation on SO_2...HF using a much smaller basis (23) predicted a near-linear S—O...H—F arrangement, midway between our two structures.

Perhaps the most interesting of the secondary structures are the bridged complexes H_2CO/HCN and CH_3F/HCN. The HCN molecule can act as both H donor and H acceptor and is long enough to form two H-bonding interactions with other ambidentate molecules. The cyclic structures correspond to an antiparallel arrangement of dipoles but the angles for the H bonds depart from the usual linear HCN..H—X which may explain why the double interaction is not the primary stable structure.

The complexes between CH_3F and HX are found to have a minimum energy when X—H...F—C—H define a plane, HF and HCl preferring the staggered structure 7*a* and HCN the eclipsed 7*b*. In fact the energy varies very little as HX moves on a cone around C—F, e.g., CH_3F...HF has an energy of $U = -0.01064$ au in conformation 7*a* which increases to $U = -0.01058$ au in 7*b*. It is therefore likely that the complex will exhibit internal rotation of the HX subunit. Propyne...HF is an example of a Van der Waals molecule where internal rotational motion of HF has been studied (24).

Based on the available evidence, Table 4 strongly suggests that our model is successful in predicting the structures of hydrogen-bonded complexes. Some regularities emerge when the results for different complexes are compared. In hydrogen bonds Z—Y...H—X the direction of approach of the proton donor H—X varies with the nature of the proton acceptor Y. Thus when Y = N as in N_2, HCN, NH_3 the complex has axial symmetry but when Y is a halogen the Y...H—X atoms are approximately collinear and lie at an angle to the Z—Y symmetry axis. A rationalization of this behaviour has been proposed by Legon and Millen (3). Their rule for H-bonded geometries is that HX attaches along the line of a nonbonded pair on the Y atom or, in the absence of a lone pair, perpendicular to the π cloud in a π-bonded system. A simple hybridization picture suggests that the direction of attack would then be: axial for Z—N (*sp*), at 120° to the Z—O axis for O(sp^2) in H_2CO, at the tetrahedral angle for O(sp^3) in H_2O or F in HF. Deviations from these angles could be explained, in qualitative terms, by differential repulsion between lone and bonding pairs, using valence-shell-electron-pair repulsion (VSEPR) arguments.

The essence of the Legon–Millen rule is that a hydrogen bond forms to a region of high electron density in the proton acceptor. It is therefore a qualitative electrostatic model of H bonding. As our model incorporates a description of lone pair, σ and π bonding distributions through the point multipoles we obtain results which may be rationalized in the same way. Our model has the additional advantages that it predicts deviations from the idealized angles of the hybridization model, for instance that ∠COF in H_2CO..HF is 110° and not 120°, decides between alternative H-bonded structures, e.g. H_3N...HF vs. HF...H_3N, and has a wider application to non-H-bonded complexes.

Although most of the complexes in Table 4 contain a hydrogen bond, some molecules of other types are included. H_2CO...F_2 and complexes of F_2, Cl_2 and ClF with NH_3 have been studied by *ab initio* calculation (25) and found to have structures in line with the predictions of the electrostatic model. Decomposition of the SCF energy shows significant electrostatic and charge-transfer interaction energies in the equilibrium geometry (25) but the angular shape of the complex is largely determined by variation of the electrostatic component (10, 25). Halogen dimers and mixed dimers are predicted in Table 4 to have floppy "L" structures, consistent with the structure of solid Cl_2 (26) and molecular beam data (27). The very simplest electrostatic model, of a point quadrupole for each molecule, would predict a "T" structure for these dimers, but a representation of the spatial distribution of the lone pair density produces the "L" structure, **9** (10). In Kollman's (10) model this was achieved by a system of point charges, in ours by atomic quadrupoles.

A contrasting example is the CO_2 dimer. Once thought to have a polar "T" structure, there is experimental and theoretical evidence suggesting that it is nonpolar (28–30). Again two point molecular quadrupoles held at fixed distance apart favour a "T" shape but our model predicts the nonpolar skew parallel

TABLE 4. Predicted structures of Van der Waals complexes; U is the total electrostatic interaction energy; the angles θ_1, θ_2 are defined differently for the various structures **1** to **12**. In **1**, θ_1 is $\angle COX$ and θ_2 is $\angle OXY$; in **2** θ_2 is $\angle AHX$; in **6**, θ_1 is $\angle SOH$ and θ_2 is $\angle OHX$; in **7** θ_2 is $\angle FXH$ and θ_1 is $\angle CFX$

Structure	Complex	Prediction	U/au	Experiment	Reference	Structure	Complex	Prediction	U/au	Experiment	Reference
1	$H_2CO\ldots HF$	$\theta_1=113°$, $\theta_2=171°$, $\angle COF=110°$	−0.01503	$\theta_1=115°$, $\angle COF=109.5°$	41	**7***a*	$CH_3F\ldots HF$	$\theta_1=68°$, $\theta_2=7°$	−0.01064		
	$H_2CO\ldots HCl$	114°, 170°	−0.01003				$CH_3F\ldots HCl$	66°, 4°	−0.00713		
	$H_2CO\ldots HCN$	129°, 174°	−0.01024			**7***b*	$CH_3F\ldots HCN$	50°, 4°	−0.00742		
	$H_2CO\ldots F_2$	110°, 179°	−0.00093			**8**	$N_2\ldots HF$	Linear	−0.00551	Linear	55
	$H_2CO\ldots Cl_2$	113°, 172°	−0.00247				$N_2\ldots HCl$	Linear	−0.00356	Linear	56
2	$H_2O\ldots HF$	60°, 172°	−0.01608	$\theta_1=46°\pm8°$	3		$N_2\ldots HCN$	Linear	−0.00307	Linear	69
	$H_2O\ldots HCl$	57°, 173°	−0.01070				$N_2\ldots F_2$	Linear	−0.00033		
	$H_2O\ldots HCN$	52°, 183°	−0.01076		42		$N_2\ldots Cl_2$	Linear	−0.00076		
	$H_2S\ldots HF$	88°, 178°	−0.01024	$\theta_1=89°$	19		$HCN\ldots HF$	Linear	−0.01246	Linear	57
	$H_2S\ldots HCl$	89°, 180°	−0.00683				$HCN\ldots HCl$	Linear	−0.00844	Linear	58
	$H_2S\ldots HCN$	84°, 177°	−0.00667	$\theta_1\sim85°$	20		$HCN\ldots HCN$	Linear	−0.00950	Linear	59
3	$H_3N\ldots HF$	C_{3v}	−0.02273	C_{3v}	43		$HCN\ldots F_2$	Linear	−0.00072		
	$H_3N\ldots HCl$	C_{3v}	−0.01510				$HCN\ldots Cl_2$	Linear	−0.00205		
	$H_3N\ldots HCN$	C_{3v}	−0.01490	C_{3v}	44		$OC\ldots HF$	Linear	−0.00649	Linear	60, 61
	$H_3N\ldots HCCH$	C_{3v}	−0.00967	C_{3v}	45		$OC\ldots HCl$	Linear	−0.00424	Linear	61, 62
	$H_3N\ldots F_2$	C_{3v}	−0.00136				$OC\ldots HCN$	Linear	−0.00371	Linear	63
	$H_3N\ldots Cl_2$	C_{3v}	−0.00355			**9**	$HF\ldots HF$	$\theta_1=72°$, $\theta_2=7°$	−0.00966	$\theta_1=60°$ to 70°	64
	$H_3N\ldots ClF$	C_{3v}	−0.00531				$HF\ldots HCl$	72°, 6°	−0.00644	$\theta_1=50°$ (estimate)	65
	$H_3P\ldots HF$	C_{3v}	−0.00900	C_{3v}	46		$HCl\ldots HCl$	87°, 5°	−0.00379	$\theta_1=83°$, $\theta_2\sim2°$	
	$H_3P\ldots HCl$	C_{3v}	−0.00601	C_{3v}	47					(*ab initio*)	66
	$H_3P\ldots HCN$	C_{3v}	−0.00602	C_{3v}	48					$\theta_1\sim90°$ (estimate)	67
	$H_3P\ldots HCCH$	C_{3v}	−0.00388				$F_2\ldots HF$	77°, 5°	−0.00130		
4	$H_4C_2\ldots HF$	C_{2v} HX at 90° to plane	−0.00929	As predicted	49		$F_2\ldots HCl$	77°, 4°	−0.00081		
	$H_4C_2\ldots HCl$	C_{2v} HX at 90° to plane	−0.00630	As predicted	50		$Cl_2\ldots HF$	77°, 4°	−0.00290		
	$H_4C_2\ldots HCN$	C_{2v} HX at 90° to plane	−0.00610	As predicted	51		$Cl_2\ldots FH$				68
5	$H_2C_2\ldots HF$	C_{2v}, planar	−0.00994	C_{2v}, planar	52		$Cl_2\ldots HCl$	76°, 4°	−0.00187		
	$H_2C_2\ldots HCl$	C_{2v}, planar	−0.00652	C_{2v}, planar	53		$F_2\ldots F_2$	58°, 35°	−0.00008		
	$H_2C_2\ldots HCN$	C_{2v}, planar	−0.00646	C_{2v}, planar	54		$Cl_2\ldots Cl_2$	59°, 32°	−0.00043		
6	$SO_2\ldots HF$	$\theta_1=118°$, $\theta_2=160°$	−0.01024				$Cl_2\ldots F_2$	65°, 24°	−0.00018		
	$SO_2\ldots HCl$	120°, 168°	−0.00673				$ClF\ldots ClF$	63°, 9°	−0.00105		
	$SO_2\ldots HCN$	230°, 178°	−0.00632								

TABLE 5. Secondary structures of Van der Waals complexes; these structures represent local minima in the electrostatic interaction energy U. The planar structures of the first six entries are

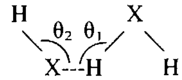

Complex	Structure	U/au
HF...H_2O	Planar $\theta_1=\angle AHX=166°$, $\theta_2=\angle HXH=100°$	−0.00842
HCl..H_2O	166°, 87°	−0.00479
HCN...H_2O	182°, 172°	−0.00937
HF...H_2S	175°, 114°	−0.00456
HCl..H_2S	175°, 97°	−0.00257
HCN..H_2S	180°, 180°	−0.00583
HF...H_3N	C_{3v}, HX below N	−0.00622
HCl..H_3N	C_{3v}, HX below N	−0.00385
F_2...H_3N	C_{3v}, HX below N	−0.00042
SO_2..HF	As in **6** $\theta_1=234°$, $\theta_2=180°$	−0.00916
SO_2..HCl	232°, 180°	−0.00617
SO_2..HCN	135°, 169°	−0.00618
H_2CO/HCN	Bridged as in **11**, ∠OCN=98°, ∠COH=97°	−0.00455
CH_3F/HCN	Bridged as in **12**, ∠FCN=84°, ∠CFH=118°	−0.00367
HF...HCN	As in **9**, $\theta_1=54°$, $\theta_2=5°$	−0.00663
HCl..HF	88°, 7°	−0.00568

TABLE 6. Effect of electron correlation on the multipole moments of CO; all quantities are in au; the origin of coordinates is the centre of mass of $^{12}C^{16}O$. The total molecular moments are μ_z(SCF) = 0.1007, θ_{zz}(SCF) = −1.4981, μ_z(SCF+MP2) = −0.1681, θ_{zz}(SCF+MP2) = −1.5013 au

		q		μ_z		θ_{zz}	
Centre	z	SCF	+MP2	SCF	+MP2	SCF	+MP2
C	1.218	0.366	−0.099	−0.398	−0.099	−1.062	−1.070
*	0.152	−0.516	0.158	−0.161	−0.160	0.585	0.501
O	−0.914	0.150	−0.059	0.430	0.134	0.128	−0.205

TABLE 7. Effect of electron correlation in CO on the electrostatic energy of CO complexes

	U/au	
Complex	SCF	+MP2
OC...HF	−0.00649	−0.00816
CO...HF	−0.00521	−0.00280
CO...HCl	−0.00424	−0.00540
OC...HCl	−0.00348	−0.00179

structure, **10**, with ∠O=C...O ≃ 110°. The same structure was predicted by Barton, Chablo, and Howard (28) using a hard dumb-bell molecular shape *plus* central point quadrupoles. Thus in this case the key factor is the inclusion of molecular shape in the model rather than an improved description of the electron density.

Taken together, these examples show that both ingredients of the model (namely, electrostatics and size and shape) are needed for a successful description of noncovalent interactions. An accurate representation of the electron density and hence of the electrostatic potential in the region of space around a molecule may be constructed in a number of ways. Bentley (31) has derived atomic multipoles by fitting to total molecular multipoles. Kollman (11) and Brobjer and Murrell (32, 33) use arrays of point charges with magnitudes and positions mimicing bonding and lone pairs. The DMA method offers advantages in that it is completely *ab initio* and therefore capable of systematic improvement and is easily implemented in a standard SCF or CI package (13, 17). The hard-sphere model of molecular shape is extremely simple but appears adequate in most cases. A possible refinement would be to use a transferable empirical repulsive potential based on crystallographic data. An alternative approach uses experimental intermolecular separations (32, 33) but this cannot predict structures of complexes not yet observed in experiment.

Having shown the successes of our simple model, it is appropriate to enquire into its limitations. The DMA point multipoles were obtained in the SCF approximation. One case where the SCF multipoles might be unreliable is the CO molecule. In Table 6 we show the DMA for CO at SCF and second-order Møller−Plesset (i.e. uncorrelated and correlated) levels (34) and in Table 7 compare the predictions of both sets for the CO/HF and CO/HCl complexes. Inclusion of correlation changes the molecular dipole from 0.1007 au (C^+O^-) to 0.1681 au (C^-O^+), so significant changes occur in the DMA, leading to changes in the calculated electrostatic interaction energy. However, although correlation enhances the relative stability of OC...HX over CO...HX by factors of more than four, the qualitative prediction of which form is the more stable is the same at SCF and MP levels, and both agree with experiment. As CO might be considered as a "worst case" for the effect of correlation this is an encouraging result.

A second limitation is our use of the sum of Van der Waals radii to set the intermolecular distances in the calculation. If the experimental structure has a much shorter distance our model may be inappropriate (35). At first sight a shortened distance might be taken to imply a "chemical" rather than a physical electrostatic explanation of the binding. One example of interest is the complex between ClF and HF (35). From experiment this has the "anti-hydrogen-bonded" structure HF...ClF (36). If we apply our model using Van der Waals radii of $\sigma(\mathrm{Cl}) = 1.80$ Å and $\sigma(\mathrm{F}) = 1.35$ Å we find that the H-bonded structure with $\angle$ClFF = 108°, $\angle$FFH = 5° has $U = -0.00443$ au while the HF...ClF structure with $\angle$FClF = 172°, $\angle$ClFH = 125° has $U = -0.00243$ au. Similarly the H-bonded ClF...HCl is predicted to be more stable than FCl...ClH. However the Cl...F distance in HF...ClF is not 3.15 Å, which is the sum of the Van der Waals radii, but only 2.76 Å (36). When a smaller separation is used the electrostatic energy switches in favour of HF...ClF at a distance close to 2.75 Å. In large-basis supermolecule calculations (25) the electrostatic energy favours the experimental structure and is the factor which discriminates between the hydrogen-bonded and "anti-hydrogen-bonded" forms (9). Thus although the electrostatic energy still explains the bonding, the assumption of hard-sphere distances needs modification in this case. Similar arguments apply to HF...Cl_2, which is found from experiments to be "anti-hydrogen-bonded" (68) but is predicted to be H-bonded (Table 4) when the F...Cl distance is fixed at 3.15 Å).

We have shown that a very simple model incorporating electrostatic interactions and hard-sphere repulsions has considerable success in describing the structures of many Van der Waals complexes. The model also enables predictions of new structures to be made, and permits the evaluation of relative stabilities of tautomeric forms of a complex and of barrier heights for transitions between these tautomers. But representation of the repulsive potential by an infinite step function is a gross approximation which will be inadequate in some cases. The hard-sphere model does not permit the repulsive forces to moderate the binding energy. And in its present form the theory excludes the mutual distortion of the interacting molecules, and therefore lacks the (attractive) induction and dispersion contributions to the well-depth. The net effect of these approximations is usually to exaggerate the well-depth, particularly in the case of hydrogen-bonded complexes.

Refinements to the basic model will be explored in later work.

Acknowledgement

It is a pleasure to express our admiration of the contributions to the subject made by Professor C. Sandorfy of the University of Montréal.

1. W. Klemperer. Faraday Discuss. **62**, 179 (1977).
2. W. Klemperer. J. Mol. Struct. **59**, 161 (1980).
3. A. C. Legon and D. J. Millen. Faraday Discuss. **73**, 71 (1982); **73**, 127 (1982); **73**, 128 (1982).
4. H. Umeyama and K. Morokuma. J. Am. Chem. Soc. **99**, 1316 (1977).
5. R. R. Lucchese, K. Haber, and H. F. Schaefer. J. Am. Chem. Soc. **98**, 7617 (1976).
6. A-M. Sapse and J. M. Howell. J. Chem. Phys. **78**, 5738 (1983).
7. A. D. Buckingham. *In* Intermolecular interactions — from diatomics to biopolymers. *Edited by* B. Pullman. Wiley, 1978.
8. C. A. Coulson. Research, **10**, 149 (1957).
9. P. Schuster. *In* The hydrogen bond. I. Theory. *Edited by* P. Schuster, G. Zundel, and C. Sandorfy. North-Holland, Amsterdam. 1976.
10. P. Kollman. J. Am. Chem. Soc. **99**, 4875 (1977).
11. P. Kollman. Acc. Chem. Res. **10**, 365 (1977).
12. A. D. Buckingham and P. W. Fowler. J. Chem. Phys. **79**, 6426 (1983).
13. A. J. Stone. Chem. Phys. Lett. **83**, 233 (1981).
14. P. W. Fowler and A. D. Buckingham. Mol. Phys. **50**, 1349 (1983).
15. H-J. Werner and W. Meyer. Mol. Phys. **31**, 855 (1976).
16. L. Pauling. The nature of the chemical bond. 3rd ed. Cornell University. 1960.
17. R. D. Amos. The Cambridge analytical derivatives package. SERC, U.K., 1984.
18. G. G. Bacskay. J. Chem. Phys. **79**, 2090 (1983).
19. R. Viswanathan and T. R. Dyke. J. Chem. Phys. **77**, 1166 (1982).
20. E. J. Goodwin and A. C. Legon. J. Chem. Soc. Faraday II, **80**, 1669 (1984).
21. G. L. Johnson and L. Andrews. J. Am. Chem. Soc. **105**, 163 (1983).
22. E. Knözinger and R. Wittenbeck. J. Chem. Phys. **80**, 5979 (1984).
23. M. E. Friedlander, J. M. Howell, and A-M. Sapse. Inorg. Chem. **22**, 100 (1983).
24. J. A. Shea, R. E. Bumgarner, and G. Henderson. J. Chem. Phys. **80**, 4605 (1984).
25. H. Umeyama, K. Morokuma, and S. Yamabe. J. Am. Chem. Soc. **99**, 330 (1977).
26. R. W. G. Wyckoff. Crystal structures. Interscience, New York. 1963.
27. S. J. Harris, S. E. Novick, J. S. Winn, and W. Klemperer. J. Chem. Phys. **61**, 3866 (1974).
28. A. E. Barton, A. Chablo, and B. J. Howard. Chem. Phys. Lett. **60**, 414 (1979).
29. N. Brigot, S. Odiot, S. H. Walmsley, and J. L. Whitten. Chem. Phys. Lett. **49**, 157 (1977).
30. N. Brigot, S. Odiot, and S. H. Walmsley. Chem. Phys. Lett. **88**, 543 (1982).
31. J. Bentley. *In* Chemical applications of atomic and molecular electrostatic potentials. *Edited by* P. Politzer and D. G. Truhlar. Plenum, New York. 1981.
32. J. T. Brobjer. Faraday Discuss. **73**, 128 (1982).
33. J. T. Brobjer and J. N. Murrell. J. Chem. Soc. Faraday Trans. II, **78**, 1853 (1982).
34. P. W. Fowler and S. F. O'Shea. Unpublished data.
35. F. A. Baiocchi, W. Reiher, and W. Klemperer. J. Chem. Phys. **79**, 6428 (1983).
36. S. E. Novick, K. C. Janda, and W. Klemperer. J. Chem. Phys. **65**, 5115 (1976).
37. M. Alderton and A. J. Stone. To be published.
38. P. W. Fowler. Unpublished data.
39. R. D. Amos. Chem. Phys. Lett. **108**, 185 (1984); **113**, 19 (1985).
40. P. W. Fowler. Mol. Phys. **47**, 355 (1982).
41. F. A. Baiocchi and W. Klemperer. J. Chem. Phys. **78**, 3509 (1983).
42. A. J. Fillery-Travis, A. C. Legon, and L. C. Willoughby. Chem. Phys. Lett. **98**, 369 (1983).
43. B. J. Howard. To be published.
44. G. T. Fraser, K. R. Leopold, D. D. Nelson, A. Tung, and W. Klemperer. J. Chem. Phys. **80**, 3073 (1984).
45. G. T. Fraser, K. R. Leopold, and W. Klemperer. J. Chem. Phys. **80**, 1423 (1984).
46. A. C. Legon and L. C. Willoughby. Chem. Phys. **74**, 127 (1983).
47. A. C. Legon and L. C. Willoughby. J. Chem. Soc. Chem. Commun. 997 (1982).
48. A. C. Legon and L. C. Willoughby. Chem. Phys. **85**, 443

(1984).
49. J. A. SHEA and W. H. FLYGARE. J. Chem. Phys. **76**, 4857 (1982).
50. P. D. ALDRICH, A. C. LEGON, and W. H. FLYGARE. J. Chem. Phys. **75**, 2126 (1981).
51. S. G. KUKOLICH, W. G. READ, and P. D. ALDRICH. J. Chem. Phys. **78**, 3552 (1983).
52. W. G. READ and W. H. FLYGARE. J. Chem. Phys. **76**, 2238 (1982).
53. A. C. LEGON, P. D. ALDRICH, and W. H. FLYGARE. J. Chem. Phys. **75**, 625 (1981).
54. P. D. ALDRICH, S. G. KUKOLICH, and E. J. CAMPBELL. J. Chem. Phys. **78**, 3521 (1983).
55. P. D. SOPER, A. C. LEGON, W. G. READ, and W. H. FLYGARE. J. Chem. Phys. **76**, 292 (1982).
56. R. S. ALTMAN, M. D. MARSHALL, and W. KLEMPERER. J. Chem. Phys. **79**, 57 (1983).
57. A. C. LEGON, D. J. MILLEN, and S. C. ROGERS. Proc. R. Soc. London Ser. A **370**, 213 (1980).
58. A. C. LEGON, E. J. CAMPBELL, and W. H. FLYGARE. J. Chem. Phys. **76**, 2267 (1982).
59. A. C. LEGON, D. J. MILLEN, and P. J. MJÖBERG. Chem. Phys. Lett. **47**, 589 (1977).
60. A. C. LEGON, P. D. SOPER, and W. H. FLYGARE. J. Chem. Phys. **74**, 4944 (1981).
61. A. C. LEGON, P. D. SOPER, M. R. KEENAN, T. K. MINTON, T. J. BALLE, and W. H. FLYGARE. J. Chem. Phys. **73**, 583 (1980).
62. P. D. SOPER, A. C. LEGON, and W. H. FLYGARE. J. Chem. Phys. **74**, 2138 (1981).
63. E. J. GOODWIN and A. C. LEGON. Chem. Phys. **87**, 81 (1984).
64. T. R. DYKE, B. J. HOWARD, and W. KLEMPERER. J. Chem. Phys. **56**, 2442 (1972).
65. K. C. JANDA, J. M. STEED, S. E. NOVICK, and W. KLEMPERER. J. Chem. Phys. **67**, 5162 (1977).
66. C. VOTAVA, R. ALRICHS, and A. GEIGER. J. Chem. Phys. **78**, 6841 (1983).
67. N. OHASHI and A. S. PINE. J. Chem. Phys. **81**, 73 (1984).
68. F. A. BAIOCCHI, T. A. DIXON, and W. KLEMPERER. J. Chem. Phys. **77**, 1632 (1982).
69. E. J. GOODWIN and A. C. LEGON. To be published.

Selective photoinduced Ca^{2+} diffusion in rhodopsin–lipid bilayers: an internal transmitter hypothesis

N'SUAVI KOSSI N'SOUKPOÉ AND ROGER M. LEBLANC

Centre de recherche en photobiophysique, Université du Québec à Trois-Rivières, Trois-Rivières (Qué.), Canada, G9A 5H7

Received August 6, 1984

This paper is dedicated to Professor Camille Sandorfy on the occasion of his 65th birthday

N'SUAVI KOSSI N'SOUKPOÉ and ROGER M. LEBLANC. Can. J. Chem. **63**, 2026 (1985).

Triton X-100 purified rhodopsin has been incorporated into lipid bilayer membranes prepared by the combined lifting-and-touching method. The illumination of the membranes with white light and monochromatic light of λ = 498 nm resulted in a high selective increase of Ca^{2+} diffusion through the lipid bilayers compared to Na^+ and K^+. The stoichiometric ratios of photoinduced ion diffusion were found to be more than 888 Ca^{2+} Rh^{*-1} s^{-1} and 166 Na^+ Rh^{*-1} s^{-1} at 290 K using the white light, and 1 277 Ca^{2+} Rh^{*-1} s^{-1}, 96 K^+ Rh^{*-1} s^{-1}, and 50 Na^+ Rh^{*-1} s^{-1} at 276 K using the monochromatic light. It was inferred that Ca^{2+} is an excellent candidate as internal transmitter in the visual photo-transduction.

N'SUAVI KOSSI N'SOUKPOÉ et ROGER M. LEBLANC. Can. J. Chem. **63**, 2026 (1985).

On a incorporé de la rhodopsine purifiée au Triton X-100 dans des membranes de doubles couches de lipides préparées par la méthode combinant le soulèvement et le toucher. L'illumination des membranes par de la lumière blanche et de la lumière monochromatique de λ = 498 nm provoque une augmentation importante, si on la compare aux ions Na^+ et K^+, de la diffusion sélective du Ca^{2+} à travers les doubles couches de lipides. On a trouvé que les valeurs des rapports stoïchiométriques de diffusion ionique photoinduite sont égales à 888 Ca^{2+} Rh^{*-1} s^{-1} et 166 Na^+ Rh^{*-1} s^{-1}, à 290 K et sous l'influence de la lumière blanche, et 1277 Ca^{2+} Rh^{*-1} s^{-1}, 96 K^+ Rh^{*-1} s^{-1} et 50 Na^+ Rh^{*-1} s^{-1}, à 276 K et sous l'influence de la lumière monochromatique. On en déduit que le Ca^{2+} est un excellent candidat comme transmetteur interne dans la photo-transduction visuelle.

[Traduit par le journal]

Introduction

All the vertebrate photoreceptors share the ability to respond to light absorption by a change in ionic conductance of the plasma membrane.

If we consider the vertebrate rods, there exists a steady electric current in the darkness, the "dark current", which enters the outer segment, flows axially through the cytoplasm of the outer and inner segments, the nuclear and synapse regions, and returns to the outer segment via the intercellular space (1–4).

Membrane potential recordings (5–8) have revealed that light causes the plasma membrane to hyperpolarize from −40 mV to −60 mV. The "dark current" seems to be carried by Na^+ since the photo-response is suppressed by a complete removal of Na^+ from the external medium (9, 10) and the "dark current" is reduced in the presence of ouabain (3, 10). Most researchers agree that the effect of light, most likely, is to cause reduction of the sodium conductance (5, 9, 10, 11) by means of liberation of an internal transmitter which can block sodium channels present in the plasma membrane (10, 12, 13). The efficiency of light is so great that a single absorbed photon can transiently reduce a rod's "dark current" by about 3% (14). The very nature of the transmitter has not yet been clearly established. Experimental data are accumulating and there is a sounding indication that Ca^{2+} is the internal transmitter (15–24). But there also exists a possibility that *c*-GMP could be the internal transmitter (25–31). This point is not quite clear as yet. All that we know for sure is that (*i*) the presence of a transmitter is necessary for connecting the disc membrane (the site of excitation of the visual pigment) with the plasma membrane (the site of the electric response), disc and plasma membranes being structurally (32), osmotically (33), and electrically (14, 34) uncoupled and (*ii*) the transmitter should be released at a rate of $\sim 10^3$ molecules per excited pigment per second (35), may be less, $\sim 10^2$ (10).

In a previous paper (36) we have described an especial experimental procedure for preparing rhodopsin–lipid bilayer membranes by the monolayer technique. We have also presented the application of these lipid bilayers to the study of the ionic aspects of the visual process. Here, we are giving more details about the results obtained in relevance to the possible involvement of Ca^{2+} as an internal transmitter in the visual transduction.

Materials

Chemicals

Ethanol is purchased from Fisher Chem. Co., Montréal, Qué. Phosphatidylethanolamine (PE), phosphatidylcholine (PC), and phosphatidylserine (PS) extracted from bovine tissues are used as bought from Applied Sci. Lab., State College, PA, without further purification. Cholesterol is supplied by Sigma Co., St. Louis, MO. Fresh bovine eyes, obtained from a local slaughter-house, are dark-adapted for whole night at 277 K and the retinae dissected and kept frozen at 253 K until use. Water for the monolayer work is deionized and distilled through a quartz double distillation system (Brinkman Instruments Can. Ltd., Toronto, Ont.): the specific resistivity is greater than 18 MΩ cm and surface tension higher than 71 mN m^{-1} at 298 K.

Ion diffusion system

The ion diffusion measurements have been performed in a double compartment system (36) composed of two beakers connected together with Teflon joints, the contacts of which are sealed with O-rings and vacuum silicone grease. The whole device is carefully shielded against light with black tape except for the light-irradiation window (5 cm in diameter) on the side of compartment-I. The ionic activities are to be measured in compartment-II, using Orion ion specific electrodes (Fisher Sci. Co., Montréal, Qué.) connected with a pH meter (type PHM26, Radiometer, Copenhagen, Denmark), set as closer as possible to the membrane that will be placed between the two compartments. The capacity of compartment-I is 135 cm^3 and that of compartment-II is 75 cm^3.

Methods

Extraction and purification of rhodopsin

The rod outer segments (ROS) are isolated from the dark-adapted

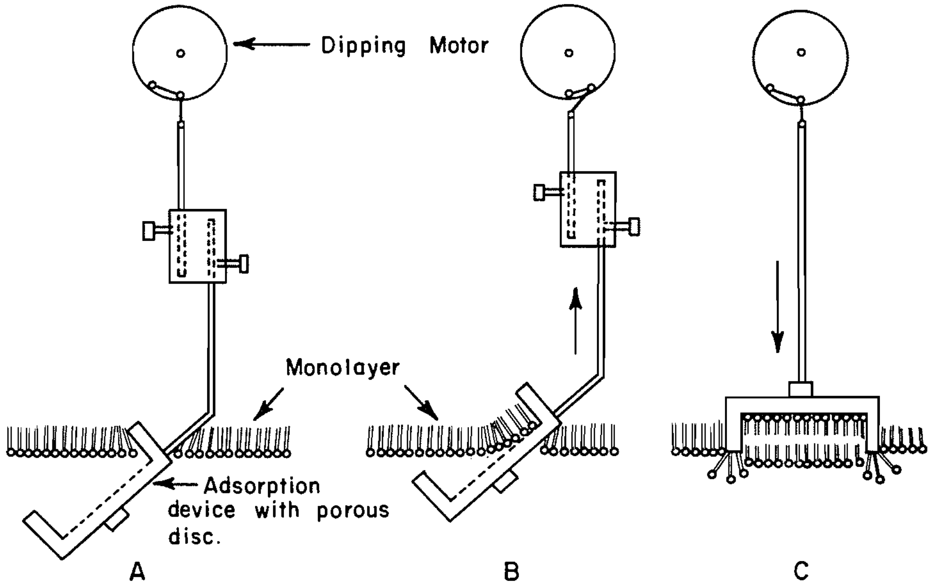

FIG. 1. Schematical representation of the combined lifting-and-touching method. (*A*): The adsorption device is immersed in the subphase (Tris-HCl, 2×10^{-3} mol dm^{-3}, pH: 7.2) while the rhodopsin-lipid monolayer is formed at the air–aqueous interface. (*B*): The adsorption of the first monolayer is shown during the lifting process. We see the hydrophilic adsorbing surface of the porous disc in broken line. (*C*): The touching process illustrates the formation of the bilayer (issued from ref. 36).

retinae using the sucrose gradient method described by Applebury *et al.* (37). The purified ROS are solubilized over a night by gentle agitation in 2% solution of Triton X-100 in Tris-HCl buffer (2×10^{-3} mol dm^{-3}, pH: 7.2). Rhodopsin solution is then centrifuged for 1 h at 40 000 g. The clear supernatant is adsorbed on top of an Ecteola cellulose column according to Osborne, Sardet, and Helenius (38). Purified rhodopsin is eluted with 2% solution of Triton X-100, Tris-HCl 2×10^{-3} mol dm^{-3}, NaCl 0.1 mol dm^{-3}, pH: 7.2. The purified rhodopsin solution is then diluted 1 : 1 with buffer and reconcentrated by the aid of an Immersible Molecular Separator Kit (Millipore, Mississauga, Ont.). This procedure repeated two or three times is aimed to remove a large amount of Triton X-100 from the rhodopsin solution. Then, the final removal of the detergent is effected by adsorption on bio-beads SM-2 using the inversion method as described by Holloway (39). Since rhodopsin is practically insoluble in water, it is important not to eliminate Triton X-100 over a certain critical point at which the pigment precipitates and most of the time gets denatured. The bio-beads treatment is accomplished stepwise in the sense that, after 1 h of continuous adsorption on bio-beads, the procedure is pursued at intervals of 2 min, measuring the elimination of the detergent by its absorption spectrum and simultaneously testing the surface pressure (Π) at the air-aqueous interface of a monolayer trough until the spreading of 100 μL of the rhodopsin solution does not show a significant initial surface pressure (i.e., $\Pi < 1$ mN m^{-1}). Usually, the solution is then centrifuged 30 min at 40 000 g to eliminate any small suspended particles in the solution.

Purified rhodopsin at air–aqueous interface

The "detergent-free" rhodopsin is spread at air-aqueous interface of a Langmuir type film balance (40), by means of the glass rod method described by Trurnit (41), the subphase being Tris-HCl 2×10^{-3} mol dm^{-3}, pH: 7.2. This spreading technique lessens the loss of material in the subphase. About 100 μL of rhodopsin solution 10^{-6}–10^{-5} mol dm^{-3} are used at a time. The concentration of rhodopsin is concurrently determined using the absorbance change ($\Delta A_{498\ \mathrm{nm}}$) before and after complete bleaching of the pigment, and by protein content measurement by Bio-Rad Protein Assay (Bio Rad Laboratories Canada, Ltd, Mississauga, Ont.).[1] The spread molecules are compressed uniformly and continuously at a speed of 17×10^6 Å^2 min^{-1} with a glass barrier moved by an electric compression motor provided with a rheostat for speed control. The limiting molecular area value has been used to evaluate rhodopsin cross section at the air-aqueous interface.

Preparation of the rhodopsin-containing lipid bilayers

The lipid bilayer membranes have been prepared by the combined lifting-and-touching method. An especially designed adsorption device has been used for this purpose. The device composed of a porous disc which was fixed to a Teflon block with a Teflon ring such as to expose one face of the porous disc to the preparation of the bilayer. The rhodopsin–lipid solutions used were prepared in 8% ethanol (v/v) according to their weight ratios in the native bovine rod outer segment disc membranes (42), i.e., 50.0% rhodopsin, 23.0% PE, 12.5% PC, 6.5% PS, and 8.0% cholesterol. The procedure for the preparation of the membrane is described by Kossi and Leblanc (36). Briefly, a porous disc made of triacetate cellulose, supported by a Teflon block (Fig. 1) was immersed in the subphase of a Langmuir trough which consisted of Tris buffer 2×10^{-3} mol dm^{-3}, pH: 7.2. The rhodopsin–lipid monolayer was spread at the air–aqueous interface and compressed at constant speed of 17×10^6 Å^2 min^{-1} to a pressure of 32 mN m^{-1}. The adsorption device was then lifted slowly and simultaneously compressing the monolayer to counterbalance the drop of the surface pressure due to the adsorption of a monolayer on the surface of the porous disc. After 5 min stabilization, the adsorption device was set parallel to the air–aqueous interfacial monolayer and allowed to come into contact with the monolayer horizontally. By raising the adsorption device, a second monolayer was adsorbed on the first one in a tail-to-tail fashion. Lipid bilayer membranes incorporated with rhodopsin prepared by this combined lifting-and-touching method have been used to study the photoinduced ion diffusion. Note that the membranes were prepared and transferred into the diffusion system under a dim red light. This technique makes it possible to obtain large membranes (14.82 cm^2).

Ionic permeability experiments

The artificial membrane supported by the porous disc was inserted in between a double compartment system which was sealed with vacuum silicone grease and filled with Tris-HCl (2×10^{-3} mol dm^{-3}, pH: 7.2). To measure the net photoinduced ion diffusion, the experiments have been performed in three irradiation conditions: (*i*) at 290 K by irradiating the membranes with an incandescent white light (300 W) placed at a distance of 60 cm away from the diffusion apparatus;

[1] Issued from Bio-Radiations, No. 25, September 1977, p. 4.

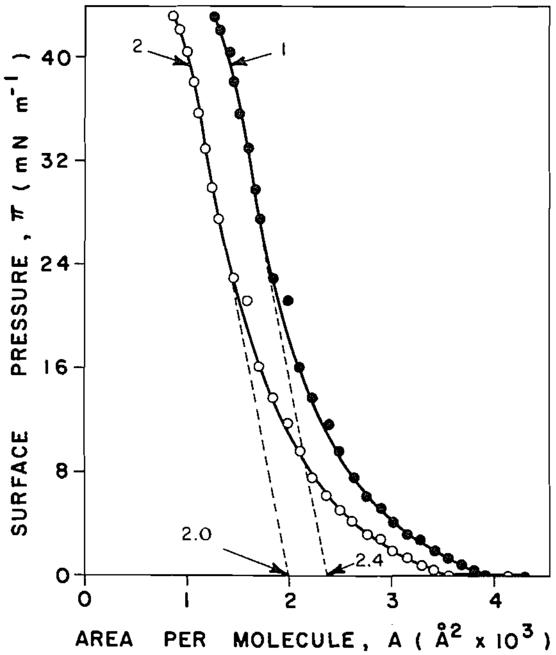

FIG. 2. Surface pressure–area isotherms of purified rhodopsin. The subphase is Tris-HCl buffer 2×10^{-3} mol dm^{-3}; pH: 7.2; T = 290 K. Curve 1 (●) is the isotherm obtained when using $\Delta A_{498\ nm}$ to calculate rhodopsin concentration. Curve 2 (○) is the isotherm obtained when using protein content values for rhodopsin concentration.

(*ii*) at 290 K by irradiating with the same light source filtered through a Corning colour filter (No. 2-61, Esco Products, Oak Ridge, NJ) the absorbance of which is 2 for $\lambda \leq 607$ nm; the purpose of using this safety light of $\lambda \geq 607$ nm is to test an eventual heating effect of the light source on the ion diffusion; and (*iii*) at 276 K by irradiating with a monochromatic light ($\lambda = 498 \pm 2$ nm) by means of a monochromator (Ser. No. 665 Am. ISA Inc., Metuchers, NJ). The light intensity was 2×10^{13} photons cm^{-2} s^{-1} as measured by a power meter (Model 21A, Optikon Ltd., Sci. Instr., Waterloo, Ont.). The membranes contained $3.5 \pm 0.1 \times 10^{13}$ rhodopsin molecules (23.6×10^{11} Rh cm^{-2}) as determined by the deposition ratios. The irradiation started 3 min after the ion under study was added to compartment-I, the ionic concentration of which was made 18.51×10^{-3} mol dm^{-3}. Both compartments were buffered with Tris-HCl 2×10^{-3} mol dm^{-3}, pH: 7.2. The illumination was kept on continuously through the measurements. The ionic activity resulting from photoinduced ion diffusion was measured in compartment-II using ion selective electrodes. A minimum of three measurements were run for each ion (i.e., Na^+, K^+, and Ca^{2+}) on three different membranes. The mean ion flux was plotted against time for the kinetic study of the ion diffusion induced by monochromatic beam (λ = 498 nm).

Results

Spectral properties of the purified rhodopsin

The Triton X-100 purification yielded 10^{-6}–10^{-5} mol dm^{-3} rhodopsin solutions as calculated from the absorbance difference at 498 nm before and after bleaching, using $\epsilon_{498\ nm}$ = 40 600 dm^3 mol^{-1} cm^{-1} (43). The spectral ratio $A_{278\ nm}/A_{498\ nm}$ was 2.0 ± 0.2, with 2 phospholipids per rhodopsin molecule as revealed by the phosphorus determination method developed by Fiske and Subbarow (44). The removal of the detergent proved very satisfactory as can be seen from the surface pressure-area isotherm (Π–A curves) of rhodopsin at air–aqueous interface (Fig. 2). This point will be elaborated in the following section.

Monolayer properties of the purified rhodopsin

When working with rhodopsin monolayer, it is of extreme importance to characterize the behaviour of this pigment at the air–water interface. The spreading of aqueous rhodopsin at air–water interface needs a special care in order to avoid loss of material in the subphase. The method developed by Trurnit (41) is suitable for rhodopsin solution nearly free from detergent. Indeed, we did not find any solubilization effect of rhodopsin in the subphase on the Π–A curves shown in Fig. 2. The Π–A curves rise monotonously as the molecules are gradually compressed. In Fig. 2, curve 1 is obtained by calculating rhodopsin concentration from the absorption data (i.e., $\Delta A_{498\ nm}$, $\epsilon_{498\ nm}$ = 40 600 dm^3 mol^{-1} cm^{-1}), and curve 2 was plotted using the protein content of rhodopsin solution. The extrapolation of the steep region of the Π–A curves to pressure zero gives the limiting molecular area which is 2 400 ± 120 Å^2 in the case of curve 1 and 2 000 ± 100 Å^2 for curve 2. Assuming that the cross section of rhodopsin at the air–aqueous interface is a circle as it seems to be by our own electron microscope observation (unpublished data) and from the literature (45, 46), and neglecting the contribution of the remaining Triton X-100 and phospholipids to the measured limiting area because of their small size compared to that of rhodopsin, the diameter would be 55.3 ± 1.3 Å and 50.4 ± 1.2 Å, respectively, when employing the former and latter limiting molecular areas. Values ranging between 40 Å and 80 Å have been obtained for rhodopsin diameter by Heller (46), Blasie *et al.* (45) and Darszon *et al.* (47). Many other works have been done on rhodopsin at air–aqueous interface (48–53) but the Π–A curve of rhodopsin appeared only in two papers: that of Hyono *et al.* (48) and that of Azuma and Takagi (49). The Π–A curve reported by Hyono *et al.* (48) was in arbitrary units, and accordingly, is useless for comparison. In Azuma and Takagi paper (49), the minimum extrapolated molecular area, obtained on pure water was found to be 4 000 Å^2 giving 71.3 Å for the diameter of rhodopsin; this work was performed with membrane fragments. Other works (54, 55) have shown that rhodopsin can be somewhat elongated.

Now, there is a significant difference between the limiting molecular areas when using the $\Delta A_{498\ nm}$ or the protein content determination methods to calculate the concentration of rhodopsin solutions. It makes clear that some bleaching of rhodopsin occurs during the numerous manipulations related to the purification of rhodopsin and to the removal of the detergent. This bleaching is possibly due to the elimination of the detergent since the use of Ecteola cellulose should have separated rhodopsin from contaminating opsin during the purification.

We can estimate rhodopsin activity in terms of spectral activity by the ratio of the two values for the limiting molecular areas (2 000/2 400) that gives 0.83. Therefore, any quantitative work involving the biological activity of rhodopsin should be based on its absorbance difference whereas size measurements are to be done on the basis of protein content analysis as far as monolayer work is concerned. The actual cross section of rhodopsin molecule should be equated to 2 000 Å^2 according to our determinations.

Photoinduced ion diffusion through the artificial membranes

From the light-effect experiments, it was observed as general features that, the white light and the monochromatic light of λ = 498 nm triggered the permeability of rhodopsin-containing lipid bilayers to ions, whereas light of $\lambda > 607$ nm, not absorbed by rhodopsin, had no detectable effect on the ion dif-

TABLE 1. Effect of light on the ion fluxes (ϕ) (number of ions per second)

	$\phi_{Na^+} \times 10^{-17}$		$\phi_{K^+} \times 10^{-17}$		$\phi_{Ca^{2+}} \times 10^{-17}$	
t (s)	White light	λ = 498 nm	White light	λ = 498 nm	White light	λ = 498 nm
0	—	—	—	—	—	—
60	0.00	0.00	4.30	0.00	0.00	0.00
120	0.00	0.00	2.90	0.00	0.00	0.00
180 ($h\nu$)	0.00	0.00	3.60	0.00	0.00	0.00
240	0.00	0.90	3.60	1.80	0.00	21.20
300	6.80	0.70	3.60	1.30	23.00	28.80
360	6.10	0.30	4.10	1.70	19.00	17.30
420	0.70	0.60	3.20	1.50	7.20	5.70
480	2.80	0.50	3.00	1.80	15.40	0.00
540	3.80	0.50	3.30	0.90	8.60	2.70
600	4.30	0.80	3.30	1.60	9.00	2.30
660	—	0.40	—	1.40	19.40	0.00
720	—	0.40	—	2.80	21.70	0.00

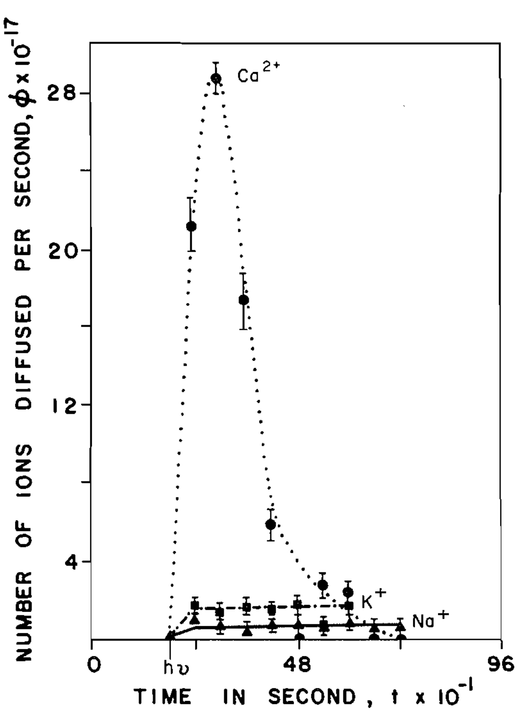

FIG. 3. Photoinduced ion diffusion curves using monochromatic light (λ = 498 nm) at 276 K for Na^+ flux (▲), K^+ flux (■), and Ca^{2+} flux (●).

fusion.

The mean ion fluxes are shown in Table 1; t measures the time (s) after the ion to be used was added to compartment-I. We can note that the variation of the fluxes with time is very irregular for Na^+ and Ca^{2+} ions with white light, and that only dark leakage of K^+ occurred in these conditions. The irregularity of the flux with the white light could simply be due to variations in the intensity of the incandescent lamp. The irradiation with monochromatic light (λ = 498 nm), most representative for bovine rhodopsin (λ_{max} = 498 nm), evoked a constant rate diffusion of Na^+ and K^+ as shown in Fig. 3. It could be also observed that Ca^{2+} flux curve clearly stands out from the others. It is concluded that the illumination of the membranes selectively increases the permeability to Ca^{2+} compared to Na^+ and K^+. The ion flux for Ca^{2+} (Fig. 3) presents an important jump at the beginning followed by an exponential decrease until electrochemical equilibrium is reached. The ion diffusion evoked by the 498 nm beam indicates that the excitation of rhodopsin is responsible for the effect observed.

The initial slopes of the diffusion curves (Fig. 3) can be used to calculate the stoichiometric ratios of the photoinduced ion diffusion. In our experiments, it was not possible to measure the exact number of rhodopsin molecules bleached during the irradiation because the porous disc is not transparent. To give an idea of the stoichiometry of the ion diffusion, we have assumed that most of rhodopsin molecules were bleached at the very beginning of the illumination. Based on this assumption, the white light induced ion diffusion rates were 166 Na^+ Rh^{*-1} s^{-1}, and 888 Ca^{2+} Rh^{*-1} s^{-1} at 290 K; at 276 K, the stoichiometric rates for the ion diffusion induced by the monochromatic light (λ = 498 nm) were found to be: 1 277 Ca^{2+} Rh^{*-1} s^{-1}, 96 K^+ Rh^{*-1} s^{-1} and 50 Na^+ Rh^{*-1} s^{-1}. The mean relative error is 10%. Since it is more likely that the number of molecules of rhodopsin effectively bleached is less than what has been assumed, the stoichiometric ratios reported here should be considered as minimum values.

To summarize, the results show that (i) light that does not excite rhodopsin ($\lambda \geq 607$ nm) has no effect on the lipid bilayer permeability; (ii) rhodopsin-exciting light (λ = 498 nm) causes the lipid bilayer permeability to increase for Na^+, K^+, and Ca^{2+} (except for K^+ at 290 K), with a marked selectivity for Ca^{2+}. This selectivity at 498 nm is 13:1 at 276 K for Ca^{2+} as compared with its nearest neighbour (i.e., K^+). The absorption of light energy by rhodopsin therefore does selectively evoke ion diffusion through the artificial membranes prepared by the combined lifting-and-touching method. Preliminary observations about ion diffusion through the porous disc alone do not show any apparent selectivity for the ions studied. Thus it clearly appears that the selectivity observed comes from rhodopsin present in the lipid bilayer.

Discussion

The conservation of the structural and physiological integrity, and the purification of extracted membrane proteins have long been a hard task. The common practice is not only to solubilize the membrane in a strong solvent such as detergents but also in a non-denaturing detergent so as to lessen the damage to the protein, which presents some problems. These problems are further complicated by the tension-interfering effect of detergents as far as monolayer work is concerned.

Thus, not only are we to choose a detergent which can highly purify the lipoprotein, rhodopsin, but also a detergent which would not affect much the structure and activity of rhodopsin, and above all, a detergent which can be removed easily to allow the air-aqueous interface experiments.

Many detergents have been used for these purposes such as digitonin (56–60), Emulphogene BC (61), cholic acid (62), and Triton X-100 (63, 64). We have chosen Triton X-100 for its removability and for the ease of following its removal by the absorbance decrease at 275 nm. The 17% loss of rhodopsin activity following the removal of Triton X-100, though not dramatic but significant, is unavoidable since we absolutely need a very low level of Triton X-100 in the rhodopsin solution for the monolayer work to be possible. However, the purity is good as indicated by $A_{278\ \mathrm{nm}}/A_{498\ \mathrm{nm}} = 2.0 \pm 0.2$ and by the $\Pi-A$ curves with a calculated diameter of 50.4 ± 1.2 Å in accordance with other results, e.g. 40–50 Å (45), 46 Å (46). Rhodopsin prepared in this way is stable for a few days to a week and should not be frozen in order to avoid precipitation. Note that our rhodopsin monolayer films contained traces of phospholipids (2 molecules of phospholipid per molecule of rhodopsin) and of Triton X-100. Accordingly, the calculated diameter which has been equated with that of rhodopsin represents a maximum value. However, the discrepancy from the true value should be negligible due to the small dimension of the contaminating molecules which are expected to act as space filler for rhodopsin molecules.

The results obtained from the light-effect experiments are quite encouraging. The bleaching of a single molecule of active rhodopsin is responsible for the diffusion of at least 50 Na^+, 96 K^+, and 1 277 Ca^{2+} ions per second at 276 K with 498 nm beam. This selective and amplified response could not but support the functional integrity of the pigment extracted. The lack of light-effect on K^+ diffusion at 290 K could be due to masking effect of K^+ diffusion induced by traces of all-*trans* retinal (50, 65, 66), which is not the case at 276 K since $t_{1/2}$ for the transition Metarhodopsin-I → Metarhodopsin-II is 160 min at 277 K (67). These results agree well with those obtained elsewhere on rhodopsin-containing vesicles: short light flashes promoted a steady release of Ca^{2+} from preloaded vesicles (23, 24), the diffusion of about 184 Na^+ per bleached rhodopsin and a greater stoichiometric ratio for Ca^{2+} (19). We have observed for the photoinduced ion diffusion, a latency of about 60 s. This latency should be considered as an apparent one mostly due to the delay time of the electrode response and to the distance to be run by the ions before reaching the electrodes.

Now, that light induces Ca^{2+} diffusion up to a rate of 1 277 ions per bleached rhodopsin per second is of great importance for the hypothesis that Ca^{2+} is the internal transmitter for the visual process. Cone (35) stated that the internal transmitter should have a stoichiometric release of 10^3 molecules per bleached rhodopsin per second. The high Ca^{2+} diffusion rate obtained here strongly suggests that Ca^{2+} is an excellent candidate for the internal transmitter. Thus, on the absorption of a photon, a single rhodopsin molecule among 10^6–10^9 in the vertebrate rod will form a unimolecular transmembrane channel (68) releasing over 10^3 Ca^{2+} per second that will diffuse to the plasma membrane where they will block sodium channels. The overall results will be a 3% reduction of the dark current (14). The Ca^{2+} will then be reconcentrated in the discs by means of a Ca^{2+} activated pump (69).

As such, the results obtained on artificial membranes are very suggestive for the Ca^{2+} hypothesis. The only disagreement is the varying and very low stoichiometry of Ca^{2+} photoinduced diffusion observed for isolated rod outer segments (15, 16, 21, 70, 71) and for isolated rod outer segment discs (20). Could this be due to the difficulties encountered in integral isolation (i.e., without loss of Ca^{2+} before the illumination) of these sub-cellular structures, or to some difference between the structural state of rhodopsin in these sub-cellular fractions and that in model systems? One thing is remarkable. Most of sub-cellular structures, if not all, show very small and slow photoinduced Ca^{2+} flux while model systems as this and others (19, 23, 24) present a steady and large Ca^{2+} flux evoked by illumination except one on rhodopsin-containing vesicles (72). If swelling of discs occurs during isolation as it is usually the case (73), one may question the physiological intactness of the isolated structures since disc membranes may be partially disrupted, probably releasing a great amount of their Ca^{2+} content. Isolation of rod outer segments might meet with the same problem too. On the other hand, rhodopsin in artificial membranes does respond to light by a large Ca^{2+} diffusion in accordance with the Ca^{2+} hypothesis, except for the delay time in some cases. Montal, Darszon, and Trissl (74) observed a latency of ca. 100 s which they attributed to the time required for different rhodopsin molecules to aggregate and form "multimolecular" channels for ion flux. This delay time will become shorter as rhodopsin molecules get more concentrated in the membranes. In our experiments, some 60 s delay was sometimes observed which is due, not only to the diffusion through the lipid bilayer, but much more to the distance separating the ion selective electrode from the bilayer. If one could record the ionic activity immediately on release of the cation from these artificial membranes, the latency would then shorten enough to be of physiological relevance.

If the role of rhodopsin on bleaching is to trigger the release of Ca^{2+}, then the visual pigment seems to work better in model systems than in sub-cellular ones: which looks strange. It appears necessary to find out what could be the cause of such a discrepancy. We are waiting for studies on the structural state of rhodopsin in our bilayer membranes to compare with that *in vivo*, and on the physiological intactness of the isolated structures used in calcium photoinduced diffusion experiments. The work done by George and Hagins (75) is noteworthy. They observed a large photoinduced Ca^{2+} release from isolated rod outer segment discs exceeding 10 000 ions in some trials in 90 s, in accordance with the Ca^{2+} hypothesis.

Conclusion

We have demonstrated the possibility to study the ionic aspects of the visual process on a new lipid bilayer model membrane obtained by the combined lifting-and-touching method. The effect of light resulted in a high increase of ion diffusion with a marked selectivity for Ca^{2+} relatively to Na^+ and K^+, suggesting that Ca^{2+} is the internal transmitter. We hope that these positive results obtained on artificial systems will encourage pursuing the work on living systems in order to confirm the Ca^{2+} hypothesis in the visual transduction process. Further work is required to elucidate the very mechanism of release of this transmitter.

Acknowledgements

The authors thank Dr. F. Boucher for helpful discussions. This work was supported by the Natural Sciences and Engineering Research Council of Canada and the Ministère de l'Education du Québec.

1. R. D. PENN and W. A. HAGINS. Nature (London), **223**, 201 (1969).
2. W. A. HAGINS, R. D. PENN, and S. YOSHIKAMI. Biophys. J. **10**, 380 (1970).
3. R. ZUCKERMAN. J. Physiol. (London), **235**, 333 (1973).
4. W. ERNST, W. S. JAGGER, and C. BAUMANN. Nature (London), **248**, 253 (1974).
5. T. TOMITA. Q. Rev. Biophys. **3**, 179 (1970).
6. D. BAYLOR and M. G. F. FUORTES. J. Physiol. (London), **207**, 77 (1970).
7. D. BAYLOR and A. L. HODGKIN. J. Physiol. (London), **234**, 163 (1973).
8. J. E. BROWN and L. H. PINTO. J. Physiol. (London), **236**, 575 (1974).
9. A. J. SILLMANN, H. ITO, and T. TOMITA. Vision Res. **9**, 1443 (1969).
10. S. YOSHIKAMI and W. A. HAGINS. *In* Biochemistry and physiology of visual pigments. *Edited by* H. Langer. Springer Verlag, New York. 1973. pp. 245–255.
11. J. TOYODA, H. NOSAKI, and T. TOMITA. Vision Res. **9**, 453 (1969).
12. W. A. HAGINS and S. YOSHIKAMI. Ann. N.Y. Acad. Sci. **264**, 314 (1975).
13. W. A. HAGINS, W. E. ROBINSON, and S. YOSHIKAMI. *In* Energy transformation in biological systems. Ciba Foundation Symposium. Vol. 31. Published by ASP. Elsevier, Excepta Medica, North Holland, Amsterdam. 1975. pp. 169–189.
14. R. D. PENN and W. A. HAGINS. Biophys. J. **12**, 1073 (1972).
15. E. Z. SZUTS and R. A. CONE. Fed. Proc. **33**, 1471 (1974).
16. T. HENDRIKS, F. J. M. DAEMEN, and S. L. BONTING. Biochim. Biophys. Acta, **345**, 468 (1974).
17. P. A. LIEBMAN. Invest. Ophthalmol. **13**, 700 (1974).
18. M. WELLER, N. VIRMAUX, and P. MANDEL. Nature, **256**, 68 (1975).
19. A. DARSZON and M. MONTAL. *In* Mitochondria: bioenergetics, biogenesis, and membrane structure. *Edited by* L. Parker and A. Gomez. Academic Press Inc., New York. 1976. pp. 389–401.
20. H. SMITH, R. S. FAGER, and B. LITMAN. Biochemistry, **16**, 1399 (1977).
21. U. B. KAUPP and W. JUNGE. FEBS Lett. **81**(2), 229 (1977).
22. U. B. KAUPP, P. P. M. SCHNETKAMP, and W. JUNGE. Biochim. Biophys. Acta, **552**, 390 (1979).
23. W. L. HUBBELL, B. FUNG, Y. CHEN, and K. HONG. *In* Vertebrate photoreception. *Edited by* H. B. Barlow and P. Fatt. Academic Press, London. 1977. pp. 41–59.
24. D. F. O'BRIEN. Photochem. Photobiol. **29**, 679 (1979).
25. R. T. FLETCHER and G. J. CHADER. Biochem. Biophys. Res. Commun. **70**, 1297 (1976).
26. H. T. ORR, O. H. LOWRY, A. I. COHEN, and J. A. FERRENDELLI. Proc. Natl. Acad. Sci. U.S.A. **73**, 4442 (1976).
27. C. GORRIDIS. Exp. Eye Res. **24**, 171 (1977).
28. M. L. WOODRUFF, D. BOWNDS, S. H. GREEN, J. L. MORRISEY, and A. SHEDLOVSKY. J. Gen. Physiol. **69**, 667 (1977).
29. R. YEE and P. A. LIEBMAN. J. Biol. Chem. **253**, 8902 (1978).
30. W. H. MILLER and G. D. NICOL. Nature, **280**, 64 (1979).
31. P. A. LIEBMAN and E. N. PUGH, JR. Vision Res. **19**, 375 (1979).
32. A. I. COHEN. Vision Res. **10**, 445 (1970).
33. J. I. KORENBROT, D. T. BROWN, and R. A. CONE. J. Cell Biol. **56**, 389 (1973).
34. H. RÜPPEL and W. A. HAGINS. *In* Biochemistry and physiology of visual pigments. *Edited by* H. Langer. Springer-Verlag, New York. 1973. pp. 257–261.
35. R. A. CONE. *In* Biochemistry and physiology of visual pigments. *Edited by* H. Langer. Springer-Verlag, New York. 1973. pp. 245–255.
36. C. N. KOSSI and R. M. LEBLANC. J. Colloid Interface Sci. **80**, 426 (1981).
37. M. L. APPLEBURY, D. M. ZUCKERMAN, A. A. LAMOLA, and T. M. JOVIN. Biochemistry, **13**, 3448 (1974).
38. H. B. OSBORNE, C. SARDET, and A. HELENIUS. Eur. J. Biochem. **44**, 383 (1974).
39. P. W. HOLLOWAY. Anal. Biochem. **53**, 304 (1973).
40. S. HOTCHANDANI, R. M. LEBLANC, and F. BOUCHER. Vision Res. **15**, 605 (1975).
41. H. J. TRURNIT. J. Colloid Sci. **15**, 1 (1960).
42. H. SHICHI. J. Biol. Chem. **246**, 6178 (1971).
43. G. WALD and P. K. BROWN. J. Gen. Physiol. **37**, 189 (1953–54).
44. C. H. FISKE and V. SUBBAROW. J. Biol. Chem. **66**, 375 (1925).
45. J. K. BLASIE, M. M. DEWEY, A. E. BLAUROCK, and C. R. WORTHINGTON. J. Mol. Biol. **14**, 143 (1965).
46. J. HELLER. Biochemistry, **8**, 675 (1969).
47. A. DARSZON, C. A. VANDENBERG, M. SCHOENFIELD, M. H. ELLISMAN, N. C. SPITZER, and M. MONTAL. Proc. Natl. Acad. Sci. U.S.A. **77**(1), 239 (1980).
48. A. HYONO, S. KURIYAMA, K. TSUJI, and Y. HOSOYA. Nature, **193**, 679 (1962).
49. K. AZUMA and M. TAKAGI. Ann. Rep. Biol. Works, Fac. Sci., Osaka Univ. **14**, 73 (1966).
50. S. L. BONTING and A. D. BANGHAM. Exp. Eye Res. **6**, 400 (1967).
51. M. MONTAL and J. I. KORENBROT. Nature, **246**, 219 (1973).
52. H. I. KARAN, R. E. HIRSCH, and S. S. BRODY. Z. Naturforsch. **33c**, 317 (1978).
53. J. I. KORENBROT and O. JONES. J. Membr. Biol. **46**, 239 (1979).
54. C.-W. WU and L. STRYER. Proc. Natl. Acad. Sci. U.S.A. **69**, 1104 (1972).
55. C. SARDET, A. TARDIEU, and V. LUZZATI. J. Mol. Biol. **105**, 383 (1976).
56. K. TANSLEY. J. Physiol. (London), **71**, 442 (1931).
57. R. HUBBARD and G. WALD. J. Gen. Physiol. **36**, 269 (1952).
58. A. KROPF and R. HUBBARD. Ann. N.Y. Acad. Sci. U.S.A. **74**, 266 (1958).
59. R. G. MATTHEWS, R. HUBBARD, P. K. BROWN, and G. WALD. J. Gen. Physiol. **47**, 215 (1963).
60. W. E. ABRAHAMSON and S. E. OSTROY. Prog. Biophys. Mol. Biol. **17**, 179 (1967).
61. H. SCHICHI, S. M. LEWIS, F. IRREVERE, and A. L. STONE. J. Biol. Chem. **244**, 529 (1969).
62. M. MAKINO, T. HAMANAKA, Y. ORII, and Y. KITO. Biochim. Biophys. Acta, **495**, 299 (1977).
63. F. CRESCITELLI. Vision Res. **7**, 685 (1967).
64. C. N. KOSSI, G. MUNGER, and R. M. LEBLANC. Vision Res. **17**, 917 (1977).
65. G. DUNCAN, F. J. M. DAEMEN, and S. L. BONTING. Fed. Proc. **28**, 331 (1969).
66. S. L. BONTING. Nova Acta Leopoldina, **208**, 53 (1973).
67. S. E. OSTROY, F. ERHARDT, and E. W. ABRAHAMSON. Biochim. Biophys. Acta, **112**, 265 (1966).
68. W. L. HUBBELL and B. K.-K. FUNG. *In* Membrane transduction mechanisms. *Edited by* R. A. Cone and J. E. Dowling. Raven Press, New York. 1979. pp. 17–25.
69. W. E. ROBINSON and W. A. HAGINS. Photochem. Photobiol. **29**, 693 (1979).
70. H. G. GOLD and J. L. KORENBROT. Invest. Ophtalmol. Vis. Sci. **18**, 4a (1979).
71. N. YA. ORLOV, A. G. GASPARYAN, and E. E. FESENKO. Biofizika, **25**(1), 63 (1980).
72. P. N. TYMINSKI, R. T. KLINGBIEL, R. A. OTT, and D. F. O'BRIEN. Biochemistry, **21**(6), 1197 (1982).
73. E. Z. SZUTS. J. Gen. Physiol. **76**, 253 (1980).
74. M. MONTAL, A. DARSZON, and H. W. TRISSL. Nature, **267**, 221 (1977).
75. J. S. GEORGE and W. A. HAGINS. Nature (London), **303**, 344 (1983).

Antibonding σ^* orbitals in molecular spectroscopy

M. B. ROBIN
AT&T Bell Laboratories, Murray Hill, NJ 07974, USA

Received August 1, 1984

This paper is dedicated to Professor Camille Sandorfy on the occasion of his 65th birthday

M. B. ROBIN. Can. J. Chem. **63**, 2032 (1985).

This paper discusses the role of σ^* antibonding valence MO's in the electronic spectra of large molecules. Using the term value and antishielding concepts, molecular absorption patterns terminating at σ^* MO's are systematized and rationalized; the frequencies of such excitations correlate with the ground-state bond strengths of the bonds giving rise to the σ^* MO's. In unsaturated systems, the $\pi \rightarrow \sigma^*$ and $np \rightarrow \sigma^*$ excitations can be distinguished on the basis of their term values. Confusion in the past regarding the existence of excitations to σ^* relates to the fact that σ^* MO's often can be totally mixed into the surrounding sea of Rydberg levels of the same symmetry, and for all practical purposes can cease to exist except as perturbations on the Rydberg levels. For nonpenetrating Rydberg manifolds there is little or no mixing with σ^* MO's of the same symmetry, setting the stage for the appearance of valence-shell excitations to σ^* in high-symmetry molecules which are analogous to the $d \rightarrow f$ inner-well giant resonances of atomic spectroscopy.

M. B. ROBIN. Can. J. Chem. **63**, 2032 (1985).

Dans ce travail, on discute du rôle des OM de valence antiliante σ^* dans les spectres électroniques des grosses molécules. Utilisant les concepts de valeur de terme et d'antiblindage, on systématise et on rationalise les types d'absorptions moléculaires qui se terminent au niveau des OM σ^*; il existe une corrélation entre les fréquences de telles excitations et les longueurs de liaisons dans l'état atomique fondamental qui donne lieu aux OM σ^*. Dans les systèmes non-saturés, on peut distinguer les excitations $\pi \rightarrow \sigma^*$ des excitations $np \rightarrow \sigma^*$ en se basant sur leurs valeurs de terme. La confusion qui a été observée dans le passé relativement à l'existence d'excitations vers les niveaux σ^* provient du fait que les OM σ^* peuvent souvent être complètement confondues avec les niveaux de Rydberg de même symétrie qui les entourent et, à toutes fins pratiques, elles cessent d'exister, excepté comme perturbations des niveaux de Rydberg. Pour les états non-pénétrants de Rydberg, il y peu ou pas du tout de mélange avec les OM σ^* de même symétrie et ceci permet, dans les molécules de haute symétrie, de noter l'apparition d'excitations des couches de valence vers les états σ^* qui sont semblables aux résonances géantes $d \rightarrow f$ de la spectroscopie atomique.

[Traduit par le journal]

I. Introduction

All molecules — from H_2 to DNA — have one aspect in common: a σ bond between two or more atoms, where "σ" expresses the local symmetry of the bonding orbital. In a molecular orbital description of the bonding, these σ bonding MO's unavoidably have valence-shell σ^* antibonding MO's associated with them, many of which are unoccupied in the ground state. Spectroscopic intuition suggests that transitions terminating at the various vacant σ^* MO's can be among the most intense electronic transitions in molecules, should appear in both the vapor-phase and condensed-phase spectra of all molecules regardless of size, polarity, geometry or degree of unsaturation, and will be intimately involved in every molecule's photochemistry. In this we include not only $\sigma \rightarrow \sigma^*$ excitations but those originating at π and np lone-pair orbitals as well.

Being an unavoidable component of every molecule's electronic spectrum, transitions to σ^* should have the highest priority for study by spectroscopists, photochemists, and theorists. Strange then that so very little is known about valence-shell transitions terminating at σ^* in molecules. In a spectroscopic literature replete with experimental and theoretical papers on $\pi \rightarrow \pi^*$ and Rydberg excitations, the transitions to σ^* orbitals are only indirectly mentioned, if at all. Indeed, there is a gaping hole in our understanding of molecular excited states which is both embarrassing to admit and tempting to jump into for the new insights it might yield. Chemists have hesitated to jump for two reasons: (*1*) those far from the field consider the situation obvious and so would not bother with it and (*2*) those close to the field consider it opaque and too difficult to deal with. As always, the truth lies somewhere in between, in this case, closer to point (*2*) than to point (*1*).

In this paper, I attempt to sketch the big picture for molecular excitations terminating at σ^* MO's. For this, an outline is constructed which uses the byproducts of many other studies, most often carried out for other reasons. Because we are interpreting very incomplete data, the approach used here is a qualitative one, aimed at better-defining the problems rather than rigorously solving them. Hopefully, others will pursue these qualitative ideas and test them more fully. The material discussed here is abstracted from a larger study (1), and the interested reader is referred to that work for more details. Since one of the few serious attempts at understanding the σ spectra of polyatomic molecules was that of Camille Sandorfy (2), and because a large volume of work on the problem has since come out of his laboratory, it is fitting that this paper is dedicated to him on his 65th birthday.

Our discussion centers upon a description of the spectral properties of the valence-shell excitations terminating at σ^* MO's called *A* bands. We focus first upon *A* bands, for the data are relatively copious here and trustworthy; much of what is learned from studying the *A* bands then is transferable to other transitions terminating at σ^*.

II. *A*-bands and term values

II.A. Definitions

The *A* bands of the alkyl halides are the best known molecular excitations involving σ^* MO's. The prototypical *A* band in the molecule R—$\ddot{X}$ is due to the excitation of an electron from the *np* lone-pair orbital on $\ddot{X}$ to the σ^*(R—X) antibonding MO involving the halogen and the radical bound to it, Fig. 1. Simply termed an *A* band in the past (3, 4), we now classify this excitation as an $A(np,\sigma^*)$ band. We further broaden the *A*-band definition by including as *A* bands the outer-shell valence ex-

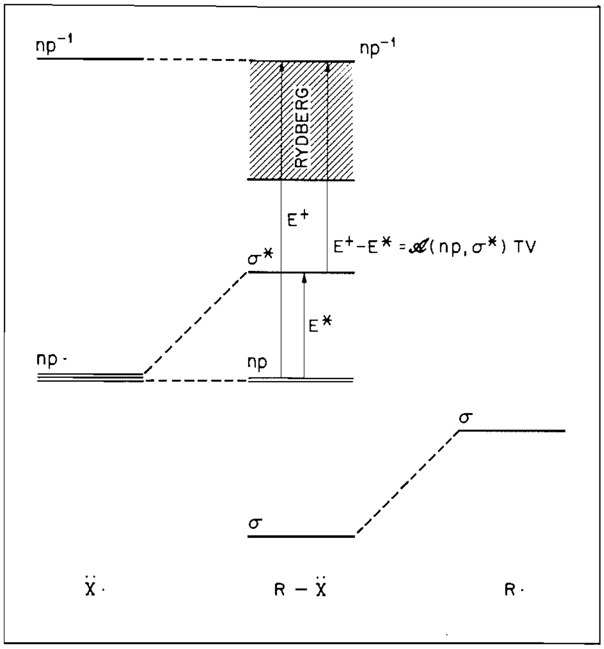

FIG. 1. Definition of the A-band term value in alkyl halides.

citations originating at nonbonding lone-pair orbitals in any system having such an orbital (e.g., trimethyl arsine, acetone, hexachlorobenzene, trimethylene sulfide, etc.). Inasmuch as all inner-shell orbitals in a spectroscopic sense are nonbonding and so also are lone pairs, all inner-shell valence transitions terminating at σ^* are hereby deemed to be A bands. In contrast to the A bands in which the originating orbital is essentially nonbonding and localized, the originating orbitals for $\pi \rightarrow \pi^*$ and $\sigma \rightarrow \sigma^*$ types of valence-shell bands are strongly bonding and delocalized; for these we maintain the time-honored $N \rightarrow V_n$ designation of Mulliken. See Section II.F for a discussion of A-band terminology in unsaturated systems.

Very early on, Mulliken (5) recognized the close similarity in nodal patterns between certain antibonding valence-shell orbitals and the lowest Rydberg orbitals of the same symmetry. Thus for example, the $a_1\sigma^*$ valence and $3sa_1$ Rydberg orbitals of methane both are totally symmetric with each having two radial nodes while in ethylene for example, the π^* valence and $3d_{xz}$ Rydberg orbitals each have two perpendicular nodal planes and no radial nodes. Though Mulliken's point of view has been that the differences between such look-alike pairs of Rydberg and valence-shell orbitals is only a semantic one, we consider configurations such as (ϕ_i, $3sa_1$) and (ϕ_i, $a_1\sigma^*$) to be distinct zero-order functions, with transitions imaginable to each separately or to their linear combinations if they are mixed. (See Section III.A for a short discussion on this point.) Pairs of terminating orbitals such as $a_1\sigma^*$ and $3sa_1$ are called "Rydberg/valence-shell conjugates" (1, 4). The $A(\phi_i, \sigma^*)$ levels of interest in this paper are the valence conjugates to either the (ϕ_i, ns), (ϕ_i, np), (ϕ_i, nd) or (ϕ_i, nf) Rydberg configurations of the system, depending upon the symmetry of a particular σ^*.

In attempting to gain some understanding of A-band spectra, we use an approach which has proved to be quite successful for identifying and correlating molecular Rydberg transitions: that of the molecular term value. In the case of Rydberg transitions, this approach is natural since the term value, $R/(n - \delta)^2$, appears prominently in the Rydberg formula describing the energetics of Rydberg series members. In this expression, R is the Rydberg constant, n is the principal quantum number of the Rydberg orbital, and δ in the quantum defect. Alternatively, being the difference between the ground-state ionization potential and the Rydberg excitation energy, the Rydberg term value can be interpreted as the Rydberg excited-state ionization potential. For a valence excited state (ϕ_i,σ^*), the term value has no meaning in the Rydberg sense since there is no convergent series of valence-shell states. However, the $A(\phi_i,\sigma^*)$ band term value as defined in Fig. 1 (the difference between the ϕ_i^{-1} ionization potential of energy E^+ and the $A(\phi_i,\sigma^*)$ band excitation energy E^*) does have meaning when viewed as the ionization potential of an electron in σ^* when promoted from ϕ_i. Thus we hope to learn something about σ^* orbitals by comparing their ionization potentials in groups of related (excited) molecules.

Data on A-band frequencies and term values in several classes of molecules are assembled in Tables 1, 2, and 3(1). Perusing this data, it is obvious that there is considerable regularity among the term values even though the transition is valence shell rather than Rydberg. In some cases the term-value trends parallel those of Rydberg excitations, while in others the trends are opposite. The A-band data in the tables lead to several conclusions, as discussed in the following sections.

II.B. Term-value trends and bond strengths

It is readily seen from Table 1 that the term values for the $A(np,\sigma^*)$ outer-shell transitions in the alkyl halides vary in a regular manner as one halide is replaced by another. For purposes of identifying such A bands in more complex systems, it is useful to note that the chloroalkane term values are in the 30 000 – 38 000 cm^{-1} range, with the bromo and iodoalkane term values some 3 000–6 000 cm^{-1} higher. In all cases, the A-band term value of a particular alkyl halide increases with increasing halogenation. Both this and the term-value increase in the Cl, Br, I monohalide series are counter to the trends observed for the conjugate (np,(n + 1)s) Rydberg excitations (4). These two trends of opposite sign cross between F and Cl, so that in the alkyl halides RCl, RBr, and RI the level ordering is A-band-below-conjugate-Rydberg, whereas in RF the ordering is conjugate-Rydberg-below-A-band. Other A-band term-value trends are discussed in Sections II.C and II.D.

As shown in Fig. 1, the interaction between the σ orbitals on R and X upon forming the R—X bond elevates σ^*, thereby reducing the $A(np,\sigma^*)$ term value. Since the σ^* level is raised more, the stronger the R—X bond, one expects the $A(np,\sigma^*)$ term values to vary *inversely* with the R—X bond strengths within a class of closely related molecules. Looking first at the methyl halides, Fig. 2, one notes the increasing (np,σ^*) term values in the series CH_3Cl, CH_3Br, and CH_3I, whereas the C—X bond strengths are decreasing in the same order. From this simple relationship we can extrapolate to a ($2p$,σ^*) term value of 26 800 cm^{-1} in CH_3F. Inasmuch as the ($2p$,$3s$) Rydberg term value is 33 000 cm^{-1} in CH_3F, it is now clear why A bands are not observed in the alkyl fluorides: the C—F bonds are so strong that σ^* lies within the thicket of Rydberg excitations. Again, there is a monotonic increase of the lowest (np,σ^*) term value as one goes from CH_3X to CX_4 for X = Cl, Br, and I, in inverse order of their C—X bond strengths.

A trend identical to that of the outer-shell term values is seen as well in the inner-shell ($1s_C$,σ^*) term values of the methyl halides, Fig. 2, with the ($1s_C$,σ^*) term value for a particular compound approximately 8 000 cm^{-1} larger than that for

TABLE 1. Outer-shell $A(np,\sigma^*)$-band term values in saturated, halide-containing molecules (1)

Molecule	Frequency, cm^{-1}	Ionization potential, cm^{-1}	Term value, cm^{-1}
CH_3Cl	58 800	90 980	32 200
CH_2Cl_2	58 800	92 800	34 000
$CHCl_3$	57 200	93 200	36 000
CCl_4	57 100	95 100	38 000
C_2H_5Cl	59 000	89 020	30 000
n-C_3H_7Cl	58 600	87 840	29 200
i-C_3H_7Cl	57 700	87 270	29 600
n-C_4H_9Cl	58 200	87 760	29 600
CH_2FCl	62 500	94 700	32 200
CHF_2Cl	66 200	101 600	35 400
CF_3Cl	65 300	104 900	39 600
CF_2BrCl	61 000	104 000	43 000
CF_2Cl_2	56 500	99 200	42 700
$CFCl_3$	55 860	96 000	40 140
C_2F_5Cl	66 700	104 500	37 800
CH_3CF_2Cl	63 900	100 800	36 900
CF_3CHCl_2	57 100	96 800	39 700
CF_3CCl_3	57 500	95 200	37 700
$CF_2ClCFHCl$	57 500	96 800	39 300
$CFCl_2CF_2Cl$	55 000	97 190	42 200
$CF_3CHBrCl$	59 500	90 100	30 600
$CH_3OCF_2CHCl_2$	57 500	92 800	35 300
HCF_2OCF_2CHFCl	57 500	98 400	40 900
$GeCl_4$	56 800	97 800	41 000
$SnCl_4$	50 200	97 600	47 400
PCl_3	57 000	94 450	37 450
CH_3Br	50 000	85 000	35 000
CH_2Br_2	45 500	85 600	40 100
$CHBr_3$	41 200	84 500	43 300
CBr_4	39 500	83 800	44 300
CF_2Br_2	44 000	90 200	46 200
CF_3Br	48 850	96 800	47 950
CF_2ClBr	48 800	95 400	46 600
$CF_3CHClBr$	49 000	90 300	41 300
SiH_3Br	52 400	89 000	36 600
$SiBr_4$	51 300	87 500	36 200
$GeBr_4$	40 800	87 100	46 300
$SnBr_4$	38 000	88 700	50 700
CH_3I	38 500	77 030	38 530
C_2H_5I	38 500	75 380	36 880
n-C_3H_7I	38 500	74 610	36 110
i-C_3H_7I	38 500	74 120	35 620
t-C_4H_9I	37 000	73 240	36 240
C_5H_9I	38 500	73 200	34 700
$C_6H_{11}I$	38 500	71 860	33 360
CI_4	25 800	76 000[a]	50 000
CF_3I	37 700	85 580	47 880
C_2F_5I	37 000	85 620	48 600

[a] No ionization potential data available; value taken from X-α scattered wave calculation.

(np,σ^*). The extrapolated $(1s_C,\sigma^*)$ term value for methyl fluoride is 36 500 cm^{-1}, a value which is very close to that for the $(1s_C,3s)$ inner-shell Rydberg state. Thus it is not surprise that these conjugate levels are found to be nearly degenerate in the inner-shell spectrum of CH_3F (1).

The influence of bond strength on the A-band frequencies also appears prominently in the spectra of the Group IV tetrachlorides MCl_4, Fig. 3, where $A(3p,\sigma^*)$ bands are readily observed in CCl_4, $GeCl_4$, and $SnCl_4$, but not in $SiCl_4$ (6). In this group, the M—Cl bond is especially strong in $SiCl_4$ (88 kcal/mol) compared to the others (*ca.* 72 kcal/mol), thereby elevating the $3p \rightarrow \sigma^*$ excitations of $SiCl_4$ among the Rydberg excitations where they are lost from view. At the opposite extreme, the Sn—Cl bond strength in $SnCl_4$ is only 68 kcal/mol, and its $A(3p,\sigma^*)$ bands are at the lowest frequencies observed for tetrachlorides.

Because the bond strength in BF_3 is very large (153 kcal/mol), the $A(1s_B,\sigma^*)$ term value is so far diminished as to become negative. That is, the $1s_B \rightarrow \sigma^*$ excitation in BF_3 is at higher frequency than the $1s_B^{-1}$ ionization potential (by 18 500 cm^{-1}), and consequently appears as a shape resonance (7). There is a strong possibility that the outer shell $A(2p_F,\sigma^*)$ band of BF_3 also will lie above the $2p_F^{-1}$ ionization limit. At the opposite extreme, in a molecule such as NF_3 (4) where the N—F bond strength is only 67 kcal/mol, the $A(2p_N,\sigma^*)$ term value is correspondingly elevated to 40 100 cm^{-1}, so that the A band precedes the Rydberg parade. In the $1s_N$ and $1s_F$ spectra of NF_3, the $(1s,\sigma^*)$ term values of the A bands increase to 52 000 cm^{-1}, as anticipated from the antishielding argument (Section II.D).

Whereas the term value of the $(np,(n+1)s)$ Rydberg configuration is understandable in terms of the core penetration of an essentially nonbonding $(n+1)s$ Rydberg orbital, in the case of the (np,σ^*) conjugate configuration the term value will strongly reflect the antibonding nature of the σ^* MO and therewith, the strength of the relevant σ bond.

II.C. Alkylation and fluorination effects on term values

The larger the R group in RX, the weaker the R—X bond. As in Section II.B above, this would tend to increase the (np,σ^*) term value. On the other hand, large R groups strongly stabilize the np^{-1} ionic state by hyperconjugation, thereby decreasing the (np,σ^*) term value. The latter factor is dominant. The effects of alkylation on the (np,σ^*) term value are seen most clearly in the iodides, Table 1. The $A(5p,\sigma^*)$ band falls consistently at 38 500 cm^{-1} in the alkyl iodides while the ionization potential decreases from 77 030 cm^{-1} in methyl iodide to 71 860 cm^{-1} in cyclohexyl iodide. As a result of this overwhelming stabilization of the cation by the hyperconjugative alkyl groups, the $(5p,\sigma^*)$ term value steadily drops from a value of 38 500 cm^{-1} in methyl iodide to 33 360 cm^{-1} in cyclohexyl iodide. In the alkyl chlorides, the same trend is evident, though with a smaller slope. The depressing effect of the alkyl group on A-band term values is evident as well in the inner-shell term values of HCl ($2p_{Cl}$, 47 500 cm^{-1}), CH_3Cl ($1s_C$, 40 000 cm^{-1}), and C_2H_5Cl ($1s_C$, 38 700 cm^{-1}). This trend parallels that for the corresponding conjugate Rydberg absorptions.

Fluorination of an alkyl halide acts in a direction opposite to that of alkylation, increasing the (np,σ^*) term values, as is also the case with the conjugate Rydberg excitations. The term-value effects of replacing hydrogen by fluorine on several valence excitations are summarized in Table 2. One sees that in the case of the halide A bands, fluorination shifts the outer-shell A band term value to higher frequencies by up to 12 000 cm^{-1}, but an average value is more like *ca.* 8 000 cm^{-1}. A similar positive increment applies to the inner-shell $(2p,\sigma^*)$ term values in the SiH_4/SiF_4 pair, the only one for which inner-shell data is available. A sampling of spectroscopic frequencies in highly fluorinated hypervalent species such as SF_6, XeF_6, etc., reveals A-band term values as large as 80 000 cm^{-1} for inner-shell transitions, consonant with the low M—F bond energies

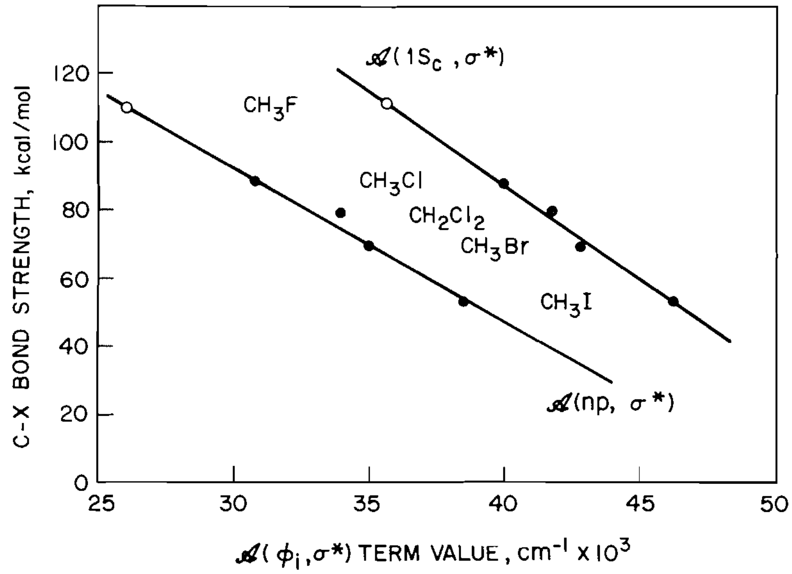

FIG. 2. Variation of the $A(np,\sigma^*)$ term values with C—X bond strength in the methyl halides.

TABLE 2. Fluorination effects on valence shell A-band term values (1)

Upper-state configuration	H compound	Term value, cm^{-1}	F compound	Term value, cm^{-1}
$(2p,\sigma^*)$	SiH_4	35 000	SiF_4	45 500
$^3(\pi,\pi^*)$	$H_2C{=}CH_2$	49 950	$F_2C{=}CF_2$	47 200
$^1(\pi,\pi^*)$	$H_2C{=}CH_2$	23 050	$F_2C{=}CF_2$	13 600
$^3(\pi,\pi^*)$	$H_2C{=}CHCl$	49 200	$F_2C{=}CFCl$	47 400
$^1(\pi,\pi^*)$	$H_2C{=}CHCl$	26 700	$F_2C{=}CFCl$	20 200
$(3p,\sigma^*)$	CH_3Cl	31 000	CF_2HCl	35 400
			CF_3Cl	39 500
$(3p,\sigma^*)$	CH_2Cl_2	35 900	CF_2Cl_2	43 100
$(3p,\sigma^*)$	$CHCl_3$	36 000	$CFCl_3$	40 400
$(3p,\sigma^*)$	C_2H_5Cl	30 000	CH_3CF_2Cl	36 900
			C_2F_5Cl	37 800
$(4p,\sigma^*)$	CH_3Br	34 000	CF_3Br	46 800
$(4p,\sigma^*)$	CH_2Br_2	40 000	CF_2Br_2	46 200
$(5p,\sigma^*)$	CH_3I	39 000	CF_3I	46 200
$(1s,\pi^*)$	$CH_3CH{=}CHCH_3$	46 000	$CF_3CF{=}CFCF_3$	54 800

in these molecules. It appears that the (np,σ^*) term-value decrease on alkylation of an alkyl halide is due largely to the alkyl group's effect on the np^{-1} ionization energy, whereas the increase of this term value on fluorination is due to the inductive lowering of the σ^* level.

II.D. Antishielding in the inner-shell spectra

The ionization energy (term value) in an $A(\phi_i,\sigma^*)$ configuration will depend not only upon the $\sigma-\sigma^*$ split as evidenced by the bond strength, but also upon the effective nuclear charges of the AO's in the σ^* MO. In the A-band upper state, the optical electron is electrostatically bound to the core due to the imperfect shielding of the nucleus by the valence electrons. The shielding of the σ^* orbital from the nucleus is more efficiently performed by the inner-shell electrons ($1s$) than the outer-shell electrons ($2s$ and $2p$) because the inner-shell orbitals are less easily penetrated by an electron in σ^*. Consequently, when the electronic configuration is changed from an outer-shell one such as $(2p,\sigma^*)$ to an inner-shell one such as $(1s,\sigma^*)$ the shielding of the σ^* orbital from the nucleus decreases and the term value rises. Looked at another way, the effective nuclear charge for a $2p$ orbital on C^+ in the outer-shell configuration $1s^22s^22p$ is 3.25 according to Slater's rules whereas for a $2p$ orbital in the $1s2s^22p^2$ inner-shell configuration, it is 3.75. This increased binding of the optical electron as the hole descends to a lower level we call "*antishielding*". The antishielding increment for inner-shell excitation over outer-shell excitation will be much larger for a σ^* MO than for a Rydberg orbital since σ^* MO's are more penetrating. Exchange effects also contribute somewhat to the larger term values of inner-shell A bands (8).

One sees in Table 3 that for excitation from the various halogen AO's into σ^*(C—X) of the halomethanes, the (ϕ_i,σ^*) term value indeed drops as the energy of ϕ_i descends, in accord with the antishielding concept. Moreover, a hole in $1s_C$ is about equivalent in antishielding to a hole in $2p_{Cl}$, but is much less antishielding than when ϕ_i is $2s_{Cl}$ or $1s_{Cl}$. For a given inner-shell originating orbital ϕ_i, there is also an increase of the (ϕ_i,σ^*) term value as the methane molecule is successively chlorinated, Table 3. This can be explained as due in part to a weakening of the C—Cl bond with chlorination and also to C—Cl/C—Cl interactions which split the σ^*(C—Cl) man-

TABLE 3. $A(\phi_i,\sigma^*)$-band term values in the halomethanes, CH_xX_{4-x} (1)

	$(1s_C,\sigma^*)$	$(1s_X,\sigma^*)$	$(2s_X,\sigma^*)$	$((n-1)p_X,\sigma^*)^a$	$(np_X,\sigma^*)^a$	$((n-1)d_X,\sigma^*)^a$
CH_3F	36 500[b]	—	—	—	26 800[b]	—
CH_3Cl	40 000	45 500	44 000	42 400	32 200	—
CH_2Cl_2	41 100	—	53 500	42 200	34 000	—
$CHCl_3$	46 800	—	58 400	49 600	36 000	—
CCl_4	50 800	—	57 600	51 200	38 000	—
CH_3Br	42 700	—	—	—	35 000	44 400[c]
CH_3I	45 600	—	—	—	38 530	48 800[d]

[a]The highest filled halogen lone-pair orbital is assigned quantum number n.
[b]Extrapolated values from Fig. 2.
[c]Term value for the $A(3d_1,\sigma^*)$ band.
[d]Average of the two $(4d_1,\sigma^*)$ spin–orbit components having term values of 49 200 and 48 400 cm^{-1}.

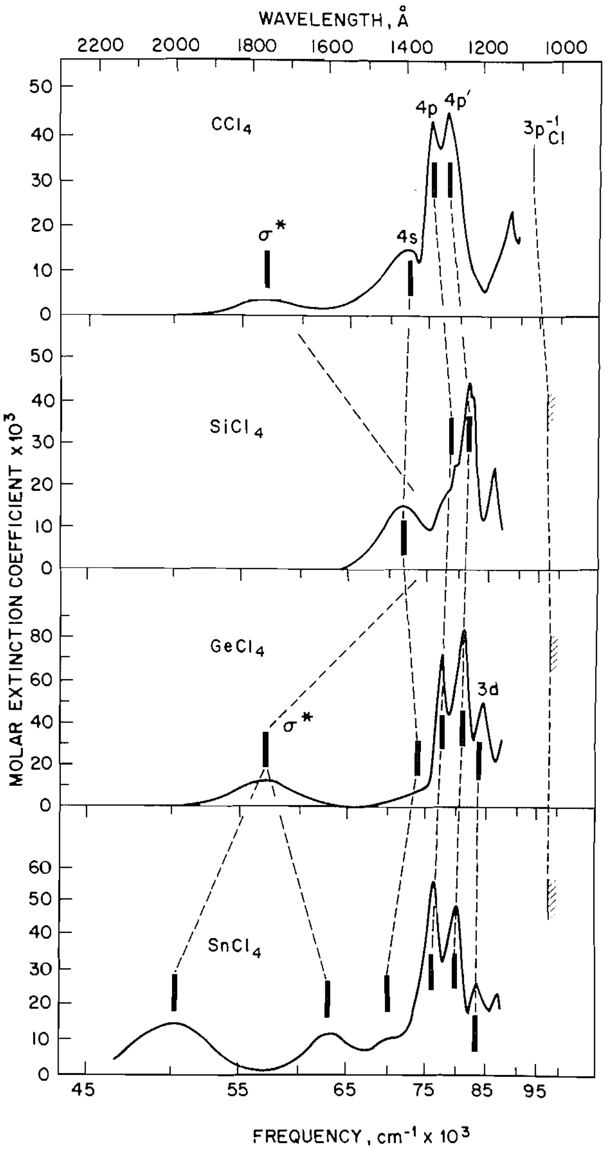

FIG. 3. Assignments of the outer-shell spectra of the Group IV tetrachlorides (redrawn from ref. 6).

ifold into several components, the lowest of which is progressively stabilized upon further chlorination. This stabilization is most evident in the valence temporary-negative-ion (TNI) resonances of the chloromethanes, in which a resonance measures the energy necessary to attach an electron to the molecule via the σ^* MO's (9). Thus between CH_3Cl and CCl_4 there is a monotonic decrease of the lowest valence TNI resonance frequency from 27 800 cm^{-1} to a figure which is actually just slightly negative. The antishielding enhancement of inner-shell term values is dramatically illustrated by the case of $SiCl_4$, where the $A(2p_{Si},\sigma^*)$ band is prominent as the lowest excitation, having a 51 000 cm^{-1} term value (4), in strong contrast to the $A(3p_{Cl},\sigma^*)$ band of the outer shell which is lost among the Rydberg bands and so must have a term value which is less than 25 000 cm^{-1}.

II.E. A *Bands in nonhalide systems*

All of the A-band trends quoted above are deduced from data on the alkyl halides. What now if the halogen and its lone pair in R—X are replaced by one of the groups —OH, —SCH$_3$, —NH$_2$, etc., so as to form alcohols, thioethers, amines, etc.? There is no choice but to follow the scheme of Fig. 1 and to consider $A(np,\sigma^*)$ and $A(1s,\sigma^*)$ bands in these substances as well. Though these systems are chemically different from the alkyl halides, one expects that their $A(np,\sigma^*)$ bands nonetheless will behave spectroscopically as described above, with the understanding however, that they will not necessarily lie below the Rydberg manifold. From this point of view, it is clear for example, that the weak transition in CF_3OF having a term value of 55 000 cm^{-1} with respect to the $2p_O^{-1}$ ionization potential (10) is an $A(2p_O,\sigma^*)$ band of extraordinarily large term value thanks to an O—F bond strength of only 43.5 kcal/mol . In H_2O_2, where the O—O bond strength is only 37 kcal/mol, a low-lying $A(2p_O,\sigma^*)$ band absorption likely is responsible for the observed dissociation into OH radicals with unit quantum yield at 2537 Å. However, given molecules having more normal bond strengths, one most often does not find $A(np,\sigma^*)$ bands in the outer-shell spectra of molecules bearing lone pairs on O, S, N, P, etc. For this, one must go to the X-ray spectra, thereby taking advantage of the inner-shell antishielding which increases the A-band term value (Section II.D). We defer discussion of the fate of outer-shell A bands in the nonhalides to Section III.B.

Since the antishielding effect operates more strongly on valence states than on Rydberg states, and more strongly in the inner-shell spectra than in the outer shell, $A(\phi_i,\sigma^*)$ bands are more often visible below their Rydberg conjugates in the inner-shell spectrum. The relative ease of spotting A bands in the inner-shell spectra is also promoted by the fact that outer-shell $A(np,\sigma^*)$ excitations for overlap reasons are among the weaker transitions in the outer-shell spectrum. Consequently such bands are visible only when their terms values are much larger than those of the similarly weak but far-more-numerous Rydberg bands in the same spectral region. On the other hand,

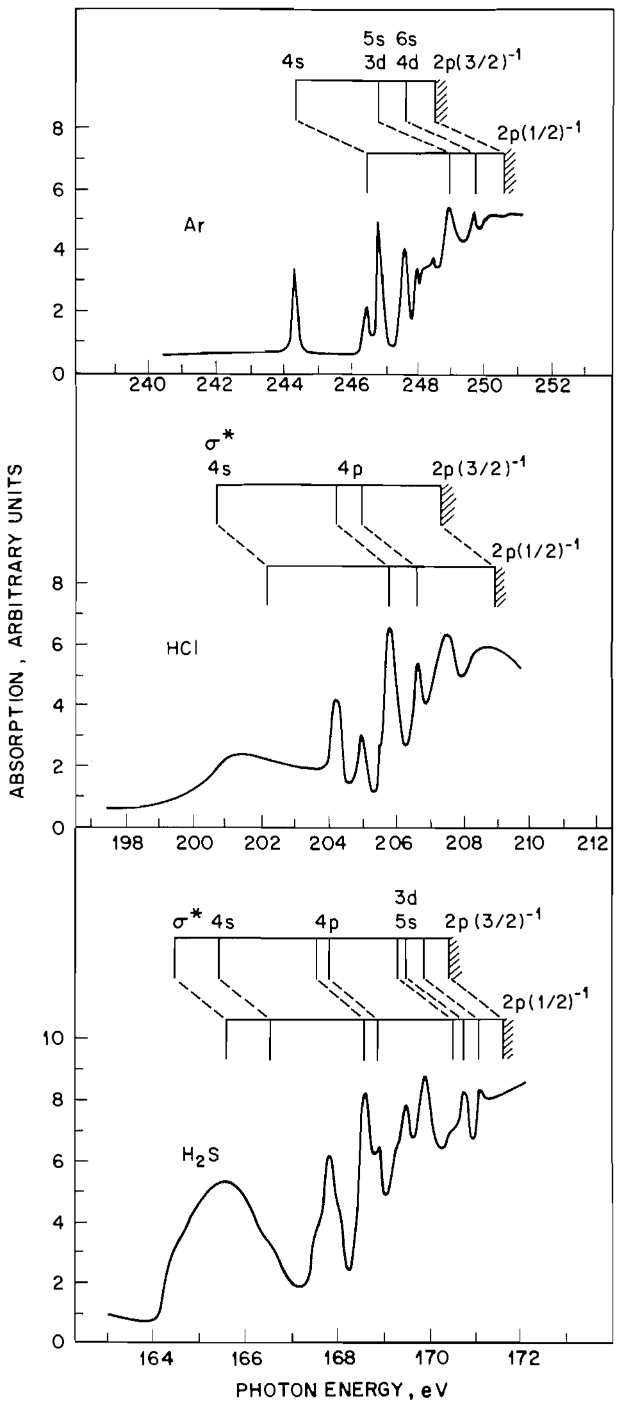

FIG. 4. Development of the $A(3p,\sigma^*)$ band in the isoelectronic series Ar, HCl, H_2S (redrawn from ref. 11).

$A(1s,\sigma^*)$ bands are among the most intense in the inner-shell spectrum, again for reasons of overlap between the originating and terminating orbitals.

It is easiest to see how σ* MO's influence molecular spectra by comparing the inner-shell spectra of several molecular hydrides with that of their isoelectronic united atom. Thus in Fig. 4, the $2p$ molecular spectra of HCl and H_2S are compared with that of Ar (see, for example, ref. 11), revealing a number of differences. Interpretation of these spectra requires an allowance for the $2p_{3/2}$–$2p_{1/2}$ spin–orbit splitting of the core in each case. First, we note that the very broad transitions about 50 000 cm^{-1} below the $2p^{-1}$ ionization limits in the molecular spectra do not appear in the spectrum of the isoelectronic atom, and hence must involve molecular σ* MO's, which is to say, these are $A(2p,\sigma^*)$ bands. Next, the sharp $2p \rightarrow 4s$ transition of the atom is barely detectable in the molecular spectra, suggesting appreciable mixing between the $(2p,a_1\sigma^*)$ and $(2p,4sa_1)$ conjugate configurations such that the former is intensified and the latter diminished. Finally, whereas the $2p \rightarrow 4p$ transition is absolutely forbidden in the atom, it is an allowed transition in the molecular case. Once beyond the transitions to $4p$, the Rydberg spectra of the Ar atom and its isoelectronic molecular hydrides are quite comparable, except for certain small core splittings in the latter. The $2p$ spectra of PH_3 and SiH_4 closely follow the pattern of molecular transitions described above for HCl and H_2S; however, the outer-shell transitions to σ* in PH_3 and SiH_4 do *not* precede the lowest Rydberg excitations, contrary to the ordering for HCl and H_2S in the outer-shell spectra.

II.F. A *band varieties in unsaturated systems*

When the group bearing the lone pair is bonded directly to an unsaturated center as in $H_2C{=}CHX$, the *A*-band possibilities are manifold. As in alkyl halides, there is an $A(np,\sigma^*)$ band present. However the $A(np,\sigma^*)$ band in unsaturated systems generally is not the lowest-frequency *A* band, for there generally are occupied π MO's above *np* in these compounds. In such a case, the lowest *A* band is $A(\pi,\sigma^*)$ in an obvious notation. $A(np,\sigma^*)$ and $A(\pi,\sigma^*)$ bands appear in the outer-shell spectrum with separations nearly equal to the difference of np^{-1} and π^{-1} ionization potentials, with each occupied π MO in the molecule responsible for a specific $A(\pi,\sigma^*)$ band. Two other transitions are possible here: $\pi \rightarrow \pi^*$ and $np \rightarrow \pi^*$. Since both of these are encompassed in the well-known V_n notation of $\pi \rightarrow \pi^*$ excitations, they have not been renamed to fit into the *A*-band scheme. The inner-shell spectra of such unsaturated systems will commence with $\phi_i \rightarrow \pi^*$ transitions, followed by $\phi_i \rightarrow \sigma^*$ and Rydberg excitations.

By way of example, note that the 43 500-cm^{-1} band of tetrachloroethylene must be valence shell as witnessed by its frequency and by its behavior in condensed phases (12), and involves either $3p\pi_{Cl}$ or $\pi(C{=}C)$ as originating MO's and either $\pi^*(C{=}C)$ or $\sigma^*(C{-}Cl)$ as terminating MO's. Since the $\pi(C{=}C)$ MO is above the uppermost $3p\pi_{Cl}$ MO by 17 000 cm^{-1} in tetrachloroethylene, one concludes that the lowest valence transition in tetrachloroethylene will originate at $\pi(C{=}C)$. Since the $\pi \rightarrow \pi^*$ assignment is preempted by the intense band at 47 600 cm^{-1}, we must assign the 43 500-cm^{-1} band of tetrachloroethylene as originating at $\pi(C{=}C)$ and terminating at $\sigma^*(C{-}Cl)$, i.e., it is an $A(\pi,\sigma^*)$ band analogous to those of the fluoroethylenes in the 55 000 – 57 000 cm^{-1} region. Another likely *A* band appears in tetrachloroethylene at 61 900 cm^{-1} as a sharp but unstructured feature. Dauber and Brith (8) observed this band clearly in the neat crystal and in a Kr matrix where it is shifted to the low-frequency side of the vapor-phase band, as is the $\pi \rightarrow \pi^*$ valence-shell band at 47 600 cm^{-1}. By contrast, the $\pi \rightarrow 4s$ Rydberg excitation between 50 000 and 57 000 cm^{-1} is high-frequency shifted in a Kr matrix, and does not appear at all in the spectrum of the neat crystal. Though it is clear from this that the 61 900-cm^{-1} band of tetrachloroethylene is a valence excitation, it can be assigned as either $3p_{Cl} \rightarrow \pi^*$ or $3p_{Cl} \rightarrow \sigma^*$. We note, however, that the $A(\pi,\sigma^*)$ and $A(np,\sigma^*)$ band term values of the haloethylenes are quite constant (28 000 ± 1 500 cm^{-1}), irrespective of the halogen's atomic number or the extent of halogenation (1). Assignment of the 61 900-cm^{-1} feature of tetrachloroethylene as an $A(np,\sigma^*)$ band results in a 30 000 cm^{-1} term value, just equal to that of the $A(\pi,\sigma^*)$ band. Looked at from the point of view of the ground state, the transitions to (π,σ^*) and to $(3p,\sigma^*)$ differ by exactly the difference between the π^{-1} and $3p^{-1}$ ionization potentials. The implication from such simple one-electron-like behavior of the A band energies is that such states are much better described at the Hartree–Fock level (along with $n \rightarrow \pi^*$ and Rydberg excitations) than are the singlet configurations (π,π^*) and (σ,σ^*).

II.G. A *bands in transition-metal complexes*

The arguments of previous sections also apply to the case where the central atom is a transition metal and the ligands again carry lone-pair electrons as in WF_6 or CrO_2Cl_2. For octahedral or tetrahedral symmetry, the virtual *nd* valence orbitals split into π^* and σ^* sets with π^* lower. The lowest transitions originating at *np* will be $np \rightarrow \pi^*$, but these will be followed by $A(np,\sigma^*)$ bands. For transitions terminating at π^*, the spectral splittings closely reflect those among the *np* orbitals as observed in the photoelectron spectrum (1), which is to say, the (np,π^*) term values are constant; similar splittings appear among the A band transitions to σ^*. The difference of (np,π^*) and (np,σ^*) term values relates closely to $10Dq$ in these compounds.

Note that in the case of WF_6 for example, the lowest *nd* orbitals ($n = 5$) of W are involved in bonding to the F atoms, and so are part of the virtual π^*/σ^* valence-orbital set, thereby making $(n + 1)d$ the lowest *d*-type Rydberg orbital. In SF_6 however, the lowest *nd* orbitals ($n = 3$) do not participate in the bonding of the ground state and so the $3d$ orbitals are part of the Rydberg manifold instead.

II.H. General factors influencing observation of A *bands*

In a practical sense, the largest difficulty with spectroscopy terminating at σ^* is that the spectral bands are continuous and so are both difficult to separate from other continua in the same region and do not allow for vibronic or rotational analysis. For the $A(np,\sigma^*)$ transitions, the excitation can be phrased in terms of valence-bond structures

$$\mathrm{R}\cdot\cdot\ddot{\mathrm{X}} \xrightarrow{h\nu} \mathrm{R}\cdot:\dot{\mathrm{X}}$$

which clearly show why the upper state is dissociative. In fact, there are no known $A(np,\sigma^*)$ band excitations which show any vibronic structure whatsoever. On the other hand, for $\sigma \rightarrow \sigma^*$ excitation the appropriate valence-bond structures are:

$$\mathrm{R}\cdot\cdot\ddot{\mathrm{X}} \xrightarrow{h\nu} \{\mathrm{R}:^-\ \ddot{\mathrm{X}}^+ \leftrightarrow \mathrm{R}^+:\ddot{\mathrm{X}}^-\}$$

the upper state of which is not necessarily dissociative considering the Coulomb attraction between the R and X fragments. Indeed, the $\sigma \rightarrow \sigma^*$ excitations of the hydrogen halides (13) are highly nonvertical but vibrationally structured!

In general, one can say that A bands involving σ^* can be observed in inner- and outer-shell spectra when the single bond of interest is weak (bond strength less than 85 kcal/mol) so that the A band falls below the Rydberg traffic, or is very strong (approximately 125 kcal/mol or more) so that it lies above the ionization limit. Most interesting is the intermediate situation appropriate to molecules such as CH_4, CF_4, H_2O, PF_3, and BCl_3 in which the transitions to σ^* fall among the Rydberg excitations originating at the same lone pair MO. The ramifications of this situation are discussed in the next Section.

III. Valence miscibility with the Rydberg sea

III.A. Reality and coexistence of valence/Rydberg conjugates

The question of the mixing of valence/Rydberg conjugate orbitals and the real or imagined existence of such conjugate pairs remains unsettled in the literature (14–17), however, it is our position that pairs of conjugate orbitals do coexist. In support of the simultaneous reality of conjugate Rydberg and valence-shell states, we first quote the numerous highly accurate calculations on a variety of molecules which predict their existence. Thus for example, in HF, Bettendorf *et al.* (18) calculate that the valence $A(2p\pi,\sigma^*)$ band will be centered at 84 040 cm^{-1} with the upper state being repulsive, whereas the conjugate Rydberg transition to $(2p\pi,3s)$ is predicted to fall at 105 400 cm^{-1} with a bound upper-state surface. These predicted transitions of HF are closely parallel to the $A(5p\pi,\sigma^*)$ and Rydberg $5p\pi \rightarrow 6s$ conjugate bands of methyl iodide, about which there is no question. Interestingly, X-α calculations on H_2S which do not employ the LCAO format at all nonetheless predict the separate existence of $(5a_1,\sigma^*)$ and $(5a_1,3p\sigma)$ conjugate excited states (19). Finally, we mention that the inner-shell spectra of several second-row hydrides (Fig. 4, for example) clearly and indisputably show that conjugate valence shell and Rydberg excitations are seen in the same spectrum. Note also that conjugate valence shell and Rydberg excitations are well-documented in atomic spectra (20). Of course, the observation of both $A(np,\sigma^*)$ valence-shell bands and $np \rightarrow (n + 1)s$ Rydberg bands in a huge number of alkyl halides (cf. Table 1, for example) is even better evidence for the simultaneous existence of conjugate upper states.

III.B. Conjugate mixing and its consequences

Having stated our point of view as regards the reality of distinct valence-shell and Rydberg conjugate states, we next consider the possibility of their mixing. Unfortunately, the most revealing calculations on this point involve π^* upper orbitals rather than σ^*, however we believe the phenomenon applies to both and so present a discussion of the former as illustrative of the latter. Buenker and Peyerimhoff (21, 22) explain that in ethylene the (π,π^*) valence state and the conjugate $(\pi,3d_{xz})$ Rydberg state are mixed so that each becomes an approximately 50:50 mixture. The higher component in which (π,π^*) and $(\pi,3d_{xz})$ are out-of-phase, in a sense is the valence conjugate of the $(\pi,4d_{xz})$ Rydberg level and again there is strong mixing between these. In this way, significant (π,π^*) valence character is dispersed throughout the entire (π,nd_{xz}) Rydberg manifold. In the above example, the lowest level retains sufficient (π,π^*) character after mixing to be labelled as such, however, this is not necessarily always the case. As a counterexample, the $(1b_1,a_1\sigma^*)$ valence configuration of water is calculated to be so thoroughly mixed into the $(1b_1,ns)$ levels of the Rydberg sea (23) that it no longer contributes enough to any one state to merit calling that state "$(1b_1,a_1\sigma^*)$". This extreme miscibility of the valence-shell level and its conjugate Rydberg manifold is most apparent in the outer-shell spectra of the first-row and second-row hydrides, excepting the hydrogen halides. Note too that the miscibility of σ^* valence orbitals with the conjugate Rydberg sea can be selective, for in H_2S, the $a_1\sigma^*$ MO is totally miscible (as in H_2O), whereas the $b_2\sigma^*$ MO is not.

It is a fascinating question as to when an interloping valence level will be totally dissolved in the Rydberg sea and when it is only dampened by it. It is our experience that the miscibility of a valence level with its conjugate Rydberg sea is governed by two factors: energy and symmetry. Looking at the spectra and calculations, it appears that the distinct transitions to such valence-shell levels still appear when they are energetically at the edges of the sea and so only get their feet wet, i.e., when the interlopers precede the Rydberg parade (as in the alkyl halides), and when they follow it as shape resonances (as in BF_3). In the intermediate region, valence levels find themselves in a high density of symmetry-compatible Rydberg levels and so might readily lose their valence identity through mixing. This is reasonable in light of the inherently small mixing element that exists between large-radius Rydberg and small-radius valence-shell wavefunctions, meaning that wavefunction mixing can be effective only when the levels are near-degenerate. Because the valence interloper will fall below the Rydberg parade when its term value is significantly larger than that of the lowest conjugate Rydberg level, weak σ bonds, fluorination of the molecule or exciting from inner-shell orbitals will promote the appearance of such *A* bands.

Symmetry is the second important factor in determining the miscibility of a valence level with the conjugate Rydberg sea. Note that the valence/Rydberg mixing occurs at the MO level, and so will depend upon the overlap of these orbitals. If a particular manifold of Rydberg orbitals has a very high angular momentum then the orbitals will not penetrate the core and so will have a greatly diminished tendency to mix with the conjugate antibonding valence MO. Generalizing, an antibonding valence MO of *s* symmetry will be most likely to dissolve in the conjugate *ns* Rydberg sea when dipped into it, whereas *p*-symmetry and *d*-symmetry antibonding valence MO's will be much less apt to dissolve in their less-penetrating Rydberg manifolds. Thus we have a natural explanation for why the $(1b_1,a_1\sigma^*)$ valence configuration of water dissolves completely in the conjugate $(1b_1,nsa_1)$ Rydberg manifold whereas the (π,π^*) valence configuration of ethylene does not dissolve completely in the conjugate $(\pi,3d_{xz})$ Rydberg manifold. An antibonding MO of *f* symmetry offers the extreme case, for the *nf* Rydberg orbitals are quite nonpenetrating and there will be very little tendency indeed for overlap and dissolution. However, the symmetry of the molecule also must be high if the *f*-type valence orbital is to retain totally its valence character, for only in high-symmetry systems will the more-penetrating *ns* and *np* Rydberg seas have symmetry representations different from that of one or more components of *nf*. Examples of these principles at work are discussed below (cf. Section III.D).

Yet another factor working in the same direction as symmetry is that of the width of the Rydberg sea. Since this is typically 35 000 cm^{-1} for the *ns* Rydberg manifold but only 6 400 cm^{-1} for *nf*, one sees that the near-degeneracy criterion for strong mixing will be easier to fulfill for σ^* levels of *s* symmetry than for σ^* levels of *f* symmetry.

Consideration of the two factors discussed above leads to the conclusion that complete miscibility of the valence level $(a\sigma^*)$ with the conjugate Rydberg sea occurs when a totally symmetric valence level falls within a sea which is both totally symmetric and penetrating (*nsa*). In this case, the σ^* level no longer is a distinct entity, but exists only as a perturbation of the conjugate Rydberg orbitals. If the valence level is either above or below the Rydberg manifold and/or has a symmetry such that its conjugate Rydberg levels are less penetrating, as with *np*, *nd*, or *nf* orbitals, then the mixing is correspondingly reduced and a distinct σ^* valence-shell level exists.

Experimental proof of the complete dissolution of a valence orbital in the Rydberg sea will be difficult, for it is not easy to ascertain if a distinct σ^* level still exists among the Rydberg levels, or if it exists above them as a shape resonance. Perhaps only a high-quality calculation can settle the question in any particular case. Note however that the valence/Rydberg nature of a nominally valence-shell configuration cannot be assessed correctly by calculation unless the basis set is rather complete in the conjugate Rydberg orbitals. This is in contrast to the approach often used of implementing the Rydberg basis only when concerned directly with calculating the higher Rydberg states.

Because the properties of Rydberg and valence-shell states are so different, mixing of these two types of configurations can produce profound effects. The consequences of Rydberg/valence shell mixing are best illustrated by calculations on the $^1(\pi,\pi^*)$ and $^1(\pi,3d_{xz})$ configurations of ethylene (22, 24). Again, these are presented as illustrative of what effects Rydberg/valence miscibility might have on transitions to σ^* orbitals. Calculations show that the mixing matrix element between Rydberg and valence-shell configurations generally is largest when the two configurations differ by a one-electron promotion, i.e., when they are conjugate. In the case of ethylene, mixing with the $^1(\pi,nd_{xz})$ manifold lowers the $^1(\pi,\pi^*)$ frequency by ca. 7 000 cm^{-1}, and results in a final V-state orbital which has 45–50% Rydberg character. For reasons of spatial overlap, the $\pi \rightarrow \pi^*$ valence excitation of ethylene is far more intense than the conjugate $\pi \rightarrow nd_{xz}$ Rydberg excitations, and consequently the calculated *f* value for the $\pi \rightarrow \pi^*$ excitation decreases from 0.485 to 0.293 upon admitting nd_{xz} orbitals into the calculation. Though the "missing" oscillator strength is donated to the Rydberg excitations, it is not very noticeable in any one of them since it is distributed among all of the $\pi \rightarrow nd_{xz}$ transitions. The importance of Rydberg/ valence-shell mixing on the *f* values in atoms also has been noted (20).

As expected, the values of $\langle x^2 \rangle$ for the out-of-plane *x* coordinate computed for valence shell and Rydberg MO's in planar molecules vary sharply depending upon orbital type. Thus for the π^* valence MO in the $^3(\pi,\pi^*)$ state of ethylene, $\langle x^2 \rangle$ is $3.88a_0^2$, while for $3d_{xz}$ in $^1(\pi,3d_{xz})$ it swells to $53.6a_0^2$; the π^* MO of mixed character in $^1(\pi,\pi^*)$ has the intermediate value $24.3a_0^2$. Another measure of spatial extent is offered by the Coulomb self-energy integral J_{jj} in the (ϕ_i,ϕ_j) configuration; the value of J_{jj} decreases with increasing ϕ_j orbital size, and in fact can be used as a criterion on which to base a Rydberg/ valence-shell assignment. One sees that valence-shell excitations terminating both at π^* and σ^* have computed upper orbital self-energies in the 70 000 – 95 000 cm^{-1} range whereas the Rydberg orbital self-energies occupy the 0 – 32 000 cm^{-1} range, depending upon their term values (1). Interestingly, the π^* self-energy of the $^1(\pi,\pi^*)$ valence-shell configuration after mixing, 32 500 cm^{-1}, is far below that normally assigned to valence-shell states, but at the top of the Rydberg range, a clear indication of its heavy Rydberg admixture. In contrast, the π^* self-energy for the $^1(1s,\pi^*)$ level of ethylene, 93 600 cm^{-1}, is solidly in the valence-shell camp, as appropriate for a purely valence configuration. With the exception of the $^1(\pi,\pi^*)$ level, the J_{jj} self-energies of (ϕ_i,ϕ_j) configurations of ethylene are very much independent of the open-shell orbital ϕ_i.

It is generally true that the Franck–Condon envelopes of the lowest Rydberg excitation in a molecule and the corresponding photoelectron band are identical (4). However, if a (ϕ_i,σ^*) valence level is strongly mixed with the (ϕ_i,ns) conjugate Rydberg levels such that they are dissociative and rapidly

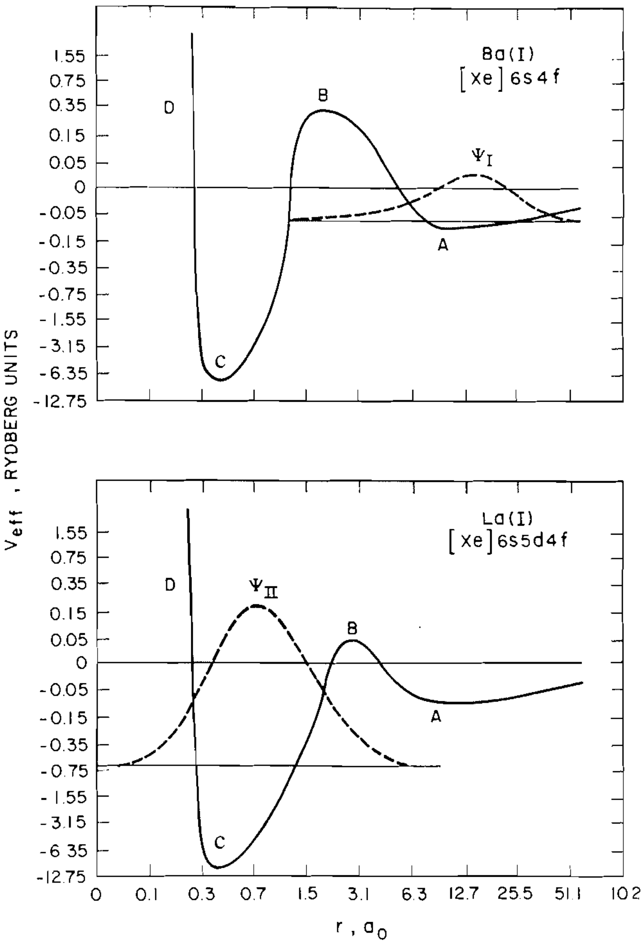

FIG. 5. Inner and outer wells and their wavefunctions.

deRydbergize with distance whereas the ϕ_i^{-1} ion is not so mixed, then the vibronic envelopes for the $\phi_i \rightarrow 3s$ and $\phi_i \rightarrow \infty$ transitions will be noticeably different. Thus, for example, the extreme differences of the $\phi_i \rightarrow 3s$ Rydberg and ϕ_i^{-1} photoelectron band profiles in H_2O, CH_4, H_2S, and HCOOH result from the strong mixing of their lowest Rydberg levels with their valence conjugates. On the other hand, such mixing is much weaker in NH_3 and effectively nonexistent in the alkyl chlorides, bromides, and iodides, for example.

If the $\phi_i \rightarrow a_1\sigma^*$ excitation is not observed below the Rydberg bands originating at ϕ_i, and does not mix with them as evidenced by the close similarity of the $\phi_i \rightarrow 3s$ and ϕ_i^{-1} band shapes, then it seems safe to conclude that $a_1\sigma^*$ is suspended in the ϕ_i^{-1} ionization continuum as a shape resonance. This argument does not hold for σ^* MO's which are less than totally symmetric, for these cases the conjugate Rydberg orbitals are only weakly penetrating and do not mix very well with σ^* regardless of their relative frequencies.

III.C. Conjugate unmixing

Provided the Rydberg/valence-shell mixing is not too extreme, it is possible to experimentally deperturb these levels. Thus any of the well-known external perturbations which are so effective in helping to distinguish valence-shell from Rydberg excitations (4) also are effective in removing the effects of Rydberg perturbations on valence-shell transitions. Interacting Rydberg and valence-shell levels also can be deperturbed by first producing an inner-shell hole which then shifts the offending Rydberg levels of the resulting ion far out of resonance with the valence-shell level of interest.

In addition to configurational mixing, it is now well documented that the mixing and unmixing of Rydberg and valence conjugates in molecules can be induced by changes of internuclear distance. Thus, for example, in each of the hydrides CH_4, C_2H_5, SiH_4, NH_3, PH_3, CH_3, and H_2O it has been computed that at the ground-state geometry, the first excited state of the same spin multiplicity is overwhelmingly Rydberg, as measured by any criterion. However, as either a hydrogen atom or a hydrogen molecule leaves the molecule, the Rydberg state in question rapidly evolves into a valence-shell state of the system, passing through all degrees of mixture on the way to total separation (deRydbergization). In this case, the increasing bond length leads to a decreasing $\sigma \rightarrow \sigma^*$ split. Consequently, the σ^* level quickly drops below the band of conjugate Rydberg levels, the mixing is turned off, and the eventual dissociation products have valence-shell configurations (17). It may also happen that at the ground-state equilibrium geometry, the σ^* valence MO is above the block of Rydberg levels so that $\phi_i \rightarrow \sigma^*$ is a shape resonance. In this case, as the relevant bond is lengthened, σ^* first comes into resonance with the Rydberg sea and assumes a strong Rydberg character before passing out the other side and becoming valence again at very large distances. These aspects of Rydberg/valence shell mixing are of extreme importance to a discussion of photochemistry in the vacuum ultraviolet, and the interested reader is referred to a number of papers in which the subject is explored in depth (17, 25–28). The rapidly changing Rydberg/valence-shell character of a potential surface raises a question of semantics for the photochemist who is concerned with its broadest reaches, however this is not as confounding for the spectroscopist who works closely in the vicinity of the ground-state R_e. Nonetheless, we must emphasize that even at R_e the mixing may be such that neither "valence" nor "Rydberg" designations are adequate.

III.D. Molecular giant resonances as manifestations of σ^* immiscibility

There is a fascinating development taking form in atomic spectroscopy which not only appears to have strong parallels in the area of molecular Rydberg/valence mixing, but impacts directly on the question of observing $\sigma \rightarrow \sigma^*$ valence shell excitations in saturated molecules. Consider the effective radial potential in an atom (V_{eff}) as consisting of a Coulombic term $(-1/r)$ and a centrifugal term $l(l+1)/r^2$ as plotted in Fig. 5 for the $4f$ orbital of lanthanum in the [Xe]$6s5d4f$ configuration. As Connerade explains (29, 30), in region A the Coulombic part of the potential is dominant, however as r decreases, the centrifugal effect acts to raise the potential, as in region B. Once into region B however, the electron then is able to penetrate the core more effectively, thereby experiencing a higher effective nuclear charge and so lowering the potential again, as in region C. Finally, at very short distances, region D, the $1/r^2$ dependence of the centrifugal potential overcomes the $-1/r$ dependence of the Coulombic potential and V_{eff} rises abruptly. The net result of these two competing potential terms in the case of atomic orbitals having $l \geqslant 2$ is a double-well effective potential. The hump in region II is called the centrifugal barrier, but in fairness it must be noted that it is due equally to the effect of penetration, and does not even appear in the hydrogen atom where penetration is not possible.

Figure 5 shows the double-well V_{eff} for $4f$ orbitals in the excited states of both the lanthanum and barium atoms, and as expected for neighboring atoms in the periodic table, the curves are semiquantitatively alike. What is most surprising to see is that the corresponding $4f$ wavefunctions are exceedingly different, with that in the [Xe]$6s4f$ configuration of Ba occupying the outer well and peaked at ca. $15a_0$, whereas that in the [Xe]$6s5d4f$ configuration of La occupies the inner well and is peaked at less than $1a_0$!! The $4f$ orbital in the Ba excited state is properly termed a Rydberg orbital due to its size and due to the fact that its energy is dictated largely by the $-1/r$ part of the potential. On the other hand, this is clearly not the case for the $4f$ orbital of La trapped in the inner well of region C, and so this is termed a "nonRydberg" orbital (29). Moreover, as is known for double-well potentials in general, even slight differences between the two well profiles are sufficient to shift the electron from one well to the other. Wavefunction collapse results from the transfer of the electron from the outer to the inner well. Only with very fine tuning is one able to get the wavefunction to occupy both wells simultaneously. Considerable theoretical and experimental work on atoms is now available to support the notion of large-l wavefunction collapse under relatively small perturbation.

In our attempt to apply this type of reasoning to molecules we first must discard the centrifugal potential because we wish to apply the double-well concept to states where l may equal zero or to low-symmetry molecules in which the angular momentum is quenched (31). In its place, we invoke a spatial modulation of the potential due to the spatially extended nature of the molecular core. In the molecular case, the repulsive hump comes not from the combination of centrifugal force and penetration, but from the orthogonality to the molecular bonds in the core. Depending upon the details of the potential, the lowest level may be strongly compressed (Ψ_I) or expanded (Ψ_{II}); after proper orthogonalization to the occupied core orbitals, these functions are seen to be antibonding valence-shell orbitals (σ^*, π^*, δ^*, etc., depending upon unspecified angular factors) and their Rydberg conjugates (*ns*, *np*π, *nd*δ, etc.), respectively. Arguing as in the atomic case, we expect that relatively small changes of potential will suffice to change drastically the nature of the lowest bound level, and in certain conditions can lead to a wavefunction which is a linear combination of Ψ_I and Ψ_{II}.

We have forced a parallel between the atomic and molecular potentials and then argued for analogous behavior in the two models largely because there are notable similarities in the experimental observations on Rydberg/nonRydberg spectra in atoms and on Rydberg/valence-shell mixing and ordering in molecules. Following the description of the atomic spectra given by Connerade (29) we note the following analogies:

(*i*) In atoms, the two states of the double-well potential are small radius (nonRydberg) and large radius (Rydberg). In molecules, the two states of the double-well potential are small radius (antibonding valence shell) and large radius (Rydberg).

(*ii*) As the effective potential for an atom is varied, the lowest level in the outer well may collapse into the inner well. As the M—H bond in a molecule is continuously lengthened, the lowest Rydberg level may be rapidly transformed (deRydbergized) into an antibonding valence level.

(*iii*) Atomic resonances to inner-well levels (*giant resonances*) are much more intense than transitions to outer-well levels (Rydberg excitations) for reasons of spatial overlap between the originating and terminating orbitals. Inner-shell molecular transitions to valence levels are much more intense than transitions to Rydberg levels for reasons of spatial overlap.

(*iv*) Atomic transitions to inner-well levels (giant resonances) appear in solids whereas those to outer-well Rydberg levels generally do not. This parallels exactly the behavior of valence-shell and Rydberg upper states in molecules.

(*v*) When the outer-well wavefunction in an atom collapses to the inner well, the next higher outer-well level moves down and then plays the role of the lowest outer-well level. Energetically, this lowest level can be close to the position of the lowest level before collapse, however, by its node count it is one higher. Thus there is a semantic problem as to whether the lowest outer-well function after collapse should be assigned principal quantum number n or $n + 1$. Exactly the same problem has been pointed out in regard the numbering of Rydberg levels when preceded by a conjugate valence level (cf. ref. 4, p. 26, for example).

(*vi*) In atoms, the inner-well levels may be below (bound levels) or above the relevant ionization limit (resonantly localized continuum levels). A similar situation holds for the valence states of molecules.

In view of the many similarities between the atomic and molecular cases, it is important to point out an essential difference as well. In the atomic case, a double-well effective potential is inappropriate for s or p symmetries because of their zero or small l values. In contrast, s and p electrons in molecules may move in a double-well effective potential with distinct inner-well and outer-well wavefunctions provided the inner-well wavefunction does not dissolve completely in the sea of outer-well functions.

Much of what we are saying here is either explicitly or implicitly contained in Dehmer's original discussion (32) of the double-well model for molecular excited states. What we want to emphasize is that the inner well is associated with antibonding valence MO's and that relatively small differences of the shape of the effective potential can make the lowest level appear as Rydberg, antibonding valence, or a mixture of these.

By way of example, let us now apply this to a molecular system. In certain hydrides (alkanes) of high symmetry, there can be an antibonding valence MO with symmetry conjugate *only* to one of the *nf* Rydberg orbitals, which orbitals in turn are notoriously poor at penetration. In these cases the inner-well antibonding MO (χ^*) will not be mixed with its conjugate Rydberg levels even if quasi-degenerate with them. In this case, the allowed electric-dipole excitations to the χ^* level must originate at an MO (χ) having a d orbital or g orbital nodal pattern, and will be very intense compared to the Rydberg transitions terminating at the conjugate *nf* Rydberg orbitals for reasons of spatial overlap. Additionally, such $\chi \rightarrow \chi^*(d \rightarrow f)$ molecular giant resonance will not be perturbed on going from the vapor to a condensed phase since the terminating level does not have an expanded wavefunction. We must point out how unusual this situation is, for virtually all discrete absorptions in alkanes have been assigned successfully as Rydberg transitions (1, 4).

Just such a giant resonance can be found in the D_{3h} molecule cyclopropane. The uppermost filled MO of cyclopropane has E' symmetry and a few of the lower $3e' \rightarrow ns$ and $3e' \rightarrow np$ Rydberg excitations have been identified in the 50 000 – 70 000 cm^{-1} region (33), Fig. 6. Following these, there is a broad and very intense feature centered at 82 000 cm^{-1} which has been calculated to be a valence shell $3e' \rightarrow 1a_2'$ excitation. We note here that the oscillator strength of 0.7 observed for this band is unusually high in the extreme for an alkane (the absorption

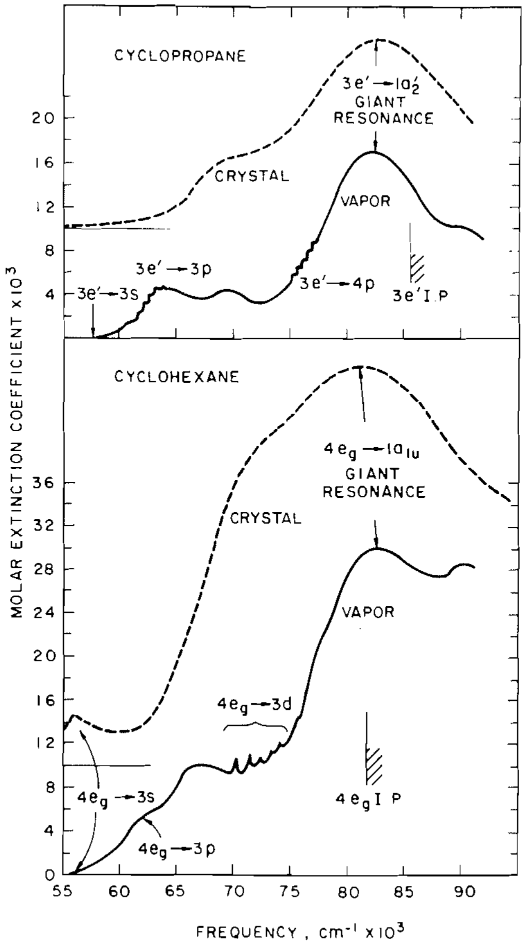

FIG. 6. The assignment of giant molecular resonances in the spectra of cyclopropane and cyclohexane (34).

cross section at the maximum is 68 Mb), and that spectra of thin films of cyclopropane, Fig. 6, show the band in question shifted slightly to 80 000 cm^{-1} but otherwise unperturbed. Finally, the χ^* MO of a_2' symmetry belongs to a representation which is unique to f orbitals in D_{3h}, whereas the $3e'$ MO has the symmetry of an atomic d orbital. Thus we see that the 82 000-cm^{-1} excitation of cyclopropane has the nodal properties of a $d \rightarrow f$ transition, however, since the a_2' terminating orbital is of the inner-well type the transition appears as a molecular giant resonance and is nonRydberg, *i.e.*, valence shell. It is amazing that the molecular analog of the $d \rightarrow f$ giant resonance of lanthanum at *ca.* 100 eV is to be found in cyclopropane at 10 eV! It also may be significant that both are found centered just at or above the ionization thresholds of the originating orbitals.

Arguing backward, the key features leading to a giant resonance in a polyatomic molecule are seen to be:

(*1*) The presence of an antibonding valence-shell orbital in the molecule which transforms like one of the components of the *nf* orbital manifold.

(*2*) Sufficiently high molecular symmetry so that the components of the *ns*, *np*, and *nd* Rydberg manifolds have symmetries different from that of the *f*-like antibonding valence-shell orbital and hence cannot mix with it.

(*3*) An originating valence MO of *d*-like atomic symmetry, thereby resulting in intense $d \rightarrow f$ dipole excitation.

Using the above criteria, we have searched for other $d \rightarrow f$ giant resonances in polyatomic molecules, and feel that others exist in cyclohexane (Fig. 6) and uranium hexafluoride (34).

III.E. Other cases of low-lying σ^* orbitals

We have established the idea that excitations to σ^* levels will lie below the Rydberg manifold and not be mixed with it provided the $\sigma \rightarrow \sigma^*$ split is not too large. This comes about not only when the M—X bond is inherently weak, but also when the molecule is severely strained. Thus a low-lying $\sigma \rightarrow \sigma^*$ excitation of strong valence character is expected in a molecule such as quadricyclane with its very long base bonds. There is no spectral data available as yet on systems such as this.

Yet another mechanism by which σ^* can be made relatively low-lying is by fluorinating a planar unsaturated system. In this case, the perfluoro effect (35) acts to dramatically lower the σ and σ^* manifolds with respect to π and π^*. This relative shift of *ca.* 2 eV between the centers of gravity of the π/π^* and σ/σ^* orbital sets is enough to bring $\pi \rightarrow \sigma^*$ out of the Rydberg woods and into the open. As examples, we note the prominent $\pi \rightarrow \sigma^*$ valence-shell bands in the spectra of the fluoroethylenes and in the fluorobenzenes (1, 36). Note however, that if the system is nonplanar, as in CH_3-containing olefins for example, both the π/π^* and σ/σ^* manifolds are depressed upon fluorination, with little or no depression of the $\pi \rightarrow \sigma^*$ interval.

A rare but well-documented example of a $\sigma \rightarrow \sigma^*$ excitation in a polyatomic molecule is the $3\sigma_g \rightarrow 3\sigma_u^*$ transition of acetylene at 107 500 cm^{-1}. In this case, the transition is just below the conjugate ($3\sigma_g$, *np*) Rydberg levels, and though it must be mixed somewhat with them, it has resisted total dissolution for reasons having to do both with frequency and symmetry. Less well-documented as $\sigma \rightarrow \sigma^*$ excitations are the intense transitions in the longer perfluoroalkanes (4); solid-film spectra of these systems would be most interesting. In π-electron systems, the fate of $\sigma \rightarrow \sigma^*$ excitations is especially cloudy inasmuch as there is strong mixing of (σ,σ^*) configurations with the highly polar (π,π^*) configurations, as discussed by Mulliken (37).

IV. Conclusions

Our overall study of excitations to σ^* lead us to a number of conclusions:

(*i*) Term values are of great use in correlating *A*-band transitions terminating at σ^*, even though these are valence excitations and the concept usually is reserved for Rydberg excitations.

(*ii*) The *A*-band term value is strongly dependent upon the strength of the σ bond appropriate to σ^*.

(*iii*) The *A*-band term values of the outer shell are enhanced in the inner-shell spectra by antishielding, *i.e.*, an enhanced effective nuclear charge for σ^* in the inner-shell spectra.

(*iv*) There is considerable evidence in favor of the simultaneous existence of both valence-shell states terminating at σ^* and their Rydberg conjugates.

(*v*) Contrary to expectations, *A* bands do not always appear in molecular spectra. Their appearance is strongly affected by the extent of valence/Rydberg miscibility, which in turn depends upon how closely the *A* band and Rydberg manifold match in frequency, and upon the ability of the Rydberg levels to overlap the valence level via penetration.

(*vi*) The $\sigma \rightarrow \sigma^*$ valence excitations are rare, but can appear as giant resonances in certain molecules of high symmetry.

(*vii*) Excitations of the sort $\pi \rightarrow \sigma^*$ in planar unsaturated systems are a regular feature in halogen-substituted systems. Heavy fluorination accentuates the prominence of $\pi \rightarrow \sigma^*$ excitations.

1. M. B. ROBIN. Higher excited states of polyatomic molecules. Vol. III. Academic Press. 1985.
2. C. SANDORFY. *In* Sigma molecular orbital theory. *Edited by* O. Sinanoglu and K. B. Wiberg. Yale University Press, New Haven. 1970. p. 130.
3. K. KIMURA and S. NAGAKURA. Spectrochim. Acta. **17**, 166 (1961).
4. M. B. ROBIN. Higher excited states of polyatomic molecules. Vol. I. Academic Press. 1974.
5. R. S. MULLIKEN. J. Chem. Phys. **3**, 517 (1935).
6. G. C. CAUSLEY and B. R. RUSSELL. J. Electron Spectrosc. Related Phenomena, **11**, 383 (1977).
7. E. ISHIGURO, S. IWATA, Y. SUZUKI, A. MIKUNI, and T. SASAKI. J. Phys. B: At. Mol. Phys. **15**, 1841 (1982).
8. H. FRIEDRICH, B. SONNTAG, P. RABE, W. BUTSCHER, and W. H. E. SCHWARZ. Chem. Phys. Lett. **64**, 360 (1979).
9. P. D. BURROW, A. MODELLI, N. S. CHIU, and K. D. JORDAN. J. Chem. Phys. **77**, 2699 (1982).
10. M. B. ROBIN and N. A. KUEBLER. J. Electron Spectrosc. Related Phenomena, **1**, 13 (1972).
11. W. H. E. SCHWARZ. Chem. Phys. **9**, 157 (1975).
12. P. DAUBER and M. BRITH. Chem. Phys. **11**, 143 (1975).
13. J. G. STAMPER, and R. F. BARROW. J. Phys. Chem. **65**, 250 (1961).
14. R. S. Mulliken. Acc. Chem. Res. **9**, 7 (1976).
15. R. S. MULLIKEN. Chem. Phys. Lett. **46**, 197 (1977).
16. O. SINANOGLU. *In* Chemical spectroscopy and photochemistry in the vacuum-ultraviolet. *Edited by* C. Sandorfy, P. J. Ausloos, and M. B. Robin. D. Reidel, Dordrecht. 1974. p. 337.
17. J.-P. MALRIEU. Theoret. Chim. Acta, **59**, 251 (1981).
18. M. BETTENDORF, R. J. BUENKER, S. D. PEYERIMHOFF, and J. RÖMELT. Z. Phys. **304A**, 125 (1982).
19. R. ROBERGE and D. R. SALAHUB. J. Chem. Phys. **70**, 1177 (1979).
20. W. L. LUKEN. Chem. Phys. Lett. **61**, 162 (1979).
21. R. J. BUENKER and S. D. PEYERIMHOFF. Chem. Phys. Lett. **36**, 415 (1975).
22. S. D. PEYERIMHOFF. Gazz. Chim. Ital. **108**, 411 (1978).
23. V. STAEMMLER, R. JAQUET, and M. JUNGEN. J. Chem. Phys. **74**, 1285 (1981).
24. H. NAKATSUJI. J. Chem. Phys. **80**, 3703 (1984).
25. E. M. EVLETH and E. KASSAB. *In* Computational theoretical organic chemistry. *Edited by* I. G. Csizmadia and R. Daudel. D. Reidel, Dordrecht. 1981. p. 379.
26. E. M. EVLETH and E. KASSAB. *In* Quantum theory of chemical reactions. Vol. II. *Edited by* R. Daudel, A. Pullman, L. Salem, and A. Veillard. D. Reidel, Dordrecht. 1980. p. 261.
27. C. SANDORFY. Z. Phys. Chem. **101**, 307 (1976).
28. C. SANDORFY. Prog. Theoret. Org. Chem. **2**, 384 (1977).
29. J. P. CONNERADE. Contemp. Phys. **19**, 415 (1978).
30. J. P. CONNERADE. J. Less Common Metals, **93**, 171 (1983).
31. C. R. NATOLI. *In* EXAFS and near edge structure. *Edited by* A. Bianconi, L. Incoccia, and S. Stipcich. Springer, New York. 1983. p. 43.
32. J. L. DEHMER. J. Chem. Phys. **56**, 4496 (1972).
33. H. BASCH, M. B. ROBIN, N. A. KUEBLER, C. BAKER, and D. W. TURNER. J. Chem. Phys. **51**, 52 (1969).
34. M. B. ROBIN. To be published.
35. C. R. BRUNDLE, M. B. ROBIN, N. A. KUEBLER, and H. BASCH. J. Am. Chem. Soc. **94**, 1451 (1972).
36. J. PHILIS, A. BOVOLINOS, G. ANDRITSOPOULOS, E. PANTOS, and P. TSEKERIS. J. Phys. B.: At. Mol. Phys. **14**, 3621 (1981).
37. R. S. MULLIKEN. Chem. Phys. Lett. **25**, 305 (1974).

Molecular conformation of ozone and thiozone: the transition state method

WILLIAM G. LAIDLAW
Chemistry Department, University of Calgary, Calgary, Alta., Canada T2N 1N4
AND
MILAN TRSIC
Instituto de Fisica e Quimica de Sao Carlos, University of Sao Paulo, P.O. Box 369, 13560 Sao Carlos, SP, Brazil

Received January 11, 1985

This paper is dedicated to Professor Camille Sandorfy on the occasion of his 65th birthday

WILLIAM G. LAIDLAW and MILAN TRSIC. Can. J. Chem. **63**, 2044 (1985).

The relative energy of the closed and open forms of ozone and thiozone are calculated using the HFS DVM transition state method. For ozone the open form is lower by some 21 kcal/mol and for thiozone the open form is some 11 kcal/mol lower.

WILLIAM G. LAIDLAW et MILAN TRSIC. Can. J. Chem. **63**, 2044 (1985).

Utilisant la méthode de l'état de transition de HFS DVM, on a calculé les énergies relatives des formes ouvertes et fermées de l'ozone et de la thiozone. Les niveaux énergétiques des formes ouvertes de l'ozone et de la thiozone sont respectivement 21 kcal/mol et 11 kcal/mol plus faibles que ceux des formes fermées.

[Traduit par le journal]

Introduction

By the mid 1970's the Hartree Fock Slater (HFS) method had been applied, with considerable success, to the calculation of ionization energies, electron excitation energies, and other one-electron properties (1). In 1978 we explored the use of the HFS "total statistical energy" as a measure of the expectation value of the hamiltonian by calculating the single determinant statistical energy for various conformations of ozone and thiozone (2). We utilized a STO double ζ basis set (3) augmented with a $3d$ orbital on sulfur (exponent 1.71 (2)) and employed several calculational techniques such as diophantine numerical integration and a fitting procedure for the electron density which had been pioneered by Ziegler, Baerends, and co-workers (1*a*–*d*). We refer to this algorithm as the HFS DVM scheme and utilize an exchange coupling of $\alpha = 0.7$. The energy contributions which appeared sensitive to the numerical integration steps were calculated analytically following a method of Baerends and Ros (4). Our results indicated that the closed form (all three nuclei equidistant from one another) of both ozone and thiozone were lower in energy than the open form by some 40 kcal/mol. This result for ozone was certainly at variance with its known conformation (5). However, our results were comparable to rather good quality HF single determinant calculations which also predicted the closed form for these molecules (6). We concluded that the HFS statistical energy was at least as good a predictor as the Hartree Fock energy.

In the past half dozen years the evaluation of the energy in the Hartree Fock Slater context has received additional attention. The transition state method of Ziegler and co-workers (7) has shown great promise, especially for larger systems (8). Most recently the calculations of Morin, Foti, and Salahub (9) for the statistical energy of ozone and thiozone, using their HFS (LCAO-Xα and LCAO-Local Density (10)) procedures; renewed our interest in the problem. Consequently we have investigated the conformational energy of ozone and thiozone using, now, the transition state method (7).

The transition state method

The essence of the transition state method for bond energy is the *direct* calculation of the difference in energy of the molecule and the chosen reference fragments (usually atoms). In other words, one does *not* calculate separately the energy of molecule and the energy of its reference and then subtract the two. Rather one derives an expression for the energy difference and calculates this directly. The critical step in this procedure, for a molecule AB, is the introduction of the atomic (i.e. fragment) densities ρ_A and ρ_B, the molecular density $\rho_{\overline{AB}}$ and a transition state density

$$\rho_T = \frac{1}{2}(\rho_A + \rho_B + \rho_{\overline{AB}})$$

Since the statistical energy (the HFS representation of the expectation value of the hamiltonian H) is a functional of the density, the energy difference, $\Delta E = E_{AB} - (E_A + E_B)$, is a direct function of ρ_A, ρ_B, and $\rho_{\overline{AB}}$. Ziegler and Rauk (7) have shown that

$$[1] \quad \Delta E = -E_{cl} - \Delta E_{cx} - \sum_{ij} F_{ij}\Delta P_{ij}$$

where E_{cl} is the classical electronic energy of two distributions ρ_A and ρ_B and their associated nuclear repulsions, ΔE_{cx} is the difference between the HFS exchange interaction of $\rho_{\overline{AB}}$ and that of ρ_A and ρ_B and F_{ij} is a Taylor expansion around the transition state of matrix elements of the one-electron HFS hamiltonian operator h. The result given in eq. [1] is correct to third order in a Taylor expansion around the transition state density ρ_T.

Results

Using the same basis set and the same frozen core approximation as in our earlier work we calculated the bond energy ΔE of eq. [1] directly for both thiozone and ozone. Two electronic configurations $a_1^8a_2^2b_1^6b_2^2$ and $a_1^8a_2^2b_1^4b_2^4$ were considered and both the bond lengths and the bond angles were varied within C_{2v} symmetry to obtain the minimum bond energy ΔE (note, ΔE is negative). The result obtained for ozone showed that the minimum ΔE for the open form,

$$a_1^8a_2^2b_1^6b_2^2 \equiv 1a_1^2\ 1b_2^2\ 2a_1^2\ 2b_2^2\ 1b_1^2\ 3a_1^2\ 1a_2^2\ 3b_2^2\ 4a_1^2 \quad \text{(i.e., } 4\pi)$$

is obtained at a central angle of 120° and bond length 1.30 Å whereas the minimum ΔE for the closed form

$$a_1^8a_1^2b_1^4b_2^4 \equiv 1a_1^2(2a_1^2\ 1b_2^2)3a_1^2\ 1b_1^2(2b_2^2\ 4a_1^2)\ (1a_2^2\ 2b_1^2)(\text{i.e. } 6\pi)$$

was obtained for an equilateral form with a bond length of 1.45 Å. The open form is the lower by some 21 kcal/mol. The recent calculation by Morin *et al.* (9) using their versions of the HFS procedure favours the open form of ozone by some 45 kcal/mol whereas rather sophisticated CI treatments give the open form as lower by some 21 ± 5 kcal/mol (11*a*) or 28 kcal/mol (11*b*) or 38 kcal/mol (11*c*). The bond length 1.30 Å and bond angle 120° for the open form of ozone are to be compared to the experimental values in the range 1.28 Å for the bond lengths and 117° for the central angle (5). For thiozone a similar calculation for the minimum ΔE yields an open form,

$$a_1^8a_2^2b_1^6b_2^2 \equiv 1a_1^2\ 1b_2^2\ 2a_1^2\ 2b_2^2\ 1b_1^2\ 3a_1^2\ 1a_2^2\ 3b_2^2\ 4a_1^2$$

with a bond length of 1.95 Å and central angle of 120° whereas the closed form

$$a_1^8a_2^2b_1^4b_2^4 \equiv 1a_1^2(2a_1^2\ 1b_2^2)3a_1^2\ 1b_1^2(4a_1^2\ 2b_2^2)\ (2b_1^2\ 1a_2^2)$$

minimum has the equilateral form with a bond length of 2.06 Å. The open form of thiozone is lower than the closed form by some 11 kcal/mol which may be compared with 15 kcal/mol obtained by Morin *et al.* (9) and with the 17 kcal/mol results given in recent CI calculations (11*c*).

These results are in contrast to that reported in our earlier calculation (2) and are in contrast to the HF single determinant results, cf. ref. 6. However, they show the same preference for the open form given recently by Morin *et al.* (9) using their version of the HFS approach and of course are consistent with the known form for ozone (5) and with CI calculations for ozone (11*a*, 11*b*) and for thiozone (11*c*).

Discussion

The HFS SCF DVM scheme represents the molecular orbitals as an expansion in a chosen basis set (e.g. the Double ζ STOs) and develops the variational SCF problem in terms of the chosen basis set. However, for the sake of efficiency (a major consideration in the large molecules to which this procedure has been applied (8)) the density is always fitted by a least-squares procedure to a set of "fit functions". Further, the integrations required in the HFS SCF procedure are obtained numerically (diophantine point selection). We referred to this routine as the HFS DVM procedure.

It is relatively straightforward to increase the number of points in a numerical integration until stability is ensured and typically 1000 points per atom is sufficient for stability of one-electron properties. The generation of the best fit functions, although less direct, can be accomplished by using a family of STO *s, p,d*, etc. orbitals on each center with exponents chosen to span the space from diffuse to contracted. Again the precise choice does not materially affect one-electron properties. However, the numerical integration and fitting procedure do have serious implications for the calculation of the total energy of the system.

In 1978, Baerends and Ros (4) pointed out that the sensitivity to the number of points in the numerical integration can be overcome by evaluating all terms in the SCF energy except the exchange contribution by analytical rather than numerical integration. That is, the SCF electron density is fitted using the fit functions and inserted into the integrals contributing to the energy and these terms are then evaluated analytically. This reduces the sensitivity such that again about 1000 points per atom is sufficient for stability of the numerical integration. The sensitivity of the total statistical energy to the choice of fit functions can not so easily be removed since there is no straight forward criteria which can be applied, *a priori*, for all molecules. Consequently calculations of the total statistical energy by both Baerends and Ros (4) and by ourselves (2) were limited and all that appeared possible was that the results for total statistical energy using the HFS DVM algorithm were at least comparable to the Hartree Fock results.

However, the picture is much more positive using the transition state approach with the HFS DVM. We have already observed that certain terms in the total energy viz., the exchange term, ΔE_{ex}, were relatively insensitive to the numerical integration and fitting procedures. So also Ziegler and Rauk (7) found that the additional terms which are generated by the Taylor expansion in ΔE, i.e. the terms F_{ij}, in eq. [1], are relatively insensitive to the number of points in the numerical integration (in all cases tested 1000 points per atom achieved an accuracy to within 2 kcal per mol).[1]

The sensitivity to fit functions arises primarily through the term E_{el}. In the case of the transition state method, with atoms as fragments, E_{el} requires only atomic distributions. It is always easy to obtain optimum fit functions for atomic distributions (for the fit functions are generated automatically within the suite of programs and they are always *s*-type as befits a spherical distribution). The additional requirements that the molecular situation places on fit functions are not nearly as severe with the transition state calculation of ΔE as they were for the total statistical energy E. Nevertheless, we have augmented the standard fit set referred to above with fit functions including sets of *p* and *d* orbitals on each centre to generate an "extended molecular fit set". We have added yet more fit functions to our extended fit set and found no change in ΔE and we have *deleted* fit functions (e.g., *d*) and found some change (e.g., for thiozone deletion of *d* fit functions changed ΔE from −256 to −258 kcal/mol for the open form and from ΔE = −247 to −257 kcal/mol for the closed form for a change of about 4% in ΔE for the highly strained closed form where clearly the added flexibility of the expended fit set is necessary). We concluded that an extended set of fit functions are still essential and that our extended molecular fit set was approaching an optimal choice for thiozone.

This leaves choice of basis functions and the truncation procedure itself. Certainly the basis must be chosen with some care and perhaps the best criteria is comparison of experimental and calculated results. For diatomics the comparison of even just a DZ HFS basis vs. extended basis HF calculations as against experimental results is in favour of the HFS procedure and of course an extended basis HFS is normally an improvement (see Table 2 of ref. 7 for calculation results with DZ, and extended basis and comparison to HF and experimental results). In the calculations reported here the basis set is of DZ quality augmented by *d* functions.

Turning to the truncation procedure itself, perhaps the most telling point of the efficacy of the transition state method is

[1] See Table 1 of ref. 7 for calculations using 10^3, 10^4, 10^5 points for F_2. These results show that the term E_{el} is responsible for slow convergence and that the remaining terms in eq. [1] stabilize with, of the order of, 10^3 points. Our own tests, on thiozone with 1000, 2000, and 4000 points per atom gave values of ΔE of −247, −246, and −247 kcal/mol at R_{SS} = 2.1 Å for the closed form and −256, −255, and −256 kcal/mol at R_{SS} = 2.0 Å for the open form. This is a variation of ΔE of less than 2 kcal/mol.

comparison to experimental results for a variety of molecules. Rauk and Ziegler have shown in a number of cases, that the transition state method provides accurate representations of the bond energy when complete schemes, such as the HF, do not give the correct answer (see Table 2 of ref. 7 and also ref. 8). Indeed our calculation, giving the open form of ozone lower than the closed form by some 21 kcal/mol, compares favourably with the results of an extended CI calculation (11*a*). Consequently the truncation scheme appears to be satisfactory.

With these comments on numerical integration, fit functions, basis sets and truncation, in mind, we believe that eq. [1] is an appropriate representation of the bond energy, ΔE, in the HFS DVM scheme. That it is an adequate HFS probe of conformational energy is demonstrated by noting that it predicts that the open form is lower in energy than the closed for both thiozone and ozone — a result qualitatively similar to that of Salahub and co-workers (9) using their version of the HFS procedure.

Acknowledgements

The authors are pleased to acknowledge valuable conversations with Tom Ziegler and the use of programs developed by him and by the Amsterdam group of E. Baerends. We would also like to thank Dennis Salahub for stimulating us to repeat our work on S_3/O_3 and for his willingness to discuss, openly, his results prior to publication. Kim Wagstaff assisted with the calculations.

1. (*a*) E. J. BAERENDS, D. E. ELLIS, and P. ROS. Chem. Phys. **2**, 41 (1973); E. J. BAERENDS and P. ROS. Chem. Phys. **2**, 52 (1973); (*b*) E. J. BAERENDS and P. ROS. Chem. Phys. **8**, 412 (1975); M. TRSIC, T. ZIEGLER, and W. G. LAIDLAW. Chem. Phys. **15**, 383 (1976); (*c*) T. ZIEGLER, A. RAUK, and E. J. BAERENDS. Chem. Phys. **16**, 209 (1976); (*d*) T. ZIEGLER, A. RAUK, and E. J. BAERENDS. Theoret. Chim. Acta, (Berlin), **43**, 261 (1977); (*e*) M. TRSIC and W. G. LAIDLAW. Can. J. Chem. **56**, 1582 (1978).
2. W. G. LAIDLAW and M. TRSIC. Chem. Phys. **36**, 323 (1979).
3. E. CLEMENTI and C. ROETTI. At. Nucl. Data Tables, **14**, 177 (1974).
4. E. J. BAERENDS and P. ROS. Intl. J. Quantum Chem. Symp. **12**, 169 (1978).
5. G. HERZBERG. Electronic spectra of polyatomic molecules. Van Nostrand, Princeton. 1966.
6. N. R. CARLSEN and H. SCHAEFER. Chem. Phys. Lett. **48**, 390 (1977).
7. T. ZIEGLER and A. RAUK. Theoret. Chim. Acta, (Berlin), **46**, 1 (1977).
8. T. ZIEGLER. J. Am. Chem. Soc. **105**, 7543 (1983).
9. M. MORIN, A. E. FOTI, and D. R. SALAHUB. Can. J. Chem. **63**, 1982 (1985).
10. (*a*) H. SAUBE and R. H. FELTON. J. Chem. Phys. **62**, 1122 (1975); (*b*) B. I. DUNLAP, J. W. D. CONNOLLY, and J. R. SABIN. J. Chem. Phys. **71**, 3396 (1970); **71**, 4993 (1970).
11. (*a*) ROBERT R. LUCCHESE and H. F. SCHAEFFER, III. J. Chem. Phys. **67**, 848 (1977); (*b*) P. J. HAY and T. H. DUNNING JR. J. Chem. Phys. **67**, 2290 (1977); (*c*) W. L. FENG, O. NOVARRO, and J. GARCIA-PRIETO. Chem. Phys. Lett. **111**, 297 (1984).

Raman investigations of collective vibrational motions in van der Waals liquids[1]

S. BRATOS AND G. TARJUS

Laboratoire de Physique Théorique des Liquides,[2] Université Pierre et Marie Curie, Paris, France

Received December 11, 1984

This paper is dedicated to Professor Camille Sandorfy on the occasion of his 65th birthday

S. BRATOS and G. TARJUS. Can. J. Chem. **63**, 2047 (1985).

Recent investigations of collective vibrational motions in pure van der Waals liquids and in their isotopic mixtures are reviewed. Experimental data are enumerated first. The theory is presented later, separately, for non-composite and composite bands of both isotropic and anisotropic Raman spectra. It is shown that isotropic Raman processes are partially coherent and contain information about collective vibrational motions in liquids. In turn, anisotropic Raman processes are incoherent in the zero-order description and their study is less important in the present context.

S. BRATOS et G. TARJUS. Can. J. Chem. **63**, 2047 (1985).

Les études récentes des mouvements vibrationnels collectifs dans des liquides de van der Waals purs et dans leurs mélanges isotopiques sont examinées. Les données expérimentales sont décrites d'abord. La théorie est présentée ensuite, séparément pour les bandes Raman composées et pour les bandes Raman non-composées, tant isotropes qu'anisotropes. On montre que les processus Raman isotropes sont partiellement cohérents et qu'ils contiennent des informations relatives aux mouvements vibrationnels collectifs dans les liquides. Par contre, les processus Raman anisotropes sont incohérents, dans la description d'ordre zéro au moins, et leur étude est moins importante dans le présent contexte.

[Traduit par le journal]

1. Introduction

Considerable interest has been manifested over the last decade in studying collective vibrational and rotational motions in liquids by Raman spectroscopy. The possibilities offered by this technique were not immediately recognized. In fact, the phases of molecular vibrations in dense fluids were considered in the early work to be randomly distributed, an assumption called the random phase assumption. A Raman process was thus believed to be intrinsically incoherent, incapable of giving any information about collective motions in liquids. However, recent investigations have shown that these processes may, in fact, be partially coherent. Raman spectroscopy was thus adopted, over the last few years, by scientists studying this problem. The purpose of the present paper is to review this subject, currently in rapid evolution. It will be shown that, although considerable progress has been made, the field still is far from maturity. For general reviews on vibrational spectroscopy of dense fluids see, e.g., refs. 1 and 2.

2. Experimental data

It is convenient to start this discussion by briefly presenting the basic experimental material submitted to a theoretical analysis in later sections. In the early work, collective vibrational effects were studied by diluting the liquid progressively in the usual "chemical" solvents (3–10). Unfortunately, diluting a liquid modifies the force law and the answer is rarely nonambiguous. All modern work thus employs the isotopic dilution technique, which is free of this complication (11–19). Progress has been accelerated by the existence of theories which influenced the proper choice of experiment. The main experimental data collected in this way are described below. They refer to pure liquids and to their isotopic solutions, if not stated otherwise.

The main characteristics of isotropic spectra are enumerated first. (*i*) Their bands are broader in pure liquids than in dilute solutions. This was shown quantitatively by Oehme and Klostermann (20) for the ν HBr and ν DBr bands in mixtures HBr/DBr and by Pinan-Lucarré (21) for the ν_2 band of CD_3I in mixtures CD_3I/CH_3I; see also ref. 22. (*ii*) The position of an isotropic Raman band is a linear function of concentration of the active species, whereas its half-width may exhibit a nonlinear concentration dependence. First discovered in "chemical" solvents by Bondarev and Mardaeva (23), Fujiyama *et al.* (24), Arndt and co-workers (25–27), Yarwood, Ackroyd *et al.* (28), and Scheibe (29), it was also reported by Kamoun and Mirone (30), Döge *et al.* (31), and Oehme and Klostermann (20) in the case of isotopic solutions. (*iii*) The half-width of an isotropic Raman band varies with temperature, but no simple rule seems to exist. The constant pressure and variable temperature experiment by Döge *et al.* (32) on the ν_1, ν_2, and ν_3 bands of liquids CH_3I showed that some bands narrow with increasing temperature, whereas some others broaden.

As far as the anisotropic spectra are concerned, they show a noticeably different behavior. (*i*) Little broadening of these bands takes place when going from dilute solutions to pure liquids. This observation due to Pinan-Luccaré and to Oehme and Klostermann was described in the papers cited earlier. (*ii*) The peak frequency of an anisotropic Raman band is much less concentration dependent than the peak frequency of the corresponding isotropic Raman band (20). (*iii*) The isotropic and anisotropic Raman bands do not coincide; this effect is called the "non-coincidence effect". First observed in pure liquids by Schwartz and Wang (33), it was studied in liquids and binary mixtures by Fini and Mirone (34), Perchard and Perchard (35), Korsunskii *et al.* (36), Mirone and Fini (37), and by Desbat and Huong (38); to our knowledge, it has not yet been examined in isotopic mixtures. The result from these data is that resonant interactions in pure liquids and isotopic mixtures affect differently the isotropic and anisotropic Raman spectra. For some reason, their action is quenched to a considerable extent in the latter case. One of the tasks with which the theory is confronted is to explain this difference.

[1]This paper was presented to the EMLG conference "Beyond the Monomolecular Approach" which took place in Nice, from September 3 to 8, 1984.

[2]Equipe Associée au CNRS.

3. Theory. Non-composite Raman bands of pure liquids

(a) *Generalities*

Although the essential role of the resonant intermolecular coupling was correctly understood as early as 1960 (39), the theory of Raman bands of pure van der Waals liquids really started only thirteen years later. The first contribution was due to Döge, who proposed a crude picture of vibrational exciton transfer effects in Raman spectra (40). Later, Lynden-Bell showed how these effects are influenced by the symmetry of molecular vibrations (41). Analytical theories of band shapes appeared in 1977–1978, proposed nearly simultaneously by Wang (42), Wertheimer (43), and Oxtoby (1). They all concern the case of rapidly modulated isotropic Raman bands. Computer simulation techniques were introduced in this field in 1978 by Oxtoby *et al.* (44). Finally, the theory was extended in 1981 by Bratos and Tarjus (45); it applies to isotropic Raman spectra of arbitrary modulation speed and to anisotropic Raman spectra. These theories will be discussed in the present paper by taking the Bratos–Tarjus theory as a basis of discussion. In fact, this theory is general enough to encompass all previous work.

(b) *Method of calculation*

(1) The theory to be presented concerns a diatomic molecular liquid, the simplest prototype of molecular liquids. This choice is imposed by the need to eliminate, in a first analysis, such complicating features as harmonic and anharmonic coupling between various molecular vibrators, existence of different energy relaxation mechanisms, etc. A proper account of these effects seems beyond the scope of the majority of cases.

If an electromagnetic wave of frequency ω_0 is scattered from such a system, the isotropic and the anisotropic Raman differential cross-sections may be written

$$[1a]\quad \left[\frac{\partial^2\sigma}{\partial\omega\partial\Omega}\right]_{\text{iso}} = \frac{1}{2\pi} K_s^4 \int_{-\infty}^{+\infty} \mathrm{d}t\, e^{-i\omega t} \sum_{i,j} \langle a_{0i}^{(0)}(0)\, a_{0j}^{(0)}(t)\rangle$$

$$[1b]\quad \left[\frac{\partial^2\sigma}{\partial\omega\partial\Omega}\right]_{\text{ani}} = \frac{1}{2\pi} K_s^4 \int_{-\infty}^{+\infty} \mathrm{d}t\, e^{-i\omega t} \sum_{i,j} \langle a_{0i}^{(2)}(0)\, a_{0j}^{(2)}(t)\rangle$$

In these formulas, $a_{0i}^{(0)}$, $a_{0j}^{(0)}$, $a_{0i}^{(2)}$, $a_{0j}^{(2)}$ represent spherical components of the Raman polarizability tensors of various molecules. Moreover, ω is the difference between the frequencies of the scattered and incident light. Equations [1*a*, *b*] represent the basis of the subsequent discussion.

(2) The following model is used in this section. (*i*) The molecules are executing anharmonic vibrations described by internal vibrational coordinates $r = (r_1, r_2, \ldots, r_N)$. They are perturbed by a stochastic potential $V(r,t)$ expressing molecular interactions. The corresponding semi-classical Hamiltonian can be written:

$$[2]\quad H(r,t) = \left[\frac{1}{2}\sum_{i=1}^{N} p_i^2 + \frac{1}{2}\sum_{i=1}^{N} K r_i^2 + \frac{1}{6}\sum_{i=1}^{N} f r_i^3 + \ldots\right] + \left[\sum_{i=1}^{N} V_i(t) r_i + \frac{1}{2}\sum_{i,j=1}^{N} V_{ij}(t) r_i r_j + \frac{1}{6}\sum_{i,j,k=1}^{N} V_{ijk}(t) r_i r_j r_k + \ldots\right]$$

$V_i(t)$, $V_{ii}(t)$, $V_{iii}(t)$, etc. give rise to environmental fluctuations of vibrational frequency whereas $V_{ij}(t)$, $V_{ijk}(t)$, etc. describe the resonant intermolecular coupling. (*ii*) The molecules of the liquid are executing stochastic reorientations and translations. (*iii*) The correlation between vibrations and rotations, although present, is weak. (*iv*) There is no collision-induced scattering.

The validity of these assumptions merits discussion. The assumptions (*i*) and (*ii*) are of general use in the spectroscopy of liquids and are justified in the majority of cases of practical interest. The assumption (*iii*) is much more questionable. It was studied by Levesque *et al.* who employed molecular dynamics techniques (46) and by Tarjus and Bratos who used analytical methods (47). These investigations showed that the simple product approximation is surprisingly accurate and that the use of assumption (*iii*) is legitimate. Unfortunately, no definite statement can be made about assumption (*iv*). The error introduced by treating collision-induced processes separately is totally unknown.

(3) The central part of the present problem is to calculate the vibrations of a set of N-coupled vibrators evolving in a spatially and temporally disordered medium. Its counterpart in the ordered crystalline phase has been carefully examined by Born and Huang, Davidov, and many others. The basic equations are the Heisenberg equations of motion for the variables r_i. Then, (*i*) choosing a basic set composed of non-excited and mono-excited anharmonic vibrator wave functions, (*ii*) defining a frequency matrix where $\hbar\,\Omega_{st} = \langle s|V|t\rangle - \delta_{st}\langle 0|V|0\rangle$, (*iii*) suppressing in the Hamiltonian matrix all elements which connect vibrational states of different degree of excitation, and (*iv*) considering the basic equations [1*a*, *b*] of the theory, there results:

$$[3a]\quad G^{(0)}(t) = \sum_{ij} \langle a_{0i}^{(0)}(0)\, a_{0j}^{(0)}(t)\rangle = \frac{N\hbar}{2\mu\omega_0}\left(\frac{\partial\alpha}{\partial r}\right)_0^2 e^{i\omega_0 t} \sum_{ij} \left\langle \exp_0\left[i\int_0^t \mathrm{d}t_1\, \Omega(t_1)\right]\right\rangle_{ij}$$

$$\begin{aligned}[3b]\quad G^{(2)}(t) &= \sum_{ij} \langle a_{0i}^{(2)}(0)\, a_{0j}^{(2)}(t)\rangle \\ &= \frac{2}{15}\frac{N\hbar}{2\mu\omega_0}\left(\frac{\partial\beta}{\partial r}\right)_0^2 e^{i\omega_0 t} \sum_{ij}\Bigg[\langle D_{00}^{(2)}(\theta_i(0))\, D_{00}^{(2)}(\theta_j(t))\rangle \left\langle \exp_0\left[i\int_0^t \mathrm{d}t_1\, \Omega(t_1)\right]\right\rangle_{ij} \\ &\quad + i\int_0^t \mathrm{d}\tau \sum_{ijk} \langle\langle D_{00}^{(2)}(\theta_i(0))\, D_{00}^{(2)}(\theta_j(t))\rangle\, (\Omega_{jk}(\tau) - \langle\Omega_{jk}\rangle)\rangle \left\langle \exp_0\left[i\int_0^t \mathrm{d}t_1\, \Omega(t_1)\right]\right\rangle_{ki} + \ldots\Bigg] \\ &= G^{(20)}(t) + G^{(21)}(t) + \ldots\end{aligned}$$

In these equations $D_{st}^{(2)}(\theta)$ are elements of the Wigner rotation matrix $D^{(2)}(\theta)$, α is the mean Raman polarizability and β the Raman anisotropy of a diatomic molecule, whereas all other terms have their usual meaning. One notices that $G^{(2)}(t)$, contrary to $G^{(0)}(t)$, appears in the form of a series. Its leading term is the well-known product of rotational and vibrational functions, whereas the remaining terms provide a higher-order description of the rotation–vibration correlation effects. The assumption (*iii*) reduces the expansion of $G^{(2)}(t)$ to $G^{(20)}(t)$ and the subsequent theory is a zero-order theory. It should be emphasized, however, that the terms which couple rotations and vibrations are still present in the Hamiltonian and affect even this zero-order theory.

(4) The expressions [3*a*, *b*] contain ordered exponentials, objects which are difficult to handle. However, a considerable simplification is obtained by using symmetry arguments. In fact, a sample of pure liquid transforms into itself if two, three, or several molecules are permuted. The exact Hamiltonian of such a system is thus invariant under the operations of the full N-symmetric group; this is also true, mutatis mutandis, for the approximate Hamiltonian of eq. [2]. It then turns out that all ensemble-average matrices which enter into the calculation commute. They can always be diagonalized, whatever their order. The presence of this symmetry thus makes calculations practicable.

The theoretical method to be employed depends on the strength of molecular interactions. If they are weak, as for example in van der Waals liquids, the following procedure may be adopted. Vibrational correlation functions contained in eqs. [3*a*, *b*] are calculated by applying the cumulant expansion techniques (48, 49). Their use is particularly simple in the present case where all matrices commute after averaging. Thus generalized cumulants may be replaced by ordered cumulants and ordered exponentials by ordinary exponentials. In turn, rotational correlation functions involved in eq. [3*b*] are determined by supposing that the composite variable $A = (D^{(2)}_{00}(\theta_1), D^{(2)}_{00}(\theta_2), \ldots, D^{(2)}_{00}(\theta_N))$ obeys a simple Langevin equation with a constant $N \times N$ friction matrix. The following results are then found, valid for all modulation speeds:

$$[4a] \quad G^{(0)}(t) = \frac{N\hbar}{2\mu\omega_0}\left(\frac{\partial\alpha}{\partial r}\right)_0^2 e^{i\omega_0 t}\, e^{\lambda_1(t)}$$

$$[4b] \quad G^{(0)}_{\mathrm{S}}(t) = \frac{N\hbar}{2\mu\omega_0}\left(\frac{\partial\alpha}{\partial r}\right)_0^2 e^{i\omega_0 t}\, e^{\lambda_2(t)}$$

$$[4c] \quad G^{(0)}_{\mathrm{D}}(t) = \frac{N\hbar}{2\mu\omega_0}\left(\frac{\partial\alpha}{\partial r}\right)_0^2 e^{i\omega_0 t}\,(e^{\lambda_1(t)} - e^{\lambda_2(t)})$$

$$[4d] \quad G^{(20)}(t) = G^{(20)}_{\mathrm{S}}(t) = \frac{2}{15}\frac{N\hbar}{2\mu\omega_0}\left(\frac{\partial\beta}{\partial r}\right)_0^2 e^{i\omega_0 t}\, e^{\lambda_2(t) - \rho_2 t}$$

$$[4e] \quad G^{(20)}_{\mathrm{D}}(t) = 0$$

$$[4f] \quad \lambda_1(t) = i\int_0^t dt'\,[\langle\Omega_{11}(t')\rangle + N\langle\Omega_{12}(t')\rangle] + i^2\int_0^t dt'\int_0^{t'} dt''\,\{\langle\Delta\Omega_{11}(t')\Delta\Omega_{11}(t'')\rangle$$
$$+ N[\langle\Delta\Omega_{11}(t')\Delta\Omega_{12}(t'')\rangle + \langle\Delta\Omega_{12}(t')\Delta\Omega_{11}(t'')\rangle + \langle\Delta\Omega_{12}(t')\Delta\Omega_{12}(t'')\rangle] + N^2\langle\Delta\Omega_{12}(t')\Delta\Omega_{13}(t'')\rangle\} + \ldots$$

$$[4g] \quad \lambda_2(t) = i\int_0^t dt'\,\langle\Omega_{11}(t')\rangle + i^2\int_0^t dt'\int_0^{t'} dt''\,\{\langle\Delta\Omega_{11}(t')\Delta\Omega_{11}(t'')\rangle + N\langle\Delta\Omega_{12}(t')\Delta\Omega_{12}(t'')\rangle\} + \ldots$$

In these equations the subscripts S, D indicate the self- and distinct pair components, respectively, of $G^{(0)}(t)$, $G^{(20)}(t)$, $\Delta\Omega_{ij} = \Omega_{ij} - \langle\Omega_{ij}\rangle$, and ρ_2 is the $(N-1)$-fold degenerate root of the friction matrix. $\lambda_1(t)$ then represents the cumulant series describing collective vibrations in liquids and $\lambda_2(t)$ is its self-vibration analogue. All these equations are valid in the thermodynamic limit $N \to \infty$, $V \to \infty$, $N/V = \rho$, where ρ is a finite quantity.

If molecular interactions are strong enough, as for example in hydrogen bonded liquids, the convergence of the cumulant series is slow and may even become doubtful. Equations [4*a*–*g*] then break down and entirely different methods must be invented in order to carry out the averaging of ordered exponentials in eqs. [3*a*, *b*]. This problem, particularly acute in the presence of molecular associations, is currently under active investigation.[3]

(c) *Results and discussion*

(1) Spectral properties of isotropic Raman spectra may be described either by the correlation function $G^{(0)}(t)$ or by its Fourier transform; compare with eqs. [4*a*], [4*b*], [4*c*], [4*f*], [4*g*]. The following conclusions, valid for a diatomic molecular liquid, may be reached theoretically. (*i*) The isotropic Raman process is a partially coherent process. This can be seen by noticing that, in eq. [4*c*], the distinct pair correlation function, $G^{(0)}_{\mathrm{D}}(t)$, is generally non-vanishing. This result is prior to the Bratos–Tarjus theory. Implicit in papers by Valiev (39), Tokuhiro and Rothschild (15), Rothschild (51), and Döge (40, 52), the coherence effect was treated explicitly in papers by Vincent-Geisse (53), Lynden-Bell (41, 54), Wang (42), Wertheimer (43, 55), and Oxtoby (1); see also the coherent exciton scattering approach due to Knapp (56). Its existence was confirmed by computer simulation studies due to Oxtoby and coworkers (44, 46). (*ii*) Distinct pair correlation functions give no contribution to the integrated intensity of an isotropic Raman band. This statement, due to Wang (42), can be proven by considering eq. [4*c*] and by noticing that the integrated intensity is proportional to $G^{(0)}(0)$. (*iii*) The temperature variation of an isotropic Raman band depends on that of $\lambda_1(t)$. More specifically, according to Wang, its half-width decreases with increasing temperature if the modulation is fast (42). All these predictions are in excellent agreement with experimental data enumerated in Section 2.

(2) Anisotropic Raman band profiles are described by eqs. [4*d*], [4*e*], [4*f*], and [4*g*]. The theory leads to the following conclusions. (*i*) In the zero-order approximation, an anisotropic Raman process is completely incoherent. This can be shown by noticing that the distinct pair correlation function, $G^{(20)}_{\mathrm{D}}(t)$, vanishes in this approximation. However, a small amount of coherence is reintroduced in higher order approximations (57). (*ii*) Only minor changes of the band shape are expected when going from a dilute isotopic solution to a pure liquid. In fact, not only does the distinct pair correlation function vanish, but also the self-contribution is virtually unaffected by dilution. This latter statement can be proven by assuming

[3] D. E. Logan, private communication.

the potential energy V of the system to be pair additive, $V = \sum_{i<j} v_{ij}$. Then

$$[5a] \quad \Omega_{ii} = \sum_{j \neq i} \omega_{ij}^{\mathrm{EF}} = \sum_{j \neq i} \frac{1}{2\mu\omega_0}\left[-\frac{f}{K}\left(\frac{\partial v_{ij}}{\partial r_i}\right)_0 + \left(\frac{\partial^2 v_{ij}}{\partial r_i^2}\right)_0\right]$$

$$[5b] \quad \Omega_{ij} = \omega_{ij}^{\mathrm{RT}} = \frac{1}{2\mu\omega_0}\left(\frac{\partial^2 v_{ij}}{\partial r_i \partial r_j}\right)_0$$

$$[6a] \quad \langle\Delta\Omega_{11}(t')\,\Delta\Omega_{11}(t'')\rangle = N\langle\Delta\omega_{12}^{\mathrm{EF}}(t')\,\Delta\omega_{12}^{\mathrm{EF}}(t'')\rangle + N^2\langle\Delta\omega_{12}^{\mathrm{EF}}(t')\,\Delta\omega_{13}^{\mathrm{EF}}(t'')\rangle$$

$$[6b] \quad N\langle\Delta\Omega_{12}(t')\,\Delta\Omega_{12}(t'')\rangle = N\langle\Delta\omega_{12}^{\mathrm{RT}}(t')\,\Delta\omega_{12}^{\mathrm{RT}}(t'')\rangle$$

where $\omega_{ij}^{\mathrm{EF}}$ describe the effect of environmental fluctuations of the transition frequency, whereas $\omega_{ij}^{\mathrm{RT}}$ take account of the resonant transfer of the vibrational energy. As for all diatomics, the anharmonicity of the diatomic vibrator makes $\omega_{ij}^{\mathrm{EF}}$s about an order of magnitude larger than $\omega_{ij}^{\mathrm{RT}}$s and, in addition, $\langle\Delta\Omega_{12}(t')\,\Delta\Omega_{12}(t'')\rangle$ is quadratic in $\omega_{ij}^{\mathrm{RT}}$s, the object [6*b*] is quite small as compared with the object [6*a*], which proves the statement (57). (*iii*) The isotropic and anisotropic Raman bands of liquids do not coincide. In the lowest order description, their first moments differ by $N\langle\Omega_{12}\rangle$. The exact expressions for those, and the second, spectral moments are available as well and are due to Wang and McHale (58) and McHale (59). (*iv*) The difference in the action of resonant coupling mechanisms in isotropic and anisotropic Raman spectra has its ultimate origin in the permutational symmetry of the liquid sample. For preliminary work on this problem, see the papers by Döge (40, 52) and Lynden-Bell (41). All these theoretical predictions are in an excellent agreement with the experimental data of Section 2. It is even astonishing that the zero-order theory can do so much.

(3) This section may be concluded by examining the possibility of an experimental determination of self- and distinct pair correlation functions. Two different procedures may be envisaged in the frame of the present theory. (*i*) In the first procedure the isotropic Raman spectrum is recorded for a pure liquid; its Fourier transform gives $G^{(0)}(t)$. Next, the isotropic and anisotropic Raman spectra of a dilute isotopic solution are measured. Applying standard VV–VH separation techniques and Fourier transforming the result gives the vibrational and rotational correlation functions of the active molecule in solution. The latter is equal to that of the pure liquid if rotational motions are not altered by the isotopic substitution. Finally, the anisotropic Raman spectrum of a pure liquid is experimentally determined and is Fourier transformed. Dividing by the rotational correlation function of the solution then gives $G_{\mathrm{S}}^{(0)}(t)$. (*ii*) In the second method, the isotropic Raman spectrum is recorded for a pure liquid and for a dilute isotopic solution. Then the Fourier inverted solution spectrum gives $G_{\mathrm{S}}^{(0)}(t)$ whereas the Fourier inverted liquid–solution difference spectrum gives $G_{\mathrm{D}}^{(0)}(t)$. The second procedure is much simpler, but relies on the identification of the vibrational correlation function of the dissolved molecule with the vibrational self-correlation function of the pure liquid. No assumption of this sort is required in the first procedure. At the present time, the practical use of either of these methods is handicapped by difficulties encountered in measuring weak Raman spectra of dilute solutions.

4. Theory. Non-composite Raman bands of isotopic mixtures

(a) *Generalities*

The study of this problem was initiated in 1973 by Bondarev and Mardaeva (23) and, later, by Fujiyama *et al.* (24) who proposed a simple model in which spectral effects in binary mixtures were interpreted in terms of concentration fluctuation of particles on a fictitious space lattice. More recently, in 1978, Knauss (60) and Wertheimer (61) examined the same problem in the framework of the Zwanzig–Mori theory of Brownian motion. Limited to the fast modulation regime, these theories emphasize the role of structure breaking in the usual solvents and its absence in isotopic solvents. Finally, in 1982, Knapp and Fischer (62) elaborated a kinetic model which accounts for both static and dynamic properties of the system and for concentration fluctuations around the reference molecule. All this work led to a partial analysis of Raman processes in binary mixtures. For reasons explained earlier in this paper, the subsequent discussion remains limited, basically, to the isotopic mixtures, and the usual "chemical" mixtures will be only briefly mentioned. Here again, the description is based on the Bratos–Tarjus theory (63) which encompasses, and generalizes, the results reached by previous authors.

(b) *Method of calculation*

The system under consideration contains N_{A} and N_{B} diatomic molecules of isotopic species A and B, respectively, $N_{\mathrm{A}} + N_{\mathrm{B}} = N$. Moreover, this mixture is such that there is no overlap of Raman bands of these isotopic species. This choice permits us to eliminate all complications due to the intra- or intermolecular energy relaxation, the anharmonic coupling of normal modes, etc. Equations [1*a*, *b*] still remain basic equations of the theory, as do the assumptions of the model described in Section 3b(2). However, they apply now to that one of the two isotopic species which is submitted to spectral examination. The potential energy $V(r, t)$ of an isotopic mixture is the same as that of a pure liquid; this is a consequence of the well-known Born–Oppenheimer theorem. Finally, the only difference is that the frequency matrix $\Omega(t)$ has the dimension $N_{\mathrm{A}} \times N_{\mathrm{A}}$ rather than $N \times N$, supposing the species A has been chosen for spectral investigation. The elements of this frequency matrix, both diagonal and non-diagonal, coincide with the corresponding elements of the frequency matrix of the pure liquid. Equations [4*a*–*h*] can then readily be modified to apply to isotopic mixtures. It is sufficient to replace N by $N_{\mathrm{A}} = c_{\mathrm{A}}N$, where c_{A} is the number density of the isotopic species A. The following results are easily obtainable in this way:

$$[7a] \quad G^{(0)}(c_{\mathrm{A}}, t) = c_{\mathrm{A}} \frac{N\hbar}{2\mu\omega_0}\left(\frac{\partial\alpha}{\partial r}\right)_0^2 e^{i\omega_0 t}\, e^{\lambda_1(c_{\mathrm{A}}, t)}$$

$$[7b] \quad G_{\mathrm{S}}^{(0)}(c_{\mathrm{A}}, t) = c_{\mathrm{A}} \frac{N\hbar}{2\mu\omega_0}\left(\frac{\partial\alpha}{\partial r}\right)_0^2 e^{i\omega_0 t}\, e^{\lambda_2(c_{\mathrm{A}}, t)}$$

$$[7c] \quad G_{\mathrm{D}}^{(0)}(c_{\mathrm{A}}, t) = c_{\mathrm{A}} \frac{N\hbar}{2\mu\omega_0}\left(\frac{\partial\alpha}{\partial r}\right)^2 e^{i\omega_0 t}\,(e^{\lambda_1(c_{\mathrm{A}}, t)} - e^{\lambda_2(c_{\mathrm{A}}, t)})$$

$$[7d] \quad G^{(20)}(c_{\mathrm{A}}, t) = G_{\mathrm{S}}^{(20)}(c_{\mathrm{A}}, t) = c_{\mathrm{A}} \frac{2}{15} \frac{N\hbar}{2\mu\omega_0}\left(\frac{\partial\beta}{\partial r}\right)_0^2 e^{i\omega_0 t}\, e^{\lambda_2(c_{\mathrm{A}}, t) - p_2 t}$$

$$[7e] \quad G_{\mathrm{D}}^{(20)}(c_{\mathrm{A}}, t) = 0$$

$$[7f]\quad \lambda_1(c_A,t) = i\int_0^t dt'\,\{[\langle\Omega_{11}(t')\rangle] + c_A[N\langle\Omega_{12}(t')\rangle]\} + i^2\int_0^t dt'\int_0^{t'} dt''\,\{[\langle\Delta\Omega_{11}(t')\,\Delta\Omega_{11}(t'')\rangle]$$
$$+ c_A[N\langle\Delta\Omega_{11}(t')\,\Delta\Omega_{12}(t'')\rangle + N\langle\Delta\Omega_{12}(t')\,\Delta\Omega_{11}(t'')\rangle + N\langle\Delta\Omega_{12}(t')\,\Delta\Omega_{12}(t'')\rangle] + c_A^2[N^2\langle\Delta\Omega_{12}(t')\,\Delta\Omega_{13}(t'')\rangle]\} + \ldots$$

$$[7g]\quad \lambda_2(c_A,t) = i\int_0^t dt'\,\{[\langle\Omega_{11}(t')\rangle]\} + i^2\int_0^t dt'\int_0^{t'} dt''\,\{[\langle\Delta\Omega_{11}(t')\,\Delta\Omega_{11}(t'')\rangle] + c_A[N\langle\Delta\Omega_{12}(t')\,\Delta\Omega_{12}(t'')\rangle]\} + \ldots$$

Similar equations are valid for the isotopic species B. It should be stressed that there is no hidden concentration dependence through the pair and three-body time-dependent distribution functions that are needed to calculate the correlation functions of eqs. [7*a*–*g*]. This is due to the absence of structure breaking in an isotopic dilution process.

(c) *Results and discussion*

The above zero-order theory of Raman processes in isotopic mixtures leads to the following results. (*i*) The peak frequency of an isotropic Raman band is a linear function of the concentration of the active species. This result, prior to the Bratos–Tarjus theory, is due to Wertheimer (61). On the other hand, the position of an anisotropic Raman band is independent of concentration. (*ii*) The variation of the half-width of an isotropic Raman band with concentration strongly depends on the speed of vibrational modulation. If it is fast, the half-width is a quadratic function of the concentration; if it is slow, it depends on the square root of this function. The former of these limits has already been discussed by Wertheimer (61) and Knauss (60), and the latter in the model due to Bondarev and Mardaeva (23) and Fujiyama *et al.* (24); see also Knapp and Fischer (62). (*iii*) The half-width of an anisotropic Raman band is a linear function of concentration if the vibrational modulation is fast and it depends on the square root of this function if it is slow. (*iv*) The c_A^2 term of $\lambda_1(c_A,t)$ and the c_A term of $\lambda_2(c_A,t)$ are expected to be small for all diatomics. The argument is the same as that of Section 3c(2). The half-width of an anisotropic Raman band is thus virtually independent of the concentration. These theoretical predictions conform to the data of Section 2.

The present discussion may be closed with some brief comments relative to non-isotopic mixtures. In this case, the fluctuation of the chemical composition of the first solvation shell of the reference molecule is the main source of the additional band broadening. Both $\lambda_1(c_A,t)$ and $\lambda_2(c_A,t)$ contain large c_A^2 dependent terms. Moreover, when the liquid is progressively diluted, the structure breaking occurs; the distribution functions may be strongly concentration dependent, particularly if the two species differ much in their dimensions and in their chemical properties. The models by Bondarev and Mardaeva (23), Fujiyama *et al.* (24), and Knapp and Fischer (62) describe this complicated situation in a rough manner. The only quantitative approach is due to Knauss (60), but its application remains difficult. Finally, the vibrational dephasing of Raman active ions in aqueous electrolyte solutions was studied by Kato (64).

5. Theory. Composite Raman bands of liquids and isotopic mixtures

(a) *Generalities*

The study of composite bands was initiated fifty years ago by analysing the structure of ν OH bands in hydrogen bonded liquids. Their properties were examined experimentally in several thousands of publications. Moreover, statistical theories of the band shape in dilute solutions were proposed as well; review papers are given in refs. 65 and 66. Contrasting with this situation is that relative to the composite Raman bands of pure van der Waals liquids and of their isotopic mixtures. The quantitative experimental work is virtually non-existent and only a few theories have been published. They are due to Wertheimer (61, 67, 68) and to McHale and Wang (69) who examined, between 1978 and 1980, three types of composite bands: hot bands corresponding to the transitions $0 \to \nu$ and $\nu' \to \nu' + \nu$ (67, 68), doublets produced by the Fermi resonance (69), and interacting fundamentals $0 \to \mu$ and $0 \to \nu$ of a given mode in isotopic mixtures (61). At the present time, the coverage of this field is fragmentary. The importance of these problems should by no means be underestimated: the majority of Raman bands of polyatomic molecules are overlapping composite bands.

(b) *Method of calculation*

The theories for this group are quantum mechanical in principle although, in practice, non-vibrational degrees of freedom are treated classically. The following model is used in these theories. (*i*) The Hamiltonian of a pure liquid is written $H = H_{KIN} + H_{POT} + H_{VIB}$ where H_{KIN} represents the translational and rotational kinetic energy of the fluid, H_{POT} describes molecular interactions, whereas H_{VIB} is the Hamiltonian of a system of non-interacting vibrators. The Hamiltonian of an isotopic binary mixture is written similarly, the indices J,K distinguishing its various components:

$$[8]\quad H = \sum_{J=1}^{2} H_{KIN}^{J} + \sum_{J,K=1}^{2} H_{POT}^{J,K} + \sum_{J=1}^{2} H_{VIB}^{J}$$

(*ii*) Thermal fluctuations of the bath are fast on the time scale of the experiment. (*iii*) Collision-induced contributions to the mean polarizability are neglected.

The assumptions (*i*) and (*iii*) above, as well as that postulating a classical thermal bath, were already examined in Section 3b(2) and do not need to be reexamined. On the contrary, assumption (*ii*) is new and limits the theory to rapidly modulated Raman processes. This restriction means that, in practice, only weakly interacting van der Waals liquids may be treated by the above theories. It should also be emphasized that, in polyatomic molecules, assigning a small set of transitions to a given composite band generally represents an approximation. It is in fact difficult to take into account all secondary energy and phase relaxation mechanisms contributing to the profile.

The calculation employs the Zwanzig–Mori theory of Brownian motion. The basic set of dynamical variables $a_i(t)$ is that of collective vibrational transition operators between the states to which the band is assigned. For example, in the problem of two overlapping fundamentals of an isotopic mixture, one has:

$$[9]\quad a_1 = (Nc_1)^{-1/2}\sum_j \sigma_{\mu 0}^{1j}; \quad a_2 = (Nc_2)^{-1/2}\sum_k \sigma_{\nu 0}^{2k}$$

In eqs. [9], $\sigma_{\mu 0}^{1j}$ is the transition operator for the $0 \rightarrow \mu$ transition of jth molecule of the species 1, $\sigma_{\nu 0}^{2k}$ that for the $0 \rightarrow \nu$ transition of kth molecule of the species 2, N the total number of molecules, and c_1, c_2 the concentrations of the two species. Furthermore, in refs. 61, 67, and 68 the frequency and the memory matrix were calculated by suppressing H_{POT} in the expressions for the density matrix and the projected propagator. Finally, simple models were employed in estimating the role of various band shaping exchange mechanisms.

(c) *Results and discussion*

The following results may be reached from these theories. As far as the $0 \rightarrow \nu$, $\nu' \rightarrow \nu + \nu'$ isotropic Raman bands are concerned (67, 68), the theory showed that the interaction between individual resonances originates essentially in intermolecular vibrational correlations. Moreover, various energy redistribution processes are spectrally active and may involve both low and high vibrational energy levels. The coupling mechanism produces a frequency shift, a broadening or narrowing, and an asymmetry of individual vibrational lines. It also leads to a redistribution of spectral intensity among various components. All these processes are thermally activated and vanish at low temperatures. Similar problems were investigated by Harris, Shelby and Cornelius (70, 71) and by Abbot and Oxtoby (50). However, the resonant interaction between molecules was not explicitly included in their calculations.

Intermolecular couplings were also introduced, in addition to intramolecular couplings, into the theory of the Fermi-resonance doublet (69). According to this theory, the spectral behavior is strongly concentration dependent. If the Fermi resonance is weak, the peaks of the coupled bands shift in opposite directions as the concentration is increased. If it is strong, the Fermi interaction parameter has a non-linear concentration dependence. This mechanism was also studied by Abbot and Oxtoby (50) in the case of dilute solutions.

Finally, it was found in isotropic Raman spectra of binary isotopic mixtures (61) that vibrational motions of different molecular species may be significantly coupled. This is due to the action of distinct vibrational correlations. The coupling, however, occurs only for weakly separated or overlapping bands. Moreover, the correlation time of vibrational self-coorelation functions turns out to be essentially independent of concentration. This result has its origin in the fact that the nearly resonant transfer between molecules of different types is almost as fast as the resonant transfer between molecules of the same species. A similar behavior of isolated isotropic Raman bands was discussed in Section 3c(2). It is probable that the majority of results cited here are of general validity, although the theories of this section are fast-modulation theories.

6. Conclusions

A first important conclusion of this review is that the random phase approximation can not be retained in its simple form. Intermolecular forces introduce a correlation between phases of individual vibrators and, in the absence of any complicating factor, distinct pair vibrational correlation functions survive. This is why isotropic Raman processes are partially coherent. However, though they are collective, rotational motions destroy these correlations if the rotation–vibration coupling is small enough. The coherence of anisotropic Raman processes, which can only be transmitted by this mechanism, thus remains small and resonance transfer effects are quenched correspondingly.

A second conclusion concerns the nature of collective processes accessible to a study by Raman spectroscopy. As shown earlier, isotropic Raman spectroscopy permits an analysis of a variety of dephasing and energy relaxation processes. The former can most conveniently be examined in the case of high frequency fundamentals where they alone are present. On the other hand, both phase and energy relaxation processes affect composite bands and cannot easily be disentangled from each other; the theory still remains fragmentary at this point. Resonance transfer and environmental fluctuation processes never act independently of each other; their interference in fact is usually the main source of the band broadening when going from dilute isotopic solutions to pure liquids. Using "chemical" solvents complicates the analysis to a considerable extent. Three new effects appear in this case: change of the force law, breaking of the liquid structure in the dilution process, and concentration fluctuations modifying the local chemical composition of the solution. From the other side, anisotropic Raman spectroscopy is not well adapted, by its nature, to the study of collective vibrational and rotational processes in liquids; it can be employed, however, to separate collective and monomolecular motions from one another. As a whole, the field is still far from maturity.

Finally, it is interesting to ask why spectacular spectroscopic features observed in quasi-elastic light scattering spectra, features such as the Rayleigh–Brillouin triplet or those resulting from the reorientation – shear wave coupling, have never been reported for non-elastic Raman spectra. The reasons for this non-observation are not known. However, the coherence of isotropic Raman spectra may not be sufficient to guarantee the existence of similar effects; this is still more true for the anisotropic Raman spectra. A further study of this problem certainly merits attention.

1. D. W. OXTOBY. Adv. Chem. Phys. **40**, 1 (1978).
2. S. BRATOS. *In* Vibrational spectroscopy of molecular liquids and solids. *Edited by* S. Bratos and R. M. Pick. Plenum Press, New York. 1980. p. 43.
3. G. DÖGE. Z. Naturforsch. Teil A, **23**, 1405 (1968).
4. M. LAFAIX and J. VINCENT-GESSE. Spectrochim. Acta Part A, **29**, 177 (1973).
5. A. M. AMORIM DA COSTA, M. A. NORMAN, and J. H. R. CLARKE. Mol. Phys. **29**, 191 (1975).
6. C. K. CHEUNG, D. R. JONES, and C. H. WANG. J. Chem. Phys. **64**, 3567 (1976).
7. N. N. NEUMAN and G. C. TABISZ. Chem. Phys. **15**, 195 (1976).
8. A. MORADI-ARAGHI and M. SCHWARTZ. J. Chem. Phys. **71**, 166 (1979).
9. T. KATO and T. TAKENAKA. Chem. Phys. Lett. **62**, 77 (1979).
10. W. SCHMITZ. Nuovo Cimento B, **63**, 386 (1981).
11. T. T. WALL. J. Chem. Phys. **52**, 2792 (1970).
12. W. C. MUNDI, L. GUTIERREZ, and F. H. SPEDDING. J. Chem. Phys. **59**, 2173 (1973).
13. P. C. M. VAN WOERKOM, J. DE BLEISER, and J. C. LEYTE. Chem. Phys. Lett. **20**, 592 (1973).
14. P. C. M. VAN WOERKOM, J. DE BLEISER, M. DE ZWART, P. M. J. BURGERS, and J. C. LEYTE. Ber. Bunsenges. Phys. Chem. **78**, 1303 (1974).
15. T. TOKUHIRO and W. G. ROTHSCHILD. J. Chem. Phys. **62**, 2150 (1975).
16. J. E. GRIFFITHS, M. CLERC, and P. M. RENTZEPIS. J. Chem. Phys. **60**, 3824 (1974).
17. J. SCHROEDER, V. H. SCHIEMANN, P. T. SHARKO, and J. JONAS. J. Chem. Phys. **66**, 3215 (1977).
18. R. LE SAR and R. KOPELMAN. J. Chem. Phys. **66**, 5035 (1977).
19. J. LAANE and W. KIEFER. J. Chem. Phys. **73**, 4971 (1980).

20. K. L. OEHME and K. KLOSTERMANN. J. Chem. Phys. In press.
21. J. P. PINAN-LUCARRÉ. Chem. Phys. Lett. **98**, 195 (1983).
22. G. DÖGE and A. KHUEN. J. Mol. Struct. **45**, 101 (1978).
23. A. F. BONDAREV and A. I. MARDAEVA. Opt. Spectrosc. USSR, **35**, 167 (1973).
24. T. FUJIYAMA, M. KAKIMOTO, and T. SUZUKI. Bull. Chem. Soc. Jpn. **49**, 606 (1976).
25. J. YARWOOD, R. ARNDT, and G. DÖGE. Chem. Phys. **25**, 387 (1977).
26. R. ARNDT and R. E. D. MCCLUNG. J. Chem. Phys. **69**, 4280 (1978).
27. G. DÖGE, R. ARNDT, H. BUHL, and G. BETTERMANN. Z. Naturforsch. Teil A, **35**, 468 (1980).
28. J. YARWOOD, R. ACKROYD, K. E. ARNOLD, G. DÖGE, and R. ARNDT. Chem. Phys. Lett. **77**, 239 (1981).
29. D. SCHEIBE. J. Raman Spectrosc. **13**, 103 (1982).
30. M. KAMOUN and P. MIRONE. Chem. Phys. Lett. **75**, 287 (1980).
31. G. DÖGE, R. ARNDT, and J. YARWOOD. Mol. Phys. **52**, 399 (1984).
32. G. DÖGE, R. ARNDT, and A. KHUEN. Chem. Phys. **21**, 53 (1977).
33. M. SCHWARTZ and C. H. WANG. Chem. Phys. Lett. **25**, 26 (1974).
34. G. FINI and P. MIRONE. J. Chem. Soc. Faraday Trans. 2, **70**, 1776 (1974).
35. C. PERCHARD and J. P. PERCHARD. Chem. Phys. Lett. **27**, 445 (1974).
36. V. I. KORSUNSKII, N. L. LAVRIK, and YU. NABERUKHIN. Opt. Spectrosc. USSR, **41**, 468 (1976).
37. P. MIRONE and G. FINI. J. Chem. Phys. **71**, 2241 (1979).
38. B. DESBAT and P. V. HUONG. J. Raman Spectrosc. **8**, 1 (1979).
39. K. A. VALIEV. Opt. Spectrosc. USSR, **11**, 253 (1961).
40. G. DÖGE. Z. Naturforsch. Teil A, **28**, 919 (1973).
41. R. M. LYNDEN-BELL. Mol. Phys. **33**, 907 (1977).
42. C. H. WANG. Mol. Phys. **33**, 207 (1977).
43. R. K. WERTHEIMER. Mol. Phys. **35**, 257 (1978).
44. D. W. OXTOBY, D. LEVESQUE, and J. J. WEIS. J. Chem. Phys. **68**, 5528 (1978).
45. S. BRATOS and G. TARJUS. Phys. Rev. A, **24**, 1591 (1981).
46. D. LEVESQUE, J. J. WEIS, and D. W. OXTOBY. J. Chem. Phys. **79**, 917 (1983).
47. G. TARJUS and S. BRATOS. Phys. Rev. A, **30**, 1087 (1984).
48. R. KUBO. J. Phys. Soc. Jpn. **17**, 1100 (1962).
49. N. G. VAN KAMPEN. Physica (Utrecht), **74**, 215 (1974).
50. R. J. ABBOT and D. W. OXTOBY. J. Chem. Phys. **70**, 4703 (1979).
51. W. G. ROTHSCHILD. J. Chem. Phys. **65**, 2958 (1976).
52. G. DÖGE. *In* Molecular motions in liquids. *Edited by* J. Lascombe. D. Reidel Publ. Comp., Dordrecht. 1974. p. 225.
53. J. VINCENT-GEISSE. Spectrochim. Acta Part A, **24**, 1 (1968).
54. R. M. LYNDEN-BELL. Mol. Phys. **36**, 1529 (1978).
55. R. K. WERTHEIMER. Mol. Phys. **38**, 797 (1979).
56. E. W. KNAPP. J. Chem. Phys. **81**, 643 (1984).
57. S. BRATOS and G. TARJUS. *In* Raman spectroscopy. *Edited by* J. Lascombe and P. V. Huong. J. Wiley and Sons, New York. 1982. p. 317.
58. C. H. WANG and J. MCHALE. J. Chem. Phys. **72**, 4039 (1980).
59. J. L. MCHALE. J. Chem. Phys. **75**, 30 (1981).
60. D. C. KNAUSS. Mol. Phys. **36**, 413 (1978).
61. R. K. WERTHEIMER. Mol. Phys. **36**, 1631 (1978).
62. E. W. KNAPP and S. FISCHER. J. Chem. Phys. **76**, 4730 (1982).
63. S. BRATOS and G. TARJUS. Phys. Rev. A. In press.
64. T. KATO. Mol. Phys. **39**, 559 (1980).
65. C. SANDORFY. *In* The hydrogen bond. *Edited by* P. Schuster, G. Zundel, and C. Sandorfy. North Holland Publ. Comp., Amsterdam. 1976. p. 613.
66. S. BRATOS, J. LASCOMBE, and A. NOVAK. *In* Molecular interactions. *Edited by* H. Ratajczak and W. J. Orville-Thomas. John Wiley, Chichester. 1980. p. 301.
67. R. K. WERTHEIMER. Chem. Phys. **41**, 229 (1979).
68. R. K. WERTHEIMER. Chem. Phys. **45**, 415 (1980).
69. J. L. MCHALE and C. H. WANG. J. Chem. Phys. **73**, 3600 (1980).
70. C. B. HARRIS, R. M. SHELBY, and P. A. CORNELIUS. Chem. Phys. Lett. **57**, 8 (1978).
71. R. M. SHELBY, C. B. HARRIS, and P. A. CORNELIUS. J. Chem. Phys. **70**, 34 (1979).

^{1}H and ^{13}C nmr study of exchange and isomerism in dimethylsulphoxide solutions of neutral methylmercury–xanthosine complexes

FRANÇOIS ALLAIRE, MICHEL SIMARD, AND ANDRÉ L. BEAUCHAMP[1]
Département de Chimie, Université de Montréal, C.P. 6210, Succ. A, Montréal (Qué.), Canada H3C 3V1

Received September 25, 1984

This paper is dedicated to Professor Camille Sandorfy on the occasion of his 65th birthday

FRANÇOIS ALLAIRE, MICHEL SIMARD, and ANDRÉ L. BEAUCHAMP. Can. J. Chem. **63**, 2054 (1985).

The xanthosine (H_2Xan) complexes $(CH_3Hg)(HXan)$ and $(CH_3Hg)_2(Xan)$ have been studied in $(CD_3)_2SO$ solution at room temperature by ^{1}H (90 MHz) and ^{13}C nmr (20.1 MHz) spectroscopy. For $(CH_3Hg)_2(Xan)$, where the N1-H and N3-H protons have been substituted by CH_3Hg^+ groups, individual ^{1}H and ^{13}C resonances from the unequivalent CH_3Hg^+ groups indicate that these cations do not exchange rapidly between the two sites. For solutions of $(CH_3Hg)(HXan)$, in which only one of the N—H protons has been substituted, both types of spectra show two sets of resonances for the purine unit as well as for the CH_3Hg^+ groups. This indicates that the 1:1 complex exists as two linkage isomers (N3—H, N1—Hg) and (N3—Hg, N1—H) in slow exchange. These two isomers are formed in equal amounts. When free xanthosine is added, the N3-mercurated complex exchanges rapidly with the free ligand, whereas the N1-mercurated complex does not exchange.

FRANÇOIS ALLAIRE, MICHEL SIMARD et ANDRÉ L. BEAUCHAMP. Can. J. Chem. **63**, 2054 (1985).

Les complexes $(CH_3Hg)(HXan)$ et $(CH_3Hg)_2(Xan)$ de la xanthosine (H_2Xan) ont été étudiés en solution dans $(CD_3)_2SO$ à température ambiante par rmn ^{1}H (90 MHz) et ^{13}C (20.1 MHz). Pour $(CH_3Hg)_2(Xan)$, composé dans lequel les protons N1-H et N3-H ont été substitués par des groupes CH_3Hg^+, les deux groupes CH_3Hg^+ non équivalents produisent des résonances ^{1}H et ^{13}C distinctes, ce qui indique que ces cations ne s'échangent pas rapidement entre les deux sites. Dans le cas des solutions de $(CH_3Hg)(HXan)$, où un seul proton N—H a été substitué, les deux sortes de spectres comportent deux séries de signaux tant pour le résidu purinique que pour les groupes CH_3Hg^+. Ceci montre que le complexe 1:1 existe sous forme de deux isomères de liaison (N3—H, N1—Hg) et (N3—Hg, N1—H) en échange lent. Ces deux isomères se forment en quantités égales. Si l'on ajoute de la xanthosine libre à la solution, on constate que le composé mercurié en N3 s'échange rapidement avec le ligand libre, tandis que le composé mercurié en N1 ne s'échange pas.

Introduction

Our laboratory has been examining the reactions of the CH_3Hg^+ cation with DNA constituents for several years. In a recent report (1), we described and structurally characterized a series of CH_3Hg^+ complexes of xanthine, a nucleobase related to guanine. That work was being extended to the analog nucleoside xanthosine (H_2Xan), **A**, when we became aware that a similar study was underway in another laboratory. The latter study by Buncel, Norris, and co-workers (2) has now been published. These authors have prepared a number of xanthosine compounds in which the CH_3Hg^+ cation has been shown to react by coordination of the N7 lone pair and by substitution of the N1-H and N3-H protons. These workers also obtained C8-methylmercurated derivatives. In our preliminary work on the CH_3Hg^+–xanthosine system, we had already isolated by slightly different methods the neutral $(CH_3Hg)(HXan)$ and $(CH_3Hg)_2(Xan)$ compounds and unusual peak splitting had been noted in the ^{1}H and ^{13}C nmr spectra of these compounds in $(CD_3)_2SO$. These observations have now been confirmed and they reveal interesting details pertaining to the exchange of the CH_3Hg^+ cation in these systems. These results are discussed in the present paper.

Experimental section

Xanthosine (Aldrich) and CH_3HgOH (Alfa, 1 *M* aqueous solution) were used without further purification. C, H, and N were analyzed by Schwarzkopf Laboratories, New York. The CH_3Hg^+ group was titrated potentiometrically with 0.05 *M* KCl (Ag/AgCl electrode) in an ethanol–water mixture, as described earlier (1, 3).

Nuclear magnetic resonance measurements

The ^{1}H nmr spectra were recorded with a Bruker WH-90 instrument and the ^{13}C spectra with a Bruker WH-80 instrument operating at 20.1 MHz, both at ambient probe temperature (28°C). Me_4Si was used as internal reference. In all cases, the compounds were dissolved in $(CD_3)_2SO$ (Merck, Sharp and Dohme, Canada). The solutions were prepared by dissolving ~150 mg of complex per mL.

Preparations

The methylmercury complexes were first reported by Buncel, Norris, and co-workers (2). They are prepared here by slightly different methods, yielding hydrated forms.

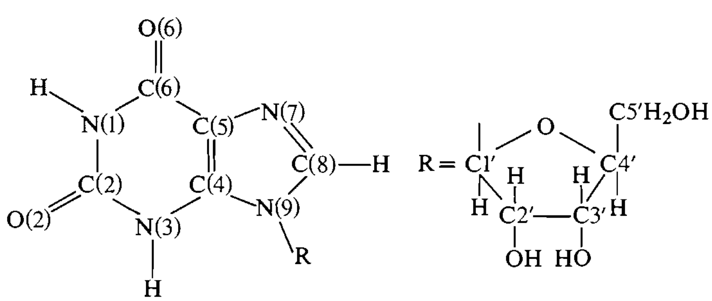

A

[1] To whom all correspondence should be addressed.

TABLE 1. ^1H nmr results for xanthosine and its CH_3Hg^+ complexes[a]

Complex	δ (ppm) N1-H	C8-H	$CH_3(Hg)$	$^2J(^1H—^{199}Hg)$[b]
H_2Xan (**A**)	10.94	7.91	—	—
$(CH_3Hg)(HXan)$ (N1, **C***a*)	—	7.80	0.78	196
$(CH_3Hg)(HXan)$ (N3, **C***b*)	10.77	7.88	0.82	220
$(CH_3Hg)_2(Xan)$ (**B**)	—	7.65	0.83	220 (N3)
			0.74	195 (N1)

[a] In $(CD_3)_2SO$, referenced to internal Me_4Si, 298 K, 90 MHz.
[b] ^2J coupling constant in Hz.

$(CH_3Hg)_2(Xan)\cdot H_2O$, ***B***. Xanthosine **A** (0.64 g, 2.0 mmol) was dissolved in a boiling mixture of 4.0 mL of 1 *M* CH_3HgOH and 60 mL of water. The hot solution was stirred for 1 h and allowed to cool. After 3 days, the solid was filtered, washed with ethanol, and dried at room temperature *in vacuo*. Yield: 1.26 g, 85%. The solid dried under these conditions is a monohydrate. *Anal.* calcd. for $C_{12}H_{18}Hg_2N_4O_7$: Hg 54.84, C 19.70, H 2.48, N 7.66; found: Hg 54.86, C 19.79, H 2.18, N 7.86. Substitution of both the N1-H and N3-H protons in this compound is evidenced from the shift of the whole carbonyl infrared absorption of xanthosine from ~1700 cm^{-1} to ~1635 cm^{-1}, as noted when the same two sites of xanthine are substituted (1).

$(CH_3Hg)(HXan)\cdot 2H_2O$, ***C***. Xanthosine **A** (0.64 g, 2.0 mmol) was dissolved in a boiling mixture of 2.0 mL of 1 *M* CH_3HgOH and 60 mL of water, and subsequently treated in the same way as above. Yield: 0.30 g, 28%. *Anal.* calcd. for $C_{11}H_{18}HgN_4O_8$: Hg 37.50; found: Hg 37.73. The ir spectrum shows carbonyl bands at ~1690 and ~1640 cm^{-1}, indicating that substitution has taken place at only one of the N—H sites, as found for an analogous substitution pattern in xanthine (1).

Results and discussion

Xanthosine (A)

The free nucleobase **A** contains two acidic protons attached to the pyrimidine ring. The N3-H proton dissociates first, with a pk_a values of 5.6, whereas the N1-H proton is less acidic (pk_a = 9.9) (4, 5).

The ^1H nmr data for xanthosine in $(CD_3)_2SO$ (Table 1 and Fig. 1*d*) are in good agreement with those previously reported (2). The C8-H proton produces a sharp resonance at 7.91 ppm. The spectrum also contains signals for the ribose protons, which will not be discussed here. At low field, a broad signal at 10.94 ppm, integrating for one proton, is due to N1-H (6). The N3-H proton should also give a resonance at still lower field, but it is not observed in this case. A similar situation was encountered for the N7-H proton of xanthine (pk_a = 7.7) (1), which was found to appear in the spectra of very dry $(CD_3)_2SO$, but to disappear when the amount of water in $(CD_3)_2SO$ increased, owing to exchange with the protons of water (6). The N3-H proton of xanthosine is more acidic and, therefore, probably more labile than the N7-H proton of xanthine, so that the absence of the N3-H resonance here is likely to result from fast exchange with water.

The ^{13}C spectrum of xanthosine (Table 2 and Fig. 2*d*) is in accord with the previous report (2).

*$(CH_3Hg)_2(Xan)$ (**B**)*

In this compound, two CH_3Hg^+ groups have substituted the N1-H and N3-H protons of xanthosine. Structure **B** is supported by the carbonyl stretching region of the ir infrared spectrum, which is similar to those observed for xanthine complexes in which both pyrimidine protons had been substituted (1).

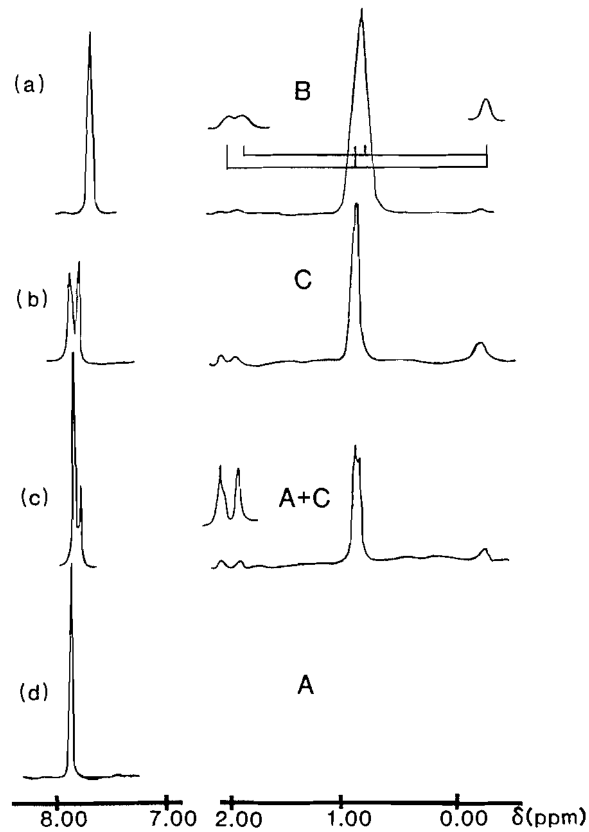

FIG. 1. C8-H (left) and CH_3Hg^+ (right) regions of the ^1H nmr spectra in $(CD_3)_2SO$ at room temperature. Chemical shifts referenced to Me_4Si. (*a*) $(CH_3Hg)_2(Xan)$ (**B**); (*b*) $(CH_3Hg)(HXan)$ (**C**); (*c*) 30:70 mixture of xanthosine (**A**) and $(CH_3Hg)(HXan)$ (**C**); and (*d*) xanthosine (**A**).

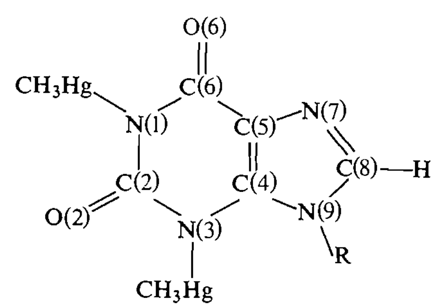

B

In agreement with this structure, the N1-H signal is absent from the ^1H spectrum of the complex. The C8-H signal has shifted upfield by 0.26 ppm compared to xanthosine (Fig. 1*a* and Table 1).

TABLE 2. ^{13}C nmr results for xanthosine and its CH_3Hg^+ complexes[a]

Complex	δ (ppm)										
	C2	C4	C5	C6	C8	CH_3(Hg)	C1′	C2′	C3′	C4′	C5′
H_2Xan (**A**)	150.4	139.3	116.2	157.7	135.6	—	88.7	73.9	70.8	86.1	61.3
(CH_3Hg)(HXan) (N1, **C***a*)	157.2[b]	143.1	116.2	161.7	134.1	1.4	87.4	73.8	70.4	86.1	61.3
(CH_3Hg)(HXan) (N3, **C***b*)	154.2	144.5	116.2	158.1[b]	134.1	−0.4	87.4	73.8	70.4	86.1	61.3
$(CH_3Hg)_2$(Xan) (**B**)	160.3	146.9	118.1	161.8	132.4	1.3 (N1) −0.7 (N3)	86.3	74.2	70.2	86.3	61.1

[a]In $(CD_3)_2SO$, referenced to internal Me_4Si, 298 K, 20.11 MHz.
[b]Assignments for these two signals could be interchanged.

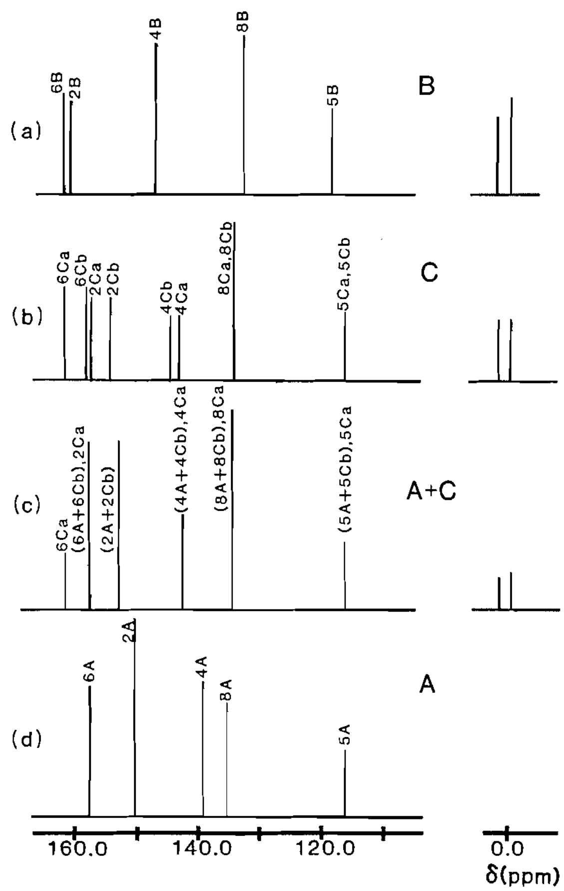

FIG. 2. Purine (left) and CH_3Hg^+ (right) regions of the ^{13}C nmr spectra in $(CD_3)_2SO$ at room temperature. Chemical shifts referenced to Me_4Si. (*a*) $(CH_3Hg)_2$(Xan) (**B**); (*b*) (CH_3Hg)(HXan) (**C**); (*c*) 30:70 mixture of xanthosine (**A**) and (CH_3Hg)(HXan) (**C**); and (*d*) xanthosine (**A**).

The most unusual feature of this spectrum is found in the high-field region, where the resonances for the CH_3Hg^+ groups appear (Fig. 1*a*). The methyl signal centered at 0.78 ppm is broader than usually found for similar systems (1, 8–12). The presence of two unresolved signals under this broad peak is indicated by the shape of the satellites due to coupling between the methyl protons and ^{199}Hg (17% abundance). Figure 1*a* clearly shows that the satellite at low field contains two equal components. This region can be interpreted in terms of a first resonance at 0.74 ppm with a ^2J(^{1}H—^{199}Hg) constant of 195 Hz, and a second component with the same intensity at 0.83 ppm with a ^2J constant of 220 Hz. This particular combination of chemical shifts and coupling constants produces two distinct peaks for the low-field satellites, but accidental coincidence of the components for the high-field satellites.

The presence of two distinct signals for N-bonded CH_3Hg^+ groups is unusual, since purine and pyrimidine complexes containing more than one type of CH_3Hg^+ groups commonly show only a single sharp resonance due to fast exchange of the CH_3Hg^+ groups between the various sites at room temperature (1, 7–12). The presence of two signals has been observed by Buncel, Norris, and co-workers (2, 8, 10–12) when N-bonded and C-bonded CH_3Hg^+ groups are simultaneously present, the latter being known to be non-labile. The presence of C-bonded groups in the present case can be ruled out, as this type of group should produce a resonance at higher field (~0.55 ppm) with a ^2J coupling constant of ~157 Hz (2, 8, 12). Therefore, in contrast by most similar systems, the two CH_3Hg^+ groups in the present compound do not exchange rapidly between the two coordination sites.

This interpretation is supported by the ^{13}C spectrum (Fig. 2*a* and Table 2), which also contains two resolved resonances at 1.3 and −0.7 ppm for the methyl carbons of CH_3Hg^+ groups in slow exchange. The remaining ^{13}C signals are in good agreement with those reported earlier (2), except for the weak C2 signal, which we have found to occur 2 ppm downfield from the reported value. The large downfield shifts of 9.9, 7.6, and 4.1 ppm on C2, C4, and C6, respectively, confirm the substitution of the N1-H and N3-H protons.

Rabenstein (13) examined CH_3HgL complexes with a series of ligands L by ^{1}H nmr spectroscopy and found that the ^2J coupling constant decreases linearly as a function of log *K* (where *K* is the formation constant of CH_3HgL). In fact, the "log *K*" term is used as a measure of the nucleophilic character of L with respect to the CH_3Hg^+ ion. Other workers (11, 14) have proposed a similar relation between ^2J and, this time, the pK_a value (where k_a is the ordinary dissociation constant of the ligand conjugated acid HL), which also measures the nucleophilic character of L, but with respect to H^+. The ^2J value was shown to decrease as the pk_a of the conjugated acid increased. This dependence of ^2J on the pk_a allows us to assign the signal at 0.74 ppm (^2J = 195 Hz) (Table 1) to the N1-bound CH_3Hg^+ group, whereas the other resonance at 0.83 ppm (^2J = 220 Hz) is due to the N3-bound group. In a second step, the ^{13}C signals for the CH_3Hg^+ groups can be assigned, since Buncel, Norris, and co-workers (2) have shown that the ^{13}C chemical shift increases as the ^2J constant decreases. Therefore, the ^{13}C signal at 1.3 ppm (Table 2) is assigned to the N1-bound CH_3Hg^+ group, while the −0.7 ppm resonance is due to the N3-bound group.

(CH_3Hg)(HXan) (C)

The high-field regions of the ^{1}H and ^{13}C nmr spectra (Figs.

1*b* and 2*b*, respectively) indicate that two types of slowly exchanging CH_3Hg^+ groups are again present. The ^{13}C spectrum exhibits two resolved signals. In some high-quality ^1H spectra, small splitting of the main signal at 0.81 ppm could be detected, but the presence of two unequivalent CH_3Hg^+ groups is evidenced mainly, as in the previous case, from the two components of the low-field satellite for $^1H-^{199}Hg$ coupling. The chemical shifts and coupling constants are close to those found for $(CH_3Hg)_2(Xan)$, indicating that the slowly exchanging CH_3Hg^+ groups are probably similar to those identified in **B**. However, the present system differs markedly from the previous case by the fact that the ligand signals provide evidence for two types of differently coordinated xanthosines in slow exchange. For instance, the C8-H resonance (Fig. 1*b*) exists as two discrete signals of roughly equal intensities at 7.80 and 7.88 ppm. The ^1H spectrum also includes a broad peak at 10.77 ppm (Table 1), whose integration corresponds to only one half of the combined integrations of both C8-H signals. This broad signal is very likely due to the N1-H proton in a species representing only one half of total xanthosine present. In the ^{13}C spectrum (Fig. 2*b*), the peaks for C5 and C8 at 116.2 and 134.1 ppm, respectively, are not split, but a total of six signals are found above 140 ppm, where only the ligand C2, C4, and C6 resonances are expected.

At first, it was believed that one set of signals could originate from $(CH_3Hg)_2(Xan)$ impurity. However, this assumption was ruled out, since the C8-H signal of **B** should occur at 7.65 ppm (Table 1). ^{13}C spectra of solutions of **C** containing added **B** led to the same conclusion.

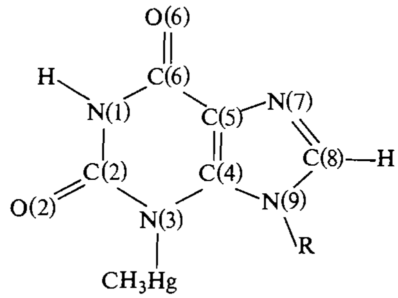

C*b*

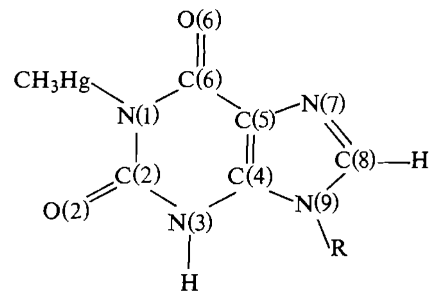

C*a*

Our results can be explained if the $(CH_3Hg)(HXan)$ complex exists as two linkage isomers, labelled **C***a* and **C***b*, corresponding to the two possible distributions of one H^+ and one CH_3Hg^+ ions on N1 and N3. The ^1H and ^{13}C resonances for the CH_3Hg^+ groups were interpreted by comparison with those deduced above for **B**. The broad signal at 10.77 ppm was assigned to the N1-H proton of **C***b*, whereas the analog N3-H resonance for **C***a* is believed to be absent from the spectrum, as for xanthosine, because of fast exchange with the protons of the water present in $(CD_3)_2SO$. The remaining ^1H signals and the ^{13}C resonances, except those of C8 and C5 which were unsplit, could not be unambiguously assigned at this stage. However, spectra of $(CH_3Hg)(HXan)$ in presence of uncomplexed xanthosine allowed us to remove this ambiguity because the two isomer exchange differently with free xanthosine.

Adding xanthosine **A** to a solution of **C** did not introduce a new set of ^{13}C peaks at the positions already observed in the spectrum of **A**. However, most of the purine resonances of **C** were displaced (Fig. 2*c*). Therefore, some exchange process involving free and complexed xanthosine must take place to produce signal averaging. Figure 2*c* corresponds to a 30:35:35 mixture of **A**, **C***a* and **C***b*. The signal observed at 152.9 ppm for the mixture results from averaging of the C2 resonances of xanthosine and one of the isomers of **C** in fast exchange. The fast-exchanging isomer will be identified as **C***b* later. The expected average chemical shift $(30 \times 150.4 + 35 \times 154.2)/65 = 152.4$ ppm) is in good agreement with the observed chemical shift. However, this exchange process cannot involve the other isomer, since the C6 resonance of **C** at 161.7 ppm is not displaced in the presence of free xanthosine, but simply loses intensity. This resonance is assigned to the non-exchanging isomer, to be later identified as **C***a*. The remaining signals above 130 ppm all contain overlapping peaks originating from **C***a* and the averaged signal for (**A** + **C***b*). For instance, the (**A** + **C***b*) signal for C6 expected to occur at 157.9 ppm and the C2 resonance of **C***a* at 157.2 ppm produce a broad signal at 157.9 ppm. Similarly, the (**A** + **C***b*) signals expected at 142.1 (C4) and 134.8 ppm (C8) are too close to the corresponding resonances of **C***a* (143.1 and 134.1 ppm, respectively) to give resolved peaks, and the mixture gives broad resonances centered at 142.7 and 134.7 ppm (Fig. 2*c*). As to the C5 signals, they occur at 116.2 ppm for the three species and they are not sensitive to exchange.

The ^1H spectrum (Fig. 1*c*) is consistent with the above interpretation. The C8-H peak at 7.80 ppm is assigned to **C***a*, since it occurs at the same position before and after the addition of free xanthosine. In the spectrum of the mixture, the 7.80 ppm peak is much weaker than the broad 7.88 ppm resonance due to (**A** + **C***b*).

The above discussion allowed us to distribute the ^1H and ^{13}C resonances observed in the spectrum of **C** (Figs. 1*b* and 2*b*) into two sets corresponding to a fast-exchanging isomer and a slow-exchanging isomer, respectively. However, the correspondence between each set and one isomer of **C** was not yet established. Final identification was based on the ^{13}C chemical shifts. It has been shown that substitution of an N—H proton by a CH_3Hg^+ ion in molecules of this type leads to large downfield shifts on both adjacent carbons (1, 8, 9). No clear conclusions could be drawn from the resonance of C2 (Table 2), which is adjacent to both N1 and N3. The C4 signal was affected almost to the same extent in both complexes and could not provide direct evidence. However, the C6 resonance of xanthosine was displaced downfield by 4.0 ppm for the non-exchanging isomer and remained essentially unmoved for the other. Therefore, the non-exchanging isomer must have C6 adjacent to the substituted N—H proton, and it is formally identified as **C***a*.

Concluding remarks

^{1}H and ^{13}C nmr spectroscopy shows that in contrast with most other systems containing more than one type of N-bonded CH_3Hg^+ ions, the neutral $(CH_3Hg)_2(Xan)$ compound gives rise to slow exchange of the CH_3Hg^+ groups on the nmr time scale at room temperature (90 MHz ^{1}H and 20.1 MHz ^{13}C). The $(CH_3Hg)(HXan)$ complex exists as two linkage isomers **C***a* and **C***b* because exchange of the CH_3Hg^+ groups between the N1 and N3 positions is also slow. However, the N3-Hg/N1-H isomer **C***b* exchanges rapidly with uncomplexed xanthosine, whereas the N1-Hg/N3-H isomer **C***a* does not. The greater lability of the N3-bound CH_3Hg^+ group is in good correlation with the fact mentioned earlier that the N3-H proton is more labile than the N1-H proton.

Another peculiar result revealed by this study is the constant values for the chemical shifts (both ^{1}H and ^{13}C) and ^{2}J coupling constants for CH_3Hg^+ groups bonded to a given site, no matter if the other site is occupied by another CH_3Hg^+ group or by a proton. For instance, the ^{1}H resonance of the N3-bound CH_3Hg^+ group occurs at 0.82 ppm with a ^{2}J coupling constant of 220 Hz for both **B** and **C***b*, in spite of the fact that the N1-H proton is present in **C***b* but substituted by another CH_3Hg^+ group in **B**. This suggests that at least in this system, the electronegativity difference between H and Hg does not lead to dramatic changes in electron distribution and basicity for the other coordination sites in the purine moiety.

Acknowledgments

We are grateful to E. Buncel and A. R. Norris for providing preprints of their work on the CH_3Hg^+ complexes with xanthosine (ref. 2) and other ligands. We wish to thank R. Mayer for his technical assistance in recording the nmr spectra. The financial support of the Natural Sciences and Engineering Research Council of Canada and the Ministère de l'Education du Québec is gratefully acknowledged.

1. F. ALLAIRE and A. L. BEAUCHAMP. Can. J. Chem. **62**, 2249 (1984).
2. E. BUNCEL, B. K. HUNTER, R. KUMAR, and A. R. NORRIS. J. Inorg. Biochem. **20**, 171 (1984).
3. F. BÉLANGER-GARIÉPY. M.Sc. Thesis, University of Montreal, Montreal, P.Q. 1981.
4. J. J. CHRISTENSEN, J. H. RYTTING, and R. M. IZATT. Biochemistry, **9**, 4907 (1970); R. R. REDDY, K. W. REDDY, and M. M. T. KHAN. J. Inorg. Nucl. Chem. **38**, 1923 (1976); **40**, 1265 (1978).
5. D. LICHTENBERG, F. BERGMANN, and Z. NEIMAN. J. Chem. Soc. C, 1676 (1971).
6. L. M. TWANMOH, H. B. WOOD, JR., and J. S. DRISCOLL. Heterocyclic Chem. **10**, 187 (1973).
7. L. PRIZANT, R. RIVEST, and A. L. BEAUCHAMP. Can. J. Chem. **59**, 2290 (1981).
8. A. R. NORRIS, R. KUMAR, E. BUNCEL, and A. L. BEAUCHAMP. J. Inorg. Biochem. **21**, 277 (1984).
9. J. P. CHARLAND and A. L. BEAUCHAMP. In preparation.
10. A. R. NORRIS, E. BUNCEL, and S. E. TAYLOR. J. Inorg. Biochem. **16**, 279 (1982).
11. S. E. TAYLOR, E. BUNCEL, and A. R. NORRIS. J. Inorg. Biochem. **15**, 131 (1981).
12. E. BUNCEL, A. R. NORRIS, W. J. RACZ, and S. E. TAYLOR. Inorg. Chem. **20**, 98 (1981).
13. D. L. RABENSTEIN. Acc. Chem. Res. **11**, 100 (1978).
14. A. J. CANTY and A. MARKER. Inorg. Chem. **15**, 425 (1976).

Vibrational intensities in molecules with strained bonds: cyclopropane

M. GUSSONI

CNR, Unita' di Spettroscopia Molecolare in Milano dell' Istituto di Chimica Fisica Applicata dei Materiali di Genova, Politecnico di Milano, Piazza L. da Vinci, 32. Milano, Italy

AND

C. CASTIGLIONI AND G. ZERBI

Dipartimento di Chimica Industriale e Ingegneria Chimica, Politecnico di Milano, Piazza L. da Vinci, 32. Milano, Italy

Received October 25, 1984

This paper is dedicated to Professor Camille Sandorfy on the occasion of his 65th birthday

M. GUSSONI, C. CASTIGLIONI, and G. ZERBI. Can. J. Chem. **63**, 2059 (1985).

Static and dynamic electronic charges in cyclopropane are derived from infrared intensities using parametric methods already successfully tested on many other organic molecules. Rigorous and somewhat simpler methods are adopted and the results compared. It is shown that, because of the presence of strained CC bonds in the molecule, the electrical behaviour of the C—H groups approaches that of C—H bonds in $=CH_2$ groups. Comparison of data from cyclopropane and ethylene oxide is made.

M. GUSSONI, C. CASTIGLIONI et G. ZERBI. Can. J. Chem. **63**, 2059 (1985).

Utilisant des méthodes paramétriques que l'on a déjà vérifiées avec succès sur d'autres molécules organiques et se basant sur les intensités des bandes infrarouges, on a calculé les charges électroniques statiques ainsi que dynamiques du cyclopropane. Des méthodes rigoureuses et quelque peu plus simples ont été adaptées et l'on compare les résultats. On démontre que, à cause de la présence dans le cyclopropane de liaisons CC tendues, le comportement électrique des groupements C—H ressemble à celui des liaisons C—H des groupements $=CH_2$. On présente une comparaison des données relatives au cyclopropane et à l'oxyde d'éthylène.

[Traduit par le journal]

1. Introduction

The study of infrared intensities is a powerful tool to derive an *experimental distribution* (static and dynamic) of the electronic charge in molecules (1). The success of the use of infrared intensities in understanding the electrical behaviour of molecules heavily depends on the model adopted in the analysis of the experimental data. Of the various models proposed in the past few years the one based on the so-called electrooptical parameters (EOP) (2), seems to provide the most acceptable results. In the EOP model, the molecular dipole moment $\boldsymbol{M}$ is expressed as a sum of bond contributions, according to a valence representation:

$$\boldsymbol{M} = \Sigma_k \mu_k \boldsymbol{e}_k$$

Here μ_k is the bond dipole moment of the kth bond, whose direction is that of the unit vector $\boldsymbol{e}_k$.[1] Under this assumption it is possible to derive a set of electrooptical parameters such as the equilibrium dipole moments (μ_k^0) and their derivatives with respect to any internal or symmetry coordinate ($\partial\mu^k/\partial R_t$) from the intensities of the fundamental bands.[2]

From EOP it is also possible to derive, *unequivocally*, another set of parameters, even more meaningful, namely the equilibrium atomic charges (q_α^0) and charge fluxes ($\partial q_\alpha/\partial R_t$) (ECCF) (3). Due to their localization, EOP (and ECCF) are the parameters most suitable to be transferred from molecule to molecule and have been shown to be very useful in predicting spectra (4, 5). Moreover, it seems that they have a sound physical meaning (6) from the evidence so far collected; indeed they correlate with various experimental physical quantities independent of ir intensities (6) and allow the understanding of phenomena related to intra- and intermolecular electrical interactions (7–11).

Unfortunately, the derivation of EOP from ir intensities is not immediate: their derivation requires several intermediate steps (and assumptions) that sometimes undermine the reliability of the resulting parameters. The basic requirements to be fulfilled in order to derive "good" parameters are the following (5): (*i*) very accurate measurements of absolute intensities (A_i) must be carried out of all fundamental ir bands, and, possibly, of various isotopic derivatives; (*ii*) a reliable force field must be used; and (*iii*) safe procedures in the determination of the signs of $\partial\boldsymbol{M}/\partial Q_i$ ($A_i = |\partial\boldsymbol{M}/\partial Q_i|^2$) must be adopted, including the comparison of quantum mechanical calculations.

When the above requirements are satisfied *the* set $\partial M/\partial S_i$ (S_i = symmetry coordinate) is definitively determined. However, there is still another important weakness in the determination of EOP. In general, the number of EOP exceeds the number of experimental data. The problem is then to choose among the various sets, the set of EOP which is more likely to describe the characteristics of the molecular charge distribution. This difficulty can be overcome by the simultaneous analysis of the intensities of large classes of molecules: the parameters relative to the same atomic groups in similar or in different molecular environments must be compared and the "trends" suggested by EOP in relation to physical and chemical known properties must be analyzed.

Several sets of reliable EOP have been determined this way for several molecules. An extensive work has been carried out in the case of hydrocarbons with or without substituents (5–14). From these studies a detailed understanding of the electrical properties of C—H bonds at equilibrium and during vibration has been obtained. Some conclusions of general validity are as follows:

[1]The assumption that the bond dipole lies on the internuclear axis is the most naive, but it is necessary in order to avoid an arbitrary splitting of $\mu^k_{\mathrm{longitudinal}}$ and $\mu^k_{\mathrm{transverse}}$.

[2]R_t are vibrational coordinates such as bond stretching, angle deformation, or torsion about a bond. Linear combinations of R_t dictated by symmetry, are also used.

(*i*) All the hydrogens involved in C—H bonds are positive. This means that the carbon atom, when forming the bond, withdraws electrons from H. (See Appendix for a further discussion.)

(*ii*) q_H^0 is very sensitive to the state of hybridization of the adjacent carbon atom q_H^0 in ≡CH bonds is more positive than that in =CH_2 bonds; q_H^0 in =CH_2 bonds is more positive than that in >CH_2 and —CH_3 bonds; q_H^0 in hyperconjugated methyl groups (such as in propylene, propyne, acetone) have intermediate values.

(*iii*) The charge flux on the hydrogen, when the C—H bond stretches, is negative and practically the same ($\partial q^H/\partial r = -0.2$ e Å^{-1}) for all the H atoms bonded to carbons both in sp^2 and sp^3 hybridization.

(*iv*) In the presence of π electrons there are relevant charge fluxes with in-plane bending motions, one order of magnitude larger than those in unsaturated compounds. This fact has been shown to be relevant in the interpretation of the spectra of a number of molecules (8, 14).

Recently we have proposed simple rules for deriving directly some qualitative information on EOP from the intensity pattern of bands and not just from single isolated bands. It has been shown that in the case of H atoms bonded to C(sp^2) or C(sp^3) the sum of the C—H stretching intensities per C—H (ΣI^{str}/CH) increases when q_H^0 decreases, while the sum of bending intensities per C—H (ΣI^{def}/CH) decreases when q_H^0 decreases. This has been found and rationalized in a number of cases and is thoroughly discussed in refs. 9 and 14. These criteria have been very useful in the study of those cases where only "limited" intensity data were available, namely, when overlapped bands need to be measured, when a reliable force field is not available or when it is impossible to measure the *absolute intensities* of the bands. Recently, the use of the quantity $\Sigma I^{def}/\Sigma I^{str}$ has allowed the problem of lack of experimental data on absolute intensities to be bypassed and has provided good results in the study of complex molecules such as polyacetylene. Finally, $\Sigma I^{def}/\Sigma I^{str}$ seems to be a very sensitive indicator of the differences in the charge distribution in the various C—H bonds.

On these grounds we discuss in this paper the infrared intensities of cyclopropane (15) and derive a set of EOP. The objectives of this paper are (*i*) to clarify the influence of the presence of strained CC bonds on the charge distribution in the C—H bonds and (*ii*) to show the importance of the parallel use of qualitative information such as intensity ratios, together with the detailed analysis of EOP (see discussion above).

2. Cyclopropane

The infrared intensities of C_3H_6 and C_3D_6 have been accurately determined by Levin and Pearce (LP) (15). On the basis of the highly reliable force field of Duncan and Burns (16), using the isotopic invariance criterion and a comparison with quantum mechanical calculations for the choice of the signs of the $\partial M/\partial Q_i$, LP derive the experimental $\partial M/\partial S_i$ and the corresponding atomic polar tensor (APT) for cyclopropane. Our analysis is based both on the direct use of the experimental intensities and on the EOP that can be derived. Geometry, axes and definition of coordinates are the same as those reported in ref. 15.[3]

[3]Except for the (internal and symmetry) bending coordinates that we define in radians and not, as in ref. 15, in Å. r_{CH}^0 = 1.082 Å should be used for the conversion.

TABLE 1. Observed (15) infrared intensities of cyclopropane

ν^{obs} (cm^{-1})		A^{obs} (darks)
3100.7	r^-	3021
854	P	49.5
3024.4	r^+	3853
1437.7	α	181
1028.4	W	2032
868.5	R	3114

TABLE 2. Comparison of experimental data of propane (CH_2), cyclopropane, and ethylene

	Value		
Parameter	Propane	Cyclopropane	Ethylene
ΣI^{str}/CH[a]	2812[e]	1146[f]	960[g]
ΣI^{def}/CH[b]	409[e]	896[f]	2251[g]
$\Sigma I^{def}/\Sigma I^{str}$	0.14	0.78	2.38
ν_{CH}^{is} [c]	2920	3056	3055
r_{CH}^0 [d]	1.109	1.085	1.085
α_{HCH}	106.1	116.5	117.4

[a]Sum of the CH stretching intensities per CH bond. Units are darks.
[b]Sum of bending intensities per CH bond. Units are darks.
[c]Isolated CH stretching frequency, derived by selective deuteration (18).
[d]Interatomic CH distances. Units are in Å.
[e]Reference 20.
[f]Reference 15.
[g]Reference 19.

In Table 1, we have reported the observed (15) infrared intensities of C_3H_6. The first step is to compare infrared intensities of C_3H_6 with those of *n*-paraffins and those of ethylene since it turns out from quantum chemistry (17) that the orbitals of C_3H_6 possess intermediate properties. In Table 2 the sum of the CH stretching intensities per C—H bond (ΣI^{str}/CH) and the sum of CH bending intensities per C—H bond (ΣI^{def}/CH) of propane, cyclopropane, and ethylene are reported. It becomes apparent that the intensities of cyclopropane have an intermediate behaviour between propane and ethylene. Moreover, ΣI^{str}/CH suggests that the charge distribution of CH bonds in cyclopropane is more similar to that of ethylene; this agrees with other experimental data, such as isolated CH frequency and interatomic CH distance. The latter have been shown (18) to be very sensitive to the electrical nature of the bond. If we compare $\Sigma I^{str}/\Sigma I^{def}$ for cyclopropane, ethylene, and propane (see Table 2), we conclude that $q_H^0(C_2H_4) > q_H^0(C_3H_6) > q_H^0(C_3H_8)$ (see Introduction).

In Table 3 we report the expressions of $\partial M/\partial S_i$ of cyclopropane as a function of EOP. For a direct comparison, it is useful to introduce in these expressions the values of the electrooptical parameters of ethylene and of propane (see Table 4). In Table 5 the resulting $(\partial M/\partial S_i)^{calcd}$ and the corresponding infrared intensities A_i^{calcd} are reported and compared with the experimental values. It is apparent that $\partial M/\partial S_6$ predicted from propane is too large; therefore ΣA_{calcd}^{str} predicted from C_3H_8 is also too large. This indicates that the q_H^0 transferred from propane is too small (see Introduction). The same trend is suggested by the small values calculated for $\partial M/\partial S_{10}$ and for

TABLE 3. Analytical expressions for the $\partial M/\partial S_i$ of cyclopropane as a function of electrooptical parameters; see drawings for the definition of the parameters

$\partial M^z/\partial S_6$	$= \sqrt{6}\,(\partial\mu/\partial r - \partial\mu/\partial r')\sin(\alpha/2)$	$= -0.809$ D Å^{-1}
$\partial M^z/\partial S_7$	$= (2\sqrt{3})\sin(\alpha/2)\partial\mu/\partial P - 1.102\,\mu^0$	$= -0.094$ D
$\partial M^y/\partial S_8$	$= -\sqrt{3}\,(\partial\mu/\partial r + \partial\mu/\partial r')\cos(\alpha/2) + (3/2)\partial M/\partial r$	$= 0.731$ D Å^{-1}
$\partial M^y/\partial S_9$	$= -\sqrt{6}\cos(\alpha/2)\,\partial\mu/\partial\alpha - (3/2)\,\partial M/\partial\alpha + 0.663\,\mu^0$	$= 0.011$ D
$\partial M^y/\partial S_{10}$	$= -(\sqrt{3}/\sqrt{2})\,\partial M/\partial W - 2.180\,\mu^0$	$= -0.926$ D
$\partial M^y/\partial S_{11}$	$= \sqrt{2}\,\partial M/\partial R' - 0.248\,\mu^0/r^0$	$= -1.881$ D Å^{-1}

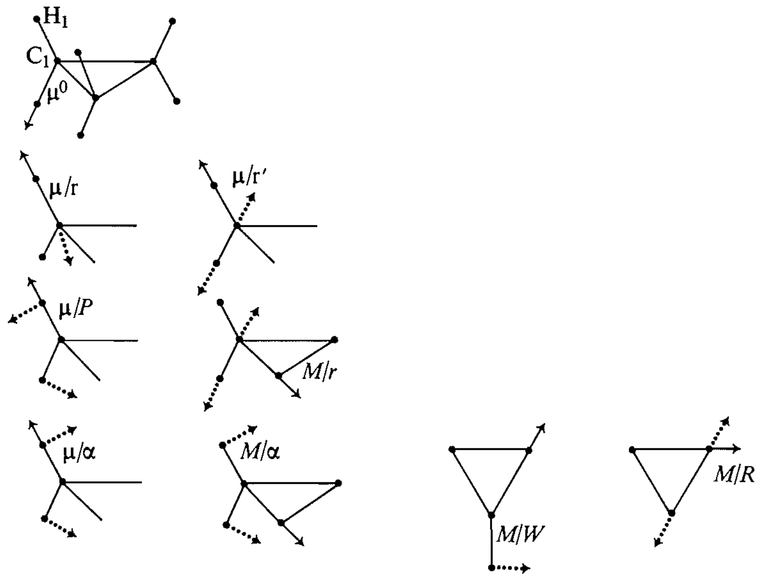

$\Sigma A^{\mathrm{def}}_{\mathrm{calcd}}$. Opposite characteristics are shown by the values calculated from ethylene; while the values of $(\partial M/\partial S_{\mathrm{str}})^{\mathrm{calcd}}$ are comparable with the experimental ones, as confirmed by the calculated values of stretching intensities, the $\Sigma A^{\mathrm{def}}_{\mathrm{calcd}}$ is very large, due to the large values assumed by $(\partial M/\partial S_{10})^{\mathrm{calcd}}$ and $(\partial M/\partial S_9)^{\mathrm{calcd}}$. The leading term in $\partial M/\partial S_{10}$ and $\partial M/\partial S_9$ is the C—H equilibrium dipole moment, that is $q^0_{\mathrm{H}} r^0_{\mathrm{CH}}$. In conclusion also a detailed transferring of EOP indicates that $q^0_{\mathrm{H}}(C_3H_8) < q^0_{\mathrm{H}}(C_3H_6) < q^0_{\mathrm{H}}(C_2H_4)$. From Table 5 one can observe that $\partial M/\partial S_{11}$ is heavily underestimated in both calculations: this indicates a large value of $\partial M^{\mathrm{CC}}/\partial R'$ in C_3H_6, suggesting the presence of a very mobile charge along the C—C bonds. It is also interesting to note that the values of the bending $\partial M/\partial S_i$ calculated from propane (i = 7, 9, 10) have the same order of magnitude. On the contrary, the corresponding experimental $\partial M/\partial S_i$ have very different values (compare $\partial M/\partial S_{10}$ with $\partial M/\partial S_7$, $\partial M/\partial S_9$). Experimental $\partial M/\partial S_i$ show similar behaviour as those calculated from ethylene. As the following will show, this behaviour can be ascribed to the presence of relevant charge fluxes on the hydrogens during bending motions, both in C_3H_6 and in C_2H_4.

We now proceed to derive a set of electrooptical parameters for C_3H_6. At this stage of the work some remarks on the determination of $\partial M/\partial S_i$ for cyclopropane are required. The positive sign chosen by LP for $\partial M/\partial S_7$ is anomalous when compared with the corresponding quantity in several other hydrocarbons: the sign of $\partial M/\partial S_i$ (S_i = bending coordinate) turns out to be the same as the sign of the deformation contribution. This also happens in C_3H_6 for all the bending $\partial M/\partial S_i$ determined by LP for the E species. We would therefore expect a negative sign for $\partial M/\partial S_7$. In the analysis of the problem we found that the L^{-1} matrix for the A species, used and published by LP, seems incorrect; the correct one is reported in Table 6. As it can be seen in Table 6, the use of the correct L^{-1} matrix modifies the results of the test of the isotopic invariance, indicating a preference, even if very slight, for the negative sign.

TABLE 4. Experimental electrooptical parameters of ethylene (13) and propane (12)

Parameter	Value: Ethylene	Value: Propane	Unit
μ^0	0.701	0.242	D
$\partial\mu/\partial r$	−0.506	−0.843	D Å^{-1}
$\partial\mu/\partial r'$	−0.067	−0.008	D Å^{-1}
$\partial M/\partial r$	—	—	D Å^{-1}
$\partial\mu/\partial P$	0.260	0.038	D rad^{-1}
$\partial\mu/\partial\alpha$	0.224	0.024	D rad^{-1}
$\partial M/\partial\alpha$	—	−0.026	D rad^{-1}
$\partial M/\partial W$	—	−0.167	D rad^{-1}
$\partial M/\partial R'$	—	−0.079	D Å^{-1}
q^0_{H}	0.134	0.045	e
$\partial q_{\mathrm{H}}/\partial r_{\mathrm{CH}}$	−0.220	−0.200	e Å^{-1}

Our analysis starts then from the $\partial M/\partial S_i$ derived by LP for the E species and from those derived for the A species with our sign choice. We work with nine unknown parameters (see Table 3), while there are only six experimental data. In general this problem is overcome by neglecting some parameters. Let us consider the bending $\partial M/\partial S_i$. As a first approximation let us retain only the terms containing μ^0. We thus have only one unknown in three equations, which turn out to be strongly incompatible ($\partial M/\partial S_7$ provides μ^0 = 0.112 D; $\partial M/\partial S_9$ provides μ^0 = 0.016 D, and $\partial M/\partial S_{10}$ provides μ^0 = 0.424 D).

TABLE 5. Comparison between the experimental $\partial M/\partial S_i$ and the infrared intensities A_i of cyclopropane and the same quantities calculated by transferring EOP from ethylene and propane; units are D Å^{-1} for $\partial M/\partial S_i$ (i = 6, 8, 11) and D for $\partial M/\partial S_i$ (i = 7, 9, 10); intensities are in darks

i	From ethylene $(\partial M/\partial S_i)^{calcd}$	Cyclopropane $(\partial M/\partial S_i)^{exp}$	From propane $(\partial M/\partial S_i)^{calcd}$
6	−0.914	−0.809	−1.739
7	−0.007	−0.094	−0.155
8	0.522	0.731	0.776
9	0.176	0.011	0.185
10	−1.528	−0.926	−0.323
11	−0.161	−1.881	−0.167

i	From ethylene A_i^{calcd}	Cyclopropane A_i^{exp}	From propane A_i^{calcd}
6	3905	3021	13958
7	1	49.5	137
8	2782	3853	5114
9	763	181	587
10	11717	2032	312
11	31	3114	38
ΣA^{str}	6687	6874	19072
ΣA^{def}	12512	5376	1074

TABLE 6. Application of isotopic invariance criterion for the A species

$$\mathbf{L}^{-1}_{C_3H_6}\ (A\ \text{species}) = \begin{array}{c|cc} & S_6 & S_7 \\ Q_6 & 0.9476 & -0.0047 \\ Q_7 & 0.0713 & 0.8407 \end{array}$$

$\partial M^z/\partial Q_6 = \pm\ 0.846$ $\qquad \partial M^z/\partial Q_7 = \pm\ 0.109$

	C_3H_6		C_3D_6	
	(−+)	(−−)	(−−)	(−+)
$\partial M^z/\partial S_6$	−0.794	*−0.809*	−0.763	*−0.795*
$\partial M^z/\partial S_7$	0.096	*−0.087*	0.113	*−0.099*

This fact indicates that angular fluxes are relevant in cyclopropane, as already suggested by previous comparison with ethylene. However, we have five angular EOP (μ^0, $\partial\mu/\partial P$, $\partial\mu/\partial\alpha$, $\partial M^{CC}/\partial\alpha$, $\partial M^{CC}/\partial W$) and three experimental data ($\partial M/\partial S_7$, $\partial M/\partial S_9$, $\partial M/\partial S_{10}$). $\partial M/\partial S_{10}$ depends only on μ^0 and $\partial M^{CC}/\partial W$. The wagging motion ($W$) of cyclopropane is similar to the out-of-plane CH deformation in ethylene, which, for symmetry reasons, is independent of any charge flux parameter. It then seems reasonable to assume that $\partial M/\partial S_{10}$ (C_3H_6) is due to a pure deformation. With this assumption $\mu^0(C_3H_6)$ = 0.425 D and therefore $q_H^0(C_3H_6)$ = 0.082 e. It is important to verify whether the assumption $\partial M^{CC}/\partial W = 0$ is reasonable. In Table 7 we have compared the values of the equilibrium hydrogen charges of several hydrocarbons with $\Sigma A^{def}/\Sigma A^{str}$. It becomes apparent that q_H^0 and $\Sigma A^{def}/\Sigma A^{str}$ indicate the same trend; notice that also q_H^0 = 0.082 e of cyclopropane is perfectly in agreement with this trend.

In Table 8 we report EOP and ECCF derived using q_H^0 = 0.082 e. From $\partial M/\partial S_9$ we have derived two possible sets of charge fluxes with angular α deformation; the correct solution is, probably, intermediate. However, we notice that all the angular fluxes are relevant (compare with the values of ethylene and of propane in Table 4): this is a peculiar characteristic of systems containing π electrons (8). Moreover, $\partial M^{CC}/\partial R'$ is very high, as expected. As for the CH stretching $\partial M/\partial S_i$ (i = 6, 8), we have two experimental data and three parameters to be determined. We choose to set $\partial M^{CC}/\partial r_{CH}$ to 0, because the alternative solution $(\partial\mu^k/\partial r_j) = 0$ provides a too low value of $\partial\mu^k/\partial r_k$ (= −0.389 e Å^{-1}). This implies a charge flux $\partial q^H/\partial r_{CH}$ = −0.150 e Å^{-1}, which is low with respect to the standard value for hydrocarbons ($\partial q^H/\partial r_{CH}$ = −0.2 e Å^{-1}).

TABLE 7. Comparison of experimental equilibrium hydrogen charge and intensity ratios for several hydrocarbons, charges are in electrons

Compound	q_H^0	$\Sigma I^{def}/\Sigma I^{str}$
C_2H_6	0.05	0.14
CH_4	0.06	0.48
CH_3CHCH_2	0.07	0.53
C_3H_8	0.08	0.78
CH_3CCH	0.10	0.95
C_6H_6	0.12	1.83
C_2H_4	0.13	2.30
C_3H_4	0.15	3.48

In conclusion, the EOP derived for cyclopropane are in agreement with the general ideas obtained from direct analysis of the intensity data; they suggest that, in the presence of strained CC bonds, the C—H bonds behave almost as =CH_2 bonds.

3. Comparison with ethylene oxide

We feel that this work may add more confidence in the direct use of intensity data to detect some general electrical characteristics of the C—H bonds. Using the same criteria it might even be possible to have an idea of the electrical behaviour of C—H bonds in other cyclic compounds. In Table 9 we report the ratio $\Sigma I^{def}/\Sigma I^{str}$ for some cyclic hydrocarbons. It is apparent that only cyclopropane has $\Sigma I^{def}/\Sigma I^{str}$ very different from the typical values of n-alkanes (see also Table 7). Also from this view point we conclude that the behaviour of the infrared intensities of cyclopropane, very similar to that of ethylene, is due to the occurrence of strained CC bonds.

It might be even more interesting to extend these considerations to compounds with electron-withdrawing substituents. Let us compare the intensities of cyclopropane with those of ethylene oxide (23). We have already faced the same question comparing ethylene and formaldehyde. In formaldehyde the presence of the oxygen alters the charge distribution in the C—H bonds; $q_H^0(CH_2O)$ is less positive than $q_H^0(C_2H_4)$ due to the back-donation of electronic charge from the oxygen lone pairs. The effect (see Table 10) is a weakening of C—H bonds of CH_2O (see r^0_{CH}, ν^{is}_{CH}, k_{CH}) and an enhancement of the CH stretching intensities as a consequence of the decrease in q_H^0 (see Discussion). From Table 10 one derives the indication of back-donation from oxygen lone pairs also in the case of ethylene oxide. The CH stretching intensities per CH of C_2H_4O is twice as large as that of C_3H_6; bond length and CH force constant are respectively larger and smaller in ethylene oxide than in cyclopropane. Therefore, we expect $q_H^0(C_2H_4O)$ to be

TABLE 8. Electrooptical parameters and electronic charges and charge fluxes for cyclopropane (see drawings in Table 3)

$\partial M/\partial W$	= 0	D rad^{-1}		$\partial Q^{C}/\partial W$	= 0	e rad^{-1}
μ^0	= 0.425	D		$\overset{0}{q}_H$	= 0.082	e
$\partial\mu^k/\partial r_k$	= −0.595	D Å^{-1}		$\partial q^H/\partial r_{CH}$	= −0.190	e Å^{-1}
$\partial\mu^k/\partial r_j$	= −0.207	D Å^{-1}		$\partial q^H/\partial r'_{CH}$	= −0.040	e Å^{-1}
$\partial\mu/\partial\alpha$	= 0.210;	0 D rad^{-1}		$\partial q^H/\partial\alpha$	= 0.040;	0 e rad^{-1}
$\partial M/\partial\alpha$	= 0;	0.128 D rad^{-1}		$\partial Q^{C1}/\partial\alpha$	= 0;	−0.018 e rad^{-1}
$\partial\mu/\partial P$	= 0.127	D rad^{-1}		$\partial q^H/\partial P$	= 0.024	e rad^{-1}
$\partial M/\partial R'$	= −1.261	D Å^{-1}		$\partial Q^{C1}/\partial R'_{CC}$	= −0.175	e Å^{-1}

TABLE 9. Comparison of the intensity ratios $\Sigma I^{def}/\Sigma I^{str}$ for some cyclic hydrocarbons

	$\Sigma I^{def}/\Sigma I^{str}$	Source of data
[Ethylene	2.30]	Ref. 19
Cyclopropane	0.78	Ref. 15
Cyclobutane	0.20	Ref. 21
Cyclopentane	0.06	Ref. 22
Cyclohexane	0.10	Ref. 22
[Ethane	0.14]	Ref. 23

less positive than $\overset{0}{q}_H$ (C_3H_6). Nevertheless, we still have a too-limited set of experimental data on cyclopropane and ethylene oxide to state safely that backdonation takes place in ethylene oxide. For instance, ν^{is}_{CH} has not been measured for C_2H_4O (ν^{is}_{CH} is *directly* derived from the ir spectra of selectively deuterated compounds and is *very sensitive* to electronic interactions such as backdonation (9, 18)). Therefore it is necessary to use microwave measurements of C—H bond lengths, which, unexpectedly, turn out to be less precise with respect to those determined by McKean from ν^{is}_{CH}. The CH force constant, k_{CH}, even if it measures the strength of the bond, is not a physical observable, but derives from a, perhaps arbitrary, parametrization of the vibrational frequencies. In conclusion, the study of back-donation in C_2H_4O requires a further determination of related physical quantities, in particular of ν^{is}_{CH}, and/or a detailed analysis of infrared intensities in terms of EOP.

On the other hand, we observe that, even if the increase of the CH stretching intensities of C_2H_4O is due to backdonation, still this effect is less pronounced than in the case of CH_2O. Two reasons, in principle, can be offered to rationalize such behaviour. In C_2H_4O there are *four* C—H bonds for one oxygen and all these bonds are equivalent with respect to the oxygen lone pairs; in CH_2O the hydrogens are only *two*. Moreover, it has been shown that back-donation is a *trans* effect, that is it involves only C—H bonds trans to lone pairs (this is the case of CH_3OH and of several polysacharides). In the case of ethylene oxide, no C—H are perfectly in a *trans* position with respect to lone pairs, a requirement certainly verified in the case of formaldehyde.

1. W. B. PERSON and G. ZERBI (*Editors*). Vibrational intensities in infrared and Raman spectroscopy. Elsevier, Amsterdam. 1982.
2. L. A. GRIBOV. Intensity theory for infrared spectra of polyatomic molecules. Consultants Bureau, NY. 1972.
3. A. J. VANSTRATEN and W. A. SMIT. J. Mol. Spectrosc. **62**, 297 (1976); J. C. DECIUS. J. Mol. Spectrosc. **57**, 384 (1975).
4. G. ZERBI, M. GUSSONI, S. ABBATE, and P. JONA. *In* Vibrational intensities in infrared and Raman spectroscopy. *Edited by* W. B. Person and G. Zerbi. Elsevier, Amsterdam. 1982. Chapt. 15.
5. M. GUSSONI. J. Mol. Structure **113**, 323 (1984).
6. M. GUSSONI, C. CASTIGLIONI, and G. ZERBI. J. Phys. Chem. **88**, 600 (1984).
7. M. GUSSONI, P. JONA, and G. ZERBI. J. Chem. Phys. **78**, 6802 (1983).
8. C. CASTIGLIONI, M. GUSSONI, and G. ZERBI. J. Chem. Phys. In press.
9. C. CASTIGLIONI, M. GUSSONI, and G. ZERBI. J. Am. Chem. Soc. To be published.
10. M. GUSSONI, C. CASTIGLIONI, and G. ZERBI. Chem. Phys. Lett. **99**, 101 (1983); C. CASTIGLIONI, M. GUSSONI, and G. ZERBI. J. Chem. Phys. **80**, 3916 (1984); C. CASTIGLIONI, M. GUSSONI, and G. ZERBI. J. Mol. Struct. **115**, 315 (1984).
11. M. GUSSONI, C. CASTIGLIONI, and G. ZERBI. J. Chem. Phys. **80**, 1377 (1984).
12. M. GUSSONI, S. ABBATE, and G. ZERBI. J. Mol. Struct. **87**, 87 (1982). M. GUSSONI, S. ABBATE, R. SANVITO, and G. ZERBI. J.

TABLE 10. Comparison of physical quantities indicating backdonation of electronic charge in C—H bonds of formaldehyde and ethylene oxyde

	$\overset{0}{q}_H$ (e)	ΣI^{str}/CH (darks)	$\overset{0}{r}_{CH}$ (Å)	$\overset{0}{k}_{CH}$ (mdyn/Å)	$\overset{0}{\nu}_{CH}$ (cm^{-1})	ΔE_{CH} (kcal/mol)
Ethylene	0.134	960	1.085[a]	5.598	3055	108
Formaldehyde	0.097	8155	1.111[a]	4.880	2813	87

	ΣI^{str}/CH (darks)	$\overset{0}{r}_{CH}$ (Å)		$\overset{0}{k}_{CH}$ (mdyn/Å)
Cyclopropane	1145	1.085[a]	1.082[b]	5.125
Ethylene oxyde	2025	—	1.085[c]	5.061

[a]From ν^{is}_{CH}, see ref. 18.
[b]From microwave, see ref. 25.
[c]From microwave, see ref. 26.

Mol. Struct. **75**, 177 (1981).
13. P. JONA, M. GUSSONI, and G. ZERBI. J. Chem. Phys. **75**, 1667 (1981).
14. M. GUSSONI, C. CASTIGLIONI, M. MIRAGOLI, G. LUGLI, and G. ZERBI. Spectrochim. Acta. In press.
15. I. W. LEVIN and R. A. R. PEARCE. J. Chem. Phys. **69**, 2196 (1978).
16. J. L. DUNCAN and G. R. BURNS. J. Mol. Spectrosc. **27**, 117 (1968).
17. R. HOFFMANN and R. B. DAVIDSON. J. Am. Chem. Soc. **93**, 5699 (1971).
18. D. C. MCKEAN. Chem. Soc. Rev. **7**, 399 (1968).
19. C. GOLIKE, I. MILLS, W. B. PERSON, and B. CRAWFORD. J. Chem. Phys. **25**, 1266 (1959).
20. S. KONDO and S. SAEKI. Spectrochim. Acta, A**29**, 1753 (1973).
21. E. P. KRAINOV, N. I. PROKOF'EVA, and L. M. SVERDLOV. Opt. Spektr. **16**, 566 (1964).
22. A. G. FINKEL and N. I. PROKOF'EVA. Opt. Spektr. **7**, 588 (1959).
23. I. M. NYQUIST, I. M. MILLS, W. B. PERSON, and B. CRAWFORD. J. Chem. Phys. **26**, 552 (1957).
24. T. NAKANAGA. J. Chem. Phys. **74**, 5384 (1981).
25. W. J. JONES and B. P. STOICHEFF. Can. J. Phys. **42**, 2259 (1964).
26. T. E. TURNER and J. A. HOWE. J. Chem. Phys. **24**, 924 (1956).
27. K. B. WIBERG and J. WENDOLOSKI. J. Phys. Chem. **88**, 587 (1984).

Appendix

The fact that all μ^0_{CH} are positive is unequivocal if the signs indicated for $\partial M/\partial S_i$ by isotopic invariance (*and* by "*ab initio*" calculations) for a large number of saturated and unsaturated hydrocarbons is assumed and if the hypothesis of alignment of the bond dipole moment with the internuclear axis is retained. Recently Wiberg (27), using the method of Bader, has pointed out that "*ab initio*" calculations do not confirm the validity of this approximation: they say that a component of the bond dipole perpendicular to the bond may exist. On this assumption, even a positive $\partial M/\partial S_{bend}$ may be split into a negative μ^0_{CH} and a positive flux of charge perpendicular to the bond. We are aware of this new line in the *interpretation* of the $\partial M/\partial S_i$ and we are grateful to the referee who has explicitly required a mention to this problem. Since Wiberg's approach so far has been applied only to a few molecules (ethylene, acetylene) with a somewhat arbitrary localization of the charges forming the bond dipoles, we believe that a larger number of molecules should be studied before introducing these concepts also in a phenomenological approach such as ours. In this case one should drop the assumption reported in the first paragraph of the Introduction and use also $\mu^k_{transverse}$. However, let us stress that the approach based on only $\mu^k_{longitudinal}$ has allowed us to explain successfully several inter- and intramolecular properties (5, 6, 10, 11).

Magnesium–nucleotide interaction. Synthesis, structure, ^{1}H, ^{13}C nuclear magnetic resonance and Fourier transform infrared studies of Mg-inosine-5′-monophosphate complexes

H. A. TAJMIR-RIARI AND T. THEOPHANIDES[1]

Department of Chemistry, Université de Montréal, C.P. 6210, Succ. A, Montréal (Qué.), Canada H3C 3V1

Received August 10, 1984

This paper is dedicated to Professor Camille Sandorfy on the occasion of his 65th birthday

H. A. TAJMIR-RIARI and T. THEOPHANIDES. Can. J. Chem. **63**, 2065 (1985).

The reaction of inosine-5′-monophosphate acid ($IMPH_2$) with hydrated magnesium chloride $MgCl_2 \cdot 6H_2O$ gives complexes of the type $Mg(IMP) \cdot 5H_2O$ and $Mg_2(IMP)_3 \cdot 15H_2O$. The FT-IR spectra of $Mg(IMP) \cdot 5H_2O$ in the region 1800–400 cm^{-1} showed marked similarities with that of the structurally characterized N_7-bound $Ni(IMP) \cdot 5H_2O$ and $Co(IMP) \cdot 5H_2O$ complexes, while $Mg_2(IMP)_3 \cdot 15H_2O$ exhibited distinct spectral similarities with the known $Cd_2(IMP)_3 \cdot 12H_2O$ and $Ca(IMP) \cdot 6.5H_2O$ compounds, where a direct metal–phosphate and metal–sugar binding as well as metal–N_7-coordination has been shown crystallographically. The Mg(II) ion in $Mg(IMP) \cdot 5H_2O$ is N_7-bound with an indirect metal–phosphate and metal–carbonyl interaction through a coordinated water molecule and in the $Mg_2(IMP)_3 \cdot 15H_2O$ compound it binds directly to the phosphate and to the sugar moiety as well as to the N_7-site of the purine ring system.

H. A. TAJMIR-RIARI et T. THEOPHANIDES. Can. J. Chem. **63**, 2065 (1985).

La réaction de l'acide inosinemonophosphate-5′ ($IMPH_2$) avec le chlorure de magnésium hydraté ($MgCl_2 \cdot 6H_2O$) conduit à la formation de complexes des types $Mg(IMP) \cdot 5H_2O$ et $Mg_2(IMP)_3 \cdot 15H_2O$. Le spectre IR par transformation de Fourier du complexe $Mg(IMP) \cdot 5H_2O$ dans la région de 1800 à 400 cm^{-1} présente des similitudes marquées avec ceux des complexes $Ni(IMP) \cdot 5H_2O$ et $Co(IMP) \cdot 5H_2O$ qui sont liés par le N_7 et qui ont été caractérisés du point de vue de la structure; par ailleurs le spectre du complexe $Mg_2(IMP)_3 \cdot 15H_2O$ présente des similarités spectrales distinctes avec les composés connus $Cd_2(IMP)_3 \cdot 12H_2O$ et $Ca(IMP) \cdot 6{,}5H_2O$ pour lesquels il a été démontré par cristallographie qu'il existe des liaisons directes métal–phosphate et métal–sucre ainsi qu'une coordination métal–N_7. L'ion Mg(II) du $Mg(IMP) \cdot 5H_2O$ est lié au N_7 par le biais d'une interaction indirecte métal–phosphate et métal–carbonyl impliquant une molécule d'eau coordonée; par ailleurs, dans le composé $Mg_2(IMP)_3 \cdot 15H_2O$, le Mg(II) se lie directement au phosphate ainsi qu'au sucre et au site N_7 du système cyclique de la purine.

[Traduit par le journal]

Introduction

There is little information on magnesium–IMP complexes. Our recent reports (1–5) showed that the Mg(II) ion behaves as a "soft" and "hard" acid by binding to the N_7-atom or to the phosphate oxygen atoms of guanosine-5′-monophosphate (GMP), deoxyguanosine-5′-monophosphate (dGMP), adenosine-5′-monophosphate (AMP), and xanthosine-5′-monophosphate (XMP) molecules under different chemical reaction conditions.

In the present work we describe the isolation and characterization of two Mg–IMP complexes synthesized at neutral pH values and we analyse the ^{1}H, ^{13}C nmr and Fourier Transform Infrared (FT-IR) spectra. Furthermore, having at our disposal unambiguous structural information on $Ni(IMP) \cdot 5H_2O$ (6), $Co(IMP) \cdot 5H_2O$ (6), $[Cu(IMP)]_n$ (7), $[Zn(IMP)]_n$ (8), $Cd_2(IMP)_3 \cdot 12H_2O$ (9), and $Ca(IMP) \cdot 6.5H_2O$ (10) we have examined the FT-IR spectra of these compounds hoping to detect characteristic features for the two structural types of Mg-complexes. In addition, we have established a correlation between spectral changes and coordination sites. The structure and the numbering scheme for 5′-$IMPH_2$ is shown below:

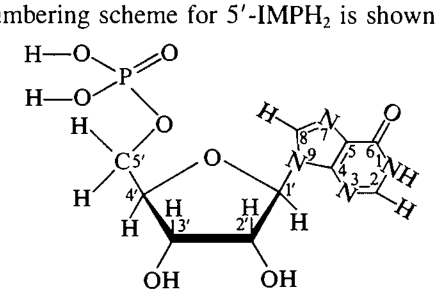

5′-$IMPH_2$

[1] To whom all correspondence should be addressed.

Experimental

Materials

The IMP acid and sodium salt were purchased from Sigma Chemical Company. D_2O (99.8%) and DMSO-d_6 (99.8%) were from Cambridge Isotope Laboratories. Hydrated magnesium chloride was from Baker Chemical Company. All the other chemicals were reagent grade and were used as supplied.

Preparation of magnesium complexes

A water solution of $MgCl_2 \cdot 6H_2O$ (1 mmol) was added to a solution of $IMPH_2$ (1 mmol) in H_2O. The pH of the solution was adjusted to 7.5 by addition of NaOH. An ethanolic solution was then used to precipitate the complex formed which was washed with alcohol several times and dried over $CaCl_2$. *Anal.* calcd. for $Mg(IMP) \cdot 5H_2O$: C 26.05, H 4.56, N 12.16, Mg 5.32; found: C 26.56, H 5.03, N 11.50, Mg, 5.15. In another attempt $MgCl_2 \cdot 6H_2O$ (2 mmol) in water was added to a solution of $IMPH_2$ (1 mmol) in H_2O and the pH was again adjusted to 7.5 with NaOH. The solution was left at room temperature for a week. Colourless crystals were separated, which were filtered off and washed with cold water and dried over $CaCl_2$. *Anal.* calcd. for $Mg_2(IMP)_3 \cdot 15H_2O$ (it should be noted that one of the IMP molecules is in the form of $IMPNa_2$): C 25.68, H 4.44, N 11.98, Mg 3.49; found: C 24.94, H 4.30, N 11.71, Mg 3.40. The two compounds are soluble in hot water and slightly soluble in hot DMSO, but are not soluble in other common organic solvents. The molar conductivities 120–200 $mol^{-1}\ \Omega^{-1}\ cm^2$ were obtained in H_2O solutions and are indicative of 2:2 electrolytes.

The structurally known complexes, $Ni(IMP) \cdot 5H_2O$, $Co(IMP) \cdot 5H_2O$, $[Cu(IMP)]_n$, $[Zn(IMP)]_n$, $Cd_2(IMP)_3 \cdot 12H_2O$, and $Ca(IMP) \cdot 6.5H_2O$ were prepared and recrystallized as reported (6–10).

^{1}H and ^{13}C nuclear magnetic resonance spectra

The spectra were recorded on a Bruker WP-80 spectrometer. Routine ^{1}H nmr spectra for analytical purposes were taken on a Varian EM 360–60 MHz. The solutions were D_2O and DMSO-d_6 containing Me_4Si or DDS as references (δ = 0.00 ppm).

TABLE 1. ^{13}C and ^{1}H nmr chemical shifts of 5′-$IMPH_2$ and its metal adducts in D_2O and DMSO solutions

	δ (ppm)									
Compound[a]	C_8	C_6	C_5	C_4	C_2	$C_{1'}$	$C_{2'}$	$C_{3'}$	$C_{4'}$	$C_{5'}$
5′-$IMPH_2$	139.37	158.20	123.10	148.70	146.40	87.50	70.50	74.60	84.30	63.60
5′-$IMPNa_2$	140.61	159.33	124.13	149.30	147.30	88.25	71.41	75.64	85.50	64.30
Mg(IMP)·$5H_2O$	140.75	159.20	123.60	149.20	147.24	88.33	71.41	75.60	85.26	64.41
$Mg_2(IMP)_3$·$15H_2O$	140.90	159.50	123.80	149.50	147.20	88.40	71.90	75.60	85.40	64.20
Ca(IMP)·$6.5H_2O$[c]	140.88	159.65	123.90	149.40	147.25	88.25	71.40	75.60	85.43	64.40

	δ (ppm)				δ (ppm)			
Compound[a]	H_8	H_2	$H_{1'}$	Compound[b]	H_8	H_2	NH	$H_{1'}$
5′-$IMPH_2$	9.00	8.36	6.25	5′-$IMPH_2$	8.33	8.07	12.40	5.90
5′-$IMPNa_2$	8.65	8.26	6.15	Mg(IMP)·$5H_2O$	8.45	8.20	12.50	6.00
Mg(IMP)·$5H_2O$	8.60	8.17	6.10	$Mg_2(IMP)_3$·$15H_2O$	8.45	8.15	12.50	6.00
$Mg_2(IMP)_3$·$15H_2O$	8.66	8.25	6.15	Ca(IMP)·$6.5H_2O$[c]	8.40	8.10	12.50	5.90
Ca(IMP)·$6.5H_2O$[c]	8.60	8.20	6.17					

[a] In D_2O solution.
[b] In DMSO solution.
[c] Structurally known compound; 5′-$IMPNa_2$ is not soluble in DMSO.

Fourier transform infrared spectra (FT-IR)

Infrared spectra were recorded on a DIGILAB FTS-15C/D Fourier transform infrared interferometer equipped with HgCdTe detector (Infrared Associates, New Brunswick, NJ), a beam splitter, and a Globar source. The spectra were obtained as KBr pellets with a resolution of 4 to 2 cm^{-1}.

X-ray powder diagrams

These were taken for comparative purposes by using a powder camera (Philips, Debye, Scherrer) with K_α-radiation and nickel filters.

Conductance measurements

The conductivity was measured with a Conductoscop E365B METROHM.

Elemental analysis

Mg(II) content was determined gravimetrically. C, H, and N were analysed at Schwarzkopf Microanalytical Laboratories (USA).

Results and discussion

Nuclear magnetic resonance spectra

The ^{13}C and ^{1}H nmr chemical shifts for 5′-$IMPH_2$ and some of its metal adducts in D_2O and DMSO solutions are given in Table 1. Unfortunately, the Na–, Mg–, and Ca–IMP compounds are not very soluble in DMSO to obtain their ^{13}C nmr spectra. The other structurally known divalent, Co–, Ni–, Cu–, Zn–, and Cd–IMP complexes (recrystallized from acidic solutions, pH = 4.5–3.8) are also not soluble in D_2O or DMSO for proton and carbon nmr spectra. We have therefore, compared the nmr spectra of only the soluble Mg–IMP compounds with the nmr spectra of the structurally characterized, Ca(IMP)·$6.5H_2O$ compound (Table 1). The nmr assignments shown here are in agreement with previously published reports (11, 12). Recently (5, 13, 14), ^{13}C and ^{1}H nmr spectroscopy was often used to characterize the nature of the interactions of alkaline-earth metals with nucleotides. The ^{13}C nmr results in D_2O (Table 1) showed that metalation (Na, Mg, and Ca) of 5′-$IMPH_2$ produces almost similar effects on the base and the sugar spectra. The largest chemical shifts observed (1 to 1.5 ppm) are for C_8, C_6, C_5, $C_{2'}$, $C_{3'}$, and $C_{4'}$ in the Na–, Mg–, and Ca–IMP compounds. On the other hand, X-ray structural analysis showed that $IMPH_2$ is N_7-protonated (15), while in $IMPNa_2$ (16) and IMPHNa (17) the Na^+ ions are coordinated to H_2O molecules and to the sugar hydroxyl groups. The N_7-site and the carbonyl group (C_6=O) are hydrogen bonded to coordinated water molecules. It has been also shown by X-ray crystal structure analysis (9) that the Ca(II) ion in Ca(IMP)·$6.5H_2O$ is directly bound to the N_7-atom of the purine ring and to the sugar hydroxyls, as well as, to water molecules.

The small chemical shifts observed for C_8, C_6, C_5, $C_{2'}$, $C_{3'}$, $C_{4'}$, and the marked nmr spectral similarities of $IMPNa_2$ (which is not N_7-coordinated in the solid state) with that of Mg(II)– and Ca–IMP complexes are indicative of coordination of these metal cations to water molecules in aqueous solution. The Ca–IMP is N7-bound in the solid state; however, in water solution the ^{13}C nmr spectra show that it is similar to $IMPNa_2$. The Ca—N7 bond must be dynamic and reversible. It is also interesting to note that the ^{1}H nmr results in D_2O did not show considerable changes for the H_8 chemical shift in the metal–IMP complexes (Table 1) and this is consistent with the ^{13}C nmr results.

The important feature of ^{1}H nmr results is the large downfield shift of the H_8 resonance when the spectra of the free acid ($IMPH_2$) are compared to those of the metalated species (Table 1). The proton downfield shift observed for H_8 in the free acid is mainly due to the protonation of the N_7-site of the purine ring. This is consistent with the presence of a zwitterionic form in the free acid both in solid state shown by crystallography (15) and in aqueous solution here. The results show a strong N_7-proton interaction in aqueous solution in contrast to the corresponding hydrated metal compounds. In DMSO solutions the H_8 resonance shows considerable downfield shift for the Mg(II)– and Ca(II)–IMP compounds compared to the free acid ($IMPH_2$). The large shift observed is consistent with a direct strong N_7–metal interaction for both Mg(II) and Ca(II) complexes (Table 1). The greater stability of the N_7–metal interaction in DMSO compared to the stability of the same species in aqueous solution (Table 1) is a solvent effect. In DMSO solution protonation of the N_7-site (ionization of the phosphate group) does not occur, while such protonation was easily observed in D_2O solutions (Table 1).

The N_1H chemical shift at 12.40 ppm did not show major changes in the nmr spectra of Mg(II)– and Ca(II)–IMP compounds (Table 1) which suggests that the N_1H group is not ionized and that it does not participate in metal–ligand bonding. More conclusive evidence regarding the nature of the metal–IMP interaction here is given from infrared spectroscopic studies discussed in the following section.

FT-IR spectra

Structurally known $Ni(IMP)\cdot 5H_2O$ and $Co(IMP)\cdot 5H_2O$ complexes showed (6) that Ni(II) and Co(II) are directly bound to the N_7-atom of the purine ring and coordinated to five H_2O molecules. The carbonyl and the phosphate groups are indirectly bound to the metal ions through coordinated water molecules by hydrogen bonding (5). On the other hand, X-ray structural analysis of the complexes, $[Zn(IMP)]_n$ (7) and $[Cu(IMP)]_n$ (8) showed that the Zn(II) and Cu(II) ions are directly linked to the oxygen atoms of the phosphate group and to the N_7-site of the ring system. In the corresponding, $Cd_2(IMP)_3\cdot 12H_2O$ (9) and $Ca(IMP)\cdot 6.5H_2O$ (10) metal complexes the metals exhibited direct metal–phosphate, metal–N_7, and metal–sugar ($O_{2'}H$ and $O_{3'}H$) binding. Furthermore, X-ray crystal structural studies on $IMPH_2$ (15) and its sodium salts ($IMPNa_2\cdot 7H_2O$ and $IMPHNa\cdot 6H_2O$) (16, 17) showed that the free acid exists in the zwitterionic form, protonated at N_7 and with a negative charge on a phosphate oxygen atom. In the disodium salt structure of IMP^{2-} the sodium ions are sugar and water coordinated (16, 17), whereas the N_7-site, the carbonyl group and the phosphate group are hydrogen bonded with water molecules (17). The FT-IR spectra of the above Cd, Ca, and Na, complexes have been recorded in the region 4000–400 cm^{-1} and compared with the corresponding Mg(II) compounds prepared in this work. The result of the spectroscopic analysis is described here.

In the region 3500 to 2500 cm^{-1} due to the presence of the strong hydrogen bonding network in the free nucleotide (15) and its metal-complexes (6–10) it is very difficult to draw conclusions on the nature of the metal–ligand bonding. The symmetric and asymmetric stretching vibrations of NH, OH, CH, and CH_2 groups of the free nucleotide occur in this region (18–20) and show no considerable changes upon nucleotide–metal complexation.

In the region 1800–400 cm^{-1} one finds drastic spectral changes in the spectra of the complexes, which are discussed below: (*a*) pyrimidine and purine ring vibrations, (*b*) phosphate vibrations, and (*c*) sugar vibrational frequencies.

(*a*) *Pyrimidine and purine ring vibrations.* A broad and strong absorption band at 1682 in the spectra of $IMPNa_2$ assigned to the $C_6{=}O$ stretching frequency (18–20) slightly shifted to higher frequencies in the spectra of Mg(II) and Ni(II) metal complexes except for Cd– and Ca–IMP compounds, where this band appeared at 1663 and 1674 cm^{-1}, respectively (Fig. 1 and Table 2). X-ray structural analysis of the known complexes showed that the carbonyl group was hydrogen bonded with outersphere coordinated water molecules ($M{-}OH_2\cdots O{=}C_6$). The small shift of the $C_6{=}O$ stretching frequency by $\Delta\bar{\nu}$ = 10–20 cm^{-1} is attributed to hydrogen bonded carbonyl or crystal packing effects. Similar spectral changes were observed in the spectra of the new Mg–IMP compounds synthesized here.

The medium intensity band at about 1640 cm^{-1} in all the spectra of N_7-bonded complexes which is not present in the spectrum of the sodium salt, most likely masked by the carbonyl band, could be assigned to the skeletal $C_6{=}C_5$ double bond stretching and to H_2O bending vibration (18–20). The NH bending vibration of the free base was observed at 1590 cm^{-1} and showed only slight changes in the spectra of the N_7-bonded complexes. In the spectrum of the $IMPH_2$ (acid) this band is not observable (Table 2). The absence of this band in the free acid spectrum (N_7-protonated) could be due to the strong and broad carbonyl absorption frequency which obscures the NH bending vibration or to the strong hydrogen bonding of the NH group in the crystal structure of the free acid (15) which could shift the NH bending towards higher frequencies and fall under the carbonyl band. The slight change of the NH bending in the spectral of Ca(II)– and Mg(II)–IMP compounds is consistent with the ^1H nmr chemical shifts of the N_1H group obtained in DMSO solution for the free acid (12.40 ppm), calcium (12.50 ppm) and magnesium (12.50 ppm) mononucleotide complexes (Table 1). It is worth noting that deprotonation of the NH group in inosine at a pH = 9–10 showed (21) disappearance of the NH stretching at 3300 cm^{-1} and the NH bending at 1590 cm^{-1}. The absorption bands at 1550 and 1519 cm^{-1} in the spectra of the free $IMPNa_2$ assigned to ring skeletal vibrations (18–20) showed a small shifting upon ligand metalation (Fig. 1 and Table 2). The shifts are mainly due to protonation or metalation of the N_7-site of the purine ring which perturbs the electronic distribution within the ring system and alters the ring skeletal frequencies.

The medium intensity band at 1481 cm^{-1} in the spectrum of $IMPNa_2$ shifted to lower frequencies at about 1475–1450 cm^{-1} upon nucleotide complexation. Since this absorption band was tentatively assigned (22) to the purine ring $N_7{-}C_8$ stretching and $C_8{-}H$ bending vibrations N_7-metalation or protonation perturbs these vibrations. The frequency changes observed ($\Delta\bar{\nu}$ = 5–30 cm^{-1}) are diagnostic of N_7-coordination of the imidazol ring to the metal, shown from crystallographic analysis (6–10). The N_7-binding of the Mg(II) ion was also demonstrated by proton nmr results obtained in DMSO solution. The chemical shifts of the H_8 of the purine ring in Mg–IMP compounds were similar to those of the corresponding N_7-coordinated, $Ca(IMP)\cdot 6.5H_2O$ compound (Table 1).

The bands centered at about 1370, 1360, 1350, 1250, 1238, and 1216 cm^{-1} in the free base spectrum assigned to the purine ring vibrational frequencies (20, 23) exhibited major intensity changes and shifting in the spectra of the N_7-coordinated complexes (Fig. 1 and Table 2). The assignment of the above bands to $N_7{-}C_5$, $N_7{-}C_8$, $N_9{-}C_8$, N_9—sugar stretchings and $C_8{-}H$ bending motion is in agreement with previous assignments (1–4). However, it seems that the N_7-electrophile bound perturbs the electron distribution in the ring system, where the vibrations are mostly localized and causes a distortion of the imidazol ring. These vibrations are also diagnostic of N_7-coordination.

The ring breathing mode at 692 cm^{-1} (20) in the spectrum of the sodium salt shifts to lower or higher frequencies depending on the nature of interaction, ie., metal–N_7, metal–phosphate, or metal–sugar interaction (Table 2). This band is sensitive to the nature of N_7-coordination and to the sugar conformational geometry (24).

(*b*) *The phosphate vibrations.* Recently we have reported (1) the vibrational frequencies of the PO_3^{2-} in mononucleotides. The infrared spectrum of 5′-$IMPNa_2$ shows five absorption bands in the region of 1100–400 cm^{-1} which are characteristic of the phosphate group (16, 19). The degenerate and symmetric stretchings of PO_3^{2-} are observed as sharp and strong absorption bands at 1090 and 977 cm^{-1}, respectively, while the P—O asymmetric stretching occurs at about 800–700 cm^{-1}. The

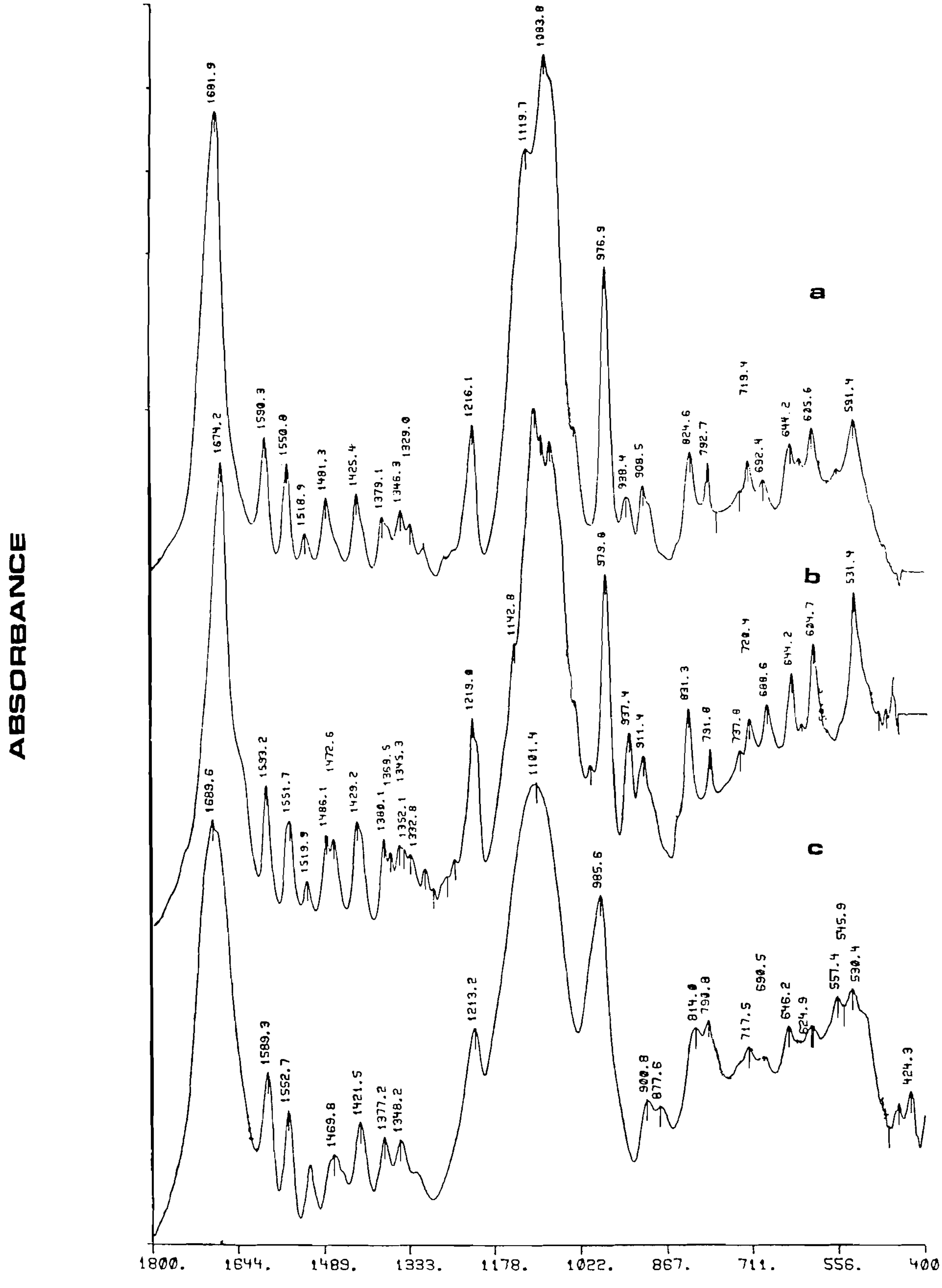

FIG. 1. FT-IR spectra of 5′-IMPNa$_2$ and its metal complexes in the region 1800–400 cm^{-1} for *a*, 5′-IMPNa$_2$; *b*, Ca(IMP)·6.5H$_2$O; *c*, Mg(IMP)·5H$_2$O; *d*, Mg$_2$(IMP)$_3$·15H$_2$O; *e*, Cd$_2$(IMP)$_3$·12H$_2$O; and *f*, Ni(IMP)·5H$_2$O.

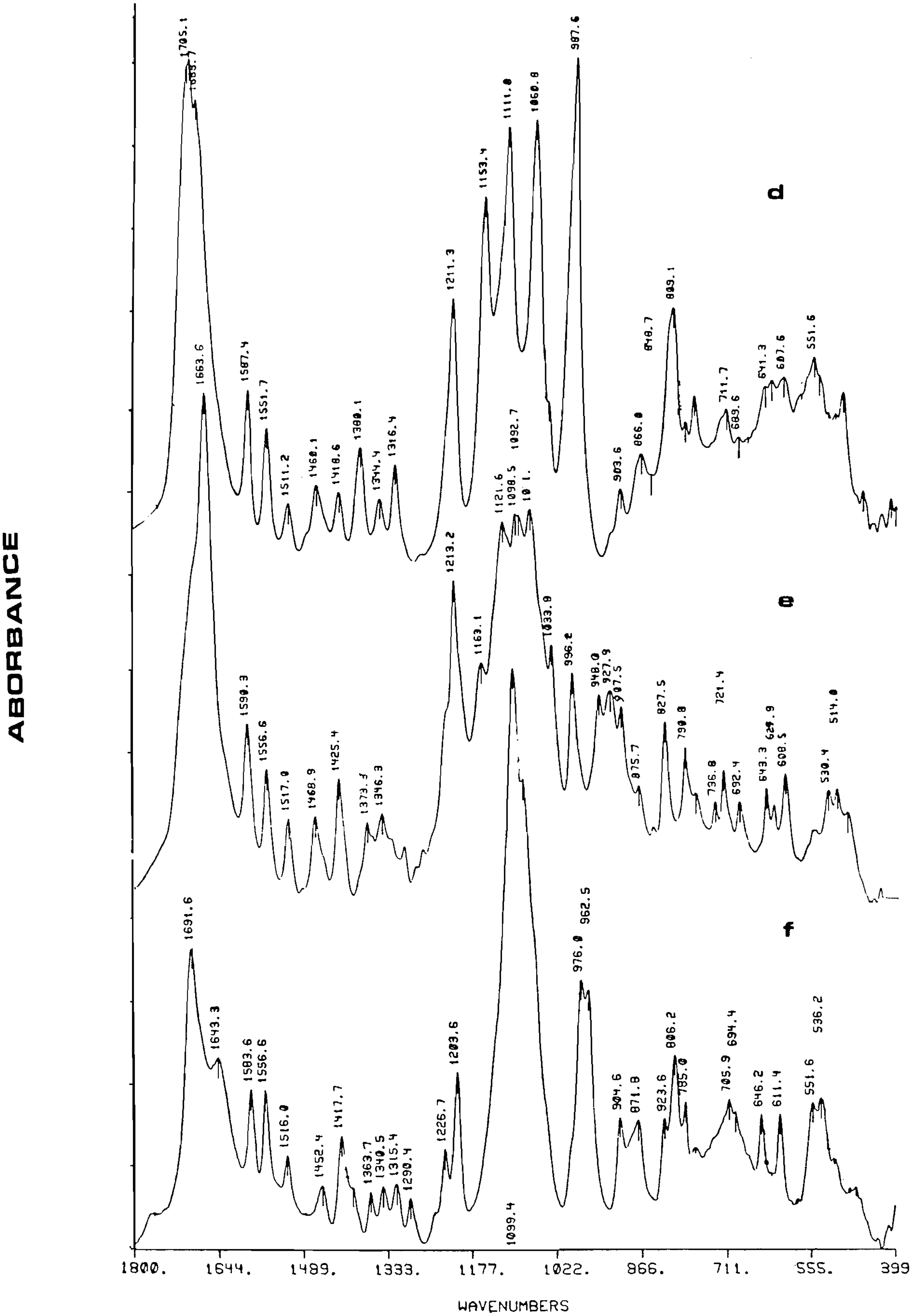

FIG. 1 (*Concluded*)

TABLE 2. FT-IR absorption bands (cm^{-1}) of the free 5-IMP and its metal complexes[a]

FT-IR absorption band								Possible assignments (18–20, 22, 23, 27)
5′-IMPNa$_2$·7H$_2$O	5′-IMPH$_2$	Ni(IMP)·5H$_2$O	[Cu(IMP)]$_n$	Cd$_2$(IMP)$_3$·12H$_2$O	Ca(IMP)·6.5H$_2$O	Mg(IMP)·5H$_2$O	Mg$_2$(IMP)$_3$·15H$_2$O	
1682 bs	1712 bs	1692 vs	1711 vs	1675 sh	1674 vs	1690 vs	1705 vs	$\nu C_6{=}O$
				1664 vs				
—	1644 sh	1463 m	1645 s	—	1645 sh	1674 sh	1688 sh	$\nu C_6{=}C_5$, δH_2O
1590 s	—	1584 s	1579 s	1590 s	1593 s	1589 s	1587 s	δNH
1550 s	1569 s	1557 s	1564 s	1557 s	1552 m	1553 m	1552 s	$\nu C_4{-}C_5$ +
1519 w	1515 sh	1516 m	1520 m	1517 m	1520 w	1517 w	1511 w	$\nu C_4{-}N_3$ + $\nu C_4{-}N_9$
1481 m	1463 w	1452 m	1475 m	1469 m	1486 m	1470 m	1460 m	$\nu N_7{-}C_8$ +
				—	1473 m	1459 sh	—	$\nu C_8{-}H$
1425 m	1422 m	1417 s	1433 s	1425 s	1429 m	1421 m	1419 w	δCH_2 + δCH
		1396 sh	1381 s	1373 m	1380 m	1377 m	1380 m	$\nu N_7{-}C_5$ +
1379 m	1363 sh	1364 w	1356 m	1362 sh	1368 w	1348 m	1344 w	$\nu N_7{-}C_8$
1360 s	1356 s	—	—	—	1352 w	—	—	
1346 m	—	1340 w	—	1346 m	1342 w	—	—	$\nu N_9{-}C_8$ +
1329 sh	1312 vw	1315 w	1315 m	1320 sh	1332 sh	—	—	
1300 w	—	1290 w	1279 m	1300 vw	1307 w	1310 sh	1316 m	$\delta C_8{-}CH$ +
1250 sh	1262 sh	1244 sh	1253 w	1260 vw	1251 sh	—	—	νN_9-sugar
1238 sh	—	1226 m	1230 sh	1220 sh	1219 s	1215 s	1211 s	
1216 s	1209 s	1204 s	1209 s	1213 vs	1206 sh	—	—	
1120 s	1112 vs	—	1132 vs	1163 s	1124 sh	—	1153 s	$\nu C{-}O$ (sugar)
				1121 vs	1106 vs	—	1111 vs	
1090 vs	1080 s	1099 bs	1082 vs	1098 vs	1094 vs	1101 bs	—	PO_3^{2-} deg.
1082 sh	1065 s	1082 s	1059 m	1065 vs	1078 vs	—	1060 vs	
1034 sh	1030 sh	—	1038 s	1034 s	1036 sh	—	—	Ribose–phosphate str.
977 s	993 s	976 s	995 vs	996 s	1005 m	—	—	
938 m	957 s	962 s	974 sh	948 s	980 vs	986 vs	987 vs	νPO_3^{2-} sym.
908 m	903 vw	904 m	—	927 s	937 s	—	920 sh	
			902 s	907 m	911 s	900 m	903 w	Ribose–phosphate str.
885 sh	870 vw	872 m	—	875 sh	—			
824 m	816 m	823 sh	843 m	850 vw	840 sh	878 m	866 m	Ribose–phosphate str.
	806 s							
792 m	788 sh	785 sh	810 s	827 s	832 s	814 s	809 s	
			787 w	791 m	792 m	790 s	787 w	
737 sh	735 sh	768 vw	771 w	772 sh	738 sh	771 sh	771 m	$\nu P{-}O$
719 m	713 m	706 m	719 m	721 m	720 m	717 m	718 m	NH out-of plane vibration
692 w	695 sh	694 sh	665 sh	692 m	688 m	640 w	689 vw	Ring breathing mode
644 m	645 w	646 m	642 m	643 m	627 vw	646 m	641 sh	
629 vw	—	626 vw	621 sh	629 w	605 s	605 m	608 m	Skeletal def.
605 m	616 s	611 m	613 s	608 m				
501 vw	555 w	562 m	563 s	560 sh	500 sh	557 m	551 s	
531 m	515 m	536 m	525 m	530 m	531 s	530 s	543	PO_3^{2-} symmetric def.
—	—	511 sh	497 s	514 m	487 sh	480 sh	499 m	Ribose def.
470 w	—	472 w	466 sh	495 sh	460 m	446 w	462 w	PO_3^{2-} deg. def.
—	—	—	412 m	—	—	424 m	410 w	

[a] s, strong; b, broad; m, medium; w, weak; ν, very; s, strong; ν, stretching; δ, bending.

other two bands are observed at 530 and 470 cm^{-1} and are assigned to the PO_3^{2-} symmetric and degenerate deformation modes, respectively (1). The two bands at 1090 and 977 cm^{-1} show major modifications (shifting and splitting) upon direct metal–phosphate bonding. In the spectra of $[Cu(IMP)]_n$, $[Zn(IMP)]_n$, $Cd_2(IMP)_3\cdot 12H_2O$, and $Ca(IMP)\cdot 6.5H_2O$ complexes which by X-ray structural analysis (7–10) showed direct metal–phosphate binding, the bands at 1090 and 977 cm^{-1} exhibited shifting and splitting as well as major intensity changes (Fig. 1 and Table 2). The above bands did not show considerable changes in the spectra of $Ni(IMP)\cdot 5H_2O$ and $Co(IMP)\cdot 5H_2O$ complexes, where an indirect metal–phosphate interaction via two coordinated water molecules ($P—\bar{O} \cdots H_2O—M—OH_2 \cdots \bar{O}—P$) was shown by X-ray analysis (6) (Fig. 1 and Table 2). The phosphate vibrational frequencies in the spectra of $Mg_2(IMP)_3\cdot 15H_2O$ showed marked similarities with the spectra of the crystallographically studied Cd(II), Ca(II), Zn(II), and Cu–IMP complexes (Fig. 1 and Table 2). This is indicative of a direct Mg—phosphate binding for $Mg_2(IMP)_3\cdot 15H_2O$, whereas the spectrum of $Mg(IMP)\cdot 5H_2O$ exhibited distinct spectral similarities with the spectra of the corresponding Ni(II) and Co(II) compounds (Fig. 1) which contain an indirect metal—phosphate linkage through coordinated water molecules. Similar observations (1) were made for the PO_3^{2-} vibrational frequencies at 1090 and 977 cm^{-1} in the spectra of $Cu_3(GMP)_3\cdot 8H_2O$, where a direct Cu—phosphate binding as well as, N_7-coordination were reported from X-ray crystal analysis (25). On the other hand, no considerable changes were observed for these vibrational frequencies in the spectra (1) of $Ni(GMP)\cdot 5H_2O$ and $Co(GMP)\cdot 5H_2O$ complexes (26).

(*c*) *Sugar vibrational frequencies*. The symmetric and asymmetric stretching vibrations of the sugar OH, CH, and CH_2 groups in mononucleotides have been observed (18, 19, 27) in the region 3600–2700 cm^{-1} overlapping with the NH, NH_2 stretchings of the base moiety and the H_2O of the metal-hydrated water molecules. Other vibrational frequencies related to the ribose ring are also appearing as sharp and fine absorption bands in the region 1400–400 cm^{-1} which are also obscured by the strong and broad absorption bands of the phosphate group and the base moiety. The assignment of the absorption bands related to the sugar frequencies is a difficult task. Metalation of the phosphate group in mononucleotides was found to be helpful in assigning the phosphate vibrational frequencies (1–4). The sodium ions in both $IMPNa_2$ and IMPHNa (16, 17) are bound directly to $O_{2'}H$ and $O_{3'}H$ of the sugar hydroxyl groups and to four water molecules (no direct interaction with the phosphate group or the N_7-atom of the base moiety exists here). The Cd(II) and Ca(II) cations are directly bound to the $O_{2'}H$ and $O_{3'}H$ hydroxyl groups as well as to the N_7-site and the phosphate oxygen atoms in $Cd_2(IMP)_3\cdot 12H_2O$ and $Ca(IMP)\cdot 6.5H_2O$ complexes (9, 10). On comparison of the infrared spectra of the Na–, Cd–, and Ca–IMP compounds with the corresponding Ni and Co complexes they showed no metal–sugar interaction (6). One can see the presence of a strong absorption band at 1120 cm^{-1} in the spectrum of the sodium salt which is not present in the spectra of Ni– and Co–IMP compounds. This band splits into two strong components in the spectra of the Cd– and Ca–IMP compounds (Fig. 1). The shifting and splitting of this band in the spectra of Cd and Ca complexes is characteristic of sugar coordination and thus the band at 1120 cm^{-1} is assigned to the sugar C—O stretching frequency. It is interesting to note that the infrared spectra of $Mg_2(IMP)_3\cdot 15H_2O$ showed marked similarities with the corresponding Cd complex (shifting and splitting of the band at 1120 cm^{-1} to 1153 and 1111 cm^{-1}) indicating a direct Mg–sugar interaction, through the hydroxyl groups. On the other hand in the spectra of the $Mg(IMP)\cdot 5H_2O$ compound only the strong and broad absorption band of the PO_3^{2-} degenerate frequency was observed (Fig. 1) as in the case of the $Ni(IMP)\cdot 5H_2O$ which contains no metal–sugar interaction. Other sugar–phosphate bands (27) in the region 900–600 cm^{-1} also exhibited splitting and shifting as well as intensity changes (Fig. 1 and Table 2) depending upon the nature of metal–ligand bonding (N_7-, phosphate or sugar). These changes can be related to conformational changes in the sugar ring upon complexation (24). It should be added that the infrared spectra of $Co(IMP)\cdot 5H_2O$ was similar to that of $Ni(IMP)_5\cdot 5H_2O$ and that of $[Zn(IMP)]_n$ was similar to $[Cu(IMP)]_n$ also studied in this work.

The proposed coordination of the Mg(II) ion in $Mg(IMP)\cdot 5H_2O$ is similar to the well known $Ni(IMP)\cdot 5H_2O$ and $Co(IMP)\cdot 5H_2O$ complexes. The $Mg_2(IMP)_3\cdot 15H_2O$ compound is similar to crystallographically known $Cd_2(IMP)_3\cdot 12H_2O$. One Mg(II) ion binds to two N_7-atoms and to a phosphate oxygen atom as well as to H_2O molecules, whereas the second Mg(II) ion is linked directly to the $O_{2'}H$ and $O_{3'}H$ sugar hydroxyl groups and to the N_7-atom as well and to water molecules as in the case of Cd (9).

The reactions of $MgCl_2\cdot 6H_2O$ with $IMPH_2$ are summarized as follows:

$$MgCl_2\cdot 6H_2O + IMPH_2 \xrightarrow[pH\,=\,7.5]{NaOH} \begin{cases} \xrightarrow{2:3} Mg_2(IMP)_2(IMPNa_2)\cdot 15H_2O + 4NaCl \\ \xrightarrow{1:1} Mg(IMP)\cdot 5H_2O + 2NaCl \end{cases}$$

Summary

Correlation between X-ray structural information and infrared spectroscopic changes in the Ni–, Co–, Cu–, Zn–, Cd–, Ca– (N_7-coordinated) and Na–IMP (free from N_7-coordination) compounds investigated here allow assignment of the vibrational frequencies in IMP^{2-}. It is known that the purine ring vibrational frequencies are strongly coupled and that an individual assignment of each band is difficult to make. However, the unambiguous X-ray structural results of several N_7-metal coordinated compounds together with their spectra helped us to make the following findings:

(*1*) The N_7-metal bound IMP^{2-} anion shows considerable changes in the bands centered around 1480–1217 cm^{-1} which originate from the purine ring vibrational frequencies,

(*2*) The indirect metal–carbonyl interaction via a metal-coordinated water molecule only slightly shifts the carbonyl stretching frequency to lower frequencies,

(*3*) The direct coordination of the phosphate oxygen atoms

to the metal ion causes shifting and splitting of the phosphate bands at 1090 and 977 cm^{-1}, while the indirect metal–phosphate interaction through metal-coordinated water molecules does not perturb considerably the positions of these absorption bands,

(*4*) The absorption band at 1120 cm^{-1} in the spectrum of $IMPNa_2$ is definitely assigned to the sugar C—O stretching frequency, and

(*5*) The X-ray powder diagrams of the Mg–IMP complexes showed no isomorphic features with that of the corresponding Ca-compound. This is most likely due to the smaller coordination number (28) of the Mg(II) ion (C.N. = 6) in the above compound compared to the Ca(II) ion (C.N. = 8). On the other hand, there were marked similarities between the X-ray powder diagrams of $Mg_2(IMP)_3 \cdot 15H_2O$ with that of the $Cd_2(IMP)_3 \cdot 12H_2O$, indicating similar coordination environments in these metal complexes.

Acknowledgement

We are grateful to the Natural Sciences and Engineering Research Council of Canada for financial support.

1. (*a*) H. A. TAJMIR-RIARI and T. THEOPHANIDES. Can. J. Chem. **61**, 1813 (1983); (*b*) T. THEOPHANIDES (*Editor*). Fourier transform infrared spectroscopy. D. Reidel Publishing Company. 1984. pp. 105–124.
2. H. A. TAJMIR-RIARI and T. THEOPHANIDES. Inorg. Chim. Acta, **80**, 183 (1983).
3. H. A. TAJMIR-RIARI and T. THEOPHANIDES. Inorg. Chim. Acta, **80**, 223 (1983).
4. E. SCHERER, H. A. TAJMIR-RIARI, and T. THEOPHANIDES. Inorg. Chim. Acta, **92**, 285 (1984).
5. (*a*) M. POLISSIOU and T. THEOPHANIDES. *In* Proceedings of the SUNYA. Conversation in biomolecular stereodynamics. Vol. 1. *Edited by* R. H. Sarma. Adenine Press, New York, NY. 1981. pp. 487–498; (*b*) M. POLISSIOU and T. THEOPHANIDES. Inorg. Chim. Acta, **56**, L1–L3 (1981); (*c*) M. MANFAIT and T. THEOPHANIDES. Magnesium, **2**, 323 (1983).
6. K. AOKI. Bull. Chem. Jpn. **48**, 1260 (1975).
7. K. AOKI. J. Chem. Soc. Chem. Commun. 600 (1977); G. R. CLARK, J. D. ORBELL, and J. M. WATERS. Biochim. Biophys. Acta, **562**, 361 (1979).
8. P. DE MEESTER, D. M. L. GOODGAME, T. J. JONES, and A. C. SKAPSKI. Biochim. Biophys. Acta, **353**, 392 (1974).
9. D. M. L. GOODGAME, I. JEEVES, C. D. REYNOLDS, and A. C. SKAPSKI. Nucleic Acid Res. **2**, 1375 (1975).
10. E. A. BROWN and C. E. BUGG. Acta Crystallogr. B**36**, 2597 (1980).
11. D. E. DORMAN and J. D. ROBERTS. Proc. Natl. Acad. Sci. USA, **65**, 19 (1970).
12. C. D. JARDETZKY and O. JARDETZKY. J. Am. Chem. Soc. **82**, 222 (1960); **82**, 229 (1960).
13. L. G. MARZILLI, B. DE CASTRO, and C. SOLORZANO. J. Am. Chem. Soc. **104**, 461 (1982).
14. S. SHIMOKAWA, H. FUKUI, H. SOHMA, and K. HOTTA. J. Am. Chem. Soc. **95**, 1777 (1973).
15. M. SUNDARALINGAM and P. PRUSINE. Nucleic Acid Res. **5**, 4375 (1978); Acta Crystallogr. B**30**, 320 (1974).
16. N. NAGASHIMA and Y. IITAKA. Acta Crystallogr. B**24**, 1136 (1968).
17. S. T. RAO and M. SUNDARALINGAM. J. Am. Chem. Soc. **91**, 1210 (1969).
18. R. C. LORD and G. J. THOMAS. Spectrochim. Acta, **23**A, 2551 (1967).
19. M. TSUBOI. Infrared and Raman spectroscopy in basic principles in nucleic acid chemistry. Vol. 1. Academic Press. 1974. pp. 399–452; Adv. Chem. Phys. **7**, 435 (1964).
20. M. TSUBOI, S. TOKAHOSHI, and I. HORADA. Physicochemical properties of nuclei acid. Vol. 2. *Edited by* J. Dunhense. Academic Press. 1973. pp. 91–145.
21. J. BARIYANGA and T. THEOPHANIDES. To be published.
22. S. MANSY and W. L. PETICOLAS. Biochemistry, **15**, 2650 (1975).
23. L. CHINSKY, P. Y. TURPIN, and J. BRAHMS. Biopolymers, **17**, 1347 (1978).
24. T. THEOPHANIDES and H. A. TAJMIR-RIARI. Structure and dynamics in nucleic acids and proteins. *Edited by* S. E. Clementi and R. H. Sarma. 1985. p. 184.
25. K. AOKI, G. R. CLARK, and J. D. ORBELL. Acta Crystallogr. B**34**, 2119 (1978).
26. P. DE MEESTER, D. M. L. GOODGAME, A. C. SKAPSKI, and T. SMITH. Biochim. Biophys. Acta, **340**, 113 (1974); Acad. Sci. Paris, **279**, 667 (1974).
27. M. J. LANE and G. J. THOMAS, JR. Biochemistry, **18**, 3839 (1979); S. A. Ferreira and G. J. THOMAS. J. Raman Spectrosc. **11**, 508 (1981); **12**, 122 (1982).
28. H. A. TAJMIR-RIARI and M. LOTFIPOOR. Spectrochim. Acta, **39**A, 167 (1983).

Electronic excitations of the free-base porphine–Ar van der Waals complex

UZI EVEN AND JOSHUA JORTNER
Department of Chemistry, Tel Aviv University, 69978 Tel Aviv, Israel

AND

ZIVA BERKOVITCH-YELLIN
Department of Structural Chemistry, The Weizmann Institute of Science, Rehovot 76100, Israel

Received October 31, 1984

This paper is dedicated to Professor Camille Sandorfy on the occasion of his 65th birthday

UZI EVEN, JOSHUA JORTNER, and ZIVA BERKOVITCH-YELLIN. Can. J. Chem. **63**, 2073 (1985).

In this paper we report on the excited-state energetics of the two lowest-lying intravalence electronic excitations $S_0 \rightarrow S_1^x$ and $S_0 \rightarrow S_1^y$ of a large van der Waals complex, consisting of Ar bound to free-base porphine (H_2P). $H_2P \cdot Ar_n$ complexes were synthesized and interrogated by laser-induced fluorescence in seeded supersonic expansions of Ar and He/Ar. Diagnostic methods, which were based on the dependence of the intensity of the spectral features on the stagnation pressure and on spectroscopy in He(99%)/Ar(1%) mixtures, were utilized for the identification of the vibrationless electronic excitations of $H_2P \cdot Ar_1$. The spectroscopic data were supplemented by model calculations of the potential surface, which demonstrate that the single equilibrium configuration of $H_2P \cdot R_1$ (R = Ne, Ar, Kr, and Xe) corresponds to the R atom being located at the twofold symmetry axis perpendicular to the porphyrin ring. While the intense $S_0 \rightarrow S_1^y$ transition of $H_2P \cdot Ar_1$ exhibits a red, dispersive, microscopic solvent shift ($\delta\nu = -24$ cm^{-1}), the $S_0 \rightarrow S_1^x$ transition is characterized by a blue microscopic spectral shift ($\delta\nu = +8$ cm^{-1}), which provides a unique example for excited-state destabilization, originating from intramolecular configurational changes induced by van der Waals binding in a large complex.

UZI EVEN, JOSHUA JORTNER et ZIVA BERKOVITCH-YELLIN. Can. J. Chem. **63**, 2073 (1985).

On a déterminé les niveaux d'énergie de l'état excité des deux excitations électroniques intravalence ayant les plus bases énergies, soit $S_0 \rightarrow S_1^x$ et $S_0 \rightarrow S_1^y$, d'un vaste complexe de van der Waals qui comprend du Ar lié à de la porphine (H_2P) existant sous une forme libre. On a synthétisé les complexes $H_2P \cdot Ar_n$ et on les a examiné à l'aide de fluorescence induite par un laser dans des expansions supersoniques ensemencées de Ar et de He/Ar. Dans le but d'identifier les excitations électroniques sans vibrations de $H_2P \cdot Ar_1$, on a utilisé des méthodes d'évaluation qui sont basées sur la relation qui existe entre l'intensité des caractéristiques spectrales et la pression de stagnation ainsi que sur la spectroscopie dans des mélanges à 99% He/1% Ar. On a utilisé les données spectrales de concert avec des calculs modèles de la surface de potentiel qui démontrent que la seule configuration d'équilibre du $H_2P \cdot R_1$ (R = Ne, Ar, Kr et Xe) correspond à celle dans laquelle l'atome R se trouve au niveau de l'axe de symétrie binaire qui est perpendiculaire au noyau de la porphyrine. Alors que la transition intense $S_0 \rightarrow S_1^y$ du $H_2P \cdot Ar_1$ présente un déplacement microscopique dû au solvant qui soit dispersif et qui se déplace vers le rouge ($\delta\nu = -24$ cm^{-1}), la transition $S_0 \rightarrow S_1^x$ est caractérisée par un déplacement spectral microscopique vers le bleu ($\delta\nu = +8$ cm^{-1}); ces résultats correspondent à un exemple unique de déstabilisation de l'état excité provenant de changements configurationnels intramoléculaires qui sont induits par un couplage de van der Waals dans un vaste complexe.

[Traduit par le journal]

I. Introduction

We have recently explored the excited-state energetics and dynamics of large van der Waals (vdW) complexes ($M \cdot R_n$), consisting of rare-gas (R) atom(s) bound to a large aromatic hydrocarbon (M), which were synthesized and interrogated in supersonic expansions (1–4). The microscopic solvent shift (1), $\delta\nu$, for the electronic origin of the $S_0 \rightarrow S_1$ intravalence $\pi\pi^*$ transition of such vdW complexes originates from the following additive effects (1–4): (1) dispersive interactions, providing an extra stabilization of S_1 which results in a red spectral shift. These are exhibited for vdW complexes containing the heavy rare gases, e.g., Ne, Ar, Kr, and Xe; (2) short-range repulsive interactions which result in a blue spectral shift. This effect dominates the spectral shifts of $M \cdot He$ complexes for which the effects of dispersive interactions are minor.

The complexing of porphyrins and the elucidation of microscopic solvent effects on their excited-state energetics and dynamics is a subject of considerable physical, chemical, and biophysical interest. With this goal in mind, we have extended our studies of vdW complexes to investigate the electronic–vibrational excitations of complexes of porphyrins with molecular ligands (5) and with rare-gas atoms. Our studies of the electronic excitations of the complexes of porphyrins with molecular ligands (5) resulted in a wealth of information regarding microscopic spectral shifts. From the point of view of general methodology, the elucidation of the spectroscopy of porphyrin – rare-gas complexes will be of considerable interest. In this paper we report on the two lowest-lying electronic excitations of the $H_2P \cdot Ar$ complex, consisting of Ar bound to free-base porphine (H_2P). This system is of interest for several reasons. Firstly, from the spectroscopic point of view, H_2P is the most interesting porphyrin, so that spectroscopic studies of its vdW complexes are pertinent. Secondly, spectroscopy of large vdW complexes combined with theoretical simulations of their potential surfaces (2, 3) are expected to provide information pertaining to the structure of these complexes and bears on the question of the existence of chemical isomers of large vdW molecules (1–3). It will be interesting to extend the scope of previous studies for aromatic hydrocarbons to porphyrins. Thirdly, the energetics of the electronic excitations of porphyrin–R complexes will result in novel information on microscopic solvent spectral shifts.

II. Experimental

We have studied the laser-induced fluorescence (LIF) excitation spectra of H_2P and its Ar complexes in pulsed, seeded, supersonic expansions of He, Ar, and He + Ar mixtures, utilizing the techniques

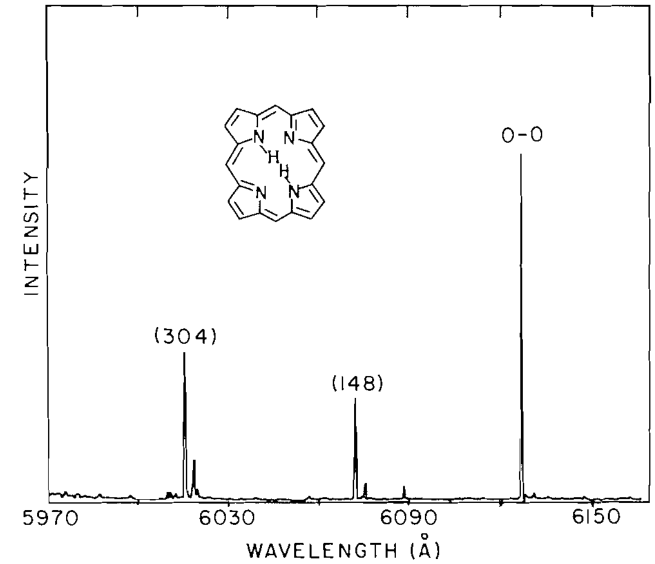

FIG. 1. The LIF spectrum in the region 5970–6160 Å of the H_2P molecule seeded in pulsed supersonic expansions of He. H_2P was heated in the nozzle chamber to 330°C, seeded in He at p = 2000 Torr, and expanded through the 0.06-cm nozzle. The exciting dye laser crossed the jet at 12 mm down the nozzle.

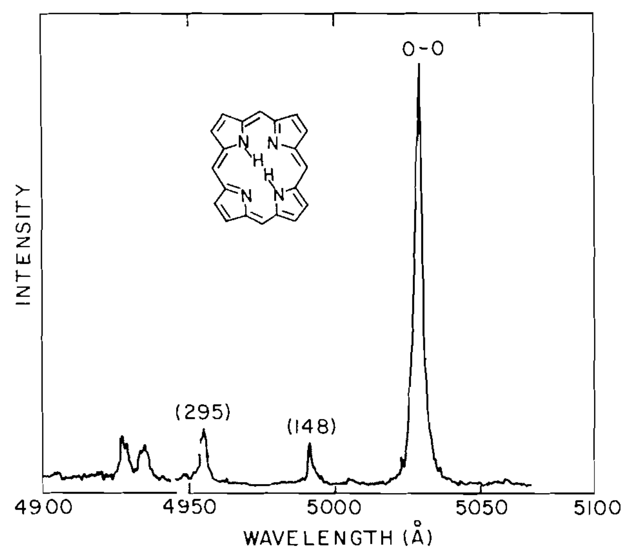

FIG. 2. The LIF spectrum in the region 4900–5100 Å of H_2P in pulsed supersonic expansions of He. Experimental conditions as in Fig. 1.

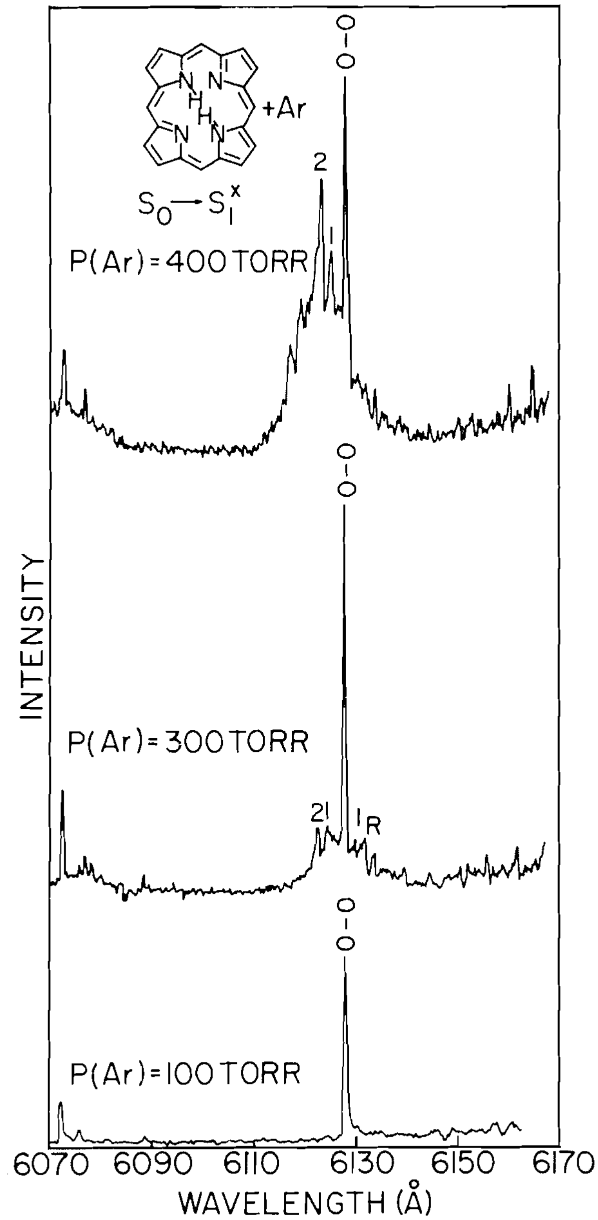

FIG. 3. The LIF spectra of H_2P in the range 6070–6170 Å in pulsed jets of Ar. The stagnation pressures of Ar are indicated on the spectra. All other experimental conditions as in Fig. 1. The $S_0 \rightarrow S_1^x$ electronic origin of the bare molecule is labelled 0–0. The spectral feature (1_R) corresponds to a hot band and the spectral features (1 and 2) attributed to the $S_0 \rightarrow S_1^x$ transition of $H_2P \cdot Ar_n$ (n = 1, 2) are marked.

previously described (6–8). A solid sample of H_2P (commercially obtained from Porphyrin Products, U.S.A.) was heated in the nozzle chamber to 330°C (vapor pressure 0.2 Torr (9); (1 Torr = 133.3 Pa). The H_2P molecule could effectively be cooled in supersonic expansions of Ar at the stagnation pressure p = 100–150 Torr and in He at p = 1500–2500 Torr, with the nozzle diameter being D = 600 μm. The LIF spectra obtained under these conditions correspond to the bare H_2P molecule, rather than to rare-gas – H_2P vdW complexes, as the spectra were identical in He and Ar. No spectroscopic evidence was obtained for the formation of He–H_2P vdW complexes under our experimental conditions. Ar–H_2P vdW complexes were synthesized in the following jets: (1) seeded expansions of Ar at p = 150–1500 Torr, and (2) seeded expansions of Ar + He mixtures containing 1–10% Ar expanded at p = 1500–2200 Torr. This preparation method results in the formation of $H_2P \cdot Ar_n$ vdW complexes with a low coordination number n, yielding preferably to complexes with n = 1. In addition, work on other large complexes (10) indicates that this preparation method allows for effective internal cooling of the vdW complex.

III. The $S_0 \rightarrow S_1^x$ transition of the $H_2P \cdot Ar_1$ complex

The lowering of the D_{4h} symmetry of the porphyrin ring by the H···H proton axis in H_2P results in the splitting of the Q band into two electronic transitions, ie., the $S_0 \rightarrow S_1^x$ transition (the Q_x band) and the $S_0 \rightarrow S_1^y$ transition (the Q_y band) (11). Figures 1 and 2 show portions of the LIF excitation spectrum of H_2P in the spectral ranges 5970–6140 Å and 4900–5050 Å, which exhibit the electronic origin of the $S_0 \rightarrow S_1^x$ transition (Fig. 1) at 16 320 cm^{-1} and the electronic origin of the $S_0 \rightarrow S_1^y$ transition (Fig. 2) located at 19 884 cm^{-1}, together with the lowest vibrational excitations in these two electronic states. Figure 3 shows the LIF spectrum of H_2P in Ar at p = 100–400

TABLE 1. Excitation energies $\delta\nu^a$ and relative intensities I^b for the 0–0 $S_0 \rightarrow S_1^x$ excitations of $H_2P \cdot Ar_n$ complexes

Label[c]	$\delta\nu^d$ (cm^{-1})	He + Ar (1%) p = 2200 Torr	Ar p = 200 Torr	Ar p = 300 Torr	Ar p = 400 Torr	Assignment
1_R	−10.6		I = 0.08	I = 0.10		
1	+8.0	I = 0.07	I = 0.06 Broad background	I = 0.15	I = 0.40	$H_2P \cdot Ar_1$
2	+13.3			I = 0.16	I = 0.71	$H_2P \cdot Ar_2$ (?)

[a]$\delta\nu$: energy relative to the electronic origin of the $S_0 \rightarrow S_1^x$ transition of the bare H_2P molecule. Accuracy of $\delta\nu$ is ± 1 cm^{-1}.
[b]I: peak intensity of the spectral feature of the complex relative to the peak intensity of the origin of the bare molecule. Accuracy of I is ±25%.
[c]See Fig. 3.
[d]Positive and negative values of $\delta\nu$ refer to blue and red spectral shifts, respectively.

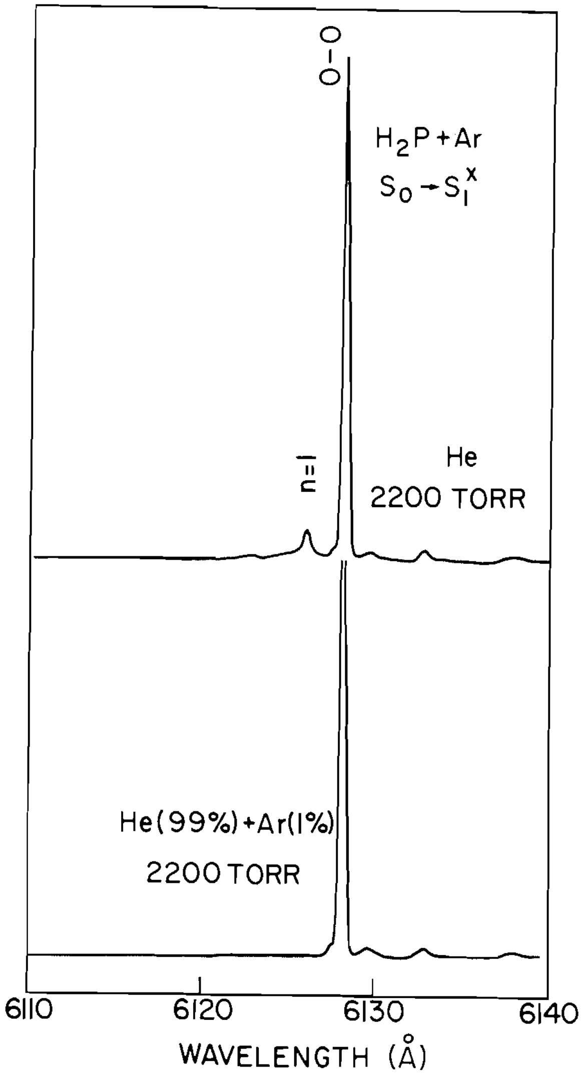

FIG. 4. The LIF spectrum of H_2P in pulsed jets of He (upper spectrum) and in a mixture of He (99%) + Ar (1%) (lower spectrum). The $S_0 \rightarrow S_1^x$ origin of $H_2P \cdot Ar_1$ is marked $n = 1$.

Torr over the range 6050–6170 Å. At p = 100 Torr only the electronic origin of the $S_0 \rightarrow S_1^x$ transition of the bare H_2P molecule is exhibited. With increasing stagnation pressure new spectral features are exhibited in Fig. 3, which involve the following two distinct types.

1. A low-energy absorption, which is red-shifted relative to the 0–0, whose relative intensity depends very weakly on the stagnation pressure (Table 1). Such low-energy absorption, which is almost devoid of any pronounced structure except a feature at $\delta\nu = -10.6$ cm^{-1}, is tentatively attributed to sequence bands and (or) hot bands of the complexes. This low-energy absorption becomes somewhat more pronounced at higher stagnation pressures of Ar due to local heating effects accompanying the formation of $H_2P \cdot Ar_n$ complexes.

2. Satellite bands appearing on the high-energy side of the electronic origin. These distinct spectral features (Fig. 3) are characterized by the following features: (*i*) their intensities depend strongly on the stagnation pressure; (*ii*) at higher pressures the spectral features at higher energies become more prominent. These properties are characteristic of vdW complexes. Accordingly, the high-energy satellite bands (Table 1) are attributed to the electronic origins of the $S_0 \rightarrow S_1^x$ transitions of $H_2P \cdot Ar_n$ vdW complexes, where the H_2P molecule within the complex is retained in its vibrationless state.

The spectroscopic data in Ar jets are insufficient to provide information concerning the composition of the $H_2P \cdot Ar_n$ vdW complexes. A conclusive spectroscopic identification of the spectral features of the $H_2P \cdot Ar_1$ complex was obtained from the spectra of H_2P seeded supersonic expansions of 99% He plus 1% Ar. From Fig. 4 it is evident that a new spectral feature at the high energy side of the electronic origin of the bare molecule is exhibited in the He + Ar mixture, which is absent in the bare molecule spectrum. As this new spectral feature appears in an He–Ar diluent of low Ar content (1%), it is attributed to the $H_2P \cdot Ar_1$ complex. As is apparent from Table 1, the energy of this spectral feature, corresponding to $H_2P \cdot Ar_1$ synthesized in an He + Ar mixture, coincides within experimental uncertainty with the energy of the lowest-lying excitation of the $H_2P \cdot Ar_n$ complexes of an unidentified composition observed in the pure Ar diluent. We also note in Fig. 4 the absence of any type 1 absorption on the low energy side of the bare molecule cooled in He + Ar. The absence of type 1 absorption in the He + Ar diluent provides some additional support to the assignment of this structureless low-energy absorption in Ar to sequence and (or) hot bands of $H_2P \cdot Ar_n$ complexes. The cooling accomplished in the He + Ar (1%) at p = 2200 Torr mixture is more efficient in precluding the appearance of these sequence and (or) hot bands.

On the basis of the identification of the spectral feature of the $H_2P \cdot Ar_1$ complex in He + Ar (1%) diluent, we can assign the excitation of this vdW complex in pure Ar (Fig. 3 and Table 1).

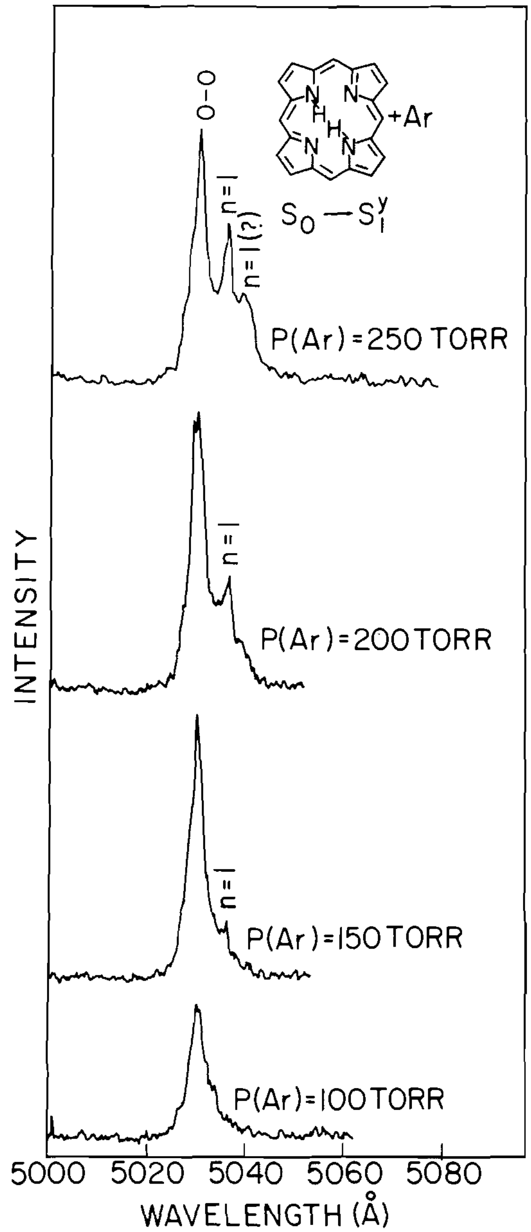

FIG. 5. The LIF spectrum of H_2P in the range 5000–5080 Å in pulsed jets of Ar. The Ar stagnation pressures are indicated on the spectra. The $S_0 \rightarrow S_1^y$ electronic origin of the bare molecule is labelled 0–0. $n = 1$ marks the spectral features attributed to the $S_0 \rightarrow S_1^y$ excitation of $H_2P \cdot Ar_1$.

The spectra of H_2P in Ar (Fig. 3) reveal additional satellite bands (Fig. 3 and Table 1) on the high energy side of the $H_2P \cdot Ar_1$ excitation, which are due to $H_2P \cdot Ar_n$ complexes with a higher $n > 1$, as yet unspecified, coordination number. A serious problem, which precludes the identification of the electronic origins of the $S_0 \rightarrow S_1^x$ transition of $H_2P \cdot Ar_n$ complexes ($n > 1$) in the Ar diluent, involves the excessive line broadening of their spectral features relative to the origin of the bare molecule (Fig. 3). This line broadening of the spectral features of the $S_0 \rightarrow S_1^x$ transition of $H_2P \cdot Ar_n$ complexes originates from: (*1*) rotational broadening effects, which are not expected to differ significantly from those of the bare molecule; (*2*) sequence and hot vibrational transitions involving the intermolecular low frequency vibrations of the Ar atoms(s) relative to the H_2P ring. The internal cooling of the intermolecular vibrational degrees of freedom of the complexes in the Ar diluent is insufficient to eliminate this thermal inhomogeneous broadening. It appears that the internal cooling in the He + Ar diluent (Fig. 4) is superior, providing a safe assignment of the electronic origin of $H_2P \cdot Ar_1$.

The identification of the spectral feature of the origin of the $S_0 \rightarrow S_1^x$ transition of $H_2P \cdot Ar_1$ (Table 1) leads to the following conclusions: (a) only a single spectral feature is exhibited; (b) the microscopic solvent shift of the electronic origin of the $S_0 \rightarrow S_1^x$ transition of H_2P in the $H_2P \cdot Ar_1$ complex relative to the bare molecule is $\delta\nu = +8 \pm 1$ cm^{-1} towards higher energies. Before alluding to the nature of this blue spectral shift, it is imperative to obtain supplementary information about the energetics of the electronic origin of the $S_0 \rightarrow S_1^y$ second electronic excitation of $H_2P \cdot Ar_1$.

IV. The $S_0 \rightarrow S_1^y$ transition of the $H_2P \cdot Ar_1$ and higher complexes

The electronic–vibrational excitations within the S_1^y manifold of bare H_2P exhibit appreciable line broadening due to intramolecular $S_1^y \rightarrow S_1^x$ electronic relaxation, the homogeneous linewidth of the electronic origin being $\delta = 11$ cm^{-1}, which corresponds to an intramolecular relaxation lifetime of 0.5 ps (8). This homogeneous relaxation line broadening is expected to be exhibited also for the $S_0 \rightarrow S_1^y$ transition of $H_2P \cdot Ar_n$ complexes and may mask the spectral features of these vdW molecules. Fortunately, we have found that the energetic separation between the electronic origin of the $S_0 \rightarrow S_1^y$ transition of bare H_2P and its complexes with Ar is sufficiently large relative to δ, so that well-characterized spectral features of the $S_0 \rightarrow S_1^y$ transition of $H_2P \cdot Ar_n$ complexes are amenable to observation and analysis.

In Figs. 5 and 6, we present the LIF spectra of H_2P in the vicinity of the electronic origin of the $S_0 \rightarrow S_1^y$ transition. These spectra of H_2P in Ar jets (Fig. 5) and in He + Ar jets (Fig. 6) clearly exhibit new spectral features on the low energy side of the electronic origin of the bare molecule, which are attributed to the vibrationless $S_0 \rightarrow S_1^y$ excitation of $H_2P \cdot Ar_n$ complexes. The intensities of these spectral features exhibit a strong dependence on the stagnation pressure, p, in Ar jets (Fig. 5) and on the partial pressure of Ar, p(Ar), in He + Ar jets. This pressure dependence enabled us to identify and characterize these well-resolved spectral features.

The two highest-energy spectral features corresponding to the $S_0 \rightarrow S_1^y$ vibrationless excitations of $H_2P \cdot Ar_n$ complexes are located at the energies -24 ± 1 cm^{-1} and -34 ± 1 cm^{-1} below the electronic origin of the bare molecule (Figs. 5 and 6 and Table 2). As is apparent from Fig. 7, the peak intensity, I, of the prominent spectral feature at -24 cm^{-1} relative to the peak intensity of the 0–0 transition of the bare molecule is given by the simple relations $I \propto p^2$ for pure Ar and $I \propto p$(Ar) for the He + Ar diluent. Accordingly, the -24-cm^{-1} feature, labelled as vdW(1), is attributed to the $H_2P \cdot Ar_1$ complex, which is formed by the three-body collision process

$$[1] \quad H_2P + Ar + Ar \rightarrow H_2P \cdot Ar_1 + Ar$$

in pure Ar, and

$$[2] \quad H_2P + Ar + He \rightarrow H_2P \cdot AR_1 + He$$

in He + Ar. The weaker spectral feature at -34 cm^{-1}, labelled as vdW(2), seems to exhibit qualitatively the same dependence on the stagnation pressure as vdW(1) (Fig. 7), and is tentatively also attributed to $H_2P \cdot Ar_1$ (Table 2). At high pressures of the

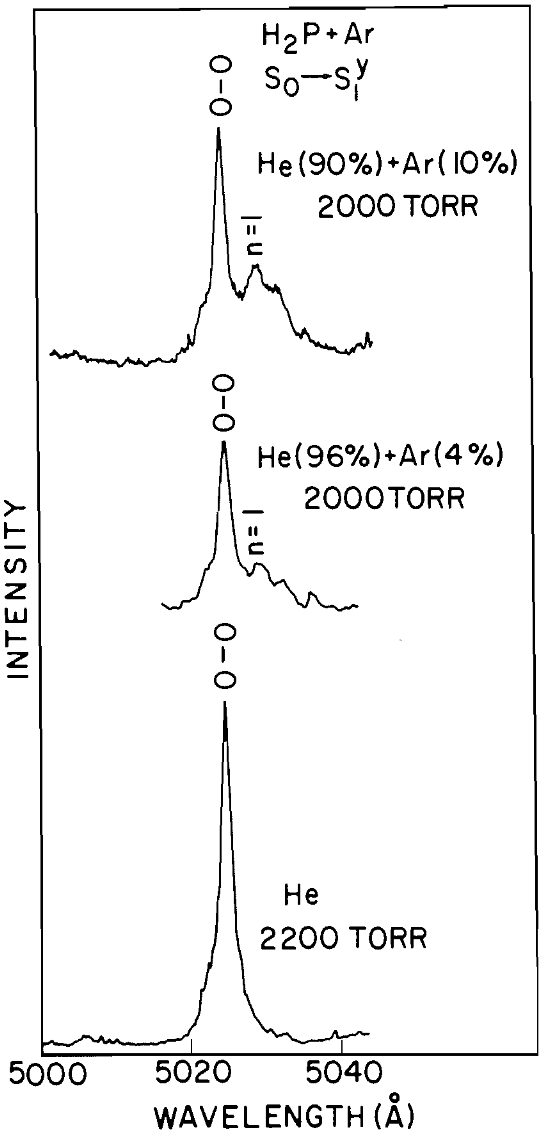

FIG. 6. The LIF spectra of H_2P in pulsed jets of He and of He/Ar mixtures at the compositions marked on the spectra. Labelling of the spectral features as in Fig. 5.

Ar diluent the lower energy features become more prominent (Fig. 8). At p = 300 Torr (Fig. 8) spectral structures due to excitations of individual $H_2P \cdot Ar_n$ complexes are well exhibited. On the basis of its order of appearance (1, 2), we tentatively attribute the spectral feature at -42 cm^{-1} below the electronic origin of bare H_2P to the $H_2P \cdot Ar_2$ complex. At higher pressures of Ar, p = 600–1200 Torr (Fig. 8), extensive complexing with Ar is exhibited, as is evident from the disappearance of the 0–0 excitation of the bare molecule. The spectra in this high p range are broad and structureless. The maximum of the broad band shifts gradually to lower energies with increasing p (Table 2). These spectra are attributed to large $H_2P \cdot Ar_n$ clusters with a high ($n > 2$) coordination number. The excessive line broadening originates from three causes: (*1*) inhomogeneous broadening originating from the overlap of spectral features of a variety of $H_2P \cdot Ar_n$ complexes with various coordination numbers; (*2*) homogeneous broadening due to phonon broadening effects of the absorption of $H_2P \cdot Ar_n$ molecules with a well-characterized structure and coordination number n; (*3*) homogeneous broadening due to intramolecular re-

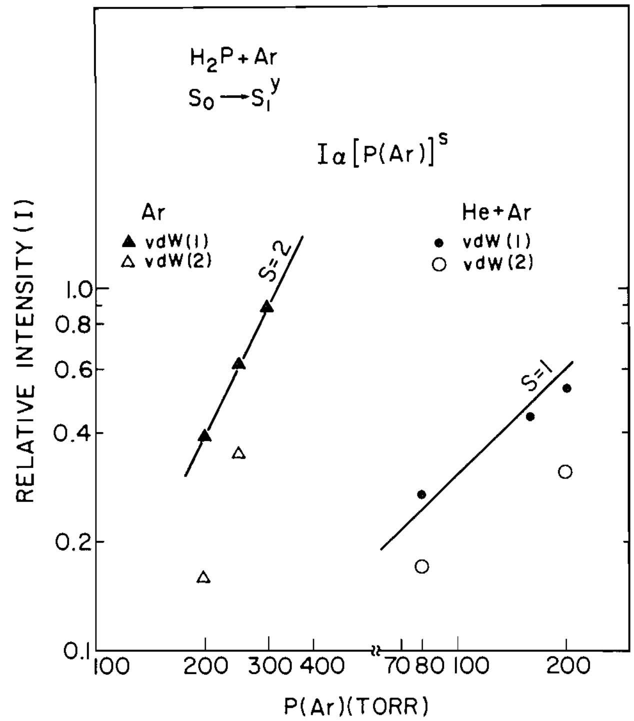

FIG. 7. The dependence of the peak intensities of the spectral features, which correspond to the $S_0 \rightarrow S_1^y$ electronic excitations of $H_2P \cdot Ar_n$ complexes on the stagnation pressure of Ar (in Ar jets) and on the partial stagnation pressure of Ar (in He + Ar) jets. The pressure dependence of both features (vdW(1)) and vdW(2)) is identical.

TABLE 2. $S_0 \rightarrow S_1^y$ excitation energies of $H_2P \cdot Ar_n$ complexes

Diluent	$\delta\nu$ (cm^{-1})[a]	Assignment
He + Ar (4%) p = 2000 Torr	−24 −35	vdW(1) vdW(2)
He + Ar (10%) p = 2000 Torr	−24 −35	vdW(1) vdW(2)
Ar p = 150 Torr	−24 −35	vdW(1) vdW(2)
Ar p = 200 Torr	−24 −35	vdW(1) vdW(2)
Ar p = 250 Torr	−24 −35	vdW(1) vdW(2)
Ar p = 300 Torr	−24 −35 −41	vdW(1) vdW(2)
Ar p = 600 Torr	−59 Broad band	$H_2P \cdot Ar_n$[b]
Ar p = 900 Torr	−112 Broad band	$H_2P \cdot Ar_n$[b]
Ar p = 1200 Torr	−147 Broad band	$H_2P \cdot Ar_n$[b]

[a] Accuracy ±1 cm^{-1}.
[b] Large vdW complexes of unspecified coordination number n.

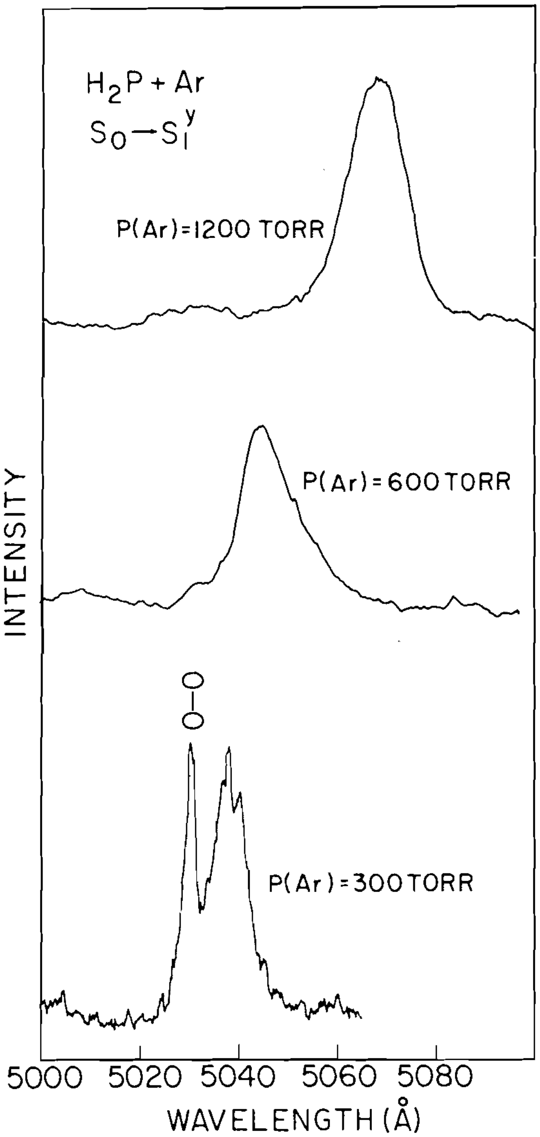

FIG. 8. The LIF spectra in the range 5000–5080 Å of H_2P in Ar jets at high stagnation pressures of Ar. Extensive complexing of Ar around H_2P is exhibited for $p(\text{Ar})$ = 600–1200 Torr.

laxation of H_2P in the complex. At present we cannot distinguish between the intermolecular contributions (*1*) and (*2*) and the intramolecular contribution (*3*) in these large clusters.

V. Potential surfaces for H_2P – rare-gas complexes

The vibrationless $S_0 \rightarrow S_1^x$ transition of $H_2P\cdot Ar_1$ exhibits a single spectral feature, while the 0–0 $S_0 \rightarrow S_1^y$ transition of this molecule reveals two spectral features. On the basis of these spectroscopic data we were unable to infer whether the multiple spectrum of the vibrationless $S_0 \rightarrow S_1^y$ transition of $H_2P\cdot Ar_1$ originates from the presence of two nearly isoenergetic chemical isomers, whose spectra overlap in the case of the $S_0 \rightarrow S_1^x$ transition, or is due, rather, to other causes (2, 3). One approach towards the elucidation of the structure of large vdW molecules, which bears on the existence of chemical isomers, rests on model calculations of the ground state intermolecular potential surfaces.

We have constructed the potential surfaces for vdW complexes between H_2P and the rare-gas atoms R(Ne, Ar, Kr, and Xe). These model calculations, which rest on the procedure of

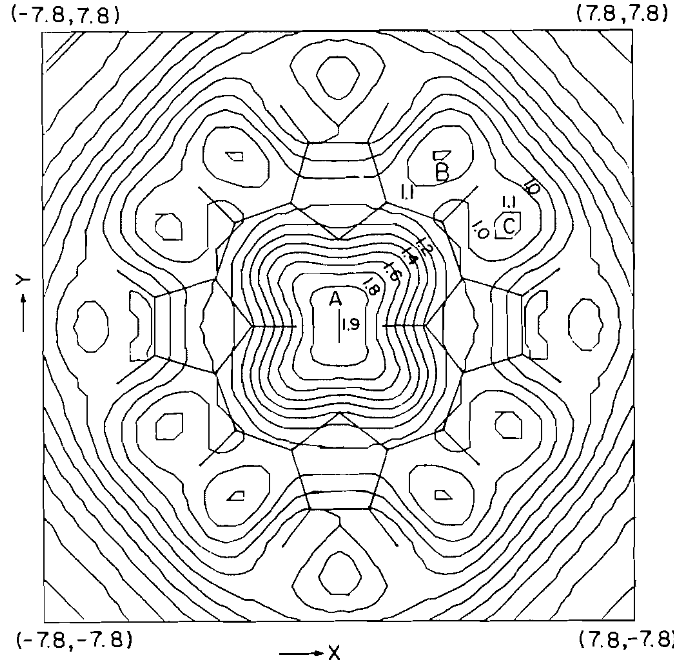

FIG. 9. Contour map for $H_2P\cdot Ar_1$ potential in the plane parallel to the porphyrin ring at a distance z = 3.2 Å from it. Distance points are given in Å units. Energies are given in kcal/mol. Points A, B, and C constitute the three points of minimum energy with point A being characterized by the lowest energy (see Table 4).

Jortner and co-workers (2, 3), provide information on the equilibrium configuration and ground-state binding energy of $H_2P\cdot R_1$ complexes and establish the energetic stability of chemical $H_2P\cdot R_1$ isomers with geometrically inequivalent sites for the R atom. The potential energy, V, for the nuclear motion of Ar in the $H_2P\cdot R_1$ complex was constructed as a superposition of pairwise atom–atom potentials between each of the C, N, and H atoms of H_2P and the R atom (3)

$$[3]\quad V(\{r_\beta\}) = \sum_\beta A_\beta\{-r_\beta^{-6} + [(r_\beta^0)^6/2]\, r_\beta^{-12}\}$$

where $r_\beta = |\boldsymbol{r} - \boldsymbol{r}_\beta|$ is the distance between the R atom located at the position $\boldsymbol{r}$, and the β-th atom of H_2P, which is located at $\boldsymbol{r}_\beta$. Three sets of potential parameters for A_β and r_β^0 were used:

Set 1: The R—C pair potential (PP) was taken from the heats of absorption of rare-gas atoms on graphite. The R—N PP was taken to be equal to the Ar—C PP. The Ar—H PPs were taken from our previous work (3).

Set 2: Using the Buckingham PP for H—H and C—C given by Mirsky (12) and the R—R potential (13), we have estimated the R—C and R—H PP using the combination rules (13). The N—R PP was taken to be equal to that of the C—R PP.

Set 3: The same as Set 1 for the C—R and the H—Ar PPs. The N—R potential was estimated from the N—N PP parameters of Hill (14).

The geometry of the H_2P ring was taken from crystallographic data. The two internal protons were assumed to be located in the porphyrin plane.

Figure 9 shows the potential surface of $H_2P\cdot Ar_1$ parallel to the H_2P xy plane at a distance of z = 3.2 Å from it, which was calculated by using Set 1 of the PPs. As is apparent from Fig. 9, three points of minimum energy are exhibited, which are labelled as A, B, and C. At this z = 3.2 Å distance, the points A, B, and C correspond to the absolute energy minima for the

TABLE 3. Test of potential parameters for $H_2P \cdot Ar_1$ by the calculation of the three points of minimum energy on the potential surface

	Set 1	Set 2	Set 3
Point A			
Energy (kcal/mol^{-1})	−1.905	−2.302	−2.221
x (Å)	0	0	0
y (Å)	0	0	0
z (Å)	3.2	2.8	3.3
Point B			
Energy (kcal/mol^{-1})	−1.131	−1.065	−1.390
x (Å)	2.4		
y (Å)	4.0		
z (Å)	3.2		
Point C			
Energy (kcal/mol^{-1})	−1.217	−1.125	−1.297
x (Å)	4.0		
y (Å)	2.6		
z (Å)	3.2		

three-dimensional potential. Point A corresponds to the Ar atom located on the central twofold symmetry axis of the porphyrin ring, while points B and C are located between the pyrole rings and the *meso* C—H group. To assess the sensitivity of the energetic data for $H_2P \cdot Ar_1$ to the PPs, we present in Table 3 the energies and positions of the minimum energy points A, B, and C. It is apparent that the gross features of the potential surfaces, the energetic data, and the geometries for $H_2P \cdot Ar_1$ are similar for the three sets of the PPs. In view of the uncertainty in the assignment of PPs for the N—Ar (and N—R) interaction, we are somewhat reluctant to use Set 3, which considers explicitly this interaction. Accordingly, all subsequent calculations reported in the present paper were conducted by using Set 1.

From the calculations of the potential surfaces of $H_2P \cdot R_1$ complexes, the following conclusions emerge.

1. For all $H_2P \cdot R_1$ complexes there are three points of minimum energy on each side of the porphyrin ring (Fig. 9 and Table 4).

2. There is a single minimum point of lowest energy (point A) on each side of the ring.

3. The energies of the points B and C, which correspond to the two local minima (Fig. 9 and Table 4), are considerably higher than the energy of point A. The energy difference ΔE_{AB} between points A and B is ΔE_{AB} = 94 cm^{-1} for Ne, ΔE_{AB} = 241 cm^{-1} for Ar, ΔE_{AB} = 262 cm^{-1} for Kr, and ΔE_{AB} = 405 cm^{-1} for Xe, while the energy difference, ΔE_{AC}, between points A and C is ΔE_{AC} = 137 cm^{-1} for Ne, ΔE_{AC} = 273 cm^{-1} for Ar, ΔE_{AC} = 318 cm^{-1} for Kr, and ΔE_{AB} = 437 cm^{-1} for Xe.

4. The energy differences ΔE_{AB} and ΔE_{AC} considerably exceed the translational energies $kT_t \simeq$ 2–5 K (15) and the intramolecular vibrational energies $kT_V <$ 10–20 K (10), which prevail in the seeded supersonic expansions utilized in our experiments. Accordingly, we expect that only a single isomer of $H_2P \cdot R_1$ corresponding to the localization of the R atom around point A is energetically stable. No other isomers, i.e., conformers corresponding to vibrationally excited states, are expected to be accessible via thermal excitation.

5. The binding energies of the $H_2P \cdot R_1$ molecules are 310 cm^{-1} for $H_2P \cdot Ne_1$, 666 cm^{-1} for $H_2P \cdot Ar_1$, 796 cm^{-1} for $H_2P \cdot Kr_1$, and 990 cm^{-1} for $H_2P \cdot Xe_1$. Although the exact numerical values are only approximate, they indicate relatively large binding energies of an R atom to large aromatic hydrocarbons.

TABLE 4. Points of minimum energy on the $H_2P \cdot R_1$ potential surface

R	Ne	Ar	Kr	Xe
Point A				
Energy (kcal/mol^{-1})	−0.883	−1.905	−2.275	−2.833
x (Å)	0	0	0	0
y (Å)	0	0	0	0
z (Å)	2.9	3.2	3.3	3.4
Point B				
Energy (kcal/mol^{-1})	−0.614	−1.217	−1.527	−1.675
x (Å)	2.2	2.4	2.2	2.6
y (Å)	4.0	4.0	3.8	4.2
z (Å)	2.9	3.2	3.4	3.4
Point C				
Energy (kcal/mol^{-1})	−0.420	−1.310	−1.366	−1.584
x (Å)	5.6	4.0	3.8	4.2
y (Å)	0	2.6	2.2	2.6
z (Å)	2.9	3.2	3.3	3.4
Point D				
Energy (kcal/mol^{-1})	−0.490			
x (Å)	0			
y (Å)	5.6			
z (Å)	2.9			

6. The equilibrium configuration of $H_2P \cdot R_1$ complexes corresponds to the R atom located at the twofold symmetry axis perpendicular to the porphyrin ring. The equilibrium distances are z = 2.9 Å for Ne, z = 3.2 Å for Ar, z = 3.3 Å for Kr, and z = 3.4 Å for Xe.

The only serious sin of omission inherent in these model calculations pertains to the role of the two internal H atoms, which were taken to be located in the porphyrin plane. In the bare H_2P molecule the two protons may be displaced out of the porphyrin plane. It is possible that the binding of an R atom to H_2P will modify the intramolecular equilibrium configuration of these two protons.

VI. Concluding remarks

Our spectroscopic studies provide quite extensive information on the $S_0 \rightarrow S_1{}^x$ and $S_0 \rightarrow S_1{}^y$ transitions of the $H_2P \cdot Ar_1$ complex with the porphyrin ring in the complex undergoing vibrationless electronic excitations. The information on microscopic spectral shifts induced by an Ar atom on the vibrationless excitations of H_2P pertains both to structural and energetic information. The facts are (*1*) a single spectral feature for the $S_0 \rightarrow S_1{}^x$ transition of $H_2P \cdot Ar_1$ was observed; (*2*) multiple spectra for the $S_0 \rightarrow S_1{}^y$ transition of $H_2P \cdot Ar_1$ were exhibited, revealing two spectral features; (*3*) the spectral features of the $S_0 \rightarrow S_1{}^x$ transition are blue shifted, being located at $\delta\nu = +8 \pm 1$ cm^{-1}; (*4*) the two spectral features of the $S_0 \rightarrow S_1{}^y$ transition of $H_2P \cdot Ar_1$ are red shifted relative to the 0–0 of the bare molecule, being located at $\delta\nu = -24 \pm 1$ cm^{-1} and at -35 ± 1 cm^{-1}. The main spectral feature is located at −24 cm^{-1}, while the −35-cm^{-1} feature is weaker, with a relative peak intensity of 25%. The observation of a single spectral feature for the $S_0 \rightarrow S_1{}^x$ transition provides (observation (*1*)) spectroscopic evidence for the existence of a single energetically stable structure of the $H_2P\cdot Ar_1$ complex. This conclusion is compatible with the results of our model calculations of the potential surface, which indicate the stability of the single configuration of this complex. Accordingly, we are reluctant to attribute the multiple spectrum consisting of two spectral features separated by 11 cm^{-1} for the $S_0 \rightarrow S_1^y$ transition (observation (*2*)) as originating from the excitation of two nearly isoenergetic isomers of $H_2P\cdot Ar_1$, because such a picture is incompatible with the results of the model calculation, as well as with observation (*1*). It should be borne in mind, however, that our model calculations disregarded the possibility of a configurational change of the H_2P induced by the binding of Ar, which may involve a displacement of the central H atoms. One may argue that the multiple spectrum of the Q_y band of $H_2P\cdot Ar_1$ originates from the contribution of two nearly isoenergetic isomers, where in both cases the Ar is located on the twofold axis of H_2P but differs in the configuration of the two protons. Obviously, observation (*1*) cannot easily be reconciled with such an assumption. The nature of the relatively weak satellite vdW(2) feature of the $S_0 \rightarrow S_1^y$ transition of $H_2P\cdot Ar_1$ requires further study.

The qualitative difference in the signs of the microscopic solvent shifts for the $S_0 \rightarrow S_1^x$ and $S_0 \rightarrow S_1^y$ transitions of $H_2P\cdot Ar_1$ (observations (*3*) and (*4*)) is of considerable interest. The spectral shift of the $S_0 \rightarrow S_1^y$ transition of the complex is $\delta\nu = -24\ cm^{-1}$. Such a red shift is characteristic of dispersive interactions, being ubiquitous in complexes of large organic molecules with heavy rare gases. The dispersive contribution to the spectral shift is expected to be determined by the polarizability α_R of R, and by the oscillator strength, f, for the corresponding electronic transition (4), i.e., $\delta\nu = -\alpha_R(a + bf)$, where a and b are constants. The $S_0 \rightarrow S_1^y$ transition of H_2P, which is characterized by a moderately large oscillator strength ($f \simeq 0.06$) (8, 11), is expected to exhibit an ordinary red spectral shift, being dominated by the dispersive contribution. On the other hand, the oscillator strength for the $S_0 \rightarrow S_1^x$ transition is low ($f \simeq 0.01$) (8, 11), and the contribution of the dispersive excited-state stabilization to the spectral shift for this transition in $H_2P\cdot Ar_1$ is expected to be small. The occurrence of a blue microscopic spectral shift $\delta\nu = +8\ cm^{-1}$ for the $S_0 \rightarrow S_1^x$ transition of $H_2P\cdot Ar_1$ clearly demonstrates that the microscopic solvent shift in this complex is not dominated by dispersive interactions. This blue spectral shift constitutes the first case of energetic destabilization of the excited state of a large vdW complex containing a heavy (Ar) R atom. The blue microscopic spectral shift for the $S_0 \rightarrow S_1^x$ origin of $H_2P\cdot Ar_1$ is attributed to configurational changes within the H_2P molecule induced by the binding of an Ar atom, which presumably involves a displacement of the central H atoms. The manifestation of this configurational change on the energetic destabilization of the electronically excited state is not masked by dispersive interactions, which are small in the present case. We were able to provide a unique example for a new contribution to a microscopic solvent spectral shift, which is due to intramolecular configurational changes induced by vdW binding in a large complex.

All the spectroscopic data for large vdW complexes reported to date pertain to intravalence electronic excitation of such systems. The extension of these studies for the interrogation of extravalence, Rydberg-type, electronic excitations of these large complexes will be of considerable interest. In this case, the major contribution to the microscopic spectral shift will originate from short-range excited-state repulsive interactions, unveiling novel features of solvent perturbations of excited-state energetics, nuclear dynamics, and intramolecular dynamics of extravalence molecular excitations. In this context, the search for Rydberg excitations of porphyrins and their vdW complexes will be of considerable intrinsic interest. It is expected that the novel spectroscopic methods in seeded supersonic jets will unveil the mystery of the Rydberg states of porphyrins, which constitute an important research area pioneered by Sandorfy and co-workers (16).

1. A. AMIRAV and J. JORTNER. J. Chem. Phys. **75**, 2489 (1981).
2. U. EVEN, A. AMIRAV, S. LEUTWYLER, M. J. ONDRECHEN, Z. BERKOVITCH-YELLIN, and J. JORTNER. Discuss. Faraday Soc. (London), **73**, 153 (1982).
3. M. J. ONDRECHEN, Z. BERKOVITCH-YELLIN, and J. JORTNER. J. Am. Chem. Soc. **103**, 6586 (1981).
4. A. AMIRAV, U. EVEN, B. DICK, and J. JORTNER. Mol. Phys. **49**, 899 (1983).
5. U. EVEN and J. JORTNER. J. Phys. Chem. **87**, 28 (1983).
6. U. EVEN, J. MAGEN, J. FRIEDMAN, and J. JORTNER. J. Chem. Phys. **77**, 4374 (1982).
7. U. EVEN, J. MAGEN, J. FRIEDMAN, and J. JORTNER. J. Chem. Phys. **77**, 4384 (1982).
8. U. EVEN and J. JORTNER. J. Chem. Phys. **77**, 4391 (1982).
9. L. EDWARDS, D. H. DOLPHIN, M. GOUTERMAN, and A. D. ADLER. J. Mol. Spectrosc. **38**, 16 (1971).
10. U. EVEN and J. JORTNER. J. Chem. Phys. **78**, 3445 (1983).
11. M. GOUTERMAN. The porphyrins. Vol. III. *Edited by* D. H. Dolphin. Academic Press, New York. 1978. p. 1.
12. A. MIRSKY. Computing in crystallography. 1978. p. 169.
13. J. O. HIRSCHFELDER, C. F. CURTISS, and R. B. BIRD. Molecular theory of gases and liquids. John Wiley and Sons, New York. 1954.
14. T. L. HILL. J. Chem. Phys. **16**, 399 (1948).
15. A. AMIRAV, U. EVEN, J. JORTNER, F. W. BIRSS, and D. A. RAMSAY. Can. J. Phys. **61**, 278 (1983).
16. P. R. DUPUIS, P. R. ROBERGE, and C. SANDORFY. Chem. Phys. Lett. **75**, 434 (1980).

Azulenium cations. An experimental and theoretical study of the cations derived from hydrocarbon derivatives of azulene

J. W. LEWIS AND R. V. NAUMAN

Department of Chemistry, Louisiana State University, Baton Rouge, LA 70803, U.S.A.

Received August 6, 1984

This paper is dedicated to Professor Camille Sandorfy on the occasion of his 65th birthday

J. W. LEWIS and R. V. NAUMAN. Can. J. Chem. **63**, 2081 (1985).

The ambient temperature ultraviolet absorption and the 77 K luminescence spectra of a series of four hydrocarbon derivatives of azulene in sulfuric acid solution are presented and discussed in detail. CNDO/S calculations have been carried out and the calculational results are compared with the experimental results. The phosphorescences of these cationic species are reported for the first time. The present results suggest that an inversion in the order of electronic states is perhaps responsible for the normal emissions of the protonated species and the anomalous emissions of the parent molecules.

J. W. LEWIS et R. V. NAUMAN. Can. J. Chem. **63**, 2081 (1985).

Opérant en solution dans de l'acide sulfurique, on a mesuré les spectres d'absorption ultraviolette à la température ambiante et les spectres de luminescence à 77 K d'une série de 4 hydrocarbures dérivant de l'azulène; on en discute en détail. On a réalisé des calculs CNDO/S et on les a comparé avec les résultats expérimentaux. On rapporte pour le premier fois l'observation de phosphorescence de ces espèces cationiques. Les résultats actuels suggèrent qu'une inversion dans l'ordre des états électroniques est peut-être responsable des émissions normales des espèces protonées et des émissions anormales des molécules mères.

[Traduit par le journal]

Introduction

The structure of azulene in strongly acidic medium has been studied for several years. Frey (1) in 1956 first attempted to use nuclear magnetic resonance (nmr) to determine the structure of the azulenium cation. Since that time several groups (2–9)

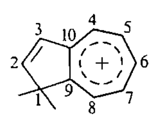

have, by means of nmr, established that the site of protonation is position one of the azulene nucleus (or, alternatively, position three of 1-substituted azulenes is protonated). These studies of the ground state structure show that the chemical shifts of protons two and three are only slightly altered by the protonation. On the other hand, those of the protons on the seven-membered ring are appreciably altered. The authors concluded that the electron deficiency is localized in the seven-membered ring and is shared almost equally throughout the ring. It is also generally established that only monoprotonation of all the hydrocarbon derivatives of azulene occurs. There is no firm evidence to support the existence of a doubly charged cation.

The azulenium cation has also been investigated theoretically and the electronic absorption spectrum was interpreted with the help of a "molecule in molecule" calculational model (10, 11). These calculations predict transitions at 352.1, 323.6, 259.1, 227.3, and 211.9 nm. These authors concluded that the lowest energy singlet–singlet transition has at least 60% charge-transfer character.

The luminescence of azulenium cations has not been systematically investigated previously. Heilbronner *et al.* (10, 12) have reported some fluorscence spectra in connection with studies of the ground and first excited singlet state pK values and of proton dissociation of the cations in the first excited singlet state. In addition, two other papers concerned with the emission of protonated azulenes have appeared (13, 14). The emissions reported in the literature (14) are normal $S_1 \rightarrow S_0$ fluorescences and they appear to be broad, structureless bands in the spectra recorded from room temperature solutions. There are no reports of the phosphorescence of the azulenium cations.

In the present work we present absorption and emission spectra of the cations of four hydrocarbon derivatives of azulene. We also present and discuss low temperature emission spectra of these cations and report for the first time phosphorescences of the cations. Finally, CNDO/S calculations have been carried out and the calculational results are compared with the experimental results. The calculational results appear to indicate that an inversion in the order of the two lowest energy unoccupied singlet orbitals of azulene is the most important result of protonation. The inversion in the order of these molecular orbitals is perhaps intimately related to the normal emissions of the protonated species and to the anomalous emissions of the parent species.

The CNDO/S program employed for these studies is a modified version of the modified CNDO method ((CNDO/S-CI), J. Del Bene and H. H. Jaffe, QCPE 174). This program has been modified in-house to accommodate 200 basic members and 99 atomic centers (as opposed to the 99 basic members and 31 atomic centers specified in the original version).

Experimental

The azulene and 4,6,8-trimethylazulene used in these studies are commercial products of Rutgerwerke A. G. and were prepared in 1959. The samples were subjected to three or more chromatographic separations (absorptive filtration), three crystallizations from purified hexane, and three to five vacuum sublimations. The samples treated in this manner gave no indication of the presence of naphthalene, a known photochemical product of azulene. 2-Phenylazulene was prepared by means of a modification of a literature procedure (15). 6-Phenylazulene was also prepared by means of a modification of a literature procedure (16, 17). These modifications are described in detail elsewhere (18). 2-Phenyl- and 6-phenylazulene were also subjected to the three different methods of purification employed above for azulene and were found to be spectroscopically homogeneous.

The absorption spectra were measured by means of a Cary 14 recording spectrophotometer. The emission spectra were recorded by

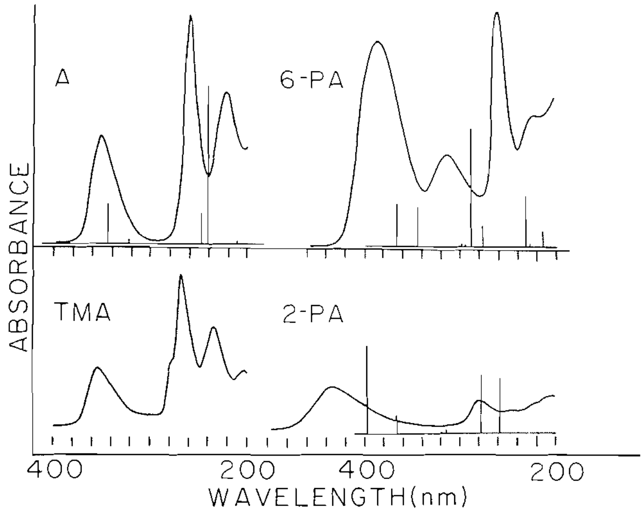

FIG. 1. Absorption spectra of the azulene derivatives in 60% H_2SO_4. The vertical lines represent the calculated transition energies (see text). The concentrations are: Azulene – 1.69×10^{-4} *M*, $\epsilon_{351\ \mathrm{nm}}$ (1.26×10^4), $\epsilon_{258\ \mathrm{nm}}$ (2.71×10^4), $\epsilon_{222\ \mathrm{nm}}$ (1.81×10^4); trimethylazulene – 1.41×10^{-4} *M*, $\epsilon_{353\ \mathrm{nm}}$ (1.50×10^4), $\epsilon_{267\ \mathrm{nm}}$ (3.83×10^4), $\epsilon_{234\ \mathrm{nm}}$ (2.52×10^4); 6-phenylazulene – 3.00×10^{-5} *M*, $\epsilon_{385\ \mathrm{nm}}$ (2.44×10^4), $\epsilon_{312\ \mathrm{nm}}$ (1.13×10^4), $\epsilon_{259\ \mathrm{nm}}$ (2.82×10^4); and 2-phenylazulene – 4.70×10^{-5} *M* $\epsilon_{438\ \mathrm{nm}}$ (3.23×10^3).

means of a home-built spectrometer system which is described elsewhere (19). A rotating dual blade phosphoroscope was installed on the spectrometer in order to obtain pure phosphorescence spectra. The reported emission spectra are not corrected for photomultiplier response, variation in the intensity of the exciting source, nor for the characteristics of the excitation and emission monochromators. Excitation was front surface for all the fluorescence measurements and was at 180 degrees to observation for all the phosphorescence measurements.

The analytical solutions of these azulene derivatives were prepared immediately prior to measurement in order to avoid some long-time chemical degradation which occurs in strongly acidic solution. The solvent in all cases consisted of 60 vol.% sulfuric acid. The solvent gave no emissions at the excitation wavelengths employed in this study. The solvent formed a partially transparent, cracked glass at 77 K.

Results

The absorption spectra recorded from ambient temperature solutions of azulene, 4,6,8-trimethylazulene (TMA), 2-phenylazulene (2-PA), and 6-phenylazulene (6-PA) in 60% sulfuric acid are reproduced in Fig. 1. The vertical lines shown in most of the spectra represent the position and relative oscillator strengths of the calculated transitions. The model chosen for the calculations is a somewhat restricted one in that the bond angles and bond distances used for the cations are identical to those of the unprotonated parent molecules. The only differences between the present model and that of the unprotonated parent molecules are rehybridization of the carbon atom at position one and delocalization of the positive charge.

The luminescence spectra recorded from solutions, maintained at 77 K, of the azulene derivatives in 60% sulfuric acid are reproduced in Fig. 2. It should be noted that the phosphorescences of the cations are much weaker than the fluorescences. The relative intensities of the two emissions are shown in the spectra of the azulenium cation. On the same scale as the fluorescence, the phosphorescence is seen as a slight bump in the baseline. (In alcoholic hydrochloric and hydrobromic acid solutions of azulene, the intensity of the phosphorescence increases appreciably.)

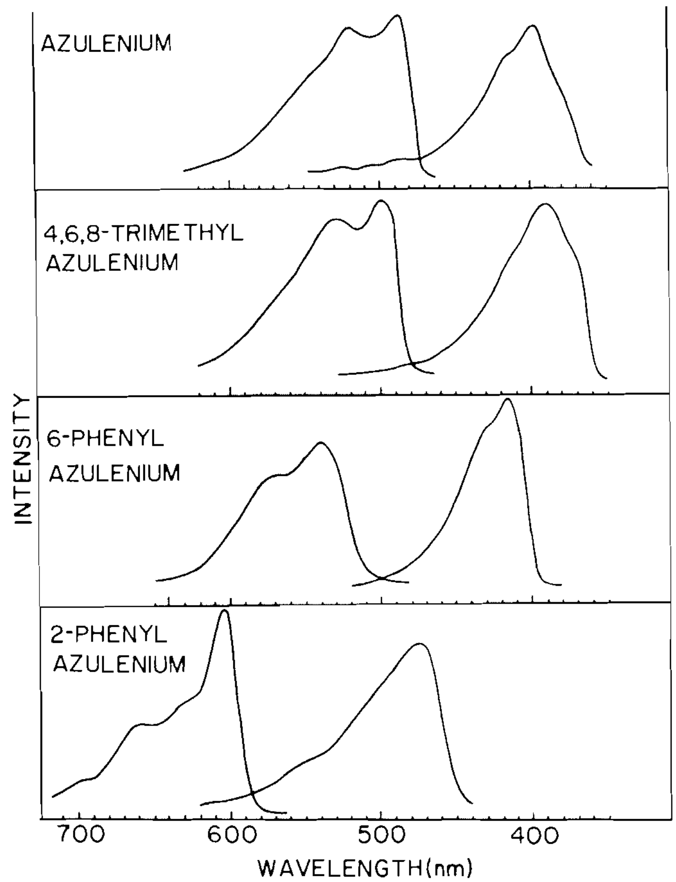

FIG. 2. Luminescence spectra of azulene derivatives in 60% H_2SO_4. The spectra are those from solutions in cracked glasses at 77 K. The concentration of each derivative is identical with that listed for the absorption spectrum. The phosphorescence appears on the left in each spectrum.

In Fig. 3 are shown the calculated transitions of three cations in the form of a transition correlation diagram. In this figure the dashed lines connect transitions of similar orbital character. In general, it can be seen that the theoretical transition energies are in excellent agreement with the experimental energies although the former are higher in every case.

Discussion

The model chosen for the CNDO/S calculations is, in some ways, a somewhat restricted one. The bond angles and bond distances of the protonated species are limited to those of the neutral parent molecules. The selected model should therefore by justified.

The azulene – azulenium cation equilibrium in solutions of various acid concentrations has been investigated by Long and Schulze (6–8) and by Challis and Long (9). In addition, Heilbronner *et al.* (11) have studied the proton dissociation of the azulenium cation in the first excited singlet state by means of flash photolytic techniques. These experiments demonstrated that one of the products produced by a flash is azulene in its ground state. A series of flashes leads to a distortion of the azulene – azulenium cation equilibrium which may be conveniently measured by monitoring the absorbance of the solution at some wavelength which corresponds to the position of the lowest energy absorption band of azulene. At higher

TABLE 1. Calculated transitions and oscillator strengths

Ion	Transition wavelength in nm (oscillator strength)					
Azulenium	345(0.141)	323(0.015)	248(0.112)	241(0.552)	213(0.105)	194(0.315)
6-Phenylazulenium	367(01.48)	345(0.135)	289(0.418)	277(0.074)	233(0.178)	227(0.199)
2-Phenylazulenium	399(0.315)	356(0.065)	270(0.213)	250(0.199)	228(0.237)	216(0.146)

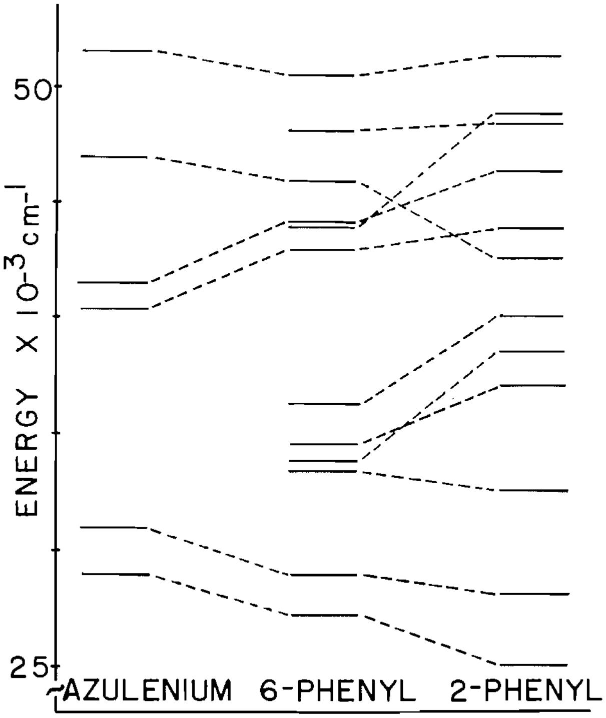

FIG. 3. Correlation diagram of the calculated transition energies of the azulenium, 6-phenylazulenium, and 2-phenylazulenium cations.

concentrations of acid, the reprotonation of azulene became too fast to measure with the equipment employed. The point, however, is that proton dissociation in the lowest energy excited state of the azulenium cation probably occurs even in very strongly acidic solutions, although the azulene molecule is not observed by means of conventional flash techniques. Since the neutral azulene molecule is produced from an excited azulenium cation by proton dissociation, it appears logical that the equilibrium geometry of the excited azulenium cation should be adequately represented by the ground state geometry of the azulene molecule. We realize, however, that this choice is not equally satisfactory for the ground state azulenium cation since the bond angles and bond distances, perhaps even the planarity, of the cation are probably relaxed upon protonation. On the other hand, the relaxed geometry of the ground state cation is not really satisfactory for the excited state cation so that a choice had to be made. The changes should have an effect only on the transition energies and not on the order of the transitions. The reasonable values of the calculated transitions and their close correspondence to the earlier values of Heilbronner *et al.* (10, 12) seem to justify the present choice of a model for the azulenium cations.

The general characteristics of the lowest energy absorption bands of all four of the hydrocarbon derivatives of azulene are very similar. The shapes of these bands in the various spectra are consistent with the presence of two electronic transitions in this wavelength region. The theoretical calculations also predict two transitions. The theoretical transitions and oscillator strengths are listed in Table 1. Comparison of these oscillator strengths for the pairs of transitions demonstrates that the higher energy transitions have the smaller oscillator strengths, thus the correct shape of the lowest energy absorption bands is also predicted by the restricted model. All these results are in excellent accord with the results of the earlier "molecule in molecule" calculations of Heilbronner *et al.* (10, 11). The pairing of transitions throughout the calculated spectrum appears to be a general phenomenon in all the azulene derivatives studied in this work. This effect was also predicted by the calculations of Heilbronner *et al.*

Although the spectra are not shown, there is a considerable difference between the locations of the wavelength maxima in the ambient temperature absorption and fluorescence excitation spectra of the azulenium and 2-phenylazulenium cations. The fluorescence excitation maximum of the first electronic transition of the azulenium cation shifts 940 cm^{-1} to lower energy relative to the maximum in the absorption spectrum and that of the 2-phenylazulenium cation shifts 825 cm^{-1} to lower energy. Ideally, of course, the fluorescence excitation maximum should be identical with the absorption maximum. Large shifts such as those listed here are normally indicative of substantial changes in geometry of the emitting species relative to that of the absorbing species. In view of our arguments given above, this latter result is entirely expected.

There is also a sizable blue shift of the fluorescence maxima of the cations as the temperature decreases. For example, the wavelength maximum of the ambient temperature azulenium fluorescence occurs at 428 nm, while that at 77 K occurs at 398 nm, which corresponds to an 1800 cm^{-1} blue shift. The shift of the fluorescence maximum of the 2-phenylazulenium cation is from 510 nm at room temperature to 475 nm at 77 K. This change corresponds to a 1450 cm^{-1} blue shift. In strongly acidic solution at room temperature azulene may be viewed as an ionic species that has a rather flexible structure and consequently gives rise to the structureless absorption and fluorescence spectra. At 77 K the structure is rigidly fixed by the solvent matrix. This rigidity is clearly demonstrated by the dramatic shift of the fluorescence to higher energy and by the increase in vibrational structure of the fluorescence.

It is found that the cations of the hydrocarbon derivatives of azulene fluoresce even more strongly at 77 K than they do at room temperature. The 77 K fluorescences have not been reported previously. Our room temperature fluorescence of azulene in 60% sulfuric acid agrees with that reported in the literature (14). The cations also exhibit phosphorescence at 77 K. Both these emissions originate from the lowest energy excited state of the appropriate multiplicity in contrast to the behavior of the parent molecules which fluoresce exclusively from the second excited singlet state (both $S_2 \rightarrow S_1$ and $S_2 \rightarrow S_0$ emissions are observed). These emissions that originate from the lowest excited singlet and triplet states would appear to suggest that the excited states of the cations are greatly different from the excited states of the parent molecules. However, an

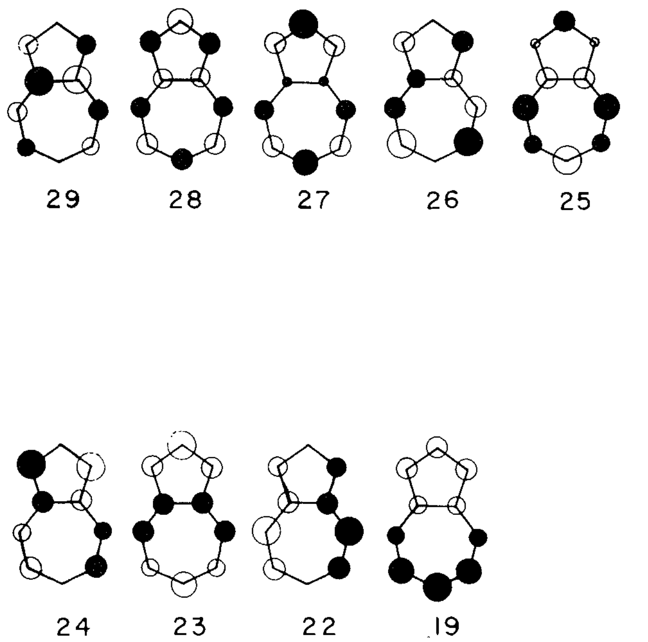

FIG. 4. The highest occupied (HOMO) and lowest unoccupied (LUMO) orbitals of azulene. Orbitals 19–24 are the HOMOs.

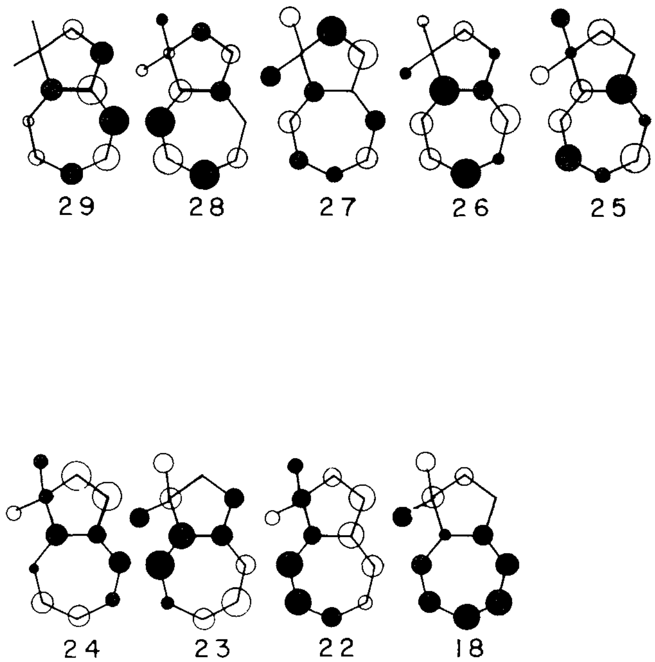

FIG. 5. The highest occupied (HOMO) and lowest unoccupied (LUMO) orbitals of the azulenium cation. Orbitals 18–24 are the HOMOs.

examination of the available information suggests that the excited singlet states of the cations and the parent molecules are somewhat similar, although the ordering of the states may be inverted. The present theoretical data indicate that a sufficient condition for normal Kasha's rule fluorescence is that the order of the two lowest energy unoccupied singlet states of azulene be reversed.

It is apparent that the association of an orbital transition, such as LUMO ← HOMO, with an electronic transition is a rather severe approximation. The incorporation of configuration interaction, such as is done in the CNDO/S procedure, somewhat lessens the severity of the approximation. The orbital representations obtained by the CNDO/S procedure are thus only an aid in the assignment of electronic transitions; however, within this degree of approximation the present calculations yield some interesting insights. Compare, for example, the orbital representations in Figs. 4 and 5. The orbitals labelled 25 and 26 represent the two lowest energy unoccupied orbitals of both the cation (Fig. 5) and the parent molecule (Fig. 4). The essential difference between the azulene orbital labelled 26 and the azulenium cation orbital labelled 25 is a small amount of electron density at positions 2 and 6 of the azulenium cation. Conversely, the azulene orbital labelled 25 is very similar to the azulenium cation orbital labelled 26. Thus, the present calculational results suggest that the order of the two lowest energy excited states of azulene is inverted upon protonation. If such is the case, then the emitting state of both species has the same orbital character and the inversion in the order of the states may explain the normal, Kasha's rule, emissions of the cations.

If one compares the absorption spectra of the azulenium ion with that of azulene (see Fig. 6), one finds that there is an amazing similarity between all the transitions, except that the first transition either does not appear in the spectrum of the azulenium ion or appears as a weak shoulder at about 320 nm in accord with the orbital inversion argument of the previous section. Very similar results are found in the spectra of all the hydrocarbon derivatives of azulene (18). This comparison suggests that the higher energy states of azulene may have geometries and charge distributions similar to those of the states of the azulenium ion and that only the first transition in azulene is unique.

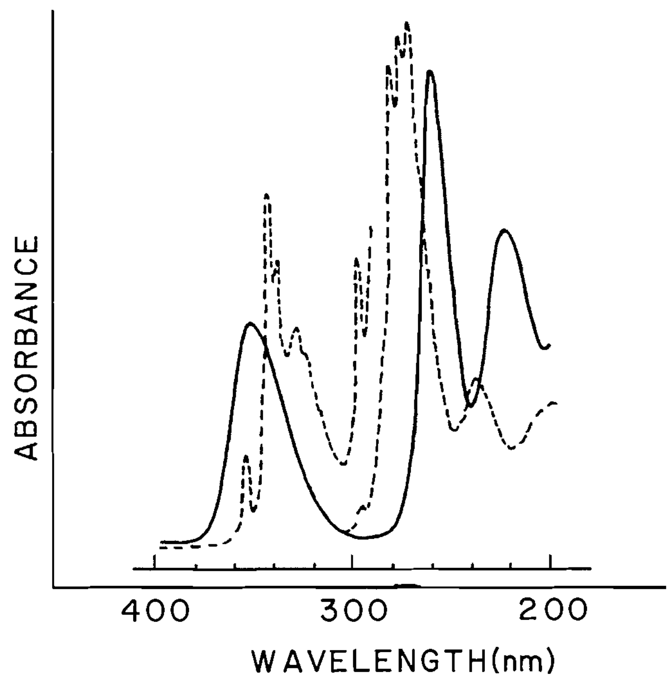

FIG. 6. Comparison of the absorption spectra of azulene (- - -) in 3-methylpentane solution (2.51×10^{-3} M and azulene (—) in 60% H_2SO_4 solution (1.69×10^{-4} M). The vertical scales for the two spectra are not the same.

In conclusion, it seems that the fluorescence emitting states of azulene and azulenium ion are very similar; perhaps the emission of azulene is not anomalous but it is the unusual first absorption that should be considered to be anomalous.

Although the photophysics of azulene has been reconsidered many times in the last twenty years, the similarity between the second excited singlet state of azulene and the first excited singlet state of the azulenium ion suggests that many phenomena should be reinvestigated; for example, is the first excited singlet state of azulene dissociative, predissociative, or an efficient sensitizer of a dissociative triplet state? Resonance Raman studies should lead to some clarification of these phenomena.

Acknowledgement

One of the authors (J.W.L.) was supported by the U.S. Department of Energy under Contract No. De-AS05-76EV-030018 during the preparation of this manuscript.

1. H. M. FREY. J. Chem. Phys. **25**, 600 (1956).
2. S. S. DANYLUK and W. G. SCHNEIDER. J. Am. Chem. Soc. **82**, 997 (1960).
3. S. S. DANYLUK and W. G. SCHMEIDER. Can. J. Chem. **40**, 1777 (1962).
4. E. HEILBRONNER, D. MEUCHE, B. B. MOLLOY, and D. H. REID. Helv. Chem. Acta, **46**, 2483 (1963).
5. J. SCHULZE and F. A. LONG. J. Am. Chem. Soc. **86**, 322 (1964).
6. F. A. LONG and J. SCHULZE. J. Am. Chem. Soc. **83**, 3340 (1961).
7. F. A. LONG and J. SCHULZE. J. Am. Chem. Soc. **86**, 327 (1964).
8. F. A. LONG and J. SCHULZE. J. Am. Chem. Soc. **86**, 331 (1964).
9. B. C. CHALLIS and F. A. LONG. J. Am. Chem. Soc. **87**, 1196 (1965).
10. E. HEILBRONNER, R. HAGEN, W. MEIER, and P. SEILER. Helv. Chem. Acta, **50**, 1523 (1967).
11. E. HEILBRONNER, W. MEIER, and D. MEUCHE. Helv. Chem. Acta, **45**, 2628 (1962).
12. E. HEILBRONNER, K. H. GRELLMANN, P. SEILER, and A. WELLER. J. Am. Chem. Soc. **90**, 4238 (1968).
13. J. A. POOLE and R. C. DHINGRA. J. Phys. Chem. **78**, 4577 (1968).
14. W. TREIBS and M. SCHOLZ. Z. Physik. Chem. **214**, 118 (1959).
15. T. NOZOE, K. TAKASE, and S. FUKUDA. Bull Chem. Soc. Jpn. **44**, 2210 (1971).
16. S. M. MAKIN, V. M. LIKHOSHERTOV, and M. I. SHELEMINA. Zh. Obshch. Khim. **34**, 1809 (1964); Chem. Abstr. **61**, 8261e (1964).
17. YU. N. PORSHNEV, E. M. TERESHCHENK, V. V. TITOV, and V. B. MOCHALIN. Zh. Org. Khim. **8**, 1989 (1972).
18. J. W. LEWIS. Ph. D. Dissertation, Louisiana State University, Baton Rouge, 1979.
19. E. HUGHES, J. H. WHARTON, and R. V. NAUMAN. J. Phys. Chem. **75**, 1097 (1971).

COMMUNICATION

Pressure broadening effects in the far-infrared vibration–rotation spectra of several alkylamines and alkylethers[1]

D. J. GERSON
IBM Instruments Inc., Orchard Park, Danbury, CT, 06810, USA

AND

W. G. FATELEY
Kansas State University, Department of Chemistry, Manhattan, KS, 66506, USA

Received August 1, 1984

This paper is dedicated to Professor Camille Sandorfy on the occasion of his 65th birthday

D. J. GERSON and W. G. FATELEY. Can. J. Chem. **63**, 2086 (1985).

The far-infrared vibration–rotation spectra of the infrared-active internal rotation mode of dimethylether, dimethylamine, methylamine, and ethylamine have been recorded at several vapor pressures. The effect of pressure broadening on the $1 \leftarrow 0$ torsional transition has been experimentally determined. It was found that the Van Vleck – Weisskopf model gave the best fit to these experimental results. It was also found that pressure broadening of the $1 \leftarrow 0$ transition did not overlap the next transition in the series at sample vapor pressures less than 50 Torr.

D. J. GERSON et W. G. FATELEY. Can. J. Chem. **63**, 2086 (1985).

Opérant à plusieurs tensions de vapeur, on a déterminé les spectres de vibration–rotation dans le proche infrarouge du mode de rotation interne, actif dans l'infrarouge, du diméthyléther, de la diméthylamine, de la méthylamine ainsi que de l'éthylamine. On a déterminé expérimentalement l'effet d'élargissement dû à la pression sur la transition de torsion $1 \leftarrow 0$. On a aussi trouvé que, dans ces séries et à des tensions de vapeur inférieures à 50 Torr, l'élargissement dû à la pression de la transition $1 \leftarrow 0$ ne se superpose pas à la transition suivante.

[Traduit par le journal]

Introduction

Recently, Durig and co-workers have presented a series of papers which have investigated the effect of top–top coupling on the observed vibration–rotation spectrum of molecules with two internal C_{3v} rotors (1). To obtain good spectra, these studies were performed using sample vapor pressures in excess of 100 Torr. At these pressures, significant amounts of vibrational fine structure is obscured by pressure broadening (2). Since the observable internal rotation torsional transitions are very narrow, the disappearance of bands due to pressure broadening could alter the vibrational assignment of the transitions and the subsequent potential function. Cooke and co-workers have shown that this occurs in dimethylether (3).

In an effort to determine the maximum vapor pressure of sample which maintains a well resolved vibration–rotation spectrum, the far-infrared spectra of dimethylether, dimethylamine, methylamine, and ethylamine were recorded at several sample vapor pressures. The resultant degradations in resolution with increased vapor pressure were compared to those expected from theory (4), and the results of these comparisons are reported herein.

Experimental

The samples of dimethylether, dimethylamine, methylamine, and ethylamine were purchased from Matheson, Inc. (East Rutherford, NJ). Samples were purified by low temperature fractional distillation and cold-trapping over 4A sieves prior to the acquisition of their spectra (5). The samples were then passed through activated molecular sieves at room temperature into the infrared vapor cell. Typical sample vapor pressures used in the analyses varied from 1 Torr to 750 Torr.

The spectra were obtained using an IBM Instruments IR/98 vacuum spectrometer equipped with mercury arc source, 500 lines/inch metal mesh beamsplitter and liquid helium cooled germanium bolometer operating below the lambda point. The samples were contained in a Wilks multipass gas cell equipped with polyethylene window lenses and vacuum fittings as supplied by IBM Instruments. The cell pathlength was fixed at 2.75 m for all spectra recorded for this study. The spectra were transformed from 512 coadded interferograms, boxcar apodized, to give an effective resolution of 0.022 cm^{-1}.

Calculations were performed using an IBM System 9001 computer system. Data analysis programs written in S9000 Pascal were used to analyze the experimental and theoretical data. The experimental data were transferred to the S9000 using standard RS232 protocol from the Aspect data system of the FTIR spectrometer.[2]

Results

The effect of increasing the sample vapor pressure on the resolution of the torsional fine structure of dimethyl ether is displayed graphically in Fig. 1. It can be seen that almost all of the observable fine structure disappears by 100 Torr of sample vapor pressure. Figure 2 shows this effect in the region of $10 \leftarrow 00$ transition.

The theoretical derivation of the Debye intensity for hard collisions between fixed dipoles has been given by Van Vleck and Weisskopf (4). In general, the net absorption coefficient, γ, is dependent upon the dipole moment of the transition, μ_{ij}, and the transition frequency, ν (eq. [1]).

[1] Presented in part at the 1983 Pittsburgh Conference on Analytical Chemistry and Applied Spectroscopy, paper 627.

[2] Program CHBOUT, ABACUS User Group (1982), as supplied by Bruker Spectrospin, Zurich, Switzerland, and Program PRTPTS, IBM User Group (1982), as supplied by IBM Instruments, Inc., Danbury, CT.

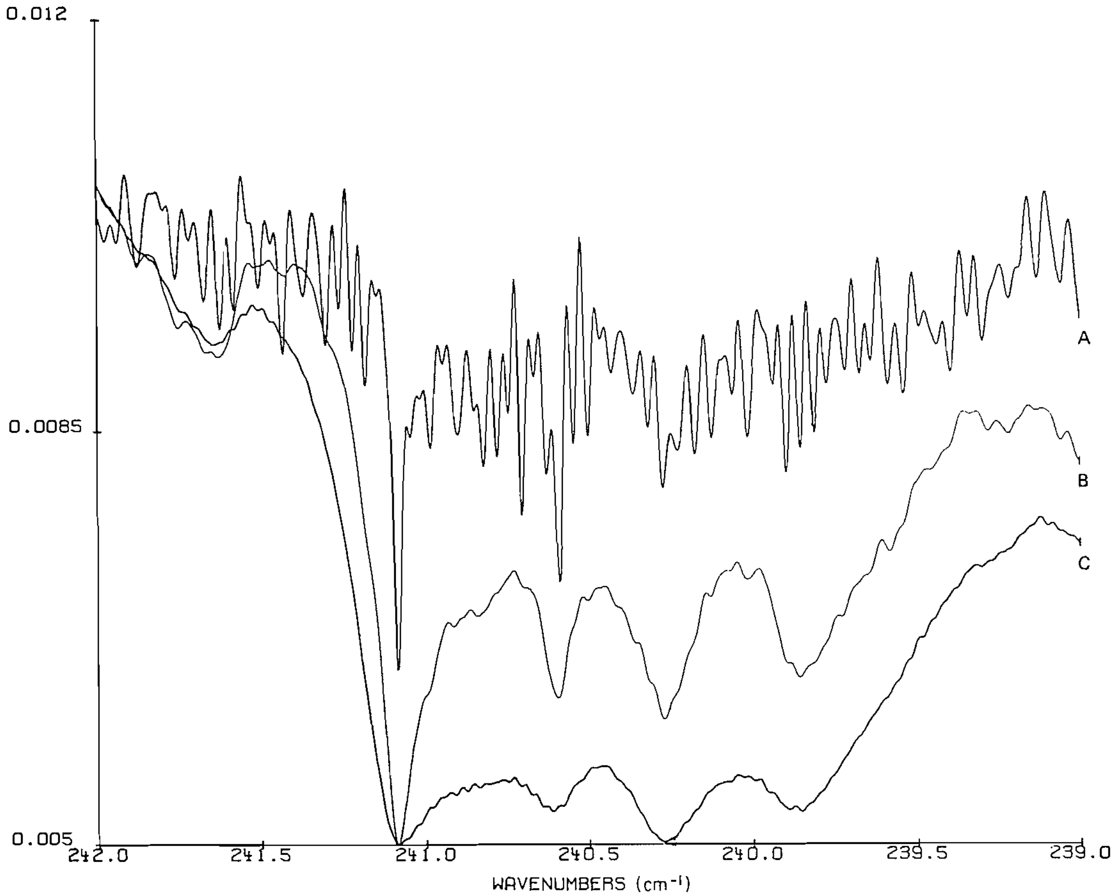

FIG. 1. Far-infrared spectral region from 242 to 239 cm^{-1} of dimethylether in the region of the torsion frequencies, ν_{26}. (*A*) 1 Torr; (*B*) 10 Torr; (*C*) 100 Torr. A Wilks multipass gas cell equipped with polyethylene lens windows was used.

$$[1] \quad \gamma = \frac{8\pi^2 N\nu^2 f}{3ckT}\left|\mu_{ij}\right|^2 \times \frac{1}{2}\pi\tau\left[\frac{1}{(\nu-\nu_0)^2+(1/2\pi\tau)^2} + \frac{1}{(\nu+\nu_0{}^2+(1/2\pi\tau)^2}\right]$$

where

$$[2] \quad |\mu_{ij}|^2 = \sum_M |u_x\langle JMJ'M'\rangle|^2 + |u_y\langle JMJ'M'\rangle|^2 + |u_z\langle JMJ'M'\rangle|^2$$

At low pressures, $\frac{1}{2}\pi\tau \ll \nu_0$, and the first term in eq. [1] predominates. If the observations are limited to the region near ν_0, eq. [1] reduces to:

$$\gamma = \frac{8\pi^2 Nf}{3ckT}\left|\mu_{ij}\right|^2 \nu^2\left[\frac{\Delta\nu}{(\nu-\nu_0)^2+(\Delta\nu)^2}\right]$$

provided $\Delta\nu \ll \nu_0$. Under these conditions, the integrated line intensity becomes

$$\gamma_I = \frac{8\pi^2 Nf}{3ckT}\left|\mu_{ij}\right|^2 \nu_0$$

and the halfwidth, $\Delta\nu$, is proportional to the sample pressure, $(1/2)\pi\tau$, for low pressures.

For the molecules examined in this study, the experimentally observed halfwidth, FWHH, and the integrated intensity, (the calculated values of the halfwidth and the relative error) are also presented in Table 1. As shown in Table 1, the differences between the calculated and observed values for the FWHH are

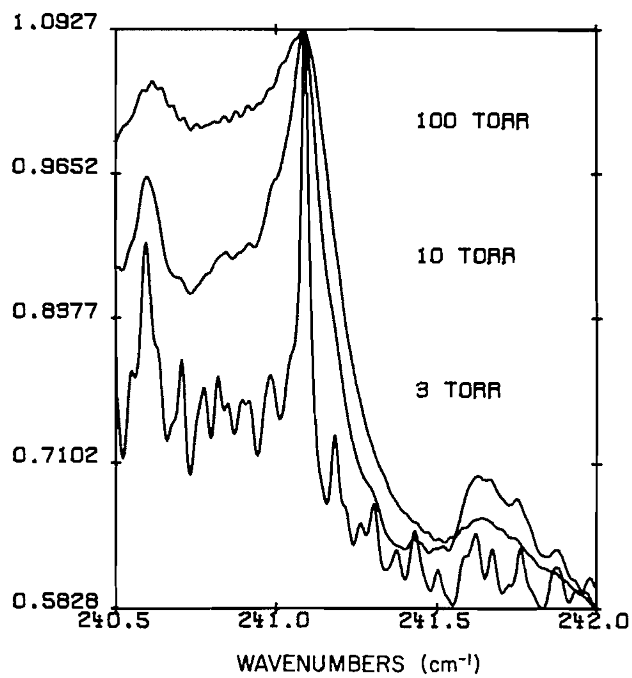

FIG. 2. Far-infrared spectrum of dimethyl ether in the region of the $1 0 \leftarrow 0 0$ transition. The same experimental conditions as in Fig. 1 are present here. The top spectrum is 100 Torr, middle spectrum is 10 Torr and the bottom spectrum is 3 Torr pressure of dimethylene.

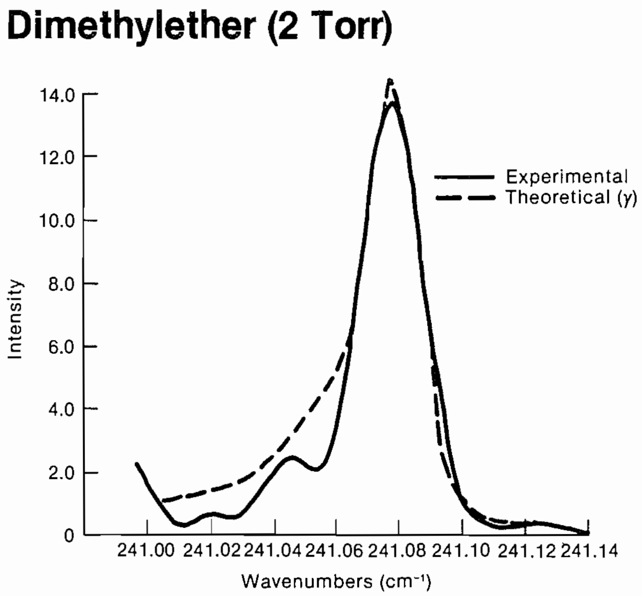

FIG. 3. Comparison of the experimental and theoretical band profile for the 10 ← 00 transition of dimethylether at 2 Torr.

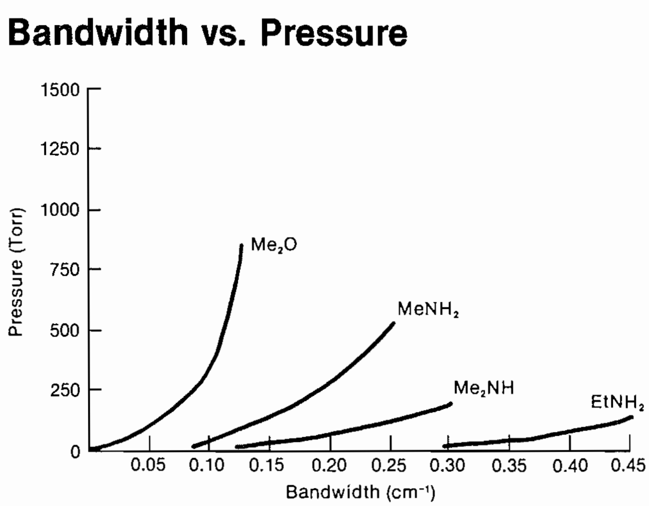

FIG. 4. Experimental pressure broadening effects for dimethylether, dimethylamine, methylamine, and ethylamine.

approximately the same as the resolution limit of the interferometer, 0.022 cm^{-1}.

Comparison of the theoretical (calculated) and experimental line shape, at low vapor pressure, for the 1 ← 0 transition of dimethylether is shown in Fig. 3. The good agreement between the experimentally observed band and the line shape calculated using eq. [4], is most probably indicative of the lack of observable intermolecular perturbations caused by the two internal rotors. At low vapor pressures, the halfwidth, $\Delta\nu$, is observed to follow a linear relationship with sample pressure. However, as shown in Fig. 4, at sample pressures greater than 100 Torr, this relationship does not hold.

TABLE 1. Experimental and calculated band width and band intensity data

Molecule	FWHH[a] (cm^{-1}) Obsd.	Calcd.	Δ	Integrated absorbance ($\times 10^2$)
CH_3OCH_3	0.080	0.062	0.018	12.0
CH_3NHCH_3	0.180	0.163	0.017	10.3
CH_3NH_2	0.130	0.103	0.027	3.2
$C_2H_5NH_2$	0.36	0.392	0.032	8.8

[a]FWHH: frequency width at half height at 10 Torr.

Conclusion

The observed pressure broadening effects in dimethylether, dimethylamine, methylamine, and ethylamine have been found to follow the Van Vleck – Weisskopf model at pressures up to 750 Torr. No significant differences were found between the calculated and observed FWHH for the dimethyl-X compounds, indicating that the interaction between the two internal rotors has little effect on intermolecular events. The maximum vapor pressure found to give resolvable fine structure was 100 Torr for the two dimethyl rotor compounds. At pressures above 100 Torr, the 2 ← 1 transition was found to be obscurred by the pressure broadened 1 ← 0 transition. For methylamine and ethylamine, this was found to occur at pressures greater than 50 Torr.

Acknowledgments

The authors would like to thank Dr. J. M. Casper, IBM Instruments, for his assistance in obtaining the spectrum of dimethylether. The authors would also like to thank Dr. D. A. C. Compton, SOHIO Research, for his constructive comments during the course of this study.

One of the authors (W.G.F.) would like to acknowledge partial support for the study from an NSF grant CHE-8109570.

1. J. R. DURIG and J. F. SULLIVAN. *In* Spectroscopy in chemistry and physics: modern trends. *Edited by* F. J. Comes, A. Muller, and W. J. Orville-Thomas. Elsevier Scientific Publishing Co., Amsterdam. 1983.
2. J. CASPER. Private communication.
3. J. COOKE, W. G. FATELEY, and J. M. CASPER. Proc. 1982 Pittsburgh Conf. on Anal. Chem. Appl. Spectrosc.
4. J. H. VAN VLECK and V. F. WEISSKOPF. Rev. Mod. Phys. **17**, 227 (1945).
5. D. J. GERSON. Ph.D. Thesis. University of South Carolina. 1980.

Réarrangement de thiophénobishomotropones en naphto[1,8-*bc*]thiophène et benzo[2,3-*b*]thiophène; études spectroscopique et mécanistique

BERNARD HANQUET, MICHEL FARNIER ET ROGER GUILARD[1]

Laboratoire de Synthèse et d'Electrosynthèse Organométallique associé au C.N.R.S. (UA 33), Faculté des Sciences "Gabriel", 6, Bd Gabriel, 21100 Dijon, France

ET

CLAUDE LECOMTE ET YVES DUSAUSOY

Laboratoire de Minéralogie et Cristallographie, Equipe de recherche associée au C.N.R.S. n° 162, Faculté des Sciences, Centre de 2ème Cycle, Boite Postale n° 239, 54506 Vandoeuvre les Nancy, France

Reçu le 25 juillet 1984

BERNARD HANQUET, MICHEL FARNIER, ROGER GUILARD, CLAUDE LECOMTE et YVES DUSAUSOY. Can. J. Chem. **63**, 2089 (1985).

Opposées à l'éthanedithiol, les thiophéno[*c*] et [*b*]bishomotropones subissent un réarrangement original conduisant à un naphto[1,8-*bc*]thiophène et (ou) à un benzo[*b*]thiophène. La structure des produits obtenus est déterminée par marquage isotopique, examen comparatif des spectres de rmn protonique, et dans le cas du diphényl-5,6 naphto[1,8-*bc*]thiophène par analyse cristallographique. Un mécanisme réactionnel est proposé impliquant au stade déterminant un transfert électronique entre un nucléophile "doux" et un acide "dur".

BERNARD HANQUET, MICHEL FARNIER, ROGER GUILARD, CLAUDE LECOMTE, and YVES DUSAUSOY. Can. J. Chem. **63**, 2089 (1985).

A non classical rearrangement is observed when thiopheno[*c*] and [*b*]bishomotropones react with ethanedithiol, leading to a naphtho[1,8-*bc*]thiophene and (or) a benzo[*b*]thiophene. The structure of the products is supported by deuterium labelling, ^{1}H nmr spectra, and X-ray analysis of 5,6-diphenyl naphtho[1,8-*bc*]thiophene. A mechanism is proposed which implies an electronic transfer between a "soft" nucleophile and a "hard" acid, in the key step.

Introduction

Dans un article antérieur nous avons décrit la réactivité singulière de la thiophénomonohomotropone **1** lorsqu'on l'oppose aux thiols (1). Nous avons montré en particulier qu'en présence d'éthanedithiol et d'acide paratoluènesulfonique (APTS), le dérivé homotroponique **1** subit un réarrangement original et conduit à un composé benzothiophénique porteur d'un groupement aldéhyde protégé par un reste dithiolanne. Le mécanisme de ce réarrangement implique entre autres la rupture d'une double liaison carbone–carbone résultant de l'action conjuguée de l'éthanedithiol – nucléophile "doux" – et du groupe carbonyle protoné – acide "dur".

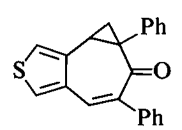

1

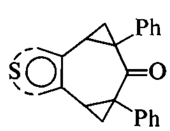

2

Or lors de la synthèse des thiophénohomotropones (2) on observe parallèlement à la formation de monohomotropones **1** celle de bishomotropones **2**. Il nous est apparu intéressant d'étudier le comportement de ces derniers composés vis-à-vis de l'éthanedithiol pour préciser le rôle joué par la présence d'un second motif cyclopropanique et de vérifier si le réarrangement original observé dans le cas de dérivés thiophénomonohomotroponiques pouvait être étendu aux thiophénobishomotropones.

Nous décrivons dans le présent mémoire les résultats de cette étude et, sur la base des diverses données expérimentales et spectroscopiques, nous discutons le mécanisme rendant compte de la formation du produit de réarrangement obtenu.

[1] Auteur à qui adresser la correspondance.

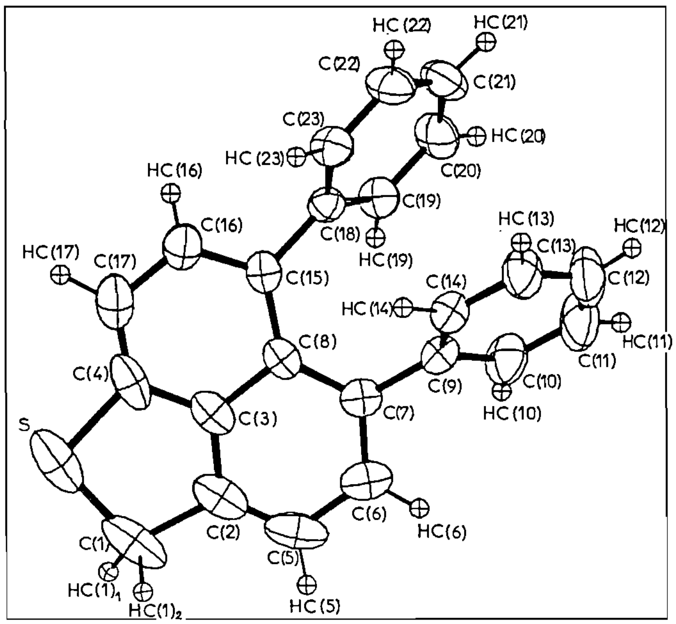

FIG. 1. Vue ORTEP de la structure cristalline de **3**.

Résultats

En opposant la thiophéno[*c*]bishomotropone **2***a* à l'éthanedithiol-1,2 en présence d'acide paratoluènesulfonique dans le toluène à reflux, on accède à un composé **3**. Les données du spectre de masse et l'analyse du spectre de rmn protonique n'apportent pas d'éléments décisifs pour la détermination de la structure. Nous avons alors été conduits à effectuer un examen radiocristallographique de **3**.

La conformation moléculaire est représentée par la fig. 1. Les distances et les angles de la molécule sont consignés dans le tableau 1. Les atomes constituant les trois cycles ortho-

TABLEAU 1. Distances et angles

Liaison	Distance (Å)	Liaisons	Angle (deg)
S—C(1)	1,819(8)	C(1)—S—C(4)	94,9(3)
S—C(4)	1,755(4)	S—C(1)—C(2)	104,8(4)
C(1)—C(2)	1,580(7)	C(1)—C(2)—C(3)	112,7(5)
C(2)—C(3)	1,391(6)	C(1)—C(2)—C(5)	127,1(4)
C(3)—C(4)	1,417(6)	C(3)—C(2)—C(5)	120,2(4)
C(2)—C(5)	1,352(7)	C(2)—C(3)—C(4)	116,2(4)
C(5)—C(6)	1,417(6)	C(2)—C(3)—C(8)	122,9(4)
C(6)—C(7)	1,377(5)	C(4)—C(3)—C(8)	120,8(5)
C(7)—C(8)	1,436(5)	S—C(4)—C(3)	111,3(4)
C(8)—C(3)	1,436(5)	S—C(4)—C(17)	127,0(4)
C(8)—C(15)	1,430(5)	C(3)—C(4)—C(17)	121,7(4)
C(15)—C(16)	1,379(5)	C(2)—C(5)—C(6)	118,8(4)
C(16)—C(17)	1,407(6)	C(5)—C(6)—C(7)	122,8(5)
C(17)—C(4)	1,335(7)	C(6)—C(7)—C(8)	119,4(4)
C(7)—C(9)	1,493(5)	C(6)—C(7)—C(9)	116,6(5)
C(15)—C(18)	1,492(5)	C(8)—C(7)—C(9)	123,7(4)
		C(3)—C(8)—C(7)	115,5(4)
		C(3)—C(8)—C(15)	116,1(4)
		C(7)—C(8)—C(15)	128,4(3)
		C(8)—C(15)—C(16)	119,6(3)
		C(8)—C(15)—C(18)	124,2(4)
		C(16)—C(15)—C(18)	116,1(4)
		C(15)—C(16)—C(17)	123,1(4)
		C(4)—C(17)—C(16)	118,3(4)
Moyenne des liaisons des cycles:		Moyenne des angles des cycles:	
C(9) . . . . . . C(14)	1,382(6)	C(9) . . . . . . C(14)	119,6(5)
C(18) . . . . . . C(23)	1,384(5)	C(18) . . . . . . C(23)	119,6(4)

TABLEAU 2. Plans moyens et angles entre plans

Plan n° 1 défini par S,C(1), C(2), C(3), C(4), C(5), C(6), C(7), C(8), C(15), C(16), C(17)

S(0,01 Å) C(1) (−0,04) C(2) (0,01) C(3) (0,01) C(4) (0,00)
C(5) (0,04) C(6) (0,00) C(7) (−0,07) C(8) (0,01) C(15) (0,06)
C(16) (0,00) C(17) (−0,04) C(9) (−0,26) C(18) (0,28)

équation $-0{,}23591x + 2{,}73996y + 0{,}36460z = 6{,}36001$

Plan n° 2 défini par C(9), C(10), C(11), C(12), C(13), C(14)

C(9) (0,01) C(10) (0,00) C(11) (−0,01) C(12) (0,01)
C(13) (0,00) C(14) (−0,01)

équation $-0{,}57348x + 0{,}72773y + 1{,}40027z = 12{,}31549$

Plan n° 3 défini par C(18), C(19), C(20), C(21), C(22), C(23)

C(18) (−0,01) C(19) (0,01) C(20) (0,00)
C(21) (−0,01) C(22) (0,01) C(23) (0,01)

équation $-1{,}12901x + 0{,}72262y + 1{,}00241z = 10{,}45987$

Angle	plan 1	plan 2	plan 3
plan 1		55,3°	55,8°
plan 2			23,5°

condensés forment un plan; l'écart maximum d'un atome au plan moyen est de 0,07 Å. Dans le cycle à cinq chaînons, les liaisons communes aux deux cycles C(3)—C(4) et C(3)—C(2) sont de 1,417(6) et 1,391(6) Å. La liaison C(1)—C(2) est simple: 1,580(7) Å. Compte tenu de la valeur des écart-types et de l'agitation thermique la différence observée entre les deux liaisons S—C est tout juste significative. Dans les deux cycles à six chaînons orthocondensés la moyenne de la longueur est de 1,398(6) Å. Toutefois, on remarque une pseudosymétrie par rapport à C(3)—C(8): trois liaisons longues autour de C(8), deux liaisons courtes C(4)—C(17) et C(2)—C(5), deux liaisons équivalentes C(6)—C(7) et C(15)—C(16), deux autres très proches C(5)—C(6) et C(16)—C(17). Les atomes C(9) et C(18) des deux groupes phényles s'écartent de part et d'autre du plan moyen moléculaire de 0,27 Å et les liaisons C(15)—C(18) et C(7)—C(9) ne sont pas parallèles mais forment un angle de 16° (voir tableau 2). Ces deux écarts à la géométrie idéale correspondant à une hybridation sp^2 de C(7) et C(15), résultent de l'empêchement stérique entre les deux noyaux phényle. Ces derniers forment un angle de 23,5° et sont inclinés dans le même sens d'un angle de 55° par rapport aux trois cycles orthocondensés.

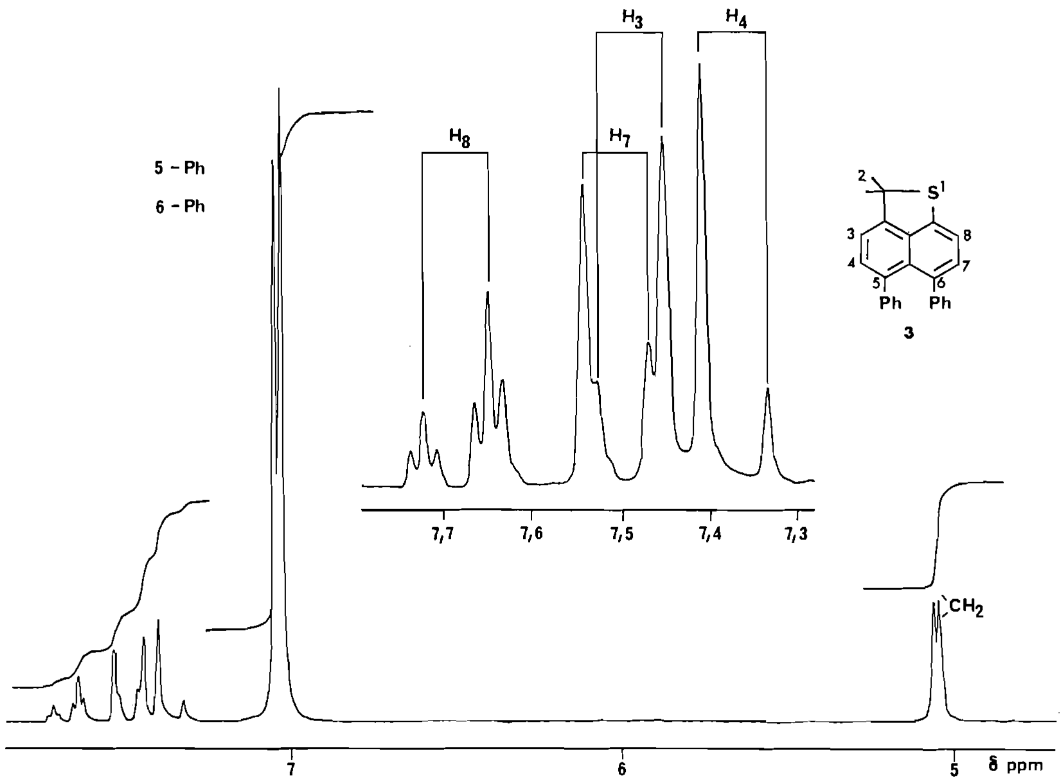

FIG. 2. Spectres rmn [1]H (100 MHz, $(CD_3)_2CO$) du naphto[1,8-*bc*]thiophène **3**.

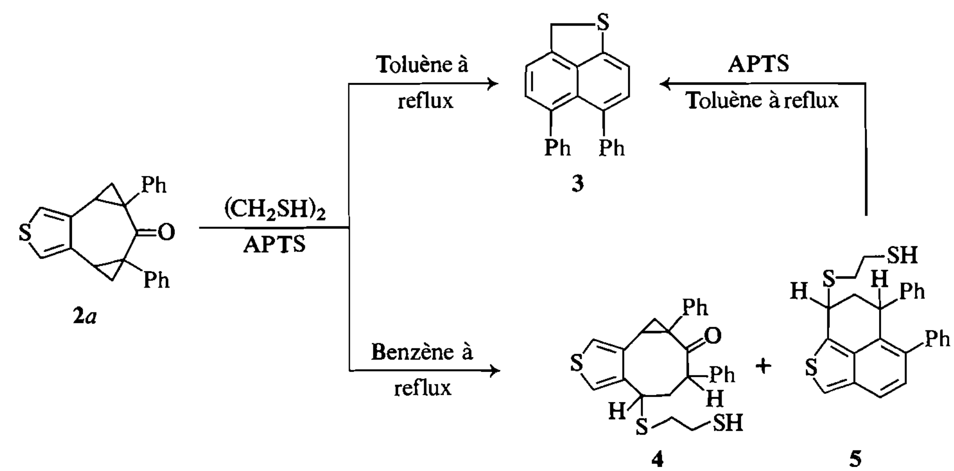

SCHÉMA 1

La structure de **3** étant établie, l'analyse de son spectre de rmn est alors très aisée (voir fig. 2).

Si la structure de ce naphto[1,8-*bc*]thiophène (3) **3** était établie sans ambiguïté, il convenait toutefois d'expliquer sa formation au départ de la thiophéno[*c*]bishomotropone et de proposer un mécanisme réactionnel rendant compte de cette transformation originale.

Étude expérimentale de la transformation des thiophénobishomotropones

Nous avons abordé l'étude du mécanisme conduisant à la formation du naphtothiophène **3** selon trois directions principales: (*i*) en étudiant l'influence des modalités opératoires sur l'évolution de la réaction; (*ii*) en mettant en oeuvre la thiophéno[*b*]bishomotropone **2***b* isomère de **2***a*; (*iii*) en procédant au départ d'analogues deutériés de **2**.

(a) *Influences de la température et du solvant*

Ces deux paramètres semblent jouer un rôle important: si on remplace le toluène par le benzène, on isole un mélange de deux produits **4** et **5** (proportions relatives 84 et 16%) différents du naphtothiophène **3** obtenu dans le toluène à reflux (voir schéma 1). La structure de **4** est déterminée par examen critique des ses données spectroscopiques. En infra-rouge on note la présence d'une bande d'intensité faible à 2570 cm^{-1} caractéristique d'un reste —SH et celle d'une vibration carbonyle à 1700 cm^{-1}. L'augmentation de la fréquence de ce vibrateur carbonyle par rapport à celle du composé de départ traduit la rupture d'un des cycles à trois chaînons, consécutive à l'addition d'une molécule d'éthanedithiol. Le spectre de masse conforte également cette hypothèse (voir partie expérimentale).

L'analyse du spectre de rmn protonique apparaît plus délicate. La partie la plus déblindée du spectre se présente sous la

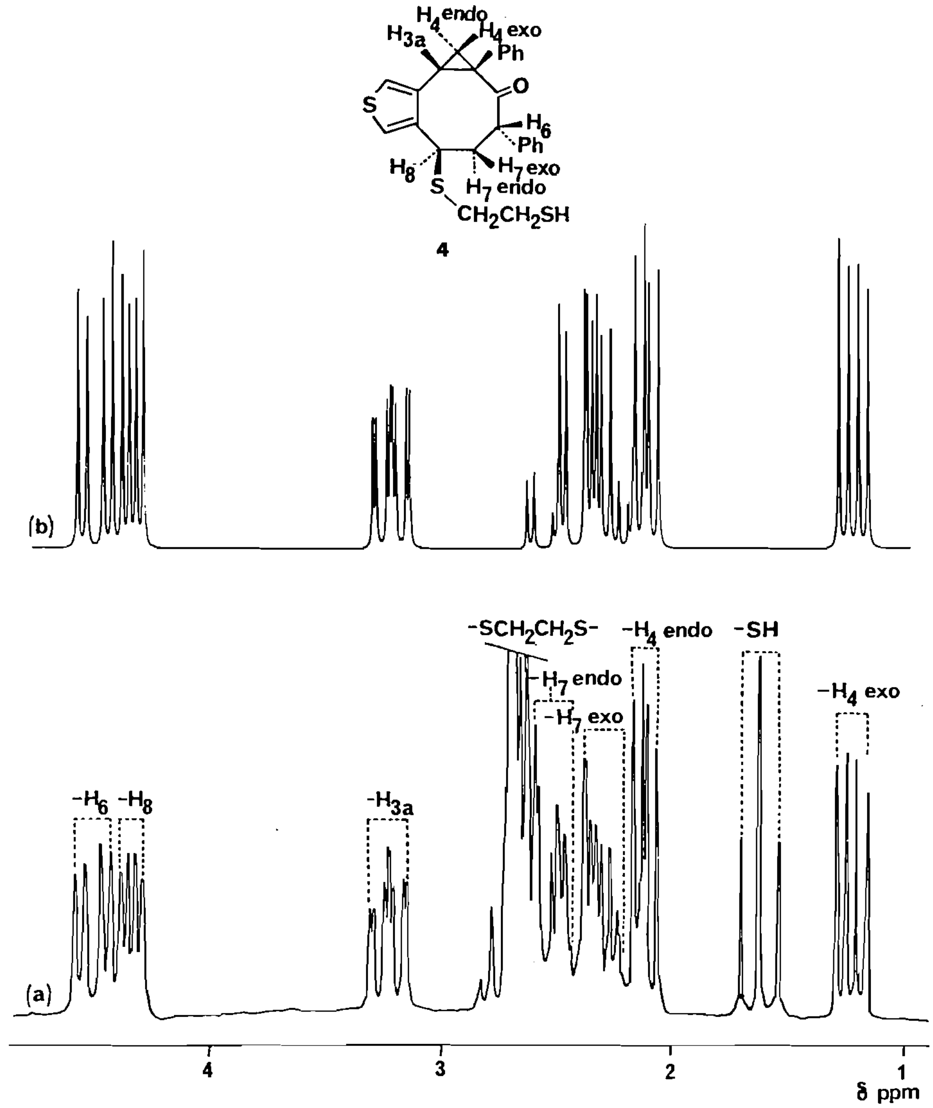

FIG. 3. (a) Spectre rmn ^1H expérimental du composé **4** (100 MHz, $CDCl_3$). (b) Spectre simulé (la partie —SCH_2CH_2SH a été volontairement omise).

forme d'un massif complexe (δ ~ 6,90–7,45 ppm) et correspond aux 12 protons des restes phényle et du noyau thiophénique. Dans le domaine 1,00 à 5,00 ppm (voir fig. 3a) apparaissent également les signaux de 12 protons: un système AMX correspond à un motif cyclopropanique, un massif complexe de 4 protons attribuable au reste —SCH_2CH_2S— et un unique proton —SH. Enfin les signaux relatifs aux quatre protons H_6, H_{7endo}, H_{7exo} et H_8 ont été analysés. Le spectre calculé coincide parfaitement avec le spectre expérimental (4) (voir fig. 3b). Il apparaît donc que **4** est l'adduit de Michael entre la thiophéno[*c*]homotropone et l'éthanedithiol-1,2. Une telle réaction est classique dans la série des cétones α,β-éthyléniques (5); dans notre cas le cycle à trois chaînons peut être assimilé à une double liaison.

Le composé **5** qui apparaît simultanément avec **4** présente certaines analogies spectroscopiques avec ce dernier: on observe une vibration —SH à 2562 cm^{-1} et l'absence de vibration associée à un reste carbonyle. Sur le spectre de masse de **5** le pic moléculaire diffère de 18 par rapport à celui de **4** par perte d'une molécule d'eau et on note la perte d'un reste $(CH_2SH)_2$. Le spectre de rmn (voir fig. 4) permet d'individualiser trois protons aromatiques: H_3 et H_4 couplés en *ortho* et H_2 qui présente un couplage à longue distance (^5J = 1,98 Hz) avec le proton résonant à 3,81 ppm. Pour ce dernier signal on note également deux autres couplages, comparables à ceux observés pour le proton H_8 de **4**. De même le massif à 4,39 ppm est attribuable à un proton —CHPh— (pour **4**, δ H_6 = 4,49 ppm). Pour le composé **5** aucun signal n'apparaît dans le domaine de résonance des protons cyclopropaniques alors que trois massifs (intensités respectives 4, 2 et 1) sont présents sur les spectres de **4** et de **5**. Ces signaux sont respectivement attribuables au motif —SCH_2CH_2S—, au méthylène "intracyclique" et enfin au proton —SH résonant à haut champ.

La structure proposée est celle d'un dihydronaphto[1,8-*bc*]-thiophène dont le squelette n'est pas sans rappeler celui de **3** obtenu dans le toluène à reflux.

Pour préciser l'influence du paramètre thermique sur l'évolution de la réaction nous avons tenté au départ de **4** d'accéder au naphtothiophène **3**. En chauffant **4** au reflux du toluène en présence d'APTS ce composé reste inaltéré, mais en revanche **5** conduit à **3** dans ces conditions de température et d'acidité.

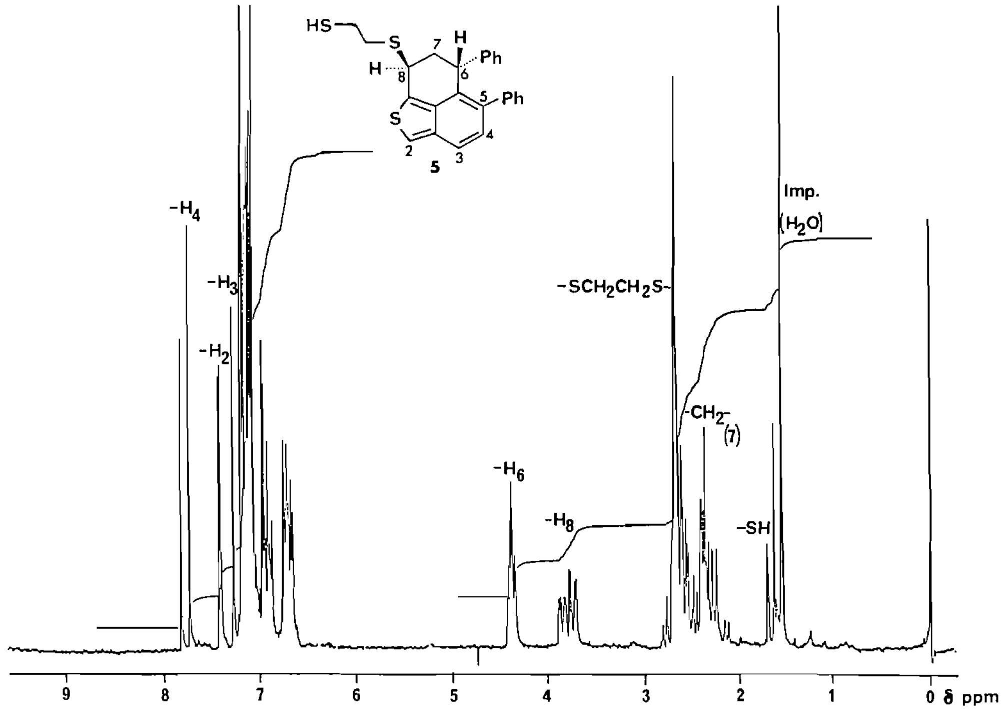

FIG. 4. Spectre rmn ^1H (100 MHz, $CDCl_3$) du composé **5**.

(b) *Synthèses au départ de la thiophéno[*b*]bishomotropone*

Comme nous l'avons indiqué plus haut il était intéressant de vérifier si une variation structurale opérée au niveau du substrat de départ pouvait conduire à des produits de réarrangement différents.

Après chauffage de la thiophéno[*b*]bishomotropone **2***b* isomère de **2***a* dans le toluène à reflux en présence d'APTS on isole le naphto[1,8-*bc*]thiophène **3** et un second produit **6** (proportions relatives: 4 et 96%; voir schéma 2).

L'analyse du spectre de masse de **6** suggère l'incorporation d'une molécule d'éthanedithiol ($M^+ = 418$), confirmée par la présence d'un fragment à 324 $[M - (CH_2SH)_2]^+$. Le spectre infra-rouge ne présente plus la vibration associée au carbonyle et l'absence de vibration —SH laisse supposer l'existence d'un aldéhyde ou d'une cétone protégée sous forme de dithiolanne. Cette hypothèse a été vérifiée en libérant le groupe aldéhyde par traitement de **6** à l'aide d'un sel mercurique (voir schéma 2). Le produit majoritaire **7** obtenu présente une bande intense à 1724 cm^{-1} caractéristique d'un aldéhyde aliphatique. De plus la désulfuration totale de **6** par le nickel de Raney permet d'accéder à **8** présentant en rmn protonique deux groupements éthyle. L'un de ces restes provient de la réduction du motif dithiolanne, l'autre de la chaîne carbonée du cycle thiophénique suggérant la présence d'un cycle benzo[*b*]thiophénique.

L'examen du spectre rmn de **6** permet de préciser la structure de ce composé: dans la partie située à haut champ on distingue 8 protons: un massif complexe de quatre protons (—SCH_2CH_2S—), un multiplet de deux protons (—CH_2—) et deux protons $H_{1'}$ et $H_{3'}$; dans la partie aromatique (voir fig. 5a) l'existence d'un motif α,β-thiophénique (respectivement H_2 et H_3) et d'un couplage orthobenzénique (H_4 et H_5) confirme le squelette benzo[*b*]thiophénique disubstitué.

L'examen attentif du signal à 7,60 ppm (voir fig. 5b) révèle l'existence de deux protons α-thiophéniques différents: le signal le plus intense (85%) est un doublet (J = 5,47 Hz) et correspond au proton H_2 de **6***a*. Sur l'autre signal (15%) apparaît un couplage supplémentaire de 0,53 Hz avec le proton H_6 de l'isomère **6***b*.

La structure de chacun des produits isolés lors des synthèses exposées plus haut étant connue, il convenait de préciser le mécanisme de réarrangement des thiophéno[*c*] et [*b*]bishomotropones; aussi avons-nous mis en oeuvre des analogues deutériés de ces différents substrats.

(c) *Synthèses au départ d'analogues deutériés de* **2**

Au départ de la thiophéno[*c*]bishomotropone D-3b,D-6a (**2***a'*) et en travaillant dans un milieu deutérié (APTS-OD, D_2O) on accède, dans le toluène à reflux, au dérivé **3'** (voir schéma 3). L'examen comparatif des spectres rmn de **3** et **3'** montre que les deux systèmes AB se simplifient en deux singulets élargis (couplage $^3J_{HD}$). On note également que le méthylène benzylique a subi, dans le milieu, une incorporation partielle de deutérium. Les atomes de deutérium initialement présents dans **2***a'* se retrouvent en position 3 et 8 du naphtothiophène **3'**: ce résultat sera mis à profit dans l'établissement du mécanisme de réarrangement.

Si la réaction est conduite dans le toluène en présence d'APTS non deutérié, on constate la perte totale des deux atomes de deutérium et on isole **3** et non **3'**. Cette donnée n'est pas en contradiction avec l'observation précédente si l'échange protonique avec le milieu réactionnel intervient lors d'un stade ultime du réarrangement. Toutefois, lors du chauffage de **3** dans le toluène en présence d'APTS-OD, D_2O, aucune incorporation de deutérium n'est constatée. L'échange H/D ne concerne donc pas le naphtothiophène lors d'un processus réversible.

En procédant au départ des mêmes réactifs on accède, dans le benzène à reflux, au dérivé **4'** analogue de **4**. Sur le spectre de rmn de l'adduit **4'** on note la conservation des deux atomes de deutérium dans les positions indiquées ainsi que l'incorporation partielle de deutérium au niveau du motif

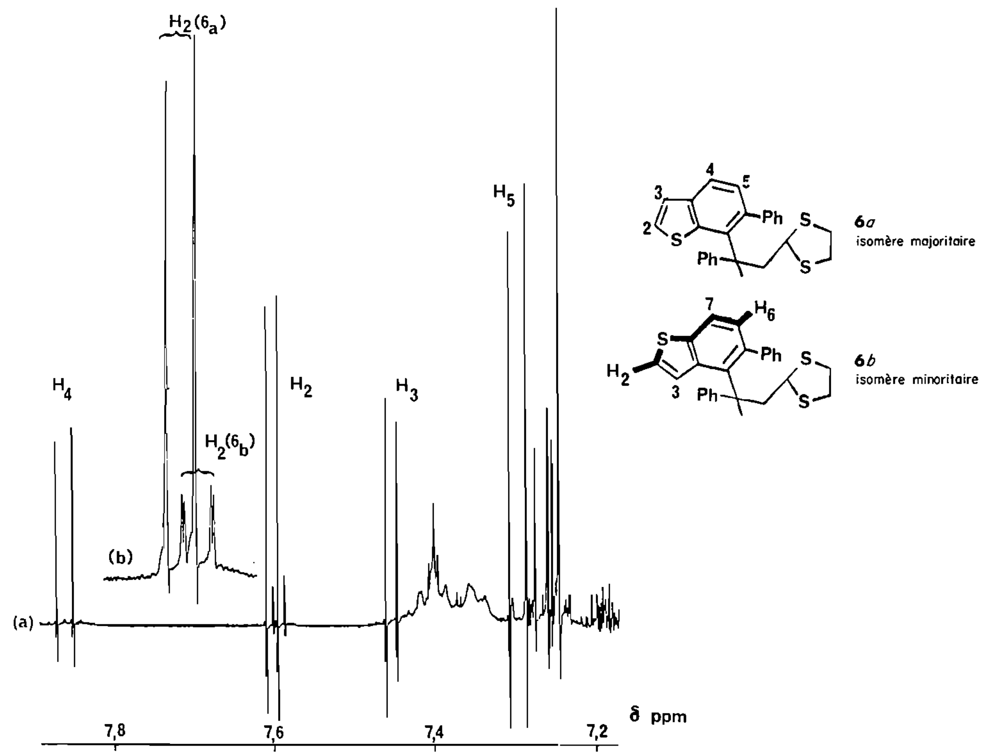

FIG. 5. Spectre rmn ¹H (400 MHz, $(CD_3)_2CO$) des composés **6*a*** et **6*b***.

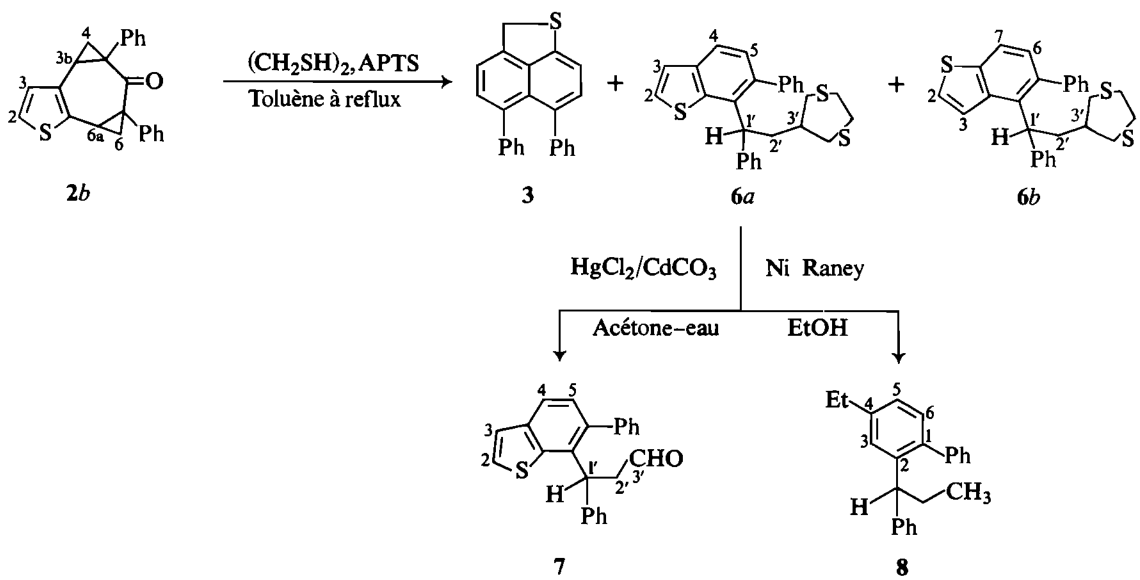

SCHÉMA 2

—CHPh— (voir schéma 3).

Nous avons également mis en oeuvre les composés **2*b*′** et **2*b*″** analogues monodeutériés de la thiophéno[*b*]bishomotropone **2*b*** (voir schéma 4).

Au départ de chacun de ces composés on isole le benzo[*b*]thiophène monodeutérié attendu (l'autre isomère n'apparaît qu'à l'état de traces) mais le naphtothiophène obtenu conjointement ne contient pas de deutéron. Les composés benzothiophéniques sont des intermédiaires monodeutériés, cependant, comme pour l'isomère [*c*], la thiophéno[*b*]bishomotropone subit, à un stade avancé du réarrangement, un échange isotopique D/H avec le milieu acide.

De l'ensemble de ces observations expérimentales, nous pensons pouvoir dégager trois points importants qui vont orienter notre analyse du mécanisme: (*i*) la thiophéno[*c*]bishomotropone livre – dans des conditions voisines – trois produits dont la formation résulte de processus successifs et compétitifs, mettant en jeu un ou deux groupes cyclopropaniques; (*ii*) la thiophéno[*b*]bishomotropone donne des produits ayant pour origine des réactions intéressant les deux sites cyclopropaniques de la molécule; (*iii*) l'analyse des résultats des réactions mettant en oeuvre des composés deutériés apporte des indications précieuses pour la formulation du mécanisme.

Mécanisme du réarrangement

À l'évidence la formation de l'adduit de Michael **4** intervient

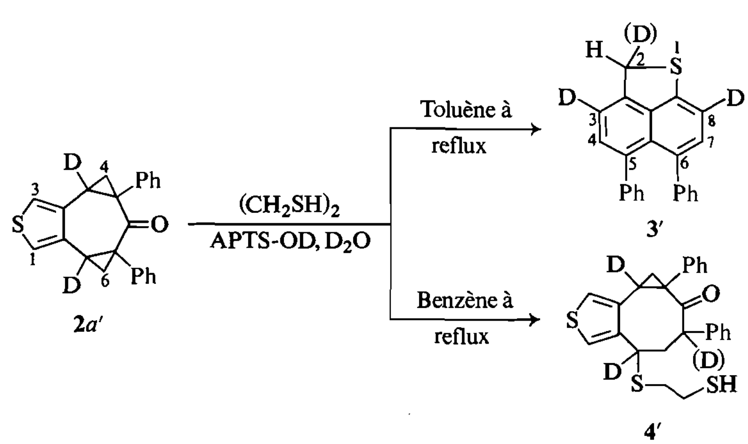

SCHÉMA 3

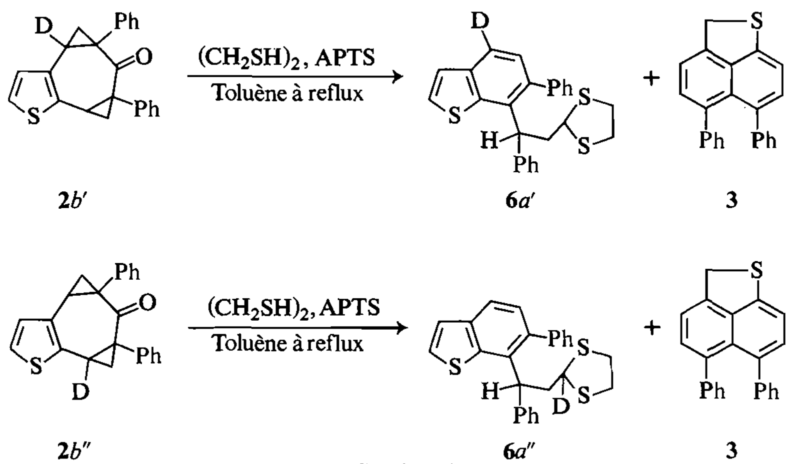

SCHÉMA 4

lors des premières étapes du réarrangement (voir schéma 5): après protonation de la bishomotropone et addition de l'éthane-dithiol, l'intermédiaire (a) subit une prototropie et l'énol protoné (b) s'équilibre en la cétone protonée (c). Après le départ d'un proton on obtient l'adduit **4**.

L'intermédiaire (c) peut évoluer différemment vers (d): l'atome de soufre peut attaquer l'atome de carbone 8 et le transfert du doublet de la liaison C_8—C_{8a} vers C_5 induit le retour du doublet du carbonyle. Cette migration transannulaire d'une liaison σ serait favorisée par l'attaque nucléophile du thiol et le caractère attracteur de l'ion oxonium. Une autre possibilité fait intervenir le cycle thiophénique qui agirait d'abord comme nucléophile. À titre d'exemple nous avons représenté sur le schéma 6 l'évolution de la thiophéno[*c*]bishomotropone dans cette hypothèse. Pour évaluer au départ de (d) le comportement spécifique de chacun des substrats lors des étapes ultérieures nous avons fait figurer les trois isomères sur le schéma 5: l'isomère thiophéno[*c*]bishomotroponique (voie A) se déshydrate avec ouverture simultanée du cycle à trois chaînons pour conduire à un benzo[*c*]thiophène non isolé. La cyclisation de ce dernier livre le naphto[1,8-*bc*]thiophène **3**; l'isomère thiophéno[*b*]bishomotroponique conduit selon la voie B au benzo[*b*]thiophène **6***b* qui se transforme *in situ* presque entièrement en naphto[1,8-*bc*]thiophène **3**; si l'attaque initiale a concerné l'autre motif cyclopropanique, la voie C conduit au benzo[*b*]thiophène **6***a* isomère du précédent qui ne peut se cycliser en naphto[1,8-*bc*]thiophène.

La différence de réactivité observée entre les deux séries isomères concerne essentiellement le passage (c) → (d). Lors de cette étape la rupture au niveau de l'hétérocycle intéresse le sommet β pour la voie A alors que cette rupture concerne le sommet α pour la voie C. La réactivité différente entre les positions α et β thiophéniques est bien connue; elle explique que la thiophéno[*b*]bishomotropone subit une attaque plus aisée sur un des deux sites cyclopropaniques, conduisant préférentiellement à **6***a*: la voie C est privilégiée par rapport à la voie B.

Il reste à préciser pourquoi la transformation conduite en milieu deutérié permet la conservation totale des deutérons, alors que ces derniers sont substitués lors de la dernière étape dans un milieu protique. Ce résultat est la conséquence d'un échange lors de la cyclisation conduisant à **3**. Un tel phénomène a déjà été observé par Cox *et al.* (6) lors de la cyclisation photochimique d'un thiobenzoylnaphtalène.

Conclusion

Le comportement des thiophéno[*c*] et [*b*]bishomotropones vis-à-vis de l'éthanedithiol en milieu acide apparaît très original. Le composé présentant un groupement carbonyle protégé n'apparaît jamais et suivant les conditions opératoires on obtient soit un adduit de Michael, soit un dérivé benzothiophénique, soit un naphtothiophène.

L'analyse du mécanisme de formation de ces dérivés a été rendue possible par la mise en oeuvre de substrats deutériés.

Ce réarrangement non classique fait apparaître – au stade déterminant – un transfert électronique concerté entre un nucléophile doux et un acide dur.

L'analyse comparative des spectres de rmn des produits et de

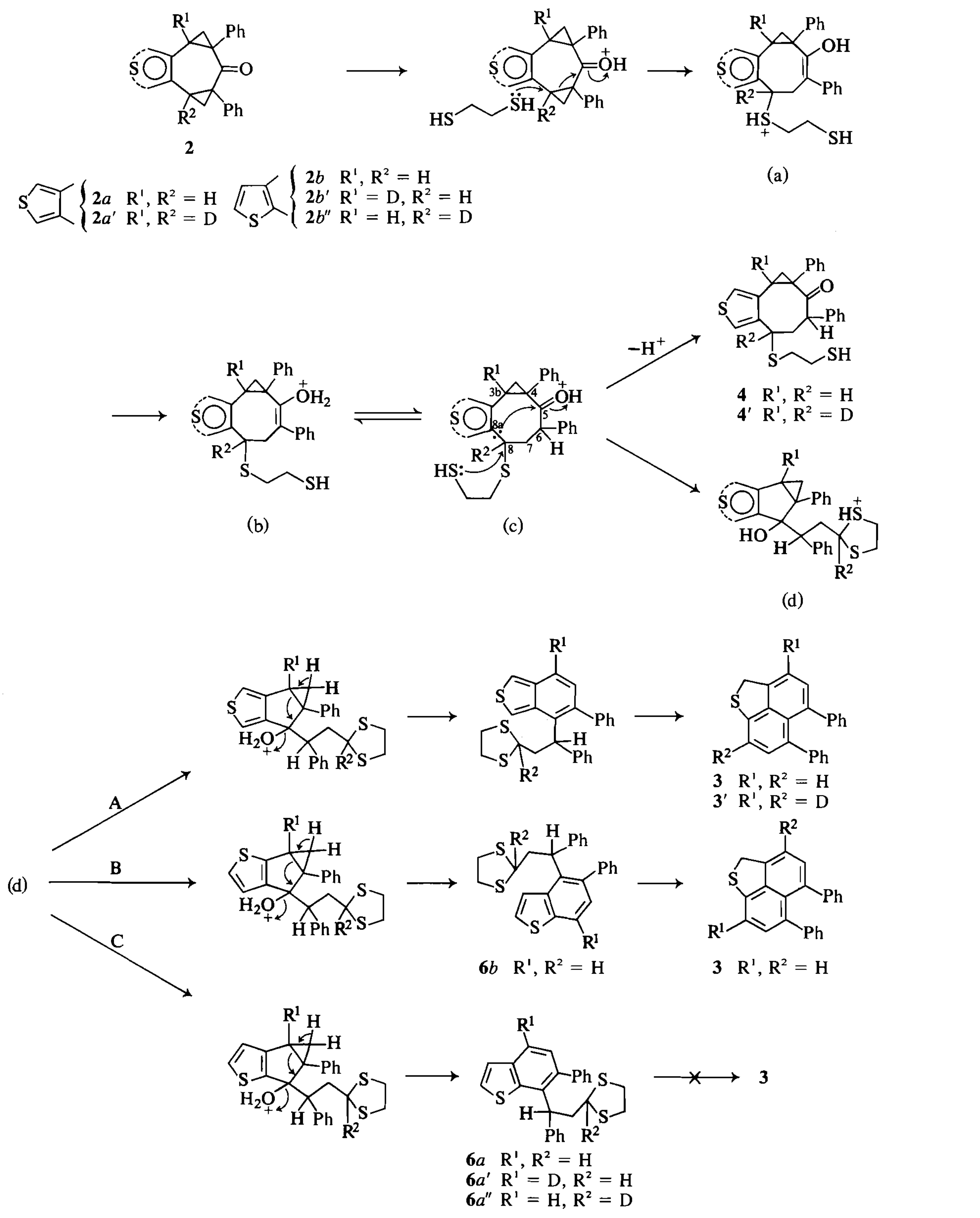

SCHÉMA 5

leurs analogues deutériés s'est révélée très précieuse et a permis de conforter de nombreuses étapes du mécanisme proposé.

Partie expérimentale

Les analyses élémentaires ont été effectuées par le Service Central d'Analyse du C.N.R.S. Les spectres de rmn ^{1}H ont été enregistrés à 100 MHz sur un appareil Jeol FX 100 et à 400 MHz sur un appareil Bruker WM 400. Un échantillon de 5 mg est – sauf indication contraire – dissous dans 0,2 cm^3 de $CDCl_3$. Les déplacements chimiques sont donnés en ppm par rapport à $SiMe_4$ et les constantes de couplage en Hz. Les multiplicités sont indiquées comme suit: s (singulet), d (doublet), t (triplet), q (quadruplet), m (multiplet). Les spectres infrarouge ont été relevés sur un appareil Perkin–Elmer 580 (2 mg de produit en suspension dans 200 mg de KBr). Les spectres de masse ont

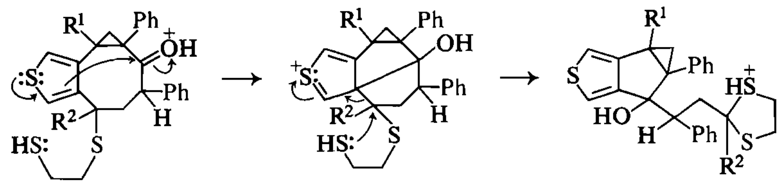

(c) (d)

SCHÉMA 6

été obtenus par impact électronique (30–70 eV) à l'aide d'un appareil Finnigan 3300.

Thiophénotropones deutériées

*Diphényl-5,7 cyclohepta[*c*]thiophénone-6 (D-4, D-8)*

La préparation a été décrite dans un article antérieur (1).

*Diphényl-5,7 cyclohepta[*b*]thiophénone-6 (D-4) et diphényl-5,7 cyclohepta[*b*]thiophénone-6 (D-8)*

On procède comme dans le cas précédent respectivement au départ de diformyl-2,3 thiophène (CDO-3) ou (CDO-2). Rdts = 68 et 79%, F = 138 et 138°C.

Thiophénobishomotropones

trans *Diphényl-4a,5a tétrahydro-4,4a,6,6a 3b*H*,5a*H*-dicyclopropa[3,4:6,7]cyclohepta[1,2-*c*]thiophénone-5 (D-3b, D-6a),* **2**a′

On procède comme pour son analogue non deutérié (2), au départ de la thiophénotropone correspondante. Rdt = 62%, F = 208°C; rmn δ: 1,43 (d, H_{4exo} et H_{6exo}, J = 6,30 Hz), 2,10 (d, H_{4endo} et H_{6endo}, J = 6,30 Hz), 7,10–7,40 (m, 12H, arom.).

trans *Diphényl-4a,5a tétrahydro-4,4a,6,6a 3b*H*,5a*H*-dicyclopropa[3,4:6,7]cyclohepta[1,2-*b*]thiophénone-5,* **2**b

On procède comme pour l'isomère [*c*] (2). Rdt = 74%, F = 190°C; rmn δ: 1,44 (dd, H_{6exo}, J = 4,49 et 8,89 Hz), 1,49 (dd, H_{4exo}, J = 4,57 et 9,08 Hz), 2,06 (dd, H_{6endo}, J = 4,49 et 6,20 Hz), 2,22 (dd, H_{4endo}, J = 4,57 et 6,64 Hz), 2,73 (dd, H_{3b}, J = 6,64 et 9,08 Hz), 2,86 (dd, H_{6a}, J = 6,20 et 8,89 Hz), 6,92 (d, H_3, J = 5,13 Hz), 7,08 (d, H_2, J = 5,13 Hz), ~ 7,30 (m, 2-C_6H_5).

trans *Diphényl-4a,5a tétrahydro-4,4a,6,6a 3b*H*,5a*H*-dicyclopropa[3,4:6,7]cyclohepta[1,2-*b*]thiophénone-5 (D-3b),* **2**b′

On procède comme pour **2**b. Rdt = 59%, F = 189°C; rmn δ: 1,44 (dd, H_{6exo}, J = 5,08 et 8,91 Hz), 1,53 (d, H_{4exo}, J = 5,40 Hz), 2,05 (dd, H_{6endo}, J = 5,08 et 6,29 Hz), 2,22 (d, H_{4endo}, J = 5,40 Hz), 2,86 (dd, H_{6a}, J = 6,29 et 8,91 Hz), 6,91 (d, H_3, J = 5,19 Hz), 7,08 (d, H_2, J = 5,19 Hz), ~ 7,30 (m, 2-C_6H_5).

trans *Diphényl-4a,5a tétrahydro-4,4a,6,6a 3b*H*,5a*H*-dicyclopropa[3,4:6,7]cyclohepta[1,2-*b*]thiophénone-5 (D-6a),* **2**b″

On procède comme précédemment. Rdt = 62%, F = 184°C; rmn δ: 1,44 (d, H_{6exo}, J = 5,09 Hz), 1,48 (dd, H_{4exo}, J = 5,22 et 9,11 Hz), 2,07 (d, H_{6endo}, J = 5,09 Hz), 2,20 (dd, H_{4endo}, J = 5,22 et 6,64 Hz), 2,74 (dd, H_{3b}, J = 6,64 et 9,11 Hz), 6,91 (d, H_3, J = 5,19 Hz), 7,08 (d, H_2, J = 5,19 Hz), ~ 7,30 (m, 2-C_6H_5).

*Réactions de l'éthanedithiol et des thiophéno[*c*]bishomotropones*

*Diphényl-5,6 2*H*-naphto[1,8-*bc*]thiophène,* **3**

On porte à reflux pendant 18 h 1,71 g (5 mmol) de bishomotropone **2**a, 0,95 g (5 mmol) d'acide *p*-toluènesulfonique (APTS) et 1,26 cm^3 (15 mmol) d'éthanedithiol-1,2 dans 50 cm^3 de toluène anhydre. Le milieu se colore progressivement en lie-de-vin. Après refroidissement, on jette le mélange réactionnel sur 100 cm^3 de soude 2 *N*, extrait à l'éther, lave les phases organiques réunies à l'eau jusqu'à neutralité. Après séchage les solvants sont évaporés sous pression réduite et l'huile résiduelle est chromatographiée sur acide silicique (éluant: chlorure de méthylène/hexane 1:1). Les premières fractions d'élution – fortement colorées en rouge-violet – sont réunies et évaporées. Elles abandonnent 0,61 g (Rdt = 38%) du composé **3** par recristallisation dans l'éther diisopropylique; F = 171°C; ir (cm^{-1}): 3052, 3019, 1579, 1501, 1491, 1441, 1412, 1348, 1183, 1173, 1093, 1073, 1031, 896, 836, 820, 794, 758, 701; rmn δ (($(CD_3)_2CO$): 5,09 (d, —CH_2—, J = 1,47 Hz), 6,86 (s, —C_6H_5), 7,08 (s, —C_6H_5), 7,41 (d, H_4, J = 7,51 Hz), 7,50 (d, H_3, J = 7,51 Hz), 7,54 (d, H_7, J = 7,39 Hz), 7,71 (dt, H_8, J = 7,39 et 1,47 Hz); *m/e*: 324 (M), 323 (M − H), 247 (M − C_6H_5), 202 (247 − CHS). *Anal.* calc. pour $C_{23}H_{16}S$: C 85,14, H 4,97, S 9,88; trouvé: C 85,13, H 4,95, S 9,79.

*Diphényl-5,6 2*H*-naphto[1,8-*bc*]thiophène (D-3, D-8),* **3′**

La préparation de **3′** est identique à celle de **3** mais elle est conduite en présence d'APTS-OD préparé en dissolvant 0,19 g (1 mmol) d'APTS dans 50 cm^3 de toluène anhydre et 5 cm^3 d'eau lourde. Après 15 min d'échange à 50°C l'eau est entrainée sous forme d'azéotrope. L'opération d'échange isotopique est renouvelée trois fois. On ajoute ensuite 0,31 g (1 mmol) de la bishomotropone **2**a′ et 1 cm^3 d'éthanedithiol-1,2 (12 mmol). Après traitement, on isole 0,02 g de **3′**. Rdt = 7%, F = 170°C; ir (cm^{-1}): 3050, 3018, 1558, 1492, 1441, 1396, 1348, 1072, 904, 754, 700; rmn δ ($(CD_3)_2CO$): 5,08 (s élargi, —CH_2—), 7,05 (s, —C_6H_5), 7,07 (s, —C_6H_5), 7,41 (s, H_4), 7,54 (s, H_7); *m/e*: 326 (M), 249 (M − C_6H_5).

*Diphényl-4a,6 (éthanedithiolyl)-8 hexahydro-4,4a,5,6,7,8 3b*H*-cyclopropa[3,4]cycloocta[1,2-*c*]thiophénone-5,* **4** *et diphényl-5,6 (éthanedithiolyl)-8 dihydro-6,7 8*H*-naphto[1,8-*bc*]-thiophène,* **5**

Après 12 h de chauffage à reflux de 1,02 g (3 mmol) de **2**a, 0,57 g (3 mmol) d'APTS et de 1,26 cm^3 (15 mmol) d'éthanedithiol dans 30 cm^3 de benzène anhydre, on obtient un mélange de deux composés principaux, séparés par chromatographie sur acide silicique (chlorure de méthylène/hexane 1:2). Les premières fractions d'élution contiennent 0,05 g (Rdt = 4%, F = 90°C) de **5**, les dernières fractions abandonnent 0,28 g (Rdt = 21%, F = 128–134°C) de **4**. *Composé 4*: ir (cm^{-1}): 3096, 3086, 2568, 1702, 1492, 1060, 802, 698; rmn δ: 1,25 (dd, H_{4exo}, J = 4,11 et 8,30 Hz), 1,63 (t, —SH, J = 7,94 Hz), 2,12 (dd, H_{4endo}, J = 4,11 et 5,98 Hz), 2,28 (ddd, H_{7exo}, J = 3,22, 6,51 et 13,72 Hz), 2,48 (ddd, H_{7endo}, J = 2,68, 11,97 et 13,72 Hz), ~2,70 (m, —SCH_2CH_2S—), 3,22 (ddd, H_{3a}, J = 1,46, 5,98 et 8,30 Hz), 4,33 (dd, H_8, J = 2,68 et 6,51 Hz), 4,49 (dd, H_6, J = 3,22 et 11,97 Hz), 6,90–7,45 (m, 12H, arom.); *m/e*: 436 (M), 375 (M − CH_2CH_2SH), 342 (M − $(CH_2SH)_2$). *Anal.* calc. pour $C_{25}H_{24}OS_3$: C 68,76, H 5,54, O 3,66, S 22,03; trouvé: C 68,96, H 5,58, O 4,17, S 21,28. *Composé 5*: ir (cm^{-1}): 3058, 3026, 2562, 1493, 1449, 1439, 824, 778, 763, 700; rmn δ: 1,62 (t, —SH, J = 8,00 Hz), 2,35 (m, CH_2(7)), 2,65 (m, —SCH_2CH_2S—), 3,81 (ddd, H_8, J = 1,98, 4,39 et 6,37 Hz), 4,39 (t, H_6, J = 3,51 Hz), 6,70–7,20 (m, 10H, arom.), 7,29 (d, H_3, J = 8,57 Hz), 7,46 (d, H_2, J = 1,98 Hz), 7,83 (d, H_4, J = 8,57 Hz); *m/e*: 418 (M), 324 (M − $(CH_2SH)_2$), 247 (324 − C_6H_5).

*Diphényl-4a,6 (éthanedithiolyl)-8 hexahydro-4,4a,5,6,7,8 3b*H*-cyclopropa[3,4]cycloocta[1,2-*c*]thiophénone-5 (D-3a, D-6, D8)* **4′**

Après échange isotopique au départ de 0,19 g (1 mmol) d'APTS dans 50 cm^3 de benzène, on ajoute au milieu réactionnel 0,34 g (1 mmol) de **2**a′ et 1 cm^3 (12 mmol) d'éthanedithiol-1,2. Les quantités mises en jeu ne permettent d'isoler que 0,21 g de **4′** analogue deutérié de **4**. Rdt = 48%, F = 136–138°C; ir (cm^{-1}): 2940, 2910, 2560, 2300, 1696, 1498, 1492, 1037, 760, 698; rmn δ: 1,23 (d, H_{4exo}, J = 4,03 Hz), 1,62 (t, —SH, J = 7,69 Hz), 2,11 (d, H_{4endo}, J = 4,03 Hz), 2,25 (d, H_{7exo}, J = 13,79 Hz), 2,46 (d, H_{7endo}, J = 13,79 Hz), ~ 2,70 (m, —SCH_2CH_2S—), 6,90 – 7,45 (m, 12H, arom.). *Anal.* calc. pour $C_{25}H_{21}D_3OS_3$: C 68,32, O 3,64, S 21,84; trouvé: C 68,30, O 4,39, S 21,36.

*Réactions de l'éthanedithiol et des thiophéno[*b*]bishomotropones*

*Phényl-6 (phényl-1' dithiolannyl-3' n-propyl)-7 benzo[*c*]thiophène,* 6*a, phényl-5 (phényl-1' dithiolannyl-3' n-propyl)-4 benzo[*c*]thiophène* 6*b et 2*H*-naphto[1,8-*bc*]thiophène,* 3

Au départ de 1,71 g (5 mmol) de la bishomotropone **2***b*, de 0,95 g (5 mmol) d'APTS et de 2,0 cm^3 (25 mmol) d'éthanedithiol-1,2 dans 60 cm^3 de toluène à reflux pendant 12 h, on isole après traitement 0,02 g du composé **3** précédemment décrit (F = 171°C, Rdt ~2%) et 1,18 g du mélange **6***a* + **6***b* (F = 132°C, Rdt = 56%); ir (cm^{-1}): 3080, 3055, 3023, 1494, 1447, 1438, 820, 746, 720, 700; rmn δ (400 MHz, $(CD_3)_2CO$): 2,75 (m, —CH_2—), ~3,10 (m, —SCH_2CH_2S—), 4,13 (dd, $H_{3'}$, J = 5,74 et 8,42 Hz), 4,84 (dd, $H_{1'}$, J = 6,71 et 8,91 Hz), 7,00 – 7,40 (m, 10H, arom.), 7,30 (d, H_5, J = 8,11 Hz), 7,45 (d, H_3, J = 5,47 Hz), 7,59 (dd, H_2 (**6***b*), J = 0,53 et 5,47 Hz), 7,60 (d, H_2 (**6***a*), J = 5,47 Hz), 7,86 (d, H_4, J = 8,11 Hz); m/e: 418 (M), 324 (M − $(CH_2SH)_2$), 300 (M − $C_4H_8S_2$), 105 ($C_3H_5S_2$). *Anal.* calc. pour **6***a* + **6***b*, $C_{25}H_{22}S_3$: C 71,72, H 5,30, S 22,98; trouvé: C 71,86, H 5,45, S 22,92.

*Phényl-6 (phényl-1' dithiolannyl-3' n-propyl)-7 benzo[*b*]thiophène (D-4),* 6*a'*

On opère comme dans le cas précédent: au départ de 1,71 g (5 mmol) de **2***b'* on isole successivement 0,008 g de **3** (Rdt ~0,5%) et 0,46 g de **6***a'* (F = 132°C, Rdt = 22%); rmn δ: 2,75 (m, —CH_2—), ~3,00 (m, —SCH_2CH_2S—), 4,15 (dd, $H_{3'}$, J = 5,80 et 8,36 Hz), 4,83 (dd, $H_{1'}$, J = 6,74 et 8,70 Hz), 7,0–7,3 (m, 13H, arom.); m/e: 419 (M), 325 (M − $(CH_2SH)_2$), 301 (M − $C_4H_8S_2$), 105 ($C_3H_5S_2$). *Anal.* calc. pour $C_{25}H_{21}DS_3$: C 71,59, S 22,89; trouvé: C 72,02, S 22,82.

*Phényl-6 (phényl-1' dithiolannyl-3' n-propyl)-7 benzo[*b*]thiophène (D-3'),* 6*a''*

De même 1,71 g (5 mmol) de **2***b''* conduisent à 0,025 g de **3** (Rdt ~1,5%) et 1,11 g de **6***a''* (F = 132°C, Rdt = 53%). rmn δ: 2,75 (m, —CH_2—), ~3,00 (m, —SCH_2CH_2S—), 4,84 (dd, $H_{1'}$, J = 6,65 et 8,72 Hz), 7,0 – 7,3 (m, 13H, arom.), 7,75 (d, H_4, J = 8,06 Hz); m/e: 419 (M), 325 (M − $(CH_2SH)_2$), 301 (M − $C_4H_8S_2$), 106 ($C_3H_4DS_2$). *Anal.* calc. pour $C_{25}H_{21}DS_3$: C 71,59, S 22,89; trouvé: C 71,65, S 22,60.

Transformations au départ des composés 6*a et* 6*b*

*Phényl-6 (phényl-1' oxo-3' n-propyl)-7 benzo[*b*]thiophène,* 7

Suivant la procédure de Wolfrom (7), on agite à la température ambiante 0,42 g (1 mmol) du mélange des dithiolannes **6***a* + **6***b*, 8,00 g (30 mmol) de chlorure mercurique dans 60 cm^3 d'acétone et 10 cm^3 d'eau distillée. On ajoute ensuite, en quatre fractions, 8,00 g (46 mmol) de carbonate de cadmium toutes les deux heures. Après traitement le résidu obtenu est chromatographié sur acide silicique (chlorure de méthylène/hexane 1:1). La transformation n'est pas totale, elle permet d'isoler 0,03 g de l'aldéhyde majoritaire **7** (F = 133°C, Rdt = 10%); ir (cm^{-1}): 3094, 3054, 1724, 1450, 1087, 752, 720, 698; rmn δ: 3,18 (ddd, $H_{2'a}$, J = 1,96, 7,30 et 16,80 Hz), 3,48 (ddd, $H_{2'b}$, J = 2,42, 8,07 et 16,80 Hz), 5,24 (dd, $H_{1'}$, J = 7,30 et 8,07 Hz), 7,0 – 7,3 (m, 13H, arom.), 7,75 (d, H_4, J = 8,05 Hz), 9,55 (dd, —CHO, J = 1,96 et 2,42 Hz); m/e: 342 (M), 324 (M − H_2O), 298 (M − C_2H_4O). *Anal.* calc. pour $C_{23}H_{18}OS$: C 80,67, H 5,30, O 4,67, S 9,36; trouvé: C 81,17, H 5,18, O 5,08, S 8,81.

Phényl-1 éthyl-4 (phényl-1' n-propyl)-2 benzène, 8

On prépare le nickel de Raney au départ de 8 g d'alliage et de 30 cm^3 de lessive de soude à 30%. On agite magnétiquement 0,35 g (0,83 mmol) du mélange des dithiolannes **6***a* + **6***b* en présence du catalyseur, dans 40 cm^3 d'éthanol. Après 16 h de reflux on élimine le nickel et on évapore le solvant. Après chromatographie sur acide silicique (chlorure de méthylène/hexane 1:1), on isole un liquide (R_f ~ 0,3), Rdt = 80%; ir (cm^{-1}): 3058, 3025, 2963, 2931, 2872, 1600, 1494, 1482, 1451, 1009, 830, 763, 700; rmn δ: 0,70 (t, $CH_3(3')$, J = 7,40 Hz), 1,19 (t, $CH_3(2'')$, J = 7,60 Hz), 1,92 (quintuplet, $CH_2(2')$, J = 7,40 Hz), 2,60 (q, $CH_2(1'')$, J = 7,60 Hz), 3,86 (t, $CH(1')$, J = 7,40 Hz), 6,8 – 7,2 (m, 13H, arom.); m/e: 300 (M), 271 (M − C_2H_5), 193 (271 − C_6H_6). *Anal.* calc. pour $C_{23}H_{24}$: C 91,95, H 8,05; trouvé: C 90,83, H 8,02.

TABLEAU 3. Coordonnées fractionnaires (×10^4) et agitation thermique équivalente

Atome	x	y	z	B_{eq}
S	1003(1)	1099(2)	5744(1)	6,74(5)
C(1)	1647(7)	1334(8)	4834(5)	6,1(2)
C(2)	3060(4)	1407(4)	5343(4)	4,4(1)
C(3)	3377(4)	1214(4)	6285(3)	3,5(1)
C(4)	2406(4)	1021(5)	6628(4)	4,4(1)
C(5)	3926(6)	1628(5)	4959(4)	4,9(2)
C(6)	5157(5)	1566(5)	5524(3)	4,1(1)
C(7)	5511(4)	1304(4)	6451(3)	3,1(1)
C(8)	4610(3)	1190(4)	6890(3)	2,8(1)
C(9)	6829(4)	1050(4)	6928(3)	3,2(1)
C(10)	7693(5)	2014(5)	6877(4)	4,7(2)
C(11)	8913(5)	1745(7)	7302(5)	6,1(2)
C(12)	9284(5)	548(7)	7785(5)	6,2(2)
C(13)	8446(4)	−412(6)	7829(4)	4,7(2)
C(14)	7230(4)	−173(4)	7397(3)	3,4(1)
C(15)	4783(3)	1029(4)	7845(3)	2,9(1)
C(16)	3797(4)	797(5)	8124(4)	4,0(1)
C(17)	2598(4)	774(6)	7516(4)	4,8(2)
C(18)	5978(4)	1156(4)	8589(3)	2,8(1)
C(19)	6691(4)	2334(4)	8665(3)	3,3(1)
C(20)	7801(4)	2420(5)	9353(4)	4,4(2)
C(21)	8217(5)	1363(6)	9970(3)	4,7(2)
C(22)	7500(5)	214(5)	9918(3)	4,5(1)
C(23)	6387(4)	113(5)	9231(3)	3,6(1)

Paramètres cristallins et groupe spatial de 3

$C_{23}H_{16}S$ m = 324

Monoclinique, a = 11,711(4), b = 9,707(6), c = 15,452(9) Å, β = 109,41(4)°, V = 1655,6 Å^3, Z = 4, D_c = 1,30, $F(000)$ = 680 e^-, CuK_α (λ = 1,54051 Å), groupe d'espace $P2_1/c$. Un cristal de dimensions 0,2 × 0,1 × 0,2 mm a été utilisé pour cette analyse. Les mesures ont été effectuées sur un diffractomètre automatique Nonius CAD4F avec un contrôle de dérive réalisé sur trois taches mesurées toutes les cent mesures. Les intensités de 3159 réflexions (1 < θ < 60°) ont été enregistrées selon la technique de balayage θ/2θ et 2118 d'entre elles ont été utilisées ($I > 2\sigma(I)$). La structure a été résolue par la méthode de détermination automatique des phases à l'aide du programme MULTAN (8). Elle a été affinée par une méthode de moindres carrés avec matrice complète (SHELX) (9). Les valeurs des facteurs de diffusion atomique sont celles de "International Tables for X-ray Crystallography". Les corrections d'extinction n'ont pas été effectuées et l'absorption a été négligée compte tenu de la taille du cristal (coefficient linéaire μ = 13 cm^{-1}). Dans l'affinement par moindres carrés la pondération w est maintenue égale à 1. La densité électronique différence observée sur la carte finale est de 0,45 e/Å^3. Les coordonnées des atomes d'hydrogène ont été déterminées à partir de section différence puis affinées avec un facteur d'agitation thermique isotrope bloqué égal à celui du carbone auquel il est attaché. Les valeurs des différentes coordonnées fractionnaires et le paramètre d'agitation thermique équivalent sont donnés dans le Tableau 3. Le facteur de reliabilité sans pondération est $R(F)$ = 0,059. Les amplitudes des facteurs de structure, les coordonnées fractionnaires des atomes d'hydrogène et les facteurs d'agitation thermique anisotropes des atomes lourds sont disponibles.[2]

1. B. HANQUET, Y. DUSAUSOY et R. GUILARD. J. Chem. Soc. Perkin Trans. 1. Sous presse.
2. B. HANQUET, R. GUILARD et P. FOURNARI. Bull. Soc. Chim. Fr. 571 (1977).

[2] Ces données ont été déposées et peuvent être obtenues à un prix nominal, en s'adressant au Dépôt de données non publiées, ICIST, Conseil national de recherches du Canada, Ottawa, Ont., Canada K1A 0S2.

3. (*a*) P. FRIEDLANDER et N. WOROSHZOW. Justus Liebigs Ann. Chem. 1 (1912); (*b*) L. F. FIESER et V. DESREUX. J. Am. Chem. Soc. **60**, 2255 (1938); (*c*) D. G. HAWTHORNE et Q. N. PORTER. Aust. J. Chem. **19**, 1909 (1966); (*d*) U. FOLLI, D. IAROSSI et F. TADDEI. J. Chem. Soc. Perkin Trans. 2, 933 (1974).
4. PANIC. Parameter Adjustment in NMR by iterative calculation. Programme Bruker Version 820601.2.
5. B. H. NICOLET. J. Am. Chem. Soc. **53**, 3066 (1931).
6. A. COX, D. R. KEMP, R. LAPOUYADE, P. DE MAYO, J. JOUSSOT-DUBIEN et R. BONNEAU. Can. J. Chem. **53**, 2386 (1975).
7. M. L. WOLFROM. J. Am. Chem. Soc. **51**, 2188 (1929).
8. P. MAIN, S. E. HULL, L. LESSINGER, G. GERMAIN, J. P. LECLERCQ et M. M. WOOLFSON. MULTAN 78. A system of computer programs for the automatic solution of crystal structures from X-ray diffraction data. Universités de York et de Louvain.
9. G. M. SHELDRICK. SHELX 76. A program for crystal structure determination. Université de Cambridge.

Towards a complete account of diastereotopic hydrogen isotope exchange of carbon acids. III. Base-catalyzed exchange of sulfoxides. Evidence for exchange by inversion

NICK HENRY WERSTIUK AND SUJIT BANERJEE[1]
Department of Chemistry, McMaster University, Hamilton, Ont., Canada L8S 4M1

Received July 16, 1984

NICK HENRY WERSTIUK and SUJIT BANERJEE. Can. J. Chem. **63**, 2100 (1985).

The rate constants for deuteroxide and hydroxide catalyzed H → D and D → H exchange of benzodihydrothiophene oxide (**1**a) and several of its deuterated analogs **1**b, **1**c, and **1**d at 30.00 ± 0.05°C are reported along with the rate constants for D → H exchange of deuterated benzyl methyl sulfoxides **2**b and **2**c. Application of the steady-state assumption to schemes involving equilibrating pyramidal anions yield equations which are used to fit experimentally determined $(k_f/k_s)^{H\rightarrow D}$ and $(k_f/k_s)^{D\rightarrow H}$ ratios. The analysis supports our view that exchange of the diastereotopic protons (deuterons) occurs by inversion. The inversion component contributes significantly to exchange of the "slow" proton (deuteron) of a diastereotopic pair and this accounts for the observation that $(k_f/k_s)^{D\rightarrow H} < (k_f/k_s)^{H\rightarrow D}$. This study establishes an upper limit of 6 kcal for the barrier to inversion of the carbanions derivable from **1** and **2**, if pyramidal anions are formed.

NICK HENRY WERSTIUK et SUJIT BANERJEE. Can. J. Chem. **63**, 2100 (1985).

Opérant à 30,00 ± 0,05°C et en présence de deutéroxyde et d'hydroxyde comme catalyseurs, on a mesuré les constantes de vitesse des réactions d'échange H → D et D → H, de l'oxyde de benzodihydrothiophène et de plusieurs de ses analogues deutérés (**1**b, **1**c et **1**d) ainsi que les constantes de vitesse des réactions d'échange D → H des benzylméthylesulfoxydes deutérés **2**b et **2**c. Si on applique l'hypothèse de l'état stationnaire aux processus impliquant un équilibre des anions pyramidaux, on obtient des équations que l'on peut utiliser pour établir une corrélation avec les rapports $(k_f/k_s)^{H\rightarrow D}$ et $(k_f/k_s)^{D\rightarrow H}$ obtenus expérimentalement. L'analyse est en accord avec notre hypothèse selon laquelle l'échange des protons (deutérons) diastéréotopes se fait par inversion. La composante de l'inversion contribue d'une façon importante à l'échange du proton (deutéron) "lent" d'une paire diastéréotope et ceci tient compte du fait que $(k_f/k_s)^{D\rightarrow H} < (k_f/k_s)^{H\rightarrow D}$. S'il se forme des anions pyramidaux, cette étude a permis d'établir à 6 kcal la limite supérieure pour la barrière d'inversion des carbanions provenant des composés **1** et **2**.

[Traduit par le journal]

Introduction

The stereochemistry of base-catalyzed hydrogen isotope exchange of carbon acids other than ketones has commanded considerable interest over the past two decades, and there have been documented numerous studies of the rates of "fast" and "slow" exchange of diastereotopic protons of sulfoxides (1−19, 33), sulfones (20−28), sulfonium salts (29−34), nitrosoamines (35−37), and other carbon acids (38, 39). Researchers were primarily interested in establishing the nature of the intermediate carbanions − planar or rapidly equilibrating − and the factors which control their stability.

By studying H → D and D → H exchange of bicyclo[2.2.1]-heptan-2-one we established that exchange of diastereotopic protons (deuterons) is quite complex − exchange of the "slow" proton (deuteron) by inversion is very important and is manifest in a $(k_f/k_s)^{D\rightarrow H}$ ratio which is considerably smaller than the $(k_f/k_s)^{H\rightarrow D}$ ratio (40). We assumed that a common enolate was generated by abstraction of a fast (*exo*) proton or slow (*endo*) proton and developed equations which related the observed rate ratios, $(k_f/k_s)^{H\rightarrow D}$ and $(k_f/k_s)^{D\rightarrow H}$, to the intrinsic selectivity, the primary and secondary kinetic isotope effects (KIEs) for deprotonation and protonation, and the solvent isotope effects (SIEs) (41).

In this paper we deal with more complex exchange schemes which include pyramidal diastereotopic carbanions as intermediates. We report the rate constants for H→D and D→H exchange of benzodihydrothiophene oxide (**1**a) and several of its deuterated analogs **1**b, **1**c, and **1**d, the rate constants for D → H exchange of benzyl methyl sulfoxide-d_2, and consider exchange data for labelled benzyl methyl sulfoxides published

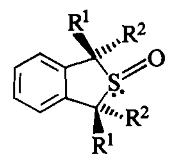

1

a $R^1 = R^2 = H$
b $R^1 = R^2 = D$
c $R^1 = D$, $R^2 = H$
d $R^1 = H$, $R^2 = D$

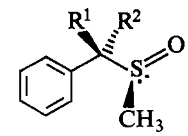

2

a $R^1 = R^2 = H$
b $R^1 = R^2 = D$
c $R^1 = H$, $R^2 = D$

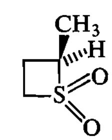

3

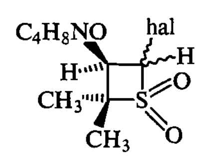

4

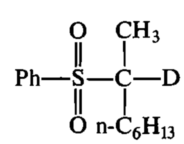

5

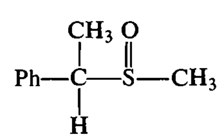

6

by Fraser and Ng (18). It is clear, based on our analysis, that exchange of the slow proton of sulfoxides also occurs by inversion to a considerable extent.[2] We place an upper limit

[1]Present address: Safety and Environmental Protection Division, Brookhaven National Laboratory, Upton, New York 11973.

[2]For the purposes of simplicity our treatment ignores the fact that exchange of the fast proton must also occur by inversion to a very minor extent. This relates to $k_f^{H\rightarrow D}$ and $k_f^{D\rightarrow H}$ used in subsequent derivations. Also, when $k_f \gg k_s$, $k_{f_{obs}}^{H\rightarrow D} \simeq k_1 V_D$.

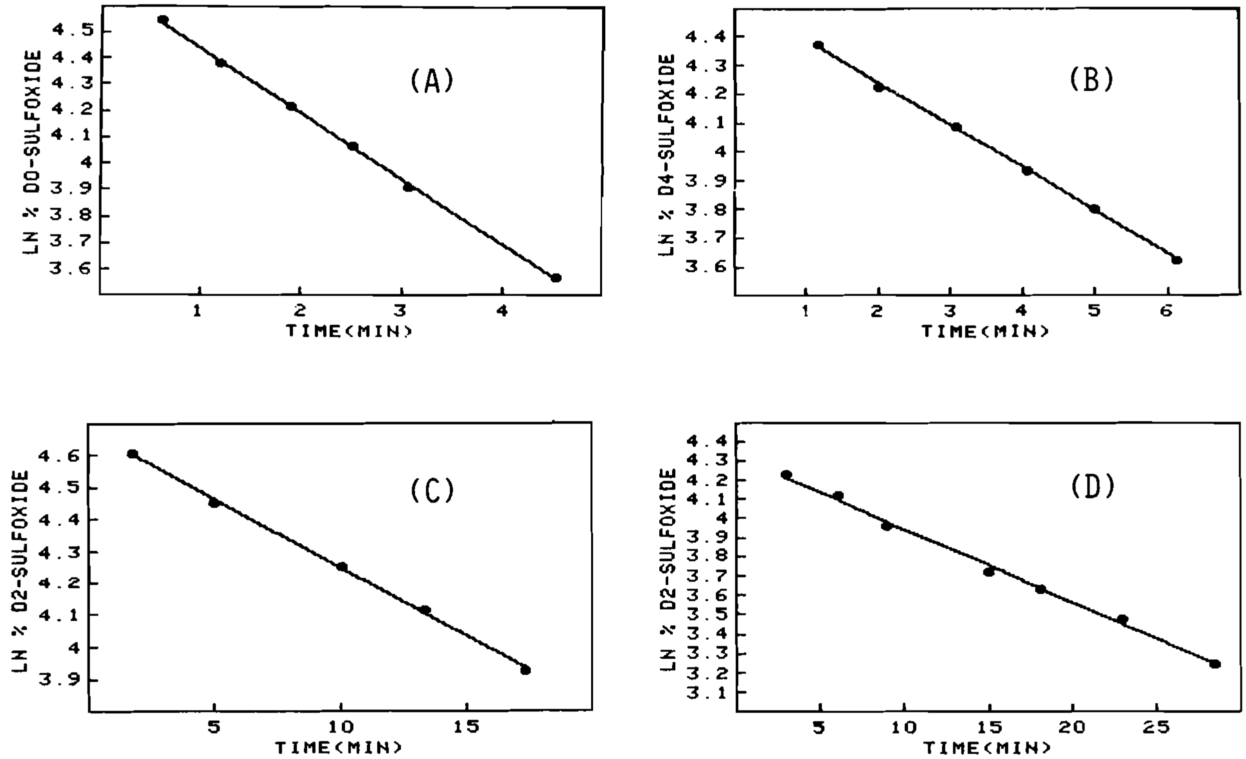

FIG. 1. (A) Plot of ln % d_0-sulfoxide versus time for exchange of **1***a* in 0.0064 *M* NaOD−D_2O at 30.00 ± 0.05°C. (B) Plot of ln % d_4-sulfoxide versus time for exchange of **1***b* in 0.0233 *M* NaOH−H_2O at 30.00 ± 0.05°C. (C) Plot of ln % d_2-sulfoxide versus time for exchange of **1***a* in 0.0064 *M* NaOD−D_2O at 30.00 ± 0.05°C after a 4-min interval. (D) Plot of ln % d_2-sulfoxide versus time for exchange of **1***b* in 0.0233 *M* NaOH−H_2O at 30.00 ± 0.05°C after a 40-min interval.

TABLE 1. Second-order rate constants for hydroxide (deuteroxide)-catalyzed hydrogen isotope exchange of benzodihydrothiophene oxide at 30.00 ± 0.05°C

Exchange[a]	k (M^{-1} min^{-1})[b] per H(D)	k_f/k_s
trans H→D (**1***a*)[c]	19.54±0.57	59.2±3.5
cis H→D (**1***d*)[d]	0.33±0.01	
trans D→H (**1***b*)[e]	2.94±0.01	17.3±2.3
cis D→H (**1***c*)[f]	0.17±0.01	

[a]Exchange *cis* and *trans* to the sulfoxide oxygen.
[b]Errors given are twice the standard deviation.
[c][Base] = 0.0064 *M*; average of two determinations.
[d][Base] = 0.0064 *M*; average of two determinations.
[e][Base] = 0.0233 *M*; average of three determinations.
[f][Base] = 0.0233 *M*; average of two determinations.

on the barrier to inversion of diastereotopic anions if they are generated from **1** or **2**. Our analysis, however, points to involvement of a single intermediate in the exchange of **1** and **2**.

Results

The kinetics of H → D and D → H exchange of benzodihydrothiophene oxide (**1***a*) and its deuterated analogs **1***b*, **1***c*, and **1***d* were studied in NaOD−D_2O and NaOH−H_2O solutions, respectively, at 30.00 ± 0.05°C. D → H exchange studies of benzyl methyl sulfoxide-d_2 and benzyl methyl sulfoxide-d_1 were also undertaken. The sulfoxides were dissolved in the appropriate base solution; aliquots were withdrawn at suitable intervals, quenched by a buffer, and extracted with ether. Deuterium analyses were carried out mass spectrometrically at low voltage and the rate data were uncorrected for dilution due to exchange (42). The results for **1***a*, **1***b*, **1***c*, and **1***d* are given in Table 1 along with the $(k_f/k_s)^{H\to D}$ and $(k_f/k_s)^{D\to H}$ ratios, which are 59.2 ± 3.5 and 17.3 ± 2.3, respectively. Figures 1(A) and 1(B) show typical computer-generated plots, including the linear-least-square lines, for *trans* H → D exchange of **1***a* and D → H exchange of **1***b*. Figures 1(C) and 1(D) show the plots for *cis* H → D and D → H exchange of **1***c* and **1***d*, respectively. Our value of 59.2 ± 3.5 for $(k_f/k_s)^{H\to D}$ compares favourably with the value of 67 at 5°C reported by King and du Manoir, who established that the

TABLE 2. Second-order rate constants for hydroxide-catalyzed D → H exchange of deuterated benzyl methyl sulfoxides at 30.00 ± 0.05°C

Substrate	k (M^{-1} min^{-1}) × 10^2[a,b]	$(k_f/k_s)^{D\to H}$
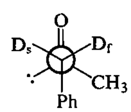 **2***b*	4.73±0.44[c]	10.8±1.3
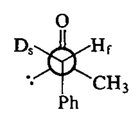 **2***c*	0.437±0.011[d]	

[a]Exchanges were carried out in 0.68 *M* NaOH−H_2O.
[b]Errors are expressed as twice the standard deviation.
[c]Average of two determinations.
[d]Single determination.

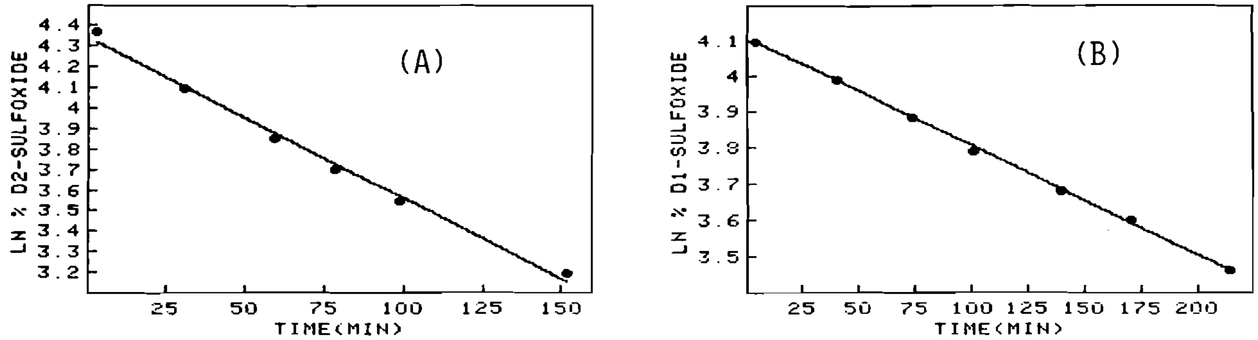

FIG. 2. (A) Plot of ln % d_2-sulfoxide versus time for exchange of **2*a*** in 0.68 *M* NaOH−H_2O at 30.00 ± 0.05°C. (B) Plot of ln % d_1-sulfoxide versus time for exchange of **2*b*** in 0.68 *M* NaOH−H_2O at 30.00 ± 0.05°C after a 100-min interval.

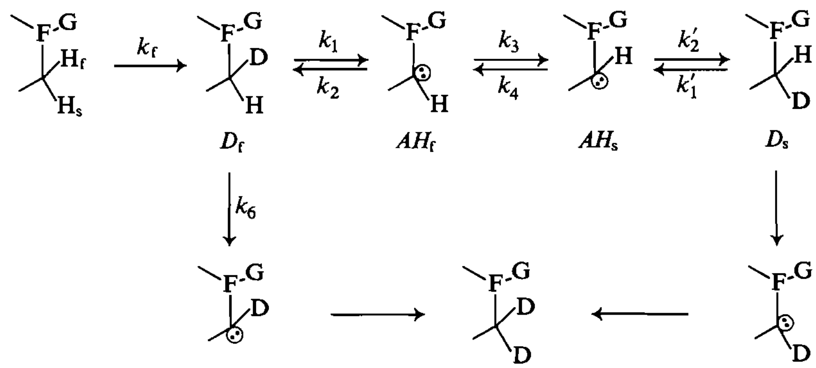

SCHEME 1

hydrogens *trans* to the oxygen of **1*a*** exchange faster than the *cis* hydrogens (15). Table 2 gives the data for exchange of **2*b*** and **2*c*** and $(k_f/k_s)^{D\to H}$ that is 10.8 ± 1.3. Figures 2(A) and 2(B) are typical computer-generated plots for exchange of **2*b*** and **2*c***, respectively. In **2** it is the pro-*R* hydrogen of *S* that exchanges faster than the pro-*S* hydrogen (7). The $(k_f/k_s)^{D\to H}$ ratios determined by ourselves and Fraser and Ng (9.9 ± 0.03) (18) compare very favourably.

Discussion and conclusions

Derivations of equations for H−D exchange

If Scheme 1 (F-G = functional group) is considered for H → D exchange of a carbon acid involving diastereotopic pyramidal anions as intermediates, then a steady-state treatment using AH_f, AH_s, and D_s as steady-state intermediates yields the expression given in eq. [1] for $k_s^{H\to D}$.[3] Rewriting eq. [1] with C given by eq. [2] yields eq. [3].

$$[1]\quad k_{s_{obs}}^{H\to S} \simeq k_6 + k_1\left\{1 - k_2\left[\frac{k_5(k_2' + k_4) + k_1'k_4}{k_2k_4(k_1' + k_5) + k_2'k_5(k_2 + k_3)}\right]\right\}$$

$$[2]\quad C = k_2'k_5 + k_4k_5 + k_1'k_4$$

$$[3]\quad k_{s_{obs}}^{H\to D} \simeq k_6 + k_1\left[1 - \frac{C}{C + \frac{k_3}{k_2}(k_2'k_5)}\right]$$

When k_3/k_2 is small − the barrier to inversion of AH_f is high − $k_{s_{obs}}^{H\to D} \simeq k_6$. However, if the barrier to inversion is low and k_3 is comparable to or larger than k_2, then I, given by eq. [4], corresponds basically to an inversion component of slow proton (deuteron) exchange and makes a substantial contribution to $k_{s_{obs}}^{H\to D}$ with the result that $k_{s_{obs}}^{H\to D} > k_6$. Clearly, under

$$[4]\quad I = k_1\left[1 - \frac{C}{C + \frac{k_3}{k_2}(k_2'k_5)}\right]$$

these circumstances, $(k_f/k_s)_{obs}^{H\to D}$ does not provide an accurate measure of the intrinsic selectivity. If S_D is the intrinsic selectivity in deuterated medium, V_D and L_D are the primary KIEs for "fast" and "slow" deprotonations, V_D' and L_D' are the primary KIEs for protonation, and v_D and l_D are the secondary KIEs, then the following relationships obtain:

$$S_D \simeq k_4k_2V_D'/k_3k_2'L_D' \simeq k_1V_Dk_1'L_D \simeq k_5v_D/k_6l_D,\qquad k_5 \simeq k_1V_D/v_D$$

If two terms a_D and b_D defined as $a_D = k_3/k_2V_D'$ and $b_D = k_4/k_2'L_D'$ are used, then $b_D = a_DS_D$. Substitution of the appropriate terms into eq. [1], and simplification, yields eq. [5].

$$[5]\quad k_{s_{obs}}^{H\to D} \simeq k_6 + k_1\left[\frac{a_DS_DL_DV_D'}{S_D(b_DL_DL_D' + a_DV_D'L_D + L_D) + b_Dv_DL_D'}\right]$$

Since $k_6 \simeq k_5v_D/S_Dl_D \simeq k_1V_D/S_Dl_D$ and $k_f^{H\to D} \simeq k_1V_D$, eq. [5] yields eq. [6][2] that can be rewritten as eq. [7] since $b_D = a_DS_D$.

$$[6]\quad k_{s_{obs}}^{H\to D} \simeq k_{f_{obs}}^{H\to D}\left\{\frac{1}{S_Dl_D} + \frac{V_D'}{V_D}\left[\frac{a_DS_DL_D}{S_D(b_DL_DL_D' + a_DV_D'L_D + L_D + b_Dv_DL_D'}\right]\right\}$$

[3]As discussed in our preceding paper (41), it is likely that more complex alternatives, perhaps more quantitative analyses of the exchange of diastereotopic protons (deuterons, tritons), are possible. However, in our view, our analysis is a viable approach when $k_f \gg k_s$ and D_s and H_s can be considered as steady-state intermediates.

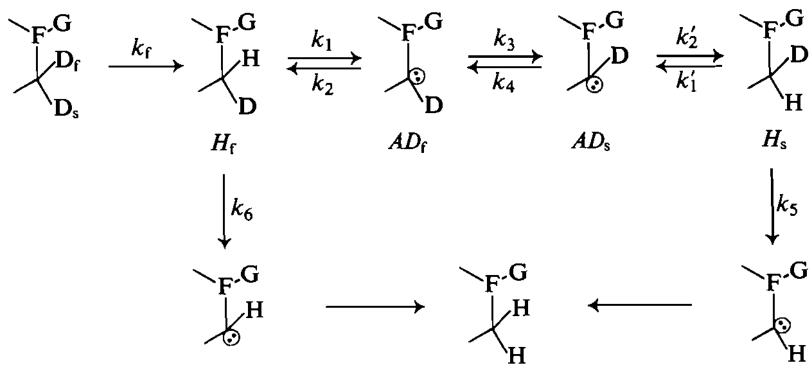

SCHEME 2

$$[7]\quad \left(\frac{k_f}{k_s}\right)_{obs}^{H\to D} \simeq \frac{l_D S_D\left(a_D L_D' S_D + a_D V_D' + \frac{a_D v_D L_D'}{L_D} + 1\right)}{a_D L_D' S_D + a_D V_D' + \frac{a_D v_D L_D'}{L_D} + \frac{a_D l_D S_D V_D'}{V_D} + 1}$$

If a_D is small ($k_3 \ll k_2$) or equal to 0 — the barrier to inversion is high or non-inverting anions are formed — then eq. [7] simplifies into eq. [8], exactly what would be expected if diastereomeric anions were formed and fast and slow exchange occurred only by retention.

$$[8]\quad \left(\frac{k_f}{k_s}\right)_{obs}^{H\to D} \simeq l_D S_D$$

In the case where a_D is large — the barrier to inversion is considerably smaller than the barrier to protonation — and $S_D > V_D > v_D$, eq. [9] obtains.

$$[9]\quad \left(\frac{k_f}{k_s}\right)_{obs}^{H\to D} \simeq \frac{l_D L_D' S_D}{L_D' + \frac{V_D'}{V_D} l_D}$$

That eq. [9] is exactly what is obtained in a simpler treatment when only a single intermediate is considered, i.e., ketones (40, 41), provides support for the validity of our analysis: the case where a_D is large ($k_3 \gg k_2$) is equivalent to the case where a single intermediate is generated. If the deprotonation and protonation KIEs are similar in magnitude — $V_D \simeq V_D' \simeq L_D \simeq L_D'$ — and set equal to i and the secondary KIEs are $\simeq 1$, eq. [9] simplifies to eq. [10].

$$[10]\quad \left(\frac{k_f}{k_s}\right)_{obs}^{H\to D} \simeq \frac{S_D i}{i+1}$$

Presently there is no information available on the relative magnitudes of the isotope effects although it is expected that the protonation KIEs should be equal to or less than the deprotonation KIEs. Limited data available for ketones (41) indicate that the protonation KIEs are equal to or less than the deprotonation KIEs.

Derivation of equations for D → H exchange

If Scheme 2 is considered for D → H exchange of a carbon acid where diastereotopic pyramidal carbanions are intermediates, then a steady-state treatment involving AD_f, AD_s, and H_s as steady-state intermediates yields expression [11] for $k_{s_{obs}}^{D\to H}$.

$$[11]\quad k_{s_{obs}}^{D\to H} \simeq k_6 + k_1\left\{1 - k_2\left[\frac{k_5(k_2' + k_4) + k_1'k_4}{k_2k_4(k_1' + k_5) + k_2'k_5(k_2 + k_3)}\right]\right\}$$

If C' is the collection of constants given by eq. [12], then eq. [11] can be rewritten as eq. [13].

$$[12]\quad C' = k_2'k_5 + k_4k_5 + k_1'k_4$$

$$[13]\quad k_{s_{obs}}^{D\to H} \simeq k_6 + k_1\left[1 - \frac{C'}{C' + \frac{k_3}{k_2}(k_2'k_5)}\right]$$

When the barrier to inversion of AD_f is high — k_3/k_2 is small — then $k_{obs}^{D\to H} \simeq k_6$. However, if the barrier to inversion is low and $k_3 \gg k_2$, then $k_{obs}^{D\to H} > k_6$. If S_H is the intrinsic selectivity, V_H and L_H are the primary KIEs for fast and slow deprotonation, respectively, in non-deuterated medium, v_H and l_H are the corresponding secondary KIEs, and, given that $S_H \simeq k_4k_2l_H/k_3k_2'v_H \simeq k_1v_H/k_1'l_H \simeq k_5V_H/k_6L_H$, $k_5 \simeq k_1v_H/V_H$, $a_H = k_3v_H/k_2$, $b_H = k_4l_H/k_2'$, and $b_H = a_HS_H$, eq. [14] obtains.

$$[14]\quad k_{obs}^{D\to H} \simeq k_6 + k_1\left(\frac{a_HS_Hl_H^2}{a_HS_HV_Hv_H + a_HS_H^2v_Hl_H + S_Hv_Hl_H^2 + a_HS_Hl_H^2}\right)$$

Since $S_H \simeq k_5V_H/k_6L_H$ and $k_5 \simeq k_1v_H/V_H$, eq. [14] can be rewritten as eq. [15].

$$[15]\quad k_{s_{obs}}^{D\to H} \simeq k_1\left[\frac{a_HV_Hv_H^2 + a_HS_Hv_H^2l_H + v_H^2l_H^2 + a_Hv_H^2l_H^2 + a_HS_HL_Hl_H^2}{S_HL_H(a_Hv_HV_H + a_HS_Hv_Hl_H + v_Hl_H^2 + a_Hl_H^2)}\right]$$

Since $k_1 \simeq k_f^{D\to H}V_H$, eq. [15] can be rewritten as eq. [16].[2]

$$[16]\quad \left(\frac{k_f}{k_s}\right)_{obs}^{D\to H} \simeq \frac{L_H}{V_H}\left[\frac{S_H(a_HV_Hv_H + a_HS_Hv_Hl_H + v_Hl_H^2 + a_Hl_H^2)}{a_HV_Hv_H^2 + a_HS_Hv_H^2l_H + v_H^2l_H^2 + a_Hv_H^2l_H^2 + a_HS_HL_Hl_H^2}\right]$$

TABLE 3. Hydrogen isotope exchange of benzyl methyl sulfoxide[a]

Substrate	Medium	k (M^{-1} min^{-1}) × 10^2 H	D	T
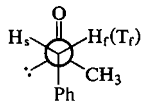	NaOD–D_2O (0.04 M)	21.6±0.3		7.22±0.06
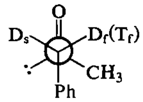	NaOH–H_2O (0.04 M)		5.41±0.08	3.90±0.03
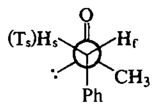	NaOD–D_2O[b] (0.48 M)	0.942		0.330±0.004
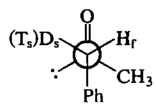	NaOH–H_2O (0.48 M)		0.545	0.392±0.004

[a]Taken from ref. 18.
[b]Exchange actually occurs on the D_f substituted species because $k_f = 21.6\ k_s$.

If the barrier to inversion of AD_f is high ($k_3 \ll k_2$ and a_H approaches 0) or exchange occurs only by retention, then eq. [16] reduces to eq. [17]. The result is exactly what would be expected for those cases. When a_H is large – the barrier to inversion is considerably smaller than the barrier to protonation – and S_H is larger than the KIEs, eq. [17] reduces to eq. [18]. If the deprotonation and protonation KIEs

$$[17]\quad \left(\frac{k_f}{k_s}\right)^{D\to H}_{obs} \simeq \frac{S_H L_H}{V_H \nu_H}$$

$$[18]\quad \left(\frac{k_f}{k_s}\right)^{D\to H}_{obs} \simeq \frac{S_H L_H \nu_H}{V_H(L_H l_H + \nu_H^2)}$$

are similar in magnitude and set equal to i and the secondary KIEs ≃ 1, eq. [18] further reduces to eq. [19].

$$[19]\quad \left(\frac{k_f}{k_s}\right)^{D\to H}_{obs} \simeq \frac{S_H}{i+1}$$

That eqs. [18] and [19] are identical to the equations for $(k_f/k_s)^{D\to H}_{obs}$ obtained previously, utilizing a scheme where a single intermediate (40, 41) is generated, i.e., from ketones, establishes the validity of our approach and the equations generated therefrom.

When a ratio of [10]/[19] is taken, eq. [20] results.

$$[20]\quad \frac{\left(\frac{k_f}{k_s}\right)^{H\to D}_{obs}}{\left(\frac{k_f}{k_s}\right)^{D\to H}_{obs}} \simeq \frac{\frac{S_D i_D}{i_D + 1}}{\frac{S_H}{i_H + 1}} \simeq \left(\frac{S_D i_D}{i_D + 1}\right)\left(\frac{i_H + 1}{S_H}\right)$$

Since $S_D = S_H$ and $i_D \simeq i_H$ are set equal to i, eq. [20] reduces to eq. [21].

$$[21]\quad \frac{\left(\frac{k_f}{k_s}\right)^{H\to D}_{obs}}{\left(\frac{k_f}{k_s}\right)^{D\to H}_{obs}} \simeq i$$

From the data in Table 1 the ratio given by eq. [21] for **1** is 3.41 ± 0.66, a reasonable value for i (*vide infra*). In Table 3 are listed data for hydrogen isotope exchange of benzyl methyl sulfoxide and its deuterated and tritiated analogs published by Fraser and Ng (18). The $(k_f/k_s)^{H\to D}$, $(k_f/k_s)^{D\to H}$, $(k_f/k_s)^{H\to T}$, and $(k_f/k_s)^{T\to H}$ ratios calculated from the data are 22.9 ± 0.7, 9.9 ± 0.03, 21.8 ± 0.2, and 10.0 ± 0.02, respectively. The H → D/D → H ratio for **2** is 2.31 ± 0.14. Since $(k_H/k_T)_f$ = 2.99, application of the Swain–Schaad relationship yields a value of 2.2 for $(k_H/k_D)_f$. Since $(k_H/k_D)_f \simeq i$, the correlation between the value of the ratio (i) given by eq. [21] and the experimentally obtained isotope effect for **2** is noteworthy and confirms the validity of our treatment.

Since eq. [22] holds for fast exchange of **2** in deuterated and non-deuterated medium ($SIE_f \simeq SIE_1$)

$$[22]\quad \frac{k_f^{H\to D}}{k_f^{D\to H}} = 3.99 \simeq V_H \nu_H\ SIE_f$$

and $V_H \simeq V_D = 2.2$, and ν_H the secondary KIE in non-deuterated medium should fall in the range of 1.1–1.2, SIE_f can range from 1.81–1.51, mid-range being around 1.6. The range evaluated for SIE_f is reasonable, based on the solvent isotope effects[4] that have been determined for a variety of carbon acids. The analysis also establishes that the secondary KIE for fast deprotonation (ν_D) is in the range expected for an $sp^3 \to$ "sp^2-like" process. A mid-range value of 1.15 will be used in subsequent discussions and calculations and it is assumed that $\nu_D \simeq l_D \simeq \nu_H \simeq l_H$. Since $k_f^{D\to H}$ is obtained from exchange of **1***b* that has two β-deuterons, assuming that the β-KIEs are cumulative, the H → D/D → H ratio for **1** is given by eq. [23].

[4]The SIEs for hydroxide-catalyzed reactions of nitroethane, 2-nitropropane, acetone, phenylacetylene, *tert*-butylmalononitrile, 9-fluoroenylmethane, and 1,4-dicyano-2-butene are 1.40, 1.35, 1.47, 1.33, 1.72, 1.49, and 1.38, respectively (43). Based on our analysis, values of 1.4 and 2.4 reported by Rauk *et al.* (44) for the secondary KIE and SIE, respectively, seem unusually high.

$$[23]\quad \frac{k_f^{H\to D}}{k_f^{D\to H}} = 6.6 \simeq V_H \nu_H (\nu_H^{\beta})^2 \mathrm{SIE_f}$$

Since ν_H^{β} should range between 1 and 1.1, V_H for **1** should fall in the range of 3.6–3.0 assuming that $\mathrm{SIE_f} \simeq 1.6$ (*vide supra*). The correlation between V_H evaluated using eq. [23] and *i* obtained from eq. [21] is significant and provides additional support for the validity of this treatment. There is a significant inversion component to the exchange of the slow proton (deuteron or triton) of a diastereotopic pair.

Derivation of equations for H → D exchange including solvent isotope effects

Although our analysis adequately accounts for the difference between the $(k_f/k_s)^{H\to D}$ and $(k_f/k_s)^{D\to H}$ ratios, it is necessary, in principle, to include solvent isotope effects for fast and slow exchange to obtain a more accurate measure of the intrinsic selectivity. It should be noted, however, that the effect on the rate ratio is minimal if $\mathrm{SIE_f} \simeq \mathrm{SIE_s}$, which is most likely in these cases because the fast–slow reactivities for **1** and **2** are not vastly different. Given the expressions for S_D developed for H → D exchange (*vide supra*) and since $\mathrm{SIE}'_1 \simeq \mathrm{SIE}_6$ and $\mathrm{SIE}_5 \simeq \mathrm{SIE}_1$, assuming that the SIEs for inversion of the diastereomeric anions are negligibly small, substitution of the appropriate terms for S_D, a_D, and b_D, which now include the SIEs,[5] into eq. [1] yields eq. [24]. If a_D is small – the barrier to inversion is high or two non-inverting anions are generated – then eq. [24] reduces to eq. [25],

$$[24]\quad \left(\frac{k_f}{k_s}\right)^{H\to D}_{obs} \simeq \frac{(l_D S_D)\left(a_D L'_D S_D \mathrm{SIE}_1^2 + \dfrac{a_D V'_D \mathrm{SIE}_1^2 \mathrm{SIE}'_2}{\mathrm{SIE}_2} + \mathrm{SIE}_1^2\mathrm{SIE}'_2 + \dfrac{a_D V_D L'_D \mathrm{SIE}_1 \mathrm{SIE}_6}{L_D}\right)}{a_D L'_D S_D \mathrm{SIE}_1\mathrm{SIE}_6 + \dfrac{a_D V'_D \mathrm{SIE}_1 \mathrm{SIE}'_2 \mathrm{SIE}_6}{\mathrm{SIE}_2} + \mathrm{SIE}_1\mathrm{SIE}'_2\mathrm{SIE}_6 + \dfrac{a_D \nu_D L'_D \mathrm{SIE}_6^2}{L_D} + \dfrac{a_D l_D V'_D S_D \mathrm{SIE}_1^2 \mathrm{SIE}'_2}{V_D \mathrm{SIE}_2}}$$

$$[25]\quad \left(\frac{k_f}{k_s}\right)^{H\to D}_{obs} \simeq \frac{l_D S_D \mathrm{SIE}_1}{\mathrm{SIE}_6}$$

exactly what would be expected for those cases. If a_D is large – the barrier to inversion is less than the barrier to protonation – and $S_D > V'_D$, L'_D, SIE_1, SIE_6, or ν_D, eq. [24] simplifies to eq. [26].

$$[26]\quad \left(\frac{k_f}{k_s}\right)^{H\to D}_{obs} \simeq \frac{l_D L'_D S_D \mathrm{SIE}_1}{\left[L'_D + \dfrac{\mathrm{SIE}_1}{\mathrm{SIE}_6}\dfrac{\mathrm{SIE}'_2}{\mathrm{SIE}_2}\left(\dfrac{l'_D V'_D}{V_D}\right)\right]\mathrm{SIE}_6}$$

From eqs. [18] and [26] we obtain eq. [27].

$$[27]\quad \left(\frac{k_s}{k_f}\right)^{H\to D}\left(\frac{k_f}{k_s}\right)^{D\to H} \simeq \frac{\left[L'_D + \left(\dfrac{\mathrm{SIE}_1\mathrm{SIE}'_2}{\mathrm{SIE}_6\mathrm{SIE}_2}\right)\left(\dfrac{l_D V'_D}{V_D}\right)\right]\mathrm{SIE}_6}{l_D L'_D S_D \mathrm{SIE}_1}\left[\frac{S_H L_H \nu_H}{V_H(L_H l_H + \nu_H^2)}\right]$$

Since $\mathrm{SIE}_1 \simeq \mathrm{SIE_f}$, on the assumption that $V_D \simeq V'_D \simeq L'_D \simeq L_H$, and l_D, ν_H, and $l_H \simeq 1$, and $\mathrm{SIE}_1 \simeq \mathrm{SIE}_6$, $\mathrm{SIE}_2 \simeq \mathrm{SIE}'_2$, eq. [27] can be transformed into eq. [28] using eq. [23]. Since $\mathrm{SIE}_1 \simeq \mathrm{SIE_f}$ was shown to be in the region of 1.6 (*vide supra*) and

$$[28]\quad \frac{k_s^{H\to D}}{k_s^{D\to H}} \simeq \nu_H(\nu_H^{\beta})^2\mathrm{SIE}_6$$

$\mathrm{SIE}_1 \simeq \mathrm{SIE}_6$, and since k_f and k_s are not vastly different, $k_s^{H\to D}/k_s^{D\to H}$, given by eq. [28], should be in the region of 1.8–2.2 if ν_H is set equal to 1.15 and ν_H^{β} lies between 1 and 1.1. The experimental values of the ratio for **1** and **2**, 1.94 ± 0.19 and 1.73, respectively, are in excellent agreement with the predicted value. If exchange of the slow proton (deuteron) occurs only by retention, then the $k_s^{H\to D}/k_s^{D\to H}$ ratio derived from eq. [29] – a ratio of eqs. [17] and [25] – would be expected to be considerably larger than the value predicted by our analysis. Given eq. [22], eq. [29] can be rearranged into

$$[29]\quad \frac{\left(\dfrac{k_f}{k_s}\right)^{H\to D}}{\left(\dfrac{k_f}{k_s}\right)^{D\to H}} \simeq \frac{\dfrac{l_D S_D \mathrm{SIE}_1}{\mathrm{SIE}_6}}{\dfrac{S_H L_H}{V_H \nu_H}}$$

eq. [30] ($S_H = S_D$). Using a value of 1.15 for l_D, 2.2 for V_H,

$$[30]\quad \frac{k_s^{H\to D}}{k_s^{D\to H}} \simeq \frac{L_H \mathrm{SIE}_6}{l_D}$$

and 1.6 for SIE_1, we calculate a ratio of 3.1 for **2** if exchange occurs only by retention. For **1**, since $V_H \simeq 3.3$, the ratio is predicted to be near 4.6.

By neglecting solvent isotope effects, using eqs. [8] and [17] for the cases where exchange occurs only by retention, and eqs. [7], [9], [16], and [18] for the cases where exchange by inversion is included, it is possible to evaluate the intrinsic selectivities and $(k_f/k_s)^{D\to H}$ ratios from the $(k_f/k_s)^{H\to D}_{obs}$ ratios. The experimental value for $(k_f/k_s)^{H\to D}$, the KIEs, and the inversion protonation parameters a_D and a_H were used to calculate S_R (selectivity calculated using eq. [8] assuming exchange with retention), S_I (selectivity calculated using eq. [7] including inversion), R_R ($(k_f/k_s)^{D\to H}$ calculating using eq. [17] assuming exchange with retention), and R_I ($(k_f/k_s)^{D\to H}$ calculated using eq. [16] assuming exchange by inversion). The data for **1**, using $(k_f/k_s)^{H\to D}_{obs} = 59.2$, are given in Table 4. As expected, S_R and R_R are invariant with a_D and a_H, and it is clear that the calculated $(k_f/k_s)^{D\to H}$ ratio ($R_I = 16.1$) corresponds closely to

[5] $S_D \simeq k_4 k_2 V'_D \mathrm{SIE}'_2 / k_3 k'_2 L'_D \mathrm{SIE}_2 \simeq k_1 V_D \mathrm{SIE}_6 / k'_1 L_D \mathrm{SIE}_1 \simeq k_5 \nu_D \mathrm{SIE}_6 / k_6 l_D \mathrm{SIE}_1$, $a_D = k_3 \mathrm{SIE}_2 / k_2 V'_D$ and $b_D = k_4 \mathrm{SIE}'_2 / k'_2 L'_D$ and $b_D = a_D S_D$.

TABLE 4. Calculated intrinsic selectivity and $(k_f/k_s)^{D\rightarrow H}$ for exchange of benzodehydrothiopene oxide

	Calculated selectivity		Calculated $(k_f/k_s)^{D\rightarrow H}$	
a_D	S_R[a]	S_I[a]	R_R[a,b]	R_I[a,b]
10^{-6}	51.5	51.5	44.8	44.7
10^{-5}	51.5	51.5	44.8	44.6
10^{-4}	51.5	51.8	44.8	42.9
10^{-3}	51.5	54.2	44.8	32.9
10^{-2}	51.5	63.4	44.8	19.2
10^{-1}	51.5	68.3	44.8	16.4
1	51.5	69.0	44.8	16.1
10	51.5	69.1	44.8	16.1
100	51.5	69.1	44.8	16.1
1000	51.5	69.1	44.8	16.1

[a]The constants used to evaluate the parameters were $(k_f/k_s)^{H\rightarrow D}$ (59.2), V_D, L_D, V'_D, L'_D, V_H, and L_H (all set at 3.3), ν_D, l_D, ν_H, and l_H (all sets at 1.15).
[b]It can be shown (*vide supra*) that $a_H = 3.8 \times a_D$ for **1** if $V_D \simeq 3.3$ and $\nu_H = 1.15$. A value of $3.8 \times a_D$ was used to evaluate R_R and R_I.

TABLE 5. Calculated intrinsic selectivities and rate ratios for D → H exchange of benzyl methyl sulfoxide

a_D	Calculated selectivity[a] S_I	Calculated $(k_f/k_s)^{D\rightarrow H}$[b,c] R_I
10^{-6}	19.9	17.3
10^{-5}	19.9	17.3
10^{-4}	20.0	17.2
10^{-3}	20.4	16.4
10^{-2}	23.4	13.2
10^{-1}	28.5	9.8
1	29.7	9.4
10	29.8	9.4
100	29.8	9.4
1000	29.8	9.4

[a]The other parameter S_R had the value 19.9.
[b]The other parameter R_R had the value 17.3.
[c]It can be shown (*vide supra*) that $a_H = 2.5 \times a_D$ for **2** when $V'_D = 2.2$ and $\nu_H = 1.15$. A value of $2.5 \times a_D$ was used for a_H in the calculation of R_I.

the observed value (17.3 ± 2.3) when inversion is included and $a_D \geq 0.1$. This is not the case if exchange is assumed to occur only with retention – $(k_f/k_s)^{D\rightarrow H}$ would have a much larger value of 44.8. Based on our analysis, the intrinsic selectivity is in the region of 68, 35% larger than the value of 51.5 calculated on the assumption that exchange occurs only with retention. An identical analysis carried out for **2** yielded the data listed in Table 5. As in the case of **1**, the calculated $(k_f/k_s)^{D\rightarrow H}$ ratio R_I (9.8–9.4) corresponds closely to the experimentally observed values of 10.8 ± 1.3 (this work) and 9.9 ± 0.03 (Fraser and Ng) when $a_D \geq 0.1$. The analysis establishes that the intrinsic selectivity for hydrogen isotope exchange of the diastereotopic protons of **2** is ≃29, approximately 45% larger than the value (19.9) which is obtained on the assumption that exchange occurs only with retention. That the calculated selectivity S_I and the $(k_f/k_s)^{D\rightarrow H}$ ratio R_I are not sensitive to the values for the protonation isotope effects V'_D and L'_D was established by using $V'_D = L'_D = 2.5$ and 3.8 for **2** and $V'_D = L'_D = 1.5$ and 3.0 for **1**. The differences in the calculated values were minimal. It is important to note that for both **1** and **2** S_I approaches S_{obs} and R_I approaches $(k_f/k_s)_{obs}^{D\rightarrow H}$ when $a_D \geq 0.1$. Consequently, when the barrier to inversion is comparable to the barrier to protonation, exchange of diastereotopic protons (deuterons) by inversion cannot be distinguished from a mechanism where a single intermediate is involved.

From the intrinsic selectivities for **1** (68) and **2** (29), the primary and secondary KIEs and the inversion–protonation parameters a_D and a_H, it is possible to calculate expected $(k_f/k_s)^{H\rightarrow D}$ and $(k_f/k_s)^{D\rightarrow H}$ ratios. Using eq. [1], a value of 3.3 for V_D, V'_D, L_D, and L'_D, a value of 1.15 for ν_D and l_D, we calculated $(k_f/k_s)^{H\rightarrow D}$ ratios for values of a_D which ranged from 10^{-6} to 10^3. A plot of the calculated values as a function of a_D given in Fig. 3(A) illustrates the variation of the observed rate ratio with a variation in the barrier to inversion. Similar calculations using eq. [16], values of 3.3 for V_H and L_H and 1.15 for ν_H and l_H, and a_H[6] that ranged from 3.8×10^{-6} to 3.8×10^3 were carried out to obtain $(k_f/k_s)^{D\rightarrow H}$. A plot is given in Fig. 3(B). Identical calculations were carried out for **2** using the appropriate parameters – $V_D = V'_D = L_D = L'_D = V_H = L_H = 2.2$, $\nu_D = l_D = l_H = 1.15$, a_D ranging from 10^{-6} to 10^{-3}, and a_H ranging from 2.5×10^{-6} to 2.5×10^3. Plots of the calculated $(k_f/k_s)^{H\rightarrow D}$ and $(k_f/k_s)^{D\rightarrow H}$ values versus a_D and a_H, respectively, are shown in Figs. 4(A) and (B). That the observed rate ratios plateau when $a_D(a_H)$ values are large and small is quite clear. The calculated values for $(k_f/k_s)^{H\rightarrow D}$ and $(k_f/k_s)^{D\rightarrow H}$ for **1** and **2** correspond closely to the observed values when $a_D(a_H) \geq 0.1$.

While it would be interesting to compare the rate ratios for H→D and D→H exchange of a carbon acid where diastereotopic anions with a high barrier to inversion ($a_D < 10^{-2}$) are generated, in practice it will be difficult to obtain such a substrate. Even 4-membered-ring sulfones have k_e/k_α values around 1. For example, thietane-1,1-dioxide **3** exhibits a k_e/k_α of 0.60–0.67 in $(CH_3)_3COD-(CH_3)_3COK$ (26) and 2-halogeno-3-morpholinothietane-1,1-dioxides of the type **4** exhibit k_e/k_α values around 1 in CD_3CN-D_2O (28).

Again, it is noteworthy that our analysis yields values of $(k_f/k_s)^{D\rightarrow H}$ for **1** and **2** that compare very well with the experimental values when the inversion–protonation parameter a_D is ≃ 0.1. This result is in accord with stereochemical studies of hydrogen isotope exchange of **5** (21) and **6** (14) where rates of exchange and racemization can be determined directly. For the $R-R$ and $R-S$ diastereomers of **5** the k_e/k_α ratios are 1.2 and 3.6, respectively, in $(CH_3)_3COK-(CH_3)_3COH$ at 60°C. For **6**, that is a particularly good model for **1** and **2**, $k_e/k_\alpha = 1.3$ in $NaOD-D_2O$ at 56°C. Since a k_e/k_α value of less than 2 signifies that inversion occurs more rapidly than reprotonation of the anion, the results establish the validity of our analysis and show that the stereochemical aspects of exchange of **1** and **2** are similar to **6**. From a_D it is possible to set an *upper limit* to the barrier of inversion of the diastereotopic anions, if they are intermediates. By using the Arrhenius equation and the fact that $k_{3(\mathrm{inv})}/k_{2(\mathrm{prot})} = a_D V'_D$, eqs. [31] and [32] obtain.

$$[31] \quad \ln a_D V'_D \simeq \ln \frac{A_{\mathrm{inv}}\, e^{\frac{-E_{\mathrm{inv}}}{RT}}}{A_{\mathrm{prot}}\, e^{\frac{-E_{\mathrm{prot}}}{RT}}}$$

[6]It can be shown that $a_H \simeq 3.8 \times a_D$ for **1** and $2.2 \times a_D$ for **2** (*vide supra*).

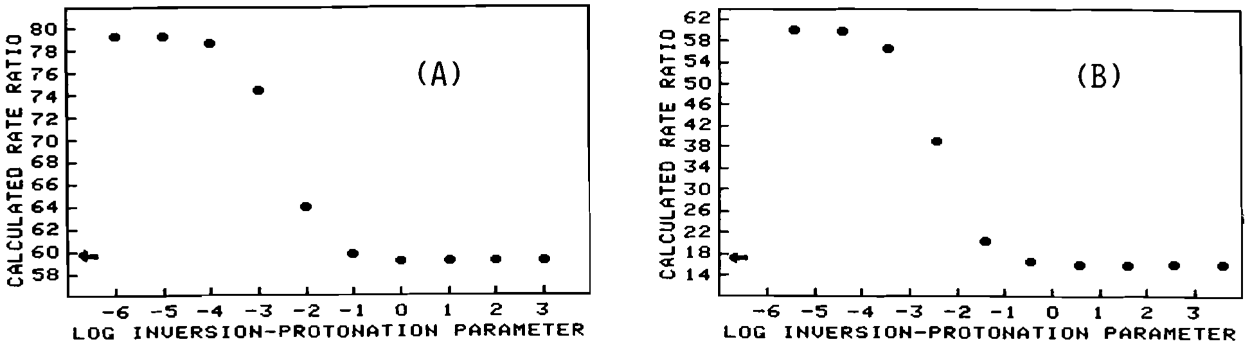

FIG. 3. (A) Plot of the calculated $(k_f/k_s)^{H\to D}$ ratio versus a_D for exchange of **1***a*. The bold-faced arrow indicates the experimentally determined value. (B) Plot of the calculated $(k_f/k_s)^{D\to H}$ ratio versus a_H for exchange of **1***b*. The bold-faced arrow indicates the experimentally determined value.

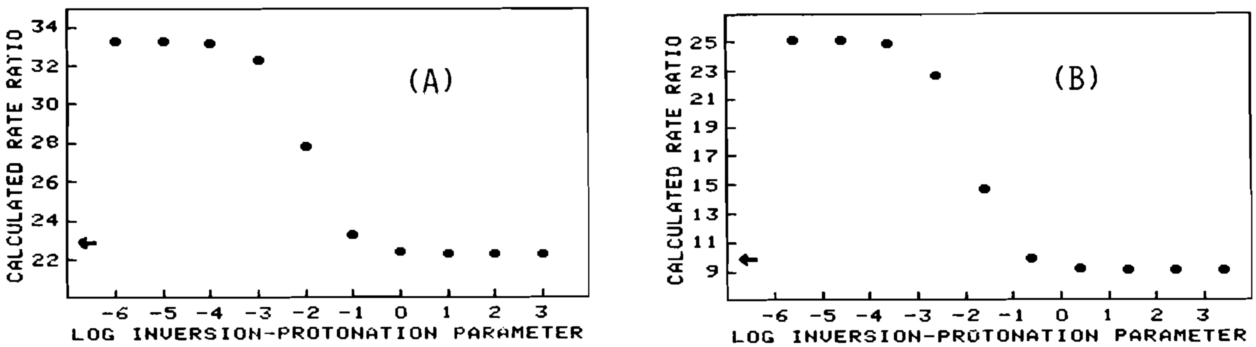

FIG. 4. (A) Plot of the calculated $(k_f/k_s)^{H\to D}$ ratio versus a_D for exchange of **2***a*. The bold-faced arrow indicates the experimentally determined value. (B) Plot of the calculated $(k_f/k_s)^{D\to H}$ ratio versus a_H for exchange of **2***b*. The bold-faced arrow indicates the experimentally determined value.

TABLE 6. Estimated inversion barriers for anions at 30°C

		Calculated inversion barrier (kcal)	
Protonation barrier (kcal)	k_{prot} (M^{-1} s^{-1})	1	2
3.0	2.1×10^9	4.8	5.0
4.0	4.1×10^8	5.8	6.0
5.0	7.8×10^7	6.8	7.0
6.0	1.5×10^7	7.8	8.0
7.0	2.9×10^6	8.8	9.0

$$[32] \quad E_{inv} \simeq RT\left(\ln A_{inv} - \ln A_{prot} + \frac{E_{prot}}{RT} - \ln a_D V'_D\right)$$

With $a_D = 0.1$, $V'_D = 3.3$ and 2.2 for **1** and **2**, respectively, $T = 303$, and estimates for E_{prot}, A_{inv} ($\sim 1 \times 10^{14}$) (45, 46), and A_{prot} ($\sim 3 \times 10^{11}$) (45, 46),[7] E_{inv} can be obtained (Table 6). If k_{prot} for the carbanions derived from **1** and **2** is $\geq 10^8$ (47) and if pyramidal diastereotopic anions are involved as intermediates in the exchange of **1** and **2**, then the inversion barriers must be ≤ 6 kcal. This is in keeping with current views on the barriers to inversion of carbanions (48).

It is clear from our analysis[8] that the diastereotopic hydrogens of **1** and **2** undergo exchange by inversion and that the inversion component contributes significantly to $k_s^{H\to D}$ and $k_s^{D\to H}$, yielding a $(k_f/k_s)^{D\to H}$ ratio that is substantially less than $(k_f/k_s)^{H\to D}$. Consequently, the Streitweiser–Swain method (49, 50) used to determine the extent of internal return for H → D(T) exchange of carbon acids should be applied with caution to cases where diastereotopic hydrogens, deuterons, or tritons are exchanged. This is so because k_s^H, k_s^D, and k_s^T used to obtain k_H/k_T and k_D/k_T can be significantly affected by the inversion component (*vide supra*), and the determination of the degree of internal return is particularly sensitive to the k_H/k_T and k_D/k_T values.

To illustrate the problem, consider the data (Table 3) for **2** accumulated by Fraser and Ng and used to establish that there is 3% and 12% internal return for exchange of the fast and slow protons, respectively. The only way we can reasonably account for the fact that $k_{T(s)}$ (0.392 ± 0.004) for exchange of **2**-H_f-T_s in NaOH–H_2O is greater than $k_{T(s)}$ (0.330 ± 0.004) for **2**-D_f-T_s in NaOD–D_2O is to invoke a larger component of inversion to exchange of **2**-H_f-T_s,[9] a reasonable consideration since $k_{H(f)}/$

[7]These are average values for the frequency factors for first-order and second-order processes.

[8]All derivations of equations have been deposited as Supplementary Material. Copies may be obtained, at a nominal charge, from the Depository of Unpublished Data, CISTI, National Research Council of Canada, Ottawa, Ont., Canada, K1A 0S2.

[9]Since SIE ≃ 1.6 and the secondary KIE ≃ 1.15, $k_{T(s)}$ for **2**-D_f-T_s should be 1.4 times larger than $k_{T(s)}$ for **2**-H_f-T_s. In the case of fast exchange of **2**, $k_{T(f)}$ for **2**-T_f-H_s in NaOD–D_2O is, as expected, approximately 1.6 × 1.15 times as fast as $k_{T(f)}$ for **2**-T_f-D_s in NaOH–H_2O).

$k_{D(f)} = 2.2$. The alternative is to assume that $SIE_s \simeq 1.0$, an unlikely situation because k_f and k_s are not vastly different. The transition states should not differ greatly and the degree of solvation of the base, the substrate, and the transition states should be comparable in each case.

Experimental

Preparation of substrates

Benzodihydrothiophene oxide (**1***a*) was prepared according to the method described by King and du Manior (15).

The tetradeuterated oxide **1***b* was prepared by exchange of **1***a* (1 g) in 0.1 *M* $NaOD-D_2O$ (25 mL) at 50°C for 1 h. The reaction mixture was extracted with ether (5 × 10 mL), the combined extracts were dried over $MgSO_4$, and the solvent was removed on the rotatory evaporator. Recrystallization of the residue from benzene–pentane gave **1***b* (0.8 g), mp 89–90°C. Mass spectral analysis showed that the d_4-species constituted 90.9% of the mixture.

Deuterated benzyl methyl sulfoxide **2***b* was prepared by treating **2***a* (0.25 g) in 1 *M* $NaOD-D_2O$ for 3 h at 70°C. The mixture was cooled and extracted with methylene chloride (4 × 2 mL). The combined extracts were dried over $MgSO_4$, the solvent was removed on the rotatory evaporator, and the residue was sublimed under aspirator vacuum to yield **2***b* (0.16 g), mp 52–53°C. Mass spectral analysis established that the d_2-species constituted 75.9% of the mixture.

Exchange kinetics

Benzodihydrothiophene oxide

To obtain the rate constant for *trans*-H → D (fast) exchange of **1***a*, **1***a* (5–10 mg) was dissolved in 1.5 mL of 0.0064 *M* $NaOH-H_2O$ that was equilibrated in a constant temperature bath maintained at 30.00 ± 0.05°C, and 5–7 aliquots (~0.1 mL) were removed at appropriate intervals and quenched in 1.5 mL of a dipotassium hydrogen phosphate buffer of pH 7.0 and ether (2 mL). The aliquots were extracted by repeatedly withdrawing and expelling the ether layer through the aqueous layer with a Pasteur pipette. The ether layer was dried, the solvent was evaporated, and the decrease in d_0-species was monitored mass spectrometrically at low voltage (12–15 eV). The peak intensities for each aliquot were obtained as an average of at least three scans.

To obtain the rate constant for *cis*-H → D (slow) exchange of **1***d*, **1***a* was exchanged as described above and the decrease of d_2-species was monitored mass spectrometrically by withdrawing aliquots after a 4-min interval.

The rate constant for *trans*-D → H (fast) exchange was obtained by exchanging **1***b* (3–5 mg) in 1.5 mL of 0.0233 *M* $NaOH-H_2O$ and the decrease in d_4-species with time was monitored mass spectrometrically in the usual manner.

To obtain the rate constant for *cis*-D → H (slow) exchange, **1***b* was exchanged in 0.0233 *M* $NaOH-H_2O$ as described above and the decrease of d_2-species with time was monitored mass spectrometrically after a 40-min interval.

Benzyl methyl sulfoxide

To obtain the rate constant for fast D → H exchange of dideuterated benzyl methyl sulfoxide **2***b*, **2***b* (10–15 mg) was dissolved in 1.5 mL of 0.6 *M* $NaOH-H_2O$ at 30.00 ± 0.05°C and aliquots were removed at appropriate periods, quenched with dipotassium hydrogen phosphate buffer (2 mL), and extracted with ether (2 mL). The decrease in d_2-species with time was monitored mass spectrometrically as described above.

The rate constant for slow D → H was obtained by exchanging **2***b*. Aliquots (5–6) were removed after an interval of ~100 min and the decrease in d_1-species with time was monitored mass spectrometrically as described above.

Acknowledgement

We thank the Natural Sciences and Engineering Research Council of Canada for financial support.

1. E. BUNCEL, E. A. SYMONS, and A. W. ZABEL. Chem. Commun. 173 (1965).
2. A. RAUK, E. BUNCEL, R. V. MOIR, and S. WOLFE. J. Am. Chem. Soc. **87**, 5448 (1965).
3. S. WOLFE and A. RAUK. Chem. Commun. 778 (1966).
4. R. STEWART and J. R. JONES. J. Am. Chem. Soc. **87**, 5069 (1966).
5. E. BULLOCK, J. M. W. SCOTT, and P. D. GOLDING. Chem. Commun. 168 (1967).
6. M. NISHO. Chem. Commun. 562 (1968).
7. J. E. BALDWIN, R. E. HACKLER, and R. M. SCOTT. Chem. Commun. 1415 (1969).
8. R. R. FRASER and F. J. SCHUBER. Chem. Commun. 397 (1969).
9. B. J. HUTCHINSON, K. K. ANDERSEN, and A. R. KATRITZKY. J. Am. Chem. Soc. **91**, 3839 (1969).
10. J. DURST, K. R. FRASER, M. R. MCCLORY, R. B. SWINGLE, R. VIAU, and Y. Y. WIGFIELD. Can. J. Chem. **48**, 2148 (1970).
11. R. R. FRASER, F. J. SCHUBER, and Y. Y. WIGFIELD. J. Am. Chem. Soc. **94**, 8775 (1972).
12. K. NISHIHATA and M. NISHO. J. Chem. Soc. Perkin Trans. 2, 1730 (1972).
13. R. VIAU and T. DURST. J. Am. Chem. Soc. **94**, 1346 (1973).
14. M. B. D'AMORE and J. I. BRAUMAN. J. Chem. Soc. Chem. Commun. 398 (1973).
15. J. F. KING and J. R. DU MANOIR. Can. J. Chem. **51**, 4082 (1973).
16. U. FOLLI, D. IAROSSI, I. MORETTI, F. TADDEI, and G. TORRE. J. Chem. Soc. Perkin Trans. 2, 1655 (1974).
17. U. FOLLI, D. IAROSSI, and F. TADDEI. J. Chem. Soc. Perkin Trans. 2, 1658 (1974).
18. R. R. FRASER and L. K. NG. J. Am. Chem. Soc. **98**, 4334 (1976).
19. F. A. CAREY, O. D. DAILEY, JR., and O. HERNANDEZ. J. Org. Chem. **41**, 3974 (1976).
20. E. J. COREY and E. T. KAISA. J. Am. Chem. Soc. **83**, 490 (1961).
21. D. J. CRAM, D. A. SCOTT, and W. D. NIELSEN. J. Am. Chem. Soc. **83**, 3696 (1961).
22. H. L. GOERING, D. L. TOWNS, and B. DITTMAR. J. Org. Chem. **27**, 736 (1962).
23. D. J. CRAM, R. D. TREPKA, and P. ST. JANIAK. J. Am. Chem. Soc. **88**, 2749 (1966).
24. F. G. BORDWELL, D. D. PHILLIPS, and J. M. WILLIAMS, JR. J. Am. Chem. Soc. **90**, 426 (1968).
25. R. R. FRASER and F. J. SCHUBER. Chem. Commun. 1474 (1969).
26. L. A. PAQUETTE, J. P. FREEMAN, and M. J. WYVRATT. J. Am. Chem. Soc. **93**, 3216 (1971).
27. F. HIBBERT. J. Chem. Soc. Perkin Trans. 2, 1289 (1973).
28. S. BRADAMENTE, P. DEL BUTTERO, D. LANDINI, and S. MALORAMA. J. Chem. Soc. Perkin Trans. 2, 1676 (1974).
29. G. BARBARELLA, A. GARBESI, and A. FAVA. Helv. Chim. Acta, **54**, 341 (1971).
30. G. BARBARELLA, A. GARBESI, and A. FAVA. Helv. Chim. Acta, **54**, 2297 (1971).
31. G. BARBARELLA, A. GARBESI, A. BOICELLI, and A. FAVA. J. Am. Chem. Soc. **95**, 8051 (1973).
32. O. HOFER and E. L. ELIEL. J. Am. Chem. Soc. **95**, 8045 (1973).
33. G. BARBARELLA, A. GARBESI, and A. FAVA. J. Am. Chem. Soc. **97**, 5883 (1975).
34. G. BARBARELLA, P. DEMBECH, A. GARBESI, F. BERNARDI, A. BOTTONI, and A. FAVA. J. Am. Chem. Soc. **100**, 200 (1973).
35. R. R. FRASER and Y. Y. WIGFIELD. Tetrahedron Lett. **27**, 2515 (1971).
36. R. R. FRASER, T. B. GRINDLEY, and S. PASSANNANTI. Can. J. Chem. **53**, 2473 (1975).
37. R. R. FRASER and L. K. NG. J. Am. Chem. Soc. **98**, 5895 (1976).
38. J. M. BROWN, E. H. CAIN, and M. C. MCIVOR. J. Chem. Soc. (B), 730 (1971).
39. D. H. HUNTER, Y-T. LIN, A. L. MCINTYRE, D. J. SCHEARING, and M. ZVAGULIS. J. Am. Chem. Soc. **95**, 8327 (1973).
40. S. BANERJEE and N. H. WERSTIUK. Can. J. Chem. **53**, 1099

(1975).
41. N. H. WERSTIUK and S. BANERJEE. Can. J. Chem. **63**, 534 (1985).
42. N. H. WERSTIUK, R. TAILLEFER, and S. BANERJEE. Can. J. Chem. **56**, 1140 (1978).
43. J. R. JONES. The ionization of carbon acids. Academic, London. 1973. p. 203.
44. A. RAUK, S. WOLFE, and I. G. CSIZMADIA. Can. J. Chem. **47**, 113 (1969).
45. E. A. MOELWYN-HUGHES. The kinetics of reactions in solution. Oxford, London. 1947.
46. A. A. FROST and R. G. PEARSON. Kinetics and mechanism. 2nd ed. Wiley, New York. 1961.
47. F. HIBBERT. *In* Comprehensive chemical kinetics. *Edited by* C. H. Bamford and C. F. H. Tipper. Elsevier, Amsterdam. 1977. Chapt. 2.
48. P. R. PEOPLES and J. B. GRUTZNER. J. Am. Chem. Soc. **102**, 4709 (1980).
49. A. STREITWIESER, W. B. HOLLYHEAD, H. H. PUDJAATMAKA, P. H. OWENS, T. L. KRUGER, P. A. RUBENSTEIN, R. H. MACQUARRIE, M. L. BROWSKA, W. K. C. CHU, and H. H. NIEMEYER. J. Am. Chem. Soc. **93**, 5088 (1971).
50. A. STREITWIESER, P. H. OWENS, G. SONNICHSEN, W. K. SMITH, G. R. ZILER, H. M. ZILER, H. M. NIEMEYER, and T. L. KRUGER. J. Am. Chem. Soc. **95**, 4254 (1973).

Fractionation of organic extracts of environmental water samples by low pressure column chromatography and high performance liquid chromatography techniques

R. A. MOORE AND F. W. KARASEK[1]
Department of Chemistry, University of Waterloo, Waterloo, Ont., Canada N2L 3G1

Received August 10, 1984

R. A. MOORE and F. W. KARASEK. Can. J. Chem. **63**, 2110 (1985).

Prefractionation procedures based on high performance liquid chromatography (hplc) and low pressure column chromatography (lpcc) were developed and applied to the separation of components in extracts of environmental samples. Effective fractionation was obtained using solvent systems based on hexane, carbon tetrachloride, dichloromethane, and ether for elution on lpcc Florisil and hplc silica columns. This facilitated the identification of over thirty compounds consisting mainly of aliphatic and polyaromatic hydrocarbons, phthalate esters, phenols, and pesticides in environmental samples extracted from water. Chromatographic background levels were minimized, and compounds whose chromatographic peaks were unresolved before fractionation were isolated into separate fractions. This afforded more highly reliable gc/ms identifications. Prefractionation also served to retard the rapid degradation of capillary columns which was caused by the injection of unfractionated samples.

R. A. MOORE et F. W. KARASEK. Can. J. Chem. **63**, 2110 (1985).

On a mis au point des méthodes de préfractionnement basées sur la chromatographie liquide à haute performance (clhp) et sur la chromatographie sur colonne à basse pression (ccbp) et on les a utilisées pour fractionner des extraits d'échantillons provenant de l'environnement. On a pu faire des séparations efficaces en utilisant des systèmes de solvants comportant de l'hexane, du tétrachlorure de carbone, du dichlorométhane et de l'éther comme éluants pour des colonnes de Florisile en ccbp et de silice en clhp. Ceci facilite l'identification de plus de trente composés constitués principalement d'hydrocarbures aliphatiques et polyaromatiques, de phtalates, de phénols et de pesticides dans des échantillons provenant de l'environnement et extraits de l'eau. On a minimisé les niveaux chromatographiques de base et on a obtenu des fractions séparées pour des composés dont les pics chromatographiques n'étaient pas résolus avant le fractionnement. Le préfractionnement permet également de retarder la dégradation rapide des colonnes capillaires qui est provoquée par l'injection d'échantillons non fractionnés.

[Traduit par le journal]

Introduction

Organic extracts of water samples are often directly analyzed by gas chromatography (gc), and combined gas chromatography – mass spectrometry (gc/ms) techniques without prior sample clean-up. However, the analysis of complex water samples is greatly simplified through the application of some form of fractionation to separate compounds into similar groups prior to the final determinative step. This approach overcomes difficulties caused by overlapping chromatographic peaks of the complex mixture, which make quantitation inaccurate and lead to ambiguities in mass spectral identifications.

One of the earliest classification procedures employed for environmental water samples separated the complex ether extract of organic material, which had been previously concentrated onto carbon filters, into groups consisting of neutral, basic, acidic, amphoteric, and phenolic compounds (1, 2). This was accomplished through a series of solvent extractions under various conditions.

Rosen and Middleton (3) applied a fractionation procedure based on adsorption chromatography to the neutral extract of surface waters polluted by refinery wastes. The concentrated neutral fraction was adsorbed onto the top of a silica gel column which was sequentially eluted with isooctane, benzene, and a chloroform–methanol mixture. The isooctane fraction contained aliphatic hydrocarbons, aromatic hydrocarbons eluted in the benzene fraction, and the chloroform–methanol fraction contained oxygenated compounds. Shinohara *et al.* described a similar fractionation technique for the neutral organic fraction of extracts from tap-water samples (4). The silica gel column was eluted with isooctane, isooctane–benzene (1:1), benzene – ethyl acetate (1:1), and benzene–methanol (1:1). Aliphatic hydrocarbons were recovered in the isooctane fraction and aromatic compounds were present in the isooctane–benzene fraction. The other two fractions contained several oxygenated compounds.

Leenheer and Huffman developed a procedure called "dissolved organic carbon (DOC)" fractionation analysis, whereby organic solutes are concentrated and fractionated by non-ionic and ion-exchange resin adsorbents into hydrophobic-base, -acid, and -neutral fractions (5, 6). An anion-exchange resin prepared by chloromethylation of Amberlite XAD-4 resin was used by Richard and Fritz to isolate acidic organic material from other organics in aqueous solutions (7). Both hydrophilic and hydrophobic acids were recovered using this resin.

The applicability of high performance liquid chromatography (hplc) as an efficient means of separating organics in extracts of water samples into various polarity groups was demonstrated by Thruston (8). He employed μ-Porasil columns and gradient elution with hexane and chloroform to obtain three major fractions from tap-water samples. A first fraction contained polynuclear aromatic hydrocarbons, chlorinated hydrocarbons, and aliphatic hydrocarbons, the second fraction contained several oxygenated compounds, and the final fraction contained mainly phthalate esters.

During studies of trace organics in river water samples from Trinidad it was noted that direct analysis of concentrated extracts frequently resulted in complex chromatograms in which many peaks were only partly resolved and steeply rising baselines were evident (9). The lack of resolution often resulted in ambiguous spectral interpretations. Several of these extracts were also shown to cause rapid deterioration of the capillary columns used for chromatographic analysis. Prefractionation procedures based on low pressure column chromatography (lpcc) and hplc were developed in order to overcome these

[1] Author to whom correspondence may be addressed.

TABLE 1. Florisil fractionation of standard test solution using hexane – carbon tetrachloride – ether eluting system

Pk. no.[a]	Compound	% in hexane	% in CCl_4	% in ether	Total % recovered[b]
1	n-Hexyl benzene	53	—	—	53
2	Ethyl phenol	—	—	67	67
3	Biphenyl	66	—	—	66
4	Methyl hendecanoate	10	67	—	77
5	Dimethyl naphthalene	68	—	—	68
6	Dimethyl naphthalene	71	—	—	71
7	Dimethyl naphthalene	72	—	—	72
8	Phenyl phenol	—	—	80	80
9	Methyl tetradecanoate	24	66	—	90
10	1-Naphthol	—	—	38[c]	38[c]
11	α-BHC	94	—	—	94
12	Benzyl benzoate	13	75	11	99
13	Phenanthrene	88	16	—	104
14	γ-BHC	79	24	—	103
15	Aldrin	96	—	—	96
17	Dibutyl phthalate	—	—	98	98
18	Fluoranthene	48	43	—	91
19	Dieldrin	25	78	—	103
20	Endrin	25	68	—	93
21	*o,p* DDT	103		—	103
22	Methoxychlor		92	—	92

[a]Peak number as shown in Fig. 1.
[b]Average relative standard deviation from mean of triplicate analysis = 7%; range = 4–9%.
[c]When 150 mL ether used, recovery of 1-naphthol = 54%; with 200 μL ether, recovery of 81% obtained.

difficulties. Effective fractionations were obtained using solvent systems based on hexane, carbon tetrachloride, dichloromethane, and ether for elution on lpcc Florisil columns and hplc silica columns. These fractionation procedures as applied to a standard mixture and to extracts of river water samples are the subject of this report.

Experimental

Solvents and standards

All solvents were "Distilled in Glass, UV grade" (Caledon Laboratories, Canada). Standard compounds used in the development of the fractionation procedure were obtained from U.S. Environmental Protection Agency Reference Standards Repository; Polyscience Corporation, U.S.A.; Chem. Service Inc. Pa; and Aldrich Chemical Company, Inc., Wisconsin, U.S.A. A standard test solution was prepared as described in a previous paper (10).

Low pressure column chromatographic fractionation

Florisil (60–100 mesh, Fisher Scientific Co., U.S.A.) and alumina (neutral, 80–100 mesh, Woelm Pharma, GmbH & Co., West Germany) adsorbents were heated at 300°C for 6 h prior to use. Glass columns (25 cm length id 1.0 cm), fitted with Teflon stopcocks, were dry packed with the adsorbents such that adsorbent columns of 9 cm length were obtained. Plugs of silanized glass wool which were pre-extracted with the eluting solvents were used at the top and bottom of the adsorbent columns. The column was pre-wet with the first eluting solvent prior to introduction of sample or standard to the top of the column with a Hamilton microsyringe. Fractionation was effected by the sequential addition of the required volume of each eluting solvent to the column, the solvent being allowed to percolate through the column under gravity flow. Fractions were collected in 250-mL glass round-bottom flasks and evaporated to 0.1 mL by rotary evaporation under vacuum followed by final volume reduction with a stream of high-purity nitrogen.

High performance liquid chromatographic fractionation

A Spectra-Physics SP-8000 high performance liquid chromatograph equipped with an SP-8400 uv–visible detector and SP-4100 integrator was used. The hplc column was a Spherisorb silica column (250 mm × 9.4 mm id, Terochem, Canada). A sample loop of 140 μL volume was employed for sample introduction into the hplc and a wavelength of 254 nm was used throughout for monitoring of the hplc effluent. The collected fractions were treated in the same manner as described for lpcc above, then subjected to gc and gc/ms analyses.

Gas chromatographic and mass spectral analyses

Quantitative gas chromatographic analyses were performed with a Hewlett–Packard (HP) 5880A gas chromatograph equipped with a level 4 integrator, a flame ionization detector, cool on-column injection system, and a widebore (0.32 mm × 30 m) DB-1701 fused silica capillary column (J & W Scientific Inc. Rancho Cardova, CA., U.S.A.). The gc conditions were: injection port 40°C; column temperature programmed from 40°C to 250°C at a rate of 4°C/min.; detector temperature 300°C; helium carrier gas flow rate measured at 40°C, 2 mL/min; injection volume 0.6 μL.

Capillary gc/ms analysis employing a Hewlett–Packard 5992A gc/ms calculator equipped with the same column was used to verify the identities of compounds corresponding to each gas chromatographic peak.

Results and discussion

Fractionation by low pressure column chromatography

In preliminary experiments, both alumina and Florisil were employed as adsorbents for lpcc fractionation of the test solution. However, use of alumina columns resulted in less effective overall fractionation and lower recovery of the more polar compounds compared to Florisil, for similar eluting conditions. It was therefore decided to restrict lpcc fractionation to Florisil adsorbent.

Use of hexane followed by carbon tetrachloride and ether for elution proved to be an effective method for fractionation of the test solution. Table 1 shows the results of fractionation employing this solvent sequence (50 mL of each solvent) and Florisil columns. Chromatograms of the three fractions are shown in Fig. 1.

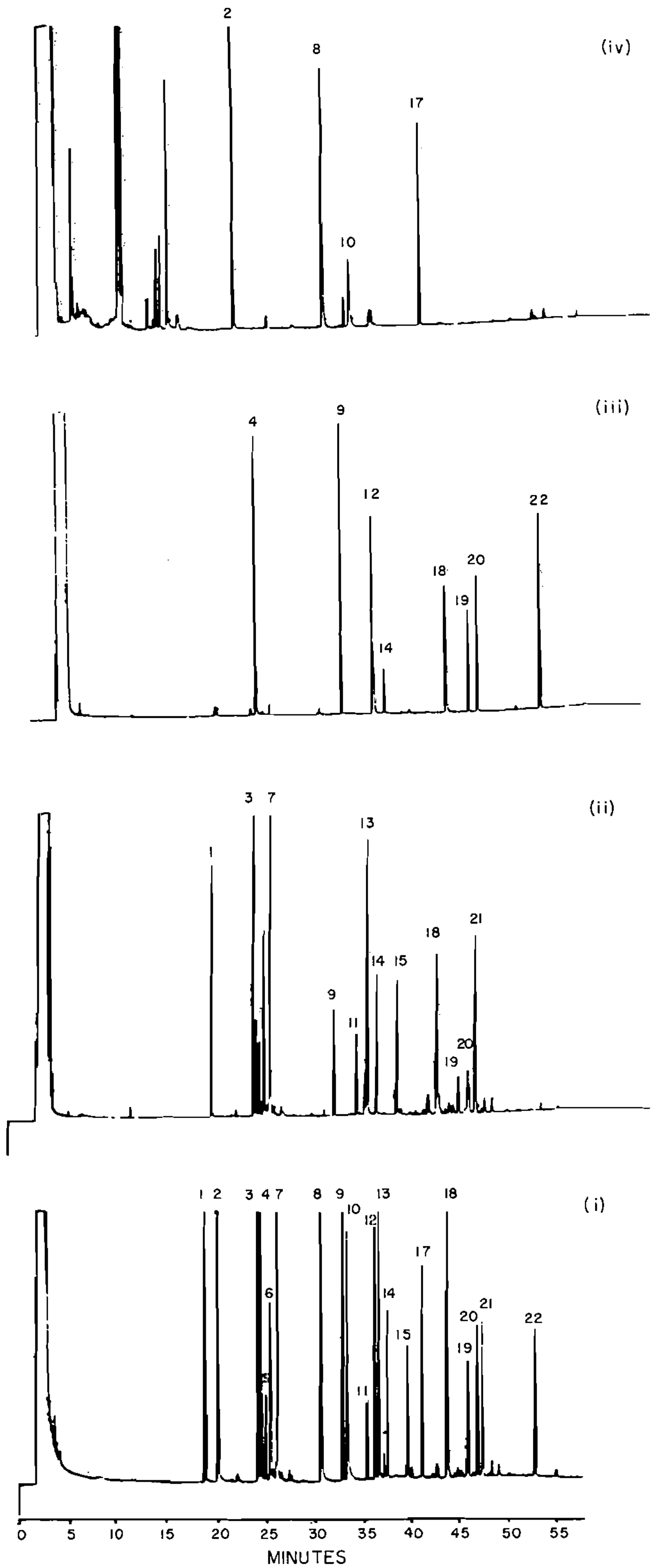

FIG. 1. Gas chromatograms of fractions obtained from lpcc separation of standard mixture. (i) Unfractionated solution. (ii) Hexane fraction. (iii) Carbon tetrachloride fraction. (iv) Ether fraction.

The phenols were confined exclusively to the ether fraction. The recovery of naphthol was, however, low (38%). The carbon tetrachloride fraction contained the major portion of endrin, dieldrin, benzyl benzoate, and the esters methyl tetradecanoate and methyl hendecanoate, and all of the methoxychlor appeared in this fraction. Fluoranthene was almost equally distributed between the hexane and carbon tetrachloride fractions. Aldrin, *o,p* DDT, α-BHC, dimethyl naphthalene, biphenyl, and n-hexyl benzene were confined to the hexane fraction; most of the phenanthrene (88%) and γ-BHC (79%) also appeared in this fraction.

Further optimization of the fractionation on Florisil required improvement in the low recovery of 1-naphthol. Increasing the volume of ether used for elution by a factor of three resulted in an improvement in the recovery of 1-naphthol from 38% to 64%, and a further increase to 79% was obtained on elution with 200 mL ether. Ether was replaced by acetone as the third eluting solvent but no compounds were recovered in the acetone. Attempts to use methanol as the third eluting solvent decreased the recovery of 1-naphthol as well as the other phenolic compounds. Severe peak distortion was also noted in the gc analysis of the methanol fraction. The system employing hexane, carbon tetrachloride, and ether was therefore adopted as our optimal low pressure chromatography fractionation procedure and applied to extracts of samples from Trinidad water systems.

Fractionation by high performance liquid chromatography

The eluting system of hexane – carbon tetrachloride – ether in a ternary gradient, which was effective for fractionation on Florisil, was investigated for the hplc fractionation of the test solution on a silica column. Use of ether as the third eluting solvent proved, however, to be unsuitable. Bubbles tended to form in the hplc system, thereby impairing the performance of the pump and impeding the flow of solvent. Further, no compounds were recovered in the ether fraction. Therefore, methylene chloride was substituted for ether as the third eluting solvent.

The gradient program illustrated in Fig. 2(i) yielded the recoveries shown in Table 2 for six collected fractions. With the exception of 1-naphthol, excellent recoveries were obtained for all compounds and the elution patterns of Table 2 indicated that a fractionation scheme based on this eluting system was feasible. It was apparent that combination of some fractions and modification of the solvent gradients could improve the overall efficiency of the hplc separation procedure. Therefore, the gradient program of Fig. 2(ii) was employed and three fractions collected at the times indicated. This scheme was very effective and yielded the results shown in Table 3. High reproducibility of fractionation was obtained and separation of compounds into fractions was very distinct, with little cross-contamination. Hexyl benzene, biphenyl, dimethyl naphthalane, phenanthrene, aldrin, fluoranthene, and *o,p* DDT were confined to the hexane fraction (fraction 1). The esters – benzyl benzoate, methyl hendecanocate, and methyl tetradecanoate, and methoxychlor, dieldrin, endrin, α-BHC, and γ-BHC eluted in fraction 2. α-BHC seemed to elute just at the beginning of fraction 2 with the result that a small increase in the volume of hexane (5 mL) causes it to elute in the first fraction. The phenolic compounds, *o*-ethyl phenol, phenyl phenol, and 1-naphthol together with dibutyl phthalate were eluted in fraction 3. The recovery of 1-naphthol increased from 36% to 57% as the volume of methylene chloride was increased from 75 mL (Table 2) to ≈150 mL (Table 3). Further increase in the methylene chloride to 200 mL improved the recovery of 1-naphthol to 81%.

Fractionation of extracts of environmental samples

The optimized lpcc and hplc fractionation schemes were

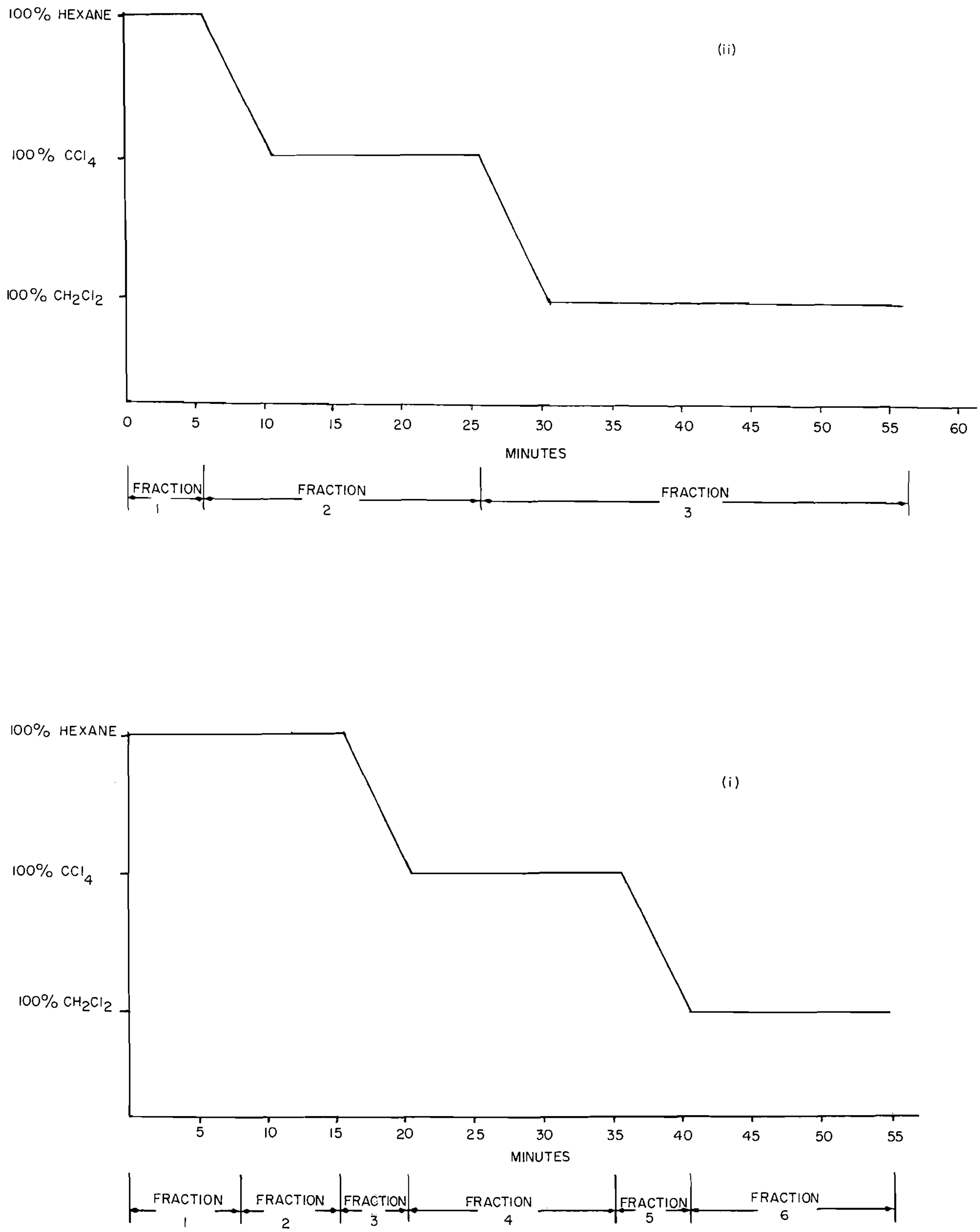

FIG. 2. Gradient programs for hplc fractionation of standard mixture.

TABLE 2. High performance liquid chromatographic fractionation (1) of standard test solution using gradient program of Fig. 2(i)

Pk. no.[a]	Compound	% Recovered						Total % Recovered
		Fraction 1	Fraction 2	Fraction 3	Fraction 4	Fraction 5	Fraction 6	
1	n-Hexyl benzene	64	—	—	—	—	—	64
2	*o*-Ethyl phenol	—	—	—	5	23	37	65
3	Biphenyl	75	—	—	—	—	—	75
4	Methyl hendecanoate	—	23	54	3	—	—	80
5	Dimethyl naphthalene	77	—	—	—	—	—	77
6	Dimethyl naphthalene	78	—	—	—	—	—	78
7	Dimethyl naphthalene	80	—	—	—	—	—	80
8	Phenyl phenol	—	—	—	11	51	28	90
9	Methyl tetradecanoate	—	28	62	4	—	—	94
10	1-Naphthol	—	—	—	—	—	36	36
11	α-BHC	59	32	—	3	—	—	94
12	Benzyl benzoate	—	38	52	—	—	—	90
13	Phenanthrene	95	—	—	—	—	—	95
14	γ-BHC	—	86	—	—	—	—	86
15	Aldrin	95	—	—	—	—	—	95
17	Dibutyl phthalate	—	—	—	—	26	80	106
18	Fluoranthene	103	—	—	—	—	—	103
19	Dieldrin	15	38	44	—	—	—	97
20	Endrin	14	44	43	—	—	—	101
21	*o,p* DDT	104	—	—	—	—	—	104
22	Methoxychlor	—	35	47	22	—	—	104

[a] Peak number as shown in Fig. 1.

TABLE 3. High performance liquid chromatographic fractionation of standard test solution using solvent gradient program of Fig. 2(ii)

Pk. no.[a]	Compound	% Recovered			
		Fraction 1	Fraction 2	Fraction 3	Total[b]
1	n-Hexyl benzene	50	—	—	50
2	*o*-Ethyl phenol	—	—	67	67
3	Biphenyl	69	—	—	69
4	Methyl hendecanoate	—	80	—	80
5	Dimethyl naphthalene	70	—	—	70
6	Dimethyl naphthalene	71	—	—	71
7	Dimethyl naphthalene	74	—	—	74
8	Phenyl phenol	—	21	63	84
9	Methyl tetradecanoate	—	95	—	95
10	1-Naphthol	—	—	57	57
11	α-BHC	11	82	—	93
12	Benzyl benzoate	—	103	—	103
13	Phenanthrene	89	—	—	89
14	γ-BHC	—	96	—	96
15	Aldrin	93	—	—	93
17	Dibutyl phthalate	—	—	88	88
18	Fluoranthene	97	—	—	97
19	Dieldrin	14	82	—	96
20	Endrin	16	77	—	93
21	*o,p* DDT	102	—	—	102
22	Methoxychlor	—	105	—	105

[a] Peak number as shown in Fig. 1.
[b] Average relative standard deviation from mean of triplicate analysis = 6%; range 4–7%.

applied to the fractionation of organic extracts of water samples from Mausica River, Trinidad (9). Figure 3 shows chromatograms of the fractions of the hplc procedure. The chromatograms obtained for the lpcc fractionation were similar to those of hplc. The hexane fraction in both cases contained the alkanes. Most of the other constituents of the unfractionated samples occurred in the ether fraction of the lpcc method and in fraction 3 of the hplc technique. These included the phenols, phthalates, benzothiazole, 6-chloro-3,4-dimethylphenol n-methyl carbamate, 1-(3*H*)-isobenzofuranone, and 1,6-dimethyl 4-isopropyl naphthalene. The lpcc carbon tetrachloride fraction and hplc fraction 2 contained virtually no compounds except for a small amount of phenols which occurred in the lpcc carbon tetrachloride fraction.

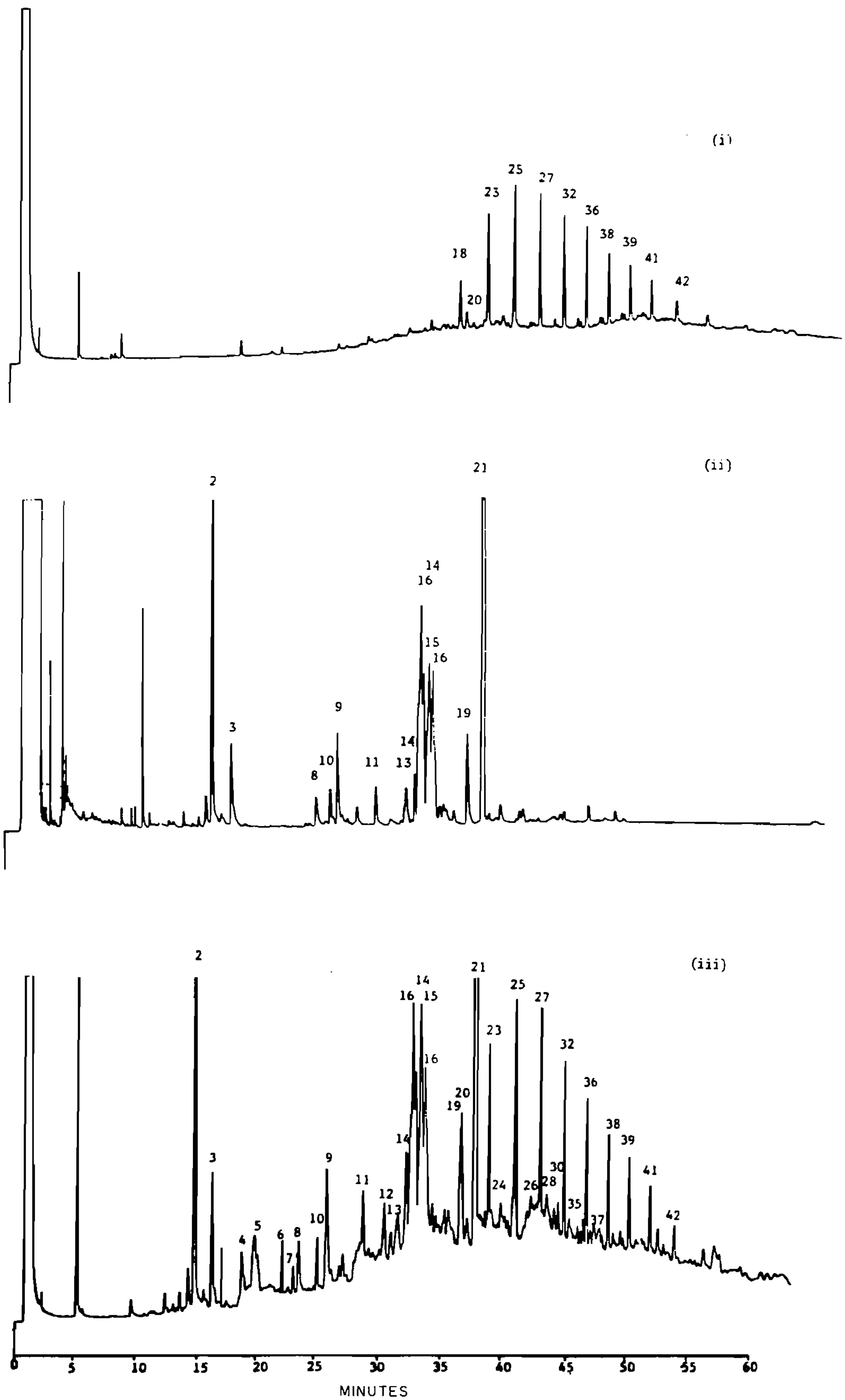

FIG. 3. Gas chromatograms of fractions obtained from hplc separation of organic extract of Mausica River sample. (i) Fraction 1. (ii) Fraction 3. (iii) Unfractionated Extract. Gradient program of Fig. 2(ii) employed.

TABLE 4. Estimated recoveries of constituents of Mausica River extract after lpcc and hplc fractionation

Pk. no.[a]	Compound	Florisil fractionation				Hplc fractionation		
		C_2H_{12}	CCl_4	Et_2O	Total	C_6H_{12}	Et_2O	Total
1	2-Ethyl-1-hexanol							
2	α-Terpineol			35	35		48	48
3	Benzothiazole			25	25		48	48
4	Unidentified							
5	Unidentified			42	42			
6	Unidentified							
7	Unidentified							
8	1-(3*H*)-Isobenzofuranone			37	37		52	52
9	6-Chloro-3,4-dimethyl phenol n-methyl carbamate		5	35	40		45	45
10	2,4-Dimethyl, 6-*t*-butyl phenol (or isomer)		10	40	50		57	57
11	Diethyl phthalate			68	68		59	59
12	*p*-Propoxy phenol	√		49	49		√	
13	Unidentified			44	44		49	49
14	*p*-Nonyl phenol or isomers		15	50	65		30	30
15	Unidentified		√	√				
16	4-(2,2,3,3-Tetramethyl butyl) phenol or isomers		15	57	72		58	58
17	Dodecyl phenol or isomer							
18	Eicosane	√				√		
19	1,6-Dimethyl 4-isopropyl naphthalene			√				
20	*S*-Hydrindacene 1,1,4,5,6,8-hexamethyl	√						
21	Dibutyl phthalate			44	44			
22	2-Hydroxy-benzothiazole							
23	Heneicosane (C_{21} alkane)	84			84	79		79
24	1-Naphthyl-n methyl carbamate			√				
25	Docosane	75			75	88		88
26	Unidentified							
27	Tricosane	73			73	91		91
28	2,6-di-*t*-butyl-4 mercaptophenol							
29	Unidentified							
30	2,6-Dinonyl phenol or isomers							
31	2,6,10-Trimethyl tetradecane							
32	Tetracosane	76			76	90		90
33	11-Cyclohexyl heneicosane							
34	9-Cyclohexyl heptadecane							
35	1-Phenanthrene carboxylic acid, 1,2,3,4,4a, 9,10,10a-octahydro-1,4a-dimethyl-7-(1-methylethyl)-methyl ester							
36	Pentacosane	77			77	95		95
37	3-Hydroxy 4-isopropyl 5,10-dimethyl decalone-1							
38	Hexacosane	78			78	101		101
39	Heptacosane	72			72	99		99
40	Di(2-ethylhexyl)phthalate							
41	Octacosane	70			70	98		98
42	Unidentified	√				99		99

[a] Peak number as shown in Fig. 3(iii); √ – present, but no estimate can be given.

Recoveries for some of the compounds in the various fractions are given in Table 4. These values are based on the integrated peak areas of the fractions compared with the corresponding peak areas of the unfractionated sample injected under the same conditions. The errors in these estimates for the peaks at retention times greater than 20 min (Fig. 3) are expected to be fairly high as a result of the low resolution of several peaks in this region of the chromatogram. The recoveries of several compounds in the ether fraction of the lpcc fractionation and fraction 3 of the hplc method were low. Increasing the volume of these eluents above the 50 mL volume which was used can be expected to result in improved recoveries.

Nonetheless, the fractionation schemes were effective in simplifying the sample extract and served to improve the reliability of mass spectral identifications. Compounds identified in extracts from the Mausica River are detailed in Table 4. Several of these compounds could not be identified from the mass spectra of the unfractionated samples because of peak overlap and high backgrounds. Their identification was facilitated by application of the fractionation procedures. Much of the unresolved "hump" evident in the chromatogram of the unfractionated sample was not seen in the chromatograms of the fractions (Fig. 3).

A further benefit of hplc and lpcc fractionation is the preservation of the chromatographic column. Figure 4 depicts the effect on the column performance of a single injection of the unfractionated sample. The lower trace represents a chromatogram of the test solution used in the earlier fractionation experiments, prior to the injection of the unfractionated sample. The

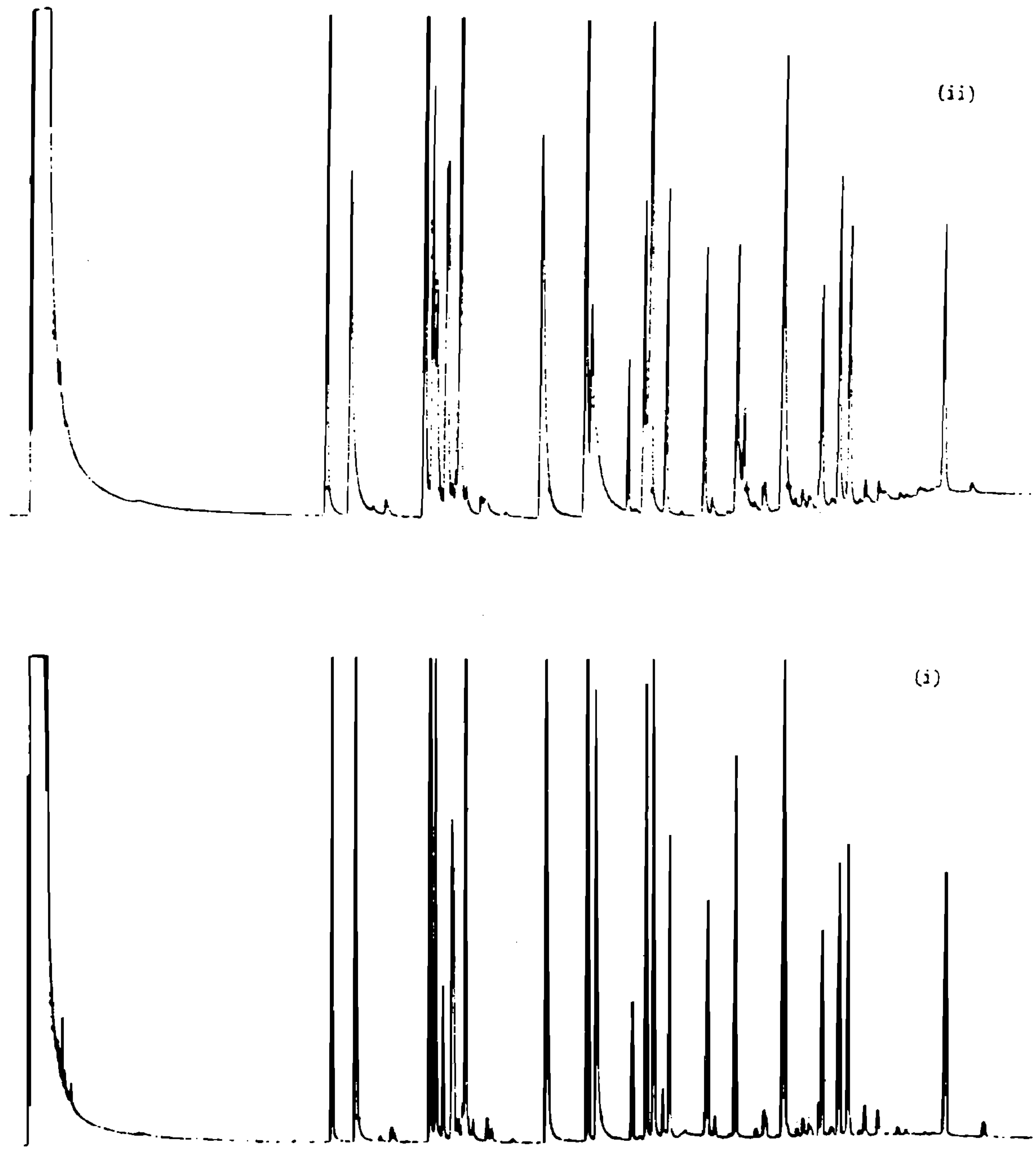

FIG. 4. Chromatograms illustrating the effect of unfractionated extracts of samples on column performance. (i) Standard mixture before injection of unfractionated extract. (ii) Standard mixture following one injection of unfractionated extract.

upper trace is the chromatogram obtained for the test solution injected immediately after the completion of the chromatographic run of the sample. The column efficiency is severely affected, as is evident from the broad tailing peaks. A portion of the front of the column had to be removed in order to restore the column performance to the original level. Column deterioriation was much slower when samples were subjected to fractionation prior to gc analysis.

Conclusion

The hplc and lpcc techniques were effectively used for fractionation of environmental water samples prior to gc and gc/ms analysis. This prefractionation afforded more highly reliable gc/ms identification of sample components and lessened degradation of the capillary columns. The hplc fractionation was faster and more highly reproducible than the lpcc technique. The effectiveness of methylene chloride for separation of the more polar components in the hplc method is advantageous compared to the lpcc method which required ether, since diethyl ether must be purified prior to being used. The lpcc method has the advantage of lower cost owing to the very simple apparatus that is required for its application.

Acknowledgements

This work was supported by a grant from the International Development Research Centre (I.D.R.C.).

1. H. BRAUS, F. M. MIDDLETON, and G. WALTON. Anal. Chem. **23**, 1160 (1951).

2. H. BRAUS, F. M. MIDDLETON, and C. C. RUCHHOFT. Anal. Chem. **24**, 1872 (1952).
3. A. A. ROSEN and F. M. MIDDLETON. Anal. Chem. **27**, 790 (1955).
4. R. SHINOHARA, A. KIDO, S. ETO, T. HORI, M. KOGA, and T. AKIYAMA. Water Res. **15**, 535 (1981).
5. J. A. LEENHEER and E. W. D. HUFFMAN, JR. J. Res. U.S. Geol. Surv. **4**, 737 (1976).
6. J. A. LEENHEER. Environ. Sci. Technol. **15**, 578 (1981).
7. J. J. RICHARD and J. S. FRITZ. J. Chromatogr. Sci. **18**, 35 (1980).
8. A. D. THRUSTON, JR. J. Chromatogr. Sci. **16**, 254 (1978).
9. R. A. MOORE and F. W. KARASEK. Int. J. Environ. Anal. Chem. **17**, 203 (1984).
10. R. A. MOORE and F. W. KARASEK. Int. J. Environ. Anal. Chem. **17**, 187 (1984).

Novel hydrogen bonding in crystalline tetra-n-butylammonium salts of catechol halides[1]

MASOOD A. KHAN, ARCHIBALD W. MCCULLOCH, AND A. GAVIN MCINNES

Atlantic Research Laboratory, National Research Council of Canada, 1411 Oxford Street, Halifax, N.S., Canada B3H 3Z1

Received August 28, 1984

MASOOD A. KHAN, ARCHIBALD W. MCCULLOCH, and A. GAVIN MCINNES. Can. J. Chem. **63**, 2119 (1985).

The crystal structures of $[N(n\text{-}C_4H_9)_4]$ [catechol...Cl] (**1**) and $[N(n\text{-}C_4H_9)_4]$ [catechol...Br] (**2**) have been determined by X-ray analysis which showed that the two structures are isomorphous, with the orthorhombic space group *Pbca*, $Z = 8$. The cell dimensions and final *R*-values are: (**1**) $a = 15.323(2)$, $b = 16.166(2)$, $c = 19.713(2)$ Å, $R = 0.048$ for 1361 observed reflections; (**2**) $a = 15.432(1)$, $b = 16.244(2)$, $c = 19.824(1)$ Å, $R = 0.041$ for 1958 observed reflections. The crystal structures consist of discrete tetra-n-butylammonium cations and catechol halide anions. Catechol forms two strong hydrogen bonds to a single halide ion giving a pattern of hydrogen bonding unique for such systems.

MASOOD A. KHAN, ARCHIBALD W. MCCULLOCH et A. GAVIN MCINNES. Can. J. Chem. **63**, 2119 (1985).

Faisant appel à la diffraction des rayons-X, on a déterminé les structures cristallines du $[N(n\text{-}C_4H_9)_4]$ [catéchol...Cl] (**1**) et du $[N(n\text{-}C_4H_9)_4]$ [catéchol...Br] (**2**) qui sont isomorphes, avec un groupe d'espace orthorhombique *Pbca* et $Z = 8$. Les dimensions de la maille et les valeurs finales de *R* sont: (**1**) a = 15,323(2), b = 16,166(2), c = 19,713(2) Å, R = 0,048 pour 1361 réflexions observées; (**2**) a = 15,432(1), b = 16,244(2), c = 19,824(1) Å, R = 0,041 pour 1958 réflexions observées. Les structures cristallines comportent des cations tétra-n-butylammonium ainsi que des anions halogénures de catéchol individuels. Le catéchol forme deux liaisons hydrogènes fortes avec un seul ion halogénure et ceci provoque la formation d'un type de liaisons hydrogènes qui est unique pour de tels systèmes.

[Traduit par le journal]

Introduction

During recent investigations of the use of the tetrabutylammonium salt of the silicon–catechol complex in silicon analysis we isolated a crystalline 2:1 complex of catechol and tetrabutylammonium hydroxide. A recent communication from this laboratory reported the synthesis and structural study of this and a series of other complexes of aromatic hydroxy compounds with ammonium salts and amines, and the existence of novel hydrogen-bonding networks in these compounds (1). We now report the preparation, characterization, and crystal structures of the tetra-n-butylammonium salts of catechol chloride **1** and catechol bromide **2**.

Experimental

The ^{1}H (80 MHz) and ^{13}C (20 MHz) nmr spectra were recorded in $CDCl_3$ on a Varian FT-80A spectrometer with internal ^{2}H lock to the solvent and a temperature of 35°C. Conditions for the ^{1}H spectra were SW 1000 Hz, AT 4.1 s (data accuracy ±0.1 Hz), FA 90°. The ^{13}C spectra were acquired with SW 4132 Hz, AT 0.99 or 1.982 s (data accuracy ±0.5 or ±0.3 Hz), FA 23° or 45°, ^{1}H irradiation at 80 Hz, (a) $\gamma H_2/2\pi \sim 4000$ Hz, modulation bandwidth 2000 Hz (broadband decoupling), (b) as for (a) but irradiating for 2.0 s between data acquisitions only to retain nOe (HR spectra). The infrared spectra were recorded on a BOMEM DA 3.02 FTIR spectrophotometer, the samples being in the form of fluorocarbon mulls sandwiched between KBr windows.

Preparation of complexes

1: A solution of tetra-n-butylammonium chloride (1.39 g) in water (15 mL) was added to a solution of 1,2-benzenediol (0.55 g) in water (10 mL). After a few minutes the aqueous mixture was extracted with CH_2Cl_2 (4 × 20 mL). Drying and evaporation followed by recrystallization from petroleum ether (bp 60–80°C)/ethyl acetate gave **1** as colorless prisms, mp 74–75°C; ν_{max}: most intense absorption at 3135 cm^{-1}; δ_H: 0.95 (12H, m), 1.40 (16H, m), 3.14 (8H, m), 6.76 (4H, centroid of AA'XX' m), 8.57 (2H, s); δ_C: 13.62 (qm), 19.57 (bt), 23.83 (bt), 58.46 (bt), 116.97 (dm, 157.7), 120.14 (dd, 160.4, 8.5), 145.16 (m).

TABLE 1. Summary of crystal data, intensity collections, and structural refinement for $C_{22}H_{42}ClNO_2$ (**1**) and $C_{22}H_{42}BrNO_2$ (**2**)

Parameters		1	2
fw		388.04	432.49
Cell constants (Å)[a] at 22°C	*a*	15.323(2)	15.432(1)
	b	16.166(2)	16.244(2)
	c	19.713(2)	19.824(1)
V (Å^3)		4883	4970
D_c (g cm^{-3})		1.056	1.156
μ (cm^{-1})		14.84	23.52
Crystal dimensions (mm)		0.15 × 0.40 × 0.40	0.24 × 0.26 × 0.26
Min/max abs. correct		1.22/1.72	1.45/1.69
2 θ angle (°): Cell const.		94–110	109–119
Data collection		4–110	4–130
Reflections measd. (h, k, l)		3077	4235
Reflections used		1361	1958
$R = [\Sigma(\lvert F_o\rvert - \lvert F_c\rvert)/\Sigma\lvert F_o\rvert)$		0.048	0.041
$R_w = [\Sigma w(F_o - F_c)^2/wF_o^2]^{1/2}$		0.057	0.048
$S = [\Sigma(F_o - F_c)^2/(m - n)]^{1/2}$		2.05	1.64
(Shift/error)$_{max}$		0.02	0.06
ρ_{max} (e Å^{-3})		0.14	0.27

[a]The cell constants were derived by least-squares analysis of the diffractometer setting of 24 well-centered high-angle reflections.

2: The corresponding bromide was prepared by analogous reaction of tetra-n-butylammonium bromide (16.14 g) and 1,2-benzenediol (5.50 g). Recrystallization from petroleum ether/ethyl acetate gave **2** as colorless prisms, mp 84–85°C; ν_{max}: most intense absorption at 3216 cm^{-1}; δ_H: 0.96 (12H, m), 1.47 (16H, m), 3.19 (8H, m), 6.81 (4H, centroid of AA'XX' m), 7.68 (2H, s); δ_C: 13.57 (qm), 19.61

[1]NRCC No. 24148.

TABLE 2*a*. Atomic parameters *x*, *y*, *z* and B_{eq}[a] for **1** (e.s.d's refer to the last digit printed)

Atom	*x*	*y*	*z*	B_{eq}, Å^2
Cl	0.13726(9)	0.18831(8)	0.00845(7)	9.6
O(1)	0.1015(2)	0.0820(2)	−0.1140(2)	8.8
O(2)	0.1831(3)	0.2388(2)	−0.1354(2)	12.1
N	0.1719(2)	0.8943(2)	0.0501(2)	6.0
C(1)	0.1093(3)	0.1185(3)	−0.1765(2)	6.8
C(2)	0.1480(3)	0.1935(3)	−0.1871(2)	8.0
C(3)	0.1513(4)	0.2258(3)	−0.2526(3)	9.8
C(4)	0.1164(3)	0.1823(3)	−0.3064(2)	9.7
C(5)	0.0790(4)	0.1072(3)	−0.2947(3)	9.7
C(6)	0.0762(3)	0.0762(3)	−0.2302(2)	8.4
C(11)	0.1747(3)	0.8089(2)	0.0813(2)	5.9
C(12)	0.0881(3)	0.7715(3)	0.1020(2)	7.0
C(13)	0.1062(3)	0.6841(3)	0.1297(2)	8.4
C(14)	0.0226(4)	0.6390(3)	0.1440(3)	11.7
C(21)	0.1370(3)	0.9584(2)	0.1012(2)	6.7
C(22)	0.1879(4)	0.9633(3)	0.1668(2)	8.6
C(23)	0.1547(4)	1.0338(3)	0.2110(3)	9.4
C(24)	0.2002(5)	1.0385(3)	0.2786(3)	11.7
C(31)	0.2649(3)	0.9140(3)	0.0299(2)	6.2
C(32)	0.2781(3)	0.9952(3)	−0.0071(2)	7.2
C(33)	0.3751(3)	1.0086(4)	−0.0194(3)	9.0
C(34)	0.3918(4)	1.0905(4)	−0.0565(3)	11.1
C(41)	0.1108(3)	0.8967(3)	−0.0103(2)	6.5
C(42)	0.1368(3)	0.8398(3)	−0.0672(2)	8.0
C(43)	0.0688(4)	0.8436(4)	−0.1227(2)	10.2
C(44)	0.0929(4)	0.7879(4)	−0.1808(3)	14.7
HO1	0.104(3)	0.115(3)	−0.069(2)	12.4
HO2	0.170(4)	0.226(3)	−0.089(3)	16.8

[a]$B_{eq} = 8\pi^2[1/3(U_{11} + U_{22} + U_{33})]$.

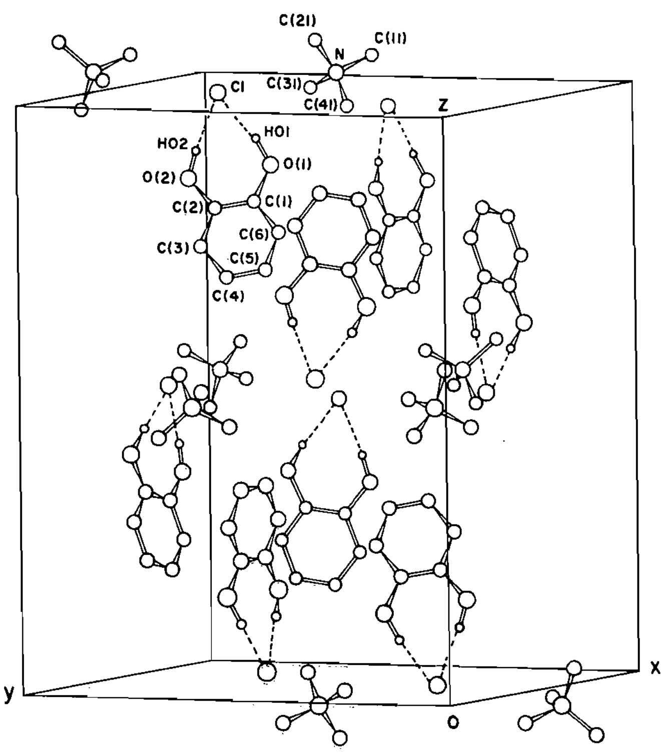

FIG. 1. Packing diagram for **1**. For clarity only one carbon atom of each butyl group is shown. Labelled atoms have the symmetry equivalent positions of $0.5 - x$, $0.5 + y$, $1 + z$ for the catechol moiety and $0.5 - x$, $-0.5 + y$, $1 + z$ for the cation.

TABLE 2*b*. Atomic parameters **2**

Atom	*x*	*y*	*z*	B_{eq}
Br	0.13387(3)	0.19095(4)	0.00888(3)	7.48
O(1)	0.1045(2)	0.0778(2)	−0.1201(2)	8.0
O(2)	0.1848(3)	0.2353(2)	−0.1441(2)	11.4
N	0.1725(2)	0.8964(2)	0.0513(2)	5.3
C(1)	0.1096(3)	0.1140(3)	−0.1822(2)	6.2
C(2)	0.1485(3)	0.1892(3)	−0.1933(2)	7.0
C(3)	0.1499(4)	0.2213(3)	−0.2577(3)	8.8
C(4)	0.1128(3)	0.1783(3)	−0.3106(2)	8.9
C(5)	0.0764(3)	0.1026(4)	−0.2987(2)	8.7
C(6)	0.0750(3)	0.0715(3)	−0.2354(2)	7.5
C(11)	0.1741(3)	0.8107(2)	0.0830(2)	5.5
C(12)	0.0878(3)	0.7748(3)	0.1033(2)	6.4
C(13)	0.1036(3)	0.6885(3)	0.1306(2)	7.6
C(14)	0.0203(4)	0.6436(3)	0.1446(3)	10.7
C(21)	0.1375(3)	0.9607(3)	0.1008(2)	6.1
C(22)	0.1853(3)	0.9664(3)	0.1674(2)	7.9
C(23)	0.1550(3)	1.0366(3)	0.2099(3)	8.6
C(24)	0.1985(4)	1.0423(4)	0.2763(3)	11.5
C(31)	0.2657(3)	0.9156(3)	0.0322(2)	5.6
C(32)	0.2794(3)	0.9959(3)	−0.0051(2)	6.4
C(33)	0.3755(3)	1.0103(3)	−0.0162(3)	7.8
C(34)	0.3930(4)	1.0897(4)	−0.0535(3)	10.2
C(41)	0.1128(3)	0.8984(3)	−0.0096(2)	6.0
C(42)	0.1377(3)	0.8407(3)	−0.0657(2)	7.4
C(43)	0.0744(4)	0.8461(4)	−0.1235(2)	9.7
C(44)	0.0959(4)	0.7879(5)	−0.1800(3)	12.8
HO1	0.115(3)	0.108(3)	−0.082(2)	12.0
HO2	0.177(3)	0.219(3)	−0.102(3)	14.1

(bt), 24.01 (bt), 58.80 (bt), 116.62 (dm, 158.2), 120.22 (dd, 160.4, 8.7), 145.01 (m).

Crystallography

Crystals of **1** and **2** are orthorhombic, space group *Pbca* (from single-crystal photographs and diffractometry), $Z = 8$. Suitable specimens were mounted on glass fibers for data collection. The relative intensities of the independent reflections were measured with a Picker four-circle diffractometer, using Ni-filtered CuK_α radiation ($\lambda K\alpha_1$ = 1.54056 Å). The $\theta - 2\theta$ scan method was used, and individual reflection profiles were analysed as described by Grant and Gabe (2). The intensities of the three monitor reflections did not change significantly during data collection. The standard deviations were evaluated from the counting statistics, and only the reflections with $I_{net} > 2\sigma(I_{net})$ were used in the subsequent analysis. Absorption correction (Gaussian integration) was applied to the intensities.

The structures were solved by the heavy atom method and refined by block-diagonal least squares, minimizing $\Sigma w(F_o - kF_c)^2$ where $w = [\sigma^2(F_o) + 0.0003F_o^2]^{-1}$. Positional and thermal parameters (anisotropic thermal motion was assumed for all non-hydrogen atoms) were refined for all the atoms, except methylene and phenyl hydrogen atoms, which were included in the idealized position (C—H = 1.08 Å) and only an individual isotropic temperature factor was refined for them.

The computer programs used for calculation have been described by Larson and Gabe (3). The atomic scattering factors[2] were taken from International Tables, Vol. IV (ref. 4).

Crystal data and some details of refinement are given in Table 1, and atomic coordinates in Table 2. Bond lengths and angles are given in Table 3, and details of hydrogen-bond interactions in Table 4. Tables of structure factors, anisotropic thermal parameters, hydrogen atom coordinates are available as supplementary data.[3]

[2]Neutral scattering curves were used for Cl and Br.

[3]Complete set of data is available upon request, at a nominal charge, from the Depository of Unpublished Data, CISTI, National Research Council of Canada, Ottawa, Ont., Canada K1S 0A2.

TABLE 3*a*. Bond distances (Å) and angles (°) for catechol

Distances	1	2
O(1)—HO(1)	1.03(4)	0.92(5)
O(1)—C(1)	1.372(5)	1.366(5)
O(2)—HO(2)	0.96(5)	0.87(5)
O(2)—C(2)	1.365(6)	1.351(6)
C(1)—C(2)	1.366(6)	1.378(6)
C(1)—C(6)	1.359(6)	1.369(6)
C(2)—C(3)	1.394(7)	1.380(7)
C(3)—C(4)	1.380(8)	1.384(8)
C(4)—C(5)	1.363(8)	1.371(8)
C(5)—C(6)	1.367(7)	1.353(7)
Angles		
C(1)—O(1)—HO(1)	122(2)	120(3)
C(2)—O(2)—HO(2)	121(3)	117(3)
O(1)—C(1)—C(2)	123.8(4)	123.4(4)
O(1)—C(1)—C(6)	116.8(4)	117.0(4)
C(2)—C(1)—C(6)	119.4(4)	119.6(4)
O(2)—C(2)—C(1)	122.2(4)	123.9(4)
O(2)—C(2)—C(3)	118.5(4)	116.8(4)
C(1)—C(2)—C(3)	119.3(5)	119.4(5)
C(2)—C(3)—C(4)	120.5(5)	120.2(5)
C(3)—C(4)—C(5)	119.1(5)	119.5(4)
C(4)—C(5)—C(6)	119.9(5)	120.1(5)
C(1)—C(6)—C(5)	121.9(5)	121.3(5)

TABLE 3*b*. Bond distances (Å) and angles (°) for the cation

Distances	1	2
N—C(11)	1.511(5)	1.528(5)
N—C(21)	1.541(5)	1.533(5)
N—C(31)	1.513(6)	1.519(5)
N—C(41)	1.517(5)	1.519(5)
C(11)—C(12)	1.514(6)	1.507(6)
C(12)—C(13)	1.540(6)	1.523(6)
C(13)—C(14)	1.502(8)	1.502(8)
C(21)—C(22)	1.513(7)	1.514(7)
C(22)—C(23)	1.521(6)	1.493(7)
C(23)—C(24)	1.507(8)	1.480(8)
C(31)—C(32)	1.515(6)	1.515(6)
C(32)—C(33)	1.523(7)	1.517(6)
C(33)—C(34)	1.533(7)	1.512(8)
C(41)—C(42)	1.504(6)	1.504(7)
C(42)—C(43)	1.513(7)	1.509(7)
C(43)—C(44)	1.503(9)	1.502(9)
Angles		
C(11)—N—C(21)	111.0(3)	111.3(3)
C(11)—N—C(31)	105.9(3)	105.9(3)
C(11)—N—C(41)	111.1(3)	110.8(3)
C(21)—N—C(31)	110.9(3)	110.8(3)
C(21)—N—C(41)	106.4(3)	106.3(3)
C(31)—N—C(41)	111.7(3)	111.8(3)
N—C(11)—C(12)	116.7(3)	116.7(3)
C(11)—C(12)—C(13)	107.7(4)	108.1(4)
C(12)—C(13)—C(14)	111.0(4)	112.1(4)
N—C(21)—C(22)	114.5(3)	115.3(3)
C(21)—C(22)—C(23)	110.9(4)	112.7(4)
C(22)—C(23)—C(24)	113.0(4)	114.1(5)
N—C(31)—C(32)	115.8(3)	115.5(3)
C(31)—C(32)—C(33)	109.3(4)	109.9(4)
C(32)—C(33)—C(34)	111.2(5)	112.2(4)
N—C(41)—C(42)	113.9(4)	114.8(3)
C(41)—C(42)—C(43)	109.3(4)	111.1(4)
C(42)—C(43)—C(44)	110.9(5)	112.7(5)

TABLE 4. Hydrogen-bonded interactions

	1	2
O(1)...X	3.014(3) Å	3.182(3) Å
O(2)...X	3.033(4)	3.215(4)
HO(1)...X	2.00(4)	2.26(4)
HO(2)...X	2.08(5)	2.35(5)
O(1)—HO(1)...X	166(4)°	176(4)°
O(2)—HO(2)...X	174(4)	170(4)

Results and discussion

The X-ray analysis of compounds **1** and **2** established that they are isomorphous and that the crystal structures consist of discrete tetra-n-butylammonium cations and catechol halide anions (Fig. 1). The structure of the tetra-n-butylammonium cation is normal and calls for no special comments (Table 3*b*).

The halide ion accepts two essentially linear hydrogen bonds from the same catechol (Fig. 1; Table 4). The O...Cl distances are at the lower end of the range of reported values (3.045(3)−3.317(2) Å (5)), while the O...Br distances are in the usual range (3.19(1)−3.22(1) Å (6, 7)). These distances are smaller than the corresponding sums of van der Waals radii (3.27 Å for **1**, 3.37 Å for **2** (8)); the differences are 0.24 and 0.26 Å for **1**, and 0.16 and 0.19 Å for **2**. These results indicate that hydrogen bonding is stronger in **1** than in **2**. This is substantiated by their ir spectra which are identical except in the region of the OH stretching modes. The OH stretching absorption band for **2** occurs at 3216 cm^{-1}, and that for **1** at 3135 cm^{-1}, 81 cm^{-1} lower.

The pattern of hydrogen bonding found in **1** and **2** appears to be unique for such systems. In a number of catecholamine halides (refs. 6, 9−11) the hydroxyl groups are hydrogen bonded to two different halogens, as in **3**. Moreover, in these

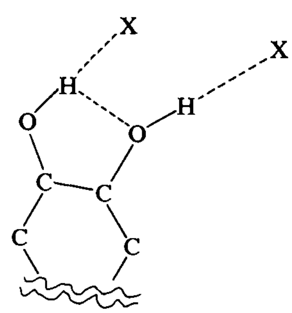

3

compounds, as in native catechol (12), and in the tetraethylammonium salt (1), one hydrogen atom lies outside the sector bounded by the C—O vectors, while the other lies inside, often forming an intramolecular bond (see, **3**). The pattern of hydrogen bonding in **1** and **2**, in which the halide ion accepts two bonds from the same catechol, requires that both hydrogen atoms lie inside the sector (Fig. 1) with unusually short non-bonded distances of 2.10(6) Å for **1** and 2.09(7) Å for **2**. Crystal packing may be the determining factor for such an unusual hydrogen-bond configuration, since it would otherwise be unstable, because of the repulsion of the similarly charged hydrogen atoms (13). This repulsion causes the oxygen atoms to be farther apart than they would otherwise be, with an increase of the C(1)—C(2)—O(2) and C(2)—C(1)—O(1) angles (Fig. 1; 122.2(4) to 123.9(4)°), and a decrease of the C(3)—C(2)—O(2) and C(6)—C(1)—O(1) angles (116.8(4) to 118.5(4)°) from the ideal value of 120°.

Our studies of hydrogen bonding in these complexes are continuing. If indeed crystal packing forces dictate the unusual pattern observed in **1** and **2**, substitution of a smaller cation may result in restoration of the more usual hydrogen-bonding network. We are also studying the nature of hydrogen bonding of **1** and **2** in solution.

Acknowledgements

We wish to thank Dr. A. W. Hanson and Dr. M. Falk for helpful discussions. Our thanks go also to P. F. Seto for ir data. M.A.K. thanks NSERC for the award of a visiting fellowship.

1. A. W. HANSON, A. W. MCCULLOCH, and A. G. MCINNES. Tetrahedron Lett. **23**, 607 (1982).
2. D. F. GRANT and E. J. GABE. J. Appl. Crystallogr., **11**, 114 (1978).
3. A. C. LARSON and E. J. GABE. Computing in crystallography. Delft University Press, Delft, Holland. 1978. pp. 81–89.
4. International tables for X-ray crystallography. Vol. IV. Kynoch Press, Birmingham. Table 2.2B ("SDS" for H, "RAF" otherwise); Table 2.3.1 for halogen dispersion correction (1974).
5. P. SCHUSTER, G. ZUNDEL, and C. SANDORFY (*Editors*). The hydrogen bond. Vol. II, North Holland Publishing Company, Amsterdam. 1976. pp. 440–456.
6. J. GIESECKE. Acta Crystallogr. Sect. B, B**32**, 2337 (1976).
7. D. L. WARD, K. WEI, J. G. HOOGERHEIDE, and A. I. POPOV. Acta Crystallogr., Sect. B, **34**, 110 (1978).
8. A. BONDI. J. Phys. Chem. **68**, 441 (1964).
9. J. GIESECKE. Acta Crystallogr. Sect. B, **36**, 178 (1980).
10. J. GIESECKE. Acta Crystallogr. Sect. B, **29**, 1785 (1973).
11. D. CARLSTROM. Acta Crystallogr., Sect. B, **29**, 161 (1973).
12. VON H. WUNDERLICH and D. MOOTZ. Acta Crystallogr. Sect. B, **27**, 1684 (1971).
13. L. PAULING. The nature of the chemical bond. Cornell University Press, Ithaca, NY. 1960. pp. 494–495.

The reaction of 3-methyltricarballylic acid with acetic anhydride: three products of acylative decarboxylation[1]

GEORGE M. STRUNZ, GESSIE BRISARD,[2] AND PIERRE GIGUÈRE
Maritimes Forest Research Centre, Canadian Forestry Service, P.O. Box 4000, Fredericton, N.B., Canada E3B 5P7

Received September 20, 1984

GEORGE M. STRUNZ, GESSIE BRISARD, and PIERRE GIGUÈRE. Can. J. Chem. **63**, 2123 (1985).

Three products, 2-acetonyl-2-methylsuccinic anhydride (**5**), 2,7-dioxa-1,5-dimethylbicyclo[3.2.1]octane-3,6-dione (**6**), and 3-acetonyl-3,5-dimethyl-2(3*H*) furanone (**7**) were identified from the base-catalysed reaction of 3-methyltricarballylic acid with acetic anhydride. These compounds arise as a result of acylative decarboxylation of 3-methyltricarballylic acid.

GEORGE M. STRUNZ, GESSIE BRISARD et PIERRE GIGUÈRE. Can. J. Chem. **63**, 2123 (1985).

On a identifié trois produits de la réaction de l'acide tricarballylique-3-méthyle avec l'anhydride acétique sous catalyse basique: l'anhydride succinique acétonyl-2 méthyl-2 (**5**), le bicyclo[3.2.1] octane dioxa-2,7 dicéto-3,6 diméthyl-1,5 (**6**), et le 2(3*H*) furanone acétonyl-3 dimethyl-3,5 (**7**). Ces composés résultent de la décarboxylation acylative de l'acide tricarballylique-3-méthyle.

In 1901, Rudolph Fittig reported that reaction of the sodium salt of tricarballylic acid with acid anhydrides afforded bislactones of structure **1** (1). We have been interested in the potential of these compounds (and of the spiro bislactone **2**) as precursors for the synthesis of 1,4-diketones, hence of substituted cyclopentenones (2, 3).

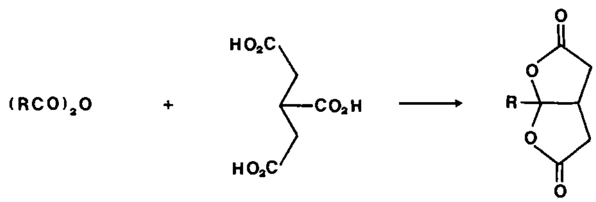

1

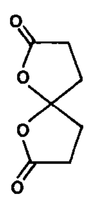

2

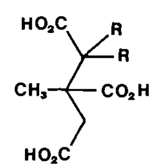

3

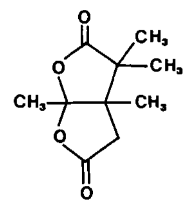

4

In contemplating the mechanism by which the bislactones **1** are formed, Fittig (1) recognized that acylation of tricarballylic acid (or a derivative) at C-3 would afford a β-ketoacid which could readily undergo decarboxylation to a ketodicarboxylic acid capable of cyclization to **1**. To test whether this was indeed the course of the transformation, he selected a tricarballylic acid derivative, camphoronic acid **3** (R = CH_3), which could not undergo direct acylation at C-3 prior to decarboxylation, and subjected its salt similarly to reaction wih acetic anhydride. The isolation in low yield of a crystalline product, which he considered to be the bislactone **4**, led Fittig to propose that the reaction proceeded instead by extrusion of carbon dioxide from a mixed anhydride, involving the carboxyl group at C-3 (Fig. 1). The first mechanism, which can be formulated in several essentially equivalent ways (e.g., Scheme 1 (R = H)[3,4]; cf. ref. 4) appears to provide a more plausible pathway to the bislactones (1), notwithstanding its inability to account for the formation of **4** from camphoronic acid. We report herein our parallel studies on the reaction of the related, simpler and more readily available[5] 3-methyltricarballylic acid **3** (R = H) with acetic anhydride. The results suggest an alternative interpretation of Fittig's observations in the camphoronic acid experiment.

In his pioneering studies, Fittig obtained optimum results when he treated the sodium salt of tricarballylic acid with 1.5 equivalents of anhydride (1). Later workers found that enhanced yields of the bislactones were obtained when the free acid was used with a larger excess of anhydride (5), particularly in the presence of powdered soft glass or employing a reaction vessel which was previously washed with a strongly alkaline detergent (6). Our own studies demonstrated that pyridine can be an effective catalyst for the process (2).

When 3-methyltricarballylic acid **3** (R = H) was heated under reflux with an excess of acetic anhydride in the presence of a catalytic amount of pyridine, evolution of carbon dioxide was sluggish. A more expeditious reaction occurred when 4-dimethylaminopyridine (7) was employed as catalyst. The attendant, initially vigorous, evolution of carbon dioxide moderated with time, and was quite slow after 4.5 h, when the reaction was terminated by removal of volatile material under reduced pressure. After charcoal treatment, the crude residue solidified, and afforded a pure product, A, by crystallization from ethyl acetate. Flash chromatography (8) of the mother liquor augmented the yield of A (total 42%), and gave two additional (incompletely resolved) products, designated B and C in order of increasing chromatographic mobility. Product B could be isolated by crystallization of material from the appropriate chromatographic fractions, while the minor component C required further chromatographic purification.

[1] Presented in part at the CAN–AM Chemical Congress, Montreal, June 6, 1984.

[2] Undergraduate cooperative program participant from Université de Sherbrooke.

[3] Acylation might be intermolecular, but a possible mode of intramolecular acylation is shown in Scheme 1.

[4] We thank a referee for suggesting modifications to the mechanistic scheme originally depicted.

[5] Commercially available.

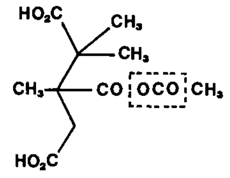

FIG. 1

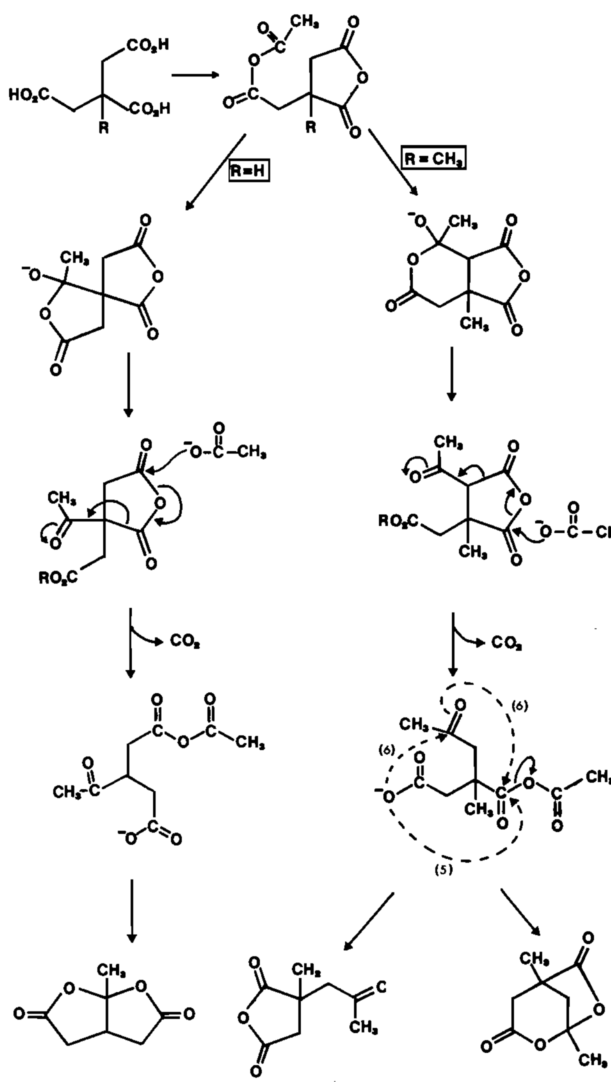

1 5 6

SCHEME 1

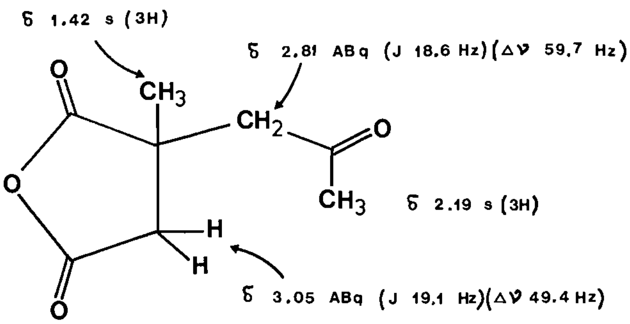

FIG. 2

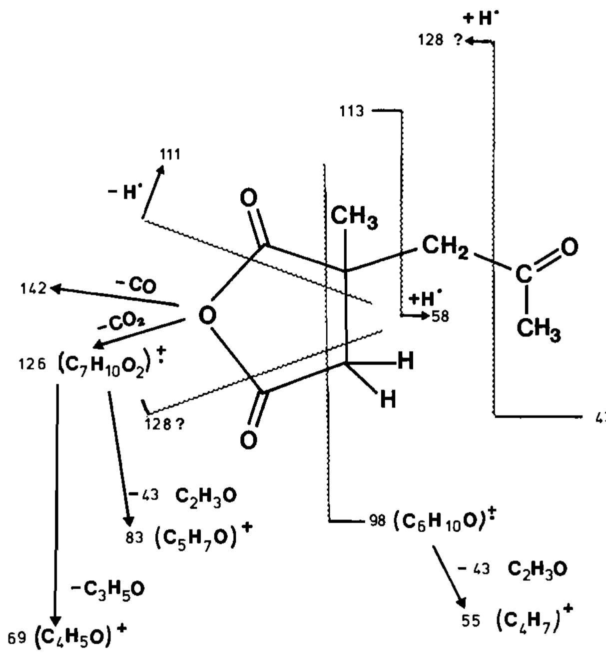

FIG. 3

The most abundant and least mobile product A, $C_8H_{10}O_4$, was readily identified as 2-acetonyl-2-methylsuccinic anhydride, **5**, by analysis of its spectra. Thus, the infrared spectrum ($CHCl_3$) demonstrates the presence of a five-membered cyclic anhydride by bands at 1864 and 1787 cm^{-1} (9) and the ketone is manifested as a peak at 1718 cm^{-1}.

Signals in the 200-MHz ^{1}Hmr spectrum and their assignments are indicated in Fig. 2. Mass spectral fragmentations are proposed in Fig. 3 (sequence not implied).

A mechanism involving acylation at C-2 of a suitable derivative of 3-methyltricarballylic acid could account for the formation of **5** (cf. Scheme 1 (R = CH_3)).[3,4]

The crystalline product B (obtained in 7.4% yield) is isomeric and interconvertible with the anhydride A (**5**), *vide infra*. Spectroscopic and chemical evidence indicates that it possesses the bridged bislactone structure **6**. Infrared bands associated with the bislactone system are found at 1812, 1792, and 1760 cm^{-1}. The 200-MHz ^{1}Hmr spectrum shows three-proton singlets at δ 1.38 and 1.81, corresponding to the hydrogens of the two methyl groups. The spectrum is also characterized by AB patterns centred at δ 2.30 ($|J_{AB}|$ 12.5 Hz; $\Delta\nu_{AB}$ 16.3 Hz) and δ 2.82 ($|J_{AB}|$ 19.0 Hz; $\Delta\nu_{AB}$ 45.7 Hz) attributable to the pairs of geminal hydrogens on the two methylene carbons. A structurally diagnostic feature of the spectrum is the long-range "*W*-coupling" (10) (1.9 Hz) exhibited by the lower field proton of each pair (H-4β and H-8β). The mass spectrum of B (*m/e* 170 ($M^{+\cdot}$); 98 (M − CO_2 and CO)$^{+\cdot}$ base peak) appears to be fully consistent with structure **6**. Such a structure may be derived from the same type of intermediate as **5** (cf. Scheme 1). Furthermore, acid-catalysed dehydration of the ketodiacid obtained by hydrolysis of either anhydride **5** or bislactone **6** produced a mixture of **5** and **6**, confirming the structural relationship between these compounds and providing additional support for formulation **6**.

The third product C, $C_9H_{12}O_3$ (~1% yield) was readily identified as **7** by spectroscopic analysis. Thus, the enol lactone and ketone functionality are manifested in the infrared spectrum by

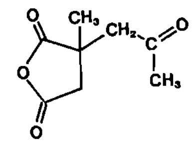

5

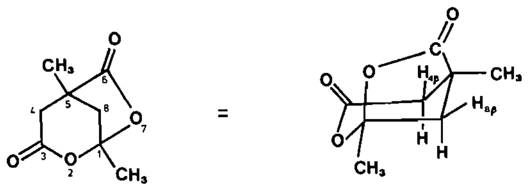

6

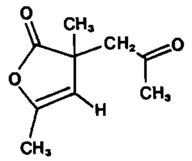

7

bands at 1793 and 1721 cm^{-1}, respectively (9). In the 200-MHz ^{1}Hmr spectrum, the hydrogens of the angular methyl group and methyl ketone give rise to singlets at δ 1.29 and 2.11, respectively. The vinylic methyl group is represented by a three-proton doublet at δ 2.00, displaying coupling (J 1.5 Hz) with the vinyl hydrogen at δ 5.16 (q, J 1.5 Hz). The geminal methylene protons α to the ketone appear as an AB quartet at δ 2.83 ($|J_{AB}|$ 17.9 Hz; $\Delta\nu$ = 21.5 Hz). The mass spectrum (m/e 168 ($M^{+\cdot}$); 111 ($M - C_3H_5O)^+$; 83 ($M - C_3H_5O$ and $CO)^+$ base peak) is in accord with the assigned structure.

The formation of C (**7**), may be rationalized in terms of a double acylation–decarboxylation process leading to 4-carboxy-4-methyl-heptane-2,6-dione or an acid anhydride thereof, which cyclizes to the enol lactone product.

Although the substrate and conditions examined in the present study differ from those investigated by Fittig, we note that homologues of **5** and **6**, bearing *gem*-dimethyl groups at the appropriate position, (C-3 and C-4, respectively) could in principle be formed by similar acylative decarboxylation of camphoronic acid. Such compounds are isomeric with the putative bislactone **4**, and the three structures could not readily have been distinguished on the basis of the data and methodology available to Fittig.

Experimental

Melting points were determined on a hot-stage apparatus and are uncorrected. Infrared spectra were recorded on a Beckman Acculab 2 spectrophotometer. Nuclear magnetic resonance spectra were run on a Varian XL-200 instrument. Mass spectra were obtained with an Hitachi Perkin Elmer RMU-6D mass spectrometer. High resolution mass spectra were provided by Mr. A. I. Budd, University of Alberta. Microanalyses were performed by Spang Microanalytical laboratory, Eagle Harbor, MI.

Reaction of 3-methyltricarballylic acid with acetic anhydride

To freshly distilled acetic anhydride (20 mL) containing 4-dimethylaminopyridine (200 mg, 1.64 mmol) was added 3-methyltricarballylic acid (1.95 g, 10.26 mmol). The solution was heated under reflux, and CO_2 evolution was periodically monitored by the precipitation of carbonate from a solution of barium hydroxide. The initially fairly vigorous evolution of CO_2 moderated with time, and was quite slow after 4.5 h, when the reaction was terminated by distillation of the volatile material under reduced pressure (water pump; bath temperature ambient to 95°C). (In some runs, the mixture was allowed to cool and set aside for several hours before distillation.) The dark brown residue was dissolved in ethyl acetate and treated with activated charcoal. After removal of the charcoal by filtration, evaporation of the solvent *in vacuo* yielded an orange-colored residue. Crystallization from ethyl acetate afforded almost colorless crystals of A, contaminated by a small amount of a second product. Compound A (**5**) was rendered colorless and pure by recrystallization from ethyl acetate, dimorphic crystals, mp 112–117°C and 149–151°C; ir ($CHCl_3$), inter alia: 1864, 1787, 1718 and 1010 cm^{-1}; nmr ($CDCl_3$, 200 MHz), see Fig. 2; mass spectrum (inter alia), m/e (relative intensity) (ion): 170.0577 (7) $(C_8H_{10}O_4)^{+\cdot}$ ($M^{+\cdot}$), 142.0632 (11) $(C_7H_{10}O_3)^{+\cdot}$, 128.0484 (24) $(C_6H_8O_3)^{+\cdot}$, 126.0680 (9) $(C_7H_{10}O_2)^{+\cdot}$, 124.0524 (12) $(C_7H_8O_2)^{+\cdot}$, 113.0245 (26) $(C_5H_5O_3)^+$, 111.0453 (44) $(C_6H_7O_2)^+$, 98.0733 (100) $(C_6H_{10}O)^{+\cdot}$, 83.0510 (56) $(C_5H_7O)^+$, 82.0434 (33) $(C_5H_6O)^{+\cdot}$, 69.0344 (9) $(C_4H_5O)^+$, 58.0448 (15) $C_3H_6O)^{+\cdot}$, 55.0572 (34) $(C_4H_7)^+$. *Anal.* calcd. for $C_8H_{10}O_4$: C 56.46, H 5.92; found: C 56.88, H 6.08.

The yield of A was augmented to a total of 738 mg (42%) by additional material obtained from flash chromotography (8) of the mother liquor. The eluent was chloroform – ethyl acetate in a stepwise gradient from 95:5 to 88:12.

Earlier fractions from the chromatography contained components B (**6**) and C (**7**) which were not completely resolved. Fractions richest in component B were combined and evaporated to dryness *in vacuo*. Crystallization from cyclohexane–toluene yielded 130 mg (7.4%) of bislactone B (**6**), mp 101–103°C. A sample recrystallized from toluene had mp 102–104°C; ir (KBr): 3000, 2965, 2945, 2925, 2885, 1812 (s), 1792, 1760 (s), 1455, 1412, 1390, 1350, 1322, 1290, 1265, 1172, 1142, 1122, 1077, 1034, 986, 974, 925, 902, 894, 800, and 735 cm^{-1}; nmr ($CDCl_3$, 200 MHz), see text; mass spectrum (inter alia), m/e (relative intensity) (ion): 171.0662 (0.65) $(C_8H_{11}O_4)^+$ (MH^+), 170.0563 (0.24) $(C_8H_{10}O_4)^{+\cdot}$ ($M^{+\cdot}$), 126.0682 (75) $(C_7H_{10}O_2)^{+\cdot}$, 111.0446 (5) $(C_6H_7O_2)^+$, 100.0524 (8) $(C_5H_8O_2)^{+\cdot}$, 98.0732 (100) $(C_6H_{10}O)^{+\cdot}$, 83.0499 (54) $(C_5H_7O)^+$, 69.0343 (13) $(C_4H_5O)^+$, 55.0566 (23) $(C_4H_7)^+$. *Anal.* calcd. for $C_8H_{10}O_4$: C 56.46, H 5.92; found: C 56.54, H 5.96.

Mother liquors from crystallization of B were combined with the chromatographic fractions containing C, and the resulting mixture was chromatographed on a column of Lichroprep Si 60 (Merck), eluting with hexane – ethyl acetate (7:3) under a pressure of 0.2 kg cm^{-2}, flow rate 2 mL min^{-1}. The olefin C (**7**) was obtained in about 1% yield as a pale yellow oil which set on standing to a soft white solid. The product resisted further purification attempts by recrystallization or preparative layer chromatography and the persistence of some minor contaminants could be detected in the mass and nmr spectra, as well as by gc: ir ($CHCl_3$), inter alia: 1793, 1721 cm^{-1}; nmr ($CDCl_3$, 200 MHz), see text; mass spectrum, m/e (relative intensity) (ion), inter alia: 208.0733 (2.4) ($C_{11}H_{12}O_4$ – contaminant), 194.0573 (1.4) ($C_{10}H_{10}O_4$ – contaminant), 168.0784 (6.9) $(C_9H_{12}O_3)^{+\cdot}$ ($M^{+\cdot}$), 153.0550 (2) $(C_8H_9O_3)^+$, 125.0604 (33) $(C_7H_9O_2)^+$, 124.0890 (32) $(C_8H_{12}O)^{+\cdot}$, 111.0444 (36) $(C_6H_7O_2)^+$, 109.0654 (19) $(C_7H_9O)^+$, 98.0730 (22) $(C_6H_{10}O)^{+\cdot}$, 97.0653 (16) $(C_6H_9O)^+$, 83.0498 (100) $(C_5H_7O)^+$.

*Interconversion of bislactone **6** and anhydride **5***

The bislactone **6** (65.0 mg, 0.38 mmol) was suspended in distilled water (20 mL) and the system was gradually brought to reflux temperature. At about 50°C all solid material had dissolved, and test paper indicated a pH of approximately 5, which dropped to about 3 as the temperature increased. The solution was heated under reflux for 3 h, after which it was evaporated to dryness under reduced pressure. To the resulting crude ketodiacid was added toluene (30 mL) and p-toluenesulfonic acid (3.0 mg), and the solution was heated under reflux with a Dean–Stark water separator for 3 h. Preparative layer chromatography of the product afforded 26 mg of the anhydride **5**, identified by comparison with an authentic sample, and 12 mg of regenerated bislactone **6**. Similar results were obtained with the ketodiacid obtained from hydrolysis of the anhydride **5**.

Acknowledgement

The authors are indebted to Mr. L. Calhoun, University of New Brunswick, for providing the 200-MHz nmr spectra.

1. R. FITTIG. Justus Liebigs Ann. Chem. **314**, 1 (1901).
2. G. M. STRUNZ and G. S. LAL. Can. J. Chem. **60**, 2528 (1982).
3. G. M. STRUNZ, P. GIGUÈRE, and M. EBACHER. Synth. Commun. **13**, 823 (1983).
4. G. C. SMITH and D. M. FAHEY. J. Am. Chem. Soc. **81**, 3391 (1959).
5. A. LAWSON. J. Chem. Soc. 144 (1957).
6. W. L. PARKER and F. JOHNSON. J. Org. Chem. **38**, 2489 (1973).
7. W. STEGLICH and G. HÖFLE. Angew. Chem. Int. Ed. Engl. **8**, 981 (1969).
8. W. C. STILL, M. KAHN, and A. MITRA. J. Org. Chem. **43**, 2923 (1978).
9. K. NAKANISHI. Infrared absorption spectroscopy, practical. Holden–Day Inc., San Francisco, CA. 1962.
10. (*a*) L. M. JACKMAN and S. STERNHELL. Applications of nuclear magnetic resonance spectroscopy in organic chemistry. Pergamon Press, New York. 1969; (*b*) A. J. G. BAXTER and A. B. HOLMES. J. Chem. Soc. Perkin Trans. 1, 2343 (1977).

The kinetics of the reactions of atomic hydrogen with halo-ethylenes

Mahmooda G. Ahmed[1] and William E. Jones
Department of Chemistry, Dalhousie University, Halifax, N.S., Canada B3H 4J3

Received November 2, 1984

Mahmooda G. Ahmed and William E. Jones. Can. J. Chem. **63**, 2127 (1985).

The absolute rate constants for the addition of H atoms to C_2H_3F, 1,1-$C_2H_2F_2$, C_2HF_3, C_2H_3Cl, 1,1-$C_2H_2Cl_2$, C_2HCl_3, and C_2H_3Br have been determined at 298 ± 2 K over the pressure range 0.70−1.35 Torr. For each of the compounds, the rate constants are found to undergo a modest increase with pressure. At 1.00 Torr the values determined for the rate constants are: C_2H_3F, (8.86 ± 1.12) × 10^{-14}; 1,1-$C_2H_2F_2$, (8.16 ± 0.66) × 10^{-14}; C_2HF_3, (6.21 ± 0.53) × 10^{-14}; C_2H_3Cl, (27.0 ± 0.5) × 10^{-14}; 1,1-$C_2H_2Cl_2$, (59.6 ± 3.4) × 10^{-14}; C_2HCl_3, (10.4 ± 0.8) × 10^{-14}; C_2H_3Br, (27.8 ± 2.5) × 10^{-14}; in units of cm^3 $molecule^{-1}$ s^{-1}.

Mahmooda G. Ahmed et William E. Jones. Can. J. Chem. **63**, 2127 (1985).

Opérant à 298 ± 2 K et à des pressions allant de 0,70 à 1,35 Torr, on a déterminé les constantes absolues des vitesses d'additions d'atomes de H aux C_2H_3F, $C_2H_2F_2$-1,1, C_2HF_3, C_2H_3Cl, $C_2H_2Cl_2$-1,1, C_2HCl_3 et C_2H_3Br. Pour chacun des composés, on a trouvé que les constantes de vitesse augmentent légèrement avec une augmentation de la pression. A 1,00 Torr, les valeurs déterminées pour les constantes de vitesse sont les suivantes: C_2H_3F, (8,86 ± 1,12) × 10^{-14}; $C_2H_2F_2$-1,1, (8,16 ± 0,66) × 10^{-14}; C_2HF_3, (6,21 ± 0,53) × 10^{-14}; C_2H_3Cl, (27,0 ± 0,5) × 10^{-14}; $C_2H_2Cl_2$-1,1, (59,6 ± 3,4) × 10^{-14}; C_2HCl_3, (10,4 ± 0,8) × 10^{-14}; C_2H_3Br, (27,8 ± 2,5) × 10^{-14}; les unités étant cm^3 $molécule^{-1}$ s^{-1}.

[Traduit par le journal]

Introduction

While much work has been published on the reactions of hydrogen atoms with ethylene (1, 2), there have been few reports on the kinetics of the reactions of hydrogen atoms with halo-substituted ethylenes.

Teng and Jones (3, 4) have discussed in detail the mechanisms for the reactions of H atoms with fluoro-ethylene and 1,1-difluoro-ethylene. From an analysis of the products formed in a normal fast flow system and using computer simulation, they calculated rate constants for each of the steps in the mechanisms of these reactions. The absolute rate constants for the addition of H atoms to ethylene and fluorinated ethylenes have been reported by Sugawara *et al.* (5). They observed a decrease in the value of the absolute rate constant as the substitution by fluorine increased. A similar trend was observed by Kilcoyne and Jennings (6), in their study of the relative rates of the addition of hydrogen atoms to fluorinated ethylenes. However, work by Penzhorn and Sandoval (7) did not indicate the same regular increase in relative rates from ethylene to tetrafluoro-ethylene.

To date, there have been two studies reported on the reaction of atomic hydrogen with chloro-substituted ethylenes. Rennert and Wijnen (8), from their study of the reaction with vinyl chloride suggested that the abstraction of a chlorine from the vinyl chloride was faster than the addition of an hydrogen atom to the vinyl chloride. Tanner and Jamieson (9), by trapping products formed in a flow system, determined independent rate constants for the formation of HCl and hydrocarbons (C_2H_4 and C_2H_6).

In the present study, the absolute rate constants for the addition of hydrogen atoms to chloro-ethylene, 1,1-dichloro-ethylene, and trichloro-ethylene have been measured using a fast flow vacuum system coupled to a mass spectrometer. In addition, the reaction of H atoms with vinyl fluoride, 1,1-difluoro-ethylene, and trifluoro-ethylene have been measured and are reported for comparison with previous measurements and with the chloro compounds. The absolute rate constant for the addition of H atoms to vinyl bromide has also been measured and is reported for the first time. Each of the rates have been measured for at least three pressures and a definite dependence on pressure is indicated.

Experimental

The reactions were studied in a typical fast flow vacuum system coupled to a mass spectrometer. A portion of the reaction mixture passed directly into the mass spectrometer ionization chamber through a line of sight double pinhole system. Details of the flow system, the pinhole region, the mass spectrometer, and the data acquisition system are described elsewhere (10).

Hydrogen atoms were produced by passing a mixture of molecular hydrogen and helium through a 2450-MHz electrodeless discharge sustained by a 100-W Kiva MPG-2 generator. Typical flow conditions were: He, 3 × 10^{-4} mol s^{-1}; H_2, 1.8 × 10^{-5} mol s^{-1}. The reaction tube was coated with ortho-phosphoric acid, in order to minimize heterogeneous wall recombination.

The concentration of hydrogen atoms was measured by NO_2 titration. An excess of NO_2 at a known pressure was introduced to the stream of H atoms. The decay of NO_2^+ (m/z = 46) was then followed with time as the flow of NO_2 was allowed to decrease. The end point was determined as the flow of NO_2 at which the NO_2^+ signal became constant or was essentially zero. A typical titration curve is shown in Fig. 1. The flow rate of H atoms was determined from the flow rate of NO_2 at the end point on the assumption that $[H]/[NO_2]$ = 1:1.5 (11). The usual correction for the NO_2/N_2O_4 equilibrium was applied to the calculation of the flow rate of NO_2.

The concentration of H atoms was also determined directly from the extent of H_2 conversion to H by monitoring the change in the molecular H_2 peak height when the microwave discharge was on and off. The maximum deviation between the direct measurement and the titration method was approximately 8%. The change in the concentration of hydrogen atoms along the reaction tube was found to be less than 3% as calculated by the titration method at different reactant inlet jets.

Helium and molecular hydrogen were obtained from Linde. Vinyl fluoride, vinyl chloride, vinyl bromide, and NO_2 were obtained from Matheson of Canada Ltd. All condensable gases were purified by bulb-to-bulb distillation, until no impurity could be detected mass spectrometrically. NO_2 was treated with molecular oxygen and

[1]Present address: Department of Chemistry, Jahangirnagar University, Savar Dhaka, Bangladesh.

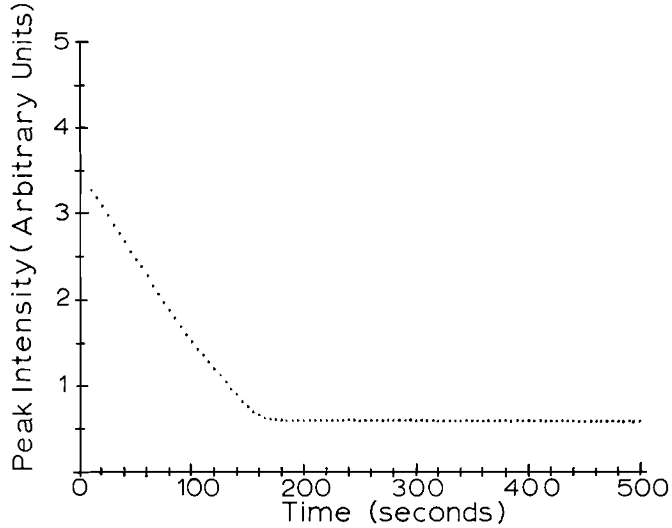

FIG. 1. A typical titration curve for the determination of the concentration of atomic hydrogen with NO_2. The curve indicates the decay of NO_2^+ as the flow of NO_2 is decreased regularly with time.

purified by trap-to-trap distillation *in vacuo*.

Since the present experiments required very low concentrations of halo-ethylene, about 1% of the H atom concentration, a mixture of 1% halo-ethylene in helium was prepared and admitted through the reactant inlet at a flow rate which provided the required concentration of halo-ethylene. This procedure also prevented back diffusion of H atoms into the reactant inlet which might have occurred if very low flow rates of halo-ethylene had been added directly.

Room temperature, 298 ± 2 K, was used for all experiments. The heat generated in the experiment was considered to be negligible since the halo-ethylene concentration was small relative to the amount of gas flowing in the tube. The reaction pressure was measured by a mercury McLeod gauge. The axial pressure gradient in the reactor was less than 2% of the total pressure. The pressure in the mass spectrometer was approximately 2×10^{-5} Torr (1 Torr = 133.3 Pa). The ionization voltage was maintained at 50 eV. The reaction time was calculated from the distance between the point of mixing of the reactants and the glass pinhole, on the assumption that the reaction stopped when the pressure dropped to approximately 5×10^{-5} Torr at this point. Under the experimental conditions used, a plug flow condition could be assumed and the time was calculated as $t = d/v$, where v is the linear flow velocity of reactant gases, and d is the distance from the reactant jet to the glass pinhole. The halo-ethylene molecular ion peak was monitored as the halo-ethylene was admitted to the stream of H atoms through each reactant inlet. From these measurements the variation of the concentration of the halo-ethylene with reaction time was obtained.

Results

A simplified scheme for the bimolecular reaction between hydrogen atoms and halo-ethylenes, RX, may be represented as

$$\mathrm{H} + \mathrm{RX} \rightarrow \text{products}$$

On the assumption that the H atom concentration is constant, the integrated rate expression for this reaction is given by

$$\ln\,[\mathrm{RX}]_t = -k[\mathrm{H}]t + \ln\,[\mathrm{RX}]_0$$

where k is the apparent bimolecular rate constant, and $[\mathrm{RX}]_t$ and $[\mathrm{RX}]_0$ are the concentrations of halo-ethylene at time t and 0, respectively. Under pseudo-first-order conditions, i.e., $[\mathrm{H}] \gg [\mathrm{RX}]$, the integrated equation becomes;

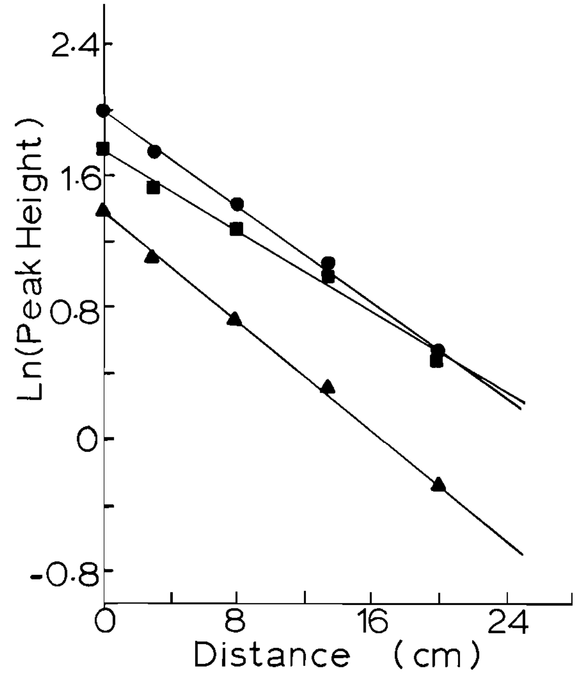

FIG. 2. A sample plot showing the variation of ln (peak height) of the halo-ethylene molecular ion peak with distance of the inlet from the sampling pinhole. (Vinyl chloride is the sample halo-ethylene.) ■ 1.35 Torr $F_H = 7.35 \times 10^{-6}$ mol s^{-1}; $k = 2.87 \times 10^{-13}$ cm^3 molecule^{-1} s^{-1}. ● 1.00 Torr $F_H = 6.88 \times 10^{-6}$ mol s^{-1}; $k = 2.63 \times 10^{-13}$ cm^3 molecule^{-1} s^{-1}. ▲ 0.70 Torr $F_H = 7.54 \times 10^{-6}$ mol s^{-1}; $k = 2.14 \times 10^{-13}$ cm^3 molecule^{-1} s^{-1}.

$$\ln\,[\mathrm{RX}]_t = -k_{\mathrm{obs}}t + \ln\,[\mathrm{RX}]_0$$

where k_{obs} is the pseudo-first-order rate constant. It is assumed in this equation that the rate constant k_{obs} is independent of the mode of loss of H atoms and that halo-ethylene is lost only through its reaction with H atoms and is not consumed or regenerated in subsequent reactions. These assumptions have been verified for all the halo-ethylenes used. The concentration of halo-ethylene was varied threefold and the rate constant was found to be independent of the initial concentration of the halo-ethylene. Analysis of the products also showed that the halo-ethylene was not consumed in secondary reactions.

A plot of $-\ln\,[\mathrm{RX}]$ vs. time t gives the pseudo-first-order rate constant k_{obs}. The value of k is then calculated using the value of [H].

The variation with distance (equivalent to reaction time) of ln (peak height) of the molecular ion of the halo-ethylene was monitored using computer assisted data acquisition. A sample plot for vinyl chloride is shown in Fig. 2. After conversion of the distance axis to time, the slope of the line provides the pseudo-first-order rate constant. From the concentration of the H atoms, the apparent bimolecular rate constant k is determined.

The values for the bimolecular rate constant for each of the reactants C_2H_3Cl, $C_2H_2Cl_2$, C_2HCl_3, C_2H_3F, $C_2H_2F_2$, C_2HF_3, and C_2H_3Br are given in Table 1.

Discussion

A comparison of the products resulting from the reaction of hydrogen atoms with the various halo-ethylenes indicated that a general mechanism analogous to that for the reaction of H atoms with ethylene (3, 4) may be applicable to the H atom –

TABLE 1. Apparent bimolecular rate constants for the addition of hydrogen atoms (temperature 298 ± 2 K)

Pressure (Torr)	Reactant (k in units of cm^3 $molecule^{-1}$ s^{-1} $\times 10^{14}$)						
	$C_2H_3F^a$	$1,1\text{-}C_2H_2F_2^b$	$C_2HF_3^b$	$C_2H_3Cl^a$	$1,1\text{-}C_2H_2Cl_2^b$	$C_2HCl_3^c$	$C_2H_3Br^a$
0.70±0.05	7.64±0.78	7.32±0.29	5.17±0.35	21.2±1.6	47.3±3.1	9.2±0.8	24.6±1.4
1.00±0.05	8.86±1.12	8.16±0.66	6.21±0.53	27.0±0.5	59.6±3.4	10.4±0.8	27.8±2.5
1.30±0.05	10.80±0.90	10.47±0.41	7.30±0.46	30.3±3.9	63.8±3.5	11.9±1.6	38.3±1.8

NOTE: For C_2Cl_4 an upper limit for k at 1.30 Torr was found to be 1.3×10^{-14} cm^3 $molecule^{-1}$ s^{-1}.
[a]Twenty determinations at each pressure.
[b]Ten determinations at each pressure.
[c]Five determinations at each pressure.

halo-ethylene reaction as follows:

$$[1]\quad H + RX \xrightarrow{k_1} RHX^*$$

$$[2]\quad RHX^* \xrightarrow{k_2} RX + H$$

$$[3]\quad RHX^* + M \xrightarrow{k_3} RHX + M$$

$$[4]\quad H + RHX \rightarrow RH_2X \rightarrow RH + HX \quad (k_4)$$

where RX is the halo-ethylene molecule with X as F, Cl, or Br and M is a third body. The addition of an H atom to RX produces a vibrationally excited RHX* radical which can decompose to H and RX, or to be stabilized through collision as in eq. [3]. The stabilized radical can react with an H atom as in eq. [4] to produce an excited molecule which will decompose to produce RH and HX.

Applying the steady state treatment to the above mechanism, the rate of disappearance of RX may be shown to be:

$$-d[RX]/dt = (k_1 [H] [RX] \times k_3[M])/(k_2 + k_3[M])$$

which gives the apparent bimolecular rate constant k as:

$$k = (k_1 \times k_3[M])/(k_2 + k_3[M])$$

If $k_2 = 0$ or if $k_2 \ll k_3[M]$, k is equal to k_1 at any pressure. If neither of these conditions exists, the value of k will increase with pressure.

The experimental values of k for the addition of H atoms to C_2H_3F, $1,1\text{-}C_2H_2F_2$, C_2HF_3, C_2H_3Cl, $1,1\text{-}C_2H_2Cl_2$, C_2HCl_3, and C_2H_3Br presented in Table 1 show a modest increase with increasing pressure over the limited pressure range 0.7−1.35 Torr used in this work.

The value of the rate constant for the addition of H atoms to C_2H_3F at a pressure of 1.00 Torr is $8.82 \pm 1.12 \times 10^{-14}$ cm^3 $molecule^{-1}$ s^{-1}, which is in reasonable agreement with the value 4.53×10^{-14} determined by Teng and Jones (3). Sugawara *et al.* (5) obtained a value of 5.2×10^{-13} cm^3 $molecule^{-1}$ s^{-1} at a pressure greater than 180 Torr. From the steady state treatment it can be seen that a plot of k^{-1} against P^{-1} or $[M]^{-1}$ should be linear. An extrapolation of this plot to 180 Torr gives a value of approximately 2×10^{-13} which, at about half the value of Sugawara *et al.*, is quite satisfactory agreement considering the length of the extrapolation.

Successive substitution of F atoms for H atoms in ethylene has been found to decrease the rate constant for the addition of H atoms to the resulting fluoro-ethylene (4−6). A similar trend has been observed in the present study, as may be seen in Table 1.

The only value available for the rate constant for the addition of H atoms to C_2H_3Cl is 6.90×10^{-14} cm^3 $molecule^{-1}$ s^{-1} as given by Rennert and Wijnen (8), which is somewhat smaller than the value calculated in the present work.

To our knowledge, there is no previous report in the literature which gives the rate constant for the reaction of H atoms with C_2H_3Br.

The values of the rate constants given in Table 1 for C_2H_3F, C_2H_3Cl, and C_2H_3Br tend to increase from C_2H_3F to C_2H_3Br. A similar trend in reactivity has been observed for the reaction of O atoms with these same molecules (12−15). This has been explained by considering two opposing influences created by the substituted halogen atom on the reactivity of the olefin. These influences can be attributed to the strong negative inductive effect ($-I$) due to the electronegativity of the halogen, and the positive inductive effect ($+I$) as a result of the repulsion of π electrons present in the p orbitals of the halogen atom and the mesomeric ($+M$) effect, as distinguished by Clark *et al.* (16). When an F atom is substituted in C_2H_4, a deactivation of the double bond occurs due to the combined effects described above, and the reaction of H atoms with C_2H_3F becomes slower than that for the reaction with the C_2H_4 molecule.

The donation of the unshared electrons from the substituted halogen to the double bond increases along the series H < F < Cl < Br while the electronegativities of the atoms decrease along the series F > Cl > Br > H. These combined effects cause a change in the reactivity when F is substituted for Cl or Br. A change in the reactivity is also observed with an increase in the number of substituents (4−6). The rate constants presented in Table 1 indicate that as fluorine substitution increases the rate constants decrease. For chlorine substitution, an increase in the rate constants occurs between C_2H_3Cl and $1,1\text{-}C_2H_2Cl_2$, but substitution of a third Cl atom decreases the rate constant. Preliminary results indicate that further substitution by a Cl atom further decreases the rate constant.

Acknowledgements

We acknowledge financial support from the Natural Sciences and Engineering Research Council of Canada in the form of an operating grant to W. E. J., and from the Faculty of Graduate Studies of Dalhousie University for a fellowship to M.G.A. We thank D. Burkholder for his advice and assistance in the maintenance and operation of the mass spectrometer system.

1. W. E. JONES, S. D. MCKNIGHT, and L. TENG. Chem. Rev. **73**, 407 (1973).
2. C. A. COWFER and J. V. MICHAEL. J. Chem. Phys. **62**, 3504 (1975).
3. L. TENG and W. E. JONES. J. Chem. Soc. Faraday Trans. 1, **68**, 1267 (1972).

4. L. TENG and W. E. JONES. J. Chem. Soc. Faraday Trans. 1, **69**, 189 (1973).
5. K. SUGAWARA, K. OKAZAKI, and S. SATO. Bull. Chem. Soc. Jpn. **54**, 358 (1981).
6. J. P. KILCOYNE and K. R. JENNINGS. J. Chem. Soc. Faraday Trans. 1, **70**, 379 (1974).
7. R. D. PENZHORN and H. W. SANDOVAL. J. Phys. Chem. **74**, 2065 (1970).
8. A. M. RENNERT and M. H. J. WIJNEN. Ber. Bunsenges. Phys. Chem. **72**, 222 (1968).
9. J. S. TANNER and J. W. S. JAMIESON. Can. J. Chem. **49**, 1023 (1971).
10. L. RAMALEY, K. LING, D. BURKHOLDER, M. IEKI, and W. E. JONES. Chem. Biomed. Environ. Instrum. **9**, 335 (1979).
11. L. F. PHILLIPS and H. I. SCHIFF. J. Chem. Phys. **37**, 1233 (1962).
12. I. R. SLAGLE, D. GUTMAN, and J. R. GILBERT. 15th Int. Symp. Combustion. The Combustion Institute. 1974. pp. 785.
13. R. ATKINSON and J. N. PITTS, JR. J. Chem. Phys. **67**, 2488 (1977).
14. R. E. HUIE, J. T. HERRON, and D. D. DAVIS. Int. J. Chem. Kinet. **4**, 521 (1972).
15. R. ATKINSON and J. N. PITTS, JR. Int. J. Chem. Kinet. **8**, 475 (1976).
16. D. J. CLARK, J. N. MURRELL, and J. M. TEDDER. J. Chem. Soc. 1250 (1963).

Organic reactions in liquid crystalline solvents. 1. The thermal *cis–trans* isomerization of a bulky olefin in cholesteric liquid crystalline solvents

WILLIAM J. LEIGH,[1] DEBBIE T. FRENDO,[2] AND PAUL J. KLAWUNN
Department of Chemistry, McMaster University, Hamilton, Ont., Canada L8S 4M1

Received October 5, 1984

WILLIAM J. LEIGH, DEBBIE T. FRENDO, and PAUL J. KLAWUNN. Can. J. Chem. **63**, 2131 (1985).

The effect of cholesteric liquid crystalline solvents on the energetics of rotational thermal *cis–trans* isomerization of olefins has been examined. Rate constants have been obtained over a 70-degree temperature range for isomerization of *trans*-1,2-di-(4-cyanophenyl)-1,2-diphenylethylene in two isotropic solvents and three cholesteric liquid crystals and the Arrhenius parameters determined. The rates of isomerization are found to be consistently slower in the liquid crystalline phases compared to the isotropic solvents. The Arrhenius parameters for isomerization of the olefin in the isotropic solvents (E_a = 34.8 ± 0.3 kcal/mol; $\Delta S^{\neq}$ = −1.5 ± 0.5 e.u.) compare favourably with reported values for its isomerization in benzene solution. In the cholesteric phases, E_a is consistently 1–1.5 kcal/mol higher and $\Delta S^{\neq}$ slightly more positive than the corresponding values for the isotropic solvents. The results are tentatively rationalized in terms of disruption of liquid crystalline order as the olefin twists from its pseudo-planar, ground state geometry through the globular, twisted transition state. The magnitude of this effect is proposed to depend on both the difference in steric bulk of the ground and transition states and the "tightness" of the solvation shell seen by the isomerizing molecule. It is believed that in the present case the observed effects are somewhat truncated as a result of rather poor solvation of the bulky olefin in the liquid crystalline phases.

WILLIAM J. LEIGH, DEBBIE T. FRENDO et PAUL J. KLAWUNN. Can. J. Chem. **63**, 2131 (1985).

On a étudié l'effet des solvants cholestériques cristaux-liquides sur les niveaux énergétiques de l'isomérisation *cis–trans* thermique de rotation des oléfines. Opérant sur une plage de température de 70 degrés, on a obtenu les constantes de vitesse d'isomérisation du di-(cyano-4 phényl)-1,2 diphényl-1,2 éthylène dans deux solvants isotropes ainsi que dans trois cristaux liquides cholestériques et on a aussi déterminé les paramètres d'Arrhénius. On a trouvé que les vitesses d'isomérisation sont systématiquement plus lentes dans les phases de cristaux liquides que dans les solvants isotropes. Les paramètres d'Arrhénius pour l'isomérisation de l'oléfine dans les solvants isotropes (E_a = 34,8 ± 0,3 kcal/mol; $\Delta S^{\neq}$ = −1,5 ± 0,5 u.e.) se comparent favorablement avec les valeurs rapportées antérieurement pour son isomérisation en solution dans le benzène. Dans les phases cholestériques, les valeurs de E_a sont systématiquement de 1 à 1,5 kcal/mol plus élevées et la valeur du $\Delta S^{\neq}$ est légèrement plus positive que les valeurs correspondantes pour les solvants isotropes. D'une façon préliminaire, on rationalise les résultats en fonction d'une dislocation de l'ordre du liquide cristallin alors que l'oléfine se déplace de la géométrie pseudo-planaire de son état fondamental vers l'état de transition globulaire qui a subi une torsion. On croit que l'amplitude de cet effet dépend à la fois de la différence entre les encombrements des états fondamental et de transition et de la nature compacte du noyau de solvatation ressenti par la molécule qui s'isomérise. Dans le cas présent, on croit que les effets observés sont un peu tronqués à cause de la mauvaise solvatation de l'oléfine encombrée dans les phases liquides cristallines.

[Traduit par le journal]

Introduction

The use of thermotropic liquid crystals as solvents for thermal and photochemical reactions has been the subject of numerous reports in recent years (1–13). Most commonly, these investigations have examined the effects of these materials on unimolecular processes which involve some degree of distortion of an oriented solute's molecular framework. Examples include the Claisen rearrangement in nematic solvents (1), intramolecular excimer formation in cholesterics (2), and the Norrish Type II reaction in cholesteric and smectic solvents (3). The common thread in each of these examples is that the reaction or process in question involves cyclization of an oriented, rod-like solute; if this results in disruption of liquid crystalline order, then some effect on the rate of the process is generally observed.

Increasing attention is being focussed on the effects of liquid crystalline solvents on the dynamics of bimolecular reactions (4–8), and Samori and co-workers have noted that the largest effects on reactivity are to be expected for reactions whose energetics are dominated by entropy factors (8), that is, in reactions which are subject to rather severe orientational constraints in the transition state. The systems which have been investigated to date have used liquid crystals to control the mutual orientations of the reactive solutes, the idea being that reaction efficiency should be greater when the reactive moieties are held in the optimum mutual orientation for interaction. Examples include the photodimerizations of acenapthylene (6) and tetraphenylbutatriene (4), pyrene excimer and exciplex formation (7), and sulfonate ester rearrangements (8).

Several years ago, Nerbonne and Weiss reported an investigation of the effects of cholesteric liquid crystalline solvents on the energetics of the thermal *cis–trans* isomerization of azobenzene (9*a*), in an attempt to elucidate the mechanism of this process, whether via bond rotation or nitrogen inversion. The transition states for these two mechanisms differ considerably in their shapes, and thus might be expected to be solvated somewhat differently in a liquid crystal. It was suggested that isomerization by bond rotation should be impeded in a liquid crystalline solvent as a result of the disruptive effects of the bulky, globular transition state on solvent order. Isomerization by nitrogen inversion, on the other hand, should not be affected by liquid crystalline solvents, since passage through this transition state involves a change in solute geometry which is more compatible with the macroscopic solvent "structure". This idea that transition states of different steric shape might be solvated somewhat differently in a liquid crystalline solvent is

[1] Author to whom correspondence may be addressed.
[2] Natural Sciences and Engineering Research Council Summer Student, 1984.

TABLE 1. Transition temperatures for pure and doped cholesteric liquid crystals[a]

Liquid crystal	Wt.% **1**	K → Ch[b]	Ch → I[c]
Cholesteryl benzoate (CB)	0	149–151	178–180
	0.5	148–150	174–176.5
Cholesteryl 4-chlorobenzoate (CCB)	0	169.5–171	247–248.5
	0.5	168–170	246–247.5
Cholesteryl 6-methoxy-2-naphthoate (CMN)	0	182–183	285–290
	1.0	181–182	275–283
Cholestanyl 4-methylbenzoate (CT)	0	172–173	228–229
	0.5	172–174	227–228

[a] In °C, corrected; measured by thermal microscopy.
[b] Solid to cholesteric transition.
[c] Cholesteric to isotropic transition.

directly analogous to the known behaviour of liquid crystals with respect to the differences in their ability to solvate planar or rod-like solutes and non-planar or globular ones (14). The result that both the activation energy and entropy for the isomerization of azobenzene were significantly more positive in a cholesteric liquid crystal compared to isotropic solvents was taken as evidence for the bond rotation mechanism for this isomerization (9*a*). Since that time, a number of studies have provided rather convincing evidence in favour of the bond inversion mechanism (15). Otruba and Weiss have recently reported a correction to their earlier report (9*b*). They have found that the energetics of the thermal *cis–trans* isomerization of azobenzene and a series of substituted derivatives are in fact *not at all affected* by liquid crystalline solvents; they conclude that azobenzene must therefore isomerize via the more widely accepted (15) nitrogen inversion mechanism.

The proposal that a liquid crystalline solvent might be able to distinguish between rotational and inversion transition states in the azobenzene isomerization, while seemingly viable, remains unproven. No reliable indication exists of the potential magnitude of the effect on the energetics of rotational *cis–trans* isomerization of olefins by liquid crystalline solvents. A report of a two-fold enhancement in the rate of thermal *cis–trans* isomerization of *cis*-stilbene in a nematic solvent relative to that in isotropic media (16) must be viewed as suspect, since at the temperature examined (156°C), the isomerization rates are grossly incompatible with the known activation parameters for the uncatalysed thermal isomerization of this olefin (17).

We wish to report the results of our study of the kinetics of the thermal *cis–trans* isomerization of 1,2-di-(4-cyanophenyl)-1,2-diphenylethylene (**1**) in cholesteric liquid crystalline

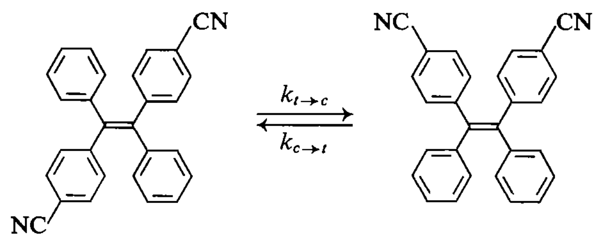

1

and isotropic solvents. Our results suggest that cholesteric liquid crystals are indeed capable of affecting the energetics of rotational *cis–trans* isomerization, although the observed effect is small and it is difficult to derive definitive conclusions with regard to its origins. The magnitude of the effect which is observed in this system can be explained as being the result of several factors, all of which derive from the manner in which this solute is solvated in the liquid crystalline environment.

Results

Transition temperatures for the liquid crystalline materials used in this study were measured by thermal microscopy for both the pure materials and the doped mixtures used in the kinetic studies. These are collected in Table 1. The **1**-doped samples were prepared by evaporation of methylene chloride solutions of **1** and the aromatic esters under vacuum to ensure intimate mixing of the two components. While the substantial effects on both the K → Ch and Ch → I transition temperatures indicate that the olefin is, presumably, soluble in each of the mesophases employed, this was further corroborated by simple monitoring of the dissolution of a small crystal of *trans*-**1** in the cholesteric phase of each of these materials by thermal microscopy. In each case, dissolution appeared to be complete within ca. 5 min at a temperature ca. 10°C above that of the K → Ch transition.

The rates of isomerization of *trans*-**1** were measured over the temperature range 170–245°C as the rates of approach to equilibrium, according to published procedures (18). The data were analysed according to eq. [1], in which X_0^T, X_t^T, and X_e^T are the mole fractions of the *trans*-isomer initially, at time *t*, and at

$$[1] \quad \ln (X_t^T - X_e^T) = \ln (X_0^T - X_e^T) - kt$$

equilibrium, respectively, and *k* represents the sum of the rate constants for the forward and reverse reactions. Equilibrium compositions were established from both directions in order to ensure complete equilibration. At a given temperature, the equilibrium composition for **1** did not vary significantly as a function of solvent. Rate and equilibrium data for the thermal isomerization of **1** as 0.5 or 1.0 wt.% solutions in cholesteryl benzoate (CB), 3β-cholestanyl 4-toluate (CT), cholesteryl 4-chlorobenzoate (CCB), cholesteryl 6-methoxy-2-naphthoate (CMN), and n-decyl 4-anisoate (DA) are collected in Table 2. The quoted errors in the rate constants have been estimated as the standard deviations, obtained from weighted linear least-squares analyses of the data according to eq. [1]. Representative plots are shown in Fig. 1 for the isomerization of *trans*-**1** in the cholesteric phase of CCB and the isotropic phase of CB at 200°C.

Kinetic runs using DA and CMN as solvents were performed simultaneously at each temperature; thus, differences in the rate constants at each temperature are more meaningful for these two solvents than for the other three. The runs using CB, CT, and CCB as solvents were done separately, and the temperature varied by ±1° from run to run. While the temperatures

TABLE 2. Rates and equilibria for the thermal *cis–trans* isomerization of *trans*-**1** in various solvents[a]

Temperature (°C)[b]	DA	CMN	CB	CT	CCB	K^c
170	—	—	0.103 ±0.005	—	0.090 ±0.002	0.711
180	—	—	0.27 ±0.01	—	0.20 ±0.01	0.715
190	0.56 ±0.03	0.42 ±0.04	0.75 ±0.06	0.59 ±0.05	0.40 ±0.05	0.720
200	1.52 ±0.03	0.92 ±0.12	1.58 ±0.05	1.19 ±0.08	1.12 ±0.07	0.725
210.4	3.22 ±0.05	2.30 ±0.18	3.94 ±0.16	2.90 ±0.22	3.04 ±0.09	0.731
220	6.03 ±0.04	4.46 ±0.18	7.25 ±0.20	5.54 ±0.43	5.71 ±0.18	0.762
225	8.74 ±0.18	6.81 ±0.09	—	8.91 ±0.47	—	0.763
230	12.1 ±0.5	10.9 ±0.8	14.9 ±0.3	13.6 ±0.5	12.7 ±0.5	0.763
235	16.7 ±0.3	12.5 ±0.3	—	—	—	0.746
240	24.7 ±0.5	19.8 ±0.5	26.2 ±0.6	28.9 ±0.5	22.0 ±1.5	0.775
245	32.4 ±1.4	26.8 ±0.7	41.3 ±1.6	39.0 ±1.2	—	0.772

[a]In units of 10^{-4} s^{-1}. Errors quoted as $\pm\sigma$.
[b]±1.0°C.
[c]$K_e = k_{t\to c}/k_{c\to t} = 1/X_e^T - 1$. The values represent the average of all measurements at a single temperature; the measured values varied by less than ±0.05 from solvent to solvent.

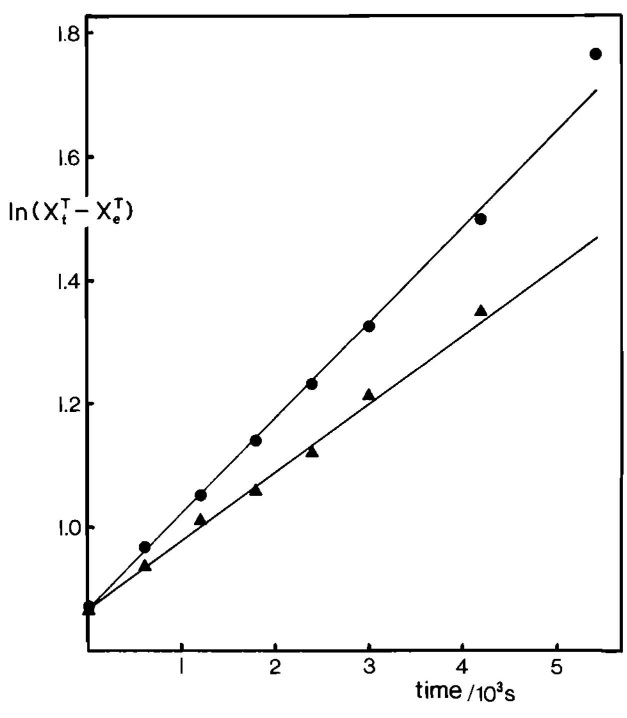

FIG. 1. Mole fraction vs. time data, plotted according to eq. [1], for the thermal *cis–trans* isomerization of *trans*-**1** in CB (●, isotropic) and CCB (▲, cholesteric) at 200°C.

recorded in Table 2 do not reveal these minor differences, they were in fact incorporated in the Arrhenius plots and calculations discussed below.

A sample of DA was heated at 230°C for 35 h and examined by ^{1}Hmr spectroscopy in order to ensure that solvent decomposition does not occur to any significant extent at these temperatures during the times required for the kinetic analyses. *p*-Anisic acid could not be detected in the nmr spectrum of DA after being subjected to this treatment.

TABLE 3. Transition temperatures and rate constants for thermal isomerization of *trans*-**1** in cholesteric CMN at 210°C as a function of concentration

	Transition temperature (°C)[a]		
Wt.% **1**	K → Ch	Ch → I	10^4 k (s^{-1})
0	182–183	285–290	—
0.2	181–183	283–287	2.15 ± 0.09
0.5	181–183	277–284	2.11 ± 0.03
1.0	181–183	275–283	2.30 ± 0.19
2.0	180–183	270–276	2.32 ± 0.06

[a]Measured by thermal microscopy.

Mesophase stability over the time periods necessary for the kinetic analyses was verified for each of the liquid crystals employed, by visual inspection of **1**-doped samples in a thermal microscope held at 240°C (220°C for CT) for 3 h.

The rates of isomerization of *trans*-**1** in CMN at 210°C were measured using samples containing 0.2, 0.5, 1.0, and 2.0 wt.% **1**. These data are collected in Table 3, along with the measured transition temperatures for each of the mixtures.

Arrhenius plots for our data are shown in Figs. 2 and 3. Least-squares analysis of each yielded the Arrhenius parameters collected in Table 4. The insert in Fig. 3 shows a plot which illustrates the dependence of the ratio of the rate constants in isotropic DA and cholesteric CMN on inverse temperature; such a plot gives a better indication of the differences in the Arrhenius parameters obtained, along with the estimated errors in these differences. Least-squares analysis of this plot

TABLE 4. Arrhenius parameters for the thermal *cis–trans* isomerization of **1** in cholesteric and isotropic media[a]

Solvent	Phase	E_a[b]	ln A[c]	$\Delta S^{\neq}$ (200°)[d]
CB	Isotropic	35.0 ± 0.6	28.56 ± 0.64	−1.4 ± 0.6
CCB	Cholesteric	36.4 ± 0.8	29.79 ± 0.93	−0.2 ± 0.9
CB/CT/CCB	Isotropic	34.8 ± 0.2	28.42 ± 0.53	−1.5 ± 0.5
CB/CT/CCB	Cholesteric	36.0 ± 0.3	30.41 ± 0.61	−0.5 ± 0.6
DA	Isotropic	34.6 ± 0.5	27.95 ± 0.56	−2.0 ± 0.5
CMN	Cholesteric	36.3 ± 0.6	29.45 ± 0.63	−0.5 ± 0.6
Benzene[e]	Isotropic	35.0 ± 0.5	28.25 ± 0.56	−1.7 ± 0.5

[a] Errors quoted as $\pm\sigma$.
[b] In kcal/mol.
[c] In s^{-1}.
[d] In e.u.
[e] Calculated from the rate constant data in ref. 18, using our linear least-squares program.

yields the differences in the Arrhenius parameters for isomerization of **1** in the two solvents: $\Delta E_a = 2.5 \pm 1.2$ kcal/mol and $\Delta(\Delta S^{\neq}) = 2 \pm 2$ e.u. ($R^2 = -0.83$).

Discussion

Liquid crystals are ordered fluids, with properties intermediate between those of an isotropic liquid and a crystalline solid, and are characterized according to the degree and type of orientational and translational ordering of their constituent molecules (19*a*).[3] The primary requirement met by all thermotropic liquid crystals (with the exception of discotics) is that the molecular shape of the component molecules be rod-like (19). The order in nematic liquid crystals is purely orientational; the constituent molecules are, on the average, oriented with their long molecular axes parallel to one another. Unlike the more highly ordered smectic types, there is no translational ordering in nematics, and hence these are the most fluid type of liquid crystalline phase.

Cholesteric phases are formed by optically active molecules (such as cholesteryl esters) or by nematics doped with an optically active solute (20). The structure of cholesterics is best described as "twisted nematic"; that is, the ordering is nematic, with a gradual twist in the orientational alignment (characterized by the director, *n*) as one proceeds through the bulk of the sample (21). This gradual twist in the director describes a helix, the period of which typically proceeds over a few thousand angstroms, and this imparts a macroscopic chirality to the liquid crystal. Cholesterics are widely described as being layered, consisting of a series of nematic "sheets" which are stacked such that the director twists slightly upon proceeding from layer to layer (2, 20*b*). While this description of cholesterics perhaps aids in the visualization of the nature of their optical activity, it must be emphasized that it is *only* an approximation (21), insofar as crystallographic studies do not substantiate the presence of discrete layers in these materials.[4]

Solubilization of solutes in liquid crystals occurs so as to incorporate the solute with a minimal amount of disruption of the surrounding crystalline lattice, and appears to be governed primarily by steric factors (14, 19).[5] A solute whose molecular shape is similar to that of the solvent molecules is more effectively solubilized and creates less disruption of liquid crystalline order than one which is grossly dissimilar in structure (14).[5] If the solute undergoes some unimolecular reaction which involves a change in shape as it proceeds through the transition state, then some effect on the energetics of the reaction is expected as a result of the necessary disruption of the ordered solvation shell. The magnitude of this effect will depend on how tightly the solute (in its ground state geometry) is solubilized in the liquid crystal, as well as the degree of distortion which the molecule must undergo (and hence the extent of disruption it imposes on solvent order) in order to reach the transition state.

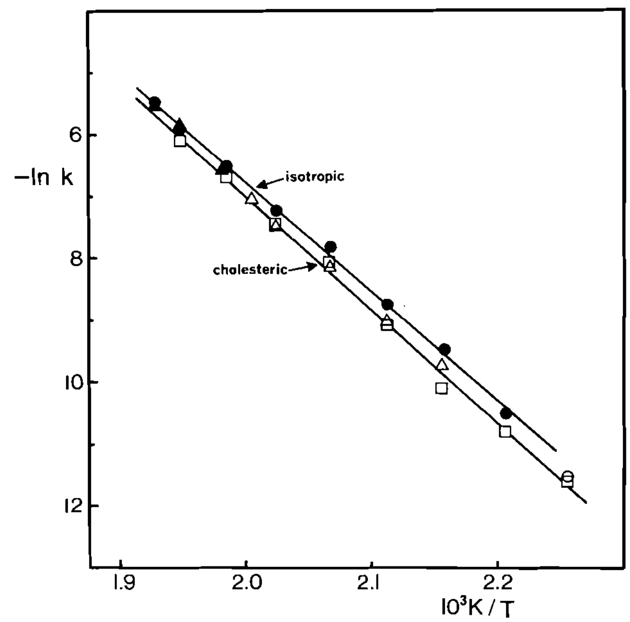

FIG. 2. Arrhenius plots for the thermal *cis–trans* isomerization of **1** in the isotropic and cholesteric phases of CB (chol. ○; isot. ●), CT (chol. △; isot. ▲), and CCB (chol. □). The lines drawn represent those obtained from least-squares analysis of the two sets of the *combined* data.

A number of examples of the effects of liquid crystalline order on the energetics of unimolecular reactions have been reported (1–3, 9–13), and it is clear that the effects on reactivity are greatest when the solute is well oriented in the liquid crystal (12). For rod-like reactants, the solvation shell is reasonably tight, and reaction involves "dragging" portions of the solute's framework out of their solvent-induced orientations. Reactivity is affected as a result of the solvent's ability to orient

[3] For comprehensive descriptions of the structure and properties of liquid crystals, see ref. 19*a–c*.
[4] Reference 19*b*, Chapt. 5.2, and references cited therein; cf. however, ref. 22.
[5] Reference 19*b*, Chapt. 9.1, and references cited therein.

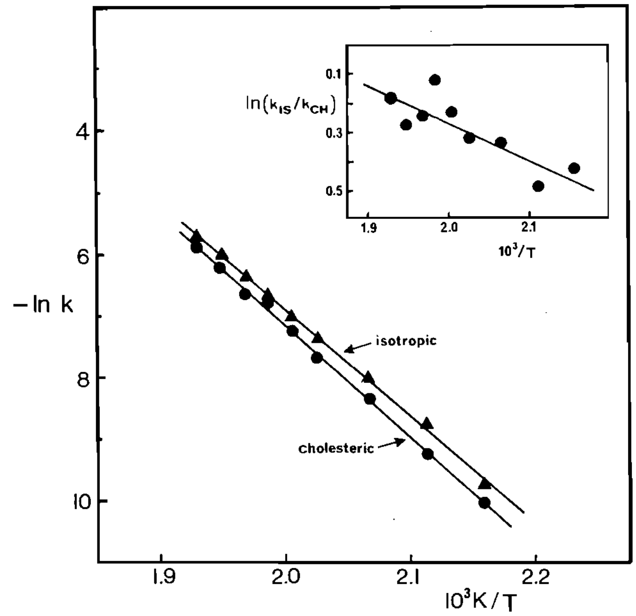

FIG. 3. Arrhenius plots for the thermal *cis–trans* isomerization of **1** in isotropic DA (▲) and cholesteric CMN (●). Insert: Arrhenius-type plot using the ratios of the rate constants in CMN and DA (k_{CH}/k_{IS}).

the solute and inhibit molecular motions which deviate from that orientation. Tetraphenylethylene is disc-like in shape, and therefore is expected to be oriented in a cholesteric phase with its molecular plane parallel to the long molecular axes of the surrounding solvent molecules (23). As a result of its disc-like shape, it will not be as tightly solvated in a cholesteric phase as would be a rod-like solute. Nevertheless, twisting about the double bond in the course of *cis–trans* isomerization does involve rather substantial changes in molecular shape, and this should result in disruption of whatever solvent order exists in, or surrounding, the primary solvation shell.

There is a slight variation in the rate of isomerization of **1** as a function of solvent for the two isotropic solvents examined, n-decyl anisoate (DA) and cholesteryl benzoate (CB) (see Table 2), the rates being consistently slower in the former at each of the temperatures examined. The origin of this solvent effect, if it is real, is not clear. It is not the result of differences in solvent polarity, since the rates in the more polar DA correlate better with those in benzene (calculated from the published Arrhenius parameters). It is possible that the somewhat faster rates in CB are the result of catalysis by trace impurities, although the rate of isomerization of **1** at 220°C did not vary using a more rigorously purified sample of that solvent.

It is important to note that the rates of isomerization of **1** in isotropic CB agree rather well with those in isotropic cholestanyl toluate (CT) (>225°C). Furthermore, the rates of isomerization in the cholesteric phases of CT (<225°C) and CB (170°C) are identical to those in cholesteric CCB at the same temperatures. Thus, the rate data for isomerization of **1** in CB, CT, and CCB, at least, appear to be internally consistent.

It is well known that the density and viscosity of a liquid crystalline phase vary significantly over the temperature range at which it exists; hence for a particular liquid crystal, the mesophase will be more "rigid" the closer it is to its K → Ch transition temperature (i.e., the lower its solvent reduced temperature, T/T_I, where T_I represents the mesophase → isotropic transition temperature).[6] Furthermore, mesogens of similar structure tend to show the same dependencies on reduced temperature with respect to these properties and other properties related to them (24). We wondered if the magnitude of the effect of cholesteric order on the rate of isomerization of **1** would depend on the "rigidity" of the liquid crystalline phase, and the three cholesterics used in the present study were chosen with this in mind. Thus, CT (chol. 172–228°C (25)), CCB (chol. 169–248°C (26)), and CMN (chol. 182–290°C (27)) were chosen so as to provide cholesteric phases which are at the upper end, in the middle, and at the lower end of their mesophase temperature ranges, respectively, over the temperature range at which our rate measurements were carried out. While the significantly slower rates of isomerization in CMN may indicate that there is in fact some dependence of rate on mesophase rigidity, this interpretation must be viewed with caution. Firstly, if it is correct, then a significant difference is expected in the rates of isomerization of **1** in CB and CCB at 170°C (these two are at the extreme high and low ends of their mesophase ranges, respectively, at this temperature). This is clearly not the case. We note that the differences in the rates in CMN relative to CT and CCB are of a similar magnitude to those observed for the isotropic solvents DA and CB. Thus, it appears likely that the same sort of solvent effect responsible for the difference in the rates of isomerization of **1** in DA and CB is operating in the cholesteric phases as well. For the purposes of discussion, it seems prudent to restrict comparison of the data in CMN to those in DA, and consider the CB/CT/CCB rate data as a separate set.

The data in Table 2 demonstrate that at every temperature, the rate of thermal *cis–trans* isomerization of **1** is significantly (and reproducibly) slower in the cholesteric solvents than in the corresponding model isotropic solvents throughout the temperature range examined, by 10–35%. Clearly, rotation about the carbon–carbon double bond in this olefin is inhibited in the ordered liquid crystalline phases relative to isotropic media.

The Arrhenius plots in Fig. 2 demonstrate more clearly the relationship between the measured rates of isomerization of **1** in CB, CT, and CCB. The lines drawn in Fig. 2 represent those obtained from least-squares analysis of the *combined* data for these three solvents. Analysis of the data for the isotropic solvents yields E_a = 34.8 ± 0.3 kcal/mol and $\Delta S^{\neq}$ (200°) = −1.5 ± 0.5 e.u., in excellent agreement with the parameters reported previously for isomerization of this olefin in benzene solution (18). Similar analysis of the data for the cholesteric phases of CB, CT, and CCB yields E_a = 36.0 ± 0.2 kcal/mol and $\Delta S^{\neq}$ (200°) = −0.5 ± 0.6 e.u. The correlation coefficients for the two analyses were better than 0.999 in both cases. Figure 3 shows the Arrhenius plots for DA and CMN, and the calculated Arrhenius parameters for these solvents are collected in Table 4.

While these plots clearly demonstrate that there is *some* difference between the energetics of *cis–trans* isomerization in the cholesteric and isotropic solvents, it is difficult to get a clear idea of the origin of this effect (whether enthalpic, entropic, or both) from the calculated Arrhenius parameters, considering the magnitude of the errors. The differences in $\Delta S^{\neq}$ certainly cannot be considered to be significant. An Arrhenius-type plot using the ratios of the rate constants in cholesteric CMN and isotropic DA, shown as an insert in Fig. 3, gives a somewhat more sensitive indication of the significance of the differences

[6] Reference 19*b*, chapt. 8, and references cited therein.

in the Arrhenius parameters. Keeping in mind that the errors in the calculated rate ratios are much larger than those in the rate constants themselves, the trend in the plot is clearly consistent with a slightly higher activation energy for isomerization of **1** in the cholesteric phase relative to the isotropic solvent.

It is tempting to ascribe the slightly higher activation energy for thermal isomerization of **1** in the cholesteric phases to the effects of liquid crystalline order on the transition state for *cis–trans* isomerization. If the change in shape from the "plate-like" ground state geometry of **1** to the globular 90°-twisted transition state is accompanied by some disruption of local solvent order, then increases in both the energy and entropy of activation for the process relative to their values in isotropic solvents are expected. Considering the sizeable difference in the shapes of the "planar" and twisted geometries of **1**, the magnitude of the observed effect in the present case is, however, clearly not large. The reason for this can be rationalized on the basis of how effectively **1** is expected to be solvated in the cholesteric phases examined.

Crystallographic data show that tetraphenylethylene is a rather bulky molecule in its ground state geometry. The phenyl groups are situated in a propeller-like arrangement, and the double bond is twisted by ca. 8° (28). As the data in Table 1 show, incorporation of as little as 0.5 wt.% (ca. 0.015 *M*) *trans*-**1** has a fairly substantial effect on the Ch → I transition temperatures of each of the cholesterics employed in the present study. Thus, the presence of **1** in even low concentrations disrupts cholesteric order to a significant extent, with the result that **1** is rather poorly solvated in these liquid crystals. Indeed, while the bulk mixtures remain liquid crystalline even at olefin concentrations up to 2%, it is possible that local disruption of solvent order is so severe that the effective solvation of individual solute molecules is almost isotropic. Further support for this idea derives from the lack of variation in the rate of isomerization of **1** as a function of either its concentration (Table 3) in the cholesteric phases or the rigidity of the mesophase.[7] Thus, as **1** isomerizes, any further disruption of solvent order is of a secondary nature, and the isomerization is inhibited to only a small extent.

Intimately related to this explanation is the possibility that the observed differences are the result of viscosity effects. Liquid crystals are highly viscous fluids in the bulk, and on a microscopic level their viscosity is highly anisotropic (19). The hindered rotation about the double bond in **1** in the cholesteric phases might then be attributed to viscous drag effects. However, to the extent that overcoming this viscous drag must involve disruption of solvent order, such a distinction seems superfluous. There is, nonetheless, another possible explanation for the observed effect, which is based on solvent viscosity arguments. It is reasonable to expect that the viscosity in an isotropic "microdroplet" which is surrounded by an ordered environment might be considerably higher than that in the bulk isotropic phase. The primary solvation shell of **1** in a cholesteric liquid crystal might then be viewed as a highly viscous, isotropic solvent, and it is this high effective viscosity which inhibits the isomerization, *not* the necessity of disrupting solvent order beyond the primary solvation shell. In order to account for the observed rate effects, the effective viscosity in the isotropic microdomains containing the solute must then be several orders of magnitude larger than that in the bulk isotropic phase, since the Arrhenius parameters for isomerization of **1** in the isotropic phase of cholesteryl benzoate are the same as those reported for that in benzene solution, and the bulk viscosities of these two solvents differ by at least two orders of magnitude at 180°C (29).

The "twisted nematic" description of the macroscopic order in cholesterics, insofar as it implies overall nematic order with no discrete solvent layering (30), leads to the expectation that **1** is oriented in the liquid crystal with its molecular plane held (on the average) parallel to the long molecular axes of the surrounding solvent molecules (23). The same orientation is expected in nematic and smectic liquid crystals. According to this picture, one would then expect that *any* liquid crystalline phase should produce an effect on the energetics of thermal isomerization of **1**, with the magnitude of the effect correlating with the degree of mesophase order. Thus, it would be predicted that nematic phases should produce an effect similar to that of cholesterics on the Arrhenius parameters for isomerization of **1**, while the effect of smectic phases might be somewhat greater owing to their higher degree of order and rigidity. The reported effect of a nematic solvent on the rate of isomerization of *cis*-stilbene (16) is consistent with this idea. Unfortunately, it is difficult to test this hypothesis with the present system, owing to the unavailability of nematic and smectic solvents in the temperature range required to observe the isomerization of **1**. These ideas clearly deserve systematic investigation.[8]

Despite our uncertainties with respect to the precise nature of the effect of cholesteric solvation on the energetics of *cis–trans* isomerization of **1**, the fact that an effect is observed at all indicates that cholesteric liquid crystals are indeed capable of inhibiting processes which involve a substantial change in molecular shape in the transition state, even for solutes which are not particularly well solvated in the liquid crystal. In the case of azobenzene, which is incorporated much more effectively in these media (32), it is probable that rotational *cis–trans* isomerization, if it occurred, could in fact be detected in cholesteric liquid crystalline solvents. We believe that the result that the energetics of isomerization of azobenzene are unaffected in cholesteric liquid crystals relative to their magnitude in isotropic solvents (9*b*) indicates that the bond inversion mechanism is indeed the operative mechanism for *cis–trans* isomerization of this molecule. However, it is difficult to predict what magnitude of an effect would obtain for bond rotation in this system, if it did occur. While azobenzene is solubilized more effectively than **1** in a liquid crystal (allowing potentially more disruption of solvent order in the course of bond rotation), the change in its shape as it approaches the rotational transition state is much less substantial.

Our observation that cholesteric liquid crystalline solvents are able to affect the dynamics of a solute's unimolecular reaction involving formation of a globular transition state from a relatively poorly solvated, disc-like ground state may illustrate the potential of these media towards controlling chemical reactivity in a useful manner. For example, it may be possible to use liquid crystals to exert stereochemical control on bimolecular reactions which normally yield some variety of products through transition states of grossly different shape, as a result of differences in liquid crystalline transition state solvation. Work in this area is currently in progress and will be reported in the near future.

[7] We thank one of the referees for pointing this out.

[8] While this paper was being reviewed, a report appeared describing substantial inhibition of bond rotation in 4-(dimethylamino)pyrimidine in a nematic solvent (see ref. 31).

Experimental

Melting points and transition temperatures were measured on a Reichert micro-hot stage microscope with polarizing lenses and are corrected. The [1]Hmr spectra were recorded in deuteriochloroform solution on a Varian EM390 nmr spectrometer. A Jumo-MS D.B.P. mercury thermoregulator, a Fisher Model 32 transistor relay, and an insulated silicon oil (Dow Corning 710) bath were used for temperature control in the kinetic studies. Temperatures were recorded with a Leeds & Northrup Model 8692 temperature potentiometer and a copper–constantan thermocouple, or a Cole–Parmer Model 8110-10 Type K thermocouple thermometer, and did not vary by more than 0.4°C during any particular run. Temperatures are considered accurate to ±1.0°C.

Analyses of mixtures of *cis*- and *trans*-**1** were performed using a Gilson isocratic hplc (high performance liquid chromatography) system, consisting of a Model 302 pump, Model 802B manometric module, Holochrome variable wavelength detector, a Rheodyne Model 7125 loop injection valve, and a Varian Model A-6 strip chart recorder, in conjunction with a 25 × 0.46 cm Merck Hibar Si60 (10 μ) analytical column. Dichloromethane was used as eluant, with a flow rate of 1.0 mL/min, and an analytical wavelength of 300 nm was used for all analyses. Preparative lc (liquid chromatography) was performed using the same system, in conjunction with 24 × 1.1 cm or 31 × 2.5 cm Merck Lobar Si60 (40–63 μ) glass columns. The detector was interfaced to a Unitron microcomputer via an Adalab data acquisition/control card (Interactive Microware, Inc.), after amplification of the 10-mV signal with an Adaamp analog amplifier. Chromatogram acquisition, analysis, and storage were performed using the Chromatochart (Interactive Microware, Inc.) software. Apparent mole fractions of the *trans* isomer so obtained were then converted to true mole fractions with a working curve, constructed with eleven standard solutions of accurately weighed mixtures of pure *cis*- and *trans*-**1**.

n-Decanol was used as received from BDH Chemicals, Ltd. Cholesterol (BDH) was recrystallized once from 95% ethanol. 3β-Cholestanol (Aldrich) was recrystallized once from 95% ethanol. Cholesteryl benzoate (Aldrich) was recrystallized twice from n-pentanol (33), and finally from ligroin/ethanol. A more highly purified sample was prepared by column chromatography (silica gel; hexanes) followed by one further recrystallization from ligroin/ethanol. Dichloromethane was Caledon HPLC grade and used as received. Hexanes (Caledon reagent grade) was distilled before use.

4-Anisoyl chloride, 4-toluoyl chloride, 4-chlorobenzoyl chloride, and 6-methoxy-2-naphthoyl chloride were prepared by refluxing the corresponding carboxylic acid in thionyl chloride for 2–8 h, followed by removal of excess thionyl chloride by vacuum distillation. The acid chlorides were used without further purification. 6-Methoxy-2-naphthoic acid was synthesized according to published procedures (34), and was recrystallized thrice from 95% ethanol (mp 197–198°C (lit. (34) mp 202°C)).

n-Decyl anisoate (DA) was prepared by refluxing n-decanol (16 g, 0.1 mol) and 4-anisoyl chloride (17 g, 0.1 mol) in freshly distilled *N,N*-dimethylaniline (60 mL) for 3 h (27). After cooling, the reaction mixture was poured onto crushed ice, and extracted with ether (5 × 50 mL). The combined ether extracts were washed with 5% aqueous hydrochloric acid (7 × 30 mL), 10% aqueous sodium hydroxide (5 × 30 mL), and water (5 × 30 mL). Drying over anhydrous magnesium sulfate, followed by evaporation of solvent, afforded a brown oil which was chromatographed on silica gel, using hexanes as the eluant, to yield a yellow oil which subsequently crystallized. Two recrystallizations from methanol afforded colourless crystals (7.5 g, 0.026 mol, 26%) of n-decyl anisoate (mp 28–29°C; bp 155–156°C (0.01 Torr; 1 Torr = 133.3 Pa)), assigned on the basis of its [1]Hmr and infrared spectra.

Cholesteryl 6-methoxy-2-naphthoate (CMN) was prepared in similar fashion, and was obtained in 21% yield after four recrystallizations from chloroform/ethanol (1:1). The product was further purified by preparative lc, using hexanes as the eluant, followed by one further recrystallization from chloroform/ethanol, yielding colourless crystals. Transition temperatures are listed in Table 1 (lit. (27): K → Ch, 183°C; Ch → I, 302.5°C). Better yields (>80%) were obtained using pyridine as solvent in the preparation, according to the procedure outlined below for CCB and CT.

Cholesteryl 4-chlorobenzoate (CCB) and cholestanyl 4-toluate (CT) were prepared by heating mixtures of cholesterol and 3β-cholestanol, respectively, with the appropriate acid chloride in pyridine for 12 h at 50–60°C. The reaction mixtures were quenched with water, extracted with dichloromethane, and the organic extracts were washed successively with 5% aqueous HCl, 10% aqueous sodium hydroxide, and water (five times each). The solutions were dried over anhydrous magnesium sulfate and the solvent was evaporated. The resulting solids were then chromatographed on silica gel using hexanes as eluant. CCB was further purified by recrystallization from ethanol, n-pentanol, and again from ethanol to yield colourless crystals (22%), the transition temperatures for which are listed in Table 1 (lit. (26): K → Ch, 165°C; Ch → I, 240°C). CT was further purified by recrystallization from n-pentanol, preparative lc (hexanes as eluant), and final recrystallization from chloroform/ethanol (1:2), to yield colourless crystals (18%). The transition temperatures are listed in Table 1 (lit. (25): K → Ch, 172°C; Ch → I, 225°C).

The stability of these materials towards thermolysis at the temperatures employed in the kinetic studies was examined by heating a sample of DA in a sealed tube at 230°C for 35 h. The [1]Hmr spectrum of the contents of the tube had not changed perceptibly from that recorded before this treatment.

The *cis*- and *trans*-**1** were prepared according to the published procedure (18). The crude yellow solid obtained from the preparation was chromatographed on a silica gel column, eluting with hexane/benzene (1:9). The mixture of olefins obtained as the first fraction from this column was then separated by semi-preparative lc, using dichloromethane as eluant. The first component collected was recrystallized from chloroform/ethanol, affording *trans*-**1** as slightly yellow needles (mp 204–206°C (lit. (18) mp 203–204°C)). The second component collected was recrystallized as well from chloroform/ethanol to yield slightly yellow needles of *cis*-**1** (mp 247–249°C (lit. (18) mp 247–249°C)). The hplc analyses of the two indicated them to be >99% isomerically pure in each case.

Solutions of *cis*- and *trans*-**1** for the kinetic measurements were prepared by adding an appropriate aliquot of a 0.1 *M* solution of the olefin in benzene to 0.6-g portions of each of the esters, dissolving the mixtures in dichloromethane, evaporating the solvent on the rotary evaporator, and finally pumping on the mixtures under high vacuum for 3 h to remove final traces of volatile solvents. Portions (5–7 mg) were placed in 7-mm Pyrex tubes (soaked in 10% sodium hydroxide (2 h), rinsed four times with distilled water, and finally oven-dried), the tubes were evacuated on a vacuum line to ca. 10^{-5} Torr, cooled in liquid nitrogen, and sealed.

Eight or nine tubes containing the *trans*-isomer, and one containing the *cis*, were then placed simultaneously in the preset insulated kinetic bath. In runs carried out above 210°C, the tubes were prewarmed briefly (ca. 1 min) in another oil bath set at 150°C before placing them in the kinetic bath, in order to prevent drastic temperature fluctuation. The temperature of the kinetic bath did not vary by more than 1° during the addition of the sample tubes, and recovered to its original value within 1.5 min. Samples were removed after suitable time intervals, quenched in an ice-bath, opened, and the contents were dissolved in benzene or dichloromethane and analysed by hplc. In all cases, the esteric solvents eluted well before the isomeric olefins, and their presence in such large quantities was shown to have no effect on the relative peak areas of *cis*- and *trans*-**1** by injection of standard mixtures. In no case did the hplc traces of the heated mixtures change during the course of a run, other than in the relative amounts of the isomeric olefins. Several of the unheated sealed tubes were used to check the initial composition of the samples to ensure that no accidental heating had occurred during the sealing process. The *cis* sample and one of the *trans* samples were heated for extended periods of time to evaluate the equilibrium composition in each solvent at each temperature examined. The equilibrium constants recorded in Table 2 are the average of all determinations at a given temperature.

Rate constants ($k_{c \to t} + k_{t \to c}$) were determined by weighted linear least-squares analyses of the mole fraction vs. time data according to eq. [1], and are collected in Table 2. Arrhenius parameters were determined by linear least-squares analyses of the rate data according to the Arrhenius equation, and are collected in Table 4.

Acknowledgements

We wish to thank the Natural Sciences and Engineering Research Council of Canada for its generous financial support of this work, and Dr. R. G. Weiss of Georgetown University, Washington, D.C. for valuable correspondence.

1. (*a*) W. E. BACON and G. H. BROWN. Mol. Cryst. Liq. Cryst. **12**, 229 (1971); (*b*) M. J. S. DEWAR and B. D. NAHLOVSKY. J. Am. Chem. Soc. **96**, 460 (1974).
2. (*a*) V. C. ANDERSON, B. B. CRAIG, and R. G. WEISS. J. Phys. Chem. **86**, 4642 (1982); (*b*) Mol. Cryst. Liq. Cryst. **97**, 351 (1983).
3. (*a*) J. M. NERBONNE and R. G. WEISS. Isr. J. Chem. **18**, 266 (1979); (*b*) D. A. HROVAT, J. H. LIU, N. J. TURRO, and R. G. WEISS. J. Am. Chem. Soc. **106**, 7033 (1984).
4. G. AVIV, J. SAGIV, and A. YOGEV. Mol. Cryst. Liq. Cryst. **36**, 349 (1976).
5. T. KUNIEDA, T. TAKAHASHI, and M. HIROBE. Tetrahedron Lett. **24**, 5107 (1983).
6. (*a*) J. M. NERBONNE and R. G. WEISS. J. Am. Chem. Soc. **100**, 2571 (1978); (*b*) J. Am. Chem. Soc. **101**, 402 (1979).
7. (*a*) V. C. ANDERSON, B. B. CRAIG, and R. G. WEISS. J. Am. Chem. Soc. **103**, 7169 (1981); (*b*) J. Am. Chem. Soc. **104**, 2972 (1982).
8. (*a*) B. SAMORI and L. FIOCCO. J. Am. Chem. Soc. **104**, 2634 (1982); (*b*) P. DE MARIA, A. LODI, B. SAMORI, F. RUSTICHELLI, and G. TORQUATI. J. Am. Chem. Soc. **106**, 653 (1984).
9. (*a*) J. M. NERBONNE and R. G. WEISS. J. Am. Chem. Soc. **100**, 5953 (1978); (*b*) J. P. OTRUBA and R. G. WEISS. J. Org. Chem. **48**, 3448 (1983).
10. (*a*) C. ESKENAZI, J. F. NICOUD, and H. B. KAGAN. J. Org. Chem. **44**, 995 (1979), and references cited therein; (*b*) P. SEURON and G. SOLLADIE. J. Org. Chem. **45**, 715 (1980); (*c*) Y. TANAKA, T. CHIYO, S. IIJIMA, T. SHIMIZU, and T. KUSANO. Mol. Cryst. Liq. Cryst. **99**, 255 (1983).
11. E. G. CASSIS, JR. and R. G. WEISS. Photochem. Photobiol. **35**, 439 (1982).
12. J. P. OTRUBA and R. G. WEISS. Mol. Cryst. Liq. Cryst. **80**, 165 (1982).
13. S. MELONE, V. MOSINI, R. NICOLETTI, B. SAMORI, and G. TORQUATI. Mol. Cryst. Liq. Cryst. **98**, 399 (1983).
14. (*a*) J. M. SCHNUR and D. E. MARTIRE. Mol. Cryst. Liq. Cryst. **26**, 213 (1974); (*b*) G. A. OWEIMREEN, G. C. LIN, and D. E. MARTIRE. J. Phys. Chem. **83**, 2111 (1979); (*c*) D. E. MARTIRE. *In* The molecular physics of liquid crystals. *Edited by* G. W. Gray and G. R. Luckhurst. Academic Press, New York. 1979. Chapt. 11; (*d*) G. A. OWEIMREEN and D. E. MARTIRE. J. Chem. Phys. **72**, 2500 (1980); (*e*) P. J. PORCARO and P. SHUBIAK. J. Chromatogr. Sci. **9**, 690 (1971).
15. (*a*) S. SHINKAI, T. OGAWA, T. NAKAJI, T. KUSANO, and O. MANABE. Tetrahedron Lett. 4569 (1979); (*b*) S. SHINKAI, T. NAKAJI, Y. NISHIDA, T. OGAWA, and O. MANABE. J. Am. Chem. Soc. **102**, 5860 (1980); (*c*) H. RAU and E. LUDDECKE. J. Am. Chem. Soc. **104**, 1616 (1982); (*d*) T. ASANO, T. YANO, and T. OKADA. J. Am. Chem. Soc. **104**, 4900 (1982).
16. S. I. TORGOVA, E. I. KOVSHEV, and V. V. TITOV. J. Org. Chem. USSR, **12**, 1569 (1976).
17. A. V. SANTORO, E. J. BARRETT, and H. W. HOYER. J. Am. Chem. Soc. **89**, 4545 (1967).
18. W. J. LEIGH and D. R. ARNOLD. Can. J. Chem. **59**, 609 (1981).
19. (*a*) F. D. SAEVA (*Editor*). Liquid crystals. The fourth state of matter. Marcel Dekker, Inc., New York. 1979; (*b*) H. KELKER and R. HATZ. Handbook of Liquid crystals. Verlag Chemie, Weinheim, Deerfield. 1980; (*c*) G. H. BROWN, J. W. DOANE, and V. D. NEFF. A review of the structure and properties of liquid crystals. Chemical Rubber Company Press, Cleveland. 1971.
20. (*a*) H. H. GIBSON. *In* Liquid crystals. The fourth state of matter. *Edited by* F. D. Saeva. Marcel Dekker, Inc., New York. 1979. Chapt. 4; (*b*) F. D. SAEVA. Pure Appl. Chem. **38**, 25 (1974).
21. (*a*) G. W. GRAY. *In* The molecular physics of liquid crystals. *Edited by* G. R. Luckhurst and G. W. Gray. Academic Press, London. 1979. Chapt. 1; (*b*) H. SCHRODER. Chapt. 5; (*c*) B. W. VAN DER MEER and G. VERTOGEN. Chapt. 6.
22. J. H. WENDORFF, and F. P. PRICE. Mol. Cryst. Liq. Cryst. **24**, 129 (1973).
23. E. SACKMANN, P. KREBS, H. U. REGA, J. VOSS, and H. MOHWALD. Mol. Cryst. Liq. Cryst. **24**, 283 (1973).
24. S. G. CARR, S. K. KHOO, G. R. LUCKHURST, and H. J. SMITH. Mol. Cryst. Liq. Cryst. **45**, 161 (1978).
25. C. WIEGAND. Z. Naturforsch. Teil B, **4**, 249 (1949).
26. E. M. BARRELL II, K. E. BREDFELDT, and M. J. VOGEL. Mol. Cryst. Liq. Cryst. **18**, 195 (1972).
27. J. S. DAVE and G. KURIAN. Pramana, Suppl. 1, 427 (1975).
28. A. HOEKSTRA and A. VOS. Acta Crystallogr. Sect. B, **31**, 1716 (1975); **31**, 1722 (1975).
29. C. G. KARTHA and R. K. L. P. AGARWAL. J. Phys. Soc. Jpn. **28**, 470 (1970).
30. P. N. KEATING. *In* Liquid crystals 2, Part II. *Edited by* G. H. Brown. Gordon and Breach, London. 1970. p. 279.
31. B. M. FUNG, R. V. SIGH, and M. M. ALCOCK. J. Am. Chem. Soc. **106**, 7301 (1984).
32. E. SACKMANN. J. Am. Chem. Soc. **93**, 7088 (1971).
33. G. J. DAVIS and R. S. PORTER. Mol. Cryst. Liq. Cryst. **6**, 377 (1970).
34. C. TARD, H. LAPIN, and A. HOREAU. C. R. Acad. Sci. **246**, 3644 (1958).

Synthetic study on *N*-hydroxyaspartic acid

T. KOLASA[1]

Department of Organic Chemistry, Technical University of Gdansk, 80-952 Gdansk, Poland

Received August 10, 1984

T. KOLASA. Can. J. Chem. **63**, 2139 (1985).

The synthesis of *N*-acyl derivatives of *N*-hydroxyaspartic acid was achieved by use of *N*-benzyloxyaspartic acid esters as starting material. The preparation of *N*-benzyloxyaspartic acid is described.

T. KOLASA. Can. J. Chem. **63**, 2139 (1985).

Utilisant des esters de l'acide *N*-benzoyloxyaspartique comme produit de départ, on a réussi la synthèse de dérivés *N*-acylés de l'acide *N*-hydroxyaspartique. On décrit la préparation de l'acide *N*-benzyloxyaspartique.

[Traduit par le journal]

Introduction

The naturally occurring hydroxamic acids are *N*-acyl derivatives of *N*-hydroxyamino acids. Although free *N*-hydroxyamino acids have not been found in living cells, these compounds have been isolated from the parent hydroxamic acids after hydrolysis.

In this manner, the most frequently isolated *N*-hydroxyamino acids are ω-*N*-hydroxyamino acids, such as ε-*N*-hydroxylysine and δ-*N*-hydroxyornithine (1). The α-*N*-hydroxyamino acids appear very rarely, and until now the presence of only a few α-*N*-hydroxyamino acids in nature has been confirmed. These include *N*-hydroxyglycine in hadacidin (2), α-*N*-hydroxytyrosine and α-*N*-hydroxyalanine in mycelianamide (3), α-*N*-hydroxyisoleucine in aspergillic acid (4), α-*N*-hydroxyleucine in pulcherrimin (5), and *N*-hydroxyaspartic acid in peptide hydroxamates isolated from cultures of *Corynebacterium kutscheri* (6) and *Mycobacterium avium* (7).

Several experimental approaches to the synthesis of α-*N*-hydroxyamino acids have been developed (8–11). While most α-*N*-hydroxyamino acids, including many naturally occurring derivatives have been prepared, *N*-hydroxyaspartic acid has not been synthesized previously.

Emery (12) showed that enzyme extracts from *Bacillus cadaveris* or *Proteus vulgaris* synthesize *N*-hydroxyaspartic acid from fumaric acid and hydroxylamine. Unfortunately, in spite of unquestionable confirmation of the appearance of that amino acid, an extensive effort to isolate and purify it was unsuccessful. Similarly, attempted chemical syntheses of *N*-hydroxyaspartic acid by the reaction of bromosuccinic acid with hydroxylamine and the reaction of hydroxylamine with fumaric acid were unsuccessful. Furthermore, efforts to synthesize *N*-hydroxyaspartic acid acyl derivatives have not been successful. In addition, the attempted isolation of *N*-hydroxyaspartic acid through acidic hydrolysis of the naturally occurring dipeptide, L-α-asparaginyl-L-α-(*N*-hydroxy)asparagine, was also unsuccessful (7).

The problems described above, plus the unique structure of the peptide hydroxamates isolated by McCullough and Merkal (6, 7) prompted our synthetic studies.

Results and discussion

This work describes the synthesis of *N*-hydroxyaspartic acid derivatives through an application of the benzyl group for protection of the hydroxylamine moiety.

The synthesis of α-*N*-benzyloxyamino acids (10) and their application to the synthesis of *N*-acyl-α-*N*-hydroxyamino acids (13) and α-*N*-hydroxypeptides (14) has been described earlier. Thus, treatment of bromosuccinic acid with *O*-benzylhydroxylamine was anticipated to provide *N*-benzyloxyaspartic acid. Unfortunately, instead of the desired material, two other products were isolated. First, compound A, mp 160–161°C, precipitated from aqueous solution at pH 4, while the second compound B, mp 110–112°C, separated at pH 3. Compound A was the main product of the reaction.

The nmr spectra of both compounds were identical and the elementary analyses indicated the same formulas. A comparison of the ir spectra of both products indicated that compound A is characterized by two carbonyl absorption bands at 1710 and 1670 cm^{-1}, while compound B has only one carbonyl absorption band at 1715 cm^{-1}. Furthermore, the hydrogenolysis of compound A gave a hydroxamic acid (positive $FeCl_3$ test), while a product of the hydrogenolysis of compound B appeared to have an *N*-hydroxyamine group (positive $AgNO_3$ test).

Structural assignment of the compounds based on elemental analysis, ir and ^{1}H nmr spectroscopy, as well as chemical properties, showed that compound A is a β-*N*-benzyloxyamide of malic acid and compound B is *N*-benzyloxyaspartic acid. Hence the reaction of bromosuccinic acid with *O*-benzylhydroxylamine can be represented by Scheme 1.

The literature (15, 16) describes many examples of formation of the β-hydroxyacid amides during the reaction of β-bromoacids with ammonia and suggests that they are formed from intermediate β-lactones. Recently, the β-lactones of malic acid were used in the process of synthesis of the β-lactam ring (17, 18). It has also been shown that the β-lactone of *N*-protected threonine reacts very smoothly with *O*-benzylhydroxylamine to provide the *N*-benzyloxyamide (19).

These results suggested that protection of the carbonyl groups was necessary. Indeed, the reaction of bromosuccinic acid esters with *O*-benzylhydroxylamine gave the desired products, *N*-benzyloxyaspartic acid esters, with good yields. Thus, the dimethyl, diethyl, and di-*tert*-butyl esters of *N*-benzyloxyaspartic acid were obtained from bromosuccinic acid as well as *O*-tosyl malic acid diesters. In addition, the free *N*-benzyloxyaspartic acid is a stable compound and can be easily prepared from the di-*tert*-butyl esters. The *N*-hydroxyaspartic acid, obtained from *N*-benzyloxyaspartic acid by hydrogenolysis, is very unstable. Efforts to isolate and purify it were unsuccessful, as were the attempts of Emery (12). Unlike the unstable free *N*-hydroxyaspartic acid, the di-*tert*-butyl ester is

[1]Present address: Department of Chemistry, University of Notre Dame, Notre Dame, Indiana 46556, U.S.A.

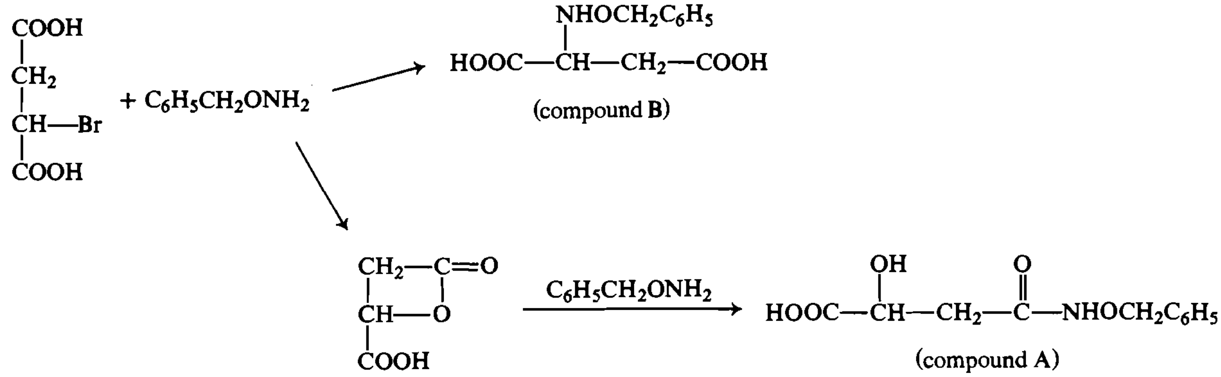

SCHEME 1

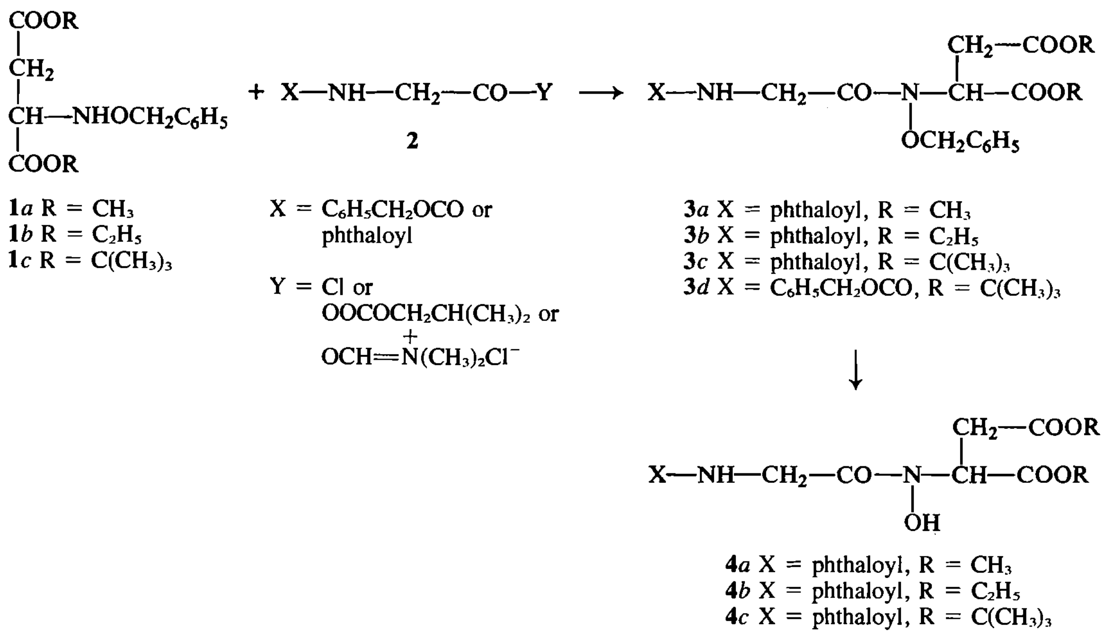

SCHEME 2

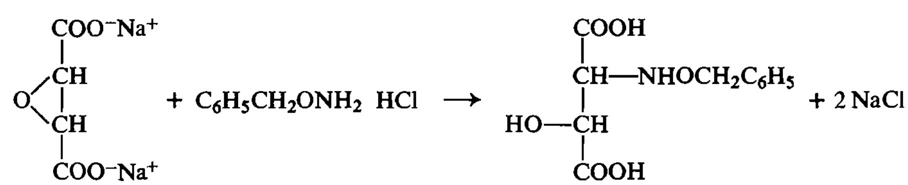

SCHEME 3

stable and can be stored at room temperature.

According to Emery (12), the synthesis of *N*-hydroxyaspartic acid *N*-acyl derivatives through acylation of free *N*-hydroxyaspartic acid did not give the desired products. Therefore, direct use of *N*-benzyloxyaspartic acid diesters as the starting materials seemed to be more attractive. Based on the above considerations, the *N*-formyl and *N*-acetyl-*N*-hydroxyaspartic acid diesters were synthesized earlier (13). Described here are the syntheses of the *N*-hydroxypeptides (Scheme 2).

As has been shown earlier (14), the preparation of *N*-benzyloxypeptides with *N*-terminal glycine proceeds with good yields, but with other *N*-terminal amino acids the yields are very low. Therefore, a new method was utilized for the synthesis of *N*-benzyloxyamides (20). Use of iminochlorides as activating agents of the carboxyl groups afforded the *N*-benzyloxypeptides in good yields. The *N*-benzyloxypeptides can be readily converted to the corresponding *N*-hydroxypeptides by hydrogenation.

Additionally, *threo*-β-hydroxy-*N*-benzyloxyaspartic acid has been synthesized by the reaction of *cis*-epoxysuccinic acid with *O*-benzylhydroxylamine (Scheme 3). Initially, the direct preparation of β-hydroxy-*N*-hydroxyaspartic acid was attempted by reaction of hydroxylamine hydrochloride with the disodium salt of *cis*-epoxysuccinic acid. Unfortunately, although many products were found, none was the desired one, probably because of decomposition. Also, the attempted isolation of the product of hydrogenolysis of β-hydroxy-*N*-benzyloxyaspartic acid was unsuccessful.

Experimental

All melting points are uncorrected. The nmr spectra were obtained with a Tesla BS 487 spectrometer 80 MHz. The L- and D-bromosuccinic acids were prepared from the corresponding aspartic acids according to the procedure of Testa *et al.* (21).

β-N-Benzyloxyamide of malic acid

To a solution of bromosuccinic acid (19.7 g, 0.1 mol) in ethanol (100 mL) was added *O*-benzylhydroxylamine (61.5 g, 0.5 mol). The reaction mixture was kept at room temperature for 10 days and then concentrated *in vacuo*. The residue was dissolved in ethyl ether and washed several times with 10% $NaHCO_3$. The water solution was acidified with 2 *N* HCl to pH 4, to precipitate 19.1 g of compound A (80%), mp 160–161°C (EtOH); ^{1}H nmr (in DMSO-d_6) δ: 2.5 (2H, d, J = 7 Hz, —CH_2—), 4.2 (1H, m, —CHO—), 4.82 (2H, s, —CH_2O—), 7.38 (5H, s, aromatic). *Anal.* calcd. for $C_{11}H_{13}NO_5$: C 55.23, H 5.44; N 5.86%; found: C 55.57, H 5.09, N 6.07%. Further acidification to pH 3 gave a compound B (1.2 g, 5%), mp 110–112°C; ^{1}H nmr (in DMSO-d_6) δ: 2.66 (2H, dd, J = 7 Hz, 3 Hz, —CH_2—), 4.0 (1H, t, J = 7 Hz, —CHN—), 4.72 (2H, s, —CH_2O—), 7.38 (5H, s, aromatic). *Anal.* calcd. for $C_{11}H_{13}NO_5$: C 55.23, H 5.44, N 5.86%; found: C 54.89, H 5.24, N 5.66%.

*N-Benzyloxyaspartic acid esters **1**a, **1**b, and **1**c*

To a solution of bromosuccinic acid (or *O*-tosyl malic acid) esters (0.1 mol) in 100 mL of ethanol was added *O*-benzylhydroxylamine (0.3 mol). The reaction was kept at room temperature for 10 days. Then the solution was concentrated *in vacuo*, dissolved in ethyl ether, and washed with 2 *N* HCl (or 5% citric acid in the case of *tert*-butyl esters) and water. The organic layer was dried ($MgSO_4$) and concentrated *in vacuo*. The oily residue was treated with an ethereal solution of HCl (in the case of *tert*-butyl esters, silica gel column chromatography with benzene as eluent was used); after cooling, the hydrochlorides were filtered off and crystallized from EtOH–Et_2O. The yields and properties are given below.

N-Benzyloxy-D-aspartic acid dimethyl ester was prepared from L-bromosuccinic acid dimethyl ester in 87% yield, $[\alpha]_D^{20}$ +2.0 (*c* 7, CH_3OH); mp (hydrochloride) 115–116°C; ^{1}H nmr (in DMSO-d_6) δ: 3.1 (2H, d, J = 7 Hz, —CH_2—), 3.72 (3H, s, —OCH_3), 3.85 (3H, s, —OCH_3), 4.58 (1H, t, J = 7 Hz, —CHN—), 5.12 (2H, s, —CH_2O—), 7.5 (5H, s, aromatic), 10.05 (2H, broad s, NH_2^+). *Anal.* calcd. for $C_{13}H_{18}NO_5Cl$: C 51.40, H 5.92, N 4.61%; found: C 51.12, H 6.07, N 4.89%.

This compound has also been synthesized from *O*-tosyl-L-malic acid dimethyl ester in 80% yield, $[\alpha]_D^{20}$ +2.3 (*c* 7, CH_3OH); mp (hydrochloride) 113–115°C. *Anal.* calcd. for $C_{13}H_{18}NO_5Cl$: N 4.61; found: N 4.65%.

N-Benzyloxy-L-aspartic acid dimethyl ester was synthesized from D-bromosuccinic acid dimethyl ester in 93% yield, $[\alpha]_D^{25}$ = −2.7 (*c* 7, CH_3OH); mp (hydrochloride) 116–117°C; ^{1}H nmr (in DMSO-d_6) δ: 3.05 (2H, d, J = 7 Hz, —CH_2—), 3.7 (3H, s, —OCH_3), 3.8 (3H, s, —OCH_3), 4.5 (1H, t, J = 7 Hz, —CHN—), 5.03 (2H, s, —CH_2O—), 7.43 (5H, s, aromatic), 11.23 (2H, broad s, NH_2^+). *Anal.* calcd. for $C_{13}H_{18}NO_5Cl$: N 4.61%; found: N 4.72%.

N-Benzyloxy-DL-aspartic acid dimethyl ester was prepared from *O*-tosyl-DL-malic acid dimethyl ester in 82% yield, mp (hydrochloride) 108–110°C; ^{1}H nmr (in TFA) δ: 3.1 (2H, m, —CH_2—), 3.42 (3H, s, —OCH_3), 3.6 (3H, s, —OCH_3), 4.8 (1H, m, —CHN—), 5.2 (2H, s, —CH_2O—), 7.3 (5H, s, aromatic). *Anal.* calcd. for $C_{13}H_{18}NO_5Cl$: N 4.61%; found: N 4.44%.

N-Benzyloxy-DL-aspartic acid diethyl ester was synthesized from *O*-tosyl-DL-malic acid diethyl ester in 78% yield, mp (hydrochloride) 98–100°C; ^{1}H nmr (in DMSO-d_6) δ: 1.3 (6H, q, J = 7 Hz, 2 × —CH_3), 3.08 (2H, d, J = 7 Hz, —CH_2—), 4.24 (4H, dt, J = 7 Hz, 2 × —OCH_2—), 4.53 (1H, m, —CHN—), 5.13 (2H, s, benzylic), 7.5 (5H, s, aromatic), 11.0 (2H, broad s, NH_2^+). *Anal.* calcd. for $C_{15}H_{22}NO_5Cl$: C 54.29, H 6.64, N 4.22%; found: C 53.98, H 6.39, N 4.46%.

This compound was also prepared from DL-bromosuccinic acid diethyl ester in 88% yield, mp (hydrochloride) 103–105°C; ^{1}H nmr (in $CDCl_3$) δ: 1.0 (6H, q, J = 7 Hz, 2 × —CH_3), 3.0 (2H, m, —CH_2—), 3.95 (4H, dt, J = 7 Hz, 2 × —OCH_2—), 4.52 (1H, m, —CHN—), 5.18 (2H, s, benzylic), 7.13 (5H, s, aromatic), 8.85 (2H, broad s, NH_2^+). *Anal.* calcd. for $C_{15}H_{22}NO_5Cl$: N 4.22%; found: N 4.48%.

*N-Benzyloxy-D-aspartic acid di-*tert*-butyl ester* was obtained from L-bromosuccinic acid di-*tert*-butyl ester in 74% yield, mp (hydrochloride) 73–75°C; $[\alpha]_D^{20}$ +6.0 (*c* 6, CH_2Cl_2); ^{1}H nmr (in $CDCl_3$) δ: 1.3 (9H, s, —$C(CH_3)_3$), 1.36 (9H, s, —$C(CH_3)_3$), 2.4 (2H, dd, J = 7 Hz, 4 Hz, —CH_2—), 3.75 (1H, q, J = 7 Hz, —CHN—), 5.05 (2H, s, —CH_2O—), 6.08 (1H, d, J = 7 Hz, —NH—) 7.17 (5H, s, aromatic). *Anal.* calcd. for $C_{19}H_{29}NO_5$: C 64.96, H 8.26, N 3.99%; found: C 64.68, H 8.40, N 4.20%.

*N-Benzyloxy-L-aspartic acid di-*tert*-butyl ester* was synthesized from D-bromosuccinic acid di-*tert*-butyl ester in 72% yield, mp (hydrochloride) 78–80°C; $[\alpha]_D^{20}$ −5.6 (*c* 6, CH_2Cl_2); ^{1}H nmr (in $CDCl_3$) δ: 1.3 (18H, s, 2 × —$C(CH_3)_3$), 2.4 (2H, dd, J = 7 Hz, 4 Hz, —CH_2—), 3.72 (1H, q, J = 7 Hz, —CHN—), 5.0 (2H, s, —CH_2O—), 6.05 (1H, d, J = 7 Hz, —NH—), 7.25 (5H, s, aromatic). *Anal.* calcd. for $C_{19}H_{29}NO_5$: N 3.99%; found: N 4.07%.

*N-Benzyloxy-DL-aspartic acid di-*tert*-butyl ester* was prepared from DL-bromosuccinic acid in 63% yield, mp (hydrochloride) 69–71°C; ^{1}H nmr (in $CDCl_3$) δ: 1.42 (18H, s, 2 × —$C(CH_3)_3$), 2.66 (2H, dd, J = 7 Hz, 3 Hz, —CH_2—), 4.0 (1H, t, J = 7 Hz, —CHN—), 5.34 (2H, s, —CH_2O—), 7.0 (1H, broad s, —NH—), 7.65 (5H, s, aromatic). *Anal.* calcd. for $C_{19}H_{29}NO_5$: N 3.99%; found: N 4.39%.

N-Benzyloxy-D-aspartic acid

To *N*-benzyloxy-D-aspartic acid di-*tert*-butyl ester (3.51 g, 10 mmol) was added 4 mL of trifluoroacetic acid and after 30 min the reaction mixture was concentrated *in vacuo*. To the residue, 10 mL of water was added and the solution was cooled in an ice bath. The solution was then filtered, and washed with cold water to give the product (2.1 g, 90%), mp 120–121°C (EtOH–H_2O); $[\alpha]_D^{25}$ +6.3 (*c* 6, MeOH); ^{1}H nmr (in DMSO-d_6) δ: 2.68 (2H, dd, J = 7 Hz, 4 Hz, —CH_2—), 3.97 (1H, t, J = 7 Hz, —CHN—), 4.7 (2H, s, —CH_2O—), 7.4 (5H, s, aromatic). *Anal.* calcd. for $C_{11}H_{13}NO_5$: N 5.86%; found: N 5.82%.

*N-Hydroxy-DL-aspartic acid di-*tert*-butyl ester*

To a solution of *N*-benzyloxy-DL-aspartic acid di-*tert*-butyl ester (1.76 g, 5 mmol) in ethanol (10 mL) was added 10% Pd/C (50 mg) and hydrogen was passed through the solution for 1 h. Then the filtered solution was evaporated to dryness, redissolved in chloroform, and purified on a silica gel column, using $CHCl_3$–MeOH (9:1) as eluent to give an oily product (2.07 g, 83%); ^{1}H nmr (in $CDCl_3$) δ: 1.3 (9H, s, —$C(CH_3)_3$), 1.33 (9H, s, —$C(CH_3)_3$), 2.58 (2H, d, J = 7 Hz, —CH_2—), 3.75 (1H, t, J = 7 Hz, —CHN—). *Anal.* calcd. for $C_{12}H_{23}NO_5$: N 5.37%; found: N 5.62%.

N-Carbobenzoxy-N-benzyloxy-DL-aspartic acid

To a solution of *N*-benzyloxy-DL-aspartic acid di-*tert*-butyl ester (3.51 g, 10 mmol) in CH_2Cl_2 (20 mL) was added solid $NaHCO_3$ (1.26 g, 15 mmol) and 11 mmol of carbobenzoxy chloride. The reaction mixture was stirred at room temperature overnight, and then was washed with water, dried ($MgSO_4$), and concentrated *in vacuo*. Then 3 mL of trifluoroacetic acid was added and after 30 min the solvent was evaporated to dryness. The residue was dissolved in ethyl ether and washed with 10% $NaHCO_3$. The water solution was acidified to pH 4 and the precipitated product filtered off to provide a white powder (2 g, 54%), mp 123–125°C (EtOAc – petroleum ether 30–60°C); ^{1}H nmr (in DMSO-d_6) δ: 3.0 (2H, dd, J = 7 Hz, 4 Hz, —CH_2—), 4.82 (1H, t, J = 7 Hz, —CHN—), 4.97 (2H, s, —CH_2O—), 5.3 (2H, s, —CH_2O—), 7.35 (5H, s, aromatic), 7.44 (5H, s, aromatic). *Anal.* calcd. for $C_{19}H_{19}NO_7$: N 3.75%; found: N 3.99%.

threo-β-Hydroxy-N-benzyloxy-DL-aspartic acid was obtained in 60% yield, according to the known procedure for preparation of β-hydroxyaspartic acid (22, 23), mp 150–152°C; ^{1}H nmr (in TFA) δ: 5.3 (2H, s, —CH—CH—), 5.4 (2H, s, —CH_2O—), 7.6 (5H, s, aromatic). *Anal.* calcd. for $C_{11}H_{13}NO_6$: N 5.49%; found: N 5.40%.

N-*Phthaloylglycyl*-N-*benzyloxyaspartic acid esters* **3**a, **3**b, **3**c were synthesized according to the standard procedures already used for the preparation of *N*-benzyloxypeptides (14).

N-*Phthaloylglycyl*-N-*benzyloxy*-D-*aspartic acid dimethyl ester* was prepared by the acid chloride method in 66% yield, mp 58–59°C (EtOAc – pet. ether 30–60°C), $[\alpha]_D^{20}$ −6.0 (*c* 6, $CHCl_3$); ^{1}H nmr (in $CDCl_3$) δ: 2.83 (2H, t, *J* = 7 Hz, —CH_2—), 3.45 (3H, s, —OCH_3), 3.53 (3H, s, —OCH_3), 4.38 (2H, s, —CH_2N—), 4.9 (2H, s, —CH_2O—), 5.05 (1H, t, *J* = 7 Hz, —CHN—), 7.1 (5H, s, aromatic), 7.5 (4H, m, aromatic). *Anal.* calcd. for $C_{23}H_{22}N_2O_8$: C 60.79, H 4.84, N 6.17%; found: C 61.02, H 4.98, N 6.50%.

N-*Phthaloylglycyl*-N-*benzyloxy*-DL-*aspartic acid diethyl ester* was synthesized as an oily compound in 85% yield by the acid chloride method and in 78% yield by the mixed anhydride method; ^{1}H nmr (in $CDCl_3$) δ: 1.05 (6H, dt, *J* = 7 Hz, 3 Hz, 2 × —CH_3), 2.87 (2H, t, *J* = 7 Hz, —CH_2—), 4.0 (4H, dq, *J* = 7 Hz, 3 Hz, 2 × —CH_2O—), 4.35 (2H, s, —CH_2N—), 4.9 (2H, s, benzylic), 5.0 (1H, t, *J* = 7 Hz, —CHN—), 7.2 (5H, s, aromatic), 7.5 (4H, s, aromatic). *Anal.* calcd. for $C_{25}H_{26}N_2O_8$: C 62.24, H 5.39, N 5.81%; found: C 62.03, H 5.13, N 5.84%.

N-*Phthaloylglycyl*-N-*benzyloxy*-DL-*aspartic acid di*-tert-*butyl ester* was obtained by the acid chloride method in 63% yield, mp 72–73°C (EtOAc – pet. ether 30–60°C); ^{1}H nmr (in $CDCl_3$) δ: 1.32 (18H, s, 2 × —$C(CH_3)_3$), 2.78 (2H, t, *J* = 7 Hz, —CH_2—), 4.38 (2H, s, —CH_2N—), 4.92 (3H, s + m, —CH_2O—, —CHN—), 7.3 (5H, s, aromatic), 7.58 (4H, m, aromatic). *Anal.* calcd. for $C_{29}H_{34}N_2O_8$: C 64.68, H 6.32, N 5.20%; found: C 64.33, H 6.58, N 5.40%.

N-*Phthaloylglycyl*-N-*benzyloxy*-D-*aspartic acid di*-tert-*butyl ester* was prepared by the acid chloride method in 65% yield, mp 69–70°C (EtOAc – pet. ether 30–60°C), $[\alpha]_D^{20}$ +11.0 (*c* 4, acetone); ^{1}H nmr (in $CDCl_3$) δ: 1.3 (18H, s, 2 × —$C(CH_3)_3$), 2.73 (1H, d, *J* = 7 Hz, 1/2 × —CH_2—), 2.9 (1H, d, *J* = 7 Hz, 1/2 × —CH_2—), 4.37 (2H, s, —CH_2N—), 4.97 (3H, s + m, —CH_2O—, —CHN—), 7.27 (5H, s, aromatic), 7.6 (4H, m, aromatic). *Anal.* calcd. for $C_{29}H_{34}N_2O_8$: N 5.20%; found: N 5.37%.

N-*Carbobenzoxyglycyl*-N-*benzyloxy*-DL-*aspartic acid di*-tert-*butyl ester* **1**d was synthesized by the mixed anhydride method as an oily compound in 76% yield; ^{1}H nmr (in $CDCl_3$) δ: 1.27 (18H, s, 2 × —$C(CH_3)_3$), 2.7 (1H, d, *J* = 7 Hz, 1/2 × —CH_2—), 2.85 (1H, d, *J* = 7 Hz, 1/2 × —CH_2—), 4.0 (2H, m, —CH_2N—), 4.8 (2H, s, —CH_2O—), 4.95 (2H, s, —CH_2O—), 5.2 (2H, m, —CHN—), 7.17 (5H, s, aromatic), 7.22 (5H, s, aromatic). *Anal.* calcd. for $C_{29}H_{38}N_2O_8$: C 64.20, H 7.01, N 5.16%; found: C 63.93, H 7.23, N 5.26%.

This compound was also prepared by the iminochloride method (20) in 82% yield. *Anal.* calcd. for $C_{29}H_{38}N_2O_8$: C 64.20, H 7.01, N 5.16%; found: C 64.01, H 7.12, N 5.13%.

N-*Phthaloylglycyl*-N-*hydroxyaspartic acid esters* **4**a, **4**b, **4**c were synthesized by hydrogenation of *N*-benzyloxypeptides according to an earlier described procedure (14).

N-*Phthaloylglycyl*-N-*hydroxy*-D-*aspartic acid dimethyl ester* was obtained in 97% yield, mp 172–173°C (EtOAc – pet. ether 30–60°C), $[\alpha]_D^{20}$ −9.0 (*c* 4, acetone–DMF 4:1); ^{1}H nmr (in $CDCl_3$ + a few drops of TFA) δ: 3.05 (2H, d, *J* = 7 Hz, —CH_2—), 3.6 (3H, s, —OCH_3), 3.67 (3H, s, —OCH_3), 4.75 (2H, s, —CH_2N—), 5.5 (1H, t, *J* = 7 Hz, —CHN—), 7.65 (4H, m, aromatic). *Anal.* calcd. for $C_{16}H_{16}N_2O_8$: N 7.69%; found: N 7.94%.

N-*Phthaloylglycyl*-N-*hydroxy*-DL-*aspartic acid diethyl ester* was prepared in 82% yield, mp 108–109°C (EtOAc – pet. ether 30–60°C); ^{1}H nmr (in $CDCl_3$) δ: 1.12 (6H, dt, *J* = 7 Hz, 3 Hz, 2 × —CH_3), 2.85 (2H, d, *J* = 7 Hz, —CH_2—), 4.05 (4H, dq, *J* = 7 Hz, 3 Hz, 2 × —CH_2O—), 4.65 (2H, s, —CH_2N—), 5.3 (1H, t, *J* = 7 Hz, —CHN—), 7.68 (4H, m, aromatic). *Anal.* calcd. for $C_{18}H_{20}N_2O_8$: N 7.18%; found: N 6.91%.

N-*Phthaloylglycyl*-N-*hydroxy*-DL-*aspartic acid di*-tert-*butyl ester* was isolated in 90% yield, mp 167–168°C (EtOAc – pet. ether 30–60°C); ^{1}H nmr (in DMSO-d_6) δ: 1.3 (18H, s, 2 × —$C(CH_3)_3$), 2.95 (2H, d, *J* = 7 Hz, —CH_2—), 4.8 (2H, s, —CH_2N—), 5.25 (1H, t, *J* = 7 Hz, —CHN—), 7.62 (4H, m, aromatic). *Anal.* calcd. for $C_{28}H_{28}N_2O_8$: N 6.25%; found: N 6.13%.

Glycyl-N-*hydroxy*-DL-*aspartic acid* was obtained from *N*-carbobenzoxyglycyl-*N*-benzyloxy-DL-aspartic acid di-*tert*-butyl ester as described earlier (14) (by removing *tert*-butyl groups with trifluoroacetic acid, followed by simultaneous hydrogenation of the carbobenzoxy and benzyl groups) in 72% yield; mp 164–167°C dec. (H_2O–EtOH); ^{1}H nmr (in D_2O) δ: 2.97 (2H, d, *J* = 7 Hz, —CH_2—), 4.1 (2H, s, —CH_2N—), 5.2 (1H, t, *J* = 7 Hz, —CHN—). *Anal.* calcd. for $C_6H_{10}N_2O_6$: N 13.59%; found: 13.33%.

N-*Formyl*-N-*hydroxy*-L-*alanyl*-N-*hydroxy*-L-*aspartic acid dimethyl ester*

To a solution of absolute DMF (9.2 mL, 0.12 mol) in dry CH_2Cl_2 (50 mL) was added dropwise at −10 to −5°C freshly distilled oxalyl chloride (4 mL, 0.048 mol). After 15 min, the *N*-formyl-*N*-benzyloxy-L-alanine (6.6 g, 30 mmol) was added. The reaction mixture was stirred for 30 min at −15 to −5°C and then *N*-benzyloxy-L-aspartic acid dimethyl ester hydrochloride (9.1 g, 30 mmol) in pyridine (22 mL, 0.25 mol) was added. After 2 h at −5 to 0°C and 2 h at room temperature water was added and the methylene chloride solution was separated. The organic layer was washed with water, dried ($MgSO_4$), and concentrated *in vacuo*. The oily residue was dissolved in MeOH, 10% Pd/C (100 mg) was added, and hydrogen was passed through the solution for 2 h. After filtration and removing methanol under reduced pressure, the product was purified on a silica gel column using $CHCl_3$–MeOH (8:1) as the eluent to yield an oily product (4.5 g, 52%); ^{1}H nmr (in $CDCl_3$) δ: 1.25 (3H, m, —CH_3), 2.84 (2H, d, *J* = 7 Hz, —CH_2—), 3.46 (6H, s, 2 × —OCH_3), 4.4 (1H, m, —CHN—), 4.9 (1H, t, *J* = 7 Hz, —CHN—), 7.93 (0.5H, s, 1/2 × H—C=O), 8.1 (0.5H, s, 1/2 × H—C=O). *Anal.* calcd. for $C_{10}H_{16}N_2O_8$: N 9.59; found: N 9.40%.

Acknowledgement

This work was supported by grant MR-12 from the Polish Academy of Science.

1. H. Maehr. Pure Appl. Chem. **28**, 603 (1971).
2. E. A. Kaczka, C. O. Gitterman, E. L. Dulaney, and K. Folkers. Biochemistry, **1**, 340 (1962).
3. A. J. Birch, R. A. Massey-Westropp, and R. W. Rickards. J. Chem. Soc. 3717 (1956).
4. J. Dutcher. J. Biol. Chem. **171**, 321 (1947); **171**, 341 (1947).
5. A. J. Kluyver, J. P. van der Walt, and A. J. van Triet. Proc. Natl. Acad. Sci. U.S.A. **39**, 583 (1953).
6. W. G. McCullough and R. S. Merkal. J. Bacteriol. **137**, 243 (1979).
7. W. G. McCullough and R. S. Merkal. J. Bacteriol. **128**, 15 (1976).
8. T. Polonski and A. Chimiak. J. Org. Chem. **41**, 2092 (1976).
9. T. Polonski and A. Chimiak. Tetrahedron Lett. 2453 (1974).
10. T. Kolasa and A. Chimiak. Tetrahedron, **30**, 3591 (1974).
11. M. Milewska, T. Kolasa, and A. Chimiak. Pol. J. Chem. **55**, 2215 (1981).
12. T. F. Emery. Biochemistry, **2**, 1041 (1963).
13. T. Kolasa. Tetrahedron, **39**, 1753 (1983).
14. T. Kolasa and A. Chimiak. Tetrahedron, **33**, 3285 (1977).
15. G. Senter and A. M. Ward. J. Chem. Soc. **127**, 1847 (1925).
16. H. E. Zaugg. Org. React. **8**, 305 (1954).
17. M. J. Miller, J. S. Bajwa, P. G. Mattingly, and K. Peterson. J. Org. Chem. **47**, 4928 (1982).
18. J. S. Bajwa and M. J. Miller. J. Org. Chem. **48**, 1114 (1983).
19. E. M. Gordon, M. A. Ondetti, J. Pluscec, C. M. Cimarusti, D. P. Bonner, and R. B. Sykes. J. Am. Chem. Soc. **104**, 6053 (1982).
20. P. A. Stadler. Helv. Chim. Acta, **61**, 1675 (1978).
21. E. Testa, B. J. R. Nicolaus, L. Mariani, and G. Pagani. Helv. Chim. Acta, **46**, 766 (1963).
22. C. W. Jones III, D. E. Leyden, and C. H. Stammer. Can. J. Chem. **47**, 4363 (1969).
23. T. Kolasa and E. Gross. Int. J. Pept. Protein Res. **20**, 254 (1982).

Application of ^{13}C nuclear magnetic resonance to the conformational analysis of vicinally di- and trisubstituted cyclohexanes: halohydrins, methoxyhalohydrins, and their acetates

G. W. BUCHANAN[1]
Ottawa–Carleton Institute for Research and Graduate Studies in Chemistry, Carleton University, Ottawa, Ont., Canada K1S 5B6

J. W. BOVENKAMP,[1] A. RODRIGUE, AND R. A. B. BANNARD
Defence Research Establishment Ottawa, Ottawa, Ont., Canada K1A 0Z4

AND

R. Y. MOIR
Department of Chemistry, Queen's University, Kingston, Ont., Canada K7L 3N6

Received November 13, 1984

G. W. BUCHANAN, J. W. BOVENKAMP, A. RODRIGUE, R. A. B. BANNARD, and R. Y. MOIR. Can. J. Chem. **63**, 2143 (1985).

Low temperature ^{13}C nuclear magnetic resonance spectroscopy has been employed to obtain the chemical shifts and to examine the conformational equilibria of the four chlorohydrins and bromohydrins of 3-methoxycyclohexene. The corresponding acetates and the unsubstituted halohydrins have also been examined. The observed chemical shifts were compared with those calculated from additivity considerations. Limitations of this approach are discussed. Relative peak area measurements have been used to obtain conformational free energies in favourable cases.

G. W. BUCHANAN, J. W. BOVENKAMP, A. RODRIGUE, R. A. B. BANNARD et R. Y. MOIR. Can. J. Chem. **63**, 2143 (1985).

On a fait appel à résonance magnétique nucléaire du ^{13}C pour déterminer les déplacements chimiques et pour évaluer l'équilibre conformationnel de quatre chlorohydrines et bromohydrines du méthoxy-3 cyclohexène. On a aussi examiné les spectres des acétates correspondants ainsi que ceux des halohydrines qui ne sont pas substituées. On a comparé les déplacements chimiques observés avec ceux calculés à l'aide de considérations d'additivité. On discute des limitations de cette approche. Dans des cas favorables, on a utilisé des mesures d'intensités relatives des pics pour obtenir les énergies libres conformationnelles.

[Traduit par le journal]

Introduction

The compounds shown in Fig. 1 have been the subject of several previous investigations (1, 2). The most recent work (1) involved a study of the kinetics of formation of the *cis*- and *trans*-3-methoxycyclohexane epoxides from the halohydrins **3**, **8**, **5**, and **10** and **2**, **7**, **4**, and **9**, respectively, as well as the kinetics of scission of these epoxides by hydrogen chloride. Earlier studies were concerned with elaboration of the regio- and stereochemistry of the latter reactions, by the separation and characterization of isomeric chlorohydrins **2**–**5** and isomeric bromohydrins **7**–**10**. Structural proofs for these compounds relied very heavily on the use of the splitting pattern of the methine protons in the proton magnetic resonance spectra of the corresponding acetates **12**–**15** and **17**–**20** (3–5).

In this paper, a low-temperature ^{13}C nmr study of the four *trans*-chlorohydrins (**2**–**5**) and the four *trans*-bromohydrins (**7**–**10**) derived from 3-methoxycyclohexene is described. Results for the unsubstituted halohydrins (**1** and **6**), as well as those for the corresponding acetates (**11**–**20**), are also reported. Predicted ^{13}C chemical shifts calculated from additivity considerations derived from monosubstituted cyclohexanes are compared with the observed chemical shifts. The equilibrium constants, from which the conformational free energy differences were calculated, were obtained from the relative peak area measurements of the resonances of individual conformers at 178 K.

Results and discussion

The structures and numbering schemes for the twenty compounds studied are depicted in Fig. 1. Tables 1–4 contain the ^{13}C nmr chemical shifts observed at room temperature as well as those for individual conformations A and B, obtained at 178 K. Parenthesized values denote ambiguous assignments, while A and B describe the less and more stable conformations, respectively. For the all *trans*-substituted compounds **2**, **7**, **12**, **17**, **5**, **10**, **15**, and **20**, only conformer B could be detected. We estimate our detection limit as 1%.

(a) *Resonance assignments*

A variety of techniques were used for ^{13}C signal assignments. Resonances for CH_3, CH_2, CH, and quaternary carbons were distinguished by single frequency off-resonance ^1H decoupling or APT (6) experiments. Distinction between CH carbons bonded to OMe, OH, and OAc was made via selective ^1H decoupling, since the methine proton resonances are well separated, and have characteristic chemical shifts (7). For compounds such as **1**, the assignment of room temperature methylene carbon resonances was made unambiguously via two-dimensional, double quantum coherence spectra, i.e. 2D-INADEQUATE experiments (8).

In order to aid assignments of pairs of resonances due to conformational isomers, detailed studies of the spectra near the coalescence temperatures (typically 200–233 K) were carried out. Extensive use was made of the fact that the larger the chemical shift difference between an exchanging pair of resonances, the higher will be the observed coalescence temperature.

(b) *Chemical shifts*

A model compound approach can be successfully used to predict the resonance positions for *unsubstituted* ring carbons

[1]Authors to whom correspondence should be addressed.

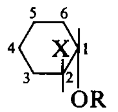

1 X = Cl, R = H
6 X = Br, R = H
11 X = Cl, R = Ac
16 X = Br, R = Ac

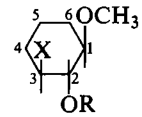

2 X = Cl, R = H
7 X = Br, R = H
12 X = Cl, R = Ac
17 X = Br, R = Ac

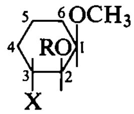

3 X = Cl, R = H
8 X = Br, R = H
13 X = Cl, R = Ac
18 X = Br, R = Ac

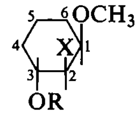

4 X = Cl, R = H
9 X = Br, R = H
14 X = Cl, R = Ac
19 X = Br, R = Ac

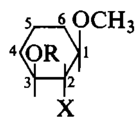

5 X = Cl, R = H
10 X = Br, R = H
15 X = Cl, R = Ac
20 X = Br, R = Ac

FIG. 1. Structures and numbering schemes for **1–20**.

TABLE 1. ^{13}C chemical shifts for chlorohydrins **1–5** (δ_C from TMS $\pm$ 0.01)‡

Compound	C-1	C-2	C-3	C-4	C-5	C-6	OCH_3
1	75.49	67.69	35.58	25.93	24.31	33.67	
1A*	n.o.†	n.o.†	28.05	(19.80)	(19.80)	n.o.†	
1B*	74.95	67.15	35.75	25.81	24.27	34.14	
2	83.47	79.09	63.20	35.47	22.26	28.75	57.39
2A*	n.o.†	n.o.†	n.o.†	n.o.†	n.o.†	n.o.†	n.o.†
2B*	83.19	77.84	63.37	35.24	21.87	28.21	57.28
3	79.14	75.21	62.54	33.72	19.55	26.55	56.83
3A*	76.69	69.02	60.54	27.19	18.69	24.56	56.25
3B*	79.80	76.29	63.24	35.64	19.56	26.04	56.68
4	79.40	70.93	68.41	32.21	18.58	27.81	57.21
4A*	75.71	61.24	70.72	25.50	18.60	25.47	55.81
4B*	80.00	70.13	69.36	34.23	18.22	27.18	56.86
5	82.50	71.14	74.19	32.61	19.54	30.28	
5A*	n.o.†	n.o.†	n.o.†	n.o.†	n.o.†	n.o.†	
5B*	81.94	71.98	73.78	32.72	19.58	29.94	

*At 178.0 $\pm$ 2.0 K.
†n.o. ≡ not observable.
‡0.8 *M* solutions in CD_2Cl_2.

to within $\pm$1.0 ppm, on the average, of those observed for both major and minor conformations. Available ^{13}C data (9–11) for individual conformers of monosubstituted cyclohexanes (Table 5) were employed along with additivity considerations to give the calculated ring carbon chemical shifts shown in Table 6. If one regards substitution of a group X as depicted below, one

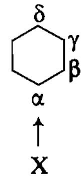

TABLE 2. ^{13}C chemical shifts for bromohydrins **6–10** (δ_C from TMS $\pm$ 0.01)‡

Compound	C-1	C-2	C-3	C-4	C-5	C-6	OCH_3
6	75.57	62.25	36.69	27.00	24.47	34.13	
6A*	69.03	n.o.†	n.o.†	20.46	19.57	n.o.†	
6B*	75.11	61.92	36.75	26.90	24.40	34.55	
7	83.58	79.09	55.85	36.51	23.66	28.99	57.54
7A*	n.o.†	n.o.†	n.o.†	n.o.†	n.o.†	n.o.†	n.o.†
7B*	83.29	77.88	56.16	36.19	23.26	28.42	57.42
8	79.19	75.38	56.09	34.73	20.49	26.71	56.82
8A*	76.61	69.07	n.o.†	27.62	19.59	24.69	56.52
8B*	79.98	76.33	56.66	36.59	20.48	26.13	57.02
9	79.59	63.34	70.96	32.65	18.70	28.23	57.16
9A*	75.32	56.61	71.02	25.72	18.77	26.34	55.64
9B*	80.38	63.98	70.26	34.95	18.35	27.55	57.04
10	82.66	65.48	74.07	33.64	19.76	30.74	57.50
10A*	n.o.†	n.o.†	n.o.†	n.o.†	n.o.†	n.o.†	n.o.†
10B*	82.38	65.11	73.51	34.25	19.67	30.34	57.42

*At 178.0 $\pm$ 2.0 K.
†n.o. ≡ not observable.
‡0.8 *M* solutions in CD_2Cl_2.

can then employ the known substituent induced shifts for α_{ax}, α_{eq}, β_{ax}, β_{eq}, γ_{ax}, γ_{eq}, δ_{ax}, and δ_{eq} sites, for X = Cl, Br, OAc, OH, and OMe (9–11).

The additivity approach is illustrated below for the C-3 and C-4 sites of the major conformation of **1**, starting with a shift

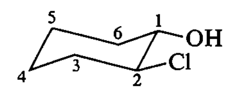

1B

of 27.7 ppm for cyclohexane itself. Thus, for C-3, one predicts $\delta_C = 27.7 + \beta_{eq}(Cl) + \gamma_{eq}(OH)$; i.e. $\delta_C = 27.7 + 10.5 - 2.7 = 35.5$. The observed shift is 35.75, in excellent agreement with that predicted. Similarly for C-4 one predicts $\delta_C = 27.7 + \gamma_{eq}(Cl) + \delta_{eq}(OH) = 27.7 - 0.6 - 2.0 = 25.1$, in good agreement with the observed chemical shift of 25.81 ppm.

For substituted ring carbons, one cannot reliably employ such a pairwise additivity approach. Table 7 illustrates the differences between calculated and observed ^{13}C shieldings for a typical series **4**, **9**, **14**, and **19**, depicted in Fig. 1. Clearly the agreement between calculated and observed shifts for a particular carbon depends on the stereochemistry. This is most dramatically apparent at C-2, the halogenated carbon.

The additivity approach fails to take into account the γ–*gauche* interactions between the vicinal substituents, which are expected to lead to observed shifts which are upfield from those predicted (i.e. positive differences in Table 7). There is ample literature precedent for this observation (12, 13). Also, the additivity approach assumes that the addition of a polar group to cyclohexane would cause the same chemical shift effect as the addition of a polar group to a cyclohexane ring in which the ring carbons are subjected to the inductive effect of existing substituents. Note that although the values in Table 7 are generally positive, some negative values are also present.

Recently, Schneider *et al.* (14) have studied a series of vicinally substituted dihalocyclohexanes. In agreement with our findings, they observe differences of up to ca. 9 ppm between the observed ^{13}C shifts, and those calculated from pairwise additivity for the halogenated carbons. They interpret

TABLE 3. ^{13}C chemical shifts for **11–15** (δ_C from TMS ± 0.01)‡

Compound	C-1	C-2	C-3	C-4	C-5	C-6	OCH_3	$\overset{O}{\overset{\|}{\mathrm{C}}}\mathrm{-CH_3}$	
11	75.84	61.04	35.12	24.81	23.54	30.98		169.73	21.01
11A*	70.96	56.68	28.44	(19.98)	(19.02)	n.o.†		171.33	n.o.†
11B*	76.22	61.72	35.82	25.51	23.83	31.86		170.20	21.35
12	81.32	78.72	60.17	35.41	21.97	29.40	57.42	170.01	20.99
12A*	n.o.†	n.o.†	n.o.†	n.o.†	n.o.†	n.o.†	n.o.†	n.o.†	n.o.†
12B*	80.61	78.00	59.95	34.91	21.53	28.60	57.30	170.40	21.17
13	77.34	76.30	57.81	34.18	19.50	27.53	57.32	169.78	20.88
13A*	74.33	69.24	57.25	27.89	18.47	n.o.†	56.17	170.24	n.o.†
13B*	77.45	77.21	58.25	35.53	19.22	26.15	56.56	170.57	21.41
14	78.87	62.60	72.83	29.06	18.57	27.27	56.93	169.47	20.93
14A*	75.75	58.16	72.49	23.52	18.54	25.04	55.53	169.84	n.o.†
14B*	79.69	64.57	72.19	31.76	17.93	27.34	57.04	169.88	21.18
15	82.96	66.34	75.10	(31.40)	19.81	(30.61)	57.85	169.97	21.01
15A*	n.o.†	n.o.†	n.o.†	n.o.†	n.o.†	n.o.†	n.o.†	n.o.†	n.o.†
15B*	82.29	66.20	74.67	(31.20)	19.49	(29.89)	57.65	170.38	21.40

*At 178.0 ± 2.0 K.
†n.o.† ≡ not observable.
‡0.8 *M* solutions in CD_2Cl_2.

TABLE 4. ^{13}C chemical shifts for **16–20** (δ_C from TMS ± 0.01)‡

Compound	C-1	C-2	C-3	C-4	C-5	C-6	OCH_3	$\overset{O}{\overset{\|}{\mathrm{C}}}\mathrm{-CH_3}$	
16	75.90	53.36	36.02	25.84	23.63	31.50		169.78	21.09
16A*	71.11	50.05	28.91	n.o.†	19.78	n.o.†		n.o.†	n.o.†
16B*	76.06	54.08	36.73	26.56	23.92	32.42		169.69	21.27
17	81.59	78.73	51.46	36.31	23.36	29.50	57.46	169.92	21.10
17A*	n.o.†	n.o.†	n.o.†	n.o.†	n.o.†	n.o.†	n.o.†	n.o.†	n.o.†
17B*	80.93	78.13	51.68	35.86	23.00	28.79	57.48	170.48	21.45
18	76.27	77.36	50.04	34.92	20.40	27.57	57.30	169.71	20.93
18A*	74.37	69.38	49.62	28.32	19.36	26.34	56.31	169.91	n.o.†
18B*	77.60	77.33	50.44	36.47	20.24	26.55	56.76	170.15	21.30
19	78.68	55.79	72.89	29.23	18.69	27.64	56.77	169.44	21.03
19A*	75.27	52.78	72.96	23.68	19.12	25.95	55.47	169.86	n.o.†
19B*	79.78	57.55	71.94	32.35	17.91	27.46	56.96	169.90	21.36
20	82.70	58.81	75.00	31.79	19.76	30.84	57.51	169.66	20.99
20A*	n.o.†	n.o.†	n.o.†	n.o.†	n.o.†	n.o.†	n.o.†	n.o.†	n.o.†
20B*	82.18	58.94	74.58	31.71	19.53	30.28	57.45	169.92	21.30

*At 178.0 ± 2.0 K.
†n.o. ≡ not observable.
‡0.8 *M* solutions in CD_2Cl_2.

their results in terms of a linear electric field theory (15) for ^{13}C shieldings, in which enhanced electron flow to the carbon bearing the substituent of highest polarizability is predicted. The calculations of Schneider *et al.* (14), however, lead to the conclusion that carbons bearing the substituents of highest polarizability are in fact *deshielded*, rather than shielded, as one might expect on the basis of intuitive electron density arguments.

Applying such an approach to our compounds, one would then suggest that the halogenated carbons should show the lowest positive values in Table 7, since halogens are more polarizable than oxygen. In the conformers "B" of Table 7, this is indeed true, i.e. C-2 shows the lowest +'ve difference.

In the "A" conformers of Table 7, however, just the opposite result is found, with the halogenated carbon showing the largest positive deviation between calculated and observed ^{13}C shifts.

It is evident that several factors must be contributing to the observed ^{13}C shifts in these 1,2,3-trisubstituted cyclohexanes. It would be valuable to examine 1,3-disubstituted cyclohexanes in the future, to delineate the role of 1,3 interactions to the observed shifts.

In addition to ring carbon chemical shift differences between conformational isomers, the methoxyl carbon resonances show consistent stereochemical dependence. For the series of materials **3**, **8**, **13**, and **18** the "A" isomers (below) all have equatorial

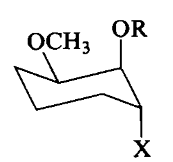

3, 8, 13, 18A

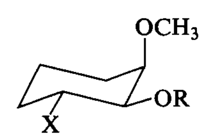

B

TABLE 5. Stereochemical dependence (9–11) of substituent induced chemical shifts* (in ppm from cyclohexane; δ_C = 27.7)

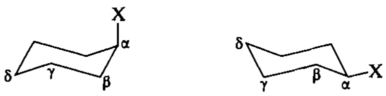

ax eq

X	Conformation	α	β	γ	δ
Cl	ax	32.3	6.7	−7.1	−1.4
	eq	32.3	10.5	−0.6	−2.2
Br	ax	27.5	7.2	−6.5	−1.5
	eq	24.6	11.2	0.3	−2.5
OCH_3	ax	47.1	1.8	−7.2	−1.4
	eq	51.8	4.5	−2.8	−1.8
OAc	ax	42.1	2.8	−6.4	
	eq	45.8	5.0	−2.4	−1.7
OH	ax	37.7	5.1	−6.9	−0.4
	eq	42.6	8.0	−2.7	−2.0

*Positive sign denotes downfield shift; negative sign denotes upfield shift.

TABLE 6. Calculated (from additivity) ring carbon chemical shifts (δ_C from TMS)

Conformation	C-1	C-2	C-3	C-4	C-5	C-6
1A			27.5	20.2	19.4	
1B	80.8	68.0	35.5	25.1	22.8	35.1
2B	86.9	85.3	65.2	33.7	22.3	27.3
3A	77.5	76.6	62.3	25.7	17.4	23.9
3B	82.2	82.6	60.8	34.1	17.9	24.6
4A	79.3	69.6	69.3	23.9	16.4	24.7
4B	82.6	69.8	73.6	33.7	15.6	26.9
5B	87.3	72.4	78.0	33.3	20.0	29.6
6A	72.6			20.8	19.3	
6B	81.5	60.3	36.2	26.0	22.5	36.0
7B	87.8	86.0	57.4	34.4	23.2	27.0
8A	78.1	77.1		26.2	18.0	23.8
8B	83.1	83.3	53.1	34.8	18.8	24.3
9A	79.8	64.8	69.8	24.5	16.5	25.3
9B	83.3	62.1	74.3	34.6	15.3	27.8
10B	88.0	64.8	78.7	34.2	19.7	30.5
11A	76.5	62.8	28.0	20.6	19.9	
11B	84.0	64.9	35.8	25.4	23.1	32.1
12B	83.9	88.5	62.2	34.0	22.6	27.6
13A	75.2	81.0	60.0	26.2	18.8	
13B	79.2	85.8	57.8	34.4	18.2	24.9
14A	79.8	67.3	73.7	21.6	17.1	25.1
14B	82.9	66.8	76.8	30.7	15.9	27.2
15B	87.6	69.5	81.2	30.3	20.3	29.9
16A	77.0	58.0	28.5		19.8	
16B	84.7	57.3	36.5	26.3	22.8	33.0
17B	84.8	89.2	54.5	34.7	23.5	27.4
18A	75.8	81.5	55.2	26.7	18.4	24.3
18B	80.1	86.5	50.1	35.1	19.1	24.6
19A	80.3	62.5	74.2	22.2	17.0	25.7
19B	83.6	59.1	77.5	31.6	15.6	28.1
20B	88.3	61.8	81.9	31.2	20.0	30.8

OCH_3 groups which are shielded by 0.39–0.50 ppm relative to the axial OCH_3 functions of the "B" isomers respectively.

Similarly in the series **4**, **9**, **14**, and **19**, the equatorial OCH_3 groups of the "A" isomers are again shielded relative to their axial counterparts, the differences ranging from 1.05 to 1.51 ppm.

TABLE 7. Calculated minus observed ^{13}C chemical shifts for the methine ring carbons of **4**, **9**, **14**, and **19***

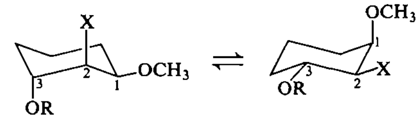

"A" "B"

	C-1		C-2		C-3	
	A	B	A	B	A	B
4 X = Cl, R = H	+3.6	+2.6	+8.4	−0.3	−1.4	+4.2
9 X = Br, R = H	+4.5	+2.9	+8.2	−1.9	−1.2	+4.0
14 X = Cl, R = Ac	+4.0	+3.2	+9.1	+2.2	+1.2	+4.6
19 X = Br, R = Ac	+5.0	+3.8	+9.7	+1.5	+1.2	+5.6
Average	+4.3	+3.1	+8.9	+0.4	−0.1	+4.6

*A positive sign denotes that the observed shift is upfield from that calculated.

TABLE 8. Equilibrium constants* and conformational free energies†

Compound	K(A⇌B)	Number of determinations	$-\Delta G^0$ (kcal/mol)
1,2-Disubstituted			
1	60.0	2	1.45±0.07
6	91.7	3	1.60±0.06
11	18.0	6	1.02±0.08
16	27.2	4	1.17±0.10
1,2,3-Trisubstituted (methoxyl *cis* to adjacent OH or OAc)			
3	4.7	7	0.55±0.04
8	5.0	6	0.57±0.07
13	5.3	5	0.59±0.10
18	6.2	6	0.65±0.06
1,2,3-Trisubstituted (methoxyl *cis* to adjacent Cl or Br)			
4	3.0	4	0.39±0.07
9	3.0	5	0.39±0.05
14	3.2	6	0.41±0.03
19	1.8	7	0.23±0.02

*The equilibrium constants for **2**, **7**, **12**, **17**, and **5**, **10**, **15**, and **20** were >99.0.
†At 178.0 ± 2.0 K.

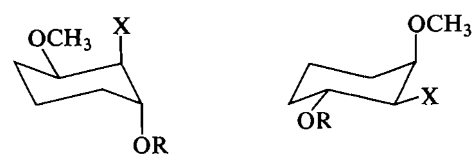

4,9,14,19A **B**

It is interesting to note that for methoxycyclohexane itself (9) the axial and equatorial OCH_3 groups were found to have identical chemical shifts (δ_C = 55.05) at 180 K in CF_2Cl_2 solvent.

Separate carbonyl carbon resonances for *O*-acetyl groups for both conformations were observed for compounds **11**, **13**, **14**, **18**, and **19**. For compounds bearing methoxyl groups, the carbonyl carbon of the axial OAc is shielded relative to its equatorial counterpart. In **11**, however, the carbonyl carbon of the equatorial OAc group is more shielded, by 1.13 ppm. For acetoxycyclohexane itself at 180 K, no chemical shift difference between conformers was detected (9).

In the case of the CH_3 groups of the OAc moieties, we were unable to detect separate resonances for axial and equatorial substituents, in accord with previous observations for acetoxycyclohexane (9).

(c) *Conformational free energies*

The equilibrium constants collected in Table 8 were calculated from relative peak area measurements of resonances for individual conformers. Values for $-\Delta G^0$, the conformational free energy difference, were subsequently calculated using the equation $-\Delta G^0 = RT \ln K$. Error limits in $-\Delta G^0$ were obtained from the standard deviations in the equilibrium constants derived from individual resonances.

Initially, in discussing the $-\Delta G^0$ data, it is important to note that relatively concentrated solutions (0.8 *M* in CD_2Cl_2) are necessary for this work. As a result, materials in which there can be intermolecular association (such as alcohols) will tend to show a larger preference for the equatorial OH conformation (especially for alcohols without significant γ−*gauche* interactions) than would be the case at lower solute concentrations. This is due to the higher spatial accessibility of an equatorial OH relative to its axial counterpart for intermolecular hydrogen bonding.

The low temperature ^{13}C results for cyclohexanol itself illustrate this point. To date, we have not been able to detect ^{13}C resonances for the axial conformer (under the conditions used for the other compounds in this study), presumably due to the above-mentioned dimerization effects which stabilize the equatorial conformation. Since our limit of detection is ca. 1%, we estimate K for cyclohexanol itself to exceed 99 under the present experimental conditions. Schneider and Hoppen (9) also were not able to detect the axial conformer in CF_2Cl_2, although Subbotin and Sergeyev (11) succeeded in detecting it in CS_2 solution.

It is interesting for both *trans* halohydrins **1** and **6**, that the minor diaxial conformers *can* be detected by ^{13}C nmr at low temperature. The increased preference for the "A" conformations, bearing two axial substituents, may be due to destabilization of the "B" conformers resulting from dipole−dipole repulsion between the neighbouring polar groups. Such

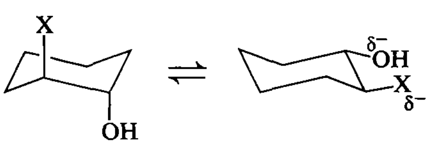

1, 6, A **B**

dipolar effects are well known in *trans*-1,2-dibromocyclohexane and lead to a preference for the diaxial form in CCl_4 and benzene solution (16). Also, the spatial accessibility of the equatorial OH and thus its capability to take part in intermolecular hydrogen bonding is probably reduced by the γ−*gauche* interaction with the chlorine substituent.

For the corresponding acetates **11** and **16**, the equilibria are further biased towards the diaxial conformer (reductions of 0.43 kcal/mol in $-\Delta G^0$ for both comparisons). Since the conformational free energies of OH and OAc are expected to be close (17), the main reason for this is presumed to be that intermolecular hydrogen bonding stabilizes the diequatorial conformers of the alcohols but not those of the acetates.

For the second series of molecules depicted in Fig. 1, i.e. **2**, **7**, **12**, and **17**, no spectra of the minor conformations were obtainable.

Introduction of a methoxyl group *cis* to the OR function,

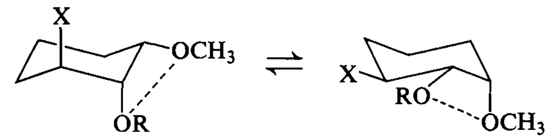

3, 8, 13, 18 A **B**

as in the series **3**, **8**, **13**, and **18** (Fig. 1 and Table 8), considerably enhances the amount of conformer A present in the equilibrium. Since the γ−*gauche* interaction (depicted above) between an equatorial methoxyl and an axial OR is expected to be essentially the same as that between an axial methoxyl and an equatorial OH, the conformational free energy difference between pairs of conformers (e.g., $-\Delta G^0$ for **1** minus $-\Delta G^0$ for **3**) is expected to be approximately 0.75 kcal/mol (9) on the introduction of the methoxyl group in **3**, **8**, **13**, and **18**. (The same argument holds for **4**, **9**, **14**, and **19** where the methoxyl is introduced *cis* to the halogen.) The other interactions involving halogen and OR with each other and with the remainder of the ring are expected to cancel when the $-\Delta G^0$ values of corresponding compounds in Table 7 with and without methoxyl are subtracted.

For the alcohols **3** and **8**, as compared to **1** and **6** respectively, the $-\Delta G^0$ values decrease by 0.90 and 1.03 kcal/mol. These larger than expected differences in $-\Delta G^0$ values require comment. A possible interpretation might involve intramolecular hydrogen bonding between the methoxyl and the *cis* hydroxyl. However, even larger differences in $-\Delta G^0$ values are found when **4** and **9** are compared with **1** and **6** and in these comparisons hydrogen bonding differences are unlikely to be significant (*vide infra*). For the acetates **13** and **18**, as compared to **11** and **16**, respectively, the $-\Delta G^0$ values decrease by 0.43 and 0.52 kcal/mol. These are smaller than the 0.75 kcal/mol decrease expected.

The equilibria of **4**, **9**, **14**, and **19** exhibit more conformer A than any of the other compounds shown in Fig. 1. In these cases, the methoxyl is introduced *cis* to the halogen and again the approximate difference in $-\Delta G^0$ values from the corresponding compounds without the methoxyl group (**1**, **6**, **11**, and **16**) should be about 0.75 kcal/mol. The actual differences are 1.06, 1.21, 0.61, and 0.94 kcal/mol respectively. Again, it is the chloro- and bromohydrins which have the largest differences in $-\Delta G^0$ values. As pointed out above, the addition of a methoxyl *cis* to the halogen should not interfere with the hydrogen bonding characteristics of the halohydrins.

Finally, it is interesting to note that the bromoacetate **19** has significantly more conformer A than the chloroacetate **14**, whereas in the other two pairs of acetates (i.e. **11** vs. **16** and **13** vs. **18**) it is the chloroacetate which has relatively more A conformer present.

To summarize, it is evident that ^{13}C nmr represents an interesting addition to available techniques for examining stereochemical properties of these molecules. It is also clear, however, that further efforts in this field will be necessary in order to delineate more properly the influences of hydrogen bonding and dipolar effects on the observed ^{13}C chemical shifts and conformational equilibria.

To these ends, other series of appropriately 1,2 and 1,3-disubstituted cyclohexanes are under examination.

Experimental

(a) *Spectra*

The ^{13}C spectra were obtained at 50.3 MHz using a Varian XL-200 spectrometer. Sample concentrations were 0.8 *M* in CD_2Cl_2 solutions contained in 10-mm od tubes. Routinely, spectra were obtained with complete ^1H noise decoupling. Normal conditions were as follows: sweep width = 10 000 Hz, number of data points = 32 000, pulse width = 7.0 μs (45°), acquisition time = 1.6 s, and repetition rate = 1.0 s. The number of accumulations for the low temperature spectra was typically 2000.

The equilibrium constants were calculated from relative peak area measurements, which were made electronically. No significant difference in *K* values resulted from spectra obtained with the above conditions as opposed to those recorded under suppressed $^1H-^{13}C$ nuclear Overhauser effect conditions.

The 2D INADEQUATE spectra (8) were obtained using the CCC2D pulse sequence of the XL-200 software. For **1** the sweep width in each domain was 3741 Hz. A 560 × 256 data point matrix was used, transforming 1024 and 512 points respectively.

(b) *Materials*

The compounds **1**−**20**, which were available (1−5) from previous studies, were redistilled or recrystallized before use. Purities were determined by gas−liquid chromatography (Perkin-Elmer model Sigma 1B, equipped with a thermal conductivity detector (250°C) and dedicated computer with built-in recorder; column: 10-ft glass (2-mm id) packed with 10% UCW-98 on Gas-Chrom. Q 80/100 mesh; flow rate of carrier gas (He) was 20 mL/min; oven temperature was 150°C). The purities were determined as: 99.9% (**1**, **3**, **10**, **12**, **15**, and **20**), 99.8% (**2** and **7**), 99.7% (**6**, **8**, and **17**), 99.6% (**5**, **11**, and **16**), 99.2% (**14**), 99.1% (**13**), 98.6% (**18**), 98.3% (**19**), and 97.8% (**4** and **9**). See ref. 18 for a detailed analysis of the glc retention time behaviour of these compounds.

Acknowledgements

We thank Mr. K. Bourque for his expert technical assistance. Financial support (GWB) from NSERC is also gratefully acknowledged.

1. J. W. Bovenkamp, E. J. Langstaff, R. Y. Moir, and R. A. B. Bannard. Can. J. Chem. **57**, 2444 (1979).
2. J. W. Bovenkamp, R. Y. Moir, and R. A. B. Bannard. Can. J. Chem. **55**, 4144 (1977).
3. R. U. Lemieux, R. K. Kullnig, and R. Y. Moir. J. Am. Chem. Soc. **80**, 2237 (1958).
4. E. J. Langstaff, E. Hamanaka, G. A. Neville, and R. Y. Moir. Can. J. Chem. **45**, 1907 (1967).
5. R. A. B. Bannard. Can. J. Chem. **44**, 775 (1966).
6. S. L. Patt and J. N. Shoolery. J. Magn. Reson. **46**, 535 (1982).
7. E. L. Eliel and M. H. Gianni. Tetrahedron Lett. 97 (1962).
8. A. Bax, R. Freeman, T. A. Frenkiel, and M. H. Levitt. J. Magn. Reson. **43**, 478 (1981).
9. H. J. Schneider and V. Hoppen. Tetrahedron Lett. 579 (1974).
10. H. J. Schneider and V. Hoppen. J. Org. Chem. **43**, 3866 (1978).
11. O. A. Subbotin and N. M. Sergeyev. J. Chem. Soc. Chem. Commun. 141 (1976).
12. K. Laihia, J. Paasivirta, H. Pikkarainen, and S. Aho-Pulliainen. Org. Magn. Reson. **22**, 117 (1984).
13. O. A. Subbotin, N. M. Sergeyev, V. N. Chlopkov, N. G. Nikishova, and Y. G. Bundel. Org. Magn. Reson. **13**, 259 (1980).
14. H.-J. Schneider, G. Becker, W. Freitag, and V. Hoppen. J. Chem. Res. (S), 14−15 (1979).
15. H.-J. Schneider and W. Freitag. J. Am. Chem. Soc. **99**, 8363 (1977).
16. P. Klaeboe, J. J. Lothe, and K. Lunde. Acta. Chem. Scand. **11**, 1677 (1957).
17. E. L. Eliel, N. L. Allinger, S. J. Angyal, and G. A. Morrison. Conformational analysis. Interscience, New York, NY. 1965. pp. 44−45.
18. J. W. Bovenkamp, R. Y. Moir, A. A. Casselman, and R. A. B. Bannard. J. Chromatogr. **118**, 345 (1976).

Synthesis and biological activity of nucleoside analogs involving modifications in the carbohydrate ring

WALTER A. SZAREK, B. MARIO PINTO, AND MASAHARU IWAKAWA
Carbohydrate Research Institute and Department of Chemistry, Queen's University, Kingston, Ont., Canada K7L 3N6
Received October 20, 1983[1]

WALTER A. SZAREK, B. MARIO PINTO, and MASAHARU IWAKAWA. Can. J. Chem. **63**, 2149 (1985).

The synthesis of a variety of nucleoside analogs involving modifications in the carbohydrate ring is described. In particular, 6-substituted purin-9-yl derivatives of 1-oxa-4-thiacyclohexane and 1,4-dioxacyclohexane have been synthesized. A number of 6-chloropurin-9-yl derivatives of substituted 1-oxa-4-thiacyclohexane have also been derived from the parent compounds by way of a Pummerer rearrangement. A route to nucleoside analogs of 1-oxa-4-thiacyclohexane from naturally occurring nucleosides is illustrated for the case of inosine. A route to nucleoside analogs in which the carbohydrate moiety is replaced by an acyclic moiety bearing α,β-unsaturated esters is also illustrated for the case of uridine. The results of biological screening of these analogs and others previously synthesized in our program against leukemia L-1210 cells in vitro are presented; some of these compounds showed marginal antitumor activity. The screening results of selected compounds against the human HeLa cell line in vitro are also presented; none of the compounds that were tested showed significant inhibitory activity of cell growth.

WALTER A. SZAREK, B. MARIO PINTO et MASAHARU IWAKAWA. Can. J. Chem. **63**, 2149 (1985).

On décrit une synthèse de divers analogues des nucléosides qui fait appel à des modifications du cycle du sucre. On a ainsi synthétisé des dérivés purinyl-9 substitués en position 6 de l'oxa-1 thia-4 cyclohexane et du dioxa-1,4 cyclohexane. Une transformation de Pummerer sur des composés apparentés permet d'obtenir des dérivés chloro-6 purinyl-9 de l'oxa-1 thia-4 cyclohexane substitué. Utilisant l'inosine comme exemple, on illustre une voie d'accès aux analogues oxa-1 thio-4 cyclohexanes des nucléosides en faisant appel à des nucléosides réactionnels comme produits de départ. Utilisant l'uridine comme exemple, on propose une méthode d'obtenir des analogues de nucléosides dans lesquels on a remplacé l'unité d'hydrate de carbone par une unité acyclique comportant une unité d'esters α,β insaturés. On présente les résultats obtenus lors d'une évaluation biologique in vitro de ces analogues et d'autres synthétisés antérieurement au cours de notre programme contre les cellules L-1210 de la leucémie. Quelques uns de ces composés présentent une activité anti-tumorale faible. On présente également les résultats obtenus lors d'évaluations in vitro de composés choisis pour leur activité contre la lignée de cellules HeLa humaines. Les composés étudiés ne montrent aucune activité inhibitrice significative sur la croissance des cellules.

[Traduit par le journal]

Introduction

In recent years an active area of research in this laboratory has been the synthesis of nucleoside analogs involving modifications in the carbohydrate ring. As part of this program, the synthesis of nucleoside analogs containing more than one heteroatom in the "carbohydrate" ring has been undertaken. The stimulus for this aspect of nucleoside chemistry was provided by the reported biological activity of the adduct of periodate-oxidized adenosine with isonicotinic acid hydrazide (1) and the interesting biological properties exhibited by ribonucleoside dialdehydes themselves (2). The latter compounds exist in solution as several hydrated species, one of which possesses a 1,4-dioxacyclohexane structure (3). Thus far, reports (4) from this laboratory have described the synthesis of 6-substituted purin-9-yl derivatives of 1-oxa-4-thiacyclohexane, 1,4-dithiacyclohexane, 1,4-dioxacyclohexane, 1-oxa-4-azacyclohexane, and 1-thia-4-azacyclohexane (**1–10**), and of some corresponding pyrimidine derivatives. In addition, the synthesis of nucleoside analogs in which the sugar moiety is replaced by thiazolidine derivatives (**11**, **12**) has also been reported (5). Since that time, McCormick and McElhinney have reported (6) the synthesis of nucleoside analogs of 6-substituted purinyl derivatives in which the carbohydrate moiety is replaced by substituted 1-thia-4-azacyclohexane derivatives and Dvonch and Alburn (7) have reported the synthesis and antileukemic activity of nucleoside analogs derived from the reaction of ethanol or methanol with periodate-oxidized inosine, adenosine, or cytidine. The latter compounds possess 1,4-dioxane structures. Furthermore, periodate-oxidized 5′-deoxyinosine has recently

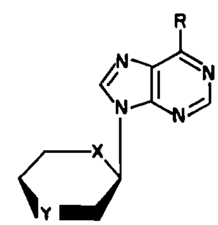

1 X = O, Y = S, R = Cl
2 X = O, Y = S, R = NH_2
3 X = O, Y = S, R = SH
4 X = S, Y = O, R = Cl
5 X = Y = S, R = Cl
6 X = Y = S, R = NH_2
7 X = Y = S, R = SH
8 X = Y = O, R = Cl
9 X = O, Y = N-Bz, R = Cl
10 X = S, Y = N-Bz, R = Cl
13 X = S, Y = O, R = NH_2
14 X = S, Y = O, R = SH
15 X = Y = O, R = NH_2
16 X = Y = O, R = SH

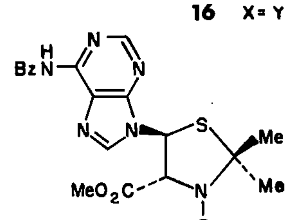

11

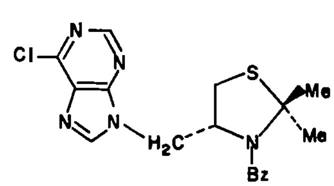

12

[1]Revision received July 26, 1984.

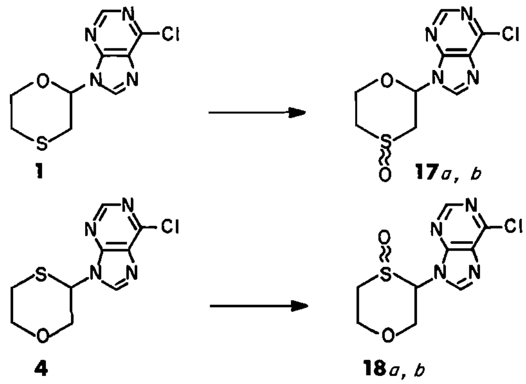

SCHEME 1

been reported (8) to be a more potent antitumor agent than inosine dialdehyde.

As a further extension, we now report the synthesis of 9-(1-oxa-4-thiacyclohexan-3-yl)adenine (**13**) and 9-(1-oxa-4-thiacyclohexan-3-yl)-9*H*-purine-6(1*H*)-thione (**14**) from **4** and of 9-(1,4-dioxacyclohexan-2-yl)adenine (**15**) and 9-(1,4-dioxacyclohexan-2-yl)-9*H*-purine-6(1*H*)-thione (**16**) from **8**. In addition, a number of 6-chloropurin-9-yl derivatives of substituted 1-oxa-4-thiacyclohexane have been synthesized from **1** and **4** in order to evaluate the effects of substituents, if any, on the biological activity of these compounds. Furthermore, a general route to nucleoside analogs of 1-oxa-4-thiacyclohexane from naturally occurring nucleosides is illustrated for the case of inosine; this approach is patterned after the work of Foster and co-workers (9) on the conversion of suitably protected glycopyranosides into derivatives of 2-hydroxy-1-oxa-4-thiacyclohexane.

Since inosine dialdehyde has been shown (10) to contain two aldehyde groups which can cross-link protein molecules, the synthesis of nucleoside analogs bearing functionality that is capable of reacting in similar fashion with functional groups in proteins is also of interest. A route to novel nucleoside analogs bearing such functionality is illustrated, therefore, for the case of uridine.

We also now report the results of biological screening of some of the nucleoside analogs synthesized in our program.

Results and discussion

(a) *Synthesis*

Treatment of **4** with methanolic ammonia gave crystalline 9-(1-oxa-4-thiacyclohexan-3-yl)adenine (**13**) in 83% yield whereas the use of methanolic potassium hydrosulfide afforded crystalline 9-(1-oxa-4-thiacyclohexan-3-yl)-9*H*-purine-6(1*H*)-thione (**14**) in 87% yield. Similarly, compound **8** was converted into crystalline 9-(1,4-dioxacyclohexan-2-yl)adenine (**15**) in 81% yield and into crystalline 9-(1,4-dioxacyclohexan-2-yl)-9*H*-purine-6(1*H*)-thione (**16**) in 92% yield. Compounds **13**, **14** and **15**, **16** exhibited conformational behaviour that was similar to that observed (11) for the parent, 6-chloro derivatives, **4** and **8**, respectively.

6-Chloro-9-(1-oxa-4-thiacyclohexan-2-yl)-9*H*-purine (**1**) was converted into a mixture of isomeric sulfoxides (**17***a*, **17***b*) by oxidation with sodium metaperiodate according to the method of Leonard and Johnson (12) (Scheme 1). The ^{1}H nmr spectrum indicated the presence of two isomeric sulfoxides in a ratio of 3.2:1, as estimated by integration of the corresponding signals for H-2′. Recrystallization from ethanol resulted in

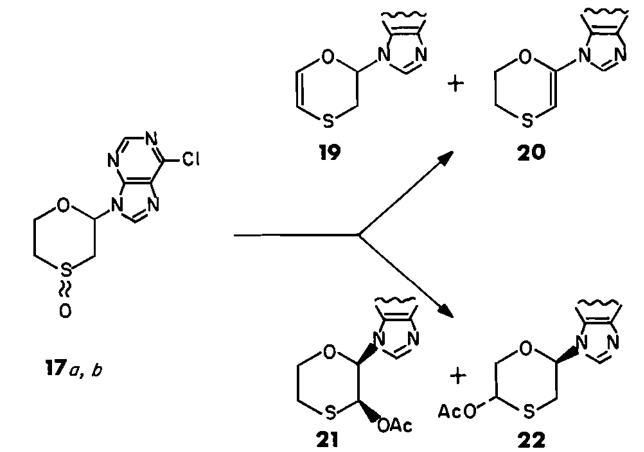

SCHEME 2

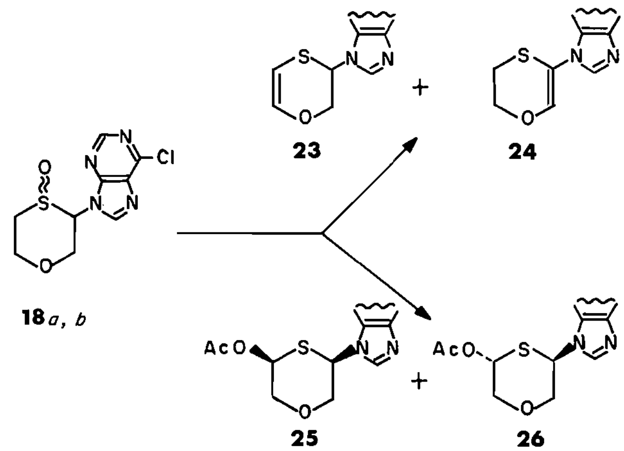

SCHEME 3

a mixture that was highly enriched in the major isomer (**17***a*). The major and minor isomers were assigned the *trans* and *cis* stereochemistry, respectively, on the basis of their nmr spectra. The detailed examination of the configurations and conformations of these derivatives and others reported below will be described in a subsequent paper (13).

Oxidation of 6-chloro-9-(1-oxa-4-thiacyclohexan-3-yl)-9*H*-purine (**4**) with sodium metaperiodate afforded a mixture of the isomeric sulfoxides **18***a* and **18***b* in a ratio of 1.2:1, as indicated by its ^{1}H nmr spectrum (Scheme 1). Recrystallization from ethanol–hexane afforded white prisms which were shown by ^{1}H nmr spectroscopy to consist predominantly of the major isomer (**18***a*); thus, the unambiguous assignment of signals to the two isomers **18***a* and **18***b* could be made in the ^{1}H nmr and ^{13}C nmr spectra of the isomeric mixture of sulfoxides. Compound **18***a* was assigned the *cis* stereochemistry and **18***b* was assigned the *trans* stereochemistry (13).

Treatment of a mixture of the isomeric sulfoxides **17** with an excess of acetic anhydride in benzene containing a trace of *p*-toluenesulfonic acid monohydrate at 60–70°C afforded a mixture of four components, two of which were identified as being acetoxy derivatives and two of which were identified as being the products of elimination reactions (see Scheme 2). The structures of the olefins were readily established by nmr spectroscopy and the compounds were identified as being 6-chloro-9-(1-oxa-4-thiacyclohex-5-en-2-yl)-9*H*-purine (**19**)

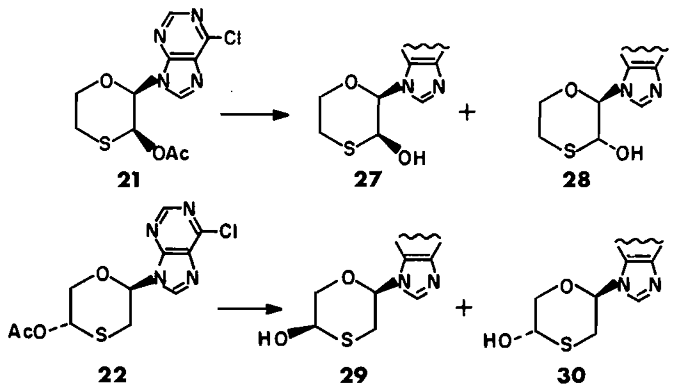

SCHEME 4

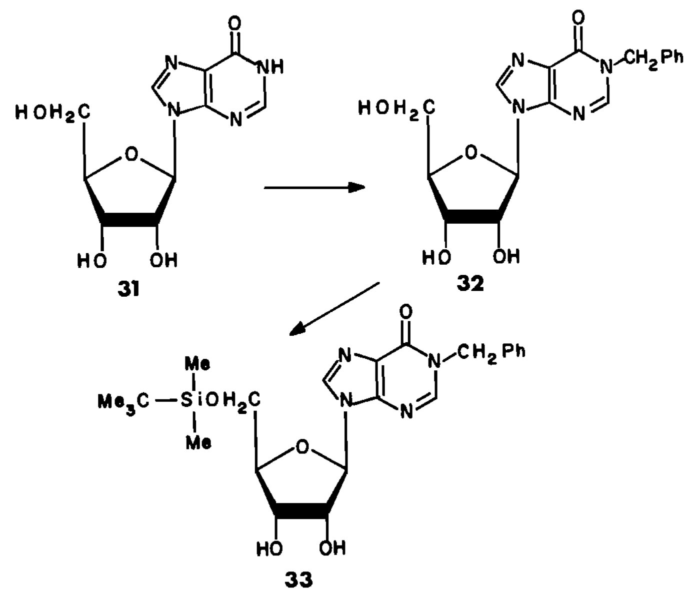

SCHEME 5

and 6-chloro-9-(1-oxa-4-thiacyclohex-2-en-2-yl)-9*H*-purine (**20**). The constitution and stereochemistry of the acetoxy derivatives were also established by nmr spectroscopy (13). Compound **21** was identified as being *cis*-6-chloro-9-(3-acetoxy-1-oxa-4-thiacyclohexan-2-yl)-9*H*-purine and compound **22** was identified as being *trans*-6-chloro-9-(5-acetoxy-1-oxa-4-thiacyclohexan-2-yl)-9*H*-purine (13). The *cis*-3′-acetoxy derivative (**21**), the *trans*-5′-acetoxy derivative (**22**), the 2′,3′-olefin (**20**), and the 5′,6′-olefin (**19**) were obtained from the Pummerer reaction of **17** in a ratio of 12:2:2.4:1, respectively.

Treatment of a mixture of isomeric sulfoxides **18** with an excess of acetic anhydride in benzene containing a trace of *p*-toluenesulfonic acid monohydrate at 60–70°C afforded a solid which was revealed by tlc, after multiple development of the plate, to consist of four components (see Scheme 3). The individual components were isolated after tedious preparative thin-layer chromatography in which the plate was subjected to multiple development. The two faster-moving components were readily identified by means of ^{1}H nmr spectroscopy as being the unsaturated compounds, namely 6-chloro-9-(1-oxa-4-thiacyclohex-5-en-3-yl)-9*H*-purine (**23**), and 6-chloro-9-(1-oxa-4-thiacyclohex-2-en-3-yl)-9*H*-purine (**24**) (see Scheme 3). The two slower-moving components were isolated as crystalline solids and were identified as being the *cis*- and *trans*-5′-acetoxy derivatives by nmr spectroscopy (13).

Treatment of the acetate **21** with sodium borohydride in methanol afforded a solid which was identified as being a mixture of *cis*- and *trans*-6-chloro-9-(3-hydroxy-1-oxa-4-thiacyclohexan-2-yl)-9*H*-purine, **27** and **28**, respectively (see Scheme 4).

Treatment of the regioisomeric acetate **22** with sodium borohydride in methanol afforded a solid which was identified as being a mixture of *cis*- and *trans*-6-chloro-9-(5-hydroxy-1-oxa-4-thiacyclohexan-2-yl)-9*H*-purine, **29** and **30**, respectively (see Scheme 4).

Treatment of a mixture of *cis*- and *trans*-6-chloro-9-(5-acetoxy-1-oxa-4-thiacyclohexan-3-yl)-9*H*-purine (**25**, **26**) with sodium borohydride did not furnish the expected hydroxy derivatives. Thin-layer chromatography indicated the absence of uv-active components other than that at the origin. Presumably, the products decompose with loss of 6-chloropurine.

Thus far, the synthesis of nucleoside analogs from noncarbohydrate precursors has been described. The method has consisted, therefore, of the appropriate functionalization of the saturated heterocycle and the subsequent coupling of this product with an appropriate nucleoside base. Modifications of the nucleoside base and of the saturated heterocyclic moiety itself have then been effected. It would be advantageous, however, to have a route to compounds of this type which would circumvent the coupling step. In particular, a synthesis which employed naturally occurring nucleosides as starting materials would be particularly useful. An entry into nucleoside analogs of 1-oxa-4-thiacyclohexanes starting from naturally occurring nucleosides is described below. The method is illustrated for the case of inosine as the starting nucleoside. A merit of using this starting material is that the hypoxanthine moiety can be readily modified to give 6-chloro, 6-amino, or 6-thiono derivatives (see, for example, ref. 14).

Treatment of inosine (**31**) with benzyl chloride and sodium hydrogen carbonate in *N*,*N*-dimethylformamide, by modification of the method of Shaw (15), afforded 1-benzylinosine (**32**) as a white crystalline solid. Protection of *N*-1 was considered necessary in order to obviate its participation in subsequent reactions. For example, it is known (16) that attempted iodination of 2′,3′-*O*-isopropylideneinosine using methyltriphenoxyphosphonium iodide gives 2′,3′-*O*-isopropylidene-3,5′-cycloinosine as the major product. Moreover, Holmes and Robins (17) have shown that 5′-*O*-*p*-tolylsulfonyl-2′,3′-*O*-isopropylideneinosine is also converted into the cyclonucleoside in refluxing dioxane, and Hampton *et al.* (18) have shown that cyclonucleoside formation accompanies bimolecular displacement reactions at C-5′ of the *p*-tolylsulfonyl derivative. Compound **32** was then treated with 1.1 equivalents of *tert*-butyldimethylsilyl chloride in dry *N*,*N*-dimethylformamide containing imidazole (19, 20) to give crystalline 1-benzyl-5′-*O*-*tert*-butyldimethylsilylinosine (**33**) (see Scheme 5). The selectivity of this reagent for reaction at the 5′-position of ribonucleosides is well documented (19).

Oxidation of **33** with sodium metaperiodate in a mixture of ethanol and water followed by borohydride reduction of the resulting "dialdehyde" **34** afforded the diol **35** (see Scheme 6). The functionalization of the diol **35** proved to be much more difficult than had been anticipated. Thus, treatment of **35** with an excess of *p*-toluenesulfonyl chloride in pyridine for an extended time period afforded a mixture of the ditosylate **36** and the monotosylate **37** in low yield (Scheme 6) but yielded mostly unreacted starting material. Other attempts to convert the hy-

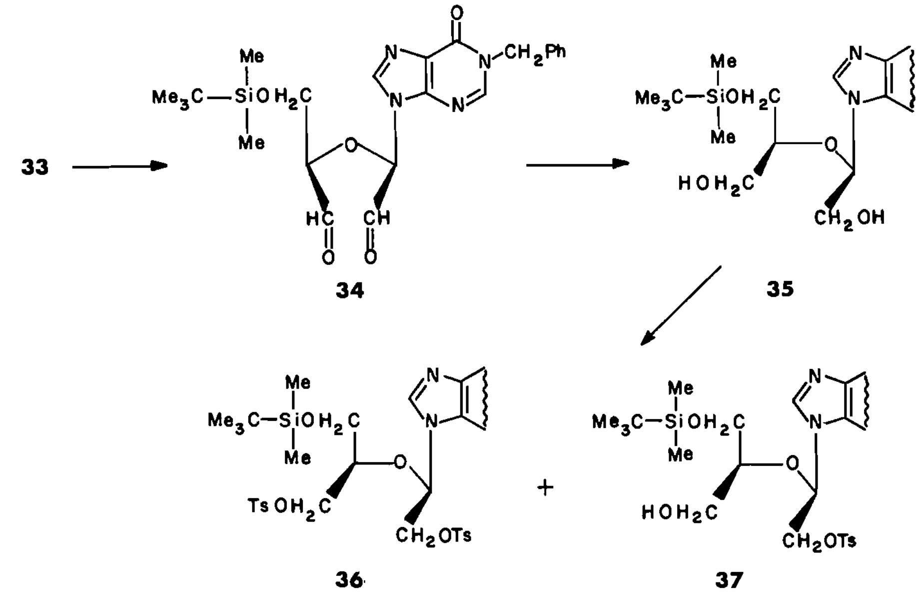

SCHEME 6

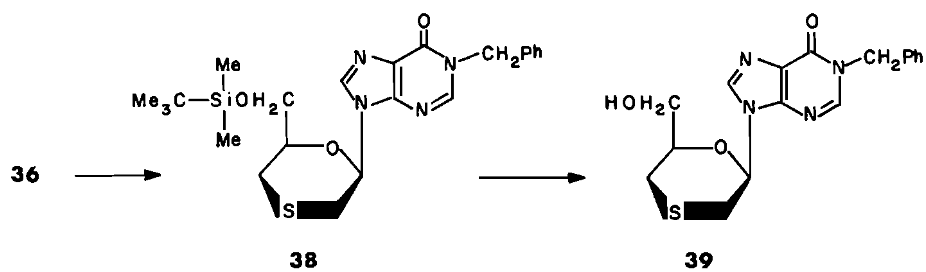

SCHEME 7

droxyl functions into suitable leaving groups did not offer a significant improvement of yield. For instance, attempts to form the dimesylate using methanesulfonyl chloride in pyridine afforded mostly starting material, even with prolonged reaction times at room temperature. Attempts to synthesize the corresponding dichloride with thionyl chloride or the corresponding dibromide using carbon tetrabromide and triphenylphosphine (21) were also unsuccessful and yielded mostly unreacted starting material. Attempted conversion of the hydroxyl functions into trifluoromethanesulfonic esters using triflic anhydride in a mixture of pyridine and methylene chloride (22) gave a product distribution similar to that observed in the reaction with *p*-toluenesulfonyl chloride. It is noteworthy that Dailey and Fuchs (23) have recently reported a similar problematic situation involving the conversion of the hydroxyl group of a "neopentyl" alcohol into a suitable leaving group. Some of the methods described above were also applied in this system, although without much success.

Treatment of the ditosylate **36** with sodium sulfide in refluxing ethanol afforded, after chromatography, a small amount of a white foam that was identified as being the desired 1-oxa-4-thiacyclohexane derivative **38** by means of nmr spectroscopy. Compound **38** is assigned the conformation in which both the purine moiety and the silyloxymethyl function adopt equatorial orientations since the signal for H-2′ in the ^{1}H nmr spectrum appears as a doublet of doublets having a value for $|J_{2',3'} + J_{2',3''}|$ of 13 Hz, a value that is typical for an axial proton coupled to the axial and equatorial protons of a vicinal methylene group, and since the sequence of reactions is expected to proceed with retention of configuration at C-1′ and C-4′ of inosine (**31**). The apparently low yield of **38** was accounted for by isolation of a second, more polar component that was identified as being the alcohol **39** resulting from desilylation of **38**. Compound **39** was also obtained as a white foam from the silyl ether **38** by treatment with tetra-*n*-butylammonium fluoride in tetrahydrofuran (20) (Scheme 7). The structure of **39** was unambiguously established by complete assignment of its ^{1}H nmr spectrum recorded in chloroform-*d* at 220 MHz (13).

The sequence of reactions outlined above could, presumably, be extended to other naturally occurring nucleosides to furnish both purine and pyrimidine derivatives of 1,4-oxathiane.

In view of the promising antitumor activity exhibited (2*d*, 24) by inosine dialdehyde and in view of its ability to cross-link proteins (10), it was felt that the synthesis of nucleoside analogs bearing functionality that could react in a similar fashion with certain functional groups in proteins would also be of interest. A synthetic scheme employing naturally occurring nucleosides as substrates would be particularly desirable. A general route to such nucleoside analogs is illustrated below for the case of uridine as the starting material. The route is analogous to that employed by Ireson *et al.* (25) in the synthesis of diolefins from methyl 4,6-*O*-benzylidene-α-D-glucopyranoside.

Treatment of uridine (**40**) with *tert*-butyldimethylsilyl chloride and imidazole in *N*,*N*-dimethylformamide (19, 20) af-

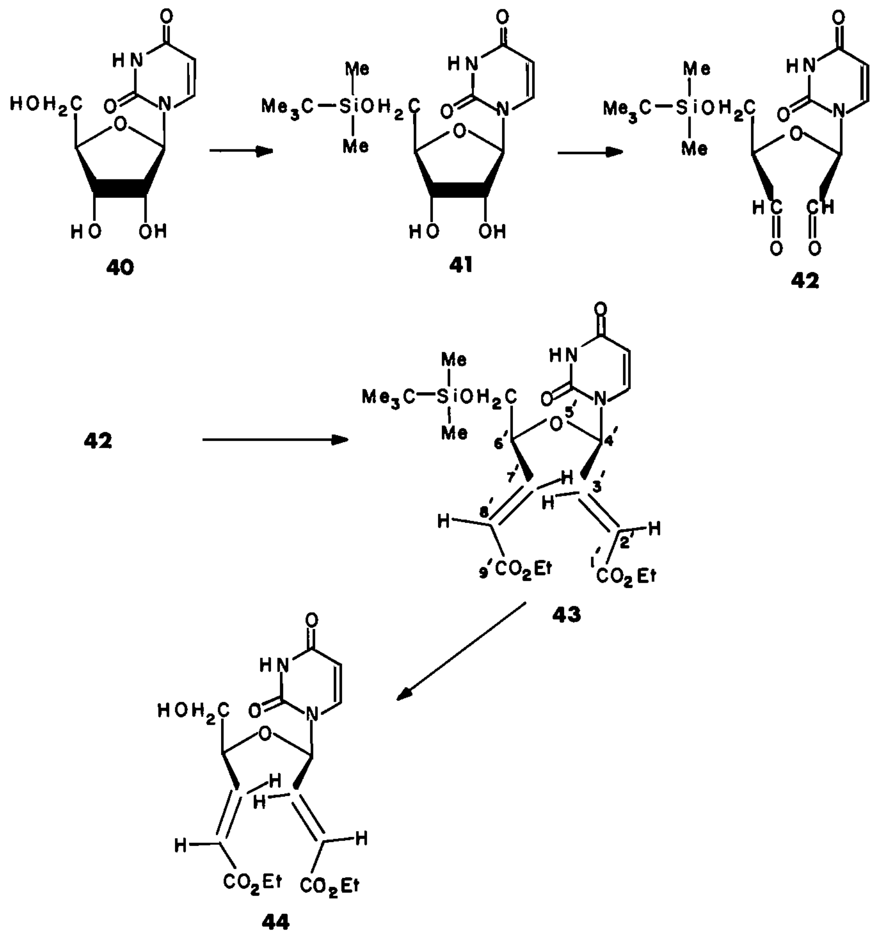

SCHEME 8

forded solid 5′-*O*-*tert*-butyldimethylsilyluridine (**41**) (Scheme 8). Periodate oxidation of **41** yielded the "dialdehyde" **42** which was used without further purification. Treatment of **42** with the Wittig reagent, carbethoxymethylenetriphenylphosphorane, in *N*,*N*-dimethylformamide at 95°C for 3 h (Scheme 8) afforded a syrup that was purified by high performance liquid chromatography. Compound **43** was obtained as white needles from ether–hexane. It was identified as being the (2*E*,7*E*), (4*R*,6*S*) isomer (13).

Treatment of **43** with tetra-*n*-butylammonium fluoride in tetrahydrofuran (20) afforded the alcohol **44** as a white foam. Its ^{1}H nmr spectrum recorded at 60 MHz in chloroform-*d* was similar to that of the silyl ether **43**; chemical shift assignments were made, therefore, by analogy with those (13) in the spectrum of **43**.

The α,β-unsaturated esters in compound **44** should be capable of functioning as alkylating agents since they should readily undergo conjugate addition with different nucleophiles (see ref. 25).

The route outlined above should be applicable to other suitably protected, naturally occurring nucleosides. Furthermore, this type of analog offers entry into a variety of nucleoside analogs of substituted 1-oxa-4-thiacyclohexanes and 1-oxa-4-azacyclohexanes via double conjugate addition of sodium sulfide or ammonia, respectively, as exemplified by the work of Ireson *et al.* (25).

(b) *Biological activity*

The inhibitory effects of the nucleoside analogs synthesized in this program on the growth of various mammalian tumor cell lines in vitro and on bacterial cells were investigated. The biological activity against the murine L-1210 tumor cell line, the human HeLa cell line, and the bacterial strains was evaluated by Dr. A. Bloch and co-workers of the Department of Experimental Therapeutics, Grace Cancer Drug Center at the Ros-well Park Memorial Institute. The protocol, methodology, and testing conditions have been previously reported (26–28).

The inhibitory effects that these agents exerted on the in vitro growth of murine L-1210 tumor cells are shown in Table 1. The activities of 6-chloro-9-(tetrahydropyran-2-yl)-9*H*-purine (**45**), 2′-azido-2′-deoxyarabinosylcytosine (**46**), and 2′-amino-2′-deoxyarabinosylcytosine (**47**) in the same test system are also documented for the purposes of comparison. Compounds **46** and **47** were synthesized by Bloch and co-workers (29) and have been screened under conditions identical to those used for the nucleoside analogs synthesized in this program. Compound **45** was prepared by the method of Robins *et al.* (30); this compound has been reported (31) to show significant antitumor activity.

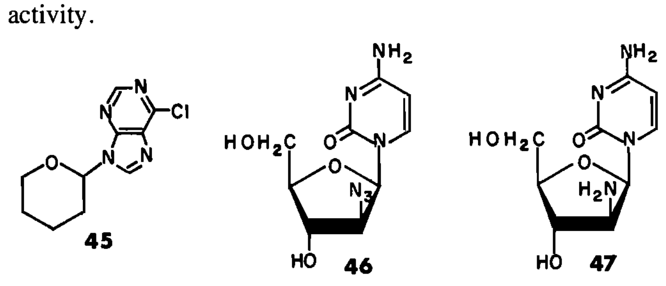

TABLE 1. Inhibitory effects of nucleoside analogs on the growth of murine leukemia L-1210 cells in vitro[a]

Compound	Molar concentration for 50% inhibition of growth[b]
1	5×10^{-5}
2	$>10^{-4}$
3	6×10^{-5}
4	4×10^{-5}
5	5×10^{-5}
6	9×10^{-5}
7	$X \times 10^{-4}$
8	8×10^{-6}
9	5×10^{-5}
10	$>10^{-4}$
11	$>10^{-4}$
12	8×10^{-5}
13	$>10^{-4}$
14	[c]
15	$>10^{-4}$
16	[c]
17	[c]
18	4×10^{-5}
20	$>10^{-4}$
21	1×10^{-5}
22	2×10^{-5}
24	6×10^{-6}
25, 26	3×10^{-5}
27, 28	3×10^{-5}
29, 30	2×10^{-5}
39	$>10^{-4}$
44	3×10^{-5}
45[d]	8×10^{-6}[e]
46	6×10^{-7}[f]
47	4×10^{-6}[f]
6-Chloropurine	$>10^{-4}$

[a] The culture conditions used have been published in ref. 28.
[b] Average value from multiple tests.
[c] Compound was insufficiently soluble in 10% dimethylsulfoxide in water to be tested.
[d] Prepared by the method of Robins *et al.* (30).
[e] Value from ref. 31.
[f] Values from ref. 29.

As shown in Table 1, the nucleoside analogs inhibit the growth of leukemia L-1210 cells in vitro at concentrations ranging from $1 \times 10^{-6}\,M$ to $> 10^{-4}\,M$. In comparison, the tetrahydropyran-2-yl derivative **45** exerts its effect at a concentration of $8 \times 10^{-6}\,M$ for 50% inhibition of growth, and 2′-azido- and 2′-amino-2′-deoxyarabinosylcytosine exert a similar effect at concentrations of $6 \times 10^{-7}\,M$ and $4 \times 10^{-6}\,M$, respectively. Comparison of the anti-proliferative activities of the 6-substituted purin-9-yl derivatives of unsubstituted 1,4-oxathiane, 1,4-dioxane, and 1,4-dithiane indicates that, in general, the 6-chloropurinyl derivatives inhibit cell proliferation more than their 6-amino and 6-thio analogs. In addition, the 6-amino derivatives, with the exception of the dithiane derivative **6**, show inhibitory effects at concentrations greater than $10^{-4}\,M$ and are considered, therefore, to be inactive. Since 6-chloropurine itself has been reported to show significant antitumor activity (14*b*) and 6-mercaptopurine is used for the treatment of acute leukemia (32), and in view of the fact that the 6-amino derivatives are inactive, it is conceivable that the activity of the 6-chloro and the 6-thio derivatives is mediated

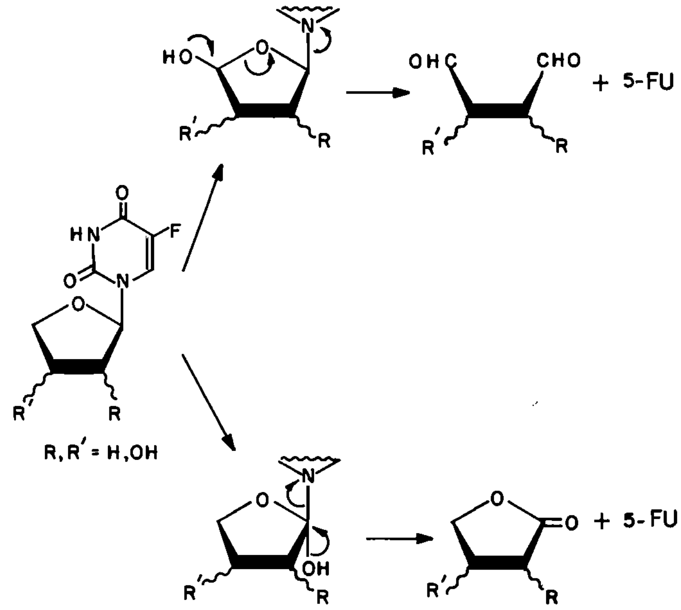

SCHEME 9

via release of the purine base. The proposed mode of action would then require metabolic activation of the nucleoside analogs to give the free bases which could either inhibit utilization of free purines or, alternatively, could be incorporated into aberrant nucleotides which could then inhibit a number of vital metabolic reactions. Within this context the nucleoside analogs could be considered to be functioning as prodrugs. However, the mechanisms by which the compounds bring about cell death are not clear, and it is also possible that the intact nucleoside analogs act as inhibitors of metabolic functions. There is ample evidence in the literature in support of both modes of action of related nucleoside analogs.

For example, the ribonucleosides containing 6-mercaptopurine, 6-thioguanine, and 5-fluorouracil exert effects similar to the free bases, mainly as a result of extensive cleavage of the nucleosides to the bases (33). The bases then undergo metabolic activation through phosphorylation and subsequent incorporation into nucleotides. However, the depot forms of the aberrant bases are sometimes advantageous in that they can provide for longer survival times (34) or can result in reduced toxicity (35) relative to the free bases. The point is further illustrated by the biological activities (36, 37) of 5-fluorouracil (5-FU) and (*R*,*S*)-1-(tetrahydrofuran-2-yl)-5-fluorouracil (ftorafur or FT) (**48**). Ftorafur has shown significant antitumor

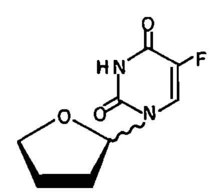

48

activity with a spectrum of activity similar to that of 5-FU, but it is less toxic than 5-FU (36). Lin *et al.* (37) have also reported that 3′- and 4′-hydroxyftorafur (hydroxylated FT metabolites that have also been isolated from patients' urine after FT administration (38)) exert inhibitory effects on HeLa cell growth equal to that of FT. These workers have suggested that the

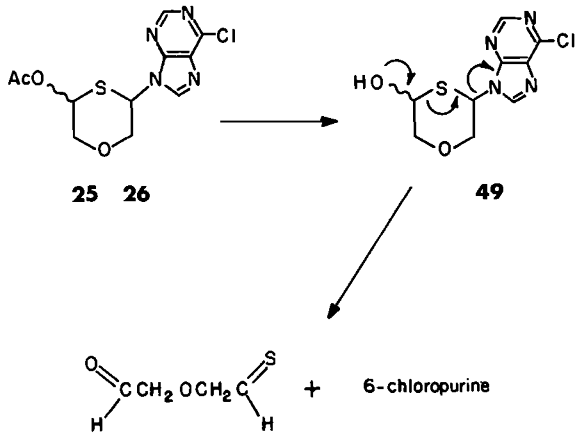

SCHEME 10

metabolic conversion of FT into 5-FU may involve hydroxylation and, in particular, hydroxylation at C-2′ or C-5′, which leads to the liberation of 5-fluorouracil, as indicated in Scheme 9. The possibility that formation of such hemiacetals or hemiketals can lead to the liberation of the base moiety is supported by one of the results presented in the preceding section. Thus, the attempted reduction of the acetoxy compounds (**25** and **26**) resulted in the liberation of 6-chloropurine. One could envisage the loss of the purine base from the hemiacetal **49** as proceeding by a mechanism analogous to that proposed by Lin *et al.* (37) (see Scheme 10).

In contrast, there is evidence that certain nucleoside analogs might exert their effects by mechanisms other than those involving the loss of the aberrant bases. For instance, 9-methyl-6-thioguanine and 9-(*n*-butyl)-6-thioguanine are active against tumor cell lines that are resistant to 6-thioguanine (39*a*, *b*). Moreover, it has been shown that 9-(*n*-butyl)-6-thioguanine is neither dealkylated nor incorporated into nucleic acid in the mouse, and that the compound may exert its effect by interference of utilization of preformed adenine for DNA synthesis (39*b*, *c*). In addition, a number of 9-alkyl derivatives of 6-thiopurine are reported to be active against 6-thiopurine-resistant tumor cell lines (40). These results suggest that the inhibitory activity of the 9-alkyl-6-substituted purines is not mediated by release of the free bases; alternatively, these compounds may act upon enzymes which have been deleted in the resistant strains (41). Similarly, 6-thio-9-(β-D-erythrofuranosyl)purine has been reported (42) to retain its activity against a strain of *S. faecium* that was resistant to the effects of 6-thiopurine or 6-thioinosine, an observation that provides evidence for a mode of action not involving liberation of 6-thiopurine.

Table 1 also shows that the concentration of 6-chloropurine required for 50% inhibition of cell growth is greater than 10^{-4} *M*. It would appear, therefore, that the saturated heterocyclic moieties in the nucleoside analogs do make a significant contribution to the activity of certain derivatives. This is particularly evident in the case of 9-(1,4-dithian-2-yl)adenine (**6**) which shows an ID_{50} of 9×10^{-5} *M*. The latter result is reminiscent of the reported activity of 9-(tetrahydrofuran-2-yl)-adenine against Adenocarcinoma 755 (43).

Interestingly, the 6-chloropurin-9-yl derivative of 4-benzoyl-1-oxa-4-azacyclohexane (**9**) inhibits cell proliferation at a concentration of 5×10^{-5} *M* whereas the corresponding 4-benzoyl-1-thia-4-azacyclohexane analog (**10**) is inactive.

The introduction of acetoxy or hydroxy substituents into the 1,4-oxathiane ring of the nucleoside analogs does not appear to affect the biological activity appreciably; the molar concentrations required for 50% inhibition of growth range from 1×10^{-5} to 3×10^{-5}. Moreover, the presence of an acetoxy group in place of a hydroxy group does not lead to any marked difference in activity of the corresponding nucleoside analogs. It is interesting to note that the acylation of nucleosides has sometimes led to an improvement of their therapeutic effectiveness (for a discussion, see ref. 44). The improvement may be attributed to the increased stabilization of the acylated compounds towards metabolic degradation as well as to their increased lipophilicity.

TABLE 2. Inhibitory effects of nucleoside analogs on the growth of human HeLa tumor cells in vitro[a]

Compound	Molar concentration for 50% inhibition of growth[b]
4	$>10^{-4}$ (40% inhibition at 10^{-4} *M*)
8	$>10^{-4}$ (35% inhibition at 10^{-4} *M*)
18	$>10^{-4}$
21	$>10^{-4}$ (30% inhibition at 10^{-4} *M*)
22	$>10^{-4}$ (40% inhibition at 10^{-4} *M*)
24	$>10^{-4}$
25, 26	$>10^{-4}$
27, 28	$>10^{-4}$
29, 30	$>10^{-4}$
46	2×10^{-7}[c]
47	3×10^{-5}[c]

[a] The culture conditions used have been published in ref. 28.
[b] Average value from multiple tests.
[c] Values from ref. 29.

The introduction of unsaturation into the 1,4-oxathiane ring provides an interesting result. Thus, 6-chloro-9-(1-oxa-4-thiacyclohex-2-en-3-yl)-9*H*-purine (**24**) inhibits the growth of leukemia L-1210 cells in vitro at a concentration of 6×10^{-6} *M* whereas the regioisomer, namely 6-chloro-9-(1-oxa-4-thiacyclohex-2-en-2-yl)-9*H*-purine (**20**), is inactive.

Oxidation of the 1,4-oxathiane moiety to give the sulfoxides furnishes nucleoside analogs which show inhibitory activity that is comparable to that of the parent compound. The result is only available for **18** since the regioisomer **17** was insufficiently soluble in 10% dimethylsulfoxide in water to be tested.

The acyclic, uracil-base nucleoside analog **44** shows an ID_{50} of 3×10^{-5} *M*.

The substituted thiazolidine derivative **12** containing 6-chloropurine inhibits the growth of L-1210 cells at a concentration of 8×10^{-5} *M* whereas the derivative **11** containing 6-benzamidopurine is inactive.

The encouraging activity exhibited by various of the nucleoside analogs against leukemia L-1210 cells in vitro prompted the screening of selected compounds in the human HeLa tumor cell line in vitro. As indicated in Table 2, none of the nucleoside analogs synthesized in this program that were tested showed significant inhibitory activity of the cell growth of HeLa cells in vitro although these compounds displayed activity in the leukemia L-1210 test system. In comparison, 2′-azido-2′-deoxyarabinosylcytosine (**46**) and 2′-amino-2′-deoxyarabinosylcytosine (**47**) inhibit the growth of HeLa cells in vitro at concentrations of 2×10^{-7} *M* and 3×10^{-5} *M*, respectively.

Various nucleoside analogs synthesized in this program were also subjected to screening against several bacterial strains, namely *Streptococcus faecium*, *E. coli* K-12, and *E. coli* B. However, none of the compounds tested showed significant activity in these bacterial systems.

Experimental

Melting points were determined with a Fisher–Johns apparatus and are uncorrected. Mass spectra were recorded on a CEC 21-104 mass spectrometer under electron-impact conditions at 70 eV ionizing voltage. Proton magnetic resonance (^{1}H nmr) spectra were recorded on a Bruker HX-60 or Varian HR-220 spectrometer. Carbon-13 magnetic resonance (^{13}C nmr) spectra were recorded on a Bruker HX-60 spectrometer equipped with a FT60M Fourier transform accessory at 15.09 MHz. Chemical shifts are given in ppm downfield from tetramethylsilane (TMS). Ultraviolet (uv) spectra were measured on a Unicam SP 800.

Analytical thin-layer chromatography (tlc) was performed on pre-coated glass plates with Merck silica gel 60F-254 as the adsorbent (layer thickness 0.25 mm). The developed plates were air-dried and exposed to uv light and (or) sprayed with a solution of cerium sulfate (1%) and molybdic acid (1.5%) in 10% aqueous sulfuric acid, and heated at 150°C. Preparative thin-layer chromatography was performed on pre-coated glass plates with Merck silica gel 60F-254 as the adsorbent (layer thickness 2 mm). Column chromatography was performed on Brinkman silica gel (70–235 mesh, E. Merck). High performance liquid chromatography was performed on a Waters Associates Prep/LC System 500. The chromatographic solvents (v/v) employed in this work are as follows: (A) benzene – ethyl acetate, 1:1; (B) 2:1; (C) *n*-propanol – ethyl acetate – water, 3:1:1; (D) ethyl acetate – ethanol, 20:1; (E) toluene – ethyl acetate, 1:1; (F) 1:2; (G) benzene – ethyl acetate, 3:1; (H) ethyl acetate.

Solvents were evaporated under reduced pressure and below 40°C.

*6-Chloro-9-(1-oxa-4-thiacyclohexan-3-yl)-9*H*-purine (4)*

The title compound was prepared from 3-hydroxy-1-oxa-4-thiacyclohexane by treatment with diethyl azodicarboxylate, methyldiphenylphosphine, and 6-chloropurine, by the method of Szarek *et al.* (4*c*, 5, 45, 46).[2]

9-(1-Oxa-4-thiacyclohexan-3-yl)adenine (13)

A solution of 6-chloro-9-(1-oxa-4-thiacyclohexan-3-yl)-9*H*-purine (**4**) (0.25 g, 0.97 mmol) in methanolic ammonia (10 mL, 10%) was heated at 90°C in a sealed glass tube for 4 h. The mixture was cooled to room temperature and then to 0°C. The crystals were removed by filtration and were identified as being 9-(1-oxa-4-thiacyclohexan-3-yl)adenine (**13**) (0.192 g, 83%), mp 199–202°C; uv λ_{max} (ethanol): 260 nm (ϵ 7,912), 229.5 (ϵ 1,846); λ_{max} (ethanol containing a trace of acid, pH 2): 260 nm (ϵ 7,912), 233 nm (ϵ 3,516); λ_{max} (ethanol containing a trace of sodium hydroxide, pH 10): 260 nm (ϵ 8,352), 232 nm (ϵ 2,593); ^{1}H nmr data (60 MHz, DMSO-d_6) δ: 2.62 (1H, d of m, J = 14 Hz, H-5′e), 3.08 (1H, m, H-5′a), 3.64–4.70 (4H, m's, 2H-2″s, 2H-6″s), 5.53 (1H, t, $|J_{3',2'} + J_{3',2''}|$ = 6.1 Hz, H-3′), 7.29 (2H, br s, NH_2), 8.17, 8.48 (2H, s's, H-2, H-8). *Anal.* calcd. for $C_9H_{11}N_5OS$: C 45.56, H 4.67, N 29.52, S 13.51; found: C 45.57, H 4.81, N 29.39, S 13.33.

*9-(1-Oxa-4-thiacyclohexan-3-yl)-9*H*-purine-6(1*H*)-thione (14)*

To a solution of 6-chloro-9-(1-oxa-4-thiacyclohexan-3-yl)-9*H*-purine (**4**) (0.31 g, 1.21 mmol) in methanol (7 mL) was added 2 mL of methanolic potassium hydrosulfide (prepared by saturating a solution of potassium hydroxide (0.3 g) in methanol (3 mL) with hydrogen sulfide at 0°C), and the mixture was heated at reflux temperature for 20 min. The mixture was cooled to room temperature and then to 0°C. The crystals were collected, and washed with cold methanol and water. The crystals were dried under vacuum over phosphorus pentoxide and were identified as being 9-(1-oxa-4-thiacyclohexan-3-yl)-9*H*-purine-6(1*H*)-thione (**14**) (0.267 g, 87%), mp 215°C (discoloring), 257°C (dec.); ^{1}H nmr data (60 MHz, DMSO-d_6) δ: 2.58 (1H, d of m, J = 14 Hz, H-5′e), 3.10 (1H, m, H-5′a), 3.5–4.25 (2H, m's, 2H-6″s), 4.15 (1H, d of d, J = 2.7, 12.4 Hz, H-2′e), 4.47 (1H, d of d, J = 2.9, 12.4 Hz, H-2′a), 5.5 (1H, t, $|J_{3',2'} + J_{3',2''}|$ = 6.0 Hz, H-3′), 8.24, 8.59 (2H, s's, H-2, H-8). *Anal.* calcd. for $C_9H_{10}N_4OS_2$: C 42.50, H 3.96, N 22.03, S 25.14; found: C 42.64, H 4.11, N 21.85, S 24.99.

9-(1,4-Dioxacyclohexan-2-yl)adenine (15)

A solution of 6-chloro-9-(1,4-dioxacyclohexan-2-yl)-9*H*-purine (**8**) (0.25 g, 1.04 mmol), prepared by the method of Szarek *et al.* (4*b*), in methanolic ammonia (10 mL, 10%) was heated at 90°C in a sealed glass tube for 4 h. The mixture was cooled to room temperature and then to 0°C. The crystals were obtained by filtration and were identified as being 9-(1,4-dioxacyclohexan-2-yl)adenine (**15**) (0.186 g, 81%), mp 185–186°C; uv λ_{max} (ethanol): 259.5 nm (ϵ 14 136), 226 nm (ϵ 1,571); λ_{max} (ethanol containing a trace of hydrochloric acid, pH 2): 259.5 nm (ϵ 14 136), 230 nm (ϵ 3,246); λ_{max} (ethanol containing a trace of sodium hydroxide, pH 10): 260 nm (ϵ 14 450), 232 nm (ϵ 4,293); ^{1}H nmr data (60 MHz, DMSO-d_6) δ: 3.80 (4H, m, 2H-5″s, 2H-6″s), 3.83–4.5 (2H, m's, 2H-3″s), 5.82 (1H, d of d, J = 3.4, 6.8 Hz, $|J_{2',3'} + J_{2',3''}|$ = 10.2 Hz, H-2′), 7.30 (2H, br s, NH_2), 8.17, 8.35 (2H, s's, H-2, H-8). *Anal.* calcd. for $C_9H_{11}N_5O_2$: C 48.86, H 5.01, N 31.66; found: C 49.20, H 5.24, N 31.38.

*9-(1,4-Dioxacyclohexan-2-yl)-9*H*-purine-6(1*H*)-thione (16)*

To a solution of 6-chloro-9-(1,4-dioxacyclohexan-2-yl)-9*H*-purine (**8**) (0.31 g, 1.29 mmol) in methanol (6 mL) was added 1.5 mL of methanolic potassium hydrosulfide (prepared by saturating a solution of potassium hydroxide (0.3 g) in methanol (3 mL) with hydrogen sulfide at 0°C), and the mixture was heated at reflux temperature for 20 min. The mixture was cooled and the crystals were collected, and washed with cold methanol and water. The crystals were dried under vacuum over phosphorus pentoxide and were identified as being 9-(1,4-dioxacyclohexan-2-yl)-9*H*-purine-6(1*H*)-thione (**16**) (0.285 g, 92%), mp 240°C (dec.); ^{1}H nmr data (60 MHz, DMSO-d_6) δ: 3.80 (4H, m, 2H-5″s, 2H-6″s), 3.83–4.42 (2H, m's, 2H-3″s), 5.83 (1H, d of d, J = 3.9, 6.1 Hz, $|J_{2',3'} + J_{2',3''}|$ = 9.8 Hz, H-2′), 8.23, 8.49 (2H, s's, H-2, H-8). *Anal.* calcd. for $C_9H_{10}N_4O_2S$: C 45.37, H 4.23, N 23.51, S 13.46; found: C 45.32, H 4.24, N 23.43, S 13.37.

Cis- *and* trans-*6-chloro-9-(1-oxa-4-oxo-4-thiacyclohexan-2-yl)-9*H*-purine (17*a*, 17*b*)*

A solution of 6-chloro-9-(1-oxa-4-thiacyclohexan-2-yl)-9*H*-purine (**1**) (0.896 g, 3.49 mmol), prepared by the method of Szarek *et al.* (4*b*), in methanol (50 mL) was added dropwise over a period of 0.5 h to a solution of sodium metaperiodate (0.822 g, 3.84 mmol) in water (40 mL) at 0°C. The mixture was stirred at 0°C for 8 h and then filtered. The methanol was evaporated, and the resulting aqueous solution was continuously extracted with chloroform (200 mL) for 4 h. The extracts were dried over anhydrous sodium sulfate, and concentrated to give a solid (0.926 g, 97%). Thin-layer chromatography (Solvent A) indicated the absence of starting material (R_f 0.56) and the presence of a component at the origin. The ^{1}H nmr spectrum indicated the presence of two isomeric sulfoxides in a ratio of 3.2:1. Recrystallization from ethanol afforded white crystals which were shown by ^{1}H nmr spectroscopy to consist of a mixture that was enriched in the major isomer **17***a*, mp 173–185°C (dec.). Compound **17***a* was identified as being *trans*-6-chloro-9-(1-oxa-4-oxo-4-thiacyclohexan-2-yl)-9*H*-purine; ^{1}H nmr data (60 MHz, DMSO-d_6) δ: 2.83–5.0 (6H, m's, 2H-3″s, 2H-5″s, 2H-6″s), 6.53 (1H, d of d, J = 2.1, 10.6 Hz, $|J_{2',3'} + J_{2',3''}|$ = 12.7 Hz, H-2′), 8.83, 8.93 (2H, s's, H-2, H-8). Compound **17***b* was identified as being *cis*-6-chloro-9-(4-oxo-1-oxa-4-thiacyclohexan-2-yl)-9*H*-purine; ^{1}H nmr data (60 MHz, DMSO-d_6) δ: 2.83–5.0 (6H, m's, 2H-3″s, 2H-5″s, 2H-6″s), 6.15 (1H, d of d, $|J_{2',3'} + J_{2',3''}|$ = 8.3 Hz, H-2′), 8.83, 9.07 (2H, s's, H-2, H-8). *Anal.* calcd. for $C_9H_9N_4O_2SCl$: C 39.64, H 3.33, N 20.54, S 11.76; found: C 39.45, H 3.59, N 20.38, S 11.64.

Cis- *and* trans-*6-chloro-9-(1-oxa-4-oxo-4-thiacyclohexan-3-yl)-9*H*-purine (18*a*, 18*b*)*

A solution of 6-chloro-9-(1-oxa-4-thiacyclohexan-3-yl)-9*H*-purine

[2] Also, M. C. Depew and W. A. Szarek, unpublished results.

(**4**) (0.295 g, 1.15 mmol), prepared from 3-hydroxy-1-oxa-4-thiacyclohexane by treatment with diethyl azodicarboxylate, methyldiphenylphosphine, and 6-chloropurine, by the method of Szarek *et al.* (4*c*, 5, 45, 46), in methanol (20 mL) was added to a solution of sodium metaperiodate (0.258 g, 1.21 mmol) in water (20 mL) at 0°C dropwise over a period of 10 min. The mixture was stirred at 0°C for 12 h and then at room temperature for 12 h. Thin-layer chromatography (Solvent A) indicated the presence of starting material (R_f 0.43). Sodium metaperiodate (0.16 g) was added and the mixture was stirred for 24 h; tlc still showed the presence of a small amount of starting material. Sodium metaperiodate (0.025 g) was added and stirring was continued for an additional 24 h; tlc (Solvent A) indicated the absence of starting material and the presence of a component having an R_f value of 0.14. The mixture was concentrated to remove methanol and was then subjected to continuous extraction with chloroform (200 mL) for 12 h. The extracts were dried over anhydrous magnesium sulfate, and concentrated to give a solid (0.29 g, 93%). The ^{1}H nmr spectrum indicated the presence of two isomeric sulfoxides in a ratio of 1.2:1. Recrystallization from ethanol–hexane afforded white prisms which were shown by ^{1}H nmr spectroscopy to consist predominantly of the major isomer (**18*a***), mp 197–204°C (dec.). Compound **18*a*** was identified as being *cis*-6-chloro-9-(1-oxa-4-oxo-4-thiacyclohexan-3-yl)-9*H*-purine; ^{1}H nmr data (100 MHz, DMSO-d_6) δ: 3.10 (1H, d of t, J = 14 Hz, $W_{1/2} \simeq 8$ Hz, H-5′e), 3.41 (1H, d of d, $J \simeq 14$, 4.2 Hz, H-5′a), 3.8–4.2 (3H, m's, H-2′e, H-6′a, H-6′e), 4.71 (1H, d of d, J = 12.4, 10 Hz, H-2′a), 5.99 (1H, d of d, J = 10.1, 4.0 Hz, $|J_{3',2'} + J_{3',2''}|$ = 14.1 Hz, H-3′), 8.70, 8.83 (2H, s's, H-2, H-8); ^{13}C nmr data (DMSO-d_6) δ: 44.85 (C-5), 57.40 (C-6), 60.77 (C-2), 62.06 (C-3), 130.3, 145.0, 151.8 (purine). Compound **18*b*** was identified as being *trans*-6-chloro-9-(1-oxa-4-oxo-4-thiacyclohexan-3-yl)-9*H*-purine; ^{1}H nmr data (60 MHz, DMSO-d_6) δ: 2.83–5.1 (6H, m's, 2H-2′′s, 2H-5′′s, 2H-6′′s), 5.58 (1H, d of d, $|J_{3',2'} + J_{3',2''}|$ = 10.5 Hz, H-3′), 8.87 (2H, s, H-2, H-8); ^{13}C nmr data (DMSO-d_6) δ: 47.44 (C-5), 61.29 (C-6), 64.07 (C-2), 68.02 (C-3), 130.7, 145.9, 149.5, 151.8 (purine). *Anal.* calcd. for $C_9H_9N_4O_2SCl$: C 39.64, H 3.33, N 20.54, S 11.76; found: C 39.32, H 3.33, N 20.36, S 11.58.

Pummerer reaction with cis- *and* trans-*6-chloro-9-(1-oxa-4-oxo-4-thiacyclohexan-2-yl)-9*H*-purine (17*a, *17*b)

A suspension of a mixture of sulfoxides (**17*a***, **17*b***) (1.58 g, 5.87 mmol) in acetic anhydride (40 mL) and benzene (100 mL), containing *p*-toluenesulfonic acid (10 mg), was heated at 60–70°C for 48 h. As the reaction proceeded, a clear solution was obtained. The mixture was cooled and was stirred with sodium hydrogen carbonate solution (150 mL) for 2 h. The layers were separated and the organic layer was washed with sodium hydrogen carbonate solution (75 mL) and then with water (75 mL), and dried over magnesium sulfate. Evaporation of the solvent afforded a solid which was revealed by tlc (Solvent B) to consist of four components having R_f values of 0.43, 0.37, 0.31, and 0.22. The mixture was chromatographed on silica gel using Solvent B as eluant. The component having an R_f value of 0.43 was obtained as a syrup and was identified as being 6-chloro-9-(1-oxa-4-thiacyclohex-5-en-2-yl)-9*H*-purine (**19**) (0.05 g, 3.3%); ^{1}H nmr data (60 MHz, $CDCl_3$) δ: 3.43 (2H, m, 2H-3′′s), 5.42 (1H, br d, J = 6.3 Hz, $W_{1/2}$ = 2.5 Hz, H-5′), 6.70 (1H, t, $|J_{2',3'} + J_{2',3''}|$ = 8.5 Hz, H-2′), 6.76 (1H, d, J = 6.3 Hz, H-6′), 8.36, 8.77 (2H, s's, H-2, H-8). The component having an R_f value of 0.37 was isolated as a solid and was recrystallized from ethanol to give white crystals (0.113 g, 8%), mp 113–135°C; it was identified as being 6-chloro-9-(1-oxa-4-thiacyclohex-2-en-2-yl)-9*H*-purine (**20**); ^{1}H nmr data (100 MHz $CDCl_3$) δ: 3.18 (2H, m, 2H-5′′s), 4.67 (2H, m, 2H-6′′s), 6.37 (1H, s, H-3′), 8.34, 8.77 (2H, s's, H-2, H-8); ^{13}C nmr data ($CDCl_3$) δ: 25.05 (C-5′), 67.69 (C-6′), 88.40 (C-3′), (C-2′ masked by $CDCl_3$), 132.0, 141.86, 152.41 (purine). *Anal.* calcd. for $C_9H_7N_4OSCl$: C 42.44, H 2.77, N 22.00, S 12.59; found: C 42.28, H 2.74, N 21.89, S 12.63.

The component having an R_f value of 0.31 was obtained as a white solid from ethanol–hexane (0.727 g, 39%), mp 157–158°C, and was identified as being *cis*-6-chloro-9-(3-acetoxy-1-oxa-4-thiacyclohexan-2-yl)-9*H*-purine (**21**); ^{1}H nmr data (100 MHz, $CDCl_3$) δ: 2.01 (3H, s, Me), 3.02 (2H, m, 2H-5′′s), 4.15 (2H, m, 2H-6′′s), 6.13 (1H, d, $J_{2',3'}$ = 5.6 Hz, H-2′ or H-3′), 6.29 (1H, d, $J_{2',3'}$ = 5.6 Hz, H-3′ or H-2′), 8.62, 8.75 (2H, s's, H-2, H-8); ^{13}C nmr data ($CDCl_3$) δ: 20.58 (Me), 25.69 (C-5′), 65.88 (C-6′), 68.47 (C-3′), 81.35 (C-2′), 143.3, 152.34 (purine), 168.5 (CO). *Anal.* calcd. for $C_{11}H_{11}N_4O_3SCl$: C 41.98, H 3.52, N 17.80, S 10.19; found: C 41.96, H 3.69, N 17.94, S 10.08.

The component having an R_f value of 0.22 was isolated as a solid and was recrystallized from ethanol to give white crystals (0.118 g, 64%), mp 147–148°C; it was identified as being *trans*-6-chloro-9-(5-acetoxy-1-oxa-4-thiacyclohexan-2-yl)-9*H*-purine (**22**); ^{1}H nmr data (100 MHz, $CDCl_3$) δ: 2.20 (3H, s, Me), 3.46 (1H, d of d, J = 14.5, 4.5 Hz, H-3′), 3.72 (1H, d of d, J = 14.5, 3.9 Hz, H-3″), 4.03 (1H, d of d, J = 13.1, 4 Hz, H-6′), 4.22 (1H, d of d, J = 13.1, 2.75 Hz, H-6″), 5.79 (1H, t, $|J_{5',6'} + J_{5',6''}|$ = 6.75 Hz, J = 2.75–3.25 Hz, H-5′), 6.36 (1H, t, $|J_{2',3'} + J_{2',3''}|$ = 8.25 Hz, J = 4 Hz, H-2′), 8.72 (2H, s, H-2, H-8); ^{13}C nmr data ($CDCl_3$) δ: 20.97 (Me), 25.89 (C-3′), 65.23 (C-6′), 67.37 (C-5′), 77.72 (C-2′), 131.57, 143.67, 152.21 (purine), 169.36 (CO). *Anal.* calcd. for $C_{11}H_{11}N_4O_3SCl$: C 41.98, H 3.52, N 17.80, S 10.19; found: C 41.63, H 3.51, N 17.68, S 10.01.

Pummerer reaction with cis- *and* trans-*6-chloro-9-(1-oxa-4-oxo-4-thiacyclohexan-3-yl)-9*H*-purine (18*a, *18*b)

An isomeric mixture of sulfoxides (**18*a***, **18*b***) (0.65 g, 2.38 mmol) in acetic anhydride (60 mL) and benzene (40 mL), containing *p*-toluenesulfonic acid (33 mg), was heated at 60–70°C for 40 h. The mixture was diluted with benzene (50 mL) and aqueous sodium hydrogen carbonate solution (50 mL) was added. The mixture was stirred for 2 h. The organic layer was separated, washed with water (50 mL), and was dried over anhydrous sodium sulfate. Evaporation of the solvent afforded a solid which was revealed by tlc (Solvent B) to consist of four components having R_f values of 0.65, 0.57, 0.48, and 0.41 after the plate had been developed three times. The aqueous layer was subjected to continuous extraction with chloroform for 12 h. The extracts were concentrated to give a solid which was identified as being unreacted starting material (**18*a***, **18*b***) (0.166 g). The crude mixture from above was applied to preparative thin-layer plates and the plates were developed five times using Solvent B as eluant. The component having an R_f value of 0.65 was isolated as a syrup and was identified as being 6-chloro-9-(1-oxa-4-thiacyclohex-5-en-3-yl)-9*H*-purine (**23**) (0.004 g, 1%); ^{1}H nmr data (60 MHz, $CDCl_3$) δ: 4.39 (1H, d of d, J = 12, 2 Hz, H-2′), 4.72 (1H, d of d, J = 12, 3 Hz, H-2″), 5.46 (1H, d of d, $J_{5',6'}$ = 7 Hz, $J_{5',3'}$ = 2 Hz, H-5′), 6.23 (1H, m, $|J_{3',2'} + J_{3',2''}|$ = 4.5 Hz, H-3′), 6.87 (1H, d, $J_{6',5'}$ = 7 Hz, H-6′), 8.47, 8.79 (2H, s's, H-2, H-8). The component having an R_f value of 0.57 was isolated as a solid and was recrystallized from ethanol to give white needles (0.062 g, 13.7%), mp 143–144°C; it was identified as being 6-chloro-9-(1-oxa-4-thiacyclohex-2-en-3-yl)-9*H*-purine (**24**); ^{1}H nmr data (60 MHz, $CDCl_3$) δ: 3.27 (2H, m, 2H-5′′s), 4.47 (2H, m, 2H-6′′s), 7.13 (1H, s, H-2′), 8.18, 8.82 (2H, s's, H-2, H-8). *Anal.* calcd. for $C_9H_7N_4OSCl$: C 42.44, H 2.77, N 22.00, S 12.59; found: C 42.38, H 2.83, N 21.77, S 12.37.

The component having an R_f value of 0.48 was isolated as a solid and was recrystallized from ethanol as white prisms (0.025 g, 4.5%), mp 160–164°C (dec.); it was identified as being *cis*-6-chloro-9-(5-acetoxy-1-oxa-4-thiacyclohexan-3-yl)-9*H*-purine (**25**); ^{1}H nmr data (100 MHz, $CDCl_3$) δ: 2.08 (3H, s, Me), 3.85–4.80 (4H, m's, 2H-2′′s, 2H-6′′s), 5.75 (2H, m, $W_{1/2}$ = 8 Hz, H-3′, H-5′), 8.74, 9.06 (2H, s's, H-2, H-8). The component having an R_f value of 0.41 was isolated as a solid and was recrystallized from ethanol to give white prisms (0.05 g, 9%), mp 144–145°C; it was identified as being *trans*-6-chloro-9-(5-acetoxy-1-oxa-4-thiacyclohexan-3-yl)-9*H*-purine (**26**); ^{1}H nmr data (100 MHz, $CDCl_3$) δ: 2.24 (3H, s, Me), 3.85–4.60 (4H, m, 2H-2′′s, 2H-6′′s), 5.97 (1H, t, $|J_{3',2'} + J_{3',2''}|$ = 4.5 Hz, H-3′), 6.19 (1H, d of d, J = 4.2, 8.4 Hz, $|J_{5',6'} + J_{5',6''}|$ = 12.6 Hz, H-5′), 8.36, 8.77 (2H, s's, H-2, H-8); ^{13}C nmr data ($CDCl_3$) δ: 20.97 (Me), 49.18 (C-3′), 70.15, 70.73, 71.12 (C-2′, C-5′, C-6′), 131.57, 143.48, 152.34 (purine), 168.5 (CO). *Anal.* calcd. for $C_{11}H_{11}N_4O_3SCl$: C 41.98, H 3.52, N 17.80, S 10.19; found (for a mixture of **25** and **26**): C 41.77, H 3.43, N 17.78, S 10.24.

Cis- *and* trans-*6-chloro-9-(3-hydroxy-1-oxa-4-thiacyclohexan-2-yl)-9*H-*purine (27, 28)*

Sodium borohydride (0.02 g, 0.53 mmol) was added to an ice-cooled solution of the acetate **21** (0.167 g, 0.53 mmol) in dry methanol (40 mL). The mixture was warmed to room temperature and was stirred for 12 h. The mixture was neutralized with moist Amberlite IRC 50 (H), the resin was removed by filtration, and the solution was concentrated to give a solid. Thin-layer chromatography (Solvent A) revealed the absence of starting material (R_f 0.53) and the presence of a component having an R_f value of 0.44. Preparative thin-layer chromatography using Solvent A as eluant afforded a white solid which was identified as being a mixture of *cis*- and *trans*-6-chloro-9-(3-hydroxy-1-oxa-4-thiacyclohexan-2-yl)-9*H*-purine (**27**, **28**) (0.097 g, 67%), mp 135–137°C; ir (KBr): 3410, 3200 (br OH), 1590, 1560, 1480 (purine ring) cm^{-1}; ^{1}H nmr data (60 MHz, $CDCl_3$ with D_2O, 300 K) *cis*-isomer **27**, δ: 2.33 (1H, d of t, H-5′e), 3.40 (1H, d of q, J = 14, 11, 4.8 Hz, H-5″a), 3.85–4.7 (2H, m's, 2H-6′′s), 4.98 (1H, br s, H-3′), 6.28 (1H, d, $J_{2',3'}$ = 1.2 Hz, H-2′), 8.60, 8.66 (2H, s's, H-2, H-8); *trans*-isomer **28**, δ: 5.34 (1H, d, $J_{2',3'}$ = 8 Hz, H-2′ or H-3′), 5.87 (1H, $J_{2',3'}$ = 8 Hz, H-3′ or H-2′); ratio of **27**:**28** = 3.25:1; (60 MHz, DMSO-d_6 with D_2O, 300 K), *cis*-isomer **27**, δ: 4.95 (1H, br s, H-3′), 6.23 (1H, br s, H-2′), 8.66, 8.80 (2H, s's, H-2, H-8); *trans*-isomer **28**, δ: 5.49 (1H, d, $J_{2',3'}$ = 8.3 Hz, H-2′ or H-3′), 5.83 (1H, d, $J_{2',3'}$ = 8.3 Hz, H-3′ or H-2′), 8.83, 8.92 (2H, s's, H-2, H-8); ratio of **27**:**28** = 1.3:1; 60 MHz, DMSO-d_6 with D_2O, 340 K), *cis*-isomer **27**, δ: 4.95 (1H, br s, H-3′), 6.23 (1H, d, $J_{2',3'}$ = 1.5 Hz, H-2′), 8.65, 8.78 (2H, s's, H-2, H-8); *trans*-isomer **28**, δ: 5.49, 5.83 (2H, d's, $J_{2',3'}$ = 8.3 Hz, H-2′, H-3′), 8.81, 8.85 (2H, s's, H-2, H-8). Ratio of **27**:**28** = 2.6:1. The ^{13}C nmr data (DMSO-d_6) **27**, δ: 20.77 (C-5′), 67.50 (C-3′), 70.86 (C-6′), 83.74 (C-2′), 145.09, 145.87, 151.76 (purine); **28**, δ: 28.60 (C-5′), 69.38 (C-3′), 69.76 (C-6′), 86.33 (C-2′); ratio of **27**:**28** 1:1; (DMSO-d_6 + $CDCl_3$), **27**, δ: 21.41 (C-5′), 68.29 (C-3′), 71.27 (C-6′), 83.88 (C-2′), 144.35, 145.0, 151.53, 151.85 (purine); **28**, δ: 28.97 (C-5′), 69.91 (C-3′), 70.43 (C-6′), 86.66 (C-2′); ratio of **27**:**28** ≃ 2:1. *Anal.* calcd. for $C_9H_9O_2SCl$: C 39.64, H 3.33, N 20.54, S 11.76; found: C 39.77, H 3.44, N 19.68, S 11.83.

Cis- *and* trans-*6-chloro-9-(5-hydroxy-1-oxa-4-thiacyclohexan-2-yl)-9*H-*purine (29, 30)*

Sodium borohydride (0.015 g, 0.39 mmol) was added to an ice-cooled solution of the acetate **22** (0.122 g, 0.39 mmol) in dry methanol (30 mL). The mixture was warmed to room temperature and was stirred for 15 h. The mixture was neutralized with moist Amberlite IRC 50 (H), filtered, and the solvent was evaporated to give a syrup. Thin-layer chromatography (Solvent B) indicated the absence of starting material (R_f 0.25) and the presence of another component having an R_f value of 0.08. Preparative thin-layer chromatography using Solvent A as eluant afforded a white solid which was identified as being a mixture of *cis*- and *trans*-6-chloro-9-(5-hydroxy-1-oxa-4-thiacyclohexan-2-yl)-9*H*-purine (**29**, **30**) (0.53 g, 50%), mp 164–166°C (dec.); ir (KBr): 3370, 3290 (br, OH), 1598, 1560, 1488 (purine ring) cm^{-1}; ^{1}H nmr data (60 MHz, $CDCl_3$, 300 K), *cis*-isomer **29** only, δ: 2.83 (1H, d of d, J = 13, 2.2 Hz, H-3′e), 3.25–4.6 (3H, m's, H-3″a, 2H-6′′s), 4.85 (1H, m, $|J_{5',6'} + J_{5',6''}|$ = 5 Hz, H-5′), 6.13 (1H, d of d, J = 10.5, 2.2 Hz, $|J_{2',3'} + J_{2',3''}|$ = 12.7 Hz, H-2′), 8.50, 8.76 (2H, s's, H-2, H-8); (60 MHz, DMSO-d_6 with D_2O, ~300 K), *cis*-isomer **29**, δ: 2.89 (1H, d of d, J = 13, 2 Hz, H-3′e), 3.5–4.4 (3H, m's, H-3″a, 2H-6′′s), 4.77 (1H, m, $|J_{5',6'} + J_{5',6''}|$ = 4.5 Hz, H-5′), 6.09 (1H, d of d, J = 10.8, 2.2 Hz, $|J_{2',3'} + J_{2',3''}|$ = 13.0 Hz, H-2′), 8.83, 8.92 (2H, s's, H-2, H-8); *trans*- isomer **30**, δ: 4.97 (1H, d of d, J = 7.5, 3.2 Hz, $|J_{5',6'} + J_{5',6''}|$ = 10.7 Hz, H-5′), 6.18 (1H, m, $|J_{2',3'} + J_{2',3''}|$ ≃ 9 Hz, partially obscured by H-2′ of **29**, H-2′); ratio of **29**:**30** = 2.7:1; (DMSO-d_6 with D_2O, 340 K), *cis*-isomer **29**, δ: 4.77 (1H, m, $|J_{5',6'} + J_{5',6''}|$ = 5.2 Hz, H-5′), 6.10 (1H, d of d, J = 10.2, 2.2 Hz, $|J_{2',3'} + J_{2',3''}|$ = 12.4 Hz, H-2′), 8.80, 8.83 (2H, s's, H-2, H-8); *trans*-isomer **30**, δ: 5.0 (1H, d of d, J = 7.3, 3.2 Hz, $|J_{5',6'} + J_{5',6''}|$ = 10.5 Hz, H-5′), ~6.2 (1H, m, H-2′); ratio of **29**:**30** = 2.2:1; (DMSO-d_6 with D_2O, 400 K), *cis*-isomer **29**, δ: 4.77 (1H, m $|J_{5',6'} + J_{5',6''}|$ = 5.2 Hz, H-5′), 6.10 (1H, d of d, J = 2.4, 10.2 Hz, $|J_{2',3'} + J_{2',3''}|$ = 12.7 Hz, H-2′), 8.74 (2H, s, H-2, H-8); *trans*-isomer **30**, δ: 5.02 (1H, d of d, J = 3.9, 7.3 Hz, $|J_{5',6'} + J_{5',6''}|$ = 11.2 Hz, H-5′), ~6.2 (1H, d of d, $|J_{2',3'} + J_{2',3''}|$ = 7–8 Hz, partially obscured by H-2′ of **29**, H-2′); ratio of **29**:**30** = 2.7:1; ^{13}C nmr data (DMSO-d_6) **29**, δ: 24.53 (C-3′), 66.01 (C-5′), 72.20 (C-6′), 81.48 (C-2′), 130.86, 145.16, 151.76 (purine); **30**, δ: 28.41 (C-3′), 68.22 (C-5′), 72.61 (C-6′), 80.44 (C-2′). *Anal.* calcd. for $C_9H_9N_4SO_2Cl$: C 39.64, H 3.33, N 20.54, S 11.76; found: C 39.53, H 3.45, N 20.35, S 11.81.

Attempted reduction of cis- *and* trans-*6-chloro-9-(5-acetoxy-1-oxa-4-thiacyclohexan-3-yl)-9*H-*purine (25, 26)*

Sodium borohydride (0.011 g, 0.3 mmol) was added to an ice-cooled solution of a mixture of the acetates **25** and **26** (0.09 g, 0.29 mmol) in dry methanol (25 mL). The mixture was warmed to room temperature and was stirred for 12 h. Thin-layer chromatography (Solvent A) indicated that the main uv-active component was present at the origin. The mixture was neutralized with Rexyn 102 (H), the resin was removed by filtration, and the solvent was evaporated to give a syrup; tlc indicated the absence of a uv-active component other than that at the origin (6-chloropurine).

1-Benzylinosine (32)

Inosine (**31**) (8.36 g, 0.031 mol) was dissolved with heating in *N*,*N*-dimethylformamide (240 mL). Sodium hydrogen carbonate (8.4 g, 0.1 mol) and benzyl chloride (8.5 mL, 0.074 mol) were added and the mixture was heated at 90°C for 6 h. The solvent was removed under reduced pressure to give a solid. Water (250 mL) was added to the residue and, after trituration, was removed under reduced pressure. The process was repeated. The residue was triturated with warm water (150 mL) and the remaining solid was collected (10.2 g, 85%), mp 215–220°C. Thin-layer chromatography (Solvent C) indicated the presence of one component having an R_f value of 0.71. Recrystallization from 95% ethanol afforded white crystals which were identified as being 1-benzylinosine (**32**), mp 221–222°C; lit. (15) mp 219–222°C; ^{1}H nmr data (60 MHz, DMSO-d_6) δ: 3.45 (br peak, OH), 3.74 (2H, m, H-5′, H-5″), 3.85–4.38 (2H, m's, H-3′, H-4′), 4.57 (1H, m, H-2′), 5.2 (br peak, OH), 5.23 (2H, s, CH_2Ph), 5.91 (1H, d, J = 5 Hz, H-1′), 7.35 (5H, s, Ph), 8.40, 8.66 (two 1H s's, H-2, H-8).

*1-Benzyl-5′-*O-tert-*butyldimethylsilylinosine (33)*

To a mixture of 1-benzylinosine (**32**) (5.85 g, 0.015 mol) and imidazole (2.15 g, 0.031 mol) in amine-free, dry *N*,*N*-dimethylformamide (250 mL) was added *tert*-butyldimethylsilyl chloride (2.72 g, 0.018 mol) with stirring. The mixture was let stand at room temperature for 12 h, after which the solvent was removed under reduced pressure. The residue was triturated with water (125 mL) and the water was carefully decanted. The process was repeated. The gummy residue was treated with ethanol (40 mL) and the remaining solid was collected. This was identified as being unreacted material (**32**) (0.46 g). The filtrate was concentrated to give a solid (6.98 g, 98%). Thin-layer chromatography (Solvent C) indicated the absence of starting material and the presence of a faster-moving component. Compound **33** was obtained from methanol as white needles, mp 204.5–206.5°C. ^{1}H nmr data (60 MHz, DMSO-d_6) δ: 0.05 (6H, s, 2-Me), 0.87 (9H, s, *t*-Bu), 3.7–4.33 (m's, H-3′, H-4′, OH), 4.5 (1H, m, H-2′), 5.24 (2H, s, CH_2Ph), 5.62 (1H, d, J = 5.8 Hz, OH), 5.90 (1H, d, J = 4.6 Hz, H-1′), 7.31 (5H, s, Ph), 8.27, 8.61 (two 1H s's, H-2, H-8). *Anal.* calcd. for $C_{23}H_{32}N_4O_5Si$: C 58.45, H 6.83, N 11.86; found: C 58.63, H 6.88, N 11.99.

*1-Benzyl-6-oxo-9-[(1*R*,3*R*)-1,3-bis(*p*-tolylsulfonyloxymethyl)-4-*tert*-butyldimethylsilyloxy-2-oxabutyl]-9*H*-purine (36)*

To a solution of 1-benzyl-5′-*O*-*tert*-butyldimethylsilylinosine (**33**) (3.0 g, 6.35 mmol) in ethanol (250 mL) at 0°C was added a solution of sodium metaperiodate (1.63 g, 7.62 mmol) in water (60 mL) with stirring. The mixture was warmed to room temperature and stirring was continued for 24 h. Barium chloride solution (10%) was added to precipitate iodate and periodate ions. The mixture was cooled and the salts were removed by filtration. The filtrate was concentrated to afford a solid which was dissolved in methanol (60 mL) and water (30 mL). The solution was cooled to 0°C and sodium borohydride (0.722 g, 19.1 mmol) was added in portions; the flask was protected from light. The mixture was gradually warmed to room temperature and stirring was continued for 12 h. The mixture was brought to pH 8 by addition of wet Amberlite IRC 50 (H). The resin was removed by filtration and the filtrate was concentrated. The residue was repeatedly concentrated from methanol to remove boric acid, and the resulting white foam was dried under vacuum. Thin-layer chromatography (Solvent D) indicated the presence of one component having an R_f value of 0.22. The foam was dissolved in pyridine and the solution was cooled to 0°C. *p*-Toluenesulfonyl chloride (4.0 g, 0.02 mol) was added in portions. The mixture was gradually warmed to room temperature and was stirred for 72 h. The mixture was poured into ice and was then extracted with methylene chloride (3 × 100 mL). The extracts were washed with sodium hydrogen carbonate solution (100 mL) and water (100 mL), and dried over anhydrous magnesium sulfate. Evaporation of the solvent afforded a foam. Thin-layer chromatography (Solvent A) indicated the presence of two major components having R_f values of 0.45 and 0.34 as well as a large amount of unreacted diol **35**. The foam was chromatographed on silica gel using Solvent E as eluant initially and then Solvent F as eluant. The component having an R_f value of 0.45 was obtained as a foam and was identified as being the ditosylate **36** (0.82 g, 17%); ^{1}H nmr data ($CDCl_3$, 60 MHz) δ: 0.02 (6H, s, $SiMe_2$), 0.87 (9H, s, *t*-Bu), 2.55, 2.60 (two 3 H s's, 2-Me), 3.08–4.83 (7H, m's, 2-CH_2OTs, CH_2OSi, H-3′), 5.37 (2H, s, CH_2Ph), 6.12 (1H, t, J = 5.2 Hz, H-1′), 7.42 (5H, s, Ph), 7.33, 7.73 (two 1H d's, J = 8 Hz, Ar), 7.42, 7.90 (two 1H d's, J = 8 Hz, Ar), 7.90, 8.15 (two 1H s's, H-2, H-8). *Anal.* calcd. for $C_{37}H_{46}N_4O_9S_2Si$: C 56.75, H 5.92, N 7.16, S 8.19; found: C 56.88, H 6.04, N 7.66, S 7.95.

The component having an R_f value of 0.34 was obtained as a syrup and was identified as being the monotosylate **37** (0.125 g, 3%); ^{1}H nmr data ($CDCl_3$, 60 MHz) δ: 0.1 (6H, s, $SiMe_2$), 0.84 (9H, s, *t*-Bu), 2.48 (3H, s, Me), 3.34–4.05 (5H, m's, CH_2OSi, CH_2OH, H-3′), 4.52 (2H, d, J = 5.8 Hz, CH_2OTs), 5.27 (2H, "s", CH_2Ph), 6.24 (1H, t, J = 5.8 Hz, H-1′), 7.26, 7.67 (two 1H d's, J = 8 Hz, Ar), 7.38 (5H, s, Ph), 7.92, 8.01 (two 1H s's, H-2, H-8).

*1-Benzyl-6-oxo-9-[(2*R*,6*R*)-6-*tert*-butyldimethylsilyloxymethyl-1-oxa-4-thiacyclohexan-2-yl]-9*H*-purine (38)*

To a refluxing solution of the ditosylate **36** (0.578 g, 0.74 mmol) in 95% ethanol (100 mL) was added a solution of sodium sulfide (0.087 g, 1.11 mmol) (freshly recrystallized from ethanol) in hot 95% ethanol (60 mL) dropwise over a period of 1 h. After 5 h tlc (Solvent A) indicated the presence of starting material as well as a slower-moving component having an R_f value of 0.39. Sodium sulfide (0.060 g) was added and refluxing was continued. After 12 h tlc (Solvent A) still showed the presence of starting material. An additional amount of sodium sulfide (0.030 g) was added and refluxing was continued for 24 h. Thin-layer chromatography indicated that the major component present was that having an R_f value of 0.39. Dry Ice was added to neutralize the mixture and the ethanol was evaporated. The residue was partitioned between methylene chloride and sodium hydrogen carbonate (150 mL/100 mL). The methylene chloride layer was dried over anhydrous sodium sulfate, and concentrated to give a syrup which was chromatographed on silica gel using Solvent E as eluant. The component having an R_f value of 0.39 was obtained as a white foam and was identified as being compound **38** (0.031 g, 9%); ^{1}H nmr data ($CDCl_3$, 60 MHz) δ: 0.02 (6H, s, 2-Me), 0.87 (9H, s, *t*-Bu), 2.47–3.17 (4H, m's, H-3′, H-3″, H-5′, H-5″), 3.17–4.2 (3H, m's, H-6′, CH_2OSi), 5.18 (2H, "s", CH_2Ph), 5.80 (1H, d of d, $J_{2',3'e}$ = 3 Hz, $J_{2',3''a}$ = 10 Hz, H-2′), 7.23 (5H, s, Ph), 7.79, 7.90 (two 1H s's, H-2, H-8); ^{13}C nmr data (in $CDCl_3$) δ: 5.37 (Me), 25.80 (*t*-Bu), 27.87 (C-5′), 31.17 (C-3′), 49.22 (CH_2OSi), 65.32 (CH_2Ph), 81.36 (C-6′), 82.39 (C-2′), 128.05, 128.96, 135.88, 137.17, 147.07, 156.38 (Ar), 204.3 (CO). *Anal.* calcd. for $C_{23}H_{32}N_4O_3SSi$: C 58.44, H 6.83, N 11.85, S 6.78; found: C 58.79, H 7.22, N 10.84, S 6.67. Mol. Wt. calcd. for $C_{23}H_{32}N_4O_3SSi$: 472.7; found: *m/e* 415 ($M^{+\cdot}$ − *t*-Bu), 358 ($M^{+\cdot}$ − *t*-BuMe$_2$Si).

After compound **38** was isolated, the column was eluted with Solvent D to yield a component having an R_f value of 0.25 (Solvent D). This component was obtained as a white foam and was identified as being the alcohol **39** resulting from desilylation of **38** (0.39, 49%).

*1-Benzyl-6-oxo-9-[(2*R*,6*R*)-6-hydroxymethyl-1-oxa-4-thiacyclohexan-2-yl]-9*H*-purine (39)*

The silyl ether **38** (0.038 g, 0.8 mmol) was treated with tetra-*n*-butylammonium fluoride (2 mL, 1.3 *N* in tetrahydrofuran) for 12 h. Thin-layer chromatography (Solvent D) indicated the absence of starting material and the presence of a more polar component having an R_f value of 0.25. The solvent was evaporated and the residue was partitioned between methylene chloride and water (20 mL/10 mL). The organic layer was dried over anhydrous sodium sulfate, and concentrated to afford a syrup. Preparative thin-layer chromatography using Solvent D as eluant yielded compound **39** as a white foam (0.026 g, 90%); ^{1}H nmr data ($CDCl_3$, 220 MHz) δ: 2.39 (1H, br d, J_{gem} = 14 Hz, $W_{1/2}$ = 5 Hz, H-5′e), 2.72 (1H, br d, J_{gem} = 13–15 Hz, $W_{1/2}$ = 5 Hz, H-3′e), 2.76 (1H, d of d, J_{gem} = 14 Hz, $J_{5''a,6'}$ = 11 Hz, H-5″a), 3.17 (1H, d of d, J_{gem} = 13 Hz, $J_{3''a,2'}$ = 11 Hz, H-3′a), 3.67 (2H, m, CH_2OH), 4.15 (1H, octet, H-6′), 5.23 (2H ABq, $J \simeq$ 14 Hz, CH_2Ph), 5.90 (1H, d of d, $J_{2',3'e}$ = 1.8 Hz, $J_{2',3''a}$ = 10.8 Hz, $|J_{2',3'} + J_{2',3''}|$ = 12.6 Hz, H-2′), 7.39 (5H, s, Ph), 7.99, 8.08 (two 1H s's, H-2, H-8).

*5′-O-*tert*-Butyldimethylsilyluridine (41)*

To a solution of uridine (**40**) (0.5 g, 2.05 mmol) and imidazole (0.31 g, 4.51 mmol) in amine-free, dry *N,N*-dimethylformamide (40 mL) at room temperature was added *tert*-butyldimethylsilyl chloride (0.34 g, 2.25 mmol). The mixture was stirred for 1 h. The solvent was evaporated under reduced pressure and water was added to the residue. The solid that formed was collected and washed with water. Compound **41** was obtained as a white solid from methanol–water (0.7 g, 95%), mp 85–88°C; ^{1}H nmr data (DMSO-d_6, 60 MHz) δ: 0.08 (6H, s, 2-Me), 0.91 (9H, s, *t*-Bu), 3.3–4.47 (6H, m, H-2′, H-3′, H-4′, H-5′, H-5″, OH), 5.59 (1H, d, J = 8.4 Hz, H-6), 5.81 (1H, d, J = 4 Hz, H-1′), 7.84 (1H, d, J = 8.4 Hz, H-5), 11.42 (1H, br peak, NH).

*5′-O-*tert*-Butyldimethylsilyluridine "dialdehyde" (42)*

To a stirred solution of *tert*-butyldimethylsilyluridine (**41**) (1.0 g, 2.79 mmol) in methanol (60 mL) at 0°C was added sodium metaperiodate (0.72 g, 3.35 mmol) in water (30 mL). The mixture was gradually warmed to room temperature and was stirred for 12 h. The solution was concentrated to a volume of 40 mL. Ethanol (100 mL) was added and the mixture was stirred for 15 min. The salts were removed by filtration and the filtrate was concentrated to afford a solid.

*1-[(2*E*,7*E*),(4*R*,6*S*)-Diethyl 6-*tert*-butyldimethylsilyloxymethyl-5-oxanona-2,7-dienoate-4-yl]uracil (43)*

A solution of the "dialdehyde" **42** (0.55 g, 1.53 mmol) and carbethoxymethylenetriphenylphosphorane (1.6 g, 4.59 mmol) in *N,N*-dimethylformamide (50 mL) was heated at 95°C for 3 h. The solvent was removed under reduced pressure to yield a syrup. Thin-layer chromatography (Solvent B) indicated the presence of one major component having an R_f value of 0.38. High performance liquid chromatography using Solvent G as eluant afforded a white solid (0.51 g, 67%). Recrystallization from ether–hexane yielded compound **43** as white needles, mp 105.5–106.5°C; ^{1}H nmr data ($CDCl_3$, 220 MHz) δ: 0.045 (6H, s, 2-Me), 0.86 (9H, s, *t*-Bu), 1.32, 1.33 (two 3H t's, 2-Me), 3.66 (2H, AB pattern, CH_2OSi), 4.24, 4.26 (two 2H q's, 2-CH_2CH_3), ~4.21 (1H, m, (obscured by CH_2CH_3 signals), H-6′), 5.81 (1H, d of d, $J_{6,5}$ = 8 Hz, $^4J_{6,4'}$ = 2 Hz, H-6), 6.11 (1H, d of d, $J_{8',7'}$ = 16 Hz, $^4J_{8',6'}$ = 1.1 Hz, H-8′), 6.31 (1H, d of d, $J_{7',8'}$ = 15.7 Hz, $J_{7',6'}$ = 2 Hz, H-7′), 6.39 (1H, d of d, $J_{4',3'}$ = 3.9 Hz, $^4J_{4',6}$ = 2 Hz, H-4′), 6.77 (1H, d of d, $J_{2',3'}$ = 15.7 Hz, $^4J_{2',4'}$ = 1.1 Hz, H-2′), 6.79 (1H, d of d, $J_{3',2'}$ = 15.8 Hz, $J_{3',4'}$ = 3.9 Hz, H-3′), 7.35 (1H, d, $J_{5,6}$ = 8 Hz, H-5), 9.46 (1H, br s, NH). *Anal.* calcd. for $C_{23}H_{36}N_2O_8Si$: C 55.62, H 7.31, N 5.64; found: C 55.56, H 7.51, N 5.41.

*1-[(2E,7E),(4R,6S)-Diethyl 6-hydroxymethyl-5-oxanona-2,7-dieneoate-4-yl]uracil (**44**)*

The silyl ether **43** (0.183 g, 0.37 mmol) was treated with tetra-*n*-butylammonium fluoride (1.5 mL, 1.3 *N* in tetrahydrofuran) for 2 h. Thin-layer chromatography (Solvent H) indicated the presence of one component having an R_f value of 0.34. The solvent was evaporated and the residue was partitioned between methylene chloride and water (20 mL/10 mL). The organic layer was dried over anhydrous magnesium sulfate, and concentrated to afford a syrup. Chromatography on silica gel using Solvent H as eluant gave a white foam which was identified as being compound **44** (0.13 g, 92%); ^{1}H nmr data ($CDCl_3$, 60 MHz) δ: 1.30, 1.32 (two 3H t's, 2-Me), 3.68 (2H, m, CH_2OH), 4.17, 4.23 (two 2H q's, 2-CH_2CH_3), ~4.2 (1H, m (partially obscured by CH_2 signals), H-6′), 5.73 (1H, d, J = 8 Hz, H-6), 6.1 (1H, d, J = 16 Hz, H-8′), 6.3 (1H, d, J = 16 Hz, H-7′), 6.38 (1H, d, $J \simeq 4$ Hz, H-4′), 6.78 (1H, d, $J \simeq 16$ Hz, H-2′), 6.83 (1H, br d, J = 16 Hz, H-3′), 7.42 (1H, d, J = 8 Hz, H-5), 10.62 (1H, br s, NH). *Anal.* calcd. for $C_{17}H_{22}O_8N_2$: C 53.40, H 5.80, N 7.33; found: C 53.38, H 6.30, N 6.93.

Acknowledgements

The authors are grateful to Dr. A. Bloch of Roswell Park Memorial Institute for performing the biological screening of the nucleoside analogs. Financial assistance from NSERC Canada in the form of grants (to W.A.S.) and a scholarship (to B.M.P.) is gratefully acknowledged. The authors also wish to thank Queen's University for financial support.

1. W. DVONCH and H. E. ALBURN. Abstr. Papers Am. Chem. Soc. Meeting, 155, C56 (1968); Chem. Eng. News, **46**, 41 (1968); U.S. Patent No. 3,542,776 (November, 1970); Chem. Abstr. **74**, 31760 (1971).
2. (*a*) J. G. CORY, M. M. MANSELL. C. B. GEORGE, and D. S. WILKINSON. Arch. Biochem. Biophys. **160**, 495 (1974); J. G. CORY and C. B. GEORGE. Biochem. Biophys. Res. Commun. **52**, 496 (1973); (*b*) J. G. CORY and M. M. MANSELL. Cancer Res. **35**, 390 (1975); (*c*) W. DVONCH, H. FLETCHER III, F. J. GREGORY, E.-M. H. HEALY, C. H. WARREN, and H. E. ALBURN. Cancer Res. **26**, 2386 (1966); (*d*) R. L. CYSYK and R. H. ADAMSON. Cancer Treat. Rep. **60**, 555 (1976).
3. F. HANSSKE, M. SPRINZL, and F. CRAMER. Bioorg. Chem. **3**, 367 (1974); F. HANSSKE and F. CRAMER. Carbohydr. Res., **54**, 75 (1977); A. S. JONES, A. F. MARKHAM, and R. T. WALKER. J. Chem. Soc. Perkin Trans. 1, 1567 (1976).
4. (*a*) D. M. VYAS and W. A. SZAREK. Carbohydr. Res. **30**, 225 (1973); (*b*) W. A. SZAREK, D. M. VYAS, and B. ACHMATOWICZ. J. Heterocycl. Chem. **12**, 123 (1975); (*c*) B. M. PINTO, D. M. VYAS, and W. A. SZAREK. Can. J. Chem. **55**, 937 (1977); (*d*) L. J. J. HRONOWSKI and W. A. SZAREK. J. Med. Chem. **25**, 522 (1982).
5. M. IWAKAWA, B. M. PINTO, and W. A. SZAREK. Can. J. Chem. **56**, 326 (1978).
6. J. E. MCCORMICK and R. S. MCELHINNEY. J. Chem. Soc. Perkin Trans. 1, 64 (1978); 500 (1978).
7. W. DVONCH and H. E. ALBURN. U.S. Patent No. 4,000,137 (December, 1976); U.S. Patent No. 4,041,037 (August, 1977); Chem. Abstr. **86**, 155900t (1977).
8. J. G. CORY and S. H. PARKER. Biochem. Pharmacol. **28**, 867 (1979).
9. K. W. BUCK, F. A. FAHIM, A. B. FOSTER, A. R. PERRY, M. H. QADIR, and J. M. WEBBER. Carbohydr. Res. **2**, 14 (1966).
10. R. L. CYSYK and R. H. ADAMSON. Cancer Treat. Rep. **60**, 563 (1976).
11. W. A. SZAREK, D. M. VYAS, A.-M. SEPULCHRE, S. D. GERO, and G. LUKACS. Can. J. Chem. **52**, 2041 (1974); W. A. SZAREK, D. M. VYAS, and B. ACHMATOWICZ. Tetrahedron Lett. 1553 (1975).
12. N. J. LEONARD and C. R. JOHNSON. J. Org. Chem. **27**, 283 (1962).
13. W. A. SZAREK, B. M. PINTO, and M. IWAKAWA. Can. J. Chem. **63**, 2162 (1985).
14. J. F. GERSTER, A. F. LEWIS, and R. K. ROBINS. J. Org. Chem. **28**, 945 (1963); A. BENDICH, P. J. RUSSELL, JR., and J. J. FOX. J. Am. Chem. Soc. **76**, 6073 (1954).
15. E. SHAW. J. Am. Chem. Soc. **80**, 3899 (1958).
16. J. P. H. VERHEYDEN and J. G. MOFFATT. J. Org. Chem. **35**, 2319 (1970).
17. R. E. HOLMES and R. K. ROBINS. J. Org. Chem. **28**, 3483 (1963).
18. A. HAMPTON, M. BAYER, V. S. GUPTA, and S. Y. CHU. J. Med. Chem. **11**, 1229 (1968).
19. K. K. OGILVIE, S. L. BEAUCAGE, D. W. ENTWISTLE, E. A. THOMPSON, M. A. QUILLIAM, and J. B. WESTMORE. J. Carbohydr. Nucleosides, Nucleotides, **3**, 197 (1976).
20. E. J. COREY and A. VENKATESWARLU. J. Am. Chem. Soc. **94**, 6190 (1972).
21. J. HOOZ and S. S. H. GILANI. Can. J. Chem. **46**, 86 (1968).
22. R. W. BINKLEY and D. G. HEHEMANN. J. Org. Chem. **43**, 3244 (1978).
23. O. D. DAILEY, JR. and P. L. FUCHS. J. Org. Chem. **45**, 216 (1980).
24. M. SLAVIK. Ann. New York Acad. Sci. **255**, 266 (1975).
25. J. C. IRESON, J. B. LEE, and M. J. TYLER. Tetrahedron, **33**, 3279 (1977).
26. M. BOBEK, R. L. WHISTLER, and A. BLOCH. J. Med. Chem. **13**, 411 (1970); **15**, 168 (1972).
27. A. BLOCH and C. COUTSOGEORGOPOULOS. Biochemistry, **5**, 3345 (1966).
28. M. BOBEK, A BLOCH, P. BERKOWITZ, and T. J. BARDOS. J. Med. Chem. **20**, 458 (1977).
29. M. BOBEK, Y. C. CHEUNG, and A. BLOCH. J. Med. Chem. **21**, 597 (1978).
30. R. K. ROBINS, E. F. GODEFROI, E. C. TAYLOR, L. R. LEWIS, and A. JACKSON. J. Am. Chem. Soc. **83**, 2574 (1961).
31. R. K. ROBINS. J. Med. Chem. **7**, 186 (1964).
32. M. D. DOWLING, JR., I. H. KRAKOFF, and D. A. KARNOFSKY. *In* Chemotherapy of cancer. *Edited by* W. H. Cole. Lea and Febiger, Philadelphia, PA. 1970. p. 1.
33. A. R. P. PATERSON and A. SUTHERLAND. Can. J. Biochem. **42**, 1415 (1964); G. D. BIRNIE, H. KROEGER, and C. HEIDELBERGER. Biochemistry, **2**, 566 (1963).
34. R. M. WHITTINGTON, S. L. RIVERS, and M. E. PATNO. Cancer Chemother. Rep. **34**, 47 (1964); I. H. KRAKOFF, R. R. ELLISON, and C. T. C. TAN. Cancer Res. **21**, 1015 (1961).
35. C. HEIDELBERGER, L. GRIESBACK, O. CRUZ, R. J. SCHNITZER, and E. GRUNBERG. Proc. Soc. Exp. Biol. Med. **97**, 470 (1958); C. HEIDELBERGER. Prog. Nucl. Acid Res. Mol. Biol. **4**, 1 (1965); A. R. CURRERI and F. J. ANSFIELD. Cancer Res. **23**, 1226 (1963).
36. N. G. BLOKHINA, E. K. VOZNY, and A. M. GARIN. Cancer, **30**, 390 (1972); N. I. KAREV, N. G. BLOKHINA, E. K. VOZNY, and M. P. PERSHIN. Neoplasma, **19**, 347 (1972); N. VALDIVIESO, G. P. BODEY, J. A. GOTTLIEB, and E. J. FREIREICH. Cancer Res. **36**, 1821 (1976).
37. A. J. LIN, R. S. BENJAMIN, P. N. RAO, and T. L. LOO. J. Med. Chem. **22**, 1096 (1979).
38. J. A. BENVENUTO, D. FARQUHAR, E. J. FREIRICH, and T. L. LOO. Proc. Am. Assoc. Cancer Res. **18**, 145 (1977).
39. (*a*) G. A. LEPAGE and M. JONES. Cancer Res. **21**, 642 (1961); (*b*) A. P. KIMBALL and G. A. LEPAGE. Cancer Res. **22**, 1301 (1962); (*c*) Proc. Am. Assoc. Cancer Res. **4**, 34 (1963).
40. G. G. KELLY, G. P. WHEELER, and J. A. MONTGOMERY. Cancer Res. **22**, 329 (1962).
41. R. W. BROCKMAN. Adv. Cancer Res. **7**, 129 (1963).
42. A. BLOCH, E. MIHICH, C. A. NICHOL, D. H. MURRAY, J. PROKOP, and R. K. ROBINS. Proc. Am. Assoc. Cancer Res. **8**, 6

(1967).
43. W. A. BOWLES, F. H. SCHNEIDER, L. R. LEWIS, and R. K. ROBINS. J. Med. Chem. **6**, 471 (1963).
44. A. BLOCH. *In* Drug design. Vol. IV. *Edited by* E. J. Ariens. Academic Press, New York, NY. 1973. Chapt. 8. p. 352.
45. W. A. SZAREK, C. DEPEW, H. C. JARRELL, and J. K. N. JONES. Chem. Commun. 648 (1975).
46. M. C. DEPEW. Ph.D. thesis, Queen's University, Kingston, Ontario, Canada, 1976.

Nucleoside analogs involving modifications in the carbohydrate ring: nuclear magnetic resonance spectroscopic studies

WALTER A. SZAREK, B. MARIO PINTO, AND MASAHARU IWAKAWA
Carbohydrate Research Institute and Department of Chemistry, Queen's University, Kingston, Ont., Canada K7L 3N6

Received October 20, 1983[1]

WALTER A. SZAREK, B. MARIO PINTO, and MASAHARU IWAKAWA. Can. J. Chem. **63**, 2162 (1985).

The concomitant use of ^{1}H nmr and ^{13}C nmr spectroscopy as a probe of structure, stereochemistry, and conformation of several nucleoside analogs derived from 1-oxa-4-thiacyclohexane is described. The ^{1}H nmr spectroscopic properties of an acyclic nucleoside analog derived from uridine are also described.

WALTER A. SZAREK, B. MARIO PINTO et MASAHARU IWAKAWA. Can. J. Chem. **63**, 2162 (1985).

On décrit l'utilisation concomitante de la spectroscopie rmn du ^{1}H et du ^{13}C comme méthode pour déterminer la structure, la stéréochimie et la conformation de plusieurs analogues nucléosides dérivant de l'oxa-1 thia-4 cyclohexane. On décrit aussi les propriétés spectroscopiques, en rmn du ^{1}H, d'un analogue acyclique nucléoside dérivé d'une uridine.

[Traduit par le journal]

Introduction

In recent years an active area of research in this laboratory has been the synthesis (1) and conformational analysis (2) of nucleoside analogs involving modifications in the carbohydrate ring. As part of this program we have recently reported (3) the synthesis and biological activity of the nucleoside analogs **1**–**12**. In this paper we describe their nuclear magnetic resonance spectroscopic properties. The concomitant use of ^{1}H nmr and ^{13}C nmr spectroscopy has proved invaluable in the proof of structure and in the investigation of stereochemistry and conformation of these compounds.

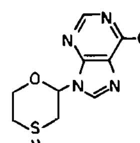

1*a, b*

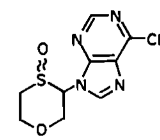

2*a, b*

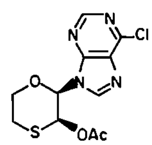

3

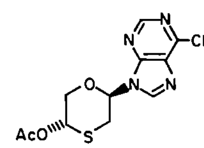

4

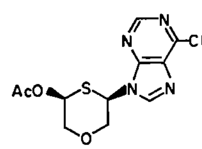

5

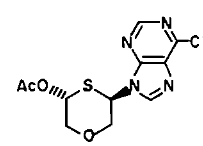

6

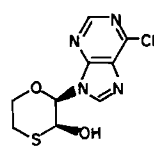

7

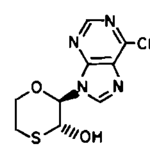

8

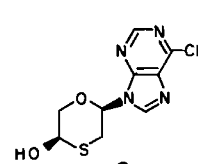

9

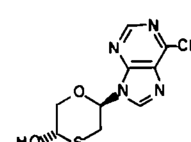

10

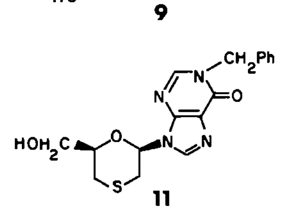

11

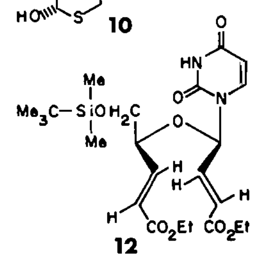

12

Results and discussion

The isomeric sulfoxides **1***a*, **1***b* were obtained by oxidation of 6-chloro-9-(1-oxa-4-thiacyclohexan-2-yl)-9*H*-purine (**13**) with sodium metaperiodate (3). The ^{1}H nmr spectrum indicated the presence of two isomeric sulfoxides in a ratio of 3.2:1, as estimated by integration of the corresponding signals for H-2′. Recrystallization from ethanol resulted in a mixture that was highly enriched in the major isomer (**1***a*). The H-2′ signal in the spectrum of **1***a* appeared as a doublet of doublets ($|J_{2',3'} + J_{2',3''}|$ = 12.7 Hz) at δ 6.53 whereas that for **1***b* appeared at δ 6.15 as a doublet of doublets ($|J_{2',3'} + J_{2',3''}|$ = 8.3 Hz). The assignment of stereochemistry and conformation in **1***a* and **1***b* was made on the basis of the signs and magnitudes of the sulfoxidation chemical-shift increments ($\Delta\delta_{H\text{-}i} = \delta_{H\text{-}i}^{S-O} - \delta_{H\text{-}i}^{S}$) of H-2′ signals in the ^{1}H nmr spectra of the two isomers. Examination of the spectra of **13** and **1***a* shows that the H-2′ signal in the spectrum of **1***a* is shifted downfield by 0.5 ppm relative to the corresponding signal in the spectrum of the sulfide **13**. This deshielding has been ascribed to electric-field effects and (or) the acetylene-like anisotropy of the S=O bond, and is consistent with a *syn*-axial relationship of H-2′ to the sulfinyl group (4–7). This assignment is supported by the observed value for $|J_{2',3'} + J_{2',3''}|$ which suggests a preponderance of the conformation in which the purine moiety is equatorially oriented. Compound **1***a* is identified, therefore, as being *trans*-6-chloro-9-(1-oxa-4-oxo-4-thiacyclohexan-2-yl)-9*H*-purine (see Fig. 1). In contrast, the H-2′ signal in the spectrum of **1***b* is shifted downfield by only 0.12 ppm relative to the corresponding signal in the spectrum of **13**, and is consistent with the assignment of the *cis*-stereochemistry to this compound. The value obtained for $|J_{2',3'} + J_{2',3''}|$ is also indicative of a preponderance of the conformer in which both the sulfinyl group and the purine moiety adopt the axial orientation (see Fig. 1). The strong preference for the axial orientation of the sulfinyl group in related sulfoxides is well documented (2*a*, 2*b*, 4–8). Compound **1***b* is identified, therefore, as being *cis*-6-chloro-9-(1-

[1] Revision received November 22, 1984.

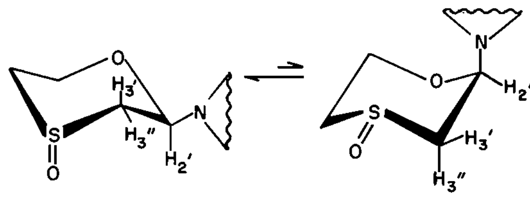

1a

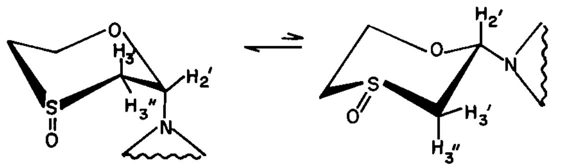

1b

FIG. 1. Conformational equilibria of the isomeric sulfoxides **1a** and **1b**.

oxa-4-oxo-4-thiacyclohexan-2-yl)-9*H*-purine. Unfortunately, the sulfoxides **1** were insufficiently soluble to permit the recording of their ^{13}C nmr spectra.

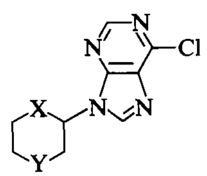

13 X = O, Y = S
14 X = S, Y = O

Oxidation of 6-chloro-9-(1-oxa-4-thiacyclohexan-3-yl)-9*H*-purine (**14**) with sodium metaperiodate (3) afforded a mixture of the isomeric sulfoxides **2a** and **2b** in a ratio of 1.2:1, as indicated by its ^1H nmr spectrum. Recrystallization from ethanol–hexane afforded white prisms which were shown by ^1H nmr spectroscopy to consist of predominantly the major isomer (**2a**); this permitted the unambiguous assignment of signals to the two isomers **2a** and **2b** in the ^1H nmr and ^{13}C nmr spectra of the isomeric mixture of sulfoxides. The H-3′ signal in the spectrum of **2a** appeared as a doublet of doublets ($|J_{3',2'} + J_{3',2''}| = 14.1$ Hz) at δ 5.99 whereas the corresponding signal in the spectrum of **2b** appeared as a doublet of doublets ($|J_{3',2'} + J_{3',2''}| = 10.5$ Hz) at δ 5.58. The observed value of $|J_{3',2'} + J_{3',2''}|$ in the spectrum of **2a** is most certainly indicative of a conformation in which the purine moiety is almost exclusively equatorially oriented whereas that observed for **2b** suggests a preponderance of a conformation in which the purine moiety is equatorial, although not nearly to the extent as is present in **2a**. It is noteworthy that the H-3′ signal in the ^1H nmr spectrum of **2a** is shifted downfield by 0.42 ppm relative to the corresponding signal in the spectrum of the parent sulfide (**14**) whereas the H-3′ signal in the spectrum of **2b** appears at virtually the same chemical shift as that in the spectrum of **14**. Examination of the ^{13}C nmr spectrum of **2a** indicates that C-2′ and C-6′ are shielded by ~10 ppm and C-3′ and C-5′ are deshielded by 12.7 ppm and 20.7 ppm, respectively, relative to the corresponding carbons in the parent sulfide **14** (see Table 1). The magnitude of the shielding of the β-carbons in six-membered, cyclic sulfoxides relative to those in the corresponding sulfides is associated with an axial disposition of the sulfinyl oxygen in the sulfoxides (**2a**, **2b**, 7–9). The ^{13}C nmr data for **2a** are consistent, therefore, with the preponderance of a conformation in which the sulfinyl group is axially disposed, and compound **2a** is identified as being *cis*-6-chloro-9-(1-oxa-4-oxo-4-thiacyclohexan-3-yl)-9*H*-purine (see Fig. 2). Consequently, compound **2b** is assigned the *trans* stereochemistry. Examination of the ^{13}C nmr spectrum of **2b** shows that C-2′ and C-6′ are shielded by ~7 ppm and C-3′ and C-5′ are deshielded by 18.6 ppm and 23.3 ppm, respectively, relative to the corresponding carbons in **14** (Table 1). The lesser shielding of C-2′ and C-6′ in **2b** as compared to that in **2a** (relative to C-2′ and C-6′ in **14**) can be taken as evidence for a lesser proportion of the conformation in which the sulfinyl group is axial in the former case. It should be noted that the equatorial disposition of the sulfinyl group in six-membered, cyclic sulfoxides also results in shielding of the β-carbons relative to those in the parent sulfides, although the magnitude of the shielding is considerably smaller than that observed in the corresponding systems having axially-disposed sulfinyl groups (7–9). It is not clear whether this is yet another example of shielding as a result of a γ-*anti* substituent effect (10, 11). Additional information about the conformational behaviour of **2b** may be obtained by comparison of the chemical-shift differences of the signals for

TABLE 1. Carbon-13 chemical-shift data[a] for saturated-ring carbons in 6-chloropurin-9-yl derivatives of 1-oxa-4-thiacyclohexane and 1-oxa-4-thiacyclohexane 1-oxide

	Carbon			
Compound[b]	C-2′	C-3′	C-5′	C-6′
14	71.1	49.4	24.1	68.1
2a	60.8	62.1	44.8	57.4
2b	64.1	68.0	47.4	61.3

[a] In ppm downfield from internal TMS; the spectrum of **14** was obtained in chloroform-*d* solution; the spectra of **2a**, **2b** were obtained in dimethylsulfoxide-d_6 solution.

[b] Chemical-shift data for 1,4-oxathiane are as follows: δ_{CDCl_3} 27.0 (C-3, C-5), 68.5 (C-2, C-6); corresponding data for 1,4-oxathiane 4-oxide are: δ_{CDCl_3} 46.2 (C-3, C-5), 59.0 (C-2, C-6) (2a).

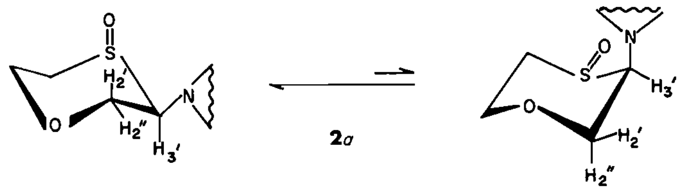

2a

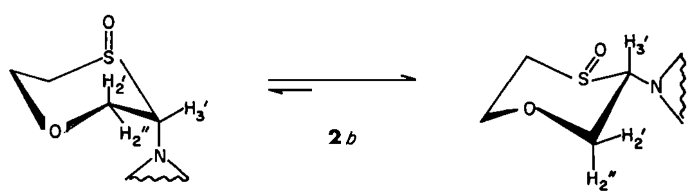

2b

FIG. 2. Conformational equilibria of the isomeric sulfoxides **2a** and **2b**.

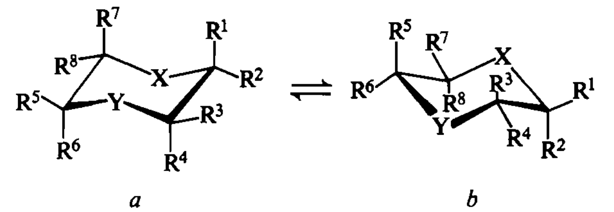

3	R^1 = 6-chloropurin-9-yl;	R^3 = OAc;	X = O;	Y = S
15	R^1 = 6-chloropurin-9-yl;	R^4 = OAc;	X = O;	Y = S
4	R^1 = 6-chloropurin-9-yl;	R^6 = OAc;	X = O;	Y = S
16	R^1 = 6-chloropurin-9-yl;	R^5 = OAc;	X = O;	Y = S
5	R^2 = 6-chloropurin-9-yl;	R^8 = OAc;	X = S;	Y = O
6	R^2 = 6-chloropurin-9-yl;	R^7 = OAc;	X = S;	Y = O
7	R^1 = 6-chloropurin-9-yl;	R^3 = OH;	X = O;	Y = S
8	R^1 = 6-chloropurin-9-yl;	R^4 = OH;	X = O;	Y = S
9	R^1 = 6-chloropurin-9-yl;	R^5 = OH;	X = O;	Y = S
10	R^1 = 6-chloropurin-9-yl;	R^6 = OH;	X = O;	Y = S

All other substituents, R = H

FIG. 3. Possible configurational and conformational isomers of 6-chloro-9-(3-acetoxy-1-oxa-4-thiacyclohexan-2-yl)-9*H*-purine (**3***a* and **3***b*, **15***a* and **15***b*), 6-chloro-9-(5-acetoxy-1-oxa-4-thiacyclohexan-2-yl)-9*H*-purine (**4***a* and **4***b*, **16***a* and **16***b*), 6-chloro-9-(5-acetoxy-1-oxa-4-thiacyclohexan-3-yl)-9*H*-purine (**5***a* and **5***b*, **6***a* and **6***b*), 6-chloro-9-(3-hydroxy-1-oxa-4-thiacyclohexan-2-yl)-9*H*-purine (**7***a* and **7***b*, **8***a* and **8***b*), and 6-chloro-9-(5-hydroxy-1-oxa-4-thiacyclohexan-2-yl)-9*H*-purine (**9***a* and **9***b*, **10***a* and **10***b*).

the β-carbons in the isomeric sulfoxides, **2***a* and **2***b*, with the corresponding differences in appropriate isomeric sulfoxides. Thus, for example, $\Delta\delta_{C\text{-}6'}$ is 3.9 ppm for **2***a* and **2***b* whereas the corresponding chemical-shift difference for the C-2 or C-6 signals in the spectra of axial and equatorial 1,4-oxathiane 4-oxides is 7.02 ppm (8), and the chemical-shift difference for the C-2 signals in the spectra of *trans*-hexahydro-1,4-benzoxathiane 4-oxides is 5.96 ppm (7). This evidence suggests that *trans*-6-chloro-9-(1-oxa-4-oxo-4-thiacyclohexan-3-yl)-9*H*-purine (**2***b*) exists as a mixture of conformers which contains a significant amount of the conformer in which the sulfinyl moiety is axially oriented (see Fig. 2). It is possible to estimate approximately the extent of this equilibrium provided that values of $|J_{2',3'} + J_{2'',3'}|$ in conformationally-locked systems are available. Using approximate values for $|J_{2',3'} + J_{2'',3'}|$ for the two conformations in which the purine moiety is either axial or equatorial (2*c*), one estimates that **2***b* exists in the conformation in which the purine moiety and sulfinyl group are both equatorial to the extent of 63%. The slight equatorial preference of the purine moiety in **2***b* and the almost exclusive equatorial orientation of the purine moiety in **2***a* contrast with the conformational behaviour of the parent sulfide (**14**). The latter compound exhibits a marked preference for the conformation in which the purine moiety is axial (89%) (2*c*).

The acetoxy derivatives **3** and **4** were obtained from the Pummerer reaction of the isomeric sulfoxides **1** (3); their constitution and stereochemistry were established as follows. The ^{1}H nmr spectrum of the major product of the reaction, **3**, showed the presence of two mutually-coupled doublets at δ 6.13 and δ 6.29 (J = 5.6 Hz), a result that is consistent with the presence of the acetoxy group at the 3′-position. The value of $J_{2',3'}$ further suggests that compound **3** is unlikely to exist to a great extent in a conformation in which H-2′ and H-3′ are *trans*-diaxially disposed (see **15***a* and **15***b* in Fig. 3). The possible configurational and conformational isomers for **3** are shown in Fig. 3. Examination of the ^{13}C nmr spectral data (Table 2) for **3** permitted the assignment of stereochemistry and preferred conformation. The chemical-shift assignments were facilitated by consideration of the substitutent effects on the ^{13}C chemical shifts in related compounds (2) and by means of gated-decoupling experiments. One would anticipate that a preferred conformation in which the acetoxy group was axially oriented would be manifested in a shielding of C-5′ by virtue of a γ-*gauche* interaction (2, 12). The data presented in Table 2 indicate that the signal for C-5′ in the spectrum of **3** appears at virtually the same chemical shift as the corresponding signal in the spectrum of **13**. This result is, therefore, inconsistent with the preference for a conformation in which the acetoxy group is axially disposed. Furthermore, the signal for C-6′ in the spectrum of **3** is shifted upfield by 4.32 ppm relative to the corresponding signal in the spectrum of **13**. This may be attributed to a γ-*gauche* interaction between the purine moiety and C-6′ (2, 12) in **3**. In contrast, the signal for C-6′ in the spectrum of **13** (which has been shown (2) to exist preponderantly in the conformation in which the purine moiety is equatorial) is shifted downfield by 1.7 ppm relative to C-2 and C-6 in 1,4-oxathiane. Compound **3** is assigned, therefore, a preponderant conformation in which the acetoxy group is equatorial and the purine moiety is axial (see **3***a*), and is identified as being *cis*-6-chloro-9-(3-acetoxy-1-oxa-4-thiacyclohexan-2-yl)-9*H*-purine. It is noteworthy that the conformational preference of the purine moiety in **3** contrasts with that observed for **13** in which the purine moiety is predominantly equatorial (2), and the conformational preference of the acetoxy group contrasts with previous examples of the anomeric effect in sulfur heterocycles (13–15). However, the preference for a *gauche* arrangement of atoms within the 1,2-disubstituted ethane-type fragment is maintained.

TABLE 2. Carbon-13 chemical-shift data[a] for saturated-ring carbons in 6-chloropurin-9-yl derivatives of some substituted 1-oxa-4-thiacyclohexanes

	Carbon			
Compound	C-2′	C-3′	C-5′	C-6′
13	82.0	31.1	25.9	70.2
3	81.35	68.47	25.69	65.88
4	77.72	67.37	25.89	65.23

[a] In ppm downfield from internal TMS in chloroform-*d*.

The structure of the second acetoxy derivative **4** was deduced in an analogous manner to that described above. The ^{1}H nmr spectrum of **4** showed the presence of two ABX systems, a result that is consistent only with the presence of the acetoxy group at the 5′-position. The possible configurational and conformational isomers for a 5′-acetoxy derivative are shown in Fig. 3. Examination of the ^{1}H nmr spectrum of **4** indicated that the signals for the methine protons appeared as triplets at δ 5.69 ($|J_{AX} + J_{BX}|$ = 6.75 Hz) and δ 6.36 ($|J_{AX} + J_{BX}|$ = 8.25 Hz). Since the signals for the methylene protons are readily assigned to H-3′, H-3″ and H-6′, H-6″, the signals at δ 5.79 and δ 6.36 are assigned to H-5′ and H-2′, respectively, on the basis of the difference in coupling constants between these protons and the corresponding methylene protons. Furthermore, examination of the AB portions of both ABX patterns indicates that all of the coupling constants to H-5′ or H-2′ are small (2.75–4.5 Hz). This suggests a preponderance of a conformation in which both methine protons are equatorially oriented (see **4***a* in Fig. 3); the conclusion is supported by the values of $|J_{2',3'} + J_{2',3''}| = 8.25$ Hz and $|J_{5',6'} + J_{5',6''}| = 6.75$ Hz (2*c*). Compound **4** is assigned, therefore, a preferred conformation in which both the acetoxy group and the purine moiety are axially disposed, and is identified as being *trans*-6-chloro-9-(5-acetoxy-1-oxa-4-thiacyclohexan-2-yl)-9*H*-purine. The assignment is further corroborated by the ^{13}C nmr data for **4** which are presented in Table 2; the chemical shift assignments were made as previously described. Thus, the signals for C-3′ and C-6′ in the spectrum of **4** are shifted upfield by 5.2 ppm and 5.0 ppm, respectively, relative to the corresponding signals in the spectrum of **13**. This result is consistent with the axial orientation of both the acetoxy group and the purine moiety, a situation which should be manifested in a shielding of C-3′ and C-6′, respectively, by virtue of the γ-*gauche* interactions (2, 12). The axial preference of the purine moiety in **4** contrasts with that observed for **13** in which the purine moiety adopts an equatorial orientation in the preferred conformation, but the axial preference of the acetoxy group is consistent with expectations based on knowledge of the anomeric effect in sulfur heterocycles (13–15).

The structures of the acetoxy derivatives **5** and **6**, obtained from the isomeric sulfoxides **2** (3), were deduced as follows. The possible configurational and conformational isomers are shown in Fig. 3. Examination of the ^{1}H nmr spectrum of the less polar (tlc) of the two acetoxy derivatives indicated that the signals for H-3′ and H-5′ overlapped to give a narrow multiplet at δ 5.75 whose width at half-height was 7 Hz. The value of $W_{1/2}$ is indicative of a preponderance of a conformation in which both H-3′ and H-5′ are equatorially oriented. This component is assigned, therefore, the *cis*-stereochemistry (see **5***b* in Fig. 3) and is identified as being *cis*-6-chloro-9-(5-acetoxy-1-oxa-4-thiacyclohexan-3-yl)-9*H*-purine (**5**). The more polar of the two acetoxy compounds is assigned, consequently, the *trans*-stereochemistry. The signal for H-3′ in the ^{1}H nmr spectrum of this component appears at δ 5.79 as a triplet whose width at half-height ($|J_{3',2'} + J_{3',2''}|$) is 4.5 Hz whereas the signal for H-5′ appears at δ 6.19 as a doublet of doublets ($|J_{5',6'} + J_{5',6''}| = 12.6$ Hz). The values of $|J_{AX} + J_{BX}|$ are indicative of a preponderance of a conformation in which the acetoxy group is equatorial and the purine moiety is axial (see **6***b* in Fig. 3) and are consistent, therefore, with the assignment of the *trans*-stereochemistry to this compound. The assignment is further corroborated by the ^{13}C nmr data for this compound. The ^{13}C nmr spectrum shows a signal at δ 49.18 and three signals at δ 71.12, 70.73, and 70.15 for the saturated-ring carbons. The signal at δ 49.18 is assigned to C-3′ by analogy with the chemical shift of C-3′ (δ 49.4) in the spectrum of **14** (2) but the latter group of signals could not be assigned to the respective carbons with certainty. However, it is obvious that the signal for C-2′ appears at virtually the same chemical shift as does the corresponding signal (δ 71.1) in the spectrum of **14**. This is consistent with a preponderant conformation in which the acetoxy group is equatorial since an axial orientation of the 5′-acetoxy substituent would be expected to be manifested in an upfield shift of the C-2′ signal by virtue of the γ-*gauche* effect (2, 12). The more polar of the two acetoxy compounds is identified, therefore, as being *trans*-6-chloro-9-(5-acetoxy-1-oxa-4-thiacyclohexan-3-yl)-9*H*-purine (**6***b*). It is noteworthy that the purine moiety adopts an axial orientation in the preponderant conformations of both **5** and **6**, a preference that is also manifested in the predominant conformation of the parent compound **14**.

Treatment of the acetate **3** with sodium borohydride (3) afforded a mixture of *cis*- and *trans*-6-chloro-9-(3-hydroxy-1-oxa-4-thiacyclohexan-2-yl)-9*H*-purine, **7** and **8**, respectively. The possible configurational and conformational isomers for the 3′-hydroxy derivative are shown in Fig. 3. The elucidation of stereochemistry and preferred conformations of **7** and **8** was effected in the following manner. Examination of the ^{1}H nmr spectrum that was obtained in chloroform-*d* containing a trace of deuterium oxide, at 300 K, revealed the presence of two sets of signals corresponding to the methine hydrogens in **7** and **8**, one set being of greater intensity than the other (3.25:1). The signals attributable to the major isomer appeared as a broadened singlet at δ 4.98 and a doublet at δ 6.28 ($J = 1.2$ Hz) whereas the corresponding signals for the minor isomer appeared as two mutually-coupled doublets at δ 5.34 and δ 5.87 with a coupling constant of 8 Hz. The value of 8 Hz obtained for $|J_{2',3'}|$ in the minor isomer is indicative of a preponderant conformation in which H-2′ and H-3′ are *trans*-diaxially disposed (see **8***b* in Fig. 3). The minor isomer is identified, therefore, as being *trans*-6-chloro-9-(3-hydroxy-1-oxa-4-thiacyclohexan-2-yl)-9*H*-purine (**8**). The major isomer must be, therefore, *cis*-6-chloro-9-(3-hydroxy-1-oxa-4-thiacyclohexan-2-yl)-9*H*-purine (**7**) (the magnitude of $|J_{2',3'}|$ in this isomer is unusually small for J_{ae} coupling). When the ^{1}H nmr spectrum of the mixture of alcohols was obtained in dimethylsulfoxide-d_6 instead of chloroform-*d*, at 300 K, the ratio of the two isomers **7**:**8** was observed to change to a value of 1.3:1, thereby suggesting that equilibration of the two isomers was taking place by way of the intermediate aldehyde. Moreover, the spectrum of the mixture that was obtained in dimethylsulfoxide-d_6 at 340 K indicated the presence of **7** and **8** in a ratio of 2.6:1.

TABLE 3. Carbon-13 chemical-shift data[a] for saturated-ring carbons in 6-chloropurin-9-yl derivatives of hydroxy-substituted 1-oxa-4-thiacyclohexanes

	Carbon			
Compound	C-2′	C-3′	C-5′	C-6′
7	83.74	67.50	20.77	70.86
8	86.33	69.38	28.60	69.76
9	81.48	24.53	66.01	75.20
10	80.44	28.41	68.22	72.61

[a]In ppm downfield from internal TMS in dimethylsulfoxide-d_6.

The carbon-13 nmr data for the saturated-ring carbons in **7** and **8** are presented in Table 3. The ^{13}C nmr spectrum, obtained in dimethylsulfoxide-d_6 at 300 K, showed the presence of two sets of peaks in a ratio of ~1:1. Chemical-shift assignments were facilitated by obtaining the spectrum in a mixture of chloroform-*d* and dimethylsulfoxide-d_6 in which the ratio of **7**:**8** was found to be 2:1. (The compounds were insufficiently soluble in chloroform-*d* alone to permit the recording of the ^{13}C spectrum in this solvent.) The chemical-shift assignments were confirmed by means of gated-decoupling experiments. Inspection of the ^{13}C nmr data for **7** (Table 3) and **13** (Table 2) indicates that the signal for C-5′ in the spectrum of **7** is shifted upfield by 5.1 ppm relative to the corresponding signal in the spectrum of **13**. This is consistent with a preponderant conformation in which the hydroxyl group is axial (see **7***b* in Fig. 3) since a shielding of C-5′ in **7***b* as compared to C-5′ in **13**, by virtue of the γ-*gauche* effect, would then be predicted. The nearly identical chemical shifts of the C-6′ signals in the spectra of **7** and **13** also suggest that the purine moiety is equatorial

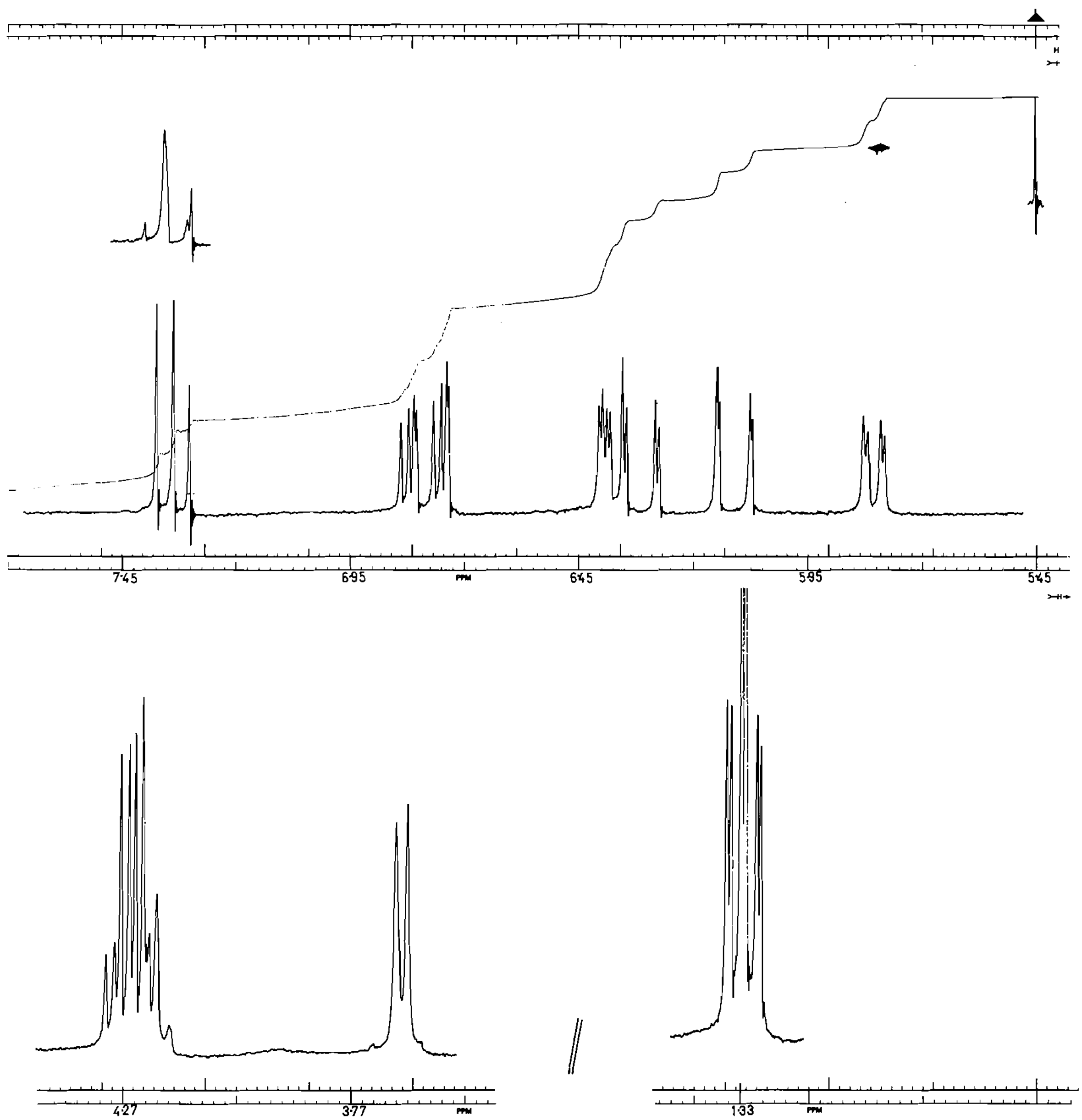

FIG. 4. The ^{1}H nmr spectrum of **12** recorded at 220 MHz in chloroform-*d*.

in the preferred conformation. The ^{13}C nmr data, therefore, support the earlier assignment of *cis*-stereochemistry in the major isomer. Similarly, the ^{13}C nmr data for **8** are also consistent with the assignment of a predominant conformation in which both the hydroxyl group and the purine moiety are equatorially oriented. For instance, the signal for C-6′ in the spectrum of **8** appears at virtually the same chemical shift as the corresponding signal in the spectrum of **13**, thereby suggesting an equatorial orientation of the purine moiety in the preferred conformation. It should be noted, however, that C-5′ in **8** is deshielded by 2.7 ppm relative to C-5′ in **13**. This result remains an anomaly in view of what is known about the γ-*anti* substituent effect in related systems (11, 16). Of particular relevance is the fact that C-5 in 2-methyl-1,4-dioxane-*2a,3e*-diol (in which the 3-OH group is *anti* to C-5) is shielded by 1.8 ppm relative to C-2 in 1,4-dioxane (16).

It is interesting to note that the *cis*-isomer **7** is preferred over the *trans*-isomer **8**. It is possible that this preference is brought about by the manifestation of the reverse anomeric effect which favours the equatorial orientation of the purine moiety, the anomeric effect which favours the axial orientation of the hydroxyl group, and an attractive *gauche* effect within the 1,2-disubstituted ethane-type fragment. Since all three conformational effects (2*b*, *c*) act in such a manner as to stabilize **7***b*, it would be the preferred conformation. However, by use of similar arguments it would also have been predicted that the corresponding acetoxy derivative **3** would exist preferentially in a conformation in which the purine moiety was equatorial and the acetoxy group was axial. As described earlier, exactly the opposite conformational behaviour was observed for **3**. The conformational preference of the *trans*-3′-hydroxy derivative **8** reflects the strong preference of the purine moiety to adopt an equatorial orientation, a preference that overrides the anomeric effect at the hemiacetal centre.

Treatment of the regioisomeric acetate **4** with sodium borohydride (3) afforded a mixture of *cis*- and *trans*-6-chloro-9-(5-

hydroxy-1-oxa-4-thiacyclohexan-2-yl)-9*H*-purine, **9** and **10**, respectively. The possible configurational and conformational isomers for the 5′-hydroxy derivative are shown in Fig. 3. Examination of the [1]H nmr spectrum of the mixture that was obtained in chloroform-*d* at 300 K indicated the presence of only one isomer. Thus, the signal for H-5′ appeared as a poorly resolved multiplet at δ 4.85 ($|J_{5',6'} + J_{5',6''}|$ = 5 Hz) and the signal for H-2′ appeared as a doublet of doublets at δ 6.13 ($|J_{2',3'} + J_{2',3''}|$ = 12.7 Hz). The values of $|J_{AX} + J_{BX}|$ are consistent with the predominance of a conformation in which the purine moiety is equatorial and the hydroxyl group is axial (see **9***b* in Fig. 3). Once again, the conformational preference is consistent with that which would be predicted on the basis of the reverse anomeric effect and the anomeric effect. This isomer is identified, therefore, as being *cis*-6-chloro-9-(5-hydroxy-1-oxa-4-thiacyclohexan-2-yl)-9*H*-purine (**9**). In contrast, the [1]H nmr spectrum of the mixture in dimethylsulfoxide-d_6 containing deuterium oxide, at 300 K, indicated the presence of two isomers, **9** and **10**, in a ratio of 2.7:1. The signal for H-5′ in the minor isomer **10** appeared as a doublet of doublets at δ 4.97 ($|J_{5',6'} + J_{5',6''}|$ = 10.7 Hz) and the signal for H-2′ appeared as a multiplet at 6.18 that was partially obscured by the signal for H-2′ of the *cis*-isomer **9**. The value for $|J_{2',3'} + J_{2',3''}|$ was estimated, consequently, as being approximately 9 Hz. The values of $|J_{AX} + J_{BX}|$ suggest that there is a predominance of the conformation in which both the purine moiety and the hydroxyl group are equatorial (see **10***b* in Fig. 3), although there is a significant contribution to the conformational equilibrium from the alternate conformation **10***a*. Thus, in the case of **10**, the reverse anomeric effect and anomeric effect oppose one another in exerting their influence on the conformational preference. Compound **10** is identified, therefore, as being *trans*-6-chloro-9-(5-hydroxy-1-oxa-4-thiacyclohexan-2-yl)-9*H*-purine. The [1]H nmr spectra in dimethylsulfoxide-d_6 at higher temperatures showed slight changes in the ratio of *cis*- and *trans*-isomers as well as slight changes in the positions of the conformational equilibria of the two isomers.

The carbon-13 nmr data for the isomeric hydroxy derivatives **9**, **10** are presented in Table 3. Comparison of the [13]C nmr data for **9** and for **13** (Table 2) indicates that the C-3′ in **9** experiences a shielding of 6.6 ppm relative to C-3′ in the parent compound **13**. The shielding is attributable to a γ-*gauche* interaction and is consistent, therefore, with the previous assignment of the hydroxyl group being in the axial orientation in the preferred conformation of **9**. The assignment of the conformational behaviour of the *trans*-isomer **10** on the basis of [1]H nmr spectroscopic evidence is further supported by the [13]C nmr data for **10**. For instance, the signal for C-3′ in the spectrum of **10** is shifted upfield by 2.7 ppm relative to the corresponding signal in the spectrum of **13**. The magnitude of the shielding can be attributed to the operation of the γ-*anti* substituent effect of the hydroxyl group in conformation **10***b* (11, 16). For example, examination of the [13]C nmr data for methyl-substituted derivatives of 1,4-dioxacyclohexane-2,3-diols (16) indicates that the γ-*anti* substituent effect of hydroxyl, acting across the ring oxygen atom, is shielding by 1.8 ppm. Should conformation **10***a* exist to an appreciable extent in the conformational equilibrium, there would result also a shielding of C-3′ in **10** relative to that in **13** by virtue of the γ-*gauche* effect. Thus, the overall effect of having a conformational equilibrium which is biased in favour of **10***b* but which contains an appreciable amount of **10***a* should be manifested in a slight shielding of C-3′ in **10** relative to C-3′ in **13**. The shielding of C-6′ in **10** relative to C-6′ in **9** can also be taken as evidence for the presence of a significant amount of **10***a* in the conformational equilibrium, given that **9** exists almost exclusively in conformation **9***b* and assuming that the magnitudes of the γ-*anti* substituent effects in **9***b* and **10***b* are approximately equal.

Since the parent nucleoside analogs **13** and **14** that were used for the elaboration of the substituted compounds, as discussed in the preceding section, were racemic mixtures, it follows that the compounds derived from **13** and **14** will also be mixtures of enantiomers. In the preceding discussion, only one enantiomeric form for each of **1**–**10** has been shown; however, these structures should be viewed as enantiomeric pairs of compounds. It should be noted also that chair conformations have been assumed to be the most stable conformations of the 6-chloropurin-9-yl derivatives described in the preceding sections, although it is recognized that bond-angle and torsional-angle distortion will undoubtedly be present in these compounds and will result, consequently, in some distortion of the six-membered ring.

It is clear from the preceding section that the concomitant use of [1]H nmr and [13]C nmr spectroscopy provides an extremely useful tool for the investigation of stereochemistry and conformation in substituted 1,4-diheterocyclohexanes. In particular, it should be noted that substituent effects on [13]C shieldings in substituted diheterocyclohexanes are at least qualitatively the same as in substituted cyclohexanes, as indicated also by the work of Ayras (16) on substituted 1,4-dioxanes. The use of the γ-*gauche* and γ-*anti* substituent effects as probes of stereochemistry and conformation is especially noteworthy.

The structure of compound **11** was unambiguously assigned by complete assignment of its [1]H nmr spectrum recorded in chloroform-*d* at 220 MHz (3). The values of $|J_{2',3'} + J_{2',3''}|$ (12.6 Hz) and $J_{5'a,6'}$ (11 Hz) leave no doubt that compound **11** exists in a conformation in which both the purine moiety and the hydroxymethyl function adopt equatorial orientations. The (2′*R*,6′*R*) stereochemistry is consistent with retention of configuration at these centres in the course of the reactions (3).

The partial [1]H nmr spectrum of **12** recorded at 220 MHz in chloroform-*d* is shown in Fig. 4. Chemical-shift assignments were readily made by first-order analysis of the spectrum and by matching of signals attributable to mutually-coupled protons; the assignments have been documented previously (3). An interesting feature of the spectrum is the appearance of the H-6 signal of the uracil moiety as a doublet of doublets. There is no doubt about the assignment since decoupling of this signal resulted in collapse of the low field doublet appearing at δ 7.35; the latter signal is assigned to H-5 of the uracil moiety. The coupling of 2 Hz in the signal for H-6 is attributed, therefore, to long-range four-bond coupling interactions between H-4′ and H-6; the signal for H-4′ at δ 6.39 also shows a coupling of 2 Hz. Long-range four-bond coupling interactions between H-8′ and H-6′ ($^4J_{8',6'}$ = 1.1 Hz) and between H-2′ and H-4′ ($^4J_{2',4'}$ = 1.1 Hz) are also observed. The [1]H nmr spectrum further indicates that $J_{2',3'}$ and $J_{7',8'}$ are about 16 Hz; this value is typical for coupling of olefinic protons having an *anti* relationship to one another (17). Compound **12** is identified, therefore, as being the (2*E*,7*E*), (4*R*,6*S*) isomer.

Experimental

All compounds were prepared as described previously (3). Proton magnetic resonance ([1]H nmr) spectra were recorded on a Bruker HX-60 or Varian HR-220 spectrometer. Carbon-13 magnetic resonance ([13]C nmr) spectra were recorded on a Bruker HX-60 spectrometer equipped with a FT60M Fourier transform accessory at 15.09 MHz. Chemical shifts are given in ppm downfield from tetramethylsilane (TMS). The complete nmr spectral data have been previously documented (3).

Acknowledgements

The authors are grateful to Dr. A. A. Grey of the Canadian 220 MHz NMR Centre for his cooperation in the acquisition of ^{1}H nmr spectra at 220 MHz. Financial assistance from NSERC Canada in the form of grants (to W.A.S.) and a scholarship (to B.M.P.) is gratefully acknowledged. The authors also wish to thank Queen's University for financial support.

1. (*a*) D. M. VYAS and W. A. SZAREK. Carbohydr. Res. **30**, 225 (1973); (*b*) W. A. SZAREK, D. M. VYAS, and B. ACHMATOWICZ. J. Heterocycl. Chem. **12**, 123 (1975); (*c*) B. M. PINTO, D. M. VYAS, and W. A. SZAREK. Can. J. Chem. **55**, 937 (1977); (*d*) M. IWAKAWA, B. M. PINTO, and W. A. SZAREK. Can. J. Chem. **56**, 326 (1978); (*e*) L. J. J. HRONOWSKI and W. A. SZAREK. J. Med. Chem. **25**, 522 (1982).
2. (*a*) W. A. SZAREK, D. M. VYAS, A.-M. SEPULCHRE, S. D. GERO, and G. LUKACS. Can. J. Chem. **52**, 2041 (1974); (*b*) W. A. SZAREK, D. M. VYAS, and B. ACHMATOWICZ. Tetrahedron Lett. 1553 (1975); (*c*) B. M. PINTO. Ph.D. Thesis, Queen's University, Kingston, Ontario, Canada, 1980.
3. W. A. SZAREK, B. M. PINTO, and M. IWAKAWA. Can. J. Chem. **63**, 2149 (1985).
4. E. JONSSON. Ark. Kemi, **26**, 357 (1967).
5. D. N. HARPP and J. G. GLEASON. J. Org. Chem. **36**, 1314 (1971).
6. A. B. FOSTER, Q. H. HASAN, D. R. HAWKINS, and J. M. WEBBER. Chem. Commun. 1084 (1968); A. B. FOSTER, T. D. INCH, M. H. QADIR, and J. M. WEBBER. Chem. Commun. 1086 (1968).
7. D. M. FRIEZE, P. F. HUGHES, R. L. MERRILL, and S. A. EVANS, JR. J. Org. Chem. **42**, 2206 (1977).
8. D. M. FRIEZE and S. A. EVANS, JR. J. Org. Chem. **40**, 2690 (1975).
9. G. W. BUCHANAN, J. B. STOTHERS, and G. WOOD. Can. J. Chem. **51**, 3746 (1973); N. K. WILSON and J. B. STOTHERS. Top. Stereochem. **8**, 1 (1974).
10. E. L. ELIEL, W. F. BAILEY, L. D. KOPP, R. L. WILSON, D. M. GRANT, R. BERTRAND, K. A. CHRISTENSEN, K. D. DALLING, H. W. DUCH, E. WENKERT, F. M. SCHELL, and D. W. COCHRAN. J. Am. Chem. Soc. **97**, 322 (1975).
11. T. P. FORREST and J. G. K. WEBB. Org. Magn. Reson. **12**, 371 (1979).
12. D. M. GRANT and B. V. CHENEY. J. Am. Chem. Soc. **89**, 5315 (1967).
13. N. S. ZEFIROV and I. V. KAZIMIRCHIK. Russ. Chem. Rev. **43**, 107 (1974).
14. M. OKI, T. SUGAWARA, and H. IWAMURA. Bull. Chem. Soc. Jpn. **47**, 2457 (1974); T. SUGAWARA, H. IWAMURA, and M. OKI. Bull. Chem. Soc. Jpn. **47**, 1496 (1974).
15. A. J. DE HOOG. Ph.D. Thesis, University of Leiden, 1971.
16. P. AYRAS. Org. Magn. Reson. **11**, 152 (1978).
17. L. M. JACKMAN and S. STERNHELL. Applications of nuclear magnetic resonance spectroscopy in organic chemistry. 2nd ed. Pergamon Press, London. 1969. p. 301.

The structure and resonance Raman spectra – structure correlations for N-benzoyl-DL-alanine ethyl dithioester[1]

R. H. ANGUS, P. R. CAREY,[2] H. LEE, A. C. STORER, AND K. I. VARUGHESE
Division of Biological Sciences, National Research Council of Canada, Ottawa, Ont., Canada K1A 0R6

Received August 9, 1984

R. H. ANGUS, P. R. CAREY, H. LEE, A. C. STORER, and K. I. VARUGHESE. Can. J. Chem. **63**, 2169 (1985).

An X-ray crystallographic analysis of *N*-benzoyl-DL-alanine ethyl dithioester demonstrates that it takes up a *B*-type conformation comparable to that found for *N*-acylglycine dithioesters in the crystalline state. *B*-conformations are characterized by small N—C—C—S(thiol) torsional angles resulting from an N···S(thiol) interaction. In the present case the N—C—C—S torsional angle is −23° and the N···S distance 2.830 Å. A Raman spectroscopic study of a single crystal and a resonance Raman (RR) spectroscopic study of powdered *N*-benzoyl-DL-alanine ethyl dithioester establish the RR signature for the compound in its *B*-form. The RR spectra of the dithioester in CCl_4 and H_2O/CH_3CN, aided by $^{13}C{=}S$ substitution, provide information on the RR signatures of *B, A,* and C_5 type conformers in solution. The *A* and C_5 signatures for the *N*-acylalanine dithioester resemble closely those for an *N*-acylglycine dithioester but the *B* signature is perturbed markedly compared to that of a glycine analog.

R. H. ANGUS, P. R. CAREY, H. LEE, A. C. STORER, and K. I. VARUGHESE. Can. J. Chem. **63**, 2169 (1985).

Une analyse des données cristallographiques obtenues par diffraction des rayons-X sur le dithioester éthylique de la *N*-benzoyl DL-alanine démontre que ce composé existe sous une conformation du type *B* comparable à celle, trouvée à l'état cristallin, des dithioesters de la *N*-acylglycine. Les conformations de type *B* sont caractérisées par de petits angles de torsion N—C—C—S(thiol) qui proviennent d'une interaction N···S(thiol). Dans le cas présent, l'angle de torsion N—C—C—S est égal à −23° et la distance N···S est égale à 2,830 Å. Une étude par spectroscopie Raman sur un cristal unique et une étude par spectroscopie Raman de résonance (RR) sur le dithioester éthylique de la *N*-benzoyl DL-alanine en poudre ont permis d'établir la signature RR du composé sous sa forme *B*. Les spectres RR du dithioester, dans le CCl_4 ainsi que dans un mélange H_2O/CH_3CN, couplés à des substitutions $^{13}C{=}S$ ont permis d'obtenir de l'information sur les signatures RR des conformères des types *B, A* et C_5 en solution. Les signatures des conformations *A* et C_5 du dithioester de la *N*-acylalanine ressemblent beaucoup à celles d'un dithioester de la *N*-acylglycine; toutefois la signature de la conformation *B* diffère passablement de celle de l'analogue de la glycine.

[Traduit par le journal]

Introduction

By reacting thionoesters, of the form $RC({=}O)NHCH_2C({=}S)OCH_3$, with cysteine proteinases such as papain it is possible to generate transient acyl–enzyme intermediates $RC({=}O)NHCH_2({=}S)S$-papain, where the substrate is linked to the enzyme by the thiol sulfur of cysteine 25. These intermediates have an intense electronic absorption band near 315 nm due to the dithioester chromophore that affords the opportunity of obtaining the resonance Raman (RR) spectrum of the dithioester group and the adjacent bonds (1). Thus, we are able to observe the vibrational spectrum of the group undergoing transformation in the active site and, by combining RR and other techniques, arrive at a detailed description of conformational events during enzymolysis.

Interpretation of the RR spectra of the enzyme–substrate intermediates has been greatly facilitated by joint Raman X-ray crystallographic studies on model compounds of the type $RC({=}O)NHCH_2C({=}S)SC_2H_5$, which have led to a set of precise spectra–structure correlations (2,3). It has also been necessary to undertake an analysis of the conformational properties of these dithioesters in solution by Raman, RR, and FTIR spectroscopy (4). Taking the crystallographic and spectroscopic results together, the findings are that in non-hydrogen bonding solvents such as CCl_4 the glycine-based dithioesters exist in a major populational state known as C_5 in which the N—H forms a hydrogen bond to the thiono sulfur and the resultant five-membered ring is essentially planar (Fig. 1). There is a minor population of a state known as conformer *B* in CCl_4 and this is the predominant form in H-bonding solvents such as H_2O. The *B*-form is also shown in Fig. 1 and has the N atom *cis* to the thiol sulfur as a consequence of a N···S interaction. This form is essentially unique to dithio- and thiolesters (5) and is of importance for the dithioacyl enzymes since it is the sole conformational state in native $RC({=}O)NHCH_2C({=}S)S$-papains (6) and other plant cysteine proteinases (7). Returning to the model compounds, there is another conformational state found in hydrogen bonding solvents. This is the *A*-form shown in Fig. 1; it is converted to the C_5 conformer by a 90° rotation about the NH—CH_2 bond, and the N—H group participates in H-bonding to solvent rather than bonding intramolecularly to the thiono sulfur (2,4).

To date, our studies have dealt with substrates and their corresponding model compounds based on glycine derivatives. Glycine is atypical among the amino acids in having a fairly unhindered conformational space (8). Moreover, it has been known for some time from kinetic studies that the reactivity of papain towards substrates based on other amino acid derivatives may vary markedly (9). Thus, it is of obvious importance to explore the conformational properties of non-glycine dithioesters both as model compounds and as enzyme–substrate intermediates. In the present work we show that *N*-benzoyl-DL-alanine ethyl dithioester takes up a conformation in the crystalline state resembling very closely the *B*-conformation that has such importance for glycine dithioesters. In addition, we establish RR spectra – structure correlations for the alanine dithioester.

Experimental

Materials

The D and L mixtures of $PhC({=}O)NHCH(CH_3)C({=}S)SC_2H_5$ and $PhC({=}O)NHCH(CH_3)^{13}C({=}S)SC_2H_5$ were prepared from their re-

[1]NRCC No. 24211.
[2]Author to whom correspondence may be addressed.

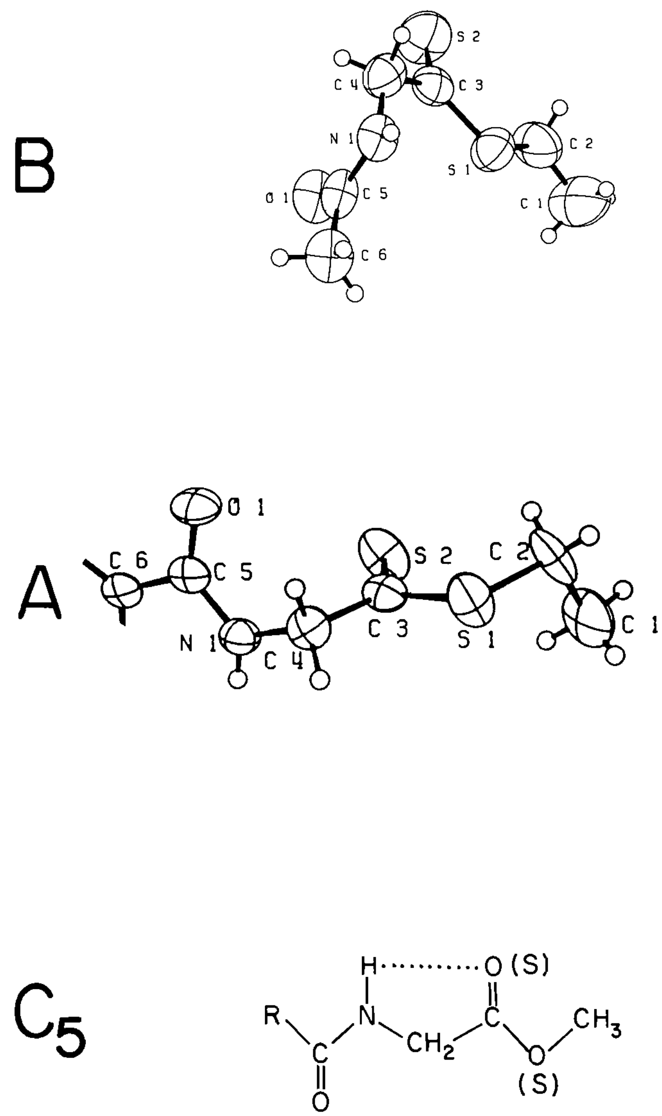

FIG. 1. The three types of conformations taken up by glycine-based dithio esters.

spective nitriles as described by Storer *et al.* (10). The *N*-benzoyl α-aminopropionitriles were obtained by modifying the synthesis of DL-alanine (11). For the unlabelled derivative, acetaldehyde (0.1 equiv.) was reacted with a mixture of ammonium chloride and an ice cold solution of sodium cyanide. (For the [^{13}C] substituted nitrile, sodium [^{13}C] cyanide (99 at.%, Merck, Sharp and Dohme, Canada) was used and the preparation was scaled down five-fold.) The mixture was brought to room temperature and stirred for 4 h. The light yellow mixture was placed in an Erlenmeyer flask, cooled, and titrated with 5 *N* NaOH to pH 10−11. Benzoyl chloride (0.1 equiv.), dissolved in ether (10% solution), was added dropwise while the pH of the mixture was maintained at 10−11. After addition was complete, the mixture was stirred for 30 min at 0°C, then for 1 h at room temperature, while the ether was removed by a stream of air. The nitrile separated out as a slightly yellow solid, which was collected by filtration, washed with cold water, and dried.

The nitrile (1.74 g, 0.01 mol) was added to a 250-mL round bottom flask with 50 mL CH_2Cl_2 and ethanethiol (1.86 g, 0.03 mol) then cooled to 0°C. Dry HCl (gas) was bubbled through this mixture for 20 min. The thioimido ester hydrochloride was precipitated by addition of anhydrous ether. The gummy solid adhered to the sides of the flask so the ethereal solution was decanted and the solid was dried under vacuum in a desiccator, as these salts are extremely hygroscopic.

Pyridine (15 mL), cooled to 0°C and saturated with H_2S (gas), was added to the flask containing the precipitated thioimido ester, then H_2S (gas) was passed through the cooled (0°C), deep yellow solution for no more than 15 min after which the solution was allowed to stand stoppered for 5 min. The cooled solution was then treated with 2 *N* HCl to neutralize the pyridine and produce a pH of approximately 1. The oily mixture was extracted with ether, then the ethereal solution was washed with 1 *N* HCl, H_2O, saturated NaCl solution, then dried over Na_2SO_4. The solution was then filtered and the ether removed by rotary evaporation. The dithioester was purified by passage down a silica gel column using ether/acetonitrile 9:1. The purity of the sample was checked by nmr and elemental analysis. The yield was 0.127 g (5% of theoretical yield based on nitrile), for the unlabelled material.

Crystal data

$C_{12}H_{15}ONS_2$ fw = 253.38
Orthorhombic, $Pca2_1$, a = 9.522 (2), b = 6.587 (1), c = 21.025 (4) Å, z = 4, ρ_c = 1.278 g cm^{-3}, λ (Mo K_α) = 0.7107 Å, μ (Mo K_α) = 3.75 cm^{-1}.

Yellow crystals of *N*-benzoyl-DL-alanine ethyl dithioester were obtained by diffusing hexane into a solution of the compound in ether. The data were measured at room temperature on an Enraf−Nonius CAD-4 diffractometer using a crystal of dimensions 0.70 × 0.40 × 0.15 mm with Zr-filtered Mo K_α radiation. The unit cell dimensions were determined using 22 well-centered reflections in the 2θ range 26−38°. The intensity data were measured to a 2θ limit of 60° by the ω/θ scan mode (Δω = 0.80 + 0.25 tan θ°) with a prescan speed of 3 1/3° per minute and the final scan with a time limit of 60 s. An empirical ϕ absorption correction was applied making use of measurements on two reflections with χ ≃ 90°. A total of 1969 unique reflections were measured of which 1641 had intensities greater than $2\sigma(I)$.

The structure was solved using the computer program MULTAN 80 (12) and refined using a block diagonal least-squares procedure. Weights for individual reflections were assigned from counting statistics. All the hydrogen atoms were located from the difference electron density map and were refined assigning isotropic thermal parameters, while non-hydrogen atoms were refined anisotropically. The scattering factors were taken from "International Tables" (13). All the 1969 unique reflections measured were used in the refinement, the final $R(\Sigma|\Delta F|/\Sigma|F_o|)$ = 0.052, $R(\Sigma w|\Delta F|/\Sigma w|F_o|)$ = 0.046, and the final electron density map was essentially featureless. The shift to σ ratios in the last cycle were all less than 0.1 and $S[\Sigma w\Delta F^2/(m-n)]^{\frac{1}{2}}$ = 1.05

Spectral data

The 647.1-nm excited Raman spectrum of a single crystal of *N*-benzoyl-DL-alanine ethyl dithioester was obtained using a Jarrell−Ash 25-400 spectrometer-based system (14); approximately 50 mW of laser power and a spectral slit of 8 cm^{-1} were used. The 324-nm excited RR spectra of *N*-benzoyl-DL-alanine ethyl dithioester in a powdered form were obtained using a multichannel system described recently (15). The solid material was used to coat the inside of a spinning quartz nmr tube and examined in the backscattering geometry. The RR spectra of *N*-benzoyl-DL-alanine ethyl dithioester in solution were obtained from 1−2 mL of solution contained in a quartz cuvette. The solution was stirred by a small Teflon-coated magnetic stirrer to obviate problems associated with photodecomposition or photo-isomerization (15), and examined in the normal 90° excitation-observation geometry. The RR spectra were obtained using approximately 70 mW of 324-nm Kr^+ excitation and a spectral slit of 12 cm^{-1}.

Results and discussion

The crystal structure of N-*benzoyl-*DL-*alanine ethyl dithioester*

Both the D and L forms of the dithioester occur in the crystal but since the cysteine proteinases exhibit a specificity for the L form of amino acid substrates the discussion will be concerned

TABLE 1(*a*). Positional and thermal parameters of non-hydrogen atoms for the L species of *N*-benzoyl-DL-alanine ethyl dithioester[a]

Code	x/a	y/b	z/c	B_{eq}
S(1)	73571(12)	8652(15)	40950(5)	4.3
S(2)	81086(22)	−32568(20)	36082(6)	7.1
O(1)	9716(2)	−1269(4)	5447(1)	4.7
N(1)	7384(2)	−939(3)	5316(1)	3.6
C(1)	9090(5)	1703(7)	3071(2)	6.6
C(2)	7598(4)	1363(5)	3257(2)	5.1
C(3)	7647(3)	−1699(4)	4163(1)	4.0
C(4)	7321(2)	−2503(4)	4829(1)	3.6
C(5)	5875(3)	−3523(5)	4836(1)	4.6
C(6)	8614(2)	−419(4)	5583(1)	3.5
C(7)	8599(2)	1267(4)	6054(1)	3.7
C(8)	7689(3)	2918(4)	5991(1)	4.4
C(9)	7792(4)	4529(6)	6418(2)	5.9
C(10)	8755(5)	4482(7)	6902(2)	6.4
C(11)	9646(5)	2839(8)	6968(2)	6.4
C(12)	9574(3)	1257(6)	6544(1)	5.0

[a]The fractional coordinates of sulfur atoms are multiplied by 10^5, the rest by 10^4. B_{eq} is calculated as $\frac{8\pi^2}{3}(U_{11} + U_{22} + U_{33})$.

TABLE 1(*b*). Positional and thermal parameters of hydrogen atoms and the bond lengths associated with them[a]

	x/a	y/b	z/c	B	Bonded to	Bond length (Å)
H(1)	674(3)	−35(4)	544(1)	1.5	N(1)	0.77(3)
H(2)	955(9)	248(12)	328(4)	6.5	C(1)	0.81(8)
H(3)	958(4)	68(5)	317(2)	2.8	C(1)	0.84(4)
H(4)	922(7)	210(8)	264(3)	4.9	C(1)	0.96(6)
H(5)	716(7)	20(9)	301(3)	4.8	C(2)	1.02(6)
H(6)	707(5)	257(7)	316(2)	4.0	C(2)	0.96(5)
H(7)	791(4)	−345(6)	492(2)	2.8	C(4)	0.86(4)
H(8)	581(4)	−450(5)	454(2)	2.8	C(5)	0.90(4)
H(9)	516(3)	−254(4)	472(1)	1.8	C(5)	0.97(3)
H(10)	564(3)	−398(4)	526(1)	1.7	C(5)	0.96(3)
H(11)	688(4)	295(6)	567(2)	3.0	C(8)	1.02(4)
H(12)	721(4)	570(5)	636(2)	3.0	C(9)	0.96(4)
H(13)	889(9)	551(11)	714(4)	6.1	C(10)	0.86(8)
H(14)	1030(7)	290(9)	730(3)	5.3	C(11)	0.94(6)
H(15)	1011(5)	18(7)	660(2)	3.7	C(12)	0.88(5)

[a]The fractional coordinates are multiplied by 10^3.

primarily with the L enantiomer. In the crystal structure the L and D forms are symmetry related. The positional parameters, the torsion angles, etc. reported in this paper are for the L form. The positional and thermal parameters of non-hydrogen atoms and hydrogen atoms in the *N*-benzoyl-L-alanine ethyl dithioester are shown in Tables 1*a* and 1*b*,[3] respectively, and its structure is depicted in Fig. 2. Some relevant torsional angles are given in Table 2 and bond distances and bond angles are given in Fig. 3.

An important finding is that the *N*-benzoyl-DL-alanine ethyl dithioester assumes a *B*-type conformation. The characteristics of a *B* conformer are a small N—C—C—S(thiol) torsional angle resulting from an N···S interaction, and nearly orthogonal amide and ester planes. The N—C(4)—C(3)—S(1) (ψ') and C(6)—N—C(4)—C(3) (ϕ') torsional angles are −23.0° and −84.0°, respectively, and the N···S distance is 2.830 Å.

[3]Tables of observed and calculated structure factors and anisotropic temperature factors are available at a nominal charge, from the Depository of Unpublished Data, CISTI, National Research Council of Canada, Ottawa, Ont., Canada K1A 0S2.

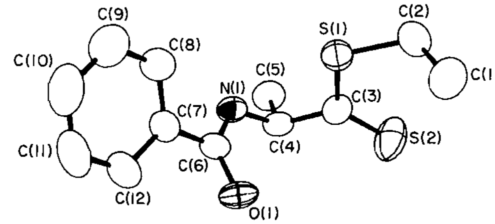

FIG. 2. The thermal ellipsoid plot of *N*-benzoyl-L-alanine ethyl dithioester.

TABLE 2. Selected torsional angles (deg) for the L species of *N*-benzoyl-DL-alanine ethyl dithioester

Angles	Deg
C(8)—C(7)—C(6)—N(1)	−34.5 (4)
C(8)—C(7)—C(6)—O(1)	144.9 (3)
C(7)—C(6)—N(1)—C(4)	177.0 (3)
C(6)—N(1)—C(4)—C(3)	−84.0 (3)
N(1)—C(4)—C(3)—S(1)	−23.0 (3)
N(1)—C(4)—C(3)—S(2)	160.7 (3)
C(5)—C(4)—C(3)—S(2)	−76.0 (3)
C(4)—C(3)—S(1)—C(2)	−173.1 (3)
C(3)—S(1)—C(2)—C(1)	−84.8 (5)

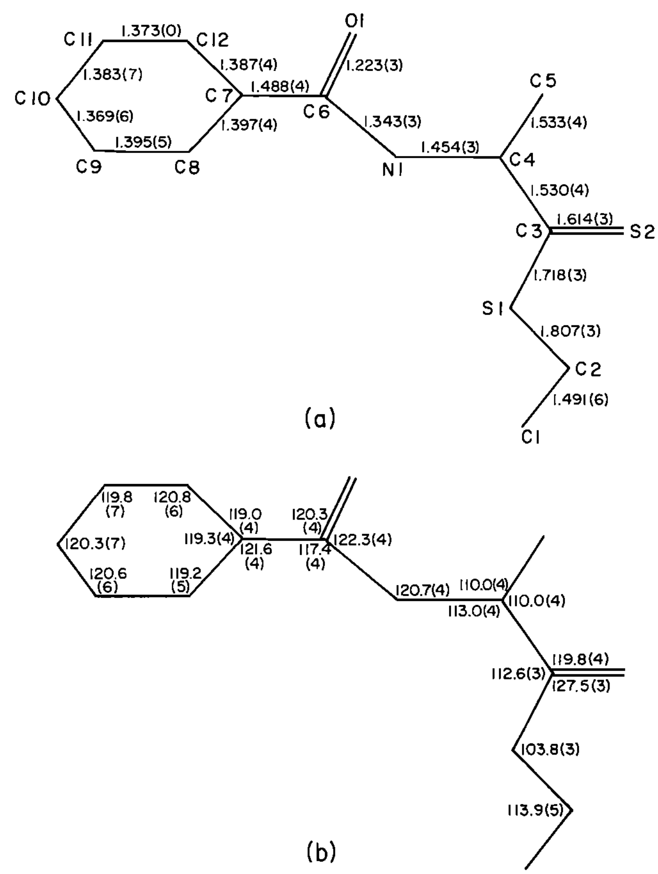

FIG. 3. (*a*) Bond lengths and (*b*) angles for *N*-benzoyl-L-alanine ethyl dithioester.

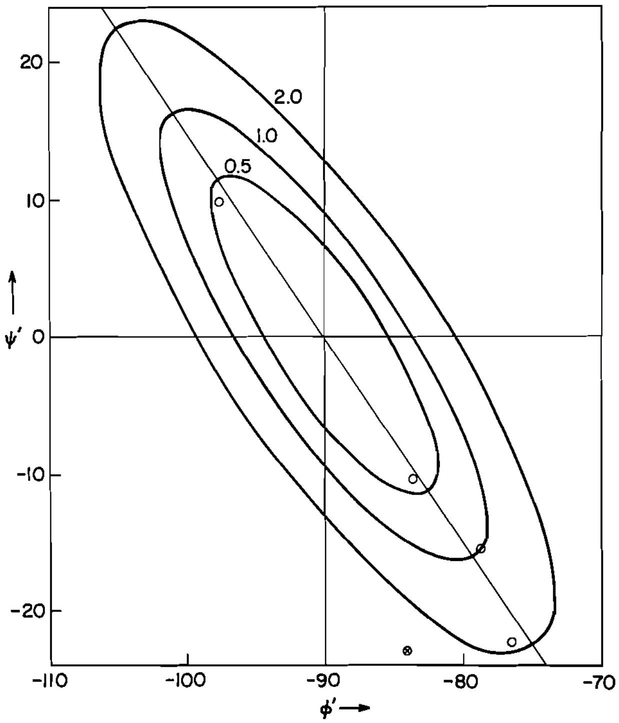

FIG. 4. The θ plot. The contours represent Δθ (deviations from θ minimum = 20.1°) of 0.5°, 1.0°, and 2.0°. The open circles represent the ψ',ϕ' values for four glycine dithioesters. The ψ',ϕ point for *N*-benzoyl-L-alanine ethyl dithioester is marked as ⊗.

B-type conformations are a favored conformational state of dithio- and thiol-esters of glycine but are essentially absent for glycine dioxygen esters (5). The pertinent structural parameters for *N*-benzoyl-DL-alanine ethyl dithioester are compared to those for various glycine dithio- and thiol-esters in Table 3. It is seen that the ψ', ϕ' angles, the N···S distance, and the bond lengths around the dithioester chromophore fall within, or close to, the range delineated for glycine dithioesters. Therefore, alanine dithioesters (and in all likelihood alanine thiolesters) can take up a *B*-type conformation very similar to that found for glycine based dithioesters and thiolesters. This finding is significant in view of the fact that substitution at the α carbon atom greatly restricts the conformational space available to dipeptides and depsipeptides (8).

In a recent publication (3) it was shown that the ϕ', ψ' angles of four glycine dithioesters are correlated, a plot of ϕ' vs. ψ' for the four dithioesters lying close to a straight line. These results demonstrated that there is a strongly preferred line of approach of the nitrogen to the thiol sulfur atom, which is retained over a fairly wide range of values for ϕ' and ψ'. The correlation is illustrated in Fig. 4 which also plots the contours for θ, which is defined as the angle between the N···S direction and the normal to the amide plane at the nitrogen atom (3). On purely geometrical grounds it can be shown that the smallest value of θ possible is about 20.1°, and Fig. 4 demonstrates that the glycine dithioester points all lie close to the θ minimum. For the present structure the ϕ', ψ' point lies slightly off the line defined by the glycine dithioester conformations (Fig. 4). However, the deviation from θ_{min} is less than 3° and clearly the line of approach of N to S (thiol) is very similar in the present alanine case to that found for the glycine dithioesters. This small deviation is most probably due to the steric effect of introducing the β CH_3 group in the alanine case. Further evidence for a strong N···S interaction is found in the N···S distance of 2.830 Å (Table 3). This is the shortest N···S distance found to date, in this class of compound, and should be compared to the sum of the van der Waals radii of 3.35 Å (16).

For *N*-benzoyl-DL-alanine ethyl dithioester the benzene ring is tilted by about 35° from the plane of the carbonyl. The C(1)—C(2) bond is essentially *gauche* with respect to the C(3)—S(1) bond; the torsional angle C(1)—C(2)—S(1)—C(3) is −84.8°. Values close to +80°, −80°, and 180° have been found for this angle in dithio- and thiol-esters and are probably selected by crystal packing forces. The bonds meeting at C(3) and at C(6) are planar and thus there is no evidence for pyramidalization at either atom. As is normal for molecules containing the peptide linkage, there is an intermolecular N—H···O hydrogen bond. The N—H distance is 0.77(3) Å, the N···O distance 2.941(3) Å, and the N—H···O angle 161(5)°.

Resonance Raman signatures for N-*benzoyl*-DL-*alanine ethyl dithioester in its* B *and non-B conformations*

The RR signature for *N*-benzoyl-DL-alanine ethyl dithioester in its *B* form can be obtained by comparing the Raman spectrum of a single crystal of the compound (Fig. 5) with the RR spectrum of the powdered material (Fig. 6). Under the experimental conditions employed in this work, the Raman, or RR, spectrum of the D form is identical to the spectrum of the L form. Thus, the spectral data for the DL mixture may be correlated immediately to the structure of the L form given emphasis here. The Raman spectrum was obtained from the same crystal used for X-ray crystallographic analysis and the conformationally sensitive bands in the RR spectrum at 1091, 683, and 566 cm^{-1} in all likelihood correspond to the bands seen in the Raman spectrum at 1086, 680, and 562 cm^{-1}. The correspondence between the Raman spectrum of the single crystal and the RR spectrum of the powdered material is supported by the results for the $PhC(=O)NHCHCH_3{}^{13}C(=S)SC_2H_5$ compound. The RR results (Fig. 6) indicate that the 1091 cm^{-1} band is a composite feature, the most intense part of which shifts to 1063 cm^{-1}. Similarly the feature at 1086 cm^{-1} in the single crystal spectrum (Fig. 5) is probably made up of more than one band and its major contributor shifts to 1066 cm^{-1} upon $^{13}C{=}S$ substitution (data not shown). The band near 682 cm^{-1} is unshifted in both the Raman and RR spectra upon $^{13}C{=}S$ substitution and the band near 504 cm^{-1} shifts to lower frequency by 4−5 cm^{-1} in both cases. Since the single crystal is known to be in the *B*-form, the correspondence between the Raman and RR spectra establishes that the powdered material is also in the *B* form and that the RR *B*-signature of *N*-benzoyl-DL-alanine ethyl dithioester is that seen in Fig. 6.

The relationship between RR spectral signature and conformations is fairly well understood for glycine-based dithioesters (1−4). This class of molecules in the *B*-form has an intense RR band near 1130 cm^{-1}, designated Band II (10), which has major contributions from $\nu_{C=S}$ and ν_{C-C} (from the C—C(=S) linkage) motions. For the alanine derivative, the 28 cm^{-1} shift seen in the 1091 cm^{-1} band upon $^{13}C{=}S$ substitution (Fig. 6) makes it probable that the 1091 cm^{-1} feature corresponds to Band II for this molecule. The 1169 cm^{-1} feature (Fig. 6) is probably analogous to the highly delocalized mode seen in this region in glycine derivatives (3). RR features are also seen near 1040 and 685 cm^{-1} for both glycine and alanine dithioesters (Figs. 5 and 6, and ref. 3) and it is likely

TABLE 3. Pertinent structural and Raman data for *N*-acylglycine dithioesters and thiolesters and *N*-benzoyl-L-alanine ethyl dithioester

Compound	Conformer	N···S[a]	C—C[b]	C═S	C—S[d]	S—C[e]	φ′	ψ′	Band II	$\nu_{C—S}$[f]	$\nu_{S—C}$[g]	C—S—C—C
N-(*p*-nitrobenzoyl) glycine ethyl dithioester (ref. 2)	*A*	3.043	1.516(4) Å	1.615(3) Å	1.727(3) Å	1.791(4) Å	−86.2°	−171.7°	1169[c]	660	680	−83.9
N-benzoylglycine ethyl dithioester I (ref. 3)	*B*	2.866	1.522(3)	1.615(3)	1.710(3)	1.804(3)	−78.7	−15.5	1120	600	700	−176.1
N-benzoylglycine ethyl dithioester II (ref. 3)	*B*	2.846	1.522(3)	1.624(3)	1.711(3)	1.804(3)	−83.5	−10.5	1120	600	700	+178.8
N-(*p*-chlorobenzoyl) glycine ethyl dithioester (ref. 3)	*B*	2.851	1.518(3)	1.618(3)	1.710(3)	1.820(3)	−97.1	+9.5	1124	587	681	−88.7
N-acetylglycine ethyl dithioester (ref. 2)	*B*	2.891	1.504(11)	1.635(5)	1.700(6)	1.807(9)	−76.3	−22.2	1143	584	698	−168.5
N-benzoyl-L-alanine ethyl dithioester	*B*	2.830	1.530(4)	1.614(3)	1.718(3)	1.807(3)	−84.0	−23.0	1086	562	680	−84.8
N-benzoylglycyine ethyl thiolester (ref. 5)	*B*	2.879	1.521(7)	—	1.722(5)	1.802(5)	−88.7	+5.4	—	621[h]	678[h]	−79.0
N-(β-phenylpropionyl) glycine ethyl thiolester (ref. 5)	*B*	2.930	1.492(4)	—	1.764(4)	1.809(4)	−84.8	−15.4	—	606[h]	672[h]	+79.1

[a]Sulfur *cis* to N. In conformer *A* it is thione and for the remaining it is thiol.
[b]C—C(═S) bond.
[c]Band I, band positions are for crystalline form.
[d]C(═S)—S bond.
[e]S—C_2H_5.
[f]$\nu_{C—S}$ is an intense mode in the RR spectrum which contains contributions from stretching motions of the C—C(═S)—S group.
[g]$\nu_{S—C}$ is a fairly localized motion of the S—C linkage.
[h]Unpublished work, this laboratory.

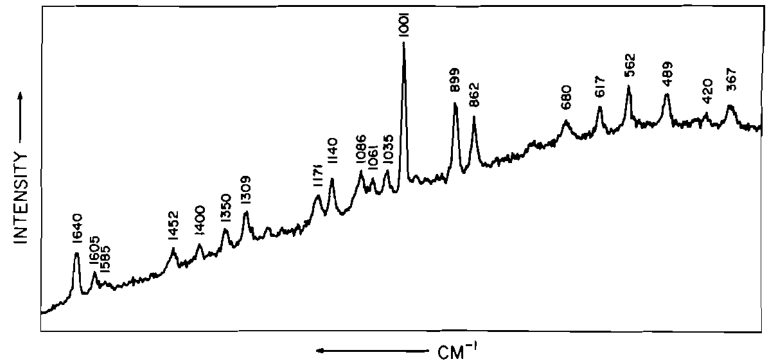

FIG. 5. The 654.1-nm excited Raman spectrum of a single crystal of *N*-benzoyl-DL-alanine ethyl dithioester.

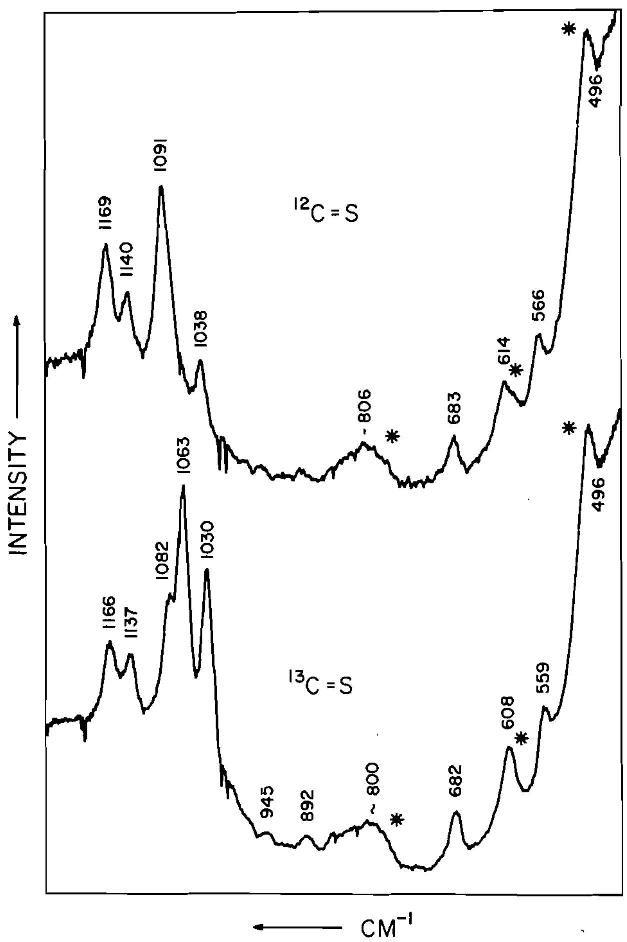

FIG. 6. Resonance Raman spectra of powdered *N*-benzoyl-DL-alanine ethyl dithioester. The quartz of the sample tube makes a contribution in the regions marked with an asterisk.

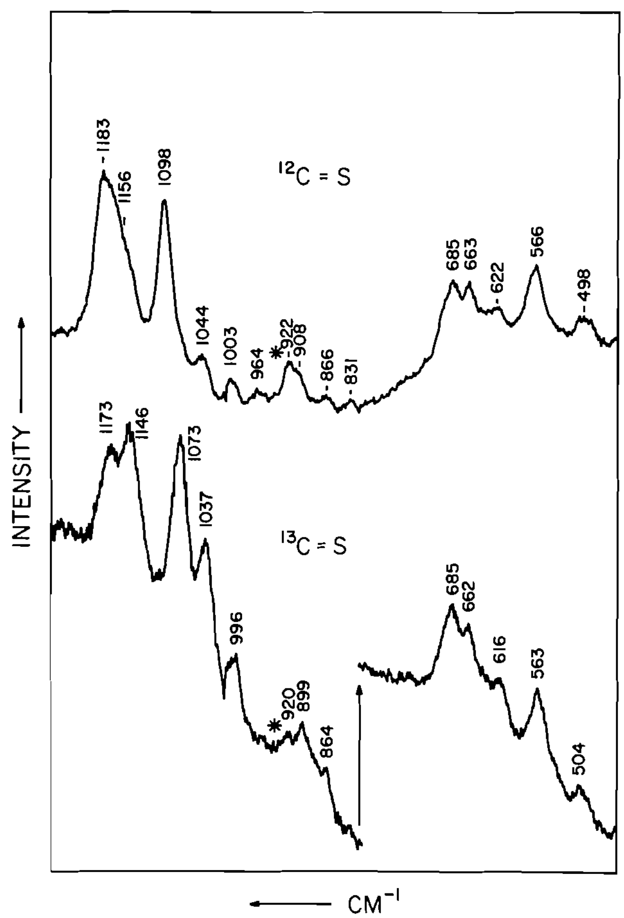

FIG. 7. Resonance Raman spectra (324-nm excitation) of ~2 × 10^{-4} *M* *N*-benzoyl-DL-alanine ethyl dithioester in CH_3CN/H_2O (1:200 v/v). The feature marked with an asterisk is due to CH_3CN.

that the latter band has a major contribution from ν_{S-C} (from the S—CH_2 bond) in both cases. The RR peak near 565 cm^{-1} (Figs. 5, 6) probably corresponds to the conformationally sensitive mode seen near 600 cm^{-1} for glycine dithioesters (4), neither feature being very sensitive to $^{13}C{=}S$ substitution. Thus, both the conformationally sensitive features, one in the 1100 and the other in the 600 cm^{-1} region, appear at approximately 30 cm^{-1} lower in the alanine case. Since the crystallographic results indicate that bond lengths are very similar in the glycine and alanine derivatives, it is unlikely that the frequency differences are due to a change in bond order. Rather, it is likely that the lowering of the frequencies is brought about by the change in the potential energy distribution as a consequence of the insertion of the methyl group at the α carbon. In this regard, it is noteworthy that the most intense features in the RR spectra of ethyl dithiotrimethyl acetate occur at atypically low frequencies for a dialkyl dithioester, namely at 1108 and 573 cm^{-1} (17).

Figure 7 demonstrates that the *B*-signature, and thus the conformation, is similar in H_2O/CH_3CN solution to that in the solid phase. The conformationally sensitive *B*-markers occur at 1098 and 566 cm^{-1} in CH_3CN/H_2O, close to the 1091 and 566 cm^{-1} values found for the solid. Moreover, the 25 cm^{-1} shift

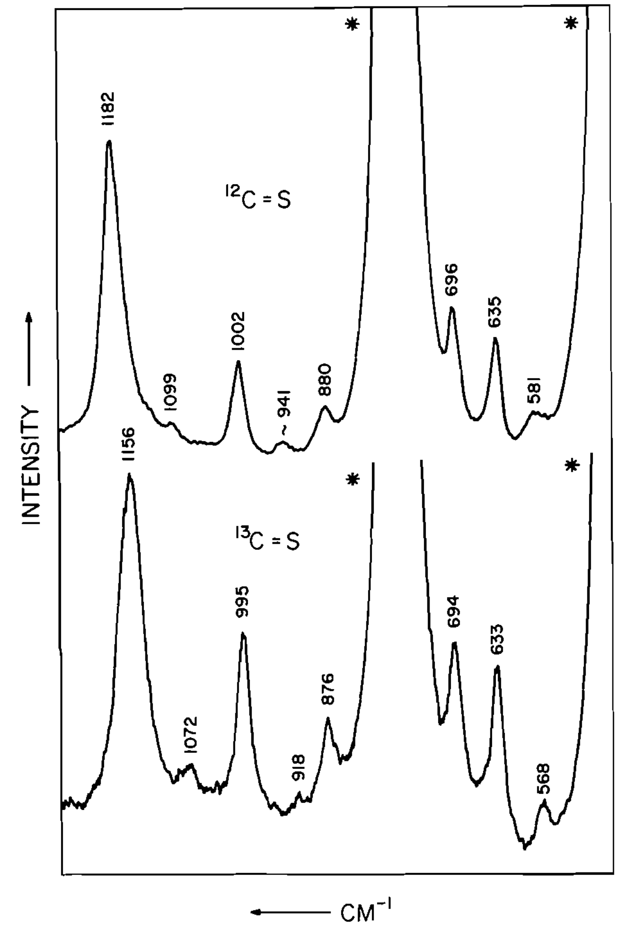

FIG. 8. Resonance Raman spectra (324-nm excitation) of ~8 × 10^{-4} *M* *N*-benzoyl-DL-alanine ethyl dithioester in CCl_4. Features marked with an asterisk are due to CCl_4.

in the 1098 cm^{-1} feature and the 3 cm^{-1} shifts in the 563 cm^{-1} feature upon $^{13}C{=}S$ substitution (Fig. 7) mimic closely the behaviour of the solid material. Additionally, there are several bands seen in the solution RR spectra which are not present in the spectrum of the solid. In particular, the intense band in the 1175 cm^{-1} region and the less intense feature occurring at 663 cm^{-1} are characteristic *A* conformer markers in the case of glycine-based dithioesters. Although the band profile in the 1175 cm^{-1} region is complex due to the overlap of *A* and *B* conformer bands, it is probable that the "centre of gravity" of the composite feature moves to lower wavenumbers upon $^{13}C{=}S$ substitution due to a substantial shift in the "*A* peak" near 1180 cm^{-1}. (There is further evidence for this in the RR spectrum of *N*(β-phenylpropionyl)alanine ethyl dithioester, unpublished work, this laboratory.) For glycine based dithioesters the predominant species in non-hydrogen bonding solvents such as CCl_4 is the C_5 conformer (Fig. 1). The RR spectra of *N*-benzoyl-DL-alanine ethyl dithioester and its $^{13}C{=}S$ analog in CCl_4 (Fig. 8) are very similar to those of a glycine dithioester in a C_5 type conformer. The 1182 and 635 cm^{-1} features are C_5 conformer markers and the similarity of *A* and C_5 marker bands in the 1175 cm^{-1} region adds weight to the argument for assigning a band near 1175 cm^{-1} in the spectra from H_2O/CH_3CN solution to an *A* conformer. The band near 1000 cm^{-1} seen in Fig. 8 is not present in the spectra of glycine derivatives in CCl_4 and it is suggested that it has some ν_{C-C} character from the C_α—CH_3 bond.

It follows from the above discussion that vibrational coupling involving the C_α—CH_3 group modifies the RR signature of the *B* conformer, but not the C_5 (and probably not the A) form. Thus, considering a Newman projection along C4—C3 the potential energy distribution is modified for

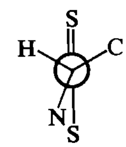

conformer *B*

but not for

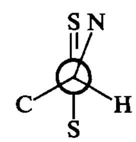

conformer C_5

One outcome of the present work will be that the characteristic signatures for C_5 (and *A*) and *B* type conformers of the alanine dithioester established here can be used in future investigations of acyl-papains in which the alanine moiety is bound to cysteine-25 in papain's active site.

1. P. R. CAREY and A. C. STORER. Acc. Chem. Res. **16**, 455 (1983).
2. C. P. HUBER, Y. OZAKI, D. H. PLIURA, A. C. STORER, and P. R. CAREY. Biochemistry, **21**, 3109 (1982).
3. K. I. VARUGHESE, A. C. STORER, and P. R. CAREY. J. Am. Chem. Soc. **106**, 8252 (1984).
4. H. LEE, A. C. STORER, and P. R. CAREY. Biochemistry, **22**, 4781 (1983).
5. C. P. HUBER, P. R. CAREY, S. HSI, H. LEE, and A. C. STORER. J. Am. Chem. Soc. **106**, 8263 (1984).
6. A. C. STORER, H. LEE, and P. R. CAREY. Biochemistry, **22**, 4789 (1983).
7. P. R. CAREY, Y. OZAKI, and A. C. STORER. Biochem. Biophys. Res. Commun. **117**, 725 (1983).
8. G. E. SCHULZ and R. H. SCHIRMER. Principles of protein structure. Springer Verlag, New York. 1979. p. 22.
9. A. WILLIAMS, E. C. LUCAS, A. R. RIMMER, and H. C. HAWKINS. J. Chem. Soc. Perkin Trans. 2, 627 (1972).
10. A. C. STORER, Y. OZAKI, and P. R. CAREY. Can. J. Chem. **60**, 199 (1982).
11. E. C. KENDALL and B. F. MCKENZIE. Org. Synth. Coll. Vol. 1, 21 (1964).
12. P. MAIN, S. J. FISKE, S. E. HULL, L. LESSINGER, G. GERMAIN, J-P. DECLERCQ, and M. M. WOOLFSON. MULTAN 80. A System of computer programs for automatic solution of crystal structures from X-ray diffraction data. University of York, England and University of Louvain, Louvain, Belgium (1980).
13. International tables for X-ray crystallography. Vol. III. Kynoch Press, Birmingham, U. K. 1962. p. 202.
14. K. KUMAR and P. R. CAREY. J. Chem. Phys. **63**, 3697 (1975).
15. P. R. CAREY and L. R. SANS CARTIER. J. Raman Spectrosc. **14**, 271 (1983).
16. A. BONDI. J. Phys. Chem. **68**, 441 (1964).
17. Y. OZAKI, A. C. STORER, and P. R. CAREY. Can. J. Chem. **60**, 190 (1982).

Structure and nuclear magnetic resonance spectra of 6-bromo-3,3′,4′,5,7-penta-O-methylcatechin

F. W. B. EINSTEIN,[1] E. KIEHLMANN,[1] AND E. K. WOLOWIDNYK
Department of Chemistry, Simon Fraser University, Burnaby, B.C., Canada V5A 1S6

Received September 12, 1984

F. W. B. EINSTEIN, E. KIEHLMANN, and E. K. WOLOWIDNYK. Can. J. Chem. **63**, 2176 (1985).

The title compound has been synthesized by selective debromination of 6,8-dibromocatechin and indirect methylation of the resulting 6-bromocatechin via its pentaacetate. The structure of $C_{20}H_{23}BrO_6$ has been determined by X-ray crystallography. The compound crystallizes in the space group $P1$ with $a = 9.589(3)$ Å, $b = 11.576(3)$ Å, $c = 11.326(3)$ Å, $\alpha = 118.80(3)°$, $\beta = 93.23(3)°$, $\gamma = 111.44(3)°$, $\rho_c = 1.481$ g cm^{-3}, and $Z = 2$. Intensities were measured for 2584 independent reflections ($2\theta < 45°$) of which 2213 were observed ($I > 3.0\sigma(I)$) and used in subsequent refinement (final R values were $R = 0.0268$ and $R_w = 0.0344$). Crystallographic and pmr data confirm the position of the bromine atom at C-6, the *trans*-diaxial arrangement of H-2/H-3 and the quasi-equatorial orientation of the 3,4-dimethoxyphenyl group (ring B). The two heterocyclic ring conformations are consistent with the expected flexibility of the molecule.

F. W. B. EINSTEIN, E. KIEHLMANN et E. K. WOLOWIDNYK. Can. J. Chem. **63**, 2176 (1985).

On a synthétisé le composé mentionné dans le titre par une débromation de la dibromo-6,8 catéchine et par une méthylation indirecte de la bromo-6 catéchine qui en résulte, via son pentaacétate. On a déterminé la structure du composé $C_{20}H_{23}BrO_6$ par diffraction des rayons x. Le composé cristallise dans le groupe d'espace $P1$, avec $a = 9{,}589(3)$ Å, $b = 11{,}576(3)$ Å, $c = 11{,}326(3)$ Å, $\alpha = 118{,}80(3)°$, $\beta = 93{,}23(3)°$, $\gamma = 111{,}44(3)°$, $\rho_c = 1{,}481$ g cm^{-3} et $Z = 2$. On a mesuré les intensités pour 2584 réflexions indépendantes ($2\theta < 45°$) desquelles 2213 ont été observées ($I > 3\sigma(I)$) et utilisées pour l'affinement jusqu'à des valeurs finales de $R = 0{,}0268$ et $R_w = 0{,}0344$. Les données cristallographiques et de rmn du ^{1}H confirment la position de l'atome de brome en C-6, l'arrangement *trans*-diaxial des H-2/H-3 et l'orientation quasi-équatoriale du groupement diméthoxy-3,4 phényle (cycle B). Les conformations des deux hétérocycles sont en accord avec la flexibilité attendue de la molécule.

[Traduit par le journal]

Introduction

The regiochemistry of electrophilic substitution of the phloroglucinol ring (ring A) of flavan-3,5,7-triols continues to attract attention in view of its importance in determining the structure and conformations of condensed tannins. The first halogenations of catechin derivatives were reported by Liebermann and Tauchert (1) who obtained monochloro- and monobromocatechin pentaacetates from catechin pentaacetate and molecular halogen in glacial acetic acid, and by Kostanecki and co-workers (2) and Freudenberg and co-workers (3) who halogenated methylated catechins by the same procedure. Weinges and co-workers (4) claimed in 1968 that electrophilic substitution occurs preferentially at C-8; however, the techniques of structure determination available at that time did not permit a clear distinction between two regio-isomeric monosubstitution products. It was not until 1977 that the configuration of 8-bromo-tetra-O-methylcatechin was proven by X-ray structure analysis (5), the pmr parameters of a series of chemically correlated 8-substituted catechins were recorded and the first 6-bromo derivative was synthesized by partial debromination of the corresponding 6,8-dibromo compound (6), as shown in route *a* of reaction [1]

[1]

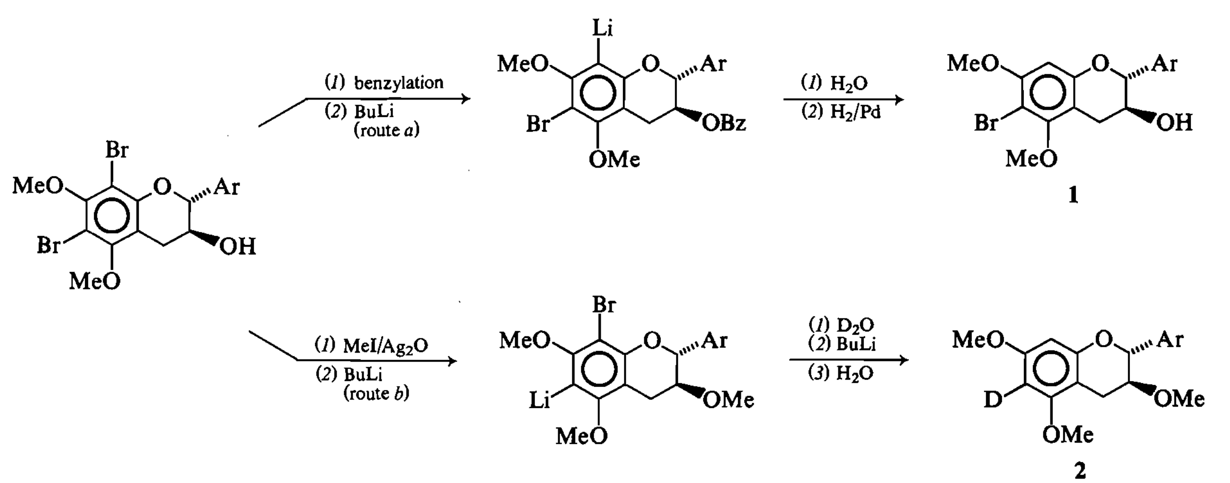

Ar = 3,4-dimethoxyphenyl

[1]To whom correspondence may be addressed.

TABLE 1. Atomic parameters and B_{eq}'s of non-hydrogen atoms; esd's refer to the last digit printed*

Atom	x	y	z	B_{eq}	Atom	x	y	z	B_{eq}
Br(A6)	0.75340(9)	0.81878(7)	0.78216(9)	4.98(8)	Br(B6)	1.50000	1.50000	0.75000	4.01(6)
O(A1)	1.2278 (8)	1.4534 (8)	1.0592 (8)	3.7 (4)	O(B1)	1.0222 (8)	0.8723 (9)	0.4685 (8)	4.1 (5)
O(A131)	1.7583 (8)	1.9277 (9)	1.2470 (8)	4.6 (4)	O(B131)	0.5182 (9)	0.4067 (9)	0.2967 (8)	5.1 (4)
O(A141)	1.6684 (9)	2.1236 (8)	1.3943 (7)	4.0 (4)	O(B141)	0.5755 (8)	0.1899 (8)	0.1430 (7)	4.0 (4)
O(A31)	1.0589 (9)	1.6001 (9)	0.9082 (8)	4.9 (5)	O(B31)	1.2020 (9)	0.7035 (9)	0.5889 (8)	4.8 (4)
O(A51)	0.7287 (8)	1.0492 (8)	0.7354 (7)	3.9 (5)	O(B51)	1.5159 (7)	1.2637 (8)	0.7908 (7)	3.7 (4)
O(A71)	1.0630 (9)	0.9755 (9)	0.9901 (9)	4.8 (5)	O(B71)	1.1908 (8)	1.3484 (9)	0.5480 (9)	5.0 (5)
C(A2)	1.2156 (8)	1.5398 (7)	1.0039 (8)	3.2 (4)	C(B2)	1.0778 (8)	0.7670 (7)	0.4561 (8)	3.5 (4)
C(A11)	1.3307 (10)	1.6977 (10)	1.1151 (9)	2.8 (4)	C(B11)	0.9448 (11)	0.6165 (11)	0.3708 (9)	3.2 (5)
C(A12)	1.4886 (12)	1.7355 (12)	1.1312 (10)	3.3 (5)	C(B12)	0.7920 (12)	0.5860 (12)	0.3774 (11)	3.6 (6)
C(A13)	1.6013 (11)	1.8802 (11)	1.2282 (9)	2.7 (5)	C(B13)	0.6729 (13)	0.4474 (16)	0.3014 (12)	4.2 (8)
C(A131)	1.8086 (14)	1.8241 (15)	1.1593 (12)	6.1 (7)	C(B131)	0.4763 (14)	0.5237 (15)	0.3821 (14)	6.4 (8)
C(A14)	1.5483 (12)	1.9849 (13)	1.3069 (11)	3.4 (7)	C(B14)	0.6999 (11)	0.3269 (12)	0.2126 (10)	3.0 (6)
C(A141)	1.6269 (15)	2.2400 (13)	1.4781 (13)	5.6 (7)	C(B141)	0.6035 (14)	0.0668 (13)	0.0533 (11)	4.4 (6)
C(A15)	1.3969 (13)	1.9438 (12)	1.2981 (10)	3.5 (6)	C(B15)	0.8538 (12)	0.3524 (10)	0.2059 (9)	3.2 (5)
C(A16)	1.2884 (10)	1.8022 (10)	1.2006 (9)	3.2 (5)	C(B16)	0.9739 (10)	0.4987 (10)	0.2826 (8)	3.2 (5)
C(A3)	1.0482 (10)	1.5068 (11)	0.9576 (9)	3.4 (5)	C(B3)	1.1564 (10)	0.8125 (10)	0.6039 (9)	3.4 (5)
C(A31)	0.9131 (11)	1.5947 (10)	0.8660 (10)	5.5 (6)	C(B31)	1.2592 (15)	0.7192 (12)	0.7111 (12)	7.6 (8)
C(A4)	0.9497 (12)	1.3509 (11)	0.8459 (11)	3.2 (6)	C(B4)	1.2949 (12)	0.9695 (14)	0.6764 (12)	4.3 (7)
C(A5)	0.8759 (11)	1.1011 (11)	0.8245 (10)	2.8 (5)	C(B5)	1.3759 (11)	1.2099 (12)	0.7024 (10)	3.1 (7)
C(A51)	0.7207 (16)	0.9801 (17)	0.5910 (12)	5.3 (8)	C(B51)	1.5282 (15)	1.3304 (15)	0.9357 (12)	5.2 (8)
C(A6)	0.9011 (11)	1.0146 (12)	0.8620 (10)	3.2 (7)	C(B6)	1.3442 (11)	1.3024 (11)	0.6696 (11)	3.3 (6)
C(A7)	1.0405 (11)	1.0726 (13)	0.9652 (10)	3.4 (6)	C(B7)	1.2072 (12)	1.2506 (12)	0.5776 (11)	3.1 (7)
C(A71)	1.2010 (15)	1.0317 (17)	1.0902 (17)	6.4 (10)	C(B71)	1.0519 (16)	1.3009 (15)	0.4490 (15)	5.7 (9)
C(A8)	1.1479 (12)	1.2212 (14)	1.0242 (11)	3.7 (6)	C(B8)	1.0999 (11)	1.1080 (11)	0.5088 (10)	3.0 (6)
C(A9)	1.1151 (12)	1.3049 (11)	0.9837 (10)	2.9 (6)	C(B9)	1.1297 (10)	1.0135 (13)	0.5391 (11)	3.4 (6)
C(A10)	0.9797 (11)	1.2474 (13)	0.8815 (10)	3.1 (6)	C(B10)	1.2645 (11)	1.0638 (11)	0.6373 (11)	2.9 (6)

*B_{eq} is the arithmetic mean of the principal axes of the thermal ellipsoid.

In this reaction, lithiation was postulated to occur regioselectively at the sterically less hindered C-8 position, based on the measured pmr parameters of **1**, though Weinges, in a related study (7), had claimed lithiation at C-6 of 6,8-dibromopenta-*O*-methylcatechin under comparable conditions (reaction [1], route *b*). To resolve this discrepancy, rule out epimerization as competing reaction and to obtain an authentic sample of a 6-substituted catechin for chemical and spectral correlation, we decided to prepare 6-bromopenta-*O*-methylcatechin by a new route and determine its structure by X-ray diffraction.

Discussion

6-Bromocatechin was synthesized by regioselective debromination of 6,8-dibromocatechin as described in the literature (10). Although direct pentamethylation with methyl iodide and silver oxide (11) is possible, we chose Freudenberg's acetylation–methylation sequence (12) in order to compare the pmr parameters of the resulting intermediates with published literature values. In the event, we found reasonable agreement for 6-bromocatechin pentaacetate and excellent agreement of the chemical shifts and coupling constants reported for 6-bromotetra-*O*-methylcatechin (13). Since the latter compound has been previously prepared under much milder reaction conditions, i.e., methylation of 6-bromocatechin with diazomethane (13) and catalytic hydrogenolysis of the corresponding 3-*O*-benzyl ether (6*b*), our results demonstrate that epimerization is not a significant side reaction in the conversion of 6-bromocatechin pentaacetate to 6-bromo-tetra-*O*-methylcatechin with dimethyl sulfate and strong base. This procedure may, therefore, be used to derivatize flavanoids which give low yields and/or mixtures of partially methylated products with diazomethane or dimethyl sulfate/potassium carbonate. 6-Bromo-3′,4′,5(or 7)-tri-*O*-methyl-7(or 5)-*O*-acetylcatechin was identified as byproduct.

While the major product of partial debromination of 3-*O*-benzyl-6,8-dibromo-3′,4′,5,7-tetra-*O*-methylcatechin with *n*-butyl lithium, followed by protonation of the lithiated intermediate (reaction [1], route *a*) and chromatographic purification (6), is indeed 3-*O*-benzyl-6-bromo-3′,4′,5,7-tetra-*O*-methylcatechin as evidenced by the identity (melting point, pmr) of its hydrogenolysis product with the 6-bromotetra-*O*-methylcatechin prepared independently by the afore-mentioned route, the 8-bromo isomer is also formed but retained longer on the chromatography column. Thus, the isolation of 6-deutero-8-bromopenta-*O*-methylcatechin (**2**) from the partial lithiation and deuteration of 6,8-dibromopenta-*O*-methylcatechin (reaction [1], route *b*) by Weinges *et al.* (7) appears to be simply a consequence of its lower solubility in ethanol (relative to the 6-bromo isomer). It may, therefore, be concluded that the 6- and 8-position of alkylated 6,8-dibromocatechins do not differ significantly in their reactivity toward *n*-butyl lithium. Our finding that catechin pentaacetate undergoes predominantly 6-bromination provides further proof that steric accessibility (favoring C-8 over C-6) is not the only factor determining the orientation in substitution reactions of ring A of catechin derivatives.

Methylation of the 3-hydroxy group was achieved by Purdie's method (11), thus completing the synthesis of this new compound (reaction [2]).

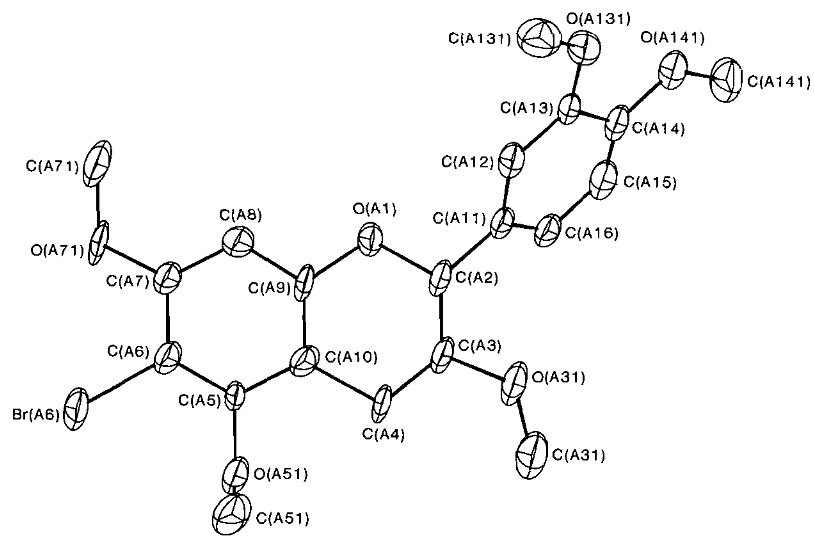

FIG. 1. Snoopi diagram showing molecule A viewed normal to the fused ring system.

[2]

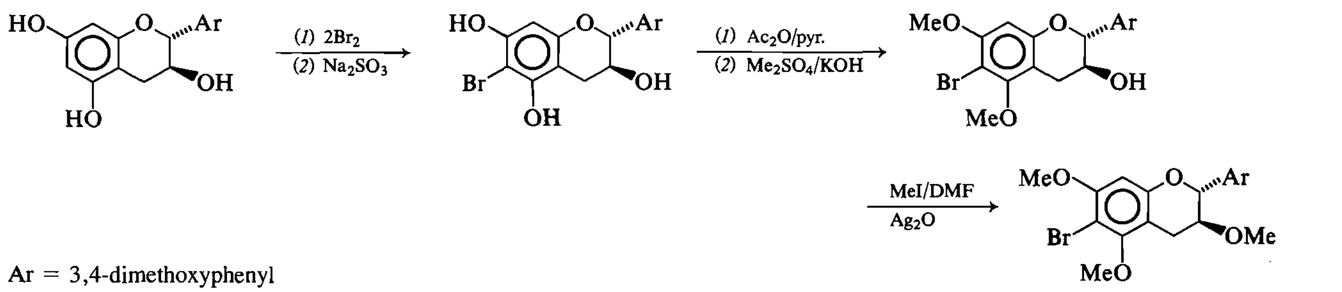

Ar = 3,4-dimethoxyphenyl

3

Detailed analysis of the pmr spectrum (in $CDCl_3$) of 6-bromopenta-*O*-methylcatechin (**3**), including computer simulation, permitted for the first time the assignment of all resonances to specific protons with the exception of the two methoxy peaks of ring B. The heterocyclic ring protons absorb at 4.892 (H-2), 3.689 (H-3), 3.051 (H-4 equatorial) and 2.770 (H-4 axial) ppm, with coupling constants of 7.2 (J_{23}), 5.0 (J_{34e}), 7.7 (J_{34a}), and 16.3 Hz (J_{44}). The large values for J_{23} and J_{34a} are indicative of *trans*-diaxial arrangements in a half-chair conformation. Decoupling experiments showed that H-2 is long-range coupled to H-4a (J = 0.4 Hz) and H-6′ (J = 0.6 Hz), and that both H-4a and H-4e are weakly coupled to H-8 (line broadening). The aromatic protons of ring B resonate at 6.895 (H-2′), 6.876 (H-5′), and 6.941 ppm (H-6′), with coupling constants of 2.0 ($J_{2'6'}$) and 8.2 Hz ($J_{5'6'}$); the line widths of the H-2′ and H-5′ signals indicate weak *para* coupling. Irradiation of H-8 (δ 6.379 ppm) leads to NOE enhancement of the singlet at 3.828 ppm which can, therefore, be assigned to the methoxy group at C-7 (14). Line shape analysis reveals that of the five methoxy peaks only three are broadened due to long-range spin coupling to the respective *ortho*-hydrogens (J approx. 0.2 Hz) thus permitting their assignment to MeO-7 (3.828 ppm) and MeO-3′,4′ (3.887 and 3.875 ppm) and the assignment of the singlets at 3.817 and 3.251 ppm to MeO-5 and MeO-3, respectively.

The unit cell contains two molecules which differ in the conformation of the heterocyclic ring.[2] While C-2 is above and C-3 below the plane of ring A in both molecules, the heavy atoms attached at these two positions (C-11 at C-2 and O at C-3) are located above this plane in molecule B ("sofa") and below in molecule A ("half-chair"), indicating a high degree of conformational flexibility (see Tables 4 and 5) (Fig. 1). The dihedral angles measured for the "sofa" conformation are very close to the values reported in the literature (5) for 8-bromo-tetra-*O*-methylcatechin. The O/C-2/C-3/C-4 dihedral angle of 60° shows the *trans*-diaxial arrangement of H-2 and H-3 and the quasi-equatorial position of ring B in both molecules.

[2]The complete set of data can be purchased from the Depository of Unpublished Data, CISTI, National Research Council of Canada, Ottawa, Ont., Canada K1A 0S2.

Experimental

Mass spectra were recorded on an HP-5985 quadrupole instrument, nmr spectra on a Bruker spectrometer (400 MHz); chemical shifts (in $CDCl_3$) are reported in ppm downfield from TMS.

6-Bromocatechin was prepared as described in the literature (10) and acetylated with acetic anhydride and pyridine (13). The pentaacetate (290 mg), mp 146–149°C (lit. (13) 149–151°C) was dissolved in methanol (1.5 mL) and methylated with dimethyl sulphate (0.70 mL) and 50% aqueous KOH (added dropwise over a 1-h period) according to Freudenberg's procedure (12). The usual workup gave a mixture (133 mg) containing 6-bromotetra-*O*-methylcatechin (**1**) as major product, with melting point (126–128°C) and pmr spectrum of a purified sample identical to the values reported in the literature (6, 13), and 6-bromo-3′,4′,5(or 7)-tri-*O*-methyl-7(or 5)-*O*-acetylcatechin as minor product, identified by its pmr parameters: δ 6.980/6.936/6.894 (3H, dd/d/d, J = 2.0 and 8.2 Hz, H-2′/5′/6′), 6.454 (s, H-8), 4.653 (d, J = 8.6 Hz, H-2), 4.06 (m, H-3), 3.887/3.821 (s, 9H, 3 × OMe), 2.97/2.62 (m, 2H, H-4), and 2.360 (s, 3H, OAc).

Exhaustive methylation (11) of the mixture (42 mg) in DMF (0.40 mL) with silver oxide (50 mg) and methyl iodide (0.16 mL, added in four portions over a period of six days) gave the title compound in 93%

TABLE 2. Bond distances

Bonds	Distance (Å)	
	Molecule A	Molecule B
Br(6)—C(6)	1.869(11)	1.906(9)
O(1)—C(2)	1.444(11)	1.452(11)
O(1)—C(9)	1.406(13)	1.338(13)
O(31)—C(3)	1.414(11)	1.420(12)
O(31)—C(31)	1.421(11)	1.359(13)
O(51)—C(5)	1.416(12)	1.353(12)
O(51)—C(51)	1.415(13)	1.413(14)
O(71)—C(7)	1.365(14)	1.381(14)
O(71)—C(71)	1.397(15)	1.426(14)
O(131)—C(13)	1.363(12)	1.372(13)
O(131)—C(131)	1.409(15)	1.452(15)
O(141)—C(14)	1.368(13)	1.366(12)
O(141)—C(141)	1.442(14)	1.432(14)
C(2)—C(11)	1.515(11)	1.487(11)
C(2)—C(3)	1.504(11)	1.539(11)
C(11)—C(12)	1.388(13)	1.391(14)
C(11)—C(16)	1.356(13)	1.389(13)
C(12)—C(13)	1.396(14)	1.356(17)
C(13)—C(14)	1.408(16)	1.401(17)
C(14)—C(15)	1.333(15)	1.410(14)
C(15)—C(16)	1.367(14)	1.412(13)
C(3)—C(4)	1.473(14)	1.554(14)
C(4)—C(10)	1.545(15)	1.468(17)
C(5)—C(6)	1.349(15)	1.409(16)
C(5)—C(10)	1.385(15)	1.391(15)
C(6)—C(7)	1.419(14)	1.356(15)
C(7)—C(8)	1.409(17)	1.349(14)
C(8)—C(9)	1.372(17)	1.405(16)
C(9)—C(10)	1.387(14)	1.382(15)

yield, mp 140−142°C after recrystallization from EtOH. *Anal.* calcd. for $C_{20}H_{23}BrO_6$: C 54.68, H 5.28; found: C 54.47, H 5.28. Mass spectrum (70 eV): molecular ion at *m/e* 438 (4.0) and 440 (3.3), 289 (7.2), 287 (7.0), 195 (11.5), 194 (100), 179 (16.0), and 151 (7.0). Cmr (100.6 MHz) δ 25.0 (C-4), 56.0, 56.4, 57.4 (ArO*Me*), 60.2 (RO*Me*), 76.5 (C-3), 80.0 (C-2), 96.9 (C-8), 98.2 (C-6), 107.7 (C-10), 110.1, 111.4 (C-2′, C-5′), 119.4 (C-6′), 131.3 (C-1′), 149.2 (C-3′, C-4′), 154.7, 156.0 (C-5, C-7), and 156.5 (C-9).

Structure determination

Crystal data fw = 439.14

$C_{20}H_{23}BrO_6$

Triclinic $P1$, a = 9.589(3) Å, b = 11.576(3) Å, c = 11.326(3) Å, α = 118.80(3)°, β = 93.23(3)°, γ = 111.44(3)°, V = 982.8 Å^3, ρ_c = 1.481 g cm^{-3}, Z = 2, μ = 20.998 cm^{-1}, γ (MoKα_1) = 0.70930 Å, F(000) = 451.94.

A colourless rectangular shaped crystal (0.28 × 0.22 × 0.40 mm) was mounted on a Nonius CAD4F diffractometer with a graphite monochromator. Cell dimensions were determined using 25 independent reflections (2θ = 17−31°). The take-off angle was 2.9° and a symmetrical θ−2θ scan of (1.3 + 0.692 tan θ)° was used. Intensity data were collected in the 2θ ≤ 45° region at a variable speed (minimum 2°θ min^{-1}). The intensities of two standards were measured every 100 reflections and they were used to scale the data (±3.5%). Amongst 2584 independent reflections, 2213 were observed ($I > 3.0\sigma(I)$), and the structure analysis is based on them. Analytical absorption corrections were applied by the method of Tompa (τ = 0.524−0.659) (8*a*).

Conventional Patterson and Fourier methods were used to solve the structure. Refinement by full-matrix least-squares proceeded slowly. The chirality of the molecule was confirmed prior to inclusion of the hydrogen atoms and anisotropic refinement of the lighter atoms. Several cycles of refinement, not including anomalous scattering, were followed by two independent refinements (for each band), the difference in results being R = 0.0617, R_w = 0.0685 and GOF = 9.53 for the correct (indicated) model and R = 0.0629, R_w = 0.0703 and GOF = 9.78 for the alternative. $R = \Sigma||F_o| - |F_c||/\Sigma|F_o|$, $R_w = [\Sigma_w(|F_o| - |F_c|)^2/\Sigma_w|F_o|^2]^{1/2}$, and GOF $= (\Sigma_w(|F_o| - |F_c|)^2/(N_{obs} - N_{var}))^{1/2}$. Hydrogen atoms were mostly located from electron density difference maps and in all cases recalculated with a C—H distance of 0.95 Å. The temperature factors assigned were 7.11 Å^2 for methyl hydrogen atoms and 4.74 Å^2 for the remainder.

TABLE 3. Bond angles

Bonds	Angle (deg)	
	Molecule A	Molecule B
C(2)—O(1)—C(9)	115.9(7)	116.0(8)
C(3)—O(31)—C(31)	113.5(7)	115.3(8)
C(5)—O(51)—C(51)	113.9(8)	117.4(8)
C(7)—O(71)—C(71)	116.8(9)	119.5(9)
C(13)—O(131)—C(131)	117.3(8)	117.0(9)
C(14)—O(141)—C(141)	117.0(9)	117.4(8)
O(1)—C(2)—C(11)	105.3(6)	108.5(7)
O(1)—C(2)—C(3)	111.1(6)	109.2(7)
C(11)—C(2)—C(3)	117.8(7)	114.8(6)
C(2)—C(11)—C(12)	117.4(8)	123.3(9)
C(2)—C(11)—C(16)	124.0(8)	118.9(8)
C(12)—C(11)—C(16)	118.6(9)	117.8(9)
C(11)—C(12)—C(13)	120.6(9)	122.5(10)
O(131)—C(13)—C(12)	124.3(9)	126.9(11)
O(131)—C(13)—C(14)	118.1(9)	112.4(11)
C(12)—C(13)—C(14)	117.6(9)	120.7(10)
O(141)—C(14)—C(13)	112.4(9)	117.5(9)
O(141)—C(14)—C(15)	126.7(10)	123.7(9)
C(13)—C(14)—C(15)	120.7(10)	118.7(9)
C(14)—C(15)—C(16)	120.4(9)	119.1(9)
C(11)—C(16)—C(15)	121.7(8)	121.2(8)
O(31)—C(3)—C(2)	103.2(6)	107.9(7)
O(31)—C(3)—C(4)	111.1(8)	113.8(8)
C(2)—C(3)—C(4)	112.5(8)	108.0(7)
C(3)—C(4)—C(10)	111.1(8)	113.3(8)
O(51)—C(5)—C(6)	119.8(9)	119.2(10)
O(51)—C(5)—C(10)	116.1(9)	122.0(10)
C(6)—C(5)—C(10)	123.7(9)	118.7(9)
Br(6)—C(6)—C(5)	121.0(7)	119.3(8)
Br(6)—C(6)—C(7)	119.1(8)	120.0(8)
C(5)—C(6)—C(7)	119.9(10)	120.7(9)
O(71)—C(7)—C(6)	116.5(10)	116.1(9)
O(71)—C(7)—C(8)	126.0(9)	121.9(10)
C(6)—C(7)—C(8)	117.3(11)	121.7(10)
C(7)—C(8)—C(9)	120.3(10)	118.4(9)
O(1)—C(9)—C(8)	113.6(9)	117.2(9)
O(1)—C(9)—C(10)	124.0(10)	121.2(11)
C(8)—C(9)—C(10)	122.3(10)	121.6(10)
C(4)—C(10)—C(5)	124.6(9)	118.6(10)
C(4)—C(10)—C(9)	118.8(10)	122.7(10)
C(5)—C(10)—C(9)	116.5(10)	118.7(10)

Final full-matrix least-squares refinement was carried out for all non-hydrogen atoms (anisotropic temperature factors). The final agreement was R = 0.0268 and R_w = 0.034 and GOF = 1.48 for 484 variables. A weighting scheme of the form $w = 1/(\sigma^2(F_o) + kF_o^2)$ was applied (where k = 0.0004) and did not show any systematic trends as a function of $|F_o|$, sin θ/λ or h, k, l. The final difference map had, as its only major feature, six peaks and troughs (max. 0.38(5), −0.22(5) e/Å^3) around the bromine atoms.

The atomic scattering factors, including anomalous scattering, were taken from ref. 9. The computer programs used are those from ref. 8. Final coordinates are listed in Table 1, and interatomic distances and angles are listed in Tables 2 and 3.

TABLE 4. Deviations of heterocyclic ring atoms from the mean plane of the fused benzene ring

(*a*) Equations of the best planes

Plane	Equation	χ^2
(*1*)	$-0.6737x + 0.1164y + 0.7228z + 2.600 = 0$	8.9
(*2*)	$-0.6621x + 0.0782y + 0.7442z - 1.697 = 0$	7.0

(*b*) Deviations from the best plane (Å)

	Deviation	
Atom	Plane (*1*) Molecule A	Plane (*2*) Molecule B
O(1)	0.10(2)	−0.06(2)
O(31)	0.15(3)	−0.34(3)
C(2)	−0.16(2)	−0.61(2)
C(11)	0.22(3)	−0.62(3)
C(3)	0.50(2)	0.18(2)
C(4)	0.01(2)	0.05(2)
C(9)	0.01(2)	−0.02(2)
C(10)	−0.03(2)	0.00(2)

TABLE 5. Dihedral angles in heterocyclic ring

	Angle (deg)	
Bonds	Molecule A	Molecule B
O(1)—C(2)—C(3)—C(4)	−60(1)	−60(1)
C(2)—C(3)—C(4)—C(10)	+46(1)	+34(1)
C(3)—C(4)—C(10)—C(9)	−17(2)	−4(2)
C(4)—C(10)—C(9)—O(1)	+1(2)	−4(2)
C(10)—C(9)—O(1)—C(2)	−14(2)	−24(2)
C(9)—O(1)—C(2)—C(3)	+42(1)	+56(1)

Acknowledgements

We wish to thank D. Cherniwchan for technical assistance and NSERC for financial support.

1. C. LIEBERMANN and TAUCHERT. Chem. Ber. **13**, 694 (1880).
2. (*a*) ST. V. KOSTANECKI and R. G. KREMBS. Chem. Ber. **35**, 2410 (1902); (*b*) ST. V. KOSTANECKI and V. LAMPE. Chem. Ber. **39**, 4007 (1906); **40**, 4910 (1907).
3. (*a*) K. FREUDENBERG, L. ORTHNER, and H. FIKENTSCHER. Liebigs Ann. Chem. **436**, 286 (1924); (*b*) K. FREUDENBERG and L. PURRMANN. Liebigs Ann. Chem. **437**, 274 (1924).
4. K. WEINGES, W. KALTENHAEUSER, H.-D. MARX, E. NADER, F. NADER, J. PERNER, and D. SEILER. Liebigs Ann. Chem. **711**, 184 (1968).
5. D. W. ENGEL, M. HATTINGH, H. K. L. HUNDT, and D. G. ROUX. J. Chem. Soc. Chem. Commun. 695 (1978).
6. (*a*) H. K. L. HUNDT and D. G. ROUX. J. Chem. Soc. Chem. Commun. 696 (1978); (*b*) H. K. L. HUNDT and D. G. ROUX. J. Chem. Soc. Perkin Trans. 1, 1227 (1981).
7. K. WEINGES, W. EBERT, D. HUTHWELKER, H. MATTAUCH, and J. PERNER. Liebigs Ann. Chem. **716**, 114 (1969).
8. (*a*) J. DEMEULENAER and H. TOMPA. Acta Crystallogr. **19**, 1014 (1965); (*b*) A. C. LARSON and E. J. GABE. Computing in crystallography. *Edited by* H. Schenk *et al.*, Delft University Press, Holland, 1978. p. 81.
9. D. T. CROMER and J. T. WABER. International tables for X-ray crystallography. Vol. IV. Kynoch Press, Birmingham, England. 1974.
10. E. KIEHLMANN, P. J. VAN DER MERWE, and H. K. L. HUNDT. Org. Prep. Proc. Int. **15**, 341 (1983).
11. T. PURDIE and J. C. IRVINE. J. Chem. Soc. **83**, 1021 (1903).
12. K. FREUDENBERG. Liebigs Ann. Chem. **433**, 230 (1923).
13. G. W. MCGRAW and R. W. HEMINGWAY. J. Chem. Soc. Perkin Trans. 1, 973 (1982).
14. G. SCHILLING. Liebigs Ann. Chem. 1822 (1975).

A vanadium-51 nuclear magnetic resonance investigation of vanadate oxyanions in a lyotropic liquid crystalline bilayer system

ALAN S. TRACEY[1] AND KEITH RADLEY

Department of Chemistry, Simon Fraser University, Burnaby, B.C., Canada V5A 1S6

Received August 7, 1984

ALAN S. TRACEY and KEITH RADLEY. Can. J. Chem. **63**, 2181 (1985).

The vanadate ion VO_4H^{2-} and two of its polymeric forms contained in mixed lyotropic mesophase prepared from potassium dodecanoate/*n*-alkyltrimethylammonium bromide in water have been investigated by ^{51}V nuclear magnetic resonance spectroscopy. The results indicate that the tetrahedral ion interacts with the micellar surface through the hydrating water associated with this ion. The ion undergoes strong interactions with the carboxylate headgroup of the dodecanoate as well as with the headgroup of the alkyltrimethylammonium detergent, which of course is of opposite charge. The other two species investigated have previously been assigned by various workers to $V_2O_7^{4-}$ and its cyclic dimer $V_4O_{12}^{4-}$. The results obtained here are not consistent with those assignments but rather with more symmetrical compounds such as the tetrahedral uncharged molecule V_4O_{10} and a higher analogue of this, respectively. The nmr spectra from these latter species show that they undergo, at best, extremely weak interactions with the cationic surface but strong interactions with an anionic one. The behaviour of the quadrupole splittings observed is consistent with specific interactions to the carboxylate moiety. The observation of an induced chemical shift separation between vanadium resonances from the same highly symmetric species confirms that binding of this compound is very strong.

ALAN S. TRACEY et KEITH RADLEY. Can. J. Chem. **63**, 2181 (1985).

Faisant appel à la rmn du ^{51}V, on a étudié l'ion vanadate VO_4H^{2-} et deux de ses formes polymériques contenus dans une mésophase lyotrope préparée à partir de dodecanoate de potassium/bromure de *n*-alkyltriméthylammonium dans de l'eau. Les résultats indiquent que l'ion tétraédrique interagit avec la surface micellaire par le biais de l'eau hydratante qui est associée avec cet ion. L'ion subit de fortes interactions du groupe carboxylate du dodécanoate de même que du groupe alkyltriméthylammonium du détergent qui est de charge opposée. Pour les deux autres espèces étudiées, divers auteurs leurs avaient antérieurement attribué les structures suivantes: $V_2O_7^{4-}$ et son dimère cyclique $V_4O_{12}^{4-}$. Les résultats obtenus dans notre travail ne sont pas en accord avec ces attributions; ils favorisent plutôt des structures plus symétriques comme celles d'une molécule tétraédrique ne portant pas de charge, V_4O_{10}, ainsi que celle d'un de ses analogues supérieurs. Les spectres rmn de ces espèces montrent que, dans les meilleures conditions, ils ne subissent que de faibles interactions avec la surface cationique alors qu'ils subissent de fortes interactions avec la surface anionique. Le comportement observé pour les couplages quadrupolaires est en accord avec les interactions spécifiques de la portion carboxylate. La présence d'une séparation induite par le déplacement chimique, entre les diverses résonances du vanadium des mêmes espèces hautement symétriques, confirme que la coordination de ce composé est très forte.

[Traduit par le journal]

Introduction

The oxyanions of vanadium (V) display a complex chemistry in aqueous solution, forming an extensive array of anionic forms varying from the monomeric VO_4^{3-} to the polymeric decavanadate $V_{10}O_{28}^{6-}$. These ions have been investigated by ^{51}V nuclear magnetic resonance (nmr) spectroscopic techniques and structures have been assigned to most of the observed resonances (1−6).

Vanadate oxyanions are of great importance to the life processes of biological systems, vanadium apparently being an essential nutrient which appears to have its major effect on the action of enzymes (7). However, its function is not well understood.

In view of both the intrinsic interest in vanadate anions themselves and of their importance in living systems, it was decided to investigate the behaviour of these ions in the liquid crystalline bilayer system prepared from potassium dodecanoate/*n*-alkyltrimethylammonium bromide combined in various proportions in D_2O. This system is particularly useful since the charge on the bilayer surface can be varied as desired. Details of ion binding interactions not otherwise readily available can be obtained via the nuclear quadrupole splitting (8, 9).

Vanadium-51 is a spin 7/2 nucleus and therefore has an electric nuclear quadrupole moment. As a consequence of the quadrupole moment, ^{51}V provides nmr spectra characterized by a chemical shift and a quadrupole splitting when contained in an anisotropic solvent. The quadrupole splitting, $\Delta\nu$, is dependent on the partial alignment of the quadrupolar nucleus with respect to the applied magnetic field of the nmr spectrometer, so that eq. [1] is obtained, where Q_v is the quadrupole coupling constant for ^{51}V in the chemical species of interest and

$$[1] \quad \Delta\nu = \frac{Q_v}{2I(2I-1)}(3S'_{zz} + \eta(S'_{xx} - S'_{yy}))$$

I is the nuclear spin (10). η is a measure of the asymmetry in Q_v and this term is not important for the highly symmetrical species investigated here. The various S'_{ii} are order parameters describing the partial alignment of the molecular fixed electric field gradients, which alignment gives rise to the quadrupole splitting. The S'_{ii} can be written in terms of a molecular based coordinate system but this transformation is not necessary for this study.

Quadrupole splittings from molecular or ionic species with tetrahedral or higher symmetry can only arise by distorting the highly symmetric shape to lower symmetry. Specific interactions (11, 12) including those resulting from ion binding (11) can cause distortions, therefore giving rise to such splittings. If the molecule being investigated has symmetry lower than tetrahedral, the forces within the liquid crystal will impose a partial alignment and quadrupole splittings will be obtained. The imposition of alignment may be taken to represent the fact that the three spatial coordinate axes are not equivalent. The

[1]Author to whom correspondence may be addressed.

TABLE 1. Mesophase compositions and observed quadrupole splittings from the various components in this liquid crystalline system

	Composition[a]				Spectral parameters (Hz)[b]				
X	K Dodec[c]	TDTMABr[d]	DTMABr[e]	Decanol	$\Delta\nu$ (D)	$\Delta\nu$ (Na)	$\Delta\nu_1$ (V)	$\Delta\nu_2$ (V)	SW_2 (V)
0.0	—	336	—	50	25	709	174	—	66
0.1	24	303	—	35	22	409	154	—	54
0.2	47	270	—	20	17	34	144	—	59
0.3	71	236	—	0	1	386	119	—	99
0.4	95	—	168	25	17	953	104	—	270
0.5	119	—	140	10	51	1812	124	—	613
0.6	143	—	112	10	93	1747	101	—	969
0.7	166	—	84	0	124	824	76	—	1028
0.8	190	67	—	10	155	605	81	221	1418
0.9	214	34	—	30	209	3679	85	298	1792
1.0	238	—	—	50	253	7002	94	340	2114

[a]Compositions are given in mg. The amount of D_2O used was 880 mg for each sample (D_2O contained 7.5 wt.% CsCl and 2.5 wt.% Na_3VO_4). X is the mole fraction of potassium dodecanoate in total detergent.
[b]$\Delta\nu$ (x) gives the quadrupole splittings observed for the nucleus x, while SW_2 gives the spectral width observed for the vanadium resonance of species 2.
[c]Potassium dodecanoate.
[d]Tetradecyltrimethylammonium bromide.
[e]Decyltrimethylammonium bromide.

liquid crystalline materials used here have a unique axis, the optic axis.

At the vanadate concentration and pH of the solutions investigated here three species are observable. The two major components correspond in chemical shift to those ions assigned to VO_4H^{2-} and $V_2O_7^{4-}$ while the minor component corresponds to $V_4O_{12}^{4-}$ (3–5). VO_4H^{2-} is the monoprotonated derivative of the tetrahedral ion VO_4^{3-} while $V_2O_7^{4-}$ and $V_4O_{12}^{4-}$ are the dimer and tetramer of this ion, the vanadium atoms being linked through oxygen.

Experimental

The liquid crystalline materials used in this study have been described elsewhere and the procedure used here differs little from that previously reported (8, 9, 13). The compositions for the various mesophases studied are given in Table 1. ^{51}V and ^{17}O nmr spectra were obtained at 30°C from a 400-MHz broadband nmr spectrometer operating unlocked in the FT mode at ambient temperature.

The assignment of ^{51}V resonances in the liquid crystal spectra was carried out by comparison of those spectra to spectra from aqueous solutions of varying composition and pH. The relevant spectra were distinguished only by minor differences from those given in ref. 4. No significant chemical shift differences between isotropic and anisotropic spectra were observed.

Spectra were also obtained from solutions similar to those of the bottom entry of Table 1, except that decanol was not included in the preparation so that the solution was isotropic. The two major ^{51}V signals were studied as a function of vanadate concentration.

A solution similar to the top entry of Table 1 was prepared using ^{17}O enriched H_2O (15 at.% ^{17}O) but with no decanol, so that the solution was isotropic. Several ^{51}V and ^{17}O spectra were obtained and carefully integrated. The requisite quantity of decanol was then added to the sample so as to form the nematic material. Further ^{17}O and a ^{51}V spectrum were obtained. ^{17}O assignments were taken from ref. 4.

Vanadium chemical shifts are reported relative to $VOCl_3$ prepared as an external reference, while oxygen shifts are relative to the ^{17}O of the water.

Results and discussion

The results of this study are summarized in Table 1. Figure 1 shows the various vanadium spectra obtained on proceeding through the series of mesophases starting with 100% anionic amphiphile (potassium dodecanoate) to 100% cationic amphiphile (tetradecyltrimethylammonium bromide). There are various puzzling features of these spectra which must be explained.

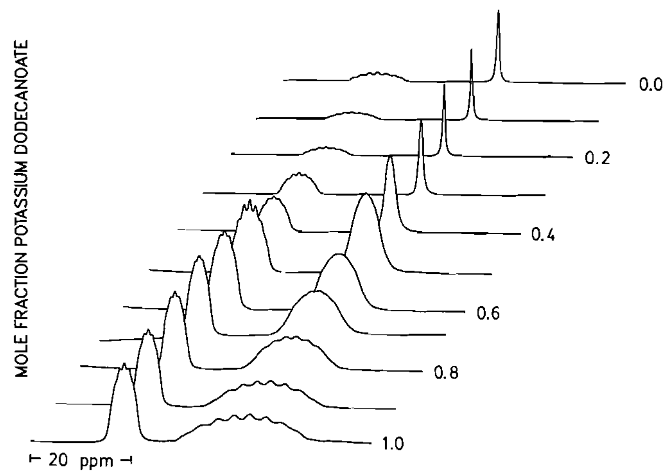

FIG. 1. The ^{51}V nmr spectra obtained from the vanadate species as the mole fraction, X, of anionic detergent in total detergent was varied from $X = 0$ to $X = 1$.

Turning first to the quadrupole splittings for Na^+ and D_2O contained in the various samples (Table 1), it is observed that the values are typical for these materials (8, 9, 13). Some minor problems were encountered with the formation of 50 and 60 mol% phases, as seen in Fig. 1, but this is not important here. It is important to note that quadrupole splittings of up to several kHz were induced in the nominally spherical hydrated sodium ion by interactions with the anisotropic solvent.

From Fig. 1 it is observed that one vanadate species provides quadrupole splittings throughout the range of compositions. From its chemical shift, −537.5 ppm, and from dilution and pH studies in aqueous solution this resonance is assigned to VO_4H^{2-}, which is in agreement with the detailed work of other groups (2–6). The magnitude of the quadrupole splittings is

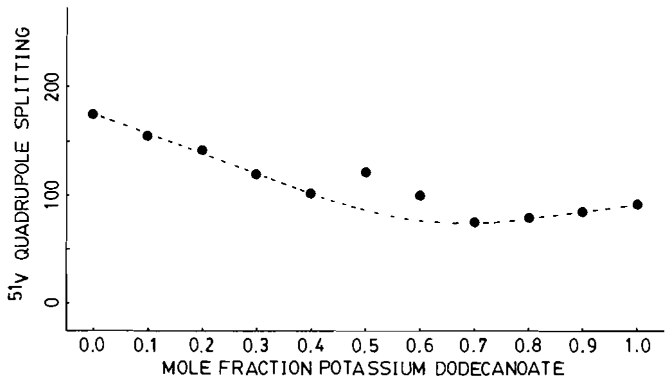

FIG. 2. The variation in the ^{51}V quadrupole splitting from the VO_4H^{2-} ion throughout the range of compositions of mesophases employed in this study. The dashed line has no theoretical significance.

small, as expected from a vanadium nucleus in a tetrahedral environment. In fact the magnitude of the splitting is consistent with an ion that is very close to perfectly tetrahedral, which indicates that the proton of this ion, VO_4H^{2-}, is probably only associated with the ion through the waters of hydration, so that tetrahedral symmetry is not lost.

Figure 2 shows the variation of quadrupole splitting from the VO_4H^{2-} ion as the charge on the micellar surface is varied from fully positive, $X = 0$, to fully negative, $X = 1.0$. The jog in the figure at $X = 0.5$ and $X = 0.6$ is associated with mesophase formation problems, probably a result of the alkaline conditions employed. On proceeding from the anionic mesophase $X = 1$ to $X = 0.7$ there is a gradual decrease in the quadrupole splitting. A minimum is reached between $X = 0.5$ and 0.6, at which point the splitting begins to increase, reaching a maximum at $X = 0$, the cationic mesophase. The magnitude of the maximum change in quadrupole splittings, about a factor of two, is not indicative of major changes in the mechanism of binding to the interface. The presence of a minimum in the curve may indicate that this ion, although carrying a negative charge, undergoes positive interactions with both the cationic and the anionic surfaces, although three-site binding cannot be ruled out. It has previously been found that the negatively charged aluminum ion, $Al(OH)_4^-$, interacts strongly in a positive manner with carboxylate groups (8). It was suggested in that case that binding to the carboxylates occurred through the hydrating water. A similar mechanism may be operative here.

On turning to Fig. 1 it is clear that the second resonance investigated here, which occurs at −552.1 ppm, shows a much different behaviour from that of the vanadate ion. This resonance corresponds to that which has been assigned to the $V_2O_7^{4-}$ ion. Because of the low symmetry of such an ion the forces of the anisotropic solvent should easily align it to give quadrupole splittings, particularly in the cationic mesophase. ^{51}V quadrupole splittings not only are not observed in that mesophase but the measured linewidths are not significantly different from those in normal aqueous medium, being about 60 Hz in either case. Furthermore, quadrupole splittings, as evidenced by increasing linewidth, for this species arise only when a signitficant proportion (≈40%) of cationic amphiphile has been replaced by the anionic material. Since quadrupole splittings were not resolved in the majority of the spectra, Fig. 3 shows the total linewidth of this resonance as a function of the mole fraction of potassium dodecanoate. The spectral width when corrected for the linewidth of a single transition,

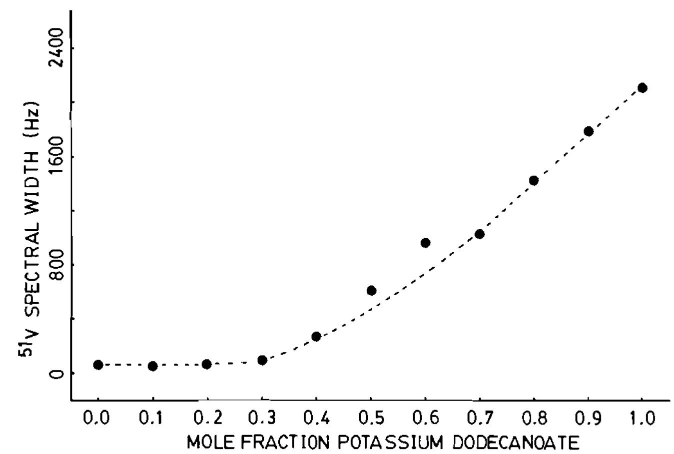

FIG. 3. The spectral width variation of the ^{51}V resonance from the second component observed in this study. No theoretical significance should be attached to the dashed line.

then divided by six, is a reasonable approximation to the quadrupole splitting, as is easily verified from Table 1.

It is possible to provide rational arguments, based on structure and orientation, to explain the absence of ^{51}V quadrupole splittings from this ion. Such arguments cannot simultaneously account for the absence of dipolar couplings between the two vanadium nuclei. In addition the ^{17}O spectrum from an ^{17}O-enriched sample showed no quadrupole splitting from the oxygens of this ion. It can only be that the ion is not being aligned by the anisotropic forces of the cationic solvent. It is extremely difficult to rationalize this conclusion in terms of the $V_2O_7^{4-}$ ion. Some information concerning this species is provided by comparing oxygen and vanadium spectra of an isotropic solution prepared according to the composition of the top entry of Table 1, but without the decanol. From several independent vanadium spectra, a ratio of intensities for the −537 and −562-ppm resonances of 1:0.82 ± 0.02 was obtained. The corresponding ratio in the oxygen spectrum was 1:0.54 ± 0.02, where the errors represent the maximum deviation from the mean. From these values and assuming that VO_4H^{2-} is the correct structural assignment for the −537 and 574.5-ppm resonances of the vanadium and oxygen spectra, respectively, a ratio of 2:5.3 ± 0.2 for V to O is obtained. This provides the possible formulae $n(V_2O_5)$ and $n(V_4O_{11})$. Interestingly enough, if it is assumed that the species presumed to be VO_4 is actually VO_6, then a ratio of vanadium to oxygen for the second species of 1:4.0 ± 0.2 is obtained. The oxygen signal of this second compound occurs at 696.8 ppm. Two other signals are observed which occur at 407 and 713 ppm. The former has previously been assigned to the bridging oxygen of $V_2O_7^{4-}$, the latter has not previously been reported. It is not clear that either are associated with the much more intense 696.8-ppm resonance. The 713-ppm ^{17}O resonance may be associated with the low intensity ^{51}V signal not yet discussed.

The third ^{51}V species investigated in this study, occurring at −573.1 ppm but not seen in Fig. 1 because of its low concentration, also shows no quadrupole splittings in the $X = 0$ to $X = 0.3$ range of the nematic solutions. This latter species has been tentatively identified as the cyclic tetramer $V_4O_{12}^{4-}$ (4). Again, the absence of partial alignment is difficult to accept. There are various lines of evidence which point to the high symmetry of the species giving rise to the −562.1-ppm ^{51}V resonance. They include the ^{51}V linewidth of about 60 Hz, which is comparable to that of the −537.5 ppm (VO_4H^{2-}) resonance. Narrow linewidths derive from inefficient quadrupole relaxation, a consequence of high symmetry. The most compelling evidence for high symmetry is the fact that there is no alignment of this compound in the cationic liquid crystalline solution. No compound of other than tetrahedral or higher symmetry has been observed not to align in a liquid crystalline medium and even such highly symmetrical species almost invariably give rise to quadrupole or dipole splittings because of distortion forces. In this vanadium case, we have not one but two species which are not aligned yet have been assigned structures not compatible with that finding. It is therefore proposed that the second species being observed is V_4O_{10}, the tetrahedral uncharged dimer of $V_2O_7^{4-}$, while the third species is a higher analogue. V_4O_{10} will have vanadium at the vertices of a tetrahedron with linkages occurring through oxygen. Like other tetrahedral species, quadrupole splittings can only be observed if the molecule is distorted from its high symmetry by interactions with the solvent.

Irrespective of identity, it is clear that this compound undergoes extremely weak if not repulsive interactions with the positively charged surface and only begins interacting with the interface when about 40% of the amphiphilic headgroups in the interface are carboxylates. There follows an approximately linear increase in quadrupole splitting with dodecanoate concentration, which indicates that specific interactions between the carboxylate groups of potassium dodecanoate and this vanadate species occur. An important aspect of the signal is the apparent lack of resolution until high concentrations of carboxylate are employed, at which point not seven but eight transitions occurring in pairs of equal intensity were obtained. This behaviour can be seen, although not clearly, in Fig. 1. Such a spectrum can only be ascribed to two superimposed, equally intense spectra chemically shifted from each other by about one quadrupole splitting. Spectra simulation served to confirm this conclusion. Heating the sample until it became isotropic (337 K) caused collapse of the spectrum to a single transition. Furthermore, preparation of samples similar to the bottom entry of Table 1 for which the composition was unchanged, except for the absence of decanol (thus providing an isotropic solution), also provided a single transition for this species. From this it is apparent that collapse of this spectrum to a single transition results from the loss of an induced shift because of the change to isotropic medium. Liquid crystals can induce chemical shifts because the shift is a tensor quantity and, like quadrupole splittings, is orientation dependent (14, 15).

It is clear from these results that this species interacts very strongly with the carboxylate headgroups of the bilayer interface. The binding is sufficient to slow exchange enough to see signals from two types of vanadium nuclei in the same molecule via an induced chemical shift. These nuclei would be identical if the molecule was not bound. This accounts for the broadness of the transitions in the intermediate regions of Fig. 1, where exchange occurs at a rate comparable to chemical shift.

Dilution studies were carried out for preparations in which decanol was not included. While the other components were kept at constant proportions the vanadate concentration was decreased by factors of 2 to a total change of 64. The relative proportions of the two components were obtained from the nmr spectra. Comparison of these proportions with those calculated from a simple equilibrium expression indicated the presence of an equilibrium of the type $3V_1 \leftrightarrows 2V_2$, where V_1 corresponds to vanadium resonance 1 and V_2 to resonance 2. These results apparently rule out an equilibrium of the type $4VO_4 \leftrightarrows V_4O_{10}$ and may indicate that resonance 1, ascribed to VO_4H^{2-}, has been incorrectly described.

The results of this dilution study are ambiguous, the situation no doubt being complicated by the presence of potassium dodecanoate. Considerably more work is required for this vanadate system, particularly in an aqueous system free from the complicating influence of detergents and electrolytes. The species assigned here and by others as VO_4H^{2-} must be unequivocally identified. Independent evidence for the structure of V_4O_{10} is also required since the results here, although indicating a highly symmetric species, do not specify the number of vanadium nuclei in that compound. Work aimed at providing an unambiguous identification of these and the various other vanadium resonances observed in aqueous solution is in progress.

Acknowledgements

Thanks are gratefully extended to the Natural Sciences and Engineering Research Council of Canada for its financial support of this work.

1. D. REHDER. Bull. Magn. Reson. **4**, 33 (1982).
2. M. T. POPE and B. W. DALE. Q. Rev. Chem. Soc. (Lond.), **22**, 527 (1968).
3. S. E. O'DONNELL and M. T. POPE. J. Chem. Soc. Dalton Trans. 2290 (1976).
4. E. HEATH and O. W. HOWARTH. J. Chem. Soc. Dalton Trans. 1105 (1981).
5. O. W. HOWARTH and R. E. RICHARDS. J. Chem. Soc. 864 (1975).
6. M. A. HABAYEB and O. E. HILEMAN, JR. Can. J. Chem. **58**, 2255 (1980).
7. T. RAMASARMA and F. L. CRANE. Curr. Top. Cell. Regul. **20**, 247 (1981).
8. A. S. TRACEY and T. L. BOIVIN. J. Am. Chem. Soc. **105**, 4901 (1983).
9. A. S. TRACEY and T. L. BOIVIN. J. Phys. Chem. **88**, 1017 (1984).
10. C. L. KHETRAPAL, A. C. KUNWAR, A. S. TRACEY, and P. DIEHL. NMR: Basic Princ. Prog. **9**, 14 (1975).
11. H. WENNERSTRÖM, G. LINDBLOM, and B. LINDMAN. Chem. Scr. **6**, 97 (1974).
12. D. BAILEY, A. D. BUCKINGHAM, F. FUJIWARA, and L. W. REEVES. J. Magn. Reson. **18**, 344 (1975).
13. L. HECKER, L. W. REEVES, and A. S. TRACEY. Mol. Cryst. Liq. Cryst. **53**, 77 (1979).
14. P. DIEHL and C. L. KHETRAPAL. NMR: Basic Princ. Prog. **1**, 11 (1969).
15. C. L. KHETRAPAL and A. C. KUNWAR. Adv. Magn. Reson. **9**, 320 (1977).

The molecular conformations of 8,11-dimethyl-5,6-benzo-2-oxo-1,3,2-dioxathiepin and 4,4-dimethyl-5,6-benzo-2-oxo-1,3,2-dioxathiepin

A. LACHAPELLE AND M. ST-JACQUES[1]

Département de Chimie, Université de Montréal, C.P. 6210, Succ. A, Montreal (Qué.), Canada H3C 3V1

Received September 19, 1984

A. LACHAPELLE and M. ST-JACQUES. Can. J. Chem. **63**, 2185 (1985).

The conformational properties of 8,11-dimethyl-5,6-benzo-2-oxo-1,3,2-dioxathiepin (**5**) and of 4,4-dimethyl-5,6-benzo-2-oxo-1,3,2-dioxathiepin (**6**) have been investigated using ^{1}H and ^{13}C dnmr as well as ir spectroscopy. Analysis of low temperature nmr spectra (down to −148°C) and of S═O stretching vibrations in room temperature ir spectra indicates that the most stable conformations detected for solutions in CHF_2Cl/CD_2Cl_2 (80:20) are TB (83%) and C-a (17%) for **5** and only the TB **7** for **6**. Substituent effects of methyl groups at the *peri* and the benzylic positions on the conformational properties of the seven-membered sulfites are discussed.

A. LACHAPELLE et M. ST-JACQUES. Can. J. Chem. **63**, 2185 (1985).

Les propriétés conformationnnelles de la diméthyl-8,11-benzo-5,6-oxo-2-dioxathiépine-1,3,2 (**5**) et de la diméthyl-4,4-benzo-5,6-oxo-2-dioxathiépine-1,3,2 (**6**) ont été étudiées à l'aide de la spectroscopie rmn dynamique ^{1}H et ^{13}C, ainsi que de la spectroscopie ir. L'analyse des spectres de la rmn à basse température (jusqu'à −148°C) et des fréquences de vibration d'élongation du lien S═O à température de la pièce indique que les conformations les plus stables en solution dans un mélange CHF_2Cl/CD_2Cl_2 (80:20) sont TB (83%) et C-a (17%) pour le composé **5** et seulement la forme TB **7** pour le composé **6**. Les effets de groupements méthyles en position *péri* ou benzylique sur les propriétés conformationnelles des sulfites à sept chaînons sont discutés.

Introduction

The conformational properties of six-membered cyclic sulfites have been thoroughly studied during the last two decades (1–8), while those of seven-membered and larger ring homologs were scarcely investigated (9–15). Recently, St-Jacques and co-workers (15) showed that enlargement from six to seven-membered ring, resulting from the replacement of the 5 methylene unit in 2-oxo-1,3,2-dioxathiane (**1**) by a benzo group, led to a change from the single C-a form, observed for **1**, to a 1:1 mixture (C-a ⇌ TB) for **2**, in CHF_2Cl, at −100°C. Further investigations (16) of methyl derivatives of **2**, using room temperature ir as well as low temperature ^{1}H and ^{13}C nmr methods, indicated that the presence of a methyl group, at the 4 position, *cis* to the S═O double bond (**3**), shifted the equilibrium toward the TB form (96% TB-*c*-Me_e and 4% TB-*c*-Me_a[2] in CHF_2Cl, at −80°C) because of severe 1,3-diaxial interactions in the C-a form. In contrast, a methyl group *trans* to the S═O double bond, at the same 4 position (**4**), unexpectedly shifted the equilibrium toward the C-a form (82% C-a and 18% TB-*t*-Me_e[2] in CHF_2Cl, at −80°C).

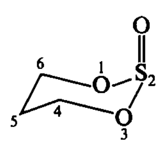

1

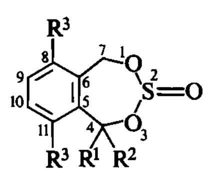

2 $R^1 = R^2 = R^3 = H$
3 $R^1 = CH_3, R^2 = R^3 = H$ (*cis*)
4 $R^1 = CH_3, R^2 = R^3 = H$ (*trans*)
5 $R^1 = R^2 = H, R^3 = CH_3$
6 $R^1 = R^2 = CH_3, R^3 = H$

These results, together with our general interest in the conformational properties of seven-membered rings, led us to investigate the conformational properties of 8,11-dimethyl-5,6-benzo-1,3,2-dioxathiepin (**5**) and of 4,4-dimethyl-5,6-benzo-1,3,2-dioxathiepin (**6**), which combine some of the structural characteristics of both compounds **3** and **4**. The additional data obtained shed some light into the nature of the interactions of methyl groups situated near the junction of the seven-membered and the aromatic rings.

TABLE 1. Infrared spectral data for the S═O stretching band of compounds **2**, **5**, and **6** in CS_2 and in CH_3CN

Compound	Solvent	(S═O) stretching band (cm^{-1})	Relative integration (%)
2	CS_2[a]	1223(S); 1184(S)[b]	46:54
	CH_3CN[a]	1210(S); 1179(S)	55:45
5	CS_2	1222(S); 1184(M)	70:30
	CH_3CN	1213(S); 1182(M)	81:19
6	CS_2	1217(S)	~100
	CH_3CN	1208(S)	~100

[a] The data for this compound were taken from ref. 16.
[b] The letters S and M refer to strong and medium intensities respectively.

Results

Infrared spectra

The ir spectra of 0.05 *M* solutions of compounds **5** and **6** were recorded both in CS_2 and in CH_3CN; they showed characteristic stretching vibrations for the S═O bond in the 1175–1230 cm^{-1} region, as reported in Table 1. Compound **5** showed two bands of unequal intensity in both solvents, a strong band at 1222 cm^{-1} and a weaker band at 1184 cm^{-1} in CS_2 in the ratio 70:30, while in CH_3CN the relative proportions of the strong band at 1213 cm^{-1} and of the weaker band at 1182 cm^{-1} are 81:19. Compound **6**, on the other hand, showed only a single strong band at 1217 cm^{-1} in CS_2; it shifted to 1208 cm^{-1} in CH_3CN.

Nuclear magnetic resonance spectra

High field ^{1}H (400 MHz) and ^{13}C (100 MHz) nmr spectra of compounds **5** and **6** were taken at different temperatures be-

[1] Author to whom correspondence should be addressed.
[2] The letters "*c*" and "*t*" refer to the *cis* and *trans* relations between the methyl group and the S═O double bond, while the letters "a" and "e", placed as subscript after Me, refer to the equatorial and axial orientations of the methyl groups in the various conformations.

TABLE 2. Carbon-13 chemical shifts and dynamic data for compounds **5** and **6** at high and low temperatures[a]

Compound	Temperature (°C)	C-4 (ppm)	C-5	C-6	C-7	C-8	C-9	C-10	C-11	CH_3	$\Delta G^{\neq}$ (kcal/mol)
5	−20	60.75	135.10[b]	135.10[b]	60.75	135.32[b]	131.23	131.23	135.32[b]	19.93	
											9.5 ± 0.3 (−58°C)
	−80	61.87[c]	134.29[b]	134.29[b]	61.87	134.54[b]	130.73	130.73	134.54[b]	20.26[c]	
		57.71	137.40[b]	137.40[b]	57.71	136.68[b]	132.19	132.19	136.68[b]	20.3[d]	
	−125	[c,e]	134.19[b]	134.19[b]	[e]	134.67[b]	130.75	130.75	134.67[b]	20.48[c]	
		57.85	136.85[b]	136.85[b]	57.85	137.29[b]	132.29	132.29	137.29[b]	20.5[d]	
											6.5 ± 0.3 (−125°C)
	−148[f]	64.02[c]	—	—	60.30	—	—	—	—		
		—	—	—	—	—	—	—	—	—	
6	−10	87.17	146.38	134.43	64.43	128.26	128.50	130.00	130.20	31.29; 32.46	
	−125	87.30	145.91	133.74	64.30	128.26	128.50	130.00	130.20	31.14; 31.92	

[a] Unless otherwise mentioned, the spectra were recorded at 100.62 MHz in CHF_2Cl (80%)/CD_2Cl_2 (20%) with internal TMS.
[b] The assignment of peaks may be reversed.
[c] The first row of chemical shifts corresponds to the most intense set of signals.
[d] This peak is hidden under the major methyl peak.
[e] Very broad line centered at 62 ppm.
[f] The spectrum was recorded at 20.13 MHz.

TABLE 3. ^1H nuclear magnetic resonance spectral parameters of the benzylic and methyl protons for compounds **5** and **6** at high and low temperatures[a]

Compound	Temperature (°C)	H-4 (ppm)	H-4′ (ppm)	H-7 (ppm)	H-7′ (ppm)	$^2J_{44'}$ (Hz)	$^2J_{77'}$ (Hz)	CH_3 (ppm)	$\Delta G^{\neq}$ (kcal/mol)
5	−10	4.96	5.81	4.96	5.81	−14.6	−14.8	2.29	9.8 ± 0.3 (−70°C)
	−95	5.06[b]	5.53	5.06	5.53	−14.7	−14.7	2.27[b]	
		4.72	6.39	4.72	6.39	−13.4	−13.4	2.40	6.3 ± 0.2 (−130°C)
	−140	5.1[b]	5.1	5.2	5.90	[c]	[c]	2.28[b]	
		4.74	6.38	4.74	6.38	−13.7	−13.7	2.42	
6	−15	—	—	4.10	6.23	—	−14.0	1.83	
								1.90	
	−130	—	—	4.62	6.25	—	−13.9	1.85	
								1.91	

[a] The spectra were recorded at 400 MHz in CHF_2Cl (80%)/CD_2Cl_2 (20%) with internal TMS.
[b] The first row of chemical shifts corresponds to the less intense set of signals.
[c] The presence of broad peaks does not allow determination of the coupling constants.

tween −15 and −140°C. Tables 2 and 3 summarize the pertinent parameters.

Compound **5** revealed two spectral modifications in both ^1H and ^{13}C spectra recorded in a CHF_2Cl/CD_2Cl_2 solvent mixture (80:20) at low temperatures, as shown in Fig. 1. The ^{13}C spectrum at −20°C shows five well-resolved signals (chemical shifts are given in Table 2), most of which were assigned from a consideration of methyl substituent effects on the parameters of the parent compound **2** (16). All carbon signals broaden at lower temperatures and give at −80°C two sets of signals in the ratio 83:17 (the letter "b" identifies the set of taller signals while the letter "c" refers to the set of weaker signals). The free activation energy for the underlying process is estimated at 9.5 ± 0.3 kcal/mol (40 ± 1 kJ/mol) at −58°C, using standard equations (17) and a transmission coefficient of 1.

At −125°C, all the minor "c" signals remain sharp, while appreciable broadening occurs for one of the major "b" quaternary carbons signals (134.54 ppm at −80°C) as well as for the major "b" benzylic carbon signal (61.87 ppm). This last signal, when recorded at 20 MHz down to −148°C, splits into two lines of equal intensities, as shown in the inset of Fig. 1. A free activation energy of 6.5 ± 0.3 kcal/mol (27 ± 1 kJ/mol) at −125°C was estimated for that second process, using a method similar to that for the higher energy process.

The ^1H spectrum of compound **5** at −10°C, on the right hand side of Fig. 1, reveals a low-field averaged AX pattern (H-4 and H-7 methylene protons) and a high-field singlet (methyl protons) whose parameters are given in Table 3. The AX pattern undergoes two major modifications at lower temperatures. First, a process transforms the four methylene lines into eight lines at −85°C consisting of a minor AX pattern, labelled "c", and a major AB pattern labelled "b". The left side of that AB pattern further broadens at lower temperatures to give, at −140°C, two broadened peaks at 5.9 and 5.1 ppm, as illustrated by the splitting diagram. The signal at 5.1 ppm is partially obscured from overlap with the right half of the AB pattern observed at −85°C and which has only broadened at −140°C. A free activation energy of 6.3 ± 0.3 kcal/mol (26 ± 1 kJ/mol) was estimated for that last process at −130°C.

In contrast, the ^1H methyl signal undergoes only one spectral change at lower temperatures, whereby the singlet at −20°C splits into two lines (also labelled "b" and "c") of unequal

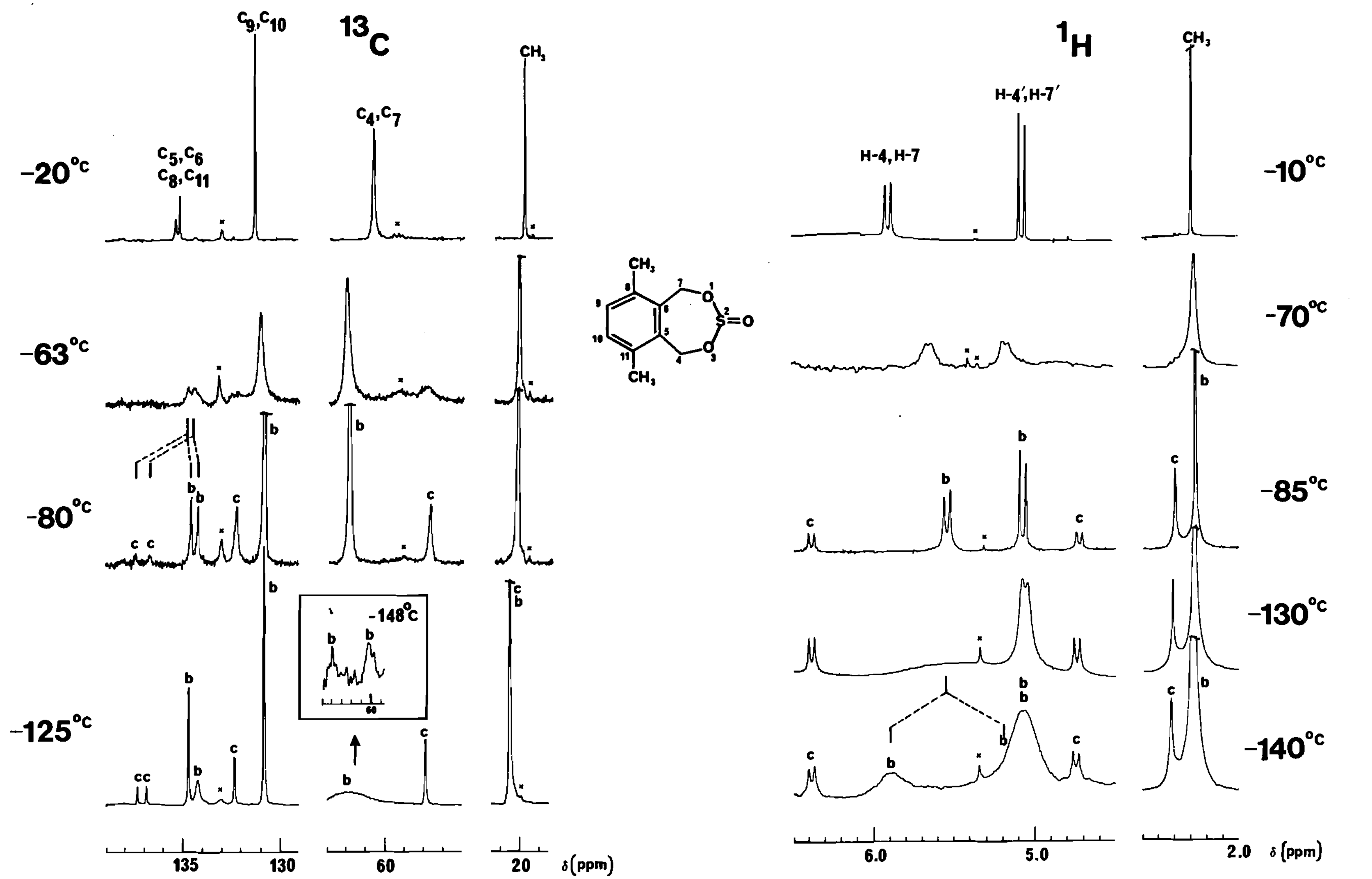

FIG. 1. Partial 100.6-MHz ^{13}C (left-hand side) and 400.1-MHz ^{1}H (right-hand side) nmr spectra of **5** in CHF_2Cl/CD_2Cl_2 (80:20) at several temperatures. The meaning of the letters b and c is given in the text. Small impurity signals are denoted by X. The origin of the signals in the inset on the bottom left-hand side is discussed in the text.

intensities at −85°C. A free activation energy of 9.8 ± 0.3 kcal/mol (41 ± 1 kJ/mol) was estimated for the underlying process at −70°C. Further lowering of the temperature down to −140°C only broadens these two unequal lines.

By comparison, compound **6** showed no spectral modification down to −125°C, for both ^{1}H and ^{13}C spectra taken in a CHF_2Cl/CD_2Cl_2 solvent mixture (80:20). The ^{13}C spectrum at −10°C reveals ten signals which were readily identified using the same procedure as for compound **5**. Table 2 contains the pertinent ^{13}C chemical shift parameters. The ^{1}H spectrum of **6** at −15°C shows a low-field AX pattern (H-7 methylene protons) and two high-field singlets (methyl protons). All signals broadened at low temperature, but no ^{1}H spectral splitting was observed down to −125°C. Table 3 contains the pertinent ^{1}H parameters.

Discussion

Ring conformation from infrared spectra

Extensive infrared investigations of six-membered cyclic sulfites revealed that specific frequency domains, associated with the S=O stretching vibration, are characteristic of each of the three possible spatial arrangements for the sulfite moiety (axial, isoclinal, or equatorial) (1). This relation holds only when molecular association effects are negligible, as for concentrations of 0.05 *M* or less. These frequency domains later proved to be equally applicable to seven-membered cyclic sulfites (11, 15) for which the straightforward observation of the S=O stretching bands in the 1150–1300 cm^{-1} region constitutes a direct probe for the conformational disposition of the sulfite moiety. This information then permits unambiguous identification of chair (C) or twist-boat (TB) ring geometries.

The ir spectra of **5**, for example, reveal two bands in both CS_2 and CH_3CN, as summarized in Table 1. The most intense band (1222 cm^{-1} in CS_2), is characteristic of an isoclinally oriented sulfite moiety (TB form) while the less intense band at 1184 cm^{-1}, in the same solvent, is characteristic of an axially oriented sulfite moiety (C-a or B-a form). Previous results for **2** (15) indicate that the B-a form is not likely to exist in such a system. The induced solvent shifts of 9 cm^{-1} (major band) and of 2 cm^{-1} (minor band) on going from CS_2 to CH_3CN follow trends similar to those observed in six-membered rings (1) for TB and C-a forms respectively. Finally, the increase in the population of the major band (TB) in a more polar solvent (CH_3CN) confirms the above conformational assignments because TB is more polar than C-a (15).

The presence of only one band at 1217 cm^{-1} in the ir spectrum of **6**, in CS_2, and the induced solvent shift of 9 cm^{-1} on going from CS_2 to CH_3CN identifies the TB form as the only detectable conformation for this compound. It is, however, important to point out that the geminal methyl groups of compound **6** can be located at two different benzylic positions in the TB conformation, that is, either *anti* (**7**) or *syn* (**8**) to the S=O double bond. Although ir methods fail to distinguish between these two possibilities, ^{1}H and ^{13}C nmr techniques provide parameters capable of probing the difference between **7** and **8** and thereby complement the conformational information deduced from the ir spectra.

Conformational features from nmr spectra

Proton and carbon-13 nmr parameters have been used extensively to define the orientation of the sulfite moiety as well as the spatial arrangement of nearby substituents. Data for each nucleus derive their utility from different characteristics of the sulfite function, which affect nearby nuclei.

Proton nmr, for example, can help differentiate between axial, isoclinal, and equatorial orientations of the S=O double bond through anisotropy effects on adjacent methylene protons. The effect decreases with a change of the S=O position from axial to equatorial in the chair form of six-membered cyclic sulfites (6). The chemical shift difference between geminal protons γ to the S=O double bond can therefore act as a useful conformational probe. By comparison, ^{13}C nmr parameters, especially through the γ effect (which represents the shift produced by the S=O bond on the γ carbon), can be utilized to deduce stereochemical relationships and thereby discriminate between various orientations of the S=O bond in the different conformations possible.

The averaged ^{1}H and ^{13}C spectra (Fig. 1) of **5** at −10°C have changed, at intermediate temperatures (−80°C for ^{1}H and −85°C for ^{13}C), into two sets of signals of unequal intensities. The minor set (labelled "c") remains unchanged down to −148°C; this observation is consistent with a rigid conformation possessing a plane of symmetry, most probably the chair form. Moreover, the large ^{1}H chemical shift difference ($\Delta\delta$ = 1.67 ppm) observed at −85°C between the two geminal benzylic protons (H-4 or H-7) of that minor C form indicates a large S=O anisotropy effect. Furthermore, the chair geometry explains the highly shielded C-4,7 carbon-13 signals (57.71 ppm at −80°C) relative to 76.25 ppm for the same carbons in 5,6-benzo-1,3-dioxepin (18). This large upfield shift (18.54 ppm) cannot be accounted for solely by the γ effect of the *peri* methyl groups as indicated by the fact that a similar γ effect in 1-methylnaphthalene is only 3.7 ppm (19). Such a high degree of shielding must also involve a *gauche* effect relative to the S=O band. These combined arguments, together with the symmetrical nature of the conformation, support the conclusion that C-a is the minor conformation of **5**, as was deduced from ir data.

The major sets of signals, labelled "b" both in the ^{1}H spectrum at −85°C and in the ^{13}C spectrum at −80°C, undergo additional changes as the temperature is lowered. The low-field half of the ^{1}H "b" pattern broadens extensively, splits, and gives, at −140°C, two distinct but broadened "b" peaks as illustrated by the splitting diagram. These two peaks, together with the high-field signal labelled "bb" which has only broadened at −140°C, indicate that the underlying conformation has at least three (and very likely four) chemically non-equivalent benzylic protons. This result suggests that the major conformation of **5** lacks a plane of symmetry, and is therefore a TB form. This conclusion is confirmed by the observation at −148°C of two chemically non-equivalent benzylic carbon-13 signals for the major conformation (Fig. 1, inset), again characteristic of the TB form.

Symmetry arguments, however, cannot be used for compound **6** because all conformations possible are inherently devoid of symmetry. Proton and carbon-13 nmr data can, however, be used to distinguish between the two possible TB forms, namely **7** or **8**.

The absence of change noted for the ^{1}H and ^{13}C spectra of **6** down to −125°C can be explained in one of the two following ways: either only one TB form (**7** or **8**) exists very predominantly or, alternatively, compound **6** exists as a mixture of **7** and **8** still undergoing rapid pseudorotation at −125°C. Close examination of results for related compounds helps resolve this ambiguity. First, St-Jacques and co-workers (16) have found that the C-7 signals for the TB forms of *cis*-4-methyl-5,6-

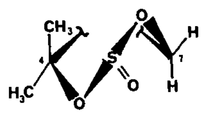

7

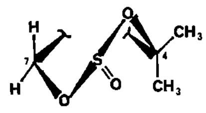

8

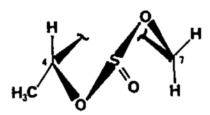

9

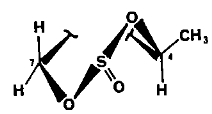

10

benzo-1,3,2-dioxathiepin (**9**) and of *trans*-4-methyl-5,6-benzo-1,3,2-dioxathiepin (**10**) have distinct chemical shifts at −125°C (63.91 and 67.19 ppm respectively). Next, the examination of structures **7**, **8**, **9**, and **10** indicates that the **7**–**9** pair and the **8**–**10** pair differ only by the addition of an axial methyl group at C-4 to **9** and **10**. Molecular models show that these axial methyl groups are quite remote from C-7, so that the C-7 chemical shifts obtained for **9** and **10** could be used as probes for the geometry of the TB form of **6** (**7** or **8**). The observation that the chemical shift of the C-7 signal of **6**, (64.30 ppm at −125°C) lies fairly close to the C-7 chemical shift of **9** (63.91 ppm at −125°C) (16) therefore points to the TB form **7**.

The above suggestion is further corroborated by the proton spectrum of **6** at −125°C, which reveals a chemical shift difference of 1.63 ppm for the two H-7 methylene protons. Corresponding values (15) for the benzylic protons of the TB form of **2** show that striking differences exist between the chemical shift difference of the CH_2 group *syn* ($\Delta\delta$ = 1.2 ppm) and *anti* ($\Delta\delta$ = 0.3 ppm) to the S═O bond, as a consequence of a stronger anisotropy effect for the *syn* CH_2 group. Therefore, the value ($\Delta\delta$ = 1.63 ppm) obtained for the geminal H-7 protons of **6** not only points to **7** as the preferred TB form for compound **6**, but also suggests the existence of some distortion around the *syn* C-7 carbon, which would lead to a stronger anisotropy effect in **7** than in **2**, and also in **9**, for which $\Delta\delta$ = 1.33 ppm (16).

Characteristics of methyl interactions

Although the results thus far presented for compounds **5** and **6** indicate a similar shift towards the TB form (relative to the 50:50 C-a/TB conformational equilibrium of compound **2** (15)), the methyl interactions governing those conformational preferences differ significantly for the two compounds on hand.

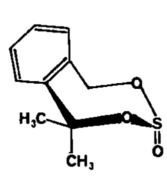

11

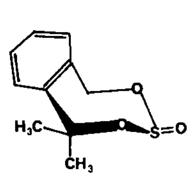

12

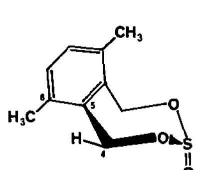

13

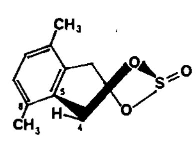

14

For example, compound **6** can exist as four possible conformers: two TB forms (**7** and **8**), a C-a form (**11**) and a C-e form (**12**). Among them, the C-a form **11** and the TB form **8** exhibit severe steric interactions between the axial methyl group (pseudoaxial in **8**) and the S═O bond. The C-e form **12**, on the other hand, is destabilized by an unfavorable electronic arrangement of the sulfite function (15) and by a 1,5 steric interaction between the axial methyl group and the axial H-7 proton. These unfavorable interactions in **8**, **11**, and **12** therefore explain the fact that the TB form **7** is found to be most stable for compound **6**.

In contrast, compound **5** exhibits particular methyl hydrogen interactions involving the two rings of the molecule. Molecular models show that the introduction of methyl groups at positions 8 and 11 of the parent compound **2** creates strong interactions between those methyl groups and one of the adjacent benzylic protons. Furthermore, examination of the C(4)—C(5)—C(8) plane of the same models indicates that the angle between the *peri*-methyl group and the equatorial H-4 proton is smaller in the C-a form (**13**) than in the TB form (**14**). This should result in a significantly stronger steric CH_3–H-4_e interaction in the C-a form than in the TB form. Consequently, the changes in the ^{13}C data whereby the γ' methyl effect on C(4) (or C(7)) is greater for the C-a form (−4.72 ppm) than for the TB form (−2.59 ppm) are compatible with the above.

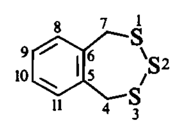

15

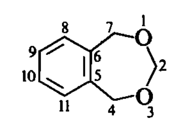

16

Similar increases in TB population were also noted upon introduction of methyl groups at the *peri* positions of other closely related systems (20),[3] namely 5,6-benzo-1,2,3-trithiacycloheptene (**15**) and 5,6-benzo-1,3-dioxepin (**16**). The above arguments suggest that these molecules should also exhibit stronger *peri* interactions in the C-a form.

Finally, it is informative to analyse the conformational effect associated with a "reverse" *peri* interaction, involving an equatorial benzylic methyl group and a *peri* aromatic proton. Compound **4**, for example, provides such a case. Even though ^{13}C parameters (16) suggest that the interaction between the methyl group and the *peri* aromatic proton is stronger in the C-a form that in the TB form, compound **4** unexpectedly favours the C-a form. The nature of the CH_3---H interaction is either not simple or solely operative in **4** so that the concept of "reversibility" is not applicable in such circumstances.

Experimental

Melting points are uncorrected and were determined using a Buchi melting point apparatus. High resolution spectra at 70 eV were recorded using a modified MS-9 spectrometer. Flash chromatography was performed on 230–400 mesh silica gel under standard conditions described by Still and co-workers (21). Anhydrous ether was taken directly from a freshly opened sealed can (Fisher), while thionyl chloride was distilled from quinoline, and triethylamine from calcium oxide.

The ir spectra of compounds **5** and **6** were taken as 0.05 *M* solutions in CS_2 and in CH_3CN, using a 0.05-mm KBr cell (nominal value), and were recorded on a Digilab FTS-15C/D Fourier transform infrared spectrometer, equipped with a wide-range photoconductive mercury

[3] Also, R. St-Amour and M. St-Jacques, unpublished results.

cadmium telluride detector, a KBr beam splitter, and a Lobar source. The instrument was purged with nitrogen before use. Typically, 200 interferograms of 2096 points each, recorded with a maximum optical retardation of 0.50 cm^{-1} and an optical velocity of 1.2 cm^{-1}, were co-added, apodized with a triangular function, and Fourier transformed with 8 levels of zero filling, resulting in a spectral resolution of 2 cm^{-1}. The base line was corrected using multiple linear least-square functions. Integrations were performed using a PEAKAREA program (Digilab), which leads to approximate values in the case of partially overlapping peaks.

Routine ^1H nmr spectra were taken on a Bruker WH-90 spectrometer: solutions were typically 10% (w/v) in $CDCl_3$ containing Me_4Si as reference. The following abbreviations will be used to describe the peaks: s = singlet, m = multiplet, br = broad. Routine ^{13}C nmr spectra were taken on a Bruker WP-80 spectrometer; solutions were typically 15% (w/v) in $CDCl_3$ containing Me_4Si as reference.

The variable temperature ^1H nmr spectra at 400 MHz and ^{13}C nmr spectra at 100.62 MHz were obtained using a Bruker WH-400 spectrometer equipped with a variable temperature unit B-VT-1000. Calibration using a thermocouple inside a solvent-containing nmr tube indicates that the low temperatures reported are exact within 2°C.

The ^1H spectra were recorded as solutions in chlorodifluoromethane (10 mg in 0.55 mL of solution) containing Me_4Si and about 15–20% of CD_2Cl_2 (for locking purposes), in standard 5-mm tubes which had been degassed and sealed. The following parameters were used: flip angle: 60–65°; SW = 4000 Hz; pulse delay = none; data size 4K; acquistion time = 0.512 s. The ^{13}C spectra were recorded with proton noise decoupling for solutions in chlorodifluoromethane (150 mg in 2.2 mL of solution) containing Me_4Si and about 15–20% of CD_2Cl_2, as locking agent, in standard 10-mm tubes which were degassed and sealed. The following instrumental parameters were used: flip angle = 65–70°; SW = 17 000 – 22 000 Hz; data size = 16K; acquisition time = 0.323–0.482 s; pulse delay = none.

The rate constants were determined at the coalescence temperature using the equation $k = \pi\Delta\nu\sqrt{2}$ for singlet to doublet splitting in ^1H (methyl signal of **5**) and ^{13}C nmr spectra (the equation provides an acceptable estimate for lines of unequal intensity (22)). The free energy barriers were calculated from standard equations (17) using a transmission coefficient of 1.

2,5-Dimethylphthalic anhydride

This compound was prepared by a Diels–Alder reaction between 2,5-dimethylfuran (Aldrich) and maleic anhydride, followed by dehydration with concentrated sulfuric acid, as described by Newman and Lord (23). The white solid was characterized by its melting point (139–142°C), which was identical with that published, and by its ^1H nmr (90 MHz, $CDCl_3$) spectrum: δ 2.67 (s, 6H), 7.53 (s, 2H).

*2,5-Dimethyl-(*o*)-benzenedimethanol*

To a mixture of 2.5 g $LiAlH_4$ in 30 mL of boiling anhydrous THF was added dropwise, under argon, a solution of 7.0 g of 2,5-dimethylphthalic anhydride in 70 mL of anhydrous THF. The resultant solution was refluxed during 48 h and then cooled to room temperature. The excess hydride was decomposed cautiously with 5 mL of 10% H_2SO_4 and filtered through sintered glass. The filtrate was then evaporated, giving 3.8 g (58% yield) of a white solid, which was characterized by its melting point (69–70°C), identical with that published (24), and by its ^1H nmr (90 MHz, $CDCl_3$) spectrum: δ 2.37 (s, 6H), 3.25 (br, 2H, exchangeable with D_2O), 4.71 (s, 4H), 7.05 (s, 2H).

8,11-Dimethyl-5,6-benzo-2-oxo-1,3,2-dioxathiepin (5)

To a mixture of 1.5 g of 2,5-dimethyl-(*o*)-benzenedimethanol, and 2.8 mL of triethylamine (2 equiv.) in 20 mL of anhydrous ether, at 0°C, was added dropwise, under argon, a solution of 0.72 mL (1 equiv.) of thionyl chloride in 20 mL of anhydrous ether. A white precipitate (triethylammonium chloride) appeared at the beginning of the addition and became more abundant as the reaction proceeded. After the addition was completed, the solution was stirred an additional 1.5 h, warmed to room temperature, then filtered on a Büchner funnel and evaporated, giving an oil which was triturated in hexane: 1.0 g (52% yield) of a white powder was thus obtained. This crude material was purified by flash chromatography on silica gel, using CH_2Cl_2 as eluent, giving, in the media fraction, analytically pure white crystals (mp 48°C). The ^1H and ^{13}C nmr spectra (Tables 2 and 3), as well as the high resolution mass spectrum confirm its identity. *Mol. Wt.* calcd. for **5**, $C_{10}H_{12}O_3S$: 212.0507; found (mass spectrum at 70 eV): 212.0510.

*α,α-Dimethyl-*o*-xylene α,α'-diol*

This compound was prepared from phthalide (Aldrich) by a procedure similar to the one of Goldschmidt and Zoebelein (25) in 58% yield. Analytically pure material was obtained by distillation under reduced pressure (100°C/0.3 Torr; 1 Torr = 133.3 Pa), giving an oil which crystallized on standing (mp 62–63°C); ^1H nmr (90 MHz, $CDCl_3$): δ 1.59 (s, 6H), 4.71 (s, 4H), two of which are exchangeable with D_2O, 7.22 (m, 4H, aromatic protons).

4,4-Dimethyl-5,6-benzo-2-oxo-1,3,2-dioxathiepin (6)

To a mixture of 1.5 g of α,α-dimethyl-*o*-xylene α,α'-diol, and 6.3 mL (5 equiv.) of triethylamine in 25 mL of anhydrous ether, at 0°C, was added dropwise a solution of 0.7 mL (1 equiv.) of thionyl chloride in 25 mL of anhydrous ether. The solution was then allowed to warm at room temperature, and stirred during 96 h. Filtration of the salts followed by evaporation under reduced pressure yielded 1.42 g (74% yield) of a yellow oil. Flash column chromatography on 40–63 μm silica gel (Merck no. 9385) using dichloromethane as solvent gave, in the middle fractions, pure **6** as a white powder (mp 48°C). Its identity was later confirmed by its ^1H and ^{13}C nmr spectra (Tables 2 and 3) as well as by its high resolution mass spectrum. *Mol. Wt.* calcd. for **6**, $C_{10}H_{12}O_3S$: 212.0507; found (mass spectrum at 70 eV): 212.0500.

Acknowledgements

We wish to acknowledge the technical assistance of Mr. Jean-Claude Bolduc of the "Laboratoire de spectroscopie infrarouge par transformée de Fourier" and of Dr. Phan Viet Minh Tan of the "Laboratoire régional de RMN à haut champ", both situated at the Université de Montréal. We are grateful to Y. Aubin for assistance in preparing the dimethyl derivatives **5** and **6**. We wish to thank the National Research Council of Canada for its financial assistance.

1. L. Cazaux, J. D. Bastide, G. Chassaing, and P. Maroni. Spectrochim. Acta Part A, **35**, 15 (1979), and references cited.
2. G. W. Buchanan and D. G. Hellier. Can. J. Chem. **54**, 1428 (1976).
3. G. W. Buchanan, C. M. E. Cousineau, and T. C. Mundell. Can. J. Chem. **56**, 2019 (1978).
4. D. G. Hellier and A. M. Philips. Org. Magn. Reson. **18**, 178 (1982).
5. C. H. Green and D. G. Hellier. J. Chem. Soc. Perkin Trans. 2, 190 (1975), and references cited.
6. G. Wood, J. M. McIntosh, and M. H. Miskow. Can. J. Chem. **49**, 1202 (1971).
7. (*a*) H. Nikander, K. Pihlaja, and T. Virtanen. Acta Chem. Scand. Ser. B, **36**, 117 (1982); (*b*) T. Virtanen, H. Nikander, and K. Pihlaja. Tetrahedron, **38**, 2821 (1982).
8. Y. Y. Samitov, L. K. Ulldasheva, and I. V. Anonikova. Zh. Org. Khim. **18**, 406 (1982).
9. (*a*) R. Riemchneider and V. Wuscherpfennig. Z. Naturforsch. Teil B, **17**, 516 (1962); (*b*) **17**, 585 (1962).
10. S. E. Forman, A. J. Burbetaki, M. C. Cohen, and R. A. Olofson. J. Org. Chem. **30**, 169 (1965).
11. A. C. Guimaraes, J. B. Robert, L. Cazaux, C. Picard, and P. Tisnes. Tetrahedron Lett. **21**, 1039 (1980).
12. T. Nishiyama, Y. Nakai, H. Shishibori, and F. Yamada. Bull. Chem. Soc. Jpn. **54**, 1410 (1981).
13. B. A. Arbusov, E. N. Kumovitskii, A. B. Remigov, A. V.

AGANOV, I. V. ANONIMOVA, G. N. SERGEEVA, and V. V. KLOGHKOV. Dokl. Akad. Nauk SSSR, **239**, 109 (1979).
14. A. C. GUIMARAES, P. DE ALMEIDA, M. BALTAS, and L. CAZAUX. Org. Magn. Reson. **21**, 711 (1983).
15. H. FAUCHER, A. C. GUIMARAES, J. B. ROBERT, F. SAURIOL, and M. ST-JACQUES. Tetrahedron, **37**, 689 (1981).
16. A. C. GUIMARAES, P. DE ALMEIDA, A. LACHAPELLE, and M. ST-JACQUES. Can. J. Chem. **61**, 2244 (1983).
17. F. A. L. ANET, P. J. DEGEN, and J. KRANE. J. Am. Chem. Soc. **98**, 2059 (1976).
18. A. BLANCHETTE, F. SAURIOL-LORD, and M. ST-JACQUES. J. Am. Chem. Soc. **100**, 4055 (1978).
19. T. DRAKENBERG, J. SANDSTROM, and J. SEITA. Org. Magn. Reson. **11**, 243 (1978).
20. S. KABUSS, A. LUTTRINGHAUS, H. FRIEBOLIN, H. G. SCHMID, and R. MECKE. Tetrahedron Lett. **7**, 719 (1966).
21. A. MITRA, M. KAHN, and W. C. STILL. J. Org. Chem. **43**, 2923 (1978).
22. D. KOST, E. H. CARLSON, and M. RABAN. Chem. Commun. 656 (1971).
23. M. S. NEWMAN and B. T. LORD. J. Am. Chem. Soc. **66**, 733 (1944).
24. V. E. BUCHTA and G. LOWE. Ann. **597**, 123 (1955).
25. S. GOLDSCHMIDT and A. ZOEBELEIN. Chem. Ber. **94**, 169 (1961).

Photocyclization of 2-vinylbiphenyls: stereochemistry of the triplet state cyclization

RENÉ LAPOUYADE, CLAUDE MANIGAND, AND AZIZ NOURMAMODE

Laboratoire Associé au CNRS N° 348 et Ecole Nationale Supérieure de Chimie et de Physique de Bordeaux, Université de Bordeaux 1, 33405 Talence Cédex, France

Received July 19, 1984

This paper is dedicated to Professor Paul de Mayo on the occasion of his 60th birthday

RENÉ LAPOUYADE, CLAUDE MANIGAND, and AZIZ NOURMAMODE. Can. J. Chem. **63**, 2192 (1985).

The photochemistry of five- to eight-membered ring containing 2-cycloalkenyl biphenyls was examined under direct and sensitized irradiation. From the singlet excited state only *trans* 9,10-cycloalkyl-9,10-dihydrophenanthrenes were obtained. From the triplet state the *trans* isomer was exclusively formed from 2-cyclopentenyl and 2-cyclohexenyl biphenyls while the *cis* isomer also appeared with 2-cycloheptenyl and 2-cyclooctenyl biphenyls. We propose that the *cis* isomers resulted from the cyclization of the perpendicular triplet of cycloheptenyl biphenyl and from the perpendicular and *trans* triplet of cyclooctenyl biphenyl. Whereas the photocyclization of 2-vinylbiphenyls was regarded as a singlet-state reaction, the quantum yields of reaction of 2-cycloalkenyl biphenyls, from both singlet and triplet states, were high ($\Phi_S = 0.20–0.26$; $\Phi_T = 0.15–0.46$).

RENÉ LAPOUYADE, CLAUDE MANIGAND et AZIZ NOURMAMODE. Can. J. Chem. **63**, 2192 (1985).

On a étudié, par irradiation directe et sensibilisée, la photoréactivité de quatre cycloalcényl-2 biphényles où le groupe cycloalcène varie du cyclopentène au cyclooctène. Par l'état excité singulet, il ne se forme que les cycloalkyl-9,10 dihydro-9,10 phénanthrènes *trans*. Par l'état triplet, l'isomère *trans* est obtenu seul dans le cas des cyclopenténуl-2 et cyclohexényl-2 biphényles, alors que l'isomère *cis* apparaît avec les cycloheptényl-2 et cyclooctényl-2 biphényles. Les isomères *cis* sont attribués à la cyclisation des cycloalcènes perpendiculaires et du cyclooctényl *trans* à l'état triplet. Alors que la cyclisation des vinyl-2 biphényles était considérée comme une réaction de l'état singulet, les rendements quantiques de réaction sont élevés, aussi bien par le triplet que par le singulet ($\Phi_S = 0{,}20–0{,}26$; $\Phi_T = 0{,}15–0{,}46$).

Introduction

Mechanistic interpretations of the complicated photochemistry of conjugated hexatrienes have been discussed recently (1). The number of reactive pathways was dramatically reduced by incorporating two consecutive double bonds in benzene rings; namely, with 2-vinylbiphenyls only *cis–trans* photo-izomerization and -cyclization were observed. With *Z*(*E*)-1-biphenyl-2-yl-1-phenylpropene **1** we reported (2) a stereoselective singlet cyclization, as anticipated for a concerted conrotatory [6π] electrocyclic ring closure, and a nonstereoselective triplet cyclization which was no less expected, since in order to be concerted a triplet electrocyclic reaction either would have to produce a triplet product or possess a mechanism for efficient intersystem crossing to the ground state of the product (3). We interpreted the unchanged stereochemistry of the triplet cyclization, whatever the isomer irradiated by a cyclization through a common intermediate, as possibly a perpendicular triplet state.

But it has now been established that a fast equilibrium between the planar and perpendicular triplet states occurs with stilbene, and naphthyl- and biphenyl-substituted olefines (4–6), so that the identical stereochemistry of triplet cyclization of **1***E* and **1***Z* could also be explained by a cyclization from planar triplets **1***E* and **1***Z* in equilibrium.

With a view to determining at which point along the excited singlet and triplet surfaces the new bond is made, we have now measured the efficiency and determined the stereochemistry of cyclization of a series of 2-vinylbiphenyls where the double bond is inserted in five- to eight-membered rings whose effect on the geometry of the triplet state we have previously discussed for α-naphthyl (6) and β-naphthyl (7) ethylene derivatives.

Results

I. *Synthesis of photochemical reactants*

Compound **1** was prepared from 2-benzoylbiphenyl by a Wittig reaction with the "instant ylide" ethyltriphenylphosphonium bromide – sodium amide, developed by Schlosser and Schaub (8): the two isomers (9) were formed in equal amounts and separated by flash chromatography (10). 1-(2-Biphenyl)-cycloalkenes (**2–5**) (11) were obtained by reaction of 2-lithiobiphenyl with appropriate cycloalkanones and dehydration of the resulting alcohols with thionyl chloride in pyridine (12) (Scheme 1). Only the cyclopentyl derivative was not satisfactorily dehydrated by this method, and P_2O_5 in CCl_4 was used. When an acidic dehydrating agent was employed, the desired products were contaminated with the corresponding spirocycloalkane fluorenes (13). We verified that compounds **2–5** were quantitatively cyclized to spirocycloalkane fluorenes by refluxing a benzene solution with a catalytic amount of *p*-toluenesulfonic acid (Scheme 1).

II. *Photolysis of* **2–5** *and identification of the photoproducts*

1. *Direct irradiation*

Under preparative conditions the direct irradiation (313 nm) of degassed cyclohexane solutions of **2** and **3** (5×10^{-3} *M*) afforded only one isomer of the corresponding 9,10-cycloalkyl-9,10-dihydrophenanthrenes. Irradiation of argon degassed solutions of **4** and **5** gave the two isomers in a ratio of 86:14 for **4** and 80:20 for **5**. But by adding piperylene (10^{-3} *M*) the previously minor isomer disappeared completely for **4** while 5% remained with the irradiation of **5**. The ratio of the photoproducts was not altered by an extended irradiation.

2. *Isomerization of the photoproducts and assignment of their configuration*

We assigned a *trans* configuration to the single isomers obtained by direct irradiations of **2–5** for the following reasons:

(*a*) A conrotatory ring closure followed by a suprafacial [1,5] sigmatropic hydrogen shift is the accepted mechanism of the singlet cyclization of 2-vinylbiphenyls. It has accounted for the stereoselectivity observed by several authors (2, 14) (Scheme 2).

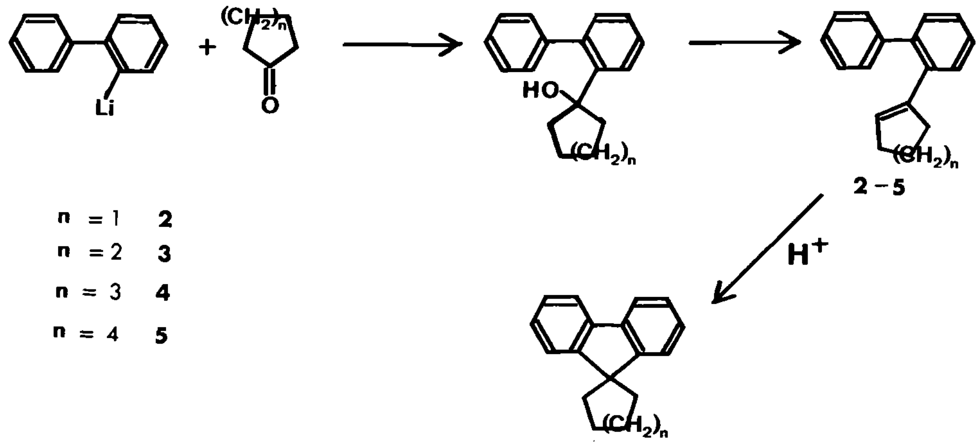

SCHEME 1. Synthesis of 1-(2-biphenyl)-cycloalkenes.

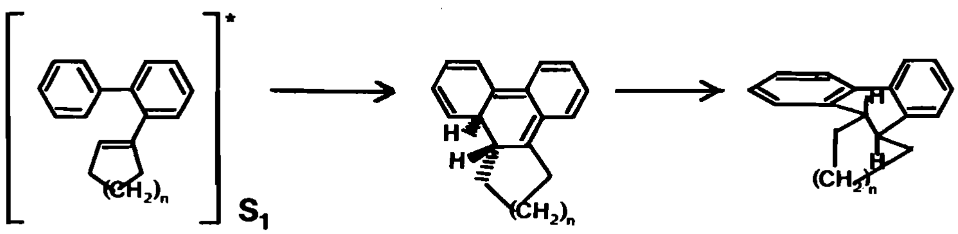

2 – 5 TRANS 6 – 9

SCHEME 2. Singlet cyclization of 1-(2-biphenyl)-cycloalkenes.

(b) We have isomerized the photoproducts via the carbanion generated with nBuli in diethyl ether with six equivalents of HMPA. Rabideau and Harvey (15) had already observed a 100% *cis* stereoselectivity for the protonation from the pseudo-axial direction of 9,10-dialkyl-9-lithio-9,10-dihydrophenanthrenes, while the vicinal alkyl group assumed the relatively unhindered axial position. We thought that with a fully HMPA solvated cation the axial protonation of the planar carbanion might be favoured (16–19), while the large solvated cation, maintained in the vicinity of the anion by the low polarity of the solvent, could add to the perihydrogen interaction to favour an axial position for the vicinal cycloalkyl substitution and, as a consequence, the *cis* isomer would result (Scheme 3). In fact, the photoisomers were all converted to the other isomers, which became predominant. Since the reaction mixture is not equilibrating, the observed ratios of isomers do not reflect the relative thermodynamic stability but, rather, the stereochemistry of kinetic protonation of the unstable carbanions.

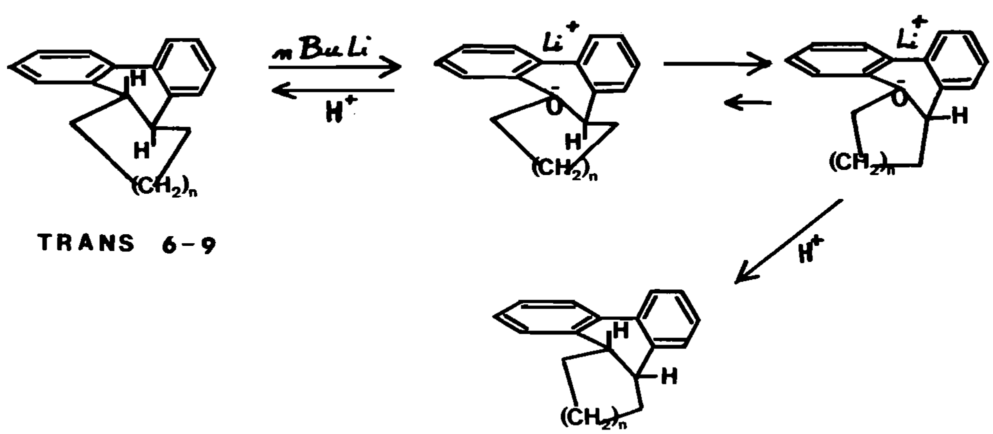

CIS 6 – 9

Reactants	Products (%)
trans **6**	*trans* **6** (25), *cis* **6** (75)
trans **7**	*trans* **7** (36.5), *cis* **7** (63.5)
trans **8**	*trans* **8** (7), *cis* **8** (93)
trans **9**	*trans* **9** (13), *cis* **9** (87)

SCHEME 3. *trans–cis* Isomerization of 9,10-cycloalkyl-9,10-dihydrophenanthrenes with nBuli in ether–HMPA.

(c) Since direct irradiation of **2–5** gave only one isomer of **6–9** but base isomerization afforded the other isomer we were able to compare the properties of configurational isomers for each couple. The nmr analysis of the benzylic hydrogen signals of 9,10-dihydrophenanthrenes has proved useful for configurational and conformational studies (18, 20) but extension to compounds **6–9** was not straightforward, since if one could assume that the *cis* isomers (Scheme 3) were rapidly interconverting and averaging the axial and equatorial benzylic hydrogens, after inspection of molecular models it appeared that the *trans* isomers could only present the saturated ring bisequatorially fused to the 9,10 bond (Scheme 3), whereas Harvey showed that *trans*-9,10-dialkyl-9,10-dihydrophenanthrenes preferred the diaxial conformation. Furthermore, axial and equatorial hydrogens cannot be distinguished on the basis of chemical shift alone and coupling constants are not easily available for these structurally (*cis*) or dynamically (*trans*) symmetrically substituted 9,10-dihydrophenanthrenes. Nevertheless we observed a complete homogeneity from **6** to **9** for the chemical shift of benzylic hydrogens: the photoproducts (*trans* isomers, axial hydrogens) are shielded relative to their isomers (*cis* isomers, axial and equatorial hydrogens) (see Experimental).

The photoproducts are eluted after their isomers on silica gel, and have a longer retention time on gas chromatography with a column of 3% OV1 on Chromosorb W-HP.

Dehydrogenation of dihydroaromatic hydrocarbons over 10% Pd/C in refluxing diglyme has already been observed to be slower for the isomer where the substituents interfere with adsorption on the catalyst surface (21). In this regard we expected a faster dehydrogenation for the *cis* isomer, where one face presents the two hydrogens accessible to the catalyst. In fact, after 2 h of reflux an equivalent mixture of *cis*- and *trans*-**7** has been transformed to triphenylene and unaffected *trans*-**7**.

3. *Sensitized cyclization*

In contrast to direct irradiations, xanthone (2×10^{-3} *M*) sensitized irradiations of nitrogen degassed benzenic solutions of **2–5** (2.25×10^{-3} *M*) led to a different stereochemistry of cyclization, depending on the size of the cycloalkene ring: with cyclopentene (**2**) and cyclohexene (**3**) only one isomer was formed, which was identical with the one obtained by direct irradiation, consequently the *trans*-isomer; with cycloheptene (**4**) the *trans* isomer was predominant (65%) but the *cis* was also formed (35%); and with cyclooctene, at the beginning of the irradiation (see quantum yields) the ratio *cis*/*trans* was 54:46, while further irradiation increased the *cis* proportion, which reached 85:15 when the cyclization was complete.

We also observed a reduced proportion of *cis*-**8** when the irradiated acetonitrile solution of **4** was saturated with air or oxygen: *trans*/*cis* = 65:35 (nitrogen saturated), 67:33 (air saturated), 73:27 (oxygen saturated) when the conversion was approximately 20%.

As for direct excitation, prolonged irradiations did not change the ratio of the photoproduct isomers.

4. *Quantum yields of direct and sensitized photocyclizations*

Quantum yields (Tables 1 and 2) were determined using an optical bench with a 2-kW xenon lamp and a Jobin–Yvon HL monochromator. Aberchrome 540 ($\phi = 0.20$) (22) was used to measure the intensity of the incident light at 315 nm (direct irradiations) and 340 nm (sensitized irradiations). The concentrations of **2–5** were such that more than 98% of the incident light was absorbed (direct irradiations, concentration = 5×10^{-2} *M*) or complete triplet quenching of the sensitizer occurred (sensitized reactions, concentration = 5×10^{-2} *M*). After irradiation, the degree of reaction and the amount of photoproducts were determined by vapor phase chromatography using a 25-m fused silica capillary column packed with CP Sil 8 CB. The internal standard was *m*- or *p*-terphenyl. The conversions never exceeded 2%.

TABLE 1. Quantum yields for direct irradiations

		Quantum yields of photoproducts		
Compounds	Additive	*trans*	*cis*	*trans* + *cis*
2	—	0.31	—	0.31
2	Piperylene	0.20	—	0.20
3	—	0.36	—	0.36
3	Piperylene	0.20	—	0.20
4	—	0.26	—	0.26
4	Piperylene	0.24	—	0.24
5	—	0.21	0.02	0.23
5	Piperylene	0.19	0.01	0.20

λ_{excit} = 315 nm; solvent: acetonitrile; **2–5** conc. = 5×10^{-2} *M*; nitrogen degassed.

TABLE 2. Quantum yields for xanthone sensitized cyclizations

	Quantum yields of photoproducts		
Compounds	*trans*	*cis*	*trans* + *cis*
2	0.46	—	0.46
3	0.37	—	0.37
4	0.19	0.11	0.30
5	0.07	0.08	0.15

λ_{excit} = 340 nm; solvent: acetonitrile; **2–5** conc. 5×10^{-2} *M*; xanthone conc. = 4×10^{-4} *M*, degassing with four freeze–thaw cycles.

Interpretative discussion

Singlet cyclization

The stereochemistry of the singlet cyclization of 2-vinylbiphenyls was well accounted for by a concerted conrotatory ring closure followed by a suprafacial 1,5 hydrogen shift (2, 14, 23–25). From 2-cycloalkenylbiphenyls **2–4**, which are only stable in the *cis* configuration in the ground state, the exclusive formation of the *trans* photoproducts, as also the relatively constant quantum yields, denote a cyclization from the *cis* isomer without a concurrent isomerization in the excited state. The *cis* photoproduct (~5%) obtained with **5** could arise from a small amount of *trans*-**5** already present before irradiation. We shall not discuss further the singlet cyclization of these compounds since we have now observed a biexponential decay of their fluorescence, so that the principle of nonequilibration of excited rotamers (26) (NEER) should apply and the quantum yield of reaction should be highly dependent on the reactive conformer proportion.

Triplet cyclization

We have not yet been able to differentiate the triplet state conformers but if the NEER principle is maintained during the triplet lifetime, as we have shown in the β-naphthalene series (7), we might emphasize the high efficiency of the sensitized reactions, since the quantum yield of cyclization of the reactive conformer would be still higher than the measured quantum yield. As for the singlet cyclization, it is possible that differential population of the conformers contributes to the observed quantum yield trends, but in the triplet state the appearance of *cis* photoproduct is indicative of an initial photoisomerization; therefore we will discuss the relation between the size of the cycloalkene and the efficiency and the stereochemistry of the cyclization. Biphenyl has an intermediate triplet energy (65–66 kcal mol^{-1}), between fluorene (68 kcal mol^{-1}) and naphthalene (61 kcal mol^{-1}) (27). Thus at room temperature, we could anticipate a fast interconversion between planar and perpendicular conformations of the triplet state for 2-vinylbiphenyls, as directly observed by Tokumaru and co-workers with unreactive 4-vinylbiphenyls (5). For 2-cycloalkenyl biphenyls the relative populations of planar and perpendicular triplets might be in the order of those described for 1-cycloalkenyl naphthalenes (6), with perhaps an increase in the percentage of the perpendicular triplets as a result of the higher triplet energy of biphenyl vs. naphthalene. Thus one may expect an exclusively planar triplet for **2** and **3** and a fast equilibrium between planar and perpendicular triplet for **4**. With **5** a *trans* triplet can also be expected. The observed increase in efficiency of the cyclization, with the hindering of isomerization from **5** to **2**, is consistent with an efficient cyclization from a planar triplet in competition with a decay from twisted configurations with the latter becoming faster with increasing size of the cycloalkene. The stereochemistry of the reaction of **2** and **3** is the same as that observed from the singlet state; a concerted mechanism and consequently perhaps adiabatic cyclization from a planar *cis* triplet can be inferred.

The formation of the *cis* photoproducts from **4** can only be explained by a cyclization from the perpendicular triplet state since a *trans* triplet state is not expected on energetic grounds (6), and a *trans* ground state, if it cyclized thermally, would give the *trans* photoproduct by disrotatory cyclization.

With **5** the *cis* photoproduct can also result from the cyclization of the perpendicular triplet but the increase of the *cis* proportion with conversion indicates the participation of a concerted cyclization following excitation of the *trans* ground state.

Depending on the size of the cycloalkenes, we have found products resulting from the cyclization of three different triplet conformations: (*i*) with smaller cycloalkenes, **2** and **3**, an efficient cyclization occurs from the planar *cis* triplet state; (*ii*) with the cycloheptenyl derivative **4**, the perpendicular triplet state is attainable and can explain the appearance of the *cis* photoproduct; the *trans* photoproduct could result from the cyclization of the planar *cis* and the perpendicular triplet conformers; (*iii*) the stereochemistry of cyclization of the cyclooctenyl derivative **5** is accounted for by the participation of the three triplet conformers (*cis*, perpendicular, and *trans*).

For unstrained acyclic 2-vinylbiphenyls, we can foresee a fast equilibrium between the three conformers of the triplet state consistent with the unchanged stereochemistry of cyclization, whatever the isomer irradiated (2), but the discovery of the more reactive conformers must await further investigations.

Experimental

The ^1H nmr spectra were recorded on either Hitachi–Perkin–Elmer R 24 B (60 MHz) or Brücker WH 90 (90 MHz) Instruments. Chemical shifts were given in δ (ppm) relative to tetramethylsilane (TMS) as the internal reference. Mass spectra were taken on a VG Micromass 16 F. The ^{13}C nmr spectra were obtained on a Brüker WP 60 (15.08 MHz) spectrometer equipped with a Nicolet BNC 12 calculator (4K programme, 8K acquisition) using 10–15% (w/v) solutions in chloroform-*d* containing 0.5% TMS. The individual carbon shieldings were measured from noise-decoupled spectra. nBuli from Aldrich was used as received. Diethyl ether was dried over sodium and stored under nitrogen over 4 Å molecular sieves. Hexamethylphosphoric triamide (HMPT) was distilled over calcium hydride and stored over 4 Å molecular sieves. All reactions were stirred magnetically and carried out under an atmosphere of nitrogen in flame dried glassware.

1-(2-Biphenyl)-cycloalcenes

1-(2-Biphenyl)-cyclopentene, **2**, and 1-(2-biphenyl)-cyclohexene, **3**, were known (11); we prepared these compounds according to the procedure described for **4**.

1-(2-Biphenyl)-cycloheptene, 4

To 2-biphenyllithium, prepared from 2-bromobiphenyl (1.11 g, 5×10^{-2} mol) in ether (50 mL) and a 1.5 *M* solution of n-butyllithium (5 mL) was added slowly at 0°C a solution of cycloheptanone (0.84 g, 7.5×10^{-2} mol) in ether (20 mL). The mixture was stirred for 1 h at room temperature, refluxed for 3 h, hydrolyzed with cold aqueous 10% ammonium chloride (50 mL), and extracted with ether (2 × 20 mL). The residue from evaporation of the dried (magnesium sulfate) ethereal extracts was chromatographed on a silica gel column. Petroleum ether elution gave 110 mg of biphenyl and diethylether elution gave 950 mg of an oil. This oil was dissolved in 30 mL of dry pyridine, chilled to −5°C, and 3 mL of thionylchloride was added. The mixture was allowed to stand at 10°C for 4 h, and then poured into ice water. The oily mixture was extracted with 100 mL of ether, the extract was washed with saturated saline solution, and dried and evaporated under reduced pressure. Chromatography on a silica gel column and elution with petroleum ether of the residue gave 760 mg (64%) of 1-(2-biphenyl)-cycloheptene in oil; nmr (CCl_4): 1–2.4 (m, 10H), 5.8 (t, 1H, *J* = 6.8 Hz), 7.1–7.5 (m, 9H). *Anal.* calcd. for $C_{19}H_{20}$: C 91.93, H 8.06; found: C 91.66, H 7.89.

1-(2-Biphenyl)-cyclooctene, 5

According to the procedure given for **4**, we obtained 820 mg (65%) of **5** (oil); nmr (CCL_4): 1.1–2.47 (m, 12H), 5.7 (t, 1H, *J* = 7.8 Hz), 7.03–7.48 (m, 9H). *Anal.* calcd. for $C_{20}H_{22}$: C 91.6, H 8.41; found: C 91.48, H 8.28.

Spiro[cycloalkane-9,9 fluorenes]

All 1-(2-biphenyl)-cycloalkenes gave quantitatively the corresponding spiro[cycloalkane-9,9 fluorenes] when treated as described for the cyclohexenyl derivative.

Spiro[cyclohexane-9,9 fluorene]

1-(2-Biphenyl)-cyclohexene, **3** (234 mg), was refluxed in benzene (1 h) with a catalytic amount of paratoluene sulfonic acid. Thin-layer chromatography on silica gel developed with light petroleum ether showed only one spot in uv light with a slightly shorter R_f than **3**. Chromatography on a silica gel column gave 198 mg (84%) of spiro[cyclohexane-9,9 fluorene] (13) which was recrystallized from 95% ethanol to afford white crystals, mp 82–83°C; ^1H nmr (CCl_4): 0.8–2.16 (m, 10H), 7.16–7.87 (m, 8H); ^{13}C nmr ($CDCl_3$): 153.036 ($C_{4a,b}$), 139.525 ($C_{8a,9a}$), 126.682 ($C_{2,3,6,7}$), 124.248 ($C_{1,8}$), 119.622 ($C_{4,5}$), 50.116 (C_9), 35.509 ($C_{10,14}$), 25.466 (C_{12}), 22.545 ($C_{11,13}$); mass spectra *m/e* (calcd. for $C_{18}H_{18}$: 234): 235 (12.8, M + 1), 234 (68, M), 191 (41, M − ($CH_2{=}CH_2$ + $^{\bullet}CH_3$), 178 (100, M − $2CH_2{=}CH_2$, phenanthrene).

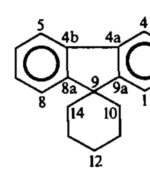

General procedure for preparative irradiations

Preparative irradiations were carried out in a Rayonet RPR-100 reactor at 300 nm with a quartz tube for direct irradiations, or at 350 nm in a Pyrex vessel for sensitized reactions with xanthone. In direct photolysis, solutions of 1-(2-biphenyl)-cycloalkenes (5×10^{-3} *M*) in cyclohexane (100 mL) were purged with argon for 30 min and irradiated 4 h. Sensitized reactions were conducted in degassed benzene solution (100 mL) with 2.25×10^{-3} *M* of reactant and 2×10^{-3} *M* of xanthone; after 4 h of irradiation, all the reactants had been cyclized and the relative amounts of the photoproduct isomers were estimated by comparing the integrations of the corresponding peaks in glc.

trans-*9,10-Cyclopentyl-9,10-dihydrophenanthrene* t-***6***

Direct and sensitized irradiation gave only one isomer (glc). The solutions were evaporated and chromatographed on a silica gel column. Elution with petroleum ether, followed by recrystallization from methanol, afforded 86% (direct) and 88% (sensitized) of *trans*-9,10-cyclopentyl-9,10-dihydrophenanthrene as white needles, mp 155°C; ^{1}H nmr (CCl_4): 1.3–2.5 (m, 6H), 2.62 (m, 2H), 7–7.5 (m, 6H), 7.5–7.96 (m, 2H); mass spectra, *m/e* (calcd. for $C_{17}H_{16}$: 220): 221 (18.7, M + 1), 220 (100, M), 192 (70.9, M − $CH_2{=}CH_2$), 191 (97.9, M − CH_3 − CH_2), 178 (40.5, phenanthrene). *Anal.* calcd. for $C_{17}H_{16}$: C 92.73, H 7.27, found: C 92.19, H 7.26.

trans-*9,10-Cyclohexyl-9,10-dihydrophenanthrene t-7*

Direct and sensitized irradiations gave only the *trans* isomer (glc). Chromatography from a silica gel column, with petroleum ether as eluent, afforded 82% (direct) and 85% (sensitized) of *trans*-9,10-cyclohexyl-9,10-dihydrophenanthrene. Recrystallization from methanol gave white crystals, mp 90°C; ^{1}H nmr (CCl_4): 1.2–2.2 (m, 8H), 2.4 (m, 2H), 7–7.3 (m, 6H), 7.4–7.8 (m, 2H); mass spectra, *m/e* (calcd. for $C_{18}H_{18}$: 234): 235 (31.1, M + 1), 234 (100, M), 192 (52.4), 191 (96.2), 178 (29). *Anal.* calcd. for $C_{18}H_{18}$: C 92.31, H 7.69; found: C 91.96, H 7.93.

trans-*9,10-Cycloheptyl-9,10-dihydrophenanthrene,* t-***8***

Direct irradiation of **4** in a standard solution as described above, but containing also 10^{-3} *M* of piperylene, gave only *trans*-9,10-cycloheptyl-9,10-dihydrophenanthrene (glc) as an oil (78%); ^{1}H nmr (CCl_4): 1.6–2.5 (m, 10H), 2.53 (m, 2H), 7.1–7.5 (m, 6H), 7.6–7.9 (m, 2H); mass spectra, *m/e* (calcd. for $C_{19}H_{20}$: 248): 249 (13.6, M + 1), 248 (65.4, M), 192 (49), 191 (100), 178 (42.4). *Anal.* calcd. for $C_{19}H_{20}$: C 91.93, H 8.06; found: C 91.68, H 8.01.

trans-*9,10-Cyclooctyl-9,10-dihydrophenanthrene,* t-***9***

Direct irradiation of **5** in the standard solution containing 10^{-3} *M* piperylene gave a mixture of *trans* (95%) and *cis* (5%) **9** (glc). Chromatography on silica gel impregnated with 10% caffeine gave first a mixture of *trans* and *cis* **9** and then pure *trans*-**9**, mp 104°C; ^{1}H nmr (CCl_4): 1.4–2.5 (m, 12H), 2.88 (m, 2H), 7–7.5 (m, 6H), 7.5–7.9 (m, 2H); mass spectra, *m/e* (calcd. for $C_{20}H_{22}$: 262): 263 (16.6, M + 1), 262 (76, M), 192 (60.1), 191 (100), 178 (47). *Anal.* calcd. for $C_{20}H_{22}$: C 91.6, H 8.41; found: 91.48, H 8.26.

Base isomerization of trans-*9,10-cycloalkyl-9,10-dihydrophenanthrenes, **6–9***

By treating, at 0°C and under nitrogen, a solution of 5 mmol of *trans*-9,10-cycloalkyl-9,10-dihydrophenanthrene in 80 mL of diethyl ether and 6.4 mL (60 mmol) of HMPT with 10 mmol of nBuli in hexane for 4 h we obtained, after hydrolysis with methanol, a mixture of *trans* and *cis* **6–9** where the *cis* isomer is always dominant (see table, Scheme 3). The *cis* isomers have always a shorter retention time and the relative amounts are estimated from the corresponding areas in glc. Chromatography on silica gel impregnated with 10% caffeine, with petroleum ether as eluent, gave pure cis **6–9**. The *cis* isomers have the same mass spectra as the *trans* isomers.

cis-*9,10-Cyclopentyl-9,10-dihydrophenanthrene, c-**6***, mp 72°C; nmr (CCl_4): 1.3–2.5 (m, 6H), 3.23 (m, 2H), 7.1–7.4 (m, 6H), 7.5–7.94 (m, 2H). *Anal.* calcd. for $C_{17}H_{16}$: C 92.73, H 7.27; found: C 92.49, H 7.16.

cis-*9,10-Cyclohexyl-9,10-dihydrophenanthrene,* c-*7*, oil; nmr (CCl_4): 1.3–2.2 (m, 8H), 3.07 (m, 2H), 7.1–7.4 (m, 6H), 7.5–7.94 (m, 2). *Anal.* calcd. for $C_{18}H_{18}$: C 92.31, H 7.69; found: C 92.08, H 7.57.

cis-*9,10-Cycloheptyl-9,10-dihydrophenanthrene,* c-***8***, oil; nmr (CCl_4): 1.4–2.4 (m, 10H), 3.11 (m, 2H), 7.1–7.5 (m, 6H), 7.5–7.9 (m, 2H). *Anal.* calcd. for $C_{19}H_{20}$: C 91.63, H 8.06; found: C 91.60, H 7.89.

cis-*9,10-Cyclooctyl-9,10-dihydrophenanthrene,* c-***9***, oil, nmr (CCl_4): 1.4–2.5 (m, 12H), 3.15 (m, 2H), 7–7.5 (m, 6H), 7.5–7.9 (m, 2H). *Anal.* calcd. for $C_{20}H_{22}$: C 91.6, H 8.41; found: C 91.59, H 8.48.

Dehydrogenation of cis- *and* trans-*9,10-cyclohexyl-9,10-dihydrophenanthrene*

An equimolar mixture of *cis* and *trans*-9,10-cyclohexyl-9,10-dihydrophenanthrene (214 mg) dissolved in diglyme (50 mL) containing 20 mg of 10% Pd/C were refluxed under nitrogen. After 2 h a glc control showed that approximately half of the *cis* isomer had been dehydrogenated to tetrahydrotriphenylene and triphenylene while the *trans* isomer was unchanged. After refluxing overnight, the solvent was removed under vacuum and the residue chromatographed on a silica gel column. Elution with petroleum ether gave 82 mg of *t*-**7** and 108 mg of triphenylene.

1. W. G. Dauben, E. L. McInnis, and D. M. Michno. *In* Rearrangements in ground and excited states. Vol. 3. *Edited by* P. de Mayo. Academic Press, New York. 1980. Chapt. 15. p. 91.
2. R. Lapouyade, R. Koussini, A. Nourmamode, and Ch. Courseille. J. Chem. Soc. Chem. Commun. 740 (1980).
3. N. J. Turro. Modern molecular photochemistry. The Benjamin Cummings Publishing Company Inc., Menlo Park, California. 1978.
4. H. Gorner, D. W. Eaker, and J. Saltiel. J. Am. Chem. Soc. **103**, 7164 (1981).
5. T. Arai, T. Karatsu, H. Sakuragi, and K. Tokumaru. Chem. Lett. 1377 (1981).
6. S. Lazare, R. Bonneau, and R. Lapouyade. J. Phys. Chem. **88**, 18 (1984).
7. S. Lazare, R. Lapouyade, and M. P. Robert. Nouv. J. Chim. **8**, 407 (1984).
8. M. Schlosser and B. Schaub. Chimia, **36**, 396 (1982).
9. A. Nourmamode, R. Lapouyade, B. Barbe, and M. Petraud. Bull. Soc. Chim. Fr. II, 207 (1981).
10. W. C. Still, M. Kahn, and A. Mitra. J. Org. Chem. **43**, 2923 (1978).
11. C. K. Bradsher. J. Am. Chem. Soc., **61**, 3131 (1939).
12. W. S. Allen and S. Bernstein. J. Am. Chem. Soc. **77**, 1028 (1955).
13. W. E. Bachmann and M. C. Kloetzel. J. Am. Chem. Soc. **59**, 2207 (1937).
14. P. G. H. op het Veld and W. H. Laarhoven. J. Chem. Soc. Perkin Trans. 2, 915 (1978).
15. P. W. Rabideau and R. G. Harvey. J. Org. Chem. **35**, 25 (1970).
16. E. J. Panek and T. D. Rodgers. J. Am. Chem. Soc. **96**, 6921 (1974).
17. M. Daney, R. Lapouyade, and H. Bouas-Laurent. Tetrahedron Lett. 783 (1978).
18. F. D. Lewis and R. J. Devoe. J. Org. Chem. **47**, 888 (1982).
19. P. W. Rabideau, D. M. Wetzel, C. A. Husted, and J. R. Lawrence. Tetrahedron Lett. **25**, 31 (1984).
20. P. W. Rabideau, R. G. Harvey, and J. B. Stothers. J. Chem. Soc. Chem. Commun. 1005 (1969).
21. P. P. Fu and R. G. Harvey. Chem. Rev. **78**, 317 (1978).
22. H. G. Heller and J. R. Langan. J. Chem. Soc. Perkin Trans. 2, 341 (1981).
23. W. H. Laarhoven. Recl. Trav. Chim. Pays-Bas, **102**, 185 (1983); **102**, 241 (1983).
24. R. Koussini, R. Lapouyade, and Ph. Fornier de Violet. J. Am. Chem. Soc. **100**, 6679 (1978).
25. A. Padwa, Ch. Doubleday, and A. Mazzu. J. Org. Chem. **42**, 3271 (1977).
26. H. J. C. Jacobs, J. W. J. Gielen, and E. Havinga. Tetrahedron Lett. 4013 (1981).
27. S. L. Murov. Handbook of photochemistry. Marcel Dekker, New York. 1973.

Chemistry of amido radicals: intramolecular hydrogen abstraction as related to amido radical configurations

YUAN L. CHOW,[1] THOMAS W. MOJELSKY, AND LEON J. MAGDZINSKI
Department of Chemistry, Simon Fraser University, Burnaby, B.C., Canada V5A 1S6

AND

M. TICHÝ
Institute of Organic and Biochemistry, Czechoslovak Academy of Science, Prague, Czechoslavakia

Received August 10, 1984

YUAN L. CHOW, THOMAS W. MOJELSKY, LEON J. MAGDZINSKI, and M. TICHÝ. Can. J. Chem. **63**, 2197 (1985).

Model bromamides were photolysed to investigate the reactivity of intramolecular C-5 hydrogen abstraction (from the nitrogen atom) of the corresponding amidyl radicals and of the cyclization of the resulting C-bromides. The observed results are discussed in terms of stereoelectronic as well as energetic considerations. In the former C-5 hydrogen abstraction, the reactivity difference between semi-rigid *trans* and *cis*-oriented reaction centers is only slightly in favor of the latter; the small difference is interpreted as due to the planar ground state Π amidyl radical structure with a low N—CO twisting barrier (4–5 kcal/mol). This interpretation is supported by the efficient C-5 hydrogen abstraction in *N*-bromo-*N*-alkyltoluamides, since a rigid planar amidyl radical does not allow the methyl C—H bond to colinearly approach the Π orbital. In marked contrast, there are large reactivity differences in the cyclization of C-bromides derived from these intramolecular H—Br exchanges; these arise from the requirement of colinearity of the approaching and departing bonds. Thus this requires the coplanar orientation of the C—CH_3 and C—CO bonds and this is the source of the reactivity differences.

YUAN L. CHOW, THOMAS W. MOJELSKY, LEON J. MAGDZINSKI et M. TICHÝ. Can. J. Chem. **63**, 2197 (1985).

On a effectué la photolyse de bromamides modèles dans le but d'étudier la réactivité, vis-à-vis de l'enlèvement intramoléculaire de l'hydrogène en C-5 (par rapport à l'atome d'azote), des radicaux amidyles correspondants ainsi que la cyclisation des C-bromures qui en résultent. On discute des résultats observés en fonction de considérations tant stéréoélectroniques qu'énergétiques. Dans le cas de l'enlèvement des hydrogènes en position C-5, la différence de réactivité entre les centres réactionnels semi-régides orientés en *cis* ou en *trans* ne favorise que légèrement les premiers; on peut interpréter la différence minime en supposant que l'état fondamental planaire Π de la structure radicalaire amidyle comporte une barrière à la rotation N—CO qui est faible (environ 4 à 5 kcal/mol). Cette interprétation est en accord avec le fait que l'enlèvement des hydrogènes en position C-5 des *N*-bromo *N*-alkyltoluamides est une réaction efficace et que ce résultat est dû à l'existence d'un radical amidyle planaire rigide qui ne permet pas à la liaison C—H du méthyle de s'approcher colinéairement de l'orbitale Π. Par opposition, il existe de grandes différences dans la réactivité des cyclisations des C-bromures qui dérivent de ces échanges H—Br intramoléculaires; ces différences proviennent du fait qu'il doit y avoir une colinéarité entre les liens qui approchent et ceux qui partent. Ceci requiert donc une orientation coplanaire des liaisons C—CH_3 et C—CO et ceci est la source des différences dans les réactivités.

[Traduit par le journal]

Amidyl radicals, RCON̈R′ (for reviews, see ref. 1), may have the Σ or Π electronic configurations as shown in **A** and **B**, assuming a sp^2 hybridization of the nitrogen atom. An N—CO bond twisted structure from **B** (Π configuration) is shown in **D**. If *sp* hybridization of the nitrogen atom is assumed, three non-bonded electrons are located in two *p*-orbitals as in **C**, which structurally resembles the Σ configuration.

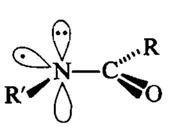

A

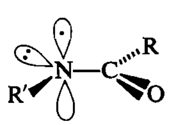

B

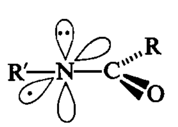

C

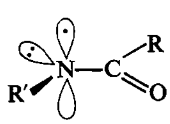

D

About 15 years ago, we (2) showed that amidyl radicals do not react from the O-centered radical, but rather from the N-centered radical, and that amidyl radicals preferentially abstract the C-5 hydrogen (from the N-center) from the alkyl side chain rather than from the acyl side chain (3–5). On the basis of the Π electronic configuration of amidyl radicals indicated by esr (electron spin resonance) (6) and ^{13}C CIDNP (7) evidence we have proposed, after extensive model analyses, that amidyl radicals can twist around the N—CO bond with a small energy barrier (8) which causes the observed preference in intramolecular H-abstraction from the alkyl side chain. Later, using stereochemical considerations to explain the intramolecular additions of amidyl radicals to olefinic (9) and aryl groups (10, 11), others proposed the Σ (or Π) electronic configuration for the reactive state of amidyl radicals, which is generally the ground state unless special conditions prevail. While theoretical calculations on this question have been inconclusive (12, 13), detailed esr studies by Ingold's group (14–16) have finally confirmed that simple amidyl radicals have the Π radical ground state, which has either a planar or a twisted N—CO conformation with a low energy barrier (14). The latter had previously been generally neglected in considering the stereochemical implications of amidyl radical additions (9–11). As it is now possible to present a definite discussion, we deem it worthwhile to publish these old results describing intramolecular H-abstraction reactivities involving acyl chains as related to the amidyl radical configurations.

[1] Author to whom correspondence may be addressed.

Results

The plan of this investigation was to generate the amidyl radicals by photolysis of *N*-bromamides **2**, **7**, and **14** and to examine the facility of intramolecular H-abstraction by product pattern analysis. Each amidyl radical should undergo intramolecular H-abstraction preferentially from the CH_3 group located at the C-5 position in the acyl side chains. Their efficiencies are expected to be controlled by the geometry of the methyl and carboxamide groups attached on rigid or semi-rigid ring systems.

The *N-tert*-butyl carboxamides **1***a* and **6***a* of *trans*- and *cis*-2-methylcyclohexane carboxylic acids were brominated with *tert*-butylhypobromite and the bromamides **2***a* and **7***a* were photolyzed in benzene by a procedure similar to that described before (8). In contrast to the excellent yields of bromide **3***a* from *trans*-bromamide **2***a*, the irradiation of *cis*-bromamide **7***a* gave more than 14 compounds; among them were amide **6***a* (33%) and iminolactones **9***a*, **11**, and **12**. These iminolactones were not isolated in pure states, but lactone **10** was obtained after vigorous hydrolysis of a mixture of iminolactones. The

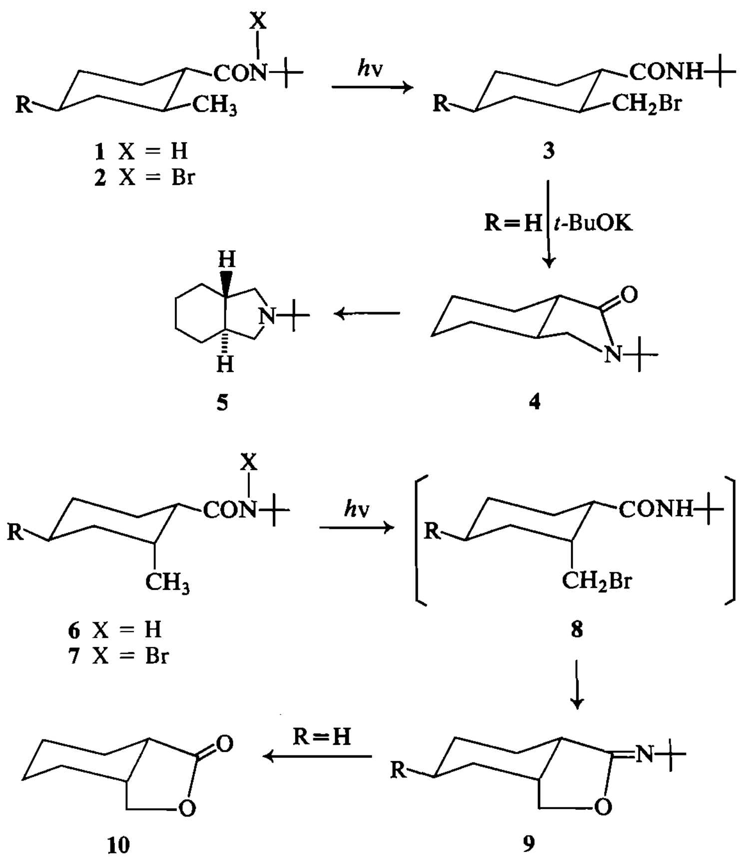

Series *a* R = H; series *b* R = *t*-Bu

C-bromide **3***a* did not cyclize on heating but did so under the effect of hot *t*-BuOK to give lactam **4***a*, which was reduced to give pyrrolidin derivative **5***a*; this proved the lactam formation instead of the iminolactone formation which has been shown to be facile in acyclic bromamide photolysis (4, 8). The formation of iminolactones **11** and **12** and the complexity of the product pattern indicate that the *cis*-1,2-disubstituted cyclohexane ring must have a substantial population of the alternate chair conformation in which the *t*-BuN(X)CO group takes the axial conformation,[2] allowing H-abstraction from the C(3)-axial and C(5)-axial hydrogen to occur (see Discussion).

The use of 4-*tert*-butyl group substituted semi-rigid carboxamides **1***b* and **6***b* prevented the ring inversion to occur and gave cleaner results; in these models the cyclohexane ring is anchored on one side but the opposite side is flexible enough to do flattening and puckering. Photolysis of bromamide **2***b* gave a stable C-bromide **3** in about 90% yield, with small amounts of **1***b* and three by-products. Photolysis of *cis*-bromamide **7***b* gave more than 92% of the hydrobromide of iminolactone **9**, obviously formed from the primary photoproduct C-bromide **8***b*, and gave the free base **9** on neutralization. The structures of both **3***b* and **9***b* were decided by the fact that the nmr signals of the methyl groups in the starting bromamides were replaced by CH_2 signals with magnetically nonequivalent protons at the expected chemical shifts.

Either bromamides **14***a* or **14***b*, derived from *N*-methyl- or *N-tert*-butyltoluamides, were photolyzed in benzene or benzene containing 10% cyclohexane to give essentially quantitative yields of iminolactones **16***a* and **16***b* via the intermediacy of unisolated C-bromides **15***a* and **15***b*. In the presence or absence of a bromine atom and bromine scavenger, the product patterns were not affected, indicating that intramolecular hydrogen abstraction by the amidyl radicals from the *ortho*-methyl group is extremely efficient and operates cleanly.

[2] Using *cis*-ethyl-4-methylcyclohexane carboxylate as an approximate model, the population of the conformational isomer corresponding to **6***a* (or **7***a*) is 28% (17).

TABLE 1. Competitive inter- and intramolecular hydrogen abstraction by the amido radicals **17** and **18**

Solvent: % (v/v) cyclohexane in benzene	% Recovered amides (% of products)[a]	
	trans-**1***b* (% **3***b*)[a]	*cis*-**6***b* (% **9***b*)[a]
100	96 (≈2.5)	91 (≈8)
26.7	37 (63)	22 (77)
12.0	32 (68)	17 (83)
8.3	28 (72)	13 (87)
0.0	<5 (≈90)[b]	0 (>92)[b]

[a]The yields of the products were taken as (100% − % of recovered amides) and were also checked against their vpc peaks. These are shown in the brackets.
[b]The % yields of the products were determined from the isolation and confirmed by vpc analysis.

The competitive inter- versus intra-molecular H-abstraction of the amidyl radicals **17** and **18** (R = *tert*-butyl) generated from *cis*- and *trans*-bromamides **2***b* and **7***b* was investigated in solvent mixtures of cyclohexane–benzene. With increasing amounts of cyclohexane, intermolecular H-abstraction increased to afford more parent amides **1***b* and **6***b* in competition with the formation of **3***b* and **8***b* (i.e., **9***b*, see Table 1). The extent of the formation of these products should vary depending on the energetics (or the geometry) of the transition states in H-abstraction. In addition, the extent of the former, **1***b* and **6***b*, also depends on the concentrations of cyclohexane. Since quantitative gc analysis of **3***b* and **9***b* was frustrated by the broad and unsymmetrical peaks, the % yields of the parent amides **1***b* and **6***b* were analysed against an internal standard.

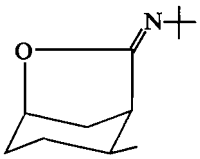

11

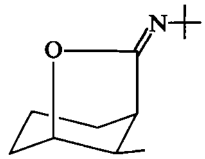

12

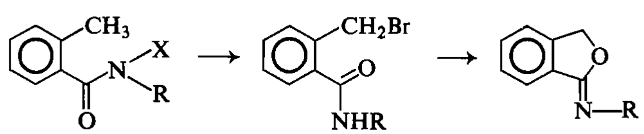

13 X = H
14 X = Br

15

16

phthalide

Series *a* R = CH_3; series *b* R = $(CH_3)_3C$—

The photolysis conditions were kept constant except for solvent variations, and the starting bromamides were examined with ir to make sure no starting amides were left unbrominated. The lack of the starting materials prevented us from getting more points, but each point was repeated twice to give average values. Because of many steps taken in working up to give gc analytical samples, estimations of degree of accuracy were not easy. But the trend of decreases could be easily discerned.

Discussion

While intramolecular H-abstraction from the C-5 hydrogen of the acyl side chain in acyclic flexible amidyl radicals is relatively ineffective (3, 4, 8), the model amidyl radicals **17** and **18** generated from **1** and **6** in the present case undergo such H-abstraction very efficiently, at least in benzene, a poor H-atom donating solvent. This efficiency no doubt arises from the fact that the reacting carboxamide and methyl groups are held in a semi-rigid framework and that β-elimination, which has been shown to occur more readily than this type of intramolecular H-abstraction (3, 8), is blocked. Similar intramolecular H-abstraction in the aromatic amidyl radicals **20** generated from **13** is more efficient since even where the β-elimination is not blocked (with —$\dot{N}$—CH_3 from **13***a*) and intermolecular H-abstraction is possible, the intramolecular H-abstraction has prevailed over other possibilities. That functionalization at the methyl group of toluamide does not arise from a bromine atom chain reaction is demonstrated by the lack of effects on the pattern of the reaction in the presence of a bromine atom (or Br_2) scavenger, *tert*-butylethylene.

Table 1 shows the comparison of the efficiency of the intramolecular H-abstraction in *trans*- and *cis*-amidyl radicals **17***b* and **18***b* (k_t and k_c) using the independent competitions against intermolecular H-abstraction from cyclohexane (k_i[cyclohexane]) as the standard. This comparison is based on the assumption that intermolecular H-abstractions from cyclohexane by **17***b* and **18***b* occur with approximately the same rate constant, as both *N*-*tert*-butyl carboxamide groups have approximately, but not exactly, the same environment. This assumption is reasonable since the steric effects of the *N*-*tert*-butyl group exert such overwhelming influences on intermolecular H-abstraction that those of others become insignificant. While the difference in the intramolecular H-abstractions in **17***b* and **18***b* are small, **18***b* with the *cis*-configuration does so more efficiently, as shown by the two trends in Table 1. The smallness of the observed difference is a critical phenomenon which requires discussion.

The intramolecular H-transfers between an alkoxy (18–21) or aminium (22) radical and a C-5 hydrogen bond are generally evaluated with the O···C (or N^+···C) distance in an appropriate conformation. Owing to the definite structure assumed, and

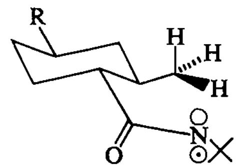

17

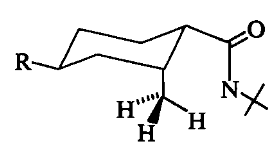

18

R = H

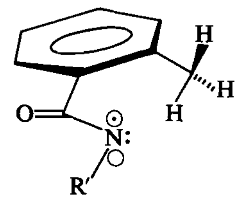

20

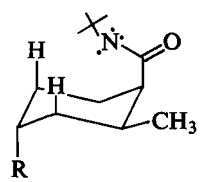

19

accepted, in amidyl radicals, the orientation of the interacting orbital containing the unpaired electron and the C—H bond has to be considered in various probable conformations. Studies of Dreiding models have indicated that should amidyl radicals react in the Σ configuration, the observed small reactivity difference could be interpreted readily: in either *trans*-**17***b* or *cis*-**18***b*, the carboxamide and methyl groups could rotate to orient the sp^2-orbital and a C—H bond in a N···C distance of

2.5–2.6 Å with near colinear orientation without imposing much strain on the cyclohexane ring. Undoubtedly, similar considerations in the intramolecular addition reaction had led other groups to come to the conclusion that amidyl radicals might have the reactive state Σ configuration (9). This would be reasonable if the esr results were not known (14), since in the Π-configuration such close proximity and colinearity of the interacting centers could not be achieved. Model studies of the more rigid aromatic amidyl radical **20** shows these features more clearly; the Π radical has no chance for intramolecular H-transfer. But, *this argument is faulty in assuming that the* Π *configuration is planar and rigid, or planar and having an energy barrier of twisting higher than the activation energy of intramolecular H-abstraction.*

Electron spin resonance evidence from Ingold's group leaves no doubt that amidyl radicals, RCOṄR′, have the Π ground state configuration (14). If twisting of the N—CO bond with a low energy barrier (8, 14) is accepted for the Π-radicals, it is readily seen that the intramolecular H-transfer in models **17** and **18** occurs without perceivable efficiency difference between the *cis*- and *trans*-configurations. Dreiding models show the interacting orbitals can be near colinear, with the N···C distance about 2.5 Å, by twisting the N—CO bond for both. Early esr work also established that the delocalization of the unpaired electron to a CO or electron-withdrawing group in various radicals is minimal (6, 23); thus a low energy barrier (of N—CO twisting) and, also, the lack of the O-radical behavior for amidyl radicals are supported. Experimental activation energies (16) may be used to estimate the N—CO twisting energy barrier. We have proposed that the overwhelming preference (by a factor of at least 100) for abstraction of an acyl C-5 hydrogen over an alkyl C-5 hydrogen in an intramolecular competition arises primarily from the requirement to twist the N—CO out of the plane (8); this assumption has led us to estimate the energy barrier of twisting to be 3–4 kcal/mol. The difference of activation energies (16) in the two types of intramolecular H-abstractions is 1.4 kcal/mol, probably the lower limit of the twisting barrier; the necessity for this barrier to be lower than the activation energy of acyl C-5 hydrogen abstraction (9.1 kcal/mol) (16) can place the upper limit of this barrier at this figure. Thus, 4–5 kcal/mol for the N—CO twisting barrier is reasonable and surprisingly low in comparison to the N—CO twisting barrier of amides, determined to be ≈16–22 kcal/mol by variable temperature nmr studies (24).[3]

We now consider the *slightly* more efficient intramolecular C-5 hydrogen abstraction in *cis*-**18** than in *trans*-**17**. The transition state of the intramolecular H-abstraction can be facilitated by moving the C—CH_3 and C—CO bonds in the e,e-orientation in *trans*-**17***b* and those in the e,a-orientation in *cis*-**18***b* closer from the normal dihedral angles of 65° and 55°, respectively.[3] This motion is possible in *cis*-**18***b* since it causes flattening of the cyclohexane ring, but it is prohibited in *trans*-**17***b* since the motion causes the puckering of the ring (25). Thus, the smallness in the efficiency difference between two series of experiments (Table 1) indicates that coplanarity (21, 22) of these two bonds is not important; otherwise the difference will be substantial, as shown in the ring closure of C-bromides **3***b* and **8***b* discussed below.

[3]In the transition state of radical H-abstraction from a C-5 hydrogen, coplanarity requirements are also considered (see refs. 19 and 23).

The great efficiency difference in the ring closure of **3***b* and **8***b* to the iminolactones is a nice contrast to the intramolecular H-abstraction discussed above. For the iminolactone formation, the C=O has to approach the rear end of the C—Br bond in the transition state in which the colinearity of the interacting orbitals is the best geometry, minimizing the energy requirement. Similar Dreiding model studies show that such transition states require bringing the C—CO and C—CH_2Br bond close to coplanar orientation, which means the puckering of the cyclohexane ring in **3***b* (compare **17***b*). As this motion requires a large energy expenditure, the corresponding iminolactone is not formed even under forced conditions. Similar coplanarity requirements in **8***b* mean the flattening of the cyclohexane ring (compare **18***b*), which demands a relatively small energy expenditure (<10 kcal/mol), thus the facile formation of iminolactone **9***b* from **8***b* (25). For the unisolated aromatic C-bromide **15** from **14**, the cyclization is even more facile since the two relevant bonds are already held in coplanar orientation; the ring closure is spontaneous.

Though iminolactones **11** and **12** have not been isolated, their formation on irradiation of **7***a* is certain. From the consideration of conformation free energies, the alternative conformation to **6***a* and **7***a* should exist to a certain extent (17) and should generate amidyl radical **19** which undergoes intramolecular H-abstraction from the C(3)- and C(5)-axial hydrogens as discussed above. In the present H-abstraction, since the C—H bonds are semi-rigid, the requirement of the N—CO twisting in the Π amidyl radical is more obvious than ever. It should be noted that the cyclohexane ring inversion **18***a* ⇄ **19** is quite likely much slower than intramolecular H-abstraction from energetic considerations. The activation energies of the latter have been shown to be 9.1 kcal/mol in acyclic amidyl radicals (16) and, in the present case, probably <9.0 kcal/mol because of semi-rigid model **6***a*. In contrast, the activation energies for the former are generally ≈10 kcal/mol (25) and in **18***a* ⇄ **19** it should be higher than this value because of the eclipsing of 1,2-disubstituents in the transition state.

The small difference in intramolecular H-abstraction between *trans*-**17***b* and *cis*-**18***b* is surprising and has been explained by the Π amidyl radical configuration having a low energy barrier for twisting around the N—CO bond; undoubtedly, the esr results (14–16) provide us some confidence in arriving at this conclusion. However, another explanation is possible, though more speculative in nature. For this, we assume that Π and Σ radical configurations (i.e., **B** and **A**) as the ground and lowest excited state electronic configurations of amidyl radicals, and that the energy split between the two states is fairly small, say < 9.1 kcal/mol, in other words, much less than the activation energy for intramolecular H-abstraction from acyl chains (16). Under such a circumstance, intramolecular H-abstraction from acyl chains must involve the transition of the Π radical configuration **B** to the Σ radical configuration **A**. As such, no significant stereoelectronic control of the intramolecular H-abstraction can be observed with the model amidyl radicals used in the present study.

While the model systems adapted in the present study are inadequate to give us a finite solution, they have led us to recognize immensely intricate electronic configurations of amidyl radicals in their static and dynamic (reactive) states. The challenge led us to extend considerations to other reactive radicals with possibilities of delocalization, such as carboxyl and nitrogen dioxide radicals.

Experimental

The conditions and equipment are the same as those given in ref. 8. The samples of *trans*-4-*tert*-butyl-*trans*-2-methylcyclohexanecarboxylic acid and its *cis* isomer were obtained from the synthetic scheme published previously (26). The carboxylic acids were treated with $SOCl_2$ followed by *tert*-butylamine to afford the *N-tert*-butylcarboxamides **1***b* and **6***b*.

Photolysis of trans-*bromamide* **2**b

To a 25-mL aluminum foil-protected Erlenmeyer flask was added the *t*-BuOBr solution (5 mL) and **1***b* (0.148 g), which were stirred for 2 h at 0°C. After 2 h reaction, an aliquot was tested by ir spectroscopy for the absence of the 1500 cm^{-1} peak. The resulting crude solid was dissolved in anhydrous benzene (120 mL) placed a Pyrex photocell kept at 20°C. A 200-W medium pressure Hanovia lamp was used as the irradiation source. The photolysis was carried out for 45 min but the reaction was essentially complete in 30 min, as shown by KI–AcOH tests. The benzene solution was concentrated to give a solid residue (0.220 g); ir: 3430 (m), 3300 (m), 1665, 1505 (m) cm^{-1}; nmr: 5.7 (b, 1H), 4.5 (bs, 2H), 1.4 (s), 0.9 (s) ppm. Vapor phase chromatography (vpc) showed that the product had one major peak (90%) and four small peaks, of which one was the amide **1***b*.

A portion (0.180 g) of this photoproduct was subjected to preparative tlc on silica gel plates with 2% CH_3OH in $CHCl_3$ as the eluting solvent. The appropriate portion of the plates was scraped off and the silica gel was extracted with 15 mL CH_3OH for 1 h. The material recovered from the CH_3OH solution was taken up in $CHCl_3$ (2 mL) and was filtered through a short column containing neutral alumina (2 g) and further eluted with $CHCl_3$ (100 mL). Evaporation of $CHCl_3$ left a solid (0.130 g) which was recrystallized from acetone/petroleum ether (1:9) to give white crystals of **3***b*, mp 134–135°C; ir: 3430 (m), 1665, 1505 (m) cm^{-1}; ms *m/e*: 333 (M^+, 27), 331 (M^+, 27), 318 (18), 316 (18), 276 (64), 274 (59), 252 (100). *Anal.* calcd. for $C_{16}H_{30}NOBr$: C 57.84, H 9.10, N 4.22; found: C 57.78, H 9.04, N 4.25.

Compound **3***b* (30 mg) was refluxed in 20 mL benzene for 2 h. No change was observed in the ir spectrum of the residue.

Photolysis of cis-*bromamide* **7**b

The *N*-bromamide was prepared from **6***b* (0.147 g) and *t*-BuOBr in the usual manner to give **7***b* as a yellow solid (0.232 g). This material was dissolved in anhydrous benzene (120 mL) and photolyzed in the usual manner for 45 min. The photolysate was evaporated to give the solid HBr salt of **9***b* (0.233 g); ir: 3350 (m), 2950, 2860, 2750, 2670 (m), 1675, 1510 (w) cm^{-1}; nmr: 7.0 (bs, 1H), 4.7 (m, 1H), 3.9 (m, 1H), 2.7 (m, 1H), 1.55 (s), 0.9 (s) ppm. Irradiation at ca. 1.7 ppm changed the 4.7 and 3.9 ppm signals to an unsymmetrical AB quartet (J = 17 Hz).

The photoproducts (0.160 g) were taken up in 25 mL saturated Na_2CO_3 solution which was extracted with $CHCl_3$ (3 × 10 mL). The combined organic extracts were worked up to give, upon evaporation, a solid (0.076 g), which on gc showed one major peak (>92%) and three minor peaks, none of which corresponded to the starting amide **6***b*. The solid was subjected to preparative tlc on silica gel with 2% $CH_3OH - CHCl_3$ as eluent. After the usual extraction process, it gave a solid residue (0.06 g) which was recrystallized from $CHCl_3$/acetone (3:1) mixture to yield **9***b*, mp 92–93°C; ir: 1700, 1505, 1235, 1010 cm^{-1}; ms *m/e*: 251 (M^+, 10), 237 (54), 236 (100), 194 (15), 180 (11), 84 (47). *Anal.* calcd. for $C_{16}H_{29}NO$: C 76.44, H 11.63, N 5.57; found: C 76.71, H 11.65, N 5.39.

Quantitative analysis of cis- *and* trans-*bromamide photolyses*

Amide **1***b* or **6***b* (50.0 mg) and the *tert*-butylhypobromite solution (4 mL) were reacted as described before. After 2 h reaction time, a sample was taken for ir spectrum examination. Once the absence of absorption at 1500 cm^{-1} had been confirmed, the solution was concentrated at 0°C to a constant weight of residue while taking precautions to avoid exposure to light. The solid was then dissolved in the solvent mixture (120 mL) and was photolyzed under the conditions previously described.

For the photolysate obtained from amide **1***b*, 0.2 mL of the internal standard (*N-tert*-butyltoluamide 9.7 mg/5.0 mL $CHCl_3$) and sufficient photolysate were mixed to make exactly 5.0 mL solution, which was then concentrated on the rotary evaporator (15°C water bath temperature) until all the solvent was removed. Then 0.25 mL $CHCl_3$ was added and the resulting solution was analyzed by vpc (15% DEGS column at 180°C). The ratio of the area for amide **1***b* to internal standard was calculated and, with the assistance of a previously prepared calibration curve, the quantity of **1***b* in the solution was determined.

The photolysate obtained from amide **6***b* was treated with Na_2CO_3 solution. After drying, 5.0 mL of the photolysate was withdrawn and concentrated on the rotary evaporator (water bath at 15°C). To the residue was added 0.25 mL 2-phenylpropanone internal standard solution (concentration 0.268 mg/mL). The solution was analysed by vpc as above.

Photolysis of trans-*bromamide* **2**a

Sodium and isoamyl alcohol reduction of *o*-toluic acid according to the published method (27) gave *trans*-2-methylcyclohexanecarboxylic acid, mp 41–43°C; anilide mp 147–148°C (lit. (27) mp 148°C). The *N-tert*-butylamide **19** was recrystallized from aqueous ethanol; mp 159–160°C; ir (CCl_4): 3455, 1670, 1510 cm^{-1}; nmr: 0.87 (d, J = 5 Hz, 3H), 1.27 (s, 9H) ppm. *Anal.* calcd. for $C_{12}H_{23}NO$: C 73.04, H 11.75, N 7.10; found: C 72.96, H 11.55, N 7.23.

The usual bromination of **1***a* with *t*-BuOBr afforded bromamide **2***a*; ir (CCl_4): 1664, 1450 cm^{-1}; nmr: 0.93 (d, J = 6 Hz, 3H), 1.45 (s, 9H). This bromamide (870 mg) in benzene (30 mL) was photolyzed for 30 min, and the photolysate was evaporated under vacuum. The residue was chromatographed on silicic acid to give amide **1***a* (33 mg) and impure C-bromo compound **3***a* (662 mg); ir: 3440, 1640, 1510 cm^{-1}; nmr: 3.41 (bd, 2H); ms *m/e*: 377, 375, 260, 262, 220, 222, 203, 205, 196, 140, 95. Heating of the latter fraction in benzene caused darkening of the solution and gave **3***a* on work-up.

The residue obtained from photolysis of **2***a* (652 mg) was refluxed with *t*-BuOK (230 mg) in *t*-BuOH (6 mL) for 2 h. The product was analyzed by vpc showing **4** (66%, RT 7 min), **1***a* (16%, RT 4.8 min), and some unreacted **3***a*. Silicic acid chromatography of the product gave lactam **4** (196 mg); ir: 1690, 1400, 1365 cm^{-1}; nmr: 1.37 (s, 9H), 3.39 (dd, J = 9 and 5.5 Hz, 1H), 2.98 (dd, J = 9 and 2 Hz, 1H) ppm; ms *m/e*: 195 (M^+, 16), 180 (100), 178 (55), 152 (53), 58 (19).

The lactam **4** was reduced with LAH to pyrrolidine **5** which gave a picrate, mp 155–157°C. *Anal.* calcd. for $C_{18}H_{26}N_4O_7$: C 52.68, H 6.39, N 13.65; found: C 52.83, H 6.44, N 13.58.

Photolysis of cis-*bromamide* **7**a

Hydrogenation of *o*-toluic acid in the presence of PtO_2 in acetic acid followed by fractional distillation (28) gave a fraction boiling at 106–108°C/0.5 Torr (1 Torr = 133.3 Pa). The methyl ester of the fraction was analyzed by vpc showing the presence of 95% of *cis*-2-methylcyclohexanecarboxylic acid and 5% of the *trans* isomer. The corresponding amide had mp 151–152°C (lit. (28) mp 151–153°C); ir: 3360, 3180, 1660, 1620; nmr: 0.91 (d, J = 6 Hz, 3H), 2.57 (m, $W_{1/2}$ = 15 Hz, 1H) ppm. The corresponding anilide had mp 119–122°C (lit. (28) mp 68°C); ir: 3325, 1655, 1600, 1520. *N-tert*-butylamide **6***a* was recrystallized from a pet. ether – benzene mixture giving white crystals, mp 111–112°C; ir: 3320, 1645, 1550 cm^{-1}; nmr: 0.92 (d, J = 7 Hz, 3H), 1.38 (s, 9H) ppm. *Anal.* calcd. for $C_{12}H_{23}NO$: C 73.04, H 11.75, N 7.10; found: C 73.01, H 11.68, N 7.28.

Amide **6***a* (0.5 g) was brominated and photolyzed as described above. The crude product showed more than 10 spots on tlc analysis. The crude product was separated by silicic acid chromatograph to give fractions 1 (228 mg), 2 (192 mg), and 3 (50 mg). Fraction 1 contained the parent amide **6***a* (33% overall estimated from peak areas) and several minor components as shown by vpc. Fraction 2 was rechromatographed to give an amorphous solid; ir: 1705, 1460, 1310, 1140; nmr: 4.67 (t, J = 4), 4.35 ($W_{1/2}$ = 7 Hz), 3.25 ($W_{1/2}$ = 7 Hz), 2.33 ($W_{1/2}$ = 8 Hz), 0.97 (d, J = 6.5 Hz), 1.02 (d, J = 6.5 Hz) ppm.

This amorphous solid was assumed to be a mixture of iminolactones **11** and **12**. On attempted recrystallization from a benzene–ethanol mixture, the ir and nmr of the recovered solid exhibited patterns similar to those of fraction 3, which was believed to be an isomeric mixture of hydrolysis products of **11** and **12**. Another portion obtained from this chromatography exhibited the nmr signal at 4.1 (dd, J = 9 and 3.5 Hz) and 4.0 (J = 9 and 2 Hz) ppm due to **9***a*.

A combined fraction 2 (626 mg) was hydrolyzed in hot 4 N HCl solution for 20 h. The product was separated into an acidic fraction (126 mg) and a neutral fraction (310 mg). The acidic fraction was chromatographed on silicic acid to afford lactone **10** (66 mg); ir: 2875, 1780, 1140, 950 cm^{-1}; nmr: 4.09 (dd, J = 9 and 4 Hz, 1H), 3.80 (dd, J = 9 and 1 Hz, 1H) ppm. An authentic lactone **10** was synthesized from LAH reduction of *cis*-1,2-cyclohexanedicarboxylic acid and showed identical ir and nmr spectra with those obtained from the photolysis sample.

Photolysis of N-*bromo*-N-*methyltoluamide* *14*a

The toluamide **13***a* (0.23 g) and *t*-BuOBr (6 mL) were reacted to give a bromamide **14***a* (0.37 g) which was taken up in benzene (120 mL) and irradiated as above at 20°C for 1 h. The photolysate was evaporated to afford a residue (0.31 g) which was recrystallized three times from $CHCl_3$–acetone (1:3) to give the hydrobromide of iminolactone **16***a*, mp 205–206°C; ir: 3460 (m), 2700 (m), 1700; nmr (D_2O): 7.9 (4H, m), 6.0 (2H, s), 3.4 (3H, s) ppm. *Anal.* calcd. for $C_9H_{10}NOBr$: C 47.39, H 4.42, N 6.14; found: C 47.47, H 4.51, N 6.25.

The residue from the mother liquor was treated with saturated Na_2CO_3 solution (20 mL) and extracted with CH_2Cl_2. Work-up of the extracts gave iminolactone **16***a* (0.113 g); ir: 1700 cm^{-1}; nmr: 7.5 (4H, m), 5.3 (2H, s), 3.18 (3H, s) ppm; ms m/e (%): 148 (M^+, 16), 147 (100), 146 (84), 118 (77). The solid in pet. ether was chromatographed on neutral alumina to give, as the only solid, phthalide, mp 69–71°C (lit. (29) mp 72–73°C); ir and nmr spectra were identical with those of another sample.

In a separate experiment, bromamide **14***a* (0.32 g) was photolyzed in 5% cyclohexane – benzene (120 mL) containing 3 drops of *tert*-butylethylene. The crude product before or after basification, or after chromatography, did not yield the starting amide **13***a*.

Photolysis of N-*bromo*-N-tert-*butyltoluamide* *14*b

The parent amide, **13***b*, (0.22 g) was treated with *t*-BuOBr (6 mL) to give *N*-bromamide **14***b* (0.33 g) which was photolyzed as above for 1 h at 20°C and evaporated to give a residue (0.25 g). Part of this (0.13 g) was recrystallized from acetone–$CHCl_3$ (3:1) to give the hydrobromide of iminolactone **16***b*, mp 110–111°C; ir: 1675 cm^{-1}; nmr: 7.8 (4H, m), 5.9 (2H, s), 1.75 (9H, s) ppm. The residue (0.12 g) was treated with saturated Na_2CO_3 solution (10 mL) and extracted with CH_2Cl_2 to give iminolactone **16***b* (0.07 g); ir: 1700, 1650 cm^{-1}; nmr: 7.8 (4H, m), 5.25 (2H, s), 1.4 (9H, s); ms m/e (%): 189 (M^+, 12), 174 (100), 134 (71).

Attempts to reduce iminolactone **16***b* with an excess of LAH gave only **16***b*. Iminolactone **16***b* (0.05 g) in 20% H_2SO_4 was refluxed for 3 h. The solution was extracted with $CHCl_3$. The extracts were evaporated to give phthalide (0.03 g), mp 72–73°C (29), as the only peak shown in gc analysis.

In a separate experiment, bromamide **14***b* (0.22 g) was photolyzed in 5% cyclohexane – benzene containing 3 drops of *tert*-butylethylene. The photolysate was neutralized, extracted, and worked up to give iminolactone **16***b* without contamination.

Acknowledgement

The authors from Simon Fraser University are much indebted to the Natural Sciences and Engineering Research Council of Canada, Ottawa for financial support of this project.

1. R. S. NEALE. Synthesis, 1 (1971); P. A. MACKIEWICZ and R. FURSTOSS. Tetrahedron, **34**, 3241 (1978); W. C. DANEN and F. A. NEUGEBAUER. Angew. Chem. Int. Ed. Engl. **14**, 783 (1975).
2. Y. L. CHOW and T. C. JOSEPH. J. Chem. Soc. Chem. Commun. 490 (1969).
3. Y. L. CHOW, J. N. S. TAM, and A. C. H. LEE. Can. J. Chem. **47**, 2441 (1969); Y. L. CHOW and A. C. H. LEE. Can. J. Chem. **45**, 311 (1967).
4. R. S. NEALE, N. L. MARCUS, and R. G. SCHEPERS. J. Am. Chem. Soc. **88**, 3051 (1966).
5. R. A. JOHNSON and F. D. GREENE. J. Org. Chem. **40**, 2186 (1975).
6. W. C. DANEN and R. W. GELLERT. J. Am. Chem. Soc. **94**, 6853 (1972).
7. C. BROWN and A. J. LAWSON. Tetrahedron Lett. 191 (1975).
8. T. C. JOSEPH, J. N. S. TAM, M. KITADANI, and Y. L. CHOW. Can. J. Chem. **54**, 3517 (1976).
9. P. MACKIEWICZ, R. FURTOSS, B. WAEGELL, R. COTE, and J. LESSARD. J. Org. Chem. **43**, 3746 (1978).
10. S. A. GLOVER and A. GOOSEN. J. Chem. Soc. Perkin Trans. 1, 1348 (1977).
11. A. R. FORRESTER, A. S. INGRAM, and R. H. THOMPSON. J. Chem. Soc. Perkin Trans. 1, 2847, (1972).
12. N. C. BAIRD and H. B. KATHPAL. J. Am. Chem. Soc. **98**, 753 (1976); N. C. BAIRD and K. F. TAYLOR. Can. J. Chem. **58**, 733 (1980).
13. M. J. S. DEWAR, A. H. PAKIARI, and A. B. PIERINI. J. Am. Chem. Soc. **104**, 3234 (1982).
14. R. SUTCLIFFE, D. GRILLER, J. LESSARD, and K. U. INGOLD. J. Am. Chem. Soc. **103**, 624 (1981); J. LESSARD, D. GRILLER, and K. U. INGOLD. J. Am. Chem. Soc. **102**, 3269 (1980).
15. R. SUTCLIFFE, M. ANPO, A. STOLOW, and K. U. INGOLD. J. Am. Chem. Soc. **104**, 6064 (1982).
16. R. SUTCLIFFE and K. U. INGOLD. J. Am. Chem. Soc. **104**, 6071 (1982).
17. E. L. ELIEL, N. L. ALLINGER, S. J. ANGYAL, and G. A. MORRISON. Conformational analysis. Interscience Publishers, New York. 1966. p. 36.
18. M. AKHTAR. *In* Advances in photochemistry. Vol. 2. *Edited by* W. A. Noyes, Jr., G. S. Hammond, and J. N. Pitts, Jr. Interscience, New York. 1964. p. 263.
19. K. HEUSLER and J. KALVODA. Angew. Chem. Int. Ed. Engl. **3**, 525 (1964); J. KALVODA and K. HEUSLER. Synthesis, 501 (1971).
20. R. H. HEESE. Advances in free radical chemistry. Vol. 3. *Edited by* G. H. Williams. Logos Press, New York. 1969. p. 83.
21. C. WALLING and A. PADWA. J. Am. Chem. Soc. **85**, 1597 (1963).
22. E. J. COREY and W. R. HERTLER. J. Am. Chem. Soc. **82**, 1657 (1960).
23. G. A. RUSSELL and J. LOKENSGARD. J. Am. Chem. Soc. **89**, 5059 (1967).
24. D. A. R. WILLIAMS and F. G. RIDDEL. J. Chem. Soc. Perkin Trans. 2, 567 (1973).
25. G. BINSCH. *In* Topics in stereochemistry. Vol. 3. *Edited by* E. L. Eliel and N. L. Allinger. Interscience Publishers, New York. 1968. p. 97.
26. J. SICHER, M. TICHY, and F. SIPOS. Collect. Czech. Chem. Commun. **31**, 2238 (1966).
27. F. W. KAY and W. H. PERKIN, JR. J. Chem. Soc. **87**, 1067 (1905).
28. A. K. MACBETH, J. H. MILLS, and D. H. SIMMONDS. J. Chem. Soc. 1011 (1949).
29. J. N. S. TAM, T. MOJELSKY, K. HANAYA, and Y. L. CHOW. Tetrahedron, **31**, 1123 (1975).

Chemistry of amidyl radicals: intramolecular reactivities of alkenyl amidyl radicals

YUAN L. CHOW[1] AND RICHARD A. PERRY[2]

Department of Chemistry, Simon Fraser University, Burnaby, B.C., Canada V5A 1S6

Received August 10, 1984

YUAN L. CHOW and RICHARD A. PERRY. Can. J. Chem. **63**, 2203 (1985).

Amidyl radicals possessing $\Delta^{4,5}$, $\Delta^{5,6}$, and $\Delta^{6,7}$ double bonds were generated from the photodecomposition of nitrosamides and chloramides and the products were identified. Dichotomies of amidyl radical reactivities were discovered and compared with published kinetic rate constants. In complete reversal to intermolecular reactivities, intramolecularly the alkenyl amidyl radicals preferentially add to the double bonds rather than abstract a C-5 hydrogen even if it is allylic. In intramolecular competition, amidyl radicals add to an acyl side chain double bond more efficiently than to an alkyl one; this is just the opposite to intramolecular H-abstraction of amidyl radicals. Taken together with the published results, it is established that, in intramolecular attacks of double bonds, amidyl radicals selectively undergo the *propia*-addition to generate an *exo*-cyclic radical rather than the *longa*-addition to an *endo*-cyclic radical: this rule should replace the old one that amidyl radicals preferentially cyclize to form five-membered rings if choices are available.

YUAN L. CHOW et RICHARD A. PERRY. Can. J. Chem. **63**, 2203 (1985).

On a généré des radicaux amidyles possédant des doubles liaisons $\Delta^{4,5}$, $\Delta^{5,6}$ et $\Delta^{6,7}$ en faisant appel à la photodécomposition de nitrosamides et de chloramides et on a identifié les produits obtenus. On a découvert les dichotomies des réactivités des radicaux amidyles et on les a comparé avec les constantes de vitesses cinétiques publiées antérieurement. En opposition complète avec les réactivités intermoléculaires, les radicaux amidyles alkényles s'additionnent préférentiellement d'une façon intramoléculaire sur les doubles liaisons plutôt que d'enlever un hydrogène en C-5, même s'il est allylique. Dans une compétition intramoléculaire, les radicaux amidyles s'additionnent plus facilement à une double liaison d'une chaîne latérale acyle qu'à une chaîne alkyle; ce résultat est justement l'opposé de ce qui se produit lors d'un enlèvement intramoléculaire de H des radicaux amidyles. Si l'on prend ces résultats avec ceux qui ont été publiés antérieurement, on peut établir que, lors d'attaques intramoléculaires sur des doubles liaisons, les radicaux amidyles subissent sélectivement une addition *propia* conduisant à un radical cyclique *exo* plutôt qu'une addition *longa* conduisant à un radical cyclique *endo*: cette règle devrait remplacer la règle antérieure selon laquelle les radicaux amidyles se cyclisent préférentiellement pour former des cycles à cinq chaînons, s'ils en ont le choix.

[Traduit par le journal]

Chemistry of amidyl radicals has attracted much attention in the last two decades (1–11) and been reviewed (1–4). The major interest has been the electronic configuration from which amidyl radicals (RCOṄR) (12–20) react with substrates and its relation to amidyl radical reactivities. Fifteen years ago, we found that *N*-alkylamidyl radicals interact with an olefin (e.g., 1,3-pentadiene and cyclohexene) by exclusive allylic hydrogen abstraction but no addition (21, 22);[3] this preference was totally reversed in intramolecular reactivity, e.g., addition to the C(5)-atom of the olefinic bond prevailed over H-abstraction from the C(5)-allylic hydrogen (24). These observations have led us to an extensive investigation of the intramolecular reactivity of amidyl radicals (25). In the meantime, while arguments on the Σ and Π amidyl radical configurations continued inconclusively, several works (14–18) on intramolecular reactivities, in particular cyclizations of alkenyl amidyl radicals, were published and interpreted in favor of Σ and (or) Π electronic configurations as the reactive state. Theoretical calculations (19, 20) on the $\Sigma-\Pi$ structure of amidyl radicals have not been able to give a definitive answer (19). Recently, Ingold's group (26–29) has extended the esr observations reported earlier by Danen and Gellert (12), and proven convincingly that amidyl radicals (RCOṄR) possess Π structure in their ground state; they have also determined many valuable rate constants of amidyl radical reactions by kinetic esr spectroscopy (27, 29). The availability of these finite parameters allows us to discuss our old results more intelligently. We wish to publish this work now.

Results

The general plan was to generate amidyl radicals carrying a $\Delta^{4,5}$, $\Delta^{5,6}$, or $\Delta^{6,7}$ (from the N center) olefinic bond either in N-alkyl or N-acyl chains and investigate competing intramolecular H-abstraction from the C(5)-hydrogens and additions to the double bonds. It should be noted that intramolecularly, amidyl radicals preferentially abstract the C-5 hydrogens on the alkyl side chain of the N-center rather than those from the acyl side chain (9, 14), and do so from the nitrogen center but not from the amide oxygen center (14, 15).

The required amides **1***a*–**6***a* were prepared by the usual reactions and the details of their preparation have been described in the thesis submitted by one of the authors (25). Nitrosamides **1***b*–**6***b* were prepared by nitrosation with either $NaNO_2$ in $AcOH-Ac_2O$ or N_2O_4 in CH_2Cl_2 and the crude products were utilized in photolysis without purification since nitrosamides are generally sensitive to heat and light (9, 30). By either method, one of the side reactions was the addition of N_2O_4 or N_2O_3 to the double bond. While this addition was slower than the nitrosamide formations in general, some of these nitrosamides were contaminated with a small amount of the addition products (see Table 1). In the preparation of **4***b* and **6***b* the contaminants amounted to as much as 15% and were clearly observable in the nmr and ir spectra. Therefore, all these nitrosamide samples were closely monitored with ir and nmr spectra before photolysis and the light source was filtered with $NaNO_2$ – sodium naphthalate filter solution to cut off the energy <400 nm in order to avoid excitation of nitro or nitrite

[1] Author to whom correspondence may be addressed.

[2] Present address: Merck Sharpe & Dohm, Stable Isotopes, P.O. Box 899, Point Clair – Dorval, P.Q., Canada H9R 4P7.

[3] A similar phenomenon was also observed, see ref. 23.

TABLE 1. Spectral data of *N*-nitrosamides and *N*-chloramides

Compound	Nuclear magnetic resonance (ppm in $CDCl_3$)			Infrared (liquid film) (cm^{-1})	Ultraviolet (in benzene) nm (ϵ)
	CH=*CH*	*CH*—CONH—*CH*			
1*b*	5.70(m)	3.80(m)	3.10(s)	1725, 1500	428(90), 408(85), 392(60), 375(50)
1*c*	5.77(m)	3.10(m)	3.40(s)	1660, 1440[c]	—
2*b*	5.82(m)	4.40(m)	3.10(s)	1725, 1500[c]	422(50), 403(55), 387(40), 372(25)
3*b*	3.75(m)	3.33(m)	3.08(s)	1725, 1500	423(95), 404(90), 385(55), 374(40)
4*b*	5.67(m)[b]	3.15(fd)	3.12(s)	1720, 1500[c]	421(80), 402(80), 386(60), 370(20)[a]
5*b*	5.57(m)[b]	2.79(s)	3.72(bd)	1725, 1640[c]	426(90), 407(85), 391(50), 376(30)
6*b*	5.71(m)[b]	2.66(s)	4.30(m)	1730, 1515[c]	423(6), 405(55), 390(40), 366(25)
6*c*	5.61(m)[b]	2.24(s)	4.55(m)	1670	—

[a]This uv spectrum was taken in CCl_4.
[b]The integrations were less than 2H due to addition reaction.
[c]Weak absorptions due to the parent amides ($\approx$1640 and $\approx$1550 cm^{-1}) were observed.

groups. The filter system allows us to selectively excite the $n \rightarrow \pi^*$ transition band of nitrosamides and gives cleaner product formation, as demonstrated in earlier studies (30). The preparation of nitrosamides **1***b*–**6***b* and chloramides **1***c* and **6***c* was described in the thesis (25). Their physical data are given in Table 1.

Photolysis of nitrosamides under nitrogen generally gives the C-nitroso compounds as the primary photoproducts that are in equilibrium with their dimer and also tautomerize to the corresponding *syn*- and *anti*-oximes[4] with a slower rate. Depending on the photolysis conditions, the C-nitroso dimer absorption in the 300-nm region can be observed and the dimers can be isolated if the photolysates are worked up quickly (9). In general, the photolysates were kept at room temperature for a long time to allow their tautomerization to oximes as shown below. The structures and stereochemistry of *syn*- and *anti*-oximes were determined from chemical shifts and coupling patterns of the neighboring protons (e.g., N—CH_3, N—CH, etc.) and characteristic ir absorptions; the correlations were well established from our previous work (31).

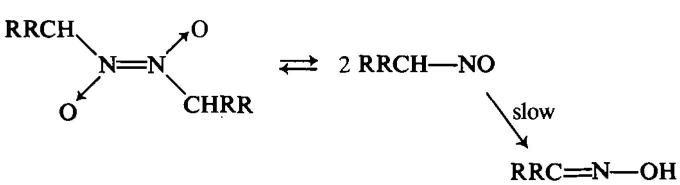

Photolysis of **1***b* in benzene under nitrogen gave *anti*- and *syn*-oximes **6** (2:1 ratio, up to 68%), ketolactam **7** (18%), and a mixture of *syn*- and *anti*-enone oximes **11** (6%); about 4% of nitratolactam **9** was also detected. The crude product contained the corresponding C-nitroso dimer and could be hydrolysed by sodium bisulfite to give ketolactam **7** in 56% yield. As *syn*-**6** was slowly isomerized to *anti*-**6** on standing, a sample of *syn*-oxime was obtained as a mixture with *anti*-**6**. Their configurations were clearly indicated by the N−CH and N−CH_3 protons at 3.90 and 2.82 ppm for *anti*-**6** as compared to those at 4.65 and 2.89 ppm for *syn*-**6**. The ketolactam **7** was reduced with $NaBH_4$ to *endo*- and *exo*-hydroxylactams **10**, and with LAH followed by Jones' oxidation to aminoketone **8**, the structure of which was established previously (32). Enone oxime **11** could not be separated to its *syn* and *anti* isomers, but showed ir absorptions at 1670 and 1550 cm^{-1} for a secondary amide and the chemical shifts of the olefinic protons at 6.3 and 5.8 ppm regions assignable to such conjugated oximes (33).

Photolysis of **1***b* under oxygen, other conditions being the same, was straightforward, giving the *exo*- and *endo*-isomeric pair of nitratolactams **9** (51%) and that of hydroxylactams **10** in addition to nitrolactams as the minor products, in agreement with the oxidative photoreaction of nitrosamides shown previously (30). The nitrolactams were obtained in only small amounts and could not be isolated. The structures of **9** and **10** were related to ketolactam **7** and aminoketone **8** by a series of hydrolysis, reduction, and oxidation as described in the Experimental. The *endo*- and *exo*-nitratolactams **9** showed the expected ir bands at 1690, 1630, 1280, and 860 cm^{-1} and similar ms fragmentation patterns; the *endo* and *exo* configurations were confirmed by the proton signals of CH—ONO_2; the former gave a double doublet at 5.1 ppm (J = 9 and 7 Hz) for the axial H and the latter a narrow signal at 5.26 ppm ($W_{1/2}$ = 9 Hz) for the equatorial H.

Photolysis of chloramide **1***c* was also investigated under nitrogen to give *endo*- and *exo*-chlorolactams **12** (33 and 39% isolated yields), both of which showed well-defined nmr spectra and the same ms pattern; the former showed an axial proton (for CHCl) at 4.25 ppm (ddd with J = 9, 7 and 1 Hz) and the latter an equatorial proton at 4.32 (dd, with J = 6 and 3 Hz). Chlorolactams **12** were easily reduced to chloroamines **14**, but only *endo*-**14** could be isolated. The *exo*-**14** was unstable and reduced by LAH much more rapidly (than *endo*-**14**) to the known amine **13** (34), due to the efficient participation of the amine in displacing the chloride; the intermediate, aziridinium ion, was obviously reduced to give the azabicyclic[3.2.1] system as in **13**.

Photolysis of nitrosamide **2***b* under nitrogen gave *syn*-β-lactam oxime **15** (44%) and the corresponding keto-β-lactam (7%); a β-lactam was indicated by the ir peak at 1725 cm^{-1}. By decoupling experiments, the low-field doublet (C(1)−H) and triplet (C(6)−H) were shown to be coupled to each other with J = 5 Hz, in analogy to nmr data of a *cis*-fused lactam ring system (35). This, together with the fact that the C(1)−H is shown not to be coupled to other high-field protons, virtually eliminates the alternate structure **16** as the product. The assignment of the *syn* orientation was based on the low chemical shift of C(1)−H at 4.05 ppm and relatively high chemical shift of C(3)-equatorial hydrogen at 2.6 ppm in accordance with the

[4]Following the previous definition (30), the *syn*-oxime is the one possessing the oximino OH on the side of the lactam ring and the *anti*-oxime is the one possessing that on the opposite side.

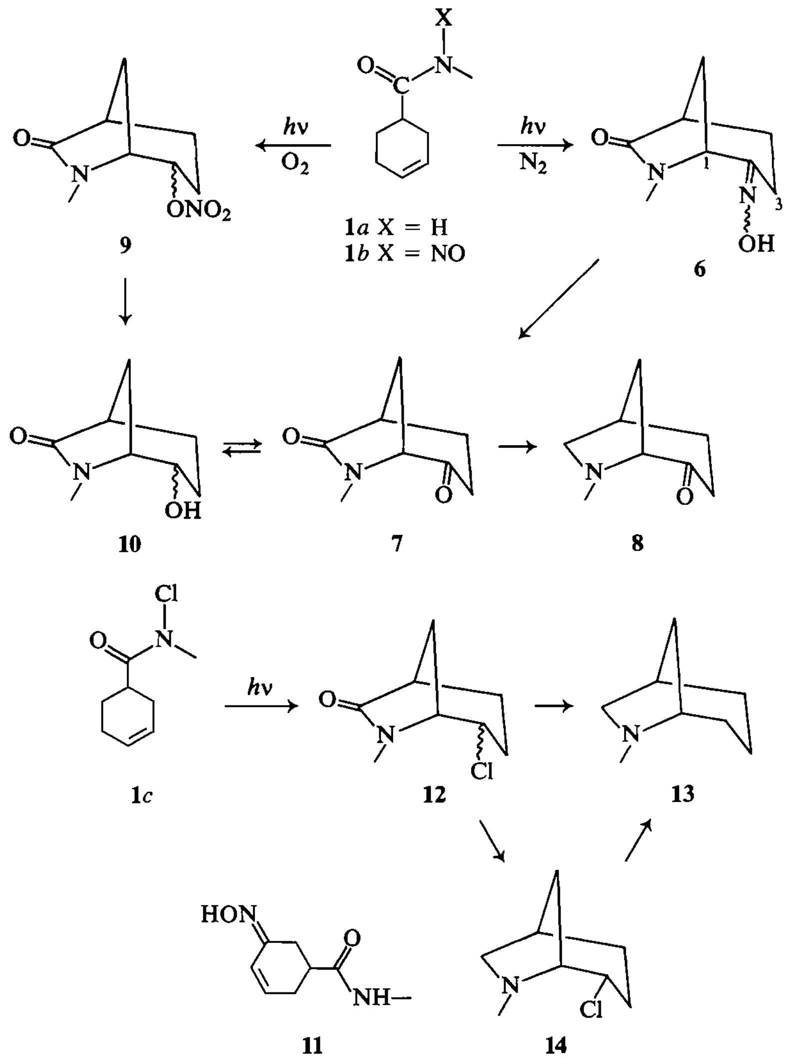

previous correlation (31). The keto-β-lactam was not isolated in the pure state.

Successful use of $BrCCl_3$ as a radical trapping agent (32) led us to photolyze nitrosamide 3*b* in $BrCCl_3$ whereby single *exo*-bromolactam **17** was isolated in 89% yield. In the process, CCl_3NO was also formed, as shown by the uv absorption (32) at 580 nm. The nmr spectrum became well separated on addition of $Eu(fod)_3$; decoupling experiments on this spectrum (see Experimental) clarified the coupling patterns of the protons. The coupling constants of $J_{1,5}$ = 8 Hz and $J_{1,8}$ = 1.5 Hz are in good agreement with other azabicyclo[3.3.0] derivatives (36) and confirm the *exo*-bromo orientation in **17**. LAH reduction of **17** to the known amine **18** completed the proof of the structure (37).

The preparation of nitrosamide 4*b* was accompanied by N_2O_4 addition to the double bond. The best sample contained a small amount of the starting amide 4*a* and some N_2O_4 adducts (ca. 10%); this material was used in the photolysis under nitrogen. The crude product was a complex mixture but gave *anti*-oxime **19** (25%) and a fraction tentatively assigned to enone oxime **21** (≈7%) after extensive chromatography. The *anti*-oxime **19** was the only *tertiary* amide obtained, showing a low amide CO stretching frequency at 1605 cm^{-1} and the OH signal at 10 ppm. The nmr triplet at 3.85 ppm indicated a more symmetrical skeleton of the [3.3.1] system than the [4.2.1] system. This chemical shift, together with the multiplet at 3.25 ppm for the equatorial C(7)−H, indicated the *anti*-oxime configuration. The ketolactam was reduced with LAH and oxidized by Jones' reagent to give aminoketone **22**.[5] All other fractions were secondary amides (ca. 1640, 1550 cm^{-1}) that did not show typical olefinic proton signals, except for one which exhibited ir absorptions at 1635 and 1550 cm^{-1}, and olefinic proton signals for an enone oxime (33) at the 6.2 and 6.8 ppm regions. This compound could be the oxime **21**. Various difficulties prevented us from continuing the work.

Photolysis of 5*b* under nitrogen gave *syn*- and *anti*-oximino-amides **23** (49%) and ketoamide **24** (14%). The C-nitroso dimer was also detected during irradiation (λ_{max} 295 nm) and tautomerized slowly to the oximes. In spite of extensive search for enone oximes, only the starting amide 5*a* (8%) was obtained from the crude product. The *syn*-oxime **23** was not isolated in the pure state but as a mixture with *anti*-**23**. This mixture was hydrolysed to ketoamide **24** as the only product. The oximes *anti*-**23** and *syn*-**23** exhibited the expected nmr signals (31) for the C(1)−H at 4.39 ppm (dd, J = 5.5 and 1 Hz) and 5.40 ppm (broad d, J = 5.5), respectively.

Nitrosation of acetamide 6*a* was contaminated with ca. 10% of the N_2O_4 addition products as the best sample ever obtained.

[5]It should be mentioned that aminium radicals preferentially add to a double bond, either in intermolecular or intramolecular reactions (38).

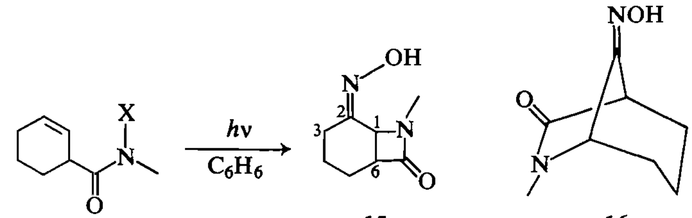

2*a* X = H
2*b* X = NO

15

16

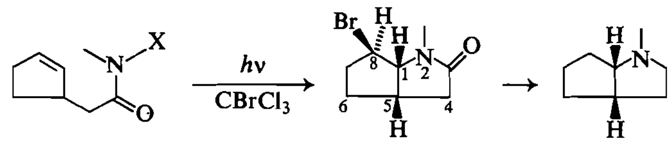

3*a* X = H
3*b* X = NO

17

18

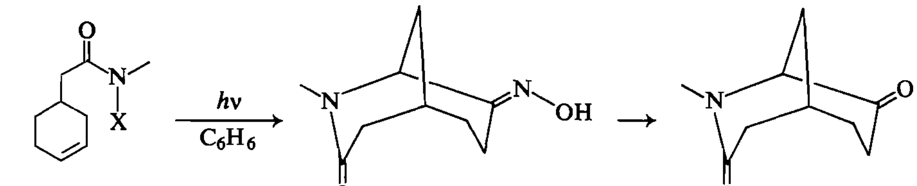

4*a* X = H
4*b* X = NO

19

20

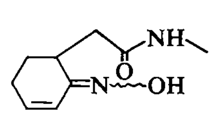

21

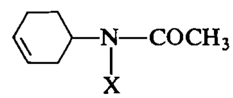

6*a* X = H
6*b* X = NO
6*c* X = Cl

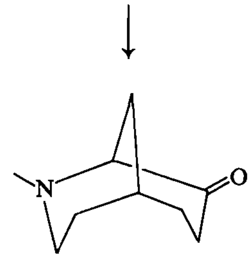

22

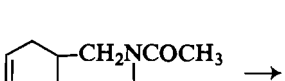

5*a* X = H
5*b* X = NO

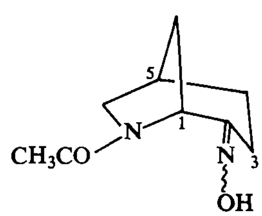

23

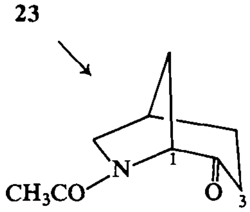

24

This sample decomposed slowly in benzene in the dark. Photolysis of this sample showed no formation of C-nitroso compound, and the crude product gave **6***a* (37%) and 4-acetoxycyclohexene (9%) in addition to many minor products. The preparation and photolysis of *N*-chloramide **6***c* were even more complicated, giving at least 14 compounds in the 5−10% yield range after photolysis. As in neither photolysis was a bicyclic acetamide detected, the work was not pursued further.

Discussion

Three general conclusions can be drawn from the intramolecular reactions presented here and published in the literature (17, 18). First of all, in contrast to the intermolecular reactivities reported before (21−23), intramolecular addition of amidyl radicals preferentially occurs to suitably located double bonds (e.g. $\Delta^{3,4}$, $\Delta^{4,5}$, and $\Delta^{5,6}$ from nitrogen) either in acyl or alkyl side chains to form 4, 5, and 6-membered rings, rather than to abstract C-5 hydrogens, even if these hydrogens are allylic. Secondly, the attack on these double bonds always occurs specifically in the *propia*-mode (i.e. attack at the nearest end of the double bond) to generate *exo*-cyclic C-radicals rather than in the *longa*-mode (i.e. attack at the further removed end of the double bond).[6] It is now established that for amidyl

[6]The new term *propia−longa* addition is derived from the Latin adjectives *propius* (near) and *longus* (far) to describe the point of attack during the course of reactions. This term is preferred over that of the *exo−endo* cyclization (refs. 29 and 39) since conceptually the latter can give alternative pathways and cause ambiguity in the formation of polycyclic systems.

radicals *propia*-cyclization takes precedence over ring size considerations: e.g., $\Delta^{4,5}$, $\Delta^{5,6}$, and $\Delta^{6,7}$-alkenyl amidyl radicals cyclize to give four, five, and six-membered rings, respectively. Similar preference for *propia*-addition has been reported for the kinetically controlled cyclization of alkenyl C-radicals (39). Thirdly, the *propia*-cyclization of amidyl radicals involving the acyl chain occurs more efficiently than that involving an alkyl chain; this is in sharp contrast to the pattern of the intramolecular H-abstraction reactivity of amidyl radicals (14).

These conclusions can be expanded for individual cases with reference to kinetic data reported for intramolecular reactions of amidyl radicals (27, 29). As these kinetic data were obtained with open chain amidyl models, comparisons with them have to take into account semi-flexible cyclic alkenyl groups in the amidyl models used in these studies.

The activation energy for intramolecular H-abstraction is 6–9 kcal/mol ranging from C-5 allylic to C-5 methyl hydrogen, and that for the *propia*-cyclic addition 5–8 kcal/mol in the addition to C-5 and C-6 olefinic carbons (29); it is expected that corresponding reactions in intermolecular modes will require even higher activation energies, as their rate constants of H-abstraction by amidyl radicals suggest ($\approx 10^4\ M^{-1}\ s^{-1}$) (21, 29). As some cyclohexene derivatives are shown to have the activation energy of inversion (e.g. **25** ⇄ **26**) of 5–6 kcal/mol (40), the cyclohexene ring inversion can be faster than any

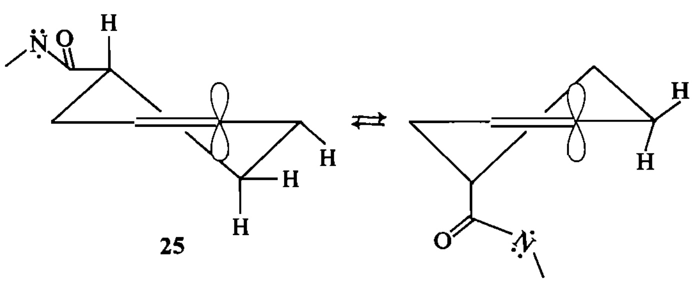

25 **26**

inter- and intramolecular reactions. As such, the requirement for the axial orientation of the amidyl radical side chain as in **26** would not be expected to be the rate limiting factor in the intramolecular reactions.

The second conclusion is best illustrated by cycloaddition of **2*b***, where a strained β-lactam is formed without a trace of a γ-lactam, and is also shown in the *N*-chloramide cyclizations of **27** and **28** reported by Kuehne and Horne (18). The cyclization in **28** to a four-membered ring obviously requires so high an activation energy that intermolecular reactions supersede the overall pattern; unfortunately, H-abstraction from C-5 allylic hydrogen was not carefully investigated. With two distinct exceptions involving bicyclo[3.3.1]non-6-en-3-yl amidyl radical systems, chromous chloride promoted cyclization of *N*-chloramides mostly follows this rule (41), indicating that chromous ions may have not changed the behavior of amidyl radicals by coordination.

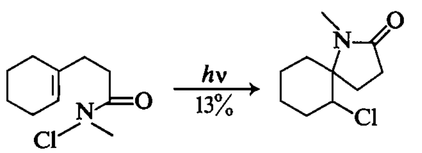

27

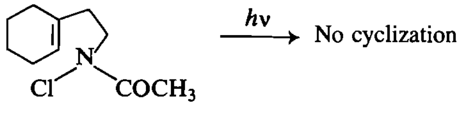

28

The first conclusion is amply substantiated by **1*b***, **1*c***, and **5*b*** in this paper and other chloramides reported by others (17, 18): intramolecular addition to the C-5 olefinic carbon always occurs preferentially over H-abstraction from the C-5 allylic hydrogen. The published kinetic data on open chain amidyl radical reactions (29) show that the ratio of rate constants for the former addition to the latter H-abstraction is ≥2 in the competition involving acyl chains. A similar ratio for the competition involving alkyl chains is estimated[7] to be $5 \times 10^4/1 \times 10^7 = 1/200$, which is dramatically different from the nil H-abstraction observed in **5*b*** and similar *N*-chloramide decompositions (17, 18). The kinetic data (29) also indicate the rate constant ratio of addition to the C-6 of a $\Delta^{6,7}$ olefinic bond to H-abstraction from a C-5 allylic hydrogen to be $1 \times 10^6/5 \times 10^6 = 1/5$, when involving acyl chain reactions. The observed results from the decompositions of **4*b*** and *N*-chloramide **29** are just the reverse, e.g., the addition to form the six-membered ring occurs preferentially over H-abstraction from the allylic C-5 hydrogens in acyl chain reactions (though less efficiently than $\Delta^{5,6}$ cyclization in **1*b*** and **1*c***). There is a curious lack of H-abstraction from the C-5 allylic hydrogens located on the alkyl side of amidyl radicals generated from *N*-chloramide **30**, even when the addition to the $\Delta^{6,7}$ double bond does not occur (17).

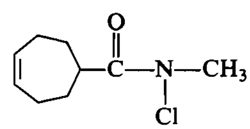

29

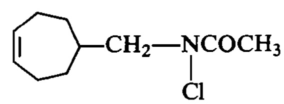

30

The third conclusion is demonstrated by the better yields of the cyclization products from **1*b*** and **1*c*** in comparison to the poorer yield of those from **5*b***. This is more dramatically demonstrated in the benzoyl peroxide initiated decomposition of three series of *N*-chloramides (e.g. **29** vs. **30**) previously reported (17), and is also supported by kinetic data (29). It is noteworthy that amidyl radical intramolecular H-abstraction from C-5 hydrogen is far more (at least 100 times) efficient with those hydrogens in an alkyl chain than those in an acyl chain (14), just the reverse of the observed intramolecular addition reactivity.

While the diverse reactivity differences described above should be intrinsically related to the Σ–Π radical structures of amidyl radicals, it is difficult to provide convincing explanations for all cases. As suggested by Waegel, Lessard, and co-workers (17), the Σ configuration of the amidyl radical could provide some rationale, *albeit* weak, for the observed geometry of the cyclizations. The esr results of the Π-configuration with twisting of the N—CO bond open up

[7]The rate constant of intramolecular hydrogen abstraction by amidyl radicals from C-5 allylic —CH_2— in alkyl side chains is estimated from ref. 29 as follows. The rate ratio of abstraction from C-5 methyl hydrogens in alkyl side chains to those in acyl side chains is calculated to be 2.5. The multiplication of this ratio with the rate constant of intramolecular hydrogen abstraction from C-5 allylic (CH_2) hydrogen in an acyl side chain ($5 \times 10^6\ M^{-1}\ s^{-1}$) is taken as the corresponding rate constant involving an alkyl side chain.

wide possibilities for interpretation and they indicate that the model amides used in this and other investigations (17) are utterly powerless to correlate the reactivities with electronic configurations. Nevertheless, one suggestion can be made to rationalize the amidyl radical intramolecular reactivities, i.e., preference in addition over H-abstraction and that for acyl over alkyl side chains. It is envisaged that the amide carbonyl, being scarcely conjugated (42), may have some attractive interaction with a suitably located double bond to facilitate intramolecular addition of the nitrogen radical center. The CO group in **5** and **30** apparently has difficulties in assuming a favored conformation for such interactions; this may arise from the small barrier required for the N—CO bond twisting as proposed before (14).

The observed reactivity discrepancy between esr kinetic results (28, 29) and the results from product analysis (*vide supra*) could arise from the fact that the rate constants are determined for individual model compounds and their comparisons are intermolecular, i.e., between two different compounds. In this study, the comparisons involve intramolecular competitions in which conditions are the same for addition and abstraction reactivities. Indeed, in the kinetic studies by esr signal decays, Ingold's group (28, 29) has concluded that intramolecular reactions of amidyl radicals are very sensitive to steric factors that may still be significant over surprisingly large distances. If so, comparisons of amidyl radical reactivities even by intramolecular competitions within a molecular framework, such as in **1**, **4**, or **5**, may also be subject to subtle remote steric effects. Therefore, even if these results from product analysis are experimentally meaningful, their interpretations are beyond our present understanding. In short, the flexible and semi-flexible models utilized so far in this paper and others (17, 18), although synthetically useful, are not adequate to elucidate the details of the transition state in amidyl radical reactions and are likewise powerless to probe the electronic configurations of amidyl radicals.

Experimental

Unless otherwise specified, nmr spectra were recorded with a Varian A56/60 spectrometer in $CDCl_3$ using TMS as the internal standard. Infrared spectra were recorded as Nujol mulls or neat liquids with a Perkin Elmer model 457 grating spectrophotometer, uv spectra with a Unicam SP800 spectrometer, and mass spectra with a Hitachi–Perkin–Elmer RMU-6E instrument at 80 eV. Melting points were recorded with a Fisher Johns hot stage apparatus and were uncorrected. Microanalyses were performed by Mr. M. K. Yang, Department of Biological Sciences, Simon Fraser University.

Preparation of nitrosamides and chloramides

The required amides **1***a*–**6***a* were prepared by the usual methods and described in the thesis (25). Nitrosation of amides followed published methods (9, 32, 38) using $NaNO_2$ in $AcOH-Ac_2O$ or N_2O_4 in CH_2Cl_2. In certain cases, the addition of N_2O_4 to the alkenyl bonds also occurred to give nitrosamides contaminated by such by-products. The nitrosamides **1***b*–**6***b* obtained from the preparation were examined with ir and nmr spectroscopy to see the extent of the addition to double bond. These crude nitrosamide specimens were characterized by spectroscopic data (Table 1) and were used without purification.

N-Chloramides were prepared by standard procedure using sodium hypochlorite (or Purfex bleach) (5, 14) and the spectroscopic data are given in Table 1. The crude products were used for photolysis without purification.

Photolysis of alkenyl nitrosamides

A nitrosamide (1–15 mmol) in redistilled benzene (230 mL) was irradiated with a Hanovia medium pressure Hg lamp through a $NaNO_2$ – sodium naphthalate filter solution (<400-nm cut-off) (30) while the solution was purged with dry nitrogen and cooled externally with an ice bath. At intervals, samples were taken to examine decreases of the absorption at the 405-nm region; in some cases, the intense absorption of the dimer of the C-nitroso compounds at λ_{max} 290 nm appeared. In all cases, a small sample was set in a dark place at the same temperature as the dark reaction; no decrease of the uv absorption was observed. When the 405-nm absorption disappeared (1–4 h), the photolysates were evaporated and crude products were chromatographed or treated further accordingly.

1. N-*Nitroso*-N-*methyl-3-cylcohexene-1-carboxamide* (**1***b*)

(a) *Under nitrogen*

Nitrosamide **1***b* prepared from **19** (2.2 g) in benzene (230 mL) was photolyzed to give a crude product which contained a C-nitroso dimer (ir 1220 cm^{-1}, λ_{max} 295 nm, and an nmr singlet at 2.91 ppm). On standing, the dimer disappeared. Recrystallization from $EtOH-H_2O$ gave a solid (730 mg) which was recrystallized to give *anti*-oxime **6**, mp 203–205°C; ir (KBr): 3300 (b), 3100 (m), 1670, 1230, 950, 920 cm^{-1}; nmr (pyridine-d_5): 4.09 (1H, dd, J = 5.5 and 1 Hz), 3.6–3.3 (1H, m), 2.74 (3H, 8), 2.52 (1H, m), 2.2–1.6 (5H, m) ppm; ms (130°C), m/e (%): 168(M^+, 14), 152(14), 151(100), 123(14), 110(37), 98(26), 94(14), 42(40). *Exact Mass* calcd. for $C_8H_{12}N_2O_2$: 168.0898; found (ms): 168.0882. *Anal.* calcd. for $C_8H_{12}N_2O_2$: C 57.14, H 7.14, N 16.67; found: C 57.27, H 7.17, N 16.60. Decoupling experiments showed that neither signal at 4.08 and 2.52 ppm was coupled to the equatorial C(3)–H at 3.5 ppm.

In a separate experiment, the crude residue obtained from photolysis of nitrosamide **1***b* (amide **1***a*, 2 g, as the starting material) was heated in 50% EtOH (60 mL) with sodium bisulfite (35 g). The solution was made basic (pH 9), and was extracted with CH_2Cl_2 and chromatographed on alumina to give the first fraction, which was distilled at 84–85°C/5 Torr (1 Torr = 133.3 Pa) to give ketolactam **7** (1.23 g); ir (CCl_4): 1735 (sh), 1715, 1645, 1400 cm^{-1}; nmr: 3.70 (1H, dd, J = 5 and 2 Hz), 2.86 (3H, s), 2.8–1.85 (7H, m) ppm; ms (30°C), m/e (%): 153(M^+, 64), 137(11), 125 (44), 110(22), 109(17), 97(100), 96(44), 80(28), 79(22), 69(67), 68(42), 42(92). *Exact Mass* calcd. for $C_8H_{11}NO_2$: 153.0789; found (ms): 153.0744. The ketolactam **7** (1.03 g) in ether (150 mL) was refluxed with LAH (2 g, 0.05 mol) for 48 h. The ether extracts were carefully distilled with a Vigreux column to afford the corresponding volatile alcohols (32). The alcohol mixture (150 mg) was oxidized with a Jones' reagent for 20 min to give, after work-up, aminoketone **8** (90 mg); the ir, nmr, and mass spectra were identical with those of the authentic sample (32). Ketolactam **7** was reduced by $NaBH_4$ to give a mixture of *exo*- and *endo*-hydroxylactam **10** (*vide infra*).

A crude residue (2.4 g) from another photolysis was chromatographed on basic alumina (120 g) in the CH_2Cl_2-MeOH solvent system. Ketolactam **7** (510 mg) contaminated by a small amount of nitratolactams **9** was eluted with CH_2Cl_2. The second fraction (80 mg) was a mixture of *syn*- and *anti*-oxime **11**; ir: 3400 (b), 1670 (s), 1550 (m), 1400, 1070 (m), 1050 (m); nmr: ≈6.3 (1H, m), 5.75 (1H, m), 3.8–3.3 (2H, m), 2.79 (3H, s); ms (30°C), m/e (%): 168(M^+, 67), 137(90), 109(27), 96(67), 80(87), 79(100), 55(33), 42(47). The third fraction (430 mg) was a complex mixture containing the C-nitroso dimer, **6**, and **11**. The fourth fraction eluted with 2–3% MeOH – CH_2Cl_2 was *anti*-oxime **6** (310 mg). The following fractions (810 mg) were mixtures of *syn*-oxime **6** (4.65 and 2.89 ppm) and *anti*-oxime **6** (3.90 and 2.82 ppm). A mixture of the oximes **6** (120 mg) was treated with sodium bisulfite in ethanol to afford ketolactam **7** (105 mg).

(b) *Under oxygen*

Crude nitrosamide **1***b* prepared from 1.2 g amide **1***a* was irradiated in benzene (230 mL) as above except that oxygen, instead of nitrogen, was bubbled through the solution. No uv absorption of the C-nitroso dimer at 295 nm was observed. The photolysate was evaporated and the crude oil chromatographed on neutral silica (65 g) eluted with 0.5% MeOH – CH_2Cl_2 to afford a mixture (970 mg) of *endo*- and *exo*-nitratolactam **9** (2:1 ratio) contaminated with **1***a* (8%): nmr singlets at 2.95, 2.92, and 2.81 ppm. The second fraction (200 mg) was a mixture of *exo*- and *endo*-hydroxylactams **10**; ir: 3400 (b), 1670, 1070 cm^{-1}; nmr: 4.3 (m), 3.9 (m), 2.86 (s), 2.83 (s) ppm. The last fraction (500 mg) was mainly **10** contaminated by nitro compounds, as shown by ir absorptions at 1680, 1550; *m/e* at 184; and nmr multiplet at 4.7 ppm. A portion of this fraction (90 mg) was oxidized with Jones' reagent and chromatographed to give ketolactam **7**, but nitrolactam could not be isolated. The first fraction was chromatographed again to afford two nitratolactams:

Exo-**9**; ir: 1690, 1630, 1280, 860 cm^{-1}; nmr: 5.26 (1H, m, $W_{1/2}$ = 9 Hz), 3.82 (H, m), 2.92 (3H, s), 3.0−1.5 (8H, m) ppm; ms (80°C), *m/e*(%): 200(M^+, 1), 168(4), 154(52), 138(19), 126(17), 110(89), 98(81), 81(22), 69(33), 55(33), 42(100).

Endo-**9** has the same ir pattern as *exo*-**9**; nmr: 5.10 (1H, dd, *J* = 9 and 7 Hz), 3.85 (1H, bd, *J* = 6), 2.95 (3H, s), 2.8−1.4 (8H, m) ppm; ms (75°C), *m/e*(%): 154(58), 138(17), 126(17), 110(100), 98(89), 83(17), 81(17), 69(33), 55(28), 42(100); ms(70°C), *m/e*(%): 200(M^+, 1), 154(63).

Hydrolysis of a mixture of *exo*- and *endo*-**9** with dilute NaOH in $EtOH-H_2O$ (0.1 *N*) gave a mixture of *exo*- and *endo*-**10** which was oxidized by Jones' reagent to ketolactam **7**. A mixture of *exo*- and *endo*-**9** was reduced by LAH in ether for 48 h, followed by oxidation with Jones' reagent to give aminoketone **8**.

N-Nitroso-N-methyl-2-cyclohexene-1-carboxamide (**2***a*)

The crude nitrosamide (obtained from 450 mg of **2***a* without purification) was photolyzed as above under nitrogen to give a residue (450 mg) which was recrystallized from benzene twice to give *syn*-oxime **15** (150 mg), mp 145−150°C (dec.); ir (KBr): 3200 (b), 3080 (m), 1725 (s), 1650 (m), 1440, 935 cm^{-1}; nmr: 8.7 (OH), 4.02 (1H, d, *J* = 5 Hz), 3.55 (1H, t, *J* = 5 Hz), 2.82 (3H, s), 2.8−1.3 (6H, m) ppm; ms (100°C), *m/e*(%): 169(M^+ + 1, 7), 168(M^+, 4), 151(5), 140(5), 112(36), 111(100), 110(27), 94(48), 67(39), 66(63), 42(36); ms (30°C), *m/e*(%): 169(M^+ + 1, 2), 168(M^+, 9). *Exact Mass* calcd. for $C_8H_{12}N_2O_2$: 168.0899; found (ms): 168.0856. *Anal.* calcd. for $C_8H_{12}N_2O_2$: C 57.13, H 7.19, N 16.66; found: C 56.94, H 7.36, N 16.86.

The mother liquor was chromatographed on neutral alumina eluted with 0−0.5% $CH_3OH-CH_2Cl_2$ to give the first fraction (100 mg) containing **2***a* and the ketolactam of **15** (ir 1745 cm^{-1}, and nmr 3.6 (m) and 1.90 (s) ppm). Elution with 5−20% MeOH − CH_2Cl_2 gave *syn*-oxime **15** (90 mg). Hydrolysis of **15** with sodium bisulfite gave a complex mixture.

N-Nitroso-N-methyl-(2-cyclopenten-1-yl)acetamide (**3***b*)

Crude nitrosamide **3***b* (640 mg) in $BrCCl_3$ (230 mL) was photolyzed under nitrogen in the usual manner. The distilled solvent showed a uv absorption at 580 nm due to CCl_3NO. The residue was chromatographed to give **3***a* and *exo*-bromolactam **17** (730 mg) which was distilled; ir: 1685 (s), 1400 (s), 1255 (s), 600 (m); nmr: 4.2 (2H, m), 2.92 (3H, s), 3.15−1.8 (6H, m), 1.5 (1H, m) ppm: gc−ms *m/e*(%): 219(M^+, 37), 217(37), 138(10), 110(100), 96(25), 82(16), 68(23), 42(29). *Exact Mass* calcd. for $C_8H_{12}NOBr$: 217.0103; found (ms): 217.0054. LAH reduction of **17** gave the amine **18**; the picrate from ethanol, mp 204−207°C (dec.) (lit. (37) mp 207°C).

Exo-bromolactam **17** (20 mg) and Eu(fod) (3 mg) in $CDCl_3$ exhibited a well-separated spectrum shown in the thesis (25). Irradiation of C(5)−H (4.6 ppm) collapsed C(1)−H (6.25 ppm) to singlet and the *endo*- and *exo*-C(4)−H (7.1 and 8.15 ppm) to an AB quartet (*J* = 18.5 Hz); the C(6)−H (3.15 and 3.75 ppm) coupling patterns were also changed. Irradiation of the *endo*-C(4)−H changed the *exo*-C(4)−H to a doublet (10 Hz) and C(5)−H to doublet of quartet (*J* = 8.9 and 3 Hz). Irradiation of *exo*-C(7)−H (3.0 ppm) changed *endo*-C(8)−H (6.05 ppm) to a double doublet (*J* = 3.5 and 1.5 Hz).

N-Nitroso-N-methyl-(3-cyclohexen-1-yl)acetamide (**4***b*)

A crude nitrosamide **4***b* contained by-products (ca. 15%) arising from the addition of N_2O_4 to the double bond, as shown by the nmr and ir spectra. This nitrosamide (1.39 g) in benzene was photolyzed as shown above. The crude product was chromatographed on neutral alumina to afford a mixture of unidentified secondary amides containing no double bond (290 mg) as the first fraction. The second fraction eluted with 1% MeOH − CH_2Cl_2 was recrystallized from acetone to give *anti*-oxime **19** (250 mg), mp 165−167°C (dec.); ir (CCl_4): 3200 (b), 3100 (b), 1605, 930 cm^{-1}; nmr: 10.0 (OH), 3.85 (1H, t, *J* = 3 Hz), 3.25 (1H, m), 2.88 (3H, s), 2.85−1.2 (9H, m); ms (110°C), *m/e*(%): 182(M^+, 10), 165(60), 150(40), 123(35), 110(35), 108(50), 95(10), 73(100), 58(35). *Anal.* calcd. for $C_9H_{14}N_2O_2$: C 59.32, H 7.74, N 15.37; found: C 59.50, H 7.80, N 15.27. The remaining fractions showed ir bands at 1640 and 1550 cm^{-1} and only one nmr signal in the 6.0−5.0 ppm region. This fraction (75 mg) was contaminated by other components and showed ir peaks at 3300 (b), 1635, 1550, 985, 970 cm^{-1}; nmr: ≈6.8 (m), 6.2 (m), 2.78 (d, on addition of D_2O collapsed to singlet); ms (180°C), *m/e*(%): 182(5), 165(32), 151(21), 134(21), 124(32), 106(100), 91(86), 79(36), 77(36), 73(79), 58(68), 45(36). It decomposed to a complex mixture on attempted bulb-to-bulb distillation at ≈100°C.

The *anti*-oxime **19** (80 mg) was treated with sodium bisulfite in aqueous ethanol to give ketolactam **20**; ir: 1720, 1625, 1395 cm^{-1}; ms (65°C), *m/e*(%): 167(M^+, 34), 139(20), 123(51), 110(100), 82(24), 73(17), 68(20), 59(37), 57(29), 42(37). Ketolactam (50 mg) was reduced in ether with LAH (150 mg) and the residue was oxidized with Jones' reagent to give the known (38) aminoketone **22** (28 mg): the picrate mp 205−210°C; an identical ir spectrum with that of an authentic sample (38).

N-Nitroso-N-(3-cyclohexen-1-ylmethyl)acetamide (**5***b*)

Crude nitrosamide (1.25 g) in benzene was irradiated for 1.75 h under normal conditions to show a C-nitroso dimer uv absorption at ca. 300 nm. The crude product was chromatographed on basic alumina. The parent amide **5***a* and ketoamide **24** were eluted as mixtures with 0.5−1% MeOH − CH_2Cl_2: this was rechromatographed to give **1***a* (75 mg) and **24** (200 mg) which was distilled at 1 Torr; ir: 1725 (s), 1630 (s); nmr: 4.14 (d, *J* = 6 Hz), 3.65 (d, *J* = 3 Hz), 6.57 (bs, $W_{1/2}$ = 5 Hz); ms (100°C), *m/e*(%): 167(M^+, 28), 139(25), 126(50), 110(50), 68(100), 43(56). The remaining fractions (580 mg) were mixtures of *anti*- and *syn*-oxime **23** (4:1 ratio). The *anti*-oxime **23** was recrystallized from acetone, mp 160−163°C (dec.); ir (KBr): 3300 (b), 1615 (s), 1460, 1420, 955, 940 cm^{-1}; nmr: 9.5 (OH), 4.39 (1H, bd, *J* = 5.5 Hz), 3.51 (1H, m), 2.55 (1H, m), 2.07 (3H, s), 2.4−1.4 (6H, m); ms (90°C), *m/e*(%): 182(M^+, 25), 165(8), 123(100), 85(40), 83(52), 80(17), 68(17), 59(33), 43(54). *Exact Mass* calcd. for $C_9H_{14}N_2O_2$: 182.1055; found (ms): 182.1009. *Anal.* calcd. for $C_9H_{14}N_2O_2$: C 59.32, H 7.74, N 15.37; found: C 59.18, H 7.80, N 15.40. Rechromatography of the residue gave a fraction containing *syn*-oxime **23** as the major component (ca. 80%) and showed an nmr doublet at 5.40 (*J* = 5.5 Hz).

A mixture of *syn*- and *anti*-oxime **23** in 6 *N* HCl (20 mL) was heated on a water bath for 5 h. The crude products were chromatographed to give ketoamide **24** (60 mg) and the starting oximes (25 mg).

Photolysis of N-chloro-N-methyl-3-cyclohexene-1-carboxamide (**1***c*)

N-Chloramide **1***c* (1.2 g) in benzene (250 mL) was photolyzed through a Vycor filter under nitrogen for 4 h. The crude product showed an nmr singlet at 3.05 (*endo*-**12**), 2.88 (*exo*-**12**), and 2.81 (for **1***a*) in a ratio of 41:53:6 and three gc peaks at 5.7, 5.0, and 3.5 min (for **1***a*) in a ratio of 44:49:7. The crude product (1.4 g) was chromatographed on silicic acid (50 g) eluted with 0−3% MeOH − CH_2Cl_2 to give an oil which was distilled at 5 Torr to give *exo*-chlorolactam **12** (700 mg); ir: 1690, 1450, 815 cm^{-1}; nmr: 4.32 (1H, dd, *J* = 6.0 and 3.0 Hz), 3.70 (1H, t, *J* = 4 Hz), 2.88 (3H, s), 2.5 (1H, bm, $W_{1/2}$ = 7 Hz), 2.45−1.5 (6H, m) ppm; ms (100°C), *m/e*(%): 175(M^+, 23), 173(M^+, 67), 138(68), 110(100), 96(64), 83(22), 68(30), 53(29), 42(42). *Exact Mass* calcd. for $C_8H_{12}NO^{35}Cl$: 173.0607; found (ms): 173.0602. The fractions eluted with 3% MeOH − CH_2Cl_2 (700 mg) contained *endo*-chlorolactam **12** and **1***a* and were rechromatographed to give *endo*-**12**; ir: 1690, 1450, 765, 750 cm^{-1}; nmr: 4.25 (1H, ddd, *J* = 9, 7, and 1 Hz), 3.86 (1H, dd, *J* = 5.5 and 1 Hz), 3.05 (3H, s), 2.5−1.5 (7H, m) ppm; ms showed the same pattern as that of *exo*-**12**.

An ether solution of *exo*-**12** (100 mg) and LAH (0.8 g) in ether was set aside for 5 days. The crude oil obtained was treated with picric acid in benzene; the precipitate was recrystallized from EtOH to afford the picrate of bicyclic amine **13**, mp 255°C (dec.) (lit. (34) mp 250°C). *Anal.* calcd. for $C_{14}H_{18}N_4O_7$: C 47.46, H 5.08, N 15.82; found: C 47.69, H 5.12, N 15.59.

A crude product (1.2 g) containing *exo*-**12**, *endo*-**12**, and **1***a* in a ratio of 48:42:10 in ether was stirred with LAH (3 g) and aliquots were removed at intervals for work-up and examined with gc. In 10 h, the above three peaks disappeared and were replaced by peaks at 1.7 (**13**), 1.8 (methyl-3-cyclohexenylmethylamine), and 3.5 (*endo*-chloramine **14**) min. After this, the peak of **13** gradually increased at the expense of the peak of *endo*-**14**. In 30 h, the latter disappeared to give only the former peak. LAH reduction of a crude product was stopped at 10 h, and the reaction was worked up to give a crude product that was chromatographed to give *endo*-chloramine **14** (360 mg); ir: 1450, 780 cm^{-1}; nmr: 3.2 (h, ddd, J = 9, 7 and 1.5 Hz), 2.96 (2H, m), 2.52 (3H, s), 2.45 (1H, b, $W_{1/2}$ = 5), 2.7−1.2 (7H, m) ppm; ms (100°C), m/e(%): 161(M^+, 12), 159(M^+, 32), 124(22), 96(32), 82(100), 67(16), 55(18), 42(50). The ir and nmr spectra were superimposable with an authentic sample (42). Further elution afforded amine **12** and *N*-(3-cyclohexenyl)methylmethylamine.

When *exo*-chlorolactam **12** (180 mg) was reduced with LAH (1 g) for 5 h in ether, it gave **13** and what appeared to be the *exo*-chloramine **14** as a 1:3 mixture; ir: 1450, 760 cm^{-1}; nmr: 4.3 (2H, m), 2.8 (1H, m), 2.43 (3H, s), 2.5−1.1 ppm (8H, m) ppm. This compound decomposed on standing at room temperature.

Acknowledgement

The authors are grateful to the Natural Sciences and Engineering Research Council of Canada, Ottawa, for generous financial aid for this project.

1. R. S. NEALE. Synthesis, 1 (1971).
2. W. C. DANEN and F. A. NEUGEBAUER. Angew. Chem. Int. Ed. Engl. **14**, 783 (1975).
3. Y. L. CHOW. *In* N-Nitrosamines. *Edited by* J. P. Anselme. ACS Symposium Series, No. 101, A.C.S., Washington, D.C., 1979. p. 1.
4. P. MACKIEWICZ and R. FURSTOSS. Tetrahedron, **34**, 3241 (1978).
5. R. S. NEALE, N. L. MARCUS, and R. G. SCHEPERS. J. Am. Chem. Soc. **88**, 3051 (1966); R. S. NEALE and N. L. MARCUS. J. Org. Chem. **34**, 1808 (1969).
6. O. E. EDWARD, J. M. PATON, M. H. BENN, R. E. MITCHELL, C. WATANOTADA, and K. M. VOHRA. Can. J. Chem. **49**, 1648 (1971).
7. E. FLESIA, A. CROATTO, P. TORDO, and J. M. SURZUR. Tetrahedron Lett. 535 (1972).
8. B. DANIELI, P. MANITTO, and G. RUSSO. Chem. Ind. 203 (1971).
9. Y. L. CHOW, J. N. S. TAM, M. and A. C. H. LEE. Can. J. Chem. **47**, 2441 (1969).
10. D. H. R. BARTON, A. L. J. BECKWITH, and A. GOOSEN. J. Chem. Soc. 181, 1965.
11. L. P. KUHN, G. G. KLEINSPEHN, and A. C. DUCKWORTH. J. Am. Chem. Soc. **89**, 3858 (1967).
12. W. C. DANEN and R. W. GELLERT. J. Am. Chem. Soc. **94**, 6853 (1972).
13. E. HEDAYA, R. L. HINMAN, V. SCHOMAKER, S. THEODOROPOULOS, and L. M. KYLE. J. Am. Chem. Soc. **89**, 4875 (1967).
14. T. C. JOSEPH, J. N. S. TAM, M. KITADANI, and Y. L. CHOW. Can. J. Chem. **54**, 3517 (1976); Y. L. CHOW and T. C. JOSEPH. J. Chem. Soc. D, 490 (1969).
15. R. A. JOHNSON and F. D. GREENE. J. Org. Chem. **40**, 2186 (1975); **40**, 2192 (1975).
16. C. BROWN and A. J. LAWSON. Tetrahedron Lett. 191 (1975); S. A. GLOVER and A. GOOSEN. J. Chem. Soc. Perkin Trans. 1, 1348 (1977); 653 (1978).
17. P. MACKIEWICZ, R. FURSTOSS, B. WAEGELL, R. COTE, and J. LESSARD. J. Org. Chem. **43**, 3746 (1978).
18. M. KUEHNE and D. A. HORNE. J. Org. Chem. **40**, 1287 (1975).
19. N. C. BAIRD, and H. B. KATHPAL. J. Am. Chem. Soc. **98**, 7532 (1976); N. C. BAIRD, R. R. GUPTA, and K. F. TAYLOR. J. Am. Chem. Soc. **101**, 4531 (1979); T. KOENIG, J. A. HOOBLER, C. E. KLOPFENSTEIN, G. HEDEN, F. SUNDERMAN, and B. R. RUSSELL. J. Am. Chem. Soc. **96**, 4573 (1974).
20. M. J. S. DEWER, A. H. PAKIARI, and A. B. PIERINI. J. Am. Chem. Soc. **104**, 3242 (1982).
21. J. N. S. TAM, R. W. YIP, and Y. L. CHOW. J. Am. Chem. Soc. **96**, 4543 (1974).
22. J. N. S. TAM. Ph.D. Thesis, Simon Fraser University, 1970.
23. J. LESSARD, Y. COUTURE, M. MONDON, and D. TOUCHARD. Can. J. Chem. **62**, 105 (1984); J. LESSARD, M. MONDON, and D. TOUCHARD. Can. J. Chem. **59**, 431 (1981).
24. Y. L. CHOW and R. A. PERRY. Tetrahedron Lett. 531 (1972).
25. R. A. PERRY. Ph.D. Thesis, Simon Fraser University, 1974.
26. J. LESSARD, D. GRILLER, and K. U. INGOLD. J. Am. Chem. Soc. **102**, 3262 (1980).
27. R. SUTCLIFFE, D. GRILLER, J. LESSARD, and K. U. INGOLD. J. Am. Chem. Soc. **103**, 624 (1981).
28. R. SUTCLIFFE, M. ANPO, A. STOLOW, and K. U. INGOLD. J. Am. Chem. Soc. **104**, 6064 (1982).
29. R. SUTCLIFFE and K. U. INGOLD. J. Am. Chem. Soc. **104**, 6071 (1982).
30. Y. L. CHOW and J. N. S. TAM. J. Chem. Soc. C, 1138 (1970); Y. L. CHOW, J. N. S. TAM, C. J. COLON, and K. S. PILLAY. Can. J. Chem. **51**, 2469 (1973).
31. Y. L. CHOW and C. J. COLON. J. Org. Chem. **33**, 2598 (1968).
32. R. A. PERRY, R. W. LOCKHART, M. KITADANI, and Y. L. CHOW. Can. J. Chem. **56**, 2906 (1978).
33. Y. L. CHOW, C. J. COLON, and D. W. L. CHANG. Can. J. Chem. **48**, 1664 (1970).
34. R. FURSTOSS, P. TEISSIER, and B. WAEGELL. Chem. Commun. 384 (1970).
35. A. K. BASE, H. P. S. CHAWLA, B. DOYAL, and M. S. MANHAS. Tetrahedron Lett. 2503 (1973); Y. BECKER, A. EISENSTADT, and Y. SHUO. Tetrahedron Lett. 3183 (1973).
36. K. FUJITA, K. HALA, R. ODA, and I. TABUSHI. J. Org. Chem. **38**, 2640 (1973).
37. A. BERTHO and G. RODL. Chem. Ber. **92**, 2218 (1954).
38. R. A. PERRY, S. C. CHEN, B. C. MENON, K. HANAYA, and Y. L. CHOW. Can. J. Chem. **54**, 2385 (1976).
39. A. L. J. BECKWITH, C. S. EASTON, and A. K. SERELIS. J. Chem. Soc. Chem. Commun. 482 (1980); A. L. J. BECKWITH, T. LAWRENCE, and A. K. SERELIS. J. Chem. Soc. Chem. Commun. 484 (1980).
40. F. A. L. ANET and M. Z. HAQ. J. Am. Chem. Soc. **87**, 3147 (1965); F. R. JENSEN and C. H. BUSHWELLER. J. Am. Chem. Soc. **87**, 3285 (1965).
41. J. LESSARD, R. COTE, P. MACKIEWICZ, R. FURSTOSS, and B. WAEGELL. J. Org. Chem. **43**, 3750 (1978).
42. G. A. RUSSELL and J. LOKENSGARD. J. Am. Chem. Soc. **89**, 5059 (1967).

Shielding anisotropy in tin compounds: spectroscopic studies of alkyltin cations in strong acid solutions

THOMAS BIRCHALL[1] AND VEERAGATHY MANIVANNAN
Department of Chemistry, McMaster University, Hamilton, Ont., Canada L8S 4M1

Received May 4, 1984[2]

THOMAS BIRCHALL and VEERAGATHY MANIVANNAN. Can. J. Chem. **63**, 2211 (1985).

We have observed that the ^{119}Sn nmr spectra of dialkyltin cationic species in highly acidic solutions are strongly field dependent. Relaxation time measurements at three different magnetic fields have established that the dominant spin-lattice relaxation mechanism for these species at high magnetic field is shielding anisotropy. A comparison of T_1^{-1} and T_2^{-1} values indicates that at room temperature a rapid chemical exchange process is occurring. In the case of the $(CH_3)_2Sn(SO_3F)_2-HSO_3F$ system variable temperature ^{119}Sn nmr reveals the presence of three tin species which are involved in this exchange process.

THOMAS BIRCHALL et VEERAGATHY MANIVANNAN. Can. J. Chem. **63**, 2211 (1985).

On a observé que les spectres rmn du ^{119}Sn d'espèces cationiques dialkylétain, en solutions dans des milieux fortement acides, dépendent beaucoup du champ. Des mesures de temps de relaxation à trois champs magnétiques différents ont permis d'établir que, pour ces espèces soumises à un champ magnétique élevé, le mécanisme principal de relaxation spin-réseau est l'anisotropie de blindage. Une comparaison des valeurs de T_1^{-1} et T_2^{-1} indique que, à température ambiante, il se produit un processus rapide d'échange chimique. Dans le cas du système $(CH_3)_2Sn(SO_3F)_2-HSO_3F$, la rmn du ^{119}Sn à température variable permet de révéler la présence de trois espèces d'étain qui sont impliquées dans ce processus d'échange.

[Traduit par le journal]

Introduction

A number of dimethyl- and trimethyl-tin derivatives of substituted sulphuric acids have been isolated as solids and characterized by Mössbauer and vibrational spectroscopy (1, 2). In one case, dimethyltin(IV) fluorosulphate, an X-ray crystal structure has been reported (3). The nature of these species in solution prior to crystallization has been studied by ^{1}H nmr and frozen solution ^{119}Sn Mössbauer spectroscopy and the structures in solution inferred from this data (4). This present study was initially aimed at measuring one-bond spin–spin coupling constants, $^1J_{^{119}Sn-^{13}C}$, in order to correlate these values with the Mössbauer data for these species. In so doing we observed that the ^{119}Sn nmr signal line width increased dramatically with the field of the instrument used to make the measurements. This led us to carry out relaxation time measurements at three different magnetic fields. There have been relatively few reports of relaxation time measurements on the ^{119}Sn nucleus and most of these studies have been made on relatively small and nearly symmetrical molecules (5, 6*a*). In these latter cases the dominant relaxation mechanisms are dipolar, spin-rotation, and scalar relaxation. Recently Blunden *et al.* (6*b*) have measured ^{119}Sn spin lattice relaxation times, and nuclear Overhauser enhancement (nOe) factors, for some organotin compounds. Although their T_1 and η values for $Bu_2Sn(OAc)_2$ were found to be field dependent, they attributed this to an exchange process. Here we present data which shows that for the $[(CH_3)_2Sn]^{2+}$ species shielding anisotropy (SA) is the dominant relaxation mechanism in ^{119}Sn nmr at high magnetic field. The complete dominance of the SA mechanism has been observed for several heavy nuclei such as ^{195}Pt (7), ^{199}Hg (8), ^{205}Tl (9), and ^{207}Pb (10), particularly in cases where there is a large asymmetry at the nucleus of interest. Also we have been able to observe, by variable temperature ^{119}Sn nmr, the presence of three tin species in solution that are involved in an exchange process.

[1]Author to whom correspondence may be addressed.
[2]Revision received January 17, 1985.

Experimental

Dimethyl- and trimethyl-tin species in sulphuric acid were prepared following the published procedure (4). The diethyltin species in sulphuric acid was prepared by the dissolution of diethyltin dichloride in 100% H_2SO_4 at room temperature (RT). The triethyltin species in fluorosulphuric acid was prepared by the reaction of tetraethyltin in HSO_3F at -30°C. The dibutyltin species was obtained by reacting $(n-C_4H_9)_6Sn_2$ with 100% H_2SO_4 at room temperature.

Tin-119 nmr spectra were recorded at operating frequencies of 33.56, 93.27, and 149.21 MHz on Bruker WH-90, WM-250, and WH-400 instruments respectively. Samples were contained in 10-mm (od) round bottomed tubes without a lock substance on the WM-250 and WH-400 instruments. For spectra recorded on the WH-90, samples were contained in an 8-mm (od) round bottomed tube which was placed concentrically into a 10-mm outer tube containing D_2O as the lock substance. Chemical shifts were measured relative to an external reference of neat $(CH_3)_4Sn$.

All spin-lattice relaxation times were measured using the inversion recovery technique and calculated using a three-parameter fitting procedure (11). The lengths of the 90° pulses used were 36 μs (WH-90), 28 μs (WM-250), and 29 μs (WH-400). The operating temperatures were 24°C and 22°C for the WM-250 and WH-400, respectively except for the variable temperature work. The estimated errors in T_1 measurements are less than 10%. The nOe measurements were obtained on the WH-90 by the gated decoupling technique with a minimum delay of 10 T_1. All samples were degassed by bubbling dry nitrogen through the sample.

Results and discussion

Dialkyltin sulphates have been produced by the solvolysis of R_4Sn, R_3SnX, or R_2SnX_2 with sulphuric or substituted sulphuric acids (1). The compounds isolated from these solutions have been examined by a variety of spectroscopic methods, and it was concluded that the tin environment was distorted octahedral with four equatorial oxygens, from sulphate groups, and *trans* axial alkyl groups completing the coordination (1, 2). This has been confirmed for $(CH_3)_2Sn(SO_3F)_2$ (3). Frozen solution ^{119}Sn Mössbauer data and ^{1}H nmr spectroscopy, of solutions of these species in strong acids, suggested that this

TABLE 1. ^{119}Sn line widths and relaxation time measurements for dialkyltinsulphates in 100% sulphuric acid

Compound	ν_0^2	T_1 (s)	η	T_1^{-1} (s^{-1})	T_{1DD}^{-1} (s^{-1})	T_{1SA}^{-1} (s^{-1})	$\Delta W_{1/2}$ (Hz)	T_2^{-1} (s^{-1})
$(CH_3)_2Sn(SO_4)$	1126.3	0.054	−0.20	18.5	2.7	15.8	85*	267
0.8 $M\ L^{-1}$	8699.3	0.009		109.9	(0.2)	(109.7)	450*	1414
	22263.6	0.0056		178.5	(0.1)	(178.5)	990*	3110
$(C_2H_5)_2Sn(SO_4)$	1126.3	0.035	−0.29	28.5	7.4	21.1	75†	236
1.20 $M\ L^{-1}$	8699.3	0.0087		114.9	—	(114.9)	670†	2105
	22263.6	0.0063		158.7	—	(158.7)	720†	2262
$(C_4H_9)_2Sn(SO_4)$	1126.3	0.0038	−0.27	26.3	—	—		
0.4 $M\ L^{-1}$	22263.6	0.0064		156.2	—	—		

NOTE: All measurements were made at room temperature.
*These measurements were carried out at a concentration of 1.2 $M\ L^{-1}$. Linewidths are fitted using "Numarit: Iterative N.M.R. Spectral Analysis Program", K. M. Worvill and J. S. Martin (1975), a development of NUMAR (ref. 16).
†Full width at half height.

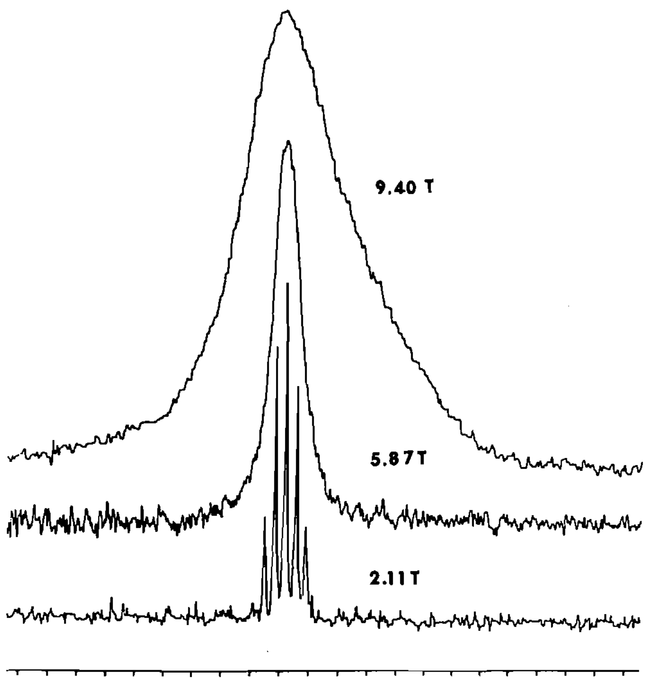

FIG. 1. ^{119}Sn nmr spectra of 0.8 M^{-1} $[(CH_3)_2Sn][SO_4]$ in 100% H_2SO_4 at field strengths of 2.11 T, 5.87 T, and 9.40 T.

geometry was preserved in solution (4). Since Mössbauer isomer shifts (δ) measure the s electron density at the tin nucleus, the participation of s electrons in the tin–ligand bonds will be reflected in a change in these isomer shifts (8). In the nmr experiment one might expect the $^{119}Sn-^{13}C$ coupling constant to be sensitive to the s character of the tin–carbon bond, if the Fermi contact term is the dominant contributor. Therefore there should be a relationship between δ and $^1J_{^{119}Sn-^{13}C}$. With this in mind we set out to measure $^1J_{^{119}Sn-^{13}C}$ for a series of alkyltin species in an attempt to correlate these values with ^{119}Sn Mössbauer data. Tin-119 nmr spectra of the sulphuric acid solutions, recorded at 33.56 MHz (2.114 T), showed the expected multiplet patterns due to coupling with the protons from the alkyl groups, though the individual lines were broad (Fig. 1). It was not, however, possible to observe the ^{13}C satellite peaks in the hydrogen decoupled spectrum, and $^1J_{^{119}Sn-^{13}C}$ values were subsequently obtained from the ^{13}C spectra. In an attempt to obtain better spectra, ^{119}Sn nmr data were recorded at higher magnetic fields (5.872 T and 9.40 T). This had the effect of broadening the ^{119}Sn lines so that the spin–spin coupling of the protons to the tin nucleus was obscured, Fig. 1. It became obvious that an accurate measure of both T_1 and T_2, the spin-lattice and spin–spin relaxation times, would be necessary before a satisfactory explanation of these spectra could be obtained.

There are several possible mechanisms which contribute to spin-lattice relaxation, namely (*i*) dipole–dipole, $T_{1(DD)}^{-1}$; (*ii*) spin-rotation, $T_{1(SR)}^{-1}$; (*iii*) scalar relaxation $T_{1(SC)}^{-1}$; and (*iv*) shielding anisotropy $T_{1(SA)}^{-1}$ (12). Of these, the spin-rotation mechanism is likely to be a minor contributor because of the large size of these solvated tin cations. Scalar relaxation usually occurs through a modulation of the scalar coupling via interaction with a nucleus having a short relaxation time, usually a quadrupolar nucleus. This leaves dipole–dipole and SA as the main line-broadening mechanisms, eq. [1], and these have been measured and tabulated in Table 1. From these data it is clear that T_1 for all three species is field dependent and de-

$$[1]\quad T_1^{-1} = T_{1(DD)}^{-1} + T_{1(SA)}^{-1}$$

creases with increasing field strength. It is interesting to note that at 2.114 T the relaxation time of the methyl species is much longer than for either the ethyl or butyl species, but as the field strength increases the difference decreases, until at 9.40 T the ethyl and butyl have longer relaxation times than the methyl species.

In order to obtain an estimate of $T_{1(DD)}^{-1}$, nOe measurements were made. The nOe is defined as the ratio of the double resonance intensity to the single resonance intensity and, since ^{119}Sn has a negative magnetogyric ratio, this results in a diminution of this nOe ratio (12). The nOe operates by cross relaxation between the two spin systems and the main contributor is from dipole–dipole coupling, except when there can be scalar coupling modulated by chemical exchange. Since, in these systems, the alkyl groups are not directly involved in any exchange process, scalar coupling can be eliminated.

Figure 2 shows plots of T_1^{-1} versus ν_0^2 for the dimethyl and diethyl species in 100% H_2SO_4: the T_1^{-1} values, at zero field (ν_0

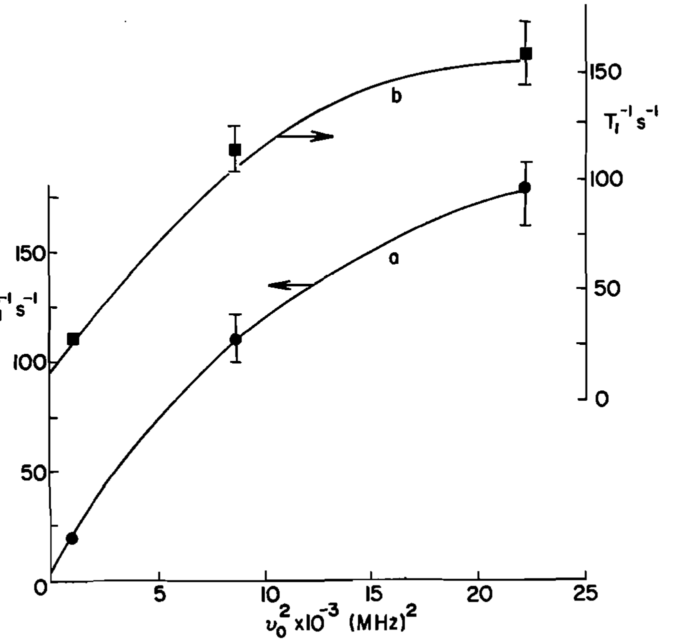

FIG. 2. Plots of T_1^{-1} versus ν_0^2 for: (a) $[(CH_3)_2Sn][SO_4]$ (L.H.S.) ● and (b) $[(C_2H_5)_2Sn][SO_4]$ (R.H.S.) ⊞ in 100% H_2SO_4.

= 0) are obtained by extrapolation. When B_0 approaches zero field strength, the effect of SA is negligible and the main contributors to the relaxation can only be dipolar, since the spin rotation mechanism can be neglected because of the large size of the solvated cation. Therefore, for the dimethyltin species at zero field, $T_1^{-1} = T_{1(DD)}^{-1} = 3.3\ s^{-1}$ and the corresponding value for the diethyltin species is $15.0\ s^{-1}$. Under extreme narrowing conditions, the relaxation rate of spin I, due to intramolecular dipole–dipole interactions with spin S, $T_{1(DD)}^{-1}$ (intra) is independent of frequency and is given by eq. [2] (12).

$$[2] \quad T_{1(DD)}^{-1}\ (\text{intra}) = \frac{\mu_0^2\gamma_I^2\gamma_S^2 h^2 s(s+1)}{12\pi^2 \sum_i r_{IS_i}^6}\tau_c$$

where μ_0 is the permeability of a vacuum, h is Planck's constant, r_{IS_i} is the internuclear distance between nucleus of spin I and S_i, and τ_c is the molecular tumbling correlation time.

Using eq. [2], and the above values for $T_{1(DD)}^{-1}$, τ_c is estimated to be 3.0×10^{-9} s and 1.3×10^{-8} s for the dimethyltin and diethyltin species respectively. With these τ_c values the magnitudes of $(\omega_0\tau_c)^2$, at three different fields 2.114 T, 5.872 T and 9.401 T, were found to be $(CH_3)_2Sn^{2+}$: 0.40, 3.09, 7.91; $(C_2H_5)_2Sn^{2+}$: 7.50, 58.04, 148.50, respectively. From these values it is clear that these systems deviate from the extreme narrowing condition even at 2.114 T, and the general equation must be used to calculate $T_{1(DD)}^{-1}$.

Werbelow (13) has established an expression for the frequency dependence of the nOe effect for coupled nuclei with gyromagnetic ratios of opposite sign. Using the equation given in this reference (13), η_{max} can be calculated using the estimated τ_c for the dimethyltin and diethyltin species at 2.114 T. From the experimentally measured nOe factors at 2.114 T, $T_{1(DD)}^{-1}$ was calculated using eq. [3]

$$[3] \quad \text{nOe} = 1 + \eta, \quad \eta = \eta_{max}\frac{T_1}{T_{1(DD)}}$$

The $T_{1(DD)}^{-1}$ values at zero field are different from those at 2.114 T. This difference is expected since these systems are outside the extreme narrowing condition.

The increased dipolar contribution in the diethyl species compared to the dimethyl may be attributed to its lower mobility, longer τ_c, and to the contribution from the additional protons. For the di-n-butyl case, we believe that its effective solvated size may not be very different from that of the diethyl species in these solutions and the increased number of protons in the former case will have little additional effect due to the r^{-6} dependence. Spin-lattice relaxation time and nOe measurements, made for the dimethyltin species in D_2SO_4 solution, were found to be the same as in H_2SO_4, indicating that intermolecular dipole–dipole relaxation is not significant in this system.

At 9.40 T we were unable to detect a nOe effect, indicating that the SA mechanism is the dominant one at high magnetic fields, whereas at lower fields dipolar mechanisms play a significant role for these species. Therefore it is reasonable to assume, at 5.872 T and 9.40 T, that the measured T_1^{-1} is equal to $T_{1(SA)}^{-1}$. Note the large increase in SA contribution as the field is increased from 2.114 T through 5.872 T to 9.40 T.

To our knowledge this is the first documented case of SA for the ^{119}Sn nucleus, though the effect has been noted for ^{195}Pt (7), ^{199}Hg (8), ^{205}Tl (9), and ^{207}Pb (10). In these latter cases the molecules studied are quite asymmetric and it is under these situations that nmr spectra obtained at high magnetic fields will be broadened due to SA. For the dialkyltin species the effect is dramatic (Fig. 1) and no useful spin–spin coupling information could be obtained by recording spectra at high fields. However, this broadening is augmented considerably by chemical exchange processes, which are discussed in the next section. That these molecules are very asymmetric at the tin nucleus has been demonstrated by ^{119}Sn Mössbauer measurements, which show very large quadrupole splittings (4). When the molecules are less asymmetric the broadening at high field is less serious and, for the triethyltin species in fluorosulphuric acid at 5.872 T, some spin–spin coupling can be resolved. Mössbauer measurements show that the trialkyltin compounds have a smaller quadrupole splitting than the corresponding (*trans*) dialkyltin molecules (4).

The SA contribution to T_1 is given by eq. [4]

$$[4] \quad \frac{1}{T_1}(\text{SA}) = \frac{1}{15}(\gamma_I B_0)^2(\Delta\sigma)^2\left[\frac{(2\tau_c)}{1+\omega_0^2\tau_c^2}\right]$$

where $\Delta\sigma$ is the shielding anisotropy. Using the above value for τ_c and the ^{119}Sn T_1 measured at 9.40 T, for the $(CH_3)_2Sn^{2+}$ and diethyl species, one arrives at values of 2005 ppm and 4478 ppm respectively for $\Delta\sigma$. These values are not unreasonable considering the large range for ^{119}Sn chemical shifts. They may be compared with the values obtained for other cases, e.g. $(CH_3)_2Hg$ $\Delta\sigma = 6100$ ppm (8). However, care should be taken in considering the magnitude of this value since the rotational correlation time may not be the same as that which modulates the SA. This estimate is further clouded by the fact that the tin is involved in a chemical exchange process (see below). For some cobalt systems it has been suggested that this correlation time is associated with the lifetime of hydrogen bonded second sphere complexes (14), and there is no doubt that hydrogen bonding will be extensive in our systems, between the coordinated sulphate groups and the solvent.

From the simple theory of the SA effect under extreme narrowing conditions one would have expected a linear plot of $T_{1(SA)}^{-1}$ versus ν_0 (2). However, our experimental data do not

TABLE 2. Concentration and temperature dependence of the ^{119}Sn chemical shifts and line widths for dialkyltinsulphonates in 100% HSO_3X (X = OH, F)

Compound	Concentration ($M\ L^{-1}$)	Temperature (°C)	δ* (ppm)	$\Delta W_{1/2}$ (Hz)
$(CH_3)_2Sn(SO_4)$‡	1.20	RT	−155	1160(990)†
	0.80	RT	−156	1850
	0.40	RT	−182	4100
$(C_2H_5)_2Sn(SO_4)$‡	1.20	RT	−267	720
	0.80	RT	−247	1160
	0.40	RT	−263	700
$(C_4H_9)_2Sn(SO_4)$‡	0.40	RT	−252	460
	0.20	RT	−252	410
$(CH_3)_2Sn(SO_3F)_2$	1.16	RT	−106	366
		−80	−218	5829
	0.40	RT	−144	414
		−80	−225	2200
$(C_2H_5)_2Sn(SO_3F)_2$	1.4	RT	−235	57.5
		−80	−264	1150

*Measured at ν_0 = 149.21 MHz.
†Fitted line width.
‡Because of the high freezing point of 100% H_2SO_4 (10.657°C) it was not possible to record spectra at low temperature.

TABLE 3. ^{119}Sn nuclear magnetic resonance chemical shifts and spin–spin coupling constants for alkyltinsulphonates in acid solutions

Compound	Concentration ($M\ L^{-1}$)	Temperature (°C)	$\delta_{^{119}Sn}$ (ppm)	$\Delta W_{1/2}$ (Hz)	^1J* (Hz)	^2J (Hz)	^3J (Hz)
In H_2SO_4							
$(CH_3)_3Sn(HSO_4)$ (92%)	0.96	0	194	—	409	65	
$(C_2H_5)_2Sn(SO_4)$	1.2	Amb	−268	—	516	68	188
$(CH_3)_2Sn(SO_4)$	1.2	Amb	−154	—	627	97	
In HSO_3F							
$(C_2H_5)_3Sn(SO_3F)_2$	1.4	−20	288	—	330	49	147
$(C_2H_5)_2Sn(SO_3F)_2$	1.4	Amb	−253	—	428	61	184
		0	−242	—		58	189
		−20	−248				
		−60	−259	~650			
		−80	−264	~1150	440		
		−85	−265	~1625			
$(CH_3)_2Sn(SO_3F)_2$ (at 93.2 MHz)	1.16	Amb	−106	460	558		
		−20	−113	846			
		−40	−119	1720	571		
		−60	−128	5070	573		
		−70	−158	8330			
			8.2	1600			
		−75	−201	6795			
			~−14	9770			
			7.3	978			
		−80	−219	5830	575		
			~5	7960			
			6.2	610			
		−90	−232	~5860	566		
			38	353			
			32	~4030			
$(CH_3)_2Sn(SO_3F)_2$ (at 149.2 MHz)		−80	−238	~7500			
			4.2	375			
			28.8	~4990			
		−90	3.3	420			
			32.3	~7140			

*Measured from the ^1H decoupled ^{13}C spectra. The ^{117}Sn and ^{119}Sn satellite peaks were not resolved and this is the average coupling. $^1J = J_{^{119}Sn-^{13}C}$; $^2J = J_{^{119}Sn-C-^1H}$; $^3J = J_{^{119}Sn-C-C-^1H}$.

follow a straight line (Fig. 2) because, for the systems studied here, the conditions for extreme narrowing do not apply at the higher magnetic field.

Chemical exchange

The measured line widths of the ^{119}Sn signals in 100% H_2SO_4 varied considerably with applied magnetic field (Table 1). These measured widths at half height are inversely proportional to the spin–spin relaxation times T_2 ($\Delta W_{1/2} = 1/\pi T_2$) so that it is possible to estimate T_2^{-1} after allowance has been made for $^2J_{^{119}\text{Sn}-\text{C}-^1\text{H}}$. Even though there are large errors associated with these estimates, it is apparent that T_2^{-1} is much larger than T_1^{-1} in all cases. There are three possible sources for these differences, namely (*i*) scalar relaxation, which is not possible here for the reasons given above; (*ii*) SA, which would lead to differences between T_1^{-1} and T_2^{-1}. Since these systems are outside the extreme narrowing condition, $T_{2(\text{SA})}^{-1}$ is estimated using the general equation (12). This leads to values of 73.1 s^{-1}, 434.8 s^{-1}, and 1021.0 s^{-1} for the dimethyltin species at 2.114 T, 5.872 T, and 9.40 T respectively. The differences observed between T_1^{-1} and T_2^{-1} are much greater than can be accounted for by the SA contribution. This leaves (*iii*) chemical exchange broadening as the source of the difference between T_1 and T_2.

Tin-119 nmr spectra for the dimethyltin and diethyltin species in 100% H_2SO_4 were recorded at three different magnetic fields and at two or three different concentrations. Spectra for the dibutyltin species were obtained at 9.40 T at two concentrations. The line widths and chemical shifts are recorded in Table 2. It is apparent that, in addition to the increased line broadening with field, there is also a marked increase in line width with increasing dilution, with the exception of the dibutyltin case where no significant change was observed. These changes with dilution support the idea that chemical exchange is occurring and that the rate of exchange is dependent upon the nature of the alkyl group. As the size of the alkyl group increases, the width at half height of the ^{119}Sn resonance decreases. Since there is only one tin signal observed in these solutions, these line width changes suggest that the rate of exchange is faster for the butyl than for the ethyl derivative and that the dimethyltin species is involved in the slowest exchange process.

Solutions in 100% sulphuric acid are not very suitable for variable temperature nmr studies, since these solutions freeze at ~10°C, but fluorosulphuric acid solutions can be studied down to ~−90°C. A solution of the dimethyltin species in fluorosulphuric acid was examined at 5.872 T and a single broadened resonance was observed δ = −106 ppm (Table 3). On cooling to −70°C a new tin resonance appeared at ~8.2 ppm, which increased in intensity on further cooling. By −80°C a third broad resonance was clearly visible at ~5 ppm. During this cooling the intensity of the high field signal decreased as the signals at lower field increased in intensity (Fig. 3). Cooling to −90°C produced no further changes and the sample was frozen below this temperature. These observations clearly confirm that an exchange process (or processes) is involved in these solutions. At 9.40 T the spectra are very similar, except that at −90°C the high field signal has now disappeared and only two broad signals remain. From these observations it is apparent that there are at least three distinct dimethyltin species present. For a solution of the diethyltin species in HSO_3F only one broad ^{119}Sn resonance was ever observed, even at −80°C. This is consistent with the earlier

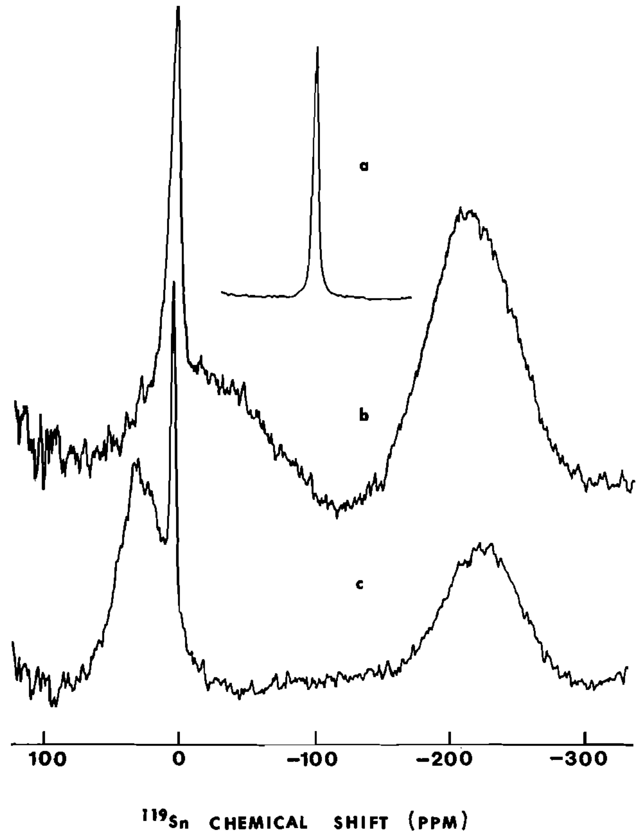

FIG. 3. ^{119}Sn nmr spectra of a 1.16 M^{-1} solution of $[(CH_3)_2Sn]\cdot[SO_3F]$ in HSO_3F at (a) 24°C, (b) −75°C, and (c) −90°C at a magnetic field strength of 5.87 T.

discussion, and confirms that the exchange process is faster for the diethyl- than for the dimethyltin case.

The concentration and temperature dependence of $^1J_{^{13}\text{C}-^{119}\text{Sn}}$ was found by recording ^{13}C nmr spectra (see Table 3). A small increase of ~15 Hz is noted over the temperature range studied. Under these conditions the ^{119}Sn spectra indicate the presence of three tin species, but at the ^{13}C resonance frequency these three species are not resolvable and only an average $^1J_{^{117,119}\text{Sn}-^{13}\text{C}}$ is measurable. Since this increase in the spin–spin coupling is only ~2.5% we conclude that the exchanging tin species have very similar geometries. Changes in the tin environment produce substantial changes in $^1J_{^{117,119}\text{Sn}-^{13}\text{C}}$. For example $(CH_3)_4Sn$ has $^1J_{^{119}\text{Sn}-^{13}\text{C}} = 335$ Hz, five-coordinate tin has a coupling of ~400 Hz, while for six-coordinate tin the value is often in excess of 600 Hz. These trends are in qualitative agreement with an increasing *s* character to the C—Sn bonds, i.e. from sp^3 in R_4Sn, through sp^2 in $[R_3Sn]^+$, to sp in $[R_2Sn]^{2+}$ in the solvated cationic species. The $^2J_{^{119}\text{Sn}-\text{C}-^1\text{H}}$ couplings follow the same trend. For the ethyl derivative it is interesting to note that $^3J_{^{119}\text{Sn}-\text{C}-\text{C}-^1\text{H}}$ is much larger in magnitude than $^2J_{^{119}\text{Sn}-\text{C}-^1\text{H}}$ though these probably have opposite signs (15). The ^{119}Sn chemical shifts and $^1J_{^{119}\text{Sn}-^{13}\text{C}}$ coupling constants found for the trialkyl- and dialkyltin species in strong acids are consistent with the idea that these species are strongly solvated and have trigonal bipyramidal and *trans* octahedral geometries respectively in solution (4). Dimethyltin(IV) fluorosulphate in the solid state has been shown to have an octahedral geometry with *trans* CH_3 groups (3). It had been concluded earlier (4) that this *trans* octahedral geometry was preserved in solution.

Since the ^{119}Sn nmr shows that more than one tin species is present in the low temperature HSO_3F solutions, we decided to reexamine the frozen solutions by more careful Mössbauer measurements. A two-line spectrum was observed, but the two lines do not have the same intensity or width. Many reasons exist for such spectra but, in view of the nmr evidence, we conclude that these spectra arise from overlapping quadrupole split doublets. However, we were only able to fit two doublets to the absorption envelopes (δ_1, 1.94 mm s^{-1}; Δ_1, 5.51 mm s^{-1}; δ_2, 1.73 mm s^{-1}; Δ_2, 5.08 mm s^{-1}, where δ is the Mössbauer isomer shift, relative to $CaSnO_3$, and Δ is the quadrupole splitting parameter). The sets of parameters indicate that the two tin environments are very similar to that found for $(CH_3)_2Sn(SO_3F)_2$ in the solid state (3). These two overlapping spectra must arise from the two tin species which dominate the low temperature ^{119}Sn nmr spectrum shown in Fig. 3. Presumably the tin species, giving rise to the highest field nmr resonance at more elevated temperatures, is no longer present in the frozen Mössbauer samples.

Clearly there are at least three different tin species present in these strong acid solutions that are involved in equilibria which, on the nmr time scale, average the tin environments. Aubke and co-workers (2) have shown that dimethyltin sulphonates, in the parent acid, are not completely ionized according to eq. [5] even in dilute solution. Both nmr and Mössbauer evidence indicate that the tin species in these solu-

$$[5]\quad (CH_3)_2SnSO_4 + H_2SO_4 \rightleftarrows \underset{\mathbf{I}}{[(CH_3)_2Sn]^{2+}} + [2HSO_4]^-$$

tions are six coordinate, and eq. [5] should perhaps be rewritten as eq. [6]

$$[6]\quad \underset{\mathbf{II}}{(CH_3)_2Sn(HSO_4)_2(H_2SO_4)_2} + 2H_2SO_4 \rightleftarrows \underset{\mathbf{III}}{[(CH_3)_2Sn(H_2SO_4)_4]^{2+}} + 2[HSO_4]^-$$

with the equilibrium lying heavily to the left. Since proton transfer processes are extremely fast it is unlikely that cooling, even to −90°C, will result in resolvable signals for **II** and **III**, but the equilibrium would be displaced towards **II** and account for the shift of the ^{119}Sn nmr signal to higher magnetic field, **II** being more shielded than **III**. This would also be consistent with the observation that the tin-119 nmr line widths become broader on dilution.

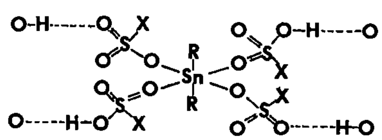

IV

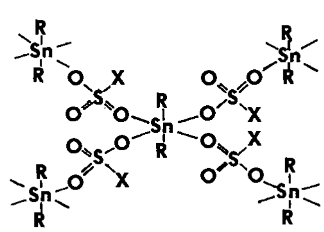

V

At low temperature, species less shielded than **II** are present and since the $^1J_{^{117,119}Sn-^{13}C}$ values change only marginally, the difference in shielding must come from a redistribution of electron density from the sulphonate ligands. We believe that **II** is an isolated species linked to other units or solvent by hydrogen bonding and that each $[SO_3X]^-$ or HSO_3X ligand is monodentate. At lower temperatures these weak hydrogen bonded interactions must be converted to stronger linkages via sulphonate bridges, and result in the deshielding observed. We suggest that the peak in the ^{119}Sn nmr spectrum at ~4 ppm arises from a polymeric species **IV** while that at lowest field, ~29 ppm, has the polymeric units of **IV** cross linked to give **V**, which is the structure observed in the solid state for $(CH_3)_2Sn(SO_3F)_2$ (3). The two ^{119}Sn Mössbauer doublets observed in the frozen solution of $(CH_3)_2Sn(SO_3F)_2$ in HSO_3F we attribute to species **IV** and **V**.

Acknowledgements

We wish to thank Prof. R. F. Lenkinski, of the S.W. Ontario N.M.R. Centre at Guelph, for recording spectra on the WH-400 and for his suggestion to measure relaxation times, and to Mr. B. G. Sayer for help with the other nmr spectra and for his sound advice. The Natural Sciences and Engineering Research Council of Canada is also thanked for financial support.

1. P. A. Yeats, B. F. E. Ford, J. R. Sams, and F. Aubke. J. Chem. Soc. Chem. Commun. 791 (1969).
2. P. A. Yeats, J. R. Sams, and F. Aubke. Inorg. Chem. **10**, 1877 (1971).
3. F. H. Allen, J. A. Lerbscher, and J. Trotter. J. Chem. Soc. (A), 2507 (1971).
4. T. Birchall, P. K. H. Chan, and A. R. Pereira. J. Chem. Soc. Dalton Trans. 2157 (1974).
5. R. R. Sharp and J. W. Tolan. J. Chem. Phys. **65**, 522 (1976).
6. (*a*) C. R. Lassigne and E. J. Wells. Can. J. Chem. **55**, 927 (1977); (*b*) S. J. Blunden, A. Frangou, and D. G. Gillies. Org. Magn. Reson. **20**, 170 (1982).
7. J. Y. Lallemand, J. Soulié, and J. C. Chattard. J. Chem. Soc. Chem. Commun. 436 (1980).
8. R. E. Wasylishen, R. E. Lenkinski, and C. Rogers. Can. J. Chem. **60**, 2113 (1982).
9. F. Brady, R. W. Matthews, M. J. Foster, and G. D. Gillies. Inorg. Nucl. Chem. Lett. **17**, 155 (1981).
10. G. R. Hayes, D. G. Gillies, L. P. Blaauw, and A. D. H. Claque. J. Magn. Reson. **45**, 102 (1981).
11. N. R. Draper and H. Smith. Applied regression analysis. 2nd ed. Wiley, New York. 1981. Chapt. 10.
12. G. A. Webb. *In* N.M.R. and the periodic table. *Edited by* R. K. Harris and B. E. Mann. Academic Press, New York. 1978. pp. 78–84.
13. L. Werbelow. J. Magn. Reson. **57**, 136 (1984).
14. S. C. F. Au-Yeung and D. R. Eaton. J. Magn. Reson. **52**, 366 (1983).
15. L. Verdonck and G. P. van der Kelen. Ber. Bunsenges. Phys. Chem. **69**, 478 (1965).
16. A. R. Quirt and J. S. Martin. J. Magn. Reson. **5**, 318 (1971).

$^5J(CH_3,SH)$ as a negative proximate or as a positive $\sigma-\pi$ coupling in 2-methylthiophenol derivatives

TED SCHAEFER, JAMES PEELING,[1] RUDY SEBASTIAN, AND JAMES D. BALEJA
Department of Chemistry, University of Manitoba, Winnipeg, Man., Canada R3T 2N2

Received November 5, 1984

TED SCHAEFER, JAMES PEELING, RUDY SEBASTIAN, and JAMES D. BALEJA. Can. J. Chem. **63**, 2217 (1985).

Analyses of the ^1H nmr spectra of 6-chloro-2-methylthiophenol and of 4-*tert*-butyl-2-methylthiophenol in CCl_4 solution, together with double irradiation experiments, show that $^5J(CH_5,SH)$ in the former compound is -0.66 Hz and is $+0.47$ Hz in the latter. In the chloro compound, the sulfhydryl group spends relatively little time in out-of-plane conformations at 300 K. The negative coupling is a consequence of a through-space or proximate coupling mechanism. In the other compound, the sulfhydryl group samples many out-of-plane conformations but relatively few in which the S—H bond lies near the methyl group. Therefore $^5J(CH_3,SH)$ is now dominated by a $\sigma-\pi$ electron mechanism and is positive. Probably by coincidence, $^4J(H,SH)$ in this compound is equal in magnitude but opposite in sign to $^5J(CH_3,SH)$.

TED SCHAEFER, JAMES PEELING, RUDY SEBASTIAN et JAMES D. BALEJA. Can. J. Chem. **63**, 2217 (1985).

L'analyse des spectres rmn du ^1H du chloro-6 méthyl-2 thiophénol et du *tert*-butyl-4 méthyl-2 thiophénol, en solutions dans du CCl_4 et faite de concert avec des expériences de double irradiation, permet de montrer que la valeur de $^5J(CH_5,SH)$ dans le premier composé est égale à $-0,66$ Hz alors qu'elle est égale à $+0,47$ dans le dernier composé. À 300 K, le groupement sulfhydryle du composé chloré n'est pratiquement jamais dans le conformation hors-plan. La constante de couplage négative serait une conséquence d'une mécanisme de couplage à travers l'espace ou par proximité. Dans l'autre composé, le groupement sulfhydryle pourrait occuper plusieurs conformations hors-plan; toutefois, il en existe relativement peu dans lesquelles la liaison S—H se situerait près du groupement méthyle. Donc, le couplage $^5J(CH_3,SH)$ est dominé par un mécanisme électronique $\sigma-\pi$ et il est positif. Probablement dû à une coïncidence, la valeur de $^4J(H,SH)$ dans ce composé est d'amplitude égale mais de signe opposé à la valeur de $^5J(CH_3,SH)$.

[Traduit par le journal]

Introduction

The long-range spin–spin coupling constants, $^nJ(H,SH)$, between the sulfhydryl and ring protons in thiophenol and various of its derivatives are moderately well understood as conformational indicators (1–6). $^6J(H,SH)$, involving the *para* proton, depends on $\sin^2\theta$, where θ is the angle by which the S—H bond twists out of the benzene plane, and is therefore a so-called $\sigma-\pi$ coupling. $^5J(H,SH)$ is a composite of $\sigma-\pi$, depending on $\sin^2\theta$, and σ, proportional to $\sin^2(\theta/2)$, interactions among nuclear and electronic angular momenta. Such couplings can be employed in the derivation of expectation values of the angular functions which, in turn, can be related to the internal barrier to rotation about the C—S bond. The assumption that $^4J(H,SH)$ is also predominantly a $\sigma-\pi$ coupling allows a reasonable description of the change in internal barrier caused by electronic perturbations from the *para* substituent in a number of thiophenol derivatives (3, 5).

One test for a predominant $\sigma-\pi$ mechanism relies on the "methyl group replacement" technique (7), in which a ring hydrogen is replaced by a methyl group. The test implies, for example, that $^6J(H,CH_3) = -^7J(CH_3,CH_3) = -0.62$ Hz in toluene and *p*-xylene if a $\sigma-\pi$ mechanism accounts for ^6J. This equality is borne out by experiment (8, 9). However, the corresponding relationship does not hold for *o*-xylene (8, 9) in which $^5J(CH_3,CH_3)$ is $+0.45(2)$ Hz (9), whereas $^4J(H,CH_3)$ is $-0.75(3)$ Hz in toluene (10). Of course, it might appear that the $\sigma-\pi$ component of $^4J(H,CH_3)$ is -0.45 Hz. This appearance is very likely misleading, primarily because of the likelihood of a "through-space" or proximate coupling component in $^5J(CH_3,CH_3)$. A proximate mechanism implies spin polarization transmitted via interactions between electron orbitals in proximate bonds or even between orbitals centered on the coupled nuclei (11). Therefore, $^5J(CH_3,CH_3)$ may measure a composite of $\sigma-\pi$ and proximate mechanisms. Judging from a proximate coupling like $^5J(H,CH_3)$ in anisole (12–14), the proximate component of $^5J(CH_3,CH_3)$ in *o*-xylene may well be negative, implying a rather larger $\sigma-\pi$ component of $^4J(H,CH_3)$ than would be deduced from an uncritical use of the methyl replacement procedure. Computations of $^5J(CH_3,CH_3)$ support (15) the existence of a proximate component but, probably because of the local threefold symmetry of each methyl group and the concomitant averaging over so many couplings (three protons in each group), experimental proof of its existence has not been forthcoming.

If one of the methyl groups is replaced by a sulfhydryl group and if the latter can be held at various orientations with respect to the methyl moiety (preferred θ values), then the existence of a $\sigma-\pi$ component in $^5J(CH_3,SH)$, having a maximum at $\theta = 90°$, *and* of a proximate component, with a maximum magnitude (perhaps of opposite sign to the $\sigma-\pi$ component) when the S—H bond lies near the methyl group, may be demonstrable. In this paper we show that $^5J(SH,CH_3)$ is negative in 6-chloro-2-methylthiophenol, **1**, and is positive in 2-methyl-4-*tert*-butylthiophenol, **2**.

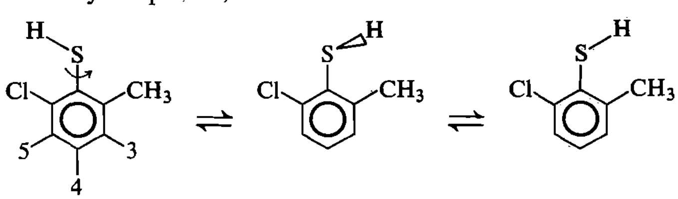

1*a* $\theta = 0°$ **1***b* $0 \le \theta \le 180°$ **1***c* $\theta = 180°$

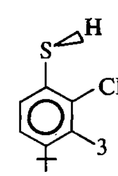

2

[1]University of Petroleum and Minerals, Saudi Arabia.

TABLE 1. The ^{1}H nmr spectral parameters for 6-chloro-2-methylthiophenol, **1**, and 2-methyl-4-*tert*-butylthiophenol, **2**, in CCl_4 solution

Parameter	Value 1[a]	Value 2[b]	Parameter	Value 1[a]	Value 2[b]
ν_{SH}	1257.571(1)[c]	298.791(4)[c]	$^{4}J(H,CH_3)$	−0.725(1)	−0.714(3)
ν_{CH_3}	704.719(1)[d]	230.234(3)[d]	$^{5}J(H,CH_3)$	0.306(1)	0.406(4)
ν_3	2093.634(1)	706.760(3)	$^{6}J(H,CH_3)$	−0.606(1)	−0.587(3)
ν_4	2069.267(1)	—	$^{4}J(H,SH)$	—	−0.477(6)
ν_5	2159.911(1)	698.146(3)	$^{5}J(H,SH)$	0.531(2)	0.423(5)
ν_6	—	709.542(5)	$^{5}J(H\text{-}5,SH)$	0.247(2)	0.286(5)
$^{3}J_{34}$	7.550(2)	—	$^{6}J(H,SH)$	−0.097(2)	—
$^{3}J_{45}$	8.046(2)	—	$^{5}J(CH_3,SH)$	−0.659(1)	0.469(4)
$^{3}J_{56}$	—	8.133(5)	rms deviation	0.007	0.017
$^{4}J_{35}$	1.385(2)	2.292(5)			
$^{5}J_{36}$	—	0.379(5)			

[a]For a 2.5 mol% solution in CCl_4, containing some cyclohexane-d_{12} and at 300 K.
[b]For a 3.0 mol% solution in CCl_4, containing some tetramethylsilane and at 305 K.
[c]The shifts are given in Hz at 300.135 MHz relative to internal TMS for **1** and at 100.001 MHz (centerband) for **2**.
[d]For **1** the numbers in parentheses are probable errors while for **2** they are standard deviations.

Experimental

6-Chloro-2-methylthiophenol, **1**, from Fairfield Chem. Co. was prepared as a 2.5 mol% solution in CCl_4, which also contained 0.6 mol% cyclohexane-d_{12}. A 3.0 mol% solution of 2-methyl-4-*tert*-butylthiophenol, **2**, from Aldrich, in CCl_4 contained some tetramethylsilane. These samples were transferred to 5-mm od nmr tubes, which were degassed by numerous freeze–pump–thaw cycles and were then flame-sealed.

The ^{1}H nmr spectrum of **2** was calibrated by a procedure previously described (16) on an HA100 spectrometer at a probe temperature of 305 K. Because the existence of small, unresolvable couplings between the protons of the *tert*-butyl group and the ring protons led to increased linewidths for the peaks of H-3 and H-5, the calibration procedure was performed during irradiation of the *tert*-butyl proton peak at δ 1.268. The calibration gave peak frequencies with standard deviations of ≤0.02 Hz.

The ^{1}H nmr spectrum of **1** was obtained on an AM300 spectrometer at a probe temperature of 300 K. Typically, 8 scans were acquired using quadrature detection. In order to obtain a digital resolution of 0.01 Hz/point, narrow sweepwidths, say 300 Hz, and acquisition times of 27.3 s were used.

The signs of $^{5}J(CH_3,SH)$ in **1** and **2** were obtained by weak double irradiation methods. For **1** it proved most convenient to record the CH_3 peaks while perturbing selected peaks in the H-3 multiplet. Among other sign ratios so determined, it was shown that $^{5}J(H,SH)/{}^{5}J(CH_3,SH) < 0$. $^{5}J(H,SH)$ is positive (2). For **2**, irradiation of selected peaks in the CH_3 multiplet led to perturbations of certain peaks in the H-6 region, which showed that $^{4}J(H,SH)/{}^{5}J(CH_3,SH) < 0$. $^{4}J(H,SH)$ is negative (2). The positive sign of $^{5}J(CH_3,SH)$ was confirmed by experiments in which $^{4}J(H,SH)$ and $^{5}J(H,SH)$ had their signs determined relative to those of the long-range couplings between the methyl and ring protons. The latter are known (17).

STO 3G MO computations (18) were performed with the geometry optimization algorithm of the program MONSTERGAUSS (19). INDO MO FPT (20, 21) calculations of coupling constants assumed the STO 3G MO geometries.

Results and discussion

Spectral analysis

Because almost all the expected peaks in the ^{1}H nmr spectrum of **1** at 300 MHz were resolved, the analysis with the program PANIC (part of the software on the AM300) was straightforward. The spectral parameters are given in Table 1. Figure 1 displays the ^{1}H nmr spectrum of the sulfhydryl proton, illustrating resolution of the smallest proton–proton coupling in **1**.

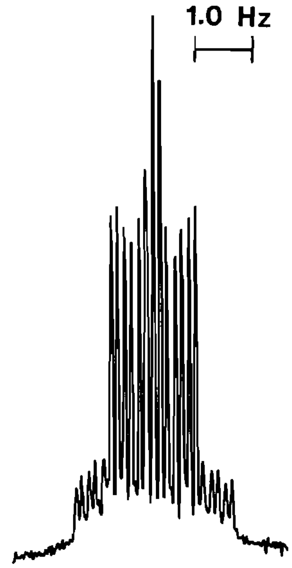

FIG. 1. The ^{1}H nmr spectrum of the sulfhydryl proton at 300.135 MHz and 300 K for a 2.5 mol% solution of 6-chloro-2-methylthiophenol in CCl_4 solution. The smallest splitting has a magnitude of 0.097(2) Hz and represents the coupling between the sulfhydryl proton and H-4, six bonds away.

The ^{1}H nmr spectrum of **2** was analyzed with the program LAME (22, 23), having been calibrated in the cw mode at 100 MHz while irradiating the transitions of the *tert*-butyl protons. The ring protons are fairly tightly coupled, leading to somewhat lower precision in the spectral parameters in Table 1 than for **1**, which displayed an essentially first-order spectrum at 300 MHz.

Both analyses assumed signs of coupling constants consistent with the double resonance experiments described above.

$^{5}J(CH_3SH)$ in 6-chloro-2-methylthiophenol, 1

If $^{6}J(H,SH)$ were zero, then a discussion in terms of planar conformations **1***a* and **1***c* would be adequate. In fact, $^{6}J(H,SH)$ vanishes or is very small in 2,6-dichlorothiophenol (3), in which intramolecular hydrogen bonding may help to stabilize the planar conformation, and is -0.97 Hz in 2-hydroxythiophenol (4), where the S—H bond is held in a plane nearly perpendicular to the molecular plane by a stereospecific O—H...S hydrogen bond involving the 3*p* lone-pair on sulfur. These data are consistent with a $\sigma-\pi$ mechanism for ^{6}J(H,SH), obeying $-0.97 \langle \sin^2 \theta \rangle$, angular brackets indicating an average over all the populated hindered rotor states of the S—H group. Then the observed ^{6}J(H,SH) of -0.097 Hz in **1** implies $\langle \sin^2 \theta \rangle$ as 0.10. If the barrier to rotation about the C—S bond in **1** were twofold, then its magnitude would be about 16 kJ/mol (5, 24) and a discussion in terms of a **1***a* $\rightleftarrows$ **1***c* equilibrium would be adequate at 300 K, V_2 being much larger than *kT*.

Of course, a substantial V_1 component exists, as indicated by the relative magnitudes of ^{5}J(H,SH) in **1**. In terms of the two-site equilibrium, one may write (3) $\Delta G_{300} = -RT \ln K = -RT \ln (0.531/0.247) = -1.9$ kJ/mol, favoring **1***a* ($K = 2.1_5$). A proper treatment would involve computations of the change in $\langle \sin^2 \theta \rangle$ caused by the presence of V_1, yielding a correction to V_2. However, because V_2 is nearly an order of magnitude larger than V_1, the perturbation would be small, as would the correction to V_1 caused by a finite $\langle \sin^2 \theta \rangle$.

Because (4) ^{4}J(H,SH) is near -1.1 Hz at $\theta = 90°$, it follows that as a $\sigma-\pi$ coupling its value would be about -0.11 Hz in the hypothetical molecule containing no methyl group but otherwise obeying the approximate potential function derived from ^{6}J(H,SH) and ^{5}J(H,SH). Hence ^{5}J(CH_3,SH) would be about $+0.11$ Hz if it were measuring the $\sigma-\pi$ component of ^{4}J(H,SH). The actual value of ^{5}J(CH_3,SH) is $-0.65(1)$ Hz in **1**.

The most likely source of this large negative coupling is the proximate coupling mechanism. The following approach was taken to the computation of the proximate interaction. The optimized geometry of 2-methylthiophenol, **3**, obtained from

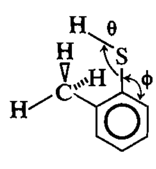

3

STO 3G MO computations, was used to calculate ^{5}J(CH_3,SH) by the INDO MO FPT approach. For $\theta = 98.0°$ and $\phi = 114.9°$, the computations gave ^{5}J(CH_3,SH) as -1.28 Hz. An increase of 2° in ϕ resulted in a calculated coupling of -1.73 Hz whereas a decrease of 2° in θ yielded -1.52 Hz. For the planar *trans* form of 2-methylthiophenol, the optimized geometry yielded ^{5}J(CH_3,SH) as 0.21 Hz. In **1**, the latter conformation is about 68% abundant. Therefore, a naive approach yields ^{5}J(CH_3,SH) as $0.68\ (0.21) + 0.32\ (-1.28)$ or -0.28 Hz. Of course, the *ortho* chlorine substituent will very likely cause a somewhat more compressed geometry of the SH and CH_3 groups in **1***c* than in 2-methylthiophenol, leading to a larger magnitude of the coupling. Furthermore, the coupling **1** contains some nonplanar populations, **1***b*. It seem bootless to compute further in an attempt to match the computed coupling in **1** to its observed value of -0.65 Hz, but it is also eminently reasonable that this sizeable negative number is indeed the consequence of a proximate mechanism. The discussion now turns to the coupling in **2**, in which the large populations of conformers containing out-of-plane SH groups should entail a dominant $\sigma-\pi$ mechanism and hence a positive sign.

*^{5}J(CH_3,SH) in 2-methyl-4-*tert*-butylthiophenol, 2*

To within experimental error, ^{4}J(H,SH) and ^{5}J(CH_3,SH) are equal and opposite in sign, as expected if ^{4}J(H,SH) is a $\sigma-\pi$ coupling and ^{5}J(CH_3,SH) is now also a $\sigma-\pi$ coupling, in contrast to the situation in **1**. In **2**, nonplanar SH conformations are predominant, in contrast to **1**, and $\langle \sin^2 \theta \rangle$ is 0.43 because ^{4}J(H,SH) is -1.1 Hz at $\theta = 90°$ (4, 5). Consequently, it is a poor approximation to employ ^{5}J(H,SH) in the estimation of an equilibrium between planar conformations, as was done for **1** above. For nonplanar conformations, ^{5}J(H,SH) has a significant $\sigma-\pi$ component (5), varying as $\sin^2 \theta$, while the σ component varies as $\sin^2 (\theta/2)$. Hence ^{5}J(H-5,SH) may be appreciable in **2** (it is 0.29 Hz compared to 0.42 Hz for ^{5}J(H-3,SH)) without the necessity for a significant population of type **1***c*.

The STO 3G MO computations on 2-methylthiophenol, when corrected for the fact that they overestimate the twofold barrier in thiophenol by about 10 kJ/mol (4), imply that the SH group spends only 10% of its time in conformations characterized by $120° < \theta < 180°$. Consequently, the negative proximate component of ^{5}J(CH_3,SH) will be small.

On the other hand, the conformation with $\theta = 0°$ is of lowest energy and the computed coupling at this angle is 0.21 Hz (see previous section). Therefore it is difficult to disentangle the components of ^{5}J(CH_3,SH) in **2** and its observed equality in magnitude with ^{4}J(H,SH) must be regarded as a coincidence. Nevertheless, the large magnitude of the coupling strongly suggests a major $\sigma-\pi$ component and is compatible with the large out-of-plane excursions of the SH bond predicted by the MO results.

Acknowledgements

We are grateful to Kirk Marat for advice on spectral data accumulations and for the maintenance of the AM300, and to the Natural Sciences and Engineering Research Council of Canada for essential financial assistance.

1. W. J. E. PARR and T. SCHAEFER. J. Magn. Reson. **25**, 171 (1977).
2. T. SCHAEFER and W. J. E. PARR. Can. J. Chem. **55**, 552 (1977).
3. T. SCHAEFER and W. J. E. PARR. Can. J. Chem. **57**, 1421 (1979).
4. T. SCHAEFER, T. A. WILDMAN, and S. R. SALMAN. J. Am. Chem. Soc. **102**, 107 (1980).
5. T. SCHAEFER and T. A. WILDMAN. Chem. Phys. Lett. **80**, 280 (1981).
6. T. SCHAEFER, T. A. WILDMAN, and R. SEBASTIAN. Can. J. Chem. **60**, 1924 (1982).
7. R. A. HOFFMAN. Mol. Phys. **1**, 326 (1958).
8. C. J. MACDONALD and W. F. REYNOLDS. Can. J. Chem. **48**, 1002 (1970).
9. J. B. ROWBOTHAM and T. SCHAEFER. Can. J. Chem. **52**, 489 (1974).
10. M. P. WILLIAMSON, R. KOSTELNIK, and S. M. CASTELLANO. J. Chem. Phys. **49**, 2218 (1968).
11. M. BARFIELD and M. KARPLUS. J. Am. Chem. Soc. **91**, 1 (1969).
12. H. A. GAUR, J. VRIEND, and W. G. B. HUYSMANS. Tetrahedron Lett. 1999 (1969).
13. T. SCHAEFER and R. LAATIKAINEN. Can. J. Chem. **61**, 224 (1983).
14. T. SCHAEFER, T. A. WILDMAN, and J. PEELING. J. Magn. Reson. **56**, 144 (1984).
15. R. WASYLISHEN and T. SCHAEFER. Can. J. Chem. **50**, 1852 (1972).
16. T. SCHAEFER and R. SEBASTIAN. J. Magn. Reson. **41**, 395 (1980).

17. G. KOTOWYCZ and T. SCHAEFER. Can. J. Chem. **44**, 2743 (1966).
18. W. J. HEHRE, R. F. STEWART, and J. A. POPLE. J. Chem. Phys. **51**, 2657 (1969).
19. M. R. PETERSEN and R. A. POIRIER. MONSTERGAUSS, Department of Chemistry, University of Toronto, Toronto, Ontario, 1981.
20. J. A. POPLE, J. W. MCIVER, and N. S. OSTLUND. J. Chem. Phys. **49**, 2960 (1968).
21. P. DOBOSH and N. S. OSTLUND. QCPE, **11**, 281 (1975).
22. S. M. CASTELLANO and A. A. BOTHNER-BY. J. Chem. Phys. **41**, 3863 (1964).
23. C. W. HAIGH. Annu. Rep. Nucl. Magn. Reson. Spectrosc. **4**, 311 (1971).
24. W. J. E. PARR and T. SCHAEFER. Acc. Chem. Res. **13**, 400 (1980).

Branched-chain sugars in asymmetric synthesis. Total synthesis of marine antibiotic (−)-malyngolide

PAK-TSUN HO[1] AND SIMMIE WONG

Guelph–Waterloo Centre for Graduate Work in Chemistry, University of Waterloo, Waterloo, Ont., Canada N2L 3G1

Received October 25, 1984

PAK-TSUN HO and SIMMIE WONG. Can. J. Chem. **63**, 2221 (1985).

Marine antibiotic (−)-malyngolide has been stereospecifically synthesized in about 25% overall yield from 2,3-*O*-isopropylidene-D-apiose, easily prepared from D-mannose.

PAK-TSUN HO et SIMMIE WONG. Can. J. Chem. **63**, 2221 (1985).

Utilisant comme produit de départ l'*O*-isopropylidène-2,3-D-apiose que l'on peut facilement préparer à partir du D-mannose, on a réalisé une synthèse stéréospécifique (rendement global de 25%) de l'antibiotique marin, (−)-malyngolide.

[Traduit par le journal]

Marine antibiotic (−)-malyngolide **1**, which was isolated in 1979 by Moore and co-workers (1) from a variety of the alga *Lyngbya majuscula*, exhibits significant activity against *Mycobacterium smegmatis* and *Streptococcus pyogenes* (2). A number of syntheses of malyngolide have been recently recorded (3), since its structure determination was reported (1).

In connection with our interest in the use of branched-chain sugars as chiral synthons for the asymmetric synthesis of natural products (4), we consider that the configuration at C-5 of (−)-malyngolide is derived from a C-3-hydroxymethyl branched-chain sugar as illustrated by the analysis in Scheme 1. Thus, bond disconnection at C-2 and C-3 of (−)-malyngolide generates a D-apiose derivative. Our synthesis started with D-mannose and converged to 2-*C*-(hydroxymethyl)-2,3-*O*-isopropylidene-D-mannofuranose **2**, which has been prepared by a one-step methodology developed in our laboratory (5). Transformation of **2** to 2,3-*O*-isopropylidene-D-apiose **3** has been accomplished in a simple one-pot operation in excellent yield (6).

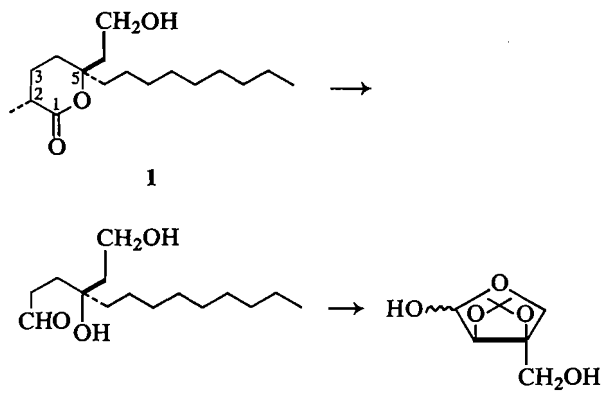

1

3

SCHEME 1

Reaction of compound **3** with tosyl chloride (1 equiv.) in dichloromethane in the presence of pyridine at 5°C gave the crystalline tosylate **4** in quantitative yield, mp 104°C. Treatment of compound **4** with *p*-toluenesulfonic acid (20% by weight) in anhydrous methanol at refluxing temperature for $2\frac{1}{2}$ days, followed by addition of methanolic potassium hydroxide to pH 10 at ice temperature, led to the formation of the epoxide **5** in 80% yield after chromatographic purification. The proton nuclear magnetic resonance spectrum of the substance fully corroborated the structural assignment (see experimental section).

The stage was set for the attachment of the hydrocarbon side chain by a cuprous iodide catalyzed Grignard reaction. Reaction of the epoxide **5** with octylmagnesium bromide (2.5 equiv.) in the presence of 10% cuprous iodide in tetrahydrofuran at −40°C afforded quantitatively the tertiary alcohol **6**. The use of tetrahydrofuran as the solvent for this reaction is essential. Any other solvent, such as diethyl ether or DME, used for this reaction gave either extremely low yield or no formation of the desired product.

Completion of the synthesis of the marine antibiotic required removal of the hydroxyl function at the C-2 carbon of compound **6**. Conversion of the diol **6** to compound **7** was accomplished in 89% overall yield by standard procedures, acetylation of the secondary alcohol (acetic anhydride, pyridine, room temperature), formation of the methylthiomethyl ether (acetic anhydride, dimethyl sulfoxide, room temperature), and generation of the secondary alcohol by mild alkali hydrolysis. Thiocarbonylation of compound **7** with thiocarbonyl diimidazole in tetrahydrofuran at 60°C afforded the thiocarbonate **8**. When this material was allowed to react with excess of tri-n-butyltin hydride (2 equiv.) in benzene in the presence of a catalytic amount of radical initiator α,α′-azobisisobutyronitrile at refluxing temperature, the deoxygenated product **9** was smoothly formed in 82% yield (7). Exposure of compound **9** to acidic conditions (in aqueous hydrochloric acid, acetone) resulted in the isolation of the desired furanose derivative **10** in 75% yield after purification.

Further elaboration of the cyclic hemiacetal **10** was accomplished in the following way. Wittig reaction of **10** with carbethoxyethylidene triphenylphosphorane (2 equiv.) in acetonitrile at 50°C yielded presumably the *trans* isomer **11** as the sole product in 72% yield. Its proton nuclear magnetic resonance spectrum shows a broad triplet (J = 10 Hz) at δ 6.97, a doublet (J = 10 Hz) at δ 2.40, and a broad singlet at δ 1.87. These values are in agreement with the assigned structure. The unsaturated ester was hydrogenated in quantitative yield to a diastereoisomeric mixture of the esters **12** in a ratio of 1:1 based on steric reasoning and its proton nuclear magnetic resonance spectrum and these two isomers were not separated at this stage. The corresponding acids **13** were obtained quantitatively by reaction of compunds **12** with potassium hydroxide in aqueous methanol at room temperature. Finally, the acids **13**, on treatment with either dicyclohexylcarbodiimide and

[1]Author to whom correspondence may be addressed at: Penninsula Laboratories Inc., 611 Taylor Way, Belmont, CA 94002, U.S.A.

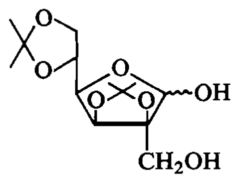

2

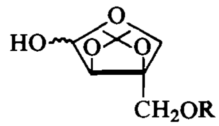

3 R = H
4 R = Ts

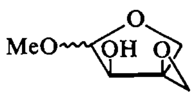

5

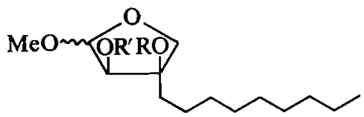

6 R′ = R = H
7 R′ = H, R = CH_2SMe
8 R′ = C(=S)—Im, R = CH_2SMe

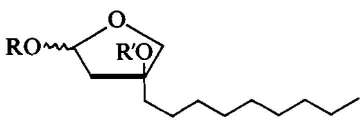

9 R = Me, R′ = CH_2SMe
10 R = R′ = H

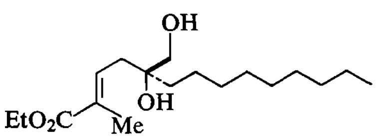

11

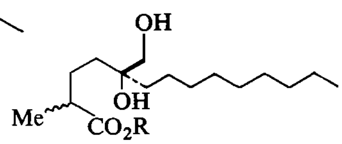

12 R = Et
13 R = H

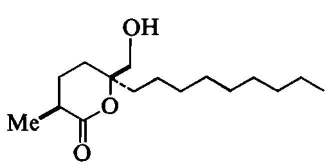

14

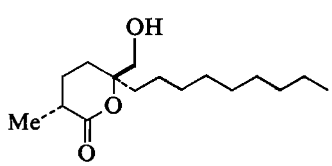

1

pyridine in benzene at room temperature (8), or dipyridyl disulfide and triphenylphosphine in benzene at room temperature (9), were converted in 90% yield to the epimeric lactones **14** and **1**, easily separable by chromatography on silica gel (5% acetone in hexane and dichloromethane). The proton nuclear magnetic resonance spectrum of the lactone **1** exhibits a pair of doublets (J = 12 Hz) at δ 3.7 and δ 3.47 ppm for the isolated hydroxymethyl and is completely identical with the spectrum reported for the naturally occurring (−)-malyngolide, $[\alpha]_D$ −12.8° (c 0.8, chloroform) (lit. (1) $[\alpha]_D$ −13° (c 2, chloroform)). Compound **14**, which is (+)-epimalyngolide, shows a broad singlet at δ 3.61 ppm for the methylene of the isolated primary alcohol in its proton nuclear magnetic resonance spectrum and exhibits a specific rotation of $[\alpha]_D$ +17.6° (c 1.1, chloroform) (lit. (3) $[\alpha]_D$ +17°). The epimalyngolide, on treatment with potassium *tert*-butoxide in dimethylsulfoxide (3), has been easily epimerized to the natural (−)-malyngolide. Thus, the synthesis of (−)-malyngolide was stereospecific.

Experimental

General

Melting points were determined on a Reichert hot stage apparatus and are uncorrected. Optical rotations were determined by a Karl–Zeiss model LEP 370740 polarimeter at 546 and 578 nm at room temperature. Infrared spectra were recorded on a Beckmann model IR-10 spectrometer using chloroform as solvent. Proton nuclear magnetic resonance (^{1}H nmr) spectra were measured with Bruker spectrometers, models WP-80 or WH-400, using deuteriochloroform with tetramethylsilane as internal standard unless otherwise specified. Thin layer and preparative layer chromatography were done using silica gel containing fluorescent indicator (G_{254}).

Tosylation of 2,3-O-isopropylidene-D-apiose 3

To a stirred solution of compound **3** (13.7 g, 7.2 mmol) and anhydrous pyridine (27 mL, 21.6 mmol) in anhydrous dichloromethane (150 mL) at 5°C, tosyl chloride (14.8 g, 7.8 mmol) was added. The mixture was left overnight at the same temperature, after which time the mixture was diluted with diethyl ether (300 mL). A standard work-up gave the crystalline tosylate **4** in quantitative yield, mp 104°C; $[\alpha]_D$ −43° (c 2.0, chloroform); ir (chloroform): 3500 (hydroxyl) cm^{-1}; ^{1}H nmr δ: 7.81 and 7.35 (2d, 4H, aromatic protons), 5.34 (s, 1H, C-1 proton), 4.30 (s, 1H, C-2 proton), 4.22 (s, 2H, C-4 protons), 3.93 (s, 2H, C-3′ protons), 2.44 (s, 3H, methyl), 1.3 and 1.40 (2s, 6H, 2 methyls). *Anal.* calcd. for $C_{15}H_{20}O_7S$: C 52.31, H 5.86; found: C 52.26, H 5.92.

Preparation of the epoxide 5

A solution of compound **4** (17.3 g, 50.3 mmol) and *p*-toluenesulfonic acid (3.4 g, 20% by weight) in anhydrous methanol (500 mL) was refluxed for 2½ days. The reaction mixture was then cooled to 0°C and methanolic potassium hydroxide was added until the solution became pH 10. The mixture was stirred at room temperature for 2 h, after which time it was carefully neutralized with *p*-toluenesulfonic acid. Removal of the white precipitates and evaporation of the solvent gave a residue. Flash chromatography of the crude product on silica gel using 10% diethyl ether in chloroform as solvent afforded the epoxide **5** (5.88 g, 80%) as a homogeneous syrup, $[\alpha]_D$ −95° (c 1.13, chloroform); ir (chloroform): 3500 (hydroxyl) cm^{-1}; ^{1}H nmr δ: 4.97 (s, 1H, C-1 proton), 4.06 (q, 2H, J = 13 Hz, C-4 protons), 3.94 (s, 1H, C-2 proton), 3.41 (s, 3H, methoxyl), 3.06 (dd, 2H, J = 8 Hz, epoxide). *Anal.* calcd. for $C_6H_{10}O_4$: C 49.31, H 6.89; found: C 49.36, H 6.87.

Preparation of compound 6

Cuprous iodide (0.1 g, 0.51 mmol) was added to the well-stirred Grignard reagent prepared from octyl bromide (0.99 g, 5.14 mmol) and magnesium metal (0.13 g, 5.15 mmol) in 20 mL of dry tetrahydrofuran at −40°C under argon. The mixture was stirred at the same temperature for 2 h and the solution of compound **5** (0.3 g, 2.05 mmol) in 10 mL of tetrahydrofuran was added dropwise over a period of 30 min. The resulting yellow solution was warmed up to room temperature and stirred for 15 min. Saturated aqueous ammonium chloride and ether were added successively and the layers were separated. The aqueous layer was extracted with ether and the combined extracts were washed with saturated aqueous ammonium chloride and dried over anhydrous magnesium sulfate. Removal of the solvent provided an oil which was purified by flash chromatography on silica gel to give the desired product **6** in quantitative yield; $[\alpha]_D$ −74° (c 1.18, chloroform); ir (chloroform): 3500 (hydroxyl) cm^{-1}; ^{1}H nmr δ: 4.85 (s, 1H, C-1 proton), 3.95 (s, 1H, C-2 proton), 3.85 (s, 2H, C-4 proton), 1.25 (m, 16H, methylene protons), 0.88 (t, 3H, methyl). *Anal.* calcd. for $C_{14}H_{28}O_4$: C 64.58, H 10.84; found: C 64.59, H 10.82.

Preparation of the hydroxyl methylthiomethyl ether 7

Acetylation of compound **6** (1.12 g, 4.55 mmol) under standard conditions gave the hydroxyl acetate in quantitative yield; ^{1}H nmr δ: 4.90 (s, 2H, C-1 and C-2 protons), 3.86 (s, 2H, C-4 protons), 3.37

(s, 3H, methoxyl), 2.13 (s, 3H, acetate), 1.25 (m, 16H, methylene protons), 0.88 (t, 3H, methyl).

The hydroxyl acetate was mixed with dimethyl sulfoxide (5 mL) and acetic anhydride (5 mL). The mixture was stirred at room temperature for 3 days, after which time removal of the solvents under vacuum gave an oily material. This material was dissolved in 10% aqueous methanol (5 mL), followed by the addition of potassium carbonate (0.25 g). The solution was stirred at room temperature for 5 h and 10 mL of water was added. The reaction mixture was extracted with ether (3 × 4.0 mL) and the combined extracts were washed with brine water, dried over anhydrous magnesium sulfate, and concentrated to a syrup. Chromatography of the crude product **7** on silica gel yielded a pure product **7** (1.23 g, 89%); $[\alpha]_D$ −57° (*c* 1.3, chloroform); ir (chloroform): 3500 (hydroxyl) cm^{-1}; ^{1}H nmr δ: 4.84 (broad s, 1H, C-1 proton), 4.64 (s, 2H, —O—CH$_2$—S—), 3.96 (dd, 2H, *J* = 16 Hz, C-4 protons), 3.85 (br s, 1H, C-2 proton), 3.37 (s, 3H, methoxyl), 2.17 (s, 3H, methyl), 1.25 (m, 16H, methylene protons), 0.88 (t, 3H, methyl). *Anal.* calcd. for $C_{16}H_{32}O_4S$: C 59.94, H 10.10; found: C 59.90, H 10.18.

*Thiocarbonylation of compound **7** to compound **8***

Compound **7** (1.07 g, 3.5 mmol) and 1,1′-thiocarbonyl diimidazole (0.75 g, 7 mmol) were dissolved in 20 mL of anhydrous tetrahydrofuran. The solution was heated under reflux for 1 h, after which time removal of the solvent gave a yellow residue. Flash chromatography of the yellow material on silica gel using 5% diethyl ether in dichloromethane as solvent yielded compound **8** (1.27 g, 87%) as a homogeneous syrup, $[\alpha]_D$ −24° (*c* 1.8, chloroform); ^{1}H nmr δ: 7.33 (br s, 1H, imidazole proton), 7.10 (br s, 1H, imidazole proton), 5.73 (s, 1H, C-2 protons), 5.10 (s, 1H, C-1 proton), 4.58 (s, 2H, —O—CH$_2$—S—), 4.15 (dd, 2H, *J* = 16 Hz, C-4 protons), 3.37 (s, 3H, methoxyl), 2.17 (s, 3H, methyl), 1.25 (m, 16H, methylene protons), 0.88 (t, 3H, methyl). *Anal.* calcd. for $C_{20}H_{34}O_4S_2N_2$: C 55.79, H 7.97; found: C 55.68, H 7.92.

*Deoxygenation of compound **8** to compound **9***

To a hot (80°C) stirred solution of tri-*n*-butyltin hydride (0.25 mL, 1.02 mmol) and a catalytic amount of α,α′-azobisisobutyronitrile in anhydrous benzene (5 mL) under an atmosphere of argon was added dropwise a solution of the thiocarbonate **8** (0.282 g, 0.68 mmol) in 20 mL of anhydrous benzene. The solution was stirred under reflux for additional $\frac{1}{2}$ h and concentrated under vacuum to an oily material. The crude product was purified by flash chromatography on silica gel using 5% ethyl acetate in hexane as eluant to afford the desired product **9** (0.181 g, 82%) as a homogeneous syrup; $[\alpha]_D$ −56.5° (*c* 1.2, chloroform); ^{1}H nmr δ: 5.07 (m, 1H, C-1 proton), 4.47 (s, 2H, —O—CH$_2$—S—), 3.86 (dd, 2H, *J* = 14 Hz, C-4 protons), 3.37 (s, 3H, methoxyl), 2.17 (s, 3H, methyl), 1.87 (m, 2H, C-2 protons), 1.25 (m, 16H, methylene protons), 0.88 (t, 3H, methyl). *Anal.* calcd. for $C_{16}H_{32}O_3S$: C 63.12, H 10.60; found: C 63.11, H 10.63.

*Hydrolysis of compound **9** to furanose derivative **10***

A solution of compound **9** (0.2 g, 0.69 mmol) in 5 mL of 1 *N* aqueous hydrochloric acid and 8 mL of acetone was stirred at 70°C for $2\frac{1}{2}$ h. The reaction mixture was neutralized with aqueous sodium bicarbonate to pH 7. Removal of the solvent gave a residue which was extracted with dichloromethane. The combined extracts were dried over anhydrous magnesium sulfate and concentrated to a syrup. Chromatography of the syrup on silica gel using 3% methanol, 27% ether, and 70% dichloromethane as eluant yielded the desired product **10** as a homogeneous syrup (0.113 g, 75%); $[\alpha]_D$ +21° (*c* 1.0, chloroform); ir (chloroform): 3550−3480 (hydroxyl) cm^{-1}; ^{1}H nmr δ: 5.43 (br t, 1H, C-1 proton), 3.82 (dd, 2H, *J* = 18 Hz, C-4 protons), 2.00 (br m, 2H, C-2 protons), 1.25 (m, 16H, methylene protons), 0.88 (br t, 3H, methyl). *Anal.* calcd. for $C_{13}H_{26}O_3$: C 67.79, H 11.38; found: C 67.73, H 11.29.

*Preparation of the hydroxyl unsaturated ester **11***

A solution of compound **10** (87 mg, 0.38 mmol) and carboethoxyethylidene triphenylphosphorane (274 mg, 0.76 mmol) in 5 mL of anhydrous acetonitrile was stirred at 50°C under argon for $2\frac{1}{2}$ h. After removal of the solvent, flash chromatography of the crude product on silica gel using 10% acetone in chloroform as eluant afforded the pure unsaturated ester **11** (85 mg, 72%) as a homogeneous syrup; $[\alpha]_D$ −2.5° (*c* 1.0, chloroform); ir (chloroform): 3500−3300 (hydroxyl), 1720 (unsaturated ester) cm^{-1}; ^{1}H nmr δ: 6.97 (br t, 1H, *J* = 10 Hz, vinyl proton), 4.27 (dd, 2H, *J* = 8 Hz, —CH$_2$—O—CO—), 3.53 (s, 2H, hydroxymethylene), 2.40 (d, 2H, *J* = 10 Hz, allylic protons), 1.87 (br s, 3H, methyl), 1.25 (m, 16H, methylene protons), 0.88 (t, 3H, methyl). *Anal.* calcd. for $C_{18}H_{34}O_4$: C 68.74, H 10.91; found: C 68.72, H 10.93.

*Hydrogenation of compound **11** to the saturated esters **12***

A solution of compound **11** (76 mg, 0.24 mmol) in 6 mL of ethanol in the presence of 10% palladium on activated carbon (10 mg) was hydrogenated at atmospheric pressure for 3 h. Removal of the catalyst and solvent yielded a pair of the diastereoisomeric esters **12** in quantitative yield; ir (chloroform): 3500−3300 (hydroxyl), 1731 (ester) cm^{-1}; ^{1}H nmr δ: 4.13 (q, 2H, *J* = 8 Hz, —CH$_2$—O—CO—), 3.40 (br s, 2H, hydroxymethylene), 1.25 (m, 19H, methylene and methyl), 0.88 (t, 3H, methyl). *Anal.* calcd. for $C_{18}H_{36}O_4$: C 68.31, H 11.47; found: C 68.39, H 11.44.

*Formation of the hydroxyl carboxylic acid **13***

The ester **12** (68 mg, 0.22 mmol) was hydrolyzed in 50% aqueous methanol (5 mL) with potassium hydroxide (0.3 g) at room temperature for 3 h. The solution was then acidified to pH 3 with aqueous hydrochloric acid and extracted with dichloromethane (3 × 10 mL). The combined extracts were dried over anhydrous magnesium sulfate and removal of the solvent afforded the desired product **13** in quantitative yield; ir (chloroform): 3500−2500 and 1710 (carboxylic acid) cm^{-1}; ^{1}H nmr δ: 3.47 (br s, 2H, hydroxymethylene), 1.25 (m, 23 H, methylene and methyl), 0.88 (t, 3H, methyl). *Anal.* calcd. for $C_{16}H_{32}O_4$: C 66.61, H 11.20; found: C 66.58, H 11.12.

*Preparation of (−)-malyngolide **1** and (+)-epimalyngolide **14***

(a) A solution of compound **13** (56 mg, 0.20 mmol), triphenylphosphine (79 mg, 0.3 mmol), and 2,2′-dipyridyldisulfide (66 mg, 0.3 mmol) in benzene (3 mL) was stirred at room temperature for 3 h. Removal of the solvent gave the epimeric lactones (ratio 1:1), which were separated with preparative tlc on silica gel using 5% acetone in hexane and dichloromethane (50:50) as solvent to yield (−)-malyngolide **1** and its epimeric lactone **14** (52 mg, 90%).

(b) When a solution of compound **13** (56 mg, 0.20 mmol), dicyclohexylcarbodiimide (62 mg, 0.3 mmol), and pyridine (32 mg, 0.4 mmol) in 3 mL of anhydrous benzene was stirred at room temperature overnight, a similar result was obtained.

(−)-Malyngolide exhibited infrared and ^{1}H nmr spectra identical with those of the natural product; $[\alpha]_D$ −12.8° (*c* 0.8, chloroform); ir (chloroform): 3500−3400 (hydroxyl), 1731 (lactone) cm^{-1}; ^{1}H nmr δ: 3.71 and 3.47 (2d, 2H, *J* = 12 Hz, hydroxymethylene), 2.41 (m, 1H, —*CH*—CO—), 2.20−1.45 (m, 4H, methylene protons), 1.25 (m, 19H, methylene and methyl), 0.88 (t, 3H, methyl). *Anal.* calcd. for $C_{16}H_{30}O_3$: C 71.07, H 11.18; found: C 71.01, H 11.26. (+)-Epimalyngolide: $[\alpha]_D$ +17.5° (*c* 1.1, chloroform); ir (chloroform): 3500−3400 (hydroxyl), 1731 (lactone) cm^{-1}; ^{1}H nmr δ: 3.60 (s, 2H, hydroxymethylene), 2.45 (m, 1H, —*CH*—CO—), 2.10−1.45 (m, 4H, methylene protons), 1.25 (m, 19H, methylene and methyl), 0.86 (t, 3H, methyl). *Anal.* calcd. for $C_{16}H_{30}O_3$: C 71.07, H 11.18; found: C 70.98, H 11.09.

Acknowledgments

We thank the Natural Sciences and Engineering Research Council of Canada for financial support of this work, and Dr. P. Sinay for sending us various spectra of synthetic and natural malyngolide for comparison.

1. J. H. Cardllina II, R. E. Moore, E. V. Arnold, and J. Clardy. J. Org. Chem. **44**, 4039 (1979).

2. T. J. STARR, E. F. DIEG, K. K. CHURCH, and M. B. ALLEN. Tex. Rep. Biol. Med. **20**, 271 (1962).
3. T. KOGURE and E. L. ELIEL. J. Org. Chem. **49**, 576 (1984), and references cited therein.
4. P. T. HO. Can. J. Chem. **58**, 858 (1980).
5. P. T. HO. Tetrahedron Lett. 1623 (1978).
6. P. T. HO. Can. J. Chem. **57**, 381 (1979).
7. (*a*) D. H. R. BARTON and W. B. MOTHERWELL. Pure Appl. Chem. **53**, 15 (1981); (*b*) J. R. RASMUSSEN, C. J. SLINGER, R. J. KORDISH, and D. D. NEWMAN-EVANS. J. Org. Chem. **46**, 4831 (1981).
8. R. B. WOODWARD, F. E. BADER, H. BICKEL, A. J. FREY, and R. W. KIERSTEAD. Tetrahedron, **2**, 1 (1958).
9. E. J. COREY and K. C. NICOLAOU. J. Am. Chem. Soc. **96**, 5614 (1974).

A nuclear magnetic resonance study of the equilibria and kinetics of the reaction of penicillamine with cystine and related disulfides

YVON THERIAULT AND DALLAS L. RABENSTEIN[1]

Department of Chemistry, University of Alberta, Edmonton, Alta., Canada T6G 2G2

Received October 29, 1984

YVON THERIAULT and DALLAS L. RABENSTEIN. Can. J. Chem. **63**, 2225 (1985).

The thiol/disulfide exchange reactions of penicillamine (PSH) with cystine and several related disulfides (RSSR) have been studied by ^{1}H nmr. The reactions take place in two steps:

$$PSH + RSSR \rightleftarrows PSSR + RSH$$
$$PSH + PSSR \rightleftarrows PSSP + RSH$$

The equilibria and kinetics of the reactions of PSH with cystine were characterized over the pH range 5–8, while the reactions with the disulfides of cysteamine, homocysteine, 2-mercaptoethanol, mercaptoacetic acid, 3-mercaptopropionic acid, and mercaptosuccinic acid were studied at neutral pH. From the pH dependence of the rate of the reaction of PSH with cystine, the reactive species are identified as penicillamine with its amino group protonated and its thiol group deprotonated and cystine and penicillamine–cysteine mixed disulfide with their amino groups protonated. For all the disulfides studied, the extent to which the first reaction occurs is within a factor of 2–3 of that predicted by a random distribution, while the extent to which the second reaction occurs is considerably less than for a random distribution. This is attributed to steric effects due to the two methyl groups next to the sulfur of penicillamine.

YVON THERIAULT et DALLAS L. RABENSTEIN. Can. J. Chem. **63**, 2225 (1985).

Faisant appel à la rmn du ^{1}H, on a étudié les réactions d'échange thiol/disulfure de la pénicillamine (PSH) avec la cystéine et plusieurs disulfures (RSSR). Les réactions se produisent en deux étapes

$$PSH + RSSR \rightleftarrows PSSR + RSH$$
$$PSH + PSSR \rightleftarrows PSSP + RSH$$

On a caractérisé les équilibres et les cinétiques des réactions de la PSH avec la cystéine dans un intervalle de pH allant de 5 à 8 tandis qu'on a étudié les réactions avec les disulfures de la cystéamine, de l'homocystéine, du mercapto-2 éthanol, de l'acide mercaptoacétique, de l'acide mercapto-3 propionique et de l'acide mercaptosuccinique à des pH neutres. L'effet du pH sur la vitesse de réaction de la PSH avec la cystéine a permis d'identifier, comme espèces réactives, la pénicillamine avec son groupe amino protoné et son groupe thiol déprotoné ainsi que le disulfure mixte pénicillamine–cystéine avec leur groupe amino protoné. Pour tous les disulfures étudiés, une comparaison des taux de réactions observés avec les taux prévus en se basant sur une distribution au hasard indique que dans le cas de la première réaction le facteur est égal à 2–3 alors que pour la deuxième réaction, le taux est beaucoup plus faible que celui prévu sur cette base. On attribue ceci aux effets stériques des deux groupes méthyles présents au voisinage du soufre de la pénicillamine.

[Traduit par le journal]

Introduction

Penicillamine (PSH, **1**), is widely used in medicine (1, 2) for the treatment of cystinuria (3), Wilson's disease (4), heavy metal poisoning (5, 6), and rheumatoid arthritis (7–10). In the treatment of cystinuria, the mechanism of action is the reaction of penicillamine with relatively insoluble cystine[2] (CSSC, **2**) to form penicillamine–cysteine mixed disulfide (PSSC, **3**).

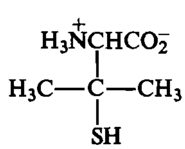

1

Because PSSC is somewhat more soluble than CSSC, treatment with penicillamine results in decreased formation of cystine stones in the kidneys of cystinuric patients (1, 3).

Penicillamine reacts with CSSC to form PSSC by the thiol/disulfide exchange reaction:

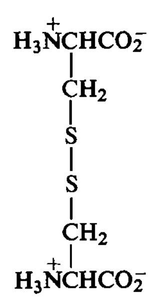

2

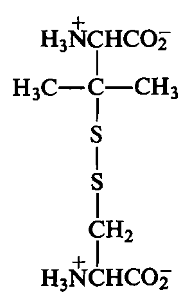

3

[1] $PSH + CSSC \rightleftarrows PSSC + CSH$

A second thiol/disulfide exchange can also take place, yielding the symmetrical disulfide PSSP.

[2] $PSH + PSSC \rightleftarrows PSSP + CSH$

These thiol/disulfide exchange reactions are important not only because they form the basis for the treatment of cystinuria with penicillamine, but also because they represent a major pathway by which penicillamine is metabolized in all patients who are given penicillamine (10).

In this paper, we report the results of a detailed study of the reaction of PSH with cystine and several related disul-

[1]Author to whom correspondence may be addressed at the Department of Chemistry, University of California–Riverside, Riverside, CA 92521, U.S.A.

[2]CSSC has a solubility of 2.8×10^{-4} *M* at pH 6.95 and 25°C (11).

fides. Equilibrium and kinetic data were obtained by ^1H nuclear magnetic resonance (nmr) spectroscopy over a wide pH range. Resolved resonances were obtained for the various penicillamine-containing species, making it possible to characterize separately the two steps in the thiol/disulfide exchange. From the pH dependence of the equilibrium and kinetic data, the reactive species are identified and pH independent equilibrium and rate constants are evaluated.

Experimental

D-Penicillamine and cysteine were obtained from Sigma Chemical Co. D-Penicillamine disulfide, 2-hydroxyethyldisulfide, cystamine, and cysteamine were obtained from Aldrich Chemical Co. Cystine and homocystine were from ICN Pharmaceuticals, and homocysteine was from Nutritional Biochemical Corp. For most experiments, the thiols and disulfides were used as received. In several experiments, solutions of penicillamine were electrolyzed over a Hg pool electrode (12) to reduce traces (<1%) of penicillamine disulfide.

The pH measurements were made at 25°C with a Fisher Accumet pH meter equipped with a standard glass electrode and a fiber-tipped, saturated calomel reference electrode, or a microcombination electrode. The ^1H nmr spectra were measured at 200 MHz and 25°C on a Bruker WH-200 nmr spectrometer operating in the pulse/Fourier transform mode. All nmr spectra were measured on aqueous solutions. To avoid the dynamic range problem, the water resonance was reduced in intensity by saturating it with a decoupler pulse applied at the water resonance frequency for 2 s prior to the observation pulse. The spectrometer was run in the unlocked mode. The ^1H chemical shifts were measured relative to the methyl resonance of *tert*-butanol (TBA) which was added to the solutions at a concentration of 0.001–0.01 *M*, depending on the thiol and disulfide concentrations. Chemical shifts are reported relative to the methyl resonance of sodium-2,2-dimethyl-2-silapentane-5-sulfonate (DSS). So that quantitative information could be obtained from resonance intensities, the repetition time was at least 5 times the longest T_1 of the methyl resonances of interest. T_1 values were measured by the inversion–recovery method.

Solutions were prepared in water which had been purified by distilling it twice and then passing it through a Barnstead D8902 Ultrapure mixed-bed ion exchange resin. KCl (1 *M*) and EDTA (0.003 *M*) were added for ionic strength control and to complex traces of heavy metals which would catalyze the air oxidation of thiols (13). The solvent mixture was deoxygenated by bubbling with argon or nitrogen before addition of thiol to minimize oxidation by dissolved oxygen. Inert gas was blown over the solution during adjustment of pH, and nmr tubes were flushed with gas before transfer of an aliquot of solution to the tube. For solutions which required more than several hours to come to equilibrium, the solution was degassed by taking it, in an nmr tube, through at least three freeze–pump–thaw cycles on a vacuum line. The nmr tube was then sealed while still on the vacuum line.

Results

Reaction of penicillamine with cystine

In Fig. 1 are shown ^1H nmr spectra of PSH (A), CSSC (B), CSH (D), and PSSP (E), and of a solution prepared from PSH and CSSC (C). The ^1H nmr spectrum of PSH consists of a singlet at 3.29 ppm from the methine proton on C_α, and two singlets at 1.27 and 1.55 ppm from the two methyl groups. The two methyl groups give two separate resonances due to the asymmetric carbon at C_α. The resonance at 1.2397 ppm in spectrum A is from TBA. The same assignment applies to the resonances in the spectrum of PSSP. The spectrum of CSH consists of an ABX pattern. The AB part is centered at 2.8 ppm and is from the two nonequivalent methylene protons on C_β, while the X part from the methine proton on C_α is centered at 3.50 ppm. The spectrum for CSSC also consists of an ABX pattern, and the assignment is the same.

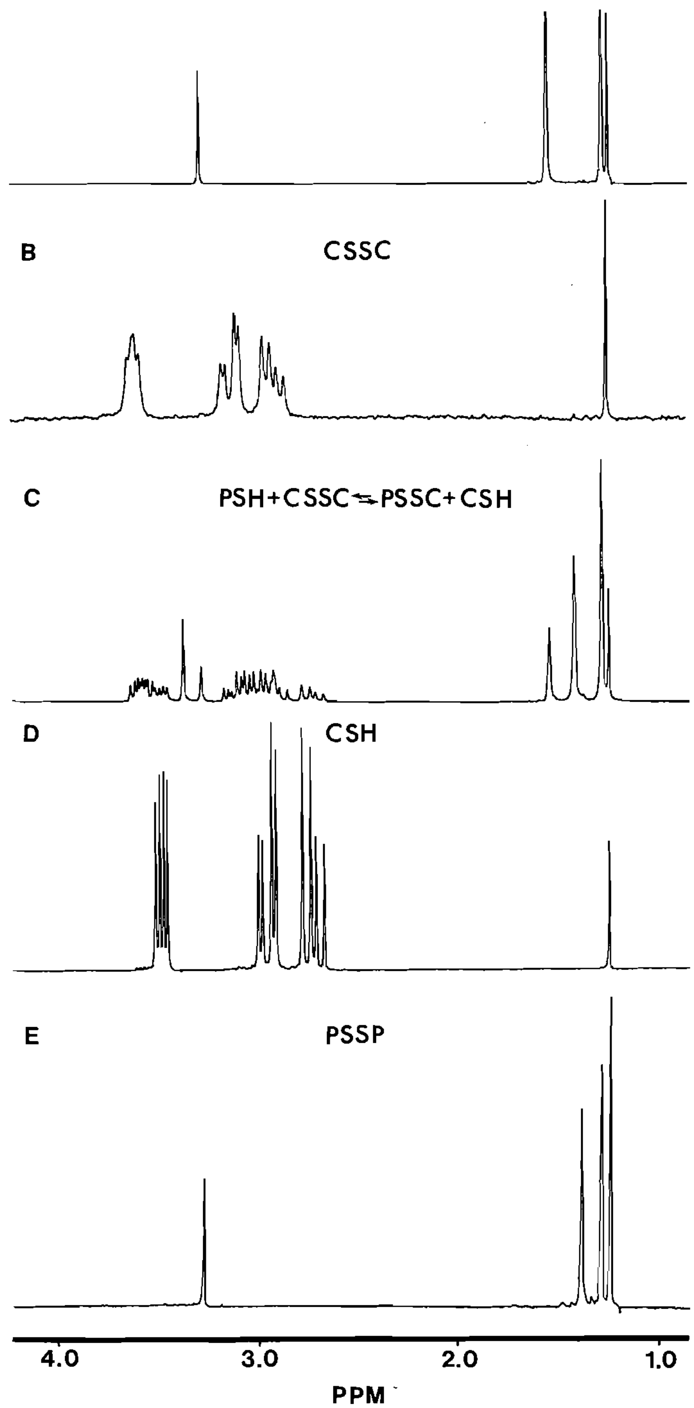

FIG. 1. The 200-MHz ^1H nmr spectra of (A) 0.20 *M* PSH, (B) 0.18 *M* CSSC, (C) a solution which contained initially 0.10 *M* PSH and 0.090 *M* CSSC, (D) 0.45 *M* CSH, and (E) 0.010 *M* PSSP at 23°C. All solutions were in D_2O and contained *tert*-butanol. pH = 10.0.

In spectrum C, there are resonances in addition to those from PSH and CSSC. These are assigned to PSSC and CSH, the products of the thiol/disulfide exchange reaction between PSH and CSSC. Under these solution conditions, there is negligible reaction of PSSC with PSH to form PSSP. There is considerable overlap of the resonances in the ABX patterns of CSH, CSSC, and PSSC. However, the singlet methine and methyl

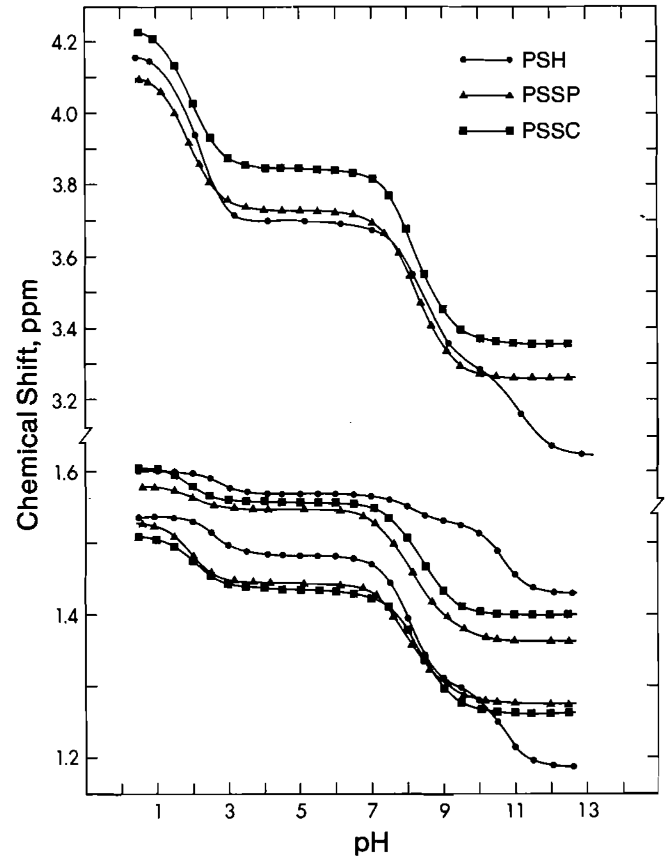

FIG. 2. Chemical shifts of the methine (top) and methyl (bottom) protons of PSH, PSSP, and the PSH part of PSSC as a function of pH.

resonances of PSH, PSSP, and PSSC are resolved over a wide pH range, as shown by the chemical shift data plotted in Fig. 2. The equilibria and kinetics of the thiol/disulfide exchange reactions were characterized using the methine and methyl resonances.

The reaction of PSH with CSSC takes place in two steps:

$$[3]\quad PSH_t + CSSC_t \underset{k_{2c}}{\overset{k_{1c}}{\rightleftarrows}} PSSC_t + CSH_t$$

$$[4]\quad PSH_t + PSSC_t \underset{k_{4c}}{\overset{k_{3c}}{\rightleftarrows}} PSSP_t + CSH_t$$

where PSH_t, $PSSC_t$, etc. represent the total concentrations of the various protonated forms of PSH, PSSC, etc., at a particular pH, and $k_{1c}-k_{4c}$ are conditional rate constants, i.e. rate constants for the thiol/disulfide exchange reactions for those conditions. The two stepwise reactions are described by the conditional equilibrium constants, K_{1c} and K_{2c}, which are defined as:

$$[5]\quad K_{1c} = \frac{[PSSC_t][CSH_t]}{[PSH_t][CSSC_t]}$$

$$[6]\quad K_{2c} = \frac{[PSSP_t][CSH_t]}{[PSH_t][PSSC_t]}$$

The conditional equilibrium constants were determined over a wide range of solution pH from the intensities of the methyl resonances in solutions prepared from PSH and CSSC. First, the concentrations of PSH, PSSC, and PSSP, if present, were calculated from the initial PSH concentration and the relative areas of the methyl resonances, and then the concentrations of

TABLE 1. Conditional equilibrium constants for penicillamine–cystine thiol/disulfide exchange reactions[a]

pH	[PSH][b] (mM)	[CSSC][b] (mM)	K_{1c}	K_{2c}
5.96	1.01	1.02	4.48	—
7.95	1.01	1.02	4.78	—
8.77	3.55	4.49	3.70	0.0279
8.93	5.07	3.00	5.08	0.0470
9.07	3.55	4.49	5.40	0.0544
9.46	3.55	4.49	5.57	0.0427
10.00	5.07	3.00	5.48	—
10.02	3.55	4.49	6.19	0.0423

[a]25°C; 1 M KCl; 0.003 M EDTA.
[b]Initial concentrations.

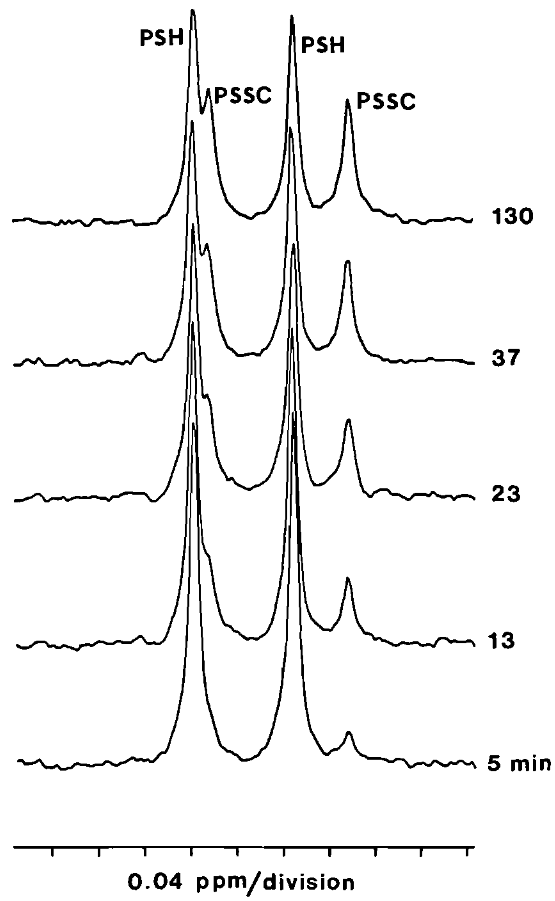

FIG. 3. The 200-MHz ^{1}H nmr spectra of the methyl groups in a solution which contained initially 0.00504 M PSH and 0.00297 M CSSC as a function of time. 1 M KCl, 0.003 M EDTA. pH = 5.94, 24°C.

CSH and CSSC were obtained by difference. To minimize air oxidation of thiol, the solutions were contained in nmr tubes which were degassed and sealed under vacuum. Spectra were obtained for each solution at intervals of 2–3 days until there were no further changes in resonance intensities. The concentrations of PSH and CSSC used and the conditional equilibrium constants obtained are given in Table 1. The conditional equilibrium constants for the reaction of PSH with CSSC at pH 7.4 and 37°C have also been estimated by Eldjarn and Hambraeus (15) using radioactive isotope tracer methods. They estimated K_{1c} to be 0.13 and K_{2c} to be ~0.01, both of which differ

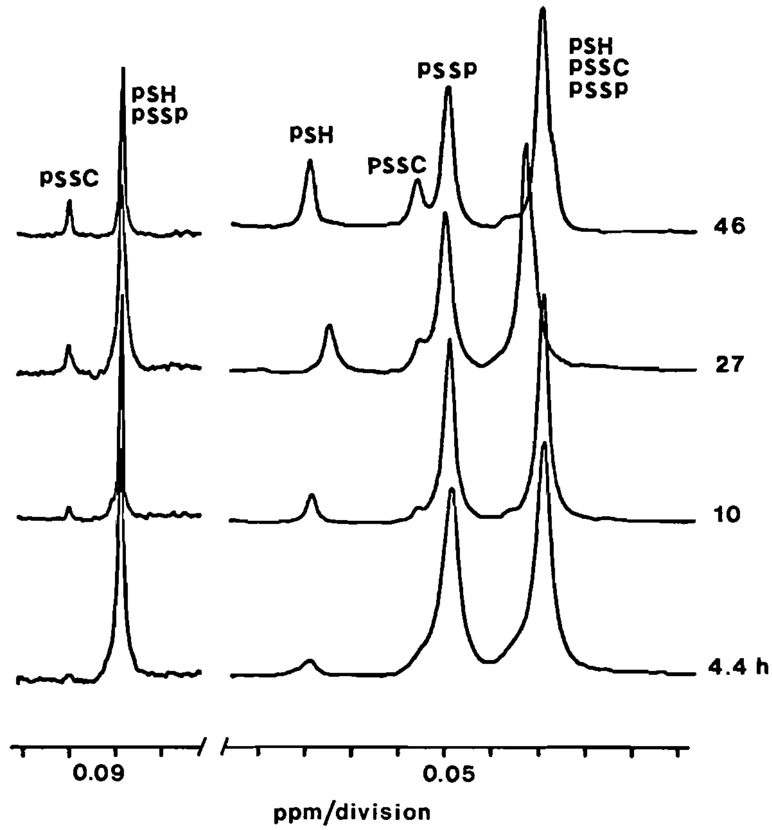

FIG. 4. The 200-MHz ^{1}H nmr spectra of the methine (left) and methyl (right) protons of PSH, PSSP, and PSSC in a solution which contained initially 0.102 M CSH and 0.100 M PSSP. The reaction was run at pH = 12.44, aliquots were quenched by lowering the pH to ~0.5, and then the pH was raised to ~9 when nmr spectra were run so that resolved resonances would be obtained for the various species. The pH was not identical for each nmr sample.

considerably from the values determined in the present work. The large differences may result from their experimental method which used radioactively-labelled cystine. Products of the reaction of PSH with labelled CSSC were separated by electrophoresis and then CSSC, PSSC, and CSH were determined by measuring the radioactivity. However, there was uncertainty in the results because CSSC and PSSC migrated together, and also the concentration of PSSP, which our work shows to be very small, had to be calculated by taking the difference between larger numbers of similar magnitude.

Spectra measured as a function of time in the equilibrium study indicate that the reaction of PSH with CSSC (eq. [3]) is much faster than the subsequent reaction of PSH with PSSC (eq. [4]). Thus, the kinetics of the two reactions were characterized separately. Figure 3 shows spectra obtained in a typical kinetics experiment. Rate constant k_{1c} was obtained by fitting time course data of this type by nonlinear least-squares calculations (14) to eq. [7], which is the integrated form of the rate expression for a second order, reversible reaction.

$$[7] \quad X = \frac{A_0B_0X_e\left(1 - \exp\left(\frac{k_{1c}t}{A}\right)\right)}{X_e(A_0 + B_0) - A_0B_0\left(1 + \exp\left(\frac{k_{1c}t}{A}\right)\right)}$$

where

$$[8] \quad A = \frac{X_e}{2A_0B_0 - X_e(A_0 + B_0)}$$

X and X_e are the concentrations of PSSC at time t and at equilibrium, and A_0 and B_0 are the initial concentrations of PSH and CSSC. k_{1c} and X_e were both treated as unknowns in the nonlinear least-squares calculations. The experimental conditions and the values obtained for k_{1c} from kinetic data covering the pH range 5–8 are given in Table 2.

TABLE 2. Conditional rate constants for the reaction of PSH with CSSC[a]

pH	$[PSH]_0$[b] (mM)	$[CSSC]_0$[b] (mM)	k_{1c}[c] (M^{-1} min^{-1})
5.07	3.02	1.98	1.22±0.16
5.89	5.04	1.12	7.75±0.37
5.94	5.04	2.97	8.35±0.33
6.72	5.04	1.12	46.2±3.7
6.93	3.02	1.98	97.2±4.6
8.05	2.00	2.00	465±130

[a]25°C; 1 M KCl; 0.003 M EDTA.
[b]Initial concentrations.
[c]Uncertainties are the linear estimate of the standard deviation from the nonlinear least-squares fits.

The rate of the reaction of CSH with PSSP is slow, and to bring it onto a time scale convenient for study a combination of high pH (pH 10–12) and high reactant concentrations was used. Typical time course data are shown in Fig. 4. The concentration of PSSC was obtained from the methine resonances while the concentration of PSH was obtained from the methyl resonances. The values obtained by the initial slope method for k_{4c} from time course data of this type are (pH, k_{4c}): 10.39, 0.0052 M^{-1} min^{-1}; 10.73, 0.0037 M^{-1} min^{-1}; 11.95, 0.0033

TABLE 3. Conditional equilibrium and rate constants for the reaction of penicillamine with selected disulfides at pH 7.4[a]

RSSR	pH[b]	K_{1c}	K_{2c}	K_{3c}	$\Delta E^{o\prime}$,[c] (V)	k_{1c},[d] (M^{-1} min^{-1})	k_{2c},[e] (M^{-1} min^{-1})
Cysteamine disulfide	7.4	1.78±0.10	0.031±0.006	0.0552	−0.0371	152±3	85.3
Homocysteine disulfide	7.0	1.24	0.033	0.0409	−0.0410	—	—
2-Mercaptoethanol disulfide	7.5	1.86±0.11	0.027±0.002	0.0502	−0.0383	12.2±0.9	6.56
Mercaptoacetic acid disulfide	7.4	2.49±0.05	—	—	—	43.6±3.2	17.1
3-Mercaptopropionic acid disulfide	7.4	1.40±0.19	0.027±0.003	0.0378	−0.0420	17.5±1.1	12.5
Mercaptosuccinic acid disulfide	7.4	2.04±0.23	0.025±0.004	0.0510	−0.0381	0.181±0.008	0.0886
Cystine[f]	7.4	4.66	0.024	0.116	−0.0281	210	40.9
Glutathione disulfide[g]	7.4	1.36	0.039	0.0530	−0.0376	36.6	26.9

[a]25°C; 1 M KCl; 0.003 M EDTA.
[b]pH at which K_{1c} and K_{2c} measured experimentally.
[c]$E^{o\prime}_{RSSR/RSH} - E^{o\prime}_{PSSP/PSH}$; eq. [17].
[d]Uncertainties are linear estimates of the standard deviations from the nonlinear least-squares fits.
[e]Calculated from K_{1c} and k_{1c}; $k_{2c} = k_{1c}/K_{1c}$.
[f]Values listed for K_{1c}, K_{2c}, and k_{1c} were calculated from pH-independent constants given in text.
[g]Reference 23.

M^{-1} min^{-1}; 12.44, 0.0029 M^{-1} min^{-1}. The initial concentrations of CSH and PSSP in the four experiments were 0.102 M and 0.100 M respectively.

Reaction of penicillamine with other disulfides

The conditional equilibrium constants K_{1c} and K_{2c} and the conditional rate constant k_{1c} were measured for the reaction of PSH with the disulfides of cysteamine (CySSCy), homocysteine (HSSH), 2-mercaptoethanol (ESSE), mercaptoacetic acid (MSSM), 3-mercaptopropionic acid (PrSSPr), and mercaptosuccinic acid (SuSSSu) at pH values in the pH range 7–8. The equilibrium data were obtained from solutions which were degassed in the nmr tube by the freeze–pump–thaw method and then the nmr tube was sealed. Spectra were measured at various times up to 200 h after mixing to ensure that the two thiol/disulfide exchange reactions had come to equilibrium. The conditional equilibrium constants at pH 7.4 calculated from the intensities of the methyl resonances by the methods described in the previous section are given in Table 3.

Conditional rate constant k_{1c} was also determined for these thiols by fitting the concentrations of the mixed disulfides, RSSP, as determined from the relative intensities of the methyl resonances for PSH and RSSP as a function of time, to eq. [7]. The reaction of PSH with RSSP is much slower than its reaction with RSSR, and the collection of kinetic data was stopped before detectable PSSP had formed. The k_{1c} values, and the values calculated for k_{2c} from k_{1c} and K_{1c}, at pH 7.4, are also given in Table 3.

Discussion

Thiol/disulfide exchange reactions proceed via the thiolate anion (11, 15–23). For PSH, there are two thiolate anion species possible: PS^-, in which the thiol group is deprotonated and the ammonium group protonated, and PS^{2-}, in which both groups are deprotonated. Both are present at low concentrations over the pH range 5–8; however, the dependence of their concentrations on pH is different. The logarithms of the fractional concentrations (α) of these two species, as calculated from pK_A values for PSH (24), are plotted as a function of pH over the pH range 5–8 in Fig. 5. The slope of the log α_{PS^-} vs. pH plot is one, over the pH range 5–7, while that of the log $\alpha_{PS^{2-}}$ vs. pH plot is two. Also plotted in Fig. 5 is log k_{1c} for the reaction of PSH with cystine (Table 2) vs. pH. The parallel dependence of log k_{1c} and log α_{PS^-} on pH indicates PS^- to be the reactive species.

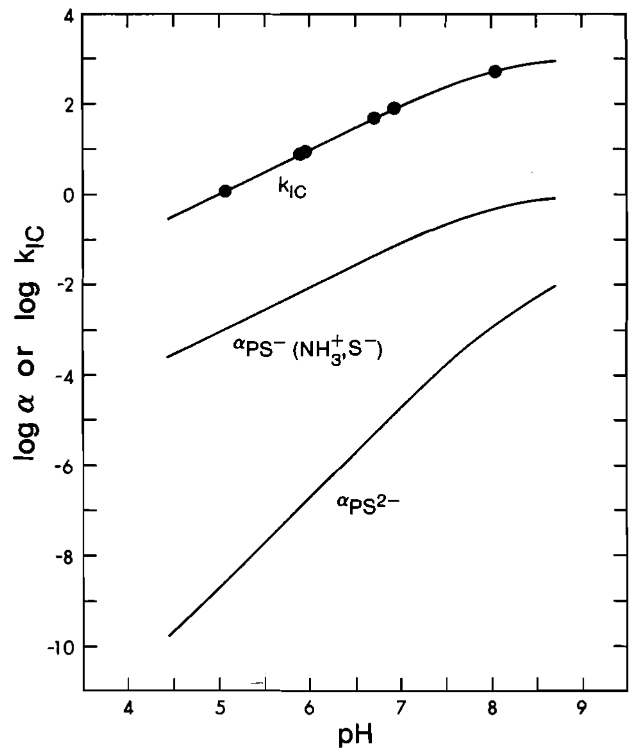

FIG. 5. The logarithm of the fractional concentration, α, of penicillamine in the amino-protonated, thiol-deprotonated (PS^-) and amino-deprotonated, thiol-deprotonated (PS^{2-}) forms and of the conditional rate constant k_{1c} for the reaction of PSH with CSSC as a function of pH. The solid curve through the experimental points is the theoretical curve predicted by a single pH-independent rate constant. See text for details.

The pH-independent rate constant for the reaction of PS^- with cystine is related to k_{1c} by eq. [9].

$$[9] \quad k_{1c} = k_1 \left(\frac{k_{a12} a_H}{a_H^2 + a_H K_{A2} + K_{A2} K_{A3}} \right)$$

where K_{A2} and K_{A3} are acid dissociation constants for PSH and a_H is activity of hydrogen as calculated directly from the pH meter reading. k_{a12} is the microscopic acid dissociation constant for the deprotonation of the thiol group of the PSH species in which both the amino and thiol groups are protonated (24). A value of 1090 ± 53 M^{-1} min^{-1} was obtained for k_1 by a nonlinear least-squares fit (14) of the data in Table 2 to eq. [9]. The straight line through the experimental data in Fig. 5 is the theoretical curve predicted by this value for k_1.

There is also the possibility that the rate constant depends on the protonation state of CSSC. However, the excellent agreement between the experimental data in Fig. 5 and the theoretical curve predicted by a single rate constant, k_1, indicates that either there is no dependence of k_{1c} on the protonation state of CSSC over the pH range 5–8 or the fractional concentration of the reactive CSSC species is constant over this pH range. The fractional concentration of the carboxylate-deprotonated, amino-protonated form, $CSSC^{\circ}$, varies from 1 to 0.4 over this pH range, while that of the species having only one amino group protonated, $CSSC^-$, varies from 0.001 to 0.6. The good fit of the experimental data in Fig. 5 to a single rate constant suggests that the rate constants for the reaction of PS^- with $CSSC^{\circ}$ and $CSSC^-$ are similar.

Assuming the reactive PSH species in the other thiol/disulfide exchange reactions to also be PS^-, pH-independent rate constants can be calculated using eq. [9]. The results are: CySSCy, k_1 = 800 ± 230 M^{-1} min^{-1}; ESSE, k_1 = 63.3 ± 3.0 M^{-1} min^{-1}; MSSM, k_1 = 230 ± 27 M^{-1} min^{-1}; PrSSPr, k_1 = 92 ± 6 M^{-1} min^{-1}; SuSSSu, k_1 = 0.95 ± 0.05 M^{-1} min^{-1}.

The equilibrium constants in Tables 1 and 3 are pH-dependent conditional equilibrium constants in terms of all the species present at the particular pH values. pH-independent equilibrium constants, K_1 and K_2, for the PSH–cystine thiol/disulfide exchange reactions in terms of the reactive species, eq. [10]–[13],

[10] $PS^- + CSSC^{\circ} \rightleftarrows PSSC^{\circ} + CS^-$

[11] $PS^- + PSSC^{\circ} \rightleftarrows PSSP^{\circ} + CS^-$

[12] $$K_1 = \frac{[PSSC^{\circ}][CS^-]}{[PS^-][CSSC^{\circ}]}$$

[13] $$K_2 = \frac{[PSSP^{\circ}][CS^-]}{[PSSC^{\circ}][PS^-]}$$

are related to the values for K_{1c} and K_{2c} by eqs. [14] and [15].

[14] $$K_1 = K_{1c}\frac{\alpha_1\alpha_2}{\alpha_3\alpha_4}$$

[15] $$K_2 = K_{2c}\frac{\alpha_2\alpha_5}{\alpha_1\alpha_3}$$

where α_1 is the fraction of $PSSC_t$ that is in the form $PSSC^{\circ}$, α_2 and α_3 the fractions of CSH_t and PSH_t that are in the amino-protonated, thiol-deprotonated forms, and α_4 and α_5 the fractions of $CSSC_t$ and $PSSP_t$, respectively, that are in the $CSSC^{\circ}$ and $PSSP^{\circ}$ forms. α_1–α_5 were calculated from the acid dissociation constants of the different species (25). Values of 5.36 ± 0.42 and 0.0198 ± 0.0028 were obtained for K_1 and K_2 by fitting the K_{1c} and K_{2c} values in Table 1 to eqs. [14] and [15]. pH-independent equilibrium constants for the reactions written in terms of all the reactants and products in their fully deprotonated forms can also be calculated from the results in Table 1. The values obtained are 12.0 ± 1.5 and 0.099 ± 0.012 for the first and second reactions, respectively.

The pH-independent equilibrium constants for the reactions written in terms of the reactive species cannot be calculated from the conditional equilibrium constants in Table 3 for the other disulfides studied because the acid dissociation constants of the various mixed disulfides are not known.

The equilibrium constant for the overall reaction of PSH with CSSC, K_3, is calculated to be 0.106 using the relation

[16] $2PS^- + CSSC^{\circ} \rightleftarrows PSSP^{\circ} + 2CS^-$

$K_3 = K_1K_2$. If the equilibrium positions in the two stepwise reactions were governed by random distribution, K_1 and K_2 would be 2 and 0.5, respectively, and K_3 would be 1. The values obtained for the analogous thiol/disulfide exchange reactions involving penicillamine and glutathione disulfide are K_1 = 0.56 ± 0.02, K_2 = 0.0143 ± 0.0014, and $K_3 = 8.0 \times 10^{-3}$ (23). For both systems, K_1 differs from the random distribution value of 2 by a factor of 2–3, although in opposite directions, whereas K_2 and K_3 are considerably less than the random distribution values. In contrast, K_1 = 1.27, K_2 = 0.27, and K_3 = 0.34 for the analogous thiol/disulfide exchange reactions involving cysteine and glutathione disulfide (20). These results, along with the values for K_{2c} in Table 3, indicate that PSH has considerably less tendency to react with its mixed disulfides to form the symmetrical disulfide PSSP than predicted by random distribution. As compared to cysteine, this is presumably due to steric effects from the replacement of the two hydrogens on the β carbon of cysteine by the two methyl groups of PSH. Similar steric effects have been reported previously for thiol/disulfide exchange reactions involving a series of alkyl thiols and disulfides (26), a series of substituted 2-aminoethane thiols and 4,4′-dithiobis(benzene sulfonate) (19) and glutathione reacting with a series of mercaptoalkane–cysteine mixed disulfides (27).

The values listed in Table 3 for the conditional equilibrium constant K_{1c} for the reaction of PSH with the eight disulfides are quite similar, as are the eight values for K_{2c}. However, the values for the conditional rate constant k_{1c} cover a wide range, with that for mercaptosuccinic acid disulfide a factor of approximately 1000 less than those for cystine and cysteamine disulfide. It is not possible to identify the factors which govern the rates of reaction from these results, although they do suggest that the total charge on the disulfide is important; mercaptosuccinic acid disulfide has a charge of −4 at pH 7.4, whereas the disulfides for which k_{1c} is in the intermediate range have total charges of −2 or 0 at this pH, and cystine and cysteamine disulfide have total charges of 0 and +2, respectively. Since the pH is the same, the reactive penicillamine species in each reaction is presumably the same, with a charge of −1.

The values in Table 3 for the overall equilibrium constant K_{3c} are related to the differences between the formal electrode potential $E^{\circ\prime}$ for the various RSSR/RSH redox couples and that of the PSSP/PSH couple according to eq. [17].

[17] $$\Delta E^{\circ\prime} = E^{\circ\prime}_{RSSR/RSH} - E^{\circ\prime}_{PSSP/PSH} = \frac{RT}{nF}\ln K_{3c}$$

Listed in Table 3 are the differences, $\Delta E^{\circ\prime}$, calculated from the values determined for K_{3c}. The values for $\Delta E^{\circ\prime}$ are all negative, indicating that the thiol forms of all seven molecules have slightly greater reducing power at physiological pH than does PSH. The small values for K_{2c} indicate that the smaller overall reducing power of PSH is due to its much smaller tendency to form its symmetrical disulfide. The values for $\Delta E^{\circ\prime}$ for the seven thiols are similar, indicating that they have similar reducing strength at physiological pH. However, for this to be the case, their intrinsic reducing strengths must increase in the order 3-mercaptopropionic acid > mercaptosuccinic acid > mercaptoethanol > glutathione > cysteamine ~ cysteine, i.e. the order in which the thiol pK_A values decrease (24), since the thiolate species is the active form in the reduction of disulfide by thiol.

Acknowledgements

This research was supported by the Natural Sciences and Engineering Research Council of Canada, the Alberta Heritage Foundation for Medical Research, and the University of Alberta. Financial support of Y.T. by an AHFMR Studentship is gratefully acknowledged.

1. J. C. CRAWHALL, D. LECAVALIER, and P. RYAN. Biopharm. Drug Dispos. **1**, 73 (1979).
2. W. L. LYLE and R. L. KLEINMAN (*Editors*). Penicillamine at 21: its place in therapeutics now. Proc. R. Soc. Med. **70**, Suppl. 3, 1977.
3. J. C. CRAWHALL, E. F. SCOWEN, and R. W. E. WATTS. Br. J. Med. **1**, 588 (1963).
4. J. M. WALSHE. Am. J. Med. **21**, 487 (1956).
5. A. GOLDBERG, J. A. SMITH, and A. LOCKHEAD. Br. J. Med. **1**, 1270 (1963).
6. J. T. MACGREGOR and T. W. CLARKSON. Adv. Exp. Med. Biol. **48**, 463 (1974).
7. F. M. ANDREWS, A. J. CAMP, A. T. DAY, A. M. FREEMAN, D. N. GOLDING, J. R. GOLDING, A. G. S. HILL, E. LEWIS-FANNING, and W. H. LYLE. Lancet, **1**, 275 (1973).
8. E. JELLUM and S. SKREDE. *In* Penicillamine research in rheumatoid disease. *Edited by* E. Munthe. Fabritius and Sonner, Oslo. 1976. p. 68.
9. E. MUNTHE (*Editor*). Penicillamine research in rheumatoid disease. Fabritius and Sonner, Oslo. 1976.
10. I. A. JAFFE. *In* Penicillamine research in rheumatoid disease. *Edited by* E. Munthe. Fabritius and Sonner, Oslo. 1976. p. 11.
11. I. M. KOLTHOFF, W. STRICKS, and R. C. KAPOOR. J. Am. Chem. Soc. **77**, 4733 (1955).
12. R. SAETRE and D. L. RABENSTEIN. Anal. Chem. **50**, 276 (1978).
13. J. F. ROESLER, J. LESLIE, and G. GORIN. J. Org. Chem. **29**, 1488 (1964).
14. J. L. DYE and V. A. NICELY. J. Chem. Educ., **48**, 443 (1971).
15. L. ELDJARN and L. HAMBRAEUS. Scand. J. Clin. Lab. Invest. **16**, 153 (1964).
16. P. JOCELYN. Eur. J. Biochem., **2**, 327 (1967).
17. L. ELDJARN and A. PIHL. J. Am. Chem. Soc. **79**, 4589 (1957).
18. L. ELDJARN and A. PIHL. J. Biol. Chem. **225**, 499 (1957).
19. G. GORIN, G. DOUGHTY, and R. GIDEON. J. Chem. Soc. B, 729 (1967).
20. G. GORIN and G. DOUGHTY. Arch. Biochem. Biophys. **126**, 547 (1968).
21. J. M. WILSON, R. J. BAYER, and D. J. HUPE. J. Am. Chem. Soc. **99**, 7922 (1977).
22. R. P. SZAJEWSKI and G. M. WHITESIDES. J. Am. Chem. Soc. **102**, 2011 (1980).
23. D. L. RABENSTEIN and Y. THERIAULT. Can. J. Chem. **62**, 1672 (1984).
24. R. S. REID and D. L. RABENSTEIN. Can. J. Chem. **59**, 1505 (1981).
25. Y. THERIAULT, B. V. CHEESMAN, A. P. ARNOLD, and D. L. RABENSTEIN. Can. J. Chem. **62**, 1312 (1984).
26. G. DALMAN, J. MCDERMED, and G. GORIN. J. Org. Chem. **29**, 1480 (1964).
27. U. WEBER, P. HARTTER, and L. FLOHÉ. Hoppe-Seyler's Z. Physiol. Chem. **351**, 1389 (1970).

Synthesis and ¹³C nuclear magnetic resonance assignments of cannithrene 1: a cannabis constituent

FAROUK S. EL-FERALY,[1] STEVE F. CHEATHAM, AND JAMES D. MCCHESNEY
Department of Pharmacognosy, School of Pharmacy, University of Mississippi, University, MI 38677, U.S.A.

Received October 12, 1984

FAROUK S. EL-FERALY, STEVE F. CHEATHAM, and JAMES D. MCCHESNEY. Can. J. Chem. **63**, 2232 (1985).

Two synthetic approaches to cannithrene 1 (**1**) have been explored. One-pot annelation of 6,8-dimethoxytetralone by first forming a β-keto sulfoxide, then addition of methyl vinyl ketone, gave, unexpectedly, after elimination of the sulfoxide, the naphthol (**10**). The successful route to cannithrene 1 (**1**) involved regiospecific demethylation of 6,8-dimethoxytetralone, then its conversion to enone **16**. Pyridinium bromide perbromide provided the necessary aromatization to give cannithrene 1 (**1**) after deprotection by hydrogenolysis. The ^{13}C nmr assignments of **1** were made.

FAROUK S. EL-FERALY, STEVE F. CHEATHAM et JAMES D. MCCHESNEY. Can. J. Chem. **63**, 2232 (1985).

On a évalué deux approches différentes pour la synthèse du cannithrène 1 (**1**). D'une façon surprenante, l'annellation dans un seul récipient de la diméthoxy-6,8 tétralone impliquant en premier lieu la formation d'un β-cétosulfoxyde, puis l'addition de méthylvinylcétone ne conduit, après l'élimination du sulfoxyde, qu'au naphtol **10**. La façon d'obtenir le cannithrène 1 (**1**) implique une déméthylation régiospécifique de la diméthoxy-6,8 tétralone, puis sa conversion en énone **16**. Après une déprotection par hydrogénolyse, l'aromatisation conduisant au cannithrène 1 (**1**) se fait sous l'influence du perbromure du bromure de pyridinium. On a fait les attributions des carbones du composé **1** dans le spectre rmn du ^{13}C.

[Traduit par le journal]

Cannabis sativa (marihuana) contains a group of dihydrostilbenes (1−3) like dihydroreserveratrole (**2**) and its monomethyl ether **3** which seem to be important precursors to various other stilbenoid derivatives. Thus, biogenetic phenol−phenol coupling could lead to cannabispiradienone (**4**) and cannabispiran (**5**) and its dehydro analog **6** and also could possibly lead

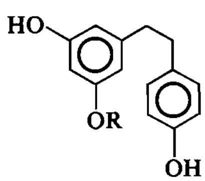

2, R = H
3, R = ME

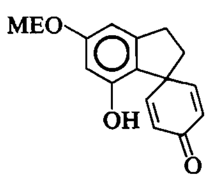

4

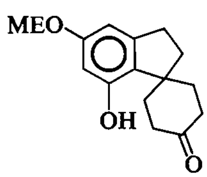

5

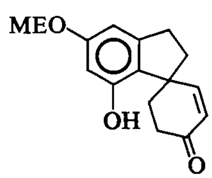

6

biogenetically to cannithrene 1 (**1**), another cannabis constituent. Indeed, Crombie *et al.* (4) have shown that heating **4** above its melting point caused the dienone−phenol rearrangement to give cannithrene 1 (**1**).

Cannithrene 1 (**1**) was obtained in only 4 mg per kg yield from *Cannabis*. Because of its structural similarity to the orchid phytoalexins (5), a study of its antimicrobial (especially its antifungal) properties was deemed important. This necessitated the development of an unambiguous synthetic route to this compound. Furthermore, a readily available supply of **1** was expected to make it possible to evaluate it biologically for many of the pharmacologic effects of marihuana.[2]

The synthetic plan for cannithrene 1 (**1**) depended upon first synthesizing 6,8-dimethoxytetralone (**7**), followed by addition of the mono oxygenated aromatic ring by a Robinson-type annelation. Thus, commercially available 3,5-dimethoxycinnamic acid was catalytically hydrogenated to its dihydro derivative, which was converted to the acid chloride by treatment with oxalyl chloride. Arndt−Eistert homologation of the acid chloride furnished the methyl ester which was hydrolyzed to the free acid **8**, then cyclized to 6,8-dimethoxytetralone (**7**) using polyphosphoric acid.[3]

The most appropriate conditions for the annelation of **7** appeared to be the one-pot annelation conditions reported by Boger *et al.* (6). This annelation sequence involved first forming the β-keto phenyl sulfene **9** by sulfenylating the lithium enolate of **7** with diphenyldisulfide. The product **9** was

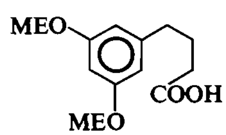

8

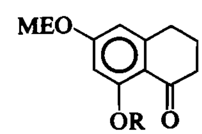

7, R = CH_3
12, R = H

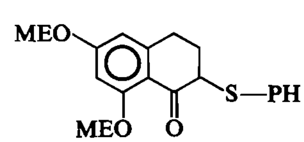

9

oxidized to the sulfoxide with sodium periodate and then reacted immediately with methyl vinyl ketone in the presence of sodium methoxide. Unfortunately, the isolated phenolic product turned out to be the naphthol **10** and not cannithrene 1 (**1**). The structure of **10** was established, based on its spec-

[1]Author to whom correspondence may be addressed.

[2]The results of screening cannithrene 1 (**1**) for antimicrobial and antiglaucoma activities will be reported elsewhere.

[3]Direct rearrangement of the diazo ketone to the free acid was possible using silver oxide in aqueous dioxane, but the yield was lower than the overall yield obtained by rearrangement in methanol and subsequent hydrolysis of the resulting ester.

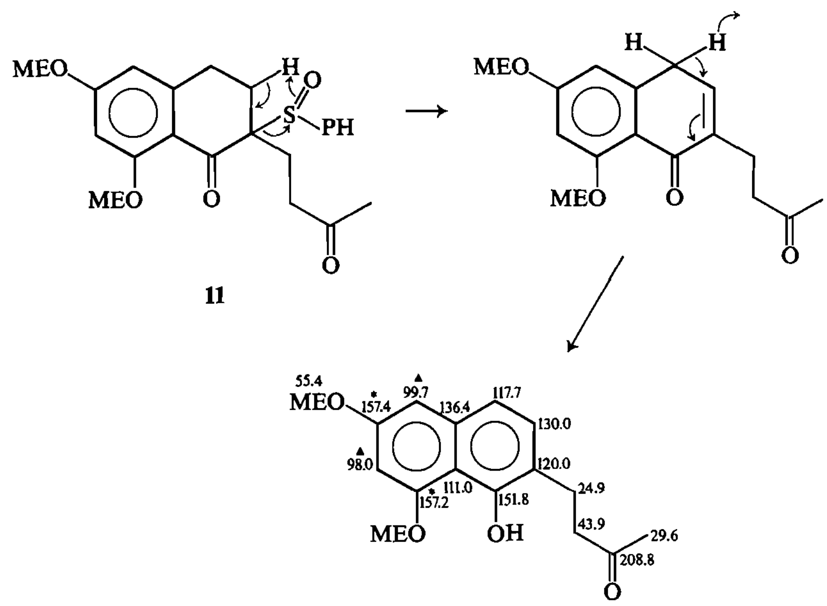

10
SCHEME 1

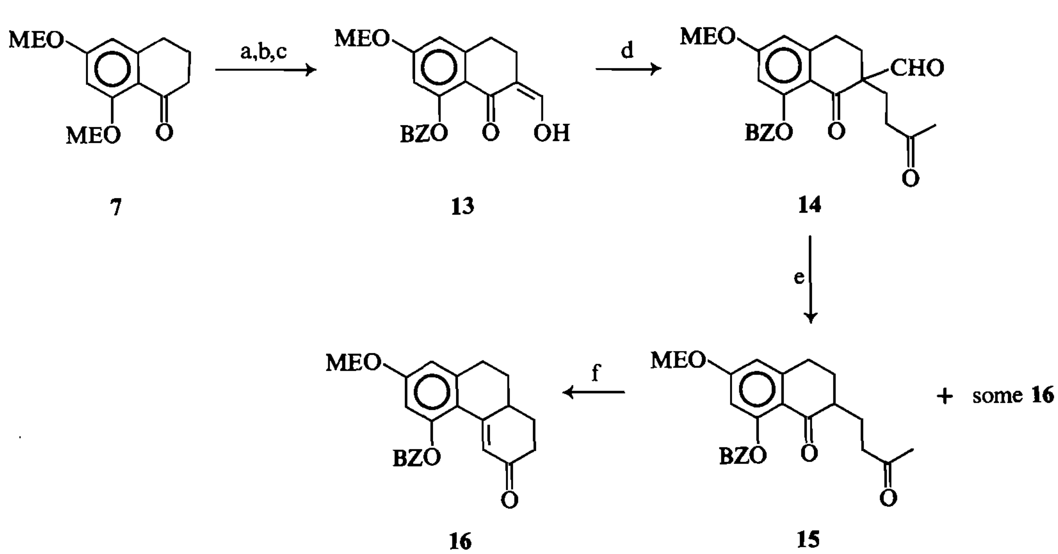

a: BCl_3/CH_2Cl_2 (77%); b: benzylbromide/K_2CO_3 (95%); c: ethylformate/$NaOCH_3$ (100%); d: methyl vinyl ketone/$N(Et)_3$ (100%); e: $NaOCH_3$; f: NaH (60% from **14**)

SCHEME 2

troscopic properties (see Experimental) including its ^{13}C nmr signals (see structure **10** in Scheme 1). The unexpected formation of **10** may be rationalized by a consideration of the reaction conditions and the mechanism proposed by Boger *et al.* (6) for the annelation reaction. For a dihydrophenanthrene to be formed, aldolization should precede the sulfoxide elimination. Apparently the reverse took place and this led to the formation of the naphthol **10**. The driving force for the facile elimination of the sulfoxide group in **11** is probably the formation of the aromatic system (Scheme 1).

The successful synthetic approach to cannithrene 1 (**1**) depended on, first, regiospecific demethylation of 6,8-dimethoxytetralone (**7**) to 8-hydroxy-6-methoxytetralone (**12**) using boron trichloride in methylene chloride. The ir spectrum of the product **12**, when compared to that of the starting material **7**, showed that the carbonyl peak had shifted approximately 30 cm^{-1}, from 1654 cm^{-1} in **7** to 1623 cm^{-1} in **11**, which is consistent with the formation of an intramolecular hydrogen bond. Protection of the hydroxyl group in **12** by benzylation, and formylation using ethyl formate and excess sodium methoxide, provided the intermediate **13**. Crude **13** was treated with methyl vinyl ketone to give the alkylated product **14** quantitatively. Smooth cyclization of **14** was accomplished after considerable experimentation by first briefly treating **14** with sodium ethoxide to give **15**, and usually a small amount of **16**, followed by treatment of the mixture with sodium hydride to furnish **16** (Scheme 2).

The aromatization of **16** to a dihydrophenanthrene proved to be a formidable task. Treatment with 2,3-dichloro-5,6-dicyano-1,4-benzoquinone (DDQ), chloranil (tetrachloro-1,4-benzoquinone), or Pd/C did not yield the desired product. Treatment with pyridinium bromide perbromide (7), on the

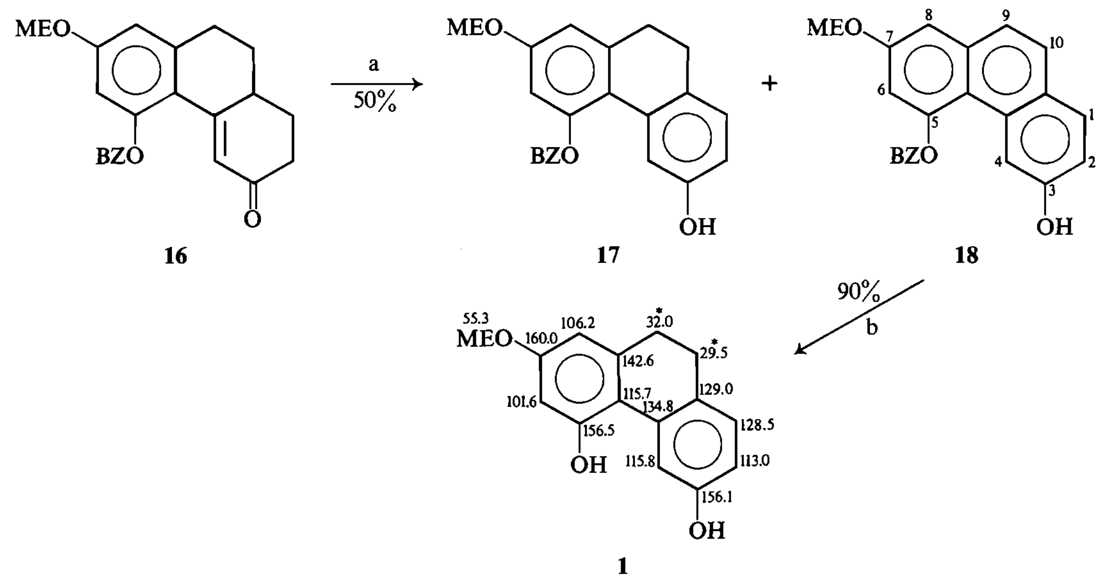

a: Pyridinium bromide perbromide; b: 10% Pd/C (90%)

SCHEME 3

other hand, gave a mixture of benzyl cannithrene 1 (**17**) and the corresponding phenanthrene **18** as based on ^{1}H nmr analysis of the mixture. Hydrogenation of this mixture using 10% palladium on carbon as catalyst gave a single product identical with cannithrene 1 (**1**), based on spectral comparisons.

The previously unreported ^{13}C nmr assignments for cannithrene 1 (**1**) are listed in Scheme 3. The ^{13}C nmr assignments were made by inspecting the coupled spectrum. Cannithrene 1 (**1**) exhibited three oxygenated aromatic signals at δ 160.0, 156.5, and 156.1. The signal at δ 160.0 appeared as a quartet (J = 2.0 Hz) in the coupled spectrum because of three-bond coupling to the methoxy protons. This confirmed that the signal at δ 160.0 was due to C-7. The signal at δ 156.5 appeared as a singlet (no three-bond coupling) and was assigned to C-5, leaving the signal at δ 156.1 (partially masked by the signal at δ 156.5) to be assigned to C-3. Of the aromatic singlets in the off-resonance spectrum, carbon-8a has no three-bond couplings and is the singlet at δ 142.6. Carbon-4a occurred as a doublet (J = 6.8 Hz) in the coupled spectrum at δ 139.4 due to three-bond coupling to H-1. The signal at δ 129.0 is a triplet (J = 6.8 Hz) in the coupled spectrum and was unambiguously assigned to C-10a due to three-bond coupling to both H-2 and H-4. The final aromatic singlet occurred at δ 115.7 and appeared as a multiplet in the coupled spectrum and was assigned to C-4b. Most of the aromatic doublets in the off-resonance spectrum could also be assigned by inspection of the coupled spectrum. The signal at δ 128.5 was a doublet (J = 156 Hz) with no further three-bond couplings and was assigned to C-1. The other two off-resonance doublets which could be assigned based on the coupled data were the signals at δ 106.2 and 101.6, ascribed to C-8 and C-6, respectively. This assignment was consistent with the former signal being a doublet (J = 158 Hz) with unresolved three-bond coupling (to H-6 and C-9 protons), while the latter was only three-bond coupled to H-8 and appeared as a sharp double doublet (J = 158, 4.9 Hz). The assignments of C-8 and C-6 were also consistent with their chemical shift values, as the more shielded of the two (C-6) is *ortho* to two oxygen functions, while the other (C-8) is *ortho* to only one oxygen function. The signals at δ 115.8 and 113.0 could not be assigned on the basis of the coupled data and assignments were made by selective proton decoupling. Irradiation at δ 7.94 (H-4) caused the carbon signal at δ 115.8 to collapse to a singlet, whereas the signal at δ 113.0 remained a doublet. Likewise, irradiation at δ 6.58 caused the signal at δ 113.0 to collapse, while the signal at δ 115.8 remained a doublet. This confirmed the assignment of C-2 to the signal at δ 113.0 and C-4 to the signal at δ 115.8.

In addition to the above signals, the methoxy carbon was found to resonate at δ 55.3, and the two methylene triplets, which could not be distinguished, resonated at δ 32.0 and 29.4.

Experimental

Melting points (mp, °C) were determined on a Thomas–Hoover melting point apparatus and are uncorrected. The ir spectra (cm^{-1}) were obtained on a Perkin–Elmer 281B spectrophotometer and measured in a KBr disk or as 10% solution in $CHCl_3$. The ^{1}H nmr spectra were recorded on JEOL C-60 HL, Varian EM-390, and JEOL JNM-FX 60 spectrometers using tetramethylsilane (TMS) as internal standard; chemical shifts were reported in δ (ppm) units. The ^{13}C nmr spectra were taken on a JEOL JNM-FX 60 (15.03 MHz) and the chemical shifts are also reported in δ (ppm) units. Coupled spectra were recorded using gated decoupling with 16K data points (decoupler off during data aquisition) and integrations recorded with decoupler on during data aquisitions and long pulse delays. Mass spectral data were obtained on a Finnigan 3200 spectrometer with an INCOS data system.

4-(3,5-Dimethoxyphenyl)butyric acid (8) and its methyl ester

The acid chloride of 3-(3,5-dimethoxyphenyl) propionic acid (8) was prepared by dissolving the acid (5 g, 22.3 mmol) in 50 mL of benzene containing four drops of DMF, followed by the addition of 10 mL of oxalyl chloride (54.15 mmol). The mixture was stirred at room temperature for 0.5 h. Removal of the benzene left the crude acid chloride which was dissolved in 25 mL of ether and added to 250 mL of an ethereal solution of diazomethane (excess). Evaporation of the ether left the diazoketone as a reddish oil which was dissolved in MeOH (400 mL) and stirred for 3 h at 60°C with freshly prepared Ag_2O, prepared by adding 10 mL of 25% aqueous KOH to 2.5 g of $AgNO_3$ in 10 mL of H_2O. Filtration and evaporation of the MeOH phase left a black oil that was dissolved in $CHCl_3$ and filtered over a short column of SiO_2. Evaporation of $CHCl_3$ left 4.93 (87%) of the methyl ester of **8** as a pale yellow oil; ir ($CHCl_3$): 1730, 1600; ^{1}H nmr ($CDCl_3$): 1.97 (m, 2H), 2.34 (t, 2H, J = 7.0 Hz), 2.60 (t, 2H, J = 7.0 Hz), 3.67 (s, 3H), 3.77 (s, 6H), 6.33 (s, 3H); ^{13}C nmr ($CDCl_3$): 173.8 (s), 161.1 (s), 143.9 (s), 106.8 (d), 98.4 (d), 55.2 (q), 51.3 (q), 35.4 (t), 33.4 (t), 26.3 (t); ms: M^+ at m/z 238 (28%). *Anal.* calcd. for $C_{13}H_{18}O_4$ (238): C 65.53, H 7.61; found: C 65.66, H 7.89.

The same reaction was tried following a general literature (9) procedure starting with 0.5 g of the above acid chloride, but the rearrangement of the acid chloride was carried out in aqueous dioxane and the product crystallized from ether–hexane to give colorless needles of **8** (290 mg, 55%), mp 64–65°C; ir ($CHCl_3$): 3300–2400, 1708, 1593; ^{1}H nmr ($CDCl_3$): 1.98 (m, 2H), 2.37 (t, 2H, J = 7.0 Hz), 2.62 (t, 2H, J = 7.0 Hz), 3.76 (s, 6H), 6.34 (s, 3H), 9.77 (br s, exchangeable); ^{13}C nmr ($CDCl_3$): 179.2 (s), 161.0 (s), 143.7 (s), 106.8 (d), 98.3 (d), 55.2 (q), 35.3 (t), 33.3 (t), 26.1 (t); ms: M^+ m/z 224 (34%). *Anal.* calcd. for $C_{12}H_{16}O_4$ (224): C 64.27, H 7.19; found: C 64.50, H 7.37.

The same acid was obtained by stirring for 3 h under N_2 a solution of the ester obtained above (4.8 g) in MeOH (50 mL) to which was added a solution of KOH (5 g) in 15 mL of H_2O. Removal of the MeOH and $CHCl_3$ extraction of the acidified residue gave 4.33 g (96%) of this acid.

6,8-Dimethoxytetralone (7)

The acid **8** (3.76 g) was added with stirring to polyphosphoric acid (60 g) heated to 100–110°C and stirring continued for 4 h. Work-up by addition of ice and $CHCl_3$ extraction furnished a product that was subjected to flash chromatography (10) using acetone–CH_2Cl_2 (1:9) as solvent to give 3.0 g (87%) of 6,8-dimethoxytetralone (**7**), crystallizing as yellow plates from ether–hexane, mp 64–65°C (lit. (11) mp 65°C); ir ($CHCl_3$): 2920, 1654, 1592; ^{1}H nmr ($CDCl_3$): 1.71 (m, 2H), 2.56 (t, 2H, J = 6.5 Hz), 2.88 (t, 2H, J = 6.5 Hz), 3.83 (s, 3H), 3.87 (s, 3H), 6.33 (s, 2H); ^{13}C nmr ($CDCl_3$): 195.3 (s), 163.9 (s), 162.6 (s), 149.1 (s), 116.5 (s), 104.9 (d), 97.3 (d), 55.9 (q), 55.3 (q), 40.8 (t), 31.5 (t), 22.9 (t); ms: M^+ m/z 206 (60%).

Sulfenylation of 6,8-dimethoxytetralone (7) to 9

Diisopropylamine (0.25 mL) was added to a flame dried flask under N_2 in a Dry Ice – acetone bath. Dry THF (1 mL) was added, followed by 1.2 mL of 1.6 *M* *n*-butyllithium in cyclohexane. This mixture was stirred for 0.25 h, then 200 mg of 6,8-dimethoxytetralone (**7**) in 1 mL of THF was added. Stirring was continued for 1 h, then a solution of 425 mg of diphenyldisulfide in 1 mL of THF was added. Stirring was continued for 2 h in a Dry Ice – CCl_4 bath and for 1 h at room temperature. After normal work-up and flash chromatography (10) of the crude product using acetone–$CHCl_3$ (1:9) as solvent, 237 mg (78%) of **9** were obtained as an oil, homogenous on tlc (one spot, R_f 0.52 on SiO_2 plates using 10% acetone in $CHCl_3$ as solvent); ir ($CHCl_3$): 3000, 1660; ^{1}H nmr ($CDCl_3$): 2.0–3.43 (m, 4H), 3.82 (s, 3H), 3.86 (s, 3H), 4.03 (dd, 1H, J = 7.5, 4.0 Hz), 6.30 (2H, J = 1.0 Hz), and the 5 aromatic protons from 7.2 to 7.6; ^{13}C nmr ($CDCl_3$): 191.5 (s), 164.3 (s), 163.4 (s), 147.6 (s), 134.4 (s), 132.3 (d), 128.9 (d), 127.3 (d), 115.4 (s), 104.8 (d), 97.7 (d), 56.0 (q), 55.4 (q), 29.1 (t), 28.3 (t); ms: M^+ m/z 314 (5%). *Anal.* calcd. for $C_{18}H_{18}O_3$ (314): C 68.77, H 8.39, S 10.20; found: C 68.60, H 8.59, S 10.49.

Attempted annelation of 9; isolation of 10

The sulfenylated ketone **9** (265 mg) was dissolved in MeOH (4 mL) and chilled in an ice bath. Sodium periodate (174 mg) in a minimum amount of H_2O was added. After 22.5 h, when the reaction went to completion, the mixture was filtered and MeOH was evaporated, leaving 300 mg of a residue which was dissolved in 10 mL of THF–MeOH (1:1), and 0.04 mL of a 25% $NaOCH_3$ solution in MeOH was added. Methyl vinyl ketone (0.1 mL) was added to the mixture which was chilled to 0°C for 24 h. Excess $NaOCH_3$ solution was added (0.25 mL) and stirring continued for 31 h. The usual work-up and extraction of the product with $CHCl_3$ furnished 286 mg of a dark oil that was chromatographed over 50 g of SiO_2 using 1% acetone in $CHCl_3$ as solvent to give 48 mg (23%) of **10**, as an oil that was homogeneous on tlc; ir ($CHCl_3$): 3400, 1708, 1630, 1590; ^{1}H nmr ($CDCl_3$): 2.10 (s, 3H), 2.90 (m, 4H), 3.88 (s, 3H), 4.01 (s, 3H), 6.47 (d, 1H, J = 2.5 Hz), 6.70 (d, 1H, J = 2.5 Hz), 7.10 (d, 1H, J = 8.0 Hz), 7.23 (d, 1H, J = 8.0 Hz), 9.30 (s, 1H, exchangeable); ^{13}C nmr ($CDCl_3$): see structure **10**; ms: M^+ m/z 274 (40%). *Mol. Wt.* calcd. for $C_{16}H_{18}O_4$: 274.1205; found: 274.1207.

8-Hydroxy-6-methoxytetralone

6,8-Dimethoxytetralone (**7**) (2.0 g) was dissolved in 20 mL CH_2Cl_2 under N_2 and the solution was cooled to −78°C. BCl_3 (30 mL of a 1 *M* solution in CH_2Cl_2) was added dropwise to the solution. The Dry Ice – acetone bath was then removed, and the solution stirred 0.5 h while returning to room temperature. Work-up and extraction with ethyl acetate provided 1.44 g (77%) of 8-hydroxy-6-methoxytetralone, which crystallized from ether–hexane to give the analytical sample, mp 68–69°C; ir ($CHCl_3$): 3250–3020, 1623; ^{1}H nmr ($CDCl_3$): 2.02 (m, 2H), 2.61 (t, 2H, J = 6.0 Hz), 2.84 (t, 2H, J = 6.0 Hz), 3.79 (s, 3H), 6.24 (s, 2H), 12.83 (s, 1H exchangeable); ^{13}C nmr ($CDCl_3$): 202.9 (s), 165.8 (s), 165.6 (s), 147.2 (s), 111.6 (s), 106.6 (d), 98.8 (d), 55.4 (q), 38.5 (t), 29.8 (t), 22.9 (t); ms: M^+ m/z 192 (80%). *Anal.* calcd. for $C_{11}H_{12}O_3$: C 70.58, H 5.92; found: C 70.34, H 5.76.

8-Benzyloxy-6-methoxytetralone

The hydroxy tetralone obtained above (1.6 g) was benzylated by refluxing for 24 h in acetone solution (150 mL) in the presence of K_2CO_3 (12.9 g) and benzylbromide (3.20 g). Work-up and chromatography of the product on SiO_2 using $CHCl_3$ as solvent provided 2.23 g (95%) of the benzyloxy derivative as an oil; ir ($CHCl_3$): 1663, 1595; ^{1}H nmr ($CDCl_3$): 2.00 (m, 2H), 2.59 (t, 2H, J = 7.0 Hz), 2.87 (t, 2H, J = 7.0 Hz), 3.76 (s, 3H), 5.12 (s, 2H), 6.29 (d, 1H, J = 2.0 Hz), 6.33 (d, 1H, J = 2.0 Hz), 7.20–7.70 (m, 5H); ^{13}C nmr ($CDCl_3$): 195.4 (s), 163.8 (s), 161.6 (s), 149.1 (s), 137.0 (s), 128.5 (d), 127.6 (d), 126.8 (d), 117.2 (s), 105.5 (d), 99.3 (d), 70.7 (t), 55.3 (q), 40.9 (t), 31.6 (t), 22.9 (t); ms: M^+ m/z 282 (14%). *Anal.* calcd. for $C_{18}H_{18}O_3$: C 76.57, H 6.43; found: C 76.39, H 6.76.

Hydroxymethylation of 8-benzyloxy-6-methoxytetralone to 13

A solution of 8-benzyloxy-5-methoxytetralone (2.58 g) in ethyl formate (5 mL) was stirred overnight with a mixture of solid $NaOCH_3$ (2.5 g) and dried ethyl formate (20 mL). Acidification and chloroform extraction gave 2.89 g (100%) of **13**, which crystallized from MeOH to afford slightly yellow clusters, mp 96–99°C; ir ($CHCl_3$): 2370, 1630, 1595; ^{1}H nmr ($CDCl_3$): 2.42 (t, 2H, J = 7.0 Hz), 2.82 (t, 2H, J = 7.0 Hz), 3.80 (s, 3H), 5.20 (s, 2H), 6.34 (d, 1H, J = 2.5 Hz), 6.43 (d, 1H, J = 2.5 Hz), 7.24–7.76 (m, 5H), 8.10 (bs, 1H), 14.6 (bs, exchangeable); ^{13}C nmr ($CDCl_3$): 185.7 (s), 172.2 (d), 163.8 (s), 146.8 (s), 136.5 (s), 128.6 (d), 127.9 (d), 126.9 (d), 105.8 (d), 99.3 (d), 70.8 (t), 55.4 (q), 31.1 (t), 23.1 (t); ms: M^+ m/z 310 (1%). *Mol. Wt.* calcd. for $C_{19}H_{18}O_4$: 310.1205; found: 310.1200.

Alkylation of 13 to 14

The crude ketone **13** (1.2 g) was dissolved in benzene (12 mL) and stirred for 7 days with methyl vinyl ketone (0.5 mL) and 0.3 mL of triethylamine. The usual work-up using benzene gave 1.5 g (100%) of adduct **14** that proved to be unstable; ir ($CHCl_3$): 1710, 1648; ^{1}H nmr ($CDCl_3$): 1.68–2.57 (m, 7H), 2.07 (s, 3H), 3.77 (s, 3H), 5.16 (s, 2H), 6.26 (d, 1H, J = 2.5 Hz), 6.38 (d, 1H, J = 2.5 Hz), 7.25–7.67 (m, 5H), 9.71 (s, 1H); ^{13}C nmr ($CDCl_3$): 207.0 (s), 201.7 (d), 193.7 (s) due to the 3 carbonyl groups. The material was used in the next step without further purification.

Cyclization of 14 to 16 using NaOEt–NaH

To a solution of 980 mg of crude **14** in absolute EtOH (20 mL) cooled in an ice bath was added 180 mg NaOEt in 20 mL of absolute EtOH. After stirring for 3 h, 0.3 mL of CH_3COOH was added and EtOH removed. The usual work-up and chromatography of the crude product on SiO_2 using 20% ethyl acetate in benzene produced: (a) **16** (41 mg) as colorless needles, mp 94–95°C; ir ($CHCl_3$): 1634, 1592, 1570; ^{1}H nmr ($CDCl_3$): 1.33–2.97 (m, 9H), 3.70 (s, 3H), 5.10 (s, 2H), 6.28 (d, 1H, J = 2.5 Hz), 6.38 (d, 1H, J = 2.5 Hz), 7.37 (bs, 5H); ^{13}C nmr ($CDCl_3$): 200.6 (s), 161.2 (s), 160.3 (s), 155.4 (s), 143.9 (s), 136.4 (s), 128.6 (d), 128.0 (d), 127.1 (d), 125.6 (d), 115.6 (s), 106.2 (d), 99.2 (d), 70.9 (d), 55.2 (q), 37.8 (d), 37.3 (t), 31.4 (t), 30.5 (t), 30.3 (t); ms: M^+ m/z 334 (1%). *Anal.* calcd. for $C_{22}H_{22}O_3$: C 79.02, H 6.63; found: C 79.30, H 6.60. (b) **15** (615 mg), crystallized from MeOH, mp 93–94°C; ir ($CHCl_3$): 1704, 1658, 1593; ^1H nmr ($CDCl_3$): 1.58–2.64 (m, 7H), 2.24 (s, 3H), 2.97 (dd, 2H, J = 7.2, 4.8 Hz), 3.78 (s, 3H), 5.14 (s, 2H), 6.24 (d, 1H, J = 3.0 Hz), 6.69 (d, 1H, J = 3.0 Hz), 7.24–7.71 (m, 5H); ^{13}C nmr ($CDCl_3$): 208.8 (s), 197.6 (s), 163.5 (s), 161.4 (s), 148.3 (s), 136.9 (s), 128.6 (d), 127.6 (d), 126.8 (d), 116.8 (s), 105.1 (d), 99.2 (d), 70.5 (t), 55.3 (q), 48.0 (d), 41.5 (t), 30.0 (t), 29.8 (q), 28.7 (t), 24.7 (t); ms: M^+ m/z 352 (3%). *Anal.* calcd. for $C_{22}H_{24}O_4$: C 74.98, H 6.86; found: C 75.02, H 6.76.

In all later runs the mixture was not separated but directly treated with NaH as follows. The mixture (3.8 g) was dissolved in THF (50 mL) and added to 240 mg of NaH in 50 mL of THF. After stirring for 24 h, the usual work-up and flash chromatography of the product gave 3.15 g of **16** (60%), identical to the material obtained above.

Cannithrene 1 (1)[4]

The enone **16** (1.0 g) was dissolved in acetic acid (300 mL) and pyridinium bromide perbromide (1.19 g) was added slowly with vigorous stirring for 10 min. The mixture was allowed to stand for 0.5 h, then evaporated. The usual work-up produced 0.94 g of a red oil that was flash chromatographed on SiO_2 using 4% ethyl acetate in benzene to give back 0.19 g of **16** and 0.48 g (50%) of a mixture of **17** and the corresponding phenanthrene **18**. Without further purification, this mixture was dissolved in 40 mL EtOH and hydrogenated in the presence of 70 mg of 10% Pd/C. After 16 h, tlc revealed the presence of a single compound, R_f 0.24 on SiO_2 plate using 20% ethyl acetate in benzene as solvent. The usual work-up provided 0.35 g (100%) of a chromatographically homogeneous light tan oil that crystallized reluctantly from ether–hexane to give 0.27 g (38% from **16**) of cannithrene 1 (**1**) as colorless needles, mp 175–180°C with darkening (lit. (3) mp 189°C with darkening). The ^1H nmr (CD_3COCD_3) spectrum of synthetic cannithrene 1 (**1**) was identical to that of the natural material, showing signals at δ 2.67 (s, 4H), 3.75 (s, 3H), 6.38 (d, 1H, J = 2.5 Hz), 6.47 (d, 1H, J = 2.5 Hz), 6.62 (dd, 1H, J = 8.0, 2.5 Hz), 7.04 (d, 1H, J = 8.0 Hz), 8.0 (d, 1H, J = 2.5 Hz), 8.72 (s, 1H exchangeable); ir ($CHCl_3$): 3320, 1600 cm^{-1}; the ^{13}C nmr assignments are shown in Scheme 3; ms: M at m/z 242 (100%). *Anal.* calcd. for $C_{15}H_{14}O_3$: C 74.36, H 5.82; found: C 74.31, H 6.03.

[4]Conditions for the aromatization of **16** were worked out using as a model compound the analog 9,10,10a-3(2*H*)-tetrahydrophenanthrene, synthesized from commercially available α-tetralone. Pyridinium bromide perbromide dehydrogenated it to 3-hydroxydihydrophenanthrene in 75% yield with a 14% yield of the analogous 2-bromo derivative.

Acknowledgements

This investigation was taken in part from the Ph.D. dissertation of S. F. Cheatham. Financial support from the Research Institute of Pharmaceutical Sciences, University of Mississippi, is gratefully acknowledged. The authors would like to thank Professor Leslie Crombie, Department of Chemistry, The University, Nottingham, U.K., for providing a copy of the ^1H nmr spectrum of cannithrene 1.

1. F. S. EL-FERALY. J. Nat. Prod. **47**, 89 (1984).
2. L. CROMBIE and S. V. JAMIESON. J. Chem. Soc. Perkin Trans. 1, 1467 (1982), and references therein.
3. L. CROMBIE and W. M. L. CROMBIE. J. Chem. Soc. Perkin Trans. 1, 1455 (1982).
4. L. CROMBIE, W. M. L. CROMBIE, and S. V. JAMIESON. Tetrahedron Lett. 661 (1979).
5. M. H. FISCH, B. H. FLICK, and J. ARDITTI. Phytochemistry, **12**, 437 (1973).
6. D. L. BOGER and M. D. MULLICAN. J. Org. Chem. **45**, 5002 (1980).
7. W. L. MEYER, B. CLEMANS, and R. A. MANNING. J. Org. Chem. **40**, 3686 (1975).
8. F. S. EL-FERALY and YEE-MING CHAN. J. Nat. Prod. **44**, 557 (1981).
9. W. E. BACHMAN and W. S. STRUVE. "Organic reactions". Vol. 1. John Wiley and Sons, Inc., 1942. p. 38.
10. W. C. STILL, M. KAHN, and A. MITRA. J. Org. Chem. **43**, 2923 (1978).
11. E. HARDEGGER, N. RIGASSI, J. SERES, C. EGLI, P. MULLER, and K. O. FITZI. Helv. Chim. Acta, **46**, 2543 (1963).

Hydride transfer reactions. A kinetic study of oxidation of 10-methyl-9-phenylacridan by some π acceptors and a one-electron oxidant

ALLAN K. COLTER, A. GREGG PARSONS, AND KAREN FOOHEY
Guelph–Waterloo Centre for Graduate Work in Chemistry, Department of Chemistry and Biochemistry, University of Guleph, Guelph, Ont., Canada N1G 2W1

Received November 2, 1984

ALLAN K. COLTER, A. GREGG PARSONS, and KAREN FOOHEY. Can. J. Chem. **63**, 2237 (1985).

The kinetics of oxidation of 10-methyl-9-phenylacridan (**1**(H)) and 9-deuterio-10-methyl-9-phenylacridan (**1**(D)) to 10-methyl-9-phenylacridinium ion (**3**) by eight oxidants have been investigated. The oxidants included the π-acceptors 1,4-benzoquinone (BQ), 7,7,8,8-tetracyanoquinodimethane (TCNQ), *p*-bromanil (BA), *p*-chloranil (CA), tetracyanoethylene (TCNE), 2,3-dicyano-1,4-benzoquinone (DCBQ) and 2,3-dichloro-5,6-dicyano-1,4-benzoquinone (DDQ) in acetonitrile (AN), BQ in 50:50 (v/v) AN–water, and the one-electron oxidant tris(2,2′-bipyridyl)cobalt(III), $Co(bipy)_3^{3+}$, in AN. The seven π acceptors cover a 10^9-fold range of reactivity from BQ to DDQ and the deuterium kinetic isotope effect varies from 11.9 (BQ in AN) to 5.8 (DDQ). For π acceptors (BQ, TCNQ, CA, TCNE, and DCBQ) previously investigated with 10-methylacridan (NMA), **1**(H) is less reactive than NMA by factors ranging from 9.1 (BQ) to 1.7×10^2 (TCNE). The isotope effects and relative reactivities for the π acceptor oxidations are most simply explained by a one-step hydride transfer mechanism.

ALLAN K. COLTER, A. GREGG PARSONS et KAREN FOOHEY. Can. J. Chem. **63**, 2237 (1985).

On a étudié les cinétiques d'oxydation, sous l'influence de huit oxydants, du méthyl-10 phényl-9 acridane (**1**(H)) et du deutéro-9 méthyl-10 phényl-9 acridane (**1**(D)) en ion méthyl-10 phényl-9 acridinium (**3**). Les oxydants comprennent des accepteurs π comme la benzoquinone-1,4 (BQ), le tétracyano-7,7,8,8 quinodiméthane (TCNQ), le *p*-bromanil (BA), le *p*-chloranil (CA), le tétracyanoéthylène (TCNE), la dicyano-2,3 benzoquinone-1,4 (DCBQ) et la dichloro-2,3 dicyano-5,6 benzoquinone-1,4 (DDQ) dans l'acétonitrile (AN), la BQ dans un mélange 50:50 (v/v) de AN–eau ainsi que par un oxydant à un électron, le tris(bipyridyl-2,2′) cobalt(III), $Co(bipy)_3^{3+}$, dans du AN. Les sept accepteurs π couvrent un domaine de réactivité de l'ordre de 10^3 allant de la BQ à la DDQ; l'effet isotopique cinétique varie de 11,9 (BQ dans AN) à 5,8 (DDQ). Pour les accepteurs π (BQ, TCNQ, CA, TCNE et DCBQ) étudiés antérieurement avec le méthyl-10 acridane (NMA), le composé **1**(H) est moins réactif que le NMA par des facteurs allant de 9,1 (BQ) à $1{,}7 \times 10^2$ (TCNE). La plus simple explication des effets isotopiques et des réactivités relatives lors d'oxydations par des accepteurs π fait appel à un mécanisme de transfert d'hydrure en une étape.

[Traduit par le journal]

Introduction

The detailed mechanisms of hydride transfer reactions of nicotinamide coenzyme models, particularly the possibility of stepwise mechanisms initiated by a single electron transfer (SET), continue to attract considerable attention (refs. 1, 2 and references cited). In earlier papers in this series (1, 3, 4) we have examined substituent, solvent, and kinetic isotope effects in oxidation of 10-alkylacridans with a number of quinone and dicyanomethylene π acceptors. The general characteristics of these oxidations remain remarkably similar in spite of rate variations of greater than 10^8-fold. Most of these results are most economically accommodated by a one-step hydride transfer mechanism, eq. [1], although the responses of the rate to changes in structure or solvent expected for eq. [1] and for a three-step e^-, H^+, e^- mechanism in which the proton transfer is rate-determining, eq. [2], are very similar.

$$[1]\quad DH + A \xrightarrow{\sim H^{-}} D^+ + AH^-$$

$$[2]\quad DH + A \underset{}{\overset{\sim e^-}{\rightleftharpoons}} DH^{+\cdot}\, A^{-\cdot} \underset{\text{slow}}{\xrightarrow{\sim H^+}} D\cdot\, AH\cdot \underset{\text{fast}}{\xrightarrow{\sim e^-}} D^+ + AH^-$$

(DH = hydride donor, A = π acceptor oxidant)

While the radical cation – radical anion intermediate, $DH^{+\cdot}\, A^{-\cdot}$, of eq. [2] can be excluded on energetic grounds for *p*-chloranil (CA) and quinones of lower reduction potential (4), a SET-initiated stepwise mechanism such as eq. [2] should become increasingly feasible with increasing acceptor reduction potential (2, 4, 5).

As part of an effort aimed at defining the range of mechanisms possible for hydride transfers from dihydropyridines and related compounds to π acceptors we have investigated the oxidation of 10-methyl-9-phenylacridan (**1**) by a series of π acceptors and a one-electron oxidant. This study was prompted

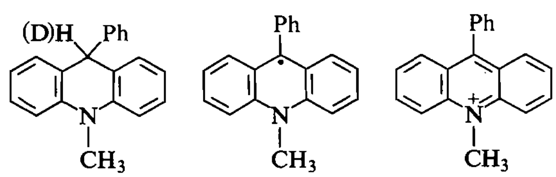

1, DH **2**, D· **3**, D^+

by the following considerations: A 9-phenyl group might be expected to favor a stepwise mechanism by steric inhibition of direct hydride transfer relative to electron transfer and by stabilization of the intermediate 9-phenyl-9-acridanyl radical (D·, **2**). This radical is long-lived, and has been produced by uv irradiation of methanolic solutions of 10-methyl-9-phenylacridinium chloride (6). The fact that **1** has a single 9-H greatly simplifies measurement of the primary kinetic deuterium isotope effect.

Results

The oxidants investigated in this work included 5 benzoquinones (**4–8**), two cyanomethylene acceptors (**9** and **10**), and the one-electron oxidant tris(2,2′-bipyridyl)cobalt(III), $Co(bipy)_3^{3+}$. BA was included to compare two different benzoquinones (BA and CA) of nearly identical oxidizing strength but different steric requirements. The lower reactivity of **1**

TABLE 1. Rates of oxidation of **1**(H) and **1**(D)[a]

Oxidant	E^0, V[c]	[Oxidant], M	$k(M^{-1}\ s^{-1})$[b] 1(H)	$k(M^{-1}\ s^{-1})$[b] 1(D)	k_H/k_D	$k_{NMA}/k_{1(H)}$[d]
BQ[e]	−0.51[g]	$(1.50–1.60) \times 10^{-1}$	$6.25 \pm 0.18 \times 10^{-5}$	$5.24 \pm 0.16 \times 10^{-6}$	11.9 ± 0.5	9.1
BQ[e, f]	−0.51[g]	1.14×10^{-1}	$2.45 \pm 0.09 \times 10^{-3}$	$2.55 \pm 0.08 \times 10^{-4}$	9.6 ± 0.5	10
TCNQ	0.19[h]	$(8.28–13.5) \times 10^{-3}$	$3.57 \pm 0.11 \times 10^{-3}$	$5.70 \pm 0.41 \times 10^{-4}$	6.3 ± 0.5	66
BA	0.00[g]	6.83×10^{-4}	$3.19 \pm 0.10 \times 10^{-1}$	$3.00 \pm 0.09 \times 10^{-2}$	10.6 ± 0.5	—
CA	0.01[g]	$(5.15–11.6) \times 10^{-2}$	$5.92 \pm 0.30 \times 10^{-1}$	$5.68 \pm 0.28 \times 10^{-2}$	10.4 ± 0.7	20
TCNE	0.24[h]	$(6.05–25.7) \times 10^{-3}$	$6.37 \pm 0.21 \times 10^{-1}$	$1.08 \pm 0.04 \times 10^{-1}$	5.9 ± 0.3	1.7×10^2
DCBQ	0.30[i]	$(2.22–9.35) \times 10^{-3}$	$8.68 \pm 0.80 \times 10^2$	$1.09 \pm 0.11 \times 10^2$	8.0 ± 1.1	13
DDQ	0.50[g]	$(9.60–31.0) \times 10^{-4}$	$7.53 \pm 0.62 \times 10^4$	$1.29 \pm 0.12 \times 10^4$	5.8 ± 0.7	ca. 25[k]
$Co(bipy)_3^{3+}$	0.235[j]	$(7.60–10.2) \times 10^{-4}$	$1.05 \pm 0.02 \times 10^{-2}$	$0.96 \pm 0.02 \times 10^{-2}$	1.08 ± 0.01	24

[a]Temperature 25.0°C. Solvent acetonitrile unless otherwise specified. [**1**] = $(2–6) \times 10^{-5}\ M$.
[b]Average of 3 to 8 determinations with standard deviations.
[c]Standard one-electron reduction potential in AN vs. SCE.
[d]Reactivity of *N*-methylacridan (1) relative to that of **1**(H).
[e]0.01 M acetic acid added.
[f]50:50 (v/v) AN–water.
[g]Reference 10, 0.1 M tetraethylammonium perchlorate.
[h]Reference 11, 0.1 M tetraethylammonium perchlorate.
[i]Reference 12, 0.1 M $LiClO_4$.
[j]Reference 13, $5 \times 10^{-3}\ M$ tetraethylammonium perchlorate.
[k]Calculated from a value of $2.9 \pm 0.1 \times 10^5\ M^{-1}\ s^{-1}$ for 9,9-dideuterio-NMA (G. Saito, unpublished work) and the rate constant for **1**(D), assuming a secondary deuterium isotope effect of 1.1 (3).

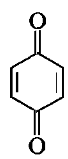
4, BQ

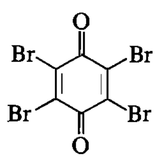
5, BA

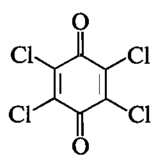
6, CA

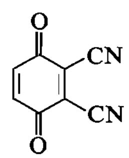
7, DCBQ

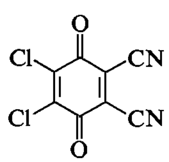
8, DDQ

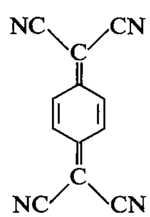
9, TCNQ

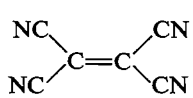
10, TCNE

compared to 10-methylacridan (NMA) made it possible to extend the kinetic measurements to DDQ. The other six oxidants have been investigated earlier with NMA (3, 7).

The reactions of **1** with the oxidants included in this study are identical to the corresponding reactions of NMA (1, 3, 7, 8). Quantitative oxidation of **1** to **3** was confirmed by uv–visible spectral examination of kinetic solutions for all oxidants except TCNQ, where the spectrum of **3** is masked by that of the radical ion $TCNQ^{\cdot-}$, produced in equimolar quantities to the **1** consumed. The oxidation product, **3**, was also isolated in greater than 90% yields as the perchlorate or chloride salt using DDQ oxidant. As discussed earlier (1, 3, 4), the reduction product of the π acceptors, as well as the overall stoichiometry, depends on the extent to which the rapid reaction of the product of hydride transfer, AH^-, with unreacted acceptor ($2AH^- + A \rightleftharpoons AH_2 + 2A^{\cdot-}$) occurs. This reaction occurs to a slight extent with CA and BA, and essentially completely with DCBQ and DDQ.

The kinetic results for reaction of **1**(H) and **1**(D) with the eight oxidants in acetonitrile (AN) and with BQ in 50:50 v/v AN–water are summarized in Table 1. Rate measurements with all oxidants except BA and $Co(bipy)_3^{3+}$ were carried out under pseudo first-order conditions using a 30-fold or greater excess of oxidant. With BA and $Co(bipy)_3^{3+}$, lower molar ratios of oxidant to **1** were used and the data analyzed using the appropriate second-order rate equation. A first-order dependence on both acridan and oxidant concentrations is well established by this and earlier work (1, 3, 4) for the π acceptors.

With $Co(bipy)_3^{3+}$ a second-order rate law was again observed under the conditions investigated. The results of our studies of oxidation of NMA by $Co(bipy)_3^{3+}$ are consistent with a mechanism involving rate-determining SET with subsequent or concurrent loss of H^+. This mechanism (1), which is analogous to that suggested by Bruice and co-workers (9) for oxidation of dihydropyridine analogs with $Fe(CN)_6^{3-}$, allows, in principle, for retardation of the rate by $Co(bipy)_3^{2+}$ produced in the reaction. At $(2–4) \times 10^{-5}\ M$ **1**, however, no measurable deviation from second-order behavior was observed. Added $Co(bipy)_3^{2+}$ at concentrations of $2 \times 10^{-4}\ M$ or higher does produce measurable decreases in rate but the interpretation of these effects is complicated by a negative salt effect. Consequently, we were unable to obtain a reliable estimate of the ratio of the rate constants for the proton-transfer and reverse electron-transfer steps, or of the deuterium isotope effect for the proton-transfer step (9).

At the beginning of this investigation we planned to examine the symmetrical hydride transfer between **1** and **3** (to regenerate **1** and **3**) for evidence for a stepwise mechanism, using esr spectroscopy to detect any D· and nmr spectroscopy to detect any H/D exchange at the 9-position in AN–D_2O solvent. However, using **1** with a $^{14}CH_3$ label and a procedure similar to that of Powell and Bruice (2), we found the hydride transfer from **1** to **3** to be too slow (at least 10^3 times slower than that between NMA and 10-methylacridinium ion (2)) to make such experiments practical.

Discussion

The primary deuterium kinetic isotope effects (kie's) (Table 1) are remarkably similar to those observed for oxidation of NMA with the same π acceptors (3). Where there are significant differences, the kie is marginally greater for **1** (viz., 10.4 ± 0.7 vs. 7.7 ± 0.4 with CA, 5.9 ± 0.3 vs. 4.8 ± 0.3 with TCNE, 8.0 ± 1.1 vs. 5.4 ± 0.4 with DCBQ). Furthermore the trends are identical, the kie decreasing from AN to AN–water with BQ and with increasing oxidizing strength within a series of structurally-related oxidants. Any differences in the steric requirements of BA and CA are not great enough to have a measurable effect on the kie.

An earlier analysis (4) led to the conclusion that the radical cation – radical anion pair intermediate, $DH^{+\cdot}\ A^{-\cdot}$, of a SET-initiated mechanism is energetically inaccessible in oxidation with BQ or CA ($E^0 = -0.51$ V and 0.01 V, respectively). These arguments lead to the same conclusion for **1**, whose one-electron oxidation potential should be slightly greater than that of NMA (below). The same analysis was used earlier by Verhoeven and co-workers (5) to exclude SET-initiated mechanisms in oxidation of *N*-benzyl-1,4-dihydronicotinamide (BNAH) by CA in AN. More recently Miller and co-workers (14) have investigated the kinetics of oxidation of NADH by a series of ferrocinium cation one-electron oxidants in aqueous 1-propanol. Their results enable them to estimate E^0 for one-electron oxidation of NADH in aqueous solution, and from it the rate constant for formation of the $DH^{+\cdot}\ A^{-\cdot}$ intermediate in oxidation of NADH by BQ. The calculated rate constant was 4×10^4 times smaller than the experimental rate constant, leading to the conclusion that oxidation of NADH by BQ in water cannot occur by a SET-initiated pathway.

Although a SET-initiated mechanism cannot be excluded by the same arguments for DCBQ ($E^0 = 0.30$ V), the relative reactivities of 2- and 3-methoxy-*N*-methoxyacridans (1) and of NMA and 10,10′-dimethyl-9,9′-biacridanyl (7) strongly indicate a synchronous mechanism for this acceptor as well. The kie in reaction of **1** with DDQ ($E^0 = 0.50$ V) remains large and is not out of line with that expected from the kie's of the less reactive benzoquinones. Consequently, although the extent of C—H bond breaking, C—O bond making, and degree of charge transfer (1) must change in a regular way from BQ to DDQ, the kie's for the benzoquinones are most simply accommodated by a mechanism in which electron and proton transfer are strongly coupled, that is, essentially a one-step hydride transfer.

It is interesting to compare the kie's observed in this work with those reported in two recent related studies. Kreevoy and co-workers (15) have reported primary kie's of 5.71 and 5.45, respectively, in oxidation of 9,9′-dideuterio-NMA by *N*-methyl- and *N*-(4-trifluoromethylbenzyl)-3-cyanoquinolinium ions in 4:1 2-propanol – water at 25°C. The measured equilibrium constants for the two oxidations are 0.70 and 28, respectively, and therefore these kie's would be expected to be close to the theoretical maximum. Interestingly, several of the kie's observed in oxidation of **1** and NMA (3) by uncharged π acceptors in AN are considerably larger. Further work is required to determine the reasons for these differences.

In a second related study Tanaka and co-workers (16) measured kie's in oxidation of BNAH with a series of benzoquinones ranging in reactivity from trimethyl-1,4-benzoquinone ($E^0 = -0.75$ V, $k_H/k_D = 5.61$) to DDQ ($E^0 = 0.51$ V, $k_H/k_D = 1.5$) in AN at 25°C. A bell-shaped dependence of the kie on E^0 was observed, with a maximum at BQ ($E^0 = -0.50$ V, $k_H/k_D = 6.2$). The results were interpreted in terms of a proton transfer within the ion pair intermediate, $BNAH^{+\cdot}A^{-\cdot}$, and the maximum kie for BQ taken to mean that the pK_a's of $BNAH^{+\cdot}$ and $BQH\cdot$ are approximately equal, i.e. that ΔG^0 for the proton transfer step is approximately zero. Aside from the prohibitively high energy expected for the $BNAH^{+\cdot}BQ^{-\cdot}$ intermediate (5) there is another problem with this explanation. The pK_a of the semiquinone radical $BQH\cdot$ is around 4.0 ± 0.1 in water (17, 18) while that of $BNAH^{+\cdot}$ has been estimated as −4 in AN (19) and as −3.5 in water (14). Clearly, $BNAH^{+\cdot}$ is close to 10^7 times as acidic as $BQH\cdot$ in water and the difference will surely be much greater in AN because $BQ^{-\cdot}$ is more strongly solvated by hydrogen bonding in water than $BNA\cdot$ (20). It is clear, therefore, that the proton transfer within a $BNAH^{+\cdot}A^{-\cdot}$ intermediate would be highly exoergic for BQ, and likely for all of the quinones investigated.

In contrast to the π acceptor results, the kie in the e^-, H^+, e^- oxidation by $Co(bipy)_3^{3+}$ indicates only minor C—H bond weakening in the transition state for the rate-determining electron transfer step. For this particular system we have not been successful in determining the kie for the proton transfer step, as has recently been accomplished for several similar $Fe(CN)_6^{3-}$ oxidations (9). Further efforts along these lines are planned.

The reactivities of **1** relative to NMA (Table 1) reflect a more complex combination of effects. NMA is more rapidly oxidized than **1** with all oxidants studied, relative reactivities varying from 9.1 to 1.7×10^2. A hydride transfer transition state is expected to be much more sensitive to the steric requirements of a C-9 substituent than an electron transfer transition state. In apparent contradiction to this expectation, the relative reactivities of NMA and **1** are nearly identical for CA and $Co(bipy)_3^{3+}$, which are known to react by one-step hydride transfer and stepwise e^-, H^+, e^- mechanisms, respectively. In attempting to understand these relative reactivities it is useful to first consider the expected electronic effect of the 9-phenyl substituent in relation to transition state structure.

The pK_{R^+} values of *N*-methylacridinium ion (NMA^+) and **3** (25°C, ionic strength 0.1) (eq. [3]) are, respectively, 10.03 and 11.01 (21). The 9-phenyl substituent therefore increases the stability of the acridinium ion oxidation product relative to the acridan, and, if the transition state resembles the acridinium ion, the electronic effect of the 9-phenyl should result in a rate

[3] 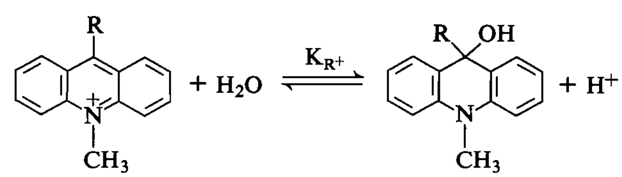

increase. A linear relationship between log k (oxidation) and pK_{R^+} was demonstrated in oxidation of a series of N-(substituted benzyl)acridans by BQ, TCNQ, CA, TCNE, and DCBQ (4). Using these relationships and the pK_{R^+} values for NMA^+ and **3**, the electronic effect of a 9-phenyl substituent should make **1** more reactive than NMA by factors of about 2.3 (BQ, AN), 3.9 (BQ, 50:50 AN–H_2O), 6.3 (TCNQ), 4.9 (CA), and 5.0 (DCBQ). In agreement with expectation, NMA^+ reacts 31 times as fast as **3** as a hydride *acceptor* with 1-benzyl-1,4-dihydronicotinamide (AN, 20°C) (22), though this difference is undoubtedly partly steric in origin.

In contrast, the anodic peak potential for (essentially reversible) one-electron oxidation of 9,9-diphenyl-NMA in AN occurs at 0.13 V higher potential than that of 9,9-dimethyl-NMA (23). From the σ_I values of H, CH_3, and phenyl (0.00, −0.04, and 0.10, respectively (ref. 20, p. 98)), we estimate that replacement of a single 9-H by phenyl should result in an increase in the one-electron oxidation potential of ca. (0.13/2)

$\times (0.10/0.14) = 4.6 \times 10^{-2}$ V. If the full influence on ΔG^0 for electrochemical oxidation is felt in $\Delta G^{\ddagger}$ for oxidation by $Co(bipy)_3^{3+}$, the electronic effect of the 9-phenyl substituent would lead to a rate decrease of ca. 6-fold.

For the benzoquinones the rate ratios (NMA vs. **1**) are approximately constant (within a factor of about 2). Given the other evidence for a one-step mechanism for these oxidations (above), these ratios are believed to reflect a combination of electronic rate enhancement and steric retardation by the 9-phenyl substituent. The estimates of electronic rate enhancements (above) lead to estimates of steric retardation factors of $9.1 \times 2.3 = 21$ (BQ), 98 (CA), and 65 (DCBQ). The reactivities of NMA relative to **1** toward TCNQ and TCNE are larger, leading by the same procedure to estimates of steric retardation factors of ca. 4.2×10^2 (TCNQ) and 5.6×10^2 (TCNE). The larger steric effects with the dicyanomethylene acceptors may be a result of greater steric requirements of a dicyanomethylene carbon vs. a carbonyl oxygen. The observed rate ratio with $Co(bipy)_3^{3+}$ reflects both electronic and steric retardation so that the steric retardation factor is estimated to be around $24/6 = 4$. More systematic investigations of steric effects in hydride transfer reactions and their use in defining the mechanism are in progress.

Experimental

Melting points were measured in open capillary tubes and are uncorrected. Proton nmr spectra were measured using a Varian EM-360 spectrometer. Chemical shifts are reported in δ units, with tetramethylsilane as internal standard. Ultraviolet–visible spectra were obtained using a Cary 118C spectrophotometer and mass spectra with a VG 7070G spectrometer. Elemental microanalyses were performed by Guelph Chemical Laboratories, Guelph, Ontario.

Reagents and solvents

BQ, TCNQ, CA, TCNE, DCBQ, and $Co(bipy)_3(ClO_4)_3 \cdot 3H_2O$ were obtained and purified as described earlier (1, 3). BA was prepared from hydroquinone following Torrey and Hunter (24) and purified by crystallization from benzene, mp 304–305°C (lit. (25) mp 300°C). DDQ (Aldrich) was purified by crystallization from benzene followed by drying under vacuum, mp 215–217°C (lit. (26) mp 215–217°C).

10-Methyl-9-phenylacridan (**1**(H)) was obtained, along with variable amounts of 10,10′-dimethyl-9,9′-biacridanyl by reaction of *N*-methylacridinium iodide (3) with phenylmagnesium bromide in anhydrous ether (27) and purified by recrystallizing twice from ethanol, mp 104–106°C (lit. (27) mp 104°C); nmr ($CDCl_3$) δ: 3.3 (s, 3H, N-CH_3), 5.10 (s, 1H, 9-H), 6.67–7.32 (m, 13H, aromatic). Mass spectrum (*m/e*): 271 (M^+), 194 (M^+ − phenyl). *Anal.* calcd. for $C_{20}H_{17}N$: C 88.52, H 6.31, N 5.16; found: 88.54, H 6.25, N 5.30.

9-Deuterio-10-methyl-9-phenylacridan (**1**(D)) was obtained by reduction of 10-methyl-9-phenylacridinium perchlorate with sodium borodeuteride (min. 98 at.% D) as described earlier for reduction of *N*-methylacridinium perchlorate (3) and purified by recrystallizing 3 times from absolute ethanol, mp 107–108°C. The yield of purified product was 37%. Its nmr spectrum indicated about 5% H at the 9 position. 10-Methyl-9-phenylacridinium perchlorate was obtained in yields over 90% by oxidation of **1** with DDQ in ether solution as described earlier for oxidation of NMA (3).

Kinetic measurements

Kinetics of oxidation were measured spectrophotometrically using methods and instrumentation described earlier (1, 3). The progress of the reaction was followed at the 10-methyl-9-phenylacridinium ion maximum at 361 nm (22) for all oxidants except TCNQ, where the formation of $TCNQ^{\cdot -}$ was followed at 680 or 740 nm. Measurements were carried out under pseudo first-order conditions using a 30-fold or greater excess of oxidant over acridan with all oxidants except BA and $Co(bipy)_3^{3+}$, where lower ratios (Table 1) were used and the data analyzed using the appropriate second-order rate equation (1). $Co(bipy)_3^{3+}$ rates were run under N_2 atmosphere after degassing.

Acknowledgements

Financial support from the Natural Sciences and Engineering Research Council of Canada is gratefully acknowledged. We wish to thank R. E. Berry for technical assistance and R. J. Balahura for the use of stopped flow equipment.

1. A. K. COLTER, P. PLANK, J. P. BERGSMA, R. LAHTI, A. A. QUESNEL, and A. G. PARSONS. Can. J. Chem. **62**, 1780 (1984).
2. M. F. POWELL and T. C. BRUICE. J. Am. Chem. Soc. **105**, 7139 (1983).
3. A. K. COLTER, G. SAITO, and F. J. SHAROM. Can. J. Chem. **55**, 2741 (1977).
4. A. K. COLTER, C. C. LAI, T. W. WILLIAMSON, and R. E. BERRY. Can. J. Chem. **61**, 2544 (1983).
5. F. M. MARTENS, J. W. VERHOEVEN, R. A. GASE, U. K. PANDIT, and TH. J. DEBOER. Tetrahedron, **34**, 443 (1978).
6. A. CASTELLANO, J. P. CATTEAU, and A. LEBLANCHE-COMBIER. J. Phys. Chem. **80**, 2614 (1976).
7. A. K. COLTER, C. C. LAI, A. G. PARSONS, N. B. RAMSEY, and G. SAITO. Can. J. Chem. **63**, 445 (1985).
8. G. SAITO and A. K. COLTER. Tetrahedron Lett. **38**, 3325 (1977).
9. M. F. POWELL, J. C. WU, and T. C. BRUICE. J. Am. Chem. Soc. **106**, 3850 (1984).
10. M. E. PEOVER. J. Chem. Soc. 4540 (1962).
11. M. E. PEOVER. Trans. Faraday Soc. **58**, 2370 (1962).
12. R. M. SCRIBNER. J. Org. Chem. **31**, 3671 (1966).
13. N. TANAKA and Y. SATO. Bull. Chem. Soc. Jpn. **41**, 2059 (1968).
14. (*a*) B. W. CARLSON and L. L. MILLER. J. Am. Chem. Soc. **105**, 7453 (1983); (*b*) B. W. CARLSON, L. L. MILLER, P. NETA, and J. GRODKOWSKI. J. Am. Chem. Soc. **106**, 7233 (1984).
15. D. OSTOVIĆ, R. M. G. ROBERTS, and M. M. KREEVOY. J. Am. Chem. Soc. **105**, 7629 (1983).
16. S. FUKUZUMI, N. NISHIZAWA, and T. TANAKA. J. Org. Chem. **49**, 3571 (1984).
17. K. B. PATEL and R. L. WILLSON. J. Chem. Soc. Faraday Trans. 1, **69**, 814 (1973).
18. D. VELTWISCH and K.-D. ASMUS. J. Chem. Soc. Perkin Trans. 2, 1147 (1982).
19. F. M. MARTENS and J. W. VERHOEVEN. Recl. Trav. Chim. Pays-Bas, **100**, 229 (1981).
20. J. HINE. Structural effects on equilibria in organic chemistry. John Wiley and Sons, New York, NY. 1975. p. 133.
21. J. W. BUNTING and W. G. MEATHRELL. Can. J. Chem. **51**, 1965 (1973).
22. A. VAN LAAR, H. J. VAN RAMESDONK, and J. W. VERHOEVEN. Recl. Trav. Chim. Pays-Bas, **102**, 157 (1983).
23. H. STURM, H. KIESELE, and E. DALTROZZO. Chem. Ber. **111**, 227 (1978).
24. H. A. TORREY and W. H. HUNTER. J. Am. Chem. Soc. **34**, 702 (1914).
25. C. GRAEBE and L. WELTNER. Ann. **263**, 31 (1891).
26. P. W. D. MITCHELL. Can. J. Chem. **41**, 550 (1963).
27. M. FREUND and G. BODE. Ber. **42**, 1746 (1909).

Stéréochimie de la réduction des α-iminocétones. Étude de l'effet des substituants par une approche quantitative des facteurs gouvernant la stéréosélectivité

BENITO ALCAIDE, CARMEN L. MARDOMINGO, RAFAEL PÉREZ-OSSORIO ET JOAQUÍN PLUMET[1]
Departamento de Química Orgánica, Facultad de Química, Universidad Complutense, Ciudad Universitaria, 28040 Madrid, Espagne

ET

ROGER PHAN-TAN-LUU[1] ET MICHELLE SARGENT
Laboratoire de Prospective Réactionnelle et d'Analyse de l'Information, Université d'Aix-Marseille III, Rue Henri Poincaré, 13397 Marseille, France

Reçu le 21 septembre 1984

BENITO ALCAIDE, CARMEN L. MARDOMINGO, RAFAEL PÉREZ-OSSORIO, JOAQUÍN PLUMET, ROGER PHAN-TAN-LUU et MICHELLE SARGENT. Can. J. Chem. **63**, 2241 (1985).

À partir du rapport *RR,SS*/*RS,SR* des 2-aminoéthanols isomères obtenus par réduction de 24 α-iminocétones ($LiAlH_4$) les auteurs ont étudié l'influence des substituants sur la stéréochimie de la réaction en postulant un modèle mathématique à 7 coefficients. Les valeurs de ces coefficients calculées par regression multilinéaire sont d'accord avec le mécanisme de réduction postulé précédemment et mettent en évidence quelques conclusions additionnelles. L'application des méthodes modernes de construction de matrices d'expériences permet d'en choisir 10 d'un ensemble de 24 expériences et montre que ce sous-ensemble permet d'extraire des informations de la même qualité.

BENITO ALCAIDE, CARMEN L. MARDOMINGO, RAFAEL PÉREZ-OSSORIO, JOAQUÍN PLUMET, ROGER PHAN-TAN-LUU, and MICHELLE SARGENT. Can. J. Chem. **63**, 2241 (1985).

Using the isomeric ratio of *RR,SS* to *RS,SR* of a series of 2-aminoethanols obtained by the $LiAlH_4$ reduction of 24 α-iminoketones we propose a mathematical model with 7 coefficients for the effect of substituent on the stereochemical course of the reaction. The values of these coefficients obtained by multilinear regression analysis are in agreement with the previously proposed mechanism for reduction but allow for some additional conclusions. The use of modern methods for the construction of experimental matrices allows us to choose 10 from a total of 24 experiments and shows that information of the same quality can be obtained from this subset.

[Journal translation]

Introduction

La réduction des α-iminocétones par l'action de l'hydrure de lithium-aluminium (HAL) conduit à la formation de mélanges de 2-aminoéthanols stéréoisomères (1, 2).

L'étude du cours du processus permet d'établir que la stéréochimie de la réaction est le résultat d'une compétition entre deux chemins réactionnels formulés dans la fig. 1. Le chemin **a** est le résultat de l'attaque préalable du groupement carbonyle conduisant à l'isomère *RR,SS*, et le chemin **b**, issu de l'attaque préalable du groupement imino conduisant à l'isomère *RS,SR*. Cette simplification fondée sur les données expérimentales dans le cas des α-iminocétones dérivées des systèmes benzyliques[2] et raisonnablement étendue aux autres α-iminocétones[3] a été expliqué précédemment à l'aide des modèles stéréochimiques qui rendent compte du résultat du processus (2).

L'objectif de ce travail est de déduire une équation multiparamétrique, en utilisant les données expérimentales disponibles et qui nous permettra d'établir quantitativement l'influence de la modification structurelle des α-iminocétones sur la stéréochimie de la réduction. Dans ce but, nous avons fait varier les substituants R^1 et R^2 (Ph ou Me, fig. 1), et R^3 par le changement de la nature et de la position (*m* ou *p*) du substituant aromatique X. Pour caractériser ce substituant, nous avons choisi deux paramètres électroniques qui décrivent les effets inductif et de résonance que nous voulons considérer. Finalement nous effectuerons une critique méthodologique "a posteriori" de la démarche suivie dans le traitement du problème.

Modèle mathématique

Notre modèle mathématique est une équation dont la réponse étudiée est le pourcentage du stéréoisomère *RR,SS*, et qui comprend quatre termes du premier degré, traduisant l'effet global des variables étudiées et deux termes d'intéraction qui tiennent compte de la possibilité de que l'effet de la nature du substituant R^3 n'est pas indépendant de la nature du substituant R^2. L'effet global de R^3 est décrit par les paramètres σ_0^R et σ_I (5).

Le modèle peut donc s'écrire:

$$[1] \quad Y = (\%RR,SS) = a_0 + a_1(R^1) + a_2(R^2) + a_3(\sigma_0^R \text{ de X}) + a_4(\sigma_I \text{ de X}) + a_{23}(R^2)(\sigma_0^R \text{ de X}) + a_{24}(R^2)(\sigma_I \text{ de X})$$

Nous avons réuni l'ensemble de 24 molécules dont on a étudié la réduction avec HAL/Et_2O dans le tableau 1, ainsi que les valeurs des variables correspondantes et la réponse expérimentale obtenue. Pour éviter le danger d'une interprétation du modèle exprimé avec des variables naturelles, nous utilisons pour le facteur R^3 des variables codées (6) qui sont obtenues à partir de la transformation:

$$[2] \quad \text{variable codée} = (\text{variable naturelle} - \text{centre})/\text{pas}$$

Pour chaque variable, le centre choisi est la valeur médiane et le pas de variation est tel que la variable codée est comprise entre +1 et −1. Le tableau 2 résume les valeurs du centre et

[1] Auteurs auxquels la correspondence peut être adressée.
[2] L'hydrogénation catalytique d'iminocétones benzyliques et la réduction ultérieure des aminocétones intermediaires avec HAL conduit exclusivement à l'isomère *RS,SR* (3, 4).
[3] B. Alcaide, R. Pérez-Ossorio et J. Plumet: résultats non publiés.

TABLEAU 1. Réaction de réduction de α-iminocétones avec HAL/Et_2O. Paramètres descripteurs du substituant R^3

N°	R^1	R^2	R^3	σ_0^R	σ_I	%*RR*,*SS*
1	Ph	Ph	C_6H_5	0,00	0,00	63,9
2	Ph	Ph	pFC_6H_4	−0,34	0,51	89,6
3	Ph	Ph	$pClC_6H_4$	−0,20	0,47	74,4
4	Ph	Ph	$pBrC_6H_4$	−0,16	0,45	81,0
5	Ph	Ph	pIC_6H_4	−0,12	0,39	56,1
6	Ph	Ph	$pMeOC_6H_4$	−0,41	0,26	95,0
7	Ph	Ph	$pMeC_6H_4$	−0,10	−0,05	79,6
8	Ph	Ph	$pMe_2NC_6H_4$	−0,52	0,05	97,5
9	Ph	Ph	$mClC_6H_4$	0,00	0,47	55,9
10	Ph	Ph	$mMeC_6H_4$	0,00	−0,05	75,1
11	Ph	Me	C_6H_5	0,00	0,00	31,0
12	Ph	Me	$pMeC_6H_4$	−0,10	−0,05	25,9
13	Ph	Me	$pMeOC_6H_4$	−0,41	0,26	23,1
14	Ph	Me	pFC_6H_4	−0,34	0,51	29,5
15	Ph	Me	$pClC_6H_4$	−0,20	0,47	29,5
16	Ph	Me	$pMe_2NC_6H_4$	−0,52	0,05	20,0
17	Me	Me	C_6H_5	0,00	0,00	33,8
18	Me	Me	$pMeC_6H_4$	−0,10	−0,05	30,1
19	Me	Me	pFC_6H_4	−0,34	0,51	28,1
20	Me	Me	$pClC_6H_4$	−0,20	0,47	30,1
21	Me	Me	$pBrC_6H_4$	−0,16	0,45	31,0
22	Me	Me	pIC_6H_4	−0,12	0,39	32,1
23	Me	Me	$pMeOC_6H_4$	−0,41	0,26	28,1
24	Me	Me	$pMe_2NC_6H_4$	−0,52	0,05	23,7

pas choisies pour chaque variable.

L'équation [1] peut alors s'écrire:

$$[3] \quad Y = b_0 + b_1x_1 + b_2x_2 + b_3x_3 + b_4x_4 + b_{23}x_2x_3 + b_{24}x_2x_4$$

Nous donnons dans le tableau 3 la matrice d'expériences exprimée en variables codées.

Les valeurs trouvées pour les facteurs d'inflation[4] étant satisfaisantes (tableau 4), nous pouvons calculer par la méthode des moindres carrés des estimations valables des coefficients du modèle:

$$[4] \quad Y = 55{,}7 - 1{,}1x_1 + 27{,}9x_2 - 6{,}9x_3 - 1{,}5x_4 - 11{,}6x_2x_3 - 3{,}2x_2x_4 \quad (R_A^2 = 0{,}96)^5$$

Interprétation

Nous pouvons constater la faible influence de la variable x_1 ($b_1 = -1{,}1$). Les autres coefficients b_2, b_3 et b_4, respectivement égaux à +27,9, −6,5 et −1,5 ne peuvent être interprétés seuls, les effets des variables x_2, x_3 et x_4 n'étant pas indépendants par hypothèse (intéractions x_2x_3 et x_2x_4). D'autre part, la haute valeur du coefficient b_{23} (−11,6) et la petite valeur (−3,2) de b_{24} sont significatives. L'intéraction la plus importante, b_{23}, correspond aux variables (R^2): (σ_0^R de X) ce qui signifie que les effets des substituants en position 3 sur la réponse étudiée ne sont pas additifs, c'est-à-dire, l'influence de σ_0^R de X sur %*RR*,*SS* n'est pas la même suivant la nature de R^2 (Me ou Ph). Ceci peut être visualisé facilement en représentant la réponse *Y* en fonction de σ_0^R de X (fig. 2).

Nous en déduisons que l'influence de σ_0^R de X sur la stéréochimie de la réaction est beaucoup plus importante dans le cas

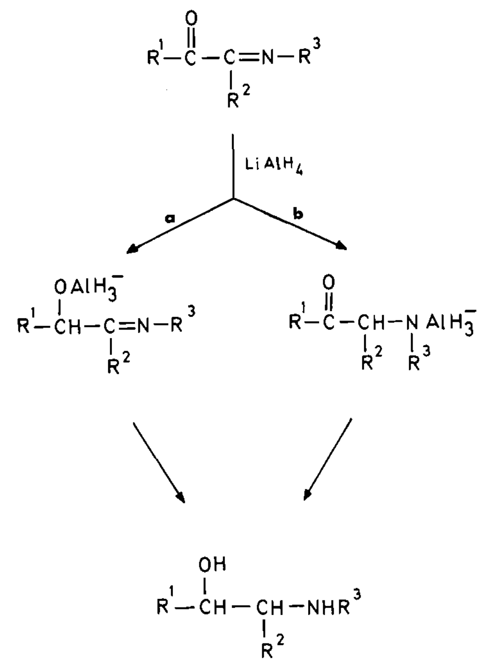

FIG. 1

TABLEAU 2. Centre et pas de variation des variables

Variable codée[a]	Variable naturelle	Centre	Pas
x_3	σ_0^R de X	0,26	0,26
x_4	σ_I de X	0,23	0,28

[a] $x_j = -1$ pour R^j = Me; $x_j = +1$ pour R^j = Ph (j = 1, 2).

TABLEAU 3. Matrice d'expériences complète (variables codées)

Exp. N°	x_1	x_2	x_3(σ_0^R de X)	x_4(σ_I de X)
1	1	1	1,0000	−0,8214
2	1	1	−0,3077	1,0000
3	1	1	0,2308	0,8571
4	1	1	0,3846	0,7857
5	1	1	0,5385	0,5714
6	1	1	−0,5769	0,1071
7	1	1	0,6154	−1,0000
8	1	1	−1,0000	−0,6429
9	1	1	1,0000	0,8571
10	1	1	1,0000	−1,0000
11	1	−1	1,0000	−0,8214
12	1	−1	0,6154	−1,0000
13	1	−1	−0,5769	0,1071
14	1	−1	−0,3077	1,0000
15	1	−1	0,2308	0,8571
16	1	−1	−1,0000	−0,6429
17	−1	−1	1,0000	−0,8214
18	−1	−1	0,6154	−1,0000
19	−1	−1	−0,3077	1,0000
20	−1	−1	0,2308	0,8571
21	−1	−1	0,3846	0,7857
22	−1	−1	0,5385	0,5714
23	−1	−1	−0,5769	0,1071
24	−1	−1	−1,0000	−0,6429

[4] On entend par facteur d'inflation le terme diagonal de la matrice inverse de la matrice de corrélation. Voir réf. 7.

[5] Pour la définition de R_A^2 voir réf. 12.

TABLEAU 4. Facteurs d'inflation pour l'éq. [3] avec la totalité de molécules (colonne a) avec la matrice optimale-D, N = 10 (colonne b)

Coeff.	Facteur d'inflation (a)	Facteur d'inflation (b)
b_1	1,60	1,40
b_2	1,68	1,45
b_3	1,09	1,09
b_4	1,06	1,07
b_{23}	1,13	1,06
b_{24}	1,06	1,05

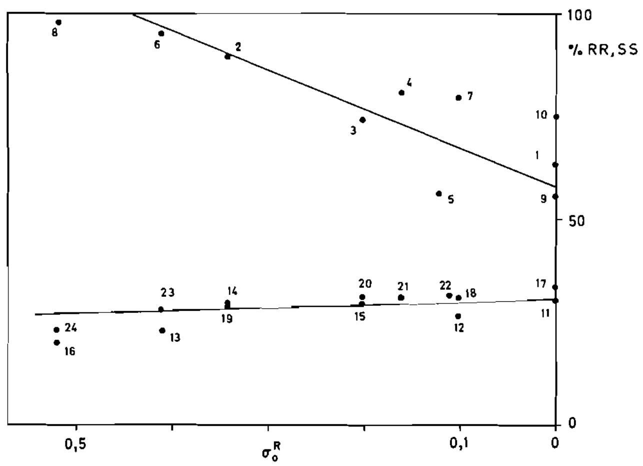

FIG. 2. La réponse (Y) en fonction de σ_0^R de X.

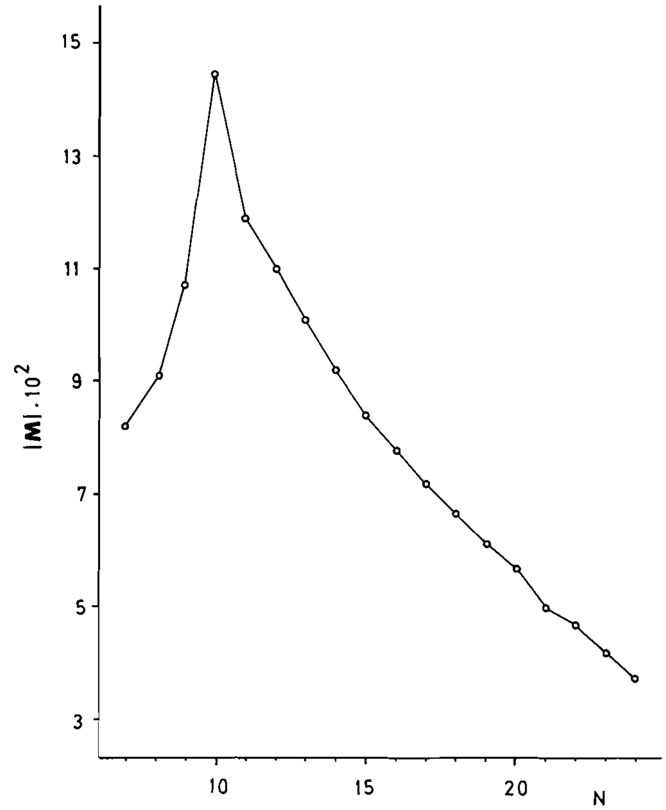

FIG. 3. La valeur du déterminant $|\mathbf{M}|$ en fonction de N.

de monoimines dérivées du benzyl (expériences 1–10, correspondant à la présence d'un groupement phényl en position 2) que dans le cas où R^2 est un groupement méthyl, expériences 11–24 pour lesquelles l'influence de σ_0^R est pratiquement nulle.

Conclusion du point de vue chimique

L'étude de la réaction de réduction réalisée sur l'ensemble de 24 α-iminocétones et celle du modèle confirment le schéma réactionnel proposé (fig. 1) et mettent en évidence le changement de mécanisme en passant des composés avec R^2 = Ph aux composés avec R^2 = Me.

Pour les molécules 1–10, le chemin de réaction **a** est choisi de préférence au chemin **b**: les caractéristiques électroniques du groupement phényl en position 2 provoquent un "durcissement" du groupement carbonyle (chemin **a**) et donc l'augmentation du pourcentage de l'isomère *RR,SS* (voir fig. 1). Ceci implique que la cétone n'est pas conjugée au groupe imino, ce qui a été confirmé pour ces composés par analyse au rayons-X (8) et rmn du carbone-13 (9).

Dans le premier groupe de molécules l'influence de la nature électronique de R^3 est confirmée (2). Plus le substituant R^3 est électrodonneur plus la conjugaison augmente, c'est-à-dire, plus grande est la planarité entre groupements aromatique R^3 et imino. Par conséquent il y a une augmentation du pourcentage de l'isomère *RR,SS*.

Par contre cette influence est nulle pour le deuxième sous-ensemble d'iminocétones (11–24, R^2 = Me). Nous constatons que la substitution d'un méthyl par un phényl en position 1, et le caractère inductif du substituant R^3 n'ont pas d'influence sur la stéreochimie de la réduction de ce genre de composés.

Présentation d'une strategie optimale

Les données que nous avons utilisées dans la première partie de cette étude ont été obtenues sans suivre une strategie bien définie, le problème se précisant au fur et à mesure de l'avancement du travail.

Nous allons illustrer l'application de la Méthodologie de la Récherche Expérimentale (10) à notre problème en supposant qu'aucune expérience n'a été faite. Nous avons à notre disposition 24 molécules candidates.

1. Cet ensemble de molécules contient-il assez d'information?

Les valeurs des coefficients d'inflation permettent de dire que cet ensemble est bien structuré et que les informations obtenues sont de bonne qualité. Rappelons que les facteurs d'inflation peuvent être calculés avant d'avoir effectué des expériences.

2. Peut-on réduire le nombre d'expériences sans affecter sensiblement la qualité des informations fournies?

Nous avons extrait de l'ensemble de 24 points candidats le meilleur sous-ensemble permettant d'étudier le modèle postulé. Le critère choisi est le critère d'optimalité-D (maximisation du déterminant de la matrice d'information normée $|\mathbf{M}|$). Pour différentes valeurs de N (N = nombre de molécules) nous avons calculé la matrice d'expériences optimale-D. Dans la fig. 3, nous montrons la variation de $|\mathbf{M}|$ en fonction de N. On peut constater l'existence d'un maximum pour N = 10. La matrice d'expériences correspondente comporte les molécules données dans le tableau 5. La valeur du déterminant normé décroit régulièrement de N = 10 à N = 24 (fig. 3). Les valeurs des facteurs d'inflation sont satisfaisantes pour la matrice d'expériences optimale-D (tableau 4).

Nous avons calculé les coefficients du modèle (éq. [3]) par la méthode des moindres carrés en utilisant le sous-ensemble des 10 molécules. Les valeurs de ces coefficients ne diffèrent

TABLEAU 5. Matrice d'expériences optimale-D ($|X'X|$ = 1 329 000, $|\mathbf{M}|$ = 0,1329, trace $(X'X)^{-1}$ = 1,06)

N	R^1	R^2	R^3
2	Ph	Ph	$p\mathrm{FC_6H_4}$
8	Ph	Ph	$p\mathrm{Me_2NC_6H_4}$
9	Ph	Ph	$m\mathrm{ClC_6H_4}$
10	Ph	Ph	$m\mathrm{MeC_6H_4}$
11	Ph	Me	$\mathrm{C_6H_5}$
14	Ph	Me	$p\mathrm{FC_6H_4}$
16	Ph	Me	$p\mathrm{Me_2NC_6H_4}$
17	Me	Me	$\mathrm{C_6H_5}$
19	Me	Me	$p\mathrm{FC_6H_4}$
24	Me	Me	$p\mathrm{Me_2NC_6H_4}$

TABLEAU 6. Estimation des coefficients obtenus par la méthode des moindres carrés avec l'ensemble des 24 expériences (coeff. 1) et avec le sous-ensemble à 10 molécules (coeff. 2)

i de b_i	Coeff. 1[a]	Coeff. 2[b]
1	−1,1	−0,9
2	27,9	27,5
3	−6,9	−5,4
4	−1,5	−1,4
23	−11,6	−10,9
24	−3,2	−3,3

[a] Coefficient de regression multiple ajusté R^2_A = 0,96.
[b] Coefficient de regression multiple ajusté R^2_A = 0,95.

pas significativement de celles que nous avons calculées plus haut avec la totalité de molécules (tableau 6).

Dans le tableau 7, nous avons réuni les valeurs expérimentales (*%RR,SS*) et les valeurs de la réponse calculées à partir des modèles à 24 et à 10 expériences. L'accord entre ces valeurs est satisfaisant.

Matrice d'expériences robuste

La structure de la matrice d'expériences optimale n'est valable que pour le modèle formulé. Si nous changeons de modèle, il est évident que la matrice d'expériences sera modifiée, les informations nécessaires n'étant pas les mêmes.

Dans une deuxième démarche, nous envisageons le cas où nous ne faisons aucune hypothèse sur le modèle. Nous avons utilisé une démarche analoge à celle de Kennard et Stone (11) qui propose une répartition uniforme de points dans le domaine expérimental. La procédure originale est insuffisante à certain niveau: elle ne donne que l'ordre d'apparition des points mais ne permet pas de mettre en évidence des arrangements de points constituants des structures optimales que nous appelons "stables". Nous avons utilisé un algorithme modifié mettant en évidence ces structures. Ceci nous permet de selectionner un sous-ensemble de points qui nous donne suffisamment d'information pour envisager une interpolation ultérieure. La meilleure distribution de points donnant une structure stable est celle donnée dans le tableau 8.

Les deux matrices obtenues comportent de nombreux points communs. Notons la proximité topologique des points 19 et 20.

TABLEAU 7. Valeurs de *%RR,SS* expérimentales et calculées par le modèle avec l'ensemble des 24 expériences (a) et avec le sous-ensemble à 10 molécules (b)

N°	*Y* (*%RR,SS*) exp.	*Y* calculée (a)	*Y* calculée (b)
1	63,9	67,9	70,2
2	89,6	83,4	82,9
3	74,4	74,5	74,8
4	81,0	71,7	72,6
5	56,1	69,8	71,1
6	95,0	92,6	91,5
7	79,6	75,8	77,3
8	97,5	103,9	101,8
9	55,9	59,9	62,3
10	75,1	68,8	71,0
11	31,0	30,0	31,5
12	25,9	27,9	29,2
13	23,1	24,1	24,7
14	29,5	26,9	27,9
15	29,5	29,2	30,6
16	20,0	20,9	21,0
17	33,8	32,6	33,2
18	30,1	30,2	30,8
19	28,1	29,1	29,6
20	30,1	31,4	32,3
21	31,0	32,0	33,0
22	32,1	32,4	33,4
23	28,1	26,4	26,5
24	23,7	23,2	22,7

TABLEAU 8. Matrice d'expériences robuste ($|X'X|$ = 1 287 500, $|\mathbf{M}|$ = 0,12875)

N	R^1	R^2	R^3
2	Ph	Ph	$p\mathrm{FC_6H_4}$
8	Ph	Ph	$p\mathrm{Me_2NC_6H_4}$
9	Ph	Ph	$m\mathrm{ClC_6H_4}$
10	Ph	Ph	$m\mathrm{MeC_6H_4}$
11	Ph	Me	$\mathrm{C_6H_5}$
14	Ph	Me	$p\mathrm{FC_6H_4}$
16	Ph	Me	$p\mathrm{Me_2NC_6H_4}$
17	Me	Me	$\mathrm{C_6H_5}$
20	Me	Me	$p\mathrm{ClC_6H_4}$
24	Me	Me	$p\mathrm{Me_2NC_6H_4}$

1. B. ALCAIDE, R. FERNANDEZ, C. LÓPEZ-MARDOMINGO, R. PÉREZ-OSSORIO et J. PLUMET. J. Org. Chem. **46**, 3234 (1981).
2. B. ALCAIDE, C. LÓPEZ-MARDOMINGO, R. PÉREZ-OSSORIO et J. PLUMET. J. Chem. Soc. Perkin Trans. 2, 1649 (1983).
3. B. ALCAIDE, G. ESCOBAR, C. LÓPEZ-MARDOMINGO, R. PÉREZ-OSSORIO et J. PLUMET. Tetrahedron Lett. 2033 (1982).
4. B. ALCAIDE, G. ESCOBAR, R. PÉREZ-OSSORIO et J. PLUMET. Org. Prep. Proc. Int. (Brief), **14**(3), 220 (1982).
5. N. B. CHAPMAN et J. SHORTER. Correlation analysis in chemistry. Plenum Press, New York. 1978. p. 439.
6. D. MATHIEU. Thèse d'Etat. Université d'Aix-Marseille III, 1981.
7. S. CHATTERJEE et B. PRICE. Regression analysis by example. Wiley, New York. 1977. p. 182.
8. I. FONSECA, S. GARCÍA-BLANCO et S. MARTINEZ. Acta Crystallogr. Sect. B, **35**, 2643 (1979).
9. J. L. GARCÍA RUANO, R. HARO, C. PASCUAL, R. PÉREZ-OSSORIO et J. PLUMET. An. Quim. **75**, 165 (1979).
10. NEMROD. New Efficient Methodology of Research using Optimal Design. 1981.
11. R. W. KENNARD et L. A. STONE. Technometrics, **11**, 137 (1969).
12. R. D. SNEE. J. Qual. Technol. **3**, 159 (1971).

Étude cinétique de l'ouverture thermique de la liaison C—C d'aziridines et d'époxydes dipôles-1,3 potentiels: I. Méthode d'étude expérimentale

AÏCHA DERDOUR ET FERNAND TEXIER

Laboratoire de synthèse organique, ONRS 75B/033, Institut de Chimie, Université d'Oran, Es-Sénia, Algérie

Reçu le 25 septembre 1984

AÏCHA DERDOUR et FERNAND TEXIER. Can. J. Chem. **63**, 2245 (1985).

Les cyano-2 aziridines **1**, les alcoxy carbonyl-2 aziridines **2**, les aroyl-2 aziridines **3** et les dicyano-2,2 aryl-3 oxiranes **4** s'ouvrent thermiquement entre les deux carbones pour donner respectivement un ylure d'azométhine et un ylure de carbonyle. La réaction de ces ylures d'azométhine avec l'ACDM (acétylène dicarboxylate de méthyle) conduit à une pyrroline-3 qui évolue, selon les substituants, en pyrroline-2 ou en pyrrole. L'addition des ylures de carbonyle donne des dihydrofuranes. Le traitement cinétique de l'addition de ces hétérocycles **1** à **4** à l'ACDM permet la détermination de la constante de vitesse d'ouverture de la liaison C—C (k_1). La réaction est suivie à l'aide de l'ir dans le cas des aziridines **1** et de la hplc dans tous les autres cas. La constante expérimentale de vitesse (k_{ex}) est toujours d'ordre 1 par rapport à l'hétérocycle. Dans le cas des *N*-cyclohexyl cyano-2 alkyl-3 aziridines et de la *N*-cyclohexyl carbométhoxy-2 phényl-3 aziridine, k_{ex} dépend de la concentration en ACDM, ce qui implique que la cycloaddition de l'ylure d'azométhine et sa refermeture en aziridine ont des vitesses comparables. Dans les autres cas, k_{ex} est indépendante de la concentration en ACDM, ce qui correspond à une lente transformation de l'hétérocycle en dipôle-1,3 suivie d'une cycloaddition rapide, $k_{ex} \simeq k_1$.

AÏCHA DERDOUR and FERNAND TEXIER. Can. J. Chem. **63**, 2245 (1985).

The thermolysis of the 2-cyanoaziridines (**1**), 2-alkoxycarbonylaziridines (**2**), 2-arylaziridines (**3**), and 2,2-dicyano-3-aryloxiranes (**4**) leads to a rupture of the carbon–carbon bond yielding an azomethine ylide and the ylide of a carbonyl. The reaction of these ylides of azomethine with methyl acetylene dicarboxylate (MADC) leads to the formation of a 3-pyroline, which is transformed, according to the substituants, to a 2-pyrroline or to pyrrole. The addition of the ylides of carbonyl leads to the formation of dihydrofurans. Through the kinetic treatment of the addition of these heterocyclic compounds (**1** to **4**) to MADC, it is possible to determine the rate constants for the opening of the C—C bond (k_1). In the case of the aziridines **1**, the rates have been determined by ir while hplc has been used in the other cases. Relative to the heterocyclic compounds, the order of the experimental rate constants (k_{ex}) is always equal to one. In the cases of the *N*-cyclohexyl-2-cyano-3-alkylaziridines and of the *N*-cyclohexyl-2-carbomethoxy-3-phenylaziridine, k_{ex} varies with the concentration of MADC and this implies that the rate constants for the cycloaddition of the ylide of azomethine and its reclosing to give aziridine are similar. In the other cases, k_{ex} is independent of the concentration of MADC and this implies that the heterocyclic compounds are slowly transformed into 1,3-dipoles, followed by a rapid cycloaddition, $k_{ex} \simeq k_1$.

[Journal translation]

Introduction

Les aziridines et époxydes convenablement substitués s'ouvrent thermiquement entre les deux carbones (1, 2). Les dipôles-1,3 ainsi formés ne sont pas isolés, mais ils peuvent être additionnés à différents dipolarophiles permettant ainsi la synthèse d'hétérocycles à cinq chaînons variés (schéma 1).

Malgré la diversité des réactions de cycloaddition d'ylures d'azométhine et d'ylures de carbonyle obtenus par thermolyse du petit cycle à trois chaînons correspondant, l'étude cinétique de ces réactions n'a été que partiellement abordée (3, 4) et le but recherché par ces auteurs n'était pas l'étude des facteurs qui favorisent l'ouverture électrocyclique.

La stéréochimie de l'ouverture de ces petits cycles en dipôles-1,3 est bien expliquée par les règles de Woodward et Hoffmann (5). Par contre, les facteurs qui favorisent ces réactions ne semblent pas avoir été clairement dégagés malgré quelques tentatives faites par Epiotis (6) et Carpenter (7); récemment, l'un d'entre nous a tenté d'interpréter la réactivité péricyclique des cycles à trois chaînons à l'aide de la méthode des relaxations (8). C'est pourquoi, nous nous sommes proposés d'étudier la vitesse d'ouverture des aziridines **1**, **2** et **3** substituées respectivement en 2 par un nitrile, un ester ou une cétone, et des époxydes **4** substitués en 2 par deux nitriles; en effet, selon la littérature, l'ouverture péricyclique des aziridines et époxydes est facilitée par des substituants électro-attracteurs sur les carbones (1, 2, 8):

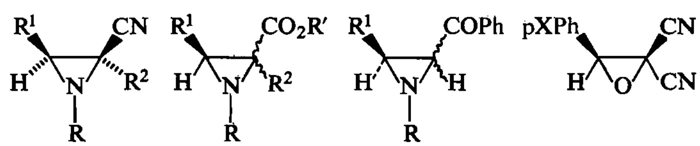

1 **2** **3** **4**

1. Position du problème

Les ylures d'azométhine ainsi que les ylures de carbonyle obtenus par ouverture thermique des hétérocycles à trois chaînons correspondants sont des intermédiaires réactionnels qui ne sont mis en évidence que par leurs produits de cycloaddition. L'équilibre aziridine ⇄ ylure d'azométhine est considérablement déplacé vers l'aziridine (9), de telle sorte que les ylures d'azométhine ne sont pas détectables par les méthodes spectroscopiques usuelles. Cependant, il peut être démontré, grâce à des études cinétiques, que l'addition d'une aziridine, ou

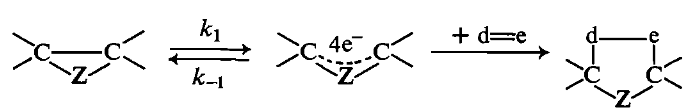

[Z = N—R: ylure d'azométhine
Z = O: ylure de carbonyle]

SCHÉMA 1

d'un époxyde, à un dipolarophile est précédée de la formation réversible d'un intermédiaire d'énergie élevée (3, 9, 10). C'est la raison pour laquelle nous avons étudié la cinétique de l'addition des aziridines **1** à **3** et des époxydes **4** à l'acétylène dicarboxylate de méthyle (ACDM) afin de déterminer les constantes de vitesse correspondant à l'ouverture thermique de la liaison C—C.

D'une manière générale, l'addition d'une aziridine ylure d'azométhine potentiel à un dipolarophile peut être schématisée comme suit (schéma 2):

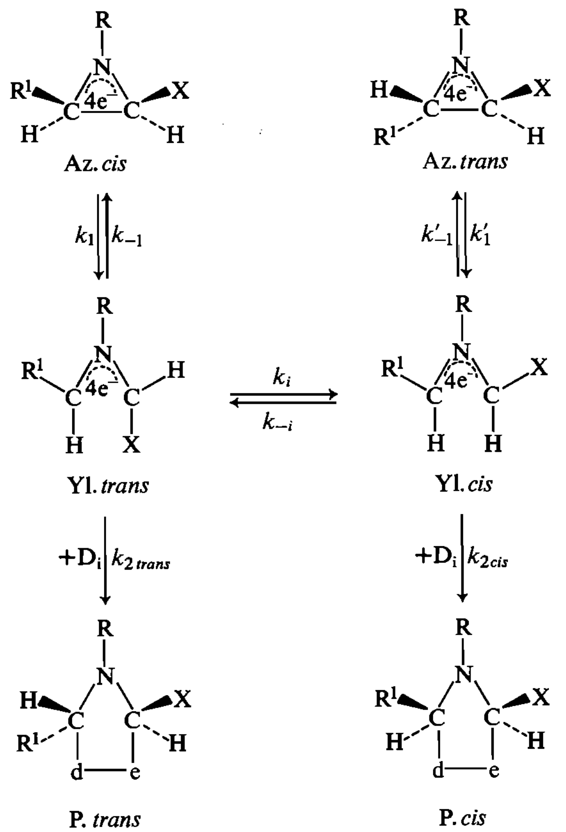

k_1, k'_1: constantes cinétiques d'ouverture des aziridines
k_{-1} k'_{-1}: constantes cinétiques de refermeture des ylures
k_{2trans}, k_{2cis}: constantes cinétiques de la cycloaddition
k_i, k_{-i}: constantes d'isomérisation
P_{cis}, P_{trans}: produits d'addition
D_i = dipolarophile (d═e)
Az: aziridine
Yl: ylure d'azométhine

SCHÉMA 2

Si l'on considère une aziridine *cis*, son ouverture conrotatoire,[1] dont la constante de vitesse est k_1, conduit à l'ylure d'azométhine *trans*. En l'absence de dipolarophile, l'ylure *trans* peut s'isomériser en ylure *cis*; ce dernier peut se cycliser en aziridine *trans*. Ce phénomène explique l'isomérisation thermique des aziridines ylures d'azométhine potentiels (10–12). En présence d'un dipolarophile si la cycloaddition est rapide par rapport à l'isomérisation, c'est-à-dire lorsque $k_2\,[D_i] \gg k_i$, l'isomérisation de l'ylure peut être ignorée. C'est la raison pour laquelle nous avons utilisé l'ACDM qui est l'un des meilleurs dipolarophiles vis-à-vis des ylures d'azométhine et de carbonyle. Dans ces conditions l'ouverture thermique des aziridines peut se mettre sous la forme:

$$\mathrm{Az} \underset{k_{-1}}{\overset{k_1}{\rightleftharpoons}} \mathrm{Yl} + \mathrm{D_i} \xrightarrow{k_2} \mathrm{P}$$

Az: aziridine; Yl: ylure d'azométhine; D_i: dipolarophile; P: produit d'addition.

La vitesse de la réaction s'exprime de la manière suivante:

$$[1]\quad v = +\frac{dP}{dt} = k_2\,[\mathrm{Yl}]\,[\mathrm{D_i}]$$

En appliquant le principe de l'état stationnaire au réactif intermédiaire (ylure), on obtient l'éq. [2]

$$[2]\quad v = +\frac{dP}{dt} = \frac{k_1 k_2 [\mathrm{Az}][\mathrm{D_i}]}{k_{-1} + k_2[\mathrm{D_i}]}$$

Cette expression de la vitesse peut s'écrire:

$$[3]\quad v = +\frac{dP}{dt} = k_{ex}\,[\mathrm{Az}]$$

avec

$$k_{ex} = \frac{k_1 k_2 [\mathrm{D_i}]}{k_{-1} + k_2[\mathrm{D_i}]}$$

ou

$$k_{ex} = k_1 - \frac{k_{-1}}{k_2}\cdot\frac{k_{ex}}{[\mathrm{D_i}]}$$

La constante expérimentale de vitesse correspond à une réaction du pseudo ordre 1 et varie avec la concentration en ACDM. La courbe représentant $k_{ex} = f(k_{ex}/[D_i])$ est une droite de pente k_{-1}/k_2 et d'ordonnée à l'origine k_1, la constante cinétique d'ouverture de l'aziridine.

L'expression de la vitesse peut encore être simplifiée lorsque $k_{-1} \ll k_2[D_i]$, c'est-à-dire dans le cas où la vitesse de refermeture de l'ylure en aziridine est faible devant la vitesse de cycloaddition.

La vitesse s'exprime alors par:

$$[4]\quad v = k_1\,[\mathrm{Az}]$$

Dans ce cas, la constante cinétique de la réaction n'est autre que la constante d'ouverture k_1 de l'aziridine. Celle-ci est alors indépendante de la concentration en dipolarophile.

2. Méthode d'étude

La détermination des constantes d'ouverture (k_1) des hétérocycles **1** à **4** se résume donc à suivre la vitesse de disparition de l'aziridine ou de l'époxyde lors de sa réaction avec l'ACDM et d'appliquer, selon le cas, l'éq. [3] ou [4]. La cinétique d'ouverture des cyano-2 aziridines **1** a été suivie à l'aide de l'ir (infrarouge), dans les autres cas, nous avons utilisé la chromatographie en phase liquide (cpl).

2.1. Utilisation de l'infra-rouge

L'addition des ylures d'azométhine **5** résultant de l'ouverture thermique des cyano-2 aziridines **1**, à l'ACDM, conduit à des pyrroles **7** qui proviennent de l'élimination spontanée de HCN à partir du produit de cycloaddition **6**, une pyrroline-3 (12) (schéma 3).

Après avoir vérifié que les aziridines **1** suivent la loi de Lambert–Beer, nous avons suivi la disparition de **1** en me-

[1] L'ouverture conrotatoire peut se faire a priori de deux manières différentes conduisant à deux isomères conformationnels de l'ylure d'azométhine (10, 13).

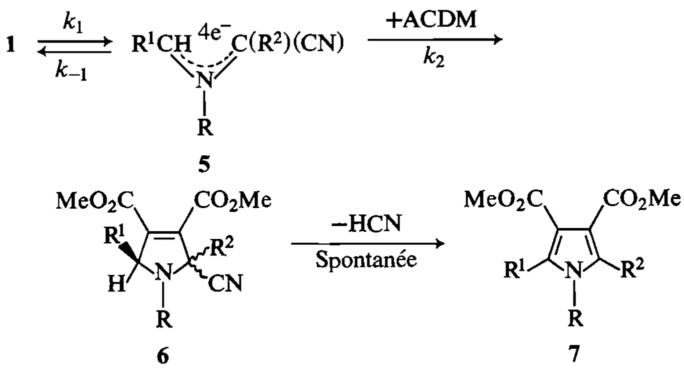

SCHÉMA 3

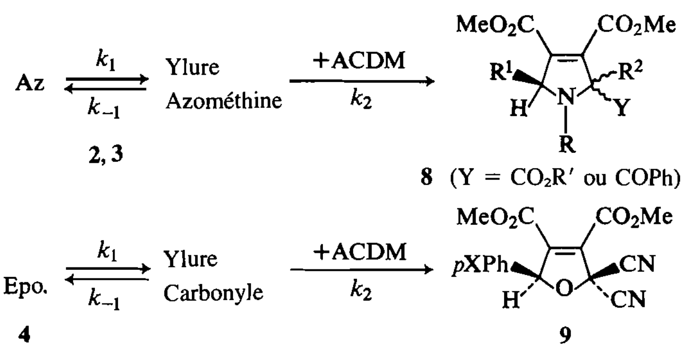

SCHÉMA 4

surant la transmission de la bande d'absorption $\nu C{\equiv}N$ vers 2240 cm^{-1}; HCN absorbe à 2095 cm^{-1} et il n'y a pas de chevauchement des bandes de l'aziridine et des produits formés. La constante expérimentale de vitesse k_{ex} est déterminée graphiquement, après avoir fait pour chaque pointe un minimum de trois mesures de la transmission. La précision de la mesure de la transmission étant de 1% (voir la partie expérimentale pour l'appareillage), k_1 est déterminée avec une précision de l'ordre de 10% après calcul de régression linéaire. Malgré l'importance relative de l'erreur commise sur k_1 (ceci étant dû à la méthode utilisée), les valeurs obtenues avec les aziridines diversement substituées sont suffisamment différentes pour qu'elles puissent être discutées.

2.2. Utilisation de la chromatographie en phase liquide

L'addition des aziridines **2** et **3** et des époxydes **4** conduit respectivement à des pyrrolines-3 **8** (1, 11, 15), qui parfois sont isomérisées en pyrrolines-2, et à des dihydrofuranes **9** (16) (schéma 4).

Une étude ir et uv (ultraviolet) s'est avérée impossible à cause des chevauchements des bandes d'absorption des produits initiaux et des produits formés, c'est pourquoi nous avons suivi la vitesse de disparition des composés **2**, **3** et **4** en les dosant tout au long de la réaction à l'aide de la cpl. Les constantes expérimentales de vitesse sont obtenues avec un pourcentage d'erreur inférieur à 5%.

Nous avons vérifié que les constantes de vitesse ainsi obtenues sont tout à fait comparables à celles obtenues par ir, comme le montre l'exemple de l'aziridine **1***a*; les valeurs obtenues sont pratiquement les mêmes, compte tenu des pourcentages d'erreur inhérents à chaque méthode.

3. Résultats et discussion

Les différents époxydes et aziridines dipôles-1,3 potentiels

TABLEAU 1. Répertoire des aziridines **1**, **2**, **3** utilisées au cours de ce travail

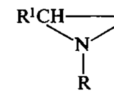

1: Y = CN
2: Y = CO_2R'
3: Y = COPh

N° Composé	R	R¹	R²	Méthode[a]	Référence
1*a* (*cis*)	C_6H_{11}	Ph	H	A	12
1*b* (*cis*)	C_6H_{11}	*p*ClPh	H	A	[b]
1*c* (*cis*)	C_6H_{11}	*p*MeOPh	H	A	[b]
1*d* (*cis*)	C_6H_{11}	*p*NO_2Ph	H	A	[b]
1*e* (*cis*)	C_6H_{11}	*p*CNPh	H	A	[b]
1*f* (*cis*)	C_6H_{11}	*p*BrPh	H	A	[b]
1*g* (*cis*)	C_6H_{11}	*p*Me_2NPh	H	A	[b]
1*h* (*cis*)	C_6H_{11}	Me_2CH—	H	A	[b]
1*i*	C_6H_{11}	Me	H	A	[b]
1*j*	C_6H_{11}	H	H	A	17
1*k*	Ph	H	Me	C	18
2*a*	C_6H_{11}	Ph	H	A	15, 19
2*b* (*trans*)	Ph	Ph	H	D[c]	11
2*c*	Ph	CO_2Me	CO_2Me	C	20
3*a* (*cis*)	C_6H_{11}	Ph	H	A et B	21
3*b* (*trans*)	C_6H_{11}	Ph	H	B	21
3*c* (*trans*)	C_6H_{11}	Ph	H	B[d]	[b]
3*d* (*trans*)	C_6H_{11}	Ph	H	B[e]	[b]

[a] A: Méthode de Cromwell; B: méthode de Southwick; C: thermolyse de la triazoline; D: méthode de Deyrup.
[b] Ce travail.
[c] Ester éthylique R′ = Et.
[d] Y = COPh*p*OMe.
[e] Y = COPh*p*NO_2.

TABLEAU 1 bis. Répertoire des époxydes **17** utilisés au cours de ce travail (22)

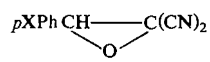

17

N° du composé:	4*a*	4*b*	4*c*	4*d*
X:	H	Cl	MeO	NO_2

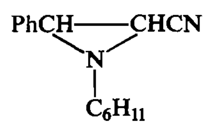

1*a*

Solvant: toluène;
k_1 (ir) $29{,}0 \times 10^{-5}$ s^{-1}
$T = 121{,}5 \pm 0{,}1$°C
k_1 (cpl) $28{,}8 \times 10^{-5}$ s^{-1}

étudiés au cours de ce travail sont répertoriés dans les tableaux 1 et 1 bis; ils sont préparés en utilisant des méthodes connues et décrites dans la littérature.

Toutes les aziridines **1** utilisées au cours de ce travail n'ont pas été étudiées précédemment, c'est pourquoi, avant l'étude cinétique, nous avons vérifié que l'addition à l'ACDM conduit dans chaque cas à un pyrrole **7** (14) selon la réaction décrite par Merah et Texier (12).

La réactivité des époxydes **4** vis-à-vis de l'ACDM a été étudiée par Robert *et al.* (16); toutefois, celle de l'époxyde **4***d* (X = NO_2) est si faible que le produit d'addition n'avait pas été isolé. Nous avons vérifié que la réaction conduit bien au dihydrofurane correspondant **9***d* (X = NO_2) que nous avons isolé et purifié. Les caractéristiques des nouveaux pyrroles **7** et du

TABLEAU 2. Influence de la concentration en ACDM sur k_{ex} (cas des aziridines **1**h, **1**i et **1**j, T = 121,5 ± 0,1°C, solvant: toluène)

Composé	R^1	k_1[a]	[ACDM][b]	k_{ex}[a]
1h	$CH(Me)_2$	0,10	8,16	0,16
			16,32	0,23
			24,48	0,29
			32,8	0,31
1i	Me	0,90	8,16	0,28
			16,32	0,43
			32,8	0,55
			53	0,64
1j	H	3,50	8,16	0,60
			28,6	1,70
			36,7	1,90
			45,3	2,38

[a] k_1: 10^5 s^{-1}; k_{ex}: 10^5 s^{-1}.
[b] [ACDM]: 10^2 mol L^{-1}.

TABLEAU 3. Influence de la concentration en ACDM sur k_{ex} (cas des aziridines **1**a à **1**g et **1**k, T = 121,5 ± 0,1°C, solvant: toluène)

		[ACDM] × 10^2 (mol L^{-1})			
		8,16	16,32	24,48	32,64
Aziridine	k_1 (10^5 s^{-1})	k_{ex} (10^5 s^{-1})			
1a	29,2	28,8	29,0	29,1	29,1
1b	27,8	27,6	26,9	27,7	28,9
1c	57,5	57,4	56,9	57,6	57,8
1d	25,1	24,8	25,2	24,9	25,6
1e	26,2	25,9	26,3	26,0	26,4
1f	27,5	27,5	27,8	26,3	27,6
1g	129,0	128,7	129,2	129,2	129,0
1k	1,51	1,51	1,54	1,49	1,50
3a *cis*	43,4	43,51	43,40	43,20	43,20
3b *trans*	36,04	35,74	35,78	36,04	36,06
3c *trans*	422,0	420,8	422,0	421,1	422,0
3d *trans*	153,3	153,2	153,35	153,15	153,45

composé **9**d sont rassemblées dans la partie expérimentale.

Pour toutes les aziridines **1** et **3**, l'isomérisation de l'ylure d'azométhine peut être négligée (k_2/[D_i] >> k_i). Les époxydes **4** portent deux substituants identiques sur le carbone 2 et le problème d'isomérisation ne se pose pas.

Lorsque R et R^1 sont des alkyles (composés **1**h à j), la constante expérimentale de vitesse k_{ex} dépend de la concentration en ACDM (tableau 2) et la constante k_1 est déterminée graphiquement en résolvant l'éq. [3]. Ces résultats montrent que dans ces cas, la cycloaddition de l'ylure d'azométhine et sa refermeture en aziridine ont des vitesses comparables.

Lorsque R ou R^1 est un aryle, la constante expérimentale de vitesse k_{ex} est pratiquement indépendante de la concentration en ACDM, comme le montrent les résultats rassemblés dans les tableaux 3 et 4. Ceci correspond au fait que $k_{-1} \ll k_2$[ACDM]; dans ces conditions, $k_{ex} = k_1$, la constante d'ouverture de l'hétérocycle. Ces résultats impliquent une lente transformation de l'hétérocycle en dipôle-1,3 suivie d'une cycloaddition rapide.

Les aziridines **2** (Y = CO_2R') ont un comportement particulier. La vitesse d'isomérisation des composés **2**a et **2**b est du même ordre de grandeur que la vitesse d'addition de l'ylure d'azométhine à l'ACDM et de ce fait, elle ne peut être négligée.

TABLEAU 4. Influence de la concentration en ACDM sur k_{ex} (cas des époxydes **4**a à **4**d; T = 121,5 ± 0.1°C, solvant: CCl_4)

		[ACDM] × 10^2 (mol L^{-1})		
		2	4	6
Epoxyde	$k_1 \times 10^5$ (s^{-1})	$k_{ex} \times 10^5$ (s^{-1})		
4a	19,20	19,17	19,20	19,23
4b	22,50	22,60	21,50	22,40
4c	76,73	76,67	76,70	76,82
4d	13,67	13,42	13,80	13,80

TABLEAU 5. Constantes de vitesse d'ouverture k_1 mesurées en cinétique initiale de l'aziridine **2**b à différentes températures[a]

	T (°C)			
	60	82,5	105	121,5
$k_I \times 10^4$ (s^{-1})	0,7	1,9	10,1	43,1
$k_{-I} \times 10^4$ (s^{-1})	0,8	1,8	9,8	39,9
$K = k_I/k_{-I}$	0,98	1,07	1,03	1,08
$k_1 \times 10^4$ (s^{-1})	2,9	8,2	34,1	100,0

[a] K: constante de vitesse globale d'isomérisation; k_I et k_{-I} constantes directe et inverse d'isomérisation.

gée. À titre d'exemple, nous avons rassemblé dans le tableau 5 les constantes de vitesse globale d'isomérisation de l'aziridine **2**b *cis*. La constante k_1 doit donc être déterminée en cinétique initiale à partir de l'équation:

$$V_0 = \frac{d[P trans]}{dt} = k_2[Yl \cdot trans]\,[ACDM]$$

De plus, la constante k_{ex} (déterminée en vitesse initiale) de l'aziridine **2**a (R = C_6H_{11}) dépend de la concentration en ACDM, k_1 est obtenue en traçant la courbe $k_{ex} = f(k_{ex}/$[ACDM]). Dans le cas des composés **2**b et **2**c, l'éq. [6] est applicable, $k_{ex} \simeq k_1$. Avec l'aziridine **2**c nous avons observé un phénomène particulier, la cycloaddition est réversible[2] et l'addition de l'aziridine à l'ACDM est équilibrée, ce qui explique que, dans les conditions de synthèse, le rendement en pyrroline-3 est toujours médiocre (23). La constante de vitesse doit donc être déterminée également en vitesse initiale; les différentes constantes de vitesse ainsi obtenues sont rassemblées dans le tableau 6.

Une partie des effets de substituant a été discutée dans deux courtes communications (24). Une discussion détaillée est effectuée dans l'article suivant, à partir des paramètres d'activation déterminés après avoir mesuré la constante d'ouverture k_1 à différentes températures.

Partie expérimentale

Les aziridines **1**a, **1**j, **1**k, **2** et **3** et les époxydes **4** sont connus. Ils sont préparés selon le mode opératoire décrit dans la référence correspondante du tableau 1.

Les aziridines **1**b à **1**i sont obtenues en appliquant la méthode de Cromwell, selon le mode opératoire décrit par Merah et Texier pour

[2] La réversibilité de la cycloaddition dipôlaire-1,3 a été observée avec divers dipôles-1,3 (26) parmi lesquels les ylures d'azométhine, mais à notre connaissance, aucune rationalisation de ces résultats n'a été tentée.

TABLEAU 6. Influence de la concentration en ACDM sur k_{ex} (cas des aziridines esters **2***a* à **2***c*; T = 121,5 ± 0,1°C, solvant: toluène)

		[ACDM] × 10^2 (mol L^{-1})					
		5	7	10	13,8	15	27,6
Aziridine	$k_1 \times 10^5$ (s^{-1})	$k_{ex} \times 10^5$ (s^{-1})					
2*a*	6,35	—	2,5	—	3,7	—	5,0
2*b*	100,0	—	—	99,8	—	100	—
2*c*	10,3	10,2	—	10,35	—	10,3	—

TABLEAU 7. Pourcentage relatif aziridine **1**/enamine **11**; solvant: benzène

X:	CN	Cl	MeO	Me_2N	H	Br
% Rel.[a]	65:35	57:43	73:27	61:39	70:30	70:30

[a] Dosage à l'aide de la rmn du produit brut de la réaction.

la synthèse de l'aziridine **1***a* (12).

Deux équivalents de cyclohexylamine (R = C_6H_{11}) sont ajoutés goutte à goutte aux oléfines α-bromées **10**, en solution dans le benzène ou l'éther lorsque R[1] est un aroyle (soit 0,1 mol de cyclohexylamine dans 100 mL de solvant), dans l'acétonitrile lorsque R[1] est un alkyle. La température est maintenue entre 5 et 10°C. Le mélange est alors abandonné à la température ambiante, dans l'obscurité. L'état d'avancement de la réaction est suivi par pesée du bromhydrate qui précipite. Finalement, le solvant est évaporé et le résidu est recristallisé dans l'éthanol à 95%. L'aziridine **1***b* a été purifiée par chromatographie sur colonne d'alumine (80 g/1 g d'huile) avec éther/éther de pétrole 50:50 comme éluant.

La synthèse des cyano-2 aziridines pour lesquelles R[1] est un substituant aromatique s'accompagne toujours de la formation d'énamines **11** isomères (12). Dans tous les cas, l'aziridine précipite en premier, et par recristallisation fractionnée dans l'éthanol à 95°C, on obtient parfois l'énamine qui précipite à partir du 3ème jet de cristallisation. Le pourcentage relatif aziridine/énamine, déterminé par analyse rmn (résonance magnétique nucléaire) du produit brut réactionnel, est donné dans le tableau 7, mais nous n'avons pas cherché à isoler et purifier l'énamine **11** dans tous les cas.

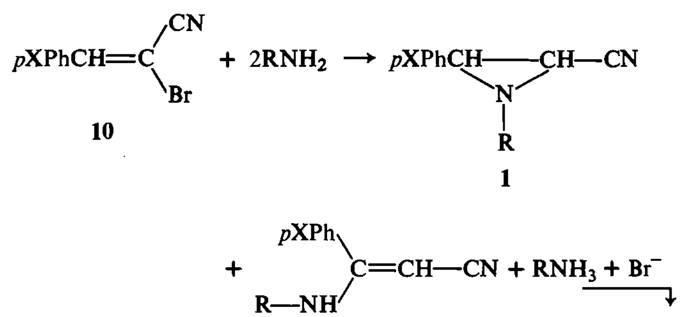

10 **1** **11**

Toutes les aziridines **1** ainsi obtenues pour lesquelles R[1] est un substituant aryle ont la configuration *cis* (R[1] par rapport à CN). Les caractéristiques physiques des aziridines ainsi que les rendements en produits isolés sont rassemblés dans le tableau 8, les résultats des analyses centésimales figurent au tableau 9.

Synthèse des pyrroles 7

L'aziridine **1** (1 g) et l'ACDM en quantité stoechiométrique sont portés à l'ébullition dans 30 cm^3 de toluène anhydre, pendant 24 h. Le

TABLEAU 8. Propriétés physicochimiques des aziridines

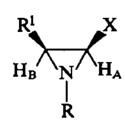

N°	Rdt%[c]	Durée (jour)	F (°C) ou Eb (°C/Torr)[d]	Infrarouge ($CHCl_3$) νC≡N ou νC=O	Résonance magnétique nucléaire ($CDCl_3$); δ (TMS) H_A	H_B	Me	$J_{H_AH_B}$
1*a*	86	21	114	2236	2,31	2,88		5,9
1*b*	87	21	137	2245	2,32	2,85		5,8
1*c*	85	21	120	2244	2,16	2,72	3,66	5,4
1*d*	70	28	143	2242	2,54	3,07		6
1*e*	82	21	121	2247, 2267	2,48	3		
1*f*	71	21	141	2250	2,41	2,92		6,08
1*g*	72	28	127	2243	2,20	2,82	3,04	6,02
1*h*[a]	43	28		2238	Multiplet entre 1 et 2 ppm			
1*i*[b]	61	28	61	2245				
3*c*	75	28	133	1645	3,58	3,58	3,88	
3*d*	64	28	126	1655	3,55	3,55		

[a] L'aziridine **1***h* a été purifiée par chromatographie sur colonne d'alumine (80 g/1 g d'huile), éluant: éther/éther de pétrole (50:50).

[b] Les protons cycliques et ceux du cyclohexyle résonnent entre 1 et 2 ppm.

[c] Les rendements sont calculés par rapport au pourcentage relatif en aziridine (**1***a* à **1***g*) donné par rmn. Pour les aziridines **1***h* et **1***i* par rapport à l'oléfine α bromée.

[d] 1 Torr = 133.3 Pa.

TABLEAU 9. Analyse centésimale des aziridines

		C%		N%		H%		O%	
N°	Formule brute	Calc.	Tr.	Calc.	Tr.	Calc.	Tr.	Calc.	Tr.
1*b*	$C_{15}H_{17}N_2Cl$	69,09	69,15	10,75	11,02	6,53	6,59	—	—
1*c*	$C_{16}H_{20}N_2O$	75,00	74,94	10,94	10,78	—	—	6,25	6,22
1*d*	$C_{15}H_{17}N_3O_2$	66,42	66,59	15,5	15,37	6,27	—	11,81	12,09
1*e*	$C_{16}H_{17}N_3$	76,49	76,37	16,73	16,81	6,77	6,78	—	—
1*f*	$C_{15}H_{17}N_2Br$	59,02	59,15	9,18	9,16	5,57	5,63	—	—
1*g*	$C_{17}H_{23}N_3$	75,84	75,92	15,61	15,85	8,55	8,61	—	—
1*i*	$C_{10}H_{16}N_2$	73,17	73,19	17,07	17,06	9,76	9,86	—	—
3*c*	$C_{22}H_{25}NO_2$	78,80	78,90	4,17	4,20	7,46	7,51	9,55	9,40
3*d*	$C_{21}H_{22}N_2O_3$	72,00	71,89	8,00	7,93	6,28	6,31	13,71	13,86

TABLEAU 10. Caractéristiques des pyrroles **7** (R^2 = H)

						Infrarouge (cm^{-1})	Résonance magnétique nucléaire ($CDCl_3$); δ (TMS)	
N°	R	R^1	R^2	Rdt[a] (%)	F (°C)	νC=O	Me(esters)	H(cycl.)
7*b*	C_6H_{11}	*p*ClPh	H	84	128–129	1715	(3,62; 3,75)	(7,22)
7*c*	C_6H_{11}	*p*MeOPh[(c)]	H	87	100–101	1690	(3,80; 3,90)	(7,21)
7*d*	C_6H_{11}	*p*(O_2N)Ph	H	87	180	1700	(3,72; 3,88)	(7,38)
7*e*	C_6H_{11}	*p*NCPh	H	88	147–148	1713	(3,65; 3,80)	(7,30)
7*f*	C_6H_{11}	*p*BrPh	H	86	129–130	1702	(3,65; 3,83)	(7,25)
7*g*	C_6H_{11}	*p*$(Me)_2$NPh	H	89	168	1710	(3,72; 3,83)	(7,30)

[a] L'analyse rmn du produit réactionnel brut montre que la réaction est pratiquement quantitative. Les rendements indiqués dans le tableau sont les rendements en produit récupéré et recristallisé.

TABLEAU 11. Analyse centésimale des pyrroles **7**

		C%		H%		N%		O%	
N°	Formule brute	Calc.	Tr.	Calc.	Tr.	Calc.	Tr.	Calc.	Tr.
7*b*	$C_{20}H_{22}O_4NCl$	63,92	63,78	5,86	5,79	3,73	3,82	17,42	17,51
7*c*	$C_{21}H_{25}O_5N$	67,93	67,73	6,74	6,79	3,77	3,69	21,56	21,41
7*d*	$C_{20}H_{22}O_6N_2$	62,18	62,33	5,70	5,82	7,25	7,27	24,87	24,48
7*e*	$C_{21}H_{22}O_4N_2$	68,85	68,72	6,02	5,94	7,65	7,72	17,48	17,30
7*f*	$C_{20}H_{22}O_4NBr$	57,14	57,28	5,23	5,21	3,33	3,50	15,23	15,20
7*g*	$C_{22}H_{28}O_4N_2$	68,75	68,80	7,29	7,28	7,29	7,17	16,66	16,74
7*k*	$C_{15}H_{15}O_4N$	65,93	65,44	5,49	5,55	5,13	4,76	23,44	23,45

TABLEAU 12. Conditions expérimentales utilisées pour le dosage des aziridines et époxydes **1** à **4** par hplc

	Composé											
Paramètre	**1***a*	**2***a*	**2***b*	**2***c*	**3***a*	**3***b*	**3***c*	**3***d*	**4***a*	**4***b*	**4***c*	**4***d*
Concentration initiale (10^4 mol L^{-1})	70	60	40	70	30	30	30	25	20	30	25	20
Eluant	n-hexane	MeOH	MeOH/eau (50:50)	MeOH/eau (80:20)	MeOH	MeOH	THF	THF	THF	THF	THF	THF
Vitesse d'élution (mL/min)	2,0	0,5	1,0	1,0	1,0	1,0	1,0	1,0	2,0	2,0	2,0	2,0
Références des colonnes[a]	A	B	B	B	B	B	B	B	C	C	C	C

[a] A: Bondapak – CN; φ: 3,9 mm; B: Bondapak – C_{18}; φ: 3,9 mm; C: Styragel de 100 Å, 500 Å, 10^3 Å, 10^4 Å, placées en série; φ = 7,8 mm.

solvant est distillé et le résidu dissous dans le minimum de méthanol. Par refroidissement, le produit d'addition cristallise; il est essoré, lavé puis séché. Les caractéristiques des pyrroles ainsi que les rendements sont consignés dans le tableau 10; leurs analyses centésimales sont rassemblées dans le tableau 11.

Synthèse du dihydrofurane 9d *(X = NO_2)*

L'époxyde **4***d* (1 g) est additionné à 0,66 g d'ACDM dans 30 cm^3 de xylène anhydre. La solution est portée à reflux pendant 30 h. Après distillation du solvant, le résidu est dissous dans le minimum de méthanol chaud. Par refroidissement, le dihydrofurane **9***d* précipite.

Après recristallisation dans le méthanol, il fond à 124–125°C; ir: 1744 et 1758 cm^{-1} (νC═O ester), 2250 (νC≡N); rmn ($CDCl_3$): 3,85 et 4,05 (s, méthyles ester), 6,95 (H, s). *Anal.* calc. pour $C_{16}H_{11}N_3O_7$: C 53,78, N 11,77, O 31,37; tr.: C 53,50, N 11,70, O 31,48.

Solvants et ACDM

Les solvants utilisés pour les études cinétiques sont purifiés selon les méthodes décrites dans la littérature (25) et utilisés fraîchement distillés.

L'ACDM est un produit commercial Fluka purissimum.

Méthodes d'analyse

L'infra-rouge

L'appareil utilisé est un spectrophotomètre Perkin–Elmer 457 à double faisceau. La longueur d'onde est celle de la bande d'absorption du nitrile, vers 2240 cm^{-1}.

Après avoir vérifié que les aziridines **1** suivent la loi de Lambert–Beer, une courbe d'étalonnage est établie pour chaque cas.

La solution est préparée par dissolution de l'aziridine dans 9 cm^3 de solvant contenant l'ACDM à la concentration de 8×10^{-4} mol L^{-1}. La concentration initiale en aziridine est mesurée par ir, elle est déduite de la courbe d'étalonnage, elle est choisie de façon à obtenir une densité optique initiale D_0 voisine de 0,75. Suivant l'aziridine, la concentration varie de 0,2 à $0,4 \times 10^{-4}$ mol L^{-1}. Cette solution est partagée en 10 fractions qui sont placées dans des tubes en verre de 2 cm^3. Ces derniers sont scellés et placés au temps $t = 0$ dans un bain thermostaté. Les tubes, prélevés au cours du temps sont refroidis immédiatement dans l'azote liquide et dosés par ir.[3]

Nous avons vérifié pour chaque aziridine qu'elle ne se dégrade pas au cours du temps à la température de l'expérience. Pour celà, l'aziridine est placée dans un tube témoin, sans ACDM, dans les mêmes conditions de T (°C), concentration et solvant. Le dosage ir permet de s'assurer que la dégradation est négligeable aux températures utilisées.

Détermination expérimentale de k_{ex}

La vitesse globale de la réaction d'ouverture est d'ordre 1 par rapport à la concentration en aziridine, elle s'exprime à l'aide de l'éq. [3]

$$[3] \quad v = \frac{dx}{dt} = k_{ex}[\mathrm{Az}]$$

À l'instant $t = 0$, $[\mathrm{Az}] = [\mathrm{Az}]_0$ et l'expression peut s'écrire:

$$[5] \quad \frac{dx}{[\mathrm{Az}]_0 - x} = k_{ex}\, dt$$

et

$$\log [\mathrm{Az}]_0 - \log ([\mathrm{Az}]_0 - x) = k_{ex}\, t$$

En appliquant la loi de Beer–Lambert, nous pouvons écrire:

$$[6] \quad \log D = \log \epsilon\, l + \log [\mathrm{Az}]$$

D étant la densité optique, ϵ le coefficient d'extinction, et l la largeur de la cuve. À $t = 0$:

$$[7] \quad \log D_0 = \log \epsilon\, l + \log [\mathrm{Az}]_0$$

En comparant les équations [5] et [7], on en déduit l'éq. [8].

$$[8] \quad \log D_0 - \log D = k_{ex}t$$

La constante expérimentale de vitesse est déterminée graphiquement à partir de la pente de la droite $-\log D = f(t)$; elle est précisée par un calcul de régression linéaire. Dans tous les cas, le coefficient de correlation est de l'ordre de 0,999.

[3] L'ouverture des aziridines **1** en ylures d'azométhine est négligeable à la température ambiante, l'addition à l'ACDM ne se produit que lorsque la solution est mise dans le bain thermostaté. Aussi, après refroidissement, la solution peut être conservée au froid plusieurs heures avant d'effectuer le dosage ir.

TABLEAU 13. Détermination des constantes globales d'équilibre de l'addition de **2***c* à l'ACDM à différentes températures

$$2c + \mathrm{ACDM} \underset{K_{-1}}{\overset{K_1}{\rightleftharpoons}} \text{pyrroline-3}$$

T (°C):	60	78,5	105	121,2	138,5
$K = \dfrac{K_1}{K_{-1}}$:	1,20	1,24	1,25	1,48	1,54

Méthode chromatographique

L'appareil utilisé est un Waters 440, ayant un système de détection uv à 254 nm. Les références des colonnes utilisées, de longueur 30 cm, ainsi que les éluants sont donnés dans le tableau 12.

Le facteur de sensibilité de l'appareil est donné par la relation [9], il est déterminé pour chaque produit.

$$[9] \quad f_p = \frac{A_p}{A_i} \cdot \frac{m_i}{m_p}$$

m_p: masse du composé p (g), m_i: masse de l'étalon interne, A_p: surface de pic du composé, A_i: surface de pic de l'étalon interne. Connaissant différentes masses m_i, m_p et leurs surfaces correspondantes, on en déduit f_p.

La quantité d'aziridine (tableau 12) pesée exactement est dissoute dans 5 cm^3 de solution, 0,5 cm^3 est utilisé comme référence et dans le reste de la solution, on ajoute en excés (10:1) la quantité d'ACDM. Cette solution est répartie dans 10 tubes en verre qui sont scellés et plongés à $t = 0$ dans un bain thermostaté à la température désirée.

Les tubes sont prélevés à différents temps et refroidis dans l'azote liquide. Ensuite ils sont dosés après y avoir ajouté une quantité bien déterminée d'étalon interne.

Notre choix s'est porté sur le méthacrylate de dodécyle qui a un volume de rétention très différent des produits réactionnels. Nous avons préféré ajouter l'étalon interne après réaction pour éviter de fausser l'effet du solvant. Mais il est vrai que les erreurs engendrées par cette manière d'opérer ne sont pas négligeables, et nous avons comparé la précision des mesures à celle obtenue par un dosage statistique (injection d'une même quantité de solution à plusieurs reprises) en mesurant directement la surface du pic. Il s'est avéré, après calcul de régression linéaire, que la précision des mesures par ces deux méthodes était comparable.

Cas particulier: L'addition de l'ACDM à l'aziridine **2***c* est réversible et équilibrée. Dans le tableau 13 nous avons rassemblé les constantes d'équilibre à différentes températures. La variaiton de $-\log [\mathrm{Az}] = f(t)$ permet d'obtenir k_1 en prenant la tangente à l'origine de la courbe représentative. La variation de $\log [\mathrm{Az}]_e/[\mathrm{Az}_e - \mathrm{Az}] = f(t)$ permet de calculer k_{-1}, qui correspond à la constante de vitesse de cycloréversion.

1. J. W. LOWN. Rec. Chem. Prog. **32**, 51 (1971).
2. R. M. KELLOGG. Tetrahedron, **32**, 2165 (1976).
3. (*a*) R. HUISGEN et H. MADER. J. Am. Chem. Soc. **93**, 1777 (1971); (*b*) R. HUISGEN. Angew. Chem. Int. Ed. Engl. **16**, 572 (1977).
4. A. C. OEHLSCHLAGER, A. S. YIM et M. H. AKHTAR. Can. J. Chem. **56**, 273 (1978).
5. R. B. WOODWARD et R. HOFFMANN. The conservation of orbital symmetry. Academic Press, New York. 1970.
6. N. D. EPIOTIS. Angew. Chem. Int. Ed. Engl. **13**, 751 (1974).
7. B. K. CARPENTER. Tetrahedron, **34**, 1877 (1978).
8. O. HENRI-ROUSSEAU, P. PUJOL et F. TEXIER. Bull. Soc. Chim. Fr. II, 496 (1980).
9. H. HERMANN, R. HUISGEN et H. MADER. J. Am. Chem. Soc. **93**, 1779 (1971).
10. (*a*) R. HUISGEN, W. SCHEER et H. MADER. J. Am. Chem. Soc. **89**, 1753 (1967); (*b*) Angew. Chem. Int. Ed. Engl. **8**, 602 (1969); (*c*) R. HUISGEN. Angew. Chem. Int. Ed. Engl. **16**, 572 (1977);

(*d*) R. HUISGEN et H. MADER. Angew. Chem. Int. Ed. Engl. **8**, 604 (1969).
11. J. A. DEYRUP. J. Org. Chem. **34**, 2724 (1969).
12. B. MERAH et F. TEXIER. Bull. Soc. Chim. Fr. II, 553 (1980).
13. F. TEXIER et R. CARRIÉ. Bull. Soc. Chim. Fr. 310 (1974).
14. A. DERDOUR. Thèse de doctorat d'état, Oran, 1982.
15. P. B. WOLLER et N. H. CROMWELL. J. Org. Chem. **35**, 888 (1970).
16. A. ROBERT, J. J. POMMERET et A. FOUCAUD. C.R. Acad. Sci. Ser. C, **270**, 1739 (1970).
17. TH. WAGNER-JAUREGG. Helv. Chim. Acta, **5**, 1237 (1961); **5**, 1249 (1961).
18. P. BARET. Thèse de doctorat d'état, Grenoble, 1975.
19. L. WARTSKI et C. WAKSELMANN. Bull. Soc. Chim. Fr. 1478 (1972).
20. M. S. OUALI, M. VAULTIER et R. CARRIÉ. Bull. Soc. Chim. Fr. II, 633 (1979).
21. N. H. CROMWELL, R. D. RABSON et C. F. HARRIS. J. Am. Chem. Soc. **65**, 3120 (1943).
22. (*a*) J. J. POMMERET et A. ROBERT. Tetrahedron, **27**, 2977 (1971); (*b*) A. ROBERT et A. FOUCAUD. Bull. Soc. Chim. Fr. 2354 (1969).
23. M. VAULTIER. Thèse de doctorat d'état, Rennes, 1977.
24. (*a*) A. DERDOUR et F. TEXIER. C. R. Acad. Sci. Ser. C, **291**, 101 (1980); (*b*) A. DERDOUR, O. HENRI-ROUSSEAU et F. TEXIER. C. R. Acad. Sci. Ser. C, **296**, 553 (1983).
25. A. I. VOGEL. A textbook of practical organic chemistry. 2ème ed. Longmans, London. 1956.
26. (*a*) R. HUISGEN, H. HAUCK, R. GRASHEY et H. SEIDL. Chem. Ber. **101**, 2568 (1968); (*b*) J. W. LOWN et K. MATSUMOTO. Can. J. Chem. **50**, 534 (1972); (*c*) M. JOUCLA, J. HAMELIN et R. CARRIÉ. Bull. Soc. Chim. Fr. 3116 (1973); (*d*) F. TEXIER et J. BOURGOIS. J. Heterocycl. Chem. **12**, 505 (1975); (*e*) G. LEFEVRE et J. HAMELIN. Tetrahedron Lett. 1757 (1979); (*f*) G. GUIHENEUF, C. LAURENCE et A. R. KATRITSKY. J. Chem. Soc. Perkin Trans. 2, 1829 (1976).

Six-bond ^{1}H,^{1}H and ^{1}H,^{19}F spin coupling constants as indicators of geometry in aniline and *p*-fluoroaniline

TED SCHAEFER AND GLENN H. PENNER
Department of Chemistry, University of Manitoba, Winnipeg, Man., Canada R3T 2N2

Received November 16, 1984

TED SCHAEFER and GLENN H. PENNER. Can. J. Chem. **63**, 2253 (1985).

The long-range coupling constants between amino protons and the ring proton or fluorine nucleus in the *para* position of aniline and *p*-fluoroaniline imply that, in benzene solution, the geometry at the amino group is very similar in the two compounds. The ratio of the two coupling constants is consistent with potential functions for inversion at nitrogen derived from far infrared data, but inconsistent with microwave spectra which indicate that the angle defining the intersection of the amino and benzene planes differs by 9° in these two compounds.

TED SCHAEFER et GLENN H. PENNER. Can. J. Chem. **63**, 2253 (1985).

Les constantes à longue distance entre les protons du groupe amino et les protons du cycle ou les noyaux de fluor en position *para* de l'aniline et de la *p*-fluoroaniline impliquent que, en solution dans le benzène, la géométrie du groupe amino de chacun de ces deux composés est très semblable. Le rapport entre les deux constantes de couplage est en accord avec les fonctions de potentiel pour l'inversion au niveau de l'azote que l'on peut dériver à partir de données obtenues par des spectres dans l'infrarouge lointain; toutefois le rapport n'est pas en accord avec les spectres de microondes qui indiquent que l'angle défini par l'intersection entre le plan du groupe amino et celui du benzène diffère de 9° dans ces deux composés.

[Traduit par le journal]

Introduction

The nonplanarity of aniline, **1**, is well established (1–6). Considered as a derivative of pyramidal ammonia, this nonplanarity is entirely reasonable and can be defined by the angle in **1***a*, measuring the intersection between the HNH and benzene planes. The corresponding angle in ammonia itself is

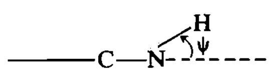

1*a*

53.8°, corresponding to the equilibrium configuration (7). Conjugation of the lone pair on nitrogen with the π electron system of the aromatic nucleus leads to a decrease of ψ relative to its value in ammonia. A rather full substitution structure for aniline in the gas phase yields ψ as 37.5 ± 2°, the error indicating the difficulty with which the amino hydrogen atoms are determined from microwave spectroscopy (4). Ultraviolet absorption (2) and fluorescence (3) spectra of aniline imply 47° and 42°, respectively, for ψ, and the spectra for aniline in argon matrices suggest a lowering of ψ. Far infrared gas spectra of aniline (5) are used to deduce a ψ of 42.2°, together with a potential for the inversion at nitrogen. The barrier to inversion of 6.3 kJ/mol agrees very well with that obtained from another study of the far infrared spectrum (6).

The presence of a substituent in the *para* position should alter the extent of conjugation across the C—N bond in aniline and therefore should cause a change in ψ. Fluorine is a π electron donor. Consequently, in *p*-fluoroaniline, **2**, ψ should be larger than in aniline and, indeed, the microwave spectra of this compound (8) and its NHD isotopic derivative are interpreted to mean that ψ is 46.4°. This corresponds to a change of 9° relative to aniline and, at first sight, appears rather large. The far infrared spectrum (5) yields ψ as 42.7°; in the same work that gave 42.2° for aniline. By way of comparison, the microwave spectra of six isotopic species of *p*-chloroaniline imply ψ as 42.5° (9). A study of *p*-bromoaniline partly oriented in a nematic solvent suggests that ψ is 40.2° and that it is 33.4° for *p*-nitroaniline (10). STO 3G MO calculations indicate very small differences in ψ for aniline and *p*-fluoroaniline (11). Our own optimized geometries yield ψ near 52° for **1** and **2**. It is well known that rather larger basis sets are needed if a correct geometry is to be calculated at nitrogen in ammonia and its derivatives (12, 13).

MINDO computations indicate that ψ increases by 3° in the presence of a *p*-fluoro substituent (14). A correlation of $^1J(^1\mathrm{H},^{15}\mathrm{N})$ values and the N—H stretching frequencies places *p*-fluoroaniline well on the regression line (15). However, when its microwave geometry is used to calculate the bond order of the N—H bond, *p*-fluoroaniline deviates significantly from the correlation between the bond order and $^1J(^1\mathrm{H},^{15}\mathrm{N})$. This result is reasonable because $^1J(^1\mathrm{H},^{15}\mathrm{N})$ is -78.6 ± 0.2 Hz for aniline in chloroform solution (16) and -78.9 Hz in benzene solution (17), and changes very little, to -77.8 ± 0.2 Hz (16) for *p*-fluoroaniline in chloroform solution, the same value we measure in benzene solution. $^1J(^1\mathrm{H},^{15}\mathrm{N})$ is linearly related to the hybridization at nitrogen (18), % *s* character = $-0.43\ ^1J(^1\mathrm{H},^{15}\mathrm{N}) - 6$, so that the couplings imply only a small change in geometry at nitrogen in **1** and **2**.

Long-range couplings and amino group geometry

Because of the disagreement among the various approaches to the determination of ψ and because the geometry may well be different in solution and the vapor phase, it appears useful to examine other molecular properties which depend on the geometry of the molecule. One such property is the long-range coupling interaction between nuclei, transmitted by the intervening electrons.

For example, in toluene the coupling over six formal bonds between methyl protons and the ring proton in the *para* position, $^6J^{\mathrm{H,H}}$, is -0.62 Hz (19). It can be written (20) as $^6J^{\mathrm{H,H}} = {}^6J_{90}^{\mathrm{H,H}} \langle \sin^2 \theta \rangle$, where $^6J_{90}$ is the value at $\theta = 90°$ in **3** and $\langle \sin^2 \theta \rangle$ is the expectation value of $\sin^2 \theta$. This quantity can be

X = C, N, etc.

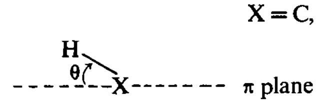

3

calculated, classically or quantum mechanically (21), if the potential function for the internal rotation about the exocyclic C—C bond is known. Alternatively, if ${}^6J_{90}^{\mathrm{H,H}}$ is known and ${}^6J^{\mathrm{H,H}}$ is measured, then $\langle \sin^2 \theta \rangle$ can be used to find the internal barrier. In toluene the latter is only 0.058 kJ/mol, $\langle \sin^2 \theta \rangle$ becomes 0.5 at ambient temperatures, and ${}^6J_{90}$ is therefore -1.24 Hz.

In *p*-fluorotoluene, ${}^6J^{\mathrm{H,F}}$ is 1.15 Hz (22, 23). Because ${}^6J^{\mathrm{H,H}}$ and ${}^6J^{\mathrm{H,F}}$ are examples of $\sigma-\pi$ couplings (23), they can be expressed as ${}^6J^{\mathrm{H,H}} \propto Q_{\mathrm{CCH}}^{\mathrm{H}} Q_{\mathrm{CH}}^{\mathrm{H}}$ and ${}^6J^{\mathrm{H,F}} \propto Q_{\mathrm{CCH}}^{\mathrm{H}} Q_{\mathrm{CF}}^{\mathrm{F}}$. In these expressions, $Q_{\mathrm{CH}}^{\mathrm{H}}$ represents the hyperfine coupling parameter (spin polarization) determining the magnitude of the interaction between an electron spin in the π system and the proton in the C—H bond, $Q_{\mathrm{CF}}^{\mathrm{F}}$ is the analogous quantity for a C—F bond, and $Q_{\mathrm{CCH}}^{\mathrm{H}}$ represents the β-interaction for the CH bond in the sidechain with the π electrons. It is the latter quantity which introduces the θ dependence of ${}^6J$. For toluene and *p*-fluorotoluene, then, ${}^6J^{\mathrm{H,H}}/J^{\mathrm{H,F}} = -0.62/1.15 = -0.539 \propto Q_{\mathrm{CH}}/Q_{\mathrm{CF}}$. A similar result should hold for **1** and **2**. A study of radicals containing aniline and *p*-fluoroaniline adducts suggests $Q_{\mathrm{CF}}^{\mathrm{F}} \sim -2Q_{\mathrm{CH}}^{\mathrm{H}}$ (24). In **1** in benzene-d_6 solution (17), ${}^6J^{\mathrm{H,H}}$ is $-0.137(3)$ Hz while ${}^6J^{\mathrm{H,F}}$ for **2** in benzene-d_6 solution is $+0.26(2)$ Hz; both numbers are measured at 305 K. Their ratio is -0.523, a hint that perhaps the ground state geometry is very similar for the two molecules in benzene solution.

A more quantitative approach goes as follows. The angle ψ is related to the angle θ to a good approximation by $\tan \theta = \mathrm{ctn}(\phi/2) \sin \psi$ in which φ is the HNH bond angle (12). Now, because the barrier to rotation about the C—N bond in **1** and **2** is near 21 kJ/mol (5), the dependence of $\langle \sin^2 \theta \rangle$ on torsion about this bond is very small at 305 K (21). Accordingly, we calculate $\langle \sin^2 \theta \rangle$ for the available potential functions given by Larsen *et al.* (5). These are $V(\psi)$ (kJ mol^{-1}) $= 138.8(1 - \cos \psi) \times 46.8(1 - \cos 2\psi)$ for aniline and $148.8(1 - \cos \psi) - 50.6(1 - \cos 2\psi)$ for *p*-fluoroaniline. These functions are evaluated at intervals of 5° and a classical averaging procedure yields $\langle \sin^2 \theta \rangle$ as 0.148_4 and 0.154_1 for **1** and **2**, respectively, at 350 K. The value of θ is derived for a given ψ from the above formula and φ is estimated from a fit of values of φ and ψ known at ψ = 0, 38, 46, and 53.8°. The fit is $\phi = 120.6 - 4.44 \times 10^{-3} \psi^2$ and is sufficiently accurate for our purposes.

The ratio of the $\langle \sin^2 \theta \rangle$ values is 0.963 and implicitly assumes values of ψ of 42.2° and 42.7° at the minimum of the potentials above. Again, the corresponding ratio involving ${}^6J^{\mathrm{H,H}}$ and ${}^6J^{\mathrm{H,F}}$ is $({}^6J^{\mathrm{H,H}}/J^{\mathrm{H,F}})\,({}^6J_{90}^{\mathrm{H,F}}/{}^6J_{90}^{\mathrm{H,H}}) = (-0.137/0.264)(2.30/-1.24) = 0.963$. Here ${}^6J_{90}^{\mathrm{H,F}}/{}^6J_{90}^{\mathrm{H,H}}$ is equivalent to $Q_{\mathrm{CH}}^{\mathrm{H}}/Q_{\mathrm{CF}}^{\mathrm{H}}$ and is derived from toluene, as discussed above.

The good agreement is emphasized by the following comparison. If it were assumed that the equilibrium ψ values of 42.2° and 42.7° for **1** and **2** defined rigid molecules, then $\sin^2 \theta$ would be 0.166_5 and 0.170_5. These numbers are about 10% larger than the more precise $\langle \sin^2 \theta \rangle$ values found from the averaging procedure. If the ψ values for **1** and **2** differed by 9° in solution, then (using 38° and 46°) an estimated corrected ratio of $\langle \sin^2 \theta \rangle$ values for the two molecules would be 0.664 and not 0.963.

Now, the present arguments are not meant to imply that ψ is nearly 42° for both molecules in solution, *only* that ψ must have very similar values in solution. A full substitution structure for *p*-fluoroaniline in the gas phase would be of interest.

A check on the $\sigma-\pi$ nature of ${}^6J^{\mathrm{H,H}}$ and ${}^6J^{\mathrm{H,F}}$, which should vanish at θ = 0°, is available from the unobservable ${}^6J^{\mathrm{H,H}}$ in 2,6-dibromoaniline (25), the ±0.08 ± 0.02 Hz for ${}^6J^{\mathrm{H,F}}$ in 2,4,6-trifluoroaniline (see below), and the unobservable ${}^6J^{\mathrm{H,F}}$ in 2,6-dibromo-4-fluoroaniline. The *ortho* substituents cause a flattening of the pyramid at nitrogen, as indicated by ${}^1J({}^1\mathrm{H},{}^{15}\mathrm{N})$, probably because of intramolecular hydrogen bonding. The difference of 1 Hz in the ${}^1J({}^1\mathrm{H},{}^{15}\mathrm{N})$ in the two molecules can be accommodated by a difference of 0.4 in the % *s* character at nitrogen (18), corresponding to a change of 0.6° in the HNH bond angle, which, in the vicinity of 40°, translates into a change of 1.5° in ψ. That is, ${}^1J({}^1\mathrm{H},{}^{15}\mathrm{N})$ is consistent with only a slightly larger value of ψ in *p*-fluoroaniline. The far infrared spectra in the gas phase imply a difference of 0.5° in ψ. Both these values are consistent with ${}^6J^{\mathrm{H,H}}$ and ${}^6J^{\mathrm{H,F}}$.

Also consistent with similar ψ values in the two compounds are the ${}^5J^{\mathrm{H,H}}$ of 0.296(3) and 0.300(2) Hz in aniline and *p*-fluoroaniline. It is very likely that ${}^5J^{\mathrm{H,H}}$ can be written as $A\langle \sin^2 \theta \rangle + B\langle \sin^2 \theta/2 \rangle$, just as for toluene (26) and thiophenol (27). Consequently a difference of 9° in ψ should yield rather different ${}^5J^{\mathrm{H,H}}$ numbers because θ changes by 4° for such a change in ψ. Near ψ = 40°, the ratio of the $\langle \sin^2 \theta \rangle$ values would be 0.76 and a significant difference in ${}^5J^{\mathrm{H,H}}$ would be expected. Similar remarks hold for the ${}^4J^{\mathrm{H,H}}$ values of $-0.189(3)$ and $-0.209(2)$ Hz for **1** and **2**, although the θ dependence of ${}^4J^{\mathrm{H,H}}$ is somewhat more ambiguous.

Finally, it may be noted that our INDO MO FPT computations of ${}^6J^{\mathrm{H,H}}$ in **1** and of ${}^6J^{\mathrm{H,F}}$ in **2** yield a $\sin^2 \theta$ dependence and that ${}^6J_{90}^{\mathrm{H,H}}$ is -1.08 ± 0.10 Hz for a statistical fit and ${}^6J_{90}^{\mathrm{H,F}}$ is 1.68 ± 0.05 Hz. The $\langle \sin^2 \theta \rangle$ value of 0.148_4 obtained for **1** from the potential functions above implies a ${}^6J_{90}^{\mathrm{H,H}}$ of -1.08 Hz. For **2** $\langle \sin^2 \theta \rangle$ was found as 0.154_1 above and suggests a ${}^6J_{90}^{\mathrm{H,F}}$ of 0.262/0.154 or 1.70 Hz, probably in accidental agreement with the INDO result because INDO MO FPT calculations underestimate ${}^6J_{90}^{\mathrm{H,F}}$ in *p*-fluorotoluene (20).

Conclusions

The long-range nuclear spin–spin coupling constants for aniline and *p*-fluoroaniline in benzene-d_6 solution imply very similar amino group geometries in the two molecules. This result is consistent with the interpretation of the far infrared spectra of these molecules in the gas phase and, in quantitative detail, with the potential functions for inversion derived from the infrared data. Apparently, intermolecular association or perturbations in solution do not significantly alter the geometry nor the inversion rates, perhaps because the nuclear (proton) motions involved in the inversion can proceed with minimal changes in the effective volume of the molecules.

However, the microwave spectrum of *p*-fluoroaniline suggests rather a large change in the geometry at nitrogen relative to aniline. If a full substitution structure were to bear out this suggestion, then the agreement between nmr and infrared data above would presumably be coincidental.

Experimental

p-Fluoroaniline, **2**, 2,4,6-trifluoroaniline, **4**, and 2,4-difluoroaniline came from Aldrich Chemical Co. Bromination of the latter compounds yielded 2-bromo-4,6-difluoroaniline, **5**. Solutions (5 mol%) of **2**, **4**, and **5** were prepared in benzene-d_6 solution. Intermolecular amino proton exchange was retarded as described previously (17). Samples contained a drop of tetramethylsilane and were transferred to 5-mm od nmr tubes. The samples were degassed by the freeze–pump–thaw procedure and were flame sealed.

The ^{1}H and ^{19}F nmr spectra were recorded with a Bruker WH-90-DS at a probe temperature of 305 K and in a manner recently described in detail (28). The sign of ${}^6J^{\mathrm{H,F}}$ in **2** was determined by weak ${}^{19}\mathrm{F}\{{}^1\mathrm{H}\}$ irradiation experiments (29) which showed that ${}^6J^{\mathrm{H,F}}/{}^5J^{\mathrm{H,NH}} > 0$.

TABLE 1. The ^{1}H and ^{19}F spectral parameters for a 5 mol% solution of *p*-fluoroaniline, **2**, in benzene-d_6 at 305 K

Parameter	Value	Parameter	Value
ν_{amino}	300.0	$^{4}J^{H,NH}$	−0.209(2)
$\nu_2 = \nu_6$	546.569(1)[a]	$^{5}J_{25}$	0.357(1)
$\nu_3 = \nu_5$	603.656(1)[a]	$^{5}J^{H,NH}$	0.300(2)
$^{3}J_{23}$	8.743(2)[b]	$^{6}J^{F,NH}$	0.262(2)
$^{3}J_{34}$	8.523(2)	Transitions calcd.	256
$^{4}J_{24}$	4.474(2)	Transitions assigned	189
$^{4}J_{26}$	2.990(2)	Largest difference	0.028
$^{4}J_{35}$	2.987(2)	Root mean square error	0.010

[a]In Hz at 90.023 MHz relative to internal TMS. The ^{19}F spectrum was recorded at 84.700 MHz.
[b]The numbers in parentheses are the standard deviations from the NUMARIT analysis. No amino proton transitions were assigned, of course.

$^{5}J^{H,NH}$ is positive (30). For **4**, decoupling experiments and linewidth simulations demonstrated that $^{6}J^{H,F} = \pm 0.08 \pm 0.01$ Hz. For **5** no broadening of the F-4 spectrum due to $^{6}J^{H,F}$ could be detected and $^{6}J^{H,F}$ must be less than 0.05 Hz in magnitude.

The ^{1}H and ^{19}F nmr spectra of **2**, **4**, and **5** were analyzed with the computer programs LAME (31, 32) and NUMARIT (33). Table 1 gives the spectral data for **2** and shows the precision obtained in the analyses. Amino proton transitions were not assigned in any of the analyses because the ^{1}H nmr spectra of these protons are broad bands caused by intermediate rates of spin-lattice relaxation of the quadrupolar ^{14}N nucleus.

Acknowledgments

We are grateful to the Natural Sciences and Engineering Research Council of Canada for financial assistance.

1. D. G. LISTER and J. K. TYLER. J. Chem. Soc. Chem. Commun. 152 (1966).
2. J. C. D. BRAND, D. R. WILLIAMS, and T. J. COOK. J. Mol. Spectrosc. **20**, 359 (1966).
3. M. QUACK and M. STOCKBERGER. J. Mol. Spectrosc. **43**, 87 (1972).
4. D. G. LISTER, J. K. TYLER, J. H. HØG, and N. W. LARSEN. J. Mol. Struct. **23**, 253 (1974).
5. N. W. LARSEN, E. L. HANSEN, and F. M. NICOLAISEN. Chem. Phys. Lett. **43**, 584 (1976).
6. R. A. KYDD and P. J. KRUEGER. J. Chem. Phys. **69**, 827 (1978).
7. K. KUCHITSU, J. P. GULLORY, and L. S. BARTELL. J. Chem. Phys. **49**, 2488 (1968).
8. A. HASTIE, D. G. LISTER, R. L. MCNEIL, and J. K. TYLER. J. Chem. Soc. Chem. Commun. 108 (1970).
9. A. NONAT, A. BOUCHY, and G. ROUSSY. J. Mol. Struct. **116**, 227 (1984).
10. G. FRONZA, R. MONDELLI, F. LELI, E. W. RANDALL, and C. A. VERACINI. J. Magn. Reson. **37**, 275 (1980).
11. W. J. HEHRE, L. RADOM, and J. A. POPLE. J. Chem. Soc. Chem. Commun. 669 (1972).
12. A. WOLF, U. VOETS, and H.-H. SCHMIDKE. Theor. Chim. Acta (Berl.), **54**, 229 (1980).
13. A. SZABO and N. S. OSTLUND. Modern quantum chemistry. Macmillan, New York. 1982. p. 202.
14. W. J. E. PARR and R. E. WASYLISHEN. J. Mol. Struct. **38**, 272 (1977).
15. M. TAKASUKA and Y. TERUI. J. Chem. Soc. Perkin Trans. 2, 1545 (1984).
16. T. AXENROD, P. S. PREGOSIN, M. J. WIEDER, and G. W. A. MILNE. J. Am. Chem. Soc. **91**, 3681 (1969).
17. R. WASYLISHEN, J. B. ROWBOTHAM, L. ERNST, and T. SCHAEFER. Can. J. Chem. **50**, 2575 (1972).
18. G. BINSCH, J. B. LAMBERT, B. W. ROBERTS, and J. D. ROBERTS. J. Am. Chem. Soc. **86**, 5564 (1964).
19. M. P. WILLIAMSON, R. KOSTELNIK, and S. M. CASTELLANO. J. Chem. Phys. **49**, 2218 (1968).
20. R. E. WASYLISHEN and T. SCHAEFER. Can. J. Chem. **50**, 1852 (1972).
21. W. J. E. PARR and T. SCHAEFER. Acc. Chem. Res. **13**, 400 (1980).
22. T. SCHAEFER, W. DANCHURA, W. NIEMCZURA, and J. PEELING. Can. J. Chem. **56**, 2442 (1978).
23. R. WASYLISHEN and T. SCHAEFER. Can. J. Chem. **49**, 94 (1971).
24. C. CHACHATY, A. FORCHIONI, and J. VIRLET. Can. J. Chem. **53**, 648 (1975).
25. R. WASYLISHEN and T. SCHAEFER. Can. J. Chem. **48**, 1263 (1970).
26. T. SCHAEFER and R. LAATIKAINEN. Can. J. Chem. **61**, 2785 (1983).
27. T. SCHAEFER, T. A. WILDMAN, and R. SEBASTIAN. Can. J. Chem. **60**, 1924 (1982).
28. T. SCHAEFER and R. SEBASTIAN. J. Magn. Reson. **41**, 395 (1980).
29. R. FREEMAN and W. A. ANDERSON. J. Chem. Phys. **37**, 2053 (1962).
30. T. SCHAEFER and R. WASYLISHEN. Can. J. Chem. **48**, 1343 (1970).
31. S. M. CASTELLANO and A. A. BOTHNER-BY. J. Chem. Phys. **41**, 3863 (1964).
32. C. W. HAIGH. Annu. Rep. Nucl. Magn. Reson. Spectrosc. **4**, 311 (1971).
33. A. R. QUIRT and J. S. MARTIN. J. Magn. Reson. **5**, 318 (1971); J. S. MARTIN, A. R. QUIRT, and K. E. WORVILL. The nmr program library. Daresbury Laboratory, Daresbury, U.K.

The conformational behaviour of 2-fluoro and of 2,6-difluoroacetophenone implied by proximate spin–spin coupling constants and MO calculations

TED SCHAEFER, GLENN H. PENNER, TIMOTHY A. WILDMAN, AND JAMES PEELING[1]

Department of Chemistry, University of Manitoba, Winnipeg, Man., Canada R3T 2N2

Received December 12, 1984

TED SCHAEFER, GLENN H. PENNER, TIMOTHY A. WILDMAN, and JAMES PEELING. Can. J. Chem. **63**, 2256 (1985).

The temperature dependence of ${}^5J_o^{\mathrm{F,CH_3}} \equiv {}^5J$, the nuclear spin–spin coupling constant over five formal bonds between the methyl protons and the ^{19}F nucleus in 2-fluoroacetophenone and 2,6-difluoroacetophenone, is modelled on the assumption that ${}^5J$ is a proximate coupling and that the STO 3G MO potential functions describe the population distributions of the rotamers defined by rotation about the exocyclic sp^2–sp^2 carbon–carbon bond. It is assumed that ${}^5J$ has a $\cos^4\theta$ dependence between 0 and 90°, where θ is the angle by which the acetyl group twists out of the plane of the benzene plane. The potential function is obtained from extensive geometry optimization procedures for a range of θ values. At 305 K, nonplanar conformations are substantially populated in 2-fluoroacetophenone, according to this model, which is also consistent with the idea that the 2,6-difluoro derivative has a markedly nonplanar ground state. The model reproduces the large ${}^5J$ in the monofluoro relative to the difluoro compound, as well as the much larger temperature dependence in the former.

TED SCHAEFER, GLENN H. PENNER, TIMOTHY A. WILDMAN et JAMES PEELING. Can. J. Chem. **63**, 2256 (1985).

On explique l'effet de la température sur les constantes de couplage nucléaire ${}^5J_o^{\mathrm{F,CH_3}} \equiv {}^5J$, à travers 5 liaisons formelles entre les protons du méthyle et le noyau de ^{19}F de la fluoro-2 acétophénone et de la difluoro-2,6 acétophénone, en se basant sur l'hypothèse que ${}^5J$ est un couplage dû à un effet de proximité et que les fonctions de potentiel des orbitales moléculaires STO 3G décrivent bien les distributions de population des rotamères définis par la rotation autour de la liaison exocyclique carbone–carbone sp^2–sp^2. On suppose que, entre 0 et 90°, il existe une relation entre ${}^5J$ et le $\cos^4\theta$, où θ est l'angle formé par le plan du groupe acétyle et le plan du benzène. On obtient la fonction de potentiel à partir de méthodes étendues d'optimisation de la géométrie pour une large échelle de valeurs de θ. À 305 K, ce modèle suggère que les proportions de fluoro-acétophénone qui existent dans des conformations qui ne sont pas planes sont assez importantes; ceci est également en accord avec l'idée que l'état fondamental du dérivé difluoro-2,6 est nettement non planaire. Le modèle reproduit l'importante valeur de ${}^5J$ du composé monofluoré par rapport au composé difluoré ainsi que l'effet beaucoup plus grand de la température dans le cas du composé monofluoré.

[Traduit par le journal]

Introduction

The conformational preference of the acetyl group in 2-fluoroacetophenone, **2**, has been discussed extensively (1–7). For the parent compound, **1**, an adequate discussion has been done in terms of a **1***a* ⇌ **1***b* equilibrium (8–11) at ambient or lower temperatures. The barrier to rotation about the

1 $R^2 = R^6 = H$
2 $R^2 = F$, $R^6 = H$
3 $R^2 = R^6 = F$

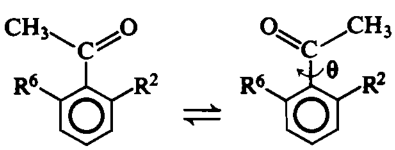

θ = 180° — *a*; θ = 0° — *b*

Csp^2—Csp^2 exocyclic bond is estimated as 13 kJ/mol from torsional frequencies in the vapor (12) and as 22.4 kJ/mol from dynamic nmr experiments in solution (13). For **2**, various techniques purport to find preferences ranging from all *a* (1), through markedly nonplanar froms (5*a*, *b*) intermediate between *a* and *b*, to a possibly all *b* (3, 7). A recent paper (7) reviews the previous work and, on the basis of dipole moment and Kerr constant measurements in CCl_4 solution, concludes that *b* is present to the extent of 95 ± 5% at 298 K and that the angle of twist, θ, about the exocyclic Csp^2—Csp^2 bond is 10 ± 10°. This conclusion assumes the same out-of-plane angles in *a* and *b*.

For 2,6-difluoroacetophenone, an estimate of 40° for θ is based on ^{19}F nmr chemical shifts (5*a*), but is predicated on a value of 33 to 40° for θ in 4-fluoroacetophenone. The latter value is intuitively doubtful in that the π electron donating fluorine substituent should increase the double bond character of the exocyclic C—C bond. Now, one of the most striking properties of the ^{1}H nmr spectrum of **2** is the large magnitude of the formally five-bond coupling, ${}^5J_o^{\mathrm{F,CH_3}}$, between the methyl protons and the *ortho* ^{19}F nucleus. It is reported as 4.80 Hz at 305 K in $CDCl_3$, C_6D_6, and $C_6D_5CD_3$ solutions, and as 4.20 Hz in DMSO at 305 K (14). In $C_6D_5CD_3$ solution, ${}^5J_o^{\mathrm{F,CH_3}}$ is 6.50 Hz at 203 K and 4.20 Hz at 383 K (15). It is also reported as 6.2 Hz at 210 K and 4.1 Hz at 423 K, but it is unclear in what solvent these couplings were obtained (4). In a 30 mol% solution in $(CH_3)_2C{=}O$, ${}^5J_o^{\mathrm{F,CH_3}}$ is 4.72 Hz (2) at about 300 K.

${}^5J_o^{\mathrm{F,CH_3}} \equiv {}^5J$ in **2** is assumed (14) to be a "through-space" or proximate coupling. Such couplings are remarkably sensitive to the distance between the bonds carrying the coupled nuclei (16, 17) and hence ${}^5J$ is taken as evidence for a preponderance of *b* in the *a*/*b* equilibrium (2, 4, 15). It is also suggested (15) that the observed ${}^5J$ is a measure of this equilibrium, although ${}^5J_a$ and ${}^5J_b$ are as yet unknown.

One difficulty with the application of such an assumption is the distance sensitivity of proximate coupling mechanisms. Thus, a thorough theoretical study (18) of the proximate coupling, ${}^5J_o^{\mathrm{H,CH_3}}$, in anisole and its comparison with experiment (18, 19) shows that its magnitude drops rapidly as the methyl group twists out of the benzene plane. When the angle of twist about the Csp^2—O bond reaches about 60°, ${}^5J_o^{\mathrm{H,CH_3}}$ is very nearly zero. If ${}^5J_o^{\mathrm{F,CH_3}}$ behaves in a similar manner, then a simple *a*/*b* equilibrium no longer suffices as a model because values of θ other than zero, as in *b*, and 180°, as in *a*, must surely be represented at temperatures above absolute zero.

[1] Present address, University of Petroleum and Minerals, Saudi Arabia.

In this paper, certain assumptions about the θ dependence of ^5J together with MO calculations of $V(\theta)$, the potential function for the conformation of the acetyl group, are combined with the observed temperature dependence of ^5J, to show that a simple a/b equilibrium is an inadequate description for **2**. True, b is the low-energy form for **2**, but many other conformers corresponding to various θ values are appreciably populated at temperatures between 180 and 423 K. For **3**, similar considerations also provide an estimate of θ for the preferred nonplanar conformation of the acetyl moiety.

Experimental

Unlabelled and methyl-^{13}C-enriched 2-fluoroacetophenone were obtained by addition (20) of 2-fluorobenzaldehyde (Aldrich) to ethereal methyl magnesium iodide to yield 1-(2-fluorophenyl) ethanol. A solution of the crude alcohol in CH_2Cl_2 was added to a mixture of pyridinium chlorochromate (21) in CH_2Cl_2, and the crude product of 2-fluoroacetophenone, **2**, was chromatographed on silica gel plates with hexanes containing a small amount of ether. The product contained some residual 2-fluorobenzaldehyde, but was used without further purification, spectral analysis proceeding without difficulties. The 2,6-difluoroacetophenone, **3**, came from Maybridge and the 2,3,4,5,6-pentafluoroacetophenone from Fairfield. Methyl iodide (95% ^{13}C) was obtained from Stohler.

Solutions for nmr analysis were prepared by weight in acetone-d_6, were transferred to 5-mm od nmr tubes by filtering through cotton wool, and were degassed by eight freeze–pump–thaw cycles before the tubes were flame sealed.

The ^{1}H nmr spectrum of a 4.9 mol% solution of 2-fluoroacetophenone-α-^{13}C was calibrated at a probe temperature of 305 K on an HA100 nmr spectrometer by a procedure whose details have been described (22). The ^{1}H nmr spectrum of a 5.3 mol% solution of 2-fluoroacetophenone was accumulated on a pulsed Bruker WH90 instrument at 305 K, again by methods previously described (22).

Weak double irradiation experiments (23) on the enriched **2**, in which the ^{1}H nmr peaks of the methyl protons were perturbed while observing the ^{19}F nmr spectrum, demonstrated that $^1J(^1\text{H},^{13}\text{C})/^4J(^{13}\text{C},^{19}\text{F}) > 0$. Since $^1J(^1\text{H},^{13}\text{C})$ is positive (24), so is $^4J(^{13}\text{C},^{19}\text{F})$. A second set of experiments involved the observation of the methyl ^{13}C nmr spectrum while the transitions of the methyl ^{1}H nmr spectrum were weakly perturbed. It followed that $^4J(^{13}\text{C},^{19}\text{F})/^5J(^1\text{H},^{19}\text{F})$ was positive. Consequently the proximate coupling $^5J(^1\text{H},^{19}\text{F}) = {}^5J_o^{\text{F,CH}_3} \equiv {}^5J$ is positive.

The ^{1}H spectrum of a 3 mol% solution of 2,6-difluoroacetophenone, **3**, was accumulated at 90 MHz and at a probe temperature of 305 K. The ^{19}F nmr spectrum was also recorded.

Variable temperature experiments employed the Bruker B-ST100/700 temperature controller and the digital resolution was about 0.05 Hz/real point. Samples were equilibriated for at least 15 min at each temperature. The temperature control unit was calibrated with a copper–constantan thermocouple immersed in CH_2Cl_2 between 170 and 305 K.

STO 3G MO computations (25) utilized an Amdahl 470/V8 system with the program MONSTERGAUSS (26). INDO MO FPT calculations (27) of spin–spin coupling constants were also performed using the program FINDO,[2] a version (28) of CNINDO/74 (29) containing numerous options including the modification of Fock matrix elements.

Results and discussion

Spectral analyses

The ^{1}H nmr spectra of **2** at 90 and 100 MHz were both analyzed with the computer program LAME (30, 31). As many as 873 transitions were assigned in these analyses, the standard deviations in the spectral parameters all being below 0.005 Hz.

[2] R. Laatikainen, unpublished.

TABLE 1. $^5J_o^{\text{F,CH}_3} \equiv {}^5J$ at various temperatures for 2-fluoroacetophenone-α-^{13}C, **2**, and 2,6-difluoroacetophenone, **3**

	^5J			^5J	
T^a	**2**^{b}	**3**^{c}	T^a	**2**^{b}	**3**^{c}
305	+4.51^d	1.56^{e,f}	230	5.33	1.68
290	4.65	1.58	220	5.46	—
280	4.75	1.60	211	5.58	—
270	4.86	1.61	202	5.74	—
260	4.97	1.63	192	5.88	1.76$_5$
250	5.09	1.65	182	5.99	—
240	5.21	1.66			

^{a} Accurate to at least 1 K.
^{b} For a 4.9 mol% solution in acetone-d_6.
^{c} For a 3 mol% solution in acetone-d_6.
^{d} These numbers are reproduced by the equation ^5J (Hz) = $8.15_2 - 0.012_1\,T$ (r = 0.9971).
^{e} These numbers are reproduced by ^5J (Hz) = $2.11_1 - 1.83_9 \times 10^{-3}\,T$ (r = 0.9971).
^{f} For a 4.7 mol% solution of pentafluoroacetophenone in acetone-d_6, ^5J is 1.887, 1.861, 1.823, and 1.777 Hz at 280, 290, 305, 315, and 325 K, respectively. These numbers are reproduced by ^5J (Hz) = $2.57_1 - 2.44_7 \times 10^{-3}\,T$ (r = 0.9996).

These parameters are not reproduced here because previous values are available (4). However, ^5J was +4.48(2) Hz for the enriched sample and 4.510(1) Hz for the unenriched. The former gave $^1J(^1\text{H},^{13}\text{C})$ as 128.246(2) Hz, while $^5J(\text{H-5},^{13}\text{C})$ and $^4J(\text{H-6},^{13}\text{C})$ were ± 0.399(2) and ±0.105(2) Hz, respectively, and of the same sign, as determined by $^1\text{H}\{^1\text{H}\}$ experiments.

The ^{1}H and ^{19}F nmr spectra of **3** were analyzed, assigning a total of 474 transitions. Only $^5J_p^{\text{H,F}}$ differed by more than 0.1 Hz from a previous analysis (32), the present value being −1.183(2) Hz. For the 3 mol% solution in acetone-d_6, the ^{19}F chemical shift is 50.15 ppm to low field of internal C_6F_6 at 305 K.

The analyses confirm that the identification of ^5J with the observed splitting of the methyl ^{1}H nmr peaks in **2** and **3** is valid and therefore that the measured temperature dependence of ^5J from splittings is reliable.

The temperature dependence of $^5\text{J} \equiv {}^5\text{J}_o^{\text{F,CH}_3}$

Table 1 presents ^5J as a function of temperature for **2** and **3**. The coupling increases as the temperature decreases, as anticipated for a proximate coupling if the drop in temperature entails a decreased average distance between the methyl group and the C—F bond. The simplest approach to the data for **2** assumes a two-site equilibrium, say a/b, with a temperature independent energy difference between a and b. A good fit[3] of ^5J to K^{-1} is found, with a rms deviation of 0.01_1 Hz for 13 points between 182 and 305 K. The model yields a value of $3.1_4 \pm 0.2_6$ kJ/mol for the energetic preference of conformer b, an intuitively reasonable value. However, it also gives ^5J as $7.4_9 \pm 0.2_2$ Hz for b and $-5.8_2 \pm 0.3_4$ Hz for a (90% confidence level). This latter number is most likely absurd and emphasizes the inadequacy of the model. Accordingly it is rejected, even though the energy difference obtained from it happens to agree with the *ab initio* MO calculations below. Furthermore, a two-

[3] Using the computer program, THERMO, by R. Laatikainen; unpublished.

TABLE 2. INDO MO FPT computations of $^5J \equiv {}^5J_o^{F,CH_3}$ in 2-fluoroacetophenone[a]

	^5J (Hz)			
θ (deg)[b]	Total[c]	No F,CH_3[d]	No CF[e]	No HF[f]
0	0.18[g]	−0.56	−0.45	5.84
	4.81[h]	−0.95	−0.67	3.11
	2.14[i]	−0.36	−0.64	7.21
15	−2.47	−0.48	−6.00	4.64
30	−4.79	−0.29	−6.23	2.36
45	−2.93	−0.02	−3.31	0.91
60	−0.75	0.23	−0.80	0.45
75	0.16	0.39	0.18	0.42
90	0.41	0.46	0.42	0.45
120	0.32	0.33	0.33	0.33
150	0.13	0.14	0.13	0.14
180	0.03	0.03	0.02	0.03

[a] The geometry is near that from a partially optimized structure for *b* (see text) with bond lengths in pm as C1C (153.1), CCα(154.3), CαH(108.6), CO(139.1), C1C2(140.0), C1C6(140.0), C2F(135.6) and bond angles in degrees as C1CCα(118.8), C1CO(120.0), C2C1C(120.0), CCαH(110.1), FC2C1(120.0), H6C6C1(120.0).

[b] The angle by which the acetyl group twists about the Csp^2—Csp^2 bond. At θ = 180° the methyl group lies *trans* to the C—F bond.

[c] No off-diagonal Fock matrix elements are omitted.

[d] All off-diagonal Fock matrix elements between orbitals on F and the methyl group are set to zero.

[e] No Fock elements between orbitals on F and the methyl C.

[f] No Fock elements between orbitals on F and methyl H.

[g] It is known that one C—H bond of the methyl group lies in the plane of the benzene ring, pointing away from the *ortho* C—H (C—F) bond (9). The value of 0.18 Hz is the average over the three C—H bonds.

[h] For the proton in the C—H in the plane of the ring and pointing away from C—F.

[i] For the other two C—H bonds.

site model for **3** is hardly sensible, yet ^5J in **3** also depends on temperature.

An n*-site model*

A rigorous description of the variation of ^5J with temperature demands a knowledge of the potential energy surface for the movement of the acetyl group relative to the benzene ring considered as a frame (including rotational and vibrational motion of the methyl group), of how this surface changes with temperature in the presence of solvent molecules, and of how ^5J depends on this potential surface. Here we take a simple approach designed to reproduce semiquantitatively, first, the large magnitude of ^5J in **2** relative to **3** and, second, the larger absolute changes in ^5J in **2** caused by temperature changes.

Evidence that ^5J is a proximate coupling can be adduced via INDO MO FPT computations as follows, in spite of the well-known failures (33–36) of this technique for certain proximate H,F couplings. In Table 2 such computations of ^5J are found. As expected from calculations of couplings with a large proximate component in other molecules, such as 2-fluorotoluene (35) and 2-methylbenzoylfluoride (34), ^5J is calculated as either very small or as large and negative when the methyl group lies near the C—F bond, that is, for small θ values. Using Barfield's procedure (37), in which certain off-diagonal matrix elements in the Fock matrices are held at zero throughout the iterative cycles, one may attempt to identify the source of the qualitative discrepancy between theory and experiment. For example, in Table 2 the third column represents the couplings computed when no spin state information is allowed to be transmitted *directly* between orbitals centered on fluorine and those centered on the atoms of the methyl group. Up to a point, these numbers yield the couplings transmitted via the intervening bonds. In the fourth column, all elements between the orbitals on fluorine and the methyl carbon are forced to vanish. The large negative ^5J numbers for small θ imply that it is H,F interactions which are incorrectly given by theory. Indeed, in the last column of Table 2 large positive ^5J numbers appear when the Fock matrix elements involving fluorine and methyl hydrogen orbitals are absent. Furthermore, ^5J drops rapidly from 5.84 Hz at θ = 0° to 0.45 Hz at θ = 60°, qualitatively as expected for a proximate coupling.

The results are reminiscent of those obtained in a detailed study of $^5J_o^{H,CH_3}$ in anisole (18), in which the observed negative and proximate coupling is quantitatively reproduced by the INDO MO FPT approach. $^5J_o^{H,CH_3}$, as calculated, very closely approximates a $\cos^4\theta$ function.

The assumption is now made that ^5J in **2** also follows $\cos^4\theta$ as in $^5J = {}^5J_o \cos^4\theta$ (defined for $0 \le \theta \le 90°$), where ^5J_o is that at θ = 0. The ^5J values at θ = 0 in Table 2 are not reliable in view of the above discussion. A more reliable ^5J_o must be sought in experiment. For **2** in Table 1, ^5J is given as $8.15_2 - 0.012_1\ T$ (r = 0.997). This empirical linear dependence on temperature is assumed to give ^5J_o as 8.15_2 Hz.

A potential function for the rotation of the acetyl group in **2** was obtained via the geometry optimization routine in the program MONSTERGAUSS. Bond lengths and bond angles were optimized as θ changed in steps of 15° between 0 and 180° with the proviso, however, that the benzene core remain a hexagon. The calculated energies can be fitted to give $V(\theta)$ (kJ) = $(3.0 \pm 0.2)\sin^2(\theta/2) + (9.9 \pm 0.3)\sin^2\theta - (1.4 \pm 0.3)\sin^2(2\theta)$ at the 95% confidence interval. In other words, *b* is more stable than *a* by 3.0 kJ/mol, rather close to the 3.1 kJ/mol predicted by the inadequate 2-site model above. It is clear, however, that $V(\theta)$ implies substantial populations of nonplanar forms at the temperatures given in Table 1, although conformer *b* is confirmed as that of lowest energy.

A simple calculation of ^5J at a given temperature proceeds by weighting each ^5J at a given θ with the population implied by $V(\theta)$ and the appropriate Boltzmann factor. In Table 3 the results of this procedure applied to **2** are given at three temperatures. At 305 K, ^5J is calculated as 4.88 Hz, the observed value being 4.51 Hz. At 240 K, the calculated and measured values are 5.37 and 5.21 Hz, respectively, while at 182 K they are 6.08 and 5.99 Hz. The agreement between the model and experiment improves at the lower temperatures. The improvement is *not* to be taken as proof that the model is correct at lower temperatures. An adjustment of $V(\theta)$, no doubt itself a function of temperature in solution, and (or) of ^5J_o could be made so as to produce a better match between observed and model-derived ^5J values at the 13 temperatures in Table 1. Such adjustments were abjured because even an exact fit would not *prove* the $\cos^4\theta$ dependence of ^5J nor its ^5J_o value, nor, for that matter, the exactness of $V(\theta)$.

That $V(\theta)$ is dependent on solvent is indicated by the solvent dependence of ^5J, described above. Using the $V(\theta)$ above and ^5J (θ = 0) as 8.15_2 Hz, the calculated ^5J at 203, 305, and 383 K becomes 5.79, 4.88, and 4.23 Hz, respectively. The observed values in toluene solution are 6.50, 4.80, and 4.20 Hz at these temperatures (15). In this solvent the calculated and observed couplings agree better at higher temperatures, in contrast to the acetone solution above. At 305 K, ^5J is 4.80 Hz in $CDCl_3$, toluene, and benzene solutions (14).

TABLE 3. The STO 3G MO energies, populations, and ^5J values as a function of θ for 2-fluoroacetophenone, **2**

		$P(\theta)^c$			$^5J(\theta) \times P(\theta)$ (Hz)^d		
θ (deg)^a	E (kJ)^b	305 K	240 K	182 K	305 K	240 K	182 K
0	0.00	0.280	0.332	0.399	2.28	2.71	3.26
15	0.39	0.240	0.273	0.309	1.70	1.94	2.19
30	1.78	0.139	0.136	0.123	0.64	0.62	0.57
45	4.06	0.057	0.043	0.027	0.16	0.09	0.06
60	6.76	0.019	0.011	0.005	0.01	0.01	0.00
75	9.88	0.006	0.002	0.001	0.00	0.00	0.00
90	11.48	0.003	0.001	0.000	0.00	0.00	0.00
105	10.83	0.004	0.001	0.000	—	—	—
120	8.77	0.009	0.004	0.001	—	—	—
135	6.31	0.023	0.014	0.006	—	—	—
150	4.17	0.054	0.041	0.025	—	—	—
165	3.14	0.081	0.069	0.050	—	—	—
180	3.06	0.084	0.072	0.053	—	—	—

^{a}The angle of twist about the Csp^2—Csp^2 bond, and $\theta = 0$ defines the conformation *b* in the text in which the methyl group lies nearest the C—F bond.

^{b}The energy of the conformer with $\theta = 0$ is $-475.165{,}556$ hartrees. The relative energies of the other conformers are from the actual STO 3G values.

^{c}Fractional populations based on a Boltzmann distribution using the E values in the second column.

^{d} $^5J(\theta)$ is not tabulated and is calculated from $^5J_o^{F,CH_3} \equiv {}^5J$ (Hz) $= 8.15_2 \cos^4 \theta$, defined between $\theta = 0$ and 90°. ^5J is assumed to be zero for $\theta > 90°$.

TABLE 4. The STO 3G energies, populations, and ^5J values for 2,6-difluoroacetophenone, **3**

		$P(\theta)^c$		$^5J(\theta) \times P(\theta)$ (Hz)^d	
θ (deg)^a	E (kJ)^b	305 K	192 K	305 K^f	192 K^f
0	1.9	0.117	0.092	0.96	0.75
15	1.1	0.161	0.152	1.14	1.08
30	0.0^e	0.248	0.303	1.14	1.39
45	0.1	0.239	0.285	0.49	0.58
60	1.4	0.143	0.126	0.07	0.06
75	3.8	0.056	0.028	0.00	0.00
90	4.9	0.036	0.014	0.00	0.00

^{a}For $\theta = 0$ the molecule has all heavy atoms in a plane.

^{b}The energy at $\theta = 30°$ is $-572.622{,}066$ hartrees.

^{c}Calculated as explained in Table 3.

^{d}Calculated as in Table 3 with $^5J_o = 8.15_2$ Hz.

^{e}The minimum energy occurs at 39° for the fitted equation in the text, but note the small difference in the calculated energies at $\theta = 30$ and 45°. The equation in the text yields the energy at 39° as 0.3 ± 0.3 kJ/mol lower than at 30°.

^{f}Note that the sum of the ^5J values must be divided by two to make a comparison with the observed ^5J.

Another test of the model may be had in the temperature dependence of ^5J in 2,6-difluoroacetophenone, **3**. The STO 3G optimized energies yield $V(\theta)$ (kJ) $= 1.8 + (3.0 \pm 0.2) \sin^2 \theta - (3.4 \pm 0.2) \sin^2 (2\theta)$ at the 95% confidence level. Clearly, the (flat) minimum in energy occurs in the vicinity of 39°, a distinctly nonplanar conformation. Table 4 gives the actual calculated energies as a function of θ as well as the calculations of ^5J by the procedure used for **2**. At 305 K the calculated and observed values are 1.90 and 1.56 Hz, respectively; they are 1.93 and 1.77 Hz at 192 K. The important point is that the model predicts small ^5J values, relative to **2**, and also a much smaller temperature dependence of ^5J than in **2**; both predictions are correct.

The observed temperature dependence of ^5J in Table 1 for **3** is empirically given by $^5J = 2.11_1 - 1.83_9 \times 10^{-3}\, T$ ($r = 0.997_1$). The value of 2.11 Hz is reproduced by the $\cos^4 \theta$ dependence at $\theta = 44.5°$, yielding 2.81 Hz at 40° and 1.39 Hz at 50°. The computed $V(\theta)$ is flat in this region, differing by only 0.1 kJ/mol between $\theta = 30$ and 45°. The model is consistent with the idea that **3** is a nonplanar molecule and that the preferred value of θ lies in the vicinity of 45°.

Although $V(\theta)$ was not calculated for pentafluoroacetophenone, its ^5J values between 280 and 325 K (Table 1) are given by ^5J (Hz) $= 2.57_1 - 2.44_7 \times 10^{-3}\, T$ ($r = 0.999_6$), implying that its nonplanarity is not quite as pronounced as for **3**. The empirical ^5J dependence on θ implies θ as 41° when ^5J is 2.57 Hz. The *para* fluorine substituent should act to increase the conjugation of the acetyl group with the π system of the ring, thereby decreasing the expectation value of θ (13), but the *meta* substituents *may* act in the opposite direction.

The vapor pressure of 2-fluoroacetophenone at ambient temperatures is very small because its normal boiling point lies near 473 K. Nevertheless, an ^{1}H nmr gas phase spectrum was obtained on a Bruker AM300 spectrometer from a sample containing some gaseous TMS and sufficient SF_6 to give a total gas pressure of 2500 to 3000 Torr (1 Torr = 133.3 Pa). The presence of the SF_6 increased T_2 (38) sufficiently to produce a linewidth at half height of 1.1 Hz for the TMS peak. Under these conditions, the linewidth of the methyl proton resonance was 2.5 Hz. Naturally, the intrinsic linewidth of the methyl proton resonance need not be the same as the TMS resonance, and may well be larger. Nevertheless, an upper limit of not more than 1.5 Hz for $^5J(F,CH_3)$ is indicated by these results.

It follows from the present coupling model that the molecule is no longer planar in its conformation of lowest energy. A rough estimate is that the angle of twist, θ, for the acetyl group lies in the vicinity of 50°. In that event, the conjugational energy of the acetyl group with the π system of the benzene nucleus is reduced by about 50%. Indeed, our measurements indicate that the shift range of the ring protons is about 0.2 ppm, as compared to 0.6 ppm in acetone-d_6 solution.

Furthermore, the available data for acetophenone indicate an internal barrier of 13 kJ/mol in the gas phase (39) and 22.4 kJ/mol in solution (40). Then, perhaps, the present gas phase data for 2-fluoroacetophenone become less puzzling. Indeed, speculations about solvent-assisted charge separation are tempting and suggest a number of measurements on other molecules.

Acknowledgments

We are grateful to the Natural Sciences and Engineering Research Council of Canada for financial assistance.

1. A. R. KATRITZKY, M. V. SINNOTT, T. T. TIDWELL, and R. D. TOPSOM. J. Am. Chem. Soc. **91**, 628 (1969).
2. E. BOCK, R. WASYLISHEN, B. E. GABOURY, and E. TOMCHUK. Can. J. Chem. **51**, 1906 (1973).
3. P. J. KRUEGER. Can. J. Chem. **51**, 1363 (1973).
4. W. B. SMITH, D. L. DEAVENPORT, and A. M. IHRIG. J. Am. Chem. Soc. **94**, 1959 (1972).
5. (*a*) M. G. BELSHAM, A. R. MUIR, M. KINNS, L. PHILLIPS, and L.-M. TWANMOH. J. Chem. Soc. Perkin Trans. 2, 119 (1974); (*b*) A. LEWIN. J. Am. Chem. Soc. **86**, 2304 (1964).
6. T. E. ST. AMOUR, M. I. BURGAR, B. VALENTINE, and D. FIAT. J. Am. Chem. Soc. **103**, 1128 (1981).
7. D. MIRARCHI and G. L. D. RITCHIE. J. Mol. Struct. **118**, 303 (1984).
8. D. MIRARCHI and G. L. D. RITCHIE. Aust. J. Chem. **34**, 1443 (1981), and references therein.
9. P. DIEHL, H. HUBER, A. C. KUNWAR, and M. REINHOLD. Org. Magn. Reson. **9**, 374 (1977).
10. Y. TANIMOTO, H. KOBAYASHI, S. NAGAKURA, and Y. SAITO. Acta Crystallogr. Sect. B, **29**, 1822 (1973).
11. T. SCHAEFER, T. A. WILDMAN, and R. SEBASTIAN. J. Mol. Struct. **89**, 93 (1982).
12. F. A. MILLER, W. G. FATELEY, and R. E. WITTKOWSKI. Spectrochim. Acta, Part A, **23**, 891 (1967).
13. T. DRAKENBERG, J. SOMMER, and R. JOST. J. Chem. Soc. Perkin Trans. 2, 363 (1980).
14. W. ADCOCK, D. G. MATTHEWS, and S. Q. A. RIZVI. Aust. J. Chem. **24**, 1829 (1971).
15. W. ADOCK and S. Q. A. RIZVI. Aust. J. Chem. **26**, 2659 (1973).
16. J. D. ROBERTS, D. R. DAVIES, and R. P. LUTZ. J. Am. Chem. Soc. **83**, 246 (1961).
17. J. HILTON and L. H. SUTCLIFFE. Prog. Nucl. Magn. Reson. Spectrosc. **10**, 27 (1975).
18. T. SCHAEFER and R. LAATIKAINEN. Can. J. Chem. **61**, 224 (1983).
19. T. SCHAEFER, T. A. WILDMAN, and J. PEELING. J. Magn. Reson. **56**, 144 (1984).
20. M. KHARASCH and O. REINMUTH. Grignard reactions of nonmetallic substances. Prentice Hall, New York. 1954.
21. E. J. COREY and J. W. SUGGS. Tetrahedron Lett. 2647 (1975).
22. T. SCHAEFER and R. SEBASTIAN. J. Magn. Reson. **41**, 395 (1980).
23. R. FREEMAN and W. A. ANDERSON. J. Chem. Phys. **37**, 2053 (1962).
24. G. ENGLERT and A. SAUPE. Mol. Cryst. **1**, 503 (1966).
25. W. J. HEHRE, R. F. STEWART, and J. A. POPLE. J. Chem. Phys. **51**, 2657 (1969).
26. M. R. PETERSEN and R. A. POIRIER. MONSTERGAUSS. Department of Chemistry, University of Toronto, Toronto, Ontario, Canada. 1981.
27. J. A. POPLE, J. W. MCIVER, and N. S. OSTLUND. J. Chem. Phys. **49**, 2965 (1968).
28. R. LAATIKAINEN. J. Magn. Reson. **52**, 293 (1983).
29. P. DOBOSH and N. S. OSTLUND. QCPE, **11**, 281 (1975).
30. S. CASTELLANO and A. A. BOTHNER-BY. J. Chem. Phys. **41**, 3863 (1964).
31. C. W. HAIGH. Annu. Rep. NMR Spectrosc. **41**, 311 (1971).
32. R. J. ABRAHAM, D. B. MACDONALD, and E. S. PEPPER. J. Chem. Soc. B, 835 (1967).
33. R. E. WASYLISHEN and M. BARFIELD. J. Am. Chem. Soc. **97**, 4545 (1975).
34. T. SCHAEFER, S. R. SALMAN, and T. A. WILDMAN. Can. J. Chem. **58**, 2364 (1980).
35. T. SCHAEFER, R. SEBASTIAN, R. P. VEREGIN, and R. LAATIKAINEN. Can. J. Chem. **61**, 29 (1983).
36. M. BARFIELD, S. R. WALTER, K. A. CLARK, G. W. GRIBBLE, K. W. HADEN, W. J. KELLY, and C. S. LE HOULLIER. Org. Magn. Reson. **20**, 92 (1982).
37. M. BARFIELD. J. Am. Chem. Soc. **102**, 1 (1980).
38. N. S. TRUE and B. D. ROSS. J. Phys. Chem. **88**, 3216 (1984).
39. F. A. MILLER, W. G. FATELEY, and R. E. WITTKOWSKI. Spectrochim. Acta, Part A, **23**, 891 (1967).
40. T. DRAKENBERG, R. JOST, and J. SOMMER. Org. Magn. Reson. **8**, 529 (1976).

Rhenium and manganese carbonyl compounds incorporating tridentate chelating pyrazolyl gallate ligands

Brenda M. Louie, Steven J. Rettig, Alan Storr, and James Trotter
Department of Chemistry, University of British Columbia, 2036 Main Mall, Vancouver, B.C., Canada V6T 1Y6

Received August 23, 1984

Brenda M. Louie, Steven J. Rettig, Alan Storr, and James Trotter. Can. J. Chem. **63**, 2261 (1985).

The coordinating properties of a variety of unsymmetrical uninegative tridentate chelating "pyrazolylgallate" ligands have been studied using the tricarbonyl moieties "$M(CO)_3$", where M = Mn or Re, as acceptor species. A series of monomeric, pseudo octahedral complexes has been characterized and a *fac* mode of coordination established for the tridentate gallate ligands from ^1H nmr, ir measurements, and X-ray structure determinations. Nitrosylation of a selection of the rhenium tricarbonyl compounds has yielded a number of cationic rhenium mononitrosyl dicarbonyl species. The reactivity of these cations towards reducing agents has been investigated.

Brenda M. Louie, Steven J. Rettig, Alan Storr et James Trotter. Can. J. Chem. **63**, 2261 (1985).

On a étudié les propriétées coordinantes d'une variété de ligands chélatants, tridentates, univalents et non-symétriques du type "pyrazolylgallate" en utilisant des unités tricarbonyles "$M(CO)_3$", dans lesquelles M = Mn ou Re, comme accepteurs. On a caractérisé une série de complexes monomères, pseudooctaédriques et, faisant appel à des mesures ir et rmn du ^1H ainsi que des déterminations de structures par diffraction des rayons X, on a établi que le mode de coordination est *fac*. La nitrosylation de composés rhénium tricarbonyles choisis conduit à un certain nombre d'espèces cationiques rhénium mononitrosyle dicarbonyles. On a étudié la réactivité de ces cations avec des agents de réductions.

[Traduit par le journal]

Introduction

In our continuing investigations of anionic tridentate chelating pyrazolylgallate ligands a number of new rhenium and manganese carbonyl derivatives have been prepared using a variety of three atom donor ligands of the general formula:

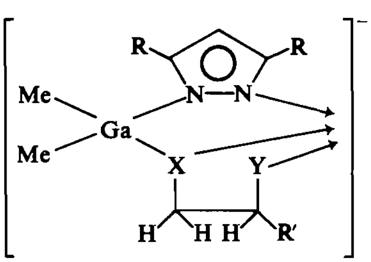

1

X = O or S; Y = NMe_2 or NH_2; R′ = H; R = H or Me
X = O; Y = SEt or SPh; R′ = H; R = Me
X = O; Y = NH_2; R′ = Me or Et; R = Me

This report introduces the ligands where X = S, and the ligands incorporating the chiral amino alcohols (R′ = Me or Et), for the first time. In addition to the complexes bearing the ligands **1**, the complex $[MeGa(N_2C_3H_3)_3]Re(CO)_3$ has been prepared and characterized. The configuration of the tridentate ligands in the complexes has been determined from infrared and ^1H nmr measurements, and the reactivity of a selection of the Re tricarbonyl compounds towards nitrosylation and subsequent reduction procedures has been probed. Definitive X-ray structural results are presented for four representative compounds.

Experimental

Starting materials

Air-sensitive materials were handled in oxygen-free dry nitrogen. Tetrahydrofuran (THF) and benzene were dried by refluxing over sodium/benzophenone and molten potassium, respectively. Methylene chloride and acetonitrile were each dried over P_2O_5 prior to distillation. All distilled solvents were stored under dry nitrogen following distillation. $Mn(CO)_5Br$ (1) and $[Re(CO)_4Cl]_2$ (2) were prepared from the corresponding $[M(CO)_5]_2$ compounds (M = Mn or Re) (Strem) by standard routes. L-2-amino-1-propanol (Aldrich), *d*-2-amino-1-butanol (Aldrich), *l*-2-amino-1-butanol (Aldrich), nitryl hexafluorophosphate (Alpha), and nitrosyl tetrafluoroborate were used as supplied. Nitrosyl hexafluorophosphate (Alpha) was dried *in vacuo* over P_2O_5 before use. Iodosobenzene (ICN) was used as supplied. Lithium triethylborohydride and potassium tri-*sec*-butylborohydride were purchased as 1 *M* solutions in THF (Aldrich) and used as supplied.

Ligand synthesis

All the ligands **1** were prepared as standard solutions in THF. The ligands involving (X = O; Y = NH_2; R′ = Me or Et) and (X = S; Y = NH_2 or NMe_2) were prepared by refluxing $Na^+[Me_3Ga(N_2C_3H_3)]^-$ or $Na^+[Me_3Ga(N_2C_5H_7)]^-$ with the appropriate chiral amino alcohol or amino thiol in THF until cessation of methane evolution. The resulting ligand solution was then made up to standard volume and aliquots used in subsequent reactions. The remaining ligands **1** and the ligand $Na^+[MeGa(N_2C_3H_3)_3]^-$ were prepared as described earlier (3–6).

Preparation of manganese and rhenium tricarbonyl complexes

The general method employed for the preparation of the complexes **1–16** listed in Table 1, together with analytical and ir data, and the complex **17** $[MeGa(N_2C_3H_3)_3]Re(CO)_3$ (*Anal.* calcd. for $[MeGa(N_2C_3H_3)_3]Re(CO)_3$: C 28.06, H 2.16, N 15.11; found: C 27.95, H 2.13, N 14.90. ν_{CO} 2028, 1918 cm^{-1} (cyclohexane). ^1H nmr (C_6D_6), τ = 10.04s (Ga—Me), 4.20t (pz-H^4), 3.09d (pz-H^5), 2.22d (pz-H^3) (τ values refer to $\tau_{C_6H_6}$ = 2.84 ppm, pz = pyrazolyl, $N_2C_3H_3$, J_{HCCH} = ~2 Hz for pz protons), was to react one or two molar equivalents of the appropriate ligand with ~0.5 g of $Mn(CO)_5Br$ or $[Re(CO)_4Cl]_2$, respectively, dissolved in ~75 mL THF. The mixture was refluxed overnight and the THF subsequently removed *in vacuo*. The solid remaining was then extracted with ~20 mL benzene and the mixture filtered. Slow evaporation of the benzene from the filtrate resulted in either well-formed crystalline products or amorphous solids in ~55–80% yields. The latter were either recrystallized from benzene/CH_2Cl_2 mixtures or dried by pumping *in vacuo* at ~50°C. ^1H nmr data for the complexes are collected in Tables 2 and 3.

Nitrosylation of selected rhenium tricarbonyl complexes

In general a slight excess of NO_2PF_6 dissolved in CH_2Cl_2/acetonitrile was added dropwise to ~0.3 g of $LRe(CO)_3$ {L = $[MeGa(N_2C_3H_3)_3]$, $[Me_2Ga(N_2C_3H_3)(OCH_2CH_2NMe_2)]$, or [Me$_2$Ga-

TABLE 1. Melting points, analytical and ir data for

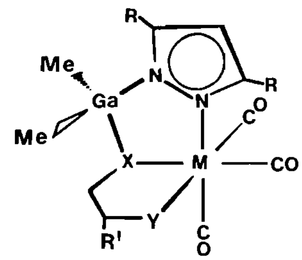

No.	M	R	R′	X	Y	Melting point (°C)	Calculated (%) C	H	N	Found (%) C	H	N	ν_{CO} (cm^{-1}) C_6H_{12}
1	Mn	H	H	S	NH_2	*	31.44	3.93	11.00	31.20	4.00	11.15	2031, 1940, 1919
2	Mn	H	H	S	NMe_2	*	35.15	4.64	10.25	35.56	4.67	10.79	2030, 1938, 1915
3	Mn	Me	H	S	NH_2	*	35.15	4.64	10.25	35.45	4.68	9.91	2028, 1938, 1914
4	Mn	Me	H	S	NMe_2	*	36.84	5.48	8.92†	36.57	5.40	8.92	2030, 1935, 1907
5	Re	H	H	O	NH_2	159–160	24.15	3.02	8.45	24.02	2.99	8.23	2030, 1920, 1900
6	Re	H	H	O	NMe_2	123–125	27.43	3.62	8.00	27.48	3.59	7.88	2015, 1926, 1905
7	Re	Me	H	O	NH_2	172–174	27.43	3.62	8.00	27.69	3.63	7.67	2025, 1920, 1898
8	Re	Me	H	O	NMe_2	158–159	30.39	4.16	7.60	30.50	4.28	7.54	2028, 1917, 1891
9	Re	H	H	S	NH_2	*	23.40	2.92	8.19	23.98	3.08	7.98	2029, 1926, 1908
10	Re	H	H	S	NMe_2	*	26.62	3.51	7.76	26.96	3.71	7.98	2031, 1926, 1905
11	Re	Me	H	S	NH_2	160–163	26.62	3.51	7.76	26.40	3.74	7.46	2031, 1926, 1904
12	Re	Me	H	S	NMe_2	109–112	29.53	4.04	7.38	29.61	4.28	7.09	2027, 1925, 1900
13	Re	Me	H	O	SPh	170–172	34.95	3.56	4.53	34.96	3.63	4.53	2028, 1940, 1916
14	Re	Me	H	O	SEt	136–138	29.47	4.91	3.86	29.32	4.77	3.75	2030, 1925, 1901
15	Re	Me	Me	O	NH_2	178–181	28.95	3.90	7.79	28.96	4.07	7.69‡	2029, 1918, 1895
16	Re	Me	Et	O	NH_2	157–160	30.39	4.19	7.59	30.33	4.23	7.36§	2026, 1920, 1898
										30.28	4.11	7.40‖	

*Decomposes before melting.
†Calculated for $[Me_2Ga(N_2C_5H_7)(SCH_2CH_2NMe_2)]Mn(CO)_3 \cdot H_2O$.
‡Starting amino alcohol = L-2-amino-1-propanol.
§Starting amino alcohol = *d*-2-amino-1-butanol.
‖Starting amino alcohol = *l*-2-amino-1-butanol.

TABLE 2. ^1H nmr data for

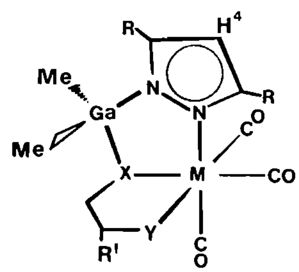

No.	M	R	R′	X	Y	τ (ppm) in C_6D_6* Ga–Me	H^4	R	Y
1	Mn	H	H	S	NH_2	9.83s, 10.11s	3.87t	2.49d, 2.68d	
2	Mn	H	H	S	NMe_2	9.92s, 10.09s	3.86t	2.24d, 2.65d	8.08s, 8.59s
3	Mn	Me	H	S	NH_2	9.75s, 10.11s	4.27s	7.88s, 7.94s	
4	Mn	Me	H	S	NMe_2	9.98s, 10.03s	4.25s	7.58s, 7.92s	8.03s, 8.60s
5	Re	H	H	O	NH_2	9.88s, 10.33s	3.95t	2.49d, 2.85d	
6	Re	H	H	O	NMe_2	9.92s, 10.26s	3.97t	2.43d, 2.83d	7.76s, 8.44s
7	Re	Me	H	O	NH_2	9.80s, 10.28s	4.34s	7.80s, 8.04s	
8	Re	Me	H	O	NMe_2	9.92s, 10.20s	4.32s	7.70s, 8.03s	7.70s, 8.32s
9	Re	H	H	S	NH_2	9.87s, 10.14s	4.04t	2.47d, 2.83d	
10	Re	H	H	S	NMe_2	9.91s, 10.06s	4.01t	2.40d, 2.83d	7.91s, 8.33s
11	Re	Me	H	S	NH_2	9.76s, 10.09s	4.39s	7.87s, 7.99s	
12	Re	Me	H	S	NMe_2	10.01s, 10.07s	4.37s	7.66s, 7.83s	7.98s, 8.41s
13	Re	Me	H	O	SPh	9.79s, 10.27s	4.34s	7.74s, 8.02s	3.10m
14	Re	Me	H	O	SEt	9.77s, 10.30s	4.34s	7.62s, 8.04s	~7.62m, ~7.84m, 9.23t

*$\tau_{C_6H_6}$ = 2.84 ppm; s = singlet, d = doublet (J ~2 Hz), t = triplet (J ~2 Hz), m = multiplet.

TABLE 3. ^{1}H nmr data for 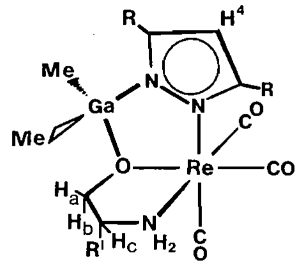

No.	R	R′	Approximate isomer ratio	Predicted position of R′†	τ (ppm) in C_6D_6* Ga—Me		R		H^4	Ha	Hb	Hc	R′	N—H_2
15	Me	Me	3	*trans*	9.76s	10.22s	7.69s	7.99s	4.30s	6.34dd‡	7.12t§	8.43m‖	10.01d	8.58m 8.93m
			1	*cis*	9.60s	10.08s	7.77s	7.99s	4.30s	6.74dd‡	7.45t§	¶	10.13d	¶
16	Me	Et	3	*trans*	9.74s	10.20s	7.67s	8.00s	4.31s	6.18dd‡	7.10t§	8.42m	9.81t ~9.65m	~8.51m 8.75m
			1	*cis*	9.58s	10.09s	7.76s	8.00s	4.31s	6.61dd‡	7.29t§	¶	9.83t ~9.65m	¶

*$\tau_{C_6H_6}$ = 2.84 ppm; s = singlet, d = doublet, t = triplet, dd = doublet of doublets, m = multiplet.
†*trans* = position on opposite side of metal as pyrazolyl group, *cis* = position on same side of metal as pyrazolyl group.
‡J_{ab} = 11.2 Hz, J_{ac} = 4.0 Hz.
§J_{ba} = 11.2 Hz, J_{bc} = 11.2 Hz.
‖J_{ca} = 4.0 Hz, J_{cb} = 11.2 Hz, $J_{c\text{-}NH_2} \sim$ 4 Hz, $J_{c\text{-}Me}$ = 7.2 Hz.
¶Not discernible.

$(N_2C_5H_7)(OCH_2CH_2NMe_2)]\}$ dissolved in ~50 mL CH_2Cl_2. The addition caused rapid evolution of CO and a change of the solution from colorless to brown. After stirring the reaction mixture for 5 min ~200 mL of anhydrous Et_2O was added resulting in the immediate precipitation of a dark orange–brown solid. The solvents were decanted off and the solid dried for ~12 h *in vacuo* at ~50°C. When L = $[MeGa(N_2C_3H_3)_3]$ the very air-sensitive nitrosylated product formed in 20% yield. For the remaining two tridentate ligands yields varied between 30 and 70%.

$NOPF_6$ and $NOBF_4$ could also be used as nitrosylating agents but longer reaction times of ~8 h were necessary. Physical data for the rhenium nitrosyl cations prepared, as well as for the starting tricarbonyl complexes in the same solvents, are tabulated in Table 4.

Spectra

Mass spectra were recorded on either a Varian MAT CH4B (Mn complexes) or AES MS 50 (Kratos) (Re complexes) spectrometer operating at 70 eV. Representative data for three of the complexes together with typical assignments are tabulated in Table 5. Infrared spectra were recorded on a Perkin-Elmer 598 spectrometer. ^{1}H nmr spectra were obtained on either a Varian XL-100 or Bruker WP80 instrument using FT techniques.

X-ray crystallographic analyses of *$[Me_2Ga(N_2C_5H_7)(OCH_2CH_2NMe_2)]Re(CO)_3$, 8, $[Me_2Ga(N_2C_5H_7)(OCH_2CH_2SPh)]Re(CO)_3$, 13, $[Me_2Ga(N_2C_5H_7)(OCH_2C(H)EtNH_2)]Re(CO)_3$, 16, and $[MeGa(N_2C_3H_3)_3]Re(CO)_3$, 17*

Crystallographic data are presented in Table 6. Unit-cell parameters were refined by least-squares on 2 sin θ/λ values for 25 reflections with 2θ = 40–50° measured with Mo-K_{α_1} radiation. The intensities of three standard reflections, measured every hour throughout the data collections, showed only small random fluctuations in each case. The data were processed[1] and corrected for absorption using the Gaussian integration method (7, 8) for compounds **8**, **16**, and **17** (224, 208, and 216 integration points, respectively) and the analytical method (7, 9) for compound **13**.

The structure of **13** is isomorphous with that of the manganese analog (10), the refinement initiated with the coordinates of non-hydrogen atoms determined for $[Me_2Ga(N_2C_5H_7)(OCH_2CH_2SPh)]$-$Mn(CO)_3$ (10). The three remaining structures were solved by conventional heavy-atom methods, the Re and Ga coordinates being determined from the Patterson functions and those of the remaining non-hydrogen atoms from subsequent difference maps. In the case of **17**, the non-centrosymmetric space group $Pn2_1a$ was indicated by *E*-statistics and by the Patterson function. In each case the non-hydrogen atoms were refined (full-matrix) with anisotropic thermal parameters. For **8**, **13**, and **17** the hydrogen atoms were included as fixed contributors in idealized positions (based on observed positions with C(sp^2)—H = 0.97 and C(sp^3)—H = 0.98 Å). The scattering factors of ref. 11 were used for the non-hydrogen atoms and those of ref. 12 for hydrogen atoms. Anomalous scattering corrections (13) were applied for Re, Ga, and S atoms. The absolute configuration of **16** is determined by that known for the chiral starting material. In the case of **17** attempts to determine the polarity by parallel refinement were unsuccessful.

The final positional and equivalent isotropic thermal parameters for non-hydrogen atoms appear in Table 7. Bond lengths, bond angles, and intra-annular torsion angles are given in Tables 8–10, respectively. Calculated hydrogen parameters, anisotropic thermal parameters, and complete listings of torsion angles (Tables 11–13) have been placed in the Depository for Unpublished Data[2] along with measured and calculated structure factor amplitudes for the four compounds.

Results and discussion

Analysis of mass spectral, ir, and ^{1}H nmr data for the complexes listed in Table 1 and also for the compound $[MeGa(N_2C_3H_3)_3]Re(CO)_3$ points to the monomeric octahedral structures for the whole series of compounds studied. Unlike the $[MeGa(N_2C_3H_3)_3]^-$ ligand (5) and the related pyrazolylborate ligands, $[RB(N_2C_3H_3)_3]$ (R = H, alkyl, aryl) (14–16), which coordinate exclusively in a *fac* conformation due to

[1]The computer programs used include locally written programs for data processing and locally modified versions of the following: ORFLS, full-matrix least-squares, and ORFFE, function and errors, by W. R. Busing, K. O. Martin and H. A. Levy; Patterson and Fourier syntheses, by A. Zalkin; ORTEP II, illustrations, by C. K. Johnson.

[2]The structure factor tables and other material mentioned in the text are available, at a nominal charge, from the Depository of Unpublished Data, CISTI, National Research Council of Canada, Ottawa, Ont., Canada K1A 0S2.

TABLE 4. Infrared and ^1H nmr data for $LRe(CO)_3 \rightarrow LRe(CO)_2(NO)^+PF_6^-$
I → II

No.	Compound	L	R	Infrared (cm^{-1}) ν_{CO}	Infrared (cm^{-1}) ν_{NO}	^1H nmr in $(CD_3)_2CO$, τ (ppm)* Ga—Me	H^4	R	—NMe_2
17	I	$MeGa(N_2C_3HR_2)_3$	H	2028, 1910†		9.32s	3.52t	1.83d, 2.05d	
18	II	$MeGa(N_2C_3HR_2)_3$	H	2038, 1921†	1827†	10.01s,	3.28t	1.79d, 2.10d	
6	I	$Me_2Ga(N_2C_3HR_2)(OCH_2CH_2NMe_2)$	H	2020, 1898, 1873‡		10.19s, 10.28s	3.50t	2.06d, 2.16d	6.73s, 7.51s
19	II	$Me_2Ga(N_2C_3HR_2)(OCH_2CH_2NMe_2)$	H	2040, 1930‡	1815‡	9.98s	2.87§	1.33§, 1.79§	6.74s, 6.78s
8	I	$Me_2Ga(N_2C_3HR_2)(OCH_2CH_2NMe_2)$	Me	2015, 1894, 1869‡		10.17s, 10.31s	3.95s	6.74s, 7.52s	7.46s, 7.7s
20	II	$Me_2Ga(N_2C_3HR_2)(OCH_2CH_2NMe_2)$	Me	2035, 1920‡	1816‡	10.03s	2.57s	6.79s, 7.89s	6.76s

*$\tau_{(CH_3)_2CO}$ = 7.89 ppm; s = singlet, d = doublet (J ~ 2Hz), t = triplet (J ~ 2 Hz).
†MeCN.
‡Nujol.
§Poor resolution.

TABLE 5. Mass spectral data of 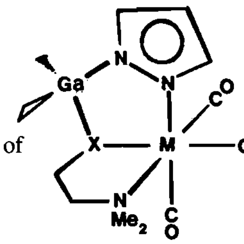 ≡ **P**

Assignment	Relative intensities (*i*) M = Re X = O	(*ii*) M = Re X = S	(*iii*) M = Mn X = S
P^+	25.0	18.0	5.6
$P - Me^+$	100.0	100.0	2.6
$P - CO^+$	2.3	0.0	0.0
$P - Me - CO^+$	0.9	1.4	Trace*
$P - 2CO^+$	2.0	0.0	0.0
$P - Me - 2CO^+$	4.5	7.3	3.9
$P - 3CO^+$	Trace	2.4	100.0
$P - Me - 3CO^+$	1.4	3.1	8.7
$P - 2Me - 3CO^+$	Trace	1.5	2.2
$P - Me - 3CO - pz^+$	Trace	73.0	81.8
M^+	Trace	Trace	4.0
Me_2Ga^+	10.5	30.3	16.1
Ga^+	11.1	24.4	38.2
pzH^+	1.7	3.6	4.7

*Trace = <0.5.

geometric constraints, the unsymmetric ligands **1** can potentially coordinate in either a *fac* or *mer* configuration (4, 17). However, in each of the complexes described in this paper, the transition metal is coordinated entirely by a *fac* arrangement of **1**. This arrangement of the ligating atoms is evident from both the ir and the ^1H nmr results and has been confirmed by crystal structure determinations for complexes **8**, **13**, **16**, and **17** (see below).

[$Me_2Ga(N_2C_3HR_2)(XCH_2CH_2NR''_2)$]$M(CO)_3$ (R, R″ = H or Me; X = O or S; M = Re) or (R, R″ = H or Me; X = S; M = Mn)

Three strong bands in the ν_{CO} region (see Table 1) for each of the complexes **1–16** indicate that the pyrazolylgallate tridentate ligand occupies three facial positions in the octahedral structures, with the three CO groups occupying the remaining set of facial positions. A *mer* arrangement for the unsymmetrical pyrazolylgallate ligand in these complexes would lead to two weak ν_{CO} bands and one strong ν_{CO} band in the ir of the complexes (18). The ^1H nmr spectra for the complexes (Table 2) also supports the *fac* conformation for the chelating ligands in the complexes with two sharp Ga—Me signals observed in each case. A *mer* arrangement would make the two Ga—Me groups equivalent and hence just one signal would be observed in this region of the spectrum. The X-ray crystal structure of the complex where R = R″ = Me, X = O, and M = Re is shown in Fig. 1.

Mass spectral data obtained for the complexes (Table 5) reveal interesting behavioural differences between the Re and Mn derivatives. Although the fragmentation patterns appear very similar for the three complexes the relative intensities of the signals differ sharply. Thus while the strongest signal is assignable to the P − Me^+ ion (P = parent) for the Re compounds, this signal is of much lower intensity for the valence

TABLE 6. Crystallographic data*

Parameter	Value†			
	$L^1Re(CO)_3$	$L^2Re(CO)_3$	$L^3Re(CO)_3$	$L^4Re(CO)_3$
Formula	$C_{14}H_{23}GaN_3O_4Re$	$C_{18}H_{22}GaN_2O_4ReS$	$C_{14}H_{23}GaN_3O_4Re$	$C_{13}H_{12}GaN_6O_3Re$
fw.	553.27	618.37	553.27	556.20
Crystal system	Monoclinic	Triclinic	Orthorhombic	Orthorhombic
Space group	$P2_1/c$	$P\bar{1}$	$P2_12_12_1$	$Pn2_1a$§
a	7.8271(4)	10.4892(14)	7.3661(3)	13.8978(5)
b	9.7730(3)	11.630(2)	14.7287(5)	15.4267(5)
c (Å)	24.6403(13)	9.5855(13)	17.8928(13)	8.0228(2)
α	90	111.508(7)	90	90
β	92.302(3)	97.567(9)	90	90
γ (deg)	90	86.217(10)	90	90
V (Å^3)	1883.3(2)	1078.2(3)	1941.2(2)	1720.0(1)
Z	4	2	4	4
D_c (g/cm^3)	1.951	1.905	1.893	2.148
$F(000)$	1064	596	1064	1048
μ(Mo$-K_\alpha$) cm^{-1}	79.6	70.5	77.2	87.1
Crystal dimensions (mm)	0.13×0.16×0.52	0.13×0.28×0.30	0.10×0.19×0.38	0.42×0.45×0.50
Transmission factors	0.176−0.476	0.118−0.371	0.243−0.531	0.036−0.110
Scan type	$\omega-2\theta$	$\omega-2\theta$	$\omega-2\theta$	$\omega-2\theta$
Scan range (deg in ω)	0.65+0.35tanθ	0.65+0.35tanθ	0.62+0.35tanθ	0.80+0.35tanθ
Scan speed (deg/min)	0.69−10.06	0.84−10.06	1.01−10.06	1.55−10.06
Data collected	$+h, +k, \pm l$	$\pm h, \pm k, +l$	$+h, +k, +l$	$+h, +k, +l$
$2\theta_{max}$ (deg)	60	60	60	60
Unique reflections	5458	6250	3203	2579
Reflections with $I \geq 3\sigma(I)$	3091	4111	1774	1856
Number of variables	208	244	208	216
R	0.043	0.036	0.035	0.053
R_w	0.050	0.040	0.041	0.059
S	0.936	1.651	1.780	2.519
Mean Δ/σ (final cycle)	0.02	0.01	0.04	0.04
Max Δ/σ (final cycle)	0.13	0.09	0.42	0.14
Residual density (e/Å^3)‖	−3.8 to +3.8	−3.3 to +2.0	−1.7 to +1.3	−7.6 to +3.3

*Temperature 22°C, Enraf-Nonius CAD4-F diffractometer, Mo-K_α radiation ($\lambda_{K_{\alpha 1}}$ = 0.70930, $\lambda_{K_{\alpha 2}}$ = 0.71359 Å), graphite monochromator, takeoff angle 2.7°, aperture (2.00 + tan θ) × 4.0 mm at a distance of 173 mm from the crystal, scan range extended by 25% on both sides for background measurement, $\sigma^2(I) = S + 2B + [0.04(S - B)]^2$ (S = scan count, B = normalized background count), function minimized $\Sigma w(|F_o| - |F_c|)^2$ where $w = 1/\sigma^2(F)$, $R = \Sigma||F_o| - |F_c||/\Sigma|F_o|$, $R_w = (\Sigma w(|F_o| - |F_c|)^2/\Sigma w|F_o|^2)^{1/2}$, $S = (\Sigma w(|F_o| - |F_c|)^2/(m - n))^{1/2}$. Values given for R, R_w, and S are based on those reflections with $I \geq 3\sigma(I)$.

†L^1 = $[Me_2Ga(N_2C_5H_7)(OCH_2CH_2NMe_2)]$, L^2 = $[Me_2Ga(N_2C_5H_7)(OCH_2CH_2SPh)]$, L^3 = $[Me_2Ga(N_2C_5H_7)(OCH_2C(H)EtNH_2)]$, L^4 = $[MeGa(N_2C_3H_3)_3]$.

‡Reduced cell, conventional orientation.

§Non-standard setting of $Pna2_1$, equivalent positions: (x, y, z; $-x$, $1/2 + y$, $-z$; $1/2 - x$, $1/2 + y$, $1/2 + z$; $1/2 + x$, y, $1/2 - z$).

‖Largest peaks near Re atoms in every case, the maps were essentially featureless away from the heavy atoms.

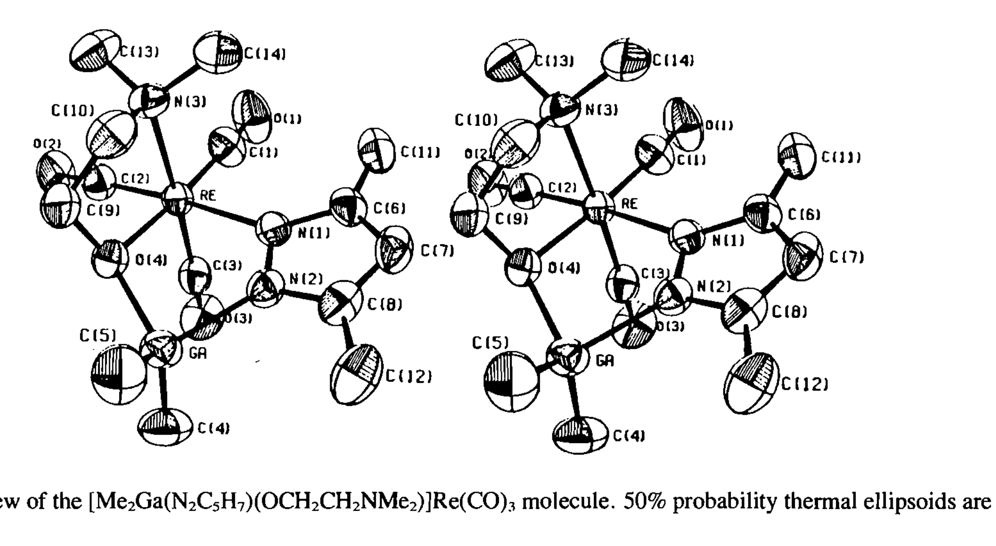

FIG. 1. Stereoscopic view of the $[Me_2Ga(N_2C_5H_7)(OCH_2CH_2NMe_2)]Re(CO)_3$ molecule. 50% probability thermal ellipsoids are shown for the non-hydrogen atoms.

TABLE 7. Final positional (fractional × 10^4; Re, Ga, and S × 10^5) and isotropic thermal parameters ($U \times 10^3$ Å^2) with estimated standard deviations in parentheses*

Atom	x	y	z	U_{eq}	Atom	x	y	z	U_{eq}
	$[Me_2Ga(N_2C_5H_7)(OCH_2CH_2NMe_2)]Re(CO)_3$					$[Me_2Ga(N_2C_5H_7)(OCH_2C(H)EtNH_2)]Re(CO)_3$			
Re	49020(4)	42246(3)	34142(1)	37	Re	44010(6)	53818(3)	47928(3)	59
Ga	32381(14)	12207(10)	39175(4)	48	Ga	39517(19)	41045(9)	31815(7)	64
O(1)	6476(12)	7075(8)	3518(3)	88	O(1)	4948(21)	5637(10)	6444(7)	146
O(2)	6911(11)	4031(8)	2377(3)	74	O(2)	2859(22)	7298(8)	4850(11)	165
O(3)	8204(9)	3187(9)	3977(3)	76	O(3)	549(14)	4784(9)	5163(7)	113
O(4)	3687(7)	2273(6)	3275(2)	43	O(4)	4241(12)	5302(5)	3590(5)	70
N(1)	3470(9)	4169(7)	4159(3)	41	N(1)	5491(13)	3610(5)	3999(5)	54
N(2)	2785(9)	2950(7)	4321(3)	42	N(2)	5585(12)	4036(5)	4659(4)	46
N(3)	2393(10)	4868(8)	2967(3)	50	N(3)	7188(14)	5837(7)	4431(9)	88
C(1)	5876(13)	6005(10)	3494(4)	55	C(1)	4796(23)	5477(14)	5819(9)	131
C(2)	6116(13)	4106(9)	2759(4)	51	C(2)	3514(26)	6578(9)	4796(12)	106
C(3)	6925(12)	3571(10)	3779(4)	50	C(3)	2082(17)	4967(10)	5023(8)	74
C(4)	5387(16)	431(12)	4183(5)	74	C(4)	5182(27)	4061(10)	2187(9)	101
C(5)	1138(16)	152(12)	3817(5)	75	C(5)	1404(18)	3751(11)	3348(9)	83
C(6)	3099(11)	5116(10)	4539(4)	46	C(6)	6494(15)	2823(7)	4030(7)	59
C(7)	2141(12)	4486(11)	4934(4)	54	C(7)	7204(16)	2743(7)	4747(9)	70
C(8)	1978(11)	3140(11)	4790(4)	49	C(8)	6604(16)	3498(7)	5126(8)	64
C(9)	2407(13)	2370(10)	2852(4)	55	C(9)	5534(33)	5915(9)	3260(10)	113
C(10)	1316(13)	3613(12)	2948(4)	63	C(10)	7384(31)	5754(14)	3554(13)	128
C(11)	3634(13)	6583(11)	4525(4)	60	C(11)	8565(70)	6668(20)	3206(18)	224
C(12)	1106(15)	1993(13)	5065(4)	74	C(12)	10015(54)	6393(25)	3347(30)	299
C(13)	2708(15)	5357(13)	2410(4)	72	C(13)	6638(23)	2162(10)	3364(10)	97
C(14)	1429(16)	5949(13)	3248(5)	77	C(14)	6948(20)	3751(10)	5941(7)	79
	$[Me_2Ga(N_2C_5H_7)(OCH_2CH_2SPh)]Re(CO)_3$					$[MeGa(N_2C_3H_3)_3]Re(CO)_3$			
Re	78170(2)	81977(2)	65502(2)	49	Re	34576(3)	35000	28221(7)	31
Ga	66578(6)	65640(6)	28115(7)	57	Ga	36330(14)	11806(16)	25710(24)	37
S	68915(12)	102423(13)	65478(15)	55	O(1)	4870(13)	4818(11)	1329(26)	74
O(1)	8908(5)	5629(5)	6321(8)	99	O(2)	3455(14)	4578(13)	6048(25)	80
O(2)	7780(5)	8862(6)	9938(6)	100	O(3)	1834(12)	4671(11)	1513(27)	68
O(3)	10630(4)	8981(5)	7221(6)	84	N(1)	2531(10)	1678(9)	3695(19)	40
O(4)	7739(3)	7884(3)	4184(4)	51	N(2)	2434(9)	2558(8)	3764(16)	29
N(1)	5824(4)	7612(4)	5852(5)	54	N(3)	3559(9)	1855(10)	514(19)	35
N(2)	5534(4)	6761(4)	4395(5)	59	N(4)	3505(9)	2743(9)	564(18)	31
C(1)	8456(6)	6585(6)	6389(7)	66	N(5)	4617(10)	1824(10)	3686(22)	43
C(2)	7768(6)	8602(7)	8659(7)	70	N(6)	4622(9)	2707(11)	3780(19)	40
C(3)	9572(5)	8701(5)	6967(6)	57	C(1)	4379(13)	4294(13)	1914(27)	51
C(4)	7602(7)	5001(6)	2341(9)	82	C(2)	3442(14)	4153(15)	4869(33)	59
C(5)	5674(7)	7114(6)	1229(7)	75	C(3)	2439(14)	4261(15)	1967(26)	51
C(6)	4779(5)	7696(6)	6562(6)	58	C(4)	3838(21)	−67(12)	2406(27)	57
C(7)	3843(5)	6906(6)	5604(8)	65	C(5)	1769(13)	1328(14)	4448(26)	48
C(8)	4365(5)	6324(6)	4242(8)	65	C(6)	1148(14)	1938(17)	5023(33)	63
C(9)	7851(5)	8978(5)	3862(6)	53	C(7)	1604(13)	2704(13)	4596(28)	45
C(10)	6832(6)	9907(5)	4538(6)	60	C(8)	3569(12)	1586(15)	−1107(24)	47
C(11)	8095(5)	11381(5)	7427(6)	56	C(9)	3536(14)	2286(20)	−2093(19)	52
C(12)	8662(6)	11981(6)	6681(7)	70	C(10)	3512(13)	2963(15)	−1022(25)	45
C(13)	9551(7)	12894(7)	7500(11)	87	C(11)	5423(14)	1521(16)	4533(32)	62
C(14)	9868(7)	13185(7)	9013(11)	93	C(12)	5925(13)	2287(23)	5131(31)	71
C(15)	9300(8)	12571(7)	9746(9)	95	C(13)	5390(14)	2937(14)	4637(29)	54
C(16)	8410(7)	11692(6)	8967(7)	80					
C(17)	4692(6)	8567(8)	8159(7)	81					
C(18)	3817(8)	5370(8)	2817(11)	98					

*U_{eq} = (1/3) trace U_{diag}.

isoelectronic Mn compound, which displays as its most intense signal that arising from the P − 3CO$^+$ ion. This difference in behaviour reflects stronger M—CO bonds for the Re complexes when compared to the Mn species. In support of this conjecture an examination of the ν_{CO} stretching frequencies for the compounds (Table 1) reveals repeatedly lower ν_{CO} values for the Re complexes than the corresponding Mn compounds. This can only result from stronger back bonding to the carbonyl ligands in the Re species, which leads to stronger "Re—CO" bonds.

Three general points can be made from a comparison of the complexes **1**−**12** and the four related Mn compounds where X = O; R, R″ = H or Me (19). Firstly, complexes where M = Re are air-stable while the corresponding complexes where M = Mn tend to be air-sensitive. Secondly, complexes where X = O show greater air stability than the corresponding

TABLE 8. Bond lengths (Å) with estimated standard deviations in parentheses

Bond	Length (Å)	Bond	Length (Å)
$[Me_2Ga(N_2C_5H_7)(OCH_2CH_2NMe_2)]Re(CO)_3$			
Re —O(4)	2.153(6)	O(4)—C(9)	1.419(10)
Re —N(1)	2.189(7)	N(1)—N(2)	1.372(9)
Re —N(3)	2.300(7)	N(1)—C(6)	1.358(11)
Re —C(1)	1.907(10)	N(2)—C(8)	1.352(11)
Re —C(2)	1.910(10)	N(3)—C(10)	1.488(14)
Re —C(3)	1.899(10)	N(3)—C(13)	1.483(13)
Ga —O(4)	1.933(6)	N(3)—C(14)	1.485(14)
Ga —N(2)	2.000(7)	C(6)—C(7)	1.394(13)
Ga —C(4)	1.940(11)	C(6)—C(11)	1.494(14)
Ga —C(5)	1.955(12)	C(7)—C(8)	1.368(14)
O(1)—C(1)	1.146(11)	C(8)—C(12)	1.490(14)
O(2)—C(2)	1.151(11)	C(9)—C(10)	1.510(15)
O(3)—C(3)	1.158(11)		
$[Me_2Ga(N_2C_5H_7)(OCH_2CH_2SPh)]Re(CO)_3$			
Re —S	2.5091(14)	O(4)—C(9)	1.430(6)
Re —O(4)	2.152(3)	N(1)—N(2)	1.392(6)
Re —N(1)	2.183(4)	N(1)—C(6)	1.344(6)
Re —C(1)	1.908(6)	N(2)—C(8)	1.328(7)
Re —C(2)	1.907(6)	C(6)—C(7)	1.384(9)
Re —C(3)	1.915(6)	C(6)—C(17)	1.505(9)
Ga —O(4)	1.931(4)	C(7)—C(8)	1.398(9)
Ga —N(2)	1.982(5)	C(8)—C(18)	1.481(10)
Ga —C(4)	1.941(7)	C(9)—C(10)	1.499(8)
Ga —C(5)	1.996(6)	C(11)—C(12)	1.373(8)
S —C(10)	1.814(6)	C(11)—C(16)	1.384(8)
S —C(11)	1.783(6)	C(12)—C(13)	1.393(9)
O(1)—C(1)	1.162(8)	C(13)—C(14)	1.363(12)
O(2)—C(2)	1.148(7)	C(14)—C(15)	1.376(13)
O(3)—C(3)	1.147(7)	C(15)—C(16)	1.363(10)
$[Me_2Ga(N_2C_5H_7)(OCH_2C(H)EtNH_2)]Re(CO)_3$			
Re —O(4)	2.158(9)	O(4)—C(9)	1.44(2)
Re —N(2)	2.179(7)	N(1)—N(2)	1.339(11)
Re —N(3)	2.254(11)	N(1)—C(6)	1.375(13)
Re —C(1)	1.864(14)	N(2)—C(8)	1.374(14)
Re —C(2)	1.880(12)	N(3)—C(10)	1.58(3)
Re —C(3)	1.860(13)	C(6)—C(7)	1.39(2)
Ga —O(4)	1.921(8)	C(6)—C(13)	1.54(2)
Ga —N(1)	1.989(9)	C(7)—C(8)	1.37(2)
Ga —C(4)	2.00(2)	C(8)—C(14)	1.53(2)
Ga —C(5)	1.970(14)	C(9)—C(10)	1.48(3)
O(1)—C(1)	1.15(2)	C(10)—C(11)	1.72(4)
O(1)—C(2)	1.17(2)	C(11)—C(12)	1.17(6)
O(3)—C(3)	1.188(15)		
$[MeGa(N_2C_3H_3)_3]Re(CO)_3$			
Re —N(2)	2.170(12)	N(1)—C(5)	1.33(2)
Re —N(4)	2.157(15)	N(2)—C(7)	1.35(2)
Re —N(6)	2.169(15)	N(3)—N(4)	1.37(2)
Re —C(1)	1.92(2)	N(3)—C(8)	1.36(2)
Re —C(2)	1.93(2)	N(4)—C(10)	1.32(2)
Re —C(3)	1.96(2)	N(5)—N(6)	1.37(2)
Ga —N(1)	1.936(15)	N(5)—C(11)	1.39(2)
Ga —N(3)	1.95(2)	N(6)—C(13)	1.32(2)
Ga —N(5)	1.91(2)	C(5)—C(6)	1.36(3)
Ga —C(4)	1.95(2)	C(6)—C(7)	1.38(3)
O(1)—C(1)	1.16(2)	C(8)—C(9)	1.34(3)
O(2)—C(2)	1.15(3)	C(9)—C(10)	1.35(3)
O(3)—C(3)	1.11(2)	C(11)—C(12)	1.45(4)
N(1)—N(2)	1.37(2)	C(12)—C(13)	1.31(3)

complexes where X = S. In addition, the presence of an alkyl group at the R and R″ positions of the tridentate ligand also resulted in some stabilization of the complexes, an effect observed in other compounds incorporating this type of ligand (19, 20).

$[Me_2Ga(N_2C_5H_7)(OCH_2CH_2SR''')]Re(CO)_3$ (R‴ = Et or Ph)

The complexation of the tridentate "SR‴" ligands to various transition metal moieties has been detailed previously (6, 10). These ligands reacted readily with $[Re(CO)_4Cl]_2$ forming colorless crystalline tricarbonyl complexes (Tables 1 and 2). The mass spectra of both the "S—Et" and "S—Ph" species were dominated, like the Re complexes discussed above, by the signal attributable to the $P - Me^+$ ion (100%). The highest m/e signals recorded corresponded to the parent ions (P^+, 20%), with weak signals (<3%) assignable to successive loss of CO from both the P^+ and $P - Me^+$ ions being recorded. The X-ray crystal structure of the complex where R‴ = Ph is shown in Fig. 2.

$[Me_2Ga(N_2C_5H_7)(OCH_2C(H)R'NH_2)]Re(CO)_3$ (R′ = Me or Et)

A chiral carbon centre was incorporated into the unsymmetric pyrazolylgallate ligand by reacting the appropriate chiral amino alcohols with $Na^+[Me_3Ga(N_2C_5H_7)]^-$. The resulting ligands reacted readily with $[Re(CO)_4Cl]_2$ to form air-stable, crystalline, monomeric products. The resulting tricarbonyl complexes may be formed as two possible diastereoisomers (see Fig. 3). These have been designated "*cis*' when the R′ group is on the same side of the transition metal as the "pyrazolyl" group and "*trans*" when the R′ group is on the opposite side. The ^1H data for these complexes are tabulated in Table 3. The assignment of the aminoalcohol protons was established by double resonance experiments. From steric arguments the "*trans*" isomer is favored over the "*cis*" isomer and indeed a crystal structure determination (R′ = Et) has confirmed this arrangement in the solid state (Fig. 4). The ^1H nmr results suggest a mixture of isomers to be present in solution with the ratio varying with the solvent. Thus, dissolving the sample used for the X-ray crystal structure determination in C_6D_6, resulted in two sets of signals in the ratio of ~3:1. In d_6-acetone the ratio was ~10:1. It is conjectured that the predominant isomer in solution is the *trans* isomer and that interconversion between this isomer and the *cis* form may result from initial breaking of the Re—N bond to give a five coordinate intermediate followed by inversion about the oxygen atom, and reforming of the Re—N bond. A relatively weak "M—N" bond (M = transition metal) has been suggested in several other related complexes containing unsymmetric pyrazolylgallate ligands, complexes which also exhibit fluxional behaviour in solution (6, 20–22).

$[MeGa(N_2C_3H_3)_3]Re(CO)_3$

This tricarbonyl complex containing the symmetric methyl tris(1-pyrazolyl) gallate ligand crystallized as large colorless cubic crystals from benzene. The facial coordination of the gallate ligand and the three CO groups was evident from the ν_{CO} vibrations which consisted of two bands in the predicted intensity pattern for such an octahedral complex (18). An X-ray crystal structure determination has confirmed this arrangement in the solid state (Fig. 5). The mass spectrum of the complex displayed a prominent signal due to the parent ion, P^+ (50%), with other strong signals due to the ions $P - Me^+$ (92%), $P - CO^+$ (27%), $P - 2CO^+$ (24%), $P - 3CO^+$ (100%), $P - Me - 3CO^+$ (9%), and Ga^+ (30%).

TABLE 9. Bond angles (deg) with estimated standard deviations in parentheses

Bonds	Angle (deg)	Bonds	Angle (deg)	Bonds	Angle (deg)	Bonds	Angle (deg)
	$[Me_2Ga(N_2C_5H_7)(OCH_2CH_2NMe_2)]Re(CO)_3$				$[Me_2Ga(N_2C_5H_7)(OCH_2C(H)EtNH_2)]Re(CO)_3$		
O(4)—Re—N(1)	82.8(2)	Re—N(1)—N(2)	119.0(5)	O(4)—Re—N(2)	82.1(3)	Ga—O(4)—C(9)	119.5(9)
O(4)—Re—N(3)	78.6(3)	Re—N(1)—C(6)	133.9(6)	O(4)—Re—N(3)	77.3(4)	Ga—N(1)—N(2)	120.5(6)
O(4)—Re—C(1)	175.8(4)	N(2)—N(1)—C(6)	107.1(7)	O(4)—Re—C(1)	174.0(6)	Ga—N(1)—C(6)	130.1(8)
O(4)—Re—C(2)	92.5(3)	Ga—N(2)—N(1)	120.7(5)	O(4)—Re—C(2)	92.0(6)	N(2)—N(1)—C(6)	109.4(9)
O(4)—Re—C(3)	97.6(3)	Ga—N(2)—C(8)	129.7(6)	O(4)—Re—C(3)	98.8(5)	Re—N(2)—N(1)	120.1(6)
N(1)—Re—N(3)	87.2(3)	N(1)—N(2)—C(8)	109.3(7)	N(2)—Re—N(3)	82.8(3)	Re—N(2)—C(8)	132.6(7)
N(1)—Re—C(1)	98.7(3)	Re—N(3)—C(10)	105.2(6)	N(2)—Re—C(1)	96.6(6)	N(1)—N(2)—C(8)	107.1(8)
N(1)—Re—C(2)	175.0(3)	Re—N(3)—C(13)	111.1(6)	N(2)—Re—C(2)	173.0(7)	Re—N(3)—C(10)	110.2(10)
N(1)—Re—C(3)	92.3(3)	Re—N(3)—C(14)	114.3(6)	N(2)—Re—C(3)	95.3(5)	Re—C(1)—O(1)	172(2)
N(3)—Re—C(1)	97.5(4)	C(10)—N(3)—C(13)	110.5(8)	N(3)—Re—C(1)	96.8(7)	Re—C(2)—O(2)	174(2)
N(3)—Re—C(2)	93.2(4)	C(10)—N(3)—C(14)	107.7(9)	N(3)—Re—C(2)	92.2(7)	Re—C(3)—O(3)	173.8(14)
N(3)—Re—C(3)	176.2(3)	C(13)—N(3)—C(14)	108.0(8)	N(3)—Re—C(3)	175.8(6)	N(1)—C(6)—C(7)	108.1(10)
C(1)—Re—C(2)	86.1(4)	Re—C(1)—O(1)	176.9(9)	C(1)—Re—C(2)	88.9(8)	N(1)—C(6)—C(13)	122.5(12)
C(1)—Re—C(3)	86.3(4)	Re—C(2)—O(2)	177.1(9)	C(1)—Re—C(3)	87.1(7)	C(7)—C(6)—C(13)	129.3(11)
C(2)—Re—C(3)	86.9(4)	Re—C(3)—O(3)	176.4(8)	C(2)—Re—C(3)	89.3(8)	C(6)—C(7)—C(8)	105.4(10)
O(4)—Ga—N(2)	90.0(3)	N(1)—C(6)—C(7)	108.5(8)	O(4)—Ga—N(1)	89.6(3)	N(2)—C(8)—C(7)	110.1(11)
O(4)—Ga—C(4)	107.7(4)	N(1)—C(6)—C(11)	124.7(9)	O(4)—Ga—C(4)	108.5(5)	N(2)—C(8)—C(14)	122.0(10)
O(4)—Ga—C(5)	111.1(4)	C(7)—C(6)—C(11)	126.8(8)	O(4)—Ga—C(5)	106.9(5)	C(7)—C(8)—C(14)	128.0(12)
N(2)—Ga—C(4)	109.7(4)	C(6)—C(7)—C(8)	106.9(8)	N(1)—Ga—C(4)	112.6(6)	O(4)—C(9)—C(10)	111.3(14)
N(2)—Ga—C(5)	110.5(4)	N(2)—C(8)—C(7)	108.2(8)	N(1)—Ga—C(5)	109.6(5)	N(3)—C(10)—C(9)	105(2)
C(4)—Ga—C(5)	122.9(5)	N(2)—C(8)—C(12)	121.7(9)	C(4)—Ga—C(5)	124.0(7)	N(3)—C(10)—C(11)	110(2)
Re—O(4)—Ga	115.7(3)	C(7)—C(8)—C(12)	130.2(9)	Re—O(4)—Ga	115.8(4)	C(9)—C(10)—C(11)	102(2)
Re—O(4)—C(9)	110.6(5)	O(4)—C(9)—C(10)	109.0(7)	Re—O(4)—C(9)	109.8(10)	C(10)—C(11)—C(12)	96(3)
Ga—O(4)—C(9)	119.4(5)	N(3)—C(10)—C(9)	110.2(8)				
	$[Me_2Ga(N_2C_5H_7)(OCH_2CH_2SPh)]Re(CO)_3$				$[MeGa(N_2C_3H_3)_3]Re(CO)_3$		
S—Re—O(4)	80.24(10)	Re—N(1)—N(2)	117.3(3)	N(2)—Re—N(4)	87.1(5)	N(1)—N(2)—C(7)	105.7(14)
S—Re—N(1)	83.46(12)	Re—N(1)—C(6)	135.4(4)	N(2)—Re—N(6)	89.3(5)	Ga—N(3)—N(4)	120.6(12)
S—Re—C(1)	175.4(2)	N(2)—N(1)—C(6)	106.2(4)	N(2)—Re—C(1)	177.4(7)	Ga—N(3)—C(8)	130.0(15)
S—Re—C(2)	94.5(2)	Ga—N(2)—N(1)	120.6(3)	N(2)—Re—C(2)	92.6(7)	N(4)—N(3)—C(8)	109(2)
S—Re—C(3)	95.3(2)	Ga—N(2)—C(8)	128.7(4)	N(2)—Re—C(3)	92.9(7)	Re—N(4)—N(3)	124.5(12)
O(4)—Re—N(1)	81.38(14)	N(1)—N(2)—C(8)	109.8(5)	N(4)—Re—N(6)	88.3(6)	Re—N(4)—C(10)	132.2(13)
O(4)—Re—C(1)	95.7(2)	Re—C(1)—O(1)	176.4(6)	N(4)—Re—C(1)	90.4(7)	N(3)—N(4)—C(10)	103(2)
O(4)—Re—C(2)	174.5(2)	Re—C(2)—O(2)	177.7(6)	N(4)—Re—C(2)	178.3(8)	Ga—N(5)—N(6)	123.2(12)
O(4)—Re—C(3)	93.1(2)	Re—C(3)—O(3)	178.6(5)	N(4)—Re—C(3)	93.0(7)	Ga—N(5)—C(11)	129.1(14)
N(1)—Re—C(1)	93.8(2)	N(1)—C(6)—C(7)	110.1(5)	N(6)—Re—C(1)	89.8(8)	N(6)—N(5)—C(11)	108(2)
N(1)—Re—C(2)	96.3(2)	N(1)—C(6)—C(17)	122.6(5)	N(6)—Re—C(2)	90.0(8)	Re—N(6)—N(5)	122.6(11)
N(1)—Re—C(3)	174.5(2)	C(7)—C(6)—C(17)	127.4(5)	N(6)—Re—C(3)	177.6(7)	Re—N(6)—C(13)	129.6(15)
C(1)—Re—C(2)	89.4(3)	C(6)—C(7)—C(8)	105.7(5)	C(1)—Re—C(2)	89.8(9)	N(5)—N(6)—C(13)	108(2)
C(1)—Re—C(3)	87.1(2)	N(2)—C(8)—C(7)	108.2(5)	C(1)—Re—C(3)	88.1(10)	Re—C(1)—O(1)	174(2)
C(2)—Re—C(3)	89.2(2)	N(2)—C(8)—C(18)	121.7(6)	C(2)—Re—C(3)	88.7(10)	Re—C(2)—O(2)	176(2)
O(4)—Ga—N(2)	91.2(2)	C(7)—C(8)—C(18)	130.1(6)	N(1)—Ga—N(3)	98.1(6)	Re—C(3)—O(3)	177(2)
O(4)—Ga—C(4)	109.8(3)	O(4)—C(9)—C(10)	110.0(4)	N(1)—Ga—N(5)	98.2(7)	N(1)—C(5)—C(6)	112(2)
O(4)—Ga—C(5)	109.5(2)	S—C(10)—C(9)	111.3(4)	N(1)—Ga—C(4)	122.5(9)	C(5)—C(6)—C(7)	102(2)
N(2)—Ga—C(4)	110.2(3)	S—C(11)—C(12)	123.9(5)	N(3)—Ga—N(5)	99.0(7)	N(2)—C(7)—C(6)	112(2)
N(2)—Ga—C(5)	108.6(3)	S—C(11)—C(16)	116.2(5)	N(3)—Ga—C(4)	118.4(8)	N(3)—C(8)—C(9)	108(2)
C(4)—Ga—C(5)	122.9(3)	C(12)—C(11)—C(16)	119.8(6)	N(5)—Ga—C(4)	116.1(10)	C(8)—C(9)—C(10)	104.4(15)
Re—S—C(10)	97.4(2)	C(11)—C(12)—C(13)	118.9(7)	Ga—N(1)—N(2)	119.4(11)	N(4)—C(10)—C(9)	114(2)
Re—S—C(11)	108.4(2)	C(12)—C(13)—C(14)	121.0(7)	Ga—N(1)—C(5)	132.8(13)	N(5)—C(11)—C(12)	106(2)
C(10)—S—C(11)	105.7(3)	C(13)—C(14)—C(15)	119.6(7)	N(2)—N(1)—C(5)	107.8(15)	C(11)—C(12)—C(13)	104(2)
Re—O(4)—Ga	116.7(2)	C(14)—C(15)—C(16)	120.1(7)	Re—N(2)—N(1)	126.0(10)	N(6)—C(13)—C(12)	114(2)
Re—O(4)—C(9)	114.3(3)	C(11)—C(16)—C(15)	120.6(7)	Re—N(2)—C(7)	128.3(12)		
Ga—O(4)—C(9)	119.8(3)						

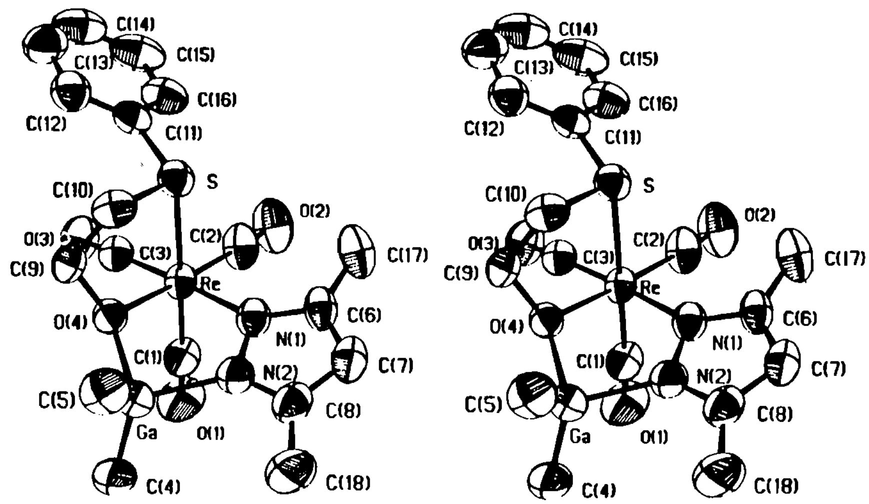

FIG. 2. Stereoscopic view of the $[Me_2Ga(N_2C_5H_7)(OCH_2CH_2SPh)]Re(CO)_3$ molecule. 50% probability thermal ellipsoids are shown for the non-hydrogen atoms.

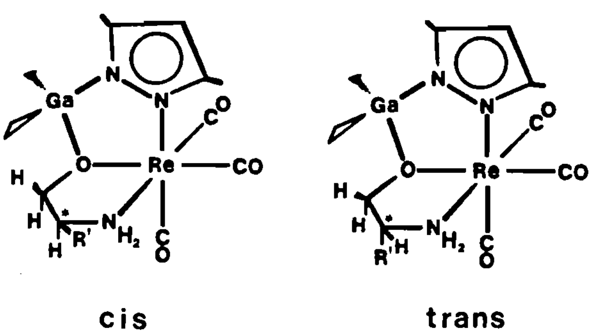

FIG. 3. Diastereoisomers formed in octahedral complexes incorporating facial tridentate pyrazolyl gallate ligands derived from chiral amino alcohols.

Reactivity of selected $LRe(CO)_3$ complexes {L = $[MeGa(N_2C_3H_3)_3]$ or $[Me_2Ga(N_2C_3HR_2)(OCH_2CH_2NMe_2)]$ (R = H or Me)}

(a) Nitrosylation

The reactions of the selected $LRe(CO)_3$ complexes with NO_2PF_6, $NOPF_6$, or $NOBF_4$ resulted in air-sensitive orange–brown powders of the corresponding nitrosyl cations $LRe(CO)_2(NO)^+$ in variable yields. These cations differ from their air-stable cyclopentadienyl analogs, $(\eta^5\text{-}C_5H_5)Re(CO)_2(NO)^+$, which can be prepared in near quantitative yields by similar reaction procedures (23, 24).

The $LRe(CO)_2(NO)^+$ cations were shown to be fluxional in d_6-acetone solution by variable temperature ^{1}H nmr experiments. When L = $[MeGa(N_2C_3H_3)_3]$ two different types of pyrazolyl rings should be evident in a ratio of 2:1 for a rigid species as observed for the isoelectronic complexes $[MeGa(N_2C_3H_3)_3]M(CO)_2(NO)$ (where M = Mo or W) (5). However, the ^{1}H nmr spectrum of $[MeGa(N_2C_3H_3)_3]Re(CO)_2(NO)^+$ displayed only one set of pyrazolyl resonances in d_6-acetone at room temperature. These resonances showed considerable broadening at lower temperatures (Fig. 6) but no clear splitting of the signals was observed. The room temperature spectrum can be explained by a rapid rotation of the tridentate ligand about the Re...Ga axis or alternatively by a rapid ligand rearrangement occurring via a 5-coordinate intermediate in which the chelating ligand coordinates in a bidentate fashion. A similar mechanism has been proposed recently to account for the solution behaviour of $[B(N_2C_3H_3)_4]Rh$(diene), (where diene = duroquinone, 1,5-cyclooctadiene or norbornadiene) (25).

The nitrosylation of $LRe(CO)_3$ when L is an unsymmetrical ligand can occur theoretically at any one of the three possible sites A, B, C in Fig. 7. For any rigid isomer produced, the ^{1}H nmr spectrum should display two equally intense Ga—Me singlets, giving a maximum of six Ga—Me singlets if all three isomers are formed. The actual room temperature ^{1}H nmr spectra of the two complexes $LRe(CO)_2(NO)^+$ {L = $[Me_2Ga(N_2C_3HR_2)(OCH_2CH_2NMe_2)]$ where R = H or Me} both display but one Ga—Me singlet, which, although broadened at −70°C, could not be resolved into separate signals. The room temperature spectra can be explained by the presence of a fluxional species in solution which interconverts via a 5-coordinate intermediate as shown in Fig. 8. Thus in the 5-coordinate intermediate the Ga—Me groups become equivalent, producing one signal in the ^{1}H nmr spectra. This explanation presumes that the nitrosylation has occurred solely at position C (Fig. 7) since substitution at the A or B positions would leave the Ga—Me groups inequivalent even in the proposed 5-coordinate intermediate unless a concomitant scrambling of the nitrosyl and carbonyl groups was also occurring.

(b) Attempted hydride reduction of a coordinated carbonyl ligand

Recently the ability of the $(\eta^5\text{-}C_5H_5)Re(CO)_2(NO)^+$ cation to be converted into unusually stable complexes having coordinated organic functional groups has been recognized (23, 24, 26, 27). Thus the hydride reduction of the cation results in a series of relatively stable neutral complexes (23), i.e.

$$L'Re{-}CO^+ \rightarrow L'Re{-}CHO \rightarrow L'Re{-}CH_2OH \rightarrow L'Re{-}CH_3$$
$$[L' = (\eta^5\text{-}C_5H_5)(CO)(NO)]$$

It has been suggested earlier that hydride reduced metal carbonyl species should become more stabilized by increasing the electron density on the transition metal centre in the precursor species (24, 27). It is well known that pyrazolylgallate ligands have a greater propensity to fulfill this function than the cyclopentadienyl ligand in metal carbonyl species (5, 19), as reflected in lower ν_{CO} stretching frequencies for the former complexes. Thus it was anticipated that the $LRe(CO)_2(NO)^+$ cations produced in this study might well undergo ready conversion to stable, neutral organo rhenium derivatives. How-

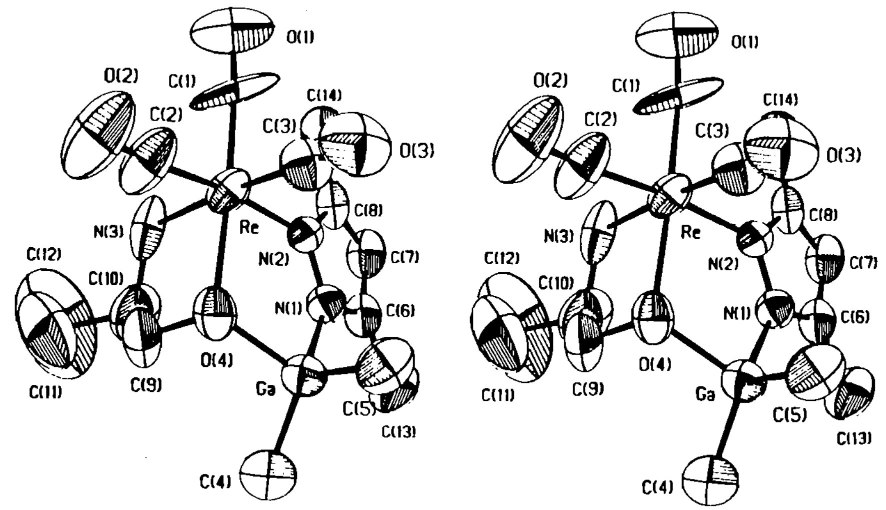

FIG. 4. Stereoscopic view of the $[Me_2Ga(N_2C_5H_7)(OCH_2C(H)EtNH_2]Re(CO)_3$ molecule. 50% probability thermal ellipsoids are shown for the non-hydrogen atoms.

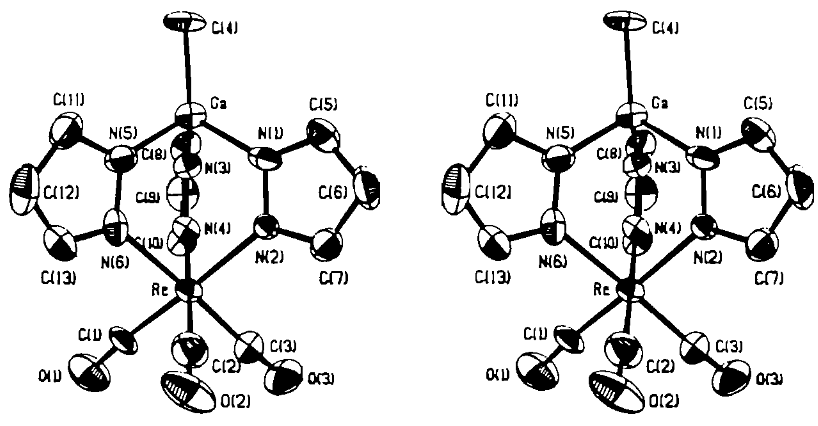

FIG. 5. Stereoscopic view of the $[MeGa(N_2C_3H_3)_3]Re(CO)_3$ molecule. 50% probability thermal ellipsoids are shown for the non-hydrogen atoms.

ever, despite repeated attempts with a variety of reducing agents (e.g., $LiEt_3BH$, K(*sec*-Bu)$_3$BH) at −78°C to room temperature no organo rhenium species was identified. Indeed ir and ^{1}H nmr measurements did not indicate the presence of either a reduced coordinated carbonyl ligand or a rhenium hydride species. It appeared instead that the pyrazolylgallate ligands themselves were unstable under the reaction conditions.

(c) Attempted substitution of a carbonyl with a tertiary phosphine

(η^5-C_5H_5)Re(CO)$_2$(PPh$_3$) can be prepared by the uv irradiation of (η^5-C_5H_5)Re(CO)$_3$ and PPh$_3$ in THF (28). The substituted nitrosyl cations (η^5-C_5H_5)Mn(CO)(NO)(L″)$^+$ and (η^5-C_5H_5)Re(CO)(NO)(L″)$^+$ (where L″ = a neutral two-electron donor ligand) have been prepared by refluxing (η^5-C_5H_5)M(CO)$_2$(NO)$^+$ (M = Mn or Re), and L″ in the presence of Et_3N/acetone (29) or iodosobenzene/MeCN (24), respectively. In contrast to these results it was found that the carbonyl ligands in both the LRe(CO)$_3$ and LRe(CO)$_2$(NO)$^+$ complexes were inert with respect to substitution with $PR_3^†$ ($R^†$ = Ph, OPh or OMe). This observed non-lability of the coordinated carbonyl groups may result from the superior electron-donating strength of pyrazolylgallate ligands compared to the cyclopentadienyl ligand (5, 19).

*Crystal structures of **8**, **13**, **16**, and **17***

In each of the four molecules the tridentate gallate ligand is facially coordinated, the geometry about the rhenium atom being irregular octahedral. Deviations from "ideal" geometry are smallest for **17** in which no five-membered chelate rings are formed. The average D—Re—D (D = N, O or S), OC—Re—CO, *cis*- and *trans*-D—Re—CO angles are 82.9, 86.4, 95.3 and 175.7° for **8**; 81.7, 88.6, 94.8 and 174.8° for **13**; 80.7, 88.4, 95.3 and 174.7° for **16**; 88.2, 88.9, 91.5 and 177.8° for **17**. All bond distances involving Re lie within the normal ranges. The Re—O and Re—N(pz) distances in **8**, **13**, and **16** are equal within experimental error, the mean values (with rms deviations from the mean in parentheses) being 2.154(3) and 2.184(5) Å, respectively. The mean Re—N(pz) distance of 2.165(7) Å in **17**, involving unsubstituted pyrazolyl groups, is marginally (2σ) shorter. The mean Re—CO distance of 1.94(2) Å in **17** is ~2σ longer than the corresponding values of 1.905(6), 1.910(4), and 1.87(1) Å in **8**, **13**, and **16**, respectively. The Re—S distance in **13** is 2.509(1) Å and, as expected, the "Re—NMe$_2$" distance of 2.300(7) Å in **8** is longer than the "Re—NH$_2$" distance of 2.254(11) Å in **16**. With the exception of parameters involving the poorly defined (and possibly disordered) ethyl side chain in **16**, bond lengths and angles in all four structures are as expected.

TABLE 10. Intra-annular torsion angles (deg) with standard deviations in parentheses

Atoms	Angle (deg)
$[Me_2Ga(N_2C_5H_7)(OCH_2CH_2NMe_2)]Re(CO)_3$	
N(1)—Re —O(4)—Ga	−31.5(3)
N(2)—Ga —O(4)—Re	34.5(3)
O(4)—Ga —N(2)—N(1)	−24.0(6)
Re —N(1)—N(2)—Ga	4.8(8)
O(4)—Re —N(1)—N(2)	15.3(5)
N(3)—Re —O(4)—C(9)	19.7(6)
Re —O(4)—C(9)—C(10)	−46.9(9)
O(4)—C(9)—C(10)—N(3)	58.5(10)
Re —N(3)—C(10)—C(9)	−38.1(9)
O(4)—Re —N(3)—C(10)	10.6(6)
$[Me_2Ga(N_2C_5H_7)(OCH_2CH_2SPh)]Re(CO)_3$	
N(1)—Re —O(4)—Ga	−33.4(2)
N(2)—Ga —O(4)—Re	27.4(2)
O(4)—Ga —N(2)—N(1)	−3.1(4)
Re —N(1)—N(2)—Ga	−21.9(5)
O(4)—Re —N(1)—N(2)	31.5(3)
S —Re —O(4)—C(9)	28.6(3)
Re —O(4)—C(9)—C(10)	−56.2(4)
O(4)—C(9)—C(10)—S	55.4(5)
Re —S —C(10)—C(9)	−28.1(4)
O(4)—Re —S —C(10)	0.8(2)
$[Me_2Ga(N_2C_5H_7)(OCH_2C(H)EtNH_2)]Re(CO)_3$	
N(2)—Re —O(4)—Ga	29.9(4)
N(1)—Ga —O(4)—Re	−34.5(5)
O(4)—Ga —N(1)—N(2)	27.1(8)
Ga —N(1)—N(2)—Re	−9.6(10)
O(4)—Re —N(2)—N(1)	−11.6(7)
N(3)—Re —O(4)—C(9)	−24.9(10)
Re —O(4)—C(9)—C(10)	54(2)
O(4)—C(9)—C(10)—N(3)	−55(2)
Re —N(3)—C(10)—C(9)	31(2)
O(4)—Re —N(3)—C(10)	−4.2(11)
$[MeGa(N_2C_3H_3)_3]Re(CO)_3$	
N(4)—Re —N(2)—N(1)	47.5(13)
Ga —N(1)—N(2)—Re	−3(2)
N(3)—Ga —N(1)—N(2)	−48.7(13)
N(1)—Ga —N(3)—N(4)	52.0(11)
Ga —N(3)—N(4)—Re	−1.6(15)
N(2)—Re —N(4)—N(3)	−43.7(11)
N(6)—Re —N(2)—N(1)	−40.8(14)
Ga —N(1)—N(2)—Re	−3(2)
N(5)—Ga —N(1)—N(2)	51.7(13)
N(1)—Ga —N(5)—N(6)	−53(2)
Ga —N(5)—N(6)—Re	4(2)
N(2)—Re —N(6)—N(5)	39.9(15)
N(6)—Re —N(4)—N(3)	45.6(11)
Ga —N(3)—N(4)—Re	−1.6(15)
N(5)—Ga —N(3)—N(4)	−47.6(11)
N(3)—Ga —N(5)—N(6)	46(2)
Ga —N(5)—N(6)—Re	4(2)
N(4)—Re —N(6)—N(5)	−47.3(15)

Pyrazolyl and phenyl rings are all planar within experimental error ($\chi^2 = 0.2-4.3$). The five-membered chelate rings in **8**, **13**, and **16** are all significantly non-planar and have either envelope or irregular puckered conformations (see Table 10). The three six-membered chelate rings in **17** have slightly irregular boat conformations. The non-bonded Re···Ga separations are 3.459(1), 3.4780(6), 3.459(1), and 3.592(3) Å, respectively, for **8**, **13**, **16**, and **17**.

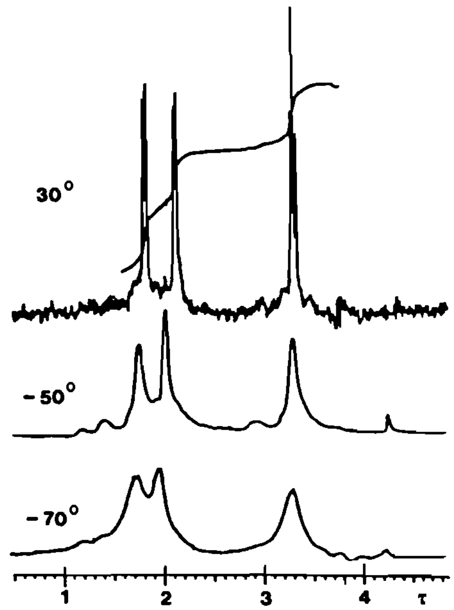

FIG. 6. Variable temperature 80 MHz ^1H nmr spectra of $[MeGa(N_2C_3H_3)_3]Re(CO)_2(NO)^+$ in d_6-acetone (pyrazolyl protons only).

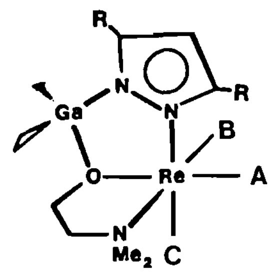

FIG. 7. Three possible sites (A, B, C) for carbonyl substitution in $LRe(CO)_3$ complexes (L = unsymmetrical tridentate ligand).

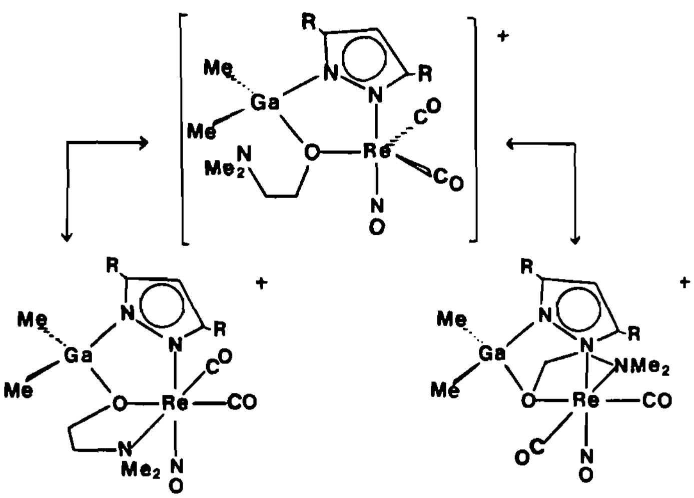

FIG. 8. Proposed fluxional behaviour of nitrosyl cations in solution at room temperature.

The structure of **8** consists of discrete molecules, all intermolecular distances being greater than the sum of van der Waals radii. In **13** and **17** there are possible weak intermolecular interactions: C(10)—H(10a)···S($1-x, 2-y, 1-z$) (H···S = 3.00, C···S = 3.905(6) Å, C—H···S = 153°) in **13**;

C(4)—H(4b)···O(1) ($1 - x, y - 1/2, -z$), C(10)—H(10)···O(2) ($x, y, z - 1$), and C(11)—H(11)···O(2) ($1 - x, y - 1/2, 1 - z$) (H···O = 2.57, 2.58, 2.50, C···O = 3.50(3), 3.43(3), 3.41(3) Å, C—H···O = 158, 147, 154°) in **17**. Molecules of **16** are each linked to two others by inferred N—H···O(carbonyl) hydrogen bonds: N(3)···O(2) ($1/2 + x, 3/2 - y, 1 - z$) = 3.07(2) Å and N(3)···O(2) ($1 + x, y, z$) = 3.20(2) Å.

Summary

The reactions between a variety of tridentate pyrazolylgallate anionic ligands and $[Re(CO)_4Cl]_2$ or $Mn(CO)_5Br$ have been described. In all compounds isolated the chelating ligand was found to coordinate in a facial manner. The reactivity of selected pyrazolylgallate rhenium species has also been probed. Presently we are investigating a series of rhodium complexes in which the unsymmetric tridentate ligands are meridionally coordinated in both four and five-coordinate species.

Acknowledgements

We thank the Natural Sciences and Engineering Research Council for financial support, Mr. P. Borda for elemental analyses, and the University of British Columbia Computing Centre for assistance.

1. R. B. KING. Organometallic synthesis. Vol. 1. Academic Press, New York. 1965. p. 174.
2. G. DOLCETTI and J. R. NORTON. Inorganic synthesis. Vol. 16. Academic Press, New York. 1976. p. 35.
3. K. S. CHONG, S. J. RETTIG, A. STORR, and J. TROTTER. Can. J. Chem. **55**, 4166 (1977).
4. K. S. CHONG, S. J. RETTIG, A. STORR, and J. TROTTER. Can. J. Chem. **56**, 1212 (1978).
5. K. R. BREAKELL, S. J. RETTIG, D. L. SINGBEIL, A. STORR, and J. TROTTER. Can. J. Chem. **56**, 2099 (1978).
6. K. S. CHONG and A. STORR. Can. J. Chem. **59**, 1331 (1981).
7. P. COPPENS, L. LEISEROWITZ, and D. RABINOVICH. Acta Crystallogr. **18**, 1035 (1965).
8. W. R. BUSING and H. A. LEVY. Acta Crystallogr. **22**, 457 (1967).
9. J. DE MEULENAER and H. TOMPA. Acta Crystallogr. **19**, 1014 (1965).
10. K. S. CHONG, S. J. RETTIG, A. STORR, and J. TROTTER. Can. J. Chem. **59**, 2391 (1981).
11. D. T. CROMER and J. B. MANN. Acta Crystallogr. Sect. A, **24**, 321 (1968).
12. R. F. STEWART, E. R. DAVIDSON, and W. T. SIMPSON. J. Chem. Phys. **42**, 3175 (1965).
13. D. T. CROMER and D. LIBERMAN. J. Chem. Phys. **53**, 1891 (1970).
14. S. TROFIMENKO. Acc. Chem. Res. **4**, 17 (1971).
15. S. TROFIMENKO. Chem. Rev. **72**, 497 (1972).
16. A. SHAVER. J. Organomet. Chem. Library, **3**, 157 (1977).
17. K. S. CHONG, S. J. RETTIG, A. STORR, and J. TROTTER. Can. J. Chem. **57**, 3113 (1979).
18. D. M. ADAMS. Metal−ligand and related vibrations. Edward Arnold, London. 1967.
19. K. S. CHONG and A. STORR. Can. J. Chem. **57**, 167 (1979).
20. K. S. CHONG. Ph.D. Thesis. University of British Columbia. 1980.
21. K. S. CHONG, S. J. RETTIG, A. STORR, and J. TROTTER. Can. J. Chem. **57**, 3107 (1979).
22. K. S. CHONG, S. J. RETTIG, A. STORR, and J. TROTTER. Can. J. Chem. **59**, 518 (1981).
23. C. P. CASEY, M. A. ANDREWS, D. R. MCALISTER, and E. RINZ. J. Am. Chem. Soc. **102**, 1927 (1980).
24. W. TAM, G. Y. LIN, W. K. WONG, W. A. KIEL, V. K. WONG, and J. A. GLADYSZ. J. Am. Chem. Soc. **104**, 141 (1982).
25. M. COCIVERA, G. FERGUSON, F. J. LALOR, and P. SZCECINSKI. Organometallics, **1**, 1139 (1982).
26. J. R. SWEET and W. A. G. GRAHAM. Organometallics, **1**, 982 (1982).
27. J. R. SWEET and W. A. G. GRAHAM. J. Am. Chem. Soc. **104**, 2811 (1982).
28. A. N. NESMEYANOV, N. E. KOLOBOVA, Y. V. MAKAROV, B. V. LOKSHIN, and E. B. RUSACH. Izv. Akad. Nauk. S.S.S.R., Ser. Khim. (Engl. Transl.), 612 (1975).
29. T. A. JAMES and J. A. MCCLEVERTY. J. Chem. Soc. (A), 850 (1970).

The preparation of bis(perfluoroethyl) tellurium difluoride and dichloride, *trans* perfluoroethyl tellurium monochloride tetrafluoride, *trans* bis(perfluoroethyl) tellurium tetrafluoride; and the preparation and X-ray crystal structure of perfluoroethyl tellurium trifluoride

CLEMENT LAU, JACK PASSMORE, E. KEITH RICHARDSON, TOM K. WHIDDEN, AND PETER S. WHITE
Department of Chemistry, University of New Brunswick, Fredericton, N.B., Canada E3B 6E2

Received August 13, 1984

CLEMENT LAU, JACK PASSMORE, E. KEITH RICHARDSON, TOM K. WHIDDEN, and PETER S. WHITE. Can. J. Chem. **63**, 2273 (1985).

The reaction of $(C_2F_5)_2Te$ and XeF_2 in a slurry of SO_2ClF yielded $(C_2F_5)_2TeF_2$ essentially quantitatively. Chlorine and $(C_2F_5)_2Te$ gave $(C_2F_5)_2TeCl_2$. Both $(C_2F_5)_2TeF_2$ and $(C_2F_5)_2TeCl_2$ were assigned a trigonal bipyramidal geometry, on the basis of their ^{19}F nmr and vibrational spectra, with the lone pair and C_2F_5 groups in equatorial, and the halogens in the axial positions. Perfluoroethyl tellurium trifluoride was prepared essentially quantitatively by the reaction of $C_2F_5TeTeC_2F_5$ and XeF_2 in liquid SO_2F_2. The generally inert SO_2ClF was found to react with $C_2F_5TeTeC_2F_5$ to give $C_2F_5TeCl_xF_{3-x}$ and sulphur dioxide. The structure of $C_2F_5TeF_3$ was determined by X-ray diffraction. The crystals are tetragonal with a = 10.129(4), c = 25.561(6) Å, and Z = 16. The structure was refined in space group $I4_1/a$ to a conventional R factor of 0.051 for 901 observed reflections with $I \geq 3\sigma(I)$. Each tellurium atom is surrounded by two terminal fluorine atoms and two bridging fluorine atoms and a C_2F_5 group in an axial position around the apex of a distorted square pyramid. The square-pyramidal units are linked by symmetrical *cis* bridging atoms into endless chains with bridging angles of 180° and 177°. The geometry of the $(C_2F_5TeF_4)$ group is consistent with steric activity of the non-bonded electron pair. The ^{19}F nmr and Raman spectra of $C_2F_5TeF_3$ were recorded and the Raman spectrum assigned. *trans*-$C_2F_5TeClF_4$ was prepared by the reaction of $C_2F_5TeTeC_2F_5$, and an excess of ClF. The *trans* octahedral geometry of $C_2F_5TeClF_4$ was unambiguously assigned from its ^{19}F nmr and vibrational spectra. A mixture of *trans*-$(C_2F_5)_2TeF_4$ and *trans*-$C_2F_5TeClF_4$ was obtained from the reaction of $(C_2F_5)_2Te$ and an excess of ClF. *Trans* geometry of $(C_2F_5)_2TeF_4$ was unambiguously assigned from its ^{19}F nmr spectrum.

CLEMENT LAU, JACK PASSMORE, E. KEITH RICHARDSON, TOM K. WHIDDEN et PETER S. WHITE.Can. J. Chem. **63**, 2273 (1985).

La réaction du $(C_2F_5)_2Te$ et du XeF_2 dans une pâte de SO_2ClF donne du $(C_2F_5)_2TeF_2$ avec un rendement essentiellement quantitatif. Le chlore et le $(C_2F_5)_2Te$ donnent du $(C_2F_5)_2TeCl_2$. En se basant sur leurs spectres de rmn du ^{19}F et sur leurs spectres vibrationnels, on attribue une géométrie pyramidale trigonales aux composés $(C_2F_5)_2TeF_2$ et $(C_2F_5)_2TeCl_2$; le doublet libre et les groupes C_2F_5 seraient en position équatoriale, alors que les halogènes seraient en position axiale. On a préparé le trifluorure du perfluroéthyle de tellure avec un rendement essentiellement quantitatif en faisant réagir le $C_2F_5TeTeC_2F_5$ avec le XeF_2 dans du SO_2F_2 liquide. On a trouvé que le SO_2ClF, généralement inerte, réagit avec le $C_2F_5TeTeF_5$ pour donner du $C_2F_5TeCl_xF_{3-x}$ et du bioxyde de soufre. On a déterminé la structure du $C_2F_5TeF_3$ par diffraction de rayons X. Les cristaux sont tétragonaux, avec a = 10,129(4), c = 25,561(6) Å et Z = 16. On a affiné la structure dans le groupe d'espace $I4_1/a$ jusqu'à un facteur conventionnel R de 0,051 pour 901 réflexions observées avec $I \geq 3\sigma(I)$. Chaque atome de tellure est entouré par deux atomes terminaux de fluor, deux atomes de fluor en position de pont et un groupe C_2F_5 en position axiale autour du sommet d'une pyramide carrée déformé. Les unités pyramides carrées sont liées par des atomes *cis* symétriques en position de pont dans des chaînes sans fin avec des angles de liaison de 180° et de 177°. La géométrie du groupe $C_2F_5TeF_4$ est en accord avec une activité stérique de la paire d'électrons non liés. On a enregistré les spectres de rmn du ^{19}F et les spectres Raman du $C_2F_5TeF_3$ et on a attribué les pics du spectre Raman. On a préparé le $C_2F_5TeClF_4$-*trans* par réaction du $C_2F_5TeTeC_2F_5$ avec un excès de ClF. On lui a attribué sans équivoque une géométrie octaédrique en se basant sur son spectre de rmn du ^{19}F et sur son spectre vibrationnel. On a obtenu un mélange de $(C_2F_5)_2TeF_4$ *trans* et de $C_2F_5TeClF_4$ *trans* en faisant réagir le $(C_2F_5)_2Te$ avec un excès de ClF. Les spectres de rmn du ^{19}F et Raman ont permis d'attribuer sans équivoque une géométrie *trans* au $(C_2F_5)_2TeF_4$.

[Traduit par le journal]

Introduction

In the course of our investigations of the chemistry of homopolyatomic cations of sulphur, selenium, and tellurium (1–4), we found that $(C_2F_5)_2Te_n$ (n = 1, 2) could be prepared in reasonable yields by the reaction of $Te_4(AsF_6)_2$ and C_2F_4. The only report of a perfluoroalkyl of tellurium prior to this work was $(CF_3)_2Te_2$ (5), prepared in small amounts by the reaction of CF_3 radicals with a tellurium film. Perfluoroalkyl derivatives of sulphur and selenium tetrafluorides and hexafluorides had been readily prepared in good yield by the oxidations of $(C_2F_5)_2Se_n$ (n = 1, 2) (6), and R_fS_n (n = 1, 2) (R_f various perfluoroalkyls) (7, 8) with chlorine monofluoride. Perfluoroalkyl derivatives of tellurium tetrafluoride and hexafluoride were unknown and therefore $(C_2F_5)_2Te_n$ (n = 1, 2) were reacted with the fluorinating agents chlorine monofluoride and xenon difluoride, leading to compounds listed in the title. A preliminary report of this work has been published (9) and a full account is given below. *trans*-$C_2F_5TeClF_4$ and *trans*-$(C_2F_5)_2TeF_4$ are the only known organic derivatives of TeF_6. The related *cis*- and *trans*-$(MeO)TeClF_4$ have been prepared (10). Since our preliminary report was published, $(CF_3)_2Te_n$ (n = 1, 2) have been prepared by a variety of routes (11–14). Bis(perfluoromethyl) telluride has been oxidised to $(CF_3)_2TeF_2$ (15), $(CF_3)_2TeX_2$ (X = Cl, Br (12, 16) and CF_3TeX_3 (X = Cl, Br (17)).

Diorganotellurium(IV) dihalides of the type R_2TeX_2 (X = F, Cl, Br), e.g. $(C_6H_5)_2TeX_2$ (X = F, Cl, Br), $(CH_3)_2TeCl_2$, $(C_{12}H_8O)_2TeCl_2$ are established as having simple molecular structures with some tellurium–halogen intermolecular association (18, 19). The structure of the difluoride appears to show the least secondary interactions, and it is therefore not surprising that the structures of $(C_2F_5)_2TeF_2$ (below) and $(CF_3)_2TeF_2$ (15) are readily assigned in V.S.E.P.R. terms (20) as having AX_2Y_2E geometries on the basis of their vibrational spectra and ^{19}F nmr spectroscopy, with two fluorine

TABLE 1. Vibrational spectrum $(C_2F_5)_2TeF_2$[a]

Raman			
Single crystal	Liquid	Infrared[b]	Tentative assignments
1384 v, w, br	1384 w, br		
		1320 s	C—F stretching and combination modes
1334 v, w, br	1334 w, br		
1204 w, br	1206 w, dp	1252 s	
		1229 s	
1122 w, br	1124 w, dp		
		1140 m	
1110 w, br	1110 w, dp		
930 w, br	942 w, dp		
913 m	924 w, p		C—C stretch
	912 w, dp	912 s	
748 vs	746 s, p	745 m	(C_2F_5) def.
629 w	629 w, p	620 vw	(C_2F_5) def.
583 vw	592 vw, dp		
539 w			
520 s	540 s, p	565 s	Te—F asym. str.
506 s	500 s, br, p[c]	540 m	Te—F sym. str.
481 sh			?
440 vw	436 vw, dp		
368 w	385 vw, dp 368 w, p		C_2F_5 rock
303 w	303 s, dp		
285 vw	287 w, p 268 sh		
251 s			Te—C asym. str.
	250 m, dp		
235 m			Te—C sym. str.
	235 s, p		
224 w			Te—C str.
212 s	211 s, dp		TeF sym. bend?
198 sh 176 sh	174 vw		?
128 m, br 120 m, br	129 sh ? 113 m, p		?

[a]Frequencies are quoted in cm^{-1}: m = medium, s = strong, w = weak, sh = shoulder, br = broad, p = polarised, dp = depolarised, vw = very weak, vs = very strong.
[b]Infrared of gas obtained in a 10 cm cell equipped with AgCl windows.
[c]The broad peak spans the range 450–520 cm^{-1} and may be indication of intramolecular fluorine bridging in the liquid state.

atoms occupying axial positions of the trigonal bipyramid. The organo tellurium trichlorides, $RTeCl_3$ (R = C_6H_5, OC_6H_4, $ClCH_2CH_3$) have chlorine bridged polymeric structures (18), tellurium tetrafluoride (21) is an associated *cis*-bridged polymer and the properties of $C_2F_5TeF_3$ suggested it was also polymeric. The structure of $C_2F_5TeF_3$ was not unambiguously deduced from its vibrational spectrum, or ^{19}F nmr. We therefore determined the single crystal X-ray structure of this compound and the results are reported below. As far as we are aware, this is the first report of an X-ray structural determination of a perfluoro-organic derivative of TeF_4, and the first report of a structure of an organic derivative of the type $RTeF_3$.

Experimental

Apparatus and techniques have been described (4, 6). $(C_2F_5)_2Te_n$ n = 1, 2, were prepared according to ref. 4, and their purity established by vpc and mass spectra. The ditelluride decomposes into the monotelluride and elemental tellurium on exposure to light, therefore $(C_2F_5)_2Te_2$ was stored in the dark at −78°C and experiments involving

TABLE 2. ^{19}F nmr data of perfluoroethyl tellurium compounds

Compound	Chemical shift (ppm)[a]	Coupling constant (Hz)
$(C_2F_5)_2TeCl_2$[b]	$\delta_{CF_3} = -77.4(3)$[c]	$J_{CF_3—CF_2} = 2.67$
	$\delta_{CF_2} = -93.17$	
$(C_2F_5)_2TeClF$[b]	$\delta_{CF_3} = -78.6(6)$ (d)	$J_{CF_3—TeF} = 9.5$
	$\delta_{CF_2} = -97.4(4)$ (d)	$J_{CF_2—TeF} = 50.5$
	$\delta_{TeF} = -87.8(1)$ (t, q)	
$(C_2F_5)_2TeF_2$[b]	$\delta_{CF_3} = -80.2(3)$ (t)	
	$\delta_{CF_2} = -100.8(2)$ (t)	$J_{CF_3—TeF_2} = 7.0$
	$\delta_{TeF_2} = -116.9(1)$ (p, s)	$J_{CF_2—TeF_2} = 9.3$
$C_2F_5TeF_3$[d]	$\delta_{CF_3} = -80(3)$ (t)	$J_{CF_3—CF_2} = 2.1$
	$\delta_{CF_2} = -114(2)$ (q?)	
	$\delta_{TeF_3} = -78(3)$	
trans-$(C_2F_5)_2TeF_4$[b]	$\delta_{CF_3} = -80.4(3)$ (t, p)	$J_{CF_3—CF_2} = 2.71$
	$\delta_{CF_2} = -96.7(2)$ (q, p)	$J_{CF_3—TeF_4} = 5.42$
	$\delta_{TeF_4} = -67.2(2)$ (p, s)	$J_{CF_2—TeF_4} = 12.15$
		$J_{Te^{125}—F_{eq}} = 3276$
trans-$C_2F_5TeClF_4$[b]	$\delta_{CF_3} = -80.6(3)$ (t, p)	$J_{CF_3—CF_2} = 2.70$
	$\delta_{CF_2} = -96.2(2)$ (q, p)	$J_{CF_3—TeF_4} = 5.40$
	$\delta_{TeF_4} = -11.92(4)$ (t, q)	$J_{CF_2—TeF_4} = 12.82$
		$J_{Te^{125}—F_{eq}} = 3740$
		$J_{Te^{123}—F_{eq}} = 3287$

[a]Chemical shifts are quoted relative to CCl_3F, signs are in accordance with IUPAC convention.
[b]Freon 11 is used as a solvent and internal standard.
[c]Values in parentheses stand for area under the peak; t = triplet, q = quartet, p = pentet, and s = septet.
[d]SO_2 solvent, CCl_3F external standard.

this compound carried out in the dark. XeF_2 was prepared photochemically (22). The SO_2F_2, SO_2ClF, and CCl_3F were stored over 3 Å molecular sieves prior to use. Reactions were carried out in glass vessels connected to a metal vacuum line via a 1KS4 stainless steel Whitey valve. Volumes of vessels containing XeF_2 as a reagent were such that the final pressure was less than 4 atm. Xenon was sometimes removed prior to the addition of the final aliquots of telluride. Caution must be exercised in all these reactions to prevent overheating and subsequent explosions.

Preparation of $(C_2F_5)_2TeF_2$

In a typical reaction $(C_2F_5)_2Te$ (2.67 g, 7.30 mmol) was condensed onto a slurry of XeF_2 (1.13 g, 6.67 mmol) and SO_2ClF (1.60 g) in six aliquots. The mixture was kept at −45°C for 1 h prior to the addition of the next aliquot. After complete addition of $Te(C_2F_5)_2$ the mixture was allowed to warm slowly from −45°C to room temperature over a period of 12 h. The materials, volatile at −95°C (0.75 g), −22°C (1.85 g), and room temperature (0.30 g), were mixtures of Xe, SO_2ClF, and C_2F_6; C_2F_6, C_2F_5Cl, $(C_2F_5)_2Te$, $(C_2F_5)_2TeF_2$, and SO_2F_2; and $(C_2F_5)_2TeF_2$ with traces of $(C_2F_5)_2Te$, respectively. The remaining product 2.56 g (6.34 mmol assuming $(C_2F_5)_2TeF_2$) was a white highly crystalline solid, mp 57°C, shown to be pure by ^{19}F nmr spectroscopy. The vibrational spectrum is given in Table 1, and the ^{19}F nmr spectral results summarised in Table 2. Sizable single translucent crystals were obtained in low yield in a similar reaction with CH_3CN replacing SO_2ClF as solvent.

Preparation of $(C_2F_5)_2TeCl_2$

Chlorine (0.251 g, 3.54 mmol) was condensed on $Te(C_2F_5)_2$ (0.941 g, 2.57 mmol) in six aliquots. The vessel was held at −78°C for 15 min, and then warmed to room temperature prior to the addition of the next aliquot. A crystalline white solid (1.07 g, 2.45 mmol assuming $(C_2F_5)_2TeCl_2$), and a yellow volatile liquid (0.085 g), C_2F_5Cl and Cl_2 were obtained. Sublimation of the solid *in vacuo* at 40°C led to a highly crystalline product. The solid had a small vapour pressure at room temperature and a melting point of 45°C. *Anal.* calcd. for $(C_2F_5)_2TeCl_2$: C 11.00, F 43.53, Te 29.23, Cl 16.14; found: C 11.24, F 43.85, Te 28.82, Cl 16.01. The Raman spectrum is

TABLE 3. Vibrational spectrum of $(C_2F_5)_2TeCl_2$

Infrared (cm^{-1})[a]	I	Raman (cm^{-1})[b]	I	Tentative assignment
		1328	2 vw	
1310	s			C—F stretching and
1215	s	1211	2 vw	combination modes
1130	ms	1135	2 vw	
1105	s	1104	2 vw	
905	vw	909	2 vw	C—C stretching vibrations
880	s	879	5 w	
740	s	742	9 w	
		731	2 vw	
622	m	622	1 vw	C_2F_5 deformation
590	vw	590	1 vw	
542	w	540	3 vw	
		435	1 vw	
		370	3 vw	C_2F_5 rocking
		300	6 w	
		285	100 vs	$TeCl_{ax.}$ sym. str.
		267	4 vw	$TeCl_{ax.}$ asym. str. (?)
		237	26 m	C—Te str. (?)
		226	23 m	C—Te str. (?)
		154	45 m	C—Te—C deform. (?)
		127	15 m	Cl—Te—Cl bend (?)

[a]Solid between AgCl plates.
[b]The Raman spectrum of single crystals was similar to that of the powder. The spectra were not of high quality.

given in Table 3, and the ^{19}F nmr spectral results are summarised in Table 2.

Preparation of $C_2F_5TeF_3$

In a typical experiment, $(C_2F_5)_2Te_2$ (0.784 g, 1.59 mmol) was condensed in two aliquots onto a slurry of XeF_2 (0.730 g, 4.31 mmol) and SO_2F_2 (5.53 g) in a Monel vessel (vol. ca. 50 mL) and held at −45°C after the addition of each aliquot, and finally allowed to slowly warm to room temperature over a period of 12 h. The volatiles (5.86 g) contained SO_2F_2, Xe, unreacted $(C_2F_5)_2Te_2$, and traces of C_2F_6. The remaining solid (0.65 g) (2.14 mmol assuming $C_2F_5TeF_3$) was identified as $C_2F_5TeF_3$ by its Raman and ^{19}F nmr spectra and melting point.

In another experiment $(C_2F_5)_2Te_2$ (1.07 g, 2.16 mmol) was condensed into a slurry of XeF_2 (1.06 g, or 6.26 mmol) and SO_2ClF (1.54 g) in a glass vessel in three aliquots and treated as described above. The volatiles (2.43 g) contained Xe, SO_2ClF, and traces of SO_2 and C_2F_6. The white microcrystalline solid 1.23 g (4.05 mmol assuming $C_2F_5TeF_3$) was identified as such by ^{19}F nmr and Raman spectroscopy. A saturated solution of $C_2F_5TeF_3$ in SO_2 when left for 2 h yielding rectangular crystals. The solution was decanted into a separate vessel and traces of solvent removed by evacuation. Some of these white translucent crystals were mounted in Pyrex capillaries in a Vacuum Atmosphere Dry-Box and flame sealed. A suitable single crystal was then chosen for the X-ray diffraction studies. *Anal.* calcd. for $C_2F_5TeF_3$; C 7.90, F 50.06, Te 42.03; found (bulk material): C 7.66, F 49.68, Te 42.42. The Raman spectrum is listed in Table 4 and ^{19}F nmr spectrum in Table 2. The mp of the single crystals (142−143°C), ir, and Raman spectra, and ^{19}F nmr of the crystals in SO_2 solution were identical to those of the bulk material produced in both reactions (SO_2F_2 and SO_2ClF as dilutents for XeF_2).

Reaction of SO_2ClF and $(C_2F_5)_2Te_2$

Sulphuryl chlorofluoride (1.71 g, 14.45 mmol) was condensed onto $(C_2F_5)_2Te_2$ (0.191 g, 0.38 mmol) in a glass vessel giving a red−brown solution. After 1 h, small amounts of white precipitate were observed, and after 12 h, a clear solution over a white solid. The volatile material was SO_2 and SO_2ClF (ir, ^{19}F nmr) and the white solid (0.252 g) was $C_2F_5TeCl_xF_{3-x}$ (ir, Raman, ^{19}F nmr and mp). The experiment was repeated under conditions identical to those of the synthesis of $C_2F_5TeF_3$ using SO_2ClF as a diluent for XeF_2. Ninety percent of the $(C_2F_5)_2Te_2$ was recovered from the reaction, 10% had reacted to give traces of SO_2 (ir, Raman) and $(C_2F_5)TeCl_xF_{x-3}$.

TABLE 4. Raman spectrum of $C_2F_5TeF_3$

Raman single crystal[a]	Tentative assignments
1320 vw, vbr	
1214 w, vbr	C—F stretching and combination bonds
1118 m, br	
944 m, br	C—C stretch
750 s	C_2F_5 def.
632 s	TeF stretches
594 m, br	TeF stretches
540 m	C_2F_5 def.
399 sh, w	C_2F_5 rock and/or TeF_2
371 m	bridging sym. and
354 vw	asym. stretch
316 vw	C_2F_5 rock
287 w	C_2F_5 rock
260 vs	C_2F_5 rock
240 w	Sym. Te—C stretch
220 m, w	

[a]Similar to that of a bulk sample.

Preparation of trans-$C_2F_5TeClF_4$

(*a*) By the reaction of $(C_2F_5)_2Te_2$ with an excess of ClF. In a typical experiment ClF (0.95 g, 17.5 mmol) was reacted with $(C_2F_5)_2Te_2$ (0.67 g, 1.36 mmol) in eight aliquots in a Kel-F vessel of ca. 20 mL volume. The mixture was held at −78°C for about 10 min and then the vessel warmed in order to let any solid materials on the sides of the vessel, or on the top of the reactants, melt prior to the addition of the next aliquot. A white solid was formed when the ratio of ClF:$(C_2F_5)_2Te_2$ was about 6:1. The solid remained on further additions of ClF aliquots. The solid gradually disappeared, and the product became a yellow liquid, on standing at room temperature for 3 h. The volatile material at −78°C contained Cl_2, C_2F_6, C_2F_5Cl, $TeClF_5$, *trans*-$C_2F_5TeClF_5$, and ClF. The involatile fraction melted to a clear liquid (0.95 g) at room temperature, consisting of *trans*-$C_2F_5TeClF_4$ and small amounts of $TeClF_5$ and C_2F_5Cl. Pure *trans*-$C_2F_5TeClF_4$ was obtained from the least volatile fraction of this mixture. *Anal.* calcd. for $C_2F_5TeClF_4$: C 6.70, F 47.7, Te 35.64, Cl 9.90; found: C 6.53, F 45.98, Te 35.07, Cl 10.07. The clear colourless liquid has a vapour pressure of ca. 70 Torr at room temperature. At −78°C it is a gel-like solid. It was stable in a Kel-F vessel at room temperature over several months. The ir and Raman spectra are listed in Table 5, and ^{19}F nmr spectral data given in Table 2.

It is noted that in order for a good yield of *trans*-$C_2F_5TeClF_4$, ClF must be added in small aliquots and the temperature raised slowly. Reaction with addition of a large amount of ClF and held at room temperature was extremely exothermic. In a reaction of $(C_2F_5)_2Te_2$ (1.39 g, 2.82 mmol) and ClF (1.46 g, 26.8 mmol) were condensed into a Monel vessel held at room temperature overnight. The vessel bomb initially becomes hot to the touch and the products were identified as C_2F_6 and TeF_6 (1.75 g) (ir) and a solid mixture of $TeCl_4$ and TeF_4 (ca. 1.1 g) (Raman).

(*b*) By the reaction of $C_2F_5TeCl_xF_{3-x}$ ($1 > x > 0$) with ClF. Chlorine monofluoride (0.26 g, 4.8 mmol) was added in one aliquot onto $C_2F_5TeCl_3F_{3-x}$ (0.34 g). The solid gradually disappeared on standing at room temperature giving a yellow liquid after 4 h. The materials volatile at −78°C, contained C_2F_4, CF_4, C_2F_5Cl, $TeClF_5$ (ir, ^{19}F nmr), and probably Cl_2. The material volatile at room temperature

TABLE 5. Vibrational spectrum of *trans*-$C_2F_5TeClF_4$

Infrared		Raman			
Frequency (cm^{-1})	I	Frequency (cm^{-1})	I	pol. (1/11)	Tentative assignments
1322	m	1324	vw	dp(1.0)	C—F stretching and combination modes
1305	w, sh				
1252	s				
1232	s	1227	vw	dp(0.75)	
1203	m				
1128	m	1128	vw	dp(1.0)	
942	m	940	vw	dp(0.9)	C—C stretch
752	w	750	w	p(0.10)	C_2F_5 deformation
682	vs	683	w	p(0.1)	ν asym. TeF_4
630	vw, sh	629	w	p(0.50)	C_2F_5 deformation
612	w	606	vs	p(0.03)	ν sym. TeF_4
590	vw	589	vw	p(0.6)	C_2F_5 deformation
		569	vvw	dp(0.9)	TeF_4 out-of-phase
535	vw	541	vw	p(0.3)	C_2F_5 deformation
		440	vw	dp(0.80)	C_2F_5 rock
		414	m		Te—^{35}Cl
		407	w	p(0.2)	Te—^{37}Cl
		365	vw	p(0.15)	C_2F_5 rock
		306	m	p(0.5)	TeF_4 out-of-plane
		290	vw	dp(0.9)	C_2F_5 rock
		274	vw	dp(1.0)	Sym. TeF_4 in-plane
		251	w	dp(0.8)	Asym. TeF_4 in-plane
		219	s	p(0.3)	C—Te?
		133	vw	p(0.5)	C_2F_5 rock. + $ClTeF_4$?
		93	vw	dp(0.9)	C_2F_5 torsion?

contained mainly *trans*-$C_2F_5TeClF_4$, traces of $TeClF_5$ and some unidentified material as indicated by the ^{19}F nmr spectrum.

Preparation of a mixture of trans-$C_2F_5TeClF_4$ *and* trans-$(C_2F_5)_2TeF_4$

In typical reaction, ClF (0.59 g 10.8 mmol) was reacted in eight aliquots with $(C_2F_5)_2Te$ (0.76 g, 2.08 mmol) in a Kel-F vessel. On addition of each aliquot the mixture was held at −78°C for a few minutes and then briefly allowed to warm to room temperature to enable the solid product to melt. Finally the vessel was left standing for 1 h at room temperature. The volatile material at −78°C contained C_2F_6, C_2F_5Cl, $FClO_2$ (impurity in the ClF), and small amounts of $TeClF_5$ and *trans*-$C_2F_5TeClF_5$ (ir) and probably chlorine. The material volatile at room temperature (0.90 g) contained a 2:1 mixture of *trans*-$C_2F_5TeClF_5$ and *trans*-$(C_2F_5)_2TeF_4$ and traces of C_2F_5Cl and $TeClF_5$. The ^{19}F nmr data for *trans*-$(C_2F_5)_2TeF_4$ is given in Table 2. In other similar reactions, the ratios of *trans*-$C_2F_5TeClF_4$ and *trans*-$(C_2F_5)_2TeF_4$ varied, and small amounts of other unidentified species were also detected by ^{19}F nmr.

Reactions of trans-$C_2F_5TeClF_4$ *with ClF*

Chlorine monofluoride (0.08 g, 1.4 mmol) was reacted with *trans*-$C_2F_5TeClF_4$ (0.40 g, 1.1 mmol) in a Monel vessel at 90°C overnight. The products were *trans*-$C_2F_5TeClF_4$, a small amount of $TeClF_5$ (ir, ^{19}F nmr) and an unidentified material. Chlorine monofluoride and $C_2F_5TeClF_5$ did not appear to react at room temperature.

X-ray crystal structure of $C_2F_5TeF_3$

Preliminary precession photographs showed the space group to be $I4_1/a$ (hkl, $h + k + l = 2n$; $hk0$, $h = 2n$ and $k = 2n$; hhl, $l = 2n$; $00l$, $l = 4n$). The crystal was mounted on a Picker FACS-I diffractometer equipped with graphite monochromated MoKα radiation. Cell data and an orientation matrix were obtained from a least squares fit to the coordinates of 15 Friedel pairs of centered reflections in the range $30 \leq 2\theta \leq 40°$. Intensity data were collected using an $\omega-2\theta$ scan, for $2\theta \leq 55°$. The background intensity was estimated by standing counts of 1/10 of the scan time at each end of the scan; if the reflection was considered significant ($I > 2\sigma(I)$) the scan profile was

TABLE 6. Fractional atomic coordinates (esd's in parentheses)

Atom	x/a	y/b	z/c
Te	0.21366(8)	0.28588(8)	0.33327(3)
F1	0.25	0.25	0.25
F2	0.1179(11)	0.5604(11)	0.1483(4)
F3	0.3807(8)	0.3644(9)	0.3334(4)
F4	0.5	0.25	0.1638(6)
Cl	0.1260(21)	0.4649(18)	0.2989(8)
F11	0.0529(9)	0.4275(12)	0.2563(4)
F12	0.0312(15)	0.5161(17)	0.3349(6)
C2	0.2120(34)	0.5724(20)	0.2816(12)
F21	0.1259(15)	0.6723(11)	0.2676(6)
F22	0.2886(12)	0.5233(14)	0.2472(4)
F23	0.2664(14)	0.6154(12)	0.3276(5)

analysed to provide a better estimate of the background. The relevant crystallographic data are:

$C_2F_5TeF_3$ fw = 303.6

Tetragonal, space group $I4_1/a$, a = 10.129(4), c = 25.561(6) Å, V = 2622(3) Å^3, Z = 16, $F(000)$ = 2032, D_{calcd} = 3.076 Mg m^{-3}, crystal size 0.26 × 0.25 × 0.14 mm, μ(MoKα) = 4.82 mm^{-1}, λ(MoKα) = 0.71069 Å. Number of unique reflections measured = 1516, number observed ($I \geqq 3\sigma(I)$) reflections = 901 (59%).

The structure was solved using the MULTAN (23) direct methods program, correction for absorption (transmission factors 0.30−0.48) and initial refinement was performed using Larson and Gabe's program (24) for the PDP8/A computer. Final full-matrix least-squares refinement was performed on a Wicat Systems computer using SHELX-76 (25). Scattering factors were taken from the International tables for X-ray crystallography (26) and were corrected for anomalous dispersion. The final agreement factors were $R = \Sigma|\Delta F|/\Sigma|F|$ = 0.051 and $R_w = \Sigma w^{1/2}|\Delta F|/\Sigma w^{1/2}|F|$ = 0.056 with weights based on counter statistics. A difference synthesis showed no unexpected features and had a maximum electron density of 1.18 $e^-/Å^3$ at a position 0.7 Å from the tellurium. The final atomic coordinates are given in Table 6.[1]

Results and discussion

Preparation and characterisation of $(C_2F_5)_2TeF_2$ and $(C_2F_5)_2TeCl_2$

Careful addition of $(C_2F_5)_2Te$ in small aliquots to XeF_2 in a slurry of SO_2ClF according to eq. [1] led to $(C_2F_5)_2TeF_2$ in essentially quantitative yield.

[1] $(C_2F_5)_2Te + XeF_2 \xrightarrow[\text{low temp}]{SO_2ClF} (C_2F_5)_2TeF_2 + Xe$

Single crystals of $(C_2F_5)_2TeF_2$ had a melting point of 57°C. In our preliminary communication we had reported $(C_2F_5)_2TeF_2$ to be a liquid (9). This material was in fact a mixture of $(C_2F_5)_2TeF_2$, $(C_2F_5)_2TeClF$, and $(C_2F_5)_2TeCl_2$. We note that the melting point of $(CF_3)_2TeF_2$ is reported to be 185–195°C (15), higher than that (130°C (27)) of TeF_4.

The ^{19}F nmr spectrum of $(C_2F_5)_2TeF_2$ (Table 2) is consistent with the presence of two equivalent fluorine atoms and two equivalent C_2F_5 groups. The spectrum is first order and indicative of free rotation of the C_2F_5 groups about the tellurium atom, in contrast to the ^{19}F nmr spectrum of $(C_2F_5)_2SeF_2$ which is more complicated and may suggest restricted rotation of C_2F_5 about the selenium–carbon bond (7). The vibration spectrum of liquid and solid $(C_2F_5)_2TeF_2$ (Table 1) showed peaks attributable to C_2F_5 that were similar to $(C_2F_5)_2SeF_2$ (6), in addition peaks at ca. 520 and 500 cm^{-1} (see Table 1) that are reasonably assigned to asymmetric and symmetric axial F—Te—F stretches by comparison with monomeric TeF_4 in a solid N_2 matrix (axial F—Te—F asym. 587, sym. 572) (28). The vibrational spectrum of $(CF_3)_2TeF_2$ (15) had peaks (ir 485, Raman 493, 542) in a similar region that are likely similar tellurium–fluorine stretching frequencies. The structure of $(C_2F_5)_2TeF_2$ may therefore reasonably be assigned as **1** with the two fluorine atoms in the axial positions. Bis(perfluoroethyl) tellurium difluoride has a sufficient vapour pressure at room temperature to allow an infrared spectrum to be recorded (Table 1). Thus, its physical properties, ^{19}F nmr and vibrational spectrum, indicate that $(C_2F_5)_2TeF_2$ has the molecular structure (**1**), although some weak intermolecular association cannot be ruled out.

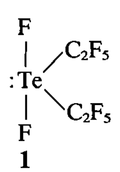

1

Bis(perfluoroethyl) tellurium dichloride was prepared essentially quantitatively by the careful addition of chlorine to $(C_2F_5)_2Te$, and was purified by sublimation. It was characterised by chemical analyses and ^{19}F nmr (Table 2). The strong peak in the Raman spectrum at 284 cm^{-1} is indicative of a Cl—Te—Cl axial symmetric stretch, by comparison with the vibrational spectrum of $(CH_3)_2TeCl_2$ (27) and $(CF_3)_2TeCl_2$ (16).

[1]Tables of anisotropic thermal parameters, and observed and calculated structure factors are available, at a nominal charge, from the Depository of Unpublished Data, CISTI, National Research Council of Canada, Ottawa, Ont., Canada K1A 0S2.

Attempts to prepare $(C_2F_5)_2TeF_2$ by the reaction of $(C_2F_5)_2Te$ and chlorine monofluoride under a variety of conditions, led to mixtures of $(C_2F_5)_2TeF_2$, $(C_2F_5)_2TeClF$, $(C_2F_5)_2TeCl_2$, $C_2F_5TeCl_xF_{3-x}$, C_2F_5Cl, $TeClF_5$, and *trans*-$C_2F_5TeClF_4$.

The reaction of $(CF_3)_2Te$ and chlorine monofluoride (15) in a diluent at −78°C led to a mixture of $(CF_3)_2TeCl_xF_{2-x}$ ($x = 0, 1, 2$). Our reaction of $(C_2F_5)_2Te$ and chlorine monofluoride was carried out under less mild conditions, i.e., in a neat reaction, with some cleavage of tellurium–carbon bonds and oxidation of tellurium to Te(VI).

We note that the analogous reactions of $(C_2F_5)_2Se$ and $(C_2F_5Se)_2$ and chlorine monofluoride at room temperature were much less exothermic than the tellurium reactions, and led quantitatively to $(C_2F_5)_2SeF_2$ and $C_2F_5SeF_3$, respectively. At 80°C $(C_2F_5)_2SeF_2$ and $C_2F_5SeF_3$ reacted with chlorine monofluoride giving *trans*-$C_2F_5SeClF_4$ in good yield (6).

Preparation and characterisation of $C_2F_5TeF_3$

Perfluoroethyl tellurium trifluoride was prepared essentially quantitatively by the careful addition of $(C_2F_5)_2Te_2$ to XeF_2 in a slurry of SO_2F_2 according to reaction [2].

[2] $(C_2F_5)_2Te_2 + 3XeF_2 \xrightarrow[-45°C]{SO_2F_2} 2C_2F_5TeF_3 + Xe$

A similar experiment, but using SO_2ClF as a slurry for XeF_2, led to some SO_2 in the product. A blank reaction of SO_2ClF and $(C_2F_5)_2Te_2$ led to reaction of 10% of the ditelluride with formation of a $C_2F_5Cl_xF_{3-x}$ mixture according to reaction [3].

[3] $(C_2F_5)_2Te_2 + 3SO_2ClF \rightarrow 3SO_2 + 2C_2F_5TeCl_xF_{3-x}$ (average $x \approx 1.5$)

SO_2ClF is generally chemically very inert and is used as an unreactive solvent. However it has been used to convert $R_3P{=}X$ (R = alkyl or alkoxy, X = S) to fluorinated organophosphorus compounds (29). The $C_2F_5TeF_3$ produced in the presence of SO_2ClF appeared to be identical to that with SO_2F_2. It is therefore likely that reaction [2] was faster than reaction [3]. It is possible that reaction [3] proceeds via the TeC_2F_5 radical in equilibrium with $(C_2F_5)_2Te_2$ or by the direct reaction of SO_2ClF and $(C_2F_5)_2Te_2$.

The melting point of $C_2F_5TeF_3$ is 142–143°C. The material we previously reported as $C_2F_5TeF_3$ (mp ca. 95°C (9)) was in fact $C_2F_5TeF_xCl_{3-x}$. The ^{19}F nmr of $C_2F_5TeF_3$ in SO_2 solution (Table 2) showed the presence of C_2F_5 and Te—F, but no coupling was observed presumably due to exchange. The Raman spectrum of solid $C_2F_5TeF_3$ (Table 3) shows peaks attributable to C_2F_5, and tellurium–fluorine stretches (632(s), 594 m(br)), that are similar to those assigned to the equatorial tellurium–fluorine stretches (621 msh, 603 ms, 572 ms) in TeF_4 (28). This is consistent with the X-ray structure of $C_2F_5TeF_3$ (see below).

Attempts to prepare pure $C_2F_5TeF_3$ by the reaction of $(C_2F_5)_2Te_x$ $x = 1, 2$ and ClF under a variety of conditions, lead to $C_2F_5TeCl_3F_{3-x}$, C_2F_5Cl, and *trans*-$C_2F_5TeClF_4$.

The preparation and characterisation of trans-$C_2F_5TeClF_4$ *and* trans-$(C_2F_5)_2TeF_4$

The colourless liquid *trans*-$C_2F_5TeClF_4$ is prepared by the careful addition of ClF in a number of small aliquots at low temperature to $(C_2F_5)_2Te_2$ in ca. 90% yield according to reaction [4]

[4] $(C_2F_5)_2Te_2 + 8ClF \rightarrow 2C_2F_5TeClF_4 + 3Cl_2$

It can also be prepared from $C_2F_5TeCl_xF_{3-x}$ presumably accord-

TABLE 7. Bond distances (Å) for $C_2F_5TeF_3$ (esd's in parentheses)

Atoms	Distance
Te—F1	2.190(1)
Te—F2	1.874(7)
Te—F3	1.870(7)
Te—F4	2.196(8)
Te—C1	2.20(2)
C1—F11	1.37(2)
C1—F12	1.43(2)
C1—C2	1.46(3)
C2—F21	1.38(2)
C2—F22	1.27(4)
C2—F23	1.37(3)
Intermolecular ≤ 3.0 Å	
Te—F3′	3.168(9)
Intramolecular non-bonded ≤ 3.0 Å	
Te—F11	2.928(9)
Te—F12	2.976(12)

ing to reactions [5] and [6].

[5] $C_2F_5TeClF_2 + ClF \rightarrow C_2F_5TeF_3 + Cl_2$

[6] $C_2F_5TeF_3 + ClF \rightarrow C_2F_5TeClF_4$

The minor products C_2F_5Cl and $TeClF_5$ are also observed. *trans*-$C_2F_5TeClF_4$ and ClF do not react at room temperature. Chlorine monofluoride does react with TeF_4 and $TeCl_4$ at room temperature to yield $TeClF_5$ (31). It is possible that $TeClF_5$ and C_2F_5Cl are formed by reactions of chlorine with perfluoroethyl tellurium species, e.g., according to reactions [7]–[9].

[7] $C_2F_5TeF_3 + Cl_2 \rightarrow C_2F_5Cl$ + "$TeClF_3$"

[8] "$TeClF_3$" $+ ClF \rightarrow Cl_2 + TeF_4$

[9] $TeF_4 + ClF \rightarrow TeClF_5$

The analogous reactions of chlorine with CF_3TeCl_3 has been reported (17) to proceed according to reaction [10].

[10] $CF_3TeCl_3 + Cl_2 \rightarrow TeCl_4 + CClF_3$

The octahedral *trans*-$C_2F_5TeClF_4$ symmetry **2** is readily assigned by means of ^{19}F nmr (Table 2) and from vibration spectra (Table 5). A comparison, and assignment, of the $ClTeF_4$ vibrational frequencies in *trans*-$C_2F_5TeClF_4$, $TeClF_5$, and *trans*-$CH_3OTeClF_4$ have been given in ref. 10.

A careful reaction at low temperature of $(C_2F_5)_2Te$ and chlorine monofluoride in a 1:5 mole ratio led to a 2:1 ratio of *trans*-$C_2F_5TeClF_4$ (**2**),

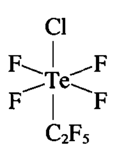

2

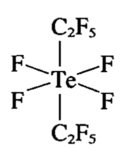

3

and *trans*-$(C_2F_5)_2TeF_4$ (**3**). The products were unambiguously identified by their ^{19}F nmr spectra (Table 2), although pure *trans*-$(C_2F_5)_2TeF_4$ was not isolated.

Crystal structure of $C_2F_5TeF_3$

The crystal packing of $C_2F_5TeF_3$ is illustrated in Fig. 1, and the coordination of atoms around tellurium are shown in Fig. 2. Bond distances and angles are given in Tables 7 and 8,

TABLE 8. Relevant bond angles (deg) in $C_2F_5TeF_3$ (esd's in parentheses)

Atoms	Angle
F1—Te—F2	163.2(4)
F3	85.4(3)
F4	99.9(5)
C1	79.4(5)
F2—Te—F3	85.8(6)
F4	85.1(6)
C1	86.3(7)
F3—Te—F4	164.2(3)
C1	90.9(8)
F4—Te—C1	75.7(7)
Te—C1—F11	108(1)
F12	108(1)
C2	120(2)
F11—C1—F12	104(2)
C2	107(2)
F12—C1—C2	109(2)
C1—C2—F21	104(2)
F22	106(2)
F23	102(2)
F21—C2—F22	120(2)
F23	104(2)
F22—C2—F23	118(3)
Intermolecular	
F3—Te—C1	153.9(7)
F11	179.5(3)
Bridging	
Te—F1—Te′	180
Te—F4—Te′	177(1)

respectively. Solid $C_2F_5TeF_3$, like TeF_4 (21), has a *cis*-fluorine bridged polymeric structure, but unlike TeF_4, the structure consists of mutually perpendicular polymeric chains (see Fig. 1). Each tellurium, in VSEPR terms (20), has an AX_4YE geometry (X = F, Y = C_2F_5, E, lone pair), see Figs. 2 and 3. The four fluorine atoms are planar within ±0.13 Å, and the lone pair is *trans* to the C_2F_5 group. Consistently, the four fluorine atoms are bent back from the lone pair, with the tellurium atom 0.26 Å above the plane of the four fluorine atoms. The geometries of the atoms around tellurium in $C_2F_5TeF_3$ and TeF_4 are similar, with the C_2F_5 group of $C_2F_5TeF_3$, in the position of the axial fluorine atom in TeF_4, and are compared in Fig. 3. The tellurium atoms in $C_2F_5TeF_3$ are linked by two essentially linear (see Table 8 and Fig. 2) *cis*-fluorine bridges, giving the chains a square wave shape (Fig. 1). The fluorine bridges in TeF_4 are neither linear (TeFTe 159(2.5)° (21)), nor symmetrical (TeF (bridging) 2.08(3), 2.26(3) Å). Thus, $C_2F_5TeF_3$ is more nearly polymeric, and TeF_4 more nearly a strong interacting molecular solid. Consistently, the melting point of $C_2F_5TeF_3$ (142–143°C) is higher than that of TeF_4 (130°C). The C_2F_5 groups and lone pairs in adjacent $C_2F_5TeF_4$ groups, and axial fluorine atoms and lone pairs in TeF_4, are *trans* to one another. Chains are linked by a weak tellurium fluorine interaction (Te—F3′, 3.168(9) Å, sum of van der Waals radii (Pauling) 3.55 Å) illustrated in Fig. 2. Chains in TeF_4, are linked by two stronger contacts (2.94(3), 3.01(3) Å), reflecting the greater partial positive charge on the tellurium atom, in tellurium tetrafluoride. The geometries of various related $RTeX_3$ (X =

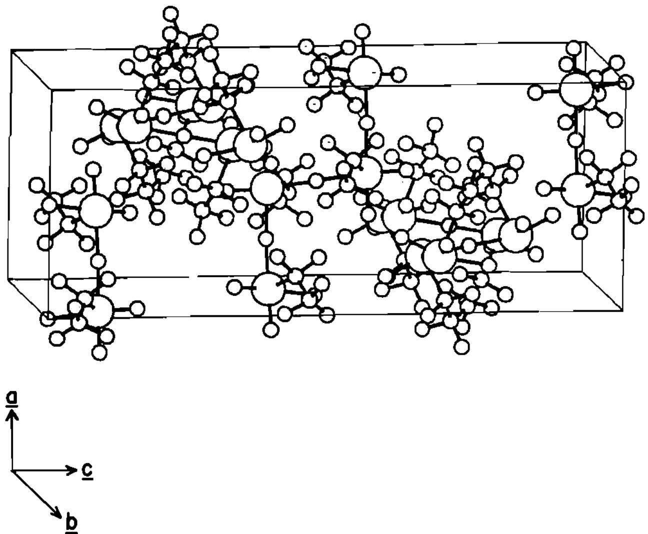

FIG. 1. Crystal packing in $C_2F_5TeF_3$.

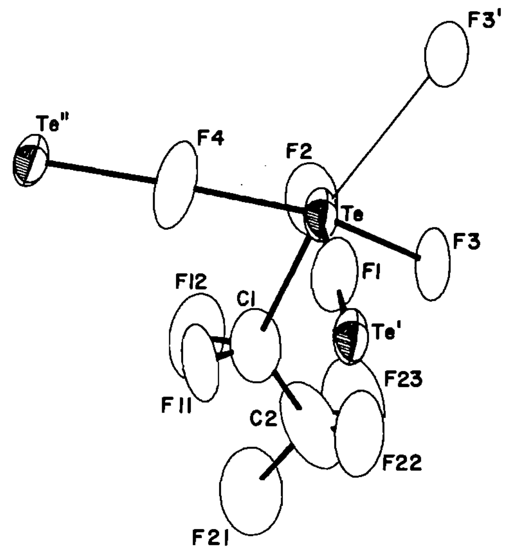

FIG. 2. The structure of $C_2F_5TeF_3$.

TABLE 9. Selected tellurium–carbon distances

Compound/species	Te—C (Å)	Reference
$C_2F_5TeF_3$	2.20(2)	This work
$Te(CH_3)_3^+$ in $Te(CH_3)_3BPh_4$	2.14(1) (mean)	33
$(CH_3)_2TeI_4$	2.14(1) (mean)	34
$(CH_3)_2TeCl_2$	2.09(3) (mean)	35
α-$(CH_3)_2TeI_2$	2.12(3) (mean)	34
$ClC_2H_4TeCl_3$	2.16(1)	36

Cl(18), Br(30), I(31)) have been determined, and discussed.

The average equatorial tellurium–fluorine terminal and bridging bonds in TeF_4 (1.90(2), 2.17(3) Å) and $C_2F_5TeF_3$ (1.872(7), 2.193(5) Å) are similar in length. The average FTeF angles within the equatorial TeF_4 base, are also similar in TeF_4 (88.8(2.4)° and $C_2F_5TeF_4$ 89.0(6)°). If the lone pair in $C_2F_5TeF_3$ were perfectly opposite the C_2F_5 group, then the angles within the TeF_4 base would be determined solely by the strengths of the tellurium fluorine bonds, and in the order F2TeF3 > F3TeF1 ≈ F2TeF4 > F4TeF1. This is not the case, and presumably the lone pair is displaced towards F4 and F1, reflecting a contribution of the valence bond structures $C_2F_5TeF2F3^+F4^-$ and $C_2F_5TeF2F3^+F1^-$, to the overall bonding in the polymer. The average C1TeF (basal) angle of 83.2(6)° is similar to the average F (axial) TeF (basal) (82.0(2.3)°) angle in TeF_4. Both are less than 90° consistent with the presence of a lone pair opposite the axial ligand. C1TeF (bridging) angles are, as anticipated by VSEPR (20) theory, smaller than C1TeF (terminal) angles. The two terminal fluorine bond distances, and, the two bridging bond distances are essentially equal, therefore it would be expected that C1TeF2 would equal C1TeF3, and C1TeF4 equal C1TeF1. However, this is not the case (see Fig. 3).

The tellurium carbon bond distance (2.20(2) Å) is likely longer than that reported for other tellurium carbon bond distances (see Table 9, and refs. 18, 30–32). Oberhammer (36) has examined the effect of substitution of methyl by perfluoromethyl in $O(CH_3)_2$, $S(CH_3)_2$, $N(CH_3)_3$, and $P(CH_3)_3$, and concluded that lengthening occurs when the central atom has an electronegativity less than 2.5 (Pauling scale). Tellurium has an electronegativity on the Pauling scale of 2.34, and length-

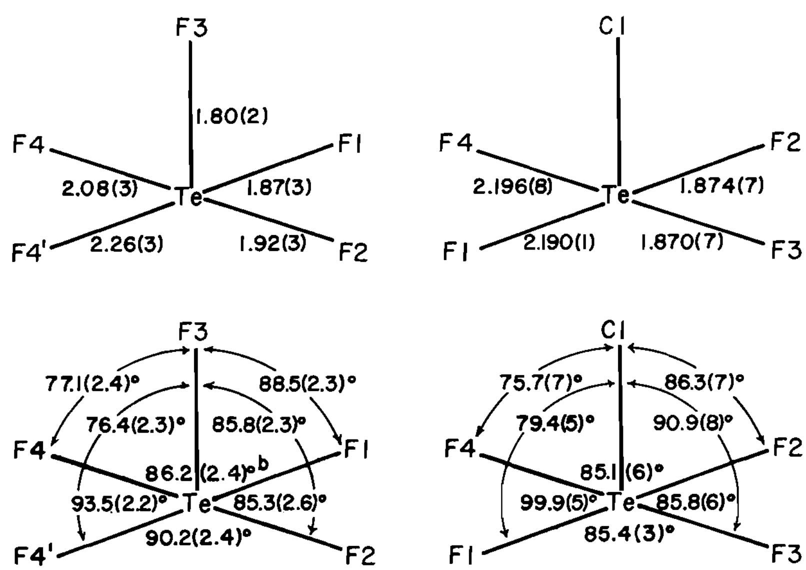

FIG. 3. A comparison of the geometries about tellurium in TeF_4 and $C_2F_5TeF_3$. Bond distances in Å.

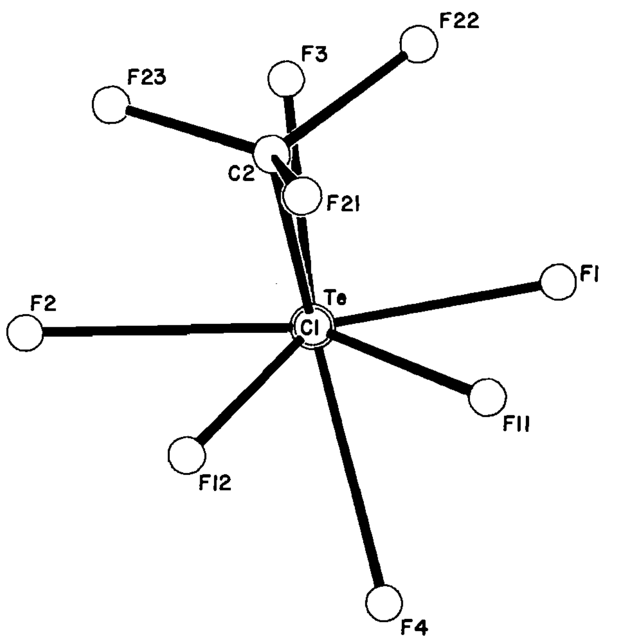

FIG. 4. View of the $C_2F_5TeF_3$ moiety projected along the Cl—Te bond.

ening is therefore expected.

Figure 4 shows a view of the $C_2F_5TeF_3$ moiety as projected along the C1—Te bond. The fluorine atoms of the C_2F_5 group and those of the basal TeF_4 are staggered relative to one another. The two fluorine atoms of the CF_2 groups have contacts to tellurium (2.93(9), 2.98(1), that are considerably less than the sum of the corresponding van der Waals radii (3.55 Å), and likely represent very weakly bonding interactions. The high standard deviations, and high thermal parameters of the atoms of the C_2F_5 group do not allow a detailed comparison with related molecules (e.g. C_2F_5I (37), *trans*-$PtClC_2F_5(PMePh_2)_2$ (38)). The TeC1C2 angle (123(2)°), which is substantially larger than the expected tetrahedral angle of 109° (28), is similar to that observed in a variety of related compounds (ref. 38 and references quoted therein) including C_2H_5 derivatives of transition metals, and it has been suggested that the opening of the MC1C2 angle may be caused by ligand–ligand interaction and/or molecular packing forces.

Acknowledgement

We thank the Natural Sciences and Engineering Research Council of Canada for financial support.

1. R. J. GILLESPIE and J. PASSMORE. Adv. Inorg. Radiochem. **17**, 49 (1975).
2. H. L. PAIGE and J. PASSMORE. Inorg. Chem. **12**, 593 (1973).
3. C. D. DESJARDINS and J. PASSMORE. Can. J. Chem. **55**, 3136 (1977).
4. C. D. DESJARDINS, H. L. PAIGE, J. PASSMORE, and P. TAYLOR. J. Chem. Soc. Dalton Trans. 488 (1975) and references therein.
5. T. N. BELL, B. J. PULLMAN, and B. O. WEST. Aust. J. Chem. **16**, 722 (1963).
6. C. LAU and J. PASSMORE. J. Fluorine Chem. **7**, 261 (1976).
7. D. T. SAUER and J. M. SHREEVE. J. Fluorine Chem. **1**, 1 (1971/72).
8. T. ABE and J. M. SHREEVE. J. Fluorine Chem. **3**, 187 (1973/74).
9. C. D. DESJARDINS, C. LAU, and J. PASSMORE. Inorg. Nucl. Chem. Lett. **10**, 151 (1974).
10. L. J. LAWLOR and J. PASSMORE. Can. J. Chem. In press.
11. S. HERBERG and D. NAUMANN. Z. Anorg. Allg. Chem. **492**, 95 (1982) and references therein.
12. M. SCHMEISSER, R. WALTER, and D. NAUMANN. Z. Anorg. Allg. Chem. **464**, 233 (1980).
13. T. J. JUHLKE, R. W. BRAUN, T. R. BIERSCHENK, and R. J. LAGOW. J. Am. Chem. Soc. **101**, 3229 (1979).
14. R. J. LAGOW, L. L. GERCHMAN, R. A. JACOB, and J. A. MORRISON. J. Am. Chem. Soc. **97**, 518 (1975).
15. D. NAUMANN and S. HERBERG. J. Fluorine Chem. **19**, 205 (1982).
16. S. HERBERG and D. NAUMANN. Z. Anorg. Allg. Chem. **494**, 151 (1982).
17. S. HERBERG and D. NAUMANN. Z. Anorg. Allg. Chem. **494**, 159 (1982).
18. N. W. ALCOCK and W. D. HARRISON. J. Chem. Soc. Dalton Trans. 251 (1982) and references therein.
19. F. J. BERRY and A. J. EDWARDS. J. Chem. Soc. Dalton Trans. 2306 (1980).
20. R. J. GILLESPIE. Molecular geometry. Van Nostrand Reinhold, London. 1972.
21. A. J. EDWARDS and F. I. HEWAIDY. J. Chem. Soc. A, 2977 (1968).
22. S. M. WILLIAMSON. Inorg. Synth. **11**, 147 (1968).
23. G. GERMAIN, P. MAIN, and M. M. WOOLFSON. Acta Crystallogr. Sect. A, **27**, 368 (1971).
24. A. C. LARSON and E. J. GABE. *In* Computing in crystallography. *Edited by* H. Schenk, R. Olthof-Hazekamp, H. van Koningsveld, and G. C. Bassi. Delft University Press, The Netherlands. 1978. pp. 81–89.
25. G. M. SHELDRICK. SHELX-76. A program for crystal structure determination. University of Cambridge, England. 1976.
26. International Tables for X-ray crystallography. Vol. IV. Kynoch Press, Birmingham. 1974.
27. G. C. HAYWARD and P. J. HENDRA. J. Chem. Soc. A, 643 (1967).
28. C. J. ADAMS and A. J. DOWNS. Spectrochem. Acta, **28**A, 1841 (1972).
29. A. LOPUSINSKI and J. MICHALSKI. J. Am. Chem. Soc. **104**, 290 (1982).
30. N. W. ALCOCK and W. D. HARRISON. Acta Crystallogr. **B38**, 2677 (1982).
31. N. W. ALCOCK and W. D. HARRISON. J. Chem. Soc. Dalton Trans. 869 (1984).
32. G. Y. CHAO and J. D. MCCULLOUGH. Acta Crystallogr. **15**, 887 (1962).
33. L. Y. Y. CHAN and F. W. B. EINSTEIN. J. Chem. Soc. Dalton Trans. 316 (1972).
34. G. D. CHRISTOFFERSON, R. A. SPARKS, and J. D. MCCULLOUGH. Acta Crystallogr. **11**, 782 (1958).
35. D. KOBELT and E. F. PAULUS. Angew. Chem. Int. Ed. Engl. **10**, 74 (1971).
36. H. OBERHAMMER. J. Mol. Struct. **28**, 349 (1975).
37. A. L. ANDREASSEN and S. H. BAUER. J. Chem. Phys. **56**, 3802 (1972).
38. M. A. BENNETT, HO-KIN CHEE, and G. B. ROBERTSON. Inorg. Chem. **18**, 1061 (1979).

The photoreactions of 2-isopropoxy-1,4-naphthoquinone in the presence of cobalt acetylacetonate and other organometallics: an esr and CIDEP study

M. Catherine Depew, B. B. Adeleke, Allison Rutter, and J. K. S. Wan
Department of Chemistry, Queen's University, Kingston, Ont., Canada K7L 3N6

Received July 23, 1984

M. Catherine Depew, B. B. Adeleke, Allison Rutter, and J. K. S. Wan. Can. J. Chem. **63,** 2281 (1985).

2-Isopropoxy-1,4-naphthoquinone has been used as a photoredox reagent in non-silver imaging process. The present study showed that the photoreactions of this quinone are very sensitive to solvent due to the competing intramolecular hydrogen abstraction from the isopropoxy group. The presence of cobalt acetylacetonate often modifies the reactions which leads to a very high quantum efficiency of producing the radical intermediates. The ether oxygen in the 2-substituent provides a further coordinating site for organometallic compounds and the quinone behaves as a 1,2-quinone when interacting with metals.

M. Catherine Depew, B. B. Adeleke, Allison Rutter et J. K. S. Wan. Can. J. Chem. **63,** 2281 (1985).

On a utilisé l'isopropoxy-2 naphtoquinone-1,4 comme agent photoréducteur dans un processus de formation d'image n'impliquant pas l'argent. Notre étude a démontré que les photoréactions de cette quinone sont très sensibles à la nature du solvant et ce fait est dû à une réaction compétitive d'enlèvement intramoléculaire d'hydrogène du groupe isopropoxyle. La présence d'acétylacétonate de cobalt modifie souvent les réactions et ceci conduit à une efficacité quantique très élevée pour la production d'intermédiaires radicalaires. L'oxygène de l'éther du substituant en position 2 fournit un nouveau site de coordination pour les composés organométalliques et la quinone se comporte comme une quinone-1,2 lorsqu'elle interagit avec les métaux.

[Traduit par le journal]

Introduction

The photochemistry of quinones has long been a subject of many studies. Much of the chemical information has been utilized when we initiated quinones as model systems for CIDEP (chemically induced dynamic electron polarization) and CIDNP (chemically induced dynamic nuclear polarization) studies (1). As well, quinones have been extensively explored as reagents to interact with metal ions and organometallics (2, 3). In recent years the use of some substituted quinones as photoredox agents in non-silver imaging processes has led to the development of a novel high gain photothermographic imaging process by the Eastman Kodak Company (4, 5). In this paper we report some of esr and CIDEP results of the photoredox reactions of 2-isopropoxy-1,4-naphthoquinone and the subsequent interactions with cobalt compounds and other organometallics. The photochemical reactions of this quinone are strongly solvent dependent; the presence of the Co(III)–acetylacetonate often modifies the esr observations of the quinone radical intermediates by secondary redox reactions. With the 2-isopropoxy substituent, the 1,4-quinone behaves efficiently as a 1,2-quinone in which the ether oxygen serves as an additional coordinating site with a number of organometallic compounds, including the manganese and rhenium carbonyls. The results will shed some light on the extremely high quantum efficiency of this quinone in the photothermographic imaging process.

Experimental

2-Isopropoxy-1,4-naphthoquinone (INQ) and 3-chloro-2-isopropoxy-1,4-naphthoquinone (CINQ) were gifts from Dr. Thap Dominh of the Eastman Kodak Company. Cobalt salts and many of the organometallics used were supplied by Aldrich Chemicals. Organic solvents were purified by appropriate methods before use. Sample solutions were all deoxygenated by purging with nitrogen gas immediately before use. In cw experiments samples were irradiated with a super pressure mercury lamp with Pyrex optics directly within the microwave cavity of an X-band esr spectrophotometer with a 100 kHz field modulation. Microwave frequency was monitored by a Hewlett Packard 5432 frequency counter and the magnetic field was measured by a Bruker nmr oscillator calibrated against DPPH. In CIDEP experiments the transient spin-polarised radicals were produced by laser photolysis using a Molectron 1 MW nitrogen laser and dc detection. The CIDEP apparatus and the method of estimating T_1 from the experimental data were described previously in detail (6).

Results and discussion

1. Photolysis of INQ and CINQ in benzene solution

The photolysis of INQ in benzene solution at room temperature produced a well resolved esr spectrum of a radical intermediate which can be assigned to the following structure (**I**):

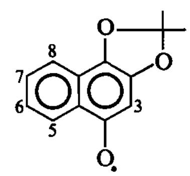

I

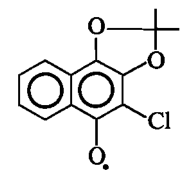

II

The photolysis of CINQ led to the observation of radical **II**. The assignments of both radicals **I** and **II** are given in Table 1.

It is obvious that both radicals are necessarily the result of some secondary photochemical reactions. In benzene solution the only primary photochemical reactions of INQ and CINQ are the intramolecular hydrogen abstraction from the 2-isopropoxy group. Similar photochemical reactions of 2-substituted quinones have been well characterized (7–9). The photolysis of INQ in acetic anhydride led to the formation of the rearranged product **III** (10):

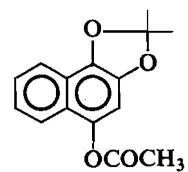

III

Thus it is reasonable that radical **I** is formed as shown in the following scheme:

TABLE 1. The esr parameters of INQ radicals generated in the photolysis of INQ in various solvents at 23°C

Radical	Solvent	g-factor	Proton hyperfine coupling constants* (G)
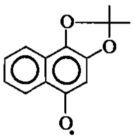 (I)	Benzene	2.0041±0.0002	a_3 = 4.90; a_6 = a_8 = 2.94; a_5 = a_7 = 0.98
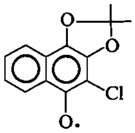 (II)	Benzene	2.0034	a_6 = a_8 = 2.78; a_5 = a_7 = 0.76
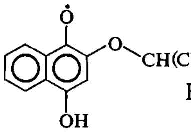 (VIII)	EPA	2.0044	$a_H^{(O—CH—)}$ = 2.37; a_{OH} = a_6 = a_8 = 1.22; a_3 = a_7 = 0.30

*Refer to diagrams in text for proton positions.

[1] INQ + $h\nu$ $\xrightarrow{\text{benzene}}$ ^{3}(INQ)*

[2] 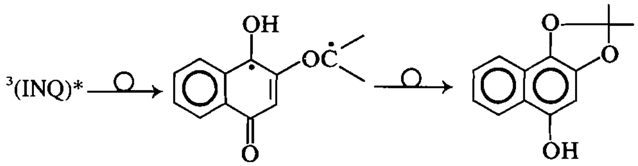

IV

[3] ^{3}(INQ)* + **IV** ⟶ Radical $\dot{\text{I}}$* + INQH$^{\bullet}$

where ^{3}(INQ)* indicates a spin-polarized triplet. Photolysis of CINQ would be expected to result in the formation of radical **II** in an analogous fashion. This reaction scheme is further supported by two sets of experiments. In the first set, the addition of some di-*t*-butylperoxide to the photolysed INQ benzene solution greatly enhanced the esr intensity of radical **I**, due to the efficient reaction

[4] R$\dot{\text{O}}$ + **IV** → $\dot{\textbf{I}}$ + ROH

In the second set of experiments, flash laser photolysis was employed in the CIDEP mode of detection. When a fresh benzene solution of INQ was flash photolysed, no radicals could be observed. However, when the solution was pre-irradiated for 3 min and then subjected to laser flash photolysis, radical **I** was immediately detected in a totally emissive mode. The polarization was strong at room temperature and can be accounted for by the triplet mechanism associated with intersystem crossing and subsequent reaction of the spin-polarized triplet in reactions [1] and [3]. The T_1 of radical **I** in benzene solution at room temperature was estimated at 2.8 μs.

Similar polarization of radical **II** was observed when CINQ in benzene was photolysed. As expected the T_1 of radical **II** is similar to that of radical **I**.

The rearrangement in reaction [2] presumably involves a biradical intermediate as proposed by Farid (8). In the photoreaction of *t*-butyl-*p*-benzoquinone, Farid (8) has used sulfur dioxide to trap the biradical which led to the formation of sultone (**V**) as the major product. In the photolysis of some cyclic ketones believed to involve a biradical as an intermediate, Scaiano (11) has successfully trapped such biradicals with nitric oxide to yield a relatively persistent nitroxide radical. In our experiments, when a benzene solution of INQ saturated with nitric oxide was photolysed, the formation of radical **I** was quenched and in its place a nitroxide radical was observed. The new nitroxide radical had the following spectral parameters: g = 2.0064; a_N = 11.6 G. Consistent with Farid's (8) observation, we have *tentatively* assigned the nitroxide radical to the structure **VI**. Prolonged irradiation further led to the

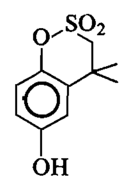

V

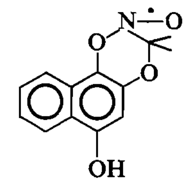

VI

observation of an additional triplet with a larger splitting of 29.9 G which is characteristic of an iminoxy type of radical. The identity of this second radical remains uncertain. However, identical experiments performed with 1,4-naphthoquinone did not yield any nitroxide radicals; this result is not unexpected since no biradical intermediates would have been involved.

2. The effect of addition of Co(III) acetylacetonate

Radicals **I** and **II** generated during the photolysis at room temperature disappeared immediately upon termination of irradiation. When Co(III) acetylacetonate was added to the benzene solution of INQ and photolysed, the esr spectrum of the radical could be observed hours after the light was turned off. In a typical experiment, the photolysis of a benzene solution containing CINQ, Co(III) acetylacetonate greatly enhanced the steady state esr signal intensity of radical **II**. A complementary examination of the photolyzed solution by uv–visible spectrometry showed a new absorption band at 490 nm. The experimental results can be explained by the following cycle, similar to that proposed by DoMinh (4) in his photothermographic imaging process:

[5] 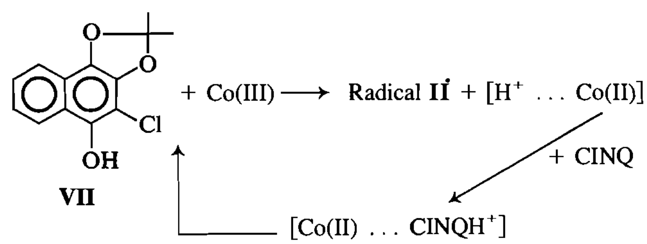

The new absorption band at 490 nm can be associated with the Co(II) complex with the protonated CINQ which further undergoes a redox reaction to yield Co(III) and the product **VII** to complete the cycle. Experimentally, the initial effect on the magnitude of radical enhancement was found to depend upon the concentration of Co(III) added. The cycle can continue in the dark to "maintain" the concentration of radicals for esr observation many hours after the termination of irradiation. In effect, the quantum yield of the radical formation was greatly magnified.

3. Photolysis of INQ in an EPA solution

A mixed solvent system containing ether, isopentane, and ethanol (EPA, 2:2:5 by volume) was used in the low temperature photolysis of INQ because of its good optical quality in the glassy state. The purpose of the experiment, carried out at 77 K, was to trap the biradical intermediate of the INQ for direct esr observation. The experiment was not successful, as neither the $M_s = 2$ nor the $M = 1$ transitions could be detected.

However, when INQ was photolysed in EPA solution at room temperature, a well-resolved esr spectrum was observed. The spectrum cannot be ascribed to the same radical **I** formed in benzene. Furthermore, the spectrum exhibited total emission immediately upon laser flash photolysis. This observation indicates that the radical is a primary polarized intermediate resulting directly from the reaction of a spin-polarized INQ triplet with the solvents. The esr parameters of this radical (given in Table 1) can be assigned to the semiquinone radical **VIII** with polarization being accounted for by the following mechanism:

[1] $\text{INQ} + h\nu \xrightarrow{\text{ISC}} {}^3(\text{INQ})^*$

[6] ${}^3(\text{INQ})^* + \text{RH (EPA solvent)} \longrightarrow$

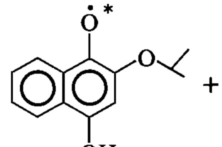

$+ \text{R}^{\bullet *}$

VIII

Under the experimental conditions, the counter radical R$_*$ was not observed. It is therefore not known which component of the EPA system reacted with the INQ triplet. However, abstraction of a hydrogen atom from ethers by quinone triplets has been observed in other systems (12).

Because of the strong polarization observed in radical **VIII**, it follows that reaction [6] must have taken place faster than the spin lattice relaxation time of the polarized INQ triplet, which in liquid solution is normally in the order of 10^{-9} s. Furthermore, since radical **I** was not observed simultaneously during the cw photolysis of INQ in EPA solvent, it appears that reaction [6] competes favorably with the intramolecular hydrogen abstraction, in reaction [2].

The photolysis of INQ was also carried out at room temperature in a number of different solvents, which can react directly with the excited triplet INQ. In THF solvent, the predominant radical intermediate was the radical anion of INQ, which also exhibited strong polarization in the emissive mode. In 2-propanol solvent, the abstraction reaction was not expected to be as fast and only a weak esr signal of the radical **VIII** was observed in cw photolysis. The CIDEP data showed that the radical **VIII** in alcoholic solvents possessed a longer spin lattice relaxation time (3.5 μs) compared to that of radical **I** in benzene (2.8 μs). This difference, however, is not due to the structural variations between the two radicals. Rather, the difference is mainly due to the different nature of the solvents with the alcoholic solvents being capable of forming hydrogen bonds with the radical **VIII**.

4. Organometallic radical adducts of INQ and CINQ

Photolysis of a number of organometallic compounds in benzene in the presence of either INQ or CINQ led to the formation of corresponding radical–quinone adducts. It is well known that for 1,2-quinones the two carbonyl oxygens both participate in the coordination. Although INQ and CINQ are

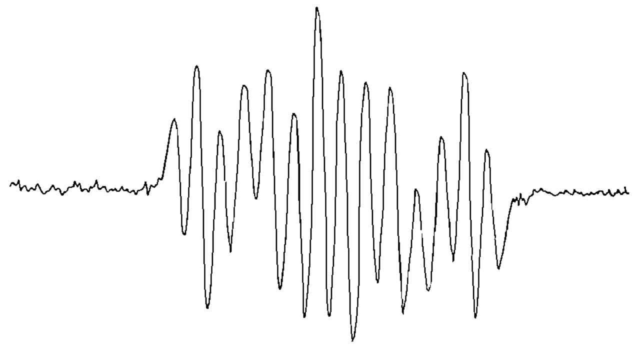

FIG. 1. Electron spin resonance spectrum obtained during cw photolysis of INQ in benzene at 23°C. CIDEP experiments showed that all hyperfine lines in the spectrum were in the emissive mode.

TABLE 2. Electron spin resonance parameters of some metal carbonyl radical adducts of INQ and CINQ in benzene at 23°C

Metal carbonyl	Organic moiety	g-factor	Metal hyperfine couplings (G)
$Re(CO)_4$, 1:1	INQ	2.0032	$a_{Re} = 15.69$
	CINQ	2.0035	$a_{Re} = 15.71$
	1,2-Naphthoquinone	2.0030	$a_{Re} = 24.2$
$Re(CO)_4$, 1:2	INQ	2.0025	$a_{Re} = 19.10$
	CINQ	2.0035	$a_{Re} = 20.19$
$Mn(CO)_4$	INQ	2.0030	$a_{Mn} = 4.75$
	CINQ	2.0030	$a_{Mn} = 6.05$
$C_5H_5V(CO)_2$	INQ	1.9750	$a_V = 82.5$
	CINQ	1.9684	$a_V = 85.8$
$C_5H_5Mo(CO)_2$	INQ	1.9666	$a_{Mo} = 35.2$
	CINQ	1.9678	$a_{Mo} = 37.8$

1,4-quinones they possess a 2-isopropoxy substituent. The results indicate that the 2-ether oxygen participates efficiently in the coordination and both INQ and CINQ thus both behave as 1,2-quinones towards the formation and stabilization of organometallic radical adducts. However, a significantly different behavior was observed between 1,2-naphthoquinone and INQ when they reacted with $Re(CO)_5$. Our previous studies (13, 14) of rhenium carbonyl – quinone (or diketone) radical adducts showed that only 1:1 adducts were observed. In only one case, when 1,10-phenanthroline was used, was a 1:2 radical complex formed. In the present system using INQ, both the 1:1 *and* the 1:2 radical complexes were simultaneously formed and observed during the photolysis. The relative intensities of the two radical complexes followed the relative concentrations of the two reagents, INQ and $Re(CO)_{10}$. It is therefore rather simple to assign the two spectra to the respective radical complexes. Although relatively persistent compared to the other INQ–organometallic adducts formed in this study, these rhenium–INQ radical adducts were still not sufficiently long-lived for isolation and further characterization. The spectral parameters for these and several other organometallic radical adducts are given in Table 2.

Laser flash photolysis experiments were also carried out in these systems where the organometallic radical adducts were formed. No CIDEP was observed in any of the radical adducts.

Acknowledgments

We are grateful to Dr. T. DoMinh of the Eastman Kodak Company for his assistance and enlightening discussion. This research is supported by the Natural Sciences and Engineering Research Council of Canada. Some of the preliminary experiments were performed by Mr. Liu Zhongli.

1. J. K. S. Wan. Adv. Photochem. **12**, 283 (1980).
2. C. G. Pierpont and R. M. Buchanan. Coordination Chem. Rev. **38**, 45 (1981).
3. K. A. M. Creber, T. I. Ho, M. C. Depew, D. Weir, and J. K. S. Wan. Can. J. Chem. **60**, 1504 (1982) and references therein.
4. T. DoMinh. Abstr. 65th Can. Chem. Conf. PH22-5, 1982.
5. T. DoMinh. U.S. Patent 4308341, (1982); Chem. Abstr. **96**, P113563 (1982); **95**, P106385 (1981).
6. J. W. M. deBoer, T. Y. C. Chung, and J. K. S. Wan. Can. J. Chem. **57**, 2971 (1979) and references therein.
7. S. Farid. Chem. Commun. 303 (1970).
8. S. Farid. Chem. Commun. 73 (1971).
9. T. Foster, A. J. Elliot, B. B. Adeleke, and J. K. S. Wan. Can. J. Chem. **56**, 869 (1978).
10. T. DoMinh. Private communication.
11. J. C. Scaiano. J. Phys. Chem. **82**, 1588 (1978) and references therein.
12. K. S. Chen, T. Foster, and J. K. S. Wan. J. Phys. Chem. **84**, 2473 (1980).
13. T. Foster, K. S. Chen, and J. K. S. Wan. J. Organomet. Chem. **184**, 113 (1980); K. A. M. Creber. Ph. D. thesis, Queen's University. 1982.
14. K. A. M. Creber and J. K. S. Wan. J. Am. Chem. Soc. **103**, 2101 (1981); Chem. Phys. Lett. **81**, 453 (1981).

Mechanism of the oxidation of triphenyl derivatives of P, As, and Sb by peroxodiphosphate

C. SRINIVASAN AND K. PITCHUMANI
School of Chemistry, Madurai Kamaraj University, Madurai – 625 021, India

Received August 30, 1984

C. SRINIVASAN and K. PITCHUMANI. Can. J. Chem. **63**, 2285 (1985).

Rate coefficients have been determined for the oxidation of Ph_3M (M = P, As, Sb) by potassium peroxodiphosphate. The reaction is found to follow second-order kinetics, first order in each in the oxidant and Ph_3M. $[H^+]$ has a pronounced accelerating effect on the reaction rate. An interesting dependence of the active species on the nature of the substrate has been observed. The reaction rate is influenced by changing the ionic strength of the medium. Acrylonitrile has no effect on the rate of oxidation. On the basis of the kinetic evidence, a general mechanism involving a biomolecular nucleophilic displacement of the substrate on the peroxo ion has been proposed. The relative rate order is found to be $Ph_3P > Ph_3Sb > Ph_3As$ and an explanation has been offered for the transposition of Ph_3Sb and Ph_3As.

C. SRINIVASAN et K. PITCHUMANI. Can. J. Chem. **63**, 2285 (1985).

On a déterminé les coefficients de vitesse pour les réactions d'oxydation des Ph_3M (M = P, As, Sb) par le peroxodiphosphate de potassium. On a trouvé que la cinétique de la réaction est du deuxième ordre, soit du premier ordre dans chacun des réactifs (oxydant et Ph_3M). La concentration en H^+ provoque une accélération importante de la vitesse. On a observé une relation intéressante entre les espèces actives et la nature du substrat. La réaction est influencée par des changements dans la force ionique du milieu réactionnel. L'acrylonitrile n'a pas d'effet sur la vitesse de la réaction. Si on se base sur les données cinétiques, on peut proposer une mécanisme général impliquant une substitution nucléophile bimoléculaire du substrat sur l'ion peroxo. On a trouvé que les vitesses relatives de réaction sont $Ph_3P > Ph_3Sb > Ph_3As$ et on offre une explication pour la transposition du Ph_3Sb et du Ph_3As.

[Traduit par le journal]

Introduction

The reactions of organic peroxides with triphenyl derivatives of Group V elements have been the subject of several investigations (1–3). They depend on the nature of both the peroxide and of the element. Though there are some kinetic studies on the oxidation of Ph_3M (M = P, As, Sb) by organic peroxides, notably by Hiatt *et al.* (4, 5), more investigations with inorganic peroxo compounds are desirable. Recently we have reported on the kinetics and mechanism of peroxodisulfate (PS) oxidation of Ph_3M in acetonitrile–water mixture (7), and on the substituent effect in the PS oxidation of triphenylarsines (8). The present paper summarizes the results of our kinetic studies of the oxidation of triphenyl derivatives of P, As, and Sb by potassium peroxodiphosphate (PP).

Experimental

Materials

Triphenylphosphine (Riedel, Prosynth) and triphenylarsine (Fluka, Purum) were recrystallized from ethanol. Triphenylstibine was prepared by the Grignard addition of phenyl magnesium bromide to antimony trichloride (9) and recrystallized from ethanol. Tetrapotassium peroxodiphosphate (FMC corporation) was used after repeated recrystallization from methanol–water mixture. A commercial sample of acetonitrile was purified by standard procedure. All the other chemicals used were of AnalaR grade.

Kinetics

Rate coefficients have been determined for the oxidation of Ph_3M (M = P, As, Sb) in 60% acetonitrile – 40% water (v/v) mixture at constant ionic strength (maintained by the addition of sodium perchlorate) and at constant $[H^+]$ under pseudo first-order conditions with a large excess of the oxidant concentration. The reaction was followed by estimating the unreacted triphenylphosphine (TPP) or triphenylarsine (TPA) by an iodometric method (10, 11). In the case of triphenylstibine (TPS), since it does not undergo instantaneous reaction with iodine, a spectrophotometric method was adopted. Rates were determined by monitoring the disappearance of the uv absorption characteristic of TPS (λ_{max} = 255 nm) using a Perkin–Elmer model 402 uv–visible spectrophotometer provided with thermostated silica cells. The alkalinity of PP was always taken into account in the calculation of $[H^+]$. Reactions were generally followed to >60% completions; reproducible results giving good first-order plots (correlation coefficient $r > 0.995$) were obtained for reactions run in duplicate or triplicate. Rate constants were calculated by the least-squares technique using a Micro 2200 computer (Hindustan Computers Ltd.,). The precision of k values is given in terms of 95% confidence limit, calculated with "Student t".

Product studies

The reaction mixture was monitored by tlc (silica gel). The product of the reaction was found to be the respective oxide in the case of TPP and TPA oxidations. Oxidations of TPS gave only a crystalline antimony product that does not melt even after heating to 280°C and liberates free iodine from potassium iodide in glacial acetic acid. This is consistent with the characteristics of a polymeric material (oxide) produced by the oxidation of TPS by hydrogen peroxide (12) and not the monomeric triphenylstibine oxide prepared by McEwen *et al.* (13). In the reaction of TPS with *tert*-butylhydroperoxide, a polymeric product is also obtained (6, 14).

The product studies were also confirmed by the uv absorption characteristics of the respective oxides (15), as the products gave peaks similar to those obtained for authentic samples of the respective oxides.

Results and discussion

Rate coefficients for different concentrations of PP and Ph_3M at constant ionic strength and $[H^+]$ are presented in Table 1. Plots of log $[Ph_3M]$ versus time yield good straight lines, from the slopes of which k_1 are calculated (Fig. 1). The linearity of the rate profiles indicates that the reaction is first order in substrate. From the double logarithmic plots of the initial rate versus initial concentrations of PP, the order with respect to PP has also been evaluated and is found to be unity in all the three cases.

TPP: slope = 0.99 ± 0.02, $r = 0.999$, $s = 0.002$
TPA: slope = 1.01 ± 0.08, $r = 0.999$, $s = 0.01$
TPS: slope = 1.06 ± 0.17, $r = 0.996$, $s = 0.02$

TABLE 1. Effect of varying [PP] and $[Ph_3M]$ on the reaction rate in 60% acetonitrile – 40% water (v/v) mixture

$[PP]_0$ (10^2 mol/L)	$[Ph_3M]$ (10^4 mol/L)	k_1‡ (10^5 s^{-1})	k_2‡ (10^3 L mol^{-1} s^{-1})
		TPP*	
1.00	10.0	5.50 ± 0.09	5.50 ± 0.09
1.50	10.0	8.23 ± 0.24	5.49 ± 0.16
2.00	10.0	10.9 ± 0.08	5.45 ± 0.04
2.50	10.0	13.5 ± 0.40	5.40 ± 0.16
3.00	10.0	16.4 ± 0.32	5.47 ± 0.11
2.00	5.00	10.8 ± 0.08	5.40 ± 0.04
2.00	15.0	11.8 ± 0.37	5.90 ± 0.19
2.00	20.0	11.0 ± 0.29	5.50 ± 0.15
2.00	25.0	10.8 ± 0.18	5.40 ± 0.09
		TPA	
0.50†	5.00	13.4 ± 0.74	26.8 ± 1.5
0.75	5.00	20.4 ± 0.54	27.2 ± 0.72
1.00	5.00	27.6 ± 1.7	27.6 ± 1.7
1.25	5.00	33.7 ± 1.1	27.0 ± 0.88
2.50§	5.00	4.56 ± 0.15	1.82 ± 0.06
2.50	10.0	4.44 ± 0.14	1.78 ± 0.06
2.50	15.0	4.33 ± 0.06	1.73 ± 0.02
2.50	20.0	4.29 ± 0.03	1.72 ± 0.01
2.50	25.0	4.20 ± 0.02	1.68 ± 0.01
		TPS‖	
0.10	1.00	6.17 ± 0.26	61.7 ± 2.6
0.15	1.00	9.51 ± 0.13	63.4 ± 0.87
0.20	1.00	12.3 ± 0.21	61.5 ± 1.1
0.25	1.00	17.3 ± 1.4	69.2 ± 5.6
0.30	1.00	19.2 ± 0.57	64.0 ± 1.9
0.30	1.50	18.3 ± 0.78	61.0 ± 2.6
0.30	2.00	18.8 ± 0.53	62.7 ± 1.8
0.30	2.50	18.5 ± 0.37	61.7 ± 1.2
0.30	3.00	19.2 ± 0.30	64.0 ± 1.0

*I = 0.36 M; $[H^+]$ = 0.00 M; t = 40°C.
†I = 0.2 M; $[H^+]$ = 0.02 M; t = 40°C.
‡The error quoted in k is the 95% confidence limit of the "Student t".
§I = 0.36 M; $[H^+]$ = 0.01 M; t = 40°C.
‖I = 0.1 M; $[H^+]$ = 0.006 M; t = 35°C.

In each substrate the plot of k_1 versus [PP] gives a good straight line passing through the origin (TPP: r = 0.999, TPA: r = 0.999, TPS: r = 0.993) showing the second-order nature of the reaction, which is also confirmed by the constancy of second-order rate constants obtained from the pseudo first-order rate constants as $k_2 = k_1/[PP]$ (Table 1).

Hydrogen ion dependence and active species

The rate of oxidation of Ph_3M by PP increases significantly with increase in $[H^+]$ at constant ionic strength. The results are presented in Table 2.

A plot of log k_1 against log $[H^+]$ gave a good straight line with a slope of 0.94 ± 0.03 (r = 0.999, s = 0.003) (Fig. 2) showing the near first-order dependence in $[H^+]$ in the oxidation of TPP. It is also confirmed from the constant values of the third-order rate constants (k_3). A plot of k_1 against $[H^+]$ is linear (r = 0.999) with an intercept indicating the presence of uncatalysed oxidation (Fig. 3).

In the oxidation of TPA, a second-order dependence in $[H^+]$ was observed when the log k_1 values are plotted against the log $[H^+]$ values (slope = 1.99 ± 0.03, r = 0.999, s = 0.01) (Fig. 2). Further, an excellent correlation is found to exist between k_1 and $[H^+]^2$ (r = 0.999) and the linear plot passes

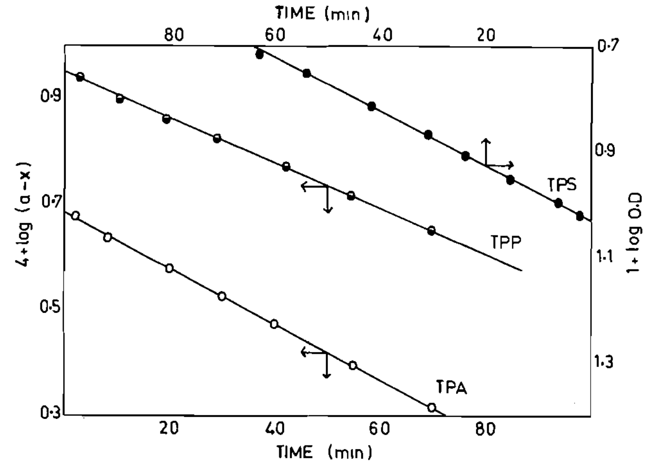

FIG. 1. Pseudo first-order plot for the oxidation of Ph_3M by PP. TPP: Plot of log $(a-x)$ versus time. [PP] = 0.03 M, [TPP] = 0.001 M, I = 0.36 M, t = 40°C. TPA: Plot of log $(a-x)$ versus time. [PP] = 0.0075 M, [TPA] = 0.0005 M, I = 0.2 M, $[H^+]$ = 0.02 M, t = 40°C. TPS: Plot of log O.D. versus time. [PP] = 0.003 M, [TPS] = 0.0001 M, I = 0.1 M, $[H^+]$ = 0.006 M, t = 35°C.

through the origin (Fig. 3). The constant values of $k_1/[H^+]^2$ (Table 2) also indicate the second-order dependence on $[H^+]$.

In the oxidation of TPS, a slope of 1.03 ± 0.09 (r = 0.998, s = 0.02) is obtained from the log–log plot of rate constants and $[H^+]$ (Fig. 2). Constant values of third-order rate constants are obtained, thus confirming the first-order dependence in $[H^+]$ (Table 2). Further, a good straight line (r = 0.998) passing almost through the origin is obtained (Fig. 3), showing that the reaction is completely acid dependent.

Active species

Peroxodiphosphate anion is tetranegative and is extensively protonated in acid medium. Hence, the various species[1] which are likely to be present are $P_2O_8^{4-}$, $HP_2O_8^{3-}$, $H_2P_2O_8^{2-}$, $H_3P_2O_8^-$, and $H_4P_2O_8$, and their relative concentration as a function of pH has been discussed by Crutchfield (16). In the present study, the pH has been maintained in the range 1–3, in which the three species, viz., $H_2P_2O_8^{2-}$, $H_3P_2O_8^-$, and $H_4P_2O_8$ may be present (16, 17) in solution. Hence the total concentration of PP is given by eq. [1]:

$$[1]\quad [PP]_T = [H_2P_2O_8^{2-}] + [H_3P_2O_8^-] + [H_4P_2O_8]$$

If all the three species are considered to contribute to the rate with respect to PP, the rate expression for the disappearance of PP can be represented (16–19) by eq. [2].

$$[2]\quad -\frac{d[PP]}{dt} = k_1'[H_2P_2O_8^{2-}] + k_2'[H_3P_2O_8^-] + k_3'[H_4P_2O_8]$$
$$= [PP]_T\frac{(k_1' + k_2'K_1[H^+] + k_3'K_1K_2[H^+]^2)}{1 + K_1[H^+] + K_1K_2[H^+]^2}$$

where k_1', k_2', and k_3' are the rate constants for the disappearance of $H_2P_2O_8^{2-}$, $H_3P_2O_8^-$, and $H_4P_2O_8$ respectively, and K_1 and K_2 represent the equilibrium constants for the protonation of $H_2P_2O_8^{2-}$ and $H_3P_2O_8^-$ respectively.

It is possible (18) to simplify the rate expression into eq. [3] by neglecting the second and third terms in the denominator in comparison to unity (17–19). Hence

[1] It is presumed that the same trend of pK_a values will be maintained in acetonitrile – water mixture as in water.

TABLE 2. Effect of $[H^+]$ on the oxidation of Ph_3M

Rate constants	$[H^+]$ (10^3 mol/L)					
	0.00	5.00	10.0	15.0	18.0	
TPP*						
k_1 (10^5 s^{-1})	6.12 ± 0.23	27.3 ± 0.99	53.1 ± 0.98	76.7 ± 1.0	91.6 ± 1.1	
k_3 (10^1 L^2 mol^{-2} s^{-1})		5.46 ± 0.20	5.31 ± 0.98	5.11 ± 0.68	5.09 ± 0.61	
	2.00	4.00	10.0	14.0	18.0	
TPA*						
k_1 (10^5 s^{-1})	0.32 ± 0.01	1.27 ± 0.02	7.69 ± 0.30	15.2 ± 0.31	25.9 ± 1.9	
$k_l/[H^+]^2$ (10^1 L^3 mol^{-3} s^{-1})	8.03 ± 0.25	7.94 ± 0.13	7.69 ± 0.30	7.76 ± 0.16	7.99 ± 0.59	
	2.00	4.00	6.00	8.00	12.0	18.0
TPS†						
k_1 (10^5 s^{-1})	6.18 ± 0.24	12.0 ± 0.21	18.1 ± 0.57	27.9 ± 1.4	37.8 ± 0.99	57.1 ± 1.3
k_3 (10^1 L^2 mol^{-2} s^{-1})	1.03 ± 0.04	1.01 ± 0.02	1.07 ± 0.03	1.16 ± 0.06	1.05 ± 0.03	1.06 ± 0.02

*General reaction conditions: $[PP]_0 = 0.01$ M and $[Ph_3M] = 0.001$ M in 60% acetonitrile – 40% water (v/v) mixture at 40°C at $I = 0.2$ M.
†$[PP]_0 = 0.03$ M, [TPS] = 0.0001 M at $I = 0.1$ M in 60% acetonitrile – 40% water (v/v) mixture at 35°C.

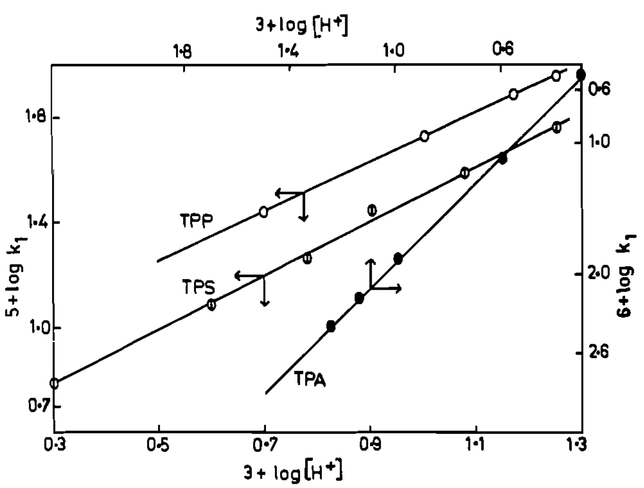

FIG. 2. Order plot for $[H^+]$. TPP: slope = 0.94 ± 0.03; r = 0.999; s = 0.003. TPA: slope = 1.99 ± 0.03; r = 0.999; s = 0.01. TPS: slope = 1.03 ± 0.09; r = 0.998; s = 0.02.

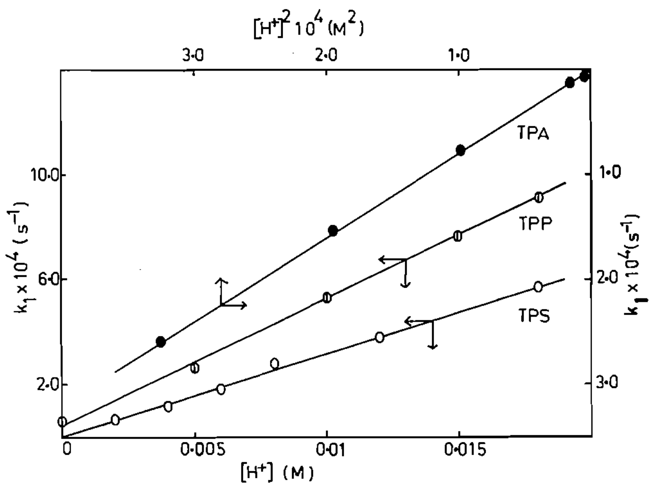

FIG. 3. Variation of k_1 with $[H^+]$ or $[H^+]^2$. TPP: r = 0.999. TPA: r = 0.999. TPS: r = 0.998.

$$[3] \quad -\frac{d[PP]}{dt} = [PP]_T\,(k_1' + k_2'K_1[H^+] + k_3'K_1K_2[H^+]^2)$$
$$= [PP]_T\, k_1 \text{ at constant } [H^+]$$

where k_1 is the pseudo first-order rate constant.

An interesting feature has been noticed here, viz., the active species in each case depends on the nature of the substrate. The nature of the active species of PP may be arrived at on the basis of the dependence of the reaction rate on $[H^+]$ and also from the plots of k_1 versus $[H^+]$ or $[H^+]^2$. The plot of k_1 versus $[H^+]$ (Fig. 3) gives a straight line with a finite intercept and eq. [3] indicates that $H_2P_2O_8^{2-}$ and $H_3P_2O_8^-$ are the active species in the oxidation of TPP. Similar analysis with Fig. 3 and eq. [3] indicates that $H_4P_2O_8$ is the active species in the oxidation of TPA. However, in the oxidation of TPS, as the least-squares analysis gives an intercept of 1.35×10^{-6} for the plot of k_1 versus $[H^+]$, the major active species will be $H_3P_2O_8^-$ with a minor contribution from $H_2P_2O_8^{2-}$.

An analysis of the dependence on $[H^+]$ and the nature of the active species of PP involved in the oxidation reveals the relative rates of oxidation[2] are TPP > TPS > TPA. An explanation for this anomalous behaviour is offered (*vide infra*).

Effect of ionic strength

In the case of TPP, there is no appreciable effect on the rate when the ionic strength is varied, while in the case of TPA and TPS the logarithm of the rate constants decreases linearly with an increase in the ionic strength of the medium (Fig. 4). The overall effect of ionic strength would be determined by eqs. [4]–[6] (*vide infra*). Steps [4] and [5] in the mechanism predict a decrease in rate with increasing ionic strength while the second-order rate constant of the rate-limiting step [6] may not be very sensitive to the change in the ionic strength since it involves a neutral species.

In the case of TPP, $H_2P_2O_8^{2-}$ is the main oxidizing species. Hence the protonation equilibria [4] and [5] do not play any role, thereby rendering the reaction insensitive to ionic strength variation. In TPA and TPS oxidations, $H_4P_2O_8$ and $H_3P_2O_8^-$

[2] We have studied the rates of oxidation of Ph_3M under identical conditions (Table 3) and the results also reveal that the relative rates of oxidation follows the same order TPP > TPS > TPA.

TABLE 3. Effect of temperature on the rate* of oxidation and activation parameters

t°C	k_2 (10^3 L mol^{-1} s^{-1}) TPP	TPA	TPS
20	20.2 ± 1.8		
25	39.4 ± 3.3	9.00 ± 0.58	19.0 ± 0.50
30	73.3 ± 3.6	13.0 ± 0.80	34.7 ± 1.6
35		20.8 ± 1.2	64.0 ± 1.9
$\Delta H^{\neq}$† (kJ mol^{-1})	92.4 ± 10.9	61.3 ± 6.54	90.1 ± 5.20
$\Delta S^{\neq}$† (J deg^{-1} mol^{-1})	38.1 ± 37.9	−78.6 ± 22.3	24.4 ± 17.7

*$[PP]_0 = 0.003$ M; $[Ph_3M]_0 = 0.0001$ M; $[H^+] = 0.006$ M; $I = 0.1$ M in 60% acetonitrile – 40% water (v/v) mixture.

†The precision of $\Delta H^{\neq}$ and $\Delta S^{\neq}$ values was calculated using the method of Petersen *et al.* (26).

respectively (formed by the protonation equilibrium steps [4] and [5]) are the active species of PP involved in the oxidation. Here the protonation constants K_1 and K_2 may decrease with increasing ionic strength, setting the same trend for the combined constants $k_2'K_1$ and $k_3'K_1K_2$ (18, 19).

The rate constants for the oxidation of Ph_3M (M = P, As, Sb) are unaffected by the presence of acrylonitrile (AN), indicating that the oxidations of Ph_3M do not involve any free radical intermediates. Since AN was found to undergo polymerization in the presence of TPP (20), an indirect method has been resorted to in order to study the effect of AN on the oxidation of TPP by PP. A blank run without PP and another with PP, TPP, and AN were carried out. Using the rate expression

$$-\frac{dx}{dt} = k[\mathrm{TPP}][\mathrm{PP}] + k_3'[\mathrm{TPP}][\mathrm{AN}]$$

the rate constant k was calculated. This compares well with the second-order rate constant obtained in the absence of AN under identical conditions. Hence it is concluded that the effect of AN on the oxidation of TPP by PP is negligible and a free-radical mechanism is ruled out.

The dependence of rate constants on temperature at constant $[H^+]$ and ionic strength was measured at three temperatures (Table 3). The activation parameters are calculated and are listed.

Mechanism and rate law

On the basis of the foregoing kinetic evidence, a general polar mechanism may be envisaged for all the triphenyl derivatives of Group V elements:

$$[4] \quad H_2P_2O_8^{2-} + H^+ \rightleftharpoons H_3P_2O_8^-$$

$$[5] \quad H_3P_2O_8^- + H^+ \rightleftharpoons H_4P_2O_8$$

$$[6] \quad Ph_3\ddot{M} + H_{4-n}P_2O_8^{n-} \xrightarrow[\text{slow and rate-determining}]{k'} \text{Intermediate} \xrightarrow[\text{fast}]{H_2O} \text{Products}$$

where n = 0, 1, or 2. For example, when n = 2,

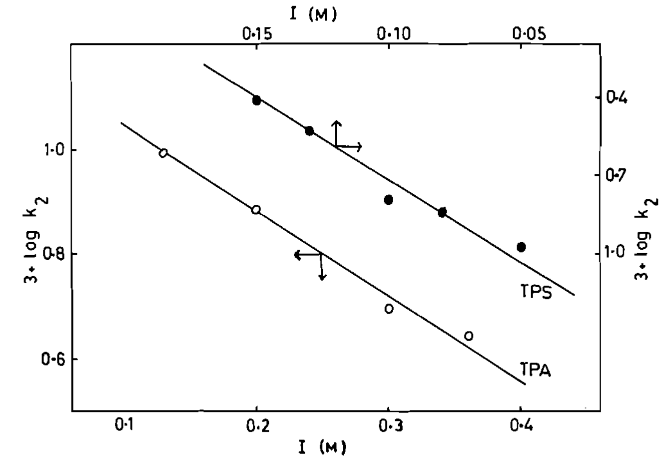

FIG. 4. Influence of ionic strength on PP oxidation of Ph_3M. TPA: r = 0.993. TPS: r = 0.978.

$$[7] \quad Ph_3\ddot{M} + H_2P_2O_8^{2-} \xrightarrow[\text{slow and rate-determining}]{k'}$$

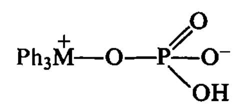

I

[8]

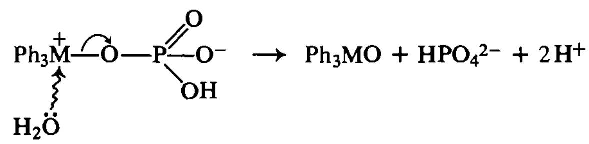

[9]

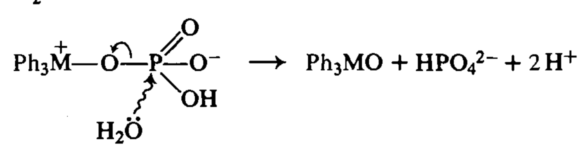

The proposed mechanism involves a bimolecular nucleophilic displacement of the substrate on the peroxide molecule in the rate-determining step [7], resulting in the formation of intermediate **I**, which then may decompose to give the oxide by the attack of water as indicated in step [8] or [9]. The question regarding the origin of the oxide oxygen, whether from solvent water or from PP, has not been solved. In a recent study (21) of the PS oxidation of TPP where the product triphenylphosphine oxide was analysed by using the ^{18}O isotope effect in ^{31}P nmr spectroscopy, it has been shown that the oxygen originates from PS.

The proposed mechanism accounts for (*i*) the second-order nature of the reaction at constant $[H^+]$ and ionic strength, (*ii*) the dependence of rate on the variation of $[H^+]$, and (*iii*) the lack of influence of acrylonitrile on the rate of oxidation. The rate law can be written as

$$[10] \quad -\frac{d[Ph_3M]}{dt} = -\frac{d[PP]}{dt} = k_2\,[Ph_3M][PP]_T$$

at constant $[H^+]$. The stoichiometry of the reaction was found to be 1 : 1 and the stoichiometric equation can be represented as

$$[11] \quad Ph_3M + H_{4-n}P_2O_8^{n-} \rightarrow Ph_3MO + 2H_{3-n}PO_4^{n-} + nH^+$$

The stoichiometric studies also confirm the proposed mechanism of the oxidation studies.

Relative reactivities

The observed order of reactivity (Table 3), TPP > TPS > TPA, is interesting because of the transposition of TPA and TPS. In the reactions of *tert*-butylhydroperoxide with Ph_3M (5, 14) and also in the PS oxidation (7) the same order of reactivity has been observed. Hiatt *et al.* (14) attribute this order to two conflicting trends, availability of *d* orbitals for π-bonding with peroxide oxygen and the Group V element-to-oxygen bond strength. The reactivity order in PS oxidation (7) has also been attributed to the above two conflicting trends.

The simultaneous considerations of the shift of electron density from the phenyl group towards the P, As, and Sb atoms via their *d* orbitals (which increases with the atomic number of M in Ph_3M) (22, 23) and the strength of the M-to-oxygen bond (the P—O bond is strong and both the As—O and Sb—O bonds are weak) (24) will account for the trend of the reactivity pattern observed in the PP oxidation. The reactivity is also in agreement with the charge density on the heteroatom in Ph_3M (25). We have determined the activation parameters under identical conditions (Table 3). The same trend of $\Delta H^{\neq}$ and $\Delta S^{\neq}$ values with TPP and TPS may be due to the involvement of the same active species in these oxidations. The repulsion between the negatively charged oxygen atom of the active species (see mechanism) and the π-electrons of the phenyl rings in the transition state may presumably be the cause of the positive entropy of activation. The absence of such a repulsion in the reaction of TPA with $H_4P_2O_8$ leads to a negative entropy of activation.

Acknowledgements

We thank Prof. N. Arumugam for helpful discussions, Prof. N. R. Subbaratnam for his interest, and Dr. M. Inbasekaran, Princeton University for a gift sample of potassium peroxodiphosphate. K. P. thanks the CSIR, New Delhi for the award of a Senior Research Fellowship.

1. R. F. HUDSON. Structure and mechanism in organophosphorus chemistry. Academic Press, London and New York. 1965. p. 4.
2. G. A. RUZUVAEV, V. A. SHUSHUNOV, V. A. DODONOV, and T. G. BRILKINA. Organic peroxides. Vol. 3. *Edited by* D. Swern. Wiley–Interscience, New York. 1972. p. 141.
3. J. I. G. CADOGEN. Q. Rev. **16**, 208 (1962).
4. R. HIATT, R. J. SMYTHE, and C. MCCOLEMAN. Can. J. Chem. **49**, 1707 (1971).
5. R. HIATT and C. MCCOLEMAN. Can. J. Chem. **49**, 1712 (1971).
6. J. I. SHULMAN. J. Org. Chem. **42**, 3970 (1977).
7. C. SRINIVASAN and K. PITCHUMANI. Int. J. Chem. Kinet. **14**, 1315 (1982).
8. C. SRINIVASAN and A. CHELLAMANI. Indian J. Chem. **23A**, 684 (1984).
9. G. S. HIERS. *In* Organic Synthesis. Coll. Vol. I. John Wiley, New York. 1956. p. 550.
10. P. D. BARTLETT and G. MEGUERIAN. J. Am. Chem. Soc. **78**, 3710 (1956).
11. A. J. SPEZIALE and L. J. TAYLOR. J. Org. Chem. **31**, 2450 (1966).
12. G. O. DOAK and L. D. FREEDMAN. Organometallic compounds of arsenic, antimony and bismuth. Wiley, New York. 1970. p. 303.
13. W. E. MCEWEN, G. H. RILES, and D. N. SCHULTZ. Phosphorus, **2**, 147 (1972).
14. R. HIATT, C. MCCOLEMAN, and G. R. HOWE. Can. J. Chem. **53**, 559 (1975).
15. H. H. JAFFE. J. Chem. Phys. **22**, 1430 (1954).
16. M. M. CRUTCHFIELD. Peroxide reaction mechanisms. *Edited by* J. O. Edwards. Interscience, New York. 1962. p. 41.
17. S. KAPOOR and Y. K. GUPTA. J. Chem. Soc. Dalton Trans., 862 (1977).
18. C. SRINIVASAN, P. KUTHALINGAM, and N. ARUMUGAM. J. Chem. Soc. Perkin Trans. 2, 170 (1980).
19. C. SRINIVASAN and S. RAJAGOPAL. React. Kinet. Catal. Lett. **12**, 45 (1979).
20. M. M. BAIZER and J. D. ANDERSON. J. Org. Chem. **30**, 1357 (1965).
21. J. M. RISLEY and R. L. VAN ETTEN. Int. J. Chem. Kinet. **16**, 1167 (1984).
22. T. P. DEBIES and J. W. RABALAIS. Inorg. Chem. **13**, 308 (1974).
23. G. DISTEFANO, S. PIGNATARO, L. SZEPES, and J. BOROSSAY. J. Organomet. Chem. **102**, 313 (1975).
24. N. P. BORISOVA and L. N. PETROV. Zh. Strukt. Khim. **13**, 701 (1972).
25. R. T. SANDERSON. Inorganic chemistry. Affiliated East–West Press Pvt. Ltd, New Delhi. 1971. p. 391.
26. R. C. PETERSEN, J. H. MARKGRAF, and S. D. ROSS. J. Am. Chem. Soc. **83**, 3819 (1961).

Physical changes in $BaSO_4$ caused by K^+ and Fe^{3+} ions

L. V. HALEY, T. A. MATTIOLI, AND D. R. WILES
Chemistry Department, Carleton University, Ottawa, Ont., Canada K1S 5B6

Received October 10, 1984

L. V. HALEY, T. A. MATTIOLI, and D. R. WILES. Can. J. Chem. **63**, 2290 (1985).

The effects of coprecipitated K^+ and Fe^{3+} ions on the nature of freshly precipitated $BaSO_4$ were studied. The presence of K^+ in the precipitate is seen to have a pronounced effect on crystal habit and increases the specific surface area of the crystals. Micro-Raman measurements show a progressive shift in the SO_4^{2-} ν_1 band for precipitates doped with potassium. This shift is seen to be a linear approach toward the ν_1 frequency of K_2SO_4. X-ray diffraction studies indicate no marked changes in cell parameters but do reveal changes in relative intensities in the diffraction patterns of potassium-doped precipitates. In the concentration ranges studied, ferric ions show no marked changes in any of the above properties. The changes are interpreted as being due to the formation of solid solution of potassium with barium sulphate, while iron is adsorbed onto the crystal surfaces. This is seen as a novel use of micro-Raman spectroscopy in the study of doped crystals.

L. V. HALEY, T. A. MATTIOLI et D. R. WILES. Can. J. Chem. **63**, 2290 (1985).

On a étudié les effets des ions K^+ et Fe^{3+} coprécipités sur la nature du $BaSO_4$ fraîchement précipité. La présence de K^+ dans le précipité semble provoquer un effet important sur les habitudes des cristaux et semble augmenter la surface spécifique des cristaux. Des mesures de micro-Raman permettent de mettre en évidence un déplacement progressif de la bande ν_1 des SO_4^{2-} dans les précipités dopés au potassium. On croit que ce déplacement présente une approche linéaire avec la fréquence ν_1 du K_2SO_4. Des études par diffraction des rayons-X n'indiquent pas de changements importants dans les paramètres de la cellule; on note toutefois des changements dans les intensités relatives des patrons de diffraction des précipités dopés au potassium. A l'intérieur des limites de concentration étudiées, les ions ferriques ne semblent pas provoquer des changements importants dans les propriétés mentionnées plus haut. On interprète les changements en fonction d'une formation de solutions solides de potassium avec le sulfate de baryum alors que le fer serait adsorbé sur les surfaces cristallines. On croit que ceci est une nouvelle méthode d'utiliser la spectroscopie micro-Raman pour étudier des cristaux dopés.

[Traduit par le journal]

Introduction

Recent studies on the use of $BaSO_4$ as a carrier in ^{230}Th determination have shown that $BaSO_4$ is an effective carrier for traces of thorium (1), but only if a sufficient quantity of potassium is present in the precipitation solution. Preliminary studies have shown (2) that both surface area and surface activity were affected by the presence of K^+ in the crystals themselves. The effect of ferric ions on the carrying of thorium with $BaSO_4$ was shown (1) to be one of suppression but up until now the properties of iron-doped $BaSO_4$ have not been studied in order to account for this interference. The present study applies Raman spectroscopy in a novel fashion, as well as electron microscopy and X-ray diffraction, to assist in discovering the nature of the influences of K^+ and Fe^{3+}.

It is known that K^+ ions and Fe^{3+} (and Fe^{2+}) ions coprecipitate with barium sulphate (3, 4). If this is so, then clearly the nature of the resultant precipitate will be altered as it will possess physical and chemical properties different from those of the pure precipitate. For instance, it is generally accepted that the coprecipitation of K^+ with barium sulphate is probably due to mixed crystal formation (3) while the Fe^{3+} coprecipitates with barium sulphate via adsorption processes (4). The possibility that potassium forms mixed crystals with barium sulphate was also recognized by Walton and Walden (5) using precision X-ray diffraction techniques and also by Ambe and Lieser (6) who were studying the coprecipitation of K^+ and Th^{4+} with $BaSO_4$.

With these different coprecipitation mechanisms, the effects of each cation upon certain properties of barium sulphate are not expected to be similar or occur to the same extent. For instance, a cation which is actually incorporated into the crystal lattice is expected to change the properties of the resulting precipitate markedly since its incorporation will cause structural changes in the crystal. The same cannot be said for impurities which are merely adsorbed or occluded in the crystal since they should not affect the fundamental structure of lattice.

The present study attempts to show that the analytical and other effects of potassium in $BaSO_4$ are symptoms of a more fundamental change in the crystal lattice. The formation of mixed crystals of K^+ with $BaSO_4$ results in changes in the precipitate's crystal habit, surface area, X-ray diffraction patterns, and Raman spectral properties. The coprecipitation of Fe^{3+} ions with $BaSO_4$ results in very small, if any, observable changes in the above mentioned properties. This is consistent with an adsorption or occlusion mechanism. The results of studies on other properties such as isotopic exchange behaviour (7) and K^+ and Fe^{3+} coprecipitation behaviour (8) are consistent with those presented here but are discussed elsewhere.

During the course of this study, we have investigated the effects of a solid solute on the Raman spectrum of a solid. This novel application of micro-Raman spectroscopy shows promise of being widely applicable to the study of coprecipitation phenomena.

Experimental

Materials

All reagents used were of the highest available purity and were used without further purification. Barium sulphate crystals were prepared by the addition of 50 mg Ba^{2+} and 2.0 mL of 9 *M* H_2SO_4 to a stirred 100 mL solution 0.1 *M* in HNO_3, and held constant at 25.0°C. The crystals were filtered on a 0.45 μm membrane (Gelman DM-450) and washed with 0.1 *M* HNO_3 and with distilled water. Potassium and ferric ion was added as needed to the solution prior to the addition of H_2SO_4. The concentrations of potassium and iron in the crystals were determined by direct analysis (7).

Raman spectroscopy

The spectroscopic studies were done on small samples mounted on a microscope slide under the 4880.0 Å beam of an argon ion laser. The beam was focussed through a Zeiss–Winkel microscope down to a

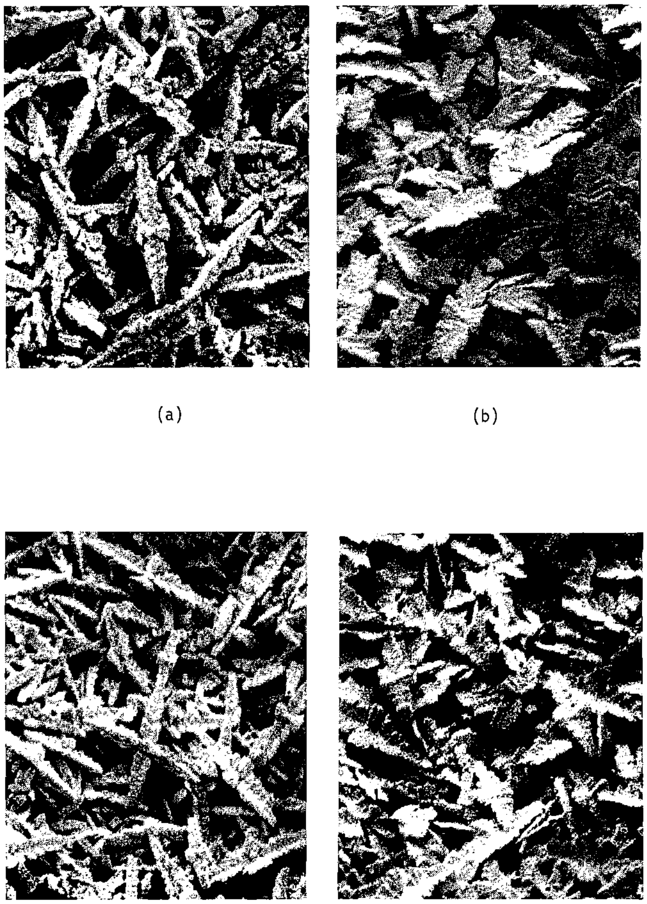

(a) (b) (c) (d)

FIG. 1. Electron micrographs (× 3000) of $BaSO_4$ crystals freshly precipitated from 0.1 *M* HNO_3 plus (*a*) nothing, (*b*) K^+ 5×10^{-3} *M*, (*c*) Fe^{3+} 5×10^{-3} *M*, (*d*) K^+ and Fe^{3+}, both 5×10^{-3} *M*.

diameter of about 1 μm. This gave the opportunity to scan various regions of small crystals which, though not essential to the present work, enabled us to examine several portions of the crystals to check for inhomogeneities. The technique is more fully described elsewhere (9, 10).

The ν_1 band of SO_4^{2-} was selected for this study because of its prominence and because it was found to display an obvious dependence on potassium concentration. Quantitative determination of the spectral parameters was done using a Hewlett-Packard 9111A graphics digit tablet connected to a Hewlett-Packard 9836 minicomputer.

Results and discussion

Crystal habit

It is well known that the conditions of precipitation of an ionic solid greatly affect the appearance or habit of the crystals formed. Particularly, it is known (11) that the presence of foreign ions influences crystal habit. It has been pointed out by Walton (12) that foreign ions which are known to form mixed crystals with the precipitate being formed caused definite changes in habit modification and that, in general, ions which are only adsorbed onto the crystal surface do not cause major changes in habit.

Scanning electron micrographs show quite clearly that potassium ions have a pronounced effect upon the morphology of $BaSO_4$ crystals (2). This has been confirmed in the present work. Fig. 1*a* shows a representative electron micrograph of

TABLE 1. Lattice parameters of $BaSO_4$ precipitates*

Sample	*a*	*b* (±0.01 Å)	*c*	Volume (±0.5 Å^3)
1	7.155	8.881	5.451	346.37
2	7.162	8.901	5.449	347.42
3	7.156	8.891	5.438	345.99
4	7.158	8.884	5.453	346.70
5	7.156	8.892	5.446	346.54
6	7.151	8.886	5.442	345.83
7	7.156(3)	8.811(4)	5.4541(3)	346.65
K_2SO_4(II)	7.456	10.08	5.776	434.10

*Sample descriptions: 1, $BaSO_4$ — 10 mg of Ba^{2+} in 100 mL 0.1 *M* HNO_3 precipitated with 2 mL of 9 *M* H_2SO_4; 2, same as 1 except p[K^+] = 1.5; 3, same as 1 except p[K^+] = 0.0; 4, same as 1 except p[Fe^{3+}] = 2.3; 5, same as 1 except p[Fe^{3+}] = 1.5; 6, same as 1 except p[Fe^{3+}] = 0.0; 7, N.B.S. standard: $BaCO_3$ treated with H_2SO_4; excess H_2SO_4 was fumed off and the sample was annealed overnight at 690°C.

barium sulphate crystals precipitated from 0.1 *M* HNO_3 solution (10 mg Ba^{2+} per 100 mL of solution). The crystal habit is the same as that reported by Fischer and Rheinehammer (11) for the precipitation conditions used. The effect of potassium ions at $pK^+ = 2.3$ is seen in Fig. 1*b* to increase lateral growth from the main axis of the crystal. It also appears that dendritic growth is increased as well as particle size and, perhaps, specific surface area.

The effect of ferric ions is not as pronounced as those of potassium. The electron micrograph in Fig. 1*c* shows $BaSO_4$ crystals precipitated in the presence of ferric ions. Here the Fe(III) concentrations were comparable to those of potassium ions in the solution from which the crystals in Fig. 1*b* were formed. The precipitate formed in the presence of ferric ions (p[Fe^{3+}] = 3.0 in solution) closely resembles the precipitate formed in the absence of K^+ and Fe^{3+} ions, and in fact, are almost indistinguishable. It is interesting to note that at the same concentration of potassium ions (i.e. p[K^+] = 3.0 in solution) Burk and Wiles (2) were still able to observe changes in the crystal habit.

As a note of further interest, the effects of the ferric ions on morphology may be examined in a different manner. When both K^+ and Fe^{3+} are present in solution, the crystal of the resulting precipitate (Fig. 1*d*) is changed in the manner consistent with potassium ions (Fig. 1*b*), although it is seen that the change in crystal habit due to potassium ions is not as pronounced when ferric ions are also present in solution.

Surface area measurement

As we previously mentioned, the potassium-doped $BaSO_4$ crystals appeared on visual inspection of the photomicrographs to possess a greater specific area than did the undoped crystals. To confirm this visual observation, the surface area of various $BaSO_4$ preparations were measured. The results are given below:

Sample	Surface area (m^2 g^{-1})
$BaSO_4$ (no added K^+ or Fe^{3+})	1.9±0.2
$BaSO_4$ (p[K^+] = 1.6)	3.6±0.1
$BaSO_4$ (p[Fe^{3+}] = 2.0)	1.8±0.2

The values in the parentheses indicate the cation concentration in the precipitation solution. Measurements were made using the Micrometrics Model 2200 High Speed Surface Analyser employing the BET method. Purified N_2 gas was used

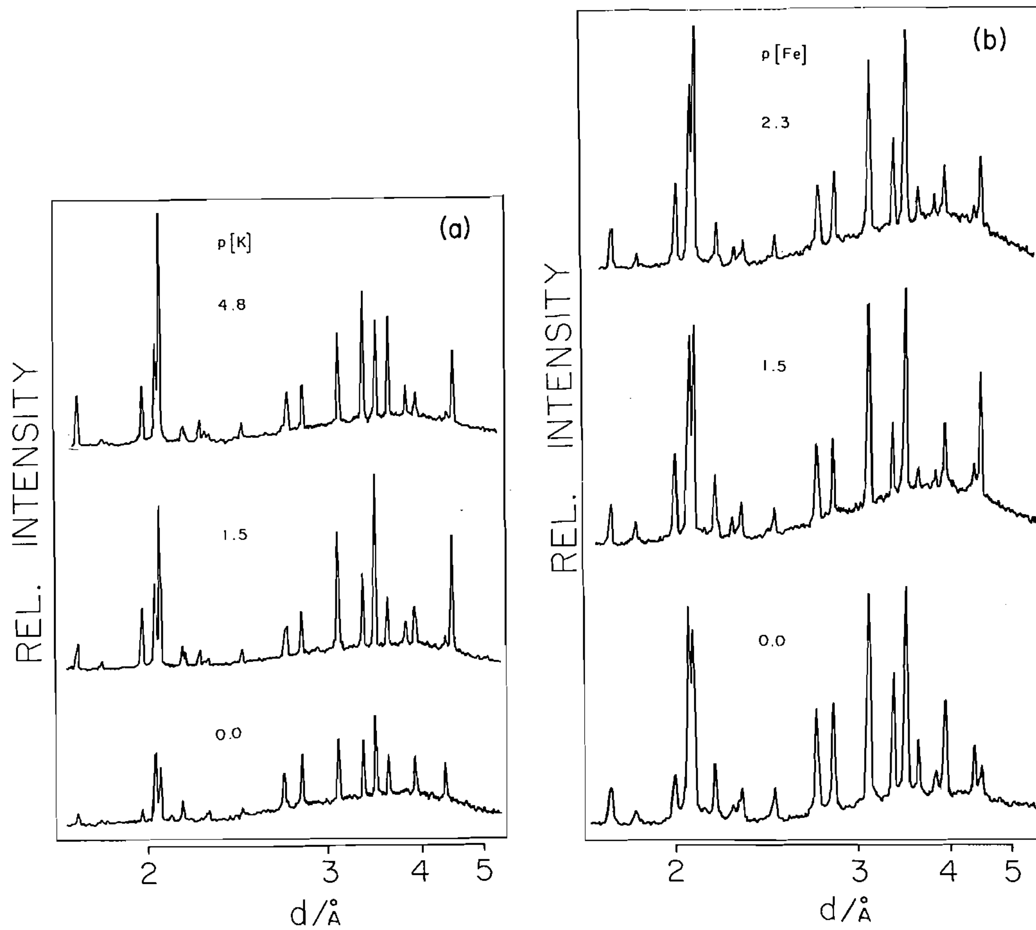

FIG. 2. (*a*) X-ray diffract ion patterns for K^+-doped $BaSO_4$. The values of p[K^+] in the precipitating solutions and given in the Figure. (*b*) X-ray diffraction patterns for the Fe^{3+}-doped $BaSO_4$. The values of p[Fe^{3+}] in the precipitating solutions are given in the figure.

as the adsorbent.

The above data clearly show that the presence of potassium results in a precipitate with greater surface area, while the presence of ferric ions is seen to have only a negligible effect on the surface area.

X-ray diffraction study

The X-ray diffraction patterns obtained for various barium sulphate precipitates containing potassium and ferric ions showed no lines other than those of barium sulphate. This corroborates observations made by Ambe and Lieser (6). Table 1 lists the observed lattice parameters and unit cell volumes of various barium sulphate precipitates.

Since K^+ ions have nearly the same ionic radii as barium ions, 1.33 Å and 1.34 Å, respectively, one would expect the lattice parameters of the potassium-doped barium sulphate to remain essentially the same if the simplistic replacement of one K^+ for one Ba^{2+} is assumed. For ferric ion, however, the ionic radius is considerably smaller than that of barium (0.64 Å for Fe^{3+} as compared to 1.34 Å for Ba^{2+}). Thus, if Fe^{3+} ions were becoming incorporated into the $BaSO_4$ lattice, one would expect changes in the lattice parameters.

It is clear from Table 1 that no trend is shown in the lattice parameters for the iron-doped precipitates. Any variation is within the expected uncertainty limits. While no conclusion can be drawn with any confidence, the results are again consistent with the anticipated effects of potassium ions being in the lattice, but not iron.

The respective diffraction patterns are given for visual comparison in Fig. 2. Although new lines were not observed, changes in their relative intensities are quite evident for those precipitates containing potassium (Fig. 2*a*). The iron-doped precipitates, on the other hand, gave patterns whose relative intensities did not show marked changes (Fig. 2*b*). To prove that the changes in relative intensities were not due to sample preparation, two separate samples were prepared and each sample was rotated 90° within the diffractometer. These precautions did not change the relative intensities of the pattern lines, verifying that the observed effect was not an artifact introduced through the sample preparation.

Structure factors were calculated for those planes which, according to Fig. 2*a*, seemed to show significant changes in intensity. These structure factors did not reveal any structural regularity and thus failed to indicate preference of certain planes for potassium substitution. The intensity changes were therefore interpreted as being due to changes in crystal habit. This interpretation is supported by the electron micrographs which were discussed above. The virtual absence of fluctuations in line intensities of the iron-doped precipitates is also consistent with this interpretation. Isotopic-exchange data (2, 7) indicate that the number of Ba^{2+} exchange sites in K^+-doped $BaSO_4$ is greater than can be explained by the increase in surface area which suggests crystallographic faces which are rich in Ba^{2+} sites are being exposed to greater degrees.

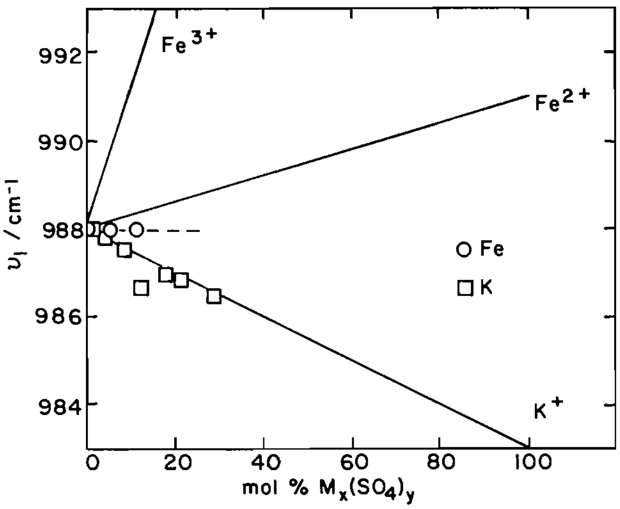

FIG. 3. Raman frequencies of the SO_4^{2-} ν_1 lines in $BaSO_4$ crystals as a function of mole percent K^+ and Fe^{3+}. See the text for a brief discussion of the anomalous point.

Micro-Raman spectroscopy study

Line frequencies in the Raman spectrum of an ion such as SO_4^{2-} will be sensitive to the electrostatic environment in the lattice which, in turn, will depend on the extent of randomly spaced substitute cations. While a mixture of $BaSO_4$ and K_2SO_4 crystals will give the two superimposed spectra, the spectrum of a true solid solution of K_2SO_4 in $BaSO_4$ should show the effect of a weighted average lattice. One can envisage various types of behaviour of the line frequency as a function of concentration. Most simply is the direct linear relationship as in this study. More likely, especially if the ionic sizes are less closely similar, will be a positive or negative deviation from the straight line. Furthermore, one can expect discontinuous behaviour when the limit of solid solubility has been exceeded with probable strong deviations just before and after the discontinuity. Finally, one can expect no change in the Raman frequencies in cases where the impurity remains in a phase distinct from the major lattice.

The observed Raman spectra for potassium-doped $BaSO_4$ crystals showed a marked shift in the frequency of the ν_1 vibrational mode of the SO_4^{2-} ion. The shift appeared to be essentially a linear function of the concentration of potassium present in the crystals for the concentration ranges studied. The results for the iron-doped $BaSO_4$ crystals were quite different, in that the ν_1 band frequency was essentially unaffected by the presence of Fe^{3+} in the precipitate.

These frequency data are plotted in Fig. 3. In this figure, three hypothetical straight lines are given which join the SO_4^{2-} ν_1 frequencies of pure $BaSO_4$ with those in pure K_2SO_4, $FeSO_4.H_2O$ and $Fe_2(SO_4)_3.H_2O$, respectively. It is evident from this diagram that the relationship is convincingly linear for the $BaSO_4-K_2SO_4$ system. The $Ba(Fe)SO_4$ data, on the other hand, show no distinct change of frequency and are not at all close to the $BaSO_4-FeSO_4$ line or to the $BaSO_4-Fe_2(SO_4)_3$ line. It is clear, therefore, that the two dopant ions interact differently with the lattice, in agreement with conclusions drawn from other experiments as described above. Potassium seems to be present in the lattice as a direct replacement for Ba^{2+} while Fe^{3+} is not. The only conjecture which can be made about the iron is that it may be adsorbed on the surface, or perhaps occluded as a separate impurity phase.

We wish to draw attention to the one point in Fig. 3 whose value puts it well below the straight line. That particular sample showed anomalous behaviour in several ways and tempted us to look for a sharp discontinuity at this composition. Since the data on both sides are directly on the proper straight line, it may rather be that the analytical data are in error. For the present we can only speculate as to whether the point as it is shown is real or not.

If the effect described here is general, and it is found that mixed crystals produced by coprecipitation always display a Raman spectrum whose line frequencies are simple functions of the mole fraction of impurity cations, then a new method will be available to investigate the nature of coprecipitated ions. This will be of considerable interest in analytical chemistry, radiochemistry, preparative inorganic chemistry, mineralogy, and in other areas of solid state chemistry. We expect to publish further reports on this subject in the near future.

Summary

Precipitates of barium sulphate containing potassium show changes in properties such as morphology and specific surface area whereas those containing iron do not, at least to the same extent, under the conditions used.

Raman data show structural changes in potassium-doped $BaSO_4$ which X-ray diffraction data could not. The progressive shift in the ν_1 frequency of the SO_4^{2-} ion suggests that mixed crystal formation is occurring. The invariance of the ν_1 frequency for iron-doped precipitates indicates that iron is present in such a manner which does not detectably affect the SO_4^{2-} environment and that solid solution is not occurring. It is suggested that this provides a new tool for the study of doped or contaminated crystals.

The state of the iron impurities is less certain than that of potassium. It can be said, however, that iron is present in such a manner as not to alter the SO_4^{2-} environment in the lattice which excludes the possibility of mixed crystal formation or incorporation into the $BaSO_4$ lattice. We conclude that the iron is adsorbed or occluded within the crystals.

Acknowledgements

We are grateful to Professors G. Y. Chao and J. A. Koningstein for the use of their X-ray and Raman spectrometers, respectively, and for helpful discussions and to Professor R. G. Barradas for the use of his computing facilities. The work was supported by the Natural Sciences and Engineering Research Council of Canada and by Carleton University.

1. R. C. BURK, I. G. DE JONG, and D. R. WILES. J. Radioanal. Chem. **78**, 81 (1983).
2. R. C. BURK and D. R. WILES. J. Radioanal. Chem. **79**, 185 (1983).
3. A. WINZER and R. GEYER. Z. Chem. **17**, 116 (1977).
4. A. GEYER and R. WINZER. Neue Hütte, **21**, 49 (1976).
5. G. WALTON and G. H. WALDEN, JR. J. Am. Chem. Soc. **68**, 1742 (1946).
6. S. AMBE and K. H. LIESER. Radiochim. Acta, **25**, 93 (1978).
7. T. MATTIOLI and D. R. WILES. To be published.
8. T. MATTIOLI and D. R. WILES. Inorg. Chim. Acta. In press.
9. L. V. HALEY, I. W. WYLIE, and J. A. KONINGSTEIN. J. Raman Spectrosc. **13**, 203 (1982).
10. B. W. COOK and J. D. LOUDEN. J. Raman Spectrosc. **8**, 279 (1979).
11. R. B. FISCHER and R. B. RHINEHAMMER. Anal. Chem. **25**, 1544 (1953).
12. A. G. WALTON. The formation and properties of precipitates. Wiley and Sons, New York. 1967. p. 151.

Sulfur trioxide sulfonation of the five alkanonaphthalenes acenaphthene, perinaphthane, 1,2,3,6,7,8-hexahydropyrene, 5,6,7,8-tetrahydrocyclohepta-acenaphthene, and 1,2,3,4,7,8,9,10-octahydrodicyclohepta[*de,ij*]naphthalene[1]

PETER DE WIT AND HANS CERFONTAIN[2]
Laboratory for Organic Chemistry, The University of Amsterdam, Nieuwe Achtergracht 129, 1018 WS Amsterdam, The Netherlands

AND

ALFRED FISCHER
Department of Chemistry, University of Victoria, Victoria, B.C., Canada V8W 2Y2

Received November 26, 1984

PETER DE WIT, HANS CERFONTAIN, and ALFRED FISCHER. Can. J. Chem. **63**, 2294 (1985).

The mono- and di-sulfonation of the 1,8-alkano- and 1,8:4,5-dialkano-naphthalenes **1–5** with SO_3 in dioxane and nitromethane as solvent have been studied and the results compared with those of 1,8-di- (**6**) and 1,4,5,8-tetramethylnaphthalene (**7**). The most reactive position of 1,8-ethano- (**1**), 1,8-propano-naphthalene (**2**), and **6** is the 4-position. Sulfonation adjacent to the 1,8-ethano bridge can be effected with SO_3 in dioxane as reagent, whereas sulfonation *ortho* to the longer alkano bridges requires the more reactive reagent SO_3 in nitromethane. Disulfonation of the 1,8:4,5-dialkanonaphthalenes **3–5** leads to the predominant formation of the "noncrossed" (i.e. the 2,7-) disulfonic acid due to the substituent effect of the 2-sulfonic acid group. The isomer distribution data for the sulfonation of the arenes and their monosulfonic acids show that the steric hindrance increases in the order ethano $\ll$ propano $\leq$ butano and propano $<$ *peri* dimethyl.

PETER DE WIT, HANS CERFONTAIN et ALFRED FISCHER. Can. J. Chem. **63**, 2294 (1985).

Opérant dans le dioxanne et dans le nitrométhane comme solvants, on a étudié les mono- et di-sulfonations des alkano-1,8 et dialkano-1,8:4,5 naphtalènes (**1–5**) par le SO_3; on compare les résultats avec ceux obtenus antérieurement avec les diméthyl-1,8 et tétraméthyl-1,4,5,8 naphtalènes (**6** et **7**). La position la plus réactive des éthano-1,8 (**1**), propano-1,8 (**2**) et diméthyl-1,8 (**6**) naphtalènes est la position 4. On peut effectuer une sulfonation sur la position adjacente du pont éthano-1,8 si l'on opère avec du SO_3 dans le dioxanne; toutefois, pour effectuer des sulfonations en *ortho* des ponts alkano plus longs on doit utiliser du SO_3 dans le nitrométhane qui est un réactif plus énergique. La disulfonation des dialkano-1,8:4,5 naphtalènes **3–5** conduit à la formation préférentielle de l'acide disulfonique "non croisé" (comme le -2,7) à cause de l'effet de substituant du groupement acide sulfonique-2. Les données sur la distribution des isomères pour la sulfonation des arènes et de leurs acides monosulfoniques montre que l'empêchement stérique augmente dans l'ordre suivant: éthano $\ll$ propano $\leq$ butano et propano $<$ *péri*-diméthyle.

[Traduit par le journal]

On disulfonation of 1,4-di-, 1,5-di-, 1,4,5-tri-, and 1,4,5,8-tetramethylnaphthalene there is a strong preference for the formation of the "noncrossed" 2,7-disulfonic acid over the "crossed" 2,6-disulfonic acid (2, 3). This was explained in terms of a larger degree of destabilization of the σ-complex for the sulfonation of the 6- than of the 7-position of the 2-sulfonic acid, due to the strong electron-withdrawing effect of the sulfo group (3, 4). In order to obtain more information on the factors governing the formation of the "crossed" and "noncrossed" disulfonic acids, we have extended our studies on the sulfonation of polymethylnaphthalenes (2, 3) to a series of alkanonaphthalenes, viz. acenaphthene (**1**), perinaphthane (**2**), 1,2,3,6,7,8-hexahydropyrene (**3**), 5,6,7,8-tetrahydrocyclohepta-acenaphthene (**4**), and 1,2,3,4,7,8,9,10-octahydrodicyclohepta[*de,ij*]naphthalene (**5**).[3]

Results

The hydrocarbons **1–5** have been sulfonated with SO_3 in $[^2H_8]$dioxane and (or) $[^2H_3]$nitromethane or nitromethane. The resulting sulfo products were assigned on the basis of the ^1H nmr data listed in Table 1. The sulfonic acid product compositions for the various sulfonations are collected in Table 2, together with those of 1,8-dimethylnaphthalene (**6**) (2) for comparison. The very predominant formation of the 2,7-disulfonic acid with **4** and **5** was further substantiated by 250-MHz ^{13}C nmr spectroscopy of the isolated dipotassium salts. The disulfonate of **5** showed ten signals (viz. at 139.9, 139.3, 139.1, 137.5, 137.0, 125.4, 33.5, 29.6, 25.7, and 25.0 ppm), whereas the 2,6-isomer would exhibit only nine signals. Similarly the disulfonate of **4** exhibits nine signals (viz. at 145.8, 143.1, 141.9, 136.3, 135.8, 127.7, 34.4, 33.1, and 28.8), illustrating the formation of a "non-crossed" disulfonate (the "crossed" isomer would exhibit sixteen signals). In view of steric hindrance (see later), the sulfonation will be very much slower adjacent to the seven- than to the five-membered ring,

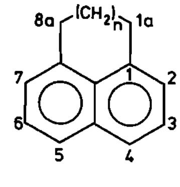

1 n = 0
2 n = 1

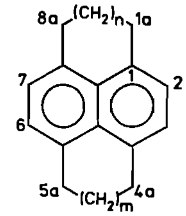

3 n = m = 1
4 n = 0; m = 2
5 n = m = 2

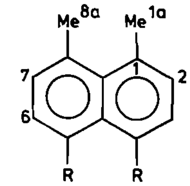

6 R = H
7 R = Me

[1] Aromatic sulfonation, part 95. Preceding paper: see ref. 1.
[2] Author to whom correspondence may be addressed.
[3] In view of the objective of the present study, the compounds **1–5** are considered substituted naphthalenes. For reasons of convenience, the aromatic ring positions of the sulfonic acid products have been numbered as for the parent alkanonaphthalenes.

TABLE 1. ^{1}H nuclear magnetic resonance chemical shifts (ppm) of the potassium sulfonates of **1**–**5**[a, b]

Hydrocarbon	Position of SO_3^-	Methylene hydrogens								Aromatic hydrogens					
		1a	1b	4a	4b	5a	5b	8a	8b	2	3	4	5	6	7
1	2	3.52						3.37			7.78	7.55	7.48	[c]	[c]
	4	3.16						3.16		7.30	7.97		8.15	7.61	7.19
	2,4	3.30						2.72			8.41		8.03	7.33	6.72
	2,5	3.30						2.72			8.03	8.33		7.91	6.79
	2,4,7	3.74						3.74			8.59		[d]	[d]	
2	4	2.82	1.73					2.82		7.16	7.80		8.25	7.38	7.07
	2,4	3.23	1.68					2.64			8.42		8.25	7.36	7.01
	2,5	3.23	1.68					2.64			7.83	8.40		7.95	6.94
3	2	3.44	1.98	2.80	1.80	2.66		2.92			7.73			7.23	7.58
	2,6	3.53	2.08	3.10	2.08	3.53		3.10			7.88				7.88
	2,7	3.60	2.20	2.92	1.80	2.92		3.60			7.88			7.88	
4	2	3.76		3.39	2.19	3.39	2.19	3.50			7.67			7.43	7.36
	3									7.86					
	2,7	3.30		2.65	1.51	2.65	1.51	3.30			7.25			7.25	
5	2,6	3.20	1.70	2.86	1.47	3.20	1.70	2.86	1.47		7.53				7.53
	2,7	3.23	1.70	2.64	1.47	2.64	1.47	3.32	1.70		7.49			7.49	

[a] $[^2H_2]O$ was used as solvent, except for the 2-sulfonic acid of **4** which was recorded in $[^2H_8]$dioxane.
[b] The $J_{1,2}$ coupling constants for the methylene hydrogens were 6.0–7.0 Hz and for the aromatic ones 8.0–9.0 Hz.
[c] The 6- and 7-H absorb in the region of the 2- and 7-H of the 5-sulfonate.
[d] The 5- and 6-H absorb in the region of the low field signals of the 2,4- and 2,5-disulfonates.

TABLE 2. Sulfonic acid product composition for the sulfonation of **1**–**6**

Substrate	Reagent[a] (equiv.)	Temp (°C)	Reaction time (min)	Reaction conditions[b]	Substrate conversion (%)	Product composition (%)[c]				
1	A (1.0)	15	60	P	>98	2(20)	4(80)			
	B (1.0)	10	300	P	81	2(<2)	4(76)	2,4(11)	2,5(13)	
	B (3.0)	20	45	P	>98			2,4(42)	2,5(55)	2,4,7(3)
	D (1.0)	20	10	R	>95	2(12)	4(88)			
2	A (1.0)	25	50	P	5		4(>96)			
			1400	P	44		4(>96)			
	A (4.0)	25	50	P	35		4(>96)			
			1600	P	97		4(>96)		2,5(≤3)	
	C (1.0)	0	30	R	85		4(83)	2,4(3)	2,5(14)	
	C (4.0)	0	20	R	>95			2,4(27)	2,5(73)	
3	C (1.0)	0	30	Q	57	2(25)		2,6(8)	2,7(67)	
	C (1.9)	0	30	Q	>95	2(7)		2,6(10)	2,7(83)	
4	A (2.0)	25	30	P	95	2(>97)	3(0.7)			
	C (4.0)	25	30	R	>95			2,6(<2)	2,7(>98)	
5	C (4.0)	25	30	R	>95			2,6(13)	2,7(87)	
6[d]	B (1.0)	0	50				4(95)			
	B (3.0)	12	50					2,4(20)	4,7(80)	

[a] A–D stand for SO_3 in $[^2H_8]$dioxane, SO_3 in nitromethane, SO_3 in $[^2H_3]$nitromethane, and trimethylsilyl chlorosulfate (5), respectively.
[b] P, Q, and R stand for homogeneous, heterogeneous due to the limited substrate solubility, and heterogenous due to precipitation of sulfonic acid products.
[c] The first number gives the position(s) of the sulfo substituent(s) and the one in parentheses the relative yield in %.
[d] See ref. 2.

rendering the formation of the 3,6-disulfonate as alternative for the assigned 2,7-isomer highly improbable.

The substrates **3** and **5** did *not* react with SO_3 in dioxane at 25°C over a period of 27 h.

The isomer distributions of the disulfonic acids on sulfonation of the various arenemonosulfonic acids, estimated from the product composition of Table 2, are collected in Table 3, together with reported data for 1,8-dimethylnaphthalene-4-sulfonic acid and 1,4,5,8-tetramethylnaphthalene-2-sulfonic acid.

Discussion

Arenemonosulfonation

The partial rate factor ratio f_2/f_4 for the sulfonation of acenaphthene (**1**) with SO_3 in dioxane as reagent is 0.25 and with trimethylsilyl chlorosulfate 0.14 (Table 2). These values are comparable to the value obtained with chlorosulfuric acid in nitrobenzene at 0°C (~0.3, based on 75% of isolated 4-sulfonic acid) (refs. 6–8), but are significantly smaller than that obtained using 95% H_2SO_4 as reagent at 25°C (2.1) (ref. 8).[4] The large dependence of the f_2/f_4 ratio on the nature of the reagent was also observed for the bromination of **1**, the degree of 2-substitution varying from 3.2 to 32.4% (ref. 11). The higher reactivity of the 4- as compared with the 2-position was also observed in protiodetritiation, f_2/f_4 being 0.37 (refs. 12–14),

[4] For toluene, f_2/f_4 is also much greater for 95.8% H_2SO_4 as reagent (1.69) (ref. 9) than for SO_3 in nitromethane (0.13) (ref. 10).

TABLE 3. Isomer distribution of the disulfonic acids formed by sulfonation of the sulfonic acids of **1**–**6**[a]

Substrate	Sulfonation isomer distribution (%)[b]	
1-2-SO_3H	2,4(46)	2,5(54)
1-4-SO_3H	2,4(42)	4,7 = 2,5(58)
2-4-SO_3H	2,4(27)	2,5(73)
3-2-SO_3H	2,6(11)	2,7(89)
4-2-SO_3H	2,6(<2)	2,7(>98)
5-2-SO_3H	2,6(13)	2,7(87)
6-4-SO_3H[c]	2,4(20)	4,7 = 2,5(80)
7-2-SO_3H[d]	2,6(5)	2,7(95)

[a]For the sulfonation conditions, see Table 2.
[b, c]See footnotes *c* and *d* of Table 2, respectively.
[d]See ref. 4.

for which reaction there is no evidence whatsoever of any steric hindrance (15), and was further observed in the nitration with nitric acid and in acetic anhydride (16) and the chlorination with chlorine in carbon tetrachloride – acetic acid (17). The f_2/f_4 ratios are rather similar for the chlorination (17) of **1**, **2**, and **6**, as are the f_2/f_4 ratios for the bromination of these three substrates (11).

The absence of sulfonation of the 2-position with **2** and **6** is ascribed to steric hindrance,[5] the C(1a)—C(1)—C(2) angle of **1** and **6** being 132.8 and 116.2° respectively (11), whereas that of **2** is in between these two extremes (12).

The argument of steric hindrance also explains the observation that SO_3 in *dioxane* leads to 2-substitution – i.e. adjacent to the alkano bridge – only with **1** and **4**, both of which contain an 1,8-ethano bridge. In fact, **3** and **5** are unreactive towards SO_3 in dioxane, and **2** gives only 4-substitution. Sulfonation adjacent to the 1,8-propano and 1,8-butano bridges is inhibited due to steric hindrance, but can be effected using the more reactive SO_3 in *nitromethane*.

Reaction of **1** with 1.0 equiv. of SO_3 in dioxane yields only monosulfonic acids, but by using 1.0 equiv. of the more reactive SO_3 in nitromethane a substantial amount of disulfonic acids (19%) is obtained. The yield of disulfonic acids is far more pronounced in the (heterogeneous) sulfonation of **3** with 1.0 equiv. of SO_3 in nitromethane (43%). The formation of disulfonic acids under conditions of monosulfonation was observed before with some polymethylnaphthalenes (3), polymethylphenanthrenes (19), pyrene and perylene (20), using SO_3 in nitromethane, and for azulene and 1,3-di-*tert*-butylazulene with SO_3 in dioxane as reagent (21). It may be explained in terms of the mixing-disguised competitive, consecutive reaction model advanced by Rys (22), as discussed before (19–21). The higher yield of disulfonation of **3** may be explained in part by assuming that the rate of sulfonation of the monosulfonic acid is higher than the rate of dissolving of the substrate.

Arenesulfonic acid sulfonation

With the monosulfonic acids of **1**, **2**, and **6**, the very substantial degree of sulfonation of the ring containing the original sulfo substituent is remarkable in view of the strong deactivating effect of the primary sulfonic acid substituent, which is only partially of conjugative origin (23). In fact, with the two naphthalenesulfonic acids, the sulfonation in the ring containing the primary sulfo group is at best very low.[6] Apparently the selectivity of the sulfonation is reduced as a result of the activating 1,8-alkano and 1,8-dimethyl substituents. The content of the 2,4-disulfonic acid product decreases in the substrate order **1**-4-SO_3H > **2**-4-SO_3H > **6**-4-SO_3H. This order reflects the enhanced steric restrictions for sulfonating the 2-position (see before), as the f_2/f_4 ratio for protiodetritiation of the parent hydrocarbons – which reaction is devoid of steric hindrance (15) – exhibits a different order, viz. **6** > **1** ≃ **2** (ref. 12).

The disulfonation of the symmetrically substituted 1,8:4,5-dialkanonaphthalenes **3** and **5** leads very predominantly to the "non-crossed" disulfonic acids, the 2,6- to 2,7-disulfonic acid ratio being 0.12 and 0.15, respectively. The preference for the "noncrossed" disulfonic acid may be explained in terms of the higher energy content of the σ-complex for the 7- as compared with the 6-substitution, due to the larger degree of destabilization by the initial sulfonic acid substituent of which the sulfur is electropositive toward the surrounding oxygens, as discussed at length elsewhere (4).

The f_6/f_7 ratios are somewhat greater for the 2-sulfonic acids of **3** (0.12) and **5** (0.15) than for that of 1,4,5,8-tetramethylnaphthalene (**7**) (0.08) (ref. 3). The lower ratio for the latter sulfonic acid is ascribed to a relative increase in the rate of 7-substitution, as will now be discussed. The steric hindrance for sulfodeprotonation of the 2-position of the alkylated naphthalenes is greater for **7** than for **3** and **5** (see before). Accordingly, the steric strain in the 2-sulfonic acid of **7** is greater than in those of **3** and **5**. To accommodate (part of) the *ortho* and *peri* strain in the 2-sulfonic acid, C(1a) will be bent out of the plane of the naphthalene skeleton in the opposite direction to the adjacent 2-SO_3H and C(8a).[7] The steric hindrance for sulfonation of the 7-position will thus be more reduced for the 2-sulfonic acid of **7** than for those of **3** and **5**, leading to a higher f_6/f_7 ratio for **7**-2-SO_3H, as observed.

The f_6/f_7 ratio is very much smaller for the 2-sulfonic acid of **4** (<0.02) than for that of **5** (0.15), due to the lesser steric hindrance for sulfonating the 7-position – i.e. adjacent to the five-membered ring – of the former sulfonic acid.

We have indicated before, for the sulfonation of polymethylnaphthalenes with SO_3, that the alternative for the direct sulfodeprotonation, viz. initial *ipso*-attack, followed by a 1,2-sulfo shift, can not be excluded (2, 3). Again in this study there is no evidence in favour of this additional sulfonation route, but it is of interest that Fischer and Leonard observed *ipso*-attack in the nitration of **3** and **4** with nitric acid in acetic anhydride (27).

Experimental

Materials

Acenaphthene was Puriss grade (Rütgerswerke, FRG), **2** (28) and **4** (29) were prepared by known procedures, **3** was obtained as a gift, and the synthesis of **5** was described before (30).

[5]The steric requirements for substitution increase in the order hydrogen exchange << chlorination < nitration < bromination < sulfonation (15, 18).

[6]Sulfonation of naphthalene-1-sulfonic acid in 98.5% H_2SO_4 at 25°C does not yield any detectable amount of 1,3-disulfonic acid, whereas the 2-sulfonic acid yields only 4% of that isomer (24). Sulfonation of naphthalene with 1.0 equiv. of SO_3 in nitromethane yields ≃90% 1- and ≃10% 2-sulfonic acid and, with 4.0 equiv. of SO_3, 48% 1,6-, 25% 1,5-, and 5% 1,7-disulfonic acid with, as additional products, the 1,3-, 2,6-, and 2,7-disulfonic acids and (possibly some) 1,3,6- and 1,3,7-trisulfonic acids (P. de Wit and H. Cerfontain, unpublished results).

[7]The methyls of octamethylnaphthalene (25) and the methyl and sulfonate groups of dipotasisum mesitylenedisulfonate (26) are displaced alternately above and below the mean molecular plane.

Sulfonations

The procedures of the sulfonation with SO_3, the working up of the reaction mixture, and the product analyses were performed as described previously (21, 31). The sulfonation of acenaphthene with trimethylsilyl chlorosulfate (Fluka) was carried out following the standard procedure (5).

Acknowledgements

The authors thank Dr. C. Tintel (University of Leiden) for a generous gift of **3**, Dr. H. J. A. Lambrechts for a preliminary study on **3**, Mr. N. J. Coenjaarts for assistance, and Prof. K. Lammertsma for a valued correspondence.

1. A. KOEBERG-TELDER, H. J. A. LAMBRECHTS, and H. CERFONTAIN. J. Chem. Soc. Perkin Trans. 2. In press.
2. K. LAMMERTSMA and H. CERFONTAIN. J. Chem. Soc. Perkin Trans. 2, 673 (1979).
3. H. J. A. LAMBRECHTS and H. CERFONTAIN. Tetrahedron, **38**, 1667 (1982).
4. H. CERFONTAIN. J. Org. Chem. **47**, 4680 (1982).
5. K. HOFMANN and G. SIMCHEN. Justus Liebigs Ann. Chem. 282 (1982).
6. K. DZIEWONSKI and T. STOLLYHWO. Chem. Ber. **57**, 1531 (1924); K. DZIEWONSKI, H. GALITZEROWNA, and A. KOEWA. Bull. Int. Acad. Pol. Sci. Lett. Ser. A, 209 (1926); Chem. Abstr. **22**, 1154 (1928).
7. C. M. SUTER. The organic chemistry of sulfur. John Wiley and Sons, Inc., New York. 1944. p. 276.
8. H. CERFONTAIN and Z. R. H. SCHAASBERG-NIENHUIS. J. Chem. Soc. Perkin Trans. 2, 989 (1974).
9. H. CERFONTAIN, F. L. J. SIXMA, and L. VOLLBRACHT. Recl. Trav. Chim. Pays-Bas, **82**, 659 (1963).
10. H. CERFONTAIN, A. KOEBERG-TELDER, and E. VAN KUIPERS. J. Chem. Soc. Perkin Trans. 2, 2091 (1972).
11. I. K. LEWIS, R. D. TOPSOM, J. VAUGHAN, and G. J. WRIGHT. J. Org. Chem. **33**, 1497 (1968).
12. M. C. A. OPIE, G. J. WRIGHT, and J. VAUGHAN. Aust. J. Chem. **24**, 1205 (1971).
13. H. V. ANSELL and R. TAYLOR. Tetrahedron Lett. **52**, 4915 (1971).
14. B. N. MCMASTER, M. C. A. OPIE, and G. J. WRIGHT. Tetrahedron Lett. **22**, 2191 (1972).
15. R. BAKER, C. EABORN, and R. TAYLOR. J. Chem. Soc. 4927 (1961).
16. G. T. MORGAN and H. A. HARRISON. J. Soc. Chem. Ind. **49**, 413T (1930).
17. H. SUZUKI, K. KAWAMURA, and T. SUGIYAMA. Bull. Inst. Chem. Res. Kyoto Univ. **51**, 186 (1973); Chem. Abstr. **79**, 136151p (1973).
18. C. K. INGOLD. Structure and mechanism in organic chemistry. 2nd ed. Cornell University Press, Ithaca. 1969. pp. 306 and 320.
19. H. CERFONTAIN, A. KOEBERG-TELDER, K. LAALI, and H. J. A. LAMBRECHTS. J. Org. Chem. **47**, 4069 (1982).
20. H. CERFONTAIN, K. LAALI, AND H. J. A. LAMBRECHTS. Recl. Trav. Chim. Pays-Bas, **102**, 210 (1983).
21. P. DE WIT and H. CERFONTAIN. Recl. Trav. Chim. Pays-Bas, **104**, 25 (1985).
22. P. RYS. Acc. Chem. Res. **9**, 345 (1976); Angew. Chem. **16**, 847 (1977); F. NABHOLZ, R. J. OTT, and P. RYS. Helv. Chim. Acta, **60**, 2926 (1977); F. NABHOLZ and P. RYS. Helv. Chim. Acta, **60**, 2937 (1977).
23. H. CERFONTAIN and Z. R. H. SCHAASBERG-NIENHUIS. J. Chem. Soc. Perkin Trans. 2, 1780 (1976); T. A. KORTEKAAS, H. CERFONTAIN, and J. M. GALL. J. Chem. Soc. Perkin Trans. 2, 445 (1978).
24. P. DE WIT and H. CERFONTAIN. Can. J. Chem. **61**, 1453 (1983).
25. D. M. DONALDSON and J. MONTEATH ROBERTSON. J. Chem. Soc. 17 (1953).
26. M. A. M. MEESTER and H. SCHENK. Recl. Trav. Chim. Pays-Bas, **91**, 213 (1972).
27. A. FISCHER and D. R. A. LEONARD. Can. J. Chem. **50**, 3367 (1972).
28. L. F. FIESER and M. D. GATES, JR. J. Am. Chem. Soc. **62**, 2338 (1940).
29. L. F. FIESER and M. A. PETERS. J. Am. Chem. Soc. **54**, 4347 (1932).
30. A. FISCHER, D. R. A. LEONARD, and D. A. R. HAPPER. Can. J. Chem. **48**, 1446 (1970).
31. H. CERFONTAIN, A. KOEBERG-TELDER, H. J. A. LAMBRECHTS, and P. DE WIT. J. Org. Chem. **49**, 4917 (1984).

Interaction of strong acids with a conjugated imine

MARTINE BISSONNETTE, HOA LE THANH, AND DANIEL VOCELLE[1]
Département de chimie, Université du Québec à Montréal (Qué.), Canada H3C 3P8

Received July 13, 1984

MARTINE BISSONNETTE, HOA LE THANH, and DANIEL VOCELLE. Can. J. Chem. **63**, 2298 (1985).

The state of protonation of a Schiff base, *trans-trans*-heptadienylidene *tert*-butylamine (HBA) was evaluated by uv and ^{1}H nmr spectroscopies. Using three strong acids, HCl, HBr, HI and by taking spectra at low temperatures, it was found that in a non-polar solvent like chloroform (or $CDCl_3$), no proton exchange occurred between the iminium ion and the halide anion. In contrast, CD_3OH induced a leveling effect and some proton transfer occurred between the iminium ion and the solvent for the HBr and HI salts. No proton exchange was present for the HBA:HCl salt. The interaction of trichloroacetic acid with HBA was also studied: full proton exchange occurred between the iminium ion and CD_3OH. In $CDCl_3$, proton transfer was also present between the iminium ion and the carboxylate anion. These facts are discussed in relation with the controversy surrounding the true state of protonation of rhodopsin.

MARTINE BISSONNETTE, HOA LE THANH et DANIEL VOCELLE. Can. J. Chem. **63**, 2298 (1985).

La protonation d'une base de Schiff, la *trans-trans*-heptadiénylidène *tert*-butylamine (HBA) a été étudiée par les spectroscopies ultraviolette et de résonance magnétique nucléaire. Par l'emploi de trois acides forts, HCl, HBr, HI et par l'obtention de spectres à basses températures, il est démontré qu'aucun échange de proton entre l'ion iminium et l'anion halogénure se produit lorsque le solvant est le chloroforme. Par contre, lorsque CD_3OH est utilisé comme solvant, un début d'échange protonique entre le solvant et l'ion iminium peut être noté. Toutefois, pour HCl, aucun échange a pu être observé. Finalement, lorsque l'acide trichloroacétique a été utilisé en conjonction avec HBA, la présence d'un transfert complet de proton a pu être observé entre l'ion iminium et CD_3OH. Dans le $CDCl_3$, un échange de proton est également présent mais cette fois-ci, entre l'ion iminium et l'anion carboxylate. Ces observations sont discutées en relation avec le problème concernant l'état de protonation de la rhodopsine.

Introduction

In the photoconversion of rhodopsin to bathorhodopsin the question of the protonation of the retinal Schiff base is still problematic (1). The most accepted model concerning the structure of rhodopsin's chromophore is the external point charge theory proposed by Nakanishi (2).

Recently, we have developed our own model of rhodopsin consisting of a dienylidene Schiff base (e.g. RCH=CH—CH=CH—CH=N—R′) and substituted acetic acids (XCH_2CO_2H). When studied by uv and ^{1}H nmr spectroscopies, this simple model indicated, among other things, that an equilibrium such as the one shown in reaction [1] was possible for certain carboxylic acids in a non-polar solvent like chloroform.

[1]

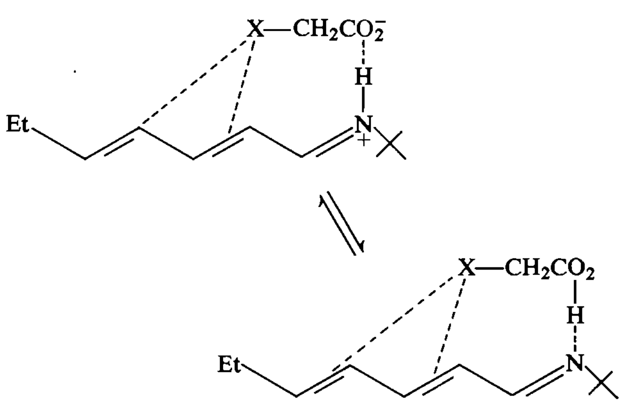

Was this equilibrium possible because of the presence of the X group of acetic acid (similar to the point charge proposed by Nakanishi) or could it exist without it? Since acetic acid or propionic acid cannot protonate a Schiff base like *trans-trans*-2,4-heptadienylidene *tert*-butylamine (HBA) (3), we thought using strong mineral acids like HCl, HBr, and HI which could fully protonate the azomethine without the help of an external point charge. Two solvents were used: chloroform (or $CDCl_3$) for a non-polar solvent and methanol (or CD_3OH) for a more polar one.

Experimental

Blatz and co-workers (4) have previously studied the interactions of these acids with N-retinylidene *n*-butylamine (NRBA) in the same two solvents. They concluded from their studies in $CHCl_3$ that the λ_{max} of NRBA depended on the distance between the protonated Schiff base nitrogen and the counter-ion. In methanol, there was a leveling effect which meant that all data in that solvent were identical. It became interesting, then, to use our model with the same acids and to study the nmr spectra and in particular, the behavior of H_7 (see Table 1 for the numbering of the hydrogens in HBA), the aldimine hydrogen —C*H*=N—, when the Schiff base is fully protonated. For an unprotonated HBA, H_7 appears as a doublet because of the

$$\begin{array}{c} \ \ \ H \\ \ \ \ | \\ —CH=C—C=N— \\ \ \ | \\ \ \ H \end{array}$$

system; for a protonated HBA, H_7 should become a doublet of doublets (5). The splitting of H_7 is then related to the state of protonation of the Schiff base and as such should give precious information on this vital problem in the chemistry of visual pigments (1).

Materials and methods

Preparation and purification of *trans-trans*-2,4-heptadienylidene *tert*-butylamine (HBA) have been described before (3). Preparation of the salts was easy: it consisted in the bubbling gazeous HCl, HBr, and HI, respectively, into an ether solution of HBA. The salt was filtered, washed with ether, and dried *in vacuo*. Gazeous HBr and HI were prepared according to classical methods (6). Solutions of the salts in chloroform or in methanol are somewhat unstable to oxygen, light and especially water. Fresh solutions are mandatory and special precautions must be taken such as working in an anhydrous atmosphere (dry box). Concentrations were always in the same range: 10^{-4} *M* for uv studies and 10^{-2} *M* for nmr. Chloroform was first percolated in a

[1]To whom all correspondence should be addressed.

TABLE 1. Chemical shifts of H_3 to H_7 of HBA and its salts in $CDCl_3$ and CD_3OH; values of the deshielding due to the acids used are in parentheses

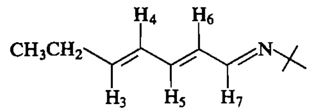

Solvent	Compounds	H_7	H_6	H_5	H_4	H_3
	HBA	8.04	6.32	6.85	6.33	6.16
CD_3OH	HBA/HCl	8.68(0.64)	6.69(0.37)	7.73(0.88)	6.62(0.29)	6.79(0.63)
	HBA/HBr	8.72(0.68)	6.69(0.37)	7.77(0.92)	6.69(0.29)	6.80(0.64)
	HBA/HI	8.67(0.63)	6.62(0.30)	7.74(0.89)	6.63(0.30)	6.80(0.64)
	HBA/TCA	8.64(0.60)	6.66(0.34)	7.69(0.84)	6.60(0.27)	6.77(0.61)
	HBA	7.87	6.26	6.57	6.18	5.95
$CDCl_3$	HBA/HCl	8.19(0.32)	7.26(1.00)	7.35(0.78)	6.37(0.19)	6.49(0.54)
	HBA/HBr	8.15(0.28)	7.38(1.12)	7.38(0.81)	6.44(0.26)	6.55(0.60)
	HBA/HI	8.41(0.54)	7.36(1.10)	7.61(1.24)	6.46(0.28)	6.69(0.74)
	HBA/TCA	7.97(0.10)	6.94(0.68)	7.19(0.62)	6.35(0.17)	6.44(0.49)

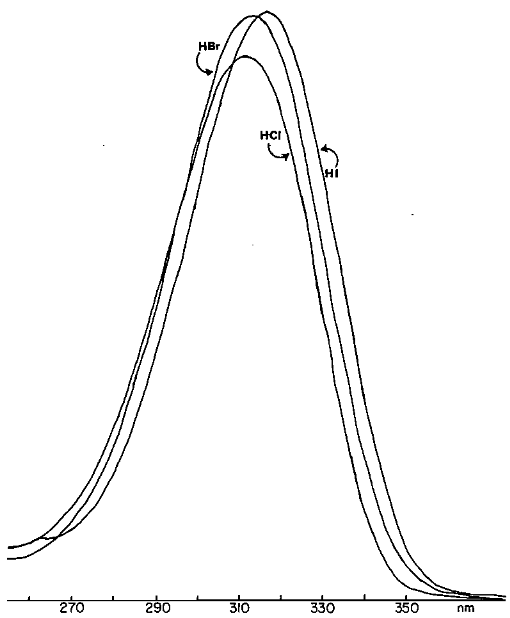

FIG. 1. Ultraviolet spectra of the hydrochloride, hydrobromide, and hydroiodide salts of HBA in chloroform.

basic alumina column and then dried over 4A molecular sieves. With this procedure, chloroform is perfectly dried and free from ethanol. The purity of this solvent was checked by gas chromatography (Varian instrument, model 3700 equipped with an 8 foot OV-101 column). Since it is extremely difficult to have completely dry methanol, CD_3OH obtained from Merck, Sharp and Dohme, was used in both uv and nmr studies.

Ultraviolet studies were made on a Cary 17 instrument while ^1H nmr spectra were recorded on a Bruker WH 400/DS (400 MHz) instrument. Assignments of chemical shifts to proper ethylenic hydrogens were done using double resonance technique.

Results and discussion

The electronic spectra of the HBA salts are simple: they consist of a single band with absorption maxima ranging from 306 to 317 nm depending on the counter-ion and the solvent used. Figure 1 shows the spectra of HBA with HCl, HBr, and HI in chloroform.

These results indicate full protonation and are in agreement with those obtained by Blatz (4) which noted the same order in the red shift of NRBA salts: iodide having a bigger shift than bromide than chloride. In methanol (CD_3OH), NRBA salts gave uv spectra consisting of a single band with λ_{max} at 306, 307, and 306 nm for the iodide, bromide, and chloride anions, respectively. This last result indicates a leveling effect by methanol. The same effect has been noted previously by Blatz (4) and also by us (3).

The nmr spectra are far more interesting. Figure 2 *a* and *b* show the 400 MHz nmr spectra of HBA and of its hydrochloride salt in $CDCl_3$ while Table 1 gives the chemical shifts of all ethylenic hydrogens (H_3 to H_7) of HBA salts in $CDCl_3$ and CD_3OH. The data for equimolar concentrations of trichloroacetic acid and HBA are also given for reasons which will be discussed later on.

It will be noted by looking at Fig. 2 *a* and *b* that the acids are inducing a pronounced deshielding especially on H_5 and H_6 in $CDCl_3$ and H_6 in CD_3OH. Nuclear magnetic resonance techniques are thus very revealing of the interactions of an acid on the hydrogens of a Schiff base. From Table 1, it is readily noticeable that a leveling effect is present in CD_3OH since the chemical shifts are all very similar, thus confirming the uv spectral data. On the basis of this effect and following Blatz's (4) explanations, it follows that the protonated azomethine is separated from the anion (Cl^-, Br^-, I^-) by at least one molecule of CD_3OH. Solvation of protonated HBA means that there must exist a rapid exchange between the hydrogens of the solvent and the acidic proton (5) as in reaction [2] and H_7 should appear as a doublet.

$$[2] \quad R{-}CH{=}CH{-}CH{=}\overset{H^*}{\underset{\oplus}{N}}{-}C(CH_3)_3 + CD_3OH \rightleftharpoons RCH{=}CH{-}CH{=}\overset{H}{\underset{\oplus}{N}}{-}C(CH_3)_3 + CD_3OH^*$$

Figure 3*a* shows the splitting of H_7, in CD_3OH, for the three salts and for the TCA:HBA system.

The hydrochloride salt of HBA indicates a doublet of doublets for H_7 while for the hydrobromide and hydroiodide, it

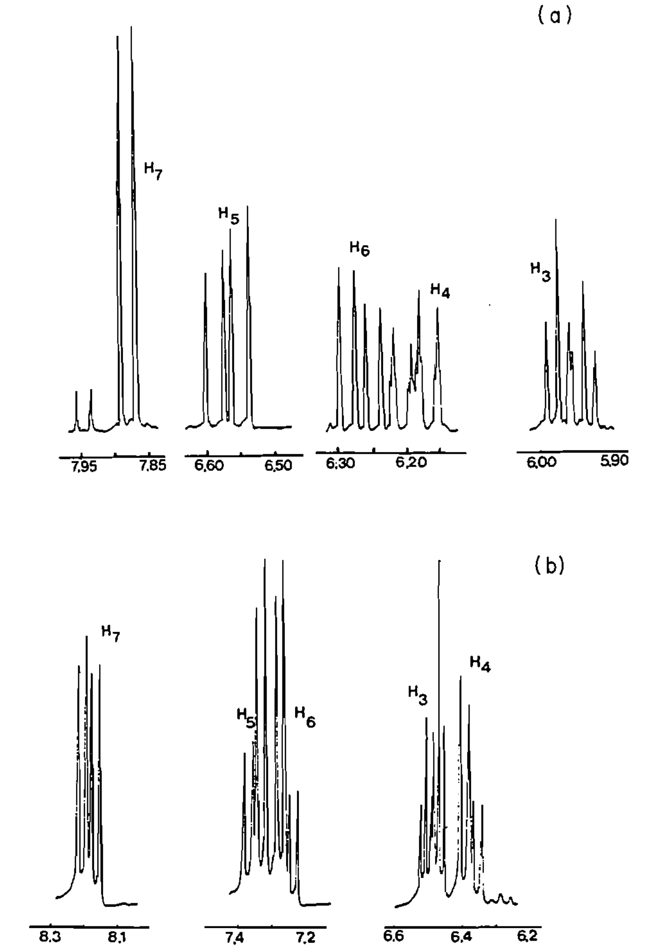

FIG. 2. ^{1}H nmr (400 MHz) spectra of (*a*) HBA in $CDCl_3$ and (*b*) HBA·HCl salt in $CDCl_3$.

is a poorly resolved multiplet. By comparison, TCA produces a well-defined doublet for H_7 and yet it has the same chemical shift (Table 1) and the same uv spectral data (for a 1:1 ratio of HBA and TCA, uv spectrum indicates one single band with a λ_{max} = 307 nm) as with the mineral acids.

To understand more fully the significance of these results, the hydroiodide solution and the TCA:HBA system were studied by nmr at different temperatures. Figure 4 *a* and *b* shows the results.

By lowering the temperature, H_7 for the HI:HBA system becomes a doublet of doublets at a temperature of 5°C while for TCA:HBA, it must reach −30°C. A doublet of doublets signifies that a proton is located on the nitrogen of the azomethine while a doublet means that a rapid exchange is present. At room temperature then, the hydroiodide and hydrobromide are exchanging protons with the solvent while the hydrochloride is not. With TCA, the exchange is more complete (faster) than with the hydroiodide and a well-defined doublet is obtained. From these results and explanations and remembering that all acids (including HCl) induce almost identical deshielding on the hydrogens of HBA, it must be inferred that in methanol: (*a*) with HCl, a tight-ion pair must exist between the chloride anion and the *solvated* cation so that proton exchange is minimal; (*b*) with HBr and HI, the ion pair is more loosely held together and some proton exchange is present; and (*c*) with TCA, there is no ion pair and both the anion and cation are fully solvated and proton exchange occurs readily.

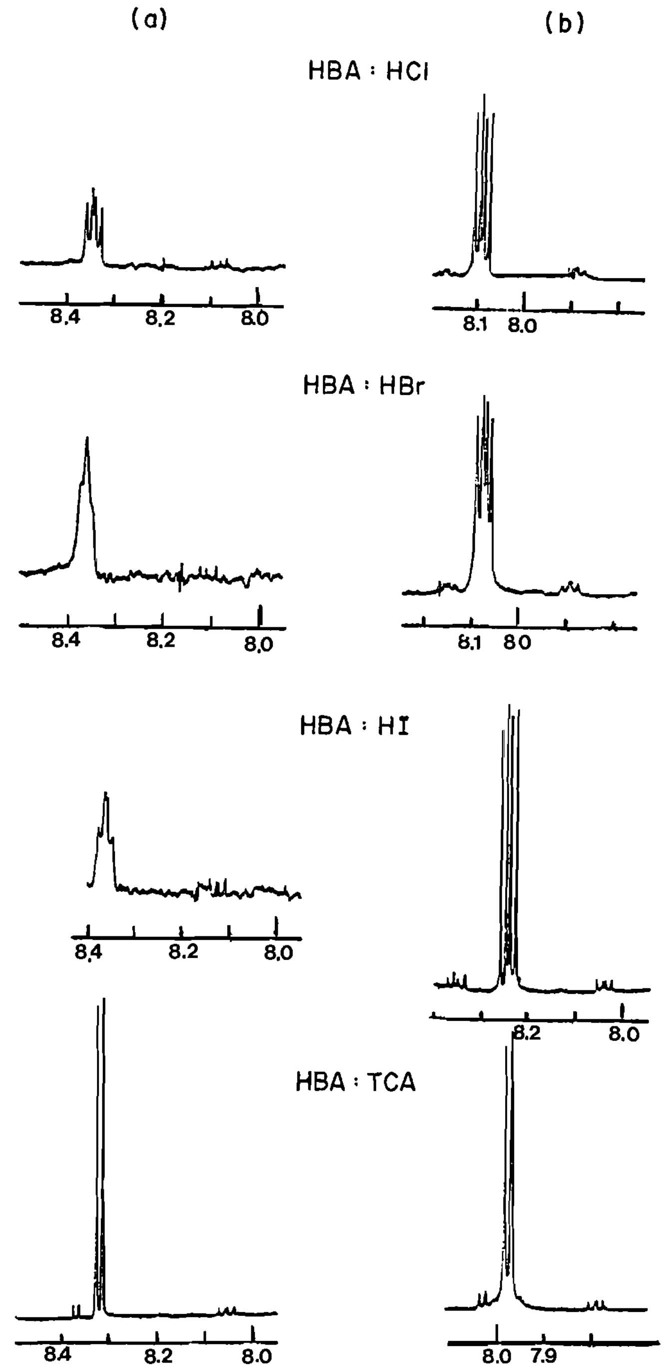

FIG. 3. Spin–spin couplings of H_7 for HBA salts: (*a*) in CD_3OH and (*b*) in $CDCl_3$.

In deuterated chloroform, the solvent being non-polar and having a low dielectric constant, ion pairs must be expected. Table 1 shows that the chemical shifts are different and thus, no leveling effects seems to exist. Acids cause a pronounced deshielding on H_6 and this deshielding vary according to the size of the anion as anticipated (4). Figure 3*b* shows the splitting of H_7 in $CDCl_3$. The three strong acids protonate fully the Schiff base and the acidic proton sits on the nitrogen without proton exchange, so that a doublet of doublets is the results. However, TCA is protonating fully HBA as shown by the uv spectrum (one band only with a λ_{max} = 310 nm) and yet H_7 appears as a doublet. This can be explained by invoking an equilibrium between unprotonated and protonated HBA (see

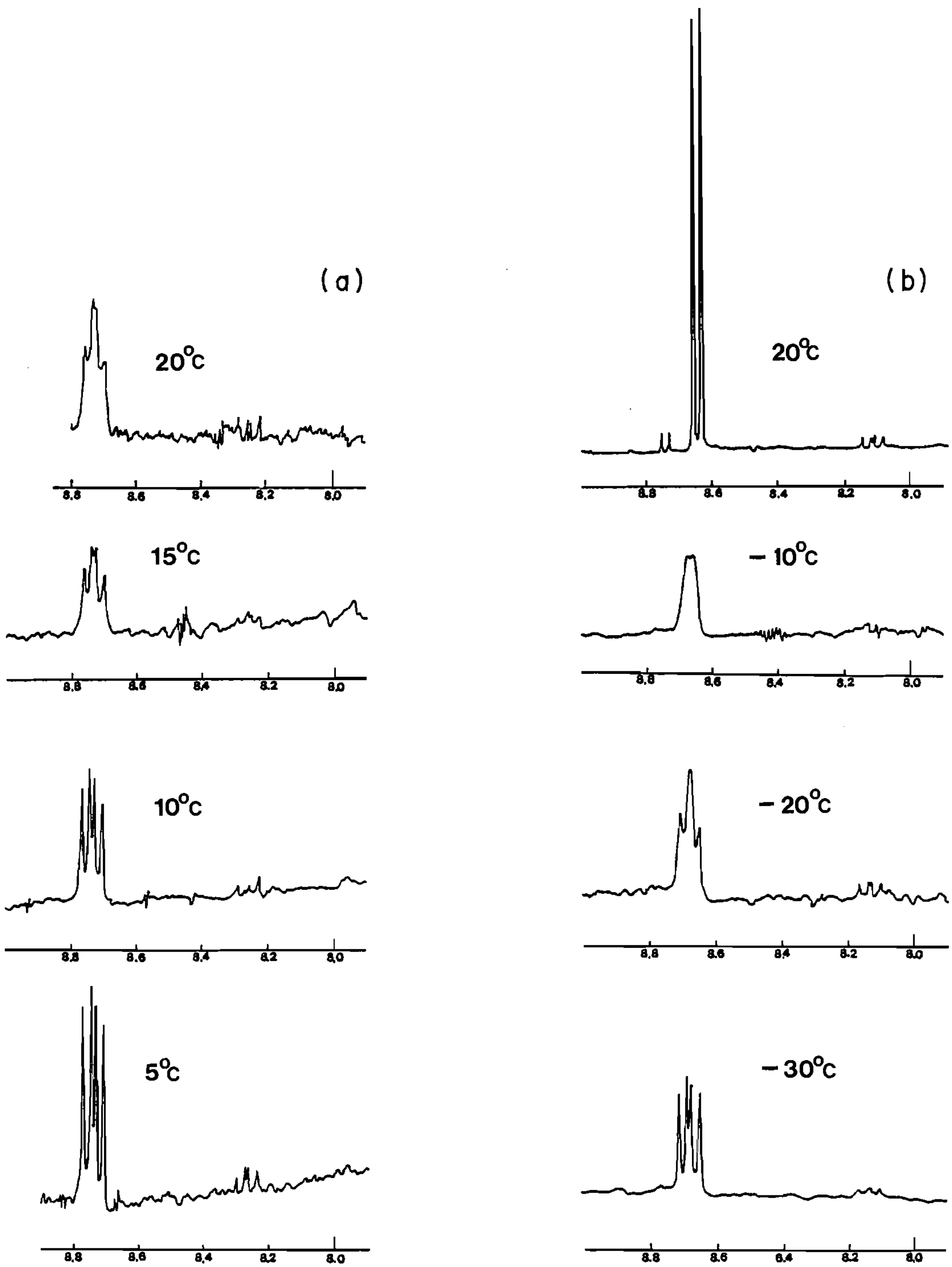

FIG. 4. Spin–spin couplings of H_7 for (*a*) HBA:HI, (*b*) TCA:HBA at different temperatures in CD_3OH.

reaction [1]). Nuclear magnetic resonance spectra in $CDCl_3$ at different temperatures show the same pattern as before in CD_3OH (Fig. 4). At −25°C, a doublet of doublets is obtained. In our previous work with halogenated carboxylic acids (3), similar conclusions were drawn. In deuterated chloroform, acids like the mono-, di-, and tri-halogenated acetic acids induced a pronounced deshielding on H_5 and H_6 while H_7 always appeared as a doublet. By increasing the proportion of acid toward the imine, a doublet of doublets was obtained for H_7. This result is analogous to the one reported here by lowering the temperature of the TCA–imine system and it confirms the fact that in chloroform, the acidic proton is wandering between the carboxylate anion and the Schiff base. Surprisingly enough, uv spectroscopy is insensitive to the proton transfer.

In conclusion, this study shows that the acidic proton on a protonated Schiff base is very labile and moves constantly between the imine group and the solvating species (if the medium is polar) or the counter-ion if it is a carboxylate anion and the milieu is non-polar. Extrapolation of our results to rhodopsin is too risky to be done since it was shown, quite recently, by two-proton spectroscopic measurements (ref. 7*a*, for a comment of one of the referees, see ref. 7*b*) that the degree of protonation did vary according to the existing milieu. This fact seems also verified by ^{13}C nmr studies done on samples of bacteriorhodopsin whose preparations were different (8). This being the case, it is nevertheless interesting to note the great lability of the acidic proton in our model and the effect of lowering the temperature which freezes the proton exchange and permits the acidic proton to be located solely on the Schiff base nitrogen.

Acknowledgements

The authors are most grateful to Professor Camille Sandorfy for helpful discussions and to the Laboratoire Régional de RMN à haut champ (Dr Phan Viet Minh Tan) of University of Montreal for all the 400 MHz nmr spectra. We acknowledge the financial help of the National Research Council of Canada (grant A0943) and of the Université du Québec à Montréal. We owe many thanks also to Ms. Danielle Sabourin for typing this manuscript.

1. V. BALOGH-NAIR and K. NAKANISHI. *In* New comprehensive biochemistry. Vol. 3. *Edited by* Ch. Tamm. Elsevier Biomedical Press, New York. 1982.
2. (*a*) M. ARNABOLDI, G. MOTTO, K. TSUJIMOTO, V. BALOGH-NAIR, and K. NAKANISHI. J. Am. Chem. Soc. **101**, 7082 (1979); (*b*) K. NAKANISHI, V. BALOGH-NAIR, M. ARNABOLDI, K. TSUJIMOTO, and B. HONIG. J. Am. Chem. Soc. **102**, 7945 (1980); (*c*) S. MORDECHAI and K. NAKANISHI. J. Am. Chem. Soc. **105**, 4033 (1983).
3. (*a*) M. BISSONNETTE and D. VOCELLE. Spectrosc. Int. J. **2**, 120 (1983); (*b*) M. BISSONNETTE, H. LETHANH, and D. VOCELLE. Can. J. Chem. **62**, 1459 (1984).
4. (*a*) J. O. ERICKSON and P. E. BLATZ. Vision Res. **8**, 1367 (1968); (*b*) P. E. BLATZ, J. H. MOHLER, and H. V. NAVANGUL. Biochemistry, **11**, 848 (1972); (*c*) P. E. BLATZ and J. H. MOHLER. Biochemistry, **14**, 2304 (1975); (*d*) P. E. BLATZ and J. H. MOHLER. Biochemistry, **11**, 2340 (1972).
5. G. M. SHARMA and O. A. ROELS. J. Org. Chem. **38**, 3648 (1973).
6. A. I. VOGEL. Text book of practical organic chemistry. 3rd ed. Longmans. p. 182.
7. (*a*) R. R. BIRGE, B. M. PIERCE, and L. P. MURRAY. *In* The proceedings of the NATO advanced study Institute on the Spectroscopy of Biological Molecules. *Edited by* C. Sandorfy and T. Theophanides. D. Reidel Publ. Co., Boston. 1984, pp. 468–481; (*b*) R. R. BIRGE, L. P. MURRAY, B. M. PIERCE, L. FINDSEN, V. BALOGH-NAIR, and K. NAKANISHI. To be published.
8. (*a*) G. D. HARBISON, S. O. SMITH, J. A. PARDOEN, P. P. J. MULDER, J. LUGTENBURG, J. HERZFELD, R. MATHIES, and R. G. GRIFFIN. Biochemistry, **23**, 2662 (1984); (*b*) G. D. MATEESCU, W. G. COPAN, D. D. MUCCIO, D. V. WATERHOUS, and E. W. ABRAHAMSON. *In* Proceedings of the International Symposium on Synthesis and Applications of Isotopically Labeled Compounds. Elsevier, Amsterdam. 1983. pp. 123–132.

A Raman spectroscopic study of the equilibria in aqueous solutions of Hg(II) chloride

PATRICE B. BENTHAM, CYNTHIA G. ROMAK, AND HERBERT F. SHURVELL[1]
Department of Chemistry, Queen's University, Kingston, Ont., Canada K7L 3N6

Received September 25, 1984

PATRICE B. BENTHAM, CYNTHIA G. ROMAK, and HERBERT F. SHURVELL. Can. J. Chem. **63**, 2303 (1985).

The techniques of factor analysis (principal component analysis) and band contour resolution have been applied to Raman spectra obtained from seven aqueous solutions of $HgCl_2$ with various amounts of HCl added to increase the chloride to mercury ratio. The digitized spectra of the Hg—Cl stretching region (200−380 cm^{-1}) were subjected to baseline fitting and removal, and normalization using the ν_2 band of ClO_4^- (380−530 cm^{-1}) as an internal intensity standard. Factor analysis indicated the presence of three scattering components in the Hg—Cl stretching band envelope. Band resolution gave the positions of peaks assigned to $HgCl_2$, $HgCl_3^-$, and $HgCl_4^{2-}$ at 320, 290, and 269 cm^{-1}, respectively. Approximate values for equilibrium constants for the equilibria present in the system have been calculated from the resolved band areas.

PATRICE B. BENTHAM, CYNTHIA G. ROMAK et HERBERT F. SHURVELL. Can. J. Chem. **63**, 2303 (1985).

On a appliqué les techniques d'analyse factorielle (analyse du composant principal) et de résolution du coutour de la bande aux spectres Raman obtenus à partir de sept solutions aqueuses de $HgCl_2$ dans lesquelles on a ajouté diverses quantités de HCl dans le but d'augmenter le rapport chlorure/mercure. On a soumis les spectres digitalisés de la région d'élongation Hg—Cl (200−380 cm^{-1}) à un ajustement et une élimination de la ligne de base, puis à une normalisation faisant appel à la bande ν_2 du ClO_4^- (380−530 cm^{-1}) comme standard interne. Dans l'enveloppe de la bande d'élongation Hg—Cl, l'analyse factorielle suggère la présence de trois composantes qui diffusent. À l'aide de la résolution des bandes, on a pu attribuer les bandes à 320, 290 et 269 cm^{-1} respectivement aux entités $HgCl_2$, $HgCl_3^-$ et $HgCl_4^{2-}$. En se basant sur les bandes résolues, on a déterminer les valeurs approximatives des constantes d'équilibre pour l'équilibre présent dans le système.

[Traduit par le journal]

Introduction

Factor analysis (or principal component analysis) and band contour resolution techniques have been useful in the infrared studies of various equilibria in CCl_4 solutions (1, 2). The method was later adapted for Raman studies, and successfully used in the investigation of aqueous In(III) chloride solutions (3) and aqueous Zn(II) chloride solutions (4). A review of the procedure with applications has been published (5). As a further extension of the method, it was decided to examine the Raman spectra of aqueous Hg(II) chloride solutions with chloride added to vary the Cl^- to Hg ratio.

Aqueous mercury(II) chloride solutions have been the subject of numerous investigations (6−19). It is generally agreed that the main aquated species present in aqueous solutions of mercury(II) chloride with concentrations of free chloride in the range 10^{-3} to 1 *M*, are $HgCl_2$, $HgCl_3^-$, and $HgCl_4^{2-}$. There is some disagreement in the literature over the assignment of the Hg—Cl stretching frequencies of the various complexes. The reported wavenumbers are compared in Tables 1, 2, and 3.

Detailed resolution of the Hg—Cl stretching band in aqueous mercury(II) chloride solutions using modern computing methods has not been attempted previously and it was felt that such a study would provide useful information on this system.

In the present study, we have recorded digitally the Hg—Cl stretching band of solutions with various *R* (chloride : mercury) ratios. By means of factor analysis and band resolution techniques, it has been possible to identify the complexed species, obtain wavenumbers for the symmetric Hg—Cl stretching modes of these species, and obtain approximate values for the equilibrium constants of the following reactions:

[1] $HgCl_2 + Cl^- \rightleftharpoons HgCl_3^-$

[2] $HgCl_3^- + Cl^- \rightleftharpoons HgCl_4^{2-}$

[3] $HgCl_2 + 2Cl^- \rightleftharpoons HgCl_4^{2-}$

[1]To whom all correspondence should be addressed.

TABLE 1. Position of the symmetric stretching vibration of $HgCl_2$ for various solvents and *R* (chloride : mercury ratios)

Solvent[a]	*R*	ν_1 (cm^{-1})[b]
Aqueous (10)	2.3	314−321 s, p
Aqueous (17)	0.34	325 w, p
Aqueous (15)	2.3	312 m, br − 322 m
Aqueous (this work)	2−4.64	320 s, p
TBP (10)	2	317 s, p
TBP (18)	—	320
TBP (19)	—	328 s, p
Melt (12)	2	313 s, p
Melt (11)	2	313 s, p
Dioxane (13)	2	319 —
Benzene (13)	2	339 —
Methanol (16)	2−3	321 —

[a]Reference numbers in parentheses.
[b]s = strong, p = polarized, w = weak, br = broad.

Experimental

Reagent grade mercuric chloride (Pfaltz and Bauer) was used to prepare a near-saturated aqueous stock solution. This was filtered to remove suspended particles and solutions containing 0.172 *M* $HgCl_2$, 1.59 *M* $HClO_4$, and varying concentrations of HCl were prepared. Details of the seven solutions used are given in Table 4.

Raman spectra of the seven solutions were recorded at 22 ± 1°C using a Jarrell-Ash 25-100 double Czerny-Turner monochromator, a RCA 30032-02 photomultiplier tube together with photon counting electronics. Raman spectra were excited by the 514.5 nm line of a Spectra-Physics Model 171 Ion laser. Laser powers between 200 and 500 mW at the sample were used. The sample was contained in a 5 mm × 5 mm × 50 mm silica cell. Two regions were scanned during the course of the study: 200 cm^{-1} to 380 cm^{-1} (the Hg—Cl stretching region) and 380 cm^{-1} to 500 cm^{-1} (the ν_2 region of the ClO_4^- ion used as an internal intensity standard). Duplicate spectra were recorded. Any spectra showing intensity variations greater than 1% between consecutive scans were rejected. The spectra were calibrated using emission lines from a neon lamp and the wavenumbers reported from

TABLE 2. Position of the symmetric stretching vibration of the $HgCl_3^-$ ion for various solvents and R (chloride : mercury ratios)

Solvent[a]	R	ν_1 (cm^{-1})[b]	Proposed structure
Aqueous (15)	2.8	285–288 w	
Aqueous (this work)	2–4.64	290 s, p	Planar
TBP (10)	3.22	294 s, p	Planar
TBP (18)	—	294 s, p	
TBP (19)	3	296 vs, p	
Melt (12)[c]	—	282 s, p	Planar
Methanol (16)	2.5–3	292 —	

[a]Reference numbers in parentheses.
[b]v = very, s = strong, p = polarized, w = weak.
[c]ν_3 = 287 cm^{-1}, ν_4 = 210 cm^{-1}.

TABLE 3. Position of the symmetric stretching vibration of the $HgCl_4^{2-}$ ion for various solvents and R (chloride : mercury ratios)

Solvent[a]	R	ν_1 (cm^{-1})[b]
Aqueous (10)	3.22	269 s, d–272 s, p
Aqueous (14)	8.0	269 —
Aqueous (15)	2.88–9.0	270–275 s, p
Aqueous (this work)	2–4.64	269 s, p
TBP extract of halogen acid (18)	?	272 s, p
Melt (12)[c]	?	267 —
Methanol (16)	2.5–6.0	268 —

[a]Reference numbers in parentheses.
[b]s = strong, d = diffuse, p = polarized, w = weak.
[c]ν_2 = 100 cm^{-1}, ν_3 = 276 cm^{-1}, ν_4 = 192 cm^{-1}.

the present work in Tables 1, 2, and 3 are believed to be accurate to within ± 1 cm^{-1}.

Computing methods

(i) Digitization

All spectra were digitized by computer. The output from the photon counting system was interfaced to a PDP11 computer. Spectra recorded in this manner were permanently stored on floppy disks as well as being transferred to the IBM 4341 computer for further processing.

(ii) Baseline removal

Duplicate spectra were averaged. A plot of a typical raw spectrum obtained in this study is shown in Fig. 1. Removal of the baseline was accomplished using a revised version of the program BSLINE (20). Three types of baseline fits were used, either an exponential baseline was fitted across the entire spectrum, or the spectrum was arbitrarily divided at 380 cm^{-1} and a linear baseline fitted to the reference peak, while an exponential-quadratic baseline was fitted to the band envelope. These three types of fits are illustrated in Figs. 1, 2 and 3*a*, respectively. The fitted baselines were subtracted from the raw spectra to give the baseline removed spectra. An example is shown in Fig. 3*b*.

(iii) Treatment of spectra

The seven baseline removed spectra were subjected to factor analysis (principal component analysis) using the program CHISQ (5). Band resolution was accomplished using a version of the program PC116 originally written by Jones *et al.* (21), but modified here for fitting Raman bands. Details of the modifications are available from the authors on request. Areas of the component bands were determined and used to calculate the equilibrium constants.

Results and discussions

(i) Factor analysis

Factor analysis (principal component analysis) (1, 5) has been applied to the Raman band envelope in the Hg—Cl stretching region of the seven solutions of 0.172 M $HgCl_2$ with added HCl, listed in Table 4. The analysis indicates that there are three scattering components contributing to the band envelope.

TABLE 4. Composition of the seven samples[a]

Solution number	Added [Cl^-] from HCl (M)	Total [Cl^-] (M)	R ([Cl^-]:[Hg^{2+}])
1	0.0	0.344	2.0
2	0.113	0.454	2.66
3	0.170	0.514	2.99
4	0.227	0.571	3.32
5	0.214	0.628	3.65
6	0.340	0.665	3.86
7	0.454	0.798	4.64

[a]Each solution was 0.17 M in $HgCl_2$ and 1.59 M in $HClO_4$. Total volume of each solution was 10.0 mL.

TABLE 5. Results of the square root of variance test

Square root of variance	Eigenvalues
0.022575	21.378387
0.027875	4.748066
0.024463	0.119980
0.023302	0.027180
0.024443	0.007961
0.021098	0.002203
0.023143	0.001380

TABLE 6. Factor analysis of seven solutions of $HgCl_2$; comparison of observed and regenerated transmittance matrix

	Distribution of misfits (number of points)					
Number of eigenvectors (m)	Number of standard deviations				χ^2	
	0–1	1–2	2–3	>3	Calcd.	Expectation value
1	462	162	113	537	114897.5	1086.0
2	700	325	151	98	3724.7	900.0
3	1035	209	28	2	817.2	716.0
4	1204	70	0	0	305.4	534.0
5	1261	13	0	0	111.3	354.0
6	1272	2	0	0	38.5	176.0
7	1274	0	0	0	0	0

In principal component analysis, the matrix $\mathbf{Q} = \mathbf{I}^T\mathbf{I}$, where $\mathbf{I}$ is the Raman intensity matrix and $\mathbf{I}^T$, its transpose, is formed. The number of scattering components is taken to be the number of non-zero eigenvalues of $\mathbf{Q}$. Due to experimental and computational errors, statistical tests must be employed to determine which eigenvalues are really non-zero.

One criterion is the square root of variance test. The number of scattering components is taken as the number of eigenvalues greater than the square root of their variance. The results of this criterion are shown in Table 5, where it is seen that the first three eigenvalues are larger than their variance.

Two further criteria are the regeneration of the intensity matrix using the minimum number of eigenvectors and the estimation of χ^2_m. When m equals the number of components, χ^2_m should have a value near the expectation value (22) which, in the present case, is given by $(N_W - m)(N_S - m)$ (23), where

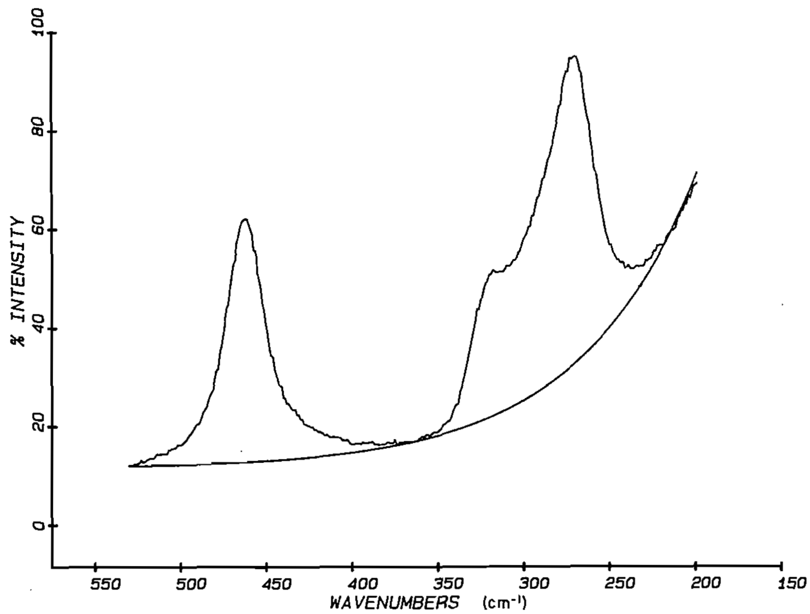

FIG. 1. The raw spectrum from sample 6 (R = 3.86) with a fitted exponential baseline.

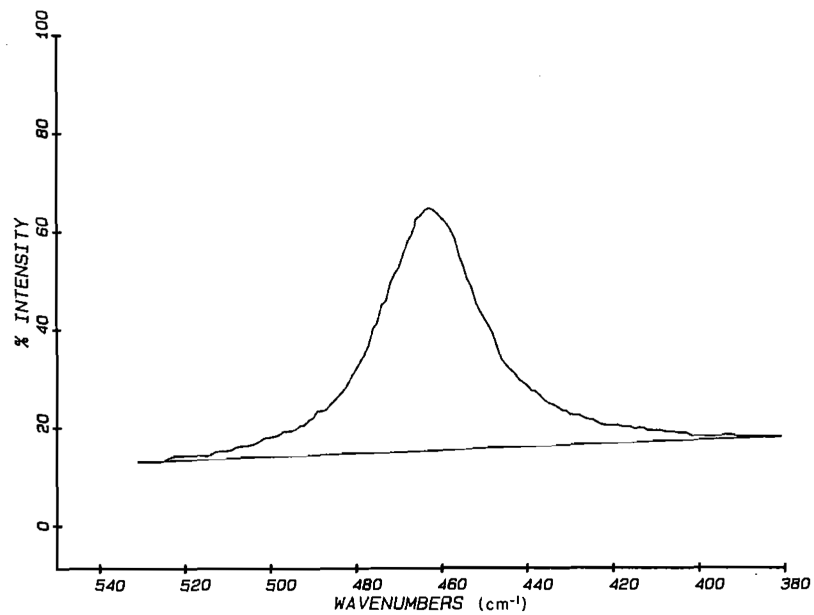

FIG. 2. A linear baseline fitted to the reference band (ν_2 of ClO_4^-) from sample 1.

N_W is the number of digitized points in the spectrum and N_S the number of solutions. The results of these two criteria are given in Table 6.

It can be seen that three eigenvectors are needed to regenerate the intensity matrix with 1272 out of 1274 points within three standard deviations of the experimental values. The χ^2 test also indicates three components, since the calculated χ_2^2 for two components is greater than the expectation value, while χ_3^2 is comparable to the expectation value.

Band resolution

Band resolution of the seven spectra was carried out. The results for solution 3 (R = 2.99) and solution 7 (R = 4.64) are shown in Figs. 4 and 5. It was found that the three bands required by the factor analysis were centered at 320 cm^{-1}, 290 cm^{-1}, and 269 cm^{-1}. The band at 320 cm^{-1}, which predominates at low chloride to mercury ratios was assigned to $HgCl_2$. The band at 269 cm^{-1} which predominates at high R values was assigned to $HgCl_4^{2-}$. The middle band, centered at 290 cm^{-1}, was assigned to $HgCl_3^-$.

Calculation of equilibrium constants

The equilibrium constants for the reactions $HgCl_2 + Cl^- \rightleftharpoons HgCl_3^-$, $HgCl_3^- + Cl^- \rightleftharpoons HgCl_4^{2-}$, and $HgCl_2 + 2Cl^- \rightleftharpoons HgCl_4^{2-}$ may be calculated from the following equations:

$$[4] \quad K_3 = \frac{[HgCl_3^-]}{[HgCl_2][Cl^-]}$$

$$[5] \quad K_4 = \frac{[HgCl_4^{2-}]}{[HgCl_3^-][Cl^-]}$$

$$[6] \quad K_3K_4 = \frac{[HgCl_4^{2-}]}{[HgCl_2][Cl^-]^2}$$

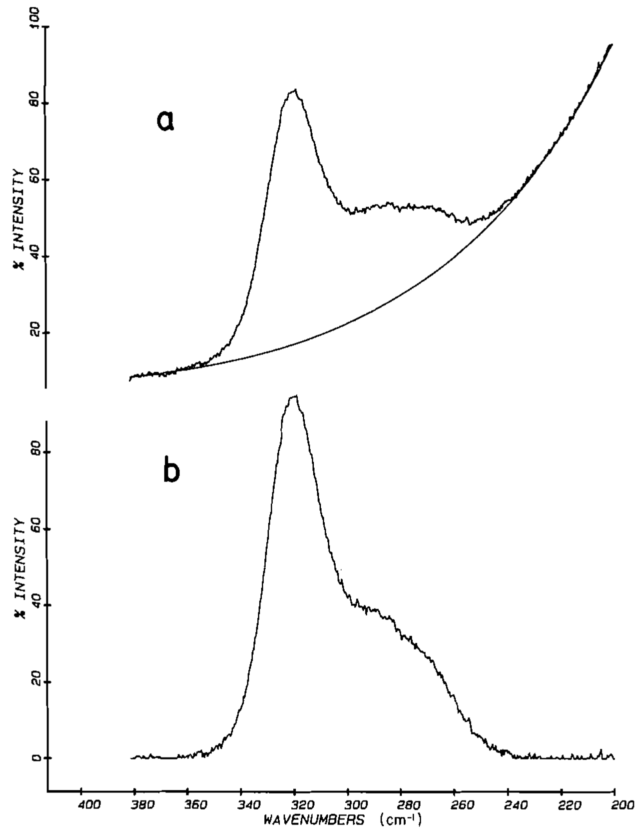

FIG. 3. The Hg—Cl stretching band from sample 2 (R = 2.66): (a) with a fitted exponential-quadratic baseline, (b) the baseline-removed band.

where the square brackets represent the concentrations of the respective species. Concentrations (C_i) may be related to resolved band areas (A_i) by the relationship:

$$[7] \quad A_i = J_iC_i$$

where J_i is a molar scattering coefficient. An approximate

TABLE 7. Results of band fitting and Cl^- ion-selective electrode measurements

Solution	Area (320 band)	Area (290 band)	Area (269 band)	$[Cl^-]$ (M)
2	498.31	313.90	113.93	0.007
3	449.85	327.95	242.13	0.004
4	674.57	469.79	532.98	0.046
5	489.84	553.84	859.51	0.064
6	321.00	562.09	963.66	0.072
7	167.62	435.62	1079.06	0.121

calculation of equilibrium constants can be made if it is assumed that the molar scattering coefficients (J_i) for the symmetric stretching bands of $HgCl_2$, $HgCl_3^-$, and $HgCl_4^{2-}$ are equal. In this case, we replace the concentrations in eqs. [4], [5], and [6] by resolved normalized band areas. The concentration of the free Cl^- ion was measured independently using a Cl^- ion-selective electrode. Table 7 lists the areas of the various bands as well as the free Cl^- ion concentration, as measured by the ion-selective electrode for each solution. All activity coefficients were assumed to be unity in this work.

Table 8 compares the values of $\log_{10} K$ for the various stepwise equilibria present in the Hg(II)/Cl^- system studied in this work with those obtained by other workers. Sillen and Ciavatta used electrochemical techniques, while Marcus employed a solvent (benzene) distribution method. The values determined here, for the equilibrium constants (eqs. [4], [5], and [6]) listed in Table 8, are somewhat higher than the literature values. However, our values would be a little lower and hence closer to the literature values if we were to make the assumption that the molar scattering coefficients (J_i) are in the ratio 2:3:4 rather than 1:1:1. This is not an unreasonable assumption, since the J_i could increase with increasing number of HgCl bonds.

Conclusions

Principal component analysis and Raman band contour resolution has shown that three scattering species are present in

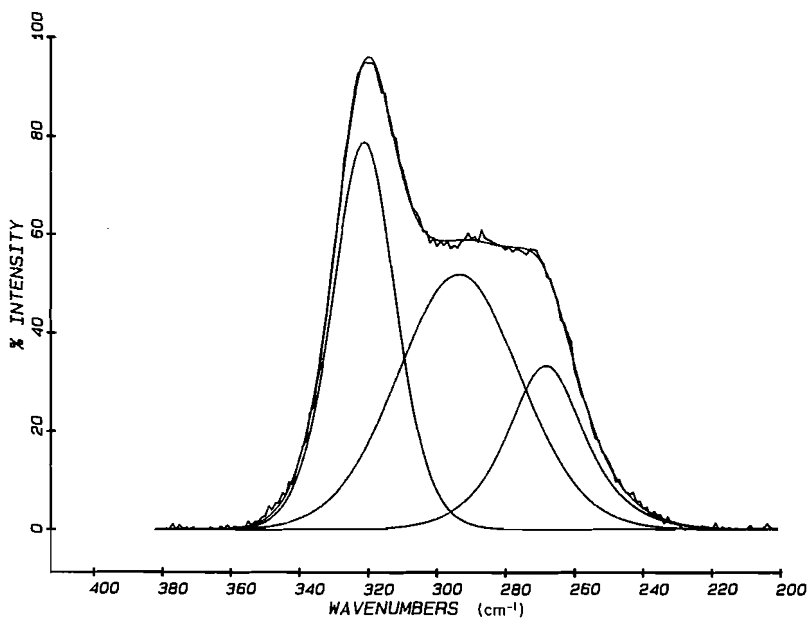

FIG. 4. The fitted Hg—Cl stretching band envelope for sample 3 (R = 2.99).

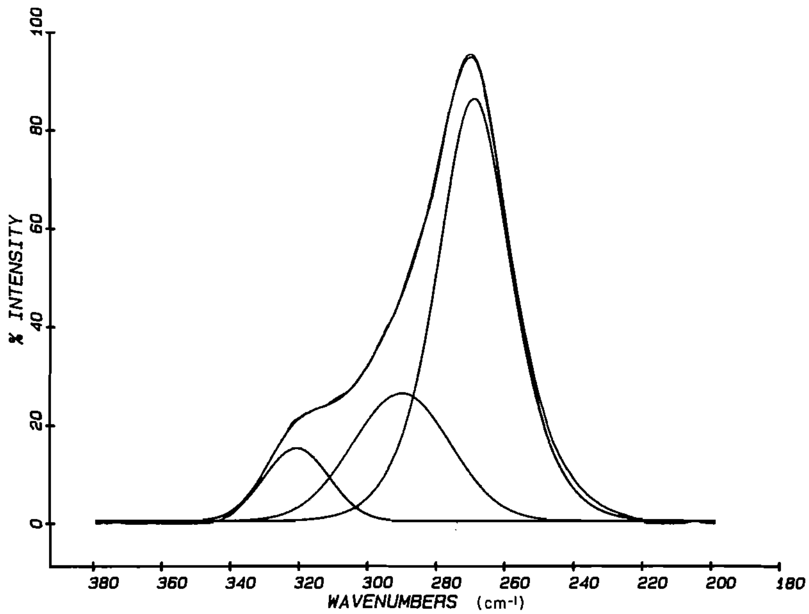

FIG. 5. The fitted Hg—Cl stretching band envelope for sample 7 (R = 4.64).

TABLE 8. Values of $\log_{10} K$ for various stepwise equilibria in Hg^{2+} system with added Cl^-

Reaction	Constant	Sillén (6) (25°C)	Marcus (8) (25°C)	Ciavatta (9) (25°C)	This work (22 ± 1°C)
$Hg^{2+} + Cl^- = HgCl^+$	$\log K_1$	6.73±0.018	—	6.72±0.02	—
$HgCl^+ + Cl^- = HgCl_2$	$\log K_2$	—	6.30±0.02	—	—
$HgCl_2 + Cl^- = HgCl_3^-$	$\log K_3$	0.85±0.15	0.95±0.03	1.00±0.01	1.29±0.25
$HgCl_3 + Cl^- = HgCl_4^{2-}$	$\log K_4$	—	—	—	1.36±0.25
$HgCl_2 + 2Cl^- = HgCl_4^{2-}$	$\log K_3K_4$	0.85±0.05	2.00±0.05	1.97±0.025	2.65±0.50

solutions of $HgCl_2$ containing added chloride ion. It is concluded that the three species are $HgCl_2$, $HgCl_3^-$, and $HgCl_4^{2-}$. The totally symmetric stretching frequencies of these species are 320 cm^{-1}, 290 cm^{-1}, and 269 cm^{-1}, respectively.

A value of 1.29 ± 0.25 was obtained for $\log_{10} K_3$, 1.36 ± 0.25 for $\log_{10} K_4$, and 2.65 ± 0.50 for $\log_{10} K_3K_4$. These values are somewhat higher than literature values. The discrepancies are most probably due to the assumptions that the molar scattering coefficients of the symmetric stretching modes of the three species were equal and that all activity coefficients were unity. The different techniques employed and different concentration ranges studied also may have contributed to the differences between our values and previous values for the equilibrium constants.

Acknowledgements

This work was supported by grants from the Natural Sciences and Engineering Research Council of Canada and Queen's University.

1. J. T. BULMER and H. F. SHURVELL. J. Phys. Chem. **77**, 256 (1973).
2. H. F. SHURVELL, K. CHITUMBO, K. A. DUNHAM, and L. CHAPPELL. Can. J. Spectrosc. **21**, 53 (1976).
3. J. JAN, J. T. BULMER, and D. E. IRISH. J. Phys. Chem. **81**, 649 (1977).
4. H. F. SHURVELL and A. DUNHAM. Can. J. Spectrosc. **23**, 5 (1978).
5. H. F. SHURVELL and J. T. BULMER. *In* Vibrational spectra and structure. Vol. 6. *Edited by* J. R. Durig. Elsevier, Amsterdam. 1977. pp. 91–172.
6. L. SILLÉN. Acta Chem. Scand. **3**, 539 (1949).
7. B. LINDGREN, A. JOHNSON, and L. SILLÉN. Acta Chem. Scand. **1**, 479 (1947).
8. Y. MARCUS. Acta Chem. Scand. **11**, 599 (1957).
9. L. CIAVATTA and H. GRIMALDI. J. Inorg. Nucl. Chem. **30**, 197 (1968).
10. J. E. D. DAVIES and D. A. LONG. J. Chem. Soc. A, 2564 (1968).
11. G. JANZ and D. W. JAMES. J. Chem. Phys. **38**, 902 (1963).
12. G. JANZ and D. W. JAMES. J. Chem. Phys. **38**, 905 (1963).
13. J. BRILL. J. Chem. Phys. **57**, 1534 (1972).
14. J. A. ROLFE, D. E. SHEPPARD, and L. A. WOODWARD. Trans. Faraday Soc. **50**, 1275 (1954).
15. H. SANDSTROM. Acta Chem. Scand. **31A**, 141 (1977).
16. Z. KECHI. Spectrochim. Acta, **18**, 1165 (1962).
17. J. CLARK and L. WOODWARD. Trans. Faraday Soc. **61**, 207 (1965).
18. E. SHORT, D. WATERS, and D. MORRIS. J. Inorg. Nucl. Chem. **26**, 902 (1964).
19. D. WATERS, E. SHORT, M. THARWAT, and D. MORRIS. J. Mol. Struct. **17**, 389 (1973).
20. T. JARV. M.Sc. Thesis. University of Waterloo, Waterloo, Ont. 1975.
21. J. PITHA and R. N. JONES. National Research Council of Canada Bulletin No. 12. 2nd ed. *In* Computer Programs for Infrared spectrophotometry. Vol. II. *Edited by* R. N. Jones. National Research Council of Canada. 1976.
22. L. G. PARAT. Probability and experimental errors in science, an elementary survey. J. Wiley, New York. 1961. p. 188.
23. J. T. BULMER. Ph.D. Thesis. Queen's University, Kingston, Ont. 1973. Appendix A.3.

A comparison of the electron impact and fast atom bombardment mass spectra of some group IV organometallic halides

JACK M. MILLER AND ADRIAN FULCHER

Department of Chemistry, Brock University, St. Catharines, Ont., Canada L2S 3A1

Received October 15, 1984

JACK M. MILLER and ADRIAN FULCHER. Can. J. Chem. **63**, 2308 (1985).

The positive ion fast atom bombardment (FAB) mass spectra of a series of group IV organometallic halides, $(phenyl)_3MCl$ (M = Ge, Sn, Pb), $(phenyl)_3PbX$ (X = Cl, Br, I) and $Sn(phenyl)_nCl_{4-n}$ are reported in a sulfolane matrix, and compared to their corresponding EI spectra. The use of other matrix liquids such as glycerol thioglycerol, diamylphenol, 18-crown-6/tetraglyme, and *p*-nitrophenyloctylether are discussed. Disappointingly FAB, like EI, does not produce significant parent ions for group IV organometallics. The FAB and EI spectra are remarkably similar with one major exception. In EI, the loss of a phenyl is preferred over the loss of a halide, while in FAB the reverse is the case, strongly suggesting that the primary ionization occurs in the condensed phase.

JACK M. MILLER et ADRIAN FULCHER. Can. J. Chem. **63**, 2308 (1985).

Opérant dans des matrices de sulfolane, on a déterminé les spectres de masse, par bombardement avec des atomes rapides d'ions positifs, d'une série d'halogénures de composés organométalliques du groupe IV, soit les $(phényl)_3MCl$ (M = Ge, Sn, Pb), les $(phényl)_3PbX$ (X = Cl, Br, I) et les $SN(phényl)_nCl_{4-n}$; on compare les spectres obtenus grâce à cette technique avec ceux obtenus par IE. On discute aussi de l'utilisation d'autres liquides matriciels comme le glycérol, le thioglycérol, le diamylphénol, l'éther 18-couronne-6/tétraglyme et l'éther *p*-nitrophénoxyoctane. Les spectres obtenus à l'aide de cette technique moderne sont désappointants puisque les quantités d'ions parents qui sont obtenues sont aussi faibles que celles obtenues sous IE et que les deux séries de spectres sont très semblables, à une exception près. Dans les spectres sous IE, la perte du phényle se fait plus facilement que celle de l'halogénure alors que c'est l'inverse dans les spectres par bombardement avec des atomes rapides; ceci suggère fortement que l'ionisation primaire se produit dans la phase condensée.

[Traduit par le journal]

Introduction

While the use of fast atom bombardment (FAB) mass spectrometry by organic and biochemists grew rapidly immediately after the discovery of the technique, inorganic and organometallic chemists have been slower to apply this important new soft ionization technique — even though at first glance the method should solve many problems associated with thermally labile, unstable, or relatively involatile organometallics. One of the drawbacks is that, unlike polar biochemical species which have an excellent chance of yielding good FAB spectra in a glycerol or thioglycerol matrix, organometallics, with a wide range of polarities, reactivities, Lewis acidities, and susceptibility to hydrolysis do not automatically yield a molecular or quasi-molecular ion on the first try in FAB with the most common and easily used matrix liquids. In addition, just as applications of EI mass spectrometry to organometallics lagged behind application to organics because it was difficult for organometallic chemists to gain access to instruments and because there are more complex rules for understanding the spectra, application of FAB to organometallics is also being delayed for the same reasons. The new very high mass (10 000 Daltons and higher) mass spectrometers now becoming available, have for the most part been installed in labs with a biomedical orientation and have been less accessible to the inorganic chemist.

However, inorganic, organometallic, and coordination chemical applications of FAB are now multiplying (1, 2). Although papers have been published on transition metal organometallics also containing group IV elements (3, 4), no details of a systematic FAB study on simple group IV organometallics have been reported in the primary literature (5). We present such a study here. The EI spectra of many of these compounds have previously been reported by Glockling and co-workers (6, 7) or obtained by us as part of an earlier EI study of some HMPA adducts (8, 9), but with one exception, they are repeated here so that we have comparisons on the same samples run in EI and FAB on the same instrument with the same geometry and under the same experimental conditions.

Experimental

Samples used were commercially available organometallics (Alfa). They were used without further purification if the melting points corresponded with those in the literature and if the mass spectra were free of obvious impurity peaks. The matrix liquids, sulfolane, diamylphenol, thioglycerol, 18-crown-6, tetraglyme (Aldrich), glycerol (BDH), and *p*-nitrophenyloctylether (Fluka) were used without further purification.

Mass spectra were obtained on a Kratos (AEI) MS30 mass spectrometer, interfaced to a Kratos DS55 data system. EI spectra were obtained from beam 2 of the MS30 with a source temperature of 180°C, samples being evaporated from a direct insertion probe heated just enough to maintain adequate sample pressure. A 4 kV accelerating voltage was used at resolution 1000, with a 300 μA regulated trap current. The FAB source was a Kratos retrofit to beam 1 of the MS30, involving the addition of fast pumping for the source, an Ion Tech Fast Atom Gun in place of the normal direct insertion lock, and a modified source endplate with a rear entry lock for the FAB probe. Argon, or preferably xenon, was used as the bombarding gas with atom gun energies of 6−8 kV and a gun current of approximately 1 mA, and a source pressure with bombarding gas flowing and evaporating matrix liquid of $1-2 \times 10^{-5}$ Torr. Samples dissolved in the matrix liquid were placed on the 2 mm diameter beveled stainless steel probe tips. The source was operated at room temperature, with the same resolution and accelerating voltage as for the EI spectra. The data system was calibrated with PFK (perfluorokerosine) for the EI spectra with real time, time to mass conversion. For FAB, perfluoroheptatriazine was used for the calibration, and data were acquired as time files and converted to mass off line, since we were not certain of having a lock mass. The matrix background could be subtracted by the data system, leaving the spectrum of the organometallic. At low masses in particular, the matrix subtraction did not always completely remove the matrix peaks, a result of the variation of the matrix spectrum with concentration. The data presented are for metal-containing ions only, normalized to 100%. Ion intensities are summed over all isotopic contributions.

TABLE 1. Comparison of the EI and FAB mass spectra of $(phenyl)_3MCl$ (M = Ge, Sn, Pb)*

	Ion abundance as % of total metal-containing ions					
	M = Pb		M = Sn		M = Ge	
Ion$^+$	EI	FAB	EI	FAB	EI	FAB
$M_2(phenyl)_5$	—	—	—	—	—	2.4
Molecular ion	—	—	0.4	—	4.4	—
$M(phenyl)_3Sulf_2$	—	—	—	—	—	1.4
$M(phenyl)_3Sulf$	—	2.6	—	2.0	—	2.0
$M(phenyl)_3$	5.1	21.9	2.7	50.6	15.4	45.2
$M(phenyl)_2ClSulf$	—	4.3	—	3.2	—	2.8
$M(phenyl)_2Cl$	20.4	9.1	45.4	12.0	40.5	15.1
$M(phenyl)_2 - H$	—	—	2.4	—	9.4	12.7
M(phenyl)Sulf	—	7.0	—	—	—	—
M(phenyl)	17.3	25.1	12.9	13.2	18.1	18.3
MClSulf	—	7.0	—	2.5	—	—
MCl	25.6	3.7	28.5	2.5	12.1	—
MSulf	—	5.9	—	—	—	—
M	31.3	12.3	5.7	15.4	—	—

*Sulf = sulfolane, the FAB matrix liquid.

TABLE 2. Comparison of the EI and FAB mass spectra of $(phenyl)_3PbX$ (X = Cl, Br, I)*

	Ion abundance as % of total metal-containing ions					
	X = Cl		X = Br		X = I	
Ion$^+$	EI	FAB	EI	FAB	EI	FAB
$(Phenyl)_2PbXSulf$	—	4.3	—	5.7	—	1.3
$(Phenyl)_2PbX$	20.4	9.1	20.4	20.0	1.0	5.8
$(Phenyl)_3PbSulf$	—	2.6	—	3.0	—	3.2
$(Phenyl)_3Pb$	5.1	21.9	5.5	14.1	32.2	24.3
(Phenyl)PbX − H	0.3	—	0.4	—	—	—
(Phenyl)PbSulf	—	7.0	—	4.9	—	5.8
(Phenyl)Pb	17.3	25.1	18.0	24.2	23.7	31.0
$(Sulf)_2PbX$	—	<1.1	—	<0.8	—	—
(Sulf)PbX	—	7.0	—	6.0	—	3.2
PbX	25.6	3.7	24.4	4.5	8.9	2.6
PbSulf	—	5.9	—	4.2	—	6.5
Pb	31.3	12.3	31.2	11.7	33.9	16.1

*Sulf = sulfolane, the FAB matrix liquid.

For the bulk of the study in sulfolane matrix, the matrix solutions were saturated with the organometallic. For the comparison of the various matrix liquids, samples were prepared with 100 mg of organometallic dissolved in 100 μL of matrix liquid.

Results and discussion

a. Comparisons of EI mass spectra with FAB mass spectra in sulfolane

In the first series of EI/FAB comparisons, Table 1 shows the differences occurring when the group IV metal is changed from lead, to tin, and then to germanium, for their respective triphenylmetalchloride derivatives. Two things stand out immediately. FAB mass spectra of these group IV organometallics show no molecular ions, quasi-molecular ions, or molecular ions coordinated to a molecule of the matrix liquid, and thus appear to be somewhat of a disappointment to those who hoped for a soft ionization technique which would readily provide a molecular ion for species such as the group IV organometallics which have notoriously weak, or absent parent ions. Only the EI spectra of the tin and germanium derivatives showed weak molecular ions. The FAB spectrum in the germanium case showed a digermanium species, presumably as a result of ion/molecule reactions occurring immediately on sputtering in the region near the matrix surface where the concentration of ions and molecules is quite high.

Two obvious differences are quickly apparent on comparison of these FAB and EI data. First there is the presence in FAB of ions involving a molecule (or even two molecules) of matrix liquid coordinated to an ion fragment, which is itself observed in both EI and FAB, the unsolvated fragment always being of greater intensity than the solvated one. The second striking difference is the relatively low abundance of organometallic ions containing the chloride, or metal chloride ions for that matter, in FAB compared to EI. Basically it appears that in FAB mass spectra of these derivatives, chloride is lost in preference to a phenyl group, whereas in EI the phenyl is lost preferentially. This might suggest that there is a pre-equilibrium or pre-ionization step in solution. Examples of pre-ionization could include protonation, i.e. a pseudo chemical ionization. A R_3MXH^+ ion thus formed could readily lose HX. Alternately, a molecule of matrix liquid could displace a halide ion giving R_3MMat^+. Under these circumstances, with energy supplied to the solution by the bombarding atoms, a cation can be formed directly by chloride loss from the parent molecule. A chloride ion might be more readily lost in solution (with a polar matrix molecule being available to solvate it) than would a phenyl anion or radical. Phenyl loss would still require a subsequent ionization step for the remaining organometallic radical species. In EI, however, in the gas phase ionization process, there is simple competition between the strength of the metal carbon and metal halogen bonds without any possibility of solvation entering the picture.

This relative halide/phenyl loss is most apparent for the triphenyl−metal ions vs. diphenyl − metal-chloride ions, where, for each metal, the FAB abundances of the former ions are virtually interchangeable with the EI intensities of the latter. The metal chloride ions themselves are also greatly reduced in FAB, to the extent of being absent for germanium. The simple phenyl M ion is reasonably consistent between EI and FAB and for each metal. The bare metal ions themselves are only observed for lead and tin, the FAB/EI ratio being reversed for the two metals. Germanium ions are absent. Another ion of interest is that due to the loss of a benzene molecule from the triphenyl germanium and tin ions. This species, appearing one mass unit below the expected mass of the essentially absent diphenyl−metal species, is observed in the EI spectrum of the tin and germanium derivatives; it being much stronger in the latter, which also shows this species as an abundant ion in its FAB spectrum.

A similar comparison on changing the halide from chloride to bromide to iodide is shown in Table 2 for the triphenyllead halides. Again we do not see parent ions in either EI or FAB, and again some preference for loss of halide is observed in FAB in comparison to the EI loss of phenyl, though this difference is less for the bromide than for the chloride. In the case of the iodide, this behavior is not apparent for the organometallic species, but still prevails for the simple lead iodide. For much of the data, the chlorides and bromides behave very much alike. With the exception of the species corresponding to tri-coordinate lead, the trends observed in the EI spectra are

TABLE 3. Comparison of the EI and FAB mass spectra of $(phenyl)_nSnCl_{4-n}$ (n = 1–4)*

	Ion abundance as % of total metal-containing ions							
	n = 4		n = 3		n = 2		n = 1	
Ion$^+$	EI	FAB‡	EI	FAB	EI	FAB	EI	FAB
Molecular ion	0.1	—	0.4	—	9.6	—	15.4	9.4
Molecular ion − H	2.1	—	—	—	—	—	—	—
$Sn(phenyl)_3Sulf$	—	9.3	—	2.0	—	—	—	—
$Sn(phenyl)_3$	42.3	35.9	2.7	50.6	—	1.9	—	—
$Sn(phenyl)_2ClSulf$	—	—	—	3.2	—	18.2	—	—
$Sn(phenyl)_2Cl$	—	—	45.4	10.6	9.1	24.3	—	—
$Sn(phenyl)_2$	16.7	—	—	—	—	—	—	—
$Sn(phenyl)_2$ − H	1.5	2.2	2.4	—	—	—	—	—
$SnCl_3Sulf$	—	—	—	—	—	—	—	1.0
$SnCl_3$	—	—	—	—	—	—	1.1	4.7
$Sn(phenyl)Cl_2Sulf$	—	—	—	—	—	10.0	—	6.8
$Sn(phenyl)Cl_2$	—	—	—	—	12.9	4.4	21.7	20.5
Sn(phenyl)Cl	—	—	—	—	18.5	—	1.8	—
Sn(phenyl)Sulf	—	4.6	—	—	—	4.2	—	—
Sn(phenyl)	17.5	31.4	12.9	13.2	3.6	7.5	2.5	4.2
$SnCl_2$	—	—	—	—	—	—	2.1	—
$SnCl(Sulf)_2$	—	—	—	—	—	6.2	—	2.5
SnClSulf	—	—	—	2.5	—	11.9	—	10.1
SnCl	—	—	28.5	2.5	39.0	7.5	40.5	28.6
Sn	18.6	10.4	5.7	15.4	7.3	4†	9.5	14†

*Sulf = sulfolane, the FAB matrix liquid.
†Tin ions are partially masked by sulfolane matrix, values calculated from ^{116}Sn.
‡Taken from ref. 6.

reflected in the FAB data. Formation of free lead cations is twice as probable in the EI spectra as in the FAB, and is not dependent on the halide.

As a potential analytical technique for this series of compounds, there is nothing to choose between the two ionization techniques. Essentially all important ions seen by one technique are seen by the other, with the exception of the coordination of matrix molecules. As the matrix is known, these are easily predictable.

When we look at a series in which the number of phenyls on tin is varied from four down to one, we observe the data shown in Table 3. The EI spectra all show parent ions, with intensities increasing as the chloride content rises, all of them quite weak except for the trichloride. In the latter case the FAB spectrum as well shows a parent molecular ion, though only two thirds the intensity of that observed in the EI spectrum. In the case of the trihalide, the generalization made above about loss of halide for the FAB spectrum in comparison with the EI spectrum breaks down to some extent, tin trichloride species in FAB being more abundant than in EI, but so too are the diphenyltin chloride containing ions. Interestingly, though FAB usually seems to lead to the loss of a halide in preference to a phenyl, the presence of three chlorides leads to the observation of a molecular ion. It is also interesting to note that it is a true molecular ion, not a quasi-molecular ion that is observed in the FAB spectrum.

FAB spectra show more metal-containing ions than the corresponding EI spectra except for the case of the tetraphenyl derivative. This difference is usually due to the presence of ions solvated by the matrix sulfolane.

b. Comparisons of various matrix liquids

In Table 4 we show the effect of changing the matrix liquid on the FAB spectra of triphenyl tin chloride. Since the concentration was kept approximately constant for the comparison of the various matrix liquids, the sulfolane data are repeated, once as the saturated solution, and once as a slightly more dilute sample. There is some variation, rather more than might be expected on repeat runs of an EI spectra, but there are no significant inversions of ion intensities. All the spectra in the matrix comparison were run on the same day with identical instrument settings, source and atom gun conditions, and with the same operator. The EI data are presented in the first column for comparison purposes. There is really no single matrix liquid which gives a FAB spectrum most closely resembling the EI spectrum, though the glycerol spectrum is clearly the farthest from the EI.

The data are presented with the matrix liquids in approximately decreasing order of polarity, with the three having acidic protons being presented first. Of these thioclycerol gave the triphenyltin cation as the base peak, i.e. not just the most intense metal-containing ion, but the most intense ion in the whole spectrum, i.e. including matrix peaks, and one to two orders of magnitude greater than that observed for diamylphenol or glycerol itself. The thioglycerol had few simple matrix ions in the spectrum, but did have some unidentified high mass species. Of the non-protic matrix liquids, only the sulfolane gave the triphenyltin cation as the base peak, with both the nitrophenyloctylether and crown ethers having low mass matrix fragments as the base peaks. Thioglycerine and sulfolane give remarkably similar spectra. As one moves across the table, with the exception of "Dap", the triphenyltin cation relative abundance decreases, and the diphenyltinchloride ion increases, though only for NPOE does the intensity invert, with the halide being more intense. In this sense, perhaps the NPOE matrix most closely resembles the EI data.

TABLE 4. Comparison of the EI and FAB mass spectra of $(C_6H_5)_3SnCl$ in various matrix liquids*

Ion$^+$	EI	Gl FAB	Dap FAB	Thio FAB	Sulf FAB	Sulf† FAB	NPOE FAB	Crown FAB
$(C_6H_5)_3SnCl$	0.4	—	—	—	—	—	—	—
$(C_6H_5)_3SnMat$	—	—	4.3	—	2.0	2.8	2.9	2.1
$(C_6H_5)_3Sn$	2.7	66.	44.4	60.0	50.6	40.2	23.5	27.9
$(C_6H_5)_2SnClMat$	—	—	4.3	—	3.2	4.3	10.3	3.5
$(C_6H_5)_2SnCl$	45.4	—	32.1	7.4	12.0	15.1	34.8	18.8
$(C_6H_5)_2Sn - H$	—	—	—	—	2.5	4.9	2.9	—
SnClMat	—	—	—	—	—	—	1.8	9.0
SnCl	28.5	—	—	2.5	2.5	4.3	7.9	6.4
C_6H_5SnMat	—	—	—	—	—	—	1.6	6.8
C_6H_5Sn	12.9	34.0	15.0	21.1	13.2	20.4	14.2	15.0
SnMat	—	—	—	—	—	—	—	3.9
Sn	5.7	—	—	9.1	15.4	7.9	—	6.4
R_3Sn^+/base peak	1.0	0.02	0.1	1.0	1.0	1.0	0.13	0.23
Base peak, m/z	‡	93	43	‡	‡	‡	43	45
Absolute R_3Sn order		6	4	1	3	3	5	2

*Mat = coordinated matrix liquid, Gl = glycerol, Dap = di-*t*-amylphenol, Thio = thiophenol, Sulf = sulfolane, NPOE = 2-nitrophenyloctylether, Crown = 18-crown-6/tetraglyme.

†The second sulfolane run was at a slightly reduced concentration, such that the same approximate concentration was used for all the samples in this run, which were run the same day with the same operator, with the same instrument settings, gain etc.

‡R_3Sn.

TABLE 5. Positive ion FAB mass spectrum in a glycerol matrix of $(C_6H_5)_3SnEC_6F_5$, E = O, S, for metal-containing ions*

O			S	
EI	FAB	Ion$^+$	EI	FAB
0.6	—	M	0.2	—
—	0.5	(M+2Gl − 2H)	—	—
55.1	60.1	Ph_3Sn	55.7	60.3
7.5	1.2	Ph_2Sn	5.2	—
18.9	26.8	PhSn	21.6	25.5
17.9	7.9	Sn	17.2	14.2
—	3.9	(Sn+Gl − H)	—	—

*Gl = glycerol matrix.

TABLE 6. Comparison of the positive FAB of $(benzyl)_2SnCl_2$ and $(phenyl)_2SnCl_2$ in sulfolane

Intensity		
R=Benzyl	R=Phenyl	Ion$^+$
8.1	—	$RSn(sulfolane)_3$
6.2	—	$R_3Sn(sulfolane)$ — a redistribution ion
17.8	18.2	$R_2SnCl(sulfolane)$
16.7	1.9	R_3Sn — a redistribution ion
7.6	24.3	R_2SnCl
—	10.0	$RSnCl_2(sulfolane)$
—	4.4	$RSnCl_2$
5.4	4.2	RSn(sulfolane)
—	6.2	$SnCl(sulfolane)_2$
12.9	11.9	SnCl(sulfolane)
21.8	7.5	RSn
—	7.5	SnCl
—	4.	Sn

Though the sulfolane spectrum gave the triphenyltin ion as the overall base peak, in absolute intensity (counts of the digitizer) terms, it was more intense in both the thioglycerol and crown matrices. In terms of apearance, the NPOE (only 5th in R_3Sn^+ intensity) and Crown (2nd) gave spectra more readily interpretable at a glance than did either sulfolane (3rd) or thioglycerol (1st in absolute intensity). However, these factors do not appear to seriously affect the actual ion intensities, the consistency rather than the differences between the matrix liquids being the more remarkable. There are differences due to solvation, and ionic equilibria, but on the whole they are less than the differences between the EI and FAB data.

c. *Other systems*

Though for the halide systems, glycerol was the worst matrix investigated, we show in Table 5 that for a non-halogenated tin, glycerol is an adequate matrix for organometallics. The EI (10) and FAB spectra are compared for the triphenyltin derivatives of pentafluorophenol and pentafluorothiophenol. If we compare the metal-containing species in both cases, the EI and FAB data are remarkably similar.

In Table 6 we compare the effect of changing the organic group from phenyl to benzyl in the R_2SnCl_2 system using a sulfolane matrix. The benzyl group appears to redistribute in the matrix under FAB conditions much more so than does a phenyl group. Loss of halide is also much more prevalent in the benzyl case. These data suggest that a study of organic exchange reactions by FAB may well be feasible if the ligands are sufficiently labile.

In conclusion, FAB appears to be a useful way to study group IV organometallics. It is, in fact, somewhat worse than EI mass spectrometry, in observing a molecular ion of the species of interest, a notoriously difficult problem for compounds of this type. However, the fragmentation appears to be similar to, though not exactly the same as, that observed in EI spectra. Thus FAB can be used for identification of known species or investigation of unknowns, especially systems not likely to be volatile or thermally stable in conventional EI inlet systems. Certainly FAB is complementary to EI data. The matrix liquids have some effect on the spectrum, but basically, if a spectrum is obtainable, the data are interpretable. Protic matrix liquids do not cause particularly serious problems with halides that are potentially hydrolytically unstable.

Acknowledgements

We wish to thank NSERC of Canada for a research grant to J.M.M. and a summer studentship to A.F., and NSERC and a Joseph H. DeFrees Grant of Research Corporation for aid in acquiring our FAB facilities.

1. J. M. MILLER. J. Organomet. Chem. **249**, 299 (1983).
2. J. M. MILLER. *In* Advances in inorganic chemistry and radiochemistry. *Edited by* H. J. Emeleus and A. G. Sharpe. Academic Press, NY. In press.
3. M. BARBER, R. S. BARDOLI, and R. D. SEDGWICK. *In* Soft ionization biological mass spectrometry. *Edited by* H. R. Morris. Heyden, London. 1981. p. 137.
4. M. BARBER, R. S. BARDOLI, R. D. SEDGWICK, and A. N. TYLER. Nature, London, **293**, 270 (1981).
5. J. M. MILLER. Paper presented at the Conference on the Organometallic and Coordination Chemistry of Ge, Sn, and Pb, Montreal, Aug. 1983.
6. D. B. CHAMBERS, F. GLOCKLING, and M. WESTON. J. Chem. Soc. A, 1759 (1967).
7. F. GLOCKLING. *In* Mass spectrometry of metal compounds. *Edited by* J. Charlambous. Butterworths, London. 1975. Chapt. 5.
8. I. WHARF, M. ONYSZCHUK, D. M. TALLETT, and J. M. MILLER. Can. J. Spectrosc. **24**, 123 (1979).
9. I. WHARF, M. ONYSZCHUK, J. M. MILLER, and T. R. B. JONES. J. Organomet. Chem. **190**, 417 (1980).
10. G. F. LANTHIER, J. M. MILLER, and A. J. OLIVER. Can. J. Chem. **51**, 1945 (1973).

Reactions of amines with β-(phenylseleninyl)vinyl sulfones derived from the selenosulfonation of acetylenes. Formation of enamine sulfones[1]

THOMAS G. BACK,[2] SCOTT COLLINS,[3] AND KWOK-WAI LAW
Department of Chemistry, University of Calgary, Calgary, Alta., Canada T2N 1N4

Received October 3, 1984

THOMAS G. BACK, SCOTT COLLINS, and KWOK-WAI LAW. Can. J. Chem. **63**, 2313 (1985).

β-(Phenylseleno)vinyl sulfones **2** were prepared from the selenosulfonation of acetylenes and were oxidized to the corresponding selenoxides **3**. These were treated *in situ* with morpholine (**4**) or pyrrolidine (**5**) to afford the corresponding enamine sulfones **6** and, in those cases where **3** were derived from terminal acetylenes, their selenenylated analogues **7**. The formation of the latter was enhanced by adding benzeneselenenyl chloride to the reaction mixture, and suppressed by the presence of selenenic acid scavengers such as enamine **10** or ethyl vinyl ether. In several instances the enamine sulfones were hydrolyzed to β-keto sulfones prior to work-up. A mechanistic rationale for the formation of **6** and **7** is presented. Selenoxide **3***f* behaved anomalously when treated with pyrrolidine and underwent isomerization to an allyl selenoxide, followed by [2,3] sigmatropic rearrangement to produce allyl alcohol **18**. Selenoxide **3***f* was reduced by *N*,*N*-dimethylhydrazine to the selenide **2***f*.

THOMAS G. BACK, SCOTT COLLINS et KWOK-WAI LAW. Can. J. Chem. **63**, 2313 (1985).

La sélénosulfonation des acétylènes a fourni les β-(phénylséléno)sulfones **2** qui ont été oxydés en sélénoxydes **3**. Le traitement de ces derniers composés *in situ* avec la morpholine (**4**) ou la pyrrolidine (**5**) a donné les énamines sulfones **6** et, dans les cas où les sélénoxydes **3** ont été dérivés des acétylènes monosubstitués, les analogues séléniés **7**. Les rendements de **7** ont été augmentés par l'addition du chlorure benzènesélénénique au mélange de la réaction et diminués par la présence des agents de trappement de l'acide benzènesélénénique, comme l'éther éthylique vinylique ou l'énamine **10**. Dans quelques cas, les énamines sulfones **6** ont été hydrolysées en sulfones β-cétoniques avant l'isolation. Une explication mécanique pour la formation de **6** et **7** est présentée. Le comportement du sélénoxyde **3***f* en présence de la pyrrolidine était anomal. Une isomérisation en sélénoxyde allylique, suivie par un réarrangement [2,3] sigmatropique, a produit l'alcool allylique **18**. Le même sélénoxyde **3***f* a été réduit par la *N*,*N*-diméthylhydrazine en séléniure **2***f*.

Introduction

The free-radical additions of selenosulfonates to olefins (1−3), allenes (4), diazomethane (5), and acetylenes (6−8) have recently been reported. In particular, the selenosulfonation of acetylenes with Se-phenyl *p*-tolueneselenosulfonate (**1**) provides an efficient route to β-(phenylseleno)vinyl sulfones **2**, which can in turn be oxidized to the corresponding selenoxides **3** (6−8) (eq. [1]). As part of our studies of selenosulfonation and its synthetic applications, we have been interested in the reactions of **2** and **3** with nucleophiles. For instance, selenides **2** undergo substitution with alkyl selenocuprates (9) (eq. [2]), and selenoxides **3** react with alcohols via Michael addition (6) to form enol ethers or ketals (eq. [3]).

[1] 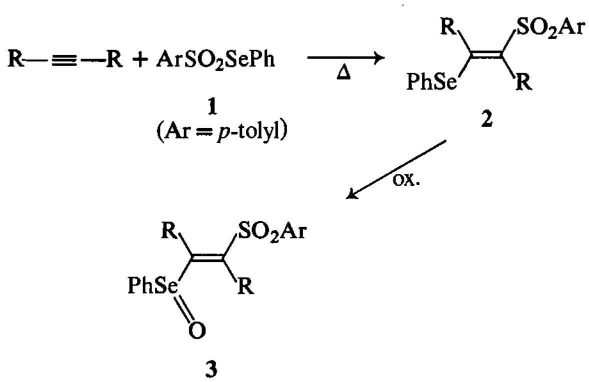

[2] 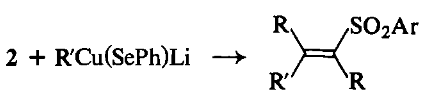

[3] 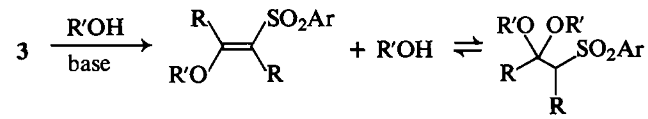

The present work is concerned with the extension of these studies to the reactions of selenoxides **3** with amines such as morpholine (**4**), pyrrolidine (**5**), and several related nucleophiles. By analogy with eqs. [2] and [3], the expected products are enamine sulfones **6** (eq. [4]). These compounds are, with some exceptions (10), unavailable from the condensation of amines with β-keto sulfones, as the latter undergo facile base-catalyzed C—C bond cleavage (11). Alternatively, the formation of enamine sulfones has been previously noted from the addition of amines to acetylenic sulfones (12−14), and from their reactions with 2-chlorovinyl (15) or 2,2-dichloroethyl sulfones (16). We now report that the aminolysis of selenoxides **3** provides enamine sulfones **6**, their selenenylated products **7**, or the corresponding β-keto sulfones, depending upon the substrate and conditions.

[4] 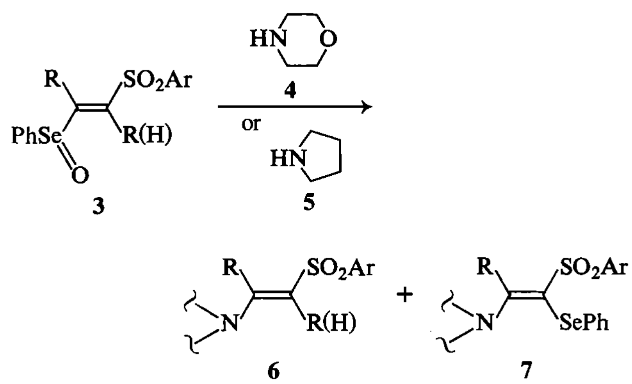

Ar = *p*-tolyl

[1]Taken in part from the Ph.D. Thesis of S. Collins, University of Calgary, 1983.
[2]Author to whom correspondence should be addressed.
[3]Recipient of an NSERC Postgraduate Scholarship and an Honorary Killam Scholarship.

TABLE 1. Reaction of selenoxides **3** with amines and enamines

	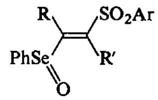 **3**					Products (% yield)[b]	
Entry	No.	R	R′	Nucleophile (equiv.)	Method[a] (time, h)	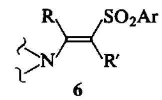 **6**	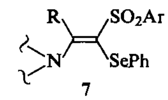 **7**
1	**3***a*	H	H	**4** (2.4)	A (1)	28	50
2		H	H	**4** (2.4)	B (1)	—	86
3		H	H	**5** (2.4)	A (0.25)	—	79
4		H	H	**10** (2.4)	A (0.25)	83	—
5	**3***b*	Ph	H	**4** (2.4)	A (24)	—	75
6		Ph	H	**4** (3.8)	C (26)	90	—
7		Ph	H	**5** (4)	C (22)	76	—
8	**3***c*	n-C_8H_{17}	H	**5** (12)	D (5)	54[c]	36[c]
9	**3***d*	n-Bu	n-Bu	**5** (12)	D (18)	83[c]	—
10	**3***e*	MeO_2C	CO_2Me	**5** (12)	A (5)	72	—
11	**3***f*	Ph	Me	**5** (12)	A (24)		[d]

[a]All experiments were conducted at room temperature. Method A: THF solvent. Method B: (*i*) THF solvent, (*ii*) excess PhSeCl added. Method C: THF solvent in presence of excess ethyl vinyl ether. Method D: (*i*) Et_2O solvent; (*ii*) H_3O^+.
[b]Isolated yields reported.
[c]Isolated as the β-keto sulfone.
[d]Product **18** (eq. [5]) was isolated in 70% yield.

Results and discussion

The results of the reactions of selenoxides **3***a*–**3***f* with morpholine (**4**) and pyrrolidine (**5**) are summarized in Table 1. Selenoxide **3***a* reacted rapidly with morpholine to afford **6** and **7** (R = R′ = H) as the minor and major products, respectively (entry 1). Only the selenenylated product **7** was obtained when the reaction mixture was further treated with benzeneselenenyl chloride (PhSeCl), or when pyrrolidine was employed instead of morpholine (entries 2 and 3). A plausible mechanism for these transformations is shown in path A of Scheme 1, in which **3***a* undergoes Michael addition of the amine to the vinyl sulfone moiety (17), followed by selenoxide elimination (18) to

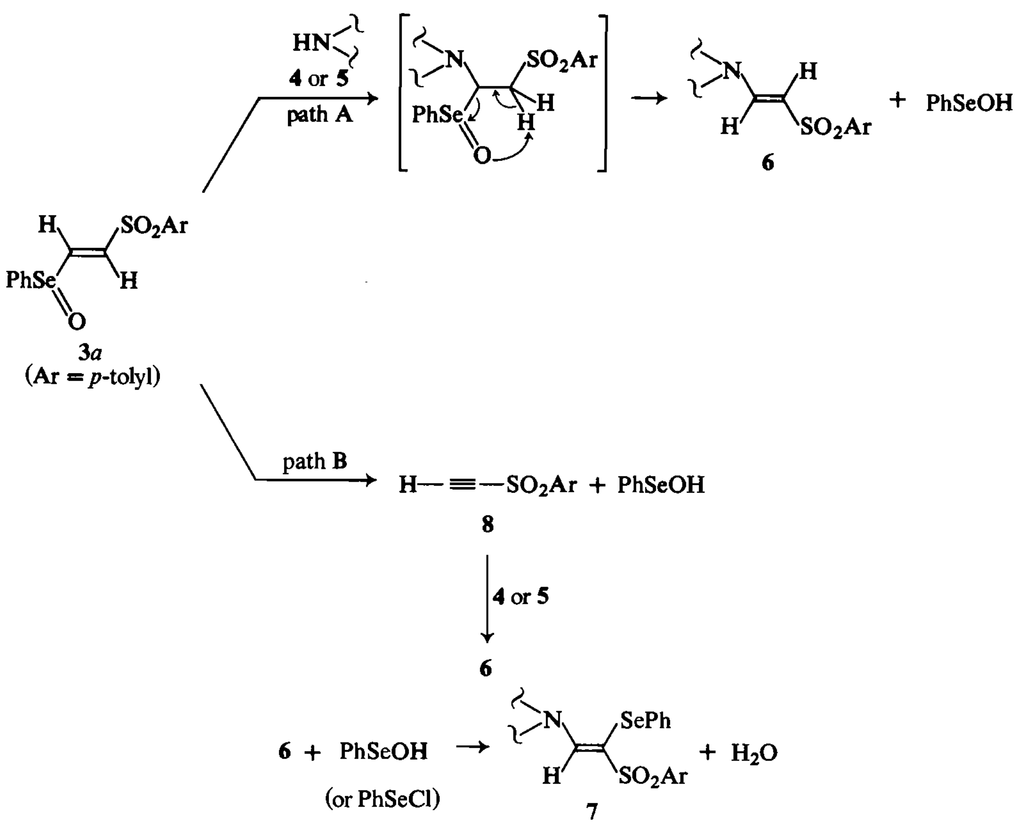

3 PhSeOH ⇌ PhSeSePh + $PhSeO_2H$ + H_2O

SCHEME 1

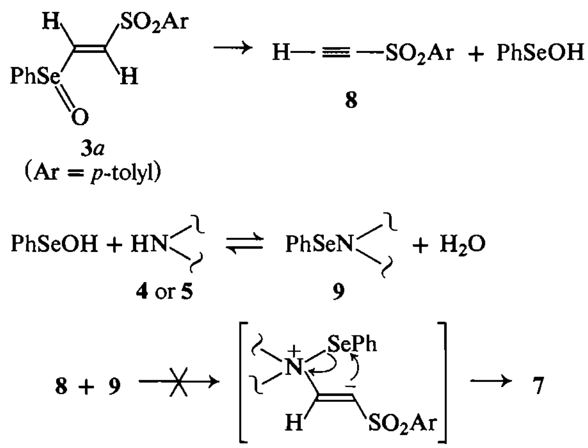

SCHEME 2

afford **6** and benzeneselenenic acid (PhSeOH). Selenoxides such as 3*a*, where R′ = H, are known to eliminate particularly rapidly under base-catalyzed conditions (6). It is therefore possible that in such systems elimination precedes Michael addition (path B) and involves intermediate acetylenic sulfones **8**, which are known to produce enamine sulfones in the presence of amines (12−14). Clearly the latter mode of reaction is precluded for those selenoxides in Table 1 where R′ ≠ H, as the absence of a vinylic hydrogen atom prevents elimination from becoming the initial step. The by-product selenenic acid (19) or a related electrophile such as the corresponding anhydride PhSeOSePh (20) can then react with the enamine sulfone to afford the selenenylated product **7**. Similar reactions of other enamines with selenenic electrophiles have been previously reported (21) and provide a precedent for this step. Any selenenic acid not consumed by the transformation of **6** to **7** disproportionates to benzeneseleninic acid and diphenyl diselenide (19), with the latter observed as a minor by-product. The addition of an excess of a selenenylating agent such as PhSeCl after the initial reaction effects the complete conversion of **6** to **7** (entry 2).

An alternative mechanism for the formation of **7** must also be considered. The selenenic acid which is produced together with the acetylenic sulfone **8** during the fragmentation of selenoxide 3*a* is expected to react with the amine to generate selenenamide **9** (22) (Scheme 2). The further reaction of this species with **8** would then afford the selenenylated product **7** via a sequential Michael addition and intramolecular selenenylation, analogous to the reactions of selenenamides with enones (22) and dimethyl acetylenedicarboxylate (23) previously reported by Reich *et al.* However, when the reaction in entry 1 was carefully monitored by ^{1}H nmr spectroscopy, it became evident that the enamine sulfone **6** is formed first and that the selenenylated product **7** arises subsequently at its expense. This observation is more consistent with Scheme 1, where **6** is the direct precursor of **7**, than with Scheme 2 where the formation of **6** and **7** proceeds independently.

The reaction of selenoxide 3*a* with excess 1-(*N*-morpholino)cyclohexene (**10**) was also investigated. Previous workers had demonstrated the additions of several enamines to vinyl sulfones (24), and the analogous process was expected to produce the corresponding γ-sulfonyl enone **13** in the present instance. Instead, however, the principal products were the enamine sulfone **6** and 2-phenylselenocyclohexanone **12**, each formed in 83% yield based on 3*a* (Scheme 3 and entry 4,

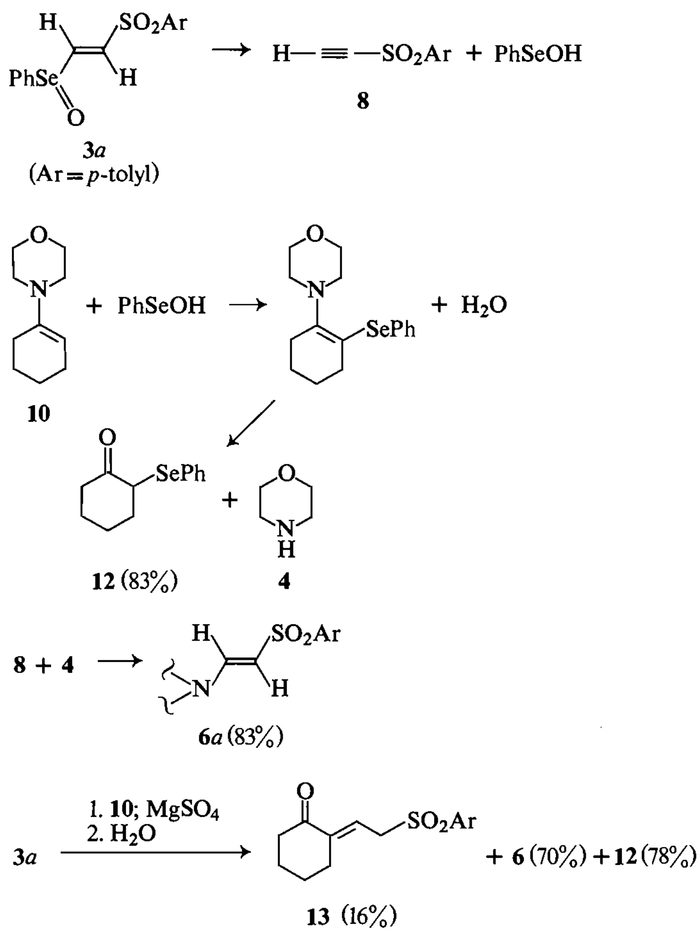

SCHEME 3

Table 1). This suggests that enamine **10** reacts not with selenoxide 3*a*, but rather with the benzeneselenenic acid produced during the fragmentation of 3*a* to the acetylenic sulfone **8**. Hydrolysis of the resulting intermediate **11** *in situ* then affords the α-seleno ketone **12**, and simultaneously liberates morpholine which adds to **8** in the usual manner to provide **6**. When the reaction was repeated under anhydrous conditions in the presence of magnesium sulfate to remove liberated water, it proceeded more slowly and the γ-sulfonyl enone **13** was obtained in a low yield of 16%; however, the previous products **6** and **12** continued to dominate. Thus, although the reactions of selenoxides **3** with enamines do not appear promising as a practical route to enones such as **13**, the present example did furnish the originally sought enamine sulfone **6**. Other attempts to efficiently convert 3*a* to **6** by blocking the subsequent selenenylation step through the *in situ* removal of the benzeneselenenic acid with a large excess of amine (25), or by its further oxidation to the corresponding seleninic acid (25), proved unsuccessful.

Entries 5 and 6 in Table 1 further illustrate the effect of a selenenic acid scavenger. The reaction of selenoxide 3*b* with morpholine (**4**) in THF produced the selenenylated enamine **7** as the only isolable product. However, when the reaction was repeated in the presence of a large excess of ethyl vinyl ether, the enamine sulfone **6** was obtained in excellent yield. It therefore appears that the nucleophilic enol ether, like enamine **10** in entry 4, is an effective trapping agent for the selenenic acid and prevents the further selenenylation of the enamine sulfone **6**.

The stereochemistry of addition of amines to acetylenic sulfones has been studied in detail by Truce *et al.* (12) and Stirling and co-workers (13, 14). When secondary amines (except aziridine) are employed, the product enamine sulfones are formed by *cis* addition to afford exclusively products with the *E*-configuration. It has been demonstrated that *Z*-products are formed kinetically, but isomerize readily to their *E*-counterparts, which are favoured because of the opposing dipoles and absence of nonbonded interactions between the amino and sulfone groups (14). The additions of secondary amines **4** and **5** to selenoxides **3** in Table 1 also proceed in a highly stereoselective manner, producing in each case only one geometric isomer of the corresponding enamine sulfone **6**. The configuration of the product **6** obtained from selenoxide **3***a* and morpholine is unequivocally established as *E* on the basis of the large vinylic coupling constant of 13 Hz. Unambiguous evidence for the configurational assignment of the other enamine sulfones in Table 1 is lacking as a result of the unavailability of both isomers for comparison. However, on the basis of the previous arguments, it is reasonable to assume that they too are the *E*-isomers. The selenenylated products **7** were also formed in a highly stereoselective manner and similar lines of reasoning suggest that they might possess the *Z*-configuration, where the amino group and sulfone moiety are once again *trans*-oriented. Such conclusions are tentative, however, in the absence of more concrete evidence.

Selenoxide **3***c* reacted with pyrrolidine to produce the expected mixture of the corresponding products **6** and **7** (entry 8, Table 1). The presence of the former compound was clearly evident from a vinylic signal at δ 4.8 in the ^{1}H nmr spectrum of the reaction mixture. However, the products could not be separated by crystallization and underwent partial hydrolysis to the corresponding β-keto sulfones **14** and **15** upon flash, column, or preparative thin-layer chromatography on either silica gel or alumina. Consequently the hydrolysis was deliberately allowed to proceed to completion and Table 1 lists the yields of the resulting β-keto sulfones. The crude enamine sulfone from selenoxide **3***d* (entry 9) also proved difficult to purify and so was similarly converted to β-keto sulfone **16** prior to isolation.

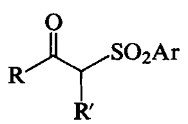

14 R = *n*-C_8H_{17}; R′ = H
15 R = *n*-C_8H_{17}; R′ = SePH
16 R = *n*-Bu = R′

An anomalous, though not entirely surprising result occurred when selenoxide **3***f* was treated with pyrrolidine (entry 11, Table 1). Base-catalyzed isomerization of **3***f* to the corresponding allylic selenoxide **17**, followed by [2,3] sigmatropic rearrangement, afforded the allylic alcohol **18** (eq. [5]). The same product has been previously observed (7) when **3***f* was allowed to react with KOH and 18-crown-6.

[5]

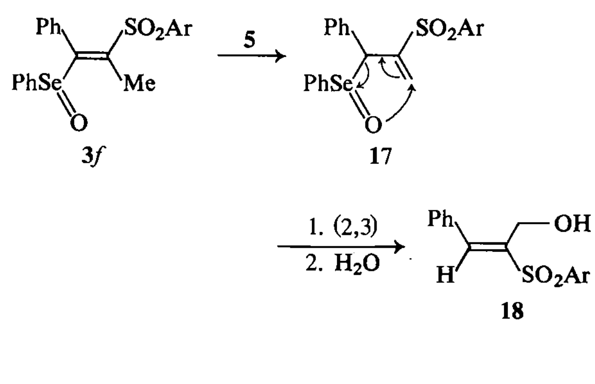

The reaction of selenoxide **3***f* with *N*,*N*-dimethylhydrazine was also investigated. Instead of addition, a redox process occurred which resulted in the formation of the corresponding selenide in nearly quantitative yield (eq. [6]). Several other oxidations of nitrogenous compounds with selenoxides are known (26).

[6] $3f + Me_2NNH_2 \longrightarrow$

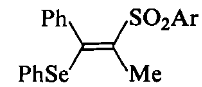

2*f*

These experiments indicate that acetylenes can in many instances be efficiently converted to enamine sulfones **6** by the sequence of selenosulfonation, oxidation, and aminolysis. When terminal acetylenes are employed as precursors, selenenylated enamines **7** generally dominate unless steps are taken to trap the electrophilic by-product, benzeneselenenic acid, as it is formed.

Experimental

Melting points were obtained on an A. H. Thomas hot-stage apparatus and are uncorrected. The ir spectra were recorded on a Perkin–Elmer 467 spectrometer. The nmr spectra were obtained on a Hitachi Perkin–Elmer R24B or a Varian XL-200 spectrometer. All nmr spectra were run in $CDCl_3$ solution and are reported in ppm downfield from tetramethylsilane. Mass spectra were recorded on a Varian MAT CH5 or a Kratos MS 80 instrument. Preparative tlc was performed on Analtech 20 × 20 cm glass plates coated with silica gel GF (1000 μm) unless otherwise noted. Ether and THF solvents were dried over $LiAlH_4$; morpholine and pyrrolidine were distilled when discolouration was apparent and were stored over KOH or molecular sieves. All other reagents, unless otherwise noted, were purchased from commercial sources and used without further purification.

Preparation of selenides 2

Selenides **2***a*–**2***d* and **2***f* were prepared from the selenosulfonation of the corresponding acetylenes as described previously (6, 7). Selenide **2***c*, formerly reported as an oil (6), was crystallized from hexane, mp 38–40°C.

Selenide 2e

Dimethyl acetylenedicarboxylate (1.42 g, 10 mmol) and Se-phenyl *p*-tolueneselenosulfonate **1** (27) (1.56 g, 5 mmol) were refluxed 48 h in 15 mL of benzene. Several portions (ca. 5 mg each) of azobis(isobutyronitrile) were added during this time. The product was evaporated *in vacuo* and crystallized from chloroform–hexane to afford 1.59 g (70%) of **2***e*, mp 172–173.5°C; ir (Nujol): 1730, 1689, 1595, 1307, 1160 cm^{-1}; nmr: 7.8–7.0 (complex 9H), 3.60 (s, 3H), 3.08 (s, 3H), 2.28 (s, 3H); mass spectrum, *m/e* (relative intensity, %): 454 (M^+, ^{80}Se, 22), 452 (M^+, ^{78}Se, 12). *Anal.* calcd. for $C_{19}H_{18}O_6SSe$: C 50.33, H 4.00, S 7.06; found: C 50.26, H 3.98, S 6.95.

Preparation of selenoxides 3a–3f

Selenoxides **3***a*–**3***f* were prepared on a scale of 0.5–1.0 mmol *in situ* just prior to use by treating the corresponding selenides **2***a*–**2***f* with a small excess (10–20%) of *m*-chloroperbenzoic acid (MCPBA) in THF or ether; tlc analysis after ca. 10 min indicated complete consumption of the selenide. In some cases the by-product *m*-chlorobenzoic acid was removed prior to use by washing the solution with aqueous K_2CO_3.

Reactions of selenoxides 3 with amines (See Table 1)

Selenoxide 3a with morpholine (4) (entry 1 and 2)

(a) Selenoxide **3***a* (0.50 mmol) and morpholine (104 mg, 1.20 mmol) were stirred for 1 h in 10 mL of THF. The solution was diluted with ether, washed with aqueous NaCl, dried over anhydrous $MgSO_4$, and concentrated *in vacuo*. Preparative tlc in 5% methanol–benzene provided 37 mg (28%) of *E*-1-(*N*-morpholino)-2-(*p*-toluenesulfonyl)-

ethene (**6**, R = R′ = H), R_f 0.42; mp 131–132°C (from dichloromethane–hexane) (lit. (15) mp 136°C); ir (KBr): 1610, 1317, 1302, 1293, 1270, 1130 cm^{-1}; nmr: 7.60 (d, J = 8 Hz, 2H), 7.10 (two superimposed d, J = 8, 13 Hz, total 3H), 4.92 (d, J = 13 Hz, 1H), 3.57 (m, 4H), 3.04 (m, 4H), 2.28 (s, 3H); mass spectrum, *m/e* (relative intensity, %): 267 (M^+, 23). A more mobile band afforded 104 mg (50%) of 2-(*N*-morpholino)-1-(phenylseleno)-1-(*p*-toluenesulfonyl)ethene (**7**, R = H), R_f 0.58; mp 160–162°C (from dichloromethane–hexane); ir (KBr): 1590, 1279, 1140 cm^{-1}; nmr: 7.91 (s, 1H), 7.58 (d, J = 8 Hz, 2H), 7.1–6.8 (complex, 7H), 3.7–3.2 (complex, 8H), 2.18 (s, 3H); mass spectrum, *m/e* (relative intensity, %): 423 (M^+, ^{80}Se, 47), 421 (M^+, ^{78}Se, 24), 268 ($M^+ - SO_2Ar$, ^{80}Se, 100). *Anal.* calcd. for $C_{19}H_{21}NO_3SSe$: C 54.03, H 5.01, N 3.32, S 7.59; found: C 54.11, H 4.99, N 3.08, S 7.34.

(b) The above procedure was repeated, except that 2.6 equivalents of PhSeCl were added to the reaction mixture prior to work-up. The product **7** (R = H) was isolated as before in 86% yield.

(c) Selenoxide **3***a* (42 mg, 0.12 mmol) and 22 mg (0.25 mmol) of morpholine were allowed to react in 1 mL of $CDCl_3$ while the reaction was monitored by ^{1}H nmr spectroscopy. After 5 min at room temperature the ratio of the signal at δ 4.92 (vinylic H of **6**) to that at δ 7.91 (vinylic H of **7**) was 4:1. It gradually decreased to 0.36:1 after 18 h.

Selenoxide 3a *with pyrrolidine (5) (entry 3)*

The reaction was performed as in entry 1. Preparative tlc in 5% methanol–benzene afforded 79% of 1-(phenylseleno)-2-(*N*-pyrrolidino)-1-(*p*-toluenesulfonyl)ethene (**7**, R = H), R_f 0.66; mp 180–182°C (from dichloromethane–hexane); ir (KBr): 1601, 1281, 1140 cm^{-1}; nmr: 8.19 (s, 1H), 7.62 (d, J = 8 Hz, 2H), 7.2–6.8 (complex, 7H), 3.7–3.4 (m, 4H), 2.19 (s, 3H), 1.9–1.6 (m, 4H); mass spectrum, *m/e* (relative intensity, %): 407 (M^+, ^{80}Se, 31), 405 (M^+, ^{78}Se, 18), 252 ($M^+ - SO_2Ar$, ^{80}Se, 100). *Anal.* calcd. for $C_{19}H_{21}NO_2SSe$: C 56.15, H 5.21, N 3.45, S 7.89; found: C 56.36, H 5.21, N 3.11, S 7.71.

Selenoxide 3a *with enamine* **10** *(entry 4)*

(a) The reaction was performed as in entry 1. Preparative tlc in 2% methanol–benzene provided 83% of 2-(phenylseleno)cyclohexanone (**12**) (28), identified by its ir, nmr, and mass spectra, and 83% of the enamine sulfone **6**, identical to the product of entry 1.

(b) The above reaction was repeated in oven-dried apparatus under dry N_2 in the presence of 0.5 g of anhydrous $MgSO_4$. It was necessary to reflux the solution for 1 h in order to effect the complete consumption of selenoxide **3***a*. Work-up as in entry 1 afforded **12** (78%), **6** (70%), and a band of intermediate mobility which provided 16% of the γ-sulfonyl enone **13**, mp 95–98°C; ir ($CHCl_3$): 1690, 1618, 1595, 1325, 1150 cm^{-1}; nmr: 7.72 (d, J = 8 Hz, 2H), 7.34 (d, J = 8 Hz, 2H), 6.32 (tt, J = 8.2, 2.1 Hz, 1H), 3.90 (d, J = 8.2 Hz, 2H), 2.5–2.0 (s at δ 2.42 superimposed on m, total 7H), 2.0–1.5 (complex, 4H); mass spectrum, *m/e* (relative intensity, %): 278 (M^+, 2), 123 ($M^+ - ArSO_2$, 100). *Anal.* calcd. for $C_{15}H_{18}O_3S$: C 64.72, H 6.52; found: C 64.33, H 6.67.

Selenoxide 3b *with morpholine (4) (entry 5 and 6)*

(a) The reaction was performed as in entry 1. Preparative tlc in 40% ethyl acetate – hexane provided 75% of 1-(*N*-morpholino)-1-phenyl-2-(phenylseleno)-2-(*p*-toluenesulfonyl)ethene **7** (R = Ph) as a yellow gum, R_f 0.45; ir (Nujol): 1597, 1578, 1300, 1285, 1268, 1136, 1120 cm^{-1}; nmr: 7.9–6.9 (complex, 14H), 3.7–2.7 (complex, 8H), 2.36 (s, 3H); mass spectrum, *m/e* (relative intensity, %): 499 (M^+, ^{80}Se, 26), 497 (M^+, ^{78}Se, 14), 344 ($M^+ - SO_2Ar$, ^{80}Se, 100). *Exact Mass*, high resolution mass spectrum, calcd. for $C_{25}H_{25}NO_3SSe$: 499.0720; found: 499.0748.

(b) Selenoxide **3***b* (255 mg, 0.60 mmol) and morpholine (0.2 mL, 2.28 mmol) were stirred 26 h in 5 mL of THF and 3 mL of ethyl vinyl ether. Volatile material was then removed *in vacuo* and preparative tlc on alumina GF with 50% ethyl acetate – hexane afforded 1-(*N*-morpholino)-1-phenyl-2-(*p*-toluenesulfonyl)ethene **6** (R = Ph), R_f 0.50, mp 121–122.5°C (from dichloromethane–hexane); ir (Nujol): 1594, 1310, 1135 cm^{-1}; nmr: 7.2–6.6 (complex, 9H), 5.28 (s, 1H), 3.36 (crude t, 4H), 2.71 (crude t, 4H), 2.11 (s, 3H); mass spectrum, *m/e* (relative intensity, %): 343 (M^+, 10), 188 ($M^+ - SO_2Ar$, 100). *Anal.* calcd. for $C_{19}H_{21}NO_3S$: C 66.45, H 6.16, N 4.08, S 9.33; found: C 66.45, H 6.29, N 3.96, S 9.59.

Selenoxide 3b *with pyrrolidine (5) (entry 7)*

The reaction was performed as in entry 6. The reaction mixture was concentrated and crystallized from dichloromethane–hexane to afford 76% of 1-phenyl-1-(*N*-pyrrolidino)-2-(*p*-toluenesulfonyl)ethene **6** (R = Ph), mp 192–193°C (lit. (29) mp 192–194°C); ir (Nujol): 1598, 1288, 1138 cm^{-1}; nmr: 7.3–6.7 (complex, 9H), 5.06 (s, 1H), 2.85 (m, 4H), 2.20 (s, 3H), 1.70 (m, 4H); mass spectrum, *m/e* (relative intensity, %): 327 (M^+, 15), 172 ($M^+ - SO_2Ar$, 100).

Selenoxide 3c *with pyrrolidine (5) (entry 8)*

The selenoxide (0.50 mmol) and pyrrolidine (0.5 mL, 6.0 mmol) were stirred 5 h in 5 mL of ether. The solution was evaporated *in vacuo* and the nmr spectrum of the residue revealed the presence of the enamine sulfone **6** (R = n-C_8H_{17}, R′ = H) by the presence of a prominent signal at δ 4.80 (vinylic H). The product was dissolved in 5 mL of THF and 2 mL of 3 *N* HCl were added. After 1 h, the mixture was diluted with ether, washed with water, then with aqueous K_2CO_3, dried over anhydrous $MgSO_4$, and evaporated to dryness. Preparative tlc in 20% ethyl acetate – hexane afforded 83 mg (54%) of β-keto sulfone **14**, R_f 0.37, identical to an authentic sample (6) (mp, ir, nmr, mass spectrum). A more mobile band furnished 83 mg (36%) of the α-phenylseleno derivative **15** as a pale yellow oil, R_f 0.50; ir (film): 1702, 1599, 1580, 1307, 1155 cm^{-1}; nmr: 7.9–7.1 (complex, 9H), 4.78 (s, 1H), 2.75 (t, J = 7 Hz, 2H), 2.45 (s, 3H), 1.8–1.1 (complex, 12H), 0.88 (t, J = 5 Hz, 3H), (signals from an unidentified impurity were observed at δ 5.45 and 5.20); mass spectrum, *m/e* (relative intensity, %): 466 (M^+, ^{80}Se, 7), 464 (M^+, ^{78}Se, 6), 91 ($C_7H_7^+$, 100). *Exact Mass*, high resolution mass spectrum, calcd. for $C_{23}H_{30}O_3SSe$: 466.10805; found: 466.1082.

Selenoxide 3d *with pyrrolidine (5) (entry 9)*

The reaction and hydrolysis were performed as in entry 8. Preparative tlc with dichloromethane afforded 83% of β-keto sulfone **16** as a pale yellow oil, R_f 0.77; bp (bulb-to-bulb) 120°C at 0.05 Torr (1 Torr = 133.3 Pa); ir (film): 1720, 1600, 1306, 1150 cm^{-1}; nmr: 7.60 (d, J = 8 Hz, 2H), 7.25 (d, J = 8 Hz, 2H), 4.03 (t, J = 7 Hz, 1H), 2.62 (t, J = 6 Hz, 2H), 2.42 (s, 3H), 2.1–0.7 (complex, 16 H); mass spectrum, *m/e* (relative intensity, %): 310 (M^+, 0.2), 85 ($nBu\overset{+}{C}{=}O$, 100). *Anal.* calcd. for $C_{17}H_{26}O_3S$: C 65.77, H 8.44, S 10.31; found: C 65.39, H 8.41, S 10.40.

Selenoxide 3e *with pyrrolidine (5) (entry 10)*

The reaction was performed as in entry 1. Flash chromatography over 20 g of alumina (elution with dichloromethane) provided 72% of dimethyl 2-(*N*-pyrrolidino)-3-(*p*-toluenesulfonyl)fumarate **6** (R = R′ = CO_2Me), mp 148–149°C (from chloroform–hexane); ir (Nujol): 1738, 1680, 1600, 1316, 1147 cm^{-1}; nmr: 7.82 (d, J = 8 Hz, 2H), 7.25 (d, J = 8 Hz, 2H), 3.98 (s, 3H), 3.55 (s, 3H), 3.42 (m, 4H), 2.40 (s, 3H), 1.96 (m, 4H); mass spectrum, *m/e* (relative intensity, %): 367 (M^+, 2), 85 (71), 83 (100). *Anal.* calcd. for $C_{17}H_{21}NO_6S$: C 55.57, H 5.76, N 3.81, S 8.73; found: C 55.82, H 5.83, N 3.90, S 8.62.

Selenoxide 3f *with pyrrolidine (5) (entry 11)*

The reaction was performed as in entry 1. Preparative tlc in 5% methanol–benzene afforded 70% of alcohol **18**, R_f 0.53, identical to an authentic sample (7) (mp, ir, nmr). A more polar band furnished 8% of the starting selenoxide.

Reaction of selenoxide 3f *with* N,N-*dimethylhydrazine*

Selenoxide **3***f* (0.50 mmol) and *N*,*N*-dimethylhydrazine (0.5 mL, 6.6 mmol) were allowed to stand for 3 days in 5 mL of THF. The solution was then diluted with ether, washed once with aqueous NaCl and 3 times with aqueous K_2CO_3. It was dried over anhydrous $MgSO_4$, evaporated to dryness, and recrystallized from ether–hexane to afford 205 mg (96%) of selenide **2***f*, identical in all respects with the original starting material.

Acknowledgements

We thank the Natural Sciences and Engineering Research Council for financial support. We are grateful to Drs. R. Yamdagni and W. S. Lin for mass spectra and elemental analyses.

1. T. G. BACK and S. COLLINS. J. Org. Chem. **46**, 3249 (1981); Tetrahedron Lett. **21**, 2215 (1980).
2. R. A. GANCARZ and J. L. KICE. J. Org. Chem. **46**, 4899 (1981); Tetrahedron Lett. **21**, 4155 (1980); Y.-H. KANG and J. L. KICE. J. Org. Chem. **49**, 1507 (1984).
3. L. A. PAQUETTE and W. A. KINNEY. Tetrahedron Lett. **23**, 5127 (1982); L. A. PAQUETTE and G. D. CROUSE. J. Org. Chem. **48**, 141 (1983).
4. Y.-H. KANG and J. L. KICE. Tetrahedron Lett. **23**, 5373 (1982).
5. T. G. BACK. J. Org. Chem. **46**, 5443 (1981).
6. T. G. BACK, S. COLLINS, and R. G. KERR. J. Org. Chem. **48**, 3077 (1983); T. G. BACK and S. COLLINS. Tetrahedron Lett. **22**, 5111 (1981).
7. T. G. BACK, S. COLLINS, U. GOKHALE, and K.-W. LAW. J. Org. Chem. **48**, 4776 (1983).
8. T. MIURA and M. KOBAYASHI. J. Chem. Soc. Chem. Commun. 438 (1982).
9. T. G. BACK, S. COLLINS, and K.-W. LAW. Tetrahedron Lett. **25**, 1689 (1984).
10. S. FATUTTA, G. PITACCO, C. RUSSO, and E. VALENTIN. J. Chem. Soc. Perkin Trans. 1, 2045 (1982).
11. J. J. LOOKER. J. Org. Chem. **31**, 2714 (1966).
12. W. E. TRUCE and D. W. ONKEN. J. Org. Chem. **40**, 3200 (1975); W. E. TRUCE and L. D. MARKLEY. J. Org. Chem. **35**, 3275 (1970).
13. S. T. MCDOWELL and C. J. M. STIRLING. J. Chem. Soc. (B), 351 (1967).
14. C. H. MCMULLEN and C. J. M. STIRLING. J. Chem. Soc. (B), 1217 (1966); C. J. M. STIRLING. J. Chem. Soc. 5863 (1964).
15. L. MARCHETTI and V. PASSALACQUA. Ann. Chim. **57**, 1275 (1967); Chem. Abstr. **68**, 95612s (1968).
16. S. STEFANIAK. Chem. Stosow. **22**, 143 (1978); Chem. Abstr. **89**, 163191q (1978).
17. S. T. MCDOWELL and C. J. M. STIRLING. J. Chem. Soc. (B), 343 (1967); 348 (1967).
18. D. LIOTTA. Acc. Chem. Res. **17**, 28 (1984); H. J. REICH. Acc. Chem. Res. **12**, 22 (1979); H. J. REICH. *In* Oxidation in organic chemistry. Part C. *Edited by* W. S. Trahanovsky. Academic Press, New York. 1978. Chapt. 1; D. L. J. CLIVE. Tetrahedron, **34**, 1049 (1978).
19. O. BEHAGHEL and H. SEIBERT. Ber. **66**, 708 (1933); H. J. REICH, S. WOLLOWITZ, J. E. TREND, F. CHOW, and D. F. WENDELBORN. J. Org. Chem. **43**, 1697 (1978); T. HORI and K. B. SHARPLESS. J. Org. Chem. **43**, 1689 (1978).
20. J. L. KICE, F. MCAFEE, and H. SLEBOCKA-TILK. Tetrahedron Lett. **23**, 3323 (1982); H. J. REICH, W. W. WILLIS, JR., and S. WOLLOWITZ. Tetrahedron Lett. **23**, 3319 (1982).
21. T. G. BACK, N. IBRAHIM, and D. J. MCPHEE. J. Org. Chem. **47**, 3283 (1982); K. ANZAI. J. Heterocycl. Chem. **16**, 567 (1979); D. R. WILLIAMS, B. A. BARNER, K. NISHITANI, and J. G. PHILLIPS. J. Am. Chem. Soc. **104**, 4708 (1982).
22. H. J. REICH and J. M. RENGA. J. Org. Chem. **40**, 3313 (1975).
23. H. J. REICH, J. M. RENGA, and J. E. TREND. Tetrahedron Lett. 2217 (1976).
24. F. BENEDETTI, S. FABRISSIN, and A. RISALITI. Tetrahedron, **39**, 3887 (1983); **40**, 977 (1984); S. FABRISSIN, S. FATUTTA, and A. RISALITI. J. Chem. Soc. Perkin Trans. 1, 109 (1981); S. FABRISSIN, S. FATUTTA, N. MALUSA, and A. RISALITI. J. Chem. Soc. Perkin Trans. 1, 686 (1980).
25. H. J. REICH, J. M. RENGA, and I. L. REICH. J. Am. Chem. Soc. **97**, 5434 (1975).
26. K. BALENOVIC, R. LAZIC, V. POLAK, and P. STERN. Bull Sci. (Cons. Acad. Sci. Arts RSF Yougosl. Sect A), **17**, 147 (1972); Chem. Abstr. **77**, 139499c (1972); N. BREGANT, I. PERINA, and K. BALENOVIC. Bull Sci. (Cons. Acad. Sci. Arts RSF Yougosl. Sect A), **17**, 148 (1972); Chem. Abstr. **77**, 152092j (1972); I. PERINA, N. BREGANT, and K. BALENOVIC. Bull Sci. (Cons. Acad. Sci. Arts RSF Yougosl. Sect A), **18**, 3 (1973); Chem. Abstr. **79**, 5096b (1973); M. POJE and K. BALENOVIC. Bull Sci. (Cons. Acad. Sci. Arts RSF Yougosl. Sect A), **20**, 1 (1975); Chem. Abstr. **83**, 43558u (1975); K. BALENOVIC, N. BREGANT, and I. PERINA. Synthesis, 172 (1973).
27. T. G. BACK and S. COLLINS. Tetrahedron Lett. **21**, 2213 (1980).
28. D. L. J. CLIVE. J. Chem. Soc. Chem. Commun. 695 (1973).
29. N. GURUSWAMY, C. R. DHARMARAJ, and K. RAMALINGAM. Ind. J. Chem. **11**, 882 (1973).

Multicomponent diffusion of aqueous sodium carbonate and aqueous sodium bicarbonate

DEREK G. LEAIST[1] AND ROBERT A. NOULTY
Department of Chemistry, University of Western Ontario, London, Ont., Canada N6A 5B7

Received September 18, 1984

DEREK G. LEAIST, and ROBERT A. NOULTY. Can. J. Chem. **63**, 2319 (1985).

Diffusion coefficients of Na_2CO_3 + H_2O and $NaHCO_3$ + H_2O have been measured by a conductimetric technique at 25°C. Above 0.1 mol L^{-1}, diffusion of aqueous Na_2CO_3 is typical of a simple binary electrolyte. At lower concentrations a significant proportion of the Na_2CO_3 component diffuses as $NaHCO_3$ and NaOH produced by hydrolysis: $Na_2CO_3 + H_2O \rightleftarrows NaHCO_3 + NaOH$. Because OH^- is more mobile than $HCO_3{}^-$, binary Na_2CO_3 + H_2O solutions undergoing diffusion separate spontaneously into two ternary solutions: Na_2CO_3 + NaOH + H_2O ahead of the diffusion boundary and Na_2CO_3 + $NaHCO_3$ + H_2O left behind the boundary. A procedure is developed for measuring multicomponent diffusion coefficients of hydrolyzing salts. Results for Na_2CO_3 are in satisfactory agreement with predicted ternary values. As a consequence of the disproportionation reaction: $2NaHCO_3 \rightleftarrows CO_2 + Na_2CO_3 + H_2O$, diffusion of aqueous $NaHCO_3$ is formally a ternary process. However, because reactants and products have similar mobilities and because only about 1% of the salt disporportionates, diffusion of aqueous $NaHCO_3$ is effectively binary.

DEREK G. LEAIST et ROBERT A. NOULTY. Can. J. Chem. **63**, 2319 (1985).

Utilisant une technique de conductimétrie à 25°C, on a mesuré les coefficients de diffusion du Na_2CO_3 + H_2O et du $NaHCO_3$ + H_2O. Au-dessus d'une concentration de 0,1 mol/L, la diffusion du Na_2CO_3 aqueux est typique d'un électrolyte binaire simple. À une concentration plus faible, une proportion notable de Na_2CO_3 diffuse sous la forme de $NaHCO_3$ et de NaOH produits par l'hydrolyse $Na_2CO_3 + H_2O \rightleftarrows NaHCO_3 + NaOH$. Puisque l'ion OH^- est plus labile que l'ion $HCO_3{}^-$, les solutions binaires de Na_2CO_3 + H_2O subissent une diffusion et se séparent spontanément en deux solutions ternaires, Na_2CO_3 + NaOH + H_2O en avant de la frontière de diffusion et Na_2CO_3 + $NaHCO_3$ + H_2O en arrière de cette frontière. On a mis au point une méthode de mesure des coefficients de diffusion dans des systèmes à plusieurs composants de sels subissant une hydrolyse. Les résultats obtenus avec le Na_2CO_3 s'accordent de façon satisfaisante avec les valeurs ternaires prévues. La réaction de dismutation $2NaHCO_3 \rightleftarrows CO_2 + Na_2CO_3 + H_2O$ implique que la diffusion du $NaHCO_3$ aqueux est formellement un processus ternaire. Cependant, en raison du fait que les réactifs et les produits ont des mobilités analogues et en raison du fait que seulement 1% du sel se dismute, la diffusion du $NaHCO_3$ aqueux est effectivement un processus binaire.

[Traduit par le journal]

1. Introduction

Aqueous solutions containing carbonate and bicarbonate salts are of biological, geological, and practical interest. Diffusion data for these electrolytes are thus essential in order to understand the transport properties of many important systems. Nevertheless, reliable diffusivities for carbonates or bicarbonates have not been published (1*a*, 2, 3).

This study was undertaken to determine accurate diffusion coefficients of Na_2CO_3 + H_2O and $NaHCO_3$ + H_2O. The sodium salts were chosen because of their general importance. Recently, activity coefficients for these systems were reported over wide ranges of composition (4, 5). With activity data, a more detailed interpretation of diffusion is possible.

Like many other important electrolytes, dilute carbonates are extensively hydrolyzed (5)

$$[\mathrm{I}]\quad CO_3^{2-} + H_2O \rightleftarrows HCO_3^- + OH^-$$
$$K_h(25°C) = 2.15 \times 10^{-4}\ \mathrm{mol\ L^{-1}}$$

Hydroxide is several times more mobile than bicarbonate. Therefore, when Na_2CO_3 diffuses in water, the total flow of NaOH should exceed the equimolar flows of $NaHCO_3$ and NaOH that are transported as the hydrolyzed portion of the Na_2CO_3 component. These considerations have led to speculation that isothermal diffusion in "binary" Na_2CO_3 + H_2O solutions is actually a multicomponent process described by a flow of partially hydrolyzed Na_2CO_3 together with a coupled flow of NaOH (6). Diffusion of Na_2CO_3 + H_2O would then be governed by ternary equations

$$[1]\quad -J_1 = D_{11}\nabla c_1 + D_{12}\nabla c_2$$

$$[2]\quad -J_2 = D_{21}\nabla c_1 + D_{22}\nabla c_2$$

rather than simpler binary expressions such as $-J = D\nabla c$ used previously (1*a*).

This paper presents an experimental procedure for measuring multicomponent diffusion coefficients of hydrolyzing salts. Results for aqueous sodium carbonate are used to establish by experiment whether or not diffusion of a hydrolyzing salt is a ternary process.

The effects of the disproportionation reaction (5)

$$[\mathrm{II}]\quad 2HCO_3^- \rightleftarrows CO_2 + CO_3^{2-} + H_2O$$
$$K(25°C) = 1.04 \times 10^{-4}$$

on diffusion of aqueous sodium bicarbonate are also discussed.

2. Experimental

Diffusion coefficients were measured at 25°C using a simplified version of Harned's conductimetric procedure (7). Initial concentrations were formed by injecting 0.1–0.4 mL of electrolyte solution into the bottom of a solution-filled channel (12.70 mm diameter, 45.63 ± 0.02 mm height). Diffusion was followed for 5–6 days by monitoring changes in electrical conductance at levels one-sixth of the distance from the top and bottom of the channel. Details of the equipment and procedure have been described (7–9).

The conductimetric technique was chosen so that measurements could be made at low concentrations where hydrolysis of Na_2CO_3 is extensive. Until very recently this technique was unreliable for studies of alkaline solutions because of errors caused by adsorption of OH^- (10) or leaching (11) of glass diffusion cells (7) during the long experiments. To avoid these problems, the cells used in this work were

[1]To whom correspondence should be addressed.

TABLE 1. Comparison of observed and predicted diffusion coefficients of aqueous $NaHCO_3$ at 25°C

c (10^{-3} mol L^{-1})	D (10^{-9} m^2 s^{-1})	D_{calcd} (10^{-9} m^2 s^{-1})	$(\Delta_1 + \Delta_2)^a$	$-c$ d ln $y_{\pm}/dc$
0.00	—	1.255	0.000	0.000
9.92	1.199	1.202	0.009	0.049
15.6	1.197	1.192	0.012	0.059
19.9	1.185	1.187	0.014	0.065
35.4	1.162	1.173	0.020	0.080
42.5	1.164	1.168	0.022	0.085
49.7	1.160	1.163	0.023	0.090
56.7	1.151	1.160	0.025	0.094
63.8	1.150	1.156	0.026	0.097
82.2	1.145	1.149	0.029	0.105
99.2	1.134	1.143	0.030	0.111

[a]Calculated with $a = 4 \times 10^{-10}$ m for the mean distance of closest approach of the ions.

constructed from high density polyethylene and fitted with very small (1 mm diameter) platinum electrodes (8, 9).

Binary diffusion coefficients

Conductances were measured five or six times per day. By pairing each reading with the corresponding reading taken on the following day, 18–24 values of the binary diffusion coefficient were calculated for each experiment using the difference relation (7, 9, 12, 13)

$$[3] \quad D = -\frac{A^2}{\pi^2} \frac{\Delta \ln (rK_B - K_T)}{\Delta t}$$

in which A is the length of the diffusion channel, $r = k_B/k_T$ is the ratio of cell constants of the bottom (B) and top (T) electrode pairs, and K_B and K_T denote conductances measured at time t.

For each $NaHCO_3$ experiment and for each Na_2CO_3 experiment above 0.1 mol L^{-1}, the standard deviation of the D values calculated from eq. [3] was 0.1–0.2%. The absence of a discernible trend in D over 5-6 days indicated that the measured diffusion coefficients corresponded to binary differential values at the final cell composition (12, 13).

Ternary diffusion

On the other hand, values of D computed from eg. [3] for dilute Na_2CO_3 solutions drifted downward by several percent over the duration of each experiment. The trend was most pronounced at 0.005 mol L^{-1}, the lowest concentration studied. This behavior was consistent with anticipated ternary diffusion (6): the apparent rate of diffusion of dilute Na_2CO_3 was initially high as NaOH produced by hydrolysis diffused rapidly along the column, while diffusion of slower Na_2CO_3 dominated the later stages of the experiment. Accordingly, diffusion of dilute Na_2CO_3 solutions was also analyzed as ternary diffusion of $Na_2CO_3(c_1)$ + NaOH$(c_2 = 0)$ + H_2O mixtures.

In order to measure ternary diffusion of this system it was necessary to run experiments with the initial gradient in the NaOH component (7, 9) for average cell compositions Na_2CO_3 + H_2O free of added NaOH. This was accomplished by introducing Na_2CO_3 + NaOH solutions into the bottom of diffusion channels filled with Na_2CO_3 + $NaHCO_3$ solutions. The concentrations were adjusted to that the amount of added NaOH component introduced into the cell at the start of the experiment was identical to the amount of added $NaHCO_3$ component initially in the cell above the injected layer. As the two solutions interdiffused, the neutralization reaction $NaHCO_3$ + NaOH $\rightleftarrows$ $2Na_2CO_3$ ensured that the final solution in the cell had binary composition Na_2CO_3 + H_2O. At 0.0500 mol L^{-1} Na_2CO_3, for example, 0.250 mL of solution containing 0.0100 mol L^{-1} Na_2CO_3 and 0.924 mol L^{-1} NaOH was injected into a cell filled with 5.53 mL of solution containing 0.0100 mol L^{-1} Na_2CO_3 and 0.0418 mol L^{-1} $NaHCO_3$; after diffusion, the final composition of solution in the cell was 0.050 mol L^{-1} Na_2CO_3.

At the same final cell composition, experiments were also run with the initial gradient in the Na_2CO_3 component. The conductance decay curves for the Na_2CO_3-gradient and the NaOH-gradient experiments were analyzed for ternary diffusion by an eigenvalue procedure. Details of this procedure have been reported (9). Each ternary experiment was run in triplicate.

Reagents

Na_2CO_3 and $NaHCO_3$ were A.C.S. reagent grade. Solutions of the salts were freshly prepared by weight prior to each run. Solutions of sodium hydroxide were prepared by dilution of highly pure saturated solutions. Winkler analyses indicated that the purified product contained negligible carbonate (<0.05% Na_2CO_3 based on total alkali). Hydroxide solutions were stored in polyethylene containers that were protected from atmospheric carbon dioxide. Concentrations of NaOH were determined by titration of potassium hydrogen phthalate.

3. Results and discussion

Aqueous sodium bicarbonate

The mean diffusion coefficients determined for this system are given in Table 1. Although the precision of D values from each run was 0.1 to 0.2% uncertainties in both the cell constant ratio and the length of the diffusion channel limited the reproducibility from run to run to ±0.5%.

At low ionic strengths the concentration-dependence of the diffusion coefficient of a strong 1:1 electrolyte is described by the Onsager–Fuoss equation (14, 15)

$$[4] \quad D(c) = (D^0 + \Delta_1 + \Delta_2)(1 + c \, d \ln y_{\pm}/dc)$$

where $y_{\pm}$ is the mean ionic activity coefficient on the molar concentration scale and D^0 is the limiting diffusion coefficient calculated from limiting ionic conductances and Nernst's expression

$$[5] \quad D^0 = \frac{RT}{F^2} \frac{\nu_+ + \nu_-}{\nu_+ z_+} \frac{\lambda_+^0 \lambda_-^0}{\lambda_+^0 + \lambda_-^0}$$

Allowance is made for the effects of ion–ion interactions using first and second order electrophoretic corrections calculated from (15)

$$[6] \quad \Delta_1 = -\frac{kT}{6\pi\eta} \frac{(z_+ t_-^0 + z_- t_+^0)^2}{|z_+ z_-|} \frac{\kappa}{1 + \kappa a}$$

$$[7] \quad \Delta_2 = -\frac{e^2}{12\pi\eta\epsilon} \frac{(z_+^2 t_-^0 + z_-^2 t_+^0)^2}{|z_+ z_-|} \left(\frac{\kappa e^{\kappa a}}{1 + \kappa a}\right)^2 \times \left[0.5772 + \ln (2\kappa a) + \sum_{n=1}^{\infty} \frac{(-2\kappa a)^n}{n(n!)}\right]$$

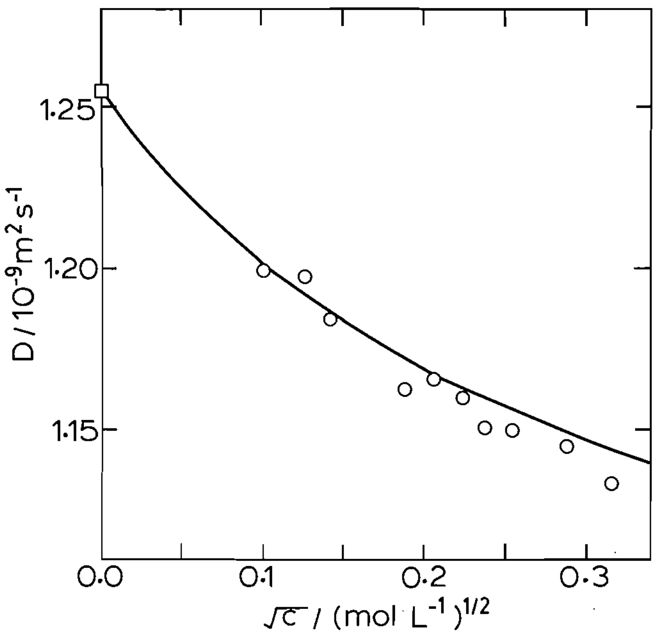

FIG. 1. Comparison of observed and predicted diffusion coefficients of aqueous $NaHCO_3$ solutions at 25°C.

in which

$$[8] \quad \kappa^2 = \frac{4\pi Ne^2}{1000\epsilon kT}(\nu_+ z_+^2 + \nu_- z_-^2)c$$

The remaining symbols appearing in eqs. [4]–[6] follow accepted electrochemical usage (15).

From the limiting ionic conductances (16*a*, 17–19) $\lambda_+^0(Na^+) = 0.005010$ and $\lambda_-^0(HCO_3^-) = 0.00445$ m² S equiv.$^{-1}$ we obtain $D^0 = 1.255 \times 10^{-9}$ m² s^{-1} for the limiting diffusion coefficient of aqueous sodium bicarbonate at 25°C and infinite dilution. The thermodynamic term $c\,d\ln y_\pm/dc$ was evaluated using activity coefficients derived by Pitzer and Peiper (4) from electrochemical-cell data. The reported molal activity coefficients ($\gamma_\pm$) were converted to molar activity coefficients required here using published densities (1*b*) and the relation (16*b*)

$$[9] \quad y_\pm = (md_0/c)\gamma_\pm$$

where m is the molality and d_0 is the density of pure water. Calculated values of the thermodynamic term are listed in Table 1.

In Table 1 observed diffusion coefficients for $NaHCO_3$ are compared with values predicted by eq. [4]. As shown in Fig. 1, agreement is especially good below 0.02 mol L^{-1}. In this region predictions made by the Onsager–Fuoss equation for 1:1 salts are generally reliable. At higher concentrations the observed diffusion coefficients are about 0.5% lower than the predicted curve. However, the discrepancy is small.

Vinograd and McBain (2) have used a porous diaphragm cell technique to measure diffusion of aqueous $NaHCO_3$. For 0.1 mol L^{-1} $NaHCO_3$ diffusing into pure water at 25°C, they report the integral diffusion coefficient 1.22×10^{-9} m² s^{-1}. The present conductimetric results over this range are consistent with an integral coefficient of about $1.16\ 10^{-9}$ m² s^{-1}, a value 5% lower. However, the diaphragm cell measurements were made before reliable procedures for calibration or stirring had been developed (20, 21). Also, diaphragm cell measurements on dilute solutions generally lead to high values of D (3). The conductimetric results are probably more reliable.

TABLE 2. Diffusion coefficients of aqueous Na_2CO_3 at 25°C

c (mol L^{-1})	D (10^{-9} m² s^{-1})	β
0.005	~1.15[a]	0.16
0.01	~1.10[a]	0.12
0.05	~1.00[a]	0.05
0.101	0.947	0.03
0.101	0.939	0.03
0.202	0.885	0.02
0.301	0.834	0.02
0.403	0.796	0.01
0.506	0.742	0.01

[a]Apparent values.

In addition to Na^+ and HCO_3^-, aqueous solutions of sodium bicarbonate contain small amounts of CO_3^{2-} and CO_2 produced by disproportionation (reaction [II]). The conditions of electroneutrality and local chemical equilibrium place two restrictions on fluxes of the four solute species. Nevertheless, two solute fluxes are independent. Therefore, strictly speaking, isothermal diffusion in aqueous solutions of sodium bicarbonate is a ternary process. In practice though, only about 1% ($\sim K^{1/2}$) of the salt disproportionates (5). Furthermore, reactants and products have similar diffusivities (16*a*, 17–19, 22, 23): $D(Na^+) = 1.33 \times 10^{-9}$, $D(HCO_3^-) = 1.18 \times 10^{-9}$, $D(CO_3^{2-}) = 0.92 \times 10^{-9}$, and $D(CO_2) = \sim 1.9 \times 10^{-9}$ m² s^{-1}. For these two reasons disproportionation is not expected to have significant effects on diffusion of sodium bicarbonate. The excellent agreement between observed diffusion coefficients and predicted binary values supports the idea that diffusion in aqueous sodium bicarbonate solutions is effectively a binary process.

Aqueous sodium carbonate

Diffusion coefficients were measured for Na_2CO_3 solutions over the range 0.005–0.5 mol L^{-1}. The results are listed in Table 2. Values for the degree of hydrolysis of the salt (5)

$$[10] \quad \beta = \frac{[OH^-]}{[CO_3^{2-}] + [OH^-]}$$

are also tabulated. D drops steadily with concentration. This behavior has been observed for aqueous Na_2SO_4 and other strong electrolytes of the 2:1 or 1:2 category (3).

In order to determine the effects of hydrolysis on the diffusional properties of the salt, it is informative to compare the measured diffusion coefficients with values predicted under the assumption of hydrolysis-free conditions. In the absence of hydrolysis or ion association, the diffusion coefficient of a dilute, unsymmetrical electrolyte is given by the expression (15)

$$[11] \quad D = (D^0 + \Delta_1)(1 + c\,d\ln y_\pm/dc)$$

(Following Stokes (15), the second order electrophoretic term, Δ_2, has been omitted for reasons of self-consistency.) Upon substitution into eq. [5] of $\lambda_-^0(CO_3^{2-}) = 0.00693$ m² s^{-1} equiv.$^{-1}$ (16*a*, 23) and the value of $\lambda_+^0(Na^+)$ quoted previously, we obtain $D^0 = 1.162 \times 10^{-9}$ m² s^{-1} for the limiting diffusion coefficient of a hypothetical solution of unhydrolyzed Na_2CO_3 at 25°C.

Goldberg (24) has derived activity coefficients of aqueous

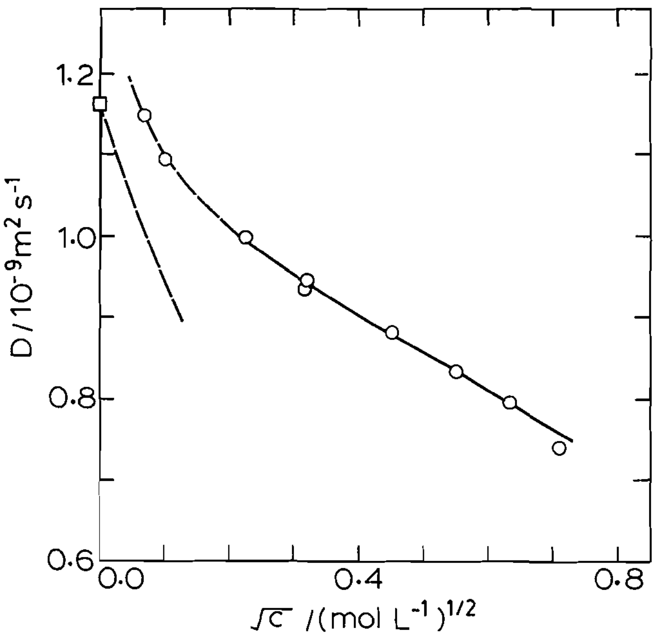

FIG. 2. Diffusion coefficients of aqueous Na_2CO_3 solutions at 25°C. Upper curve: observed values. Lower curve: predicted by eq. [11] for hydrolysis-free salt.

Na_2CO_3 from isopiestic measurements. Since hydrolysis was omitted from the analysis, diffusion coefficients of hydrolysis-free Na_2CO_3 can be estimated by evaluating the thermodynamic term in eq. [11] using Goldberg's activity data. The results of the calculations are given by the lower curve in Fig. 2.

It is evident from Fig. 2 that measured values of D are larger than anticipated for the unhydrolyzed salt. Although data above 0.1 mol L^{-1} appear to extrapolate to a limiting value close to 1.16×10^{-9} m^2 s^{-1}, results obtained below this limit curve sharply upward. In this region hydrolysis produces a significant proportion of highly mobile hydroxide ion ($D = 5.28 \times 10^{-9}$ m^2 s^{-1}).

Precise binary diffusion coefficients could not be determined at concentrations below 0.1 mol L^{-1}. For those solutions, D computed from eq. [3] was not a well-defined diffusion coefficient, but rather a time-dependent apparent binary diffusion coefficient of the mixed electrolyte Na_2CO_3 + $NaHCO_3$ + NaOH. Although the apparent molar conductance of dilute Na_2CO_3 can be interpreted by the relation (10)

$$[12] \quad \Lambda_a = (1 - \beta)\Lambda(Na_2CO_3) + \beta\Lambda(NaHCO_3) + \beta\Lambda(NaOH)$$

no simple additive rule exists to interpret the apparent diffusion coefficient of the partially hydrolyzed salt (6).

Diffusion of aqueous Na_2CO_3 produces fluxes of four solute species: Na^+, CO_3^{2-}, HCO_3^-, and OH^-. After electroneutrality and local chemical equilibrium of the hydrolysis reaction are taken into account, two solute flows must be specified to give a precise description of isothermal diffusion in aqueous solutions of the salt. We will analyze the diffusional properties of the system in terms of the molar flux J_1 of the partially hydrolyzed Na_2CO_3 component and molar flux J_2 of the NaOH component (6). (Note that J_2 is the flux of NaOH in excess of NaOH transported with $NaHCO_3$ as the hydrolyzed fraction of the Na_2CO_3 component, not the total NaOH flux.) The ternary

TABLE 3. Ternary diffusion coefficients of dilute aqueous $Na_2CO_3(c_1)$ + NaOH(c_2=0) at 25°C[a]

D_{ik}		Value		
		$c_1 = 0.005$	$c_1 = 0.010$	$c_1 = 0.050$
D_{11}	obsd.	1.04±0.02	1.05±0.02	1.01±0.03
	calcd.	0.90	0.94	0.91
D_{12}	obsd.	−0.53±0.10	−0.64±0.08	−0.53±0.03
	calcd.	−0.60	−0.66	−0.67
D_{21}	obsd.	0.22±0.04	0.14±0.04	−0.01±0.03
	calcd.	0.48	0.26	0.09
D_{22}	obsd.	3.06±0.15	3.65±0.08	3.44±0.08
	calcd.	3.22	3.22	3.13

[a]Units: c_i in mol L^{-1}, D_{ik} in 10^{-9} m^2 s^{-1}.

diffusion coefficients of the components are defined by eqs. [1] and [2]. Cross-coefficient D_{21} measures the flux of the NaOH component produced per unit gradient in concentration of the Na_2CO_3 component.

Ternary diffusion coefficients were measured at three compositions: 0.005, 0.01, and 0.05 mol L^{-1} Na_2CO_3. The results of the experiments are summarized in Table 3. Although D_{21} is zero within experimental error at 0.05 mol L^{-1} Na_2CO_3, the highest concentration studied, positive values of D_{21} observed at lower concentrations confirm that diffusion of dilute Na_2CO_3 generates concurrent transport of NaOH.

At 0.005 mol L^{-1} Na_2CO_3 the magnitude of D_{21} is about one-fifth that of D_{11}, the main diffusion coefficient of the Na_2CO_3 component. This means that the initial gradient in Na_2CO_3 produces a simultaneous flow of NaOH that is one-fifth as large as the flow of Na_2CO_3 even though the solution is free of added NaOH. Because the conductance of NaOH is large, the experimental procedure used in the present study is well-suited to the task of measuring the coupled flow of NaOH. The measurements demonstrate conclusively the ternary nature of diffusion in dilute Na_2CO_3 solutions.

The observed values of D_{22}, the main diffusion coefficient of the NaOH in aqueous Na_2CO_3, range from $3.0-3.7 \times 10^{-9}$ m^2 s^{-1}. At equivalent ionic strengths the binary diffusion coefficient of NaOH + H_2O solutions is significantly lower: $1.9-2.0 \times 10^{-9}$ m^2 s^{-1} (25, 26). In binary solutions, however, OH^- is constrained by electroneutrality to diffuse at the same rate as less-mobile Na^+. This restriction does not apply to diffusion of NaOH in aqueous Na_2CO_3 since OH^- is able to diffuse more rapidly than Na^+ while still maintaining electroneutrality by generating coupled flows of CO_3^{2-} and HCO_3^- in the opposite direction. In this instance the electric field set up by diffusion of NaOH which slows down highly mobile OH^- also drives countertransport of CO_3^{2-} and HCO_3^-. Cross-coefficient D_{12} which determines the coupled flow of the Na_2CO_3 component produced per unit gradient in NaOH is thus large and negative.

A procedure has been developed for predicting multicomponent diffusion coefficients of hydrolyzing salts (6). First, knowledge of the concentrations and diffusion coefficients of the various solute species is used to estimate Onsager transport coefficients defined by the flow equations

$$[13] \quad -J_i = \sum_k L_{ik} \nabla \mu_k$$

TABLE 4. Parameters used to predict ternary diffusion coefficients of aqueous Na_2CO_3 (c_1) + NaOH(c_2 = 0) at 25°C[a]

Parameter	Value		
	c_1 = 0.005	c_1 = 0.010	c_1 = 0.050
RTL_{11}[b]	2.62	4.85	21.3
RTL_{12}[b]	−1.86	−2.63	−5.37
RTL_{21}[b]	−1.86	−2.63	−5.37
RTL_{22}[b]	5.05	7.16	14.6
$(\partial\mu_1/\partial c_1)/RT$[c]	0.557	0.267	0.0486
$(\partial\mu_1/\partial c_2)/RT$[c]	0.300	0.134	0.0246
$(\partial\mu_2/\partial c_1)/RT$[c]	0.300	0.134	0.0246
$(\partial\mu_2/\partial c_2)/RT$[c]	0.748	0.499	0.223

[a]Units: c_i in mol L^{-1}, RTL_{ik} in 10^9 mol m^{-1} s^{-1}, $(\partial\mu_i/\partial c_k)/RT$ in m^3 mol^{-1}.
[b]Equations [29]–[31], ref. 6.
[c]Reference 5.

Diffusion coefficients of the components are then estimated from the relation

$$[14] \quad D_{ik} = \sum_m L_{im}\partial\mu_m/\partial c_k$$

Table 4 lists calculated values of L_{ik} and $\partial\mu_m/\partial c_k$. The latter were derived from activity coefficients reported by Peiper and Pitzer (5). (Hydrolysis was included in their analysis.)

Observed and predicted ternary diffusion coefficients of dilute Na_2CO_3 solutions are compared in Table 3. Since it is difficult to make accurate predictions of transport coefficients for unsymmetric mixtures (15, 27) (especially for systems such as the one under discussion in which the ions have widely different mobilities (28)), agreement can be considered satisfactory. The agreement lends support to the correctness of the measured ternary diffusion coefficients.

Bearing in mind that diffusion is usually regarded as a mixing process, it is noteworthy that diffusion causes binary $Na_2CO_3 + H_2O$ solutions to spontaneously separate into two ternary solutions: $Na_2CO_3 + NaOH + H_2O$ ahead of the diffusion boundary and $Na_2CO_3 + NaHCO_3 + H_2O$ remaining behind the boundary. Although ternary diffusion of Na_2CO_3 is important only for relatively dilute solutions, strongly hydrolyzing electrolytes such as phosphates and salts of transition metals should display ternary behavior at much higher concentrations.

Acknowledgement

Support by the Natural Sciences and Engineering Research Council of Canada is gratefully acknowledged.

1. E. W. WASHBURN (*Editor*). International critical tables. McGraw Hill, New York. 1926 (*a*) Vol. V. p. 67. (*b*) Vol. III. p. 82.
2. J. R. VINOGRAD and J. W. MCBAIN. J. Am. Chem. Soc. **63**, 2008 (1941).
3. J. A. RARD and D. G. MILLER. J. Solution Chem. **8**, 755 (1979).
4. K. S. PITZER and J. C. PEIPER. J. Phys. Chem. **84**, 2396 (1980).
5. J. C. PEIPER and K. S. PITZER. J. Chem. Thermodyn. **14**, 613 (1982).
6. D. G. LEAIST. Can. J. Chem. **61**, 1494 (1983).
7. D. G. LEAIST and P. A. LYONS. Aust. J. Chem. **33**, 1869 (1980).
8. D. G. LEAIST and P. A. LYONS. J. Solution Chem. **13**, 77 (1984).
9. D. G. LEAIST and R. A. NOULTY. Can. J. Chem. **63**, 476 (1985).
10. L. S. DARKEN and H. F. MEIER. J. Am. Chem. Soc. **64**, 621 (1942).
11. A. K. COVINGTON, M. I. A. FERRA and R. A. ROBINSON. J. Chem. Soc. Faraday Trans. 1, **11**, 1721 (1977).
12. H. S. HARNED and D. M. FRENCH. Ann. N.Y. Acad. Sci. **46**, 267 (1945).
13. H. S. HARNED and R. L. NUTTALL. J. Am. Chem. Soc. **71**, 1460 (1949).
14. L. ONSAGER and R. M. FUOSS. J. Phys. Chem. **26**, 2689 (1932).
15. R. H. STOKES. J. Am. Chem. Soc. **75**, 4563 (1953).
16. R. A. ROBINSON and R. H. STOKES. Electrolyte solutions. 2nd ed. Academic Press, New York. 1959. (*a*) Appendix 6.1. (*b*) p. 31.
17. T. SHEDLOVSKY. J. Am. Chem. Soc. **54**, 1411 (1932).
18. T. SHEDLOVSKY and D. A. MACINNES. J. Am. Chem. Soc. **57**, 1705 (1935).
19. G. C. BENSON and A. R. GORDON. J. Chem. Phys. **13**, 473 (1945).
20. R. H. STOKES. J. Am. Chem. Soc. **72**, 763 (1950).
21. R. H. STOKES. J. Am. Chem. Soc. **73**, 3527 (1951).
22. C. B. MONK. J. Chem. Soc. 429 (1949).
23. Y. P. TANG and D. M. HIMMELBLAU. Chem. Eng. Sci. **20**, 7 (1965).
24. R. N. GOLDBERG. J. Phys. Chem. Ref. Data, **10**, 671 (1981).
25. A. D. FARY, JR. Ph.D. Thesis, Institute of Paper Chemistry (affiliated with Lawrence College), Wisconsin. 1966.
26. R. A. NOULTY and D. G. LEAIST. J. Solution Chem. **13**, 767 (1984).
27. R. P. WENDT. J. Phys. Chem. **69**, 1227 (1965).
28. D. G. LEAIST. Can. J. Chem. **62**, 1692 (1984).

Studies of infrared multiphoton dissociation rates of protonated aliphatic alcohol dimers

ALEXANDER BALDWIN YOUNG,[1] RAYMOND EVANS MARCH,[2] AND RICHARD JAMES HUGHES
Department of Chemistry, Trent University, Peterborough, Ont., Canada K9J 7B8

Received October 24, 1984

ALEXANDER BALDWIN YOUNG, RAYMOND EVANS MARCH, and RICHARD JAMES HUGHES. Can. J. Chem. **63**, 2324 (1985).

The rates of photodissociation induced by absorption of infrared radiation of protonated dimers of 2-propanol and its deuterated analogues are reported. Protonated alcohol dimer ions created in a quadrupole ion store (QUISTOR) were irradiated in isolation and as a function of parent gas pressure and added collision gas (N_2). The relative weights and nature of ionic photoproducts were determined by mass spectrometry. The effect upon photolysis of collisions both prior to and during irradiation were examined. Photodissociation rates were defined by σ_D, which is the measured photodissociation rate constant normalized to the laser intensity. Nascent dimer ions which can possess up to 130 kJ mol^{-1} internal energy dissociated readily with σ_D of 15.8×10^{-21} cm^2 extrapolated to collision-free conditions. Photodissociation products from nascent dimer ions were produced via two major reaction channels. As the number of collisions suffered by the nascent dimer ion prior to irradiation was increased, the value of σ_D diminished and a single reaction channel became more prevalent. After some 270 collisions the ions appear to be collisionally relaxed prior to photolysis. The value of σ_D of 13.1×10^{-21} cm^2 extrapolated to collision-free conditions was obtained. The products from photodissociation of relaxed ions were obtained from a single reaction channel. An increase in σ_D values obtained with added nitrogen collision gas indicated a blockage or "bottleneck" in multiphoton absorption which is attributed to rotational population depletion. Three deuterated analogues of 2-propanol showed similar behaviour to that of 2-propanol with the exception that deuteron-bound dimers formed from 2-propanol (OD) and perdeutero-2-propanol failed to show rotational population depletion. The apparent lack of a "bottleneck" in multiphoton absorption by deuteron bound dimers is attributed to the diminished spacings between rotational levels of these species compared with the rotational level spacings for proton-bound dimers. Proton-bound ethanol dimers were selected for the examination of temperature effects upon photodissociation rates. While values for σ_D, extrapolated to collision-free conditions, of 15.6×10^{-21} cm^2 at 321 K (in agreement with the 2-propanol results obtained solely at this temperature) and 8.55×10^{-21} cm^2 at 293 K were obtained, the precise interpretation of such a marked temperature effect is not immediately obvious.

ALEXANDER BALDWIN YOUNG, RAYMOND EVANS MARCH et RICHARD JAMES HUGHES. Can. J. Chem. **63**, 2324 (1985).

On a mesuré les vitesses de photodissociations, induites par adsorption de radiation infrarouge, de dimères protonés du propanol-2 et de ses analogues deutérés. Opérant d'une manière isolée ainsi qu'en fonction de la pression du gaz parent et du gaz additionné (N_2), on a irradié des ions dimères d'alcool protoné créés dans un piège d'ions quadrupolaires. Faisant appel à la spectroscopie de masse, on a déterminé les masses relatives ainsi que la nature des photoproduits ioniques. On a évalué l'effet sur la photolyse de collisions qui précèdent l'irradiation ou qui lui sont concurrentes. On a défini les vitesses de photodissociations par σ_D qui est la constante de vitesse de photodissociation mesurée normalisée pour l'intensité du laser. Les ions dimères naissants, qui peuvent posséder jusqu'à 130 kJ mol^{-1} d'énergie interne, se dissocient facilement avec un σ_D de $15{,}8 \times 10^{-21}$ cm^2 si l'on extrapole aux conditions ou il n'y a pas de collisions. Les produits de photodissociations des ions dimères naissants proviennent de deux voies réactionnelles principales. Lorsqu'on augmente le nombre des collisions auxquelles sont soumis les ions dimères naissants avant l'irradiation, la valeur de σ_D diminue et une voie réactionnelle devient alors plus prévalente. Après environ 270 collisions, les ions semblent avoir atteint un état de relaxation complète avant la photolyse. On a obtenu une valeur de σ_D de $13{,}1 \times 10^{-21}$ cm^2 par extrapolation à des conditions où il n'y a pas de collisions. Les produits de photodissociations des ions dans un état de relaxation complète ont été obtenus pour une seule voie réactionnelle. Par addition azote, il se produit une augmentation des valeurs de σ_D provenant de collisions avec le gaz et indiquant un bloquage ou un "étranglement" dans l'absorption multiphoton qui est attribué à une diminution de la population rotationnelle. Trois analogues deutérés du propanol-2 présentent des comportements similaires à celui du propanol-2, à l'exception du fait que les dimères liés par un deutérium et formés à partir du propanol-2 (OD) et du perdeutéropropanol-2 ne présentent pas de diminution de la population rotationnelle. On attribue ce manque apparent d'"étranglement" dans l'absorption multiphoton par des dimères liés par des deutérium à des diminutions dans les écarts entre les niveaux rotationnels de ces espèces comparées avec les écarts entre les niveaux rotationnels dans les dimères liés par des protons. On a choisi les dimères d'éthanol liés par des protons pour examiner l'effet de la température sur les vitesses de photodissociations. Les valeurs de σ_D, extrapolées à des conditions où il n'y a pas de collisions, sont de $15{,}6 \times 10^{-21}$ cm^2 à 321 K (en accord avec les valeurs obtenues avec le propanol-2 à cette température) et de $8{,}55 \times 10^{-21}$ cm^2 à 293 K; l'interprétation précise d'un tel effet marqué de la température n'est pas immédiatement évident.

[Traduit par le journal]

Introduction

Single species photochemistry of a molecule or ion cannot be ascertained unambiguously unless the mean time between collisions is greater than that required for excitation and unimolecular decomposition. Likewise, single species chemistry induced by multiphoton absorption can only be ascertained unambiguously when the overall rate of photoexcitation and unimolecular dissociation exceeds that of a known collision rate. A novel dimension is added when the ion of interest is generated *in situ* through exoergic ion/molecule reactions, wherein the nascent ion can contain some 130 kJ mol^{-1} of internal energy as prevails for the protonated dimers of aliphatic alcohols (1). Previous studies employing slow Infrared Multiphoton Dissociation (IRMPD) as a probe of activation energy hierarchies in the gas phase photolysis of proton-bound

[1] Registered in the Ph.D. programme in Chemistry of Queen's University, Kingston, Ont., Canada.

[2] Adjunct Professor, Department of Chemistry, Queen's University, Kingston. Ont., Canada.

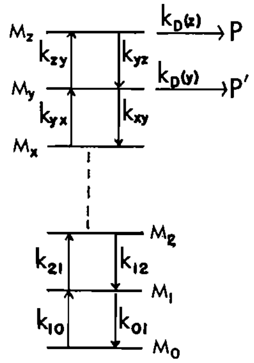

FIG. 1. Master equation approach to IRMPD.

dimers have been carried out with each of 2-propanol (2–5), ethanol (6), and I-butanol (7). It has been shown that the relative weights of reaction pathways followed by an ion excited through the absorption of several photons change with the number of collisions suffered by the nascent ion prior to irradiation. We have set out to explore the effects of collisional deactivation prior to and during irradiation through variation of parent molecule pressure, added collision gas pressure and relaxation time.

A simple physical model (8) for Infrared Multiphoton Dissociation (IRMPD) is depicted in Fig. 1, wherein the rates of population of excited levels of the specie, M, compete with the rates of depopulation. For levels with internal energy in excess of the unimolecular dissociation threshold ($E_{int} \geqslant yh\nu$) depopulation can also occur via product formation with rate constant $k_d(y)$. The difficulty in applying this treatment to experimental data from IRMPD lies in the lack of knowledge of the individual rate constants required to solve the master equation. In IRMPD the dissociation yield is measured as a function of fluence at a specified pressure and wavelength (pulsed CO_2 laser) or as a function of irradiation time at a specified pressure, wavelength and intensity (CW CO_2 laser).

It has been demonstrated (9, 10) that absorption involving only incoherent, single photon transitions between vibrational levels leads to an overall rate of dissociation which can be adequately described by a unimolecular rate law. Large polyatomic species exhibit such absorption processes due to the proximity of the quasi-continuum region of vibrational states to the ground vibrational state at ambient temperature. In these species the rate of photon absorption is much slower than the rate of intramolecular v → v transfer and the internal energy distribution can be described as ergodic, or characterized by a mean vibrational temperature (8, 9). At internal energy levels above the threshold for dissociation, the relative magnitudes of the overall rate of excitation and the rate of unimolecular dissociation affect the extent of further photon absorption of a species prior to dissociation. Quack (11) examined the case where the rate of excitation ≪ rate of dissociation and developed the equation:

$$[1] \quad k_{uni}^{ss} = \frac{-\mathrm{d}\ln(1 - F_D)}{\mathrm{d}(It)}$$

where k_{uni}^{ss} is the steady state, unimolecular dissociation rate constant; F_D is the fraction of molecules or ions decomposed by the laser; I is the measured laser intensity, and t is the duration of irradiation. Equation [1] predicts that a plot of $-\ln(1 - F_D)$ vs. fluence ($I \times t$) should produce a straight line of slope k_{uni}^{ss}; deviations from linearity are regarded by Quack as evidence that a steady state condition does not exist. In the experiments to be described, the CW CO_2 laser intensity is constant; the extent of IRMPD of the protonated alcohol dimer is measured as a function of irradiation time. In these experiments, a plot of $-\ln(1 - F_D)$ vs. time produces a straight line of slope k_{uni}^{ss}. The rate constant may also be expressed (8, 9, 12, 13) as:

$$[2] \quad k_{uni}^{ss} = \sigma_D \Phi$$

where Φ is the photon flux and σ_D is a phenomenologically defined photon absorption cross-section. The photon flux is calculated:

$$[3] \quad \Phi = \frac{I\lambda}{hc}$$

where λ is the wavelength of the laser, h is Planck's constant, and c is the speed of light. The σ_D values are thus proportional to the unimolecular rate constant, k_{uni}^{ss}, normalized to the laser intensities employed.

Experimental

Although the apparatus has been described in detail previously (2–4) some modifications have been made.

In the experiments described, a square wave generator (Heathkit) was employed to drive a mechanical chopper (PAR 222), typically with a 1:1 wheel and phase-locked to the input signal. The output signal from the chopper triggers the creation pulse (Hewlett-Packard 214A; typically +60 V/100 μs) which was applied to a gate biased at −100 V to bar filament electrons (−70 V) from the trap. The creation pulse was used to trigger a linear gate/scan delay generator combination (Ortec Brookdeal 9415 and 9425A), and the output pulse from the scan delay generator triggered an extraction pulse (Hewlett-Packard 214B; typically −40 V/5 μs) concomitantly with the detection pulse. The scan delay generator was operated via an ISAAC/APPLE IIe interface and the signal intensity of the ion of interest signal averaged and displayed on an XY recorder.

In the experiments described the signal intensity of the protonated alcohol dimer was monitored with concomitant resonance ejection (14, 15) (QRE) of the protonated parent alcohol. Four sweeps were averaged from 50 to 100 ms with and without the laser (944 cm^{-1}). Laser power was measured both before and after the experiment (Optical Engineering, Laser Power Probe). Pressures were measured via a capacitance manometer (MKS Baratron).

In those experiments which examined the extent of laser-wrought dissociation of the protonated dimer in the presence of added buffer gas (N_2), a heated inlet system connected to a 6 L glass bulb with a septum attachment was employed. Buffer gas quantities were measured by an aneroid pressure gauge (Matheson); alcohol volumes were measured via syringe and the corresponding pressure increment recorded. The bulb temperature was maintained at a temperature identical to that of the heated sidearm inlet system (50°C) used for pure alcohol introduction. In these ethanol experiments labelled "cold", the sidearm and tank were maintained at ambient temperature (~20°C). All other experiments were performed with a heated tank (48°C).

The laser power within the QUISTOR was measured via a calibrated homemade thermocouple. Reported photodissociation cross-sections were corrected for laser intensity losses due to the NaCl entrance window and the 3.0 mm aperture in the ring electrode of the QUISTOR.

Results and discussion

Protonated alcohols are formed in the gas phase via proton transfers between primary ionic fragments and the neutral alcohol. In the 2-propanol system, α-cleavage of the molecular ion produces protonated ethanal:

$$[4] \quad (CH_3)_2CHOH^{+\cdot} \rightarrow CH_3CHOH^+ + \cdot CH_3$$

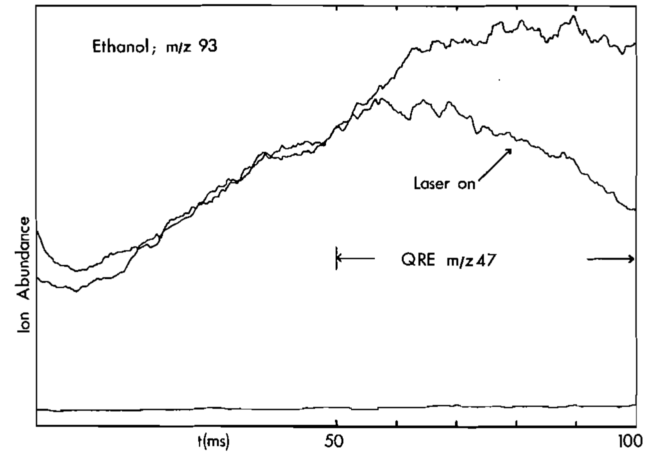

FIG. 2. Single ion monitoring trace of the protonated dimer of ethanol (m/z 93) with concomitant resonance ejection of the precursor protonated alcohol (m/z 47). Two experiments are depicted: laser on refers to 50 ms of laser irradiation at 944 cm^{-1}; in the other trace the laser is blocked.

which transfers a proton to the neutral alcohol (16):

[5] $CH_3CHOH^+ + (CH_3)_2CHOH \rightarrow CH_3CHO + (CH_3)_2CHOH_2^+$ (m/z 61)

The protonated parent alcohol reacts with another neutral alcohol, forming an excited proton-bound dimer, which may then be collisionally or radiatively relaxed:

[6] $[(CH_3)_2CHOH]_2H^{+*} \xrightarrow[{[M]}]{-h\nu} [(CH_3)_2CHOH]_2H^+$

Three reaction channels are available to the relaxed dimer:

[7] $[(CH_3)_2CHOH]_2H^+ \rightarrow (CH_3)_2CHOH_2^+ + (CH_3)_2CHOH$
m/z 61

[8] $[(CH_3)_2CHOH]_2H^+ \rightarrow (CH_3)_2CHOH_2^+ \cdot H_2O + C_3H_6$
m/z 79

[9] $[(CH_3)_2CHOH]_2H^+ \rightarrow [(CH_3)_2CH]_2OH^+ + H_2O$
m/z 103

No activation energy in excess of reaction endothermicity is expected for reaction [7]; the reported ΔH of -130 kJ mol^{-1} (1) corresponds to the absorption of 12 photons of wavelength 10.6 μm. The enthalpies of reactions [8] and [9] may be calculated from thermodynamic data (17), and are 92 kJ mol^{-1} and 79 kJ mol^{-1}, respectively. The corresponding activation energies are unknown.

The analogous reactions leading to dimer formation in deuterated 2-propanols resulted in a proton-bound dimer for 2-d_1-2-propanol and deuteron-bound dimers for 2-propanol (OD) and perdeutero-2-propanol. The proton-bound dimer derived from ethanol exhibited solely the reactions analogous to [7] and [9] upon photolysis.

Ethanol

A typical experiment is shown in Fig. 2; the resulting plot of $-\ln(1 - F_D)$ vs. time is depicted in Fig. 3. Least-squares linear regression analysis is used to calculate the slope of the best fit straight line through the data (k_{uni}^{ss}). The calibrated laser (944 cm^{-1}) intensity within the QUISTOR (beam diameter of 3 mm) is employed to calculate the phenomenologically defined photodissociation cross section, σ_D. In Table 1, values of σ_D versus pressure and collision rate are listed for a series of hot (48°C) and cold (20°C) tank experiments.

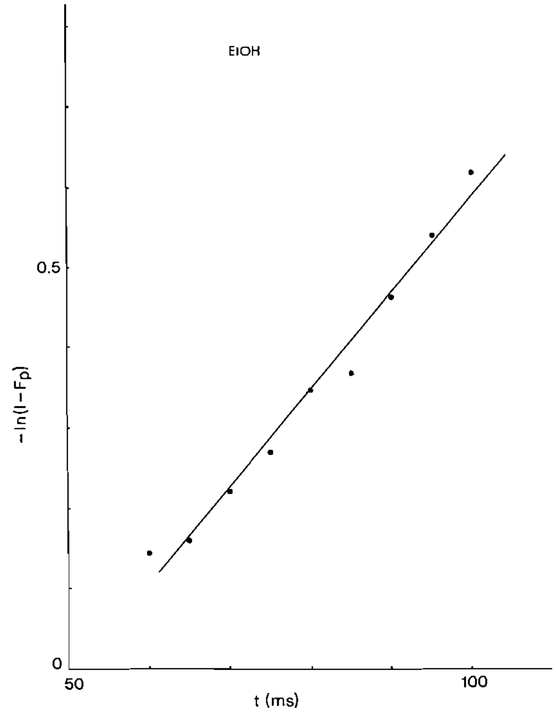

FIG. 3. Plot of $-\ln(1 - F_D)$ vs. time of the experimental data of Fig. 2.

TABLE 1. σ_D values and experimental parameters for IRMPD of protonated ethanol dimers

	Pressure (Pa)	Thermal collision rate (ms^{-1})	Dehmelt collision rate (ms^{-1})	$\sigma_D \times 10^{21}$ (cm^2)	Correlation factor
Hot	6.7×10^{-4}	0.31	1.6	13.1	0.976
	1.9×10^{-3}	0.88	4.4	10.1	0.970
	2.7×10^{-3}	1.26	6.3	6.1	0.959
	3.5×10^{-3}	1.63	8.2	5.4	0.989
	5.3×10^{-3}	2.63	13	3.6	0.971
Cold	2.7×10^{-4}	0.13	0.65	8.7	0.981
	1.3×10^{-3}	0.66	3.3	6.8	0.967
	2.7×10^{-3}	1.32	6.6	6.0	0.933

The collision rate and number of collisions prior to photolysis are calculated using Dehmelt velocities and a cross-section of 1 nm^2. The actual velocities of the trapped ions in the QUISTOR are not known precisely, however a Dehmelt potential well calculation (18) indicates that initial, collision-free ion velocities are approximately five times those derived thermally. A more recent study (8) showed that approximately 80 collisions were required to remove $\leq$ 100 kJ mol^{-1} of excess internal energy by resonant v ← v transfer which suggests that the thermal collision rate and number of collisions should be increased by at least a factor of 2 in light of the relaxation studies on the protonated dimer of 2-propanol (*vide infra*).

In Fig. 4, it can be seen that σ_D for the ethanol protonated dimer decreases with increasing collision rate. Furthermore, at low collision rates, the rate of σ_D increase is greater than for the cold experiments.

The results are difficult to rationalize as calculations of the thermal energy contribution to the internal energy of the

TABLE 2. σ_D values and experimental parameters for IRMPD of protonated 2-propanol dimers

Experimental conditions	Pressure (Pa) Alcohol	Total	Collision rate (ms^{-1})	Collisions prior to photolysis	$\sigma_D \times 10^{21}$ (cm^2)	Correlation factor
100 ms total	5.3×10^{-4}		1.1	55	13	0.997
50 ms L (944 cm^{-1})	8.0×10^{-4}		1.65	85	10.3	0.994
2-propanol only	1.6×10^{-3}		3.3	165	6.25	0.990
	2.9×10^{-3}		6.0	305	5.60	0.982
	4.0×10^{-3}		8.2	415	5.45	0.996
	6.9×10^{-3}		14.3	715	2.93	0.920
100 ms total	8.8×10^{-4}	2.1×10^{-3}	1.8	90	8.16	0.971
50 ms L (944 cm^{-1})	2.4×10^{-3}	5.9×10^{-3}	5.0	250	9.65	0.992
2-propanol/N_2 (1:1)	3.9×10^{-3}	9.3×10^{-3}	8.0	400	7.58	0.983
	5.5×10^{-3}	1.3×10^{-2}	11.3	565	6.71	0.981
200 ms total	6.7×10^{-4}		1.4	225	13.3	0.965
40 ms L (944 cm^{-1})	1.1×10^{-3}		2.2	350	10.8	0.985
2-propanol only	1.9×10^{-3}		3.6	615	8.63	0.985
	2.9×10^{-3}		6.0	960	6.62	0.954

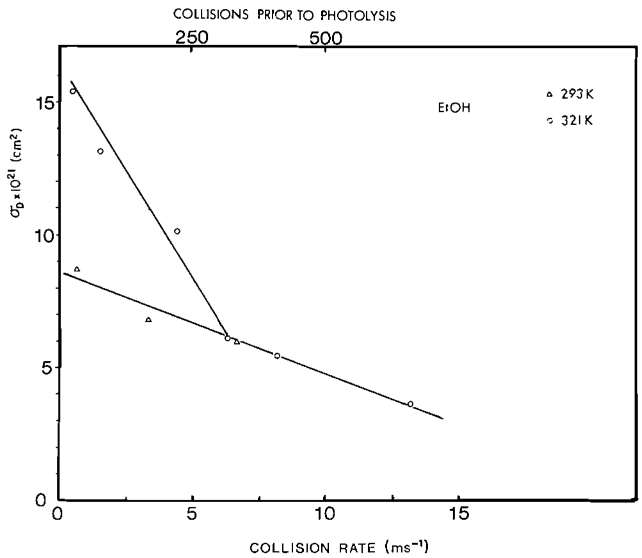

FIG. 4. Plot of σ_D vs. collision rate and number of collisions prior to photolysis for $(EtOH)_2H^+$.

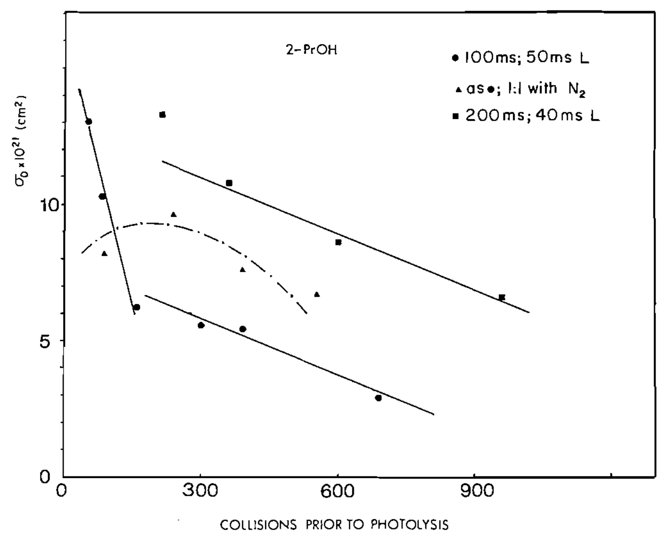

FIG. 5. Plot of σ_D vs. number of collisions prior to photolysis for $(2\text{-PrOH})_2H^+$.

proton-bound dimer show ~9 kJ mol^{-1} average vibrational energy is contributed at 293 K and ~12 kJ mol^{-1} at 321 K. The latter amount is the equivalent of the absorption of one photon at 944 cm^{-1}; however, this is insufficient to place the dimer in the quasi-continuum prior to photolysis. Calculations performed using the well-known Whitten–Rabinovitch approximation (19, 20) and the frequencies for ethanol (21) with frequencies for the proton bridge derived from the study of Bowers and co-workers (22) predict that the density of vibrational states corresponding to the absorption of 1 photon is 5.0×10^{-1} states/cm^{-1}. Using the assumption of Beauchamp and co-workers (13) that the quasi-continuum is not attained until the density of vibrational states $\gtrsim 10^3$ states/cm^{-1} due to the narrow line width of the CW CO_2 laser, this condition is fulfilled for the proton bound dimer of ethanol only after the absorption of four 944 cm^{-1} photons whereupon the density of vibrational states is 2.1×10^3 states/cm^{-1}. Anharmonicity in the vibrational mode (944 cm^{-1}) may be more easily overcome when only 3 photons are required to populate the quasi-continuum (23) by absorption initially via the P branch of the mode. The subsequent 2 photons may be absorbed in the Q and R branches, respectively; however, due to the small internal energy difference between the dimers at the two temperatures, this possibility seems tenuous.

Best fit straight lines through the data points give σ_D values in the absence of collisions when extrapolated, yielding values of 15.6×10^{-21} cm^2 and 8.55×10^{-21} cm^2 for the "hot" and "cold" proton-bound ethanol dimers, respectively.

2-Propanol

Three sets of experiments, all performed at 321 K, are reported. The first two sets comprised 50 ms of dark period followed by 50 ms of laser irradiation (944 cm^{-1}); one series examining protonated dimers formed in a pure alcohol system, the other protonated dimers formed in a 1:1 mixture of alcohol and nitrogen. The third series of experiments employed a dark period of 160 ms followed by 40 ms of laser irradiation. The protonated dimers were formed in an alcohol only system. In Table 2 measured σ_D values are reported. The data in Table 2 are plotted as σ_D vs. collisions prior to photolysis and σ_D vs.

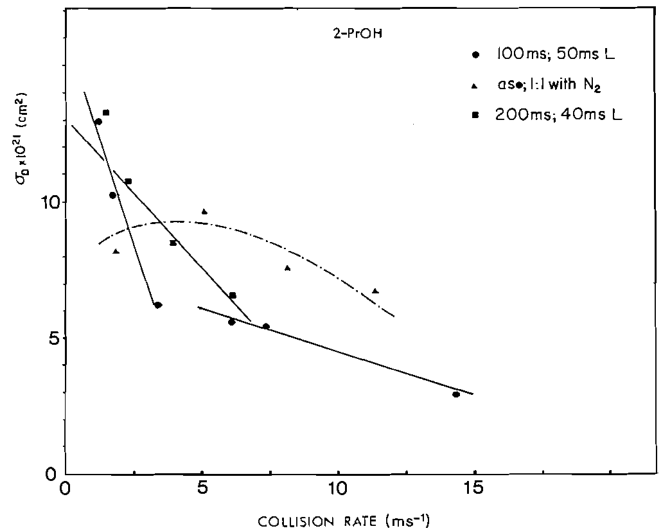

FIG. 6. Plot of σ_D vs. collision rate for IRMPD of $(2\text{-PrOH})_2H^+$.

collision rate in Figs. 5 and 6, respectively. The data obtained from the alcohol : N_2 (1 : 1) experiments are plotted as a function of Dehmelt collision rates (corrected for molecular flow) of the dimer and the neutral alcohol only.

In Fig. 5, the data for the 100 ms experiments employing the alcohol only exhibit a linear dependence of σ_D with the number of collisions prior to photolysis, albeit divided into two regions. At few collisions of the dimer before laser irradiation, the data extrapolate to a collision-free σ_D value of 15.8×10^{-21} cm²; here, the dimer population has suffered too few collisions prior to the photolysis to be fully relaxed. The steep decrease in σ_D with the number of collisions in this region is attributed to an increase in the number of photons required to effect dissociation in competition with increasing collisional deactivation (Fig. 6).

At more than about 250 collisions (*vide infra*), the dimer is fully relaxed and the path of lowest E_a is followed exclusively. The decrease in σ_D is attributed to collisional deactivation during photolysis (Fig. 6). The data in this region extrapolate to a collision-free σ_D of 8.0×10^{-21} cm².

Three of the data points from the 200 ms experiments were also fitted to a straight line and extrapolated to a collision-free σ_D value of 13.1×10^{-21} cm². Photodissociation product analysis revealed the protonated diisopropyl ether as the dominant (~95%) product from three experiments. A small amount (~5%) of protonated alcohol was also produced — presumably via photolysis of the hot protonated ether (4, 24). The lowest E_a pathway only is accessed by the laser in these experiments (24), and the proton-bound dimer ions are fully collisionally relaxed at the onset of irradiation. Although product analysis was not performed for the data point corresponding to $\sigma_D = 13.3 \times 10^{-21}$ cm², previous work (4) showed that 250 to 300 collisions prior to photolysis were required to relax fully the dimer as shown in Fig. 7. From the data in Table 2, the requisite number of collisions have not occurred for the latter dimer, hence it was not included in the calculation of the best fit straight line. The fully relaxed data from the 200 ms experiments are obtained at lower collision rates than those from the 100 ms experiments (Fig. 6); the data from the former are expected to extrapolate to a higher collision-free σ_D value. The roughly parallel nature of the decrease of σ_D with the increase in the number of collisions is due to the fact that at identical

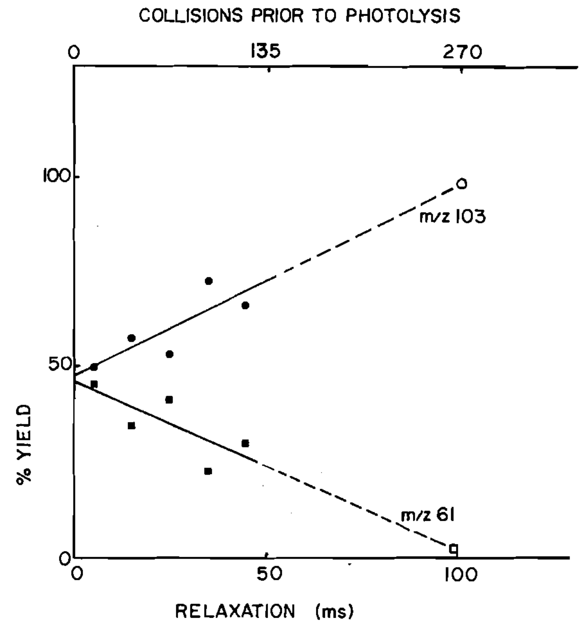

FIG. 7. Plot of IRMPD product % yield vs. relaxation time prior to photolysis of the proton-bound dimer of 2-propanol. M/z 103 is the protonated diisopropyl ether product; m/z 61 is the protonated parent alcohol. The data are extrapolated, assuming a linear fit to the yields observed in an ICR cell (24) at differing relaxation times and numbers of collisions than those employed in this study. The ICR cell yields are depicted as open symbols and are attributed to photolysis of fully relaxed dimer ions.

numbers of collisions prior to photolysis, the fully relaxed dimers from the 100 ms experiments have experienced a three-fold increase in the collision rate during photolysis. The decrease in σ_D with increasing numbers of collisions in both cases is due to an increase in collisional deactivation during photolysis, while displacement of the 200 ms results from those at 100 ms reflects the greater collision rate during photolysis of the latter resulting in a correspondingly reduced total energy increment supplied by the laser.

The data obtained from photodissociation of dimers formed in a 1 : 1 mixture of 2-propanol and nitrogen are plotted as σ_D vs. the number of collisions of the dimer with the neutral alcohol only. If nitrogen has no effect upon the photodissociation of the protonated dimers, then the data points obtained experimentally should mimic the behaviour of those obtained from the 100 ms experiments utilizing solely 2-propanol. The data are characterized by a decreased σ_D value at low numbers of collisions and enhanced σ_D values at higher collision values.

Similar behaviour has been previously reported (25–27). The enhancement has been attributed to collisional repopulation of rotational levels depleted by laser-pumping effected by collisions with the buffer gas. The data indicate that the bottleneck occurs at a low level of internal excitation of the dimer i.e. after the dimer has experienced a large number of collisions prior to photolysis.

In Fig. 6, the effect upon σ_D of the collision rate during photolysis is examined. The data obtained in the 100 ms experiments using 2-propanol only are fitted to two straight lines according to the rationale outlined previously. The steep portion of the slope corresponds to proton-bound dimers with low collision rates during photolysis and excess ($\leqslant$ 131 kJ mol⁻¹) (1) internal energy. The rapid decrease of σ_D with increasing

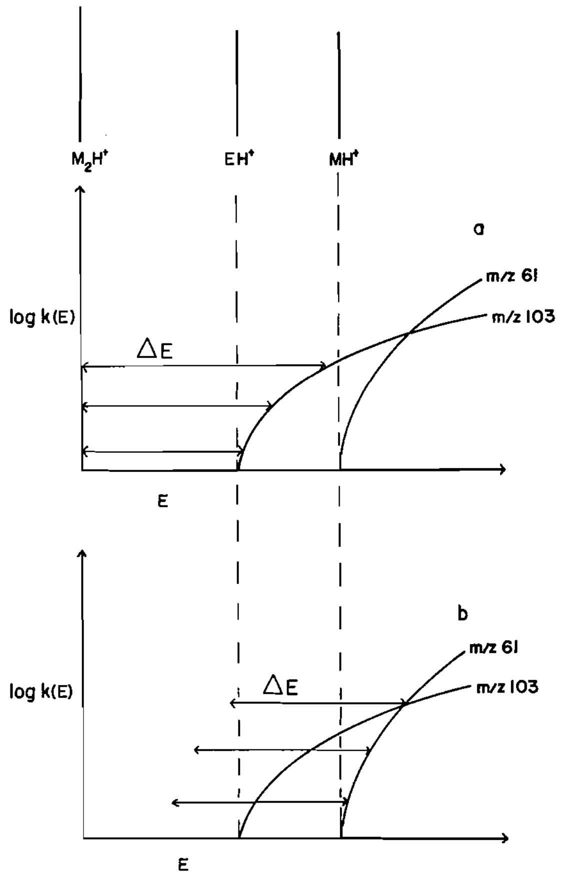

FIG. 8. Plot of log $k(E)$ vs. internal energy for the two reaction pathways of $(2\text{-PrOH})_2H^+$ upon photolysis. The symbols used are defined as follows: M_2H^+, protonated dimer; MH^+ protonated alcohol (m/z 61); EH^+, protonated ether (m/z 103); ΔE, total energy supplied by the laser.

collision rates is due to both collisional deactivation during and diminished internal energy at the onset of photolysis. At higher ($\geqslant 5$ ms^{-1}) collision rates, the decrease in σ_D is less pronounced. This is attributed to a fully relaxed dimer population at the onset of irradiation; thus laser-pumping starts at the same level of internal excitation. Furthermore, as the lowest E_a pathway only is accessed, the sole variable in the data is that of collisional deactivation which is proportional to the collision rate.

For the 200 ms results, only those experiments which produced the lowest E_a pathway exclusively were used to calculate a best fit straight line (*vide supra*). The data indicate a greater decline of σ_D with collision rates ($\leqslant 5$ ms^{-1}) than the data derived from fully relaxed dimers in the 100 ms experiments at higher collision rates (>5 ms^{-1}). Complete relaxation of the protonated dimers at the onset of irradiation in the two sets of experiments is supported by the similarity in σ_D values (within the limits of experimental error) at identical collision rates of 6 ms^{-1}, despite a threefold difference in the number of collisions prior to photolysis (Fig. 5).

In Fig. 8, the variation of log $k(E)$ is plotted as a function of internal energy, E (28, 29). The curves as drawn are of a qualitative nature and the corresponding energy spacings in the proton-bound dimer are depicted above. Case (a) corresponds to the fully relaxed situation wherein the collision rate during photolysis affects the overall energy increment (ΔE) supplied by the laser. Case (b) depicts a constant total energy increment;

TABLE 3. Calculated dissociation rates for the reaction pathway of lowest E_a of the proton-bound dimer of 2-propanol

n	m	s	ω (s^{-1})	k (s^{-1})
9	9	69	2.83×10^{13}	176
10	9	69	2.83×10^{13}	1.5×10^{3}
10	10	69	2.83×10^{13}	22.5
11	10	69	2.83×10^{13}	216
11	11	69	2.83×10^{13}	3.2
12	11	69	2.83×10^{13}	33.1
12	12	69	2.83×10^{13}	4.8×10^{-1}

however, laser-pumping starts at differing levels of internal energy of the dimer above ground state.

The collision-free σ_D value derived for fully relaxed 2-propanol dimers and leading to the protonated ether product solely is 13.1×10^{-21} cm^2. This value corresponds to a unimolecular dissociation rate constant of 29 s^{-1} calculated from eq. [2]; this rate constant may then be expressed using the Kassel form of RRKM theory (20) as:

$$[10] \quad \text{Rate} = \omega \frac{n!(n - m + s - 1)!}{(n - m)!(n + s - 1)!}$$

where n is the total number of photons absorbed by the ion, m is the number of photons required for reaction, s is the number of vibrational degrees of freedom of the ion, and ω is the laser photon frequency. For the proton-bound 2-propanol dimer, s is equal to 69, and when k_{diss} is assumed to be much greater than the overall rate of multiphoton excitation, n is equal to m. The photon employed corresponds to a frequency of 2.83×10^{13} s^{-1}. In Table 3, calculated values for the rate constant are given, along with the values of n, s, m, and ω used for the calculation.

Comparison of the calculated rate constants in Table 3 with the experimental value of 29 s^{-1} suggests an E_a for the dehydration reaction:

$$[11] \quad (2\text{-PrOH})_2H^+ + mh\nu \rightarrow 2\text{-}Pr_2OH^+ + H_2O$$

of 10 or 11 photons, of energy 11.3 kJ mol^{-1}. The E_a thus lies in the range 113 to 124 kJ mol^{-1}. In comparison, Bowers *et al.* (22) calculated an activation energy for the reaction:

$$[12] \quad (MeOH)_2H^+ \rightarrow Me_2OH^+ + H_2O$$

of 105 kJ mol^{-1}.

Deuterated 2-propanols

The observed increase in σ_D in the dimer derived from 2-propanol with added N_2 has been attributed to collisional repopulation of rotational levels which are resonant with the laser photon employed. As previously noted (25–27) such behaviour has been observed in other molecules upon ir laser photolysis. When a depletion of rotational levels which are resonant with the laser leads to a bottleneck in the IRMPD process, then the rotational level spacings should have an effect upon the magnitude of the bottleneck. Substitution of deuterium for hydrogen reduces the rotational level spacing, thus the effect of added N_2 upon σ_D values obtained from the IRMPD of various deuterated 2-propanols was investigated. In the experiments with a mixture of alcohol and nitrogen, the collision rates pertain only to collisions between the neutral alcohol and the protonated dimer. If nitrogen has no effect upon σ_D, then the data should mimic that obtained from the alcohol-only experiments.

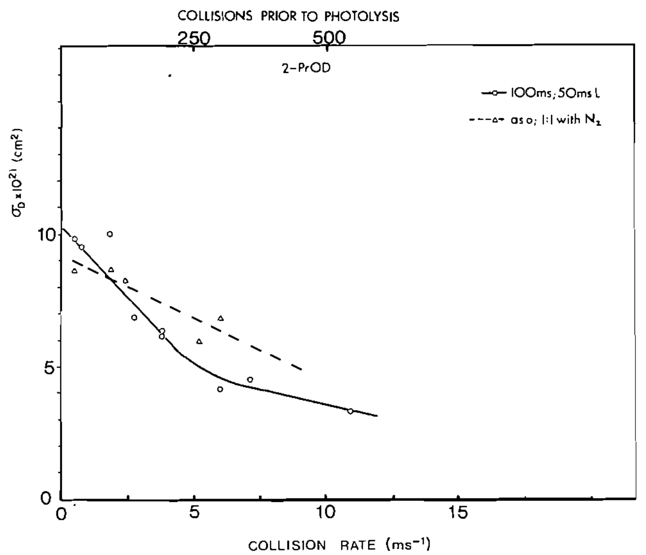

FIG. 9. Plot of σ_D vs. collision rate and number of collisions prior to photolysis for the protonated dimer of 2-propanol (OD), 2-PrOD.

2-Propanol (OD)

In Fig. 9, the results from two sets of experiments are shown as σ_D vs. collision rate. The data from the added N_2 experiments are plotted as a function of collisions of the dimer with the neutral alcohol only.

In the alcohol-only system, the decline in σ_D at low ($\leqslant 5$ ms^{-1}) collision rates is due to both the decrease in internal energy content of the dimer prior to and the increase in collisional deactivation during photolysis. At collision rates $\geqslant 5$ ms^{-1}, the dimers have experienced the requisite number of collisions for complete relaxation prior to irradiation and the gentler decline of σ_D with the increased collision rate results from collisional deactivation during photolysis. The collision-free σ_D value is 10.25×10^{-21} cm^2.

The σ_D values obtained in the alcohol and nitrogen experiments (1:1) show a small enhancement at collision rates $\geqslant 5$ ms^{-1}. At a collision rate of 5 ms^{-1}, the deuteronated dimers have suffered an average of 250 resonant collisions prior to photolysis. Evidence from the 2-propanol system suggests that these dimers are fully relaxed prior to irradiation. The alcohol/N_2 experiments indicate a smaller bottleneck than in the 2-propanol system which occurs at or near the ground state of the dimer.

2-d$_1$-2-Propanol

Three sets of experiments were performed and the results are plotted as σ_D vs. collision rate in Fig. 10. Despite fewer data points, the observed decrease of σ_D with increasing collision rate in the alcohol-only system is qualitatively similar to that observed in the previous alcohol dimers. The collision-free σ_D value is 16.1×10^{-21} cm^2.

The 1:1 mixture of alcohol and nitrogen exhibits a large increase in σ_D indicating a blockage of IRMPD in the protonated alcohol dimer. The bottleneck appears to occur at or near the ground state of the dimer.

The 1:4 mixture of alcohol and nitrogen shows essentially no enhancement of σ_D. As the data correspond to only 70 and 140 resonant collisions with the neutral alcohol, the dimers have excess internal energy and are being pumped from a level above the bottleneck.

No allowance for collisional deactivation of the dimers by non-resonant processes involving N_2 has been made. Such an allowance would shift the data points to higher collision rates.

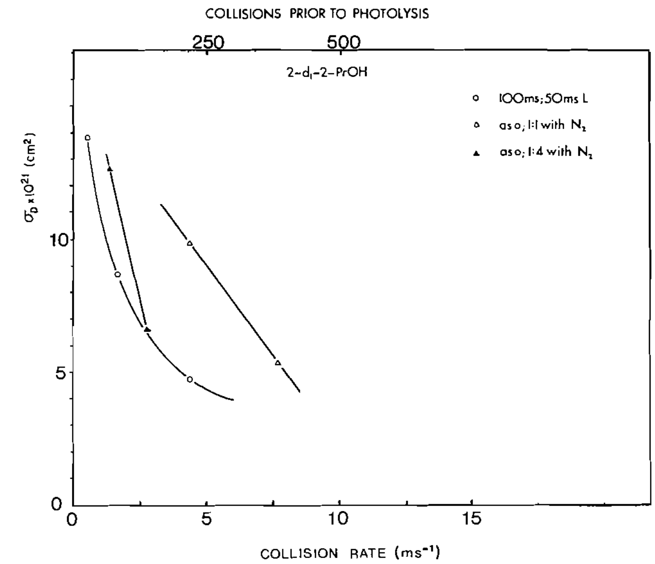

FIG. 10. Plot of σ_D vs. collision rate and number of collisions prior to photolysis for the protonated dimer of 2-d_1-2-propanol.

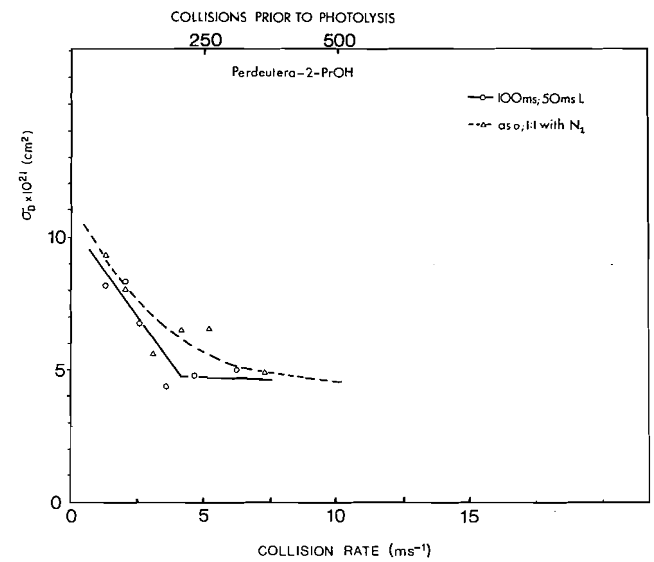

FIG. 11. Plot of σ_D vs. collision rate and number of collisions prior to photolysis for the protonated dimer of perdeutero-2-propanol.

Perdeutero-2-propanol

The results of two sets of experiments are shown in Fig. 11. Proton-bound dimers produced in the alcohol-only system exhibit the usual initial steep decrease of σ_D at low collision rates and a very gentle decrease of σ_D at higher collision rates. The collision-free σ_D is 10.5×10^{-21} cm^2.

Dimers produced in a 1:1 mixture of alcohol and nitrogen show a small increase in σ_D at collision rates = 5 ms^{-1}. Such behaviour indicates a small bottleneck in the IRMPD process occurring at or near the ground state of the deuteronated dimer.

Conclusion

Based on the results of the IRMPD studies, the four 2-propanols may be divided into two groups: those with proton-bound dimers and those with deuteron-bound dimers. The latter group exhibit both smaller collision-free σ_D values and smaller increases in σ_D when nitrogen is added to the system.

The lower collision-free σ_D value is attributed to a decrease in the rate constants for both the dehydration and scission reactions due to deuterium substitution in an active vibrational mode for product formation (30).

The smaller increase in σ_D of the deuteron-bound dimers when nitrogen is added is presumably due to a decrease in the spacing of rotational levels by deuterium substitution in the mode being pumped by the laser. The most probable identity of the vibrational mode initially pumped by the laser is the OH in plane bend at ~1385 to 1250 cm^{-1} in primary and secondary aliphatic alcohols (31). This mode shifts by a factor of approximately $(\sqrt{2})^{-1}$ upon the substitution of D for H in perdeutero and 2-propanol (OD); such a "red" shift moves the OD in plane bend into resonance with the laser operating at 944 cm^{-1}, and the smaller rotational spacings provide less of an impediment to IRMPD via anharmonic energy mismatching.

In the IRMPD of the protonated dimer of 2-propanol RRKM calculations employing the simple quantum Kassel equation suggested an activation energy of 113 to 124 kJ mol^{-1} for the reaction pathway leading to the production of protonated diisopropyl ether.

Acknowledgements

The authors acknowledge with thanks the financial support of the Natural Sciences and Engineering Research Council of Canada (for operating and equipment grants), Queen's University for a Graduate Student Assistantship, and Trent University Fund for Excellence. We acknowledge also the technical assistance of K. Fowler, W. King, J. C. S. Stuart, and J. Tomlinson. We are greatly appreciative of the cooperation of Drs. C. W. Willis and D. M. Rayner of the National Research Council of Canada for the loan of the CO_2 laser.

1. P. KEBARLE. Ann. Rev. Phys. Chem. **28**, 445 (1977); J. W. LARSON and T. B. MCMAHON. J. Am. Chem. Soc. **104**, 6255 (1982).
2. R. J. HUGHES, R. E. MARCH, and A. B. YOUNG. Int. J. Mass Spectrom. Ion Phys. **42**, 255 (1982).
3. R. J. HUGHES, R. E. MARCH, and A. B. YOUNG. Proc. 9th Int. Mass Spec. Conf., Vienna. Aug. 29 – Sept. 3, 1982. Int. J. Mass Spectrom. Ion Phys. **47**, 85 (1983).
4. R. J. HUGHES, R. E. MARCH, and A. B. YOUNG. Can. J. Chem. **61**, 834 (1983).
5. R. E. MARCH. Ionic processes in the gas phase. *Edited by* M. A. Almoster-Ferreira. D. Reidel Publishing. 1984. p. 359.
6. R. E. MARCH, R. J. HUGHES, and A. B. YOUNG. Proc. 13th Conf. British Mass Spec. Soc. Warwick Univ. U.K. Sept. 19–22, 1983.
7. R. J. HUGHES, R. E. MARCH, and A. B. YOUNG. Proc. 31st Ann. Conf. Am. Soc. Mass Spectrom. Boston. 1983. p. 747.
8. J. M. JASINSKI, R. N. ROSENFELD, F. K. MEYER, and J. I. BRAUMAN. J. Am. Chem. Soc. **104**, 652 (1982); F. K. MEYER, J. M. JASINSKI, R. N. ROSENFELD, and J. I. BRAUMAN. J. Am. Chem. Soc. **104**, 663 (1982); R. N. ROSENFELD, J. M. JASINSKI, and J. I. BRAUMAN. J. Am. Chem. Soc. **104**, 658 (1982).
9. J. G. BLACK, E. YABLONOVITCH, N. BLOEMBERGEN, and S. MUKAMEL. Phys. Rev. Lett. **38**, 1131 (1977).
10. N. BLOEMBERGEN and E. YABLONOVITCH. Phys. Today **31**(5), 23 (1978).
11. M. QUACK. J. Chem. Phys. **70**, 1069 (1979).
12. D. S. BOMSE, R. L. WOODIN, and J. L. BEAUCHAMP. Chemical and bio-chemical applications of lasers. Vol. IV. *Edited by* C. B. Moore. Academic Press, NY. 1979.
13. D. S. BOMSE, R. L. WOODIN, and J. L. BEAUCHAMP. J. Am. Chem. Soc. **101**, 5503 (1979).
14. M. A. ARMITAGE, J. E. FULFORD, D. N. HOA, R. J. HUGHES, and R. E. MARCH. Can. J. Chem. **57**, 2108 (1979).
15. J. E. FULFORD, D. N. HOA, R. J. HUGHES, R. E. MARCH, R. F. BONNER, and G. J. WONG. J. Vac. Sci. Technol. **17**, 829 (1980).
16. J. L. BEAUCHAMP and R. C. DUNBAR. J. Am. Chem. Soc. **92**, 1477 (1970); T. A. LEHMAN, T. A. ELWOOD, J. T. BURSEY, M. M. BURSEY, and J. L. BEAUCHAMP. J. Am. Chem. Soc. **93**, 2108 (1971).
17. H. M. ROSENSTOCK, K. DRAXL, B. W. STEINER, and J. T. HERRON. J. Phys. Chem. Ref. Data, Vol. 6, Supplement 1. NBS (1977); R. A. KELLER (*Editor*). Basic tables in chemistry. McGraw-Hill. 1967; J. L. HOLMES, M. FINGAS, and F. P. LOSSING. Can. J. Chem. **59**, 80 (1981).
18. R. F. BONNER and R. E. MARCH. Int. J. Mass Spectrom. Ion Phys. **25**, 411 (1977).
19. G. Z. WHITTEN and B. S. RABINOVITCH. J. Chem. Phys. **38**, 2466 (1963).
20. P. J. ROBINSON and K. A. HOLBROOK. Unimolecular reactions. Wiley-Interscience, New York, New York. 1972.
21. S. C. SCHUMANN and J. G. ASTON. J. Chem. Phys. (*a*) **6**, 480 (1938); (*b*) **6**, 485 (1938).
22. L. M. BASS, R. D. CATES, M. F. JARROLD, N. J. KIRCHNER, and M. T. BOWERS. J. Am. Chem. Soc. **105**, 7024 (1983).
23. V. S. LETOKHOV. Phys. Today, **33**(11), 34 (1980).
24. D. S. BOMSE and J. L. BEAUCHAMP. J. Am. Chem. Soc. **103**, 3292 (1981).
25. G. P. QUIGLEY. J. Photochem. **9**, 177 (1978).
26. P. J. PAPAGIANNAKOPOULOS, K. KOSNIK, and S. W. BENSON. Int. J. Chem. Kinet. **14**, 327 (1982).
27. R. D. MCALPINE, D. K. EVANS, and H. M. ADAMS. J. Chem. Phys. **78**, 5990 (1983).
28. R. D. LEVINE and R. B. BERNSTEIN. Molecular reaction dynamics. Oxford University Press, New York. 1974. p. 105.
29. F. W. MCLAFFERTY. Interpretation of mass spectra. 2nd ed. W. A. Benjamin Inc., MA. 1973. pp. 204, 208.
30. K. J. LAIDLER. Chemical kinetics. 2nd ed. McGraw-Hill. 1965. pp. 90–98.
31. H. A. SZYMANSKI. Interpreted infrared spectra. Vol. 2. Plenum Press. 1967.

The stereochemistry of some 7-hydroxyindene dimers: applications of ^{1}H nuclear magnetic resonance relaxation pathway analysis

WALTER J. CHAZIN AND LAWRENCE D. COLEBROOK[1]
Department of Chemistry, Concordia University, 1455 de Maisonneuve Blvd. W., Montreal, P.Q., Canada H3G 1M8

AND

BRIAN R. DAVIS, I. ROSS N. MCCORMICK, AND STEPHEN J. JOHNSON
Chemistry Department, University of Auckland, Private Bag, Auckland, New Zealand

Received October 6, 1983[2]

WALTER J. CHAZIN, LAWRENCE D. COLEBROOK, BRIAN R. DAVIS, I. ROSS N. MCCORMICK, and STEPHEN J. JOHNSON. Can. J. Chem. **63**, 2332 (1985).

^{1}H spin-lattice relaxation rates and nuclear Overhauser effect difference spectra have been measured (at 400 MHz) for six dimers derived from methyl-substituted 7-hydroxyindenes. Used in combination, these measurements identify the relaxation pathways available to all of the protons in the molecules. Analysis of these pathways has permitted assignment of all chemical shifts, and identification of the relative stereochemistry at all chiral centres.

WALTER J. CHAZIN, LAWRENCE D. COLEBROOK, BRIAN R. DAVIS, I. ROSS N. MCCORMICK et STEPHEN J. JOHNSON. Can. J. Chem. **63**, 2332 (1985).

On a mesuré les vitesses de relaxation spin-réseau du ^{1}H et les différences d'effet Overhauser nucléaire dans les spectres, à 400 MHz, de six dimères obtenus à partir d'hydroxy-7 indènes substitués par des groupes méthyles. Si on les combine, ces mesures permettent d'identifier les diverses voies de relaxation de tous les protons de ces molécules. Une analyse de ces diverses voies de relaxation a permis d'attribuer tous les déplacements chimiques et d'identifier les stéréochimies relatives de tous les centres chiraux.

[Traduit par le journal]

Introduction

The analysis of ^{1}H nuclear magnetic resonance spin-lattice relaxation parameters, which can be conveniently and efficiently measured using a modern pulse Fourier transform nmr spectrometer, can provide a significant amount of information about the structure and stereochemistry of organic molecules (1–3). In this report, we describe the solution structure determination of a series of methyl-substituted 7-hydroxyindene dimers, **1–6**, by nmr analysis of their ^{1}H relaxation pathways.

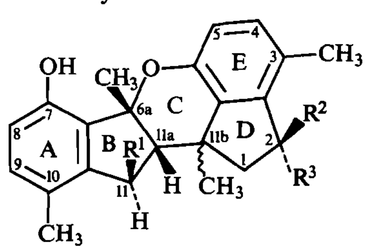

	11b	R^{1}	R^{2}	R^{3}
1	β	H	H	H
2	α	H	H	H
3	β	CH_3	CH_3	H
4	β	CH_3	H	CH_3
5	α	CH_3	H	CH_3
6	α	CH_3	CH_3	H

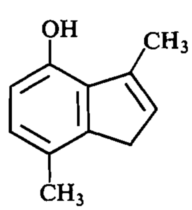

7

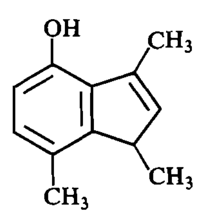

8

One of these compounds, **5**, was originally obtained as a mixture with its C-11 epimer, together with the expected tertiary alcohol, on the treatment of 3,4-dimethyl-7-hydroxyindan-1-one with methylmagnesium iodide. The structure of **5** was initially assigned (4) on the basis of its 60-MHz ^{1}H nmr spectrum, and was confirmed by an X-ray diffraction study of its 8-bromo derivative (5). Subsequent investigation resulted in the synthesis and isolation of the remaining compounds (6). In general, the dimers were prepared by treatment of the relevant indene (**7** or **8**) in chloroform with 0.5% trifluoroacetic acid. Of the tetramethyl dimers, **1** and **2**, prepared from **7**, **1** was the kinetic product, and **2** the thermodynamic product of the dimerization reaction. Compounds **1** and **2** were readily separated by chromatography. The hexamethyl dimers, **3–6**, prepared from **8**, were obtained as the kinetic product, **3**, and the successive isomerization products, **4**, **5**, and **6**, on longer acid treatment. Fractional crystallization was employed to separate **4** from **3**, and **6** from **5**.

Preliminary stereochemical assignments were made largely on the basis of the ^{13}C nmr spectra, by considering the effects of adding methyl groups, e.g. γ–*gauche* and δ–synaxial effects. The ^{13}C chemical shift assignments were made by comparison between the two series (tetra- and hexamethyl), by experiments in which the 1-methyl of the hydroxyindene was enriched in ^{13}C, and by the analysis of spectra of some mixed dimers in which an n-butyl group was substituted for the 6a-methyl group. These assignments were in complete agreement with the X-ray crystallographic analysis of the 8-bromo derivative of **5**, and have been verified by the present study. Details of these related studies will be published elsewhere (7).

The dimeric nature of these compounds creates difficulties in the application of standard ^{1}H nmr techniques to their unambiguous structure determination. In particular, the assignment of ^{1}H chemical shifts to corresponding protons in each half of the dimer is difficult because of only very slight differences in shielding. High field ^{1}H spectra (Fig. 1) were neces-

[1] Author to whom correspondence should be addressed.
[2] Revision received December 14, 1984.

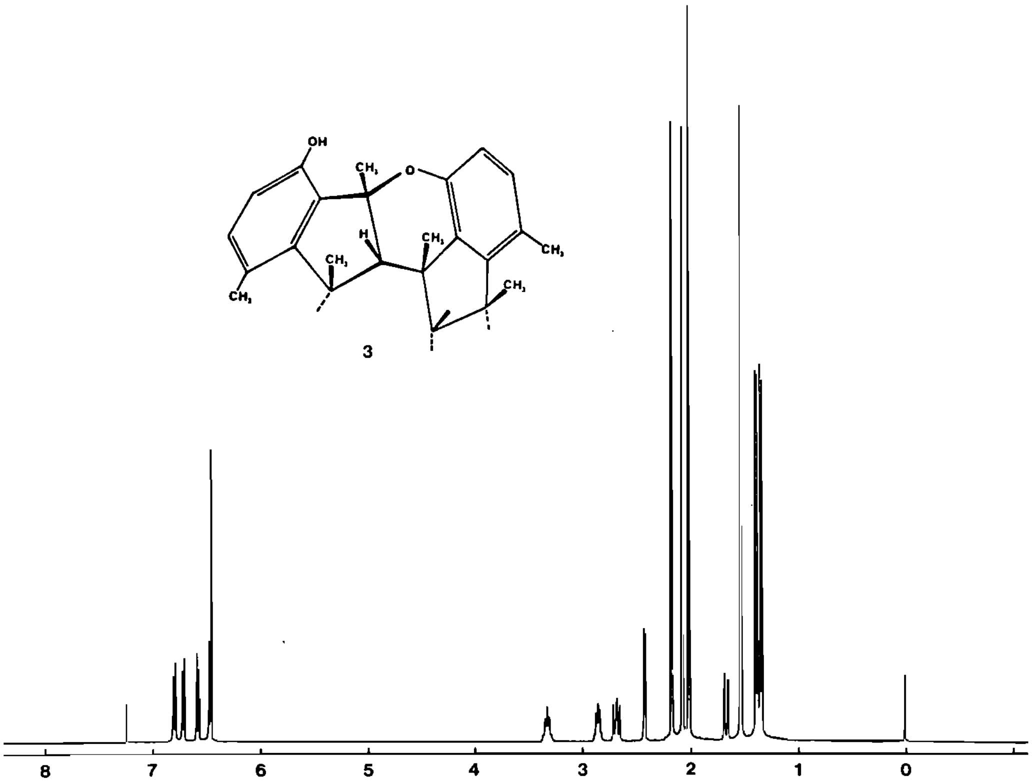

3

FIG. 1. The 400-MHz ^{1}H nmr spectrum of **3**, 0.1 *M* in $CDCl_3$.

sary to provide sufficient chemical shift dispersion to resolve all of the signals, while relaxation pathway analysis was critical for chemical shift assignment, and for the determination of stereochemistry at the chiral centres. Complete analysis of the spectral parameters of all proton signals, including differentiation of all methylene signals, and identification of the stereochemistry at all (three or five) chiral centres, has been achieved. The solution structure and stereochemistry of **5**, as determined by nmr techniques, was completely consistent with the X-ray crystallographic structure determination of the bromo derivative (5).

Relaxation pathway analysis

Proton spin-lattice relaxation in molecules of m.wt. < 1000 d, in 0.1 *M* solution in a non-viscous perdeuterated solvent, occurs predominantly by intramolecular dipolar interactions with other protons. The dipolar relaxation rate (R_{1d}) of a proton depends on the numbers of other protons in the molecule, and their distances, according to eq. [1]:

$$[1] \quad R_{1d_j} = K\left[\gamma 4 \sum_i (1/r_{ij})^6 \tau_{c_{ij}}\right] \qquad (i \neq j)$$

K is a constant, γ is the magnetogyric ratio for the proton, r_{ij} is the distance between protons i and j, and $\tau_{c_{ij}}$ is the rotational correlation time for the ij interproton vector. The τ_c term in eq. [1] contains contributions associated with segmental motion, e.g. of methyl groups, in addition to the effects of tumbling of the molecule as a whole. When a molecule tumbles isotropically, the values of τ_c are all equivalent, and a very simple relationship exists between R_1 values for any two protons:

$$[2] \quad \frac{R_{1_j}}{R_{1_k}} = \frac{\sum_i (1/r_{ij})^6 \qquad (i \neq j)}{\sum_i (1/r_{ik})^6 \qquad (i \neq k)}$$

A related parameter is the nuclear Overhauser effect (nOe) enhancement (8), which is a measure of the efficiency of the dipolar interaction between two specific nuclei. Relative nOe enhancements may be predicted in a similar manner, by calculating the contribution of each $(1/r_{ij})^6$ term to the overall sum.

The inverse sixth power dependence on internuclear distance implies that relaxation contributions are significant only for the nearest neighbors of a particular proton. In consequence, R_1 values and nOe enhancement factors are extremely sensitive to local structure and stereochemistry. Due to the unique location of each proton in the molecule, there is a unique set of relaxation pathways which characterize each proton. The various relaxation pathways to and from a particular proton can be found through the use of nOe and R_1 measurements, thereby establishing its identity.

In a relaxation pathway analysis of a complex molecule, some form of modelling is required to aid in interpretation of the data. The simple model employed uses interproton distances measured from Dreiding molecular models of possible molecular structures, and the assumption that molecular tumbling is isotropic. The latter is a reasonable approximation for these molecules at the semi-quantitative level of the analysis. This approach had worked well for some strychnos alkaloids (3). Due to the difficulties in accurately predicting the relaxation contributions from the numerous methyl groups in these molecules, calculations could only be used as a qualitative guide to the interpretation of the data.

Prediction of nOe enhancements provided guidance in the selection of key nOe experiments necessary to assign stereochemistry and corroborate chemical shift assignments. The qualitative outcome of such experiments could, in all cases, be adequately interpreted by inspection of molecular models. The small differences in chemical shifts of corresponding resonances in each half of the dimer required that subsaturating

TABLE 1. 7-Hydroxy indene dimer ^1H R_1 values[a]

Compound	R_1 (s^{-1}) 1	2	3	4	5	6
H-1α	1.67	1.70	2.16	2.11	1.82	1.88
H-1β	1.61	1.79	1.70	1.64	2.11	2.00
H-2α	1.48	1.68	0.71	—	—	0.82
CH_3-2α	—	—	—	1.40	1.45	—
H-2β	1.19[b]	1.60	—	0.69	0.80	—
CH_3-2β	—	—	1.32	—	—	1.58
CH_3-3	0.69	0.83	0.76	0.86	0.98	1.02
H-4	0.379	0.437	0.412	0.458	0.512	0.528
H-5	0.342	0.401	0.373	0.408	0.453	0.460
CH_3-6aβ	1.28	1.98	1.52	1.57	1.99	2.01
OH-7	0.341	0.311	0.38[b]	0.43[b]	0.374	0.380
H-8	0.326	0.333	0.334	0.364	0.386	0.376
H-9	0.368	0.389	0.409	0.436	0.449	0.451
CH_3-10	0.68	0.72	0.80	0.80	0.84	0.83
H-11α	1.33	1.71	0.92	0.96	0.98	1.02
H-11β	1.37	1.64	—	—	—	—
CH_3-11β	—	—	1.36	1.42	1.48	1.43
H-11aβ	0.97	0.92	0.90	0.92	0.99	0.99
CH_3-11bα	1.82	—	1.87	1.87[b]	—	—
CH_3-11bβ	—	1.95	—	—	1.81	2.12

[a] R_1 values are calculated by two-parameter non-linear regressional analysis, to a precision of ± 0.01 s^{-1}.
[b] R_1 determined by the null point method because of signal overlap.
α = alpha face, β = beta face.

power levels (soft experiments) be used in the nOe experiments in order to achieve adequate selectivity. This restriction prohibited quantitative comparisons between calculated and experimental nOe enhancements, and hence the measurement of interproton distances.

Results and discussion

The strategy adopted in this study was to first carry out non-selective ^1H spin-lattice relaxation measurements, then to use selected nOe difference (nOed) (9–11)[3] measurements to identify specific relaxation pathways.

Relaxation measurements provide a fast, efficient aid to the assignment of proton chemical shifts, since the R_1 value of a particular proton is strongly dependent on its environment. The relatively isolated, and hence slowly relaxing, OH and aromatic protons have the lowest R_1 values (0.3–0.4 and 0.3–0.5 s^{-1}, respectively). The other methine protons relax more efficiently since they have a larger number of near neighbors (R_1 values of 0.7–1.0 s^{-1}). Due to their close proximity, the methylene protons relax each other very efficiently, and have higher R_1 values (1.1–2.0 s^{-1}). Under most circumstances, methyl group relaxation is also dominated by dipolar effects. Since the methyl group protons are close to each other, they relax so efficiently that they experience little dipolar relaxation from other protons in the molecule. Interpretation of methyl group R_1 values can, therefore, be based on analysis of motional effects. This implies that, for any particular molecule, differences in methyl R_1 values can be attributed to different rates of methyl rotation. The aryl methyl groups, which are relatively free to rotate about the C—CH_3 bond axis, have R_1 values of 0.7–1.0 s^{-1}. In contrast, the alkyl methyl groups, whose rotation is evidently more restricted in these compounds, relax more efficiently, with R_1 values of 1.3–2.1 s^{-1}.

[3] Also, W. J. Chazin and L. D. Colebrook, this laboratory.

TABLE 2. Selected nOe enhancements which provide stereochemical information for *cis*-fused dimers (**1**, **3**, **4**)

Irradiated proton		Observed enhancements[a]
H-1	α	1(β), 2(α), 11(α), 11(β)
H-1	β	1(α), 2(β), 11a(β), CH_3-11b(β)
H-2	α	1(α), 2(β), CH_3-3
H-2	β	1(β), 2(α), CH_3-3
CH_3-6a	β	OH-7, 11a(β), CH_3-11b(β)
H-11	α	1(α), 11(β), CH_3-10
H-11	β	11(α), 11a(β)
H-11a	β	11(β), CH_3-6a(β), CH_3-11b(β)
CH_3-11b	β	1(β), 11a(β), CH_3-6a(β)

[a] The substituents at 2 and 11 vary from compound to compound, so the enhancements are indicated by position only.

TABLE 3. Selected nOe enhancements which provide stereochemical information for *trans*-fused dimers (**2**, **5**, **6**)

Irradiated proton		Observed enhancements[a]
H-1	α	1(β), 2(α), 11(α), CH_3-11b(α)
H-1	β	1(α), 2(β), 11a(β), 11(β)
H-2	α	1(α), 2(β), CH_3-3, CH_3-11b(α)
H-2	β	1(β), 2(α), CH_3-3
CH_3-6a	β	OH-7, 11(β), 11a(β)
H-11	α	1(α), 11(β), CH_3-10, CH_3-11b(α)
H-11	β	2(β), 11(α), 11a(β)
H-11a	β	1(β), 11(β), CH_3-6a(β)
CH_3-11b	α	1(α), 2(α), 11(α)

[a] The substituents at 2 and 11 vary from compound to compound, so the enhancements are indicated by position only.

Stereochemical determinations

Differentiation of methine from methylene protons at C-1, C-2, C-11, and C-11a was easily made by consideration of ^1H R_1 values (Table 1), since methylene protons in these compounds generally relax about twice as fast as the methine protons. Tentative assignments were made by consideration of chemical shifts and coupling constants, assisted by spin-decoupling experiments. The stereochemistry at positions 1, 2, 11, 11a, and 11b was then determined relative to that of the methyl group at position 6a (designated as being located on the upper (β) face of the molecules (5)), by relaxation pathway analysis. In all cases, H-11a was on the same (β) side of the molecule as CH_3-6aβ, as evidenced by the substantial nOe enhancements between the two (Figs. 2 and 3, Tables 2 and 3). In a similar manner, the relative stereochemistry at position 11b could be determined from the magnitudes of nuclear Overhauser effects between CH_3-11b and H-11aβ. A large nOe established the ring fusion as *cis* (compounds **1**, **3**, and **4**, Fig. 2); a small nOe, determined under similar conditions, established the ring fusion as *trans* (compounds **2**, **5**, and **6**, Fig. 3). The proton or methyl group in the β-position at C-11 was clearly distinguished from the α-position substituent by significant nOe enhancements to and from both H-11aβ and CH_3-6aβ. For all hexamethyl dimers, the 11-methyl group was identified as having β-stereochemistry.

The assignments at C-1 and C-2 were carried out in a similar manner, but required more careful consideration of the relaxation data and close inspection of molecular models. For the compounds which have *trans*-geometry of rings B and D (**2**, **5**,

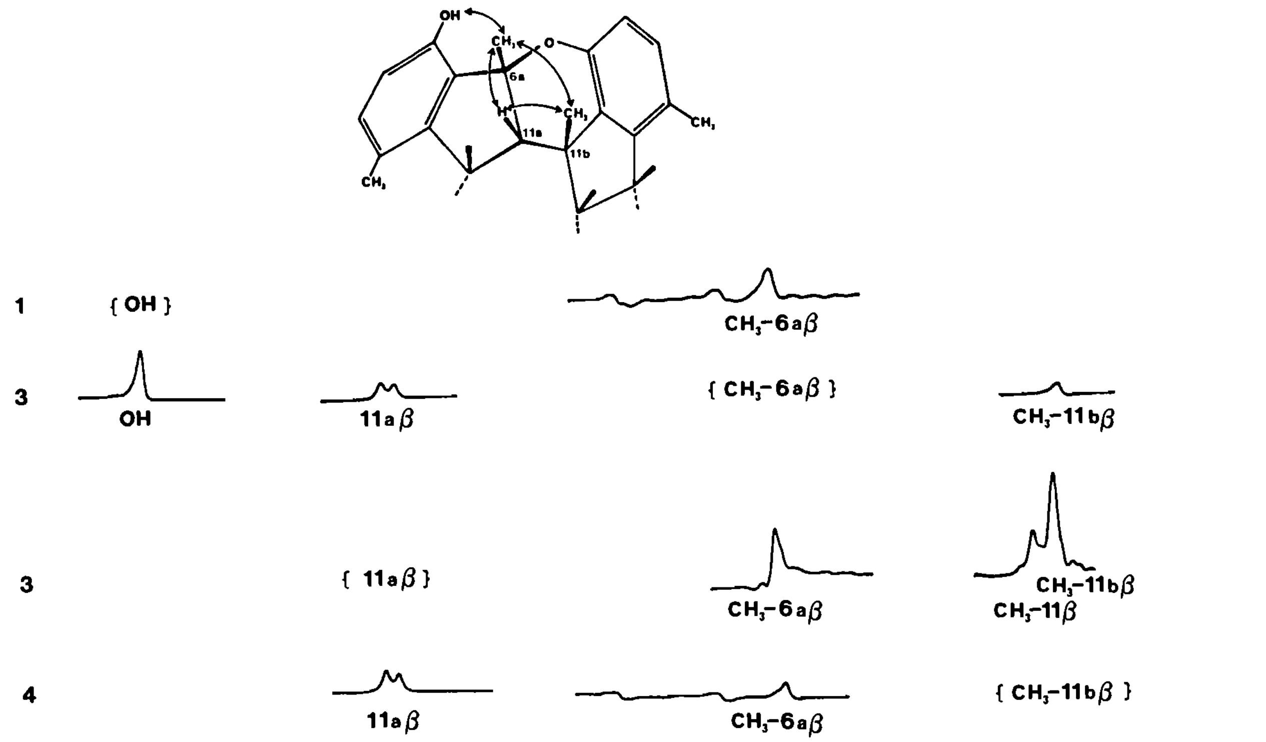

FIG. 2. Relaxation pathways (arrows), and partial nOed spectra used to determine ring fusion in *cis*-fused compounds. Transitions irradiated are indicated {}.

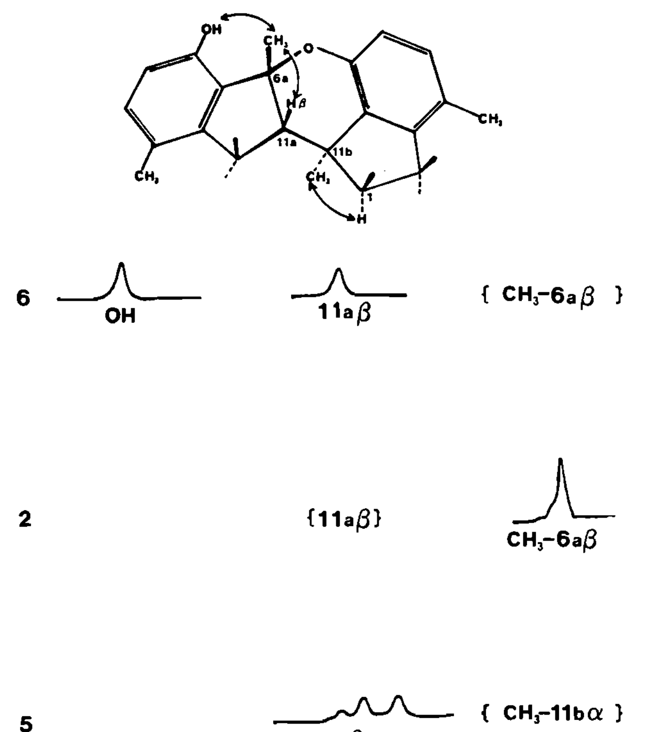

FIG. 3. Relaxation pathways (arrows), and partial nOed spectra used to determine ring fusion in *trans*-fused compounds. Transitions irradiated are indicated {}.

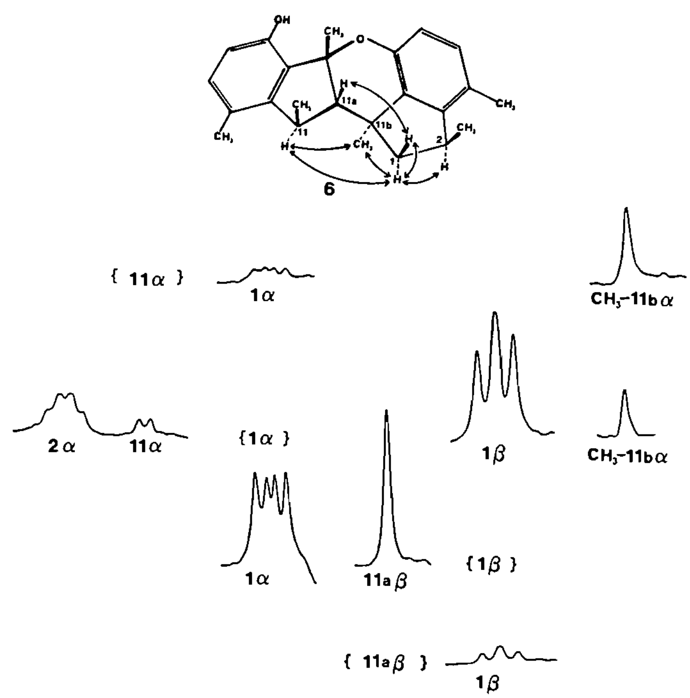

FIG. 4. Relaxation pathways (arrows), and partial nOed spectra used to determine C-1 and C-2 stereochemistry in a *trans*-fused compound, **6**. Transitions irradiated are indicated {}.

and **6**), the relaxation pathway between CH_3-11bα and the C-1 proton on the same side of the molecule serves to distinguish between the two C-1 protons (see Fig. 4). The relative magnitudes of the nOe enhancement to and from the C-1 substituents and the previously assigned C-11 substituents corroborate these assignments. The assignments at C-2 were then made by relaying the stereochemical assignments at C-1 through the relative magnitudes of the nOe enhancements (large values for adjacent substituents on the same face of the molecule, Fig. 4).

For compounds with *cis*-geometry of rings B and D (**1**, **3**,

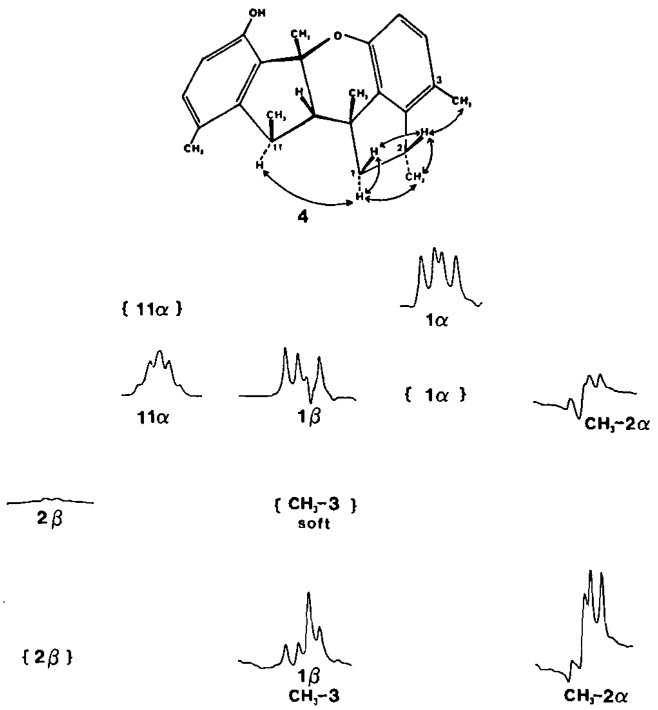

FIG. 5. Relaxation pathways (arrows), and partial nOed spectra used to determine C-1 and C-2 stereochemistry in a *cis*-fused compound, **4**. Transitions irradiated are indicated {}.

and **4**), the relaxation pathway between CH_3-11bβ and the C-1 protons (Fig. 5) clearly differentiates between the two protons. In these molecules, there is also a significant nOe between the substituents in the α-positions of C-1 and C-11, verifying the assignment and reflecting the folded geometry of the molecules. The assignments at C-2 were again made by relaying the stereochemistry established at C-1, through the magnitudes of the nOe enhancements.

Assignments in aromatic rings

The signals (400 MHz) arising from ring A protons could be distinguished from the corresponding ring E signals by a combination of chemical shift arguments, double resonance, and, in particular, by relaxation pathway analysis. The hydroxyl proton signals were readily identified as the slowly relaxing singlets at 6.1–6.8 ppm. H-8 may be distinguished from H-9, and H-4 from H-5 on the basis of the greater shielding effect in the *ortho* position from the oxygen substituents (OH-7 and OR-5a), and by the higher relaxation rates of the 4 and 9 protons resulting from significant contributions from the adjacent 3 and 10 methyl groups.

A definitive distinction between the ring A and ring E aromatic signals was established by identification, through nOed experiments, of consecutive relaxation pathways originating on the previously assigned C-2 and C-11 protons. Saturation of the H-11α resonance gave an enhancement of CH_3-10, while irradiation of the H-2α and (or) H-2β transitions gave an enhancement of CH_3-3 (Fig. 6). Since the chemical shifts of the two methyl resonances were very different ($\Delta\delta = 0.2$ ppm), these nOe enhancements gave the methyl assignments unambiguously. The H-4 and H-9 resonances could then be assigned from the nOe enhancements observed upon irradiation of CH_3-3 and CH_3-10, respectively (Fig. 6). The completion of the aromatic proton relaxation sequences to the 8 and 5 protons:

TABLE 4. ^{1}H chemical shifts[a] of compounds **1–6**

Proton	Chemical shift 1[b]	2[c]	3[b]	4[b]	5[c]	6[c]
H-1α	2.20	2.14	2.68	1.85	1.87	2.38
H-1β	1.97	1.88	1.67	2.21	2.29	1.54
H-2α	2.78	2.93	3.32	—	—	3.48
CH_3-2α	—	—	—	1.33	1.32	—
H-2β	2.96	2.80	—	3.51	3.36	—
CH_3-2β	—	—	1.39	—	—	1.40
CH_3-3	2.13	2.22	2.17	2.20	2.26	2.31
H-4	6.76	6.92	6.72	6.72	6.92	6.89
H-5	6.51	6.70	6.47	6.48	6.71	6.68
CH_3-6aβ	1.99	1.57	2.01	2.01	1.63	1.70
OH-7	6.14	6.80	6.46	6.47	6.74	6.74
H-8	6.58	6.69	6.58	6.59	6.71	6.71
H-9	6.83	6.96	6.80	6.82	6.98	6.97
CH_3-10	2.03	2.21	2.08	2.11	2.27	2.26
H-11α	2.90	2.90	2.85	3.07	3.36	3.36
H-11β	2.52	3.02	—	—	—	—
CH_3-11β	—	—	1.35	1.36	1.34	1.37
H-11aβ	2.97	2.38	2.42	2.43	1.91	2.03
CH_3-11bα	1.40	—	1.53	1.35	—	—
CH_3-11bβ	—	0.71	—	—	0.92	0.73

[a] In ppm from TMS. α = lower face, β = upper face.
[b] *cis* Fusion of rings B and C.
[c] *trans* Fusion of rings B and C.

$$CH_3\text{-}3 \leftrightarrow \text{H-4} \leftrightarrow \text{H-5} \qquad CH_3\text{-}10 \leftrightarrow \text{H-9} \leftrightarrow \text{H-8}$$

was trivial, so chemical shifts of all aromatic resonances were assigned.

With this information, the structural analysis was complete, and the full set of assignments of the nmr parameters could be made. These were refined by computer simulation when necessary, and are listed in Table 4. The stereochemistry of all six compounds was consistent with the coupling constants measured directly, or obtained using computer simulation.

Conclusion

By utilizing the relaxation pathway analysis technique outlined in the Introduction, it was possible to assign all the signals in the ^{1}H nmr spectrum of the six 7-hydroxyindene dimers, including the diastereotopic methylene protons. In addition, by careful analysis of nOe enhancements with the aid of molecular models, it was possible to determine ring fusion, and to assign the stereochemistry at all three or five chiral centres. This report demonstrates the power of the relaxation pathway technique for the analysis of the solution structure of organic molecules, even in situations where detailed quantitative analysis is not possible.

Experimental

Solutions for nmr studies were made 0.1 *M* in $CDCl_3$, without degassing, since this has been shown to be unnecessary for qualitative studies of this type (2). Spectra (eight transients) were acquired into 32K (standard spectra and R_1 measurements) or 16K (nOed spectra) data blocks over a spectral range of 3800 Hz on a Bruker WH-400 spectrometer (Montreal Regional High Field NMR Laboratory). All spectra were acquired at ambient temperature (292 K). Spectral simulations were carried out on a Hewlett–Packard 1000 computer, using a modified LAOCOON III (12) program.

R_1 values were measured using the standard inversion–recovery pulse sequence (13). The 180° pulse-width was checked at the beginning of each experiment. R_1 data within the initial slope region (14)

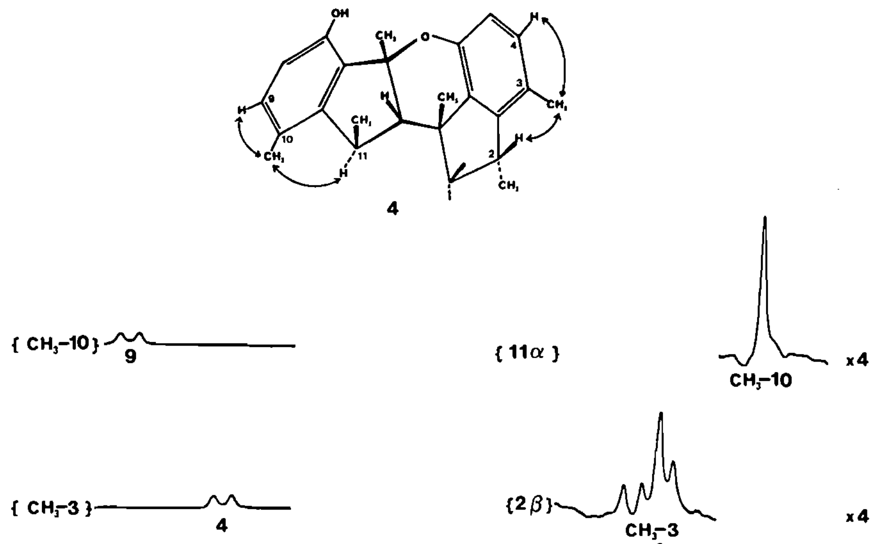

FIG. 6. Relaxation pathways (arrows), and partial nOed spectra used to distinguish between aromatic ring signals in **4**. Transitions irradiated are indicated {}.

were calculated by two-parameter, non-linear regressional analysis on the HP-1000 computer. The absolute accuracy of R_1 measurements is typically ±10% but, within a single experiment, the relative R_1 values can be determined to a precision of better than ±5%.

Theoretical R_1 values and nOe enhancements were calculated for the model described by eq. [2], using the HP-1000 computer.

The nOe enhancements were measured by the sensitive difference method using a modification, which has been described previously (3), of the procedure reported by Hall and Sanders (9). A full $5 \times T_1$ preparation period was allowed before each scan, although it is now firmly established that the use of a $1-3 \times T_1$ preparation period is more efficient when carrying out qualitative studies (11). In several of the nOe difference experiments, the use of subsaturating power levels (soft experiments) was not sufficient to ensure selectivity. In these cases, additional experiments were carried out to determine the influence of decoupler power and decoupler frequency offset on observed nOe enhancements, thereby verifying the origin of the enhancements. Although the nOed technique has been shown to be sensitive down to the order of a few tenths of a percent (11), in those instances when irradiation selectivity was a problem, only relatively large enhancements (>1%) were considered to be sufficiently reliable.

Mass spectra were recorded at 12 or 70 eV. Peak positions (m/e) are followed by relative abundances in parentheses.

Synthetic procedures

*(6aβ,11aβ,11bβ)-1,2,6a,11,11a,11b-Hexahydro-3,6a,10,11b-tetramethyldiindeno[7,1-*bc*:2′,1′-*e*]pyran-7-ol (1)*

A solution of trifluoroacetic acid in chloroform (5% v/v, 0.02 mL) was added to indenol **7** (100 mg) in chloroform (0.5 mL) at room temperature. After 90 min the mixture was worked up to give the crude product (100 mg) which was purified by preparative thin-layer chromatography (ptlc) to give the dimer **1** (60 mg), mp 130–130.5°C (from n-pentane); m/e (12 eV): 320 (6, M$^+$), 160 (34), 159 (100). *Anal.* calcd. for $C_{22}H_{24}O_2$: C 82.5, H 7.6; found: C 82.4, H 7.7.

*(6aβ,11aβ,11bα)-1,2,6a,11,11a,11b-Hexahydro-3,6a,10,11b-tetramethyldiindeno[7,1-*bc*:2′,1′-*e*]pyran-7-ol (2)*

Trifluoroacetic acid (0.025 mL) was added to the indenol **7** (100 mg) in chloroform (0.5 mL) at room temperature. After 30 min the mixture was diluted with ether and worked up to give crude product (100 mg). Chromatography and recrystallization gave the dimer **2** (60 mg), mp 157–158°C (from n-hexane); m/e (12 eV): 320 (3, M$^+$), 160 (53), 159 (100). *Anal.* calcd. for $C_{22}H_{24}O_2$: C 82.5, H 7.6; found: C 82.6, H 7.5.

*(2β,6aβ,11β,11aβ,11bβ)-1,2,6a,11,11a,11b-Hexahydro-2,3,6a,10,11,11b-hexamethyldiindeno[7,1-*bc*:2′,1′-*e*]pyran-7-ol (3)*

A solution of trifluoroacetic acid in carbon tetrachloride (5% v/v, 0.1 mL) was added to indene **8** (0.30 g) in chloroform (2.5 mL). After 35 min the solution was diluted with ether (25 mL), shaken with 5% sodium bicarbonate solution (20 mL), and worked up to give the crude product (0.30 g). Purification by ptlc gave the main component (0.20 g) which was recrystallized from n-hexane to give dimer **3** (0.17 g, 57%), mp 155–157°C; m/e (12 eV): 348 (4, M$^+$), 174 (100); (70 eV): 348 (2, M$^+$), 175 (50), 174 (72), 159 (100). *Anal.* calcd. for $C_{24}H_{28}O_2$: C 82.72, H 8.10; found: C 82.97, H 8.36. The residue from the crystallization (approximately 0.03 g) was a 2:1 mixture of dimer **3** and the C-2 epimer, dimer **4**.

*(2α,6aβ,11β,11aβ,11bβ)-1,2,6a,11,11a,11b-Hexahydro-2,3,6a,10,11,11b-hexamethyldiindeno[7,1-*bc*:2′,1′-*e*]pyran-7-ol (4)*

The indene **8** (250 mg) in chloroform (1 mL) was mixed with trifluoroacetic acid (0.01 mL) in chloroform (1 mL) at room temperature. After 1 h, work-up gave a product mixture (250 mg) which was separated by ptlc to give a fraction containing dimer **5** (60 mg) and a lower R_f fraction consisting of a 1:1 mixture of dimers **3** and **4** (150 mg). Recrystallization of this mixture from n-pentane gave crystals enriched in dimer **3**. Successive fractional recrystallizations were performed, and when the concentration of dimer **4** in the residue exceeded 65%, this dimer became concentrated in the crystals and eventually dimer **4** was obtained pure, mp 131–132.5°C; m/e (12 eV): 348 (12, M$^+$), 174 (100). *Anal.* calcd. for $C_{24}H_{28}O_2$: C 82.72, H 8.10; found: C 82.89, H 8.16.

*(2α,6aβ,11β,11aβ,11bα)-1,2,6a,11,11a,11b-Hexahydro-2,3,6a,10,11,11b-hexamethyldiindeno[7,1-*bc*:2′,1′-*e*]pyran-7-ol (5)*

Trifluoroacetic acid (0.025 mL) was added to the indene **8** (75 mg) in chloroform (0.5 mL). Work-up of the reaction mixture after 30 min and separation by ptlc gave the main component (40 mg, 54%), a 10:1 mixture of dimer **5** and the C-2 epimer, dimer **6**. Recrystallization gave pure dimer **5**, mp 167–169°C (from n-hexane); m/e (12 eV): 348 (5, M$^+$), 175 (30), 174 (100); (70 eV): 348 (3, M$^+$), 175 (100), 174 (80), 159 (43). *Anal.* calcd. for $C_{24}H_{28}O_2$: C 82.72, H 8.10; found: C 82.56, H 8.02.

*(2β,6aβ,11β,11aβ,11bα)-1,2,6a,11,11a,11b-Hexahydro-2,3,6a,10,11,11b-hexamethyldiindeno[7,1-*bc*:2′,1′-*e*]pyran-7-ol (6)*

Trifluoroacetic acid (0.2 mL) was added to the dimer **5** (0.50 g) in chloroform (5 mL) and the dark red solution was heated under reflux for 2 h. Work-up and ptlc gave a 1:1 mixture of dimers **5** and **6** (0.30

g) and a 1 : 1 mixture of dimers **3** and **4** (0.04 g). The mixture of dimers **5** and **6** (0.30 g) in methanol (20 mL) was mixed with trifluoroacetic acid (1 mL) and the solution was heated under reflux for 30 min. Work-up and ptlc gave a 1:7 mixture of dimers **5** and **6** (90 mg). Recrystallization gave pure dimer **6**, mp 173–174°C; *m/e* (12 eV): 348 (14, M^+), 175 (68), 174 (100), 159 (20); (70 eV): 348 (7.5, M^+), 175 (100), 174 (55), 159 (47). *Anal.* calcd. for $C_{24}H_{28}O_2$: C 82.72, H 8.10; found: C 83.10, H 8.41.

Acknowledgements

This work was supported in part by grants from the Natural Sciences and Engineering Research Council of Canada (NSERC), who also supplied funding towards the purchase and operation of the 400-MHz spectrometer. W.J.C. wishes to thank the Ministry of Education, Province of Quebec, and NSERC, for Fellowships.

1. L. D. HALL. Chem. Soc. Rev. **4**, 401 (1975); L. D. HALL. Chem. Can. **28**, 19 (1976); K. BOCK, L. D. HALL, and C. PEDERSON. Can. J. Chem. **58**, 1923 (1980); N. NICCOLAI, H. K. SCHOES, and W. A. GIBBONS. J. Am. Chem. Soc. **102**, 1513 (1980); N. NICCOLAI, V. GARSKY, and W. A. GIBBONS. J. Am. Chem. Soc. **102**, 1517 (1980); L. D. COLEBROOK, M. A. KHADIM, and L. D. HALL. J. Heterocycl. Chem. **17**, 651 (1980); L. D. COLEBROOK, J-M. NAVARRE, and L. D. HALL. Org. Magn. Reson. **14**, 410 (1980); L. D. COLEBROOK and L. D. HALL. Org. Magn. Reson. **21**, 532 (1983); S. PEIRIS and L. D. COLEBROOK. Org. Magn. Reson. **22**, 228 (1984).
2. L. D. COLEBROOK and L. D. HALL. Can. J. Chem. **58**, 2016 (1980).
3. W. J. CHAZIN, J. T. EDWARD, and L. D. COLEBROOK. Can. J. Chem. **61**, 1749 (1983).
4. B. R. DAVIS and I. R. N. MCCORMICK. J. Chem. Soc. Perkin Trans. 1, 3001 (1979).
5. A. W. KING, L. J. MCDONALD, J. M. WATERS, and T. N. WATERS. Cryst. Struct. Commun. **3**, 681 (1974).
6. S. J. JOHNSON. Ph.D. Thesis, University of Auckland. 1983.
7. B. R. DAVIS and S. J. JOHNSON. J. Chem. Soc. Perkin Trans. 1. Submitted.
8. J. H. NOGGLE and R. E. SCHIRMER. The nuclear Overhauser effect. Academic Press, New York. 1971.
9. L. D. HALL and J. K. M. SANDERS. J. Am. Chem. Soc. **102**, 5703 (1980).
10. W. A. GIBBONS, D. CREPEAUX, J. DELAYRE, J. J. DUNAND, G. HADJUKOVIC, and H. R. WYSSBROD. *In* Peptides, chemistry, structure, biology. *Edited by* R. Walter and J. Meinhofer. Ann Arbor Science Publications, Ann Arbor, Michigan. 1975. pp. 127–137; C. R. JONES, C. T. SIKAKANA, S. HEHIR, M. C. KUO, and W. A. GIBBONS. Biophys. J. **24**, 815 (1978); C. R. JONES, C. T. SIKAKANA, M. C. KUO, and W. A. GIBBONS. J. Am. Chem. Soc. **100**, 5960 (1978); C. R. JONES, C. T. SIKAKANA, S. P. HERIR, and W. A. GIBBONS. Biochem. Biophys. Res. Commun. **83**, 1380 (1978); M.-C. KUO and W. A. GIBBONS. J. Biol. Chem. **254**, 6278 (1979).
11. J. K. M. SANDERS and J. D. MERSH. Prog. Nucl. Magn. Reson. Spectrosc. **15**, 353 (1982).
12. S. CASTELLANO and A. A. BOTHNER-BY. J. Chem. Phys. **41**, 3863 (1964).
13. M. L. MARTIN, G. J. MARTIN, and J. J. DELPUECH. Practical NMR spectroscopy. Heyden, London. 1980. p. 254.
14. R. FREEMAN, S. WITTEKOEK, and R. R. ERNST. J. Chem. Phys. **52**, 1529 (1970).

COMMUNICATIONS

A laser interferometric study of sessile drop shape and contact angle

R. N. O'BRIEN AND PAUL SAVILLE
Department of Chemistry, University of Victoria, Victoria, B.C., Canada V8W 2Y2

Received March 26, 1985

R. N. O'BRIEN and PAUL SAVILLE. Can. J. Chem. **63**, 2339 (1985).

Small contact angles, such as water on glass, have been shown to be measurable interferometrically using fringes of equal thickness after the fashion of Newton's rings. The measured angle for the water on glass system was 0.049 ± 0.006 degrees of arc.

R. N. O'BRIEN et PAUL SAVILLE. Can. J. Chem. **63**, 2339 (1985).

On montre qu'on peut faire appel à l'interférométrie pour mesurer les petits angles de contact, tel celui de l'eau avec le verre, en utilisant des franges d'égale épaisseur à la manière des anneaux de Newton. L'angle de contact de l'eau avec le verre est de 0,049 ± 0,006.

[Traduit par le journal]

The contact angle of pure water on clean smooth glass has been the subject of investigation by many methods and over many years (1, 2). Contact angles are important for many reasons, not the least of which are those related to adhesion and biological aspects.

Probably the contact angle of water (on a variety of substrates) has been most often studied and especially on glass and siliceous materials generally (3, 4). For this reason it was decided to attempt to obtain the profile of a sessile drop on glass by interferometric means. A first trial was made using holographic interferometry. The interferogram was measurable but of poor quality. The technique was difficult and time consuming, and the measurements made from them were not totally convincing. A simpler method using fringes of equal thickness after the fashion of Newton's rings (Fig. 1(*a*)) where instead of a thin lens convex side down there was a "thin" drop of water convex side up. All of the other optical arrangements in Fig. 1 produced Fresnel fringes as well as true interference fringes but the Fresnel fringes are of so much greater definition (contrast between constructive and destructive interference) that the true interference fringe system was unusable. Figure 2 is an example of such a combined system produced by the optical system in Fig. 1(*b*). Fresnel fringes should have a bright spot in the centre and the fringes should be at r (the radius) = $\sqrt{1}$, $\sqrt{2}$, $\sqrt{3}$ etc. (5). Figure 2 clearly does not show this type of periodicity and this will be the subject of further research.

A series of interferograms made using the optical arrangement in Fig. 1(*a*) is shown in Fig. 3. These interferograms were taken with a 35 mm camera. The whole sequence was also recorded with a color video-recorder/camera and the monitor then photographed for measuring and reproduction. The interferograms were taken with a guard ring to avoid stray air currents and unsymmetrical evaporation (which was observed) and at room temperature (22°C ± 0.5). The parallel straight fringes interrupted by the drop's fringes are the result of the non-parallel sides of the glass flat.

A series of 12 drops were measured from opposite sides, that is the distance between fringes was measured. Each successive fringe from the edge of the drop (which could be unambiguously located) was located and the results averaged. The glass was float glass, expected to be 1/4 λ flat over 3 mm cleaned with Sparkleen laboratory detergent. The water was NANOpure water.

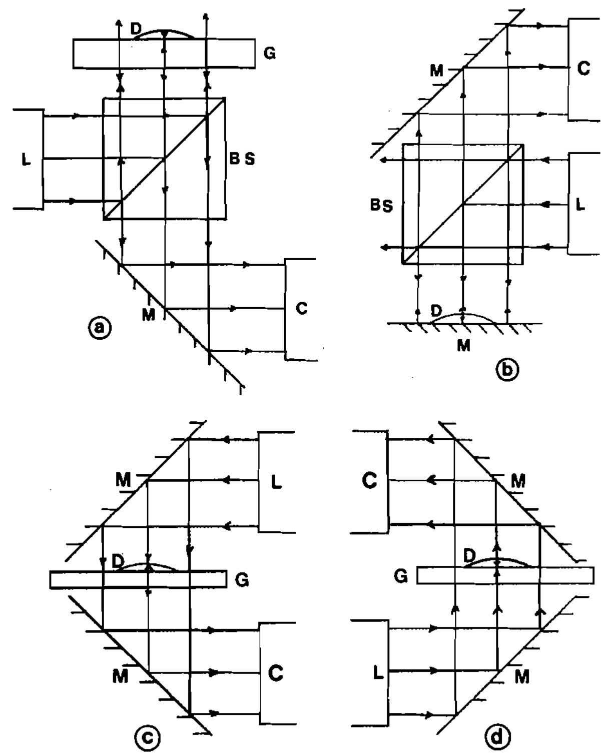

FIG. 1. Schematic diagrams of four candidate optical arrangements for interferometric determination of drop contours; (*a*) and (*b*) results are shown in Figs. 2 and 3, (*c*) and (*d*) produced similar results to (*b*). The parts are labelled L for laser (He Ne gas laser nominal 5 mW), C for camera (35 mm or video), M for first surface mirror, D for drop, and G for glass flat.

The measured contact angle was 0.049 ± 0.006 deg of arc. This agrees reasonably well with Irons (3) and Stepanov *et al.* (4) and with the general consensus that the contact angle is very small. There are even those (6) who say the angle is a "non-angle". The textbook approach is that the angle is zero or so close to it that any measurement is suspect as likely to be within the uncertainty of measurement with previously available methods. To the best of our knowledge this is the first measurement where the value is not obscured by the uncertainty of measurement.

Further work is planned in which specially prepared glass

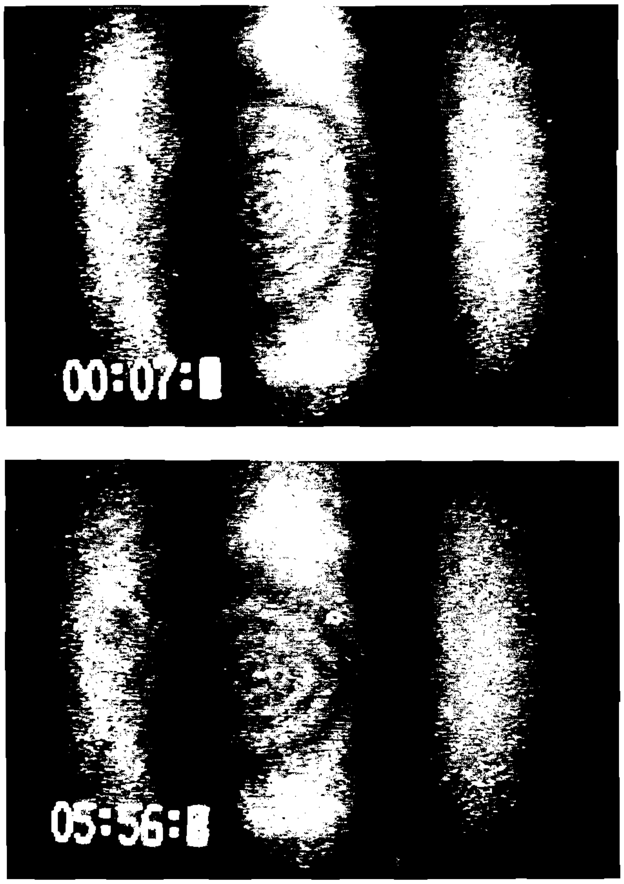

FIG. 2. Two interferograms photographed from the video monitor at the times shown after drop deposit from a drawn capillary. Note these are 5 fringes in the top frame and 4 in. in the bottom, or the drop depth has decreased by $\lambda/2$ or 316.4 nm approximately.

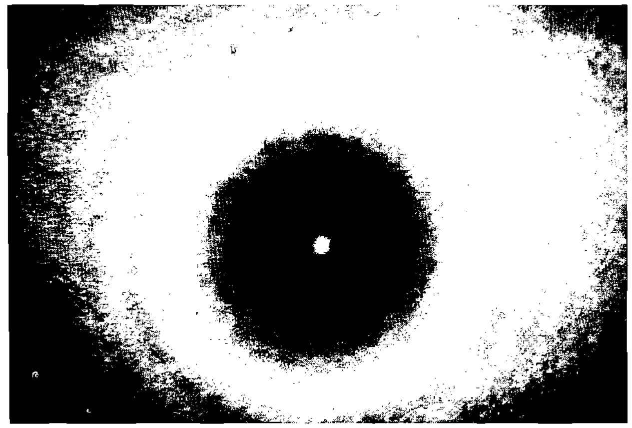

FIG. 3. An interferogram made using the optical arrangement in Fig. 1(*b*) containing a bright Fresnel diffraction pattern obscuring the fringes of equal thickness shown in Fig. 2.

flats with a minimum surface roughness will be used. Specially purified water will be tested with controlled amounts of various solutes and an attempt to add to a drop as well as to allow it to evaporate to measure advancing and retreating drop edges.

1. A. W. ADAMSON. Physical chemistry of surfaces. 4th ed. Wiley, New York. p. 338 et seq.
2. G. E. P. ELLIOTT and S. C. RIDDIFORD. Contact angles in recent progress in surface science #2. *Edited by* J. F. Danielle, T. G. H. Parkhurst, and A. E. Riddiford. Academic, New York. 1964. p. 111 et seq.
3. E. J. IRONS. Philos. Mag. **34**, 614 (1943).
4. V. G. STEPANOV, L. D. VOLYAK, and YU. V. TARLAKOV. J. Eng. Phys. **32**, 646 (1977).
5. J. MORGAN. Introduction to geometrical and physical optics. McGraw-Hill, New York. 1953. p. 268.
6. D. M. GANS. J. Phys. Chem. **49**, 165 (1945).

Radical ions in photochemistry. 16. The photosensitized (electron transfer) carbon–carbon bond-cleavage reaction of radical cations

AKIO OKAMOTO[1] AND DONALD R. ARNOLD[2]
Department of Chemistry, Dalhousie University, Halifax, N.S., Canada B3H 4J3

Received January 14, 1985

AKIO OKAMOTO and DONALD R. ARNOLD. Can. J. Chem. **63**, 2340 (1985).

The photosensitized (electron transfer) carbon–carbon bond cleavage of 1,1,2,2-tetraphenylethane (**1***b*), 2-(4-methoxyphenyl)-1,1-diphenyl-2-methylpropane (**1***c*), 1,1,2-triphenyl-2-methylpropane (**1***d*), and 2-(4-trifluoromethylphenyl)-1,1-diphenyl-2-methylpropane (**1***e*) has been studied with 1,4-dicyanobenzene (**2**) serving as the electron-accepting sensitizer. The oxidation potential of **1***b–e* have been measured by cyclic voltammetry. Estimation of the free-energy associated with the electron transfer between these donors (**1***b–e*) and the first excited singlet state of **2**, using the Weller equation, indicates the process is favorable in every case. There is, in every case, a one-to-one correspondence of products derived from reaction of the carbocation fragment and from the carbanion derived from the initially formed radical fragment. The efficiency of the reaction of **1***b*, which gives a good yield of diphenylmethane (**3**) and methyl diphenylmethyl ether, has been studied as a function of temperature. The observed activation energy (7.2 kcal mol^{-1}) is equated to the bond dissociation energy of the central bond of the radical cation ($1b^{+\cdot}$). The ratio of products from the unsymmetric compounds is dependent upon the redox potentials of the fragment radicals and carbocations.

[1] On leave from the Institute of Interdisciplinary Research, Faculty of Engineering, University of Tokyo, Tokyo, Japan.
[2] To whom all correspondence should be addressed.

AKIO OKAMOTO et DONALD R. ARNOLD. Can. J. Chem. **63**, 2340 (1985).

Utilisant le dicyano-1,4 benzène (**2**) comme sensibilisateur accepteur d'électrons, on a étudié la réaction photosensibilisée (transfert d'électrons) de clivage de la liaison carbone–carbone du tétraphényl-1,1,2,2 éthane (**1***b*), du (méthoxy-4 phényl)-2 diphényl-1,1 méthyl-2 propane (**1***d*) et du (trifluorométhyl-4 phényl)-2 diphényl-1,1 méthyl-2 propane (**1***e*). On a mesuré les potentiels d'oxydo-réduction des composés (**1***b–e*) par voltamétrie cyclique. L'évaluation, à l'aide de l'équation de Weller, de l'énergie libre associée au transfert d'électron entre ces donneurs **1***b–e* et le premier état singulet excité indique que dans tous les cas le processus est favorisé. Dans chaque cas, il y a une correspondance du type 1 à 1 des produits provenant d'une part de la réaction de la portion carbocationique et d'autre part du carbanion issu du fragment radicalaire qui se forme initialement. On a étudié, en fonction de la température, l'efficacité de la réaction du composé (**1***b*) qui donne avec un bon rendement du diphénylméthane (**3**) et du méthoxydiphénylméthane. La valeur de l'énergie d'activation (7,2 kcal mol^{-1}) est égale à l'énergie de dissociation de la liaison centrale du cation radicalaire **1***b*$^{+\cdot}$. Le rapport des produits provenant des composés asymétriques dépend des potentiels rédox respectifs des fragments radicalaire et carbocationique.

[Traduit par le journal]

Cleavage of radical cations to the fragments, radical and carbocation, is an important general reaction, not only in the gas phase where it accounts for most of the fragments in a mass spectrum, but also in solution (1–4). Our interest in this area stems from the observed cleavage of the radical cation of methyl 2,2-diphenylethyl ether (**1***a*) generated by photosensitization (electron transfer) using electron-accepting sensitizers, e.g., 1,4-dicyanobenzene (**2**) (reaction [1]). The good yield of diphenylmethane and the acetal of formaldehyde were

$$[1]\quad \underset{\mathbf{1}a}{(C_6H_5)_2CHCH_2OCH_3} \xrightarrow[CH_3CN/CH_3OH]{h\nu\,(\text{sens. }(\mathbf{2}))} \underset{\mathbf{3}}{(C_6H_5)_2CH_2} + \underset{\mathbf{4}}{CH_3OCH_2OCH_3}$$

accounted for by Scheme 1, involving the diphenylmethyl radical (R$^\cdot$) and the α-oxycarbocation fragments (R$'$ = CH_2OCH_3) (1). We have now extended this study to a series of compounds which have in common the diphenylmethyl fragment (reaction [2]). The results, which are summarized in Table 1, indicate:

$$[a]\quad \text{Sens. (A)} \xrightarrow{h\nu} A^*$$

$$[b]\quad A^* + R\text{—}R' \rightarrow A^{-\cdot} + R\text{—}R'^{+\cdot}$$

$$[c]\quad R\text{—}R'^{+\cdot} \rightarrow R^\cdot + R'^+$$

$$[d]\quad R^\cdot + R'^+ \rightleftarrows R^+ + R'^\cdot$$

$$[e]\quad R'^+ + Nu^- \rightarrow R'\text{—}Nu$$

$$[f]\quad R^\cdot + A^{-\cdot} \rightarrow R^- + A$$

$$[g]\quad R^- + H^+ \rightarrow R\text{—}H$$

SCHEME 1

(*1*) there is a one-to-one correspondence between product derived from the carbocation and that derived from the anion via the radical; (*2*) cleavage of the radical cation can be a thermally activated process; and, (*3*) the product ratio is dependent upon the relative redox potential of the fragment radical and carbocation.

$$[2]\quad \underset{\mathbf{1}}{(C_6H_5)_2CH\text{—}R'} \xrightarrow[CH_3CN/CH_3OH]{h\nu\ (\mathbf{2})\ \ 18\,\text{h at }10^\circ\text{C}\,(80^\circ\text{C})} \begin{array}{l}(C_6H_5)_2CH_2 + R'\text{—}OCH_3\\ (C_6H_5)_2CH\text{—}OCH_3 + R'\text{—}H\end{array}$$

b: R$'$ = $CH(C_6H_5)_2$
c: R$'$ = $C(CH_3)_2C_6H_4$-4-OCH_3
d: R$'$ = $C(CH_3)_2C_6H_5$
e: R$'$ = $C(CH_3)_2C_6H_4$-4-CF_3

In this series, **1***b* represents the standard; this molecule is symmetric so only two fragments can be formed (Scheme 1, step *c*). Although **1***b* is not cleaved upon irradiation at 10°C, reaction does produce diphenylmethane and methyl diphenylmethyl ether in essentially quantitative yield at 33% conversion after irradiation for 18 h at 80°C.[3] Plotting the relative efficiency of this reaction as a function of temperature, between 50–80°C, we derived an activation energy of 7.2 kcal/mol (r = 0.989) for the rate-determining step. We suggest that this represents a minimum value, close to the bond dissociation energy for the central carbon–carbon bond in the radical cation of **1***b*.

NOTE ADDED IN PROOF: The kinetic analysis used to estimate the activation energy requires several assumptions (that the temperature dependence reflects a variation in the rate of the cleavage process, that the maximum quantum yield is one, and that the actual quantum yield is low). A more thorough analysis is in progress.

Using the oxidation potentails of **1***a–e*, listed in Table 2, in the Weller equation (5), gives an indication that electron transfer between these donors and the first excited singlet state of **2** as the acceptor is favorable in every case. The results also suggest that changing the singly occupied molecular orbital from the diphenylmethyl moiety in **1***d* and **1***e* to the methoxy-substituted ring in **1***c* has no effect.

[3] There is no reaction at 80°C without irradiation or upon irradiation without the photosensitizer.

The photosensitized (electron transfer) irradiation of **1***b* in *oxygenated* acetonitrile at ca. 40°C gives benzophenone (2*a*). The mechanism of this reaction may be more complex than simply reaction of the diphenylmethyl radical with some oxygen species.

Flash photolysis studies (temperature unspecified) involving the radical cation of **1***b* indicate formation of a transient with an intense absorption band at 330 nm which was attributed to the diphenylmethyl radical (2*b*). The radical formed by deprotonation of the radical cation should, however, have a similar absorption spectrum.

TABLE 1. The photosensitized bond-cleavage reaction of $(C_6H_5)_2CH—R'$[a]

	Conversion%		Product ratio[b]						
Product	10°C	80°C	$(C_6H_5)_2CH_2$	:	CH_3OR'	:	$(C_6H_5)_2CHOCH_3$	:	HR'
1*b*	0	30	1		—		1		—
1*c*	90	100	1		1		0		0
1*d*	40	65	1		1		Trace		Trace
1*e*	40	50	1		1		1		1

[a]All irradiations were carried out on nitrogen-purged CH_3CN/CH_3OH (3/1) solutions of $(C_6H_5)_2CH—R'$ (0.2 *M*) and (**2**) (0.05 *M*) in Pyrex tubes using a 450-W medium-pressure mercury vapor lamp (Hanovia) through Pyrex glass filters for 18 h. Extent of reaction and the product ratio were determined by ^1H nmr and are accurate to 5%. Essentially all the starting material consumed was accounted for by the products listed.

[b]The efficiency of the cleavage is temperature dependent but the ratio of products is not.

TABLE 2. Oxidation potentials measured by cyclic voltammetry[a]

Compound	$E_{1/2}$/V vs. sce
1*a*	2.15[b]
1*b*	2.01 ± 0.05
1*c*	1.5 ± 0.1
1*d*	1.97 ± 0.05
1*e*	2.1 ± 0.1
$HCH(C_6H_5)_2$	2.15 ± 0.05
$HC(CH_3)_2C_6H_4$-4-OCH_3	1.57 ± 0.05
$HC(CH_3)_2C_6H_5$	2.31 ± 0.05
$HC(CH_3)_2C_6H_4$-4-CF_3	2.7 ± 0.1

[a]In acetonitrile containing 0.1 *M* tetraethylammonium perchlorate. The anodic process is irreversible; this accounts for $E_{1/2}$ being taken as 0.03 V cathodic from the anodic peak position.

[b]Reference 1.

While the oxidation potentials of the intermediate radicals are not known, it seems likely that the substituent effect on the carbocation (6) is greater than that on the radical (7); the oxidation potentials for the intermediate cumyl radicals should therefore increase in the order *para*-methoxy < unsubstituted < *para*-trifluoromethyl (8). We see (Table 1) that the product ratios depend upon the difference in the oxidation potentials of the two fragment radicals. If electron transfer rapidly equilibrated the radicals and carbocations (Scheme 1, step *d*) so that the product ratio would depend upon the relative rate of reaction of the two possible carbocations with the nucleophile, the less stable carbocation would react more rapidly (9); such is obviously not the case.

We will investigate further the kinetics of the photosensitized (electron transfer) bond-cleavage reaction and also attempt to measure the oxidation potentials of the intermediate radicals to compare with the product ratios.

Acknowledgments

This work was supported by a grant from the Natural Sciences and Engineering Research Council of Canada. The authors thank D. D. M. Wayner for helpful discussions and the assistance of M. S. Snow with the syntheses of **1***b*–*e*.

1. D. R. ARNOLD and A. J. MAROULIS. J. Am. Chem. Soc. **98**, 5931 (1976).
2. (*a*) L. W. REICHEL, G. W. GRIFFIN, A. J. MULLER, P. K. DAS, and S. N. EGE. Can. J. Chem. **62**, 424 (1984); (*b*) H. L. DAVIS, P. K. DAS, L. W. REICHEL, and G. W. GRIFFIN. J. Am. Chem. Soc. **106**, 6968 (1984).
3. D. M. CAMAIONI and J. A. FARANZ. J. Org. Chem. **49**, 1607 (1984).
4. D. F. EATON. Pure Appl. Chem. **56**, 1191 (1984).
5. D. REHM and A. WELLER. Isr. J. Chem. **8**, 259 (1970).
6. (*a*) G. A. OLAH, M. B. COMISAROW, and C. J. KIM. J. Am. Chem. Soc. **91**, 1458 (1969); (*b*) H. C. BROWN, D. P. KELLY, and M. PERIASAMY. Proc. Natl. Acad. Sci. USA, **77**, 6956 (1980).
7. (*a*) J. M. DUST and D. R. ARNOLD. J. Am. Chem. Soc. **105**, 1221 (1983); **105**, 6531 (1983); (*b*) D. R. ARNOLD, A. M. DE P. NICHOLAS, and M. S. SNOW. Can. J. Chem. In press.
8. A. G. HARRISON, P. KEBARLE, and F. P. LOSSING. J. Am. Chem. Soc. **83**, 777 (1961).
9. J. P. RICHARD and W. P. JENCKS. J. Am. Chem. Soc. **104**, 4689 (1982).

Interaction entre le groupe carbonyle et les hétéroatomes des acétates d'éthyle α-substitués

GEORGES GUIHÉNEUF,[1] CHRISTIAN BÉNARD ET ABDELJALIL LACHKAR
Laboratoire de Chimie Physique Organique, Université Cadi Ayyad, BP S15, Marrakech, Maroc
ET
MARYVONNE LUÇON
Laboratoire de Spectrochimie Moléculaire, Université de Nantes, 44072 Nantes Cédex, France

Reçu le 26 avril 1984[2]

GEORGES GUIHÉNEUF, CHRISTIAN BÉNARD, ABDELJALIL LACHKAR et MARYVONNE LUÇON. Can. J. Chem. **63**, 2343 (1985).

Les spectres infrarouges des α-aminoacétates d'éthyle présentent trois bandes dans la région ν_{CO}. Les effets de solvant ont montré qu'il ne s'agit pas de résonance de Fermi. Ces spectres ont été interprétés à partir d'un modèle qui tient compte des interactions entre le doublet des électrons non liés de l'azote et le groupe carbonyle. On prévoit l'existence d'équilibres entre les conformères résultant de l'orientation variable du doublet de l'azote par rapport au groupe CO. Ce modèle a permis l'interprétation des absorptions ν_{CO} des acétates d'éthyle substitués en α par les groupes méthoxy et éthoxy.

GEORGES GUIHÉNEUF, CHRISTIAN BÉNARD, ABDELJALIL LACHKAR, and MARYVONNE LUÇON. Can. J. Chem. **63**, 2343 (1985).

Infrared spectra of ethyl α-aminoacetates show three bands in the carbonyl region. Solvent effects show that this is not due to Fermi resonance. These spectra can be interpreted using a model that considers the interactions between the nitrogen lone pair and the carbonyl group. The existence of an equilibrium between the conformers caused by the different orientations of the nitrogen lone pair with respect to the carbonyl group can be forecast. This model enables the interpretation of the carbonyl absorptions of the α-substituted (methoxy and ethoxy) ethyl acetates.

[Journal translation]

Les spectres infrarouges des composés carbonylés α-halogénés présentent un dédoublement de la band ν_{CO}. Ce phénomène, également observé avec les α-aminocétones (1, 2), α-méthoxy et α-méthylthiocétones (3, 4), a été interprété à partir de l'existence de deux conformations énergétiquement favorisées, résultant de la rotation du groupe CH_2X par rapport à la liaison $C_{(carbonyle)}$— C_α (1–13).

Nous avons constaté l'apparition de trois bandes dans le domaine d'absorption ν_{CO} de cinq α-aminoacétates d'éthyle. L'analyse des effets de solvant sur ces spectres nous a permis de mettre en évidence un équilibre conformationnel et de proposer un modèle d'interaction applicable à d'autres types de substituants.

Résultats

Les spectres infrarouges des cinq α-aminoacétates d'éthyle suivants: α-*N*,*N* diméthylamino (**1**), α-*N*,*N* diéthylamino (**2**), α-pipéridino (**3**), α-morpholino (**4**), et α-pyrrolidino (**5**) ont été enregistrés en solution dans divers solvants entre 1900 et 1650 cm^{-1}. Quelques enregistrements sont reproduits sur les figures 1 et 2.

En raison de la proximité des trois pics d'absorption, il est préférable de procéder à une décomposition de la bande complexe. Cette séparation a été réalisée en utilisant la procédure proposée par Pitha et Jones (14); le profil des bandes correspond au produit d'une fonction de Cauchy par une fonction de Gauss. On obtient ainsi les valeurs des maxima d'absorption de chaque bande et les intensités relatives (caractérisées par l'absorption au maximum de chacune d'elles), réunies dans le tableau 1. Pour comparaison, les fréquences ν_{CO} de l'acétate d'éthyle, du propionate d'éthyle, des α-fluoro, α-chloro et α-iodo acétates d'éthyle, déterminées dans les mêmes conditions, sont rassemblées dans le tableau 2.

La précision des positions et des intensités des bandes séparées varie avec l'importance de leur recouvrement. L'accord entre les absorptions expérimentales et calculées est caractérisé par l'écart moyen et par l'écart maximum entre ces deux grandeurs. L'écart moyen est compris entre 3×10^{-3} et 10^{-3} unité de densité optique; l'écart maximum est toujours inférieur à

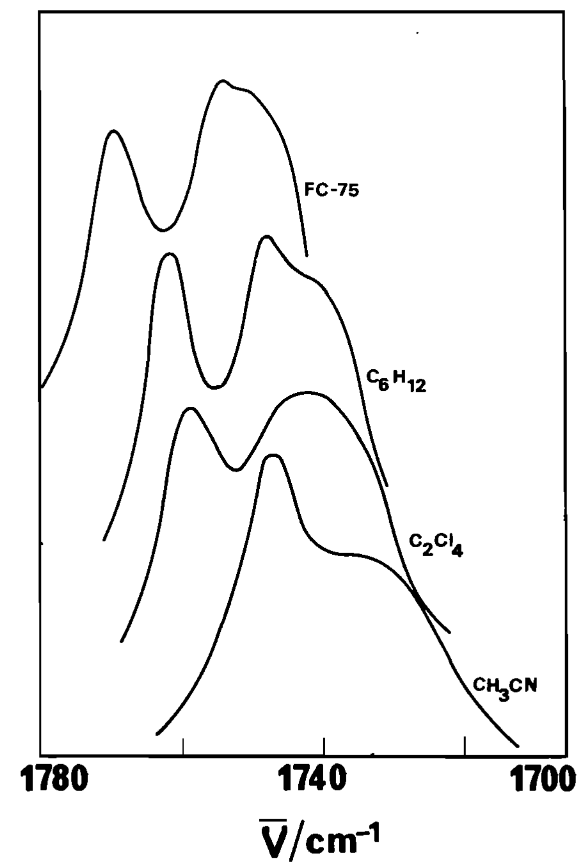

FIG. 1. Spectres de l'α-*N*,*N* diéthylamino acétate d'éthyle, **2**, en solution dans divers solvants.

[1]Auteur à qui adresser la correspondance.
[2]Revision reçue le 19 octobre 1984.

TABLEAU 1. Fréquences ν (cm^{-1}) et intensités relatives I^a des absorptions ν_{CO} des α-*N,N* diméthylamino (**1**), α-*N,N* diéthylamino (**2**), α-pipéridino (**3**), α-morpholino (**4**), α-pyrrolidino (**5**) acétates d'éthyle

		Solvants							
Composés	Paramètres	FC.75[b]	C_5H_{12}	C_7H_{16}	C_6H_{12}	C_2Cl_4	CCl_4	CS_2	CH_3CN
1	ν_A	1767	1763	1762,5	1761,5	1758,5	1757	1754	1747,5
	ν_B	1753	1749	1748,5	1748	1745,5	1745	1739	1734,5
	ν_C	1744,5	1740,5	1739,5	1738,5	1735,5	1734,5	1730,5	1726,5
	$I\nu_B$	0,9	1,15	1,05	0,9	1,15	0,75	0,9	0,35
	$I\nu_C$	0,85	1,15	1,1	1,45	1,35	1,1	1	0,75
2	ν_A	1767	1763	1762	1761	1757,5	1756	1754,5	1748
	ν_B	1751,5	1748	1747	1746,5	1743,5	1742,5	1741,5	1736
	ν_C	1742	1737,5	1736,5	1736	1731,5	1730,5	1729,5	1723
	$I\nu_B$	1,95	2,55	3,1	2,15	2,4	1,8	1,3	1
	$I\nu_C$	1,5	2,15	1,65	2,2	2,15	1,8	1,5	1
3	ν_A		1763,5	1763	1761,5	1758	1757	1754	1748,5
	ν_B		1748,5	1748	1748	1745	1744	1742	1741
	ν_C		1741	1740	1740	1735,5	1735	1733,5	1731,5
	$I\nu_B$		0,55	0,65	0,6	0,6	0.8	0,4	0,3
	$I\nu_C$		0,7	0,6	0,75	0,85	0,75	0,75	0,7
4	ν_A		1763,5	1762,5	1761,5	1758	1757,5	1755	1749,5
	ν_B		1751,5	1750,5	1749,5	1748	1747	1744,5	1740
	ν_C		1743,5	1742,5	1741	1738	1736	1735	1731
	$I\nu_B$		0,4	0,4	0,45	0,3	0,6	0,3	0,15
	$I\nu_C$		0,55	0,4	0,5	0,65	0,6	0,55	0,65
5	ν_A		1763,5	1762,5	1761,5	1758	1757,5	1755	1749
	ν_B		1749	1748,5	1748	1745	1743,5	1742	1740
	ν_C		1741,5	1740,5	1741,5	1738	1734	1732,5	1732
	$I\nu_B$		0,65	0,6	0,45	0,45	0,9	0,65	0,05
	$I\nu_C$		0,35	0,35	0,55	0,65	0,45	0,3	0,65

[a]Pour chaque solvant, l'intensité de la bande ν_A est prise comme référence.
[b]Mélange d'isomères du perfluoro-n-propyloxane.

TABLEAU 2. Fréquences ν_{CO} (cm^{-1}) des composés $XCH_2COOC_2H_5$

	X				
Solvants	H	CH_3	F[b]	Cl[b]	I
FC.75[a]	1756,6	1752,9	1786–1757	1778–1754,5	1750,8
C_5H_{12}	1751,1	1747,6	1781–1752	1773,5–1749	1746
C_7H_{16}	1749,8	1747,1	1780–1751,5	1773–1749	1744,8
CCl_4	1742,6	1739,5	1774–1746	1767–1742,5	1739,5
CS_2	1741,3	1738,7	1772–1745	1764,5–1742	1737,6
CH_3CN	1736,5	1733,5	1764,5–1743,5	1758–1738,5	1734

[a]Mélange d'isomères du perfluoro-n-propyloxane.
[b]Après séparation des deux bandes.

2×10^{-2} unité de densité optique. Le spectre expérimental est donc reproduit avec une bonne précision. Nous avons vérifié que le choix des paramètres initiaux, nécessaires au calcul, n'influait pas sur les résultats. Les tests effectués ont montré que les positions des maxima d'absorption sont reproductibles à mieux que 0,5 cm^{-1} près et que l'écart sur les intensités est inférieur à 10%.

Bien que des décompositions totalement indépendantes conduisent à des positions de maxima d'absorption très voisines pour les cinq composés, il n'est pas exclu qu'une décomposition puisse accidentellement introduire une erreur supérieure à la limite de 0,5 cm^{-1}. C'est pourquoi un résultat n'est jamais exploité isolément. Seules les variations progressives sont prises en considération.

Pour les cinq α-aminoacétates d'éthyle nous avons retenu la présence de trois bandes, même si, parfois, il était possible, au vu des spectres, de se limiter à deux. Les calculs dans cette hypothèse donnent les résultats suivants: la position de la bande

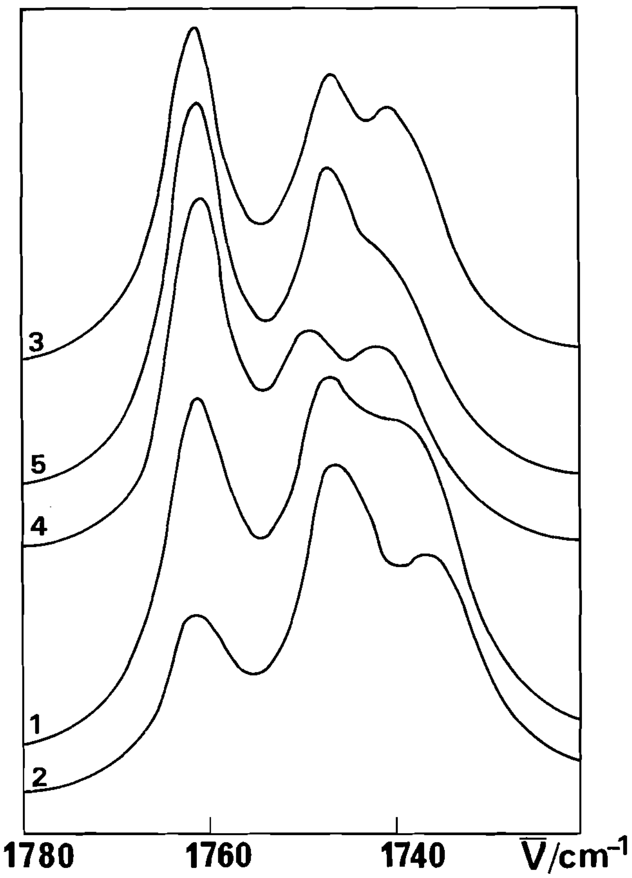

FIG. 2. Spectres des α-*N,N* diméthylamino (**1**), α-*N,N* diéthylamino (**2**), α-pipéridino (**3**), α-morpholino (**4**), α-pyrrolidino (**5**) acétates d'éthyle, en solution dans le cyclohexane.

de plus haute fréquence n'est pas modifiée mais la largeur à mi-hauteur de la deuxième bande est supérieure aux largeurs habituellement observées et son maximum après décomposition est plus proche de la première bande que le maximum apparent alors que l'on doit toujours obtenir l'inverse. Le passage à trois bandes permet d'éliminer ces anomalies.

Discussion

Dans un solvant donné, les intensités relatives des absorptions varient d'un composé à l'autre; mais dans les solvants apolaires (hydrocarbures et CCl_4) les maxima d'absorption des cinq composés se retrouvent pratiquement aux mêmes fréquences.

Nous désignerons par ν_A la bande de plus haute fréquence, par ν_B celle de fréquence intermédiaire et par ν_C la bande dont la fréquence est la plus basse. En solution dans l'heptane, par exemple, la bande ν_A est proche, pour les cinq composés, de 1763 cm^{-1}; ν_B est voisine de 1748 cm^{-1}; la dernière, ν_C, se situe vers 1740 cm^{-1}, à l'exception de **2** pour lequel la valeur est légèrement inférieure.

Cette homogénéité ne peut être fortuite et nous conduit à une première remarque: *le même phénomène doit être à l'origine de l'apparition des trois bandes pour les cinq produits étudiés.*

En solution dans l'acétonitrile, l'accord entre les positions des bandes ν_B et ν_C est moins bon. Dans ce cas, les interactions soluté–solvant sont fortes. La structure des substituants, en particulier leur encombrement, peut modifier sensiblement ces interactions et, en conséquence, les fréquences ν_B et ν_C.

Pour tous les solvants, les solutions utilisées sont très diluées et les intensités relatives des bandes sont indépendantes des concentrations. Nous pouvons donc exclure l'éventualité d'associations intermoléculaires. Trois hypothèses peuvent alors être formulées pour expliquer cette multiplicité: (a) une double résonance de Fermi entre la transition ν_{CO} et deux transitions interdites (15–17); (b) un équilibre conformationnel entre deux formes, associé à une résonance de Fermi affectant la transition ν_{CO} d'un seul des conformères; (c) un équilibre faisant intervenir trois conformations.

TABLEAU 3. Coefficients de corrélation des relations entre les fréquences ν_{CO} dans les différents solvants: α-*N,N* diméthylamino (**1**), α-*N,N* diéthylamino (**2**), α-pipéridino (**3**), α-morpholino (**4**), α-pyrrolidino (**5**) acétates d'éthyle

Corrélation de:	1	2	3	4	5
ν_B avec ν_A	0,987	0,999	0,97	0,994	0,988
ν_C avec ν_A	0,995	0,998	0,99	0,985	0,96
ν_A avec $\nu_{CH_3COOC_2H_5}$	0,965	0,99	0,987	0,99	0,987

1. *Hypothèses faisant intervenir une résonance de Fermi*

Les fréquences ν_{CO} d'un composé quelconque, en solution dans une série de solvants, sont linéairement reliées aux fréquences ν_{CO} d'un produit de référence, en solution dans les mêmes solvants (18–20). Une résonance de Fermi entraîne, pour l'une des bandes, des déviations systématiques à la relation linéaire et, en général, l'absence totale de relation pour les autres (16, 17, 21). Il n'existe pas de relation entre les fréquences des bandes du composé considéré.

En prenant l'acétate d'éthyle pour référence, chaque bande suit une relation satisfaisante et pour chaque composé les fréquences des bandes sont liées entre elles (tableau 3).

Ces résultats vont donc à l'encontre de l'hypothèse d'une résonance de Fermi.

L'analyse qualitative des variations des intensités relatives des bandes avec le solvant va dans le même sens: dans le cas d'une résonance de Fermi, la bande qui comporte la plus forte contribution de la transition fondamentale est la plus intense. L'origine de la multiplicité étant la même pour tous les produits, cette absorption, dans un solvant donné, devrait s'identifier à une même bande: ν_A, ν_B ou ν_C. Or la bande la plus intense est tantôt ν_A, tantôt ν_B et parfois ν_C. Ces observations sont incompatibles avec l'hypothèse d'une résonance de Fermi simple ou double. Il faut donc attribuer l'origine de la multiplicité ν_{CO} à un équilibre entre trois conformères.

2. *Hypothèse d'un équilibre conformationnel*

Les équilibres habituellement retenus dans le cas des molécules XCH_2COR sont les suivants[3] (fig. 3):

Les conformations où la liaison C—X, ou une liaison C—H, éclipse la liaison C═O sont plus stables que les conformations décalées (22–24): si, à l'état gazeux, la forme *anti* est prépondérante pour le chloroacétaldéhyde (25) et la fluoroacétone (26), seules les conformations *gauche* et *syn* apparaissent lorsque les molécules XCH_2COR (X = halogène) sont en solution (3–13, 25).

L'effet du substituant NR_2, en fonction de son orientation, peut être analysé uniquement à partir des interactions orbitalaires, spatiales ou à travers les liaisons, et de l'hyperconjugaison du NR_2 avec le système π du carbonyle. Il est possible

[3]Nous avons préféré les appellations *syn* et *anti* à *s-cis* et *s-trans*, souvent utilisées.

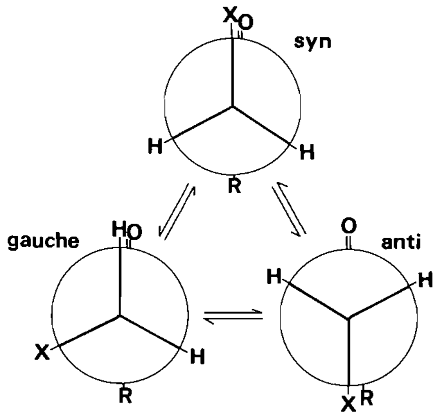

FIG. 3. Conformations privilégiées des composés XCH_2COR.

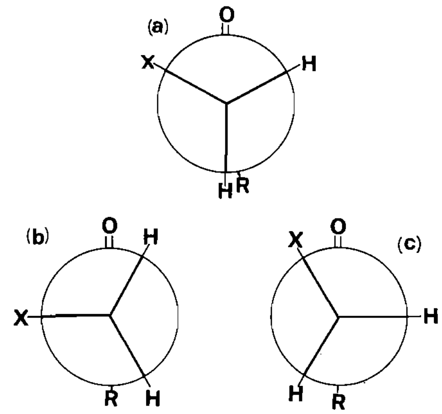

FIG. 4. Conformations décalées des composés XCH_2COR.

d'expliquer ainsi les déplacements de la transition $n - \pi$ des α-aminocétones (24). Les différences d'énergie entre les conformères, dans l'état fondamental, sont faibles et jusqu'à présent on a préféré se référer aux effets inductifs et interactions dipolaires et d'hyperconjugaison pour interpréter les variations de la fréquence ν_{CO}. Il faut remarquer que, qualitativement, les conclusions ne dépendent pas du modèle choisi.

Récemment, l'importance de l'hyperconjugaison de X avec le système π du carbonyle a été soulignée, dans le cas des cétones XCH_2COCH_3 (3). Ainsi, la variation de la fréquence ν_{CO} de 1720 cm^{-1} à 1717 cm^{-1} et à 1713 cm^{-1} dans la série X = CH_3, NMe_2, I a été attribuée, pour l'essentiel, à l'hyperconjugaison. Il ne semble pas nécessaire de prendre cet effet en considération dans la série $XCH_2COOC_2H_5$. Pour les trois mêmes substituants, on relève les valeurs suivantes: 1739,5; 1734,5 et 1739,5 cm^{-1}. La comparaison des deux séries montre que le rôle de l'hyperconjugaison est très certainement secondaire dans les acétates d'éthyle α-substitués.

L'interaction dipolaire entre les groupes CO et CX est donc le facteur primordial; elle varie avec l'orientation relative des deux dipôles et provoque le dédoublement de la bande ν_{CO}. Cet effet est maximum pour le conformère *syn*: la bande ν_{CO} de cette forme doit être située à une fréquence supérieure à celle de l'ester non substitué. Par ailleurs, la proportion de ce conformère doit augmenter avec la polarité du solvant (6, 13). Au contraire, l'interaction est faible dans la conformation *gauche* et la fréquence ν_{CO} doit être pratiquement celle de la molécule non substituée.

Ces remarques pourraient nous permettre de procéder aux corrélations suivantes: ν_A et *syn*, ν_B et *gauche*, ν_C et *anti*; mais les attributions de la bande ν_B à la forme *gauche* et de la bande ν_C à la forme *anti* sont en contradiction avec les effets de solvant. La forme *gauche* étant plus polaire que la forme *anti*, l'intensité relative de la bande correspondante (ν_B) devrait croître avec la polarité du solvant. L'inverse est observé. La considération de formes décalées parfois proposées (fig. 4) ne saurait apporter une solution satisfaisante puisqu'elles impliquent des fréquences ν_{CO} supérieures ou égales à celle de la forme *gauche*. L'hyperconjugaison maximum pour B pourrait provoquer un abaissement de la fréquence ν_{CO}, mais nous avons montré précédemment que cet effet est négligeable.

Devant l'insuffisance de ces modèles, nous proposons l'introduction d'un nouveau facteur: l'orientation du doublet d'électrons non liés de l'azote par rapport au carbonyle. Le dipôle du groupe C—X résulte de la combinaison du dipôle de la liaison C—X et du dipôle dû aux électrons non liés de X.

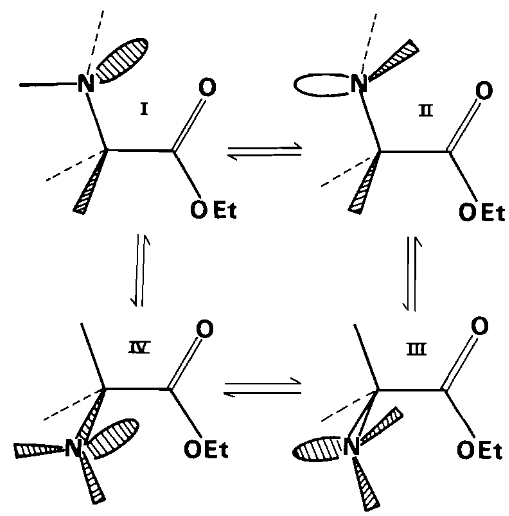

FIG. 5. Conformations des amino acétates d'éthyle.

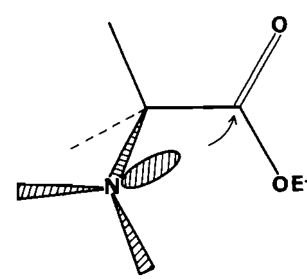

FIG. 6. Effet transannulaire dans les composés carbonylés α-aminés.

Lorsque X est un halogène, ce dipôle est dirigé selon l'axe de la liaison C—X. Ce n'est plus le cas pour X = NR_2; de plus, le dipôle formé par la liaison C—N est faible; en effet, la différence d'électronégativité entre l'atome d'azote et le carbone substitué est diminuée par le groupe CO attracteur. Le moment dipolaire du group C—NR_2 est donc essentiellement lié à l'orientation du doublet non liant de l'azote. Si, à partir des conformations *syn* et *gauche*, on envisage les diverses orientations[4] du groupe NR_2 par rapport à la liaison C—N, on

[4]Ces orientations peuvent être obtenues par rotation du groupe amino autour de la liaison C—N ou par inversion de l'azote; nos conclusions ne s'en trouvent pas modifiées.

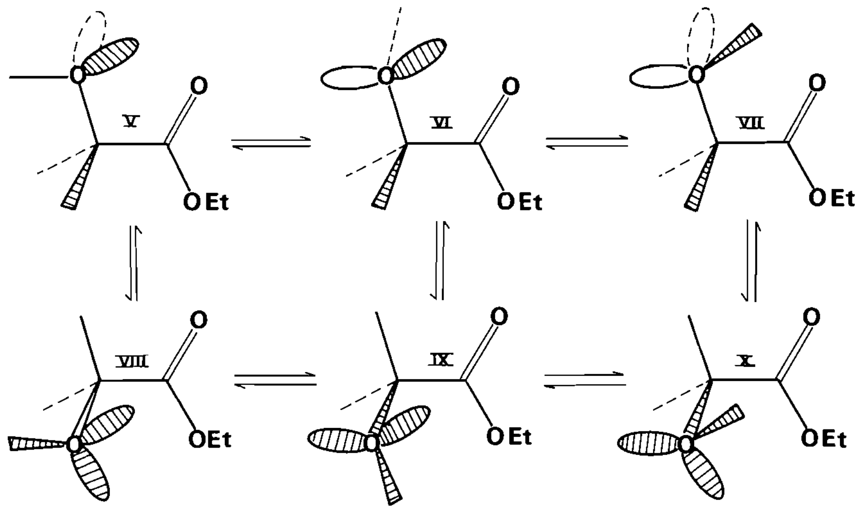

FIG. 7. Conformations des composés **6** : $CH_3OCH_2COOC_2H_5$ et **7** : $C_2H_5OCH_2COOC_2H_5$.

aboutit aux équilibres suivants (fig. 5) entre les quatre conformères I à IV: Nous avons retenu des conformations décalées pour le groupe CH_2NH_2 par analogie avec les résultats obtenus avec les amines (27), les α-aminocétones et les α-aminoaldéhydes (24).

3. *Test de validité du modèle*

Deux facteurs doivent être pris en considération: la direction relative des dipôles et leur distance (28). Le dipôle C—N étant négligeable, l'interaction est maximale pour le conformère I: en effet, l'angle dièdre entre le doublet et la liaison C=O est nul et la distance entre les deux groupes est minimale. Ce conformère est celui qui possède le moment dipolaire global le plus grand. Nous prévoyons que la fréquence ν_{CO} de I sera la plus élevée et qu'en passant d'un solvant apolaire à un solvant polaire la proportion de ce conformère augmentera, entraînant un accroissement de l'intensité relative de la bande correspondante.

Le doublet non liant de l'azote, dans la conformation II est dirigé quasi-perpendiculairement au groupe CO et la distance est plus grande que dans I. On n'attend pas d'interaction pour cette forme. Le moment dipolaire de II sera plus faible que celui de I. Le même raisonnement s'applique à III, la distance entre les dipôles étant encore plus importante. Nous ne pouvons pas espérer distinguer ces deux conformations. Les fréquences ν_{CO} de II et III doivent être confondues et semblables à celle de l'acétate d'éthyle. Par ailleurs, l'intensité relative de cette bande doit diminuer avec la polarité du solvant. Enfin, l'interaction dipolaire sera faible dans la forme IV, mais ce conformère présente la particularité d'autoriser un effet transannulaire (29) (fig. 6), déjà envisagé pour les α-morpholino et pipéridinoacétophénone (2) et prévu dans le modèle des interactions orbitalaires spatiales (24). Il en résulte un abaissement de la bande ν_{CO} correspondante par rapport à celle de l'acétate d'éthyle et la polarité attendue doit être supérieure à celle de II ou III.

Sur la base de ce modèle nous pouvons donc attendre trois bandes ν_{CO} distinctes:

La première, due aux conformations II et III, sera située à la même fréquence que celle de l'acétate d'éthyle.

La seconde, située à une fréquence supérieure, correspondra à la conformation I.

La troisième, de plus basse fréquence, sera attribuée à IV.

L'intensité relative de la bande intermédiaire devra diminuer lorsque la polarité du solvant augmentera. Les intensités des bandes extrêmes devront varier dans une faible proportion, celle de plus haute fréquence étant probablement favorisée par les solvants les plus polaires.

La confrontation de nos résultats expérimentaux avec ces prévisions montre une bonne concordance et justifie l'utilisation de ce modèle. La bande ν_A peut être attribuée à la conformation I, la band ν_B aux conformations II et IV, et la bande ν_C à la conformation III. L'évolution des intensités relatives de ces bandes en fonction du solvant confirme ces attributions: quel que soit le substrat, on note un accroissement des bandes ν_A et ν_C par rapport à ν_B lorsque la polarité du solvant augmente. Dans certains cas la bande ν_B est pratiquement absente. On note aussi que ν_A augmente légèrement plus que ν_C.

4. *Extension aux substituants méthoxy et éthoxy*

Le modèle que nous proposons doit pouvoir s'appliquer à d'autres types de substituants, en particulier aux groupes $—OCH_3$ ou $—OC_2H_5$. Les conformations à envisager doivent tenir compte de l'existence de deux doublets non liés sur l'atome d'oxygène (fig. 7).

Le moment dipolaire du conformère V est particulièrement élevé et, compte tenu des résultats obtenus pour les composés **1** et **2**, il est peu vraisemblable que la bande correspondante apparaisse, même dans les solvants les plus polaires. Les conformations VI et VII sont de ce point de vue équivalentes, de même que VIII et IX, avec une possibilité d'un effet transannulaire. Il n'existe pas de conformère analogue à II, c'est-à-dire *syn*, sans interaction dipolaire. Enfin, dans le conformère X il existe une contrainte assez forte entre les groupes CH_3 ou C_2H_5 et l'oxygène de l'ester: cette forme est vraisemblablement défavorisée.

En conséquence, nous prévoyons deux bandes principales pour les α-méthoxy (**6**) et α-éthoxy (**7**) acétates d'éthyle. La première est due aux conformères VI et VII: en négligeant le dipôle de liaison C—O et l'effet du doublet perpendiculaire au groupe C=O, nous attendons cette bande à la même position que la bande ν_A des α-aminoacétates d'éthyle. La seconde doit être située à une fréquence inférieure à celle de la molécule non substituée. Toutefois le caractère donneur de l'oxygène est moins marqué que celui de l'azote et l'effet transannulaire doit être moindre. L'abaissement de fréquence sera moins impor-

TABLEAU 4. Fréquences (cm^{-1}) et intensitiés relatives[a] des absorptions ν_{CO} des composés **6** et **7**[c]

		Solvants							
Composés	Paramètres	FC.75[b]	C_5H_{12}	C_7H_{16}	C_6H_{12}	C_2Cl_4	CCl_4	CS_2	CH_3CN
6	ν_A	1768,5	1764,8	1763,5	1763	1760	1759	1757,5	1752
	ν_C	1749,5	1744,8	1743,5	1743	1739	1737,5	1737	1733
	I_C	0,43	0,6	0,55	0,5	0,5	0,5	0,45	0,4
7	ν_A	1769	1764,5	1764	1763,5	1760	1759	1757	1753
	ν_C	1749	1744	1743,5	1742,5	1738,5	1737	1736,5	1732,5
	I_C	0,47	0,47	0,45	0,45	0,45	0,5	0,4	0,4

[a]Pour chaque solvant, l'intensité de la bande ν_A est prise comme référence.
[b]Mélange d'isomères du perfluoro-n-propyloxane.
[c]Composé **6**: $CH_3OCH_2COOC_2H_5$; composé 7: $C_2H_5OCH_2COOC_2H_5$.

tant que pour les substituants amino. Par ailleurs l'influence des solvants doit être comparable à celle que nous observons pour les bandes ν_A et ν_C des dérivés aminés.

Les résultats expérimentaux pour **6** et **7** sont conformes à cette attente et apportent une confirmation satisfaisante au modèle retenu (tableau 4).

Partie expérimentale

Tous les produits sont commerciaux, à l'exception de **3**, **4** et **5** qui ont été préparés par les méthodes habituelles. Ils ont été purifiés immédiatement avant usage (30).

Les deux spectrophotomètres utilisés pour l'enregistrement des spectres ont été étalonnés, dans la gamme 1600–1800 cm^{-1} par rapport au spectre de la vapeur d'eau. Les écarts sont inférieurs à 0,2 cm^{-1} pour le spectrophotomètre Beckman IR 9 et 0,5 cm^{-1} pour le Perkin–Elmer 683. Les reproductibilités des nombres d'ondes sont respectivement de 0,1 et 0,2 cm^{-1}.

Les spectres sont enregistrés en double faisceau, le solvant étant placé en référence. Les concentrations des produits dans les solutions varient de 2×10^{-2} à 5×10^{-3} mol L^{-1}. Les épaisseurs des cellules, équipées de fenêtres KBr ou NaCl, sont comprises entre 0,25 et 1 mm. Les conditions de concentration et d'épaisseur de cellule sont déterminées par la solubilité du produit et la transparence du solvant dans le domaine spectral étudié.

Des cellules à épaisseur variable (0–6 mm) ont été utilisées pour l'étude de l'effet des concentrations (10^{-1} à 10^{-3} mol L^{-1}) sur l'absorption ν_{CO}.

1. A. GASET, A. VERDIER, J. BONNET et A. LATTES. Spectrochim. Acta Part A, **31**, 715 (1975); et **31**, 727 (1975).
2. N. H. CROMWELL, R. E. BRAMBURY et J. L. ADELFANG. J. Am. Chem. Soc. **82**, 4241 (1960).
3. S. A. GUERRERO, J. R. T. BARROS, B. WLADISLAW, R. RITTNER et P. R. OLIVATO. J. Chem. Soc. Perkin Trans. 2, 1053 (1983).
4. B. WLADISLAW, H. VIERTLER, P. R. OLIVATO, I. C. C. CALEGAO, V. L. PARDINI et R. RITTNER. J. Chem. Soc. Perkin Trans. 2, 453 (1980).
5. N. L. ALLINGER, J. ALLINGER, L. E. FREIBERG, R. F. CZAJA et N. A. LE BEL. J. Am. Chem. Soc. **82**, 5876 (1960).
6. L. J. BELLAMY et R. L. WILLIAMS. J. Chem. Soc. 4294 (1957).
7. R. N. JONES et E. SPINNER. Can. J. Chem. **36**, 1010 (1958).
8. A. CARISTAN et H. BODOT. Bull. Soc. Chim. Fr. 3227 (1967).
9. J. BELLANTANO et J. R. BARCELLO. Spectrochim. Acta, **16**, 1333 (1960).
10. M. L. JOSIEN et C. CASTINEL. Bull. Soc. Chim. Fr., 801 (1958).
11. J. RADDELL et M. J. HARRAH. J. Chem. Phys. **36**, 1571 (1962).
12. T. L. BROWN. Spectrochim. Acta, **18**, 1615 (1962).
13. L. J. BELLAMY et R. L. WILLIAMS. J. Chem. Soc. 3465 (1958).
14. J. PITHA et R. N. JONES. Computer programmes for infrared spectroscopy, National Research Council of Canada. 1974.
15. H. LEE et J. K. WILHURST. J. Chem. Soc. 3590 (1965).
16. G. GUIHÉNEUF et C. LAURENCE. Spectrochim. Acta Part A, **34**, 15 (1978).
17. C. LAURENCE, M. BERTHELOT, M. LUÇON et G. GUIHÉNEUF. Spectrochim. Acta Part A, **33**, 353 (1977).
18. L. J. BELLAMY et R. L. WILLIAMS. Trans. Faraday Soc. **55**, 14 (1959).
19. H. P. FIGEYS et J. NASIELSKI. Spectrochim. Acta Part A, **23**, 465 (1967).
20. K. J. MORGAN et N. UNWIN. J. Chem. Soc. (B), 1336 (1967).
21. J. F. BERTRAN, L. BALLESTER, L. DOBRIHALOVA, N. SANCHEZ et R. ARRIETA. Spectrochim. Acta Part A, **24**, 1785 (1968).
22. G. J. KARABATSOS et N. HSI. J. Am. Chem. Soc. **87**, 2864 (1965).
23. G. J. KARABATSOS et D. J. FENOGLIO. J. Am. Chem. Soc. **91**, 3577 (1969).
24. C. C. LEVIN, R. HOFFMANN, W. J. HEHRE et J. HUDEC. J. Chem. Soc. Perkin Trans. 2, 210 (1973).
25. G. LUCAZEAU et A. NOVAK. J. Chim. Phys. **67**, 1614 (1970).
26. G. A. CROWDER et P. PRUETTIANGKURA. J. Mol. Struct. **15**, 197 (1973).
27. S. WOLFE, A. RAUK, L. M. TEL et I. G. CSIZMADIA. J. Chem. Soc. (B), 136 (1971).
28. J. CANTACUZENE. J. Chim. Phys. **66**, 1569 (1969).
29. N. J. LEONARD, R. C. FOX, M. OKI et S. CHIAVARELLI. J. Am. Chem. Soc. **76**, 630 (1954).
30. C. BENARD. Thèse, Toulouse (1974).

The mechanism of the oxidative deamination and decarboxylation of serine and threonine by periodate in acid medium

ROSA PASCUAL[1] AND MIGUEL A. HERRÁEZ
Departamento de Química Física, Facultad de Química, Universidad de Salamanca, Salamanca, España

Received July 12, 1984[2]

ROSA PASCUAL and MIGUEL A. HERRÁEZ. Can. J. Chem. **63**, 2349 (1985).

The kinetics of oxidation of serine and threonine by periodate have been investigated in acid medium at 10°C. The reaction rate is first order in both periodate and amino acid, and the overall reaction follows second-order kinetics. The rates decrease with increase in $[H^+]$. A catalytic effect of the buffers was not observed in the oxidation process. An analysis of the dependence of the rate on $[H^+]$ reveals that the reactive species under the experimental conditions are periodate monoanion and dianion and the dipolar form of the amino acid. The mechanism proposed and the derived rate law are consistent with the observed kinetics. The rate constants predicted using the derived rate law are in agreement with the observed rate constants, thus justifying this rate law and hence the proposed mechanistic scheme.

ROSA PASCUAL et MIGUEL A. HERRÁEZ. Can. J. Chem. **63**, 2349 (1985).

Opérant à 10°C et dans un milieu acide, on a étudié la cinétique de l'oxydation de la sérine et de la thréonine par le periodate. La réaction est du premier ordre tant en periodate qu'en acide aminé et l'ensemble de la réaction est du deuxième ordre. Les vitesses diminuent avec une augmentation de l'acidité. On n'a pas observé d'effet catalytique des tampons sur les processus d'oxydation. Une analyse de la relation entre les vitesses de réaction et la concentration en H^+ révèle que les espèces réactives dans ces conditions expérimentales sont les monoanion et dianion du periodate et la forme dipolaire de l'acide aminé. Le mécanisme proposé ainsi que l'équation de vitesse qui en dérive sont en accord avec les cinétiques observées. Les constantes de vitesse que l'on peut prévoir en se basant sur l'équation de vitesse que l'on a obtenu sont en accord avec les constantes de vitesses observées et ces résultats justifient cette équation de vitesse et donc le schéma mécanistique proposé.

[Traduit par le journal]

Introduction

It is known that periodate is used for identifying compounds which have hydroxyl, carbonyl, or amino groups on adjacent carbon atoms, and it is a clean and relatively selective reagent for their oxidative carbon–carbon cleavage. The literature on the kinetics of the periodic acid oxidation of glycols (1, 2) is quite extensive but the kinetics of the periodate oxidation of amino alcohols (3), dicarbonyl compounds (4), and amino acids (5), however, has received much less attention. Although the oxidative capacity of this reagent has been widely utilized for the quantitative determination of serine and threonine, no kinetic investigation has been attempted in order to understand the mechanistic aspects of these reactions. It has been reported (6–8) that the reaction between periodate and serine or threonine follows the scheme:

$$CH_2(OH)\text{—}CH(NH_2)\text{—}CO_2H + 2IO_4H \rightarrow CH_2O + H\text{—}CO_2H + NH_3 + CO_2 + 2IO_3H$$

$$CH_3\text{—}CH(OH)\text{—}CH(NH_2)\text{—}CO_2H + 2IO_4H \rightarrow CH_3\text{—}CHO + H\text{—}CO_2H + NH_3 + CO_2 + 2IO_3H$$

Because serine and threonine contain groups toward which periodate is highly specific and because of the various possibilities for reaction between the different species of both periodate and amino acid that can exist in aqueous solution, it seemed that an investigation of the oxidation of β-hydroxy-α-amino acids would be of interest.

Experimental

Materials

All the chemicals were obtained from Merck, and all were of analytical grade. Doubly distilled water from alkaline permanganate was used to prepare all solutions. In each series of experiments the initial pH was maintained constant throughout each reaction by use of acetate or chloroacetate buffers. The ionic strength of the system was kept at a constant value (0.20 *M*) by the addition of sodium perchlorate. Standard stock solutions of amino acids were prepared by dissolving accurately weighed amino acid in buffer solution. Sodium periodate solution was prepared in water and titrated (9) with sodium arsenite.

Kinetic method

Reaction rates were measured by following the decrease of periodate concentration with time. The iodometric determination method of unreacted periodate in a measured aliquot of the reaction mixture at different intervals of time was found unsatisfactory. Therefore a spectrophotometric procedure was utilized and the reactions were followed by measuring the absorbance of the unreacted periodate from time to time at 310 nm, using a Pye–Unicam SP600 UV instrument. Although the absorption maximum of periodate (10) is at 222 nm, this wavelength was not of practical use because of interfering absorption by other compounds in the reaction mixture. The molar absorptivities at 310 nm were obtained at all pHs used in the experiments. Reactions were followed to ca. 80–90% conversion of the initial periodate concentration. In all cases 2–3 runs were carried out.

Stoichiometry

Varying ratios of periodate to amino acid, keeping [periodate] > [amino acid] in all buffers, were allowed to stand until the completion of the reaction. Estimation of residual oxidant showed that 2 moles of periodate are consumed per mole of amino acid. Formaldehyde was detected among the reaction products of serine (11). Since glyoxylic acid has been detected as an intermediate during the periodic acid oxidation of serine and threonine (12), the stoichiometry of the periodate–glyoxylic reaction was determined through the same procedure[3] and it was found to be 1 : 1. Carbon dioxide and formic acid were detected (13) in the reaction mixture. It was observed that no visible polymerization occurs in the presence of acrylonitrile during the course of reactions. Thus, the presence of free-radical intermediates is unlikely.

[1]Author to whom correspondence should be addressed.
[2]Revision received January 23, 1985.

[3]E. Calle, R. Pascual, and M. A. Herráez. Unpublished results.

TABLE 1. Effect of varying reactant concentration on the reaction rate[a]

		Serine		Threonine	
10^3 [Per]$_0$ (M)	10^3 [AA]$_0$ (M)	$10^4\ k'_\psi$ (s^{-1})	$10^3\ k''_\psi$ (L $mol^{-1}\ s^{-1}$)	$10^4\ k'_\psi$ (s^{-1})	$10^3\ k''_\psi$ (L $mol^{-1}\ s^{-1}$)
12.0	84.0	25.2	29.1	33.3	39.3
11.0	84.0	25.1	28.9	33.2	40.0
10.0	84.0	24.9	29.4	33.3	39.5
9.00	84.0	22.9	27.6	33.5	40.3
8.00	84.0	23.7	29.0	33.4	39.9
7.00	84.0	24.4	29.6	33.6	39.7
6.00	84.0	23.9	28.8	33.1	41.2
8.00	128	36.5	28.8	51.6	40.6
8.00	112	32.1	29.3	44.7	40.3
8.00	96.0	26.6	28.5	37.3	39.4
8.00	80.0	22.1	28.9	32.5	41.2
8.00	64.0	19.0	29.5	25.7	40.8
8.00	48.0	14.3	29.2	18.9	40.2
8.00	32.0	9.53	29.1	12.6	40.6
8.00	16.0	4.52	28.5	6.22	40.5
8.00	8.00	2.24	29.2	2.89	41.2

[a]Temperature 10°C; pH 4.00; ionic strength 0.20 M.

Results

The kinetics of oxidation of serine and threonine by periodate was investigated at several initial concentrations of the reactants in acid media at pH 2.1−5.0.

At constant pH with the amino acid in excess, plots of log [periodate]$_0$/[periodate] vs. time were linear, indicating that the reactions are first-order in periodate concentration [Per]. The pseudo first-order rate constants, k'_ψ, are given in Table 1. This was also confirmed by varying the periodate concentration, which did not show any change in the pseudo first-order rate constants (Table 1). The values of k'_ψ increase with amino acid concentration. Plots of log k'_ψ vs. log [amino acid]$_0$ are linear (Fig. 1) with a slope of unity in both cases, thus indicating a first-order dependence on the amino acid concentration [AA]. Under these conditions the constancy of the second-order rate constants, k''_ψ, was checked. Plots of k'_ψ against the amino acid concentration were linear with intercepts close to zero, and their slopes gave the second-order rate constants for oxidation of the amino acids. It was observed that pH changes have a marked effect on the rates of oxidation of the amino acids. The rate increases with increase in pH of the system. The plot of the observed rate constants as a function of pH is shown in Fig. 2. In this pH range the rate is unaffected by general acids or bases. This was verified by showing that the rate of oxidation of amino acids in chloroacetate or acetate buffers at constant pH, is independent of the buffer concentration (Table 2).

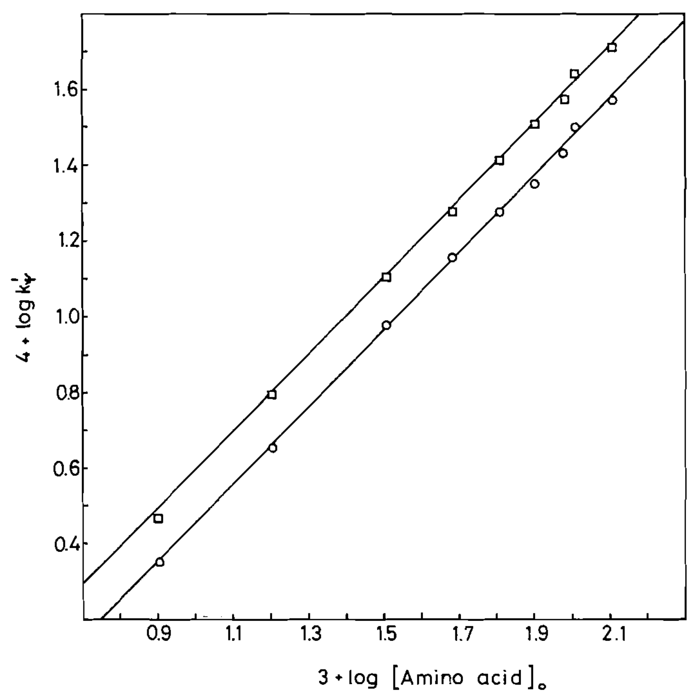

FIG. 1. Plot of log k'_ψ vs. log [amino acid]$_0$; [IO_4Na]$_0$ = 8.00 × 10^{-3} M; pH = 4.00; I = 0.20 M; temperature = 10°C; ○ serine; □ threonine.

Discussion

Aliphatic amino acids in water are known (14) to exist almost entirely in the dipolar ionic form. The equilibrium involved in acidic media is:

$$[1]\quad \underset{AA^{\pm}}{R{-}CH(NH_3^+){-}CO_2^-} + H^+ \overset{K_a}{\rightleftharpoons} \underset{AA^+}{R{-}CH(NH_3^+){-}CO_2H}$$

In acid aqueous periodate solutions, equilibria:

$$[2]\quad H_5IO_6 \overset{K_1}{\rightleftharpoons} H_4IO_6^- + H^+$$

$$[3]\quad H_4IO_6^- \overset{K_D}{\rightleftharpoons} IO_4^- + 2H_2O$$

$$[4]\quad H_4IO_6^- \overset{K_2}{\rightleftharpoons} H_3IO_6^{2-} + H^+$$

have been detected (10) and the several equilibrium constants determined.

The results suggest that the oxidation of serine and threonine by periodic acid involves multisteps. The first-order dependence of the rate on amino acid and periodate concentration, suggests the interaction between the effective species of the reactants in the rate-limiting step.

TABLE 2. Absence of buffer catalysis in the oxidation of amino acids[a]

10 $[CH_3—CO_2^-]$ (M)	0.112	0.224	0.448	1.12	1.41	1.79
10 $[CH_3—CO_2H]$ (M)	0.448	0.869	1.79	4.48	5.64	7.17
$10^2\ k''_\psi$ (ser) (L mol^{-1} s^{-1})	2.80	2.78	2.82	2.81	2.77	2.79
$10^2\ k''_\psi$ (thre) (L mol^{-1} s^{-1})	3.95	3.97	3.93	3.94	3.96	3.96
10 $(ClCH_2—CO_2^-]$ (M)	0.161	0.326	0.643	1.01	1.41	1.91
10 $[ClCH_2—CO_2H]$ (M)	0.333	0.674	1.33	2.08	2.91	3.95
$10^3\ k''_\psi$ (ser) (L mol^{-1} s^{-1})	4.54	4.52	4.50	4.56	4.51	4.55
$10^3\ k''_\psi$ (thre) (L mol^{-1} s^{-1})	6.96	6.98	6.97	6.94	6.95	6.98

[a]$[Per] = 8.00 \times 10^{-3}\ M$; $[AA] = 4.00 \times 10^{-2}\ M$; $I = 0.20\ M$; temperature = 10°C.

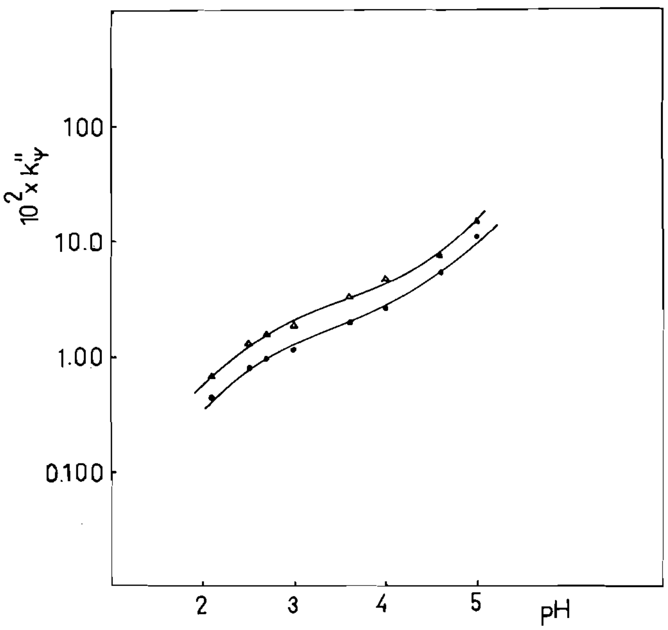

FIG. 2. Dependence of second-order rate constants on pH; ● serine; △ threonine. $[Per] = 8.00 \times 10^{-3}\ M$; $[AA] = 4.00 \times 10^{-2}\ M$; $I = 0.20\ M$; temperature = 10°C.

For the purpose of the kinetic treatment, the following scheme can be proposed:

$$[5]\quad AA + Per \underset{k_-}{\overset{k}{\rightleftharpoons}} C_1$$

$$[6]\quad C_1 \xrightarrow{k_1} Gly + aldehyde + NH_3 + IO_3H$$

$$[7]\quad Gly + Per \underset{k_{-2}}{\overset{k_2}{\rightleftharpoons}} C_2$$

$$[8]\quad C_2 \xrightarrow{k_3} CO_2 + H—CO_2H + IO_3H$$

(Per represents the totality of periodic acid and its anions.) We assume that the amino acid and periodate can reversibly form a complex (C_1) which decomposes giving the intermediate glyoxylic acid (Gly), the aldehyde (formaldehyde or acetaldehyde from serine and threonine respectively), ammonia, and iodate. Glyoxylic acid has been detected as an intermediate during the periodic acid oxidation of serine and threonine (12), and it has been reported (15) that the reaction between glyoxylic acid and periodate leads to a cyclic intermediate which undergoes disproportionation to give the products.

The observation of overall second-order kinetics under all conditions tested can be interpreted as an indication that there is not accumulation of a periodate − amino acid complex. We accept that the concentrations of C_1, Gly, and C_2 are low and that we can apply the steady-state approximation to them. In

TABLE 3. Equilibrium constants

	Periodic acid	Serine	Threonine
K_1 (mol L^{-1})	1.52×10^{-2}	—	—
K_2 (mol L^{-1})	4.79×10^{-9}	—	—
K_D	15.1	—	—
K_a (L mol^{-1})	—	$10^{-2.21}$	$10^{-2.15}$

TABLE 4. Rate constants for the periodate oxidation of amino acids[a]

Amino acid	$10^2\ k^-$ (L mol^{-1} s^{-1})	$10^{-2}\ k^{2-}$ (L mol^{-1} s^{-1})
Serine	1.60 ± 0.08	2.04 ± 0.12
Threonine	2.50 ± 0.23	2.52 ± 0.18

[a]Mean values calculated from those reported in the text.

addition, if C_1 decomposes to products so rapidly that the rate of reaction is formation of C_1; i.e., $k_1 \gg k_-$, the kinetics expression for the reaction is:

$$[9]\quad -\frac{d[Per]}{dt} = k[AA][Per]$$

In order to understand the process by which periodate oxidizes serine and threonine, it is necessary to know what species of periodate are active in these reactions. The observation that the rate of oxidation increases with decrease in pK_a value of amino acid led us to consider the dipolar ionic form of the substrate as its reactive species. The pH−rate profiles for the reactions (Fig. 2), together with the pK values of Table 3, suggest that, around pH 5, the decline in rate constant as we get to higher acidities must be due to the periodate dianion, which declines in significance in that region. In the lower pH range the oxidation of substrate must be brought about by the periodate monoanion, and the rate of this reaction should be lower than the rate of reaction of periodate dianion. Then, moving further to lower pH, the second steep decline in rate constant around pH 2 can only be due to the beginning of the decline in the zwitterions of the substrates.

In analyzing the variation of reaction rate with pH, we consider that the effective reactants are the monoanion ($H_4IO_6^-$ + IO_4^-) and dianion ($H_3IO_6^{2-}$) of periodate and the dipolar ionic form of the amino acid. Thus, for the overall rate equation, we can write:

$$[10]\quad k''_\psi[Per][AA] = [k^-(Per^-) + k^{2-}(Per^{2-})][AA^\pm]$$

where (Per^-) and (Per^{2-}) represent the various periodate species for the charges represented, and k^- and k^{2-} the rate constants for reaction between dipolar amino acid and periodate monoanion and dianion respectively.

In formulating eq. [10], we assume that the rate of reaction between the undissociated periodic acid (Per^0) and dipolar ami-

TABLE 5. Dependence of k''_ψ on $[H^+]$[a]

pH	$10^6 f_b(H^+)$	Serine: $10^2 k''_\psi$ (expt.) ($L\ mol^{-1}\ s^{-1}$)	Serine: $10^2 k''_\psi$ (calcd.) ($L\ mol^{-1}\ s^{-1}$)	Threonine: $10^2 k''_\psi$ (expt.) ($L\ mol^{-1}\ s^{-1}$)	Threonine: $10^2 k''_\psi$ (calcd.) ($L\ mol^{-1}\ s^{-1}$)
5.00	0.152	10.7	11.4	13.9	14.5
4.60	0.383	5.44	5.47	7.76	7.28
4.00	1.53	2.80	2.56	3.95	3.68
3.60	3.88	2.01	1.96	3.14	2.93
3.00	16.2	1.28	1.37	1.88	2.15
2.70	34.3	0.960	1.10	1.56	1.76
2.50	58.1	0.802	0.892	1.30	1.45
2.10	184	0.454	0.463	0.696	0.778

[a] $[Per] = 8.00 \times 10^{-3}\ M$; $[AA] = 4.00 \times 10^{-2}\ M$; $I = 0.20\ M$; temperature = 10°C.

no acid is negligible. Our kinetic treatment does not distinguish between the hydrated ($H_4IO_6^-$) and dehydrated (IO_4^-) forms of the periodate monoanion. The total concentration of periodate [Per] and amino acid [AA] over the acid range:

$$[11]\quad [Per] = [Per^0] + [Per^-] + [Per^{2-}]$$

$$[12]\quad [AA] = [AA^\pm] + [AA^+]$$

From the dissociation equilibria [1]–[4] and eqs. [11] and [12], eq. [9] becomes:

$$[13]\quad -\frac{d[Per]}{dt} = k''_\psi[AA][Per]$$

where:

$$[14]\quad k''_\psi = \frac{k^-K_1[H^+] + k^{2-}K_1K_2}{[H^+]^2 + K_1[H^+] + K_1K_2}\cdot\frac{K_a}{K_a + [H^+]}$$

In order to calculate the values of k^- and k^{2-} in eq. [14], we will consider the various pH regions separately. In treating the results we use values of K_1 and K_2, the apparent first and second dissociation constants of periodic acid (Table 3) expressed in terms of concentrations. They were determined for the ionic strength 0.20 M and 10°C from existing results (10).

At pH 2.1–3.0, we can ignore reactions of the periodate dianion (Per^{2-}) and eq. [14] reduces to:

$$[15]\quad k''_\psi = \frac{k^-K_1K_a}{[H^+]^2 + [H^+](K_1 + K_a) + K_1K_a}$$

Using the values of k''_ψ from Table 5 for pH ≤ 3.0 and eq. [15] in the form:

$$[16]\quad k''_\psi \cdot f_a(H^+) = k^-K_1K_a$$

where:

$$[17]\quad f_a(H^+) = [H^+]^2 + [H^+](K_1 + K_a) + K_1K_a$$

we obtain the value of $10^2 k^- = 1.52$ and $2.27\ L\ mol^{-1}\ s^{-1}$ for serine and threonine respectively. The constancy of $k''_\psi \cdot f_a[H^+]$ supports the assumption of negligible reaction between the amino acid and undissociated periodic acid in this pH range.

At pH 3.6–5.0 we consider all the amino acid to be in the dipolar ionic form, and eq. [14] becomes:

$$[18]\quad k''_\psi = \frac{k^-K_1[H^+] + k^{2-}K_1K_2}{[H^+]^2 + K_1[H^+] + K_1K_2}$$

or:

$$[19]\quad k''_\psi \cdot f_b(H^+) = k^-K_1[H^+] + k^{2-}K_1K_2$$

where:

$$[20]\quad f_b(H^+) = [H^+]^2 + K_1[H^+] + K_1K_2$$

The function $k''_\psi \cdot f_b(H^+)$ plotted against $[H^+]$ gives a straight line. From the slope and the intercept of the line, values of the individual rate constants for the oxidation of amino acids were found to be: $k^- = 1.68 \times 10^{-2}\ L\ mol^{-1}\ s^{-1}$ and $k^{2-} = 2.04 \times 10^2\ L\ mol^{-1}\ s^{-1}$ for serine and $k^- = 2.73 \times 10^{-2}\ L\ mol^{-1}\ s^{-1}$ and $k^{2-} = 2.52 \times 10^2\ L\ mol^{-1}\ s^{-1}$ for threonine.

To check the validity of eq. [14], we used it to calculate the rate constants as $[H^+]$ varies. The rate constants were evaluated from the constants in Table 4, values of $f_b(H^+)$, and corrections made for the concentration of amino acid in the dipolar form. The values of $f_b(H^+)$, and calculated values of k''_ψ are shown in Table 5, along with the experimentally observed values of k''_ψ.

In the treatment given, it has been assumed that the reaction could be represented by a summation of bimolecular reactions, each involving one molecule of periodate in one of its stages of ionization and one molecule of amino acid in the dipolar form. The data have been fitted with this assumption to within the experimental error. As calculations show, the periodate dianion is more reactive than the monoanion. A similar result has been observed (4) in the oxidation of 1,2-dioxo compounds by periodate, where an increase of the reaction rate with increase in the charge of the periodate species was shown.

Our kinetic analysis includes an attack of periodate on amino acid to form a complex. We have found no evidence for the formation of a kinetically detectable concentration of complex in the oxidation of amino acids by periodate. However, this does not rule out the possibility that substrate–periodate complexes are intermediates in oxidation if their formation, rather than their decomposition to products, is rate controlling.

1. (*a*) F. R. DUKE. J. Am. Chem. Soc. **69**, 3054 (1947); (*b*) F. R. DUKE and V. C. BULGRIN. J. Am. Chem. Soc. **76**, 3803 (1954).
2. (*a*) G. J. BUIST and C. A. BUNTON. J. Chem. Soc. 1406 (1954); 4580 (1957); J. Chem. Soc. (B), 2117 (1971); (*b*) G. J. BUIST, C. A. BUNTON, and J. H. MILES. J. Chem. Soc. 4567 (1957); 4575 (1957); 743 (1959); (*c*) S. SENENT, M. PÉREZ, and P. ESCUDERO. An. R. Soc. Esp. Fis. Quim. Ser., B **57**, 153 (1961); (*d*) G. J. BUIST, C. A. BUNTON, and J. LOMAS. J. Chem. Soc. (B), 1094 (1966); 1099 (1966); (*e*) G. J. BUIST and J. D. LEWIS. J. Chem. Soc. (B), 90 (1968); (*f*) G. J. BUIST, C. A. BUNTON, and W. C. P. HIPPERSON. J. Chem. Soc. (B), 2128 (1971).
3. (*a*) G. DAHLGREN and J. HODSON. J. Phys. Chem. **68**, 416 (1964); (*b*) G. DAHLGREN and E. RAND. J. Phys. Chem. **71**, 1955 (1967); (*c*) L. MAROS, I. MOLNÁR-PERL, E. SCHISSEL, and V. SZERDAHELYI. J. Chem. Soc. Perkin Trans. 2, 39 (1980).

4. (*a*) V. SHINER and C. WASSMUTH. J. Am. Chem. Soc. **81**, 37 (1959); (*b*) G. DAHLGREN and K. REED. J. Am. Chem. Soc. **71**, 1380 (1967).
5. (*a*) SUSHILA and K. GROVER. J. Indian Chem. Soc. **54**, 1159 (1977); (*b*) M. PRASADA RAO, B. SETHURAM, and N. NAVANEETH RAO. J. Indian Chem. Soc. **57**, 149 (1980).
6. B. NICOLET and L. SHINN. J. Am. Chem. Soc. **61**, 1615 (1939).
7. A. MARTIN and R. SYNGE. Biochem. J. **35**, 294 (1941).
8. D. MORTIMER. Can. J. Biochem. Physiol. **37**, 919 (1959).
9. D. SKOOG and D. WEST. Fundamentos de química analítica. Reverté, Barcelona. 1970.
10. C. CROUTHAMEL, H. MEEK, D. MARTIN, and C. BANKS. J. Am. Chem. Soc. **71**, 3031 (1949); C. CROUTHAMEL, A. HAYES, and D. MARTIN. J. Am. Chem. Soc. **73**, 82 (1951).
11. D. A. MCFADYEN. J. Biol. Chem. **158**, 107 (1945).
12. D. SPRINSON and E. CHARGAFF. J. Biol. Chem. **164**, 433 (1946).
13. E. KNAPPE and D. PETERI. Z. Anal. Chem. **188**, 184 (1962).
14. J. GREENSTEIN and M. WINITZ. Chemistry of the amino acids. John Wiley, Sons, Inc., New York. 1961.
15. L. MAROS, I. MOLNAR-PERL, and L. KOVER. J. Chem. Soc. Perkin Trans. 2, 1337 (1976).

Synthèse d'aryl nitronorbornènes par cycloaddition de Diels–Alder entre les aryl-nitroéthylènes et le cyclopentadiène. Justification de la stéréochimie et de la réactivité relative observées par la méthode CNDO/II. Obtention d'aryl aminonorbornènes

JEAN BOURGUIGNON, GILLES LE NARD ET GUY QUEGUINER[1]

Laboratoire de Chimie Organique Hétérocyclique, Institut National Supérieur de Chimie Industrielle de Rouen, 76130 – Mont Saint Aignan, France

Reçu le 23 mai 1984[2]

JEAN BOURGUIGNON, GILLES LE NARD et GUY QUEGUINER. Can. J. Chem. **63**, 2354 (1985).

Les synthèses d'un certain nombre d'aryl-2 nitroéthylènes (nitrostyrènes) ont été optimisées. Les nitrostyrènes ont été opposés au cyclopentadiène dans des cycloadditions de type Diels–Alder, et les aryl-3 nitro-2 norbornènes obtenus ont été réduits en aryl-3 amino-2 norbornènes. Ces composés sont susceptibles de posséder une activité dopaminergique. La stéréochimie des adduits obtenus dans les réactions de Diels–Alder a été déterminée par rmn de ^1H. Ce résultat et la réactivité relative des nitrostyrènes vis-à-vis du cyclopentadiène ont été confirmés par des calculs théoriques basés sur la méthode CNDO/II.

JEAN BOURGUIGNON, GILLES LE NARD, and GUY QUEGUINER. Can. J. Chem. **63**, 2354 (1985).

Syntheses of numerous 2-aryl nitroethylenes (nitrostyrenes) have been optimized. The nitrostyrenes have been reacted with cyclopentadiene in Diels–Alder cycloadditions and the 3-aryl 2-nitronorbornenes obtained have been reduced into 3-aryl 2-aminonorbornenes. These compounds are potentially dopaminergic molecules. The stereochemistry of the adducts obtained in the Diels–Alder reaction has been determined by ^1H nmr. The stereochemistry and the relative reactivity of the nitrostyrenes versus cyclopentadiene have been confirmed by theoretical calculations based on the CNDO/II method.

Les aryl-2 nitroéthylènes **1** ou nitrostyrènes sont facilement préparés par action de nitroalcanes sur des aldéhydes aromatiques. Les produits ainsi obtenus, opposés au cyclopentadiène dans les réactions de type Diels–Alder, conduisent à des aryl-3 nitro-2 bicyclo[2,2,1]heptènes-5 ou aryl-3 nitro-2 norbornènes **2**. La réduction du groupe nitro de ces composés fournit les amines correspondantes **3** qui possèdent l'enchaînement Ar—C—C—N susceptible de leur conférer une activité antiparkinsonienne (1).[3]

$$ArCHO + \underset{\displaystyle R}{\underset{|}{C}}H_2—NO_2 \longrightarrow ARCH(OH)—CH(R)—NO_2 \xrightarrow{-H_2O}$$

(R = H ou CH_3)

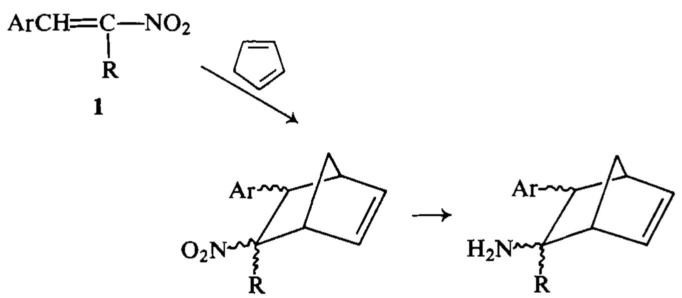

1 **2** **3**

Le premier β-nitrostyrène a été préparé en 1884 par deshydratation du nitroalcool résultant de la condensation du benzaldéhyde et du nitrométhane (2). Depuis, cette réaction a été effectuée dans des conditions très variées: utilisation de catalyseurs basiques divers pour réaliser la condensation, deshydratation dans des conditions très différentes les unes des autres, etc. . . . (3). Les rendements sont parfois faibles ou les procédés quelquefois difficiles à mettre en oeuvre: nous avons simplifié et amélioré les méthodes permettant de préparer les aryl-2 nitroéthylènes que nous souhaitions obtenir.

La réaction de Diels–Alder conduisant aux aryl nitronorbornènes **2** est une réaction stéréospécifique. Au départ d'un nitrostyrène de configuration donnée, elle peut donner plusieurs isomères selon la position des substituants par rapport au système bicyclique ponté: une étude spectroscopique nous a permis de préciser la structure des produits obtenus.

Nous avons par ailleurs constaté expérimentalement une réactivité très différente des nitrostyrènes vis-à-vis du cyclopentadiène. Ceci nous a incité à effectuer une étude théorique (utilisant la méthode CNDO/II). Cette étude montre une excellente corrélation entre les calculs et les résultats observés. De plus, la théorie permet aussi de justifier la stéréochimie de la réaction.

Enfin la réduction des nitronorbornènes **2** en aryl amino norbornènes **3** a été réalisée par l'intermédiaire de $LiAlH_4$ qui laisse intacte la double liaison du norbornène.

I. Synthèse des aryl-2 nitroéthylènes, aryl nitro et aryl amino norbornènes

1. *Aryl-2 nitroéthylènes 1*

$$ArCHO + CH_3NO_2 \longrightarrow \underset{\textbf{1}}{ArCH{=}CH—NO_2} + H_2O$$

Au départ du nitrométhane les aryl-2 nitroéthylènes (ou nitrostyrènes) ont été obtenus par l'une des trois méthodes suivantes: passage par un intermédiaire nitronate transformé "*in situ*" en nitrostyrène (méthode A (4)); formation d'une imine et obtention de la double liaison en milieu tamponné (méthode B (5a, 5b)); mise en oeuvre de méthodes particulières pour les aldéhydes pyridiniques (méthode C (voir partie expérimentale)).

Les rendements obtenus par l'une ou l'autre méthode sont en général supérieurs à ceux donnés dans la littérature. En série pyridinique nous avons considérablement amélioré les méthodes décrites: la réaction a lieu en quelques heures au lieu de plusieurs jours (6). Les produits obtenus sont rassemblés dans

[1]Auteur à qui adresser la correspondance.
[2]Revision reçue le 8 février 1985.
[3]Les amines seront testées au laboratoire du Professeur Costentin de la Faculté de Pharmacie de Rouen.

le tableau 1.[4]

À partir du nitroéthane, nous avons préparé des β-méthyl β-nitrostyrènes (ou aryl-3 nitro-2 propènes-2) par une méthode très voisine de la méthode B (voir partie expérimentale).

$$ArCHO + CH_3CH_2NO_2 \longrightarrow ArCH{=}C(CH_3){-}NO_2$$

Ar = phényle-1: **1***o*; thiényle-2: **1***p*

Le manque de réactivité de ces composés lors des cycloadditions de Diels–Alder ne nous a pas incité à préparer d'autres composés de ce type.

Les nitrostyrènes obtenus sont facilement identifiés en spectroscopie ir et rmn de ^{1}H. On observe en effet un couplage de 14 Hz entre les protons éthyléniques caractéristique de la configuration *E*. Par ailleurs, l'attribution au proton éthylénique voisin du cycle aromatique du déplacement chimique le plus élevé a été faite: (*i*) par comparaison avec le déplacement chimique du proton en α du cycle des β-méthyl β-nitrostyrènes $Ar{-}C(H){=}C(CH_3){-}NO_2$; (*ii*) par application de la formule de Pascual (7*a*, *b*) δ (C=C—H) = 5,28 + ΣZ_i qui permet de prévoir les déplacements chimiques du proton éthylénique selon la configuration de la double liaison (ΣZ_i étant la somme des incréments des divers groupements voisins du proton étudié).

2. *Aryl nitronorbornènes 2*

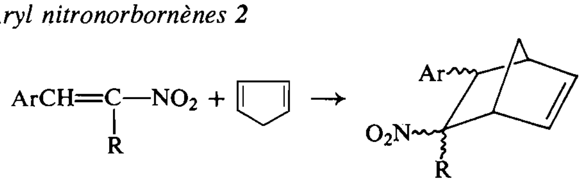

2

Les conditions expérimentales mises en jeu pour réaliser la cycloaddition sont de deux types: Catégorie A: réaction à température ambiante; Catégorie B: réaction vers 110 à 120°C. Certains composés n'ont pas réagi, nous les avons rangé dans la catégorie C.

Remarque: La réaction de Diels–Alder est une réaction réversible (retro Diels–Alder) lorsqu'on élève la température. Ceci nous a posé des problèmes pour purifier certains adduits par distillation (voir partie expérimentale).

Lors de la cycloaddition, la configuration *s-trans* de la partie de l'adduit correspondante au nitrostyrène peut donner deux structures différentes selon que le groupe nitro par exemple est en position "*endo*" ou "*exo*" par rapport au système bicyclique ponté.

Noland *et al.* (10) ont effectué une étude détaillée des spectres de rmn de ^{1}H des deux isomères *endo* et *exo* dans le cas du nitro-2 phényl-3 bicyclo[2,2,1]heptène-5 **2***a*. Ils n'ont pas attribué tous les signaux observés mais il apparaît cependant que le signal du proton H_2 permet de repérer sans ambiguïté les deux isomères: dans le composé "*endo*", il se présente sous la forme d'un triplet possédant un déplacement chimique de 4,18 ppm alors que dans l'isomère "*exo*" il se présente sous forme d'un quadruplet à 4,41 ppm.

L'examen de la courbe d'intégration du produit obtenu directement à partir du milieu réactionnel brut de réaction nous a permis de préciser les pourcentages des deux isomères obtenus (Tableau 1).

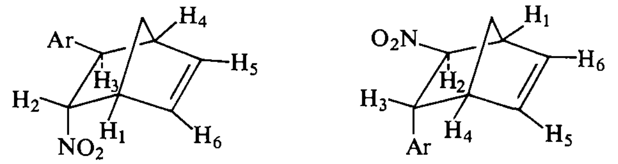

Remarque: Nous avons utilisé deux solvants différents, le toluène et l'acide acétique. Nous n'avons pas trouvé de différence entre les pourcentages des deux isomères *endo* et *exo*.

On remarque que l'on obtient de manière prépondérante l'isomère nitro "*endo*". Généralement après purification l'isomère minoritaire est éliminé. Jusqu'à présent on expliquait cette prépondérance de l'isomère nitro "*endo*" par le fait que le groupement nitro est plus petit que le groupement phényle (11). Nous verrons plus loin que l'on peut confirmer ce résultat par le calcul.

3. *Aryl aminonorbornènes 3*

La réduction du groupement nitro des aryl nitronorbornènes donne lieu à des molécules possédant l'enchaînement Ar—C—C—NH_2. Les composés possédant cet enchaînement, en particulier sous la forme "*s-trans*", sont connus pour posséder fréquemment des activités dopaminergiques et notamment antiparkinsonienne. Citons, par exemple, les plus connues de ces molécules: la dopamine, l'apomorphine, ...

Nous avons effectué la réduction du groupe nitro en utilisant $LiAlH_4$. La réaction ne pose guère de problèmes.

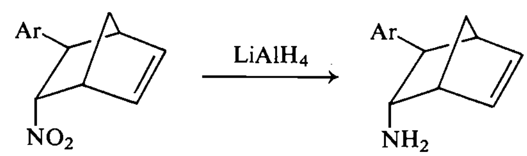

2 **3**

Les réductions ont été effectuées dans l'éther éthylique ou dans le tétrahydrofuranne (THF) suivant la solubilité des réactifs nitrés (Tableau 1).

L'hydrolyse du mélange réactionnel a été effectuée selon la séquence suivante: eau, puis soude, puis eau. L'hydroxyde d'aluminium est ainsi filtré facilement et la solution est évaporée laissant un produit purifiable soit par distillation, soit par chromatographie sur colonne.

Tous les produits obtenus présentent en spectroscopie infrarouge une bande intense à environ 3400 cm^{-1} correspondant à la vibration du groupe NH_2. En spectroscopie de résonance magnétique nucléaire du proton, on note le glissement d'environ 1,5 ppm vers les champs forts du proton H_2 par rapport au déplacement chimique du même proton dans le composé nitré initial (adjacent au nitro, puis après réduction à l'amino).

II. Étude de la réactivité et de la stéréospécifité lors de la réaction de Diels–Alder par la méthode CNDO/II

1. *Introduction*

La réaction de Diels–Alder est une cycloaddition qui fait intervenir un diène et un diénophile. L'étude des mécanismes de cette réaction a été fortement influencée par les règles de Woodward–Hoffmann (8). La réaction se passe en général sous contrôle orbitalaire frontalier: la plus haute orbitale occupée (H.O.) de l'un des réactifs interagit en général avec la plus basse vacante (B.V.) de l'autre réactif. Dans certains cas les

[4] Les produits préparés sont repérés par une lettre indiquée en indice après le numéro du composé. Cette lettre est utilisée pour désigner le groupe Ar et sert à identifier les divers composés **1**, **2** et **3**.

TABLEAU 1. Nitrostyrènes, nitro et aminonorbornènes

Substituant	Indice	Aryl-2 nitro ethylènes (*) **1**	Arylnitro norbornènes (†) **2**		Arylamino norbornènes (‡) **3**
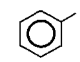	a	A	A	85	A
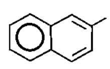	b	A	A	92	A
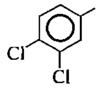	c	A	A	>95	B
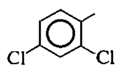	d	A	A	>95	B
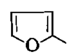	e	A	A	90	A
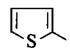	f	A	A	>95	A
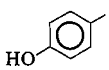	g	B	B	>95	A
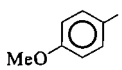	h	B	B	>95	A
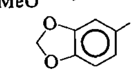	i	B	B	>95	A
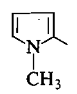	j	B	C	—	—
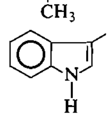	k	B	C	—	—
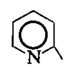	l	C	A	>95	A
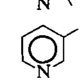	m	C	A	>95	A
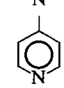	n	C	A	90	A

*Méthode d'obtention du nitrostyrène.
†Conditions dans laquelle la réaction de Diels–Alder a été effectuée et pourcentage d'isomère "*endo*".
‡Solvant dans lequel la réduction a été effectuée. A: éther B: THF.

deux H.O. et B.V. de chacun des deux composés peuvent interagir si le diène et le diénophile ont des orbitales frontières de niveau d'énergie voisins (9).

La cycloaddition fait intervenir les carbones 1 et 4 du diène et les carbones 1 et 2 du diénophile (voir schéma 1). L'équation simplifiée ci-dessous exprime les interactions orbitalaires:

$$\Delta E = \frac{(C_{1\,\mathrm{H.O.}} \cdot C_{1\,\mathrm{B.V.}}\ \beta_{1.1} + C_{4\,\mathrm{H.O.}} \cdot C_{2\,\mathrm{B.V.}}\ \beta_{4.2})^2}{E_{\mathrm{H.O.\ (diène)}} - E_{\mathrm{B.V.\ (diénophile)}}} + \frac{(C_{1\,\mathrm{B.V.}} \cdot C_{1\,\mathrm{H.O.}}\ \beta_{1.1} + C_{2\,\mathrm{H.O.}} \cdot C_{4\,\mathrm{B.V.}}\ \beta'_{2.4})^2}{E_{\mathrm{H.O.\ (diénophile)}} - E_{\mathrm{B.V.\ (diène)}}}$$

$C_{1\,\mathrm{H.O.}}$: coefficient de l'orbitale atomique du carbone 1 dans l'orbitale H.O. et $\beta_{1.1}$: intégrale de résonance.

Lorsqu'on étudie le comportement d'un diène unique vis-à-vis d'une série homogène de diénophiles on peut alors simplifier encore ΔE jusqu'à l'expression ci-dessous (9):

(a) (b)

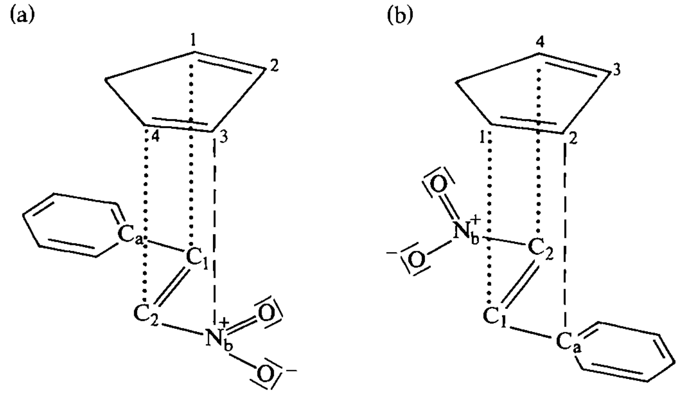

SCHÉMA 1

$$\Delta E = k - \frac{1}{E_{\mathrm{H.O.}} - E_{\mathrm{B.V.}}}$$

La réaction de Diels–Alder que nous étudions est probablement du type dit "normal". Ce diénophile comprend un groupe électroattracteur (le groupe nitro) et un cycle aromatique qui étend la conjugaison. Le niveau énergétique des orbitales vacantes doit donc être normalement considérablement abaissé. C'est ce que nous nous proposons de montrer par le calcul.

La connaissance du terme $E_{\mathrm{H.O.}} - E_{\mathrm{B.V.}}$ doit donc nous permettre en plus de comparer la réactivité de divers nitrostyrènes vis-à-vis du cyclopentadiène.

En ce qui concerne l'aspect stérique de la réaction, on sait que dans le cas des diènes cycliques le composé obtenu est majoritairement le composé "*endo*". On justifie ce résultat en examinant les interactions secondaires qui peuvent se produire à côté des interactions primaires responsables de la cycloaddition. Dans le cas de la réaction étudiée ici, ces interactions secondaires peuvent concerner soit l'azote N_b du groupe nitro soit le carbone C_a du cycle aromatique du nitrostyrène.

Le terme représentant cette interaction secondaire se trouve cette fois au numérateur de l'équation développée initiale. L'énergie de perturbation sera d'autant plus importante que le coefficient orbitalaire de l'atome considéré du diénophile (C_a ou N_b) sera plus élevé.

Pour évaluer ces différents termes nous permettant de répondre aux questions posées concernant la réactivité des divers nitrostyrènes et la stéréochimie de la réaction, nous avons effectué les calculs par la méthode CNDO/II: dans le cas d'une famille homogène, cette méthode fournit d'excellents éléments de comparaison (12).

On peut négliger le rôle du solvant car c'est une réaction concertée (13).

2. *Résultats*

À partir des données géométriques fournies par la littérature (14) le calcul donne par exemple les résultats suivants dans le cas du composé **1***m* et du cyclopentadiène.

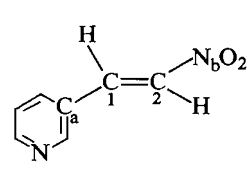

1*m*

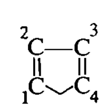

$E_{\mathrm{H.O.}} = -12{,}76$ eV $\quad E_{\mathrm{H.O.}} = 12{,}35$ eV
$E_{\mathrm{B.V.}} = 0{,}5$ eV $\quad E_{\mathrm{B.V.}} = 3{,}05$ eV

Coefficients des orbitales frontières:

B.V.: $C_a = 0{,}2172$ $C_1 = 0{,}4828$
$C_2 = -0{,}3673$ $N_b = -0{,}3702$
H.O.: $C_a = 0{,}0199$ $C_1 = -0{,}0145$
$C_2 = -0{,}0189$ $N_b = 0{,}0087$

H.O.: $C_1 = -0{,}5778$ $C_2 = -0{,}4078$
$C_3 = 0{,}4078$ $C_4 = 0{,}5778$

3. *Discussion*

La différence $E_{H.O.} - E_{B.V.}$ la plus faible en valeur absolue est obtenue en faisant intervenir (comme prévu) la B.V. du nitrostyrène et la H.O. du cyclopentadiène: 12,85 eV contre 15,81 eV dans l'autre cas. On confirme ainsi que l'on a affaire à une réaction de Diels–Alder "normale" (9).

Par ailleurs, on observe que le coefficient orbitalaire de l'azote N_b dans le B.V. du diénophile est plus élevé que celui du carbone C_a. L'interaction secondaire attractive avec le carbone C_2 (ou C_3) du cyclopentadiène sera donc plus forte si on considère l'azote N_b et il est donc normal que l'on obtienne préférentiellement l'isomère "*endo*" nitro.

Remarque: Ce résultat est confirmé par l'examen des coefficients de l'azote N_b et du carbone C_a dans l'orbitale H.O. du diénophile: dans ce cas on observe que le coefficient du carbone C_a est plus élevé en valeur absolue que celui de l'azote N_b. L'interaction secondaire repulsive est donc plus forte si on considère le carbone C_a ce qui défavorise l'obtention de l'isomère "*endo*" aryl (15).

Nous donnons dans le tableau 2, la valeur $E_{H.O.} - E_{B.V.}$ calculée pour tous les nitrostyrènes ainsi que les valeurs absolues des coefficients orbitalaires de l'azote N_b et du carbone C_a dans les orbitales B.V. et H.O. du diénophile.

Les valeurs de $E_{H.O.} - E_{B.V.}$ permettent de déduire l'échelle de réactivité suivante:

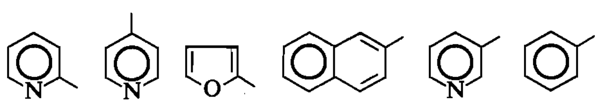

1*l* **1***n* **1***e* **1***b* **1***m* **1***a*

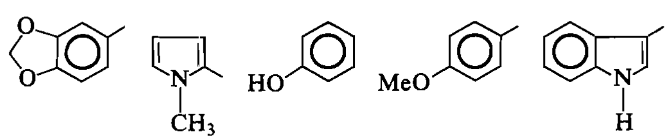

1*i* **1***j* **1***g* **1***h* **1***k*

Cette séquence permet de justifier les observations expérimentales concernant les conditions dans lesquelles les divers nitrostyrènes pouvaient réagir avec le cyclopentadiène.

On peut en effet remarquer que les composés **1***a*, **1***b*, **1***e*, **1***l*, **1***m* et **1***n* qui réagissent à température ordinaire sont ceux pour lesquels $E_{H.O.} - E_{B.V.} < 12{,}91$ (catégorie A).

Les nitrostyrènes **1***g*, **1***h* et **1***i* qui réagissent à 110–120°C sont ceux pour lesquels $12{,}91 < E_{H.O.} - E_{B.V.} < 13{,}07$ (catégorie B).

Les nitrostyrènes **1***j* et **1***k* n'ont pas réagi dans les conditions utilisées. Pour **1***j* cela peut sembler anormal ($E_{H.O.} - E_{B.V.} = 13{,}01$) mais pour **1***k* cela paraît tout à fait justifié ($E_{H.O.} - E_{B.V.} = 13{,}39$).

On peut donc dire que mis à part le composé **1***j* on constate qu'il existe une très bonne corrélation entre les valeurs calculées et les résultats expérimentaux.

Nous avons pu vérifier la validité de la méthode en l'appliquant au dérivé *N*-acétylé du composé **1***k* qui réagit avec le cyclopentadiène uniquement à température élevée comme l'ont montré Royer et Beugelmans-Verrier (16). Le calcul de $E_{H.O.} - E_{B.V.}$ donne une valeur de 13,06 eV ce qui place bien ce composé dans la catégorie B.

Enfin dans le cas du β-méthyl β-nitrostyrène **1***o* le calcul de $E_{H.O.} - E_{B.V.}$ montre que l'on obtient sensiblement la même valeur lorsqu'on fait intervenir les orbitales H.O. et B.V. du diène ou du diénophile (12,90 et 13,01 eV respectivement). La réaction est alors "à demande neutre en électrons" et elle est plus difficile à réaliser (9). Ceci explique que nous n'ayons pas obtenu d'adduit avec le cyclopentadiène.

Partie expérimentale

Les points de fusion ont été déterminés sur un banc de Kofler et n'ont pas été corrigés.

Les spectres ir ont été enregistrés soit avec un spectrographe Perkin–Elmer 237 soit avec un spectrographe Beckman IR 4250: les solides sont dispersés dans du KBr sous forme de pastilles et les liquides sont insérés dans des fenêtres de NaCl sous forme de film.

Les spectres de rmn de ^1H ont été enregistrés sur un appareil Varian A60 ou Varian T60. La double irradiation a été effectuée sur un appareil Bruker WH 90D par Mme Chapelle du Service Commun de l'Université de Rouen que nous remercions à cette occasion.

Les microanalyses ont été réalisées sur un appareil Technicon. Dans les tableaux récapitulatifs, les produits pour lesquels la formule brute est donnée ont fourni des résultats corrects à l'analyse.

A. *Synthèse des nitrostyrènes*

I. *Méthode A: méthode à froid*

Dans un tricol muni d'une agitation et d'un thermomètre, on introduit 200 mL de méthanol, 61 g (1 mol) de CH_3NO_2 et 2 mL d'une solution de soude 10,5 *M*. On ajoute ensuite goutte à goutte à l'aide d'une ampoule de coulée, 1 mol d'aldéhyde en maintenant la température inférieure ou égale à 10°C. On abaisse alors la température du mélange à 5°C, puis on introduit goutte à goutte 98 mL de soude 10,5 *M* en maintenant la température inférieure à 15°C. Il se forme alors un précipité de plus en plus épais (un ajout de méthanol peut être nécessaire pour rendre le milieu plus fluide).

Après 30 min d'agitation, on introduit 350 mL d'un mélange eau–glace qui fait passer la pâte en solution. Celle-ci est alors ajoutée goutte à goutte à 100 mL d'acide chlorhydrique concentré et 150 mL d'eau. Il se forme un précipité qui est filtré, puis lavé à l'eau jusqu'à disparition de l'acidité. On recristallise dans l'éthanol.

II. *Méthode B: méthode à chaud*

Dans un ballon de 250 mL, on introduit 24,4 g (0,4 mol) de nitrométhane, 0,4 mol d'aldéhyde, 50 mL d'isopropanol puis 2,8 g de benzylamine et 2,4 g d'acide acétique glacial. Le mélange est porté 1 h à reflux. Il y a apparition d'un précipité que l'on filtre et qui est recristallisé dans l'éthanol. Dans le cas du *N*-méthyl formyl-2 pyrrole et du formyl-3 indole, le mode opératoire a été modifié comme suit: À 200 mL de nitrométhane sont ajoutés 0,1 mol d'aldéhyde et 4 g d'acétate d'ammonium. Le mélange est alors porté, sous agitation, à la température de reflux pendant une demi-heure, puis refroidi. Le nitrostyrène est alors filtré, puis recristallisé dans l'éthanol absolu.

III. *Méthode C: méthodes particulières*

1. *Synthèse de la (nitro-2 éthényl)-3 pyridine* **1**m

Dans un tricol muni d'une agitation, on introduit successivement 25 mL d'éthanol absolu, 8,6 g (0,14 mol) de nitrométhane, 0,2 g de chlorhydrate de méthylamine et 0,04 g de carbonate de sodium

TABLEAU 2. $E_{H.O.} - E_{B.V.}$ et valeurs absolues des coefficients orbitalaires de l'azote N_b et du carbone C_a dans la B.V. et la H.O. du diénophile

Nitrostyrène	$E_{H.O.} - E_{B.V.}$	Orbitale B.V. N_b	Orbitale B.V. C_a	Orbitale H.O. N_b	Orbitale H.O. C_a
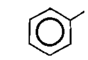 1*a*	12,91	0,3711	0,2276	0,0090	0,0231
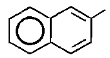 1*b*	12,83	0,3378	0,2450	0,0205	0,3364
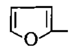 1*e*	12,78	0,3731	0,1993	0,0309	0,4908
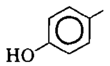 1*g*	13,03	0,3778	0,2055	0,0353	0,4489
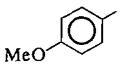 1*h*	13,07	0,3794	0,2038	0,0315	0,4410
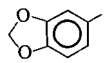 1*i*	12,92	0,3622	0,2276	0,0177	0,2434
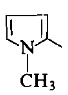 1*j*	13,01	0,3663	0,1780	0,0294	0,4875
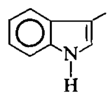 1*k*	13,39	0,3933	0,1487	0,0195	0,4734
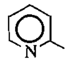 1*l*	12,54	0,3386	0,2558	0,0124	0,0515
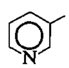 1*m*	12,85	0,3702	0,2172	0,0087	0,0199
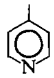 1*n*	12,59	0,3542	0,2609	0,0085	0,0112

anhydre. On ajoute alors à cette solution vigoureusement agitée 15 g (0,14 mol) de formyl-3 pyridine. Trois jours plus tard, le mélange refroidi est filtré. Le solide jaune est alors lavé avec de l'éther sulfurique puis séché dans un dessiccateur. On obtient ainsi 11,6 g de (nitro-2 éthényl)-3 pyridine **1***m*. F = 141°C. Rendement = 55%; cristaux jaunes.

2. *Synthèse de la (nitro-2 éthényl)-2 pyridine 1*l

(*a*) Dans un ballon contenant 180 mL de nitrométhane refroidi par un bain de glace, on ajoute 53,8 g (0,5 mol) de formyl-2 pyridine. Le mélange est agité vigoureusement, et l'on ajoute 2,7 g de carbonate de potassium. On laisse réagir 15 h à 0°C puis l'on ajoute 200 à 300 mL d'éthanol absolu. On fait alors passer dans la solution un courant d'acide chlorhydrique sec, provoquant la précipitation du chlorhydrate de (nitro-2 éthanol-1)-2 pyridine qui est filtré et séché sous vide. F = 138°C. Rendement = 85%.

(*b*) À une solution de 50 mL d'anhydride acétique contenant 20,4 g (0,1 mol) de chlorhydrate de (nitro-2 éthanol-1)-2 pyridine, on ajoute 16,4 g (0,2 mol) d'acétate de sodium. Le mélange est agité et placé dans un bain de glace pendant 24 h. Il est ensuite versé dans 300 mL d'eau glacée et extrait au chloroforme. Les phases organiques rassemblées sont lavées avec une solution saturée en hydrogénocarbonate de sodium, puis avec de l'eau. Elles sont ensuite séchées sur sulfate de magnésium et évaporées sous vide à température ambiante. Le solide ainsi recueilli est dissous dans du tétrachlorure de carbone et la solution est filtrée deux fois sur charbon actif, puis évaporée à sec laissant 8,5 g d'un solide jaune: la (nitro-2 éthényl)-2 pyridine **1***l*. F = 73°C. Rendement = 57%; rendement global = 48%.

TABLEAU 3. Nitrostyrènes

Ar = (R = H)	Méthode	Rdt	F (°C) Trouvé	F (°C) Litt.
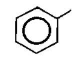 1*a*	A	84	57	57 (17*a*)
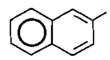 1*b*	A	80	122	122 (17*b*)
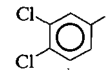 1*c*	A	63	89	85 (17*b*) 89 (17*c*)
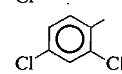 1*d*	A	68	113	116 (17*b*) 113 (17*c*)
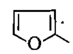 1*e*	A	63	74	74 (17*d*)
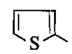 1*f*	A	64	80	79 (17*e*)
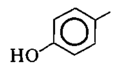 1*g*	B	82	162	171 (17*f*)
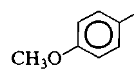 1*h*	B	70	86	86 (17*g*)
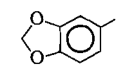 1*i*	B	77	158	158 (17*g*)
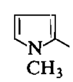 1*j*	B	72	102	(17*h*)
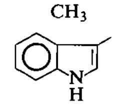 1*k*	B	83	174	171–172 (17*i*)
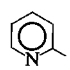 1*l*	C	48	73	73 (17*j*)
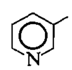 1*m*	C	55	141	141 (17*k*)
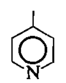 1*n*	C	69	110	
Ar = (R = CH_3)				
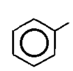 1*o*	B	51	64	65 (17*l*)
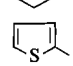 1*p*	B	47	69	68,5 (17*m*)

3. *Synthèse de la (nitro-2 éthényl)-4 pyridine 1*n

(*a*) À une solution de 100 mL de nitrométhane contenant 30 g (0,28 mol) de formyl-4 pyridine fraîchement distillée, on ajoute 1,5 g de carbonate de potassium en agitant fortement. La température monte à environ 35°C et le mélange est alors placé 30 min dans un bain de glace tout en maintenant l'agitation. Le solide blanc formé est alors extrait dans du méthanol, plus filtré. La solution recueillie est évaporée à sec à température ambiante laissant 41 g d'un solide blanc: la (nitro-2 éthanol-1)-4 pyridine. F = 95°C. Rendement = 90%.

(*b*) À 10 g (0,06 mol) de (nitro-2 éthanol-1)-4 pyridine en suspension dans 50 mL d'anhydride acétique sont ajoutés 9,8 g (0,12 mol) d'acétate de sodium. Le mélange est agité fortement sur bain de glace pendant quelques heures, puis versé dans 250 mL d'eau glacée. La solution obtenue est extraite au chloroforme, les phases organiques rassemblées sont lavées à l'eau, séchées sur sulfate de magnésium et

TABLEAU 4. Arylnitronorbornènes

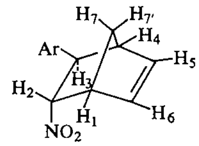

Ar		Catégorie	Méthode de purification	Rdt (%)	F/E	Litt. ou microanalyses (voir tableau 6)	rmn ^{1}H du cycle norbornène							Solvant
							H_1	H_2	H_3	H_4	H_5	H_6	$H_7H_{7'}$	
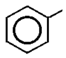	2*a*	A	1	80	$E_{0,5}=124$	$E_1=145(10)$ (18*a*)	3,84	4,81	3,39	3,09	6,5	6,0	1,74	a
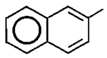	2*b*	A	2(CCl_4)	57	Huile	$C_{17}H_{15}NO_2$	3,79	4,92	3,41	3,12	6,47	6,02	1,68	b
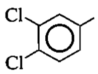	2*c*	A	3	46,5	$F=120$	119–120(18*b*)	3,5	5,53	3,30	3,0	6,40	6,13	1,63	c
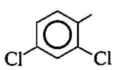	2*d*	A	3	42	$F=105$	105–106(18*b*)	3,67	5,73	3,40	3,0	6,73	6,13	1,57	c
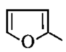	2*e*	A	1	78	$E_{0,8}=100$	$E_{0,8}=100$(18*c*)	3,50	5,03	3,35	3,02	6,44	5,93	1,68	b
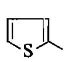	2*f*	A	1	85	$E_{0,7}=115$	$E_{0,65}=129$(18*c*)	3,49	4,93	3,49	3,04	6,60	6,10	1,75	a
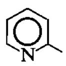	2*l*	A	1	65	$E_{0,1}=128$	$C_{12}H_{12}N_2O_2$	3,60	5,90	3,47	2,97	6,53	6,07	2,13 et 1,45	a
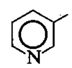	2*m*	A	1	90	$E_{0,3}=161$	$C_{12}H_{12}N_2O_2$	3,57	5,0	3,33	3,13	6,57	6,17	1,75	b
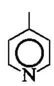	2*n*	A	1	70	$E_{0,1}=140$	$C_{12}H_{12}N_2O_2$	3,93	5,50	3,60	3,21	6,70	6,08	1,93	b
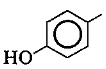	2*g*	B	2(Et_2O)	68	Gel	$C_{13}H_{13}NO_3$	3,50	5,30	3,13	2,93	6,60	6,08	1,63	c
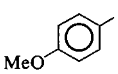	2*h*	B	1	47	$E_1=150$	$C_{14}H_{15}NO_3$	3,50	4,87	3,27	3,03	6,53	6,07	1,73	b
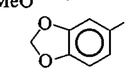	2*i*	B	2(Et_2O)	72	Huile	$C_{14}H_{13}NO_4$	3,40	5,27	3,12	2,88	5,97	6,45	1,63	c

NOTES: Spectres de rmn: échantillons mis en solution dans CCl_4 (a), $CDCl_3$ (b), DMSO-d_6 (c).

évaporée sous vide à température ambiante, laissant 6,84 g de cristaux bruns. Rendement = 76,5%; rendement global = 69%.

IV. *Synthèses des* β*-méthyl* β*-nitrostyrènes*

Dans un ballon de 250 mL on introduit 30 g (0,4 mol) de nitroéthane, 0,4 mol d'aldéhyde, 50 mL d'isopropanol, puis 1,9 g de n-butylamine et 2,4 g d'acide acétique glacial. Le mélange est porté à reflux pendant une nuit, puis refroidi. Le solide formé est filtré, lavé à l'éthanol puis recristallisé dans du méthanol.

Les caractéristiques des nitrostyrènes préparés sont indiquées dans le tableau 3.

B. *Synthèse des aryl-3 nitro-2 bicyclo*[2,2,*1*]*heptènes-5 ou arylnitronorbornènes*

Remarque: dans un souci de cohérence et de simplicité nous avons systématiquement placé le cycle avant le nitro dans l'appellation des arylnitronorbornènes sans tenir compte de l'ordre alphabétique.

Les nitrostyrènes peuvent être classés en trois catégories:

I. *Catégorie A*

Dans un erlen muni d'une agitation magnétique, on verse successivement 100 mL de toluène, 0,1 mol de nitrostyrène et 0,1 mol de cyclopentadiène fraîchement distillé. Le flacon est bouché hermétiquement et le mélange agité est laissé réagir pendant un temps variant de une journée à trois jours suivant le nitrostyrène de départ. Le toluène est alors éliminé sous vide et le résidu est purifiée par l'une des trois méthodes suivantes dans le but d'obtenir les arylnitronorbornènes purs:

méthode 1 : distillation sous vide
méthode 2 : chromatographie sur colonne
méthode 3 : filtration

II. *Catégorie B*

Dans un tricol muni d'une agitation et d'un réfrigérant, on verse 100 mL de toluène ou d'acide acétique, 0,1 mol de nitrostyrène et 0,1 mol de cyclopentadiène fraîchement préparé. Le mélange est porté à ébullition pendant environ 20 h. Le solvant est alors évaporé et la solution obtenue est traitée par distillation ou chromatographie sur colonne d'alumine.

TABLEAU 5. Aminonorbornènes

Ar		Méthode de purification	Rdt (%)	F/E	Litt. ou microanalyses (voir tableau 6)	rmn ^{1}H du cycle norbornène							Solvant
						H_1	H_2	H_3	H_4	H_5	H_6	H_7H_7'	
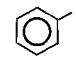	3*a*	1	92	E_1=114	19*a*	2,07	3,33	2,87	2,87	6,50	6,17	1,67	a
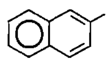	3*b*	2(CCl_4)	85	Huile	$C_{17}H_{17}N$	2,13	3,48	2,88	2,88	6,46	5,95	1,67	a
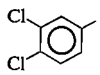	3*c*	2(MeOH)	65	Huile	$C_{13}H_{13}Cl_2N$	2,80	3,26	2,71	2,71	6,12	6,01	1,62	b
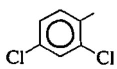	3*d*	2(MeOH)	62	Huile	$C_{13}H_{13}Cl_2N$	2,40	3,40	2,40	2,68	6,37	6,10	1,33	b
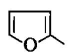	3*e*	1	83	E_1=85	$C_{11}H_{13}NO$	2,97	3,47	2,83	2,83	6,34	5,93	1,64	a
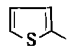	3*f*	1	85	$E_{0,4}$=106	$C_{11}H_{13}NS$	2,84	3,42	2,25	2,84	6,48	6,18	1,67	a
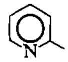	3*l*	2($CHCl_3$)	86	Huile	$C_{12}H_{14}N_2$	2,13	4,32	2,81	2,81	6,21	5,92	1,68	b
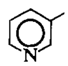	3*m*	2($CHCl_3$)	90	Huile	$C_{12}H_{14}N_2$	2,22	4,12	2,76	2,76	6,05	5,82	1,68	a
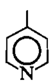	3*n*	2($CHCl_3$)	78	Huile	$C_{12}H_{14}N_2$	2,42	4,37	2,83	2,83	6,20	5,70	1,40	b
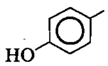	3*g*	2($Et_2O/CHCl_3$)	72	Gel	$C_{13}H_{15}NO$	2,60	3,37	2,73	2,73	6,32	5,98	1,58	a
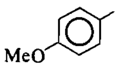	3*h*	2(Et_2O)	78	Gel	19*b*	2,58	3,40	2,68	2,68	7,37	5,82	1,62	a
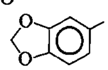	3*i*	2($Et_2O/CHCl_3$)	75	Gel	$C_{14}H_{15}NO_2$	2,62	3,32	2,72	2,72	6,28	5,84	1,61	a

Spectres de rmn: échantillons mis en solution dans $CDCl_3$ (a) ou DMSO (b).

III. *Catégorie C*

Les nitrostyrènes suivants n'ont pas réagi dans les conditions ci-dessus

Ar	R	Composé
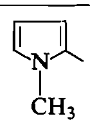	H	1*j*
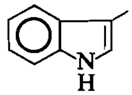	H	1*k*
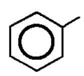	CH_3	1*o*
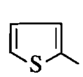	CH_3	1*p*

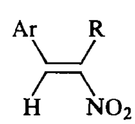

C. *Synthèse des aryl-3 amino-2 bicyclo*[2,2,1]*heptènes-5 ou aryl aminonorbornènes*

Dans un ballon tricol muni d'une agitation et d'un condenseur, on

TABLEAU 6. Microanalyses des arylnitro et aminonorbornènes

	Composé	Valeurs calculées			Valeurs trouvées		
		% C	% H	% N	% C	% H	% N
2*b*	$C_{17}H_{15}NO_2$	76,98	5,66	5,28	77,1	5,7	5,1
2*l*	$C_{12}H_{12}N_2O_2$	66,66	5,55	12,96	66,9	5,2	13,2
2*m*	$C_{12}H_{12}N_2O_2$	66,66	5,55	12,96	66,4	5,3	13,0
2*n*	$C_{12}H_{12}N_2O_2$	66,66	5,55	12,96	66,7	5,3	12,8
2*g*	$C_{13}H_{13}NO_3$	70,59	5,88	6,33	70,7	5,9	6,4
2*h*	$C_{14}H_{15}NO_3$	68,57	6,12	5,71	68,8	6,0	5,7
2*i*	$C_{14}H_{13}NO_4$	64,86	5,02	5,41	64,9	5,0	5,5
3*b*	$C_{17}H_{17}N$	84,81	7,23	5,96	84,8	7,0	6,0
3*c*	$C_{13}H_{13}Cl_2N$	61,42	5,12	5,51	61,3	5,5	5,4
3*d*	$C_{13}H_{13}Cl_2N$	61,42	5,12	5,51	61,5	5,2	5,5
3*e*	$C_{11}H_{13}NO$	75,43	7,43	8,00	75,2	7,4	7,9
3*f*	$C_{11}H_{13}NS$	69,11	6,81	7,33	69,1	6,9	7,3
3*l*	$C_{12}H_{14}N_2$	84,70	8,24	16,47	84,9	8,0	16,6
3*m*	$C_{12}H_{14}N_2$	84,70	8,24	16,47	85,0	8,3	16,7
3*n*	$C_{12}H_{14}N_2$	84,70	8,24	16,47	84,7	8,1	16,5
3*g*	$C_{13}H_{15}NO$	77,61	7,46	6,97	78,0	7,5	6,7
3*i*	$C_{14}H_{15}NO_2$	73,36	6,55	6,11	73,4	6,6	6,0

verse 500 mL d'éther éthylique (ou de tétrahydrofuranne). L'ensemble est placé dans un bain de glace et l'on introduit 5,7 g (0,15 mol) d'hydrure d'aluminium en poudre.

On fait alors couler goutte à goutte, à l'aide d'une ampoule à brome, 0,1 mol de nitrostyrène dissous dans 100 mL de solvant. La température est maintenue inférieure à 30°C. On laisse alors réagir 30 min supplémentaires, puis on introduit successivement, avec précaution, 5,7 mL d'eau, 5,7 mL de soude à 15% et 17,1 mL d'eau. La solution est alors filtrée, séchée sur sulfate de magnésium et évaporée sous vide. Le produit obtenu est alors purifié soit par distillation (méthode 1) soit par chromatographie sur colonne d'alumine (méthode 2).

Remerciements

Il nous est agréable de remercier le Dr. André Loupy pour les discussions fructueuses que nous avons eues avec lui. Nous remercions également la Société Chimique de la Grande Paroisse pour l'aide financière nous permettant de réaliser ce travail et qui nous a approvisionné en nitroalcanes.

1. R. J. MILLER, P. H. KELLY et J. L. NEUMEYER. Eur. J. Pharmacol. **27**, 212 (1975).
2. B. PRIEBS. Justus Liebigs Ann. Chem. **225**, 319 (1884).
3. G. JONES. Organic reactions. Vol. 15. John Wiley and Sons, New York. 1967 p. 254.
4. D. E. WORRALL. Org. Synth. Coll. Vol. 1. John Wiley and Sons, New York. 1941. p. 413.
5. (*a*) G. A. ALLES. J. Am. Chem. Soc. **54**, 271 (1932); (*b*) J. PATAI. The chemistry of alkenes. Wiley Interscience, New York. 1964. p. 258.
6. (*a*) K. W. MERZ. Arch. Pharm. **292**, 496 (1959); **297**, 307 (1964); (*b*) F. ZYMALKOKSKI. Arch. Pharm. **289**, 52 (1956).
7. (*a*) C. PASCUAL, J. MEIER et W. SIMON. Helv. Chim. Acta, **49**, 164 (1966); (*b*) U. E. MATTER, C. PASCUAL, E. PRETSCH, A. PROSS, W. SIMON et S. STRERNHELL. Tetrahedron, **25**, 691 (1969); **25**, 2033 (1969).
8. R. B. WOODWARD et R. HOFFMANN. The conservation of orbital symmetry. Verlag Chemie, Weinheim. 1970; Angew. Chem. Int. Ed. Engl. **8**, 781 (1969).
9. (*a*) J. SAUER et R. SUSTMANN. Angew. Chem. Int. Ed. Engl. **19**, 779 (1980); (*b*) R. SUSTMANN. Tetrahedron Lett. 2721 (1971).
10. W. E. NOLLAND, B. A. LANGAGER, J. W. MANTHEY, A. G. ZACCHEI, D. L. PETRAK et G. L. EIAN. Can. J. Chem. **45**, 2969 (1967).
11. G. I. POOS, J. KLEIS, R. R. WITTEKIND et J. D. ROSENAU. J. Org. Chem. **26**, 4898 (1961).
12. (*a*) J. A. POPLE, D. P. SANTRY et G. A. SEGAL. J. Chem. Phys. **43**, 5129 (1965); (*b*) J. A. POPLE et G. A. SEGAL. J. Chem. Phys. **43**, 5136 (1965); (*c*) **44**, 3299 (1966).
13. (*a*) J. SAUER. Angew. Chem. Int. Ed. Engl. **6**, 16 (1967); (*b*) L. ANDREWS et E. M. KEEFER. J. Am. Chem. Soc. **77**, 6284 (1955).
14. J. A. POPLE et M. GORDON. J. Am. Chem. Soc. **89**, 1254 (1967).
15. A. LOUPY, J. M. LEFOUR, B. DESCHAMPS et J. SEYDEN-PENNE. Nouv. J. Chim. **4**, 121 (1980).
16. J. ROYER et M. BEUGELMANS-VERRIER. Nouv. J. Chim. **5**, 581 (1981).
17. (*a*) D. E. WORRALL. Organic synthesis. Vol. 15. John Wiley and Sons, New York. 1941. p. 254. (*b*) Brevet Français n° 2115 089 (1972); (*c*) M. E. NEHER, E. W. GOLBERG et R. W. FAIRCHILD. J. Org. Chem. **26**, 5220 (1961); (*d*) L. BOUVEAULT et A. WAHL. C.R. Acad. Sci. **135**, 41 (1902); (*e*) W. J. KING et F. F. NORD. J. Org. Chem. **14**, 405 (1949); (*f*) O. SCHALTES et H. A. GRAEFE. J. Am. Chem. Soc. **74**, 4486 (1952); (*g*) O. M. LERNEG. Zh. Prikl. Khim. **31**, 663 (1958); Chem. Abstr. **52**, 18271h (1958); (*h*) R. S. HOSMANE, S. P. HIREMATH et S. W. SCHNELLER. J. Chem. Soc. Perkin Trans. 1, 2450 (1973); (*i*) E. H. P. YOUNG. J. Chem. Soc. 3493 (1958); (*j*) K. MERZ et H. J. HANSSEN. Arch. Pharm. **297**, 307 (1964); Chem. Abstr. **61** 4306d (1964); (*k*) A. DORMON et F. BOBERG. Ann. **578**, 101 (1952); (*l*) KNOEVENAGEL et WALTER. Ber. **37**, 4502 (1904) ou F. BOBERG et G. R. SCHULTZE. Ber. **90**, 1221 (1957); (*m*) R. T. GILSDORF et F. F. NORD. J. Org. Chem. **15**, 807 (1950).
18. (*a*) C. F. H. ALLEN et A. BELL. J. Am. Chem. Soc. **61**, 521 (1939); (*b*) M. A. NEHER, E. W. GOLBERG et R. W. FAIRCHILD. J. Org. Chem. **26**, 5220 (1961); (*c*) C. F. H. ALLEN, A. BELL et J. N. GATES. J. Org. Chem. **8**, 373 (1943).
19. (*a*) E. G. KATRAEV et P. S. MATVEEVA. Zh. Obshch. Khim. **23**, 405 (1953); (*b*) T. WEINSTOCK, N. SCHWARZ et M. F. KORMENDY. J. Org. Chem. **26**, 5247 (1961).

Some reactions of 1-methyl-1,2-dihydropyridines with organic azides. Synthesis and reactions of 1,2,5,6-tetrahydropyridylidene-2-cyan(sulfon)amides and piperidylidene-2-cyan(sulfon)amides

THEODORE A. ONDRUS, PURUSHOTTAM R. PEDNEKAR, AND EDWARD E. KNAUS[1]
Faculty of Pharmacy and Pharmaceutical Sciences, University of Alberta, Edmonton, Alta., Canada T6G 2N8

Received August 7, 1984

THEODORE A. ONDRUS, PURUSHOTTAM R. PEDNEKAR, and EDWARD E. KNAUS. Can. J. Chem. **63**, 2362 (1985).

The regiospecific 1,3-dipolar cycloaddition reaction of 1,2-dihydropyridines **2** with organic azides **3** affords 2,7-diazabicyclo[4.1.0]hept-4-enes **4**. Treatment of **4***a* with neutral aluminum oxide opened the aziridine ring to afford the 1,2,5,6-tetrahydropyridylidene-2-cyanamide **5**. Catalytic hydrogenation of **4** and **5** using palladium-on-charcoal and hydrogen yielded the 1-methyl-2-piperidylidenes **6**. Oxidation of 1-methyl-1,2,5,6-tetrahydropyridylidene-2-cyanamide (**5**) with alkaline hydrogen peroxide yielded the oxirane **7** arising from epoxidation of the 3,4-olefenic bond, whereas oxidation of the bicyclic aziridine **4***a* with *m*-chloroperbenzoic acid resulted in epoxidation of the 4,5-olefenic bond and opening of the aziridine ring to give the oxirane 3-methyl-3-aza-7-oxabicyclo[4.1.0]heptylidene-4-cyanamide (**10**). Base-catalyzed abstraction of the C-3 proton of 1-methyl-2-piperidylidenes **6** yielded the 3-lithio analogs which, after bromination, were converted to the target compounds **18** upon condensation with 4-[(2-aminoethyl)thiomethyl]-5-methylimidazole.

THEODORE A. ONDRUS, PURUSHOTTAM R. PEDNEKAR et EDWARD E. KNAUS. Can. J. Chem. **63**, 2362 (1985).

La réaction de cycloaddition dipolaire-1,3 régiospécifique des dihydro-1,2 pyridines **2** avec les azotures organiques **3** conduit aux diaza-2,7 bicyclo[4.1.0]heptènes-4 **4**. L'alumine neutre provoque l'ouverture du cycle de l'aziridine du composé **4***a* et conduit au tétrahydro-1,2,5,6 pyridylidènecyanamide-2 **5**. L'hydrogénation catalytique des composés **4** et **5** en présence de palladium déposé sur du charbon permet d'accéder aux méthyl-1 pipéridylènes-2 **6**. L'oxydation du méthyl-1 tétrahydro-1,2,5,6 pyridylènecyanamide-2 **5** par de l'eau oxygénée en milieu alcalin conduit à l'oxirane **7** qui provient de l'époxydation de la liaison oléfinique en positions 3 et 4 tandis que l'oxydation de l'aziridine bicyclique **4***a* par l'acide *m*-chloroperbenzoïque conduit à l'époxydation de la liaison oléfinique en positions 4 et 5 et l'ouverture du cycle de l'aziridine donne l'oxirane méthyl-3 aza-3 oxa-7 bicyclo[4.1.0]heptylidènecyanamide-2 (**10**). L'enlèvement d'un proton en C-3 des méthyl-1 pipérylidènes-2 **6**, catalysé par une base, fournit les analogues lithiés-3 qui, après bromation et condensation sur le [(amino-2 éthyl)thiométhyl]-4 méthyl-5 imidazole, conduisent aux composés **18** attendus.

[Traduit par le journal]

The discovery of histamine H_2-receptor antagonists led to the development of cimetidine (**1***a*), which is used widely as a clinically effective inhibitor of gastric acid secretion in the treatment of duodenal ulcers and related conditions (1, 2). More recently, the development of etintidine (**1***b*) (3), oxmetidine (**1***c*) (4), and the 3,4-diamino-1,2,5-thiadiazole 1-oxide analog (**1***d*) (5) has demonstrated the potential for an increase in potency relative to cimetidine while still maintaining high H_2-receptor specificity.

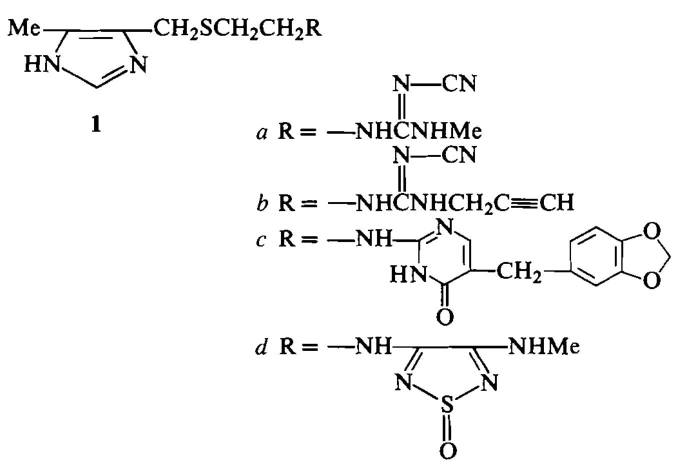

In an earlier study, we showed that the regiospecific 1,3-dipolar cycloaddition reaction of 2-substituted-1,2-dihydropyridines with azides afforded diazabicyclo[4.1.0]hept-4-enes in quantitative yield (6). It was therefore of interest to investigate the 1,3-dipolar cycloaddition reaction of 1-methyl-1,2-dihydropyridines **2** with selected organic azides **3** as a method for the synthesis of 2-methyl-2,7-diazabicyclo[4.1.0]-hept-4-enes **4** for elaboration to 1-methyl-1,2,5,6-tetrahydropyridylidene-2-cyanamide **5** and 1-methyl-2-piperidylidenes **6***a*–*d*. The piperidylidenes **5** and **6***a* bear some structural similarity to the cyanoguanidine (*a*, *b*), isocytosine (*c*), and aminothiazole (*d*) R-moieties of **1**. It was therefore of interest to prepare compounds of general structure **1** utilizing **5** and **6** as potential heterocyclic pharmacophores of *a*–*d*. We now describe some chemical studies directed toward the utilization of **5** and **6** as novel heterocyclic pharmacophores for the synthesis of new heterocycles with potential H_2-receptor antagonistic activity.

Reaction of 1-methyl-1,2-dihydropyridines **2** with organic azides **3** proceeded rapidly at 0°C with evolution of nitrogen to yield 2-methyl-2,7-diazabicyclo[4.1.0]hept-4-enes (**4**) in good yield (see Scheme 1). Treatment of **4***a* with neutral aluminum oxide (Brockman Activity 1) in methylene chloride at 25°C afforded **5** (82%). Hydrogenation of either 1-methyl-1,2,5,6-tetrahydropyridylidene-2-cyanamide (**5**) or 2-methyl-2,7-diazabicyclo[4.1.0]hept-2-enes (**4***a*–*d*) using 10% palladium-on-charcoal and hydrogen gas at 35 psi (1 psi = 6.9 kPa) afforded the respective 1-methyl-2-piperidylidenes **6***a*–*d* in quantitative yield.

Treatment of **5** with alkaline hydrogen peroxide afforded the bicyclic oxirane 3-methyl-3-aza-7-oxabicyclo[4.1.0]heptylidene-2-cyanamide (**7**) in 99% yield. In contrast, reaction of **5** with *m*-chloroperbenzoic acid in methylene chloride gave only a trace yield of **7** along with unreacted **5**. Reaction of **7** with

[1]Author to whom correspondence should be addressed.

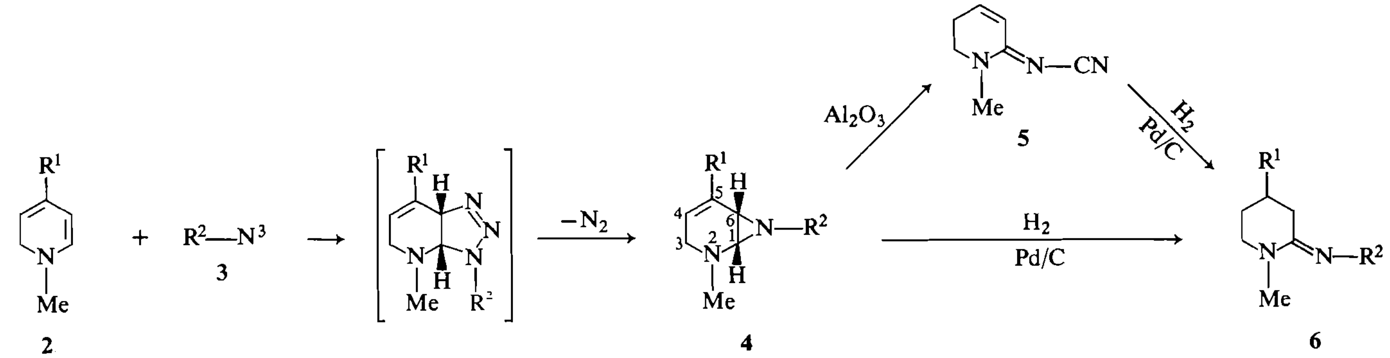

2: *a* R^1 = H; *b* R^1 = Me

3: *a* R^2 = CN; *b* R^2 = $PhSO_2$; *c* R^2 = CF_3SO_2

4: *a* R^1 = H, R^2 = CN; *b* R^1 = Me, R^2 = CN; *c* R^1 = H, R^2 = $PhSO_2$; *d* R^1 = H, R^2 = CF_3SO_2

6: *a* R^1 = H, R^2 = CN; *b* R^1 = Me, R^2 = CN; *c* R^1 = H, R^2 = $PhSO_2$; *d* R^1 = H, R^2 = CF_3SO_2

SCHEME 1

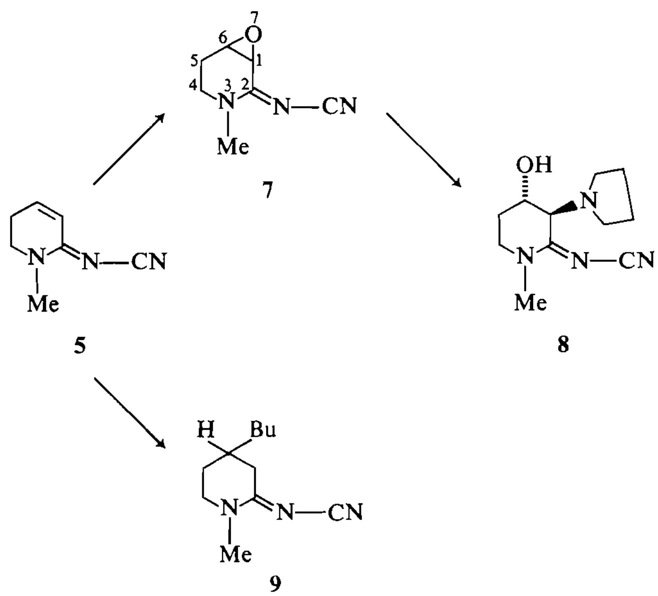

SCHEME 2

pyrrolidine as solvent and nucleophile yielded the expected *trans*-aminoalcohol **8** in 95% yield due to regiospecific nucleophilic attack at the more electropositive C-1 position. The *trans*-aminoalcohol **8** exhibited a $J_{3,4}$ coupling constant of 3.75 Hz, which is consistent with either a $J_{3,4}$ eq−eq or ax−eq coupling (7). On this basis, it was expected that **7** would serve as a useful intermediate for incorporation of the 5-methylimidazol-4-ylmethylthioethylamino moiety into the C-1 position of **7**. However, reaction of **7** with the less reactive 4-[(2-aminoethyl)thiomethyl]-5-methylimidazole in tetrahydrofuran at reflux temperature did not occur and **7** was recovered unchanged. The Michael reaction of n-butyllithium with **5** yielded **9** (89%) (see Scheme 2).

Oxidation of **4***a* with *meta*-chloroperbenzoic acid yielded the bicyclic oxirane **10** (93%) (see Scheme 3). The allylic alcohol **11** (98%) was obtained when a solution of **10** in methanol containing suspended neutral aluminum oxide was stirred at 25°C for 18 h. This reaction represents an alternative procedure to effect the oxirane-to-allylic alcohol transformation (8). The C-4 cyanamide substitutent of **10** exerts an influence in this transformation, presumably by increasing the acidity of the C-5 methylene protons, since treatment of the bicyclic oxirane **7** with neutral aluminum oxide in methylene chloride gave a complex mixture of at least five products. Reaction of **10** with sodium thiophenolate gave **12***a* and **13***a* in a ratio of 1 : 1. When the more nucleophilic sodium thiophenolate is used, **12** may be formed by either a Michael addition to **11** or by nucleophilic attack at the C-6 position of **10**. Compound **13** is formed by nucleophilic attack at the C-1 position of **10**. A similar reaction of **10** with morpholine in tetrahydrofuran at 25°C afforded a mixture of **12***b* and **13***b* (88%) which could not be separated by tlc. The bicyclic oxirane **10** is much more reactive to morpholine than is the bicyclic oxirane **7**, since **7** did not react in refluxing tetrahydrofuran.

It was expected that the C-3 position of 1-methyl-2-piperidylidenes **6** would be an active methylene. Incorporation of a suitable C-3 substituent would provide the required intermediates for condensation with 4-[(2-aminoethyl)thiomethyl]-5-methylimidazole to prepare the target compounds. Thus, reaction of **6***a* with n-butyllithium and quenching with deuterium oxide yielded **14***a*, having a C-3 deuterium substituent (see Scheme 4). Addition of the 3-lithio derivative of **6***a*, obtained from the reaction of **6***a* with n-butyllithium, to a solution of *N*-bromosuccinimide at −77°C yielded the 3-bromo derivative **14***b* (71%) together with the dimeric product **15** (22%). A similar reaction using molecular bromine afforded **14***b* (67%) and **15** (12%). The temperature and mode of addition influence the product ratios since addition of *N*-bromosuccinimide to the 3-lithio analog of **6***a* at 0°C gave **14***b* (15%) and **15** (79%). The 3-bromo derivatives **14***c* (91%) and **14***d* (90%) were prepared from **6***c* and **6***d* respectively, using *N*-bromosuccinimide. The dimeric product **15** likely arises from the subsequent reaction of **14***b* with 1-methyl-3-lithiopiperidylidene-2-cyanamide.

The preparation of 1-methyl-3-aminopiperidylidene-2-cyanamide (**14**, R^1 = NH_2, R^2 = CN) was investigated, since the 3-amino substituent would be amenable to condensation with a variety of 5-methylimidazol-4-ylmethylthioethyl agents having a good leaving substituent at the terminal position of the ethyl chain. Several attempts to prepare **14** (R^1 = NH_2, R^2 = CN) by reaction of the corresponding 3-lithio derivative with chloroamine, methoxylamine, or hydroxylamine-*O*-sulfonic acid were unsuccessful. On the other hand, reaction of the 3-bromo derivative **14***b* with sodium azide afforded the 3-azido analog **16** (100%). The reduction of the 3-azido substituent of **16** using lithium aluminum hydride or 10% palladium-on-charcoal and

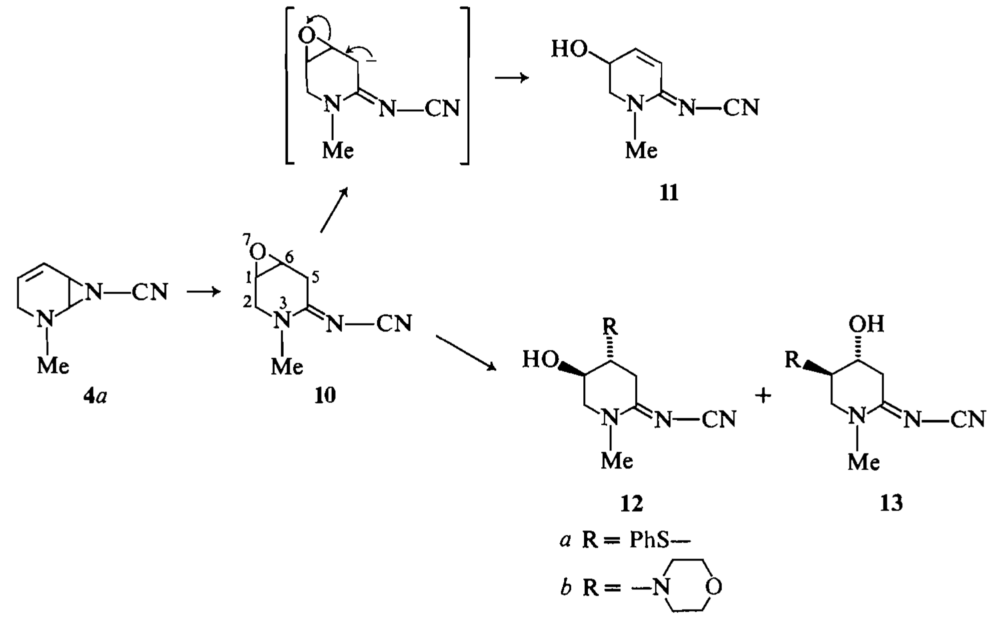

SCHEME 3

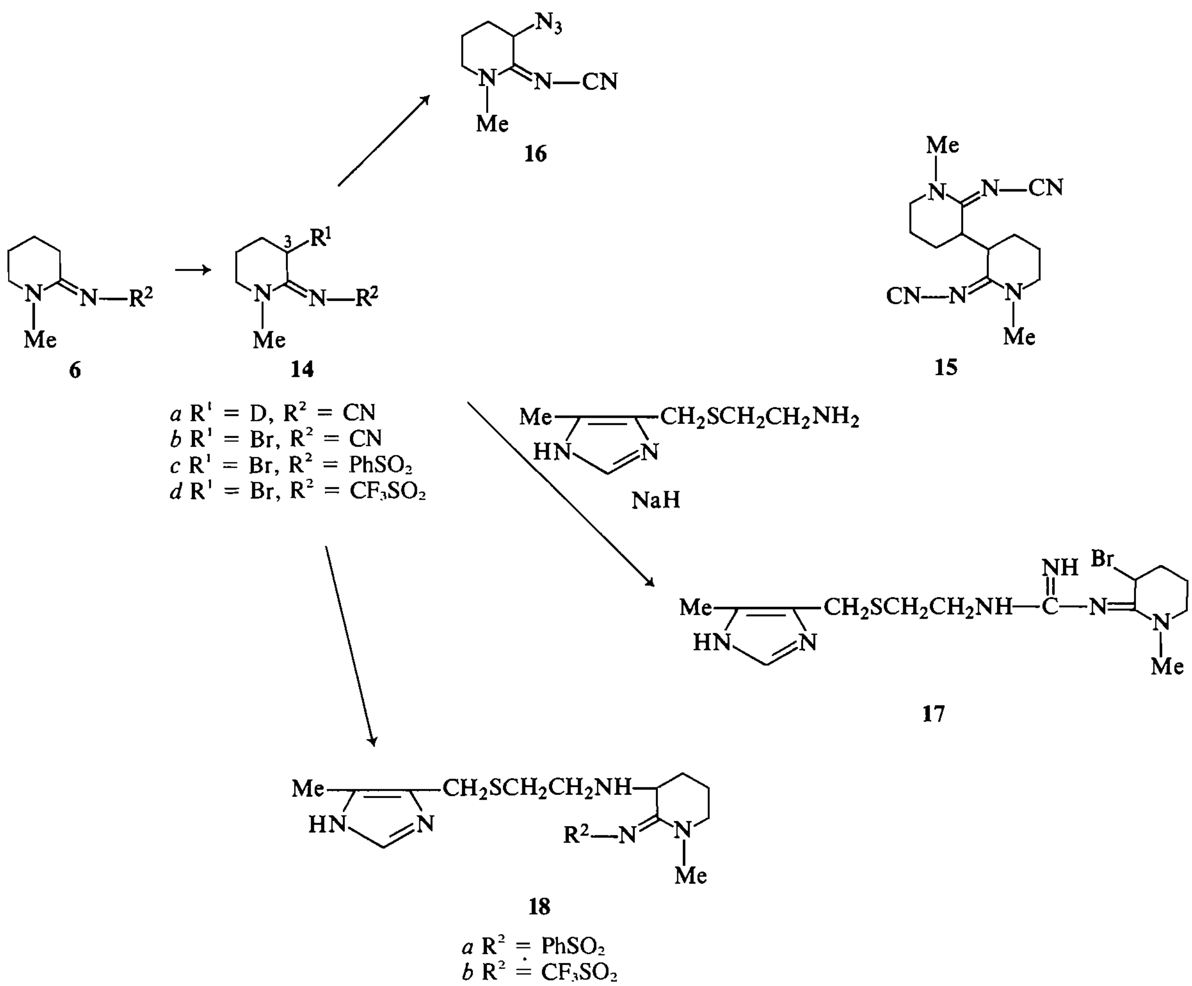

SCHEME 4

H_2 gas at 35 psi proceeded rapidly to afford a complex mixture of products from which the desired 3-amino product could not be isolated.

The reaction of the 3-bromo derivative **14***b* with 4-[(2-aminoethyl)thiomethyl]-5-methylimidazole dihydrobromide and excess sodium hydride was investigated, since nucleophilic displacement of the 3-bromo substituent of **14***b* would provide the target compound in one step. When this reaction was performed, a product which exhibited spectral and microanalytical data consistent with structure **17** (90%) was obtained. The ir spectrum of **17** did not show an absorption due to nitrile stretching but it did exhibit two C=N absorptions at 1595 and 1645 cm^{-1}, indicating that the cyano moiety had participated in the reaction. Kosasayama *et al.* have reported that the bicyclic compound **20** may be formed by intramolecular addition of the hydroxy substituent to the cyanamide moiety of **19** (9). The 3-bromopiperidylidenes **14***c* (R^1 = $PhSO_2$) and **14***d* (R^2 = CF_3SO_2) were therefore prepared in order that the undesired reaction involving the cyano group of **14***b* could be precluded.

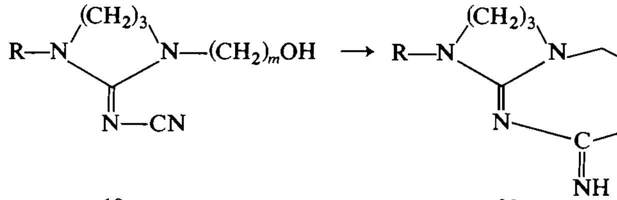

19 20

Condensation of **14***c* and **14***d* with 4-[(2-aminoethyl)thiomethyl]-5-methylimidazole in ethanol at reflux afforded the target compounds **18***a* (43%) and **18***b* (36%) respectively.

The benzenesulfonyl analog **18***a* was evaluated as an antagonist of the positive chronotropic action of histamine in the isolated guinea pig right atrium, which is a standard assay for histamine H_2-receptor antagonists, and was found to be inactive at a concentration of 3×10^{-4} molar.

Experimental

Melting points were determined with a Büchi capillary apparatus and are uncorrected. Infrared spectra (potassium bromide unless otherwise noted) were taken on a Unicam SP 1000 or Nicolet 5DX FT spectrometer. Nuclear magnetic resonance spectra were determined for solutions in deuterochloroform, unless otherwise stated, with a Bruker AM 300, WH 200, or Varian EM 360A spectrometer and these exact mass measurements are in some instances used in lieu of elemental analysis. All of the products described gave rise to a single spot on tlc, using a solvent system less polar and more polar than the specific solvent system described for purification of the reaction mixture. No residue remained after combustion of the products purified by chromatographic procedures. Mass spectra were measured on an AEI MS-50 mass spectrometer. Preparative high pressure liquid chromatography was performed using a Water's Prep LC/System 500 A using Prep Pak-500 silica cartridges. 1,2-Dihydropyridines **2***a*,*b* were prepared according to the procedure of Fowler (10). The azides **3***b*,*c* were prepared from the reaction of the respective sulfonyl chloride with five equivalents sodium azide in acetonitrile. **Warning: Cyanogen azide is a hazardous material**. It should be handled only in solution. Concentration to pure material will result in violent detonation by heat or shock (11).

*2-Methyl-7-cyano-2,7-diazabicyclo[4.1.0]hept-4-ene (4*a*)*

A solution of 1-methyl-1,2-dihydropyridine (**2***a*, 6.18 g, 65 mmol) in 100 mL of dry ether was added slowly with stirring to a solution of cyanogen azide (65 mmol), prepared from cyanogen bromide (6.89 g, 65 mmol) and sodium azide (22.1 g, 0.325 mol), as reported previously (6), in 150 mL of acetonitrile under a nitrogen atmosphere at 0°C. The reaction mixture was allowed to warm to 25°C during 15 min. Removal of the solvent *in vacuo* gave a solid which was redissolved in 200 mL of methylene chloride. This solution was washed with water (2 × 75 mL) and the water washes were extracted with 75 mL of methylene chloride. The combined organic extracts were dried ($MgSO_4$) and the solvent removed *in vacuo* to give a pale brown solid which on recrystallization from ether–methanol (4:1 v/v) afforded **4***a* (7.11 g, 81%); mp 118°C; ir: 1560 (C=C), 2160 (CN) cm^{-1}; ^1H nmr δ: 3.18 (s, 3H, Me), 3.41 (m, 2H, H-1, H-6), 4.06 (m, 2H, H-3), 5.83 (m, 2H, H-4, H-5). *Exact Mass* calcd. for $C_7H_9N_3$: 135.0796; found (high resolution ms): 135.0796.

*2,5-Dimethyl-7-cyano-2,7-diazabicyclo[4.1.0]hept-4-ene (4*b*)*

Reaction of **2***b* (9.69 g, 65 mmol) with cyanogen azide (5.1 g, 75 mmol), using the procedure outlined for the preparation of **4***a*, gave **4***b*, yield (76%); mp 117°C; ir: 2175 (CN) cm^{-1}; ^1H nmr δ: 1.8 (s, 3H, C(5)-Me), 3.17 (s, 3H, N-Me), 3.3 (m, 2H, H-1, H-6), 4.01 (m, 2H, H-3), 5.52 (m, 1H, H-4). *Exact Mass* calcd. for $C_8H_{11}N_3$: 149.0953; found (high resolution ms): 149.0951.

*2-Methyl-7-benzenesulfonyl-2,7-diazabicyclo[4.1.0]hept-4-ene (4*c*)*

A solution of **2***a* (20 mmol) in 100 mL of ether was added to a solution of **3***b* (20 mmol) in 5 mL of ether and the reaction was completed as outlined for the preparation of **4***a*, to give a red viscous product (5.4 g). The product was purified by preparative tlc, using eleven 200 × 200 mm silica gel G plates, 1.0 mm in thickness, with benzene – ethyl acetate (1:1 v/v) as development solvent. Extraction of the band having R_f 0.45 yielded **4***c* (2.58 g, 51%); mp 78°C; ir: 1570 (C=C) cm^{-1}; ^1H nmr δ: 3.08 (s, 3H, Me), 3.6 (m, 2H, H-1, H-6), 3.95 (m, 2H, H-3), 5.7 (m, 2H, H-4, H-5), 7.5 (m, 3H, *meta* and *para* phenyl hydrogens), 8.0 (m, 2H, *ortho* phenyl hydrogens). *Exact Mass* calcd. for $C_{12}H_{14}N_2O_2S$: 250.0756; found (high resolution ms): 250.0766.

*2-Methyl-7-trifluoromethanesulfonyl-2,7-diazabicyclo[4.1.0]hept-4-ene (4*d*)*

Reaction of **2***a* (20 mmol) with **3***c* (30 mmol), using the procedure outlined for the preparation of **4***a*, gave a red viscous oil (3.35 g) which was purified by preparative tlc using twelve 200 × 200 mm silica gel G plates, 0.75 mm in thickness, with benzene – ethyl acetate (1:1 v/v) as development solvent. Extraction of the band having R_f 0.6 yielded **4***d* (2.0 g, 41%); mp 70°C; ir: 1605 (C=C) cm^{-1}; ^1H nmr δ: 3.25 (s, 3H, Me), 3.66 (m, 2H, H-1, H-6), 4.17 (m, 2H, H-3), 5.86 (m, 2H, H-4, H-5). *Exact Mass* calcd. for $C_7H_9N_2O_2SF_3$: 242.0337; found (high resolution ms): 242.0332.

1-Methyl-1,2,5,6-tetrahydropyridylidene-2-cyanamide (5)

A mixture of **4***a* (2.0 g, 14.8 mmol) and neutral aluminum oxide (10 g, Brockman Activity 1) suspended in 50 mL of methylene chloride was stirred for 24 h at 25°C. The alumina was filtered and washed with 200 mL of ethyl acetate. Removal of the solvent from the combined organic extracts *in vacuo* afforded a white solid (1.6 g) which was shown by ^1H nmr to consist of 82% **5** and 18% **4***a* as determined from the integrals of H-4 and H-5 at 5.83 δ for **4***a* and of H-3 and H-4 at 6.63 δ for **5**. A pure sample of **5** was obtained by preparative hplc (1.55 g reaction mixture) using ethyl acetate – methylene chloride (1:9 v/v) as eluant at a flow rate of 250 mL min^{-1}. Collection of the first 1500 mL eluant gave **5** (0.531 g); mp 66°C; ir: 2150 (CN), 1555 (C=N) cm^{-1}; ^1H nmr δ: 2.53 (m, 2H, H-5), 3.13 (s, 3H, Me), 3.57 (m, 2H, H-6), 6.63 (m, 2H, H-3, H-4). *Exact Mass* calcd. for $C_7H_9N_3$: 135.0797; found (high resolution ms): 135.0797. Collection of the 1500 to 2500-mL eluant gave 0.848 g of a mixture of **5** and **4***a* in a ratio of 4.55:1, as determined by ^1H nmr integrals. The 2500 to 3500-mL fraction gave 0.145 g of a mixture of **5** and **4***a* in a ratio of 1.6:1, as determined by ^1H nmr integrals.

*1-Methylpiperidylidene-2-cyanamide (6*a*)*

Method A

Hydrogenation of **5** (0.0675 g, 0.5 mmol) in 75 mL of methanol using 30 mg of 10% palladium-on-charcoal and hydrogen gas at 35 psi for 4 h at 25°C, followed by filtration and removal of the solvent *in vacuo*, afforded **6***a* (68.5 mg, 100%); mp 98°C; ir: 2160 (CN) and 1590 (C=N) cm^{-1}; ^1H nmr δ: 1.9 (m, 4H, H-4, H-5), 2.82 (m, 2H, H-3), 3.13 (s, 3H, Me), 3.47 (m, 2H, H-6). *Exact Mass* calcd. for $C_7H_{11}N_3$: 137.0952; found (high resolution ms): 137.0952.

A similar hydrogenation of the mixture **4***a* and **5**, obtained by treatment of **4***a* with neutral aluminum oxide as described above, also yielded **6***a* in quantitative yield.

Method B

Hydrogenation of **4***a* (0.135 g, 1 mmol) in 25 mL of methanol using

50 mg of 10% palladium-on-charcoal and hydrogen gas at 35 psi for 4 h at 25°C, as described in Method A above, also afforded **6***a* (0.137 g, 100%).

*1,4-Dimethylpiperidylidene-2-cyanamide (***6**b*)*

Reduction of **4***b* (2.23 g, 15 mmol) in 50 mL of methanol using 400 mg of 10% palladium-on-charcoal and hydrogen gas at 35 psi for 24 h, as described in Method A, gave **6***b* (2.26 g, 100%) as a white solid; mp 94°C; ir: 2180 (CN) and 1598 (C=N) cm^{-1}; ^{1}H nmr δ: 1.04 (d, J = 5 Hz, 3H, C(4)-Me), 1.2–2.15 (m, 3H, H-4, H-5), 2.35 (m, 1H, H-3), 2.9 (m, 1H, H-3), 3.05 (s, 3H, N-Me), 3.44 (m, 2H, H-6). *Exact Mass* calcd. for $C_8H_{11}N_3$: 151.1109; found (high resolution ms): 151.1107.

*1-Methylpiperidylidene-2-benzenesulfonamide (***6**c*)*

The reduction of **4***c* (76 mg, 0.304 mmol) in 25 mL of methanol using 50 mg of 10% palladium-on-charcoal and hydrogen gas at 35 psi for 3 h at 25°C, as outlined in Method A, yielded **6***c* (77 mg, 100%) as a white solid; mp 104°C; ir: 1580 (C=N) cm^{-1}; ^{1}H nmr δ: 1.6–1.89 (m, 4H, H-4, H-5), 2.89–3.2 (m, 5H, H-3, Me), 3.2–3.5 (m, 2H, H-6), 7.48 (m, 3H, *meta* and *para* phenyl hydrogens), 7.96 (m, 2H, *ortho* phenyl hydrogens). *Anal.* calcd. for $C_{12}H_{16}N_2O_2S$: C 57.12, H 6.39, N 11.10; found: C 56.80, H 6.57, N 11.14. *Exact Mass* calcd. for $C_{12}H_{16}N_2O_2S$: 250.0767; found (high resolution ms): 250.0766.

*1-Methylpiperidylidene-2-trifluoromethylsulfonamide (***6**d*)*

Hydrogenation of **4***d* (0.3 g, 1.24 mmol) in 50 mL of methanol using 100 mg of 10% palladium-on-charcoal and hydrogen gas at 35 psi for 3 h, as described in Method A, afforded **6***d* (0.303 g, 100%) as a colorless oil; mp ≃ 20°C; ir: 1600 (C=N) cm^{-1}; ^{1}H nmr δ: 1.82 (m, 4H, H-4, H-5), 3.0 (m, 2H, H-3), 3.12 (s, 3H, Me), 3.5 (m, 2H, H-6). *Exact Mass* calcd. for $C_7H_{11}N_2O_2SF_3$: 244.0493; found (high resolution ms): 244.0493.

3-Methyl-3-aza-7-oxabicyclo[4.1.0]heptylidene-2-cyanamide (7)

Hydrogen peroxide (1.3 mL of 30%, 11.6 mmol) was added slowly with stirring to a solution of **5** (1.05 g, 7.7 mmol) in 50 mL of methanol at 0°C. A solution of sodium hydroxide (3.85 mL of 1 *M*, 3.85 mmol) was added slowly with stirring and the reaction mixture was stirred for 15 min at 0°C prior to pouring onto 100 mL of ice water. The mixture was neutralized (38.5 mL of 0.1 *N* hydrochloric acid), extracted with methylene chloride (3 × 100 mL), the extract dried ($MgSO_4$), and the solvent removed *in vacuo* to afford **7** as a white solid (1.14 g, 99%); mp 111°C; ir: 2200 (CN) and 1595 (C=N) cm^{-1}; ^{1}H nmr δ: 1.85–2.75 (complex m, 2H, H-5), 3.13 (s, 3H, Me), 3.0–3.75 (complex m, 2H, H-4), 3.82 (m, 1H, H-6), 4.22 (d, $J_{1,6}$ = 4 Hz, 1H, H-1). *Exact Mass* calcd. for $C_7H_9N_3O$: 151.0746; found (high resolution ms): 151.0747.

trans-*1-Methyl-3-(1-pyrrolidinyl)-4-hydroxypiperidylidene-2-cyanamide (8)*

A solution of **7** (0.151 g, 1 mmol) in 50 mL of pyrrolidine was heated at reflux for 20 h and the solvent was removed *in vacuo* to yield a yellow semi-solid. The reaction product was purified on four 200 × 200 mm silica gel G plates, 1.0 mm in thickness, with methylene chloride – methanol (19:1 v/v) as development solvent. Extraction of the fraction having R_f 0.49 yielded **8** (0.193 g, 95%); mp 105°C; ir: 3305 (OH), 2210 (CN), and 1598 (C=N) cm^{-1}; ^{1}H nmr δ: 1.75 (m, 4H, H-3 and H-4 of pyrrolidine ring), 2.0–2.6 (m, 2H, H-5), 2.6–3.0 (m, 4H, H-2 and H-5 of pyrrolidine ring), 3.1 (s, 3H, Me), 3.51 (m, 2H, H-6), 3.88 (d, $J_{3,4}$ = 3.75 Hz, 1H, H-3), 4.3 (m, 1H, H-4, coupled to C(4)-OH), 4.53 (br s, 1H, OH, exchanges with deuterium oxide). *Exact Mass* calcd. for $C_{11}H_{18}N_4O$: 222.1480; found (high resolution ms): 222.1479.

1-Methyl-4-n-butylpiperidylidene-2-cyanamide (9)

A solution of **5** (0.162 g, 1 mmol) in 10 mL of dry tetrahydrofuran was added slowly with stirring to a solution of n-butyllithium (1 mmol) in 25 mL of dry tetrahydrofuran under a nitrogen atmosphere at −77°C. The reaction mixture was allowed to warm to 25°C during 20 min and then 50 mL of water was added. Extraction with methylene chloride (2 × 50 mL), drying the organic extract ($MgSO_4$), and removal of the solvent *in vacuo* afforded an orange oil. Preparative silica gel G tlc on four 200 mm × 200 mm plates, 1.0 mm in thickness, was performed using methylene chloride – methanol (19:1 v/v) as development solvent. Extraction of the band having R_f 0.81 yielded **9** as a colorless oil (0.145 g, 89%); ir (film): 2185 (CN) and 1598 (C=N) cm^{-1}; ^{1}H nmr δ: 0.9 (t, J = 7 Hz, 3H, —$(CH_2)_3$*CH_3*), 1.32 (m, 6H, —*$(CH_2)_3$*CH_3), 1.5–2.2 (m, 3H, H-4, H-5), 2.37 (m, 1H, H-3), 3.1 (s, 3H, N-Me), 2.85–3.2 (m, 1H, H-3), 3.43 (m, 2H, H-6). *Exact Mass* calcd. for $C_{11}H_{19}N_3$: 193.1579; found (high resolution ms): 193.1580.

3-Methyl-3-aza-7-oxabicyclo[4.1.0]heptylidene-4-cyanamide (10)

The bicyclic compound **4***a* (0.54 g, 4 mmol) was added to a suspension of *meta*-chloroperbenzoic acid (2.43 g of 85%, 12 mmol) in 75 mL of methylene chloride at 25°C with stirring. The reaction mixture was heated at reflux for 72 h and, after cooling, the stoppered vessel and contents were placed in the freezer for 2 h. The reaction mixture was filtered to remove the acids present (1.21 g). The filtrate was evaporated *in vacuo* to give a pale yellow solid, which was partitioned between 75 mL of ether and 75 mL of water. The aqueous fraction was extracted with a further 75 mL of ether and the combined ether extracts were washed with water. Removal of the water from the aqueous fraction *in vacuo* (<40°C) afforded a yellow product, which was dissolved in methylene chloride (5 mL) and the solvent removed *in vacuo* to yield **10** as a pale yellow solid (0.559 g, 93%); mp 106°C; ir: 2180 (CN) and 1603 (C=N) cm^{-1}; ^{1}H nmr δ: 3.02 (m, J_{5gem} = 20 Hz, 1H, H-5), 3.07 (s, 3H, N-Me), 3.5 (m, 2H, H-1, H-6), 3.63 (m, J_{5gem} = 20 Hz, 1H, H-5′), 3.78 (m, J_{2gem} = 15 Hz, 1H, H-2), 3.88 (m, J_{2gem} = 15 Hz, 1H, H-2′). *Exact Mass* calcd. for $C_7H_9N_3O$: 151.0746; found (high resolution ms): 151.0742.

1-Methyl-5-hydroxy-1,2,5,6-tetrahydropyridylidene-2-cyanamide (11)

A solution of **10** (0.151 g, 1 mmol) in 5 mL of methanol was added to a suspension of neutral aluminum oxide (5 g, Brockman Activity 1) in 25 mL of methanol with stirring. The mixture was stirred for 18 h at 25°C, filtered, and the solvent removed *in vacuo* to yield a white solid. Dissolution in 10 mL of methylene chloride, filtration, and removal of the solvent *in vacuo* afforded **11** as a pale yellow solid (0.148 g, 98%); mp 141°C; ir: 3340 (OH), 2090 (CN), 1655 (C=C), and 1585 (C=N) cm^{-1}; ^{1}H nmr (DMSO-d_6) δ: 3.03 (s, 3H, Me), 3.51 (m, 2H, H-6), 4.32 (d, $J_{5,OH}$ = 6 Hz of d, $J_{5,6}$ = 5 Hz of d, $J_{4,5}$ = 4.5 Hz, 1H, H-5), 5.59 (d, $J_{5,OH}$ = 6 Hz, 1H, OH, exchanges with deuterium oxide), 6.42 (d, $J_{3,4}$ = 10 Hz, 1H, H-3), 6.8 (d, $J_{3,4}$ = 10 Hz of d, $J_{4,5}$ = 4.5 Hz, 1H, H-4). *Exact Mass* calcd. for $C_7H_9N_3O$: 151.0746; found (high resolution ms): 151.0743.

trans-*1-Methyl-4-phenylthio-5-hydroxypiperidylidene-2-cyanamide (***12**a*) and* trans-*1-methyl-4-hydroxy-5-phenylthiopiperidylidene-2-cyanamide (***13**a*)*

A solution of **10** (0.151 g, 1 mmol) in 2 mL of dry tetrahydrofuran was added slowly with stirring to a suspension of sodium thiophenolate (1.1 mmol) in 25 mL of tetrahydrofuran at −77°C under a nitrogen atmosphere. After 30 min, the reaction mixture was allowed to warm to 25°C during 30 min, at which time all material dissolved. The reaction mixture was acidified (11 mL of 0.1 *N* HCl) and the solvent removed *in vacuo* to yield a semi-solid. Extraction with 5 mL of methylene chloride, filtration, and removal of the solvent *in vacuo* afforded a solid, which was purified by preparative silica gel G tlc on three 200 × 200 mm plates, 1.0 mm in thickness, with ether–methanol (10:1 v/v) as development solvent. Extraction of the band having R_f 0.41 yielded **12***a* (0.159 g, 49%); mp 135°C; ir: 3345 (OH), 2195 (CN), and 1615 (C=N) cm^{-1}; ^{1}H nmr (DMSO-d_6) δ: 2.96 (s, 3H, N-Me), 2.4–4.08 (complex m, 5H, H-3, H-5, H-6), 4.12 (m, 1H, H-4), 5.72 (m, 1H, OH, exchanges with deuterium oxide), 7.4 (m, 5H, Ph). *Anal.* calcd. for $C_{13}H_{15}N_3OS$: C 59.75, H 5.78, N 16.08; found: C 59.35, H 5.65, N 16.14. Extraction of the fraction having R_f 0.58 afforded **13***a* (0.168 g, 51%); mp 98°C; ir: 3430 (OH), 2180 (CN), and 1603 (C=N) cm^{-1}; ^{1}H nmr δ: 3.03 (s, 3H, N-Me), 2.58–3.32 (m, 2H, H-3), 3.32–3.82 (m, 3H, H-5, H-6), 3.97 (m, 1H, H-4), 4.8 (br s, 1H, OH, exchanges with deuterium oxide), 7.38

(m, 5H, Ph). *Anal.* calcd. for $C_{11}H_{15}N_3OS$: C 59.75, H 5.78, N 16.08; found: C 59.73, H 5.63, N 16.17.

trans-1-Methyl-4-(4-morpholino)-5-hydroxypiperidylidene-2-cyanamide (12b) and trans-1-methyl-4-hydroxy-5-(4-morpholino)piperidylidene-2-cyanamide (13b)

Morpholine (0.18 mL, 2 mmol) was added to a solution of **10** (0.151 g, 1 mmol) in 50 mL of dry tetrahydrofuran with stirring. The reaction was allowed to proceed for 25 h at 25°C. Removal of the solvent *in vacuo* gave an oily brown solid, which was subjected to preparative silica gel G tlc on four 200 × 200 mm plates, 1.0 mm in thickness, with methylene chloride – methanol (15:1 v/v) as development solvent. Extraction of the band having R_f 0.25 gave a mixture of **12*b*** and **13*b*** (0.21 g, 88%); mp 135–139°C; ir: 3380 (OH), 2095 (CN), and 1601 (C=N) cm^{-1}; ^{1}H nmr (300 MHz) δ: 2.63 (m, morpholino H-3, H-5), 3.08 and 3.10 (two singlets, 3:1 ratio, 3H, N-Me), 3.73 (m, 4H, morpholino H-2, H-6), 3.97 (br s, 1H, OH, exchanges with deuterium oxide), 3.15–4.37 (complex m, 5H, H-3, H-4, H-5, H-6). The ^{13}Cmr spectrum ($CDCl_3$) exhibited dual resonances at 26.74 and 28.81 (3:1 ratio), 48.7 and 50.4 (3:1 ratio), 54.43 and 55.2 (1:3 ratio), and 66.89 and 67.13 (1:3 ratio), which indicates the product was a mixture of **12*b*** and **13*b***. *Exact Mass* calcd. for $C_{11}H_{18}N_4O_2$: 238.1429; found (high resolution ms): 238.1427.

1-Methyl-3-deuteriopiperidylidene-2-cyanamide (14a)

n-Butyllithium (2 mmol) in hexane (0.82 mL) was added dropwise to a suspension of **6*a*** (0.274 g, 2 mmol) in 50 mL of dry tetrahydrofuran at −77°C under a nitrogen atmosphere with stirring. The resulting solution was maintained at −77°C for 10 min prior to warming to 0°C during 10 min and addition of deuterium oxide (0.4 mL, 20 mmol). The reaction mixture was allowed to warm to 25°C and 50 mL of water was added. Extraction with methylene chloride (3 × 50 mL), drying ($MgSO_4$), and removal of the solvent *in vacuo* yielded **14*a*** (0.257 g, 93%); ^{1}H nmr δ: 1.87 (m, 4H, H-4, H-5), 2.82 (m, 1H, H-3), 3.10 (s, 3H, Me), 3.42 (m, 2H, H-6).

1-Methyl-3-bromopiperidylidene-2-cyanamide (14b) and 3,3′-bis(1-methylpiperidylidene-2-cyanamide (15)

Method A

n-Butyllithium (2 mmol) in hexane (0.83 mL) was added to a suspension of **6*a*** (0.274 g, 2 mmol) in 50 mL of dry tetrahydrofuran at −77°C under a nitrogen atmosphere with stirring and the reaction was allowed to proceed for 10 min. *N*-Bromosuccinimide (0.356 g, 2 mmol) was dissolved in 50 mL of dry tetrahydrofuran under a nitrogen atmosphere and the solution was cooled to −77°C. The former solution of the organolithium reagent was added slowly during 20 min, with stirring at −77°C, to the *N*-bromosuccinimide solution. The reaction was allowed to warm to 25°C and 50 mL of water was added. Extraction with methylene chloride (2 × 75 mL), washing the organic extract with 50 mL of water, drying the organic extract ($MgSO_4$), and removal of the solvent *in vacuo* afforded a pale yellow solid. The products were purified by preparative silica gel G tlc using four 200 × 200 mm plates, 1.0 mm in thickness, with methylene chloride – methanol (15:1 v/v) as development solvent. Extraction of the band having R_f 0.68 with 50 mL of methanol afforded **14*b*** (0.231 g, 71%); mp 116–118°C; ir: 2160 (CN) and 1600 (C=N) cm^{-1}; ^{1}H nmr δ: 1.7–2.45 (m, 4H, H-4, H-5), 3.12 (s, 3H, Me), 3.56 (m, 2H, H-6), 5.11 (m, 1H, H-3, collapses to a singlet upon irradiation of H-4 and H-5 at 2.2 δ). *Exact Mass* calcd. for $C_7H_{10}N_3{}^{79}Br$: 215.0058; found (high resolution ms): 215.0055. Extraction of the band having R_f 0.54 gave **15** (0.045 g, 22%); mp 219°C (dec.); ir: 2170 (CN) and 1605 (C=N) cm^{-1}; ^{1}H nmr δ: 1.7–2.7 (m, 8H, H-4, H-5, H-4′, H-5′), 3.1 (s, 6H, Me), 3.15–4.05 (m, 6H, H-3, H-3′, H-6, H-6′). *Exact Mass* calcd. for $C_{14}H_{20}N_6$: 272.1749; found (high resolution ms): 272.1751.

Method B

A solution of the organolithium reagent (2 mmol) in 50 mL of tetrahydrofuran was added slowly to a solution of bromine (0.512 mL, 10 mmol) in 25 mL of dry tetrahydrofuran at −77°C under nitrogen with stirring, as described in Method A. The reaction was allowed to proceed at −77°C for 15 min prior to warming to 25°C. The reaction was completed according to Method A. The orange oil obtained was dissolved in 100 mL of methylene chloride, washed with water (2 × 100 mL), and the solvent from the organic fraction was removed *in vacuo* to give an orange semi-solid. Purification, as outlined in Method A, using methylene chloride – absolute ethanol (15:1 v/v) was performed. Extraction of the band having R_f 0.55 gave **14*b*** (0.125 g, 67%) and R_f 0.3 yielded **15** (0.014 g, 12%), which exhibited the same physical and spectral properties as **14*b*** and **15** obtained by Method A.

1-Methyl-3-bromopiperidylidene-2-benzenesulfonamide (14c)

Addition of the organolithium reagent, prepared by reaction of **6*c*** (2 mmol) with n-butyllithium (2 mmol), to a solution of *N*-bromosuccinimide (2 mmol) and completion of the reaction as outlined in Method A for the preparation of **14*b*** gave a yellow semi-solid. Preparative silica gel G tlc was effected on ten 200 × 200 mm plates, 0.75 mm in thickness, with methylene chloride – methanol (19:1 v/v) as development solvent. Extraction of the band having R_f 0.83 afforded **14*c*** (0.491 g, 91%); mp 94–96°C; ir: 1580 (C=N) cm^{-1}; ^{1}H nmr δ: 1.6–2.7 (m, 4H, H-4, H-5), 2.95 (s, 3H, Me), 3.5 (m, 2H, H-6), 6.05 (m, 1H, H-3), 7.46 (m, 3H, *meta* and *para* phenyl hydrogens), 7.95 (m, 2H, *ortho* phenyl hydrogens). *Exact Mass* calcd. for $C_{12}H_{15}N_2O_2SBr$: 330.0064; found (high resolution ms): 330.0025.

1-Methyl-3-bromopiperidylidene-2-trifluoromethanesulfonamide (14d)

Addition of the organolithium reagent, prepared by reaction of **6*d*** (2 mmol) with n-butyllithium (2 mmol) to a solution of *N*-bromosuccinimide (2 mmol) in dry tetrahydrofuran (50 mL) and completion of the reaction as outlined in Method A for the preparation of **14*b*** gave a yellow oil. Silica gel flash chromatography using ethyl acetate – petroleum oil (1:1 v/v) as eluant afforded **14*d*** (0.581 g, 90%); mp 134°C; ir: 1605 (C=N) cm^{-1}; ^{1}H nmr δ: 2.2 (m, 2H, H-4, H-5), 3.12 (s, 3H, N-Me), 3.6 (m, 2H, H-6), 5.75 (m, 1H, H-3). *Exact Mass* calcd. for $C_7H_{10}N_2O_2SBrF_3$: 321.9605; found (high resolution ms): 321.9606.

1-Methyl-3-azidopiperidylidene-2-cyanamide (16)

Sodium azide (0.326 g, 5 mmol) was added to a solution of **14*b*** (0.216 g, 1 mmol) in 50 mL of dry acetonitrile and the reaction was allowed to proceed for 20 h at 25°C with stirring. The fine solid was filtered and the solvent removed *in vacuo* to yield a yellow oil containing a white suspended solid. This was extracted with 5 mL of methylene chloride, filtered, and the solvent removed *in vacuo* to give **16** as a yellow oil that solidified (0.178 g, 100%); mp 62°C; ir (neat): 2190 (CN), 2115 (N_3), and 1605 (C=N) cm^{-1}; ^{1}H nmr δ: 2.03 (m, 4H, H-4, H-5), 3.1 (s, 3H, Me), 3.48 (m, 2H, H-6), 4.81 (m, 1H, H-3). *Exact Mass* calcd. for $C_7H_{10}N_6$: 178.0967; found (high resolution ms): 178.0969.

N-[2-(1-Methyl-3-bromo-2-piperidylidene)]-N′-[2-[(5-methylimidazol-4-yl)methylthio]ethyl]guanidine (17)

Sodium hydride (0.24 g, 5 mmol) was added to a solution of 4-[(2-aminoethyl)thiomethyl]-5-methylimidazole dihydrobromide (12) (0.832 g, 2.5 mmol) in 100 mL of dry tetrahydrofuran with stirring and the reaction mixture was heated at reflux for 2 h. After cooling to 25°C a solution of **14*b*** (0.54 g, 2.5 mmol) in 100 mL of dry tetrahydrofuran was added and the reaction was heated at reflux for 24 h. Removal of the solvent *in vacuo* yielded 1.6 g of crude material, which was purified by preparative silica gel G tlc. Chromatography was performed using eighteen plates 200 × 200 mm, 1.0 mm in thickness, with methylene chloride – methanol (3:1 v/v) as development solvent. Extraction of the fraction having R_f 0.56–0.61 afforded **17** (0.87 g, 90%); mp 248°C (dec.); ir: 3120 and 3240 (NH), 1645, and 1595 (C=N) cm^{-1}; ^{1}H nmr (DMSO-d_6) δ: 1.4 (m, 1H, H-4), 1.9 (m, 2H, H-5), 2.16 (s, 3H, ≻—Me), 2.46 (m, 1H, H-4′), 2.72 (m, 2H, SCH_2CH_2N), 3.12 (s, 3H, N-Me), 3.48 (m, 2H, H-6), 2.56 (m, 1H, S*CH*(H′)CH_2N), 3.74 (s, 2H, ≻—CH_2—S), 3.83 (m, 1H, S*CH*′(H)CH_2N), 4.7 (d, $J_{3,4}$ = 11 Hz of d, $J_{3,4'}$ = 6.5 Hz, 1H, H-3), 7.48 (s, 1H, H-2 of imidazole), 8.95 and 9.7 (br s, 2H, NH, exchange with deuterium oxide). These assignments were confirmed by double resonance studies. *Anal.* calcd. for $C_{14}H_{23}N_6SBr$: C 43.4, H 6.0, N 21.7, S 8.3, Br 20.6; found: C 43.22, H 5.89, N 21.63, S 8.38, Br 20.64.

*1-Methyl-3-[(5-methylimidazol-4-yl)methylthioethylamino)]-piperidylidene-2-benzensulfonamide (18*a*)*

Potassium carbonate (20 mL of a 25% v/v solution) was added with stirring to a solution of 4-[(2-aminoethyl)thiomethyl]-5-methylimidazole dihydrobromide (5.0 g, 15 mmol) in 25 mL of water. The solvent was removed *in vacuo* at 45°C and the residue was extracted with 50 mL of isopropanol. Filtration and removal of the solvent *in vacuo* gave a white solid (4.1 g), which was purified by silica gel flash chromatography with isopropanol−methanol (4:1 v/v) as eluant to give pure 4-[(2-aminoethyl)thiomethyl]-5-methylimidazole. A solution of the latter (0.171 g, 1 mmol) in 20 mL of ethanol was added to a solution of **14***c* (0.331 g, 1 mmol) in 35 mL of ethanol and the reaction mixture was heated at reflux for 24 h with stirring. Removal of the solvent *in vacuo* gave a brown oil, which was purified by silica gel flash chromatography with ethyl acetate − methanol (1:1 v/v) as eluant to afford **18***a* (0.179 g, 43%); ^{1}H nmr (DMSO-d_6) δ: 1.61 and 1.82 (m, 2H each, H-4, H-5 of piperidine), 2.1 (s, 3H, imidazole C-5 *Me*), 2.44 (m, 2H, SCH_2CH_2NH), 2.66 (m, 2H, SCH_2CH_2NH), 2.96 (s, 3H, N-*Me*), 3.47 (m, 2H, H-6 of piperidine), 3.62 (s, 2H, ≻—CH_2—S—), 4.23 (m, 1H, H-3 of piperidine), 7.38 (s, 1H, H-2 of imidazole), 7.53 (m, 3H, *meta* and *para* phenyl hydrogens), 7.82 (d, 2H, *ortho* phenyl hydrogens), 8.78 (m, 1H, imidazole NH, exchanges with deuterium oxide). *Exact Mass* calcd. for $C_{19}H_{27}N_5O_2S_2$: 421.1644; found (high resolution ms): 421.1641. *Anal.* calcd. for $C_{19}H_{27}N_5O_2S_2.H_2Cl_6Pt$: C 27.44, H 3.49, N 8.42; found: C 28.22, H 3.49, N 8.46.

*1-Methyl-3-[(5-methylimidazol-4-ylmethylthioethylamino)]-piperidylidene-2-trifluoromethanesulfonamide (18*b*)*

A solution of 4-[(2-aminoethyl)thiomethyl]-5-methylimidazole (0.171 g, 1 mmol) in 20 mL of absolute ethanol, prepared as described in the synthesis of **18***a*, was added to a solution of **14***d* (0.323 g, 1 mmol) in 35 mL of absolute ethanol with stirring and then the reaction mixture was heated at reflux for 24 h. Removal of the solvent *in vacuo* gave a brown oil. Purification by flash silica gel column chromatography with ethyl acetate − methanol (1:1 v/v) as eluant afforded **18***b* (0.149 g, 36%); ^{1}H nmr (DMSO-d_6) δ: 1.92 (m, 4H, H-4, H-5 of piperidine), 2.23 (s, 3H, ≻—CH_3), 2.73 (m, 2H, SCH_2CH_2NH), 2.84 (m, 2H, SCH_2CH_2NH), 3.18 (s, 3H, N*Me*), 3.5 (m, 2H, H-6), 3.78 (s, 2H, ≻—CH_2—S), 4.08 (m, 1H, H-3 of piperidine), 5.8 (m, 2H, NH, exchanges with deuterium oxide), 7.63 (s, 1H, H-2 of imidazole). *Exact Mass* calcd. for $C_{14}H_{22}N_5O_2S_2F_3$: 413.1167; found (high resolution ms): 413.1223. Compound **17***b* was quite unstable, as it decomposed slowly upon standing under nitrogen at freezer temperature.

Acknowledgement

We are grateful to the Medical Research Council of Canada (MT-4888) for financial support of this research.

1. J. W. Black, W. A. M. Duncan, G. J. Durant, C. R. Ganellin, and M. E. Parsons. Nature, **236**, 385 (1972).
2. J. S. Fordtran and M. I. Grossman. Gastroenterology **74**, 337 (1978).
3. R. L. Cavanagh, J. J. Usakewicz, and J. P. Buyniski. J. Pharmacol. Exp. Therap. **224**. 171 (1983).
4. R. C. Blakemore, T. H. Brown, G. J. Durant, J. C. Emmett, C. R. Ganellin, M. E. Parsons, and A. C. Rasmussen. Brit. J. Pharmacol. **70**, 105P (1980).
5. A. A. Algieri, G. M. Luke, R. T. Standridge, M. Brown, R. A. Partyka, and R. R. Crenshaw. J. Med. Chem. **25**, 210 (1982).
6. T. A. Ondrus and E. E. Knaus. Can. J. Chem. **57**, 2342 (1979).
7. L. M. Jackman and S. Sternhell. Nuclear magnetic resonance spectroscopy in organic chemistry. 2nd ed. Pergamon Press, Toronto. 1969. p. 288.
8. G. A. Kraus and K. Frazier. J. Org. Chem. **45**, 2579 (1980).
9. A. Kosasayama, T. Konno, K. Higashi, and F. Ishikawa. Chem. Pharm. Bull. **27**, 841 (1979).
10. F. W. Fowler. J. Org. Chem. **37**, 1321 (1972).
11. M. E. Hermes and F. D. Marsh. J. Org. Chem. **37**, 2969 (1972).
12. G. J. Durant, J. C. Emmett, C. R. Ganellin, P. D. Miles, M. E. Parsons, H. D. Prain, and G. R. White. J. Med. Chem. **20**, 901 (1977).

A spectroelectrochemical study of the technetium(IV)/technetium(III) couple in bicarbonate solutions[1]

JEAN PAQUETTE AND WARWICK E. LAWRENCE

Research Chemistry Branch, Atomic Energy of Canada Limited, Whiteshell Nuclear Research Establishment, Pinawa, Man., Canada R0E 1L0

Received November 5, 1984

JEAN PAQUETTE and WARWICK E. LAWRENCE. Can. J. Chem. **63**, 2369 (1985).

Spectroelectrochemistry at an optically transparent electrode, in conjunction with controlled potential coulometry, has been used to study the Tc(IV)/Tc(III) redox couple in aqueous bicarbonate solutions. The complexation provided by bicarbonate/carbonate ions was found to stabilize both Tc(IV) and Tc(III). The uv–visible absorption spectra for technetium(III) and technetium(IV) carbonate complexes are described. The redox potential for the Tc(IV)/Tc(III) couple, as well as the number of electrons, the number of carbonate groups, and the number of hydroxyl groups exchanged during the redox process in bicarbonate media are reported.

JEAN PAQUETTE et WARWICK E. LAWRENCE. Can. J. Chem. **63**, 2369 (1985).

Nous avons utilisé des mesures spectroélectrochimiques, ainsi que la coulométrie à potentiel controlé, pour étudier le couple oxydo-réducteur Tc(IV)/Tc(III) en milieu aqueux contenant des ions bicarbonates. On a trouvé que la complexation par les ions carbonates stabilise le Tc(IV) et le Tc(III). Les spectres d'absorbtion uv–visible du technétium(III) et (IV) sont décrits. Le potentiel oxido-réducteur du couple Tc(IV)/Tc(III), ainsi que le nombre d'électrons, le nombre d'ions carbonates et le nombre d'ions hydroxyles échangés lors de la réduction en milieu bicarbonate sont rapportés.

Introduction

Despite the wide use of ^{99m}Tc in nuclear medicine, the aqueous chemistry of technetium remains poorly understood, particularly in its lower oxidation states. In the past few years, the need for reliable chemical data for compounds and complexes of this element has increased, as attempts are made to assess the probable behaviour of encapsulated high-level radioactive wastes, in contact with groundwater in deep underground disposal vaults. Such facilities would contain relatively large quantities of the long-lived isotope ^{99}Tc.

Deep groundwater systems are often reducing. Although there are reports in the literature of the existence of complexes of reduced technetium with simple inorganic ions such as fluoride, chloride, sulphate, and phosphate (1), there is no report of the occurrence of complexes between reduced technetium and the geochemically important carbonate/bicarbonate ions. As part of a broader radioactive waste management program (2), we have examined the chemistry of technetium in its low oxidation states in bicarbonate media using spectroelectrochemical techniques. Spectral and electrochemical information on the various oxidation states of technetium in these media is critical to both the qualitative and quantitative understanding of its behaviour in geological environments being considered for nuclear waste disposal.

Experimental

Electrodes

An optically transparent electrode was made from 10 pore-per-inch reticulated vitreous carbon (RVC), obtained from Normar Industries, Anaheim, California. RVC is a glassy carbon material with a porous three-dimensional structure and good electrochemical properties. It has a free void volume of over 95% and a surface area of about 60 cm^2/cm^3. Due to the weak light absorption of the solutions used in this study, a 1-cm thick slice was used instead of the more typical 1–2 mm thickness. The RVC was fitted into a square 1-cm spectrophotometric quartz cell (Helma 100-QS). Electrical contact was made by means of a platinum wire attached to the electrode with conducting glue. The reference electrode was a miniature Ag/AgCl flexible electrode (−0.044 V vs. SCE) from Microelectrodes Inc., modified by replacing the ceramic junction with a Vycor plug. The counter-electrode was a platinum mesh enclosed in Teflon tubing, and separated from the solution by a Vycor plug. The resistance between the reference and the working electrode was about 3 kΩ. The cell had provisions for gas purging. All potentials will be quoted versus the SCE.

Apparatus

Electrochemical measurements were performed with an EG&G Princeton Applied Research Model 173/179 potentiostat/coulometer coupled to a Hewlett–Packard Model 7100B recorder. The pH measurements were made with an Orion Model 701A ionalyzer and a Microelectrodes Inc. microcombination pH electrode. Spectra were recorded in digital form, using a Hewlett–Packard Model 8450A double-beam diode array uv–visible spectrophotometer.

Reagents

The ^{99}Tc was obtained from New England Nuclear as a 0.33 mol dm^{-3} NH_4TcO_4 solution. The ammonium pertechnetate was converted to the potassium salt, which was purified by recrystallization from water, according to the procedure described by Boyd (3). A 0.1 mol dm^{-3} stock solution was then prepared and used in all experiments. Other stock solutions were made from standard ACS-grade reagents, and distilled, deionized water, without further purification. The CO_2 and Ar gases, from Canadian Liquid Air, were passed through a solid catalyst (Oxy-trap, Alltech Associates) to remove oxygen, and then through a water saturator.

Procedure

The ionic strength was maintained constant at 1.0 mol dm^{-3}, using sodium trifluoromethanesulfonate; the more customary sodium perchlorate and sodium nitrate salts were found to reoxidize reduced technetium. The solutions were purged with a CO_2–Ar mixture. The partial pressure of CO_2 needed to maintain a given $[H^+]$ and total carbonate concentration can be calculated from

$$[1] \quad pCO_2 = \frac{[H^+]C_T}{K_1 K_H}$$

which is valid for $[H^+]$ between 10^{-7} and 10^{-9} mol dm^{-3}. Here K_H is the Henry's law constant for CO_2 solubility, K_1 is the first acidity constant for carbonic acid, and C_T is the total carbonate concentration. The two constants depend on the ionic strength and on the medium used. Since their values are not known accurately for a CF_3SO_3Na

[1]Issued as AECL-8529.

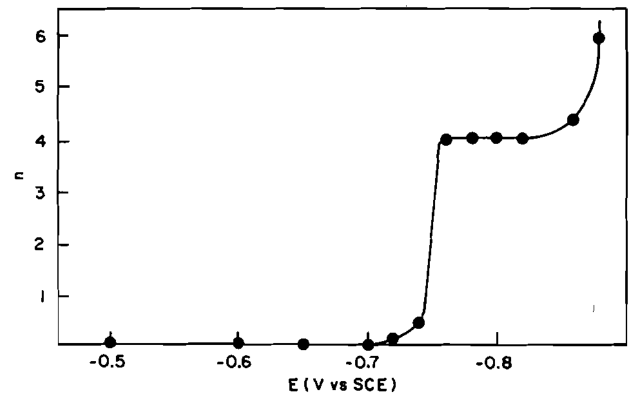

FIG. 1. Number of electrons transferred as a function of the applied potential, for a 1.2×10^{-4} mol dm^{-3} TcO_4^- solution in 0.5 mol dm^{-3} HCO_3^- medium, pH 8, at a RVC electrode.

medium, the following approach was used. A solution containing a mixture of $NaHCO_3$ and CF_3SO_3Na at an initial pH of 8 was equilibrated at a fixed partial pressure of CO_2 for 72 h. The hydrogen-ion concentration was then measured and the total carbonate concentration was obtained by titration with CF_3SO_3H, allowing the determination of K_1K_H, using eq. [1]. This value of K_1K_H was then used to calculate the required pCO_2 for various $[HCO_3^-]$ and $[H^+]$ values.

The optically transparent cell, with all electrodes in place, was fitted in the light path of the spectrophotometer and purged with the appropriate mixture of Ar and CO_2. An identical cell was placed on the reference side of the instrument, and the baseline recorded. Typically, 2 cm^3 of carefully purged HCO_3^-/TcO_4^- solution was transferred to the sample cell. The reference cell was similarly filled with a bicarbonate solution at the same concentration. Reducing potentials were applied to the sample cell, and the current, as well as the spectrum of the solution in the region between 200 and 800 nm, were monitored as a function of time and applied potential. Forty spectra were obtained and averaged at each potential.

Results and discussion

The three-dimensional structure of RVC permits a large electrode surface/solution volume ratio, and thus complete electrolysis of an electroactive species can be accomplished in a short time. Due to its open pore structure, RVC is optically transparent, with an essentially constant transmittance throughout the entire uv–visible spectral region. These properties make RVC a very useful material for *in situ* spectral monitoring of electrochemical reactions, and for the study of a variety of oxidation–reduction systems (4).

With solutions initially 1.2×10^{-4} mol dm^{-3} in TcO_4^- and 0.5 mol dm^{-3} in HCO_3^- (pH adjusted to 8.00), no significant current was observed at the RVC electrode for applied potentials above −0.62 V. At potentials below −0.70 V, the solution rapidly turned pink and then pale blue, indicating a chemical transformation. The number of electrons (n) transferred during the reduction was measured coulometrically as a function of the electrode potential. The results are shown in Fig. 1. The curve of n against applied potential displays a plateau from −0.76 to −0.82 V, corresponding to a transfer of 4.1 electrons. At more reducing potentials, n increases rapidly due to catalytic hydrogen evolution.

The reduced solution was found to be very sensitive to air oxidation, turning rapidly from blue to pink upon brief exposure to air. The same behaviour was observed on applying −0.4 V to the electrode. The number of electrons exchanged during the reoxidation was 0.9. The pink solution could be

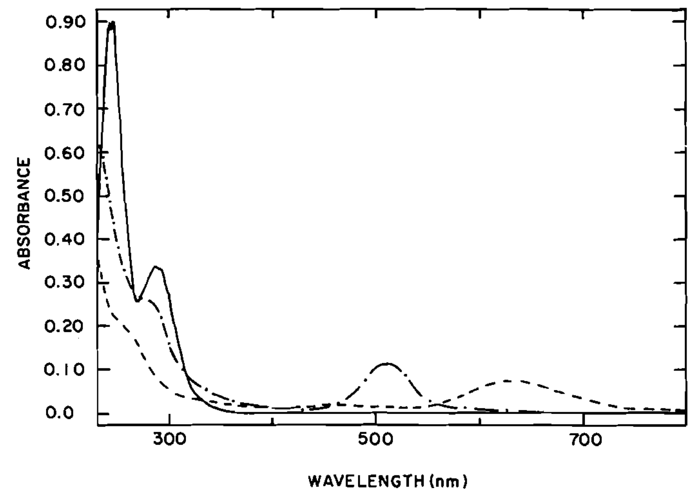

FIG. 2. Ultraviolet–visible absorption spectra for TcO_4^- (full line), Tc(IV), Tc(III) (dashed line), all at 1.2×10^{-4} mol dm^{-3} in 0.5 mol dm^{-3} HCO_3^- medium, pH 8.

rereduced at a potential of −0.75 V, with a color change to blue and an n value of 1.1.

Similar behaviour was observed at a mercury electrode. This behaviour is consistent with TcO_4^- being reduced to Tc(III) at RVC and mercury electrodes in bicarbonate media. This agrees with previous observations for a mercury electrode in various phosphate, EDTA, and DTPA solutions near neutral pH (5).

Reduction of pertechnetate at a pH of 8, in the absence of bicarbonate ions, results in precipitation of $TcO_2 \cdot 2H_2O$. Technetium(III), obtained by reduction at a pH value of one, disproportionates if the pH is raised above a value of three. Thus, soluble reduced species obtained in bicarbonate media are very likely bicarbonate/carbonate complexes of reduced technetium.

The uv–visible absorption spectra for the reduced bicarbonate species are shown in Fig. 2, together with the spectrum for TcO_4^-. The fine-structured charge transfer bands at 240 nm and 290 nm, characteristic of TcO_4^-, are replaced by intense bands with maxima below 230 nm. Both reduced species show a shoulder at 280 nm, which is more obvious for Tc(IV). The reduced species also display weaker bands in the visible, which are responsible for the color of the solutions. These are located at 512 nm for Tc(IV) and at 470 nm and 630 nm for Tc(III).

The bands in the uv region of the spectrum have high intensities and most likely belong to charge-transfer transitions. The bands in the visible region have extinction coefficients of about 800 dm^3 mol^{-1} cm^{-1}, which is too high a value for a d–d transition in a complex having a high degree of symmetry, such as octahedral or tetrahedral. If these bands were due to intrasubshell d–d transitions, then the complexes should possess a low symmetry, i.e. no center of inversion, or a distorted square planar symmetry.

The kinetics of reduction of TcO_4^- to Tc(III) in 0.5 mol dm^{-3} HCO_3^-, at a pH value of 8, have been followed *in situ* by applying a potential of −0.76 V to the RVC electrode and recording the spectra between 210 and 800 nm as a function of time. The matrix multicomponent analysis routine resident in the HP-8450A spectrophotometer was then used, together with the spectra for TcO_4^-, Tc(III), and Tc(IV), to calculate the concentration of the three species as a function of time. The results are shown in Fig. 3.

Since the RVC electrode does not have a well-defined geom-

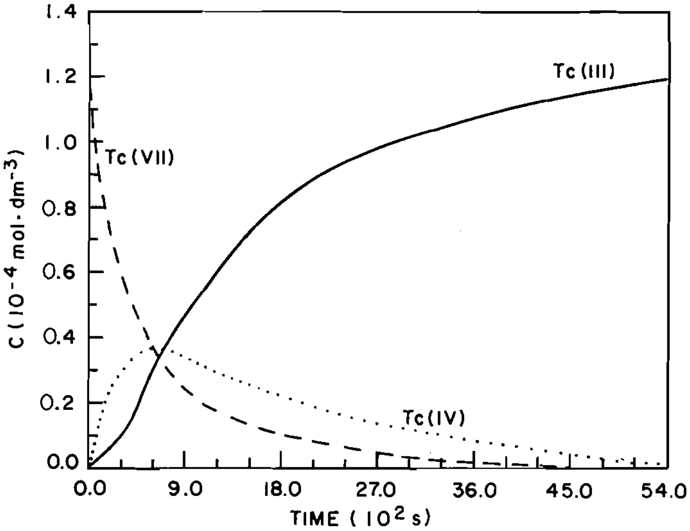

FIG. 3. Kinetics of reduction of TcO_4^- at a RVC electrode in 0.5 mol dm^{-3} HCO_3^- medium, pH 8.

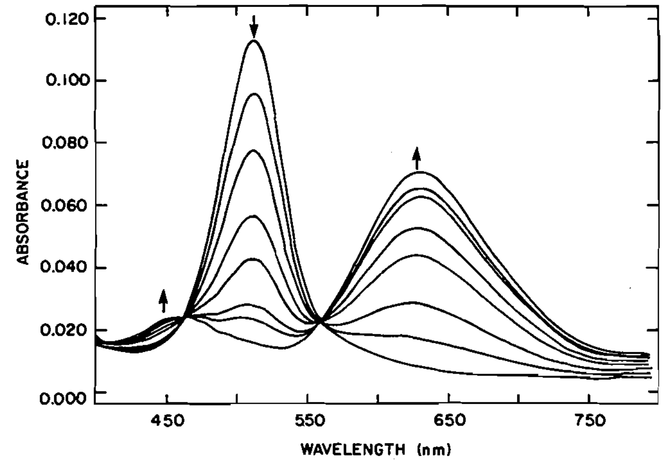

FIG. 4. Visible spectra obtained by successive application of a series of potentials from −0.5 V down to −0.78 V to a 1.2×10^{-4} mol dm^{-3} Tc(IV) solution at a pH of 8, in 0.5 mol dm^{-3} HCO_3^- medium. Arrows indicate the directions the peaks moved with decreasing potential.

etry, a quantitative calculation of the kinetic parameters was not attempted. However, some qualitative conclusions can be drawn. The concentration of TcO_4^- decreases with time, whereas the concentration of Tc(III) increases. The concentration of Tc(IV) goes through a maximum. This is typical of an A → B → C mechanism. The reduction of TcO_4^- appears to be diffusion controlled, i.e. a plot of the concentration of TcO_4^- against the square root of time is linear, for times up to 10 min. Figure 3 confirms the visual observation of the color changes during the reduction process (colorless to pink to blue) and indicates that the rate of reduction of Tc(IV) to Tc(III) is faster than the overall rate of reduction of TcO_4^- to Tc(IV). No spectral change was observed on mixing TcO_4^- with Tc(III), ruling out a reaction between them as a source of Tc(IV).

Figure 4 shows spectra obtained by successive application of a series of potentials, from −0.5 V down to −0.78 V, to a 1.2×10^{-4} mol dm^{-3} Tc(IV) solution at a pH value of 8, in 0.5 mol dm^{-3} bicarbonate medium. About 20 min were required at each potential to obtain a stable spectrum. The absorbance at 512 nm decreased, while that at 630 nm increased, with decreasing potential. Well-defined isobestic points could be observed at 470 and 560 nm. The spectra were found to be linearly dependent. That is, for the function

$$[2] \quad \delta = (1 - b)A_{\lambda,E_1} + bA_{\lambda,E_2} - A_{\lambda,E_3}$$

where A_{λ,E_i} are absorbances at fixed wavelength λ and potential E_i, there exists a value of b, for each possible combination of three spectra, that makes δ equal to zero, within experimental error, at all wavelengths except the isobestic points. In other words, any one spectrum at a particular potential is a linear combination of any two other spectra at two different potentials. This, together with the presence of isobestic points, is an indication that only two interrelated light-absorbing species are present (6), and that no significant loss of materials is occurring through precipitation or plating on the electrode.

The above behaviour implies a reversible or quasi-reversible electrochemical system, in which case the Nernst equation can be written as (7)

$$[3] \quad E = E^{0'} + \frac{0.059}{n} \log \frac{A_2 - A_1}{A_3 - A_2}$$

In eq. [3], E is the applied potential, $E^{0'}$ is the formal reduction potential, n is the number of electrons exchanged, A_1 is the absorbance for the reduced form, A_3 is the absorbance for the oxidized form, and A_2 is the absorbance for the mixture of reduced and oxidized forms. A plot of the applied potential, E, against $\log \frac{A_2 - A_1}{A_3 - A_2}$ should be a straight line with a slope of $0.059/n$ and an intercept of $E^{0'}$. Figure 5 shows plots of E versus $\log \frac{A_2 - A_1}{A_3 - A_2}$ obtained by starting with a potential at which only the oxidized form (Tc(IV)) was present, and then decreasing the potential stepwise to generate the reduced form. The plots are linear as expected from eq. [3]. The slopes correspond to an n value of 0.9 ± 0.1, as expected from the coulometric measurements, and the intercept is −0.625 V.

At constant pH and bicarbonate concentration, the redox equilibrium can be written as

$$[4] \quad \sum_{m=1}^{M} j\mathrm{Tc}_i(\mathrm{IV}) + \sum_{m=1}^{M} jie^- \rightleftharpoons \sum_{n=1}^{N} k\mathrm{Tc}_l(\mathrm{III})$$

and the electrochemical potential as

$$[5] \quad E = E^{0'} + 0.059 \log \frac{\prod_{m=1}^{M} [\mathrm{Tc}_i(\mathrm{IV})]^j}{\prod_{n=1}^{N} [\mathrm{Tc}_l(\mathrm{III})]^k}$$

where i, j, k, and l are stoichiometric coefficients, and m and n are the number of Tc(IV) and Tc(III) species present. The experimentally accessible variable is the absorbance of the solutions, given by

$$[6] \quad A_{(\mathrm{T},\lambda)} = \sum_{m=1}^{M} \epsilon_{m,\lambda}\mathrm{Tc}_i(\mathrm{IV}) + \sum_{n=1}^{N} \epsilon_{n,\lambda}\mathrm{Tc}_l(\mathrm{III})$$

where $A_{(\mathrm{T},\lambda)}$ is the total absorbance at wavelength λ, and $\epsilon_{m,\lambda}$ and $\epsilon_{n,\lambda}$ are the extinction coefficients for species m and n at wavelength λ. The fact that a plot using eq. [3] gives a straight line with a reasonable intercept and with the expected slope of 0.059 is a good indication that only one oxidized and one reduced species are present in the system, and that both of these species are mononuclear. This conclusion is consistent with the

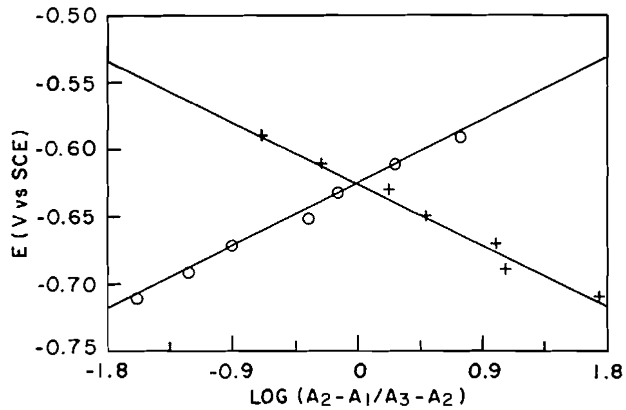

FIG. 5. Plots of applied potential against log [Tc(IV)]/[Tc(III)] for the spectra in Fig. 4. Data obtained at: + = 512 nm; ○ = 630 nm.

presence of isobestic points. The existence of only two mononuclear species was further demonstrated by increasing the initial Tc concentration from 1.2×10^{-4} mol dm^{-3} to 3.5×10^{-4} mol dm^{-3} and repeating the step reduction at the same pH and bicarbonate concentration. The same values for n and $E^{0'}$ were obtained at the higher concentration. Also, the isobestic points remained at the same wavelengths. Furthermore, the initial Tc(IV) and the final Tc(III) absorbances were equal, within experimental error, to 2.9 times the low concentration absorbance, over the 210 to 800-nm wavelength range.

For variable pH and carbonate concentration, the redox equilibrium is then given by

$$[7] \quad \mathrm{Tc(OH)}_p(\mathrm{CO_3})_q^{4-p-2q} + r\mathrm{CO_3^{-2}} + m\mathrm{H_2O} + 1e^- \rightleftharpoons \mathrm{Tc(OH)}_{p+m}(\mathrm{CO_3})_{q+r}^{3-(p+m)-2(q+r)} + m\mathrm{H^+}$$

The complexes could also be written as $\mathrm{Tc(OH)}_x(\mathrm{CO_2})_y$. By using a spectroelectrochemical method only, one cannot, from a mathematical viewpoint, distinguish between the two entities. We have chosen to use the first notation for convenience. The electrochemical potential can be rewritten as

$$[8] \quad E = E^0 + 0.059 \log \frac{[\mathrm{Tc(OH)}_p(\mathrm{CO_3})_q][\mathrm{CO_3}]^r}{[\mathrm{Tc(OH)}_{p+m}(\mathrm{CO_3})_{q+r}][\mathrm{H^+}]^m}$$

or

$$[9] \quad E = E^{0'} + 0.059 \log \frac{[\mathrm{Tc(IV)}]}{[\mathrm{Tc(III)}]}$$

where:

$$[10] \quad E^{0'} = E^0 + 0.059(r \log [\mathrm{CO_3^{-2}}] + m\,\mathrm{pH})$$

A plot of $E^{0'}$ as a function of log [$\mathrm{CO_3^{-2}}$], at constant pH, should have a slope of $0.059r$. Similarly, a plot of $E^{0'}$ as a function of pH, at constant [$\mathrm{CO_3^{-2}}$], should have a slope of $0.059m$. Combining the results from the two plots allows the calculation of E^0. The value of $E^{0'}$ was found to be independent of the bicarbonate concentration, at a constant pH of 8 and a constant ionic strength of 1 mol dm^{-3}. Hence, r is equal to zero, i.e. the two species contain the same number of carbonate ions per molecule. The slope of $E^{0'}$ against pH at constant bicarbonate concentration is 0.0585, giving a value of 0.99 for m. Hence, the Tc(III) bicarbonate species contains one more hydroxyl group than the Tc(IV) species. In that case, combining eqs. [6] and [8] gives

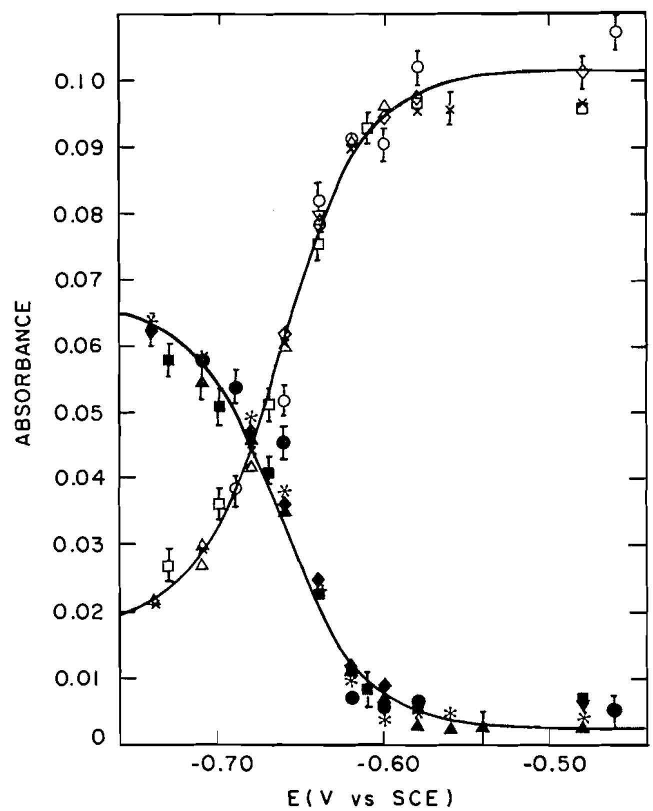

FIG. 6. Absorbance vs. applied potential at a pH value of 8. The curves have been calculated with $E^0 = -1.131$ V in eq. [11]. Open symbols are data obtained at 512 nm. Closed symbols are data obtained at 630 nm. Bicarbonate concentrations: □, 0.5 mol dm^{-3}; ▽, 0.625 mol dm^{-3}; *, ◇, 0.8 mol dm^{-3}; ○, △, 1.0 mol dm^{-3}.

$$[11] \quad A_{(\mathrm{T},\lambda)} = \frac{[\mathrm{Tc}]\epsilon_{\mathrm{IV},\lambda} \cdot 10^{E-E^0-0.059\mathrm{pH}} + [\mathrm{Tc}]\epsilon_{\mathrm{III},\lambda}}{1 + 10^{E-E^0-0.059\mathrm{pH}}}$$

where [Tc] is the total technetium concentration, $\epsilon_{\mathrm{IV},\lambda}$ is the extinction coefficient for the Tc(IV) species at wavelength λ, and $\epsilon_{\mathrm{III},\lambda}$ is the extinction coefficient for the Tc(III) species at wavelength λ.

The experimental data, plotted in Fig. 6 as absorbance vs. applied potential, fall, within experimental error, on single curves, confirming the validity of the model. A non-linear, least-squares-fitting routine was used to calculate E^0 and the extinction coefficients, giving: $E^0 = -1.131$ V; $\epsilon_{\mathrm{IV},512} = 680$; $\epsilon_{\mathrm{III},512} = 120$; $\epsilon_{\mathrm{IV},630} = 14$; and $\epsilon_{\mathrm{III},630} = 430$.

Using the above determined potential, it can be calculated that, in carbonated groundwater with a pH of 8 and a redox potential of −0.300 V (a reasonable value, if the redox potential is controlled by the Fe(III)/Fe(II) mineral equilibria), the ratio [Tc(III)]/[Tc(IV)] would be equal to 10^{-6}. Thus, soluble Tc(III) carbonate species are not expected to be important in the transport of technetium in groundwater.

The charge sign of the Tc(IV) carbonate complex was determined using a simple electromigration technique. An H-shaped cell with three compartments separated by glass frits was used. The two outer compartments were fitted with platinum electrodes and filled with bicarbonate solution. The central compartment contained a Tc(IV) bicarbonate solution. A potential of 15 V was applied between the two platinum electrodes, and the two outer compartments were analyzed for Tc by liquid scintillation counting. Tests with $\mathrm{TcO_4^-}$ showed that, in the absence of an applied potential, natural migration is insignificant over a period of 24 h, but that TcO_4^- migrates rapidly to the anode side when a potential of 15 V is applied. In all cases, the Tc(IV) carbonate complex migrated to the anode; no migration to the cathode occurred. Thus, the Tc(IV) complex is negatively charged. This was confirmed using ion-exchange resins. Technetium(IV) was quickly removed from bicarbonate solutions by an anion-exchange resin (DOWEX 1X8), but not by a cation-exchange resin (AG-50W-X8). Thus, $p + 2q$ in eq. [7] and following is greater than four. Unfortunately, the sign of the Tc(III) complex could not be measured reliably due to its rapid oxidation to Tc(IV).

Conclusions

Spectroelectrochemical techniques have been found useful for elucidation of the behaviour of reduced technetium in bicarbonate solutions. The existence of a reversible, or quasi-reversible, Tc(IV)/Tc(III) couple in these media was demonstrated. The redox potential for the couple and also the number of carbonate and hydroxyl ions exchanged during the reduction were determined. The redox equilibrium is

$$[12] \quad Tc(OH)_p(CO_3)_q^{4-p-2q} + H_2O + 1e^- \rightleftharpoons Tc(OH)_{p+1}(CO_3)_q^{3-(p+1)-2q} + H^+$$

where $p + 2q$ is greater than four. It appears that soluble Tc(IV) carbonate species would be more important than Tc(III) carbonate species in the transport of technetium in groundwater. Experiments to determine the stoichiometry and the stability of the complexes are underway.

Acknowledgements

The authors thank Dr. D. W. Shoesmith for numerous discussions, and Dr. R. J. Lemire for purifying the potassium pertechnetate salt. We also thank Mr. M. G. Bailey for assistance with some of the experiments.

1. J. GRASSI, J. DEVYNCK, and B. TRÉMILLON. Anal. Chim. Acta, **107**, 47 (1979).
2. E. L. J. ROSINGER and R. S. DIXON. Fourth Annual Report of the Canadian Nuclear Fuel Waste Management Program. Atomic Energy of Canada Limited Report, AECL-7793 (1982).
3. G. E. BOYD. J. Solution Chem. **7**, 229 (1978).
4. V. E. NORVELL and G. MAMANTOV. Anal. Chem. **49**, 1470 (1977).
5. C. D. RUSSELL. Int. J. Appl. Radiat. Isot. **28**, 241 (1977).
6. J. BRYNESTAD and G. P. SMITH. J. Phys. Chem. **72**, 296 (1968).
7. T. P. DEANGELIS and W. R. HEINEMAN. J. Chem. Educ. **53**, 594 (1976).

Oriented collisions in the recombination and disproportionation of free radicals

L. K. COHEN AND H. O. PRITCHARD
Centre for Research in Experimental Space Science, York University, Downsview, Ont., Canada M3J 1P3

Received October 10, 1984

L. K. COHEN and H. O. PRITCHARD. Can. J. Chem. 63, 2374 (1985).
It is shown that there will be strong orienting effects in the collision of two radicals which will invalidate attempts to calculate disproportionation–recombination ratios by simple geometric arguments.

L. K. COHEN et H. O. PRITCHARD. Can. J. Chem. 63, 2374 (1985).
On démontre qu'il existe des effets directifs importants dans la collision de deux radicaux et que ces effets rendent invalides tous les essais de calculer les rapports de disproportionation–recombinaison par des arguments géométriques simples.
[Traduit par le journal]

It is possible to take two extreme views of the disproportionation process which occurs between a pair of alkyl radicals, e.g.

$$CH_3 + CF_2H \rightarrow CH_4 + CF_2$$

At one extreme, one can consider that the methyl radical abstracts a hydrogen atom from the difluoromethyl radical (1); at the other extreme, that the products are the "dissociated" species in a chemical activation process, with the recombined product ($C_2H_4F_2$ in this case) being the "stabilised" fraction of the initial flux (2). It is the purpose of this note to throw some light on the mechanisms of these processes by performing trajectory calculations for the approach of two bodies under the influence of a strongly directional attractive potential, such as is characteristic of a *p*-orbital in an aliphatic free radical. We find that in such collisions, provided that the radicals are not rotating too strongly, there is a propensity for them to orient themselves so that they are "facing" each other. Thus, rather like a pair of dancers, they remain facing each other during the whole of the intimate encounter, regaining independent rotational motion only after they have receded beyond a critical value of the interparticle separation; however (to continue with the dancing analogy), collisions in which one radical "turns its back" on the other are not entirely excluded. These observations complicate attempts, such as those of Benson recently (3), to calculate disproportionation–recombination ratios by simple geometric arguments based on the spatial characteristics of the radicals.

We are faced with a multitude of possible disproportionation reactions (4) and so, for our first examination of this problem, we restrict ourselves to a carefully chosen model of the collision between two methyl radicals which retains, we believe, sufficient physical reality to enable the salient physical effects to be discerned; extension to real reactive systems is then only a matter of detail and of computational complexity.

The model and the potential

The dominant interactions are the bonding attraction between the two radical centres, and the non-bonded repulsions between the valence-saturated atoms in the system. For the attractive potential we chose, simulating ethane, a Morse curve

$$[1a] \quad V_-(r) = D_e\{\exp[-2a(r - r_e)] - 2\exp[-a(r - r_e)]\}$$

with $D_e = 88.6$ kcal mol^{-1}, $r_e = 1.54$ Å, and $a = 1.885$ Å^{-1}, derived from $D_0 = 87.2$ kcal mol^{-1} and a vibration frequency of 995 cm^{-1} (5, 6).

The repulsive potential was chosen in such a way that there was little or no repulsion beyond interparticle distances (r_i) of 5 Å, but a strong repulsion occurred for $r_i \leq 2$ Å: the simple form

$$[1b] \quad V_+(r_i) = 0.25\, D_e\{\exp[-a(r_i - r_e)]\}$$

gave rise to an empirical potential which was qualitatively satisfactory.

In order to test our conjecture that most, if not all, of the initial rotational angular momentum is converted into overall angular momentum during closest approach, it is not necessary to perform a full three-dimensional calculation with two radicals: the physical picture remains the same if one of the radicals is replaced by an atom and, further, there is no loss of physical insight if the motion is confined to two dimensions. Figure 1 shows the final mechanical system used in these model calculations: one methyl radical is splayed out flat with a mass of 12 amu at the centre, and three masses each of 1 amu located at $l = 1.1$ Å away, disposed at $i\pi/2$ ($i = 1, 2, 3$) with respect to the centreline of the nascent C—C bond, and it is considered to be rigid; the other methyl radical is replaced by a structureless mass of 15 amu. The total potential is then

$$[1] \quad V(r, \psi) = V_-(r) + \sum_i V_+(r_i)$$

where

$$r_i = [r^2 + l^2 + 2rl \sin(\psi + i\pi/2)]^{1/2}$$

and in which ψ, the angle of alignment, is the difference of the two inertial angular coordinates $\phi-\theta$; some sections of $V(r, \psi)$ are shown in Fig. 2 for three different values of the distance between the bonding centres. In the repulsive region, there are two minima which actually become weakly attractive at some distances: we regard this as reasonable, since the tetrahedral methyl group will exert strong replusions along the lines of the C—H bonds, but in the angles between each pair the repulsions will be weaker, and in the basin lying symmetrically between the three C—H bonds; also, the real potential becomes weakly attrractive in some non-bonding orientations, corresponding to the existence of Van der Waals forces. If our model did not exhibit these secondary minima in directions away from the bonding axis, then every collision would be oriented;[1] an oriented collision is defined as one in which the closest approach occurs for values of $-\pi/2 < \psi < \pi/2$ i.e. in the sector containing the normal C—C bond direction.

[1] Except at very high rotational rates, c.f. discussion of Fig. 5.

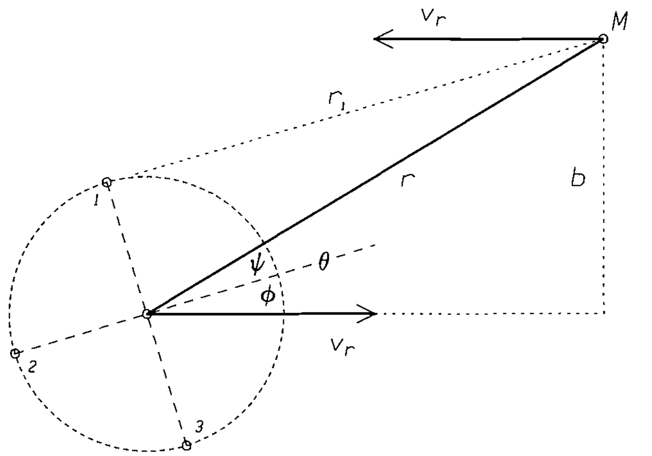

FIG. 1. Definition of the model collision system. The left-hand (distributed) particle consists of four mass points, one of 12 amu at the centre and three, each of 1 amu, held rigidly at a distance of 1.1 Å with a $\pi/2$ separation between them; the right-hand particle M is a point mass of 15 amu. Particle M interacts with the distributed particle via an attractive potential with the 12 amu mass point (eq. [1*a*]) and a repulsive potential with each of the 1 amu mass points (eq. [1*b*]). An additional simplification of the algorithm was achieved by considering that the mass of the three light particles was uniformly distributed on the circumference of a circle of radius 1.1 Å leaving only their force centres at the positions shown; this causes the centre of mass of the distributed particle to coincide with the position of the heavy mass point.

The equations of motion

In the centre-of-mass coordinates, the Hamiltonian is

$$[2] \quad H = \frac{p^2}{2\mu} + \frac{s(s+1)\hbar^2}{2I} + V(r, \psi)$$

where p is the linear momentum, μ is the reduced mass of the system, s is the rotational quantum number of the methyl radical, I is its moment of inertia, and $V(r, \psi)$ is as already defined. The canonical coordinate pairs for the system are (r, p) and (ϕ, j) where

$$[3] \quad p' = -\frac{\partial H}{\partial r}, \; r' = \frac{\partial H}{\partial p}, \; j' = -\frac{\partial H}{\partial \phi}, \; \phi' = \frac{\partial H}{\partial j}$$

with the primes denoting differentiation with respect to time. The use of the Hamiltonian $H_s = s(s+1)\hbar^2/2I$ for the angular component of the motion leads, with $s = I\phi'/\hbar$, to

$$H_s = (1/2)\frac{\partial H_s}{\partial j}\left(\frac{I\partial H_s}{\partial j} + \hbar\right)$$

which does not have a simple solution; however, by making the usual classical approximation (7) that $H_s = s^2\hbar^2/2I$, then

$$H_s = (1/2)\, I\left(\frac{\partial H_s}{\partial j}\right)^2$$

which integrates readily to $j^2/2I$, and so $j = s$ and $\phi' = j'/I$. With this simplification, all the derivatives in [3] can be evaluated analytically from [1] and [2] and the integration becomes straightforward.

Integration and selection of trajectories

The integration was performed by using a third-order Runge–Kutta method in combination with a 5-point Adams–Moulton predictor–corrector procedure. Conservation of energy was required to within 6×10^{-3} kcal mol^{-1}, which leads to the requirement of step lengths in the range 4×10^{-16} to 3×10^{-14} s; the total angular momentum, i.e.

$$\boldsymbol{J} = \boldsymbol{L} + \boldsymbol{S} = \boldsymbol{r} \times \boldsymbol{p} + \boldsymbol{\phi}'I$$

was conserved to within $10^{-4}\hbar$, always.

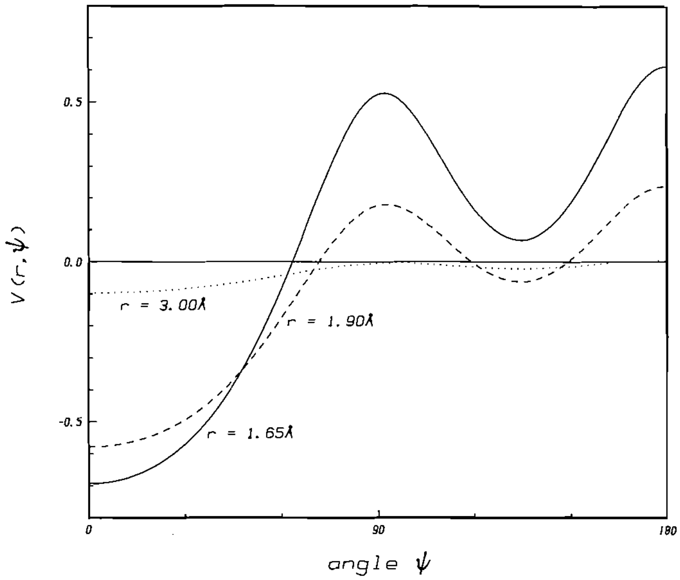

FIG. 2. Three sections through the potential surface, eq. [1], at r = 1.65, 1.9, and 3.0 Å; notice that for all angles $-\pi/2 < \psi < \pi/2$, the torque is such as to pull the system towards $\psi = 0$ where the potential is a minimum. The scale of the vertical axis is $1.0 \equiv D_e$.

Initial trajectories were chosen to sample the important regions of phase space for the recombination of two methyl radicals at 300 K, and some 2000 trajectories were examined; only integral values of s were used in the starting conditions. Figure 3 shows two typical trajectories, one in which the expected orientation occurs, and one in which it does not; the incoming segment of each trajectory is shown as a solid line, the departure path after encounter is shown broken and the dotted lines separate regions of ψ corresponding to alignment or non-alignment, as we have defined it. A qualitative time scale is shown on each trajectory, each marker denoting the time at which completed *free* rotations would have occurred in the absence of any fields; thus, the straight line sections of these graphs correspond to free rotation of the radical. It can be seen that the rotation is essentially free until a distance of between 5 and 6 Å is reached. The interaction begins to take effect at this separation and the particles are pulled towards each other; those which make their closest approach in the bond direction generally reach a turning point of within 1.2–1.3 Å of each other (depending of course upon the initial relative energy), but those which make their closest approach in a non-bonding direction do not often approach closer than 1.95 Å. There is no requirement in this calculation that the final rotational motion shall be quantised, but it is clear that these two trajectories are essentially elastic.

Since we spent most of our effort in probing the dividing lines between the aligned and the non-aligned collisions, we encountered a significant number of unusual trajectories, two of which are shown in Fig. 4: partial trapping occurs in one of these two trajectories, and it is much more inelastic, with an interconversion of translational and rotational energy taking

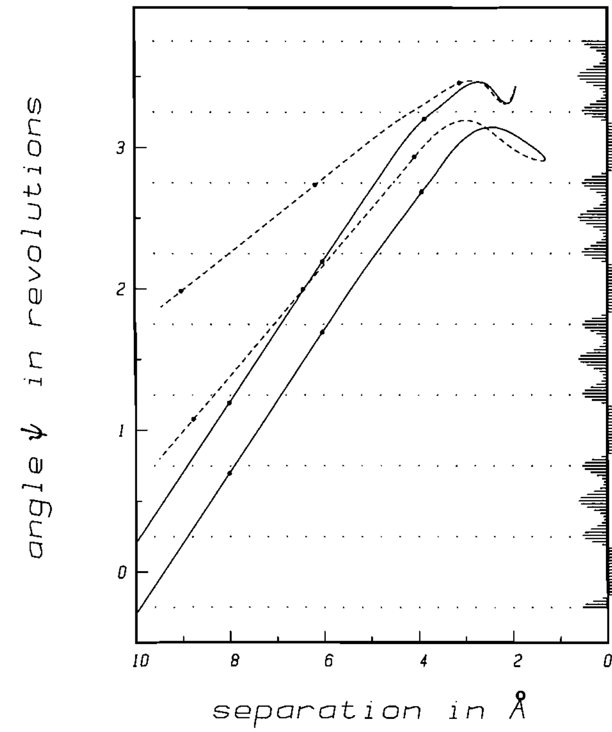

FIG. 3. A pair of typical trajectories: approach is represented by solid lines and departure by dashed lines; markers on the trajectories represent the time scale, the space between each marker representing the time taken for one *free* revolution of the distributed particle, given its initial angular momentum. The right-hand ordinate shows a schematic representation of the potential, with repulsion to the left and attraction to the right, and the regions in which the torque pulls towards $\psi = 0$ or $\pi/2 < \psi < 3\pi/2$ are separated by dotted lines. The initial conditions for all trajectories are: velocity $v_0 = \bar{v}$ (the average relative velocity for particles of mass 15 amu at 300 K); angular momentum for distributed particle = 9 $\hbar$.

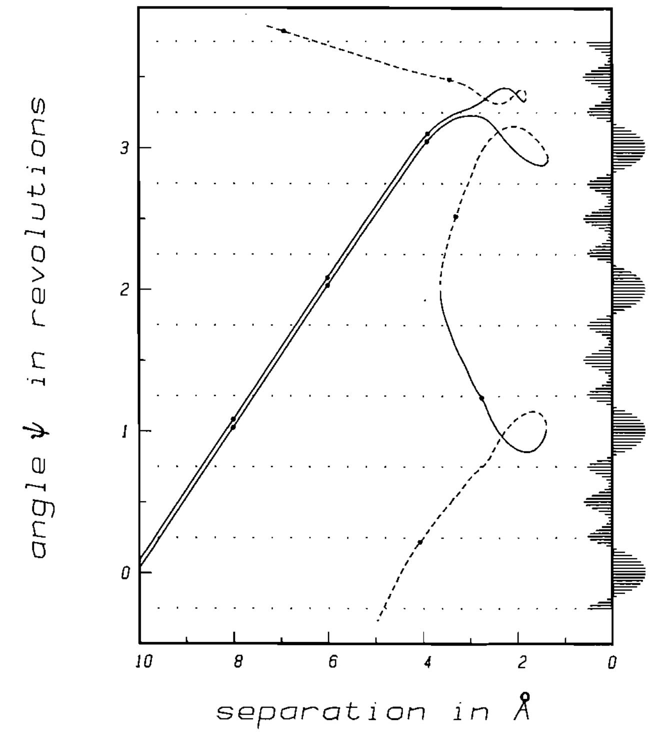

FIG. 4. A pair of atypical trajectories: see legend to Fig. 3 for further details.

place; the other is a double collision.[2]

Figure 5 shows, for a fixed initial approach velocity equal to be average value for 300 K, the fraction of non-aligned collisions as a function of the initial rotational quantum number s of the radical, in the interesting range of values of s. For the rotationless radical, $s = 0$, the probabilities of alignment and non-alignment are equal because the potential has maxima at $\psi = \pm\pi/2$. On the other hand, for exceedingly large values of s, usually $s > 50$, no collisions lead to close encounters because the radical is rotating so quickly that the attractive part of the potential does not have time to draw the particles significantly closer together before the next repulsive impulse occurs. In the important region, however (most probable value of $s \approx 3$), significant preference for oriented collisions appears, in the sense that about 70% of the collisions occur in the bonding direction and about 30% in the non-bonding direction. Results are similar at other approach velocities, with the exception of very low ones ($v_0 \leq \bar{v}/4$) where the graph exhibits considerable structure. Table 1 shows for each initial approach velocity, v_0, the mean fraction of repulsive collisions, obtained from diagrams analogous to Fig. 5 by integrating over the normal distribution of rotational quantum numbers of 300 K in this system; although the details of these curves differ somewhat with v_0, the fraction of repulsive collisions remains remarkably constant. Thus, when averaged over the appropriate Boltzmann distri-

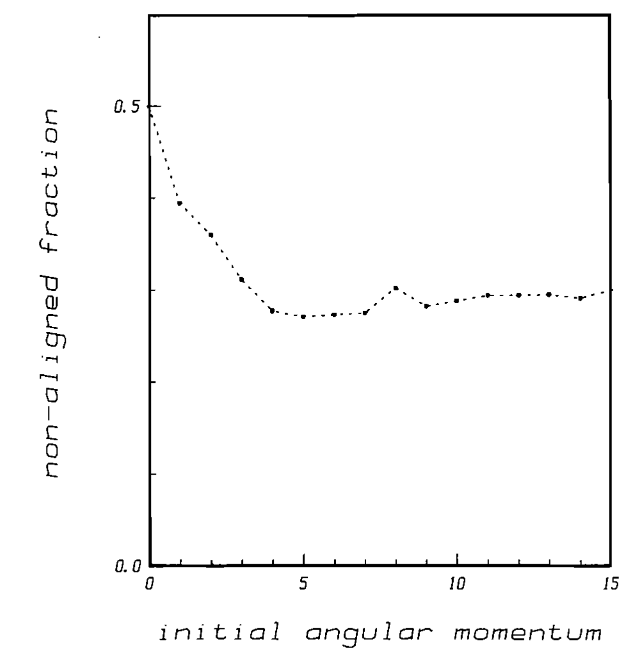

FIG. 5. Plot of the fraction of non-aligned collisions for initial approach velocity $\bar{v}$, as a function of initial angular momentum in the distributed particle. The physically interesting range at 300 K is $0 \leq s < 10$; note that as $s \rightarrow \infty$, the curve will tend to a limiting value of unity, as explained in the text. All points on this graph are determined to better than ± 0.001.

[2] Trajectories which were even more complex than this were found, but we do not reproduce them here; one, for example was initially similar to the non-aligned trajectory in Fig. 4, but on outward path, at a separation of about 4.5 Å, it was turned completely around and entered the alignment region again, approaching to within 1.3 Å before receding finally.

TABLE 1. Fraction of non-aligned collisions as a function of initial approach velocity*

v_0	Fraction
$\bar{v}/4$	0.218
$\bar{v}/2$	0.274
$\bar{v}/\sqrt{2}$	0.296
$\bar{v}$	0.320
$1.31\,\bar{v}$	0.323
$1.61\,\bar{v}$	0.369
$2.06\,\bar{v}$	0.393

* $\bar{v}$ is the average approach velocity for a pair of masses of 15 amu at 300 K, and the fraction is averaged over the rotational distribution for that temperature.

bution of approach fluxes, we find that oriented collisions are favoured in the ratio of 2.17 to 1, whereas the phase-space theory of Benson (3) would distribute the collisions equally between oriented and non-oriented. Notice that the insensitivity of the rotationally averaged alignment ratio to the initial approach velocity (in conjunction with the broad nature of the minimum found in Fig. 5 and others like it) means that the overall alignment ratio will change very little with temperature, which is a reasonable result.

Conclusions

Arguments concerning the ratio of disproportionation to recombination in alkyl radical systems cannot be based solely upon geometric considerations, since there is a strong propensity for colliding radicals to orient themselves in the bonding configuration. We have chosen a very simple model as an illustration of this point. More realistic calculations would take into consideration the three-dimensional quality of the real problem, and should allow for the fact that the radicals may deform under the influence of neighbouring particles. This is especially so in the case of methyl radicals: we have chosen to mimic the behaviour as though the methyl radical were fixed rigidly in its tetrahedral configuration (so that our conclusions would apply more generally to most radical systems), but the methyl radical is free to invert itself; our model is too simple to deal with this problem, for it would lead to the conclusion that *every* collision would be oriented at reasonable values of v_0 and s (the only exception being at very high rotational rates, as already explained in the preceding paragraph).

Unfortunately, at the present level of oversimplification, these calculations do not permit us to eliminate either of the two models of disproportionation mentioned in the Introduction: if approaches in the non-bonding directions are allowed, then abstraction is possible, but if deformation were to be so easy as to preclude such approaches, then elimination would be the only permissible mechanism.

Acknowledgement

This work was supported by the Natural Sciences and Engineering Research Council of Canada.

1. T. MINATO, S. YAMABE, H. FUJIMOTO, and K. FUKUI. Bull. Chem. Soc. Jpn. **51**, 1 (1979).
2. H. O. PRITCHARD. Quantum theory of unimolecular reactions. Cambridge University Press. 1984. p. 124.
3. S. W. BENSON. Can. J. Chem. **61**, 881 (1983).
4. J. A. KERR. Handbook of bimolecular and termolecular gas reactions. Vol. II. CRC Press, Boca Raton, FL. 1981. pp. 52–99.
5. Selected values of chemical thermodynamic properties. Technical Note 270-3, NBS. Washington. 1968.
6. T. SHIMAMOUCHI. Tables of molecular vibration frequencies. NSRDS-NBS 39, NBS Washington. 1972.
7. J. C. LIGHT. J. Chem. Phys. **40**, 3221 (1964).

Substituent effects on benzylic radical hydrogen hyperfine coupling constants. Part 4. The effect of branching of the alkyl substituent

DANIAL D. M. WAYNER[1] AND DONALD R. ARNOLD[2]
Department of Chemistry, Dalhousie University, Halifax, N.S., Canada B3H 4J3

Received November 2, 1984

DANIAL D. M. WAYNER and DONALD R. ARNOLD. Can. J. Chem. **63**, 2378 (1985).

The effects of substituents in the *meta* and *para* positions of the benzyl radical on the α-hydrogen hyperfine coupling constants (hfc's) are discussed. The electron spin resonance (esr) spectra of the *para*-methyl, ethyl, isopropyl, and *tert*-butyl substituted benzyl and cumyl radicals are analysed. Hyperconjugation involving the C—C bond is 40–60% as effective as C—H hyperconjugation for delocalizing spin density. This conclusion is supported by INDO molecular orbital calculations. Similar analysis of the ^{13}Cmr spectra of the *para*-alkyl substituted cumyl carbocations provides evidence that C—C hyperconjugation is 75–90% as effective as C—H hyperconjugation for delocalizing charge density.

DANIAL D. M. WAYNER et DONALD R. ARNOLD. Can. J. Chem. **63**, 2378 (1985).

On discute des effets des substituants en positions *méta* et *para* des radicaux benzyles sur les constantes de couplage hyperfin (chf) des hydrogènes en α. On a analysé les spectres de résonance paramagnétique électronique (rpe) des radicaux cumyles et benzyles substitués en position *para* par des groupements méthyle, éthyle, isopropyle ou *tert*-butyle. L'efficacité de l'hyperconjugaison impliquant la liaison C—C n'est que 40–60% de celle de l'hyperconjugaison C—H pour relocaliser la densité de spin. Cette conclusion est en accord avec des calculs d'orbitales moléculaires INDO. Une analyse similaire des spectres rmn du ^{13}C de carbocations cumyles substitués en position *para* par des substituants alkyles suggère que l'efficacité de l'hyperconjugaison C—C est environ 75–90% de celle de l'hyperconjugaison C—H pour délocaliser la densité de charge.

[Traduit par le journal]

Introduction

The variation in carbocation stability as a function of the degree of branching of an adjacent alkyl group has received considerable attention over a period extending back more than fifty years, to the original proposal of hyperconjugation (1). The problem, of course, is assessing the relative importance of steric and electronic effects from relative rate data (2). In addition, both C—H and C—C hyperconjugation are possible and sorting out the relative contributions of each of these effects has created some controversy (3–5).

In comparison, little is known about the effect of variation in alkyl branching on the stability of an adjacent radical centre. This may be a result of the justifiable realization that the effect of adjacent alkyl branching on the rate of most free radical reactions will be small, too small, perhaps, to be accurately measured by kinetic methods. For example, the variation in activation energy for decomposition of the symmetric azoalkanes from azo-2-methyl-2-propane to azo-2-*tert*-butyl-2-propane is too small to be critically analysed in view of the rather large experimental error (6).

The study of *para*-substituted benzyl and cumyl radicals avoids many of the difficulties, such as steric and anchimeric effects, associated with systems which have the substituent directly bonded to the reaction centre. The α-H hyperfine coupling (α-hfc) in substituted benzyl radicals has been used to define a substituent parameter (eq. [1], Table 1) which reflects the effect of the substituent on the spin density at the benzylic position (7). It is generally believed that the extent of spin delocalization away from the benzylic position should be reflected in decreased reactivity (i.e. increased stability). This reasoning has now been applied to determine the effect of branching of a *para*-alkyl substituent on the delocalization of spin density in benzyl and cumyl radicals. These results are then compared to the effect of *para*-alkyl substituents on the charge density of the cumyl carbocation.

$$[1] \quad (\sigma_\alpha^\bullet)_X = 1 - \alpha\text{-hfc}_X/\alpha\text{-hfc}_H$$

Results

The observed hyperfine coupling constants (hfc's) for several alkyl substituted benzyl and cumyl radicals are shown in Table 2. The radicals were generated by hydrogen atom abstraction from the corresponding toluene or by bromine atom abstraction from the corresponding benzylic bromide. The hfc's were estimated by initial measurement of the line positions from the signal averager and refined by computer simulation (8).

The observed ^{13}Cmr chemical shifts of the *para*-alkyl substituted cumyl carbocations are shown in Table 3. The ions were generated from the cumyl chlorides in a mixture of SbF_5/FSO_3H/SO_2ClF at −40°C as outlined by Kelly and Brown (9).

Discussion

There are some general features of the $\sigma_\alpha^\bullet$ scale which give valuable insight into the mode of interaction of substituents with the benzylic radical center.

Most of the *para* substituents delocalize spin density more effectively than the unsubstituted radical ($\sigma_\alpha^\bullet > 0$). These substituents fall into two classes. Those with non-bonding lone pairs can interact by donating an electron (Fig. 1a). In this case, the substituent is a β-spin donor. Unsaturated substituents, on the other hand, can interact by accepting an electron (Fig. 1b). In this case, the substituent is an α-spin acceptor. The orbital interactions can be represented using simple perturbation molecular orbital theory. For the β-spin donors, the orbital interactions are two-orbital, three-electron interactions and lead to a net one-electron stabilization (10). For the α-spin acceptors, the orbital interactions are three-electron, three-orbital interactions and lead to a net two-electron stabilization (10).

[1]Present address: National Research Council of Canada, Ottawa, Ont., Canada K1A 0R6.

[2]Author to whom correspondence may be addressed.

TABLE 1. $\sigma_\alpha^\bullet$ values[a]

Substituent	$\sigma_\alpha^\bullet$	Substituent	$\sigma_\alpha^\bullet$
4-SMe	0.063	4-Cl	0.011
4-COMe	0.060	4-i-Pr	0.009
4-SPh	0.058	4-*t*-B	0.008
4-COPh	0.055	4-S(O$_2$)Me	0.005
4-COOMe	0.043	3-Me	0.002
4-CN	0.040	4-OCOPh	0.000
4-SCOMe	0.029	H	0.000
4-S(O)Ph	0.026	3-OMe	−0.001
4-OMe	0.018	3-OPh	−0.002
4-OPh	0.018	4-OCOMe	−0.005
4-S(O)Me	0.018	3-Cl	−0.007
4-S(O$_2$)Ph	0.018	3-F	−0.009
4-SiMe$_3$	0.017	4-CF$_3$	−0.009
4-S(O)OMe	0.016	4-F	−0.011
4-Me	0.015	3-COOMe	−0.014
4-S(O$_2$)OMe	0.013	3-CF$_3$	−0.017
4-Et	0.012	3-CN	−0.026

[a]Calculated from eq. 1. ref. 7.

TABLE 2. Hyperfine coupling constants for alkyl substituted benzyl and cumyl radicals at −40°C[a]

Radical	*X*	a_α or a_β[b]	a_o	a_m	a_p	a_X[c]
Benzyl	H	16.25	5.10	1.70	6.13	—
	3-Me	16.22	5.15, 5.00	1.75	6.15	3.38
	4-Me	16.00	5.05	1.60	—	6.50
	4-Et	16.05	5.00	1.85	—	3.25
	4-*i*-Pr	16.10	5.10	1.80	—	2.85
	4-*t*-Bu	16.12	5.10	1.75	—	—
Cumyl[d]	H	16.28	4.70	1.65	5.55	—
	4-Me	16.10	4.70	1.60	—	5.80
	4-Et	16.13	4.60	1.60	—	2.90
	4-*i*-Pr	16.17	4.75	1.55	—	2.35[e]
	4-*t*-Bu	16.17	4.75	1.55	—	—

[a]All values in G. The uncertainty is ±0.03 G.
[b]a_α for benzyl radical, a_β for cumyl radicals.
[c]β Hydrogen(s) of alkyl substituents.
[d]From ref. 20.
[e]a_X = 2.25 at −60°C.

From this simple treatment, some qualitative predictions can be made. For the β-spin donors, the stabilization energy will depend on the energy of the lone pair. As the energy of the lone pair decreases, the ionization potential increases, and the contribution of the valence bond structure in Fig. 1a will decrease. This rationale leads to the prediction that the order of increasing spin delocalization should be —F < —Cl < —OR < —SR, which is the order observed.

Similarly, as the energy of the π (or σ)-orbital of the α-acceptors decreases, spin delocalization in the benzyl radical also should decrease. This, again, leads to the correct qualitative prediction that, for these substituents, spin delocalization should increase in the order —CF$_3$ < —CH$_3$ < —CN < —COR. The *para*-CF$_3$ and *para*-CH$_3$ substituents are considered to be α-acceptors since interaction with filled σ-orbitals is possible. In this case, the stabilizing effect of course will be much smaller since the energy separation between these orbitals is much greater (11).

This approach assumes that hydrogen as a substituent has no stabilizing effect. As a result, the relative stabilization of the benzyl radical by a *para* substituent can be predicted, but it is

TABLE 3. ^{13}C magnetic resonance chemical shifts of 4-alkylcumyl carbocations in SbF$_5$/FSO$_3$H/SO$_2$ClF at −40°C[a,b]

X	C$^+$	C (CH$_3$)	C$_1$	C$_{2,6}$	C$_{3,5}$	C$_4$	C$'_\alpha$[c]	C$'_\beta$[c]
H	254.3	32.1	139.8	140.8	131.8	154.5	—	—
4-Me	241.0	30.3	137.2	140.6	132.7	174.0	23.4	—
4-Et	241.6	30.1	137.5	141.0	131.6	179.1	30.8	12.2
4-*i*-Pr	241.3	29.9	137.6	141.1	130.2	183.0	36.7	20.6
4-*t*-Bu	242.3	30.1	137.4	140.8	129.4	185.0	38.1	28.4

[a]Chemical shifts are ±0.1 ppm downfield from external TMS.
[b]Similar data have been reported by Brown *et al.* (ref. 23).
[c]C′ is the carbon atom(s) of the 4-alkyl substituent.

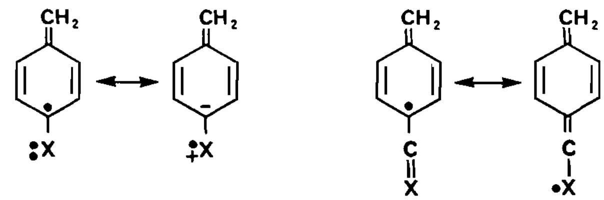

a b

FIG. 1. Substituent interactions in benzyl radicals; (a) β-spin donating substituent; (b) β-spin accepting substituent.

impossible to predict *a priori* where hydrogen will fit in the series. Furthermore, it is not possible to rank the relative effect of the β-spin donors against the α-spin acceptors.

So far, only effects on the π-system have been considered; effects on unpaired electron delocalization through the σ-framework have been ignored. Since the *meta* substituents do not interact directly with the benzylic carbon through the π-system, these substituted radicals can be used to assess the effect of substitution on delocalization in the σ-framework.

Most of the *meta* substituents delocalize spin density less effectively than the unsubstituted benzyl radical ($\sigma_\alpha^\bullet < 0$). This can be explained in terms of an inductive effect. Correlation of the α-H hfc's with σ_m, in fact, gives a straight line with a slope of 0.6 having a correlation coefficient (r) of 0.927 with the ten available points (Fig. 2). The correlation of the *meta*-substituted derivatives with σ_m also was noted by Creary from his study of the rearrangement of 2-aryl-3,3-dimethylmethylenecyclopropanes (12). This correlation can be related to the electrophilic nature of the radical.

The decreased delocalization by inductive withdrawal of electrons must not be unique to the *meta* substituents. The three *para* substituents which lead to decreased delocalization (relative to the unsubstituted radical) are all inductively withdrawing substituents; the σ values for *para*-CF$_3$, *para*-F, and *para*-OCOCH$_3$ are 0.53, 0.15, and 0.31 respectively (13). Certainly, in the case of *para*-F and *para*-CF$_3$, delocalization involving the π-system is expected to be small (14).

The decrease in spin delocalization as substituents become more electron withdrawing in nature should not come as a complete surprise. The electrophilic nature of the benzylic radical is well known (15) and, while this has often been considered to be a transition state polar effect (16), it is not unreasonable that the benzyl radical should be intrinsically electron deficient.

The mechanism by which the inductive withdrawal of electron density can lead to a decrease in spin delocalization is not so easily visualized. There is an excess of β-charge density at the *meta* position in the benzyl radical. Inductive withdrawal of

TABLE 4. Calculated (INDO) hyperfine coupling constants for some substituted benzyl radicals[a]

Substituent	a_1	a_2	a_3	a_4	a_5	a_6
4-CN	−16.73	−6.52	3.98	1.22	3.98	−6.52
	(0.932)	(0.767)	(0.447)	(0.786)	(0.447)	(0.767)
4-Me	−16.86	−6.43	3.67	7.18	3.67	−6.43
	(0.949)	(0.790)	(0.436)	(0.905)	(0.436)	(0.790)
4-Et	−16.86	−6.38	3.66	[b]	3.66	−6.38
	(0.952)	(0.783)	(0.505)		(0.505)	(0.783)
4-*i*-Pr	−16.86	−6.39	3.70	[b]	3.70	−6.39
	(0.954)	(0.798)	(0.486)		(0.486)	(0.798)
4-*t*-Bu	−16.86	−6.38	3.72	[b]	3.72	−6.38
	(0.956)	(0.799)	(0.470)		(0.470)	(0.799)
4-F	−16.92	−6.51	3.63	13.43	3.63	−6.51
	(0.970)	(0.814)	(0.482)	(1.074)	(0.482)	(0.814)
3-Me	−17.00	−6.55	−3.74	−5.75	3.64	−6.51
	(0.954)	(0.786)	(0.904)	(1.070)	(0.481)	(0.768)
H	−17.01	−6.43	3.61	−5.63	3.61	−6.43
	(0.955)	(0.793)	(0.471)	(1.089)	(0.471)	(0.793)
3-F	−17.03	−6.45	−7.70	−5.56	3.69	−6.51
	(0.962)	(0.767)	(0.613)	(1.113)	(0.488)	(0.791)
3-CN	−17.05	−6.84	−1.72	−5.94	3.78	−6.65
	(0.978)	(0.767)	(0.417)	(1.040)	(0.475)	(0.744)

[a]The ratio of the experimental hfc to the calculated hfc is in parentheses.
[b]These hfc's depends on the preferred conformation of the C—H bond with respect to the aryl ring.

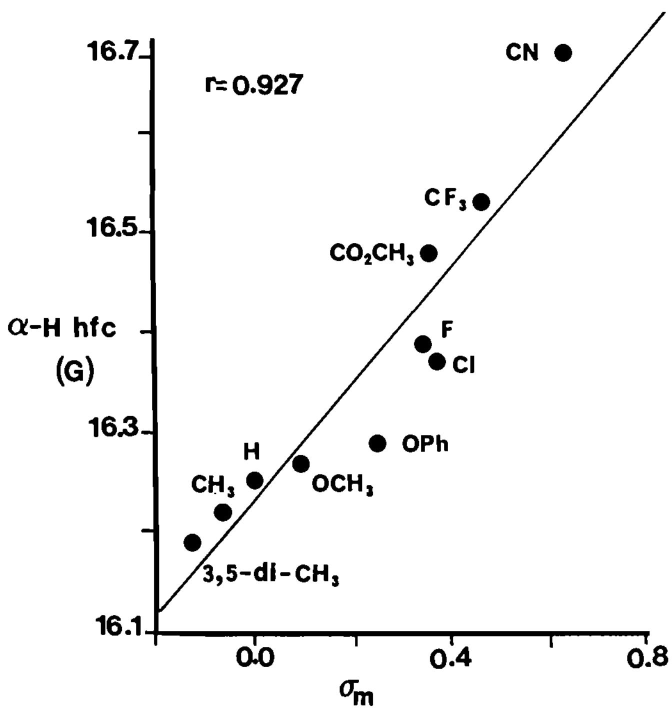

FIG. 2. Plot of α-H hfc versus σ_m for the *meta*-substituted benzyl radicals.

an excess of β-charge density by a substituent can lead to a net donation of β-charge density by the benzylic carbon into the ring. In this case, the apparent decrease in spin delocalization would be because of a net withdrawal of β-charge density from the benzylic position. For inductively donating substituents such as *meta*-CH_3, the apparent increase in spin delocalization could then be the result of a net increase in β-charge density at the benzylic carbon.

It should be noted that while this explanation accommodates the observed "*meta* effect", it cannot be used to rationalize the effect of the three *para* substituents with negative $\sigma_\alpha^\bullet$ values. If, however, the McConnell relationship applies to the entire series of benzyl radicals, the usefulness of the $\sigma_\alpha^\bullet$ scale as a reactivity parameter is not diminished, since relative reactivity will be proportional to the α-spin density (in the absence of transition state polar effects).

The calculated (INDO) hfc's for several *meta*- and *para*-substituted benzyl radicals are shown in Table 4. The ratio of the experimental hfc to the calculated hfc is approximately constant for most of the radicals. It is clear, however, that the spin distribution in the benzyl radical is not adequately reproduced for quantitative evaluation of the effects. The general trends are reproduced, but the *meta* effect is underestimated and the decreased delocalization in the *para*-fluorobenzyl radical is not predicted.

One of the difficulties with the molecular orbital approach is that complete geometry optimization of each structure is not feasible. The inductive withdrawal of electron density from the σ-framework may have the effect of lengthening the bond between the benzylic carbon and the aryl ring. This of course would lead to a decreased orbital overlap between the carbons and, consequently, a larger α-H hfc. It has been found, using *ab initio* calculations (STO-3G), that small variations in this carbon−carbon bond length have a negligible effect on the electronic *energy* of the benzyl radical, but a large effect on the *spin density* on the benzylic carbon.[3] Therefore, there is a possibility that the inductive withdrawal of electron density will result in *increased* localization of α-spin density at the benzylic position either by decreasing the overlap between the interacting centres or by increasing the energy separation between the interacting systems. In other words, the electron-withdrawing groups will lower the energy of the aromatic π-system (i.e. increase the ionization potential), which, from

[3]A. M. de P. Nicholas and D. R. Arnold, Unpublished results.

simple PMO theory, results in a decreased interaction between the benzylic carbon and the aromatic system (11). This alternative explanation should be general for both *meta* and *para* substitution.

Other MO calculations by Gey *et al.* also using model geometries, failed to adequately reproduce the experimentally determined spin distribution or substituent effect (17). Inclusion of configuration interaction improved the agreement with experimental results only slightly.

While there have been numerous studies of esr spectra of alkyl radicals (5, 18), most of these studies have been directed towards the investigation of conformational preferences, which are influenced by both steric and hyperconjugative interactions. While some studies have specifically addressed the question of the effect of substitution at the β-carbon on spin delocalization (19), the effect of branching at the α-carbon of an alkyl substituent on spin delocalization in benzylic radicals is not known. This understanding is important since many free radical reactions involve this type of intermediate, and since comparison of the effect of alkyl substituents on the spin density at the benzylic carbon in the radicals to the effect on charge density (as measured by ^{13}Cmr) at the benzylic carbon in the carbocations can be made.

The order of decreasing spin delocalization by a *para*-alkyl substituent in benzyl and cumyl radicals is methyl > ethyl > isopropyl > *tert*-butyl, in accord with the Baker–Nathan order of stabilization (Table 2). Similar results have been reported for the alkyl substituted cyclopentadienyl radicals (19).

The substituent effects on the β-H hfc in the cumyl radicals (20) are only just outside the quoted experimental uncertainty (±0.03 G) for the entire range (*para*-methyl to *para-tert*-butyl). It is, therefore, difficult to draw firm conclusions from the differences between, for example, *para*-methyl and *para*-ethyl or *para*-ethyl and *para*-isopropyl. The range of α-H hfc for the benzyl radicals is larger (0.12 G) but, even here, comparisons between adjacent members in the series is difficult. It is clear, however, that the difference (>0.1 G) between *para*-methyl and *para-tert*-butyl in both radicals is real.

It is tempting to attribute all of this effect to a difference in hyperconjugative interactions with a C—C bond relative to a C—H bond. This, certainly, will not be the case since, as we have discussed above, there must be some inductive interactions. The inductive effects, however, will be comparatively small. For example, the increased delocalization, relative to the unsubstituted benzyl radical, by a *meta*-methyl substituent is only 0.03 G. If the plot of α-hfc versus σ_m for the *meta*-substituted derivatives is extrapolated, the predicted α-hfc for the *meta-tert*-butylbenzyl radical is only 0.05 G less than for the unsubstituted benzyl radical. Therefore, the ratio of α-hfc (*tert*-butyl)/α-hfc (methyl) will slightly overestimate the relative effectiveness of C—C versus C—H hyperconjugation. By taking the difference between the *para*- and the *meta*-substituted derivatives, the ratio of these differences is approximately 40%, compared to 60% obtained when correction for the inductive effect is not included. A similar upper limit is predicted for the cumyl radicals.

It is also possible to assess the relative importance of C—C and C—H hyperconjugation in benzyl radicals from the INDO calculations. The calculated spin densities on the carbon atoms of the *tert*-butyl group in the *para-tert*-butylbenzyl radical and on the hydrogens of the methyl group in the *para*-methylbenzyl radical are shown in Table 5. The contribution from spin polarization is estimated from the spin density at a dihedral angle of

TABLE 5. Hyperconjugative interactions of C—H and C—C bonds from INDO calculations

	Spin density on the β-atom		
θ (degrees)	H[a]	C[b]	Ratio[c]
0.0	0.0011	0.0011	—
30.0	0.0072	0.0052	0.67
60.0	0.0193	0.0127	0.64
90.0	0.0255	0.0163	0.62

[a]Hydrogens of the methyl group in the 4-methylbenzyl radical.
[b]Carbons of the *tert*-butyl group in the 4-*tert*-butylbenzyl radical.
[c]Calculated by subtracting the spin density from the spin polarization mechanism (θ = 0) from the spin density on the atom. The ratio of the difference is an estimate of the relative contribution of hyperconjugation.

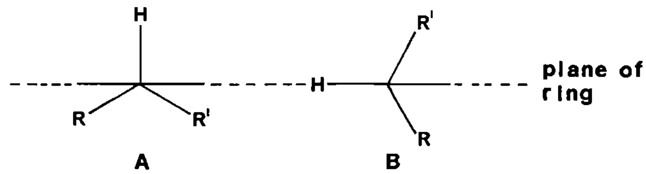

FIG. 3. Conformational preferences of *para*-alkyl substituents. (a) θ = 90° (b) θ = 0°.

0° (measured as the angle between the C—X bond and the plane of the ring), since there will be no contribution from hyperconjugation in this conformation. The results in Table 5 lead to the prediction that C—C hyperconjugation is about 65% as effective as C—H hyperconjugation. This compares favourably with the ratio estimated from the esr data.

Hyperfine coupling to the hydrogens of the alkyl substituents can give information about the conformational preference of the substituent. While the barrier to rotation of the alkyl groups is probably small, there will be preferred conformations which balance the steric interactions between the β-methyl groups and the *meta* ring hydrogens against the favourable hyperconjugative interactions (21). The magnitude of the β-hfc (of the benzylic hydrogens on the alkyl group) follows a $\sin^2 \theta$ relationship (22), where θ is the angle between the C—H bond and the plane of the ring. Two conformations are generally considered (Fig. 3). If an average angle of 45° for the *para*-methyl substituent is used, an approximate equation for the β-hfc can be determined (eq. [2]) for the cumyl radicals.

[2] $\beta\text{-hfc} \simeq 11.6 \sin^2 \theta$

From this equation an average angle (θ) of 30° is estimated for the *para*-ethyl group (at −40°C). This implies that conformation A is preferred for this substituent. For the *para*-isopropyl group, an average angle (θ) of 27° is calculated. The *para*-isopropyl benzyl radical shows a small but positive temperature coefficient (β-H hfc is 2.35 G at −40°C and 2.25 G at −60°C), which implies that, for the isopropyl group, conformation B is preferred (i.e. θ_{ave} decreases as the temperature decreases).

A comparison of the alkyl substituted cumyl radicals to the carbocations is now possible. Recently, Brown *et al.* have published the ^{13}Cmr spectra of several *para*-alkyl substituted cumyl carbocations, including -methyl, -ethyl, -isopropyl, and -*tert*-butyl (23). It was found that, in contrast to gas phase studies (4, 5) in solution, the stabilization by alkyl substituents follows the Baker–Nathan order. The differences between the gas phase and solution studies were attributed to a greater inductive contribution to the stabilization of the carbocation in the gas phase.

TABLE 6. ^{13}C-SCS of aryl ring carbons in 4-alkyl cumyl carbocations and monoalkylbenzenes[a]

	Aryl ring carbon	Substituent				
		H	Me	Et	*i*-Pr	*t*-Bu
C_1	Cumyl	0.0	−2.6	−2.3	−2.2	−2.4
	benzene	0.0	−2.9	−2.6	−2.4	−2.9
	^{13}C-SCS	0.0	0.3	0.3	0.2	0.5
$C_{2,6}$	Cumyl	0.0	−0.2	0.2	0.3	0.0
	benzene	0.0	0.0	0.0	0.1	−0.2
	^{13}C-SCS	0.0	−0.2	0.2	0.2	0.2
$C_{3,5}$	Cumyl	0.0	0.9	−0.2	−1.6	−2.4
	benzene	0.0	0.8	−0.4	−1.9	−3.1
	^{13}C-SCS	0.0	0.1	0.2	0.3	0.7
C_4	Cumyl	0.0	19.5	24.6	28.5	30.5
	benzene	0.0	9.3	15.7	20.2	22.4
	^{13}C-SCS	0.0	10.2	8.9	8.3	8.1

[a]Data for monoalkylbenzenes taken from ref. 24. For clarity the aryl carbons are numbered such that the substituent is bound to C_4.

The ^{13}Cmr spectra of the *para*-methyl, *para*-ethyl, *para*-isopropyl, and *para-tert*-butyl cumyl carbocations had also been measured in this laboratory. The observed chemical shifts are similar to those reported by Brown *et al.* (Table 3). However, our measurements were performed at −40°C, the same temperature used in the esr study. While we agree with the conclusions drawn by Brown and his co-workers, i.e., the Baker−Nathan order of stabilization is followed for the cumyl carbocations, there are other features of the ^{13}Cmr spectra which are noteworthy.

If the chemical shifts of the *meta*-methyl and *meta-tert*-butyl groups are interpolated from the plot of δ^{13}C versus σ^+, treatment similar to that used above for the radical indicates that C—C hyperconjugation is 75−90% as effective as C—H hyperconjugation. This compares very well with the 80% estimated by Brown *et al.* in their previous study of the solvolysis of cumyl chlorides (3).

Although the upfield shift of the C^+ chemical shift indicates that the cumyl carbon is becoming more shielded from *para-tert*-butyl to *para*-methyl, the effects on the ring carbon chemical shifts in some cases are in the opposite direction. The ^{13}C-SCS (substituent chemical shift) for the ring carbons of the cumyl carbocations and the monosubstituted alkyl benzenes (24), relative to the respective unsubstituted derivatives, are shown in Table 6. The differences between the two sets of numbers reveal an interesting trend. For C_1 and $C_{2,6}$ the differences indicate that there is no substituent effect on the carbocation beyond that expected by substitution of an alkyl group alone. On the other hand, $C_{3,5}$ shows an increasing effect while C_4 shows a decreasing effect. Furthermore, the difference in ^{13}C-SCS at C_4 is between 8 and 10 ppm, with methyl causing the greatest downfield shift and the other alkyl groups causing progressively smaller downfield shifts. These effects are another indication that C—H hyperconjugation is more effective than C—C hyperconjugation; in fact, this appears to be an even more sensitive probe than the chemical shift at C^+.

As the ^{13}C-SCS at C_4 decreases from methyl to *tert*-butyl, the chemical shifts of the alkyl carbons shift downfield. This also indicates that hyperconjugation to hydrogen is more effective than to carbon, since increasing the number of β-methyl groups results in less charge delocalization from C'_α, thus causing a downfield shift. The increased charge at C'_α would certainly be transmitted to C'_β.

Conclusions

The substituent effects on benzyl radical hfc's can be rationalized by simple perturbation molecular orbital theory. The interactions in the *para*-position will be predominantly either two-orbital, three-electron interactions, if the substituent has a lone pair of electrons; or three-orbital, three-electron interactions, if the substituent is unsaturated. With substitution in the *meta* position, the α-H hfc's correlate positively with σ_{meta}, indicating that the benzyl radical is intrinsically electrophilic.

The esr spectra of the *para*-alkyl substituted cumyl radicals indicate that the Baker-Nathan order of stabilization is followed. It is suggested that C—C hyperconjugation is from 40−60% as effective as C—H hyperconjugation for delocalizing spin density.

From the ^{13}Cmr spectra of the *para*-alkyl substituted cumyl carbocations, it is found that the Baker−Nathan order of stability is followed and that C—C hyperconjugation is 75−90% as effective as C—H.

Experimental

General information

The esr spectra were recorded on a Varian Associates E 109 B electron paramagnetic resonance spectrometer equipped with a liquid nitrogen variable temperature accessory. All spectra were recorded with the aid of the Nicolet 1170 signal averager. Typically, sixteen spectra were averaged (2 min per spectrum). Coupling constants were measured directly from the oscilloscope and refined by computer simulation (8) using the IBM-PC. All spectra were reproducible within the experimental uncertainty. The estimated uncertainty of ±0.03 G is the limit of resolution of the recording device used to plot the experimental spectra and the simulations. The ^{1}Hmr spectra were recorded on a Varian T-60 spectrometer and are reported in parts per million downfield from TMS. The ^{13}Cmr spectra of the cumyl cations were referenced with respect to external acetone-d_6, which has a chemical shift of 207.1 ppm downfield from TMS at −40°C. All ^{13}Cmr spectra were measured with the Atlantic Region Magnetic Resonance Centre Nicolet 360-MHz nmr spectrometer.

Di-*tert*-butyl peroxide (DTBP) and triethylsilane were obtained from Pfaltz and Bauer Inc. and were used without further purification. Hexamethylditin was obtained from Alpha Products and used without further purification. *para*-Methoxyacetophenone (PMA) was obtained from Aldrich Chemical Company Inc. and was recrystallized twice from 95% ethanol prior to use. Chlorobenzene (J. T. Baker Chemicals Inc.) was stirred over concentrated sulphuric acid, washed successively with water, saturated sodium bicarbonate, and water, dried over anhydrous magnesium sulphate, and distilled through a Vigreux column.

Preparation of benzyl bromides

The method of Grice and Owen (25) was used for the conversion of substituted benzyl alcohols to the bromides. Typically, the benzyl alcohol (0.02 mol) was dissolved in benzene (100 mL). Hydrogen bromide gas was passed through the solution for 1 h or until the solution was saturated. The reactants were heated to reflux and the water which formed was removed via a Dean−Stark trap. The solution was then dried over anhydrous magnesium sulphate, filtered, and the solvent removed at reduced pressure. The bromide was then purified by sublimation. Preparation and purification of the cumyl bromides have been described previously (7, 10).

para-*Ethylbenzylbromide*

The crude product was purified by vacuum distillation (88°C at 1 Torr; 1 Torr = 133.3 Pa) to give a 70% yield of the bromide (26); ^{1}Hmr ($CDCl_3$): 7.18 (m, 4H), 3.80 (s, 2H), 2.65 (q, 2H), 1.23 (t, 3H).

para-*(2-Propyl)benzylbromide*

The product was purified by vacuum distillation (62°C at 0.02 Torr) to give a 73% yield of the bromide (27); ^{1}Hmr ($CDCl_3$): 7.17 (m, 4H), 4.38 (s, 2H), 2.87 (m, 1H), 1.22 (d, 6H).

Electron spin resonance experiments

Toluenes

A static solution of DTBP (0.5 mL) and the toluene (100 mg) with PMA (45 mg) was irradiated in the esr spectrometer cavity using a filtered (methanol in a quartz tube) 1-kW Xe−Hg high-pressure lamp. Temperatures were controlled between 20°C and −60°C (depending on the solubility), with the majority of the samples examined at −40°C. All samples were purged with nitrogen for 5 min prior to irradiation.

Benzylbromides

Two methods were used to generate the benzyl radicals from the bromides. In method 1, a static solution of DTBP (0.2 mL), triethylsilane (0.2 mL), and the bromide (50−100 mg), diluted if necessary with chlorobenzene, was purged with nitrogen and irradiated as described above in the esr spectrometer cavity. In method 2, a solution of the bromide (50−100 mg) in *tert*-butylbenzene or chlorobenzene was continuously purged while hexamethylditin (0.1 mL) was injected via the nitrogen purge tube. It was necessary to have a glass wool plug in the purge tube to filter the hexamethylditin. This solution was irradiated as described above. The use of chlorobenzene allowed cooling of the sample to temperatures as low as −20°C without precipitation of the hexamethylditin.

Acknowledgments

This work was supported by a grant from the Natural Sciences and Engineering Research Council of Canada (including a scholarship to D.D.M.W.). The authors also acknowledge helpful discussions with R. E. Wasylishen, R. J. Boyd, and A. M. de P. Nicholas. The ^{13}Cmr spectra were obtained on the Nicolet 360-MHz spectrometer at the Atlantic Regional Magnetic Resonance Centre at Dalhousie University.

1. (*a*) R. S. MULLIKEN. J. Chem. Phys. **7**, 339 (1939); (*b*) R. S. MULLIKEN, C. A. REIKE, and W. G. BROWN. J. Am. Chem. Soc. **63**, 41 (1941).
2. J. W. BAKER. Hyperconjugation. Oxford Press, London. 1952.
3. H. C. BROWN, J. D. BRADY, M. GRAYSON, and W. H. BONNER. J. Am. Chem. Soc. **79**, 1897 (1957).
4. (*a*) E. M. ARNETT and J. W. LARSEN. J. Am. Chem. Soc. **91**, 1438 (1969); (*b*) J. W. HEHRE, R. T. MCIVNE, JR., J. A. POPLE, and P. V. R. SCHLEYER. J. Am. Chem. Soc. **96**, 7162 (1974); (*c*) W. J. ARCHER, M. A. HOUSSAINI, and R. J. TAYLOR. J. Chem. Soc. Perkin Trans. 2, 181 (1982).
5. J. C. SCHULTZ, F. A. HOULE, and J. L. BEAUCHAMP. J. Am. Chem. Soc. **106**, 3917 (1984).
6. P. S. ENGEL. Chem. Rev. **80**, 99 (1980).
7. (*a*) J. M. DUST and D. R. ARNOLD. J. Am. Chem. Soc. **105**, 1211 (1983); (*b*) **105**, 6531 (1983); (*c*) D. D. M. WAYNER and D. R. ARNOLD. Can. J. Chem. **62**, 1164 (1984).
8. U. M. OEHLER and E. G. JANZEN. Can. J. Chem. **60**, 1542 (1982).
9. D. P. KELLY and H. C. BROWN. Aust. J. Chem. **29**, 957 (1976).
10. F. BERNARDI, N. D. EPIOTIS, W. CHERRY, H. B. SCHLEGEL, M. H. WHANGBO, and S. WOLFE. J. Am. Chem. Soc. **98**, 649 (1976).
11. A. PROSS and L. RADOM. Prog. Phys. Org. Chem. **13**, 1 (1981).
12. (*a*) X. CREARY. J. Org. Chem. **43**, 1777 (1978); (*b*) **45**, 280 (1980).
13. N. B. CHAPMAN and J. SHORTER. Correlation analysis in chemistry. Plenium Press, New York. 1978.
14. L. M. STOCK and M. R. WASIELEWSKI. Prog. Phys. Org. Chem. **13**, 253 (1981).
15. W. H. DAVIS, JR. and W. A. PRYOR. J. Am. Chem. Soc. **99**, 6365 (1977).
16. W. A. PRYOR, D. F. CHURCH, F. TANG, and R. TANG. Frontiers in free radical chemistry. *Edited by* W. A. Pryor. Academic Press, New York. 1980 pp. 355−379.
17. (*a*) E. GEY and N. E. KRUGLYAK. Z. Phys. Chem. (Leipzig), **255**, 915 (1974); (*b*) **256**, 737 (1975); (*c*) E. GEY and T. TINO. Croat. Chem. Acta, **51**, 11 (1978).
18. (*a*) P. J. KRUSIC, P. MEAKIN, and J. P. JESSON. J. Phys. Chem. **75**, 3438 (1971); (*b*) P. J. KRUSIC and J. K. KOCHI. J. Am. Chem. Soc. **93**, 846 (1971); (*c*) J. LIN and F. WILLIAMS. J. Phys. Chem. **72**, 3707 (1968); (*d*) K. U. INGOLD and J. C. WALTON. J. Am. Chem. Soc. **104**, 616 (1982).
19. M. KIRA, M. WATANABE, and H. SAKURAI. J. Am. Chem. Soc. **102**, 5202 (1980).
20. D. R. ARNOLD, A. M. DE P. NICHOLAS, and M. S. SNOW. Can. J. Chem. **63**, 1150 (1985).
21. W. J. E. PARR and T. SCHAEFFER. Acc. Chem. Res. **13**, 400 (1980).
22. E. W. STONE and A. H. MAKI. J. Chem. Phys. **37**, 1326 (1962).
23. H. C. BROWN, M. PERIASAMY, and P. T. PERUMAL. J. Org. Chem. **49**, 2754 (1984).
24. D. F. EWING. Org. Magn. Reson. **12**, 499 (1979).
25. R. GRICE and L. N. OWEN. J. Chem. Soc. 1947 (1963).
26. V. I. ROZENBERG, R. I GORBACHIVA, V. A. NIKANOIOV, YU. G. BUNDEL, and D. A. REUTOV. Zh. Org. Chim. 2222 (1975).
27. J. I. CROWLEY and H. RAPOPORT. J. Org. Chem. **45**, 3215 (1980).

Étude d'α-bromo-butyrolactones; application à la préparation du méthyl-3 phényl-4 Δ^2 buténolide et du méthyl-2 phényl-1 butène-2 diol-1,4 de configuration *Z*

JOSYANE GHARBI-BENAROUS, MARTHA S. MORALES-RIOS ET GILBERT DANA[1]
Laboratoire de Stéréochimie Réactionnelle, Bât. F, Université Pierre et Marie Curie, 4 place Jussieu, 75230 Paris Cédex 05, France

Reçu le 12 septembre 1984

JOSYANE GHARBI-BENAROUS, MARTHA S. MORALES-RIOS et GILBERT DANA. Can. J. Chem. **63**, 2384 (1985).

À partir de dérivés dihydro-2,3 furanniques, on prépare successivement les bromhydrines et les bromobutyrolactones correspondantes. Une méthode d'équilibration de ces dernières par solvolyse dans le DMF est décrite. Les divers stéréoisomères sont séparés et étudiés à l'état pur. Une réaction d'élimination catalysée par les bases faibles (LiBr) conduit au buténolide correspondant avec un excellent rendement lorsque la lactone comporte un substituant en Cβ. La réaction se produit quelle que soit la configuration de l'isomère de départ. Une application de la réaction est décrite avec la synthèse stéréosélective du γ-diol du titre avec un rendement total supérieur à 85%.

JOSYANE GHARBI-BENAROUS, MARTHA S. MORALES-RIOS, and GILBERT DANA. Can. J. Chem. **63**, 2384 (1985).

Starting from 2,3-dihydrofuranic compounds, we prepare the corresponding α-bromohydrines and α-bromo-butyrolactones. A solvolytic method of equilibration of these bromolactones in DMF is described. All the stereoisomers are separated and studied. With a Cβ substituent, the elimination promoted by a weak base (LiBr) gives the Δ^2 butenolide in good yield, whatever the starting isomer configuration may be. An application is given with the stereoselective synthesis of a trisubstitued ethylenic γ-diol with a *Z* configuration.

Au cours de nos études concernant la déshydratation des α-diols éthyléniques, nous avons montré que les diols du type **1** peuvent conduire de façon quasi-exclusive (1) à des composés dihydro-2,5 furanniques **2**. Récemment, nous avons mis en évidence l'existence d'un intermédiaire réactionnel, l'α-diol éthylénique **3** de configuration *E*, isomère de **1** (2) dont la formation semble nécessiter le passage par un γ-diol insaturé, de type **4**,*Z* ou **4**,*E*.

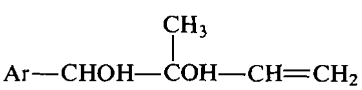

1

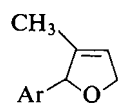

2

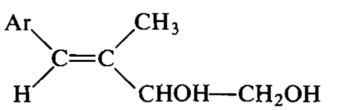

3,*E*

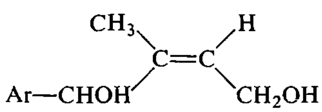

4,*Z*

Suivant sa configuration, ce diol **4** pourrait être un précurseur direct de **2** (isomère *Z*) ou un précurseur de **3** qui évolue ensuite en **2** (2). Dans le présent mémoire nous décrivons une synthèse sélective et aisée du méthyl-2 phényl-1 butène-2 diol-1,4 (**4**, Ar = C_6H_5) de configuration *Z*.

Cette synthèse consiste principalement à préparer, à partir des deux dérivés dihydro-2,3 furanniques **5** et **6** (3, 4), le buténolide **7** (schéma 1): on forme d'abord les bromhydrines correspondant aux dérivés dihydrofuranniques **5** et **6**; par oxydation ces bromhydrines donnent accès à des butyrolactones α-bromées dont la débromhydratation en Δ^2-buténolide s'est avérée facile. La réduction de ce buténolide en diol **4** de configuration *Z*, a été réalisée par action de $LiAlH_4$.

Nous discuterons la stéréochimie des différentes étapes de façon à montrer comment, partant du mélange des deux dérivés dihydrofuranniques **5** et **6** et obtenant successivement un mélange de 8 bromhydrines et de 4 bromolactones, nous avons pu préparer dans de bonnes conditions le buténolide **7** et, donc de façon rapide, efficace et stéréosélective, le diol **4**,*Z*.

[1] Auteur à qui adresser la correspondance.

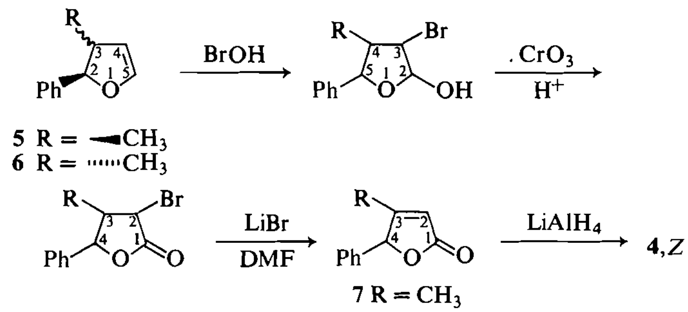

SCHÉMA 1

1. Préparation des bromhydrines

Le *N*-bromosuccinimide (NBS), en solution dans le diméthyl-sulfoxyde (DMSO) anhydre (5) réagit habituellement sur les oléfines pour former des dérivés dibromés. En présence d'humidité, le DMSO intervenant comme réactif (6) en même temps que solvant, conduit généralement par addition *anti* aux bromhydrines correspondantes, de façon stéréosélective (6, 7).

Avec les dérivés dihydrofuranniques **5** et **6**, le NBS en solution dans le DMSO humide conduit au mélange des *cis* et *trans* bromhydrines (schémas 2 et 3).

L'ion bromonium intermédiaire est en effet en équilibre avec un carbocation fortement stabilisé par les doublets libres de l'oxygène. La stéréochimie de la réaction rappelle tout à fait celle observée lors de l'étude d'autres additions électrophiles sur des éthers d'énols, linéaires (8) ou cycliques (9, 10). Comme pour les cas analogues de l'addition du chlore ou du brome (9, 11), l'entrée initiale du réactif électrophile se fait de façon largement prépondérante par la face α, opposée au noyau benzénique (~90%). Finalement chacun des composés dihydrofuranniques **5** et **6** conduit à un mélange où prédominent deux bromhydrines épimères (**8***a et* **8***b* pour **5** et **10***a* et **10***b* pour **6**, schéma 3).

La réaction est effectuée à température ambiante sur le composé dihydrofurannique **5** pur (4) ou sur des mélanges **5** et **6** (3) diversement enrichis en **6** (50 à 70%). Les bilans sont établis par rmn du proton à 80 MHz sur les produits bruts de la réaction; les spectres de certains isomères purs ont été repris à 250 MHz (tableau 1).

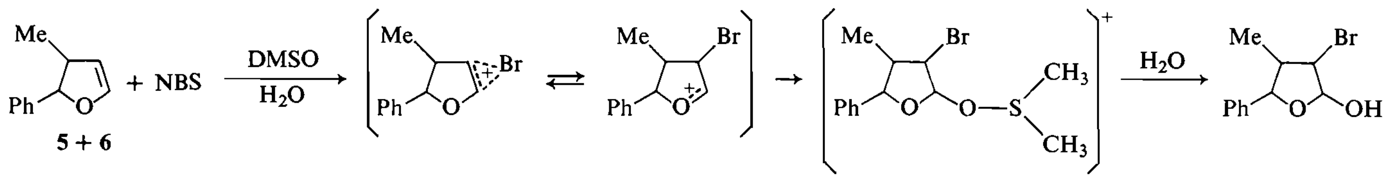

SCHÉMA 2

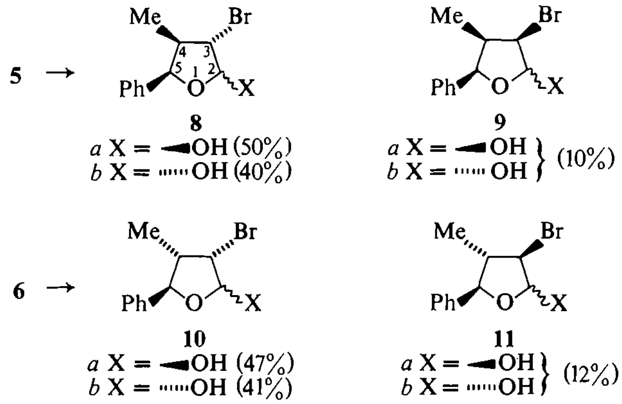

N.B.: Nous désignerons par α les substituants sur la face opposée au phényle et par β les substituants sur la même face que le phényle: *a*, X = OHβ; *b*, X = OHα

SCHÉMA 3

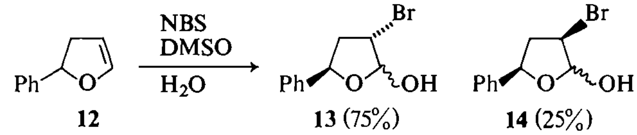

SCHÉMA 4

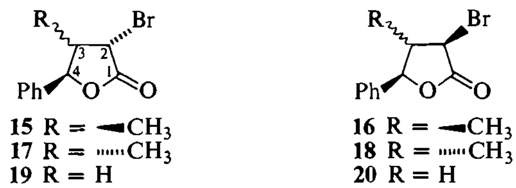

SCHÉMA 5

Par cristallisation (éther de pétrole), on isole aisément la bromhydrine **10***a* (F = 132°C). Les différents isomères peuvent être séparés par chromatographie en couche mince (ccm) sur silice, après acétylation. Les spectres rmn de chaque bromhydrine et de son acétate sont discernables principalement par le déplacement chimique du proton H2, plus déblindé de 0.7 à 1 ppm dans les acétates (tableau 1).

L'attribution des structures des différentes bromhydrines est effectuée d'une part grâce à l'analyse des couplages observés en rmn du proton (9, 12) et d'autre part grâce à l'étude des lactones préparées pour l'étape suivante de la synthèse. Nous verrons que cette oxydation supprime le centre asymétrique hémiacétalique sans altérer la configuration du carbone voisin, porteur du brome; l'analyse du mélange de lactones obtenues (schéma 5) indique donc directement l'importance relative des attaques électrophiles par la face opposée au phényle (face α) ou du côté du phényle (face β), pour chacun des composés dihydrofuranniques **5** ou **6**. Il apparaît que 10% environ d'entrée de l'électrophile Br^+ se fait par la face β du dihydrofuranne, quelle que soit l'orientation du méthyle en 3. Il peut paraître surprenant que la présence du méthyle sur l'une ou l'autre face du cycle dihydrofurannique intervienne aussi peu au cours de l'étape d'approche du réactif électrophile.

Il nous a alors paru intéressant d'examiner le cas du dérivé dihydrofurannique **12**, non méthylé en 3. On obtient de nouveau un mélange de 4 bromhydrines (schéma 4) puis de deux lactones (schéma 5) plus facilement analysable par rmn. On note alors que la lactone résultant de l'approche de l'électrophile par la face la plus encombrée **20** représente 25% du mélange. Apparemment, le méthyle en 3 intervient de façon complexe dans le problème de l'approche des réactifs, modifiant par un effet conformationnel, l'orientation du phényle.

II. Préparation des lactones bromées

Après extraction à l'éther, le mélange brut des bromhydrines est oxydé à l'aide du réactif de Jones (13). On obtient avec un rendement de 96 à 98% par rapport aux dérivés dihydrofuranniques **5** et **6** de départ, un mélange de lactones bromées séparables par ccm. La composition du mélange reflète à la fois celle des dihydrofurannes **5** et **6** de départ et, pour chacun, le pourcentage d'attaque électrophile par l'une ou l'autre face du cycle dihydrofurannique. Nous avons pu en effet montrer que les bromhydrines **8** à **11** donnent respectivement les lactones **15** à **18**.

Au cours de l'étape suivante de la synthèse (débromhydratation des lactones), nous avons mis en évidence une méthode simple d'équilibration de ces bromolactones par épimérisation du brome en α du carbonyle. Cette réaction permet d'accéder aux isomères **16** et **18** en quantité notable et de connaître la composition des mélanges à l'équilibre (**16**/**15** = 23:77 et **18**/**17** = 56:44). Nous avons pu alors vérifier que l'oxydation par le réactif de Jones de bromhydrines pures ou diversement enrichies donne bien les lactones correspondantes et que ces lactones, hors d'équilibre, n'évoluent pas dans le milieu réactionnel.

Les structures de ces lactones sont établies par rmn du proton (interprétation des déplacements chimiques et des couplages) (tableau 2).

Un certain nombre d'analyses cristallographiques de γ-lactones (14) a montré que l'hétérocycle adopte une conformation enveloppe dans laquelle le carbonyle, l'oxygène hétérocyclique ainsi que les deux carbones voisins (C2 et C4) sont coplanaires. Si la même situation prévaut dans notre cas, les lactones **15** à **18**, en solution, doivent se trouver dans un état d'équilibre conformationnel entre deux formes enveloppes non équivalentes.

L'étude des constantes de couplage vicinal J(H2H3) et J(H3H4) en rmn du proton, l'étude du déplacement chimique de l'hydrogène H4 et du méthyle 3 permettent, en même temps que la confirmation de structure des différentes lactones bromées, le choix éventuel des conformations privilégiées.

Lorsque le méthyle est *cis* par rapport au phényle, son déplacement chimique est de l'ordre de 0,7 à 0,8 ppm alors que pour les isomères *trans*, le méthyle apparaît au dessus de 1 ppm. Ceci est sans doute lié, comme dans le cas des dérivés

TABLEAU 1. Spectres rmn (^{1}H) des bromhydrines tétrahydrofuranniques méthylées en 4 et de leurs dérivés acétylés (spectres effectués à 250 MHz en solution dans $CDCl_3$, TMS interne, δ en ppm, J en Hz)

Composé	X	δ H2	δ H3	δ H4	δ H5	δ H(Me)	δ H(Ph)	δ H(OAc)	J(H2H3)	J(H3H4)	J(H4H5)	J(H4HMe)
8*a*	OHβ	5,85(d)	4,0(dd)	2,73	5,50(d)	0,72(d)	7,32	—	3,0	6,0	6,0	7,5
8*c*	OAcβ	6,42(d)	4,05(dd)	2,68	5,52(d)	0,73(d)	7,26	2,08	1,9	3,4	6,4	7,0
8*b*	OHα	5,50(d)	3,75(dd)	2,73	5,42(d)	0,60(d)	7,32	—	4,0	10,4	8,0	7,0
8*d*	OAcα	6,58(d)	3,90(dd)	(m)	5,32(d)	0,65(d)	7,26	2,08	3,3	10,5	8,8	7,0
9*b*	OHα	5,72(d)	4,30(dd)	2,89	5,32(d)	0,71(d)	7,40	—	2,0	5,7	6,0	6,3
9*d*	OAcα	6,74(d)	4,40(dd)	2,85	5,30(d)	0,72(d)	7,20	2,02	2,0	6,0	7,0	6,3
10*a*	OHβ	5,72(s)	4,35(d)	2,45	4,77(d)	1,00(d)	7,36	—	0	4,5	10,0	6,3
10*c*	OAcβ	6,50(s)	4,4(d)	2,32	4,72(d)	1,02(d)	7,26	2,10	0	4,0	10,0	6,5
10*b*	OHα	5,75(d)	3,80(dd)	(m)	4,60(d)	1,00(d)	7,36	—	4,0	10,0	10,0	6,0
10*d*	OAcα	6,55(d)	3,95(dd)	(m)	4,60(d)	1,05(d)	7,26	2,10	4,0	9,0	9,0	6,5

dihydro (15) et tétrahydrofuranniques (16) analogues, à l'anisotropie du phényle dont la rotation est gênée par la proximité des substituants en 3. Pour la même raison, l'hydrogène H4 est simultanément déplacé en sens inverse (tableau 2). On peut alors noter que dans cette série de lactones bromées le couplage J(H3H4) *cis* est plus petit que J(H3H4) *trans* indépendamment de l'orientation du brome, ce qui résulte probablement d'une abondance relativement grande des conformations **17*a*** et **18*a*** (fig. 1) comportant deux hydrogènes H3 et H4 *trans* diaxiaux.

En ce qui concerne le couplage J(H2H3), une grande valeur (11,5 Hz pour **18**) peut être associée à une orientation diaxiale des deux hydrogènes *trans* alors qu'une petite valeur (3,5 Hz pour **15**) peut être associée à leur orientation biéquatoriale (fig. 1). Les valeurs de couplages *cis* (de type équatorial–axial) sont intermédiaires (tableau 2). Il est donc probable que la lactone **15** se trouve dans la conformation **15*a*** prédominante dans laquelle le phényle équatorial, en raison de son encombrement stérique et le brome axial, en raison des effets dipolaires (17) sont le plus à l'aise; le méthyle doit alors s'accommoder d'une orientation axiale. De même, la lactone **18** doit être dans la conformation **18*a*** prédominante avec phényle et méthyle équatoriaux, le brome devant alors s'accommoder d'une orientation pseudo-équatoriale. Pour les deux autres lactones, la rmn ne permet pas de choisir une conformation prépondérante. On peut néanmoins penser que la lactone **17** se trouve dans sa conformation **17*a*** de façon probablement exclusive, ayant à la fois les substituants volumineux phényle et méthyle, équatoriaux (J(H3H4) grand) et le substituant polaire brome, en α du carbonyle, axial. Dans le cas de la lactone **16**, il est probable que les deux conformations participent à l'équilibre.

Il résulte de cette analyse que l'on doit s'attendre à ce que la lactone **17** et dans une moindre mesure, **16** (grâce à sa conformation **16*b***) soient les isomères les plus aptes à subir l'élimination E2.

III. Obtention du buténolide 7

Il était alors important de trouver des conditions équilibrantes de débromhydratation, de façon que les isomères **15** et **18** ne soient pas perdus pour la synthèse.

Les sels de lithium (LiCl, LiBr. . .) employés comme nucléophiles dans des solvants polaires aprotiques permettent d'accéder à des doubles liaisons conjuguées à des groupes attracteurs par un mécanisme d'élimination bimoléculaire (18).

Or il est connu que certains solvants aprotiques sont capables d'épimériser une bromocétone en milieu non énolisant (17) et que le DMF est le meilleur solvant pour les solvolyses en milieu aprotique (18*b*, 18*c*).

Nous avons donc soumis le mélange des bromolactones précédentes, en solution dans le DMF anhydre, à l'action de LiBr et obtenu le Δ^2 buténolide correspondant **7**, facilement identifiable par ses propriétés spectroscopiques (ir, rmn) (19). Le procédé est rapide et efficace puisque le buténolide est obtenu avec un rendement de 95% en 1 h à 120°C, indépendamment de la configuration de la bromolactone de départ. Le produit brut de la réaction d'oxydation par le réactif de Jones peut donc être utilisé sans inconvénients.

Il était alors intéressant d'examiner le comportement de chacun des isomères des bromolactones (séparés par ccm) dans le même milieu (solution dans le DMF), à 60 ou 70°C, en présence ou en l'absence de LiBr.

En l'absence de LiBr, on observe que les deux couples de lactones (**15**, **16** d'une part et **17**, **18** d'autre part) ont des réactivités nettement différentes. L'équilibre **15** ⇄ **16** s'établit

TABLEAU 2. Spectres rmn (^{1}H) des bromolactones effectués à 80 MHz en solution dans $CDCl_3$ (TMS interne, δ en ppm, J en Hz)

Composé	δ H2	δ H3	δ H4	δ H(Me)	δ H(Ph)	J(H2H3)	J(H3H4)	J(H3H(Me))
15	4,12(d)	2,86	5,76(d)	0,69(d)	7,25	3,5	6	7
16	4,87(d)	3,01	5,56(d)	0,77(d)	7,25	6,5	5,5	7
17	4,45(d)	2,37	5,06(d)	1,01(d)	7,25	5,5	9,5	6,5
18	4,30(d)	2,50	4,86(d)	1,13(d)	7,25	11,5	9,5	6,5

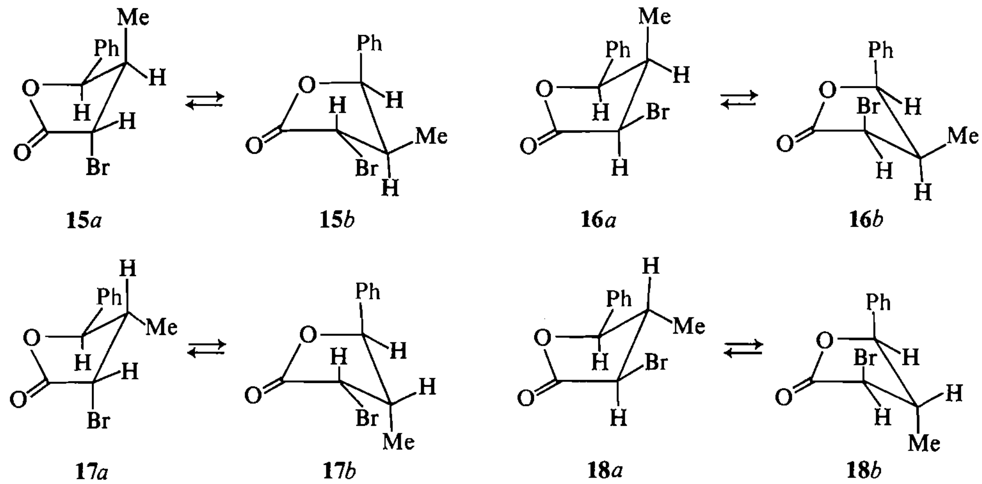

FIG. 1

plus lentement et il faut attendre environ 5 jours à 60°C pour atteindre une composition voisine de l'équilibre: **15**/**16** = 80:20 à partir de **15** ou **15**/**16** = 74:26 à partir de **16**. Au contraire l'équilibre **17** ⇄ **18** est atteint en moins de 12 h à 60°C: **17**/**18** = 42:58 à partir de **18** et **17**/**18** = 45:55 à partir de **17**. Cette équilibration dans le DMF peut en fait s'accompagner d'une lente élimination en buténolide **7**. On observe que cette nouvelle réaction est plus rapide pour les lactones **15** et **16** que pour **17** et **18**. C'est ainsi qu'à 70°C, en 1 jour, **15** et **16** ont donné 44% de buténolide alors que **17** et **18** n'en ont donnée que 6%.

En présence de LiBr, on observe les mêmes réactions d'équilibration et d'élimination; la réactivité relative des différents isomères reste la même qu'en l'absence de LiBr, avec toutefois des vitesses fortement accrues par la présence du catalyseur. Ainsi, avec une solution environ 0,15 molaire de LiBr dans le DMF, à 70°C en 1 h, les isomères **15** ou **16** ont donné 35% de buténolide alors que **17** ou **18** n'en ont donné que 8%, les lactones résiduelles étant dans un rapport **15**/**16** = 70:30 dans le premier cas et **17**/**18** = 60:40 dans le deuxième cas, à partir de chacun des quatre isomères purs.

On peut donc penser que dans le DMF pur, seules les réactions de solvolyse ont lieu, alors qu'en présence des ions Br^- apparaît la possibilité supplémentaire des réactions bimoléculaires S_N2 et E2.

Une étude plus détaillée sur le mécanisme de l'élimination et de l'isomérisation des bromolactones sera présentée dans un prochain mémoire. Nous y décrirons notamment les difficultés rencontrées dans le cas des lactones non méthylées **19** et **20**.

En conclusion, pour ce qui concerne la préparation du Δ^2-buténolide **7**, nous avons pu en réaliser une synthèse intéressante en trois étapes simples et quantitatives, ne nécessitant pas la purification ou la séparation des produits intermédiaires. On sait tout l'intérêt que suscite ce type de molécules en raison de l'abondance des buténolides parmi les substances naturelles (20) ou la variété de leur propriétés physiologiques (21). Un certain nombre d'halolactones (22) présentent également un grand intérêt au point de vue synthèse. Nous avons, quant à nous, utilisé le buténolide **7** pour préparer le γ-diol **4**, de configuration Z.

IV. Préparation du γ-diol 4,Z (Ar = C_6H_5)

Par analogie avec la réduction d'autres γ-lactones (23) la réduction du buténolide **7** par $LiAlH_4$ en suspension dans l'éther nous a fourni de façon tout à fait sélective le γ-diol insaturé **4** de configuration *Z*, avec un rendement de 90%. Le diol est purifié par cristallisation dans le mélange benzène – éther de pétrole (10:90) (*F* = 75°C) et caractérisé par ses propriétés spectroscopiques. Son isomère *E* (*F* = 122–125°C) a été récemment isolé et décrit (24).

Le diol de configuration *Z* obtenu se distingue aisément de son stéréoisomère *E* par le fait que les deux protons du groupe CH_2OH terminal ne sont pas magnétiquement équivalents en rmn. Le centre asymétrique étant séparé du CH_2 par la double liaison, on assiste à un phénomène de diastéréotopie lointain qui tient sans doute à la possibilité d'une liaison hydrogène forte.

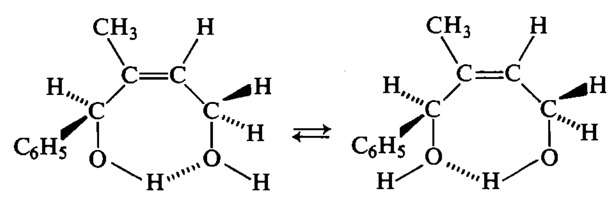

Cette structure ne peut évidemment pas exister pour l'isomère *E* (24). Le spectre ir, effectué en solution 5 × 10^{-3} molaire dans CCl_4 montre une raie fine à 3625 cm^{-1} et une bande large à 3460 cm^{-1}, l'aspect du spectre étant tout à fait analogue à celui des γ-diols saturés déjà décrits (25).

En spectrographie de masse, on note également des différences spectaculaires dans les spectres de fragmentations des isomères Z et E. Alors que l'isomère E est décrit (24) comme ne présentant pas de pic à $m/e = M - 18$, nous trouvons pour l'isomère Z que ce fragment donne le pic de base (m/e = 160:100%). D'autres pics intenses (159, 145, 116, 115, 105) n'existent pas pour l'isomère E et nous avons montré par filiation (défocalisation de métastables) qu'ils proviennent du fragment $M - 18$.

Partie expérimentale

Ce travail a été effectué à l'aide du matériel de spectroscopie et du Laboratoire de Microanalyse du Centre de Spectrochimie de Paris-Centre.

Les spectres rmn ^{1}H et ^{13}C ont été effectués sur spectrographe Bruker WP-80 et WP 250, en solution dans $CDCl_3$. Les déplacements chimiques sont exprimés en δ par rapport au tétraméthylsilane utilisé comme référence interne. Les constantes de couplage sont exprimées en hertz.

Les spectres de masse ont été réalisés avec le spectromètre Kratos MS50, les pourcentages des différents ions étant exprimés en % d'abondance relative. Les spectres ir sont faits en film liquide à l'état pur, ou en pastille KBr sur un spectrographe Perkin–Elmer modèle 357. Les points de fusion ont été déterminés sur le bloc Kofler.

Préparation des bromhydrines

À une solution refroidie à 10°C de 1 g (6,2 mmol) du mélange environ 1:1 des dérivés dihydrofuranniques **5** + **6** (3) dans 5 mL de DMSO additionné de 223 mg d'eau (2 équivalents), on ajoute sous atmosphère d'azote et sous agitation énergique, en une fois, 2,2 g de NBS. Au bout de 2 à 3 min, la solution s'échauffe légèrement et devient progressivement jaune puis orange. L'agitation est maintenue 10 à 15 min. On ajoute alors une douzaine de mL d'eau bicarbonatée. La solution s'éclaircit. On l'extrait à l'éther. Après séchage et évaporation de l'éther, le produit obtenu (1,57 g; rendement 98%) sera utilisé pour l'oxydation en lactone.

Le rendement est analogue à partir du dérivé dihydrofurannique *cis* **6** pur (4).

Hydroxy-2β bromo-3α méthyl-4α phényl-5β tétrahydrofuranne (**10***a*), F = 132°C

On dissout dans 5 mL d'éther, 850 mg de bromhydrines obtenues à partir du mélange **5** + **6**. Par addition progressive d'éther de pétrole, on obtient un précipité que l'on filtre (280 mg) et recristallise dans le même solvant: c'est l'isomère **10***a* (F = 132°C); ir: les bromhydrines présentent toujours une bande caractéristique ν_{OH} = 3400 cm^{-1} intense; rmn ^{1}H: tableau 1; ^{13}C: 12,4 (Me), 103,2 (C2), 60,5 (C3), 43,8 (C4), 87,3 (C5), 128,3 (C_p), 127,1 et 128,5 ($C_{m,o}$); masse m/e: 256 et 258 ($M^{+\cdot}$: 2%), 177 (29%), 77 (48%), 71 (100%). *Anal.* calc. pour $C_{11}H_{13}O_2Br$: C 51,36, H 5,09, Br 31,10; tr.: C 50,92, H 5,19, Br 30,79%.

Préparation des acétates des bromhydrines

On dissout 200 mg des bromhydrines dans le mélange anhydride acétique – pyridine (2 mL: 1 mL). Après 12 h à température ambiante, on hydrolyse et on extrait à l'éther. Les acétates ont été purifiés par ccm (éther/éther de pétrole 20:80). L'isomère **10***c* (X = OAcβ) cristallise (éther de pétrole/éther, F = 93°C).

Acetoxy-2β bromo-3α méthyl-4α phényl-5β tétrahydrofuranne (**10***c*), F = 93°C; ir (cm^{-1}): 1750 ($\nu_{C=O}$), 1270 (ν_{C-O}); rmn ^{1}H: tableau 1; masse m/e: 239 et 241 (7%: $M^{+\cdot} - 61$), 131 (88%), 91 (35%), 71 (55%), 43 (100%). *Anal.* calc. pour $C_{13}H_{15}O_3Br$: C 52,18, H 5,05, Br 26,70; tr.: C 52,12, H 5,12, Br 26,56%.

Les bromhydrines dérivées de **12** sont préparées de la même façon et avec des rendements analogues.

Hydroxy-2β bromo-3α phényl-5β tétrahydrofuranne (**13***a*), F = 80°C; rmn ^{1}H: 5,65 (H2α), 4,32 (H3β), 2,62 (H4α), 2,58 (H4β), 5,45 (H5α), 7,35 (H(Ph)), J(H2H3) = 0; J(H3H4α) = 0,5; J(H3H4β) = 4,25; J(H4αH4β) = −14,2; J(H5H4α) = 5,9; J(H5H4β) = 10,1. *Anal.* calc. pour $C_{10}H_{11}O_2Br$: C 49,38, H 4,53, Br 32,92; tr.: C 49,48, H 4,85, Br 32,62%.

Acetoxy-2β bromo-3α phényl-5β tétrahydrofuranne (**13***c*)

Cet ester est obtenu à partir de la bromhydrine cristallisée précédente; rmn ^{1}H: 6,5 (H2), 4,42 (H3), 2,65 (H4α), 2,55 (H4β), 5,55 (H5), 7,2 (H(Ph)), 2,08 (H(OAc)); J(H2H3) = 0,6; J(H3H4α) = 0,4; J(H3H4β) = 4,25; J(H4αH4β) = −14,4; J(H5H4α) = 5,8; J(H5H4β) = 10,2. *Anal.* calc. pour $C_{12}H_{13}O_3Br$: C 50,53, H 4,56, Br 28,07; tr.: C 50,21, H 4,69, Br 27,75%.

Préparation des bromo-lactones

Le mélange des bromhydrines (1,57 g) obtenu sous forme d'une huile claire à partir de **5** + **6** est dissous dans 30 mL d'acétone, puis refroidi à 0°C. On ajoute alors goutte à goutte, sous agitation, le réactif de Jones (13) (solution de 10,3 g CrO_3 dans 30 mL d'eau à laquelle on additionne dans la glace 8,7 mL H_2SO_4, d = 1,839) jusqu'à coloration rouge persistante. On laisse agiter 10 min puis on ajoute le minimum d'isopropanol pour revenir à la coloration verte. L'acétone est évaporée et le résidu solide, repris dans l'eau est extrait à l'éther. La solution éthérée est neutralisée (solution de bicarbonate), lavée, séchée et évaporée. Le produit huileux obtenu (1,56 g) apparaît par rmn et par ccm comme un mélange très propre de quatre lactones bien discernables (rendement 97% par rapport à **5** + **6**). Il est utilisable directement pour préparer le buténolide **7**.

Le mélange obtenu comporte deux isomères largement prédominants **15** (dérivé de **5**) et **17** (dérivé de **6**) et cristallise spontanément pour donner l'isomère **15** solide (F = 92°C).

Par isomérisation dans le DMF, on peut obtenir les deux autres lactones **16** et **18** purifiables par ccm sur silice (éther – éther de pétrole 30:70).

La formule exacte des différentes bromolactones a été confirmée par la mesure de la masse exacte de l'ion moléculaire en spectrographie de masse; ir: le spectre ir montre bien la disparition de la bande hydroxyle et la présence d'une bande double attribuable au groupe carbonyle d'une lactone α halogénée (26): 1770–1790 cm^{-1}; rmn: tableau 2.

De la même façon, le dérivé dihydrofurannique **12** conduit au mélange des deux bromolactones **19** et **20** séparables par ccm. L'isomère **19** cristallise après purification. À partir de 500 mg de **12**, on obtient 770 mg de lactones dont on extrait environ 550 mg de cristaux (F = 79°C).

Préparation du méthyl-3 phényl-4 $\Delta^{2(3)}$-butyrolactone (**7**)

Une solution de 1 g de LiBr dans 8 mL de DMF a été ajoutée à la solution de 1,56 g des bromo-lactones précédentes dans 35 mL de DMF. La solution est agitée pendant 1 h dans un bain d'huile à 120°C, sous atmosphère d'argon. Puis le mélange réactionnel est dilué avec 5 mL d'eau. Le buténolide extrait à l'éther (1,03 g) est pur. Après ccm (éther de pétrole – éther éthylique 50:50), il reste liquide (rendement final 95% par rapport au mélange **5** + **6** de départ); ir: 1760, 1645 cm^{-1}; rmn ^{1}H: 1,80 (m, 3H), 5,57 (m, 1H), 5,77 (m, 1H); J(H2H4) ≃ 0,6 Hz mesuré par découplage du méthyle. *Anal.* calc. pour $C_{11}H_{10}O_2$: C 75,86, H 5,74; tr.: C 75,77, H 5,86%.

Le même buténolide a été obtenu à partir de **6** pur: à partir de 500 mg de dérivé dihydrofurannique **6** de départ, on obtient 518 mg de buténolide **7**.

Préparation du phényl-1 méthyl-2 butène-2 diol-1,4 (**4**) (isomère Z)

Une solution de 100 mg de buténolide **7** dans l'éther anhydre est ajoutée lentement à 20 mg d'hydrure de lithium et d'aluminium en suspension dans 8 mL d'éther anhydre à 0°C. On chauffe 2–3 h à reflux sous agitation puis on hydrolyse. L'extraction à l'éther donne 98 mg du γ-diol **4** que l'on recristallise dans le mélange benzène – éther de pétrole (F = 75°C, rendement: 90% par rapport au mélange **5** + **6** de départ). Le même rendement a été obtenu sur une préparation de 4 g; ir (KBr): 1600 ($\nu_{C=C}$); 3360 (ν_{OH}). Le spectre en solution diluée dans CCl_4 a été discuté plus haut; rmn ^{1}H (à 250 MHz, $CDCl_3$): 1,60 (H(Me), s), 3,0 (H(OH), bande large), 4,18 et 4,41 (H4 et H4′), 5,61 (H3), 5,68 (H1, s), 7,30 (H(Ph)). Les protons H3, H4′ forment un système AMX, à 250 MHz, avec J(H4H4′) = 12 Hz, J(H4H3) = 6 Hz et 8 Hz; masse m/e: 178 ($M^{+\cdot}$: 1%), 160 (100%), 147 (14%), 145

(75%), 131 (47%), 129 (46%), 117 (32%), 115 (28%), 107 (41%), 105 (85%), 91 (40%); spectre de masse de l'isomère *E* (24): 178 (3%), 147 (18%), 131 (11%), 107 (24%), 105 (100%), 79 (28%), 77 (26%), 69 (11%), 51 (11%). *Anal.* calc. pour $C_{11}H_{14}O_2$: C 74,12, H 7,91; tr.: C 74,10, H 7,89%.

1. G. DANA, SA LE THI THUAN et J. GHARBI-BENAROUS. Bull. Soc. Chim. Fr. 2089 (1974); Can. J. Chem. **58**, 1451 (1980).
2. J. GHARBI-BENAROUS, M. S. MORALES-RIOS et G. DANA. J. Org. Chem. **49**, 2039 (1984).
3. A. ZYSMAN, G. DANA et J. WIEMANN. Bull. Soc. Chim. Fr. 1019 (1967); G. DANA et A. ZYSMAN. Bull. Soc. Chim. Fr. 1951 (1970); P. SCRIBE et J. WIEMANN. Bull. Soc. Chem. Fr. 2268 (1971).
4. (*a*) J. C. PALADINI et J. CHUCHE. Bull. Soc. Chim. Fr. 197 (1974); (*b*) S. HOLLAND et R. EPSZTEIN. Synthesis, 706 (1977).
5. C. T. CHENET et M. Y. WONG. Chem. Abstr. **68**, 12581 (1968).
6. D. R. DALTON, V. P. DUTTA et D. C. JONES. J. Am. Chem. Soc. **90**, 5498 (1968).
7. D. R. DALTON et V. P. DUTTA. J. Chem. Soc. (B), 85 (1971).
8. G. DANA, O. CONVERT et C. PERRIN. J. Org. Chem. **40**, 2133 (1975).
9. G. DANA et C. ROOS. Bull. Soc. Chim. Fr. 371 (1973).
10. R. U. LEMIEUX et B. FRASER-REID. Can. J. Chem. **43**, 1460 (1965).
11. C. PERRIN. Thèse d'ingénieur, Paris, 1976.
12. J. P. DECOR et G. DESCOTES. Bull. Soc. Chim. Fr. 2370 (1970).
13. (*a*) K. BOWDEN, I. M. HEILBRON, E. R. H. JONES et B. C. L. WEEDON. J. Chem. Soc. 39 (1946); (*b*) A. BOWERS, T. G. HALSALL, E. R. H. JONES et A. J. LEMIN. J. Chem. Soc. 2555 (1953); (*c*) L. F. FIESER et M. FIESER. Reagents of organic synthesis. Vol. 1. John Wiley, New York. 1967. p. 142.
14. G. A. JEFFREY et S. H. KIM. Chem. Commun. 211 (1966); P. KOLSAKER et A. S. BERG. Acta Chem. Scand. Ser. B, **33**, 755 (1979).
15. G. DANA, E. TOUBOUL et O. CONVERT. Org. Magn. Reson. **22**, 636 (1984).
16. G. DANA, E. TOUBOUL, M. MORALES-RIOS, M. PHILOCHE-LEVISALLES et C. BOIS. Can. J. Chem. **62**, 991 (1984).
17. B. MILLER et H. S. WONG. Tetrahedron, **28**, 2369 (1972).
18. (*a*) R. JOLY, J. WARNANT, G. NOMINÉ et D. BERTIN. Bull. Soc. Chim. Fr. 366 (1958); (*b*) P. BELTRAME, G. BIALE, D. J. LLOYD, A. J. PARKER, M. RUANE et S. WINSTEIN. J. Am. Chem. Soc. **94**, 2240 (1972); (*c*) W. J. FORD. Acc. Chem. Res. **6**, 410 (1973); (*d*) D. J. MCLENNAN. Tetrahedron, **31**, 2999 (1975); (*e*) H. KWART et A. GAFFNEY. J. Org. Chem. **48**, 4502 (1983).
19. (*a*) D. CAINE et A. S. FROBESE. Tetrahedron Lett. 5167 (1978); (*b*) E. J. COREY et G. SCHMIDT. Tetrahedron Lett. **21**, 731 (1980).
20. Y. S. RAO. Chem. Rev. **76**, 625 (1976); A. A. AVETISYAN et M. T. DANGYAN. Russ. Chem. Rev. **46**, 643 (1977); E. DEMOLE et D. BERTHET. Helv. Chim. Acta, **55**, 1866 (1972).
21. S. F. KRAUSER et A. C. WATTERSON, JR. J. Org. Chem. **43**, 3400 (1978); J. E. MCMURRY et S. F. DONAVAN. Tetrahedron Lett. 2869 (1977); A. COWELL et J. K. STILBE. Tetrahedron Lett. 133 (1979).
22. M. D. DOWLE et D. I. DAVIES. Chem. Soc. Rev. **8**, 171 (1979).
23. F. RAMIREZ et M. B. RUBIN. J. Am. Chem. Soc. **77**, 3768 (1955).
24. D. ANTONJUK, D. RIDLEY et M. SMAL. Aust. J. Chem. **33**, 2635 (1980).
25. L. P. KUHN, P. VON R. SCHLEYER, W. F. BAITINGER, JR. et L. EBERSON. J. Am. Chem. Soc. **86**, 650 (1964).
26. C. DAREMON, R. RAMBAUD et M. VERNIETTE. C. R. Acad. Sci. Sér. C, **277**, 255 (1973); S. CHOU, C. DAREMON et R. RAMBAUD. C. R. Acad. Sci. Sér. C, **276**, 1219 (1973).

ipso Nitration. XXVI.[1] Nitration of 1,2-dimethyl-4-nitrobenzene. Formation and reactions of adducts[2]

ALFRED FISCHER,[3] GEORGE N. HENDERSON, AND LOKANATHAN M. IYER
Department of Chemistry, University of Victoria, Victoria, B.C., Canada V8W 2Y2

Received November 16, 1984

ALFRED FISCHER, GEORGE N. HENDERSON, and LOKANATHAN M. IYER. Can. J. Chem. **63**, 2390 (1985).

Nitration of 1,2-dimethyl-4-nitrobenzene in a mixture of acetic anhydride and trifluoroacetic anhydride gives the diastereoisomers of 4,5-dimethyl-2,4-dinitrocyclohexa-2,5-dienyl acetate (50%), in addition to the 1,2-dimethyldinitrobenzenes. In moderate and more strongly acid conditions the adduct gives 4-nitro-, 3,4-dinitro-, and 3,5-dinitro-*o*-xylene. In neutral and weakly acid solutions 4-nitro- and 3,5-dinitro-*o*-xylene are formed by a radical and a sigmatropic pathway. The adduct reacts facilely with nucleophiles by allylic substitution to give a 5,6-dimethyl-6-nitrocyclohexa-2,4-dienyl derivative which, in many instances, undergoes a second allylic substitution to a new 4,5-dimethyl-2,4-dinitrocyclohexa-2,5-dienyl derivative. Depending on the nature of the introduced substituent, these 2,4- and 2,5-dienyl products may eliminate nitrous acid, under the reaction conditions, to give the corresponding aromatic compound. The dienyl acetates undergo acid-catalysed transesterification to the corresponding dienols.

ALFRED FISCHER, GEORGE N. HENDERSON et LOKANATHAN M. IYER. Can. J. Chem. **63**, 2390 (1985).

La nitration du diméthyl-1,2 nitro-4 benzène dans un mélange d'anhydride acétique et d'anhydride trifluoroacétique conduit, en plus des diméthyl-1,2 dinitrobenzènes, à la formation des diastéréoisomères de l'acétate du diméthyl-4,5 dinitro-2,4 cyclohexadiène-2,5 yle (50%). Dans des milieux modérément et plus fortement acides, l'adduit conduit aux nitro-4, dinitro-3,4 et dinitro-3,5 *o*-xylènes. Dans des milieux neutre ou légèrement acide, les nitro-4 et dinitro-3,5 *o*-xylènes se forment par un mécanisme radicalaire suivi d'une transposition sigmatropique. Par substitution allylique, l'adduit réagit facilement avec les nucléophiles et il conduit à un dérivé diméthyl-5,6 nitro-*o* cyclohexadiène-2,4 yle qui, dans plusieurs cas, subit une deuxième substitution allylique pour conduire à un nouveau dérivé diméthyl-4,5 dinitro-2,4 cyclohexadiène-2,5 yle. Dépendant de la nature des substituants introduits, ces produits diène-2,4 (ou −2,5) yles peuvent éliminer de l'acide nitreux dans les conditions de la réaction afin de conduire à la formation du composé aromatique correspondant. Les acétates de diènyles subissent des transestérifications acido-catalysées conduisant aux diénols correspondants.

[Traduit par le journal]

Nitration at a substituted position, *ipso* nitration (3), is competitive with nitration at an unsubstituted position in many aromatic compounds. The resulting *ipso*-nitrocyclohexadienyl cation is captured as a relatively stable acetate ester in acetic anhydride and can be isolated. In previous work the adduct from 3,4-dimethybenzonitrile has been obtained (4). The nitro group has directing and deactivating effects similar to those of the cyano group and it was anticipated that nitration of 1,2-dimethyl-4-nitrobenzene (4-nitro-*o*-xylene) would occur at the 2 position, *ipso* to methyl, to form an adduct.

Results and discussion

4-Nitro-*o*-xylene did not react at all when it was treated with nitric acid (5 mol ratio) in acetic anhydride (10 mol ratio) at 0°C for 48 h. Substituent constant data indicate that the nitro group is more electron withdrawing than the cyano group and this accounts for the reduced reactivity of the nitroxylene compared with the cyanoxylene. Addition of trifluoroacetic anhydride increased the reactivity of the nitrating mixture and the 4-nitro-*o*-xylene was then readily nitrated to form 3,4-dinitro- (16%), 4,5-dinitro- (12%), and 3,5-dinitro-*o*-xylene (22%), and the diastereoisomers of 4,5-dimethyl-2,4-dinitrocyclohexa-2,5-dienyl acetate (**1***am*) (40% and 10%). The reaction products were isolated by chromatography on silica and recrystallization of appropriate fractions.

Trifluoroacetic anhydride is a very effective catalyst for the nitration reaction and makes possible the nitration of deactivated substrates. 4-Nitro-*o*-xylene does not react at all in its absence, and the less deactivated 3,4-dimethylbenzonitrile, which reacts with nitric acid in acetic anhydride to the extent of 60% in 24 h, reacts to the extent of 85% in 1 h when trifluoroacetic anhydride is added.[4] In acetic anhydride nitric acid is converted into acetyl nitrate and this is accompanied by the formation of acetic acid. The trifluoroacetic anhydride would convert the acetic acid into the mixed anhydride and release trifluoroacetic acid. Since the nitration reaction is subject to acid catalysis (5), replacing the weaker acetic acid by the stronger trifluoroacetic acid would increase the rate of the reaction. Alternatively, trifluoroacetyl nitrate might be formed which would transfer nitronium ion more rapidly to the substrate and (or) exist in equilibrium with a higher concentration of nitronium ions, which react with the substrate.

Infrared, nuclear magnetic resonance, and elemental analytical data confirmed the presence of the substituents and functionalities depicted in structure **1***am*. The ultraviolet absorption maxima (*E*-**1***am* 225 nm; *Z*-**1***am* 227 nm) demonstrated that the

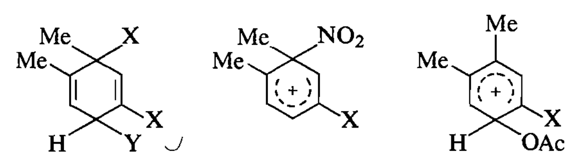

1 **2** **3**

a X = NO_2	*m* Y = OAc
b X = H	*n* Y = OMe
c X = CN	*o* Y = OH
d X = Ac	*p* Y = NO_2
e X = Bz	*q* Y = CN

[1]For Part XXV, see ref. 1.
[2]For a preliminary communication, see ref. 2.
[3]Author to whom correspondence may be addressed.
[4]D. L. Fyles and A. Fischer. Unpublished work.

TABLE 1. Relative gradients (gradient 1-$OCOCH_3$ = 1.00) of proton chemical shifts for diene adducts from the addition of Eu([$^2H_9$]fod)$_3$

Compound	1-H	3-H	4-CH_3/4-H	5-CH_3	6-H/CH_3
E*-1*am	1.62	0.24	0.16	0.03	0.70
Z*-1*am	1.57	0.28	0.09	0.06	0.69
12*m*	1.73	0.34	0.22	0.16	0.50

adducts are non-conjugated cyclohexadienes. Conjugated cyclohexadienes absorb above 250 nm (6). There are three possible locations for the double bonds in a non-conjugated cyclohexadiene derived from 4-nitro-*o*-xylene, the structures for which may be described, using the enumeration of the nitroxylene, as 1,4-, 2,5-, and 3,6-dienes. The 2,5-diene would have adjacent vinylic protons (5-H and 6-H) and these would exhibit a 10-Hz coupling which was not observed in either diene isomer. In the 1,4-diene the methyl groups would have similar magnetic environments in that each is attached to a vinylic carbon of the 1,2 double bond and each vinylic carbon is also attached to a tetrahedral carbon bearing a single hydrogen. Both methyl groups would be expected to be similarly coupled. However, only one methyl group in each isomer was split. Furthermore, the low-field proton, the 5-H in the 1,4-diene (attached to the other end of the 4,5 double bond to which the nitro group is attached), should exhibit a three-bond allylic coupling to the adjacent proton ($J \geqslant 2.6$ Hz (7)). However, in both isomers the low-field proton appeared as a singlet. Thus only the 3,6-diene arrangement of the double bonds, that shown in structure **1***am*, accounts for the ^{1}H nmr. Furthermore, only the 3,6-diene structure is in accord with the ^{13}C nmr spectra which exhibited absorptions at 61.4 and 88.9 ppm (*E*), and 60.9 and 87.7 ppm (*Z*) for the two diastereomers. These are characteristic absorptions for saturated carbon atoms. In the gated spectra the higher-field absorptions (61.4 and 60.9 ppm) were split into doublets (J = 155 Hz), indicating that in each isomer one of the atoms attached to the higher-field carbon is hydrogen, while the lower-field absorptions remained as singlets, indicating that there is no hydrogen atom attached to the lower-field saturated carbon atom. The 1,2-diene structure has one hydrogen on both saturated carbon atoms, while in the 2,5-diene neither carbon has an attached hdyrogen. Although the structure, in which the positions of the nitro and acetate are interchanged from those depicted in **1***am*, would also account for the ^{1}H nmr spectra, it would not account for the ^{13}C nmr spectra, which showed that the higher-field carbon atom, and therefore the one with acetate rather than nitro attached, is the one also attached to the hydrogen. This structure can also be rejected on the grounds that, being a secondary nitro compound, it would eliminate acetic acid exceedingly readily on treatment with base and, even if formed, would not have survived the work-up process.

The stereochemistry of the diastereoisomers was assigned on the basis of shift reagent effects. Addition of *tris*-(1,1,1,2,2,3,3-heptafluoro-7,7-[$^2H_6$]dimethyl-4,6-[$^2H_3$]octanedionato)europium(III) shifted the peaks of all protons to lower fields (Table 1). In both isomers the magnitude of the downfield shift followed the sequence 1-H > $OCOCH_3$ > 6-H > 3-H > 4-CH_3 > 5-CH_3 in accord with the expectation that the magnitude of the shift is a function of the inverse of the distance between the europium ion, attached to the acetate function, and the proton in question, and supporting the structural assignment discussed above. The shift of the 4-CH_3 protons in the major isomer (mp 95°C, eluted first) was markedly greater than that of the same protons in the minor isomer (mp 115°C, eluted second), and thus the *E* configuration (OAc *cis* to 4-CH_3) was assigned to the former and the *Z* configuration (OAc *trans* to 4-CH_3) to the latter.

Addition of nitronium ion to the 2 position of the substrate nitroxylene is the dominant nitration process. This is in accord with expectation since the nitro group is *meta* directing and, in *o*-xylene itself, *ipso* addition predominates over attack at an unsubstituted position (8). Thus, that *ipso* position which is *meta* to the nitro group is expected, and found, to be the most reactive site in 4-nitro-*o*-xylene. Calculations based on the assumed additivity of substituent effects, and using the relative partial rate factors for the nitration of toluene in acetic anhydride (9), and the isomer distribution for nitration of nitrobenzene in mixed acid (10), give the following relative extents of attack (parenthesized) at the indicated nuclear positions of 4-nitro-*o*-xylene: 1 (3), 2 (64), 3 (2), 4 (0), 5 (2), 6 (29). The observed order 2 > 6 > 3 ≈ 5 follows that calculated, but the 3 and 5 positions are much more reactive than predicted. Part of the difference between observation and calculation may lie in the fact that data for the isomer distribution for nitration of nitrobenzene in acetic anhydride is not available and data for mixed acid are used instead. However, it also appears that substituent effects in nitration are additive to only a rough approximation, at best (11, 12).

Reactions of diene 1am *with acids*

Previous studies of *ipso*-nitrocyclohexadienyl acetates have shown that the dominant reactions involve, in the initial step, either the acid-catalysed loss of acetate to (re)generate the *ipso*-nitrocyclohexadienyl cation, or the solvolysis of the nitro group, which departs as nitrite, to generate an acetoxycyclohexadienyl cation (13–16). Although the loss of nitrite is also reported to be acid-catalysed (16, 17), it is less sensitive to such catalysis than is the loss of acetate. Thus, strongly acidic conditions favour the formation of the nitrocyclohexadienyl cation, while weakly acidic, or neutral, ionizing conditions favour the formation of the acetoxycyclohexadienyl cation. The competitive balance between these two reaction pathways should be markedly affected by other substituents present in the cyclohexadiene ring. The presence of an electron-withdrawing substituent at the position *meta* to the *ipso*-nitro position results in the formation of the nitrocyclohexadienyl cation being competitive with the formation of the acetoxycyclohexadienyl cation down to lower acidity levels. The relevant cations in the case of **1***am* are **2***a* and **3***a*. Cation **3***a* is destabilized to a much greater extent by the presence of the substituent nitro group (attached to a formally positively charged centre in **3***a*) than cation **2***a* (in which the nitro goup is not attached to one of the formally positively charged centres). Similarly, the transition state leading to **3***a* is more destabilized than that leading to **2***a*. Thus the competitive balance between the two initial cation-forming reactions that exists when X = H is altered, when X = NO_2, in favour of the formation of **2***a*. In fact, cation **3***a* is so destabilized by the presence of the substituent nitro group that even at the lowest acidity levels it was not formed (none of its deprotonation product 2-nitro-4,5-dimethylphenyl acetate was detected) as other reactions intervened (*vide infra*).

Reaction of **1***am* with boron trifluoride-etherate or with trifluoroacetic acid gave the nitroxylene **6** (75%) plus the dinitroxylenes **8** and **9** (Table 2). These products arise from cation **2***a* by loss of nitronium ion, and by a sequence of 1,2 nitro shifts followed by deprotonation, respectively (Scheme 1). Myhre

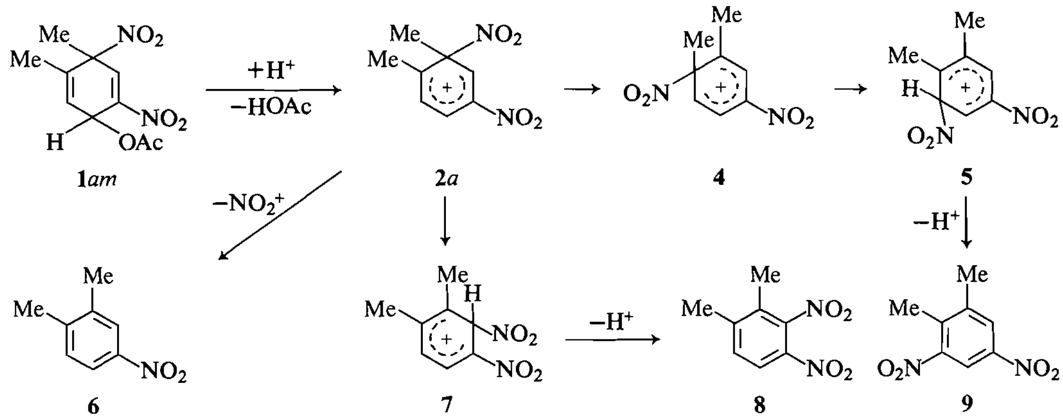

SCHEME 1

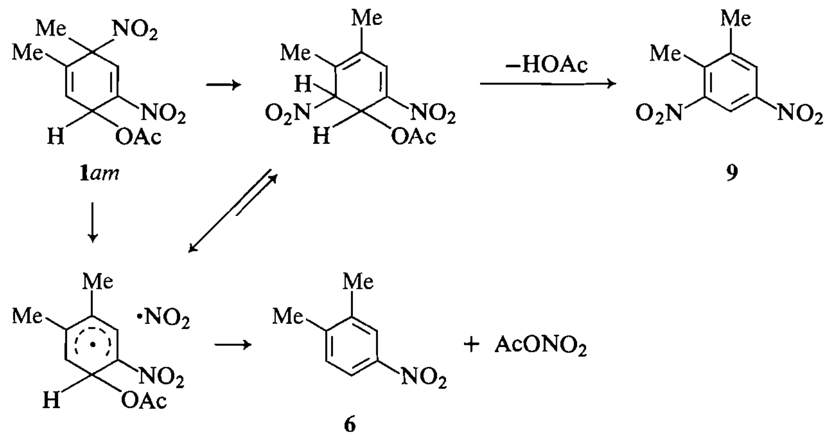

SCHEME 2

has shown that in the *ipso*-nitro cation from *o*-xylene 2*b* (2*a* and 4 are the 5-nitro and 4-nitro derivatives, respectively, of this cation) migration of the nitro group to the adjacent substituted position is fifty times faster than migration to the adjacent unsubstituted position (18). If the migration of the nitro group between the *ipso* positions of 2*a* and 4 is similarly favoured over migration to the *ortho* positions, then 2*a* and 4 should be quasi-equilibrated. At equilibrium 2*a* should be favoured because of the electronic effect of the substituent nitro group. On the other hand, the conversion of 2*a* to 7 should be inhibited by the substituent nitro group, whereas the conversion of 4 to 5 should be favoured. Thus 4, at a lower concentration, will rearrange with a higher rate constant to 5, whereas 2*a*, at a higher concentration, will rearrange with a smaller rate constant to 7. The combined effect results in the rates of formation of 5 and 7 being comparable, and thus similar amounts of 8 and 9 were obtained. Confirmation that an intermediate nitrocyclohexadienyl cation was involved in these reactions with acids was provided by repeating the reaction with boron trifluoride-etherate in the presence of mesitylene. The mesitylene captured cation 2*a* almost quantitatively to form the biphenyl **10** (19). The effect of the substituent in determining the reaction product of reactions carried out at a fixed acidity is nicely illustrated by reactions in trifluoroacetic acid. Whereas diene 1*am* gives the (di)nitroxylenes by loss of acetic acid, dienes 1*cm*, 1*dm*, and 1*em* give the aryl acetate by loss of nitrous acid (4, 20).

Reaction of 1*am* with hydrogen bromide in ether (which was not investigated in detail by glc) gave 4-nitro-*o*-xylene as the major product. In trifluoromethanesulfonic acid all three dinitro-*o*-xylenes were formed, in addition to a reduced amount of 4-nitro-*o*-xylene. An initial reaction would lead to **6**, **8**, and **9**, as in Scheme 1. In the strong acid, renitration of **6** can occur by the nitric acid liberated. If it is assumed that **6**, **8**, and **9** are initially formed in the same ratio as the average ratio of the trifluoroacetic and boron trifluoride catalysed reactions (75%, 14%, 11%) and that 44 of the 75% of **6** is renitrated to the dinitroxylenes **8**, **9**, and **11** in the same ratio that these are formed on nitration of **6** in trifluoroacetic anhydride – acetic anhydride (32:44:24), then the calculated product distribution of **6**:**8**:**9**:**11** is 31:28:30:11. The similarity to the observed ratio of 31:25:31:13 supports the proposed interpretation.

Diene 1*am* was stable to acetic acid at ambient temperature but rearomatized on heating to give **6** and **9** in nearly equal amounts. The same two products were obtained, although in a different ratio, when 1*am* was heated in toluene or pyrolyzed in the inlet of a gas chromatograph. These thermolytic reactions appear to share a common pathway. The 3,5-dinitroxylene **9** is obtained by a formal 1,3 shift of the nitro group. Such 1,3 shifts have also been observed in the rearomatization of diene adducts from dimethylbenzonitriles (4). We have shown that the adduct from 3,4-dimethylbenzonitrile (1*cm*) rearranges via a sigmatropic 1,3 nitro shift to a 2-cyano-6-nitrocyclohexa-2,4-dienyl acetate which readily eliminates acetic acid to form the 5-nitrobenzonitrile (21). The same mechanism, which also provides for the possibility of a minor contribution to the rearrangement reaction from a radical process, and which accounts for the formation of **6** and **9**, is applied to 1*am* in Scheme 2. In the presence of hydroquinone the reaction of 1*am* in acetic acid gave more **6** (68%) and less **9** (32%). Hydroquinone would act as a radical scavenger and the result suggests that a portion

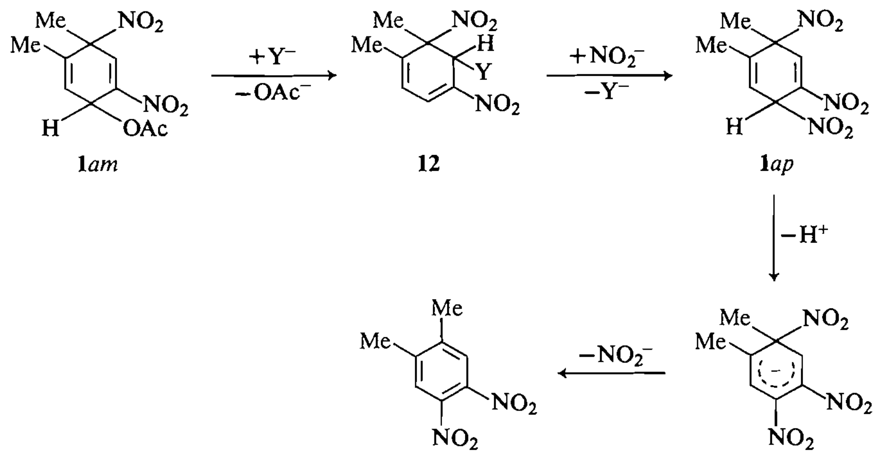

11

SCHEME 3

of the rearrangement reaction involves the radical pathway. In earlier work we suggested that such 1,3 nitro shifts occur in the *ipso*-nitro cation (4). Formal 1,3 nitro shifts do occur in the cation, as illustrated by the formation of **9** from **1***am* (Scheme 1), but these are a combination of successive 1,2 shifts and are accompanied, where possible, by the formation of the 1,2 shift product. No 3,4-dinitroxylene **8** (the 1,2 shift product) was obtained in the thermolytic reactions of **1***am* and, likewise, no 3,4-dimethyl-2-nitrobenzonitrile was obtained on the thermolysis of **1***cm*, which gave 3,4-dimethylbenzonitrile, 3,4-dimethyl-5-nitrobenzonitrile, and a trace amount of 2-cyano-3,4-dimethylphenyl acetate. It is now clear that the conditions used for the thermolytic reactions are too weakly acidic for the formation of the nitrocyclohexadienyl cation at a sufficient concentration for it to be the source of the aromatization products.

Reaction of **1***am* with 5% sulfuric acid in methanol resulted in transesterification and the formation of the *ipso*-nitrodienol **1***ao*. Because of the deactivating effect of the nitro substituent the normal $A_{AL}1$ cleavage to form **2***a*, which would give the dienyl methyl ether **1***an* and (or) **12***n*, is not competitive with $A_{AC}2$ reaction leading to the dienol. The stereochemistry at the AL chiral centre is preserved in the $A_{AC}2$ reaction and thus we were able to assign the configuration of the diastereoisomeric dienols **1***ao*: *E*-**1***am* gives *E*-**1***ao* and *Z*-**1***am* gives *Z*-**1***ao*.

Mention was made above of the effect of acidity on the competition between the formation of the ions **2***a* and **3***a* and that it appears that **3***a* is not formed even under the most favourable conditions (low acidity, ionizing solvent). Thus solvolysis of **1***am* in aqueous methanol gave **6** as the major product and no 4,5-dimethyl-2-nitrophenyl acetate (the deprotonation product of **3***a*) was obtained. As the acidity is reduced and formation of **2***a* becomes slower, **1***am* reacts by the radical and sigmatropic pathways, shown in Scheme 2, and by allylic substitution (*vide infra*). With less powerful electron-withdrawing groups than nitro, formation of the acetoxycyclohexadienyl cation **3** is more favoured and the product from this (the 2-X-3,4-dimethylphenyl acetate) begins to appear at low acidities. Thus a small amount of 2-cyano-3,4-dimethylphenyl acetate was present in the products of thermolysis of **1***cm* and, as the acidity was increased and conditions made more favourable for ionic reactions, the amount of the aryl acetate increased, becoming the major product in trifluoroacetic acid. Of course, in strongly acidic conditions the product of acetate loss and nitro migration, the dimethylbenzonitrile, should be favoured, although reaction of **1***cm* under these conditions was not investigated. The acyl-dienes **1***dm* and **1***em* gave the 2-acyl-4,5-dimethylphenyl acetate on rearomatization in neutral and weakly acid solution (i.e. on heating under reflux in toluene, acetic acid, or on standing in acetic acid (20)). No products were detected from a sigmatropic and (or) radical process, as illustrated in Scheme 2. The acyl groups are less electron-withdrawing than cyano (σ_{p-NO_2} = 0.78, σ_{p-CN} = 0.66, σ_{p-Ac} = 0.50 (22)) and the cations **3***d* and **3***e* should be more stable than **3***c*. At high acidities (boron trifluoride-etherate, 78% sufuric acid, 50% sufuric acid in acetic acid) these adducts rearomatized via cations **2***d* or **2***e* to form the 3,4-dimethylphenyl ketone and its 2-nitro and 5-nitro derivatives.

Reactions with nucleophiles

Diene **1***am* is unusual among nitronium acetate adducts in that it reacts with nucleophiles. The first such reaction was observed when we attempted to acetylate dienol **1***ao* using the acetic anhydride – pyridine reagent conventionally employed for the acetylation of hydroxyl groups (23), whence 1,2-dimethyl-4,5-dinitrobenzene (**11**) was obtained. The dienol itself was stable to pyridine, indicating that acetylation preceded aromatization, and this was confirmed by reacting the dienyl acetate **1***am* with neat pyridine to give **11** in close to quantitative yield. The reaction of **1***am* with pyridine provides a useful synthetic route to **11**.

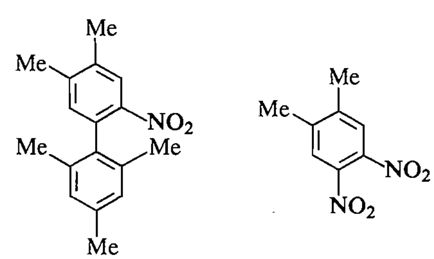

10 **11**

The mechanism shown in Scheme 3 involving consecutive S_N2' processes accounts for the apparent 1,4 migration of the nitro group (2). In the first step a general nucleophile adds at the 3 position of **1***am*, allylic to the acetate group which simultaneously departs as an anion. In the second step the general nucleophile is itself substituted at the new allylic position by the nitrite anion. For each substitution the normally unreactive (towards nucleophiles) vinyl carbon is activated by conjugation

TABLE 2. Yields of products from reactions of **1***am* (mol%)

Reagent	T(°C)	t(h)	**6**	**8**	**9**	**11**	**1**	**12**	Other
CF_3SO_3H	−20	0.1	31	25	31	13	—	—	—
CF_3CO_2H	20	18	72	15	13	—	—	—	—
BF_3OEt_2	0	0.1	78	14	8	—	—	—	—
BF_3OEt_2 Mes[a]	20	1	1	—	—	—	—	—	99 (**10**)
HBr/Et_2O	0	18	95	—	—	5	—	—	—
AcOH	100	0.3	49	—	51	—	—	—	—
$AcOH/Ac_2O$	100	0.2	44	—	56	—	—	—	—
AcOH[b]	100	0.3	68	—	32	—	—	—	—
5% H_2SO_4 MeOH	20	18	—	—	—	—	100[c]	—	—
C_5D_5N	0	0.03	3	5	—	92	—	—	—
C_5D_5N $CDCl_3$	0	18	2	3	—	95	—	—	—
$Me_2C_5H_3N$	0	0.3	2	4	—	94	—	—	—
$Me_2C_5H_3N$ $CDCl_3$	0	2	—	—	—	15	67[d]	17[e]	—
Me_3N	0	18	4	10	7	60	—	—	19[f]
KOH/MeCN[g,h]	0	0.5	—	—	—	100	—	—	—
Bu^{t}OK/MeCN	0	0.5	24	4	12	60	—	—	—
PhONa/MeCN	0	0.5	17	3	3	77	—	—	—
PhSNa/MeCN	0	0.1	1	—	—	—	—	—	99[i]
KOAc/MeCN[g,h]	0	0.1	—	—	—	100	—	—	—
KCN/MeCN[g,h]	0	0.1	—	—	—	30	—	—	70 (**14**)
KF/MeCN[g,h]	0	0.3	—	—	—	100	—	—	—
KBr/MeCN[g]	0	18	—	3	2	95	—	—	—
KBr/MeCN[g,h]	0	5	—	—	—	32	—	68[e]	—
KI/MeCN[g,h]	0	1	—	—	—	77	—	23[e]	—
KSCN/MeCN[g,h]	0	18	—	—	—	86	—	14[e]	—
NaOMe/MeOH	0	2	—	—	—	—	—	100[j]	—
KCN/MeOD[g]	0	0.5	—	—	—	6	—	—	94 (**14**)
KCN/MeOD[g] C_5H_5N	0	0.5	—	—	—	42	—	—	58 (**14**)
KNO_2/MeOD[g]	0	0.1	—	—	—	100	—	—	—
KF/MeOD[g,h]	0	20	—	—	—	28	57[k]	15[e]	—
KCl/MeOD[g,h]	20	170	—	—	—	100	—	—	—
KBr/MeOD[g,h]	20	78	—	—	—	22	45[k]	33[e]	—
KI/MeOD[g,h]	20	48	—	—	—	58	42[k]	—	—
KSCN/MeOD[g]	0	18	—	—	—	100	—	—	—
KBr/MeCN[g,h] Ac_2O	0	18	—	—	—	3	22[d]	75[e]	—
KBr/Ac_2O[g,h]	0	18	—	—	—	—	25[d]	75[e]	—
$MeOH/H_2O$	30	72	82	—	—	18	—	—	—
MeC_6H_5	110	1	78	—	22	—	—	—	—
glc	270	—	76	—	24	—	—	—	—

[a]Mesitylene.
[b]Containing hydroquinone.
[c]**1***ao*.
[d]**1***am*.
[e]**12***m*.
[f]*N-tert*-butyl-4,5-dimethyl-2-nitroaniline.
[g]Containing 18-crown-6.
[h]Nuclear magnetic resonance analysis only.
[i]4,5-Dimethyl-2-nitrophenyl phenyl sulfide.
[j]**12***n*.
[k]**1***an*.

of the double bond with the (non-migrating) vinylic nitro group. The proton α to the new nitro group in diene **1***ap* is acidic and is readily removed by base to form an anion which, in turn, rapidly loses the *ipso* nitro group as a nitrite anion (which is thus regenerated) to give **11**. The small amount of nitrite anion required to initiate the reaction could be formed by elimination of the elements of nitrous acid from **1***am* by the base. Support for the proposed mechanism is provided by the observation and isolation of the intermediate conjugated diene **12***m* and its further reaction to give **11**. It was possible to observe **12***m* as an intermediate in the reaction of **1***am* with 2,6-dimethylpyridine which reacts at ca. one-fifth of the rate of the reaction with pyridine. Thus reaction of **1***am* in chloroform with 2,6-dimethylpyridine gave, over 2 h at 0°C, unreacted **1***am* (67%) together with **12***m* (17%) and **11** (15%), whereas reaction with neat 2,6-dimethylpyridine gave **11** (94%) in 15

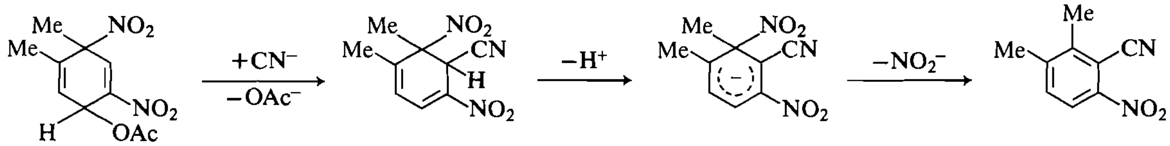

1*am* 12*q* 13 14

SCHEME 4

min. A more detailed nmr investigation of the reaction of dienol 1*ao* with acetic anhydride and pyridine at 0°C showed that acetylation to 1*am* was complete within 6 min and was accompanied by partial isomerization to give **12***m*. Formation of **11** then occurred and it was substantially complete in 1 h, during which time the intermediate formation of **12***m* was quite apparent. When 2,6-dimethylpyridine was used as the catalyst, both the acetylation and the aromatization reactions were much slower. After 24 h only 3% of **11** had been formed and the major compounds present were dienes **1***am* and **12***m*.

Generally, reaction of **1***am* with nucleophiles (Table 2) gave yields of **11** ranging from significant to substantial and indicating that nitrite anion is a very competitive nucleophile towards **12**. Thus, reaction of **1***am* in acetonitrile with hydroxide, *tert*-butoxide, phenoxide, acetate, thiocyanate, and halide ions, all gave high yields of **11**. Most notably in the reaction carried out with potassium bromide for a shorter reaction time, but also in some of the other reactions, the intermediate formation of **12***m* was apparent, supporting the mechanism outlined in Scheme 3. Thiophenoxide was an effective competitor for intermediate **12***m* in acetonitrile. Reaction of **1***am* with sodium thiophenoxide gave 4,5-dimethyl-2-nitrophenyl phenyl sulfide (99%). *tert*-Butylamine on reaction with **1***am* in chloroform gave a 19% yield of a compound tentatively identified as *N*-tert-butyl-4,5-dimethyl-2-nitroaniline, and presumably formed by attack of the amine on **12***m*, although **11** was the major product (60%). Since acetate appears to play the role of the nucleophile in the first substitution step of many of the above reactions, it is possible that this step may involve an internal concerted 1,3 migration of the ester acetate function, instigated by the addition of a nucleophile to the carbonyl carbon and thus converting the carbonyl oxygen into the more nucleophilic alkoxide. When cyanide ion was used as the nucleophile some **11** was formed, but 2,3-dimethyl-6-nitrobenzonitrile (**14**) was the major product (Scheme 4). We assume that in this case the cyanide ion successfully competes with acetate for the 3 position of **1***am*, giving **12***q*. The hydrogen atom α to the cyanide group in **12***q* is acidic and should be readily lost to give the corresponding anion **13** which would rearomatize by loss of nitrite. Cyanide is a poorer leaving group than acetate and this is another factor which would inhibit the allylic substitution of nitrite for cyanide in **12***q*, which would lead to **11**.

Acetate is liberated in the formation of **11** from **1***am* (Scheme 3) and is thus available in solution as a potential nucleophile. A striking feature of the competition between acetate and nitrite as nucleophiles is that, whereas acetate is the more effective nucleophile towards **1***am* (no intermediate **12***p* was detected, not even when **1***am* was reacted with potassium nitrite), nitrite is much more effective as a nucleophile towards **12***m*, as shown by the fact that reaction of **1***am* with potassium acetate in acetonitrile gave only **11**. Diene **12***p*, if formed, might be expected to rearomatize rapidly to **8**, but yields of this product in the nucleophilic reactions were at most very small and it is likely that these small amounts were formed by some other pathway. The 3 position in **1***am*, which is susceptible to nucleophilic attack, is flanked by methyl and nitro substituents at the quaternary centre, on one side, and by a nitro group attached to the sp^2 carbon on the other. These would hinder the approach of the bulky nitrite ion (with nitrogen acting as the nucleophilic centre). Even if this ion did add to give **12***p* it is possible that the latter would undergo rapid allylic substitution, rather than deprotonation to an anion and rearomatization to **8**, since this rearomatization process would require the newly introduced nitro group to move into the plane of the ring with increased steric interaction with the flanking groups. In contrast to nitrite, the linear (and therefore less subject to hindrance) cyanide ion readily attacked the 3 position of **1***am*, and the resulting **12***q* was readily deprotonated.

In reactions carried out in methanol there was more effective competition with nitrite for the intermediate **12**. The major product (~50%) in the reactions with potassium bromide, fluoride, and iodide was 4,5-dimethyl-2,4-dinitrocylohexa-2,5-dienyl methyl ether (**1***an*). It seems likely that the reactivity of nitrite as a nucleophile is reduced in methanol by hydrogen bonding or protonation, which allows methoxide ion or methanol to compete for the intermediate **12***m* with the small amount of available nitrite. In accordance with this suggestion, the reactions with potassium halides in methanol were much slower than reactions with potassium halides in acetonitrile. Again in these reactions the formation of **12***m* as an intermediate was apparent in the nmr spectra. Reaction of **1***am* with potassium nitrite in methanol did give **11** quantitatively, as did the reaction with potassium thiocyanate. Reaction of **1***am* with sodium methoxide in methanol at 0°C gave **12***n* in less than 5 min.

Reaction of **1***am* with potassium bromide in acetic anhydride proved to be an effective means of preparing **12***m*. In this solvent the further reaction of **12***m* with nitrite was suppressed, presumably by protonation or acetylation of the latter, and the reaction stopped at the intermediate stage. Reactions in which the conjugated diene **12***m* and its analogue **12***n* were used as substrates gave products in accord with the mechanisms outlined above (Table 3). Reaction of **12***m* with sodium methoxide in methanol gave the allylic substitution product **1***an* (77%) and **12***n* (23%). Presumably **12***n* is formed from **1***an* by a second allylic substitution. Reaction of potassium cyanide in methanol with **12***m* gave 4,5-dimethyl-2-nitrobenzonitrile and a small amount of **11**. Here the cyanide ion is able to compete effectively with nitrite (or methoxide) in the allylic substitution and the resulting **1***aq*, like **1***ap*, readily aromatizes by base-catalysed elimination of nitrous acid (cf. Scheme 3). Reaction of **12***n* with pyridine in chloroform, and with potassium iodide in acetonitrile, gave **11**. Reaction with potassium nitrite in methanol also gave **11** but, surprisingly, a substantial yield of **6** as well. Reaction with potassium cyanide in acetonitrile gave 4,5-dimethyl-2-nitrobenzonitrile and a further reaction product, 4,5-dimethyl-1,2-benzenedicarbonitrile.

Reaction of the cyanodiene **1***cm* (4) with potassium cyanide in acetonitrile gave 2-cyano-4,5-dimethylphenyl acetate (**15**)

TABLE 3. Yields of products from reactions of **1***ao*, **12***n*, and **12***m* (mol%)

Reagent	T(°C)	t(h)	6	8	9	11	1	12	Other
4% H_2SO_4[a] Ac_2O	35	0.03	82	7	11	—	—	—	—
C_5D_5N/Ac_2O[a]	0	18	—	—	—	100	—	—	—
$Me_2C_5H_3N$[a] Ac_2O	0	18	—	—	—	3	40[b]	57[c]	—
MeI/Ag_2O[a]	20	5	—	—	—	—	100[d]	—	—
BF_3OEt_2[e]	20	480	58	—	—	—	—	—	42[f]
C_5D_5N[e,g] $CDCl_3$	20	48	—	—	—	100	—	—	—
KI/MeCN[e,h]	20	18	—	—	—	100	—	—	—
KCN/MeCN[e,h]	0	0.1	—	—	—	—	—	—	70[i], 30[j]
KNO_2/MeOD[e,h]	20	360	44	—	—	56	—	—	—
glc[e]	260	—	98	—	—	—	—	—	2[k]
5% H_2SO_4[l] MeOH	20	18	—	—	—	—	—	90[m]	10[n]
NaOMe/MeOH[g,l]	0	2	—	—	—	—	77[o]	23[p]	—
KCN/MeOD[l,h]	0	2	—	—	—	13	—	—	87[i]
KI/MeOD[g,l,h]	0	18	—	—	—	100	—	—	—

[a]Substrate **1***ao*; analysis by ^{1}H nmr.
[b]**1***am*.
[c]**12***m*.
[d]**1***an*, reaction is stereospecific.
[e]Substrate **12***n*.
[f]2,3-Dimethyl-6-nitroanisole.
[g]Nuclear magnetic resonance analysis only.
[h]Containing 18-crown-6.
[i]4,5-Dimethyl-2-nitrobenzonitrile.
[j]4,5-Dimethyl-1,2-benzenedicarbonitrile.
[k]2,3-Dimethyl-6-nitroanisole.
[l]Substrate **12***m*.
[m]**12***o*.
[n]Unidentified aromatic products.
[o]**1***an*.
[p]**12***n*.

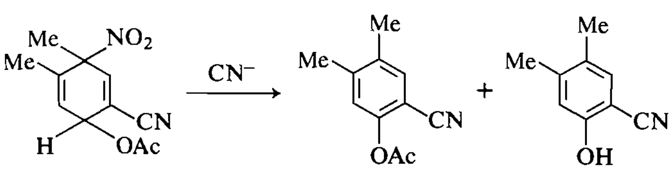

1*cm* 15 16

SCHEME 5

and its corresponding phenol **16** (Scheme 5). Evidently the 1,4 elimination of nitrous acid is preferred over the allylic substitution that occurs in **1***am*, most likely because the cyano group is less activating than nitro towards the Michael addition. Elimination to **15** also occurred, over two weeks, on reaction with sodium nitrite in methanol at 20°C. No reaction occurred between **1***cm* and pyridine in chloroform, at 20°C, over 1 week.

Other reactions

Reaction of dienol **1***ao* with sulfuric acid in acetic anhydride gave mainly **6**, together with **8** and **9**. Presumably cation **2***a* is formed as an intermediate, either directly, by acid-catalysed loss of hydroxyl, or by acetylation of **1***ao* to **1***am* followed by protonation and loss of acetic acid. Each of the diastereoisomers of **1***ao* was stereospecifically methylated with methyl iodide and silver oxide to its corresponding methyl ether. Since the stereochemistry of the dienols **1***ao* was established by the stereospecific transesterification of the acetates **1***am* (*vide supra*), the stereochemistry of the ethers was able to be determined: *E*-**1***ao* gives *E*-**1***an* and *Z*-**1***ao* gives *Z*-**1***an*.

5,6-Dimethyl-2,6-dinitrocyclohexa-2,4-dienyl methyl ether (**12***n*) reacted over 7 days with boron trifluoride-etherate, at 20°C, to give **6** and 2,3-dimethyl-6-nitro anisole. Methoxide is a poorer leaving group than acetate and the loss of nitrite from **12***n*, leading to the anisole, is competitive with loss of methoxide to form **2***a* and thence **6**. Pyrolysis of **12***n* gave mainly **6**.

5,6-Dimethyl-2,6-dinitrocyclohexa-2,4-dienyl acetate (**12***m*) underwent transesterification to the corresponding dienol (**12***o*) on treatment with sulfuric acid in methanol.

Experimental

The ir spectra, calibrated with polystyrene, were recorded as Nujol mulls or as potassium bromide discs, for solids, and as thin films between sodium chloride plates for oils, using a Pye–Unicam SP1000 or a Perkin–Elmer 283 spectrometer. The ^{1}H nmr spectra were recorded on Perkin–Elmer R32 (90 MHz) and Perkin–Elmer R12A (60 MHz) instruments. Spectra were routinely recorded in [^{2}H]chloroform, with tetramethylsilane as an internal standard. The ^{13}C nmr spectra were obtained in [^{2}H]chloroform, with tetramethylsilane as an internal reference, on a Nicolet TT14 (15.1 MHz) spectrometer. The uv spectra were recorded on a Cary-17 spectrometer, with methanol as solvent. Mass spectra were recorded on a Hitachi Perkin–Elmer RMU7 spectrometer at 70 eV. The glc analyses were performed on a Varian Aerograph 2400, using a 1.3 m × 3 mm column of 3% SE-30 on Chromosorb P at 180°C. A Finnegan 3300 system was used for combined gas chromatography and mass spectrometry of mixtures. A Waters Associates Prep LC/System 500 was employed for liquid chromatography.

1,2-Dimethyl-4-nitrobenzene was from Aldrich. Acetic anhydride was certified ACS, Fisher, and trifluoroacetic anhydride was Aldrich Gold Label (99+%). Nitric acid (300 cm^3, fuming, Fisher) was purified by distilling at 1 Torr (1 Torr = 133.3 Pa) from urea (10 g, reagent, Fisher) and sulfuric acid (500 cm^3) and stored at −25°C. Solvents used for chromatography including pentane (reagent, Fisher), anhydrous ether (reagent, Amachem), and benzene (reagent, Amachem) were further purified by drying over sodium followed by distillation and storage over molecular sieves. Non-deuterated solvents employed for spectroscopy were certified ACS, spectranalyzed (Fisher), and deuterated solvents were obtained from Merck, Sharp and Dohme. Silica gel (60–200 mesh) was Davison commercial grade H and neutral alumina (Camag, Activity I), deactivated with 3% of distilled water, was used.

In order to optimize the reaction conditions to obtain the maximum extent of diene formation on nitration, a series of reactions was carried out on a small scale (1 mmol of substrate). The reaction mixture was prepared at −78°C, the temperature then raised to 0°C, and aliquots were withdrawn at regular intervals. The ^{1}H nmr spectra of these samples were determined at −20°C. Each sample was then added to ether and neutralized with aqueous sodium bicarbonate. The ether extract was washed and dried ($MgSO_4$), the ether evaporated, and the ^{1}H nmr spectrum of the residue determined in [^{2}H]chloroform.

Small scale (nmr tube) reactions of the dienes were worked up by transferring the contents of the tube to a flask (25 cm^3), rinsing with ether, and neutralizing (where necessary) at low temperature with ammonia (for acidic reagents) or hydrochloric acid (for basic reagents). After washing with water the ether extract was dried and the ether evaporated, at 15°C, on a rotary evaporator. The product mixture was analysed by ^{1}H nmr and by glc–ms. Some reactions were only examined by ^{1}H nmr and this is indicated in the text.

*Nitration of 4-nitro-*o*-xylene*

Nitric acid (32 g, 0.51 mol) at −20°C was added cautiously and in small portions, with stirring, to a mixture of acetic anhydride (80 g) and trifluoroacetic anhydride (100 g) at −78°C.[5] The temperature of the mixture was raised to 0°C for 5 min to ensure complete reaction, and then lowered to −78°C. This nitrating mixture was added dropwise, over 10 min, to a solution of 4-nitro-*o*-xylene (**6**) (15 g, 0.1 mol) in acetic anhydride (20 g) at −78°C. The reaction temperature was then raised to 0°C and maintained for 2 h with stirring. At the end of this period, the reaction mixture was poured into a beaker containing ice (800 g) and ether (800 cm^3). Sodium bicarbonate was added to the stirred mixture until the latter was mildly alkaline (pH 8). The ether was separated and the aqueous phase extracted with ether. The combined extract was washed with water (2 × 600 cm^3), dried ($MgSO_4$), and evaporated at 15°C. Integration of the ^{1}H nmr spectrum of the crude reaction product showed that the diene adducts constituted ca. 50% of the total mixture.

The product was chromatographed on silica gel, at −40°C, using pentane–ether mixtures as eluent. Fractions eluted with up to 40% ether in pentane gave 1,2-dimethyl-3,5-dinitrobenzene (**9**) as the principal product, mp 75°C (lit. (24) mp 77°C); ir (KBr): 1520 and 1348 (NO_2) cm^{-1}; ^{1}H nmr (90 MHz, $CDCl_3$) δ: 2.46 (s, 3, 1-CH_3), 2.51 (s, 3, 2-CH_3), 8.18 (d, 1, 6-*H*), 8.35 (d, 1, 4-*H*) ppm, J_{46} = 2 Hz; ms (70 eV) *m/e* (relative intensity): 196 (40, *M*), 180 (15), 179 (100, *M* − OH), 133 (27), 132 (13), 104 (26), 103 (36), 91 (24), 78 (19), 77 (34), metastable peak at 163.5 corresponding to 196 → 179.

The 45% and 50% ether–pentane fractions gave a mixture containing 1,2-dimethyl-4,5-dinitrobenzene (**11**) (ca. 20%) and diene adducts (ca. 80%), which, on recrystallization from ether at −20°C, gave the *E* diastereomer of 4,5-dimethyl-2,4-dinitrocyclohexa-2,5-dienyl acetate (*E*-**1***am*), mp 95°C; uv (CH_3OH): 225 (775), 194 nm (1540 m^2 mol^{-1}); ir (Nujol): 1238 and 1742 ($OCOCH_3$), 1560 (NO_2) cm^{-1}; ^{1}H nmr (90 MHz, $CDCl_3$) δ: 1.88 (t, 3, 5-CH_3), 1.95 (s, 3, 4-CH_3), 2.06 (s, 3, $OCOCH_3$), 5.98 (m, 1, 6-*H*), 6.46 (m, 1, 1-*H*), 7.44 (s, 1, 3-*H*) ppm, J_{16} = 4, $J_{6,5\text{-Me}}$ = 1.5, $J_{1,5\text{-Me}}$ = 1.3 Hz. On a 300 Hz expanded spectrum, the peak due to 5-CH_3 appeared as a triplet (overlapping doublets) and the peak due to 1-H appeared as a multiplet. Irradiation of the methyl resonance at δ 1.88 collapsed the peaks at δ 5.98 and δ 6.46 ppm to two doublets. Irradiation at either δ 5.98 or δ 6.46 resulted in the collapse of 5-CH_3 to a doublet; ^{13}C nmr ($CDCl_3$) δ_C: 17.4 (5-CH_3), 20.6 ($OCOCH_3$), 23.4 (4-CH_3), 61.4 (*C*-1), 88.9 (*C*-4), 124.3 (*C*-6), 133.6 (*C*-3), 134.8 (*C*-5), 148.3 (*C*-2), 169.5 ($OCOCH_3$) ppm. *Anal.* calcd. for $C_{10}H_{12}N_2O_6$: C 46.88, H 4.72, N 10.93; found: C 47.02, H 4.70, N 10.82.

The mother liquor from these fractions was subjected to another recrystallization to give **11**, which was further recrystallized from ethanol and then had mp 118°C (lit. (24) mp 118°C); ir (KBr): 1528, 1548, 1378, and 1338 cm^{-1}; ^{1}H nmr (90 MHz, $CDCl_3$) δ: 2.37 (s, 6, 1-CH_3 and 2-CH_3), 7.63 (s, 2, 3-*H* and 6-*H*); ms (70 eV) *m/e* (relative intensity): 197 (12), 196 (100, *M*), 180 (20), 150 (14, *M* − NO_2), 108 (48), 103 (24), 92 (14), 91 (79), 80 (24), 79 (26), 78 (21), 77 (45).

The 55% ether–pentane column fraction gave a mixture of **11**, 1,2-dimethyl-3,4-dinitrobenzene (**8**), and the diene adducts in the ratio 1:4:5. This fraction was recrystallized from ether at −20°C to give the *Z*-diastereomer of **1***am*, mp 115°C (dec.); uv (CH_3OH): 227 (830), 195 nm (1620 m^2 mol^{-1}); ir (Nujol): 1240 and 1750 ($OCOCH_3$), 1560 (NO_2) cm^{-1}; ^{1}H nmr (90 MHz, $CDCl_3$) δ: 1.86 (br s, 6, 4-CH_3 and 5-CH_3), 2.04 (s, 3, $OCOCH_3$), 5.96 (m, 1, 6-*H*), 6.34 (d, 1, 1-*H*), 7.34 (s, 1, 3-*H*), J_{16} = 4 Hz, $J_{6,5\text{-Me}}$ = 1.5 Hz. Expansion of the spectrum and double resonance studies as described from *E*-**1***am* enabled the coupling constants to be determined; ^{13}C nmr ($CDCl_3$) δ_C: 17.4 (5-CH_3), 20.6 ($OCOCH_3$), 24.1 (4-CH_3), 60.9 (*C*-1), 87.7 (*C*-4), 124.3 (*C*-6), 132.8 (*C*-3), 133.9 (*C*-5), 148.4 (*C*-2), 169.8 ($OCOCH_3$). *Anal* calcd. for $C_{10}H_{12}N_2O_6$: C 46.88, H 4.72, N 10.93; found: C 46.70, H 4.72, N 10.65.

Further elution with 60% ether–pentane, followed by recrystallization of the residue from the eluate from carbon tetrachloride, gave **8**, which was further recrystallized from ethanol and then had mp 82°C (lit. (24) mp 82°C); ir (KBr): 1352 and 1540 (NO_2) cm^{-1}; ^{1}H nmr (90 MHz, $CDCl_3$) δ: 2.22 (s, 3, 1-CH_3), 2.41 (s, 3, 2-CH_3), 7.41 (d, 1, 5-*H*), 7.92 (d, 1, 6-*H*), J_{56} = 8.5 Hz; ms (70 eV) *m/e* (relative intensity): 196 (57, M), 180 (16), 179 (100, *M* − OH), 148 (13), 150 (96, *M* − NO_2), 105 (11), 104 (14), 103 (23), 92 (13), 91 (63), 79 (12), 78 (27), metastable peak at 163.5 corresponding to 196 → 179.

The separation of the diene adducts from each other and from the aromatic compounds was greatly improved using benzene as eluent at 5–10°C. The diene adducts were readily separated on the Waters liquid chromatograph.

Reactions of dienes **1**am, **12**m, *and* **12**n *with acids*

Boron trifluoride-etherate

Boron trifluoride-etherate solution (300 mm^3), at −78°C, was added to diene **1***am* (100 mg) in an nmr tube, also at −78°C. The temperature was raised to 0°C, whereupon the diene dissolved and reacted within 5 min. After work-up the products were identified as **6** (78%, *m/e* 151, *M*), **9** (8%, *m/e* 196, *M*), and **8** (14%, *m/e* 196, *M*). Diene **12***n* was treated similarly with boron trifluoride-etherate. No reaction occurred over 72 h. The mixture was worked up after 20 days at 20°C to give **6** (58%, *m/e* 151, *M*) and 2,3-dimethyl-6-nitroanisole (42%; *m/e* 181, *M*); ^{1}H nmr (90 MHz, $CDCl_3$) δ: 2.22 (s, 3, 2-CH_3), 2.29 (s, 3, 3-CH_3), 3.82 (s, 3, OCH_3), 6.95 (d, 1, 4-*H*), 7.54 (d, 1, 5-*H*), J_{45} = 9 Hz.

Boron trifluoride-etherate and mesitylene

Cold BF_3-etherate solution (250 mm^3) was added to a solution of the diene **1***am* (100 mg, 0.39 mmol) and mesitylene (250 mg, 2.1 mmol) in methylene chloride (250 mm^3) at −78°C. The solution was allowed to warm to 20°C and left to stand for 1 h. After work-up, the composition of the product was **6** (1%; *m/e* 151) and 2-nitro-2′,4,4′,5,6′-pentamethylbiphenyl (99%, *m/e* 269.143 (M_r($^{12}C_{17}{}^1H_{19}{}^{14}N^{16}O_2$) = 269.143); ^{1}H nmr (90 MHz, $CDCl_3$) δ: 1.88 (s, 6, 2′-CH_3 and 6′-CH_3), 2.25 (s, 6, 4-CH_3 and 4′-CH_3), 2.28 (s, 3, 5-CH_3), 6.81 (s, 2, 3′-*H* and 5′-*H*), 6.90 (s, 1, 6-*H*), 7.73 (s, 1, 3-*H*) ppm.

[5]**Caution**: the nitrating mixture of nitric acid in acetic anhydride and trifluoroacetic anhydride must be prepared carefully since it can spontaneously react violently.

Trifluoroacetic acid

Cold trifluoroacetic acid (450 mm^3) was added to diene **1***am* (64 mg) in an nmr tube at −78°C. No reaction occurred over 1 h after raising the temperature to 0°C. At 20°C partial rearomatization occurred over 4 h. The reaction mixture was left at 20°C for 18 h and then worked up to give a mixture of **6** (72%, *m/e* 151, *M*), **9** (13%, *m/e*, 196, *M*), and **8** (15%, *m/e* 196, *M*).

5% Sulfuric acid in methanol

Cold 5% sulfuric acid in methanol (25 cm^3) was added to diene *E*-**1***am* (600 mg), at 0°C. The mixture was allowed to warm to 20°C and the solution stirred for 18 h. The product was transferred with ether (25 cm^3) to a two-necked flask and neutralized with liquid ammonia at −78°C. The solution was filtered and the solvent removed from the filtrate at 0°C. The product was dissolved in ether (50 cm^3) and washed with water (2 × 25 cm^3). The ether extract was dried over anhydrous magnesium sulfate, filtered, and the solvent removed at 0°C to give *E*-4,5-dimethyl-2,4-dinitrocyclohexa-2,5-dien-1-ol (*E*-**1***ao*); ir (film): 3400 and 1050 (OH), 1555 (NO_2) cm^{-1}; ^1H nmr (90 MHz, $CDCl_3$) δ: 1.84 (d, 3, 5-CH_3), 1.89 (s, 3, 4-CH_3), 3.42 (s, 1, *OH*), 5.25 (d, 1, 1-*H*), 5.94 (m, 1, 6-*H*), 7.19 (s, 1, 3-*H*) ppm, J_{16} = 4, $J_{6,5\text{-Me}}$ = 1.40 Hz; ^{13}C nmr ($CDCl_3$) δ_C: 17.5 (5-CH_3), 23.5 (4-CH_3), 60.3 (*C*-1), 89.1 (*C*-4), 127.5 (*C*-6), 131.2 (*C*-3), 132.8 (*C*-5), 151.6 (*C*-2) ppm.

Under similar conditions, acetate *Z*-**1***am* gave dienol *Z*-**1***ao*; ir (film): 3420 and 1053 (OH), 1550 (NO_2) cm^{-1}; ^1H nmr (90 MHz, $CDCl_3$) δ: 1.82 (s, 6, 4-CH_3 and 5-CH_3), 3.42 (s, 1, *OH*), 5.18 (d, 1, 1-*H*), 6.00 (m, 1, 6-*H*), 7.17 (s, 1, 3-*H*) ppm, J_{16} = 4, $J_{6,5\text{-Me}}$ = 1.40 Hz; ^{13}C nmr ($CDCl_3$) δ_C: 17.4 (5-CH_3), 23.9 (4-CH_3), 60.2 (*C*-1), 88.3 (*C*-4), 127.6 (*C*-6), 130.4 (*C*-3), 132.5 (*C*-5), 151.6 (C-2) ppm.

The same reaction on diene **12***m* gave 5,6-dimethyl-2,6-dinitrocyclohexa-2,4-dien-1-ol (**12***o*); ^1H nmr (90 MHz, $CDCl_3$) δ: 1.85 (s, 3, 6-CH_3), 2.06 (d, 1, 5-CH_3), 3.80 (s, 1, *OH*), 5.43 (s, 1, 1-*H*), 6.26 (dd, 1, 3-*H*), 7.30 (d, 1, 4-*H*) ppm. A small amount (ca. 10%) of aromatic products was also formed. The dienol **12***o* was not very stable, and on vacuum drying decomposed extensively with evolution of brown fumes. It also decomposed when an attempt was made to methylate it with methyl iodide and silver oxide.

Trifluoromethanesulfonic acid

Cold trifluoromethanesulfonic acid (300 mm^3) was added to the diene **1***am* (90 mg) in an nmr tube at −78°C and the temperature was then raised to −20°C. The diene had decomposed completely in 5 min (^1H nmr). After work-up, the product composition was **6** (31%, *m/e* 151, *M*), **9** (31%, *m/e* 196, *M*), **8** (25%, *m/e* 196, *M*), and **11** (13%, *m/e* 196, *M*).

Hydrogen bromide in ether

Cold ether (500 mm^3), saturated with hydrogen bromide, was added to the diene **1***am* (64 mg) at −78°C. The temperature was raised to 0°C and, after 90 min, the ^1H nmr spectrum indicated partial rearomatization. After 18 h at 0°C, followed by work-up, **6** (95%) and **11** (5%) were obtained (^1H nmr only).

Acetic acid

Acetic acid (450 mm^3) was added to the diene **1***am* (70 mg) at 20°C. The ^1H nmr of the reaction mixture was unchanged after 30 days at 20°C. The solution was heated for 15 min at 100°C when brown fumes were evolved and after which the ^1H nmr indicated that the rearomatization was complete. After work-up the product composition was **6** (49%, *m/e* 151, *M*) and **9** (51%, *m/e* 196, *M*).

A solution of 10% (v/v) acetic anhydride in acetic acid (320 mm^3) was heated to 100°C for 10 min, cooled to 20°C, and diene **1***am* (50 mg) added. The solution was heated to 100°C for 10 min after which time ^1H nmr indicated complete rearomatization. After work-up, a mixture of **6** (44%, *m/e* 151, *M*) and **9** (56%, *m/e* 196, *M*) was obtained.

A solution of the diene **1***am* (64 mg, 0.25 mmol) and hydroquinone (28 mg, 0.25 mmol) in acetic acid (400 mm^3) was heated for 20 min at 100°C. After work-up, the product composition was **6** (68%, *m/e* 151, *M*) and **9** (32%, *m/e* 196, *M*).

Reaction of dienes **1**am, *with nucleophiles*

Pyridine and 2,6-dimethylpyridine

Cold [$^2H_5$]pyridine (315 mm^3) was added to the diene **1***am* (70 mg) in an nmr tube at −78°C. The solution turned orange-red. The temperature of the mixture was raised to 0°C and ^1H nmr, after 2 min, indicated complete rearomatization. After work-up, the product composition was **6** (3%, *m/e* 151, *M*), **8** (5%, *m/e* 196, *M*), and **11** (92%, *m/e* 196, *M*). With 2,6-dimethylpyridine rearomatization was complete after 15 min and **6** (2%, *m/e* 151, *M*), **8** (4%, *m/e* 196, *M*), and **11** (94%, *m/e* 196, *M*) were obtained.

The reaction was also carried out by adding [$^2H_5$]pyridine (21 mm^3) to a solution of the diene **1***am* (64 mg) in [^2H]chloroform (290 mm^3) at −60°C. The temperature was raised to 0°C (in 10° intervals) and the progress of the reaction monitored by ^1H nmr for 2 h. The conversion of the diene to **11** proceeded smoothly; time(min), % dienes, % arene: 30, 63, 37; 60, 43, 57; 120, 36, 64. The reaction mixture was worked up after 18 h at 0°C and the product composition was then **6** (2%, *m/e* 151, *M*), **8** (3%, *m/e* 196, *M*), and **11** (95%, *m/e* 196, *M*). Reaction of diene **12***n* with pyridine in chloroform for 48 h likewise gave **11** (~100%).

Cold 2,6-dimethylpyridine (58 mm^3) was added to a solution of diene **1***am* (64 mg) in [^2H]chloroform (290 mm^3) at −60°C. The temperature of the mixture was raised to 0°C and maintained for 2 h at this temperature. After work-up, the product composition was shown (^1H nmr) to be **11** (15%), diene **1***am* (67%), and 5,6-dimethyl-2,6-dinitrocyclohexa-2,4-dienyl acetate (**12***m*) (17%).

tert-*Butylamine*

Cold *tert*-butylamine (26 mm^3) was added to a solution of **1***am* in [^2H]chloroform. The reaction mixture was worked up after 18 h at 0°C. The product composition was **6** (4%, *m/e* 151, *M*), **9** (7%, *m/e* 196, *M*), **8** (10%, *m/e* 196, *M*), **11** (60%, *m/e* 196, *M*), and a compound tentatively identified as *N*-*tert*-butyl-4,5-dimethyl-2-nitroaniline (19%, ^1H nmr δ 1.48 ppm ($C(CH_3)_3$), *m/e* 222, *M*).

Sodium methoxide in methanol

Sodium methoxide (42 mg, 0.78 mmol) was added to a solution of the diene *E*-**1***am* (100 mg, 0.39 mmol) in methanol (350 mm^3) at −78°C. The mixture went orange-red. The temperature of the mixture was raised to 0°C for 2 h to ensure complete reaction. After work-up, the product was identified by ^1H nmr as one diastereomer of 5,6-dimethyl-2,6-dinitrocyclohexa-2,4-dienyl methyl ether (**12***n*). The reaction was repeated under similar conditions on the diastereoisomer *Z*-**1***am*, whereupon the same diastereomer of **12***n* was obtained.

Ether **12***n* was made using the crude nitration product of **6** (4 g, containing ca. 50% diene adducts). After reaction with sodium methoxide and work-up, the product was separated by hplc (Waters) using benzene as solvent. The first fraction contained mainly a mixture of aromatic compounds, present in the nitration product. The second fraction, after recrystallization from ether at −20°C, gave **12***n*, mp 69°C; uv (CH_3OH) 328 (595), 203 nm (950 m^2 mol^{-1}); ir (Nujol): 1555 (NO_2), 1090 (C—O—C) cm^{-1}; ^1H nmr (90 MHz, $CDCl_3$) δ: 1.88 (s, 3, 6-CH_3), 2.19 (d, 3, 5-CH_3), 3.55 (s, 3, OCH_3), 5.12 (s, 1, 1-*H*), 6.25 (dd, 1, 4-*H*), 7.38 (d, 1, 3-*H*) ppm, J_{34} = 6, $J_{4,5\text{-Me}}$ = 1.5 Hz. Irradiation of the 5-CH_3 (d) resonance resulted in the collapse of the 4-H (dd) resonance to a doublet. Irradiation of the 3-H (d) resonance resulted in the collapse of the 4-H (dd) resonance to a different doublet; ^{13}C nmr ($CDCl_3$) δ_C: 19.6 (6-CH_3), 20.0 (5-CH_3), 60.5 (OCH_3), 75.1 (*C*-1), 91.6 (*C*-6), 123.4 (*C*-4), 129.6 (*C*-3), 142.8 (*C*-5), 146.0 (*C*-2). *Anal.* calcd. for $C_9H_{12}N_2O_5$: C 47.37, H 5.30, N 12.27; found: C 47.55, H 5.24, N 12.14.

Acetate **12***m* was reacted similarly with sodium methoxide in methanol and gave, after work-up (^1H nmr), one diastereomer of ether **12***n* (23%) and both diastereomers of ether **1***an* (77%). The ratio of the diastereomers *E*-**1***an*/*Z*-**1***an* was 9:1, by integration of the methoxy peaks.

Sodium thiophenoxide

Sodium thiophenoxide (50 mg, 0.38 mmol) was added to a solution of diene **1***am* (64 mg, 0.25 mmol) in acetonitrile (400 mm^3) at −40°C and the temperature was raised to 0°C. After 5 min, ^{1}H nmr indicated that the diene had rearomatized. After work-up, the product composition was **6** (1%, *m/e* 151, *M*) and 4,5-dimethyl-2-nitrophenyl phenyl sulfide (99%). On recrystallization from ether, pale-yellow cubic crystals of the sulfide were obtained, mp 79°C; ^{1}H nmr (90 MHz, $CDCl_3$) δ: 2.07 (s, 3, 4-CH_3), 2.21 (s, 3, 5-CH_3), 6.60 (s, 1, 6-*H*), 7.45 (m, 5, C_6H_5), 7.96 (s, 1, 3-*H*) ppm; ms (70 eV) *m/e* (relative intensity): 259.057 (36, M_r ($C_{14}H_{13}NO_2S$) = 259.067), 199 (16), 198 (55), 196 (45), 195 (100), 182 (20), 181 (95), 166 (15).

Potassium nitrite

[$^2H_4$]Methanol (315 mm^3) was added to a mixture of the diene **1*am*** (70 mg, 0.27 mmol), potassium nitrite (35 mg, 0.42 mmol), and 18-crown-6 (35 mg, 0.41 mmol) at −78°C in an nmr tube. The ^{1}H nmr of the solution after 5 min at 0°C indicated complete rearomatization. The product, after work-up, was **11** (100%, *m/e* 196, *M*).

The reaction with potassium nitrite was carried out on the diene **12*n*** under similar conditions. The reaction mixture was left for 15 days at ambient temperature and worked up to give **6** (44%, *m/e* 151, *M*) and **11** (56%, *m/e* 196, *M*).

Potassium cyanide

Cold [$^2H_4$]methanol (315 mm^3) was added to a mixture of the diene **1*am*** (64 mg, 0.25 mmol), potassium cyanide (25 mg, 0.38 mmol), and 18-crown-6 (99 mg, 0.38 mmol) at −78°C. The mixture was warmed to 0°C for 30 min. After work-up, the products were 2,3-dimethyl-6-nitrobenzonitrile (**14**, 94%, ^{1}H nmr (90 MHz, $CDCl_3$) δ: 2.45 (s, 3, 2-CH_3), 2.60 (s, 3, 3-CH_3), 7.54 (d, 1, 4-*H*), 8.04 (d, 1, 5-*H*) ppm, J_{45} = 8.6 Hz; *m/e* 176, *M*) and **11** (6%, *m/e* 196, *M*). When the reaction was carried in acetonitrile the product ratio after work-up (^{1}H nmr) was **14**/**11** = 70:30, and in 50% (v/v) pyridine–methanol the ratio was 58:42.

Diene **12*m*** was reacted with potassium cyanide in methanol and gave 4,5-dimethyl-2-nitrobenzonitrile (87%, *m/e* 176, *M*) and **11** (13% *m/e* 196, *M*).

Diene **12*n*** on reaction with potassium cyanide in acetonitrile gave 4,5-dimethyl-2-nitrobenzonitrile (70%, ir (Nujol): 2235 (CN), 1525 and 1350 (NO_2) cm^{-1}; ^{1}H nmr (90 MHz, $CDCl_3$) δ: 2.40 (s, 3, CH_3), 2.43 (s, 3, CH_3), 7.59 (s, 1, 2-*H*), 8.05 (s, 1, 5-*H*) ppm; *m/e* 176, *M*) and 4,5-dimethyl-1,2-benzenedicarbonitrile (30%, ^{1}H nmr (90 MHz, $CDCl_3$) δ: 2.37 (s, 6, 4, CH_3 and 5-CH_3), 7.51 (s, 2, 3-*H* and 6-*H*) ppm; *m/e* 156.068 (M_r ($^{12}C_{10}{}^1H_8{}^{14}N_2$) = 156.064)).

Potassium halides

Cold methanol (400 mm^3) was added to a mixture of diene **1*am*** (64 mg, 0.25 mmol), 18-crown-6 (99 mg, 0.38 mmol), and potassium iodide (62 mg, 0.38 mmol) at −78°C. The temperature was raised to 0°C. After 1 h ^{1}H nmr showed that no reaction had occurred. The mixture was warmed to 20°C for 48 h. After work-up, ^{1}H nmr showed the products to be **11** (58%) and 4,5-dimethyl-2,4-dinitrocyclohexa-2,5-dienyl [$^2H_3$]methyl ether (**1*an***, 42%), identified by comparison of its spectrum with that of an authentic sample.

The reaction was repeated under similar conditions with potassium bromide and the mixture worked up after 78 h at 20°C to give (^{1}H nmr) **1*an*** (45%), **11** (22%), and **12*m*** (33%). The last compound was identified by comparison of its spectrum with that of an authentic sample.

With potassium chloride, and the mixture worked up after 7 days at 20°C, **1*am*** gave (^{1}H nmr) **11** as the only product.

With potassium fluoride, the product composition (^{1}H nmr) after 20 h at 0°C was **11** (28%), **1*an*** (57%), **12*m*** (15%).

[$^2H_3$]Acetonitrile (400 mm^3) was added to a mixture of potassium fluoride (22 mg, 0.38 mmol) and 18-crown-6 (99 mg, 0.38 mmol). The mixture was warmed to 50°C and the solution cooled to 0°C. Diene **1*am*** (64 mg, 0.25 mmol) was added and the reaction worked up after 20 min at 0°C to give (^{1}H nmr) **11** (ca. 100%).

With potassium bromide for 18 h at 0°C the products were **11** (95%, *m/e* 196, *M*), **8** (3%, *m/e* 196, *M*), and **9** (2%, *m/e* 196, *M*). Reaction for 5 h at 0°C gave (^{1}H nmr) **11** (32%) and **12*m*** (68%). The product mixture from this reaction on treatment with potassium iodide (62 mg, 0.38 mmol) and 18-crown-6 (99 mg, 0.38 mmol) in acetonitrile (400 mm^3) for 18 h at 0°C gave (^{1}H nmr) **11** as the main product.

With potassium iodide for 1 h at 0°C the products were (^{1}H nmr) **11** (77%) and **12*m*** (23%). The product mixture from this reaction, on further treatment with potassium iodide (62 mg, 0.38 mmol) and 18-crown-6 (99 mg, 0.38 mmol) in methanol (400 mm^3) for 18 h at 0°C, gave (^{1}H nmr) **11**. Reaction of diene **12*n*** with potassium iodide in acetonitrile for 18 h at 20°C gave (^{1}H nmr) **11**.

Cold 50% (v/v) acetic anhydride in acetonitrile (700 mm^3) was added to a mixture of potassium bromide (45 mg, 0.38 mmol) and 18-crown-6 (99 mg, 0.38 mmol) in an nmr tube. The mixture was warmed to 50°C, cooled to 0°C, and diene **1*am*** (64 mg, 0.25 mmol) added. The reaction mixture was worked up after 18 h at 0°C to give, by ^{1}H nmr, **11** (3%), diene **1*am*** (22%), and **12*m*** (75%).

In neat acetic anhydride (400 mm^3) containing potassium bromide, diene **1*am*** gave, after 18 h, a mixture of one diastereomer of **12*m*** (75%) and **1*am*** (25%).

The reaction with potassium bromide in acetic anhydride was carried out on the crude nitration product of **6** (containing ca. 50% dienes). The reaction product was worked up after 48 h at 0°C and separated by hplc using benzene as solvent. The first fraction contained mainly the aromatic compounds which were present in the original nitration product. The second fraction, after recrystallization from ether at −20°C, gave one diastereomer of **12*m***, mp 99°C; uv (CH_3OH): 325 (1145), 195 nm (1380 m^2 mol^{-1}); ir (Nujol): 1753 and 1210 ($OCOCH_3$), 1555 (NO_2) cm^{-1}; ^{1}H nmr (90 MHz, $CDCl_3$) δ: 1.78 (s, 3, 6-CH_3), 2.08 (s, 3, OCOCH_3), 2.12 (d, 3, 5-CH_3), 6.35 (dd, 1, 4-*H*), 6.93 (s, 1, 1-*H*), 7.48 (d, 1, 3-*H*) ppm, J_{34} = 7, $J_{4,5\,Me}$ = 1.5 Hz. Irradiation of the 4-H (dd) resonance resulted in the collapse of the 5-CH_3(d) resonance to a singlet and the 3-H (d) resonance to a singlet; ^{13}C nmr ($CDCl_3$) δ_C: 19.3 (6-*C*H_3), 19.8 (5-*C*H_3), 20.4 (OCO*C*H_3), 65.5 (*C*-1), 90.9 (*C*-6), 123.4 (*C*-4), 130.6 (*C*-3), 130.9 (*C*-5), 142.2 (*C*-2), 169.0 (O*C*OCH$_3$) ppm. *Anal.* calcd. for $C_{10}H_{12}N_2O_6$: C 46.88, H 4.72, N 10.93; found: C 46.80, H 4.79, N 10.82.

Other nucleophiles

The reaction of **1*am*** with potassium hydroxide, potassium *tert*-butoxide, sodium phenoxide, potassium acetate, and potassium thiocyanate, in acetonitrile, and with potassium nitrite and potassium thiocyanate in methanol, gave **11** as the major or sole product (Table 2).

Thermolysis

A solution of diene **1*am*** (64 mg) in toluene (10 cm^3) was heated under reflux for 1 h. The solvent was then removed from the yellow solution under reduced pressure. The product composition was **6** (78%, *m/e* 151, *M*) and **9** (22%, *m/e* 196, *M*). A similar result was obtained when a 1% solution of the diene **1*am*** in acetone was injected into the inlet (270°C) of a gas chromatograph.

A 1% solution of diene **12*n*** in acetone was injected into the inlet of a gas chromatograph (260°C). The products (glc–ms) were **6** (98%, *m/e* 151, *M*) and 2,3-dimethyl-6-nitroanisole (2%, *m/e* 181, *M*).

80% Methanol–water

A cold solution of 80% (v/v) methanol–water (350 mm^3) was added to the diene **1*am*** (64 mg) and the resulting mixture was left in an ultrasonic bath at ambient temperature until dissolution was complete (72 h). The ^{1}H nmr of the product indicated complete rearomatization of the diene to give **6** (82%, *m/e* 181, *M*) and **11** (18%, *m/e* 196, *M*).

*Reactions of 4,5-dimethyl-2,4-dinitrocyclohexa-2,5-dien-1-ol (***1ao***)*

Sulfuric acid in acetic anhydride

Cold 2% (v/v) sulfuric acid in acetic anhydride (250 cm^3) was added to a solution of diene **1*ao*** (90 mg), in acetic anhydride (250 mm^3) at 0°C. The temperature was raised to 35°C. After 18 h 5% rearomatization had occurred. Sulfuric acid (10 mm^3) was added to the solution at 0°C and the temperature raised to 35°C. Rearomatization was complete in 2 min and the product composition after work-up was (by ^{1}H nmr) **6** (82%), **9** (11%), and **8** (7%).

$[^2H_5]$Pyridine and acetic anhydride

Cold $[^2H_5]$pyridine (300 mm^3) was added to the diene **1***ao* (90 mg) at −78°C. The solution was warmed to 0°C and ^{1}H nmr, after 18 h, showed that no reaction had occurred. Cold acetic anhydride (450 mm^3) was added. The mixture immediately turned dark brown and ^{1}H nmr showed that no diene remained. Work-up gave (by ^{1}H nmr) **11** (~100%).

Cold $[^2H_5]$pyridine (40 mm^3, 0.5 mmol) was added to a solution of the diene **1***ao* (70 mg, 0.33 mmol) in acetic anhydride (300 mm^3) at −40°C. The temperature was raised to 0°C and the ^{1}H nmr recorded. The acetylation of **1***ao* to **1***am* was complete within 6 min, although partial isomerization to **12***m* (ca. 5%) was also observed. After 18 h at 0°C **11** was obtained on work-up (^{1}H nmr).

When 2,6-dimethylpyridine was used instead of pyridine, 50% of **1***ao* was acetylated after 150 min. Work-up after 18 h at 0°C gave (^{1}H nmr) **11** (3%), **1***am* (40%), and **12***m* (57%).

Methyl iodide and moist silver oxide

Moist silver oxide was freshly prepared as follows. Aqueous sodium hydroxide (10 cm^3, 0.05 mol) was added to a solution of silver nitrate (3.38 g) in distilled water (5 cm^3). The precipitate of silver oxide was filtered under suction and washed with distilled water (5 × 20 cm^3) to remove excess alkali.

A mixture of silver oxide (1.90 g), methyl iodide (7 cm^3), potassium hydroxide (0.01 g), and the diene *E*-**1***ao* (0.52 g) was stirred for 5 h at 20°C. The mixture was then filtered and the residue washed with ether (5 × 60 cm^3). The ether extract was dried ($MgSO_4$) and the ether and excess methyl iodide evaporated at 15°C. The product, after vacuum drying, was found to be one diastereomer of 4,5-dimethyl-2,4-dinitrocyclohexa-2,5-dienyl methyl ether (*E*-**1***an*); ^{1}H nmr (90 MHz, $CDCl_3$) δ: 1.86 (d, 3, 5-CH_3), 1.89 (s, 3, 4-CH_3), 3.35 (s, 3, OCH_3), 4.99 (d, 1, 1-*H*), 6.04 (m, 1, 6-*H*), 7.18 (s, 1, 3-*H*) ppm, $J_{16} = 4$, $J_{6,5\text{-}CH_3} = 1.35$ Hz; ^{13}C nmr ($CDCl_3$) δ_C: 17.6 (5-CH_3), 23.3 (4-CH_3), 56.8 (OCH_3), 68.0 (*C*-1), 88.9 (*C*-4), 125.5 (*C*-6), 131.6 (*C*-3), 133.6 (*C*-5), 150.4 (*C*-2) ppm.

The reaction was repeated on diene *Z*-**1***ao* to give *Z*-**1***an*; ^{1}H nmr (90 MHz, $CDCl_3$) δ: 1.86 (s, 6, 5-CH_3 and 4-CH_3), 3.30 (s, 3, OCH_3), 4.99 (d, 1, 1-*H*), 5.96 (m, 1, 6-*H*), 7.15 (s, 1, 3-*H*) ppm, $J_{16} = 4$ Hz; ^{13}C nmr ($CDCl_3$) δ_C: 18.7 (5-CH_3), 23.9 (4-CH_3), 54.9 (OCH_3), 67.1 (*C*-1), 88.1 (*C*-4), 125.9 (*C*-6), 131.4 (*C*-3), 133.7 (*C*-5), 150.3 (*C*-2) ppm.

Shift reagent studies

Eu(fod)$_3$ was added in small increments (5–10 mg) to a solution of the diene (35–50 mg) in $[^2H]$chloroform at 0°C. The weight of the reagent added and the ^{1}H nmr spectrum (tetramethylsilane reference) were determined after each addition. The volume increase resulting on addition of the reagent was ignored.

Acknowledgements

We are grateful to the Natural Sciences and Engineering Research Council of Canada for financial support and to the University of Victoria for the award of a University of Victoria Fellowship (to L.M.I.).

1. G. G. CROSS, A. FISCHER, and G. N. HENDERSON. Can. J. Chem. **62**, 2803 (1984).
2. A. FISCHER and L. M. IYER. J. Chem. Soc. Chem. Commun. 1096 (1979).
3. C. L. PERRIN and G. A. SKINNER. J. Am. Chem. Soc. **93**, 3389 (1971).
4. A. FISCHER and C. C. GREIG. Can. J. Chem. **52**, 1231 (1974).
5. A. FISCHER, A. J. READ, and J. VAUGHAN. J. Chem. Soc. 3691 (1964).
6. A. I. SCOTT. Interpretation of the ultraviolet spectra of natural products. Pergamon Press, Oxford. 1964. Chapt. 2.
7. E. W. GARBISCH, JR. J. Am. Chem. Soc. **86**, 5561 (1964).
8. D. J. BLACKSTOCK, A. FISCHER, J. VAUGHAN, and G. J. WRIGHT. Chem. Commun. 641 (1970).
9. A. FISCHER and G. J. WRIGHT. Aust. J. Chem. **27**, 217 (1974).
10. A. D. MESURE and J. G. TILLETT. J. Chem. Soc. B, 669 (1966).
11. J. W. BARNETT, R. B. MOODIE, K. SCHOFIELD, and J. B. WESTON. J. Chem. Soc. Perkin Trans. 2, 648 (1975).
12. R. S. COOK, R. PHILLIPS, and J. H. RIDD. J. Chem. Soc. Perkin Trans. 2, 1166 (1974).
13. P. C. MYHRE. J. Am. Chem. Soc. **94**, 7921 (1972).
14. T. BANWELL, C. S. MORSE, P. C. MYHRE, and A. VOLLMAR. J. Am. Chem. Soc. **99**, 3042 (1977).
15. A. FISCHER and G. N. HENDERSON. Can. J. Chem. **59**, 2314 (1981), and references cited therein.
16. C. BLOOMFIELD, R. B. MOODIE, and K. SCHOFIELD. J. Chem. Soc. Perkin Trans. 2, 1793 (1983).
17. C. BLOOMFIELD, R. B. MOODIE, and K. SCHOFIELD. J. Chem. Soc. Perkin Trans. 2, 1003 (1983).
18. C. E. BARNES and P. C. MYHRE. J. Am. Chem. Soc. **100**, 975 (1978).
19. A. FISCHER and C. C. GREIG. J. Chem. Soc. Chem. Commun. 50 (1974).
20. A. FISCHER, C. C. GREIG, and R. ROEDERER. Can. J. Chem. **53**, 1570 (1975).
21. G. S. BAPAT, A. FISCHER, G. N. HENDERSON, and S. RAYMAHASAY. J. Chem. Soc. Chem. Commun. 119 (1983); G. S. BAPAT. Ph.D. Dissertation, University of Victoria, Victoria, B.C., 1983.
22. D. H. MCDANIEL and H. C. BROWN. J. Org. Chem. **23**, 420 (1958).
23. W. J. HICKINBOTTOM. Reactions of organic compounds. 3rd ed. Longmans, London. 1962. p. 121.
24. J. BUCKINGHAM (*Editor*). Dictionary of organic compounds. 5th ed. Chapman and Hall, London. 1982. p. 2121.

Surface photochemistry: silica gel as a medium for photochemical cycloaddition of enones to allene[1]

VINOD DAVE, RAJEEV FARWAHA, PAUL DE MAYO,[2] AND J. B. STOTHERS[2]
Photochemistry Unit, Department of Chemistry, The University of Western Ontario, London, Ont., Canada N6A 5B7

Received October 19, 1984

VINOD DAVE, RAJEEV FARWAHA, PAUL DE MAYO, and J. B. STOTHERS. Can. J. Chem. **63**, 2401 (1985).

The photocycloaddition of allene to the steroidal enone **1***a*, normally occurring from the (less hindered) α side, has been directed in part to the (more hindered) β side by adsorption on the surface of silica gel. For a series of cyclic enone–allene photocycloadditions it is shown that the normally favored formation of the β,γ-regioisomeric adduct in homogeneous systems can be shifted to favor the γ,δ adduct on a silica gel surface.

VINOD DAVE, RAJEEV FARWAHA, PAUL DE MAYO et J. B. STOTHERS. Can. J. Chem. **63**, 2401 (1985).

La photocycloaddition de l'allène sur l'énone stéroïdale (**1***a*), qui se produit normalement par la face α (la moins empêchée) peut être amenée à se produire en partie par la face β (la plus empêchée) par adsorption sur une surface de gel de silice. On a montré, pour une série de photocycloadditions cycliques énone–allène, que la formation de l'adduit régioisomère-β,γ, qui est normalement favorisée dans les systèmes homogènes, peut être déplacée en faveur de l'adduit γ,δ si l'on opère sur une surface de gel de silice.

[Traduit par le journal]

Introduction

Photochemical cycloaddition between an alkene and an α,β-unsaturated cyclic ketone has proved to be a very useful tool for the synthesis of alicyclic compounds (1). Its application has been limited, however, by the lack of regio- and stereoselectivity in the reaction.

It has been known for some time that if the two faces of the double bond in the enone are stereochemically non-equivalent the major product generally arises by reaction of the olefin from the less hindered side of the enone (ref. 2, see, however, ref. 4). Recently it has been shown that such photocycloadditions can be induced on dry silica gel (3) using steroidal enones as substrates. With these compounds the α face is less hindered than the β face and thus this face is preferentially adsorbed on the gel, rendering the β face relatively more prone to attack by the olefin.

Some years ago, Wiesner and co-workers (4) proposed that the stereochemistry of the enone photocycloaddition could be predicted from the conformational posture of the enone excited state. It was postulated that the configuration of the photoadduct is controlled by a species which is trigonal in the α- and pyramidal in the β-position. This species was assumed to select the more stable configuration and thus to determine the configuration of the adduct: this resultant stereochemistry might or might not derive from the steric ease of approach of the olefin. According to the proposal, the α carbon is slightly positive in comparison to the β carbon in the transition state and an overlap of the β orbital with the terminal position of allene would be required for bond formation. Since allene addition always results in the formation of a *cis*-fused adduct, one cannot, from the stereochemistry, discuss whether α or β bond formation occurred first (1*a*, 5). The question of whether the biradical intermediate is formed by initial bond formation at C_α or C_β is not well resolved, although there is evidence that the initial bond formation can be at C_α or C_β, depending upon the structure of enone and alkene involved (ref. 6; see also refs. 1*a* and 1*d*). Several exceptions to the Wiesner proposal have recently appeared (7).[3]

As a test for his predictive guide Wiesner carried out the photocycloaddition of allene to **1** and **2** at −78°C. It was expected (4*c*) that **1** should undergo reaction on the α face, and it indeed did so, giving **3***a* (together with **4**). On the other hand, **2** was predicted to react from the β face, but the reaction could be inhibited by steric hindrance: in fact, the reaction was found to be very sluggish.

Such substances as **1** and **2** seemed of interest to test the efficiency of adsorption on silica gel for directing cycloaddition. Specifically, we were interested to know if such adsorption for **1** could lead to the formation of the hindered β adduct. This, as reported below, was found to be the case. In addition, a regioselective difference in the mode of addition to allene was observed between heterogeneous and homogeneous systems, and for this reason the study was extended to include several other enones.

Results and discussion

The photocycloaddition of 3β-acetoxy-$\Delta^{8,9}$-cholesten-7-one (**1**) and allene adsorbed on silica gel was carried out using a 450-W medium-pressure mercury lamp. The irradiation product was chromatographed to give the previously reported rearrangement product **4** and α adduct **3***a* (4*c*) in 10% and 20% yields, respectively. In addition to these known adducts, a mixture of three isomeric cycloadducts was also obtained in 70% yield. The complex mixture was not well resolved on tlc and was therefore converted to the corresponding alcohols by hydrolysis with methanolic KOH. There was obtained a new adduct as a crystalline solid[4] and a 1 : 1 mixture of alcohols identified below as **5** and **6**. This mixture was separated by flash chromatography, giving a solid and a liquid adduct. That one photoproduct, **6**, was an allene adduct followed from the mass spectrum (*m*/*e* 440); ^{1}Hmr (δ 4.49, $C{=}CH_2$) and ^{13}Cmr (δ_C: 106.3, $={CH_2}$). The head-to-head regiochemistry was re-

[1] Publication No. 340 from the Photochemistry Unit, Department of Chemistry, The University of Western Ontario, London, Ontario, Canada N6A 5B7.

[2] Authors to whom correspondence may be addressed.

[3] See also K. Wiesner, as cited by Cargill *et al.* (ref. 7*a*, footnote 12), and ref. 1*e*.

[4] The X-ray structure determination of its derived diol will be reported later.

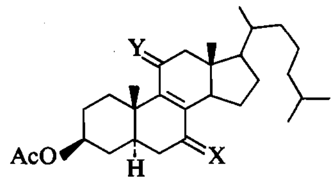

1 X = O; Y = H_2
2 X = H_2; Y = O

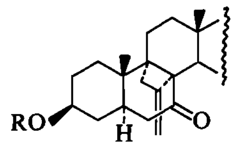

3*a* R = Ac
b R = H

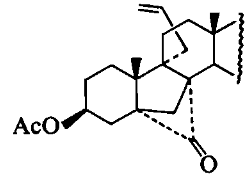

4

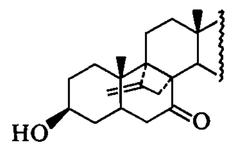

5

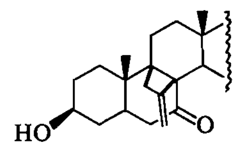

6

vealed by its medium intensity uv maximum at 290 nm (ε 96), characteristic of a β,γ-unsaturated ketone (8). The photocycloadduct **5** was also an allene adduct, as judged from the mass spectrum (*m/e* 440); the ^{1}Hmr (δ 5.17 brs, 1H and 4.93 m, 1H, —C=CH_2) and ^{13}Cmr (δ_C: 110.7 =CH_2). Cycloadduct **5** showed a very weak uv absorption maximum at 290 nm (ε 39), characteristic of an unperturbed carbonyl group, indicating it to be an γ,δ-unsaturated ketone. The stereochemistry of addition in **5** and **6** became apparent from their ^{13}Cmr spectra upon comparison with that for **3***b*. In addition to the signals for the side-chain carbons in each, there were several similarities in the spectra of **3***b* and **5** but very few for **3***b* and **6**. For **3***b* and **5** the signals for five methylene, two methine, and a quaternary centre differ by less than 0.1 ppm in the two spectra while the angular methyl, another methylene, and quaternary signals fall within 0.2 ppm (see Experimental). Thus, 12 of the 17 signals for the skeletal carbons are remarkably similar. In contrast, only a single methylene absorption for compound **6** is found within 0.1 ppm of any of those for compounds **3***b* and **5**; the quaternary centres differ by 3–8 ppm, the methines by 3–10 ppm, and the angular methyls by 1–2 ppm. On the basis of the ^{13}Cmr data, combined with the above mentioned uv absorption, it is concluded that **5** is the regioisomeric α-adduct with γ,δ-unsaturation and **6** is the β-adduct of the β,γ-unsaturated ketone.

It has been suggested that an overlap of the β orbital of the α,β-unsaturated ketone with the terminal allene carbon is required for the formation of a β,γ allene cycloadduct (4). Furthermore, it is known that ethyl, methyl, and isopropyl radicals add exclusively to the terminal carbon of allene (9). By analogy with this radical-like transition state, and *assuming that attack at the terminal position of allene is unaffected by adsorption on silica gel*, the formation of the γ,δ regioisomeric adduct **5** can be explained by assuming that initial bond formation occurs at the α carbon of the steroidal α,β-unsaturated ketone.

The photocycloaddition of 3β-acetoxy-$\Delta^{8,9}$-cholesten-11-one (**2**) and allene in methylene chloride was carried out using the reported procedure (4*c*). Thin-layer chromatography of the crude product showed the presence of mainly unreacted starting unsaturated ketone, together with a minor compound (<5%) less polar than **2**, as previously reported. Repeating this reaction on silica gel did not reveal any noticeable change.

The use of silica gel has thus induced photocycloaddition to the β face of the 8:9 double bond and, more importantly, in reasonable amount; β photoadduct **6** represents about one-third of the allene adducts formed. In addition to the exceptions reported for homogeneous systems, it appears that the proposed stereochemical rule (4) should also be applied to heterogeneous systems with caution.

The formation of the head-to-tail adduct **5** on silica gel in the photocycloaddition of steroidal enone **1** to allene encouraged us to examine the photocycloaddition reactions of some simple cyclic enones to allene under heterogeneous conditions to determine the limits and utility of the reaction. The compounds chosen for photocycloaddition were cyclohexenone (disubstituted olefin), isophorone (trisubstituted), and four bicyclic

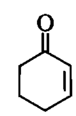

7

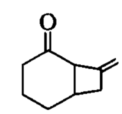

8*a*

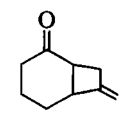

8*b*

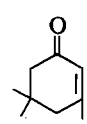

9

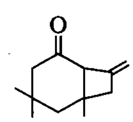

10*a*

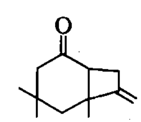

10*b*

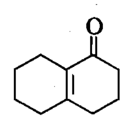

11

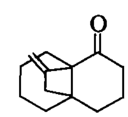

12*a*

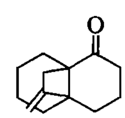

12*b*

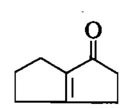

13

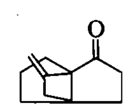

14*a*

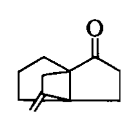

14*b*

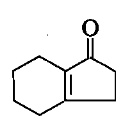

15

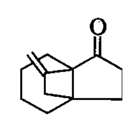

16*a*

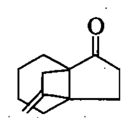

16*b*

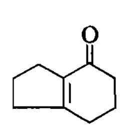

17

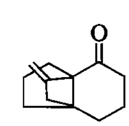

18*a*

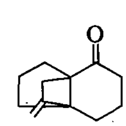

18*b*

TABLE 1. ^{13}C shielding data[a] for photoadducts

Compound	*CH*$_2$=C—	CH$_2$=*C*—	*C*=O
8*a*	108.1	144.7	208.9
8*b*	105.2	149.5	209.0
10*a*	108.2	142.3	209.8
10*b*	103.5	156.1	214.2
12*a*	105.8	147.7	212.6
12*b*	101.9	151.5	215.6
14*a*	109.8	145.4	216.5
14*b*	108.1	152.2	219.9
16*a*	106.6	145.2	219.6
16*b*	104.3	152.1	222.9
18*a*	108.1	146.3	215.1
18*b*	105.9	152.3	215.1

[a] In ppm from internal TMS in $CDCl_3$.

ketones **11**, **13**, **15**, **17** (tetrasubstituted). Their photocycloaddition reactions with allene were carried out in solution (CH_2Cl_2) and on dry silica gel. Except for the isophorone–allene cycloadduct mixture, which could be resolved on tlc, no other adduct mixtures could be resolved by glc or tlc to permit the determination of the ratio of the two regioisomeric adducts: the head-to-head (H/H)/head-to-tail (H/T) ratios in these mixtures were determined by integration of suitable signals in the ^{13}Cmr spectrum. The most reliable signal for this integration was the *sp*^{2} carbon (=CH_2) in each of the two adducts.

It is clear from the literature (1*d*) that the major product formed by photocycloaddition of allene to simple cyclopentenones and cyclohexenones *in solution* is the head-to-head adduct with a *cis* ring junction. Using this as a guide, the carbon spectra of the six unsaturated ketone–allene photocycloaddition products were examined. For the total reaction products from *solution irradiations* the spectra showed the presence of two peaks, one of high and the other of low intensity, in the region δ 104–109 ppm. These were assigned to the =CH_2 signals of the major β,γ-unsaturated ketone and the minor γ,δ-unsaturated ketone, respectively (see Table 1). These two peaks were carefully integrated to give the ratio of β,γ (head-to-head) and γ,δ (head-to-tail) adducts from the unsaturated ketones (**7**, **9**, **11**, **13**, **15**, and **17**) by solution irradiation (Table 2). The same two peaks were also integrated for the product mixtures derived from ketone–allene irradiation on dry *silica gel*. The ratios obtained are listed in Table 2.

The photocycloaddition of allene to isophorone **9** in methylene chloride and on silica gel gave two cycloadducts (**10***a* and **10***b*). Their regiochemistry was easily ascertained from their ^{1}Hmr spectra since the vinyl protons appeared as a multiplet at ~δ 5.0 in **10***a* and as two triplets at δ 4.82 and δ 4.71 in the case of **10***b*. The β,γ adduct (**10***a*) showed a low-field proton signal at δ 3.2, attributed to the methine proton at C-2: an indication of head-to-head (H/H) regiochemistry. In contrast, for **10***b* no low-field signal was detected near 3.0 ppm, which indicated head-to-tail (H/T) regiochemistry. Additional confirmation of this assignment was obtained from the ^{13}Cmr spectra of the two isomeric adducts. The assignment was made by comparisons with the data for similar analogues (Table 1).

The photocycloaddition of enones (**7**, **9**, **11**, **13**, **15**, and **17**) to allene in methylene chloride gave (H/H) regioisomers as major photoadducts with the (H/T) regioisomers present in small amounts, as shown by ^{13}Cmr. In contrast, irradiation of these enones and allene on silica produced a pronounced shift towards H/T adduct formation. The formation of the H/T product indicates a preference for reaction of the α position of the enone with the terminal allene position, or reaction at the β position of the enone with the central position of the allene. Presumably the change is caused by changes in electron distribution induced by adsorption onto the silica gel surface, but no evidence is presently available to distinguish between these possibilities. In any event the ability to change the adduct composition may be of synthetic utility.

TABLE 2. Conditions and the results of the photocycloaddition of enones to allene

Enone	System[a]	Product	Regioisomer (%)[b] H/H	H/T
7	A	**8***a*, **8***b*	94	6
	B	**8***a*, **8***b*	65	35
9	A	**10***a*, **10***b*	93	7
	B	**10***a*, **10***b*	52, 59[c]	48, 41[c]
11	A	**12***a*, **12***b*	70	30
	B	**12***a*, **12***b*	34	66
13	A	**14***a*, **14***b*	61	39
	B	**14***a*, **14***b*	46	54
15	A	**16***a*, **16***b*	75	25
	B	**16***a*, **16***b*	32	68
17	A	**18***a*, **18***b*	43	57
	B	**18***a*, **18***b*	20	80

[a] A, methylene chloride solution; B, dry silica gel.
[b] Analysed by ^{13}Cmr (see text), estimated precision ±5%.
[c] Relative ratio of isolated adducts.

In the photocycloaddition of bicyclo[4.4.0]dec-1(6)-en-one (**11**) on silica gel there was obtained, in addition to the expected adducts **12***a* and **12***b*, ~5% of a minor compound with the molecular formula $C_{13}H_{18}O$, i.e., isomeric with **12***a* and **12***b*. It appeared to contain a four-membered ring ketone since it exhibited carbonyl absorption at 1760 cm^{-1}. The ^{13}Cmr spectrum showed signals for a carbonyl carbon, two methine carbons, two quaternary carbons, and eight methylene carbons. The ^{1}Hmr spectrum contained a one-proton doublet at δ 2.7 ppm (J = 8 Hz, 1H) and a two-proton multiplet at δ 2.67–3.0 ppm (J_{AB} = 18 Hz, J_{AX} = ~2.5 Hz). To determine the origin of this product, a mixture of photocycloadducts **12***a* and **12***b* was irradiated on silica gel. The irradiation mixture was found to contain major amounts of the starting adducts **12***a* and **12***b* with 5–10% of the cyclobutanone. Thus, this compound is an over-irradiation product of **12***a* or **12***b*. Formation of this novel rearrangement product from **12***a* or **12***b* can be readily rationalized (see Scheme 1) and the structure arrived at is compatible with all the available data (but is not rigorously required by them).

Type I cleavage of **12***a*, followed by an intramolecular hydrogen transfer gives a ketene intermediate, which can subsequently undergo an allowed thermal ($2\pi_s + 2\pi_a$) cycloaddition to give the cycloadduct **12***c*. An equivalent structure can be written derived from **12***b*. Close analogy with this thermal intramolecular cycloaddition has been reported (10), see Scheme 2.

Experimental

Apparatus

Ultraviolet spectra were recorded on a Varian Cary 219 spectrophotometer. The ^{1}Hmr spectra were recorded on a Varian XL-100 (100 MHz) or an XL-200 (200 MHz). The latter instrument was used

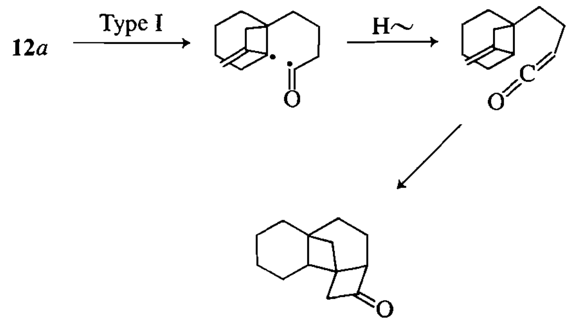

12c

SCHEME 1

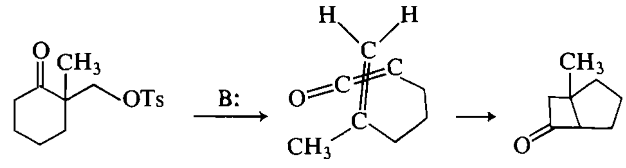

SCHEME 2

to record the ^{13}C spectra (50.3 MHz), and comparison of the fully decoupled spectra with those obtained with either the APT (11) or INEPT (12) sequence served to identify the methyl, methylene, methine, and quaternary signals. Chemical shifts are reported in parts per million (ppm) on the δ scale relative to $(CH_3)_4Si$ as internal standard. The proportions of H/H and H/T isomers in the product mixtures from irradiations of **7**, **9**, **11**,**13**,**15**, and **17** were obtained from the relative integrated intensities of the *exo*-methylene carbon signals. Measurements from spectra obtained for the same sample with 20° and 30° pulses showed good agreement (±2%); thus, the precision of the ratios is judged to be ±5%. Infrared spectra were recorded with a Beckman–Acculab 4 spectrophotometer. Mass spectra were obtained on a Varian MAT 311A system at 70 eV (direct inlet). Melting points were measured on a Reichert hot-stage apparatus and are uncorrected.

Materials

Methylene chloride was dried over CaH_2, Spectral grade methanol was used. Thin-layer chromatography (tlc) was on Kiesel gel DF-5 (Camag) plates and flash chromatography (FC) columns were prepared as described (13). Merck silica gel 60 (E. M. Merck, 35–70 mesh) was used in all irradiation experiments. The following compounds were prepared by known methods and gave satisfactory physical and spectral data: 3β-acetoxy-$\Delta^{8,9}$-cholesten-7-one (**1**) (14), 3β-acetoxy-$\Delta^{8,9}$-cholesten-11-one (**2**) (15), bicyclo[4.4.0]dec-1(6)-en-one (**11**) (16), bicyclo[0.3.3]-Δ^7-octen-1-one **13** (16), 4,5,6,7-tetrahydroindan-1-one (**15**) (16), and Δ^8-hydrindenone (**17**) (16). Allene (Canadian Liquid Air) was used as supplied.

Procedure for sample preparation and irradiation on dry silica

A preweighed sample of silica gel (~6 g) was introduced into a Pyrex tube equipped with a side arm in apparatus described elsewhere (17), and to it was added a sample of steroidal enone **1** (~0.45 mmol). The silica gel was dried at 200°C (3 h; 0.3 Torr) (1 Torr = 133.3 Pa). The silica gel was then allowed to cool to room temperature under vacuum, the enone was dropped onto the gel, and dry methylene chloride (30 mL) was condensed on to the gel by cooling the Pyrex cylinder containing the silica gel to −78°C. The slurry was shaken well in order to dissolve the enone and the methylene chloride was removed by distillation back to the original container. The silica gel was further dried in vacuum for 6 h. In the case of liquid enones **7**, **9**, **11**, **13**, **15**, and **17**, a preweighed sample (~1.0 mmol) was condensed into the Pyrex cylinder containing silica gel cooled to −78°C. The allene gas was introduced at 1 Torr (133.3 Pa) pressure into the Pyrex cylinder, containing gel and an enone, of total capacity ~43 mL at 0°C. The Pyrex cylinder was then sealed and rotated on its long axis in front of a 450-W medium-pressure Hg lamp. Irradiation times varied considerably depending upon the substrate and conversion required.

Sample analysis

The silica gel was extracted with ether and with methanol. The adduct products, except in the case of **1** and **2**, were analysed by ^{13}Cmr using the sp^2 carbon atoms (=CH_2) as probes.

Solution irradiations

A solution of enone (~0.05 *M*) in methylene chloride was irradiated while a continuous stream of allene was bubbled through the solution.

Photocycloaddition of 3β-acetoxy-$\Delta^{8,9}$-cholesten-7-one (1) to allene

Irradiation of **1** (200 mg, 0.45 mmol) and allene on 6 g of silica gave 190 mg of yellow oil which was purified by ptlc (6:4 (v/v) hexane–ether, 7 developments). The band at R_f 0.81 gave 12.3 mg of colourless solid. One recrystallization from ether–methanol gave 7.6 mg of **4**: mp 175.5–177°C (lit. (4*c*) mp 177–178°C). The band at R_f 0.74 gave 23 mg of reported (4*c*) α adduct **3*a***, mp 116–118°C (lit. (4*c*) mp 119.5–120.5°C); derived hydroxy ketone **3*b*** ^{13}Cmr ($CDCl_3$) δ_C: 22.8, 22.6, 19.1, 15.8, 12.2 (5 × CH_3), 45.3, 39.5, 38.1, 37.3, 36.1, 34.7, 30.9, 30.3, 27.6, 25.4, 23.8, 20.3 (12 × CH_2), 70.3, 55.4, 55.4, 36.0, 33.9, 28.0 (6 × CH), 60.3, 47.9, 40.3, 38.5 (4 × quat. C), 103.1 (*CH*$_2$=C—), 151.2 (CH_2=*C*—), 211.9 (C=O).

The band at R_f 0.65 gave 87 mg of colorless oil (a mixture of three adducts). This material was hydrolyzed with methanolic KOH at room temperature for 1 h. The usual work-up gave an oily solid. To this was added ether and the supernatant liquid was pipetted out leaving 21.3 mg of an unidentified adduct[4] as a colourless crystalline solid, mp 183–185°C; ir ($CHCl_3$) ν_{max}: 3400–3500, 1710 cm^{-1}; ^{1}Hmr δ: 3.52 (m, 1H); ^{13}Cmr ($CDCl_3$) δ_C: 22.8, 22.6, 19.5, 19.1, 11.7 (5 × CH_3), 49.54, 48.04, 42.5, 41.8, 39.5, 38.1, 36.1, 35.1, 32.1, 26.7, 23.8, 22.1, 19.6 (13 × CH_2), 68.3, 57.9, 55.8, 44.3, 35.7, 28.0 (6 × CH), 56.7, 56.6, 49.0, 43.1, 42.5 (5 × quat. C), 215.7 (C=O). *Exact Mass* calcd. for $C_{30}H_{48}O_2$: 440.3654; found: 440.3651. The ether soluble material (56 mg) was purified by ptlc (64:36 hexane–EtOAc, 4 developments). The band at R_f 0.51 gave 36 mg of a mixture of alcohols **5** and **6** as a colourless viscous oil. The band at R_f 0.44 gave 9.8 mg of the same unidentified cycloadduct.[4]

The acetate of the above hydroxyketone[4] was made in the usual way, giving the acetoxyketone derivative as colourless granules, mp 105–108°C (from CH_3OH); ir ($CHCl_3$) ν_{max}: 1710 cm^{-1}; ^{1}Hmr ($CDCl_3$) δ: 2.04 (s, 3H), 4.67 (m, 1H). *Exact Mass* calcd. for $C_{32}H_{50}O_2$: 482.3759; found: 482.3759.

The above acetoxyketone (33 mg, 0.07 mmol) was reduced with 60 mg (1.5 mmol) of lithium aluminium hydride in 10 mL of ether. The usual work-up gave 28 mg of diol as an oily solid. This oily solid was purified by ptlc (76:24 hexane–EtOAc, 3 developments). The band at R_f 0.53 gave 20 mg of colourless diol, mp 154°C (dec. from Et_2O – petroleum ether); ir ($CHCl_3$) ν_{max}: 3600, 3400 cm^{-1}; ^{1}Hmr ($CDCl_3$) δ: 4.08–4.1 (d, J = 6 Hz, 1H), 3.46–3.6 (m, 2H); ^{13}Cmr ($CDCl_3$) δ_C: 23.1, 22.8, 20.2, 19.4, 13.0 (5 × CH_3), 54.1, 45.8, 44.1, 43.9, 40.3, 39.0, 36.8, 36.5, 33.2, 30.6, 24.5, 23.7, 21.7 (13 × CH_2), 72.5, 68.4, 61.4, 57.5, 45.3, 36.7, 28.7 (7 × CH), 54.6, 51.8, 47.6, 47.1, 42.8 (5 × quat. C). *Exact Mass* calcd. for $C_{30}H_{50}O_2$: 442.3811; found: 442.3798.

A ~50:50 mixture of alcohols (53 mg) **5** and **6** was purified using flash column chromatography on SiO_2 (Et_2O – petroleum ether, 70:30) to give 10 mg of **6** (mp 143–146°C; ir ($CHCl_3$) ν_{max}: 3600–3400, 1705 cm^{-1}; uv (CH_3OH) λ_{max}: 290 nm (ε 96 M^{-1} cm^{-1}); ^{1}Hmr ($CDCl_3$) δ: 4.49 (brs, 2H), 3.37 (m, 1H); ^{13}Cmr ($CDCl_3$) δ_C: 22.8, 22.6, 18.8, 13.4, 11.4 (5 × CH_3), 43.0, 39.5, 38.4, 37.6, 36.2, 36.17, 31.3, 29.6, 28.5, 27.3, 25.5, 23.7 (12 × CH_2), 66.6, 54.8, 52.7, 46.2, 35.6, 28.0 (6 × CH), 54.8, 53.6, 48.6, 45.6 (4 × quat. C), 106.3 (*CH*$_2$=C—), 152.4 (CH_2=*C*—), 210.5 (C=O). *Exact Mass* calcd. for $C_{30}H_{48}O_2$: 440.3654; found: 440.3652), together with 36 mg of mixed isomers, and 8 mg of **5** as a colourless viscous oil; ir ($CHCl_3$) ν_{max}: 3400–3600, 1690 cm^{-1}; uv (CH_3OH) λ_{max}: 290 nm (ε 38.5 M^{-1} cm^{-1}); $[\alpha]^{25}$ ($CHCl_3$) −23.1°; ^{1}Hmr ($CDCl_3$) δ: 5.17 (brs, 1H), 4.93 (m, 1H), 3.04 (m, 1H); ^{13}Cmr ($CDCl_3$) δ_C: 22.8, 22.6, 19.0, 15.5, 12.5 (5 × CH_3), 44.7, 44.2, 39.5, 38.4, 37.3, 36.1, 30.9, 30.4, 27.6, 24.8, 23,7, 20.2 (12 × CH_2), 70.2, 57.4, 55.5, 36.3, 35.9, 28.0 (6 × CH), 62,3, 50.5, 40.7, 38.7 (4 × quat. C), 110.7 (*CH_2*=C—), 150.2 (CH_2=*C*—), 213.4 (C=O). *Exact Mass* calcd. for $C_{30}H_{48}O_2$: 440.3654; found: 440.3661.

Irradiation of 3β-acetoxy-$\Delta^{8,9}$-cholesten-11-one (2) and allene on silica gel

Irradiation of 3 mg of **2** and allene on 300 mg of silica gel was performed as described previously. The tlc of the crude silica irradiation product was found to be identical with the irradiation of **2** in methylene chloride at room temperature.

Irradiation of isophorone (9) and allene on silica gel

Irradiation of **9** (150 mg, 1.08 mmol) and allene on 6 g of silica gave 170 mg of oil. Chromatography of the crude irradiation product by ptlc (eluent: benzene, 4 developments) gave 78 mg of **10***a* as a colourless oil; ^{1}Hmr ($CDCl_3$) δ: 5.0–4.9 (m, 2H), 3.3–3.1 (brs, 1H), 1.3 (s, 3H), 1.12 (s, 3H), 0.85 (s, 3H); ^{13}Cmr ($CDCl_3$) δ_C: 30.9, 30.3, 27.7 (3 × CH_3), 59.7 (quat. C), 108.2 (*CH_2*=C—), 142.3 (CH_2=*C*—), 209.9 (C=O). *Exact Mass* calcd. for $C_{12}H_{18}O$: 178.1357; found: 178.1362; and 55 mg of **10***b* as a colorless oil: ^{1}Hmr ($CDCl_3$) δ: 4.90–4.78 (t, J = 2 Hz, 1H), 4.78–4.62 (t, J = 2 Hz, 1H), 1.4 (s, 3H), 1.0 (s, 6H); ^{13}Cmr ($CDCl_3$) δ_C: 30.4, 29.45, 29.3 (3 × CH_3), 47.6 (quat. C), 103.5 (*CH_2*=C—), 156.1 (CH_2=*C*—), 214.2 (C=O). *Exact Mass* calcd. for $C_{12}H_{18}O$: 178.1357; found: 178.1357.

Irradiation of bicyclo[4.4.0]dec-1(6)-en-one (11) and allene on silica gel

Irradiation of **11** (150 mg, 0.79 mmol) and allene on 5 g of silica gave 140 mg of crude oil. Chromatography of the crude oil gave 60 mg of a mixture of photocycloadducts **12***a* and **12***b*; the ^{13}Cmr data are collected in Table 2. *Exact Mass* calcd. for $C_{13}H_{18}O$: 190.1357; found: 190.1362. Also obtained was 7 mg of **12***c* as a colourless oil. A total of 33.5 mg of this material was collected from several reactions and purified by ptlc (hexane – ethyl acetate, 96:4, 3 developments) to give 20 mg of rearrangement product **12***c* as an oil; ir ($CHCl_3$) ν_{max}: 1760 cm^{-1}; ^{1}Hmr ($CDCl_3$) δ: 3.44 (d, J = 8 Hz, 1H) 3.0–2.67 (m, J_{AB} = 18 Hz, J_{AX} = ~2.5 Hz); ^{13}Cmr δ_C: 48.8, 37.6, 30.5, 29.6, 27.7, 25.0, 22.4, 21.6 (8 × CH_2), 69.6, 32.0 (2 × CH), 51.0, 45.9 (2 × quat. C), 212.6 (C=O). *Exact Mass* calcd. for $C_{13}H_{18}O$: 190.1357; found: 190.1355; oxime mp 72–82°C. *Exact Mass* calcd. for $C_{13}H_{19}ON$: 205.1466; found: 205.1469.

Irradiation of **11** and allene in methylene chloride was performed as described previously and no rearrangement product **12***c* was detected.

Photocycloaddition of 7, 9, 11, 13, 15, and 17 to allene

The photocycloaddition of the enones **7**, **9**, **11**, **13**, **15**, and **17** in methylene chloride and on silica gel was performed as previously described and products analysed by ^{13}Cmr (see Tables 1 and 2). The molecular formulae were confirmed by mass spectrometry, results for which are as follows. Mixture of **8***a* and **8***b*: *Exact Mass* calcd. for $C_9H_{12}O$: 136.0888; found 136.0893; **10***a* and **10***b*: *Exact Mass* calcd. for $C_{12}H_{18}O$: 178.1357; found 178.1362; **12***a* and **12***b*: *Exact Mass* calcd. for $C_{13}H_{18}O$: 190.1357; found 190.1362; **14***a* and **14***b*: *Exact Mass* calcd. for $C_{11}H_{14}O$: 162.1044; found 162.1040; **16***a* and **16***b*: *Exact Mass* calcd. for $C_{12}H_{16}O$: 176.1201; found 176.1201; **18***a* and **18***b*: *Exact Mass* calcd. for $C_{12}H_{16}O$: 176.1201; found 176.1200.

Acknowledgements

Two of the authors (P. de Mayo, J. B. Stothers) wish to thank the Natural Sciences and Engineering Research Council of Canada for support of this research.

1. (*a*) P. DE MAYO. Acc. Chem. Res. **4**, 41 (1971); (*b*) G. R. LENZ. Rev. Chem. Intermed. **4**, 369 (1981); (*c*) P. G. BAUSLAUGH. Synthesis, 287 (1970); (*d*) S. W. BALDWIN. Org. Photochem. **5**, 123 (1981); (*e*) A. C. WEEDON. *In* Synthetic organic photochemistry. *Edited by* W. M. Horspool. Plenum, New York. 1984. p. 61.
2. (*a*) M. B. RUBIN, I. MAYMON, and D. GLOVER. Isr. J. Chem. **8**, 7117 (1970); (*b*) G. R. LENZ. Tetrahedron, **28**, 2195 (1972); (*c*) P. SUNDER PLASSMAN, P. H. NELSON, P. H. BOYLE, A. CRUZ, J. IRIATE, P. CRABBE, J. A. ZDERIC, J. A. EDWARDS, and J. H. FRIED. J. Org. Chem. **34**, 3779 (1969).
3. R. FARWAHA, P. DE MAYO, and Y. C. TOONG. J. Chem. Soc. Chem. Commun. 739 (1983).
4. (*a*) G. MARINI-BETTOLA, S. P. SAHOO, G. A. PULTON, T. Y. R. TSAI, and K. WIESNER. Tetrahedron, **36**, 719 (1980); (*b*) K. WIESNER. Tetrahedron, **31**, 1655 (1975); (*c*) J. F. BLOUNT, G. D. GRAY, K. S. ATWAL, and K. WIESNER. Tetrahedron Lett. **21**, 4413 (1980).
5. R. O. LOUTFY and P. DE MAYO. J. Am. Chem. Soc. **99**, 3559 (1977).
6. (*a*) J. W. HANIFIN and E. COHEN. J. Am. Chem. Soc. **91**, 4494 (1969); (*b*) J. J. MCCULLOUGH, J. M. KELLY, and P. W. RASMUSSEN. J. Org. Chem. **34**, 2933 (1969).
7. (*a*) R. L. CARGILL, G. H. MORTON, and J. BORDNER. J. Org. Chem. **45**, 3929 (1980); (*b*) E. P. SEREBRYAKOV, M. I. VORONTSOVA, O. S. CHIZOV, V. A. PAVLOV, and I. M. VOLPIN. Bull. Acad. Sci. USSR, Div. Chim. Sci. **32**, 111 (1983).
8. C. J. TIMMONS. *In* "Elucidation of organic structures by physical and chemical methods. Vol. IV. Part 1. *Edited by* K. W. Bentley and G. W. Kirby. Wiley–Interscience, New York. 1972. p. 110.
9. (*a*) R. R. GETTY, J. A. KERR, A. F. T. DICKENSON, and E. DAVIES. J. Chem. Soc. (A), 979 (1967); (*b*) H. G. MEUNIER and P. I. ABELL. J. Phy. Chem. **71**, 1430 (1967).
10. S. W. BALDWIN and E. G. PAGE. J. Chem. Soc. Chem. Commun. 1337 (1972).
11. S. L. PATT and J. N. SHOOLERY. J. Mag. Reson. **46**, 535 (1982).
12. G. A. MORRIS and R. A. FREEMAN. J. Am. Chem. Soc. **107**, 760 (1979).
13. W. C. STILL, M. KAHN, and A. MITRA. J. Org. Chem. **43**, 2923 (1978).
14. L. F. FIESER. J. Am. Chem. Soc. **75**, 4395 (1953).
15. D. G. PATTERSON, C. DJERASSI, Y. YUH, and N. ALLINGER. J. Org. Chem. **42**, 2365 (1977).
16. S. B. KULKARNI and S. DEV. Tetrahedron, **24**, 553 (1968).
17. M. ABDEL-MALIK and P. DE MAYO. Can. J. Chem. **62**, 1275 (1984).

Novel sterols from the finger sponge *Haliclona oculata*

JOHN A. FINDLAY AND ASHOK D. PATIL
Chemistry Department, University of New Brunswick, Fredericton, N.B., Canada E3B 6E2

Received May 29, 1984[1]

JOHN A. FINDLAY and ASHOK D. PATIL. Can. J. Chem. **63**, 2406 (1985).

From the finger sponge, *Haliclona oculata* (Linnaeus), six new polar sterols have been isolated and their structures determined by chemical and spectroscopic means. These are 3β-hydroxy-cholesta-5,25-dien-24-one (**2**), 3β-hydroxy-24-methylene-5-cholesten-7-one (**6**), 24-methylene-5-cholesten-3β,7β-diol (**9**), 24-methylcholesta-5,22-dien-3β,7β-diol (**11**), 24-methylene-5-cholesten-3β,7α-diol (**12**), and 5β,6-epoxy-24-methylene-cholestan-3β-ol (**16**). Also shown to be present are the known monohydroxysterols (22*E*,24*S*)-24-methylcholesta-5,22-dien-3β-ol (**1**), (22*Z*)-24-norcholesta-5,22-dien-3β-ol, 24-methylene-5-cholesten-3β-ol, 24-isoethylidene-5-cholesten-3β-ol, (22*E*)-24-norcholesta-5,22-dien-3β-ol and (23*E*)-cholesta-5,23-dien-3β,25-diol. The structure **14** is tentatively proposed for a novel C_{24} sterol and **8** is suggested for the structure of a compound accompanying **6**.

JOHN A. FINDLAY et ASHOK D. PATIL. Can. J. Chem. **63**, 2406 (1985).

On a isolé six nouveaux stérols polaires de l'éponge *Haliclona oculata* (Linnaeus) et on a déterminé leurs structures par des méthodes chimiques et spectroscopiques. Il s'agit de l'hydroxy-3β cholestadiène-5,25 one-24 (**2**), de l'hydroxy-3β méthylène-24 cholestène-5 one-7 (**6**), du méthylène-24 cholestène-5 diol-3β,7β (**9**), du méthyl-24 cholestadiène-5,22 diol-3β,7β (**11**), du méthylène-24 cholestène-5 diol-3β,7α (**12**) et de l'époxy-5β,6 méthylène-24 cholestanol-3β (**16**). On a aussi montré que les monohydroxystérols connus (22*E*,24*S*) méthyl-24 cholestadiène-5,22 ol-3β (**1**), (22*Z*) nor-24 cholestadiène-5,22 ol-3β, méthylène-24 cholestène-5 ol-3β, isoéthylidène-24 cholestène-5 ol-3β, (22*E*) nor-24 cholestadiène-5,22 ol-3β et (23*E*) cholestadiène-5,23 diol-3β,25 sont aussi présents. Sur une base préliminaire, on a attribué la structure **14** à un nouveau stérol en C_{24} et la structure **8** à un composé accompagnant le composé **6**.

[Traduit par le journal]

Chemical studies on sponges have shown that they often are a source of novel sterols of biogenetic interest (1, 2). As part of a continuing study of marine natural products from Bay of Fundy organisms, we have examined the sterols of the abundant finger sponge *Haliclona oculata* (Linnaeus) and now report our findings.

Thin-layer chromatography (tlc) of fractions from silica gel column chromatography of a methanol extract of *H. oculata* showed the presence of substantial amounts of compounds more polar than the monohydroxylated sterol fraction. The five major monohydroxylated sterols were separated and identified by comparison of their spectral characteristics with literature data. The major sterol (85%) of this fraction proved to be (22*E*,24*S*)-24-methylcholesta-5,22-dien-3β-ol (22-dehydrocampesterol), **1** (3, 4), while other components were identified as (22*Z*)-24-norcholesta-5,22-dien-3β-ol (4) (1.5%), 24-methylene-5-cholesten-3β-ol (5) (2.4%), 24-isoethylidene-5-cholesten-3β-ol (isofucosterol) (4) (2.9%), and (22*E*)-24-norcholesta-5,22-dien-3β-ol (4) (0.8%).

Purification of the more polar sterols was achieved by a combination of column chromatography, preparative tlc, and high pressure liquid chromatography (hplc) on silica gel and reverse phase systems. In some cases it was necessary to separate mixtures after acetylation. In this manner we have succeeded in isolating and characterizing the six new sterols **2**, **6**, **9**, **11**, **12**, and **16**, plus the previously reported diene diol **4** (6).

The novel ketone **2** was purified as its acetate **3** whose ir spectrum ($CHCl_3$) displays strong bands at 1730 and 1670 cm^{-1} attributed to the ester and α,β-unsaturated ketone, respectively. The uv spectrum showing λ_{max} (C_2H_5OH) 223 (ε 11 440) allows placement of the enone in the sidechain. The mass spectrum of **2** shows a molecular ion *m/e* 398 ($C_{27}H_{42}O_2$) and the base peak, *m/e* 271, is attributed to loss of the sidechain plus two hydrogens. An abundant ion *m/e* 314 results from

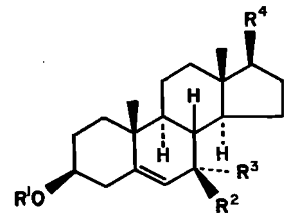

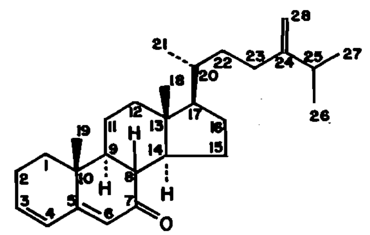

13

1 R^1,R^2,R^3 = H, R^4 = a
2 R^1,R^2,R^3 = H, R^4 = b
3 R^1 = Ac, R^2,R^3 = H, R^4 = b
4 R^1,R^2,R^3 = H, R^4 = d
5 R^1 = Ac, R^2,R^3 = H, R^4 = d
6 R^1 = H, R^2,R^3 = O, R^4 = c
7 R^1 = Ac, R^2,R^3 = O, R^4 = c
8 R^1 = H, R^2,R^3 = O, R^4 = a
9 R^1,R^3 = H, R^2 = OH, R^4 = c
10 R^1 = Ac, R^2 = OAc, R^3 = H, R^4 = c
11 R^1,R^3 = H, R^2 = OH, R^4 = a
12 R^1,R^2 = H, R^3 = OH, R^4 = c

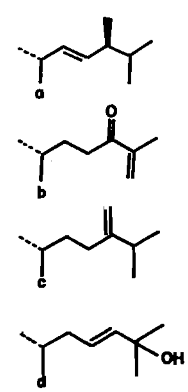

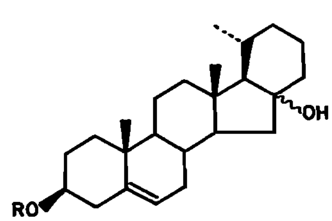

14, R = H **15**, R = Ac

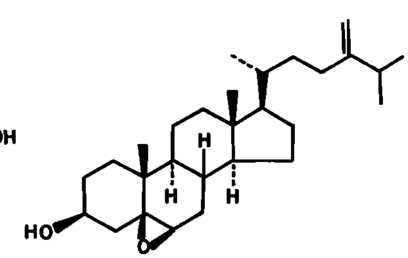

16

[1] Revision received January 24, 1985.

TABLE 1. ^{13}C Chemical shifts, multiplicities[a]

Carbon	Compounds					
	1[b]	4	7	9	12	16
1	37.34	37.23	36.01[d] T	36.94[e] T	36.92 T	37.20 T
2	31.76	31.64	27.37[c] T	31.59 T	31.55 T	31.04 T
3	71.86	71.77	72.21 D	73.36 D	73.33 D	69.44 D
4	42.36	42.28	37.75[d] T	41.74[e] T	41.71 T	42.22 T
5	140.83	140.74	163.83 S	143.47 S	143.45 S	62.89 S
6	121.72	121.65	126.71 D	125.45 D	125.43 D	63.68 D
7	31.97	31.77	201.91 S	71.45 D	71.42 D	32.60 T
8	31.97	31.77	45.42 D	40.93 D	40.90 D	29.68 D
9	50.28	50.08	49.96 D	48.26 D	48.23 D	51.32 D
10	36.57	36.48	38.33 S	36.46 S	36.41 S	34.84 S
11	21.13	21.05	21.17 T	21.08 T	21.05 T	21.97 T
12	39.76	39.66	38.67 T	39.57[c] T	39.54 T	39.82 T
13	42.36	42.34	43.16 S	42.98 S	42.94 S	39.71 S
14	56.95	56.67	49.81 D	55.32[c] D	55.29[c] D	56.21[c] D
15	24.36	24.29	26.31[c] T	26.39 T	26.35 T	24.16 T
16	28.81	28.19	28.52 T	28.54 T	28.50 T	28.11 T
17	56.08	55.78	54.63 D	55.96[c] D	55.93[c] D	56.04[c] D
18	12.10	11.89	11.99 Q	11.84 Q	11.80 Q	11.74 Q
19	19.42	18.65	18.86 Q	19.17 Q	19.13 Q	17.03 Q
20	40.26	38.79	35.68 D	35.72[d] D	35.68 D	35.68 D
21	21.05	11.38	21.27 Q	18.78 Q	18.75 Q	18.62 Q
22	136.09	42.28	30.98[e] T	30.99[c] T	30.97[e] T	30.95[e] T
23	131.91	125.46	34.69[e] T	34.70[c] T	34.68 T	34.61[e] T
24	43.10	139.38	156.75 S	156.82 S	156.83 S	156.82 S
25	33.26	70.73	33.76 D	33.81[d] D	33.78 D	33.77 D
26	19.67	29.88	21.86 Q	21.88 Q	21.83 Q	21.84 Q
27	20.15	29.88	22.00 Q	22.01 Q	21.97 Q	21.97 Q
28	18.02		106.03 T	105.98 T	105.96 T	105.92 T

[a] As determined by DEPT analysis.
[b] Assignments after Wright *et al.* (3).
[c, d, e] Assignments may be interchanged.

cleavage of the C22—C23 bond, together with a hydrogen transfer. Both of these fragments are typical of sterols possessing a cholesterol nucleus plus a double bond in the sidechain (7, 8). Confirmation of the assigned structure is available from the 200-MHz ^1H nmr spectrum, which shows signals consistent with the cholesterol nucleus plus additional methyl signals at δ 0.95 (d, J = 6 Hz) and δ 1.95 (s) assigned to the $21CH_3$ and $27CH_3$, respectively. The vinylic protons at C26 appear as singlets at δ 5.78 and δ 5.98 ppm.

The diene diol **4** displays in its mass spectrum a molecular ion m/e 400 ($C_{27}H_{44}O_2$) plus a series of fragments m/e 271, 255, and 213 consistent with its nuclear and sidechain features (7, 8). Other prominent ions m/e 382 (M − H_2O), 385 (M − CH_3), 367 (M − H_2O − CH_3), 349 (M − $2H_2O$ − CH_3) support the functionality and composition of **4**. The ^1H nmr spectrum displays a sharp singlet at δ 1.34 (6H) assigned to the terminal methyls, while the secondary methyl is seen at δ 0.92 ppm (J = 6.5 Hz). Irradiation of the allylic region (~ δ 2.0) caused the sidechain vinylic proton multiplet to collapse to an AB quartet (J_{AB} = 15.5 Hz), while the multiplicity of the $21CH_3$ was unchanged and the 3CH signal was transformed to a less complex multiplet. Thus the placement of all functional groups and the Δ^{23} geometry are established. Diene diol **4** on acetylation provided the monoacetate **5** whose infrared spectrum featured a band at 3600 cm^{-1} (tertiary OH). Comparison of the ^{13}C nmr spectrum of **4** with that of the known (3) 22-dehydrocampesterol **1** (see Table 1) provides detailed corroboration of the structure and stereochemistry of **4**, which was previously isolated from marine sources, characterized as its acetate, and designated trans-liagosterol (6).

A major component of the polar sterol fraction proved to be the novel dienone **6**, which was inseparable from a minor isomer tentatively assigned structure **8**, in view of the presence of a multiplet at δ 5.25 similar in pattern to the $\Delta^{22,23}$ proton signals in **1**. The enone feature was inferred from the infrared ($CHCl_3$) spectral features (1655 and 1640 cm^{-1}) and its ultraviolet spectrum (λ_{max} (C_2H_5OH) 238.5 (ε 15 600)). The mass spectrum exhibits a strong molecular ion m/e 412 ($C_{28}H_{44}O_2$), while an abundant ion m/e 269 results from dehydration plus loss of the sidechain from C20. An ion m/e 310 is accounted for by McLafferty rearrangement of a dehydrated species. The ^1H nmr spectrum displays singlets at δ 4.65, 4.76, and 5.64 ppm, assigned to the C24 methylene protons and the C6H, respectively, while other signals confirm the presence of two tertiary and three secondary methyls in field positions in accord with expectation (9). Distortionless enhancement bipolarization transfer (DEPT) analysis of the ^{13}C nmr spectrum of the acetate **7** of alcohol **6** shows that twenty-four of the thirty carbon atoms bear protons and, of these, eight are primary, ten are secondary, and six are tertiary. Table 1 provides assignments for the ^{13}C signals and a detailed corroboration for structures **6** and **7**. The chemical shift assignments are in close agreement with the corresponding assignments for the nuclear carbon atoms of 3β-acetoxy-cholest-5-en-7-one (12).

Hydrolysis of acetate **7** with 5% ethanolic KOH furnished the trienone **13**, which shows infrared absorption bands at

1650, 1620, and 1590 cm^{-1} and λ_{max} (C_2H_5OH) 280.5 (ϵ 15 560) in its ultraviolet spectrum, establishing the conjugated dienone features. The mass spectrum, predictably, shows prominent ions at *m/e* 269 and 310 (*vide supra*) while the ^1H nmr spectrum features a singlet at δ 5.63 (C6H) and multiplets at δ 6.08–6.28 (2H) assigned to the C3 and C4 hydrogens. The spectroscopic data are consistent with those for cholesta-3,5-dien-7-one (10) and other sterols possessing the same dienone system (11). A multiplet at δ 5.26 (0.3 H) similar in pattern to the $\Delta^{22,23}$ signal in the ^1H nmr spectrum of **1** suggests the presence (~15%) of compound **8**.

The novel diol **9** was characterized as its diacetate **10**. The mass spectrum of **9** displays a molecular ion *m/e* 414 ($C_{28}H_{46}O_2$). A prominent ion at *m/e* 253 is ascribed to a 3,5,7-triene fragment derived by loss of two molecules of water plus the sidechain, thus placing both hydroxyls in the nucleus. The relationship of functional groups in the nucleus was demonstrated by ^1H nmr experiments. Irradiation of C3H at δ 3.56 removed a coupling to the allylic hydrogen signals at δ 2.32, while irradiation at δ 1.38 (C8H) changed the C7H doublet at δ 3.84 (J = 8 Hz) to a broad singlet, thus supporting the assignment of an α configuration to the C7H. Other ^1H nmr signals are consistent with the indicated sidechain and nucleus stereochemistry. The ^{13}C nmr spectrum and DEPT analysis confirmed the number and substitution of carbon atoms in alcohol **9**, and chemical shift assignments based on comparative data for the related compound **1**, with the same skeletal ring junction stereochemistry, are given in Table 1.

The spectral characteristics of diene diol **12** are very similar to those of its C7 epimer **9**, except for the ^1H nmr signals for C6H and C7H, which appear as a doublet at δ 5.62 (J = 6 Hz) and a broad singlet at δ 3.80 ($W_{1/2}$ = 11 Hz), respectively.

The diol **11** showed a molecular ion *m/e* 416 ($C_{28}H_{48}O_2$) and a fragmentation pattern consistent with its assigned structure. The ^1H nmr spectrum displayed signals for C3H, C6H, and C8H, virtually identical with those of **9**, while the $28CH_3$ gave rise to a doublet at δ 0.88 ppm, as does the corresponding $28CH_3$ in the known compound **1** (3, 4).

The most remarkable of the polar sterols isolated from *H. oculata*, albeit in trace amounts, has the composition $C_{24}H_{38}O_2$ and features only three methyl groups, two being tertiary and giving rise to ^1H nmr signals at δ 0.68 and δ 0.96, while the third shows as a doublet at δ 0.96 (J = 6.5 Hz). These values are typical for C18, C19, and C21 methyls of the cholesterol nucleus. The absence of additional methyls, together with the elemental composition, led us to assign structure **14** to this compound on a tentative basis. The compound was converted into a monoacetate **15** whose infrared showed the presence of hydroxyl absorption.

The mass spectrum of epoxide **16** showed a molecular ion *m/e* 412 in confirmation of the composition $C_{28}H_{46}O_2$ deduced by analysis of ^{13}C nmr data (Table 1). The ion *m/e* 287, due to loss of sidechain with transfer of 2 hydrogens, and the characteristic ion at *m/e* 330, formed as a result of McLafferty rearrangement, confirm the presence of an additional oxygen in the nucleus. This is incorporated as a 5β,6-epoxide in view of ^1H nmr, which displays a broad singlet at δ 3.06 assigned to C6H and a multiplet δ 3.74 due to the C3H. The latter is found at lower field than usual due to its proximity to the epoxide. Other ^1H nmr features were consistent with the assigned structure, and the good correlation of ^{13}C nmr chemical shifts with related compounds in Table 1 provides compelling evidence in favour of structure **16**. Location of the epoxide at the 4,5-position was excluded by double irradiation experiments, and assignment of configuration is based on comparison of ^{13}C nmr chemical shift data with that of other 5β,6-epoxides (13).[2]

Experimental

General

Low resolution mass spectra were recorded with an Hitachi Perkin–Elmer RMU 6D mass spectrometer and high resolution mass spectra on an AEI-MS 50 instrument using homogeneous samples as determined by hplc and ^1H nmr. The ^1H and ^{13}C nmr spectra were recorded in $CDCl_3$ solution on a Varian XL200 instrument.

The hplc was carried out on a Waters system employing 440 absorbance and R401 refractive index detectors and using a μ-Porasil column (30 cm × 3.9 mm). Analytical and preparative tlc was performed with precoated silica gel G (Kieselgel 60, F-254) and reverse phase ($KC_{18}F$) plates. Infrared spectra were recorded on a Perkin–Elmer 598 spectrophotometer. Ultraviolet spectra were recorded on a Beckman 25 instrument and optical rotations were measured in chloroform solution using a Perkin–Elmer 241 polarimeter.

Extractions and separations

The sponge *Haliclona oculata* (Linnaeus) (3.5 kg wet weight) was collected in Passamaquoddy Bay, New Brunswick, Canada, in early spring 1982. The organisms were chopped, partially freeze-dried, and extracted in a Soxhlet with methanol. The methanolic extract (45 g), after evaporation, was chromatographed on a silica gel column (400 g, 70–200 mesh) using methanol/chloroform (1:5). Early fractions containing lipids and fats were discarded. Later fractions containing sterols and polar sterols were combined (4.5 g) and rechromatographed on a silica gel G column prepared in hexane. The free sterol fraction (1.62 g) eluted with hexane/ethyl acetate (7:3) was crystallized from methanol and acetylated with acetic anhydride/pyridine at room temperature. The steryl acetate mixture thus obtained was separated on a column of $AgNO_3$-impregnated silica gel using hexane and hexane/benzene (1:1). The individual acetates were hydrolysed with 5% ethanolic KOH to provide five known sterols which were identified by comparison of their spectral characteristics with literature data. These were: (22*E*,24*S*)-24-methylcholesta-5,22-dien-3β-ol, **1** (22-dehydrocampesterol) (85%); (22*Z*)-24-norcholesta-5,22-dien-3β-ol (1.5%); 24-methylene-5-cholesten-3β-ol (2.4%); 24-isoethylidene-5-cholesten-3β-ol (2.9%) and (22*E*)-24-norcholesta-5,22-dien-3β-ol (0.8%).

Further elution of the silica gel G column using increasing percentages of methanol in chloroform furnished several fractions which were monitored by tlc (silica gel and reverse phase). Final purifications were effected using ptlc and hplc and, in some cases, via acetates.

Compound **14** (6 mg) was eluted with methanol/chloroform (3:97) followed by **2** (23 mg), whose acetate was purified by ptlc (R_f 0.35 on silica gel using ethyl acetate/hexane, 1:10) and hplc (silica gel using ethyl acetate/chloroform, 3:97) to give pure 3β-acetoxy-cholesta-5,22-dien-24-one, **3** (26 mg) which was hydrolysed with 5% ethanolic KOH to give pure **2** (19 mg).

Other fractions also eluted with methanol/chloroform (3:97), after purification by ptlc (R_f 0.45 on silica gel using ether/hexane, 4:6), afforded 24-methylene-5-cholesten-3β-ol (47 mg).

Fractions eluted with methanol/chloroform (4:96) (53 mg), after purification via ptlc (R_f 0.50, on silica gel, methanol/chloroform, 5:95) gave pure (23*E*)-cholesta-5,23-dien-3β,25-diol, **4** (31 mg). Compound **16**, eluted immediately following **4**, was purified in similar manner.

Elution with methanol/chloroform (6:94) provided a fraction (169 mg) which after double purification by ptlc (R_f 0.43 on silica gel methanol/chloroform (9:91) and R_f 0.74 on reverse phase with ethyl acetate/ether (4:6)) afforded 3β-hydroxy-24-methylene-5-cholesten-7-one, **6** (119 mg), together with traces of the minor isomer **8**. Further

[2] The authors are grateful to a referee for drawing attention to this paper.

elution with this solvent gave a fraction (79 mg) which was acetylated and purified by ptlc (silica gel with acetone/benzene, 1:9) and hydrolysed with 5% ethanolic KOH to give a mixture of **9** (28 mg) and **11** (35 mg), separated by ptlc (reverse phase with ethyl acetate/ether, 3:7). The last fraction (37 mg) was purified on reverse phase ptlc (ethyl acetate/ether, 1:1) to provide compound **12** (29 mg) in crystalline form.

3β-Hydroxy-cholesta-5,25-dien-24-one, **2**: ir ($CHCl_3$) ν_{max}: 3600, 2950, 1695, 1670, 1450, 1370 cm^{-1}; ^1H nmr δ_{TMS}: 0.70 (s, 3H, $18CH_3$), 0.94 (d, 3H, J = 6 Hz, $21CH_3$), 1.04 (s, 3H, $19CH_3$), 1.95 (s, 3H, $27CH_3$), 3.56 (m, 1H, 3CH), 5.40 (bd, 1H, J = 4.5 Hz, 6CH), 5.78 (s, 1H, 26H), 5.98 (s, 1H, 26H); ms m/e: 398.3182 (20, M^+), 383 (13), 382 (13), 314 (9, M − C_5H_7O + H), 297 (10), 271 (100, M − $C_8H_{13}O$ − 2H), 255 (33), 213 (49).

3β-Acetoxy-cholesta-5,25-dien-24-one, **3**: ir ($CHCl_3$) ν_{max}: 2950, 1730, 1670, 1630 cm^{-1}; uv (EtOH) λ_{max}: 223 nm (ε 11 440); ^1H nmr δ_{TMS}: 0.68 (s, 3H, $18CH_3$), 0.95 (d, 3H, J = 6 Hz, $21CH_3$), 1.04 (s, 3H, $19CH_3$), 1.95 (s, 3H, $27CH_3$), 2.04 (s, 3H, CH_3CO), 4.61 (m, 1H, 3CH), 5.40 (bd, 1H, J = 4 Hz, C6H), 5.78 (s, 1H, 26CH), 5.98 (s, 1H, 26CH); ms m/e: 440 (11, M^+), 398 (63, M − C_2H_2O), 380 (100, M − CH_3COOH), 368 (31), 353 (39), 326 (5), 314 (63, 398 − C_5H_7O + H), 271 (86, 398 − $C_8H_{13}O$ − 2H), 213 (54).

(23E)-Cholesta-5,23-dien-3β,25-diol, **4**: ir ($CHCl_3$) ν_{max}: 3600, 3440, 2910, 1665, 1450, 1370 cm^{-1}; ^1H nmr δ_{TMS}: 0.70 (s, 3H, $18CH_3$), 0.92 (d, 3H, J = 6 Hz, $21CH_3$), 1.02 (s, 3H, $19CH_3$), 1.34 (s, 6H, $26CH_3/27CH_3$), 3.56 (m, 1H, 3CH), 5.38 (bd, 1H, J = 4.5 Hz, C6H), 5.61 (m, 2H, 23H/24H); ms m/e: 400 (80, M^+), 385 (18, M − CH_3), 382 (27, M − H_2O), 367 (10, M − H_2O − CH_3), 349 (5), 317 (6), 300 (25), 283 (50), 271 (100, M − sidechain − 2H), 255 (8), 213 (14), 159 (31), 145 (29), 133 (34), 81 (46).

(23E)-3β-Acetoxy-cholesta-5,23-dien-25-ol, **5**: ir ($CHCl_3$) ν_{max}: 3600, 3430, 2930, 1725, 1670, 1460, 1375 cm^{-1}; ^1H nmr δ_{TMS}: 0.69 (s, 3H, $18CH_3$), 0.91 (d, 3H, J = 6 Hz, $21CH_3$), 1.03 (s, 3H, $19CH_3$), 1.32 (s, 6H, $26CH_3/27CH_3$), 2.04 (s, 3H, CH_3CO), 4.64 (m, 1H, 3CH), 5.39 (bd, 1H, J = 4 Hz, 6CH), 6.60 (m, 2H, 23H/24H); ms m/e: 442 (5, M^+), 400 (22, M − C_2H_2O), 382 (16, M − CH_3COOH), 367 (8, M − CH_3COOH − CH_3), 349 (9, M − CH_3COOH − H_2O − CH_3), 317 (6), 300 (39), 283 (45), 271 (100, 400 − sidechain − 2H), 253 (4, 271 − H_2O), 213 (11), 159 (28), 145 (41), 133 (33).

3β-Hydroxy-24-methylene-5-cholesten-7-one, **6**: ir ($CHCl_3$) ν_{max}: 3450, 2900, 1655, 1640, 1450, 1379 cm^{-1}; uv (EtOH) λ_{max}: 238.5 nm (ε 15 620); ^1H nmr δ_{TMS}: 0.73 (s, 3H, $18CH_3$), 0.97 (d, 3H, J = 6 Hz, $21CH_3$), 1.04 (d, 6H, J = 6 Hz, $26CH_3/27CH_3$), 1.20 (s, 3H, $19CH_3$), 3.61 (m, 1H, 3CH), 4.65 (s, 1H, 28CH), 4.76 (s, 1H, 28CH), 5.64 (s, 1H, 6CH); ms m/e: 412 (5, M^+), 397 (39, M − 15), 394 (100, M − H_2O), 379 (42, M − H_2O − CH_3), 366 (34), 310 (26, M − H_2O − C_6H_{12}), 269 (22), 185 (5).

3β-Acetoxy-24-methylene-5-cholesten-7-one, **7**: ir ($CHCl_3$) ν_{max}: 2950, 1725, 1655, 1645, 1445, 1370 cm^{-1}; ^1H nmr δ_{TMS}: 0.70 (s, 3H, $18CH_3$), 0.98 (d, 3H, J = 6.5 Hz, $21CH_3$), 1.06 (d, 6H, J = 6 Hz, $26CH_3/27CH_3$), 1.23 (s, 3H, $19CH_3$), 2.08 (s, 3H, CH_3CO), 4.68 (s, 1H, 28CH), 4.75 (m, 1H, 3CH), 4.78 (s, 1H, 28CH), 5.72 (s, 1H, 6CH); ms m/e: 454.3426 (4, M^+), 394 (41, M − H_2O), 382 (41), 379 (8, M − CH_3COOH − CH_3), 310 (65, M − CH_3COOH − C_6H_{12}), 296 (33), 269 (63), 187 (83).

24-Methylenecholesta-3,5-dien-7-one, **13**

Hydrolysis of **7** (25 mg) employing 5% ethanolic KOH (5 mL) at reflux for 2 h afforded, after work-up and ptlc purification, compound **13** (17 mg): ir ($CHCl_3$) ν_{max}: 2950, 1650, 1620, 1590, 1460, 1380, 1330, 1290 cm^{-1}; uv (EtOH) λ_{max}: 280.5 nm (ε 15 560); $[\alpha]_D^{20}$ −163° (c 0.20, $CHCl_3$); ^1H nmr δ_{TMS}: 0.73 (s, 3H, $18CH_3$), 0.98 (d, 6H, J = 6.5 Hz; $26CH_3/27CH_3$), 1.05 (d, 3H, J = 6 Hz, $21CH_3$), 1.13 (s, 3H, $19CH_3$), 4.69 (s, 1H, 28CH), 4.74 (s, 1H, 28CH), 5.63 (s, 1H, 6CH), 6.08–6.28 (m, 2H, 3CH/4CH); ms m/e: 394 (100, M^+), 379 (21, M − 15), 310 (24, M − C_6H_{12}), 269 (20, M − C_9H_{17}), 199 (29), 157 (18).

24-Methylene-5-cholesten-3β,7β-diol, **9**: mp 149–151°C; ir ($CHCl_3$) ν_{max}: 3600, 3450, 2900, 1640, 1460 cm^{-1}; ^1H nmr δ_{TMS}: 0.66 (s, 3H, $18CH_3$), 0.96 (d, 3H, J = 6.5 Hz, $21CH_3$), 1.04 (d, 6H, J = 6 Hz, $26/27CH_3$), 1.06 (s, 3H, $19CH_3$), 2.32 (m, 2H, $4CH_2$), 3.56 (m, 1H, 3CH), 3.84 (bd, 1H, J = 8 Hz, C7H), 4.68 (s, 1H, 28CH), 4.74 (s, 1H, 28CH), 5.32 (s, 1H, 6CH); ms m/e: 414.3493 (12, M^+), 396 (100, M − H_2O), 384 (27), 382 (20), 312 (11, M − H_2O − C_6H_{12}).

24-Methylene-5-cholesten-3β,7β-diol diacetate, **10**: ir ($CHCl_3$) ν_{max}: 2950, 1725, 1640, 1430, 1370 cm^{-1}; ^1H nmr δ_{TMS}: 0.70 (s, 3H, $18CH_3$), 0.98 (d, 6H, J = 6.5 Hz, $26CH_3/27CH_3$), 1.02 (d, 3H, J = 6 Hz, $21CH_3$), 1.08 (s, 3H, $19CH_3$), 2.02 (s, 3H, CH_3CO), 2.03 (s, 3H, CH_3CO), 4.62 (m, 1H, 7CH), 4.67 (s, 1H, 28CH), 4.72 (s, 1H, 28CH), 5.02 (m, 1H, 3CH), 5.24 (bs, 1H, 6CH), 5.26 (m, 0.5H, 22H/23H of diacetate of **11**); ms m/e: 456 (12, M^+), 414 (8, M − C_2H_2O), 396 (100, M − CH_3COOH), 384 (49), 365 (9), 312 (21, M − CH_3COOH − C_6H_{12}), 199 (10).

24-Methylcholesta-5,22-dien-3β,7β-diol, **11**: $[\alpha]_D^{20}$ −87.1° (c 0.66, $CHCl_3$); ^1H nmr δ_{TMS}: 0.67 (s, 3H, $18CH_3$), 0.88 (d, 3H, J = 6 Hz, $28CH_3$), 0.97 (d, 6H, J = 6 Hz, $26CH_3/27CH_3$), 1.03 (d, 3H, J = 6.5 Hz, $21CH_3$), 1.06 (s, 3H, $19CH_3$), 3.54 (m, 1H, 3CH), 3.86 (m, 1H, 7CH), 5.32 (bs, 1H, 6CH); ms m/e: 414.3523 (21, M^+), 396 (100, M − H_2O), 384 (34), 382 (32), 312 (16), 271 (10), 269 (17), 211 (6).

24-Methylene-5-cholesten-3β,7α-diol, **12**: mp 129–131°C; ir ($CHCl_3$) ν_{max}: 3600, 3460, 2900, 1460 cm^{-1}; $[\alpha]_D^{20}$ +1.5° (c 1.38, $CHCl_3$); ^1H nmr δ_{TMS}: 0.69 (s, 3H, $18CH_3$), 0.96 (d, 3H, J = 6.5 Hz, $21CH_3$), 1.01 (s, 3H, $19CH_3$), 1.03 (d, 6H, J = 6 Hz, $26/27CH_3$), 3.61 (m, 1H, 3CH), 3.84 (bd, 1H, 7CH), 4.74 (s, 1H, 28CH), 4.68 (s, 1H, 28CH), 5.62 (d, 1H, J = 6 Hz, 6CH); ms m/e: 414.3495 (13, M^+), 396 (100, M − H_2O), 384 (25), 382 (31), 312 (10, M − H_2O − C_6H_{12}).

Compound **14**: ir ($CHCl_3$) ν_{max}: 3600, 3460, 2980 cm^{-1}; $[\alpha]_D^{20}$ −1.4° (c 0.5, $CHCl_3$); ^1H nmr δ_{TMS}: 0.68 (s, 3H, $18CH_3$), 0.96 (d, 3H, J = 6.5 Hz, $21CH_3$), 1.02 (s, 3H, $19CH_3$), 3.62 (m, 1H, 3CH), 5.38 (d, 1H, J = 4.5 Hz, C6H); ms m/e: 358 (8, M^+), 343 (15, M − 15), 340 (100, M − H_2O), 325 (11, M − H_2O − CH_3), 312 (4), 255 (9), 232 (12), 212 (10), 201 (14), 145 (23), 107 (26), 105 (24), 81 (34). *Monoacetate* **15**: ir ($CHCl_3$) ν_{max}: 3660, 2910, 1725, 1450, 1360 cm^{-1}; ^1H nmr δ_{TMS}: 0.68 (s, 3H, $18CH_3$), 0.93 (d, 3H, J = 6.5 Hz, $21CH_3$), 1.02 (s, 3H, $19CH_3$), 2.04 (s, 3H, CH_3CO), 4.61 (m, 1H, 3CH), 5.39 (d, 1H, J = 4.5 Hz, C6H); ms m/e: 358 (16, M − C_2H_2O), 340 (100, M − C_2H_2O − H_2O), 325 (80, 340 − CH_3), 307 (18, 325 − H_2O).

5β,6-Epoxy-24-methylenecholestan-3β-ol, **16**: ir ($CHCl_3$) ν_{max}: 3450, 2980, 1460, 1380 cm^{-1}; $[\alpha]_D^{20}$ −0.3° (c 0.75, $CHCl_3$); ^1H nmr δ_{TMS}: 0.64 (s, 3H, $18CH_3$), 0.92 (d, 6H, J = 6.5 Hz, $26CH_3/27CH_3$), 1.02 (s, 3H, $19CH_3$), 1.04 (d, 3H, J = 6 Hz, $21CH_3$), 3.06 (bs, 1H, 6CH), 3.74 (m, 1H, 3CH), 4.66 (s, 1H, 28CH), 4.71 (s, 1H, 28CH); ms m/e: 414.3521 (20, M^+), 399 (5, M − H_2O), 396 (4, M − H_2O), 386 (9), 330 (68, M − C_6H_{12}), 287 (24, M − sidechain), 190 (29).

Acknowledgements

The advice of Dr. D. Jean Burnell in some phases of this work is gratefully acknowledged. The assistance of Michael Beatty, University of New Brunswick, Saint John, in obtaining and identifying the material for this study is also gratefully acknowledged. This work was supported by a grant from the Natural Sciences and Engineering Research Council of Canada.

1. C. DJERASSI. Pure Appl. Chem. **53**, 873 (1981).
2. L. J. GOAD. *In* Marine natural products. Vol. II. *Edited by* P. J. Scheuer. Academic Press, New York. 1978. pp. 75–172.
3. J. L. C. WRIGHT, A. G. MCINNES, S. SHIMIZU, D. G. SMITH, J. A. WALTER, D. IDLER, and W. KHALIL. Can. J. Chem. **56**, 1898 (1978).
4. (*a*) I. RUBINSTEIN, L. J. GOAD, A. D. H. CLAGUE, and L. J. MULHEIRN. Phytochemistry, **15**, 195 (1976); (*b*) R. B. BATES, A. D. BREWER, B. R. KNIGHTS, and J. W. ROWE. Tetrahedron Lett. **59**, 6163 (1968); (*c*) Y. M. SHEIKH and C. DJERASSI. Tetrahedron, **30**, 4095 (1974).

5. D. R. IDLER and P. WISEMAN. Comp. Biochem. Physiol. A, **38**, 581 (1971).
6. E. FATTORUSSO, S. MAGNO, C. SANTACROCE, D. SICA, G. IMPELLIZZERI, S. MANGIAFICO, G. ORIENTE, M. PIATTELLI, and S. SCIUTO. Phytochemistry, **14**, 1579 (1975).
7. S. G. WYLLIE and C. DJERASSI. J. Org. Chem. **33**, 305 (1968).
8. B. A. KNIGHTS. J. Gas Chromatogr. **5**, 273 (1967).
9. J. ZIELINSKI, T. MILKOVA, S. POPOV, N. MAREKOV, and C. DJERASSI. Steroids, **39**, 675 (1982).
10. R. A. ABRAMOVITCH and R. G. MICETICH. Can. J. Chem. **40**, 2017 (1962).
11. N. IKEKAWA, M. MORISAKI, and K. HIRAYAMA. Phytochemistry, **11**, 2317 (1972).
12. J. W. BLUNT and J. B. STOTHERS. Org. Magn. Reson. **9**, 439 (1977).
13. H. L. HOLLAND and JAHANGIR. Can. J. Chem. **61**, 2165 (1983).

(S)-2,2,5,5-Tetramethylthiazolidine-4-carboxylic acid: a compound which exists in the amino acid rather than the zwitterion form

HELEN ELAINE HOWARD-LOCK,[1] COLIN JAMES LYNE LOCK, AND PHILIP STUART SMALLEY
Institute for Materials Research, McMaster University, Hamilton, Ont., Canada L8S 4M1

Received November 7, 1984

HELEN ELAINE HOWARD-LOCK, COLIN JAMES LYNE LOCK, and PHILIP STUART SMALLEY. Can. J. Chem. **63**, 2411 (1985).

The X-ray crystal structure of (S)-2,2,5,5-tetramethylthiazolidine-4-carboxylic acid, **1**, has been determined. Crystals are monoclinic, $P2_1$, with cell dimensions a = 11.351(4) b = 8.303(2), c = 11.969(3) Å, β = 116.69(2)°, and Z = 4. The structure was solved by standard methods and refined to R_1 = 0.0774, R_2 = 0.0670 for 2388 independent reflections. Compound **1** exists in the amino-acid form as shown by two distinctly different C—O bond lengths, 1.209 and 1.309 Å, typical of the COOH group, and by the positions of the hydrogen atoms. The amino-acid form of **1** found in the solid also exists in solution as shown by infrared and Raman spectra. The mass spectra, and ^{1}H and ^{13}C nmr spectra are reported, as well as detailed infrared and Raman spectra for the title compound and several deuterated species.

HELEN ELAINE HOWARD-LOCK, COLIN JAMES LYNE LOCK et PHILIP STUART SMALLEY. Can. J. Chem. **63**, 2411 (1985).

Faisant appel à la diffraction des rayons-X, on a déterminé la structure cristalline de l'acide (S)-tétraméthyl-2,2,5,5 thiazolidinecarboxylique-4, **1**. Les cristaux sont monocliniques, groupe d'espace $P2_1$, avec a = 11,351(4), b = 8,303(2), c = 11,969(3) Å, β = 116,69(2)° et Z = 4. On a résolu la structure par des méthodes directes et on l'a affinée jusqu'à des valeurs de R_1 = 0,0774 et R_2 = 0,0670 pour 2388 réflexions indépendantes. Le composé **1** existe sous la forme de l'acide aminé représenté; ceci est démontré par deux longueurs bien distinctes pour les liaisons C—O, 1,209 et 1,309 Å, qui sont typiques du groupe COOH ainsi que par les positions des atomes d'hydrogènes. La forme acide aminé de **1** que l'on trouve dans la forme solide se retrouverait aussi en solution si l'on se base sur les spectres infrarouge et Raman. On rapporte aussi les spectres de masse, les spectres rmn du ^{1}H et du ^{13}C ainsi que les spectres infrarouge et Raman détaillés du composé mentionné dans le titre ainsi que de plusieurs de ses dérivés deutérés.

[Traduit par le journal]

Introduction

D-Penicillamine has been used increasingly in the treatment of many diseases, of which Wilson's disease (1), rheumatoid arthritis (2), and cystinuria (3) are the best-known of several diseases (4). We have been investigating its use in rheumatoid arthritis, and establishing the spectroscopic properties and structures of its reaction products. The modes of therapeutic action and adverse side effects of the drug are based on three types of biochemical reactions: (i) the ability to form thiazolidine rings with compounds containing carbonyl groups such as ketones and aldehydes, (ii) the oxidation of the sulfhydryl group with the consequent formation of disulfide links, and (iii) the ability to chelate metals. It is reaction (i), formation of thiazolidine rings, which is the basis for the suggested use of D-penicillamine as an alcohol detoxicant (5), and for treatment of scleroderma, morphea, keloid formation, and of vitreous and scleral scarring of the eye. Interference with collagen synthesis may be responsible for reported cases of hyperextensibility of young children treated with D-penicillamine, and for a similar reason D-penicillamine has been suggested as a possible teratogen (4). Formation of thiazolidine rings is also the probable mode of action of D-penicillamine as a vitamin B6 antagonist (4, 6).

We have, therefore, been investigating (S)-2,2,5,5-tetramethylthiazolidine-4-carboxylic acid, which we first isolated when attempting to prepare crystals of D-penicillamine. Our interest was aroused because vibrational spectra suggested that the solid contained the amino-acid form rather than the zwitterion form, and that the amino-acid form existed in significant amounts in aqueous solution.

Amino acids generally exist in the zwitterion form, at least in aqueous solution. This is because the pK_a of the —COOH group is typically 2.0 and the pK_a of the —NH_3^+ group is ~10.0. Under these circumstances only about 0.01% of the compound exists as the amino-acid form in solution. We decided to investigate the problem further, particularly since the presence of the amino-acid form was not detected either in the solid state or in solution for the parent thiazolidine-4-carboxylic acid (7, 8).[2]

Experimental

(S)-2,2,5,5-tetramethylthiazolidine-4-carboxylic acid, 1

D-(−)-Penicillamine of reagent grade was supplied by Sigma Chemical Co., St. Louis, Missouri. To a saturated water solution of D-penicillamine (1.5 g, in 15 mL) was added 40 mL acetone. The mixture was evaporated under nitrogen to near dryness and filtered. The white solid (**I**) was recrystallized from acetone, and air dried. Yield 88%, mp (in air) 172–174°C (dec). The same procedure was repeated with acetone-d_6 to produce (S)-2,2-bis(trideuteromethyl)-5,5-dimethylthiazolidine-4-carboxylic acid (**2**). Compounds (**1**) and (**2**) were recrystallized from D_2O and acetone to produce (S)-3-deutero-2,2,5,5-tetramethylthiazolidine-4-carboxylic acid (-OD), **3**, and (S)-3-deutero-2,2-bis(trideuteromethyl)-5,5-dimethylthiazolidine-4-carboxylic acid (-OD), **4**. Crystals of **1** suitable for X-ray studies were slowly precipitated from an aqueous solution by vapour diffusion of acetone. The pKs of the —COOH and =NH groups were measured by titration of an aqueous solution of **1** against 0.1 N NaOH. The pHs were measured with a Corning Model 130 pH meter which was standardized with Corning potassium hydrogen phthalate buffer (pH = 4.00), BDH pH 7.00 buffer, and Fisher potassium carbonate/potassium borate/potassium hydroxide buffer (pH 10.00). The pKs of **1** were 2.8 (—CO_2H) and 5.5 (—NH—).

[1]Author to whom correspondence may be addressed.

[2]There is ambiguity in this paper about whether the structure of the (R) or (S) form was determined. There are statements "crystal structure for L-thiazolidine-4-carboxylic acid" and "values reported for L-thiazolidine-4-carboxylic acid" as compared to "the crystal structure of (S)-thiazolidine-4-carboxylic acid was determined" and the configuration shown is S. As correctly shown by Loscalzo *et al.*, the configuration of L-thiazolidine-4-carboxylic acid is R.

TABLE 1. Crystal data for 2,2,5,5-tetramethylthiazolidine-4-carboxylic acid, $C_8H_{15}NO_2S$

Parameter	Value
Formula weight	189.27
Crystal size (mm)	Plate 0.17 × 0.30 × 0.37
Space group	$P2_1$ (No. 4)
Systematic absences	O*k*O, $k = 2n + 1$
Unit cell	$a = 11.351(4)$, $b = 8.303(2)$, $c = 11.969(3)$ Å, $\beta = 116.69\ (2)°$; $V = 1007.9(5)$ Å^3, $Z = 4$
ρ (calcd.)	1.24 g cm^{-3}
ρ (obs.)	1.26(1) g cm^{-3}
Linear absorption coefficient	2.40 cm^{-1}
Max 2θ	45°
Reflections measured	$h, \pm k, \pm l$
Standrd reflections (esd)	−4 −2 −1 (0.013) −4 −2 −3 (0.014)
Temperature	22°C
Number of independent reflections	2555
Number of reflections ($I > 0$)	2388
Number of variables last cycle	157
Final R_1, $(R_2)^a$	0.0774 (0.0670)
Highest peak, location	0.6 eÅ^{-3}, 0.34, 0.08, 0.68
Lowest valley, location	0.4 eÅ^{-3}, 0.06, 0.02, −0.04
Weighting, $w = (\sigma^2 + (0.03\ F_0)^2)^{-1}$; error in an observation of unit weight	0.8672

$^aR_1 = \Sigma\|F_o| - |F_c\|/\Sigma|F_o|$; $R_2 = \{\Sigma w(|F_o| - |F_c|)^2/\Sigma_w F_o^2\}^{1/2}$.

Spectral measurements

Solutions for nmr studies were prepared in D_2O and concentrations were about 100 mg (solid) mL^{-1} of solvent. External TMS was used as the reference. Proton nmr spectra were recorded on a Varian T60 spectrometer and ^{13}C nmr spectra were recorded on a Bruker WP-80 spectrometer operating at 20.115 MHz. Mass spectra were obtained with a VG Micromass 7070F mass spectrometer with use of direct probe introduction and an ion source temperature of 200−220°C, electron potential of 70 eV, and an ionizing current of 100 A.

Infrared spectra were recorded on both Nicolet 7199 FT-IR and Perkin−Elmer Model 283 spectrophotometers. The samples were ground with KBr at a concentration of approx. 1% by weight and then pressed into pellets. To confirm that certain peaks were real, and not manifestations of the pelleting procedure, the spectra of certain samples were also run in Nujol and again in hexachlorobutadiene. For D_2O solution spectra, AgCl windows were used. Spectra were calibrated with polystyrene. For the region 500−100 cm^{-1}, the samples were prepared as Nujol mulls on polyethylene plates. Raman spectra were excited by means of the $\lambda = 5145$ Å radiation from a Spectra-Physics Model 164-02 argon ion laser and recorded on a Spex 14018 double monochromator. Solid samples were contained in glass melting point tubes, and solutions in nmr tubes. The spectrometer was calibrated regularly against an indene standard and had previously been calibrated with a neon lamp; the wavelength readout scale was found not to change (±1−2 cm^{-1}).

Collection of the X-ray diffraction data

A plate-like single crystal was sealed in a Lindemann capillary for the X-ray studies. Precession photographs showed that the crystals of **1** were monoclinic. Unit cell parameters were obtained from least-squares fit of χ, φ, and 2θ for 15 reflections in the range 19.1° < 2θ < 31.8° measured on a Nicolet P3 diffractometer having graphite-monochromated MoKα radiation (λ = 0.70926 Å at 22°C). Crystal data and other numbers related to data collection are summarized in Table 1. The density of the crystals was measured by flotation in a benzene−bromoform mixture. Intensities were also measured with use of the Nicolet P3 diffractometer and a coupled θ (crystal) − 2θ (counter) scan. The methods of selection of scan rates and initial data treatment have been described (9, 10). Corrections were made for Lorentz polarization effects but not for absorption. This will make a maximum error in F_o of 1.0%.

Solution of the structure

The sulfur atom was found from a three-dimensional Patterson synthesis and all other atoms were found from electron density difference maps. Hydrogen atoms were given temperature factors of about twice those of the atoms to which they were attached, but were not refined at this stage. Temperature factors for sulfur and oxygen atoms and adjacent carbon atoms were made anisotropic. The significance of the additional parameters was tested at each stage (11). Refinement, which minimized $\Sigma w(|F_o| - |F_c|)^2$, was continued until the maximum shift/error was 0.1. At this point, in addition to variation of all parameters for non-hydrogen atoms, x, y, z for hydrogen atoms were varied for one cycle to give a rough estimate of the hydrogen atom errors. Refinement was terminated after one further cycle with variation of only the parameters for non-hydrogen atoms. No corrections were needed for secondary extinction. Scattering curves were taken from Cromer and Waber (12) and anomalous dispersion corrections were taken from Cromer (13) and applied to the curves for S, N, O, and C. The atom parameters are listed in Table 2.[3,4]

[3]Tables of anisotropic temperature factors, H atom positions, dihedral and torsional angles, moduli of F_o and F_c, and mass spectral fragmentation patterns of **1** and **2** are available, at a nominal charge, from the Depository of Unpublished Data, CISTI, National Research Council of Canada, Ottawa, Ont., Canada K1A 0S7.

[4]All calculations were carried out on a CYBER 170/730 computer. Programs from the XRAY 76 package (14). The structure was solved by means of SHELX (15). The internally written programs CUDLS (Stephens, J.S.) and SYMFOU (Rutherford, J.S.) were used for final full-matrix least-squares and difference syntheses. The least-squares planes calculations used NRC-22 (16) and diagrams were prepared with use of ORTEP-II (17).

TABLE 2. Atomic positional parameters and temperature factors for (*S*)-2,2,5,5-tetramethylthiazolidine-4-carboxylic acid (Å^2)

Atom	x ($\times 10^4$)	y ($\times 10^4$)	z ($\times 10^4$)	U or U_{eq}*^{a} ($\times 10^3$)
S	1208(2)	0(0)	303(2)	58(1)*
C(2)	2388(6)	1696(8)	570(6)	37(4)*
N	3630(4)	884(6)	765(4)	34(1)
C(4)	3283(5)	−489(7)	−101(5)	31(1)
C(5)	2203(6)	−1515(9)	9(6)	40(4)*
C(1)	4543(7)	−1423(9)	164(7)	42(4)*
O(1)	5497(5)	−1453(7)	1139(4)	61(3)*
O(2)	4403(5)	−2245(6)	−843(4)	53(3)
C(21)	1881(7)	2770(8)	−578(6)	49(2)
C(22)	2618(7)	2630(9)	1734(6)	56(2)
C(51)	1381(7)	−2328(9)	−1198(6)	53(2)
C(52)	2778(7)	−2712(8)	1107(6)	55(2)
S′	1136(2)	−1641(3)	5135(2)	64(1)*
C(2′)	1977(6)	−3314(8)	4759(6)	38(4)*
N′	2980(4)	−2548(7)	4486(4)	35(1)
C(4′)	3544(6)	−1181(7)	5341(5)	31(1)
C(5′)	2412(6)	−130(9)	5326(6)	40(4)*
C(1′)	4438(6)	−242(9)	4956(6)	34(4)*
O(1′)	4344(4)	−255(6)	3911(4)	54(3)*
O(2′)	5308(4)	599(6)	5882(4)	54(3)*
C(21′)	2573(7)	−4454(9)	5877(6)	59(2)
C(22′)	1014(7)	−4219(10)	3601(6)	64(2)
C(51′)	2804(8)	779(11)	6546(7)	74(2)
C(52′)	1830(7)	1056(9)	4237(6)	62(2)

$^a U_{eq} = 1/3(U_{11} + U_{22} + U_{33} + 2U_{13}\cos\beta)$.

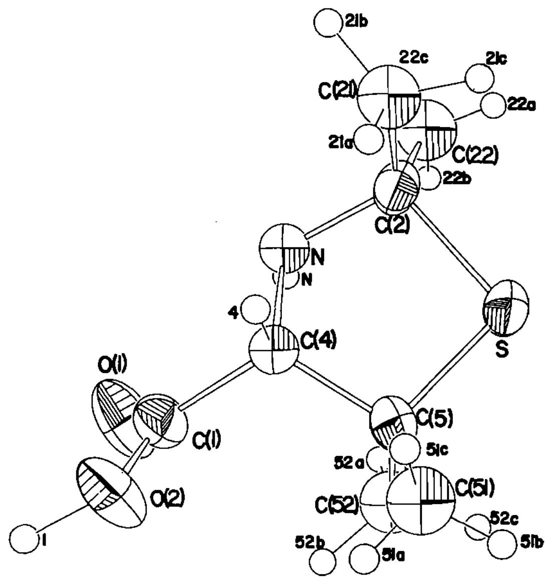

FIG. 1. The first molecule of (*S*)-2,2,5,5-tetramethylthiazolidine-4-carboxylic acid showing the atom numbering. Hydrogen atoms are indicated by affixes only in smaller letters and numbers.

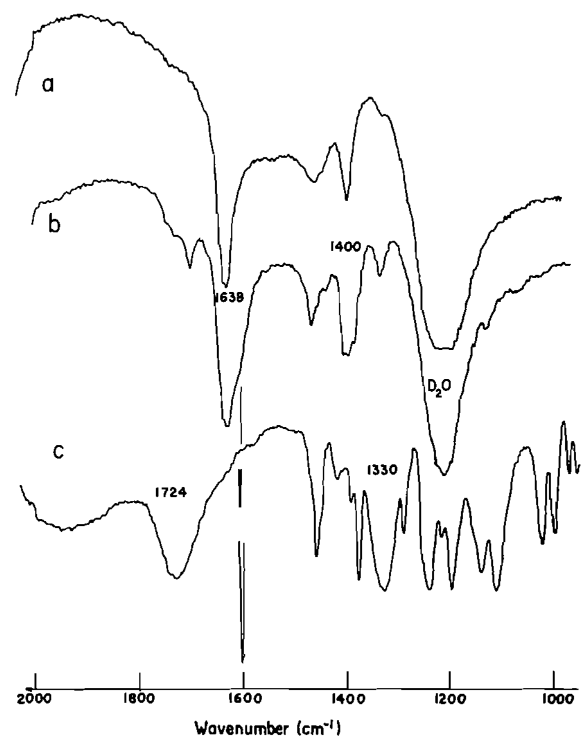

FIG. 2. Infrared spectra in the region 2000−1000 cm^{-1}: (a) thiazolidine-4-carboxylic acid, saturated D_2O solution, AgCl windows; (b) 2,2,5,5-tetramethylthiazolidine-4-carboxylic acid, D_2O solution, AgCl windows; (c) 2,2,5,5-tetramethylthiazolidine-4-carboxylic acid, solid KBr disc.

Discussion

There are two independent molecules in the unit cell, but they are very similar. One molecule is illustrated in Fig. 1, and selected interatomic distances and angles are given in Table 3. The surprising feature is that **1** has the amino-acid form rather than the zwitterion form. The carboxylate hydrogen atoms were clearly located and the presence of the hydroxyl group is reflected in the differences in the C═O (1.183(8), 1.206(7) Å) and C—OH (1.331(8), 1.307(7) Å) bond lengths. This is in contrast to thiazolidine-4-carboxylic acid, where the zwitterion is found in the solid state (7, 8). The hydrogen atoms were not detected in this case but the zwitterion form was confirmed by the near equivalence of the C—O bond lengths (1.240(8), 1.248(8) Å). It appeared that the amino-acid form of **1** might be caused by the steric hindrance of the methyl groups, but models show that it would be possible to coordinate an extra hydrogen atom at N. Further, there is strong hydrogen bonding between the carboxylic acid of one molecule and the nitrogen atom of another. The zwitterion form would be obtained if this hydrogen atom moved only 0.6 Å from the oxygen atom towards the nitrogen atom. The question arises as to whether the observed molecular structure is an artifact of the solid state or whether significant amounts of the amino-acid form exist in solution. Vibrational spectroscopy (see below) shows that small but significant amounts of **1** are present in solution. This should be reflected in the p*K*'s of the —CO_2H and —NH_2^+— sites. The fact that the p*K* of the —NH_2^+— group in the thiazolidine-4-carboxylic acid was shifted to 6.24 from the value of 10 usually found in amino acids was interpreted in terms of strain preventing the necessary sp^3 hybridization at nitrogen (18). Even greater strain is present in **1**, and this may cause the lower —NH_2^+— p*K* of 5.5. At the same time the extra methyl groups in **1** (compared to thiazolidine-4-carboxylic acid) have the normal inductive effect on the carboxylic acid function and raise its p*K* from 1.63 in thiazolidine-4-carboxylic acid to 2.8 in **1**. From these p*K* values we calculate that for thiazolidine-4-carboxylic acid, in aqueous solution, about 0.5% is present as the amino-acid form. This is a much greater amount than is present in most amino acids, but it is still undetectable by vibrational spectroscopy. As can be seen in Fig. 2a, there is no detectable carboxylic acid peak at ~1700−

TABLE 3. Selected interatomic distances (Å) and angles (deg) for (*S*)-2,2,5,5-tetramethylthiazolidine-4-carboxylic acid

Bond	Length[c]		Bond	Length		
S—C(2)	1.869(6)	1.852(8)	C(2)—N	1.484(7)	1.463(7)	
N—C(4)	1.470(7)	1.469(7)	C(4)—C(5)	1.546(8)	1.548(8)	
C(5)—S	1.827(7)	1.851(7)	C(2)—C(21)	1.518(9)	1.527(10)	
C(2)—C(22)	1.511(9)	1.523(9)	C(4)—C(1)	1.530(8)	1.507(8)	
C(1)—O(1)	1.183(8)	1.207(1)	C(1)—O(2)	1.331(8)	1.307(7)	
C(5)—C(51)	1.484(9)	1.522(9)	C(5)—C(52)	1.540(10)	1.527(9)	
Hydrogen bonds						
O(2)···N[a]	2.687(7)	O(2)—H	1.1(1)	H···N[a]	1.6(1)	156(5)
O(2′)···N′[b]	2.666(7)	O(2′)—H′	0.9(1)	H′···N′[b]	1.8(1)	150(5)

Bond	Angle[c]		Bond	Angle	
C(5)—S—C(2)	95.4(3)	94.5(3)	S—C(2)—N	104.0(4)	105.4(4)
C(2)—N—C(4)	107.9(4)	108.6(4)	N—C(4)—C(5)	109.8(5)	109.2(5)
C(4)—C(5)—S	102.7(4)	102.6(4)	S—C(2)—C(21)	109.7(4)	109.0(4)
S—C(2)—C(22)	111.0(4)	110.7(4)	N—C(2)—C(21)	110.9(5)	112.5(5)
N—C(2)—C(22)	109.3(5)	108.9(5)	N—C(4)—C(1)	108.5(5)	109.2(5)
C(5)—C(4)—C(1)	114.0(5)	112.0(5)	C(4)—C(1)—O(1)	124.9(7)	123.7(6)
C(4)—C(1)—O(2)	110.6(5)	111.9(5)	O(1)—C(1)—O(2)	124.5(7)	124.4(6)
C(4)—C(5)—C(51)	110.1(5)	112.7(6)	C(4)—C(5)—C(52)	112.3(5)	114.4(7)
S—C(5)—C(51)	109.1(5)	109.3(5)	S—C(5)—C(52)	110.0(4)	108.5(5)
C(51)—C(5)—C(52)	112.2(6)	109.1(6)	C(21)—C(2)—C(22)	111.8(6)	110.2(6)

[a,b]The atom is related to those given in Table 2 by the transformation, a, $1 - x, y - 1/2, -z$; *b*, $1 - x, 1/2 + y, 1 - z$.

[c]The second column of numbers after each bond length or angle relates to the molecule of which the atoms are designated by a prime in Table 2.

1730 cm^{-1} but the ν_a and ν_s CO_2^- peaks of the carboxylate group are clearly visible at 1638 and 1400 cm^{-1}. For **1**, however, about 5% should be present as the amino acid in aqueous solution, which is detectable by infrared (D_2O solution) spectroscopy, as shown by the weak band at 1700 cm^{-1}, Fig. 2b. Using these p*K* values, we calculate that the free energy of amino acid to zwitterion transition for thiazolidine-4-carboxylic acid is about −3.2 kcal mol^{-1}, whereas for **1** it is only −1.8 kcal mol^{-1}. This energy difference in the two forms of **1** is considerably smaller than the lattice energies, particularly in a structure in which strong hydrogen bonding is present, and we assume that the lattice energy of the amino-acid form is greater for **1**, allowing isolation of the crystalline product.

Most bond lengths and angles within the two molecules of **1** are normal. The C—S distances (mean 1.850, range 1.827(7)−1.869(6) Å) are larger than those found in (*R*)-thiazolidine-4-carboxylic acid (mean 1.799 Å) and the C—S—C angles are also larger (95.4(3), 94.5(3) vs. 89.4(4)°) (7). These differences are apparently caused by the steric requirements of the methyl groups. Similar differences in other D-penicillamine vs. L-cysteine derivatives have been noted previously. The presence of the methyl groups also affects the conformation of the thiazolidine ring. In thiazolidine-4-carboxylic acid the conformation of the ring was an envelope with the S atom 0.843 Å out of the best CNCC plane (7). In **1** the conformation is less regular and the ring flatter, but it can best be pictured as a plane defined by C(5a)SC(2)) with N (0.382(4) Å) and C(4) (0.269(5) Å) asymmetrically twisted out of the plane on opposite sides of the plane (corresponding distances for the prime molecule: N′ (0.346(4) Å), C(4′) (0.296(5) Å). Alternatively it can be considered, less satisfactorily, as an envelope with the nitrogen atom 0.563(4) Å out of the plane formed by C(2)SC(5)C(4). This is a consequence of the steric effects of the methyl groups. Figure 3 illustrates important dihedral angles in the structure. As can be seen, the two independent molecules have almost identical conformations. Very often in amino acids and particularly in derivatives of cysteine, the O(1)C(1)C(4)N-equivalent torsion angles are very small. The angles for **1** of 26.4(7) and 23.7(6)° are considerably larger than normal. Large angles have been observed previously in penicillamine (19) and its derivatives (20, 21) and have been explained in terms of non-bonding steric interactions. Similar interactions of the carboxylate group and the 5-methyl groups appear to be present here.

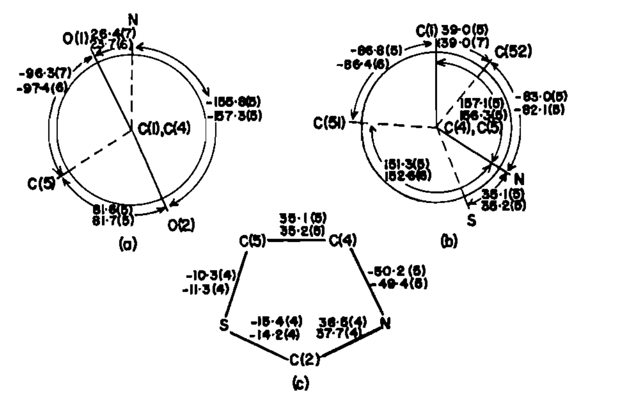

FIG. 3. Torsional angles in **1**. In (a) and (b) torsion angles are about the C(1), C(4) and C(4), C(5) bonds respectively. In (c) the torsion angles are for the two adjacent bonds about the bond to which the figures are affixed. In any pair of values, the upper refers to molecule one and the lower to molecule two (prime).

The packing in the unit cell is shown in Fig. 4. The chains of molecules up the 2_1 axes at $x = 1/2$ and $z = 0,1/2$ comprise the dominant feature of the structure. The molecules are held together by the strong hydrogen bond between the carboxylic acid group of one molecule and the amine group of the next. A question arises as to why there are two molecules in the asymmetric unit. An examination of the layers at $z = 0,1/2$ shows that the ring parts of the molecule are almost identical, except that the NH group is interchanged with the CH group. The difference lies in the COOH groups. At $x = 0$ they are arranged so that the hydrogen bonding network spirals down the 2_1 axis whereas at $x = 1/2$ the hydrogen bonding network spirals up the 2_1 axis. The CH—NH interchange, noted above, means that N—H points at the carboxyl group of an adjacent molecule whereas N′—H′ points at the sulfur atom of an adjacent molecule. In neither case is there any hydrogen bonding present, however. All other interactions are weak van der Waals forces. In the *a* direction the oxygen atoms interact with the methyl groups and in the *c* direction, the interactions are between sulfur atoms and methyl groups.

The title compound **1** is a secondary α-amino acid that is a five-membered heterocyclic molecule having no symmetry elements. There is very little published work relating to the vibrational spectra of thiazolidine-4-carboxylic acids. Some isolated C—S bond frequencies are listed by Freeman (22) for various cyclic sulfides. A study of the vibrational spectra of thiazolidine and ND thiazolidine has been reported, followed by a similar study of three monomethyl thiazolidines substituted at the C(2), C(4), and C(5) positions (23). These studies did not include work on the 4-carboxylic acids. The infrared spectra of some chelates of thiazolidine acids, including the spectra of free ligands 2-methyl-, 2,2-dimethyl-, 2,2,5,5-tetramethyl-, and 2-benzyl-thiazolidine-4-carboxylic acid have been reported for the range 4000−400 cm^{-1} (24). Our spectra of these ligands cover a greater cm^{-1} range, and they differ in many details. A detailed study of the spectra of D(−)-penicillamine and its deuterated derivatives, in solid and solution, both acid and zwitterion forms, has been reported recently (19).

The vibrational spectra and assignments for compounds **1**−**4** are shown in Table 4. The mode descriptions should be considered approximate since force constant analyses usually show considerable coupling of vibrations, particularly in the middle frequency region (800−1600 cm^{-1}). The spectra show many similarities to those for D-penicillamine and its deuterated derivatives, the main differences being (*i*) absence of ν S—H and δ S—H bands; (*ii*) replacement of bands of the NH_3^+ group by those of the NH group, and (*iii*) the presence of the three unique ring deformations δ CSC, δ CNC, and δ NCS, which are not present in D-penicillamine.

The assignment of ν N—H is unambiguous with a sharp, single band at 3262−3265 cm^{-1} in **1** and **2**. In **3** and **4** a band is observed at 2420 cm^{-1}. The isotopic shift ratio is 1.35, which is close to average for ν N—H/ν N—D ratios.

Strong, broad bands in the infrared spectrum at 2500 and 1930 cm^{-1}, which are little affected by deuterium substitution, are typical of fairly strong O—H···N bonding. These bands appear only in the infrared, and not in the Raman spectra. They are present in all samples, whether prepared as KBr discs or Nujol or hexachlorobutadiene mulls (and thus are not spurious bands from moisture in KBr).

The strong infrared bands at 1724, 1330, and 1190−1215 cm^{-1} are assigned as ν C=O, δ OH, and ν C—O respectively (see Fig. 2c). These assignments are consistent with the findings of the X-ray work indicating that **1** exists in the solid in the strongly hydrogen-bonded acid form. Deuterium exchange seems to weaken this hydrogen bonding, however, with a new band appearing at 1612 cm^{-1} (infrared); such a band in D-penicillamine was asigned to ν_a CO_2^-, and would only occur for the zwitterionic species.

The ring stretching modes can be described only very roughly as 2 ν C—S, 2 ν C—N, and ν C—C, with asymmetric stretches being more intense in the infrared, and symmetric (e.g., "ring-breathing") more intense in the Raman spectra.

We assign the strong Raman band at 580 cm^{-1} (**1**) to ν C—S; this band shows a downward shift in **2** to 537 cm^{-1}, apparently a mass effect of the CD_3 group, the isotopic ratio being 1.07. These bands also show a splitting which is attributed to Fermi resonance with the overtone of δ CCS at 294 cm^{-1} in **1**, 270 cm^{-1} in **2**. The medium intensity band at 506 cm^{-1} is assigned to the asymmetric ν C—S. These assignments are unusual and deserve discussion. Two major effects may be expected to affect the ν (C—S) frequencies. Ring strain may be expected to affect the C—S bond lengths, the C—S—C angle, and hence the C—S stretching vibrational frequency. Secondly, the C—S stretching frequency may be reduced by steric hindrance; substitution of hydrogen atoms adjacent to a C—S—C system reduces C—S stretches from 672−720 cm^{-1} (Raman, highly polarized, $\rho = 0.05-0.15$) in tetrahydrothiophene and thiazolidine to 582 cm^{-1} in di(*tert*-butyl)sulfide, 513 cm^{-1} in hexamethyl-*S*-trithiane(trithioacetone), and 547 cm^{-1} in 5-thia-10,11-diazadispiro[3.1.3.2.]undecane (22). In **1** the two effects are not independent. The substitution of the C(5) and C(2) centres with bulky methyl groups affects the conformation of the molecule **1**, in a way that seems to be a combination of the following effects: (1) the C—S bonds are lengthened as compared with both thiazolidine and D-penicillamine; (2) the C—S—C angle is increased compared to unsubstituted thiazolidine; (3) the C(2) and C(5) atoms rotate in opposite directions to minimize the C—S—C angle, for which 90° is the preferred equilibrium value.

Both the substitution and the long C—S bonds suggest that ν (C—S) should be lower than the normal range in cyclic sulfides (670−720 cm^{-1}) (22). The observed wave numbers are lower for one band but not as low as one would expect. Thus one (C—S) in **1** is higher than in D-penicillamine (580 vs. 548 cm^{-1}), close to the value for di(*tert*-butyl)sulfide. We assume the lowering effects are partially balanced by excess ring strain in **1**. The assignment of the second C—S band to 506 cm^{-1} is as expected for tetra-substituted carbons flanking the S. The assignment is supported by a weak side band of position and intensity expected for ^{34}S, which occurs on both the 506 and 473 cm^{-1} bands.

The assigned ring deformations are δ CNC at 376 cm^{-1}, δ NCS at 294 cm^{-1}, and δ CSC at 188 cm^{-1}. The deformations involving the S atom are all intense in the Raman spectrum, and all show an isotopic shift (adjacent CD_3 groups) of 1.06 to 1.07. The strong Raman band at 294 cm^{-1}, **1**; 270 cm^{-1}, **2** is not observed in unsubstituted thiazolidine-4-carboxylic acid and is therefore assigned as a δ NCS, deformation of the N—$C(CH_3)_2$—S moiety. This assignment is supported by the larger isotopic shift ratio of 1.09 for **2**.

The other assignments of bands for the methyl groups are straightforward and very similar to those for D-penicillamine. The isotopic shifts show the usual value: for the stretches they are in the range 1.33−1.40; for the deformations δ_a and δ_s they are 1.38 and 1.35, and for the rocks, ~1.2. An isotopic shift of 1.085 occurs for coupled vibrations of the C—CH_3 and C—CD_3 moieties.

The mass spectra of **1** and **2** are shown in Fig. 5. Under electron impact conditions the title compound shows a signifi-

TABLE 4. Vibrational bands of 2,2,5,5-tetramethylthiazolidine-4-carboxylic acid (**1**), its deuterated derivatives 2,2-di($^2H_3$)-methyl-5,5-dimethylthiazolidine-4-carboxylic acid (**2**), and **1** and **2** crystallized from D_2O (**3**) and (**4**)

1		**2**		**3**		**4**	
Infrared[a]	Raman[b]	Infrared	Raman	Infrared	Raman	Infrared	Assignment/remarks[c]
3440,8,200		3460,12		3440,16			
3262,66	3262,30	3265,72	3264,25	3270,59		3261	ν NH
	3006,13						associated
2990 sh	2990,36	2990 sh	2990,8	2990 sh			ν_a CH_3
			2990,17	2980,sh	2986[d]	2982	several components
2972,82	2976,100	2975,70					
2968,73	2972,14	2970,sh	2966,49	2970,100		2968	
			2962,49				
	2958,9		2955,sh				
2933,73	2934,84,25	2938,70	2935,34	2938,87	2942[d]	2932	ν_s CH_3
	2920,sh		2917,12				
	2910,sh						
2890,58,180	2886,27	2890,60	2885,22	2875,65		2885	ν CH
		2873,58,460				2869	
	2856,14		2861,9,br				
	2768,8		2769,6				
	2728,14		2725,10		2725,10		
2683,46		2665,50	2680,w	2680,sh			
2500,60,360		2500,55,360		2500,60,280		2500,br	O—H···N bonding
				2420,sh	2420,10		ν ND, $\rho = 1.35$ (3262)
			2250 sh				ν_a CD_3, $\rho = 1.33$ (2990)
		2240,40	2237,37			2235, ms	ν_a CD_3, $\rho = 1.33$ (2976)
			2229,40				ν_a CD_3, $\rho = 1.33$ (2972)
			2219,sh	2220,23			
			2175,32,20				ν_s CD_3, $\rho = 1.36$ (2958)
		2110,sh	2117,30,20				ν_s CD_3, $\rho = 1.39$ (2934)
			2085,11,60				ν_s CD_3, $\rho = 1.40$ (2920)
1930,39,200		1930,40,220		1930,49,260		1936,w,br	O—H···N bonding
1724,65,100	1710,8,55	1728,53,160	1700,7,br	1725,76,90	1710,10,35	1723,s	ν C=O
		1650,sh					
				1612,49,50		1610,m	ν_a CO_2^-
1578,sh					1590,3		
					1550,3		
				1520,6	1510,5		
1458,57	1468,46	1465,sh	1465,25	1458,59	1465,30		
1450,sh	1450,sh	1455,48	1454,sh		1448,18	1456,m	δ_a CH_3
	1440,26		1435,16		1435,20		
1416,20		1416,18,40					
1391,33	1390,9	1390,35	1387,7	1395,62	1390,9	1395,s	δ_s CH_3, out-of-phase
				1382 sh			
1373,73,shp	1370,6	1370,56	1370,6	1375,87	1368,6	1371,m	δ_s CH_3, in-phase
		1355,sh		1358,75			
1330,80,60	1322,3,30	1330,63,70	1320,3,br	1325,72	1320,15	1335,s	δ OH
				1300,51	1300,13	1298	ν_s CO_2^-
1290,45,shp	1292,5	1290,48	1289,4,br				ν CCN + δ NH
1242,83	1250,6	1240,66,60	1245,5	1240,87	1245,18	1240,s,br	ν CCN + r CH_3
1215,52	1214,10,20			1210 sh	1212,11		ν CO
			1203,13				
1196,84	1196,9,20	1195,67		1193,78	1192,6	1195,ms	ν CNC
		1180, sh				1180,sh	
1150,sh		1150,40	1153,6		1158,8	1155,w	ν CNC, $\rho = 1.05$
1143,74	1144,18,20			1140,86	1142,22		ν CCN + r CH_3
	1120,25,shp	1124,70	1127,17			1128,s	ν CCN + r CD_3, $\rho = 1.017$
1111,88	1112,38,shp			1110,100	1110,20		
		1080,55	1079,br			1084,m	
		1045,69	1050,15	1068,41		1048,m	δ_a CD_3, $\rho \simeq 1.36$
			1039,6			1031,w	
1024,63	1024,8	1025 sh	1024 sh				ν C—CH_3
				1018,48		1013,s	δ ND, $\rho = 1.27$ (1290)
	1006,6	1006,80,60	1009,20,23		1006,4	1004,s	δ_s CD_3, $\rho = 1.35$ (1376,1370)

TABLE 4. (*Concluded*)

1		2		3		4	
Infrared[a]	Raman[b]	Infrared	Raman	Infrared	Raman	Infrared	Assignment/remarks[c]
998,59		(996 sh)		998,45			r CH_3
970,34	966,24	950,sh	963,18	965,24	965,15		γ NH
	956,sh				955,sh		
940,sh	942,20	944,79	943,13	940,sh	940,24	948 m	ν C—CD_3, ρ = 1.085
						934	(1042), r CH_3
928,100	928,10	930,82	936,sh	920,97	924,14	928	ν C—CH_3 + r CH_3
				855,85	858,12	850	δ O—D---N
846,96	846,19	832,67,shp	835,12	840,86	845,10	845,m	ν CN + CH_3, ρ = 1.017
						832, m	
823,72	822,sh	815,83	817,17	812,82	812,17	820,m	Ring breathing
815,sh	818,17						
		780,30	781,5,br			780,w	r CD_3, ρ = 1.28 (998)
				762,71		761,s	δ CO_2
			756,17			759	
754,94	754,12	756,100	750,sh	745,96	745,5		r CH_3
		749,sh	738,3				
				728,sh	726,5	723,sh	γ ND
676,92	672,11	662,100	663,15	665,85	668,5	668,s	δ COOH
650,sh	650,21		650,sh	646,sh	650,12	650,sh	
		628,53				630,m	r CD_3, ρ = 1.21
	602,91,18		599,60,13		595,100,18		δ COH, acid
575,6	580,98,$^+$20	568,10		565,7	567,63,22		ν C—S, FR $^+$2 × 294, $^{++}$2 × 270
			545,98		550,sh		
546,8			537,100^{++}	540,12	532,vw,sh	535,m	ν C—S, ρ = 1.07 (580)
		520,sh,19			520		
508,w	506,33	470,15,br	473,34	510,20	500,27	475,w	ν C—S, ρ = 1.07 (506)
482,7	490,6			480,8			
445,20	448,22	444,17		440,13	440,23		δ CCC, ρ = 1.05 (448)
		425,30	425,13	428,18			
387,79	388,25	382 sh	380,11	386,80	388,20	381,ms	δ NCCO
	374,16	376,62	361,46 shp		372,13	376,s	δ CNC, ρ 1.036
		(366 m)					
356,26				355,26	354,sh		
347,28	354,5 sh	337	335,9	345,27		336,ms	
330,12	330,62,12	323,m		330,11	330,51	323,s	δ $(CH_3)_2CS$, ρ = 1.06
310 vw		313 m	311,21	309,m		313,s	
300,22		283,m		300,m			δ CCS, ring
	294,51,15	273,w	270,49,18	288,25	292,43,18	282,m	δ NCS ρ = 1.09
258,19,br	256,3	255				255,m	
		249				249,ms	
234,10	232,6		219,4		235,5	219	ρ = 1.06
		197				197,m	
191,52	188,28	182	177,20	190,s	188,23	182,s	δ CSC ρ = 1.06
169,28	160,4 br		160,12				
150,55				150	150,5	150,s	
142		142		143		142,ms	
				125			
	116,24		110,9	112		112	
102,37	103,34	104	97,25	102,w	102,24	105,s	
			91,9				
	76,19		75,12				
			67,61		70,40		

[a]Infrared notations: bands in cm^{-1}, intensities relative to strongest band = 100, half width at half maximum in cm^{-1}; s = strong, m = medium, w = weak, v = very, sh = shoulder, br = broad, shp = sharp.
[b]Raman intensities relative to the strongest Raman band with arbitrary intensity 100.
[c]Assigned notations: ν = stretching frequency, a = antisymmetric, s = symmetric, δ = deformation, r = rock, γ = out-of-plane deformation; FR = Fermi resonance; ρ = isotopic shift ratio. $^+$, $^{++}$ show which overtone bands contribute to FR.
[d]Measured from sample in D_2O solution.

cant molecular ion peak (M) at $m/z = 189$, $I = 39\%$ ($m/z = 195$, $I = 23\%$, **2**). Loss of a methyl group is shown by an $M - 15$ peak ($m/z = 174$, $I = 21\%$). That this loss is solely from C(2), and not from C(5), is confirmed by the spectrum of **2** (Fig. 5b), where only an $M - 18$ peak (loss of CD_3) at $m/z = 177$ (14%) is observed and not an $M - 15$.

Ring fragmentation patterns for thiazolidines have been studied previously and it has been found that the dominant

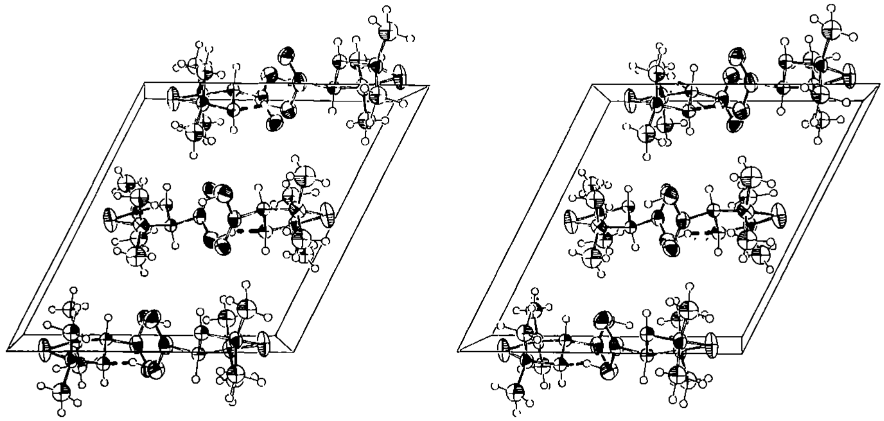

FIG. 4. The packing within the unit cell. a and c^* are parallel to the bottom and side of the page respectively and the view is down b. Hydrogen bonds are shown as dotted lines.

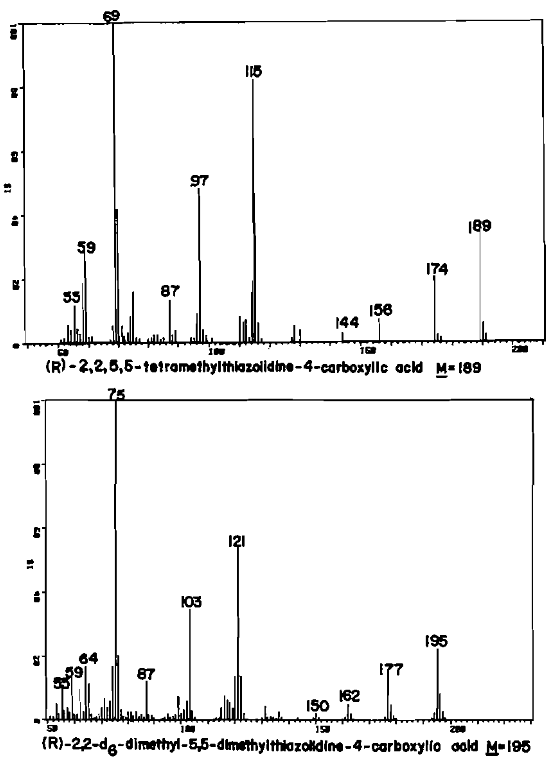

FIG. 5. The mass spectra of (S)-2,2,5,5-tetramethylthiazolidine-4-carboxylic acid and (S)-2,2-d_6-dimethyl-5,5-dimethylthiazolidine-4-carboxylic acid.

fragmentation patterns are 1,4- and 2,5-ring cleavages, with the 1,4-cleavage preferred (25). The spectrum of **1** alone does not allow differentiation between the two cleavages, but the spectrum of **2**, the deuterated analogue, shows that the 1,4-ring cleavage is highly favoured. There is a pattern of three relatively intense peaks (m/z = 115, 97, 69 in **1**; 121, 103, 75 in **2**) which arises from this 1,4-cleavage. Loss of $(CH_3)_2$ C=S leads to the intense $M - 74$ peaks at m/z = 115, **1** and 121, **2**. In **2**, there is very little loss of $(CD_3)_2$ C=S ($M - 80$, m/z = 115, 4%), which arises from 2,5-cleavage. Further fragmentation of the ions $(CX_3)C{=}\overset{+}{N}H{-}\dot{C}H\cdot CO_2H$ (X = H, m/z = 115, **1**; X = D, m/z = 121, **2**) derived from the 1,4-cleavage appears to be a two-step process, with loss of water giving $(CX_3)_2C{=}\overset{+}{N}{=}CH{-}\dot{C}{\equiv}O$ (m/z = 97, 48%, **1**; m/z = 103, 49%, **2**) followed by loss of CO to give $(CX_3)_2\dot{C}{-}\overset{+}{N}{\equiv}CH$ (m/z = 69, 100%, **1**; m/z = 75, 100%, **2**).

In both **1** and **2** the $M - 74$ peak is accompanied by an $M - 75$ peak (m/z = 114, 16% **1**; m/z = 120, 14%, **2**). Hydrogen transfer to give the $(CX_3)_2\dot{C}SH$ fragment of mass 75 comes mainly from either NH or CO_2H, since very little D transfer is apparent (m/z = 119, I = 4%) in **2**.

A 1,2-cleavage (loss of $(CX_3)_2C$, mass 42 or 48) must also occur, giving rise to a very unstable ion. No peaks were observed at m/z = 147 ($M - 42$, **1**; $M - 48$, **2**), but fragments giving peaks at m/z = 87 ($CH_3{-}\underset{\underset{S}{\|}}{C}{-}CH{=}\overset{+}{N}H$) and 55 ($CH_2{=}CH{-}CH{-}\overset{+}{N}H$) (further loss of S) for both **1** and **2** can be derived from this cleavage. Two other fragmentation patterns observed for both **1** and **2** are explained by the loss of COOH from the molecular ion ($M - 45$ peak at m/z = 144, 3%, **1**; 150, 3%, **2**) and the loss of SH ($M - 33$ peak at m/z = 156, 8%, **1**; 162, 5%, **2**).

Other peaks in the spectra can be assigned tentatively as subsequent fragmentation of the ions at m/z = 115, 121; for example, loss of COOH, gives m/z = 70, 42%, **1**; 76, 20%, **2**. The remaining significant peaks at m/z = 59 ($CH_2{=}\overset{+}{C}{-}SH$) **1** and **2** and 58, **1**, 64, **2** ($(CH_3)_2C{=}\overset{+}{N}H_2$, $(CD_3)_2C{=}\overset{+}{N}H_2$) are presumably derived from further decomposition of one of the 1,4 fragments. The various fragments suggested in the above discussion have the requisite masses and are reasonable, although other arrangements are possible.

The ^1H and ^{13}C nmr spectra for **1** and **2** and the assignments are given in Table 5. The four methyl peaks in the ^1H spectrum of **1** are resolved into two pairs (at C(2) and C(5)) by deuteration of the C(2) methyl groups. The assignment of the two peaks attached to C(5) is based on an assumed analogy to penicillin. Cooper and co-workers (26) have employed nOe experiments to study thiazolidine ring conformations in penicillin derivatives in solution and have found that the pro R methyl protons are always to high field of the pro S methyl protons. On this basis we assign the highest field resonance of **1** to the C(52), pro R, methyl group and the next highest to the C(51), pro S, methyl group. The only assignment left uncertain is the identity of the peaks arising from the methyl groups attached to C(2). In DMSO-d_6, all resonances are shifted to low field, but by unequal amounts, so that the peaks for both C(21) and C(22) methyl groups overlap.

The ^{13}C nmr spectrum of **1** also showed overlap. The normal

TABLE 5. The ^{1}H and ^{13}C nmr spectra of (*S*)-2,2,5,5-tetramethylthiazolidine-4-carboxylic acid, **1**, and (*S*)-2,2-bis(trideuteromethyl)-5,5-dimethylthiazolidine-4-carboxylic acid, **2**

Functional group	^{1}H			^{13}C	
	1 in D_2O	**1** in DMSO-d_6	**2** in D_2O	**1** in DMSO-d_6	**2** in DMSO-d_6
Pro *R*, $C(52)H_3$	1.35 (3H)	1.19 (3H)	1.35 (3H)	28.52 (q)	28.56
Pro *S*, $C(51)H_3$	1.58 (3H)	1.44 (3H)	1.58 (3H)	29.61 (q)	29.63
$C(21)H_3$ or	1.68 (3H)	1.55 (6H)		32.24 (q)	
$C(22)H_3$	1.74 (3H)			34.36 (q)	
C(5)				61.62 (s)	61.62
C(2)				73.46 (s)	73.18
C(4)—H(4)	4.26 (1H)	3.73 (H)	4.26 (1H)	73.46 (d)	73.47
COOH/NH (exchanging)		br 7.64 (2H)			
O—C(1)=O				171.31 (s)	171.40

proton decoupled spectrum consisted of seven lines for the eight carbon atoms. The resonance at 73.46 ppm was much more intense than the others, so we assumed it was two peaks overlapping. Comparison with benzoylpenicillin showed that C(2) and C(4) of the thiazolidine ring are very close in chemical shift. Since C(2) is a quaternary carbon atom and C(4) is a tertiary carbon atom, it was possible to assign these peaks by an off-resonance experiment. The overlap of C(2) and C(4) peaks also occurred in the spectrum of **2**. The two deuterated methyl groups induce a small upfield isotope shift of (6×0.25) ppm (27) but the resulting resonance of 74.68 ppm is still close enough to overlap the non-deuterated C(2) resonance at 73.46 ppm.

The ^{13}C methyl groups were again assigned by deuteration and comparison with penicillin spectra. The overall effect of deuteration is to greatly reduce the peak intensity of the deuterated carbon atoms because of decreased nOe enhancement, increased relaxation time, and dispersal of the intensity into multiplets caused by coupling between ^{13}C and ^{2}H. The results show that the resonances from the C(5) methyl groups are upfield from those on C(2), and this is presumably caused by the γ-shielding effect of the CO_2H on the C(5) methyls (27).

Acknowledgments

We thank the Natural Sciences and Engineering Research Council of Canada and the McMaster University Science and Engineering Research Board for financial support of this work.

1. J. M. WALSHE. Am. J. Med. **2**, 487 (1956).
2. A. V. CAMP. J. Rheumatol. **8** (Supp. 7) 103 (1981).
3. J. C. CRAWHALL, E. F. SCOWEN, and R. W. E. WATTS. Brit. Med. J. **1**, 588 (1963).
4. W. M. WEIGERT, H. OFFERMANNS, and P. SCHERBERICK. Angew. Chem. Int. Ed. Engl. **14**, 330 (1975).
5. H. T. NAGASAWA, D. J. W. GOON, and E. G. DEMASTER. J. Med. Chem. **21**, 1274 (1978).
6. H. E. HOWARD-LOCK, W. F. KEAN, C. J. L. LOCK, A. MEWA, and P. S. SMALLEY. Seminars in Rheumatology (1984). Submitted.
7. J. LOSCALZO, R. G. KALLEN, and D. VOET. Arch. Biochem. Biophys. **157**, 426 (1973).
8. M. GOODMAN, V. CHEN, L. BENEDETTI, C. PEDONE, and P. CORRADINI. Biopolymers, **11**, 1779 (1972).
9. B. LIPPERT, C. J. L. LOCK, B. ROSENBERG, and M. ZVAGULIS. Inorg. Chem. **16**, 1525 (1977).
10. R. P. HUGHES, N. KRISHNAMACHARI, C. J. L. LOCK, J. POWELL, and G. TURNER. Inorg. Chem. **16**, 314 (1977).
11. W. C. HAMILTON. Acta Crystallogr. **18**, 502 (1965).
12. D. T. CROMER, and J. T. WABER. International Tables for Crystallography . Vol. IV. *Edited by* J. A. Ibers and W. C. Hamilton. Kynoch Press, Birmingham, England. 1974. Table 2, 2B. pp. 99–101.
13. D. T. CROMER. In International Tables for Crystallography. Vol. IV. *Edited by* J. A. Ibers and W. C. Hamilton. Kynoch Press, Birmingham, England. 1974. Table 2.3.1 pp. 149–150.
14. J. M. STEWART. The XRAY 76 system. Tech. Rep. TR-446. Computer Science Centre, Univ. of Maryland, College Park, MD. 1976.
15. G. M. SHELDRICK. Program for crystal structure solution and refinement. Cambridge University, England. 1976.
16. M. E. PIPPY and F. R. AHMED. Program NRC-22. Mean plane and torsion angles. National Research Council of Canada, Ottawa, Canada. 1976.
17. C. K. JOHNSON. ORTEP-II. Report ORNL-5138, Oak Ridge National Laboratory, TN. 1976.
18. R. G. KALLEN. J. Am. Chem. Soc. **93**, 6227 (1971).
19. H. E. HOWARD-LOCK, C. J. L. LOCK, and P. S. SMALLEY. J. Cryst. Spectrosc. Res. **13**, 333 (1983).
20. A. CALVO, R. FAGGIANI, D. A. HARVEY, H. E. HOWARD-LOCK, W. F. KEAN, and C. J. L. LOCK. J. Cryst. Spectrosc. Res. **14**, 59 (1984).
21. R. FAGGIANI, H. E. HOWARD-LOCK, C. J. L. LOCK, M. L. MARTINS, and P. S. SMALLEY. Can. J. Chem. **62**, 1127 (1984).
22. S. K. FREEMAN. Applications of laser Raman spectroscopy. John Wiley & Sons, New York. 1974.
23. M. GUILIANO, G. DAVIDOVICS, J. CHOUTEAU, J. L. LARICE, and J. P. ROGGERO. (*a*) J. Mol. Struct. **25**, 329 (1975); (*b*) J. Mol. Struct. **25**, 343 (1975).
24. E. CATRINA. Rev. Roum. Chim. **21**, 81 (1976).
25. M. M. VESTLING and R. L. OGREN. J. Heterocycl. Chem. **12**, 243 (1975).
26. R. A. ARCHER, R. D. G. COOPER, P. V. DEMARCO, and L. F. JOHNSON. Chem. Commun. 1291 (1970).
27. R. J. ABRAHAM and P. LOFTUS. Proton and carbon-13 NMR spectroscopy. Heyden and Son Ltd., London. 1980 pp. 24–33.

Synthesis and protonation studies of a *meso*-unsubstituted surfactant porphyrin

MICHEL RINGUET AND JACQUES GAGNON

Département de chimie–biologie, Université du Québec à Trois-Rivières, C.P. 500, Trois-Rivières (Qué.), Canada G9A 5H7

Received September 5, 1984

MICHEL RINGUET and JACQUES GAGNON. Can. J. Chem. **63**, 2420 (1985).

A *meso*-unsubstituted surfactant porphyrin has been synthesized. Spectroscopic studies show that intermolecular protonation occurs between the side-chain carboxyl groups and the inner nitrogen atoms of the porphyrin, leading to the formation of a porphyrin dication. In 5×10^{-5} *M* chloroform solution, 27% of the porphyrin molecules are in the dicationic form and they are self-associated with some remaining molecules in the free base form.

MICHEL RINGUET et JACQUES GAGNON. Can. J. Chem. **63**, 2420 (1985).

On a réalisé la synthèse d'une porphyrine tensio-active qui n'est pas substituée en position *meso*. Des études spectroscopiques démontrent que la protonation intermoléculaire se produit entre les groupements carboxyliques des chaînes latérales et les atomes d'azote du coeur de la porphyrine; ceci conduit à la formation d'un dication porphyrine. En solution à 5×10^{-5} *M* dans du chloroforme, 27% des molécules de porphyrine existent sous la forme de dications et elles sont auto-associées avec quelques-unes des molécules qui restent sous la forme de bases libres.

[Traduit par le journal]

Introduction

The potential catalytic importance of porphyrins incorporated into synthetic organized molecular systems has stimulated considerable interest in the syntheses of surfactant porphyrins (1–4). These products are usually obtained by alkylation of a functionalized *meso*-tetraarylporphyrin (1–7), or esterification of natural carboxyporphyrins (8).

As part of our work on the development of a synthetic model which would mimic the primary events of green plant photosynthesis (9), the synthesis of a *meso*-unsubstituted carboxyporphyrin seemed more pertinent. This substrate would show an *etio*-type absorption spectrum, similar to the ones observed for most natural porphyrins (10), and would have the ionizable functional group needed for further studies in organized media. Hence we wish to report here the synthesis and a spectroscopic study of the protonation of a new type of surface-active porphyrin, dioctadecyldeuteroporphyrin II, **1**. Our data are consistent with an intermolecular exchange of protons between the side-chain carboxyl group of a porphyrin molecule and the inner nitrogen atom of another porphyrin ring. The nature and the extent of protonation were determined.

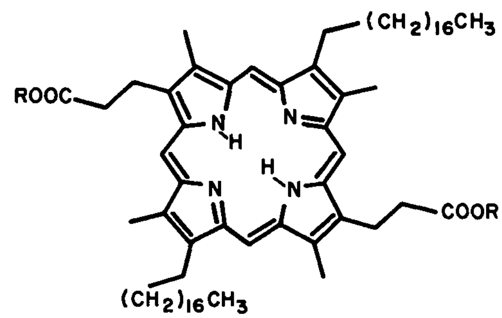

1 R = H
2 R = CH_3

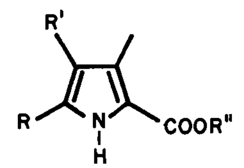

	R	R'	R"
3	CH_3	$CH_2CH_2COOCH_3$	CH_2Ph
4	CHO	$CH_2CH_2COOCH_3$	CH_2Ph
5	CH_3	H	CH_2CH_3
6	CH_3	$CO(CH_2)_{16}CH_3$	CH_2CH_3
7	CH_3	$CH_2(CH_2)_{16}CH_3$	CH_2CH_3
8	CH_3	$CH_2(CH_2)_{16}CH_3$	CH_2Ph
9	CHO	$CH_2CH_2COOCH_3$	H
10	CH_3	$CH_2(CH_2)_{16}CH_3$	H

Results and discussion

Synthesis

The porphyrin **1** is synthesized by formation and *in situ* coupling of the properly substituted 5-methyl-5′-carboxydipyrromethene, a method first reported by Chang (11).

A modification of the procedure of Clezy *et al.* (12) for the lead tetraacetate oxidation of pyrrole **3** gives the 5-formylpyrrole **4**. The long-chain substituted pyrrole **6** is prepared by acylation of pyrrole **5** with stearoyl chloride in the presence of stannic chloride. Diborane reduction of **6** affords the surfactant pyrrole **7** which is transbenzylated to give pyrrole **8**. The overall yield from pyrrole **5** to **8** is 48%. Hydrogenolysis of pyrroles **4** and **8** gives the carboxypyrroles **9** and **10** respectively, which are mixed in equimolar quantities in hot formic acid and treated with hydrobromic acid to afford the crude dipyrromethene. Self-coupling of the latter in hot formic acid in the presence of excess bromine leads to a mixture of the dicarboxyporphyrin **1**, its diester **2**, and the monoacid monoester. The mixture is then esterified to give porphyrin **2** in 8% yield from pyrrole **10**. This relatively low yield is due to the well-known lack of reactivity of long-chain substrates. Repeating the series with hexyl- rather than octadecyl-pyrrole led to a 25% yield in the last step. Hydrolysis of **2** in a mixture of water and tetrahydrofuran gives **1**.

Spectrophotometric studies

Absorption spectra of porphyrins **1** and **2** in protophylic solvents such as THF are *etio*-type (10) and follow the Beer–Lambert law over the range of concentration studied (10^{-6} to 10^{-4} *M*). In protophobic solvents, such as chloroform

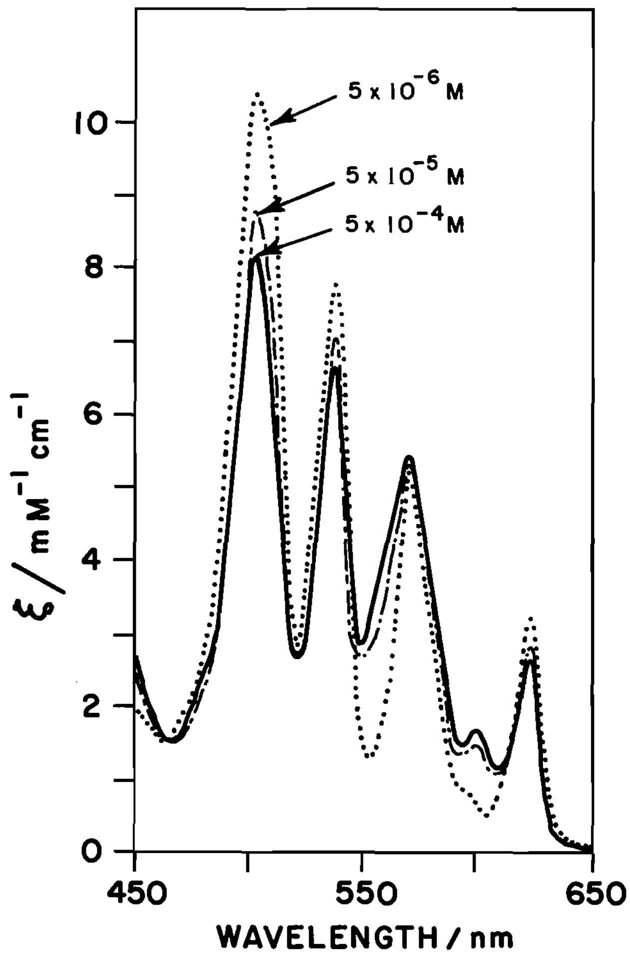

FIG. 1. Concentration dependence of the absorption spectrum of compound **1** in $CHCl_3$.

and xylene, the diester porphyrin **2** still acts in accordance with the Beer–Lambert law but the dicarboxyporphyrin **1** does not. The four maxima observed for chloroform solutions of porphyrin **1** show a concentration dependence, and a new maximum at 595 nm appears as the concentration is increased (Fig. 1).

Two different types of fluorescence spectrum are obtained by exciting a 3×10^{-5} *M* solution of compound **1** in chloroform. Excitation at 400, 485, 535, or 620 nm produces a four-band spectrum with maxima at 624, 656, 674, and 690 nm. This spectrum is similar to the ones obtained by exciting at any wavelength the 10^{-4} to 10^{-6} *M* chloroform solutions of porphyrin **2** and the 10^{-6} *M* chloroform solution of porphyrin **1**. The 10^{-4} to 10^{-6} *M* solutions of porphyrins **1** and **2** in THF give the same type of spectrum. These spectra are typical of free base porphyrins (13). The other type of spectrum has maxima at 604, 624, 664, and 690 nm and is obtained when the 3×10^{-5} *M* chloroform solution of compound **1** is excited at 420, 558, or 598 nm. These results suggest that there are two species in this solution, i.e. the free base and the protonated porphyrin, as will be shown later. This protonation is not due to HCl contamination in the chloroform since, if this was so, the protonation would also occur in the 10^{-6} *M* chloroform solution of porphyrin **1** and in the chloroform solution of porphyrin **2**. In addition, the aggregation of a carboxyporphyrin has been reported to give intermolecular protonation (4). A spectrophotometric titration from 450 to 650 nm was done with

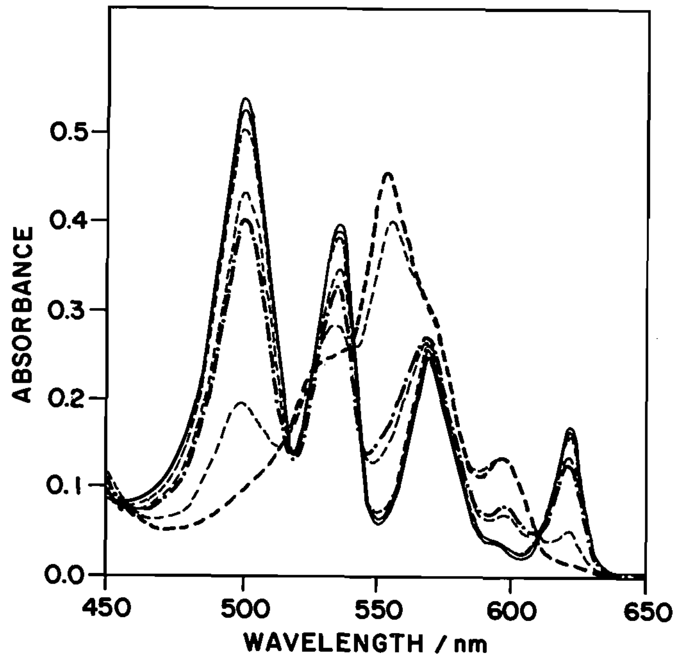

FIG. 2. Absorption spectra of a 5×10^{-5} *M* solution of compound **1** in chloroform (-··-), when titrated with triethylamine (—), and with acetic acid (......).

triethylamine (TEA) and glacial acetic acid (GAA) to identify the protonated species. Mixtures of 0.01–0.1% TEA in chloroform show the free base porphyrin spectrum, as expected. The spectrum of compound **1** was independent of solvent composition for mixtures of 0.1–10% GAA in chloroform and was also identical to the free base spectrum. At high (up to 100%) GAA concentrations, the spectra are characteristic of the porphyrin monocation, as usually found in GAA (14), with maxima at 530, 558, and 598 nm (Fig. 2). At 30% GAA in chloroform, the spectrum of compound **1** is quite similar to the one obtained with the chloroform solution.

However, the difference spectra of the chloroform solution of compound **1** relative to a solution of the free base form of the same porphyrin show the two-band spectrum typical of the dication (10). The same difference spectra for the 30% GAA in chloroform solution clearly show the three-band spectrum of the porphyrin monocation (Fig. 3). Therefore the protonated porphyrin species in the chloroform solution, a dication, is different than the monocation found in the 30% GAA in chloroform solution.

Spectrophotometric titrations with trifluoroacetic acid (TFAA) led to the formation of the dication. They were done with chloroform solutions of compound **1** to determine the percentage of dication in the solutions. These series of spectra are isosbestically related (Fig. 4). Using the method of Grigg *et al.* (14) the ratios (c_P/c_B) of the respective concentrations of the protonated and free base forms of compound **1** in chloroform were determined by eq. [1]:

$$[1] \quad (c_P/c_B) = (A - A_B)/(A_P - A)$$

where A, A_B, and A_P are the absorbance, at a particular wavelength, of a fixed concentration of the porphyrin in chloroform, in 0.1% TEA in chloroform (i.e. free base), and in 1% TFAA in chloroform (i.e. dication) respectively. The ratios were obtained for five wavelengths corresponding to the absorption maxima of either the free base (500, 530, and 622 nm) or the

TABLE 1. Extent of protonation of compound **1** in 5×10^{-5} *M* solutions

	Absorbance			
λ (nm)	1% TFAA–$CHCl_3$	0.1% TEA–$CHCl_3$	$CHCl_3$	(c_P/c_B)
500	0.059	0.539	0.403	0.39 ± 0.03
530	0.131	0.336	0.280	0.38 ± 0.06
555	0.564	0.070	0.196	0.36 ± 0.03
595	0.224	0.028	0.083	0.39 ± 0.07
622	0.024	0.168	0.128	0.38 ± 0.09

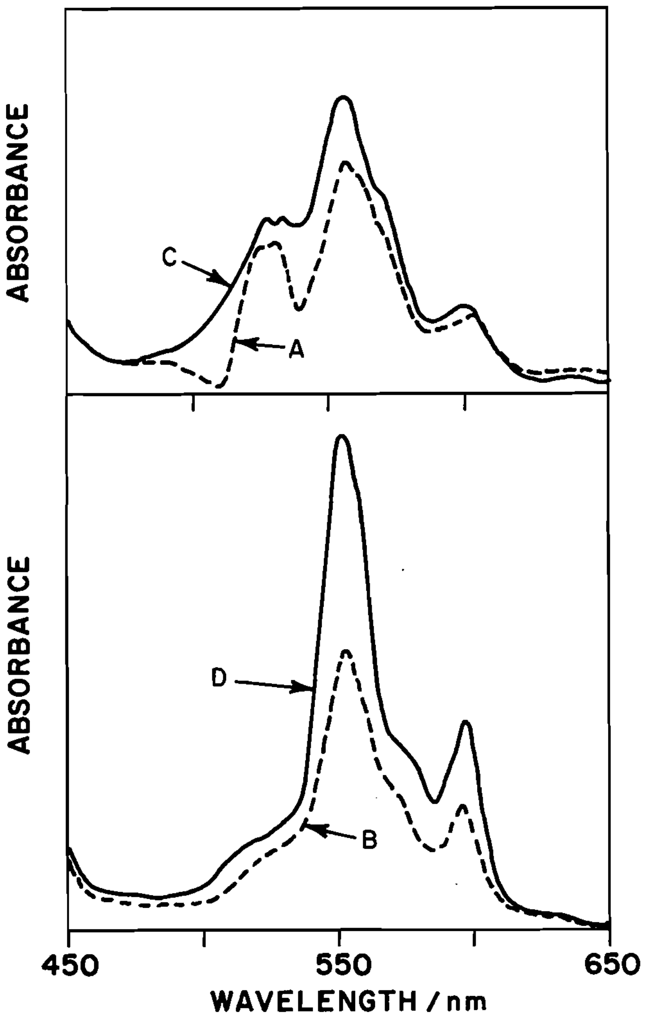

FIG. 3. Difference spectra, against free base porphyrin **1** for 5×10^{-5} *M* solutions of porphyrin **1** in 30% GAA in $CHCl_3$ (A), and in $CHCl_3$ (B). Absorption spectra of porphyrin **1** monocation (C) and dication (D).

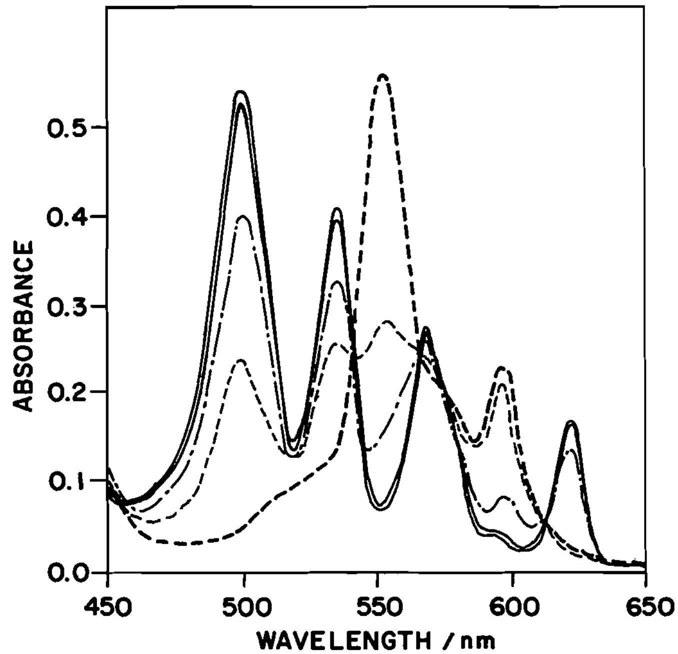

FIG. 4. Absorption spectra of a 5×10^{-5} *M* solution of compound **1** in chloroform (-·-), when titrated with triethylamine (—), and with trifluoroacetic acid (......).

dication (555 and 595 nm). Table 1 shows that 27 ± 3% of the porphyrin is in the dication form in the 5×10^{-5} *M* solution. Uniformity of the calculated ratios definitely supports the above conclusion that this chloroform solution contains an equilibrium mixture of the free base and the dication. If the same calculation is made with the monocation as the protonated reference species the ratios are sporadic. The ratios were also determined for 5×10^{-4} *M* and 5×10^{-6} *M* solutions in chloroform, which resulted in 29% and 0% dication respectively.

Molecular models show that intramolecular protonation of the inner nitrogen atoms by the side-chain carboxyl groups is not possible. So, according to our results, an aggregation phenomenon which occurs at concentrations over 5×10^{-5} *M* in chloroform leads to intermolecular protonation, the aggregates being held as ion pairs. When acetic acid is added in low concentration to the solution, the porphyrin aggregates are broken and only the free base form is observed. Neither was protonation detected in other protophylic solvents. It is noteworthy that protophobic solvents favor the ionic form while polar solvents (methanol, 10% GAA in chloroform) do not. This is in agreement with Menger's observation of a large rate enhancement for proton exchange of benzyl alcohol when catalysed by amines in benzene solvent as compared to DMSO (15). Thus, in polar solvents, the solvation of the carboxyl group by the polar solvent keeps this group from forming a hydrogen bond with the amino group which would hence lead to the ion pair.

The proximity of the porphyrin rings in the aggregates allows for the formation of the porphyrin dication, which is thermodynamically favored over the monocation but is not usually found in weak carboxylic acid solutions (10). Additional evidence of aggregation is given by vapor phase osomometry. This method gives an average molecular weight of 1313 ± 53 for porphyrin **1** in chloroform (10^{-3} *M*) as compared to a monomer molecular weight of 1016 determined by mass spectrometry. These data suggest a 1:2 dimer/monomer ratio at high porphyrin concentrations in chloroform. Assuming that the dimer is made of a dicationic porphyrin aggregated with a free base porphyrin, then this 1:2 ratio would be consistent with the approximate 1:3 dication/free base ratio found by absorption spectroscopy.

It is also noticeable that the spectrum of the chloroform solution, in which compound **1** exists as an equilibrium mixture of the free base and the dication, is isosbestically related to the set of spectra observed for the free base – monocation equilibrium. In this specific case one cannot rely on the isosbestic set of spectra to affirm that only two species are present in the mixture. Work is in progress to study this aggregation phenomenon in organized media. Preliminary results on surface pressure and surface potential of porphyrin **1** at the air–water interface show the surface properties of a surfactant.

Experimental

Instruments and method

The normal conditions and instruments for the spectra quoted in the experimental section are: uv, tetrahydrofuran solutions (ϵ_{mM} in parentheses), Cary 17D or Perkin Elmer 553; ir, Perkin Elmer 1430 or 597; nmr solutions with internal TMS standard, Varian EM 360L. Elemental analyses and vapor phase osmometry were by Schwarzkopf, New York, mass spectrometry by Université de Montréal. The solvents used in the titration study were Spectrograde and freshly distilled. Stock solutions of the porphyrin in chloroform were prepared and diluted by volume with the required solvent mixture. Only the visible region of the spectrum was retained for this study. Difference spectra were obtained by placing in the reference beam of the spectrophotometer a solution of compound **1** in its free base form (1% TEA in chloroform) at the concentration required to cancel the 500-nm band.

Benzyl 5-formyl-4-(2′-methoxycarbonylethyl)-3-methylpyrrole-2-carboxylate 4

The dimethylpyrrole **3** was prepared following essentially the procedure of Johnson *et al.* (16), yield 61%, mp 99–101°C (lit. (16) mp 99–101°C). *Anal.* calcd. for $C_{18}H_{21}NO_4$: C 68.55, H 6.71, N 4.35; found: C 68.56, H 6.69, N 4.44. Pyrrole **3** was then treated with lead tetraacetate according to Clezy *et al.* (12). Filtration over Celite of the reaction mixture before work-up led to a product which crystallized on standing. Recrystallization from ether/hexane 1:1 gave pyrrole **4**, yield 65%, mp 80–81°C (lit. (16) mp 78–79°C). *Anal.* calcd. for $C_{18}H_{19}NO_5$: C 65.64, H 5.81, N 4.25; found: C 65.57, H 5.88, N 4.05.

Ethyl 3,5-dimethyl-4-(1′-oxooctadecyl)pyrrole-2-carboxylate 6

The pyrrole **5** was prepared following the procedure of Kleinspehn (17), yield 59%, mp 124–125°C (lit. (17) mp 124–125.5°C). To pyrrole **5** (10.0 g, 60 mmol) in dry benzene (10 mL) under nitrogen was added stearoyl chloride (22.5 mL, 66 mmol). The flask contents were cooled to, and maintained at, 0°C while stannic chloride (10.5 mL, 90 mmol) was added drop by drop. The mixture was stirred for 2 h, 10% hydrochloric acid (40 mL) was added, and stirring was continued for 15 min. Chloroform extraction and recrystallization from acetone gave the pyrrole **6** (20.4 g, 47 mmol, 78%), mp 94–95°C; ν_{KBr}: 3280, 2910, 2840, 1655, 1645, 1265; δ (CCl_4): 0.85 (bt, 3H, H-18′), 1.25 (m, 30H, H-3′ to 17′), 1.30 (t, 3H, J = 7 Hz, —OCH_2CH_3), 2.50 (s, 6H, 2 × —CH_3), 2.62 (t, 2H, J = 7 Hz, H-2′), 4.23 (q, 2H, J = 7 Hz, —OCH_2—), 9.80 (bs, 1H, NH). *Anal.* calcd. for $C_{27}H_{47}NO_3$: C 74.78, H 10.92, N 3.23; found: C 74.91, H 10.75, N 3.25.

Ethyl 3,5-dimethyl-4-octadecylpyrrole-2-carboxylate 7

Pyrrole **6** (5 g, 11.5 mmol) was added to a 1 *M* solution of borane in tetrahydrofuran (60 mL, 60 mmol). The mixture was stirred under nitrogen for 12 h. Methanol was slowly added until gas formation ceased. The mixture was evaporated to dryness, methanol (60 mL) was added, and the flask contents were refluxed for 5 min. Evaporation and recrystallization from hexanes gave pyrrole **7** (4.8 g, 11.4 mmol, 99%), mp 93.5–94°C; ν_{KBr}: 3300, 2910, 2860, 1655, 1265; δ (CCl_4): 0.90 (bt, 3H, H-18′), 1.25 (m, 32H, H-2′ to 17′), 1.30 (t, 3H, J = 7 Hz, —OCH_2CH_3), 2.20 (s, 6H, 2 × —CH_3), 2.25 (bt, 2H, H-1′), 4.25 (q, 2H, J = 7 Hz, —OCH_2—), 9.00 (bs, 1H, NH). *Anal.* calcd. for $C_{27}H_{49}NO_2$: C 77.27, H 11.77, N 3.34; found: C 77.13, H 11.93, N 3.18.

Benzyl 3,5-dimethyl-4-octadecylpyrrole-2-carboxylate 8

To pyrrole **7** (5.0 g, 12 mmol) in benzyl alcohol (16 mL) was added sodium (65 mg, 3 mmol) and the mixture was heated to 80°C under reduced pressure (10 mm Hg, 1.3 kPa) for 4 h. The solvent was removed under reduced pressure. An ethanol solution of the residue was washed with water, dried, and evaporated. Recrystallization from methanol gave pyrrole **8** (3.5 g, 7.2 mmol, 61%), mp 105–106°C; ν_{KBr}: 3280, 3030, 2910, 2840, 1660, 1610, 1265; δ (CCl_4): 0.85 (bt, 3H, H-18′), 1.25 (m, 32H, H-2′ to 17′), 2.20 (s, 6H, 2 × —CH_3), 2.30 (bt, 2H, H-1′), 5.20 (s, 2H, —OCH_2—), 7.30 (s, 5H, —C_6H_5), 9.00 (bs, 1H, NH). *Anal.* calcd. for $C_{32}H_{51}NO_2$: C 79.78, H 10.67, N 2.91; found: 80.09, H 10.18, N 2.70.

Dioctadecyldeuteroporphyrin II dimethyl ester 2

The pyrrole **4** (2.9 g, 8.8 mmol) was hydrogenated at 162 kPa (1.6 atm) for 30 min in tetrahydrofuran (50 mL) containing triethylamine (0.05 mL) and 5% Pd on activated charcoal (100 mg). The mixture was filtrated over Celite and the Celite was washed with methanol (20 mL) and acetonitrile (40 mL).

The pyrrole **8** (4.3 g, 8.7 mmol) was hydrogenated as described above, with similar work-up. The two resulting solutions were mixed together and evaporated at 25°C. The residue was taken up in hot formic acid (75 mL). The mixture was stirred vigorously and 31% hydrobromic acid in glacial acetic acid (4.5 mL) was added. The mixture was refluxed for 1 h and the temperature was lowered to 25°C, bromine (1.1 mL) was added, and the reflux was continued for 2 h. The solvent was evaporated by heating under an air stream. Methanol (50 mL) containing 5% sulfuric acid was added and the mixture was stirred for 12 h. Methanol (40 mL) was evaporated from the mixture and chloroform extraction gave a dark oil which was chromatographed over silica gel. Recrystallization from chloroform/methanol 1:20 of the red fraction gave porphyrin **2** (720 mg, 0.7 mmol, 8%), mp 91–92°C; λ_{max}: 398 (120), 498 (9.8), 530 (6.2), 568 (5.7), 595 (0.8), 622 (3.8); ν_{KBr}: 3300, 2950, 2800, 1730, 1550, 1165; δ ($CDCl_3$): −4.30 (bs, 2H, NH), 0.70 (m, 6H, H-18′), 1.08 (m, 60H, H-3′ to 17′), 2.15 (bt, 4H, H-2′), 3.28 (bt, 4H, —CH_2CO—), 3.30 (s, 12H, C-CH_3), 3.45 (s, 6H, —OCH_3), 3.67 (bt, 4H, C(2)-CH_2, C(6)-CH_2), 4.01 (bt, 4H, C(4)-CH_2, C(8)-CH_2), 9.55, 9.65 (s's, 4H, *meso* protons). *Anal.* calcd. for $C_{68}H_{106}N_4O_4$: C 78.26, H 10.24, N 5.37; found: C 77.95, H 9.95, N 5.66.

Dioctadecyldeuteroporphyrin II 1

Porphyrin **2** (104 mg, 0.1 mmol) was added to a mixture of tetrahydrofuran (10 mL) and 6 *N* hydrochloric acid (10 mL). The mixture was stirred in the dark for 48 h. Brine (100 mL) was added and extraction with tetrahydrofuran gave a residue which was purified by preparative tlc on cellulose plates to give **1** (79 mg, 0.078 mmol, 78%), mp 90–91°C; λ_{max}: 398 (140), 498 (11.0), 535 (7.7), 567 (5.4), 595 (0.7), 623 (4.8); ν_{KBr}: 3300, 3100, 2950, 2920, 2800, 1715; δ ($CDCl_3$): −3.10 (bs, ≅2H, NH), 0.70 (m, 6H, H-18′), 1.08 (m, 60H, H-3′ to 17′), 2.15 (bt, 4H, H-2′), 3.30 (bt, 4H, —CH_2CO—), 3.32 (s, 12H, C-CH_3), 3.67 (bt, 4H, C(2)-CH_2, C(6)-CH_2), 4.00 (bt, 4H, C(4)-CH_2, C(8)-CH_2), 9.60 (bs, 4H, *meso* protons); m/e (FAB, crown ether): 1016. *Anal.* calcd. for $C_{66}H_{102}N_4O_4$: C 78.06, H 10.12, N 5.52; found: C 77.69, H 9.86, N 5.89.

Acknowledgements

We would like to thank Professor C. K. Chang for invaluable advice on porphyrin synthesis and Dr Surat Hotchandani for his help in the spectroscopic studies. We also thank the Natural Sciences and Engineering Research Council of Canada and the Université du Québec à Trois-Rivières for their financial support.

1. J. A. MERCER-SMITH and D. G. WHITTEN. J. Am. Chem. Soc. **101**, 6620 (1979).
2. Y. OKUNO, W. E. FORD, and M. CALVIN. Synthesis, 537 (1980).
3. A. L. MOORE, G. DIRKS, D. GUST, and T. A. MOORE. Photochem. Photobiol. **32**, 691 (1980).
4. A. RUAUDEL-TEIXIER, A. BARRAUD, B. BELBEOCH, and M. ROULLIAY. Thin Solid Films, **99**, 33 (1983).
5. J. P. COLLMAN, R. R. GAGNÉ, C. A. REED, T. R. HALBERT, G. LANG, and W. T. ROBINSON. J. Am. Chem. Soc. **97**, 1427 (1975).
6. J. H. FUHRHOP and M. BACCOUCHE. Justus Liebigs Ann. Chem. 2058 (1976).
7. T. YAMAMURA. Chem. Lett. 773 (1977).
8. G. ADLER. J. Colloid Interface Sci. **72**, 164 (1979).
9. (*a*) J.-P. DODELET, M. F. LAWRENCE, M. RINGUET, and R. M. LEBLANC. Photochem. Photobiol. **33**, 713 (1981); (*b*) M. F. LAWRENCE, J.-P. DODELET, and M. RINGUET. Photochem. Photobiol. **34**, 393 (1981); (*c*) J.-P. DODELET, H.-P. POMMIER, and M. RINGUET. J. Appl. Phys. **53**, 4270 (1982).
10. K. M. SMITH. *In* Porphyrins and metalloporphyrins. *Edited by* K. M. Smith. Elsevier, Amsterdam. 1975. Chapt. 1.
11. C. K. CHANG. J. Am. Chem. Soc. **99**, 2819 (1977).
12. P. S. CLEZY, A. J. RIEPA, A. W. NICHOL, and G. A. SMYTHE. Aust. J. Chem. **23**, 589 (1970).
13. M. GOUTERMAN. *In* The Porphyrins. Vol. III. *Edited by* D. Dolphin. Academic Press Inc., New York. 1978. pp. 44–47.
14. R. GRIGG, R. J. HAMILTON, M. L. JOZEFOWICZ, C. H. ROCHESTER, R. J. TERRELL, and H. WICKWAR. J. Chem. Soc. Perkin Trans. 2, 407 (1973).
15. F. M. MENGER, H. K. RHEE, and J. V. RHEE. J. Am. Chem. Soc. **98**, 792 (1976).
16. A. W. Johnson, E. Markham, R. Price, and K. B. SHAW. J. Chem. Soc. 4254 (1958).
17. G. G. KLEINSPEHN. J. Am. Chem. Soc. **77**, 1546 (1955).

Synthesis and nuclear magnetic resonance spectra of platinum compounds with thiourea derivatives

F. D. ROCHON, J. BARIYANGA, AND P. C. KONG

Département de chimie, Université du Québec à Montréal, C.P. 8888, Succ. A, Montréal (Qué.), Canada H3C 3P8

Received August 2, 1984

F. D. ROCHON, J. BARIYANGA, and P. C. KONG. Can. J. Chem. **63**, 2425 (1985).

Compounds of the type *trans*-$[PtL_2T_2]Cl_2$ where L = NH_3, methylamine, dimethylamine, pyridine, and 2-aminopyrimidine and T = *N*-methylthiourea and *N,N'*-dimethylthiourea and where L = NH_3 and T = *N,N,N',N'*-tetramethylthiourea have been synthesized. The ^{1}H nmr spectra have shown that the thiourea derivatives are bonded to platinum by the sulfur atom. The methyl protons of *N*-methylthiourea and one methyl group protons of *N,N'*-dimethylthiourea in the complexes, where L is aromatic, showed resonance at higher field after coordination to the metal. This was explained by an intramolecular interaction between the methyl group and the aromatic ring. The nmr spectra of the $[PtT_4]Cl_2$ compounds were also measured.

F. D. ROCHON, J. BARIYANGA et P. C. KONG. Can. J. Chem. **63**, 2425 (1985).

Les complexes de type *trans*-$[PtL_2T_2]Cl_2$ où L = NH_3, méthylamine, diméthylamine, pyridine et amino-2 pyrimidine et T = *N*-méthylthiourée, et *N,N'*-diméthylthiourée ainsi que L = NH_3 et T = *N,N,N',N'*-tétraméthylthiourée ont été synthétisés. Les spectres de résonance magnétique nucléaire ^{1}H ont montré que les dérivés de la thiourée étaient liés au platine par l'atome de soufre. Les protons de *N*-méthylthiourée et d'un groupement méthyle de *N,N'*-diméthylthiourée dans les complexes où L est aromatique, ont montré un blindage lorsque ces ligands étaient coordinés au métal. Ce blindage a été expliqué par une association intramoléculaire entre le groupement méthyle de T et le noyau aromatique. Les spectres rmn des trois composés $[PtT_4]Cl_2$ ont également été mesurés.

Introduction

Infrared studies of thiourea (tu) and its N-alkyl derivatives (T) have been reported (1, 2). The interpretation of the spectra is not easy since many absorption bands result from a mixture of vibrations. The C—N bond of thiourea and its derivatives has an appreciable double bond character. Therefore thiourea derivatives can have different conformations where the thioamide hydrogen atom and the thiocarbonyl bond are *cis* or *trans*. For *N*-alkylthiourea, there are two isomers, *trans* and *cis*, whereas for *N,N'*-dialkylthiourea, there are three isomers, *trans*−*trans*, *cis*−*cis*, and *cis*−*trans*.

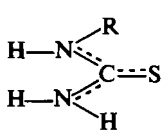

trans

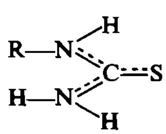

cis

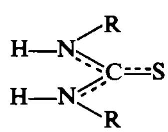

trans−*trans*

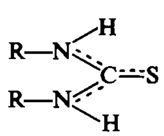

cis−*cis*

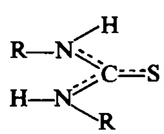

cis−*trans*

Lane *et al.* (3) studied the infrared spectra of several thiourea derivatives in the solid state. He found that *N,N'*-dimethylthiourea and *N,N'*-diethylthiourea were *trans*−*trans* isomers. *N,N'*-di-*t*-butylthiourea showed both structures *cis* and *trans*. But the authors were not able to determine whether it was the *cis*−*trans* isomer or a mixture of the *cis*−*cis* and *trans*−*trans* compounds. Methylthiourea was identified as the *trans* isomer.

Several infrared studies of $[Pt(tu)_4]Cl_2$ (4−7) have shown that thiourea was bonded to platinum through its S atom. A band between 205 and 298 cm^{-1} was assigned to the stretching Pt—S vibration. Belluco *et al.* (8) studied the infrared spectra of several platinum complexes with thiourea derivatives $[PtT_4]Cl_2$ where T = *N,N'*-dimethylthiourea (DMT), methylthiourea (MT), and tetramethylthiourea (TMT). They observe a decrease of the frequency of ν(N—H) and therefore suggested that the coordination site was N. They also assigned a new band around 350 cm^{-1} to the vibration ν(Pt—N). A year later, Gosavi *et al.* (9) showed that TMT was coordinated to platinum through its sulfur atom.

The structures of thiourea and some of its derivatives were determined. The C—N and C—S bond distances are shown on Table 1. The average C—N distance is 1.33 Å and the average C—S distance is 1.70 Å. The four atoms SCNN are in the same plane. These results confirm the double bond character of the C—N bond and show that the order of the C—S bond is less than two. The rotation around the C—N bond is partly hindered, resulting in the formation of the isomers discussed above.

The crystal structure of several metallic complexes have shown that the binding site of thiourea and its derivatives was the sulfur atom. The C—S and C—N bond distances are shown on Table 1. The average C—N distance is 1.31 Å while the average C—S distance is 1.73 Å. The C—N bond distances seem slightly shorter (0.02 Å) than in the free ligand while the C—S bond is longer (0.03 Å). These differences are relatively small but they seem significant. Therefore upon coordination, the bond order of S—C is reduced while that of C—N is slightly increased.

Very few platinum compounds of thiourea derivatives (T) have been reported. We have now synthesized several complexes of the type *trans*-$[PtL_2T_2]Cl_2$ (where L = nitrogen ligand) and $[PtT_4]Cl_2$. We have measured the infrared spectra of these compounds in the solid state, and the nmr spectra in D_2O. These results are reported below.

Experimental

trans-$[PtL_2Cl_2]$

The compounds *trans*-$[PtL_2Cl_2]$ where L = NH_3, methylamine (MA), dimethylamine (DMA), and pyridine (Py) were synthesized by the method described by Kauffman (22, 23). The compound with L = 2-aminopyrimidine (AP) was prepared by the method described by Kong and Rochon (24).

trans-$[PtL_2T_2]Cl_2$

The compound *trans*-$[Pt(NH_3)_2(MT)_2]Cl_2$ where MT = *N*-methyl-

TABLE 1. C—N and C—S bond distances (Å) in thiourea and its compounds

Compound	Bond distance		Reference
	C—N	C—S	
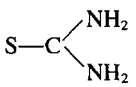	1.33(2)	1.72(2)	10
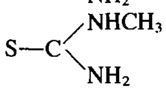	1.32(1)	1.71(1)	11
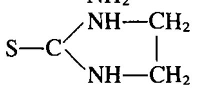	1.32(1)	1.71(1)	12
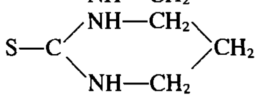	1.33(1)	1.72(1)	13
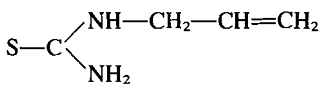	1.36(2)	1.66(2)	14
Average	1.33	1.70	
$[Pt(tu)_4]Cl_2$	1.30(1)	1.74(1)	15, 16
$[Pt(DMT)_4]Cl_2$	1.33(1)	1.74(2)	17
$[Pt(ET)_4]Cl_2$*	1.31(3)	1.74(3)	18
$[Ag(MT)_3Cl]$	1.32(1)	1.71(1)	19
$[Cu(DMT)_3Cl]^+$	1.30(1)	1.70(1)	20
$[Co(TMT)_2(NO_3)_2]$	1.33(1)	1.74(2)	21
Average	1.31	1.73	

*ET = ethylthiourea.

thiourea was prepared by the following method. *trans*-$[Pt(NH_3)_2Cl_2]$ (1 mm) was suspended in 5 mL of water. An aqueous solution of MT (4 mm in 5 mL H_2O) was added. The mixture was stirred at room temperature and after 30 min became clear. The yellow solution was filtered and evaporated to dryness under vacuum. The residue was washed with acetone and dried under vacuum for 12 h. Yield: 77%. Dec. 187−204°C. IR: 3310br, 1630s, 1550s, 970s cm^{-1}.

trans-$[Pt(NH_3)_2(DMT)_2]Cl_2$ was prepared as follows. *trans*-$[Pt(NH_3)_2Cl_2]$ (1 mm) was dissolved in 15 mL of DMF and filtered. DMT (2 mm) was added to the solution and stirred for 2 days at room temperature. The solution was kept in a refrigerator at night. More DMT (2 mm) was then added and stirred. Two hours later the precipitate was filtered and dissolved in water. The solution was filtered and evaporated to dryness under vacuum. The residue was washed with ether and dried under vacuum overnight. Yield: 50%. Dec. 195−215°C. IR: 3409m, 3325s, 3200br, 1585s, 1500s, 1275m cm^{-1}.

trans-$[Pt(NH_3)_2(TMT)_2]Cl_2$ was prepared by the following method. *trans*-$[Pt(NH_3)_2Cl_2]$ (1 mm) was dissolved in 15 mL DMF and filtered. TMT (4 mm) was added and the mixture was stirred for 24 h. Ether (20 mL) was then added and the precipitate was filtered and washed with ether. The compound was then dissolved in water and the solution was filtered and evaporated to dryness under vacuum. The residue was washed with ether and dried under vacuum overnight. Yield: 30%. Dec. 190−204°C. IR: 3250br, 3120br, 1550s, 1095s cm^{-1}.

The compounds *trans*-$[PtL_2T_2]Cl_2$ where L = MA, DMA, and Py and T = MT and DMT were prepared as follows. The compound *trans*-$[PtL_2Cl_2]$ (1 mm) was dissolved in 10 mL of DMF and filtered. An excess of T (3 mm) was added and the solution stirred until a pale yellow precipitate was obtained. After filtration, the precipitate was washed with ether and dissolved in water. The solution was filtered and evaporated to dryness under vacuum. The yellow residue was washed with ether and dried under vacuum for 12 h.

trans-$[Pt(MA)_2(MT)_2]Cl_2$: Yield: 50%. Dec. 138−160°C. IR: 3340s, 3320s, 3185br, 1665w, 1644s, 1556s, 973w cm^{-1}.
trans-$[Pt(MA)_2(DMT)_2]Cl_2$: Yield: 50%. Dec. 165−195°C. IR: 3244sh, 3170br, 3100br, 1595s, 1576s, 1495s, 1285m, 1256m cm^{-1}.
trans-$[Pt(DMA)_2(MT)_2]Cl_2$: Yield: 75%. Dec. 170−202°C. IR: 3334s, 3242s, 3200sh, 3127s, 1605s, 966m cm^{-1}.
trans-$[Pt(DMA)_2(DMT)_2]Cl_2$: Yield: 60%. Dec. 190−235°C. IR: 3195s, 3110s, 1578s, 1490s, 1283m cm^{-1}.
trans-$[Pt(Py)_2(MT)_2]Cl_2$: Yield: 60%. Dec. 190−195°C. IR: 3260br, 3170br, 1621s, 1603sh, 1556s, 958m cm^{-1}.
trans-$[Pt(Py)_2(DMT)_2]Cl_2$: Yield: 50%. Dec. 203−215°C. IR: 3120br, 1603sh, 1570s, 1270s cm^{-1}.

Complexes of the type *trans*-$[Pt(AP)_2T_2]Cl_2$ were synthesized according to the method described by Kong and Rochon (24). *trans*-$[Pt(AP)_2(MT)_2]Cl_2$: Yield, 70%. Dec. 200−208°C. IR: 3300br, 3160br, 1610s, 1580m, 1554s, 971m, 961m cm^{-1}. *trans*-$[Pt(AP)_2(DMT)_2]Cl_2$: Yield: 40%. Dec. 224−240°C. IR: 3320s, 3120br, 1615s, 1570s, 1550s, 1490s, 1270s cm^{-1}.

$[PtT_4]Cl_2$

The complexes where T = MT and DMT were prepared by the method described by Kukushkin *et al.* (25) and Kurnakov (26). Yields: 60%. mp $[Pt(MT)_4]Cl_2$: 160°C, $[Pt(DMT)_4]Cl_2$: 200°C.

$[Pt(TMT)_4]Cl_2$ was prepared as follows. K_2PtCl_4 (1 mm) was dissolved in 10 mL of water containing 3 drops of concentrated HCl. An ethanol solution of TMT (0.55 g in 5 mL ethanol) was added and stirred for 40 min. The solution was then filtered and the yellow solution was evaporated to dryness under vacuum. The residue was washed with ether and redissolved in ethanol. After filtration, the solution was evaporated to dryness under vacuum. The compound was dried at 80°C under vacuum for 12 h. Yield: 80%. Dec. 290−300°C.

The infrared spectra were measured as Nujol mulls on a P.E. 621 spectrometer. A 60 MHz Varian EM 360C was used to record the ^1H nmr spectra. The spectra were measured at 30°C in D_2O (~0.2 *M*) and a very small quantity of DSS was used as internal standard.

Discussion

The reaction between complexes of the type *trans*-$[PtL_2Cl_2]$ where L = NH_3, MA, DMA, Py, and AP and thiourea derivatives, MT, DMT, and TMT was studied. The reaction was as follows:

$$trans\text{-}[PtL_2Cl_2] + 2T \xrightarrow[\text{or DMF}]{H_2O} trans\text{-}[PtL_2T_2]Cl_2$$

trans-$[Pt(NH_3)_2(MT)_2]Cl_2$ was synthesized in water while all other complexes were synthesized in DMF. It was not possible to isolate complexes *trans*-$[PtL_2(TMT)_2]Cl_2$ for L = MA, DMA, Py, and AP probably because of steric hindrance reasons.

Compounds $[PtT_4]Cl_2$ where T = MT, DMT, and TMT were also prepared.

The results of the elemental analyses of all the compounds are shown on Table 2.

The infrared spectra of the compounds *trans*-$[PtL_2T_2]Cl_2$ were measured. The most important bands are shown in the Experimental section. Since most of the infrared bands of the thiourea derivatives are caused by combination vibrations and since there are also numerous amine bands, it was not possible to assign the vibrations observed in the infrared spectra of the compounds. Infrared spectroscopy is not an adequate method to identify the nature of the metal−ligand bond in this type of compounds. It was not possible to differentiate the —NH and —NH_2 vibrations of the T ligands from those of the amines (L). Therefore the binding site of the thiourea derivatives could not be determined by this method. Most compounds showed some weak bands between 230 and 300 cm^{-1} which might be assigned to ν(Pt—S), but the T ligands also showed some weak absorption in this region.

TABLE 2. Elemental analysis of the complexes*

Compound	Analysis (%) C	H	Cl
trans-[Pt(NH_3)$_2$(MT)$_2$]Cl_2	10.00	3.75	14.10
	9.54	3.76	14.85
trans-[Pt(MA)$_2$(MT)$_2$]Cl_2	14.17	4.33	
	14.31	4.30	
trans-[Pt(DMA)$_2$(MT)$_2$]Cl_2	17.91	4.85	
	18.32	5.28	
trans-[Pt(Py)$_2$(MT)$_2$]Cl_2	27.81	3.64	11.75
	27.34	3.78	11.86
trans-[Pt(AP)$_2$(MT)$_2$]Cl_2	22.64	3.48	11.14
	22.86	3.54	11.34
trans-[Pt(NH_3)$_2$(DMT)$_2$]Cl_2	14.17	4.36	
	14.66	4.59	
trans-[Pt(MA)$_2$(DMT)$_2$]Cl_2	17.91	4.85	
	18.32	5.03	
trans-[Pt(DMA)$_2$(DMT)$_2$]Cl_2	21.28	5.32	
	21.20	5.60	
trans-[Pt(Py)$_2$(DMT)$_2$]Cl_2	30.38	4.11	11.23
	30.10	4.12	11.77
trans-[Pt(AP)$_2$(DMT)$_2$]Cl_2	25.30	3.80	10.00
	25.00	3.75	10.23
trans-[Pt(NH_3)$_2$(TMT)$_2$]Cl_2	21.27	5.31	
	21.00	5.60	
[Pt(MT)$_4$]Cl_2	15.34	3.84	
	15.45	3.66	
[Pt(DMT)$_4$]Cl_2	21.11	4.72	
	20.99	5.02	
[Pt(TMT)$_4$]Cl_2	30.23	6.05	
	29.85	6.08	

*Calculated values in the first rows.

Nuclear magnetic resonance spectroscopy was found much more useful. The nmr spectra of the ligands and complexes where L = NH_3, MA, and DMA are shown on Table 3. All the methyl protons are shifted towards lower field upon coordination, the amine being more affected than T. The methyl protons in the amine couple with ^{195}Pt with a coupling constant of about 40 Hz. The splitting of the DMA peaks in all the complexes is caused by steric hindrance of four bulky groups, which prevents the free rotation around the Pt—N and Pt—S bonds. Therefore the environment around the two methyl groups in bonded DMA is different. For the same reasons, the DMT signals are split into two peaks in all the complexes. There is no coupling between ^{195}Pt and the methyl protons of T. Therefore the binding site of T is not the N atom, but the S atom.

The nmr spectral data of the complexes containing aromatic amines (Py and AP) are shown in Table 3. In the pyridine complexes, the $H_{2,6}$ values are shifted to a lower field by 0.7 ppm, the $H_{3,5}$ values by 0.3 ppm, and the H_4 values by 0.45 ppm. If we consider only the distances between the protons and the bonded pair of electrons on N, the sequence of deshielding should be $H_{2,6} > H_{3,5} > H_4$. But upon coordination, there is a rearrangement of the molecular orbitals and the *ortho* and *para* positions are more affected than the meta position (27). A coupling constant of 36 Hz was observed between ^{195}Pt and $H_{2,6}$.

For 2-aminopyrimidine, H_6 was most affected by the coordination to platinum, being shifted to a lower field by 0.6 ppm.

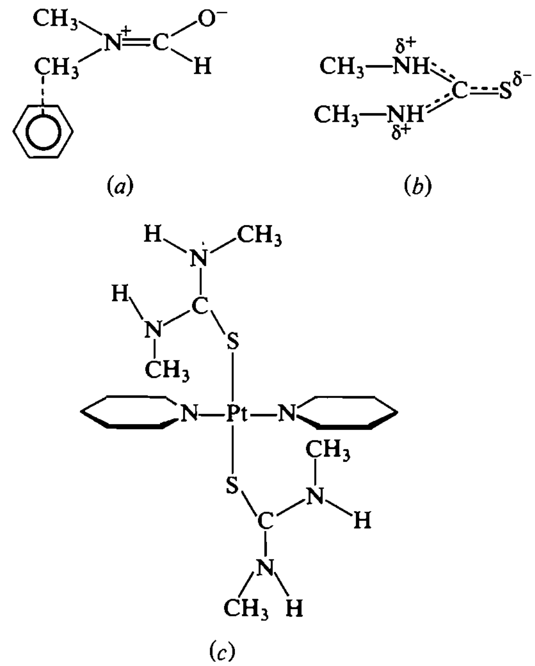

FIG. 1. (*a*) Interaction between DMF and benzene as suggested in ref. 28; (*b*) partial charges in DMT; (*c*) suggested structure for *trans*-[Pt(Py)$_2$(DMT)$_2$]$^{2+}$.

The shifts of H_5 and H_4 were 0.25 and 0.2 ppm, respectively. H_6 is coupled with ^{195}Pt (coupling constant of 36 Hz) showing that the binding site of AP is N_1. This is in agreement with the results obtained from the study of *trans*-[Pt(AP)$_2$(tu)$_2$]Cl_2 where AP was bonded to Pt through N_1 (24).

The protons of MT and of one methyl group of DMT are shifted to a higher field upon coordination to platinum. The shifts vary from 0.20 to 0.48 ppm. This observed shielding can be explained assuming the methyl group of MT and one methyl group of DMT are in the close environment of the aromatic ring of the amine. For steric reasons, the rotations around the Pt—S and Pt—N bonded are hindered and the methyl protons of T would be influenced by the π electrons of Py or AP.

A similar observation was made by Hatton and Richards (28) in a nmr study of DMF in benzene or phenol. When DMF was diluted in these solvents, the signals of the methyl protons were shifted to higher fields. This shift was explained on the base on some interaction (Fig. 1*a*) between the methyl groups of DMF and the solvent (benzene or phenol). In a similar manner, the methyl groups of MT and DMT of the platinum complexes can interact with the aromatic ring of Py and AP. Infrared and X-ray diffraction structures have confirmed the double bond character of the C—N bond, while the order of the C—S bond was considerably reduced. Therefore there is some partial charge on the T ligand, similarly to DMF (Fig. 1*b*). Therefore a close interaction between T and Py or AP would be favored because of the positive partial charge on the N atom. The structures of the compounds *trans*-[PtL_2T_2]Cl_2 where L = Py and AP and T = MT and DMT are suggested to be as on Fig. 1*c*. In this hypothesis, MT would have the *trans* conformation, while DMT could be either *trans*—*trans* or *trans*—*cis*.

The nmr spectra of the complexes were measured at different concentration in D_2O in order to confirm that these interactions were not intermolecular. There was no concentration effect on the positions of the methyl protons of MT and DMT. There-

TABLE 3. Nuclear magnetic resonance spectral data of *trans*-$[PtL_2T_2]Cl_2$

Compound		δ (ppm)				
		L			T	
L	T	Free	Complexed	J_{Pt-H} (Hz)	Free	Complexed
NH_3	MT				2.90	2.90
MA	MT	2.30	2.43	42	2.90	2.96
DMA	MT	2.30	2.52	38	2.90	2.93
			2.60	38		
NH_3	DMT				2.90	2.93
						3.03
MA	DMT	2.30	2.40	42	2.90	2.95
						3.09
DMA	DMT	2.30	2.53	39	2.90	2.95
			2.63	39		3.12
NH_3	TMT				3.05	3.30
Py	MT	7.35($H_{3,5}$)	7.58		2.90	2.58
		7.76(H_4)	8.09			
		8.40($H_{2,6}$)	8.93	36		
AP	MT	6.72(H_5)	6.90		2.90	2.63
		8.22($H_{4,6}$)	8.48(H_4)			
			8.83(H_6)	36		
Py	DMT	7.35	7.61		2.90	2.55
		7.76	8.07			3.12
		8.40	8.98	40		
AP	DMT	6.72	6.88		2.90	2.61
		8.22	8.45			3.14
			8.77	36		

TABLE 4. Nuclear magnetic resonance spectrum (δ ppm) of *trans*-$[Pt(Py)_2(DMT)_2]Cl_2$ at different temperatures

T	δ (ppm)			
(°C)	$H_{3,5}$	H_4	$H_{2,6}$	CH_3(DMT)
22	7.5	8.0	8.8	3.05
				2.50
40	7.7	8.2	9.0	3.25
				2.81
60	7.9	8.4	9.2	3.30
				2.90
80	8.1	8.6	9.4	3.40
				3.10

fore, the interactions between the methyl groups of T and the aromatic ring are of intramolecular nature.

The nmr spectrum of *trans*-$[Pt(Py)_2(DMT)_2]Cl_2$ was measured at temperatures from 22 to 80°C. Because of the small solubility of the complex, it was not possible to record the spectrum at lower temperature. All the peaks were shifted to lower fields as the temperature increased (Table 4). The two —CH_3 peaks of DMT became wider, but remained distinct.

More work is needed to confirm our hypothesis on the structures of *trans*-$[PtL_2T_2]Cl_2$ where L = Py and AP. We intend to synthesize compounds with T containing some aromatic rings, for example diphenylthiourea. We would be interested to know if the methyl groups of L could be affected by the close environment of an aromatic ring. This work is presently being done, but compounds with diphenylthiourea seem difficult to synthesize.

The nmr spectra of the $[PtT_4]Cl_2$ compounds were also measured (Table 5). All the peaks are shifted to lower field upon coordination. The shift seemed to increase with the number of C atoms (0.02, 0.05, and 0.21 ppm). All the peaks are singlets, even for the TMT complex indicating that the environment of all the methyl groups is identical.

TABLE 5. Nuclear magnetic resonance spectra of T and $[PtT_4]Cl_2$

T	δ (ppm)
MT	2.90
$[Pt(MT)_4]Cl_2$	2.92
DMT	2.90
$[Pt(DMT)_4]Cl_2$	2.95
TMT	3.05
$[Pt(TMT)_4]Cl$	3.26

1. C. N. R. RAO, R. VENKATARAGHAVAN, and T. R. KASTURI. Can. J. Chem. **42**, 36 (1964).
2. R. K. GOSAVI and C. N. R. RAO. J. Inorg. Nucl. Chem. **29**, 1937 (1967).
3. T. J. LANE, A. YAMAGUCHI, J. V. GUAGLIANO, J. A. RYAN, and S. MIZUSHIMA. J. Am. Chem. Soc. **81**, 3824 (1959).
4. A. YAMAGUCHI, R. B. PENLAND, S. MIZUSHIMA, T. J. LANE, C. CURRAN, and J. V. GUAGLIANO. J. Am. Chem. Soc. **80**, 527 (1958).
5. D. M. ADAMS and J. B. CORNELL. J. Chem. Soc. A884 (1967).
6. C. D. FLINT and M. GOODGAME. J. Chem. Soc. A744 (1966).
7. K. SWAMINATHAN and H. M. N. H. IRVING. J. Inorg. Nucl. Chem. **26**, 129 (1964).
8. U. BELLUCO, M. GRAZIANI, and P. RIGO. Inorg. Chem. **5**, 1123 (1966).
9. R. K. GOSAVI, U. AGARWALA, and C. N. R. RAO. J. Am. Chem. Soc. **89**, 235 (1967).
10. N. R. KUNCHUR and M. R. TRUTER. J. Chem. Soc. 2551 (1958).
11. M. R. TRUTER. J. Chem. Soc. 997 (1960).

12. P. J. WHEATLEY. Acta Crystallogr. **6**, 369 (1953).
13. H. W. DIAS and M. R. TRUTER. Acta Crystallogr. **17**, 937 (1964).
14. K. S. DRAGONETTE and I. L. KARLE. Acta Crystallogr. **19**, 978 (1965).
15. D. A. BERTA, N. A. SPOFFORD, P. BOLDRINI, and E. L. AMMA. Inorg. Chem. **9**, 136 (1970).
16. R. L. GIRLING, K. K. CHATTERJEE, and E. L. AMMA. Inorg. Chim. Acta, **7**, 557 (1973).
17. F. BACHECHI, L. ZAMBONELLI, and G. MARCOTRIGIANO. J. Cryst. Mol. Struct. **7**, 11 (1977).
18. R. L. GIRLING and E. L. AMMA. Inorg. Chem. **10**, 335 (1971).
19. F. C. LEE and E. L. AMMA. J. Cryst. Mol. Struct. **2**, 125 (1972).
20. F. BACHECHI and L. ZAMBONELLI. Inorg. Chim. Acta, **17**, 225 (1976).
21. A. PIGNEDOLI and G. PEYRONEL. Acta Crystallogr. B**34**, 1477 (1978).
22. G. B. KAUFFMAN and D. O. COWAN. Inorg. Synth. **7**, 239 (1963).
23. G. B. KAUFFMAN. Inorg. Synth. **7**, 249 (1963).
24. P. C. KONG and F. D. ROCHON. Can. J. Chem. **57**, 526 (1979).
25. YU. N. KUKUSHKIN, V. V. SIBIRSKAYA, V. N. SAMUSEVA, V. V. STRUKOV, V. G. POGAREVA, and T. K. MIKHALCHENKO. J. Gen. Chem. USSR, **47**, 1284 (1977).
26. N. S. KURNAKOV. J. Prakt. Chem. **50**, 481 (1894).
27. J. A. HAPPE and R. L. WARD. J. Chem. Phys. **39**, 1211 (1963).
28. J. V. HATTON and R. E. RICHARDS. Mol. Phys. **3**, 253 (1960).

Nuclear magnetic resonance and potentiometric studies of the complexation of methylmercury(II) by dithiols

ALAN P. ARNOLD AND ALLAN J. CANTY[1]
Department of Chemistry, University of Tasmania, Hobart, Tasmania, Australia 7001

AND

R. STEPHEN REID AND DALLAS L. RABENSTEIN[1]
Department of Chemistry, University of Alberta, Edmonton, Alta., Canada T6G 2G2

Received November 2, 1984

ALAN P. ARNOLD, ALLAN J. CANTY, R. STEPHEN REID, and DALLAS L. RABENSTEIN. Can. J. Chem. **63**, 2430 (1985).

Complexation of methylmercury, $CH_3Hg(II)$, by 2,3-dimercaptosuccinic acid (DMSA), 2,3-dimercaptopropanesulfonate (DMPS, Unithiol), dithioerythritol (DTE), and 2,3-dimercaptopropanol (British AntiLewisite, BAL) has been studied by ^1H nuclear magnetic resonance spectroscopy and by potentiometric titration. In the nmr study, the equilibrium constants for displacement of mercaptoacetate from its $CH_3Hg(II)$ complex by the dithiols were determined over a wide pH range, from mercaptoacetate chemical shift data. Similar competition reactions between the dithiols and mercaptoethanol were used in the potentiometric study. Using previously determined $CH_3Hg(II)$ formation constants for the competing ligands, equilibrium constants for the formation of mono- and bis-$CH_3Hg(II)$ complexes with the dithiols have been determined. The formation constants for the mono-$CH_3Hg(II)$ complexes with the vicinal dithiols BAL and DMPS are significantly higher than expected by consideration of the basicity of the sulfhydryl donors, in comparison with those for DMSA, non-vicinal DTE, and monothiols. We interpret this to indicate chelation of $CH_3Hg(II)$ by BAL and DMPS but not by DMSA. The conditional formation constants at physiological pH are discussed with reference to the effectiveness of BAL, DMPS, and DMSA as antidotes for methylmercury poisoning. In particular, the constants obtained indicate that, for dithiol antidotes at concentrations greater than that of methylmercury(II), methylmercury(II) complexes formed at physiological pH are of 1:1 stoichiometry. For BAL, a substantial proportion of the complex will be in the neutral form, in contrast to DMPS and DMSA which form anionic species only.

ALAN P. ARNOLD, ALLAN J. CANTY, R. STEPHEN REID et DALLAS L. RABENSTEIN. Can. J. Chem. **63**, 2430 (1985).

Faisant appel à la rmn du ^1H et à des titrages potentiométriques, on a étudié la complexation du méthylmercure, $CH_3Hg(II)$, par les composés suivantes: l'acide dimercaptosuccinique (ADMS), le dimercapto-2,3 propanesulfonate (DMPS, Unithiol), le dithioérythritol (DTE) et le dimercapto-2,3 propanol (British AntiLewisite, BAL). A partir des données de déplacement chimique du mercaptoacetate en rmn du ^1H, on a déterminé, sur un large intervalle de pH, les constantes d'équilibre des réactions de déplacement, par les dithiols, du mercaptoacétate de son complexe de $CH_3Hg(II)$. On a également utilisé des réactions de compétitions du même type entre des dithiols et le mercaptoéthanol, lors de l'étude potentiométrique. Faisant appel à des constantes de formation du $CH_3Hg(II)$ qui ont été déterminées antérieurement pour les ligands entrant en compétition, on a déterminé les constantes d'équilibre de formation des complexes mono- et bis-CH_3Hg avec les dithiols. Si on les compare avec les constantes de l'ADMS, du DTE (qui sont des dithiols qui ne sont pas vicinaux) ou avec celles des monothiols, les constantes de formation des complexes de mono-$CH_3Hg(II)$ avec les dithiols vicinaux BAL et DMPS sont nettement plus élevées que celles prévues en tenant compte de la basicité des sulfhydryles donneurs. Pour interpréter ces résultats, nous suggérons la présence d'une chélation du $CH_3Hg(II)$ par le BAL et le DMPS qui n'existerait pas dans le cas de l'ADMS. On discute des constantes de formation conditionnelles, à pH physiologique, en fonction d'une utilisation possible du BAL, de l'ADMS et du DMPS comme antidotes dans les empoisonnements par le méthylmercure. En particulier, les constantes obtenues indiquent que, pour des antidotes du type dithiols agissant à des concentrations supérieures à celles de méthylmercure(II), les complexes de méthylmercure formés à des pH physiologiques sont du type 1:1. Dans le cas du BAL, une proportion importante du complexe existe sous la forme neutre, contrairement au DMPS et à l'ADMS qui forment uniquement des espèces anioniques.

[Traduit par le journal]

Introduction

Methylmercury, $CH_3Hg(II)$, forms very stable complexes with monothiols (1, 2), with the result that $CH_3Hg(II)$ is thought to be essentially all thiol-bound in biological systems. For example, in human erythrocytes, $CH_3Hg(II)$ is bound almost entirely to glutathione (ca. 51%) and hemoglobin (ca. 49%) (3, 4). Complexation therapy, using monothiols such as D-penicillamine (5) or *N*-acetyl-D,L-penicillamine (5), is one of several techniques used for treatment of $CH_3Hg(II)$ poisoning; however dithiols, such as 2,3-dimercaptosuccinic acid (DMSA) (6) and 2,3-dimercaptopropanesulfonate (DMPS, Unithiol) (7) are more effective antidotes. The non-sulfonated analog of DMPS, 2,3-dimercaptopropanol (British Anti-Lewisite, BAL), is contraindicated as an antidote for $CH_3Hg(II)$ poisoning because it causes rapid redistribution of the metal into the brain (8).

Although the term "chelation therapy" is often used for such treatment, there has been no evidence that $CH_3Hg(II)$ binds simultaneously to adjacent sulfhydryl sites of these vicinal dithiols, although similar binding is found in the solid state in the 2:1 $CH_3Hg(II)$ complex of sterically rigid toluene-3,4-dithiol (9).

We have measured the equilibrium constants for the binding of $CH_3Hg(II)$ by the vicinal dithiols BAL, DMPS, and DMSA and by non-vicinal dithioerythritol (DTE) by ^1H nmr and potentiometric titration methods. The results provide evidence that BAL and DMPS do indeed chelate $CH_3Hg(II)$ in solution, whereas DMSA and DTE do not.

[1]To whom correspondence should be addressed.

TABLE 1. Acid dissociation constants of dithiols and methylmercury(II)–dithiol complexes

Acid	Abbreviated name	Acid dissociation constant	pK	
$^-O_2CCH—CHCO_2^-$ (SH, SH)	DMSA	K_3	$9.42\pm0.02^{a,b}$	9.65 ± 0.03^{d}
		K_4	11.05^{a}	11.50 ± 0.02^{d}
		$k_1{}^{c}$	9.72^{a}	9.95^{d}
		$k_2{}^{c}$	10.75^{a}	11.20^{d}
$^-O_2CCH—CHCO_2^-$ (SH, $SHgCH_3$)		k_3	9.86 ± 0.06^{a}	
CH_2CHCH_2OH (SH, SH)	BAL	K_1	$8.65\pm0.01^{d,e}$	
		K_2	10.62 ± 0.01^{d}	
		K_3	7.60 ± 0.01^{d}	
CH_2CHCH_2OH (CH_3HgS, SH) + CH_2CHCH_2OH (SH, $SHgCH_3$)				
$CH_2CHCH_2SO_3^-$ (SH, SH)	DMPS, Unithiol	K_1	$8.69\pm0.01^{d,f}$	
		K_2	$11.38\pm0.02^{d,f}$	
$CH_2CHCH_2SO_3^-$ (CH_3HgS, SH) + $CH_2CHCH_2SO_3^-$ (SH, $SHgCH_3$)		K_3	7.56 ± 0.04^{d}	
$CH_2CHOHCHOHCH_2$ (SH, SH)	DTE	K_1	9.21 ± 0.02^{a}	
		K_2	9.99 ± 0.05^{a}	
		$k_1{}^{c}$	9.51^{a}	
		$k_2{}^{c}$	9.69^{a}	
$CH_2CHOHCHOHCH_2$ ($SHgCH_3$, SH)		k_3	9.55 ± 0.03^{a}	

[a] 0.3 M KNO_3; 25°C. Uncertainties are the standard error of the estimate obtained from KINET fits.
[b] Literature values: pK_3 = 8.89, pK_4 = 10.79, 25°C, 0.1 M KNO_3 (23); pK_3 = 9.68, pK_4 = 11.14, 20°C, 0.1 M KCl (24); pK_3 = 9.44, pK_4 = 11.82, 20°C, 0.1 M KCl (25).
[c] Microscopic constant as defined in Fig. 5.
[d] 0.1 M KNO_3; 25°C. Uncertainties are one standard deviation obtained from MINIQUAD fits.
[e] Literature values: pK_1 = 8.69, pK_2 = 10.79, 25°C, 0.1 M NaCl (26); pK_1 = 8.616, pK_2 = 10.567, 25°C (27).
[f] Literature values: pK_1 = 8.84, pK_2 = 11.20 (28); pK_1 = 8.65 (2), pK_2 = 11.91 (4), 25°C, 0.1 M KCl (29).

Experimental

Chemicals

Methylmercuric iodide (Alfa Products, Morton Thiokol Inc.) was converted to stock solutions of methylmercuric hydroxide for use in ^1H nmr (1) and potentiometric titration (2) experiments. The stock solutions were standardized as described previously. Mercaptoacetic acid, 2,3-dimercaptopropanol (Aldrich), and 2-mercaptoethanol (Koch-Light) were fractionally distilled under reduced nitrogen pressure. *Meso*-2,3-dimercaptosuccinic acid (Sigma Chemical Co.), 2,3-dimercaptopropanesulfonic acid, sodium salt (Aldrich and Heyl and Co., Chem.-Pharm. Fabrik, Berlin), and dithioerythritol (Aldrich) were used as received. All thiols were stored under inert atmosphere below −4°C.

pH measurements

For the ^1H nmr study, all pH measurements were made at 25 ± 1°C with an Orion Model 701 meter equipped with either a standard glass electrode – porous ceramic junction reference electrode pair, or a microcombination electrode, in solutions containing 0.3 M KNO_3 (1). For the equilibrium potentiometric titrations, pH measurements were made at 25 ± 0.02°C with an Orion Model 701A meter equipped with a Philips glass electrode (GAT130) and glass sleeve double-junction calomel reference electrode (R44/2-SD/1) in solutions containing 0.1 M KNO_3 (2).

^1H nuclear magnetic resonance measurements

Proton nmr spectra were recorded on a Varian A60D spectrometer at a probe temperature of 25 ± 1°C with a sweep rate of 0.1 Hz/s. Chemical shifts were measured relative to either the central resonance of the triplet of tetramethylammonium ion or the singlet for 1,4-dioxane. Chemical shifts are reported relative to the methyl resonance of sodium 2,2-dimethyl-2-silapentane-5-sulfonate (DSS).

Results

Acid dissociation constants for the dithiols were determined potentiometrically in the ionic strength medium appropriate for subsequent determination of $CH_3Hg(II)$ formation constants by ^1H nmr (1) or potentiometric titration (2). Particular care was taken to preclude carbonate contamination of the titrant base, and to use values of pK_w determined under our experimental conditions. Both of these parameters significantly affect pK_a values which are determined from data above pH 10. Acid dissociation constants determined for the dithiols are listed in Table 1.

^1H nmr determination of formation constants

Formation constants for the $CH_3Hg(II)$ complexes of DMSA and DTE were determined from the exchange-averaged chemical shift of the mercaptoacetic acid (MAA) resonance in solutions containing MAA, $CH_3Hg(II)$, and the dithiol. The procedure was similar to that used to determine formation constants for monothiol–$CH_3Hg(II)$ complexes (1). Chemical shift titration data are shown in Fig. 1 for (A) a solution containing only MAA, (B) a solution containing the $CH_3Hg(II)$–MAA complex, and (C) a solution containing equimolar concentrations of MAA, $CH_3Hg(II)$, and DMSA. Curve C lies between curves A and B, indicating displacement of some of the complexed MAA by DMSA and fast exchange of MAA between its free and complexed forms. The exchange-averaged chemical shift of MAA yields directly P_f, the proportion of uncomplexed MAA (1), from which the formation constant $K_{fH,}$ defined by eq. [1],

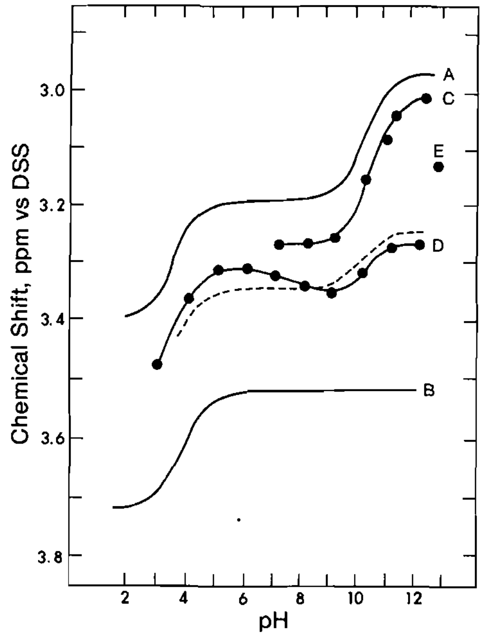

FIG. 1. pH dependence of the chemical shift of the exchange-averaged MAA resonance in solutions containing (*A*) 0.10 *M* MAA, (*B*) 0.10 *M* MAA and 0.10 *M* $CH_3Hg(II)$, (*C*) as in (*B*) plus 1 mole equivalent of DMSA, (*D*) as in (*B*) plus 0.5 mole equivalent of DMPS (—•—•— experimental and --- calculated using formation constants determined by potentiometry), and (*E*) MAA:$CH_3Hg(II)$:DTE of 2:1:1.

$$[1] \quad CH_3Hg^+ + {}^-S\,SH \rightleftarrows CH_3HgS\,SH$$

$$k_{fH} = \frac{[CH_3HgS\,SH]}{[CH_3Hg^+][{}^-S\,SH]}$$

can be calculated with eq. [2][2,3]

$$[2] \quad k_{fH}^2\,(C_M - (1 - P_f)C_{MAA} - 2C_{Dithiol})K_{dp}k_3[M]^2/[H]^2 + k_{fH}(C_M - (1 - P_f)C_{MAA} - C_{Dithiol})[M](1 + k_3/[H]) + (C_M - (1 - P_f)C_{MAA})(1 + [H]/K_3 + K_4/[H]) = 0$$

where C_M, C_{MAA}, and $C_{Dithiol}$ are the total concentrations of $CH_3Hg(II)$, MAA, and dithiol, and [M] is the concentration of free CH_3Hg^+. $[M] = (1 - P_f)/(P_f\,\alpha_{MAA}K_{fMAA})$ where K_{fMAA} is the formation constant of the $CH_3Hg(II)$−MAA complex and $\alpha = K_{aMAA}/([H] + K_{aMAA})$; K_{aMAA} is the acid dissociation constant for the thiol group of MAA (1). The equilibrium constants k_3 and K_{dp} are defined by eqs. [3] and [4].[2]

$$[3] \quad CH_3HgS\,SH \rightleftarrows CH_3HgS\,S^- + H^+$$

$$k_3 = \frac{[CH_3HgS\,S^-][H^+]}{[CH_3HgS\,SH]}$$

$$[4] \quad CH_3HgS\,S^- + CH_3HgS\,SH \rightleftarrows CH_3HgS\,SHgCH_3 + HS\,S^-$$

$$K_{dp} = \frac{[CH_3HgS\,SHgCH_3][HS\,S^-]}{[CH_3HgS\,S^-][CH_3HgS\,SH]}$$

[2] HS SH, $^-$S SH, and $^-$S S$^-$ represent dithiol, singly deprotonated dithiol, and doubly deprotonated dithiol, respectively. $CH_3HgS\,SH$ and $CH_3HgS\,S^-$ represent the 1:1 $CH_3Hg(II)$ complexes with singly and doubly deprotonated dithiol and $CH_3HgS\,SHgCH_3$ the 2:1 complex with doubly deprotonated dithiol.

[3] Lower case *k*'s are used to represent microscopic (site specific) acid-dissociation and complex formation constants.

TABLE 2. Formation constants for methylmercury(II)−dithiol complexes

Ligand	Formation constant	log (formation constant)
$^-O_2CCH(S^-)$—$CH(S^-)CO_2^-$	K_{f1}	18.4 ± 0.2^a
	K_{f2}	16.9 ± 0.2^a
	$k_{f1}^{\,b}$	18.1 ± 0.2
	$k_{f2}^{\,b}$	17.2 ± 0.2
$^-O_2CCH(S^-)$—$CH(SH)CO_2^-$	$k_{fH}^{\,b}$	17.16 ± 0.05^a
$CH_2(S^-)CH(S^-)CH_2OH$	K_{f1}	19.56 ± 0.09^c
	K_{f2}	10.46 ± 0.10^c
$CH_2(S^-)CH(SH)CH_2OH$ + $CH_2(SH)CH(S^-)CH_2OH$	K_{fH}	16.54^c
$CH_2(S^-)CH(S^-)CH_2SO_3^-$	K_{f1}	21.01 ± 0.08^c
	K_{f2}	10.26 ± 0.008^c
$CH_2(S^-)CH(SH)CH_2SO_3^-$ + $CH_2(SH)CH(S^-)CH_2SO_3^-$	K_{fH}	17.19^c
$CH_2(S^-)CHOHCHOHCH_2(S^-)$	K_{f1}	17.0 ± 0.2^a
	$k_{f1}^{\,b}$	16.7 ± 0.2
$CH_2(S^-)CHOHCHOHCH_2(SH)$	$k_{fH}^{\,b}$	16.6 ± 0.2^a

[a] Determined by nmr; 25°C, 0.3 *M* KNO_3. Uncertainties are the standard error of the estimate obtained from KINET fits.
[b] Microscopic constant as defined in Fig. 5.
[c] Determined by potentiometric titration; 25°C, 0.1 *M* KNO_3. Uncertainties are one standard deviation obtained from MINIQUAD fits.

The constants k_3 and K_{dp} were determined by titrating an equimolar mixture of $CH_3Hg(II)$ and DMSA at high pH with acid, until incipient precipitation (pH 4). A nonlinear least-squares fit of the titration data, using the rigorously weighted algorithm in KINET (10), to the algebraic model obtained from the equilibrium and mass balance equations, gave the values $pk_3 = 9.86 \pm 0.06$ and $K_{dp} = 0.6 \pm 0.2$ for DMSA. The titration data could not be fitted to a simple model involving only protonated and deprotonated 1:1 complex (eq. [3]) because the uncomplexed sulfhydryl group of the 1:1 complex still has a very high affinity for $CH_3Hg(II)$ so that, even at 1:1 $CH_3Hg(II)$:dithiol ratios, a significant amount of 2:1 complex is present.

Direct substitution of the P_f values obtained from the chemical shift titration data into eq. [2] and using these values for k_3 and K_{dp} yielded a value of log $k_{fH} = 17.16 \pm 0.05$. The formation constants calculated for the deprotonated 1:1 complex and the 2:1 complex (eqs. [5] and [6])[2]

$$[5] \quad CH_3Hg^+ + {}^-S\,S^- \rightleftarrows CH_3HgS\,S^-$$

$$K_{f1} = \frac{[CH_3HgS\,S^-]}{[CH_3Hg^+][S\,S^-]}$$

$$[6] \quad CH_3Hg^+ + CH_3HgS\,S^- \rightleftarrows CH_3HgS\,SHgCH_3$$

$$K_{f2} = \frac{[CH_3HgS\,SHgCH_3]}{[CH_3Hg^+][CH_3HgS\,S^-]}$$

using these values are listed in Table 2.

For DTE, precipitate formation in the presence of $CH_3Hg(II)$ precluded the measurement of a chemical shift titration

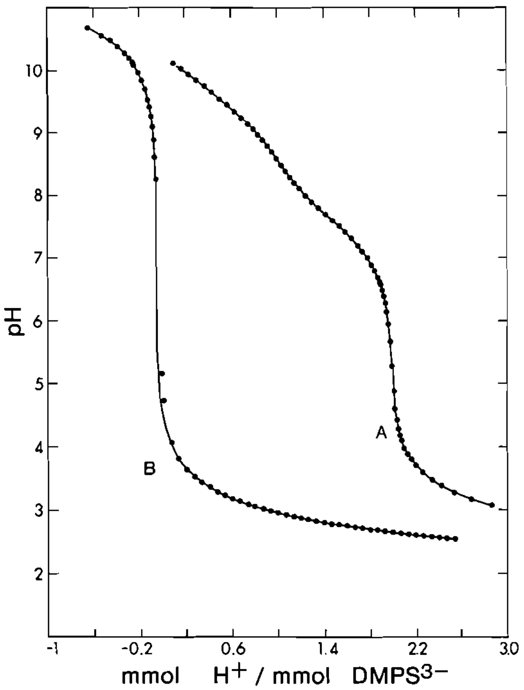

FIG. 2. Potentiometric titration curves for the $CH_3Hg(II)$-DMPS system. (A) with and (B) without ME competition. The fitted curves are calculated using the constants in Tables 1 and 2. (A) 1.186×10^{-3} M $CH_3Hg(II)$, 1.134×10^{-3} M DMPS, 3.799×10^{-3} M H^+ (total titratable), 1.178×10^{-3} M ME, (B) 2.563×10^{-3} M $CH_3Hg(II)$, 1.250×10^{-3} M DMPS, 3.168×10^{-3} M H^+ (total titratable).

curve. However, replicate measurements on a 2:1:1 MAA:$CH_3Hg(II)$:DTE solution at pH 12.2 gave a value for log k_{fH} of 16.6. The value used for k_3 in this calculation (Table 1) was calculated from pH data for the titration of an equimolar solution of DTE and $CH_3Hg(II)$ from high pH to pH 9, using a value of 0.6 for K_{dp}.

Curve D in Fig. 1 is chemical shift titration data for MAA in a solution containing MAA, $CH_3Hg(II)$, and DMPS. The intermediate chemical shift again indicates displacement of MAA by the dithiol, but because DMPS is not symmetrical, it was not possible to derive an algebraic model such as that for DMSA. However, since the MAA shift lies closer to that of $CH_3Hg(II)$−MAA, it can be concluded that the conditional formation constant, defined by eq. [7],

$$[7] \quad K_{fC} = \frac{[CH_3Hg(II) \text{ complexed by dithiol}]}{[\text{uncomplexed } CH_3Hg(II)][\text{uncomplexed dithiol SH}]}$$

is less, under these conditions, than that for the $CH_3Hg(II)$−DMSA system.

Potentiometric determination of formation constants

Formation constants for the $CH_3Hg(II)$ complexes of DMPS and BAL were determined by potentiometric titration. It has been demonstrated previously (2) that protons cannot compete effectively with $CH_3Hg(II)$ in the presence of monothiols, necessitating the use of a competitive ligand such as iodide, in order to use the potentiometric titration method. In this work, 2-mercaptoethanol (ME) was used to compete with the dithiols for $CH_3Hg(II)$. The $CH_3Hg(II)$ complex of ME has been characterized previously (log K_f = 16.13 (2), 16.12 (11)), and has no acid−base behavior, which keeps the number of species in the competition complexation model to a minimum. Representative titration data for the $CH_3Hg(II)$−DMPS system are shown in Fig. 2. Equilibrium constants were obtained from titration data using a version of MINIQUAD (12) by procedures described previously (2).

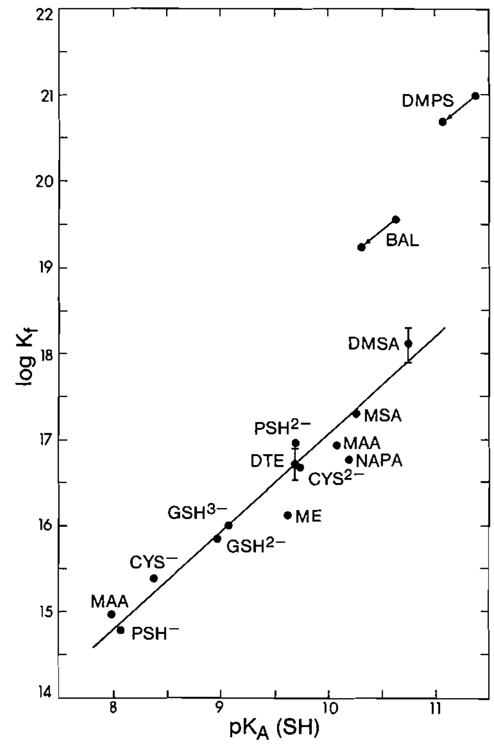

FIG. 3. Correlation between the microscopic log K_f of $CH_3Hg(II)$−thiol complexes and the microscopic pK_A of the thiol groups. ME, MAA, BAL, DMPS, DMSA, and DTE are defined in the text. O-MAA is O-methylmercaptoacetate, PSH^-, CYS^-, and GSH^{2-} the amino-protonated, thiol-deprotonated and PSH^{2-}, CYS^{2-}, and GSH^{3-} the completely deprotonated forms of penicillamine, cysteine, and glutathione, respectively, NAPA is N-acetylpenicillamine and MSA is mercaptosuccinic acid. Data for the monothiols are from [1], [2], and [4].

Potentiometric titration curves for mixtures containing equimolar amounts of BAL or DMPS and $CH_3Hg(II)$ and ME could be fitted very well to a simple model involving only protonated and deprotonated 1:1 $CH_3Hg(II)$−dithiol complexes along with the complex of ME. The values obtained for K_{fH}, K_3, and K_{f1}, eqs. [1], [3], and [5], are listed in Tables 1 and 2.

The formation constants for the 2:1 complexes of BAL and DMPS, eq. [6], were obtained from titration data of 2:1 $CH_3Hg(II)$:dithiol mixtures in the absence of ME. Under these conditions, the first sulfhydryl group is always complexed and, because of the lower affinity of the second sulfhydryl group for $CH_3Hg(II)$, the proton can compete effectively with $CH_3Hg(II)$ for this binding site. It is convenient to consider the 1:1 complex as a ligand in the presence of $CH_3Hg(II)$. The values obtained for K_{f2} for the BAL and DMPS systems are listed in Table 2.

The equilibrium constants obtained potentiometrically for the $CH_3Hg(II)$−DMPS complexes have been used to predict the chemical shift titration curve for MAA in the mixture used in the nmr study of the $CH_3Hg(II)$−DMPS system. The experimental and predicted curves are shown in Fig. 1, and the similarity between the two indicates good agreement between the nmr and potentiometric methods, considering the differences in experimental conditions.

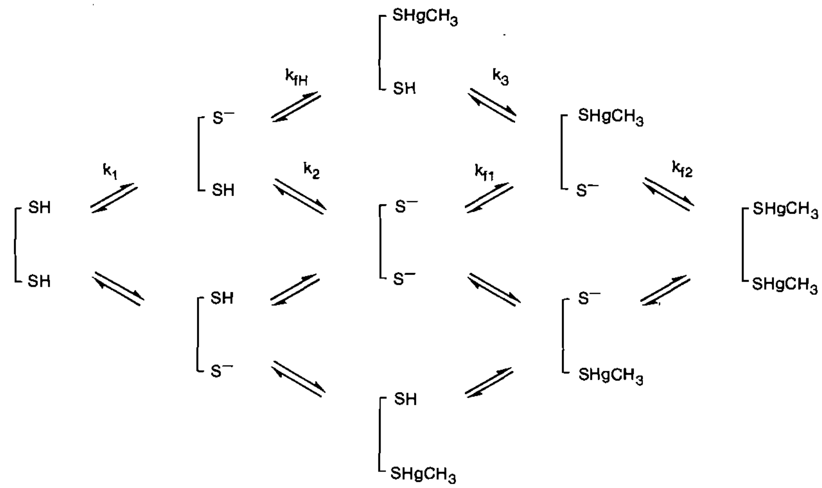

FIG. 4. Microscopic acid–base and complexation equilibria for the thiol groups of DMSA and DTE in solutions containing $CH_3Hg(II)$.

Attempts were made to determine formation constants for the $CH_3Hg(II)$–DMSA complexes by potentiometry. However, even in equimolar $CH_3Hg(II)$: dithiol solutions containing an excess of ME, significant amounts of 2 : 1 $CH_3Hg(II)$: dithiol complex are present because of the high affinity of the second sulfhydryl of DMSA for $CH_3Hg(II)$. It was not possible to refine the equilibrium constants in this system with MINIQUAD because they are too highly correlated. However, titration curves calculated with equilibrium constants obtained from the nmr study gave a good fit to the experimental pH titration curves.

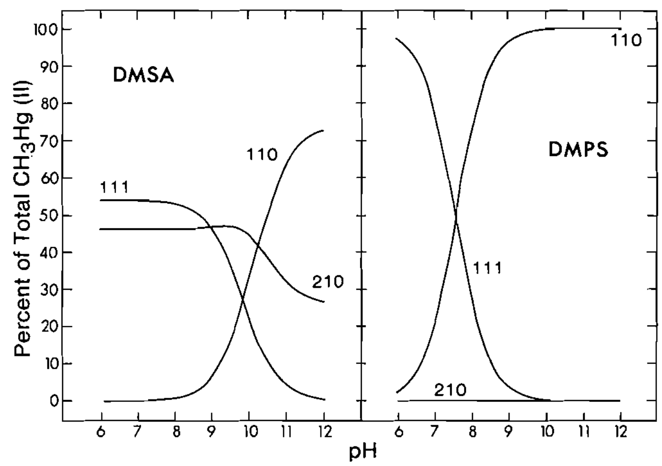

FIG. 5. Percent of total $CH_3Hg(II)$ in the various complexed forms, $M_mL_lH_h$ where m, l, and h are given by three numbers by each curve, as a function of pH in solutions containing 0.001 M $CH_3Hg(II)$ and 0.001 M dithiol. Calculated using the constants in Tables 1 and 2.

Discussion

The results in Tables 1 and 2 provide evidence for chelation in the sulfhydryl-deprotonated 1 : 1 $CH_3Hg(II)$ complexes of BAL and DMPS but not in those of DMSA and DTE. Chelation is indicated by the formation constants of the 1 : 1 deprotonated complexes, K_{f1}, which are significantly higher for the DMPS and BAL complexes than for the DMSA and DTE complexes. Figure 3 shows the relationship between the microscopic formation constant, k_{f1}, and the microscopic sulfhydryl acid dissociation constant for the $CH_3Hg(II)$ complexes of a series of monothiols (1, 2, 4) and the symmetrical dithiols DMSA and DTE. The microscopic acid dissociation and formation constants for DMSA and DTE are defined in Fig. 4, and for DMSA are related to the macroscopic constants by $k_1 = K_3/2$, $k_2 = 2K_4$, $k_{f1} = K_{f1}/2$, and $k_{f2} = 2K_{f2}$. While it was not possible to obtain the analogous microscopic constants for unsymmetrical BAL and DMPS, limits can be determined from the macroscopic constants and these are plotted in Fig. 3.

The monothiols and DMSA and DTE show the expected (1, 13) linear correlation between log K_f of their $CH_3Hg(II)$ complex and the pK_A of the coordinating group. However, it is apparent that the $CH_3Hg(II)$ complexes of BAL and DMPS are considerably more stable than would be expected by consideration of the basicity of the donor sulfur alone. We interpret this to be evidence for chelation of $CH_3Hg(II)$ in the deprotonated 1 : 1 complexes of BAL and DMPS. Chelation is also consistent with the lower sulfhydryl basicity in the deprotonated 1 : 1 complexes compared with once-protonated uncomplexed dithiol; for the protonated BAL and DMPS complexes pK_3 is significantly less than pK_1 for the doubly protonated dithiols whereas for the protonated DMSA and DTE complexes pK_3 is slightly larger. Proton displacement followed by chelation lowers pK_3 for the BAL and DMPS complexes. Alcock, Lampe, and Moore (9) have shown that $CH_3Hg(II)$ is chelated by sterically rigid vicinal dithiols in the solid state.

It seems reasonable to suggest that chelation is not present in the 1 : 1 complex of DMSA, despite the vicinal sulfhydryl groups, because of the resultant unfavorable proximity of the two deprotonated carboxylate groups which would result in this case.

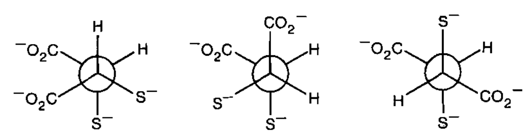

In this complex, the two sulfhydryl groups act more independently than is the case for the analogous complexes of BAL and DMPS. This is indicated by the stepwise formation constant, log K_{f2}, which for the addition of the second $CH_3Hg(II)$ cation to DMSA is 16.9 but is reduced to 10.46 and 10.26 in the BAL and DMPS complexes by chelation in the 1 : 1 complexes.

The large differences in the relative magnitudes of K_{f1}, K_{f2}, and K_{fH} for the DMSA, BAL, and DMPS complexes result in quite different distributions of $CH_3Hg(II)$ among the possible complexes, as illustrated by the species distribution diagrams in Fig. 5 for the DMSA and DMPS complexes. For the DMSA system, a large fraction of the $CH_3Hg(II)$ is present as the 2:1 complex whereas, for the DMPS system, the 2:1 complex represents <0.1% for the conditions in Fig. 5.

Since BAL, DMPS, and DMSA have all been used as antidotes for various forms of heavy-metal poisoning, it is appropriate to consider the nature of the $CH_3Hg(II)$–dithiol species expected to be present under physiological conditions. Using the equilibrium constants determined in this study, and a [dithiol]:[$CH_3Hg(II)$] ratio of 20:1, the following complexed dithiol species are expected at pH 7.4:

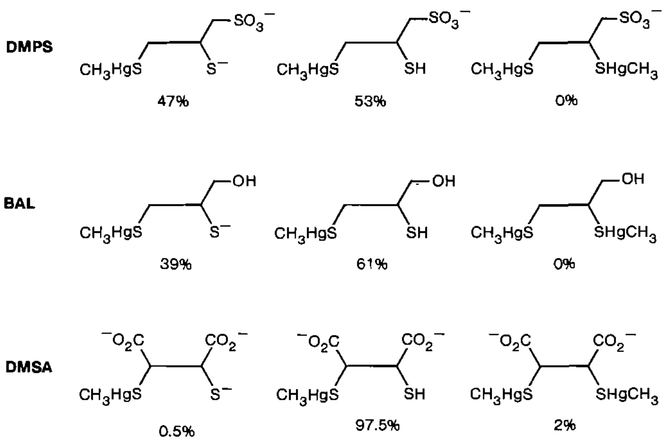

Mono-$CH_3Hg(II)$ species dominate for all the dithiols. For BAL and DMPS, about half of the complexed dithiol has a deprotonated sulfhydryl, while for DMSA, the analogous site is almost completely protonated. For DMSA and DMPS, all the major species are negatively charged. This is consistent with observed removal of $CH_3Hg(II)$ via the kidney by these dithiols (6, 7, 14). It is also known that these dithiols do not cross the red blood cell membrane, but do rapidly mobilize intracellular $CH_3Hg(II)$ (15 and footnote 4). Both are effective antidotes for $CH_3Hg(II)$ poisoning (6, 7, 15).

On the other hand, a large fraction of $CH_3Hg(II)$ complexed BAL is in the form of a neutral species under these conditions. Consistent with the expected lipophilic character of neutral BAL complexes, 1-octanol/water partition coefficients, $[CH_3Hg(II)]_{octanol}/[CH_3Hg(II)]_{water}$ for [dithiol]:[$CH_3Hg(II)$] ratios of 1:1 at pH 6.9, are ca. 10^4 greater for BAL than for DMSA and DMPS (16). Although this dithiol is an effective antidote for many other metals, including inorganic Hg(II), it redistributes $CH_3Hg(II)$ across the blood-brain barrier into the brain, and is contraindicated in cases of $CH_3Hg(II)$ toxicity.

The effectiveness of DMSA and DMPS as antidotes for $CH_3Hg(II)$ toxicity when administered orally with food, as judged by the removal of $CH_3Hg(II)$ from the brain and blood of mice, is DMSA > DMPS (14). Although factors other than formation constants are expected to be important in the effectiveness of antidotes, e.g. metabolism of antidotes and their $CH_3Hg(II)$ complexes, and the solubility properties of complexes discussed above, it is appropriate to consider possible effects of the constants determined in this study.

Since $CH_3Hg(II)$–thiol binding is extremely labile (3, 13, 17), it is likely that $CH_3Hg(II)$ in biological systems is distributed among the various intra- and extra-cellular and membrane bound sulfhydryl groups and those of antidote molecules according to an equilibrium model. If so, the relative effectiveness of DMSA and DMPS as antidotes may be related to the conditional formation constants, defined by eq. [7], of their $CH_3Hg(II)$ complexes and those of endogenous thiols at physiological pH. The dependence of the conditional formation constants of the DMSA and DMPS complexes on dithiol: $CH_3Hg(II)$ ratio is shown in Fig. 6, together with log K_{fc} for the $CH_3Hg(II)$ complexes of glutathione (GSH). Glutathione is the most abundant nonprotein thiol in biological systems (18), and has been identified as $CH_3Hg(II)$ binding site in red blood cells (3, 19) and liver cytosol (20), and 30% of rat cerebral soluble $CH_3Hg(II)$ is in a GSH complex (21). The curves illustrate the complexity of the situation, since at high dithiol:$CH_3Hg(II)$ ratios such as those expected under antidotal conditions, log K_{fc}(DMPS) > log K_{fc}(DMSA) > log K_{fc}(GSH) but at low ratios the order is altered to log K_{fc}(DMSA) > log K_{fc}(GSH) > log K_{fc}(DMPS). At low dithiol:$CH_3Hg(II)$ ratios, ^1H nmr studies of the removal of $CH_3Hg(II)$ from hemolyzed human erythrocytes (22) indicate that DMSA competes more effectively with intracellular thiols for $CH_3Hg(II)$ than DMPS.

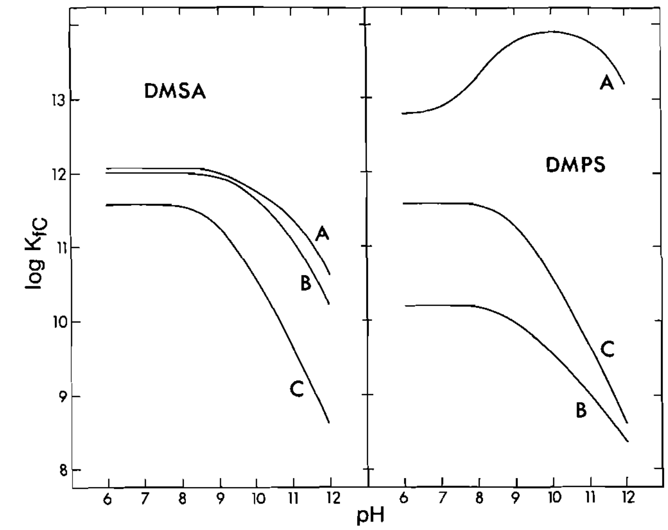

FIG. 6. pH and concentration dependence of the conditional formation constants for the $CH_3Hg(II)$–dithiol complexes and pH dependence of the conditional formation constant for the $CH_3Hg(II)$–GSH complex (*A*) 0.001 *M* $CH_3Hg(II)$, 0.01 *M* dithiol, (*B*) 0.001 *M* $CH_3Hg(II)$, 0.001 *M* dithiol. (*A*) and (*B*) were calculated with constants in Tables 1 and 2, the GSH curve (*C*) was calculated with constants in [4].

Acknowledgements

This research was supported in part by the Natural Sciences and Engineering Research Council of Canada through its Strategic Grants Program and by the University of Alberta, and in part by the National Health and Medical Research Council (Australia).

A Commonwealth Postgraduate Research Award to A.P.S., and an I. W. Killam Fellowship to R.S.R. are gratefully acknowledged.

1. R. S. REID and D. L. RABENSTEIN. Can. J. Chem. **59**, 1505 (1981).
2. A. P. ARNOLD and A. J. CANTY. Can. J. Chem. **61**, 1428 (1983).
3. D. L. RABENSTEIN, A. A. ISAB, and R. S. REID. Biochim. Biophys. Acta, **696**, 53 (1982).

[4] A. P. Arnold, R. Guy, and D. L. Rabenstein. Unpublished result.

4. R. S. REID and D. L. RABENSTEIN. J. Am. Chem. Soc. **104**, 6733 (1982).
5. J. AASETH. Acta Pharmacol. Toxicol. **39**, 289 (1976).
6. L. MAGOS. Brit. J. Pharmacol. **56**, 479 (1976).
7. B. GABARD. Acta Pharmacol. Toxicol. **39**, 250 (1976).
8. M. BERLIN, L.-G. JERKSELL, and G. NORDBERG. Acta Pharmacol. Toxicol. **23**, 312 (1965).
9. N. W. ALCOCK, P. A. LAMPE, and P. MOORE. J. Chem. Soc. Dalton Trans. 1471 (1980).
10. J. L. DYE and V. A. NICELY. J. Chem. Educ. **48**, 443 (1971).
11. G. SCHWARZENBACH and M. SCHELLENBERG. Helv. Chim. Acta, **48**, 28 (1967).
12. A. SEBATINI, A. VACCA, and P. GANS. Talanta, **21**, 53 (1974); R. N. SYLVA and M. R. DAVIDSON. J. Chem. Soc. Dalton Trans. 465 (1979).
13. D. L. RABENSTEIN. Acc. Chem. Res. **11**, 100 (1978).
14. J. AASETH and E. A. H. FRIEDHEIM. Acta Pharmacol. Toxicol. **42**, 248 (1978).
15. J. AASETH, J. ALEXANDER, and J. DEVERILL. Chem.-Biol. Interactions, **36**, 287 (1981).
16. A. P. ARNOLD, A. J. CANTY, P. W. MOORS, and G. B. DEACON. J. Inorg. Biochem. **19**, 319 (1983).
17. D. L. RABENSTEIN and R. S. REID. Inorg. Chem. **23**, 1246 (1984).
18. P. C. JOCELYN. Biochemistry of the SH group. Academic Press, New York. 1972. p. 10.
19. A. NAGANUMA and N. IMURA. Toxicol. Appl. Pharmacol. **47**, 613 (1979).
20. S. OMATA, K. SAKIMURA, T. ISHII, and H. SUGANO. Biochem. Pharmacol. **27**, 1700 (1978).
21. D. J. THOMAS and J. C. SMITH. Toxicol. Appl. Pharmacol. **47**, 547 (1979).
22. D. L. RABENSTEIN, R. S. REID, and A. A. ISAB. J. Inorg. Biochem. **18**, 241 (1983).
23. G. R. LENZ and A. E. MARTELL. Inorg. Chem. **4**, 378 (1965).
24. I. E. OKONISHNIKOVA, L. G. EGORVA, V. L. NIRONBERG, and I. Y. POSTOVSKII. Khim.-Farm. Zh. **4**, 21 (1970).
25. A. AGREN and G. SCHWARZENBACH. Helv. Chim. Acta, **38**, 1920 (1955).
26. D. L. LEUSSING and J. P. MISLAN. J. Phys. Chem. **64**, 1908 (1960).
27. P. J. ANTIKAINEN and K. TEVANEN. Suomen Kemi. **35B**, 224 (1962).
28. A. T. PILIPENKO and O. P. RYABUSHKO. Ukrain. Khim. Zh. **32**, 622 (1966).
29. P. J. ANTIKAINEN and V. M. K. ROSI. Suomen Kemi. **36B**, T32 (1963).

The influence of ammonium lignosulphonate as an expander on the formation of $PbSO_4$ on lead amalgam electrodes

R. G. BARRADAS, D. A. RENNIE, AND T. J. VANDERNOOT

The Ottawa–Carleton Institute for Research and Graduate Studies in Chemistry, Carleton University, Ottawa, Ont., Canada K1S 5B6

Received November 9, 1984

R. G. BARRADAS, D. A. RENNIE, and T. J. VANDERNOOT. Can. J. Chem. **63**, 2437 (1985).

Linear potential sweeps and potentiostatic pulse perturbations have been employed to investigate the influence of the expander ammonium lignosulphonate, on the anodic formation of $PbSO_4$ on lead amalgam electrodes in sulphuric acid solutions at 24°C. It was found that the expander strongly adsorbs onto the clean amalgam surface thus affecting the formation of the $PbSO_4$ film. The expander increased the charge necessary for passivation, inhibited the cathodic reduction of the film, and produced a more porous film. Evidence is given for the presence of an optimum concentration of expander. Some speculations concerning the mode of action of the expander onto the amalgam surface are presented.

R. G. BARRADAS, D. A. RENNIE et T. J. VANDERNOOT. Can. J. Chem. **63**, 2437 (1985).

Opérant à 24°C et dans des solutions d'acide sulfurique, on a utilisé des balayages linéaires de potentiel ainsi que des perturbations potentiostatiques pulsées pour étudier l'influence du lignosulfate d'ammonium sur la formation anodique du $PbSO_4$ sur des électrodes d'amalgame de plomb. On a trouvé que l'expanseur s'adsorbe fortement sur la surface propre d'amalgame et que ceci affecte la formation du film de $PbSO_4$. L'expanseur augmente la charge nécessaire à la passivation, inhibe la réduction cathodique du film et provoque la production d'un film plus poreux. On présente des données suggérant la présence d'une concentration optimale d'expanseur. On présente aussi quelques spéculations sur le mode d'action de l'expanseur sur la surface d'amalgame.

[Traduit par le journal]

Introduction

Much of the previous work in the literature relating to the formation of $PbSO_4$ in sulphuric acid in the presence of expanders has dealt with solid lead electrodes. During the discharge process, the expander affects the $PbSO_4$ film formed making it more porous (1–3). The $PbSO_4$ crystals were more loosely attached and they extended further from the electrode surface (1). The size of the $PbSO_4$ crystals was also reduced due to the adsorption of the expander onto the growing $PbSO_4$ crystal (3). It was also found that the expander increased the amount of charge required for passivation (3–5). The expander inhibited the cathodic reduction of the $PbSO_4$ film (3, 4, 6, 7).

Amalgam electrodes are advantageous in that they give reproducible smooth fresh surfaces which are free from surface defects and have accurately known areas. Amalgam electrodes have been employed in studies of $PbSO_4$ formation (6, 8) with and without battery expander. In the present article, the effect of the organic additive, ammonium lignosulphonate, as an expander on the formation of $PbSO_4$ on a lead amalgam electrode in sulphuric acid solutions was investigated at 24°C. An extensive set of results from sweep and step perturbations are presented for various concentrations of expander. Double layer capacitance measurements have been used to show the adsorption of the expander onto the amalgam surface. As well, the capacitance and resistance of completed $PbSO_4$ films formed in the presence of the expander have been used to make inferences concerning the film structure.

Experimental

A lead amalgam of 1.26% by weight of lead was prepared by dissolving lead beads (99.999%, Cominco of Canada Ltd.) in ultrapure mercury (99.9998% Alfa Inorganics). One millilitre of a very dilute solution of perchloric acid was kept over the amalgam to maintain it free of organic contaminants prior to use.

All solutions were prepared with ARISTAR sulphuric acid and triply distilled water. Separate deoxygenated solutions of 0.0, 0.72, 7.89, 17.45, and 76.60 ppm of ammonium lignosulphonate (Lignosol C-16, Lignosol Chemicals Ltd., Quebec) in 1.30 molal sulphuric acid were prepared. The concentrations (in ppm) are with respect to the weight of the 1.30 molal sulphuric acid solution. The composition of ammonium lignosulphonate may be found in ref. 9. The solutions were deaerated for 15 min prior to the commencement of the experiment with purified nitrogen and deaeration was continued throughout the experiment. All experiments were carried out at 24°C.

The cell body and lid were cylindrical and machined from Teflon. A hole in the bottom of the cell allowed a syringe to be inserted into the cell body. The cell body and lid were cleaned using a solution of potassium hydroxide, rinsed with thrice distilled water, and then left to soak in concentrated sulphuric acid. Prior to use, they were thoroughly rinsed again with triply distilled water followed by further cleaning in a nitrogen plasma whereby the free nitrogen radicals attack any existing organic contaminants on the surface of the cell.

The reference electrode was a Hg/Hg_2SO_4 electrode in the same acidic solution and all potentials are quoted with respect to it. A Luggin capillary was used to minimize uncompensated solution resistance.

The counter electrode was a cylindrical Pt gauze that completely surrounded the working amalgam electrode.

The needle from a glass capillary syringe (Hamilton gas tight, 50 μL) was removed and the end pulled to a very fine tip whose inner diameter was 331 μm. The working electrode consisted of a small amalgam drop that was extruded on the upturned tip. Prior to an experiment, the tip was thoroughly cleaned in potassium hydroxide, dilute nitric acid, followed by a thorough rinse in triply distilled water, and further cleansing in a nitrogen plasma. After cleaning the tip, it was rendered hydrophobic to avoid solution creepage into the tip by soaking in a solution of dimethyldichlorosilane in CCl_4. The plunger of the syringe was controlled by a micrometer (Moore and Wright, Sheffield, England) which was securely attached to the body of the syringe. The Teflon tip on the plunger of the syringe was cut away to expose the tip of the stainless steel plunger. This allowed electrical contact to be made with the amalgam electrode. Each drop was maintained at −1100 mV before a linear potential sweep or potential step was carried out.

The potentiostat was a Stonehart BC 1200 used in conjunction with a PAR model 175 programmer. An HP model 3310B function generator was used to supply a 3.98 mV rms sinusoidal signal to the

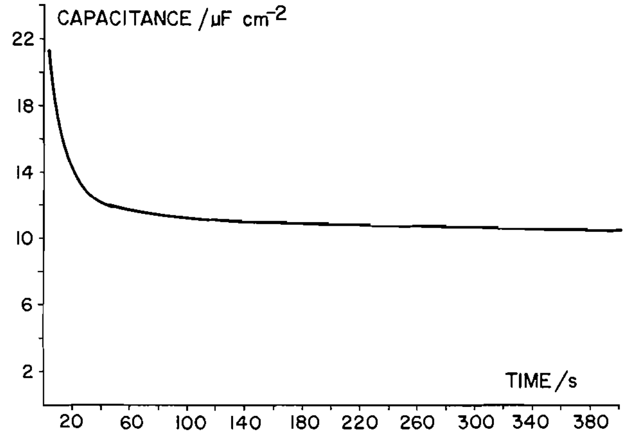

FIG. 1. A plot of the double layer capacitance as a function of time for a fresh amalgam drop in 17.45 ppm of expander. The capacitance was measured at −1100 mV vs. Hg/Hg_2SO_4.

electrode and the in-phase and out-of-phase components of admittance were measured using a PAR model 128A Lockin Amplifier. The current transients in response to potential sweeps or steps were recorded on a Nicolet 3091 digital oscilloscope and then plotted on an HP model 7047A x-y plotter. A Harrick model PDC-3XG plasma cleaner was used for cleaning.

The size of the amalgam drop was accurately determined from a calibration curve of the double layer capacitance of the drop as a function of drop size. When the drop was dislodged, the amalgam would break off inside the capillary of the tip. A new drop was slowly extruded and the capacitance recorded as a function of micrometer travel. The capacitance was relatively constant while the amalgam was still inside the capillary, and increased sharply as the drop began to form on the tip. The point when the capacitance changed sharply was taken to be the capacitance of a hemisphere of amalgam which could subsequently be employed to obtain the area of a spherical sessile drop. A calibration curve was obtained for each solution used. Fresh amalgam drops were used for each individual measurement and were all of the same approximate area (4.5×10^{-3} cm^2) in order to give a consistent geometry of the drop and capillary tip. The sessile drops were assumed to be sections of a sphere.

The expander was found to adsorb onto the electrode surface causing a change in the double layer capacitance of the drop. It was therefore necessary to wait a sufficient period of time to let the expander adsorb onto the electrode surface to its equilibrium value before the transients were obtained. This occurred when the double layer capacitance became constant. For 0.72 ppm the amount of adsorption was so small, and so slow that it was essentially equivalent to no expander being present. Therefore, for 0.0 and 0.72 ppm the transients were recorded immediately after extrusion of a drop. The higher concentrations of expander had appreciable amounts of adsorption which occurred fairly quickly. For these solutions the drops were maintained at −1100 mV until adsorption was complete.

The uncompensated resistance, Ru, was measured by applying a 50 kHz sinusoidal voltage input (3.98 mV rms) to the drop and recording the in-phase current using the lockin amplifier. The uncompensated resistance included the resistance of the Hg in the syringe. The value of Ru was checked independently by observing at what value of ohmic compensation the potentiostat began oscillating. Any overcompensation would have been obvious had it been present.

Results and discussion

(a) Adsorption of expander

The double layer capacitance of a drop was measured as a function of time at −1100 mV to determine what effect the addition of the expander had on the amalgam electrode. Figure 1 illustrates that the double layer capacitance decreases with time in a solution containing 17.45 ppm of expander. A decrease in the double layer capacitance with time in the presence of an expander has been reported previously (4, 7). It has been suggested (4, 7, 10) that the decrease in the double layer capacitance is due to the presence of an adsorbed layer of the expander on the electrode surface. At higher concentrations of expander, the double layer capacitance decreases much more quickly indicating that the rate at which the expander adsorbed onto the electrode was increased. In 1.30 molal sulphuric acid with no expander, the double layer capacitance was constant with time, and in 0.72 ppm there was a very slow decrease in the double layer capacitance. The final double layer capacitance decreased from 17 μF cm^{-2} for 0.0 ppm to 8 μF cm^{-2} for 76.60 ppm of expander. It has been suggested (4, 5, 10) that the expander forms thick multilayers on the surface of the electrode with increasing concentration, and our observations are consistent with multilayer adsorption of the expander onto the amalgam surface.

(b) Potential step dependence

The geometric models for 2D and 3D nucleation and growth of anodic films that have been developed (11, 12) treat the growth kinetics in terms of two growth rates and the nucleation rate. The growth rates involved are the lateral growth rate, k_1, representing the crystal growth parallel to the plane surface of the electrode, and the vertical growth rate, k_2, describing the growth perpendicular to the electrode surface.

The potential dependence of the kinetics of nucleation and growth of the $PbSO_4$ film on the amalgam electrode in the presence of the expander has been investigated by potential steps. The equation describing the current response due to the nucleation and growth of a 3D deposit is (12)

$$[1] \quad i = nFk_2[1 - \exp(-\pi M^2k_1^2At^3/3\rho^2)] \times \exp\left[\frac{-\pi M^2k_1^2At^3}{3\rho^2}\right]$$

where i is the current, n is the number of electrons, F is Faraday's constant, k_2 is the vertical growth rate, M is the molecular weight, k_1 is the lateral growth rate, A is the nucleation rate, t is the time, and ρ is the density of the deposit. Experimental transients can be analyzed to give values for the parameters k_2 and k_1^2A from the current maximum in the transient, i_m, and the time to the current maximum, t_m. For 3D nucleation and growth the equations for i_m and t_m are, (12)

$$[2] \quad i_m = nFk_2/4$$

$$[3] \quad t_m = \left[\frac{3\rho^2 \ln 2}{\pi M^2k_1^2A}\right]^{1/3}$$

There have been some discussions concerning the validity of certain aspects of the 3D model (13) but this article will not deal with this question.

A sample transient where the potential was stepped from −1100 to −874 mV in 7.89 ppm solution is given in Fig. 2. The falling currents before the maximum are due to lead dissolution and plots of i versus $t^{-1/2}$ are linear. The shape of the transient is characteristic for that of 3D nucleation and growth electrocrystallisation processes since the charges passed are too large for 2D monolayer formation. As the concentration of the expander was increased, the transient broadened and the tail became longer as demonstrated in the reduced variable plot of Fig. 3. The trend observed for the various concentrations of expander in Fig. 3 was also observed in the formation of thick layers of $PbCl_2$ on a lead amalgam (9). The trend may result

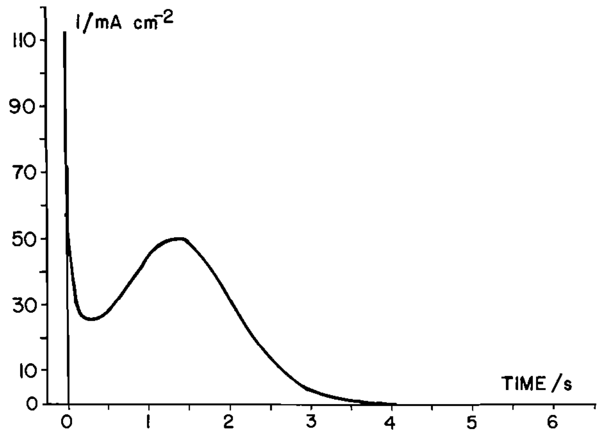

FIG. 2. A sample potential step transient where the potential was stepped from −1100 to −874 mV in 7.89 ppm of expander. Note the large initial lead dissolution current before the onset of electrocrystallisation.

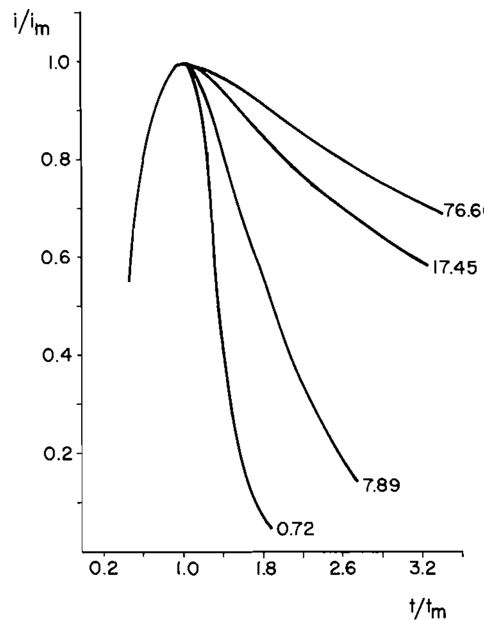

FIG. 3. Potentiostatic current−time transients plotted in nondimensional form. The numbers at the end of the curves are the expander concentrations in ppm. The curve for 0.0 ppm is not shown because it was essentially the same as that for 0.72 ppm. A single curve for the rising portion of the transients was drawn rather than the separate curves for each concentration since these portions of the transients were all very close to one another.

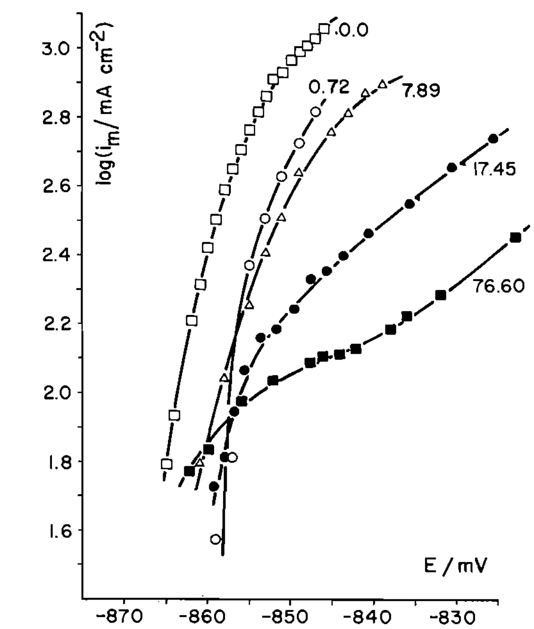

FIG. 4. A semilog plot of the maximum current, i_m, as a function of potential, E, for the potentiostatic transients. The numbers beside the curves represent the expander concentrations.

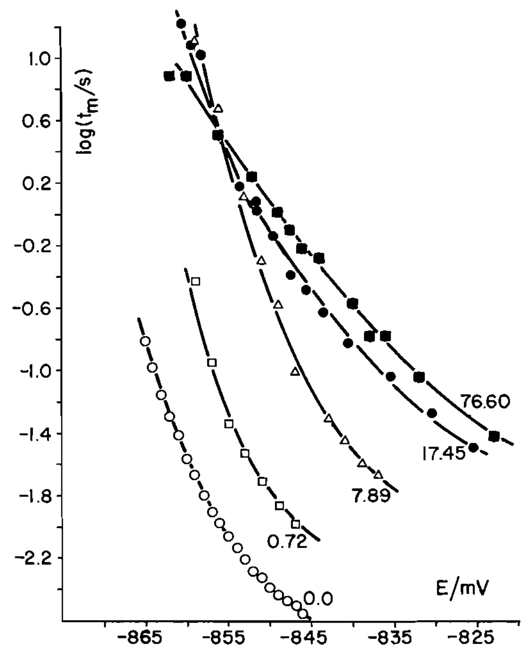

FIG. 5. A semilog plot of t_m as a function of potential, E, for the potentiostatic transients. The numbers beside the curves represent the expander concentrations.

from changes in the nucleation rate, or the lateral growth rate, or both. However, at times greater than t_m, the nucleation in terms of centres that could grow to an appreciable size is effectively over. Therefore, beyond t_m the growth of the already existing centres predominates. Since the shape of the rising portions of the curves before t_m are essentially the same for all concentrations of expander, the nucleation rate is probably unaltered by the expander. But, the tails of the transients are vastly different which suggests that the lateral growth rate must be affected by the expander.

The semilog plot of the maximum current, i_m, as a function of potential, E, is given in Fig. 4. From eq. [2] it can be seen that i_m is a function of the vertical growth rate. At low overpotentials there is not a large change in the i_m values with different concentrations of expander. However, the effect is more severe at higher overpotentials and concentrations of expander. This suggests that the expander does have some effect on the vertical growth rate and its dependence on potential at higher overpotentials and concentrations of expander.

Equation [3] shows that the time at which the maximum current occurs, t_m, is inversely proportional to the square of the lateral growth rate times the nucleation rate. Figure 5 illustrates that for a given potential, for example, −845 mV, the expander

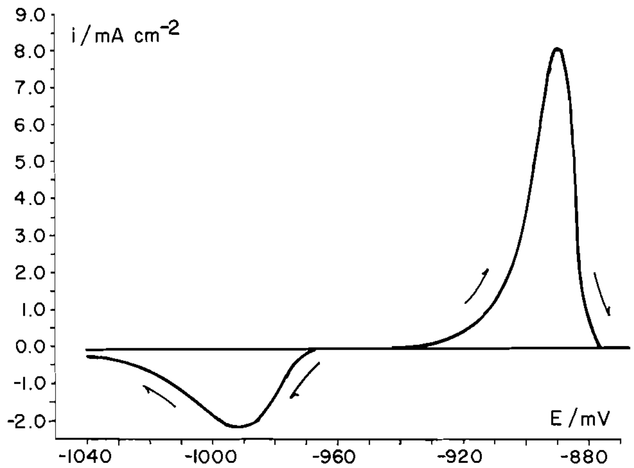

FIG. 6. A linear potential sweep at 20 mV s^{-1} in 1.30 molal H_2SO_4 with no expander added. The potential was swept anodically from −1100 to −850 mV, reversed and swept cathodically back to −1100 mV. Only the potential range from −1040 to −870 mV has been shown in the diagram.

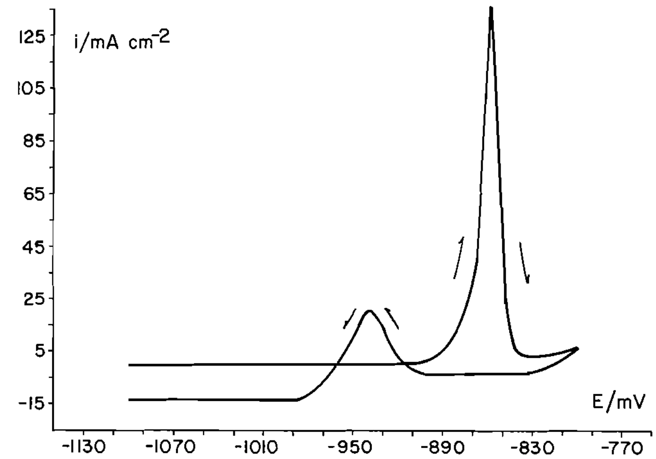

FIG. 7. A linear potential sweep at 20 mV s^{-1} in 7.89 ppm of expander. The potential was swept anodically from −1100 to −800 mV, reversed and swept cathodically to −1700 mV, again reversed and swept anodically to −1100 mV. Only the potential range from −800 to −1100 mV is shown. The current on the axes as indicated is the anodic current. The current on the reverse sweep has been expanded by a factor of 10. Note the small reduction current that is independent of potential, and the small anodic peak on the reverse sweep.

has a greater dependence on t_m than on i_m, thus affecting the lateral growth rate of the $PbSO_4$ film and/or the nucleation rate. A 1 decade change in i_m corresponds to a 1 decade change in k_2, whereas a 1 decade change in t_m corresponds to a 3 decade change in k_1^2A as indicated by eqs. [2] and [3]. Since the expander is adsorbed onto the amalgam surface it could inhibit the nucleation rate by allowing less free surface to be available for $PbSO_4$ seed nuclei. The lateral growth rate could be decreased if the expander is adsorbed onto kink sites where incorporation of $PbSO_4$ molecules occurs. It would not take a large amount of expander to block these kink sites. This is consistent with Sharpe's results (14) where it was reported that the adsorption of expander onto $PbSO_4$ was much less favourable than onto the metallic lead surface. It should be pointed out that Sharpe observed the effects on $PbSO_4$ powder and not on a growing film of $PbSO_4$ but the results are still applicable. It would be harder to prove that the expander affects the lateral growth rate than the nucleation rate since very little expander would be involved in the adsorption. It is important to point out that the relative changes of k_1 and k_2 may vary depending on the electrode substrate. The lateral growth rate k_1 should be different on the solid lead compared to the amalgam, but k_2 should be the same for both systems.

In both Figs. 4 and 5 the slopes for the curves for the lower concentrations of expander are very steep indicating electrocrystallisation. This high potential dependence of i_m and t_m at low overpotentials has been observed for both 2D and 3D systems (13).

On the basis of our results, it is not possible to conclude exactly which kinetic parameters are affected and to what degree. The general effect of the expander was to lower i_m and increase t_m which means the electrode is slower to passivate. However, the charges passed are higher, therefore, more Pb^{2+} ions must be diffusing away towards the solution side of the interphase.

(c) Linear potential sweep dependence

Figure 6 depicts a linear potential sweep at 20 mV s^{-1} in 1.30 molal sulphuric acid with no expander added. The potential was swept anodically from −1100 to −850 mV, reversed and swept cathodically back to −1100 mV. The sweep shows the presence of an anodic peak in the region of −940 to −820 mV resulting from the formation of a $PbSO_4$ film, and a cathodic peak resulting from the reduction of the film. The potential region of film formation is consistent with earlier results on solid electrodes (15−20). The equilibrium potential of the sulphated amalgam electrode in 1.30 molal sulphuric acid was calculated to be −970 mV vs. Hg_2SO_4. As seen from Fig. 6, the reduction of the $PbSO_4$ film begins at −970 mV, but a larger overpotential is necessary for the $PbSO_4$ film formation to begin.

This sweep can be compared to a similar sweep done at 20 mV s^{-1} in 7.89 ppm of expander as shown in Fig. 7. The current scale on the reverse sweep has been expanded by a factor of 10. The significant differences are the larger anodic peak current which has been shifted anodically, the presence of a small anodic peak on the reverse sweep, and the small reduction current that is independent of potential out to the region of hydrogen evolution. The absence of a reduction peak has been previously reported (3, 4, 7). It is possible that the presence of the adsorbed expander on the bare portions of the electrode inhibits the cathodic reduction of Pb^{2+} ions.

The following explanation is offered as a possible reason for the small anodic peak on the reverse sweep. A preliminary experiment investigating the double layer charging on a mercury drop in the presence of expander indicates some sort of desorption or re-orientation of the absorbed expander film in the same potential region as the small anodic peak. If desorption or re-orientation is occurring, then it is possible that bare portions of the electrode are being generated allowing for further oxidation of lead.

The linear potential sweeps in pure sulphuric acid often exhibited a sharp transition or "kink" separating the regions of lead dissolution and nucleation and growth. The lead dissolution region showed a rising curve which broke sharply at the onset of nucleation and growth. The kink was not evident on the transients from any of the solutions containing the expander.

If the potential is swept anodically from −1100 to −800 mV

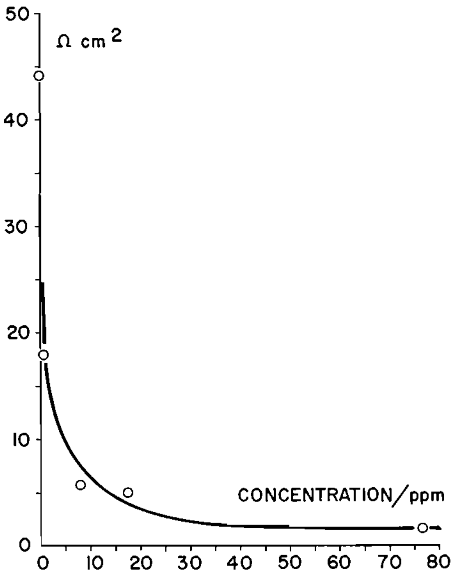

FIG. 8. The resistance of the $PbSO_4$ film measured at −800 mV as a function of expander concentration. The resistance has been multiplied by the area of the drop. The average drop area was 4.47×10^{-3} cm^2.

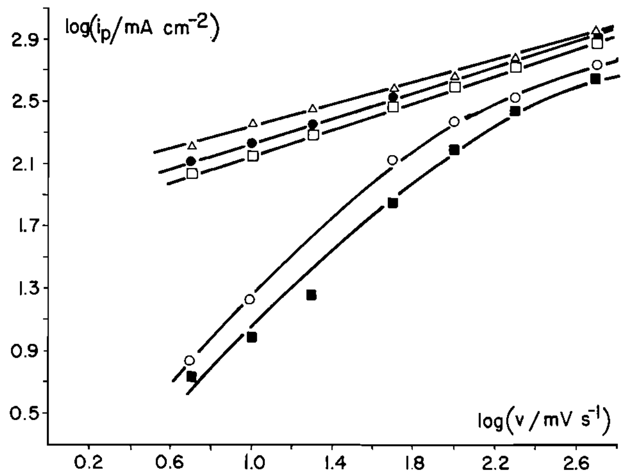

FIG. 9. A log−lot plot of the anodic peak current, i_p, as a function of sweep rate, v, for the various concentrations of expander. The symbols are ■ for 0.0 ppm, ○ for 0.72 ppm, □ for 76.60 ppm, ● for 17.45 ppm, and △ for 7.89 ppm.

to form a film of $PbSO_4$ and kept at −800 mV, the capacitance and resistance of the film can be measured. An increase in the concentration of the expander caused a small change from 0.82 to 1.99 $\mu F\ cm^{-2}$ in the capacitance of the film but a larger change in the resistance of the film occurs as shown in Fig. 8. The resistances as shown in the figure have been mutiplied by the area of the drop which is equivalent to the product of the intrinsic resistivity and the thickness of the layer. The decrease in the resistance of the film with an increase in the concentration of the expander may be due to the formation of a more porous film. An increase in the porosity of the film with the addition of expanders has been previously reported (1−3, 21, 22) and was attributed to the change in the lead sulphate crystal structure. The porosity of the film will increase if there are empty spaces or voids in the deposit. If the growth of the deposit is not complete enough for the electrode surface to be completely covered, then voids will form in the deposit. This

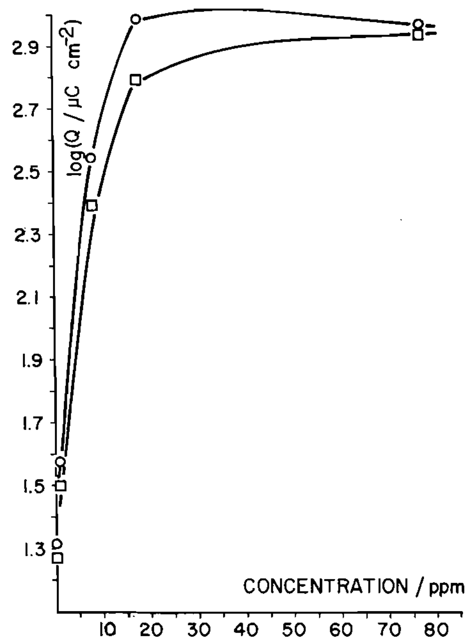

FIG. 10. A semilog plot of charge, Q, as a function of expander concentration for the sweep rates of 10 and 20 mV s^{-1}. The symbols are ○ for 10 mV s^{-1} and □ for 20 mV s^{-1}.

incomplete growth will result if the lateral growth rate is inhibited in some way.

The Tafel plots obtained from low current regions prior to onset of $PbSO_4$ nucleation and growth sweeps at 10 mV s^{-1} for 0.0 and 17.45 ppm of expander added gave linear relationships in which the slopes were 27.37 and 30.26 mV dec^{-1}, respectively. These slopes are very close to that expected (29.58 mV dec^{-1}) for a reversible 2 electron transfer reaction. In sulphuric acid solutions slopes of this magnitude have been previously reported (8, 16, 23).

The log−log dependence of the anodic peak current, i_p, as a function of sweep rate, v, is shown in Fig. 9. The slopes of the curves for 7.89, 17.45, and 76.60 ppm are less than one half. The reaction is diffusion-controlled for these concentrations as indicated by linear i_p versus the square root of the sweep rate plots. However, the plots had positive intercepts which was due to the contribution of spherical diffusion at low sweep rates. For 0.0 and 0.72 ppm the steep slopes in Fig. 9 indicates that the process is not controlled by diffusion but electrocrystallization.

An interesting feature to note is the fact that the curves for 17.45 and 76.60 ppm lie below that of 7.89 ppm. This suggests the existence of an optimum concentration of expander as reported by Mahato (5) who found 20 ppm as the optimum concentration and beyond that the expander exhibited an inhibitory effect. Pierson *et al.* (21) also mentioned that a small amount of an organic material will produce an expander effect and an excess adversely affects the functioning of the electrode.

A further effect of the expander was to increase the amount of charge required for passivation as the concentration of the expander increased as previously reported (3, 4, 6). Figure 10 depicts the increase in charge for sweep rates of 10 and 20 mV s^{-1} as a function of expander concentration. The charge required for passivation is larger but the rate of growth of the $PbSO_4$ film has decreased as expander concentration is increased. Therefore, there will be more Pb^{2+} ions diffusing into solution which increases the charge. Fewer Pb^{2+} ions will be

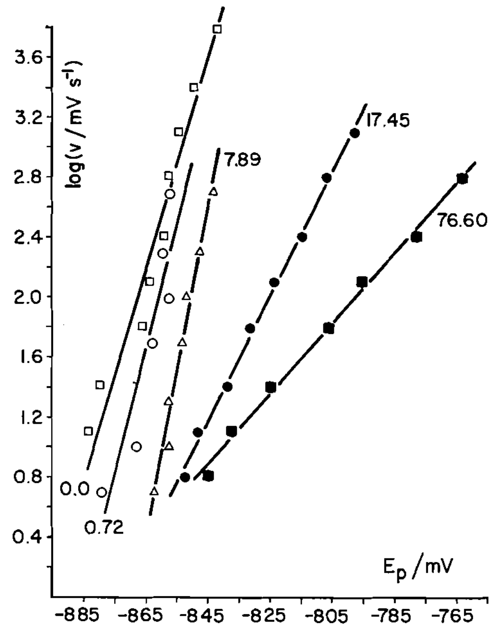

FIG. 11. A semilog plot of sweep rate, v, as a function of peak potential, E_p. The numbers beside each line represents the expander concentration in ppm. The steepness of the slopes of the curves at low concentrations of expander are characteristic of an electrocrystallisation process.

incorporated into the $PbSO_4$ film, thereby reducing the charge efficiency into the film. The expander may also help to stabilize the Pb^{2+} ions by forming complexes with the ions in solution. The inhibitory effect of the expander is evident as shown by the decrease in the curves toward 76.60 ppm. Mahato (5) observed a decrease of 37% in the charge passed when the concentration of expander was increased from 20 to 40 ppm. He attributed the charge inhibition to the multilayer surface adsorption of the expander and/or the expander's orientation on the electrode surface.

Figure 11 shows a semilog plot of the peak potential, E_p as a function of sweep rate, v. An increase in the expander concentration produces an anodic shift in the peak potential as demonstrated previously by Archdale and Harrison (6). The slopes for 0.0 and 7.89 ppm are very steep which is characteristic of rate control by electrocrystallisation. The slope of 42.37 mV dec^{-1} for 76.60 ppm is greater than 30 mV dec^{-1} that would have been expected for a 2 electron diffusion controlled process. This larger slope represents further evidence of the inhibitory effect of the expander, Archdale and Harrison have also observed a slope in the order of 30–40 mV dec^{-1} (6).

The semilog plot of anodic peak current, i_p, as a function of the peak potential, E_p, shown in Fig. 12 demonstrates similar features as that described for Fig. 11, namely the anodic shift in the potentials and the steep slopes at low concentrations of expander indicating electrocrystallisation. The inhibitory effect of the expander is evidenced by the decreasing slopes for higher concentrations of expander.

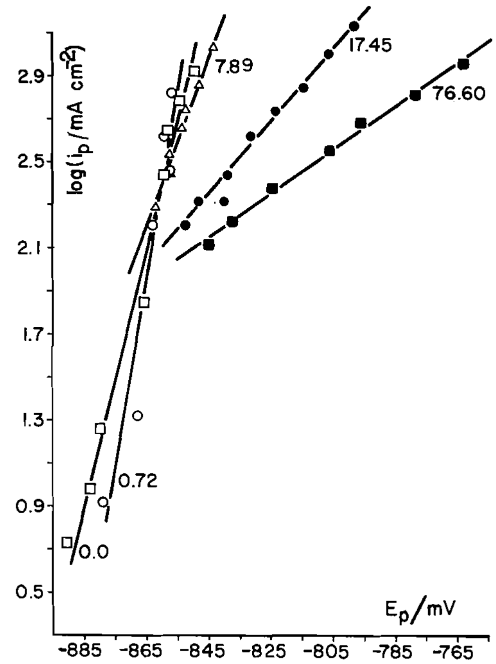

FIG. 12. A semi-log plot of the anodic peak current, i_p, as a function of peak potential, E_p. The numbers beside each line represent the expander concentrations in ppm. The steepness of the slopes at the low expander concentrations are characteristic of electrocrystallisation.

Summary

The following results were obtained in the presence of an expander at 24°C.

(*1*) The expander strongly adsorbed onto the clean amalgam surface.

(*2*) The anodic currents were increased in the presence of the expander.

(*3*) The amount of charge required for passivation was increased.

(*4*) The cathodic reduction of the $PbSO_4$ layer was inhibited.

(*5*) The resistance of the film decreased with increasing concentrations of expander, suggesting the formation of a more porous film.

(*6*) The results are consistent with the existence of an optimum concentration of expander which lies between 17.45 and 76.6 ppm.

Acknowledgements

This work has been supported by a grant from the Natural Sciences and Engineering Research Council (NSERC) of Canada. One of us (T.J.V.) is grateful to Carleton University and NSERC for the award of scholarships.

1. A. C. SIMON, S. M. CAULDER, P. J. GURLUSKY, and J. R. PIERSON. J. Electrochem. Soc. **121**, 463 (1974).
2. I. A. AGUF, W. A. DASOYAN, L. A. IVANENKO, E. V. PARSHIKOVA, and K. M. SOLOV'EVA. Sov. Electrochem. **6**, 1591 (1970).
3. B. K. MAHATO. J. Electrochem. Soc. **127**, 1679 (1980).
4. M. P. J. BRENNAN, and N. A. HAMPSON. J. Electroanal. Chem. **48**, 465 (1973).
5. B. K. MAHATO. J. Electrochem. Soc. **128**, 1416 (1981).
6. G. ARCHDALE, and J. A. HARRISON. J. Electroanal. Chem. **47**, 93 (1973).
7. T. F. SHARPE. J. Electrochem. Soc. **116**, 1639 (1969).
8. G. ARCHDALE, and J. A. HARRISON. J. Electroanal. Chem. **43**, 321 (1973).
9. R. G. BARRADAS, S. FLETCHER, and J. D. PORTER. J. Power Sources **2**, 137 (1977/78).
10. E. G. YAMPOL'SKAYA and B. N. KABANOV. J. Appl. Chem. USSR, **37**, 2501 (1964).
11. M. FLEISCHMANN, and H. R. THIRSK. *In* Advances in electrochemistry and electrochemical engineering. Vol. 3. *Edited by*

P. Delahay, Interscience, New York. 1963.
12. R. D. ARMSTRONG, M. FLEISCHMANN, H. R. THIRSK. J. Electroanal. Chem. **11**, 208 (1966).
13. R. G. BARRADAS, and J. D. PORTER. Electrochim. Acta, **27**, 541 (1982).
14. T. F. SHARPE. Electrochim. Acta, **14**, 635 (1969).
15. G. ARCHDALE, and J. A. HARRISON. J. Electroanal. Chem. **39**, 357 (1972).
16. L. M. BAUGH, K. L. BLADEN, and E. L. TYE. J. Electroanal. Chem. **145**, 355 (1983).
17. A. N. FLEMING, and J. A. HARRISON. Electrochim. Acta, **21**, 905 (1976).
18. N. A. HAMPSON and J. B. LAKEMAN. Surf. Technol. **9**, 97 (1979).
19. N. A. HAMPSON, J. B. LAKEMAN. J. Electroanal. Chem. **107**, 177 (1980).
20. D. PAVLOV. Electrochim. Acta, **23**, 845 (1978).
21. J. R. PIERSON, P. J. GURLUSKY, A. C. SIMON, and S. M. CAULDER. J. Electrochem. Soc. **117**, 1463 (1970).
22. A. C. SIMON, S. M. CAULDER, P. J. GURLUSKY, and J. R. PIERSON. Electrochim. Acta, **19**, 739 (1974).
23. G. ARCHDALE, and J. A. HARRISON. J. Electroanal. Chem. **34**, 21 (1972).

Iodine chemistry in the +1 oxidation state. I. The electronic spectra of OI^-, HOI, and H_2OI^+ [1,2]

JEAN PAQUETTE AND BEVERLY L. FORD

Research Chemistry Branch, Atomic Energy of Canada Limited, Whiteshell Nuclear Research Establishment, Pinawa, Man., Canada R0E 1L0

Received December 4, 1984

JEAN PAQUETTE AND BEVERLY L. FORD. Can. J. Chem. **63**, 2444 (1985).

Electronic spectra are reported for the hypoiodite ion (OI^-), hypoiodous acid (HOI), and its conjugate acid (H_2OI^+) in aqueous media. Iodine in the +1 oxidation state was produced by either of the two rapid reactions

$$HOCl + I^- \rightarrow HOI + Cl^-$$

or

$$ICl(g) + H_2O \rightarrow HOI + Cl^- + H^+$$

Spectroscopic evidence of the disproportionation of $OI^-/HOI/H_2OI^+$ to iodide and iodate in basic media, and to iodine and iodate in acid media, was obtained. The results are consistent with previously reported values for the pK_a of HOI and H_2OI^+.

JEAN PAQUETTE et BEVERLY L. FORD. Can. J. Chem. **63**, 2444 (1985).

Les spectres électroniques de l'ion hypoiodite (OI^-), de l'acide hypoiodeux (HOI), et de son acide conjugué (H_2OI^+) sont décrits. L'iode dans l'état d'oxidation +1 a été obtenu en utilisant les deux réactions rapides

$$HOCl + I^- \rightarrow HOI + Cl^-$$

et

$$ICl(g) + H_2O \rightarrow HOI + Cl^- + H^+$$

La dismutation de $OI^-/HOI/H_2OI^+$ en iodure et iodate en milieu basique, et en iode et iodate en milieu acide a pu être mise en évidence. Les résultats sont en accord avec les valeurs obtenues précédemment pour le pK_a de HOI et de H_2OI^+.

Introduction

Although the iodine/water system has been studied extensively in the past (1), the aqueous chemistry of iodine in the +1 oxidation state is still not clearly understood. This is largely due to the relative instability of this oxidation state in aqueous media. The use of water-cooled nuclear reactors to produce electricity has rekindled interest in this subject, since radioactive iodine is one of the more toxic nuclear fission products. In order to design effective measures to prevent the release of volatile iodine species into the environment, a knowledge of the nature and concentration of the various iodine species in solution is essential.

In this context, the hydrolysis and disproportionation equilibrium [1] is important, since it involves the conversion of a reactive and volatile species into non-reactive, involatile species:

[1] $$3I_2 + 3H_2O \rightleftharpoons 5I^- + IO_3^- + 6H^+$$

By analogy with the other members of the halogen family, reaction [1] is thought to be, in fact, a two-step process involving the +1 oxidation state species HOI as an intermediate:

[2] $$I_2 + H_2O \rightleftharpoons HOI + I^- + H^+$$

followed by

[3] $$3HOI \rightarrow 2I^- + IO_3^- + 3H^+$$

The first step is known to be rapid (2), while the second is believed to be slower. Hypoiodous acid has not been positively identified in solution, although there is much circumstantial evidence for its existence. A positive identification of HOI is central to a full understanding of the kinetics and mechanism of reaction [1]. In this publication, we report the results of a spectrophotometric study of iodine in the +1 oxidation state in basic and acidic aqueous solutions.

The electronic spectrum of hypoiodite, OI^-, in strongly basic solutions has been described by Haimovich and Treinin (3) and by Chia (4). Although both authors agree on the general shape of the spectrum, there is disagreement on the relative intensities. Haimovich (3) obtained the OI^- spectrum by dissolving $I_2(s)$ in 4 mol dm^{-3} NaOH and Chia (4) by diluting an I_3^- solution with NaOH, or by reacting hypochlorite with an excess of iodide and extrapolating the resulting spectra to zero time. In both studies, a substantial amount of I^- would have been present, which could have distorted the spectrum below 290 nm and increased the probability of producing other iodine compounds, in particular I_3^-.

To avoid these problems and to generate iodine in the +1 oxidation state in aqueous media, we have used the following two reactions:

[4] $$HOCl + I^- \rightarrow HOI + Cl^-$$

[5] $$ICl(g) + H_2O \rightleftharpoons HOI + Cl^- + H^+$$

Reaction [4] has a rate constant of 3.3×10^8 dm^3 mol^{-1} s^{-1} at 25°C and is, thus, very rapid for pH values below 12 (5). Equilibrium [5] is rapidly established and is completely to the right at pH values greater than 2 (6).

Experimental

Materials

The sodium iodide was of ACS grade and was used without further

[1]Part of this work was funded jointly by AECL and Ontario Hydro under the CANDEV agreement.

[2]Issued as AECL-8593.

purification. The hypochlorite was obtained either as a stock solution from the Fisher Scientific Company or generated by slowly bubbling chlorine gas, from Canadian Liquid Air, into a cold 1 mol dm^{-3} NaOH solution. The iodine was resublimed ACS grade and was used as such. The iodine monochloride was obtained from the J. T. Baker Chemical Company and was used as received. Other stock solutions were prepared from ACS-grade chemicals and distilled deionized water.

The hypochlorite stock solutions were analyzed by titration with NaI in 0.01 mol dm^{-3} H_2SO_4 using an Orion iodide-specific electrode (Model 94-53) as an end-point indicator. An Orion double-junction electrode (Model 90-02) was used for reference. The OCl^- absorption band at 290 nm (ϵ = 350)[3] was also used to analyze for hypochlorite.

Apparatus and procedures

All spectra were recorded in digital form, using a double-beam diode array spectrophotometer (Hewlett-Packard Model 8450A), and stored on flexible discs. The pH measurements were made with an Orion Model 701A ionalyzer using a Microelectrodes Inc. micro-combination pH electrode.

Spectra involving I_2 in NaOH solutions were obtained by injecting an iodine solution, using a glass syringe, into an equal volume of sodium hydroxide solution contained in a spectrophotometric cell. A sodium hydroxide/sodium iodide solution was used on the reference side of the spectrophotometer to balance out the absorption due to I^-.

For reactions involving $HOCl/OCl^-$ and I^-, equal volumes of equimolar solutions in the appropriate buffer (phosphate or borate) were similarly mixed, using glass syringes, in the spectrophotometric cell, and the resulting spectra were recorded as a function of time. Sodium chloride solutions, in the appropriate buffer, were used on the reference side of the spectrophotometer. Some spectra were obtained at short reaction times by using a flow system. The two reagents were driven by a double-syringe pump into a Plexiglass mixing chamber, and then into a small-volume flow cell. A stopped-flow mixing device was also used for some experiments. The spectra were recorded with the solutions flowing and could be obtained at various reaction times by changing the flow rate.

Initial experiments with ICl were attempted by quickly adding a buffer solution to ICl crystals in a spectrophotometric cell. The results were erratic, due to the slow rate of dissolution of ICl(s), and to the production of high local concentrations, leading to the formation of undesired iodine compounds. An alternative technique was then adopted whereby the cell atmosphere was first saturated with ICl vapour. The buffer solution was then introduced and the cell shaken for a few seconds to ensure good mixing between the gaseous and aqueous phases. The total iodine concentrations in these experiments were determined at the end of the reaction by adding 1 cm^3 of an acid hydrazine solution to the cell and measuring the concentration of the resulting I^- by its absorbance at 225 nm.

An ion-exchange technique was used to remove chloride ions from low pH solutions, in order to displace equilibrium [5] to the right. The anion exchange resin (Analytical Grade Dowex 1X8, 100–200 mesh, from Bio-Rad Laboratories) was converted from the chloride to the sulfate form, by elution with a large volume of a 0.5 mol dm^{-3} Na_2SO_4 solution that had been adjusted to a pH value of 2 with H_2SO_4. The elution was continued until no precipitate could be detected in the eluate after the addition of a few drops of an $AgNO_3$ solution. Immediately after contact with ICl(g), the buffer solutions were quickly passed through 2 cm^3 of the sulfate resin contained in a plastic syringe. We verified that this procedure was capable of removing most of the chloride ions by using 10^{-3} mol dm^{-3} NaCl solutions in pH 2 sulfate buffer as test solutions, and an Ag/AgCl electrode coupled to a saturated calomel electrode as a chloride detector. We also checked that this procedure did not produce any unwanted absorbance in the 200 to 800 nm spectral region.

Results

Figure 1 shows the electronic spectrum obtained by reacting

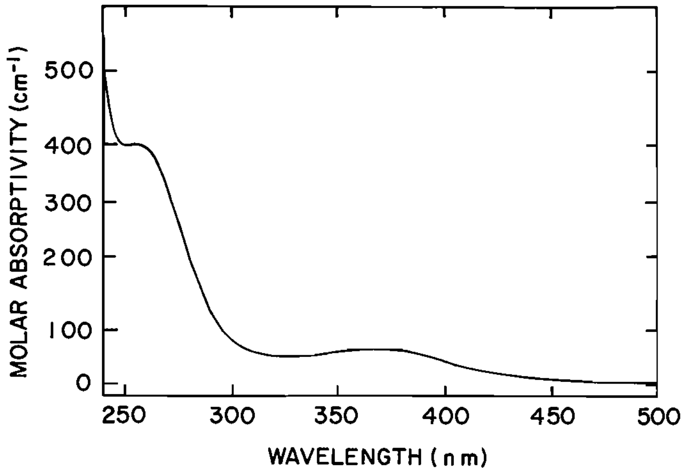

FIG. 1. The electronic spectrum for OI^- in basic solution.

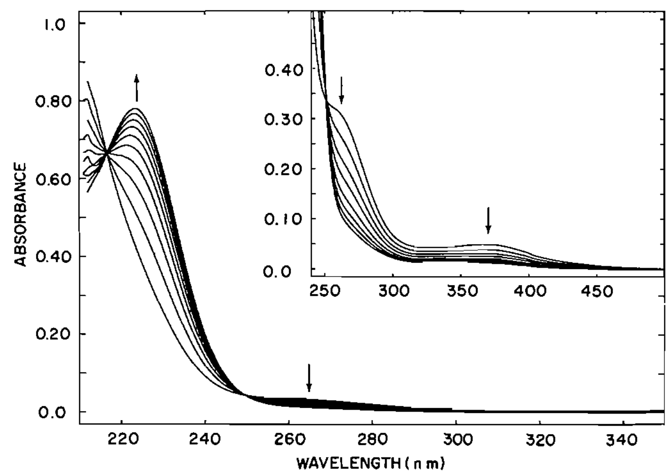

FIG. 2. Spectra as a function of time obtained after reacting ICl(g) with a borax buffer solution at a pH of 12. Arrows indicate the direction the peaks moved with time. The time between each spectrum is 200 s and the total iodine concentration is 1×10^{-4} mol dm^{-3}. The insert was obtained with a cell having a 10-cm path length.

ICl(g) with a 2 mol dm^{-3} NaOH solution (reaction [5]). An identical spectrum was obtained by diluting an I_2 solution with NaOH (reaction [2]) and using an equimolar concentration of I^- in 2 mol dm^{-3} NaOH on the reference side of the spectrophotometer, to balance out the absorption due to I^-. The spectrum is similar to those reported previously for OI^- (3, 4), but is better defined at low wavelengths. The main features of our spectrum are a weak band at 370 nm (ϵ = 60), a shoulder at 260 nm (ϵ = 400), and a sharp increase in absorbance below 260 nm. Here, ϵ is calculated in the usual manner, assuming that all of the light absorption is due to iodine in the +1 oxidation state. The spectrum changes very slowly with time at the low total concentration of iodine (5×10^{-4} mol dm^{-3}) used. Essentially identical spectra were obtained by reacting ICl(g) with 1 mol dm^{-3} and 0.1 mol dm^{-3} NaOH solutions.

Reactions [4] and [5] were used at a pH value of 12 (borax buffer) and gave identical spectra. A typical series of spectra as a function of time, obtained using reaction [5], is shown in Fig. 2. The band growing with time at 225 nm is characteristic of I^-. The spectrum obtained shortly after mixing is similar to the one obtained in 2 mol dm^{-3} NaOH and is thus attributed to OI^-. The presence of the 225 nm band and of two isobestic

[3]Throughout this paper, ϵ is the molar absorptivity, in units of mol^{-1} dm^3 cm^{-1}.

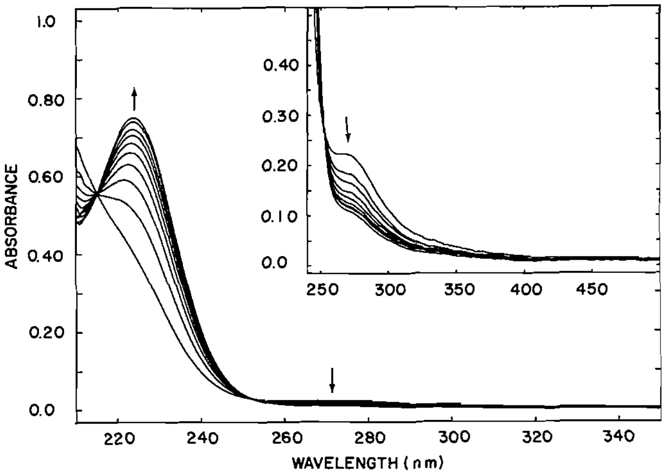

FIG. 3. Spectra as a function of time obtained after mixing equimolar solutions of I^- and OCl^- in phosphate buffer at a pH of 9. The time between each spectrum is 20 s and the total iodine concentration is 1×10^{-4} mol dm^{-3}. The insert was obtained with a cell having a 10-cm path length.

points at 215 ± 1 nm and 248 ± 1 nm is consistent with the reaction

[6] $3OI^- \rightarrow 2I^- + IO_3^-$

Figure 3 shows a series of spectra obtained as a function of time after mixing equimolar concentrations of OCl^- and I^-, at a pH value of 9, using a phosphate buffer. Identical results were obtained from reaction [5]. At this pH value, HOI would be expected to predominate over OI^- since the pK_a value for HOI is approximately 11 (4). The growing I^- band at 225 nm and the presence of two isobestic points are consistent with the occurrence of the disproportionation reaction [3].

The spectrum obtained shortly after mixing is subtly different from the spectra obtained at a pH of 12 and in NaOH solutions. The weak band previously observed at 370 nm is absent. The shoulder observed previously at 260 nm has shifted to 270 nm and the absorbance is lower at all wavelengths. Also, the two isobestic points are shifted and are now located at 210 ± 1 nm and 255 ± 1 nm.

At pH values between 8 and 7, substantial equilibrium amounts of I_2 (via reaction [2]) and I_3^- would be present, masking the spectral features of the +1 oxidation state. Therefore, this pH range was not investigated. Under more acidic conditions, the hydrolysis equilibrium [2] is very much in favour of I_2, and the following reaction sequence is expected to hold:

[4–5] $HOCl + I^-$ (or $ICl + H_2O$) $\rightarrow HOI + Cl^-$ $(+H^+)$ (fast)

[3] $3HOI \rightarrow 2I^- + IO_3^- + 3H^+$ (slow)

[2] $HOI + I^- + H^+ \rightarrow I_2 + H_2O$ (fast)

with the overall reaction being

[7] $5HOI \rightarrow 2I_2 + IO_3^- + 2H_2O + H^+$

Figure 4(a) shows spectra obtained as a function of time, at a pH of 4 (phosphate buffer). These spectra were obtained using reaction [5]; reaction [4] gave identical spectra. Two isobestic points can be observed at 260 ± 1 nm and 375 ± 1 nm. The absorbance at 285 nm decreases with time, whereas that at 460 nm increases with time. The latter band is characteristic of I_2. These observations are in agreement with the overall reaction [7]. It can be noted that some elemental iodine

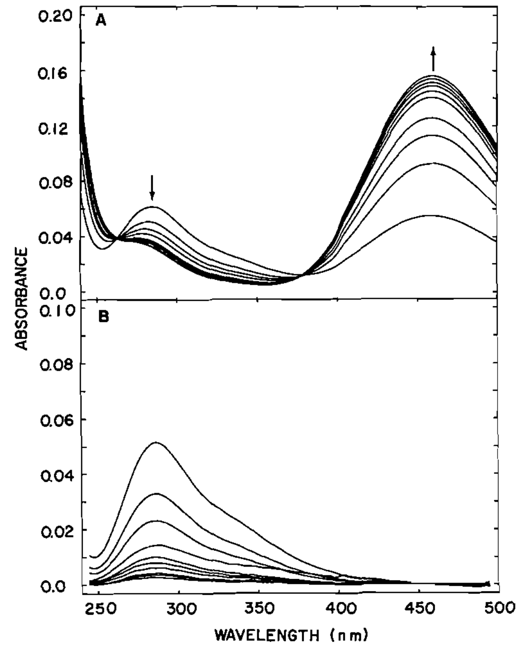

FIG. 4. (a) Spectra as a function of time obtained after reacting ICl(g) with a phosphate buffer solution at a pH of 4. The time between each spectrum is 20 s and the total iodine concentration is 5×10^{-4} mol dm^{-3}; (b) Fig. 4(a) spectra minus the ($I_2 + \frac{1}{2}IO_3^-$) spectrum scaled according to the I_2 absorbance at 460 nm.

is already present at short reaction times. In the case of reaction [5], it takes about 5 s to mix the vapour and aqueous phases. Since the subsequent disproportionation reaction is relatively rapid, some I_2 will already be present at the first measurement. For reaction [4], the reaction of HOCl with I^-, and that of HOI with I^-, have comparable rate constants (2, 5). As soon as some HOI is formed from HOCl and I^-, some reaction with the remaining I^- will occur, producing I_2. To resolve this problem, the ($I_2 + \frac{1}{2}IO_3^-$) spectrum, scaled according to the I_2 absorbance at 460 nm, was subtracted from the Fig. 4(a) spectra. The required ($I_2 + \frac{1}{2}IO_3^-$) spectrum was obtained simply by recording the spectrum at long reaction time where only I_2 and IO_3^- are present in a two-to-one ratio. The result of this subtraction process is shown in Fig. 4(b). Similar spectra were obtained at pH values of 5 and 6. These spectra are characterized by a band at 285 nm (ϵ = 200) and a weaker band at 345 nm (ϵ = 60).

Reaction [4] cannot be used at pH values below 3 due to the equilibrium formation of chlorine. To avoid this problem, only reaction [5] was used at pH values of 3 or less. Iodine monochloride is not completely hydrolyzed at low pH values and small amounts of ICl_2^- and I_2Cl^- can be formed (7). To minimize this problem, the solutions were rapidly passed through an anion exchange resin in the sulfate form to remove most of the chloride ions and displace equilibrium [5] to the right, as described in more detail in the Experimental section. Spectra obtained in this manner at pH values of 3 and 2 (sulfate buffer) were identical to the ones obtained at pH values of 4, 5, and 6.

Figure 5(a) shows a series of spectra that were obtained, as a function of time, after contacting ICl(g) with a 0.05 mol dm^{-3} H_2SO_4 solution, and passing the solutions through an anion exchange resin in the sulfate form. An isobestic point can be observed at 398 ± 1 nm. The characteristic I_2 band at 460 nm increases in intensity with time, whereas the absorbance at 310 nm decreases with time. Figure 5(b) represents the same

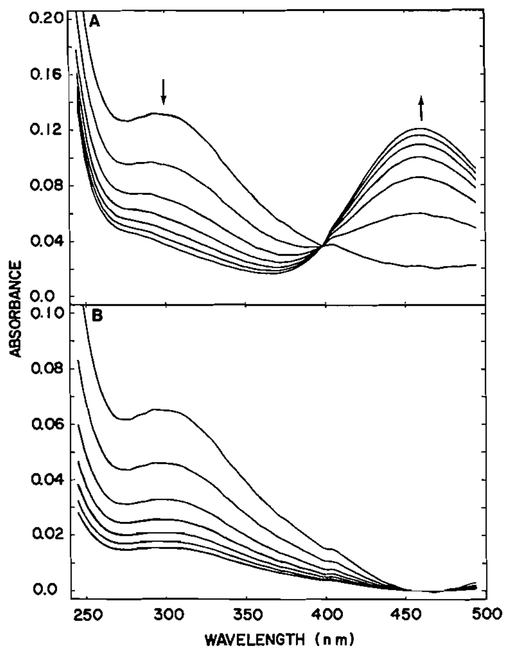

FIG. 5. (a) Spectra as a function of time obtained after reacting ICl(g) with 0.05 mol dm^{-3} H_2SO_4, and flowing the resulting solution through an anion exchange resin. The time between each spectrum is 100 s and the total iodine concentration is 5×10^{-4} mol dm^{-3}; (b) Fig. 5(a) spectra minus the ($I_2 + \frac{1}{2}IO_3^-$) spectrum scaled according to the I_2 absorbance at 460 nm.

spectra after subtraction of the ($I_2 + \frac{1}{2}IO_3^-$) spectrum, scaled according to the I_2 absorbance at 460 nm. The spectra are different from the spectra obtained at higher pH values (Fig. 4(b)), and are characterized by a single band at 310 nm (ϵ = 200). It is worth noting that spectra obtained at this acid concentration, without using the anion exchange resin, showed a conspicuous band at 335 nm, which is likely due to undissociated ICl(aq) (ref. 6, p. 574).

Discussion

We attribute the spectra obtained in NaOH solutions and at a pH of 12 to the hypoiodite ion, OI^-. Chia (4) reports a value of $(5.6 \pm 0.6) \times 10^{-3}$, based on spectrophotometric measurements, for the equilibrium quotient of the reaction

[8] $IO^- + 2I^- + H_2O \rightleftharpoons I_3^- + 2OH^-$

This value is not expected to be affected very much by the ionic strength, since the reaction is isocoulombic, and can be considered equal to the equilibrium constant. The above value, combined with the value given by Burger and Liebhafsky (8) for the equilibrium constants for reaction [2] and for the tri-iodide ion formation, leads to 10.6 ± 0.8 for the pK_a of HOI. If this value is correct, and if HOI has a spectrum markedly different from OI^-, then spectral changes would be expected to take place as the pH is lowered below 11.

This is indeed what we observed. Although there is no noticeable change in the iodine (I) spectra in solutions containing OH^- in the concentration range from 0.01 to 2 mol dm^{-3}, spectral modifications are noticeable at a pH of 9, and become very obvious at a pH of 6. From a comparison of Figs. 1, 3, and 4, the spectrum obtained at a pH of 9 is a combination of that obtained at lower pH values and that obtained in very basic solutions. We attribute the spectrum obtained at pH values between 2 to 6 to hypoiodous acid, HOI. A matrix multicomponent analysis routine was used, together with the spectra obtained in 2 mol dm^{-3} NaOH and at a pH of 4, to deconvolute the spectrum obtained at a pH of 9 into its OI^- and HOI components. An $[OI^-]/[HOI]$ ratio of 0.1 ± 0.01 was obtained. This amounts to a pK_a value of 10.0 ± 0.3 for HOI, in reasonable agreement with the value of 10.6 ± 0.8 derived from Chia's data, considering that ionic strength effects would tend to lower the pK_a. Our spectroscopic assignment is also supported by the observation of a sharp increase in the rate of decay of the spectra, as the pH is lowered below 11.

Bell and Gelles (9) determined an equilibrium constant of $(1.2 \pm 0.3) \times 10^{-11}$ at 25°C, from emf measurements, for the reaction

[9] $I_2 + H_2O \rightleftharpoons H_2OI^+ + I^-$

This value, combined with that given by Burger and Liebhafsky (8) for the equilibrium constant of reaction [2], leads to a pK_a value of 1.4 ± 0.3 for H_2OI^+. Thus, if the spectrum for H_2OI^+ is substantially different from the spectrum for HOI, spectral changes would be expected to occur as the pH is lowered below 2. This agrees well with our observations. As can be seen by comparing Figs. 4 and 5, the spectrum obtained in 0.05 mol dm^{-3} H_2SO_4 is markedly different from that obtained in the pH region from 2 to 6. We attribute the spectrum obtained in 0.05 mol dm^{-3} H_2SO_4 to protonated hypoiodous acid, H_2OI^+. This puts the pK_a for H_2OI^+ between 1 and 2, in agreement with the value of 1.4 ± 0.3 given above. This assignment is also supported by the observation of a sharp decrease in the rate of decay of the spectra as the pH is lowered below 2. It is also worth mentioning that none of the other iodine species that could be present in these solutions has an absorbance at 310 nm; ICl_2^- has a band at 345 nm (ϵ = 243) (7), I_2Cl^- has a band at 437 nm (ϵ = 1 100) (7), and ICl(aq) absorbs at 335 nm (ϵ = 250) (ref. 6, p. 574). Thus, the 310 nm band must be due to H_2OI^+.

Hypochlorite, hypobromite, and hypoiodite have low-intensity bands at 290 nm (10), 330 nm (11), and 370 nm (this work), with molar absorptivities of 350, 305, and 60, respectively. Hypochlorous, hypobromous, and hypoiodous acids have low intensity spectra that are very similar in shape. Hypochlorous acid has bands at 235 nm (ϵ = 100) and 290 nm (ϵ = 27) (10), hypobromous acid has bands at 260 nm (ϵ = 160) and 315 nm (ϵ = 35) (11), and from this work, hypoiodous acid has bands at 285 nm (ϵ = 200) and 345 nm (ϵ = 60). Thus, both the hypohalites and the hypohalous acids form remarkably regular series.

The hypohalites and the hypohalous acids have valence shells that are isoelectronic with those of the halogen molecules and of the ClF molecule. As is the case for the halogens and for ClF, the lowest energy band for the hypohalites and the hypohalous acids is likely due to the transition $^3\pi \leftarrow {}^1\Sigma^+$. For the hypohalites, the $^1\Sigma^+$ ground state correlates with $O^-(^2P)$ and $X(^2P)$, and the $^3\pi$ excited state correlates with $O(^3P)$ and $X^-(^1S)$. If the above is correct, then the potential energy curves should cross, since the electron affinity of the oxygen is smaller than that of the halogens. The dissociation products would then have high kinetic energies and, as a result, the hypohalites would be expected to decompose when irradiated in their low-intensity bands. For the hypohalous acids, the singlet ground state correlates with $OH(^2\pi)$ and $X(^2P)$. The triplet excited state may decompose to yield $OH(^2\pi)$ and $X(^2S)$. Thus, the hypohalous acids would also be expected to be photosensitive when irradiated in their low-intensity bands.

Conclusion

The use of both reaction [4] and reaction [5] has been found useful for elucidating the behaviour of iodine in the +1 oxidation state in aqueous media. The electronic spectra for OI^-, HOI, and H_2OI^+ were obtained. The results are consistent with previously reported values for the pK_a of HOI and H_2OI^+. Spectroscopic evidence of the disproportionation of iodine(I) to iodide and iodate in basic media, and to iodine and iodate in acid media, was also obtained. These reactions, coupled to uv–visible spectrophotometry, offer an ideal way of examining the kinetics of disproportionation of iodine(I). A full kinetic study will be described in a forthcoming publication.

Acknowledgements

The authors thank Dr. W. J. Fletcher of Chalk River Nuclear Laboratories for suggesting the use of reaction [5], as well as Dr. L. M. Toth of the Oak Ridge National Laboratory and Dr. D. J. Wren of the Whiteshell Nuclear Research Establishment for numerous discussions. We also thank Ontario Hydro for financial support through the CANDEV agreement.

1. A. J. DOWNS and C. J. ADAMS. The chemistry of chlorine, bromine, iodine and astatine. Pergamon Press, New York. 1973.
2. M. EIGEN and K. KUSTIN. J. Am. Chem. Soc. **84**, 1355 (1962).
3. O. HAIMOVICH and A. TREININ. Nature, **207**, 185 (1965).
4. Y.-T. CHIA. Thesis, UCRL, No. 8311 (1958).
5. M. W. LISTER and P. ROSENBLUM. Can. J. Chem. **41**, 3013 (1963).
6. P. PASCAL. Nouveau Traité de Chimie Minérale. Vol. XVI. Masson et Cie, Paris. 1960.
7. D. L. CASON and H. M. NEUMANN. J. Am. Chem. Soc. **83**, 1822 (1961).
8. J. D. BURGER and H. A. LIEBHAFSKY. Anal. Chem. **45**, 600 (1973).
9. R. P. BELL and E. GELLES. J. Chem. Soc. 2734 (1951).
10. J. C. MORRIS. J. Phys. Chem. **70**, 3798 (1966).
11. M. SOULARD, F. BLOC, and A. HATTERER. J. Chem. Soc. Dalton, 2300 (1981).

Époxydes α-éthyléniques et phénate de sodium: accès à des éthers phénoliques et phénols *ortho*-allyliques

MICHÈLE DAVID, JEAN SAULEAU ET ARMELLE SAULEAU

Laboratoire de chimie pharmaceutique, U.E.R. médico-pharmaceutiques, avenue du Professeur Léon Bernard, 35043 Rennes Cédex, France

Reçu le 4 juillet 1984[1]

MICHÈLE DAVID, JEAN SAULEAU et ARMELLE SAULEAU. Can. J. Chem. **63**, 2449 (1985).

L'ouverture d'époxydes α-éthyléniques par le phénate de sodium conduit à un mélange de composés. Les attaques nucléophiles qui entrent en compétition (composés A au niveau du carbone le moins substitué du cycle ou composés B et C au niveau du carbone β-éthylénique) peuvent être résolues par un choix judicieux des conditions opératoires (solvant, stéréochimie des époxydes). La régiosélectivité de l'attaque nucléophile est sous la dépendance d'états de transition impliquant une faible gêne stérique et une conjugaison oxiranne – double liaison.

MICHÈLE DAVID, JEAN SAULEAU, and ARMELLE SAULEAU. Can. J. Chem. **63**, 2449 (1985).

The ring cleavage reactions of α-ethylenic epoxides by sodium phenoxide afforded a mixture of products. Problems of competitive attack by this nucleophile, at the less substituted carbon (compounds A) or at the β-ethylenic carbon atom (compounds B and C), were encountered and could be resolved by judicious choice of reaction conditions (solvents, stereochemistry of the oxiranes). The regioselectivity of the attack was dependent on the transition states, implying weak steric hindrance and a conjugation oxirane – double bond.

Introduction

L'action de phénols en milieu alcalin sur des époxydes à restes saturés ou aromatiques a déjà été étudiée (1–4). Dans ce travail, nous envisageons le cas d'époxydes α-éthyléniques qui ne semble pas avoir fait l'objet d'une étude systématique, puisque les seuls exemples mentionnés dans la littérature sont ceux d'Al-bitskaya *et al.* (5) rapportés schéma 1.

Nous montrons ici que le bilan réactionnel est plus complexe; la nature, la géométrie R^*R^*,R^*S^* des époxydes insaturés, la qualité du solvant utilisé, influent en effet sur la régiosélectivité de l'attaque nucléophile par l'anion phénoxy.

Résultats

Trois composés notés A, B et C sont le plus fréquemment obtenus lors de la réaction phénol–sodium, époxydes α-insaturés (schéma 2).

Ce schéma fait ainsi apparaître une nette différence entre nos résultats et ceux d'Al'bitskaya. Si comme cet auteur, nous observons une ouverture C(1)—O époxydique (obtention de A), aucune attaque nucléophile sur le carbone-2 n'est mise en évidence. Par contre, les composés B et C formés résultent d'une attaque nucléophile sur le carbone sp_2, en β de la chaîne insaturée (cf. Discussion).

Les résultats des condensations réalisées dans le *dioxanne* (tableau 1) font apparaître les influences du degré de substitution du cycle époxydique et de sa stéréochimie.

Si les produits A sont préférentiellement formés avec les époxydes primaires–tertiaires **1***a* et **1***b*, on constate que pour **3**, la substitution du carbone-1 époxydique, sa géométrie R^*R^*, favorisent l'obtention de B et C accompagnés d'une certaine proportion de composés d'hétérocyclisation.[2] L'importance de la nature du solvant de condensation apparaît dans le tableau 1 à propos de l'époxyde **1***a* le plus facilement accessible. La compétition alcoylation O/C peut être orientée selon le solvant et l'on compare alors les taux relatifs de A, B et C.

Dans les *solvants polaires*, la régiosélectivité élevée—formation majoritaire des produits A + B d'alcoylation O—s'explique par l'accroissement de la nucléophilie de l'anion phénoxy. Avec les *solvants protiques*, les résultats corroborent ce qui est connu sur les anions ambivalents phénoxy (6, 7). La solvatation de l'oxygène époxydique et de l'anion, par interactions ion–dipole et par liaisons hydrogènes, favorise cette fois la nucléophilie du site *ortho*-carboné benzénique. Les phénols C (alcoylation C) deviennent majoritaires et ceci d'autant plus que le solvant est acide, assertion que l'on peut vérifier avec l'éthanol et le trifluoroéthanol, solvants de pK_a très différents (8).

Discussion

Pour que l'on observe une attaque nucléophile sur le carbone sp_2, en β du cycle oxiranne, l'époxyde doit pouvoir se présenter dans une conformation où le système éthylénique et le cycle oxiranne sont conjugés: coplanarité des liaisons C(1)—C(2)—C_α—C_β pour un recouvrement maximum des orbitales. Tout effet stérique empêchant ou diminuant cette conjugaison modulera alors l'attaque précitée et favorisera le site carbone-1 époxydique (formation de A).

Cas des époxydes secondaires–tertiaires 3a($R''' = H$), 3b($R''' = CH_3$) R*R* *et* R*S*

Nous envisageons deux des rotamères possibles **3′** et **3″** pour chacune des configurations R^*R^* et R^*S^* (schéma 3).

Pour les isomères R^*S^* le méthyle en C(1) et le reste éthylénique sont en position *cis*: Quand $R''' = H$, le rotamère **3′** est à exclure compte tenu de la forte gêne stérique qui implique la perte totale de la conjugaison. Seul le rotamère **3″**, moins contraint, reste à envisager; la coplanarité pouvant être atteinte, on conçoit alors la formation majoritaire de B et C de géométrie uniquement *E*. Lorsque $R''' = CH_3$, la gêne stérique dans chacun des rotamères **3′** et **3″** est telle que la conjugaison cycle – double liaison n'a pas lieu. L'attaque β est alors exclue: seul C(1) peut être attaqué (formation unique de A).

Dans les configurations R^*R^*, les conformations **3′** et **3″**, favorables à la conjugaison précitée, rendent majoritaire l'attaque du site β: obtention d'un mélange *Z*/*E* où *E* est préférentiel.

Avec le rotamère **3′** (rapprochement oxygène époxydique –

[1] Révision reçue le 4 janvier 1985.

[2] Il s'agit de dihydro-2,3 benzo[*b*] furannes.

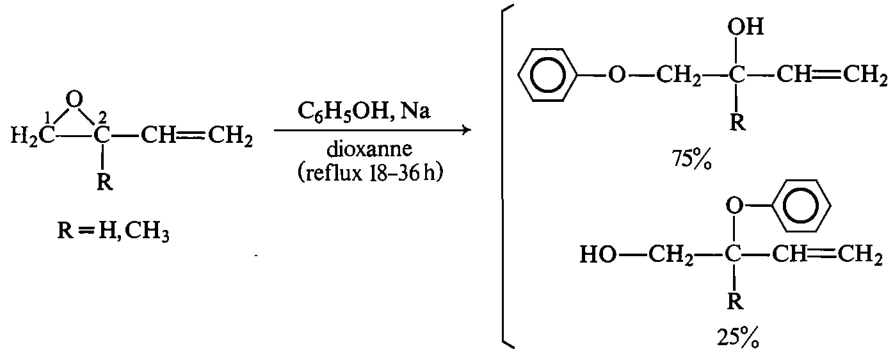

SCHÉMA 1

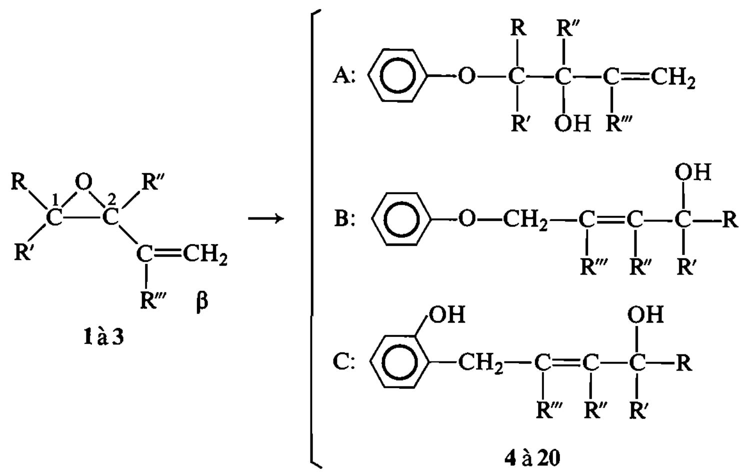

SCHÉMA 2

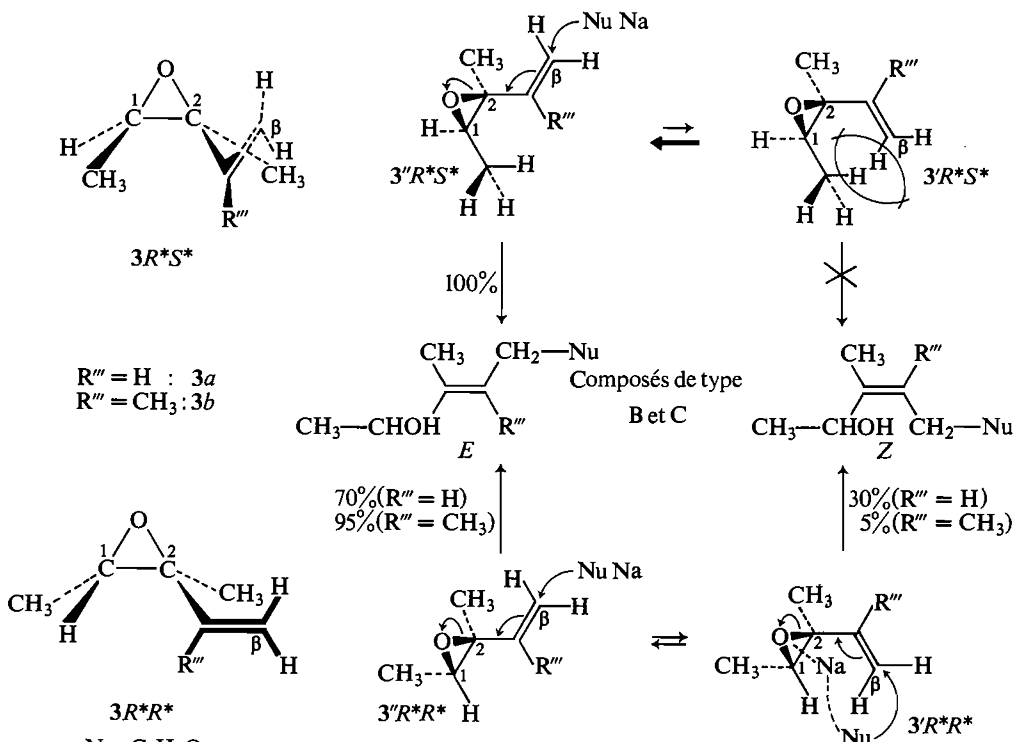

SCHÉMA 3

TABLEAU 1. Réaction phénol–sodium, époxydes

Epoxydes 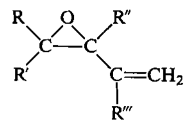	Solvant	Produits (% relatifs) Géométrie Z/E (%) A	B	C	Rdt% global
	Dioxanne	**4** (88)	**11** (2)	**16** (10)	55
			Z/E 30:70		
1*a* R = R′ = R‴ = H; R″ = CH_3	DMSO	**4** (100)			61
	C_6H_5OH	**4** (49)	**11** (6)	**16** (45)	43
	C_2H_5OH	**4** (76)	**11**	**16** (24)	62
	CF_3CH_2OH	**4** (20)	**11** (4)	**16** (76)	53
1*b* R = R′ = H; R″ = R‴ = CH_3	Dioxanne	**5** (100)			55
2 R = R′ = R‴ = H; R″ = C_6H_5	Dioxanne	**6** (38)[a]	**12** (46)	**17** (12)	30[a]
			Z/E 25:75		
3*a* R = R″ = CH_3; *R*R** R′ = R‴ = H	Dioxanne	**7** (18)	**13** (42)	**18** (20)[b]	74
			Z/E 30:70		
3*a* R = R‴ = H; *R*S** R′ = R″ = CH_3	Dioxanne	**8** (33)	**14** (22)	**19** (11)[c]	63
			Z/E 0:100		
3*b* R = R″ = R‴ = CH_3; *R*R** R′ = H	Dioxanne	**9** (25)	**15** (30)	**20** (17)[d]	51
			Z/E 5:95		
3*b* R = H; *R*S** R′ = R″ = R‴ = CH_3	Dioxanne	**10** (100)			74

[a] Présence de OCH—C(C_6H_5) = CH—CH_3 (4%): Eb 80°C/0,1 Torr (1 Torr = 133,3 Pa); rmn ^{1}H: 1,80 (d, 3H, J = 7 Hz), 6,80 (q, 1H), 9,50 (s, CHO), 6,80–7,30 (m, 5H).
[b] Produits d'hétérocyclisation: 20%.
[c] Produits d'hétérocyclisation: 34%.
[d] Produits d'hétérocyclisation: 25%.

double liaison), on peut invoquer une complexation contre ion–oxygène plus facilement atteinte lorsque R‴ = H (30% de Z). Avec R‴ = CH_3, plus volumineux, 5% de Z sont obtenus. Signalons que ce type de système cyclique a été invoqué lors de la réaction époxydes β-éthyléniques – hydrures ou thiolates (9, 10). Le conformère **3″** reste cependant privilégié: le système plus étendu, permettant une meilleure délocalisation des charges lors de l'attaque nucléophile, explique le taux majoritaire en isomère *E*.

Cas des époxydes primaires–tertiaires 1 et 2 (tableau 1)

Avec les oxirannes **1**, l'absence d'encombrement du carbone-1 (contrairement à **3**) fait de ce carbone un site d'attaque préférentiel (obtention de A) par rapport au carbone β, bien que la conjugaison soit ici possible. Le taux (12%) de produits B et C obtenus pour **1***a* se justifie par une coplanarité cycle – double liaison plus facilement atteinte que dans **1***b* (aucune attaque β) où, comme nous l'avons montré par calculs théoriques et rmn ^{17}O (11), une légère gêne stérique intervient. Il ne s'agit pas d'un effet de température, puisque des essais réalisés à 150°C, pendant 3 jours, ne modifient pas les pourcentages obtenus avec **1***a*.

Le cas de leurs homologues phénylés **2** est particulier: formation préférentielle de B et C (tableau 1). Si l'on considère le modèle oxyde de styrène (4, 12, 13) où l'électrophilie du carbone-2 oxiranique favorise son attaque nucléophile, on interprète les résultats. Puisque l'ouverture C(2)—O ne peut ici se concevoir (forte gêne reste phénylé – groupe éthylénique), la délocalisation de la charge positive de ce carbone vers la double liaison explique l'attaque nucléophile en β.

Conclusion

La réaction étudiée permet l'accès à des éthers phénoliques et (ou), des phénols *ortho*-allyliques en proportions variables selon les choix du substrat, de son éventuelle géométrie et du solvant. Cette réaction est d'ailleurs généralisable puisque l'utilisation de divers phénols substitués conduit, dans le dioxanne, aux composés A, B et C, sans changement notable dans leurs pourcentages.

Partie expérimentale

Les spectres infra-rouge (solvant CCl_4) sont enregistrés sur un appareil Perkin–Elmer 377. Les spectres ($CDCl_3$) rmn ^{1}H sont réalisés sur un appareil Varian EM 360 L (60 MHz). Pour la rmn ^{13}C, on utilise un appareil Brücker 20,1 MHz à transformée de Fourier. Les valeurs des déplacements chimiques sont à ±0,05 ppm et les constantes de couplage à ±1 Hz.

Un contrôle de pureté est réalisé sur chacun des produits par chromatographie en phase vapeur (Fractovap GT Carlo Erba, colonne SE30) et (ou) par chromatographie sur gel de silice HF254 (type 60 Merck). Pour la spectrométrie de masse, un appareil Varian MAT 311 avec procédé M.I.K.E. est utilisé.

Les époxydes α-éthyléniques sont préparés selon une méthode mise au point au laboratoire (14). Les oxirannes **3***a* et **3***b*, *R*R** et *R*S** sont séparés par distillation du mélange des stéréoisomères, au moyen d'une colonne à bande tournante Perkin–Elmer (200 plateaux théoriques).

Identification spectrale de A, B et C

L'infra-rouge met en évidence les produits de type A par leur reste vinyle terminal (905 et 970 cm^{-1}).

En rmn ^{1}H, les valeurs différentes observées dans les déplacements

TABLEAU 2. Caractéristiques physiques et spectrales des composés de type A:

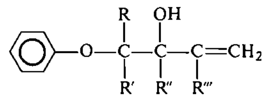

N°	Eb (°C/Torr) F (°C)	Résonance magnétique nucléaire de ^{1}H (δ ppm) R	R′	R″	R‴	—C=CH$_2$	C$_6$H$_5$	ms, m/e (intensité relative %)
4	74/0,4		3,75(s)	1,26(s)		5,00–5,28(m) 5,80–6,00(m)	6,70–7,20(m)	$C_{11}H_{14}O_2$ 178 (M$^+$, 19), 108 (70), 94 (89), 71 (100)
5	81/0,3		3,86(AB) J = 9,2 Hz	1,36(s)	1,80(m)	4,90–5,10(m)	6,80–7,50(m)	$C_{12}H_{16}O_2$ 192 (M$^+$, 13), 108 (92), 99 (18), 94 (67), 85 (100), 77 (20), 43 (44)
6	148–151/0,4		4(s)	6,50–7,40(m)		4,80–6,20(m)	6,50–7,40(m)	$C_{16}H_{16}O_2$ 240 (M$^+$, 4), 222 (9), 209 (20), 207 (44), 146 (27), 133 (100), 115 (71), 94 (26), 77 (55)
7	75/0,3	1,20(d)	4,20(q) J = 6,6 Hz	1,40(s)		5,00–5,50(m) 5,70–6,30(m)	6,80–7,30(m)	$C_{12}H_{16}O_2$ 192 (M$^+$, 4), 121 (100), 99 (40), 94 (70), 77 (39), 71 (15), 43 (38)
8	75/0,3	4,40(d)	1,23(d) J = 6,5 Hz	1,36(s)		5,00–5,80(m) 5,70–6,30(m)	6,80–7,30(m)	
9	70/0,1	1,20(d)	4,36(q) J = 6,2 Hz	1,43(s)	1,83(m)	4,90–5,20(m)	6,75–7,46(m)	$C_{13}H_{18}O_2$ 206 (M$^+$, 5), 121 (100), 113 (54), 94 (75), 85 (35), 84 (25), 77 (43), 43 (76)
10	70/0,1	4,46(q)	1,26(d) J = 6,4 Hz	1,36(s)	1,80(m)	4,96–5,20(m)	6,75–7,50(m)	

TABLEAU 2 (suite). Caractéristiques physiques et spectrales des composés de types B et C:

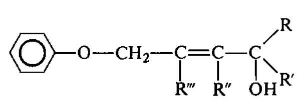

B

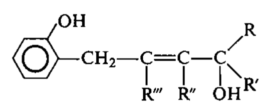

C

N°	Eb (°C/Torr) F (°C)	Résonance magnétique nucléaire de ^{1}H (δ ppm/TMS) R	R′	R″	R‴	CH$_2$	ms, m/e (intensité relative %)
E		3,90(s)		1,80(s)	5,50(t)	4,45(d) J = 6,6 Hz	$C_{11}H_{14}O_2$
11	130–135/0,2						178 (M$^+$, 3), 150 (5), 147 (10), 84 (40), 94 (100)
Z		4,03(s)		1,80(s)	5,45(t)	4,45(d) J = 6,6 Hz	
E	72(CCl$_4$)	4,50(s)		6,8 à 7,4(m)	6,00(t)	4,90(d) J = 6,4 Hz	$C_{16}H_{16}O_2$ 240 (M$^+$, 1,5), 222 (9), 209 (10), 146 (38), 117 (100), 94 (90), 91 (41)
12							
Z	148/0,3	4,60(s)		6,8 à 7,4(m)	5,90(t)	4,70(d) J = 6,4 Hz	
E	103–104/0,3	1,20(d) J = 6,4 Hz	4,20(q)	1,70(m)	5,70(t)	4,50(d) J = 6,8 Hz	$C_{12}H_{16}O_2$ 192 (M$^+$, 3), 174 (1,5), 147 (14), 145 (78) 119 (8), 98 (3), 94 (100), 43 (39)
13 **14**							
Z	104/0,3	1,20(d) J = 6,4 Hz	4,70(q)	1,75(m)	5,50(t)	4,50(t) J = 6,8 Hz	
E		1,20(d) J = 6,6 Hz	4,70(q)	1,75(m)	1,75(m)	4,40(s)	$C_{13}H_{18}O_2$ 188 (M$^+$ − H$_2$O, 10), 173 (10), 95 (44), 94 (100), 77(14), 43 (61)
15	106–110/0,1						
Z		1,25(d) J = 6,6 Hz	4,75(q)	1,75(m)	1,75(m)	4,50(s)	

TABLEAU 2 (suite). Caractéristiques physiques et spectrales des composés de types B et C

N°		Eb (°C/Torr) *F* (°C)	Résonance magnétique nucléaire de ^1H (δ ppm/TMS) R	R′	R″	R‴	CH_2	ms, *m*/*e* (intensité relative %)
16	*E*	76(CCl_4)	3,95(s)		1,70(s)	5,50(t)	3,30(d) *J* = 7,2 Hz	$C_{11}H_{14}O_2$ 178 (M^+, 3), 160 (86), 147 (35), 145 (100), 131 (15), 115 (15), 107 (46), 91 (29)
	Z	143/0,2	4,20(s)		1,75(s)	5,25(t)	3,30(d) *J* = 7,2 Hz	
17	*E*	128(CCl_4)	4,25(s)		6,5 à 7,4(m)	5,90(t)	3,30(d) *J* = 6,8 Hz	$C_{16}H_{16}O_2$ 240 (M^+, 1), 222 (100), 209 (30), 207 (48), 145 (28), 107 (37), 91 (57)
	Z	165/0,3	4,25(s)		6,5 à 7,4(m)	6,00(t)	3,30(d) *J* = 6,8 Hz	
18	*E*		1,20(d) *J* = 6,8 Hz	4,15(q)	1,60(s)	5,50(t)	3,30(d) *J* = 7,4 Hz	$C_{12}H_{16}O_2$ 192 (M^+, 3), 174 (62), 159 (68), 145 (37), 107 (26), 94 (100), 91 (10)
19	*Z*	150–153/0,2	1,20(d) *J* = 6,8 Hz	4,60(q)	1,75(s)	5,30(t)	3,30(d) *J* = 7,4 Hz	
20	*E*		1,20(d) *J* = 6,4 Hz	4,70(q)	1,70(m)	1,70(m)	3,30(s)	[a]
	Z	149–151/0,1 [a]	1,25(d) *J* = 6,4 Hz	4,75(q)	1,75(m)	1,75(m)	3,35(s)	

[a] Souillé de produit d'hétérocyclisation (cf. partie expérimentale).

TABLEAU 3. Résonance magnétique nucléaire de ^{13}C (δ ppm/TMS)

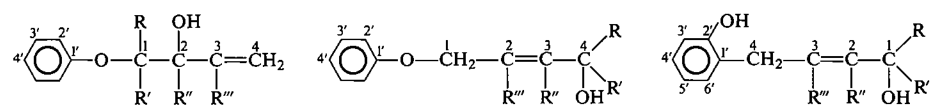

A B C

Carbones	N° 4	12 Z^a	13 E^b	13 E^c	15 *E*	15 *Z*	16 E^d	17 E^e
1	75	60,5	64,5	63,6	67	66,6	68,7	67,9
2	72,5	126,4	119,8	121,2	121,2	120,9	136	138,1*
3	145	143,4*	143,6	143,4	138,3	137,5	124	128,8
4	113,9	64,6	72,6	66,1	68,2	69,4	28,8	29,6
1′	158,9	158,6	158,9	158,5	159,1	159,1	124,3	126,1
2′	114,9	115	114,8	114,8	115,1	114,9	154,1	153,9
3′	129,6	129,6	129,5	129,6	129,6	126,3	115,7	115,6
4′	121,2	121,3	120,9	120,8	121,1	125,3	127,5	127,7
CH_3(2)	24,5				17,9	15,6	13,8	
CH_3(3)			12,7	21,4	12,3	11,2		
CH_3(4)			21,6	17,7	21,4	20,8		
5′							120,8	121
6′							130,1	130

[a] C1″: 140,1*; C2″: 126,7; C3″: 128,7; C4″: 127,9, $^3J(CH_2OH(4)-H(2))$ = 8,8 Hz.
[b] $^3J(CH_3(3)-H(2))$ = 8,8 Hz.
[c] $^3J(CH_3(3)-H(2))$ = 6,8 Hz.
[d] $^3J(CH_3(2)-H(3))$ = 7,8 Hz.
[e] C1″: 141,9*; C2″, C3″, C4″: 126,1*, 128,8*, 126,5*; $^3J(CH_2OH(1)-H(3))$ = 6,8 Hz.
* Quaternaires pouvant être inversés.

chimiques des restes méthylènes suffisent à différencier les trois types de produits (tableau 2). L'intégration de ces signaux, entre autre, permet de déterminer les pourcentages de chacun de ces composés dans les mélanges bruts réactionnels, ainsi que les proportions alcoylations O/C.

La rmn ^{13}C réalisée sur quelques échantillons confirme les données de rmn ^1H et permet l'attribution certaine de la géométrie *E*/*Z* de la double liaison dans B et C (tableau 3); par exemple, l'effet γ *gauche* subit par le carbone hydroxylé (pour B et C), uniquement dans les géométries *Z*, explique le blindage réciproque des carbones-1 et -4, et est en accord avec des données de la littérature (15–17) à propos d'alcools allyliques.

Enfin, la synthèse de l'éther phénolique **21**, réalisée par transposition allylique de **4** selon Babler (18), prouve sans ambiguïté la structure de la chaîne éthylénique de B et C. **21**: ϕ—O—CH_2—$C(CH_3)$ = CH—CH_2OH; rmn ^1H: 1, 70 (m, 3H), 4,00 (d, 2H, *J* =

7 Hz), 4,33 (s, 2H), 5,66 (t, 1H), 6,70–7,20 (m, 5H).

Condensation époxydes–phénol–sodium

Du phénol (0,05 mol) dissous dans 15 mL de solvant et 0,013 mol de sodium sont chauffés au reflux du solvant jusqu'à disparition du sodium. Après refroidissement puis introduction de 0,05 mol d'époxydes **1***a* ou **1***b* ou **2**, on chauffe à 120°C (bain thermostaté) jusqu'à disparition quasi complète de l'époxyde. L'avancement de la réaction est suivi en chromatographie à phase gazeuse.

Avec les époxydes **3**, le mélange réactionnel précédent est chauffé à 150°C pendant 3 jours dans un autoclave Mécabar (Prolabo, 250 mL) équipé d'un dispositif d'agitation et muni d'un régulateur de température.

Quelle que soit la technique, après retour à température ambiante, le milieu réactionnel versé sur 20 mL d'alcali de Claisen (35 g KOH en pastilles, 25 mL d'eau, quantité suffisante pour 100 mL CH_3OH absolu) atteint un pH ~13. Après extractions à l'éther éthylique, les phases éthérées alcalines sont successivement lavées par une solution de NH_4OH 2 *N* puis de NaOH 2 *N*. Après séchage et évaporation sous vide, les spectres rmn montrent qu'il s'agit des éthers de type A et B (très peu souillés de C).

La séparation de ces produits est réalisée par distillation sous pression réduite et (ou) par chromatographie sur plaque. Pour les éthers dérivés des époxydes **1** et **2**, on utilise le système benzène – acétate d'éthyle (70:30); pour ceux dérivés de l'époxyde **3**, on utilise $CHCl_3$.

La phase aqueuse alcaline est acidifiée à froid (HCl concentré) jusqu'à pH ~1. Après extraction éthérée, séchage, on isole les composés C toujours souillés de phénol résiduel; celui-ci éliminé par passage de la solution éthérée à pH ~5 (NaOH, 1 *N*). Les produits C sont distillés et isolés à l'état pur, exception faite pour **20** très facilement hétérocyclisable dont seul le spectre rmn ^1H a pu être réalisé.

La séparation des isomères géométriques *E*/*Z* des composés B et C (mis à part pour **15** et **20**) est effectuée par chromatographie sur gel de silice, avec le système de solvant benzène – acétate d'éthyle (70:30).

1. (*a*) D. R. Boyd et E. R. Marle. J. Chem. Soc. **105**, 2117 (1914); (*b*) D. R. Boyd et D. F. Thomas. J. Chem. Soc. **115**, 1239 (1919).
2. A. R. Sexton et E. C. Britton. J. Am. Chem. Soc. **70**, 3606 (1948).
3. G. P. MacSweeney, L. F. Wiggins et D. J. C. Wood. J. Chem. Soc. 37 (1952).
4. (*a*) C. O. Guss. J. Am. Chem. Soc. **71**, 3460 (1949); (*b*) J. Org. Chem. **16**, 1809 (1951); (*c*) J. Org. Chem. **17**, 678 (1952).
5. V. M. Al'bitskaya, A. A. Petrov et E. M. Blyakhman. Zh. Obshch. Khim. **31**, 2166 (1961); Chem. Abstr. **56**, 2363e (1962).
6. B. Tchoubar. Bull. Soc. Chim. 2069 (1964).
7. N. Kornblum, P. J. Berrigan et W. J. Lenoble. J. Am. Chem. Soc. **85**, 1141 (1963).
8. M. L. Sinnott et W. P. Jencks. J. Am. Chem. Soc. **102**, 2026 (1980).
9. R. S. Lenox et J. A. Katzenellenbogen. J. Am. Chem. Soc. **95**, 958 (1973).
10. A. Yasuda, M. Takahashi et H. Takaya. Tetrahedron Lett. **22**, 2413 (1981).
11. (*a*) J. P. Monti, R. Faure, A. Sauleau et J. Sauleau. Org. Magn. Reson. **21**, 403 (1983); (*b*) J. Etrillard, J. Sauleau, J. Huet et R. Lissilour. J. Chim. Phys. **77**, 875 (1980).
12. R. E. Parker et N. S. Isaacs. Chem. Rev. **59**, 737 (1959).
13. R. Guyon et P. Villa. Bull. Soc. Chim. 2584 (1975).
14. (*a*) J. Huet, H. Bouget et J. Sauleau. C.R. Acad. Sci. Sér. C, **271**, 430 (1970); (*b*) J. Sauleau, H. Bouget et J. Huet. C.R. Acad. Sci. Sér. C, **279**, 887 (1974); (*c*) J. Sauleau. Thèse de Doctorat ès-Sciences Physiques, Rennes, n° 250. 1976.
15. M. Schlosser et D. Coffinet. Synthesis, **7**, 380 (1971).
16. D. J. Faulkner. Synthesis, **7**, 175 (1971).
17. U. Vogeli et W. Vonphilips Born. Org. Magn. Reson. **7**, 617 (1975).
18. J. H. Babler. J. Org. Chem. **41**, 1262 (1976).

Open-chain nitrogen compounds. Part VIII.[1] 1-(2′-Acetylphenyl)-3-alkyltriazenes with reactive substituents in the alkyl group: synthons for five- and six-membered nitrogen heterocycles

KEITH VAUGHAN,[2] RONALD J. LAFRANCE, AND YORK TANG
Department of Chemistry, Saint Mary's University, Halifax, N.S., Canada B3H 3C3

AND

DONALD L. HOOPER
Department of Chemistry, Dalhousie University, Halifax, N.S., Canada B3H 4J3

Received October 11, 1984

KEITH VAUGHAN, RONALD J. LAFRANCE, YORK TANG, and DONALD L. HOOPER. Can. J. Chem. **63**, 2455 (1985).

The synthesis of a series of 1-(2′-acetylphenyl)-3-alkyltriazenes, with electron-withdrawing α-substituents in the alkyl moiety, is described. The structure of the products from the reaction of 2-acetylbenzenediazonium ion (**1**) with methylamine has been reinvestigated using high field (360 MHz) nmr spectroscopy. The 2-acetylphenyltriazenes undergo cyclization to five- or six-membered heterocycles, depending on the substituent present in the alkyl group. Attack by N-3 of the triazene on the *ortho*-acetyl group leads to a 4-methylenetriazine, which can undergo oxidation to a benzotriazinone or acid-catalysed rearrangement to a 4-alkylaminocinnoline. The reaction of **1** with alkylamines also affords red products, which have been identified as 4-arylazomethylenetriazines and fully characterized by ^{1}H and ^{13}C nmr spectroscopy. The formation of these azo compounds is consistent with the enamine character of the 4-methylenetriazines. The introduction of a CO_2Et group at the α-position of the alkyl moiety provides a competing cyclization pathway to give a five-membered heterocycle, a 5-hydroxytriazole. In this case the cyclization pathway to the six-membered heterocycle is favoured, whereas the introduction of a CN group can lead to exclusive triazole formation. The reaction of the nitrile (**2*c***) with alumina in chloroform leads to a new heterocycle, a quinazolinotriazole; in DMSO solution, **2*c*** prefers the alternative pathway and gives only the 3-cyanomethyl-4-methylenetriazine. Introduction of a benzoyl group in the alkyl moiety gives an unstable triazene; it reacts with alumina in chloroform to give a triazole, which in turn rearranges to a novel diazoalkane.

KEITH VAUGHAN, RONALD J. LAFRANCE, YORK TANG et DONALD L. HOOPER. Can. J. Chem. **63**, 2455 (1985).

On décrit la synthèse d'une série de (acétyl-2′ phényl)-1 alkyl-3 triazènes portant, en position α de la chaîne alkylée, des substituants électro-affinitaires. Faisant appel à la rmn à haut champ (360 MHz), on a réétudié la structure des produits obtenus par la réaction de l'ion acétyl-2 benzènediazonium (**1**) avec la méthylamine. Dépendant de la nature des substituants présents sur le groupe alkyle, les acétyl-2 phényltriazènes subissent une cyclisation conduisant à des hétérocycles à cinq ou à six chaînons. Une attaque du N-3 du triazène sur le groupe *ortho*-acétyle conduit à une méthylène-4 triazine qui peut subir soit une oxydation conduisant à une benzotriazinone soit une transposition acido-catalysée conduisant à une alkylamino-4 cinnoline. La réaction de **1** avec des alkylamines conduit aussi à des produits rouges que l'on a identifié comme étant des arylazométhylène-4 triazines et qui ont été complètement caractérisées en faisant appel à la rmn du ^{1}H et du ^{13}C. La formation de ces composés azo est en accord avec le caractère ènamine des méthylène-4 triazines. L'introduction d'un groupement CO_2Et en position α de la portion alkyle fournit une voie de réaction compétitive qui conduit à un hétérocycle à cinq chaînons, un hydroxy-5 triazole. Dans ce cas, la voie provoquant une cyclisation en un hétérocycle à six chaînons se trouve favorisée; par ailleurs, l'introduction d'un groupement CN peut conduire à la formation exclusive de triazole. La réaction du nitrile (**2*c***) avec de l'alumine dans le chloroforme conduit à la formation d'un nouvel hétérocycle, une quinazolinotriazole; en solution dans le DMSO, le composé **2*c*** suit plutôt une autre voie conduisant uniquement à la cyanométhyl-3 méthylène-4 triazine. L'introduction d'un groupement benzoyle dans la portion alkyle de la molécule conduit à un triazène instable; il réagit avec l'alumine dans le chloroforme pour donner un triazole qui, à son tour, se transpose en un nouveau diazoalkane.

[Traduit par le journal]

Introduction

1-Aryl-3-alkyltriazenes with appropriate substituents in the aryl and alkyl groups (X or Y) have been used as precursors for a variety of heterocyclic systems, Scheme 1. Interaction of a reactive *ortho*-substituent (X) in the aryl group with N-3 of the triazene chain, path (a), leads to 1,2,3-triazine derivatives, such as benzotriazinones (X = CO_2Et) (1), 4-iminobenzotriazines (X = CN) (2), 4-methylenebenzotriazines (X = $COCH_3$) (3), and 4-hydroxybenzotriazines (X = CHO or COAr) (4). Alternatively, if the alkyl group at N-3 has a reactive α-substituent (Y), then interaction with N-1 of the triazene chain, path (b), leads to 1,2,3-triazole derivatives. The latter method has successfully been applied to the synthesis

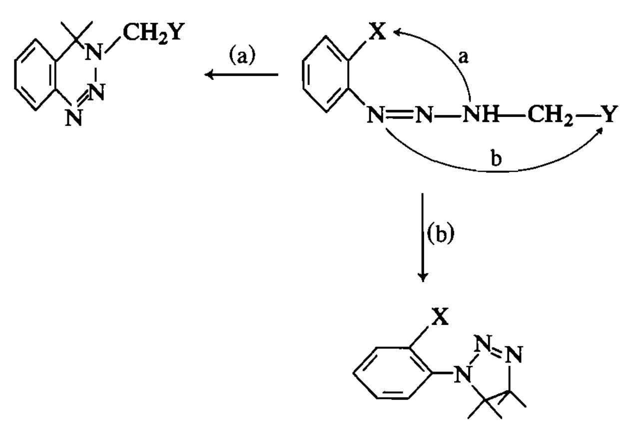

SCHEME 1

[1]For Part VII, see ref. 17; for Part VI, see ref. 18.
[2]Author to whom all correspondence should be addressed.

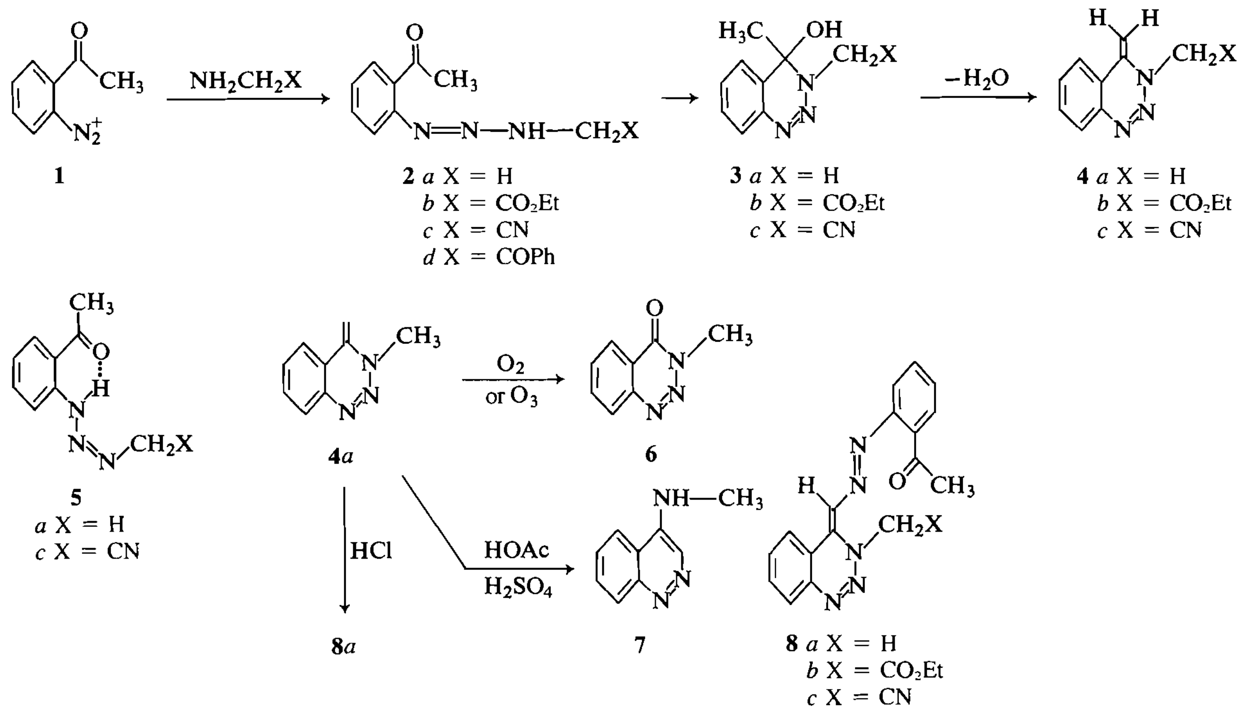

of 5-hydroxytriazoles (Y = CO_2Et) (5) and 5-aminotriazoles (Y = CN) (6).

As part of our continuing interest in the applications of open-chain nitrogen compounds as precursors for heterocyclic molecules, we report here a study of the synthesis and reactions of triazenes of this type with an acetyl group at the X-position and a variety of substituents at the Y-position (H, CO_2Et, CN, COPh). In a previous study (3), the synthesis of 4-methylene-3-alkyl-3,4-dihydro-1,2,3-benzotriazines of type **4** was achieved by spontaneous cyclization of 1-(2′-acetylphenyl)-3-alkyltriazenes (e.g. **2***a*). Reaction of *o*-acetylbenzenediazonium ion (**1**) with methylamine was reported to afford a mixture of the expected triazene (**2***a*) and its cyclization products (**3***a* and **4***a*); the cyclodehydration of **2***a* → **3***a* → **4***a* was shown to be a facile process and was most conveniently carried to completion by addition of neutral alumina to a chloroform solution of the crude reaction product. The spontaneity of the dehydration step has also been observed during an alternate synthetic route to triazines of type **3** by the reaction of a methyl Grignard reagent with benzotriazinones (7), which also affords methylenetriazines (**4**).

Subsequently we have shown (4) that stable 4-hydroxytriazines of type **3** can be prepared from the coupling reaction of alkylamines with *o*-acylbenzenediazonium ions, which lack α-hydrogen atoms in the acyl group (such as —CHO and —COAr). These 4-hydroxy-3,4-dihydrobenzo-1,2,3-triazines are stable compounds since they are unable to undergo the dehydration step to the methylenetriazine; the heterocyclic structure of compounds of type **3** has been verified by X-ray crystal structure determination (8).

Results and discussion

Coupling the diazonium ion **1** with methylamine by our reported method (3) affords an unstable orange-red coloured compound, as previously observed. The Nujol ir spectrum of this product clearly shows that it is the 4-hydroxytriazine (**3***a*), the expected cyclization product of the initially formed triazene (**2***a*). In the ir spectrum, **3***a* shows a strong band at 3160 cm^{-1} for the OH group and carbonyl absorption is completely absent, eliminating the open-chain triazene structure (**2***a*) for this product, at least in the solid state. The situation is different in solution, however, since the nmr spectrum in $CDCl_3$ clearly shows that the equilibrium **2***a* ⇆ **3***a* is quickly established; the nmr also shows that the dehydration of **3***a* → **4***a* takes place as soon as the compound is in solution. Dehydration of the solid **3***a* → **4***a* was also apparent when hours-old samples of **3***a* were examined by ^{1}H nmr. These results are consistent with our previous investigation (3) at which time only 60-MHz nmr was available to us.

We have reinvestigated the structures of these compounds by high resolution (360 MHz) nmr spectroscopy, which gives a clearer picture of the identity of the three possible components and provides useful spectroscopic information for analogues reported here. The nmr of **3***a* in $CDCl_3$ shows the N-Me protons at δ 3.66, OH at δ 3.15 (broad s), and a methyl signal at δ 1.90, assigned to the methyl at C-4, which confirms the cyclic structure. The major component of the $CDCl_3$ solution is the open-chain triazene, but the chemical shift and singlet character of the *N*-methyl group (δ 3.60) and the NH signal at δ 12.60 show without question that this triazene, like others with *ortho* substituents (9), exists as the intramolecularly H-bonded tautomer **5***a*. The growing presence of the final dehydration product (**4***a*) is indicated by the signals at δ 3.59 (s, N-Me), 3.86 (d, *J* 2.56 Hz, one vinylic CH), and 4.42 (d, *J* 2.56 Hz, the other vinylic CH). The low chemical shift of the vinylic protons of **4***a* arises from increased electron density at the exocyclic carbon atom, which indicates significant enamine character in this group. Careful control of the diazonium coupling reaction of **1** with methylamine gave a product free from the dehydrated form (**4***a*). Attempts to separate the components of the mixture by chromatography resulted in complete conversion to **4***a* (3). The dehydration process (**3***a* → **4***a*) was also observed as the major reaction pathway when the triazine (**3***a*) was dissolved in methanol. A minor pathway in the methanolic dehydration is the formation of the carbinolamine ether, 4-methoxy-3,4-dimethyl-3,4-dihydro-1,2,3-benzotriazine, where the hydroxyl

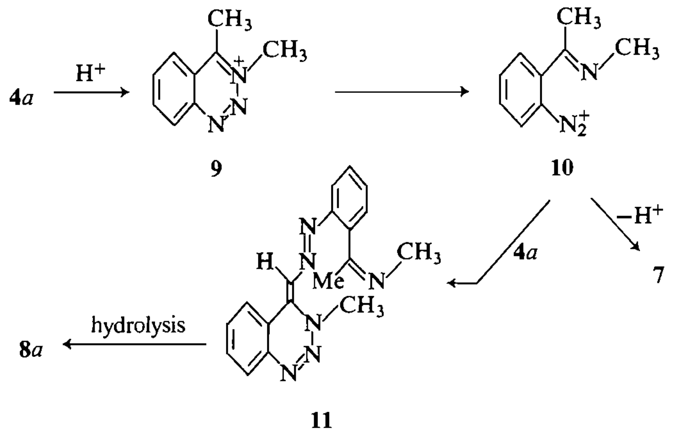

SCHEME 2

group in $3a$ is replaced by methoxyl. The formation of ethers of this type in alcoholic solution is a facile general reaction of 4-hydroxy-1,2,3-benzotriazines.[3]

The alkene character of the exocyclic C═C moiety of $4a$ is evident in reaction with ozone, which affords the benzotriazinone (**6**) in low yield; it should be emphasized that this reaction has little synthetic value since benzotriazinones are readily available by other routes (1). Oxidation of $4a$ by the atmosphere occurs slowly in chloroform solution and is also evident from nmr spectra when $4a$ is stored in the solid state for long periods; samples of $4a$ used in reactions described here are freshly prepared under a nitrogen atmosphere to minimize oxidation.

The ^{13}C nmr spectrum of $4a$ unequivocally confirms the structure, particularly with respect to the enamine character. The exocyclic vinylic methylene carbon atom gives a triplet signal at δ 75.9, which is at a relatively high field for an olefinic carbon atom. This enamine character, implied by both ^1H and ^{13}C spectra, suggests that compounds of type **4** should undergo reaction with electrophilic species at the exocyclic vinylic carbon, such as protonation to give the triazinium species (**9**) (see Scheme 2); analogous reactions are known in the chemistry of 2-methylenepyridines (10) and quinolines (11). The formation of **9** should facilitate a ring-opening pathway to the diazonium ion (**10**), which could undergo a number of synthetically useful pathways such as the Dimroth rearrangement to the methylaminocinnoline (**7**).

Indeed, reaction of $4a$ with a hot mixture of acetic and sulphuric acids gave a product which was identified by spectroscopic analysis as 4-methylaminocinnoline (**7**). The ir spectrum of **7** has an NH absorption band at 3220 cm^{-1} as the only characteristic band. The ^1H nmr spectrum of **7** provides unequivocal evidence for the structure of the rearrangement product. The *N*-methyl signal at 3.15 ppm is a clear doublet, caused by coupling to the adjacent NH proton, which appears as a broad, poorly resolved quartet at 5.2 ppm. The aromatic region of the spectrum is typical of the ABCD system of an *ortho*-substituted benzene ring, with an additional one-proton singlet at δ 8.69, arising from the uncoupled proton at C-3 of the cinnoline.

Considerable effervescent decomposition can occur during this reaction, resulting in a low yield of the cinnoline. Reaction of $4a$ with acetic acid alone afforded only an intractable tar. Nevertheless, the fact that $4a$ does rearrange to the cinnoline **7** suggests that a general synthesis of 4-alkylaminocinnolines can be developed and further investigations in this direction are being pursued. Storr and co-workers (12) have shown that the conversion $4a \rightarrow 7$ can also be achieved by flash vacuum pyrolysis.

Reaction of $4a$ with dilute hydrochloric acid affords a red compound which can also be obtained, in greater yield, by reaction of **1** with 1.33 equivalents of methylamine and neutralization with sodium carbonate or by slow addition of a large excess of methylamine to the diazonium salt solution, as also described by Treppendahl and Jakobsen (13). The structure of the red product, independently identified by us and by them, is unequivocally derived by spectroscopic analysis as 3-methyl-4-(2′-acetylphenylazo)methylenebenzotriazine ($8a$). However, the reported data (13) appear to derive from a crude product, whereas in our hands the red product recrystallizes from ether to give a higher melting point product which, although sharply melting, is not a single compound, based on nmr evidence. The components of the recrystallized red product could not be separated by repeated recrystallization and did not separate on tlc plates.

The colour of this red product, which is also observed in solution, arises from an intense band in the visible region at 430 nm (CH_3CN). The mass spectrum shows a molecular ion at m/z 305, which is consistent with a structure derived from a molecule of $4a$ coupled to the diazonium ion (**1**). The ir spectrum in Nujol shows a strong carbonyl band at 1675 cm^{-1}, which is consistent with an acetyl-carbonyl group *ortho* to an sp^2-nitrogen (14). The ^1H nmr spectrum of the recrystallized red product in $CDCl_3$ shows the presence of two components; the major component (~80%) gives ^1H signals close to the reported values (13) and consistent with the azomethylenetriazine structure ($8a$). The minor component is evident from the doubling of the acetyl-Me, N-Me, and vinylic CH signals in the ^1H spectrum; the doubling of the acetyl-Me and N-Me signals is also seen in the ^{13}C spectrum. The major component has two methyl quartets at δ 32.3 (Ac-Me) and 42.4 (N-Me), compared to 32.7 and 48.1 for the minor component. Other significant features of the ^{13}C spectrum of $8a$ are (a) a carbonyl-carbon signal at 203.35 ppm; (b) splitting of the C-10 signal (117.66 ppm) in the ^1H-coupled spectrum into a quartet (J = 6.5 Hz) by three-bond coupling to the N-Me protons; (c) assignment of the signal at 124.27 ppm to the exocyclic methylene carbon, showing as it does only the doublet (J = 166.7 Hz) splitting in the coupled spectrum.

It is tempting to suggest that the additional N-Me and acetyl-Me signals in the ^1H and ^{13}C nmr spectra of $8a$ arise from the presence of a configurational isomer with almost identical physical properties. However, variable temperature nmr studies in both $CDCl_3$ and DMSO-d_6 gave no evidence to corroborate such a suggestion.

The mechanism of formation of the azo compound ($8a$) can formally be described as coupling a mole of the 2-acetylbenzenediazonium ion (**1**) to the methylenetriazine ($4a$) at the exocyclic methylene carbon; this is the anticipated behaviour of an enamine in the presence of an electrophilic diazonium ion. This route is the most likely explanation for the formation of $8a$ during the slow treatment of **1** with $MeNH_2$ (13), when the methylenetriazine is produced in the presence of unreacted diazonium ion. (If the diazonium ion is mixed rapidly with an excess of the amine, the major product is $3a$; the orange-red colour of $3a$ may be due to trace amounts of $8a$, although the

[3]H. W. Manning, R. J. LaFrance, and K. Vaughan, unpublished results (manuscript in preparation).

latter could not be detected by nmr.)

However, this simple mechanism does not explain the formation of **8***a* when **4***a* is treated with HCl, and it is likely that an alternative mechanism (Scheme 2) is involved. Protonation of **4***a* and ring opening gives the imino-diazonium ion (**10**), which then reacts with a second molecule of **4***a* to give the azo compound (**11**); hydrolysis of the imine function to the acetyl group by the aqueous acid affords the observed product (**8***a*).

An analogous red compound is formed by the reaction of *o*-acetylbenzenediazonium chloride with ethyl glycinate hydrochloride, followed by neutralization with sodium acetate. The melting point of the crude product from this reaction is ca. 110°C, indicating that the product is the same azomethylenetriazine (**8***b*) reported (13) to have a melting point of 110–113°C. However, we have found that **8***b* can be recrystallized unchanged from ether to give red needles with mp 128–129°C.

The ir spectrum of **8***b* shows no NH or OH bands, but does have two carbonyl bands at 1750 (ester) and 1675 (ketone) cm^{-1}. The mass spectrum of **8***b* shows a molecular ion at m/z 377 consistent with structure **8***b*. The nmr analysis of **8***b* was made difficult by the instability of the compound in $CDCl_3$; decomposition in this solvent did not follow a recognizable pathway and the nmr spectra of decomposed solutions were extremely complex and unintelligible. The ^1H nmr spectrum of a fresh solution of **8***b* in $CDCl_3$ was obtained, and could be interpreted to fit structure **8***b*; however, the proton signals are broadened and doubled. The ^1H coupled ^{13}C nmr spectrum of **8***b* was assigned to a single species and gives an excellent fit to structure **8***b*; most of the signals in the spectrum of **8***b* are also found in the analogous spectrum of **8***a*. However, interpretable coupled spectra of **8***b* could not be obtained due to the decomposition taking place over the time required to record the coupled spectrum. Furthermore, **8***b* did not give measurable doubling of the methyl signals, unlike **8***a*, and **8***b* appears to be a single unstable species in $CDCl_3$.

The azomethylenetriazines **8***a* and **8***b* possess some chemical reactivity not shown by the methylenetriazines of type **4**. The visible spectra of **8***a* and **8***b* change significantly when their solutions are made acidic. Thus the strong band at 420 nm in the spectrum of **8***b* in CH_3CN shifts to 489 nm, and intensifies, when hydrochloric acid is added to the solution. The species responsible for the 489-nm band is unstable; the initial deep red colour of the HCl/CH_3CN solution fades slowly to pink and then to colourless. An analogous shift, from 430 to 477 nm, is observed when HCl is added to an ethanolic solution of **8***a*; in this case the acidified species is more stable and precipitates from the HCl/EtOH solution of **8***a* as deep-red crystals. The methylenetriazines of type **4** and the azomethylenetriazines (**8**) also differ in reactivity towards warm alcohols; triazines of type **4** are inert to reaction with alcohols, whereas those of type **8** react with alcohols under mild thermal conditions to give metastable 1:1 alcohol–triazine adducts. The structures of these adducts, and of the hydrochloride salt of **8***a*, are currently being investigated and will be reported in a later paper in this series.

The spontaneous formation of **8***b* during the coupling of ethyl glycinate with **1** indicates that the cyclodehydration **2***b* → **3***b* → **4***b* is extremely facile and also shows that the methylenetriazine (**4***b*) does indeed have a high degree of enamine reactivity as predicted (Scheme 2). When **4***b* is generated in the presence of unreacted diazonium ion, diazonium coupling to the exocyclic methylene carbon is fast and leads to the observed product (**8***b*). Isolation of the intermediate triazene (**2***b*) (or the cyclic tautomer **3***b*) was achieved by slow addition of the diazonium salt to a solution of ethyl glycinate hydrochloride with a large excess of sodium carbonate. The product of this coupling is clearly a mixture of the isomers **2***b* and **3***b*; dehydration to the methylenetriazine (**4***b*) occurs slowly in the solid and in chloroform solution. The ir spectrum of **2***b* ⇋ **3***b* shows that the material is a mixture, but also shows a minor component with a band at 2110 cm^{-1}, indicating that some of **2***b* has undergone cyclization and rearrangement, via the hydroxytriazole **12**, to an α-diazoamide (5).

A good yield of **4***b* was obtained directly from the diazonium coupling by leaving the crude product mixture, **2***b* ⇋ **3***b*, in the aqueous mother liquor overnight. Compound **4***b* is a stable, crystalline solid which recrystallizes without decomposition; **4***b* is more stable than **4***a* and less prone to atmospheric oxidation. The ^1H and ^{13}C nmr spectra of **4***b* are entirely consistent with the methylenetriazine structure and give similar chemical shifts to **4***a*.

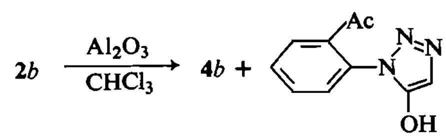

12

Cyclodehydration of **2***b* → **4***b* by the alumina/chloroform method (3) was not as clean as the conversion of **2***a* → **4***a*; a minor product of the alumina-catalysed cyclization of **2***b* was identified as the 5-hydroxytriazole (**12**) from its nmr spectrum. Similar cyclization of 3-ethoxycarbonylmethyltriazenes ($Ar.N{=}N.NH.CH_2.CO_2Et$) is a general reaction (5), but in this case the competing reaction to give the six-membered heterocycle (**4***b*) is the predominant one.

Extension of the coupling reaction of **1** to α-cyanomethylamine, which should lead to the cyanomethyltriazene (**2***c*), gave a product with ir and ^1H nmr spectra in DMSO-d_6 consistent with the cyclic structure (**3***c*). The Nujol ir spectrum of **3***c* shows a strong OH-band, and the DMSO-d_6 nmr spectrum shows a methyl signal at δ 1.77, consistent with the 4-methyltriazine structure; in $CDCl_3$ solution, the methyl group moves to the acetyl-methyl region, indicating a complete transformation to the open-chain triazene structure (**2***c*) in this solvent. This cyanomethyl compound is rare (13) among the compounds of this type in the extremity of the change from DMSO-d_6 to $CDCl_3$; most compounds in this series show equilibrium character in chloroform solution.

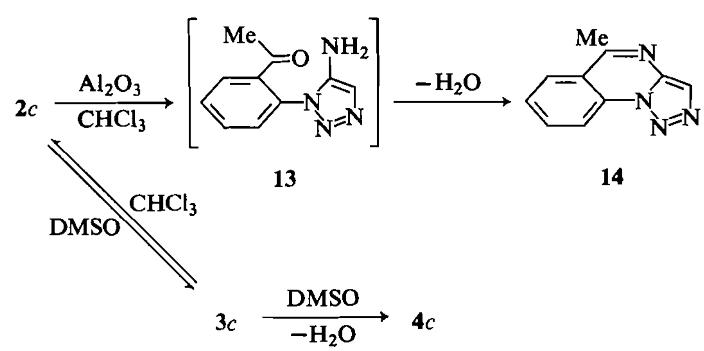

13 **14**

The ^{13}C nmr spectra of this compound in the two solvents confirm these conclusions; in $CDCl_3$, the open-chain structure is indicated by a carbonyl signal at 201.5 ppm, whereas in

DMSO-d_6 the carbonyl signal is absent and is replaced by an sp^3-carbon signal at δ 78.0 (C-4 of **3***c*). The sharpness of the signals and the singlet character of the N-CH_2 signal in the $CDCl_3$ spectrum of **2***c* show clearly that a single, intramolecularly H-bonded tautomer (**5***c*) is the preferred tautomer of the open-chain form.

A DMSO-d_6 solution of **3***c* dehydrated completely to the methylenetriazine (**4***c*) within 3 days at room temperature. However, reaction of **2***c* with alumina in chloroform followed a different route, in which cyclization to the five-membered heterocycle is favoured to afford the triazoloquinazoline (**14**). The structure of this novel tricyclic product is established unequivocally from nmr spectra: the isolated CH group at C-4 of the triazole ring gives rise to a proton singlet at δ 8.18 and a carbon doublet at δ 126.6, with a large directly-bonded coupling constant (198 Hz). The intermediate 5-aminotriazole (**13**), the initial product of a path (b) cyclization of **2***c* (6), could not be isolated. This reaction offers a new synthesis of a novel heterocyclic system and the application of this method as a general synthesis of quinazolinotriazoles is currently being investigated.[4]

The synthesis of the 3-cyanomethyl-4-arylazomethylenetriazine (**8***c*) under a variety of conditions that afforded the analogous red compounds, **8***a* and **8***b*, could not be achieved. All attempts to prepare **8***c* afforded the 4-hydroxytriazine (**3***c*), or the cyclization product (**14**) derived from **2***c*. A logical explanation for this observation is the evident reluctance of **2***c* to undergo cyclodehydration in aqueous media to the methylenetriazine (**4***c*), which is a required intermediate for the formation of **8***c*.

Further extension of this series to the coupling reaction of **1** with α-aminoacetophenone gave a very unstable triazene (**2***d*), which decomposed within hours of preparation, even when kept desiccated under vacuum. However, reaction of the freshly made triazene with alumina in chloroform did afford a mixture of two relatively stable products, which were separated by differential solubility in ether.

The major product, an ether-soluble oil, gave a characteristic ir spectrum, with strong NH and OH bands at 3450 and 3340 cm^{-1} and an intense diazo-group band at 2100 cm^{-1}, in addition to a carbonyl band at 1645 cm^{-1}. The presence of a diazoalkane group (—CHN_2) is confirmed by a one-proton signal at δ 5.9 in the ^1H nmr spectrum and a doublet carbon signal at δ 54.0 in the ^{13}C nmr with a large directly-bonded coupling constant (198 Hz) typical of diazoalkanes (15).

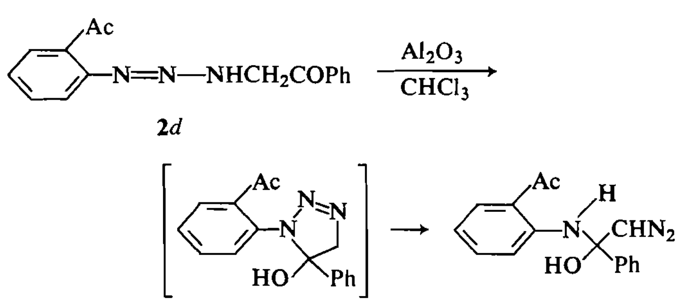

2*d* **15** **16**

Full analysis of the ir, ^1H and ^{13}C nmr spectra of this product leads to the diazoalkane-carbinolamine structure (**16**). The formation of **16** arises by a type (b) cyclization to give initially the 5-hydroxytriazolidine (**15**) and rearrangement of **15** by ring-opening at the N1—N2 bond.

Experimental

Melting points were obtained on a Kofler hot-stage apparatus and are uncorrected. Infrared spectra were recorded with Nujol mulls on a Perkin Elmer 299 grating spectrophotometer. The nmr spectra were obtained with Varian CFT20 (80 MHz) and Nicolet 360NB (360 MHz) spectrometers and mass spectra were recorded with a Dupont CEC-104 medium resolution spectrometer. Ultraviolet/visible spectra were recorded on a Cary 219 (Varian) spectrophotometer. Elemental analyses were determined by the Canadian Microanalytical Service, Vancouver, B.C., Canada.

*3,4-Dimethyl-4-hydroxy-3,4-dihydrobenzo-1,2,3-triazine (3*a*)*

2-Aminoacetophenone (1.35 g), dissolved in concentrated hydrochloric acid (3 mL) and water (25 mL), was diazotized with sodium nitrite (0.80 g) in water (15 mL) at 0°C. The mixture was stirred at 0°C for 20 min, diluted with water (30 mL), and the temperature taken down to −4°C. Aqueous methylamine (40%) (5.0 g) was added rapidly to the diazonium salt solution, so that the temperature did not rise above 5°C. The mixture was cooled quickly to −4°C over a 5-min period and the resulting orange-red precipitate was filtered and dried to afford the crude triazine (**3***a*), 1.1 g (63%), mp 85−95°C (lit. (13) mp 104−107°C); $\bar{\nu}_{max}$: 3160 cm^{-1}; δ ($CDCl_3$): 1.90 (s, CH_3 at C-4 of **3***a*), 2.60 (s, acetyl-Me, **5***a*), 3.60 (s, N-Me, **5***a*), 3.66 (s, N-Me, **3***a*), 5.15 (br s, OH, **3***a*), 6.9−7.9 (m, arom., **3***a* & **5***a*), 12.60 (s, NH, **5***a*).

*4-Methylene-3,4-dihydrobenzo-1,2,3-triazine (4*a*)*

The crude triazine (**3***a*) (0.3 g) was dissolved in chloroform and neutral alumina (9.3 g) added to the solution. After stirring at room temperature for 3.5 h, the solution was filtered and evaporated to dryness *in vacuo* to afford the pure methylenetriazine, 0.27 g (quant.), mp 64−67°C (lit. (3) mp 64−66°C): ^{13}C nmr ($CDCl_3$): 40.5 (q, *J* 140 Hz, N-CH_3), 75.9 (t, *J* 161.8 Hz, exocyclic =CH_2), 119.3 (m, C-4 of triazine), 121.1 (dd, *J* 161.5 and 7.7 Hz, arom.), 127.1 (dd, *J* 164.3 and 7.4 Hz, arom.), 130.3 (dd, *J* 163.0 and 8.25 Hz, arom.), 130.6 (dd, *J* 162.8 and 8.15 Hz, arom.), 135.7 (s, arom.), and 136.7 (m, arom.) ppm.

*Ozonolysis of 4*a

The methylenetriazine (**4***a*) (0.68 g) was dissolved in a mixture of carbon tetrachloride (75 mL) and chloroform (5 mL); the solution was filtered to remove a small amount of insoluble impurity. Ozone was passed through the solution for 1.5 h. The solution was again filtered and the filtrate evaporated to dryness under reduced pressure to afford an orange residue. Recrystallization of the crude product from 50% aqueous ethanol gave 3-methyl-1,2,3-benzotriazin-4(3*H*)-one (**6**) as colourless needles, 0.1 g (15%), mp 121−123°C; $\bar{\nu}_{max}$: 1670 cm^{-1}; δ ($CDCl_3$): 4.0 (s, 3H, N-Me), 7.7−8.2 (m, 4H, arom.). The product was identical with an authentic sample (mixture mp 121−123°C and ir spectrum) (1).

4-Methylaminocinnoline (7)

The methylenetriazine (**4***a*) (0.28 g) was treated with a warm (37°C) mixture of glacial acetic acid (2.5 mL) and conc. sulphuric acid (2.5 mL) and the mixture heated at 54°C for a few minutes. Some effervescence was evident during the reaction. The mixture was poured over ice (13 g) and the resulting solution was neutralized with 6 *M* sodium hydroxide. The mixture was filtered to remove a small amount (10 mg) of an unidentified solid, and the filtrate extracted with ether. During the ether extraction, a precipitate formed in the aqueous layer. Evaporation of the dried ether extract gave a negligible yield of an oil, whereas separation of the precipitate in the aqueous layer (after 2−3 days) afforded the 4-methylaminocinnoline (**7**), 0.04−0.15 g (12−30%), mp 238−239°C (off-white prisms from dimethylsul-

[4] It has now been shown that this method has general application to the synthesis of 5-alkyl- and 5-aryl-1,2,3-triazolo[5,1-*a*]quinazolines; the parent heterocycle can also be prepared in this manner (D. L. Hooper, H. W. Manning, R. J. LaFrance, and K. Vaughan; manuscript in preparation for this journal).

foxide) (lit. (16) mp 224°C); $\bar{\nu}_{max}$: 3220 (NH), 1580 cm^{-1}; δ ($CDCl_3$): 3.15 (3H, d, J 5.1 Hz, N-CH_3), 5.2 (1H, br, NH), 7.6 (1H, dt, J 7.1 and 1.0 Hz, arom.), 7.8 (2H, m, arom.), 8.3 (1H, dd, J 8.9 and 1.3 Hz, arom.) and 8.7 (1H, s, arom. H at C-3 of pyridazine ring).

1-(2′-Acetylphenyl)-3-ethoxycarbonylmethyltriazene (2b)

A cold solution of 2-acetylbenzenediazonium chloride (0.01 mol) in water (15 mL) was added dropwise with stirring to a cold (0°C) solution of ethyl glycinate hydrochloride (0.02 mol) and sodium carbonate (0.05 mol) in water (70 mL). The colour of the solution changes from pale yellow to bright orange-red and an orange-red oil is formed. The product was immediately extracted with chloroform and the chloroform extracts were washed (H_2O), dried, and evaporated to afford the triazene (**2*b***), 2.19 g, $\bar{\nu}_{max}$: 3460(sh), 3350(br), 3240(br), 2110(w), 1750, and 1650 cm^{-1}; δ ($CDCl_3$): 1.3 (t, J 8 Hz, C-CH_3, **4*b***), 1.33 (t, J 8 Hz, C-CH_3, **2*b***), 2.67 (s, acetyl-Me of **2*b***), 3.77 (d, J 3 Hz, vinylic proton, **4*b***), 4.30 (q, J 8 Hz, O-CH_2, **2*b*** and **4*b***), 4.5 (d, J 3 Hz, vinylic proton, **4*b***), 4.60 (s, N-CH_2, **2*b***), 4.73 (s, N-CH_2, **4*b***), 7.0–7.9 (m, arom., **2*b*** and **4*b***).

The oily product was unstable and deposited crystals within 12 h. Recrystallization of the decomposed mixture from ether afforded the methylenetriazine (**4*b***), 0.78 g, mp 91–95°C.

3-(Ethoxycarbonylmethyl)-4-methylene-3,4-dihydrobenzo-1,2,3-triazine (4b)

(a) 2-Aminoacetophenone (2.7 g) was dissolved in conc. hydrochloric acid (5.2 mL), with water (20 mL), and diazotized at 0°C with sodium nitrite (1.38 g) in water (6 mL). Sodium carbonate (10.5 g) was dissolved in water (40 mL), mixed with ethyl glycinate hydrochloride (5.6 g), and the resulting slurry, which had a pH 10, cooled to 0°C. The cold diazonium salt solution was added slowly to the ethyl glycinate slurry with vigorous stirring. After stirring for 0.5 h, the mixture was observed to contain a suspension of a pale yellow precipitate and a heavy orange oil. The oil was retained in the reaction vessel after decantation of the aqueous layer; the precipitate in the aqueous layer was found to be mainly inorganic and was discarded. The oil was kept at room temperature for 24 h, during which time it solidified to give an orange-yellow solid. Recrystallization from a mixture of ether and petroleum ether gave lustrous yellow needles of the methylenetriazine (**4*b***), 2.5 g (54%), mp 94–97°C; $\bar{\nu}_{max}$: 1750 cm^{-1}; δ (DMSO-d_6): 1.2 (3H, t, J 8 Hz, CH_3), 3.83 (1H, d, J 3 Hz, vinylic), 4.20 (2H, q, J 8 Hz, O-CH_2), 4.6 (1H, d, J 3 Hz, vinylic), 4.87 (2H, s, N-CH_2), and 7.4–7.9 (4H, m, arom.); ^{13}C nmr ($CDCl_3$): 14.07 (q, J 127 Hz, CH_3), 54.5 (t, J 141 Hz, N-CH_2), 61.7 (t, J 147 Hz, O-CH_2), 76.4 (t, J 161.6 Hz, exocyclic vinylic CH_2), 119.5 (s), 121.4 (dd, J 161 and 7 Hz), 127.7 (dd, J 164 and 6.8 Hz), 130.6 (dd, J 163.6 and 7.9 Hz), 131.2 (dd, J 162 and 7.5 Hz), 134.9 (s), 136.2 (s), and 167.6 (s, C=O) ppm. *Anal.* calcd. for $C_{12}H_{13}N_3O_2$: C 62.3, H 5.7, N 18.2%; found: C 61.93, H 5.86, N 17.71%.

(b) 1-(2-Acetylphenyl)-3-ethoxycarbonylmethyltriazene (**2*b***) (0.17 g) was dissolved in chloroform (12 mL) and neutral alumina (7 g) was added. The mixture was stirred at room temperature for 16 h, filtered to remove alumina, and the filtrate evaporated to dryness to afford a mixture of two products (0.115 g). The major component (≃80%) gave ^1H nmr signals identical to those of **4*b***, described above; the second component (≃20%) was identified as 1-(2-acetylphenyl)-5-hydroxytriazole (**12**), δ ($CDCl_3$): 2.60 (s, 3H, acetyl-Me) and 6.5–7.8 (m, 6H, arom. + OH).

3-Cyanomethyl-4-hydroxy-4-methyl-3,4-dihydrobenzo-1,2,3-triazine (3c)

A cold solution of 2-acetylbenzenediazonium chloride (0.01 mol) was added dropwise to a cold solution of aminoacetonitrile bisulphate (0.02 mol) and sodium carbonate (5.24 g) in water (40 mL). An immediate orange-red precipitate was formed; after stirring for 15 min, the precipitate was filtered to afford the triazine (**3*c***), 1.49 g (74%), mp 93–95°C (from ether/chloroform); $\bar{\nu}_{max}$: 3170 (strong and broad, OH), 1640 (w) cm^{-1}; δ (DMSO-d_6): 1.77 (3H, s, CH_3), 5.03 (2H, s, CH_2), 7.05 (1H, br s, OH), and 7.5 (4H, AA′BB′, arom.); ^{13}C nmr (DMSO-d_6): 27.3 (q, J 125 Hz, CH_3), 36.9 (t, J 148 Hz, CH_2), 78.0 (s, C-4 of triazine ring), 118.1 (t, J 8 Hz, C≡N), 124.5 (dd, J 163 and 4.5 Hz), 124.8 (s), 125.2 (dd, J 163 and 6.4 Hz), 129.4 (dd, J 163 and 7.7 Hz), 130.7 (dd, J 163 and 7.5 Hz), and 135.6 (t, J 5.8 Hz) ppm. *Anal.* calcd. for $C_{10}H_{10}N_4O$: C 59.4, H 5.0, N 27.7%; found: C 59.33, H 5.13, N 27.60%.

3-(2′-Acetylphenyl)-1-cyanomethyltriazene (5c)

This triazene was observed only in solution when the 4-hydroxytriazine (**3*c***) was dissolved in chloroform; **5*c*** gave the following nmr data: δ ($CDCl_3$): 2.62 (3H, s, CH_3), 4.6 (2H, s, CH_2), and 6.9–7.9 (5H, m, arom. + NH); ^{13}C nmr ($CDCl_3$): 28.14 (q, J 128 Hz, CH_3), 47.4 (t, J 146 Hz, N-CH_2), 114.5 (d, J 159.3 Hz), 114.9 (t, J 9.52 Hz, C≡N), 118.7 (s), 121.5 (dd, J 164.9 and 8.9 Hz), 131.6 (dd, J 158.5 and 7.9 Hz), 134.9 (dd, J 159.8 and 7.9 Hz), 142.8 (t, J 4.8 Hz), and 201.5 (d, J 4.9 Hz, C=O) ppm.

3-Cyanomethyl-4-methylene-3,4-dihydrobenzo-1,2,3-triazine (4c)

A solution of the 4-hydroxytriazine (**3*c***) in DMSO-d_6 was left at room temperature for 3 days. The nmr spectrum showed that the hydroxytriazine had undergone dehydration, cleanly and quantitatively, to give the methylenetriazine (**4*c***), which gave the following nmr spectrum: δ (DMSO-d_6): 4.27 (1H, d, J 3 Hz), 4.87 (1H, d, J 3 Hz), 5.3 (2H, s), and 7.5–8.0 (4H, m).

5-Methyl-1,2,3-triazolo[1,5-a]quinazoline (14)

The 4-hydroxytriazine (**3*c***) (0.2 g) was dissolved in chloroform (12 mL) and neutral alumina (7 g) added to the solution. The mixture was stirred vigorously at room temperature for 17 h, filtered, and evaporated to dryness to afford the triazoloquinazoline (**14**), 0.18 g (99%), mp 145°C; δ ($CDCl_3$): 2.95 (3H, s, CH_3), 7.72 (1H, dt, J 7.8 and 1.1 Hz, arom.), 7.98 (1H, dt, J 7.8 and 1.2 Hz, arom.), 8.17 (1H, dd, J 8.2 and 0.67 Hz, arom.), 8.18 (1H, s, C—H at C-4 of triazole ring), and 8.70 (1H, d, J 8.3 Hz, arom.); ^{13}C nmr ($CDCl_3$): 22.7 (q, J 130 Hz, CH_3), 115.8 (dd, J 168.6 and 7.2 Hz), 118.4 (s), 126.6 (d, J 198 Hz, C-4 of triazole), 127.0 (dd, J 162 and 7.4 Hz), 127.5 (dd, J 163 and 7.6 Hz), 132.8 (s), 134.3 (dd, J 163 and 8.0 Hz), 139.9 (d, J 14 Hz), and 161.3 (quintet, J 11.8 Hz).

1-(2′-Acetylphenyl)-3-benzoylmethyltriazene (2d)

2-Aminoacetophenone (1.35 g) was dissolved in conc. hydrochloric acid (2.6 mL), with water (10 mL), and diazotized at 0°C with sodium nitrite (0.69 g) in water (3 mL), and stirred for 0.5 h. A solution of α-aminoacetophenone hydrochloride (3.43 g) in water (70 mL) was basified with sodium carbonate (5.24 g) and the resulting yellow solution was treated slowly with the diazonium salt solution. Precipitation was immediate and, after stirring for 15 min, the product was filtered and partially dried to afford the crude triazene (**2*d***), 3.7 g, mp 80–82°C. This triazene is unstable and decomposes quickly, even when stored in a vacuum desiccator. It is used immedately after partial drying for subsequent reaction.

2-(2′-Acetylphenylamino)-2-hydroxy-2-phenyldiazoethane (16)

The crude triazene (**2*d***) (1.8 g) was dissolved in chloroform (75 mL) and mixed with neutral alumina (63 g). After stirring for 14 h, the alumina was removed by filtration and the filtrate evaporated to afford an oil, 1.72 g, which solidified partially over 24 h. Crystallization of the mixture from ether/methylene chloride afforded a low yield (0.1 g) of a crystalline product, mp 198°C, which was identified by nmr as 3,6-diphenyl-2,5-dihydropyrazine (the expected dimerization product of α-aminoacetophenone). Evaporation of the filtrate afforded the diazoethane (**16**), 1.6 g, as an oil, $\bar{\nu}_{max}$: 3450(OH), 3340(NH), 2150(sh), 2100(CN_2), and 1645(C=O) cm^{-1}; δ ($CDCl_3$): 2.60 (s, 3H, acetyl-Me), 5.9 (s, 1H, CHN_2), 6.25 (br s, 1H, OH), 6.5–6.8 (m, 2H, arom.), 7.3–8.2 (m, 7.5H, arom. + NH), and 9.1 (s, 0.5H, NH); ^{13}C nmr: 27.7 (q, J 127 Hz, acetyl-Me), 54.0 (d, J 198 Hz, CHN_2), 77.1 (s), 116.4 (d, J 8 Hz), 117.0 (dd, J 8 and 158 Hz), 118.0 (s), 126.5 (dt, J 7 and 167 Hz), 128.5 (dd, J 7.6 and 169 Hz), and 131.8 (dd, J 8 and 164 Hz), 132.5 (dt, J 7.5 and 158 Hz), 134.2 (dd, J 9.1 and 146 Hz), 136.5 (t, J 7.4 Hz), 150.1 (s), 186.1 (s), and 200.5 (s).

*3-Methyl-4-(2'-acetylphenylazo)-methylene-3,4-dihydro-1,2,3-benzotriazine (8*a*)*

(a) A solution of 2-aminoacetophenone (1.35 g) in conc. hydrochloric acid (3 mL), diluted with water (25 mL), was cooled to 0°C and diazotized with sodium nitrite (0.8 g) in water (5 mL). After stirring for 10 min, a solution of 40% aqueous methylamine (1.0 g, 1.33 equiv.) in water (10 mL) was added to the diazonium salt solution. The solution darkened in colour at this point but remained clear. The solution was neutralized with saturated sodium bicarbonate, while maintaining the temperature at 0°C, and a dark red precipitate formed immediately. The product was filtered, dried, and recrystallized from ether/chloroform to afford the azomethylenetriazine (**8***a*), 0.95 g (62%), mp 157–159°C (red needles) (Note: the reported (13) mp of **8***a* is 142°C; the crude product obtained by this method had mp 142°C); $\bar{\nu}_{max}$: 1675 cm^{-1}; λ_{max} (CH_3CN): 193(ϵ 3.37 × 10^4), 231(ϵ 2.93 × 10^4), 268(ϵ 9.2 × 10^3), 304 sh(ϵ 5.3 × 10^3), and 430(ϵ 2.8 × 10^4) nm; δ ($CDCl_3$): 2.48 and 2.60 (3H, singlets, acetyl Me), 3.94 and 4.37 (3H, singlets, N-Me), 7.36 (t, *J* 7.4 Hz, arom.), 7.43 and 7.74 (1H, singlets, vinylic =C—H), 7.52 (t, *J* 7.9 Hz, arom.), 7.55 (d, *J* 6.6 Hz, arom.), 7.58 (d, *J* 8.1 Hz, arom.), 7.68 (t, *J* 5.4 Hz, arom.), 7.68 (d, *J* 7.5 Hz, arom.), 7.83–7.86 (m, arom.), 7.91 (d, *J* 7.2 Hz, arom.), and 8.93–8.96 (m, arom.); ^{13}C nmr ($CDCl_3$): 32.3 (q, *J* 128 Hz) and 32.7 (q, *J* 128 Hz), acetyl Me; 42.38 (q, *J* 141.3 Hz), and 48.12 (q, *J* 142.7 Hz), N-Me; 117.7 (q, *J* 6.5 Hz, C-4 of triazine ring), 118.0 (weak), 119.7 (dd, *J* 162 and 8.4 Hz, arom.), 124.3 (d, *J* 167 Hz, exocyclic vinylic =CH), 128.0 (dd, *J* 162 and 7.0 Hz), 128.3 (dd, *J* 164 and 7.9 Hz, 130.2 (dd, *J* 168 and 4.3 Hz), 131.3 (dd, *J* 162 and 8.4 Hz), 132.7 (dd, *J* 164 and 8.7 Hz), 133.2 (dd, *J* 162 and 7.3 Hz), 136.6 (t, *J* 6.2 Hz), 138.0 (t, *J* 1.6 Hz), 139.3 (t, *J* 3.2 Hz), 152.1 (t, *J* 7.5 Hz, arom. C adj. to azo group), and 203.35 (s, C=O) ppm; *m*/*z*: 305(M^+), 290, 289, 278, 273, 259, 232, 220, 219, 184, 120, 92. *Anal.* calcd. for $C_{17}H_{15}N_5O$: C 66.87, H 4.95, N 22.94%; found: C 66.88, H 5.06, N 22.90%.

(b) 3-Methyl-4-methylene-3,4-dihydro-1,2,3-benzotriazine (**4***a*) (0.5 g) was dissolved in 2 *M* hydrochloric acid (10 mL), which produced an immediate pink colouration. After stirring at room temperature for 15 h, the deep-red mixture was filtered and neutralized with sodium bicarbonate. The solution turned orange and a gummy oil separated. Trituration of the oil with ether afforded a solid which was filtered to afford the azomethylenetriazine (**8***a*), 0.10 g (21%); the product was identical (ir and nmr spectra) to the sample prepared in (a).

*3-Ethoxycarbonylmethyl-4-(2'-acetylphenylazo)methylene-3,4-dihydro-1,2,3-benzotriazine (8*b*)*

2-Aminoacetophenone (3.48 g) was dissolved in 2 *M* hydrochloric acid (60 mL) and diazotized at 0°C with sodium nitrite (1.8 g) in water (8 mL). The diazonium salt solution was treated in one portion with a solution of ethyl glycinate hydrochloride (4.0 g). The resulting light yellow solution was then neutralized with an aqueous slurry of sodium acetate hydrate (40 g) and an immediate orange precipitate developed. After stirring for 20 min, the product was filtered to afford the azomethylenetriazine (**8***b*), 4.8 g (97%). Recrystallization of the crude product from ether gives red needles with mp 128–129°C (Note: the reported (13) mp of this compound is 110–113°C; the *crude* product obtained by the method described here had a mp varying from 105–108°C to 112–115°C); $\bar{\nu}_{max}$: 1750 and 1675 cm^{-1}; λ_{max}: (CH_3CN): 193(ϵ 2.67 × 10^4), 230(ϵ 2.20 × 10^4), and 420(ϵ 2.78 × 10^4) nm; λ_{max}: (CH_3CN + HCl): 192(ϵ 2.0 × 10^5) and 489(unstable) nm; δ ($CDCl_3$): 1.12(t) and 1.3(br), (3H, C-CH_3); 2.46(br) and 2.65(s), (3H, acetyl Me); 4.1(q) and 4.32(br), (2H, O-CH_2); 5.08(br) and 5.6(s), (2H, N-CH_2); 7.35–8.0(m, arom.), and 8.95(br m, arom.); ^{13}C nmr: 13.9 (q, *J* 127 Hz, Me of ethyl ester), 32.9 (q, acetyl-Me); 59.53 (t, N-CH_2), 61.5 (t, O-CH_2), 116.2 (arom., C-4 of triazine), 118.1, 119.7, 121.9, 128.0, 128.2, 128.4, 130.3, 131.0, 132.7, 133.8, 136.9, 138.3, 150.9 (arom. C adj. to azo group), 166.9 (s, ester C=O), and 203.3 (s, ketone C=O). *Anal.* calcd. for $C_{20}H_{19}N_5O_3$: C 63.65, H 5.07, N 18.56%; found: C 63.70, H 5.36, N 18.40%.

Acknowledgements

The financial assistance of the Natural Sciences and Engineering Research Council of Canada is gratefully acknowledged. The authors are also grateful to the Atlantic Regional Magnetic Resonance Center at Dalhousie University for high-field nmr spectra, to Dr. J. H. Kim at Dalhousie University for mass spectra, and to Dr. R. C. Storr (University of Liverpool, U.K.) for helpful discussion.

1. R. J. LEBLANC and K. VAUGHAN. Can. J. Chem. **50**, 2544 (1972).
2. K. VAUGHAN. Can. J. Chem. **50**, 1775 (1972).
3. H. FONG and K. VAUGHAN. Can. J. Chem. **53**, 3714 (1975).
4. P. L. FAYE, K. VAUGHAN, and D. L. HOOPER. Can. J. Chem. **61**, 179 (1983).
5. K. M. BAINES, K. VAUGHAN, D. L. HOOPER, and L. F. LEVECK. Can. J. Chem. **61**, 1549 (1983).
6. K. M. BAINES, T. W. ROURKE, K. VAUGHAN, and D. L. HOOPER. J. Org. Chem. **46**, 865 (1981).
7. J. J. A. CAMPBELL, S. J. NOYCE, and R. C. STORR. Chem. Commun. 1344 (1983).
8. K. K. LAI, C. H. SCHWALBE, K. VAUGHAN, R. J. LAFRANCE, and C. D. WHISTON. Can. J. Chem. **63**, 581 (1985).
9. K. VAUGHAN. J. Chem. Soc. Perkin Trans. 2, 17 (1977); D. L. HOOPER and K. VAUGHAN. J. Chem. Soc. Perkin Trans. 2, 1161 (1981).
10. R. A. COX, R. STEWART, M. J. COOK, A. R. KATRITZKY, and R. D. TACK. Can. J. Chem. **54**, 900 (1976).
11. G. FUKATA, C. O'BRIEN, and R. A. M. O'FERRALL. J. Chem. Soc. Perkin Trans. 2, 792 (1979).
12. S. J. NOYCE, K. R. RANDLES, and R. C. STORR. Tetrahedron Lett. **26**, 941 (1985).
13. S. TREPPENDAHL and P. JAKOBSEN. Acta Chem. Scand. (B), **38**, 185 (1984).
14. L. J. BELLAMY. Infra-red spectra of complex molecules. Vol. 1. 3rd ed. Chapman and Hall, New York. 1975. p. 150.
15. T. A. ALBRIGHT and W. J. FREEMAN. Org. Magn. Reson. **9**, 75 (1977).
16. C. M. A. ATKINSON and A. TAYLOR. J. Chem. Soc. 4236 (1955).
17. R. J. LAFRANCE, H. W. MANNING, and K. VAUGHAN. J. Org. Chem. In press.
18. H. W. MANNING, C. M. HEMENS, R. J. LAFRANCE, Y. TANG, and K. VAUGHAN. Can. J. Chem. **62**, 749 (1984).

On the electrical double layer between mercury and aqueous solutions of sodium citrate

S. GONZALEZ, S. V. ALVAREZ, AND A. ARÉVALO
Department of Physical Chemistry, University of La Laguna, Teneriffe, Canary Islands, Spain

Received February 3, 1984

S. GONZALEZ, S. V. ALVAREZ, and A. ARÉVALO. Can. J. Chem. **63**, 2462 (1985).

The adsorption of citrate ions at the Hg/aqueous $CitNa_3$ interface was studied, using both differential capacity and electrocapillary measurements. The results contrast with those obtained previously by Barradas *et al.* The hump of the C_d-E curve increases as the concentration of the solution increases to 0.5 *M*, to diminish beyond 1 *M*. The plots of ϕ^{M-2} vs. q^{-1} are linear and parallel to one another for the different values of *q*, which is in agreement with the results obtained by other authors for different anions. A Frumkin isotherm is also associated for the adsorption process and, finally, the parameters are obtained for the interface, using a type of isotherm proposed by Grahame.

S. GONZALEZ, S. V. ALVAREZ et A. ARÉVALO. Can. J. Chem. **63**, 2462 (1985).

Faisant appel à des mesures de capacité différentielle et d'électrocapillarité, on a étudié l'adsorption des ions citrates à l'interface Hg/Na_3Cit aqueux. Les résultats obtenus contrastent avec ceux obtenus antérieurement par Barradas et ses collaborateurs. La bosse qui existe dans la courbe C_d-E augmente avec une augmentation de la concentration de la solution jusqu'à une concentration de 0,5 *M*; cette particularité diminue au-delà d'une concentration de 1,0 *M*. Pour diverses valeurs de *q*, les courbes de ϕ^{M-2} en fonction de q^{-1} sont linéaires et parallèles l'une à l'autre; ceci est en accord avec les résultats obtenus par d'autres auteurs pour des anions différents. Une isotherme de Frumkin est aussi associée avec le processus d'adsorption et, utilisant un type d'isotherme proposé par Grahame, on a finalement obtenu les paramètres de l'interface.

[Traduit par le journal]

Introduction

A kinetic study of the Cu(II)−citrate system in its reduction at the dropping mercury electrode (dme) (1) pointed to the necessity of more detailed knowledge of the citrate−Hg interface. The only work related to the said interface in the literature is that of Barradas *et al.* (2). However, they operated with pH 8.8 which is a unit higher than the one we use.

Experimental

The citric acid and sodium hydroxide, both of Analytical grade, were supplied by Merck.

The differential capacity measurements were obtained with an alternate current impedance bridge, as described by Sluyters and coworkers (3). The C_d values, independent of the frequency between 100 and 10000 Hz, were measured at 1 kHz with an amplitude of 5 mV across the cell.

The measurements of surface tension were carried out with a capillary electrometer, calibrated using 0.1 *M* KCl, taking the values determined by Devanathan and Peries as reference (4). The capillary electrometer was controlled by a presostate designed by the Ruska firm. The measurements of the zero charge potential (E_z), were carried out with a streaming mercury electrode (5).

The dme capillary was internally treated with dimethyldichlorosilane vapour. The counterelectrode consisted of a pool of mercury connected to the exterior by way of a Pt wire. The reference electrode was the sce of the Ingold firm.

The pH was measured with a high precision pH meter, model pHM 84 by Radiometer, and a mixed glass electrode, model GK 2401 C.

The solutions were prepared starting from citric acid and adding carbonate-free NaOH to pH 7.80. The percentage of free Cit^{3-} was calculated at 99.8% at that moment, using the p*K* of citric acid determined by Petit-Ramel and Khalil (6). The concentrations studied cover the range $0.01-1.0$ *M*.

In an attempt to dispel the doubt due to the variation in the potential of union of liquids, E_j, a solution of 0.1 *M* of sodium citrate was kept permanently in contact with the reference electrode. The E_j of the second union, Na_3Cit 0.1 *M*/Na_3Cit *x M*, was calculated for each *x* by the Henderson equation, the E_r potential being determined in this manner.

All measurements were taken at 25 ± 0.1°C. Argon of 99.96% purity supplied by Oxican was used to eliminate oxygen from the solutions and as an inert atmosphere.

Results and discussion

Figure 1 shows the variation in C_d of the double layer as a function of the potential at all concentrations of sodium citrate studied, at pH 7.80.

The capacity minima at the most dilute concentrations take place at potentials slightly more negative than the point of zero charge, as is expected for highly asymmetric electrolytes.

The capacity of the hump increases when the concentration changes from 0.05 *M* to 0.5 *M*, decreasing later to 1 *M*. This behaviour is analogous to that of the majority of anions.

The C_d-E curves were integrated twice, taking the E_z and the surface tension corresponding to this potential as integral constants. The first integration gives the density of charge at the Hg, *q*, and the second the electrocapillary curves, which coincide with those obtained experimentally, as shown in Table 1 for the case of the 0.1 *M* solution of Na_3Cit. The coordinates of the electrocapillary maximum are presented in Table 2.

(a) Amount of specific adsorption, q^{-1}

In order to determine the q^{-1} charge due to specifically adsorbed Cit^{3-} anions, the Parsons function was adopted (7):

$$[1] \quad \xi^+ = \gamma + qE^+$$

The values of the E_r potential with regard to the reference electrode were converted to E^+ values by means of the well-known Frumkin relation (8):

$$[2] \quad E_r = E^+ + (RT/z_+F)\ln a_+ + \text{constant}$$

In the absence of data on ionic coefficients of medium activity of sodium citrate solutions, the coefficients determined for trisodium arsenate solutions (9) were taken provisionally.

The values obtained by the Parsons function, ξ^+, were interpolated for integer values of the charge.

The charge due to anions, q_-, was evaluated using the relation:

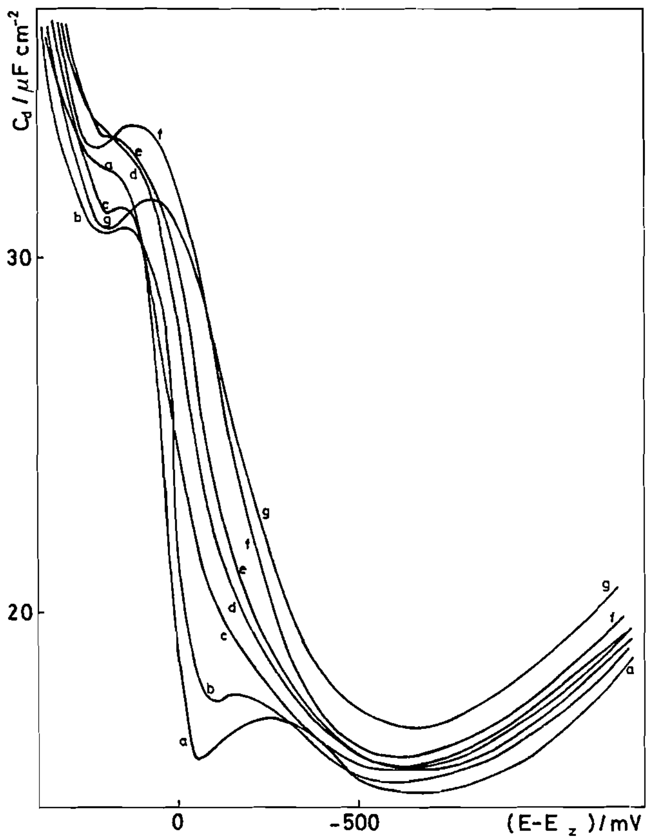

FIG. 1. Differential capacity−potential curves for Hg in aq. Na_3Cit solutions at 25°C and pH 7.80. (*a*) 0.01, (*b*) 0.02, (*c*) 0.05, (*d*) 0.1, (*e*) 0.2, (*f*) 0.5, and (*g*) 1 *M*.

$$[3] \quad q_- = -(z_- F/RT)(\partial \xi^+/\nu \partial \ln a_\pm)_q$$

The charge due to cations, q_+, was then obtained from the relation:

$$[4] \quad -q = q_s = q_+ + q_-$$

Assuming that the cation is not specifically adsorbed at all the range of potentials (i.e. $q_+ = q_+^d$), the value of ϕ_2 was calculated by means of the Gouy−Chapman theory, using the following expression resulting from the work of Grahame (10) numerically evaluated thus:

$$[5] \quad q_+^d = \frac{3RT\epsilon\epsilon_0 C}{4\pi A} \int_y^0 \frac{(3e^{-y} - 1)dy}{(3e^{-y} + e^{3y} - 4)^{1/2}}$$

where $y = F\phi_2/RT$, $A = (\epsilon\epsilon_0 RTC/2\pi)^{1/2}$, ϕ_2 is the potential at the OHP, ϵ the dielectrical constant of the solution, ϵ_0 the permittivity of the vacuum and the remaining symbols have the usual meaning.

The values of ϕ_2 were used to obtain the charge of the diffuse layer due to anions, q_-^d, evaluated from the expression by Grahame:

$$[6] \quad q_-^d = -\frac{3RT\epsilon\epsilon_0 C}{4\pi A} \int_y^0 \frac{(e^{3y} - 1)dy}{(3e^{-y} + e^{3y} - 4)^{1/2}}$$

The specifically adsorbed charge, q^{-1}, was obtained from the values of $q_-^{d'}$ and q_-, according to:

$$[7] \quad q_- = q_-^d + q^{-1}$$

Figure 2 shows the specifically adsorbed charge, q^{-1}, against the charge of the electrode at different concentrations of sodium citrate. It is evident that the curves are linear and parallel over the range of q covered. The slopes of the lines are −1, in complete agreement with the majority of anions.

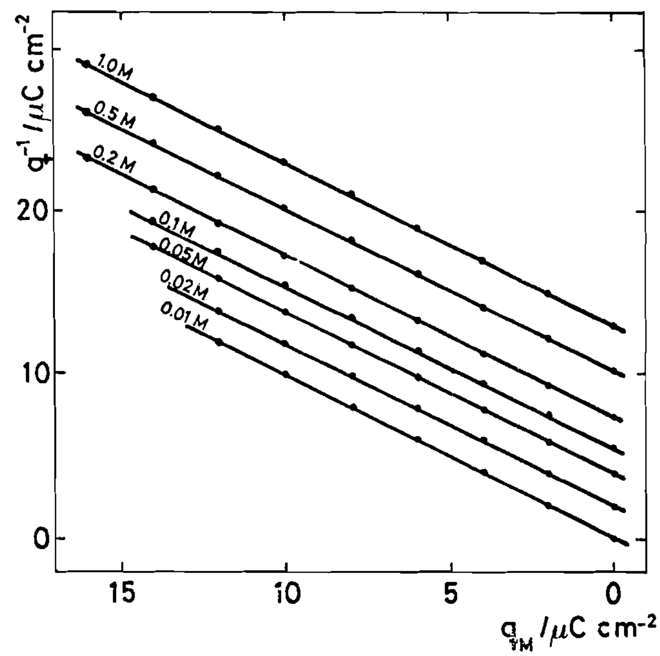

FIG. 2. Plot of charge due to specifically adsorbed citrate ions vs. electrode charge.

TABLE 1. Surface tension for solutions of sodium citrate 0.1 *M*, pH 7.80, at different potential

$E - E_z$/mV	γ_{exp}/μJ cm^{-2}	$\gamma_{calcd} - \gamma_{exp}$
400	40.00	<0.02
300	41.16	<0.02
200	41.96	<0.02
100	42.43	<0.02
0	42.58	0
−100	42.45	<0.02
−200	42.10	<0.02
−300	41.55	<0.02
−400	41.83	<0.02
−500	39.93	<0.02

TABLE 2. Coordinates of the electrocapillary maximum for solutions of aqueous sodium citrate at pH 7.80

C/mol L^{-1}	$-E_z$/V[a]	γ_z/μJ cm^{-2}	C_z/μF cm^{-2}
0.01	419	42.60	19.00
0.02	425	42.60	22.50
0.05	439	42.59	25.10
0.1	450	42.58	27.98
0.2	465	42.57	29.15
0.5	487	42.53	31.52
1.0	511	42.44	30.70

[a] E_z is the fem of the cell: Hg/Hg_2Cl_2 ‖ saturated KCl ‖ 0.1 *M* Na_3Cit ‖ *x M* Na_3Cit/Hg.

(b) Components of the differential capacity

The potential drop (ϕ^{M-2}) across the inner layer due to specific adsorption was calculated from the equation:

$$[8] \quad \phi^{M-2} = E_r - \phi_2 - K$$

where K is the value of ϕ^{M-2} corresponding to E_z in the absence

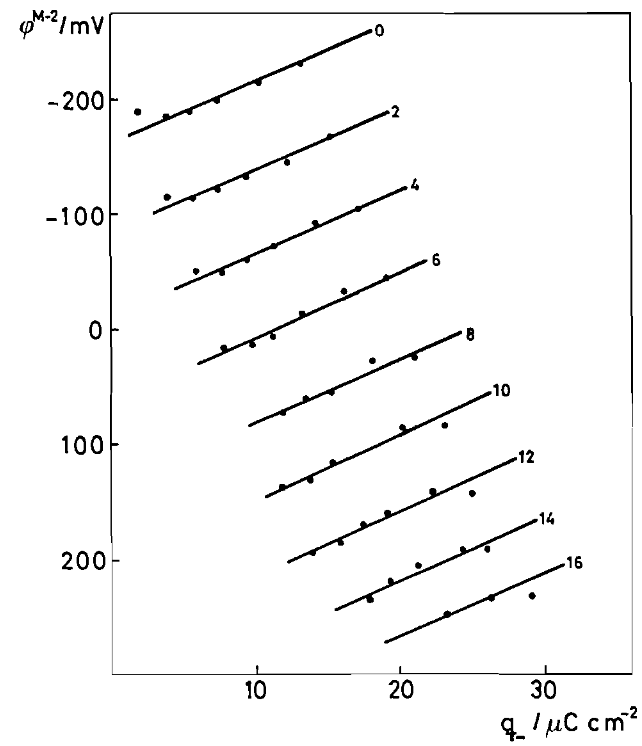

FIG. 3. Plot of potential drop across the inner layer vs charge due to specifically adsorbed citrate ions. The numbers above the lines indicate the charge on the electrode in μC cm^{-2}.

of specific adsorption.

The resulting ϕ^{M-2} values were plotted against q^{-1}, for integer values of q, as shown in Fig. 3. As observed with KCl (11), sodium benzenedisulfonate (12), and KNO_3 (13), the data determine a series of parallel straight lines. The shifts of some points is attributable to errors introduced by the graphical differentiation.

The capacity was analysed with the aid of the diffuse layer theory and the values of dq^{-1}/dq obtained by graphical differentiation of the lines in Fig. 2. The capacity of the internal region, C^i, was obtained by way of the relation:

$$[9] \quad 1/C^i = 1/C - (1/C^d)(1 + dq^{-1}/dq)$$

where C^d is the capacity of the diffuse layer, which for a 1:3 electrolyte is given by:

$$[10] \quad C^d = \frac{3AF}{2RT} \frac{e^{3y} - e^{-y}}{(e^{3y} + 3e^{-y} - 4)^{1/2}}$$

C^i was then divided into two components in accordance with:

$$[11] \quad 1/C^i = 1/{}_qC^i + (1/{}_{q^{-1}}C^i)(dq^{-1}/dq)$$

where ${}_qC^i$ is the inner layer capacity at constant specific adsorption and ${}_{q^{-1}}C^i$ the capacity at constant charge on the metal, defined respectively by:

$$[12] \quad {}_qC^i = (\partial q/\partial \phi^{M-2})_{q^{-1}}$$

and

$$[13] \quad {}_{q^{-1}}C^i = (\partial q^{-1}/\partial \phi^{M-2})_q$$

As occurs in the majority of the systems studied previously, ${}_{q^{-1}}C^i$ is independent of the amount adsorbed (in agreement with the linearity and parallelism of the plots in Fig. 3) and may therefore be substituted by the corresponding integral capacity,

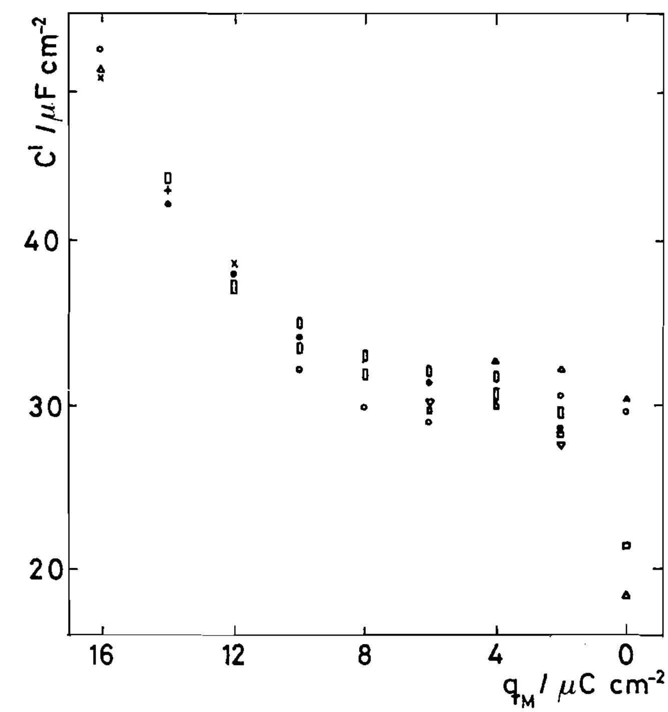

FIG. 4. Differential capacity of the inner layer of the mercury electrode in aqueous Na_3Cit as a function of the charge on the electrode and concentration of Na_3Cit: (▽) 0.01, (□) 0.02, (●) 0.05, (+) 0.1, (×) 0.2, (△) 0.5, and (○) 1 *M*.

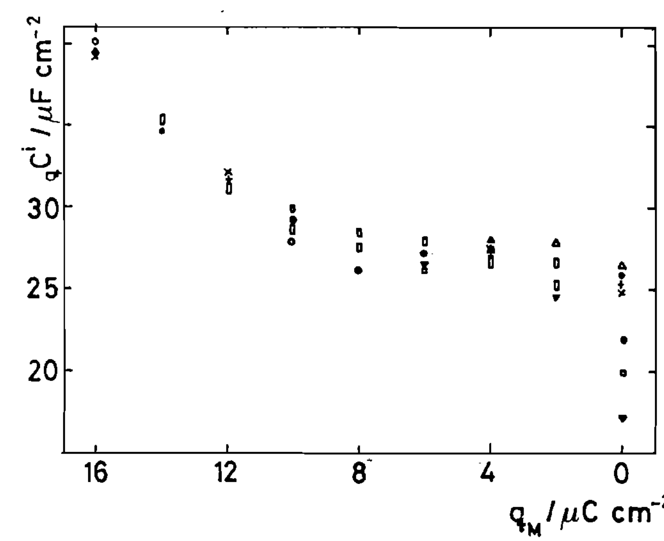

FIG. 5. Component of the capacity of the inner layer measured at constant amount adsorbed as a function of the charge on the metal and concentration of Na_3Cit: (▽) 0.01, (□) 0.02, (●) 0.05, (+) 0.1, (×) 0.2, (△) 0.5, and (○) 1 *M*.

${}_{q^{-1}}K^i$, the value of which in our system is 178 μF cm^{-2}.

The capacity of the total inner layer, C^i, and the capacity at constant charge adsorbed, ${}_qC^i$, are shown as a function of q for several concentrations of salt in Figs. 4 and 5. As can be observed, the values of both capacities depend greatly on the concentration for zero charge, but this dependence declines as the charge increases.

(c) Isotherm of adsorption

The results were fitted to a Frumkin-type isotherm as follows:

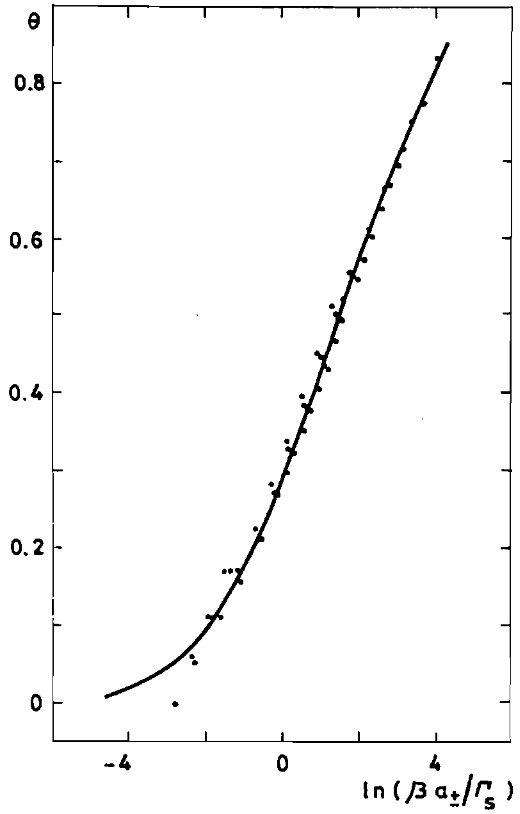

FIG. 6. Curve composed of the covering of specifically adsorbed citrate ions from solutions of Na_3Cit ($\theta = \Gamma/\Gamma_s$).

[14] $\ln [\theta/(1 - \theta)] + A\theta = \ln (\beta a_{\pm}/\Gamma_s)$

This adjustment is presented in Fig. 6, where the solid line is the theoretical curve and the values of the constants proved to be:

$A = 3$
$q_s^{-1} = 35\ \mu C\ cm^{-2}$; $\Gamma_s = 7.28 \times 10^{13}$ molecules cm^{-2}
$\ln \beta = 33.60 + 0.204q$

where A is the coefficient of lateral interaction, Γ_s the covering of saturation, q_s^{-1} equals $z_-F\Gamma_s$, and β is related with the standard free energy of adsorption at zero covering, according to:

[15] $\beta = \exp (-\Delta G^0/RT)$

The high value of the area of saturation per anion (137 Å^2/anion) suggests that the plane of the molecule is parallel to the surface of the Hg, the said orientation remaining practically constant since the results can be adjusted to a single isotherm with a constant value of the coefficient of lateral interaction, A.

In 1958, Grahame (14) proposed the use of the following adsorption isotherm:

[16] $-q^{-1} = a_{\pm} \exp (\Phi - z\phi_1 F)/RT$

where the free energy of adsorption is expressed arbitrarily as the sum of a chemical term (Φ), analogous to the potential of specific adsorption by Stern and an electrical term ($z\phi_1 F$), where ϕ_1 is the inner Helmholtz potential corresponding to the plane of the closest approach of the anion. Expression [16] was later modified by Parsons *et al.* (15) to give

[17] $(RT/z_-F) \ln (-q^{-1}/a_{\pm}) + \phi_2$
$= (\Phi/z_-F) - (q/{}_{q^{-1}}K^{i}) - (\lambda/{}_{q^{-1}}K^{i})q^{-1}$

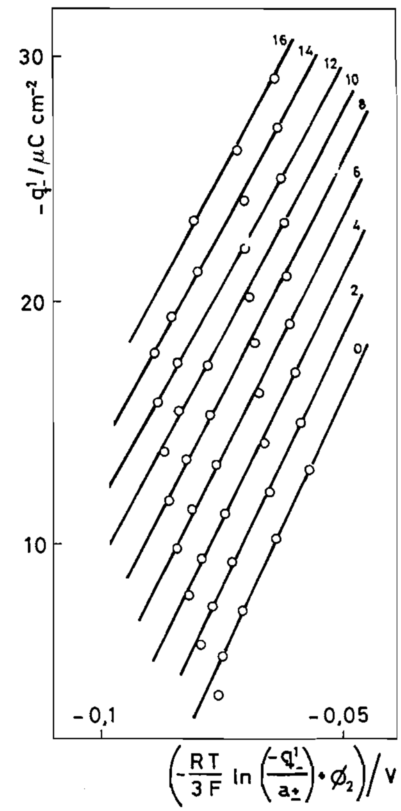

FIG. 7. Test of eq. [17] for adsorption of citrate on Hg. The numbers above the lines indicate charge on the electrode in $\mu C\ cm^{-2}$.

TABLE 3. Properties of the internal region in presence of adsorbed citrate ion

$q/\mu C\ cm^{-2}$	${}_qK/\mu C\ cm^{-2}$	$(x_2 - x_1)/x_2$	λ	g
16	29.80	0.167	0.486	0.617
14	28.50	0.160	0.495	0.601
12	27.50	0.154	0.495	0.597
10	26.91	0.151	0.474	0.614
8	26.62	0.150	0.445	0.653
6	26.27	0.148	0.445	0.651
4	25.85	0.145	0.445	0.649
2	24.61	0.138	0.445	0.644
0	23.05	0.129	0.445	0.637

where λ is defined by means of the equation:

[18] $\phi_1 - \phi_2 = [{}_q\phi^{M-2}(x_2 - x_1)/x_2] + {}_{q^{-1}}\phi^{M-2}\lambda$

The plot of the first term of eq. [17] against q^{-1} appears in Fig. 7. The adjustment of the points to straight lines supports the validity of the application of this isotherm to our system. The values of λ given in Table 3 which remain constant along the range $q = 8$ to $q = 0$, were obtained from the slopes of the lines.

The same table gives the value of $(x_2 - x_1)/x_2$, obtained by means of the expression:

[19] $(x_2 - x_1)/x_2 = {}_qK/{}_{q^{-1}}K$

together with the value of the potential of the autoatmosphere of the adsorbed ion, g, as given by:

[20] $\lambda = 1 - gx_1/x_2$

It is evident that g is smaller than the unit, as in the case of the

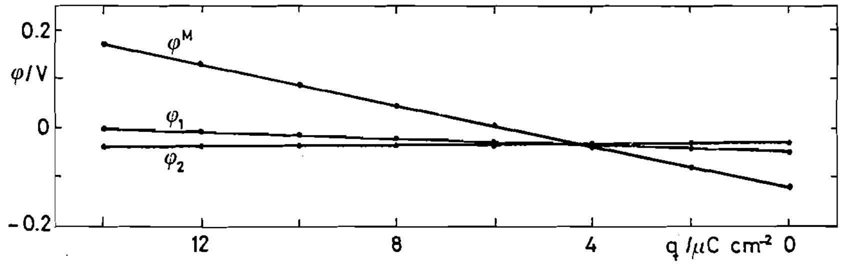

FIG. 8. Potentials in the double layer of the mercury electrode in Na_3Cit 0.1 *M* at 25°C, as a function of the charge on the electrode; ϕ^M is the part of the electrode–solution potential due to free charges, ϕ_1 is the potential of the IHP, ϕ_2 the potential of the OHP.

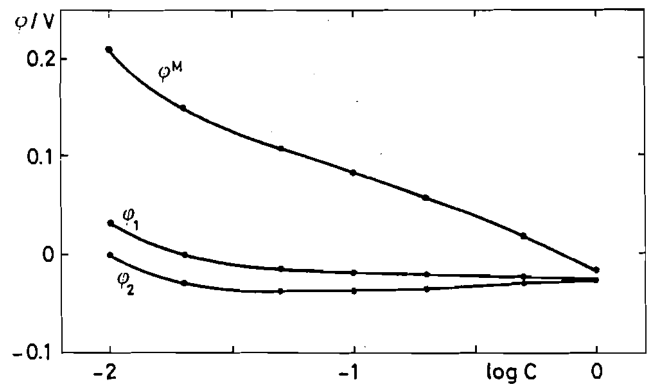

FIG. 9. Potentials in the double layer of a mercury electrode having 10 μC cm^{-2} in an aqueous solution of Na_3Cit as a function of the concentration of the solution.

azide ion (15) and the benzenedisulfonate ion (12). Given the experimental errors, g is practically independent of charge (see Table 3) supporting the prediction that the potential drop across the inner layer is additively composed of contributions from the layer on the metal and from the charge on the adsorbed layer.

The lines in Fig. 7 are parallel within the range $q = 0-16$ μC cm^{-2}. It seems reasonable therefore to conclude that the model is approximately correct in this range and that

$$g = 0.645$$
$$(x_2 - x_1)/x_2 = 0.14$$
$$\lambda = 0.445$$

The inner layer potential can be calculated from these values of the parameters by means of the equation

$$[21] \quad \phi_1 - \phi_2 = (q + \lambda q^{-1})/_{q^{-1}}K$$

The results are shown in Figs. 8 and 9; in the former they are given as a function of the charge on the mercury for a fixed concentration in the solution, while in the latter they appear as a function of the concentration for a fixed charge on the surface of the Hg. Together with ϕ_1, these figures show the external potential of Helmholtz (ϕ_2) and the part of the metal–solution potential due to free charges, ϕ^M. It should be noted that ϕ^M includes any change in potential due to the orientation of the molecules of solvent which is different from the point of zero charge.

The potential of specific adsorption, Φ, originally introduced by Stern (16), which coincides with the standard free energy of adsorption with a changed sign, can also be determined. This results in

$$\Phi = -\Delta G^0_{\text{ads}} = 20 \pm 5 \text{ kJ/mol}$$

for this system.

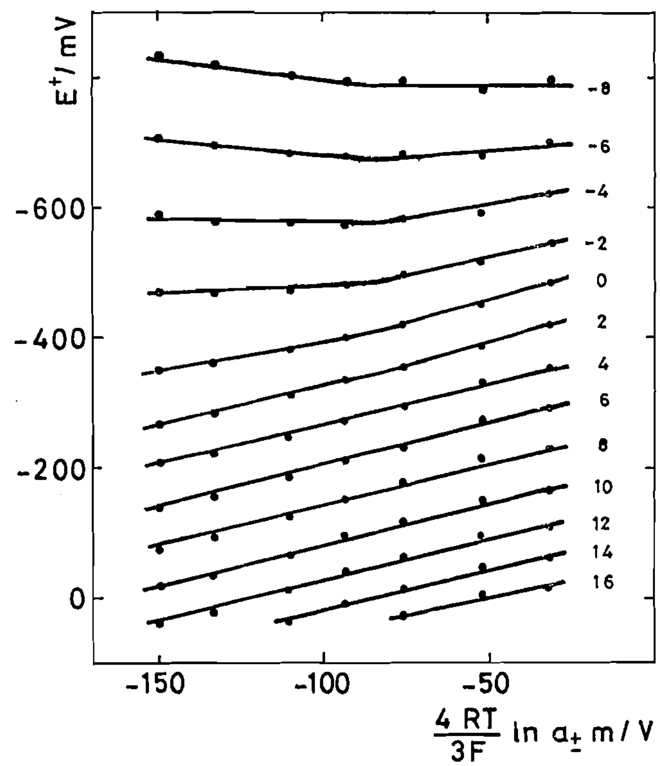

FIG. 10. Esin and Markov plots for solutions of Na_3Cit.

(d) Esin–Markov coefficient

The thermodynamic equation:

$$[22] \quad -d\xi = (4RT/3F)\Gamma_- \, d \ln a_\pm - E^+ dq$$

allows the following relation to be established:

$$[23] \quad (\partial E^+/\partial \mu)_q = -(\partial \Gamma_-/\partial q)_\mu$$

The excess of anions at the surface, Γ_-, may be separated into two contributions: that due to the specifically adsorbed charge and that due to the diffuse layer, in such a way that

$$[24] \quad z_- F(\partial E^+/\partial \mu)_q = -[(\partial q^{-1}/\partial q)_\mu + (\partial q^{\text{d}}_-/\partial q)_\mu]$$

The concentration of anions in the diffuse layer varies very little with q in the present system; the second term on the right-hand side of eq. [24] can be rejected and the Esin–Markov coefficient estimated by means of the first term.

In Fig. 10, E^+ is plotted against the chemical potential of the salt for integer values of q. The graphs are practically linear for $q > 2$ μC cm^{-2}, with slopes close to one. This is in agreement with the values obtained for $\delta q^{-1}/\delta q$ from the plots of q^{-1} vs. q (Fig. 2).

The results given above present marked differences from those obtained by other authors (2) and must be attributed to different experimental conditions.

1. S. V. ALVAREZ. Thesis. University of La Laguna, Spain. 1983.
2. R. G. BARRADAS, B. J. DONALDSON, and D. W. SHOESMITH. J. Electroanal. Chem. **41**, 243 (1973).
3. M. SLUYTERS-REHBACH, B. TIMMER, and J. H. SLUYTERS. Z. Phys. Chem. **52**, 89 (1967).
4. M. A. V. DEVANATHAN and P. PERIES. Trans. Faraday Soc. **54**, 1239 (1950).
5. D. C. GRAHAME, E. M. COFFIN, J. I. CUMMINGS, and M. A. POTH. J. Am. Chem. Soc. **74**, 1207 (1952).
6. M. M. PETIT-RAMEL and I. KHALIL. Bull. Soc. Chim. Fr. **7**, 1255 (1974).
7. R. PARSONS. Trans. Faraday Soc. **51**, 1518 (1955).
8. A. N. FRUMKIN. Z. Fiz. Khim. **30**, 2066 (1966).
9. H. S. HARNED and B. OWENS. The physical chemistry of electrolytic solutions. New York. 1958.
10. D. C. GRAHAME. J. Chem. Phys. **21**, 1054 (1953).
11. D. C. GRAHAME and R. PARSONS. J. Am. Chem. Soc. **83**, 1291 (1961).
12. J. M. PARRY and R. PARSONS. Trans. Faraday Soc. **59**, 241 (1963).
13. R. PAYNE. J. Electrochem. Soc. **80**, 4201 (1958).
14. D. C. GRAHAME. J. Am. Chem. Soc. **80**, 4201 (1958).
15. C. V. A'ALKAINE, E. R. GONZÁLEZ, and R. PARSONS. J. Electroanal. Chem. **32**, 57 (1971).
16. O. STERN. Z. Elektrochem. **30**, 508 (1924).

Charge distributions and chemical effects. XXXVII. Note on tetracyclo[4.1.0.0^{2,4}.0^{3,5}]heptane

J. BRIDET, M.-T. BÉRALDIN, AND S. FLISZÁR
Département de Chimie, Université de Montréal, C.P. 6210, Succ. A, Montréal, Qué., Canada H3C 3V1

Received October 24, 1984

J. BRIDET, M.-T. BÉRALDIN, and S. FLISZÁR. Can. J. Chem. **63**, 2468 (1985).

Full geometry and ζ optimizations are a must in the study of small cycles, as in tetracyclo[4.1.0.0^{2,4}.0^{3,5}]heptane. Indeed, nonoptimized STO-3G calculations suggest the 4-carbon to be electron richer than the carbon in 3 position, whereas the reverse is shown by optimized calculations ($q_C^{\text{Mulliken}} = -150$ vs. -138 me for C-3 and C-4, respectively). The latter result is in accord with the general trends indicating that a gain in local 2s charge is accompanied by a downfield nmr shift (δ 22.1 for C-3 and −4.0 ppm for C-4, from tetramethylsilane). These charge and shift results can be directly compared to one another because the local geometries (namely, the angles) about these two carbon atoms are very similar. This, however, is not the case with other carbon atoms of 3-membered cycloalkanes, a situation restricting the validity of simple charge–shift correlations in this class of compounds because of the changes in local geometry affecting the hybridization of carbon.

J. BRIDET, M.-T. BÉRALDIN et S. FLISZÁR. Can. J. Chem. **63**, 2468 (1985).

Il est absolument nécessaire de connaître la géométrie globale ainsi que les optimisations ζ pour étudier les petits cycles, comme le tétracyclo[4.1.0.0^{2,4}.0^{3,5}]heptane. En effet, des calculs non-optimisés au niveau STO-3G suggèrent que le carbone en 4 est plus riche en électrons que le carbone en position 3; par ailleurs, des calculs optimisés ($q_C^{\text{Mulliken}} = -150$ vs. -138 me respectivement pour les carbones en positions 3 et 4) montrent le contraire. Ce dernier résultat est en accord avec les tendances générales indiquant qu'un gain de charge locale 2s est accompagné par un déplacement vers les bas champs de la rmn (δ relatif au tétraméthylsilane de 22,1 pour C-3 et de −4,0 ppm pour le C-4). On peut comparer directement ces résultats pour les charges et les déplacements les uns aux autres parce que les géométries locales (à savoir, les angles) autour de ces deux atomes de carbones sont très semblables. Ceci n'est toutefois pas le cas avec les autres atomes de carbone des cycloalkanes à trois chaînons; cette situation restreint la validité de corrélations simples charge–déplacement dans cette classe de composés à cause des changements dans la géométrie locale affectant l'hybridisation du carbone.

[Traduit par le journal]

Introduction

The magnetic shielding of any nucleus in a molecule depends on both local and nonlocal contributions. For heavy nuclei (e.g., ^{13}C), any change in shielding accompanying structural modifications is primarily governed by its local paramagnetic part, i.e., $\Delta\sigma_{\text{total}} \simeq \Delta\sigma^{\text{p}}_{\text{local}}$: this offers a justification for postulated correlations between nuclear magnetic resonance shifts and atomic charges which, of course, are strictly local properties (1). Indeed, a number of such correlations are known for ^{13}C, ^{17}O, and ^{15}N nuclei (2–5).[1]

A case in point is that of sp^3 hybridized carbon atoms in normal and branched paraffins and in the cyclohexane series, including polycyclic hydrocarbons constructed from chair and/or boat cyclohexane rings (2–4). Their ^{13}C nmr shifts, δ_C, are accurately described (with a standard deviation of ~0.3 ppm) by the equation

$$[1] \quad \delta_C = -237.1(\Delta q_C/q_C^0) \text{ (ppm from } C_2H_6)$$

in which q_C^0 = net atomic charge of the ethane carbon (taken as reference) and Δq_C is the difference in C net charge with respect to that of ethane.[2] Note that for these carbon atoms any increase in local electron population (more negative Δq_C) results in a downfield shift (2–4).

In contrast, a remarkable study of bicyclo[n.1.0]hydrocarbons by Christl (9) reveals an anomaly in the case of tetracyclo[4.1.0.0^{2,4}.0^{3,5}]heptane **1** at carbons 3 and 4.

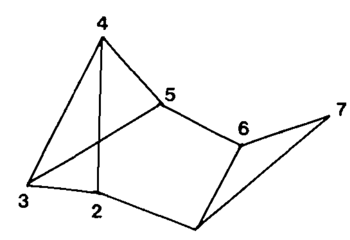

Indeed, Christl's nonoptimized STO-3G calculations suggest the 4-carbon (at −4.0 ppm from tetramethylsilane) to be

TABLE 1. Selected optimized geometry parameters^a (angles in decimal degrees, distances in Å)

Angle	Calcd.	Distance	Calcd.
$C_6C_1C_7$	59.8	C_1C_2	1.527
$C_6C_1C_2$	103.3	C_2C_3	1.540
$C_2C_1C_7$	116.6	C_2C_4	1.526
$C_3C_2C_4$	56.3	C_3C_4	1.445
$C_1C_2C_3$	108.3	C_1C_6	1.515
$C_1C_2C_4$	109.7	C_1C_7	1.506
$C_2C_3C_4 = C_4C_3C_5$	61.4	C_1H	1.082
$C_2C_3C_5$	92.0	C_2H	1.082
$C_2C_4C_3 = C_3C_4C_5$	62.4	$C_3H = C_4H$	1.077
$C_2C_4C_5$	93.1	C_7H endo	1.083
$C_1C_7C_6$	60.4	C_7H exo	1.083

^{a}Additional informations available upon request.

[1]These correlations, however, are not of a universal nature: separate correlations apply, e.g., to alkane sp^3 carbons, ethylenic or benzenic sp^2 carbons, depending on the type (σ or π) of electrons involved in the structure-dependent changes of local electron populations (2, 3). Charge-nmr shift relationships are not free from conceptual difficulties and have drawbacks of their own (2, 6–8). It is, therefore, important to be aware of the limitations restricting their utilization.

[2]The proper (*ab initio*) evaluation of charges involves careful optimizations of all variational (geometry and ζ) parameters — a task which is practically feasible only in minimal basis set calculations. Now, both Δq_C and q_C^0 are basis set dependent in numerical *ab initio* calculations, the ratio $\Delta q_C/q_C^0$, however, is not: hence our choice for the fully optimized STO-3G method.

TABLE 2. Optimized STO-3G results and nmr shifts of **1**[a]

Atom (s)	ζ_K	ζ_L	$N(1s)$	$N(2s)$	$N(2p)$	q_C	δ_C
C-1, C-6	5.70465	1.72335	1.9911	1.1446	2.9086	−44.3	17.3
C-2, C-5	5.70469	1.71731	1.9913	1.1590	2.8706	−20.9	38.4
C-3	5.70309	1.69431	1.9920	1.1754	2.9828	−150.2	22.1
C-4	5.70341	1.70087	1.9917	1.1602	2.9862	−138.1	−4.0
C-7	5.70454	1.71940	1.9911	1.1545	2.9731	−118.7	17.6

[a]The atom numbering is indicated in text. Electron populations, N, are in electron units, net atomic charges in me (= 10^{-3} e) units. The nmr shifts (ppm, downfield from tetramethylsilane) are taken from ref. 9. The hydrogen ζ's are 1.21011 (H_1), 1.22100 (H_2), 1.21193 (H_3), 1.23992 (H_4), 1.21053 (H_7*endo*), and 1.20987 (H_7*exo*).

electron richer than the carbon in 3 position (δ 22.1 from TMS), at variance with the trend indicated by eq. [1].

Of course, carbon electrons of 3- and 6-membered cycles should not be considered on the same footing because of geometry related differences in s (vs. p) character;[3] nor is it certain that positions 3 and 4 of **1** can safely be compared to one another because their local geometries and, hence, possible differences in their s character are presently not known. The apparent reversal in charge−shift trend mentioned above could thus be ascribed to a hybridization-related "special feature" regarding carbon electrons in 3-membered cycles or/and to a possible difference in local geometry about atoms 3 and 4, affecting their hybridization. Briefly, a number of reasons can be given in the present context in order to render our ignorance less visible, but they offer no replacement for an investigation into that matter.

Computational results

A standard STO-3G calculation of **1** was performed following Pople's recipe (13). Mulliken's population analysis (14) was adopted, which is reasonable because any bias possibly resulting from the half-and-half partitioning of overlap populations (which is part of this analysis) would cancel in a comparison between carbons 3 and 4. Just as in Christl's calculation (9), C-4 appeared to be somewhat electron richer than C-3, by ~10 me (10^{-3} e units).

Next, a full geometry optimization was carried out, at the STO-3G level. From the results indicated in Table 1, it is clear that the local geometries about atoms 3 and 4 are virtually the same, thus suggesting that these positions are comparable.

Finally, all ζ parameters were carefully optimized — a point which is important because atomic charges are very sensitive to the molecular environment and, hence, to ζ optimization: the most consistent charge results are obtained when this optimization is carried out at its best for each atom (or group of equivalent atoms) of the molecule under study (2, 15, 16). Each energy minimization was carried out until stable charges were obtained, within ~0.01 me. The results are indicated in Table 2.

Discussion

With charges like those described in Table 2, it is important to be aware that they should not be taken at their face value. These are Mulliken charges, including throughout a half-and-half partitioning of overlap populations in their computation. Now, this assignment of overlap terms may carry an error in situations involving heteronuclear atom pairs (as in CH bonds in the present case) — a problem discussed earlier in detail (2, 4, 15−18). (It remains true, however, that Mulliken charges are of undisputed value provided, of course, they are used with due care, in comparisons assorted with an assessment of their validity.) For this reason, the Mulliken net charge deduced for C-7, bearing two H atoms, is not to be compared to the charges of the other C atoms, bearing only one H atom.

Next, we must examine whether the other carbon charges indicated in Table 2 can all be considered on the same footing. The answer is no. Indeed, the STO-3G populations calculated for carbons 1−6 vary in an apparently uncorrelated manner both at the $2s$ and $2p$ levels. This may well be related to the local geometries (Table 1), differing for C-1,6, C-2,5, and C-3,4, i.e., to small changes in hybridization.[3] In that event, however, a comparison encompassing the charges of carbons 1−6 could be accepted only if made using results deduced from sufficiently large basis sets (e.g. 4-31 G, or larger) after configuration interaction. This is because the contribution of excited states, and the ensuing corrections in charge results following CI, depend markedly on the state of hybridization. Minor in the case of alkanes like methane, ethane, etc. (16), they are very important in unsaturated hydrocarbons like ethylene,[4] suggesting that proper inclusion of CI is also a must before valid assessments can be made regarding charge effects accompanying changes in local geometry in highly strained systems like **1**. Briefly, the STO-3G charges obtained in this work for C-1,6 and C-2,5 should not be considered on the same footing as those deduced for C-3 and C-4.

This brings us to carbon atoms 3 and 4. Their local geometries are virtually the same, meaning that these two positions can reasonably be compared to one another, without fearing any significant bias related to geometry-dependent differences in hybridization. Their $2p$ atomic populations are also almost the same, within ~3 me. These positions differ essentially in their $2s$ populations, atom 3 being ~15 me electron richer than C-4. The situation is thus similar to that encountered with paraffins and cyclohexanic hydrocarbons obeying eq. [1]: car-

[3]Del Re and co-workers (10) were concerned with the relation of s character in hybrids to bond angles and have considered hybridization as described by local orbitals, determined by requiring that hybrids on different atoms have minimal overlap unless they participate in the same bond. Alternate approaches are provided by Wiberg (11) and by Trindle and Sinanoğlu (12). Calculated p characters are in good agreement with estimates derived from nmr coupling constants (11, 12). Evaluations of hybridization are anticipated to assist in future work on charge−shift correlations in cases suspected of presenting changes in local geometry.

[4]Current work indicates that configuration interaction affects the final carbon charge of ethylene by more than 120 me at the 4-31G level (C. Mijoule, J.-M. Leclercq, and S. Fliszár, unpublished results), as compared with a correction of ~5 me for the ethane carbon atom (16).

bons 3 and 4 are virtually in the same state of hybridization and charge variations occur at the 2*s* level. In conclusion, present optimized results are now in general accord with the trend (eq. [1]) indicating that (under otherwise similar conditions) a gain in local 2*s* charge is accompanied by a downfield ^{13}C nmr shift, whereas nonoptimized calculations would suggest the contrary.

Acknowledgements

Financial support given by the National Research Council of Canada and the cooperation of the "Centre de Calcul de l'Université de Montréal" are gratefully acknowledged.

1. E. C. VAUTHIER, S. FLISZÁR, F. TONNARD, and S. ODIOT. Can. J. Chem. **61**, 1417 (1983).
2. S. FLISZÁR. Charge distributions and chemical effects. Springer-Verlag, New York, NY. 1983.
3. S. FLISZÁR, G. CARDINAL, and M.-T. BÉRALDIN. J. Am. Chem. Soc. **104**, 5287 (1982) and references therein.
4. S. FLISZÁR, A. GOURSOT, and H. DUGAS. J. Am. Chem. Soc. **96**, 4358 (1974); G. KEAN, D. GRAVEL, and S. FLISZÁR. J. Am. Chem. Soc. **98**, 4749 (1976).
5. M. COMEAU, M.-T. BÉRALDIN, E. C. VAUTHIER, and S. FLISZÁR. To be published.
6. D. G. FARNUM. Adv. Phys. Org. Chem. **11**, 123 (1975); G. L. NELSON and E. A. WILLIAMS. Prog. Phys. Org. Chem. **12**, 229 (1976).
7. G. J. MARTIN, M. L. MARTIN, and S. ODIOT. Org. Magn. Reson. **7**, 2 (1975).
8. W. J. HEHRE, R. W. TAFT, and R. D. TOPSOM. Prog. Phys. Org. Chem. **12**, 159 (1976).
9. M. CHRISTL. Chem. Ber. **108**, 2781 (1975); M. CHRISTL and W. BUCHNER. Org. Magn. Reson. **11**, 461 (1978).
10. A. VEILLARD and G. DEL RE. Theoret. Chim. Acta, **2**, 55 (1964); G. DEL RE, U. ESPOSITO, and M. CARPENTIERI. Theoret. Chim. Acta, **6**, 36 (1966).
11. K. B. WIBERG. Tetrahedron, **24**, 1083 (1968).
12. C. TRINDLE and O. SINANOĞLU. J. Chem. Phys. **49**, 65 (1968); J. Am. Chem. Soc. **91**, 853 (1969).
13. W. J. HEHRE, R. F. STEWART, and J. A. POPLE. J. Chem. Phys. **51**, 2657 (1969).
14. R. S. MULLIKEN. J. Chem. Phys. **23**, 1833 (1955); **23**, 1841 (1955); **23**, 2338 (1955); **23**, 2343 (1955).
15. S. FLISZÁR, G. KEAN, and R. MACAULAY. J. Am. Chem. Soc. **96**, 4353 (1974); G. KEAN and S. FLISZÁR. Can. J. Chem. **52**, 2772 (1974).
16. C. MIJOULE, J.-M. LECLERCQ, S. ODIOT, and S. FLISZÁR. Can. J. Chem. **63**, 1741 (1985).
17. H. HENRY and S. FLISZÁR. J. Am. Chem. Soc. **100**, 3312 (1978).
18. V. H. SMITH, JR. Phys. Script. **15**, 147 (1977).

An increased internal rotational barrier in thiophenol caused by *meta* substituents

TED SCHAEFER, JAMES D. BALEJA, AND GLENN H. PENNER
Department of Chemistry, University of Manitoba, Winnipeg, Man., Canada R3T 2N2

Received December 28, 1984

TED SCHAEFER, JAMES D. BALEJA, and GLENN H. PENNER. Can. J. Chem. **63**, 2471 (1985).

The twofold internal barriers to rotation about the C—S bond in 3,5-diX-thiophenols were determined in solution from long-range spin–spin coupling constants. They are 3.4, 4.8_5, 5.3, 6.4_5, and $7.2_5 \pm 10\%$ kJ/mol for X = H, CH_3, OCH_3, F, and Cl, respectively. In 3,5-dichloro-4-hydroxythiophenol, V_2 is −0.8 kJ/mol as compared to −1.9 kJ/mol in 4-methoxythiophenol. The *para* substituent here dominates. The observed barriers are in rough agreement with arguments based on perturbation molecular orbital theory and with MO calculations of changes in the barrier caused by substituents. The computed values appear as nearly pure twofold barriers with very small fourfold components.

TED SCHAEFER, JAMES D. BALEJA et GLENN H. PENNER. Can. J. Chem. **63**, 2471 (1985).

Faisant appel aux constantes de couplage spin–spin à longue distance et opérant en solution, on a déterminé les barrières internes binaires à la rotation autour de la liaison C—S de di-X-3,5 thiophénols. Pour des groupes X = H, CH_3, OCH_3, F et Cl, ces valeurs sont respectivement égales à 3,4, $4{,}8_5$, 5,3, $6{,}4_5$ et $7.2_5 \pm 10\%$ kJ/mol. Dans le cas du dichloro-3,5 hydroxy-4 thiophénol, la valeur de V_2 est égale à −0,8 kJ/mol; dans le cas du méthoxy-4 thiophénol, cette valeur est égale à −1,9 kJ/mol. Dans ce cas, l'influence du substituant en *para* est prédominant. Les barrières observées sont généralement en accord avec les arguments basés sur la théorie des perturbations des orbitales moléculaires ainsi qu'avec des calculs d'OM relatifs aux changements à la barrière qui seraient causés par les substituants. Il semble que les valeurs calculées soient pratiquement des barrières binaires pures et qu'elles ne contiennent que des faibles proportions de composantes quaternaires.

[Traduit par le journal]

Introduction

It is expected and observed that the barrier to rotation about the C—X bond in **1** is increased if X is a π electron acceptor such as C═O and Y is an electron donor such as OCH_3 or F (1–3). This behaviour is easily understood in terms of the increased mobile bond order of the C—X bond. More generally, the barrier to internal rotation or its equivalent, the stability of the planar conformation, will increase if X is a π electron acceptor and Y is a donor or vice versa, whereas the barrier will decrease if X and Y are both donors or both acceptors.

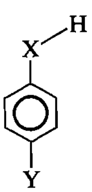

1

A good illustration is provided by *para* substituted thiophenols in which S—H is a π electron donor but conjugates relatively weakly with the π electron system of the ring. The twofold barrier to internal rotation, V_2, is only 3.4 kJ/mol (4) compared to 14.9 kJ/mol in phenol (4–7). In *p*-nitrothiophenol, V_2 rises to 9 kJ/mol, and drops to 0.4 kJ/mol in *p*-fluorothiophenol (8). In the presence of a *para* amino substituent the stable conformer becomes that in which the S—H bond prefers a plane perpendicular to the benzene plane, corresponding to a negative V_2 on this energy scale.

The barriers in the *p*-X-thiophenols are derived from $^4J^{H,H}$, the spin–spin coupling constants between the sulfhydryl and *ortho* ring protons (8), on the assumption that $^4J^{H,H} = {}^4J_{90} \langle \sin^2 \theta \rangle$. $^4J_{90}$ is the coupling when the S—H bond lies in a plane perpendicular to the benzene plane and is taken as −1.10 Hz on the basis of experimental evidence (8,9). The expectation value of $\sin^2 \theta$ is then given by $^4J^{H,H}/{}^4J_{90}$ and is related to the internal barrier to rotation about the C—S bond by a hindered rotor model (10).

It is interesting that the change in barrier, ΔV_2, computed for a series of six *p*-X-phenols (X = CH_3, OH, F, NO_2, NH_2, H) by STO 3G MO methods (11, 12), is related to ΔV_2 for the corresponding thiophenol derivatives, obtained in solution by the *J* method (8), by ΔV_2^{OH} (kJ/mol) = $0.75\, \Delta V_2^{SH} - 0.01$ (the correlation coefficient, *r*, is 0.999). Again, far infrared torsion data (5) yield ΔV_2^{OH} in cyclohexane solution. For X = F, CH_3, OCH_3, NO_2, H, these numbers are related to ΔV_2^{SH} by $\Delta V_2^{OH} = 0.72\, \Delta V_2^{SH} - 0.11$ kJ/mol ($r = 0.994$). These correlations are here taken to mean that the *J* method yields reasonable V_2 values in thiophenol derivatives and, perhaps, that the less strongly conjugated SH group is more easily perturbed by a substituent than is a hydroxyl group.

Much less is known about the perturbation of internal barriers caused by *meta* substituents. Calculations at the STO 3G level of *ab initio* molecular orbital theory (12) predict an increased barrier in phenol in the presence of σ electron withdrawing groups like F, NH_2, OH, in agreement with increased double bond character of the C—O bond. The increase is expected because the rather electronegative electron withdrawing groups lower the π* (antibonding) levels in phenol and cause enhanced conjugation of the OH group (perturbation MO model). However, although the latter is also calculated to increase in the presence of *meta* CN and NO_2 groups, the barrier itself is predicted to be lower than in phenol. Furthermore, the *meta* methyl group is also calculated to increase the barrier in phenol, yet it is hardly very electronegative. But it is a π donor. In toluene, the computed π electron densities at the *ortho* and *para* positions are higher than in benzene, but are lower at the *meta* position just as in fluorobenzene, anisole, or aniline. From this viewpoint, if F, NH_2, OH, and CH_3 groups decrease the π electron density at the *meta* position, then an increased V_2 in such phenols would be expected due to enhanced conjugation of the hydroxyl group.

The available experimental data (5) appear to relate to the torsional frequencies of some *m*-X-phenols in cyclohexane

TABLE 1. The spectral parameters for a 2.6 mol% solution of 3,5-difluorothiophenol in CCl_4, containing 10 mol% of cyclohexane-d_{12} and 0.5 mol% TMS at 298 K

Parameter	Value	Parameter	Value
ν_{SH}^{a}	1039.821(1)[b]	$^4J_{26}$	1.571(2)[c]
$\nu_2 = \nu_6$	2023.992(1)	$^4J_{35}$	7.213(1)
ν_4	1969.358(1)	$^3J_{34}$	8.853(1)
^4J(H, SH)	−0.249(1)	No. of peaks, ^{1}H	72
^5J(F, SH)	±0.066(1)	Assigned peaks	72
^6J(H, SH)	−0.248(1)	Calcd. transitions	112
$^3J_{23}$	8.463(2)	Assigned transitions	101
$^4J_{24}$	2.250(1)	rms error	0.005_4
$^5J_{25}$	−1.104(1)[c]	Largest difference	0.023

[a]Shifts are given in Hz at 300.135 MHz to low field of internal TMS.
[b]The numbers in parentheses are standard deviations in the last significant figure.
[c]$^5J_{25}$ and $^4J_{35}$ correlate with −0.50, so that only their sum or difference is known with high precision.

solution, from which it apears that NO_2, F, OCH_3, and CH_3 groups all cause an increase in V_2. The changes in V_2 are *much smaller* than for the corresponding *p*-X-phenols, being only 1.7 kJ/mol at most.

Although the J method does not lend itself to the determination of the relatively large V_2 in phenol derivatives, it is suitable for the smaller barriers in thiophenol derivatives. Accordingly, we here report on the use of ^4J and ^6J (also a $\sin^2\theta$ coupling) in the determination of V_2 in some 3,5-disubstituted thiophenol derivatives, **2**. The dinitro derivative was synthesized but its intermolecular proton exchange could apparently not be stopped in solvents in which it was sufficiently soluble for nmr measurements. $^4J^{H,H}$ was also measured in 4-chloro-3-sulfhydrylthiophenol, 3,4-dichlorothiophenol, and in 3,5-dichloro-4-hydroxythiophenol.

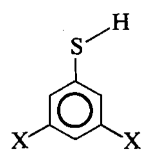

X = F, OCH_3, CH_3, Cl

2

Experimental

The asymmetric or trisubstituted thiophenols came from Aldrich. The 3,5-dichlorothiophenol was a Fairfield product. The 3,5-difluoro-, 3,5-dimethoxy-, 3,5-dinitro, and 3,5-dimethylthiophenols were prepared from the corresponding aniline derivatives via the xanthates (13, 14). A typical synthesis went as follows. 3,5-Difluoroaniline (2.58 g, 0.02 mol, Aldrich) was suspended in 16 mL H_2O containing 3.2 mL concentrated H_2SO_4. To the cooled (4°C) solution, 1.5 g $NaNO_2$ in 8 mL of water was added dropwise over 0.5 h. The solution was stirred for 1 h and was then added dropwise to a solution (50°C) of 6 g of potassium ethylxanthate in 20 mL of water over 0.5 h. The solution was stirred for 0.5 h and allowed to reach room temperature. The reddish solution was extracted with ether. The ether layer was washed twice with water, dried over $MgSO_4$, filtered, and the ether was removed to give a clear red oil. This xanthate ester was allowed to sit for 2 days over molecular sieve and was then transferred with dry ether washings to a 50-mL round bottomed flask. A suspension of $LiAlH_4$ in ether was added to the xanthate solution until frothing ceased. A little more $LiAlH_4$ was now added and the solution was stirred for 2 h. The product was extracted into ether, washed with dilute HCl, and twice with water. The ether solution was extracted into base (20% NaOH). Neutralization with concentrated HCl, extraction with ether, washing with water, and drying over $MgSO_4$ gave the product after solvent removal. An ^{1}H nmr spectrum in CCl_4 containing 10 mol% C_6D_{12} and 0.15 mol% TMS gave a spectrum characteristic of 3,5-difluorothiophenol: a δ(SH) of 3.46 together with splittings in the ring proton region due to long-range coupling to the sulfhydryl proton.

Samples for ^{1}H and ^{19}F nmr analysis were prepared in CCl_4 containing some cyclohexane-d_{12} and TMS or in benzene-d_6 containing some TMS (for chemical shift dispersion). These solutions were dried over molecular sieve and were then transferred to 5-mm od nmr sample tubes. Degassing by the freeze−pump−thaw procedure was followed by flame-sealing. Table 1 contains details about concentrations.

The ^{1}H nmr spectra were accumulated on HA100, WH90, and AM300 nmr spectrometers, following procedures recently given in detail (15, 16).

Molecular orbital calculations were performed with the program MONSTERGAUSS (17) on an Amdahl 470/V8 system.

Results and discussion

Spectral analyses

These were performed with the computer programs LAME (18, 19) and NUMARIT (20). The results of one analysis are given in Table 1, for 3,5-difluorothiophenol. Figure 1 displays the nmr spectrum of the sulfhydryl proton, illustrating the resolution of splittings as small as 0.066 Hz. Table 2 records the long-range couplings $^4J^{H,H} \equiv {}^4J$(H, SH) and $^6J^{H,H} \equiv {}^6J$(H, SH) for 8 compounds; these are the quantities of interest in this discussion.

V_2 *derived from* ^4J*(H, SH) and* ^6J*(H, SH)*

As described in detail previously (8), ^6J(H, SH) can be written as $-0.97\ \langle\sin^2\theta\rangle$ Hz where $\langle\sin^2\theta\rangle$ is the expectation value of $\sin^2\theta$ and is related to V_2, the temperature, and the reduced moment of inertia about the C—S bond; θ is the angle by which the S—H bond twists out of the ring plane. Similarly, ^4J(H, SH) is very likely given by $-1.10\ \langle\sin^2\theta\rangle$ Hz. Accordingly, for **2** one has two sources of V_2 and these are recorded in Table 2. In view of possible intrinsic substituent perturbations of ^4J and ^6J and of experimental errors in the couplings themselves, it is probably reasonable to take the mean of the two V_2 values for each compound as a basis for discussion.

Discussion of V_2 *trends*

In 4-X-thiophenol derivatives (8), V_2 is 3.4, 2.2, −1.9, 0.4, and 3.7 kJ/mol for X = H, CH_3, OCH_3, F, and Cl respectively, with errors of perhaps 10%. The strongest π electron donor, OCH_3, causes the largest decrease in V_2, as expected from the discussion above. In the corresponding 3,5-diX-thiophenol derivatives in Table 2, V_2 increases for X = CH_3, OCH_3, F, Cl

TABLE 2. Internal barriers to rotation about the C—S bond in some *meta* substituted thiophenol derivatives in solution

Compound	$-^4J^{H,H}$	$\langle \sin^2 \theta \rangle$[g]	V_2[i]	$-^6J^{H,H}$	$\langle \sin^2 \theta \rangle$[h]	V_2[i]
Thiophenol[a]	0.380(10)[f]	0.345	3.4	0.334(12)[f]	0.344	3.4
3,5-diMe[b]	0.316(5)	0.287	5.0	0.288(8)	0.296	4.7
3,5-diOCH_3[c]	0.279(10)	0.254	6.0	0.299(11)	0.308	4.6
3,5-diF[d]	0.249(1)	0.226	7.0	0.248(1)	0.256	5.9
3,5-diCl[e]	0.233(5)	0.212	7.4	0.221(5)	0.227	6.9
3,4-diCl[a]	0.376(6)[j]	0.342	3.5	—	—	—
4-Cl-3-SH[a]	0.384(5)[k]	0.354	3.2	—	—	—
3,5-diCl-4-OH[a]	0.590(2)[l]	0.537	−0.8[m]			

[a]For a 5.0 mol% solution in CCl_4 at 305 K.
[b]For a 0.5 mol% solution in benzene-d_6 at 300 K.
[c]For a 1.8 mol% solution in CCl_4 at 300 K.
[d]For a 2.6 mol% solution in CCl_4 at 298 K.
[e]For a 5.0 mol% solution in benzene-d_6 at 305 K.
[f]Numbers in parentheses are the standard deviations in the last one or two significant figures.
[g]Derived from $^4J = -1.10 \langle \sin^2 \theta \rangle$.
[h]$^6J = -0.97 \langle \sin^2 \theta \rangle$.
[i]In kJ/mol for rotation about the C—S bond.
[j]The average of −0.371 and −0.382 Hz for the two distinct *ortho* protons.
[k]The two distinct couplings to the *ortho* protons are −0.384(5) and −0.385(5) Hz.
[l]In a 4 mol% solution in $CDCl_3$, ^4J is −0.590(7) Hz, is −0.561(2) Hz in a 4 mol% solution in CS_2, −0.541(3) Hz in 5 mol% benzene-d_6, and is −0.531(4) in a 4 mol% solution in CH_2Cl_2.
[m]A negative V_2 means that the S—H bond prefers $\theta = 90°$, that is, a plane perpendicular to the benzene plane.

FIG. 1. The ^1H nmr spectrum of the sulfhydryl proton of a 2.6 mol% solution of 3,5-difluorothiophenol in CCl_4 at 298 K and 300 MHz. The splittings of 0.066 Hz caused by coupling to the two ^{19}F nuclei are clearly visible. The couplings to the *ortho* and *para* protons are almost identical, leading to the "quartet" structure in this nearly first-order spectrum.

and is largest when X = Cl, in contrast to the smallest change caused by X = Cl in the 4-X-thiophenols. Qualitatively, the increased V_2 values increase with inherent (gas) values of σ_m (21), the latter being −0.02, 0.06, 0.27, and 0.36 for CH_3, OCH_3, F, and Cl, respectively. However, on this basis the CH_3 group should cause a decrease in V_2, contrary to observation.

In terms of PMO theory (12, 22), and taking the SH group as a electron donor, the electronegative OCH_3, F, and Cl substituents lower the energy of the (almost empty) π^* orbital, leading to increased conjugation of the SH group and therefore to a higher barrier. Furthermore, considering OCH_3 and F as π electron donors, PMO theory predicts (22) an increase in π donation by both substituents (SH and the *meta* substituent) because each substituent now donates into different π^* orbitals, whose energies have been lowered by the electronegative nature of F and OCH_3. The Cl substituent is presumably a poor π electron donor (note small change in V_2 for 4-chlorothiophenol) and the large increase in V_2 must then be attributed to the first cause above. However, the CH_3 group is not very electronegative, so that the qualitative model is not entirely consistent in its predictions. Unfortunately, our attempts at the measurement of ^4J and ^6J in 3,5-dinitrothiophenol were unsuccessful. The nitro group is a π and σ electron acceptor, unlike the substituents under consideration here.

Alternatively, a simpler qualitative model recognizes that CH_3, OCH_3, and F groups, for example, while increasing π electron densities at *ortho* and *para* positions, are calculated (12, 23) to decrease them at *meta* positions. In that event, increased conjugation of the sulfhydryl group is expected, leading to a higher barrier. However, such an interpretation hardly holds for *meta* chlorine substituents.

In this connection it is interesting that the *para* substituent in 3,5-dichloro-4-hydroxythiophenol dominates as a determinant of V_2, which is −0.8 kJ/mol. Thus, in 4-methoxythiophenol (modelling a 4-hydroxy group) V_2 is −1.9 kJ/mol and in 3,5-dichlorothiophenol V_2 becomes 7.1 kJ/mol. In other words, the *meta* substituents cause only a small change in V_2 of 4-hydroxythiophenol, but a large change in V_2 in the absence of the 4-substituent. This conclusion is consistent with the observation of a V_2 of 3.5 kJ/mol in 3,4-dichlorothiophenol, it being 3.4 in thiophenol and 3.7 in the 4-chloro derivative. In a sense, the *para* substituent causes a first-order perturbation and, *in its presence*, a *meta* substituent is a second-order perturber. Although the PMO model provides *some* insight into the substituent effects on V_2 for the thiophenol derivatives in Table 2, it does not yield quantitative data. Accordingly, geometry-optimized computations of V_2 were carried out for some of the compounds.

Table 3 contains the theoretical data on the barriers to rotation about the C—S bond for a variety of subtituents. In these computations all bond angles and bond lengths were optimized with the constraint, however, that the benzene framework re-

TABLE 3. Computed barriers to rotation about the C—S bond in some thiophenol derivatives. Geometry-optimized STO 3G MO[a]

Compound[b]	A^c (kJ mol^{-1})	B^c	Compound	A^c (kJ mol^{-1})	B^c
4-H	14.74(2)	0.20(1)	3,4-diCl	16.15(1)	0.13(1)
4-CH_3	13.8	—	3,5-diCl	15.60(4)	0.09(5)
4-F	13.2	—	3,5-diCH_3	15.52(1)	0.13(1)
4-OCH_3	12.2	—	3,5-diOCH_3	17.60(1)	0.09(1)
4-OH	11.76(1)	0.26(1)	3,5-diF	16.99(2)	0.11(2)
4-NH_2	11.9	—	3-F[d]	15.90(2)	0.41(3)
4-Cl	15.9(2)	0.17(2)	3,5-diCl-4-OH	11.99(2)	0.24(1)

[a]The benzene framework is a hexagon but all other bond angles and bond lengths are optimized.

[b]The experimental values for most of the 4-X-thiophenols are given in the text. That for X = NH_2 is -2.9 ± 0.4 kJ/mol (8).

[c]$V = A \sin^2\theta + B \sin^2 2\theta$ where θ is the angle by which the S—H bond twists out of the benzene plane. Therefore A and B represent the magnitudes of the twofold and fourfold components of the barrier, respectively.

[d]The energy difference between the *cis* and *trans* planar conformers is computed as insignificant (less than 0.05 kJ/mol).

main a regular hexagon. Computations were done at 15° intervals for θ, varying the latter between 0 and 90°. The relative energies were then fit to a $A \sin^2\theta + B \sin^2 2\theta$ curve, where A represents V_2 and B represents V_4. It became clear that V_4 is rather small, so that in the interests of economy calculations were performed only at 0° and 90° for some of the 4-X-thiophenols.

Just as for phenol (11, 12), V_2 is overestimated for thiophenol at the STO 3G level of *ab initio* MO theory. Thus, the barrier in kJ/mol is calculated as $14.74(2) \sin^2\theta + 0.20(1) \sin^2 2\theta$ at the 95% confidence level, the measured value in the gas phase being 3.4 kJ/mol (4). A significant correlation exists, however, between the computed and observed changes, ΔV_2, caused by the substituents. For the 4-X-thiophenols in Table 3, ΔV_2 (theor) = $0.20 + 0.53\, \Delta V_2$ (exp) with $r = 0.956$. If all compounds, except for 3,5-dichlorothiophenol, are included in the correlation, then ΔV_2 (theor) = $0.41 + 0.63\, \Delta V_2$ (exp) with $r = 0.952$. In view of the much better correlations presented in the introduction to this paper, it may be that the theoretical values are the less reliable.

Of course, the measured barriers may well depend somewhat on solvent. Although the 3,5-dichloro compound presents problems of chemical shift dispersion, its 4-hydroxy derivative does not. Accordingly ^4J(H, SH) for the latter was also measured in CH_2Cl_2, C_6D_6, CS_2, and $CDCl_3$ solutions (apparent decomposition occurred in CH_3CN, CH_3NO_2, $(CH_3)_2C{=}O$, and DMSO solutions), yielding $-^4J$ as 0.531(4), 0.541(3), 0.561(2), and 0.590(7) Hz, respectively. These numbers correspond to an increase of 1.2 kJ/mol in V_2 on going from CCl_4 solution (Table 2) to the rather polar CH_2Cl_2 solution. Relative to the CCl_4 solution, V_2 increases by 1 kJ/mol in C_6D_6 solution. The 3,5-dichlorothiophenol spectra were measured in C_6D_6, but it would seem that only about 1 kJ/mol of the relatively large discrepancy of 2.8 kJ/mol between the experimental value and that given by the correlation above can be accounted for in this way.

The situation is unsatisfactory, particularly because such a large discrepancy between theoretical and experimental values does not exist for 3,4-dichlorothiophenol, being less than 1 kJ/mol.

The computation for 3-fluorothiophenol implies that ΔV for *meta* substituents is additive, being 1.2 kJ/mol for the mono- and 2.3 kJ/mol for the difluoro derivatives. It would be interesting to know the microwave and far infrared data for these molecules.

Finally, the barrier to rotation for the 1-SH group in 3-mercapto-4-chlorothiophenol appears to be twofold, because the two $^4J^{H,H}$ values for this group are the same, and unchanged from its value in thiophenol. Because a 4-chloro substituent perturbs V_2 very slightly, if at all (Table 2), it follows that in its presence a 3-mercapto substituent is ineffective in altering the barrier. Parenthetically, ^5J(H, SH) for the 1-SH proton is 0.259 Hz. ^5J has been written as $0.196 \langle \sin^2\theta \rangle + 0.180$ for a twofold barrier, so that ^5J is computed as 0.248 Hz, in reasonable agreement with the observed number.

Acknowledgments

We are grateful to the University of Manitoba for some computing time and to the Natural Sciences and Engineering Research Council of Canada for financial assistance. We are grateful to Dr. S. Salman for the spectral data on 3-mercapto-4-chlorothiophenol.

1. F. A. MILLER, W. G. FATELEY, and R. E. WITOWSKI. Spectrochim. Acta Part A, **23**, 891 (1967).
2. F. A. L. ANET and M. AHMAD. J. Am. Chem. Soc. **86**, 119 (1964).
3. T. DRAKENBERG, J. SOMMER, and R. JOST. J. Chem. Soc. Perkin Trans. 2, 363 (1980).
4. N. W. LARSEN and F. M. NICOLAISEN. J. Mol. Struct. **22**, 29 (1974).
5. W. G. FATELY and G. L. CARLSON. Pure Appl. Chem. **36**, 109 (1973).
6. E. MATHIER, D. WELTI, A. BAUDER, and HS. H. GÜNTHARD. J. Mol. Spectrosc. **37**, 63 (1971).
7. H. D. BIST, J. C. D. BRAND, and D. R. WILLIAMS. J. Mol. Spectrosc. **24**, 402 (1967).
8. T. SCHAEFER, T. A. WILDMAN, and R. SEBASTIAN. Can. J. Chem. **60**, 1924 (1982).
9. T. SCHAEFER, T. A. WILDMAN, and S. R. SALMAN. J. Am. Chem. Soc. **102**, 107 (1980).
10. W. J. E. PARR and T. SCHAEFER. Can. J. Chem. **13**, 400 (1980).
11. L. RADOM, W. J. HEHRE, J. A. POPLE, G. L. CARLSON, and W. G. FATELEY. J. Chem. Soc. Chem. Commun. 308 (1972).
12. A. PROSS and L. RADOM. Prog. Phys. Org. Chem. **13**, 1 (1981).

13. D. S. TARBEL and D. K. FUKUSHIMA. Org. Synth. Collect. **III**, 809 (1955).
14. E. A. BARTKUS, E. B. HOTELLING, and M. B. NEUWORTH. J. Org. Chem. **22**, 3037 (1974).
15. T. SCHAEFER and R. SEBASTIAN. J. Magn. Reson. **41**, 395 (1980).
16. T. SCHAEFER and J. D. BALEJA. J. Magn. Reson. **60**, (1984).
17. M. R. PETERSEN and R. A. POIRIER. MONSTERGAUSS, Department of Chemistry, University of Toronto, Toronto, Ontario, 1981.
18. S. CASTELLANO and A. A. BOTHNER-BY. J. Chem. Phys. **41**, 3863 (1964).
19. C. W. HAIGH. Annu. Rep. NMR Spectrosc. **4**, 311 (1971).
20. A. R. QUIRT and J. S. MARTIN. J. Magn. Reson. **5**, 318 (1971); J. S. MARTIN, A. R. QUIRT, and K. E. WORVILL. The NMR program library. Daresbury Laboratory, Daresbury, U.K.
21. M. FUJIO, R. T. MCIVER, JR., and R. W. TAFT. J. Am. Chem. Soc. **103**, 4017 (1981).
22. A. PROSS, L. RADOM, and R. W. TAFT. J. Org. Chem. **45**, 818 (1980).
23. W. J. HEHRE, L. RADOM, and J. A. POPLE. J. Am. Chem. Soc. **94**, 1496 (1972).

Volumes molaires partiels de composés tensioactifs dans les milieux salins concentrés eau–KCl

SABAH BOUGUERRA, HAMED BAHRI ET PIERRE LETELLIER[1]

Laboratoire de Physiochimie des Solutions, Université Pierre et Marie Curie, E.N.S.C.P. 11 Rue Pierre et Marie Curie, 75231 Paris Cédex 05, France

Reçu le 7 juin 1984[2]

SABAH BOUGUERRA, HAMED BAHRI et PIERRE LETELLIER. Can. J. Chem. **63**, 2476 (1985).

Les volumes molaires apparents de quatre détergents cationiques $CH_3(CH_2)_nN(CH_3)_3Br$ pour n = 9, 11, 13 et 15 ont été déterminés dans les mélanges eau – chlorure de potassium à 298 K, pour des concentrations en électrolyte support comprises entre 0,5 et 3,5 mol L^{-1}. La très faible dépendance des volumes molaires apparents des tensioactifs, *une fois micellisés*, avec la concentration du sel de fond laisse supposer que les interactions entre les amphiphiles eux-mêmes et entre les amphiphiles et leur environnement ne sont pas fondamentalement modifiées par l'addition de sel. L'utilisation de résultats antérieurs obtenus pour ces mêmes milieux, concernant le comportement des sels d'ammonium symétriques permet d'accéder aux *volumes intrinsèques* des amphiphiles et, par conséquence, d'estimer le volume réel occupé par la phase micellaire dans la solution. Des mesures des volumes molaires apparents du bromure de dodécyltriméthylammonium et du dodécylsulfate de sodium dans les mélanges eau–NaCl permettent de confirmer les rôles dissymétriques joués par les anions et les cations en milieu salin concentré.

SABAH BOUGUERRA, HAMED BAHRI, and PIERRE LETELLIER. Can. J. Chem. **63**, 2476 (1985).

Apparent molar volumes of 4 cationic detergents $CH_3(CH_2)_nN(CH_3)_3Br$ (n = 9, 11, 13, and 15) have been determined in water – potassium chloride mixtures at 298 K over a wide range of concentrations (from 0.5 to 3.5 mol L^{-1}). The small dependence of values of apparent molar volume of micellized detergent on the salt concentration suggests the interactions between amphiphiles themselves and between amphiphiles and their surroundings are not modified by the variation of KCl concentration. Previous results lead to estimates of intrinsic volumes of micellized detergents and consequently actual volumes of the micellar phase in the solution. In addition, apparent molar volumes of dodecyltrimethylammonium bromide and sodium dodecylsulfate have been determined in water – sodium chloride mixtures. The results agree fairly well with the previous conclusions and prove the dissymmetric behaviour of the anions and cations in very highly concentrated aqueous salt solutions.

L'étude des volumes molaires partiels et apparents des composés tensioactifs est généralement entreprise dans le but de déterminer avec précision des valeurs de concentration micellaire critique (cmc) (3), le phénomène de micellisation s'accompagnant le plus souvent, dans l'eau d'une importante variation des propriétés volumiques des amphiphiles.

À ce titre, différents travaux ont été réalisés dans l'eau pure, mais également en présence de faibles quantités d'additifs moléculaires (4) ou ioniques (5) dont on a pu ainsi préciser les modes d'action dans le processus de micellisation.

Peu d'études, en revanche, s'attachent à décrire le comportement volumique des détergents en milieu salin concentré, bien que de nombreux travaux se basant sur la mesure d'autres paramètres physiques (viscosité, diffusion de la lumière . . .) (6–9) montrent que les édifices micellaires sont profondément affectés par la présence d'un électrolyte concentré.

Des travaux antérieurs (1,2) nous ayant permis de préciser les *propriétés volumiques individuelles* des anions et des cations, minéraux et organiques, *mono chargés* dans les mélanges eau–KCl pour des concentrations en chlorure de potassium comprises entre 0,5 et 3,5 mol L^{-1}, nous avons entrepris l'étude des volumes molaires partiels $\bar{V}_i$ et apparents ϕ_i de composés tensioactifs dans ces mêmes milieux.

Nous nous sommes plus particulièrement intéressés à quatre halogénures d'alkyltriméthylammonium de formule générale $CH_3(CH_2)_nN^+(CH_3)_3X^-$: les bromures de décyl (n = 9) dTA, dodécyl (n = 11) DTA, tétradécyl (n = 13) TTA, hexadécyl (n = 15) HTA triméthylammonium.

Afin de juger de l'influence de la nature de l'électrolyte support et du signe de la charge portée par l'amphiphile, les comportements du dodécylsulfate de sodium DSNa et du DTA ont été également étudiés dans les milieux eau–NaCl pour une gamme de concentrations comprise entre 0,25 et 0,75 mol L^{-1} en chlorure de sodium.

I. Conditions expérimentales

Le bromure de décyltriméthylammonium est un produit Eastman Kodak; les autres détergents cationiques sont des produits Sigma. Différents essais de reproductibilité ont montré que les résultats expérimentaux obtenus avec des produits recristallisés ne différaient pas notablement de ceux obtenus à partir des produits bruts. La purification n'a donc pas été systématiquement effectuée.

Le dodécylsulfate de sodium, d'origine Prolabo RP, ne conduit en revanche à des résultats reproductibles que recristallisé au moins deux fois dans un mélange méthanol – éther éthylique. Les chlorures de potassium et de sodium sont des produits Prolabo RP. L'eau utilisée est fraichement distillée. Sa masse volumique à 298 K a été prise égale à 0,997047 g cm^{-3}. Les mesures de masses volumiques ont été réalisées au moyen d'un "densimètre vibratomètre à flux" Sodev (modèle 03D) maintenu à la température constante de 298 ± 2 × 10^{-3} K par un thermostat Setaram. Les mesures des périodes ont été effectuées sur un fréquencemètre Hewlett Packard 5315A. Le calcul de la valeur du volume molaire apparent ϕ_i du soluté i, de masse molaire M_i, à la molalité m référée à 1000 grammes de la solution eau–KCl considérée, s'effectue à partir de la relation classique:

$$\phi_i = \frac{1000}{m}\left(\frac{1}{\rho_i} - \frac{1}{\rho_0}\right) + \frac{M_i}{\rho_i}$$

ρ_i et ρ_0 sont respectivement les masses volumiques de la solution i et du solvant eau–KCl.

II. Résultats expérimentaux

II-1. *Définition des systèmes étudiés*

L'addition d'un électrolyte à une solution de tensioactif

[1]Auteur à qui adresser la correspondance.

[2]Revision reçue le 28 janvier 1985.

TABLEAU 1. Concentrations micellaires critiques des détergents étudiés (dans l'eau à 298 K)

	Détergent				
	dTA	DTA	TTA	HTA	NaDS
cmc (mol L^{-1}) (30,31)	$6,5 \times 10^{-2}$	$1,5 \times 10^{-2}$	$3,5 \times 10^{-3}$	$9,2 \times 10^{-4}$	$8,1 \times 10^{-3}$

TABLEAU 2. Volumes molaires apparents à différentes molalités du TTA dans le mélange eau−KCl 2 *M*

Molalité (mol kg^{-1})	ρ (g cm^{-3})	ϕ (cm^3 mol^{-1})
0	1,086633	—
0,0318	1,085924	328,61
0,0499	1,085524	328,74
0,0636	1,085219	328,83
0,0731	1,085017	328,76
0,0829	1,084803	328,81
0,1450	1,083499	328,82

favorise, en règle générale, le phénomène de micellisation, ce qui se traduit par un abaissement de la valeur de la cmc (10).

La technique de détermination des volumes molaires apparents mise en oeuvre dans cette étude, nécessite l'emploi d'une concentration minimale de soluté égale à 10^{-2} mol kg^{-1} (11). À cette concentration les tensioactifs utilisés, qui possèdent déjà dans l'eau des seuils critiques micellaires relativement faibles (tableau 1), se trouvent pour la plupart partiellement ou même totalement micellisés en présence de l'électrolyte support. À titre d'exemple, les variations des volumes molaires apparents du dTA en fonction de la molalité en détergent, pour différentes teneurs de la solution en chlorure de potassium, sont reportées sur la fig. 1. On peut ainsi constater que même pour la plus faible concentration de KCl utilisée, 5×10^{-1} mol L^{-1}, le dTA à 10^{-2} mol kg^{-1} est déjà partiellement associé.

Il n'est donc pas envisageable d'étudier, au moyen de la technique de mesure précédemment décrite, le comportement des amphiphiles sous leur forme monomère dans les mélanges eau−KCl.

En revanche, l'utilisation d'une concentration suffisante en détergent permet d'obtenir des systèmes *totalement micellisés* pour lesquels les propriétés physicochimiques des amphiphiles sont parfaitement définies.

C'est dans ce cadre précis que s'inclut la présente étude.

II-2. *Volumes molaires apparents des bromures d'alkyltriméthylammonium micellisés*

II-2.1. *Variations avec la molalité du tensioactif*

Les résultats expérimentaux regroupés dans le tableau 2 et illustrés par ailleurs sur la fig. 2 montrent que *dans un milieu eau−KCl donné*, une fois le système totalement micellisé, les volumes molaires apparents des détergents, de la même manière que ceux des halogènures alcalins (1), sont indépendants de leur molalité dans la gamme de concentration utilisée ($m < 3 \times 10^{-1}$ mol kg^{-1}). On pourra donc caractériser le détergent micellisé par un volume molaire apparent ϕ_m correspondant à cette valeur constante.

II-2.2 *Variations avec la concentration en KCl*

Les valeurs moyennes des volumes molaires apparents ϕ_m pour les différents détergents étudiés, à plusieurs concentrations en chlorure de potassium sont regroupées dans le tableau 3. On remarque que ces valeurs varient très peu, pour un tensioactif donné, avec la teneur de la solution en KCl. À titre de comparaison, les variations de ϕ_m pour les quatre détergents cationiques, et celles des volumes molaires apparents à dilution infinie de deux autres électrolytes KBr et $(C_4H_9)_4NBr$ sont représentées sur la fig. 3. La différence de comportement entre ces deux derniers sels a été justifiée dans une étude précédente (2).

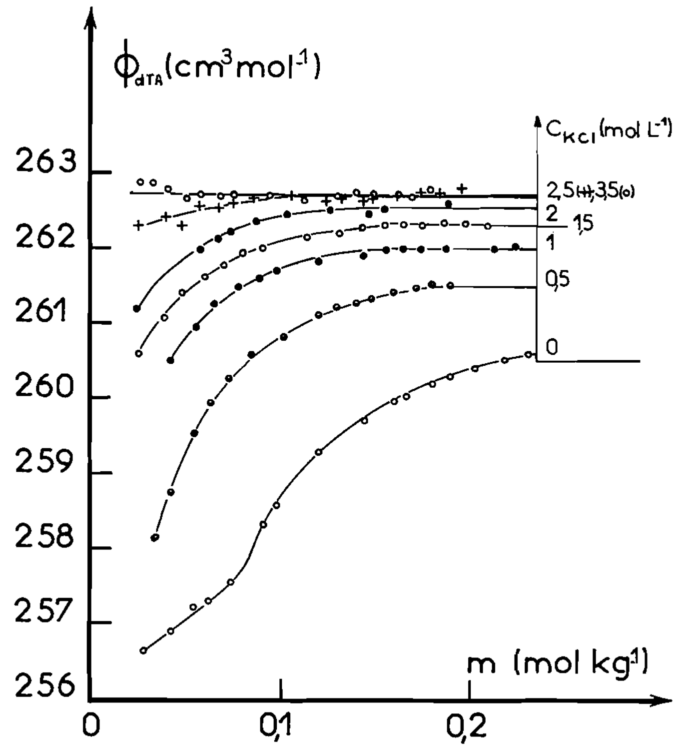

FIG. 1. Variations du volume molaire apparent du dTA avec sa molalité pour différents mélanges eau−KCl.

Les mesures réalisées avec le DSNa et le DTA dans les mélanges eau−NaCl seront évoquées ultérieurement dans le chapitre consacré à l'interprétation des résultats.

II-3. *Discussion des résultats*

La modification des propriétés structurales des systèmes micellaires, en présence de quantités variables de sel a fait l'objet de nombreux travaux et une littérature abondante existe actuellement sur ce sujet (6−9).

Nous en retiendrons les conclusions suivantes en rapport avec notre étude:

A. La création d'édifices micellaires dans l'eau pure conduit à l'apparition en solution de structures comportant un nombre élevé de charges identiques. Pour des raisons électrostatiques évidentes la majeure partie des contre-ions se trouve située dans l'environnement immédiat de la micelle.

La répartition des contre-ions s'effectue selon une loi de distribution radiale continue, partant d'une forte concentration près de la surface de la micelle qui décroit régulièrement lorsque l'on s'en éloigne (12,13).

Ce phénomène de "surconcentration" au voisinage de l'inter-

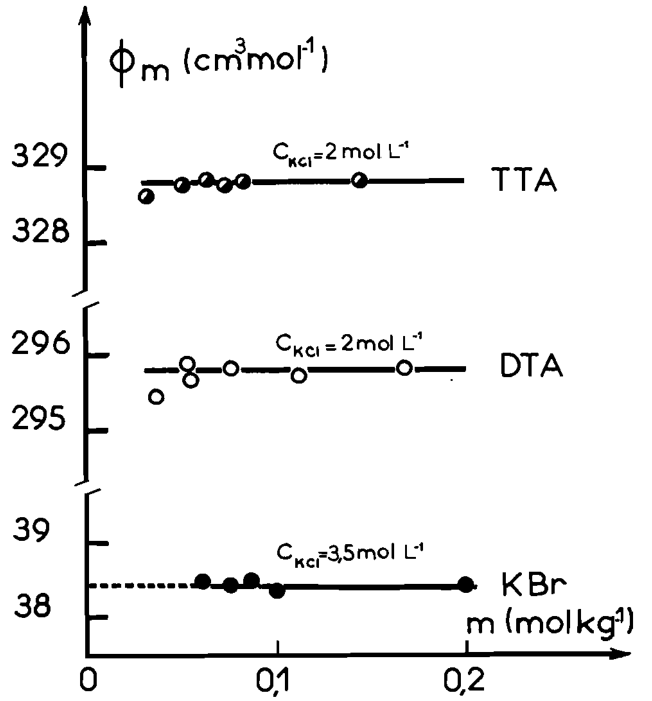

FIG. 2. Variations en fonction de leur molalité des volumes molaires apparents des détergents micellisés dans le mélange eau−KCl 2 *M* et de KBr dans le milieu 3,5 *M* en KCl.

TABLEAU 3. Valeurs des volumes molaires moyens ϕ_m des détergents micellisés dans les mélanges eau−KCl à 298 K

	Détergent			
C_{KCl} (mol L^{-1})	dTA	DTA	TTA	HTA
0	260,1	294,5	328,0	360,8
0,5	261,5	295,2	—	361,4
1	262,0	295,7	328,8	—
1,5	262,4	—	—	—
2	262,6	295,8	328,8	—
2,5	262,7	295,8	328,8	—
3	262,7	295,8	328,8	—
3,5	262,7	295,8	328,8	—

face micelle−solvant peut être traité au moyen d'un concept d'association qui suppose des contre-charges "liées" à la micelle au niveau de sa surface par l'intermédiaire d'un équilibre d'échange (14).

Cependant, la notion de "liaison" dans ce type de modèle doit être prise au sens large car elle n'implique pas l'existence de sites spécifiques sur la micelle pour le rattachement des contre-ions (15). Il en résulte que l'on ne différenciera pas au niveau de leurs propriétés thermodynamiques et en particulier de leurs volumes molaires partiels, les contre-ions qui se "fixent" sur la micelle des autres ions de la solution, cette séparation étant essentiellement formelle.

Lorsque l'on ajoute à ces solutions une quantité importante d'électrolyte, on modifie notablement la répartition des contre-ions dans l'environnement des édifices micellaires. Deux cas peuvent alors se présenter:

(a) L'électrolyte possède le même contre-ion que le détergent (ajout par exemple du sel M^+Y^- à une solution de détergent cationique T^+Y^-).

Cette opération a pour conséquence d'augmenter la concen-

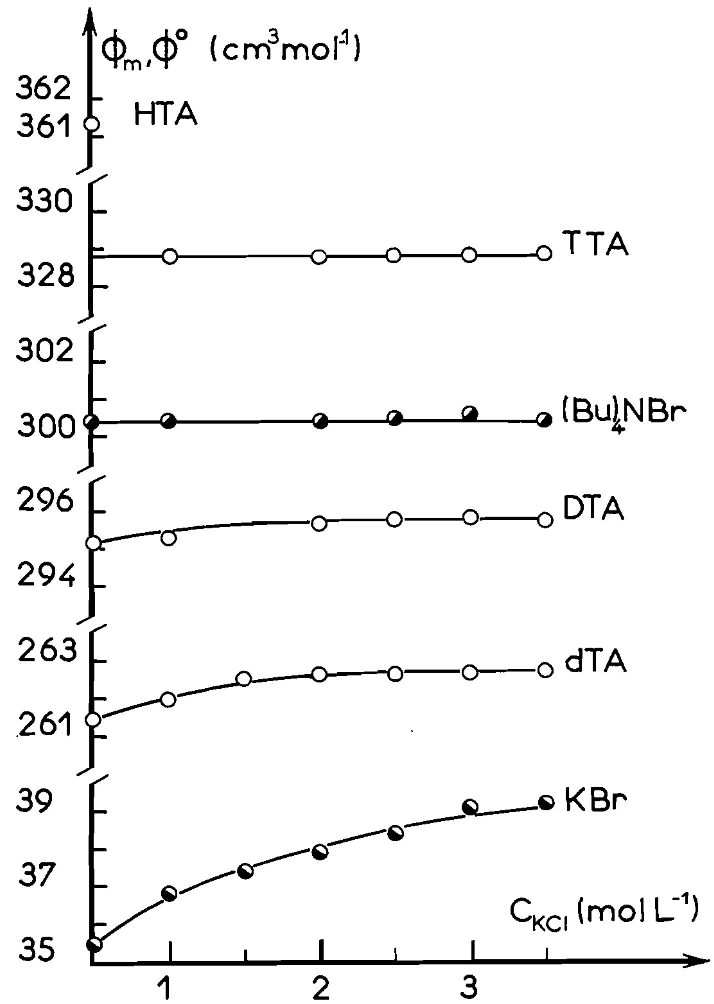

FIG. 3. Variations des volumes molaires apparents moyens ϕ_m des détergents micellisés et des volumes molaires apparents à dilution infinie ϕ^0 de KBr et $(Bu)_4NBr$ (bromure de tétrabutylammonium) dans les mélanges eau−KCl.

tration des ions Y^- dans l'environnement immédiat de la micelle. Ceci peut se traduire dans le concept de l'équilibre d'association par un déplacement de l'équilibre d'échange (contre-ions associés ⇌ contre-ions libres) vers la forme associée, ce qui correspond à une saturation en contre-ions de l'interface micelle−solvant.

Ce phénomène dont la conséquence est un affaiblissement des répulsions électrostatiques entre les "têtes" polaires des amphiphiles de la micelle est à l'origine de l'abaissement du seuil critique micellaire (16).

(b) L'électrolyte possède un contre-ion différent (par exemple l'ajout du sel M^+X^- à une solution de détergent cationique T^+Y^-).

Les ions X^- introduits tendent à participer, en concurrence avec les ions Y^-, à l'électroneutralité des édifices micellaires. Divers travaux (17−20) montrent que la répartition des ions dans le proche environnement de la micelle n'est pas controlé exclusivement par le facteur entropique, mais qu'il faut également prendre en compte la nature chimique des contre-ions.

Dans le cadre du concept de l'équilibre d'association, on considère qu'il s'établit un équilibre d'échange entre les ions X^- et Y^- plus ou moins déplacé vers l'une ou l'autre des deux formes associées (T^+,X^- et T^+,Y^-) selon la *sélectivité* relative de la micelle pour les ions X^- et Y^-.

Toutefois, en présence de fortes quantités d'électrolyte MX il se crée, par simple "effet de masse", un environnement de la micelle constitué presque exclusivement d'ions X^-.

On peut ainsi admettre que les édifices micellaires cationiques en présence de KCl à forte concentration sont associés aux ions chlorure, même si à l'origine les détergents comportaient un contre-ion différent (Br^-).

Les remarques précédentes permettent d'interpréter les propriétés des détergents cationiques dans les milieux eau−KCl et en particulier le fait que leur volume molaire apparent ϕ_m ne dépend pas de leur molalité. Ce comportement est identique à celui observé pour les halogènures alcalins mais sa justification en est différente. En effet dans le cas d'un sel minéral P^+Y^- introduit dans une solution concentrée eau−KCl, il est légitime de considérer qu'aux faibles concentrations les ions P^+ et Y^- se comportent dans le milieu comme des entités indépendantes (pas d'interactions P^+-P^+, P^+-Y^-, Y^--Y^-) (2) et en conséquence que les propriétés de ces ions peuvent être décrites par les lois des solutions diluées. La valeur du volume molaire apparent de PY est alors constante tant que la concentration du sel reste faible devant celle de l'électrolyte support. Elle s'identifie alors à sa valeur extrapolée à dilution infinie.

[1] $\phi^0_{PY} = \phi^0_{P^+} + \phi^0_{Y^-}$

Dans le cas des tensioactifs, au contraire, les cations T^+ sont agrégés sous forme d'édifices micellaires et seuls les contre-ions Y^- peuvent être supposés sans interactions réciproques tant que la concentration en détergent reste faible.

La valeur constante observée indique donc, selon toute vraisemblance, que l'intensité des interactions entre les amphiphiles T^+ eux-mêmes dans l'édifice micellaire, mais également entre T^+ et Cl^- ne varie pas lorsque la concentration du tensioactif augmente.

B. Lorsque la concentration de l'électrolyte support croit, la structure de l'édifice micellaire se modifie. La configuration initialement sphérique évolue selon la nature du détergent vers des structures de symétrie moindre (15).

Toutefois au cours des ces modifications, les interactions entre les têtes polaires des amphiphiles et les constituants du solvant ne sont pas fondamentalement modifiées, pas plus d'ailleurs que celles qui existent entre les chaînes aliphatiques regroupées au coeur de la micelle. Il faut donc s'attendre à ce que ces modifications n'entrainent pas de variations notables des volumes molaires apparents des amphiphiles micellaires.

L'indépendance des valeurs de ϕ_m, avec la concentration en KCl confirme cette hypothèse. Il a été en effet montré dans une étude précédente que les volumes molaires apparents individuels à faible concentration des halogénures Y^- s'identifiaient à leurs volumes intrinsèques ceux-ci étant eux-mêmes reliés à leurs volumes cristallins (calculés à partir des rayons de Pauling) par l'équation:

[2] $\phi_{Y^-} = V^I_{Y^-} = 1{,}92\ V^C_{Y^-}$

Les volumes molaires apparents ϕ_m des détergents T^+Y^- étant indépendants de la concentration en KCl, ϕ_{Y^-} l'étant également, il en est nécessairement de même pour les amphiphiles T^+.

Les valeurs de ϕ_m (T^+) ne varient donc pas avec la teneur de la solution en chlorure de potassium.

III. Exploitation des résultats

Une précédente étude sur le comportement des bromures de tétraalkylammonium symétriques ($(CH_3(CH_2)_x)_4NBr$) a permis

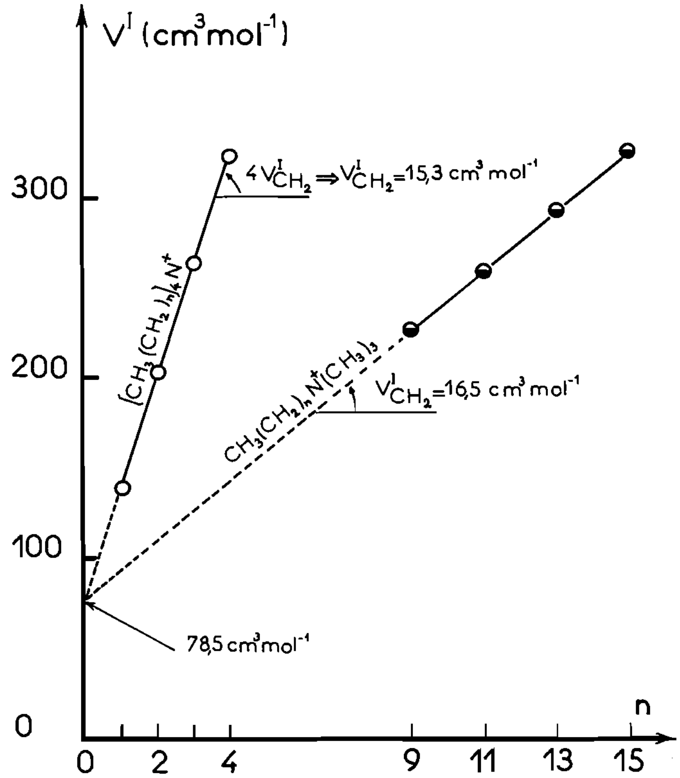

FIG. 4. Variations des volumes intrinsèques des amphiphiles micellisés $CH_3(CH_2)_nN^+(CH_3)_3$ et des volumes intrinsèques des tétra-alkylammonium $(CH_3(CH_2)_x)_4N^+$ en fonction de n ou x.

de montrer que les volumes molaires apparents des ions organiques de grande taille ($x > 2$) pouvaient être identifiés à leur volume intrinsèque en solution saline concentrée (2).

L'indépendance de ϕ_m (T^+) avec la concentration en KCl laisse supposer qu'il doit en être de même pour l'amphiphile dans l'édifice micellaire. S'il est ainsi, on peut alors écrire:

[3] $\phi_m(T^+,Br^-) = \phi_m(T^+) + \phi_{Br^-} = V^I_{T^+} + \phi_{Br^-}$

soit encore en utilisant la relation [2]:

[4] $V^I_{T^+} = \phi_m(T^+,Br^-) - 1{,}92\ V^C_{Br^-}$

Les amphiphiles étudiés appartenant à une même famille de composés $CH_3(CH_2)_nN(CH_3)_3$ (n = 9, 11, 13 et 15), il est possible de scinder leur volume intrinsèque en deux contributions: V^I_g relative au groupement polaire $(CH_3)_4N^+$, et $nV^I_{CH_2}$ relative aux n groupements CH_2 constituant la chaîne aliphatique, en supposant que chacun d'entre eux possède des propriétés voisines ($V^I_{CH_2}$).

Le volume intrinsèque de T^+ s'écrit alors:

$$V^I_{T^+} = V^I_g + n\ V^I_{CH_2}$$

soit:

[5] $V^I_{T^+} = \phi_m(T^+Br^-) - 1{,}92\ V^C_{Br^-} = V^I_g + n\ V^I_{CH_2}$

Les valeurs de $V^I_{T^+}$ ont été calculées pour les quatre détergents cationiques (tableau 4) et reportées en fonction de n sur la fig. 4. Le graphe représentatif est une droite de pente $V^I_{CH_2}$ = 16,5 cm^3 mol^{-1} et d'ordonnée à l'origine V^I_g = 78,5 cm^3 mol^{-1}.

Le volume intrinsèque de l'amphiphile $CH_3(CH_2)_nN^+(CH_3)_3$ s'écrit donc:

TABLEAU 4. Volumes intrinsèques des amphiphiles micellisés dans les milieux salins concentrés eau–KCl ($V^{I}_{Br^-}$ = 35,9 cm^3 mol^{-1})

	Détergent			
	dTA	DTA	TTA	HTA
$V^{I}_{T^+}$ (cm^3 mol^{-1})	226,8	259,9	292,9	~326

TABLEAU 5. Volumes molaires moyens de NaDS et DTA micellisés et volumes molaires apparents de NaCl et NaBr dans les mélanges eau–NaCl

	Electrolyte			
C_{NaCl} (mol L^{-1})	NaBr	NaCl	NaDS	DTA
0	23,5	16,6	249,8	294,5
0,25	25,0	17,9	250,9	295,2
0,5	25,6	18,4	251,5	295,3
0,75	26,0	19,0	252,0	295,3

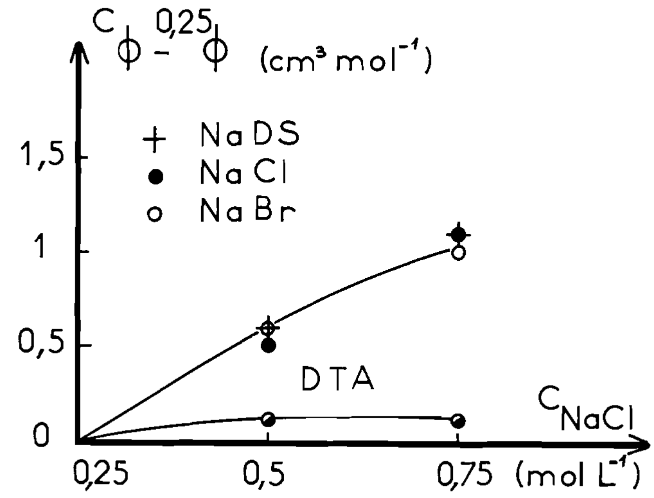

FIG. 5. Variations des volumes molaires moyens de NaDS et DTA et des volumes molaires apparents de NaCl et NaBr dans les milieux eau–NaCl à 298 K.

[6] $V^{I}_{T^+}$ (cm^3 mol^{-1}) = 78,5 + 16,5 n

La valeur trouvée pour le volume intrinsèque du groupement tétraméthylammonium (n = 0) s'identifie à celle que l'on calcule pour *l'ion tétraméthylammonium* à partir du rayon ionique proposé par Masterton *et al.* (r = 2,51 Å) (21) en appliquant la relation [2]. L'incrément de volume pour chaque CH_2 correspond à celui observé pour les alcanes purs ($8 < n < 14$) (22), laissant ainsi supposer que l'association des chaînes aliphatiques au sein de l'édifice micellaire conduit à la constitution d'un "milieu interne" dont les propriétés s'apparentent à celles des carbures saturés.

Cet incrément est nettement supérieur à celui que l'on détermine dans ce mêmes milieux pour les ions ammonium quaternaires symétriques $(CH_3(CH_2)_x)_4N^+$ pour lesquels les CH_2 possèdent un environnement aqueux (23). La représentation des variations du volume intrinsèque des cations ammonium en fonction de x conduit au tracé d'une droite de pente égale à $4V^{I}_{CH_2}$ et d'ordonnée à l'origine V^{I}_{g} relatif au même groupement tétraméthylammonium (fig. 4). On obtient:

$$V^{I}_{g} = 78{,}5 \text{ cm}^3 \text{ mol}^{-1}$$

$$V^{I}_{CH_2} = 15{,}3 \text{ cm}^3 \text{ mol}^{-1}$$

Même si l'on tient compte de la faible précision des extrapolations, il est à noter que l'on retrouve pour cette famille de composés, une valeur identique à la précédente pour le volume intrinsèque du groupement $(CH_3)_4N^+$, ce qui semble justifier les partitions des volumes telles qu'elles ont été réalisées.

La différence de volume intrinsèque observée entre les groupements —CH_2— selon qu'ils possèdent un environnement ionique aqueux ou hydrophobe est à l'origine du phénomène d'expansion lié à la micellisation qui apparaît ainsi comme une conséquence du changement d'environnement de la partie hydrophobe du détergent (24, 25).

Cas d'un détergent anionique: le dodécylsulfate de sodium

L'influence des électrolytes sur les micelles de NaDS et entre autres, les variations de la cmc avec la teneur en sel ont fait l'objet de nombreux travaux (26–29). Dans le cas du sel NaCl, il a été établi que le volume des micelles et donc leur rayon, ne varie que très faiblement (27) tant que la concentration de l'électrolyte reste inférieure à 0,45 mol L^{-1} (26,28). Au delà de cette limite la forme sphérique évolue vers une forme cylindrique (28) dont la stabilité a pu être étudiée thermodynamiquement (29). Toutefois, comme nous l'avions fait remarquer précédemment, il est probable que cette transition n'affecte pas de manière notable les volumes molaires partiels des amphiphiles et l'on pourra considérer que le volume molaire apparent de l'ion dodécylsulfate (DS^-) reste identique à son volume intrinsèque, c'est-à-dire invariant avec la teneur de la solution en électrolyte support dès que celle-ci est suffisamment importante. Il n'en sera pas de même, en revanche, pour le volume molaire apparent individuel du cation associé puisque celui-ci varie avec la teneur de la solution en électrolyte support (2). Il s'ensuit que contrairement aux détergents cationiques, il faille s'attendre à observer pour les anioniques une variation de leur volume molaire apparent avec la concentration du sel de fond.

Pour des raisons de solubilité, nous n'avons pas pu étudier le comportement de NaDS dans les mélanges eau–KCl. La vérification des hypothèses précédentes a donc été tentée dans les mélanges eau–NaCl entre 0,25 et 0,75 molaire en chlorure de sodium où nous avons étudié à titre de comparaison les volumes molaires partiels de NaDS, NaBr, NaCl, $C_{12}H_{25}N(CH_3)_3Br$.

Les résultats expérimentaux sont regroupés dans le tableau 5. Comme on peut le remarquer sur la fig. 5, le volume molaire apparent du détergent cationique est indépendant de la concentration de la solution en NaCl, alors que l'on assiste à des variations tout à fait comparables pour NaDS, NaCl et NaBr, dues essentiellement au comportement particulier de l'ion sodium.

Le volume molaire intrinsèque attribuable à l'ion dodécylsulfate est de l'ordre de 262 cm^3 mol^{-1}. Cette valeur est tout à fait comparable avec celle calculée pour le volume intrinsèque de l'amphiphile cationique, ayant même chaîne aliphatique $(CH_3(CH_2)_{11}N(CH_3)_3^+)$ qui est de l'ordre de 260 cm^3 mol^{-1}.

Ces résultats confirment les rôles dissymétriques joués par les cations et les anions dans les solutions salines concentrées.

La connaissance des valeurs des volumes intrinsèques des amphiphiles micellisés (anioniques ou cationiques) dans les mélanges eau–sel permet également d'estimer de manière précise la contribution volumique de la phase micellaire au volume total de la solution.

One-electron properties of HNO

J. ESPINOSA GARCÍA, A. LÓPEZ PIÑEIRO, AND F. J. OLIVARES DEL VALLE
Department of Physical Chemistry, University of Extremadura, Badajoz, Spain

Received May 31, 1984[1]

J. ESPINOSA GARCÍA, A. LÓPEZ PIÑEIRO, and F. J. OLIVARES DEL VALLE. Can. J. Chem. **63**, 2482 (1985).

SCF one-electron property calculations are reported for the nitroxyl molecule, using several types of Gaussian basis sets. An assessment is made of the size and type of basis set necessary to yield values for various one-electron properties that approach the best calculated or experimental results. The charge distribution is not improved by including the Gaussian lobe functions.

J. ESPINOSA GARCÍA, A. LÓPEZ PIÑEIRO et F. J. OLIVARES DEL VALLE. Can. J. Chem. **63**, 2482 (1985).

Utilisant plusieurs ensembles de base de type Gaussiens, on a effectué des calculs en champ auto-cohérent relatifs aux propriétés à un électron de la molécule de nitroxyle. On a évalué la dimension et le type d'ensemble de base nécessaire pour obtenir les valeurs de diverses propriétés à un électron qui se rapprochent le plus des résultats expérimentaux. L'inclusion des fonctions de lobe de type Gaussien n'affecte pas la distribution des charges.

[Traduit par le journal]

Introduction

The electronic structure of the nitroxyl molecule, HNO, in the ground and low-lying electronic states has been relatively well studied from an experimental (1, 2) and theoretical point of view (3). This system has been postulated as an intermediate in various photochemical and free radical reactions (2) although there is no clear evidence for the existence of free HNO. Furthermore, its structure and many of its physical and chemical properties are unknown.

Previously the study of the HNO system has been performed fundamentally on the geometry and excited states. However, the study of electronic structure and properties of the ground state has not been performed with suitable emphasis. Also, though the main characteristic of this system is its instability, HNO can form hydrogen bonded systems of an appreciable stability. In a previous work[2] this type of association has been studied.

As to the one-electron properties of HNO, very few experimental data exist (4), and no "*ab initio*" studies.

In the present paper, we report the one-electron properties for this system, analyzing the influence of the basis set. However, unfortunately it is impossible to compare our results for the HNO molecule, and we have to use a test molecule: water. Some experimental values of its one-electron properties are well determined (5), and numerous "*ab initio*" calculations have been performed. (There are several SCF computations on water. We note, among others, the ones quoted in ref. 6.)

Theoretical approach, basis set, geometry and related questions

RHF-SCF-LCAO-MO calculations were carried out using the POLYATOM V-2 (7) and GAUSSIAN 70 (8) program systems. One-electron properties were computed using the available programs as part of the POLYATOM system.

In this paper three types of Gaussian basis sets have been used: (*a*) *extended basis set* (BDZ (9, 10), DUNNING I (11), DUNNING II (12)); (*b*) *extended basis set with polarization functions*, and (*c*) *extended basis set with polarization functions and Gaussian lobe functions (13) centered off the nuclei.*

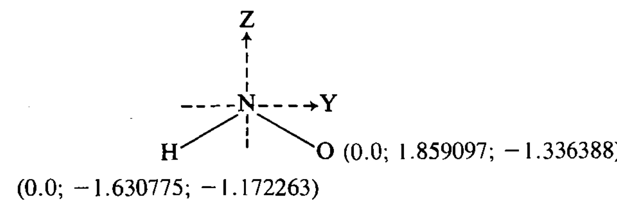

FIG. 1. Geometry and coordinates system for nitroxyl (in au).

For O and N we chose the Huzinaga and Sakai (9) basis set. This basis set includes thirteen *s*-type Gaussians and seven *p*-type Gaussians, contracted to double zeta (DZ), according to the notation {4,4,3,2;4,3}. For the hydrogen atom the basis set put forward by Basch, Robin, and Kuebler (10) has been used: four *s*-type Gaussian functions contracted to two of three and one, respectively, are used to describe the $1s$ atomic orbital (BDZ).

To study the effect of the contraction we have used the DUNNING I and II bases, which can be considered of DZ quality. Also, $3d$-type functions have been included on oxygen and nitrogen, and $2p$-type functions on hydrogen (BDZP) in order to study the effect of polarization functions.

Furthermore, the effect of the inclusion of Gaussian lobe functions, consisting of $1s$-type functions centered on the bond (BDZPL1) and the center of mass (BDZPL2) of the molecule, have also been considered.

We have used the experimental geometry for H_2O (14) and HNO (15): R(N—O) = 2.289580 au, R(N—H) = 2.008390 au and $\angle$HNO = 108.58°. See coordinate system for HNO in Fig. 1.

By convention, the multipole moments are computed relative to the center of mass of the molecule (0.0, 0.906928, − −0.727563).

Results and discussions

As numerous results exist for water (5, 6), we simply summarize, for "calibration" purposes, the values of various properties calculated with different basis sets and the corresponding experimental values in Table 1. One of the main observations that can be made is that the calculated second moments appear to agree very well with the experimental value. The results indicate that the constructed wavefunctions are remarkably successful in all cases. This is so because the second moment of the electronic distribution represents a very insensitive measure

[1]Revision received December 4, 1984.

[2]J. Espinosa García and F. J. Olivares del Valle. Unpublished results.

TABLE 1. Total energies and selected one-electron properties for water

Properties[a]	BDZ	DUNNING I	DUNNING II	BDZP	BDZPL1	BDZPL2	Exptl.
E	−76.0108	−76.0123	−76.0197	−76.0507	−76.0526	−76.0528	−76.4802[b]
$-V/T$	1.9981	1.9997	2.0001	2.0000	2.0003	2.0004	2.0000
μ_z	1.0436	1.0429	1.0685	0.8294	0.8240	0.8504	0.7296[b]
Q_{xx}	−5.3088	−5.4956	−5.5792	−5.5490	−5.5446	−5.5678	−5.563[b]
Q_{yy}	−3.1846	−3.0921	−3.0995	−3.1833	−3.1511	−3.1877	−3.108[b]
Q_{zz}	−4.3957	−4.4438	−4.5026	−4.3653	−4.3797	−4.4011	−4.416[b]
θ_{xx}	−1.5186	−1.7276	−1.7781	−1.7794	−1.7793	−1.6367	−1.86[c]
θ_{yy}	1.6677	1.8775	1.9414	1.7740	1.8110	1.7966	1.96[c]
θ_{zz}	−0.1489	−0.1499	−0.1632	−0.0009	−0.0319	−0.0235	−0.097[c]

[a]Current symbols are used for the quantities appearing in this table. All quantities here in au. Coordinates: O(0.0, 0.0, 0.0); H1(0.0, −1.431317, −1.107845); H2(0.0, 1.431317, −1.107845).
[b]See ref. 7.
[c]See ref. 6.

TABLE 2. Total energies and selected one-electron properties for nitroxyl

Properties[a]	BDZ	DUNNING I	DUNNING II	BDZP	BDZPL1	BDZPL2	Exptl.
E	−129.7344	−129.7458	−129.7524	−129.8143	−129.8197	−129.8180	−130.1212
μ_y	−0.9332	−0.8860	−0.8958	−0.7946	−0.7906	−0.7971	−0.5154±0.004[b]
μ_z	−0.3485	−0.2959	−0.3061	−0.2658	−0.2473	−0.2631	−0.4053±0.008[b]
μ	0.996	0.934	0.947	0.838	0.828	0.839	0.656[b]
Q_{xx}	−8.0320	−7.8605	−7.8554	−7.9578	−7.9700	−7.9993	
Q_{yy}	−7.5899	−7.4010	−7.3777	−7.2727	−7.2139	−7.2230	
Q_{zz}	−9.8875	−9.6919	−9.7177	−9.4919	−9.5239	−9.5280	
θ_{xx}	0.7065	0.6861	0.6975	0.4245	0.3987	0.3762	
θ_{yy}	1.3701	1.3752	1.4141	1.4521	1.5337	1.5409	
θ_{zz}	−2.0765	−2.0612	−2.1113	−1.8765	−1.9321	−1.9170	
$E(\mathrm{O})_y$[c]	0.2015	0.1787	0.0541	0.0653	0.0675	0.0657	
$E(\mathrm{O})_z$	−0.1217	−0.1083	−0.0615	−0.0413	−0.0411	−0.0428	
$E(\mathrm{N})_y$[d]	−0.0669	−0.0494	−0.0363	−0.0179	−0.0157	−0.0165	
$E(\mathrm{N})_z$	0.1900	0.1697	0.1220	0.0698	0.0668	0.0692	
$E(\mathrm{H})_y$[e]	−0.0757	−0.0679	−0.0654	0.0137	0.0165	0.0143	
$E(\mathrm{H})_z$	−0.0335	−0.0357	−0.0358	0.0071	0.0005	0.0068	
H—F_y[f]	0.0087	0.0083	0.0009	0.0033	0.0036	0.0035	
H—F_z	0.0026	0.0023	0.0026	0.0013	0.0011	0.0012	

[a]In au; 1 au = 2.54154 D; 1 au = 1.344911 Buckinghams.
[b]See ref. 5.
[c]Nuclear component: $y = 1.1683$; $z = -0.7795$.
[d]Nuclear component: $y = -1.0403$; $z = 1.0306$.
[e]Nuclear component: $y = -2.0641$; $z = -0.9777$.
[f]Sum Hellman-Feynman forces in dyn.

of the details of the electronic distribution. Even assuming all electrons to be at atomic centers may give a gross agreement with experimental values (16). However, the calculation of this property for systems for which no experimental data exist may be potentially useful.

The SCF energy and some one-electron properties of HNO are shown in Table 2. The greater flexibility of the BDZP basis with respect to BDZ is reflected in the lower E_{SCF} of the former, −129.8143 au versus −129.7344 au. However, the inclusion of Gaussian lobe functions is less critical, and the energetic improvement is small. The dipole moments calculated from the double zeta basis sets are greater than the available experimental values. However, the BDZP basis set gives the smallest values. All calculated wavefunctions yielded the correct direction for the dipole moment (4).

The second moment values indicate a general increase in the size of the electronic distribution in the z direction with an increasing number of PGTF in the bases.

For the quadrupole moment of H_2O, amongst the double zeta bases the DUNNING I or DUNNING II values are better than the Huzinaga basis. We hope, that for HNO this result will be as valid as for H_2O. The effects of polarization functions provide a strong reduction in the magnitude of the dipole and quadrupole moments.

The total electric fields at nitrogen, oxygen, and hydrogen for nitroxyl are sensitive to the basis sets and to the contraction scheme. The sums of the Hellmann−Feynman forces for the DUNNING I and II bases, for example, indicate that the latter is the best from the point of view of the accuracy of the computed electric fields.

The computed components of the electric field gradient tensors at ^{14}N, ^{17}O, and at ^{2}H are collected in Table 3 for the cartesian coordinate system. Given the nuclear quadrupole moments of the nuclei the accuracy of the computed field gradient may be determined by comparing the constants (eQq/h) with the experimentally measured values. The nuclear quadrupole moment of ^{14}N was assumed to be 1.6×10^{-26} esu cm^2 (16), the nuclear quadrupole moment of ^{17}O, -2.6×10^{-26} esu cm^2 (6), and the nuclear quadrupole moment of ^{2}H, 0.28×10^{-26} esu cm^2 (6) in order to calculate the quadrupole coupling constants (Table 3). The electric field gradients for H are less sensitive to the basis set.

TABLE 3. Fields gradients[a] and coupling constants from several basis sets

Basis sets	Oxygen (^{17}O)[b]			Nitrogen (^{14}N)[c]			Deuterium (^{2}H)[d]		
	q_{xx}	q_{yy}	q_{zz}	q_{xx}	q_{yy}	q_{zz}	q_{xx}	q_{yy}	q_{zz}
BDZ	−2.5817	0.3085	2.2169	−1.4041	−0.2557	1.6622	0.1679	−0.1894	0.0216
DUNNING I	−2.4605	0.3429	2.1206	−1.3571	−0.2577	1.6172	0.1647	−0.1851	0.0204
DUNNING II	−2.5055	0.3211	2.1662	−1.3516	−0.2790	1.6331	0.1581	−0.1757	0.0175
BDZP	−2.5453	0.3791	2.1696	−1.4577	−0.1607	1.6204	0.1329	−0.1414	0.0084
BDZPL1	−2.5155	0.3823	2.1366	−1.4553	−0.1409	1.5988	0.1311	−0.1415	0.0104
BDZPL2	−2.5360	0.3817	2.1576	−1.4519	−0.1592	1.6135	0.1327	−0.1406	0.0080

Basis sets	$(eqQ/h)^{17}O$[e]			$(eqQ/h)^{14}N$[e]			$(eqQ/h)^{2}H$[f]		
	xx	yy	zz	xx	yy	zz	xx	yy	zz
BDZ	−14.56	1.74	12.50	5.280	0.962	−6.250	−110.32	124.45	−1.42
DUNNING I	−13.88	1.93	11.96	5.103	0.968	−6.086	−108.22	121.62	−1.34
DUNNING II	−14.13	1.81	12.22	5.083	0.105	−6.143	−103.88	115.45	−1.15
BDZP	−14.35	2.14	12.24	5.480	0.604	−6.090	−87.33	92.91	−5.52
BDZPL1	−14.19	2.16	12.05	5.474	0.529	−6.013	−86.14	92.98	−6.83
BDZPL2	−14.30	2.15	12.17	5.462	0.598	−6.072	−87.19	92.38	−5.26
Exptl.[g]	—	—	—	5.1±0.2	0.4±0.5	−5.5±0.3	—	—	—

[a]In au.
[b]Nuclear component: $xx = 0.6065$, $yy = -0.6223$, $zz = 0.0158$.
[c]Nuclear component: $xx = 0.7899$, $yy = -0.7801$, $zz = -0.0098$.
[d]Nuclear component: $xx = 1.0503$, $yy = -1.2246$, $zz = 0.1742$.
[e]In MHz.
[f]In kHz.
[g]See ref. 5.

Finally, we have included $1s$ lobe functions in the BDZP basis set for comparing the effects which these functions produce. We observe that the values obtained for each of the one-electron properties are near to the values calculated with the BDZP basis set.

In conclusion, it seems that the calculated one-electron properties, where they can be compared with experimental results, fit in with these results quite reasonably. The inclusion of polarization functions has generally been found to lead to improvements in the one-electron properties calculated at a specific geometry.

Among the double zeta bases we can see that the contraction scheme is very important. Thus, the DUNNING I and II, with a smaller number of PGTF than the BDZ basis set of Huzinaga and Sakai, gives better results.

Although the BDZP with lobe functions (BDZPL1 and BDZPL2) are the best wavefunctions from an energetic point of view (only 0.0804 au above the Hartree–Fock limit), the charge distribution is not improved with respect to the BDZP basis set, and the time of calculation is much greater for the former.

1. A. B. CALLEAR and P. M. WOOD. Trans. Faraday Soc. **67**, 3899 (1971).
2. P. HATECK. Ber. B, **66**, 423 (1933); H. A. TAYLOR and C. TANFORD. J. Chem. Phys. **12**, 47 (1944); E. HINSCHLAFF and R. G. W. NORRISH. J. Chem. Soc. 1580 (1936); C. H. PURKIS and H. W. THOMSOM. Trans. Faraday Soc. **32**, 1466 (1936); J. W. C. JOHNS, A. R. W. MCKELLAR, and E. WEINBERGER. Can. J. Phys. **61**, 1106 (1983).
3. J. PESLAK, D. S. KLETT, and C. W. DAVID. J. Am. Chem. Soc. **93**, 5001 (1971); R. DITCHFIELD, J. E. DEL BENE, and J. A. POPLE. J. Am. Chem. Soc. **94**, 703 (1972); A. W. SALOTTO and L. BURNELLE. J. Chem. Phys. **52**, 2936 (1970); M. KRAUSS. J. Res. Natl. Bur. Stand. Sect. A. **73**, 191 (1969); L. E. ORGEL. J. Chem. Soc. 1276 (1953); A. A. WU, S. D. PEYERIMHOFF, and R. J. BUENKER. Chem. Phys. Lett. **35**, 316 (1975); O. NOMURA and S. IWATA. Chem. Phys. Lett. **66**, 523 (1979); O. NOMURA. Int. J. Quant. Chem. XVIII, 143 (1980); P. J. BRUNA and C. M. MARIAN. Chem. Phys. Lett. **67**, 109 (1979); E. M. SIEGBAHN, J. ALMLOF, A. HEIBER, and B. O. ROOS. J. Chem. Phys. **74**, 2384 (1981).
4. S. SAITO and K. TAKAGI. J. Mol. Spectrosc. **47**, 99 (1973).
5. J. VERHOEVEN, A. DYMANUS, and H. BLUYSSEN. J. Chem. Phys. **50**, 3330 (1969); J. VERHOEVEN and A. DYMANUS. J. Chem. Phys. **52**, 3222 (1970).
6. B. J. ROSENBERG, W. C. ERMLER, and I. SHAVITT. J. Chem. Phys. **65**, 4072 (1976); B. J. ROSENBERG and I. SHAVITT. J. Chem. Phys. **63**, 2162 (1975); H. POPKIE, H. KISTENMAYER, and E. CLEMENTI. J. Chem. Phys. **59**, 1325 (1975); D. NEUMANN and J. W. MOSKOWITZ. J. Chem. Phys. 2056 (1968).
7. D. NEUMANN, H. BASCH, R. L. KORNEGAY, L. C. SNYDER, J. W. MOSKOWITZ, C. HORNBACK, and S. P. LIEBMANN. Polyatom (V2), Q.C.P.E. **199**, Quantum Chemistry Program Exchange, Chemistry Department, Indiana University, Bloomington, IN.
8. W. J. HEHRE, W. A. LATHAN, R. DITCHFIELD, M. D. NEWTON, and J. A. POPLE. Gaussian 70, Q.C.P.E. **236**, Quantum Chemistry Program Exchange, Chemistry Department, Indiana University, Bloomington, IN.
9. S. HUZINAGA. J. Chem. Phys. **42**, 1293 (1965); S. HUZINAGA and S. SAKAI. J. Chem. Phys. **50**, 1371 (1969).
10. H. BASCH, U. B. ROBIN, and N. A. KUEBLER. J. Chem. Phys. **47**, 201 (1967).
11. T. H. DUNNING, JR. J. Chem. Phys. **53**, 2823 (1970).
12. T. H. DUNNING, JR. J. Chem. Phys. **55**, 716 (1971).
13. S. SHIH, R. J. BUENKER, S. PEYERIMHOFF, and B. WIRSAN. Theoret. Chim. Acta, **18**, 277 (1970); H. PREUSS. Z. Naturforsch, **11**, 823 (1956); J. L. WHITTEN. J. Chem. Phys. **44**, 359 (1966).
14. K. KUCHITSU and Y. MORINO. Bull. Chem. Soc. Jpn. **38**, 814 (1965).
15. F. W. DALBY. Can. J. Phys. **36**, 1336 (1958); J. L. BANCROFT, J. M. HOLLAS, and D. A. RAMSAY. Can. J. Phys. **40**, 322 (1962).
16. J. D. GODDARD and I. G. CSIZMADIA. J. Chem. Phys. **68**, 2172 (1978).

The products of hydrolysis of cyclic orthoesters as a function of pH and the theory of stereoelectronic control[1,2]

PIERRE DESLONGCHAMPS, JEAN LESSARD, AND YVES NADEAU
Laboratoire de synthèse organique, Département de Chimie, Faculté des Sciences, Université de Sherbrooke, Sherbrooke (Qué.), Canada J1K 2R1

Received November 23, 1984

PIERRE DESLONGCHAMPS, JEAN LESSARD, and YVES NADEAU. Can. J. Chem. **63**, 2485 (1985).

The acid hydrolysis of cyclic orthoesters **1**, **3–6** (R = Me), and **2** (R = Me and Et) as a function of pH was studied. The bicyclic orthoester **5** yields mainly the hydroxy-ester (less than 5% lactone), and this result is essentially independent of pH. For the other orthoesters, the relative percentage of products differs for each case and varies with pH. At pH $\leq$ 3, the percentage of lactone is always larger than at pH > 3. These results are explained on the basis of the stereoelectronic theory for the cleavage of tetrahedral intermediates.

PIERRE DESLONGCHAMPS, JEAN LESSARD et YVES NADEAU. Can. J. Chem. **63**, 2485 (1985).

On a étudié l'hydrolyse acide des orthoesters cycliques **1**, **3–6** (R = Me) et **2** (R = Me et Et) en fonction du pH. L'orthoester bicyclique **5** donne principalement l'hydroxy-ester (moins de 5% de lactone) et ce résultat est indépendant du pH. Pour les autres orthoesters, le pourcentage relatif de produits de réaction est différent dans chaque cas et varie avec le pH. À pH $\leq$ 3, le pourcentage de lactone est toujours plus grand qu'à pH > 3. On explique ces résultats en tenant compte de la théorie du contrôle stéréoélectronique dans le bris des intermédiaires tétraédriques.

The mild acid hydrolysis under kinetically controlled conditions of the five cyclic orthoesters **1–5** (R = C_2H_5) (Scheme 1) was reported by our laboratory (3) in 1975. It was found that each orthoester gave essentially only the corresponding hydroxyester; the lactone, the other possible product of the reaction, was not observed in significant quantities.[3] These results were taken as convincing evidence in favor of the theory of stereoelectronic control in hydrolytic processes (3–7).

Capon and Grieve (8) have recently reported that part of the above results were erroneous.[4] They have studied 2,2-diethoxytetrahydropyran (**2**, R = C_2H_5) and found that under our reported conditions, 20–30% of δ-valerolactone was observed by ^{1}H and ^{13}C nmr spectroscopy. They have also investigated the mild acid hydrolysis of 2,2-dimethoxytetrahydropyran (**2**, R = CH_3) under a variety of solvents and, again, they found 30–40% of δ-valerolactone.

In the meantime, McClelland and Alibhai (9) reported (in 1981) the observation that the hydroxy-ester/lactone product ratio of **10** and **9** varies as a function of pH in the course of the acid hydrolysis of the phthalide orthoester **7**. Indeed, with this compound, a quantitative analysis of the pH-dependent product ratio reveals two pH-independent regions, corresponding to the acid and base-catalyzed breakdown of the tetrahedral hemi-orthoester intermediate **8**: at pH $\leq$ 3.5, 24% of lactone **9** is produced, but above pH 3.5, only 7% of lactone **9** (and some 93% hydroxy-ester **10**) is observed.

Due to the fact that (a) part of our results are not concordant with those of Capon and Grieve (8), and (b) product ratio varies above and below pH = 3.5 as discovered by McClelland and Alibhai (9), it became necessary to repeat our investigation, especially since in our original work the acid hydrolysis of **1–5** (R = C_2H_5) was carried out with an acidic solution having a pH of about 3 (10^{-3} *M* PTSA in water).

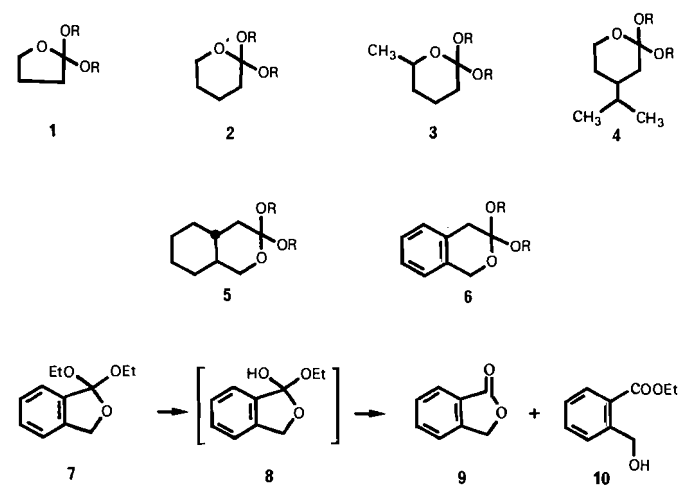

SCHEME 1

We wish now to report a product ratio study of the acid hydrolysis of cyclic orthoesters **1–6** (R = CH_3) and that of **2** (R = C_2H_5), as a function of pH. The results obtained are then rationalized on the basis of stereoelectronic principles.

Discussion

The results obtained are described in Table 1. All the cyclic orthoesters, except bicyclic orthoester **5**, show on hydrolysis two pH-independent regions for the product ratio, where the percentage of lactone is more important at pH $\leq$ 3 than at pH > 3. The bicyclic orthoester **5** behaved differently, yielding approximately 95% of hydroxy-ester between pH = 2 and 4.

The product ratio observed at pH = 4 and 5 in orthoester **2** (R = C_2H_5) is identical to the value that we originally obtained (3) by vpc analysis.[3] The product ratio observed at pH $\leq$ 3 for orthoesters **2** (R = CH_3 and C_2H_5) corresponds to the value observed by Capon and Grieve (8). The discrepancy between

[1] For general leading references on this subject, see refs. 1 and 2.

[2] Taken in part from the Ph.D. thesis of Y. Nadeau (December 1983).

[3] Analysis of the reaction products was carried out by two different methods: (a) ^{13}C nmr spectroscopy of the reaction mixture, which showed less than 1% of lactone, and (b) vpc analysis of the reaction mixture (after treatment with acetic anhydride and pyridine), which gave a ~5:95 ratio of lactone and the acetate derivative of the hydroxy-ester. Method (a) was believed to be more accurate, and it was concluded that the amount of lactone produced was negligible ($\leq$1%).

[4] We wish to thank Professor B. Capon who has communicated his results to us prior to publication.

TABLE 1. Product ratio of lactone (L) and hydroxy-ester (E) from the hydrolysis of cyclic orthoesters*

		pH 0.9	pH 1.9	pH 3	pH 4	pH 4.7
		L%/E%	L%/E%	L%/E%	L%/E%	L%/E%
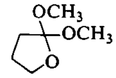	1	22:78	21:79	22:78	21:79	15:85
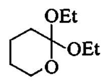	2	19:81	21:79	26:74	6:94	4:96
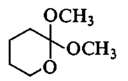	2	33:67	32:68	31:69	16:84	11:89
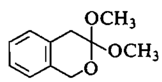	6	53:47	55:45	53:47	13:87	7:93
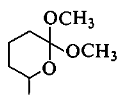	3	10:90	10:90	9:91	<5:>95	<5:>95
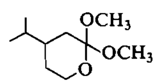	4	19:81	14:86	13:87	7:93	—
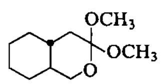	5	—	6:94	<5:>95	<5:>95	—

*The pH values refer to the pH of D_2O/DCl solutions before the mixing with the solution of orthoester in hexadeuterated acetone (see Experimental).

our results (3) and those of Capon and Grieve (8) can now be explained. In our original work, the hydrolysis must have taken place at pH higher than 3. This is highly possible because the cyclic orthoesters were stored on solid anhydrous potassium carbonate to prevent decomposition. It is also possible that the 10^{-3} *M* *p*-toluenesulfonic acid solution used had a pH higher than 3. It should be pointed out that the pH of the acidic solution was not measured because it was not an important parameter at the time of the experiments. The second method of analysis which was originally used by us (^{13}C nmr)[3] indicated less than 1% of lactone, and this result was also very likely incorrect. The standard ^{13}C nmr chemical shift values that were originally used (3) for the reaction products, i.e., δ-valerolactone and the corresponding ethyl hydroxy-ester, are essentially identical to those used by Capon and Grieve (9). Therefore, the standard values used are not the source of error and we do not know why this method did not produce the correct percentage for the lactone products.

Before continuing the discussion of the results obtained with the various orthoesters, it is now appropriate to discuss the reaction mechanism of the hydrolytic process as a function of the acidity of the medium. The large difference in rates, and the variation in product ratios observed at pH $\leq$ 3 and at pH > 3, suggest a different reaction mechanism for the breakdown of the tetrahedral intermediate at high and low acid concentration. The hydrolysis of orthoesters takes place by first producing a dialkoxycarbonium ion (Scheme 2), which is then hydrated to give a hemiorthoester tetrahedral intermediate (**11** → **12** → **13**) (10). Then, following McClelland and Alibhai (9), the cleavage of the intermediate **13** at pH $\leq$ 3 would be acid catalyzed, whereas that at pH > 3 would be hydroxide catalyzed. As a result, the two mechanisms of breakdown differ in the following way: at pH $\leq$ 3, the ester (or lactone) is ejected in its protonated form, whereas at pH > 3 it is directly produced as a non-protonated neutral species. In other words, in the acid-catalyzed process, it is the T^+ ionic form of the tetrahedral intermediate which is cleaved, producing a protonated ester, whereas in the hydroxide-catalyzed process, it is the T^0 form which is cleaved, yielding a non-protonated ester. The acid and base-catalyzed processes can be expressed by the sequences **13** → **14** → **15** and **13** → **16** → **17** respectively. We would like to point out that when an intermediate or a product is protonated, the stereoelectronic effect of one electron pair has been essentially neutralized, and this factor must be taken into consideration in order to arrive at a correct understanding of the results.

The results can now be rationalized in terms of the stereoelectronic theory for the breakdown of tetrahedral intermediates,[5] which takes into account: item (a) primary and secondary (7) stereoelectronic effects, item (b) conformational change in tetrahedral intermediate prior to breakdown, and item (c) the ionic state of tetrahedral intermediates and reaction products as a function of pH.

Items (a) and (b)

Primary and secondary stereoelectronic effects predict that a cyclic orthoester is best hydrolyzed via conformer **18** (conformer *A* in refs. 3 and 11; see also footnote 5) which gives first the *EZ* lactonium ion **19** followed by hydration to produce a

[5] See chapt. 3 in ref. 1 for a detailed analysis.

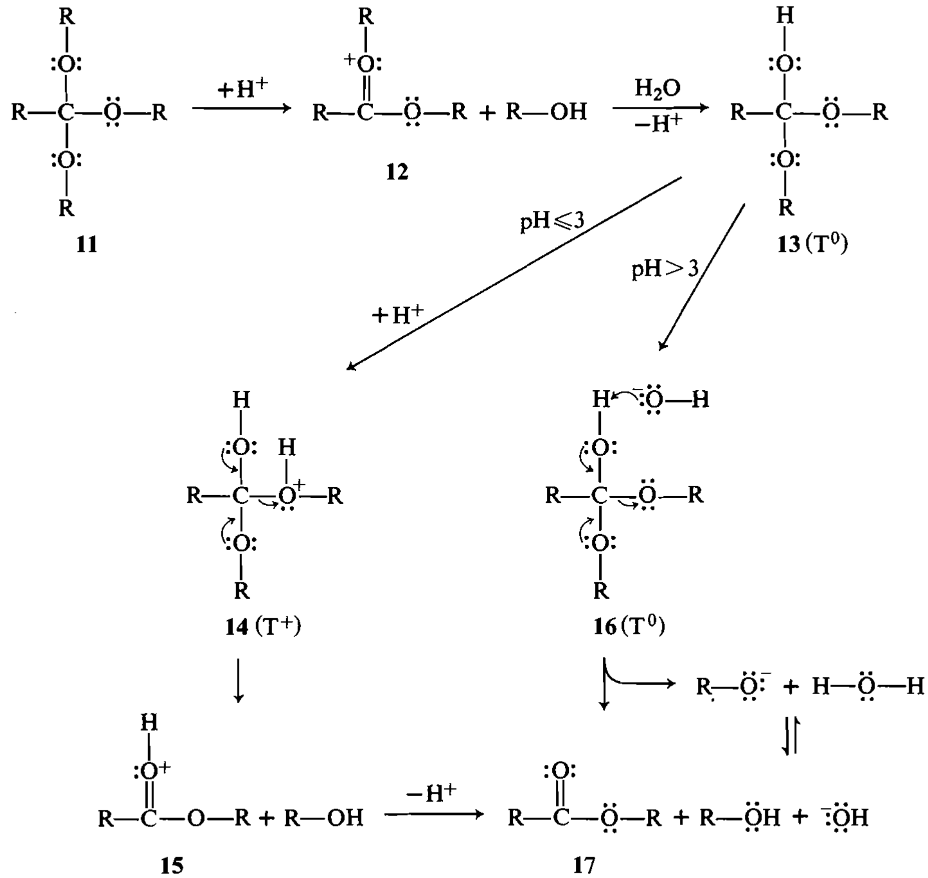

SCHEME 2

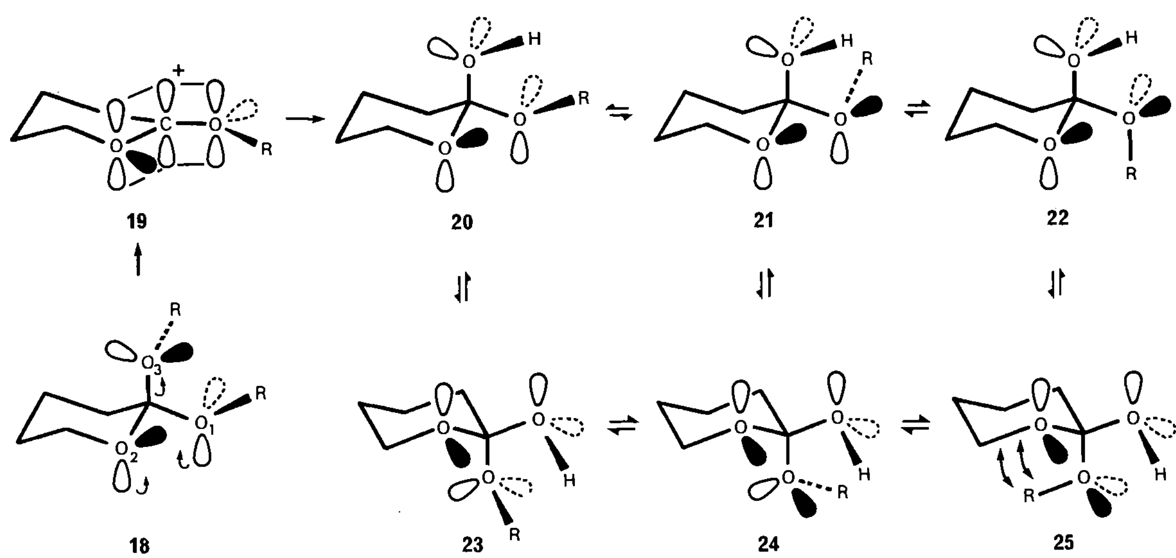

SCHEME 3

tetrahedral intermediate having conformation **20** (Scheme 3).[6] Since tetrahedral hemiorthoester intermediates have a definite lifetime under neutral or mild acid conditions (9, 12, 13), conformational equilibration then takes place to give either the three tetrahedral conformers **20**–**22** when the inversion of the chair form is not allowed or the six tetrahedral conformers **20**–**25** when chair inversion can take place with ease.

Conformer **21** cannot break down with primary stereoelectronic control (except to give back **19**), and conformer **25** is a relatively high energy conformer due to the severe steric interaction caused by the R group with the ring. These two conformers can therefore be eliminated from further consideration. The remaining four conformers **20**, **22**, **23**, and **24** can

[6] In conformation **18**, O1 and O2 each have one electron pair antiperiplanar to the axial C1—O3 bond (primary stereoelectronic effect), and O1 has one electron pair antiperiplanar to the C1—O2 bond (secondary stereoelectronic effect) (7). Thus, cleavage of the axial bond in **18** produces the *EZ* lactonium ion **19**. Following the same rule, addition of water on **19** must take place on the top face and yields a tetrahedral intermediate having the chair conformation **20**.

break down with primary stereoelectronic control. Conformers **20** and **22** can only give a hydroxy-ester, but having the *Z* and *E* configuration respectively (Scheme 4). Conformer **23** can either give the lactone or the hydroxy-ester in the *Z* conformation, whereas conformer **24** can only yield the lactone. Secondary stereoelectronic effects ease the formation of *Z* over that of an *E* ester (7). The cleavage of **20** is thus favored over that of **22**. Since lactones have the conformation of an *E* ester, formation of the hydroxy-ester in the *Z* conformation is thus electronically favored. On that basis, **23** would be more easily cleaved than **24** and would preferentially give the hydroxy-ester product. On the other hand, there is an entropy factor which favors the formation of lactone and alcohol. If this factor is as important as the secondary stereoelectronic effect, lactone formation can compete with that of the hydroxy-ester in the cleavage of **23**. On that basis, lactone formation from **24** should also be observed.[7]

Now, if we consider a cyclic orthoester (such as **2**) which can be assumed to undergo easily a conformational change via ring inversion, the following conclusion can be reached. The cation **19** will first produce **20**, which is then allowed to equilibrate to give a mixture of conformers **20**–**25**. Then, in principle, two different situations are possible. In the first one, secondary stereoelectronic effects completely overrule the entropy factor; as a result, breakdown would take place via conformers **20** and **23** yielding only the (*Z*) hydroxy-ester product. In the second situation, the secondary stereoelectronic effects cannot overrule completely the entropy factor, and breakdown could thus take place via conformers **20**, **23**, and **24**, conformer **20** yielding only the (*Z*) hydroxy-ester, conformer **23** a mixture of (*Z*) hydroxy-ester and lactone, and conformer **24** the lactone product only.[8] Thus, in the first situation, only the hydroxy-ester should be observed and, in the second, a mixture of hydroxy-ester and lactone would be expected.

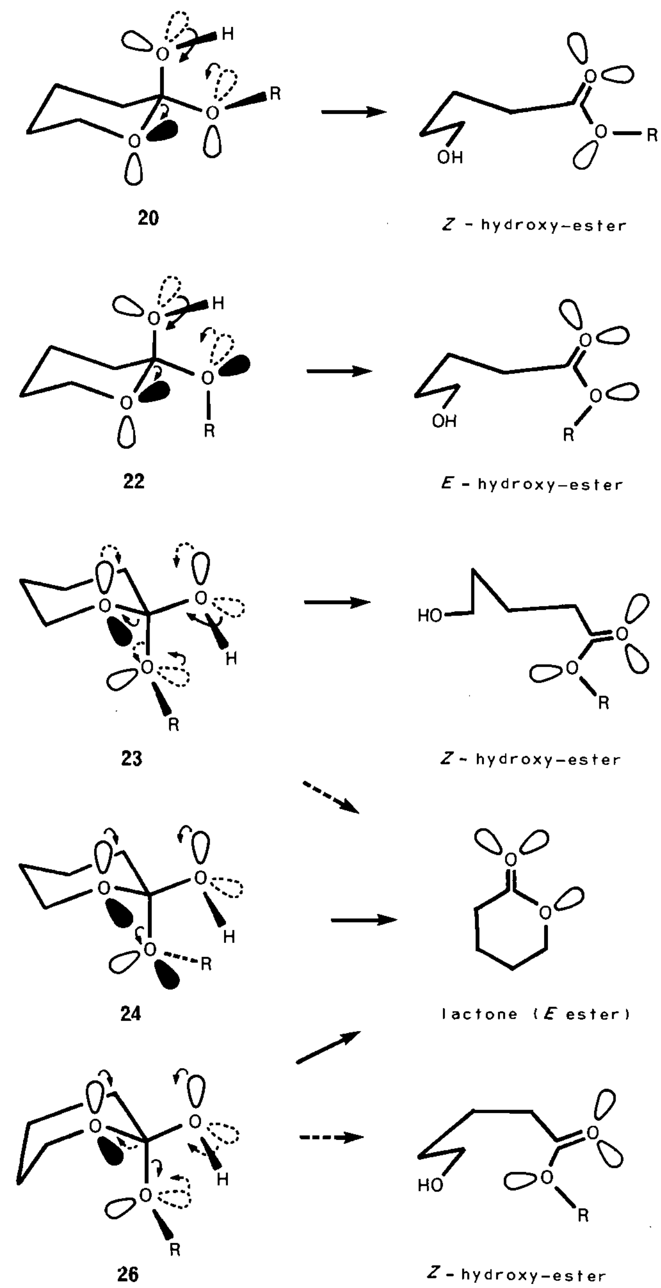

SCHEME 4

If a cyclic orthoester which cannot undergo a chair inversion (e.g. **5**) is now considered, the conclusion is the following. The cation **19** produces **20**, which is then allowed to equilibrate to give a mixture of conformers **20**–**22** only. We have already seen that with these three conformers, only **20** can break down, but to give a (*Z*) hydroxy-ester. On that basis, conformationally rigid ring orthoesters can only give the hydroxy-ester product. The only manner by which these types of orthoesters could give

[7] We have suggested (3) that the entropy release expected for a reaction involving fragmentation to give separate molecules favors the cleavage of lactone and alcohol. It was later pointed out by Kirby (see pp. 103–104 in ref. 2) that little entropy may have in fact been released by the time the transition state for C—O cleavage has been reached, and that another explanation, still based on entropy consideration, can be put forward: it involves the reversibility of ring opening in the first stage of the hydrolysis process, just before the first stable products (hydroxy-ester or lactone and alcohol) are formed. In the case of orthoesters, the first stage of the hydrolysis is the cleavage of T^+, producing (*in situ*) an R—OH group and a dialkoxycarbonium ion which are close to one another. Then two processes are possible; either the ROH group can add back on the dialkoxycarbonium ion, or the R—OH moves further away (conformational change) and becomes solvated, and concurrently the dialkoxycarbonium ion is trapped intermolecularly by water producing a hemiorthoester tetrahedral intermediate. When the ROH group is linked to the dialkoxycarbonium ion, intramolecular trapping of this ion may compete favorably with the intermolecular trapping of this ion by a molecule of solvent. With hemiorthoesters, cleavage can take place with the T^+ or the T^0 form. For the cleavage of the T^+ ionic form, the first stage is the production (nearby) of an ROH group and a protonated ester (or lactone). In the next step, either the ROH group adds back to the protonated ester or moves away and becomes solvated, and the protonated ester is concurrently deprotonated by the solvent. For the cleavage of the T^0 form, the first stage is the production (nearby) of the alkoxide ion and a non-protonated ester (or lactone). In the next step, either the alkoxide ion adds back to the ester, or moves away and becomes protonated and solvated. In both cases (T^+ or T^0), the reverse step will be more favored in an intramolecular than in an intermolecular situation. Thus, under conditions of kinetic control, i.e. when equilibration between the reaction products is not an important process, there is a factor based on entropy consideration which disfavors the formation of hydroxy-ester and favors the formation of lactone and alcohol. This effect will be referred in the text as the entropy factor.

[8] The formation of (*E*) hydroxy-ester from **22** should not be observed because this cleavage is disfavored by both the secondary stereoelectronic effects and by the entropy factor.

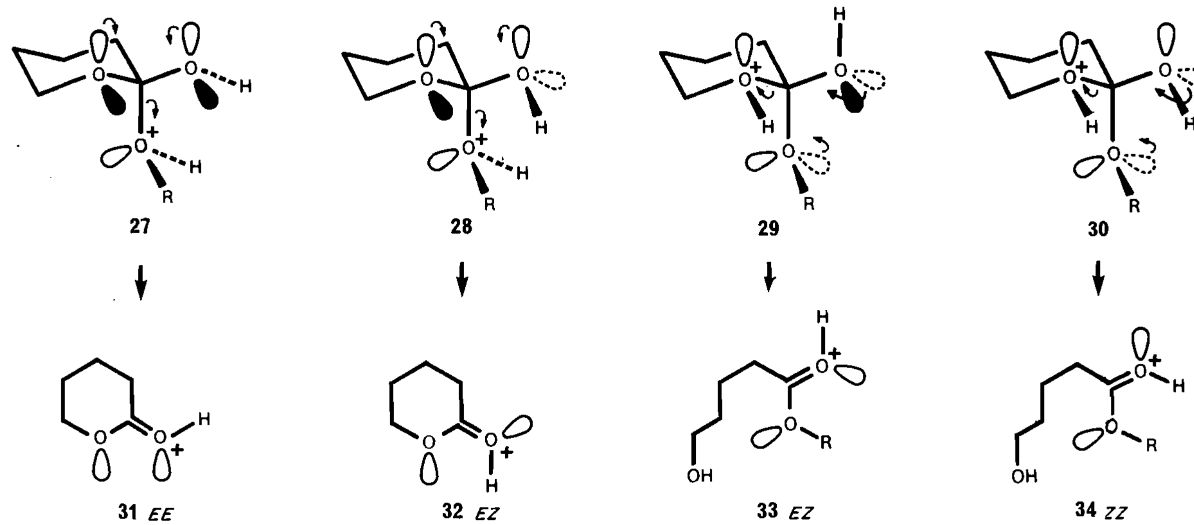

SCHEME 5

a mixture of hydroxy-ester and lactone, while respecting the stereoelectronic principles, is by undergoing a conformational change from a chair to a boat (or a twist-boat). For instance, conformer **20** could be transformed into the boat conformer **26** which can then break down to either a (*Z*) hydroxy-ester or the lactone (Scheme 4). In conclusion, orthoesters which cannot undergo a chair inversion are predicted to give mainly the hydroxy-ester because lactone formation can only occur via the cleavage of a tetrahedral intermediate having a boat conformation.[9]

Item (c)

The ionic state of tetrahedral intermediates and products as a function of pH must now be considered. The preceding discussion was concerned with cleavages of neutral tetrahedral intermediates yielding a non-protonated ester. This discussion and the conclusion reached can therefore be applied for cleavages occurring at pH > 3 (hydroxide-catalyzed breakdown of T^0 yielding a neutral ester product). It is, however, necessary to analyze the cleavages at pH ≤ 3 which take place on the T^+ form yielding a protonated product. This analysis can be done by examining the possible cleavages of the protonated forms of conformer **23** which can give either the hydroxy-ester or the lactone product. Appropriate conclusions then follow automatically for cleavages of the other intermediates **20**, **22**, and **24**.

There are four different ways by which protonated conformer **23** can break down. They correspond to **27**, **28**, **29**, and **30** (Scheme 5) depending upon which oxygen is protonated[10] (axial or ring oxygen atom), and upon the orientation of the O—H bond of the equatorial oxygen atom. The first two possibilities, **27** and **28**, give the protonated lactone in the *EE* (**31**) and *EZ* (**32**) configurations respectively, whereas the other two, **29** and **30**, lead respectively to the *EZ* (**33**) and the *ZZ* (**34**) configurations of the protonated ester.

EZ Dialkoxycarbonium ions are more stable than the corresponding *EE* isomers (16). Secondary electronic effects predict the same relative stability for protonated lactones and predict also that the process **28** → **32** (*EZ*) is energetically favored over that of **27** → **31** (*EE*). Similarly, secondary stereoelectronic effects predict that in protonated esters, the *ZZ* configuration **34** is more stable than the *EZ* configuration **33**. These effects predict also that the *ZZ* configuration **34** should be preferentially formed over the *EZ* configuration **33**. However, rigorous experimental evidence on the most stable geometry for protonated esters is lacking (17). This hypothesis is, however, supported by theoretical calculation (18) and by the fact that carboxylic acids are known to preferentially exist as cyclic hydrogen-bonded dimers having the *ZZ* configuration (19). It is therefore assumed that the process **30** → **34** (*ZZ*) is more energetically favorable than that of **29** → **33** (*EZ*). Thus, at pH ≤ 3, formation of hydroxy-ester and lactone would take place via the processes **30** → **34** (*ZZ*) and **28** → **32** (*EZ*) respectively. The former process is favored by one additional secondary stereoelectronic effect. On this basis, it should take place preferentially over the other. On the other hand, the entropy factor works in the opposite direction, favoring the process **28** → **32** (*EZ*) rather than the process **30** → **34** (*ZZ*).

It is now important to compare the cleavage of T^+ with that of T^0. In both cases, the formation of hydroxy-ester is equally favored over the formation of lactone by secondary stereoelectronic effects. In both cases also, the entropy factor favors the formation of lactone and alcohol over that of hydroxy-ester. However, this factor may play a more important role in the cleavage of T^0 than in the cleavage of T^+, resulting in a relatively larger percentage of lactone and alcohol in the cleavage of T^+. This would be due to the fact that in the first stage of the hydrolysis, before formation of the final reaction products, the reverse step (i.e. the intramolecular attack of a hydroxyl group on a protonated ester to reform T^+) would take place with greater ease than the reaction of an alkoxide ion with both a non-protonated ester and a molecule of water to reproduce T^0. As a result, a larger percentage of lactone would be observed at pH ≤ 3 (breakdown of T^+) than at pH > 3 (breakdown of T^0).

[9] Cleavage via a boat conformer is expected to be a higher energy process than that of a chair conformer. It is, however, theoretically possible that the boat formation could lie on the reaction coordinate (e.g. see ref. 14), and this process could compete with the cleavage of the chair form. The experimental results show however that this is a minor process (*vide infra*, see also ref. 15).

[10] Stereochemistry of protonation of the leaving group oxygen in **27–30** could be different than the one chosen, but the conclusion would be the same.

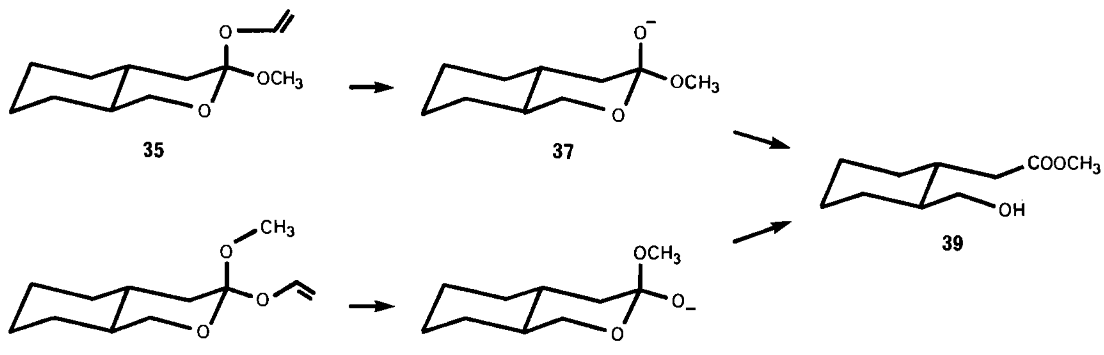

SCHEME 6

Analysis of cyclic orthoesters ***1–6***

2,2-Diethoxytetrahydropyran (**2**, R = C_2H_5) is an orthoester which can easily undergo a chair inversion; its hydrolysis must therefore take place via the breakdown of conformers **20**, **23**, and **24**. The results at pH > 3 indicate that the major fragmentation of T^0 must take place via intermediates **20** and **23**, yielding the hydroxy-ester. The small percentage of lactone would thus be the result of a minor process resulting from the cleavage of intermediates **23** and **24**. A small proportion of lactone could also come from the fragmentation of boat conformers such as **26**. The results at pH ≤ 3 indicate that the cleavage of T^+ gives more lactone than that of T^0, in accord with the preceding discussion.

The same conclusion can be reached for 2,2-dimethoxytetrahydropyran (**2**, R = CH_3). The larger percentage of lactone observed in this case by comparison with **2** (R = C_2H_5) at various pHs, can be explained by the fact that a methoxy group is considered a better leaving group than an ethoxy group. This argument is based on the fact that methanol is a stronger acid than ethanol.

The aromatic orthoester **6** (R = CH_3) is also conformationally mobile and, as predicted, there are two different product ratios with the variation of pH. The rather large proportion of lactone observed at pH ≤ 3 can be readily explained because the CH_2OH and CH_2COOMe groupings are in a *cis* arrangement due to the benzene ring. This should favor lactone formation at the transition state level.[7]

2,2-Dimethoxytetrahydrofuran (**1**, R = CH_3) is also conformationally mobile and the results obtained are in accord with the preceding general discussion. By comparison with **2** (R = CH_3), this five-membered orthoester gives slightly more lactone at pH > 3 and less at pH ≤ 3. The differences are, however, not important enough to be discussed further.

Bicyclic orthoester **5** (R = CH_3) gave essentially the same relative proportion of lactone and hydroxy-ester at low and high acid concentration. This is expected because this orthoester cannot undergo a chair inversion, and the cleavages of both, T^0 and T^+, can take place with conformer **20** only, yielding the hydroxy-ester exclusively. The small percentage of lactone must come from the cleavage of boat conformers (as T^+ or T^0) such as **26**.

The last two cyclic orthoesters **3** and **4** (R = CH_3) can be analyzed together. In these two orthoesters, a complete chair inversion process cannot be a very important process because in one conformation, the secondary methyl or isopropyl group will be in a 1,3-diaxial orientation with one of the methoxy groups. These orthoesters can, however, take a boat or twist-boat conformation much more easily than bicyclic orthoester **5** (R = CH_3). These orthoesters have therefore a lesser degree of conformational mobility than **2** or **6** (R = CH_3), but more so than **5** (R = CH_3). The product ratios obtained are in agreement with the above analysis. Orthoester **4** (R = CH_3), which produces a larger amount of lactone, appears to be more conformationally mobile than orthoester **3** (R = CH_3). But the difference in percentage of lactone could also be explained by the fact that the leaving group would be better in **4** (a primary alcohol) than in **3** (a secondary alcohol).

Conclusion

The various product ratios observed between pH 1 and 5 with cyclic orthoesters **1–6** (R = CH_3) and **2** (R = C_2H_5) are readily rationalized on the basis of the stereoelectronic theory for the cleavage of tetrahedral intermediates, which takes into account primary and secondary stereoelectronic effects, conformational changes in tetrahedral intermediates prior to breakdown, entropic factors, and the ionic state of tetrahedral intermediates and reaction products as a function of pH.

These results put this theory on a firm basis (20) and provide new information on the cleavage of cyclic hemiorthoester tetrahedral intermediates in the T^0 and the T^+ ionic forms: (a) conformer **20**, either in the T^0 or in the T^+ ionic form, yields only the hydroxy-ester; the small percentage of lactone product (≤5%) would result from a conformational change to a boat conformer (such as **26**); (b) cleavage of **23** in the T^0 neutral form preferentially yields the hydroxy-ester (>95%), and cleavage of **24** to yield the lactone product is a minor process (<5%). The formation of lactone becomes more important when the cleavage of **23** and **24** takes place on their T^+ ionic form.

A logical deduction of the above investigation is that the cleavage of negatively charged (T^-) tetrahedral intermediate should produce a product ratio similar to that predicted for T^0, i.e. mainly hydroxy-ester. This is in agreement with the fact that permanganate oxidative cleavage, under basic conditions, of axial and equatorial vinyl orthoesters **35** and **36** (Scheme 6) yields mainly the hydroxy-ester **39** via the intermediates **37** and **38** respectively (7, 21). In accord with the above rationale, γ-butyrolactone ((22, 23), D-gluconolactone (24)) and isochromane-3-one (25) do not undergo carbonyl–oxygen exchange during their basic hydrolysis.

Experimental

The ir spectra were taken on a Perkin–Elmer 681 spectrophotometer; proton nmr spectra (δ-values) were recorded on a Bruker

WX-250 spectrometer in hexadeuteroacetone.

Lactones

γ-Butyrolactone and δ-valerolactone are commercial products. Isochromanone was prepared by Baeyer–Villiger oxidation of indanone as described in ref. 26. The preparation of 5-methyl-δ-valerolactone, 3-isopropyl-δ-valerolactone, and *trans*-octahydrocoumarin was described in ref. 3.

Orthoesters 1–6

General method of preparation (3, 27)

The lactone (2 mmol) was added to a suspension of trimethyloxonium tetrafluoroborate (2 mmol) in dichloromethane (25 mL) and the mixture stirred at room temperature overnight. The resulting solution was added to sodium methoxide (3 mmol) in methanol (25 mL) cooled to −78°C. The reaction mixture was allowed to warm up to room temperature, then washed with an aqueous solution of sodium bicarbonate (10%). The organic phase was dried over potassium carbonate and the solvent evaporated. The crude orthoester was purified by distillation under vacuum and kept over potassium carbonate.

Orthoester **1** (R = CH_3): bp 62°C/10 Torr (1 Torr = 133.3 Pa); yield 82%; ir ν_{max} (film): 1000–1200 cm^{-1}; nmr δ: 3.83 (2H, multiplet, O—CH_2—), 3.18 (6H, singlet, O—CH_3), 1.17 (4H, multiplet, methylenes at C-3 and C-4).

Orthoester **2** (R = CH_3): bp 65°C/10 Torr; yield 82%; ir ν_{max} (film): 1000–1200 cm^{-1}; nmr δ: 3.67 (2H, triplet, J = 6 Hz, O—CH_2—), 3.15 (6H, singlet, O—CH_3), 1.7 (6H, multiplet, methylenes at C-3, C-4, and C-5).

Orthoester **2** (R = C_2H_5): the preparation was described in ref. 3.

Orthoester **3** (R = CH_3): bp 60°C/100 Torr; yield 86%; ir ν_{max} (film): 1000–1200 cm^{-1}; nmr δ: 3.83–3.64 (1H, multiplet, O—CH—), 3.19 (3H, singlet, O—CH_3), 3.11 (3H, singlet, O—CH_3), 1.7–1.6 (6H, multiplet, methylenes at C-3, C-4, and C-5), 1.2 (3H, doublet, J = 6 Hz, CH_3—CH—).

Orthoester **4** (R = CH_3): bp 85°C/4 Torr; yield 86%; ir ν_{max} (film): 1000–1200 cm^{-1}; nmr δ: 3.76 (1H, doublet of doublet of doublets, J = 11 Hz, 5 Hz, 2 Hz, O—CH_aH_e—), 3.58 (1H, doublet of triplets, J = 12 Hz, 2 Hz, O—CH_aH_e—), 3.21 (3H, singlet, O—CH_3), 3.11 (3H, singlet, O—CH_3), 1.9–1.5 (7H, multiplet, methylenes at C-3, C-4, and C-5, and —$CH(CH_3)_2$), 0.9 (6H, doublet, J = 5 Hz, —$CH(CH_3)_2$).

Orthoester **5** (R = CH_3): bp 80°C/0.5 Torr; yield 81%; ir ν_{max} (film): 1000–1200 cm^{-1}; nmr δ: 3.54 (1H, doublet of doublets, J = 12 Hz, 5 Hz, O—CH_aH_e—), 3.25 (1H, triplet, J = 12 Hz, O—CH_aH_e—), 3.19 (3H, singlet, O—CH_3), 3.00 (3H, singlet, O—CH_3), 1.8–1.5 (12H, multiplet).

Orthoester **6** (R = CH_3): bp 85°C/0.5 Torr; yield 80%; ir ν_{max} (film): 1000–1200 cm^{-1}; nmr δ: 7.4–7.2 (4H, multiplet, aromatic protons), 4.83 (2H, singlet O—CH_2—), 3.26 (6H, singlet, O—CH_3), 3.00 (2H, singlet, =C—CH_2—).

Orthoester hydrolysis

General procedure

From a stock solution of the orthoesters (20–40 mg) in hexadeuteroacetone (3 mL), an aliquot (0.5 mL) was transferred into a 5-mm tube in the probe of a 250-MHz spectrometer at 25°C. A dilute solution of deuterated hydrochloric acid of a given pH (measured with a pH meter: pH values of 0.9, 1.9, 3.0, 4.0, and 4.7) was then added (0.1 mL at pH = 0.9 and 1.9; 0.25 mL at pH = 3; 0.5 mL at pH = 4 and 4.7). The reaction was followed by nmr and stopped when no more orthoester was present. Two to three runs were carried out. The relative proportion of lactone and hydroxy-ester was determined by the nmr integration of well-separated and characteristic peaks of the two products.

At pH 0.9 and pH 1.9, the reaction was usually over by the time the spectrum was recorded. Spectra were recorded for an additional 15 min to check the rate of lactonization of the hydroxy-ester. Except for the hydrolysis of orthoester **5** at pH = 0.9, there was very little change in lactone/hydroxy-ester ratio between the first spectrum and that recorded after 15 min. At pH > 3, the reaction was much slower, necessitating several hours.

In these experiments, the volume ratio D_2O/CD_3COCD_3 was not kept constant since Capon and Grieve (8) had shown that it had practically no influence on the percentage of δ-valerolactone in the hydrolysis of orthoesters **2** (R = CH_3 and C_2H_5) at pH ≤ 3.

Acknowledgements

Support for this work by the Natural Sciences and Engineering Research Council of Canada (NSERCC) and by the "Ministère de l'Éducation" (FCAC), Québec, is gratefully acknowledged.

1. P. DESLONGCHAMPS. Stereoelectronic effects in organic chemistry. Organic Chemistry Series. Vol. 1. *Edited by* J. E. Baldwin. Pergamon Press, Oxford. 1983.
2. A. J. KIRBY. The anomeric effect and related stereoelectronic effects at oxygen. Springer Verlag, Berlin. 1983.
3. P. DESLONGCHAMPS, R. CHÊNEVERT, R. J. TAILLEFER, C. MOREAU, and J. K. SAUNDERS. Can. J. Chem. **53**, 1601 (1975).
4. P. DESLONGCHAMPS, P. ATLANI, D. FRÉHEL, and A. MALAVAL. Can. J. Chem. **50**, 3405 (1972).
5. P. DESLONGCHAMPS. Pure Appl. Chem. **43**, 351 (1975).
6. P. DESLONGCHAMPS. Tetrahedron, **31**, 2463 (1975).
7. P. DESLONGCHAMPS. Heterocycles, **7**, 1271 (1977).
8. B. CAPON and D. MCL.A. GRIEVE. Tetrahedron Lett. **23**, 4823 (1982).
9. R. A. MCCLELLAND and M. ALIBHAI. Can. J. Chem. **59**, 1169 (1981).
10. (*a*) E. H. CORDES. *In* Progress in physical organic chemistry. Vol. 4. *Edited by* A. Streitwieser and R. W. Taft. Interscience, New York. 1967. pp. 1–44; (*b*) E. H. CORDES and H. G. BULL. Chem. Rev. **74**, 582 (1974).
11. (*a*) G. LAMATY, C. MOREAU, and Z. MOULOUNGUI. Can. J. Chem. **61**, 2643 (1983); (*b*) G. LAMATY, P. LORENTE, and C. MOREAU. Can. J. Chem. **61**, 2651 (1983).
12. (*a*) B. CAPON, J. H. GALL, and D. MCL.A. GRIEVE. J. Chem. Soc. Chem. Commun. 1034 (1976); (*b*) B. CAPON and D. MCL.A. GRIEVE. J. Chem. Soc. Perkin Trans. 2, 300 (1980); (*c*) B. CAPON and A. K. GHOSH. J. Am. Chem. Soc. **103**, 1765 (1981); (*d*) B. CAPON, A. K. GHOSH, and D.MCL.A. GRIEVE. Acc. Chem. Res. **14**, 306 (1981).
13. (*a*) M. AHMAD, R. G. BERGSTROM, M. J. CASHEN, A. J. KRESGE, R. A. MCCLELLAND, and M. F. POWELL. J. Am. Chem. Soc. **99**, 4827 (1977); (*b*) M. AHMAD, R. G. BERGSTROM, M. J. CASHEN, Y. CHIANG, A. J. KRESGE, R. A. MCCLELLAND, and M. F. POWELL. J. Am. Chem. Soc. **101**, 2669 (1979); (*c*) R. A. MCCLELLAND and M. AHMAD. J. Org. Chem. **44**, 1855 (1979); (*d*) R. A. MCCLELLAND, M. AHMAD, J. BOHONEK, and S. GEDGE. Can. J. Chem. **57**, 1531 (1979); (*e*) R. A. MCCLELLAND and G. PATEL. J. Am. Chem. Soc. **103**, 6809 (1981); **103**, 6912 (1981).
14. (*a*) S. CHANDRASEKHAR and A. J. KIRBY. J. Chem. Soc. Chem. Commun. 171 (1978); (*b*) A. J. KIRBY and R. J. MARTIN. J. Chem. Soc. Chem. Commun. 803 (1978); (*c*) S. CHANDRASEKHAR, A. J. KIRBY, and R. J. MARTIN. J. Chem. Soc. Perkin Trans. 2, 1619 (1983); (*d*) A. J. KIRBY and R. J. MARTIN. J. Chem. Soc. Perkin Trans. 2, 1627 (1983); (*e*) A. J. KIRBY and R. J. MARTIN. J. Chem. Soc. Perkin Trans. 2, 1633 (1983); (*f*) A. J. BRIGGS, C. M. EVANS, R. GLENN, and A. J. KIRBY. J. Chem. Soc. Perkin Trans 2, 1637 (1983).
15. O. E. DESVARD and A. J. KIRBY. Tetrahedron Lett. **23**, 4163 (1982).
16. (*a*) B. G. RAMSEY and R. W. TAFT. J. Am. Chem. Soc. **88**, 3058 (1966); (*b*) R. F. BORCH. J. Am. Chem. Soc. **90**, 5303 (1968); (*c*) CH. H. V. DUSSEAU, S. E. SCHAAFSMA, H. STEINBERG, and TH. J. DE BOER. Tetrahedron Lett. 467 (1969).
17. (*a*) H. HOGEVEEN, A. F. BICKEL, C. W. HILBERS, E. L. MACKOR, and C. MACLEAN. Chem. Commun. 898 (1966); (*b*)

G. A. OLAH and A. M. WHITE. J. Am. Chem. Soc. **89**, 3591 (1967); (*c*) G. A. OLAH, D. H. O'BRIEN, and A. M. WHITE. J. Am. Chem. Soc. **89**, 5694 (1967); (*d*) H. HOGEVEEN. Recl. Trav. Chim. Pays-Bas, **87**, 1313 (1968).
18. A. SHIGIHARA, H. ICHIKAWA, and M. TSUCHIYA. Mass. Spectrosc. **30**, 145 (1982).
19. L. LEISEROWITZ. Acta Crystallogr. Sect. B, **32**, 775 (1976), and references quoted therein.
20. C. L. PERRIN and G. M. L. ARRHENIUS. J. Am. Chem. Soc. **104**, 2839 (1982).
21. P. DESLONGCHAMPS, N. BEAULIEU, R. CHÊNEVERT, and R. A. DICKINSON. Can. J. Chem. **58**, 1051 (1980).
22. F. A. LONG and L. FRIEDMAN. J. Am. Chem. Soc. **72**, 3692 (1950).
23. M. L. BENDER, H. MATSUI, R. J. THOMAS, and S. W. TOBEY. J. Am. Chem. Soc. **83**, 4193 (1961).
24. Y. POCKER and E. GREEN. J. Am. Chem. Soc. **95**, 113 (1973); **96**, 166 (1974).
25. P. DESLONGCHAMPS, U. O. CHERIYAN, A. GUIDA, and R. J. TAILLEFER. Nouv. J. Chim. **1**, 235 (1977).
26. J. H. MARKGRAF and S. J. BASTA. Synth. Commun. **2**, 139 (1972).
27. H. MEERWEIN, P. BORNER, O. FUCKS, H. J. SASSE, H. SCHRODT, and J. SPILLE. Chem. Ber. **89**, 2060 (1956).

The hydrolysis of *cis* and *trans* methoxy bicyclic and tricyclic orthoesters. Evidence for a chair–boat inversion prior to breakdown in some hemiorthoester tetrahedral intermediates

PIERRE DESLONGCHAMPS, DANIEL GUAY,[1] AND ROBERT CHÊNEVERT

Laboratoire de synthèse organique, Département de Chimie, Faculté des Sciences, Université de Sherbrooke, Sherbrooke (Qué.), Canada J1K 2R1

Received November 23, 1984

PIERRE DESLONGCHAMPS, DANIEL GUAY, and ROBERT CHÊNEVERT. Can. J. Chem. **63**, 2493 (1985).

The acid hydrolysis of *cis* and *trans* methoxy bicyclic and tricyclic orthoesters **1–4** was studied. The *trans* isomers gave only the corresponding hydroxy-lactones (**2** → **14** and **4** → **16** + **10**) whereas the *cis* isomers gave mixtures of dihydroxy-esters and hydroxy-lactones (**1** → **13** + **14**) and **3** → **15** + **16** + **10**). These results are rationalized on the basis of the stereoelectronic theory for hydrolytic processes. The fact that hydroxy-lactone **16** is produced to a larger extent than the isomeric hydroxy-lactone **10** is taken as evidence that when a tetrahedral intermediate is not allowed (stereoelectronically) to break down in a chair conformation, it will take a boat form prior to cleavage.

PIERRE DESLONGCHAMPS, DANIEL GUAY et ROBERT CHÊNEVERT. Can. J. Chem. **63**, 2493 (1985).

On a étudié l'hydrolyse en milieu acide des orthoesters bicycliques et tricycliques (**1–4**) en séries *cis* et *trans*. Les isomères *trans* ont conduit uniquement aux hydroxy-lactones (**2** → **14** et **4** → **16** + **10**) correspondantes tandis que les isomères *cis* ont donné des mélanges d'hydroxy-esters et d'hydroxy-lactones (**1** → **13** + **14** et **3** → **15** + **16** + **10**). Ces résultats sont interprétés à la lumière de la théorie du contrôle stéréoélectronique dans les processus d'hydrolyse. La formation préférentielle de l'hydroxy-lactone **16** sur son isomère **10** constitue une évidence que, ne pouvant se briser avec contrôle stéréoélectronique dans la forme chaise, un intermédiaire tétraédrique préférera le faire sous la forme bateau.

The mild acid hydrolysis of orthoesters (1) has been used as a technique to understand better the mechanism of cleavage of tetrahedral intermediates which are occurring in hydrolytic processes (2–7). Most of this work was carried out to test the validity of the theory of stereoelectronic control (8–12). In the preceding accompanying publication (13), we have shown that the results obtained so far are readily rationalized in terms of the stereoelectronic theory when it takes into account the following elements: (a) primary (2, 3, 8, 9) and secondary (10) stereoelectronic effects, (b) conformational change in tetrahedral intermediate prior to breakdown (4, 7, 14, 15), (c) an entropy factor, and (d) the ionic state of tetrahedral intermediates and reaction products as a function of pH (4, 10, 16, 17).

This theory postulates that when a tetrahedral intermediate exists in a conformation which cannot break down with primary stereoelectronic control, the intermediate will first undergo a conformational change prior to cleavage in order to fulfill the stereoelectronic requirement. When the cyclic orthoester is a conformationally mobile six-membered ring, one of the conformational changes is a chair inversion, and studies carried out so far with various orthoesters having either a mobile or a rigid conformation support this rationalization (13). This theory also predicts that when complete ring inversion is not possible, a change from a chair to a boat (or twist-boat) conformation has to take place prior to cleavage, and experimental results have been rationalized on that basis (13).

We wish now to report a study which can be taken as the first unambiguous evidence that when a hemiorthoester tetrahedral intermediate is not allowed to break down stereoelectronically in its chair conformation, it will take a boat conformation prior to cleavage. The study undertaken is the mild acid hydrolysis of *cis* and *trans* methoxy bicyclic and tricyclic orthoesters **1**, **2**, **3**, and **4** (Scheme 1).

Synthesis

Treatment of the known bromo-lactone **5** (18) (Scheme 2) with silver tetrafluoroborate gave *in situ* the lactonium salt **6** (19), which on reaction with methanol under basic conditions gave *trans* bicyclic orthoester **2** along with a small quantity (~5%) of the *cis* isomer **1**. Isomerization of **2** under anhydrous acidic conditions gave a (~1:2) mixture of isomers **1** and **2**. Each isomer was obtained pure by column chromatography using silica gel impregnated with sodium bicarbonate. The *cis* isomer **1** is a known compound and its stereochemistry is firmly established by the first synthetic route (20).

The preparation of allylic bicyclic lactone **8** from the alkylation of bicyclic lactone **7** was recently reported (18). Following a general method (3, 21), compound **8** was converted into the allylic bicyclic orthoester **9** which, after hydroboration and acid hydrolysis, gave hydroxy-bicyclic lactone **10**. Compound **10** was then converted into the bromo-bicyclic lactone **11** via the intermediate formation of a primary mesylate. Treatment of bromo-bicyclic lactone **11** with silver tetrafluoroborate gave *in situ* the corresponding tricyclic lactonium salt **12** which, on reaction with methanol under basic conditions, gave stereospecifically the *trans*-tricyclic orthoester **4**. Acid isomerization of **4** gave a mixture of *cis* and *trans* isomers **3** and **4** in a 1:5.5 ratio. The *cis* isomer was obtained pure by chromatography with silica gel impregnated with $NaHCO_3$.

Results and discussion

The theoretical products (Scheme 1) for the hydrolysis of *cis* and *trans* methoxy bicyclic orthoesters **1** and **2** are dihydroxy-ester **13** and hydroxy-lactone **14**. Those of *cis* and *trans* methoxy tricyclic orthoesters **3** and **4** are dihydroxy-ester **15** and the isomeric hydroxy-lactones **16** and **10**.

Orthoesters **1–4** were dissolved in deuterated acetone, an hydrochloric acid solution (DCl in D_2O, pH = 2) was added, and the product distribution formed in the course of the hydrolysis experiments was analyzed by 250-MHz nmr spectroscopy. The results are shown in Table 1.

[1] N.S.E.R.C.C. (Ottawa) and F.C.A.C. (Quebec) predoctoral fellowships 1982–1985.

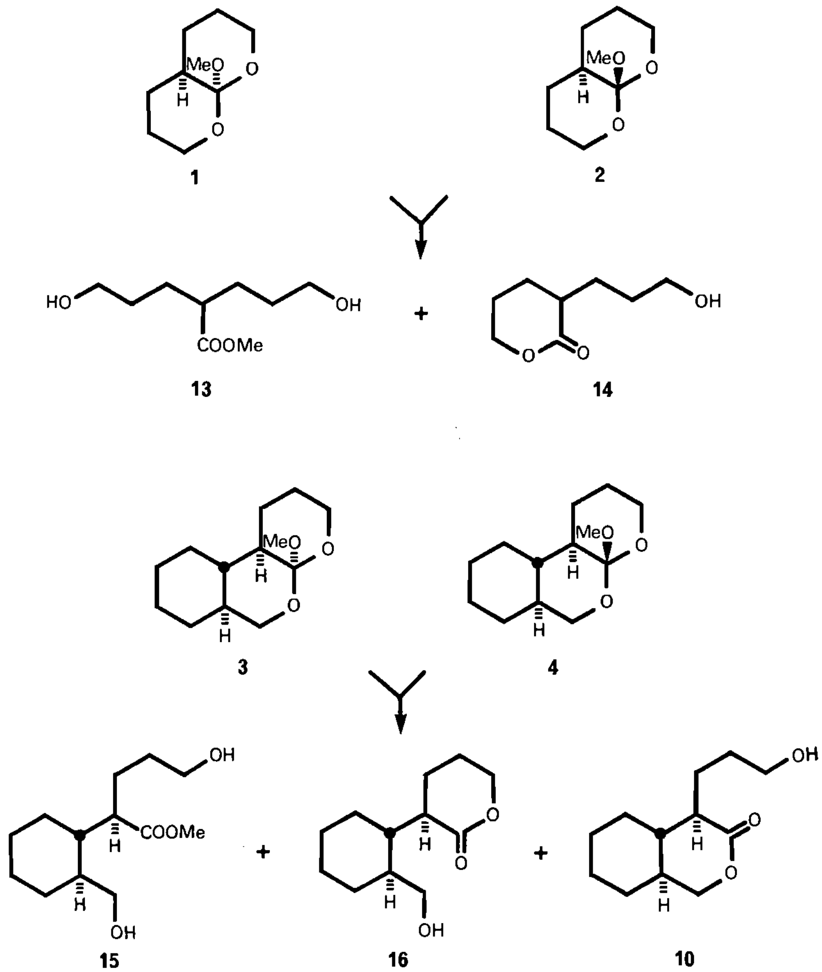

SCHEME 1

TABLE 1. Hydrolysis of *cis* and *trans* methoxy bicyclic and tricyclic orthoesters **1**, **2**, **3**, and **4**

Orthoester **1**

Time	Orthoester **1**	Dihydroxy-ester **13**	Hydroxy-lactone **14**
2 min	15	22	63
10 min	trace	33	67
25 min	0	30	70

Orthoester **2**

Time	Orthoester **2**	Dihydroxy-ester **13**	Hydroxy-lactone **14**
2 min	0	0	>99
10 min	0	0	>99

Orthoester **3**

Time	Orthoester **3**	Dihydroxy-ester **15**	Hydroxy-lactone **16**	Hydroxy-lactone **10**
2 min	>90	<5	<5	0
9 min	~30	~30	~30	~10
2 h	0	35	0	65

Orthoester **4**

Time	Orthoester **4**	Dihydroxy-ester **15**	Hydroxy-lactone **16**	Hydroxy-lactone **10**
2 min	0	0	77	23
7 min	0	0	63	37
21 min	0	0	44	56
82 min	0	0	4	96

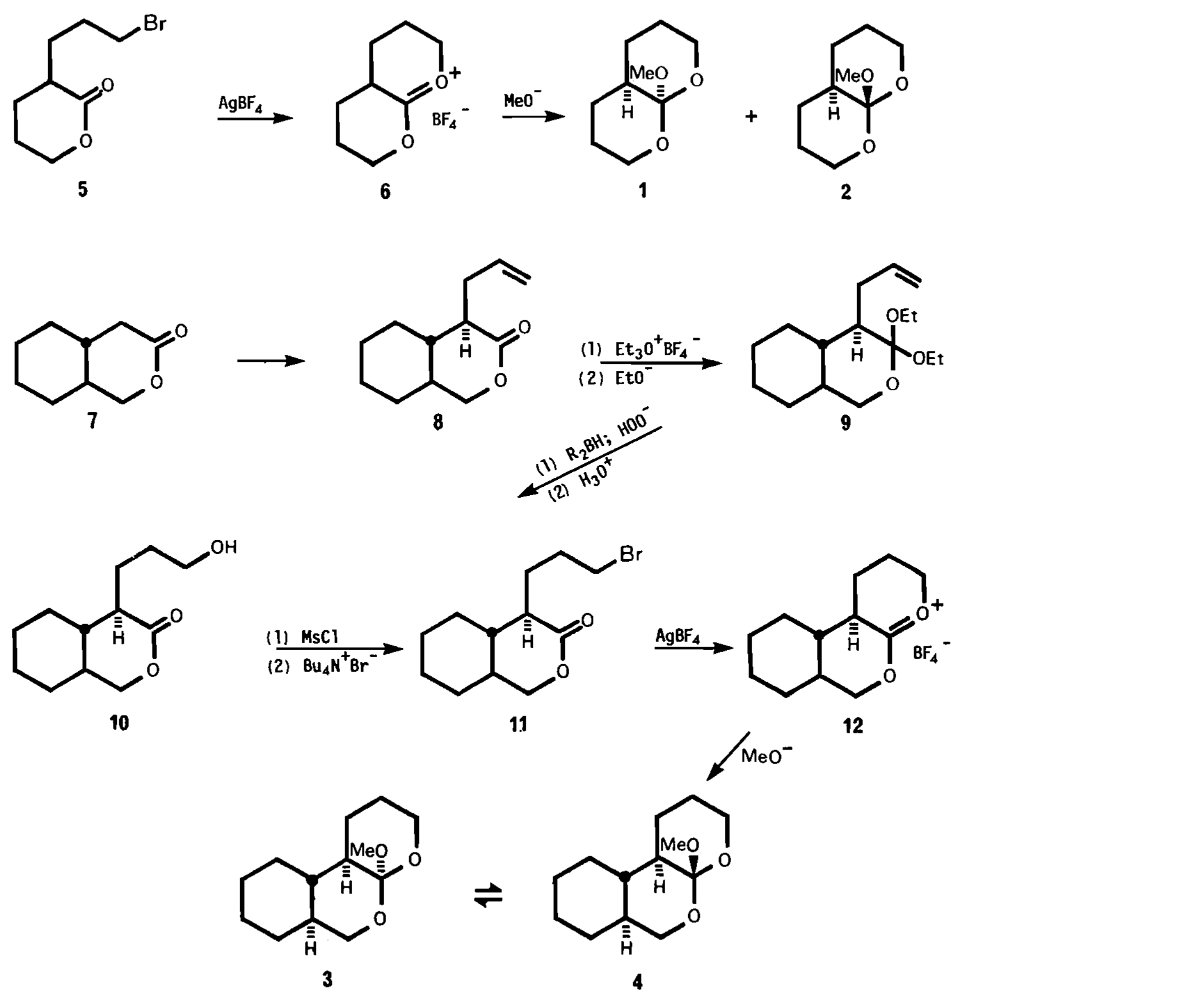

SCHEME 2

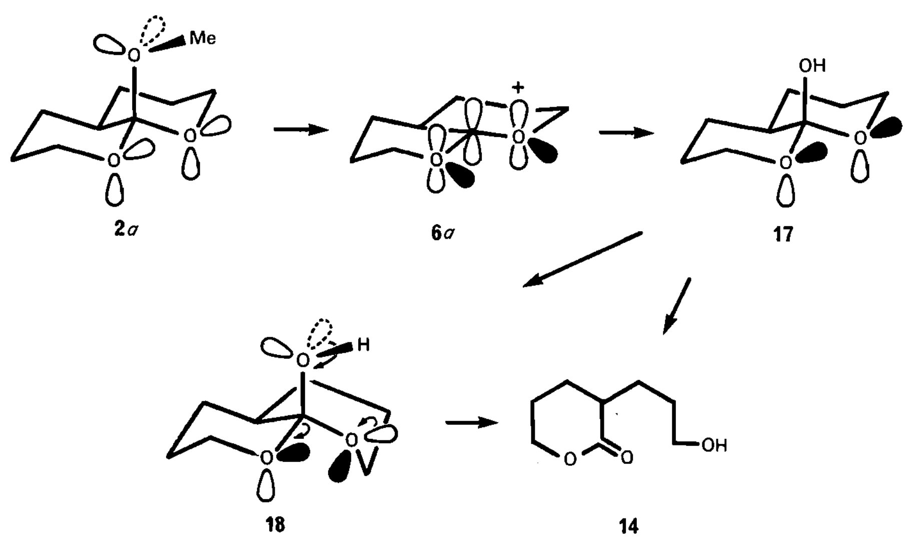

SCHEME 3

The hydrolyses of the *trans* methoxy orthoesters **2** and **4** are very fast, being complete in less than 2 min. Orthoester **2** gives only hydroxy-lactone **14**, whereas orthoester **4** produces first a mixture of hydroxy-lactones **16** and **10**, where **16** largely predominates. Hydroxy-lactone **16** is then slowly converted into the most stable hydroxy-lactone **10**. It is important to mention that the hydroxy methyl esters **13** and **15** were not observed.

The rate of hydrolysis of *cis* methoxy orthoesters **1** and **3** is slower than that of *trans* methoxy orthoesters **2** and **4**. The *cis* methoxy orthoester **1** gives a ~3:7 mixture of dihydroxy-ester **13** and hydroxy-lactone **14**. The *cis* methoxy tricyclic orthoester **3** produces first a mixture of dihydroxy-ester **15**, and hydroxy-lactones **16** and **10**. This is followed by the conversion of hydroxy-lactone **16** into the more stable isomeric hydroxy-

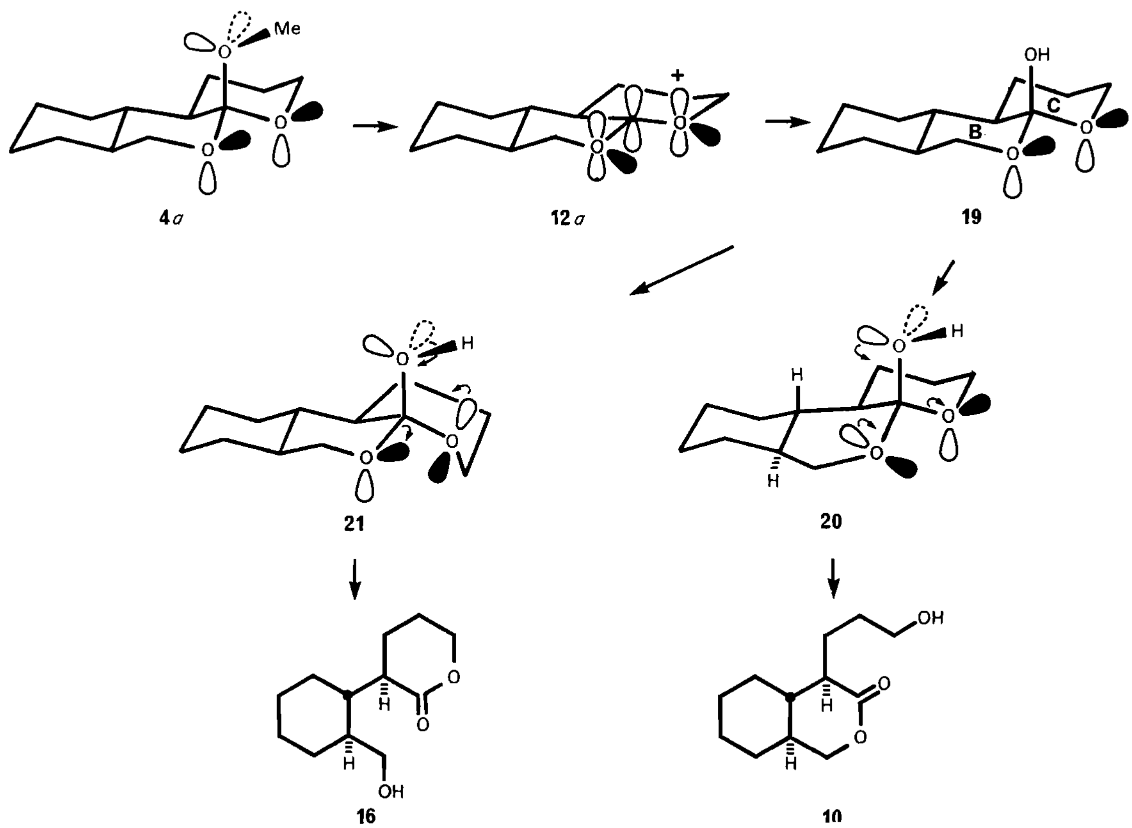

SCHEME 4

lactone **10**, but the conversion of dihydroxy-ester **15** into hydroxy-lactone **10** does not take place.[2]

Compounds **13**, **14**, **16**, and **10** were further characterized by preparation of their corresponding acetate derivative by reaction with acetic anhydride and pyridine.

The results obtained with *trans* methoxy bicyclic orthoester **2** are readily rationalized on the basis of the stereoelectronic theory. Orthoester **2** must exist in the conformation **2***a* (Scheme 3) which permits the ejection of the methoxy group yielding the bicyclic lactonium ion **6***a*. Hydration of **6***a* should give the intermediate **17**,[3] which can only give the hydroxy-lactone **14** on further cleavage. Since intermediate **17** cannot break down with stereoelectronic control, it is assumed that it will first take a boat form like **18** prior to cleavage (**17** → **18** → **14**).

Under kinetically controlled conditions, *trans* methoxy tricyclic orthoester **4** produces no dihydroxy-ester **15**, but a mixture of the two hydroxy-lactones **16** and **10**, where the less stable isomeric lactone (**16**) predominates. Orthoester **4** must exist in conformation **4***a* (Scheme 4), which can only eject the methoxy group while respecting the principle of stereoelectronic control. This reaction produces the lactonium ion **12***a*, which on hydration should give the tetrahedral intermediate **19**. This intermediate cannot break down with stereoelectronic control and must therefore undergo a conformational change prior to breakdown. In this case, ring B or ring C can take a boat form producing **20** or **21**, which on cleavage can respectively give hydroxy-lactones **10** and **16**. The preferred formation of **16** can be explained[4] by the fact that ring C is more flexible than ring B, which is fused to ring A with a *trans* junction. The resulting consequence is that boat formation will take place much more readily in ring C (→**21**) than in ring B (→**20**), and the preferential formation of hydroxy-lactone **16** is thus readily explained on that basis. This result can therefore be taken as the first experimental evidence that cleavage must take place from a boat conformation when a tetrahedral hemiorthoester intermediate is not allowed to break down in a chair conformation with stereoelectronic control.

The *cis* methoxy orthoesters **1** and **3** differ from the *trans* methoxy orthoesters **2** and **4** in the fact that they produce the corresponding dihydroxy methyl esters (**13** and **15**) along with the hydroxy-lactones (**14**, **16**, and **10**). The next operation is to analyze the cleavage of **1** and **3** on the basis of the stereoelectronic theory. The *cis* methoxy bicyclic orthoester **1** can exist in the conformations **1***a* and **1***b* (Scheme 5). Primary stereoelectronic effects predict that conformer **1***b* cannot break down (3), and cleavage should therefore take place on conformer **1***a*, which can only give the hydroxy-lactonium ion **22**. Hydration of **22** should then occur to produce the tetrahedral intermediate **23**, which is allowed to break down in only one direction, yielding the corresponding dihydroxy-ester **13**. One possible route to producing hydroxy-lactone **14** while re-

[2] A preliminary study on the acid hydrolysis of *cis* methoxy orthoester **1** led to the incorrect conclusion that **1** gave only dihydroxy methyl ester **13** (ref. 22 and pp. 80–82 in ref. 11).

[3] Hydration of **6***a* on the opposite face would produce a tetrahedral intermediate having each ring in a boat conformation. This process is thus neglected.

[4] This result cannot be explained on the basis of entropy considerations (cf. footnote 7 in ref. 13). This factor predicts that, contrary to the experimental results, the formation of hydroxy-lactone **16** should be disfavored over that of hydroxy-lactone **10** because the CH_2OH group in **16** has a lesser degree of conformational mobility than that in **10**. As a result, this is not a determining factor in the present case.

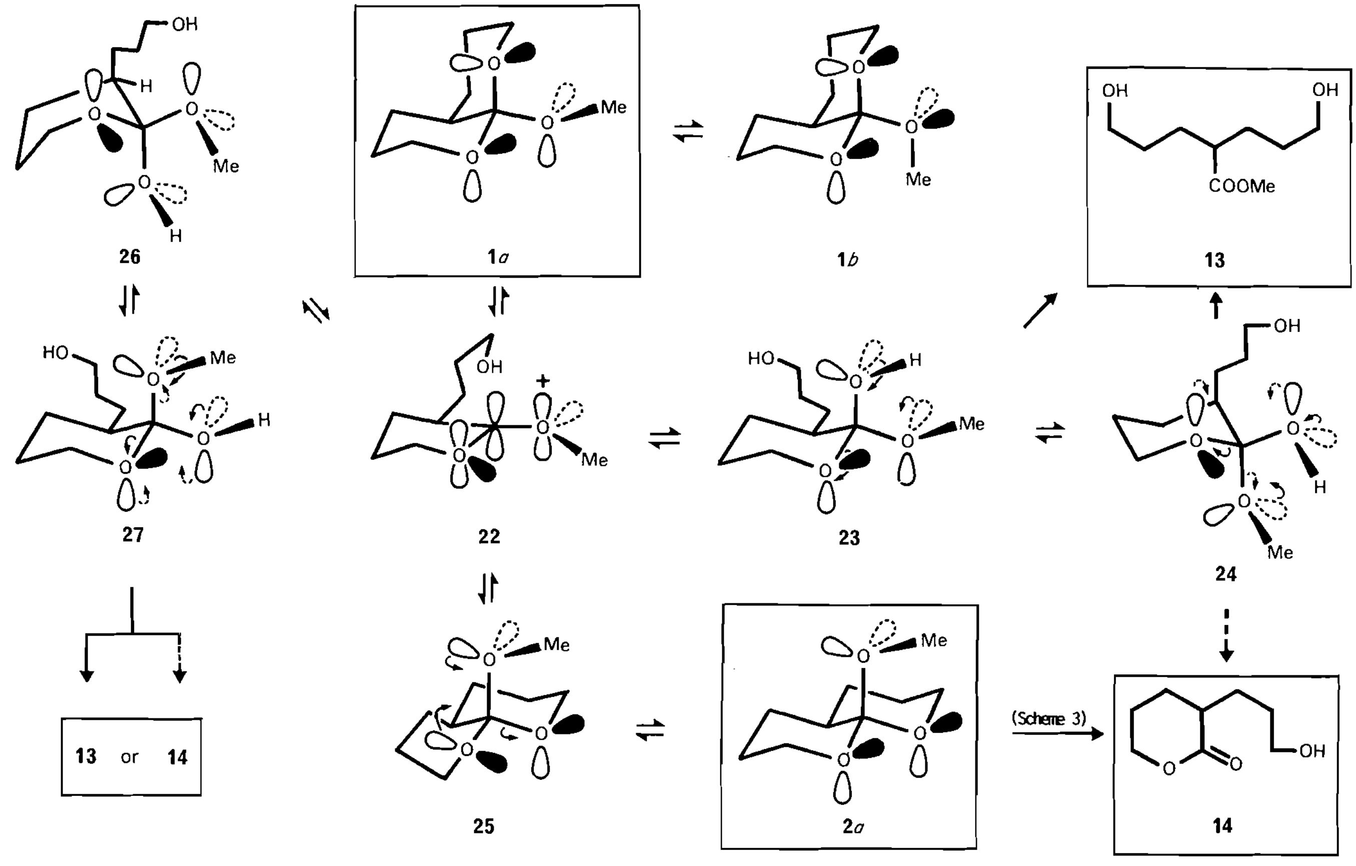

SCHEME 5

specting the principle of stereoelectronic control, is for **23** to undergo a ring inversion to give the new conformer **24**, which is allowed to produce dihydroxy-ester **13** as well as hydroxy-lactone **14**. However, conformer **24** has an axial side chain and its proportion at equilibrium with **23** will be relatively small; consequently, the route **23** → **24** → **13** + **14** cannot be expected to become an important process. The relatively large proportion of hydroxy-lactone **14** which is formed along with dihydroxy-ester **13** is thus not explained on this basis. A very similar conclusion can be reached for the *trans* methoxy tricyclic orthoester **3**. This compound should hydrolyze via a pathway which is very similar to that of **1**, i.e. **1***a* → **22** → **23** → **13**. Indeed, in this tricyclic orthoester, the ring inversion process (**23** → **24**) is not possible. Thus, again, the rationale proposed so far does not explain correctly the experimental results.

One interesting hypothesis is to assume that the isomerization of the *cis* orthoesters **1** and **3** into their corresponding *trans* orthoesters **2** and **4** can occur at a competitive rate with that of hydrolysis; indeed, on that basis, the results are readily explained because *trans* orthoesters **2** and **4** are known to give exclusively the hydroxy-lactones.

There is a good possibility that the above assumption might become the correct explanation for the following reasons. When lactonium ion **22** is produced from **1***a*, the step which follows is the nucleophilic addition of a hydroxyl group. Theoretically, there are four possibilities. This step can take place via an intramolecular process that can either give back *cis* orthoester **1***a* or produce *trans* orthoester **2***a* via the boat conformer **25**. Hydration of **22** can also take place intermolecularly by reaction with water to produce either the chair intermediate **23** or the boat intermediate **26**. The new intermediate **26** could then give the chair intermediate **27**, which is allowed stereoelectronically to cleave to either dihydroxy methyl ester **13** or hydroxy-lactone **14**.

There is no doubt that the rate of the reclosure step **22** → **1***a* must be faster than the other three competing processes. However, the reclosure step **22** → **1***a* will not influence the product ratio, but will only slow down the overall rate of hydrolysis. This is in agreement with the fact tht the *cis* orthoesters **1** and **3** are hydrolyzed at a slower rate than the *trans* isomers **2** and **4**. The second ring closure via a boat conformation (**22** → **25**) is entropically favored but it is disfavored on steric grounds. The reverse is true for the bimolecular hydration step via the chair conformer (**22** → **23**), whereas that via the boat conformer (**22** → **26**) is both sterically and entropically disfavored. The process **22** → **26** can therefore be eliminated from further consideration. As a result, there is left the possibility that the process **22** → **25** → **2***a* can compete with the hydration step **22** → **23**. If that is the case, the experimental results are readily explained. Indeed, the formation of dihydroxy methyl ester **13** would come from intermediate **23**, whereas that of hydroxy-lactone **14** would come from *trans* orthoester (**2***a*) produced from **22** via the boat intermediate **25**.

It remains to find some evidence to show that the isomerization process **22** → **25** → **2***a* can compete with that of hydrolysis (**22** → **23** → **13**). We have submitted the *cis* methoxy orthoesters **1** and **3** to acidic conditions which are similar to those for the hydrolysis, except for the fact that water was replaced by methanol. We have found that, under these conditions, isomerization from the *cis* to the *trans* orthoesters takes place rapidly. Indeed, after 5 min, it was found in both series that more than 50% of the *cis* isomer (**1** or **3**) was already converted into the corresponding *trans* orthoester (**2** or **4**). These results strongly support the preceding rationale, which clearly explains the products observed in the hydrolysis of *cis* orthoesters **1** and **3**.

Conclusion

The products of hydrolysis of *cis* and *trans* methoxy bicyclic and tricyclic orthoesters **1–4** are readily understood on the basis of the stereoelectronic theory for the cleavage of tetrahedral intermediates. This study provides also the first experimental evidence to show that when an hemiorthoester tetrahedral intermediate is not allowed to break down in a chair conformation, it will first take a boat conformation so that the cleavage can take place with ease, i.e. while following the principle of stereoelectronic control.

Experimental

The infrared (ir) spectra were taken on a Perkin–Elmer 681 spectrophotometer. Proton nuclear magnetic resonance (nmr) spectra were recorded on a Bruker WP-60 and on a Bruker WM-250 instrument. The ^{13}C nmr spectra were recorded on a Bruker WP-80SY and on a Bruker WM-250 instrument. Mass spectral assays were obtained using a Vg Micromass ZAB-1F mass spectrometer. Vapor phase chromatographic (vpc) analysis and separation were carried out on a Varian 2800 chromatograph with thermal conductivity detector (column SE-30, 10% Chromosorb W, 60–80 mesh, 5 ft × $\frac{1}{4}$ in.). The purification of orthoesters **1–4** was carried out by column chromatography with silica gel impregnated with 1% sodium bicarbonate. SiO_2–$NaHCO_3$ was prepared by mixing a saturated solution of sodium bicarbonate in methanol with silica gel followed by evaporation of the solvent with a rotatory evaporator *under vacuo*.

trans *Methoxy bicyclic orthoester 2*

Bromolactone **5** (1.07 g, 4.84 mmol) was dissolved in dichloromethane (40 mL) and benzene (5 mL) under argon. Silver tetrafluoroborate (2.18 g, 11.2 mmol) was added and the resulting mixture stirred 20 h at room temperature in absence of light. After cooling at −78°C, a solution of methanol (48 mmol), sodium methoxide (5 mmol), and diisopropylethylamine (23 mmol) in dichloromethane (10 mL) was added via syringe. The resulting mixture was allowed to warm to room temperature and stirred for 2 h. Concentration was followed by addition of aqueous sodium bicarbonate (40 mL, 5%), and ether (50 mL). The aqueous layer was extracted with ether/pentane (75%, 2 × 100 mL). The combined organic extracts were dried over potassium carbonate, filtered, and evaporated. Filtration of the residue on silica gel (20% ethyl acetate in hexane, $SiO_2/NaHCO_3$, Et_3N) afforded *trans* methoxy bicyclic orthoester **2** (318 mg, 38%) contaminated with a small amount of *cis* isomer **1** (≃5%). On attempted distillation, isomerization of the orthoester led to a mixture of **1** and **2** in the ratio of 45:55.

cis *Methoxy bicyclic orthoester 1 and* trans *methoxy bicyclic orthoester 2*

trans Methoxy bicyclic orthoester **2** (60 mg, 0.35 mmol) was dissolved in a 1:1 mixture of methanol and dichloromethane (4 mL) containing trimethyl orthoformate (10 drops). At room temperature under an argon atmosphere, acetyl chloride (1 drop) was added. The mixture was stirred 10 min before adding triethylamine (100 μL). Evaporation *in vacuo* and flash chromatography of the residue ($SiO_2/NaHCO_3$, 1:3 ethyl acetate/hexane, Et_3N) gave *cis* methoxy bicyclic orthoester **1** (13 mg, 0.076 mmol, R_f 0.45); nmr (C_3D_6O) δ: 1.2–1.8 (9H), 3.17 (3H, singlet, OCH_3), 3.61–3.77 (4H, multiplet, two CH_2O); and *trans* methoxy bicyclic orthoester **2** (27 mg, 0.15 mmol, R_f 0.35); nmr (C_3D_6O) δ: 1.3–1.7 (9H), 3.09 (3H, singlet, OCH_3), 3.53–3.71 (4H, multiplet, two CH_2O).

Allyl bicyclic orthoester 9

Triethyloxonium tetrafluoroborate (3.59 g, 0.02 mol) was added to a solution of allyl lactone **8** (1.04 g, 0.005 mol) in anhydrous dichloromethane (30 mL) under argon. After stirring 22 h at room temperature, the mixture was cooled to −78°C. Then a solution of sodium ethoxide (2.0 g, 0.03 mol) in ethanol (10 mL) was added and the mixture was left to warm up to room temperature and stirred for 40 h. The solvents were then removed *in vacuo* and a solution (50 mL) of sodium bicarbonate (2%) was added. The aqueous phase was extracted with ether (3 × 75 mL), and the organic extract was dried with potassium carbonate, filtered, and evaporated to yield crude orthoester **9** (1.32 g, 92%) as a pale yellow oil; nmr ($CDCl_3$) δ: 1.0–2.3 (13H), 1.16 (6H, triplet, J = 7.2 Hz, two CH_3—), 3.5 (4H, diffuse quadruplet, J = 7.2 Hz, two CH_3—CH_2—O), 3.5–4.25 (2H, CH_2O of the ring), 4.8–5.2 (2H, multiplet, C=CH_2), 5.5–6.2 (1H, multiplet, —CH=).

Hydroxy-bicyclic lactone 10

Borane-methyl sulfide (732 μL, 7.3 mmol) was added to a cooled (−10°C) solution of cyclohexene (1.49 mL, 14.7 mmol) in ether (5 mL) under an atmosphere of argon. After stirring 1.5 h at 0°C, the white precipitate formed was diluted with tetrahydrofuran (20 mL). To this cooled mixture was added a solution of bicyclic orthoester **9** (1.31 g, 4.88 mmol) in tetrahydrofuran (5 mL). The reaction mixture was stirred 6 h at 0°C and was then allowed to warm up to room temperature (20 min). Aqueous sodium hydroxide (1 *N*, 15 mL) was added along with hydrogen peroxide (30%, 4 mL, 40 mmol) and the reaction mixture was stirred overnight at room temperature. The solution was acidified (pH < 2) with concentrated hydrogen chloride. Hexane (30 mL) was added, and the aqueous phase was decanted and extracted with ether (3 × 30 mL). The organic extract was dried with magnesium sulfate, filtered, and evaporated. The oily residue was purified by flash chromatography (ethyl acetate/hexane/acetone, 4:5:1) to give the hydroxy-bicyclic lactone **10** (760 mg, 74%); ir (CH_2Cl_2): 3620, 3500, and 1725 cm^{-1}; nmr (C_3D_6O) δ: 0.9–2.0 (14H), 2.15–2.23 (1H, multiplet, CH—CO—O—), 2.9 (1H, broad singlet, OH), 3.51 (2H, diffuse triplet, CH_2O of the chain, J = 5.5 Hz), 3.86 and 4.15 (2H, AB part of an ABX system, J_{AB} = 11.0 Hz, J_{BX} = 4.3 Hz, J_{AB} = 10.8 Hz, CH_2O of the ring).

Bromo-bicyclic lactone 11

Mesyl chloride (280 μL, 3.6 mmol) was slowly added to a cooled (−20°C) solution of hydroxy-bicyclic lactone **10** (421 mg, 2.0 mmol) and triethylamine (560 μL, 4.0 mmol) in dichloromethane (25 mL) under an argon atmosphere. The reaction mixture was stirred at room temperature for 14 h. Hexane (20 mL) was added and the solution was washed with hydrochloric acid (1 *N*, 2 × 15 mL), then with water (10 mL). The aqueous phases were extracted with ether (2 × 10 mL) and the combined organic layers were dried over magnesium sulfate, filtered, and evaporated to yield the crude methanesulfonate lactone (650 mg). Without further purification this crude sulfonate was dissolved in benzene (45 mL) containing tetra *n*-butylammonium bromide (2.0 g, 6 mmol) under argon. The mixture was refluxed 1.5 h and then concentrated *in vacuo*. The residue was taken into ether (30 mL) and washed with water (2 × 15 mL). The aqueous phase was extracted with ether (20 mL). The organic extracts were dried over magnesium sulfate, filtered, and evaporated. Flash chromatography (30% ethyl acetate in hexane) provided the bromo-bicyclic lactone **11** (457 mg, 83%); ir (CH_2Cl_2): 1725 cm^{-1}; nmr ($CDCl_3$) δ: 0.9–2.1 (15H), 3.4 (2H, multiplet, CH_2Br), 3.85 and 4.26 (2H, AB part of an ABX system, J_{AX} = 10.7 Hz, J_{BX} = 4.4 Hz, J_{AB} = 11.1 Hz, CH_2O); ms *m/e* (70 eV): 274 and 276 (M^+). *Exact Mass* calcd.: 276.0548; found: 276.0553.

trans *Methoxy tricyclic orthoester 4*

Silver tetrafluoroborate (435 mg, 2.2 mmol) was added to a solution of bromo-bicyclic lactone **11** (410 mg, 1.5 mmol) in benzene (5 mL) and dichloromethane (5 mL). The mixture was stirred 24 h at room temperature under argon and protected from light. Then it was cooled to −78°C. A solution of sodium methoxide in methanol (105 mg NaH, 4.5 mmol) was added, followed by triethylamine (210 μL, 1.5 mmol). The resulting mixture was allowed to warm up to room temperature before filtering through Celite. The filtrate was concentrated. Aqueous sodium bicarbonate (30 mL, 2%) was added and it was extracted with ether/hexane (2:1, 3 × 20 mL). The organic layers were dried over potassium carbonate, filtered, and evaporated. Flash chromatography of the residue (15% ethyl acetate in hexane) was effected on silica gel impregnated with sodium bicarbonate and traces of triethylamine were added in solvents and test tubes. This way, *trans* methoxy tricyclic orthoester **4** (192 mg, 57%) was obtained, along with some hydroxy-lactone **10** (46 mg, 0.22 mmol). *trans* Orthoester **4**: ir (CH_2Cl_2): 1000–1200 cm^{-1}; nmr (C_3D_6O) δ: 0.9–1.8 (15H), 3.08 (3H, singlet, OCH_3), 3.25 (1H, d of d, A part of an ABX system, $J_{AB} = J_{AX} = 11.0$ Hz, one-half CH_2O), 3.48–3.70 (3H, multiplet, one and one-half CH_2O); ^{13}C nmr ($CDCl_3$) δ: 110.7, 68.2, 63.3, 47.2, 45.5, 41.8, 40.2, 28.2, 27.4, 25.7, 25.6, 25.4, 22.0; ms *m/e* (70 eV): 226 (M^+), 194 ($M^+ - CH_3OH$). *Exact Mass* calcd.: 226.1567; found: 226.1569.

cis *Methoxy tricyclic orthoester 3*

trans Methoxy tricyclic orthoester **4** (170 mg, 0.75 mmol) was dissolved in methanol (15 mL) containing trimethyl orthoformate (15 drops) under argon. Anhydrous hydrochloric acid (0.017 mmol, prepared from acetyl chloride) in methanol (60 μL) was added. After stirring 1 h: 45 min at room temperature, triethylamine (250 μL, 1.8 mmol) was added and the solution was concentrated *in vacuo*. Flash chromatography of the oily residue (10% ethyl acetate in hexane, $SiO_2/NaHCO_3$, Et_3N) afforded *trans* orthoester **4** (132 mg, 0.58 mmol, R_f 0.35) and *cis* orthoester **3** (24 mg, 0.11 mmol, R_f 0.50); ir (CH_2Cl_2): 1000–1200 cm^{-1}; nmr (C_3D_6O) δ: 0.9–1.9 (15H), 3.18 (3H, singlet, OCH_3), 3.35–3.80 (4H, multiplet, two CH_2O); ^{13}C nmr ($CDCl_3$) δ: 68.7, 64.3, 47.1, 42.7, 40.5, 38.2, 29.1, 27.6, 26.2, 25.4, 21.0, 19.5; ms *m/e* (70 eV): 226 (M^+), 194 ($M^+ - CH_3OH$). *Exact Mass* calcd.: 226.1567; found: 226.1571.

Hydrolysis of trans *methoxy bicyclic orthoester 2*

trans Methoxy bicyclic orthoester **2** (3 mg) in deuterated acetone (1 mL) was placed in an nmr tube. The pH 2 acid solution (75 μL) was added and product distribution was checked by 250-MHz nmr spectroscopy. Hydrolysis was completed within 1.5 min (see Table 1).

Hydrolysis of cis *methoxy bicyclic orthoester 1*

cis Methoxy bicyclic orthoester **1** (2 mg) was hydrolyzed under identical conditions used for the *trans* isomer **2** (above). More than 10 min were needed for complete hydrolysis (see Table 1).

Acetate of hydroxy-lactone 14 and diacetate of dihydroxy-ester 13

The *cis* methoxy bicyclic orthoester **1** (172 mg, 1 mmol) dissolved in dichloromethane (1 mL) was vigorously stirred in the presence of aqueous *p*-toluenesulfonic acid (0.5 mL, 10^{-3} *M*) at 0°C. After 10 min, the crude mixture was taken into pyridine (10 mL) and excess acetic anhydride was added (10 mL). The resulting mixture was stirred overnight at room temperature. Methanol was added at 0°C and the solvents were evaporated *in vacuo*. The products were analyzed and separated by vapor phase chromatography.

Acetate of hydroxy-lactone 14: 52%; vpc retention time, 9.5 min (175°C); ir ($CHCl_3$): 1720 and 1240 cm^{-1}; nmr ($CDCl_3$) δ: 1.5–2.1 (8H), 2.05 (3H, singlet, CH_3COO—), 2.2–2.6 (1H, multiplet, —CH—C=O), 4.15 (2H, triplet, $J = 7.0$ Hz, CH_2OAc), 4.38 (2H, triplet, $J = 6.0$ Hz, —CH_2O of the ring); ms *m/e* (70 eV): 200 (M^+), 140 ($M^+ - CH_3COOH$).

Diacetate of dihydroxy-ester 13: 48%; vpc retention time, 15.0 min (175°C); ir ($CHCl_3$): 1715 and 1240 cm^{-1}; nmr ($CDCl_3$) δ: 1.4–2.6 (9H), 2.07 (6H, singlet, CH_3COO—), 3.75 (3H, singlet, —$COOCH_3$), 3.9–4.3 (4H, multiplet, CH_2OAc).

Hydrolysis of trans *methoxy tricyclic orthoester 4*

trans Methoxy tricyclic orthoester **4** (2.5 mg) dissolved in deuterated acetone (1 mL) was placed in an nmr tube. The pH 2 acid solution was added (100 μL) and product distribution was checked by nmr spectroscopy (250 MHz). Hydrolysis was completed within 1.5 minute (see Table 1).

Hydrolysis of cis *methoxy tricyclic orthoester 3*

The hydrolysis was performed as above for the *trans* isomer **4** (see Table 1). The following nmr data were used in calculation of hydrolysis product ratios: methanol formed: 3.23 ppm; *cis* methoxy bicyclic orthoester **1**: 3.17 ppm (3H, OCH_3); *trans* methoxy bicyclic orthoester **2**: 3.09 ppm (3H, OCH_3); hydroxy-lactone **14**: 2.45–2.60 ppm (1H, —CH—CO); dihydroxy-ester **13**: 3.60 ppm (3H, $COOCH_3$), 2.28–2.38 ppm (1H, —CH—COOMe); *cis* methoxy tricyclic orthoester **3**: 3.18 ppm (3H, OCH_3); *trans* methoxy tricyclic orthoester **4**: 3.08 ppm (3H, OCH_3); hydroxy-bicyclic lactone **10**: 2.15–2.23 ppm (1H, CH—CO), 3.86 ppm (1H, CH_2OCO); hydroxy-lactone **16**: 2.8–2.95 ppm (1H, CH—CO); dihydroxy-ester **15**: 2.68–2.77 ppm (1H, CH—COOMe), 3.58 ppm (3H, $COOCH_3$).

Acetate of hydroxy-lactone 10 and acetate of hydroxy-lactone 16

trans Methoxy tricyclic orthoester **4** (18 mg, 0.08 mmol) was dissolved in dichloromethane (750 μL) and in acetone (250 μL) under argon. At room temperature, the pH 2 acid solution (150 μL) was added. After 10 minutes, tlc analysis indicated no more starting material and pyridine (2 mL) was poured in, followed by acetic anhydride (4 mL). The reaction mixture was stirred overnight at room temperature. Hexane (5 mL) and ether (10 mL) were added. The organic phase was washed with hdyrochloric acid (1 *N*, 2 × 15 mL), sodium bicarbonate (5%, 10 mL), and brine (10 mL), then dried over magnesium sulfate and filtered. The residue was purified by column chromatography (SiO_2, 40% ethyl acetate in hexane) to give the acetate of hydroxy-lactone **10** (14 mg, 0.055 mmol, R_f 0.33); ir (CH_2Cl_2): 1730 cm^{-1}; nmr (C_3D_6O) δ: 0.9–2.0 (14H), 1.97 (3H, singlet, CH_3COO), 2.17–2.25 (1H, multiplet, CH—CO—O), 4.00 (2H, triplet, $J = 6.4$ Hz, CH_2OAc), 3.88 and 4.16 (2H, AB part of an ABX system, $J_{AX} = 11.0$ Hz, $J_{BX} = 4.4$ Hz, $J_{AB} = 10.8$ Hz, CH_2O of the ring); ms *m/e* (70 eV): 255 (MH^+), 212 ($MH^+ - CH_3CO$). *Exact Mass* calcd.: 254.1518; found: 254.1510; and the acetate of hydroxylactone **16** (6 mg, 0.024 mmol, R_f 0.25); ir (CH_2Cl_2): 1730 cm^{-1}; nmr (C_3D_6O) δ: 0.9–1.9 (14H), 1.99 (3H, singlet, CH_3COO), 2.78–2.88 (1H, multiplet, CH—CO—O of the ring), 3.91 and 4.03 (2H, AB part of and ABX system, $J_{AX} = 5.8$ Hz, $J_{BX} = 4.45$ Hz, $J_{AB} = 11.3$ Hz, CH_2OAc), 4.14–4.36 (2H, multiplet, CH_2O of the ring); ms *m/e* (70 eV): 254 (M^+), 212 ($MH^+ - CH_3CO$). *Exact Mass* calcd.: 254.1518; found: 254.1510.

High resolution mass spectroscopy confirmed the 250-MHz nmr integration in that no deuterium incorporation had occurred α to the lactone during hydrolysis.

Isomerization of cis *methoxy tricyclic orthoester 3*

cis Methoxy tricyclic orthoester **3** (16 mg) was dissolved in acetone (4 mL) at room temperature under argon. Then, 75 μL of a 10^{-2} *M* acid solution (7.1 μL acetyl chloride in 10 mL methanol) were added; tlc analysis after 5 min showed that isomerization had occurred. Triethylamine (100 μL) was added and the mixture was evaporated to dryness. Dilution with ether and filtration on silica gel gave (9 mg) crude orthoesters **3** and **4** in ratios of ≃7:3 as judged by nmr (250 MHz) spectroscopy. A third compound, believed to be an isomer (3.17 ppm), was formed (≃16%) during the reaction but could not be further characterized.

Isomerization of cis *methoxy bicyclic orthoester 1*

cis Methoxy bicyclic orthoester **1** (9 mg) was dissolved in acetone (3 mL) under argon at room temperature. Then 50 μL of a 10^{-2} *M* solution of hydrochloric acid in methanol were added; tlc analysis after 5 min indicated the presence of *trans* methoxy bicyclic orthoester **2**, as confirmed by the 250-MHz nmr spectrum of the crude mixture after triethylamine quenching (*cis* **1**/*trans* **2**, ≃1:4).

Acknowledgements

Support for this work by the Natural Sciences and Engineering Research Council of Canada (NSERCC) and by the "Ministère de l'Éducation" (FCAC), Québec, is gratefully acknowledged.

1. (*a*) E. H. CORDES. Progress in physical organic chemistry. Vol. 4. *Edited by* A. Streitwieser and R. W. Taft. Interscience, New York. 1967. pp. 1–44; (*b*) E. H. CORDES and H. G. BULL.

Chem. Rev. **74**, 582 (1974).
2. P. DESLONGCHAMPS, P. ATLANI, D. FRÉHEL, and A. MALAVAL. Can. J. Chem. **50**, 3405 (1972).
3. P. DESLONGCHAMPS, R. CHÊNEVERT, R. J. TAILLEFER, C. MOREAU, and J. K. SAUNDERS. Can. J. Chem. **53**, 1601 (1975).
4. R. A. MCCLELLAND and M. ALIBHAI. Can. J. Chem. **59**, 1169 (1981).
5. B. CAPON and D.MCL.A. GRIEVE. Tetrahedron Lett. **23**, 4823 (1982).
6. (*a*) G. LAMATY, C. MOREAU, and Z. MOULOUNGUI. Can. J. Chem. **61**, 2643 (1983); (*b*) G. LAMATY, P. LORENTE, and C. MOREAU. Can. J. Chem. **61**, 2651 (1983).
7. O. E. DESVARD and A. J. KIRBY. Tetrahedron Lett. **23**, 4163 (1982).
8. P. DESLONGCHAMPS. Pure Appl. Chem. **43**, 351 (1975).
9. P. DESLONGCHAMPS. Tetrahedron, **31**, 2463 (1975).
10. P. DESLONGCHAMPS. Heterocycles, **7**, 1271 (1977).
11. P. DESLONGCHAMPS. Stereoelectronic effects in organic chemistry. Organic Chemistry Series. Vol. 1. *Edited by* J. E. Baldwin. Pergamon Press, Oxford. 1983.
12. A. J. KIRBY. The anomeric effect and related stereoelectronic effects at oxygen. Springer Verlag, Berlin. 1983.
13. P. DESLONGCHAMPS, J. LESSARD, and Y. NADEAU. Can. J. Chem. **63**, 0000 (1985).
14. (*a*) B. CAPON, J. H. GALL, and D.MCL.A. GRIEVE. J. Chem. Soc. Chem. Commun. 1034 (1976); (*b*) B. CAPON and D.MCL.A. GRIEVE. J. Chem. Soc. Perkin Trans. 2, 300 (1980); (*c*) B. CAPON and A. K. GHOSH. J. Am. Chem. Soc. **103**, 1765 (1981); (*d*) B. CAPON, A. K. GHOSH, and D.MCL.A. GRIEVE. Acc. Chem. Res. **14**, 306 (1981).
15. (*a*) M. AHMAD, R. G. BERGSTROM, M. J. CASHEN, A. J. KRESGE, R. A. MCCLELLAND, and M. F. POWELL. J. Am. Chem. Soc. **99**, 4827 (1977); (*b*) M. AHMAD, R. G. BERGSTROM, M. J. CASHEN, Y. CHIANG, A. J. KRESGE, R. A. MCCLELLAND, and M. F. POWELL. J. Am. Chem. Soc. **101**, 2669 (1979); (*c*) R. A. MCCLELLAND and M. AHMAD. J. Org. Chem. **44**, 1855 (1979); (*d*) R. A. MCCLELLAND, M. AHMAD, J. BOHONEK, and S. GEDGE. Can. J. Chem. **57**, 1531 (1979); (*e*) R. A. MCCLELLAND and G. PATEL. J. Am. Chem. Soc. **103**, 6809 (1981); **103**, 6912 (1981).
16. P. DESLONGCHAMPS, N. BEAULIEU, R. CHÊNEVERT, R. A. DICKINSON. Can. J. Chem. **58**, 1051 (1980).
17. P. DESLONGCHAMPS, U. O. CHERIYAN, A. GUIDA, and R. J. TAILLEFER. Nouv. J. Chim. **1**, 235 (1977).
18. N. BEAULIEU, R. A. DICKINSON, and P. DESLONGCHAMPS. Can. J. Chem. **58**, 2531 (1980).
19. M. K. KALOUSTIAN and F. KHOURI. J. Am. Chem. Soc. **102**, 7579 (1980).
20. S. M. MCELVAIN and G. R. MCKAY. J. Am. Chem. Soc. **77**, 5601 (1955).
21. H. MEERWEIN, P. BORNER, O. FUCKS, H. J. SASSE, H. SCHRODT, and J. SPILLE. Chem. Ber. **89**, 2060 (1956).
22. N. BEAULIEU. Ph.D. thesis. Université de Sherbrooke, Sherbrooke, Qué. 1980.

Bridged-ring steroids. III. The synthesis of bridged steroids with a bicyclo[2.2.1]heptane ring B system[1]

PETER YATES AND FRANÇOISE M. WINNIK[2]
Lash Miller Chemical Laboratories, University of Toronto, Toronto, Ont., Canada M5S 1A1

Received November 22, 1984

PETER YATES and FRANÇOISE M. WINNIK. Can. J. Chem. **63**, 2501 (1985).

Reaction of cholesta-5,7-dien-3β-yl 2-tetrahydropyranyl ether with bromoform and potassium *tert*-butoxide gave 3′,3′-dibromo-3′,6β-dihydrocyclopropa[5,6]-5a-cholest-7-en-3β-yl 2-tetrahydropyranyl ether (**1***c*), which on treatment with lithium aluminum hydride and water gave 5,8α-methano-5α-cholest-6-en-3β-yl 2-tetrahydropyranyl ether (**2***c*). This has been converted to 3β-acetoxy-5,8α-methano-5α-cholestan-6-one (**16***c*) and 3β-acetoxy-5,8α-methano-5α-cholestan-7-one (**17***c*). A preliminary investigation of the photochemistry of **16***c* and **17***c* has shown that the incorporation of the bicyclo[2.2.1]heptan-2-one system in the B ring of a steroid results in photoreactions of this system that are different from those observed in the case of simple bicyclo[2.2.1]heptan-2-ones.

PETER YATES et FRANÇOISE M. WINNIK. Can. J. Chem. **63**, 2501 (1985).

La réaction du tétrahydropyrannyloxy-2 cholestadiène-5,7 yle-3β avec le bromoforme et le *tert*-butylate de potassium conduit au tétrahydropyrannyloxy-2 dibromo-3,3′ dihydro-3′,6β cyclopropa[5,6] 5α-cholestène-7 yle-3β (**1***c*) qui, par traitement avec de l'hydrure double de lithium et d'aluminium et de l'eau, conduit au tétrahydropyrannyloxy-2 méthano-5,8α 5α-cholestène-6 yle-3β (**2***c*). Ce composé a été transformé en acétoxy-3β méthano-5,8α 5α-cholestanone-6 (**16***c*) et en acétoxy-3β méthano-5,8α 5α-cholestanone-7 (**17***c*). Une étude préliminaire de la photochimie des composés **16***c* et **17***c* a permis de montrer que l'incorporation du système bicyclo[2.2.1]heptanone-2 dans le cycle B d'un stéroïde fait que les photoréactions de ce système sont différentes de celles observées dans le cas des bicyclo[2.2.1]heptanones-2 simples.

[Traduit par le journal]

In connection with our interest in bridged steroids (1, 2), we have extended the work of Nazer (3), who was the only previous worker to synthesize bridged steroids with a bicyclo[2.2.1]heptane ring B system. In the earlier work ergosteryl tetrahydropyranyl ether was converted to its dibromocarbene adduct **1***a*, and this and its dihydro derivative **1***b* were converted to the bridged steroids **2***a* and **2***b*; the alcohol corresponding to **2***b* was epoxidized to **4***b* and this was converted to a mixture of diones **5***b* and **6***b*, which were not individually identified (Scheme 1). The α configuration was assigned to the one-carbon bridge of the bicyclo[2.2.1]heptane systems on spectroscopic and chemical grounds.

Our work was carried out in the cholestane rather than the ergostane series.[3] Cholesta-5,7-dien-3β-yl 2-tetrahydropyranyl ether was treated with bromoform and potassium *tert*-butoxide to give a dibromocarbene adduct. As in the ergostane series, a single adduct was formed and this is assigned structure **1***c* by analogy. We suggest that the high regio- and stereoselectivity in these additions is explicable in terms of the interpretation by Moss and Smudin of selectivity in the addition of dihalocarbenes to steroidal and related olefins (4). In the case of a steroid 5,7-diene two types of addition are possible (Fig. 1): α-axial attack, biased towards C-5, or β-axial attack biased towards C-8. Since the latter involves 1,3-diaxial interactions with the 18 and 19 CH_3 groups, H-11β, and pseudoaxial H-15β, while the former only involves 1,3-diaxial interactions with H-1α, H-3α, and H-9α, the two electronically equivalent additions are differentiated by steric control, greatly favoring α attack of the C-5 olefinic bond.

Our initial attempts to convert **1***c* to the bicyclo[2.2.1]heptane derivative **2***c* were disappointing. When a solution of the former in tetrahydrofuran was treated with lithium aluminum hydride under strictly anhydrous conditions, no rearrangement product could be detected and only starting material and some monobromo compound **8***c* (Scheme 2) were recovered. However, we discovered that the rearrangement occurred in good yield *when a 4:1 molar ratio of lithium aluminum hydride and water was used.* Moreover, optimal yields were obtained when the water was added in portions over a period of 2 days. It is possible that rearrangement of **1***a* and **1***b* occurred in the earlier experiments because of the inadvertent presence of water.

It is proposed that the conversion of **1***c* to **2***c* occurs by the route shown in Scheme 2. In the first step reductive dehalogenation (5) gives the intermediate **7***c*. This can either give **8***c* on protonation (*vide infra*) or proceed by loss of bromide ion to the carbene **9***c*; it is suggested that species formed by the interaction of lithium aluminum hydride and water act as Lewis acid catalysts for this step and account for the role of added water. Rearrangement of **9***c* to **10***c* is a vinylcyclopropylidene–cyclopentenylidene rearrangement and has ample precedent (6). Finally, addition of hydride to **10***c* and subsequent protonation gives **2***c*. Although the conversion of **1***c* to **2***c* is depicted as involving a stepwise series of reactions in Scheme 2, it is not excluded that some of these steps are concerted.

Nazer has reported that **11**, a ring A analogue of **1***c*, does not rearrange on treatment with lithium aluminum hydride, but gives **12** (3). In the hope that the addition of water would bring about rearrangement, we treated a mixture of **13** and **14** under the optimum conditions for the conversion of **1***c* to **2***c*. However, no rearrangement was observed under these conditions; compound **15** likewise failed to undergo rearrangement. These failures may reflect that interaction between the vacant *p* orbital of the putative carbene intermediate of type **9***c* and the olefinic π system is minimal in these cases; since such interaction is considered to facilitate the [1,3] sigmatropic rearrangement of the vinylcyclopropylidene species (6), reduction may then pre-

[1] For Parts I and II, see ref. 1.
[2] Present address: Xerox Research Centre of Canada, 2660 Speakman Drive, Mississauga, Ont., Canada L5K 2L1.
[3] The designation "*c*" is used throughout for compounds in the cholestane series.

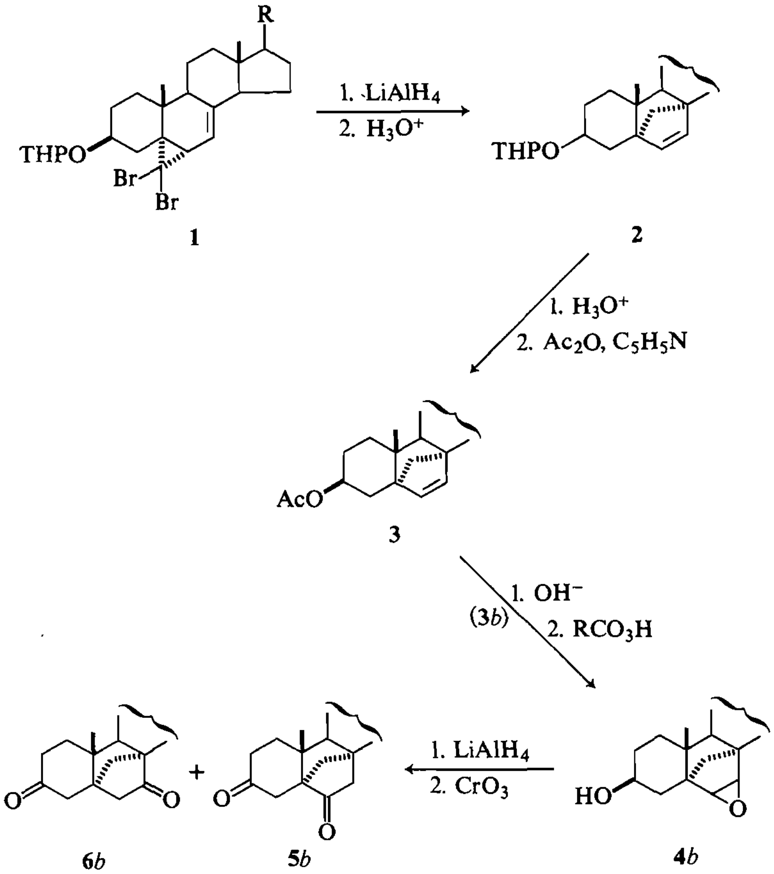

a R = $CH(CH_3)CH{=}CHCH(CH_3)CH(CH_3)_2$
b R = $CH(CH_3)CH_2CH_2CH(CH_3)CH(CH_3)_2$
c R = $CH(CH_3)CH_2CH_2CH_2CH(CH_3)_2$

SCHEME 1

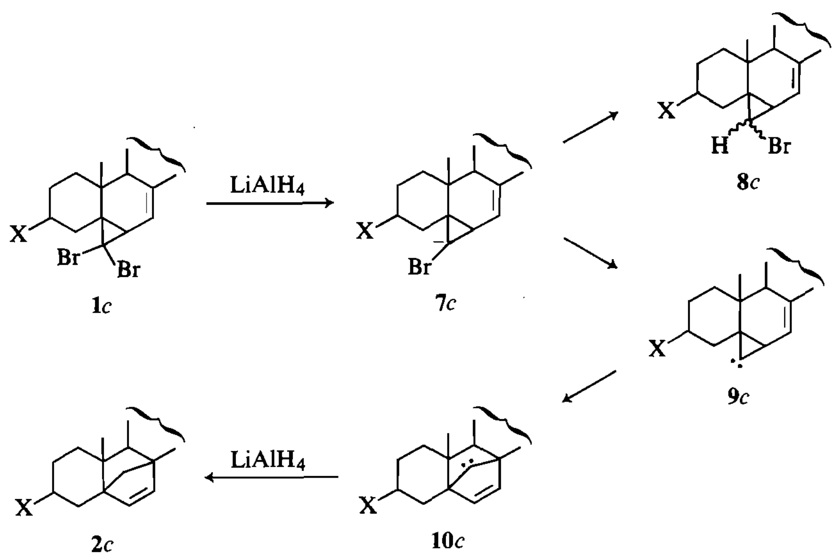

X = THPO

SCHEME 2

empt rearrangement. In the ring B cases of type **1**, rings A and C hold ring B in a conformation where the cyclopropyl ring is nearly perpendicular to the double bond and thus in an optimum geometry for rearrangement. This difference in geometry is reflected in the unusually long wavelength of the $\pi \rightarrow \pi^*$ uv maximum of **1***c* (218 nm) relative to the corresponding maxima of **11**, **13**, and **14** (<210 nm).

Compound **2***c* was converted by acid hydrolysis and acetylation to the corresponding acetate, **3***c*. Hydroboration of **3***c* followed by sequential oxidation with alkaline hydrogen per-

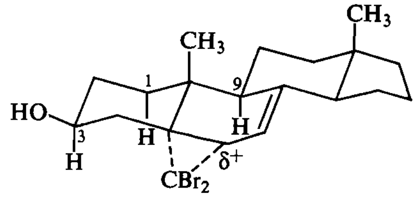

α-axial attack

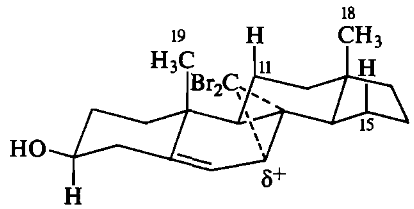

β-axial attack

FIG. 1

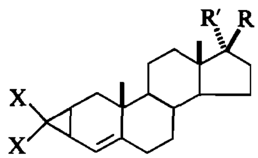

11, R = C_8H_{17}, R′ = H, X = Br
12, R = C_8H_{17}, R′ = X = H
13, R, R′ = O, X = Br

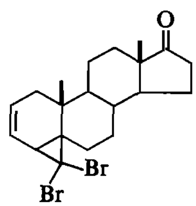

14

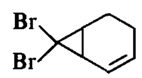

15

oxide and Jones reagent gave a mixture of **16***c* and **17***c* (Scheme 3). These were shown to be present in an approximately 1:1 ratio by vpc analysis, and were separated by painstaking chromatography on silica.

The structures of **16***c* and **17***c* were confirmed by elemental analytical and mass spectral data, bands in their ir spectra at 5.78 μm, maxima in their uv spectra at 289 (ε 29) and 302 nm (ε 25), and signals in their ^{13}C nmr spectra at δ 215.8 and 214.5.[4] However, these data did not allow individual structural assignments to be made. This was possible on the basis of comparison of the chemical shifts of the C-18 and C-19 signals in the ^1H nmr spectra of the two isomers. At 60 MHz one of the isomers shows these signals at δ 0.65 and 0.91, while the other shows superimposed signals at δ 0.92 (at 220 MHz this signal is resolved into two singlets at δ 0.916 and 0.925). Examination of molecular models (cf. Fig. 2) shows that this difference can readily be interpreted in terms of assignment of structure **16***c* to the former isomer and **17***c* to the latter. In **17***c* the C-18 methyl group is situated in the deshielding region of the C-7 carbonyl group, while in **16***c* it is too distant from the C-6 carbonyl group to be affected by it. Thus it is the signal of the C-18 methyl group that is shifted downfield in the second isomer relative to the first and the structural assignments are as given. This argument implies that the chemical shifts of the C-19 methyl signals are very similar in the two isomers, which is in accordance with the observation that the *endo*-methyl protons in 5,5-dimethyl- and 6,6-dimethylbicyclo[2.2.1]heptan-2-ones have closely similar chemical shifts (7).

[4] The ^{13}C nmr spectra of these and related compounds will be discussed in detail elsewhere.

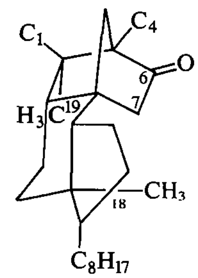

16*c*

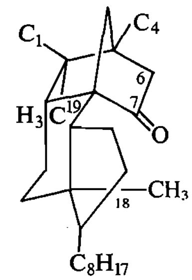

17*c*

FIG. 2

Independent chemical corroboration of the individual structural assignments was obtained as shown in Scheme 3. Treatment of the individual isomers under Haller–Bauer reaction conditions (8) gave in each case a hydroxy acid. Only one of these, that derived from **16***c*, gave on treatment with *p*-toluenesulfonic acid a γ lactone, as vouchsafed by a band at 5.66 μm in the ir spectrum of the product. Although the products were not fully characterized, it may safely be assumed that the Haller–Bauer cleavage will proceed via the more stable carbanions (8) to give the hydroxy acids **18***c* and **19***c* from **16***c* and **17***c*, respectively, and that only the former will give a γ-lactone, **20***c*, on acid treatment (Scheme 3).

In some runs for the conversion of **1***c* via **2***c* to the ketones **16***c* and **17***c* a side-product accompanied the ketones. This is considered to be the cyclopropyl ketone **21***c* on the basis of spectroscopic data (see Experimental). It must arise from **8***c* formed as a by-product in the reaction of **1***c* with lithium aluminum hydride and water (cf. Scheme 2).

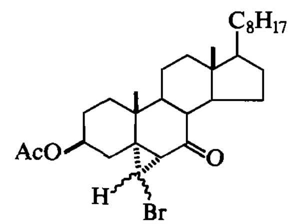

21*c*

A preliminary investigation of the photochemistry of **16***c* and **17***c* revealed an interesting difference in their photoreactivities.[5] Irradiation of **16***c* in methanol gave as the major product a methyl ester, which is considered to be **22***c* (Scheme 4), formed via Norrish Type I cleavage followed by ketene formation. The ^1H nmr spectrum of the total crude photolysate showed no evidence of enal formation. The result is unusual since, in the case of simple bicyclo[2.2.1]heptan-2-ones bearing hydrogen at the *syn*-C-7 position, enal formation proceeds to the exclusion of ketene formation after Norrish Type I cleavage (9). The selective ketene formation on irradiation of **16***c* must reflect constraints imposed by rings A and C on the biradical formed upon Norrish Type I cleavage.

On the other hand, irradiation of **17***c* in methanol gave neither enal nor ketene-derived products, as shown by the ^1H nmr spectrum of the total crude photolysate. This photolysate contained no starting material as shown by vpc analysis, but attempted purification by chromatography on silica gel gave a

[5] For discussions of the photochemistry of bicyclo[2.2.1]heptanones, see, for example, ref. 9.

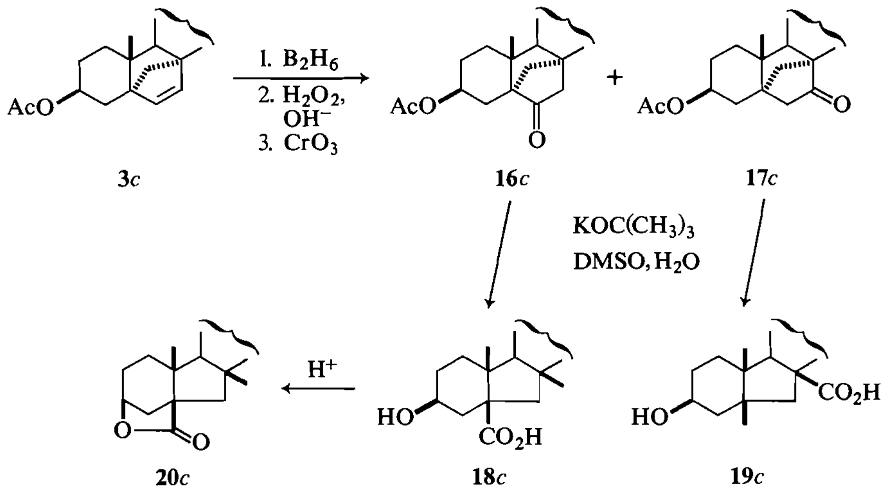

SCHEME 3

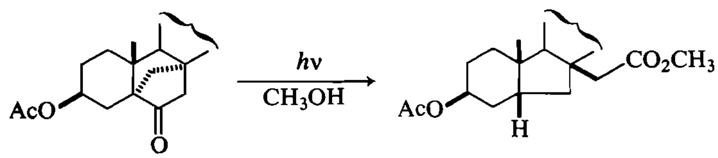

SCHEME 4

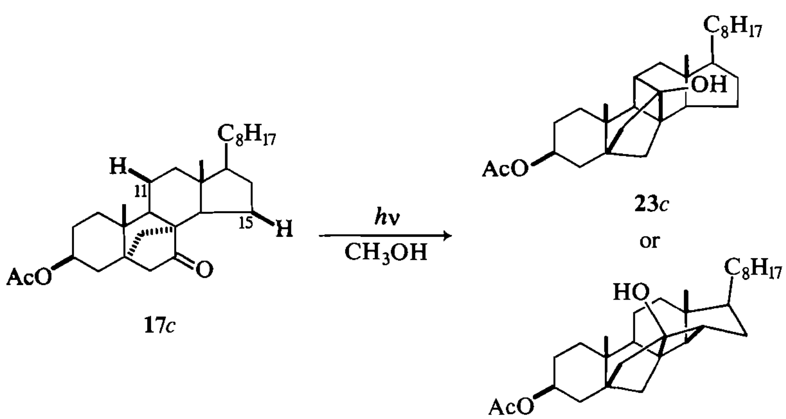

SCHEME 5

mixture whose major component was shown by vpc, tlc, and spectroscopic analysis to be **17***c*. This result can best be interpreted in terms of Norrish Type II hydrogen abstraction as the primary photochemical process followed by cyclobutanol formation (9), with the cyclobutanol reverting to the original ketone on silica gel. Examination of molecular models shows that both H-11β and H-15β, which are in the γ-relationship to the carbonyl oxygen atom, are held by the steroidal framework in very close proximity to that oxygen with a geometry that would permit ready hydrogen abstraction. We therefore postulate that the major photoproduct from **17***c* has structure **23***c* or **24***c* (Scheme 5) and that the difference in the photochemistry of **17***c* and **16***c* relates to this proximity effect.

Experimental

Melting points were determined on a Fisher–Jones apparatus and are uncorrected. Unless otherwise indicated, ir spectra were recorded in chloroform, uv spectra in cyclohexane, and ^{1}H and ^{13}C spectra in deuteriochloroform. In a standard work-up, solutions in organic solvents were washed twice with aqueous 5% sodium bicarbonate, twice with distilled water, and twice with brine, dried over anhydrous magnesium sulfate, and freed of solvent on a rotary evaporator under water aspirator pressure. Photolyses were carried out in Pyrex vessels with a Hanovia 450-W medium pressure mercury arc lamp surrounded by a quartz water-cooled jacket; photolysis solutions were flushed with dry nitrogen for 30 min immediately prior to irradiation; methanol used as solvent was boiled under reflux over magnesium and then distilled.

3′,3′-Dibromo-3′,6β-dihydrocyclopropa[5,6]-5α-cholest-7-en-3β-yl 2-tetrahydropyranyl ether (1c)

Cholesta-5,7-dien-3β-yl acetate (10) (25.0 g, 0.058 mol) was added to a solution of sodium hydroxide (5.0 g, 0.125 mol) in methanol (1 L). On heating, the solid dissolved and the solution was boiled under reflux under nitrogen for 1 h. After being kept in the refrigerator overnight, the reaction mixture was filtered to yield cholesta-5,7-dien-3β-ol (21.5 g, 96%), mp 148–150°C (lit. (11) mp 149–151°C); ir λ_{max}: 2.95 μm; ^{1}H nmr δ: 0.6–2.0 (m), 0.61 (s, 3H), 0.96 (s, 3H), 3.3–3.9 (m, 1H), 5.2–5.65 (m, 2H).

A catalytic amount of phosphorus oxychloride (20 drops) was added slowly to a stirred solution of cholesta-5,7-dien-3β-ol (21.4 g, 0.056 mol) and freshly distilled dihydropyran (22.0 mL, 0.28 mol) in dry dichloromethane (300 mL). The temperature of the solution rose from 22°C to 27°C. After 3 h the solution was diluted with diethyl ether (400 mL) and worked up in the usual manner to afford cholesta-5,7-dien-3β-yl 2-tetrahydropyranyl ether (22.4 g, 85%), recrystallized from acetone; mp 134–135°C; ir λ_{max}: 6.20 (w) μm; ^{1}H nmr δ: 0.6–2.1 (m), 0.62 (s, 3H), 0.96 (s, 3H), 3.15–4.2 (m, 3H), 4.6–4.8 (m, 1H), 5.2–5.6 (m, 2H). *Accurate Mass* calcd. for $C_{32}H_{52}O_2$ (*M*): 468.3967; found: 468.3970.

Cholest-5,7-dien-3β-yl 2-tetrahydropyranyl ether (22.3 g, 0.047 mol) was dissolved in freshly distilled, dry pentane (1 L) and the solution was poured into a 2-L three-necked round-bottomed flask fitted with a mechanical stirrer, a 100-mL addition funnel, a thermometer, and a nitrogen inlet (best yields were obtained when base-washed glassware was utilized). To the solution kept at 0°C was added potassium *tert*-butoxide (40.0 g, 0.35 mol), and then, over a period of 2 h, a solution of bromoform (35.0 g, 0.14 mol) in dry pentane (80 mL). The mixture was stirred for 2 h at room temperature and then cooled again to 0°C, and more potassium *tert*-butoxide (6.50 g, 0.058 mol) and bromoform (5.0 g, 0.019 mol) in pentane (20 mL) were added. At the end of the bromoform addition, the reaction mixture was warmed up to room temperature and filtered through alumina on a sintered-glass funnel. The solvent was evaporated to give a brown oil, which crystallized from acetone to give **1***c* as white needles (9.50 g, 31%). Recrystallization from acetone afforded **1***c* as white needles, mp 136–137°C; ir λ_{max}: 6.05 (w) μm; ^{1}H nmr δ: 0.5–2.0 (m), 0.56 (s, 3H), 1.13 (s, 3H), 3.25–4.3 (m, 3H), 5.35–5.55 (m, 1H); *m/z*: 540 (5) ($M - C_5H_{10}O_2$), 538 (10), 536 (5). *Accurate Mass* calcd. for $C_{28}H_{43}O^{81}Br$ ($C_{33}H_{52}O_2{}^{79}Br^{81}Br - C_5H_8O - H^{79}Br$ and $C_{33}H_{52}O_2{}^{81}Br_2 - C_5H_8O - H^{81}Br$), $C_{28}H_{43}O^{79}Br$ ($C_{33}H_{52}O_2{}^{79}Br^{81}Br - C_5H_8O - H^{81}Br$ and $M - C_5H_8O - H^{79}Br$): 476.2478, 474.2497; found: 476.2478, 474.2495. Chromatography or recrystallization of **1***c* led to partial hydrolysis,[6] and a satisfactory combustion analysis could not be obtained; complete hydrolysis gave the parent hydroxy compound, mp 146–148°C. *Anal.* calcd. for $C_{28}H_{44}OBr_2$: C 60.43, H 7.97, Br 28.72; found: C 60.58, H 8.07, Br 28.75.

*5,8α-Methano-5α-cholest-6-en-3β-yl acetate (3*c*)*

Compound **1***c* (11.0 g, 0.0172 mol) was dissolved in dry tetrahydrofuran (500 mL). Lithium aluminum hydride (3.1 g, 0.075 mol) was added carefully to this solution. The reaction mixture was stirred under nitrogen at room temperature for 72 h. Water (50 mg, 2.7 mmol) was added every 12 h, in five 10-μL portions. The excess hydride was destroyed by careful addition of a small amount of saturated aqueous sodium sulfate solution (3 mL). The reaction mixture was filtered, and the filtrate was diluted with diethyl ether and worked up in the usual manner. The amorphous **2***c* obtained (7.49 g, 90%) was converted into the acetate **3***c* without further purification by hydrolysis to the corresponding alcohol, followed by acetylation.

A solution of the product (7.49 g, 0.0155 mol) and concentrated aqueous hydrochloric acid (20 drops) in ethanol (75 mL) was boiled under reflux under nitrogen for 1 h. The residue after evaporation of the ethanol was taken up in diethyl ether. The usual work-up afforded the alcohol (5.89 g, 95%). A solution of the alcohol (5.89 g, 0.0148 mol) in dry pyridine (40 mL) and freshly distilled acetic anhydride (15 mL) was kept at room temperature for 16 h. The orange solution was poured over crushed ice and the mixture was neutralized with solid sodium bicarbonate. Extraction with diethyl ether, the usual work-up, and chromatography[6] on silica gel with chloroform as eluent afforded the acetate **3***c*, which was crystallized from methanol/acetone (3:1 v/v) (5.10 g, 80%); mp 92–94°C; ir λ_{max}: 5.78 μm; ^{1}H nmr δ: 0.7–2.3 (m), 0.76 (s, 3H), 0.90 (s, 3H), 2.00 (s, 3H), 4.5–5.0 (m, 1H), 5.86 and 6.31 (AB system, J = 6 Hz, 2H); *m/z*: 440 (4) (*M*). *Anal.* calcd. for $C_{30}H_{48}O_2 \cdot 0.5CH_3OH$: C 80.21, H 11.03; found: C 79.81, H 10.69. *Accurate Mass* calcd. for $C_{28}H_{44}$ ($M - C_2H_4O_2$): 380.3442; found: 380.3441.

[6] A similar observation was made in the case of **1***b* (3).

TABLE 1. Separation of compounds **16***c* and **17***c* by column chromatography

Eluent	Volume collected (mL)[a]	Weight (mg)	Composition (%)[b] 16*c*	17*c*
Benzene	400	—	—	—
Benzene – diethyl ether	1350	—	—	—
(99.5:0.5 v/v)	210	190	—	—
	840	500	—	>99
	300	79	46	54
Benzene – diethyl ether	75	21	88	12
(98:2 v/v)	75	11	90	10
	1050	350	>99	—

[a] Rate of elution 1 mL/min; 15-mL fractions collected.
[b] Determined by vpc analysis on a 3% OV-17 on Chromosorb W-HP 80/100 column at 280°C; retention times: 10.2 (**16***c*) and 8.1 min (**17***c*).

*3β-Acetoxy-5,8α-methano-5α-cholestan-6-one (16*c*) and 3β-acetoxy-5,8α-methano-5α-cholestan-7-one (17*c*)*

To a stirred solution of **3***c* (5.10 g, 0.0116 mol) in dry diethyl ether (200 mL) kept at room temperature under nitrogen was added dropwise a solution of borane – methyl sulfide (2.0 mL, 1.60 g, 0.021 mol) in dry diethyl ether (50 mL). After completion of the addition the reaction mixture was stirred at room temperature for 1 h and then was boiled under reflux for 3 h. The excess borane was destroyed with water added slowly to the reaction mixture cooled to 0°C. Oxidation was carried out with 3 *N* aqueous sodium hydroxide (5 mL) and 28% hydrogen peroxide (10 mL) at 0°C for 15 min and at room temperature for 1 h. The usual work-up afforded a mixture of alcohols (4.42 g, 83%), which was subjected immediately to further oxidation. Jones reagent (chromium trioxide (26.67 g) and concentrated sulfuric acid (230 mL) made up to 1 L with distilled water; ~15 mL) was added dropwise to a solution of the mixture of alcohols (4.42 g, 9.6 mmol) in acetone (distilled from potassium permanganate; 150 mL) until an orange brown colour persisted. The excess oxidant was destroyed with 5% aqueous sodium bisulfite (100 mL), the acetone was evaporated, and the residue was extracted with diethyl ether. The usual work-up and chromatography on silica gel with benzene/diethyl ether (97:3 v/v) as eluent gave a mixture of the two ketones **16***c* and **17***c* (2.5 g, 57%) in an approximately 1:1 ratio. The two isomers (1.7 g) were separated by column chromatography on silica gel (120 g; column diameter: 2.5 cm) as shown in Table 1. Compound **17***c* was eluted first and was recrystallized from acetone; mp 198–199°C; ir λ_{max}: 5.78 μm; uv λ_{max} (ε): 302 (25) nm; ^{1}H nmr δ: 0.65–2.1 (m), 0.92 (s, 6H), 2.01 (s, 3H), 4.5–5.2 (m, 1H); *m/z* 456 (15) (*M*). *Anal.* calcd. for $C_{30}H_{48}O_3$: C 78.90, H 10.59; found: C 78.86, H 10.48.

The isomer **16***c* was eluted last and was crystallized from acetone; mp 158–159°C; ir λ_{max}: 5.78 μm; uv λ_{max} (ε): 289 (29) nm; ^{1}H nmr δ: 0.5–2.3 (m), 0.65 (s, 3H), 0.91 (s, 3H), 2.01 (s, 3H), 4.5–5.05 (m, 1H); *m/z* 456 (5) (*M*). *Anal.* calcd. for $C_{30}H_{48}O_3$: C 78.90, H 10.59; found: C 78.82, H 10.51.

*3β-Acetoxy-3′-bromo-3′,6β-dihydrocyclopropa[5,6]-5α-cholestan-7-one (21*c*)*

In some runs the mixture of ketones **16***c* and **17***c* obtained as above was contaminated with a small amount of **21***c*, which was separated from **16***c* and **17***c* by fractional crystallization from diethyl ether; mp 206–207°C; ir λ_{max}: 5.78 μm; uv λ_{max} (ε): 297 (54) nm; ^{1}H nmr δ: 0.6–2.1 (m), 0.66 (s, 3H), 1.08 (s, 3H), 2.01 (s, 3H), 3.85–4.1 (m, 1H), 4.6–5.2 (m, 1H); *m/z*: 536 (1), 534 (1) (*M*), 395 (100). *Accurate Mass* calcd. for $C_{28}H_{43}O$ ($M - C_2H_4BrO_2$): 395.3324; found: 395.3325.

*Haller–Bauer cleavage of 16*c *and 17*c

Potassium *tert*-butoxide (freshly sublimed at 150°C/0.25 Torr (1 Torr = 133.3 Pa); 185 mg, 1.65 mmol) and dry dimethyl sulfoxide (2 mL) were stirred at room temperature under nitrogen for 30 min. Distilled water (10.8 mg, 0.60 mmol) was added slowly followed by a solution of **16***c* (68 mg, 0.15 mmol) in dimethyl sulfoxide (3 mL). The reaction mixture was stirred at room temperature for 2 h and at 45°C for 19 h. Water (5 mL) was added dropwise and the alkaline aqueous solution was extracted three times with diethyl ether. The usual work-up gave a colorless oil (12.2 mg); ir λ_{max}: 2.80 (w), 5.74 μm. The aqueous layer was acidified with concentrated hydrochloric acid (pH 1–2) and extracted five times with diethyl ether. The combined extracts were worked up in the usual manner to yield **18***c* as an oil (29 mg, 43%); ir λ_{max}: 3.0–4.2, 5.89 μm; ^{1}H nmr δ: 0.7–2.2 (m), 0.90 (s), 3.5–4.2 (m, 1H), 5.56–6.5 (m, 2H, absent after D_2O treatment). A solution of *p*-toluenesulfonic acid (dried in benzene solution by azeotropic distillation; 2 mg, 0.01 mmol) and **18***c* (29 mg, 0.067 mmol) in dry benzene (10 mL) was heated at reflux for 15 h in a Soxhlet extractor containing activated molecular sieves. The cold reaction mixture was worked up in the usual manner to give **20***c* as an oil (10 mg, 36%); λ_{max} 5.66 μm.

Similar treatment of **17***c* gave a carboxylic acid, considered to be **19***c*, which failed to give a γ-lactone.

*Irradiation of 16*c

Irradiation of **16***c* (50 mg, 0.11 mmol) in methanol (15 mL) for 3 h afforded a mixture of three compounds in the ratio ~3:1:6 as indicated by vpc analysis. The major compound **22***c* (25 mg, 46%) was isolated by chromatography on a 1-mm silica gel preparative plate eluted with chloroform and was crystallized from methanol; mp 144–147°C; ir λ_{max}: 5.78 μm; ^{1}H nmr δ: 0.8–2.8 (m), 0.88 (s, 3H), 0.96 (s, 3H), 2.01 (s, 3H), 3.61 (s, 3H), 4.5–5.25 (m, 1H); *m/z*: 488 (4) (*M*).

*Irradiation of 17*c

Irradiation of a solution of **17***c* (84 mg, 0.18 mmol) in methanol (15 mL) for 5 h afforded one major product of 68% yield with complete consumption of starting material as indicated by vpc analysis. The usual work-up gave a mixture of at least three compounds in ~1:1:1 ratio; ir λ_{max}: 5.78 μm; ^{1}H nmr δ: 0.55–2.5 (m), 0.55 (s), 0.61 (s), 0.96 (s), 1.05 (s), 2.01 (s), 4.6–5.2 (m). Chromatography on a silica gel column eluted with chloroform gave **17***c* as the major fraction (46 mg); mp 195–198°C after crystallization from methanol.

Acknowledgements

We thank the Natural Sciences and Engineering Research Council of Canada for support of this work and Messrs. Baldev Gambhir and Nick Plavac for technical assistance.

1. P. YATES and F. M. WALLISER. Can. J. Chem. **54**, 3508 (1976); P. YATES and F. M. WINNIK. Can. J. Chem. **59**, 1641 (1981).
2. F. M. WALLISER and P. YATES. Chem. Commun. 1025 (1979).
3. M. Z. NAZER. J. Org. Chem. **30**, 1737 (1965).
4. R. A. MOSS and D. J. SMUDIN. J. Org. Chem. **41**, 611 (1976).
5. C. W. JEFFORD, U. BURGER, M. H. LAFFER, and T. KABENGELE. Tetrahedron Lett. 2483 (1973).
6. W. M. JONES and U. H. BRINKER. *In* Pericyclic reactions. Vol. 1. *Edited by* A. P. Marchand and R. E. Lehr. Academic Press, New York. 1977. pp. 159–165.
7. P. YATES and G. F. HAMBLY. Can. J. Chem. **57**, 1656 (1979).
8. P. G. GASSMAN, J. T. LUMB, and F. V. ZALAR. J. Am. Chem. Soc. **89**, 946 (1967).
9. P. YATES. Pure Appl. Chem. **16**, 93 (1968); O. L. CHAPMAN and D. S. WEISS. *In* Organic photochemistry. Vol. 3. *Edited by* O. L. Chapman. Marcel Dekker, New York. 1973. Chapt. 3; P. YATES and R. O. LOUTFY. Acc. Chem. Res. **8**, 209 (1975); P. YATES. J. Photochem. **5**, 91 (1976).
10. W. G. DAUBEN and D. S. FULLERTON. J. Org. Chem. **36**, 3277 (1971).
11. S. BERNSTEIN, L. J. BINOVI, L. DORFMAN, K. J. SAX, and Y. SUBBAROW. J. Org. Chem. **14**, 433 (1949).

Proton magnetic resonance spectrum of cellulose triacetate. Temperature effects, the rotational conformation of the 6-acetoxymethyl group, and computer modelling of methyl 4,6-di-*O*-acetyl-β-glucopyranoside

VANGA S. RAO, FRANÇOISE SAURIOL, AND ARTHUR S. PERLIN
Department of Chemistry, McGill University, Montreal, P.Q., Canada H3A 2A7

AND

M. T. PHAN VIET
Laboratoire Regional de RMN, Université de Montréal, Montreal, P.Q., Canada H3C 3V1

Received November 21, 1984

VANGA S. RAO, FRANÇOISE SAURIOL, ARTHUR S. PERLIN, and M. T. PHAN VIET. Can. J. Chem. **63**, 2507 (1985).

Pronounced narrowing of the resonance signals in the 400-MHz ^{1}H nmr spectrum of cellulose triacetate in $CDCl_3$ between 25 and 50°C, as well as shielding and deshielding changes in ^{1}H chemical shifts, suggest that thermal disruption of intermolecular aggregates is accompanied by a conformational modification. Analysis of the spin–spin coupling patterns clearly evident at 50°C indicates that although there is a reversal in the chemical shifts of H-6_R and H-6_S relative to those for acetylated D-glucopyranose derivatives, the rotational conformations of the exocyclic 6-acetoxymethyl groups of the polymer and the model compounds all favor RHS and RCS rotameric forms. Supporting evidence for this conclusion is obtained from the 2-dimensional ^{1}H spectrum of a trisaccharide, *O*-β-D-glucopyranosyl-(1→3)-*O*-β-D-glucopyranosyl-(1→4)-*O*-β-D-glucopyranose undecaacetate. Computer-generated models of methyl 4,6-di-*O*-acetyl-β-glucopyranoside are examined in relation to the stereochemistry of 6-acetoxymethyl groups.

VANGA S. RAO, FRANÇOISE SAURIOL, ARTHUR S. PERLIN et M. T. PHAN VIET. Can. J. Chem. **63**, 2507 (1985).

Opérant en solution dans le $CDCl_3$ et à des températures allant de 25 à 50°C, on a déterminé les spectres rmn du ^{1}H à 400 MHz du triacétate de cellulose; la finesse des bandes ainsi que les variations dans le blindage et le déblindage des déplacements chimiques du ^{1}H suggèrent que la rupture, sous l'influence de la chaleur, des aggrégats intermoléculaires s'accompagne d'une modification de conformation. L'analyse des diagrammes de couplage spin–spin, qui sont bien évidents à 50°C, indique qu'en dépit d'une inversion des déplacements chimiques de H-6_R et de H-6_S par rapport à ceux des dérivés acétylés du D-glucopyrannose, les conformations rotationnelles des groupes acétoxyméthyles-6 exocycliques du polymère et des composés types favorisent toutes les formes rotamères RHS et RCS. Les spectres rmn du ^{1}H en deux dimensions d'un trisaccharide, l'undécaacétate du *O*-β-D-glucopyrannosyl-(1→3) *O*-β-D-glucopyrannosyl-(1→4) *O*-β-D-glucopyrannose confirme cette conclusion. On examine des modèles produits par ordinateur du di-*O*-acétyl-4,6 β-glucopyrannoside de méthyle par rapport à la stéréochimie des groupes acétoxyméthyles-6.

[Traduit par le journal]

Introduction

A recent ^{1}H nmr study on a variety of *O*-acetyl derivatives of aldohexoses and disaccharides has shown (1) that chemical shift and coupling parameters observed for the 6,6′-methylene protons of those compounds are strongly dependent upon the pattern of acetylation at O-4 and O-6 and, consequently also, on linkage position. In comparing these ^{1}H nmr characteristics with those of larger carbohydrate molecules, the spectrum of cellulose triacetate (**1**) has been examined, and is described here.

Results and discussion

The signals in the 400-MHz ^{1}H nmr spectrum of cellulose triacetate in $CDCl_3$ at 25°C (Fig. 1A) are relatively broad, and hence convey little spin–spin coupling information. However, at 50°C the resolution is improved markedly throughout (Fig. 1B), as has been observed (2) for the 220-MHz spectrum at 60°C, and, whereas the resonances of H-1 and H-6 overlap in Fig. 1A, both are now clearly evident. No peaks were detected between δ 6.3 and 5.3, the region in which the α,β-anomeric protons of reducing end residues are expected (3) to resonate, indicating that the degree of polymerization of the cellulose derivative is ≥ 100.

This pronounced increase in resolution with temperature, indicative of a phase transition, may represent disruption of intermolecular aggregates that characterize (4) solutions of cellulose acetate. Another, although not necessarily independent, possibility is a change in the conformation of the macromolecule, which is suggested by the fact that the process is accompanied by substantial variations in ^{1}H chemical shift. As shown by the data of Table 1, which compares chemical shifts over the temperature range −20 to +50°C, the positions of all resonances except those of H-5 and H-6 are displaced with temperature. The most marked changes are observed for H-1, which becomes less shielded (+36 Hz) as the temperature is raised, and for H-2, which experiences an increase in shielding (−20 Hz). Other protons exhibit a diversity of lesser influences, including those of the acetoxyl groups, which likely undergo reorientation. As the anomeric proton (H-1) is the most strongly affected, an adjustment in the orientation of the (1→4) glucosidic bond may well take place as chain mobility increases with temperature.

Vicinal coupling between ring protons, close to 9 Hz throughout (Table 2), is of the magnitude expected for β-D-glucopyranosyl residues in the $^4C_1$ conformation (**1**). Another noteworthy feature of Fig. 1B concerns the resonances of the exocyclic 6-acetoxymethyl group. That is, the downfield, H-6, signal shows a smaller coupling with H-5 than does H-6′ (Table 3), which is the converse of the relationship found for the 6-acetoxymethyl group of monomeric methyl 2,3,4,6-tetra-*O*-acetyl-β-D-glucopyranoside (**2**). Although these data may imply that **1** and **2** differ widely in rotamer populations about their exocyclic C-6/C-5 bonds, recent observations (1) on the influence of *O*-acyl groups on the chemical shifts of 6-6′-methylene protons suggest otherwise.

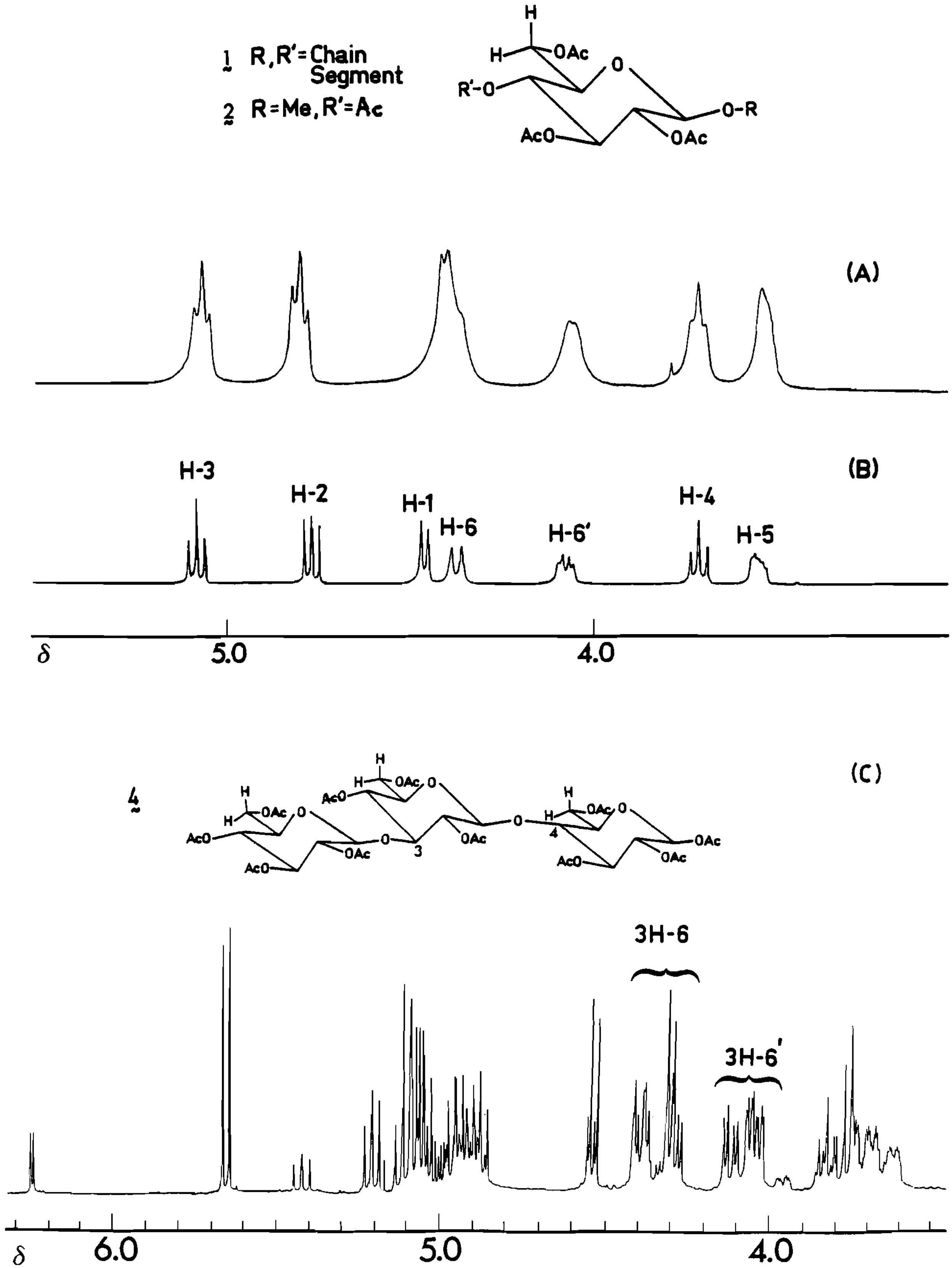

FIG. 1. The 400-MHz ^{1}H nmr spectrum of cellulose triacetate in $CDCl_3$ at (A) 25°C, (B) 50°C; signals for acetoxyl methyls are not shown (see Table 1 for chemical shift data); (C) 400-MHz ^{1}H nmr spectrum of trisaccharide derivative (4) in $CDCl_3$ at 25°C; the doublet at δ 6.25, and other minor signals, are attributable to a small proportion of the α-anomer.

TABLE 1. Effect of temperature on ^1H chemical shifts (at 400 MHz) of cellulose triacetate (**1**)

Proton	Chemical shift change (Hz)[a] 25°C	50°C
H-1	+14	+36
H-2	−10	−20
H-3	+6	+14
H-4	+10	+10
H-5	0	0
H-6	0	0
H-6′	+4	+14
OAc-2[b]	−10	−18
OAc-3[b]	−8	−12
OAc-6[b]	+4	+10

[a]Relative to the chemical shift recorded at −20°C; +, downfield displacement; −, upfield displacement.
[b]Signals at δ 2.10, 2.00, and 1.95, respectively, at 50°C; tentative assignments, based on data in refs. 1 and 5.

TABLE 2. Chemical shift and coupling data[a] for the ring protons of cellulose triacetate and trisaccharide **4**

	(δ) H-1 (*J*) (1,2)	H-2 (2,3)	H-3 (3,4)	H-4 (4,5)	H-5
Cellulose triacetate[b]	4.46 (7.6)	4.77 (9.0)	5.08 (9.0)	3.71 (9.5)	3.56
Trisaccharide **4**					
Reducing end (4-linked)	5.65 (8.3)	5.05 (9.5)	5.20 (9.5)	3.77 (8.5)	3.74
Central residue (3-linked)	4.31 (8.0)	4.95 (9.5)	3.83 (9.5)	4.92 (9.0)	3.62
Non-reducing end	4.54 (8.1)	4.88 (9.9)	5.11 (9.5)	5.09 (10.0)	3.69

[a]In $CDCl_3$.
[b]At 50°C.

Conversion of an hydroxymethyl group into an acetoxymethyl group usually leads to deshielding of the 6,6′-methylene protons by about 0.3 ppm. However, for a D-glucopyranosyl moiety esterified at O-4 as well as O-6, the effects on the methylene protons are such that the relative positions of their signals become interchanged. Hence, it has been found (1) with a variety of D-glucopyranoside derivatives that when both O-4 and O-6 bear acetyl substituents, the relative positions of the 6,6′-methylene proton resonances are analogous to those of **2**, whereas the order of their chemical shifts is reversed when either O-4 or O-6 (or both) is not acylated. A proposed (1) source of this "shift reversal" is selective deshielding of H-6_R by the 6-*O*-acetyl substituent which, presumably, is oriented appropriately through a weak interaction[1] with the 4-*O*-acetyl substituent.

This proposal can be expressed in the form of stereochemical models calculated for methyl 4,6-di-*O*-acetyl-β-glucopyranoside (**3**) (Fig. 2; for convenience, the L-enantiomer is shown). For energy minimization, three different calculations were performed with the multiple option "Maximin" program (see experimental section):

[1]For effects on ^{13}C chemical shifts of intermolecular carbonyl−carbonyl interactions, and in hydrogen-bonding solvents, see ref. 6.

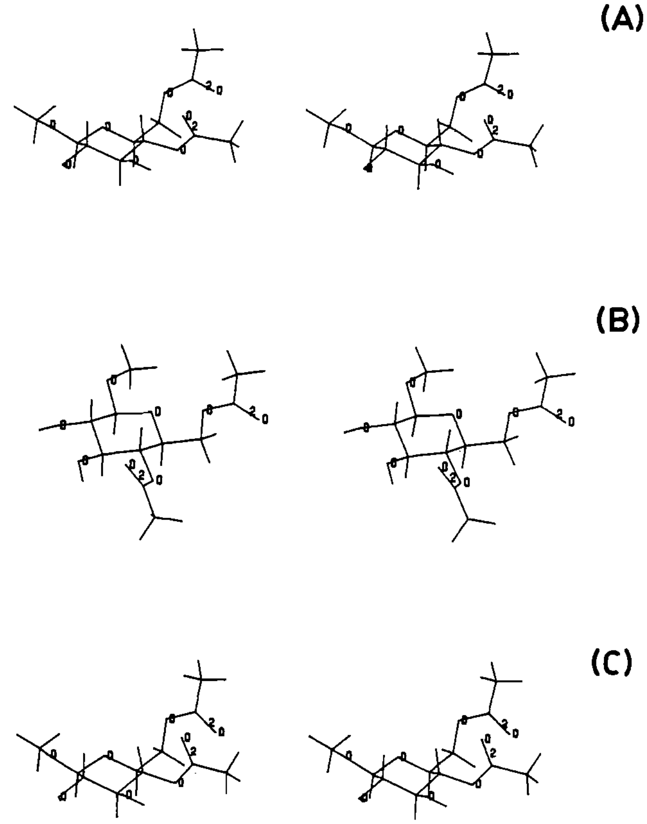

FIG. 2. Three simulated conformational models ("Maximin" minimized, 20 iterations) in *stereo* representation for methyl-4,6-di-*O*-acetyl-β-L-glucopyranoside (**3**) representing different values of E_{min}: A, −2.22 kcal/mol; B, −5.90 kcal/mol; C, 1.24 kcal/mol.

(*a*) The molecular conformation was set according to torsional angles obtained in a "search" operation, and minimization was then carried out. This procedure, which produced the structure in Fig. 2A (E_{min} = −2.22 kcal/mol), probably represents a *local*, rather than gobal, minimum energy. Altering the orientations of the individual OH groups had little or no effect on the magnitude of E_{min}.

(*b*) By allowing the five exocyclic torsional angles (see experimental section) to vary, the structure shown in Fig. 2B was obtained. Corresponding to a value of E_{min} = −5.90 kcal/mol, it is expected to represent the global minimum.

(c) A constraint was then imposed, whereby the projected angles of the two C═O groups remained fixed as in Fig. 2C during minimization, which resulted in a value of E_{min} = 1.24 kcal/mol. This increase in energy, in comparison with (b), is due mainly to a sharp rise in torsional energy, i.e, 1.97 and 7.71 kcal/mol in (b) and (c), respectively.

Energy minimization also was carried out by incorporating net atomic charges, obtained by different methods (7), for all atoms in the molecule. This treatment gave much higher total energies, attributable to the large contribution introduced by electrostatic interactions. For example, the energy (−5.90 kcal/mol) cited in (b) was raised to 1.17 kcal/mol by the incorporation of atomic charges calculated according to ref. 7(*a*), a total of 5.12 kcal/mol of this increase being due to electrostatic energy. Hence the latter accounted for most of the algebraic difference of 7.07 kcal/mol with, and without, the inclusion of atomic charges. Due to limitations in

TABLE 3. Chemical shift and spin coupling data[a] for the 6,6′-methylene protons of D-glucopyranoside peracetate residues of **1**, **2**, and **4**

	δ		^3J[b]	
	H-6	H-6′	H-6	H-6′
Cellulose triacetate (**1**)	4.38	4.08	1	5.0
Methyl 2,3,4,6-tetra-*O*-acetyl β-D-glucopyranoside (**2**)	4.29	4.15	4.6	2.5
Trisaccharide (**4**)				
Reducing end (4-linked)	4.40	4.12	2.5	4.8
Central residue (3-linked)	4.29	4.06	5.0	2.2
Non-reducing end	4.39	4.04	4.0	2.2

[a]In $CDCl_3$.
[b]Vicinal coupling with H-5.
[c]Geminal coupling (^2J) is approximately −12.5 Hz, throughout.

the computer-modelling system available, it was not feasible to separate out the local dipolar interaction of specific interest between the 4- and 6-acetoxy groups of **3** from the electrostatic interactions arising from all atoms within the molecule. Consequently, the less rigorous approach represented by (b) and (c) was adopted to provide a measure of the *magnitude* of the presumed diploar interaction between the two acetoxy groups. That is, the total energy cited in (b), calculated as a function of bond stretching, angle bending, and torsional and van der Waals energy terms, was then recalculated (c) after imposing a constraint on the orientation of the 4- and 6-C═O functions, as depicted in Fig. 2c. The energy change involved would then be expected to be, at least, compensated for by the dipolar interaction between the two carbonyl groups.

Accordingly, then, the algebraic difference in E_{min} values between (b) and (c), i.e., 7.14 kcal/mol, may be taken as an approximate measure of the stabilization energy that is entailed in the postulated dipolar attraction between the two C═O groups.

Another example in which "shift reversal" is observed is provided by a peracetylated trisaccharide, namely, *O*-β-D-glucopyranosyl-(1→3)-*O*-β-D-glucopyranosyl-(1→4)-*O*-β-D-glucopyranose undecaacetate (**4**) (8). Although the signals for the three pairs of methylene protons of **4** are not completely resolved in the 400-MHz spectrum (Fig. 1C), a full analysis was permitted by two-dimensional spectroscopy, from which the data for the ring protons and the 6,6′-methylene protons, in Tables 2 and 3, respectively, were obtained. It is seen (Table 3) that the downfield (H-6) signal of the 4-*O*-linked reducing end residue exhibits the smaller coupling with H-5 in common with cellulose triacetate. By contrast, the central, 3-*O*-linked residue and also the non-reducing end unit, both of which have O-4 and O-6 acetyl groups, are characterized by a coupling pattern closely similar to that of the glucoside (**2**). Also consistent with these findings are data reported (9) for *O*-β-D-glucopyranosyl-(1→4)-*O*-β-D-glucopyranosyl-(1→6)-*O*-β-D-glucopyranose undecaacetate: i.e., the absence of an acetyl group on O-6 of the reducing end residue, and on O-4 of the central residue, gives rise to a smaller spacing for the downfield H-6 signal in each instance, whereas the converse applies for the non-reducing end unit.

Accordingly, the fact that O-4 of cellulose triacetate is not esterified leads to the expectation that the chemical shifts of its methylenic protons should be the converse of that for **2**, which is borne out by the data of Table 3. Accepting this proposition, one may also propose assignments for the two methylene pro-

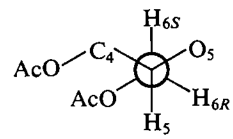

ROS

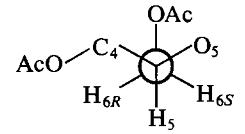

RHS

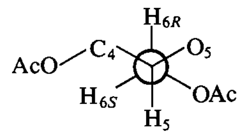

RCS

tons of the polymer, by reference to **2**, i.e., the downfield signal in Fig. 1 is due to H-6_R, and the upfield one, to H-6_S.

Based on the magnitude of coupling of H-6 and H-6′ with H-5 in D-glucopyranosides and such *O*-acetyl derivatives as **2**, it has been estimated (1) that RHS and RCS represent the major, staggered, rotamers about the C-6/C-5 bond, whereas ROS makes little or no contribution. By contrast, X-ray crystallographic studies indicate (10,11) that the 6-hydroxymethyl group of native cellulose favors the orientation represented by the ROS (tg) rotamer, and also (12) that the 6-acetoxymethyl group of solid cellulose acetate adopts principally the RHS (gg) rotameric form. However, according to the coupling data of Table 3, the RCS (gt) rotamer must contribute almost as importantly as RHS to the overall conformation of cellulose acetate in solution, as found with lower molecular weight analogs.

Experimental

Nuclear magnetic resonance spectroscopy

Proton magnetic resonance spectra were recorded with a Bruker WH-400 spectrometer, using $CDCl_3$ as solvent. Chemical shifts are reported with reference to tetramethylsilane. Analysis of the spectrum of trisaccharide peracetate **4** was facilitated by use of a two-dimensional (SECSY) technique (13).

*Molecular modelling of methyl 4,6-di-*O*-acetyl-β-glucopyranoside (**3**)*

The molecular modelling operation was performed with a "Trigraph" system, Tripos Associates, St. Louis, Mo. A model of diacetate **3** was constructed graphically from tetrahydropyran and individual atomic parameters, all of which were stored in a permanent fragment library of the system, by varying such molecular dimensions as bond length, bond angle, and torsional angle as required. The relative orientations of the exocyclic bonds (rotameric states around each rotatable bond) were adjusted according to the allowable states obtained from the "search" program, which monitors the hard-sphere van der Waals contacts between atoms. As the program contains provision for the introduction of distance constraints between atom pairs, this procedure served to screen out conformations within which the pertinent distances lay outside the regions designated. The energy minimization (14) was carried out by using the program "Maximin" (based on molecular mechanics) with multiple options, in a converging manner through optimization of molecular dimensions. It also was possible to specify molecular parts requiring optimization as a unit, e.g., the aggregate of atoms comprising the two C═O groups, as well as to preserve selected distances and angles during energy minimization. Consequently, the final energies determined are a composite of bond stretching, angle bending, and torsional and van der Waals energy terms. Negative values are obtained when there is a preponderance of residual attractive interactions (−ve) over repulsive interactions (+ve).

The search was conducted for diacetate **3** with a distance constraint range of 2.5−3.0 Å between the carbon atom of one C═O group and the oxygen atom of the other. A van der Waals factor of 0.9 and an angle increment of 15° over the range 0 to 359° were chosen for all rotatable bonds. This led to a *single* conformation with torsional

Le radical méthylènecyclopropyle: étude théorique. Chloration par *t*-BuOCl et réduction par $(n\text{Bu})_3\text{SnH}$ de dérivés cyclopropéniques

R. ARNAUD, S. CHOUBANI, R. SUBRA, M. VIDAL[1] ET M. VINCENS
Université Scientifique et Médicale de Grenoble, Laboratoire d'Études Dynamiques et Structurales de la Sélectivité (L.E.D.S.S.) IV, Bâtiment 52, Chimie Recherche, B.P. 68, 38402 Saint Martin d'Hères Cédex, France

ET

V. BARONE
Instituto Chimico, Università di Napoli, Via Mezzocannone 4, 80134 Napoli, Italy

Reçu le 19 mars 1984[2]

R. ARNAUD, S. CHOUBANI, R. SUBRA, M. VIDAL, M. VINCENS et V. BARONE. Can. J. Chem. **63**, 2512 (1985).

La chloration allylique par *t*-BuOCl des dialkyl-2,3 cyclopropene-2 carboxylates d'éthyle ou des alcools primaires et tertiaires analogues est régiosélective et hautement stéréosélective: on observe uniquement la formation du dérivé halogéné du méthylènecyclopropane dans lequel l'halogène et le groupement fonctionnel présentent une relation *trans* par rapport au cycle. La stéréochimie de la réduction par $(n\text{Bu})_3\text{SnH}$ des halogénures allyliques du méthylènecyclopropane et du cyclopropène est identique, cependant, on note également la formation de produits d'ouverture du cycle en C3. La migration exocyclique de la double liaison s'interprète par la formation intermédiaire du radical allylique. Une étude théorique par la méthode MNDO (UHF et RHF) montre que ces radicaux allyliques sont plans quel que soit le substituant. La réaction d'arrachement est toujours plus facile pour le carbone cyclique que pour le carbone exocyclique. De plus, elle est favorisée quand le carbone cyclique est substitué par un chlore au lieu d'un méthyle.

R. ARNAUD, S. CHOUBANI, R. SUBRA, M. VIDAL, M. VINCENS, and V. BARONE. Can. J. Chem. **63**, 2512 (1985).

The allylic chlorination of ethyl 2,3-dialkyl 2-cyclopropenecarboxylate or primary and tertiary alcohols is highly regio- and stereoselective. The halogenated methylenecyclopropane derivative only is observed. In that compound, the halogen substituent and the functional group are in a *trans* position with respect to the ring. The halogenated allylic compounds of methylenecyclopropane and of cyclopropene undergo reduction by $(n\text{Bu})_3\text{SnH}$ with the same stereochemistry. Products arising from ring opening are also observed. The exocyclic migration of the double bond can be related to the formation of a transient allylic radical. A theoretical study performed within the MNDO (UHF and RHF) framework leads to a planar allylic radical, whatever the substituent. The radical abstraction reaction which takes place during the reduction process is easier for a cyclic carbon atom than for an exocyclic one. In the former case, the faster reaction is obtained for a chlorinated carbon atom.

Introduction

Dans un travail récent nous avons rapporté l'étude théorique du cation méthylènecyclopropyle et précisé les conditions expérimentales qui permettent de réaliser en milieu acide, la migration intracyclique de la double liaison du méthylènecyclopropane (1, 2). Le but de ce mémoire est de résumer, d'une part, les résultats que nous avons obtenus au cours de la substitution radicalaire allylique en série cyclopropénique et d'approcher d'autre part, à l'aide d'une méthode semi-empirique, la structure de l'intermédiaire allylique: le radical méthylènecyclopropyle.

Ce type de radical a été en effet peu étudié (3); il nous a paru intéressant d'engendrer le radical méthylènecyclopropyle, non seulement à partir de précurseurs méthylènecyclopropaniques, mais également à partir des substrats cyclopropéniques isomères; dans ce cas, en effet, on peut espérer mettre en évidence l'interaction de l'électron célibataire et de la double liaison par l'intermédiaire des produits de transposition: les dérivés du méthylènecyclopropane.

Nous envisagerons successivement:

La chloration des dialkyl-2,3 cyclopropène-2 carboxylates d'éthyle et des alcools primaires et tertiaires correspondants par l'hypochlorite de tertiobutyle (4–8). Cette étude a donné lieu à une note préliminaire (9).

La réduction des halogénures méthylènecyclopropaniques et cyclopropéniques par l'hydrure de tributylétain (10–18).

L'étude théorique du radical allylique méthylènecyclopropyle (ou cyclopropénylméthyle) dont l'objectif essentiel est de préciser la nature de cette espèce intermédiaire en déterminant sa géométrie et sa structure électronique.

Partie expérimentale

Technique expérimentale

Les spectres, ir de composés purs (film) ont été enregistrés sur un appareil Perkin–Elmer 521 à réseau et double faisceau et les spectres rmn sur appareil Perkin–Elmer R 24 et sur appareil CAMECA fonctionnant à 250 MHz.

*Synthèse des esters et alcools cyclopropéniques dialkylés en position 2 et 3 **1–5**, du méthyl-2 bromométhyl-3 cyclopropènecarboxylate d'éthyle **18** et du chloro-2 méthylène-3 cyclopropanecarboxylate d'éthyle **6**:* voir références 19, 20, 22 et 23.

*Chloration des esters **1**, **4**, **5** et des alcools **2** et **3** par l'hypochlorite de tertiobutyle*

Cette réaction a été réalisée à 0°C, 40°C ou 60°C. On dissout 0,2 mol de dérivé cyclopropénique dans 150 mL de CCl_4 anhydre que l'on porte à la température voulue et on ajoute par petites quantités, 0,6 mol d'hypchlorite de tertiobutyle; après chaque addition, le mélange réactionnel est agité jusqu'à ce que la couleur jaune de *t*-BuOCl ait disparue. Une addition trop rapide du *t*-BuOCl provoque une élévation brusque de la température du mélange réactionnel. À la fin de la réaction, on évapore CCl_4 et la distillation sous pression réduite (par exemple $\theta_{eb}/0{,}4$ Torr $\simeq$ 27°C (1 Torr = 133.3 Pa) pour le mélange réactionnel de la chloration de **1** à 0°C) conduit aux esters ou alcools cyclopropylidéniques **6** et **9–15** et aux esters cyclopropaniques dichlorés **7** et **8**. Les rendements dans les différentes conditions sont mentionnés par ailleurs dans le texte.

[1] Auteur à qui adresser la correspondance.
[2] Revision reçue le 5 février 1985.

La séparation des produits de réaction a été réalisée par cpg sur colonne Carbowax-CROM WAW 20%, 1,6 m, θ(colonne) = 80°C, θ(injecteur) = 130°C.

*Chloro-2 méthyl-2 méthylène-3 cyclopropanecarboxylate d'éthyle 1*R*,2R* ***6***

Infrarouge (film): 3085 cm^{-1} $\nu(=CH_2)$, 1730 cm^{-1} $\nu(C{=}O)$; vibrations de déformation 800; 860; 920 cm^{-1}; rmn ^1H (60 MHz, CCl_4/TMS): $\delta(CH_3)$ = 1,78 ppm, 3, s; δ(▷—H) = 2,62 ppm, 1, m; δ(=—H) = 5,62 et 5,80 ppm, 2, m; $\delta(CO_2CH_2CH_3)$ = 1,26 ppm, 3, t et 4,12 ppm, 2, q; $J(CH_2CH_3)$ = 7,1 Hz; J(▷—H, =\H) = 2,3 et 2,9 Hz; rmn ^{13}C (62,86 MHz, $CDCl_3$/TMS): $\delta(C_1)$ = 33,5 ppm, d; J(C–H) = 164 Hz; $\delta(C_2)$ = 42,9 ppm, s; $\delta(C_3)$ = 135,5 ppm, s; $\delta(C_4)$ = 108,8 ppm, t, J(C–H) = 160 Hz; $\delta(—CO_2)$ = 168,2 ppm, s; $\delta(CH_2CH_3)$ = 61,1 ppm, t, J(C–H) = 147 Hz; $\delta(CH_2—CH_3)$ = 14,2 ppm, q, J(C–H) = 121 Hz; $\delta(CClCH_3)$ = 21,0 ppm, q, J(C–H) = 121 Hz. *Anal.* calc.: C 55,01, H 6,30, Cl 20,34; tr.: C 54,85, H 6,41, Cl 21,80%.

*Dichloro-2,3 diméthyl-2,3 cyclopropanecarboxylate d'éthyle 2*R*,3R* ***7***

Infrarouge (film): 1740 cm^{-1} $\nu(C{=}O)$, vibrations de déformation 840 et 920 cm^{-1}; rmn ^1H (60 MHz, CCl_4/TMS): $\delta(CH_3)$ = 1,95 ppm, 6, s–s, les 2 CH_3 sont magnétiquement non équivalents, Δδ = 2 Hz; δ(H) = 2,05 ppm, 1, s; $\delta(CO_2CH_2CH_3)$ = 1,28 ppm, 3, t et 4,11 ppm, 2, q; $J(CH_2CH_3)$ = 7,1 Hz. *Anal.* calc.: C 45,50, H 5,50, Cl 33,65; tr.: 46,10, H 5,52, Cl 32,80%.

Dichloro-2,3 diméthyl-2,3 cyclopropanecarboxylate d'éthyle meso ***8***

Infrarouge (film): 1740 cm^{-1} $\nu(C{=}O)$, vibrations de déformation 835 et 920 cm^{-1}; rmn ^1H (60 MHz, CCl_4/TMS): $\delta(CH_3)$ = 1,85 ppm, 6, s, les 2 CH_3 sont magnétiquement équivalents; δ(H) = 2,30 ppm, 1, s; $\delta(CO_2CH_2CH_3)$ = 1,30 ppm, 3, t et 4,12 ppm, 2, q; $J(CH_2CH_3)$ = 7,0 Hz. *Anal.* calc.: C 45,50, H 5,69, Cl 33,65; tr.: 45,03, H 5,37, Cl 31,96%.

*Chloro-2 méthyl-2 éthylidène-3 cyclopropanecarboxylate d'éthyle 1*R*,2R* E ***11***

Infrarouge (film): 3010 cm^{-1} $\nu(=CH)$ épaulement; 1730 cm^{-1} $\nu(C{=}O)$; rmn ^1H (60 MHz, CCl_4/TMS): $\delta(CH_3)$ = 1,80 ppm, 3, s; δ(▷—H) = 2,57 ppm, 1, d; δ(=—H) = 5,98 ppm, 1 m; $\delta(=—CH_3)$ = 1,98 ppm, 3, d; $\delta(CO_2CH_2CH_3)$ = 1,28 ppm, 3, t et 4,09 ppm, 2, q; $J(CO_2CH_2CH_3)$ = 7,1 Hz; J(=<$^{CH_3}_{H}$) = 6,7 Hz; J(=—CH_3, ▷—H) = 2,1 Hz; J(=—H, ▷—H) ≃ 2,1 Hz. *Anal.* calc.: C 57,29, H 6,90, Cl 18,83; tr.: C 56,77, H 6,42, Cl 19,35%.

*Chloro-2 méthyl-2 éthylidène-3 cyclopropanecarboxylate d'éthyle 1*R*,2R* Z ***12***

Infrarouge (film): 3010 cm^{-1} $\nu(=CH)$ épaulement; 1728 cm^{-1} $\nu(C{=}O)$; rmn ^1H (60 MHz, CCl_4/TMS): $\delta(CH_3)$ = 1,77 ppm, 3, s; δ(▷—H) = 2,55 ppm, 1, d; δ(=—H) = 6,28 ppm, 1, m; $\delta(=—CH_3)$ = 1,82 ppm, 3, d; $\delta(CO_2CH_2CH_3)$ = 1,30 ppm, 3, t et 4,12 ppm, 2, q; $J(CO_2CH_2CH_3)$ = 7,1 Hz; $J(CH_2CH_3)$ = 6,8 Hz; J(=—CH_3, ▷—H) = 1,7 Hz; J(=—H, ▷—H) ≃ 2,1 Hz. *Anal.* calc.: C 57,29, H 6,90, Cl 18,83; tr.: C 56,10, H 6,01, Cl 17,92%.

*Chloro-2 éthyl-2 méthylène-3 cyclopropanecarboxylate d'éthyle 1*R*,2R* ***13***

Infrarouge (film): 3090 cm^{-1} $\nu(=CH_2)$, 1730 cm^{-1} $\nu(C{=}O)$, vibrations de déformation: 800; 860; 890; 915 cm (large); rmn ^1H (60 MHz, CCl_4/TMS): $\delta(CH_2CH_3)$ = 2,02 ppm, 2, t et 1,10 ppm, 3, q; δ(▷—H) = 2,60 ppm, 1, m; δ(=—H) = 5,58 ppm, 1, m et 5,78 ppm, 1, m; $\delta(CO_2CH_2CH_3)$ = 1,28 ppm, 3, t et 4,08 ppm, 2, q; $J(CO_2CH_2CH_3)$ = 7 Hz; $J(CH_2CH_3)$ = 6,8 Hz; J(=CH_2, ▷—H) = 2,7 et 1,9 Hz. *Anal.* calc.: C 57,29, H 6,90, Cl 18,83; tr.: C 58,25, H 7,16, Cl 19,14%.

*Chloro-2 éthyl-2 éthylidène-3 cyclopropanecarboxylate d'éthyle 1*R*,2R* E ***14***

Infrarouge (film): 3020 cm^{-1} épaulement $\nu(=CH)$; 1732 cm^{-1} $\nu(C{=}O)$; rmn ^1H (60 MHz, CCl_4/TMS): $\delta(CH_2CH_3)$ 2 ppm, 2, t et 1,08 ppm, 3, q; δ(▷—H) = 2,55 ppm, 1, d; δ(=—H) = 6,20 ppm, 1, m; $\delta(=—CH_3)$ = 1,83 ppm, 3, m; $\delta(CO_2CH_2CH_3)$ = 1,28 ppm, 3, t et 4,10 ppm, 2, q; $J(CO_2CH_2CH_3)$ = 7,2 Hz; J(=<$^{CH_3}_{H}$) = 6,7 Hz; J(=—CH_3, ▷—H) ≃ J(=—H, ▷—H) = 2,1 Hz; $J(CH_2CH_3)$ = 7 Hz. *Anal.* calc.: C 59,26, H 7,41, Cl 17,53; tr.: 60,20, H 7,60, Cl 18,03%.

*Chloro-2 éthyl-2 éthylidène-3 cyclopropanecarboxylate d'éthyle 1*R*,2R* Z ***15***

Infrarouge (film): 3020 cm^{-1} épaulement $\nu(=CH)$; 1728 cm^{-1} $\nu(C{=}O)$; rmn ^1H (60 MHz, CCl_4/TMS): $\delta(CH_2CH_3)$ 2 ppm, 2, t et 1,10 ppm, 3, q; δ(▷—H) = 2,55 ppm, 1, d; δ(=—H) = 5,95 ppm, 1, m; $\delta(=—CH_3)$ = 1,83 ppm, 3, m; $\delta(CO_2CH_2CH_3)$ = 1,27 ppm, 3, t et 4,10 ppm, 2, q; $J(CO_2CH_2CH_3)$ = 7,1 Hz; $J(CH_2CH_3)$ = 6,9 Hz; J(=<$^{CH_3}_{H}$) = 6,7 Hz; J(=—CH_3, ▷—H) = 1,6 Hz; J(=—H, ▷—H) ≃ 2,1 Hz. *Anal.* calc.: C 59,26, H 7,41, Cl 17,53; tr.: 59,10, H 6,96, Cl 17,89%.

*(Chloro-2 méthyl-2 méthylène-3 cyclopropane 1*R*,2R**)yl méthanol* ***9***

Infrarouge (film): 3080 cm^{-1} $\nu(=CH_2)$; rmn ^1H (60 MHz, CCl_4/TMS): $\delta(CH_2OH)$ = 3,58 ppm, 2, d; $\delta(CH_3)$ = 1,69 ppm, 3, s; δ(▷—H_1) = 2,18 ppm, 1, m; δ(=—H_a) = 5,45 ppm, 1, m; δ(=—H_b) = 5,67 ppm, 1, m; $J(H_1H_a)$ = 2,2 Hz; $J(H_1H_b)$ = 3,0 Hz; $J(H_1—CH_2OH)$ = 8,5 Hz. *Anal.* calc.: C 54,34, H 6,79, Cl 26,79; tr.: C 53,82, H 7,12, Cl 25,98%.

*(Chloro-2 méthyl-2 méthylène-3 cyclopropane 1*R*,2R**)yl-2 propanol-2* ***10***

Infrarouge (film): 3080 cm^{-1} $\nu(=CH_2)$; rmn ^1H (60 MHz, CCl_4/TMS): $\delta(CMe_2OH)$ = 1,28 ppm, 3, s et 1,33 ppm, 3, s; $\delta(CH_3)$ = 1,80 ppm, 3, s; δ(▷—H) = 1,99 ppm, 1, m; δ(=—H_a) = 5,42 ppm, 1, m; δ(=—H_b) = 5,68 ppm, 1, m; $J(H_1H_a)$ = 2,4 Hz; $J(H_1H_b)$ = 3,1 Hz. *Anal.* calc.: C 59,81, H 8,10, Cl 22,12; tr.: C 59,01, H 8,60, Cl 21,45%.

Influence de l'AIBN et du galvinoxyle

On place dans un bain maintenu à 0°C (ou 60°C) trois ballons, contenant respectivement: (*i*) 1 mmol d'ester **1**, 7 mL de CCl_4; (*ii*) 1 mmol d'ester **1**, 7 mL de CCl_4 et quelques mg d'AIBN; (*iii*) 1 mmol d'ester **1**, 7 mL de CCl_4 et 1 mmol de galvinoxyle et l'on ajoute en une seule fois 3 mmol d'hypochlorite de tertiobutyle. L'avancement de la réaction est déterminé par cpg analytique sur colonne Carbowax 10%, 1,6 m.

*Action de nBu_3SnH sur les dérivés halogénés cyclopropénique **18** et cyclopropylidénique*

En tube scellé, à $0{,}85 \times 10^{-2}$ mol de dérivé halogéné **18** et 2×10^{-4} mol d'AIBN en solution dans 50 mL de benzène, on ajoute $1{,}7 \times 10^{-2}$ mol de nBu_3SnH. Le mélange réactionnel est porté à 86°C pendant 66 h. À la fin de la réaction, le benzène est évaporé, les produits distillés rapidement sous pression réduite et séparés par chromatographie cpg sur colonne UCON POLAR 25%, 3,30 mètres, θ(colonne) = 110°C et θ(injecteur) = 150°C. Les rendements sont mentionnés dans le texte.

Méthyl-3 pentadiène-2,4 oate d'éthyle E ***20***

Infrarouge (film): 3095 cm^{-1} $\nu(=CH_2)$; 1715 cm^{-1} $\nu(C{=}O)$; 1603 et 1618 $\nu(C{=}C)$; 870 et 920 cm^{-1} $\nu(HC{=}CH_2)$; uv (dans C_6H_{12}): λ_{max} = 240 cm^{-1}; ε = 19 000; rmn ^1H (250 MHz, $CDCl_3$/TMS): $\delta(CH_2CH_3)$ = 4,26 ppm, 2, q et 1,28 ppm, 3, t; $\delta(CH_3)$ = 2,26 ppm, 3, d; $\delta(H_5)$ = 5,33 ppm, 1, d; $\delta(H_5)$ = 5,59 ppm, 1, d; $\delta(H_4)$ = 6,38 ppm, 1, m; $\delta(H_2)$ = 5,96 ppm, 1, s; $J(CH_2—CH_3)$ = 7 Hz;

$J(CH_3—H_2)$ = 1 Hz; $J(H_5—H_4)$ = 10,5 Hz; $J(H_{5'}—H_4)$ = 17,4 Hz; rmn ^{13}C (62,86 MHz, $CDCl_3$/TMS): δ C_2 = 140,2 ppm; C_4 = 120,2 ppm; C_5 = 118,8 ppm; C_6 = 14,3 ou 13,5 ppm; $J(C_2—H)$ = 158 Hz; $J(C_4—H)$ = 155 Hz; $J(C_5—H)$ = 155 Hz; $J(C_6—H)$ = 126 Hz. *Anal.* calc.: C 68,57, H 8,57; tr.: C 67,92, H 8,90%.

Méthyl-3 pentadiène-2,4 oate d'éthyle Z **21**

Infrarouge (film): 3095 cm^{-1} $\nu(=CH_2)$; 1715 cm^{-1} $\nu(C=O)$; 1600 et 1620 cm^{-1} $\nu(C=C)$; 860 et 925 cm^{-1} $\nu'(HC=CH_2)$; les spectres ir de **20** et **21** présentent par ailleurs une grande similitude; rmn ^1H (250 MHz, $CDCl_3$/TMS): $\delta(CH_2CH_3)$ = 4,0 ppm, 2, q et 1,23 ppm, 3, t; $\delta(CH_3)$ = 1,95 ppm, 3, s large; $\delta(H_5) \simeq \delta(H_{5'})$ ≃ 5,30 ppm, 2, m; $\delta(H_4)$ = 7,62 ppm, 1, m; $\delta(H_2)$ = 5,50 ppm, 1, s; $J(CH_2CH_3)$ = 7 Hz; $J(H_5—H_4)$ = 10,5 Hz; $J(H_{5'}—H_4)$ = 17,4 Hz. *Anal.* calc.: C 68,57, H 8,57; tr.: 67,85, H 8,90%.

Résultats

1. *Chloration des dialkyl-2,3 cyclopropène-2 carboxylates d'éthyle **1**, **4**, **5** et des alcools primaire **2** et tertiaire **3** par l'hypochlorite de tertiobutyle*

À basse température (0°C) la chloration de l'ester **1** et des alcools **2** et **3** par *t*-BuOCl, en solution dans CCl_4, conduit avec un rendement très élevé aux dérivés du méthylènecyclopropane **6**, **9** et **10**; la H-substitution allylique présente une régiosélectivité et une stéréosélectivité très élevées: seul le carbone 2 fixe un atome de chlore d'une part et d'autre part les composés **6**, **9**, **10** ont tous la configuration relative 1*R**,2*R**; on observe également la formation de traces de dichloro-1,1 méthylène-2 cyclopropanes **7** et **8** qui résultent de l'addition du

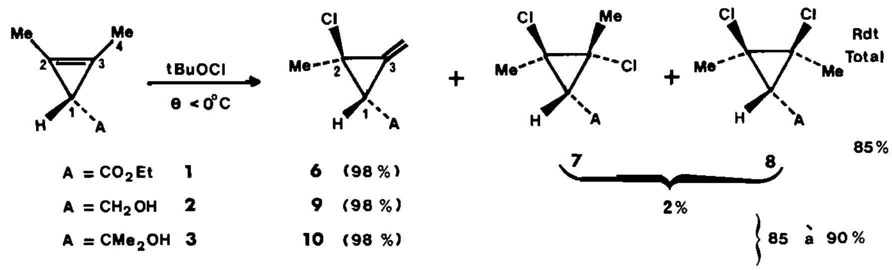

chlore sur la double liaison cyclopropénique.

À température plus élevée (65°C), le produit de H-substitution n'est plus obtenu qu'avec un rendement global de 9%, par contre la réaction d'addition du chlore sur la double liaison est nettement favorisée.

Lorsque la double liaison cyclopropénique est dissymétrique, la régiosélectivité de l'arrachement de l'hydrogène est en contradiction avec les prévisions que l'on pouvait faire à partir des réactivités comparées des liaisons C—H des carbones allyliques primaire et secondaire vis-à-vis de *t*-BuO·. À 0°C l'ester **4** conduit, en effet, préférentiellement au méthylènecyclopropane **13** avec un rendement de 40% alors que les éthylidènecyclopropanes **11** et **12** ne se forment qu'avec un rendement total de 10%; il est possible que cette inversion de la régiosélectivité soit due à une orientation défavorable des liaisons C—H du méthylène par rapport aux orbitales π. Signalons enfin que la stéréosélectivité reste, comme précédemment, très élevée et que l'addition du chlore au cycle est toujours à cette température négligeable.

L'énergie d'activation de la réaction d'arrachement du pro-

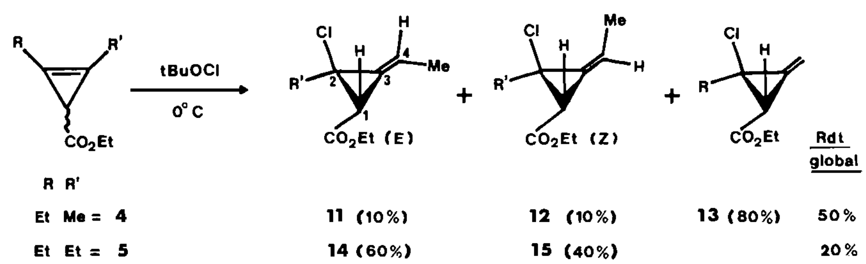

ton allylique cyclopropanique est très nettement supérieure à celle du proton allylique des substrats cyclopropéniques. Traité dans les mêmes conditions expérimentales à 0°C ou à 60°C le méthyl-2 méthylène-3 cyclopropanecarboxylate d'éthyle est retrouvé inchangé après 5 h de réaction.

Une étude détaillée de la chloration de l'ester **1** a permis de confirmer le caractère radicalaire de cette réaction: D'une part on observe l'éxistence de périodes d'induction pour les réactions de H-substitution et d'addition du chlore, la durée de la première étant nettement supérieure à celle de la seconde. D'autre part, ces réactions sont très sensibles à l'action d'inhibiteur tel que le galvinoxyle. Lorsque l'on traite à 0°C l'ester **1** (1 mol) par *t*-BuOCl (3 mol) en solution dans CCl_4 et à l'obscurité, la chloration allylique est pratiquement terminée après 4 h de réaction alors qu'en présence de galvinoxyle (1 mol) l'ester **1** est retrouvé inchangé au bout de 15 h.

Identification (stéréochimie)

En rmn, la relation *trans* du groupe méthyle et du groupement éthoxycarbonyle dans les esters **6**, **11**, **12** est établie par l'étude des glissements induits par le tris(dipivalomethanato) europium, Eu(dpm)$_3$. Nous avons observé antérieurement que le rapport des pentes $\Delta Me_2/\Delta H_1$ des droites $\delta H = f(CEu/C^0$ substrat) permet d'établir facilement la relation *cis* ou *trans* de ce méthyle et du groupement fonctionnel (21). En particulier, dans le cas du chloro-2 méthyl-2 isopropylidènecyclopropanecarboxylate d'éthyle **16** et du diméthyl-2,2 méthylène-3 cyclopropanecarboxylate d'éthyle **17** les valeurs sont les suivantes:

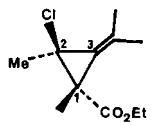

16

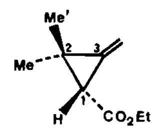

17

$\frac{\Delta \mathrm{Me}_2}{\Delta \mathrm{H}_1} = 0,66$

$\frac{\Delta \mathrm{Me}_2}{\Delta \mathrm{H}_1} = 0,69$

$\frac{\Delta \mathrm{Me}'_2}{\Delta \mathrm{H}_1} = 0,24$

Les valeurs observées dans le cas des esters **6**, **11**, **12** qui varient de 0,64 à 0,68 permettent d'attribuer sans ambiguité la configuration relative $1R^*,2R^*$ à ces composés. Une remarque identique peut être faite dans le cas des esters **13**, **14**, **15**; la valeur du rapport $\Delta(CH_2\text{—}CH_3)/\Delta H_1$, qui varie de 0,70 à 0,80, établit de même la relation *cis* des groupes Et et —CO_2Et.

Les configurations *Z* ou *E* de **11**, **12** et **14**, **15**, se déduisent également des glissements induits des méthyles vinyliques Me_4; la valeur dans le cas de la configuration *E* ($\Delta Me_4 \simeq 8$) est, comme l'on doit s'y attendre nettement supérieure à celle de la configuration *Z* ($\Delta Me_4 \simeq 1$).

Notons enfin que l'attribution des configurations relatives aux esters dichlorés **7** et **8** est fondée sur l'équivalence magnétique des deux méthyles dans **8** et leur non-équivalence dans **7**. L'effet LIS confirme ces caractéristiques d'une part et permet d'autre part, en comparant les glissements des méthyles dans ces deux composés, d'établir la relation *cis* de ces groupes et de CO_2Et dans **8**.

2. *Réduction des halogénures allyliques méthylènecyclopropanique et cyclopropénique par l'hydrure de tri-n-butylétain*

Le méthyl-2 bromométhyl-3 cyclopropènecarboxylate d'éthyle **18** traité à 86°C par nBu$_3$SnH (2 équivalents) en solution dans le benzène subit une réduction totale en 66 h; la réaction conduit au produit de H-substitution **19**, aux produits d'ouverture **20** et **21** et à un produit non identifié **22**. La réduction, dont le rendement global reste assez faible ($\simeq$50%), est très sensible à l'addition des initiateurs tel que l'azobisisobutyronitrile.

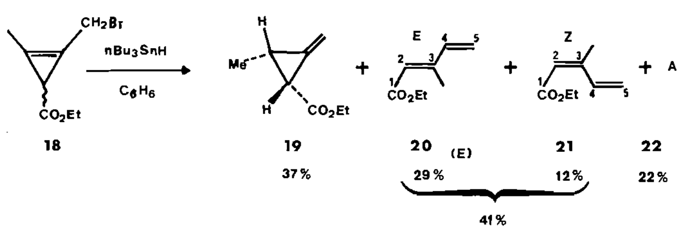

Traité dans les mêmes conditions expérimentales l'ester chloré cyclopropylidénique **6** conduit essentiellement aux composés **19**, **20** avec un rendement global de l'ordre de 50% et dans les proportions 1:3.

En l'absence de solvant, à 76°C, l'ester **6** fournit essentiellement des polymères.

L'ester **19** est identique en ir et rmn à un échantillon authentique (23, 24).

L'attribution des configurations *E* et *Z* est fondée sur l'effet anisotropique du carbonyle sur Me_3 dans **20** et sur H_4 dans **21**; le déblindage relatif de ces protons ne laisse subsister aucune incertitude quant à ces attributions. On observe en effet:

20	δ Me_3 = 2,26 ppm	**21** δ Me_3 = 1,95 ppm
	δ H_4 = 6,38 ppm	δ H_4 = 7,62 ppm

Discussion. Étude théorique

Le caractère radicalaire de la réaction de chloration des substrats cyclopropéniques par *t*-BuOCl est démontré par l'influence du galvinoxyle sur les vitesses de substitution allylique et de l'addition du chlore sur la double liaison. Le fait que la durée de la période d'induction de la chloration allylique soit supérieure à celle de l'addition sur la double liaison cyclopropénique ne peut s'interpréter que par une hypothèse analogue à celle de Walling relative aux alcynes (7) qui, compte-tenu du caractère acétylénique de la double liaison cyclopropénique n'est pas surprenante (25); notons cependant que l'attaque primaire de la double liaison peut non seulement être réalisée par *t*-BuOCl mais également par des traces de chlore moléculaire.

Addition du chlore:

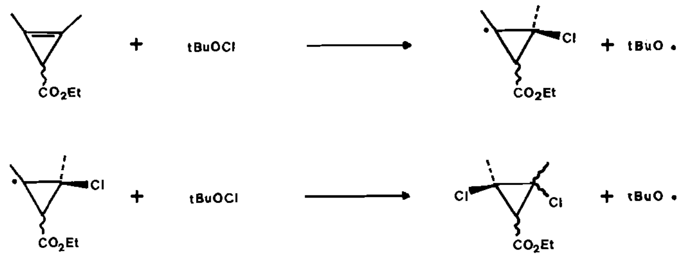

Chloration allylique:

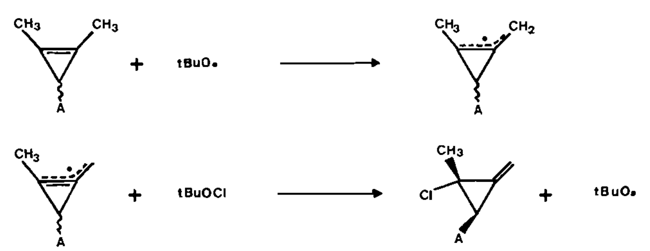

De même, comme nous l'avons vu, le caractère radicalaire de l'hydrogénolyse des liaisons C–halogène par les hydrures organostanniques est actuellement admis (réf. 3 et réf. citées). Comme précédemment la première étape de la réduction est la rupture d'une liaison allylique:

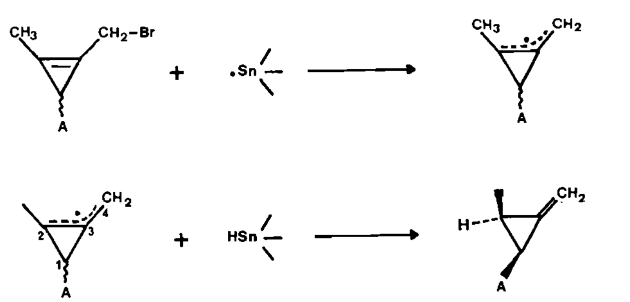

Qu'il s'agisse de la chloration par *t*-BuOCl ou de la réduction par Bu$_3$SnH des substrats cyclopropéniques, la première étape de la réaction conduit au radical (cyclopropène-1 yl)-1 alkyle (ou méthylènecyclopropyle). Ce radical peut subir une réaction d'ouverture ou arracher un atome de chlore (*t*-BuOCl) ou

TABLEAU 1. Géométries calculées pour les radicaux méthylènecyclopropyle (longueurs de liaisons en Å, angles en degrés). Les valeurs entre parenthèses sont celles obtenues par la méthode MNDO(HE)

Paramètres*	X = Y = H	X = Cl, Y = H	X = CH_3, Y = H	X = Y = CH_3
d_{12}	1,495 (1,491)	1,490 (1,488)	1,500 (1,496)	1,502 (1,499)
d_{23}	1,400 (1,393)	1,400 (1,398)	1,406 (1,398)	1,401 (1,393)
d_{34}	1,358 (1,341)	1,357 (1,337)	1,357 (1,337)	1,369 (1,360)
d_{25}	1,060 (1,060)	1,681 (1,678)	1,455 (1,453)	1,455 (1,453)
d_{46}	1,087 (1,088)	1,087 (1,088)	1,087 (1,088)	1,505 (1,507)
$\widehat{123}$	63,1 (63,4)	63,6 (63,7)	62,6 (62,8)	62,8 (63,0)
$\widehat{234}$	151,1 (151,1)	151,1 (150,7)	150,6 (150,4)	150,9 (150,9)
$\widehat{325}$	149,7 (149,6)	149,1 (149,0)	150,1 (149,9)	150,7 (150,6)

* La numérotation est celle de la fig. 1.

d'hydrogène ($HSnBu_3$); dans ce cas l'attaque est régiosélective puisque seul le carbone 2 du cycle fixera l'atome de chlore ou d'hydrogène. La réaction est par ailleurs hautement stéréosélective: le réactif approche toujours du côté le moins encombré du radical intermédiaire.

Deux types de structure peuvent être envisagés pour ce radical:

Soit une structure plane caractéristique d'un radical π de type allylique. La transposition cyclopropène → cyclopropylidène que nous avons observée au cours de la chloration et de la réduction de substrats cyclopropéniques, est en faveur d'une telle hypothèse.

Soit l'électron célibataire, dans cet intermédiaire, est localisé sur C_2; le radical est tétraédrique. Cette hypothèse est étayée par la régiosélectivité très élevée observée au cours de l'attaque des réactifs par ce radical d'une part et par la stéréochimie des produits de réduction des dibromo-1,1 méthylène-2 cyclopropanes (3).

L'étude théorique qui suit porte essentiellement sur la structure des radicaux méthylènecyclopropyle diversement substitués et sur la régiosélectivité de la réaction d'arrachement d'un atome d'hydrogène par ces radicaux.

Méthode

Compte-tenu de la complexité du problème à traiter – optimisation complète de géométrie pour l'étude de structure des radicaux et "taille" des supermolécules envisagées lors des réactions d'arrachement – nous avons choisi d'utiliser une méthode semi-empirique. Parmi celles-ci la méthode MNDO (26) permet de reproduire raisonnablement les géométries et les propriétés thermodynamiques des radicaux (27, 28); de plus, parmi les méthodes SCF semi-empiriques, cette méthode est généralement bien adaptée à l'étude des chemins réactionnels (29). Deux versions pour le traitement des systèmes à couches ouvertes ont été utilisées: MNDO "half-electron" (HE) (30) et MNDO "unrestricted" (UHF) (31). Les géométries ont été totalement optimisées en utilisant l'algorithme de Davidon–Fletcher–Powell (DFP) (32).

La localisation des états de transition a été conduite de la manière suivante (33): nous avons choisi comme variable indépendante R la distance $C_iH (i = 2,4)$ entre l'atome C_i du radical et l'atome d'hydrogène du substrat (voir fig. 4); cette distance traduit le degré d'avancement de la formation de la nouvelle liaison σ; nous avons utilisé la méthode dite de coordonnée de réaction afin d'obtenir une première localisation de l'état de transition; la structure ainsi déterminée a été utilisée comme point de départ pour la localisation définitive de l'état de transition à l'aide de la méthode décrite par McIver et Komornicki (34); la matrice des constantes de force a été calculée et nous avons vérifié qu'elle possédait une seule valeur propre négative.

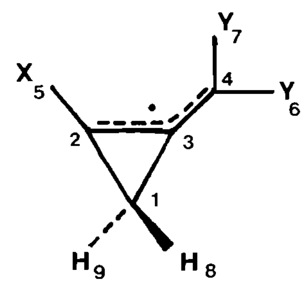

FIG. 1. Numérotation des atomes de radical méthylènecyclopropyle.

Géométries

Les principaux paramètres géométriques calculés pour les radicaux diversement substitués sont réunis dans le tableau 1; tous les radicaux sont trouvés plans (symétrie C_s); les géométries d'équilibre obtenues par les méthodes UHF et HE sont très voisines; on notera également que la présence de substituants en position 2 et 4 n'affecte que très faiblement les paramètres géométriques. Les résultats concernant les géométries d'équilibre sont en faveur d'une structure allylique: ces radicaux sont plans; les liaisons C_2—C_3 et C_3—C_4 sont intermédiaires entre une simple et une double liaison; en effet, les longueurs de ces liaisons calculées par la méthode MNDO sont comprises entre celles des hydrocarbures parents: à titre d'exemple, les liaisons C_2—C_3 et C_3—C_4 sont respectivement égales à 1,492 Å et 1,319 Å pour le méthylène-3 cyclopropane et à 1,332 Å et 1,461 Å pour le méthyl-3 cyclopropène; nous signalons que la géométrie d'équilibre calculée du méthylène-3 cyclopropane est en bon accord avec les données expérimentales (35).

On peut toutefois s'interroger sur l'aptitude de la méthode MNDO à rendre compte de l'angle de torsion α éventuel du centre radicalaire C_2. En effet, les calculs MNDO indiquent bien que les radicaux cyclopropyle (28), α-fluorocyclopropyle (α = 18,7°, déterminé dans ce travail), $\cdot CHF_2$ et $\cdot CF_3$ (27) sont pyramidaux et reproduisent correctement l'augmentation de la torsion lorsque l'on substitue les hydrogènes en α du centre

TABLEAU 2. Structure électronique et stabilité relative des radicaux méthylènecyclopropyle

Radicaux	ϵ_{SOMO} (eV)	Coefficient des OA dans la SOMO $C_{2\pi}$	$C_{4\pi}$	Indices de liaison π C_2—C_3	C_3—C_4	ΔH^* de formation (kcal mol^{-1})	Enthalpie de stabilisation* (kcal mol^{-1}) Réaction [1]	Réaction [2]
X = Y = H	−9,10	0,745	−0,639	0,611	0,778	71,0 (80,8)	—	—
X = CH_3, Y = H	−9,00	0,744	−0,594	0,565	0,806	55,7 (65,2)	8,1 (8,5)	0,7 (1,1)
X = Cl, Y = H	−9,25	0,728	−0,585	0,560	0,808	62,7 (71,9)	0,0 (0,6)	0,8 (1,3)
X = F, Y = H	−9,17	0,741	−0,576	0,536	0,818	23,4 (32,4)	2,5 (3,3)	1,8 (2,7)
X = Y = CH_3	−8,99	0,705	−0,638	0,636	0,733	38,5 (48,1)	8,4 (8,7)	11,7 (12,0)

* Les valeurs entre parenthèses sont celles obtenues par la méthode MNDO (HE).

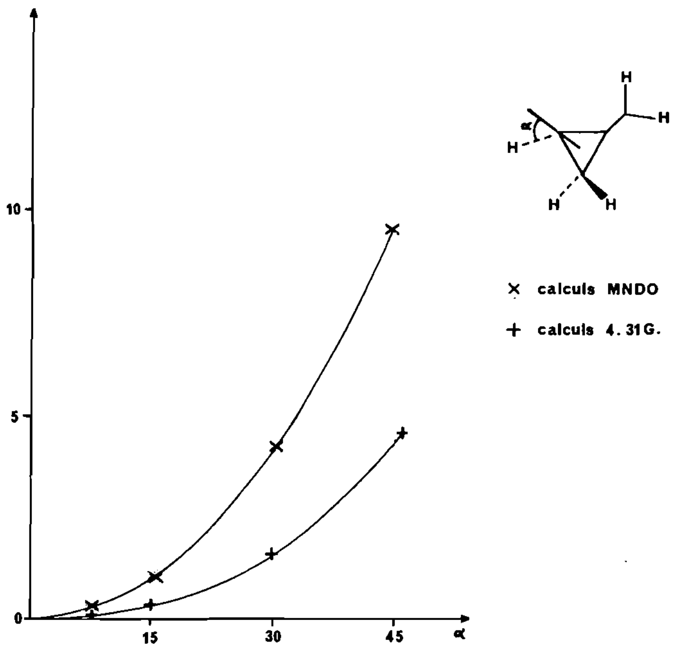

FIG. 2. Variation de l'énergie totale du radical méthylènecyclopropyle en fonction de l'angle de torsion α ($\Delta E = E_{(\alpha)} - E^0$; E^0: énergie totale du radical correspondant à α = 0°).

radicalaire par des fluors (36, 37). Cependant, les angles α ainsi obtenus semblent sous-estimés par rapport aux calculs *ab initio*: pour le cyclopropyle, α = 3° en MNDO (28) et α = 40° en *ab initio* (38); $\cdot CH_2F$, α = 0° en MNDO (27, 28) et α = 32° en *ab initio* (39). Il semble donc que la méthode sous-estime en règle générale la tendance à la pyramidalité du centre radicalaire.

Afin de mieux affiner l'analyse conformationnelle, nous avons calculé la variation de l'énergie en fonction de l'angle α (fig. 2) pour le radical méthylènecyclopropyle non substitué à l'aide des méthodes MNDO (HE) et *ab initio* (UHF) en base 4-31G: pour chaque valeur de l'angle α, nous avons fait une optimisation complète de géométrie par la méthode MNDO et les géométries obtenues ont servi à effectuer le calcul *ab initio* correspondant.

L'accord qualitatif est bon entre les deux calculs, toutefois – et ce résultat confirme notre analyse – la méthode MNDO surestime l'énergie de torsion et de ce fait, sous-estime l'angle de torsion. Le radical non substitué est donc trouvé plan aussi bien en MNDO qu'en *ab initio* au stade SCF, alors que le radical cyclopropyle est toujours trouvé pyramidal (28, 38). On peut donc s'attendre à ce que la géométrie du centre radicalaire dans les radicaux méthylènecyclopropyle diffère notablement de celle des radicaux cyclopropyles.

Structure électronique. Effet de substituant sur la stabilité des radicaux

Nous avons réuni dans le tableau 2 les principales données caractérisant la structure électronique des radicaux méthylènecyclopropyle.

L'orbitale simplement occupée a la symétrie du radical allyle; une analyse en termes d'orbitales frontières donne le centre C_2 comme étant le plus réactif ($|C_{2\pi}| > |C_{4\pi}|$); les indices de liaison π des liaisons C_2—C_3 et C_3—C_4 confirment la structure allylique de ces radicaux. Dans les deux dernières colonnes du tableau 2, nous avons fait figurer les variations d'enthalpie des réactions isodesmiques:

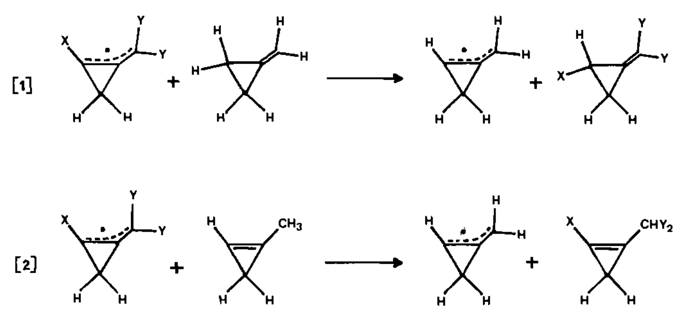

Une valeur positive de la variation d'enthalpie correspond à une stabilisation du radical substitué par rapport à l'hydrocarbure correspondant (40); la géométrie de ces derniers a été totalement optimisée par la méthode MNDO.[3]

Les variations d'enthalpie de la réaction [1] montrent: qu'un groupement méthyle en position 2 stabilise le radical; que la présence de deux substituants méthyle en position 4 n'a qu'un très faible effet sur la stabilité relative du radical.

Inversement, les variations d'enthalpie de la réaction [2] montrent que seuls les groupements méthyle en position 4 augmentent de manière sensible la stabilité relative du radical correspondant.

Ces résultats peuvent être rationalisés en termes d'interaction entre orbitales moléculaires (PMO analysis) (pour une revue, voir par exemple la réf. 41); les interactions entre orbitales frontières sont illustrées sur la figure 3; dans le cas du radical, compte-tenu de la symétrie de l'orbitale moléculaire simplement occupée (SOMO), les interactions stabilisantes ① et ②[4] sont possibles à la fois lorsque le groupement méthyle est

[3] Nous tenons à la diposition des personnes intéressées les géométries totalement optimisées des produits de substitution ainsi que celles des états de transition correspondants.

[4] Les interactions du type ① peuvent devenir déstabilisantes; le caractère déstabilisant apparaît lorsque le recouvrement intermoléculaire entre les O.M qui interagissent est introduit dans l'expression de l'énergie d'interaction (42).

en position 2 *et* en position 4; on peut prévoir que la stabilisation résultante sera plus importante lorsque le méthyle est en position 2 ($|C_{2\pi}| > |C_{4\pi}|$).

Pour les hydrocarbures correspondants, l'interaction ③ entrainera une stabilisation uniquement si le groupement méthyle est en position 2; de même l'interaction ④ ne sera importante que lorsque les groupements méthyles seront en position 4.

Ainsi les données thermodynamiques de la réaction [1] traduisent l'effet stabilisant du méthyle en position 2 (ΔH ~8 kcal mol^{-1}) qui existe pour le radical et non pour l'hydrocarbure correspondant alors que l'effet stabilisant des méthyles en position 4 n'apparaît pas car il intervient à la fois pour le radical et le dérivé méthylènecyclopropanique; de même les données thermodynamiques de la réaction [2] traduisent uniquement l'effet stabilisant des deux groupements méthyles en position 4; on notera également que l'énergie de stabilisation ramenée à *un* groupement méthyle est inférieure à celle calculée dans le cas de la réaction [1] car l'énergie d'interaction est inférieure lorsque le méthyle est substitué sur le sommet 4 ($|C_{4\pi}| < |C_{2\pi}|$).

La planéité des radicaux est apparemment en contradiction avec la très grande régiosélectivité observée dans les réactions d'arrachement d'hydrogène ou de chlore. Nous allons donc examiner dans le paragraphe suivant si malgré la planéité des radicaux, les calculs peuvent rendre compte de cette sélectivité.

Étude des réactions d'arrachement par les radicaux méthylènecyclopropyle

Les réactions élémentaires présentées dans ce paragraphe concernent uniquement l'arrachement d'un atome d'hydrogène du substrat;[5] la méthode MNDO n'étant pas paramétrisée pour l'étain, nous avons choisi comme substrat SiH_4 pour représenter $HSn(nBu)_3$.

Le formalisme MNDO a été employé par Dewar et coll. lors de l'étude d'arrachement par $\dot{C}H_3$ et $\dot{C}F_3$ d'un hydrogène de l'éthane (43) et de l'arrachement par CH_3 d'un hydrogène du méthane (note 22 de la référence 43); l'enthalpie d'activation calculée pour cette dernière réaction (28,6 kcal mol^{-1}) est supérieure à l'énergie d'activation expérimentale (14,2 kcal mol^{-1}) (44) mais comparable à celle obtenue à partir d'un calcul *ab initio* 4-31G (29,9 kcal mol^{-1}) (45); on retrouve cette tendance dans le récent travail de Pudzianowski et Loew (46): l'enthalpie d'activation correspondant à l'arrachement par l'oxygène atomique d'un atome d'hydrogène de CH_4 est de 27,4 kcal mol^{-1}, l'énergie expérimentale n'étant que de 8,4 kcal mol^{-1}. Pour compléter cette étude bibliographique, nous avons également testé la méthode MNDO sur le processus élémentaire: $\dot{C}H_3 + SiH_4 \rightarrow CH_4 + \dot{S}iH_3$; les calculs reproduisent correctement la plus grande réactivité de SiH_4 par rapport à CH_4 mais les barrières d'énergie calculées sont surestimées ($\Delta H^{\neq}$ calculé: 17,8 kcal mol^{-1}, énergie d'activation expérimentale (44): 6,9 kcal mol^{-1}).

Dans ce type de réaction où une liaison est rompue, une interaction de configuration est nécessaire ce qui explique que des calculs *ab initio* au niveau SCF surestiment l'énergie d'activation; dans le cas des méthodes semi-empiriques, une partie de l'énergie de correlation est introduite du fait de la paramétrisation et l'on aurait pu espérer un meilleur accord avec l'expérience; dans le cas de la méthode MNDO, la surestimation de l'enthalpie d'activation est attribuée (43, 46) à une surestimation des répulsions dans les interactions à trois électrons répartis sur trois centres.

[5] Une étude préliminaire de la réaction d'arrachement d'un atome de chlore (substrat modèle CH_3OCl) montre que celui-ci s'arrache plus facilement qu'un atome d'hydrogène; toutefois, nous nous sommes heurtés à des problèmes de convergence qui rendent les temps de calcul prohibitifs.

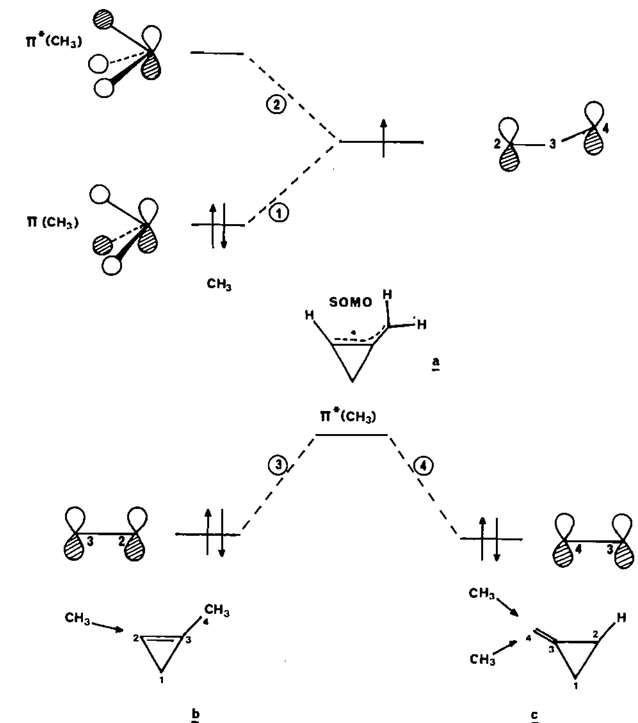

FIG. 3. Diagramme d'interaction représentant: l'interaction entre la SOMO du radical et les orbitales Π et Π* du groupement CH_3 (a); l'interaction entre la HOMO du méthyl-3 cyclopropène (b) ou la HOMO du méthylènecyclopropane (c) et l'orbitale vacante Π* (CH_3).

Le tableau 3 rassemble les valeurs des principaux paramètres géométriques calculés pour les états de transition (TS). La présence de substituants sur les centres réactifs C_2 et C_4 du radical n'entraîne que de très faibles modifications de la géométrie des états de transition.

Dans tous les cas, l'atome de carbone radicalaire, l'atome d'hydrogène (H_{10}) subissant l'arrachement et l'atome (numéroté 11) auquel il était lié dans le substrat restent alignés, le plan de symétrie du substrat bissectant les angles $\widehat{123}$ (fig. 4a) ou $\widehat{546}$ (fig. 4b); les géométries des substrats silylés ont été totalement optimisées au moyen de la méthode MNDO par Verwoerd (47).

Les états de transition apparaissent relativement tôt sur le chemin réactionnel, mais ils sont plus proches des réactants pour l'attaque en C_2(TS4a) que pour l'attaque en C_4(TS4b); notons également que la présence de méthyles sur les centres C_2 ou C_4 "retarde" l'état de transition: la liaison S_i—H(d_{10-11}) égale à 1,434 Å dans SiH_4 (47) est plus étirée lorsque l'attaque s'effectue sur le centre radicalaire C_4 et l'allongement de la liaison est plus important si les carbones 2(TS4a) ou 4(TS4b) portent un groupement méthyle; la liaison C_2—C_3 présente un allongement de ~0,05 Å (TS4a) tandis que la liaison C_3—C_4 s'allonge de ~0,07 Å (TS4b) par rapport aux liaisons correspondantes du radical (tableaux 1 et 3).

Les enthalpies d'activation sont réunies dans la dernière ligne du tableau 3; l'arrachement d'hydrogène se fait toujours à partir du centre C_2 du radical; la différence d'énergie d'activation entre les deux attaques, bien que surestimée, est

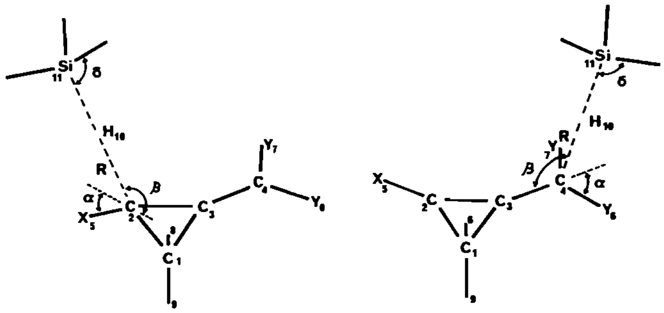

TS 4a TS 4b

FIG. 4. Numérotation des atomes et définition des paramètres géométriques utilisés pour décrire les états de transition.

suffisamment importante pour expliquer que le dérivé méthylènecyclopropanique soit le seul composé de substitution observé expérimentalement. La régiosélectivité de la réaction peut donc être expliquée sans qu'il soit nécessaire de postuler un radical pyramidal dont l'électron célibataire serait localisé en C_2.

Le radical chloré qui peut être considéré comme un modèle des radicaux étudiés par Bertrand et coll. (3) présente approximativement la même réactivité que le radical non substitué; par contre, l'effet stabilisant des substituants méthyles en C_2 ou en C_4 rend les radicaux correspondants beaucoup moins réactifs dans les réactions d'arrachement d'hydrogène et nos calculs prévoient la plus grande sélectivité pour le radical triméthylé qui peut être considéré comme un modèle des radicaux que nous avons étudiés. La réaction d'arrachement d'hydrogène par les radicaux méthylènecyclopropyle alkylés conduit à côté du dérivé méthylène cyclopropanique à des produits résultant de l'ouverture du radical; une étude complète du mécanisme de cette réaction devrait également envisager les problèmes relatifs à l'ouverture des radicaux et aux réactions d'arrachement par les radicaux non cycliques; de la compétition entre la réaction d'arrachement par le radical cyclique et l'ouverture de celui-ci va dépendre la nature des produits; notre travail permet cependant d'apporter un premier élément de réponse: le processus d'arrachement est défavorisé si le réactant est un radical cyclique alkylé en C_2 et en C_4, la régiosélectivité de la réaction étant conservée.

La polarité de l'état de transition n'est que très peu affectée par la présence de substituants sur le radical; notons toutefois que le chlore en α du centre radicalaire C_2 confère à celui-ci un faible caractère électrophile (SiH_4 porte une charge nette globale de $+0{,}013\ e^-$ dans l'état de transition, alors que la valeur correspondante pour le radical non substitué était de $-0{,}026\ e^-$).

Dans le tableau 4, nous avons rassemblé les grandeurs thermodynamiques calculées relatives au processus élémentaire d'arrachement d'un atome d'hydrogène du silane par les radicaux cycliques diversement substitués.

Si l'on admet que l'entropie d'activation varie peu dans la série envisagée, les variations de la réactivité d'un radical R· son données par: $\Delta E_i^{R} = \Delta H^{\neq}_{iR\cdot} - \Delta H^{\neq}_{i\,\text{référence}}$ (référence: radical cyclique non substitué; i: n° du centre radicalaire où s'effectue la réaction d'abstraction); les différences $\Delta(\Delta H_i) = \Delta H_{iR\cdot} - \Delta H_{i\,\text{référence}}$ traduisent les variations de l'énergie de la liaison C_i—H formée au cours de la réaction d'arrachement. Pour un substrat donné, la réactivité des radicaux varie comme $\Delta(\Delta H_i)$ (contrôle thermodynamique); de même la régiosélectivité de la

TABLEAU 3. Variation des principaux paramètres géométriques et des enthalpies d'activation des états de transition en fonction de la nature des substituants sur les centres radicalaires C_2 et C_4 (longueurs de liaison en Å, angles en degrés)

	Etat de transition 4a				Etat de transition 4b			
Paramètres*	X = Y = H	X = Cl, Y = H	X = Me, Y = H	X = Y = Me	X = Y = H	X = Cl, Y = H	X = Me, Y = H	X = Y = Me
R	1,630	1,625	1,605	1,600	1,550	1,520	1,530	1,495
d_{10-11}	1,501	1,501	1,514	1,515	1,523	1,536	1,534	1,568
d_{23}	1,439	1,450	1,450	1,448	1,347	1,346	1,351	1,345
d_{46}	1,089	1,090	1,089	1,508	1,093	1,094	1,094	1,522
d_{25}	1,071	1,721	1,476	1,476	1,062	1,686	1,459	1,453
α	31,7	37,8	32,0	31,7	26,9	28,2	28,0	29,8
β	115,9	115,3	109,8	109,7	106,0	105,9	106,1	99,1
δ	110,6	110,3	110,7	110,7	110,6	110,5	110,7	111,1
$\Delta H^{\neq}$ (kcal mol^{-1})	14,3	15,3	18,9	19,4	21,1	22,4	22,1	29,6

*Les paramètres géométriques sont définis dans la fig. 4.

TABLEAU 4. Données énergétiques relatives au diverses réactions d'arrachement d'un atome d'hydrogène par les radicaux méthylènecyclopropyle

Radicaux	ΔH_2*	ΔH_4†	Réactivité relative à SiH_4 ΔE_2^R	$\Delta(\Delta H_2)$	ΔE_4^R	$\Delta(\Delta H_4)$	Régiosélectivité ΔE^S	$\Delta H_2 - \Delta H_4$	Energie de déformation E_2^D	E_4^D
X = Y = H	−16,3	−0,4	0	0	0	0	−6,8	−15,9	$5{,}6_5$	9,0
X = Cl, Y = H	−15,6	1,0	1,0	0,7	1,3	1,4	−7,1	−16,6	$6{,}3_5$	10,6
X = CH_3, Y = H	−7,8	$0{,}7_5$	4,6	8,5	1,0	1,15	−3,2	−7,0	7,8	10,5
X = Y = CH_3	−7,6	11,6	5,1	8,7	8,5	8,5	10,2	−19,2	8,7	14,9

*Variation d'enthalpie calculée (kcal mol^{-1}) pour la réaction:

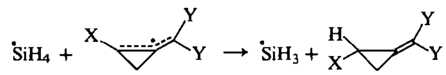

†Variation d'enthalpie calculée (kcal mol^{-1}) pour la réaction:

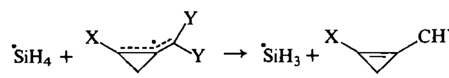

réaction $\Delta E^S = \Delta H_2^{\ddagger} - \Delta H_4^{\ddagger}$ est parfaitement corrélée par la différence des variations d'enthalpie $\Delta H_2 - \Delta H_4$. On peut vérifier également que l'état de transition apparaît d'autant plus tard sur le chemin réactionnel que la réaction d'arrachement est endothermique. Nos résultats sont en accord avec les règles énoncées par Tedder (48).

Une étude portant sur la pyramidalisation du centre C_4 (analogue à celle effectuée sur la torsion de la liaison C_2—H) dans le radical non substitué montre que la torsion des liaisons C_4—H d'un angle α correspondant au TS4b nécessite plus d'énergie que la torsion de la liaison C_2—H d'un même angle α dans le TS4a; la comparaison des énergies de déformation des réactants dans l'état de transition:

$$E_i^D = \Sigma E_{\text{réactants}}^{\text{TS}(i)} - \Sigma E_{\text{réactants}}^0$$

$E_{\text{réactants}}^{\text{TS}(i)}$: énergie de chaque réactant dans sa géométrie à l'état de transition; $E_{\text{réactants}}^0$: énergie de chaque réactant dans sa géométrie complètement optimisée) montre que celles-ci interviennent pour plus de 50% dans la différence des enthalpies d'activation $\Delta H_2^{\ddagger} - \Delta H_4^{\ddagger}$; ces différences traduisent à la fois la plus grande énergie nécessaire pour pyramidaliser le centre C_4 et l'apparition plus tardive sur le chemin réactionnel des TS de type 4b.

Conclusion

Cette étude de la chloration allylique des substrats cyclopropéniques et de la réduction de leurs dérivés bromés a permis de mettre en évidence sur le plan expérimental la migration exocyclique de la double liaison. Cette transposition s'interprète par la formation intermédiaire d'un radical plan de type allylique, l'électron célibataire étant essentiellement localisé sur les atomes C_2 et C_4.

L'étude théorique de la réactivité de ce radical montre que cette espèce se stabilise par fixation d'un atome sur le carbone C_2 quelle que soit la nature des substituants portés par le système allylique; ce résultat est en bon accord avec la régiosélectivité observée expérimentalement. Par ailleurs, la réaction d'arrachement se fait plus facilement lorsque l'on substitue en C_2 un méthyle par un atome de chlore.

Au terme de cette étude il nous apparaît que la méthode MNDO peut fournir un bon point de départ pour l'étude qualitative des réactions d'arrachement d'hydrogène d'un substrat donné par une série de radicaux. Elle permet entre autres de retrouver les règles proposées par Tedder.

1. M. VIDAL, A. DUSSAUCE et M. VINCENS. Tetrahedron Lett. 313 (1977).
2. R. ARNAUD, A. DUSSAUGE, H. FAUCHER, R. SUBRA, M. VIDAL et M. VINCENS. Tetrahedron, **40**, 315 (1984).
3. G. LEANDRI, H. MONTI et M. BERTRAND. Tetrahedron, **30**, 283 (1974).
4. J. R. KARTASHOV, V. P. PUSHKAREV et I. V. BODRIKOV. Zh. Org. Khim. **8**, 24 (1972).
5. V. R. KARTASHOV, V. P. PUSHKAREV, I. V. BODRIKOV et K. N. TISHKOV. Zh. Org. Khim. **7**, 1570 (1971).
6. C. WALLING et B. B. JACKNOW. J. Am. Chem. Soc. **82**, 6108 (1960).
7. C. WALLING et W. THALER. J. Am. Chem. Soc. **83**, 3877 (1961).
8. C. WALLING, L. HEATON et D. D. TANNER. J. Am. Chem. Soc. **87**, 1714 (1965).
9. M. VINCENS, S. CHOUBANI et M. VIDAL. Tetrahedron Lett. **22**, 4695 (1981).
10. H. G. KUIVILA. Acc. Chem. Res. **1**, 299 (1968).
11. H. G. KUIVILA. Synthesis, **10**, 499 (1970).
12. D. SEYFERTH, H. YAMAZAKI et D. L. ALLESTON. J. Org. Chem. **28**, 703 (1963).
13. D. H. LORENZ, P. SHAPIRO, A. STERN et E. I. BECKER. J. Org. Chem. **28**, 2332 (1963).
14. E. WIBERG et E. AMBERGER. Hydrides. Elsevier Publishing Company, New York. 1971. pp. 719–756.
15. J. K. CRANDALL et D. J. KEYTON. Tetrahedron Lett. **21**, 1653 (1969).
16. C. DESCOINS, M. JULIA et H. VAN SANG. Bull. Soc. Chim. Fr. 4087 (1971).
17. L. J. ALTMAN et T. R. ERDMAN. Tetrahedron Lett. 4891 (1970).
18. L. J. ALTMAN et B. W. NELSON. J. Am. Chem. Soc. **91**, 5163 (1969).
19. M. VIDAL, M. VINCENS et P. ARNAUD. Bull. Soc. Chim. Fr. 657 (1972).
20. M. VINCENS, C. DUMONT, M. VIDAL et I. DOMNIN. Tetrahedron, **39**, 4281 (1983).
21. M. VINCENS, C. DUMONT et M. VIDAL. Tetrahedron, **37**, 2683 (1981).
22. M. VINCENS, A. DUSSAUGE et M. VIDAL. Tetrahedron, **33**, 2937 (1977).
23. M. VIDAL, M. VINCENS et P. ARNAUD. Bull. Soc. Chim. Fr. 665 (1972).
24. J. L. PIERRE, M. VIDAL et P. ARNAUD. Bull. Soc. Chim. Fr. 1544 (1970).
25. G. L. CLOSS. Advances in alicyclic chemistry. Academic Press, New York. 1966.
26. M. J. S. DEWAR et W. THIEL. J. Am. Chem. Soc. **99**, 4899 (1977).
27. L. M. MOLINO, J. M. POBLET et E. CANADELL. J. Chem. Soc. Perkin Trans. 2, 1217 (1982).

28. P. BISCHOF et G. FRIEDRICH. J. Comput. Chem. **3**, 486 (1982).
29. M. J. S. DEWAR. Further perspectives in organic chemistry. Ciba Foundation Symposium 53. Elsevier, Amsterdam. 1978. p. 102.
30. (*a*) M. J. S. DEWAR, J. A. MASHMALL et G. VERIER. J. Am. Chem. Soc. **90**, 1953 (1968); (*b*) M. J. S. DEWAR et N. TRINAJSTIC. Chem. Commun. 646 (1970).
31. J. A. POPLE et R. K. NESBET. J. Chem. Phys. **22**, 571 (1954).
32. R. FLETCHER et M. J. D. POWELL. Comput. J. **6**, 163 (1963); W. C. DAVIDON. Comput. J. **10**, 406 (1968).
33. (*a*) P. BISCHOF. Computational methods in chemistry. *Édité par* J. Bargon. Plenum Press, New York. 1979. p. 133; (*b*) J. M. LLUCH et J. BERTRAN. J. Chem. Soc. Perkin Trans. 2, 1419 (1982).
34. W. MCIVER et A. KOMORNICKI. J. Am. Chem. Soc. **94**, 2625 (1972).
35. F. H. ALLEN. Tetrahedron, **38**, 645 (1982).
36. R. W. FESSENDEN. J. Phys. Chem. **71**, 74 (1967).
37. V. BARONE, F. LELJ, N. RUSSO, Y. ELLINGER et R. SUBRA. Chem. Phys. **76**, 385 (1983).
38. Y. ELLINGER, R. SUBRA, B. LEVY, P. MILLIE et G. BERTHIER. J. Chem. Phys. **62**, 10 (1975).
39. G. LEROY, D. PEETERS, C. WILANTE et M. KHALIL. Nouv. J. Chim. **4**, 403 (1980).
40. W. J. HEHRE, R. DICHFIELD, L. RADOM et J. A. POPLE. J. Am. Chem. Soc. **92**, 4796 (1970).
41. N. D. EPIOTIS, W. R. CHERRY, S. SHAIK, R. L. YATES et F. BERNADI. Top. Curr. Chem. 70 (1977).
42. F. BERNARDI, N. D. EPIOTIS, W. R. CHERRY, H. B. SCHLEGEL, M. H. WHANGBO et S. WOLFE. J. Am. Chem. Soc. **98**, 469 (1976); F. BERNARDI, W. R. CHERRY, S. SHAIK et N. D. EPIOTIS. J. Am. Chem. Soc. **100**, 1352 (1978).
43. S. B. BROWN, M. J. S. DEWAR, G. P. FORD, D. J. NELSON et H. S. RZEPA. J. Am. Chem. Soc. **100**, 7832 (1978).
44. J. M. TEDDER. Tetrahedron, **38**, 313 (1982).
45. M. T. RAYEZ-MEAUME, J. J. DANNENBERG et J. L. WHITEN. J. Am. Chem. Soc. **100**, 747 (1978).
46. A. T. PUDZIANOWSKI et G. H. LOEW. J. Phys. Chem. **87**, 1081 (1983).
47. W. S. VERWOERD. J. Comput. Chem. **3**, 445 (1982).
48. J. M. TEDDER. Angew. Chem. Int. Ed. Engl. **21**, 401 (1982).

Déplacements homolytiques intramoléculaires. 4. Thermolyse du perpentène-4 oate de *tert*-butyle dans les acides et leurs derivés: préparation de γ-butyrolactones substituées en 4 par un groupe comportant une fonction ester, acide ou nitrile

A. Kharrat

Laboratoire de chimie appliquée, Université de Bordeaux I, 351, cours de la Libération, 33405 Talence-Cédex, France

C. Gardrat

Laboratoire de chimie appliquée, Université de Bordeaux I, 351, cours de la Libération, 33405 Talence-Cédex, France

et

École nationale supérieure de chimie et de physique de Bordeaux, 351, cours de la Libération, 33405 Talence-Cédex, France

ET

B. Maillard[1]

Laboratoire de chimie appliquée, Université de Bordeaux I, 351, cours de la Libération, 33405 Talence-Cédex, France

et

Laboratoire de chimie organique des composés du silicium et de l'étain, Université de Bordeaux I, 351, cours de la Libération, 33405 Talence-Cédex, France

Reçu le 7 novembre 1984

A. Kharrat, C. Gardrat et B. Maillard. Can. J. Chem. **63**, 2522 (1985).

La thermolyse du perpentène-4 oate de *tert*-butyle **1** a été effectuée dans divers solvants ZH (acides carboxyliques, anhydrides, esters de méthyle et nitriles). Dans tous les cas, des γ-butyrolactones substituées sur le carbone 4 par le groupe ZCH_2 sont isolées, la plupart du temps avec des rendements acceptables. L'isomérisation totale des lactones **4** dérivant des acides non fonctionnels en **5** a été réalisée facilement par chauffage d'une solution tétrahydrofurannique de **4** en présence de traces d'APTS; des résultats similaires sont enregistrés à partir de solutions méthanoliques des esters lactones (**6** → **7**) en présence de traces d'APTS.

A. Kharrat, C. Gardrat, and B. Maillard. Can. J. Chem. **63**, 2522 (1985).

The thermolysis of *tert*-butylperpent-4-enoate in various solvents ZH (carboxylic acids, anhydrides, methyl esters, nitriles) led to γ-butyrolactones 4-substituted by the group ZCH_2 with good yields. The acidic treatment of the lactones **4** and **6** derived from non-functionalized alkanoic acids and methyl esters gave respectively the isomerized lactones **5** and **7**, increasing the synthetic interest of the studied homolytic reaction.

Introduction

Lors de l'étude de la thermolyse du perpentène-4 oate de *tert*-butyle **1** dans le cyclohexane (1) nous avons mis en évidence la présence du cyclohexyl-5 pentanolide-4 issu de la décomposition induite du perester insaturé par un radical cyclohexyle. La formation de la lactone se fait par une réaction en chaîne dont la phase de propagation se résume aux étapes suivantes:

[1] $Z^{\cdot} + CH_2{=}CH{-}(CH_2)_2{-}CO_3tBu$

1

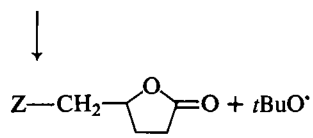

[2] $tBuO^{\cdot} + ZH \longrightarrow tBuOH + Z^{\cdot}$

avec ZH = $c\text{-}C_6H_{12}$.

Nous avons par la suite montré que ce type de réaction n'est pas particulier aux cas des cyclanes puisqu'il intervient dans les cétones (2) et les éthers (3) permettant d'accéder facilement à des γ-butyrolactones substituées en 4 par des groupes comportant des fonctions.

Les acides et leurs dérivés sont des produits qui donnent lieu à des additions radicalaires aux composés insaturés, comme le rapporte Vogel dans une mise au point ancienne (4). Dans ces conditions la thermolyse de **1** dans un acide alcanoïque ou son substitut R^1R^2CHCOY pourrait permettre d'accéder aux olides de formule générique **2**.

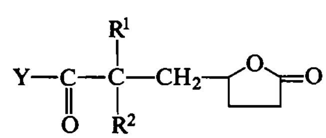

2

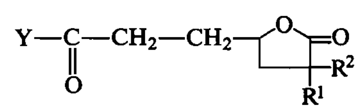

3

Une des voies d'accès les plus simples aux γ-butyrolactones consiste en l'estérification intramoléculaire d'un γ-hydroxyacide (5). Pour obtenir des lactones **4** (**2**, Y = OH) par cette voie, il faut partir d'un γ-hydroxydiacide.

Si au moins un des substituants R^1 ou R^2 n'est pas un atome d'hydrogène, une telle synthèse peut conduire a priori à deux lactones distinctes **4** (**2**, Y = OH) et **5** (**3**, Y = OH).

A notre connaissance aucune étude de ce type n'ayant été signalée dans la littérature, nous avons décidé d'effectuer la thermolyse de **1** dans les acides alcanoïques et leurs dérivés en vue de préparer sélectivement les composés **2** et de rechercher des conditions d'isomérisation de ces derniers en **3**.

Dans une première partie, après avoir défini les conditions optimales de réaction en prenant le propionate de méthyle comme composé modèle, nous avons étendu ce travail à

[1] Auteur à qui adresser toute correspondance.

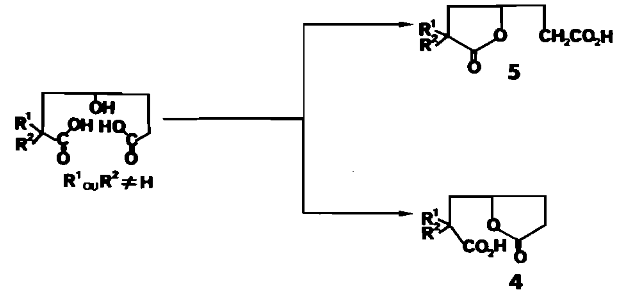

FIG. 1

d'autres esters, acides, anhydrides, amides ainsi qu'à des nitriles.[2]

Dans une deuxième partie, après avoir effectué l'étude de la lactonisation acide d'un hydroxy-4 diacide-1,7 nous avons essayé de réaliser l'isomérisation acido-catalysée de certaines γ-lactones **2** afin de voir si cela pouvait constituer une voie d'accès générale aux composés de type **3**.

Thermolyse de 1 dans les acides et leurs derivés

I. *Esters*

1. *Alcanoates de méthyle*

Les esters ont souvent été utilisés à la place des acides pour réaliser l'alkylation radicalaire de ces derniers lorsqu'il se forme des produits secondaires par réaction des acides avec les composés insaturés. Notre choix de réaliser l'étude avec les esters avant de l'entreprendre avec les acides a été dicté par une raison similaire: il semblait a priori moins facile d'avoir une isomérisation de la lactone **6** (**2**, Y = OMe) en **7** (**3**, Y = OMe) que de **4** (**2**, Y = OH) en **5** (**3**, Y = OH).[3]

Le remplacement de l'acide par un ester présente toutefois l'inconvénient d'introduire un site réactif supplémentaire: le carbone en α de l'oxygène; néanmoins, l'emploi d'un ester de méthyle limite considérablement l'attaque de la partie alcoxyle. Bien que l'acétate de méthyle soit le premier membre de la famille des esters $R^1R^2CHCO_2Me$, nous avons préféré effectuer les études préliminaires avec le propionate de méthyle afin de voir si une isomérisation de **6***b*[4] en **7***b* intervenait (dans le cas de l'acétate de méthyle, les deux formules **6***a*[4] et **7***a* correspondent au même produit).

Un essai de thermolyse de **1** dans le propionate de méthyle montre que le composé recherché **6***b* se forme. Afin de définir les conditions optimales de la réaction, nous avons effectué une étude de la décomposition de **1** dans cet ester en faisant varier la température de thermolyse, la durée et les rapports molaires.

Comme le montre le tableau 1, les conditions pour lesquelles le rendement en **6***b* est le plus élevé correspondent à un chauffage à 110°C pendant 8 h en utilisant un rapport molaire **1**/ester = 1:100.

L'étude de la thermolyse de **1** a été réalisée dans l'acétate de méthyle, le propionate de méthyle et l'isobutyrate de méthyle, ces esters possédant les différents types d'hydrogène pouvant être arrachés pour conduire à des radicaux en α du carbonyle.

[2] Les nitriles sont généralement considérés comme des dérivés d'acides. C'est pourquoi nous avons placé leur étude dans le cadre de ce travail bien qu'ils ne conduisent pas à des composés de type **2**.

[3] Les acides sont souvent transformés en esters de méthyle avant d'être analysés par cpg: cette considération a constitué un argument supplémentaire dans le choix des esters comme premiers modèles.

[4] *a*: $R^1 = R^2 = H$; *b*: $R^1 = H$, $R^2 = CH_3$; *c*: $R^1 = R^2 = CH_3$.

TABLEAU 1. Variation des rendements en **6***b* en fonction des conditions expérimentales

Rapport molaire **1**/$CH_3CH_2CO_2CH_3$	Rendement en **6***b* (%)*		
	2 h à 130°C	4 h à 120°C	8 h à 110°C
1:5	11	12	16
1:10	16	24	31
1:20	31	32	42
1:50	29	39	44
1:100	43	37	58

*Calculé par rapport au perester mis en jeu et déterminé par cpg.

Dans les deux derniers cas, les deux produits de substitution **6** (sur la partie acyle) et **8** (sur la partie méthoxyle) sont observés; les produits **6** ont toutefois été isolés facilement par chromatographie liquide–solide sur gel de silice permettant de préserver l'intérêt synthétique de la méthode.

A ces trois modèles, nous avons ajouté le cas particulier du formiate de méthyle dont l'addition radicalaire à un alcène permet d'effectuer une extension de chaîne d'un carbone (4).

Les différents composés décrits dans le tableau 2 ont été identifiés par rmn ainsi que par spectrométrie de masse. Les produits de référence **8** ont été synthétisés à partir de l'hydroxylactone correspondante **10**. Cette dernière a été obtenue à partir de la lactone ester préparée selon la réf. 6.

[3] $BrCH_2CO_2Et + CH_2{=}CH{-}(CH_2)_2OAc \xrightarrow[\text{benzoyle, 80°C}]{\text{peroxyde de}}$

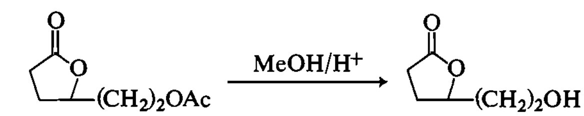

8*a* **10**

Dans le cas de la thermolyse de **1** dans l'acétate de méthyle, nous n'avons pas réussi à séparer les deux produits possibles de substitution **6***a* et **8***a*. Une estimation des proportions relatives de ces deux composés n'a également pas pu être faite bien qu'un essai de transformation du produit réactionnel par transestérification à l'aide du méthanol en présence de traces d'APTS ait été réalisé: **8***a* devrait conduire à **10** et **6***a* ne devrait pas être affecté. Si **8***a* se forme, sa proportion relative est très faible.

Comme cela avait été signalé dans le cas particulier de l'acétonylation de l'acétate de méthyle (7), nous observons une variation des proportions relatives de **6** et **8** pour les propionate et isobutyrate de méthyle selon les rapports molaires **1**/ester utilisés (Tableau 3).

Ces résultats s'accordent fort bien avec ceux des travaux antérieurs (8) indiquant que l'attaque sur les esters par les radicaux électrophiles se fait de préférence sur le groupe alcoxyle. La compétition entre la réaction [4] et la réaction d'addition à la double liaison du perester serait responsable des résultats enregistrés.

$$[4] \quad \underset{\mathbf{A}}{R^1R^2CHCO_2\dot{C}H_2} + R^1R^2CHCO_2CH_3 \longrightarrow R^1R^2CHCO_2CH_3 + \underset{\mathbf{B}}{R^1R^2\dot{C}CO_2CH_3}$$

L'existence de rendements très éloignés de 100% montre qu'il est vain de comparer entre eux les résultats obtenus pour les deux esters. Dans le cas de l'isobutyrate de méthyle, la mise

TABLEAU 2. Lactones isolées par thermolyse de **1** dans divers alcanoates de méthyle (conditions expérimentales: **1**/ester = 1 : 100; 8 h à 110°C)

Ester	$CH_3CO_2CH_3$	$CH_3CH_2CO_2CH_3$	$(CH_3)_2CHCO_2CH_3$	HCO_2CH_3
Produits	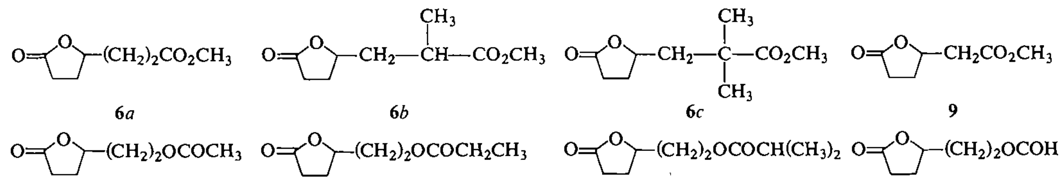 6*a*, 8*a*	6*b*, 8*b*	6*c*, 8*c*	9, 8*d*
% relatifs **6** ou **9**/**8**	*	96:4	91:9	100:0
Rdt (%)†	50	55	18	12

* Voir la discussion dans le texte.
† Déterminé sur la fraction de distillation par rapport au perester **1** mis en jeu dans la réaction.

TABLEAU 3. Variation des proportions relatives **6**/**8** en fonction des rapports molaires **1**/ester (propionate (*b*) et isobutyrate (*c*) de méthyle)* (conditions expérimentales: 8 h à 110°C)

Rapport molaire **1**/ester	1:5	1:20	1:100	1:200
6*b*/**8***b*	92:8	94:6	96:4	100:0
6*c*/**8***c*	63:37	68:32	91:9	100:0

* Dosage effectué par cpg.

en évidence de quantités non négligeables de tétraméthyl-2,2,3,3 succinate de diméthyle montre que l'addition du radical B s'effectue difficilement.

2. *Esters fonctionnels*

De nombreux esters fonctionnels (malonates, cyanoacétates, chloroacétates, acétylacétates, ω-diesters...) ont pu être substitués en α du carbonyle grâce aux réactions d'additions radicalaires (4). Nous avons effectué la thermolyse de **1** dans un ester de chacune de ces familles et avons isolé le produit de "pentanolidation". Les résultats obtenus sont rassemblés dans le tableau 4.

II. *Acides et anhydrides*

La thermolyse de **1** dans les acides et les anhydrides a été effectuée dans des conditions identiques à celles des esters (110°C, 8 h, rapport molaire **1**/solvant = 1 : 100). Elles ne sont peut-être pas optimales pour les acides et les anhydrides mais elles présentent l'avantage de permettre une comparaison des résultats obtenus à ceux des esters. La "pentanolidation" des acides acétique, propionique et isobutyrique s'effectue avec des rendements respectifs de 47%, 56% et 22%. Seuls les composés **4***a*, **4***b* et **4***c* sont obtenus. En effet, après méthylation au diazométhane, seuls **6***a*, **6***b* et **6***c* sont identifiés par comparaison en cpg à des échantillons de **6***a* (≡ **7***a*), **6***b* et **7***b*, **6***c* et **7***c*.

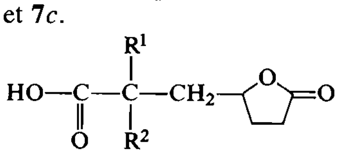

4

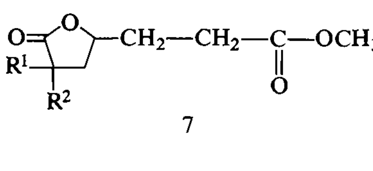

7

a $R^1 = R^2 = H$
b $R^1 = H$ $R^2 = CH_3$
c $R^1 = R^2 = CH_3$

Nous soulignerons que les rendements de fonctionnalisation des acides sont voisins de ceux des esters correspondants. En conséquence la thermolyse de **1** dans les monoesters de méthyle ne peut constituer la meilleure voie d'accès aux composés **6***a*, **6***b*, **6***c* puisque la méthylation au diazométhane des acides **4***a*, **4***b*, **4***c* (réaction quasi quantitative) permet d'accéder plus facilement aux composés recherchés et avec un meilleur rendement (dans le cas des esters une séparation des composés de type **6** et **8** est nécessaire). Cependant, dans le cas des esters fonctionnels correspondant à des acides instables dans les conditions de la réaction (acide acétylacétique, acide malonique) la "pentanolidation" de l'ester s'avère la meilleure voie d'autant qu'elle ne conduit qu'à un seul produit.

Remarque: Comme nous l'avons signalé dans le paragraphe précédent, l'addition radicalaire d'esters à des alcènes conduit généralement à des produits de substitution des deux carbones situés de part et d'autre du carbonyle, ce qui limite souvent l'intérêt synthétique de la méthode au cas des esters de méthyle. Les acides lactoniques **4** peuvent être le point de départ des composés de type **2** (Y étant un groupe alkyle quelconque); nous avons voulu voir si, en milieu non acide, il était possible de les estérifier sans isomérisation. La réactivité des azolides mise en évidence par Staab (9) a permis de préparer des esters en milieu neutre. Le traitement de l'acide lactonique **4***b* par le *N,N'*-carbonyldiimidazole permet d'obtenir l'azolide qui, par réaction sur le méthanol, conduit uniquement à **6***b*.

La thermolyse de **1** a été effectuée dans les anhydrides acétique et propionique (110°C, 8 h, **1**/anhydride = 1 : 100). Après hydrolyse du mélange réactionnel, les acides **4***a* et **4***b* sont isolés avec des rendements de l'ordre de 20%.

III. *Amides et nitriles*

La thermolyse de **1** dans le diméthylformamide et le diméthylacétamide (110°C, 8 h, **1**/amide = 1 : 100) n'a pas permis d'isoler la γ-butyrolactone fonctionnelle recherchée. Par contre, les réactions effectuées dans les mêmes conditions avec l'acétonitrile et le propionitrile ont conduit aux produits attendus **11***a* et **11***b* avec des rendements respectifs de 17% et 24%; avec l'isobutyronitrile, le tétraméthyl-2,2,3,3 succinodinitrile résultant du couplage des radicaux cyano-2 propyle-2 est le principal produit de la réaction comme lors des tentatives d'additions radicalaires de ce composé (10).

Isomérisation des lactones 4 et 6

Afin de situer notre méthode de préparation des lactones **4**

TABLEAU 4. Lactones isolées par thermolyse de **1** dans divers esters fonctionnels (conditions expérimentales **1**/ester = 1:100; 8 h à 110°C)

Ester	$CH_2(CO_2CH_3)_2$	$ClCH_2CO_2CH_3$	$CH_3COCH_2CO_2CH_3$	$(CH_2CO_2CH_3)_2$	$NCCH_2CO_2CH_3$
Produit	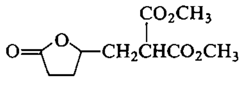 *6e*	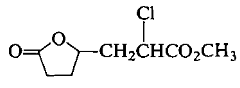 *6f*	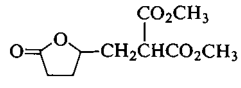 *6g*	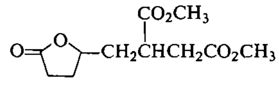 *6h*	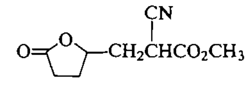 *6i*
Rdt (%)*	27	64	35	69	40

* Déterminé sur la fraction de distillation par rapport au perester **1** mis en jeu dans la réaction.

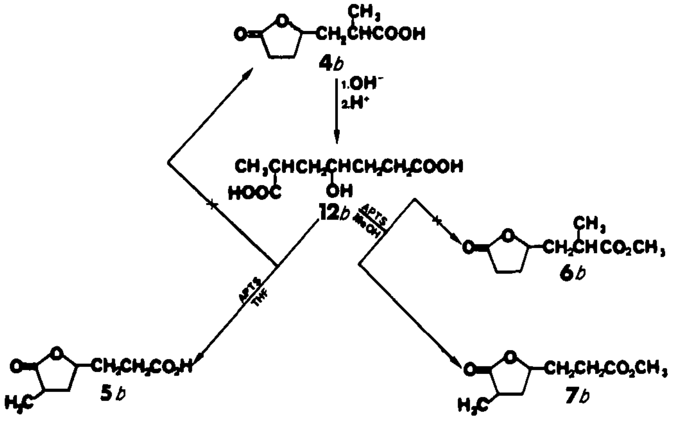

FIG. 2

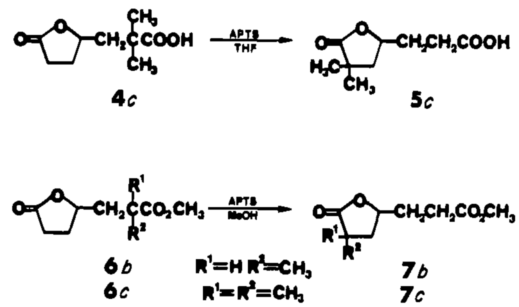

FIG. 3

relativement à la lactonisation acide à partir des hydroxydiacides, nous avons réalisé la saponification de la lactone **4***b* et isolé l'hydroxydiacide correspondant. Son traitement par l'APTS en solution dans le THF conduit à la lactone acide **5***b* isomère de **4***b*. La même réaction effectuée dans le méthanol conduit à **7***b* isomère de **6***b* (fig. 2).

Ces résultats montrent que la thermolyse de **1** dans un acide ou son ester de méthyle permet d'accéder facilement à **4** ou **6** ce qui n'est pas le cas pour la lactonisation de l'hydroxydiacide.

Il paraissait intéressant de confirmer les résultats obtenus à partir de **4***b* avec **4***c* et de voir si une isomérisation des esters **6** en composés **7** pouvait être réalisée en présence de traces d'acide dans le méthanol (fig. 3).

Le traitement de l'acide lactonique **4***c* par l'APTS dans le THF au reflux permet d'obtenir facilement l'isomère **5***c*. Les lactones **6** dérivant des monoesters conduisent à **7** (**6***b* et **6***c* donnent **7***b* et **7***c*, **6***a* et **7***a* correspondent au même composé) après un reflux de 3 h en solution méthanolique en présence de traces d'APTS.

Les composés **6***e*, **6***f*, **6***i* ne sont pas affectés même après un chauffage de 48 h. Le produit de "pentanolidation" de l'acétylacétate de méthyle **6***g* se transforme en d'autres produits que la lactone **7***g* (R^1 = H, R^2 = $COCH_3$) vraisemblablement par suite de réactions secondaires dues à la présence du carbonyle sur la chaîne latérale. La lactone **6***h* est totalement isomérisée en une autre lactone mais l'attribution de la structure de cette dernière n'a pas pu être effectuée.

Il est à noter que la thermolyse de **1** (perester brut qui contient des traces d'acide chlorhydrique) dans les monoesters et les acides conduit à un mélange de **6** et **7** ou de **4** et **5**; il est donc important que le perester soit purifié avant utilisation. La décomposition de **1** dans l'acide propionique et le propionate de méthyle en présence de faibles quantités d'APTS (2% molaire par rapport à **1**) permet d'obtenir **5***b* ou **7***b* avec des rendements équivalents à ceux obtenus sans acide pour **4***b* et **6***b*.

Conclusion

Nous retiendrons de ce travail l'intérêt synthétique de la méthode de "pentanolidation" des acides, esters de méthyle et nitriles. Dans le cas des acides et des esters de méthyle, c'est une excellente voie de préparation des lactones acides **4** et des lactones esters **6** puisque les essais de lactonisation par l'APTS de l'hydroxydiacide ont conduit uniquement aux lactones isomères **5** et **7**. La mise en évidence d'une isomérisation acidocatalysée de **4** en **5** et de **6** en **7** renforce l'aspect préparatif de la décomposition induite du perpentène-4 oate de *tert*-butyle par les radicaux dérivant des acides et des esters.

Partie expérimentale[5]

Les spectres rmn du proton ont été enregistrés sur un appareil Perkin–Elmer R 12B opérant à 60 MHz à partir de solutions à 10% dans le tétrachlorure de carbone ou le DMSO-d_6 (déplacements chimiques en δ ppm par rapport au TMS).

Les spectres rmn du ^{13}C ont été enregistrés sur un appareil Bruker WP 60 fonctionnant à 15,08 MHz équipé d'un calculateur Nicolet BNC 12 (déplacements chimiques en δ ppm par rapport au TMS) à partir de solutions dans le chloroforme deutéré.

Les spectres de masse ont été obtenus, en général, par couplage masse–cpg, sur des appareils Micromass 16 F et 70-70 sous impact électronique (70 eV). Nous n'indiquons que les pics dont l'abondance relative dépasse 10%.

L'analyse des produits par chromatographie en phase gazeuse (cpg) a été réalisée sur un appareil Intersmat IGC 112 F (ionisation de flamme; gaz vecteur: azote (débit ~30 mL/min)) équipé de colonnes en acier inox (longueur: 2 m; diamètre intérieur: 2 mm). Deux phases stationnaires ont été principalement utilisées: OV-275 (10%) sur Chromosorb WHP (80/100 mesh) et FFAP (10%) sur Chromosorb WAW (80/100 mesh). Les dosages ont été effectués par la méthode de l'étalon interne.

[5] La pureté des produits nouveaux isolés ayant été vérifiée par cpg, l'étude spectroscopique (rmn, masse) accréditant leurs structures, il ne nous a pas paru nécessaire d'effectuer leur analyse centésimale.

Les points de fusion ont été mesurés sur un appareil Mettler FP 61.

Etude des décompositions

Les études analytiques ont été réalisées en introduisant 2 cm^3 de solution dans des ampoules en Pyrex scellées placées pendant le temps adéquat dans un bain thermostaté à la température choisie (110, 120 ou 130°C).

Les études préparatives ont été effectuées sur des volumes de l'ordre de 200 cm^3 dans un autoclave de 250 cm^3 placé dans une étuve thermorégulée préalablement portée à la température souhaitée. Après élimination du solvant en excès, le produit recherché est distillé sous pression réduite puis purifié par chromatographie liquide–solide sur une colonne de gel de silice (Kieselgel 60, 35/70 mesh).

Matières premières

La préparation, la purification et le dosage du perpentène-4 oate de *tert*-butyle ont été décrits dans la réf. 1. Les esters, acides, nitriles et amides sont des produits commerciaux utilisés après distillation.

Nous avons choisi de suivre dans la partie expérimentale le même plan que pour la partie théorique.

*Thermolyse de **1** dans les acides et leurs dérivés*

1. *Alcanoates de méthyle*

Produits correspondant à l'attaque sur la partie acyle:

(Oxo-2 tétrahydrofuryl-5)-3 propionate de méthyle, **6***a*; pé 128–129°C/0,8 Torr (1 Torr = 133,3 Pa); n_D^{20} = 1,4517; rmn δ: 1,4 à 2,7 (1 massif, 8H), 3,7 (singulet, 3H), 4,1 à 4,6 (1 massif, 1H); masse m/z (abondance): 85 (100), 112 (21), 45 (16), 74 (15), 141 (14).

Méthyl-2 (oxo-2 tétrahydrofuryl-5)-3 propionate de méthyle, **6***b*; pé 128–129°C/1 Torr; n_D^{20} = 1,4562; rmn δ: 1,2 (doublet, J = 8 Hz, 3H), 1,5 à 2,9 (1 massif, 7H), 3,6 (singulet, 3H), 4,0 à 4,7 (1 massif, 1H); masse m/z (abondance): 85 (100), 88 (30), 57 (17), 56 (15), 155 (13).

Diméthyl-2,2 (oxo-2 tétrahydrofuryl-5)-3 propionate de méthyle, **6***c*; pé 130–132°C/0,8 Torr; n_D^{20} = 1,4588; rmn δ: 1,2 (singulet, 6H), 1,3 à 2,6 (1 massif, 6H), 3,6 (singulet, 3H), 4,1 à 4,7 (1 massif, 1H); masse m/z (abondance): 85 (100), 102 (38), 141 (13).

(Oxo-2 tétrahydrofuryl-5)-2 acétate de méthyle, **9**; pé 126–127°C/0,8 Torr; n_D^{20} = 1,4553; rmn δ: 1,5 à 2,6 (1 massif, 6H), 3,6 (singulet, 3H), 4,5 à 5,0 (massif, 1H); masse m/z (abondance): 85 (100), 55 (26), 43 (21), 56 (21), 59 (18).

Préparation des produits correspondant à l'attaque sur la partie méthoxyle:

Le propionate d'(oxo-2 tétrahydrofuryl-5)-2 éthyle, **8***b*, a été préparé par chauffage à 80°C pendant 24 h de 65 g de bromoacétate d'éthyle et de 5 g de propionate de butène-3 yle (synthétisé à partir de chlorure de propionyle et de butène-3 ol) en présence de 0,95 g de peroxyde de benzoyle (proportions molaires respectives 10:1:0,1). Après avoir éliminé le bromoacétate d'éthyle en excès, **8***b* est obtenu pur par passage sur gel de silice (éluant: éther de pétrole – éther) avec un rendement de 55%; n_D^{20} = 1,4604; rmn δ: 1,1 (triplet, J = 6,7 Hz, 3H), 1,5 à 2,7 (1 massif, 8H), 4,0 à 4,3 (triplet, 2H), 4,4 à 4,8 (massif, 1H); masse m/z (abondance): 57 (100), 85 (74), 112 (26), 56 (16), 84 (11).

L'(oxo-2 tétrahydrofuryl-5)-2 éthanol, **10**, a été obtenu par chauffage pendant 5 h à 65°C de 1 g de lactone **8***b* dans 20 cm^3 de méthanol en présence de traces d'APTS. Après élimination du méthanol en excès et du propionate de méthyle formé, la lactone **10** est récupérée (Rdt 85%). Aucune purification n'apparaît nécessaire; n_D^{20} = 1,4705; rmn δ: 1,5 à 2,7 (1 massif, 6H), 3,6 (triplet, J = 6,7 Hz, 2H), 4,4 à 4,9 (massif, 1H), 4,7 (singulet, 1H); masse m/z (abondance): 85 (100), 43 (85), 112 (18).

Préparation de **8***a*, **8***c* et **8***d*: dans 10 cm^3 de THF anhydre on met à température ambiante 0,25 g de *N,N'*-carbonyldiimidazole puis on ajoute goutte à goutte sous agitation la quantité d'acide correspondante (0,092 g d'acide acétique, 0,135 g d'acide isobutyrique, 0,70 g d'acide formique); au bout d'une demi-heure, on additionne 0,2 g d'hydroxylactone **10** et on laisse tourner 1 h. Après élimination du THF en excès, on purifie les lactones **8***a*, **8***c* et **8***d* par chromatographie sur gel de silice.

Acétate d'(oxo-2 tétrahydrofuryl-5)-2 éthyle, **8***a*: n_D^{20} = 1,4759; rmn δ: 1,6 à 2,8 (1 massif, 6H), 2,1 (singulet, 3H), 4,15 (triplet, J = 7,3 Hz, 2H), 4,4 à 4,9 (1 massif, 1H); masse m/z (abondance): 43 (100), 85 (98), 112 (24), 84 (13).

Isobutyrate d'(oxo-2 tétrahydrofuryl-5)-2 éthyle, **8***c*: n_D^{20} = 1,4535; rmn δ: 1,15 (doublet, J = 7,3 Hz, 6H), 1,7 à 2,9 (1 massif, 7H), 4,15 (triplet, J = 7,3 Hz, 2H), 4,4 à 4,8 (1 massif, 1H); masse m/z (abondance): 71 (100), 43 (94), 85 (80), 112 (40), 72 (24), 84 (12).

Formiate d'(oxo-2 tétrahydrofuryl-5)-2 éthyle, **8***d*: n_D^{20} = 1,4768; rmn δ: 1,5 à 2,8 (1 massif, 6 H), 4,15 (triplet, J = 7,3 Hz, 2H), 4,4 à 4,9 (1 massif, 1H), 9,1 (singulet, 1H); masse m/z (abondance): 85 (100), 68 (12), 67 (10), 112 (7).

2. *Esters fonctionnels*

(Méthoxycarbonyl)-2 (oxo-2 tétrahydrofuryl-5)-3 propionate de méthyle, **6***e*: pé 144–145°C/0,8 Torr; n_D^{20} = 1,4643; rmn δ: 1,5 à 2,7 (1 massif, 6H), 3,55 (triplet, J = 8 Hz, 1H), 3,7 (singulet, 6H), 4,2 à 4,7 (1 massif, 1H); masse m/z (abondance): 85 (100), 132 (95), 55 (31), 199 (14).

Chloro-2 (oxo-2 tétrahydrofuryl-5)-3 propionate de méthyle, **6***f*: pé 112°C/0,1 Torr; n_D^{20} = 1,4763; rmn δ: 1,7 à 2,8 (1 massif, 6H), 3,6 (singulet, 3H); 3,7 (singulet, 1H); 4,1 à 4,9 (1 massif, 1H); masse m/z (abondance): 85 (100), 74 (66), 43 (27), 59 (18), 175 (14), 177 (4,5), 108 (12), 110 (4).

Acétyl-2 (oxo-2 tétrahydrofuryl-5)-3 propionate de méthyle, **6***g*: pé 145°C/1,1 Torr; n_D^{20} = 1,4672; rmn δ: 1,6 à 2,8 (1 massif, 6H), 2,2 (singulet, 3H), 3,6 à 3,9 (1 massif, 4H), 3,7 (singulet, 3H), 4,2 à 4,7 (1 massif, 1H); masse m/z (abondance): 43 (100), 85 (56), 172 (36), 116 (21).

(Méthoxycarbonyl)-3 (oxo-2 tétrahydrofuryl-5)-4 butyrate de méthyle, **6***h*: pé 146–147°C/0,6 Torr; n_D^{20} = 1,4640; rmn δ: 1,2 à 3,1 (1 massif, 9H), 3,5 (singulet, 6H), 4,1 à 4,6 (massif, 1H); masse m/z (abondance): 59 (100), 43 (85), 97 (75), 213 (71), 85 (60), 74 (40).

Cyano-2 (oxo-2 tétrahydrofuryl-5)-3 propionate de méthyle, **6***i*: pé 158–160°C/0,05 Torr; n_D^{20} = 1,4729; rmn δ: 1,7 à 2,8 (1 massif, 6H), 3,7 à 4,1 (1 massif, 1H), 3,8 (singulet, 3H), 4,4 à 5,0 (1 massif, 1H); masse m/z (abondance): 85 (100), 99 (37), 55 (28), 68 (21).

3. *Acides et anhydrides*

Acide (oxo-2 tétrahydrofuryl-5)-3 propionique, **4***a*: pé 164–166°C/0,01 Torr; F = 62,7°C; rmn δ: 1,5 à 2,7 (1 massif, 8H), 4,2 à 4,7 (1 massif, 1H); 12,1 (singulet, 1H); masse m/z (abondance): 85 (100), 56 (17), 112 (17).

Acide méthyl-2 (oxo-2 tétrahydrofuryl-5)-3 propionique, **4***b*: pé 169–172°C/0,01 Torr; n_D^{20} = 1,4687; rmn δ: 1,0 à 1,2 (doublet, J = 6,7 Hz, 3H), 1,5 à 2,7 (1 massif, 7H), 4,2 à 4,8 (1 massif, 1H), 12,3 (singulet, 1H); masse m/z (abondance): 85 (100), 41 (24), 99 (24), 55 (16), 126 (14).

Acide diméthyl-2,2 (oxo-2 tétrahydrofuryl-5)-3 propionique, **4***c*: pé 174–177°C/0,01 Torr; n_D^{20} = 1,4694; rmn δ: 1,1 (singulet, 6H), 1,6 à 2,6 (massif, 6H), 4,2 à 4,7 (massif, 1H), 11,7 (singulet, 1H); masse m/z (abondance): 85 (100), 88 (46), 55 (41), 141 (13).

*Isomérisation des lactones **6***

Préparation des lactones **7***b* et **7***c*: les lactones **6***b* et **6***c* sont chauffées dans du méthanol au reflux pendant 2 h en présence de traces d'APTS. Après élimination du méthanol en excès, les lactones **7***b* et **7***c* sont purifiées par chromatographie sur gel de silice.

(Méthyl-3 oxo-2 tétrahydrofuryl-5)-3 propionate de méthyle, **7***b*: pé 130°C/0,8 Torr; n_D^{20} = 1,4543; rmn δ: 1,2 (doublet, J = 8 Hz, 3H), 1,5 à 2,9 (1 massif, 7H), 3,6 (singulet, 3H), 4,0 à 4,6 (1 massif, 1H); masse m/z (abondance): 99 (100), 85 (82), 74 (75), 155 (45), 126 (28).

(Diméthyl-3,3 oxo-2 tétrahydrofuryl-5)-3 propionate de méthyle, **7***c*: pé 132°C/0,8 Torr; n_D^{20} = 1,4505; rmn δ: 1,2 (singulet, 6H), 1,7 à 2,7 (1 massif, 6H), 3,7 (singulet, 3H), 4,2 à 4,7 (1 massif, 1H); masse m/z (abondance): 82 (100), 85 (65), 41 (49), 74 (23), 113 (20).

Les différences spectrales (rmn ^1H et masse) des composés **6***b* et **7***b* d'une part, **6***c* et **7***c* d'autre part ne sont pas suffisamment importantes pour confirmer leurs structures respectives. Les temps de rétention en cpg sont cependant différents. Afin de compléter l'identification de ces dérivés, nous avons effectué leur étude par rmn ^{13}C en utilisant les déplacements chimiques des différents atomes de carbone des groupes carbonyle.

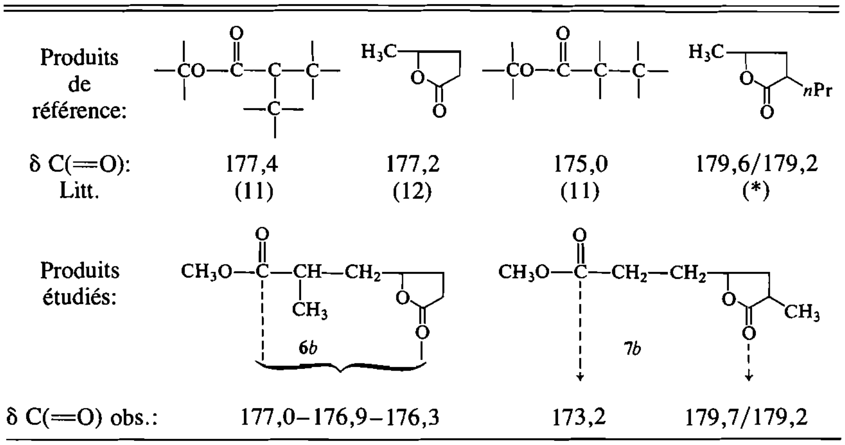

* Nous avons enregistré le spectre de ce composé.

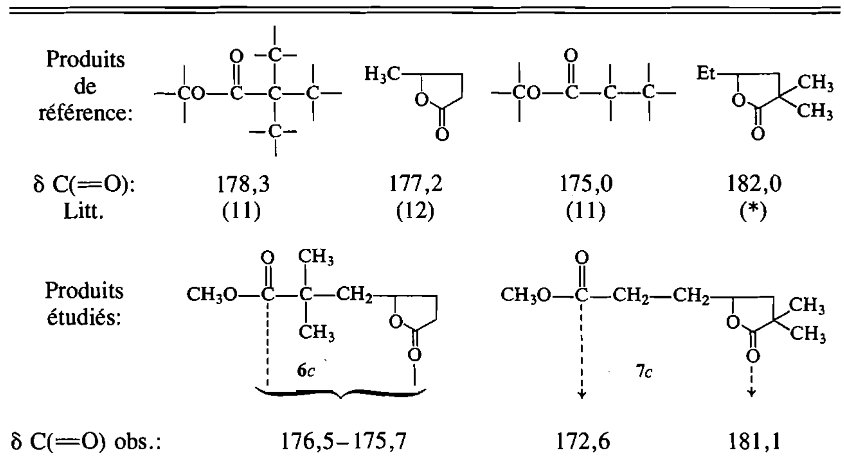

* Nous avons enregistré le spectre de ce composé.

L'étude précédente a nécessité la synthèse du diméthyl-2,2 hexanolide-4: il a été préparé à partir de 0,1 mole d'isobutyrate de méthyle et 0,1 mole d'époxyde de butène-3 yle selon la méthode générale décrite dans la réf. 14. Après acidification, extraction et distillation, la lactone est récupérée avec un rendement de 60%; pé 105–106°C/25 Torr (litt. (15) pé 89–93°C/18 Torr).

Préparation de **6*b*** à partir de **4*b***: dans 15 cm^3 de THF anhydre, on met 0,47 g de *N,N'*-carbonyldiimidazole; sous agitation et à température ambiante, on ajoute 0,5 g d'acide **4*b***. On laisse tourner une demi-heure puis on additionne lentement 0,093 g de méthanol. Une heure plus tard, on élimine le solvant, ajoute de l'eau et extrait **6*b*** à l'éther de pétrole.

Identification des produits d'addition des anhydrides: après élimination de l'anhydride en excès, on verse le résidu dans de l'eau bouillante. On laisse tourner 2 h sous agitation puis on extrait à l'éther. Après élimination du solvant, on récupère les acides **4*a*** et **4*b*** par distillation, respectivement à partir des anhydrides acétique et propionique.

4. *Nitriles*

(Cyano-2 éthyl)-5 dihydro-3,4-5*H*-furannone-2, **11*a***: pé 125–128°C/0,8 Torr; n_D^{20} = 1,4518; rmn δ: 1,5 à 2,8 (1 massif, 8H), 4,3 à 4,8 (1 massif, 1H); masse *m/z* (abondance): 85 (100), 55 (41), 41 (23), 56 (19).

(Cyano-2 propyl)-5 dihydro-3,4-5*H*-furannone-2, **11*b***: pé 131–133°C/0,8 Torr; n_D^{20} = 1,4683; rmn δ: 1,4 (doublet, *J* = 8 Hz, 3H), 1,7 à 3,1 (1 massif, 7H), 4,4 à 5,0 (1 massif, 1H); masse *m/z* (abondance): 85 (100), 55 (31), 56 (11).

Tétraméthylsuccinodinitrile: *F* = 168,5°C (litt. (13): *F* = 167–168°C).

Isomérisation des lactones 4[6]

Les lactones **4*b*** et **4*c*** (0,5 g) ont été saponifiées par chauffage en présence de potasse alcoolique (0,5 g) durant 2 h. Après extraction, acidification de la phase aqueuse, on récupère les hydroxydiacides **12*b*** et **12*c*** utilisés ensuite sans purification ultérieure (Rdt ~70%).

Acide hydroxy-4 méthyl-2 heptanedioïque, **12*b***: rmn ^{1}H: 1,85 (doublet, *J* = 8 Hz, 3H), 1,5 à 2,9 (1 massif, 7H), 4,3 à 4,8 (1 massif, 1H), 8,7 (singulet, 3H).

Acide diméthyl-2,2 hydroxy-4 heptanedioïque, **12*c***: rmn ^{1}H: 1,3 (singulet, 6H), 1,6 à 2,8 (1 massif, 6H), 4,4 à 4,9 (1 massif, 1H), 8,9 (singulet, 3H).

Les hydroxydiacides précédents (0,3 g) ont été lactonisés au reflux du THF (10 cm^3) en présence de traces d'APTS pendant 2 h. Les acides lactones **5*b*** et **5*c*** ont été obtenus après élimination du THF.

Acide (méthyl-3 oxo-2 tétrahydrofuryl-5)-3 propionique, **5*b***: rmn ^{1}H: 1,2 (doublet, *J* = 8 Hz, 3H), 1,5 à 2,8 (1 massif, 7H), 4,3 à 4,8 (1 massif, 1H), 11,1 (singulet, 1H).

Acide (diméthyl-3,3 oxo-2 tétrahydrofuryl-5)-3 propionique, **5*c***: rmn ^{1}H: 1,2 (singulet, 6H), 1,4 à 2,8 (1 massif, 6H), 4,3 à 4,8 (1 massif, 1H), 11,3 (singulet, 1H).

[6] L'isomérisation des lactones **6*b*** et **6*c*** a été décrite dans le paragraphe consacré aux acides et anhydrides.

Les lactones **5**b et **5**c ont été ensuite méthylées au diazométhane et identifiées aux lactones **7**b et **7**c par cpg.

On chauffe au reflux pendant 2 h en présence de traces d'APTS 0,5 g de lactone **4**c dans 10 cm^3 de THF. Après élimination du solvant, la lactone **5**c est isolée avec une conversion totale. Elle est transformée ensuite en lactone **7**c par traitement au diazométhane. **7**c est ensuite purifiée sur gel de silice.

Remerciements

Les auteurs remercient Monsieur le Professeur R. Lalande pour l'intérêt qu'il a porté à ce travail. Ils remercient également MM. Petraud et Barbe pour l'étude des spectres rmn ^{13}C ainsi que le Dr. Servens pour la fourniture d'un échantillon de propyl-2 pentanolide-4.

1. B. MAILLARD, A. KHARRAT et C. GARDRAT. Tetrahedron, **40**, 3531 (1984).
2. A. KHARRAT, C. GARDRAT et B. MAILLARD. Synth. Commun. **13**, 1209 (1983).
3. A. KHARRAT, C. GARDRAT et B. MAILLARD. Can. J. Chem. **62**, 2385 (1984).
4. H. H. VOGEL. Synthesis, 99 (1970) et références citées.
5. W. S. JOHNSON, V. J. BAUER, J. L. MALGRAVE, M. A. FRISCH, L. H. DREGER et W. H. HUBBARD. J. Am. Chem. Soc. **83**, 606 (1961).
6. M. S. KHARASCH, P. S. SKELL et P. FISHER. J. Am. Chem. Soc. **70**, 1055 (1948).
7. R. LALANDE, C. FILLIATRE, J-J. VILLENAVE et R. JAOUHARI. Helv. Chim. Acta, **67**, 149 (1984).
8. C. RÜCHARDT. Angew. Chem. Int. Ed. Engl. **9**, 830 (1970) et références citées.
9. H. STAAB. Angew. Chem. Int. Ed. Engl. **1**, 351 (1962).
10. M. CAZAUX et R. LALANDE. Bull. Soc. Chim. Fr. 3381 (1966).
11. P. A. COUPERUS, A. D. H. CLAGUE et J. P. C. M. WAN DONGEN. Org. Magn. Reson. **11**, 590 (1978).
12. H. PYYSALO et J. ENQVIST. Finn. Chem. Lett. 136 (1975).
13. G. S. HAMMOND, J. N. SEN et C. E. BOOZER. J. Am. Chem. Soc. **77**, 3244 (1955).
14. P. S. ENGEL et M. A. SCHEXNAYDER. J. Am. Chem. Soc. **97**, 150 (1975).
15. P. FUJITA, S. WATANABE et K. SUGA. Aust. J. Chem. **27**, 2205 (1974).

Enthalpies of interaction of aromatic solutes with organic solvents

W. KIRK STEPHENSON AND RICHARD FUCHS
Department of Chemistry, University of Houston, Houston, TX 77004, USA

Received August 20, 1984

W. KIRK STEPHENSON and RICHARD FUCHS. Can. J. Chem. **63**, 2529 (1985).

Heats of solution of several aromatic solutes (benzene, toluene, mesitylene, nitrobenzene, α,α,α-trifluorotoluene, anisole) and model compounds (*n*-butyl methyl ether, cyclohexane) in 17 organic solvents (*n*-heptane, cyclohexane, carbon tetrachloride, 1,2-dichloroethane, α,α,α-trifluorotoluene, triethylamine, butyl ether, ethyl acetate, dimethylformamide, dimethyl sulfoxide, benzene, toluene, mesitylene, *t*-butyl alcohol, 1-octanol, methanol, 2,2,2-trifluoroethanol) have been combined with solute heats of vaporization to give enthalpies of transfer from vapor to solvent ($\Delta H(v \rightarrow S)$). Differences between solute and model values ($\Delta\Delta H(v \rightarrow S) = \Delta H(v \rightarrow S)$ (aromatic solute) $- \Delta H(v \rightarrow S)$ (model) were used to evaluate aromatic solute−solvent polar interactions. Correlations of $\Delta\Delta H(v \rightarrow S)$ with solvent dipolarity−polarizability (Taft−Kamlet π^* parameter) have been determined.

W. KIRK STEPHENSON et RICHARD FUCHS. Can. J. Chem. **63**, 2529 (1985).

On a combiné les chaleurs de solution de plusieurs solutés aromatiques (benzène, toluène, mésitylène, nitrobenzène, α,α,α-trifluorotoluène, anisole) et de composés modèles (méthoxybutane, cyclohexane) dans 17 solvants organiques (heptane, cyclohexane, tétrachlorure de carbone, dichloro-1,2 éthane, α,α,α-trifluorotoluène, triéthylamine, éther butylique, acétate d'éthyle, diméthylformamide, diméthylsulfoxyde, benzène, toluène, mésytilène, alcool *tert*-butylique, octanol-1, méthanol, trifluoro-2,2,2 éthanol) avec les chaleurs de vaporisation des solutés pour obtenir les enthalpies de transfert de la vapeur au solvant ($\Delta H(v \rightarrow S)$). On a utilisé les différences entre les valeurs pour les modèles et pour les solutés ($\Delta\Delta H(v \rightarrow S) = \Delta H(v \rightarrow S)$ (soluté aromatique) $- \Delta H(v \rightarrow S)$ (modèle) pour évaluer les interactions polaires soluté−solvant. On a déterminé des corrélations entre les $\Delta\Delta H(v \rightarrow S)$ et le dipolarité−polarisabilité (paramètre π^* de Taft−Kamlet).

[Traduit par le journal]

Introduction

Aromatic solutes are capable of undergoing several types of interactions with organic solvents. Interactions with polar solvents are most commonly solute dipole − solvent dipole or solvent dipole − solute induced dipole interactions. In hydrogen-bond-donating (HBD) solvents, the rings of electron-rich aromatic compounds act as hydrogen-bond-acceptor (HBA) sites. Aromatic compounds also have the ability to form electron donor − acceptor (EDA) complexes (also known as charge-transfer or molecular complexes), in which an aromatic solute may serve as either acceptor or donor (1). EDA complexes between aromatic molecules are usually envisioned as being face-to-face.

Enthalpies of interaction of polar and nonpolar molecules with aromatic solvents have been reported (2) using the solvation enthalpy, or $\Delta\Delta H(v \rightarrow S)$, method. This method utilizes enthalpies of transfer from the vapor to solvent,

$$[1] \quad \Delta H(v \rightarrow S) = \Delta H_s - \Delta H_v = \Delta H_c + \Delta H_{int}$$

where ΔH_s is the enthalpy of solution of the liquid solute; ΔH_v, the solute heat to vaporization; ΔH_c, the enthalpy of cavity formation in the solvent; and ΔH_{int}, the enthalpy of solute−solvent interactions. For a polar aprotic solute A dissolved in a polar non-hydrogen-bond-donating solvent S, the ΔH_{int} term describes the sum of the solute−solvent dispersion (ΔH_d) and polar (ΔH_p) interactions,

$$[2] \quad \Delta H(v \rightarrow S)(A) = \Delta H_c + \Delta H_d + \Delta H_p$$

Subtraction of the solvation enthalpy of a suitable nonpolar model M ($\Delta H_p(M) = 0$) from eq. [2] gives:

$$[3] \quad \Delta\Delta H(v \rightarrow S)(A \text{ vs. } M) = \Delta\Delta H_c + \Delta\Delta H_d + \Delta H_p$$

where $\Delta\Delta H_c = \Delta H_c(A) - \Delta H_c(M)$ and $\Delta\Delta H_d = \Delta H_d(A) - \Delta H_d(M)$. It is presumed that the solute-model cavity and dispersion interaction mismatches are equal to zero so that $\Delta\Delta H(v \rightarrow S)(A \text{ vs. } M)$ is equal to ΔH_p.

The dependence of polar solute $\Delta\Delta H(v \rightarrow S)$ values on solvent "polarity" can be quantitatively expressed by equations of the form:

$$[4] \quad \Delta\Delta H(v \rightarrow S)(A \text{ vs. } M) = s\pi^* + y$$

where π^* is the Taft−Kamlet solvent dipolarity−polarizability parameter (3, 4); s, the π^* coefficient; and y, the calculated $\Delta\Delta H(v \rightarrow S)$ value in a solvent with $\pi^* = 0.00$ (y-intercept).

To investigate aromatic solute − organic solvent interactions, $\Delta\Delta H(v \rightarrow S)$ values of benzene, toluene, mesitylene, nitrobenzene (NO_2Ph), α,α,α-trifluorotoluene (CF_3Ph), and anisole in 17 organic solvents of varying polarity will be reported. Correlations of $\Delta\Delta H(v \rightarrow S)$ with solvent π^* will be determined.

Experimental

Solutes and solvents were commercial samples of 99% purity, with most exceeding 99.7%. All were stored over 4A molecular sieve, except for methanol and trifluoroethanol, which were dried over 3A molecular sieve. Purities were established by gas chromatography using a Shimadzu Mini 2 gc with a glass lined system, a 30 m × 0.25 mm id SE-30 silica capillary column, and a Hewlett-Packard 3390A integrator.

The calorimetric procedure and apparatus have previously been described (5). The calorimeter was immersed in a water bath at 25.00°C, with regulation to ±0.002°C. Liquid samples were introduced into 65−80 mL of solvent with 10-, 20-, or 50-μL syringes with immersed tips. Heats of solution were corrected (0.01−0.03 kcal/mol less endothermic) to allow for the heat capacity of the samples which were introduced at 21−23°C. The uncertainty intervals in ΔH_s (twice the standard deviation of the mean of three or more determinations) are 0.00−0.07 kcal/mol, except for four values with 0.09−0.15 kcal/mol uncertainty intervals. No effect of concentration on ΔH_s was observed.

Results and discussion

Heats of solution of several aromatic compounds (benzene, toluene, mesitylene, nitrobenzene (NO_2Ph), α,α,α-trifluoro-

TABLE 1. Solvent π^* and solute enthalpy of solution and vaporization values[a]

Solvent	Solvent π^*	Benzene	Toluene	Mesitylene	Trifluorotoluene	Nitrobenzene	Anisole	Cyclohexane	n-Butyl methyl ether
n-Heptane	−0.08	0.79±0.03[b]	0.49±0.02	0.30±0.02	1.01±0.05	2.46±0.07[b]	1.34±0.04[b]	0.19±0.02[b]	0.41±0.02[b]
c-C_6	0.00	0.91±0.02[b,c]	0.77±0.02[b,d]	0.99±0.05	1.66±0.05[b,d]	2.85±0.09[b,d]	1.72±0.03	0.00±0.02[b,d]	0.68±0.04
CCl_4	0.28	0.13±0.00	−0.04±0.00	0.18±0.02	0.77±0.01	1.28±0.03	0.41±0.00	0.20±0.00	−0.24±0.01
CF_3Ph	0.64	0.25±0.01[c]	0.05±0.00[e]	0.03±0.00[e]	0.00±0.02[b,e]	0.36±0.01[e]	0.24±0.00[e]	0.97±0.02[c]	−0.16±0.01[e]
$ClCH_2CH_2Cl$	0.81	0.12±0.02	0.10±0.01	0.57±0.02	0.95±0.01	0.10±0.01	0.00±0.05	1.77±0.02	0.23±0.01
Et_3N	0.14	0.27±0.01	0.13±0.01	0.17±0.01	0.03±0.00	1.00±0.02	0.75±0.01	0.16±0.02	0.05±0.01
Bu_2O	0.24	0.22±0.00	0.06±0.01	0.03±0.01	0.03±0.01	0.97±0.00	0.57±0.00	0.20±0.01	0.05±0.01
EtOAc	0.55	0.09±0.01	0.12±0.02	0.52±0.02	−0.03±0.05	−0.24±0.01	−0.07±0.03	1.36±0.05	0.41±0.03
DMF	0.88	0.04±0.02[b,f]	0.16±0.02[b,f]	0.83±0.03[b,f]	−0.01±0.02[b,f]	−0.19±0.02[b,f]	0.04±0.01	1.84±0.06[b,c]	0.84±0.02
DMSO	1.00	0.75±0.06	0.91±0.07	1.94±0.15	1.17±0.01	0.60±0.02	0.61±0.05	2.83±0.10	1.71±0.04
Mesitylene	0.41	0.38±0.06[e]	0.13±0.01[e]	0.00±0.00[e]	0.00±0.00[e]	0.39±0.02[b,e]	0.38±0.03[e]	0.47±0.01[e]	0.04±0.01[e]
Toluene	0.54	0.06±0.04	0.00±0.00[e]	0.17±0.00[e]	0.09±0.01	0.36±0.01[d]	0.08±0.01[d]	0.60±0.00[e]	−0.01±0.00[e]
Benzene	0.59	0.00±0.00[c]	0.12±0.02[b,d]	0.62±0.03[b,d]	0.56±0.03[b,d]	0.56±0.03[b,d]	0.04±0.01	0.87±0.03[b,c]	0.27±0.01[e]
1-Octanol	0.34[g]	0.71±0.02	0.51±0.02	0.39±0.03	0.54±0.04	1.88±0.02	1.33±0.01	0.45±0.04	0.69±0.03
t-BuOH	0.41	1.85±0.02	1.76±0.03	2.02±0.02	2.08±0.05	3.84±0.12	2.86±0.02	1.03±0.02	0.72±0.02
MeOH	0.60	0.36±0.02[b,f]	0.45±0.02[b,f]	1.04±0.03[b,f]	−0.05±0.02[b,f]	1.00±0.03[b,f]	0.85±0.01	1.18±0.04[b,c]	0.45±0.03
CF_3CH_2OH	0.73	1.47±0.06	1.46±0.01	1.95±0.06	1.18±0.06	1.57±0.07	1.27±0.02	2.60±0.05	−2.56±0.03
ΔH_v		8.09±0.01[h]	9.08±0.01[h]	11.35±0.01[h]	8.98±0.03[h]	13.15±0.05[h]	11.19±0.05[h]	7.90±0.01[h]	7.77±0.02[h]

[a] ΔH_s and ΔH_v in kcal/mol.
[b] Uncertainty interval (2 × sdm) estimated as 0.01 kcal/mol for ΔH_s between 0.00 and 0.49; 0.02 kcal/mol for ΔH_s between 0.50 and 1.00; and 3% of ΔH_s for ΔH_s greater than 1.00 kcal/mol.
[c] Reference 17.
[d] Reference 18.
[e] Reference 15.
[f] Reference 19.
[g] π^* estimated by extrapolation of methanol to 1-butanol values.
[h] Reference 20.

TABLE 2. $\Delta\Delta H$(v → S)(aromatic solute vs. model) values[a]

Solvent	Benzene vs. c-C_6	Toluene vs. benzene	Mesitylene vs. benzene	CF_3Ph vs. toluene	NO_2Ph vs. toluene	Anisole vs. toluene	Anisole vs. n-BuOMe	Anisole vs. c-C_6
n-Heptane	0.41	−1.29	−3.75	0.62	−2.10	−1.26	−2.49	−2.14
c-C_6	0.72	−1.13	−3.18	0.99	−1.99	−1.16	−2.38	−1.57
CCl_4	−0.26	−1.16	−3.21	0.91	−2.77	−1.66	−2.77	−3.08
CF_3Ph	−1.16	−0.94	−3.23	0.05	−3.76	−1.92	−3.02	−4.02
$ClCH_2CH_2Cl$	−1.84	−1.01	−2.81	0.95	−4.07	−2.21	−3.65	−5.06
Et_3N	−0.08	−1.13	−3.36	0.00	−3.20	−1.49	−2.72	−2.70
Bu_2O	−0.17	−1.15	−3.45	0.07	−3.16	−1.60	−2.90	−2.92
EtOAc	−1.46	−0.96	−2.83	−0.32	−4.43	−2.30	−3.90	−4.72
DMF	−1.99	−0.87	−2.47	−0.07	−4.42	−2.23	−4.22	−5.09
DMSO	−2.27	−0.83	−2.07	0.36	−4.38	−2.41	−4.52	−5.51
Mesitylene	−0.28	−1.24	−3.64	−0.03	−3.81	−1.86	−3.08	−3.38
Toluene	−0.73	−1.05	−3.15	0.19	−3.71	−2.03	−3.33	−3.81
Benzene	−1.06	−0.87	−2.64	0.54	−3.63	−2.19	−3.65	−4.12
1-Octanol	0.07	−1.19	−3.58	0.13	−2.70	−1.29	−2.78	−2.41
t-BuOH	0.63	−1.08	−3.09	0.42	−1.99	−1.01	−1.28	−1.46
MeOH	−1.01	−0.90	−2.58	−0.40	−3.52	−1.71	−3.02	−3.62
CF_3CH_2OH	−1.32	−1.00	−2.78	−0.18	−3.96	−2.30	0.41	−4.62

[a]In kcal/mol.

toluene (CF_3Ph), anisole) and model compounds (n-butyl methyl ether (BuOMe), cyclohexane (c-C_6)) in 17 organic solvents (n-heptane, cyclohexane, carbon tetrachloride (CCl_4), 1,2-dichloroethane ($ClCH_2CH_2Cl$), α,α,α-trifluorotoluene, triethylamine (Et_3N), butyl ether (Bu_2O), ethyl acetate (EtOAc), dimethylformamide (DMF), dimethyl sulfoxide (DMSO), benzene, toluene, mesitylene, t-butyl alcohol (t-BuOH), 1-octanol, methanol (MeOH), 2,2,2-trifluoroethanol (CF_3CH_2OH)) are listed in Table 1. Solvent π^* values and solute heats of vaporization are also given. In Table 2 are listed and calculated $\Delta\Delta H$(v → S)(aromatic solute vs. model) values.

Benzene

To investigate aromatic ring influence on the solvation process, cyclohexane ($\pi^* = 0.00$) is chosen as a model for benzene ($\pi^* = 0.59$). $\Delta\Delta H$(v → S)(benzene vs. cyclohexane) values are given in Table 2, and show a strong dependence on solvent π^* (alcohols omitted):

[5] $\Delta\Delta H(\text{v} \rightarrow \text{S})(\text{benzene vs. } c\text{-}C_6) = -2.72\pi^* + 0.47$
$n = 13$, $r = 0.971$, see $= 0.24$ kcal/mol

where n is the number of solvents in the correlations, r denotes the correlation coefficient, and see is the standard error of the estimate. Mesitylene and toluene (as solvents) are displaced endothermically from eq. [5] by 0.36 and 0.27 kcal/mol; ethyl acetate is displaced exothermically by 0.44 kcal/mol. All alcohols are displaced endothermically, but trifluoroethanol and methanol are within the see value of eq. [5]. The hydroxyl proton of phenol has been shown to interact with the benzene π cloud (6), but H-bonding between trifluoroethanol and benzene is not observed. As in the case of ketone (7, 8) and ether (8) solutes, hydrogen bonding is anticipated because the HBA basicity of benzene is greater than that of trifluoroethanol (3, 4).

Toluene and mesitylene

The solvation enthalpy of toluene in n-heptane is more exothermic than that of benzene by 1.29 kcal/mol (Table 2), a result of additional interactions of the methylene group of toluene. The methylene increment of normal alkanes (7, 8) is −1.18 kcal/mol. Correlation of toluene and benzene solvation enthalpy differences with π^* for the aprotic solvents gives:

[6] $\Delta\Delta H(\text{v} \rightarrow \text{S})(\text{toluene vs. benzene}) = 0.374\pi^* - 1.22$
$n = 13$, $r = 0.845$, see $= 0.08$ kcal/mol

The positive s value is primarily due to the slightly smaller dipolarity–polarizability of toluene relative to benzene. Molar volume difference (MV(toluene) − MV(benzene) = 17.4 mL/mol) does not appear to significantly influence eq. [6], because the inclusion of a term in δ_H (Hildebrand solubility parameter) (9), which provides a measure of the energy of cavity formation (10), does not improve the equation. The poor correlation coefficient is due largely to the nearly horizontal slope (small s value) (11).

The difference between mesitylene and benzene solvation enthalpies in n-heptane (−3.75 kcal/mol) is roughly three times the toluene–benzene difference and reflects additional methylene group interactions. $\Delta\Delta H$(v → S)(mesitylene vs. benzene) values decrease with increasing solvent polarity (alcohols omitted):

[7] $\Delta\Delta H(\text{v} \rightarrow \text{S})(\text{mesitylene vs. benzene}) = 0.44\pi^* + 0.18\delta_H - 4.91$
$n = 13$, $r = 0.891$, see $= 0.24$ kcal/mol

(δ_H^2, rather than δ_H, may be the better indicator of ΔH_c. However, r and see are unchanged if δ_H^2 is used in the correlation.) Mesitylene and benzene molar volumes differ by 50.0 mL/mol and the δ_H term is needed to account for the solute-model cavity formation mismatch. With increasing cohesiveness of the solvent ΔH_c becomes more endothermic, and this is reflected by the positive coefficient of δ_H in eq. [7]. Exclusion of the δ_H term reduces the correlation coefficient to 0.819 and increases the see value to 0.29 kcal/mol.

α,α,α-Trifluorotoluene and nitrobenzene

Trifluoro ($\sigma_p = 0.51$) and nitro ($\sigma_p = 0.78$) groups are strongly electron withdrawing (relative to hydrogen), and the rings of CF_3Ph and NO_2Ph have lower electron densities than that of toluene, which possesses an electron-donating (σ_p =

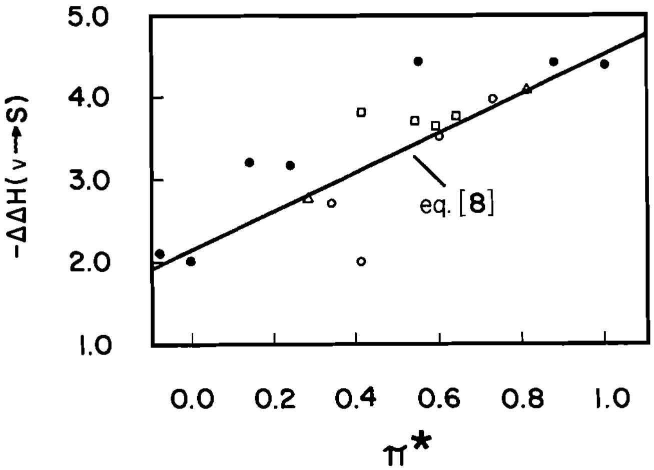

FIG. 1. Plot of $-\Delta\Delta H(\mathrm{v} \rightarrow \mathrm{S})(\mathrm{NO_2Ph}$ vs. toluene) π^* versus for select (●), chloro (△), aromatic (□), and alcohol (○) solvents.

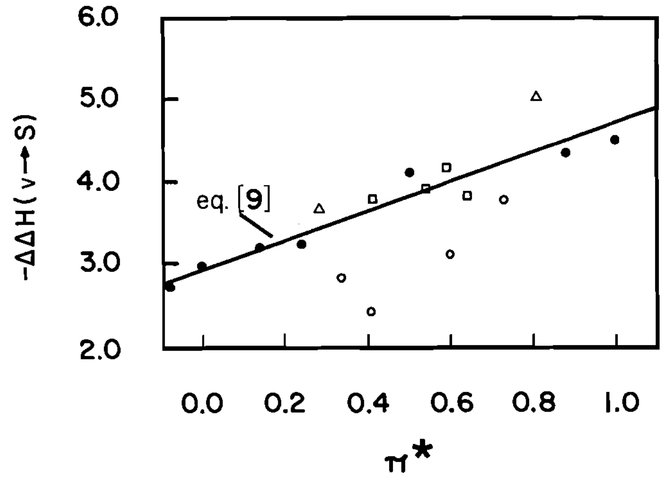

FIG. 2. Plot of $-\Delta\Delta H(\mathrm{v} \rightarrow \mathrm{S})(\mathrm{NO_2Ph}$ vs. $\mathrm{CF_3Ph}$) versus π^* for select (●), chloro (△), aromatic (□), and alcohol (○) solvents.

-0.17) methyl group. The larger π^* values of nitrobenzene ($\pi^* = 1.01$, $\mu = 3.9$ D) and trifluorotoluene ($\pi^* = 0.64$, $\mu = 2.6$ D) relative to toluene ($\pi^* = 0.54$, $\mu = 0.31$ D) are due to the greater dipolarity of the first two compounds. $\Delta\Delta H(\mathrm{v} \rightarrow \mathrm{S})(\mathrm{CF_3Ph}$ vs. toluene) values (Table 2) incorporate $\Delta\Delta H_c$, $\Delta\Delta H_d$, $\Delta\Delta H_p$(dipole−dipole), and $\Delta\Delta H_p$(dipole − induced dipole) terms; nitrobenzene and toluene have well matched molar volumes and $\Delta\Delta H_c$ will be minimal.

A plot of $\Delta\Delta H(\mathrm{v} \rightarrow \mathrm{S})(\mathrm{NO_2Ph}$ vs. toluene) versus solvent π^* is shown in Fig. 1. An unusual pattern is observed for the select solvents (SS), which are polar, monofunctional aprotic, aliphatic compounds (3). $\Delta\Delta H(\mathrm{v} \rightarrow \mathrm{SS})$ values follow the order: cyclohexane < heptane < butyl ether < triethylamine < ethyl acetate > DMF > DMSO. The maximum value is observed for ethyl acetate. Rationalization of this unusual pattern is difficult because the relative abilities of solute and model to undergo dipole−dipole and dipole − induced dipole interactions with the select solvents vary drastically; nitrobenzene favors dipolar over induction interactions, whereas the opposite is true for toluene.

The low electron density of the nitrobenzene ring suggests the possibility of electron donor − acceptor (EDA) complex formation with benzene, toluene, and mesitylene solvents. EDA complexes of polynitrobenzenes with electron donor molecules are well known, as are complexes in which benzene and methylbenzenes act as electron donors (12). The electron donor ability of methylbenzenes increases with the number of methyl groups. The free energy and enthalpy of complex formation between methylbenzenes and tetracyanoethylene become linearly more exoenergetic with decreasing arene ionization potential (13). Strong EDA complexes between trinitrobenzene and hexamethylbenzene have been reported (1), and complexes between nitrobenzene and mesitylene, although weaker as acceptor and donor molecules, are reasonable.

Hooper (14) has reported that carbon tetrachloride and *p*-xylene do not complex. The assumption that 1,2-dichloroethane also fails to complex with methylbenzenes brings the number of solvents "inert" to toluene complexation to four (cyclohexane, heptane, carbon tetrachloride, and dichloroethane). Correlation of $\Delta\Delta H(\mathrm{v} \rightarrow \mathrm{S})$ with "inert" solvent π^* gives:

[8] $\Delta\Delta H(\mathrm{v} \rightarrow \mathrm{S})(\mathrm{NO_2Ph}\text{ vs. toluene}) = -2.36\pi^* - 2.14$
$n = 4$, $r = 0.992$, see $= 0.15$ kcal/mol

Displacements of benzene, toluene, and mesitylene from the line defined by these four solvents (Fig. 1) are approximately 0.1, 0.3, and 0.7 kcal/mol. These displacements provide a crude estimate of the contribution of EDA complexing to the solvation of nitrobenzene, and are in the expected order.

$\Delta\Delta H(\mathrm{v} \rightarrow \mathrm{S})$(trifluorotoluene vs. toluene) values follow patterns identical to those of nitrobenzene for the select (cyclohexane < heptane < butyl ether < triethylamine < ethyl acetate > DMF > DMSO) and aromatic (benzene < toluene < mesitylene) solvents. Because of the similarity in π^* values for trifluorotoluene and toluene there would be little slope and poor correlation in a plot of $\Delta\Delta H(\mathrm{v} \rightarrow \mathrm{S})$ vs. solvent π^* (15).

Despite the complexity of Fig. 1, the plot of $\Delta\Delta H(\mathrm{v} \rightarrow \mathrm{S})(\mathrm{NO_2Ph}$ vs. $\mathrm{CF_3Ph}$) against solvent π^* (Fig. 2) is surprisingly simple. Correlation of the select solvent values with π^* gives:

[9] $\Delta\Delta H(\mathrm{v} \rightarrow \mathrm{S})(\mathrm{NO_2Ph}\text{ vs. }\mathrm{CF_3Ph}) = -1.78\pi^* - 2.92$
$n = 7$, $r = 0.988$, see $= 0.13$ kcal/mol

The only solvent other than the alcohols significantly out-of-line is 1,2-dichloroethane, which is displaced exothermically by 0.66 kcal/mol; other solvents are within 0.25 kcal/mol of eq. [9]. The negative slope reflects the greater dipole moment of nitrobenzene. $\Delta\Delta H(\mathrm{v} \rightarrow \mathrm{AROM})$ values are largest for benzene and smallest for mesitylene, the opposite of the trend observed with toluene as model. If EDA complexes are formed between nitrobenzene or trifluorotoluene and the methylbenzenes or benzene, the effect tends to be cancelled upon comparison of nitrobenzene with trifluorotoluene.

The well-matched molar volumes of nitrobenzene and toluene rule out a cavity formation mismatch as the source of the unusual behavior of the select solvents (SS) in Fig. 1. It is possible that $\Delta\Delta H(\mathrm{v} \rightarrow \mathrm{SS})$ values are influenced by the formation of EDA complexes in which some of the select solvents act as n donors. For example, EDA complexes of ethyl ether with tetracyanoethylene in chloroform solvent (13), diethyl ether with iodine in heptane, triethylamine with iodine in heptane, trimethylamine with sulfur dioxide in heptane, and dimethylacetamide with iodine in carbon tetrachloride (1) have been reported. However, a comparison of solvent ionization potentials suggests that nitrobenzene and trifluorotoluene do not form EDA complexes with the select solvents. For a given acceptor solute, the enthalpy of EDA complex formation is expected to increase linearly, or nearly linearly, with decreasing solvent ionization potential. The only select solvent with an ionization potential lower than those of toluene or mesitylene is triethylamine, yet butyl ether and ethyl acetate are displaced farther from the line defined by the inert solvents (Fig. 1) that is mesitylene.

Although π^* is defined as a solvent parameter, s values of $\Delta\Delta H(\mathrm{v} \rightarrow \mathrm{S})$(solute vs. model) versus solvent π^* correlation for a series of polar solutes have been shown to be proportional to the difference between solute and model π^* values (15):

$$[10] \quad \pi^*(\text{solute}) - \pi^*(\text{model}) = -0.20\, s - 0.01$$
$$n = 11,\ r = 0.978,\ \text{see} = 0.04$$

The y-intercept is within the see value of the origin, and the equation is consistent with the expectation that solvation enthalpy differences between solutes of equal polarity, or two nonpolar solutes, will not depend on solvent polarity.

The calculated π^* value (eq. [10]) for nitrobenzene (1.00) based on the s value of eq. [8] and the model (toluene) value of 0.54 (4) is in excellent agreement with the literature value (1.01) and the value calculated via eq. [9] (0.99). This gives credibility to eq. [8], which utilized only four solvents to define the dependency of $\Delta\Delta H(\mathrm{v} \rightarrow \mathrm{S})$(nitrobenzene vs. toluene) on solvent π^*.

Anisole

The π^* value of anisole (0.73) is expected to be larger than that of toluene (0.54) because of the greater dipolarity of the former ($\Delta\mu$ = 0.94 D). Differences between the solvation enthalpies (Table 2) represent, to a large extent, anisole dipolar interactions with select solvents and anisole – solvent induced dipole interactions with aromatic solvents, as well as the dispersion interaction mismatch. Solute and model molar volumes differ by only 2.3 mL/mol, and the influence of the cavity formation mismatch is minute. Correlation of the solvation enthalpy differences with solvent π^* (ethyl acetate and alcohols omitted) is given by eq. [11].

$$[11] \quad \Delta\Delta H(\mathrm{v} \rightarrow \mathrm{S})(\text{anisole vs. toluene}) = -1.12\pi^* - 1.33$$
$$n = 12,\ r = 0.969,\ \text{see} = 0.10$$

The only solvent of the 12 displaced more than 0.15 kcal/mol is benzene, which is displaced exothermically by 0.25 kcal/mol. Ethyl acetate lies 0.35 kcal/mol above the line.

Alcohol solvents exhibit behavior similar to that observed with nitrobenzene (Fig. 2) and 1-hexene (8). In each of these cases the difference between solute and model β values (Taft–Kamlet hydrogen-bond-accepting basicity parameter) (3, 4) is less than 0.30.

Evaluation of anisole induction interactions requires the use of a model with similar dipolarity, but with low polarizability. n-Butyl methyl ether has a dipole moment (μ = 1.25 D) identical to that of anisole and a molar volume which is only 9.8 mL/mol larger. The relationship of ansiole vs. n-butyl methyl ether solvation enthalpy differences with select solvent π^* is

$$[12] \quad \Delta\Delta H(\mathrm{v} \rightarrow \mathrm{S})(\text{anisole vs. } n\text{-BuOMe}) = -2.04\pi^* - 2.51$$
$$n = 7,\ r = 0.986,\ \text{see} = 0.16\ \text{kcal/mol}$$

Inclusion of the aromatic and chloro solvents reduces the correlation coefficient to 0.918. The s values of eqs. [11] and [12] suggest that anisole induction interactions contribute about 1.8 times more than anisole dipolar interactions to the solvation process.

A crude estimate of the total contribution of anisole polar interactions (induction plus dipolar) to the solvation process is obtained by adding the s value of eqs. [11] and [12]:

$$[13] \quad \Delta H_{\mathrm{p}}(\text{anisole}) = -3.16\pi^*$$

An alternative method involves the use of a nonpolar model. Cyclohexane is an excellent choice because it differs from anisole in molar volume by only 0.5 mL/mol. Correlation of $\Delta\Delta H(\mathrm{v} \rightarrow \mathrm{S})$(anisole vs. cyclohexane) with π^* of the select solvents gives:

$$\Delta\Delta H(\mathrm{v} \rightarrow \mathrm{S})(\text{anisole vs. cyclohexane}) = -3.54\pi^* - 2.14$$

or

$$[14] \quad \Delta H_{\mathrm{p}}(\text{anisole}) = -3.54\pi^*$$

The smaller s value of eq. [13] (relative to eq. [14]) is largely due to the dipolarity of toluene (μ = 0.31 D), which cancels a portion of the anisole (μ = 1.25 D) dipolar interactions. Applying a correction of 25% (0.31/1.25) to the polarity term of eq. [11] increases the s value to −1.40, which in turn increases the s value of eq. [13] to −3.44, in fair agreement with the value from eq. [14]. Our experience in this and other studies (8) suggests that satisfactory values of π^* can be calculated from eq. [10] for most compounds other than alcohols, provided that s is obtained from a good correlation ($r >$ ~0.95). The correction is based on the assumptions that solute and model dipolarities are accurately described by the dipole moments (μ for select solvents has been shown to be directly proportional to π^* (16)), and that the coefficient s reflects differences between solute and model dipolarities (eq. [10]).

The corrected values predict that anisole induction interactions are 1.5 times greater than anisole dipolar interactions with polar select solvents.

Acknowledgement

This study was supported by the Robert A. Welch Foundation (Grant E-136).

1. J. ROSE. Molecular complexes. Pergamon Press, New York. 1967.
2. R. FUCHS, L. A. PEACOCK, and W. K. STEPHENSON. Can. J. Chem. **60**, 1953 (1982).
3. M. J. KAMLET, J. L. M. ABBOUD, and R. W. TAFT. Prog. Phys. Org. Chem. **13**, 485 (1981).
4. M. J. KAMLET, J. L. M. ABBOUD, M. H. ABRAHAM, and R. W. TAFT. J. Org. Chem. **48**, 2877 (1983).
5. R. FUCHS and P. P. S. SALUJA. Can. J. Chem. **54**, 3857 (1976).
6. J. N. SPENCER, E. S. HOLMBOE, D. W. FIRTH, and M. R. KIRSHENBAUM. J. Soln. Chem. **10**, 745 (1981).
7. W. K. STEPHENSON and R. FUCHS. Can. J. Chem. **63**, 336 (1985); **63**, 349 (1985).
8. W. K. STEPHENSON. Ph.D. dissertation, University of Houston. 1984.
9. A. M. F. BARTON. Chem. Rev. **75**, 731 (1975).
10. M. H. ABRAHAM, M. J. KAMLET, and R. W. TAFT. J. Chem. Soc. Faraday Trans. 2, 923 (1982).
11. W. H. DAVIS and W. A. PRYOR. J. Chem. Ed. **53**, 285 (1976).
12. L. J. ANDREWS and R. M. KEEFER. Molecular complexes in organic chemistry. Holden-Day, San Francisco. 1964.
13. R. E. MERRIFIELD and W. D. PHILLIPS. J. Am. Chem. Soc. **80**, 2778 (1958).
14. H. O. HOOPER. J. Chem. Phys. **41**, 599 (1964).
15. R. FUCHS and W. K. STEPHENSON. J. Am. Chem. Soc. **105**, 5159 (1983).
16. J. L. M. ABBOUD and R. W. TAFT. J. Phys. Chem. **83**, 412 (1979).
17. P. P. S. SALUJA, T. M. YOUNG, R. F. RODEWALD, F. H. FUCHS,

D. KOHLI, and R. FUCHS. J. Am. Chem. Soc. **99**, 2949 (1977).
18. R. FUCHS, T. M. YOUNG, and R. F. RODEWALD. J. Am. Chem. Soc. **96**, 4705 (1974).
19. R. FUCHS and R. F. RODEWALD. J. Am. Chem. Soc. **95**, 5897 (1973).
20. J. B. PEDLEY and J. RYLANCE. Sussex-N.P.L. computer analyzed thermochemical data: organic and organometallic compounds. University of Sussex, Brighton. 1977.

Enthalpies of interaction of hydroxylic solutes with organic solvents

W. KIRK STEPHENSON AND RICHARD FUCHS
Department of Chemistry, University of Houston, Houston, TX 77004, U.S.A.

Received January 8, 1985

W. KIRK STEPHENSON and RICHARD FUCHS. Can. J. Chem. **63**, 2535 (1985).

Heats of solution of *m*-cresol, 1-butanol, 1-pentanol, *t*-amyl alcohol, and model compounds (toluene, ethyl ether, *n*-butyl methyl ether, *t*-butyl methyl ether) in 17 organic solvents (*n*-heptane, cyclohexane, carbon tetrachloride, 1,2-dichloroethane, α,α,α-trifluorotoluene, triethylamine, butyl ether, ethyl acetate, dimethylformamide, dimethyl sulfoxide, benzene, toluene, mesitylene, *t*-butyl alcohol, 1-octanol, methanol, 2,2,2-trifluoroethanol) have been combined with solute heats of vaporization to give solvation enthalpies ($\Delta H(\mathrm{v} \rightarrow \mathrm{S})$). Dependencies of solute vs. model solvation enthalpy differences on solvent dipolarity–polarizability and hydrogen-bond-accepting basicity were determined via correlations with Taft–Kamlet solvatochromic parameters (π^*, β, ξ).

m-Cresol is a substantially stronger H-bond donor than 1-butanol, 1-pentanol, and *t*-amyl alcohol, and H-bonds to acceptor solvents including alcohols. Cresol acts as an H-bond acceptor with the strong H-bond donor solvent trifluoroethanol.

W. KIRK STEPHENSON et RICHARD FUCHS. Can. J. Chem. **63**, 2535 (1985).

Dans le but de déterminer les enthalpies de solvatation ($\Delta H(\mathrm{v} \rightarrow \mathrm{S})$), on a combiné les chaleurs de solution du *m*-crésol, du butanol-1, du pentanol-1, de l'alcool *t*-amylique et de composés modèles (toluène, éther éthylique, méthoxy-1 butane, méthoxy-2 méthyl-2 propane) dans 17 solvants organiques (heptane, cyclohexane, tétrachlorure de carbone, dichloro-1,2 éthane, α,α,α-trifluorotoluène, triéthylamine, éther butylique, acétate d'éthyle, diméthylformamide, diméthylsulfoxyde, benzène, toluène, mésitylène, alcool *t*-butylique, octanol-1, méthanol, trifluoro-2,2,2 éthanol) avec les chaleurs de vaporisation des solutés. Utilisant des corrélations impliquant les paramètres solvatochromiques de Taft-Kamlet (π^*, β et ξ), on a déterminé les relations qui existent entre, d'une part, les différences d'enthalpie de solvatation des solutés vs. les modèles et, d'autre part, soit la polarisabilité–dipolarisabilité du solvant soit la basicité comme accepteur de liaisons hydrogènes.

Le *m*-crésol est un donneur de liaisons hydrogènes qui est substantiellement plus fort que le butanol-1, le pentanol-1 et l'alcool *t*-amylique; de plus, il forme des liaisons H avec les solvants accepteurs, y compris les alcools. Le crésol agit comme un accepteur de liaison H avec le solvant trifluoroéthanol qui est un donneur fort de liaison H.

[Traduit par le journal]

We have investigated enthalpies of interaction of ketone (1), aromatic (2), nitrogen base (3), and 1-octanol (4, 5) solutes with organic solvents of varying polarity. In this paper, several hydroxylic solutes (*m*-cresol, 1-butanol, 1-pentanol, and *t*-amyl alcohol (2-methyl-2-butanol)) will be examined. Enthalpies of interaction are determined by the solvation enthalpy, or $\Delta\Delta H(\mathrm{v} \rightarrow \mathrm{S})$, method. The solvation enthalpy is the enthalpy of transfer of a solute from vapor to solvent. For a solute–solvent mixture in which dispersion (d), polar (p), and hydrogen bonding (h) interactions are operative, the solvation enthalpy is

$$[1] \quad \Delta H(\mathrm{v} \rightarrow \mathrm{S}) = \Delta H_{\mathrm{s}} - \Delta H_{\mathrm{v}} = \Delta H_{\mathrm{c}} + \Delta H_{\mathrm{d}} + \Delta H_{\mathrm{p}} + \Delta H_{\mathrm{h}}$$

where s refers to the heat of solution of the liquid solute; v, the solute heat of vaporization; and c, the enthalpy of cavity formation within the solvent. ΔH_{s} and ΔH_{v} are determined experimentally. Polar and H-bonding enthalpies of interaction are presumed to be isolated by subtracting the solvation enthalpy of a suitable alkane model (M) from that of the solute (A),

$$[2] \quad \Delta\Delta H(\mathrm{v} \rightarrow \mathrm{S})(\mathrm{A\ vs.\ M}) = \Delta\Delta H_{\mathrm{c}} + \Delta\Delta H_{\mathrm{d}} + \Delta H_{\mathrm{p}} + \Delta H_{\mathrm{h}}$$

where $\Delta\Delta H(\mathrm{v} \rightarrow \mathrm{S})$, $\Delta\Delta H_{\mathrm{c}}$, and $\Delta\Delta H_{\mathrm{d}}$ refer to differences between solute and model. It has often been assumed that the first two terms on the right side of eq. [3] are equal to zero so that $\Delta\Delta H(\mathrm{v} \rightarrow \mathrm{S}) = \Delta H_{\mathrm{p}} + \Delta H_{\mathrm{h}}$, and in the absence of H-bonding, $\Delta\Delta H(\mathrm{v} \rightarrow \mathrm{S}) = \Delta H_{\mathrm{p}}$. If a model is chosen such that the solute cavity formation, dispersion, and polar interactions are cancelled, then $\Delta\Delta H(\mathrm{v} \rightarrow \mathrm{S}) = \Delta H_{\mathrm{h}}$. In practice, perfect solute and model matches are rare, and solute-model cavity formation, dispersion interaction, and/or polar interaction mismatches will be encompassed in $\Delta\Delta H(\mathrm{v} \rightarrow \mathrm{S})$ (A vs. M) values (4, 5).

Solvation enthalpy differences can be quantitatively expressed in terms of the Taft–Kamlet solvatochromic parameters (5–7),

$$[3] \quad \Delta\Delta H(\mathrm{v} \rightarrow \mathrm{S})(\mathrm{A\ vs.\ M}) = s\pi^* + b\beta + e\xi + y$$

where π^* indicates solvent dipolarity–polarizability, β represents the solvent hydrogen-bond-accepting (HBA) basicity, and ξ is the solvent coordinate covalency parameter which allows for the "family dependent" nature of enthalpies of H-bond formation (8). Parameter coefficients are s, b, and e; y is the y-axis intercept.

$\Delta\Delta H(\mathrm{v} \rightarrow \mathrm{S})$ values for *m*-cresol (vs. toluene), 1-butanol (vs. ethyl ether), 1-pentanol (vs. *n*-butyl methyl ether), and *t*-amyl alcohol (vs. *t*-butyl methyl ether) in 17 organic solvents, and correlations of the form of eq. [3], will be reported.

Experimental

Solutes and solvents were commercial samples in excess of 99% purity, with most exceeding 99.7%. Purities were established by silica capillary gas chromatography and an electronic integrator. Samples and solvents were stored over 3A or 4A molecular sieve. Triethylamine was distilled from ninhydrin to remove primary and secondary amine impurities. The calorimetric procedure and apparatus have previously been described (9).

Results and discussion

Heats of solution of *m*-cresol, 1-butanol, 1-pentanol, *t*-amyl alcohol, toluene, ethyl ether (Et_2O), *n*-butyl methyl ether (BuOMe), and *t*-butyl methyl ether (*t*-BuOMe), in organic solvents (*n*-heptane, cyclohexane, carbon tetrachloride (CCl_4), 1,2-dichloroethane ($ClCH_2CH_2Cl$), α,α,α-trifluorotoluene (CF_3Ph), triethylamine (Et_3N), butyl ether (Bu_2O), ethyl ace-

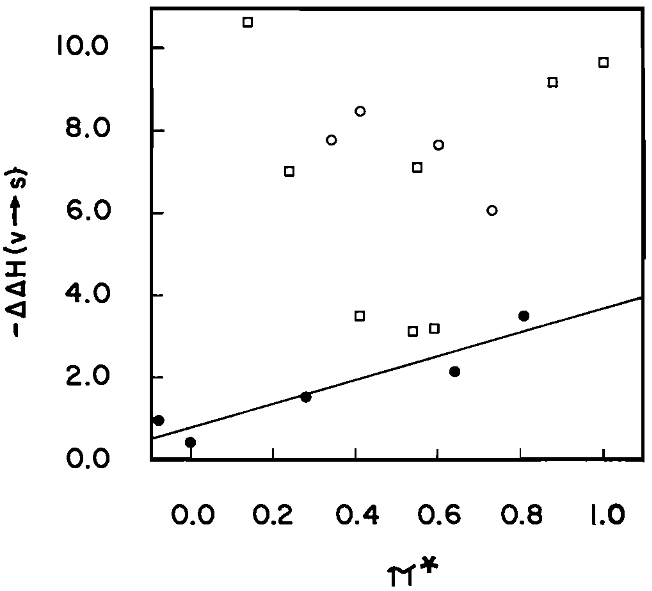

FIG. 1. Plot of $-\Delta\Delta H(\mathrm{v} \rightarrow \mathrm{S})$(*m*-cresol vs. toluene) versus π^* for NHB (●), HBA (□), and HBD (○) solvents.

tate (EtOAc), dimethylformamide (DMF), dimethyl sulfoxide (DMSO), benzene, toluene, mesitylene, 1-octanol, *t*-butyl alcohol (*t*-BuOH), methanol (MeOH), and 2,2,2-trifluoroethanol (CF_3CH_2OH)) are listed in Table 1, together with solute heats of vaporization and solvent solvatochromic parameters (π^*, β, ξ, α). Differences between alcohol solute and model solvation enthalpies are listed in Table 2.

m-*Cresol in aprotic solvents*

The correlation of $\Delta\Delta H(\mathrm{v} \rightarrow \mathrm{S})$(*m*-cresol vs. toluene) values with π^* for the five non-hydrogen-bonding solvents (*n*-heptane, cyclohexane, CCl_4, $ClCH_2CH_2Cl$, CF_3Ph) (Fig. 1) is:

[4] $\Delta\Delta H(\mathrm{v} \rightarrow \mathrm{S})(\text{cresol vs. toluene}) = -2.90\pi^* - 0.78$
$n = 5$, $r = 0.942$, see $= 0.47$ kcal/mol

where n is the number of solvents, r refers to the correlation coefficient, and see is the standard error of the estimate (10). This represents the *dipolarity–polarizability* contribution to the difference in cresol vs. toluene solvation enthalpy (the non-hydrogen-bonding baseline). Displacements of the HBA solvents from eq. [4], which represent H-bonding interactions (ΔH_h(NHBB)) (4, 6) are triethylamine, −9.46 kcal/mol; butyl ether, −5.54; ethyl acetate, −4.76; DMF, −5.86; DMSO, −5.98; mesitylene, −1.55; toluene, −0.84; benzene, −0.64; octanol, −6.00; *t*-butyl alcohol, −6.51; methanol, −5.16; and trifluoroethanol, −3.18. If H-bonding between *m*-cresol and the alcohol solvents results, in part, from the alcohols acting as H-bond donor acids and cresol as HBA base, the ΔH_h(NHBB) values will be slightly smaller than the "true" values, because the model compound toluene is a weak HBA base ($\beta = 0.11$), and toluene-solvent H-bonding will cancel a small portion of the cresol-solvent H-bonding interactions. Cresol is a stronger HBA base (than toluene) because of greater π electron density on the ring, or because the oxygen atom is a still stronger HBA center. Hydrogen bonding is strongest with triethylamine. For aromatic solvents, H-bonding decreases in the order: mesitylene > toluene > benzene > trifluorotoluene, also the order of decreasing pi electron density. The dependence of ΔH_h (NHBB) on solvent HBA basicity for the nonprotic solvents is

[5] $\Delta H_h(\text{NHBB}) = -8.22\beta - 3.47\xi - 0.30$
$n = 8$, $r = 0.986$, see $= 0.62$ kcal/mol

Addition of eqs. [4] and [5] gives a total solvatochromic equation for *m*-cresol ($n = 13$):

[6] $\Delta\Delta H(\mathrm{v} \rightarrow \mathrm{S})(\text{cresol vs. toluene}) = -2.90\pi^* - 8.22\beta - 3.47\xi - 1.08$

Single step, multiple parameter linear regression (MPLR) gives a better correlation which is in relatively poor agreement with eq. [6]:

[7] $\Delta\Delta H(\mathrm{v} \rightarrow \mathrm{S})(\text{cresol vs. toluene}) = -2.29\pi^* - 9.03\beta - 2.94\xi - 1.08$
$n = 13$, $r = 0.992$, see $= 0.51$

A total solvatochromic equation determined by MPLR using anisole ($\pi^* = 0.73$, $\beta = 0.22$, $\xi = 0.20$) rather than toluene ($\pi^* = 0.54$, $\beta = 0.11$, $\xi = 0.00$) as the model, has a π^* coefficient (−1.17) smaller than that of eq. [7] (as expected from the smaller difference in π^* between cresol and anisole). The β (−8.97) and ξ (−3.00) coefficients (and see value) are quite similar, since neither model is an H-bond donor acid.

Calculated (eqs. [6], [7]) values for non-hydrogen-bonding (NHB) and HBA solvents are within 0.75 kcal/mol of the observed values. However, differences between calculated and observed $\Delta\Delta H(\mathrm{v} \rightarrow \mathrm{S})$ values for alcohol solvents range from 0.9 to 3.4 kcal/mol.

m-*Cresol in alcohol solvents*

Alcohol solvents have the ability to interact with cresol via type A (solvent acts as a hydrogen-bond-donating (HBD) acid) and type B hydrogen bonding (solute is HBD acid). Alcohol solvent displacements from eq. [4] decrease with decreasing HBA basicity: *t*-BuOH > octanol > MeOH > trifluoroethanol, consistent with type B hydrogen bonding. This trend is opposite that observed when triethylamine is the solute in these alcohols (3). The displacement of trifluoroethanol solvent ($\beta = 0.00$) from eq. [4] is −3.18 kcal/mol, suggesting that type A hydrogen bonding is also operative. Type A hydrogen bonding is also observed for cresol in chloroform solvent ($\pi^* = 0.58$, $\beta = 0.00$, $\alpha = 0.44$), where α is the Taft–Kamlet HBD acidity parameter (6, 7). Subtraction of the estimated solvation of *m*-cresol in chloroform from that of toluene (11) gives a $\Delta\Delta H(\mathrm{v} \rightarrow \text{chloroform})$(*m*-cresol vs. toluene) value (−3.16 kcal/mol) which is displaced −0.70 kcal/mol from eq. [4] (exothermic). ($\Delta H(\mathrm{v} \rightarrow \text{chloroform})$(*m*-cresol) was estimated to be equal to the sum of the phenol (11) and calculated (5, 12) methylene group solvation enthalpies.)

Correlation of alcohol solvent (ROH) displacements from eq. [4] (Fig. 1) with solvent HBA basicity gives:

[8] $\Delta H_h(\text{NHBB})(\text{cresol vs. toluene}) = -3.23\beta - 3.17$
$n = 4$, $r = 0.999$, see $= 0.08$ kcal/mol

The excellent correlation is obtained without regard to HBD acidity (α parameter) but leads to the false conclusion that type B hydrogen bonding varies with changing ROH solvent while type A hydrogen bonding is constant. This arises from the inverse relationship between HBA basicity and HBD acidity of the four alcohol solvents:

[9] $\alpha = -1.19\beta + 1.79$
$n = 4$, $r = 0.996$, see $= 0.16$

This makes it impossible to assess the relative contributions of type A and type B interactions to the hydrogen bonding en-

TABLE 1. Solvent parameters and solute enthalpy of solution and vaporization values[a,b,c]

Solvent	π^*	α	β	ξ	*m*-Cresol	1-Butanol	1-Pentanol	*t*-Amyl alcohol	Ethyl ether	*t*-BuOMe
n-Heptane	−0.08	0.00	0.00	0.00	5.21±0.16[d]	5.80±0.17[d]	5.45±0.16[d]	5.62±0.17[d]	0.68±0.01	1.34±0.04[d]
Cyclohexane	0.00	0.00	0.00	0.00	6.02±0.18[d,e]	5.94±0.06	5.76±0.06	5.86±0.01	0.98±0.03[d]	1.54±0.01
CCl_4	0.28	0.00	0.00	0.00	4.08±0.12	4.59±0.08	4.57±0.06[f]	4.60±0.02	−0.42±0.02[d,f]	0.39±0.03
CF_3Ph	0.64	0.00	0.00	0.00	3.54±0.01[f]	4.32±0.01[f]	4.32±0.01[f]	3.86±0.01[f]	−0.29±0.01[f]	0.34±0.01[f]
$ClCH_2CH_2Cl$	0.81	0.00	0.00	0.00	2.25±0.08	3.85±0.08	3.97±0.07	3.59±0.03	0.01±0.01	−0.08±0.01
Et_3N	0.14	0.00	0.71	1.00	−4.83±0.09	−1.09±0.01	−1.04±0.01	−0.07±0.01	0.07±0.03	0.11±0.02
Bu_2O	0.24	0.00	0.46	0.20	−1.27±0.02	2.02±0.02	1.99±0.01	2.67±0.01	0.11±0.02	0.34±0.00
EtOAc	0.55	0.00	0.45	0.00	−1.33±0.05	2.09±0.09	2.27±0.05	2.07±0.03	0.28±0.00	0.25±0.01
DMF	0.88	0.00	0.69	0.00	−3.35±0.10[d,g]	0.79±0.02	1.02±0.01	0.83±0.01	0.53±0.01	0.63±0.03
DMSO	1.00	0.00	0.76	0.00	−3.07±0.06	1.09±0.05	1.42±0.06	1.30±0.05	1.33±0.08	1.48±0.01
Mesitylene	0.41	0.00	0.13[h]	0.00	2.29±0.00[f]	3.88±0.05[f]	3.89±0.08[f]	3.57±0.01[f]	0.09±0.00[f]	0.70±0.00[f]
Toluene	0.54	0.00	0.11	0.00	2.50±0.03[f]	4.05±0.04[f]	4.01±0.00[f]	3.89±0.02	−0.10±0.00[f]	0.63±0.01
Benzene	0.59	0.00	0.10	0.00	2.58±0.08[e]	4.05±0.01[f]	4.22±0.04	3.96±0.08	0.20±0.01[f]	0.62±0.00[f]
1-Octanol	0.34[h]	0.73[h]	0.90[h]	0.20	−1.57±0.03	0.09±0.02	0.06±0.01	−0.44±0.01	0.64±0.02	0.48±0.01
t-BuOH	0.41	0.68	1.01	0.20	−1.04±0.02	−0.55±0.05	−0.50±0.01	0.06±0.02	0.53±0.07	0.24±0.02
MeOH	0.60	0.98	0.62	0.20	−1.55±0.05[e]	0.21±0.00	0.38±0.02	−0.63±0.00	0.06±0.00	−0.17±0.02
CF_3CH_2OH	0.73	1.51	0.00	0.20	1.06±0.01	0.12±0.00	0.46±0.01	−0.43±0.02	−3.22±0.08	−3.76±0.07
ΔH_v					14.75±0.25[i]	12.46±0.00[f]	13.61±0.04[i]	11.94±0.02[f]	6.49±0.06[i]	7.27±0.02[i]

[a] ΔH_s and ΔH_v in kcal/mol.
[b] Solvent solvatochromic parameters from ref. 7.
[c] Toluene and *n*-BuOMe solute ΔH_s and ΔH_v values from ref. 2.
[d] Uncertainty interval (2 × sdm) estimated (2).
[e] Reference 13.
[f] Reference 14.
[g] Reference 15.
[h] Solvatochromic parameters estimated by extrapolation of methanol-1-butanol values
[i] Reference 16.

TABLE 2. $\Delta\Delta H$(v $\rightarrow$ S)(alcohol vs. model) values[a]

Solvent	Butanol vs. Et_2O	Pentanol vs. BuOMe	*t*-Amyl alcohol vs. *t*-BuOMe	*m*-Cresol vs. toluene
n-Heptane	−0.85	−0.80	−0.39	−0.95
c-C_6	−1.01	−0.76	−0.35	−0.42
CCl_4	−0.96	−1.03	−0.46	−1.55
CF_3Ph	−1.36	−1.36	−1.15	−2.18
$ClCH_2CH_2Cl$	−2.13	−2.10	−1.00	−3.52
Et_3N	−7.13	−6.93	−4.85	−10.63
Bu_2O	−4.06	−3.90	−2.34	−7.00
CH_3COOEt	−4.16	−3.98	−2.85	−7.12
DMF	−5.17	−5.66	−4.47	−9.18
DMSO	−6.04	−5.84	−4.85	−9.65
Mesitylene	−2.18	−1.90	−1.80	−3.51
Toluene	−1.82	−1.82	−1.41	−3.17
Benzene	−2.12	−1.89	−1.33	−3.21
1-Octanol	−6.52	−6.47	−5.59	−7.75
t-BuOH	−7.05	−7.06	−4.85	−8.47
MeOH	−5.82	−5.91	−5.13	−7.67
CF_3CH_2OH	−2.63	−2.63	−1.34	−6.07

[a]In kcal/mol.

thalpy. However, the order of alcohol displacements and the zero β value of trifluoroethanol suggest that the $b\beta$ portion of eq. [8] represents the minimum possible enthalpy of type B H-bond formation, whereas the *y*-intercept represents the maximum possible type A ΔH_h. The "true" type B values for the HBA alcohols will be larger because the contribution of type A H-bonding decreases as HBD acidity decreases, rather than remaining constant at the value determined by trifluoroethanol (*y*-intercept). Finally, we note that type A H-bonding by trifluoroethanol solvent (α = 1.51) to *m*-cresol should be substantially stronger than type A H-bonding by chloroform solvent (α = 0.44), as is observed.

Aliphatic alcohols

The plot of $\Delta\Delta H$(v $\rightarrow$ S)(pentanol vs. *n*-butyl methyl ether) versus solvent π^* is shown in Fig. 2 and is very similar to analogous plots for *m*-cresol (Fig. 1) and 1-octanol (4). The same is also true for 1-butanol and *t*-amyl alcohol solutes.

The correlation of 1-pentanol $\Delta\Delta H$(v $\rightarrow$ S) values with those of the NHB solvents is

[10] $\Delta\Delta H$(v $\rightarrow$ NHB)(pentanol vs. BuOMe) = $-1.32\pi^* - 0.78$
$n = 5$, $r = 0.931$, see = 0.23 kcal/mol

The expression for the dependence of HBA solvent (ROH omitted) displacements on β and ξ is

[11] ΔH_h(NHBB)(pentanol) = $-5.47\beta - 2.24\xi - 0.15$
$n = 8$, $r = 0.996$, see = 0.21 kcal/mol

The total solvatochromic equation from eqs. [10] and [11] is

[12] $\Delta\Delta H$(v $\rightarrow$ S)(pentanol vs. BuOMe) = $-1.32\pi^* - 5.47\beta - 2.24\xi - 0.63$

MPLR gives a total solvatochromic equation in good agreement with eq. [12]:

[13] $\Delta\Delta H$(v $\rightarrow$ S)(pentanol vs. BuOMe) = $-1.22\pi^* - 5.31\beta - 2.22\xi - 0.76$
$n = 13$, $r = 0.997$, see = 0.19

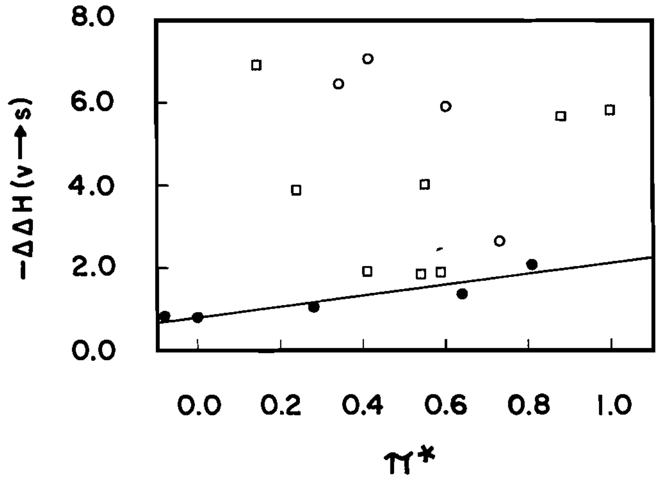

FIG. 2. Plot of $-\Delta\Delta H$(v $\rightarrow$ S)(1-pentanol vs. *n*-BuOMe) versus π^* for NHB (●), HBA (□), and HBD (○) solvents.

Total solvatochromic equations (MPLR) for 1-butanol (BuOH) and *t*-amyl alcohol are given by eqs. [14] and [15]. Alcohol solvents have been omitted.

[14] $\Delta\Delta H$(v $\rightarrow$ S)(BuOH vs. Et_2O) = $-1.07\pi^* - 5.22\beta - 2.36\xi - 0.92$
$n = 13$, $r = 0.995$, see = 0.24 kcal/mol

[15] $\Delta\Delta H$(v $\rightarrow$ S)(*t*-amyl alcohol vs. *t*-BuOMe) = $-1.12\pi^* - 4.40\beta - 1.15\xi - 0.32$
$n = 13$, $r = 0.991$, see = 0.26 kcal/mol

Based on relative β and ξ values (eqs. [13], [15]), hydrogen bonding of *t*-amyl alcohol is about 80% of that of its normal isomer. The β coefficient for *m*-cresol (eq. [6]) is almost twice as large as that of *t*-amyl alcohol, which reflects the greater HBD acidity of *monomeric* cresol (α_m) relative to monomeric alcohol solutes (Dr. Mortimer J. Kamlet, private communication).

The solvation enthalpy of *t*-amyl alcohol in *n*-heptane is less exothermic than that of 1-pentanol by 1.84 kcal/mol. The two alcohols have well matched molar volumes, and the discrepancy probably results from a dispersion interaction (rather than a cavity formation) mismatch. Approximately 0.95 kcal/mol can be attributed to the loss of quaternary carbon solvation (1, 5). The remaining 0.89 kcal/mol possibly results from a decrease in hydroxyl group solvation by dispersion interactions when hindered by an attached *t*-amyl group.

Acknowledgement

This study was supported by the Robert A. Welch Foundation (Grant E-136).

1. W. K. STEPHENSON and R. FUCHS. Can. J. Chem. **63**, 336 (1985).
2. W. K. STEPHENSON and R. FUCHS. Can. J. Chem. In press.
3. W. K. STEPHENSON and R. FUCHS. Can. J. Chem. In press.
4. W. K. STEPHENSON and R. FUCHS. Can. J. Chem. **63**, 342 (1985).
5. W. K. STEPHENSON. Ph.D. dissertation, University of Houston. 1984.
6. M. J. KAMLET, J. L. M. ABBOUD, and R. W. TAFT. Prog. Phys. Org. Chem. **13**, 485 (1981).
7. M. J. KAMLET, J. L. M. ABBOUD, M. H. ABRAHAM, and R. W. TAFT. J. Org. Chem. **48**, 2877 (1983).

8. R. W. TAFT, T. GRAMSTAD, and M. J. KAMLET. J. Org. Chem. **47**, 4557 (1982).
9. R. FUCHS and P. P. S. SALUJA. Can. J. Chem. **54**, 3857 (1976).
10. M. H. ABRAHAM. J. Am. Chem. Soc. **104**, 2085 (1982).
11. J. N. SPENCER, E. S. HOLMBOE, D. W. FIRTH, and M. R. KIRSHENBAUM. J. Soln. Chem. **10**, 745 (1981).
12. W. K. STEPHENSON and R. FUCHS. Can. J. Chem. **63**, 349 (1985).
13. R. FUCHS, T. M. YOUNG, and R. F. RODEWALD. J. Am. Chem. Soc. **96**, 4705 (1974).
14. R. FUCHS, L. A. PEACOCK, and W. K. STEPHENSON. Can. J. Chem. **60**, 1953 (1982).
15. R. FUCHS and R. F. RODEWALD. J. Am. Chem. Soc. **95**, 5897 (1973).
16. J. B. PEDLEY and J. RYLANCE. Sussex-N.P.L. computer analysed thermochemical data: organic and organometallic compounds. University of Sussex, Brighton. 1977.

Enthalpies of interaction of nitrogen base solutes with organic solvents

W. KIRK STEPHENSON AND RICHARD FUCHS
Department of Chemistry, University of Houston, Houston, TX 77004, U.S.A.

Received September 27, 1984

W. KIRK STEPHENSON and R. FUCHS. Can. J. Chem. **63**, 2540 (1985).

Heats of solution of triethylamine, aniline, pyridine, and model compounds (3-ethylpentane, benzene) in 17 organic solvents (*n*-heptane, cyclohexane, carbon tetrachloride, 1,2-dichloroethane, α,α,α-trifluorotoluene, triethylamine, butyl ether, ethyl acetate, dimethylformamide, dimethyl sulfoxide, benzene, toluene, mesitylene, *t*-butyl alcohol, 1-octanol, methanol, 2,2,2-trifluoroethanol) have been combined with solute heats of vaporization to give enthalpies of transfer from vapor to solvent ($\Delta H(\text{v} \rightarrow \text{s})$). Differences between solute and model values ($\Delta\Delta H(\text{v} \rightarrow \text{s}) = \Delta H(\text{v} \rightarrow \text{s})$ (solute) $-$ $\Delta H(\text{v} \rightarrow \text{s})$ (model)) were used to evaluate nitrogen base solute–solvent polar interactions. Correlations of $\Delta\Delta H(\text{v} \rightarrow \text{s})$ with Taft–Kamlet solvatochromic parameters (π^*, α, β) have been determined.

Aniline was found to be a better hydrogen bond donor acid than hydrogen bond acceptor base. Nevertheless, alcohols donate H-bonds to aniline. Triethylamine and pyridine are stronger HBA bases than aniline. The π^* (dipolarity–polarizability) parameter of aniline (as a solute) is calculated to be 1.10.

W. KIRK STEPHENSON et R. FUCHS. Can. J. Chem. **63**, 2540 (1985).

On a combiné les chaleurs de solution de la triéthylamine, de l'aniline, de la pyridine et de composés types (éthyl-3 pentane, benzène) dans 17 solvants organiques (*n*-heptane, cyclohexane, tétrachlorure de carbone, dichloro-1,2 éthane, α,α,α-trifluorotoluène, triéthylamine, éther butylique, acétate d'éthyle, diméthylformamide, diméthylsulfoxyde, benzène, toluène, mésitylène, alcool *tert*-butylique, octanol-1, méthanol, trifluoro-2,2,2 éthanol) avec les chaleurs de vaporisation du soluté pour obtenir les enthalpies de transfert de la vapeur au solvant ($\Delta H(\text{v} \rightarrow \text{s})$). On a utilisé les différences entre les valeurs pour les solutés et celles pour les composés modèles ($\Delta\Delta H(\text{v} \rightarrow \text{s}) = \Delta H(\text{v} \rightarrow \text{s})$ (soluté) $-$ $\Delta H(\text{v} \rightarrow \text{s})$ (modèle)) pour évaluer les interactions polaires entre le soluté (base azotée) et le solvant. On a déterminé des corrélations existant entre le $\Delta\Delta H(\text{v} \rightarrow \text{s})$ et les paramètres solvatochromiques de Taft–Kamlet (π^*, α, β).

On a trouvé que l'aniline agit mieux comme acide donneur de liaison hydrogène que comme base qui accepte des liaisons hydrogènes. Quoiqu'il en soit, les alcools donnent des liaisons hydrogènes à l'aniline. Par rapport à l'aniline, la triéthylamine et la pyridine sont des bases acceptrices de liaisons hydrogènes plus fortes. On a calculé que le paramètre π^* (dipolarité–polarisabilité) de l'aniline est égal à 1.10.

[Traduit par le journal]

We have recently studied the enthalpies of interaction of ketone (1, 2) and aromatic (2, 3) solutes with organic solvents of varying polarity, and now extend our study to several nitrogen bases, triethylamine, pyridine, and aniline. Enthalpies of interaction are determined by the solvation enthalpy, or $\Delta\Delta H(\text{v} \rightarrow \text{s})$, method. The solvation enthalpy is the enthalpy of transfer of a solute from vapor to solvent,

$$[1] \quad \Delta H(\text{v} \rightarrow \text{s}) = \Delta H_{\text{s}} - \Delta H_{\text{v}} = \Delta H_{\text{c}} + \Delta H_{\text{int}}$$

where ΔH_{s} is the heat of solution of the liquid solute; ΔH_{v}, the solute heat of vaporization; ΔH_{c}, the enthalpy of cavity formation within the solvent; and ΔH_{int}, the enthalpy of interaction of the solute with the solvent. ΔH_{s} and ΔH_{v} are determined experimentally.

In a polar hydrogen-bond-donating (HBD) solvent, triethylamine, pyridine, and aniline are capable of dispersion (d), polar (p), and hydrogen bonding (h) interactions, and the solvation enthalpy is

$$[2] \quad \Delta H(\text{v} \rightarrow \text{s}) = \Delta H_{\text{c}} + \Delta H_{\text{d}} + \Delta H_{\text{p}} + \Delta H_{\text{h}}$$

Triethylamine and pyridine are capable of type A H-bonding (solvent acts as HBD acid) only, whereas aniline is amphiprotic and might undergo either type A or type B (solvent acts as hydrogen-bond-acceptor (HBA) base) H-bonding or both. Polar and H-bonding enthalpies of interaction can, in principle, be isolated by subtracting the solvation enthalpy of a suitable model compound (M) from that of the solute (A),

$$[3] \quad \Delta\Delta H(\text{v} \rightarrow \text{s}) = \Delta\Delta H_{\text{c}} + \Delta\Delta H_{\text{d}} + \Delta H_{\text{p}} + \Delta H_{\text{h}}$$

where $\Delta\Delta H_{\text{c}}$ and $\Delta\Delta H_{\text{d}}$ refer to the difference between solute and model cavity formation and dispersion interactions, respectively. It has often been assumed that the first two terms on the right side of eq. [3] are equal to zero, and if the model is nonpolar and non-H-bonding, $\Delta\Delta H(\text{v} \rightarrow \text{s}) = \Delta H_{\text{p}} + \Delta H_{\text{h}}$, or in the absence of solute H-bonding, $\Delta\Delta H(\text{v} \rightarrow \text{s}) = \Delta H_{\text{p}}$. If a model is chosen such that the solute cavity formation, dispersion, and polar interactions cancel, then $\Delta\Delta H(\text{v} \rightarrow \text{s}) = \Delta H_{\text{h}}$. In reality perfect model compounds are likely to be rare.

Solvation enthalpy differences can be quantitatively expressed in terms of the Taft–Kamlet solvatochromic parameters (4–6),

$$[4] \quad \Delta\Delta H(\text{v} \rightarrow \text{s}) = s\pi^* + a\alpha + b\beta + y$$

where π^* provides a measure of solvent dipolarity–polarizability; α, the solvent HBD acidity; and β, the solvent HBA basicity. Parameter coefficients are s, a, and b; y is the y-axis intercept.

In this paper, $\Delta\Delta H(\text{v} \rightarrow \text{s})$ values for triethylamine (vs. 3-ethylpentane), pyridine (vs. benzene), and aniline (vs. benzene) in 17 organic solvents will be reported. Correlations having the form of eq. [4] will also be presented. Previous correlations involving triethylamine and pyridine in non-H-bond donor solvents have examined only polar effects (π^*) (7). Some values of $\Delta H(\text{v} \rightarrow \text{s})$ for triethylamine vs. tetramethyltin have been reported (8), but correlations with solvatochromic parameters were not examined.

Experimental

Solutes and solvents were commercial samples in excess of 99% purity, with most exceeding 99.7%. Purities were established by silica capillary gas chromatography and an electronic integrator. All solutes and solvents were stored over 4A molecular sieve, except for methanol

TABLE 1. Solvent parameters and solute enthalpies of solution and vaporization[a,b]

Solvent	π^*	α	β	Pyridine
n-Heptane	−0.08	0.00	0.00	1.99±0.06[c]
Cyclohexane	0.00	0.00	0.00	1.96±0.04
CCl_4	0.28	0.00	0.00	0.31±0.01[e]
CF_3Ph	0.64	0.00	0.00	0.26±0.04[e]
$ClCH_2CH_2Cl$	0.81	0.00	0.00	−0.10±0.01
Et_3N	0.14	0.00	0.71	1.02±0.02
Bu_2O	0.24	0.00	0.46	0.98±0.02
EtOAc	0.55	0.00	0.45	0.08±0.01
DMF	0.88	0.00	0.69	−0.10±0.01
DMSO	1.00	0.00	0.76	0.23±0.03
Mesitylene	0.41	0.00	(0.13)	0.73±0.01[e]
Toluene	0.54	0.00	0.11	0.19±0.01
Benzene	0.59	0.00	0.10	0.01±0.01[d]
1-Octanol	(0.34)	(0.73)	(0.90)	0.18±0.00
t-BuOH	0.41	0.68	1.01	−0.29±0.05
MeOH	0.60	0.98	0.62	−1.02±0.00
CF_3CH_2OH	0.73	1.51	0.00	−5.07±0.12
ΔH_v				9.61±0.01[g]

Solvent	Triethylamine	Aniline	Benzene	3-Ethylpentane
n-Heptane	0.08±0.01	3.59±0.11[c]	0.79±0.03[c]	0.00±0.00
Cyclohexane	0.32±0.03	4.22±0.13[c,d]	0.91±0.02[c,e]	0.23±0.01
CCl_4	−0.75±0.01	2.07±0.01	0.13±0.00	0.32±0.02
CF_3Ph	−0.24±0.03	1.97±0.00[e]	0.25±0.01[e]	0.83±0.01
$ClCH_2CH_2Cl$	0.42±0.01	0.50±0.01	0.12±0.02	1.96±0.05
Et_3N	0.00±0.00	−0.44±0.01	0.27±0.01	0.06±0.02
Bu_2O	−0.14±0.02	0.70±0.03	0.22±0.00	0.10±0.01
EtOAc	0.78±0.01	−0.84±0.01	0.09±0.01	1.47±0.01
DMF	1.35±0.07	−2.68±0.08[c,f]	0.04±0.02[c,f]	2.13±0.06
DMSO	2.23±0.05	−2.60±0.03	0.75±0.06	3.45±0.05
Mesitylene	−0.04±0.01	1.89±0.04[e]	0.38±0.06[e]	0.38±0.02
Toluene	0.27±0.01	1.40±0.02	0.06±0.04	0.72±0.02
Benzene	0.50±0.03	1.25±0.04[c,d]	0.00±0.00[e]	1.25±0.02
1-Octanol	−2.08±0.03	1.11±0.03	0.71±0.02	0.26±0.02
t-BuOH	−0.80±0.03	2.68±0.03	1.85±0.02	1.13±0.06
MeOH	−3.10±0.07	−0.62±0.03[c,f]	0.36±0.02[c,f]	1.30±0.01
CF_3CH_2OH	−17.58±0.10	−0.72±0.02	1.47±0.06	2.75±0.05
ΔH_v	8.35±0.01[h]	13.33±0.01[g]	8.09±0.01[g]	8.42±0.01[h]

[a] ΔH_s and ΔH_v in kcal/mol.
[b] Parentheses denote estimated values (ref. 5).
[c] Uncertainty interval (2 × sdm) estimated as 0.01 kcal/mol for ΔH_s between 0.00 and 0.49; 0.02 kcal/mol for ΔH_s between 0.50 and 1.00; and 3% of ΔH_s for values >1.00 kcal/mol.
[d] Reference 13.
[e] Reference 14.
[f] Reference 15.
[g] Reference 16.
[h] Reference 17.

and trifluoroethanol (3A). Triethylamine was distilled from ninhydrin to remove primary and secondary amine impurities. The calorimetric procedure and apparatus have previously been described (9).

Results and discussion

Heats of solution of triethylamine (Et_3N), pyridine, aniline (NH_2Ph), benzene, and 3-ethylpentane (Et_3CH) in 17 organic solvents (*n*-heptane, cyclohexane, carbon tetrachloride (CCl_4), 1,2-dichloroethane ($ClCH_2CH_2Cl$), α,α,α-trifluorotoluene (CF_3Ph), triethylamine (Et_3N), butyl ether (Bu_2O), ethyl acetate (EtOAc), dimethylformamide (DMF), dimethyl sulfoxide (DMSO), benzene, toluene, mesitylene, 1-octanol, *t*-butyl alcohol (*t*-BuOH), methanol (MeOH), and 2,2,2-trifluoroethanol (CF_3CH_2OH), solute heats of vaporization, and solvent solvatochromic parameters (π^*, α, β) are given in Table 1. Differences between nitrogen base and model solvation enthalpies are listed in Table 2.

Triethylamine

3-Ethylpentane (Et_3CH) is a good model for triethylamine because of the similar structural features and molar volumes ($\Delta MV = -4.4$ mL/mol). A plot of $\Delta\Delta H(v \rightarrow s)$ (triethylamine vs. 3-ethylpentane) values against solvent π^* is shown in Fig. 1. The dependence of triethylamine solvation on select solvent (4) polarity is given by eq. [5] (solvent = heptane, cyclohexane, Et_3N, Bu_2O, EtOAc, DMF, DMSO),

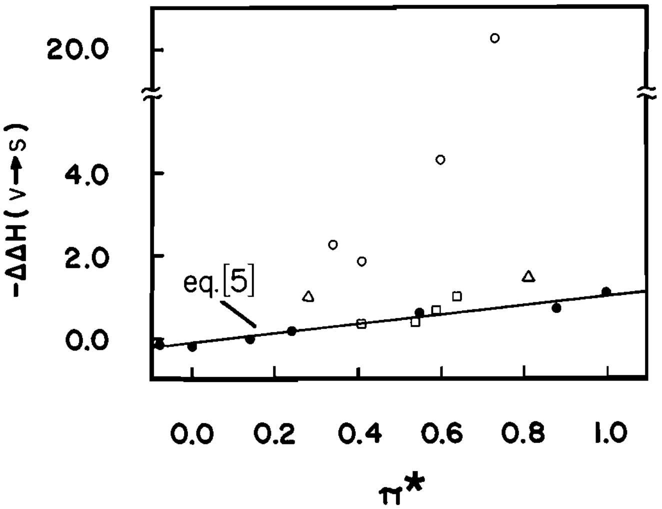

FIG. 1. Plot of $-\Delta\Delta H(\text{v} \rightarrow \text{s})(Et_3N$ vs. $Et_3CH)$ versus π^* for select (●), chloro (△), aromatic (□), and alcohol (○) solvents.

$$[5] \quad \Delta\Delta H(\text{v} \rightarrow \text{s})\ (Et_3N \text{ vs. } Et_3CH) = -1.12\pi^* + 0.11$$

$$n = 7,\ r = 0.980,\ \text{see} = 0.11 \text{ kcal/mol}$$

where n is the number of solvents, r denotes the correlation coefficient, and see refers to the standard error of the estimate (10). Mesitylene, toluene, and benzene are within 0.13 kcal/mol of eq. [5]. Trifluorotoluene is displaced exothermically by 0.39 kcal/mol, possibly due to electron donor–acceptor (charge transfer) (11) complex formation with triethylamine. Exothermic displacements of carbon tetrachloride (0.80 kcal/mol) and 1,2-dichloroethane (0.67 kcal/mol) probably result, at least partially, from a reaction with the nucleophilic amine. Reactions between amine solutes and carbon tetrachloride solvent are well documented (12).

t-Butyl alcohol, octanol, methanol, and trifluoroethanol are displaced exothermically from eq. [5] by 1.51, 2.00, 3.77, and 19.55 kcal/mol, respectively. These displacements follow the order of increasing HBD acidity:

[6] *t*-BuOH < octanol < MeOH < trifluoroethanol

and are the result of amine solute–alcohol solvent type A hydrogen bonding. $\Delta\Delta H(\text{v} \rightarrow \text{trifluoroethanol})$ is extremely large and possibly represents a proton transfer reaction in which the triethylammonium cation is formed. However, a reasonable alternative has been suggested by M. J. Kamlet (private communication). Alcohol solvents donate H-bonds to triethylamine at the expense of alcohol–alcohol H-bonds. The energy gain should depend on the HBA (β, ξ) *difference* between amine and alcohol. The difference is moderate for 1-octanol, *tert*-butyl alcohol, and methanol (vs. Et_3N), but is very large for trifluoroethanol ($\beta = 0.00$).

A total solvatochromic equation derived for the dissolution of triethylamine in select, aromatic (except trifluorotoluene), and alcohol (except trifluoroethanol) solvents using multiple parameter linear regression is

$$[7] \quad \Delta\Delta H(\text{v} \rightarrow \text{s})\ (Et_3N \text{ vs. } Et_3CH) = -1.26\pi^* - 3.19\alpha + 0.20$$

$$n = 13,\ r = 0.973,\ \text{see} = 0.32 \text{ kcal/mol}$$

The relative importance of H-bonding and polar interactions process is seen in the a/s ratio of 2.5. The π^* coefficients of eq. [5] and [7] are in fair agreement. Calculated (eq. [7]) values of $\Delta\Delta H(\text{v} \rightarrow \text{ROH})$ are more exothermic than the observed for octanol (−0.29 kcal/mol) and *t*-butyl alcohol (−0.63 kcal/mol), and more endothermic for methanol (0.65 kcal/mol). It may be that the two strongly HBA alcohols compete with solute as H-bond acceptors, whereas the weaker acceptor (methanol) does not.

TABLE 2. $\Delta\Delta H(\text{v} \rightarrow \text{s})$(nitrogen base vs. model) values[a]

Solvent	Pyridine vs. benzene	Triethylamine vs. 3-ethylpentane	Aniline vs. benzene
n-Heptane	−0.32	0.15	−2.44
Cyclohexane	−0.47	0.16	−1.93
CCl_4	−1.34	−1.00	−3.30
CF_3Ph	−1.26	−1.00	−3.27
$ClCH_2CH_2Cl$	−1.74	−1.47	−4.86
Et_3N	−0.77	0.01	−5.95
Bu_2O	−0.76	−0.17	−4.76
CH_3COOEt	−1.53	−0.62	−6.17
DMF	−1.66	−0.71	−7.96
DMSO	−2.04	−1.10	−8.59
Mesitylene	−1.41	−0.35	−3.73
Toluene	−1.39	−0.38	−3.90
Benzene	−1.51	−0.68	−3.99
1-Octanol	−2.05	−2.27	−4.84
t-BuOH	−3.66	−1.86	−4.41
MeOH	−2.90	−4.33	−6.22
CF_3CH_2OH	−8.06	−20.26	−7.43

[a]kcal/mol.

Aniline

Aniline is a solute capable of dispersion, polar, and hydrogen bonding (HBA and HBD) interactions. The cavity formation mismatch of aniline (MV = 91.2 mL/mol) vs. benzene (MV = 88.9 mL/mol) $\Delta\Delta H(\text{v} \rightarrow \text{s})$ is minimal. The plot of $\Delta\Delta H(\text{v} \rightarrow \text{s})$ vs. solvent π^* is shown in Fig. 2. The major problem in evaluating H-bonding interactions via the non-hydrogen-bonding-baseline (NHBB) method (2, 4, 6) is that a baseline cannot be clearly defined. Carbon tetrachloride and 1,2-dichloroethane possibly react with the amine, and the line defined by the alkanes and trifluorotoluene (three data points) is suspect. However, for discussion purposes, the NHB baseline will be taken as the best fit line between the five NHB solvents:

$$[8] \quad \Delta\Delta H(\text{v} \rightarrow \text{s})\ (\text{aniline vs. benzene}) = -2.55\pi^* - 2.32$$

$$n = 5,\ r = 0.891,\ \text{see} = 0.58 \text{ kcal/mol}$$

Enthalpies of H-bond formation of aniline with aromatic and dipolar aprotic solvents, as measured by displacements from eq. [8], correlate well with solvent HBA basicity (and are essentially independent of the base family dependent term ξ):

$$[9] \quad \Delta H_h(\text{NHBB})(\text{aniline}) = -5.30\beta + 0.36$$

$$n = 8,\ r = 0.992,\ \text{see} = 0.21 \text{ kcal/mol}$$

Alcohol solvents can accept or donate a hydrogen bond, but displacements from eq. [8] follow a pattern identical to that observed with triethylamine as solute (eq. [6]). If the displacements are assumed to result from type A hydrogen bonding (solvent acts as HBD acid), then for the alcohol solvents:

$$[10] \quad \Delta H_h(\text{NHBB})(\text{aniline}) = -2.37\alpha + 0.26$$

$$n = 4,\ r = 0.957,\ \text{see} = 0.34 \text{ kcal/mol}$$

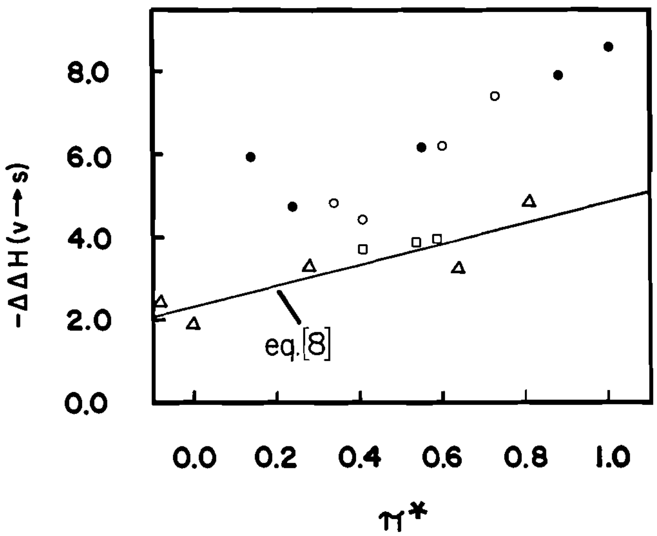

FIG. 2. Plot of $-\Delta\Delta H(v \rightarrow s)(NH_2Ph$ vs. benzene) versus π^* for H-bond acceptor (●), non-hydrogen-bonding (△), aromatic (□), and alcohol (○) solvents.

Trifluoroethanol ($\beta = 0.00$), which does not significantly undergo type B hydrogen bonding, falls well within the standard error of the estimate of eq. [10].

Addition of eq. [8]–[10] gives rise to an "all solvents" total solvatochromic equation:

$$[11] \quad \Delta\Delta H(v \rightarrow s)(\text{aniline vs. benzene}) = -2.55\pi^* -5.30\beta - 2.37\alpha - 1.70 \text{ kcal/mol}$$

where $n = 17$ and the combined see value is 0.70 kcal/mol. Multiple parameter linear regression of $\Delta\Delta H(v \rightarrow s)$ values for the same solvents gives a similar equation (β for ROH solvents assumed to be nil, i.e., aniline–alcohol solvent type B H-bonding assumed to be absent, since this would be at the expense of alcohol–alcohol H-bonding, giving no energy advantage):

$$[12] \quad \Delta\Delta H(v \rightarrow s)(\text{aniline vs. benzene}) = -2.67\pi^* -4.88\beta - 2.25\alpha - 2.16$$

$$n = 17, r = 0.985, \text{see} = 0.36 \text{ kcal/mol}$$

The dependence of aniline solvation on polar interactions is slightly larger than on type A hydrogen bonding ($s/a = 1.19$) and much smaller than type B hydrogen bonding ($s/b = 0.55$). Aniline is a considerably better hydrogen bond donor than hydrogen bond acceptor. As an acceptor aniline is considerably weaker than triethylamine (eq. [7]).

The (unreported) π^* value of aniline may be estimated from the π^* coefficients (s) in eqs. [11] and [12] as 1.09 and 1.11, based on the relationship (7) of s and the difference in π^* of solute and model.

Pyridine

Correlation of $\Delta\Delta H(v \rightarrow s)$ with π^* of the select solvents gives

$$[13] \quad \Delta\Delta H(v \rightarrow s)(\text{pyridine vs. benzene}) = -1.52\pi^* - 0.49$$

$$n = 7, r = 0.983, \text{see} = 0.13 \text{ kcal/mol}$$

Mesitylene and carbon tetrachloride are displaced exothermically by 0.30 and 0.43 kcal/mol, respectively. All other nonprotic solvents lie within 0.20 kcal/mol of eq. [13]. The negative s value is consistent with the greater polarity of pyridine ($\pi^* = 0.87$) relative to benzene ($\pi^* = 0.59$).

The four alcohol solvents are displaced exothermically from eq. [13] as a result of relatively strong type A hydrogen bonding with pyridine ($\beta = 0.64$). Displacements from eq. [13] values increase in the order octanol < MeOH < *t*-BuOH < trifluoroethanol by −1.04, −1.50, −2.55, and −6.46 kcal/mol, respectively. $\Delta\Delta H(v \rightarrow \text{ROH})$ values follow the same order and are difficult to rationalize because of the difficulty of separating the influence of ROH solvent–solvent intermolecular and pyridine–ROH solvent type A hydrogen bonding interactions. For weak HBA solutes such as 1-hexene, 1-octene, anisole, fluoro- and chlorooctane ($0.0 \leq \beta \leq 0.2$), the four alcohol solvents lie on, or endothermically displaced from, $\Delta\Delta H(v \rightarrow s)$ vs. non-HBA solvent π^* correlations (2, 3). The reason for the endothermic displacements is unknown but these possibly result from the formation of enthalpically less favorable solute – ROH solvent H-bonds at the expense of enthalpically more favorable but entropically less favorable solvent–solvent intermolecular hydrogen bonds. For slightly stronger HBA solutes (ethers, $\beta \sim 0.5$; ketones, ~ 0.5) 1-octanol, *t*-BuOH, and MeOH ($0.62 \leq \beta \leq 1.01$) lie on, or endothermically displaced from, analogous correlations; trifluoroethanol, the only ROH solvent with a β value (0.00) less than that of the solutes, is exothermically displaced. All four alcohol solvents are exothermically displaced from the triethylamine ($\beta = 0.71$), aniline, and pyridine correlations. It appears that an increase in the solute HBA basicity increases the extent to which solute–solvent H-bonding (exothermic displacements) competes with solvent–solvent intermolecular H-bonding. Because it is unknown whether enthalpies of H-bond formation with alcohol solvents are best described by displacements of $\Delta\Delta H(v \rightarrow \text{ROH})$(pyridine vs. model) values from eq. [13] or from arbitrary points endothermically displaced from eq. [13], exothermic displacements of ROH solvents (ΔH_h(NHBB)) are thought to represent minimum hydrogen bonding enthalpies. For trifluoroethanol, a weakly self-associating alcohol, the displacement from eq. [13] is probably a reasonable measure of the enthalpy of H-bond formation with pyridine.

Acknowledgement

This study was supported by the Robert A. Welch Foundation (Grant E-136).

1. W. K. STEPHENSON and R. FUCHS. Can. J. Chem. **63**, 336 (1985).
2. W. K. STEPHENSON. Ph.D. dissertation, University of Houston. 1984.
3. W. K. STEPHENSON and R. FUCHS. To be published.
4. M. J. KAMLET, J. L. M. ABBOUD, and R. W. TAFT. Prog. Phys. Org. Chem. **13**, 485 (1981).
5. M. J. KAMLET, J. L. M. ABBOUD, M. H. ABRAHAM, and R. W. TAFT. J. Org. Chem. **48**, 2877 (1983).
6. W. K. STEPHENSON and R. FUCHS. Can. J. Chem. **63**, 342 (1985).
7. R. FUCHS and W. K. STEPHENSON. J. Am. Chem. Soc. **105**, 5159 (1983).
8. M. H. ABRAHAM and A. NASEHZADEH. J. Chem. Thermodyn. **13**, 549 (1981).
9. R. FUCHS and P. P. S. SALUJA. Can. J. Chem. **54**, 3857 (1976).
10. M. H. ABRAHAM. J. Am. Chem. Soc. **104**, 2085 (1982).
11. J. ROSE. Molecular complexes. Pergamon Press, New York. 1967.

12. H. F. COLLINS. Chem. Ind. London, 704 (1957).
13. R. FUCHS, T. M. YOUNG, and R. F. RODEWALD. J. Am. Chem. Soc. **96**, 4705 (1974).
14. P. P. S. SALUJA, T. M. YOUNG, R. F. RODEWALD, F. H. FUCHS, D. KOHLI, and R. FUCHS. J. Am. Chem. Soc. **99**, 2949 (1977).
15. R. FUCHS and R. F. RODEWALD. J. Am. Chem. Soc. **95**, 5897 (1973).
16. J. B. PEDLEY and J. RYLANCE. Sussex-N.P.L. computer analysed thermochemical data: organic and organometallic compounds. University of Sussex, Brighton. 1977.
17. J. D. COX and G. PILCHER. Thermochemistry of organic and organometallic compounds. Academic Press, New York. 1970.

Synthesis, characterization, and structural studies of gallium citrate complexes

GREGORY A. BANTA, STEVEN J. RETTIG, ALAN STORR, AND JAMES TROTTER
Department of Chemistry, University of British Columbia, 2036 Main Mall, Vancouver, B.C., Canada V6T 1Y6

Received October 18, 1984

GREGORY A. BANTA, STEVEN J. RETTIG, ALAN STORR, and JAMES TROTTER. Can. J. Chem. **63**, 2545 (1985).

The synthesis and physical properties of two dimethylgallium citrate triester complexes are reported. Crystals of bis-[(trimethylcitrato)dimethylgallium(III)] are monoclinic, $a = 9.839(1)$, $b = 14.496(1)$, $c = 11.125(1)$ Å, $\beta = 108.31(1)°$, $Z = 2$, space group $P2_1/c$. The structure was solved by conventional heavy-atoms methods and was refined by full-matrix least-squares procedures to $R = 0.036$ and $R_w = 0.037$ for 1507 reflections with $I \geq 3\sigma(I)$. The structure consists of centrosymmetric dimers in which each citrate ligand is coordinated via the hydroxyl oxygen (bridging) and the C=O oxygen atom of the central ester group, forming five-membered chelate rings. Each Ga atom has irregular trigonal bipyramidal coordination geometry with Ga—O(eq) = 1.950(3), Ga—O(ax) = 2.103(3) and 2.395(3), and Ga—C(eq) = 1.953(5) and 1.947(5) Å.

GREGORY A. BANTA, STEVEN J. RETTIG, ALAN STORR et JAMES TROTTER. Can. J. Chem. **63**, 2545 (1985).

On rapporte la synthèse et les propriétés physiques de deux complexes triesters du citrate de diméthylgallium. Les cristaux de bis[(triméthylcitrato)diméthylgallium(III)] sont monocliniques, ils appartiennent au groupe d'espace $P2_1/c$ avec a = 9,839(1), b = 14,496(1), c = 11,125(1) Å, β = 108,31(1)° et Z = 2. On a résolu la structure par des méthodes conventionnelles aux atomes lourds et on l'a affinée par la méthode des moindres carrés (matrice entière) jusqu'à des valeurs de R = 0,036 et R_w = 0,037 pour 1507 réflexions avec $I \geq 3\sigma(I)$. La structure comporte des dimères centrosymétriques dans lesquels chaque ligand citrate est coordoné par le biais de l'oxygène de l'hydroxyle (pontage) et par l'atome d'oxygène du C=O du groupement ester central pour former des cycles chélatés à cinq chaînons. La géométrie de coordination de chaque atome de Ga correspond à une bipyramide trigonale irrégulière avec Ga—O(eq) = 1,950(3), Ga—O(ax) = 2,103(3) et 2,395(3) et Ga—C(eq) = 1,953(5) et 1,947(5) Å.

[Traduit par le journal]

Introduction

The importance of gallium citrate complexes in medicinal chemistry is well documented (1), but definitive structural studies in this area are lacking. In our continuing investigations of the coordination chemistry of gallium the synthesis of two crystalline dimethylgallium citrate triester complexes has been accomplished. The mode of binding of the dimethylgallium moiety in the methyl citrate triester has been determined through an X-ray structural study.

Experimental

Air-sensitive materials were handled under oxygen-free dry nitrogen. Tetrahydrofuran (THF) was dried by refluxing over sodium/benzophenone and benzene by refluxing over molten potassium. The solvents were subsequently distilled and transferred to a glove-box for immediate use.

Starting materials

The ethyl and methyl citrate triesters were prepared by the standard acid-catalyzed esterification of citric acid with 100% ethanol and methanol, respectively, using concentrated H_2SO_4. The purity of the products was checked by correlation of their ir and nmr spectra with reference data. Trimethylgallium (2) and dimethylgallium hydroxide (3) were made by standard methods.

Synthesis of (triethylcitrato)dimethylgallium(III)

This complex was prepared by two methods:

Method A: from trimethylgallium

Ethyl citrate triester (1.24 mL, 5.10 mmol) was added via a syringe to Me_3Ga (0.584 g, 5.10 mmol) in THF (50 mL). The reaction mixture was stirred at room temperature for approximately 24 h during which time methane was evolved slowly. The solvent was then removed under vacuum and the solid product recrystallized from benzene to yield large colorless crystals of the desired complex. *Anal.* calcd. for $[Me_2Ga(C_{12}H_{19}O_7)]$: C 44.83, H 6.72; found: C 44.77, H 6.61%. ^{1}H nmr (C_6D_6): τ 9.76 s ($GaMe_2$), 9.03 t (—CH_2CH_3, $J \sim 7$ Hz), 7.07 s br (—CH_2—CO_2Et), 6.04 q, 5.92 q (—CH_2CH_3, $J \sim 7$ Hz, relative intensities 2:1) (τ values refer to $\tau(C_6H_6)$ = 2.84 ppm; s = singlet, t = triplet, q = quartet, br = broad). Ir (Nujol) ν_{CO} = 1740, 1717 cm^{-1} (ν_{CO} = 1738 cm^{-1} for ethyl citrate triester), ν_{Ga-C} = 600, 536 cm^{-1}. Mp 116–118°C.

Method B: from dimethylgallium hydroxide

$[Me_2Ga(OH)]_4$ (0.52 g, 1.11 mmol) was dissolved in benzene (50 mL). Ethyl citrate triester (1.08 mL, 4.45 mmol) was injected into the reaction vessel. The ethyl citrate which is sparingly soluble in benzene dissolves slowly as it reacts with $[Me_2Ga(OH)]_4$ to produce a clear solution of the product. The reaction mixture was stirred for approximately 24 h and then the solvent was removed under vacuum. The white solid product was pumped under vacuum for several hours to ensure removal of by-product water and it was then recrystallized from benzene to yield large colorless crystals of the ester complex. These gave identical spectra and closely similar analytical results to those obtained for the product using method A above.

Synthesis of (trimethylcitrato)dimethylgallium(III)

Me_3Ga (0.403 g, 3.51 mmol) in THF (50 mL) was reacted with methyl citrate triester (0.747 g, 3.19 mmol). The reaction mixture was stirred for approximately 24 h and then the solvent was removed under vacuum. The white solid product was recrystallized from benzene to afford well-formed colorless crystals. *Anal.* calcd. for $[Me_2Ga(C_9H_{13}O_7)]$: C 39.68, H 5.75, O 33.64; found: C 39.21, H 5.89, O 33.88. ^{1}H nmr (d_6-acetone): τ 10.37 s ($GaMe_2$), 7.07 (AB)q (—CH_2—CO_2Me), 6.31 s, 6.19 s (—CO_2Me, rel. int. 2:1) (τ values refer to $\tau(d_6$-acetone) = 7.89 ppm). Ir (Nujol): ν_{CO} = 1745, 1720 cm^{-1} (ν_{CO} = 1735 cm^{-1} for methyl citrate triester) ν_{Ga-C} = 597, 536 cm^{-1}. Mp 72–75°C. Both the complexes described above are hygroscopic.

Spectra

^{1}H nmr spectra were recorded on a Bruker WP-80 instrument using FT techniques. Ir spectra were recorded on a Perkin-Elmer 598 spectrometer.

X-ray crystallographic analysis of bis[(trimethylcitrato)-dimethylgallium(III)]

The crystal selected for the X-ray study was mounted in a capillary tube under a nitrogen atmosphere and the tube was subsequently flame-sealed. The density of the material could not be measured due

TABLE 1. Final positional (fractional × 10^4, Ga × 10^5) and isotropic thermal parameters ($U \times 10^3$ Å^2) with estimated standard deviations in parentheses

Atom	x	y	z	U_{eq}*
Ga	43519(6)	39940(3)	45859(5)	43
O(1)	4503(3)	5198(2)	3855(3)	36
O(2)	5428(4)	4084(3)	1306(4)	72
O(3)	7323(4)	4897(2)	2427(4)	66
O(4)	2972(4)	3868(2)	2396(3)	52
O(5)	2282(4)	4793(2)	705(3)	60
O(6)	1191(4)	5450(3)	3000(4)	71
O(7)	1083(4)	6983(3)	2932(4)	79
C(1)	5073(5)	5611(3)	1956(4)	45
C(2)	3900(5)	5421(3)	2562(4)	38
C(3)	2976(6)	6291(3)	2405(5)	46
C(4)	5945(6)	4776(4)	1859(5)	51
C(5)	8233(7)	4120(4)	2376(7)	89
C(6)	2997(5)	4605(3)	1912(5)	44
C(7)	1475(8)	4043(4)	−39(6)	94
C(8)	1687(6)	6168(3)	2832(5)	49
C(9)	−150(8)	6956(5)	3375(8)	106
C(10)	5787(6)	3138(4)	4363(5)	69
C(11)	2623(6)	3683(4)	4995(5)	64

*U_{eq} = (1/3) trace U_{diag}.

to its sensitivity to air. A crystal bounded by the six faces (followed by their distances in mm from a common origin): ±(1 0 0), 0.038, ±(0 1 0), 0.225, ±(0 0 1), 0.238 was mounted in a general orientation. Unit-cell parameters were refined by least-squares on 2 sin θ/λ values for 25 reflections (2θ = 30−37°) measured on a diffractometer with Mo-$K\alpha$ radiation ($\lambda(K\alpha_1)$ = 0.70930, $\lambda(K\alpha_2)$ = 0.71359 Å). Crystal data at 22°C are:

$C_{22}H_{38}Ga_2O_{14}$ fw = 665.97
Monoclinic, a = 9.839(1), b = 14.496(1), c = 11.125(1) Å, β = 108.31(1)°, V = 1506.4(3) Å^3, Z = 2, ρ_c = 1.468 Mg m^{-3}, F(000) = 688, μ(Mo-$K\alpha$) = 18.4 cm^{-1}. Absent reflections: $h0l$, l odd, and $0k0$, k odd, uniquely indicate the space group $P2_1/c$ (C_{2h}^5, No. 14).

Intensities were measured with graphite-monochromated Mo-$K\alpha$ radiation on an Enraf-Nonius CAD4-F diffractometer. An ω−2θ scan at 1.55−10.06° min^{-1} over a range of (1.00 + 0.35 tan θ) degrees in ω (extended by 25% on both sides for background measurement) was employed. Data were measured to 2θ = 55°. The intensities of three check reflections, measured every 3600 s throughout the data collection, remained constant to within 1.5%. After data reduction,[1] an absorption correction was applied using the analytical method (4, 5). Transmission factors ranged from 0.481 to 0.873. Of the 3446 independent reflections measured, 1507 (43.7%) had intensities greater than or equal to 3σ(I) above background where $\sigma^2(I) = S + 2B + (0.04(S - B))^2$ with S = scan count and B = normalized background count.

The coordinates of the Ga atom were determined from the Patterson function and those of the remaining non-hydrogen atoms from a subsequent difference map. After full-matrix least-squares refinement of the non-hydrogen atoms with anisotropic thermal parameters to R = 0.053, a difference map gave the positions of most of the hydrogen atoms. In subsequent cycles of refinement the hydrogen atoms were included as fixed contributors in idealized positions (based on the observed positions with C—H = 0.98 Å). The scattering factors of ref. 6 were used for non-hydrogen atoms and those of ref. 7 for hydrogen atoms. Anomalous scattering factors from ref. 8 were used for the Ga atoms. The weighting scheme $w = 1/\sigma^2(F)$, where $\sigma^2(F)$ is derived from the previously defined $\sigma^2(I)$, gave uniform average values of $w(|F_o| - |F_c|)^2$ over ranges of both $|F_o|$ and sin θ/λ and was employed in the final stages of full-matrix refinement of 172 variables. Reflections with $I < 3\sigma(I)$ were not included in the refinement. Convergence was reached at R = 0.036 and R_w = 0.037 for 1507 reflections with $I \geq 3\sigma(I)$. For all 3446 reflections R = 0.128. The function minimized was $\Sigma w(|F_o| - |F_c|)^2$, $R = \Sigma||F_o| - |F_c||/\Sigma|F_o|$ and $R_w = (\Sigma w(|F_o| - |F_c|)^2/\Sigma w|F_o|^2)^{1/2}$.

[1]The computer programs used include locally written programs for data processing and locally modified versions of the following: ORFLS, full-matrix least-squares, and ORFFE, function and errors, by W. R. Busing, K. O. Martin, and H. A. Levy; FORDAP, Patterson and Fourier syntheses, by A. Zalkin; ORTEP II, illustrations, by C. K. Johnson.

TABLE 2. Bond lengths (Å) with estimated standard deviations in parentheses*

Bond	Length (Å)	Bond	Length (Å)
Ga —O(1)	1.950(3)	O(5)—C(6)	1.334(6)
Ga —O(4)	2.395(3)	O(5)—C(7)	1.443(6)
Ga —C(10)	1.953(5)	O(6)—C(8)	1.189(5)
Ga —C(11)	1.947(5)	O(7)—C(8)	1.342(6)
Ga —O(1)′	2.103(3)	O(7)—C(9)	1.446(7)
O(1)—C(2)	1.411(5)	C(1)—C(2)	1.533(6)
O(2)—C(4)	1.204(5)	C(1)—C(4)	1.507(7)
O(3)—C(4)	1.316(6)	C(2)—C(3)	1.532(6)
O(3)—C(5)	1.451(6)	C(2)—C(6)	1.519(6)
O(4)—C(6)	1.201(5)	C(3)—C(8)	1.498(7)

*Here and elsewhere in this report primed atoms have coordinates related to those in Table 1 by the symmetry operation (1 − x, 1 − y, 1 − z).

On the final cycle of refinement the mean and maximum parameter shifts corresponded to 0.01 and 0.07σ, respectively. The mean error in an observation of unit weight was 1.285. A final difference map showed maximum fluctuations of −1.02 to +0.41 e Å^{-3} near Ga and was essentially featureless elsewhere. The final positional and thermal parameters appear in Tables 1 and 6,[2] respectively. Measured and calculated structure factors have been placed in the Depository of Unpublished Data.[2] Bond distances, bond angles, and intra-annular torsion angles are given in Tables 2−4, respectively. Calculated hydrogen parameters (Table 5) and a complete listing of torsion angles (Table 7) are included as supplementary material.[2]

Results and discussion

The use of gallium citrate solutions is widespread in radiopharmaceutical procedures (1). Thus, since the discovery that ^{67}Ga localized in human soft tissue tumors (9) and also in inflammatory lesions (10, 11) it has been extensively used in diagnostic nuclear medicine (12). In addition ^{68}Ga has shown promise recently in positron emission tomography (PET) for medical diagnosis (13). Presently ^{67}Ga-citrate is the clinically applicable agent best suited to radionuclide tagging. The importance of this agent has prompted ^{1}H and ^{71}Ga nmr studies of gallium citrate complexes in aqueous solutions (14, 15), over a range of pH values, in an attempt to shed light on the structure of such complexes with a view to gaining a better understanding of the molecular mechanism of cellular binding of Ga and the inhibition of this process by citrate and other buffers. However, definitive structural data on gallium citrate complexes is lacking and in an effort to determine the mode of coordination of the gallium atoms by citrate species we have prepared two citrate triester complexes incorporating the dimethylgallium moiety. The complexes isolated, $Me_2Ga(C_{12}H_{19}O_7)$ and $Me_2Ga(C_9H_{13}O_7)$, are the first crystalline gal-

[2]The structure factor table, Table 6 (anisotropic thermal parameters) and other material mentioned in the text may be purchased from the Depository of Unpublished Data, CISTI, National Research Council of Canada, Ottawa, Canada K1A 0S2.

TABLE 3. Bond angles (deg) with estimated standard deviations in parentheses

Bonds	Angle (deg)	Bonds	Angle (deg)
O(1)—Ga —O(4)	74.77(11)	C(2)—C(1)—C(4)	114.3(4)
O(1)—Ga —C(10)	111.3(2)	O(1)—C(2)—C(1)	110.8(4)
O(1)—Ga —C(11)	119.4(2)	O(1)—C(2)—C(3)	110.4(4)
O(1)—Ga —O(1)′	75.77(12)	O(1)—C(2)—C(6)	107.6(4)
O(4)—Ga —C(10)	91.4(2)	C(1)—C(2)—C(3)	107.7(4)
O(4)—Ga —C(11)	87.8(2)	C(1)—C(2)—C(6)	109.9(4)
O(4)—Ga —O(1)′	150.16(11)	C(3)—C(2)—C(6)	110.4(4)
C(10)—Ga —C(11)	127.0(2)	C(2)—C(3)—C(8)	113.4(4)
C(10)—Ga —O(1)′	103.7(2)	O(2)—C(4)—O(3)	124.2(5)
C(11)—Ga —O(1)′	102.6(2)	O(2)—C(4)—C(1)	123.2(5)
Ga —O(1)—C(2)	124.6(2)	O(3)—C(4)—C(1)	112.5(5)
Ga —O(1)—Ga′	104.23(12)	O(4)—C(6)—O(5)	123.7(4)
C(2)—O(1)—Ga′	131.2(2)	O(4)—C(6)—C(2)	124.8(5)
C(4)—O(3)—C(5)	115.7(4)	O(5)—C(6)—C(2)	111.4(4)
Ga —O(4)—C(6)	107.6(3)	O(6)—C(8)—O(7)	122.8(5)
C(6)—O(5)—C(7)	116.4(4)	O(6)—C(8)—C(3)	125.7(5)
C(8)—O(7)—C(9)	116.4(4)	O(7)—C(8)—C(3)	111.3(4)

TABLE 4. Intra-annular torsion angles (deg) standard deviations in parentheses

Atoms	Value (deg)
O(4)—Ga —O(1)—C(2)	−3.0(3)
Ga —O(1)—C(2)—C(6)	6.5(5)
O(1)—C(2)—C(6)—O(4)	−9.0(7)
Ga —O(4)—C(6)—C(2)	6.8(6)
O(1)—Ga —O(4)—C(6)	−2.1(3)

lium citrate complexes to be reported and the structural characterization of the latter (see below) represents an important contribution to our knowledge in this area. The reaction employed is one of methane elimination between the hydroxyl group of the citrate triester and trimethylgallium or elimination of water between this group and the hydroxyl group of dimethylgallium hydroxide:

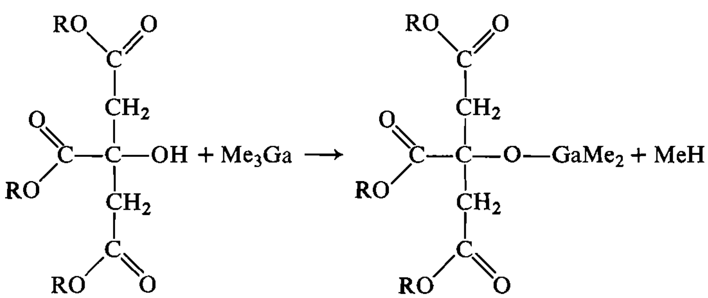

It is clear from the ir and ^{1}H nmr evidence that the hydroxyl proton of the citrate triester is removed during the reaction since the original ν_{OH} (3470 cm^{-1} (Nujol) methyl citrate triester; 3480 cm^{-1} (neat liquid) ethyl citrate triester) and τ_{OH} (5.41 τ (d_6-acetone) methyl citrate triester; obscured by other signals for the ethyl citrate triester) signals are absent in spectra of the products. The ^{1}H nmr spectra of the two products (R = Me or Et) are shown in Fig. 1. In both spectra the —GaMe$_2$ group gives a sharp singlet, indicating a symmetrical structure in solution with equivalent Ga—Me groups. The presence of two different ester groups in the ratio of 2:1 is also apparent in the spectra. These observations are in agreement with the solid-state structure of the $Me_2Ga(C_9H_{13}O_7)$ (R = Me) complex (Fig. 2) in which the —GaMe$_2$ unit is symmetrically coordinated to the oxygen atom of the triester hydroxyl group and to the carbonyl oxygen atom of the central ester function, leaving equivalent outer ester groups non-involved in the bonding. In the solid state this unit exists as a centrosymmetric dimeric species, the only distance between dimers shorter than the sum of van der Waals radii being the possible weak interaction C(5)—H(5c)···O(6) ($1 + x, y, z$) (H···O = 2.54, C···O = 3.377(7) Å, C—H···O = 144°). The dimerization occurs via the formation of a central four-membered Ga_2O_2 ring, the Ga atoms attaining 5-coordination in a trigonal-bipyramidal fashion with the two coordination polyhedra sharing an axial-equatorial edge as in numerous previous examples (16). It is interesting that the outer ester groups do not chelate the gallium atoms. Such coordination would of course lead to six-membered chelate rings, rather than the five-membered chelate rings observed in the present structure.

The splitting of the single ν_{CO} vibration in the ir spectra of the original triester compounds upon forming the dimethylgallium complexes is further evidence for non-involvement of all ester functions in the coordination to gallium. The fact that one of the ester C═O groups is coordinated via oxygen to the Ga atom, albiet weakly (Ga—O = 2.395(3) Å), must lead to the observation of two ν_{CO} bands in the ir spectrum of the product. The C═O bond lengths for the outer ester functionalities (1.204(5) and 1.189(5) Å) are equal within experimental error to that observed for the coordinated central ester group (1.201(5) Å).

The central feature of the molecular structure of bis[(trimethylcitrato)dimethylgallium(III)] is the essentially planar system of three fused rings. The central four-membered ring is exactly planar, while the five-membered chelate rings are significantly non-planar (χ^2 = 166) although each of these rings, as well as the entire fused ring system, is planar to within ±0.046(6) Å. The Ga—O distances involving the bridging alkoxide O atom (1.950(3) and 2.103(3) Å, respectively, for equatorial and axial bonds) are comparable to those observed in other dimeric alkoxo-bridged species, the corresponding ranges being 1.911(3)−1.960(8) and 2.018(2)−2.078(3) Å (16). The axial Ga—O(4) distance of 2.395(3) Å is intermediate between values of 2.127(3) for an aldehyde O atom in bis[(salicylaldehydato)dimethylgallium] and 2.695(3) Å for a carboxylato C═O atom in (L-prolinato)dimethylgallium (16).

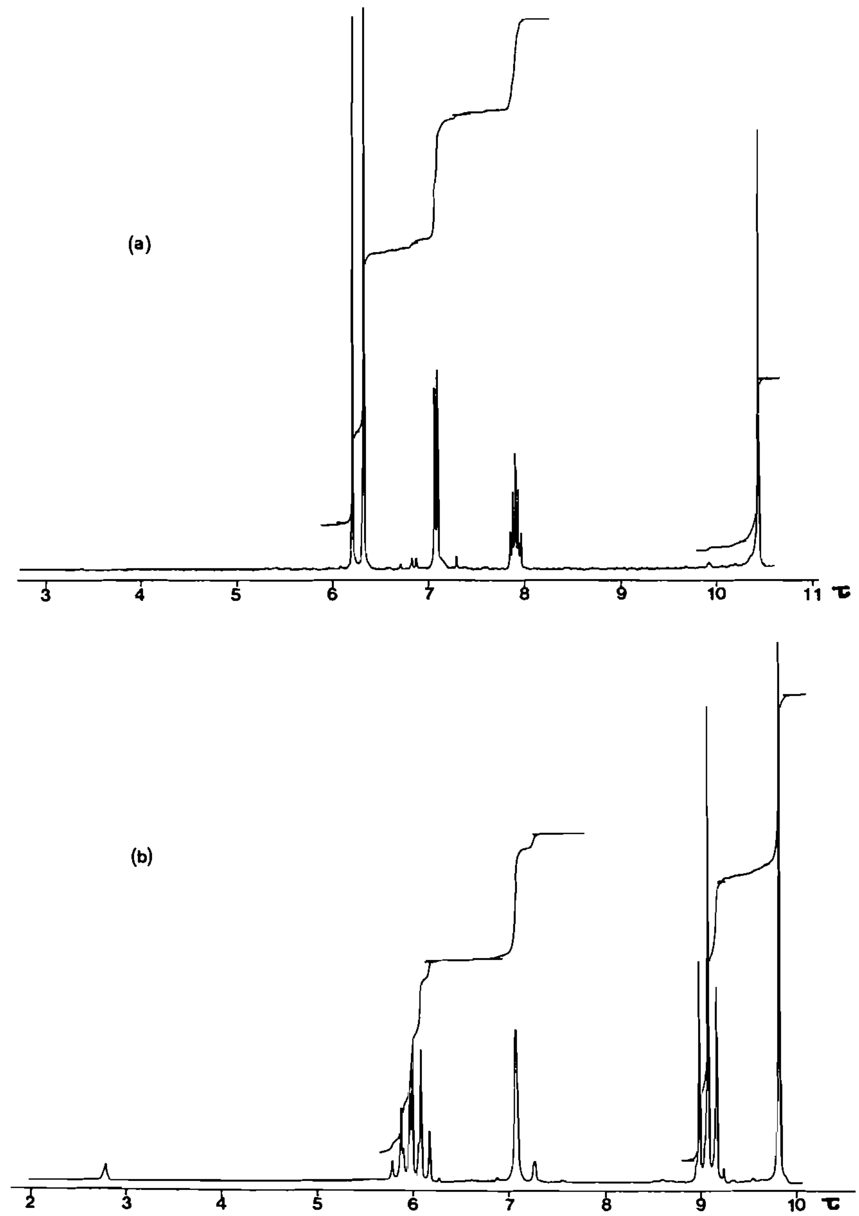

FIG. 1. 80 MHz [1]H nmr spectra of (*a*) Me_2Ga(Me citrate triester) in d_6-acetone and (*b*) Me_2Ga(Et citrate triester) in C_6D_6.

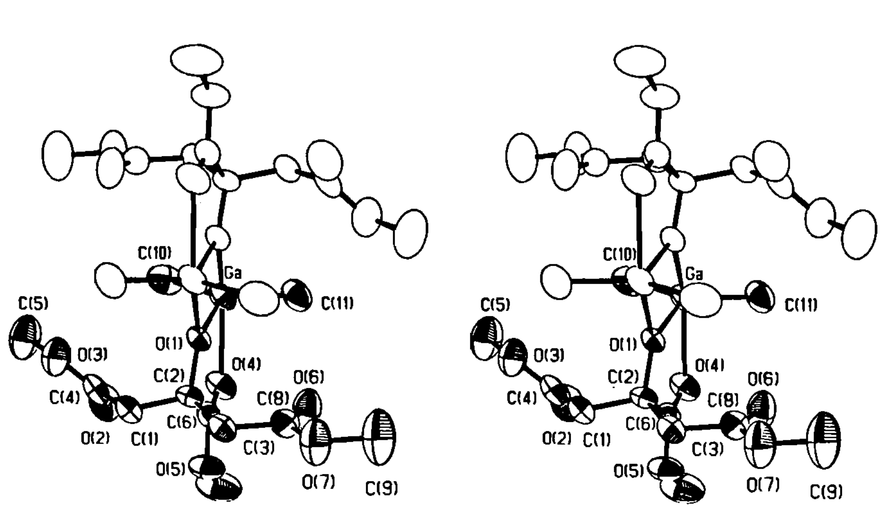

FIG. 2. Stereoscopic view of the bis[(trimethylcitrato)dimethylgallium(III)] molecule; 50% probability thermal ellipsoids are shown.

The Ga—C distances are normal as are bond lengths in the citrate moiety. Bond lengths and angles in the three ester groups are equal within experimental error, the three carboxylate groups being planar to within 0.022(5) Å with the ester methyl carbon atoms lying within 0.092(8) Å of the respective carboxylate mean planes.

Acknowledgments

We thank the Natural Sciences and Engineering Research Council of Canada for financial support and the University of British Columbia Computing Centre for assistance. We are grateful to Mr. P. Borda for the elemental analysis figures.

1. A. A. NOUJAIM. (*Editor*). Gallium-67 and related elements. Int. J. Nucl. Med. Biol. **8**, 215 (1981).
2. A. STORR and B. S. THOMAS. Can. J. Chem. **48**, 3667 (1970).
3. M. E. KENNY and A. W. LAUBENGAYER. J. Am. Chem. Soc. **76**, 4839 (1954).
4. P. COPPENS, L. LEISEROWITZ, and D. RABINOVICH. Acta Crystallogr. **18**, 1035 (1965).
5. J. DE MEULENAER and H. TOMPA. Acta Crystallogr. **19**, 1014 (1965).
6. D. T. CROMER and J. B. MANN. Acta Crystallogr. Sect. A, **24**, 321 (1968).
7. R. F. STEWART, E. R. DAVIDSON, and W. T. SIMPSON. J. Chem. Phys. **42**, 3175 (1965).
8. D. T. CROMER and D. LIBERMAN. J. Chem. Phys. **53**, 1891 (1970).
9. C. L. EDWARDS and R. L. HAYES. J. Nucl. Med. **10**, 103 (1969).
10. J. P. LAVENDER, J. P. LOWE, and J. R. BARKER. Br. J. Radiol. **44**, 361 (1971).
11. R. L. LITTENBERG, R. M. TAKETA, and N. P. ALAZRAKI. Ann. Intern. Med. **79**, 403 (1973).
12. P. B. HOFFER. J. Nucl. Med. **21**, 484 (1980a).
13. M. A. GREEN, M. J. WELCH, and J. C. HUFFMAN. J. Am. Chem. Soc. **106**, 3689 (1984).
14. J. D. GLICKSON, J. WEBB, and R. A. GAMS. Cancer Res. **34**, 2957 (1974).
15. J. D. GLICKSON, T. P. PITNER, J. WEBB, and R. A. GAMS. J. Am. Chem. Soc. **97**, 1679 (1975).
16. S. J. RETTIG, A. STORR, and J. TROTTER. Can. J. Chem. **62**, 1705 (1984) and references therein.

Synthesis and characterization of Pt(II) complexes containing the bidentate pyrazolylgallate ligand, $[Me_2Gapz_2]^-$

SOPHIA NUSSBAUM AND ALAN STORR
Department of Chemistry, University of British Columbia, 2036 Main Mall, Vancouver, B.C., Canada V6T 1Y6

Received November 2, 1984

SOPHIA NUSSBAUM and ALAN STORR. Can. J. Chem. **63**, 2550 (1985).

The complexes $[Me_2Mpz_2]Pt(Me)L$ (where L = CO, Ph_3P, or PhC≡CPh for M = Ga; L = PhC≡CPh for M = B) have been synthesized by the direct reaction of the ligands $Na[Me_2Mpz_2]$ with Pt(Me)Cl(COD) followed by the addition of ligand L. The complexes have been shown to be fluxional in solution by variable temperature ^1H nmr methods.

SOPHIA NUSSBAUM et ALAN STORR. Can. J. Chem. **63**, 2550 (1985).

On a effectué une synthèse des complexes $[Me_2Mpz_2]Pt(Me)L$ (où L = CO, Ph_3P ou PhC≡CPh, pour M = Ga; L = PhC≡CPh pour M = B) en faisant appel à une réaction directe des ligands $Na[Me_2Mpz_2]$ avec le Pt(Me)Cl(COD), suivie d'une addition du ligand L. Faisant appel à des methodes de rmn à température variable, on a montré que les complexes en solution sont fluxionels.

[Traduit par le journal]

Introduction

As part of an on-going study of the reactions of the bidentate chelating pyrazolylgallate ligand, $[Me_2Gapz_2]^-$ (where pz = pyrazolyl, $N_2C_3H_3$) (1), the reactivity of this ligand towards the platinum compound Pt(Me)Cl(COD) (where COD = 1,5 cyclooctadiene) has been examined. This same platinum compound has been reported as being unreactive towards the pyrazolyl borate ligands $[RBpz_3]^-$ and $[R_2Bpz_2]^-$ (where R = H, Ph, Et, Bu), unless the very tightly bonded COD ligand is first activated via a halogen abstraction reaction using $AgPF_6$ (2, 3). However, our studies have revealed that the $[Me_2Gapz_2]^-$ ligand reacts smoothly with Pt(Me)Cl(COD), as does its boron analogue $[Me_2Bpz_2]^-$, without the necessity of the halogen abstraction step, and producing in moderate to high yield the desired products, $[Me_2Mpz_2]Pt(Me)L$ (where L = CO, Ph_3P or PhC≡CPh for M = Ga and L = PhC≡CPh for M = B) upon subsequent addition of ligand L.

Experimental

All reactions were performed under a dry nitrogen atmosphere, using Schlenk glassware or a glove-box. Tetrahydrofuran (THF) was dried by refluxing over sodium/benzophenone and distilled prior to use. Benzene was dried by refluxing over molten potassium. Hexane was distilled from calcium sulphate, methylene chloride from calcium hydride, and ether from lithium aluminum hydride. Pt(Me)Cl(COD) was prepared from K_2PtCl_4 by a standard route (4). Ph_3P (MCB) and PhC≡CPh (Eastman Kodak Co.) were used as supplied. MeOCOC≡CCOOMe (Aldrich) was distilled prior to use. The sodium salt of the gallium ligand $[Me_2Gapz_2]^-$ was prepared as described earlier (5) and $Na[Me_2Bpz_2]$ was prepared by a literature method (6).

Reaction of Pt(Me)Cl(COD) with $Na[Me_2Gapz_2]$

Pt(Me)Cl(COD) (0.100 g, 0.282 mmol) was dissolved in THF (~10 mL) and a solution of $Na[Me_2Gapz_2]$ in THF (3.8 mL, 0.282 mmol) was added dropwise with stirring. After the addition was complete the resultant cloudy mixture, **II**, was stirred for a further 1.5 h and then used directly in the following reactions.

(a) Reaction with Ph_3P

The solvent was removed from **II** and the colorless residue suspended in CH_2Cl_2. Ph_3P (0.074 mg, 0.282 mmol) was added with stirring. After a further period of stirring (1 h), the solvent was removed under vacuo to yield an oily residue which was washed with ether, leaving behind a white solid. The ether solution, on slow evaporation of solvent, gave the desired product $[Me_2Gapz_2]Pt(Me)(Ph_3P)$ as white crystals in ~75% yield. The compound sublimed under vacuum at 60°C and had a mp of 188°C. *Anal.* calcd. for $[Me_2Gapz_2]Pt(Me)(Ph_3P)$: C 45.91, H 4.25, N 7.93; found: C 46.09, H 4.40, N 7.96%. Mass spectrum: $(P - Me)^+$ (100%), $(P - Me - pzH)^+$ (35%), $(P - Me - 2pzH)^+$ (25%), $(P - Me - 2pzH - C_6H_6)^+$ (40%) plus signals due to Ph_3P and its fragmentation (P = parent).

The white solid remaining after extraction of the original product mixture with ether was treated with THF and the solution filtered from the insoluble NaCl. The white solid obtained on removal of THF from the filtrate was recrystallized from CH_2Cl_2/hexane to yield $[Pt(Me)(Ph_3P)(\mu\text{-pz})]_2$. Yield ~ 10%, mp 223°C. *Anal.* calcd. for $[Pt(Me)(Ph_3P)(\mu\text{-pz})]_2\cdot\frac{1}{3}C_6H_{14}$: C 49.87, H 4.22, N 5.06; found: C 50.03, H 4.31, N 5.00. ^1H nmr: ($CDCl_3$ solution) τ = 9.54 dd (Pt—Me, $J_{P-Pt-CH_3}$ = 4.4 Hz, $J_{^{195}Pt-CH_3}$ = 72 Hz), τ = 4.2 q, 3.5t (pz-^{4}H), τ = 2.23–2.75 m (Ph_3P) (pz-^{3}H, pz-^{5}H obscured by Ph_3P signals). Mass spectrum: P^+ (100%), $(P - Me - MeH)^+$ (20%), $(P - Me - MeH - pzH)^+$ (61%), $(P - Me - MeH - 2pzH)^+$ (23%), $(P - Me - MeH - 2pzH - C_6H_6)^+$ (33%) plus signals due to Ph_3P and its fragmentation.

(b) Reaction with PhC≡CPh

To the stirred mixture **II** was added an equimolar amount of PhC≡CPh (0.05 mg, 0.282 mmol). The resultant solution was stirred for a further 1.5 h and the solvent then removed under vacuo. The resultant oily product mixture was then pumped for an additional 0.5 h at 40°C to remove cyclooctadiene. The remaining oil was then treated with ether and filtered. The filtrate yielded a pale yellow oil, on removal of ether solvent, which after repeated washings with hexane gave a yellow powder.[1] *Anal.* calcd. for $[Me_2Gapz_2]$Pt-(Me)(PhC≡CPh): C 44.38, H 4.02, N 9.01; found: C 41.22, H 4.16, N 8.31. Yield 89% ir (Nujol) $\nu_{C\equiv C}$ = *2069 cm^{-1}*. Mass spectrum: $(P - Me)^+$ (100%), $(P - Me - pzH)^+$ (57%), $(P - Me - 2pzH)^+$ (18%), $(P - Me - (PHC{\equiv}CPh))^+$ (40%), $(P - Me - pzH - (PhC{\equiv}CPh))^+$ (37%) plus signals due to PhC≡CPh and its fragmentation.

(c) Reaction with CO

Carbon monoxide was bubbled through the stirred mixture **II** for 1.5 h and the solvent then removed under vacuo. The oily residue was pumped on for a further 0.5 h. The oily product was then treated with CH_2Cl_2 and the mixture filtered. The CH_2Cl_2 was removed from the filtrate to yield the product as a colorless oil in approx. 40% yield. *Anal.* calcd. for $[Me_2Gapz_2]Pt(Me)(CO)$: C 25.43, H 3.18, N 11.87; found: C 25.70, H 3.29, N 11.90. Ir (CH_2Cl_2) ν_{CO} = 2085 cm^{-1}. Mass spectrum: $(P - Me)^+$ (100%), $(P - Me - CO)^+$ (35%), $(P - 2Me - CO)^+$ (8%).

[1]The product probably contains some free Pt as found by Clark *et al.* (2) in the material from the similar reaction involving the $[Et_2Bpz_2]^-$ ligand. Unfortunately, attempts to purify our product by sublimation or chromatography were unsuccessful.

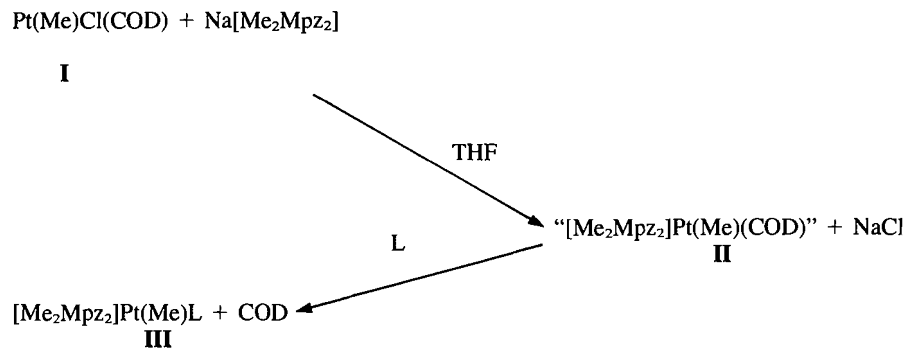

M = Ga or B; L = Ph_3P, CO, PhC≡CPh, MeOCOC≡CCOOMe

SCHEME 1

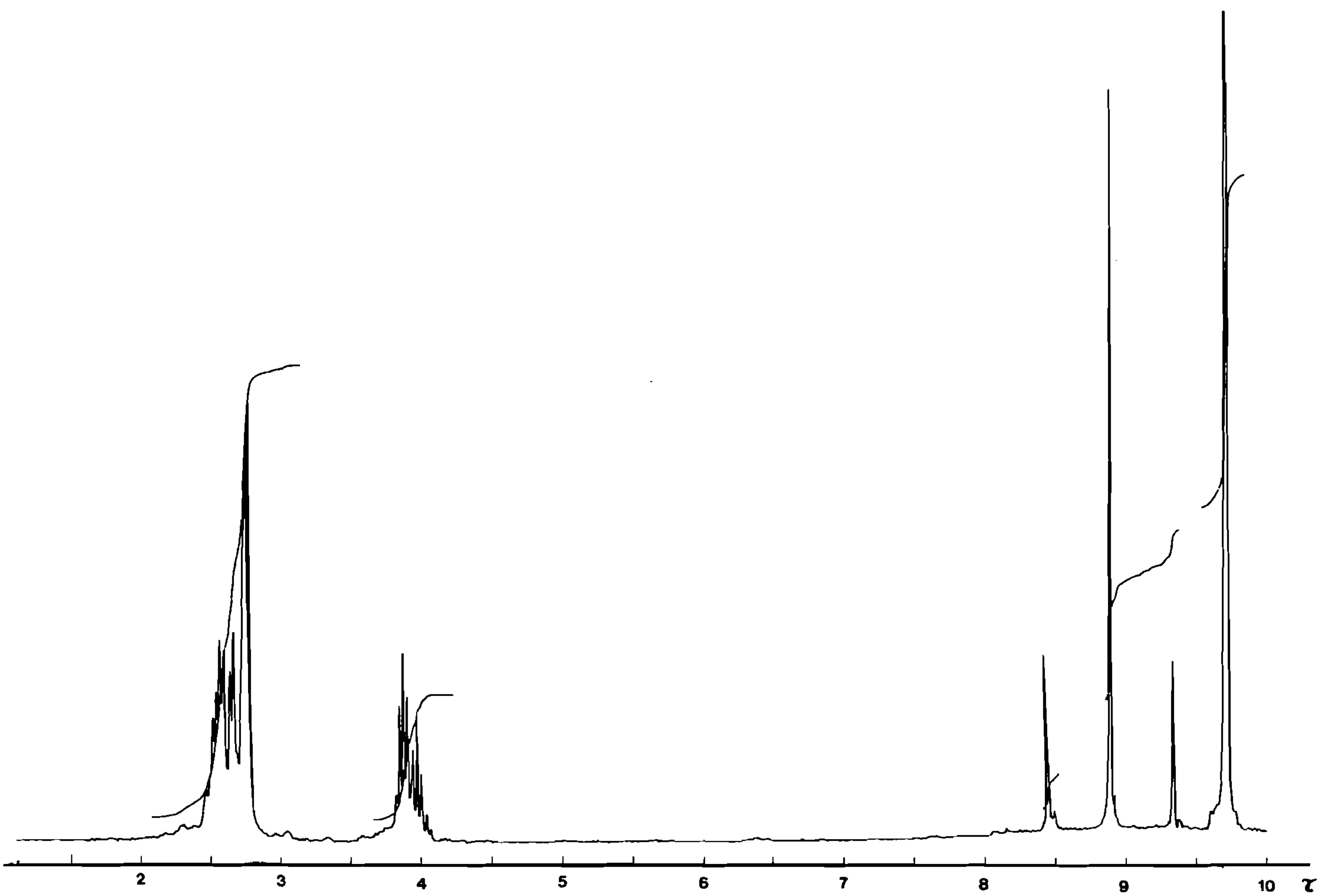

FIG. 1. Room temperature 80 MHz ^{1}H nmr spectrum of $[Me_2Gapz_2]Pt(Me)(CO)$ in C_6D_6 solution.

(d) Reaction with MeOCOC≡CCOOMe

The stirred mixture **II** was treated with an equimolar amount of MeOCOC≡CCOOMe (0.040 mg, 0.282 mmol). The reaction mixture became yellow and the color darkened slightly during the subsequent 1.5 h of stirring. The yellow oil obtained on evaporation of the solvent darkened under vacuo at ~30°C. It was then treated with CH_2Cl_2 and the mixture filtered. The yellow oil obtained on evaporation of the CH_2Cl_2 from the filtrate yielded a yellow powder on repeated washing with hexane. The characterization of this material has met with little success. Its ^{1}H nmr was very complicated although this did simplify slightly on heating the C_6D_6 solution to 70°C. Ir (CH_2Cl_2) ν_{CO} 1712, 1564 cm^{-1}, $\nu_{C=C}$ 1615 cm^{-1}.

Attempted insertion of PhC≡CPh into Pt—Me bond

(*i*) A solution of $[Me_2Gapz_2]Pt(Me)(PhC{\equiv}CPh)$ in C_6D_6 was heated to 80°C for 3 h. Some black precipitate was formed during the heating but the ^{1}H nmr spectrum of the solution remained virtually unchanged.

(*ii*) Carbon monoxide was bubbled through a solution of $[Me_2Gapz_2]Pt(Me)(PhC{\equiv}CPh)$ in benzene. The solvent was then removed under vacuum and the residue washed with hexane. $[Me_2Gapz_2]Pt(Me)(CO)$ was the only Pt-containing product formed.

Reaction of Pt(Me)Cl(COD) with Na[Me₂Bpz₂] and PhC≡CPh

Pt(Me)Cl(COD) (0.050 g, 0.14 mmol) was dissolved in 5 mL THF and a solution of $Na[Me_2Bpz_2]$ (0.028 g, 0.14 mmol) in 5 mL THF added dropwise with stirring. The mixture became cloudy immediately and was stirred for about 1.5 h. An equimolar amount of PhC≡CPh (0.025 g, 0.14 mmol) was then added and stirring was continued for a further 1.5 h. A pale yellow mixture resulted. The THF was removed to yield an oily residue which was pumped under vacuo for 1.5 h at 40°C. The residue was then extracted with CH_2Cl_2 and the mixture filtered. Addition of pentane to the filtrate and cooling to −23°C produced no crystallization of the product. The solvents were removed to yield initially a yellow oil, which transformed to a fluffy yellow solid product on brief pumping under vacuum. *Anal.* calcd. for $[Me_2Bpz_2]Pt(Me)(PhC{\equiv}CPh)$: C 49.03, H 4.44, N 9.95; found: C 49.21, H 4.52, N 9.54. Yield 83%, mp 50°C. Ir (CH_2Cl_2) $\nu_{C\equiv C}$ 1970 cm^{-1}.

Results and discussion

There have been a number of reports in the literature dealing with platinum complexes containing polypyrazolyl borate ligands (2, 3, 7−11). The reactivity of the Pt(Me)Cl(COD) complex towards such ligands has been reported to be restricted by the tightly bound COD ligand, and it was found necessary to activate the platinum complex by removal of the chloride ion using the silver salt of a non-coordinating anion (e.g. $AgPF_6$) in acetone or THF. In the resultant $[Pt(Me)(COD)(solvent)]^+$ species the COD ligand was quite labile and easily displaced (2, 3). In our studies we have examined the reactions of the $Na[Me_2Mpz_2]$ ligands (where M = Ga or B), with the Pt(Me)Cl(COD) complex and have found that the displacement of the COD ligand is quite facile without prior activation via a halide abstraction process. The synthetic route employed in the preparation of a series of platinum compounds is outlined in Scheme 1.

On addition of the pyrazolyl ligand to a solution of Pt(Me)-Cl(COD) in THF, a cloudiness occurred immediately. The resulting mixture **II** was not analyzed but, rather, used directly or after a change of solvent to CH_2Cl_2. The ligands, L, reacted smoothly with **II**, producing the complexes **III** in moderate to high yields. These were characterized by elemental analyses, mass spectra, ir, and ^1H nmr data. The ^1H nmr results are collected in Table 1 and clearly indicate the non-equivalence of the bridging pyrazolyl groups, as expected. The ^3H and ^5H proton signals appear as doublets, the ^4H proton signals as triplets. By analogy with the assignments made for the analogous complexes, $[R_2Bpz_2]Pt(Me)L$ (where R = Et or Ph; L = tertiaryphosphine, isocyanide or acetylene) (2), we assign the higher field signals to the ^4H protons on the ring *trans* to the Me group on Pt. These protons also exhibit a smaller coupling to the ^{195}Pt atoms, possibly due to the higher *trans* influence of the Me group compared to L (2).

Bimetallic species involving two bridging pyrazolyl groups usually exhibit a boat conformation for the central six-membered ring involving the two metals and the four nitrogens of the pyrazolyl rings. This arrangement has been established recently for a number of *bis* pyrazolylgallate complexes of Rh (12, 13), Re (14), Ir (15), and earlier for complexes of Mn, Mo (16), Ni (17, 18), and Cu (19). Thus the observation of a singlet for the Me_2M protons in the solution ^1H spectra at room temperature of the platinum complexes **III** led us to suspect a fluxional process for the species in solution rather than the alternate explanation of a planar M(—N—N—)$_2$Pt six-membered ring in the complexes. A representative room temperature ^1H nmr spectrum, for the complex $[Me_2Gapz_2]$-Pt(Me)(CO), is shown in Fig. 1. To confirm our prediction of a fluxional process in solution at room temperature a variable

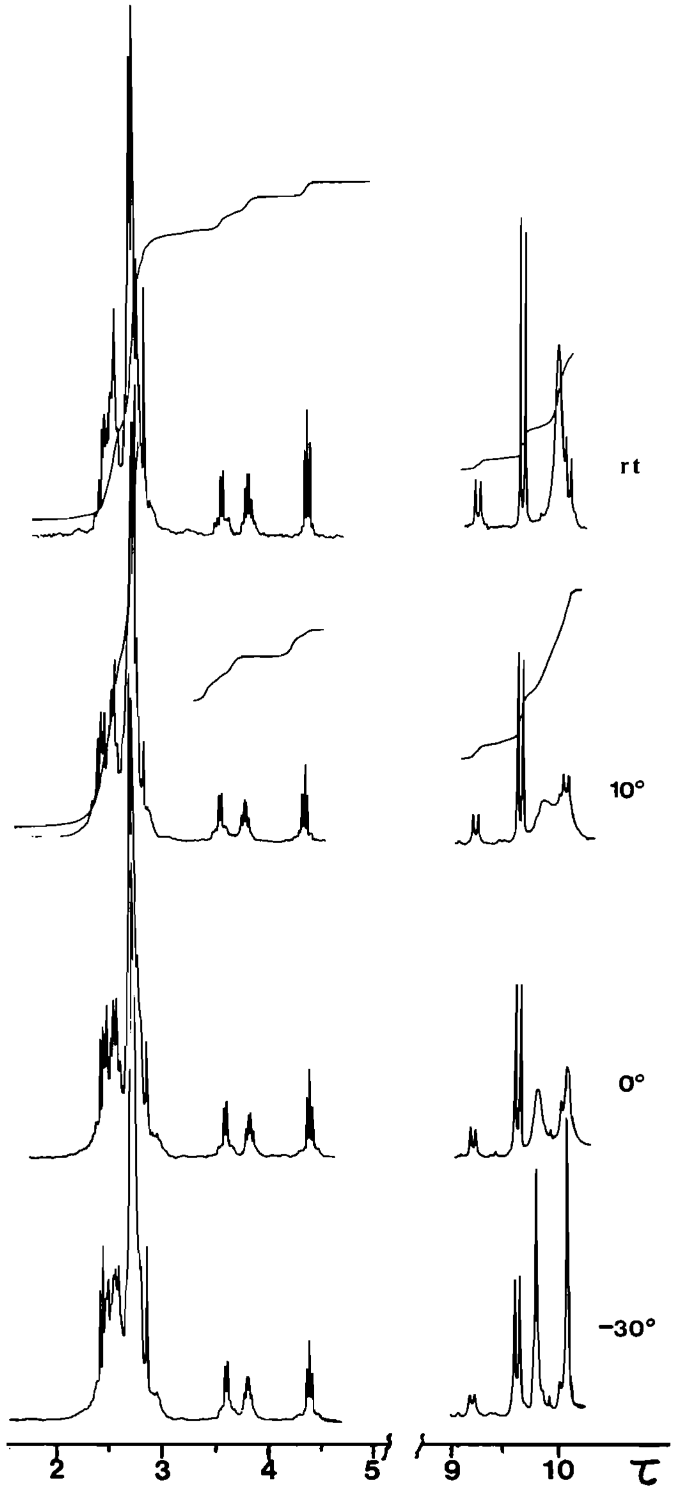

FIG. 2. Low temperature ^1H nmr spectra of $[Me_2Gapz_2]Pt(Me)$-(PPh_3) in $CDCl_3$ solution.

temperature ^1H nmr study was undertaken on the complex $[Me_2Gapz_2]Pt(Me)(PPh_3)$. This complex was chosen since the Me_2Ga singlet at room temperature was already quite broad (Fig. 2) suggesting a sluggish fluxional process even at this temperature. On cooling the solution, this signal broadened still further and eventually split into two separate signals which became quite sharp at −30°C. A fluxional process which can account for these results is shown below:

TABLE 1. ^{1}H nmr data for the complexes

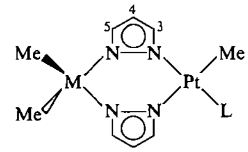

			τ (ppm)*					
M	L	Solvent	M—Me	^4H_A	^4H_B	^3H, ^5H	Pt—Me	$J_{^{195}Pt—CH_3}$
Ga	Ph_3P	$CDCl_3$	9.96s	4.37t	3.81t	3.55d + signals obscured by Ph_3P	9.63d $J_{P—Pt—CH_3}$ = 4 Hz	70
Ga	PhC≡CPh	C_6D_6	9.76s	4.11t	3.91t	2.24d, 2.56d + signals obscured by PhC≡CPh	8.94s	72
Ga	CO	C_6D_6	9.72s	3.97t	3.87t	2.52–2.70 overlapping doublets	8.90s	70
B	PhC≡CPh	C_6D_6	9.12s	4.22t	4.04t	2.30d, 2.79d + signals obscured by PhC≡CPh	8.97s	74

*τ values refer to $\tau_{C_6D_6}$ = 2.84 ppm, τ_{CHCl_3} = 2.84 ppm; J_{HCCH} ≈ 2 Hz for pz protons. H_A ring *trans* to Pt—Me, H_B ring *cis* to Pt—Me; s = singlet, d = doublet, t = triplet.

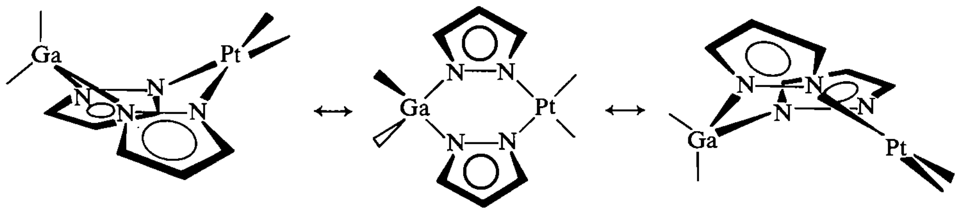

In this process the room temperature spectra result from a rapid interconversion of the extreme boat conformations via a planar intermediate. At lower temperatures the axial and equatorial Ga—Me groups become distinguishable as the fluxional process becomes slow on the nmr time scale.

In the ^{1}H nmr of all the complexes **III** the Pt—Me signal appears at ~9τ with a $J_{^{195}Pt—CH_3}$ of approximately 70 Hz, a value normally found for planar Pt(II) species. In the complex where L = Ph_3P the Pt—Me signals are split into doublets with a $J_{P—Pt—CH_3}$ of approximately 4 Hz (see Fig. 2).

Attempts to promote insertion of the PhC≡CPh ligand into the Pt—Me bond in the complex $[Me_2Gapz_2]Pt(Me)$-(PhC≡CPh) were unsuccessful. Thus prolonged refluxing of a solution of this compound in C_6D_6 caused no change in its nmr spectrum although some black precipitate suggested some decomposition. Passing carbon monoxide through a solution of the complex resulted only in displacement of the alkyne by CO and no evidence of an insertion reaction was observed. A similar reluctance to undergo insertion reactions has been observed for the related $[R_2Bpz_2]Pt(Me)$(PhC≡CPh) (where R = Et or Ph) complexes (2).

Although the reaction of **II** with the alkyne MeOCOC≡CCOOMe was complicated and gave inconclusive results it was evident that a rapid reaction had occurred, as evidenced by the immediate color change on mixing the reactants and the absence of signals due to free acetylene in the ^{1}H nmr and ir spectra of the product mixture. The ir of the product mixture exhibits a very strong band due to an uncoordinated CO group (1715 cm^{-1}) and a weaker band possibly due to a coordinated CO group (1564 cm^{-1}). A band at 1615 cm^{-1} may be due to a C=C grouping and the spectrum was blank in the region where $\nu_{C\equiv C}$ bands usually appear. Thus it appears likely that, following alkyne coordination to the Pt centre, a facile insertion of this group into the Pt—Me band may occur. A similar facile insertion has been established for the $[R_2Bpz_2]Pt(Me)$-(MeOCOC≡CCOOMe) complexes described earlier (2).

The $[Me_2Mpz_2]Pt(Me)L$ complexes, **III**, were the only Pt-containing products in all the reactions (see Scheme 1) with the exception of L = Ph_3P where **III** was formed along with a smaller amount (~10%) of the pyrazolyl-bridged platinum dimer $[Pt(Me)(Ph_3P)(\mu\text{-}pz)]_2$. (The concurrent formation of the $[Me_2Gapz_2]$ dimer was indicated in ^{1}H nmr spectra but this previously characterized compound (20, 21) was not isolated.) Both the $[Me_2Mpz_2]^-$ ligands reacted with equal facility with the Pt(Me)Cl(COD) starting material and both reaction sequences led to moderate to high yields of the final products after introduction of the ligand L. Thus it appears that the halogen abstraction step using $AgPF_6$ (2, 3) is unnecessary with these two bidentate ligand systems and perhaps by extrapolation with the $[R_2Bpz_2]^-$ ligands in general.

Acknowledgements

We thank the Natural Sciences and Engineering Research Council of Canada for financial support, Mr. P. Borda for elemental analyses, Ms. M. Austria for ^{1}H nmr spectra, and Mr. M. Lapawa for mass spectra.

1. B. M. LOUIE and A. STORR. Can. J. Chem. **62**, 1344 (1984) and references therein.
2. H. C. CLARK and K. VON WERNER. J. Organomet. Chem. **101**, 347 (1975).
3. H. C. CLARK and L. E. MANZER. Inorg. Chem. **13**, 1291 (1974).
4. H. C. CLARK and L. E. MANZER. J. Organomet. Chem. **59**, 411 (1973).

5. K. R. BREAKELL, D. J. PATMORE, and A. STORR. J. Chem. Soc. Dalton Trans. 749 (1975).
6. S. TROFIMENKO. J. Am. Chem. Soc. **84**, 6288 (1967).
7. B. W. DAVIES and N. C. PAYNE. J. Organomet. Chem. **102**, 245 (1975).
8. J. D. OLIVER and P. E. RUSH. J. Organomet. Chem. **104**, 117 (1976).
9. L. E. MANZER and P. Z. MEAKIN. Inorg. Chem. **15**, 3117 (1976).
10. F. BONATI and H. C. CLARK. Can. J. Chem. **56**, 2513 (1978).
11. A. L. BANDINI, G. BANDITELLI, G. MINGHETTI, and F. BONATI. Can. J. Chem. **57**, 3237 (1979).
12. B. M. LOUIE, S. J. RETTIG, A. STORR, and J. TROTTER. Can. J. Chem. **62**, 1057 (1984).
13. B. M. LOUIE, S. J. RETTIG, A. STORR, and J. TROTTER. Can. J. Chem. **63**, 503 (1985).
14. B. M. LOUIE, S. J. RETTIG, A. STORR, and J. TROTTER. Can. J. Chem. **63**, 703 (1985).
15. S. NUSSBAUM, S. J. RETTIG, A. STORR, and J. TROTTER. Can. J. Chem. **63**, 692 (1985).
16. S. E. ANSLOW, K. S. CHONG, S. J. RETTIG, A. STORR, and J. TROTTER. Can. J. Chem. **59**, 3123 (1981).
17. K. S. CHONG, S. J. RETTIG, A. STORR, and J. TROTTER. Can. J. Chem. **59**, 996 (1981).
18. D. F. RENDLE, A. STORR, and J. TROTTER. J. Chem. Soc. Dalton Trans. 176 (1975).
19. D. J. PATMORE, D. F. RENDLE, A. STORR, and J. TROTTER. J. Chem. Soc. Dalton Trans. 718 (1975).
20. D. F. RENDLE, A. STORR, and J. TROTTER. Can. J. Chem. **53**, 2930 (1975).
21. A. ARDUINI and A. STORR. J. Chem. Soc. Dalton Trans. 503, (1974).

The preparation and structure of methanedithiolatobis(dimethylphenylphosphine)platinum(II), $(PMe_2Ph)_2Pt(S_2CH_2)$

ALAN SHAVER[1] AND RABIN D. LAI
Department of Chemistry, McGill University, 801 Sherbrooke Street West, Montreal, P.Q., Canada H3A 2K6

AND

PETER H. BIRD[2] AND WASANTHA WICKRAMASINGHE
Department of Chemistry, Concordia University, 1455 de Maisonneuve Blvd. West, Montreal, P.Q., Canada H3G 1M8

Received October 1, 1984

ALAN SHAVER, RABIN D. LAI, PETER H. BIRD, and WASANTHA WICKRAMASINGHE. Can. J. Chem. **63**, 2555 (1985).

Attempts to prepare the complexes *cis*-$L_2Pt(SH)_2$, where L = PPh_3, $PMePh_2$, and PMePh by treatment of the appropriate dichloro complexes with NaSH in the presence of CH_2Cl_2 have resulted in the isolation of the complexes $L_2Pt(S_2CH_2)$. The X-ray structure determination of the compound for which L = PMe_2Ph confirms the presence of the $CH_2S_2^{2-}$ ligand.

ALAN SHAVER, RABIN D. LAI, PETER H. BIRD et WASANTHA WICKRAMASINGHE. Can. J. Chem. **63**, 2555 (1985).

Des essais réalisés dans le but de préparer les complexes $L_2Pt(SH)_2$-*cis*, dans lesquels L = PPh_3, $PMePh_2$ et PMe_2Ph, par la réaction des complexes dichlorés appropriés avec du NaSH en présence de CH_2Cl_2 n'ont conduit qu'à la formation de complexes $L_2Pt(S_2CH_2)$. Une détermination de la structure du composé dans lequel L = PMe_2Ph, en faisant appel à la diffraction des rayons-X, permet de confirmer la présence du ligand $CH_2S_2^{2-}$.

[Traduit par le journal]

Introduction

Compounds containing the SH^- ligand have been shown to be good precursors to complexes of catenated polysulfur ligands. Thus, $CpW(CO)_3SH$ reacts with sulfur transfer reagents of the type R—S_x—Imidyl, where x = 1, 2 and Imidyl = pthalimide, to give $CpW(CO)_3S_xR$ (1). The bisthiolo complex $Cp_2Ti(SH)_2$ reacts with the difunctional sulfur transfer reagents Imidyl—S_x—Imidyl, where x = 1, 2 to give Cp_2TiS_5, containing the cyclic S_5 ligand (2) and with R—S—Imidyl to give $Cp_2Ti(SSR)_2$, when R = alkyl and $Cp_2Ti(SR)(SSSR)$ when R = aryl (3). Thus, the reports (4–6) of the complex *cis*-$(PPh_3)_2Pt(SH)_2$, **1**, were of particular interest to us. However, despite the fact that three different preparative routes to this complex have been reported, we found it to be somewhat elusive. In this paper, we report our attempts to prepare this complex during which we have observed a novel reaction between CH_2Cl_2 and the reactants *cis*-L_2PtCl_2/NaSH, where L = PPh_3, $PMePh_2$, and PMe_2Ph, to give the complexes $L_2Pt(S_2CH_2)$, **2**–**4**. These contain the chelating ligand $CH_2S_2^{2-}$ as confirmed by the X-ray structure of complex 4.

Experimental

The general techniques used to prepare and characterize the complexes were similar to those already described (7). All solvents were of spectrograde quality. Melting points were determined in air on a Thomas-Hoover Uni-melt apparatus and are uncorrected. Proton nmr spectra were obtained on a Varian T-60 spectrometer, using $CDCl_3$ (Merck, Sharpe and Dohme of Montreal) as solvent and TMS as internal standard. Phosphorus nmr spectra were recorded using a Bruker WH-90 instrument operating in the pulsed Fourier Transform mode. The ^{31}P chemical shifts of the samples in $CDCl_3$ solution are reported in ppm upfield (negative) from 85% H_3PO_4 as external standard, using D_2O as the lock signal. Elemental analyses were performed by Midwest Microlab Ltd., Indianapolis, IN. Molecular weights were obtained in benzene or $CHCl_3$ by Spang Microanalytical Laboratory, Eagle Harbor, MI. The reactions were conducted under N_2 atmosphere with workup of the products carried out in air. The starting materials $(PPh_3)_2PtO_2$ (8) and *cis*-bis(phosphine)$PtCl_2$ (9–11) were prepared by literature methods. Technical grade (≥98.5%) dihydrogen sulfide gas (Linde) was passed through a column of "Drierite" (Anachemia) before use. Sodium hydrogen sulfide was prepared by the standard procedure (12).

A. cis-*Bis(thiolo)bis(triphenylphosphine)platinum(II),* cis-*$(PPh_3)_2Pt(SH)_2$,* ***1***

H_2S was bubbled through a THF suspension (40 mL) of $(PPh_3)PtO_2$ (0.52 g, 0.7 mmol) for 15 min. The white precipitate which formed was filtered, washed with THF and hexane, and pumped on (0.35 g, 64%).

Methanedithiolato complexes

The complexes $L_2Pt(S_2CH_2)$, where L = PPh_3, **2**; $PMePh_2$, **3**; PMe_2Ph, **4**, could be prepared by a number of similar routes as outlined in the Results section. The preparation of **4** is given as a typical example.

B. Methanedithiolatobis(dimethylphenylphosphine)platinum(II), $(PMe_2Ph)_2Pt(S_2CH_2)$, ***4***

The complex *cis*-$(PMe_2Ph)_2PtCl_2$ (0.88 g, 1.6 mmol) and NaSH (0.25 g, 45 mmol) were refluxed under nitrogen in a mixture of toluene (10 mL) and ethanol (25 mL) for 5 h. The reaction mixture was filtered in air, the filtrate evaporated in *vacuo* to a yellow oil which was extracted with a minimum amount of CH_2Cl_2, washed with 2 × 100 mL of H_2O, and dried over anhydrous $MgSO_4$. Addition of ether to the CH_2Cl_2 solution and cooling at −12°C gave **4** as yellow crystals which were collected, washed with CH_2Cl_2/Et_2O, and Et_2O, dried in a stream of N_2, and pumped on for 24 h (0.32 g, 37%).

X-ray structure determination

Crystal data:
$C_{17}H_{24}P_2PtS_2$ fw = 549.56
Monoclinic, $P2_1/c$, a = 9.555(6), b = 16.478(9), c = 13.485(8), β = 112.67(5) Å, V = 1959.1 Å^3, Z = 4, ρ_o = 1.88(2), ρ_c = 1.863 g cm^{-3}, ($MoK_\alpha\lambda$ = 0.71069 Å, 20°C, μ = 75.98 cm^{-1}).

The crystal used in the structure determination was grown from a mixture of methylene chloride and hexanes. It was a small irregularly shaped fragment with no dimension exceeding 0.1 mm. Preliminary photographic data unambiguously established the space group as monoclinic, $P2_1/c$. The unit cell was measured by accurately aligning

[1]To whom correspondence concerning the preparations should be addressed.

[2]To whom correspondence concerning the X-ray structural determination should be addressed.

TABLE 1. Analytical and physical data

Compound		mp, °C	Analysis % C Calcd.	% C Found	% H Calcd.	% H Found	% S Calcd.	% S Found	Mol. wt. Calcd.	Mol. wt. Found
cis-$(PPh_3)_2Pt(SH)_2$	**1**	215−217	55.0	53.4	4.08	4.46	8.15	8.05		
$(PPh_3)_2Pt(S_2CH_2)$	**2**	227−230	55.7	55.1	4.02	4.14	8.02	7.03		
$(PMePh_2)_2Pt(S_2CH_2)$	**3**	191−193	48.1	48.1	4.16	4.14	9.51	9.17	673	612
$(PMe_2Ph)_2Pt(S_2CH_2)$	**4**	175−177	37.1	35.8	4.37	4.34	11.7	11.9	549	520

TABLE 2. Nuclear magnetic resonance data of complexes **1**−**4** and selected literature nmr data for some other platinum(II)−thiolo complexes

Compound	S-R[a] τ	S-R[a] J(Pt—H)	S-R[a] J(P—H)
cis-$(PPh_3)_2Pt(SH)_2$	10.36	50.3	8.5
	9.82[b]	50	8.5
	8.11[c]	[d]	[d]
	8.26[e]	[d]	[d]
trans-$(PEt_3)_2Pt(SH)_2$	11.5[f]	54	10
trans-$(PPh_3)_2Pt(SH)(H)$	11.4[g]	44	10
trans-$(PBz_3)_2Pt(SH)(H)$	11.39[h]		
trans-$(PEt_3)_2Pt(SH)(H)$	10.12[i]	44	8
	11.1[f]	42	11
trans-$(PEt_3)_2Pt(SH)(I)$	10.8[f]	68	11
$(PPh_3)_2Pt(S_2CH_2)$[j]	4.33	43	1.8
$(PMePh_2)_2Pt(S_2CH_2)$[k]	4.17	39	1.7
$(PMe_2Ph)_2(S_2CH_2)$[l]	3.93	36	1.6

[a]Chemical shifts of *SH* or *CH_2*; phenyl resonances occur in the range 2−3 τ for complexes **1**−**4**; solvent is $CDCl_3$ unless stated otherwise.
[b]Reference 5, CD_2Cl_2.
[c]References 6 and 15.
[d]Not reported.
[e]Reference 16.
[f]Reference 17, CH_2Cl_2.
[g]Reference 18.
[h]Reference 19, Bz = benzyl.
[i]Reference 20, toluene.
[j]Phosphorus chemical shift (α) in ppm upfield (negative) from 85% H_3PO_4; α = −21.4, J(Pt—P) = 2979 Hz.
[k]P—CH_3: τ 8.27, J(Pt—H) = 32 Hz, J(P—H) = 9 Hz; α = −0.74, J(Pt—P) = 2854 Hz.
[l]P—CH_3: τ 8.53, J(Pt—H) = 32 Hz; J(P—H) = 10 Hz; α = 19.90, J(Pt—P) = 2815 Hz.

30 reflections on a Picker Nuclear FACS-1 fully automated diffractometer, and then performing a least-squares calculation. The data were collected using a θ−2θ scan and profile analysis (13). The scan speed was 2.0 deg min^{-1}. A unique quadrant of data was collected in the region $\pm h$, $+k$, $+l$, with three standards re-measured every 50 measurement cycles. The intensity of these standards varied randomly by less than 1%. The data were corrected for Lorentz and polarization effects, but due to the small size and poorly definable shape of the crystal no absorption correction was attempted. After data processing of 2561 measured reflections, 1883 having $I > \sigma(I)$ were retained for the structure solution. The following formulae were used for data reduction:

$$I = [N - B \cdot t_s/t_b]$$
$$\sigma(I) = [N + B(t_s/t_b)^2 + (0.02N)^2]^{1/2}$$
$$(Lp)^{-1} = \sin 2\theta_s(\cos^2 2\theta_n + 1)/(\cos^2 2\theta_m + \cos^2 2\theta_s)$$

where I is the net intensity derived from N, the measured count during the scan of duration t_s; B is the background count estimated from the peak profile analysis (13) during a time t_b; Lp is the Lorentz-polarization correction calculated using $2\theta_m$ and $2\theta_s$, the diffraction angles at the monochromator and the sample crystals, respectively.

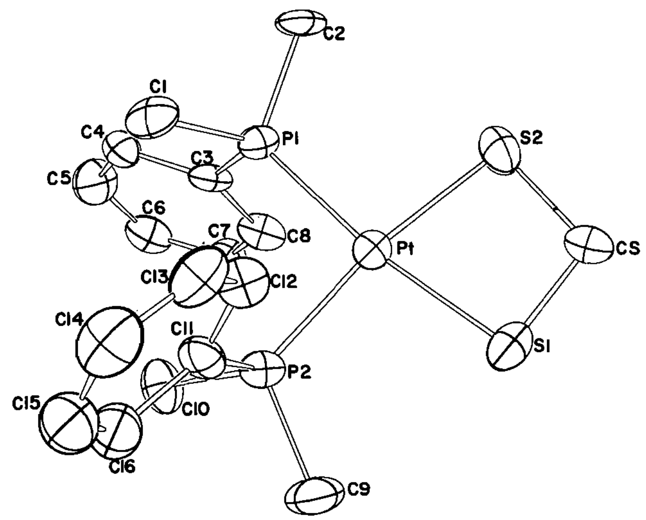

FIG. 1. The molecular configuration and numbering scheme for **4**.

TABLE 3. Final positional parameters fort **4**[a]

Atom	X	Y	Z
Pt	4797.0(6)	1094.5(3)	1589.6(4)
P1	6918(4)	1287.6(24)	1279(3)
P2	6041(5)	931.9(25)	3379(3)
S1	2426(5)	939(3)	1629(4)
S2	3171(5)	3770(3)	4814(4)
CS	1536(22)	1036(11)	178(14)
C1	8472(19)	583(9)	1886(14)
C2	6676(20)	3780(10)	4902(13)
C3	7698(17)	2295(8)	1711(10)
C4	9274(16)	2456(11)	2004(12)
C5	9791(19)	3242(12)	2379(16)
C6	8807(22)	3826(10)	2438(14)
C7	7332(18)	3666(10)	2140(13)
C8	6742(19)	2896(8)	1771(12)
C9	4851(23)	1036(12)	4148(16)
C10	7580(19)	1636(10)	4082(14)
C11	6823(17)	−77(9)	3759(11)
C12	3578(17)	4336(9)	2013(13)
C13	3087(19)	3517(10)	1684(16)
C14	2185(22)	3349(11)	692(18)
C15	1772(25)	1038(14)	4895(18)
C16	2241(20)	4753(12)	125(15)

[a]The estimated standard deviations in parentheses are right justified to the least significant digit of the preceding numbers, which have been multiplied by 10^4.

The structure was solved by conventional heavy atom methods and refined by block-diagonal least squares. All atoms were assigned anisotropic thermal parameters during the final cycles. No attempt was

TABLE 4. Bond lengths (Å) and angles (deg) for **4**

Bond	Length	Bond	Length	Bond	Length	Bond	Length
Pt—S1	2.301(5)	P1—C1	1.81(2)	C3—C4	1.43(2)	C11—C12	1.36(2)
Pt—S2	2.309(5)	P1—C2	1.78(2)	C4—C5	1.41(2)	C12—C13	1.44(2)
Pt—P1	2.244(4)	P1—C3	1.82(1)	C5—C6	1.37(3)	C13—C14	1.31(3)
Pt—P2	2.257(5)	P2—C9	1.82(2)	C6—C7	1.33(2)	C14—C15	1.41(3)
S1—CS	1.82(2)	P2—C10	1.82(2)	C7—C8	1.40(2)	C15—C16	1.37(3)
S2—CS	1.84(2)	P2—C11	1.81(2)	C8—C3	1.37(2)	C16—C12	1.45(2)

Bonds	Angle	Bonds	Angle	Bonds	Angle
S1—Pt—S2	76.1(2)	Pt—P1—C1	117.8(6)	Pt—P2—C9	114.3(7)
S1—Pt—P1	171.1(2)	Pt—P1—C2	114.9(6)	Pt—P2—C10	117.8(6)
S1—Pt—P2	94.6(2)	Pt—P1—C3	110.9(5)	Pt—P2—C11	113.6(5)
S2—Pt—P1	95.0(2)	C1—P1—C2	100.7(8)	C9—P2—C10	101.5(9)
S2—Pt—P2	170.7(2)	C1—P1—C3	106.1(7)	C9—P1—C11	101.9(8)
P1—Pt—P2	94.3(2)	C2—P1—C3	105.2(7)	C10—P2—C11	105.9(7)
Pt—S1—CS	91.3(7)	P1—C3—C4	121(1)	P2—C11—C12	118(1)
Pt—S2—CS	90.4(6)	P1—C3—C8	119(1)	P2—C11—C16	120(1)
S1—CS—S2	102.1(10)	C4—C3—C8	120(1)	C12—C11—C16	122(1)
		C3—C4—C5	117(1)	C11—C12—C13	118(1)
		C4—C5—C6	121(2)	C12—C13—C14	121(2)
		C5—C6—C7	121(2)	C13—C14—C15	120(2)
		C6—C7—C8	121(2)	C14—C15—C16	122(2)
		C7—C8—C3	119(1)	C15—C16—C11	116(2)

made to find or refine hydrogen atoms. Calculated parameters shifts were multiplied by 0.6 after each cycle and anisotropic refinement was terminated when the largest shift was less than 1/10th of the corresponding standard deviation. A final difference Fourier synthesis showed no features above 0.4 e/Å^3. The final discrepancy indices were $R_f = 0.056$, $R_{wf} = 0.077$, and the "goodness-of-fit" = 1.30. The final atomic parameters are listed in Table 1.[3] The function minimized in the least-squares refinement was: $[\Sigma w(|F_o| - |F_c|)^2]$, where $w = [(\sigma(F)^2 + 0.03\ F^2]^{-1}$. The conventional discrepancy indices are $R_f = \Sigma(||F_o| - |F_c||)/\Sigma|F_o|$, $R_{wf} = [\Sigma_w(|F_o| - |F_c|)^2/\Sigma_w|F_o|^2]^{1/2}$ and the "goodness-of-fit" is $[\Sigma_w(|F_o| - |F_c|)^2/(m - n)]^{1/2}$.

The program to control the diffractometer and the programs used for the data processing, solution and refinement of the structure were parts of the N.R.C. Package of programs wirtten for the PDP-8a minicomputer by Larson and Gabe (14).

Results

The analytical and physical data of complexes **1**−**4** are given in Table 1. The nmr data of these complexes and the data reported for some other platinum thiolo complexes are given and compared in Table 2. The preparation of **1** was a modification of a literature method (5). The use of chlorinated solvents, recommended by other reports, was found to lead to decomposition. Complex **1** reacts with CH_2Cl_2 in the presence of K_2CO_3 but the product(s) could not be identified. The routes to *cis*-$(PPh_3)_2Pt(SH)_2$ described by Schmidt and Hoffmann (6, 15) did not work in our hands. Treatment of *cis*-$(PPh_3)_2PtCl_2$ with H_2S/K_2CO_3 or with NaSH in CH_2Cl_2 gave mostly starting material plus some **2**. While it might be tempting to assign complex **1** to be *cis*-$(PPh_3)_2Pt(SH_2)$, the elemental analysis of **1**, while close to that required, was not satisfactory. The chemical shift of the S—H protons compares well to that of several other Pt—SH species but does not agree with any of the three different values reported for *cis*-$(PPh_3)Pt(SH)_2$ (5, 6, 15, 16). The values of the coupling constants between the S—H protons and the platinum and phosphorus atoms are in the range reported in the literature. However, it must be noted that **1** was quite insoluble and the nmr data may be of material extracted from the bulk and thus not representative. The infrared spectrum of **1** was not informative being similar to other platinum−sulfur systems (7, 9). Bands due to the S—H stretching vibration are often weak and difficult to detect. Reaction of **1** with sulfur transfer reagents led to intractable brown tars.

Treatment of L_2PtCl_2 with NaSH in the presence of CH_2Cl_2 led to the isolation of complexes **2**−**4**. The characterization of these complexes (Tables 1 and 2) is consistent with their formulation as compounds of the simple methanedithiolato ligand. The complexes were formed in varying yields from treatment of the dichloride with: NaSH in CH_2Cl_2, or H_2S and pulverized K_2CO_3 in CH_2Cl_2 or NaSH in toluene/ethanol followed by extraction of the dried residue with CH_2Cl_2. The latter method appears to work best. A large excess of NaSH was used since it has been found that this promotes the preparation of other MSH species. The methylene is strongly bonded to the sulfur atoms. No reaction occurred when **3** was refluxed under N_2 with lithium metal in THF for 2 h. However, benzyl chloride reacted with **3** to give the dichloride complex and presumably $PhCH_2SCH_2SCH_2Ph$; however, the latter was not isolated.

The structure of **4** consists of a square planar arrangement of two phosphine ligands and the chelating $CH_2S_2^{2-}$ ligand (Fig. 1). The final positional parameters are listed in Table 3 and the listing of the bond lengths and angles appears in Table 4. The P_2PtS_2C grouping of atom is remarkably flat, deviations from planarity being less than 0.003 Å. The phenyl rings are disposed in an *anti* fashion. Comparison of the bond lengths and angles about the coordinated atoms of **4** with those of the complex $(PPh_3)Pt(SCH_2CH_2S)$, **5** (21), which has a two carbon atom bridge between the two sulfur atoms, reveals the effect of

[3] Table 6 (temperature factors for *cis*-$(PMe_2Ph)_2Pt(S_2CH_2)$) and Table 7 (observed and calculated structure amplitudes *cis*-$(PMe_2Ph)_2Pt(S_2CH_2)$) may be purchased from the Depository of Unpublished Data, CISTI, National Research Council of Canada, Ottawa, Ont., Canada K1A 0S2.

TABLE 5. Comparison of selected average bond lengths and angles in $(PMe_2PH)_2Pt(S_2CH_2)$ and $(PPh_3)_2Pt(SCH_2CH_2S)$

Parameter	Value	
	S_2CH_2	SCH_2CH_2S[a]
Pt—P	2.251	2.289
Pt—S	2.305	2.321
C—S	1.83	1.83
S—Pt—S	76.1	87.7
S—Pt—P	94.8	86.8
P—Pt—P	94.3	99.0
Pt—S—C	90.9	102.3

[a]Reference 21.

the $CH_2S_2^{2-}$ ligand (Table 5). As expected the S—Pt—S and Pt—S—C angles are reduced in **4**. Interestingly the average Pt—P and Pt—S bond distances are also slightly shorter in **4**. The S—C—S angle in **4** (102.1) is intermediate between those for $Fe(CO)_6(S_2CH_2)$ (94.55 (22)) and $[Os_3H(CO)_{10}]_2(\mu\text{-}S_2CH_2)$ (105.3 (23)). The $CH_2S_2^{2-}$ ligand in the Osmium complex is not chelating. The S—S distance in **4** is 2.841(5) Å, which is longer than that in $Fe_2(CO)_6(S_2CH_2)$ (2.673(2)) and much longer than that in $Fe_2(CO)_6S_2$ (2.007(5)) where a S—S bond exists (24).[3]

Discussion

Since CH_2Cl_2 can, under certain circumstances, couple two thiol molecules to give a dithioacetal (25), it is tempting to suggest that complexes **2**–**4** were formed by the reaction of

$$2RSH + CH_2Cl_2 \rightarrow RS—CH_2—SR + 2HCl$$

CH_2Cl_2 with the appropriate *cis*-$L_2Pt(SH)_2$ complex. The latter, however, were not isolated except for L = PPh_3, **1**, and there remains some doubt about its characterization. Complex **1** reacts with CH_2Cl_2 but the products could not be identified. The odor of H_2S was detected during the preparations of **2**–**4** which is consistent with the reaction of the excess NaSH present with HCl produced by the reaction of CH_2Cl_2.

An alternative possibility involves the recognition (26) of the strong nucleophility of the sulfur atoms in $[Pt(\mu\text{-}S)(PPh_3)_2]_n$, **6**. This complex reacts with CH_2Cl_2 to give $[Pt_2(\mu\text{-}S)(\mu\text{-}SCH_2Cl)(PPh_3)_4]\cdot Cl$ a cation with a bridging CH_2SCl^- ligand, **7**. Complex **7** is reported to decompose in CH_2Cl_2.

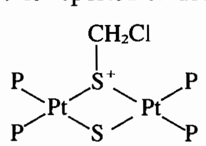

7

Complex **6** has been reported as the product upon treatment of **1** with NaOEt (15). It is possible that **1** could dimerize (7) to give **6** via elimination of H_2S. This type of reaction has been observed for $Cp_2Zr(SH)_2$ leading to $[Cp_2Zr(\mu\text{-}S)]_2$ (2). Conversion of **7** to **2** can be envisioned via internal alkylation of the bridging sulfide ligand (26).

Acknowledgements

The research was supported by grants from the Natural Sciences and Engineering Research Council of Canada and the Quebec Department of Education. Predoctoral fellowships awarded to R. D. L. by McGill University are gratefully acknowledged.

1. A. SHAVER, J. HARTGERINK, R. D. LAI, P. BIRD, and N. ANSARI. Organometallics, **2**, 938 (1983).
2. A. SHAVER and J. M. MCCALL. Organometallics **3**, 1823 (1984).
3. A. SHAVER, J. M. MCCALL, P. H. BIRD, and N. ANSARI. Organometallics, **2**, 1894 (1983).
4. B. KREUTZER, P. KREUTZER, and W. BECK. Z. Naturforsch. **27B**, 461 (1972).
5. C. E. BRIANT, G. R. HUGHES, P. C. MINSHALL, and D. M. P. MINGOS. J. Organomet. Chem. **202**, C18 (1980).
6. M. SCHMIDT and G. G. HOFFMANN. (*a*) J. Organomet. Chem. **124**, C5 (1977); (*b*) Z. Naturforsch. **33B**, 1334 (1978).
7. P. H. BIRD, U. SIRWARDANE, R. D. LAI, and A. SHAVER. Can. J. Chem. **60**, 2075 (1982).
8. C. D. COOK and G. D. JAUHAL. J. Am. Chem. Soc. **90**, 1464 (1968).
9. R. D. LAI and A. SHAVER. Inorg. Chem. **20**, 477 (1981).
10. (*a*) K. A. JENSEN. Z. Anorg. Chem. **229**, 237 (1936); (*b*) L. MALATESTA and C. CARIELLO. J. Chem. Soc. 2323 (1958); (*c*) R. UGO, F. CARIATI, and G. LAMONICA. Inorg. Synth. **11**, 105 (1968).
11. S. O. GRIM, R. L. KEITER, and W. MCFARLANE. Inorg. Chem. **6**, 1133 (1967).
12. R. E. EIBECK. Inorg. Synth. **7**, 128 (1963).
13. D. F. GRANT and E. J. GABE. J. Appl. Cryst. **11**, 114 (1978).
14. A. C. LARSON and E. J. GABE. *In* Computing in crystallography. *Edited by* H. Schenk, R. Olthof-Hazekamp, H. Van Koningsveld, and J. C. Bassi. Delft University Press, Delft, Holland. 1978. p. 81.
15. M. SCHMIDT and G. G. HOFFMANN. Z. Anorg. Allgem. Chem. **464**, 209 (1980).
16. J. A. BERTRAND and J. L. BREECE. Inorg. Chim. Acta, **8**, 267 (1974).
17. I. M. BLACKLAWS, E. A. V. EBSWORTH, D. W. H. RANKIN, and H. E. ROBERTSON. J. Chem. Soc. Dalton Trans. 753 (1978).
18. (*a*) D. MORELLI, A. SEGRE, R. UGO, G. LAMONICA, S. CENINI, F. CONTI, and F. BONATI. J. Chem. Soc. Chem. Commun. 524 (1967); (*b*) R. UGO, G. LAMONICA, S. CENINI, A. SEGRE, and F. CONTI. J. Chem. Soc. (A) 522 (1971).
19. T. MIZAMOTO. J. Organomet. Chem. **134**, 335 (1977).
20. E. A. V. EBSWORTH, J. M. EDWARD, and D. W. H. RANKIN. J. Chem. Soc. Dalton Trans. 1667 (1976).
21. S. A. BRYAN and D. M. ROUNDHILL. Acta Crystallogr. **C39**, 184 (1983).
22. A. SHAVER, P. J. FITZPATRICK, K. STELIOU, and I. S. BUTLER. J. Am. Chem. Soc. **101**, 1313 (1979).
23. R. D. ADAMS and N. M. GOLEMBESKI. J. Am. Chem. Soc. **101**, 1306 (1979).
24. C. H. WEI and L. F. DAHL. Inorg. Chem. **4**, 1 (1965).
25. (*a*) A. W. HERRIOTT and D. PICKER. Synthesis, 447 (1975); (*b*) U. SRIVASTAVA, R. H. KHAN, and S. C. BAHEL. Bokin Bobai, **7**, T414 (1979); Chem. Abstr. **92**, 146685Y (1980).
26. R. R. GUKATHASAN, R. H. MORRIS, and A. WALKER. Can. J. Chem. **61**, 2490 (1983).

Use of peak height for quantification in solvent extraction/flow injection analysis

JAMAL A. SWEILEH AND FREDERICK F. CANTWELL[1]
Department of Chemistry, University of Alberta, Edmonton, Alta., Canada T6G 2G2

Received December 5, 1984

JAMAL A. SWEILEH and FREDERICK F. CANTWELL. Can. J. Chem. **63**, 2559 (1985).

The following equation is derived which expresses peak height (P.H.) in terms of sample concentration injected (C_{SAMP}), detector sensitivity (S_F), dilution due to band dispersion (R_v), fraction extracted (ϕ), flow rates of carrier ($F_{Carrier}$), organic phase (F_o), and compensating solvent (F_c), and flow rate of organic extract through the membrane phase separator (F_M):

$$\text{P.H.} = C_{SAMP} \cdot S_F \cdot R_v \cdot \frac{F_{Carrier}}{F_o} \cdot \phi \cdot \frac{F_M}{F_M + F_c}$$

Each term in the equation is evaluated experimentally to validate the equation.

JAMAL A. SWEILEH et FREDERICK F. CANTWELL. Can. J. Chem. **63**, 2559 (1985).

On a dérivé l'équation suivante, qui exprime la hauteur des pics (H.P.) en fonction de la concentration des échantillons injectés (C_{ECHANT}), de la sensibilité du détecteur (S_F), de la dilution due à la dispersion de la bande (R_v), de la fraction extraite (ϕ), des vitesses d'écoulement du porteur ($F_{Porteur}$), de la phase organique (F_o), de la compensation par un solvant (F_c) et des vitesses d'écoulement des composés organiques à travers la membrane qui sépare les phases (F_M):

$$\text{H.P.} = C_{ECHANT} \cdot S_F \cdot R_v \cdot \frac{F_{Porteur}}{F_o} \cdot \phi \cdot \frac{F_M}{F_M + F_c}$$

On a évalué expérimentalement chacun des termes de cette équation afin de la valider.

[Traduit par le journal]

The performance of automated solvent extraction in the flow injection analysis (FIA) mode has been studied both in terms of its principles of operation and its application to quantitative determinations (refs. 1−4 and references therein). Quantification in solvent extraction/FIA is based on either peak height or peak area. In a previous paper from this laboratory the quantitative relationship between *peak area* and various system parameters was derived and experimentally verified for systems employing a concentration sensitive detector (1). The present paper deals with the quantitative relationship between *peak height* and such system parameters as detector sensitivity, peak dispersion, flow rates of aqueous and organic streams, and sample distribution coefficient.

Some types of detectors, such as molecular absorption spectrophotometers, can simply be attached to the organic extract line exiting the phase separator (1), while other detectors, such as atomic absorption spectrophotometers (AAS), may require additional plumbing to provide flow compensation to the extract entering the nebulizer (3). Furthermore, while the detector sensitivity is independent of flow rate with molecular absorption spectrophotometers, it exhibits a complex flow-rate dependence with AAS detectors (3, 5). Both situations are included in the equation which is derived and experimentally verified in the present report.

Experimental

Apparatus

Two versions of the extraction/FIA instrument are considered, one with an AAS detector and the other with a molecular absorption spectrophotometric detector. The former, which has been used in the atomic absorption determination of zinc following solvent extraction of $Zn(SCN)_2$ (3), is shown in Fig. 1. It will be referred to as Version I of the instrument. The aqueous carrier is 0.10 M HCl, the aqueous reagent is 0.50 M KSCN in 0.10 M HCl and the immiscible organic solvent is methylisobutylketone (MIBK). Carrier and reagent streams merge at the first tee junction (T_1) and the resulting combined aqueous stream merges with MIBK in the phase segmentor tee (T_2). After passing through the 3-m long Teflon extraction coil the segmented flow stream enters the membrane phase separator M from which a portion of the MIBK exits to the tee junction T_3, where it is merged with the flow of MIBK from the compensating flask. The resulting MIBK solution enters the nebulizer of the AAS detector. Carrier, reagent, and organic solvents are pumped with nitrogen pressurized constant pressure pumps (1, 3).

Samples consist of dilute solutions of Zn(II) in 0.1 M HCl which are injected via a sample injection valve V_3. During passage of the segmented aqueous−organic flow stream through the extraction coil the complex $Zn(SCN)_2$ is quantitatively extracted into MIBK. The AA signal peak is due to Zn. AA peaks are displayed on a strip chart recorder R. Details of the instrument and operation of the phase segmentor are described elsewhere (3, 4).

The aqueous flow rate F_a is the sum of carrier flow rate $F_{Carrier}$ and reagent flow rate $F_{Reagent}$; the total flow rate F_T is equal to F_a plus the MIBK flow rate F_o; flow rate of MIBK phase passing through the membrane phase separator is F_M and compensating flow rate of MIBK from the flask is F_c. It was found that use of the flow compensator resulted in the total flow rate of MIBK entering the nebulizer ($F_M + F_c$) remaining constant for a given nebulizer setting, even when F_M was purposely varied during experiments. The value of ($F_M + F_c$) is governed by the "natural" aspiration rate demanded by the particular nebulizer setting as demonstrated in this study.

The second version of the extraction/FIA instrument, called Version II, was used in studies where some flow rates were varied while others were kept constant and where it was desired to use a detector whose sensitivity is flow-rate independent. The design was similar to that in Fig. 1 except for the following changes; (*i*) the constant pressure pumps were replaced by three constant flow rate liquid chromatography pumps (Model 6000A, Waters Assoc. and Model 396 Minipump, Laboratory Data Control); (*ii*) methanol was used, instead of acetone as a flushing solvent; (*iii*) T_3 and the compensating solvent were absent; (*iv*) a uv absorbance detector (Model 770, Schoeffel Instr. Corp.) was used at 410 nm, in place of the AAS; (*v*) a peristaltic pump (Minipuls 2, Gilson Instruments) was placed in the outlet line from the detector flow cell in order to gate the flow F_M, as described previously (1); (*vi*) carrier was water, reagent was phosphate buffer,

[1]To whom all correspondence should be addressed.

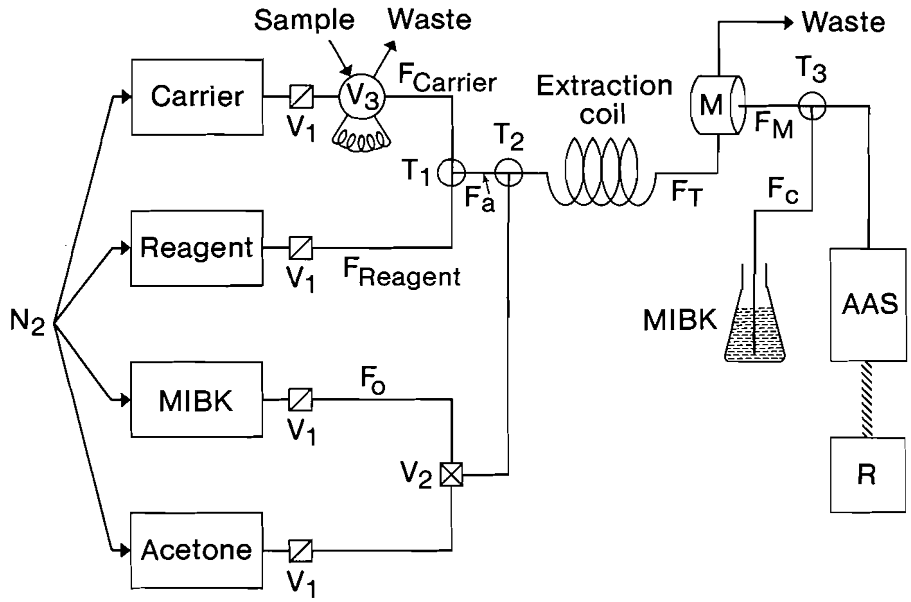

FIG. 1. Diagram of the solvent extraction/FIA instrument employing constant pressure pumping, an atomic absorption detector, and flow compensation.

organic solvent was $CHCl_3$, and the sample solution was *o*-nitroaniline in water.

In both versions of the instrument flow rates were measured by collecting the liquids in burets at the outlet end of the system. Therefore, reported values of F_{Carrier}, F_{Reagent}, F_o, F_a, and F_M are for mutually saturated phases. Also, the extraction coil was sufficiently long that extraction equilibrium was always achieved for both $Zn(SCN)_2$ and *o*-nitroaniline.

Reagents and chemicals

Ortho-nitroaniline stock solution (5.0×10^{-3} *M*) was prepared in water from the reagent grade chemical (BDH, Montreal). The sample solution (4×10^{-5} *M*) was prepared by dilution of the above stock. Phosphate buffer (0.01 *M*, pH = 7.0) was prepared in water by titrating a solution of KH_2PO_4 (McArthur Chemical Co., Montreal) to pH = 7.0 with NaOH and diluting to 2 L. Reagent grades of $CHCl_3$ (Mallinckrodt) and MIBK (Fisher Scientific Co.) were used without further purification. Other reagents and chemicals were reagent grade and have been described elsewhere (3).

Sensitivity curve

This was measured by pumping a solution of $Zn(SCN)_2$ in MIBK into the nebulizer. The "natural" aspiration rate of the nebulizer was set at 2.5 mL/min by suitable adjustment of the position of the nebulizer tip. The $Zn(SCN)_2$ solution was pumped from a constant pressure pump directly and continuously into the nebulizer — no solvent extraction or FIA was involved. $Zn(SCN)_2$ concentrations of 0.40 μg/mL and 0.70 μg/mL were used.

Effect of F_c

Variation of peak height with flow rate of compensating solvent was studied by pumping 0.4 μg/mL $Zn(SCN)_2$ solution in MIBK from a constant pressure pump through a tee junction, where it merged with the compensating flow of MIBK, and then into the nebulizer. No solvent extraction or FIA was involved in this study. The "natural" aspiration rate of the nebulizer was set at about 5 mL/min. A baseline for the AA signal was obtained by shutting off the flow of $Zn(SCN)_2$ solution so that the nebulizer aspirated only MIBK compensating solvent. The flow rate of $ZN(SCN)_2$ solution was then set, in turn, at several values by varying the nitrogen pressure in the pumps. Flow rate of the $Zn(SCN)_2$ solution from the pump was measured for each run by switching a three-way valve (No. CAV 3031, LCD) located between the pump and compensating tee so that the $Zn(SCN)_2$ solution was diverted to a measuring buret. The flow rate of compensating solvent during each run was measured as the rate of reduction in liquid level in the compensating solvent container.

Results and discussion

The derivation of an equation relating peak height to various system parameters in solvent extraction/FIA is first presented and then each of the terms in the equation is examined experimentally.

Derivation

Peak height (P.H.) is related to the maximum concentration in the sample zone (peak) entering the detector, C_{Pk}, by the expression:

$$[1] \quad \mathrm{P.H.} = S_F \cdot C_{\mathrm{Pk}}$$

in which S_F is the sensitivity of the detector in units of height per unit concentration of sample component. Depending on the detector used S_F may depend on (3, 5), or be independent of (1, 2), flow rate into the detector. The peak concentration C_{Pk} can be calculated from the concentration of sample component in the sample solution injected, C_{SAMP}, by taking into account the dilution steps, the extraction efficiency and the dilution resulting from band dispersion. These are considered here for the instrument shown in Fig. 1. Dilution resulting from merging of carrier stream with reagent stream is given by $(F_{\mathrm{Carrier}}/F_a)$. Dilution resulting from extraction into the organic phase is given by the product of the ratio F_a/F_o times the fraction of sample component extracted, ϕ. The fraction extracted can be calculated from the distribution ratio, D, and the phase ratio (1, 2):

$$[2] \quad \phi = \frac{D \cdot (F_o/F_a)}{1 + D \cdot (F_o/F_a)}$$

Dilution caused by band dispersion through the system is the result of laminar flow in connecting tubing and mixing chamber effects in the phase separator and detector (6). The relative dilution, R_v, of the sample due to dispersion is measured experimentally from a plot of peak height versus volume of sample solution injected as described below.

In flow sensitive detectors, such as an AAS, a compensating flow, F_c, merges with the flow of organic extract from the phase separator, F_M, before it enters the detector (3). Dilution of sample component concentration from this source is given by $(F_M/(F_M + F_c))$.

Combining all of the above factors accounting for dilution of the sample component allows C_{Pk} to be calculated:

$$[3] \quad C_{Pk} = C_{SAMP} \cdot R_v \cdot \frac{F_{Carrier}}{F_a} \cdot \frac{F_a}{F_o} \cdot \phi \cdot \frac{F_M}{F_M + F_c}$$

Simplifying this expression and substituting into eq. [1] gives:

$$[4] \quad \text{P.H.} = C_{SAMP} \cdot S_F \cdot R_v \cdot \frac{F_{Carrier}}{F_o} \cdot \phi \cdot \frac{F_M}{F_M + F_c}$$

The quantity ϕ depends on F_a and F_o (eq. [2]), but in the usual situation in which D is large $\phi \approx 1$ so that both ϕ and P.H. become independent of F_a. It should also be noted that with flow-rate sensitive detectors S_F depends on $(F_M + F_c)$ but, as mentioned above, when flow compensation is used with the AAS detector, $(F_M + F_c)$ remains essentially constant and equal to the "natural" aspiration rate of the nebulizer even when F_M is varied. Thus the appropriate value of S_F is read from the sensitivity curve (see below) at a flow rate equal to the nebulizer aspiration rate.

Calibration curve

Using Version I of the instrument in which an atomic absorption detector is employed, a calibration plot of peak height versus zinc concentration injected, C_{SAMP}, was found to be linear with zero intercept and a correlation coefficient of 0.9996 up to peak heights corresponding to an absorbance of about 0.5. The negative deviation observed above this absorbance is found also when samples of Zn^{2+} are aspirated directly into the flame in the normal, non-FIA manner of performing atomic absorption. This, therefore, arises from a negative deviation from Beer's Law at higher absorbances which is a well known phenomenon in atomic absorption spectroscopy. The linearity of P.H. vs. C_{SAMP} observed in the linear absorbance range of the spectrophotometer confirms the prediction of eq. [4].

Sensitivity curve

In Fig. 2 are presented plots of detector sensitivity versus flow rate into the nebulizer. The experiment was performed by pumping MIBK solutions containing two different concentrations of $Zn(SCN)_2$ directly and continuously into the nebulizer. It is seen that S_F, which is the AA signal divided by $Zn(SCN)_2$ concentration, is essentially independent of sample concentration. The general shape of this type of curve has previously been discussed (5). It clearly demonstrates the flow rate dependence of S_F for an AAS detector. Presumably, the leveling-off of the value of S_F at higher flow rates derives from the decreasing efficiency of the nebulizer at producing a fine aerosol from the aspirated liquid. The appropriate value of S_F for use in eq. [4] is read from the curve at a flow rate equal to the value of $(F_M + F_c)$ being used (i.e. at the nebulizer aspiration rate).

Relative dilution, R_v

Band dispersion resulting from flow of the sample zone through the system causes a broadening and decrease in height of the peak. In addition, as the volume of sample injected is made larger it too contributes to the width of the peak (1). To study this phenomenon both Version I and Version II instruments were used. Relative dilution R_v is evaluated from the dependence of peak height on sample volume injected. A plot of this type, for measurements made on the Version I instrument has been published (3). Three plots of this type for measurements made on the Version II instrument are presented in Fig. 3. All plots have the same general shape. The evaluation of R_v is done as follows: consider first curve A in Fig. 3. The limiting plateau seen in this curve at large injection volumes exists because the "slug" of injected sample is sufficiently long that dilution due to band dispersion does not reach the centre of the zone (1). Hence, there is no dilution due to dispersion on this plateau. For a system in which $F_o/F_a = 2.3$ the value of R_v corresponding to any injection volume is calculated as the ratio of the peak height seen in Fig. 3 at the corresponding injection volume divided by the peak height on the limiting plateau. Defined in this way R_v is the reciprocal of the "dispersion", D, used by some workers in FIA (7). The term relative dilution has been used instead of dispersion because the latter term has long been used by chromatographers to refer to bandbroadening as expressed by the standard deviation, the variance or the second central moment of the band, rather than to refer to the decrease in peak height resulting from bandbroadening.

Comparison of curves A, B, and C in Fig. 3, each of which was obtained at a different value of F_o/F_a, shows that R_v is somewhat sensitive to large changes in F_o/F_a. This is not surprising in view of the processes giving rise to band dispersion. It means, in a practical sense, that the curve used to calculate the value of R_v to be used in a given extraction/FIA determination should have been obtained under similar experimental conditions to those used in the determination. The increase in the plateau peak height seen on going from curve A to curve C is a consequence of the increase in $(F_{Carrier}/F_o)$ as seen in eq. [4] and as discussed below. (Note change in de-

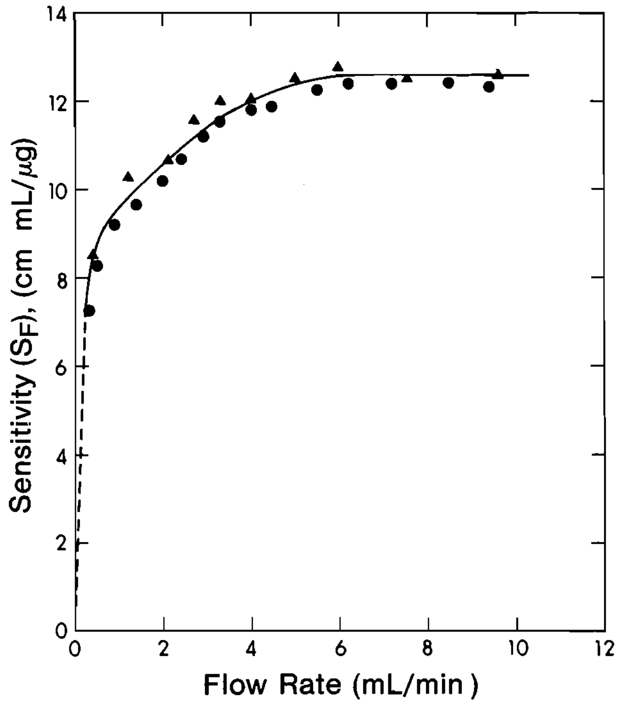

FIG. 2. Sensitivity curve for Zn obtained by pumping 0.7 μg/mL (▲) and 0.4 μg/mL (●) of $Zn(SCN)_2$ in MIBK directly into the nebulizer of the AAS. Nebulizer "natural" aspiration rate was fixed at 2.5 mL/min.

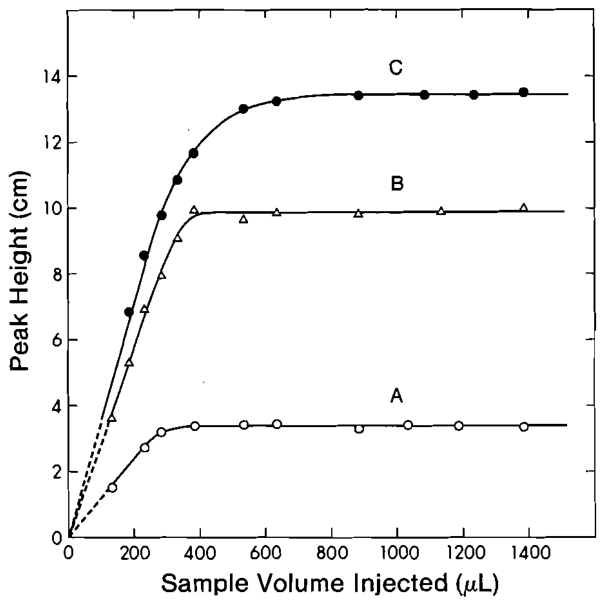

FIG. 3. Effect of sample volume injected on peak height for a sample containing 4×10^{-5} *M* *o*-nitroaniline. Version II instrument. Flow rates in mL/min are: curve *A*, $F_o = 3.0_0$, $F_{Carrier} = 0.9_0$, $F_{Reagent} = 0.4_0$, $F_M = 1.2_0$, $F_o/F_a = 2.3_1$, detector AUFS = 0.01; curve *B*, $F_o = 3.0_0$, $F_{Carrier} = 2.0_0$, $F_{Reagent} = 2.0$, $F_M = 1.1_0$, $F_o/F_a = 0.75$, detector AUFS = 0.02; curve *C*, $F_o = 1.5_0$, $F_{Carrier} = 2.0_0$, $F_{Reagent} = 2.0_0$, $F_M = 0.9_0$, $F_o/F_a = 0.37_5$, detector AUFS = 0.02.

tector sensitivity given in figure caption.) It will be recalled that, since R_v is a ratio of peak heights, it is the shapes of curves $A-C$ that relate to R_v and not the absolute values of peak heights.

Effect of $F_{Carrier}$ *on P.H.*

Equation [4] predicts a linear dependence of P.H. on $F_{Carrier}$ provided that S_F, R_v, ϕ, F_o, F_M and $(F_M + F_c)$ remain constant. This was studied using the Version II instrument. For this instrument S_F is constant, independent of flow rate. Since no compensating flow is used the last term in eq. [4] reduces to 1 and F_M is eliminated from the equation. For the sample compound *o*-nitroaniline $\phi \approx 1$ because K_D is large (8). In this experiment F_o was fixed at 3.0_0 mL/min, $F_{Reagent}$ at 0.50 mL/min and F_M at 1.0_0 mL/min while $F_{Carrier}$ was varied between 0.10 mL/min and 2.5_0 mL/min. An injection volume of 385 μL was used. Under these conditions F_o/F_a varies between 1 and 5 over the range of $F_{Carrier}$ used. Examination of Fig. 3 shows that for $F_o/F_a > 0.75$ an injection volume of 385 μL falls on the plateau so that $R_v \simeq 1$ for all values of $F_{Carrier}$ used. Thus S_F, R_v, ϕ, and F_o are constants and F_M is eliminated from eq. [4]. A plot of P.H. vs. $F_{Carrier}$ is expected to be linear. The experimentally measured plot was linear (slope = $8.3_5 \pm 0.1_2$ at 95% C.L.) with zero intercept (intercept = 0.024 ± 0.368 at 95% C.L.) and a correlation coefficient of 0.9995.

Effect of $F_{Reagent}$ *on P.H.*

According to eq. [4], P.H. should be independent of $F_{Reagent}$. The Version II instrument was used. $F_{Carrier}$ was held at 1.0_0 mL/min, F_o at 3.00 mL/min, and F_M at 1.4_5 mL/min while $F_{Reagent}$ was varied from 0.50 to 2.50 mL/min. Injection volume of *o*-nitroaniline sample solution was 385 μL. Peak height was found to be constant, independent of $F_{Reagent}$. The slope and its 95% C.L. of a plot of pH vs. $F_{Reagent}$ were 0.06 ± 0.05.

TABLE 1. Effect of compensating flow rate on signal and constancy of $(F_M + F_c)$

F_M (mL/min)	F_c (mL/min)	$(F_M + F_c)$ (mL/min)	$\frac{F_M}{(F_M + F_c)}$	AA signal (cm)
1.6_0	4.9_0	6.5_0	0.24_6	1.25
2.3_0	4.2_0	6.5_0	0.35_4	1.85
2.9_0	3.6_0	6.5_0	0.44_6	2.30
3.2_5	3.2_0	6.4_5	0.50_4	2.75
4.0_0	2.5_0	6.5_0	0.61_5	3.25
4.6_0	1.9_0	6.5_0	0.70_8	3.80
5.2_0	1.3_0	6.5_0	0.80_0	4.25
6.0_0	0.5_0	6.5_0	0.92_3	4.65
6.5_0	0.0_0	6.5_0	1.00	5.25

It should be realized that eq. [4] takes no account of the chemistry or stoichiometry of the reaction upon which an extraction/FIA determination may be based. Thus if the amount of product formed by the reaction between the sample component and the reagent is changed as a result of a change in $F_{Reagent}$, the peak height would of course change — but this effect is unrelated to the flow dependencies to which eq. [4] relates.

Effect of F_o *on P.H.*

Using the Version II instrument, $F_{Carrier}$ was fixed at 1.0_0 mL/min, $F_{Reagent}$ at 0.50 mL/min, and F_M at 1.4_5 mL/min while F_o was varied from 1.8_0 to 3.0_0 mL/min. Injection volume of *o*-nitroaniline solution was 385 μL. Since all other variables on the right-hand-side of eq. [4] are constant and F_M is eliminated as discussed earlier, a plot of P.H. vs. $1/F_o$ is expected to be linear. The experimental plot was linear (slope = 25.2 ± 1.3 at 95% C.L.) with zero intercept (intercept = 0.12 ± 1.8 at 95% C.L.) and a correlation coefficient of 0.996.

Effect of F_C *on P.H.*

Variation of peak height with the flow rate of compensating solvent was studied as described in the Experimental section. In this experiment the flow rate of $Zn(SCN)_2$ from the pump is analogous to F_M in the extraction/FIA experiment, while the flow of MIBK from the compensating flask is F_c. The results of this experiment are summarized in Table 1. It can be seen from the first three columns that, at a fixed nebulizer "natural" aspiration rate, $(F_M + F_c)$ remains constant as F_M is changed. From eq. [4] it is expected that a plot of AA signal vs $F_M/(F_M + F_c)$ should be linear. Using the data in Table 1 a plot of AA signal vs. $F_M/(F_M + F_c)$ is linear (slope = 5.17 ± 0.12 at 95% C.L.) with zero intercept (intercept = 0.05 ± 0.19 at 95% C.L.) and a correlation coefficient of 0.998.

Other studies

Several reports on the effect of flow rates on peak height in solvent extraction/FIA have previously appeared (9–12). These studies were performed as part of the optimization procedure in the development of extraction/FIA determinations. As such they were not meant to include the effects of all system parameters and, for the most part, no effort was made to keep all other system variables constant while studying the effect of one. Taking this into account, the data obtained in these studies is consistent with the predictions of eq. [4]. For example, data presented in refs. 9 and 11 give a linear plot of P.H. vs $1/F_o$

in the higher end of the range of F_0 studied, though the plots are non-linear at lower F_0. Also data in ref. 12 show that P.H. increases with an increase in aqueous phase flow rate.

Height versus area

Equation [4] is generally applicable to any detection scheme in solvent extraction/FIA in which peak height is used as the basis for quantification. Some detectors, such as an inductively coupled plasma spectrometer and amperometric detectors, exhibit a sensitivity S_F which depends on flow rate of solution into the detector, as does the atomic absorption spectrophotometer. Other detectors, such as those employing fluorescence, refractive index, or potentiometric measurements, exhibit a sensitivity that is independent of flow rate, as does the uv absorbance detector.

In several previous studies from this laboratory peak area was studied as a means of quantification in solvent extraction/FIA (1, 2, 13). On the basis of these studies and the present one it is possible to make a few observations regarding the relative advantages and disadvantages of quantification by heights and by areas. In general, under experimentally achievable optimum conditions, both area and height measurements yield a precision and accuracy of about 1%. Area measurements have the disadvantage of requiring a relatively expensive digital integration. On the other hand, area measurements are more robust than height measurements. For example, assuming that the distribution ratio is made very large so that extraction is quantitative, peak area measured in the organic phase is independent of flow rate of the aqueous phase (eq. [5], ref. 1) but peak height depends on flow rate of the aqueous carrier ($F_{Carrier}$). Thus precise control of $F_{Carrier}$ is more critical with height measurements. Another example of the robustness of area measurements is their relative independence of refractive index effects (13). The positive and negative portions of the refractive index "peak" cancel out when measurements are made over the whole peak width. In a similar way area measurements are relatively independent of the precise way in which a given volume of sample is injected (e.g. slowly or rapidly switching the injection valve).

Acknowledgements

This work was supported by the Natural Sciences and Engineering Research Council of Canada and by the University of Alberta.

1. L. FOSSEY and F. F. CANTWELL. Anal. Chem. **54**, 1693 (1982).
2. L. FOSSEY and F. F. CANTWELL. Anal. Chem. **55**, 1882 (1983).
3. J. A. SWEILEH and F. F. CANTWELL. Anal. Chem. **57**, 420 (1985).
4. J. A. SWEILEH and F. F. CANTWELL. Anal. Chem. **57**, 329 (1985).
5. J. TREIT, J. S. NIELSEN, B. KRATOCHVIL and F. F. CANTWELL. Anal. Chem. **55**, 1650 (1983).
6. J. C. STERNBERG. *In* Advances in chromatography. Vol. 2. *Edited by* J. C. Giddings and R. A. Keller. Marcel Decker, NY. 1966.
7. J. RUZICKA and E. H. HANSEN. Anal. Chim. Acta, **99**, 37 (1978).
8. A. LEO, C. HANSCH and D. ELKINS. Chem. Rev. **71**, 525 (1971).
9. F. H. BERGAMIN, J. X. MEDEIROS, B. F. REIS and A. E. G. ZAGATTO. Anal. Chim. Acta, **101**, 9 (1978).
10. B. KARLBERG and S. THELANDER. Anal. Chim. Acta, **98**, 1 (1978).
11. L. NORD and B. KARLBERG. Anal. Chim. Acta, **145**, 151 (1983).
12. O. KLINGHOFFER, J. RUZICKA and E. H. HANSEN. Talanta, **27**, 169 (1980).
13. L. FOSSEY and F. F. CANTWELL. Anal. Chem. **57**, 922 (1985).

Spectroscopic, magnetic, biological, and structural characterization of tetrakis(μ-3-chloropropanoato)bis(triphenylphosphine oxide)dicopper(II)

PATRICK SHARROCK
Département de Chimie, Université de Sherbrooke, Sherbrooke (Qué.), Canada J1K 2R1

MILAN MELNIK[1]
Department of Inorganic Chemistry, Slovak Technical University, CS81237-Bratislava, Czechoslovakia

AND

FRANCINE BELANGER-GARIEPY AND ANDRÉ L. BEAUCHAMP[2]
Département de Chimie, Université de Montréal, Montreal, (Qué.), Canada H3C 3V1

Received July 3, 1984[3]

PATRICK SHARROCK, MILAN MELNIK, FRANCINE BELANGER-GARIEPY, and ANDRÉ L. BEAUCHAMP. Can. J. Chem. **63**, 2564 (1985).

Tetrakis(μ-3-chloropropanoato)bis(triphenylphosphine oxide)dicopper(II) is formed by the reaction of the phosphine oxide on the parent copper carboxylate. It belongs to the triclinic space group $P\bar{1}$, with a = 8.603(6), b = 12.605(4), c = 12.624(5) Å, α = 76.94(3), β = 71.74(4), and γ = 74.42(4)°. The complex has the copper acetate dimer structure, in which two Cu atoms separated by 2.649(1) Å are bridged by four bidentate carboxylate groups (mean Cu—O = 1.969 Å). The Cu—O apical bond to triphenylphosphine oxide is relatively short (2.097(2) Å). The epr spectra of the solid are interpreted in terms of a dimeric species with a paramagnetic triplet state. The same signals are found in the spectra of frozen ethanol solutions, indicating that the dimer structure is retained. Magnetic susceptibility was determined in the range 81–293 K and the energy separation $-2J$ = 328(4) cm^{-1} was found between the two spin states. The phosphine oxide adduct is toxic to *Escherichia coli* with ID_{50} values near 100 μg/mL.

PATRICK SHARROCK, MILAN MELNIK, FRANCINE BELANGER-GARIEPY et ANDRÉ L. BEAUCHAMP. Can. J. Chem. **63**, 2564 (1985).

Le tétrakis(μ-3-chloropropanoato)bis(oxyde de triphénylphosphine)dicuivre(II) est produit par addition de l'oxyde de phosphine sur le sel cuivrique de l'acide 3-chloropropanoïque. La maille cristalline est triclinique, groupe spatial $P\bar{1}$, a = 8,603(6), b = 12,605(4), c = 12,624(5) Å, α = 76,94(3), β = 71,74(4) et γ = 74,42(4)°. Le complexe possède la structure dimère de l'acétate de cuivre, dans laquelle deux atomes de Cu à 2,649(1) Å l'un de l'autre sont pontés par quatre groupes carboxylate bidentates (Cu—O moyenne = 1,969 Å). La liaison Cu—O apicale avec l'oxyde de triphénylphosphine est relativement courte (2,097(2) Å). Les spectres RPE correspondent à un complexe dimère à l'état solide avec des interactions magnétiques conduisant à un état triplet paramagnétique. On retrouve les mêmes signaux dans les solutions éthanoliques gelées, ce qui indique que le dimère persiste dans ces conditions. La susceptibilité magnétique a été déterminée dans le domaine 81–293 K et une valeur $-2J$ = 328(4) cm^{-1} en a été tirée pour la différence d'énergie entre les deux états de spin. Le composé d'addition avec l'oxyde de phosphine est bactéricide envers *Escherichia coli* à des doses de 100 μg/mL.

Introduction

The spectroscopic and magnetic properties of Cu(II) carboxylates have attracted considerable attention over the years. By forming monomeric, dimeric, and polymeric structural arrangements (1–3), this class of compounds provided a variety of systems from which much of our understanding of magnetic exchange phenomena was derived.

In the past few years, we have become interested in the bactericide and fungicide properties of Cu(II) carboxylates. With a recent series of experiments (4), we have shown that antibacterial and antifungal efficiency was significantly enhanced by the presence of halogen substituents on the chain of aliphatic carboxylates. In order to extend this initial study, a broader sample of variously halogenated carboxylates is currently being investigated, and the influence of a second ligand is being examined. The triphenylphosphine oxide complex of copper(II) 3-chloropropanoate described in the present paper was isolated as part of this study. The epr spectrum of this compound in frozen ethanol solution showed signals characteristic of a carboxylate-bridged dimer. Addition of excess Ph_3PO enhanced this signal, in contrast with most similar systems, for which excess ligand results in dimer disruption (5). We therefore decided to determine the structure of this compound, since the Cu(II)–carboxylate complexes examined so far by X-ray diffraction (6–9) do not contain in apical positions bulky ligands which could distort the dimer cage (10). In addition, the compound was characterized by spectroscopic and magnetic techniques, and its antibacterial activity was measured.

Experimental section

Preparation

Copper(II) 3-chloropropanoate monohydrate was prepared from basic copper(II) carbonate and 3-chloropropanoic acid by the previously described method (11). $Cu(ClCH_2CH_2COO)_2 \cdot OPPh_3$ was prepared by combining a warm methanol solution of copper(II) 3-chloropropanoate monohydrate (together with a small amount of the corresponding free acid) and triphenylphosphine oxide Ph_3PO in a molar ratio of 1 : 1. The reaction was left to stand at room temperature. The final green product which precipitated after a few hours was filtered off, washed with cold methanol, and dried in ambient atmosphere. The compound was purified by recrystallization from methanol.

C, H, and P analyses were done by the microanalysis service of the Chemistry Department, York University, Downsview. Copper

[1] Present address: Département de chimie, Université de Sherbrooke, Sherbrooke, Qué., Canada J1K 2R1.

[2] To whom all correspondence should be addressed.

[3] Revision received March 25, 1985.

was determined volumetrically with EDTA. *Anal.* calcd. for $C_{24}H_{23}Cl_2CuPO_5$: Cu 11.41, C 51.76, H 4.16, P. 5.56; found: Cu 11.30, C 51.82, H 4.19, P 5.71.

Spectral studies

An infrared spectrum (Nujol mull) in the region 4000−400 cm^{-1} was recorded with a Perkin Elmer 621 grating infrared spectrophotometer. An electronic spectrum (Nujol mull) in the region 1.0−2.8 μm^{-1} was recorded with a Cary 14 spectrophotometer. Electron paramagnetic resonance spectra of polycrystalline samples as well as frozen solutions were recorded on a Varian model E9 spectrometer.

Magnetic measurements

Variable-temperature magnetic susceptibility measurements in the 81−293 K range were made using Gouy equipment. Magnetic susceptibility was corrected for the diamagnetism of all atoms (327×10^{-6} cm^{-3} mol^{-1}) and the temperature-independent paramagnetism of Cu(II) (60×10^{-6} cm^3 mol^{-1}) (12). The effective magnetic moment was calculated from the equation

$$\mu_{eff} = 2.82\,(\chi_M^{corr} \times T)^{1/2}.$$

Bacterial cultures

The nutrient broth used for the cultures was prepared at 8 g/L concentrations using Difco products (8 g bacto beef extract for 5 g bacto peptone). Difco bacto nutrient agar and bacto potato dextrose agar were used in colony-counting. Freeze-dried microlife cultures were from Carolina Biologicals and included *Bacillus subtilis* (no. 15-4921A) and *Escherichia coli* (no. 15-5065A). Stock cultures were prepared and renewed weekly, from which 100 μL samples were drawn for injection into 2 mL of nutrient broth contained in plastic optical cells of 1 cm optical length from Markson Science. These cultures were placed in scintillation containers and thermostated to 37°C in a Heto water-bath and shaker. Optical density was measured on a Beckman DB-G grating spectrophotometer with the wavelength set at 500 nm. Sample cells were vibrated before absorbance measurements. Calibration experiments showed successive dilutions caused linear decreases in absorbance. Agar-plating showed 1×10^6 to 4.5×10^7 colony-forming units/mL for absorbances of 0.1 to 1.0. Small samples of the compounds to be tested (100 μL) were micropipeted directly into the culture media after the lag phase, during the growth cycle of the bacteria. This had no immediate effect on the turbidimetry at the concentrations used.

Crystal data

$[Cu(ClCH_2CH_2CO_2)_2OP(C_6H_5)_3]_2$, ($C_{48}H_{46}Cl_4Cu_2P_2O_{10}$) fw = 1113.8 Triclinic, space group $P\bar{1}$, a = 8.603(6), b = 12.605(4), c = 12.624(5) Å, α = 76.94(3), β = 71,74(4), γ = 74.42(4)°, V = 1237.1 $Å^3$, Z = 1, D_c = 1.494 g cm^{-3}, F(000) = 570, λ(CuK$\bar{\alpha}$) = 1.54178 Å (graphite monochromator), t = 23°C, μ(CuK$\bar{\alpha}$) = 41.6 cm^{-1}. Crystal dimensions: 0.045 mm (between 011 and $0\bar{1}\bar{1}$) × 0.090 mm ($0\bar{1}0$ and 010) × 0.225 mm (210 and $\bar{2}\bar{1}0$).

Crystallographic measurements

The crystal was mounted on an Enraf-Nonius CAD4 diffractometer and a set of 25 reflections randomly distributed in the Laue sphere was created by the automatic search procedure. These reflections were centered and indexing yielded the above reduced triclinic cell. This cell was checked by taking along each crystallographic axis an oscillation photograph, which showed the expected layer-line spacing. The Niggli parameters clearly indicated that the lattice cannot be described within a cell of higher symmetry. The accurate cell dimensions were derived from least-squares refinement on the setting angles for the set of 25 reflections.

A total of 4665 independent CuKα reflections (hkl, $hk\bar{l}$, $h\bar{k}\bar{l}$, and $\bar{h}\bar{k}l$) within a sphere limited by 2θ = 140° were collected as described elsewhere (13). A set of 3829 reflections satisfying the criterion $I \geq 3.0\sigma(I)$ was retained for structure determination, and refinement. The intensities of three reference reflections measured every hour were used as a check on instrument and crystal stability. They showed fluctuations with 3% about respective means. The data were corrected for the Lorentz effect, polarization, and absorption (Gaussian integration, grid 10 × 10 × 10, transmission range = 0.38−0.73).

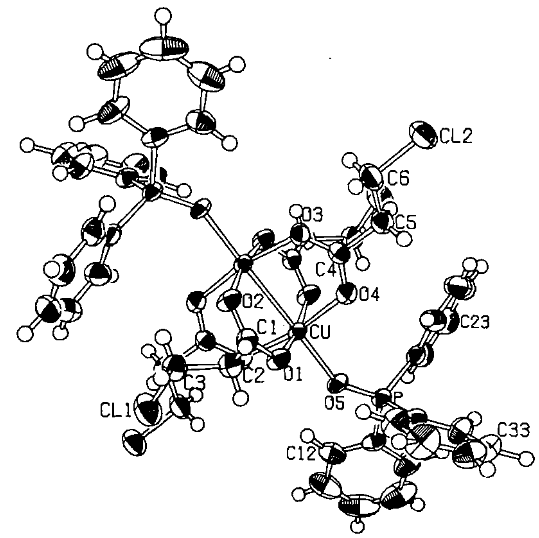

FIG. 1. ORTEP drawing of the dimeric molecule.The ellipsoids correspond to 50% probability. Phenyl ring atoms are represented by a two-digit symbol: the first digit corresponds to ring number, the second to sequential numbering around the ring, position 1 corresponding to the P-bonded carbon atom.

Resolution of the structure

The structure was solved by the heavy-atom method. The Cu and Cl atoms were located from a Patterson synthesis and the light atoms were positioned from subsequent difference Fourier (ΔF) map. Isotropic refinement of all non-hydrogen atoms by full-matrix least-squares converged to $R = \Sigma||F_o| - |F_c||/\Sigma|F_o| = 0.135$. The block-diagonal approximation was used for anisotropic refinement and the R factor reduced to 0.077. All H atoms were then located and isotopically refined. In the last cycles, individual weights w based on counting statics were applied to each reflection and a secondary extinction parameter was refined ($1.9(2) \times 10^3$). The final R factor was 0.047, whereas the weighted residual $R_w = [\Sigma w(|F_o| - |F_c|)^2/\Sigma w|F_o|^2]^{1/2}$ was 0.056, for 391 parameters refined. The goodness-of-fit ratio was 2.13. The final ΔF map showed four peaks of 0.6−1.3 e/$Å^3$ within 1.2 Å from Cu. The general background was lower than ±0.7 e/$Å^3$.

The form factors and the contributions to anomalous dispersion of Cu, Cl, and P were from standard sources (14). The programs used are listed elsewhere (15). The final coordinates and equivalent temperature factors are given in Table 1.[4]

Results and discussion

Unlike the analogous chromium(II) carboxylates, copper(II) carboxylates are not known to form adducts with phosphines. However, triphenylphosphine oxide is less sterically demanding and it reacts readily with cupric 3-chloropropanoate. No excess ligand is needed to prepare the 1 : 1 adduct.

Crystal structure

The crystal consists of dimers (Fig. 1) containing the tetrakis (μ-chloropropanoato)dimetal "windmill" cage commonly

[4]The supplementary material includes a list of observed and calculated structure factor amplitudes, the anisotropic temperature factors, the torsion angles in the carboxylate, details on least-squares plane calculations, and a table of distances and angles involving the hydrogen atoms. Complete set of data may be purchased from the Depository of Unpublished Data, CISTI, National Research Council of Canada, Ottawa, Ont., Canada K1A 0S2.

TABLE 1. Refined atomic coordinates ($\times 10^4$, H $\times$ 10^3, Cu, Cl, P $\times$ 10^5) and equivalent temperature factors ($\times 10^3$)[a]

Atom	X	Y	Z	U_{eq}
Cu(1)	50350(5)	4797(3)	8212(3)	31
Cl(1)	6325(15)	−22256(9)	26505(10)	78
Cl(2)	62718(14)	−43209(8)	38253(8)	67
P(1)	56496(10)	20655(6)	24913(6)	37
O(1)	2659(3)	416(2)	1462(2)	43
O(2)	2624(3)	−419(2)	85(2)	44
O(3)	5627(3)	−1089(2)	1522(2)	44
O(4)	5596(3)	−1902(2)	129(2)	44
O(5)	5325(3)	1137(2)	2116(2)	47
C(1)	1958(3)	−38(2)	992(2)	37
C(2)	157(4)	−100(3)	1555(3)	42
C(3)	−222(4)	−1211(3)	1629(3)	47
C(4)	5695(4)	−1916(2)	1106(2)	38
C(5)	5874(4)	−3044(3)	1845(3)	50
C(6)	6456(5)	−3064(3)	2848(3)	60
C(11)	6488(4)	1535(3)	3688(2)	43
C(12)	6765(4)	399(3)	4038(3)	55
C(13)	7405(5)	−54(4)	4974(4)	78
C(14)	7754(6)	635(5)	5537(4)	96
C(15)	7487(7)	1731(5)	5182(4)	95
C(16)	6871(6)	2218(4)	4268(3)	72
C(21)	7065(4)	2830(3)	1420(3)	42
C(22)	8714(4)	2738(3)	1437(3)	52
C(23)	9764(5)	3304(3)	544(4)	66
C(24)	9212(5)	3948(3)	−332(3)	67
C(25)	7601(6)	4033(4)	−363(3)	68
C(26)	6524(5)	3471(3)	509(3)	56
C(31)	3756(4)	3084(3)	2901(2)	41
C(32)	3775(5)	4085(3)	3183(3)	56
C(33)	2319(5)	4850(3)	3523(3)	64
C(34)	817(5)	4633(4)	3560(4)	72
C(35)	758(5)	3662(4)	3272(4)	79
C(36)	2241(4)	2875(3)	2936(3)	61
H(1)	−16(5)	6(3)	229(3)	71(12)
H(2)	−48(4)	45(3)	111(3)	47(9)
H(3)	−137(4)	−122(3)	181(3)	63(11)
H(4)	29(5)	−145(3)	93(3)	70(12)
H(5)	472(5)	−309(3)	219(4)	87(14)
H(6)	677(5)	−361(3)	142(3)	83(13)
H(7)	732(6)	−283(4)	258(4)	127(19)
H(8)	564(5)	−251(3)	327(3)	83(13)
H(12)	657(4)	−9(3)	357(3)	58(10)
H(13)	748(6)	−79(4)	524(4)	99(15)
H(14)	821(6)	40(4)	617(4)	103(16)
H(15)	767(5)	214(4)	546(4)	97(15)
H(16)	691(4)	309(3)	395(3)	65(11)
H(22)	906(4)	220(3)	205(3)	52(10)
H(23)	1069(5)	321(3)	55(3)	66(11)
H(24)	979(4)	440(3)	−91(3)	71(12)
H(25)	708(6)	448(4)	−92(4)	92(14)
H(26)	543(4)	350(3)	48(3)	47(9)
H(32)	489(5)	430(3)	294(3)	74(12)
H(33)	241(6)	567(4)	375(4)	103(16)
H(34)	−14(6)	511(4)	384(4)	112(17)
H(35)	−28(6)	334(4)	322(4)	107(16)
H(36)	223(5)	220(3)	268(3)	73(12)

[a]Hydrogens isotropically refined.

found for carboxylates of Cr(II), Cu(II), Mo(II), and Rh(II) (6). Each end of the Cu—Cu axis is occupied by the oxygen atom of a triphenylphosphine oxide ligand. The molecule possesses a crystallographic inversion center on the middle of the Cu—Cu axis. Selected interatomic distances and bond angles are listed in Table 2.

This molecule follows the trends already noted for this type of dimers. The Cu—Cu separation (2.649(1) Å) is similar to those observed in other Cu acetate or propanoate compounds (6, 16). Correlations between metal−metal separation and bond lengths or angles in the Cu—Cu—O—C—O rings have been discussed (1, 6). The Cu—Cu—O angle has been found to be the most sensitive to a change in the Cu—Cu distance. From the equation derived by Koh and Christoph (6), the distance observed here should correspond to a Cu—Cu—O angle of 84.0°, which is exactly the observed average value. Our results for other parameters compare well with those found for complexes with similar Cu—Cu separations: (averages) Cu—O, 1.969 Å; C—O, 1.256 Å; Cu—O—C, 122.9°; O—C—O, 125.9°. There exists a relation between the displacement of the copper(II) atom from the basal plane toward the apical ligand, and the increase of the copper−copper distance (1). The Cu(II) atom in the present compound is displaced 0.2063(4) Å, toward the apical oxygen atom, from the least-squares plane defined by the basal atoms, in agreement with this trend.

The cage should ideally have a four-fold axis along the Cu—Cu direction. Departure from this symmetry is significant, but not very large. The dihedral angles between adjacent Cu—Cu—O—C—O rings deviate by only 1.8° from the ideal 90° value. Some steric effect of the phenyl rings of Ph_3PO introduces small distortions. For instance, the oxygen O(5) belonging to phosphine oxide does not lie exactly along the Cu—Cu axis, the Cu—Cu—O(5) angle being 174.3(1)°. The fact that the Cu—O(3)—C(4) and Cu—O(2)—C(1) angles are ~4° greater than Cu—O(1)—C(1) and Cu—O(4)—C(4) undoubtedly results from repulsions with the nearby phosphine oxide molecule, since the O(1)···H(36) and O(4)···H(26) intramolecular contacts (2.88(4) and 2.74(3) Å, respectively) are both close to the sum of the van der Waals radii.

The Cu—O(5) bond to the apical triphenylphosphine oxide (2.097(2) Å) is noticeably shorter than the average distance of dimeric copper(II) carboxylate adducts with CuO_5 chromophores (2.16 Å) (1). Only in two examples, $Cu(2\text{-}HOC_6H_4COO)_2(C_4H_8O_2)\cdot H_2O$ (Cu—Cu = 2.64 Å) (17) and $Cu(CH_3COO)_2$ urea·H_2O (Cu—Cu = 2.637 Å) (18) is the Cu—O(apical) bond shorter than in the present case. The Cu—O(apical) distance of 1.95 Å found in $Cu(Cl_3CCOO)_2$ (2,2,6,6-tetramethylpiperidinyl-1-oxy) (8) is far shorter, but on the other hand the Cu—Cu distance (3.256(2) Å) is far longer than in any other similar dimer (1, 6). On the other hand, the Cu—O(5) distance in the present case is noticeably longer than observed in other copper(II) triphenylphosphine oxide compounds of different structural types where the metal is more accessible (19). The Cu—O(5)—P angle (149.0(2)°) lies within the wide range (140−180°) of reported metal—O—P angles (20). In all other respects, the geometry of coordinated phosphine oxide does not differ appreciably from that of the free ligand (21): P—C = 1.797 Å (av.), O—P—C = 111.6° (av.), C—P—C = 107.3° (av.). The phenyl rings are planar within 2σ (0.009 Å), with average bond lengths of 1.380 Å.

The geometry of the chloropropanoate ligand shows no unusual features. The two nonequivalent ligands present different chain conformations. In carboxylates, one of the α substituents is commonly close to an eclipsed orientation with respect to a carboxylate oxygen. In one of the ligands, O(1) is nearly eclipsed with H(1), but in the other, O(3) is eclipsed with C(6).

TABLE 2
(*a*) Interatomic distances

Bond	Distance (Å)	Bond	Distance (Å)
Cu—Cu[a]	2.649(1)	C(25)—C(26)	1.390(6)
Cu—O(1)	1.965(2)	C(26)—C(21)	1.380(5)
Cu—O(2)[a]	1.971(2)	P—C(31)	1.794(3)
Cu—O(3)	1.976(2)	C(31)—(32)	1.392(5)
Cu—O(4)[a]	1.965(2)	C(32)—C(33)	1.373(6)
Cu—O(5)	2.097(2)	C(33)—C(34)	1.376(7)
O(5)—P	1.477(3)	C(34)—C(35)	1.371(7)
P—C(11)	1.794(3)	C(35)—C(36)	1.401(6)
C(11)—C(12)	1.378(5)	C(36)—C(31)	1.383(6)
C(12)—C(13)	1.400(6)	O(1)—C(1)	1.267(4)
C(13)—C(14)	1.379(8)	O(2)—C(1)	1.249(4)
C(14)—C(15)	1.333(9)	C(1)—C(2)	1.504(5)
C(15)—C(16)	1.370(7)	C(2)—C(3)	1.498(5)
C(16)—C(11)	1.405(6)	C(3)—Cl(1)	1.784(4)
P—C(21)	1.803(3)	O(3)—C(4)	1.250(4)
C(21)—C(22)	1.399(5)	O(4)—C(4)	1.259(4)
C(22)—C(23)	1.393(6)	C(4)—C(5)	1.513(5)
C(23)—C(24)	1.350(6)	C(5)—C(6)	1.494(6)
C(24)—C(25)	1.373(7)	C(6)—Cl(2)	1.785(4)

[a]$1 - x, -y, -z$.

(*b*) Angles

Bonds	Angle (deg)	Bonds	Angle (deg)
Cu[a]—Cu—O(1)	86.28(7)	C(13)—C(14)—C(15)	119.7(5)
Cu[a]—Cu—O(2)[a]	81.72(7)	C(14)—C(15)—C(16)	122.7(5)
Cu[a]—Cu—O(3)	81.98(7)	C(15)—C(16)—C(11)	118.6(4)
Cu[a]—Cu—O(4)[a]	86.01(7)	C(16)—C(11)—C(12)	119.5(3)
Cu[a]—Cu—O(5)	174.34(7)	P—C(11)—C(16)	123.2(3)
Cu—O(5)—P	149.0(2)	O(5)—P—C(21)	114.2(1)
Cu—O(1)—C(1)	120.4(2)	P—C(21)—C(22)	122.7(3)
Cu[a]—O(2)—C(1)	126.0(2)	C(21)—C(22)—C(23)	119.4(4)
O(1)—C(1)—C(2)	117.5(3)	C(22)—C(23)—C(24)	121.1(4)
O(2)—C(1)—C(2)	116.9(3)	C(23)—C(24)—C(25)	119.9(4)
O(1)—C(1)—O(2)	125.6(3)	C(24)—C(25)—C(26)	120.5(4)
C(1)—C(2)—C(3)	114.3(3)	C(25)—C(26)—C(21)	120.0(4)
C(2)—C(3)—Cl(1)	111.1(2)	C(26)—C(21)—C(22)	119.0(3)
Cu—O(3)—C(4)	124.9(2)	P—C(21)—C(26)	118.1(3)
Cu[a]—O(4)—C(4)	120.4(2)	O(5)—P—C(31)	111.1(1)
O(3)—C(4)—C(5)	117.6(3)	P—C(31)—C(32)	121.5(3)
O(4)—C(4)—C(5)	116.2(3)	C(31)—C(32)—C(33)	121.3(4)
O(3)—C(4)—O(4)	126.2(3)	C(32)—C(33)—C(34)	119.3(4)
C(4)—C(5)—C(6)	113.4(3)	C(33)—C(34)—C(35)	120.9(4)
C(5)—C(6)—Cl(2)	111.6(3)	C(34)—C(35)—C(36)	119.9(4)
O(5)—P—C(11)	109.4(1)	C(35)—C(36)—C(31)	119.6(4)
P—C(11)—C(12)	117.3(3)	C(36)—C(31)—C(32)	119.1(3)
C(11)—C(12)—C(13)	119.4(4)	P—C(31)—C(36)	119.5(3)
C(12)—C(13)—C(14)	120.0(5)	C(11)—P—C(31)	108.2(2)
C(11)—P—C(21)	108.7(2)	C(21)—P—C(31)	105.1(2)

[a]$1 - x, -y, -z$.

The chloro substituents also adopt different orientations, the C—C—C—Cl angles being 72° for ligand 1 and 169° for ligand 2.

A stereoview of the unit cell is given in the supplementary material.[4] The molecules interact through normal van der Waals contacts.

Spectroscopic results

The ir spectrum of $Cu(ClCH_2CH_2COO)_2 \cdot OPPh_3$ shows a strong absorption band at 1188 cm^{-1} which includes the P—O stretching mode of coordinated $OPPh_3$ and an in-plane bending vibration. The shift of ν(P—O) to lower wavenumber compared with the corresponding band of free $OPPh_3$ (ν(PO) = 1193 cm^{-1}) (22) is due to the transfer of electron density from oxygen to the metal in agreement with coordination of $OPPh_3$ to copper(II) through the oxygen atom. The carboxylate stretching frequencies, $\nu_{as}(COO^-)$ at ~1630 cm^{-1} and $\nu_s(COO^-)$ at ~1415 cm^{-1}, occur at energies very similar to those reported for other copper(II) carboxylates having the dimeric copper(II) acetate structure (2, 23).

FIG. 2. Electron paramagnetic resonance spectra of the title compound. (a) Room temperature powder spectrum (b) Same sample at $\simeq$ 130 K. The inset at the right is the expanded H_{z2} signal. Microwave frequency $\nu = 9.123$ GHz. (c) Frozen ethanol solution of the complex at microwave frequency $\nu = 9.117$ GHz. The spectra are first derivative presentations of the absorptions.

The electronic absorption spectrum of the compound shows a ligand field band with a maximum at ~1.35 μm^{-1} and a shoulder at ~2.70 μm^{-1}, which is typical of bridging systems with antiferromagnetic interactions (2, 24). The position of the visible absorption band occurs at any energy slightly lower than the corresponding one found in copper(II) 3-chloropropanoate monohydrate, 1.48 μm^{-1} (11).

The epr spectra obtained for the triphenylphosphine oxide adduct are presented in Fig. 2. The absorption features of the powder at room temperature (Fig. 2a) are similar to those previously reported for dimeric copper(II) carboxylates (2, 25–27). The paramagnetic triplet state yields the absorptions at low and high field (H_{z1} and H_{z2}, respectively) and the asymmetric absorption near 4.5 kG ($H_{\perp 2}$). One absorption is missing ($H_{\perp 1}$) because $D > h\nu$ at the X-band frequency used. The spectra can be interpreted using a spin Hamiltonian for axial symmetry, where S = 1 for the thermally accessible triplet state and

$$H = g_{\|}\beta H_z S_z + g_{\perp}\beta(H_x S_x + H_y S_y) + D(S_z^2 - 2/3)$$

the other symbols have their usual meaning. We notice that a monomer signal is also present at 3.1 kG ($g_0 = 2.18$), which corresponds to a spin $S = \frac{1}{2}$ species, despite repeated purification of the complex. Bulk magnetic susceptibility indicates that this monomer "impurity" corresponds to ~0.15% of the copper present. Monomer signals are commonly found for dimeric cupric carboxylates (3, 26–28) and they may arise from defects particularly on the crystal surfaces, which are very large for the powders used in epr studies.

The low temperature powder spectrum (Fig. 2b) shows better resolution with some copper hyperfine appearing on H_{z2} and a clearly resolved seven-line pattern on H_{z1}. The observed hyperfine is consistent with coupling to two copper nuclei of spin $I = \frac{3}{2}$. The improved resolution can be attributed decreased molecular vibrations at low temperature and/or to increasing population of the diamagnetic spin-paired state at lower temperatures due to antiferromagnetic interactions.

Figure 2c presents the first frozen ethanol solution spectrum of a cupric carboxylate which shows triplet state features. The absence of $S = 1$ absorptions in liquid solution has been ascribed to the magnitude of the anisotropic zero-field parameter D (29). The frozen solution spectrum reported here demonstrates that in ethanol the complex retains the dimer structure. Furthermore, it can be seen that the width of the absorption corresponding to H_{z1} and containing unresolved hyperfine structure is similar in the frozen solution to that found at room temperature for the solid. Interdimer magnetic interactions can safely be discarded as a mechanism causing the observed line broadening in the frozen solution case.

The spin Hamiltonian parameters are classical ($g_{\perp} = 2.091$, $g_{\|} = 2.368$, $\bar{g} = 2.183$, and $A_{\|} = 125$ G) for the anisotropic frozen ethanol $S = \frac{1}{2}$ signal. The liquid solution spectrum in the same solvent is broad, with $g_0 \approx 2.20$ and $A_0 \approx 44$ G. We note that added triphenylphosphine oxide reduces the intensity of the $S = \frac{1}{2}$ signal in ethanol (at room or low temperature). From this we conclude excess ligand stabilizes the dimer structure and does not, like strong nitrogen bases, lead to monomer adducts. However, we find that water causes a dramatic increase in the $S = \frac{1}{2}$ signal intensity, pointing to water promoted dissociation of the complex. For the triplet state spectra, we find $g_{\perp} = 2.093$, $g_{\|} = 2.382$, $\bar{g} = 2.193$, and $D = 0.346$ cm^{-1}. The solid and frozen solution spectra yield identical results within experimental error. The epr parameters for the $S = 1$ and $S = \frac{1}{2}$ species are thus very similar. The hyperfine structure along H_{z1} is $A_{\|} = 60$ G, approximately half the value along $g_{\|}$ ($A_{\|} = 125$ G), in agreement with coupling to two copper atoms. Additional features include a weak half-field absorption near 1.8 kG in the frozen solution and an unexpected weak absorption on the high-field side of $H_{\perp 2}$ for the solid state spectra.

Magnetic susceptibility

The effective magnetic moment per Cu(3-chloropropanoate)$_2\cdot$OPPh$_3$ unit was measured over the range 81–293 K. It was found to decrease systematically by lowering the temperature, from 1.37 BM at 293 K to 0.23 BM at 81 K. The corresponding variation of the magnetic susceptibility, from 810×10^{-6} cm^3 mol^{-1} to 80×10^{-6} cm^3 mol^{-1} is represented in Fig. 3.

The magnetic susceptibility data of Fig. 3 were fitted to the modified Bleaney–Bowers equation (30) by a non-linear least-squares procedure:

$$\chi_M^{corr} = \frac{g_d^2 N\beta^2}{3kT}\left[1 + \frac{1}{3}\exp(-2J/kt)\right]^{-1}(1 - x) + \frac{g_m^2 N\beta^2}{4kT}x$$

In this equation, J is the exchange integral in the Heisenberg – Dirac – Van Vleck Hamiltonian ($H = -2J\hat{S}_1\cdot\hat{S}_2$), g_m and g_d are the Lande factors for the monomer and dimer, respectively, x is the molar percentage of mononuclear form, and the other symbols have their usual meanings. An epr derived Lande

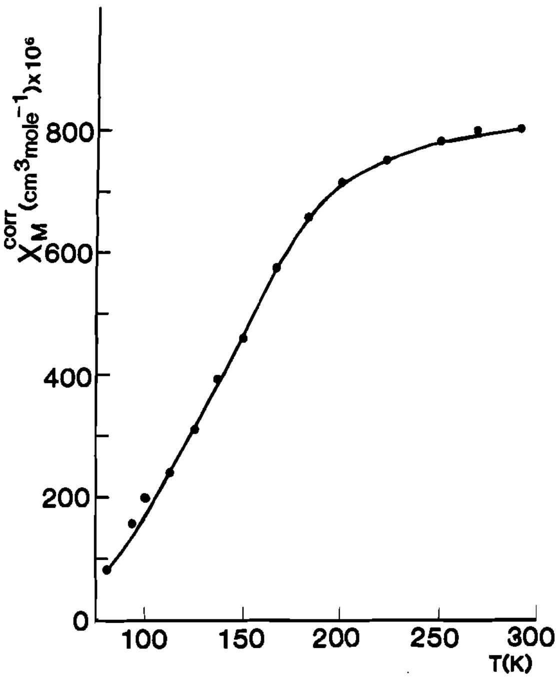

FIG. 3. Theoretical and experimental magnetic susceptibilities for the title compound. The solid line was calculated with $-2J = 328(4)$ cm^{-1} and $x = 0.15\%$.

parameter $\bar{g} = 2.19$ was used in the refinement of J and x.

The energy separation between the two spin states of the compound ($-2J = 328(4)$ cm^{-1}) indicates for this dimer an antiferromagnetic super-exchange interaction comparable with those commonly found for Cu(II) carboxylates (1−3, 26).

The magnetic data also indicate the presence of a small amount (~0.15%) of a mononuclear species in the compound. This mononuclear species produced a line at ~3.1 kG in the epr spectrum of the compound. Small amounts of monomeric "impurities" are commonly found in analytically pure Cu(II) carboxylates (3, 27−29).

Biological properties

Turbidimetric measurements carried over a 72 h period show that cupric complexes of 3-chloropropanoic acid have mild bactericidal properties. Increasing concentrations of complex lead to stronger inhibition of growth of *Escherichia coli* or *Bacillus subtilis*. The optical densities of bacterial suspensions are related to the total biomass present and the concentration needed to obtain 50% inhibition of bacterial growth can be evaluated from the reduction in absorbance resulting in the suspensions treated with bactericides (31). The dose needed for 50% inhibition of growth following a 24 h period is defined as ID_{50}^{24}.

No bactericidal effect was noted on *Bacillus subtilis*, but inhibition of growth occurs for *Escherichia coli*. The parent bis(propanoato)copper(II) monohydrate has an ID_{50}^{24} value of 50 μg/mL with an estimated error of 15% in part due to reproducibility difficulties in the age of the starting inoculum. We find that bis(3-chloropropanoato)copper(II) monohydrate is slightly more potent with $ID_{50}^{24} = 40$ μg/mL. However, the triphenylphosphine oxide adduct is much less toxic to the bacteria with $ID_{50}^{24} > 100$ μg/mL. The highest dose we used (100 μg/mL) resulted in 48% inhibition after 24 h, 66% inhibition after 48 h, and 59% after 72 h.

It may be argued that the increased molecular weight of the triphenyl phosphine oxide adduct decreases the percentage of copper in the compound, thus effectively reducing its bactericidal power. This would assume that cupric ions are the sole toxic species liberated by dissociation of the complex in water. However, we found that bis(3-chloropropanoato)copper(II) forms adducts with 4-acetylpyridine-*N*-oxide and also caffeine, with respective ID_{50}^{24} values of 50 and 75 μg/mL. Therefore, synergistic or antagonist effects between copper(II), 3-chloropropanoic acid, and added ligands may play a role in defining the biological activities of these complexes. We will report elsewhere the results obtained with similar fluoro-, bromo-, and iodocarboxylates (32).

Conclusion

X-ray diffraction shows that the 1:1 complex of triphenylphosphine oxide with $Cu(3\text{-chlopropanoate})_2$ has the copper acetate dimeric structure. The apical Ph_3PO ligands, despite their three phenyl rings, do not introduce severe distortions in the tetracarboxylate−dimetal framework. The presence of oxygen between Cu and P makes the oxide much less sterically demanding than the corresponding phosphine in the coordination sphere. However, the bulky phenyl rings may help in stabilizing the dimer by efficiently shielding the apical sites of the dimer, thereby opposing the propensity of these dimers to break into monomeric species with excess ligand. Magnetic susceptibility and epr spectra are consistent with the dimer structure in the solid, and the epr spectra indicate that the same structure is retained in frozen ethanol solution. Nevertheless, addition of water drastically changes the epr spectra, leading to features characteristic of a monomeric Cu(II) complex in solution. Therefore, the species actually responsible for the antibacterial activity is probably not the dimer originally present in the solid but some monomeric species derived therefrom.

Acknowledgments

We wish to thank M. J. Olivier who collected the X-ray data, and M. Dartiguenave and Y. Dartiguenave for very helpful discussions. Financial support from the Natural Sciences and Engineering Research Council of Canada and the Ministère de l'Education du Québec (fonds FCAC) is gratefully acknowledged.

1. M. MELNIK. Coord. Chem. Rev. **42**, 259 (1982).
2. J. CATTERICK and P. THORNTON. Adv. Inorg. Chem. Radiochem. **20**, 291 (1977).
3. M. MELNIK. Coord. Chem. Rev. **36**, 1 (1981).
4. M. MELNIK, M. AUDEROVA, and M. HOL'KO. Inorg. Chim. Acta, **67**, 117 (1982).
5. M. A. BERNARD, A. BUSNOT, D. CORNET, J. F. HEMIDY, and J. F. LEQUERLER. Rev. Chim. Miner. **19**, 80 (1982).
6. Y. B. KOH and G. G. CHRISTOPH. Inorg. Chem. **18**, 1122 (1979).
7. L. C. PORTER and R. J. DOEDENS. Inorg. Chem. **23**, 997 (1984).
8. L. C. PORTER, M. H. DICKMAN, and R. J. DOEDENS. Inorg. Chem. **22**, 1962 (1983).
9. K. SMOLANDER. Acta Chem. Scand. A**37**, 5 (1983).
10. T. ALLMAN, R. C. GOEL, N. K. JHA, and A. L. BEAUCHAMP. Inorg. Chem. **23**, 914 (1984); G. G. CHRISTOPH, J. HALPERN, G. P. KHARE, Y. B. KOH, and C. ROMANOWSKI. Inorg. Chem. **20**, 3029 (1981).
11. M. MELNIK. Acta Chem. Scand. **24**, 3243 (1970).
12. A. EARNSHAW. Introduction to magnetochemistry. Academic Press, London. 1968.
13. F. BÉLANGER-GARIÉPY and A. L. BEAUCHAMP. J. Am. Chem. Soc. **102**, 3461 (1980).

14. D. T. CROMER and J. T. WABER. Acta Crystallogr. **18**, 104 (1965); R. F. STEWART, E. R. DAVIDSON, and W. T. SIMPSON. J. Chem. Phys. **42**, 3175 (1965); D. T. CROMER. Acta Crystallogr. **18**, 17 (1965).
15. M. AUTHIER-MARTIN and A. L. BEAUCHAMP. Can. J. Chem. **55**, 1213 (1977).
16. G. SMITH, E. J. O'REILLY, and C. H. L. KENNARD. Inorg. Chim. Acta, **49**, 53 (1981).
17. A. V. ABLOV, G. A. KIOSSE, G. I. DIMITROVA, T. I. MALINOVSKII, and G. A. POPOVICH. Kristallografiya, **19**, 168 (1974).
18. YU. V. YABLOKOV, L. V. MOSINA, YU. A. SIMONOV, L. N. MILKOVA, A. V. ABLOV, and V. I. IVANOV. Zh. Strukt. Khim. **19**, 42 (1978).
19. J. A. BERTRAND, S. L. GRAHAM, H. M. DEUTSCH, and D. G. VANDERVEER. Inorg. Chim. Acta, **19**, 189 (1976); J. A. BERTRAND. Inorg. Chem. **6**, 495 (1967); J. A. BERTRAND and A. R. KALYANARAMAN. Inorg. Chim. Acta, **5**, 341 (1971).
20. G. BOMBIERI, E. FORSELLINI, G. DEPAOLI, D. BROWN, and T. C. TSO. J. Chem. Soc. Dalton Trans. 2042 (1979); J. MEUNIER-PIRET, G. GERMAIN, J. P. DECLERCQ, and M. VAN MEERSSCHE. Bull. Soc. Chim. Belge. **89**, 241 (1980).
21. G. RUBAN and V. ZABEL. Cryst. Struct. Commun. **5**, 671 (1976).
22. G. B. DEACON and J. H. S. GREEN. Spectrochim. Acta, **24A**, 845 (1968); F. A. COTTON, R. D. BARNES, and E. BANNISTER. J. Chem. Soc. 2199 (1960).
23. M. KATO, H. B. JONASSEN, and J. C. FANNING. Chem. Rev. **64**, 99 (1964).
24. L. DUBICKI and R. L. MARTIN. Inorg. Chem. **5**, 2203 (1966).
25. D. COLLISON and F. E. MABBS. J. Chem. Soc. Dalton Trans. 1565 (1982).
26. R. J. DOEDENS. Prog. Inorg. Chem. **21**, 209 (1976).
27. J. LEWIS, F. E. MABBS, L. K. ROYSTON, and W. R. SMAIL. J. Chem. Soc. A, 291 (1969).
28. M. MELNIK. J. Inorg. Nucl. Chem. **43**, 3035 (1981); M. MELNIK, M. ZIVOROVA, and J. MROZINSKI. J. Mol. Struct. **78**, 91 (1982).
29. H. GRASDALEN. J. Magn. Reson. **9**, 166 (1973).
30. B. BLEANEY and K. D. BOWERS. Proc. R. Soc. A, **214**, 451 (1952).
31. P. GERHARDT. Manual of methods for general bacteriology. Am. Soc. for Microbiol., Washington. 1981. pp. 192–196.
32. M. MELNIK and P. SHARROCK. To be published.

A theoretical study on the structures and stabilities of protonated hydrogen sulfide – hydrogen sulfide clusters

SHINICHI YAMABE,[1] TSUTOMU MINATO, AND MAKINO SAKAMOTO
Educational Technology Center, Nara University of Education, Takabatake-cho, Nara 630, Japan

AND

KIMIHIKO HIRAO
Department of Chemistry, College of General Education, Nagoya University, Nagoya 464, Japan

Received February 7, 1985

SHINICHI YAMABE, TSUTOMU MINATO, MAKINO SAKAMOTO, and KIMIHIKO HIRAO. Can. J. Chem. **63**, 2571 (1985).

An *ab initio* MO calculation is made on the $H_3S^+(H_2S)_n$ cluster ($n = 0-5$). For $n = 1$, full thermodynamic data are reproduced theoretically, and for $n = 1$, 2, and 3 the effect of *d* functions on the structure and energies is investigated. On the basis of the present results, the accuracy of two conflicting experimental data is examined.

SHINICHI YAMABE, TSUTOMU MINATO, MAKINO SAKAMOTO et KIMIHIKO HIRAO. Can. J. Chem. **63**, 2571 (1985).

On a réalisé des calculs d'OM *ab initio* sur l'aggrégat $H_3S^+(H_2S)_n$ ($n = 0-5$). Pour $n = 1$, on a pu reproduire sur une base théorique l'ensemble des données thermodynamiques; pour $n = 1$, 2 et 3, on a étudié l'effet des fonctions *d* sur la structure et les énergies. Sur la base des résultats obtenus dans présent travail, on évalue l'exactitude de deux ensembles contradictoires de données expérimentales.

[Traduit par le journal]

Introduction

The temperature dependence of the gas-phase equilibria $H_3S^+(H_2S)_{n-1} + H_2S \rightleftarrows H_3S^+(H_2S)_n$ was measured by pulsed high-pressure mass spectroscopy. Two independent thermochemical data were reported almost at the same time (1, 2). The data from the two studies, the enthalpy change ($\Delta H^0_{n-1,n}$) and the entropy change ($\Delta S^0_{n-1,n}$), are appreciably different. The $H_3O^+(H_2O)_n$ cluster has been well investigated both by experiments (3) and by theoretical calculations (4). Its geometry and energetics are now established. However, the $H_3S^+(H_2S)_n$ cluster has not yet been analyzed theoretically. One reason for this unexplored subject is the need of the large computational time, in particular, when *d* functions on the sulfur atom are included.

Since the two experimental results are somewhat conflicting (1, 2), a theoretical judgement on which data is more reliable should be informative. Also, it is of mechanistic interest to see the similarity or the difference between $H_3O^+(H_2O)_n$ and $H_3S^+(H_2S)_n$. In the present work, we carry out *ab initio* MO and CI calculations for $H_3S^+(H_2S)_n$ ($n = 1-5$).

Computational method

The GAUSSIAN 80 program (5) is used for the *ab initio* MO calculation. The 4-31G and 4-31G(*) basis sets are adopted, where in the latter the *d* orbital (exponent = 0.65) is augmented onto the sulfur atom (6). A valence-shell SD-CI calculation is performed to estimate the electron correlation effect on the $n = 1$ cluster.

To obtain the zero-point energy and the vibrational term in the entropy, vibrational analyses on the optimized geometries are made numerically. The analytical first derivatives of total energies are obtainable in the program. The second derivatives may be obtained by differentiating them numerically. They are calculated by 0.01 au displacements relative to the equilibrium points.

[1]To whom all correspondence should be addressed.

Results and discussion

First, the proton affinity (PA) of hydrogen sulfide is obtained. PA(4-31G) = 161 kcal/mol and PA(4-31G(*)) = 176, whereas PA(exptl) = 172 (7). In the formation of the smallest cluster $H_3S^+(H_2S)$ (i.e., $n = 0 \rightarrow 1$), ΔH^0 and ΔS^0 are evaluated at the full thermodynamic level. They are displayed in Table 1 together with their components. There is a large difference of $\Delta H^0_{0,1}$ between 4-31G and 4-31G(*) (−18.0 vs. −13.9). This comes mainly from that of the electronic binding energy $\Delta E_{0,1}$ and slightly from that of vibration energy ΔE_{vib}. Correlation corrections are about 2 kcal/mol for $H_3S^+ \cdots H_2S$. As for the entropy change, however, complete agreement is found (−27.0).

The huge difference of $\Delta H^0_{0,1}$ between $H_3O^+(H_2O)$ and $H_3S^+(H_2S)$ is ascribed solely to that of $\Delta E_{0,1}$ (−32.6 vs. −16.8). It is interesting to note that $\Delta S^0_{0,1}$ values of $H_3O^+(H_2O)$ and $H_3S^+(H_2S)$ are similar in spite of the remarkable difference in $\Delta E_{0,1}$.

At the right side of Table 2, the 4-31G $\Delta E_{n-1,n}$ obtained in the present work is exhibited. The 4-31G(*) values are in parentheses. The use of $\Delta E_{n-1,n}$ instead of $\Delta H^0_{n-1,n}$ is rationalized by the similar values of $\Delta H^0_{0,1}$ and $\Delta E_{0,1}$ in Table 1. As n increases, $-\Delta E_{n-1,n}$ decreases and so does $-\Delta H^0_{n-1,n}$. A large gap between $\Delta E_{2,3}$ and $\Delta E_{3,4}$ (−10.6 vs. −5.4) is found. The former corresponds to the completion of the inner solvation shell $H_3S^+(H_2S)_3$, and the latter to the attachment of an H_2S molecule at the terminal site of the shell. Such a critical gap between (2,3) and (3,4) is also shown by the $H_3O^+(H_2O)_n$ cluster. The binding energy $\Delta E_{n-1,n}$ as well as $\Delta H^0_{n-1,n}$ of $H_3O^+(H_2O)_n$ is nearly twice as large as that of $H_3S^+(H_2S)_n$. This reflects the difference of the permanent dipoles of H_2O and H_2S. μ_{H2S} = 1.78 debye(4-31G), 1.33(4-31G(*)), and 1.1(exptl). μ_{H2O} = 2.19(DZ + p) and 1.8(exptl).

The accuracy of the two experimental data $\Delta H^0_{n-1,n}$(MF) and $\Delta H^0_{n-1,n}$(HK) and two theoretical energies is examined. For (0,1) and (1,2), the 4-31G overestimates $-\Delta E_{n-1,n}$ by a few kcal/mol relative to that of 4-31G(*). This noticeable dis-

TABLE 1. Components of theoretical enthalpy and entropy changes for the gas-phase equilibrium $H_3S^+ + H_2S \rightleftarrows H_3S^+(H_2S)$ in the standard state (T = 300 K and P = 1 atm)

$$\Delta H^0_{0,1} = \Delta E_{0,1} + \Delta E_{trans} + \Delta E_{rot} + \Delta E_{vib} + \Delta(PV) + \Delta E_{correl}$$
$$\Delta S^0_{0,1} = \Delta S_{trans} + \Delta S_{rot} + \Delta S_{vib}$$

Basis set or experiment	$\Delta H^0_{0,1}$ (kcal/mol)	$\Delta E_{0,1}$	ΔE_{trans}	ΔE_{rot}	ΔE_{vib}	$\Delta(PV)$	ΔE_{correl} (CISD)
4-31G	−18.0	−16.8	−0.9	−0.9	2.9	−0.6	−1.7
DZ+p	(−35.4)[a]	(−32.6)	(−0.9)	(−0.9)	(2.5)	(−0.6)	(−2.9)
4-31G(*)	−13.9	−13.1	−0.9	−0.9	3.8	−0.6	−2.2
exptl, MF[b]	−12.8						
exptl, HK[c]	−15.4						

	$\Delta S^0_{0,1}$ (eu)	ΔS_{trans}	ΔS_{rot}	ΔS_{vib}
4-31G	−27.0	−34.5	−1.7	9.2
DZ+p	(−28.8)[a]	(−32.6)	(−3.0)	(6.8)
4-31G(*)	−27.0	−34.5	−1.3	8.8
exptl, MF[b]	−18.7			
exptl, HK[c]	−24.4			

[a]Data in parentheses are for the $H_3O^+ + H_2O \rightleftarrows H_3O^+(H_2O)$ reaction taken from ref. 4*c*.
[b]Reference 1.
[c]Reference 2.

TABLE 2. Comparison of experimental and theoretical data for the gas-phase $H_3O^+(H_2O)_n$ and $H_3S^+(H_2S)_n$ clusters. All energies are in kcal/mol. The theoretical binding energy $\Delta E_{n-1,n}$ is computed with the 4-31G basis set except those in parentheses (4-31G(*))

	$H_3O^+(H_2O)_n$		$H_3S^+(H_2S)_n$		
$(n, n-1)$	$-\Delta H^0_{n-1,n}$[a]	$-\Delta E_{n-1,n}$[b]	$-\Delta H^0_{n-1,n}$(MF)[c]	$-\Delta H^0_{n-1,n}$(HK)[d]	$-\Delta E_{n-1,n}$
(0,1)	31.6	37	12.8	$15.4_{\pm 0.5}$	16.8(13.1)
(1,2)	19.5	26	7.2	$9.1_{\pm 0.5}$	12.7(10.9)
(2,3)	17.9	22	5.4	$8.4_{\pm 0.5}$	10.6(9.3)
(3,4)	12.7	16	3.3	$6.7_{\pm 0.3}$	5.4
(4,5)	11.6	15		~6.1	4.6

[a]Reference 3.
[b]Reference 4*b*. Binding energy plus zero-point correction.
[c]Reference 1.
[d]Reference 2.

crepancy is related to the following trend. The localization of the protonic nature involved in the small species would tend to increase the 4-31G/4-31G(*) discrepancy. As another case, the charge-free system of the dimer of hydrogen sulfide $(H_2S)_2$ is considered. Its hydrogen-bond energies are calculated to be −1.9 kcal/mol (4-31G) and −1.7 (4-31G(*)). These compare favorably to −1.7 ± 0.3 by an infrared intensity measurement (8). As the cluster size becomes larger, therefore, the positive charge is dispersed and the overestimate of 4-31G gets smaller. In (2,3), the 4-31G/4-31G(*) discrepancy is only 1.3 kcal/mol. Thus, the agreement between $\Delta H^0_{n-1,n}$(HK) and the 4-31G $\Delta E_{n-1,n}$ for $n \geqq 3$ is reasonable, and overall our computational data support $\Delta H^0_{n-1,n}$(HK) rather than $\Delta H^0_{n-1,n}$ (MF). However, in $\Delta H^0_{n-1,n}$(HK), the gap between (2,3) and (3,4) appears to be slightly small (−8.4 vs. −6.7). The completion of the inner solvation shell and the soft attachment of the outer solvent would give more energetic distinction.

Figure 1 gives the optimized structures and the electron distribution of H_2S and $H_3{}^+S$. When H_2S is protonated, the positive charge is delocalized both on the three hydrogens and on the sulfur atom of H_3S^+. This is in contrast to the change of the electron density in $H_2O + H^+ \rightarrow H_3O^+$. The protonic nature is attributed to the decrease of the charge on the three hydro-

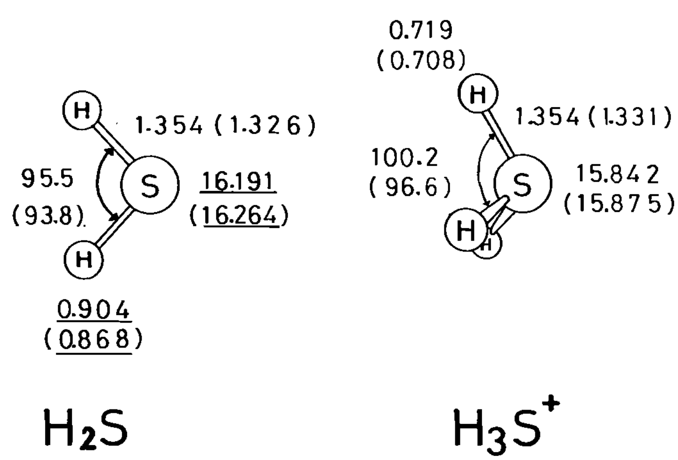

FIG. 1. The 4-31G optimized geometries of hydrogen sulfide and its protonated species. The values in parentheses are those obtained by the 4-31G(*) basis set. The bond distance is in Å and the angle in degree. Underlined numbers denote the Mulliken atom populations.

gens of H_3O^+. The small polarity of H_3S^+ as well as of H_2S is reflected in the weak strength of the hydrogen bonds in Fig. 2. In fact, the ratio of bond distances (S···H/S—H), 1.38, is

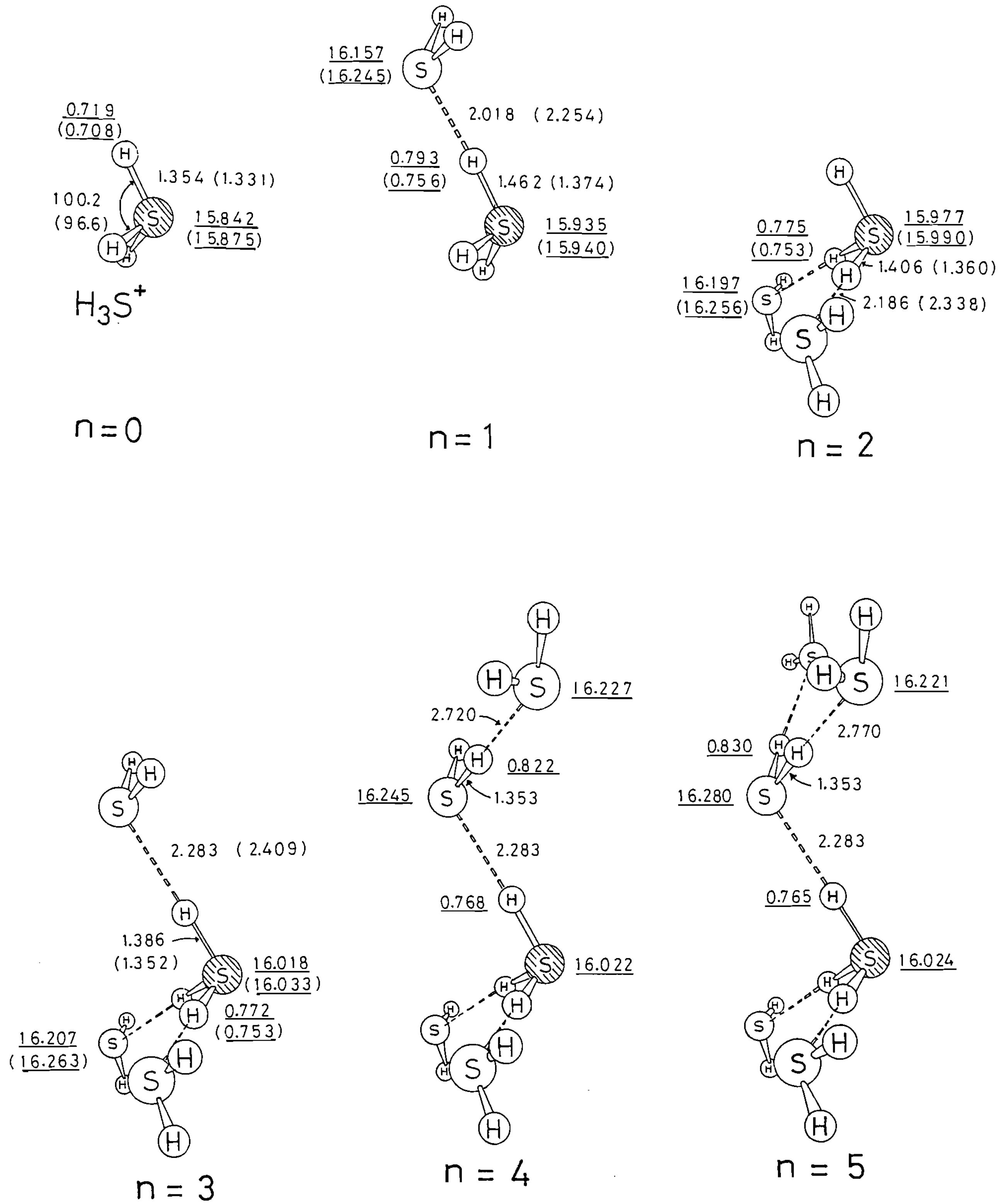

FIG. 2. The 4-31G optimized geometries of the $H_3S^+(H_2S)_n$ cluster. The structures of n = 4 and 5 are obtained by the partial optimization, where, the shell part (i.e., the n = 3 cluster) is kept constant during the optimization.

larger than that of (O···H/O—H), 1.26 (4*b*). As the cluster size grows larger, the positive (cationic) charge is dispersed and the intermolecular S···H bond becomes longer. At n = 3 and inner solvation shell completion, the electron density of the terminal hydrogen is more protonic (0.841) than that of the free H_2S molecule (0.904). Thus, $H_3S^+(H_2S)_3\cdots SH_2$ is more tightly bound than $H_2S\cdots HSH$. Even if the polarity of each species is small, the positive charge is transmitted smoothly up to terminal hydrogens in the cluster.

The effect of the *d* orbital is examined. The S—H bond of H_2S and H_3S^+ has a slightly larger polarity with 4-31G(*) than that with 4-31G. This covalent bond of 4-31G(*) is shorter than that of 4-31G. But, the intermolecular $H_2S\cdots HSH_2^+$ bond in $n = 1$ gives the opposite trend (2.254 Å by 4-31G(*) vs. 2.018 by 4-31G). This is because the intermolecular bond is composed of two bonding forces, electrostatic (ES) and charge-transfer (CT). The inclusion of the *d* orbital gives the polarization of S—H covalent bonds and enhances ES. On the other hand, it decreases CT and this is more crucial. As a net effect of these two, 4-31G(*) gives the larger intermolecular distance and smaller $-\Delta H^0_{0,1}$ (in Table 1) than 4-31G. It is well documented that the 4-31G basis set overestimates the intermolecular binding energy by a few kcal/mol due to the basis set superposition error (BSSE) (9). Generally, BSSE is recognizable in the supermolecule calculation with the basis sets of the double zeta or poorer levels. An addition of polarization functions to them diminishes the physically meaningless effect. Thus, the decrease of CT by 4-31G → 4-31G(*) may be partly ascribed to that of BSSE.

Concluding remarks

In this study, the structures and stabilities of the $H_3S^+(H_2S)_n$ clusters have been examined theoretically. Two basis sets, 4-31G and 4-31G(*), are adopted for the MO calculation. In the comparison of $\Delta H^0_{0,1}$ and $\Delta S^0_{0,1}$, the 4-31G/4-31G(*) discrepancy of the former is noticeable, but the latter term is the same. The *d* orbital on the sulfur atom enhances the polarity of H_3S^+ and H_2S, and more significantly diminishes the BSSE. As *n* increases, however, the discrepancy gets small and the use of the 4-31G basis set may be rationalized for the larger clusters.

The two conflicting experimental data are examined critically on the basis of the present results. The calculated data support $\Delta H^0_{n-1,n}$(HK) rather than $\Delta H^0_{n-1,n}$(MF). One point emerges from the former data. There would be a larger gap between $\Delta H^0_{2,3}$ and $\Delta H^0_{3,4}$ to reflect the structural differences (the inner solvation shell completion vs. the soft attachment of the H_2S).

Acknowledgments

The authors thank the Institute for Molecular Science for an allotment of CPU time on the HITAC M-200H computer. The program for the vibrational analysis has been coded by Dr. K. Yamashita, to whom they are grateful.

1. M. MEOT-NER and F. H. FIELD. J. Am. Chem. Soc. **99**, 998 (1977).
2. K. HIRAOKA and P. KEBARLE. Can. J. Chem. **55**, 24 (1977).
3. Y. K. LAU, S. IKUTA, and P. KEBARLE. J. Am. Chem. Soc. **104**, 1462 (1982) and references therein.
4. (*a*) M. D. NEWTON and S. EHRENSON. J. Am. Chem. Soc. **93**, 4971 (1971); (*b*) M. D. NEWTON. J. Chem. Phys. **67**, 5535 (1977); (*c*) S. YAMABE, T. MINATO, and K. HIRAO. J. Chem. Phys. **80**, 1576 (1984).
5. J. S. BINKLEY, R. A. WHITESIDE, R. KRISHNAN, R. SEEGER, D. J. DEFREES, H. B. SCHLEGEL, S. TOPIOL, L. R. KAHN, and J. A. POPLE. QCPE, **13**, 406 (1981).
6. W. J. PIETRO, M. M. FRANCL, W. J. HEHRE, D. J. DEFREES, J. A. POPLE, and J. S. BINKLEY. J. Am. Chem. Soc. **104**, 5039 (1982).
7. R. YAMDAGNI and P. KEBARLE. J. Am. Chem. Soc. **98**, 1320 (1976).
8. J. E. LOWDER, L. A. KENNEDY, K. G. P. SULZMANN, and S. S. PENNER. J. Quant. Spectrosc. Radiat. Transfer, **10**, 17 (1970).
9. K. MOROKUMA and K. KITAURA. Chemical applications of atomic and molecular electrostatic potentials. *Edited by* P. Politzer and D. G. Truhlar. Plenum. New York, NY. 1981. p. 215.

Metal ion biomolecule interactions. PART VII. Synthesis, spectroscopic properties and crystal structure investigations of some bis(theophyllinato)tetraaquocadmium(II) compounds

ERWIN BUNCEL,[1] RAJESH KUMAR, AND ALBERT R. NORRIS[1]
Department of Chemistry, Queen's University, Kingston, Ont., Canada K7L 3N6

AND

ANDRÉ L. BEAUCHAMP[1]
Département de Chimie, Université de Montréal, Montréal (Qué.), Canada H3C 3V1

Received September 17, 1984

ERWIN BUNCEL, RAJESH KUMAR, ALBERT R. NORRIS, and ANDRÉ L. BEAUCHAMP. Can. J. Chem. **63**, 2575 (1985).

The synthesis, ^{1}H and ^{13}C nmr and infrared spectra of the complex bis(theophyllinato)tetraaquocadmium(II), [$CdC_{14}H_{22}N_4O_5$], and its *N,N*-dimethylformamide solvates are reported. The crystals containing two molecules of *N,N*-dimethylformamide per complex belong to the monoclinic space group $P2_1/c$ with a = 10.891(3), b = 13.696(7), c = 10.110(2) Å, β = 109.03(4)°, ρ_c = 1.595 g cm^{-3}, and Z = 2. Least-squares refinement of the structure has led to a final value of the conventional R factor of 0.044 for 261 variables, using 1299 nonzero MoKα reflections. The complex consists of monomeric [$CdTh_2(H_2O)_4$] units. The cadmium lies on an inversion center. The geometry of the atoms bonded to cadmium is roughly octahedral with the two theophyllinate ions *trans* to each other and coordinated through N(7). The Cd—N(7), Cd—O(13), and Cd—O(14) distances of 2.300(5) Å, 2.346(5) Å, and 2.336(5) Å, respectively, are normal. The hydrogen bonding in the crystals is complex, with all the ligand donor and acceptor atoms participating. *N,N*-Dimethylformamide is not coordinated to cadmium, but participates in the hydrogen bonding system. The nmr spectra are consistent with theophyllinate ion being similarly bonded to cadmium in dimethyl sulfoxide solution.

ERWIN BUNCEL, RAJESH KUMAR, ALBERT R. NORRIS et ANDRÉ L. BEAUCHAMP. Can. J. Chem. **63**, 2575 (1985).

On rapporte la synthèse, les spectres rmn ^{1}H et ^{13}C et les spectres infrarouges du complexe bis(théophyllinato)tetraaquocadmium(II), [$CdC_{14}H_{22}N_4O_5$], et de ses composés solvatés avec la *N,N*-diméthylformamide. Le cristal comportant deux molécules de *N,N*-diméthylformamide par complexe appartient au groupe spatial monoclinique $P2_1/c$: a = 10,819(3), b = 13,696(7), c = 10,110(2) Å, β = 109.03(4)°, ρ_c = 1.595 g cm^{-3} et Z = 2. L'affinement par moindres carrés au moyen de 1299 réflexions MoKα significativement observées a convergé à une valeur finale de R de 0,044 pour 261 paramètres variés. Le composé est constitué de molécules monomères [$CdTh_2(H_2O)_4$]. Le cadmium se situe sur un centre de symétrie. Les atomes liés au cadmium décrivent une géométrie à peu près octaédrique, deux ions théophyllinate coordonnés par l'intermédiaire de N(7) occupant des positions *trans* l'un par rapport à l'autre. Les distances Cd—N(7), Cd—O(13) et Cd—O(14), respectivement égales à 2,300(5) Å, 2,346(5) Å et 2,336(5) Å, sont normales. Les liaisons hydrogène dans le cristal constituent un ensemble complexe auquel participent tous les atomes donneurs et accepteurs des coordinats. La *N,N*-diméthylformamide n'est pas coordonnée au cadmium, mais elle participe au réseau de liaisons hydrogène. Les spectres rmn sont en accord avec la présence d'un ion théophyllinate semblablement lié au cadmium dans la solution de diméthylsulfoxyde.

Introduction

The N(7)/O(6) portion of guanine is the region of DNA which has been the most thoroughly discussed in reference to heavy metal – DNA interactions. It is generally recognized that N(7) is the primary site of attachment of platinum antitumor drugs. Subsequent chelate formation by metal–O(6) binding has been suggested, but definitive evidence for this type of interaction is lacking (1). During the last several years, our laboratories have been actively investigating the reactions of soft mercury(II) species with nucleobases (2–4). We have recently described a number of complexes obtained with theophylline (**1**), a purine base having the same N(7)/O(6) arrangement as guanine (5, 6). The Hg^{2+} and CH_3Hg^+ cations have

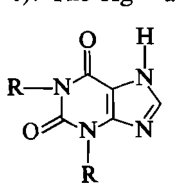

1 (R = CH_3)

been shown to bind to N(7) in all these compounds, but there was no evidence for interactions with O(6). Since Cd^{2+}, a cation noticeably harder than Hg^{2+} (7), should give rise to stronger metal–oxygen interactions, complex formation between theophylline and Cd^{2+} was examined. Our interest in this system was also stimulated by the fact that cadmium is known to be an environmental pollutant and to participate in various biological processes (8).

Crystal structure analyses on cadmium–nucleobase complexes have shown that the metal ion generally binds to the nitrogen lone pair of N(7) in purines or N(3) in pyrimidines (9–16). When a carbonyl oxygen is adjacent to these sites, it often participates in "indirect chelation" by forming hydrogen bonds with other ligands in the coordination sphere (13, 14). However, in some instances, "direct" cadmium–carbonyl interaction has been found to take place (15, 16).

In the solid state, the weakly acidic proton of neutral theophylline is bound to N(7) (17, 18). However, the comparable basicities of the imidazole N(7) and N(9) sites in purines commonly lead to a tautomeric equilibrium between the N(7)—H and N(9)—H forms. This duality manifests itself in the existence of two types of complexes with formally neutral theophylline: the metal can be bound via N(9) to the N(7)—H tautomer (19, 20), or via N(7) to the N(9)—H tautomer (21). The theophyllinium (ThH_2)$^+$ ion, in which both N(7) and N(9) bear a hydrogen atom (21, 22), has only carbonyl oxygens available for coordination and shows no pronounced affinity

[1]Correspondence to be addressed to one of these authors.

for binding to metal ions. The theophyllinate anion (Th^{-1}) derived from theophylline could, in principle, react either through N(7) or N(9), but in all the crystal structures reported so far (23–29), it was found to be bound to the metal via N(7).

As a part of our program dealing with the interactions of metal ions with nucleic acid constituents (4), we have isolated and characterized by microanalytical data, ^{1}H and ^{13}C nmr and ir spectroscopy, the novel cadmium complex bis(theophyllinato)tetraaquocadmium(II). However, the structure of this complex could not be established unambiguously by standard spectroscopic techniques, and hence, an X-ray diffraction study of the complex, crystallized from *N*,*N*-dimethylformamide/pyridine, was undertaken. The combined synthetic and structural studies are reported herein.

TABLE 1. Refined coordinates ($\times 10^4$, H $\times$ 10^3) and equivalent temperature factors ($\times 10^3$)

Atom	X	Y	Z	U_{eq}
Cd	0	5000	5000	35
O(2)	2870(5)	5312(4)	−753(5)	54
O(6)	2371(5)	3945(4)	3170(5)	52
O(10)	6498(6)	2872(4)	3694(6)	76
O(13)	1022(5)	3508(3)	4895(5)	48
O(14)	2094(5)	5487(4)	6332(5)	52
N(1)	2600(6)	4657(4)	1235(5)	37
N(3)	1400(6)	6006(4)	91(5)	43
N(7)	299(6)	5530(4)	2968(5)	37
N(9)	−146(6)	6627(4)	1145(5)	40
N(10)	5323(7)	1679(4)	2300(6)	59
C(1)	3570(10)	3922(6)	1232(8)	72
C(2)	2315(7)	5330(4)	142(6)	33
C(3)	1014(8)	6747(5)	−1034(7)	46
C(4)	794(7)	6009(4)	1083(6)	32
C(5)	1113(7)	5340(5)	2178(6)	32
C(6)	2048(7)	4602(5)	2280(7)	37
C(8)	−432(7)	6299(5)	2283(7)	40
C(10)	6215(9)	2344(7)	2646(9)	69
C(11)	4495(10)	1510(7)	3107(11)	86
C(12)	5095(11)	1072(7)	1049(9)	97
H(8)	−109(5)	656(4)	258(5)	24
H(11)	420(7)	389(5)	210(7)	69
H(12)	406(8)	410(6)	65(9)	116
H(13)	315(7)	339(5)	101(7)	81
H(31)	5(7)	697(5)	−107(7)	89
H(32)	133(7)	740(6)	−60(7)	82
H(33)	124(8)	654(6)	−160(8)	106
H(101)	686(6)	236(5)	197(6)	56
H(111)	441(8)	196(6)	362(9)	119
H(112)	339(8)	169(6)	249(9)	122
H(113)	454(8)	92(6)	347(9)	112
H(121)	513(7)	48(5)	119(7)	73
H(122)	573(6)	124(4)	61(6)	41
H(123)	426(8)	121(6)	38(8)	102
H(131)	161(6)	361(4)	454(6)	39
H(132)	55(8)	291(6)	454(9)	111
H(141)	269(7)	603(5)	623(7)	90
H(142)	230(6)	540(5)	719(6)	53

Experimental

^{1}H nmr spectra were measured in $(CD_3)_2SO$ on a Bruker HX-60 instrument operating at 60 MHz in the Fourier transform mode, using $(CH_3)_4Si$ (TMS) as internal standard. ^{13}C nmr spectra were recorded on a Bruker CXP-200 instrument operating at 50.307 MHz and were also referenced to internal TMS. All spectra were recorded at room temperature (25 ± 2°C). Infrared spectra were recorded as 1% KBr discs on a Perkin-Elmer 598 spectrometer. Microanalyses were performed by Guelph Chemical Laboratories Limited.

Commercially available theophylline (Sigma) and cadmium acetate dihydrate (BDH) were used as received.

Preparation of compounds

To a hot solution of theophylline (0.50 g, 2.77 mmol) in 50 mL of deionized water was added dropwise a solution of cadmium acetate dihydrate (0.37 g, 1.39 mmol) in 5 mL of deionized water. Immediate formation of a white precipitate resulted. After stirring the reaction mixture for 15 min at 80°C, the white solid was collected by filtration, washed with 100 mL of hot water, and dried to constant weight in a vacuum desiccator. It was crystallized once from methanol and then from a 1:5 pyridine/*N*,*N*-dimethylformamide (DMF) mixture to yield colourless crystals in 17% yield.

The analysis of the white precipitate corresponds to $[CdTh_2(H_2O)_4]$. *Anal.* calcd. for $CdC_{14}H_{22}N_8O_8$: C 30.98, H 4.09, N 20.64; found: C 31.00, H 4.36, N 20.67.

A sample of the colourless crystalline material recovered from DMF/pyridine was also submitted for elemental analysis and the results indicated a monosolvate $[CdTh_2(H_2O)_4]$.DMF. *Anal.* calcd. for $CdC_{17}H_{29}N_9O_9$: C 33.15, H 4.75, N 20.47; found: C 33.18, H 5.04, N 20.09. Single crystals taken from this sample were found to be the disolvate $[CdTh_2(H_2O)_4]$.2DMF (see below). Since the crystals deteriorate when exposed to the atmosphere for a few hours, it is likely that the material analysed had lost some DMF to give the monosolvate.

^{1}H chemical shift data

Literature values for the uncomplexed theophylline ligand are given in parentheses (5).

(*a*) For the white precipitate, $CdC_{14}H_{22}N_8O_8$: N(1)—CH_3 = 3.23 (3.26), N(3)—CH_3 = 3.45 (3.47), C(8)—H = 7.52 (8.06), N(7)—H = (13.53), H_2O = 3.52.

(*b*) For the colourless crystalline material, $CdC_{17}H_{29}N_9O_9$: N(1)—CH_3 = 3.23 (3.26), N(3)—CH_3 = 3.45 (3.47), C(8)—H = 7.52 (8.06), N(7)—H = (13.53), H_2O = 3.52, $(CH_3)_2N$— = 2.89, 2.73, —C(O)—H = 7.95.

^{13}C chemical shift data

(*a*) For the white precipitate, $CdC_{14}H_{22}N_8O_8$: N(1)—CH_3 = 27.71 (27.37), N(3)—CH_3 = 30.19 (29.36), C(2) = 151.56 (151.03), C(4) = 148.65 (147.63), C(5) = 113.56 (106.28), C(6) = 157.87 (154.18), C(8) = 147.68 (139.96).

(*b*) For the colourless crystalline material, $CdC_{17}H_{29}N_9O_9$: N(1)—CH_3 = 27.27 (27.37), N(3)—CH_3 = 29.70 (29.36), C(2) = 151.37 (151.03), C(4) = 148.60 (147.63), C(5) = 113.17 (106.28), C(6) = 157.39 (154.18), C(8) = 147.15 (139.96), $(CH_3)_2N$— = 35.62, 30.67, —C(O)—H = not observed.

Infrared absorption data:

For the white precipitate: ν(C=O) + $\delta(H_2O)$ = 1645(s); ν(C=C) + ν(C=N) = 1602(s), 1520(m). Free theophylline: 1720(s), 1680(s), 1610(w), 1560(m) (5).

Crystal data

$[CdTh_2(H_2O)_4]$.2DMF ($CdC_{14}H_{22}N_8O_8.2C_3H_7NO$) fw = 684.9

Monoclinic, $P2_1/c$, a = 10.891(3), b = 13.696(7), c = 10.110(2) Å, β = 109.03(4)°, V = 1425.6 Å^3, Z = 2, D_c = 1.595 g cm^{-3}, μ(MoKα) = 8.3 cm^{-1}, λ(MoK$\bar{\alpha}$) = 0.71069 Å (graphite monochromator), T = 23°C. Crystal dimensions: 0.12 mm × 0.14 mm × 0.15 mm.

Crystallographic measurement

The compound precipitated as colourless transparent crystals from a pyridine–DMF mixture, but these became opaque after exposure to the atmosphere for a few hours. This deterioration, which is probably due to the loss of DMF, was slowed considerably by sealing the crystal in a Lindemann capillary. Precession and cone axis photographs showed $2/m$ Laue symmetry and the systematic absences ($h0l$, $l \neq 2n$ and $0k0$, $k \neq 2n$) unambiguously defined space group $P2_1/c$.

The crystal was mounted on an Enraf-Nonius CAD-4 diffractometer. The cell parameters reported above were obtained by least-

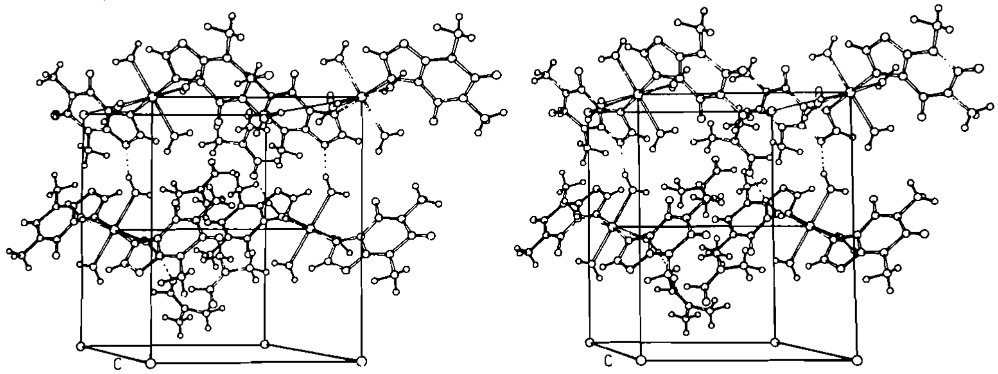

FIG. 1. Stereo view of the unit cell. The atoms are represented by spheres of arbitrary sizes. Dashed lines correspond to hydrogen bonds.

squares refinement on the setting angles of 25 reflections randomly distributed in the Laue sphere. The intensity data were collected as described elsewhere (30). The intensities of the three standard reflections decreased slowly, at the same rate, during data collection. At the end, 24% of the original intensity had been lost. The intensities were corrected accordingly at the data reduction stage. A total of 1865 *hkl* and $h\bar{k}l$ reflections were measured in the sphere limited by $2\theta \leq 45°$ (MoKα). A set of 1299 reflections with intensities $I > 3\sigma(I)$ was used to solve and refine the structure. These data were corrected for the Lorentz effect and polarization. A sample calculation showed that the transmission factor varied in the very narrow 0.85–0.89 range. Therefore, an absorption correction was deemed unnecessary.

Resolution of the structure

The structure was solved by the heavy-atom method and refined by full-matrix least-squares. The Cd atoms were positioned on equipoint 2*a* on the basis of a three-dimensional Patterson synthesis. A portion of the five-membered ring of theophylline could also be extracted from this map. These light atoms, together with Cd, were used as the initial phasing model. The remaining nonhydrogen atoms were located from subsequent structure factor and difference Fourier (ΔF) calculations. Isotropic refinement of all nonhydrogen atoms converged to $R = \Sigma||F_o| - |F_c||/\Sigma|F_o| = 0.086$ and $R_w = [\Sigma w(|F_o| - |F_c|)^2/\Sigma w|F_o|^2]^{1/2} = 0.097$. An individual weight $w = 1/\sigma^2(F)$ based on counting statistics (30) was applied to each reflection. The positions of all the hydrogen atoms were determined from the ΔF map calculated at this stage. The atoms were then anisotropically refined, except for hydrogens, which were isotropically refined. Convergence was reached for $R = 0.044$ and $R_w = 0.052$. The goodness-of-fit ratio was 1.87. The final ΔF map was essentially featureless: the general background was within $\pm$ 0.55 e Å^{-3}, but a few peaks of $\pm \sim 1$ e Å^{-3} were found near Cd.

The scattering curves were from standard sources (31). The f' and f'' contributions of Cd to anomalous dispersion were taken into account (32).

The refined coordinates are listed in Table 1. The lists of temperature factor and structure factor amplitudes are part of the supplementary material.[2]

Results and discussion

Theophylline contains four potential binding sites since the methyl groups at N(1) and N(3) effectively render these sites non coordinating. Three of these sites, i.e. C(6)═O, C(2)═O, and N(9) possess one or more lone pairs of electrons in the undissociated ligand. The N(7) atom can become a reactive site as a result of the formation of Th^{-1} via displacement of the weakly acidic N(7)—H proton (pK_a = 8.5) (33).

The solid DMF-free compound was obtained by reacting equimolar amounts of theophylline and cadmium acetate dihydrate in aqueous solution at pH 5 according to the following net reaction:

$$[1] \quad 2ThH + Cd(CH_3CO_2)_2.2H_2O \xrightarrow{H_2O} [CdTh_2(H_2O)_4] + 2CH_3COOH$$

Recrystallization of $[CdTh_2(H_2O)_4]$ from a pyridine/DMF mixture (1:5) yielded a crystalline solid whose elemental analysis was consistent with a complex containing cadmium(II), DMF, water, and theophyllinate ions. However, while the results of standard spectroscopic techniques (see below) clearly indicated that DMF was not a component of the inner coordination sphere, they were less successful in establishing unambiguously the geometrical arrangements of water and theophyllinate ions in the inner coordination sphere, the site utilized by Th^{-1} in its binding to cadmium, the state of aggregation of the complex (e.g. monomeric or dimeric), the structure of the complex and the extent (if any) of the involvement of the C(6)═O in bonding to cadmium. In order to shed some light on these problems, we undertook the X-ray crystal structure determination, the results of which are reported below.

Crystal structure of [CdTh$_2$(H$_2$O)$_4$].2DMF

Figure 1 shows an ORTEP drawing of the complex. The interatomic distances and bond angles are listed in Table 2. The structure consists of monomeric, six-coordinate molecules, $[CdTh_2(H_2O)_4]$, in which the two Th^{-1} anions are in the *trans*-positions and bound to cadmium via their N(7) nitrogens. Cadmium occupies a crystallographic inversion centre and its coordination is roughly *trans*-octahedral. Opposite Cd–ligand bonds are exactly 180° apart by symmetry. The N—Cd—O angles range from 88.4(2) to 91.6(2)°. Departure from the ideal 90° value is greater for the O—Cd—O angles (83.5(2), 96.5(2)°). The Cd—O distances of 2.346(5) and 2.336(5) Å compare well with those found in other aquo complexes (11–14). The Cd—N(7) distance (2.300(5) Å) is similar to those reported for complexes with related ligands (9–16).

N,*N*-Dimethylformamide is clearly not a constituent of the inner coordination sphere of cadmium, but rather is present in well defined lattice sites as a solvent of crystallization (Fig. 2).

As mentioned earlier, both the N(1) and N(3) sites in the theophylline are blocked by a methyl group, so coordination occurs either through N(7) or N(9) (or, perhaps, via C(6)═O or C(2)═O). In view of the observation that in neutral theophylline, the imidazole proton is bound at N(7) (17, 18), it is not surprising that, in the majority of the complexes containing

[2]Lists of anisotropic temperature factors (Table 4), weighted least-squares planes (Table 5), and observed and calculated structure factor amplitudes (Table 6) may be purchased from the Depository of Unpublished Data, CISTI, National Research Council of Canada, Ottawa, Ont., Canada K1A 0S2.

TABLE 2

(*a*) Interatomic distances

Bond	Distance (Å)	Bond	Distance (Å)
Cd—N(7)	2.300(5)	C(5)—C(6)	1.414(10)
Cd—O(13)	2.346(5)	C(6)—O(6)	1.240(8)
Cd—O(14)	2.336(5)	C(5)—N(7)	1.398(9)
N(1)—C(1)	1.460(11)	N(7)—C(8)	1.365(9)
N(1)—C(2)	1.394(8)	C(8)—N(9)	1.362(9)
N(1)—C(6)	1.377(9)	N(10)—C(10)	1.294(11)
C(2)—O(2)	1.242(9)	N(10)—C(11)	1.419(13)
C(2)—N(3)	1.349(9)	N(10)—C(12)	1.465(11)
N(3)—C(3)	1.479(8)	C(10)—O(10)	1.236(10)
N(3)—C(4)	1.369(9)	C(4)—C(5)	1.391(9)
		C(4)—N(9)	1.345(9)
C(1)—H(11)	0.92(7)	O(14)—H(141)	1.01(8)
C(1)—H(12)	0.95(9)	O(14)—H(142)	0.83(6)
C(1)—H(13)	0.85(7)	C(11)—H(111)	0.83(8)
C(3)—H(31)	1.08(8)	C(11)—H(112)	1.19(9)
C(3)—H(32)	1.01(8)	C(11)—H(113)	0.88(8)
C(3)—H(33)	0.75(8)	C(12)—H(121)	0.82(7)
C(8)—H(8)	0.93(6)	C(12)—H(122)	0.96(7)
O(13)—H(131)	0.84(6)	C(12)—H(123)	0.96(8)
O(13)—H(132)	0.97(9)		

(*b*) Bond angles

Bonds	Angle (deg)	Bonds	Angle (deg)
N(7)—Cd—O(13)	91.5(1)	N(7)—Cd—O(13)[a]	88.5(2)
N(7)—Cd—O(14)	91.6(2)	N(7)—Cd—O(14)[a]	88.4(2)
O(13)—Cd—O(14)	83.5(2)	O(13)—Cd—O(14)[a]	96.5(2)
C(1)—N(1)—C(2)	115.4(6)	C(4)—C(5)—C(6)	121.0(6)
C(1)—N(1)—C(6)	117.4(6)	C(4)—C(5)—N(7)	107.0(6)
C(2)—N(1)—C(6)	127.2(6)	C(6)—C(5)—N(7)	131.8(6)
N(1)—C(2)—O(2)	122.0(6)	C(5)—C(6)—N(1)	112.9(6)
N(3)—C(2)—O(2)	121.0(6)	C(5)—C(6)—O(6)	126.8(7)
N(1)—C(2)—N(3)	117.1(6)	N(1)—C(6)—O(6)	120.3(6)
C(2)—N(3)—C(3)	121.4(6)	C(5)—N(7)—C(8)	103.1(6)
C(2)—N(3)—C(4)	120.1(6)	C(5)—N(7)—Cd	138.8(4)
C(3)—N(3)—C(4)	118.5(6)	C(8)—N(7)—Cd	117.9(4)
N(3)—C(4)—C(5)	121.7(6)	N(7)—C(8)—N(9)	115.3(6)
N(3)—C(4)—N(9)	126.3(6)	C(4)—N(9)—C(8)	102.6(5)
C(5)—C(4)—N(9)	111.9(6)	C(10)—N(10)—C(11)	121.4(7)
		C(10)—N(10)—C(12)	122.3(7)
		C(11)—N(10)—C(12)	116.3(7)
		N(10)—C(10)—O(10)	126.8(8)
N(1)—C(1)—H(11)	110(4)	Cd—O(14)—H(141)	133(4)
N(1)—C(1)—H(12)	112(5)	Cd—O(14)—H(142)	116(5)
N(1)—C(1)—H(13)	105(5)	H(141)—O(14)—H(142)	104(6)
H(11)—C(1)—H(12)	102(7)	N(10)—C(10)—H(101)	114(3)
H(11)—C(1)—H(13)	112(7)	O(10)—C(10)—H(101)	118(3)
H(12)—C(1)—H(13)	115(7)	N(10)—C(11)—H(111)	117(6)
N(3)—C(3)—H(31)	104(4)	N(10)—C(11)—H(112)	113(4)
N(3)—C(3)—H(32)	108(4)	N(10)—C(11)—H(113)	115(6)
N(3)—C(3)—H(33)	104(6)	H(111)—C(11)—H(112)	83(7)
H(31)—C(3)—H(32)	87(6)	H(111)—C(11)—H(113)	115(8)
H(31)—C(3)—H(33)	130(8)	H(112)—C(11)—H(113)	109(7)
H(32)—C(3)—H(33)	121(8)	N(10)—C(12)—H(121)	115(5)
N(7)—C(8)—H(8)	121(3)	N(10)—C(12)—H(122)	108(4)
N(9)—C(8)—H(8)	124(3)	N(10)—C(12)—H(123)	111(5)
Cd—O(13)—H(131)	108(4)	H(121)—C(12)—H(122)	108(6)
Cd—O(13)—H(132)	123(5)	H(121)—C(12)—H(123)	107(7)
H(131)—O(13)—H(132)	112(7)	H(122)—C(12)—H(123)	107(6)

[a] $-x, 1-y, 1-z$.

TABLE 3. Geometry of the hydrogen bonds

Bond	Distance (Å)	Bonds	Angle (deg)
O(13)—H(132).....N(9)[a]			
O(13)—N(9)[a]	2.828(7)	Cd—O(13)—N(9)[a]	134.6(2)
H(132)—N(9)[a]	1.89(9)	O(13)—N(9)[a]—C(8)[a]	118.2(4)
		O(13)—N(9)[a]—C(4)[a]	136.5(4)
		O(13)—H(132)—N(9)[a]	162(8)
O(13)—H(131)....(O6) (intramolecular)			
O(13)—O(6)	2.689(8)	Cd—O(13)—O(6)	101.7(2)
H(131)—O(6)	1.89(6)	O(13)—O(6)—C(6)	123.1(5)
		O(13)—H(131)—O(6)	158(6)
O(14)—H(142)....O(2)[b]			
O(14)—O(2)[b]	2.799(6)	Cd—O(14)—O(2)[b]	119.0(2)
H(142)—O(2)[b]	1.97(6)	O(14)—O(2)[b]—C(2)[b]	135.6(5)
		O(14)—H(142)—O(2)[b]	175(6)
O(14)—H(141)....O(10)[c]			
O(14)—O(10)[c]	2.726(8)	Cd—O(14)—O(10)[c]	132.6(2)
H(141)—O(10)[c]	1.73(8)	O(14)—O(10)[c]—C(10)[c]	117.3(6)
		O(14)—H(141)—O(10)[c]	165(7)

[a] $-x, -\frac{1}{2}+y, \frac{1}{2}-z$.
[b] $x, y, 1+z$.
[c] $1-x, 1-y, 1-z$.

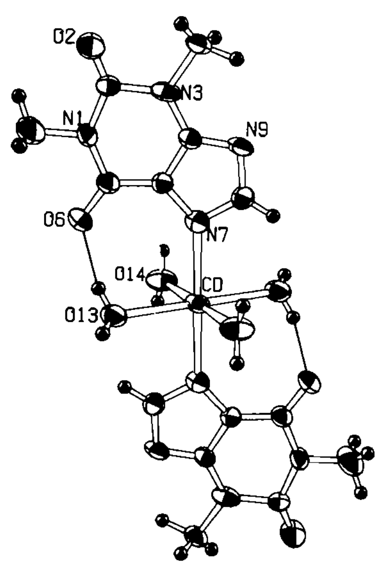

FIG. 2. ORTEP drawing of the $Cd(H_2O)_4(C_7H_7N_4O_2)_2$ molecule. The ellipsoids correspond to 50% probability, except for hydrogens, which are shown as spheres of arbitrary size. The dashed lines correspond to hydrogen bonds. The cadmium atom occupies a crystallographic inversion centre.

the theophyllinate anion, the coordination of $(Th)^{-1}$ is through N(7). Kistenmacher, Marzilli, and co-workers (23–29) reported the structures of a number of complexes with the theophyllinate anion and they invariably found the metal to be bound to N(7) rather than N(9). They also pointed out that O(6) is consistently involved in stabilizing interactions, either by weak coordination with the metal (in copper complexes), or through hydrogen bonding with other coordinated ligands. The present complex clearly belongs to the latter class. The intramolecular O(13)—H···O(6) bond is strong, with an O(13)—O(6) separation of 2.689(8) Å lying on the low side of the range (2.65–2.93 Å) proposed by Stout and Jensen for this type of H-bond (34). The hydrogen lies close to the O(13)—O(6) direction and all the angles are favorable (Table 3). On the other hand, binding via N(9) would replace this stabilizing interaction by a repulsion between water and the hydrophobic N(3)—CH_3 portion of theophylline. The so-called "indirect chelation" of O(6) appears to introduce a stabilization large enough to favor bonding to N(7) in azahypoxanthine, a ligand very similar to theophylline, in spite of the fact that N(8) and N(9) are believed to be more basic that N(7) (14). Indirect chelation also exists in the cadmium complexes of inosine monophosphate and guanosine monophosphate (13). Therefore, whenever such extra stabilization is possible, the acceptor ability of N(7) is enhanced, and both factors have to be considered when discussing the relative affinities of N(7) and N(9) in such systems.

The theophylline unit consists of two individual rings, both planar within 1.7σ (0.012 Å). The angle between the rings is 2.0° (Table 4, supplementary material). The substituents are displaced slightly, although significantly, from their respective planes: O(6), 0.047(5) Å; C(1), 0.034(9) Å; Cd, −0.137 Å. The DMF molecule (excluding the methyl hydrogens) is planar within 2σ (0.019 Å).

The hydrogen bonding in $[Th_2Cd(H_2O)_4]$.2DMF is extensive due to the presence of a number of donor and acceptor sites in the theophyllinate anion and DMF molecule. The four water molecules on the cadmium atom provide additional donor sites. The distances and angles associated with these possible hydrogen bonds are listed in Table 3. The pair of symmetry-equivalent intramolecular O(13)—H(13)···O(6) hydrogen bonds has been discussed above. The packing pattern (Fig. 2) shows some intermolecular hydrogen bonds. O(2) is involved in an intermolecular hydrogen bond with the hydrogen of an O(14) water molecule: the O(14)···O(2) distance is 2.799(6) Å, and the O(14)—H(142)—O(2) angle is 175(6)°. The theophyllinate ligands are linked together by intermolecular O(13)—H(132)···N(9) hydrogen bonds, with an O(13)—N(9) distance of 2.828(7) Å and O(13)—H(132)—N(9) angle of 162(8)°. The oxygen atom of DMF is also involved in hydrogen bonding to water molecules attached to the central metal atom.

^1H and ^{13}C nmr and ir spectroscopic analysis of the compounds

^1H and ^{13}C nmr and ir spectra of the complexes, together with comparable data for the parent theophylline, are given in the experimental section. The ^1H nmr spectrum exhibits upfield shifts of the N(1)—CH_3, N(3)—CH_3, and C(8)—H resonances, with the resonance due to N(7)—H being absent. This is consistent with theophyllinate binding via N(7) with concomitant proton displacement. The trends of the chemical shifts of the N(1)—CH_3, N(3)—CH_3, and C(8)—H are parallel to those observed in the [(CH_3Hg)Th].H_2O and [Th_2Hg].H_2O complexes, in which N(7)—Hg binding is known to occur (5). In a solution of the crystalline sample, the ^1H resonances associated with DMF are at $\delta = 2.89$ and 2.73 ppm ($N(CH_3)_2$) and $\delta = 7.95$ ppm (—C(O)—H). The water and purine resonances of the DMF solvate are relatively unchanged as compared to corresponding resonances of the noncrystalline sample. Natural abundance proton decoupled ^{13}C nmr spectra were also obtained. Signals of most interest are those which are close to the site of metallation. The resonances due to C(5) and C(8) show downfield shifts of 7.28 and 7.72 ppm together with a downfield shift of the C(6) resonance of 3.69 ppm. The other resonances are relatively unaffected in comparison to those of theophylline itself. The trend is in the same order as is observed with [(CH_3Hg)Th].H_2O and [Th_2Hg].H_2O (5). These changes in the chemical shifts of C(5) and C(8) resonances can be attributed to the transfer of charge from N(7) to the ring systems on removal of the proton (35). The change in chemical shift of the C(6) resonance could be, in part, due to the involvement of C(6)═O group in hydrogen bonding to the water groups attached to the central metal atom (see X-ray structure).

The ir spectra of the complexes show a strong multicomponent absorption at 1645 cm^{-1}. Similar strong bands, attributed to the $\delta(H_2O)$ mode and the two C═O stretching vibrations found at ~1685 and ~1635 cm^{-1}, have been found in a number of complexes containing the theophyllinate ion (5, 36). Free theophylline has corresponding absorptions at 1720 and 1680 cm^{-1}. Shifts of this magnitude in the C═O stretching modes are sometimes cited as evidence for N(7)—O(6) chelation. However, based on the X-ray results obtained in the present study and with [(CH_3Hg)Th].H_2O (5, 6), this lowering in the stretching mode is more likely a consequence of the deprotonation of the imidazole ring, with a possible contribution resulting from the involvement of the C(6)═O oxygen atom in the formation of strong hydrogen bonds with the hydrogen atom of the water molecule attached to the central metal atom.

Acknowledgments

We wish to thank M. J. Olivier for collecting the X-ray data and the Natural Sciences and Engineering Research Council of Canada for financial support.

1. J. K. BARTON and S. J. LIPPARD. Nucleic acid – metal ion interactions. Vol. 1. *Edited by* T. G. Spiro. Wiley, New York. 1980. Chapt. 2.
2. J. P. CHARLAND, M. SIMARD, and A. L. BEAUCHAMP. Inorg. Chim. Acta, **80**, L57 (1983); A. L. BEAUCHAMP. Inorg. Chim. Acta, **91**, 33 (1984); F. GUAY, A. L. BEAUCHAMP, C. GILBERT, and R. SAVOIE. Can. J. Spectrosc. **28**, 13 (1983).
3. F. GUAY and A. L. BEAUCHAMP. Inorg. Chim. Acta, **66**, 57 (1982); M. J. OLIVIER and A. L. BEAUCHAMP. Inorg. Chem. **19**, 1064 (1980).
4. A. R. NORRIS, E. BUNCEL, and S. E. TAYLOR. J. Inorg. Biochem. **16**, 279 (1982); S. E. TAYLOR, E. BUNCEL, and A. R. NORRIS. J. Inorg. Biochem. **15**, 131 (1981); E. BUNCEL, A. R. NORRIS, W. J. RACZ, and S. E. TAYLOR. Inorg. Chem. **20**, 98 (1981); E. BUNCEL, A. R. NORRIS, S. E. TAYLOR, and W. J. RACZ. Can. J. Chem. **60**, 3033 (1982); E. BUNCEL, B. K. HUNTER, R. KUMAR, and A. R. NORRIS. J. Inorg. Biochem. **20**, 171 (1984); A. R. NORRIS, R. KUMAR, and E. BUNCEL. J. Inorg. Biochem. **22**, 11 (1984).
5. A. R. NORRIS, R. KUMAR, E. BUNCEL, and A. L. BEAUCHAMP. J. Inorg. Biochem. **21**, 277 (1984).
6. A. R. NORRIS, S. E. TAYLOR, E. BUNCEL, F. BÉLANGER-GARIÉPY, and A. L. BEAUCHAMP. Inorg. Chim. Acta, **92**, 271 (1984).
7. R. G. PARR and R. G. PEARSON. J. Am. Chem. Soc. **105**, 7512 (1983).
8. G. I. EICHHORN. Inorganic biochemistry. Elsevier, Amsterdam. 1973. Chapt. 34; K. J. ELLIS, D. VARTSKY, I. ZANZI, S. H. COHN, and S. YASUMURA. Science (Washington, DC), **205**, 323 (1979); B. L. VALLEE and D. D. ULMER. Annu. Rev. Biochem. **41**, 91 (1972); M. A. SIROVER and L. A. LOEB. Science (Washington, DC), **194**, 1434 (1976); D. J. HOFFMAN and S. K. NIYOGI. Science (Washington, DC), **198**, 513 (1977); K. B. JACOBSON and J. E. TURNER. Toxicology, **16**, 1 (1980).
9. C. H. WEI and K. B. JACOBSON. Inorg. Chem. **20**, 356 (1981).
10. E. H. GRIFFITH, N. G. CHARLES, and E. L. AMMA. Acta Crystallogr. Sect. B, **38**, 942 (1982).
11. I. MUTIKAINEN and P. LUMME. Acta Crystallogr. Sect. B, **36**, 2237 (1980).
12. D. M. L. GOODGAME, I. JEEVES, C. D. REYNOLDS, and A. C. SKAPSKI. Biochem. J. **151**, 467 (1975); G. R. CLARK and J. D. ORBELL. Acta Crystallogr. Sect. B, B**34**, 1815 (1978); J. K. SHIBA and R. BAU. Inorg. Chem. **17**, 3484 (1978).
13. K. AOKI. Acta Crystallogr. Sect. B, **32**, 1454 (1976); D. M. L. GOODGAME, I. JEEVES, C. D. REYNOLDS, and A. C. SKAPSKI. Nucleic Acid Res. **2**, 1375 (1975).
14. L. G. PURNELL, E. D. ESTES, and D. J. HODGSON. J. Am. Chem. Soc. **98**, 740 (1976).
15. C. GAGNON, A. L. BEAUCHAMP, and D. TRANQUI. Can. J. Chem. **57**, 1372 (1979).
16. E. H. GRIFFITH and E. L. AMMA. J. Chem. Soc. Chem. Commun. 1013 (1979).
17. D. J. SUTOR. Acta Crystallogr. **11**, 83 (1958).
18. E. SHEFTER. J. Pharm. Sci. **58**, 710 (1969).
19. E. H. GRIFFITH and E. L. AMMA. J. Chem. Soc. Chem. Commun. 322 (1979).
20. K. AOKI and H. YAMAZAKI. J. Chem. Soc. Chem. Commun. 186 (1980).
21. M. B. CINGI, A. M. M. LANFREDI, A. TIRIPICCHIO, and M. T. CAMELLINI. Transition Met. Chem. (Weinheim, Ger.), **4**, 221 (1979).
22. C. H. KOO, H. S. SHIN, and S. S. OH. Taehan Hwahak Hoechi, **22**, 86 (1978); Chem. Abstr. **89**, 106974 (1978).
23. T. SORRELL, L. G. MARZILLI, and T. J. KISTENMACHER. J. Am. Chem. Soc. **98**, 2181 (1976).
24. T. J. KISTENMACHER, D. J. SZALDA, C. C. CHIANG, M. ROSSI, and L. G. MARZILLI. Inorg. Chem. **17**, 2582 (1978).
25. D. J. SZALDA, T. J. KISTENMACHER, and L. G. MARZILLI. Inorg. Chem. **15**, 2783 (1976).
26. D. J. SZALDA, T. J. KISTENMACHER, and L. G. MARZILLI. J. Am. Chem. Soc. **98**, 8371 (1976).
27. T. J. KISTENMACHER, D. J. SZALDA, and L. G. MARZILLI. Inorg. Chem. **14**, 1686 (1975).
28. T. J. KISTENMACHER. Acta Crystallogr. Sect. B, **31**, 85 (1975).
29. T. J. KISTENMACHER and D. J. SZALDA. Acta Crystallogr. Sect. B, **31**, 90 (1975).
30. F. BÉLANGER-GARIÉPY and A. L. BEAUCHAMP. J. Am. Chem. Soc. **102**, 3461 (1980).
31. D. T. CROMER and J. T. WABER. Acta Crystallogr. **18**, 104 (1965); R. F. STEWART, E. R. DAVIDSON, and W. T. SIMPSON.

J. Chem. Phys. **42**, 3175 (1965).
32. D. T. CROMER. Acta Crystallogr. **18**, 17 (1965).
33. D. LICHTENBERG, F. BERGMANN, and Z. NEIMAN. J. Chem. Soc. (C), 1676 (1971).
34. G. H. STOUT and L. H. JENSEN. "X-ray structure determination". Macmillan, London. 1968. p. 303.
35. L. C. SNYDER, R. G. SHULMAN, and D. B. NEUMANN. J. Chem. Phys. **53**, 256 (1970).
36. W. BECK and N. KOTTMAIR. Chem. Ber. **109**, 970 (1976).

COMMUNICATION

Facile H–D exchange of the bridgehead methyls of bicyclo[2.2.2]octan-2,5-diones. Evidence for a carbon analogue of the acyloin rearrangement

NICK HENRY WERSTIUK, GWEN IRENE WADE,[1] AND PETER JOHN JOSEPH MARTIN[2]
Department of Chemistry, McMaster University, Hamilton, Ont., Canada L8S 4M1

Received May 10, 1985

NICK HENRY WERSTIUK, GWEN IRENE WADE, and PETER JOHN JOSEPH MARTIN. Can. J. Chem. **63**, 2582 (1985).

Hexamethyltwistyl-2,5-dione **4** has been synthesized and its H–D exchange studied in *t*-BuOK/*t*-BuOD at 125°C. We find that the bridgehead methyl at C-3 undergoes exchange 7×10^5 times faster than the bridgehead methyl of bicyclo[2.2.1]heptan-2-one (fenchone). This result, along with a previous study, establishes the first examples of the carbon analogue of the acyloin rearrangement of alicyclic systems.

NICK HENRY WERSTIUK, GWEN IRENE WADE et PETER JOHN JOSEPH MARTIN. Can. J. Chem. **63**, 2582 (1985).

On a synthétisé l'hexaméthyltwistyldione-2,5 (**4**) et on a étudié son échange H–D sous l'influence du *tert*-BuOK/*tert*-BuOD, à 125°C. On trouve que la vitesse d'échange du groupement méthyle en tête de pont, en C-3, est 7×10^5 fois plus rapide que celle du groupement méthyle en tête de pont de la triméthyl-1,3,3 bicyclo[2.2.1] heptanone-2 (fenchone). Ce résultat, de même que ceux obtenus au cours d'une étude antérieure, permet d'établir les premiers exemples d'analogues carbonés d'une transposition aux acyloïnes dans des systèmes alicycliques.

[Traduit par le journal]

Numerous examples of the base-catalyzed rearrangement of α-ketols (acyloins) (Scheme 1) have been documented in the literature. The rearrangements occur readily in acyclic, monocyclic, bicylic, and polycyclic substrates (1–10).[3] The nitrogen analogue of the acyloin rearrangement has been observed in the conversion of α-lactams to α-hydroxyimines by alkyllithiums (11–13). Prior to this report, which documents the first examples of the carbon analogue of the acyloin rearrangement in alicyclic systems, Miller and Bhattacharya (14)[4] established that the anion of dienone **1** undergoes a concerted 1,2 shift of a methyl group at −10°C to yield anthrone **2** (Scheme 2).

From our studies on the homoenolization of bicyclic diones (15, 16) it was established that dione **3** undergoes facile H–D exchange of the bridgehead methyl (Table 1) at 100°C. From the unusual sequence of the deuterium incorporation we deduced that H–D exchange was not rate determining and considered a possible mechanism for the exchange based on a β-enolization.

To establish the generality of the facile exchange of the bridgehead methyl, we have synthesized hexamethyltwistyl-2,5-dione **4** and studied its H–D exchange in 1 *M* *t*-BuOK/*t*-BuOD at 125°C. It was found that the bridgehead methyl at C-3 undergoes exchange approximately 7×10^5 times faster than the bridgehead methyl of fenchone (17).[5] We propose that the exchange of the methyls of **3** and **4** does not occur via a β-enolization, but rather is a consequence of the involvement of a carbon analogue of the acyloin rearrangement (CAAR) of α-enolate **4**-*E* that locates a methyl group at the terminus of an enone (Scheme 3). Our work represents the first examples of

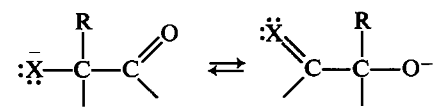

X = O, N, C
: = lone pairs or σ bonds

SCHEME 1

TABLE 1. Base-catalyzed H–D exchange of diones in *t*-BuOK/*t*-BuOD

Dione[a]	Temperature (±3°)	Time (h)	Excess D per molecule (D in methyl)[b]
3	100°C	25	2.01(0.51)
4	125	24	3.78(2.53)
4	125	44	4.35(2.40)[c]

[a] Ketone concentrations ranged between 0.1 and 0.15 *M* and the base concentrations were in the range of 1.0–1.2 *M*. The diones were recovered in 70–80% yield.
[b] Determined mass spectrometrically at low voltage.
[c] Small amounts of d_5 and d_6 species were present.

[1] NSERCC Summer Studentship awardee, 1983.
[2] NSERCC Summer Studentship awardee, 1984.
[3] The references quoted represent only a fraction of the studies of α-ketols which have been reported.
[4]

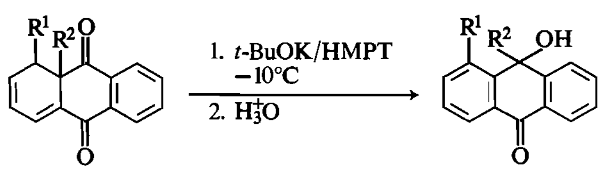

1
a R[1] = H; R[2] = CH_3
b R[1] = R[2] = CH_3

2
a R[1] = H; R[2] = CH_3

SCHEME 2

[5] Based on the fact that fenchone (1,3,3-trimethylbicyclo[2.2.1]-heptan-2-one) undergoes 7.3% exchange of the bridgehead methyl after 300 h at 220°C (17). We previously reported that the methyl of **3** exchanges 5×10^3 faster than the bridgehead methyl of fenchone. The apparent increase in the rate of exchange of **4** is predominantly due to the fact that a better estimate of the rate of exchange of the bridgehead methyl of fenchone is now available.

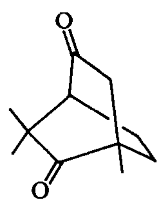

3

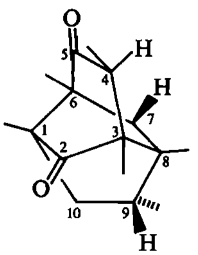

4

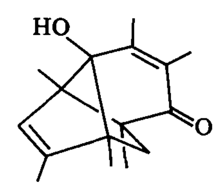

5

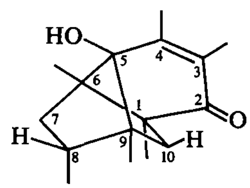

6

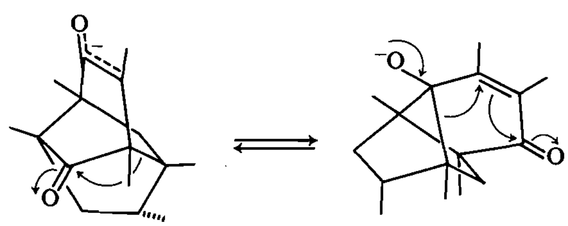

4-*E* 6-*O*

SCHEME 3

CAAR in systems lacking the driving force of a concurrent aromatization.

Dione **4** was prepared from tricyclic hydroxyenone **5** that was described previously by Scheffer and Dzakpasu (18). To avoid the possibility of ring-opening of the Δ^9-analogue of **4** during exchange, hydroxyenone **5** was converted into **6** by catalytic hydrogenation on Pd/charcoal, and **6** was rearranged to **4** by KH/THF (19).[6] The stereochemistries at C-4 and C-9 of **4** are those expected on the basis of the stereoelectronic control of protonation of the α-enolate and the steric control of the reduction, respectively. The *W*-coupling of 2 Hz between the *exo* protons at C-8 and C-10 of **6** confirms the latter expectation (in **4** the *W*-coupling between the *exo* proton at C-7 and the proton at C-9 is also clearly visible and is 1 Hz).

The ^{2}Hmr spectrum of deuterated **4** showed signals only at δ 2.2 and δ 1.1 in a ratio of 1:3. Based on the ^{1}Hmr spectrum, the resonance at δ 2.2 corresponds to the deuteron α to the carbonyl group. That the resonance at δ 1.1 corresponds to the bridgehead methyl at C-1 was established by selectively labelling the methyl group at the terminus of the enone system of **5** in NaOD/D_2O/dioxane. Trideutero-**5** was reduced to deuterated **6**, and **6** was rearranged to **4**, which exhibited a resonance at δ 1.1 in the ^{2}Hmr spectrum. In our view, the facile exchange of **4** (and **3**) can only be accounted for by invoking a rearrangement of the α-enolate **4**-*E* to **6**-*O*, the oxyanion of **6**. Base-catalyzed exchange of **6**-*O* or **6**, followed by rearrangement of **6**-*O* to deuterated **4** via a vinylogous acyloin rearrangement, can account for the experimental results. The vinylogous acyloin rearrangement, examples of which are documented in the literature (19–23), and the carbon analogue of the acyloin rearrangement are related in that the latter is the reverse of the former. Under certain circumstances the CAAR occurs at a reasonable rate but, in cases where the dione is significantly more stable than the hydroxyenone, the CAAR can only be detected by hydrogen-isotope exchange. That the α-enolates of **3** and **4** rearrange at 100–125°C and the anion of **1***a* rearranges at −10°C is a consequence of the aromatization of ring a of **1***a*. It is interesting to note that, although methyl substitution α to the carbonyl group (compare **3** and **4**) does not appear to affect the rate of rearrangement in the alicylic systems, Miller and Bhattacharya reported that dienedione **1***b* does not undergo the 1,2-methyl shift (14).

[6] The spectroscopic data for **4** and **6** were consistent with the proposed structures.

Acknowledgements

We thank the Natural Sciences and Engineering Research Council of Canada for financial support.

1. N. L. WENDLER. *In* Molecular rearrangements. *Edited by* P. de Mayo. Interscience, New York, NY. 1963. Chapt. 16.
2. A. J. WARING. *In* Advances in alicyclic chemistry. Vol. 1. *Edited by* H. Hart and G. J. Karabatsos. Academic Press, New York, NY. 1966. p. 215.
3. Y. MAZUR and M. NUSSIM. Tetrahedron Lett. 817 (1961).
4. A. NICKON, T. NISHIDA, and Y-I. LIN. J. Am. Chem. Soc. **91**, 6860 (1969).
5. W. H. URRY, J. C. DUGGAN, and M-S. H. PAI. J. Am. Chem. Soc. **92**, 5785 (1970).
6. J. V. PAUKSTELIS and D. N. STEPHENS. Tetrahedron Lett. 3549 (1971).
7. P. R. BROOKS and J. M. HARRISON. J. Chem. Soc. Chem. Commun. 997 (1972).
8. R. P. MILLER and D. DOLCE. Tetrahedron Lett. 1151 (1973).
9. W. T. BARCLAY and H. D. PATEL. J. Org. Chem. **39**, 1949 (1974).
10. D. H. D. CROUT, C. J. R. HEDGECOCK, E. L. LIPSCOMB, and F. B. ARMSTRONG. J. Chem. Soc. Chem. Commun. 304 (1980).
11. E. R. TALATY, A. R. CLAGUE, M. O. AGHO, M. N. DESHPANDE, P. M. COURTNEY, D. H. BURGER, and E. F. ROBERTS. J. Chem. Soc. Chem. Commun. 889 (1980).
12. E. R. TALATY and C. M. UNTERMOEHLEN. J. Chem. Soc. Chem. Commun. 204 (1974).
13. H. E. BAUMGARTEN, D. G. MCMAHAN, V. J. ELIA, B. I. GOLD, V. W. DAY, and R. O. DAY. J. Org. Chem. **41**, 3798 (1976).
14. B. MILLER and A. K. BHATTACHARYA. J. Am. Chem. Soc. **102**, 2450 (1980).
15. N. H. WERSTIUK and S. YEROUSHALMI. Can. J. Chem. **58**, 1601 (1980).
16. N. H. WERSTIUK and S. YEROUSHALMI. Can. J. Chem. **58**, 1604 (1980).
17. N. H. WERSTIUK and G. TIMMINS. Can. J. Chem. **63**, 526 (1985).
18. J. R. SCHEFFER and A. A. DZAKPASU. J. Am. Chem. Soc. **100**, 2163 (1978).
19. T. J. GREENHOUGH, J. R. SCHEFFER, J. TROTTER, and Y-F. WONG. J. Chem. Soc. Chem. Commun. 993 (1979).
20. E. BRAMBERGER. Chem. Ber. **33**, 3600 (1900).
21. S. GOODWIN and B. WITKOP. J. Am. Chem. Soc. **79**, 179 (1957).
22. A. NISHINAGA, T. ITAHARA, and T. MATSUURA. Chem. Ber. **109**, 1530 (1976).
23. J. R. SCHEFFER and Y-F. WONG. J. Am. Chem. Soc. **102**, 6604 (1980).

The indirect determination of trace reactive silicon in waters by neutron activation analysis

PHILLIP OLTMANN AND DOUGLAS E. RYAN[1]

Trace Analysis Research Centre, Chemistry Department, Dalhousie University, Halifax, N.S., Canada B3H 4J1

Received December 3, 1984

PHILLIP OLTMANN and DOUGLAS E. RYAN. Can. J. Chem. **63**, 2585 (1985).

Reactive silicon in waters was determined indirectly by counting ^{101}Tc after neutron activation of molybdosilicic acid (MSA) extracted with methyl isobutyl ketone (MIBK). The detection limit (defined as twice the standard deviation for the blank) was 0.2 ng mL^{-1}. The relative standard deviation was 3% at the 10 ng mL^{-1} level and 30% at the 1 ng mL^{-1} level. Phosphate, arsenate, and ferric ions did not interfere by themselves. Interference from the reduction of molybdophosphoric acid by tannic acid was eliminated through the use of dichromate. The salt effect normally encountered in the analysis of sea water was examined with particular reference to silicate content of reagent salts used in preparing synthetic sea water.

PHILLIP OLTMANN et DOUGLAS E. RYAN. Can. J. Chem. **63**, 2585 (1985).

On a déterminé les niveaux de silicium réactif présents dans des eaux en faisant appel à une méthode indirecte impliquant le comptage du ^{101}Tc après une activation neutronique de l'acide molybdisilicique (AMS) qui est extrait par de la méthyl isobutyl cétone (MIBC). La limite de détection (qui est définie comme étant le double de la déviation standard d'un blanc) est égale à 0,2 ng mL^{-1}. La déviation relative standard est égale à 3% à des concentrations de 10 ng mL^{-1} et de 30% à un niveau de 1 ng mL^{-1}. Les ions phosphate, arsénate et ferrique n'interfèrent pas directement. L'interférence provenant de la réduction de l'acide molybdophosphorique par l'acide tannique a été éliminée en utilisant du bichromate. On a étudié l'effet de sel que l'on rencontre lors de l'analyse de l'eau de mer et particulièrement en ce qui a trait au contenu en silicate des réactifs qui sont utilisés pour préparer de l'eau de mer synthétique.

[Traduit par le journal]

Introduction

Silicon is second in abundance to oxygen in the geosphere and therefore is present in other spheres including natural waters. The concentration may be high in deep sea water or undetectable in some surface waters (1, 2). Silicon in waters is essential to diatoms and planktons, the basis of the aquatic food chain (1, 3, 4). It is present in waters as silicate ions (which may be polymerized), as colloidal silicon dioxide and clays, or in plant life. Silicon is also deleterious to industrial processes (5–7) leaving hard deposits on turbine blades and piping of steam power generators resulting in reduced heat transfer and turbine efficiency; demineralization processes must reduce concentrations to less than 50 ng mL^{-1}. Chemicals such as phosphates, tannic and oxalic acids are used in piping waters to reduce corrosion and minimize deposits, and these vary with generator manufacturer. Natural waters may also contain copious amounts of phosphate, sodium chloride, or biological decay products. Methods for silicon determinations, therefore, must be selective and sensitive.

A recent paper (8) reports on the determination of silicon in waters used for washing modern integrated circuits. ASTM recommends that silicic acid concentrations be below 5 ng mL^{-1} for this application, a restraint that renders conventional analysis methods obsolete. The determination of silicon in waters is usually accomplished spectrophotometrically after reduction of molybdosilicic acid (MSA). MSA has also been applied in a flow injection system (9), in a voltammetric finish (7, 10), in a kinetic method (11), and a radioreagent method (12). Only α-MSA is formed over the pH range 3.8–4.8 in solutions 0.005 – 0.1 *M* in molybdate and only β-MSA at pH's 1.0–1.8 at the same molybdate concentrations (13). A short review of MSA production has recently been published (14).

"Reactive silica" denotes silicon species that readily react producing MSA (<20 min); these are orthosilicate and its dimer. Longer chains and colloidal silica react slowly over a period of hours or days reflecting their dissociation and dissolution. Phosphorus(V), arsenic(V), and germanium(IV) also form heteropoly acids under the β-MSA formation conditions and can produce a positive interference in spectrophotometric determinations while fluoride and tannic and humic acids (biological decay products) can produce negative interferences by inhibiting the formation of MSA. Tannic acid can produce a positive interference when present with phosphate by reducing molybdophosphoric acid.

This paper reports on the determination of reactive silicon by neutron activation of extracted MSA. The production of MSA is well defined and its separation from excess molybdate, by extraction, is readily accomplished. The SLOWPOKE reactor is particularly advantageous since direct irradiation of liquids can be done.

Experimental

Reagents and instrumentation

The following reagents were used: ammonium molybdate (Fisher certified), silicon dioxide (INC 99.999%), soidum carbonate (Thorn Smith 99.98%), sulfuric acid (Fisher 96%), MIBK (Aldrich reagent grade), and potassium hydroxide (BDH ACS grade). Ultrapure water, used to dilute reagents, was prepared by sub-boiling distillation of distilled water from a 20 L pyrex flask heated with an ir lamp. A 5 L nalgene flask cooled with ice was used for collection and the water was stored in a similar 20 L container. Teflon separatory funnels were dismantled and soaked in 50% KOH between uses to eliminate possible memory effects. A Tracor Northern TN 1700 multichannel analyzer connected to a Ge(Li) detector was employed to monitor the 307 keV photopeak of ^{101}Tc, the daughter of ^{101}Mo produced upon irradiation.

Procedure

To 50 mL water samples in 125 mL Teflon separatory funnels were added 1 mL of a freshly prepared 10% ammonium molybdate solution and 1 mL 1:5 H_2SO_4:H_2O to produce a pH of 1.2–1.4. After 20 min, any isopoly acids, molybdosphosphoric acid (MPA), and molybdoarsenic acid (MAA) present were destroyed by the addition of 20 mL of 1:1 H_2SO_4 and the MSA extracted with 2 mL MIBK. The

[1]To whom all correspondence should be addressed.

organic phase was washed once with 10 mL 1:5 H_2SO_4 and transferred to a polyvial. The vial was doubly sealed before irradiation in the SLOWPOKE II research reactor; irradiation (t_i), decay (t_d), and counting times (t_c) were 30 min, 1 min, and 30 min, respectively, at a neutron flux of 5×10^{11} n cm^{-1} s^{-1}. Quantitation was achieved by reference to an analytical curve prepared from data obtained for 0−1 μg Si added to 50 mL of ultrapure water. Sea water standards (Wako Pure Chemicals) were analyzed by using a 1 mL aliquot with 50 mL of ultrapure water. The amount of sulfuric acid needed to give the proper pH was determined in a separate experiment.

Interference study

Chemicals present in natural and industrial waters were examined for interferences on the production of MSA, for silicate content and for complexation/extraction of molybdate. The chemicals studied were ferric ammonium sulfate (McArthur Chem. Co. reagent grade), sodium chloride (BDH ACS grade), citric acid (Fisher ACS), tartaric acid (Eastman), oxalic acid (Fisher ACS), tannic acid (J. T. Baker), humic acid (Aldrich), ammonium fluoride (Analar AR grade), ammonium phosphate monobasic (B & A), phosphorous and arsenic AA standards 1000 ppm (Aldrich), sodium arsenate (Analar AR grade), and germanium dioxide (Fisher 99.99%), the latter fused as for silicon dioxide.

Possible interferences were studied under three separate reaction conditions: (*A*) molybdate was added to test ion solutions after the addition of 20 mL 1:1 H_2SO_4; (*B*) all reagents were reacted at pH 1.4 without a silicate standard; (*C*) same as (*B*) but with a silicate standard. Ions were studied further by using ^{76}As and ^{32}P labelled salts in similar experiments. The organic phases were counted for β^- emissions using a Triton X-100 cocktail (15). Equal activities of ^{76}As and ^{32}P were added directly to the cocktail and counted as a reference. Labelled salts were prepared by irradiation of ammonium arsenate and ammonium phosphate in the SLOWPOKE II reactor.

Results and discussion

The sensitivity of the method was 85.7 ± 2.1 counts per nanogram of silicon; the blank value was 1800 ± 550 counts as calculated using a least-squares analysis on 26 data points over the range 0−1 μg of silicon added. The data were obtained using two separate silicon standards and four separate molybdate preparations over a period of four days. The standard deviations listed, therefore, represent the sum of all weighing, measuring, and counting variances with the latter making the largest contribution. The blank value, equivalent to 20 ng Si, represents reactive silicon contamination in molybdate sources since the blank increased with molybdate concentration. There was also a contamination by unreactive forms of silicate since the blank value tripled when a one week old solution of molybdate was used; the blank value for Aldrich Gold Label ammonium molybdate was similar to that for the cheaper Fisher certified reagent.

The detection limit was defined as twice the standard deviation of the blank (13 ng Si). Thus for a 50 mL aliquot, the detection limit was 0.2 ng mL^{-1} (or 0.007 μg-at L^{-1} in the units used by oceanographers where 1 μg-at = 1 μmol). This detection limit is comparable to that of the most recent papers published (8, 16) and is significantly lower than a reported radioreagent method (12). The proposed method has the advantage over the latter in that one does not handle radioactive solutions, and irradiated samples can be disposed of safely without a long waiting period.

The upper limit was taken to be 1000 ng (20 ng mL^{-1}) above which the 307 keV photopeak broadened and accuracy decreased. The unsymmetrical broadening was a function of the redrifted detector and the counting system available. This upper limit can be extended by dilution of the sample with ultrapure water. Reducing the sample size, increasing the volume of MIBK used for extraction, reducing irradiation and count times or placing the sample farther from the detector also increases the upper limit but a new analytical curve must be prepared for these conditions.

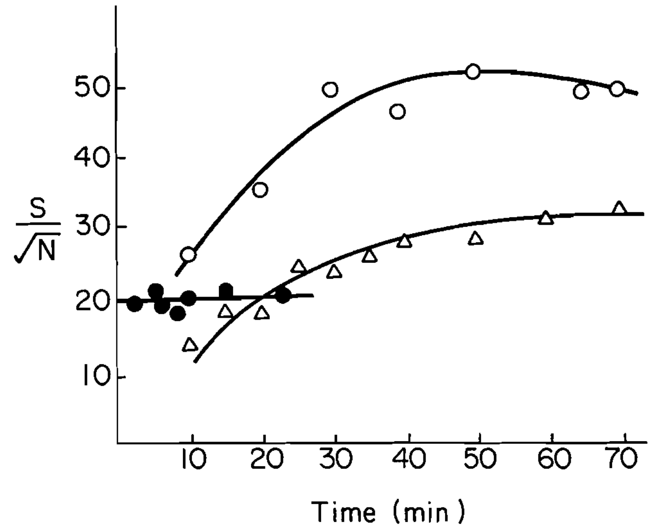

FIG. 1. Optimization curves obtained by plotting the signal to square root of noise ratio ($S/\sqrt{N}$) vs. time. ○ t_d, t_c = 1 m, 30 m, time = irradiation time; △ t_i, t_d = 15 m, 1 m, time = counting time; ● t_c = t_c = 15 m, time = decay time. N = background reading.

Figure 1 shows the data for optimizing irradiation, decay, and counting times. This was necessary because of the Compton background at 307 keV due to ^{41}Ar and ^{38}Cl; argon was present in the vial headspace and dissolved in MIBK while chlorine was present as a contaminant in the irradiation vials. The major contribution was ^{38}Cl and removal of ^{41}Ar by flushing with nitrogen was not particularly advantageous. Short variations in decay time had little affect on $S/\sqrt{N}$; this reached a maximum at an irradiation time of 30 minutes. The greatest increase in $S/\sqrt{N}$ vs. counting time is over the time interval of 0−30 min. At more than 30 min count time, little rise in $S/\sqrt{N}$ is observed. Time economy and a detectable reagent blank lead to the optimum conditions $t_i = t_c = 30$ m and $t_d = 1$ m.

Table 1 shows the results of possible interferences. Under condition *A*, heteropoly acids do not form at the acidity used. Therefore, an apparent signal indicates that a molybdenum complex, other than a heteropoly acid, was extracted. This was observed for tannic acid and high concentrations of fluoride and chloride. The positive interference of tannic acid was eliminated with dichromate. Interference by fluoride can be neglected for natural water samples since such high concentrations are not observed in nature. The interference from chloride was linear and was equivalent to 42.6 ng Si/1% NaCl. This value was used as a correction for the molybdenum chloride interaction in seawater analysis.

Reaction under condition *B* (pH 1.4) yields heteropoly acids including any MSA formed from silicate present in the salts used. All chemicals tested showed silicate contamination. Molybdogermanic acid is stable under the conditions used, but effects from germanium can normally be neglected due to its very low occurrence (17). The evidence under condition *B* was not, *on its own*, sufficiently conclusive to say that the data for phosphate and arsenate were the consequence of silicate but the

TABLE 1. Effects of possible interferences under conditions *A*, *B*, and *C**

Test species or ions	Concentration in μg/50 mL	Conditions (μg Si equivalent) A	B	C	μg Si taken	μg Si found
Citric acid	5000	<0.01	0.09	0.22	0.12	0.13
Oxalic acid	5000	—	0.08	0.21	0.12	0.13
Tartaric acid	5000	<0.01	0.09	0.20	0.12	0.11
Tannic acid	5000	0.20	—	—	—	—
As as arsenate	10 (Aldrich)	<0.01	0.15	0.27	0.12	0.12
As as arsenate	135 (Analar)	<0.01	0.06	0.16	0.08	0.10
P as phosphate	100 (Aldrich)	<0.01	0.62	0.70	0.08	0.08
P as phosphate	200 (*B* and *A*)	<0.01	0.08	0.19	0.12	0.11
Fe as ferric ion	6500	<0.01	0.05	0.14	0.08	0.09
Ge as germinate	0.26	—	0.11	0.19	0.08	0.08
Dichromate ion	215	<0.01	0.13	1.2	1.2	1.1
Sodium chloride	3.05%	0.13	0.23	0.39	0.12	0.16
	<0.31%	<0.01				
Tannic acid	5000	<0.01	0.29	0.42	0.12	0.13
Dichromate ion	215					
Hummic acid	5000	<0.01	0.18	0.31	0.12	0.13
Dichromate ion	215					
Tannic acid	5000					
P as phosphate	400	<0.01	0.42	1.7	1.2	1.3
Dichromate ion	215					
Tannic acid	5000					
As as arsenate	135	—	0.30	1.18	0.83	0.88
Dichromate ion	215					

*Reaction conditions *A*, pH ≪1 (MSA cannot form); *B*, pH = 1.4; *C*, pH = 1.4 with Si standard addition.

TABLE 2. Results from tracer studies using ^{32}P and ^{76}As reacted and extracted to separate MSA*

μg taken	Observed activity of nuclide taken	Observed activity of nuclide found	% extracted
65 μg P	1.5×10^5 cpm	<10 cpm	<0.0007%
40 μg As	3.6×10^5 cpm	120 cpm	0.03%

*Irradiated salts decayed for 2 days to eliminate ^{31}Si.

TABLE 3. Data for analysis of silicon standards with the results of two determinations

ng Si mL^{-1} taken	ng Si mL^{-1} found	σ
12.3	12.2	0.4
9.8	10.4	0.3
7.4	7.4	0.3
4.9	4.8	0.3
2.5	2.4	0.3
1.9	1.8	0.3
1.2	1.4	0.3
0.6	0.8	0.3
0.2	0.4	0.3
0.1	<0.2	0.3

results from two different sources of these ions show that there must be varying amounts of silicate present. Table 2 shows, when ^{32}P and ^{76}As are used as tracers, that <0.007% of phosphate and 0.03% arsenate are extracted and proves that the results obtained under conditions *B* for these ions must be the result of silicate contamination.

Chemicals contain silicon in both reactive and unreactive forms. The blank increased for solutions of molybdate on standing and higher values were observed for old solutions of test ions.

Low-level silicate contamination is deleterious especially when reagents contribute the same amount or more than samples. The accuracy of determinations in the interference study was therefore reduced as can be seen by comparison of values for conditions *B* and *C*; the quantity of silicon found was, of course, the difference.

Table 3 shows the accuracy of the method for the determination of silicon in standard water samples prepared in this laboratory. The lowest value (0.1 ng mL^{-1}) was below the detection limit ($2\sigma_b$, b = blank value) and at about the detection limit (0.2 ng mL^{-1}) a large error was observed and expected since meaningful data cannot be achieved below the quantitation limit ($4\sigma_b$, or 0.4 ng mL^{-1}).

Table 4 shows the applicability of the procedure to seawater analysis. The data are the mean of three replicate determinations. Values were consistently high indicating that the silicate content of the salts used in standard preparation may have been neglected by the manufacturer. The neglect of silicate contamination of salts used in preparing an analytical curve for seawater analysis has the net effect of producing slightly lower results for real samples. The methodology used here eliminates this problem.

Deionized water (Fisher high purity column), distilled water (Corning borosilicate still), and tap water were analyzed giving silicon concentrations of 1.1 ng mL^{-1}, 4.6 ng mL^{-1}, and 1.2 μg mL^{-1}, respectively. Unfortunately no standard reference ma-

TABLE 4. Analysis of sea water standards (Wako Pure Chemicals)

[Si] μg-at L^{-1}	mL used for analysis	[Si] found μg-at L^{-1}
0	50	0.29±0.07
5	1	5.25±0.32
10	1	10.2±0.6
25	1	25.4±0.8

terials were available for further testing.

The $^{101}Mo-^{101}Tc$ decay scheme was chosen over the $^{99}Mo-^{99m}Tc$ parent daughter relationship because the latter necessitates long irradiations and, therefore, the use of dry samples. Attempts to dry organic phases resulted in solvent creep and irregular deposition of the analyte on vial walls. Use of short-lived species permitted a much shorter analysis time. In addition the reagent blank determined the detection limit, not the ability to detect molybdenum and there was no advantage in using the more sensitive, but longer lived $^{99}Mo-^{99m}Tc$ parent daughter relationship.

Conclusions

The method described is applicable to water with extremely low silicon content (20−0.2 ng mL^{-1}), and is not affected by large amounts of tannic acid, arsenate, phosphate, and ferric ions or combinations of these. It is advantageous for colored samples and can determine silicate in reagent salts. Samples can be stored for long periods of time once encapsulated, since the NAA experiment does not depend on subsequent speciation changes. The detection limit could be lowered if methods of purifying molybdate sources improve.

The low operating temperature of the SLOWPOKE II reactor permits irradiation of liquids for periods up to 3 h so that samples need not be dried and short analysis times are possible.

Acknowledgements

Phillip Oltmann wishes to thank the Natural Sciences and Engineering Research Council of Canada for a post-graduate scholarship. This work was supported by a grant from the Natural Sciences and Engineering Research Council of Canada.

1. J. P. RILEY and G. SKIRROW (*Editors*). Chemical oceanography. Vol. 1. Academic Press, New York. 1965.
2. G. L. KRAUSSE, C. L. SCHELSKE, and C. O. DAVIS. Freshwater Biol. **13**, 73 (1983).
3. K. SCHWARZ. Trace element metabolism in animals -2. University Park Press, Baltimore. 1973. pp. 355−380.
4. G. BENDZ and I. LINGVIST (*Editors*). Biochemistry of silicon and related problems. Plenum Press, New York. 1978.
5. L. R. MORRISON and R. L. WILSON. Analyst, **88**, 88 (1963).
6. J. A. RAWA and E. L. HENN. Anal. Chem. **51**, 452 (1979).
7. P. VALENTA and H. W. NURNBERG. Anal. Lett. **14**, (A12), 921 (1981).
8. K. YOSHIMURA, M. MOTOMURA, T. TARUTANI, and T. SHIMONO. Anal. Chem. **56**, 2342 (1984).
9. J. THOMSEN, K. S. JOHNSON, and R. L. PETTY. Anal. Chem. **55**, 2378 (1983).
10. A. BAZZI and D. F. BOLTZ. Anal. Lett. **9**, 1111 (1976).
11. K. OHASHI, H. KAWAGUCHI, and K. YAMAMOTO. Anal. Chim. Acta, **111**, 301 (1979).
12. N. D. THAKER and D. N. PATKAR. Radiochem. Radioanal. Lett. **53**, 161 (1982).
13. V. W. TRUESDALE and C. J. SMITH. Analyst, **100**, 203 (1975).
14. A. C. BARBOSA and F. A. TOURINKO. Anal. Lett. **17**, (A10), 957 (1984).
15. H. BEM, J. HOLZBECHER, and D. E. RYAN. Anal. Chim. Acta, **152**, 247 (1983).
16. T. OKADA and T. KUWAMOTO. Anal. Chem. **57**, 258 (1985).
17. M. O. ANDREAE. Trace metals in sea water. Plenum Press, New York. 1981. p. 14.

The synthesis of 5-hydroxy chromenes[1]

J. W. ApSimon[2] and L. W. Herman

Ottawa–Carleton Institute for Graduate Studies and Research in Chemistry, Carleton Campus, Ottawa, Ont., Canada K1S 5B6

and

C. Huber

Division of Biological Sciences, National Research Council of Canada, Ottawa, Ont., Canada K1A 0R6

Received October 2, 1984

J. W. ApSimon, L. W. Herman, and C. Huber. Can. J. Chem. **63**, 2589 (1985).

The synthesis of 2,2-dimethyl-5-hydroxychromene (**1***d*) is described. The synthesis of the analogous 5,7-dihydroxy derivatives, using similar conditions, yields the adduct **9** derived via a Bucherer type reaction. X-ray analysis of **9** demonstrated that a pyrrolidine group was in the 7-position, and that the 5-hydroxyl group was involved in a strong intramolecular hydrogen bond to the 4-keto oxygen atom.

J. W. ApSimon, L. W. Herman et C. Huber. Can. J. Chem. **63**, 2589 (1985).

On décrit une synthèse du diméthyl-2,2 hydroxy-5 chromène (**1***d*). Une synthèse des dérivés dihydroxy-5,7 analogues qui fait appel à des conditions semblables ne conduit qu'à l'adduit **9** qui provient d'une réaction du type de Bucherer. Par diffraction des rayons-X on peut démontrer que, dans le composé **9**, le groupement pyrrolidine est en position 7 et que le groupement hydroxyle en position 5 est impliqué dans une forte liaison hydrogène intramoléculaire qui le lie à l'atome d'oxygène de la cétone en position 4.

[Traduit par le journal]

Introduction

In 1976, Bowers *et al.* (1) isolated two compounds from the plant *Ageratum houstanianum* which caused precocious metamorphosis, prevented ovarian development, and induced diapause in locusts and certain beetles. These natural anti-juvenile hormones, now known as Precocene I (**1***a*) and II (**1***b*),

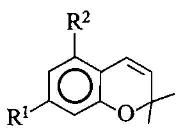

1*a* R^1 = OMe, R^2 = H
1*b* R^1 = R^2 = OMe
1*c* R^1 = R^2 = H
1*d* R^1 = H, R^2 = OH
1*e* R^1 = OTs, R^2 = H
1*f* R^1 = H, R^2 = OBn
1*g* R^1 = H, R^2 = OPhenacyl

were already named 6-demethoxy ageratochromene (2) and ageratochromene (3) by the groups who first characterized them. This family of compounds shows great promise as a new generation of insecticides: while they are deadly to the insect targets, they are non-toxic to mammals probably because of their mechanism of action, which is believed (4–7) to require in vivo activation to a reactive epoxide which easily alkylates nucleophiles (7, 8), a route that is probably responsible for the destruction of the *corpora allata*, the insect organ responsible for juvenile hormone production.

The synthesis of 2,2-dimethyl chromenes (**1***c*) may be approached either by the preparation of another related ring system with subsequent variation of functionality, or by alkylation of a free phenol followed by cyclization onto the aromatic ring. Among the former approaches, the earliest was the alkylation of a coumarin with a Grignard reagent (9). In 1962, Iwai and Ide (10) first reported the synthesis of chromenes from the Claisen rearrangement of propargyl aryl ethers, an approach later used by Hlubecek *et al.* (11) who synthesized Precocenes I and II by the O-alkylation of 3-methoxy or 3,4-dimethoxy phenol with 3-chloro-3-methyl-1-butyne, followed by cyclization in *N,N*-diethylaniline.

Chromenes may also be obtained via the corresponding chroman by dehydrogenation with DDQ (12–14, 16, 17) or halogenation–dehydrohalogenation (16). Prenylated aromatic compounds may be formed under acidic conditions, with 2-methylbut-3-en-2-ol in the presence of BF_3 etherate (16), or under basic conditions with n-BuLi and dimethallyl bromide (17). Camps *et al.* (18) used $Ni(AcAc)_2$ as a catalyst to condense phenols with 1,3-dichloro-3-methylbutane to give the chroman system. Alternatively, *ortho* prenylated phenols may be directly cyclized to chromenes using potassium dichromate in benzene in the presence of Adogen 464 ("orange benzene") (19), DDQ in ether (19), or *N*-iodosuccinimide (20).

Sartori *et al.* (21) reacted metal phenolates with α,β-unsaturated aldehydes in toluene and obtained good yields of chromenes. Titanium, magnesium, tin, and aluminum phenolates were all found to be reactive, but highly coordinating solvents (e.g. DMF, glyme, HMPA, TMEDA) caused the reaction to fail. Crombie and co-workers (22) used a masked enone synthon, 3-hydroxy-3-methyl-1,1-dimethoxybutane, to give chromenes directly from phenols. This method was used primarily on aromatic compounds with an acetyl group *para* to the free phenol.

Another straightforward route to 2,2-dimethyl chromenes is via the corresponding chromanone derivative, followed by hydride reduction and dehydration. Chromanones are formed by the condensation of a phenol with 3,3-dimethyl acrylic acid in the presence of an acid catalyst such as HF (23), zinc chloride – phosphoryl chloride (24), polyphosphoric acid (25), BF_3 etherate (26), or methanesulphonic acid (27) (which is now the reagent of choice). Alternately, pyrrolidine catalysed condensation of an *ortho*-hydroxy acetophenone with ketones also affords chromanones in high yields (28).

In a series of studies, various chromenes related to naturally occurring compounds possessing insecticidal activity were synthesized in an attempt to discover materials of greater biological activity.

[1] Taken in part from the M.Sc. thesis of L. Herman, January 1982, Carleton University, Ottawa.

[2] Author to whom correspondence may be addressed.

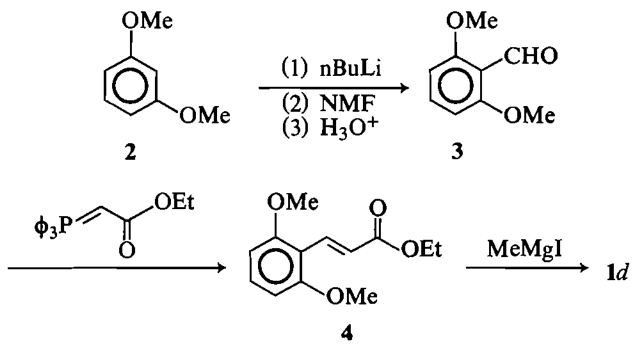

SCHEME 1

Results and discussion

Based on a report by Mechoulam and Gaoni (29) that a cannabinoid precursor was demethylated and alkylated to the corresponding phenoxy pyran, the synthesis outlined in Scheme 1 was performed. Aromatic formylation may occur in higher yields by using DMF in place of *N*-methyl formanilide. Reaction of aldehyde **3** with the stable Wittig reagent methylenecarboethoxytriphenylphosphorane occurred cleanly in high yield (85%), but the one-pot Grignard fusion methylation–dealkylation gave only ~30% of the desired product, **1***d*, along with a large amount of polymeric material.

An alternate route was followed when the synthesis of the 7-OH isomer of the desired chromene was attempted. Formation of chromanone **5***a* was achieved by the condensation of resorcinol and 3,3-dimethyl acrylic acid in the presence of $POCl_3/ZnCl_2$ (24) and, upon isolation, pure crystalline **5***a* was obtained in 67% yield. Protection of the free phenol as the *p*-toluene sulphonate followed by reduction of the carbonyl provided the desired alcohol **6***a* in 75% yield (some cleavage

5*a* R' = OH, R² = H
5*b* R' = H, R² = OH
5*c* R' = H, R² = OBn
5*d* R' = R² = OH
5*e* R' = OTs, R² = H
5*f* R' = H, R² = OTs
5*g* R' = H, R² = OAc

6*a* R' = OTs, R² = H
6*b* R' = H, R² = OBn
6*c* R' = H, R² = OH
6*d* R' = H, R² = OPhenacyl

of the tosyl group was observed). Dehydration of this alcohol using toluene sulphonic acid in refluxing toluene was quantitative; however, deprotection of the phenol with KOH/MeOH met with unexpected failure when only polymeric material was isolated. Photochemical cleavage was also ineffective. The lability of **1***e* to base, along with the total stability of **6***a* to TsOH, is unusual considering the reported compatibility of chromenes with base (15, 23) and their reactivity with respect to acids (30–32).

Several simple syntheses were next attempted in the absence of a phenol protecting group. Chroman **7***a* was synthesized as reported (15); however, treatment with DDQ gave only intractable tars. Crombie's 3-hydroxy-3-methyl-butanal dimethyl acetal (22), which reacts with some phenols to give hydroxychromenes, did not react with resorcinol.

In order to synthesize 5-OH chromanones in a regiospecific way, the method developed by Kabbe (28) was employed.

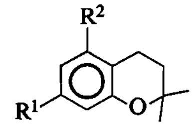

7*a* R' = OH, R² = H
7*b* R' = H, R² = OH

2,6-Dihydroxyacetophenone, synthesized via the appropriately substituted coumarin (33), was condensed with acetone, giving chromanone **5***b* in 75% yield. Because of the strong chelating effect shown by *ortho*-hydroxy aromatic ketones, the phenol could not be acylated under standard conditions (e.g. K_2CO_3/acetone/TsCl). Using conditions of anhydrous phase transfer catalysis (34), however, the *p*-toluene sulphonate and acetate esters could be formed, but reduction of these esters with a variety of hydride reagents resulted only in cleavage of the esters or re-isolation of starting materials. Chromanone **5***b* was benzylated using benzyl bromide/K_2CO_3/acetone and reduction of **5***c* with $NaBH_4$ occurred readily (30), as did the subsequent dehydration with TsOH. Unfortunately, the benzylated chromene **1***f* was not a suitable synthetic intermediate. Catalytic hydrogenation with absorption of one equivalent of hydrogen yielded only the deprotected chroman **7***b* and unreacted starting material. Subsequent attempts at dealkylation using a wide variety of reagents noted for their mildness all failed (35–39), yielding only intractable tars.

The phenacyl group (40) proved to be suitable protecting group for the desired synthesis. Reaction of chromanone **5***b* with 2-bromoacetophenone in K_2CO_3/acetone or under phase transfer conditions both failed but, after reduction of **5***b* with LAH, the corresponding chromanol **6***c* was O-alkylated with phenacyl bromide only at the phenolic site (**6***d*). This was then dehydrated with TsOH to give **1***g*, and the deprotection of the phenol effected with Zn in acetic acid. In this manner chromene **1***d* was isolated in high yield with no evidence of polymerization.

While the dehydration of unprotected chromanol **6***c* with TsOH gives only tarry material, reaction with Zn/AcOH gives the 5-OH chroman **7***b* in 67% yield.

The synthesis of 5,7-dihydroxychromenes was next investigated. Although 5,7-dihydroxy chromanones are readily available (26) by the condensation of phloroglucinol and 3,3-dimethylacrylic acid in BF_3 etherate, the applicability of the pyrrolidine catalysed route was examined.

Phloroglucinol was acetylated in good yield with acetonitrile in the presence of HCl and $ZnCl_2$ (41). Treatment of phloroacetophenone (**8**) with pyrrolidine and acetone resulted in a product **9**. This adduct probably arises as a result of initial substitution of a phenolic hydroxyl by pyrrolidine (as in the classical Bucherer reaction (42)), followed by cyclization. This was demonstrated by the sequential reaction of **8** with pyrrolidine, giving adduct **10**, followed by treatment with pyrrolidine/acetone to give chromanone **9**. Chromanone **5***d*, synthesized by another route (27), does not react with pyrrolidine in a Bucherer sense.

X-ray structural analysis was performed on a sample of **9**. Final fractional coordinates for the non-hydrogen atoms are listed in Table 1, and thermal vibration parameters have been deposited.[3] A perspective view of the molecule is shown in Fig.

[3]Tables of observed and calculated structural factors, of final parameters for the hydrogen atoms, of anisotropic thermal vibration parameters for the non-hydrogen atoms, and of bond lengths and bond angles involving hydrogen atoms may be purchased from the Depository of Unpublished Data, CISTI, National Research Council of Canada, Ottawa, Ont., Canada K1A 0S2.

TABLE 1. Fractional coordinates ($\times 10^4$) and equivalent isotropic temperature factors (Å^2) for the non-hydrogen atoms

Atom	x	y	z	B_{eq}
O(1)	3552(2)	801(3)	474(1)	4.4
O(2)	3080(2)	2635(4)	2396(1)	6.2
O(3)	1857(2)	5821(4)	1792(1)	5.6
N(1)	1247(2)	6546(4)	−685(1)	4.3
C(2)	4467(2)	147(5)	1112(1)	4.6
C(3)	3882(3)	104(5)	1728(1)	5.1
C(4)	3221(3)	2074(5)	1810(1)	4.7
C(5)	2734(2)	3253(5)	1178(1)	4.1
C(6)	2027(2)	5087(5)	1174(1)	4.3
C(7)	1520(2)	6159(5)	567(1)	4.3
C(8)	1701(2)	5452(4)	−84(1)	4.0
C(9)	2390(2)	3605(4)	−89(1)	3.9
C(10)	2898(2)	2563(4)	524(1)	3.8
C(11)	4860(3)	−2004(5)	940(2)	5.6
C(12)	5531(3)	1694(6)	1236(2)	5.8
C(13)	624(3)	8553(5)	−704(2)	5.2
C(14)	564(5)	9348(7)	−1440(2)	8.6
C(15)	625(4)	7525(7)	−1871(2)	7.6
C(16)	1321(3)	5872(5)	−1385(1)	5.0

$$B_{eq} = \frac{8}{3}\pi^2 \sum_i \sum_j U_{ij} a_i^* a_j^* \mathbf{a}_i \cdot \mathbf{a}_j.$$

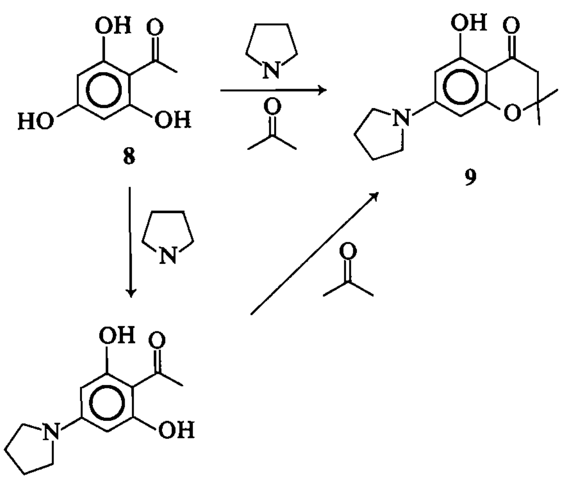

1, and the crystallographic numbering scheme and bond lengths are given in Fig. 2. The C—H bond lengths, which are not shown, vary from 0.90 to 0.99 Å, with a mean value of 0.95 Å. Bond angles are presented in Fig. 3.

With the exception of the C(12) atom, representing an axial methyl group, all the non-hydrogen atoms in the molecule are within 0.5 Å of planarity, but there are statistically significant deviations from each of the constituent mean planes mentioned below. The pyrrolidine ring has an envelope conformation with the C(14) atom displaced 0.395(6) Å from the mean plane through the other four atoms. This plane makes an angle of 6.57° with the mean plane through the benzopyrone system. The aromatic ring is nearly planar, with maximum deviations of 0.008(3) Å, while the dihydropyran ring is in the 1,2-diplanar conformation, with C(2) displaced by 0.606(3) Å from the mean plane through the other five atoms. Endocyclic torsional angles are listed in Table 2.

The bond lengths and angles in the benzopyrone moiety are generally similar to the equivalent values in 3-bromo-2,3-di-

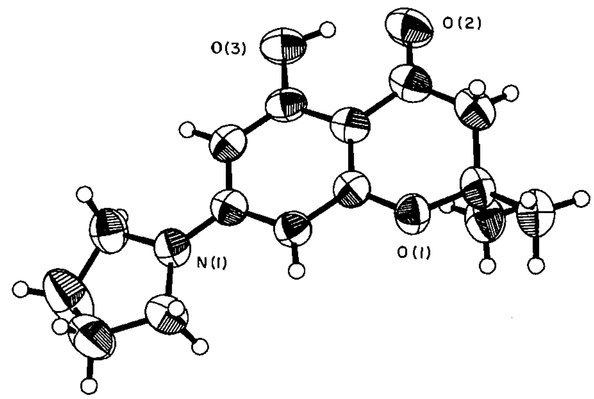

FIG. 1. A perspective view of the molecule. The thermal ellipsoids enclose 50% probability, while hydrogen atoms are shown as arbitrarily small spheres.

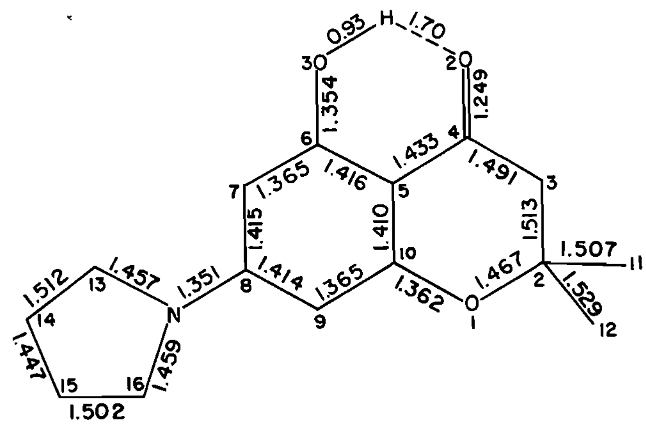

FIG. 2. Crystallographic numbering scheme and bond lengths (Å). The estimated standard deivations are 0.003–0.006 Å.

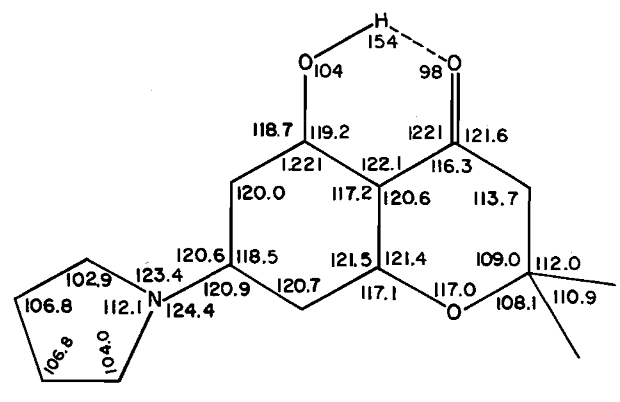

FIG. 3. Bond angles (°). The estimated standard deviations are 0.2–0.4°.

hydro-2-phenyl-4*H*-benzopyran-4-one (43), 4′-bromoflavanone (44), and (−)-2*R*-(2,3-dihydro-2*R*-isopropyl-4-oxo-4*H*-1-benzopyran-6-yl)-*N*-(1*R*-phenylethyl) propionamide (45), see Table 5. However, in the present structure the C(4)=O(2) bond is longer and the adjacent C(4)—C(5) bond is shorter than the equivalent bonds in the other structures. The aromatic ring here shows pronounced quinonoid character, with C(6)—C(7) and C(9)—C(10) significantly shorter than the other four bonds and C(6)—C(5)—C(10) and C(7)—C(8)—C(9) smaller than the other four endocyclic angles. The C(8)—N(1) bond also appears to be shorter than

TABLE 2. Endocyclic torsional angles

Bond	Angle (°)
(A) *Pyrone ring*	
O(1)—C(2)—C(3)—C(4)	−51.1(3)
C(2)—C(3)—C(4)—C(5)	28.1(4)
C(3)—C(4)—C(5)—C(10)	−0.7(4)
C(4)—C(5)—C(10)—O(1)	−2.0(4)
C(5)—C(10)—O(1)—C(2)	−24.3(4)
C(10)—O(1)—C(2)—C(3)	49.9(3)
(B) *Aromatic ring*	
C(5)—C(6)—C(7)—C(8)	−0.4(4)
C(6)—C(7)—C(8)—C(9)	1.4(4)
C(7)—C(8)—C(9)—C(10)	−1.9(4)
C(8)—C(9)—C(10)—C(5)	1.5(4)
C(9)—C(10)—C(5)—C(6)	−0.5(4)
C(10)—C(5)—C(6)—C(7)	−0.1(4)
(C) *Pyrrolidine ring*	
N(1)—C(13)—C(14)—C(15)	24.6(4)
C(13)—C(14)—C(15)—C(16)	−27.7(5)
C(14)—C(15)—C(16)—N(1)	19.4(4)
C(15)—C(16)—N(1)—C(13)	−3.6(3)
C(16)—N(1)—C(13)—C(14)	−12.6(4)

expected for a C_{sp^2}—N_{sp^2} single bond. These observations suggest that some electron polarization is occurring as indicated in **11**, an effect which would be favoured by the strong intramolecular hydrogen bond.

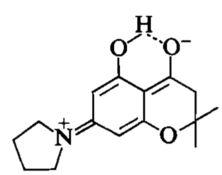

11

The C(14)—C(15) bond in the pyrrolidine group (1.447(4) Å) is very much shortened from the usual single bond length. Such an effect has been observed before in other structures; in sodium 1-pyrrolidine carbodithioate (SPCT) (46), the shortening (to 1.419 Å) is more extreme even at 150 K, while in the structure of sulpiride (47), the equivalent bond is shortened only to 1.483(10) Å. In the present structure the C(14) and C(15) atoms both have very large thermal vibration parameters, indicating that there may be some time-averaged conformational reorientation here, as in SPCT (46).

There are no intermolecular distances shorter than normal van der Waals contacts.

Experimental

Melting points were determined on a Fisher melting point block or a Mettler FP1 melting point apparatus; all melting points are expressed in degrees Celsius, and are uncorrected. The ^{1}H nmr spectra were obtained on Varian EM-360A or Varian T-60A 60-MHz spectrometers using $CDCl_3$ as solvent and tetramethylsilane (TMS) as the internal standard; shifts are expressed in the δ scale and the following abbreviations used: s, singlet; d, doublet; t, triplet; q, quartet; m, multiplet. Infrared (ir) spectra were obtained on a Perkin–Elmer 237B grating spectrophotometer using polystyrene film as a standard; absorbances are expressed in units of cm^{-1}. Mass spectra were determined with an A.E.I. M.S. 12 instrument at Trent University; values are expressed as *m/e* (relative intensity). Combustion analyses were performed by Canadian Microanalytic Laboratories at Guelph, Ontario.

Thin layer chromatographic plates were obtained from E. Merck Reagents (silica gel F-254, 0.25 mm layer thickness); preparative thick layer chromatography was performed on similar plates but with a 2-mm layer of silica gel. Products were detected by viewing under an uv source, or by spraying the plate with 1% ceric ammonium nitrate in 50% aqueous sulphuric acid followed by gentle heating. All ethereal reaction solvents (except for diethyl ether) were dried by refluxing over Na in the presence of benzophenone until a dark blue colour persisted, and then distilled. Anhydrous diethyl ether was purchased from Mallinckrodt and used directly. Spectral grade solvents were used for all other reactions where dryness was not critical.

Carbon-13 spectra were taken on a Bruker WP-80 spectrometer at the National Research Council of Canada, Ottawa, Ontario, or on a Varian CFT-20 at the University of Ottawa, Ottawa, Ontario.

Ethyl-2,6-dimethoxy-cinnamate (4) from 3

Based on a method by Mali and Yadev (48), aldehyde **3** (0.70 g, 4.4 mmol) (49) and methylenecarboethoxytriphenylphosphorane (2.3 g, 6.6 mmol) (50) were refluxed for 1 day in toluene (15 mL) under Ar. The mixture was cooled, washed with two 10-mL portions of 2 *M* HCl, passed through Florisil, and eluted with CH_2Cl_2 (75 mL). Removal of the solvent afforded 0.90 g (3.8 mmol) of cinnamate **4**, essentially pure by tlc (86% yield). The oil solidified upon standing, mp 78–80°C; ir: 1695 (α,β-unsaturated ester); nmr: 1.30 (t, 3H, J = 7 Hz, —OCH_2CH_3), 3.85 (s, 6H, —OCH_3), 4.27 (q, 2H, J = 7 Hz, —OCH_2CH_3), 6.53 (d, 2H, J = 7 Hz, H-3 and H-5), 6.87 (d, 1H, J = 16 Hz, —H), 7.25 (t, 1H, J = 7 Hz, H-4), 7.80 (d, 1H, J = 16 Hz, —H); ms: 236 (100), 205 (96), 191 (96), 177 (95), 161 (19), 148 (45), 133 (26), 105 (18), 91 (20), 77 (18). *Mol. Wt.* (high resolution ms) calcd. for $C_{13}H_{16}O_4$: 236.1098; found: 236.1073.

2,2-Dimethyl-4-keto-7-tosyloxy-benzopyran (5e) from 5d

Chromanone **5*a*** (9.7 g, 50 mmol) (38), K_2CO_3 (50 g), and *p*-toluene sulphonyl chloride (9.5 g, 50 mmol) were refluxed in acetone (100 mL) for 3 h. After cooling, the mixture was filtered and the solvent removed on a rotoevaporator. The residue was recrystallized from MeOH–H_2O, affording pure crystalline **5*e*** (14.9 g, 43 mmol, 86% yield), mp 79–80°C; ir: 1695 (C=O) cm^{-1}; nmr: 1.42 (s, 6H, C-2 *gem* dimethyls), 2.43 (s, 3H, tosyl CH_3), 2.70 (s, 2H, H-3), 6.70 (bs, 2H, H-6 and H-8), 7.35 (bd, 2H, J = 8 Hz, tosyl Ar-H's *ortho* to sulphone), 7.78 (bd, 3H, J = 8 Hz, tosyl Ar-H's *ortho* to methyl and H-5); ms: 347 (14), 346 (56), 332 (21), 331 (94), 291 (35), 155 (50), 91 (100), *m** 317.

2,2-Dimethyl-4-hydroxy-7-tosyloxy-benzopyran (6a) from 5e

To a suspension of $LiAlH_4$ (41.0 g, 10.8 mmol) in ether (50 mL) under argon at 0°C was added, dropwise, chromanone **5*e*** (5.0 g, 14.4 mmol) in dry ether (50 mL). After stirring for 4 h, the reaction was quenched with 20% (v/v) aqueous acetic acid (20 mL). The mixture was stirred until most of the solids had dissolved (about 1 h), ether (100 mL) added, and the mixture was filtered. The aqueous layer was removed, and the organic layer washed with two 100-mL portions of saturated aqueous $NaHCO_3$ solution. Evaporation followed by recrystallization from MeOH–H_2O gave 3.7 g (10.8 mmol, 75%) of pure crystalline **6*a***, mp 107°C; ir ($CHCl_3$): 3350 (phenolic OH) cm^{-1}; nmr: 1.30 (d, 6H, J = 7 Hz, C-2 *gem* dimethyls), 2.43 (s, 3H, tosyl CH_3), 4.80 (d of d, 1H, J = 6.8 Hz, H-4), 6.53 (s, 1H, H-8), 6.58 (d, 1H, J = 4 Hz, H-6), 7.36 (bd, 3H, J = 6 Hz, tosyl Ar-H's *ortho* to sulphone, H-5), 7.76 (d, 2H, J = 8 Hz, tosyl Ar-H's *ortho* to methyl); ms: 348 (52), 315 (35), 293 (36), 155 (100), 91 (87). *Mol. Wt.* (high resolution ms) calcd. for $C_{18}H_{20}O_5S$: 348.1058; found: 348.1044.

Δ^3-2,2-Dimethyl-7-tosyloxy-benzopyran (1e) from 6a

Chromanol **6*a*** (1.00 g, 2.86 mmol) and *p*-toluene sulphonic acid (20 mg) were refluxed in toluene (50 mL) for 15 min. The slightly pink solution was cooled, washed with saturated $NaHCO_3$ solution, the solvent removed, and the residue recrystallized from MeOH–H_2O. Chromene **1*e*** (0.90 g, 2.70 mmol, 94% yield) was obtained as light pink crystals, mp 102°C; nmr: 1.73 (s, 6H, C-2 *gem*-dimethyls), 2.80 (s, 3H, tosyl Ar-CH_3), 5.63 (d, 1H, J = 10 Hz, H-3), 6.40 (d, 1H,

J = 10 Hz, H-4), 6.55 (s, 1H, H-8), 6.62 (d, 1H, J = 4 Hz, H-6), 7.45 (bd, 2H, J = 6 Hz, tosyl Ar-H's *ortho* to sulphone), 7.90 (bd, 24, J = 6 Hz, tosyl Ar-H's *ortho* to methyl); ms: 330 (16), 315 (100), 160 (29), 132 (14), 91 (18); m^* 301. *Mol. Wt.* (high resolution ms) calcd. for $C_{18}H_{18}O_4S$: 330.0935; found: 330.0930.

*2,2-Dimethyl-5-hydroxy-4-keto-benzopyran (5*b*)*

Based on a procedure by Kabbe (28), 2,6-dihydroxy acetophenone (14.4 g, 98.6 mmol), pyrrolidine (12.2 g, 172 mmol), acetone (6.0 g, 103.5 mmol), and toluene (100 mL) were stirred for 4 days under Ar. The mixture was acidified with 2 *N* HCl (100 mL), the organic layer separated and washed with three 50-mL portions of saturated aqueous NaCl, and the solvent removed. The residue was dissolved in CH_2Cl_2 (50 mL), passed through Florisil, and eluted with CH_2Cl_2 (200 mL). After removal of the solvent, the residue was recrystallized from ethanol–water to give **5*b*** as yellow needles (14.0 g, 72.5 mmol, 74% yield), mp 66°C; ir: 3100 (b, w, hydrogen bonded OH), 1565 (hydrogen bonded C=O) cm^{-1}; nmr: 1.47 (s, 6H, C-2, *gem*-dimethyls), 2.75 (s, 2H, H-3), 6.43 (d, 1H, J = 8 Hz, H-6), 6.52 (d, 1H, J = 8 Hz, H-8), 7.40 (t, 1H, J = 8 Hz, H-7); ms: 192 (59), 177 (100), 137 (65), 136 (43), 108 (28). *Mol. Wt.* (high resolution ms) calcd. for $C_{11}H_{12}O_3$: 192.0840; found: 192.0813.

*2,2-Dimethyl-4-keto-5-tosyloxy-benzopyran (5*f*) from 5*b

Chromanone **5*f*** (1.0 g, 5.2 mmol), *p*-toluenesulphonyl chloride (1.1 g, 5.7 mmol), NaOH (1.0 g, 25 mmol), and TEBAC (0.13 g, 0.52 mmol) were stirred in CH_2Cl_2 (25 mL) under Ar for 6 h. The mixture was passed through Florisil, eluted with 100 mL CH_2Cl_2, the solvent removed, and the residue purified by column chromatography (silica gel) to give **5*f*** as a clear oil (1.3 g, 3.7 mmol, 72% yield); ir: 1700 (C=O) cm^{-1}; nmr: 1.33 (s, 6H, C-2 *gem* dimethyls), 2.40 (s, 3H, tosyl CH_3), 2.57 (s, 2H, H-3), 6.70–6.97 (m, 2H, H-6 and H-8), 7.33 (d, 2H, J = 8 Hz, tosyl Ar-H's *ortho* to sulphone), 7.85 (d, 2H, J = 8 Hz, tosyl Ar-H's *ortho* to methyl); ms: 346 (45), 331 (25), 291 (28), 155 (100), 91 (80). *Mol. Wt.* (high resolution ms) calcd. for $C_{18}H_{20}O_5S$: 346.0947; found: 346.0911.

*5-Acetoxy-2,2-dimethyl-4-keto-benzopyran (5*g*) from 5*b

Chromanone **5*b*** (0.10 g, 0.52 mmol), powdered NaOH (0.10 g, 2.5 mmol), and triethyl benzyl ammonium chloride (TEBAC) (0.025 g, 0.12 mmol) were stirred under Ar in dry CH_2Cl_2 (5 mL). Acetyl chloride (2 mL) was added dropwise by syringe and the mixture was stirred for 20 min. Dichloromethane (20 mL) was then added, and the mixture passed through Florisil and eluted with 50 mL CH_2Cl_2. The solvent was removed and the residue purified by thick layer chromatography to give **5*g*** (0.11 g, 0.47 mmol, 90% yield); ir: 1770 (acetate C=O), 1690 (C-4 C=O) cm^{-1}; nmr: 1.43 (s, 6H, C-2 *gem* dimethyls), 2.33 (s, 3H, acetate CH_3), 2.63 (s, 2H, H-3), 6.60 (d, 1H, J = 8 Hz, H-6), 6.83 (d, 1H, J = 8 Hz, H-8), 7.43 (t, 1H, J = 8 Hz, H-7); ms: 234 (17), 192 (72), 177 (100), 137 (57), 136 (39), 108 (27). *Mol. Wt.* (high resolution ms) calcd. for $C_{13}H_{14}O_4$: 234.0930; found: 234.0911.

*5-Benzyloxy-2,2-dimethyl-4-keto-benzopyran (5*c*) from 5*b

Chromanone **5*b*** (0.10 g, 0.52 mmol), benzyl bromide (0.10 g, 0.58 mmol), and K_2CO_3 (0.5 g) were refluxed in acetone (20 mL) for 3 days. The mixture was filtered, the solvent removed, and the residue taken up in 50 mL of ether. After washing with 2 *N* NaOH (30 mL) followed by H_2O (30 mL), the solvent was evaporated. Recrystallization from ether–hexane gave **5*c*** (0.12 g, 0.43 mmol, 83%) as white crystals, mp 128°C; ir: 1685 (C=O) cm^{-1}; nmr: 1.45 (s, 6H, C-2 *gem* dimethyls), 2.70 (s, 2H, H-3), 5.20 (s, 2H, benzylic CH_2), 6.55 (d, 2H, J = 8 Hz, H-6 and H-8), 7.20–7.73 (m, 6H, aromatic H); ms: 282 (11), 91 (100).

*5-Benzyloxy-2,2-dimethyl-4-hydroxy-benzopyran (6*b*) from 5*c

Chromanone **5*c*** (1.8 g, 6.3 mmol) in methanol (10 mL) was added dropwise to $NaBH_4$ (0.34 g, 9.2 mmol) in methanol (30 mL). After stirring overnight under Ar, the excess $NaBH_4$ was destroyed by careful dropwise addition of 2 *N* HCl (30 mL). The resulting solution was diluted with ether (100 mL) and water, and the organic layer separated and washed with a saturated sodium bicarbonate solution (2 × 50 mL). After removal of the solvent, the oily residue (1.7 g, 6.0 mmol, 95% yield) was found to be pure enough (by tlc) to proceed to the dehydration step. A small sample was purified by thick layer chromatography for analysis, confirming its identity as **6*b***; ir: 3450 (benzylic OH) cm^{-1}; nmr: 1.32 (s, 3H, C-2 methyl), 1.42 (s, 3H, C-2 methyl), 2.03 (d, 2H, J = 6 Hz, H-3), 3.37 (bs, 1H, C-4 OH), 5.10 (t, 1H, J = 6 Hz, H-4), 5.13 (s, 2H, benzyl CH_2), 6.57 (d, 2H, J = 7 Hz, H-6, and H-8), 7.30 (t, 1H, J = 7 Hz, H-7), 7.47 (s, 5H, benzyl Ar-H).

TABLE 3. Fractional coordinates ($\times 10^3$) and isotropic temperature factors (Å^2) for the hydrogen atoms

Atom	x	y	z	B_{iso}
H(3)	229(3)	488(6)	213(2)	7.9(9)
H(31)	329(2)	−104(5)	167(1)	4.7(6)
H(32)	445(3)	−11(6)	214(2)	6.5(8)
H(71)	105(2)	735(5)	57(1)	4.6(6)
H(91)	254(2)	312(4)	−49(1)	3.2(5)
H(111)	546(3)	−259(6)	133(2)	6.5(8)
H(112)	419(3)	−292(6)	79(2)	6.9(8)
H(113)	523(3)	−194(6)	53(2)	7.0(8)
H(121)	526(3)	313(5)	132(2)	6.7(8)
H(122)	587(3)	165(6)	86(2)	7.2(8)
H(123)	616(3)	121(5)	164(2)	6.0(7)
H(131)	−17	835	−63	5.8
H(132)	108	948	−34	6.0
H(141)	−15	1012	−162	9.2
H(142)	124	1021	−143	10.5
H(151)	100	780	−224	9.2
H(152)	−20	708	−209	10.4
H(161)	94	449	−150	6.6
H(162)	214	575	−141	5.8

*Δ^3-5-Benzyloxy-2,2-dimethyl-benzopyran (1*g*) from 6*b

Chromanol **6*b*** (1.6 g, 5.6 mmol) was dissolved in dry toluene (50 mL). The solution was brought to reflux under Ar, and *p*-toluene sulphonic acid (50 mg, 0.29 mmol) was added in one portion. After refluxing for 15 min, the solution was allowed to cool and washed with two 10-mL portions of 2 *N* NaOH, followed by one 50-mL portion of distilled water. The organic layer was passed through Florisil, eluted with CH_2Cl_2 (100 mL), and the solvent removed to give chromene **1*g*** (1.4 g, 5.2 mmol, 93%) as a slightly yellow oil, essentially pure by tlc. A small sample was purified further by thick layer chromatography; nmr: 1.47 (s, 6H, C-2 *gem* dimethyls), 5.13 (s, 2H, benzyl CH_2), 5.60 (d, 1H, J = 10 Hz, H-3), 6.53 (d, 1H, J = 8 Hz, H-8), 6.51 (d, 1H, J = 8 Hz, H-6), 6.82 (d, 1H, J = 10 Hz, H-4), 7.47 (s, 5Hz, benzyl Ar-H); ms: 266 (35), 251 (99), 160 (41), 91 (100), 65 (26). *Mol. Wt.* (high resolution ms) calcd. for $C_{18}H_{18}O_2$: 266.1347; found: 266.1327.

*5-Hydroxy-2,2-dimethyl-benzopyran (7*b*) from 1*g

Chromene **1*g*** (0.10 g, 0.37 mmol), Pd/C (0.1 g), and dry ethanol (5 mL) were stirred under a hydrogen atmosphere. When 8 mL of hydrogen were consumed, the reaction vessel was removed, the solution filtered, and the solvent removed. After separation by thick layer chromatography, 43 mg of starting material was recovered along with **7*b*** (32 mg, 0.18 mmol, 86% yield based on recovered starting material); ir: 3350 (b, phenolic O—H) cm^{-1}; nmr: 1.30 (s, 6H, C-2 *gem* dimethyls), 1.78 (t, 2H, J = 6 Hz, H-3), 2.67 (t, 2H, J = 6 Hz, H-4), 5.10 (bs, 1H, phenolic O—H), 6.33 (d, 1H, J = 8 Hz, H-6), 6.45 (d, 1H, J = 8 Hz, H-8), 7.00 (t, 1H, J = 8 Hz, H-7); ms: 178 (60), 163 (22), 123 (100), 94 (17). *Mol. Wt.* (high resolution ms) calcd. for $C_{11}H_{14}O_2$: 178.1028; found: 178.1011.

*4,5-Dihydroxy-2,2-dimethyl-benzopyran (6*c*) from 5*b

To a suspension of $LiAlH_4$ (0.1 g, 26.3 mmol) in anhydrous ether (50 mL) under Ar was added, dropwise, **5*b*** (504 mg, 2.23 mmol) in

TABLE 4. Anisotropic thermal parameters ($Å^2$) and their estimated standard deviations (all $\times 10^4$) for the non-hydrogen atoms

Atom	U_{11}	U_{22}	U_{33}	$2U_{23}$	$2U_{13}$	$2U_{12}$
O(1)	541(10)	562(11)	527(11)	−15(19)	119(17)	126(18)
O(2)	922(16)	965(17)	454(11)	−27(24)	292(21)	−73(28)
O(3)	832(14)	801(15)	545(11)	−229(23)	538(21)	8(24)
N(1)	578(13)	512(14)	519(13)	1(22)	205(21)	32(23)
C(2)	531(15)	566(17)	574(16)	185(29)	45(24)	3(28)
C(3)	660(18)	662(19)	559(16)	172(30)	108(28)	−147(32)
C(4)	584(16)	677(19)	476(15)	−50(29)	139(24)	−303(30)
C(5)	506(15)	569(17)	472(15)	−81(25)	210(23)	−208(27)
C(6)	540(15)	625(18)	494(15)	−226(28)	342(24)	−168(29)
C(7)	519(15)	527(16)	585(16)	−85(27)	312(24)	16(27)
C(8)	444(13)	535(16)	510(15)	−26(26)	193(22)	−153(25)
C(9)	498(14)	543(16)	450(15)	−113(25)	209(22)	−50(26)
C(10)	431(13)	494(15)	521(15)	−33(26)	189(23)	−145(24)
C(11)	658(19)	669(21)	759(20)	141(34)	144(32)	193(33)
C(12)	562(17)	737(22)	828(22)	181(36)	105(30)	−133(33)
C(13)	694(19)	549(18)	672(18)	3(31)	127(29)	52(30)
C(14)	1661(42)	727(25)	734(24)	175(42)	70(50)	193(54)
C(15)	1220(32)	968(28)	703(22)	503(45)	558(42)	347(50)
C(16)	700(18)	655(19)	528(16)	24(31)	270(27)	−102(33)

$T = \exp\left[-2\pi^2\left(U_{11}h^2a^{*2} + U_{22}k^2b^{*2} + U_{33}l^2c^{*2} + 2U_{23}klb^*c^* + 2U_{13}hla^*c^* + 2U_{12}hka^*b^*\right)\right]$.

anhydrous ether (20 mL) and stirring continued overnight. After cooling to 0°C, 1 mL of water, then 1 mL of 3 *N* NaOH, and finally 3 mL of water were added sequentially and dropwise to the reaction mixture. The solids were filtered by suction, washed with ether, and the solvent removed to give **6***c* (451 mg, 2.32 mmol, 88%) as a clear oil. Purification was unnecessary; ir: 3300 (phenolic OH, benzylic OH) cm^{-1}; nmr: 1.27 (s, 3H, C-2 methyl), 1.37 (s, 3H, C-2 methyl), 2.03 (d, 2H, J = 6 Hz, H-3), 3.77 (m, 1H, C-4 OH), 5.12 (t, 2H, J = 6 Hz, H-4), 6.42 (d, 2H, J = 8 Hz, H-6 and H-8), 7.08 (t, 1H, J = 8 Hz, H-7).

*2,2-Dimethyl-5-hydroxy-benzopyran (7*b*) from 6*c

Chromanol **6***c* (1.0 g, 5.2 mmol), Zn dust (2.0 g), and acetic acid (20 mL) were stirred overnight. After addition of methanol (100 mL), solid $NaHCO_3$ was added with vigorous stirring until no further CO_2 evolution was noted. The mixture was filtered and the solvent removed to afford 0.63 g of chroman **7***a* (3.5 mmol, 67% yield), essentially pure by tlc.

*2,2-Dimethyl-4-hydroxy-5-phenancyloxy-benzopyran (6*d*) from 6*c

Compound **6***c* (100 mg, 0.51 mmol), K_2CO_3 (1 g), and phenacyl bromide (110 mg, 0.55 mmol) were refluxed in acetone (20 mL) under Ar for 3 h. The orange solution was filtered, the solvent removed, and the residue purified by thick layer chromatography to give **6***d* (128 mg, 0.41 mmol, 81%) as a yellow oil; ir: 3450 (benzylic OH), 1700 (phenacyl C=O) cm^{-1}; nmr: 1.34 (s, 3H, C-2 methyl), 1.43 (s, 3H, C-2 methyl), 2.08 (d, 2H, J = 6 Hz, H-3), 5.13 (t, 1H, J = 6 Hz, H-4), 5.39 (5.24, benzyl CH_2), 6.41 (d, 2H, J = 8 Hz, H-6 and H-8), 6.90 (t, 1H, J = 8 Hz, H-7), 7.30–8.10 (m, 6H, phenacyl Ar-H); ms: 312 (4), 295 (100), 177 (12), 149 (85).

*Δ^3-2,2-Dimethyl-5-phenacyloxy-benzopyran (1g) from 6*d

Compound **6***d* (100 mg, 0.32 mmol) was dissolved in toluene (10 mL) and brought to reflux under Ar. *p*-Toluene sulphonic acid (1 mg) was added, and reflux was continued for 15 min. After allowing the solution to cool, it was washed with 2 *N* NaOH (20 mL), passed through Florisil, and eluted with CH_2Cl_2 (50 mL). Removal of the solvent gave chromene **1***g* (89 mg, 0.30 mmol, 93% yield), essentially pure by tlc; ir: 1700 (C=O) cm^{-1}; nmr: 1.42 (s, 6H, C-2 *gem* dimethyls), 5.25 (s, 2H, phenacyl CH_2), 5.57 (d, 1H, J = 10 Hz, H-3), 6.32 (d, 1H, J = 8 Hz, H-8), 6.34 (d, 1H, J = 8 Hz, H-6); ms: 295 (100), 294 (24), 279 (44), 223 (21), 161 (19), 105 (26).

*Δ^3-2,2-Dimethyl-5-hydroxy-benzopyran (1*d*) from 1g*

Chromene **1***g* (140 mg, 0.48 mmol) was dissolved in a mixture of H_2O (5 mL) and glacial acetic acid (15 mL). After adding zinc dust (0.13 g, 2.0 mmol) the solution was stirred under Ar overnight. The mixture was filtered, diluted with methanol (50 mL), and neutralized with solid $NaHCO_3$ under vigorous stirring until no CO_2 evolution was apparent. The mixture was again filtered, and the solvent removed. Pure **1***d* was obtained by thick layer chromatography (62 mg, 0.35 mmol, 74%) as pale white flakes. All physical and spectral data was identical to an authentic sample of **1***d*.

2,2-Dimethyl-5-hydroxy-4-keto-7-pyrrolidinyl-benzopyran (9) from 8

A mixture of acetophenone **8** (3.1 g, 19.1 mmol) (30), pyrrolidine (3.2 mL, 2.7 g, 38.0 mmol), and acetone (1.6 g, 33.3 mmol) were heated in toluene (75 mL) until all of the solids were dissolved (~40°C), under Ar. Stirring was continued for 3 days, after which the reaction was cooled, washed with 2 *N* HCl, and the solvent removed. The residue was dissolved in CH_2Cl_2, passed through Florisil, and eluted with CH_2Cl_2. After removal of the solvent, the remaining material was recrystallized from MeOH–H_2O to give pure **9** (1.9 g, 7.2 mmol, 38% yield), mp 143–144°C; ir (KBr pellet): 3450 (phenolic OH), 1665 (aromatic hydrogen bonded C=O) cm^{-1}; nmr: 1.45 (s, 6H, C-2 *gem* dimethyls), 2.00 (m, 4H, pyrrolidinyl H3 and H4), 2.63 (s, 2H, H-3), 3.35 (t, 4H, J = 6 Hz, pyrrolidinyl H2 and H5), 5.63 (bs, 2H, H-6 and H-8); ^{13}C nmr: 25.35 (9, C-2 *gem* dimethyls), 26.92 (t, pyrrolidinyl C-3 and C-4), 47.45 (t, C-3), 47.70 (9, pyrrolidinyl C-1 and C-5), 91.28 (d, C-8), 91.39 (d, C-6), 99.10 (s, C-10), 154.78 (s, C-7), 160.83 (s, C-5), 160.83 (s, C-5), 163.56 (s, C-9), 193.47 (s, C-4); ms: 262 (18), 261 (100), 246 (53), 206 (47). *Anal.* calcd.: C 68.67, H 7.70, N 5.34; found: C 68.81, H 7.44, N 5.38.

2,6-Dihydroxy-4-pyrrolidinyl-acetophenone (10) from 8

A mixture of acetophenone **8** (100 mg, 0.617 mmol) and pyrrolidine (1 mL) was stirred at 40°C under Ar for 3 days in toluene (10 mL). After cooling, the solvent was removed on the rotoevaporator and the residue dissolved in CH_2Cl_2, passed through Florisil, and eluted with more CH_2Cl_2. After removal of the solvent, purification by thick layer chromatography gave **10** as an oil (41 mg, 0.19 mmol, 31%); ir: 3300 (b, phenolic OH), 1635 (aromatic hydrogen bonded C=O) cm^{-1}; nmr: 1.80–2.16 (m, 44, pyrrolidinyl H-3 and H-4), 2.58 (s, 3H, $COCH_3$), 3.10–3.47 (m, 4H, pyrrolidinyl H-1 and H-5), 5.67 (s, 2H, H-3 and H-5); ms: 221 (52), 207 (12), 206 (100); *m** 192.

TABLE 5. Bond lengths (Å) and bond angles (°) involving H atoms

Bond	Length (Å)	Bond	Length (Å)
O(3)—H(3)	0.93(4)	C(12)—H(123)	0.98(3)
C(3)—H(31)	0.98(3)	C(13)—H(131)	0.96
C(3)—H(32)	0.91(3)	C(13)—H(132)	0.97
C(7)—H(71)	0.93(3)	C(14)—H(141)	0.94
C(9)—H(91)	0.90(2)	C(14)—H(142)	0.94
C(11)—H(111)	0.96(3)	C(15)—H(151)	0.95
C(11)—H(112)	0.94(4)	C(15)—H(152)	0.97
C(11)—H(113)	0.99(4)	C(16)—H(161)	0.98
C(12)—H(121)	0.99(4)	C(16)—H(162)	0.95
C(12)—H(122)	0.91(4)		

Bond	Angle (°)	Bond	Angle (°)
C(6)—O(3)—H(3)	104(2)	H(122)—C(12)—H(123)	107(3)
C(2)—C(3)—H(31)	111(2)	N(1)—C(13)—H(131)	110
C(2)—C(3)—H(32)	111(2)	N(1)—C(13)—H(132)	111
C(4)—C(3)—H(31)	107(2)	C(14)—C(13)—H(131)	112
C(4)—C(3)—H(32)	107(2)	C(14)—C(13)—H(132)	112
H(31)—C(3)—H(32)	107(3)	H(131)—C(13)—H(132)	109
C(6)—C(7)—H(71)	122(2)	C(13)—C(14)—H(141)	111
C(8)—C(7)—H(71)	118(2)	C(13)—C(14)—H(142)	110
C(8)—C(9)—H(91)	121(2)	C(15)—C(14)—H(141)	111
C(10)—C(9)—H(91)	118(2)	C(15)—C(14)—H(142)	109
C(2)—C(11)—H(111)	111(2)	H(141)—C(14)—H(142)	109
C(2)—C(11)—H(112)	112(2)	C(14)—C(15)—H(151)	113
C(2)—C(11)—H(113)	110(2)	C(14)—C(15)—H(152)	108
H(111)—C(11)—H(112)	111(3)	C(16)—C(15)—H(151)	111
H(111)—C(11)—H(113)	107(3)	C(16)—C(15)—H(152)	111
H(112)—C(11)—H(113)	104(3)	H(151)—C(15)—H(152)	107
C(2)—C(12)—H(121)	111(2)	N(1)—C(16)—H(161)	110
C(2)—C(12)—H(122)	109(2)	N(1)—C(16)—H(162)	111
C(2)—C(12)—H(123)	108(2)	C(15)—C(16)—H(161)	111
H(121)—C(12)—H(122)	112(3)	C(15)—C(16)—H(162)	113
H(121)—C(12)—H(123)	110(3)	H(161)—C(16)—H(162)	107

Compound **9** crystallized from ethanol as colourless translucent prisms. The specimen picked for X-ray study had dimensions 0.2 × 0.4 × 0.5 mm. It was mounted with its elongation direction parallel to the ϕ axis on an Enraf–Nonius CAD-4F diffractometer and the following data were obtained.

$C_{15}H_{19}NO_3$ f.w. 261.32

Monoclinic, $P2_1/c$, a = 11.319(1), b = 6.376(1), c = 19.563(2) Å, β = 104.59(1)°, V = 1366.3 Å^3, Z = 4, ρ_c = 1.270 g cm^{-3}, μ(MoKα) = 0.95 cm^{-1}, F(000) = 560.

Cell dimensions were measured with Ni-filtered Cu radiation ($\lambda(K\alpha_1)$ = 1.54056, $\lambda(K\alpha_2)$ = 1.54439 Å) using the θ values of 25 carefully centered reflections. The relative intensity measurements were made with monochromatized Mo radiation ($\lambda(K\bar{\alpha})$ = 0.7107 Å), using $\omega-2\theta$ scans over ω ranges of $(1.2 + 0.4 \tan\theta)°$, extended by 25% at each end for the backgrounds, at scan speeds of 0.63 to 5.03 min^{-1} in ω. A total of 2401 independent reflections in the hkl and hKl octants, $\theta \le 25°$, were measured and 1498 of these, with $I \ge \sigma(I)$, were considered observed. Two standard reflections were monitored at intervals of 100 min exposure time, and their intensities showed random fluctuations of ±2% and ±2.3%. The net intensities were corrected for Lorentz and polarization effects; no absorption correction was applied.

The structure was determined by direct methods, and refined by block-diagonal least-squares calculations, minimizing $\Sigma w(|F_o| - |F_c|)^2$. All hydrogen atoms were located on a difference map, and refined with isotropic thermal parameters, Table 3, while non-hydrogen atoms were refined anisotropically (Tables 4 and 5). However, the hydrogen atom parameters associated with the pyrrolidine group did not converge satisfactorily, and ultimately were held constant. The weighting scheme used for the final stages of refinement was: $\sqrt{w}$ = 1 if $|F_o| \le 25.0$, $\sqrt{w} = 25.0/|F_o|$ if $|F_o| > 25.0$, and $\sqrt{w} = \sqrt{w} \times \sin^2 0.0536$ if $\sin^2\theta < 0.0536$. This scheme made $\langle w(F_o - F_c)^2\rangle$ values essentially independent of $|F_o|$ and of $\sin^2\theta$. In the final least-squares cycle, the mean (shift/estimated standard deviation) was 0.03, and all shifts were less than 0.20 σ. The final R value was 0.0466 for all observed reflections, and R_w was 0.054. A difference map calculated from the final structure factors contained random densities between 0.25 and −0.19 e/Å^3. Scattering factor values for C, N, and O were taken from International Tables for X-ray Crystallography, Vol. IV (51), and values for H were taken from Stewart, Davidson, and Simpson (52).

The systematic absences are ($h0l$) if l is odd, ($0k0$) if k is odd, these specify space group $P2_1/c$ uniquely. No violations were noticed in the preliminary experimental work: for the main intensity measurement process the systematic absence conditions were incorporated into the data collection parameters.

Acknowledgements

We thank the Natural Sciences and Engineering Research Council of Canada, and Carleton University, for support of the research programme during which these observations were made.

1. W. S. BOWERS, T. OHTA, J. S. CLEERE, and P. A. MARSELLA. Science, **193**, 542 (1976).
2. T. R. KASTURI and T. MANITHOMAS. Tetrahedron Lett. 2573 (1967).
3. A. R. ALERTSEN. Acta Chem. Scand. **9**, 1725 (1955).
4. W. S. BOWERS, T. OHTA, and R. J. KUHR. J. Agric. Food Chem.

25, 478 (1977).
5. W. S. BOWERS, M. E. BURT, and R. J. KUHR. Pestic. Biochem. Physiol. **9**, 300 (1978).
6. W. S. BOWERS, M. E. BURT, and R. J. KUHR. Bull. Environ. Contam. Toxicol. **22**, 586 (1971).
7. W. S. BOWERS., D. M. SODURLAND, and A. MESSEGUER. J. Agric. Food Chem. **28**, 724 (1980).
8. R. C. JENNINGS and A. P. OTTRIDGE. J. Chem. Soc. Chem. Commun. 920 (1979).
9. J. HOUBEN. Chem. Ber. **37**, 489 (1904).
10. I. IWAI and J. IDE. Chem. Pharm. Bull. **10**, 926 (1962).
11. J. HLUBUCEK, E. RITCHIE, and W. C. TAYLOR. Tetrahedron Lett. **17**, 1369 (1969).
12. A. JAIN, R. GUPTA, and P. SARPAL. Tetrahedron, **34**, 3563 (1978).
13. A. JAIN, R. KHAZANCHI, and A. KUMAR. Tetrahedron, **34**, 3569 (1978).
14. A. JAIN, D. JULI, and R. GUPTA. Ind. J. Chem. **16B**, 611 (1978).
15. H. FUKAMI and M. NAKAJIMA. Agric. Biol. Chem. **25**, 247 (1961).
16. V. GUJRAL and S. GUPTA. Bull. Chem. Soc. Jpn. **52**, 3679 (1979).
17. C. CARDILLO, R. CRICCHIO, and L. MERLIN. Tetrahedron, **24**, 4825 (1968).
18. F. CAMPS, J. COLL, A. MESSEGUER, and M. PERICAS. J. Heterocycl. Chem. **17**, 207 (1980).
19. G. CARDILLO, M. ORENA, G. PORZI, and S. SANDRI. J. Chem. Soc. Chem. Commun. 830 (1979).
20. A. BONGINI, G. CARDILLO, M. ORENA, G. PORZI, and S. SANDRI. Tetrahedron Lett. **27**, 2545 (1979).
21. G. SARTORI, G. CASIRAGHI, L. BOLZONI, and G. CASNATI. J. Org. Chem. **44**, 803 (1979).
22. W. BANDARANAYAKE, L. CROMBIE, and D. WHITING. J. Chem. Soc. (C), 811 (1971).
23. V. MIYANO and M. MATSUI. Chem. Ber. **31**, 397 (1958).
24. P. IYER and G. SHAH. Ind. J. Chem. **6**, 227 (1967).
25. A. JEFFERSON, I. MOORE, and F. SCHEINMANN. J. Chem. Soc. (C), 151 (1967).
26. M. L. WOLFROM, J. KOMITSKY, JR., and J. H. LOOKER. J. Org. Chem. **30**, 144 (1964).
27. F. CAMPS, J. COLL, A. MESSEGUER, M. A. PERICAS, S. RICART, W. S. BOWERS, and D. M. SODERLAND. Synthesis, 725 (1980).
28. H. J. KABBE. Synthesis, 886 (1978).
29. R. MECHOULAM and Y. GAONI. J. Am. Chem. Soc. **87**, 3273 (1975).
30. H. FUKAMI, M. NAKAYAMA, and M. NAKAJIMA. Agric. Biol. Chem. **25**, 243 (1961).
31. T. R. KASTURI and T. MANITHOMAS. Tetrahedron Lett. 2573 (1967).
32. M. SCHWARZ. J. Heterocycl. Chem. **14**, 333 (1977).
33. G. C. AMIN and N. M. SHAH. Org. Synth. Coll. Vol. 3, 280 (1955).
34. V. O. ILLI. Tetrahedron Lett. **26**, 2431 (1979).
35. G. OLAH., G. K. PRAKASH, and S. C. NARANG. Synthesis, 825 (1978).
36. J. MARSH and L. GOODMAN. J. Org. Chem. **30**, 2491 (1965).
37. M. JUNG and M. LYSTER. J. Org. Chem. **42**, 3761 (1977).
38. J. MCOMIE, M. WATTS, and D. WEST. Tetrahedron, **24**, 2289 (1968).
39. K. MARKIEWITZ and C. DAWAON. J. Org. Chem. **30**, 1610 (1965).
40. J. HENDRICKSON and C. KANDALL. Tetrahedron Lett. **5**, 343 (1970).
41. A. VOGEL. Textbook of practical organic chemistry. 4th ed. Longman Group Ltd., London. 1979. p. 782.
42. Organic reactions. Vol. 1. John Wiley & Sons, Inc., New York. 1942. p. 105.
43. J. S. CANTRELL and G. S. HOCKSTEIN. Acta Crystallogr. Sect. B, **38**, 981 (1982).
44. J. S. CANTRELL, R. A. STALZER, and T. L. BECKER. Acta Crystallogr. Sect. B, **30**, 154, (1974).
45. A. J. GEDDES, B. SHELDRICK, and D. AKRIGG. Acta Crytallogr. Sect. B, **36**, 3193 (1980).
46. J. ALBERTSSON, A. OSKARSSON, K. STÅHL, C. SVENSSON, and I. YMÉN. Acta Crystallogr. Sect. B, **36**, 3072 (1980).
47. C. HOUTTEMANE, J. C. BOIVIN, G. NOWOGROCKI, D. J. THOMAS, and J. P. BONTE. Acta Crystallogr. Sect. B, **37**, 981 (1981).
48. R. S. MALI and V. J. YADAV. Synthesis, 465 (1977).
49. H. CHRISTENSEN. Synth. Commun. **5**, 65 (1975).
50. VON O. ISTLER, H. BUTMANN, M. MONTAVON, R. RUEGG, G. RYSER, and P. ZELLER. Helv. Chim. Acta, **40**, 1247 (1957).
51. International tables for X-ray crystallography. Vol. IV. Kynoch Press, Birmingham. 1974.
52. R. F. STEWART, E. R. DAVIDSON, and W. T. SIMPSON. J. Chem. Phys. **42**, 3175 (1965).

^1H nuclear magnetic resonance spectral parameters of toluene. Implications for conformational analysis and isotope shifts

TED SCHAEFER, RUDY SEBASTIAN, AND GLENN H. PENNER
Department of Chemistry, University of Manitoba, Winnipeg, Man., Canada R3T 2N2

Received December 19, 1984

TED SCHAEFER, RUDY SEBASTIAN, and GLENN H. PENNER. Can. J. Chem. **63**, 2597 (1985).

A precise analysis of the ^1H nmr spectrum of toluene as a dilute solution in carbon disulfide yields a revised set of spectral parameters. The chemical shift of the *para* proton lies 12.6 ppb to low frequency of that of the *ortho* protons at 300 K. The ring proton chemical shifts are discussed and compared with ^1H and ^3H shifts observed in carbon tetrachloride. The long-range couplings between methyl and ring protons can be said to be quantitatively understood in terms of σ and $\sigma-\pi$ electron transmitted mechanisms. The changes observed in these three couplings in phenylacetaldehyde can be quantitatively reproduced in terms of these mechanisms and also illustrate how these changes are direct measures of the conformational preferences in this molecule.

TED SCHAEFER, RUDY SEBASTIAN et GLENN H. PENNER. Can. J. Chem. **63**, 2597 (1985).

Une analyse précise des spectres rmn du ^1H du toluène, en solution diluée dans le disulfure de carbone, a permis d'obtenir un nouvel ensemble de paramètres spectraux. À 300 K, le déplacement chimique du proton *para* se situe à une fréquence de 12,6 ppb plus basse que celle des protons *ortho*. On discute des déplacements chimiques des protons du cycle et on les compare avec les déplacements des ^1H et ^3H qui ont été déterminés en solution dans le tétrachlorure de carbone. On peut dire que l'on peut expliquer quantitativement les couplages à longue distance entre les protons du cycle et ceux du groupement méthyle en faisant appel à des mécanismes impliquant que les électrons sont transmis par les liaisons σ et $\sigma-\pi$. On peut reproduire quantitativement les changements observés dans ces trois couplages du phénylacétaldéhyde en faisant appel à ces mécanismes; de plus, on peut illustrer comment ces changements sont des mesures directes des préférences conformationnelles dans cette molécule.

[Traduit par le journal]

Introduction

A remarkable early analysis of the tightly coupled ^1H nmr spectrum (1) of neat toluene yielded spectral parameters of interest in a variety of applications. The order of the chemical shifts of the ring protons is solvent dependent and is of interest from the viewpoint of the methyl group as an electron donor (2) and in the use of ^3H nmr spectroscopy (3). The coupling constants are of use in, for example, the analysis of ^{13}C nmr spectra (4–6) and in the theory of spin–spin coupling mechanisms (7–9). In particular, the long-range couplings over four, five, and six formal bonds between the methyl and ring protons, $^4J(H,CH_3)$, $^5J(H,CH_3)$, and $^6J(H,CH_3)$, constitute the reference points for theoretical computations of $\sigma-\pi$ and other coupling mechanisms (7) and for the use of these couplings as detailed conformational indicators (8–10).

With modern nmr instrumentation, the precision of calibration procedures and the chemical shift dispersion have improved significantly. It becomes desirable to provide somewhat more precise spectral parameters for toluene than could be obtained with older instruments.

Results and discussion

In Table 1 the ^1H nmr spectral parameters are given for toluene as a dilute solution in a CS_2/C_6D_{12}/TMS mixture. The precision of the parameters is understandably rather higher than that of previous analyses at lower spectrometer frequencies and some of their values differ significantly from those in the literature (1, 2, 11). Figure 1 illustrates the computed and observed ^1H nmr spectra of the methyl protons.

The chemical shifts

Solvent effects (12–14) on chemical shifts are well known, of course, particularly the large differential solvent shifts caused by aromatic solvents (12–18). The latter no doubt account for the fact that in neat toluene the *ortho* protons resonate to high field of the *para* proton, whereas in other solvents, including that in Table 1, the *para* protons are most shielded (2, 3).

The ring proton shifts, measured at 100 MHz in CCl_4, were extrapolated to infinite dilution (2), as were the ^3H nmr shifts (3). From these results it is clear that measurement at 2.0 mol% as in Table 1 yields a maximum difference of less than 0.002 ppm between these shifts and those at infinite dilution. In Table 2 are given the high field shifts, Δ, relative to benzene, caused by the methyl substituent in toluene. In CS_2 solution, Δ_P is 0.212 ppm, which may be compared with an INDO calculation (19) of 0.28 ppm. Qualitatively, the positive Δ_P is expected because the methyl group is a π electron donor. However, all the ring proton resonances shift to high field in the presence of the methyl substituent whereas the MO theories (20, 21) imply that the electron density decreases at the *meta* position relative to benzene. Furthermore, the computed π electron densities in **1** at the *para* position are too small to account for the upfield shift of 0.21 ppm, if the common proportionality (22) of about 11 ppm/electron is accepted (of course, the π electron densities at the *meta* position of common π electron donors like NH_2 or OCH_3 are also calculated to be less than in benzene, yet the *meta* proton shifts in aniline and anisole lie upfield from benzene (23)). Solvent effects are not likely the source of such discrepancies. Thus, the π charge distribution for toluene in CS_2 solution, determined from absolute infrared band intensities (25) and given in parentheses in **1**, also disagrees with a simple model of this kind. These matters have been discussed

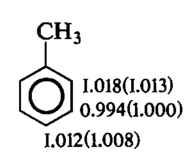

1

TABLE 1. ^{1}H nuclear magnetic resonance spectral parameters for a 2.0 mol% solution in CS_2[a] at 300 K

Parameter	Value	Parameter	Value
ν_{CH_3}	688.561(1)[b,c]	$^5J_{25}$	0.610(1)
ν_o	2106.558(1)[d]	$^4J(H,CH_3)$	−0.702(1)
ν_m	2130.281(1)	$^5J(H,CH_3)$	0.329(1)
ν_p	2102.784(2)	$^6J(H,CH_3)$	−0.602(2)
$^3J_{23}$	7.655(2)[e]	Transitions calcd.	566
$^3J_{34}$	7.417(2)	Transitions assigned	408
$^4J_{26}$	1.902(3)	Peaks observed	147
$^4J_{35}$	1.442(2)	Largest difference	0.032
$^4J_{24}$	1.273(3)	Root mean square deviation	0.013

[a]Containing also 10 mol% of C_6D_{12} and 0.5 mol% TMS.
[b]In Hz at 300.135 MHz to low field of TMS.
[c]Numbers in parentheses are standard deviations in the last significant figure.
[d]At the same concentration in this solvent, $\nu_{C_6H_6}$ is 2166.440 Hz.
[e]The largest correlations among the parameters are: ν_m/ν_p 0.19, $\nu_o/^4J_{26}$ −0.22, $\nu_p/^4J_{26}$ 0.16, $\nu_p/^3J_{34}$ 0.27, $^3J_{23}/^4J_{35}$ −0.16, $^3J_{23}/^4J_{26}$ −0.20.

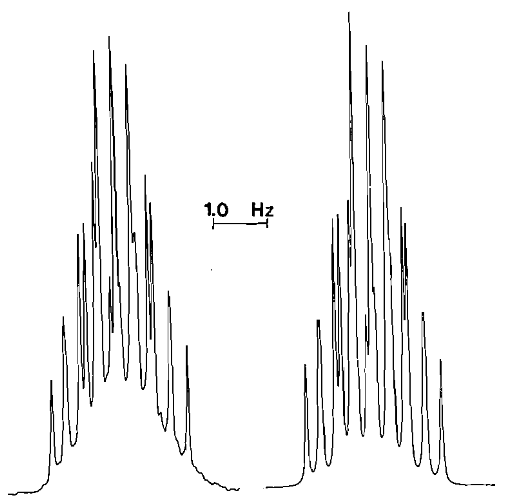

FIG. 1. The ^{1}H nmr spectrum of the methyl protons in toluene in 300 K as a 2.0 mol% solution in CS_2 and containing 10.0 mol% cyclohexane-d_{12} and 0.5 mol% tetramethylsilane. The computed spectrum assumes the spectral parameters in Table 1. The computed spectrum has lorentzian line shapes whereas the observed spectrum contains a small amount of gaussian character. In addition, the baseline of the observed spectrum is not identical to that of the computed spectrum. The discrepancies between the two spectra are only apparent in the sense that peak frequencies, on which the analysis is based, are in satisfactory agreement. The spectra were recorded on a scale of 0.5 Hz/cm.

(24) and it is shown that ^{1}H shifts at the *meta* and *para* positions can be roughly related to computed σ-electron populations at hydrogen if certain correction terms are included.

Based on somewhat complex referencing procedures (3, 26), it was concluded that aromatic tritons resonate *downfield* from aromatic protons. The Δ values in Table 2 appear to confirm this conclusion because the ^{1}H nmr shift of benzene in the appropriate solvent is used to calculate the Δ values (the shift of ^{3}H in [^{3}H]-benzene relative to the shift of ^{1}H in benzene is apparently unavailable). This isotope effect amounts to 0.04_3 ppm at each position in toluene if the data in rows 2 and 3 of Table 2 are considered to be most reliable. Note that

TABLE 2. Ring proton chemical shift changes caused by the methyl group in toluene

Solvent	Δ_o[d]	Δ_m[d]	Δ_p[d]	$\Delta_p - \Delta_o$	$\Delta_o - \Delta_m$	$\Delta_p - \Delta_m$
CCl_4[a]	0.201	0.124	0.220	0.019	0.077	0.076
CS_2[b]	0.199_5	0.120_5	0.212	0.013	0.079	0.093
CCl_4[c]	0.156	0.077	0.171	0.015	0.079	0.094

[a]Analyses at 100 MHz and extrapolation to infinite dilution, $\delta_{C_6H_6}$ is 7.262 ppm.
[b]Present results, $\delta_{C_6H_6}$ is 7.218 ppm.
[c]From ^{3}H nmr shifts, taking $\delta_{C_6H_6}$ as 7.262 ppm.
[d]A positive Δ implies a high-field shift relative to benzene.

the *differences* between the Δ values for these two rows agree rather well.

However, these results should not be taken as proof that tritons are less shielded than protons in the same position (primary isotope effect). Because the change in shielding caused by bond lengthening is negative (27), it is most likely that the aromatic tritons are more shielded than aromatic protons. Accordingly, the apparent negative isotope shift in Table 2 is a consequence of the reference procedure using tetramethylsilane and singly tritiated tetramethylsilane (26).

The long-range couplings to methyl protons

$^4J(H,CH_3) \equiv {}^4J$, sometimes called an *ortho* benzylic coupling, was originally found to be −0.75 Hz (1). Its value in Table 2 is −0.702(1) Hz. In a recent (8) detailed investigation of ^4J and its conformational dependence in aromatic systems, it was written as

$$[1] \quad {}^4J\ (\mathrm{Hz}) = 6.90\ \pi \sin^2\theta - 0.32 \cos^2\theta$$

where π is the mutual atom−atom polarizability and θ is the angle by which the α C—H bond twists out of the benzene plane. For toluene π is −0.157 and we rewrite eq. [1] as eq. [2],

$$[2] \quad {}^4J\ (\mathrm{Hz}) = -1.08\langle\sin^2\theta\rangle - 0.32\langle\cos^2\theta\rangle$$

where angular brackets indicate expectation values. The latter are 0.5 for toluene, whether or not the methyl group rotates rapidly, so that ^4J is calculated as −0.70 Hz, exactly as given in Table 1.

The INDO MO FPT computations (7) of ^4J are reproduced by eq. [3], where the indicated errors come from the 95%

$$[3] \quad {}^4J\ (\mathrm{Hz}) = -0.342(5) - 1.005(6)\sin^2\theta - 0.230(5)\sin^2(\theta/2)$$

confidence level. This equation predicts ^4J as −0.96 Hz, clearly an overestimate of its magnitude. An empirical adjustment might proceed as follows. The expectation value of $\sin^2(\theta/2)$ is again 0.5, so that eq. [3] becomes ^4J (Hz) = −0.457 − 1.005 $\sin^2\theta$. If the numbers are scaled by 0.70/0.96, one has ^4J (Hz) = −0.33 − 0.73 $\sin^2\theta$ or a value of -0.69_5 Hz. Of course, eq. [2] may also be written as ^4J (Hz) = −0.32 − 0.76 $\sin^2\theta$ for toluene (high symmetry). The angle independent term in eq. [3] does seem unsatisfactory, however.

The ring-substituent dependence of ^4J can be large because of changes in the atom−atom polarizability (8). However, in 3-fluorotoluene the ^4J values are −0.693(2) Hz for H-3 and −0.701(2) Hz for H-6, while in 2-chloro-5-fluorotoluene ^4J is −0.700(3) Hz (28). On the other hand, ^4J is −0.779(2) Hz in 2-fluorotoluene (29) and −0.714(3) Hz in 4-fluorotoluene (30). All these numbers are for CS_2 solutions.

TABLE 3. The ^{1}H spectral parameters for a 3 mol% solution of phenylacetaldehyde in benzene-d_6 at 294 K and 300.135 MHz

Parameter	Value	Parameter	Value
ν(COH)[a]	2877.281(1)[b]	^4J(H,CH$_2$)	−0.564(1)
ν(CH$_2$)	911.543(1)	$^5J_{25}$	0.606(1)
$\nu_2 = \nu_6$	2044.701(1)	^5J(H,CH$_2$)	0.282(1)
$\nu_3 = \nu_5$	2118.595(1)	^5J(H,CHO)	0.000(1)[c]
ν_4	2206.749(2)	^6J(H,CH$_2$)	−0.399(2)
^3J(H,CH$_2$)	2.357(1)	^6J(H,CHO)	0.000(1)[c]
$^3J_{23}$	7.683(1)	^7J(H,CHO)	(−)0.001(2)[c]
$^3J_{34}$	7.497(2)	Calcd. transitions	776
$^4J_{24}$	1.253(2)	Assigned transitions	403
$^4J_{26}$	1.937(2)	Largest difference	0.032
$^4J_{35}$	1.474(1)	Root mean square deviation	0.010

[a]In Hz at 300.135 MHz to low field of internal tetramethylsilane.
[b]Numbers in parentheses are the standard deviations in the last significant figure.
[c]No evidence for finite magnitudes of these couplings existed in the spectrum, but the couplings were allowed to vary in the iterations.

Turning to $^5J(\mathrm{H,CH_3}) \equiv {}^5J$, it has been proposed (9) that ^5J is given by eq. [4].

$$[4] \quad {}^5J = {}^5J^{\pi} \sin^2\theta + {}^5J^{\sigma} \sin^2(\theta/2)$$

In eq. [4] the $\sigma-\pi$ electron contribution is given by 0.336 Hz (9). Then $^5J^{\sigma}$, the σ-electron component, is 0.322 Hz because ^5J in toluene is 0.329(1) Hz in Table 1. Hence eq. [4] becomes eq. [5].

$$[5] \quad {}^5J\ (\mathrm{Hz}) = 0.336\langle\sin^2\theta\rangle + 0.322\langle\sin^2(\theta/2)\rangle$$

The observed ring substituent dependence of ^5J is relatively large (9). ^5J is 0.300(1) Hz in 3-fluorotoluene and is as large as 0.438(2) Hz in 2,6-difluorotoluene.

Unlike ^5J, the coupling over six bonds, $^6J(\mathrm{H,CH_3}) \equiv {}^6J$ is insensitive to ring substitution. ^6J in toluene is −0.602(2) Hz (Table 1) and varies from −0.584(2) Hz in 2-fluoro-6-aminotoluene to −0.622(1) Hz in 2,3,5,6-tetrafluorotoluene (29). Experimentally and theoretically it appears that eq. [6] holds for ^6J, where

$$[6] \quad {}^6J = {}^6J_{90} \sin^2\theta$$

$^6J_{90}$ is its value when the α C—H bond lies in a plane perpendicular to the benzene plane (7, 10). It appears that $^6J_{90}$ is −1.20 Hz.

A test of equations [2], [5], and [6]

For a 3 mol% solution of phenylacetaldehyde in benzene-d_6, we find ^4J, ^5J, and ^6J as −0.564(1), 0.282(1), and −0.399(2) Hz, respectively (precise analyses of benzyl compounds are scarce and therefore the spectral parameters are given in Table 3). The value of ^6J implies that **2** is the preferred conformation and that $\langle\sin^2\theta\rangle$ is −0.339/−1.20 or 0.332. With the assumption of a twofold barrier[1] to rotation about the C—C

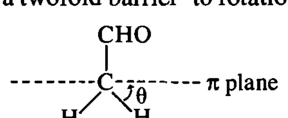

$\theta = 30°$

2

[1]An STO 3G MO computation (see Experimental) suggests that **2** is 8 kJ/mol more stable than a conformer with $\theta = 60°$ (aldehyde function in-plane).

bond to the phenyl group (10), this value of $\langle\sin^2\theta\rangle$ corresponds to 9.7 kJ/mol. It also follows that $\langle\cos^2\theta\rangle$ is 0.668 and therefore, from eq. [2], that ^4J should be −0.572 Hz. The observed value is −0.564(1) Hz. Again, from eq. [5], one has ^5J as 0.273 Hz because for a twofold barrier (31) $\langle\sin^2(\theta/2)\rangle$ is 0.5. The measured value is 0.282(1) Hz. The consistency among calculated and observed numbers is taken as adequate. The utility of these long-range couplings and its reliance on the precise values in Table 1 are thereby shown. It remains to be investigated just how sensitive the couplings are to the electronic nature of the atom attached to the methylene group.

Experimental

A 2.0 mol% solution of toluene in CS$_2$, containing 10 mol% cyclohexane-d_{12} and 0.5 mol% tetramethylsilane, was transferred to a 5-mm od nmr tube. The solution was degassed by the freeze−pump−thaw procedure and the sample tube was flame sealed. The ^{1}H nmr spectrum was accumulated at a probe temperature of 300 K on a Bruker AM300 spectrometer. A 3.0 mol% solution of phenylacetaldehyde in benzene-d_6 solution was treated similarly, except that the probe temperature was 294 K.

A wide sweepwidth survey spectrum was obtained in order to reference the spectrum with respect to TMS, and to obtain the locations of the aromatic and sidechain regions. Each region was examined in detail, with sweepwidth and data region adjusted to given acquisition times of approximately 40 s. Four to sixteen scans were acquired. Zero filling to twice the original data region was done before transforming the FIDs using a small amount of gaussian multiplication. Linewidths at half height were approximately 0.08 Hz after this resolution enhancement.

The ^{1}H nmr spectrum was analyzed with the computer program NUMARIT (32), extensively modified by R.S.

The STO 3G MO computations employed the program MONSTERGAUSS (33) and were performed on an Amdahl V8 system. Geometry optimization of all bond angles and bond lengths was done at $\theta = 0°$ and 90°. However, the phenyl framework was constrained to remain a regular hexagon.

Acknowledgments

We are grateful to the Natural Sciences and Engineering Research Council of Canada for financial assistance and to a referee for very instructive comments.

1. M. P. WILLIAMSON, R. KOSTELNIK, and S. M. CASTELLANO. J. Chem. Phys. **49**, 2218 (1968).
2. K. HAYAMIZU and O. YAMAMOTO. J. Mol. Spectrosc. **29**, 183 (1969).
3. M. A. LONG, J. K. SAUNDERS, P. G. WILLIAMS, A. L. ODELL, and R. W. MARTIN. Org. Magn. Reson. **22**, 665 (1984).
4. M. HANSEN and H. J. JAKOBSEN. J. Magn. Reson. **20**, 520 (1975).
5. L. ERNST, V. WRAY, V. A. CHERTKOV, and N. M. SERGEYEV. J. Magn. Reson. **25**, 123 (1977).
6. T. SCHAEFER, J. PEELING, and G. H. PENNER. Can. J. Chem. **61**, 2773 (1983).
7. R. WASYLISHEN and T. SCHAEFER. Can. J. Chem. **50**, 1852 (1972).
8. M. BARFIELD, C. J. FALLICK, K. HATA, S. STERNHELL, and P. W. WESTERMAN. J. Am. Chem. Soc. **105**, 2178 (1983).
9. T. SCHAEFER and R. LAATIKAINEN. Can. J. Chem. **61**, 2785 (1983).
10. W. J. E. PARR and T. S. SCHAEFER. Acc. Chem. Res. **13**, 400 (1980).
11. F. A. BOVEY, F. P. HOOD, E. PIER, and N. E. WEAVER. J. Am. Chem. Soc. **87**, 2060 (1965).
12. A. A. BOTHNER-BY and R. E. GLICK. J. Chem. Phys. **26**, 1651 (1957).

13. J. R. ZIMMERMAN and M. R. FOSTER. J. Phys. Chem. **61**, 282 (1957).
14. A. D. BUCKINGHAM, T. SCHAEFER, and W. G. SCHNEIDER. J. Chem. Phys. **32**, 1227 (1960).
15. R. WASYLISHEN, T. SCHAEFER, and R. SCHWENK. Can. J. Chem. **48**, 2885 (1970).
16. J. HOMER and C. C. PERCIVAL. J. Chem. Soc. Faraday Trans. 2, **80**, 1 (1984).
17. F. H. A. RUMMENS. *In* N.M.R. principles and progress. Vol. 10. *Edited by* P. Diehl, E. Fluck, and R. Kosfeld. Springer Verlag, Berlin. 1975.
18. P. LASZLO. Prog. Nucl. Magn. Reson. Spectrosc. **3**, 231 (1967).
19. P. A. DOBOSH, P. D. ELLIS, and Y-C. CHOU. J. Magn. Reson. **36**, 439 (1979).
20. W. J. HEHRE, L. RADOM, and J. A. POPLE. J. Am. Chem. Soc. **94**, 1496 (1972).
21. A. PROSS and L. RADOM. Prog. Phys. Org. Chem. **13**, 1 (1981).
22. T. SCHAEFER and W. G. SCHNEIDER. Can. J. Chem. **41**, 966 (1963).
23. K. HAYAMIZU and O. YAMAMOTO. J. Mol. Spectrosc. **28**, 89 (1968).
24. M. AKIYAMA. Spectrochim. Acta Part A, **40**, 781 (1984).
25. W. J. HEHRE, R. W. TAFT, and R. D. TOPSOM. Prog. Phys. Org. Chem. **12**, 159 (1976).
26. J. P. BLOXSIDGE, J. A. ELVIDGE, J. R. JONES, R. B. MANE, and M. SALJOUGHIAN. Org. Magn. Reson. **12**, 574 (1979).
27. H. J. OSTEN and C. J. JAMESON. J. Chem. Phys. **81**, 4288 (1984).
28. T. SCHAEFER, W. DANCHURA, and W. NIEMCZURA. Can. J. Chem. **56**, 2233 (1978).
29. T. SCHAEFER, R. SEBASTIAN, R. P. VEREGIN, and R. LAATIKAINEN. Can. J. Chem. **61**, 29 (1983).
30. T. SCHAEFER, W. DANCHURA, W. NIEMCZURA, and J. PEELING. Can. J. Chem. **56**, 2442 (1978).
31. T. SCHAEFER, T. A. WILDMAN, and R. SEBASTIAN. Can. J. Chem. **60**, 1924 (1982).
32. A. R. QUIRT and J. S. MARTIN. J. Magn. Reson. **5**, 318 (1971); J. S. MARTIN, A. R. QUIRT, and K. E. WORVILL. The NMR program library. Daresbury Laboratory, Daresbury, U.K.
33. M. R. PETERSEN and R. A. POIRIER. MONSTERGAUSS, Department of Chemistry, University of Toronto, Toronto, Ontario, 1981.

Réactivité du nucléophile azoture vis-à-vis de cations hétérocycliques aromatiques. VIII. Réarrangement de β-tétrazolo-*trans*-benzalacétophénones

JEAN-CLAUDE CHERTON, MARC BAZINET, MARIE-MADELEINE BOLZE, MARC LANSON ET PAUL-LOUIS DESBENE
Laboratoire de chimie organique structurale, Université de Paris VI, 8, rue Cuvier, 75230 Paris Cédex, France

Reçu le 13 novembre 1984

JEAN-CLAUDE CHERTON, MARC BAZINET, MARIE-MADELEINE BOLZE, MARC LANSON et PAUL-LOUIS DESBENE. Can. J. Chem. **63**, 2601 (1985).

Les β-tétrazolo-*trans*-benzalacétophénones (T) s'isomérisent au chauffage en iminoazides (I.A.) correspondants. Ces derniers, non isolables, subissent selon les conditions du milieu diverses évolutions. Ils peuvent être interceptés par les bases organiques comme la triphénylphosphine et la pyridine. En solvants aromatiques, ils évoluent avec perte d'azote par l'intermédiaire de diazirines et d'oxadiazépines vers des hétérocycles diazotés à cinq chaînons: pyrazoles et imidazoles *N*-benzoylés. L'emploi d'un solvant protique favorise l'isomérisation des tétrazoles en iminoazides. On observe alors la solvolyse des formes azidooxazines et même oxazinium résultant de la suite d'équilibres et réaction:

(T) $\leftrightarrows$ (I.A.) $\leftrightarrows$ azidooxazine $\rightarrow$ oxazinium.

JEAN-CLAUDE CHERTON, MARC BAZINET, MARIE-MADELEINE BOLZE, MARC LANSON, and PAUL-LOUIS DESBENE. Can. J. Chem. **63**, 2601 (1985).

β-Tetrazolyl-*trans*-benzalacetophenones (T) isomerize upon heating into the corresponding azido-azomethines (A). These non-isolable products undergo various transformations depending on the reaction conditions. With organic bases such as triphenylphosphine or pyridine, their interception can occur. In aromatic solvents, a rearrangement involving loss of nitrogen leads to five-membered diazoted heterocycles: *N*-benzoyl imidazoles and pyrazoles, via intermediate diazirines and oxazepines. Protic solvents have been found to facilitate the isomerisation of tetrazoles into azidoazomethines. Solvolysis of the azido-oxazine and in some cases of the oxazinium species resulting from the equilibrium and reaction:

(T) $\leftrightarrows$ (A) $\leftrightarrows$ azidooxazine $\rightarrow$ oxazinium

are then observed.

Dans un précédent article, nous avons décrit le comportement de cations oxaziniums-1,3 **1** (1) vis-à-vis du nucléophile azoture. Nous avons montré que la formation des β-tétrazolo-*trans*-benzalacétophénones **2** (notées plus rapidement "tétrazoles") résultait selon toute vraisemblance d'une attaque de N_3^- sur le pôle C2 du cation hétéroaromatique conduisant transitoirement aux azido-2 2*H*-oxazines-1,3 **3** correspondantes. La filiation azide **3** → tétrazole **2** était interprétée comme résultant de la superposition de deux tautoméries de type cycle–chaîne autour de l'iminoazide **4** (cf. schéma 1).

L'obtention des tétrazoles **2** constitue une dérivation au schéma réactionnel qu'on pouvait escompter en se fondant sur le comportement des pyryliums (2–4) puisqu'elle inhibe la formation des hétérocycles heptaatomiques.

Cation hétéroaromatique $\xrightarrow{N_3^-}$ azide hétérocyclique $\xrightarrow{-N_2,\,\Delta}$ hétérocycle azoté heptaatomique

Néanmoins, le mécanisme que nous proposons pour la formation des tétrazoles (cf. schéma 1) laisse entrevoir la possibilité d'un retour vers les formes azides **4** et même **3** en intervenant sur les conditions des deux tautoméries.

Le travail présenté concerne l'étude de la tautomérie iminoazide $\rightleftharpoons$ tétrazole pour le couple **4**/**2**, entreprise comme une tentative d'aboutir à un réarrangement des formes azides **4** ou **3** en hétérocycles diazotés heptaatomiques.

De telles isomérisations peuvent s'envisager soit comme des réactions électrocycliques (5) soit comme des cycloadditions dipolaires-1,5 (6) soit encore comme des cycloadditions-1,3 au cours de l'attaque d'un azide sur une imine (7). Un calcul effectué par la méthode LCAO–SCF sur le modèle le plus simple ($R^1 = R^2 = H$, cf. schéma 2) montre que dans l'isomérisation iminoazide (I.A.) $\leftrightarrows$ tétrazole (T), l'état de transition s'apparente plutôt au réactif (I.A.) (quoique plus polarisé) qu'au produit (T) (7).

Ce résultat théorique s'accorde aussi bien avec le postulat de Hammond (prédiction d'états de transition "reactant-like" pour les systèmes réactifs) qu'avec de nombreux résultats de la littérature (ainsi qu'avec nos observations) qui montrent en général une plus grande stabilité pour la forme tétrazole (7, 8).

L'examen des données de la littérature permet de distinguer deux types de facteurs jouant sur l'équilibre (I.A.) $\leftrightarrows$ (T): des facteurs structuraux (nature de R^1, R^2) et des facteurs de milieu (température, polarité et proticité du solvant).

Facteurs structuraux

La cyclisation implique une configuration *cis* entre la paire libre de l'atome imino et le reste azido. Pour les iminoazides linéaires (R^1 et R^2 non liés) cette condition implique que l'isomérisation *syn* $\leftrightarrows$ *anti* de la double liaison C=N soit possible. Une telle inversion est très rapide si R^1 est un groupe alkyle ou aryle, la forme tétrazole est alors généralement observée (9). En revanche, si R^1 est électro-donneur ($\ddot{O}R$, $\ddot{O}H$, $\ddot{S}R$, $\ddot{N}R$) l'inversion est considérablement ralentie et l'(I.A.) est la forme tautomère prépondérante (9), voire unique comme dans le cas des azidoximes (10).

Facteurs de milieu

L'emploi de solvants polaires, donc de solvants stabilisant mieux l'état de transition polarisé que la forme (I.A.) doit en principe favoriser la cyclisation en tétrazole (7), cette prévision s'accorde avec un ensemble d'observations (9).

Lorsque le groupe R^1 est susceptible de se protoner l'emploi de solvants protiques déplace par contre l'équilibre vers les formes (I.A.) (9). Enfin, bien que cette règle ne soit pas d'une généralité absolue, la formation des iminoazides est souvent endothermique (11).

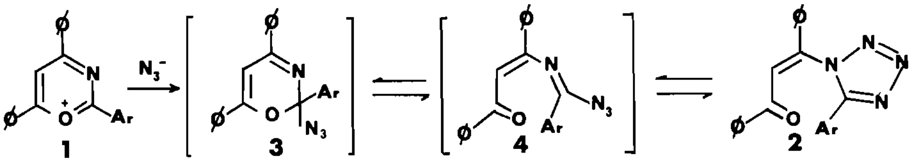

oxazinium-1,3 azido-oxazine imino-azide tétrazole

(a) Ar = C_6H_5 (b) Ar = $pCH_3OC_6H_4$ (c) Ar = $pNO_2C_6H_4$

SCHÉMA 1

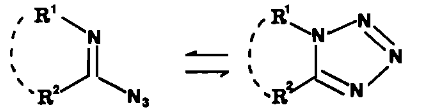

Iminoazide (I.A) tétrazole (T)

R^1 et R^2 éventuellement liés.

SCHÉMA 2

Résultats et discussion

Dans le cas des couples (I.A.)/(T) **4**/**2** les formes (I.A.) sont des formes acycliques dont le groupe R^1 n'est pas électrodonneur, il est donc normal que la forme tétrazole **2** soit la plus stable à température ambiante. Aussi n'avons nous pas tenté d'intervenir sur les facteurs de structure mais sur les facteurs de milieu, d'exploitation plus immédiate.

1. *Effets de solvant à température ordinaire*

Nous avons choisi l'infra-rouge comme méthode d'étude de l'equilibre en solution et procédé à l'enregistrement des solutions du tétrazole triphénylé **2***a* (cf. schéma 1) dans CCl_4, CH_3CN et CF_3COOH. Dans ces conditions nous n'avons décelé aucune trace d'absorption dans la région caractéristique des vibrations d'élongation asymétrique du groupe N_3 des iminoazides (2160–2120 cm^{-1}) (12).

Le facteur solvant est donc à lui seul insuffisant pour déplacer à température ambiante l'équilibre (T) $\leftrightharpoons$ (I.A.) vers les formes (I.A.).

2. *Utilisation du facteur température: thermolyse des tétrazoles 2*

On pouvait envisager pour les tétrazoles **2** une isomérisation endothermique en les iminoazides **4** correspondants. Nous avons donc procédé à une étude de la thermolyse des tétrazoles **2** dans diverses conditions (solvant, catalyseur...).

Le chauffage des tétrazoles **2** n'a pas permis d'isoler les iminoazides **4** correspondants; on observe selon la nature du solvant, aromatique ou protique, deux comportements bien typés des tétrazoles.

(a). Réarrangements thermiques en solvant aromatique

Ils conduisent par perte d'azote (~100%) à des mélanges essentiellement constitués d'hétérocycles à cinq chaînons: les pyrazoles **5** et **6** et les imidazoles **7** et **8** (schéma 3).

La transformation totale du tétrazole **2***a* nécessite un chauffage à 160°C pendant 6 h. Elle conduit à un mélange complexe d'une vingtaine de composés dont on a pu identifier ou isoler les six constituants prépondérants représentant environ 70% du bilan (cf. tableau 1 et partie expérimentale).

Le *N*-benzoyldiphényl-3,5 pyrazole **5***a* et le *N*-benzoyldiphényl-2,4 imidazole **7***a*, composés majoritaires, semblent être des produits primaires de la réaction. En revanche, le diphényl-3,5 pyrazole **6** (13) et le *N*-benzoyl-diphényl-2,5 imidazole **8** sont des produits secondaires résultants de transformations ultérieures des produits majoritaires **5** et **7** respectifs dans les conditions de la thermolyse (cf. tableau 2).

On note également la présence de traces de β-benzamido-*trans*-benzalacétophénone **9***a* "pseudo base" de l'oxazinium **1***a* (1, 14) ainsi que d'un composé **10***a* (il s'agit comme on le verra d'un photoisomère de **2***a*).

(b). Réarrangement thermique des tétrazoles en solvant protique

Le tétrazole **2***a* ne subit pratiquement aucune modification au cours d'un chauffage au reflux dans l'éthanol absolu. En revanche il se réarrange par chauffage dans l'éthanol à 95%, l'acide acétique ou l'acide trifluoroacétique. On obtient, non plus des hétérocycles azotés à cinq chaînons et de l'azote moléculaire, mais la β-benzamido-*trans*-benzalacétophénone **9***a*. Comparativement aux réarrangements en solvants aromatiques, ces réarrangements en solvants protiques sont plus rapides et s'effectuent à température modérée.

Il est à noter que lors du chauffage du tétrazole **2***a* en solution dans l'acide trifluoroacétique se développe une coloration jaune vif qui a pu être attribuée à la présence du cation oxazinium, le trifluoroacétate d'oxazinium (cf. partie expérimentale).

(c). Chauffage du tétrazole 2a en présence de réactifs spécifiques des azides organiques

L'emploi du cuivre comme éventuel catalyseur de décomposition du tétrazole **2***a* (15) diminue effectivement la température du réarrangement, mais il en modifie aussi le cours (cf. tableaux 1 et 2) puisqu'il catalyse également la débenzoylation du *N*-benzoyl-pyrazole **5** et qu'il dégrade le *N*-benzoylimidazole **7**. Ce catalyseur n'apporte donc pas d'amélioration aux réarrangements thermiques.

Nous avons également tenté de mettre en évidence le retour vers des formes azides par chauffage du tétrazole **2***a*, en opérant en présence de réactifs spécifiques d'azides organiques comme la triphénylphosphine $P(Ph)_3$ (16*a*, *b*) ou les amines aromatiques.

La triphénylphosphine est bien connue pour intercepter les azides organiques en conduisant à des adduits 1:1 plus ou moins stables à température ambiante. On constate que son emploi lors du chauffage du tétrazole **2***a* modifie le cours

$$P(Ph)_3 + R'N_3 \rightleftharpoons \left|\overset{+}{P}(Ph)_3\text{—}\overset{-}{N}\text{—}N\text{=}N\text{—}R'\right| \xrightarrow{-N_2} \overset{+}{P}(Ph)_3\text{—}\overset{-}{N}\text{—}R' \updownarrow P(Ph)_3\text{=}N\text{—}R'$$

phosphoimine

habituel des réarrangements thermiques. Ainsi, dans l'orthodichlorobenzène (ODCB) aussi bien que dans l'éthanol à 95% on observe une diminution des rendements en produits habituels, respectivement hétérocycles azotés majoritaires **5***a* et **7***a* et pseudo-base **9***a*. On note en revanche la formation de nouveaux

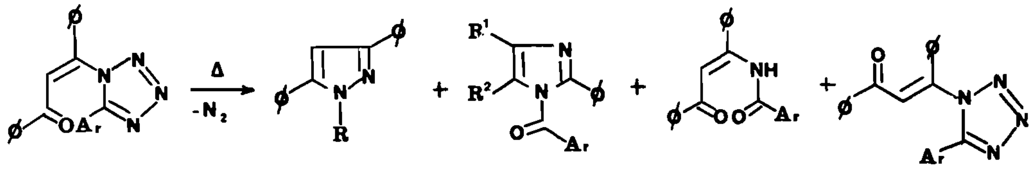

2 5 R = ArCO 6 R = H 7 R¹ = ϕ, R² = H 8 R¹ = H R² = ϕ 9 10

SCHÉMA 3

TABLEAU 1. Thermolyse des tétrazoles 2*a*–*c*

Tétrazole 2 solvant; temp. (°C); durée (h)	Composés obtenus 5	7	8	6	9	10	Autres composés
1. **2***a* Ar = C_6H_5 ODCB; 160; 6	30 (29)*	31 (29)	(7)	(1)	(2)	(0,1)	
2. **2***b* Ar = $CH_3OC_6H_4$ ODCB; 160; 6	26	†		†	†		
3. **2***c* Ar = $NO_2C_6H_4$ ODCB; 160; 6	30	†		†	†		
4. **2***a* C_6H_6, 80; 48	Traces						
5. **2***c* C_6H_6, 80; 48	20				10		
6. **2***a* EtOH abs.; 78, 48							
7. **2***a* EtOH 95%; 78; 2					95		
8. **2***a* CH_3COOH, 115; 1					65		
9. **2***a* CF_3COOH, 75; 2					65		**1***a* uv
10. **2***a* + cuivre ODCB, 120; 6	(1,5)	(0,1)	(0,5)	(10)	(9,5)		
11. **2***a* + $P(Ph)_3$ ODCB, 160; 6	18	13			2		**11** 20% $(Ph)_3PO$ 20%
12. **2***a* + $P(Ph)_3$ EtOH 95%, 78; 6	10	15			35		**11** 20% $(Ph)_3PO$ 20%
13. **2***a* + pyridine					40		**11** 11% **12** 15%

*Les rendements en % sont déterminés par ccm à l'exception de ceux entre parenthèses: dosage clhp.
† Séparation délicate.

TABLEAU 2. Thermostabilité du benzoyl-1 diphényl-3,5 pyrazole 5*a* et du benzoyl-1 diphényl-2,4 imidazole 7*a*

Conditions solvant; temp. (°C); durée (h)	Composés obtenus				
14. **5***a* ODCB, 160; 12	**5***a*	49%	**6**	4%	résines
15. **5***a* + cuivre ODCB, 160; 2	**5***a*	10%	**6**	80%	
16. **7***a* ODCB, 160; 12	**7***a*	28%	**8***a*	3%	résines
17. **7***a* + cuivre ODCB, 160; 2	**7***a*	0%	**8***a*	traces	résines
18. **7***a* + cuivre ODCB, 160; 12	Dégradation totale des produits habituels				résines

produits: oxyde de triphénylphosphine et triphényl-2,4,6 pyrimidine **11**. Enfin, l'utilisation de la pyridine comme solvant de thermolyse de **2***a* modifie également le comportement habituel; comme précédemment, on obtient de la triphényl-2,4,6 pyrimidine **11** à côté d'un composé supplémentaire: le diphényl-3,5 isoxazole **12** (17).

3. *Activation photochimique des tétrazoles*

Nous avons également envisagé d'intervenir sur l'équilibre (T) ⇆ (I.A.) par une décomposition photochimique de l'azide (2, 18).

L'irradiation donne lieu à deux types de transformations: (*i*) une activation de courte durée et peu énergétique provoque une

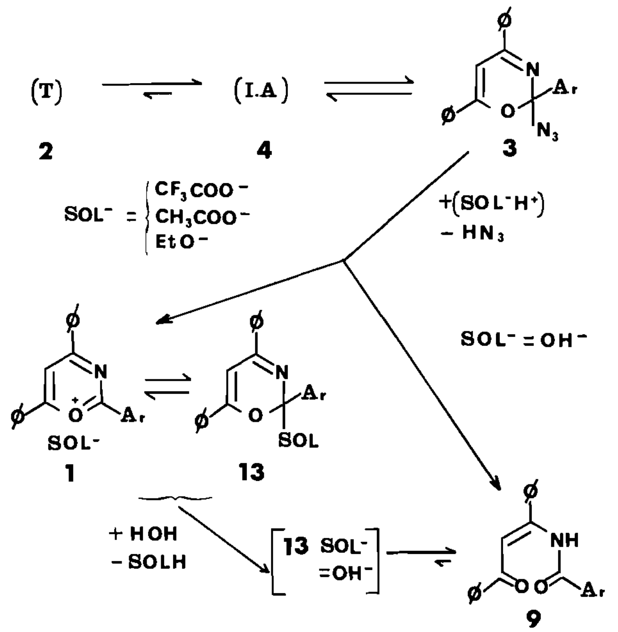

SCHÉMA 4

photoisomérisation du système énonique avec préservation du noyau tétrazole. Cette photoisomérisation **2***a* ⇆ **10***a* s'apparente à la photoisomérisation *trans* ⇆ *cis* de la benzalacétophénone (19) et, comme celle-ci, peut se produire à la lumière solaire. (*ii*) Une irradiation prolongée à plus courte longueur d'onde provoque, outre la photoisomérisation précédente, un réarrangement du motif tétrazole des deux isomères **2***a* et **10***a*. On aboutit rapidement à un mélange réactionnel beaucoup plus complexe que celui des thermolyses, les divers produits primaires pyrazoles et imidazoles devant vraisemblablement subir eux-mêmes des réarrangements photochimiques (20).

Ce mode d'activation n'a donc pas été retenu pour le réarrangement des tétrazoles.

Le noyau tétrazole est un cycle relativement stable en l'absence de substituants le rendant sensible à la chaleur (21). Ainsi, les diaryl-1,5 tétrazoles se décomposent-ils par chauffage au dessus de leurs points de fusion (220–250°C) avec perte d'azote et formation de mélange de carbodiimides et de benzimidazoles (22).

La décomposition des tétrazoles **2** semble suivre un cours différent: elle se produit à plus basse température, 160°C dans l'ODCB et même 78°C dans l'éthanol à 95%, et ne fournit pas de carbodiimide (absence de bande d'absorption N═C═N vers 2160 cm^{-1} en spectroscopie infra-rouge).

Ceci conduit à envisager pour les β-tétrazolo-*trans*-benzalacétophénones **2** plutôt qu'un réarrangement "classique" de la forme tétrazole, un réarrangement des formes azides correspondantes: (I.A.) **4** voire azido oxazine **3**. Nous proposons donc un mécanisme impliquant dans un *premier temps* la conversion des tétrazoles **2** en (I.A.) **4** correspondants,[1] ces derniers subissant dans un *deuxième temps* diverses évolutions selon les conditions de milieu.

[1] Comparativement aux diaryl-1,5 tétrazoles on peut concevoir que cette thermolyse soit favorisée par la présence d'un groupe R[1] *trans*-chalcone plus électroattracteur qu'un groupe aryle (cf. schéma 2). Il y aurait déstabilisation du noyau tétrazole réputé électroattracteur (23) et stabilisation de la forme azide électrodonneur (24).

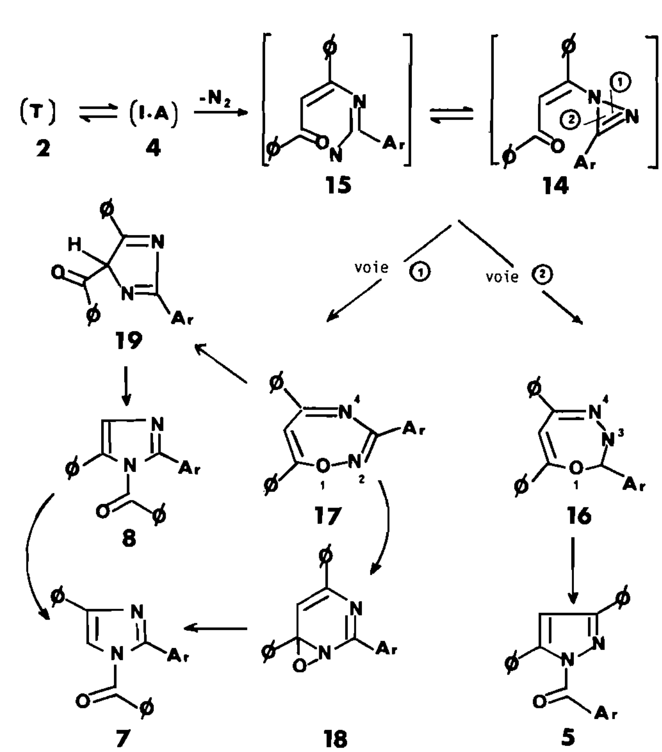

SCHÉMA 5

En solvant protique

L'obtention des pseudo-bases **9** s'interprète en admettant la solvolyse des azido-oxazines **3**. Les 2*H*-oxazines **13** résultantes peuvent même selon les cas ($sol^- = CF_3COO^-$ ou CH_3COO^-) évoluer selon une troisième dissociation d'un type nouveau (25) oxazine → oxazinium-1,3. Cette hypothèse d'une dissociation des oxazines en paires d'ions plus ou moins intimes selon la nature du solvant est confirmée par l'observation du cation oxazinium dans le cas où le solvant est CF_3COOH.

En solvant aromatique neutre

La conversion (I.A.) → (T) ne bénéficiant plus du facteur favorable de la proticité exige un chauffage plus important. En ce qui concerne le deuxième équilibre (I.A.) → azidooxazine, il est vraisemblable que c'est la forme (I.A.) qui prédomine (en raison de l'absence de solvolyse, et car c'est vraisemblablement la forme la plus stable si l'on se rapporte au système α-pyranne – diénone (26)).

Nous proposons donc de rationaliser les thermolyses en solvant aromatique à partir de la forme (I.A.) **4** avec comme étapes clés la formation d'intermédiaires tels que la diazirine[2] **14** et les oxadiazepines **16** et **17**.

La thermolyse des azides vinyliques fait intervenir des azirines formées par addition des nitrènes intermédiaires sur la double liaison (27, 28). De façon analogue on peut concevoir le passage (I.A.) **4** → cétodiazirine **14** via le nitrène **15**.

Deux évolutions vers les oxadiazépines **16** et **17** sont possibles pour cette cétodiazirine **14**, par attaque du dipôle-1,3 qu'elle constitue sur le carbonyle du système énonique (2, 4). (voies 1 et 2). Enfin, (*i*) le passage oxadiazépine-1,3,4 **16** → pyrazole **5** s'effectuerait par transposition sigmatropique d'ordre 1,3 (cf. la réf. 31 dans le cas voisin des benz(*d*)oxazépines-1,3); (*ii*) alors que l'oxadiazépine-1,2,4 **17** conduirait à l'imidazole **7** par des transpositions faisant jouer

[2] Ce type d'intermédiaire a déjà été postulé pour rendre compte de la photodécarboxylation de diverses sydnones (29, 30).

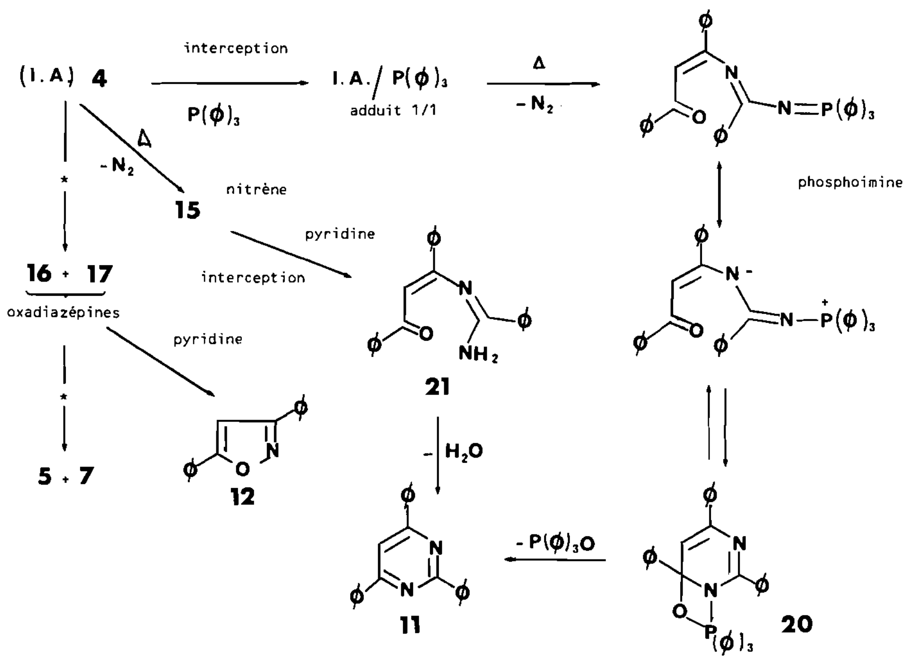

*évolution habituelle

SCHÉMA 6

l'oxirane **18** (32) ou l'imidazole *C*-benzoylé **19**.

En présence de $P(Ph)_3$ ou de pyridine

La thermolyse du tétrazole **2***a* en présence de $P(Ph)_3$ conduit aux mêmes produits $P(Ph)_3O$ et pyrimidine **11** que lors d'une attaque de NaN_3 sur l'oxazinium **1***a* effectuée en présence de $P(Ph)_3$ (1). Ceci suggère une interception du même azide: azidooxazine **3***a* ou plus vraisemblablement iminoazide **4***a*. Dans la dernière hypothèse, il s'agirait en fait d'une réaction "Wittig-like" intramoléculaire dont on connaît un précédent (33).

L'emploi de pyridine comme solvant conduit également à la formation de la pyrimidine **11**. Il s'agit vraisemblablement de l'interception de l'imidonitrène **15** avec formation de l'énamine intermédiaire **21**. Un deuxième effet de la pyridine est de limiter[3] les réarrangements des oxadiazépines **16** et **17** en pyrazoles **5** et imidazoles **7** au profit d'une autre évolution conduisant au diphényl-3,5 isoxazole **12** par perte de benzonitrile (cf. schéma 6).

Conclusion

L'étude de la tautomérie tétrazole **2** → (I.A.) **4** a montré que conformément aux prévisions la formation des (I.A.) est endothermique. En solvant aromatique, les (I.A.) évoluent comme attendu avec perte d'azote vers des hétérocycles à 7 chaînons: les oxadiazépines. Ces composés sont malheureusement instables et s'isomérisent thermiquement en pyrazoles et imidazoles *N*-benzoylés. Si l'emploi de solvants protiques favorise l'isomérisation (T) → (I.A.) il ne permet pas davantage l'isolement des oxadiazépines. En effet surviennent alors exclusivement des réactions de solvolyse de l'azidooxazine **3** résultant de l'équilibre (I.A.) $\rightleftharpoons$ **3**. S'il a été observé que l'introduction d'un groupe électroattracteur comme un *p*-nitrophényl sur le carbone du noyau tétrazolique joue dans un sens favorable à l'isomérisation (T) $\leftrightarrows$ (I.A.), l'exploitation des facteurs structuraux reste encore à approfondir. Enfin, dans le but d'éviter tout chauffage en vue d'isoler éventuellement les oxadiazépines, nous envisageons de faire appel à des azapyryliums, comme les oxaziniums-1,2 ou oxaziniums-1,4, tels que la formation de tétrazoles soit d'emblée impossible.

[3]On connaît en effet des réarrangements d'oxazépines-1,3 en *N*-benzoylpyrroles catalysés par les acides (34).

Partie expérimentale

Les spectres d'absorption ultraviolet–visible et infra-rouge ont été respectivement enregistrés sur des appareils Hewlett–Packard 8450 A ou Philips SP8-250 et Philips SP3-200. Les spectres de rmn ^1H et rmn ^{13}C ont été enregistrés sur appareil EM 360 Varian ou Bruker WP 80 et WM 250. Les spectres de masse ont été effectués par Mesdemoiselles J. Mercier et C. Lange que nous remercions, respectivement au centre de Mesures Physiques de Paris sur un spectromètre AEI MS 50 et au laboratoire sur un spectrographe quadrupôlaire Nermag R10-10C. Les analyses élémentaires ont été effectuées par le centre de Microanalyse du CNRS ou au laboratoire de Microanalyse de l'Université Pierre et Marie Curie. Les points de fusion non corrigés ont été déterminés de façon instantanée au banc de Köfler.

Le chromatographe liquide utilisé est constitué de: 2 pompes Waters modèle 6000 A pilotées par le moniteur de gradient Waters modèle 660; un injecteur universel U6 K; un détecteur uv–visible à filtres interférentiels Waters M 440.

I. *Effets de température et de solvants sur l'équilibre iminoazide $\rightleftharpoons$ tétrazole*

Les thermolyses des tétrazoles **2***a*, *b*, *c* ont été effectuées à l'abri de la lumière dans diverses conditions de température, de solvant ou de réactifs spécifiques d'azides organiques. L'évolution des réactions est suivie par chromatographie sur couche mince de silice (ccm) jusqu'à cessation du dégagement d'azote.

Thermolyse du tétrazole 2a *dans l'ODCB. Manipulation 1*

Une solution de 100 mg de tétrazole **2***a* dans 2 cm^3 d'ODCB anhydre est chauffée à 160°C pendant 6 h. La solution est concentrée puis analysée par ccm préparative sur silice (Merck) (cf. tableau 1). Une analyse qualitative par chromatographie liquide hautes performances (clhp) révèle la présence d'une vingtaine de composés. Nous avons pu procéder à la quantification de six composés majoritaires au moyen d'échantillons standards indépendamment obtenus en conjuguant la clhp *semi-préparative et la ccm.*

Conditions d'analyse clhp: *colonne*: 2 (33 × 0,46 cm) μ porasil 10μ; *solvant*: gradient n° 6 entre n-heptane et n-heptane/[CH_2Cl_2/AcOEt] (95:5) en 15 min jusqu'au mélange n-heptane/[CH_2Cl_2/AcOEt] (75:25); *débit*: 2 mL/min; détection uv à 254 nm; température ambiante.

Thermolyse des tétrazoles 2b *et* 2c *dans l'ODCB. Manipulations 2 et 3*

On opère comme précédemment. Les pyrazoles **5***b* et **5***c* sont isolés par ccm sans difficulté, par contre, les imidazoles **7***b* et **7***c* n'ont pu être suffisamment purifiés pour donner une analyse centésimale satisfaisante. Ceci est dû à la présence de produits de polarités voisines tels que pseudo-bases **9***b*, *c* et pyrazoles bases **6***b*, *c* (cf. tableau 1). La structure des produits majoritaires pyrazoles **5**, **6**, imidazoles **7**, **8** sera discutée dans le paragraphe suivant.

Thermolyse des tétrazoles dans le benzène. Manipulations 4 et 5

Le chauffage *de 100 mg de tétrazole* **2***a* (ou **2***b*) dans 2 cm^3 de benzène anhydre ne produit aucune modification en 48 h. Par contre, dans les mêmes conditions, le tétrazole **2***c* se réarrange en partie: la ccm permet d'isoler 20% de pyrazole **5***c* (19,5 mg), 10% de pseudo-base **9***c* (9,5 mg), et 40 mg de tétrazole inchangé.

Thermolyse du tétrazole 2a *en solvant protique. Manipulations 6 à 9*

On chauffe les solutions de **2***a* dans divers solvants protiques au reflux. Après traitement: lavage à l'eau, extraction à l'éther ou simplement évaporation du solvant dans le cas de l'éthanol, on purifie la pseudo-base **9***a* par ccm. Dans le cas du chauffage dans CF_3COOH, la coloration jaune vif fluorescente a été attribuée à la formation du cation oxazinium-1,3 **1***a* par spectroscopie uv–visible.

Thermolyses du tétrazole 2a *dans l'ODCB en présence de P(Ph)₃. Manipulation 11*

Le tétrazole **2***a* (186 mg, 0,5 mmol) est chauffé dans 2 cm^3 d'ODCB anhydre à 160°C pendant 6 h en présence de 131 mg (0,5 mmol) de $P(Ph)_3$. Le traitement habituel conduit à un mélange de pyrazole **5***a* (18%, 30 mg), d'imidazole **7***a* (13%, 21 mg), de pseudo-base **9***a* (2%, 2,5 mg), de triphényl-2,4,6 pyrimidine **11** (1) (20%, 31 mg) et de l'oxyde de triphénylphosphine (20%, 25 mg). On obtient le même genre de produits en opérant au reflux de l'éthanol (*manipulation 12*).

Thermolyse du tétrazole 2a *dans la pyridine. Manipulation 13*

Le tétrazole **2***a* (30 mg, 0,08 mmol) est chauffé 48 h dans 2 cm^3 de pyridine anhydre à 115°C. On obtient après traitement: de la triphénylpyrimidine **11** (11%, 3 mg), du diphényl-3,5 isoxazole **12** (17) (15%, 3,5 mg, Fi 140°C) ainsi que de la pseudo-base **10***a* (40%, 11,5 mg).

Thermostabilité du pyrazole 5a *(cf. tableau 2)*

La manipulation 14 montre que le pyrazole **5***a* n'est pas stable dans les conditions où il est produit par dégradation du tétrazole **2***a*. Il se décompose en mélange de composés dont le seul qui puisse être identifié est le pyrazole base **6***a* (4%). Cette décomposition est beaucoup plus propre et plus rapide en présence de cuivre (*manipulation 15*).

Thermostabilité de l'imidazole 7a *(cf. tableau 2)*

La manipulation 16 montre que l'imidazole **7***a* subit une dégradation importante au chauffage, le seul produit isolable étant son isomère **8***a* en faible quantité. La dégradation de **7***a* est complète en présence de cuivre même pour un chauffage de courte durée (*exp. 17 et 18*).

II. *Structure des produits issus des thermolyses*

Les pseudo bases **9***a*–*c* obtenues par chauffage des tétrazoles en solvant protique ont fait l'objet d'une étude spectroscopique dans un précédent article (1). La triphényl-2,4,6 pyrimidine **11** déjà connue (34) a été identifiée (Fi, ir) à un échantillon authentique, de même que le diphényl-3,5 isoxazole **12***a* (17).

1. *Structure des pyrazoles* **5** *et* **6**

Seul le diphényl-3,5 pyrazole **6***a* était connu, nous l'avons identifié à un échantillon obtenu par action de l'hydrazine sur l'oxazinium **1***a* (35).

(a) *Benzoyl-1 diphényl-3,5 pyrazole* 5a: À une solution de 76 mg (0,34 mmol) de pyrazole **6***a* dans 5 cm^3 d'éther anhydre, on ajoute lentement 20 μL de chlorure de benzoyle. Après lavage à l'eau jusqu'à neutralité le mélange réactionnel chromatographié (ccm sur silice) fournit 56 mg (40%) de **5***a* pur, Fi 128°C (éther); ir cm^{-1} (KBr): 1700, 1600, 1580, 900; uv ν_{max} (log ϵ_{max}) (éther): 242 (4, 53), 275 (4, 17); rmn ^1H ($CDCl_3$) δ ppm/TMS: 8,3–8,05 (m, 2H), 8,7–7,5 (m, 2H), 7,7–7,2 (m, 11H), 6,8 (s, 1H, H4); masse *m/e*: M^+ 324 (25), 296 (12), 295 (17), 220 (35), 191 (11), 165 (3), *105* (100), 77 (39); *Anal.* calc. pour $C_{22}H_{16}N_2O$: C 81,46, H 4,97, N 8,64; tr: C 81,42, H 5,01, N 8,69.

La structure des autres N*-aroyl-pyrazoles* 5b *et* 5c se fonde sur la comparaison de leurs propriétés spectroscopiques avec celles de **5***a*. En infra-rouge, la présence d'une bande d'absorption située vers 1710 cm^{-1} écarte l'hypothèse d'une structure de *C*-aroyl-pyrazole pour laquelle le carbonyle se situerait vers 1660–1665 cm^{-1} (36). Elle s'accorde en revanche avec la structure proposée de *N*-aroyl-pyrazole (37). En rmn ^1H, on constate que le déplacement chimique du proton noté H4 est pratiquement constant pour les pyrazoles **5***a*–*c*. Ce résultat établit que le groupe aryle substitué est situé dans le motif aroyle (qu'il influence d'ailleurs en ir au niveau de ν(C=O)) et non pas sur les sommets C3 ou C5. L'utilisation de la relation empirique de Tensmeyer et Ainsworth (38) donnée pour les pyrazoles-1,3,5 trisubstitués confirme nettement dans le cas de **5***a* la structure de *N*-benzoyl-diphényl-3,5 pyrazole:

δ H4	$CDCl_3$	observé 6,85	calculé 6,86
	CCl_4	observé 6,80	calculé 6,75

(b) p-*Méthoxybenzoyl-1 diphényl-3,5 pyrazole* 5b: Fi 80–82°C (éther); ir cm^{-1} (KBr): 2860, 1705, 1600, 1580, 900; rmn ^1H ($CDCl_3$) δ ppm/TMS: 8,25–7,05 (sys. AA′BB′, 4H), 8,1–7,3 (m, 10H), 6,9 (s, 1H, H4), 3,9 (s, 3H); masse *m/e*: M^+ 354 (35), 220 (80), 191 (20), 189 (12), *135* (100), 105 (5), 77 (40).

(c) p-*Nitrobenzoyl-1 diphényl-3,5 pyrazole* 5c: Fi 150–152°C (éther); ir cm^{-1} (KBr): 1715, 1600, 1575, 1350, 920; rmn ^1H ($CDCl_3$) δ ppm/TMS: 8,5–8,2 (m, 4H), 8,05–7,7 (m, 4H), 7,7–7,3 (m, 6H), 6,89 (s, 1H, H4); masse *m/e*: M^+ 369 (10), 341 (8), *220* (100), 191 (40), 189 (30), 165 (10), 150 (25), 105 (8), 77 (42). *Anal.* calc. pour $C_{22}H_{15}N_3O_3$: C 71,53, H 4,09, N 11,38; tr: C 71,68, H 4,18, N 11,55.

2. *Structure des imidazoles* 7a *et* 7b

Les preuves structurales reposent essentiellement sur des arguments chimiques. Ainsi l'hydrolyse (39) du diphényl-2,4 *N*-benzoyl-imidazole **7***a* (*F* 141°C), conduit-elle à la "base de Minovici": le diphényl-2,5 imidazole via la "base de Kunckell" (40): le diphényl-2,4 imidazole instable dans les conditions de l'hydrolyse. La benzoylation de cette dernière "base" selon la réf. 41 conduit au *N*-benzoyl-diphényl-2,5 imidazole identifié au composé **8***a* (*F* 120–121°C) obtenu lors de la thermolyse du tétrazole **2***a*.

(a) N-*Benzoyldiphényl-2,4 imidazole* 7a, obtenu par thermolyse du tétrazole **2***a* après ccm (silice): Fi 141°C (éther); ir cm^{-1} (KBr): 1715, 1600, 1580, 900; uv (éther) ν_{max} nm (log ϵ_{max}): 257 (4, 33), 2,84 (4, 34); rmn ^1H ($CDCl_3$) δ ppm/TMS: 8,0–7,1 (m); masse *m/e*: M^+ 324 (16), 220 (5), 165 (1), 106 (10), *105* (100), 77 (10). *Anal.* calc. pour $C_{22}H_{16}N_2O$: C 81,46, H 4,97, N 8,64; tr: C 81,42, H 4,91, N 8,52.

(b) *Hydrolyse du benzoyl-1 diphényl-2,4 imidazole* 7a: 23 mg de l'imidazole **7***a* sont hydrolysés selon la méthode de M. Weiss (39) en présence d'acétate d'ammonium (50 mg) et d'acide acétique (250 μL). Au cours de la réaction suivie par ccm, on constate la transformation du produit primaire d'hydrolyse **7***a* en base de Minovici **8***a* de polarité supérieure. On isole après traitement 11 mg (72%) de **8***a*, Fi 141°C, identifié à un échantillon authentique préparé indépendamment (41).

(c) *Benzoyl-1 diphényl-2,5 imidazole* 8a: 14 mg de **8***d* sont chauffés 20 min à 130°C dans 200 μL de Φ-COCl. Après refroidissement et agitation 30 min dans une solution éthanolique d'ammoniaque à 10%, on lave à l'eau et extrait à l'éther jusqu'à neutralité. On obtient après ccm sur silice 8 mg (40%) d'imidazole **8***a*, Fi 120–121°C.

Ce composé est identique à l'imidazole obtenu (7%) par thermolyse du tétrazole **2***a* dans l'ODCB ou par réarrangement thermique de l'imidazole **7***a* (cf. tableau 2); ir cm^{-1} (KBr): 1730, 1710, 1600, 1580, 900; masse *m*/*e*: M^+ 324 (10), 220 (4), 165 (1), 106 (11), *105* (100), 77 (45).

III. *Irradiation du tétrazole* **2**a

Irradiation de courte durée à $\lambda > 300$ *nm ou irradiation à la lumière solaire. Obtention du tétrazole* **10**a

La tétrazole **2***a* s'isomérise lentement à l'état solide ou en solution à la lumière du laboratoire en tétrazole **10***a* (cf tableau 1).

Une solution de 200 mg (0,57 mmol) de tétrazole **2***a* dans 100 cm^3 d'un mélange de cyclohexane–benzène (60:40) est préalablement dégazée pendant 15 min par barbotage d'azote. L'irradiation est réalisée au moyen d'une lampe de type SP 500 Philips au travers d'un filtre Pyrex ($\lambda > 300$ nm). Il semble que la réaction, suivie par ccm, donne lieu à un photoéquilibre. Au bout d'1 h on évapore le solvant et obtient après purification par ccm (silice) 150 mg (75%) de tétrazole **10***a*, Fi 116°C (éther); ir[4] cm^{-1} (KBr): 1670, 1620, 1595; uv (éther) ν_{max} nm (log ϵ_{max}): 238 (4, 38), 290 (3, 94); rmn ^1H ($CDCl_3$) δ ppm/TMS: 8,1–7,6 (m, 4H), 7,55–7,20 (m, 11H), 7,15[5] (s, 1H); rmn ^1H (C_6D_6) δ ppm/TMS: 7,9–7,7 (m, 4H), 7,2–6,65 (m, 11H), 6,6[5] (s, 1H, H5); rmn ^{13}C ($CDCl_3$) δ ppm/TMS: carbones quaternaires 191,2, 155,2, 141,8, 137,3, 133,3, 131,3, 124,6; carbones tertiaires 134,7, 132,4; masse *m*/*e*: M^+ 324 (221), 310 (9), 247 (7), *105* (100), 77 (45). *Anal.* calc. pour $C_{22}H_{16}N_4O$: C 74,98, H 4,58, N 15,90; tr: C 74,69, H 4,70, N 15,63.

1. J. C. CHERTON, P. L. DESBENE, M. BAZINET, M. LANSON, O. CONVERT et J. J. BASSELIER. Can. J. Chem. **63**, 86 (1985).
2. (*a*) J. P. LE ROUX, J. C. CHERTON et P. L. DESBENE. C.R. Acad. Sci. **280**, 37 (1975); (*b*) P. L. DESBENE, J. C. CHERTON, J. P. LE ROUX et J. J. BASSELIER. Tetrahedron, **40**, 3539 (1984).
3. P. L. DESBENE, D. RICHARD, J. C. CHERTON et P. CHAQUIN. Tetrahedron, **40**, 3549 (1984).
4. P. L. DESBENE et J. C. CHERTON. Tetrahedron, **40**, 3565 (1984).
5. J. ELGUERO. Bull. Soc. Chim. Fr. 1925 (1971).
6. H. REIMINGER. Chem. Ber. **103**, 1900 (1970).
7. L. A. BURKE, J. ELGUERO, G. LEROY et M. SANA. J. Am. Chem. Soc. **98**, 1685 (1976).
8. W. LWOWSKI. The chemistry of the azido group. *Édité par* S. Patai. Interscience, New York. 1971. p. 503.
9. B. STANOVNIK et M. TISLER. Tetrahedron, **25**, 3313 (1969).
10. F. ELOY. J. Org. Chem. **26**, 952 (1961).
11. M. TISLER. Synthesis, 123 (1973).

[4] On note entre 1340 et 690 cm^{-1} la présence d'un ensemble de bandes caractéristiques du noyau tétrazolique (1).

[5] Le recours à un réactif de déplacement chimique induisant des déplacements à champ fort $Pr(fod)_3$ a permis de localiser le proton H5 à la limite du massif aromatique vers les champs forts. Cette attribution est également confirmée par la rmn à haut champ (250 MHz).

12. G. A. REYNOLDS, J. A. VAN ALLAN et J. F. TINKER. J. Org. Chem. **24**, 1205 (1959).
13. I. SHIBUYA et M. KURABAYASHI. Bull. Chem. Soc. Jpn. **46**, 3902 (1973).
14. A. PADWA et N. EISENHARDT. J. Org. Chem. **35**, 2472 (1970).
15. K. FRAUNBERG et R. HUISGEN. Tetrahedron Lett. 2599 (1969).
16. (*a*) J. E. LEFFLER, U. HONSBERG, Y. TSUNO et I. FORSBALD. J. Org. Chem. **26**, 4810 (1961); (*b*) L. F. KASUKHIN, M. P. PONOMARCHUK, T. I. KLEPA, V. P. LYSENKO et YU GOLOBOY. Zh. Obshch. Khim. **47**, 2188 (1977).
17. C. MOUREU et M. BRACHIN. C.R. Acad. Sci. **137**, 795 (1903).
18. F. L. BACH, J. KARLINER et G. E. VAN LEAR. Chem. Commun. 1111 (1969).
19. R. E. LUTZ et R. H. JORDAN. J. Am. Chem. Soc. **72**, 4090 (1950).
20. (*a*) P. BEAK, J. L. MIESEL et W. R. MESSER. Tetrahedron Lett. 5315 (1967); (*b*) P. BEAK et W. MESSER. Tetrahedron, **25**, 3287 (1969).
21. M. C. EWAN et M. W. RIGG. J. Am. Chem. Soc. **73**, 4725 (1951).
22. P. A. S. SMITH et E. LEON. J. Am. Chem. Soc. **80**, 4647 (1958).
23. R. A. HENRY, W. G. FINEGAN et E. LIEBER. J. Am. Chem. Soc. **81**, 4671 (1959).
24. E. LIEBER, R. L. MINNIS et C. A. RAO. Chem. Rev. **65**, 377 (1965).
25. J. J. BASSELIER et J. P. LE ROUX. C.R. Acad. Sci. Ser. C, **268**, 622 (1969).
26. J. P. LE ROUX, G. LETERTRE, P. L. DESBENE et J. J. BASSELIER. Bull. Soc. Chim. 4059 (1971).
27. G. SMOLINSKY. J. Org. Chem. **33**, 2411 (1068) et réf. citées.
28. P. L. DESBENE et J. C. CHERTON. Tetrahedron, **40**, 3567 (1984).
29. H. GUTTHARD et F. REITER. Tetrahedron Lett. **29**, 2749 (1971).
30. A. CHINONE, Y. HUSEYA et M. OHTA. Bull. Chem. Soc. Jpn. **43**, 2650 (1970).
31. O. BUCHARDT, P. L. KUMLER et C. LOHSE. Acta. Chem. Scand. **23**, 2149 (1969).
32. F. BELLAMY, J. STREITH et H. FRITZ. Nouv. J. Chim. **3**, 115 (1979).
33. J. ACKRELL, E. GALEAZZI et J. M. MUCHOWSKI. Can. J. Chem. **57**, 2696 (1979).
34. T. MUKAI et S. SUKAWA. Tetrahedron Lett. 1835 (1973).
35. R. R. SCHMIDT. Chem. Ber. **98**, 334 (1965).
36. J. BASTIDE, O. HENRI-ROUSSEAU et L. APART-PASCOT. Tetrahedron, **30**, 3355 (1974).
37. G. RIO et A. LECAS-NAWROLKA. Bull. Soc. Chim. Fr. 1723 (1971).
38. L. G. TENSMEYER et C. AINSWORTH. J. Org. Chem. **31**, 1878 (1966).
39. M. WEISS. J. Am. Chem. Soc. **74**, 5193 (1952).
40. R. BURTLES et F. LEE PYMAN. J. Chem. Soc. **123**, 361 (1923).
41. O. GERNGROS. Chem. Ber. **46**, 1908 (1913).

The gas phase reactions of the trichloromethylium ion with alkyl aromatics, studied by high pressure mass spectrometry

JOHN ALFRED STONE, NANCY JOAN MOOTE, AND ANASTASIA C. M. WOJTYNIAK
Chemistry Department, Queen's University, Kingston, Ont., Canada K7L 3N6

Received August 17, 1984[1]

JOHN ALFRED STONE, NANCY JOAN MOOTE, and ANASTASIA C. M. WOJTYNIAK. Can. J. Chem. **63**, 2608 (1985).

The reactions of trichloromethylium (CCl_3^+) with benzene and the lower alkyl aromatics (ArH) have been studied by high pressure mass spectrometry at pressures in the range 2–4 Torr and temperatures from 300 to 560 K. The only two primary products are the adduct $ArHCCl_3^+$ and $ArCCl_2^+$, which is formed by loss of HCl from the adduct. The relative yields of adduct increase with increasing number of methyl substituents on the aromatic ring (benzene → mesitylene). The disappearance of CCl_3^+ is kinetically second order with specific rate constants increasing from benzene to mesitylene, the latter reacting essentially at every ion–molecule collision. All rate constants are fairly large ($>10^{10}$ cc molecule^{-1} s^{-1}) and show negative temperature coefficients. $ArCCl_2^+$ is unreactive but $ArHCCl_3^+$ reacts further by proton transfer to ArH.

JOHN ALFRED STONE, NANCY JOAN MOOTE et ANASTASIA C. M. WOJTYNIAK. Can. J. Chem. **63**, 2608 (1985).

Opérant à des pressions allant de 2 à 4 Torr et à des températures allant de 300 à 560 K et faisant appel à la spectrométrie de masse à haute pression, on a étudié les réactions de l'ion trichlorométhylium (CCl_3^+) avec le benzène et les alkylbenzènes légers (ArH). Les deux seuls produits primaires sont l'adduit $ArHCCl_3^+$ et le $ArCCl_2^+$ qui se forme à partir de l'adduit par la perte de HCl. Les rendements relatifs de l'adduit augmentent avec une augmentation du nombre de substituants méthyles sur le noyau aromatique (benzène → mésitylène). La disparition du CCl_3^+ est cinétiquement du deuxième ordre et les constantes spécifiques de vitesse augmentent lorsqu'on passe du benzène au mésitylène; ce dernier réagit essentiellement à chaque collision ion–molécule. Toutes les constantes de vitesse sont assez élevées ($>10^{10}$ cc molécule^{-1} s^{-1}) et elles présentent toutes des coefficients de température qui sont négatifs. Alors que le $ArCCl_2^+$ n'est pas réactif, le $ArHCCl_3^+$ est susceptible de donner d'autres réactions par transfert de proton vers les ArH.

[Traduit par le journal]

Introduction

The reactions of trichloromethylium, CCl_3^+, with aromatic hydrocarbons have been previously studied by mass spectrometry at low pressures (~10^{-4} Torr; 1 Torr = 133.3 Pa). Theard and Hamill (1) identified the main reaction between CCl_3^+ and benzene, in CCl_4/C_6H_6 mixtures, as

[1] $CCl_3^+ + C_6H_6 \rightarrow C_7H_5Cl_2^+ + HCl$

Virin *et al.* confirmed the occurrence of this reaction in the same system (2) and also found the analogous reactions with toluene (3) and ethylbenzene (4). The stabilized $C_6H_6CCl_3^+$ adduct was not observed. Theard and Hamill did observe several other chlorinated and non-chlorinated secondary ions, which can be ascribed to the presence of either epithermal ions caused by the ion repeller fields used or primary ions other than CCl_3^+.

Many ion–molecule reactions observed mass spectrometrically can often also be identified in radiolytic systems (5). It is therefore surprising that no chlorinated aromatic products are ascribed to the reactions of CCl_3^+ in γ-irradiated CCl_4/aromatic (100:2) mixtures at total pressures from 100 to 760 Torr and ambient temperature (6, 7). The reported yields of chlorinated benzene and toluene products are very low, the sum of *G* values (molecules of product formed per 100 eV of energy absorbed by the system) being in no system greater than 1, whereas *G* (ions) in gases is ~4 (8). The few products observed were shown to probably have free radicals (CCl_3 and Cl) as precursors. Since CCl_3^+ is the dominant ion in the low pressure mass spectrum of CCl_4 and since it is unreactive towards the parent molecule (9), much ion chemistry in dilute aromatic/CCl_4 mixtures must originate with CCl_3^+ even though none was identified.

[1]Revision received March 18, 1985.

In order to gain some insight into the radiolysis results and to obtain more information on the reactions of CCl_3^+ with aromatic compounds we have studied the behaviour of CCl_4/aromatic hydrocarbon mixtures in a high pressure (2–4 Torr) mass spectrometer ion source operated under field free conditions. Our pressure regime is between that of the earlier low pressure mass spectrometric work and the much higher pressure used in the radiolysis study.

Experimental

Materials

Methane (Matheson Ultra-high Purity) had a stated purity exceeding 99.99%; carbon tetrachloride (Fisher Spectrograde) was used as received; all aromatics were of the highest purities available. In no case were impurities, or ions attributable to impurities, observed in any of the mass spectra.

Procedure

The mass spectrometer, equipped with field free, high pressure ion source has been described previously (10). The pressure range over which the instrument gave adequate signal was 2–4 Torr. Products of ion–molecule reactions were identified in conventional chemical ionization spectra when the source was operated in a standard, continuous ionization mode. Reaction sequences were determined by pulsing the electron beam (11). After a 50-μs pulse of 2-keV electrons the temporal profile of the intensity of a selected ion was followed for up to 10 ms using an ion multiplier, ion counting equipment, and a multiscalar. Data for $1-8\times10^3$ pulses were summed. Such data for every ion observed in the CI spectrum were normalized and plotted as normalized ion intensities vs. residence time in the ion source.

Results and discussion

The formation of CCl_3^+

In order to obtain unambiguous results it was essential that CCl_3^+ ions be generated in a bath gas towards which they exhibit no reactivity. It would have been preferable to use pure

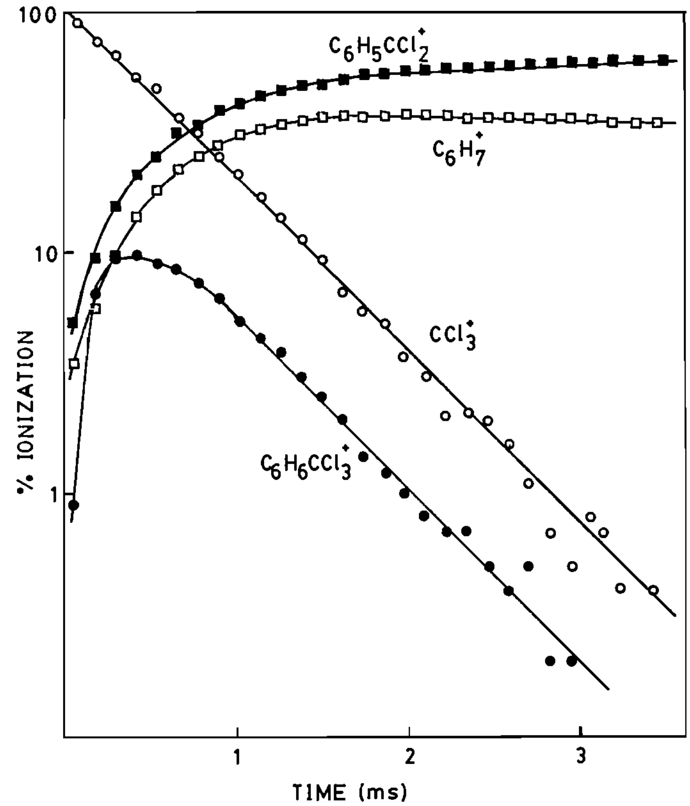

FIG. 1. Normalized ion intensities as functions of time, observed in 3.8 Torr of methane containing 3.5×10^{-4} Torr benzene and 1.0×10^{-3} Torr carbon tetrachloride at 435 K.

CCl_4 since it has been shown that CCl_3^+ generated from CCl_4 by electron impact is unreactive towards the parent molecule (9). High pressures of CCl_4 were found to inhibit the operation of the field free source. After a short time of operation, ions no longer emerged from the ion exit slit without the assistance of a repeller field. Such effects have been attributed to the formation of a semiconducting film on the edges of the slit (12). Ions were transmitted again when the source was heated to ~600 K and then cooled to the appropriate temperature but the use of pure CCl_4 again led to the disappearance of the ion beam.

CCl_3^+ was readily formed in mixtures of ~0.3 mol% CCl_4 in CH_4 and it was the only ion present 100 μs or so after a pulse of ionizing electrons at pressures above 2 Torr. The major ions present in methane alone at long reaction times are CH_5^+ and $C_2H_5^+$ (13). Both these ions react with CCl_4 to produce CCl_3^+. In addition, i-$C_3H_7^+$ produced in a CH_4/C_3H_8 mixture (20:1) also reacts with CCl_4 to produce CCl_3^+. However, neither i-$C_4H_9^+$ formed in CH_4/n-C_4H_{10} nor *t*-$C_4H_9^+$ formed in CH_4/i-C_4H_{10} mixtures was observed to react with CCl_4. These findings are in accord with those obtained using ion cyclotron resonance and substantiate the range 191–203 kcal mol^{-1} placed on $\Delta H_f^0(CCl_3^+)$ (14).

The reactions of CCl_3^+ with aromatic hydrocarbons

CCl_3^+ was found to react with benzene, toluene, the xylenes, and mesitylene. Only two initial product ions were observed with each aromatic (ArH), the adduct ion, $ArHCCl_3^+$, and the ion $ArCCl_2^+$ formed by loss of HCl from the adduct. Typical results are shown in Figs. 1–3.

Benzene + CCl_3^+

The adduct formed between C_6H_6 and CCl_3^+, $C_6H_6CCl_3^+$, is

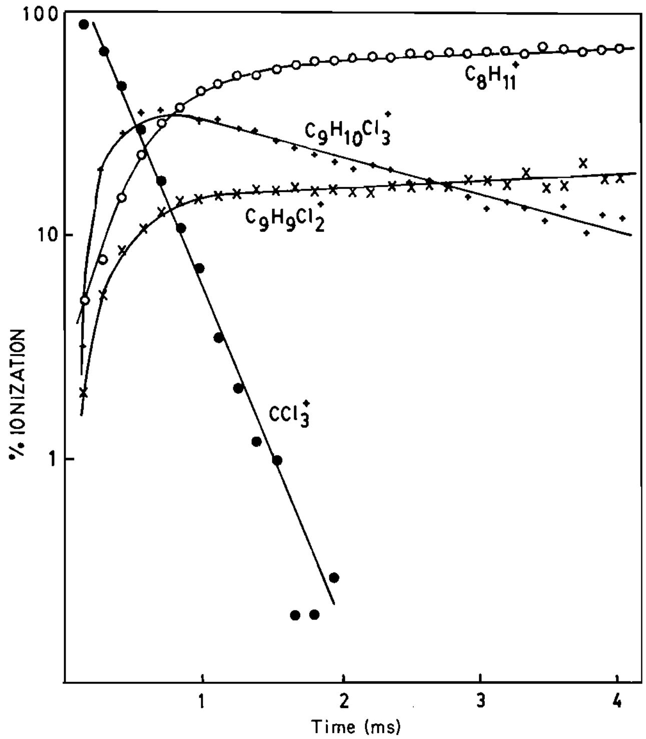

FIG. 2. Normalized ion intensities as functions of time, observed in 3.9 Torr of methane containing 1.8×10^{-4} Torr *m*-xylene and 1.0×10^{-3} Torr carbon tetrachloride at 460 K.

a major product ion only at low temperatures and, even then, only at short reaction times (Fig. 1). It is absent from the spectrum at temperatures above 500 K when $C_6H_5CCl_2^+$ is the sole product ion observed. This latter ion is always the major product at long reaction times at temperatures from 300 to 560 K. It is always the major ion in the mass spectrum.

At low temperatures, when $C_6H_6CCl_3^+$ is present, its yield maximizes after a few hundred microseconds and then decreases rapidly. $C_6H_6CCl_3^+$ is identified as an arenium ion since it transfers a proton to neutral benzene in a second-order reaction. Proton transfer to bases of higher basicity than benzene is also observed.

[2] 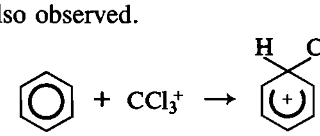 (I)

[3] 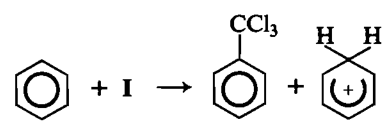

The *ipso*-protonated ion, **I**, probably rearranges rapidly by H^+ migration to more basic sites on other ring carbons prior to the occurrence of reaction [2]. The electron-withdrawing properties of the CCl_3 group will increase the acidity of the proton in **I** and its isomers to a value greater than that of protonated benzene, which explains the facile proton transfer, reaction [3].

$C_6H_5CCl_2^+$ is presumably a benzyl cation, which is the same as that observed at low pressure (1, 2) and is formed by loss of HCl from the adduct. It is not observed to react further.

[4] 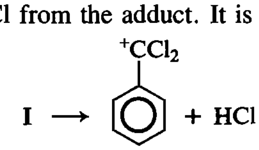

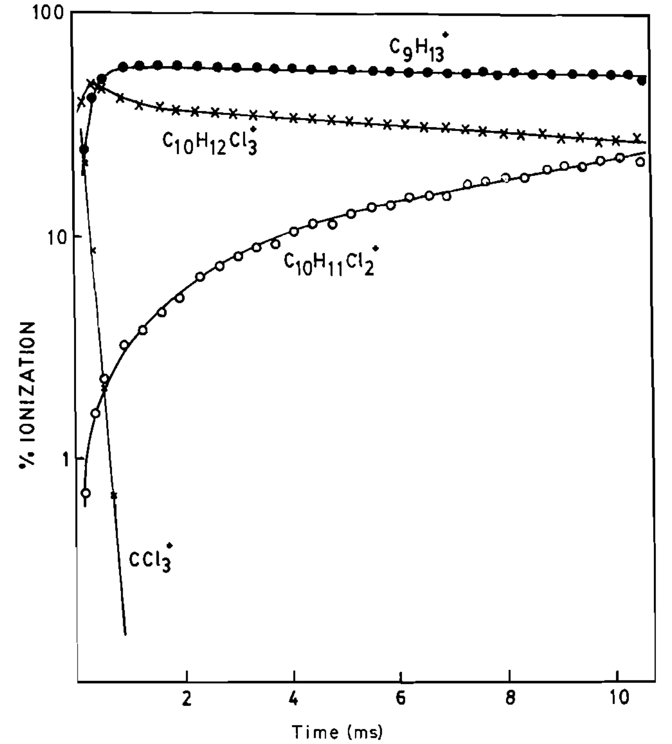

FIG. 3. Normalized ion intensities as functions of time, observed in 3.9 Torr of methane containing 1.4×10^{-4} Torr mesitylene and 1.6×10^{-3} Torr carbon tetrachloride at 300 K.

If reactions [2] and [3] were the only fate of $C_6H_6CCl_3^+$, then the ratio ($[C_6H_7^+] + [C_6H_6CCl_3^+])/[C_6H_5CCl_2^+]$ should remain constant at all times. The ratio actually declines slowly from a value of 1.2 at short reaction time to 0.53 at the longest time. At very long reaction time $C_6H_7^+$ is decreasing very slowly, while $C_6H_5CCl_2^+$ is still increasing (Fig. 1) even though CCl_3^+ and $C_6H_6CCl_3^+$ have essentially disappeared. This suggests that $C_6H_7^+$ is reacting to form $C_6H_5CCl_2^+$, presumably by reaction with CCl_4. Two possible mechanisms may be written, (a) a dissociative proton transfer (reaction [5]) generating CCl_3^+ which then reacts with C_6H_6 via reactions [2] and [4] to give $C_6H_5CCl_2^+$:

[5] $C_6H_7^+ + CCl_4 \rightarrow C_6H_6 + HCl + CCl_3^+$

and (b) a concerted reaction whereby $C_6H_6CCl_3^+$ is formed as a primary product and again decomposes to $C_6H_5CCl_2^+$:

[6] $C_6H_7^+ + CCl_4 \rightarrow C_6H_6CCl_3^+ + HCl$

With ΔH_f^0 (CCl_3^+) in the range 192–203 kcal mol^{-1}, reaction [5] is endothermic by 13–25 kcal mol^{-1} and will not be observed. Reaction [6] is less endothermic than reaction [5] by the binding energy of CCl_3^+ to C_6H_6. The latter value is not known but, considering that the methyl cation affinity of benzene calculated from the dissociation of protonated toluene is 95 kcal mol^{-1},[2] the binding energy of CCl_3^+ to C_6H_6, although less than that of CH_3^+, will be sufficiently great to make reaction [6] exothermic. The slowness of the energetically allowed reaction may be attributed to competitive dissociation of an initially formed ion–molecule complex. Entropy favours return to reactants rather than formation of products via a tight transition state.

It was not possible to experimentally ascertain whether reaction [6] occurs. A very slow ($k = 7 \times 10^{-13}$ cc molecule^{-1} s^{-1} at 468 K) disappearance of $C_6H_7^+$ was observed in a 4:1 CCl_4/C_6H_6 mixture in CH_4. A small accompanying increase in the yield of $C_6H_5CCl_2^+$ was observed at the same time but this increase was only about one-half the expected value. Some unidentified products (*m/z* 119 and 121) made up the difference. No such reaction was observed with any of the other aromatics. Such a slow reaction is at the lower limit of what can be studied by high pressure mass spectrometry. The study is doubly difficult since the product, $C_6H_5CCl_2^+$, is also formed in other reactions. Confirmation of the occurrence of reaction [6] will require a different experimental technique.

Reaction [6] is obviously too slow to account for all the large change with time of the ratio ($[C_6H_7^+] + [C_6H_6CCl_3^+])/[C_6H_5CCl_2^+]$. A slow thermal decomposition of stabilized $C_6H_6CCl_3^+$ must also be occurring. Such a reaction was found to occur with xylene and mesitylene (see later).

The $C_7H_6Cl_3^+$ formed in reaction [2] will be in an excited state and will require third body stabilization in order to be observed by the ion detection system. Prior to this stabilization it may be possible for decomposition to occur by loss of HCl, yielding $C_6H_5CCl_2^+$ (reaction [4]). It is impossible to quantitatively determine the branching ratio of decomposition to stabilization since, as discussed above, $C_6H_5CCl_2^+$ is formed in several ways. If the assumption is made that all the $C_6H_7^+$ observed has $C_7H_6Cl_3^+$ as precursor, then the following generalization may be made regarding the effects of temperature and pressure on the branching ratio. At high temperature (>500 K) and any pressure in the range 1.0–4.5 Torr the yield of $C_6H_5CCl_2^+$ constitutes more than 99% of the detected products. At 298 K and 4.0 Torr, $C_7H_6Cl_3^+ + C_6H_7^+$ account for 90% of the products observed at the shortest reaction time; at the same temperature and a pressure of 1.2 Torr the value is reduced to 75%. These percentages are only a lower limit for stabilization and it is probable that at 298 K and 2–4 Torr essentially all encounters between CCl_3^+ and C_6H_6 lead to a stabilized $C_7H_6Cl_3^+$ that either thermally decomposes or reacts by proton transfer. As the temperature is increased decomposition may occur before stabilization but, since the lifetime of the stabilized complex with respect to thermal decomposition will decrease, the two effects are inseparable.

An attempt was made to produce the adduct $C_6H_6CCl_3^+$ by protonation of α,α,α-trichlorotoluene. The only observed product of protonation by CH_5^+ and $C_2H_5^+$ was $C_6H_5CCl_2^+$. Protonation must be on chlorine rather than on the ring. α,α,α-Trichlorotoluene is formed in reaction [2] and it is at first sight surprising that this product was not observed in good yield in the γ-radiolysis of CCl_4/C_6H_6 gaseous mixtures (7). We found, however, that the following slow reaction occurs.

[7] 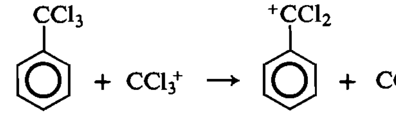

At the high total dose of 4.8 Mrad employed in the radiolysis it is possible that much of the initially formed α,α,α-trichlorotoluene is scavenged. The fate of the resulting α,α-dichlorobenzyl cation is unknown. Neutralization by a negative ion to give products that were not discovered or further reaction with

[2]Thermochemical data for neutral molecules are taken from ref. 15. Proton affinities are from ref. 16. ΔH_f^0 (CH_3^+) = 261.8 kcal mol^{-1} (ref. 24). The proton affinity values have been decreased by 2 kcal mol^{-1}, in line with the change in the accepted value of the proton affinity of ammonia from 205 to 203 kcal mol^{-1}.

benzene to give undetected high molecular weight products are possibilities.

Toluene + CCl_3^+

The reaction of toluene with CCl_3^+ was qualitatively the same as that of benzene. The $C_7H_8CCl_3^+$ adduct was a little more stable than that of benzene and a very small signal due to this ion was present (<1% total ionization) even at the elevated temperature of 560 K.

Xylenes + CCl_3^+

All the xylenes behaved in the same manner, the example of *m*-xylene shown in Fig. 2 being typical. The CCl_3^+ adducts are much more stable than those of either toluene or benzene but, again, further reaction occurs by proton transfer to yield protonated xylenes, e.g.

[8]
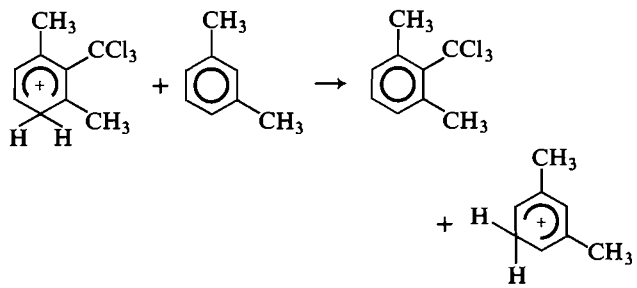

Loss of HCl from $C_9H_{10}Cl_3^+$ leads to $C_9H_9Cl_2^+$. Figure 2 shows that the yield of the latter ion reaches a maximum value of only 15% total ionization. The yield increases rapidly at short times when CCl_3^+ is still present, implying decomposition of the nascent *m*-xylene CCl_3^+ complexes. At long reaction times the $C_9H_9Cl_2^+$ curve increases slowly, even though CCl_3^+ has disappeared. This increase must be due to the thermal decomposition of the thermally stabilized complex, a reaction which is in competition with proton transfer to neutral *m*-xylene.

Mesitylene + CCl_3^+

Mesitylene yields the most stable adduct with CCl_3^+. Even at 560 K the adduct constituted about 50% of the product ions in a mass spectrum taken at 3.0 Torr for a 0.03:0.0003:1, CCl_4/mesitylene/CH_4 mixture.

[9]
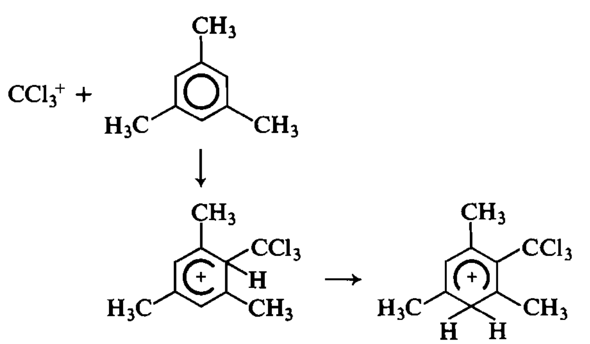

(II) (III)

The three methyl groups confer stability on $C_{10}H_{12}Cl_3^+$. Two of the methyl groups will always be *ortho* and one will be *para* to the protonated tetrahedral site even if, as is probable, rearrangement occurs from an initial *ipso* form (**II**) to a more stable structure (**III**).

The stabilization afforded by the methyl group of toluene protonated at different ring positions relative to protonated benzene has been estimated (17). The values are (kcal mol^{-1})

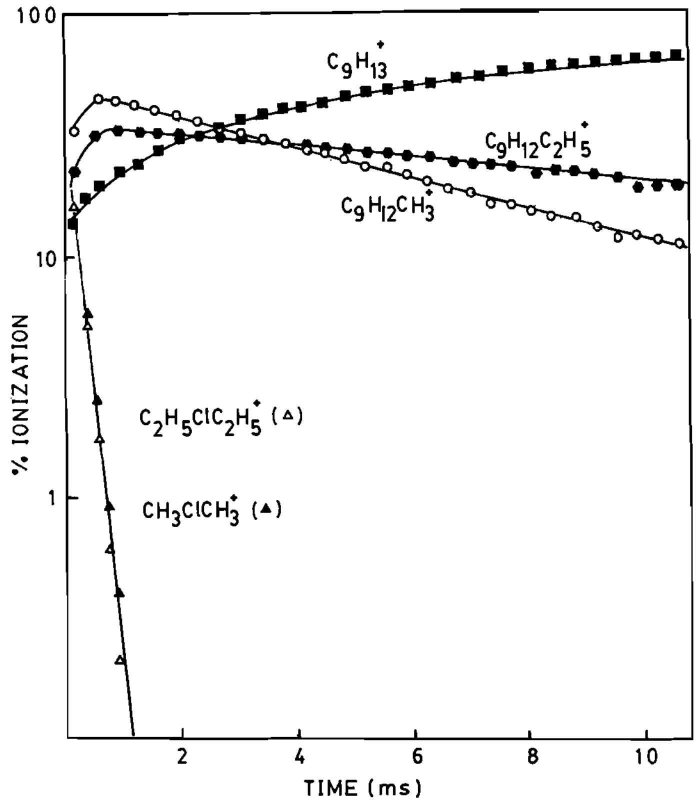

FIG. 4. Normalized ion intensities as functions of time, observed in 3.5 Torr methane containing 0.26 Torr methylchloride and 1.4 × 10^{-4} Torr mesitylene at 300 K.

ipso 0.3, *ortho* 6.5, *meta* 2.0, and *para* 8.5. On the assumption that the effects of methyl groups are additive, the calculated proton affinity of mesitylene with two methyls *ortho* and one methyl *para* to the protonation site is +21.5 kcal mol^{-1} relative to that of benzene. Experimentally the value is +17.0 kcal mol^{-1}, consistent with the estimate (17).

The most stable form of the mesitylene CCl_3^+ adduct should therefore be **III**, with the electron-withdrawing CCl_3 group *meta* to the proton site. Although its effect on proton binding energy will be least in this position, the CCl_3 group should still be destabilizing. We therefore expected a facile proton transfer to mesitylene, analogous to the reactions observed in the systems containing benzene, toluene, and the xylenes.

Figure 3 shows that at 300 K $C_{10}H_{12}Cl_3^+$ transfers a proton to mesitylene, yielding $C_9H_{13}^+$ only at relatively short reaction times when CCl_3^+ is still present. After this time the yield of $C_9H_{13}^+$ remains constant and no further reaction of this ion was observed. This was found to be the case for a variety of reagent concentrations and total pressures. The implication is that at this temperature only nascent, i.e. not fully thermalized, arenium ions are capable of protonating mesitylene. For the thermalized arenium ion, therefore, a CCl_3 substituent appears actually to decrease the acidity of protonated mesitylene.

The above observation is in contrast to that of Buttrill and co-workers (18) who found that the arenium ion resulting from the addition of mesitylene$^+$ to NO_2, $C_9H_{12}NO_2^+$, transfers a proton "very rapidly" to mesitylene. If the arenium ion has a structure analogous to **III**, with NO_2 *meta* to the site of the proton, then its destabilizing influence should not be too much greater than that of CCl_3 since at this site only the inductive effect is operative (19).

TABLE 1. Rate constants for the reaction CCl_3^+ + ArH → products

ArH	Temperature (K)	k (cc molecule^{-1} s^{-1} × 10^{10})	Reaction efficiency[a]
Benzene	560	1.0	0.09
Toluene	560	4.4	0.38
o-Xylene	560	6.5	0.55
m-Xylene	560	8.9	0.75
p-Xylene	560	6.6	0.56
Mesitylene	560	8.8	0.72
Mesitylene	298	12.7	1.04
p-Fluorotoluene	432	2.9	—

[a]Reaction efficiency = $P = k_{\text{exptl}}/k_{\text{ADO}}$.

We have previously reported (20) that when CH_3^+ or $C_2H_5^+$ adds to mesitylene, the resulting arenium ion does transfer a proton, albeit slowly, to mesitylene. We have repeated that experiment with the results shown in Fig. 4. The decays of the two arenium ions by proton transfer to mesitylene at 300 K are second order, with the very low rate constants of 1×10^{-11} (C_2H_5) and 3×10^{-11} (CH_3) cc molecule^{-1} s^{-1}. These alkyl groups *meta* to the CH_2 group will stabilize the ion by ~2 kcal mol^{-1} (17), the ethyl group being slightly more effective than the methyl. Proton transfer to mesitylene will therefore be endothermic by this amount and hence the reaction will be quite slow (21), as is observed. Comparison of the results in Figs. 3 and 4 suggests that a CCl_3 substituent is more stabilizing than either CH_3 or C_2H_5, but the effect must therefore be kinetic rather than thermodynamic.

At 468 K the mesitylene-CCl_3^+ adduct did transfer a proton to mesitylene ($k = 7 \times 10^{-11}$ cc molecule^{-1} s^{-1}), consistent with the reaction being endothermic and therefore having a positive activation energy. It is interesting that proton transfer from the $C_2H_5^+$ and CH_3^+ mesitylene adducts to mesitylene at the same and higher temperatures did not show the expected increases in rate. At 468 K the methyl and ethyl adducts had rate constants of 1.6 and 0.8×10^{-11} cc molecule^{-1} s^{-1} respectively and the values decreased further at higher temperatures. It was confirmed by equilibrium measurements that the proton affinity of 1,2,3,5-tetramethylbenzene is higher than that of mesitylene, the difference being 2.2 kcal mol^{-1}. These results suggest that the adducts formed by alkyl ions and aromatics may not be the commonly accepted arenium ions. This point is under further investigation.

Figure 3 shows that although $C_{10}H_{11}Cl_2^+$ has the mesitylene-CCl_3^+ adduct $C_{10}H_{12}Cl_3^+$ as precursor its rate of formation is very low and that it must arise from thermalized $C_{10}H_{12}Cl_3^+$. There is no dependence of yield on mesitylene concentration and a second-order transfer of CCl_3^+ to mesitylene with accompanying loss of HCl may be ruled out. Thermal decomposition of the adduct, as suggested for benzene, toluene, and the xylenes, must occur. In support of this contention, the yield of $C_{10}H_{11}Cl_2^+$ was negligibly small at 298 K. No experimental evidence was found for a reaction between protonated mesitylene and CCl_4 analogous to that suggested for benzene.

Specific rate constants for the disappearance of CCl_3^+

The reaction of CCl_3^+ with an aromatic molecule to form a stabilized adduct may be written

$$[11] \quad CCl_3^+ + ArH \underset{k_b}{\overset{k_a}{\rightleftharpoons}} (ArHCCl_3^+)^*$$

$$[12] \quad (ArHCCl_3^+)^* + M \underset{k_d}{\overset{k_c}{\rightleftharpoons}} ArHCCl_3^+ + M$$

With the usual assumptions that the excited intermediate complex achieves a steady state concentration and that k_d is negligible compared with k_c, the overall forward rate constant is given by

$$[13] \quad k_f = \frac{k_a k_c[M]}{k_b + k_c[M]}$$

When $k_b \gg k_c[M]$ the reaction is kinetically third order, whereas at higher total pressure, when $k_c[M] \gg k_b$, second-order kinetics will be observed. The disappearance of CCl_3^+ was always pseudo first order (see Figs. 1–3). Second-order rate constants were obtained from the measured slopes using the equation

$$[14] \quad \ln \frac{[CCl_3^+]_t}{[CCl_3^+]_0} = \ln \frac{i_t}{i_0} = k_f[ArH]_t$$

where i_t is the normalized CCl_3^+ ion current at time t. There was no significant change in the value of any measured second-order rate constant with pressure over the limited experimental range of 2–4 Torr. Meot-Ner has discussed in detail the available data on pressure and temperature dependences of ion–molecule association reactions (22). Although third-order behaviour has been observed for many of these reactions at pressure below 1 Torr, intermediate or second-order behaviour is often observed at higher pressure especially for more complex molecules. It is not surprising that only second-order behaviour is observed in our systems, which contain relatively large participating molecules with many degrees of freedom in their internal motions.

Second-order rate constants, obtained mainly at 560 K, are presented in Table 1. Reproducibility of a given value from day to day was better than ±15%. Also shown is the efficiency of reaction per collision, $P = k_{\text{exptl}}/k_{\text{ADO}}$, where k_{ADO} is the rate constant for ion–molecule collision calculated by the averaged dipole orientation theory (23).

The efficiency of reaction is high for all the aromatics studied and is close to unity for mesitylene at all temperatures. The efficiency of reaction increases as the number of methyl groups on the aromatic increases (benzene → mesitylene), presumably due to the stability of the arenium ion formed, i.e. there is a correlation between reaction exothermicity and reaction rate.

Figure 5 shows the effect of temperature on the specific rate constants for benzene, toluene, *m*-xylene, and mesitylene. The data points for benzene show some scatter but do encompass results for a range of benzene concentrations differing by a factor of 20 and for carbon tetrachloride by a factor of more than 100. The plot for benzene shows that the temperature dependence of the specific reaction rate constant is of the form $k \propto T^n$ with $n = -2$. *m*-Xylene and mesitylene have specific rate constants close to the collisional limit at all but the highest temperatures, when the values fall off somewhat, so that in this region again each shows a negative temperature dependence. The rate constants for toluene are between those of benzene and *m*-xylene, with a negative temperature coefficient ($n \approx -1$). It was not experimentally possible to obtain data at temperatures below 298 K.

There is therefore no energy barrier to the formation of the trichloromethylarenium ions but there are insufficient data to

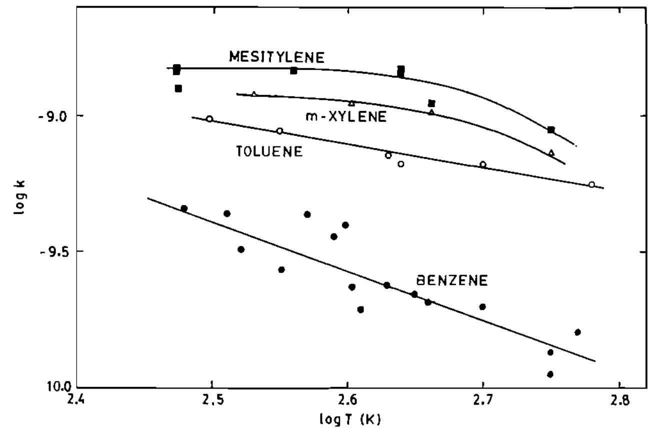

FIG. 5. The variations with temperature of the specific rate constants for the reactions of CCl_3^+ with benzene, toluene, *m*-xylene, and mesitylene. Ion source pressures 2–4.5 Torr. For *m*-xylene and mesitylene the points encompass results obtained with carbon tetrachloride in the concentration range 0.1–0.3 mol% and 4×10^{-3} mol% aromatic. For benzene and toluene the range of carbon tetrachloride concentrations is 5×10^{-3} to 0.1 mol% and aromatic 1×10^{-3} to 2×10^{-2} mol%. There are no significant trends with concentration variations.

speculate on the significance of the slopes of the plots shown in Fig. 5; suffice to say that the nature of the plots is consistent with the association mechanism postulated.

At 298 K benzene reacts with CCl_3^+ with an efficiency $P = 0.4$. This least reactive of the aromatics therefore reacts at this temperature once in every 2.5 collisions. In order to study in depth the temperature coefficients of the reactions of CCl_3^+ with aromatics it will be necessary to work with compounds of lower reactivity than benzene. The halogenated benzenes would be suitable candidates, although in this context it is interesting that no reaction was observed between CCl_3^+ and hexafluorobenzene at 463 K.

Acknowledgement

The authors thank the Natural Sciences and Engineering Research Council of Canada for financial assistance.

1. L. P. THEARD, and W. H. HAMILL. J. Am. Chem. Soc. **84**, 1134 (1962).
2. L. I. VIRIN, YU. A. SAFIN, and R. V. DZHAGATSPANYAN. Khim. Vys. Energ. **2**, 16 (1968).
3. L. I. VIRIN, YU. A. SAFIN, L. I. VIKHROVA, and R. V. DZHAGATSPANYAN. Khim. Vys. Energ. **4**, 342 (1970).
4. L. I. VIRIN, YU. A. SAFIN, and R. V. DZHAGATSPANYAN. Khim. Vys. Energ. **6**, 408 (1972).
5. S. E. LIAS and P. AUSLOOS. Ion–molecule reactions, their role in radiation chemistry. American Chemical Society, 1975.
6. R. CIPOLLINI. Radiochem. Radioanal. Lett. **16**, 193 (1974).
7. R. CIPOLLINI, G. LILLA, N. PEPE, and M. SPERANZA. J. Phys. Chem. **82**, 1207 (1978).
8. C. E. KLOTS. *In* Fundamental processes in radiation chemistry. *Edited by* P. Ausloos. Interscience, New York. 1968. p. 1.
9. N. A. MACASKILL. Aust. J. Chem. **23**, 893 (1970).
10. J. A. STONE and D. E. SPLINTER. Can. J. Chem. **59**, 1779 (1981).
11. P. KEBARLE. *In* Interaction between ions and molecules. *Edited by* P. Ausloos. Plenum Press, New York. 1975. p. 459.
12. J. V. HEADLEY, R. S. MASON, and K. R. JENNINGS. J. Chem. Soc. Faraday Trans. 1, **78**, 933 (1982).
13. F. H. FIELD and M. S. B. MUNSON. J. Am. Chem. Soc. **87**, 3289 (1965).
14. S. G. LIAS and P. AUSLOOS. Int. J. Mass. Spectrom. Ion. Phys. **23**, 273 (1977).
15. J. D. COX and G. PILCHER. Thermochemistry of organic and organometallic compounds. Academic Press, New York. 1970.
16. D. H. AUE and M. T. BOWERS. *In* Gas phase ion chemistry. Vol. 2. *Edited by* M. T. Bowers. Academic Press, New York. 1979. p. 1.
17. J. L. DEVLIN, J. F. WOLF, R. W. TAFT, and W. J. HEHRE. J. Am. Chem. Soc. **98**, 1990 (1976).
18. R. J. SMITT, S. E. BUTTRILL, and D. S. ROSS. J. Am. Chem. Soc. **106**, 926 (1984).
19. R. A. Y. JONES. Physical and mechanistic organic chemistry. Cambridge University Press, Cambridge. 1979.
20. J. A. STONE, W. M. SPLINTER, and D. E. SPLINTER. Can. J. Chem. **62**, 1373 (1984).
21. D. K. BOHME, G. I. MACKAY, and H. I. SCHIFF. J. Chem. Phys. **73**, 4976 (1980).
22. M. MEOT-NER. *In* Gas phase ion chemistry. Vol. 1. Academic Press, New York. 1979. p. 197.
23. T. SU and M. T. BOWERS. Int. J. Mass. Spectrom. Ion Phys. **12**, 347 (1973).
24. F. A. HOULE and J. L. BEAUCHAMP. J. Am. Chem. Soc. **101**, 4067 (1979).

The conformational analysis of piriprost, an inhibitor of leukotriene synthesis, based on high-field nuclear magnetic resonance studies[1]

GEORGE KOTOVYCH, HELMUT BEIERBECK, AND DAVID SALMON
Department of Chemistry, University of Alberta, Edmonton, Alta., Canada T6G 2G2

Received October 22, 1984

GEORGE KOTOVYCH, HELMUT BEIERBECK, and DAVID SALMON. Can. J. Chem. **63**, 2614 (1985).

The analysis of proton nuclear Overhauser effect data for piriprost, (6,9-deepoxy)-6,9-(phenylimino)-$\Delta^{6,8}$ prostaglandin I_1, indicates that the cyclopentene ring has the ^{11}E conformation. A long-range nOe effect indicates that the α-chain is folded near the pyrrole and the phenyl rings.

GEORGE KOTOVYCH, HELMUT BEIERBECK et DAVID SALMON. Can. J. Chem. **63**, 2614 (1985).

Une analyse des données relatives à l'effet Overhauser nucléaire du proton pour le piriprost, déépoxy-6,9 phénylimino-6,9 $\Delta^{6,8}$-prostaglandine I_1, indique que le noyau cyclopentène existe dans la conformation ^{11}E. Un effet eOn à longue distance indique que la chaîne α est repliée près des noyaux pyrrole ainsi que phényle.

[Traduit par le journal]

The leukotrienes are the products of the metabolism of arachidonic acid, which proceeds via two enzymatic processes. Cyclooxygenase transforms arachidonic acid to the prostaglandins, the thromboxanes, and prostacyclin, whereas lipoxygenases give rise to the leukotrienes. The properties and syntheses of the leukotrienes have been well reviewed (1, 2). The leukotrienes may be separated into two categories. The first series consists of leukotrienes C_4, D_4, and E_4, which collectively account for the biological activity ascribed to Slow Reacting Substances of Anaphylaxis. These compounds may therefore be important mediators of human diseases such as bronchial asthma. The second series consists of 5,12-dihydroxyeicosatetraenoic acids and one of these is leukotriene B_4, which is a potent stimulator of the movement of the leucocytes in vitro.

Over the last few years, we have been interested in the conformational analysis of the prostaglandins and leukotrienes (3, 4) as well as in quantitative nuclear Overhauser effect (nOe) studies as applied to flexible systems. In the course of these studies, we have analyzed nuclear Overhauser effect data for piriprost (6,9-deepoxy)-6,9-(phenylimino)-$\Delta^{6,8}$ prostaglandin I_1 (5), an inhibitor of leukotriene synthesis (Fig. 1). The quantitative analysis of the nOe data indicates the presence of a long-range interaction between the H-2 protons of the α chain and the pyrrole as well as the phenyl protons. These results will lead to a better understanding of structure–activity relationships.

Experimental

Piriprost was a gift from the Upjohn Company, in Kalamazoo, Michigan. The sample was prepared in glycine-d_6 buffer in D_2O, pH 9.95. The sample was frozen on the vacuum rack, the D_2O was removed, and fresh 100% D_2O was vacuum distilled into the nmr tube. The sample was then degassed, using the freeze–pump–thaw technique, and sealed. The solution concentration was ~0.005 *M* to minimize intermolecular association. About 5% EDTA was added to the solution. All glassware was cleaned extensively, including a nitric acid wash, to eliminate paramagnetic impurities.

All nmr measurements were carried out on a Bruker WH-400 FT nmr spectrometer equipped with an Aspect 2000 data system, using 16K, 32K, or 64K of memory, as required. The solvent deuterium resonances served as lock signal.

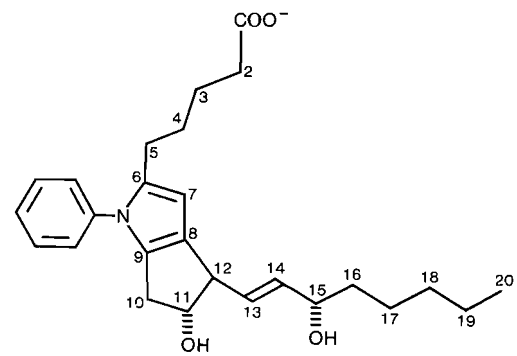

FIG. 1. The structure of piriprost.

For the determination of nonselective longitudinal ^{1}H relaxation times the $180°-t-90°$ pulse sequence was employed. Usually three M_∞ and twelve M_t measurements were taken, with $t \leq T_1$. The M_∞ and M_t represent sums of peak heights for each multiplet. Relaxation times were derived by a ln $(M_\infty - M_t)$ vs. t least-squares linear fit as well as a nonlinear least-squares fit using the Bruker DISNMR program, with good agreement. The T_1 data are averages of three determinations.

In the nOe experiments the decoupler was set to the first of three or four multiplets and four transients recorded (quadrature detection), the decoupler moved to the next multiplet, and finally far off resonance. Each multiplet was irradiated for a time $t \geq 5T_1$ with sufficient power to just saturate that signal. Each quoted nOe value is the average of three to five determinations. The quantitative nOe's were evaluated as follows. The normal and saturated spectra were simultaneously displayed on the screen and then subtracted. The difference spectrum was plotted and then the integration was performed. The intensity of the proton being saturated was used as the reference and nOe's are measured with respect to this peak.

Nuclear Overhauser effects

For the case of isotropic motion and dipole–dipole relaxation the fractional enhancement $f_d(s)$ at nucleus d on saturating signal s is given by (6)

$$[1] \quad f_d(s) = A\left[\sum_s g_d(s) - \sum_{i \neq d,s} f_i(s) g_d(i)\right] = -A \sum_{i \neq d} f_i(s) g_d(i), \qquad f_s(s) = -1$$

where $g_d(i)$ = the geometric term = $N_i\langle r_{di}^{-6}\rangle / \Sigma N_j \langle r_{dj}^{-6}\rangle$; N_j = number of magnetically equivalent nuclei j; r_{dj} = distance between protons d and j; and

[1]Paper Number 13 in a series of high-field nmr studies on the eicosanoids. Papers 11 and 12 are refs. 3 and 4.

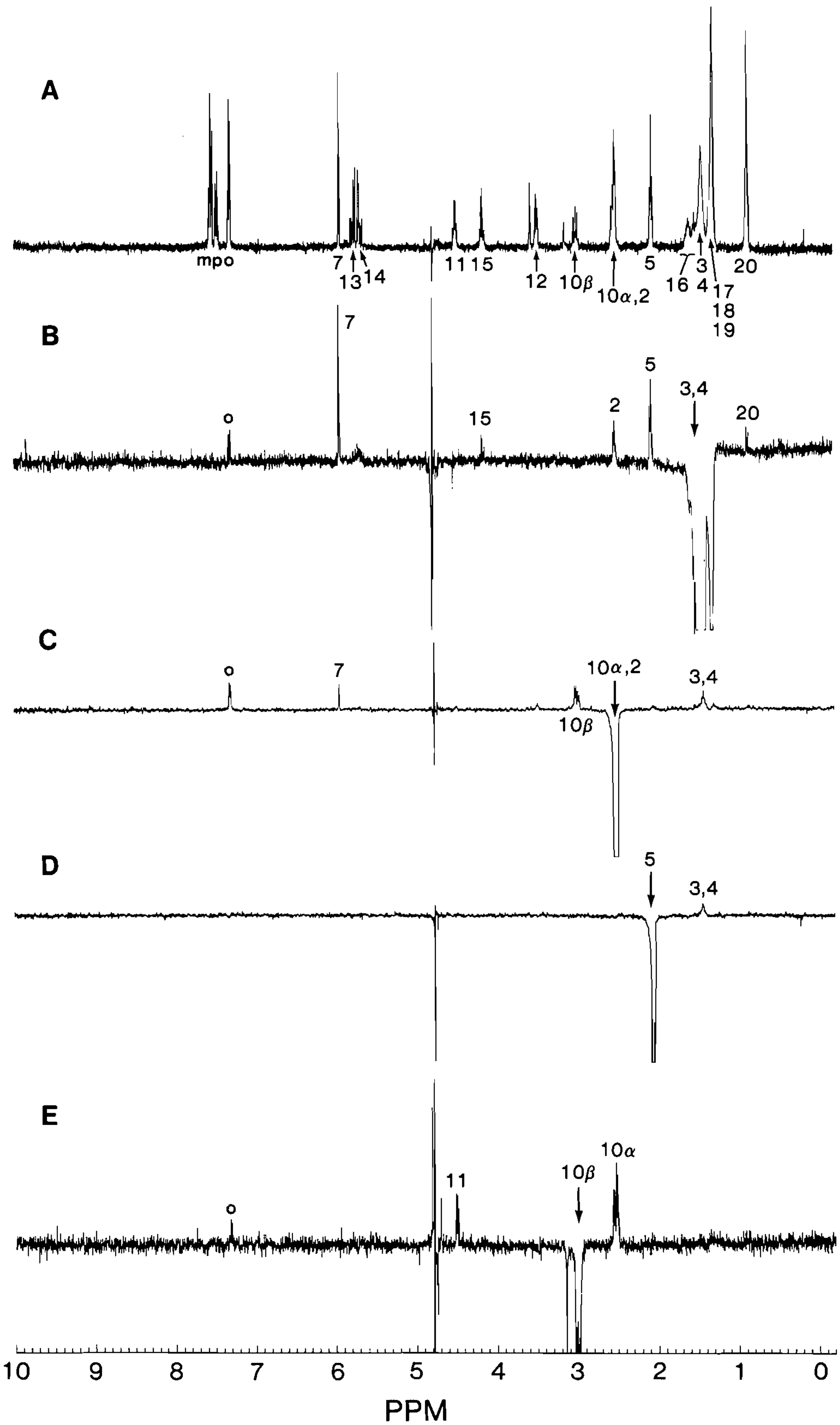

FIG. 2. The nmr spectra observed for piriprost. (A) the normal spectrum including solvent suppression, (B) saturation of the H3,4 multiplet, (C) saturation of the H10α and H2 multiplets, (D) saturation of H5, and (E) saturation of H10β.

TABLE 1. Chemical shifts (ppm) and coupling constants (Hz) for piriprost in glycine buffer, pH 9.85[a]

Protons	δ	Protons	J
2 (10α)	2.528	H2–H3	7.0
3	1.425		
4	1.432	H4–H5	7.2
5	2.060		
7	5.944		
10α (2)	2.528	H10α–H10β	15.25
10β	3.004	H10β–H11	7.2
11	4.498	H10α–H11	5.7
12	3.485		
13	5.774	H11–H12	5.5
14	5.682	H12–H13	7.1
15	4.159	H13–H14	15.3
16, 16*	~1.57	H14–H15	7.2
17–19	1.308	H15–H16	6.9
20	0.870	H19–H20	6.9

[a]The reference for the chemical shifts was internal DSS that was added after all the nOe and T_1 measurements were completed.

A = the correlation term

$$= [6\tau_c/(1 + 4\omega^2\tau_c^2) - \tau_c]/[\tau_c + 3\tau_c/(1 + \omega^2\tau_c^2) + 6\tau_c/(1 + 4\omega^2\tau_c^2)]$$

The brackets in $\langle r_{dj}^{-6}\rangle$ indicate conformational averages (7), where appropriate. The $f_d(s)$ were derived by an iterative least-squares fit of eq. [1] to the observed nOe's, treating A as an adjustable parameter.

Relaxation times

Nonselective ^{1}H relaxation times were calculated by a least-squares fit of eq. [2] (6) to the observed values, treating B as variable

$$[2] \quad T_{1i} = B/\left[\sum_{j\neq i} N_j\langle r_{ij}^{-6}\rangle + (N_i - 1)r_{ii}^{-6}\right]$$

where

$$B = 10/\{\hbar^2\gamma_H^4 \times [3\tau_c/(1 + \omega^2\tau_c^2) + 12\tau_c/(1 + 4\omega^2\tau_c^2)]\}$$

Ring conformations

The ring coordinates were based on the microwave structure of pyrrole (8) coupled with the force-field structure for cyclopentene (9).

The cyclopentene ring can only adopt the ^{11}E or $_{11}E$ conformations and the nOe data support the ^{11}E conformation. This places the ω chain as well as the C-11 OH group pseudoequatorial. The phenyl group must be nearly perpendicular to the pyrrole ring due to steric interactions from the protons at C5 and C10. In this conformation H10β is closer to the phenyl protons than H10α. X-ray data of related systems indicate that in 2,6-disubstituted biphenyl analogs the angle between the planes is either 73.9° (10) or 91.8° (11).

Side chain conformations

Coordinates and conformer populations for segment C2–C15 were needed. The conformations of the α- and ω-chains were built with C—C and C═C bond lengths of 0.154 and 0.134 nm, trigonal bond angles, and eclipsed C(sp^2)—C(sp^3) and staggered C(sp^3)—C(sp^3) rotamers. The N—C6—C5 bond angle was taken to be 120° and the C6—C5—C4 and C5—C4—C3 bond angles 112°.

Results and discussion

The 400-MHz nmr spectrum of piriprost is shown in Fig. 2 together with the multiplet assignments. These are based on decoupling experiments. Representative nOe experiments are also presented in Fig. 2. The chemical shifts and coupling constants are shown in Table 1. For the cyclopentene ring, only three vicinal coupling constants are available. On this basis, it

TABLE 2. Nuclear Overhauser effect data for piriprost in glycine buffer, pH 9.85

Irradiated proton	Detected proton[a]	Calculated[b]
2[c]	3 or 4 – 5.1	4.3
	7 – 4.5	
10α[c]	10β – 18.6	19.9
10α,2	*ortho* – 6.1	(1.0)[d]
3,4	2 – 6.4	5.0
	5 – 7.8	4.9
	7 – 8.4	—
5	3 or 4 – 3.7	4.3
	ortho – 0.0	4.4
7	3 or 4 – 1.2	—
10β	10α – 22.0	22.2
	11 – 8.9	8.9
	ortho – 1.6	0.9
11	10β – 3.1	3.7
	12 – 3.1	3.6
	13/14 – 3.0	—
12	7 – 0.9	0.8
	11 – 1.8	2.1
	13/14 – 3.6	—
13/14	11 – 4.1	10.4
	12 – 13.2	15.8
	15 – 7.6	—
	17 – 2.3	—
ortho	2 – 1.9	—

[a]The error limits on the observed nOe's are estimated to be one unit.
[b]A correlation time of 0.25 ns was used in the calculations.
[c]The 2 and 10α protons overlap but the appropriate nOe's are assigned as shown.
[d]The calculated nOe is due to the saturation of H10α.

was difficult to confirm the ring conformation. The nOe data proved most useful in showing that this ring has the ^{11}E conformation (Table 2). The nOe expression [1] is applicable to the rigid portion of the molecule, from C6 to C15, as is the case for prostacyclin and its analogs (12, 13).

Excellent agreement is observed between the observed and calculated nOe's between the ring protons, namely, H10α, H10β, 11, and 12 (Table 2) for the ^{11}E conformation of the cyclopentene ring. The phenyl group is oriented almost perpendicular to the plane of the pyrrole ring. This is supported by the fact that an nOe is not observed to the *ortho* protons on saturating H5. An nOe is not observed to H5, H10α, nor H10β on saturating the *ortho* protons. Saturation of H10β results in a small nOe (1.6%) to the *ortho* protons. Saturation of the overlapping H2 and H10α multiplet results in a 6.1% nOe to the *ortho* protons. In both cases the calculated nOe is 1%. The difference is due to the interaction between the H2 and the *ortho* protons. A wide range of calculations were carried out in which the phenyl group was placed at different positions with respect to the pyrrole ring, but the best agreement between the observed and calculated nOe values was for the perpendicular phenyl ring conformation.

The data in Table 2 show that the large long-range nOe from H2 to H7 is about 4.5%. This nOe cannot arise from saturation of H10α (which overlaps H2) because the internuclear distance across the ring is too large. Finally, saturation of the *ortho* protons results in a very small nOe to H2.

The calculated and observed T_1 data are presented in Table 3. Good agreement is observed for protons H7, H10β, H11, and H12 as well as the *meta* protons. The long T_1 for the phenyl *ortho* protons becomes 1.43 s when the phenyl ring is

TABLE 3. T_1 data for piriprost

Proton	T_1 (obs.)	T_1 (calcd.)[a]
3,4	~0.50	
5	0.75	
7	1.72	1.61
10β	0.38	0.37
11	1.18	1.09
12	1.43	1.27
13	1.14	
14	1.24	
15	0.95	
17–19	~0.90	
ortho	1.53	2.13
meta	1.64	1.65
para	2.05	1.63

[a]A correlation time of 0.10 ns was used to calculate the T_1 data. The error limits on the T_1 measurements are ±5%.

twisted 30° out of the perpendicular orientation, and then is in good agreement with the observed T_1 of 1.53 s. The longer observed T_1 for H_p is a special case because it is on an axis of rotation and hence may have a shorter correlation time. Hence these data suggest some flexibility in the conformation of the phenyl ring. Finally, the calculated T_1's are based on a correlation time of 0.10 ns, which is slightly shorter than the 0.25-ns correlation time that gives the best fit to the nOe data (Table 2). The reason for this discrepancy is not known, but was observed previously in the PGI series (13).

The ω-chain conformations are determined by the fact that acyclic C(sp^2)—C(sp^3) bonds such as C12—C13 and C14—C15 are known to prefer rotational states in which the double bond eclipses the single bond (14, 15). In this situation the C12—H and C15—H bonds would be more or less coplanar with C13—C14. The vicinal coupling constants (J(H12−H13) = 7.1 Hz and J(H14−H15) = 7.2 Hz) do not agree with an exclusive antiperiplanar conformation, for which Garbisch's equation (16) estimates a value of 11.6 Hz. Consequently, other eclipsed rotamers are significantly populated. Ideally, the nOe experiment should allow the estimation of rotamer populations. Unfortunately H13 and H14 form an AB system and only the f_i{13,14} are available. Consequently, the nOe's and T_1's in Tables 2 and 3 were calculated with the population of the preferred rotamer to be 50%, as was done with the PGI series (13). In the minor rotamers H14 comes very close to H11 and a large nOe (10.4%) is calculated for f_{11}{13,14}. The observed nOe is 4.1%. In the absence of a molecular mechanics calculation for this molecule, a computer fit to the T_1 and nOe data was not pursued beyond C14 because the range of conformers about C12—C13 could be varied, or C12—C13 may be in rotational states with an H12—H13 dihedral angle close to 150° (3).

The mobility of the α-chain, and the close approach of H2 to the *ortho* protons as well as H7 is most interesting. As there is no nOe from H5 to H7, this indicates that H5 must be as far away as possible from H7. Similarly, there is no nOe to the *ortho* protons on saturating H5. This is consistent with the nearly perpendicular orientation of the phenyl ring. However, rotation about C5—C6 is necessary. The C4—C5—C6—C7 dihedral angle of zero will explain the lack of an nOe from H5 to H7, but it will exclude an nOe from H2 to the *ortho* protons. What was done, therefore, in our calculations was to take this angle as zero and C3—C4—C5—C6, C2—C3—C4—C5, and C1—C2—C3—C4 dihedral angles all *trans*. This does not bring the H2 protons near the *ortho* nor the H7 protons to which an nOe is observed. But because of the wide range of conformations that can be adopted by this chain, coupled with the fact that the α-chain will have a shortening of the correlation times as the segmental motion increases, the above model was used in the calculations.

In Table 2, the calculated contributions to the nOe's arising from the α-chain are therefore not reported, i.e. from H2 to H7 and to the *ortho* protons, from H3,4 to H7, nor from H7 to H3,4.

In summary, a long-range nOe is observed from H2 to the *ortho* protons and the pyrrole H7 proton. In all of our previous work involving the prostaglandins, this long-range nOe was not observed, either because of multiplet overlap or due to the fact that for the prostacyclin analogs there are two geminal H7 protons. As these protons relax each other, it would be difficult to observe long-range nOe's. The ring adopts an ^{11}E conformation, which is supported specifically by the nOe data, more so than the limited coupling constant data. The phenyl ring is almost perpendicular to the plane of the rings as determined by the small nOe's between the H10 and H5 protons and the aromatic ring protons, while the T_1 data suggest some flexibility in this ring. Finally, the ω-chain conformations are similar to those observed in the prostacyclin series of compounds because the coupling constants are similar.

Acknowledgements

The authors thank Dr. John Burka of the Pharmacology Department for valuable discussions, Wayne Moffat, Dr. Gabor Toth, and Dr. H. Kawaki for their assistance in obtaining some of the spectra, Dr. M. Bach for the sample of piriprost, and Dr. L. Baczynskyj for a sample of the methyl ester, and the Natural Sciences and Engineering Research Council of Canada and the University of Alberta for generous financial assistance.

1. B. SAMUELSSON. Angew. Chem. Int. Ed. Engl. **21**, 902 (1982).
2. E. J. COREY. Experientia, **38**, 1259 (1982).
3. M. SUGIURA, H. BEIERBECK, P. C. BELANGER, and G. KOTOVYCH. J. Am. Chem. Soc. **106**, 4021 (1984).
4. M. SUGIURA, H. BEIERBECK, G. KOTOVYCH, and P. C. BELANGER. Can. J. Chem. **62**, 1640 (1984).
5. M. K. BACH, J. R. BRASHLER, H. W. SMITH, F. A. FITZPATRICK, F. F. SUN, and J. C. MCGUIRE. Prostaglandins, **23**, 759 (1982).
6. J. H. NOGGLE and R. E. SCHIRMER. The nuclear Overhauser effect. Academic Press, New York. 1971.
7. R. E. SCHIRMER, J. P. DAVIS, J. H. NOGGLE, and P. A. HART. J. Am. Chem. Soc. **94**, 2561 (1972).
8. L. NYGAARD, J. T. NIELSEN, J. KIRCHHEINER, G. MALTESEN, J. RASTRUP-ANDERSEN, and G. O. SORENSEN. J. Mol. Struct. **3**, 491 (1969).
9. O. ERMER and S. LIFSON. J. Am. Chem. Soc. **95**, 4121 (1973).
10. J. H. CARDELLINA, M. P. KIRKUP, R. E. MOORE, J. S. MYNDERSE, K. SEFF, and C. J. SIMMONS. Tetrahedron Lett. 4915 (1979).
11. L. HILTUNEN, L. NIINISTO, T. PAKKANEN, and T. PAKKANEN. Cryst. Struct. Commun. **7**, 643 (1978).
12. G. KOTOVYCH and G. H. M. AARTS. Org. Magn. Reson. **18**, 77 (1982).
13. H. BEIERBECK, G. KOTOVYCH, and M. SUGIURA. Can. J. Chem. **63**, 1143 (1985).
14. G. J. KARABATSOS and D. J. FENOGLIO. Top. Stereochem. **5**, 167 (1970).
15. H. KISHI. Aldrichimica Acta, **13**, 23 (1980).
16. E. W. GARBISCH. J. Am. Chem. Soc. **86**, 5561 (1964).

Nitro-olefin bicycloannulation: one-step synthesis of tricyclo[3.2.1.$0^{2,7}$]octan-6-ones from cyclohexenones and of tricyclo[2.2.1.$0^{2,6}$]heptan-3-ones from cyclopentenones

ROBERT M. CORY,[1] PAUL C. ANDERSON, MURRAY D. BAILEY, FRED R. MCLAREN, RICHARD M. RENNEBOOG, AND BRIAN R. YAMAMOTO

Department of Chemistry, University of Western Ontario, London, Ont., Canada N6A 5B7

Received December 19, 1984

ROBERT M. CORY, PAUL C. ANDERSON, MURRAY D. BAILEY, FRED R. MCLAREN, RICHARD M. RENNEBOOG, and BRIAN R. YAMAMOTO. Can. J. Chem. **63**, 2618 (1985).

Nitro-olefins bicycloannulate the α′-enolates of α-cyclohexenones and α-cyclopentenones by initial addition at −78°C, followed by further reaction *in situ* in the presence of hexamethylphosphoramide in refluxing tetrahydrofuran to give tricyclo-[3.2.1.$0^{2,7}$]octan-6-ones and tricyclo[2.2.1.$0^{2,6}$]heptan-3-ones in a single synthetic step. The reactions with 1-nitropropene and with a nitro-olefin having a more complex β-substituent are stereoselective, forming predominantly the tricyclic diastereomer in which the group derived from the β-substituent of the nitro-olefin is *syn* to the carbonyl bridge. Based on the isolation of intermediates and side products, the mechanism of the bicycloannulation is shown to proceed via sequential kinetically controlled conjugate addition of the enolate to the nitro-olefin at low temperatures, thermodynamically controlled intramolecular Michael addition at higher temperatures to give a bicyclo[2.2.2]octanone intermediate, and hexamethylphosphoramide-assisted expulsion of the nitro group as nitrite ion with formation of the cyclopropane ring. For the first time this type of bicycloannulation has been applied to cyclopentenones, and a one-step synthesis of tricyclenone has been carried out to demonstrate the synthetic utility of this new reaction.

ROBERT M. CORY, PAUL C. ANDERSON, MURRAY D. BAILEY, FRED R. MCLAREN, RICHARD M. RENNEBOOG et BRIAN R. YAMAMOTO. Can. J. Chem. **63**, 2618 (1985).

À −78°C, les nitro-oléfines s'additionnent sur les α′-énolates des α-cyclohexénones et des α-cyclopenténones; par réaction *in situ* en présence d'hexaméthylphosphoramide dans le tétrahydrofuranne au reflux, les produits ainsi obtenus conduisent en une seule étape à une bicycloannellation qui fournit les tricyclo[3.2.1.$0^{2,7}$]octanones-6 et les tricyclo[2.2.1.$0^{2,6}$]heptanones-3. Le nitro-1 propène et les nitro-oléfines ayant des substituants plus complexes en positions β réagissent d'une façon stéréosélective pour conduire à la formation prépondérante du diastéréoisomère tricyclique dans lequel le groupe provenant du substituant en position β de la nitro-oléfine est en position *syn* par rapport au pont carbonyle. En se basant sur la nature des intermédiaires et des produits secondaires qu'on a pu isoler, on montre que la bicycloannellation s'effectue par l'intermédiaire d'une série d'additions conjuguées sous contrôle cinétique de l'énolate sur la nitro-oléfine à basses températures et d'additions de Michael intramoléculaires à haute température sous contrôle thermodynamique qui conduisent à la bicyclo[2.2.2]octanone intermédiaire et à l'expulsion du groupe nitro sous forme de cyclopropane. On a appliqué pour la première fois ce type de bicycloannellation aux cyclopenténones et, pour démontrer l'utilité de cette nouvelle réaction, on a réalisé en une seule étape la synthèse de la tricyclénone.

[Traduit par le journal]

Introduction

The development of new methodology for the efficient construction of polycyclic systems has long been a major emphasis of research in organic synthesis. Our own contributions to this work have focussed on the discovery of new bicycloannulation reactions, in which tricyclic structures are formed in a single synthetic operation from monocyclic precursors.[2] In particular, we have reported a series of methods for the bicycloannulation of cyclohexenes (1*b*, 2) and cyclohexenones (1*a*, 3) to give tricyclo[3.2.1.$0^{2,7}$]octanes (**1**). This tricyclic system is a salient

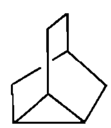

1

feature of four terpene families, including the ishwarane (4) and cycloseychellene (5) sesquiterpenes and the trachylobane (6) and helifulvane (7) diterpenes, and we have applied two of our bicycloannulation reactions to the total synthesis of ishwarane (1*b*, 2*b*) and trachyloban-19-oic acid (3*c*, *d*).

[1]Author to whom correspondence should be addressed.

[2]For the most recent previous papers in the series Bicycloannulation see ref. 1.

While recent work elsewhere has involved the construction of this tricyclo-octane system using multi-step procedures terminated by carbene insertion reactions (8),[3] our cyclohexenone bicycloannulations (Scheme 1) follow a series of three mechanistic steps, none of which involve carbenes. The α′ (kinetic) enolate (**2**) of the enone undergoes an initial conjugate addition to an activated olefin (**3**), in which Z has dual character, acting first as an electron-withdrawing group and then as a leaving group, displacement of which forms the cyclopropane ring of the tricyclo-octanone (**4**).[4] We have demonstrated that this type of bicycloannulation is successful with vinyl phosphonium salts (3*c*−*e*), vinyl sulfones (1*a*, 3*b*), and nitro-olefins (3*a*), and Hagiwara *et al.* have reported an analogous reaction of α-bromoacrylic esters, which they have used as the key step in a synthesis of ishwarane (12). Nitro-olefins, in particular, have become increasingly useful in synthesis in recent years (13−15), and we present herein a full description of our own work with these versatile reagents.

[3]We have also used a carbene strategy for a total synthesis of ishwarone (1*b*, 9). The first total synthesis of ishwarone employed a fundamentally different approach, in which the cyclopropane ring was generated by carbene addition in the *first* step of the construction of the tricyclo-octane system from a cyclohexene (10).

[4]The cyclopropane ring of this tricyclo-octanone system has also been formed by intramolecular enolate displacement of *conventional* leaving groups (11).

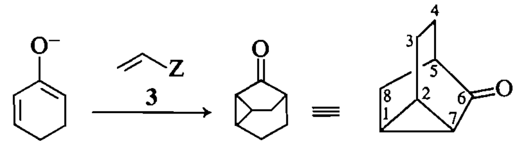

2 4

SCHEME 1. Bicycloannulation of cyclohexenone.

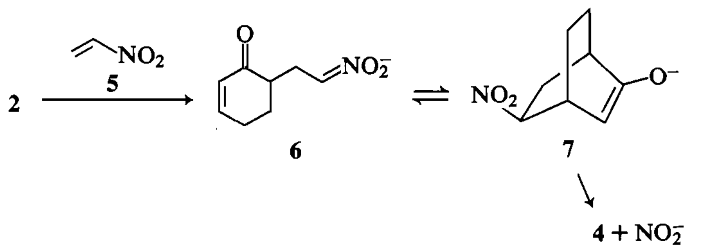

SCHEME 2. Nitro-olefin bicycloannulation.

The proposed mechanism of our bicycloannulation with nitroethylene (**5**) is shown in Scheme 2, in which the initial intermediate, nitronate **6**, closes to a bicyclo[2.2.2]octane system (**7**), followed by expulsion of nitrite ion. Conjugate addition of ketone enolates to nitro-olefins has found recent synthetic utility (13, 15*a*, *b*, *c*, *h*), and Michael addition of nitronate ions to α,β-unsaturated ketones has long been a useful tool (13, 16). The displacement of the nitro group from sp^3 carbon has received little attention (17), but a cyclopropanation method involving base-catalyzed addition of nitromethane and nitroethane to alkylidene malononitriles and malononitrile esters followed by intramolecular displacement of the nitro group has been reported (18). However, although each of the three steps in the bicycloannulation had precedent in previous studies, their combination had not been reported prior to our investigation.

Results and discussion

As in our studies of vinyl sulfones, in our initial experiments with nitro-olefins the procedure effective in bicycloannulations with vinyl phosphonium salts (3*c*) failed to provide volatile products, even with long reflux periods in tetrahydrofuran (THF). However, addition of hexamethylphosphoramide (HMPA) after addition of the nitro-olefin to the enolate, followed by a period of reflux, caused the formation of low to moderate yields of tricyclo-octanones. Polymerization of the nitro-olefin was minimized by adding it at −78°C. Thus, for example, when a solution of 1-nitropropene (**10**) in THF was added to a solution of the lithium α′-enolate (**9**) of isophorone (**8**) in THF at −78°C followed by addition of HMPA at room temperature and reflux for 16 h, there was obtained a 63% combined yield of two diastereomeric tricyclo-octanones: 58% of isomer **11**, having the 8-methyl group *syn* to the carbonyl bridge, and 5% of isomer **12**, having the 8-methyl *anti*. In addition, the nitro-bicyclo-octanone **13** was isolated in 4% yield (see entry 1, Table 1).

The stereochemistry of the major product was evident from the fact that the C-8 proton was coupled only with the 8-methyl protons in ^{1}H nmr, giving rise to a quartet at δ 2.36 with a coupling constant of 6.5 Hz. The lack of coupling of the *anti* 8-H with the bridgehead protons vicinal to it at C-1 and C-5 had been established in earlier work (3*c*). In contrast, the absorption due to the C-8 proton of epimer **12** appeared as a quartet

TABLE 1. Nitro-olefin bicycloannulation yields

Entry	Substrate	Reagent	Product	Yield, %
1	Isophorone	**10**	**11**	58[a]
2	*l*-Carvone	**10**	**22**	3[b]
3	**29**	**10**	**31**	42
4	**29**	**33**	**34**	25
5	**36**	**5**	**38**	13
6	**39**	**5**	**40**	3[c]
7	Isophorone	**5**	**42**	2[d]
8	**45**	**10**	**47**	39
9	**51**	**10**	—	0
10	**45**	**5**	**53**	22

[a]Plus **12** (5%) and **13** (4%).
[b]Plus **23** (1%).
[c]Plus **41** (7%).
[d]Plus **43** (19%).

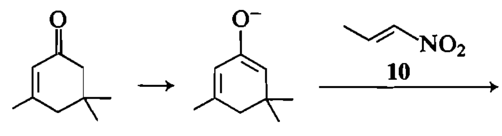

8 9

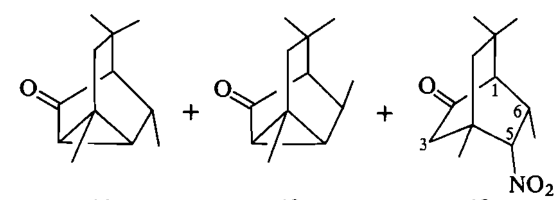

11 12 13

14 15

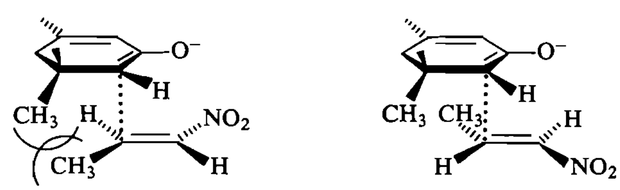

16 17

of doublets of doublets at δ 2.43, in which coupling constants of 7, 5, and 3 Hz were established by decoupling experiments to be due to coupling with the 8-methyl, C-5, and C-3 protons, respectively. These assignments were confirmed by LIS (lanthanide-induced shifts) studies, which found the ratio of Eu(fod)$_3$-induced shifts of the 8-methyl relative to the 8-H absorptions to be 1.2 for the *syn* isomer (**11**) vs. 0.42 for the *anti* isomer (**12**). For the adduct, **13**, decoupling showed the proton at C-6 (δ 2.68) to be coupled with the bridgehead proton at C-1, but with a coupling constant near zero, and also demonstrated coupling of 6-H with the proton at C-5 (δ 4.47) with J = 9 Hz. The C-5 proton also showed long range (*W*) coupling of 1 Hz with the proton at C-3 *anti* to the nitro group. These data are consistent only with the *syn-syn* stereochemistry proposed for this product.

When the reaction was quenched with acetic acid 30 min after adding the nitropropene at −78°C, two diastereomeric adducts were isolated in a combined yield of 74%. The major product (46%) was assigned to the *threo* adduct (**14**) based on the similarity of the AB pattern (part of an ABX system) in the ^{1}H nmr, due to the CH_2NO_2 protons, to that of the corresponding adduct with carvone (*vide infra*), the structure of which was unambiguously determined. These AB absorptions for **14** appeared at δ 4.60 and 4.28 with vicinal couplings of 10 and 3 Hz, respectively, and a geminal coupling constant of 13 Hz. By default the minor diastereomer (28%) was the *erythro* adduct, **15**, in the nmr of which the corresponding AB pattern at δ 4.62 and 4.36 showed vicinal couplings of 7 and 7.5 Hz, respectively, and the same geminal coupling of 13 Hz. In addition, the side-chain methyl doublet appeared at δ 1.25 in the spectrum of the *threo* diastereomer but at δ 1.00 in the case of the *erythro* adduct. Preference for the *threo* adduct has been observed previously in kinetically controlled additions of cyclohexanone enolate to a β-nitrostyrene (13, 19) and of cyclohexanone enamines to 1-nitropropene (20). This has been attributed to a combination of steric and electronic effects in the transition state and formulated by Seebach and Golinski as a "topological rule" applicable also to a variety of related reaction types (21).

Although it is the *threo* adduct (14), as the nitronate, which must give rise to the major bicycloannulation product (**11**) when HMPA is added, it should be noted that the stereoselectivity of the conjugate addition is much lower than that of the bicycloannulation itself. Furthermore, it is also much lower than that reported for cyclohexanone, which is essentially 100% (13, 19). This may be attributed to steric interference in the preferred transition state (**16**) between the methyl group of the nitro-olefin and one of the methyl groups of the enolate of isophorone, which would have the effect of raising the energy of this transition state relative to that (**17**) giving rise to the *erythro* adduct (**15**). As the temperature of the reaction mixture is raised and HMPA is added, an equilibrium is presumably set up between these adducts (as the nitronate anions) and the original enolate and nitro-olefin reactants. In turn, an equilibrium concentration of each of the bicyclo-octanes (**18** and **19**) resulting from intramolecular Michael addition of **14** and **15**, respectively, should also be established. This time it is adduct **19** in which unfavorable steric interaction between the two offending methyl groups is present. Thus, preference for the *syn* tricyclo-octanone **14** can be ascribed to an unfavorable equilibrium concentration of the *anti* adduct, **19**, relative to that of the *syn* adduct, **18**.

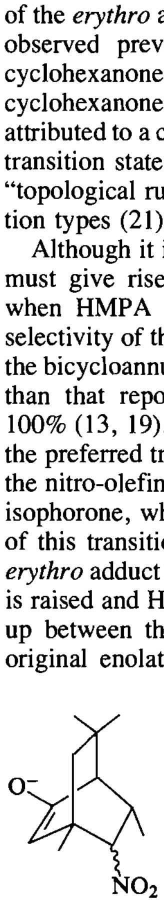

18

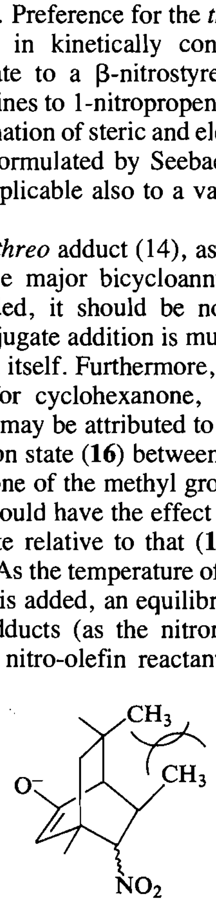

19

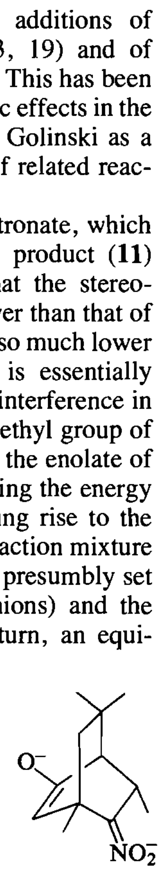

20

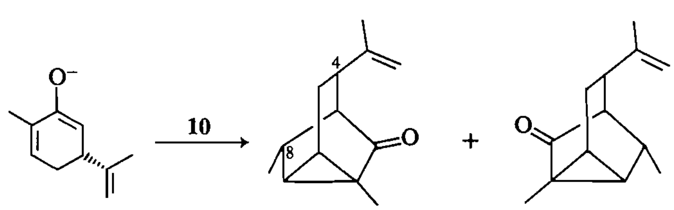

21 **22** **23**

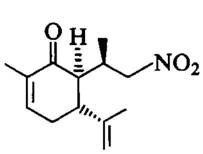

24

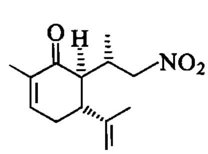

25

The formation of the annulation product, **13**, as a by-product of the bicycloannulation is understandable if one assumes that the excess LDA can remove a proton from intermediate **18** to give dianion **20**, thus removing some of **18** from the pathway leading to tricyclo-octanone **11** by preventing the final step, displacement of the nitro group, from taking place. During work-up, protonation of **20** would be expected to occur from the side of the nitronate moiety *anti* to the adjacent methyl group at C-6, thus providing the observed stereochemistry in adduct **13**. Whatever the explanation, the presence of **13** at least proves the presence of intermediate **18** in the reaction mixture and lends support to the proposed mechanism for the bicycloannulation.[5]

In our studies of vinyl phosphonium bicycloannulation a substrate providing some of the highest yields was carvone, although these were only on the order of 30−45% (3*c*). In the bicycloannulation of the same substrate with phenyl vinyl sulfone, however, only a 5% yield of tricyclo-octanone was obtained (1*a*, 3*a*). It was thus of great interest to determine if the relatively high yield obtained from the bicycloannulation of isophorone with 1-nitropropene extended also to carvone. Unfortunately, the results were even less encouraging than in the case of the vinyl sulfone. Reaction of the α-enolate (**21**) of *l*-carvone with 1-nitropropene under the same conditions as for isophorone, followed by addition of HMPA and reflux, gave only a 3% yield of the expected tricyclo-octanone, **22**, formed by attack of the nitro-olefin from the less hindered side of the enolate, and a 1% yield of tricyclo-octanone **23**, formed by attack on the *more* hindered side of the enolate. Interestingly, none of the two possible diastereomers with an *anti* 8-methyl group was detected, but in view of the low yields it is quite possible that minor amounts of other diastereomers were formed but in less than detectable quantities.

As was the case for the major product (**11**) from bicycloannulation of isophorone, the C-8 proton of *both* of the carvone-derived tricyclo-octanones gave rise to a quartet with J = 6.5 Hz in each of their nmr spectra (δ 2.11 for **22** and 2.18 for **23**), showing that the 8-methyl group in each of these diastereomers is *syn* to the carbonyl bridge. Again this assignment was confirmed by LIS, with a ratio of 0.9 for 8-methyl to 8-H for **22** and a ratio of 1.0 for **23**. Inter-compound LIS ratios for the isopropenyl groups were 2.3 for the methyl shift of **22** to that of **23**, 1.3 for the vinyl protons *trans* to the tricyclic system, and 3.2 for the *cis* vinyl protons, indicating *opposite* stereochemistry at C-4, the *syn* diastereomer being the major product, **22**. A detailed analysis of the ^{13}C nmr spectra (see Experimental) of the two tricyclo-octanones was also consistent with this stereochemical assignment.

[5]We have no evidence which would indicate the mechanism by which the nitro group is actually displaced, but the involvement of single electron transfer (SET) in this step would enable displacement even when the nitro group is *syn*, as in adduct **13**. Although an internal S_N2 type of mechanism has been proposed for cyclopropane ring formation of this type (18), a SET mechanism is preferred for most displacements of nitro groups from sp^3 carbon (17).

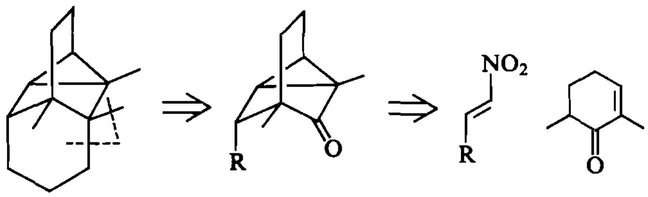

26 27 28 29

SCHEME 3. Retro-synthetic analysis.

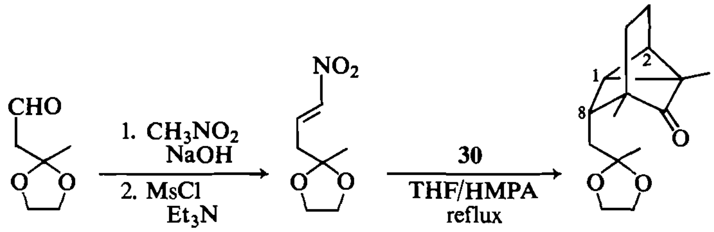

32 33 34

SCHEME 4. Synthesis of a "cycloseychellene" precursor.

In spite of the low yield of the bicycloannulation of carvone, quenching with acetic acid at −78°C gave a 4 : 1 mixture of two diastereomeric adducts from which the major one could be isolated by recrystallization from ethanol in 75% yield. A single crystal X-ray structure determination (22) proved that this adduct (**24**) had the *threo* stereochemistry with respect to the new carbon−carbon single bond, as predicted by the *topological rule*, and that addition of the nitro-olefin had occurred from the side of the enolate opposite to the isopropenyl group, as expected on steric grounds. The minor adduct (**25**) was separated from the mother liquor with difficulty by thick-layer chromatography in 7% yield. That this diastereomer had the *erythro* stereochemistry was indicated by the fact that the nmr absorption due to the CH_2NO_2 protons was an AB portion of an ABX pattern almost superimposable on that of the minor adduct (**15**) from isophorone (δ 4.91 and 4.62; J_{gem} = 13 Hz and J_{vic} = 7 and 6.5 Hz, respectively). Similarly, the AB pattern at δ 4.58 and 4.32 for the *threo* adduct (**24**) showed a geminal coupling constant of 12 Hz and vicinal ones of 9 and 4 Hz, respectively, very close to the values observed for the major isophorone adduct and thus supporting the stereochemical assignment of the latter. As with the isophorone adducts, the doublet for the methyl group of the side chain appeared at δ 1.29 and 1.00 for the *threo* and *erythro* adducts, respectively. Thus, low temperature addition of 1-nitropropene to carvone occurs exclusively from the less hindered side of the enolate, in spite of the observation that at higher temperatures and in the presence of HMPA tricyclo-octanone **23** is formed and must be derived from initial attack of the nitro-olefin from the *more* hindered side. Again, this seeming discrepancy may be attributed to kinetic control at −78°C in the absence of HMPA vs. thermodynamic control at reflux in the presence of HMPA. The greater stereoselectivity observed for addition to carvone at low temperature as compared with that for the corresponding addition to isophorone is consistent with the lack, in the transition state for carvone, of any adverse methyl−methyl steric interaction as depicted in structure **16**.

The relatively high degree of stereoselectivity found in the bicycloannulation of isophorone was attractive from the point of view of natural product synthesis, and one possibility investigated was a total synthesis of a structure (**26**) proposed for cycloseychellene, a tetracyclic patchouli oil sesquiterpene, in 1973 (23). The retro-synthetic strategy, shown in Scheme 3, involved disconnection of the two bonds indicated, giving tricyclo-octanone **27** after functionalization, where R would contain appropriate functionality for construction of the missing ring. Based on our results for nitro-olefin bicycloannulation of isophorone and carvone, this intermediate should be preparable stereoselectively from nitro-olefin **28** and cyclohexenone **29**. There were, however, two potential stumbling blocks in the path of this scheme. First, although the reasons for the low yield of the bicycloannulation of carvone are unknown, it is related to **29** in that both enones have a methyl group at the α position, as opposed to the β-methyl of the high yielding substrate, isophorone. Second, it was not known to what extent the methyl−methyl steric interaction depicted in intermediate **19** was responsible for the high stereoselectivity in the bicycloannulation of isophorone, an effect which would be absent in the addition of **28** to **29**.

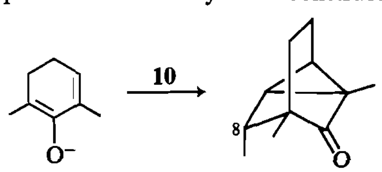

30 31

Therefore, a model study was carried out using 1-nitropropene as the bicycloannulation reagent and cyclohexenone **29** (1*b*) as the substrate. When the α'-enolate (**30**) of this ketone was treated with 1-nitropropene under the same conditions as for the other two substrates, we were gratified to discover that the desired tricyclo-octanone, **31**, was produced, apparently *with complete stereoselectivity*, in a yield of 42%! As before, the stereochemistry of the product was evident from ^{1}H nmr, in which the 8-H absorption appeared as a quartet (J = 7 Hz) at δ 2.02, and the LIS ratio of 8-methyl to 8-H was 1.0.

Whatever the reasons for this unexpected success, the stage was now set for cycloseychellene itself. The translation of a portion of the strategy implied in Scheme 3 into chemical reality was accomplished by choosing a masked acetonyl group to represent R. The conversion of tricyclo-octanone **27** into the natural product might be carried out by transforming the keto group of **27** into an acceptor containing a latent methyl group, ring closure by intramolecular attack of the enolate of the acetonyl group on this acceptor group, and methylation. Accordingly, the protected keto-nitro-olefin, **33**, was prepared by base-catalyzed nitro-aldol condensation[6] of nitromethane with keto-aldehyde, **32**, previously reported by Kelly and Tsang (25), followed by dehydration employing a modification of the method of McMurry and Melton (26) (Scheme 4). When this nitro-olefin was condensed with enolate **30** under the standard bicycloannulation protocol, the desired tricyclo-octanone, **34**, was isolated in 25% yield, none of the *anti* diastereomer being detected. The stereochemistry of this product was indicated by the presence of a sharp doublet in the nmr at δ 2.36 (J = 7.5 Hz), which could only be due to the bridgehead cyclopropyl proton at C-1 coupled with its vicinal partner at C-2 (3*c*). The lack of coupling of the 1-H with the proton at C-8 shows, as for the simpler tricyclo-octanones, that the side chain must have the *syn* configuration, as required for the total

[6]The more recent method of Wollenberg and Miller (24), employing potassium fluoride as the catalyst, proved to be capricious in this case.

synthesis. Unfortunately, it was at this point that a report by Welch and co-workers appeared, demonstrating that structure **26** was *not* the correct one for cycloseychellene and proving that the actual structure of the natural product is **35**, in which the only difference is the placement of the cyclopropane ring (5, 8*c*).[7] From a synthetic standpoint, of course, this is not a trivial change, and the course of our proposed total synthesis had to be altered completely and started over again. Our revised synthesis, which does not involve nitro-olefin bicycloannulation, is now in the final stages and will be reported separately.

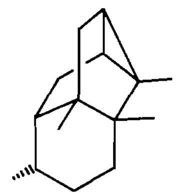

35

With the synthetic power of bicycloannulation with β-substituted nitro-olefins **10** and **33** well established, it was of interest to test the possibility that nitroethylene itself (**5**), the instability of which toward polymerization places it just within the borders of synthetic utility (14*f*, *l*), could also be used for the bicycloannulation of cyclohexenones. This would not only extend the scope of the nitro-olefin method, but would, in addition, allow an accurate comparison between the three bicycloannulation methods we have developed for cyclohexenones. We have found that *l*-carvone can readily be methylated at the α′ position (1*a*, 3*b*), and the resulting 2,6-dimethyl substituted cyclohexenone, **36**, as a mixture of diastereomers, could be converted to its α′-enolate, **37**, by reaction with LDA as usual. Treatment of this enolate with nitroethylene in the presence of HMPA using the standard bicycloannulation conditions produced a disappointingly low yield (13%) of tricyclo-octanone **38**, but in this case the reaction appeared to be completely stereoselective, only the product resulting from attack of the reagent from the less hindered side of the enolate being detected. Bicycloannulation of 3-methylcyclohexenone **39** with nitroethylene gave the annulation adduct, bicyclo-octanone **41**, as the major product, but in only 7% yield, the tricyclo-octanone (**40**) being isolated in only 3% yield. Similarly, bicycloannulation of isophorone (**8**) with the same reagent gave only a 2% yield of the desired tricyclo-octanone (**42**), the major product again being the bicyclic nitro-ketone (**43**), formed in a yield of 19%.

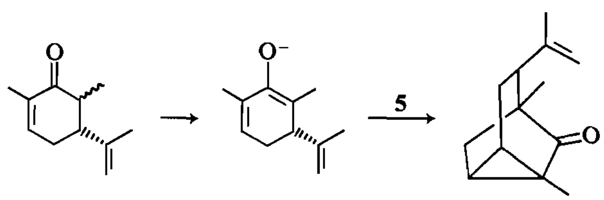

36 **37** **38**

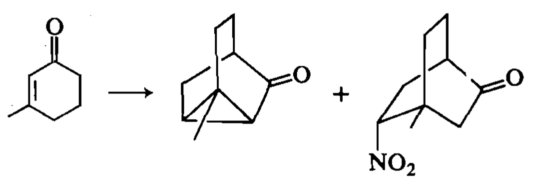

39 **40** **41**

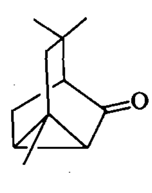

42

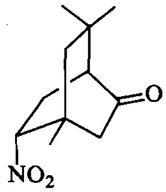

43

[7]The total synthesis of the racemic modification of cycloseychellene has recently been reported (27).

TABLE 2. Comparison of nitroethylene with vinyl sulfone and vinyl phosphonium bicycloannulations

Entry	Substrate	Reagent	Product	Yield, %
1	**39**	$CH_2{=}CHNO_2$ (**5**)	**40**	3
2	**39**	$CH_2{=}CHSO_2Ar^a$ (CVS)	**40**	19
3	**39**	$CH_2{=}CHPPh_3Br$ (VTB)	—	0
4	Isophorone	**5**	**42**	2
5	Isophorone	$CH_2{=}CHSO_2Ph$ (PVS)	**42**	38
6	Isophorone	CVS	**42**	7
7	Isophorone	VTB	**42**	16
8	**36**	**5**	**38**	13
9	**36**	PVS	**38**	17
10	**36**	CVS	**38**	20
11	**36**	VTB	**38**	65

[a]Ar = *p*-chlorophenyl.

The bicycloannulation yields for nitroethylene are summarized in Table 2 along with the corresponding data for phenyl vinyl sulfone (1*a*) and vinyltriphenylphosphonium bromide (3*c*). It is quite clear that bicycloannulation with the parent nitro-olefin, at least, does not compare favorably with the other two methods. However, it must be borne in mind that nitroethylene possesses an exceptional tendency to polymerize, so that this comparison cannot be generalized to all nitro-olefins. Unfortunately, we have no information on the abilities of *propenyl* sulfones and phosphonium salts to undergo the bicycloannulation reaction, so no comparison can be made with 1-nitropropene.

Although it would be desirable to extend these bicycloannulation methods to substrates other than cyclohexenones, our efforts toward this end were uniformly unsuccessful in the cases of the vinyl sulfones and vinyl phosphonium salts. Even cyclopentenones were uncooperative with the latter two reagents, but there still remained the possibility of success with the nitro-olefin method. In view of the variety of terpenes having the tricyclo[2.2.1.0^{2,6}]heptane ring system (**44**), including the sesquiterpenes α-santalol, α-santalene, longicyclene, cyclosativene, and cyclocopacamphene, the extension of nitro-olefin bicycloannulation to cyclopentenones would be of potential importance for the total synthesis of these natural products. Since isophorone had given the highest yields of the cyclohexenone substrates, a cyclopentenone (**45**) was chosen such that its structure approximated most closely that of isophorone. In the event, when its α'-enolate, **46**, generated in the usual way, was treated with 1-nitropropene and HMPA at reflux, a 39% yield of the desired tricyclo-heptanone (**47**) was obtained stereoselectively. The overall structure was indicated by the presence of three methyl singlets, a methyl doublet at δ 1.00, and the lack of vinyl proton absorption in the nmr, by a strong carbonyl ir absorption at 1757 cm^{-1}, and by comparison of the ^{13}C nmr data with that for related compounds (28, 29). An LIS ratio of 1.3 for 5-methyl to 5-H demonstrated the expected *syn* stereochemistry, while the latter proton gave rise to an nmr absorption which appeared to be a quartet of triplets, J = 6.5 and 1.5 Hz at δ 2.50, showing small coupling with the C-4 and C-6 protons vicinal to it.

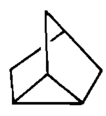

44

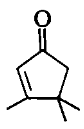

45

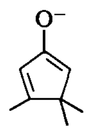

46

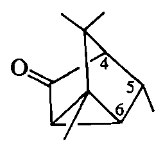

47

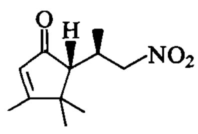

48

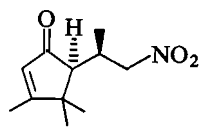

49

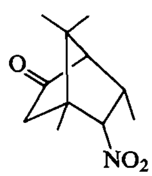

50

A low temperature quench with acetic acid after addition of the nitro-olefin gave unexpected results, the predominant adduct having the *erythro* stereochemistry (**48**), based again on ^{1}H nmr, and the minor product being the *threo* diastereomer (**49**), formed in yields of 50% and 37%, respectively. Although this stereochemistry is opposite to that observed for the cyclohexenone adducts, when it is compared with that of the adducts from isophorone, in which the corresponding yields were 28% and 46%, respectively, it can be seen that neither the selectivities nor the differences between them are very significant. Presumably, similar factors are responsible for the large proportion of *erythro* product in each case (*vide supra*). Interestingly, when the reaction was allowed to proceed at reflux, but in the *absence* of HMPA, the proportion of **48** and **49** was observed to slowly decrease at the expense of a new product. Work-up provided *none* of the tricyclo-heptanone (**47**) observed to form under the influence of HMPA, but gave a 3% yield of **49**, 6% of **48**, and 6% of what is believed to be the cyclized adduct, **50**, by analogy with adduct **13** from isophorone. The ^{1}H nmr data for the latter product were consistent with this stereochemical assignment, showing absorptions due to the C-5 proton at δ 4.76 as a doublet of doublets coupled with the vicinal 6-H (J = 6.5 Hz) and long-range (W) with the *exo* 3-H (J = 1 Hz), to the C-6 proton at δ 2.80 as a quintet coupled with both the 6-methyl and H-5 with a coupling constant of about 7 Hz, and to the C-1 bridgehead proton as a singlet at δ 2.13, $J_{1,6}$ being zero. The formation of this product only in the *absence* of HMPA and the isolation of the tricyclo-heptanone (**47**) only in the *presence* of HMPA would seem to argue for a predominant role in the *final* step of the mechanism, the displacement of the nitro group, for the facilitating effects of this cosolvent in the bicycloannulation reactions.

Although we were unsuccessful in isolating any volatile products from an attempted bicycloannulation of 3-methylcyclopentenone (**51**) with 1-nitropropene, a low temperature quench gave a 57% yield of an adduct which could not be completely purified, but the ^{1}H nmr of which was consistent with the *erythro* structure, **52**. If this assignment is correct, and we have no additional confirmation of it, it indicates that more work must be done before a firm understanding of the factors determining the stereochemistry of these adducts is at hand.

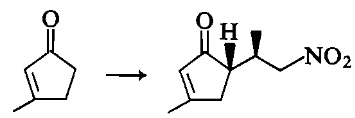

51 **52**

The success of the bicycloannulation of cyclopentenone **45** with 1-nitropropene led us to attempt a one-step synthesis of racemic tricyclenone (**53**) (30) from the same ketone. In the event, when the α'-enolate of cyclopentenone **45** was treated with nitroethylene in the presence of HMPA, the reaction required 187 h to force it to completion, but in the end a 22% yield of crystalline tricyclenone was isolated. Since tricyclenone has been converted by Wolff–Kishner reduction to tricyclene (**54**) by Nametkin and Zabrodina (31), our synthesis represents a formal two-step synthesis of this monoterpene,

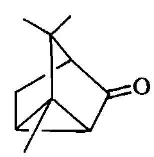

53

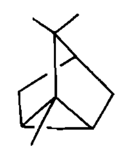

54

which occurs naturally in *Picea abies* (L.) Karsten (= *P. excelsa* Link) (32), *Picea mariana* (Mill.) (the black spruce) (33), and *Abies balsamea* (L.) Mill. (the balsam fir) (34).

In summary, although the nitro-olefin bicycloannulation method described here often gives inferior yields to those obtained by vinyl sulfone and vinyl phosphonium salts, in many cases the yields are quite acceptable, and in one specific example, the conversion of isophorone to tricyclo-octanone **11**, the yield is among the highest ever obtained for this type of reaction. Furthermore, the high degree of *syn* stereoselectivity observed when 1-nitropropene is used as the reagent is a characteristic of this method which promises to be useful in the total synthesis of natural products. The relatively inexpensive and convenient preparation of this stable nitro-olefin from cheap and readily available materials makes it all the more attractive. Finally, for the first time it is now possible to synthesize tricyclo-heptanones in a single synthetic step from cyclopentenones, although it remains to be seen how general this method will be for this purpose. Even nitroethylene gave a fairly good yield of tricyclenone, considering that the yield of this one-step procedure was higher than the overall yield of the previously reported highest-yielding multi-step one (30). The availability of these new synthetic tools greatly expands the pool of tricyclic products and intermediates within our reach, and those that we have described, as well as (by implication) a variety of related compounds, are now only a step away.

Experimental

General

All reactions were conducted under a positive pressure of argon. Ethyl ether (when used as a reaction solvent) and tetrahydrofuran were freshly distilled from sodium benzophenone ketyl, diisopropylamine was distilled from calcium hydride and stored over 4-A molecular sieves, and hexamethylphosphoramide was distilled from 13X molecular sieves. Butyllithium (in hexane) was obtained from Ventron and was titrated with 2-butanol in xylene (bipyridyl indicator) before use.

Preparative thick-layer chromatography was performed on precoated E. Merck silica gel GF (2 mm) on glass plates. Ethyl acetate was used to extract the separated components from the silica gel.

Nuclear magnetic resonance spectra were recorded on Varian Model XL-100 and XL-200 spectrometers, and ^1H and ^{13}C chemical shifts are reported in ppm (δ) downfield from internal tetramethylsilane. Infrared spectra were obtained on a Beckman Model 4250 spectrophotometer, and mass spectra were determined by electron impact on a Varian MAT Model 311A spectrometer employing an ionizing voltage of 70 eV unless stated otherwise. Melting and boiling points are uncorrected.

*Bicycloannulation procedure. 2,4,4,8(*syn*)-Tetramethyltricyclo-[3.2.1.0^{2,7}]octan-6-one (11) and 2,4,4,8(*anti*)-tetramethyltricyclo[3.2.1.0^{2,7}]octan-6-one (12)*

To a solution of 0.62 mL (0.45 g, 4.4 mmol) of diisopropylamine and 3 mg of 2,2′-bipyridyl in 4 mL of tetrahydrofuran at 0°C was added dropwise, with stirring, 2.5 mL (4.0 mmol) of 1.6 *M* *n*-butyllithium over 10 min. The resulting crimson solution was stirred at 0°C for 15 min, and a solution of 0.46 g (3.3 mmol) of isophorone (**8**) in 4 mL of tetrahydrofuran was then added dropwise, with stirring, over 45 min. After the mixture had been cooled to −78°C, a solution of 0.35 g (4.0 mmol) of 1-nitropropene[8] in 12 mL of tetrahydrofuran was added dropwise, with stirring, over 1.75 h, and the resulting yellow solution was stirred at −78°C for an additional 30 min. After the mixture had been allowed to warm to room temperature, 5 mL of hexamethylphosphoramide was added, and the mixture was then refluxed for 16 h. The cooled mixture was poured into 50 mL of saturated aqueous sodium bicarbonate, and the aqueous phase was extracted with 3 × 50 mL of petroleum ether (boiling range 30−60°C). The combined extracts were washed with 2 × 40 mL of water and 40 mL of brine and dried over anhydrous sodium sulfate. The solvent was distilled through a Vigreux column, and the residual concentrate was subjected to preparative gas chromatography[9] (140°C for 45 min; heat to 230°C at 40°C min^{-1}; 230°C) to give the following three products (yields determined by analytical gas chromatography[10] at 210°C using *n*-hexadecane as internal standard): (a) tricyclo-octanone **11**; 58%; colorless oil; gas chromatography[9] t_r = 28 min; ir ($CHCl_3$): 1720 cm^{-1}; ^1H nmr (100 MHz, $CDCl_3$) δ: [relative lanthanide-induced shifts (LIS) with added Eu(fod)$_3$ in brackets] 2.86 (d, 1H, *J* = 14 Hz), 2.83 (d, 1H, *J* = 5 Hz), 2.61 (d, 1 H, *J* = 14 Hz), 2.51 (d, 1H, *J* = 5 Hz), 2.36 [1.0] (q, 1H, *J* = 6.5 Hz), 1.26 (bs, 1H), 1.08 (s, 3H), 1.05 (s, 3H), 1.02 [1.2] (d, 3H, *J* = 6.5 Hz), 0.90 (s, 3H); mass spectrum, *m/z* (relative intensity): 178 (M$^+$, 22), 163 (7), 150 (9), 135 (19), 121 (20), 107 (41), 83 (100), 54 (22); high resolution mass spectrum, *m/z* calcd. for $C_{12}H_{18}O$: 178.1358; found: 178.1359; (*b*) tricyclo-octanone **12**; 5%; colorless oil; gas chromatography[9] t_r = 42 min; ir ($CHCl_3$): 1720 cm^{-1}; ^1H nmr (100 MHz, $CDCl_3$) δ: [relative LIS (with added Eu(fod)$_3$) in brackets] 2.43 [1.0] (qdd, 1H, *J* = 7, 5, 3 Hz), 2.04 (d, 1H, *J* = 14 Hz), 1.89 (dd, 1H, *J* = 5, 3 Hz), 1.61 (d, 1H, *J* = 5 Hz), 1.60 (d, 1H, *J* = 14 Hz), 1.51 (d, 1H, *J* = 5 Hz), 1.30 [0.42] (d, 3H, *J* = 7 Hz), 1.11 (s, 3H), 1.10 (s, 3H), 0.86 (s, 3H); mass spectrum, *m/z* (relative intensity): 178 (M$^+$, 18), 163 (6), 150 (15), 135 (21), 121 (32), 107 (43), 95 (22), 83 (100), 53 (28); high resolution mass spectrum, *m/z* calcd. for $C_{12}H_{18}O$: 178.1358; found: 178.1361; (c) 4,6(*syn*), 7,7-tetramethyl-5(*syn*)-nitrobicyclo-[2.2.2]octan-2-one (**13**); 4%; yellow oil; gas chromatography[9] t_r = 55 min; ir ($CHCl_3$): 1710, 1550 cm^{-1}; ^1H nmr (100 MHz, $CDCl_3$) δ: 4.47 (dd, 1H, *J* = 9, 1 Hz), 2.87 (bd, 1H, *J* = 19 Hz), 2.68 (bq, 1H, *J* = 8 Hz), 2.00 (bs, 1H), 1.85 (dd, 1H, *J* = 19, 1 Hz), 1.58 (d, 1H, *J* = 14 Hz), 1.41 (d, 1H, *J* = 14 Hz), 1.34 (d, 1H, *J* = 7 Hz), 1.22 (s, 3H), 1.02 (s, 3H), 0.97 (s, 3H); mass spectrum, *m/z* (relative intensity): 225 (M$^+$, 10), 178 (7), 153 (7), 135 (100), 121 (52), 109 (62), 95 (74), 83 (48), 69 (55), 55 (74); high resolution mass spectrum, *m/z* calcd. for $C_{12}H_{19}NO_3$: 225.1365; found: 225.1368.

Michael addition procedure. threo-*3,5,5-Trimethyl-6-(1-methyl-2-nitroethyl)cyclohex-2-en-1-one (14) and* erythro-*3,5,5-trimethyl-6-(1-methyl-2-nitroethyl)cyclohex-2-en-1-one (15)*

To a solution of 0.62 mL (0.45 g, 4.4 mmol) of diisopropylamine and 3 mg of 2,2′-bipyridyl in 4 mL of tetrahydrofuran at 0°C was added dropwise, with stirring, 2.5 mL (4.0 mmol) of 1.6 *M* *n*-butyllithium over 10 min. The resulting crimson solution was stirred at 0°C for 15 min, and a solution of 0.46 g (3.3 mmol) of isophorone (**8**) in 4 mL of tetrahydrofuran was then added dropwise, with stirring, over 45 min. After the mixture had been cooled to −78°C, a solution of 0.35 g (4.0 mmol) of 1-nitropropene[8] in 12 mL of tetrahydrofuran was added dropwise, with stirring, over 1.75 h. The resulting yellow solution was stirred at −78°C for an additional 30 min, after which 0.23 mL (0.24 g, 4.0 mmol) of glacial acetic acid was added rapidly, with stirring. The mixture was allowed to warm to room temperature and poured into 50 mL of water, and the aqueous phase was extracted with 3 × 50 mL of ethyl ether. The combined extracts were washed with 2 × 25 mL of water and 25 mL of brine and dried over anhydrous sodium sulfate. The solvent was evaporated under reduced pressure to give 0.83 g of crude product, of which 0.20 g was subjected to preparative thick-layer chromatography (eluting 4× with 9:1 methylene chloride/cyclohexane). Although the products were not completely separated from each other, careful dissection of the adsorbent layer provided samples enriched in each of the two major products, and integration of the nmr spectra gave approximate relative amounts from which the yields could be calculated: (a) *threo* adduct **14**; 0.34 g (46%); yellow oil; ir ($CHCl_3$): 1675, 1550 cm^{-1}; ^1H nmr (100 MHz, $CDCl_3$) δ: 5.85 (bs, 1H), 4.60 (dd, 1H, *J* = 13, 10 Hz), 4.28 (dd, 1H, *J* = 13, 3 Hz), 2.76 (m, 1H), 2.2 (m, 3H), 1.94 (bs, 3H), 1.25 (d, 3H, *J* = 7 Hz), 1.17 (s, 3H), 1.09 (s, 3H); mass spectrum (25 eV), *m/z* (relative intensity): 225 (M$^+$, 3), 191 (3), 178 (33), 162 (27), 149 (15), 136 (34), 123 (45), 97 (20), 82 (100); high resolution mass spectrum, *m/z* calcd. for $C_{12}H_{19}NO_3$: 225.1365; found: 225.1361; (*b*) *erythro* adduct **15**; 0.21 g (28%); yellow oil; ir ($CHCl_3$): 1675, 1550 cm^{-1}; ^1H nmr (100 MHz, $CDCl_3$) δ: 5.91 (bs, 1H), 4.62 (dd, 1H, *J* = 13, 7 Hz), 4.36 (dd, 1H, *J* = 13, 7.5 Hz), 2.84 (sextet of d, 1H, *J* = 7, 2.5 Hz), 2.22 (bs, 1H), 2.04 (d, 1H, *J* = 2.5 Hz), 1.94 (bs, 3H), 1.12 (s, 3H), 1.09 (s, 3H), 1.00 (d, 3H, *J* = 7 Hz; mass spectrum, *m/z* (relative intensity): 225 (M$^+$, 5), 178 (5), 163 (9), 149 (8), 123 (30), 97 (9), 82 (100), 54 (14); high resolution mass spectrum, *m/z* calcd. for $C_{12}H_{19}NO_3$: 225.1365; found: 225.1368. In addition, a small amount of an impurity (ca. 10%), tentatively assigned to 4,6(*syn*),7,7-tetramethyl-5(*anti*)-nitrobicyclo[2.2.2]octan-2-one, could be discerned in the nmr spectrum of **14**: 4.06 (bd, 1H, *J* = 6 Hz), 2.99 (b, quintet, 1H, *J* = 7 Hz), 1.01 (s, 3H), 0.97 (s, 3H).

[8] 1-Nitropropene was prepared in 36% overall yield from acetaldehyde and nitromethane using an improved procedure for the nitroaldol condensation (Henry reaction) (24). The dehydration of the nitro-alcohol (without purification of this intermediate) was carried out according to a long-standing recipe (35), which has since been optimized (36).

[9] A 0.2 in. × 10 ft copper column packed with 10% SE-30 on Diatoport S was employed with a helium flow rate of 60 mL min^{-1}.

[10] A 0.2 in. × 6 ft stainless-steel column packed with 10% Silar-5CP (Applied Science silicone ASI 50 phenyl/50 cyanopropyl) on Gas-Chrom Q (100/120 mesh) was employed with a helium flow rate of 60 mL min^{-1}.

4(syn)-Isopropenyl-7,8(syn)-dimethyltricyclo[3.2.1.0^{2,7}]octan-6-one (22) and 4(anti)-isopropenyl-7,8(syn)-dimethyltricyclo-[3.2.1.0^{2,7}]octan-6-one (23)

By the standard bicycloannulation procedure, 0.50 g (3.3 mmol) of *l*-carvone and 0.35 g (4.0 mmol) of 1-nitropropene[8] gave (gas chromatography[9] program: 170°C for 24 min; heat to 230°C at 40°C min^{-1}; 230°C) tricyclo-octanone **22**; 3%; colorless oil; gas chromatography t_r = 19.5 min; ir ($CHCl_3$): 1722, 1645 cm^{-1}; ^{1}H nmr (100 MHz, $CDCl_3$) δ: [relative LIS with added $Eu(fod)_3$ in brackets] 4.78 [0.4 and 1.6] (bs, 2H), 2.66 [1.1] (ddd, 1H, *J* = 10, 6, 2 Hz), 2.29 (ddd, 1H, *J* = 14, 10, 2.5 Hz), 2.11 [1.0] (q, 1H, *J* = 6.5 Hz), 2.08 (ddd, 1H, *J* = 14, 6, 2.5 Hz), 1.91 [2.7] (d, 1H, *J* = 2 Hz), 1.87 (d, 1H, *J* = 7 Hz), 1.68 [0.7] (bs, 3H), 1.67 (dt, 1H, *J* = 7, 2.5 Hz), 1.21 [1.2] (s, 3H), 1.04 [0.9] (d, 3H, *J* = 6.5 Hz); ^{13}C nmr (25.2 MHz, $CDCl_3$) δ: 213.4 (s), 147.3 (s), 110.4 (t), 53.3 (d), 49.3 (d), 39.4 (d), 36.7 (d), 34.5 (d), 33.2 (s), 23.9 (t), 21.3 (q), 19.9 (q), 12.9 (q) (cf. ref. 28); mass spectrum, *m/z* (relative intensity): 190 (M^+, 17), 175 (10), 147 (8), 135 (10), 122 (100), 106 (28), 94 (34), 80 (30), 67 (43); high resolution mass spectrum, *m/z* calcd. for $C_{13}H_{18}O$: 190.1358; found: 190.1356; and tricyclo-octanone **23**; 1%; colorless oil; gas chromatography t_r = 21.5 min; ir ($CHCl_3$): 1727 cm^{-1}; ^{1}H nmr (100 MHz, $CDCl_3$) δ: [relative LIS with added $Eu(fod)_3$ in brackets] 4.72 [0.3] (bs, 1H), 4.63 [0.5] (bs, 1H), 2.54 [1.8] (bt, 1H, *J* = 9 Hz), 2.18 [1.0] (q, 1H, *J* = 6.5 Hz), 1.84 [2.7] (bs, 1H), 1.7–2.3 (m, 4H), 1.61 [0.3] (bs, 3H), 1.15 [1.7] (s, 3H), 0.94 [1.0] (d, 3H, *J* = 6.5 Hz); ^{13}C nmr (25.2 MHz, $CDCl_3$) δ: 212.9 (s), 146.2 (s), 109.3 (t), 52.7 (d), 47.3 (d), 38.9 (d), 34.6 (d), 32.4 (s), 28.7 (d), 22.4 (t), 22.1 (q), 20.1 (q), 12.9 (q) (cf. ref. 28); mass spectrum, *m/z* (relative intensity): 190 (M^+, 11), 175 (6), 147 (4), 135 (8), 122 (100), 105 (20), 91 (18), 79 (17), 67 (22); high resolution mass spectrum, *m/z* calcd. for $C_{13}H_{18}O$: 190.1358; found: 190.1360.

(1′R, 5R, 6R)-5-Isopropenyl-2-methyl-6-(1′-methyl-2′-nitroethyl)-cyclohex-2-en-1-one (24) and (1′S, 5R, 6R)-5-isopropenyl-2-methyl-6-(1′-methyl-2′-nitroethyl)cyclohex-2-en-1-one (25)

By the standard Michael addition procedure, 0.50 g (3.3 mmol) of *l*-carvone and 0.35 g (4.0 mmol) of 1-nitropropene[8] gave, after recrystallization of the crude product (nmr indicated a 4:1 ratio of **24** to **25**), adduct **24**; 0.5 g (75%); colorless needles; mp 106.5–107°C (ethanol); ir ($CHCl_3$): 1670, 1550 cm^{-1}; ^{1}H nmr (100 MHz, $CDCl_3$) δ: 6.71 (bs, 1H), 4.94 (bs, 2H), 4.58 (dd, 1H, *J* = 12, 9 Hz), 4.32 (dd, 1H, *J* = 12, 4 Hz), 2.2–3.0 (m, 5H), 1.76 (bs, 6H), 1.29 (d, 1H, *J* = 7 Hz); mass spectrum, *m/z* (relative intensity): 237 (M^+, 2), 220 (2), 191 (3), 161 (2), 149 (12), 110 (9), 94 (10), 83 (100), 50 (20); high resolution mass spectrum, *m/z* calcd. for $C_{13}H_{19}NO_3$: 237.1365; found: 237.1369; single crystal X-ray structure determination (22). The mother liquor was evaporated under reduced pressure, and the residue was subjected to preparative thick-layer chromatography (eluting 2× with 9:1 methylene chloride/cyclohexane). Although the products were not completely separated from each other, careful dissection of the adsorbent layer provided a sample consisting of ca. 10% adduct **24** and ca. 90% adduct **25**; 53 mg (7%); yellow oil; ir ($CHCl_3$): 1670, 1550 cm^{-1}; ^{1}H nmr (100 MHz, $CDCl_3$) δ: 6.73 (bs, 1H), 4.91 (dd, 1H, *J* = 13, 7 Hz), 4.90 (bs, 2H), 4.62 (dd, 1H, *J* = 13, 6.5 Hz), 2.3–3.1 (m, 5H), 1.73 (bs, 6H), 1.00 (d, 3H, *J* = 7 Hz); mass spectrum (25 eV), *m/z* (relative intensity): 237 (M^+, 2), 220 (2), 204 (2), 189 (11), 175 (10), 161 (13), 149 (58), 135 (14), 121 (21), 110 (23), 83 (100).

5,7,8(syn)-Trimethyltricyclo[3.2.1.0^{2,7}]octan-6-one (31)

By the standard bicycloannulation procedure, 0.41 g (3.3 mmol) of 2,6-dimethylcyclohex-2-en-1-one (**29**) (1*b*) and 0.35 g (4.0 mmol) of 1-nitropropene[8] gave (gas chromatography[10] 210°C) tricyclo-octanone **31**; 42% (*n*-hexadecane internal standard); colorless oil; ir: 1730 cm^{-1}; ^{1}H nmr (100 MHz, $CDCl_3$) δ: [relative LIS with added $Eu(fod)_3$ in brackets] 2.02 [1.0] (bq, 1H, *J* = 7 Hz), 1.5–1.9 (m, 7H), 1.22 [1.5] (s, 3H), 0.93 [1.0] (d, 3H, *J* = 7 Hz), 0.83 [1.7] (s, 3H); ^{13}C nmr (50.4 MHz, $CDCl_3$) δ: 217.7 (s), 47.0 (s), 38.5 (t), 38.1 (d), 37.9 (d), 36.6 (d), 33.3 (s), 18.0 (q), 17.2 (t), 15.7 (q), 13.4 (q); mass spectrum, *m/z* (relative intensity): 164 (M^+, 53), 149 (15), 136 (17), 122 (33), 107 (44), 95 (100), 91 (46), 82 (84), 67 (72); high resolution mass spectrum, *m/z* calcd. for $C_{11}H_{16}O$: 164.1201; found: 164.1200.

2-Methyl-2-(3-nitro-allyl)-1,3-dioxolane (33)

To a solution of 1.0 mL (14.4 mmol) of nitromethane in 14 mL of 95% ethanol was added dropwise, with stirring, 1.5 mL of 10% aqueous NaOH. To the resulting yellow solution was added dropwise, with stirring, 1.79 g (13.8 mmol) of 2-methyl-1,3-dioxolane-2-acetaldehyde (**32**) over 15 min. After the mixture had been stirred for 24 h, 50 mL of water was added, and the aqueous phase was extracted with methylene chloride (3 × 50 mL). The combined extracts were dried over anhydrous sodium sulfate, and the solvent was evaporated under reduced pressure to give the ketal-nitro-aldol, 2-(2-hydroxy-3-nitropropyl)-2-methyl-1,3-dioxolane; 1.82 g (69%); yellow oil (from which an analytical sample was obtained by bulb-to-bulb distillation); bp 92–95°C/0.5 Torr (1 Torr = 133.32 Pa); ir: 3435, 1555 cm^{-1}; ^{1}H nmr (200 MHz, $CDCl_3$) δ: 4.63 (m, 1H), 4.45 (d, 2H, *J* = 7 Hz), 4.02 (s, 4H), 3.81 (bs, 1H), 1.95 (d, 2H, *J* = 6 Hz), 1.40 (s, 3H); mass spectrum (25 eV), *m/z* (relative intensity): 176 (20), 158 (2), 115 (3), 112 (6), 89 (5), 88 (100), 57 (3).

To a solution of 0.18 g (0.96 mmol) of the crude ketal-nitro-aldol and 0.53 mL (3.8 mmol) of triethylamine in 6 mL of methylene chloride at 0°C was added dropwise, with stirring, 0.10 mL (1.3 mmol) of methanesulfonyl chloride. After the mixture had been stirred for 30 min at 0°C, it was washed with water (2 × 50 mL) and 50 mL of brine and dried over anhydrous sodium sulfate. The solvent was evaporated under reduced pressure, and the residual oil was subjected to open-column liquid chromatography on silica gel, eluting with 1:1 cyclohexane/ethyl acetate, to give ketal-nitro-olefin **33**; 0.10 g (61%); yellow oil; ir: 1660, 1520 cm^{-1}; ^{1}H nmr (100 MHz, $CDCl_3$) δ: 7.28 (dt, 1H, *J* = 13, 7 Hz), 6.99 (d, 1H, *J* = 13 Hz), 3.97 (s, 4H), 2.59 (d, 2H, *J* = 7 Hz), 1.38 (s, 3H); mass spectrum (25 eV), *m/z*: 158, 127, 87, 43.

5,7-Dimethyl-8(syn)-(2-methyldioxol-2-ylmethyl)tricyclo-[3.2.1.0^{2,7}]octan-6-one (34)

By the standard bicycloannulation procedure (66 h reflux), 0.52 g (4.2 mmol) of 2,6-dimethylcyclohex-2-en-1-one (**29**) (1*b*) and 0.63 g (3.7 mmol) of ketal-nitro-olefin **33** gave a crude orange oil which was subjected to open-column liquid chromatography on silica gel. Elution with cyclohexane gave ketal-tricyclo-octanone **34**; 0.23 g (25%); yellow oil; ir: 1715 cm^{-1}; ^{1}H nmr (100 MHz, $CDCl_3$) δ: 3.94 (s, 4H), 2.36 (d, 1H, *J* = 7.5 Hz), 1.5–2.2 (m, 8H), 1.37 (s, 3H), 1.22 (s, 3H), 0.83 (s, 3H); mass spectrum (25 eV), *m/z* (relative intensity): 250 (M^+, 1), 235 (2), 179 (2), 149 (1), 135 (3), 124 (2), 87 (100); high resolution mass spectrum, *m/z* calcd. for $C_{15}H_{22}O_3$: 250.1569; found: 250.1574.

4(syn)-Isopropenyl-5,7-dimethyltricyclo[3.2.1.0^{2,7}]octan-6-one (38)

By the standard bicycloannulation procedure, 0.94 g (5.6 mmol) of (5*R*)-2,6-dimethyl-5-isopropenylcyclohex-2-en-1-one (**36**) (1*a*) and 1.8 mL (5.6 mmol) of 3.1 *M* nitroethylene in benzene (14*l*) gave (gas chromatography[11] 170°C) tricyclo-octanone **38**; 13%; colorless oil; ^{1}H nmr (200 MHz, $CDCl_3$) δ: 4.67 (nm, 1H), 4.60 (nm, 1H), 2.59 (dd, 1H, *J* = 10, 6 Hz), 2.31 (ddd, 1H, *J* = 15, 10, 2 Hz), 1.6–2.0 (m, 5H), 1.52 (nm, 3H), 1.24 (s, 3H), 0.87 (s, 3H; other spectral data as reported earlier (1*a*).

2-Methyltricyclo[3.2.1.0^{2,7}]octan-6-one (40)

By the standard bicycloannulation procedure, 0.25 g (2.3 mmol) of 3-methylcyclohex-2-en-1-one (**39**) and 4.3 mL (3.0 mmol) of 5% nitroethylene in benzene (14*l*) gave (gas chromatography[11] 170°C), in addition to a 12% recovery of **39**, tricyclo-octanone **40**; 2 mg (3%); colorless oil; spectral data as previously reported (1*a*); and 4-methyl-5(*syn*)-nitrobicyclo[2.2.2]octan-2-one (**41**); 30 mg (7%); yellow oil; ir: 1726, 1545 cm^{-1}; ^{1}H nmr (100 MHz, $CDCl_3$) δ: 4.42

[11] A 0.2 in. × 6 ft stainless-steel column packed with 10% OV-225 on Chromosorb W (80/100 mesh) was employed with a helium flow rate of 60 mL min^{-1}.

(m, 1H), 1.02 (s, 3H); mass spectrum, *m/z*: 183 (M^+), 164, 145, 136, 121, 109, 93, 84, 67, 55, 41; high resolution mass spectrum, *m/z* calcd. for $C_9H_{13}NO_3$: 183.0900; found: 183.0893.

*2,4,4-Trimethyltricyclo[3.2.1.0^{2,7}]octan-6-one (**42**)*

By the standard bicycloannulation procedure, 0.25 g (1.8 mmol) of isophorone (**8**) and 4.7 mL (3.2 mmol) of 5% nitroethylene in benzene (14*l*) gave (gas chromatography[11] 170°C), in addition to a 20% recovery of **8**, tricyclo-octanone **42**; 5 mg (2%); colorless oil; spectral data as previously reported (3*c*); and 4,7,7-trimethyl-5-(*syn*)-nitrobicyclo[2.2.2]octan-2-one (**43**); 72 mg (19%); yellow oil; ir: 1725, 1546 cm^{-1}; ^{1}H nmr (100 MHz, $CDCl_3$) δ: 4.57 (bdd, 1H, J = 9, 6 Hz), 1.12 (s, 3H), 1.05 (s, 3H), 1.00 (s, 3H); mass spectrum, *m/z* (relative intensity): 211 (M^+, 27), 180 (22), 165 (38), 137 (22), 121 (100), 95 (68), 81 (62), 69 (92), 55 (47), 41 (53); high resolution mass spectrum, *m/z* calcd. for $C_{11}H_{17}NO_3$: 211.1210; found: 211.1211.

*1,5(*syn*),7,7-tetramethyltricyclo[2.2.1.0^{2,6}]heptan-3-one (**47**)*

By the standard bicycloannulation procedure, 0.54 g (4.4 mmol) of 3,4,4-trimethylcyclopent-2-en-1-one (**45**) (37) and 0.43 g (4.9 mmol) of 1-nitropropene[8] gave (gas chromatography[9] program: 150°C for 3 min; heat to 210°C at 30°C min^{-1}; 210°C) tricyclo-heptanone **47**; 39% (biphenyl internal standard); colorless oil; ir: 1757 cm^{-1}; ^{1}H nmr (100 MHz, $CDCl_3$) δ: [relative LIS with added $Eu(fod)_3$ in brackets] 2.50 [1.0] (qt, 1H, J = 6.5, 1.5 Hz), 1.89 [1.0] (bd, 1H, J = 5 Hz), 1.33 [3.2] (bs, 1H), 1.20 [0.5] (s, 3H), 1.17 [1.8] (d, 1H, J = 5 Hz), 1.05 [0.8] (s, 3H), 1.03 [1.5] (s, 3H), 1.00 [1.3] (d, 3H, J = 6.5 Hz); ^{13}C nmr (25.2 MHz, $CDCl_3$) δ: 213.5 (s), 58.0 (d), 44.5 (s), 40.0 (s), 36.6 (d), 35.5 (d), 26.8 (d), 21.6 (q), 19.6 (q), 14.8 (q), 10.4 (q); mass spectrum, *m/z* (relative intensity): 164 (M^+, 18), 149 (8), 136 (12), 121 (100), 105 (29), 91 (18), 79 (21), 67 (6), 53 (9); high resolution mass spectrum, *m/z* calcd. for $C_{11}H_{16}O$: 164.1201; found: 164.1205.

threo-*3,4,4-Trimethyl-5-(1-methyl-2-nitroethyl)cyclopent-2-en-1-one (**49**) and* erythro-*3,4,4-trimethyl-5-(1-methyl-2-nitroethyl)-cyclopent-2-en-1-one (**48**)*

By the standard Michael addition procedure, 0.50 g (4.1 mmol) of 3,4,4-trimethylcyclopent-2-en-1-one (**45**) (37) and 0.44 g (5.1 mmol) of 1-nitropropene[8] gave (preparative gas chromatography[9] program: 200°C for 5 min; heat at 6°C min^{-1} to 230°C; 230°C) *threo* adduct **49**; 0.32 g (37%); yellow oil; gas chromatography t_r = 16.9 min; ir (CCl_4): 1705, 1625, 1555 cm^{-1}; ^{1}H nmr (100 MHz, $CDCl_3$) δ: 5.83 (bs, 1H), 4.91 (dd, 1H, J = 13, 4 Hz), 4.53 (dd, 1H, J = 13, 9 Hz), 2.70 (m, 1H), 2.14 (d, 1H, J = 7 Hz), 2.06 (d, 3H, J = 1 Hz), 1.29 (s, 3H), 1.26 (d, 3H, J = 7 Hz), 1.23 (s, 3H); mass spectrum (25 eV), *m/z* (relative intensity): 211 (M^+, 2), 196 (3), 180 (7), 164 (79), 150 (12), 135 (11), 124 (100), 109 (15), 85 (10), 72 (12); high resolution mass spectrum, *m/z* calcd. for $C_{11}H_{17}NO_3$: 211.1204; found: 211.1207; and *erythro* adduct **48**; 0.4 g (50%); yellow oil; gas chromatography t_r = 15.5 min; ir (CCl_4); 1707, 1627, 1554 cm^{-1}; ^{1}H nmr (100 MHz, $CDCl_3$) δ: 5.82 (bs, 1H), 4.72 (dd, 1H, J = 12.5, 7.5 Hz), 4.51 (dd, 1H, J = 12.5, 7 Hz), 2.75 (m, 1H), 2.05 (d, 3H, J = 1 Hz), 1.22 (s, 6H), 0.93 (d, 1H, J = 7 Hz); mass spectrum (25 eV), *m/z* (relative intensity): 211 (M^+, 2), 196 (4), 181 (8), 164 (20), 149 (9), 135 (9), 124 (100), 109 (30), 95 (16), 84 (14), 48 (22); high resolution mass spectrum, *m/z* calcd. for $C_{11}H_{17}NO_3$; 211.1204; found: 211.1198.

*4,6(*endo*),7,7-Tetramethyl-5(*endo*)-nitrobicyclo[2.2.1]heptan-2-one (**50**)*

To a solution of 0.85 mL (6.1 mmol) of diisopropylamine and 3 mg of 2,2′-bipyridyl in 4 mL of tetrahydrofuran at 0°C was added dropwise, with stirring, 3.7 mL (5.3 mmol) of 1.4 *M* *n*-butyllithium over 10 min. The resulting crimson solution was stirred at 0°C for 15 min, and a solution of 0.55 g (4.5 mmol) of 3,4,4-trimethylcyclopent-2-en-1-one (**45**) (37) in 8 mL of tetrahydrofuran was then added dropwise, with stirring, over 45 min. After the mixture had been cooled to −78°C, a solution of 0.50 g (5.7 mmol) of 1-nitropropene in 9 mL of tetrahydrofuran was added dropwise, with stirring, over 2.5 h, and the resulting yellow solution was stirred at −78°C for an additional 30 min. After the mixture had been allowed to warm to room temperature, it was refluxed for 20 h. The progress of the reaction was followed by gas chromatography, which indicated the presence of Michael adducts **49** and **48** plus only a relatively small amount of bicycloheptanone **50** just prior to reflux, followed by a gradual increase in the amount of **50** at the expense of the other two products during reflux. The cooled mixture was poured into 50 mL of saturated aqueous sodium bicarbonate, and the aqueous phase was extracted with 3 × 50 mL of ethyl ether. The combined extracts were washed with 50 mL of brine and dried over anhydrous sodium sulfate. The solvent was distilled through a Vigreux column, and the residual concentrate was subjected to preparative gas chromatography[9] (program: 200°C for 5 min; heat at 6°C min^{-1} to 230°C; 230°C) to give the following three major products: (a) Michael adduct **49**; 28 mg (3%); gas chromatography and spectral data as above; (b) Michael adduct **48**; 59 mg (6%); gas chromatography and spectral data as above; (c) bicycloheptanone **50**; 55 mg (6%); yellow oil; gas chromatography t_r = 13.0 min; ir (CCl_4): 1767, 1550 cm^{-1}; ^{1}H nmr (100 MHz, $CDCl_3$) δ: 4.76 (dd, 1H, J = 6.5, 1 Hz), 2.80 (quintet, 1H, J = 7 Hz), 2.31 (d, 1H, J = 19 Hz), 2.13 (s, 1H), 2.05 (d, 1H, J = 19 Hz), 1.38 (d, 3H, J = 7 Hz), 1.25 (s, 3H), 1.20 (s, 3H), 1.00 (s, 3H); mass spectrum, *m/z* (relative intensity): 211 (M^+, 5), 180 (1), 165 (4), 150 (5), 135 (23), 121 (45), 108 (31), 95 (53), 83 (100), 67 (43), 54 (61); high resolution mass spectrum, *m/z* calcd. for $C_{11}H_{17}NO_3$: 211.1204; found: 211.1206.

erythro-*3-Methyl-5-(1-methyl-2-nitroethyl)cyclopent-2-en-1-one (**52**)*

To a solution of 0.71 mL (5.1 mmol) of diisopropylamine and 3 mg of 2,2′-bipyridyl in 4 mL of tetrahydrofuran at 0°C was added dropwise, with stirring, 3.1 mL (4.4 mmol) of 1.4 *M* *n*-butyllithium over 10 min. The resulting crimson solution was cooled to −78°C and 0.59 mL (3.3 mmol) of hexamethylphosphoramide was added, resulting in a deep purple solution. After this solution had been stirred at −78°C for 15 min, a solution of 0.32 g (3.3 mmol) of 3-methylcyclopent-2-en-1-one (**51**) in 4 mL of tetrahydrofuran was then added dropwise, with stirring, over 45 min. After the mixture had been stirred at −78°C for an additional 30 min, a solution of 0.39 g (4.1 mmol) of 1-nitropropene[8] in 8 mL of tetrahydrofuran was added dropwise, with stirring, over 2.5 h. The resulting yellow solution was stirred at −78°C for an additional 30 min, after which 0.29 mL of glacial acetic acid was added rapidly, with stirring. The mixture was allowed to warm to room temperature and poured into 50 mL of ethyl ether and 50 mL of saturated aqueous sodium bicarbonate, and the aqueous phase was extracted with 2 × 50 mL of ethyl ether. The combined extracts were washed with 50 mL of brine and dried over anhydrous sodium sulfate. The solution was concentrated by distillation through a Vigreux column, and the concentrate was subjected to preparative thick-layer chromatography (eluting 2× with $CHCl_3$) to give impure adduct **52**; 0.36 g (57%); ^{1}H nmr (100 MHz, $CDCl_3$) δ: 5.59 (bs, 1H), 4.81 (dd, 1H, J = 12.5, 6.5 Hz), 4.53 (dd, 1H, J = 12.5, 7.5 Hz), 2.5−3.2 (m, 4H), 2.35 (bs, 3H), 1.08 (d, 3H, J = 7 Hz).

*Tricyclenone (**53**)*

By the standard bicycloannulation procedure (but with a 187-h reflux period, during the first 130 h of which the product gas chromatography peak was observed to increase gradually) 0.51 g (4.1 mmol) of 3,4,4-trimethylcyclopent-2-en-1-one (**45**) (37) and 2.3 mL (5.2 mmol) of 2.3 *M* nitroethylene in benzene (14*l*) gave (gas chromatography[9] 180°C) tricyclenone (**53**); 22% (diphenylmethane internal standard); colorless crystals; mp 100−106°C (lit. (38) mp 97.5−100°C); ir (CCl_4): 1758 cm^{-1} (the spectrum was superimposable on that of an authentic sample);[12] ^{1}H nmr (100 MHz, $CDCl_3$) δ: 2.06 (dt, 1H, J = 11, 1.5 Hz), 1.97 (bd, 1H, J = 5 Hz), 1.84 (bd, 1H, J = 11 Hz), 1.52 (bs, 1H), 1.23 (s, 3H), 1.19 (bd, 1H, J = 5 Hz), 1.05 (s, 3H), 1.02 (s, 3H); ^{13}C nmr (25.2 MHz, $CDCl_3$) δ: 213.6 (s), 51.5 (d), 43.9 (s), 38.7 (s), 29.4 (t), 29.3 (d), 27.9 (d), 21.3 (q), 19.3 (q), 10.2 (q).

[12]We are grateful to Professor J. K. Crandall for copies of ir and nmr spectra of tricyclenone.

Acknowledgements

We are grateful to the Natural Sciences and Engineering Research Council of Canada for financial support of this work.

1. (*a*) R. M. CORY and R. M. RENNEBOOG. J. Org. Chem. **49**, 3898 (1984); (*b*) R. M. CORY, L. P. J. BURTON, D. M. T. CHAN, F. R. MCLAREN, M. H. RASTALL, and R. M. RENNEBOOG. Can. J. Chem. **62**, 1908 (1984).
2. (*a*) R. M. CORY, L. P. J. BURTON, and R. G. PECHERLE. Synth. Commun. **9**, 735 (1979); (*b*) R. M. CORY and F. R. MCLAREN. J. Chem. Soc. Chem. Commun. 587 (1977).
3. (*a*) R. M. CORY, P. C. ANDERSON, F. R. MCLAREN, and B. R. Yamamoto. J. Chem. Soc. Chem. Commun. 73 (1981); (*b*) R. M. CORY and R. M. RENNEBOOG. J. Chem. Soc. Chem. Commun. 1081 (1980); (*c*) R. M. CORY, D. M. T. CHAN, Y. M. A. NAGUIB, M. H. RASTALL, and R. M. RENNEBOOG. J. Org. Chem. **45**, 1852 (1980); (*d*) R. M. CORY, Y. M. A. NAGUIB, and M. H. RASMUSSEN. J. Chem. Soc. Chem. Commun. 504 (1979); (*e*) R. M. CORY and D. M. T. CHAN. Tetrahedron Lett. 4441 (1975).
4. R. NISHIDA and Z. KUMAZAWA. Agric. Biol. Chem. **37**, 341 (1973); T. R. GOVINDACHARI and P. C. PARTHASARATHY. Indian J. Chem. **9**, 1310 (1971); A. K. GANGULY, T. R. GOPINATH, K. NAGARAJAN, B. R. PAI, and P. C. PARTHASARATHY. Tetrahedron, **26**, 2371 (1970); T. R. GOVINDACHARI, P. A. MOHAMED, and P. C. PARTHASARATHY. Tetrahedron, **26**, 615 (1970).
5. M. R. WILLCOTT, P. A. MORRISON, J.-M. ASSERCQ, S. C. WELCH, and R. INNERS. J. Org. Chem. **46**, 4819 (1981).
6. G. FERGUSON, R. MCCRINDLE, S. T. MURPHY, and M. PARVEZ. J. Chem. Res. 2009 (1982); B. M. FRAGA, A. G. GONZALEZ, M. G. HERNANDEZ, J. R. HANSON, and P. B. HITCHCOCK. J. Chem. Soc. Chem. Commun. 594 (1982).
7. F. BOHLMANN and W. ROTARD. Justus Liebigs Ann. Chem. 1220 (1982); F. BOHLMANN, W.-R. ABRAHAM, and W. S. SHELDRICK. Phytochemistry, **19**, 869 (1980); F. BOHLMANN, R. ZDERO, R. ZEISBERG, and W. S. SHELDRICK. Phytochemistry, **18**, 1359 (1979).
8. (*a*) H. NIWA, N. BAN, and K. YAMADA. Tetrahedron Lett. **24**, 937 (1983); (*b*) B. C. RANU, M. SARKAR, P. C. CHAKRABORTI, and U. R. GHATAK. J. Chem. Soc. Perkin Trans. 1, 865 (1982); (*c*) S. C. WELCH, J. M. GRUBER, C.-Y. CHOU, M. R. WILLCOTT, and R. INNERS. J. Org. Chem. **46**, 4816 (1981).
9. R. M. CORY, D. M. T. CHAN, F. R. MCLAREN, M. H. RASMUSSEN, and R. M. RENNEBOOG. Tetrahedron Lett. 4133 (1979).
10. E. PIERS and T.-W. HALL. Can. J. Chem. **58**, 2613 (1980); J. Chem. Soc. Commun. 880 (1977).
11. R. B. KELLY, B. A. BECKETT, J. EBER, H.-K. HUNG, and J. ZAMECNIK. Can. J. Chem. **53**, 143 (1975); R. B. KELLY, J. EBER, and H.-K. HUNG. Can. J. Chem. **51**, 2534 (1973); J. Chem. Soc. Chem. Commun. 689 (1973); W. HERZ, R. N. MIRRINGTON, H. YOUNG, and Y. Y. LIN. J. Org. Chem. **33**, 4210 (1968); W. HERZ, R. N. MIRRINGTON, and H. YOUNG. Tetrahedron Lett. 405 (1968).
12. H. HAGIWARA, H. UDA, and T. KODAMA. J. Chem. Soc. Perkin Trans. 1, 963 (1980); H. HAGIWARA, T. KODAWA, H. KOSUGI, and H. UDA. J. Chem. Soc. Chem. Commun. 413 (1976); D. SPITZNER, A. ENGLER, T. LIESE, G. SPLETTSTOSSER, and A. DE MEIJERE. Angew. Chem. Int. Ed. Engl. **21**, 791 (1982).
13. D. SEEBACH, E. W. COLVIN, F. LEHR, and T. WELLER. Chimia, **33**, 1 (1979).
14. (*a*) M. MIYASHITA, T. YANAMI, T. KUMAZAWA, and A. YOSHIKOSHI. J. Am. Chem. Soc. **106**, 2149 (1984); (*b*) T.-L. HO. Synth. Commun. **12**, 339 (1982); (*c*) N. ONO, H. MIYAKE, and A. KAJI. J. Chem. Soc. Chem. Commun. 33 (1982); (*d*) P. KNOCHEL and D. SEEBACH. Tetrahedron Lett. **23**, 3897 (1982); (*e*) S. J. BLARER, W. B. SCHWEIZER, and D. SEEBACH. Helv. Chim. Acta, **65**, 1637 (1982); (*f*) D. RANGANATHAN, S. RANGANATHAN, and S. BAMEZAI. Tetrahedron Lett. **23**, 2789 (1982); (*g*) M. MIYASHITA, T. YANAMI, and A. YOSHIKOSHI. Org. Synth. **60**, 117 (1981); (*h*) P. KNOCHEL and D. SEEBACH. Tetrahedron Lett. **22**, 3223 (1981); (*i*) E. J. COREY and H. ESTREICHER. Tetrahedron Lett. **22**, 603 (1981); (*j*) P. KNOCHEL and D. SEEBACH. Nouv. J. Chim. **5**, 75 (1981); (*k*) D. SEEBACH and J. GOLINSKI. Helv. Chim. Acta, **64**, 1413 (1981); (*l*) D. RANGANATHAN, C. B. RAO, S. RANGANATHAN, A. K. MEHROTRA, and R. IYENGAR. J. Org. Chem. **45**, 1185 (1980).
15. (*a*) T. TANAKA, T. TORU, N. OKAMURA, A. HAZATO, S. SUGIURA, K. MANABE, S. KUROZUMI, M. SUZUKI, T. KAWAGISHI, and R. NOYORI. Tetrahedron Lett. **24**, 4103 (1983); (*b*) K. COOPER and G. PATTENDEN. J. Chem. Soc. Perkin Trans. 1, 799 (1984); M. HORTON and G. PATTENDEN. J. Chem. Soc. Perkin Trans. 1, 811 (1984); (*c*) T. WELLER and D. SEEBACH. Tetrahedron Lett. **23**, 935 (1982); (*d*) D. H. R. BARTON, W. B. MOTHERWELL, and S. Z. ZARD. J. Chem. Soc. Chem. Commun. 551 (1982); (*e*) G. JUST and H. OH. Can. J. Chem. **59**, 2729 (1981); (*f*) T. KAMETANI, M. TSUBUKI, and H. NEMOTO. J. Org. Chem. **45**, 4391 (1980); (*g*) T. KAMETANI, M. TSUBUKI, and H. NEMOTO. Tetrahedron Lett. **21**, 4855 (1980); (*h*) M. MIYASHITA, T. KUMAZAWA, and A. YOSHIKOSHI. J. Org. Chem. **45**, 2945 (1980).
16. M. BRITTEN-KELLY, B. J. WILLIS, and D. H. R. BARTON. Synthesis, 27 (1980).
17. N. KORNBLUM, H. K. SINGH, and S. D. BOYD. J. Org. Chem. **49**, 358 (1984); N. KORNBLUM and A. S. ERICKSON. J. Org. Chem. **46**, 1037 (1981); M. BENN and A. C. M. MEESTERS. J. Chem. Soc. Chem. Commun. 597 (1977).
18. K. ANNEN, H. HOFMEISTER, H. LAURENT, A. SEEGER, and R. WEICHERT. Chem. Ber. **111**, 3094 (1978).
19. D. SEEBACH, H. F. LEITZ, and V. EHRIG. Chem. Ber. **108**, 1924 (1975).
20. E. VALENTIN, G. PITACCO, F. P. COLONNA, and A. RISALITI. Tetrahedron, **30**, 2741 (1974).
21. D. SEEBACH and J. GOLINSKI. Helv. Chim. Acta, **64**, 1413 (1981).
22. D. D. JOHNSTON and N. C. PAYNE. Acta Crystallogr. Sect. B, **37**, 1472 (1981).
23. S. J. TERHUNE, J. W. HOGG, and B. M. LAWRENCE. Tetrahedron Lett. 4705 (1973).
24. R. H. WOLLENBERG and S. J. MILLER. Tetrahedron Lett. 3219 (1978).
25. T. R. KELLY and W.-G. TSANG. Tetrahedron Lett. 4457 (1978).
26. J. E. MCMURRY and J. MELTON. J. Org. Chem. **40**, 2138 (1975).
27. H. NIWA, N. BAN, and K. YAMADA. Tetrahedron Lett. **24**, 937 (1983); S. C. WELCH, J. M. GRUBER, and P. A. MORRISON. Tetrahedron Lett. **25**, 5497 (1984).
28. R. M. CORY and J. B. STOTHERS. Org. Magn. Reson. **11**, 252 (1978).
29. E. LIPPMAA, T. PEHK, and J. PAASIVIRTA. Org. Magn. Reson. **5**, 277 (1973).
30. L. BOROWIECKI and M. WEŁNIAK. Rocz. Chem. **51**, 1751 (1977).
31. S. S. NAMETKIN and S. S. ZABRODINA. Dokl. Akad. Nauk SSSR, **36**, 142 (1942); Chem. Abstr. **37**, 5712 (1943).
32. I. I. BRADYSHEV and K A. CHERCHES. Sb. Nauchn. Rab. Inst. Fiz. Org. Khim. Akad. Nauk B. SSR, 96 (1959); Chem. Abstr. **55**, 3930a (1961).
33. A. C. SHAW. Can. J. Res. Sect. B, **28**, 268 (1950).
34. A. C. SHAW. Can. J. Chem. **31**, 193 (1953).
35. G. D. BUCKLEY and C. W. SCAIFE. J. Chem. Soc. 1471 (1947).
36. M. MIYASHITA, T. YANAMI, and A. YOSHIKOSHI. Org. Synth. **60**, 101 (1981).
37. J.-M. CONIA and M.-L. LERIVEREND. Bull. Soc. Chim. Fr. 2981 (1970).
38. J. K. CRANDALL, L. C. CRAWLEY, D. B. BANKS, and L. C. LIN. J. Org. Chem. **36**, 510 (1971).

A magnetically aligning lyotropic mesophase with a clay inclusion

M. A. DESANDO AND L. W. REEVES
Department of Chemistry, University of Waterloo, Waterloo, Ont., Canada N2L 3G1

Received July 3, 1984[1]

M. A. DESANDO and L. W. REEVES. Can. J. Chem. **63**, 2628 (1985).

The inclusion of clay (bentonite) (ca. 0.08–0.64 wt.%) in the lyotropic mesophase formed by potassium dodecanoate + KCl + ^2H_2O has been observed by ^2H nmr not to alter the type I CM character of the phase. Relaxation of the mesophase director has been analyzed in terms of two processes over a range of ^2H_2O concentrations. A slow process with rate constants of ca. $2 \times 10^{-4} - 8 \times 10^{-4}$ s^{-1} exists for the phase with clay over ^2H_2O concentrations of 63.9–65.9 wt.%. A tenfold increase in the rate constant with an increase in the ^2H_2O content from 62.5 to 65.5% was observed for the ternary phase at 302 K.

M. A. DESANDO et L. W. REEVES. Can. J. Chem. **63**, 2628 (1985).

Faisant appel à la rmn du ^2H, on a observé que l'inclusion d'argile (bentonite) (environ 0,08–0,64% en poids) dans la mésophase lyotrope formée par du dodécanoate de potassium + KCl + ^2H_2O n'altère pas le caractère de type I CM de la phase. Pour diverses concentrations de ^2H_2O, on a analysé la relaxation du directeur de la mésophase en fonction de deux processus. Pour la phase avec de l'argile et à des concentrations de ^2H_2O allant de 63,9 à 65,9% en poids, il existe un processus lent avec des constantes de vitesse d'environ 2×10^{-4} à 8×10^{-4} s^{-1}. Dans la phase ternaire à 302 K, la constante de vitesse est multipliée par 10 lorsque la teneur en ^2H_2O augmente de 62,5 à 65,5%.

[Traduit par le journal]

Introduction

Lyotropic mesophases which align in magnetic fields have been reported (1–6), in which the components of the micelles are of molecular dimensions, e.g., surfactants, aliphatic alcohols, and inorganic electrolytes. A novel situation exists when the size of an inclusion is larger than that of the micelles—in this work, clay particles. Intermicellar forces contribute largely to the generation of nematic order in the mesophase; thus the presence of large particles in suspension will no doubt change the order in the system, and consequently the alignment properties in a magnetic field.

A key factor in the preparation of a mesophase with large inclusion particles is the formation of a stable suspension. Clays are good examples of materials which display colloidal properties (7). The study of clay–surfactant interactions, particularly in the mesophase condition, offers interesting prospects in areas such as enhanced oil recovery, mineral processing, chemical evolution (protobiogenesis), and membrane phenomena. The dispersion of clays in a mesophase matrix not only affords information on mesophase phenomena, but also provides a novel approach to the study of clays, per se. In addition, clays are flexible chemical systems; for instance, they may be intercalated with different types of compounds, and may undergo ion-exchange reactions (7, 8).

Experimental

Bentonite (Fisher) was ground and dried in an oven at ~200°C for several days. The clay was mixed with isotopically pure deuterium oxide (^2H_2O) (99.7 at.%; Merck, Sharp and Dohme) to form a slurry which was centrifuged on an Adams Analytical centrifuge for various intervals of time to produce suspensions with clay concentrations in the range 0.09–0.98 weight percent. In each case the supernatant liquid showed a strong Tyndall effect in He–Ne laser light. The quantity of bentonite in suspension was determined gravimetrically from evaporation of the ^2H_2O.

Potassium dodecanoate was prepared by reacting equimolar quantities of dodecanoic acid and potassium hydroxide in absolute ethanol followed by several recrystallizations from ethanol. Surfactant from laboratory stock (3) was recrystallized from absolute ethanol and then dried *in vacuo*. The purity of the surfactant was checked from its proton nmr spectrum.

TABLE 1. Alignment rate constant (k) and nuclear quadrupole splitting ($\Delta\nu$) values for the type I CM lyotropic mesophases of potassium dodecanoate/potassium chloride/^2H_2O (compositions in wt.%) at 302 K

^2H_2O	Potassium dodecanoate	Potassium chloride	$10^4\ k$ (10^4 s^{-1})	$\Delta\nu$ (Hz)
62.51	34.40	3.10	1.1	727
63.37	33.61	3.03	1.9	668
63.49	33.40	3.11	3.1	636
63.78	33.23	2.99	3.5	617
63.95	32.98	3.07	3.4	585
64.18	32.82	3.00	4.8	537
64.18	32.82	3.00	5.6	536
64.63	32.45	2.92	5.7	582
64.78	32.31	2.91	5.7	575
64.91	32.18	2.91	5.7	537
65.11	32.00	2.90	7.3	549
65.30	31.83	2.87	10.0	516
65.31	31.81	2.88	11.4	515
65.38	31.75	2.87	7.3	525
65.58[a]	31.75	2.87	9.2	519

[a]At 305 K.

Mesophases were prepared with compositions, in weight percent, of potassium dodecanoate/KCl/^2H_2O, and potassium dodecanoate/KCl/^2H_2O/bentonite as listed in Tables 1 and 2. The amounts of ^2H_2O and bentonite in the phases were varied while the ratio of wt.% surfactant to electrolyte was maintained around 11.03. Experiments were performed on many different mesophases, each prepared separately by weight. Some mesophases were made of similar concentrations and some repeat experiments were carried out on the same samples in order to verify the observed alignment rate constants. All glassware were cleaned by the same procedure, that is, they were first washed with a commercial detergent solution, then rigorously rinsed with deionized water, and finally dried *in vacuo*.

The ^2H nmr spectra were recorded on a Bruker WP-80 Fourier transform spectrometer operating at 12.24 MHz with a magnetic field strength of 1.88 T. The temperature was maintained within ±1 K with a calibrated B-ST 100/700 temperature controller. Samples in 10-mm

[1]Revision received March 13, 1985.

TABLE 2. Alignment rate constants (k_1 and k_2) and deuterium nuclear quadrupole splitting ($\Delta\nu$) values of type I CM lytotropic mesophases of potassium dodecanoate/potassium chloride/^2H_2O/bentonite (compositions in wt.%) at 302 K

^2H_2O	Potassium dodecanoate	Potassium chloride	Bentonite	k_1 (10^4 s^{-1})	k_2 (10^4 s^{-1})	$\Delta\nu$ (Hz)	k_1/k_2
63.94[a]	32.50	2.93	0.63	4.1	2.8	580	1.5
63.94	32.50	2.93	0.63	3.8	2.0	588	1.9
64.21	32.21	2.94	0.64	5.1	2.5	568	2.0
64.57	32.35	2.91	0.16	3.8	2.3	586	1.7
64.67	32.31	2.91	0.17	6.7	4.4	586	1.5
64.77	32.11	2.97	0.14	6.6	5.5	529	1.2
64.91	32.05	2.89	0.16	6.9	5.0	534	1.4
65.53	31.52	2.84	0.10	12.7	7.6	515	1.7
65.53	31.52	2.84	0.10	11.3	7.4	516	1.5
65.85	31.25	2.81	0.08	12.9	6.5	515	2.0

[a]At 305 K.

od thin-wall precision nmr tubes (Wilmad) were placed in a multinuclear probehead equipped with an external deuterium lock. Mesophases were allowed to align (usually overnight) in the magnetic field until a constant deuterium nuclear quadrupole splitting was observed. Each sample was subjected to an angular displacement, in the range ca. 20–35° away from the aligned position, around the long axis of the nmr tube. A Bruker Aspect 2000 computer program was used to accumulate, transform, and store deuterium nmr spectra at various intervals of time during the course of the mesophase realignment.

References 5, 9, and 10 outline in additional detail the procedure used in the measurements of the alignment rates.

Mesophases were viewed between crossed light polarizing film (Bausch & Lomb; catalogue no. 31-52-62-26) after they were allowed to align in the 1.88-T field of a Bruker magnet and also in the 2.31-T field of a Varian magnet.

Results

Alignment of the mesophase director in a steady-state externally applied magnetic field can be followed by measuring the nuclear quadrupole splitting ($\Delta\nu$) as a function of time (9, 10). The angle (Ω) between the mesophase director (uniaxis of symmetry) and the applied field can be expressed as:

$$\Omega = \cos^{-1}\{[(2\Delta\nu)/(3\Delta\nu_0)] + (1/3)\}^{1/2}$$

where $\Delta\nu_0$ is the value of the nuclear quadrupole splitting for the mesophase director aligned parallel to the direction of the external magnetic field.

A kinetic rate expression, based on the continuum theory, may be derived to describe the discrete relaxation of the mesophase director with time (t) from its initial angular displacement (Ω_0) relative to the $\Omega = 0$ position (aligned parallel to the applied field) (10).

$$-\ln(\tan\Omega) = kt - \ln(\tan\Omega_0)$$

The continuum theory, however, neglects surface effects such as those generated by solid/liquid interfaces, e.g., glass walls and solid particulates (11–13). Other solutions of the continuum equations are therefore necessary if the alignment process involves a nonuniform distribution of micelle directors and more than one relaxation process, resulting in a nonlinear function of $-\ln(\tan\Omega)$ with time.

Rate constants were determined from linear regression analyses of the lines of best fit to the plots of $-\ln(\tan\Omega)$ versus t (see Figs. 2 and 3 for sample plots). Where nonlinear variation of $-\ln(\tan\Omega)$ with time was dominant, two rate constants were determined from the limiting slopes of the curve (see Fig. 3). The uncertainty in the rate constant within the error limits of $\Delta\nu$ and the reproducibility is ca. $\pm 0.5 \times 10^{-4}$ s^{-1}.

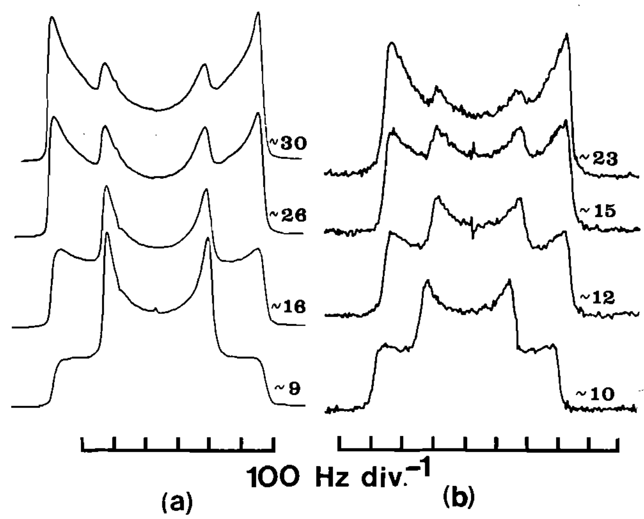

FIG. 1. Evolution of the ^2H nmr powder pattern spectra of ^2H_2O as a function of time (in min) elapsed after placement of the type I CM lyotropic mesophase in the applied magnetic field; (a) potassium dodecanoate/KCl/^2H_2O (33.40:3.11:63.49 wt.%); (b) potassium dodecanoate/KCl/bentonite/^2H_2O (32.50:2.93:0.63:63.94 wt.%).

Discussion

Analysis of the deuterium nmr signal from ^2H_2O in an aligning lyotropic mesophase allows for the characterization of the type of phase with respect to the sign of the diamagnetic susceptibility anisotropy ($\Delta\chi$) (2, 4–6). For example, the powder pattern spectra in Fig. 1 can be ascribed to type I CM (cylindrical micelle) lyomesophases, that is, liquid crystals composed of cylindrical type micelles with a positive $\Delta\chi$, i.e., with the director aligned in the direction of the applied field. This feature is a remarkable one, for mesophases may be quite sensitive to alterations in their physical and chemical constitutions. Even more interesting are the comparisons of the rate constants for alignment of the director of the mesophase with clay to those of the same phase without the clay (see Tables 1 and 2, and Figs. 2, 3, and 5).

The rate constants ($1.1 \times 10^{-4} - 11.4 \times 10^{-4}$ s^{-1} at 302 K) for the ternary phase are of the same order of magnitude as

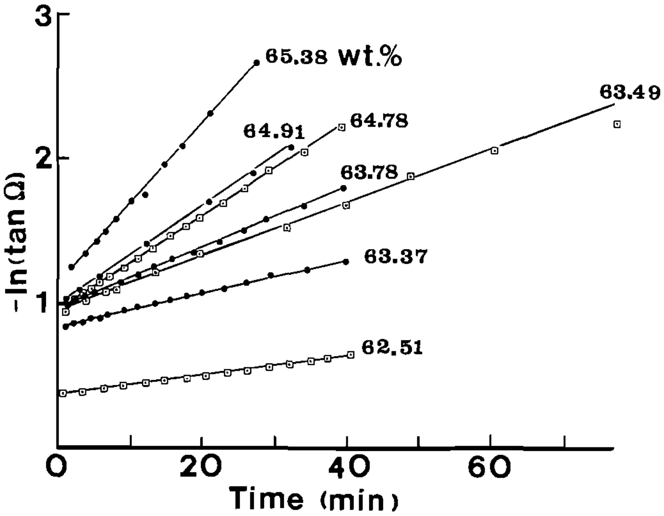

FIG. 2. Time dependence of the angular displacement (Ω) between the mesophase director and the applied magnetic field after an initial rotation of the aligned mesophase director away from the direction of the applied magnetic field, for potassium dodecanoate + KCl + ^2H_2O at different ^2H_2O concentrations (wt.%).

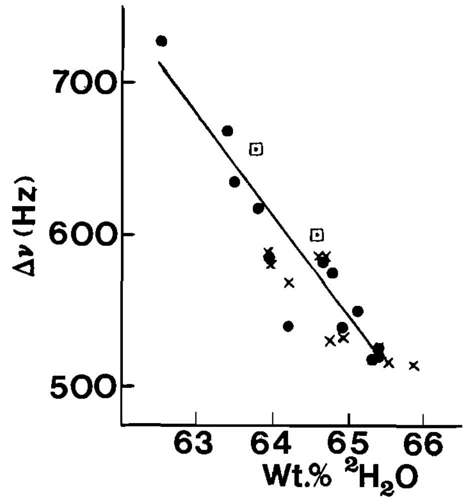

FIG. 4. Plot of nuclear quadrupole splitting (Δν) against weight percent of ^2H_2O; ●, potassium dodecanoate/KCl/^2H_2O; ×, potassium dodecanoate/KCl/^2H_2O/bentonite; ⊡, lit. value at 1.41 T and 303 K (ref. 10).

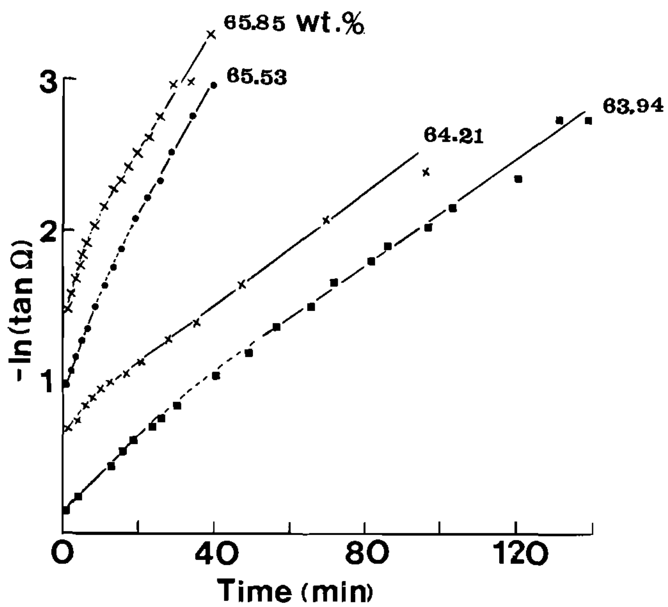

FIG. 3. Time dependence of the angular displacement (Ω) between the mesophase director and the applied magnetic field after an initial rotation of the aligned mesophase director away from the direction of the applied magnetic field, for potassium dodecanoate + KCl + ^2H_2O + bentonite at different ^2H_2O concentrations (wt.%).

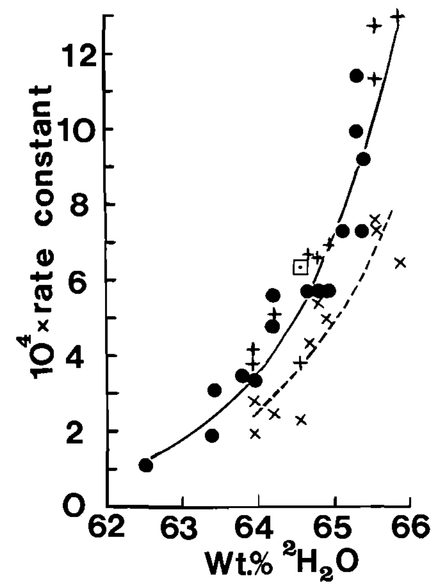

FIG. 5. Variation of the rate constants for the alignment of the mesophase director as a function of the ^2H_2O concentration; ●, k (⊡, lit. (calcd., ref. 10)), (potassium dodecanoate/KCl/^2H_2O); +, k_1; ×, k_2 (potassium dodecanoate/KCl/^2H_2O/bentonite): —— calcd. (k = exp (0.697 wt.% − 52.534)) for the ternary phase: --- calcd. (k_2 = exp (0.672 wt.% − 51.327)) for the quaternary phase.

those measured by Fujiwara and Reeves (10) at 1.44 T. The presence of the bentonite particles, which typically are disk-shaped (14) (diameter of ~2 500 to 7 000 Å) (14, 15), must perturb the order of the cylindrical micelles (length ≥ 500 Å) (16) in the mesophase, the intermicellar interactions, and consequently the order of the ^2H_2O molecules. These effects influence the pattern of flow dislocations in the mesophase, which may account for the weaker less apparent optical diffraction pattern ("schlieren" texture) (17) when the mesophase with clay (in the nmr tubes) was viewed between crossed Polaroids. This behaviour is in contrast to the ternary phase, which exhibited a clear diffraction pattern. The diffraction pattern of the former phase was observed to be far more sensitive to mechanical disturbances than the phase without the clay.

An average spatial angular distribution of the clay particles that is different from that of the surfactant micelles induces localized reordering around the inclusion particles, which in turn leads to a distribution of the diamagnetic susceptibility anisotropy in the sample ($\Delta\chi = \sum_i X_i \Delta\chi_i$; the summation is over the $\Delta\chi$ associated with mole fractions X_i of the species which are present, e.g., surfactant micelles, clay particles, hemimicelles, etc.). A consequence of the foregoing effect may be a change in the rate of alignment of the mesophase director, for $k = -\Delta\chi B^2/\lambda$ (B is the strength of the applied magnetic field and λ is a parameter related to the twist viscosity of the medium (10)). Also, an increase in λ owing to changes in the structure of the mesophase, from the bentonite, would decrease the alignment rate of the mesophase director.

A measure of local order in the system may be gained from the value of the quadrupole splitting ($\Delta\nu$)

$$\Delta\nu = (3/4)QS_a\langle(3\cos^2\Omega - 1)\rangle$$

which is related to the degree of order parameter (S_a) (2, 10, 18).

$$S_a = (1/2)\langle(3\cos^2\theta - 1)\rangle$$

In the case of the ^{2}H nmr signal of ^2H_2O, the S_a is associated with the average angle of alignment (θ) of the O—^{2}H bonds to the mesophase director. It is evident from Fig. 4 that $\Delta\nu$ decreases nearly linearly with an increase in the weight percent (W) of ^2H_2O from ca. 62.5% to 65.5% ($\Delta\nu$(Hz) = $-68.4W$ + 4990.2 for the ternary phase) and is in line with a decrease in nematic order as the isotropic micellar domain is approached at ~66 wt.% ^2H_2O.

Observations of the temporal dependence of the deuterium nuclear quadrupole splitting reveal, for the mesophases with clay, a dispersion of the alignment rate process (see Table 2 and Fig. 3). One interesting feature of the $-\ln(\tan\Omega)$ versus time plots is that there is no appreciable dispersion of the mesophase director for the ternary phase (Fig. 2).

Although the dispersion of the mesophase alignment into more than one rate process has been previously reported (10, 19) for nematic lyotropes, the nature of the relaxations is not well understood. There is evidence from the work of Fujiwara and Reeves (10) that wall effects play a role in the alignment process. Results from the present study also favour the fact that solid surfaces, e.g., clay particles, influence the relaxation of the mesophase director.

Magnetohydrodynamic relaxation of the potassium dodecanoate/KCl/^2H_2O mesophase shows a strong correlation to the amount of solvent. Notice from Fig. 5 how the rate constant (k) increases from ca. 10^{-4} to ca. 10^{-3} s^{-1} over the cylindrical micelle (CM) domain of the mesophase. Furthermore, note that the k value appears to vary nonlinearly, especially around the limits of the CM domain. A curve corresponding to the equation, $k = \exp(0.697\,W - 52.534)$, from the plot of ln k versus wt.% ^2H_2O, has been fitted to the data in Fig. 5. Even though the curve is for the rate constant (k) associated with a single process, i.e., no dispersion, nearly all of the k_1 values for the quaternary phase are on or above the curve. However, the k_2 values when clay is added to the system lie below the curve and suggest that the bentonite particles induce a slower relaxation process for the alignment of the mesophase director. Note, for example (Table 2), how the ratio of the alignment rate for the fast and slow processes (k_1/k_2) is, in most cases, around 1.5–2.0 when clay is present.

Clay particles are known to align in electric and in magnetic fields. Shah *et al.* (14, 15) have demonstrated how aqueous bentonite suspensions undergo a reversal of electro-optical birefringence with increasing electric field strength owing to the presence of permanent and induced dipole moments. In strong electric fields the bentonite particles align with the normal to the plate face perpendicular to the direction of the applied field (14, 15). The research of J. V. Champion *et al.* (20) on kaolinite, containing iron impurities, has shown that the particles possess a permanent magnetic moment susceptibility. Aqueous suspensions of bentonite are also known to exhibit magneto-optical birefringence (21).

Other important properties of clays which should be noted are their ability to (*i*) self-associate (22); (*ii*) intercalate long-chain polar molecules (23–25) and electrolytes (7, 8, 24), and (*iii*) form bilayer, multilayer, or hemimicelle clay particles (26). The physico-chemical properties of the clay, no doubt, are responsible in large part for the intriguing alignment properties of the mesophase.

Conclusion

A low concentration (ca. 0.08–0.64 wt.%) of clay (bentonite)[2] in the nematic lyomesophase formed by potassium dodecanoate/KCl/^2H_2O does not destroy the type I CM character of the phase. In the case of the ternary potassium dodecanoate/KCl/^2H_2O mesophase, the alignment rate for the mesophase director increases by about an order of magnitude from ca. 10^{-4} to 10^{-3} s^{-1} with an increase in ^2H_2O concentration from ca. 62.5 to ca. 65.5 wt.% at 302 K in a 1.88-T magnetic field.

Relaxation of the director of the aligned clay-containing mesophase has been analyzed in terms of two rate constants. The results suggest that the inclusion of the clay particles may induce a slower relaxation of the mesophase director.

Inclusions of particles of colloidal dimension, e.g., clay, in a nematic lyotropic mesophase offer a unique method for the study of clay–micelle interactions and the magnetic properties of clays.

Acknowledgement

We wish to express our gratitude to the NSERC of Canada for providing funds for the research.

1. K. RADLEY and L. W. REEVES. Can. J. Chem. **53**, 2998 (1975).
2. F. Y. FUJIWARA, L. W. REEVES, M. SUZUKI, and J. A. VANIN. *In* Solution chemistry of surfactants. Vol. 1. *Edited by* K. L. Mittal. Plenum Press, New York. 1979. p. 63.
3. M. ACIMIS and L. W. REEVES. J. Phys. Chem. **84**, 2277 (1980).
4. B. J. FORREST and L. W. REEVES. Chem. Rev. **81**, 1 (1981).
5. M. E. MARCONDES HELENE and L. W. REEVES. Chem. Phys. Lett. **89**, 519 (1982).
6. L. W. REEVES. Isr. J. Chem. **23**, 363 (1983).
7. R. E. GRIM. Clay mineralogy. McGraw–Hill, New York. 1968.
8. T. J. PINNAVAIA. Science, **220**, 365 (1983).
9. M. E. MARCONDES HELENE, L. W. REEVES, and C. ROBINSON. *In* Liquid crystals and ordered fluids. Vol. 4. Plenum Press, New York. 1982. p. 451.
10. F. Y. FUJIWARA and L. W. REEVES. Can. J. Chem. **56**, 2178 (1978).
11. F. M. LESLIE, G. R. LUCKHURST, and H. J. SMITH. Chem. Phys. Lett. **13**, 368 (1972).
12. P. G. DE GENNES. The physics of liquid crystals. Clarendon Press, Oxford. 1974.
13. S. CHANDRASEKHAR. Liquid crystals. Cambridge University Press, Cambridge. 1977.
14. M. J. SHAH. J. Phys. Chem. **67**, 2215 (1963).
15. M. J. SHAH, D. C. THOMPSON, and C. M. HART. J. Phys. Chem. **67**, 1170 (1963).
16. A. M. FIGUEIREDO NETO and L. Q. AMARAL. Acta Crystallogr. Sect. A, **39**, 651 (1983).
17. J. CHARVOLIN and Y. HENDRIKX. *In* Liquid crystals of one- and two-dimensional order. *Edited by* W. Helfrich and G. Heppke. Springer Verlag, Berlin. 1980. p. 265.

[2]The term "clay" has been applied to the dispersed colloid in the context that the aluminosilicate clay mineral, montmorillonite, is the principle component of bentonite.

18. M. E. MARCONDES HELENE and L. W. REEVES. J. Phys. Chem. **85**, 718 (1981).
19. N. BODEN, K. J. MCMULLEN, M. C. HOLMES, and G. J. T. TIDDY. *In* Liquid crystals of one- and two-dimensional order. *Edited by* W. Helfrich and G. Heppke. Springer Verlag, Berlin. 1980. p. 299.
20. J. V. CHAMPION, D. DOWNER, G. H. MEETEN, S. A. VAUDREY, and L. F. GATE. J. Chem. Soc. Faraday Trans. 2, **74**, 843 (1978).
21. R. V. MEHTA. J. Colloid Interface Sci. **42**, 165 (1973).
22. B. RAND, E. PEKENĆ, J. W. GOODWIN, and R. W. SMITH. J. Chem. Soc. Faraday Trans. 1, **76**, 225 (1980).
23. B. K. G. THENG. The chemistry of clay—organic reactions. Adam Hilger, Bristol, England. 1974.
24. H. VAN OLPHEN. An introduction to clay colloid chemistry. Interscience Publishers, New York. 1963.
25. R. A. DELLA GUARDIA and J. K. THOMAS. J. Phys. Chem. **88**, 964 (1984).
26. C. C. NUNN, R. S. SCHECHTER, and W. H. WADE. J. Phys. Chem. **86**, 3271 (1982).

Quantitative studies of the autoxidation of linoleate monomers sequestered in phosphatidylcholine bilayers. Absolute rate constants in bilayers

LAWRENCE ROSS COATES BARCLAY,[1] STEVEN JEFFREY LOCKE, JOSEPH MARK MACNEIL, AND JOANN VANKESSEL
Department of Chemistry, Mount Allison University, Sackville, N.B., Canada E0A 3C0

Received December 19, 1984

LAWRENCE ROSS COATES BARCLAY, STEVEN JEFFREY LOCKE, JOSEPH MARK MACNEIL, and JOANN VANKESSEL. Can. J. Chem. **63**, 2633 (1985).

The kinetics of autoxidation of linoleic acid in dimyristoylphosphatidylcholine (DMPC) bilayers were studied at 30°C and pH 7 under 760 Torr O_2. Reactions were initiated using either the lipid-soluble di-*tert*-butylhyponitrite (DBHN) or water-soluble azobis(2-amidinopropane)·HCl (ABAP). Rates of chain initiation, R_i, were measured with a lipid-soluble antioxidant, α-tocopherol, or a water-soluble one, 6-hydroxy-2,5,7,8-tetramethylchroman-2-carboxylate (Trolox). The slightly higher oxidizability obtained ($k_p/2k_t^{\frac{1}{2}} = 2.76 \times 10^{-2}\ M^{-\frac{1}{2}}\ s^{-\frac{1}{2}}$) compared to methyl linoleate in chlorobenzene ($k_p/2k_t^{\frac{1}{2}} = 2.18 \times 10^{-2}\ M^{-\frac{1}{2}}\ s^{-\frac{1}{2}}$) is attributed to a moderate polar solvent effect on ionized linoleate near the bilayer surface. A low initiator efficiency, $e = 0.0895$ for DBHN in DMPC, is attributed to the cage effect in the bilayer of high microviscosity. Similar autoxidation experiments on methyl linoleate in DMPC bilayers gave a lower oxidizability ($k_p/2k_t^{\frac{1}{2}} = 1.79 \times 10^{-2}\ M^{-\frac{1}{2}}\ s^{-\frac{1}{2}}$), indicating that the ester is sequestered deeper in the hydrophobic region of DMPC than is ionized linoleate. Some absolute rate constants are determined using the rotating sector technique for linoleic acid in 0.50 *M* SDS micelles, and egg lecithin and dilinoleoylphosphatidylcholine (DLPC) bilayers. A hundredfold decrease in the termination rate constant, $2k_t$, for DLPC bilayer compared to homogeneous solution is attributed to chain termination in a bilayer region of high polarity. A concomitant reduction (up to tenfold) in the propagation rate constant, k_p, is attributed to diffusion of polar peroxyl radicals away from the oxidizable region of the bilayer.

LAWRENCE ROSS COATES BARCLAY, STEVEN JEFFREY LOCKE, JOSEPH MARK MACNEIL et JOANN VANKESSEL. Can. J. Chem. **63**, 2633 (1985).

Opérant à 30°C, à un pH de 7 et sous une pression de 760 Torr d'O_2, on a étudié la cinétique de l'auto-oxydation de l'acide linoléique dans des couches doubles de dimyristoylphosphatidylcholine (DMPC). On a initié les réactions à l'aide soit de l'hyponitrite du di-*tert*-butyle (HNDB) qui est soluble dans les lipides soit le chlorhydrate de l'azo bis(amidino-2 propane) (ABAP) qui est soluble dans l'eau. On a mesuré les vitesses d'initiation de chaînes, R_i, en présence d'un antioxydant soluble dans l'eau, l'α-tocophérol, ainsi que d'un antioxydant soluble dans l'eau, l'hydroxy-6 tétraméthyl-2,5,7,8 chromanecarboxylate-2 (Trolox). L'oxydabilité est légèrement supérieure ($k_p/2k_t^{\frac{1}{2}} = 2{,}76 \times 10^{-2}\ M^{-\frac{1}{2}}\ s^{-\frac{1}{2}}$) à celle du linoléate de méthyle ($k_p/2k_t^{\frac{1}{2}} = 2{,}18 \times 10^{-2}\ M^{-\frac{1}{2}}\ s^{-\frac{1}{2}}$); on attribue ce résultat à une influence modérée du solvant polaire sur le linoléate ionisé près de la surface à couche double. On attribue la faible efficacité comme initiateur, $e = 0{,}0895$, du HNDB dans le DMPC à un effet de cage dans la double couche qui aurait une microviscosité élevée. Des expériences semblables d'auto-oxydation sur le linoléate de méthyle dans des doubles couches de DMPC donnent lieu à des oxydabilités plus faibles ($k_p/2k_t^{\frac{1}{2}} = 1{,}79 \times 10^{-2}\ M^{-\frac{1}{2}}\ s^{-\frac{1}{2}}$); ce résultat indiquerait que l'ester est plus séquestré dans la région hydrophobe du DMPC que les ions linoléates. Faisant appel à la technique des secteurs rotatifs, on a déterminé quelques constantes absolues de vitesse pour l'acide linoléique à 0,5 *M* dans des micelles de SDS et dans des doubles couches de lécithines d'oeuf et de dilinoléoylphosphatidylcholine (DLPC). On a observé que, par comparaison avec les valeurs obtenues en solutions homogènes, les constantes de vitesse de terminaison, $2k_t$, dans des doubles couches de DLPC sont cent fois moins grandes; on attribue ce résultat à des terminaisons de chaînes dans une région de la double couche de haute polarité. Une réduction concomitante (facteur allant jusqu'à dix) dans la constante de vitesse de propagation, k_p, est attribuée à la diffusion des radicaux polaires peroxyles de la région oxydable de la double couche.

[Traduit par le journal]

Introduction

Renewed interest in the autoxidation of polyunsaturated fatty acids and esters has developed because of the susceptibility of unsaturated carbon chains to peroxidation when they are incorporated into phospholipid biomembranes and the relevance of such peroxidation to various cell-damaging pathological events, including aging (1, 2), heart disease (3), and cancer (4).

We are applying *quantitative* kinetic methods to study the autoxidation of biological molecules in microenvironments such as bilayers and micelles (5–8). Autoxidation in these systems is a free-radical chain process which appears to follow the same classical rate law as in homogeneous solution (5, 8) whereby the oxygen uptake is given by eq. [1]:

$$[1]\quad -\frac{d[O_2]}{dt} = \frac{k_p}{2k_t^{\frac{1}{2}}}[RH]R_i^{\frac{1}{2}}$$

where RH is the substrate, R_i the rate of chain initiation, k_p the propagation rate constant, and $2k_t$ the chain termination rate constant. In these kinetic studies, the rate of chain initiation, R_i, is controlled by using an initiator with a known rate constant for decomposition, k_i. Not all of the radicals escape the solvent cage where they are formed; therefore the actual R_i must be measured, for example, by the inhibitor method (9) using a phenolic antioxidant such as α-tocopherol (α-T) known to trap two peroxyl radicals (10), so that R_i is given by eq. [2], where τ is the inhibition time.

$$[2]\quad R_i = 2[ArOH]/\tau$$

The efficiency of chain initiation is expressed as $e = R_i/2k_i[In]$

[1]Author to whom correspondence may be addressed.

and the radical chain length as $\nu = d[O_2]/dt/R_i$. Under such controlled conditions, the ratio of rate constants $k_p/(2k_t)^{\frac{1}{2}}$ known as the "oxidizability" of the substrate can be measured (eq. [3]):

$$[3] \quad \frac{k_p}{(2k_t)^{\frac{1}{2}}} = \frac{-d[O_2]/dt}{[RH]R_i^{\frac{1}{2}}}$$

Bilayers provide a medium for transport and solubilization of various solutes (11), including relatively large proportions of biologically important intermediates such as cholesterol (12) and fatty acids (13). Bilayer vesicles are also important as drug carriers and media for reactivity control (14) and such bilayers as the phosphatidyl cholines have important effects on free radical dynamics (15–17). It is desirable, therefore, to know what effect a bilayer might have on the chemical behavior of a substance solubilized in it. The fundamental question we address here is: *What is the effect on the oxidizability of a polyunsaturated fatty acid (or ester) when it is sequestered in a phosphatidyl choline bilayer?* We selected linoleate as the unsaturated acid/ester substrate for this kinetic study. The kinetics of autoxidation of linoleate have recently been studied in homogeneous solution (18, 19) and in micelles (5–8, 20), and Weener and Porter have reported on product studies from the cooxidation of polyunsaturated lecithins with linoleic acid (21). However, we are not aware of a quantitative kinetic study of an unsaturated fatty acid in a bilayer. In addition, we report on some *preliminary* studies of the absolute rate constants for propagation, k_p, and termination, $2k_t$, for autoxidation of linoleate in various media, and of unsaturated lecithins in bilayers using the rotating sector technique.

Experimental

1. *Materials and preparations*

Solvents

Chlorobenzene and *ortho*-dichlorobenzene, reagent grades, were dried over calcium chloride and distilled before use.

Phosphate buffer

Solutions were prepared from 0.05 *M* of each of NaH_2PO_4 and $NaHPO_4$ in glass-distilled water containing 1×10^{-4} *M* EDTA.

Tetralin

Tetralin, Fisher Purified, was distilled "*in vacuo*" under nitrogen and passed through a column of alumina to remove traces of hydroperoxides immediately before use.

Linoleic acid and *methyl linoleate* were obtained from Nu-Chek-Prep, >99% purity).

Sodium dodecyl sulfate

The SDS was electrophoresis purity grade (Bio–Rad).

Initiators

Initiators were stored at −30°C and solutions were then prepared immediately before use. Di-*tert*-butylhyponitrite (DBHN) (5) was purified by recrystallization from cold methanol. Azobis(2-amidinopropane)hydrochloride (ABAP), azobisisobutyronitrile (AIBN), azobiscyclohexylnitrile (ACHN), and 2,2′-azobis(2,4-dimethylvaleronitrile) (ADVN) were obtained from Polysciences, Inc. The latter three were recrystallized from methanol before use. The 4,4′-azobis(4-cyanovaleric acid) (ABVA) was obtained from Aldrich. The azobis(2-*n*-butylcarboxylpropane) (ABCP) was synthesized as described (15).

Phospholipids

The egg lecithin phosphatidylcholine (ELPC), dilinoleoyl phosphatidylcholine (DLPC), dipalmitoyl phosphatidylcholine (DPPC), and dimyristoyl phosphatidylcholine (DMPC) were obtained from Avanti Polar Lipids. They were stored in sealed vials at −30°C.

Inhibitors

α-Tocopherol (α-T) (Eastman–Kodak) was stored in known concentrations in hexane under argon at −30°C. The water-soluble Trolox, a gift from Hoffmann–LaRoche, Nutley, New Jersey, was used as freshly prepared solutions in phosphate buffer (pH 7.0).

Bilayers

The bilayer dispersions were prepared by vortex stirring in phosphate buffer (pH 7) containing EDTA of films of the phospholipids from evaporation of a solution in methylene chloride as described (5). Lipid-soluble initiators (DBHN, ABCP, ACHN, and ADVN) were dissolved in the bilayers by adding them to the organic solvent – phospholipid phase before evaporation to a film. Sonication of the bilayers was carried out under argon in a Bransonic 220 ultrasonic bath.

2. *Analyses*

The concentration of DBHN remaining in the bilayer was measured by hlpc analysis because of the loss of this initiator due to its volatility (5) during the bilayer preparation. An aliquot of the bilayer dispersion containing DBHN was added to three times its volume of methanol to break up the bilayer. An internal standard solution of acetanilide was then added and the DBHN concentration measured on a SP-8000 hplc using a Brownlee RP-8 column eluted with 60:40 methanol/water at 2.0 mL/min.

The particle sizes of the vesicles in the aqueous dispersions were determined by Dr. G. F. Barclay on a difference interference contrast microscope (Zeiss Nomarski) at 1250× magnification.

3. *Autoxidation procedures*

The autoxidation procedure described previously (5) was followed. In autoxidation using water-soluble initiators (ABAP, ABVA) and inhibitor (Trolox), the reaction was initiated by adding a solution of known concentration of the initiator in phosphate buffer. The rate of oxygen uptake was measured, followed by injection of a known concentration of Trolox in buffer to the same reaction to measure the R_i by the induction period method.

The rotating sector method to measure absolute rate constants has been reviewed in terms of the theory (22) and applications (23). Our procedure to obtain k_p and $2k_t$ for autoxidation was similar to that of Howard and Ingold (24). The method is based upon measurement of the lifetime of the reaction chains. For this measurement the reaction is initiated by photochemical decomposition of the initiator with a rotating sectored disc of known dimensions between the light source (in this case a focused 200-W super pressure mercury arc light filtered through Pyrex) and the reaction flask. Rates of oxygen uptake are measured at various sector speeds and the $2k_t$ calculated as described (24). The k_p is then calculated from the rate at steady illumination from eq. [1] by substituting for the measured $2k_t$ and the R_i. The variations in rates with light intensity were measured at full light and 10%, 25%, and 50% light by inserting neutral density filters into the light beam. In all cases the thermal (dark) rate remained low (less than 10%) compared to the photochemical rate on the same sample.

Results and discussion

1. *The oxidizability of methyl linoleate in homogeneous solution*

The kinetics of autoxidation of methyl linoleate initiated by azobisisobutyryl nitrile (AIBN) were studied at three concentrations in chlorobenzene and the results are shown in Table 1. The oxidizability result ($k_p/2k_t = 2.18 \pm 0.09 \times 10^{-2} M^{-\frac{1}{2}} s^{-\frac{1}{2}}$) is in good agreement with the published value of 2.10×10^{-2} $M^{-\frac{1}{2}} s^{-\frac{1}{2}}$ (25). The considerably higher oxidizability in *ortho*-dichlorobenzene ($4.08 \times 10^{-2} M^{-\frac{1}{2}} s^{-\frac{1}{2}}$) is attributed to a solvent effect since an increase in solvent polarity[2] is known to increase

[2]The dielectric constants of the solvents are C_6H_5Cl, 5.62, and o-$C_6H_4Cl_2$, 9.93 at 25°C (26).

TABLE 1. Autoxidation of methyl linoleate in organic solvents[a]

No.[b]	Substrate $M \times 10^2$	Solvent	$2k_i$ [In] $M\ s^{-1} \times 10^9$	R_i[c] $M\ s^{-1} \times 10^9$	e	$-d[O_2]/dt$[d] $M\ s^{-1} \times 10^8$	ν	$\frac{-d[O_2]/dt}{[RH]R_i^{1/2}}$ $M^{-1/2}\ s^{-1/2} \times 10^2$
1	2.26	Chlorobenzene	7.44	3.68	0.495	3.18	9	2.32
2	4.52	Chlorobenzene	7.44	3.94	0.530	6.36	16	2.24
3	9.04	Chlorobenzene	7.44	3.94	0.530	11.9	30	2.10
4	(a) 2.26	*o*-Dichlorobenzene	19.5	13.6	0.697	10.8	8	4.08
	(b) 2.26	*o*-Dichlorobenzene	19.5	13.6[e]	—	10.3	—	3.93

[a]All runs at 30°C, 760 Torr O_2 (1 Torr = 133.3 Pa).
[b]Nos. 1−3 were initiated with azobisisobutyronitrile (AIBN) $4.00 \times 10^{-2}\ M$, $k_i = 9.3 \times 10^{-8}\ s^{-1}$ (ref. 5), no. 4 with di-*tert*-butylhyponitrite (DBHN), $3.04 \times 10^{-3}\ M$, $k_i = 3.2 \times 10^{-6}\ s^{-1}$ (ref. 5).
[c]R_i was measured by the induction period with α-tocopherol.
[d]Rates are corrected for nitrogen evolution from the initiator, oxygen absorbed by the initiating radicals, and oxygen evolved in chain termination by adding $(1 - e)k_i$ [In] to the measured rate.
[e]Calculated using $e = 0.697$ from Run 4 (a).

TABLE 2. Autoxidation of linoleic acid in PPC bilayers[a]

PPC used[b]	Initiator[c] (mol × 10^6)	Inhibitor (mol × 10^8)	Induction period, s × 10^{-3}	R_i[a] $M\ s^{-1} \times 10^7$	e	$-d[O_2]/dt$[a,h] $M\ s^{-1} \times 10^6$	Chain length	Oxidizability[a] $M^{-1/2}\ s^{-1/2} \times 10^2$
DMPC	DBHN(6.66)	α-T(0.922)	6.37	1.57	0.070	5.21	29	2.97[e]
DMPC	(6.66)	Trolox(0.650)	3.17	1.64	0.096	5.10	31	2.45[e]
DMPC	(5.52)	(0.660)	4.00	1.32	0.093	4.46	34	2.35[e]
DMPC	ABAP(82.4)	Trolox(1.48)	1.18	11.2	0.453	13.7	12	2.52[f]
	(82.3)	(5.08)	3.46	11.6	0.453	19.3	17	3.49[g]
DPPC	DBHN(11.3)	α-T(3.24)	3.44	0.756	0.026	5.36	71	3.74[e]
DPPC	(7.5)	—	—	0.492[d]	[d]	4.52	92	4.00[e]

[a]1.29×10^{-5} mol, 4.0×10^{-6} L of linoleic acid and 2.12×10^{-5} L of bilayer were used in each run. The combined volume was used for the reaction volume in calculations. Reactions were carried out in 2.00 mL of phosphate buffer (pH 7.0) at 30°C.
[b]DMPC, dimyristoyl phosphatidylcholine; DPPC, dipalmitoyl phosphatidylcholine.
[c]DBHN, di-*tert*-butylhyponitrite (the amount in the bilayers determined by RP hplc analyses); ABAP, azobis(2-amidinopropane hydrochloride), $k_i = 3.82 \times 10^{-7}\ s^{-1}$ (ref. 6).
[d]The value of 0.026 was used to calculate the R_i.
[e]The bilayers were prepared by vortex stirring, giving mixtures of particle sizes up to approximately 6 μm in size.
[f]The bilayer was prepared by sonication (2 h).
[g]The bilayer was sonicated at 50°C until a nearly clear dispersion formed ($9\frac{1}{2}$ h). The particles were less than 0.2 μm in size.
[h]The same as footnote *d*, Table 1.

the oxidizability of a substrate (27−29). The results in these similar nonprotic solvents of different polarity provide a basis for comparison with the autoxidation of linoleate in micelles and bilayers.

2. *Autoxidation of linoleate in PPC bilayers*

(*a*) *The oxidizability of linoleic acid in DMPC and DPPC bilayers using lipid-soluble and water-soluble initiators and inhibitors*

We have recently shown (6) that various combinations of *lipid-soluble* and *water-soluble* initiators and inhibitors can be used for quantitative kinetic studies in micelles and bilayers whereby the same oxidizability of a substrate was obtained with the initiator or inhibitor in either the aqueous phase or the micellar or bilayer phase. The present results from the autoxidation of linoleic acid in bilayers outlined in Table 2 provide an important application of the earlier findings. Thus the oxidizability of linoleic acid in dimyristoyl phosphatidyl choline (DMPC) bilayers is the same, within experimental error, whether one uses a combination of a lipid-soluble initiator, di-*tert*-butylhyponitrite (DBHN), with a lipid-soluble inhibitor, α-tocopherol (α-T), or a water-soluble inhibitor, 6-hydroxy-2,5,7,8-tetramethylchroman-2-carboxylate (Trolox). Furthermore, similar results were obtained for the oxidizability of linoleic acid in DMPC when one initiates with a water-soluble initiator azobisamidinopropane·HCl (ABAP) and uses water-soluble Trolox to measure the R_i (Table 2). Other workers (13) report that linoleic acid readily partitions into PPC bilayers, and the fact that we obtain the same oxidizability of linoleic acid whether the initiators and inhibitors are located in the water or the bilayer is consistent with solubilization into the bilayer region.

The *magnitude* of the oxidizability of a *given* substrate is known to be increased by the polarity of the medium (27−29). This solvent effect could be exerted on a dipolar transition state of the type

$$\text{R—O—O}\cdot + \text{H—R} \xrightarrow{k_p} [\text{R—O—O}^{-}\cdot\text{H}\cdot\overset{+}{\text{R}}]$$

resulting in an increase in the propagation rate constant. However, actual measurements of propagation (k_p) and termination (k_t) rate constants for hydrocarbons in various solvents demonstrated that the solvent polarity effect is mainly on the rate of *termination* (28), which is decreased due to the fact that the polarity of peroxyl radicals (30) is destroyed in the termination step. The termination rate constants for radical recombinations

TABLE 3. Autoxidation of methyl linoleate in DMPC bilayers[a]

Substrate (mol × 10^5)	Initiator (mol × 10^5)	Inhibitor (mol × 10^8)	Induction period, s × 10^{-3}	R_i $M\,s^{-1}$ × 10^7	$-d[O_2]/dt$ $M\,s^{-1}$ × 10^6	Chain length	Oxidizability $M^{-\frac{1}{2}}\,s^{-\frac{1}{2}}$ × 10^2
1.50	ABAP[b](8.12)	α-T(5.81)	7.13	5.99	7.80	13	1.83
0.91	(8.15)	(7.75)	6.77	9.38	6.13	7	1.69
1.50	(8.08)	Trolox(4.67)	3.53	9.73	9.52	10	1.75
0.91	(8.08)	(7.71)	5.62	11.2	7.42	7	1.88
3.82	ABVA[c](0.360)	(5.20)	1.75	0.17	2.57	15	1.80

[a]See footnote *a*, Table 2.
[b]The initiator efficiency, $e = 0.438 \pm 0.027$ (ref. 6 gives $e = 0.43$).
[c]4,4′-Azobis(4-cyanovaleric acid) was decomposed photolytically.

in bilayers could similarly be suppressed if peroxyl radicals diffuse to the polar region as suggested earlier (5).

The value for the oxidizability of linoleic acid in DMPC bilayers ($2.76 \pm 0.42 \times 10^{-2}\,M^{-\frac{1}{2}}\,s^{-\frac{1}{2}}$) is somewhat higher than that found for methyl linoleate in solution in chlorobenzene. This difference could be due to the position of the linoleate chain in the bilayer. An ionized carboxylate head group in this case would tend to pull the chain out towards the aqueous surface where the dielectric constant is expected to be higher, resulting in a moderate "solvent effect". The higher oxidizability of linoleic acid in highly sonicated vesicles ($3.49 \times 10^{-2}\,M^{-\frac{1}{2}}\,s^{-\frac{1}{2}}$) appears to be due to the effect of particle size on the absolute rate constants (*vide infra*).

The rather low initiator efficiency, *e*, for the bilayer-soluble initiator, DBHN ($8.95 \pm 1.15\%$), is consistent with chain initiation in the bilayer region where the microviscosity is high. This results in a high proportion of cage recombination. Similar results were found for initiation of bilayer autoxidation in egg lecithin by DBHN, where *e* was found to be 9.1% (5).

A few autoxidation runs were carried out on linoleic acid in a bilayer below the phase transition temperature by using dipalmitoylphosphatidyl choline (DPPC, phase transition 41°C) at 30°C and typical results are included in Table 2. In this case the initiator efficiency of DBHN is even lower (2.6%), presumably due to a higher microviscosity of a bilayer below its phase transition temperature.

(b) The oxidizability of methyl linoleate in DMPC bilayers

The autoxidation of methyl linoleate was initiated in DMPC bilayers by using water-soluble initiators ABAP and 4,4′-azobis(4-cyanovaleric acid) (ABVA). The R_i was measured using either the lipid-soluble inhibitor, α-T, or water-soluble Trolox. The results of these experiments are summarized in Table 3. The oxidizability of this *neutral* linoleate chain ($1.79 \pm 0.07 \times 10^{-2}\,M^{-\frac{1}{2}}\,s^{-\frac{1}{2}}$) is only measurably lower than observed in chlorobenzene solution but it is significantly lower than that found for ionized linoleate in DMPC ($2.76 \times 10^{-2}\,M^{-\frac{1}{2}}\,s^{-\frac{1}{2}}$). We suggest that this indicates that methyl linoleate is sequestered deep in the relatively nonpolar, more fluid region (31) of DMPC where it undergoes autoxidation.

Our results outlined in Tables 2 and 3 provide interesting applications of various combinations of lipid-soluble and water-soluble initiators and inhibitors for quantitative kinetic studies in bilayers (i.e. DBHN with either α-T or Trolox, ABAP with Trolox, ABAP with α-T or Trolox[3]). This raises important questions as to how both water-soluble and lipid-soluble initiators and inhibitors exhibit the same effectiveness in initiating autoxidation and trapping radicals in bilayer autoxidation. The radical trapping effectiveness of water-soluble Trolox for radicals formed in the lipid phase is understood on the basis of our earlier postulate (5) that polar peroxyl radicals formed in the nonpolar hydrocarbon phase of a bilayer will diffuse into the more polar aqueous–lipid interfacial region. The effective radical trapping ability of Trolox for peroxyls initially formed in the bilayer from lipid-soluble DBHN confirms this postulate. Trolox in the water is expected to trap these radicals at the water–bilayer interface. It is also remarkable to find that a charged water-soluble initiator (ABAP, ABVA) and inhibitor appear to have access to the various layers of the multilamellar liposomes used, suggesting a rather fluid overall system. We are studying these phenomena in more detail by comparing the behavior of multilamellar and unilamellar systems.

3. *Absolute rate constants for propagation,* k_p, *and termination,* $2k_t$

Some exploratory experiments were conducted to (1) determine if the rotating sector technique (22), widely used to study photoinitiated reactions in homogeneous solution (33, 34) can be applied to determine absolute rate constants, k_p and $2k_t$, in microenvironments such as bilayers and micelles, and (2) to determine the applicability of water-soluble initiators and inhibitors (6) to this technique. Trial experiments carried out in homogeneous media, Table 4, Nos. 1–4, gave good agreement of the k_p and $2k_t$ for tetralin (lit. values (33) are $k_p = 6.4\,M^{-1}\,s^{-1}$ and $2k_t = 7.6 \times 10^6\,M^{-1}\,s^{-1}$) and reasonable agreement for methyl linoleate in chlorobenzene (lit. values (34) are $k_p = 62\,M^{-1}\,s^{-1}$ and $2k_t = 8.8 \times 10^6\,M^{-1}\,s^{-1}$), considering the large errors that occur in the determinations of k_p and $2k_t$ (24). For eq. [1] (Introduction) to be followed exactly, chain termination must be bimolecular and the oxidation rate must be proportional to $R_i^{\frac{1}{2}}$. This is tested by using initiators of relatively high thermal stability (Table 4) and measuring the reaction rate order, which should be half order, with respect to the light intensity. The somewhat higher order (0.57) with methyl linoleate is attributed to some first-order chain termination in addition to bimolecular chain termination.

Preliminary experiments in SDS micelles and bilayers (Table 4, Nos. 6–12) indicate that photodecomposition of azo-initiators occurs so that the rotating sector method to estimate absolute rate constants is applicable to these systems. Although bilayers are typically opaque milky dispersions, continuous shaking of the sample exposes a fresh layer to the light and permits effective photocatalytic decomposition of the initiator.

[3]ABAP has recently been reported to initiate oxidation of lecithin bilayers (32).

Furthermore, the order in light intensity is one-half, within experimental error, as required for bimolecular termination. The use of water-soluble initiators and inhibitors also makes it possible to prepare the bilayers by various techniques (vortex stirring, sonication, dialysis) *prior* to the initiation of autoxidation. The latter two procedures result in decomposition or loss of lipid-soluble initiators and inhibitors which must be inserted prior to preparation of a bilayer (5), and this decomposition makes it difficult to study unilamellar bilayer vesicles by controlled autoxidation.

The data outlined in Nos. 6–13 provide the first published evidence of absolute autoxidation rate constants in microenvironments. Although our results for the absolute rate constants are somewhat preliminary and a detailed analysis requires more data, a few interesting trends can be noted. There is a notable decrease in the termination rate constant ($2k_t$) for autoxidation of a phospholipid in bilayers compared to that in homogeneous solution (Compare Nos. 7–11 with DLPC in *tert*-butyl alcohol), and this reduction could be as much as a hundredfold for DLPC in bilayers compared to homogeneous solution. We suggest that this reduction in $2k_t$ is probably a consequence of the termination of peroxyls in the polar region of the bilayer.[4] Nevertheless the oxidizability, $k_p/2k_t^{\frac{1}{2}}$, of a bilayer remains about the same as that in homogeneous solution (compare DLPC in *tert*-butyl alcohol and in a bilayer, Nos. 5 and 9). This results from a significant *reduction* in the k_p, by as much as tenfold, as well as the noted decrease in $2k_t$. A reduction in k_p was anticipated earlier (5) when we hypothesized that polar peroxyl radicals (30) would diffuse away from the nonpolar hydrocarbon-like environment. As a result they would not readily abstract the labile CH_2 groups which are deeper in the bilayer. It also appears that the oxidizability of a substrate depends somewhat on the nature of the PPC particles employed. Thus DLPC in sonicated vesicles has about double the $k_p/2k_t^{\frac{1}{2}}$ (Nos. 10, 11) compared to multilamellar bilayers (No. 9), and methyl linoleate in highly sonicated DMPC vesicles has a significantly higher $k_p/2k_t^{\frac{1}{2}}$ value compared to that in multilamellar bilayers (Table 3). The reason for this is not entirely obvious, although it appears to result mainly from an increase in the k_p term.

Acknowledgements

We are indebted to Drs. G. W. Burton and K. U. Ingold of N.R.C.C. for their assistance with the rotating sector experiments, and to Dr. G. F. Barclay of our Biology Department for the microscopic examination of the vesicles. Financial assistance provided by the Natural Sciences and Engineering Research Council of Canada is gratefully acknowledged.

1. A. L. TAPPEL. *In* Free radicals in biology. Vol. IV. *Edited by* W. A. Pryor. Academic Press, New York. 1980. Chapt. 1. pp. 1–47.
2. J. R. WALTON and L. PACKER. *In* Vitamin E—a comprehensive treatise. Basic and clinical nutrition. Vol. 1. *Edited by* L. J. Machlin. M. Dekker, New York. 1980. pp. 495–517.
3. N. A. PORTER. *In* Free radicals in biology. Vol. IV. *Edited*

[4]If the peroxyl radicals terminate in the aqueous-lipid interface as proposed (*vide infra*), the reduction in $2k_t$ could be due to stabilization of the polar peroxyl radicals by the polar aqueous buffer and by hydrogen bonding (29):

$$R-\ddot{\underset{..}{O}}-\dot{\underset{..}{O}} \leftrightarrow R-\overset{+}{\dot{\underset{..}{O}}}-\overset{-}{\ddot{\underset{..}{O}}}:\text{---}\underset{H}{HO}$$

TABLE 4. Absolute rate constants for propagation, k_p, and termination, $2k_t$, at 30°C

No.	Substrate[a] (mol × 10^5)	Initiator[b] (mol × 10^6)	Medium[a]	Order in light intensity[c]	Inhibitor (mol × 10^8)	Induction period (s × 10^{-3})	R_i $M\,s^{-1} \times 10^7$	$-d[O_2]/dt$ $M\,s^{-1} \times 10^6$	ν	$\frac{-d[O_2]/dt}{[RH]R_i^{\frac{1}{2}}}$ $M^{-\frac{1}{2}}\,s^{-\frac{1}{2}} \times 10^2$	k_p $M^{-1}\,s^{-1}$	$2k_t$ $M^{-1}\,s^{-1} \times 10^{-6}$
1	Tetralin(1470)	ABCP(2.9)	Neat	—	α-T(9.22)	6.32	0.146	1.91	131	0.22	5.6	6.4
2	Tetralin(1470)	(2.9)	Neat	—	(9.60)	6.86	0.140	2.00	143	0.23	6.0	6.5
3	Me Lin(30.2)	ACHN(9.0)	C_6H_5Cl	0.57	(12.8)	1.128	1.13	0.940	8	1.94	31	2.7
4	Me Lin(30.2)	(9.0)	C_6H_5Cl	0.57	(12.8)	1.128	1.13	0.979	9	1.93	32	2.7
5	DLPC(6.13)	(8.2)	*tert*-Butyl alcohol	0.47	(6.4)	0.630	1.02	0.566	6	5.8	150	6.8
6	Lin A(6.43)	ABAP(3.7)	0.50 *M* SDS	0.48	Trolox(1.73)	0.228	6.05	6.85	11	3.4	15	0.20
7	ELPC(2.50)	(14.6)	Bilayer	0.51	(15.1)	0.990	122	84.0	7	2.4	10	0.16
8	ELPC(6.88)	ADVN(4.0)	Bilayer	0.51	α-T(5.76)	1.37	12.3	45.9	37	4.1	18	0.18
9	DLPC(2.50)	ABCP(14.3)	Bilayer	0.49	(5.94)	0.636	74.7	110	16	4.0	15	0.14
10	DLPC(2.50)	ABCP(14.3)	Bilayer	0.47	Trolox(25.0)	8.64	23.3	84.0	36	5.5	16	0.080
11	DLPC(2.50)	ABCP(14.6)	Bilayer[d]	0.51	(15.1)	2.23	54.2	253	47	10.9	30	0.076
12	DLPC(2.50)	(14.6)	Bilayer[d]	0.47	(15.1)	1.89	63.9	272	43	10.8	22	0.043
13	Me Lin(3.02)	ABVA(4.6)	Bilayer (DMPC)[e]	0.52	(5.2)	2.09	7.50	20.5	27	5.2	41	0.63

[a]Me Lin, methyl linoleate; Lin A, linoleic acid; DLPC, dilinoleoylphosphatidylcholine; ELPC, egg lecithin. The bulk volume was 2.0 mL in each run. The reaction volume used for calculations for 0.50 *M* SDS is 2.5×10^{-4} L (ref. 8); for Nos. 7–13 the bilayer volume is used (see Table 2, footnote *a*). Except where noted, bilayers were prepared by vortex stirring.
[b]ABCP, azobis(2-*n*-butylcarboxy)propane; ACHN, azobiscyclohexylnitrile; ADVN, 2,2′-azobis(2,4-dimethylvaleronitrile); ABVA, 4,4′-azobis(4-cyanovaleric acid).
[c]Determined by varying light intensity with neutral density filters (10%, 25%, 50%, 100%).
[d]Prepared by vortex stirring followed by 1 to 2-h sonication.
[e]Sonicated at 50°C for 5 h to give a transparent dispersion; particle sizes less than 0.2 μm.

by W. A. Pryor. Academic Press, New York. 1980. Chapt. 8. pp. 261–294.
4. B. N. AMES. Science, **221**, 1256 (1983).
5. L. R. C. BARCLAY and K. U. INGOLD. J. Am. Chem. Soc. **103**, 6478 (1981).
6. L. R. C. BARCLAY, S. J. LOCKE, J. M. MACNEIL, J. VANKESSEL, G. W. BURTON, and K. U. INGOLD. J. Am. Chem. Soc. **106**, 2479 (1984).
7. L. R. C. BARCLAY, S. J. LOCKE, and J. M. MACNEIL. Can. J. Chem. **61**, 1288 (1983).
8. L. R. C. BARCLAY, S. J. LOCKE, and J. M. MACNEIL. Can. J. Chem. **63**, 366 (1985).
9. C. E. BOOZER, G. S. HAMMOND, C. E. HAMILTON, and J. N. SEN. J. Am. Chem. Soc. **77**, 3233 (1955).
10. G. W. BURTON and K. U. INGOLD. J. Am. Chem. Soc. **103**, 6472 (1981).
11. M. K. JAIN and R. C. WAGNER. Introduction to biological membranes. Wiley–Interscience, New York. 1980.
12. U. COGAN, M. SHINITZKY, G. WEBER, and T. NISHIDA. Biochemistry, **12**, 521 (1973).
13. H. WEENEN and N. A. PORTER. J. Am. Chem. Soc. **104**, 5216 (1982).
14. J. H. FENDLER. Acc. Chem. Res. **13**, 7 (1980).
15. J. S. WINTERLE and T. MILL. J. Am. Chem. Soc. **102**, 6336 (1980).
16. R. C. PETTER, J. C. MITCHELL, W. J. BRITTAIN, T. J. MCINTOSH, and N. A. PORTER. J. Am. Chem. Soc. **105**, 5700 (1983).
17. N. A. PORTER, R. C. PETTER, and W. J. BRITTAIN. J. Am. Chem. Soc. **106**, 813 (1984).
18. Y. YAMAMOTO, E. NIKI, and Y. KAMIYA. Bull. Chem. Soc. Jpn. **55**, 1548 (1982).
19. Y. YAMAMOTO, E. NIKI, and Y. KAMIYA. Lipids, **17**, 870 (1982).
20. Y. YAMAMOTO, S. HAGA, E. NIKI, and Y. KAMIYA. Bull. Chem. Soc. Jpn. **57**, 1260 (1984).
21. H. WEENEN and N. A. PORTER. J. Am. Chem. Soc. **104**, 5216 (1982).
22. G. M. BURNETT and H. W. MELVILLE. *In* Technique of organic chemistry. Vol. VIII. Part II. *Edited by* S. L. Friess, E. S. Lewis, and A. Weissberger. Interscience, New York. 1963. Chapt. 20.
23. J. A. HOWARD. Adv. Free-Radical Chem. **4**, 49 (1972).
24. J. A. HOWARD and K. U. INGOLD. Can. J. Chem. **43**, 2729, 2737 (1965).
25. J. A. HOWARD and K. U. INGOLD. Can. J. Chem. **45**, 793 (1967).
26. R. C. WEAST (*Editor*). CRC handbook of chemistry and physics. 52nd ed. The Chemical Rubber Co., Cleveland, Ohio. 1971–1972. p. E-45.
27. J. A. HOWARD and K. U. INGOLD. Can. J. Chem. **42**, 1044 and 1250 (1964).
28. J. A. HOWARD and K. U. INGOLD. Can. J. Chem. **44**, 1119 (1966).
29. D. G. HENDRY and G. A. RUSSELL. J. Am. Chem. Soc. **86**, 2368 (1964).
30. R. W. FESSENDEN, A. HITACHI, and V. NAGARAJAN. J. Phys. Chem. **88**, 107 (1984).
31. W. L. HUBBELL and H. M. MCCONNELL. J. Am. Chem. Soc. **93**, 314 (1971).
32. Y. YAMAMOTO, E. NIKI, Y. KAMIYA, and H. SHIMASAKI. Biochim. Biophys. Acta, **795**, 332 (1984).
33. J. A. HOWARD and K. U. INGOLD. Can. J. Chem. **44**, 1113 (1966); **44**, 1119 (1966).
34. J. A. HOWARD and K. U. INGOLD. Can. J. Chem. **45**, 785 (1967).

Interactions entre les cations et les sucres. I. Évaluation de l'enthalpie libre d'interaction Ca^{2+} − D-(−)-ribose dans l'eau à 25°C

JEAN-PIERRE MOREL[1] ET CLAUDE LHERMET
Laboratoire d'Étude des Interactions Solutés–Solvants, U.A. au C.N.R.S. n° 434, Université de Clermont 2, 63170 Aubière, France

Reçu le 17 décembre 1984

JEAN-PIERRE MOREL et CLAUDE LHERMET. Can. J. Chem. **63**, 2639 (1985).

L'interaction des deux pentoses isomères D-(−)-ribose et D-(−)-arabinose avec l'ion Ca^{2+} en solution aqueuse est étudiée à l'aide de deux types de cellules électrochimiques (avec et sans jonction) comportant une électrode à membrane liquide sélective à Ca^{2+}. Certains isomères du D-(−)-ribose possèdent une séquence d'hydroxyles susceptible d'interagir spécifiquement avec le cation. La mesure de l'enthalpie libre de transfert de l'ion Ca^{2+} entre l'eau et les solutions sucrées permet de calculer un paramètre d'interaction par paire caractéristique. D'autre part, cette interaction spécifique est également caractérisée par sa constante d'association: β_1 = 0,93. Les deux approches sont étudiées et leur cohérence est démontrée.

JEAN-PIERRE MOREL and CLAUDE LHERMET. Can. J. Chem. **63**, 2639 (1985).

The interaction of the two isomeric pentoses D-(−)-ribose and D-(−)-arabinose with the Ca^{2+} ion in aqueous solution is studied with the help of two types of electrochemical cells (with and without liquid junction) including a liquid-membrane Ca^{2+}-selective electrode. Some of the D-(−)-ribose isomers contain a sequence of hydroxyl groups which can interact specifically with the cation. The measurement of the Gibbs free energy of transfer of Ca^{2+} between water and the sugar solutions allows one to calculate a characteristic pair-interaction parameter. This specific interaction can also be characterized by its association constant: β_1 = 0.93. The two approaches are studied and their coherence is shown.

Introduction

Les interactions en solution aqueuse entre les cations métalliques et les saccharides, malgré leur relative faiblesse, sont d'une grande importance pour la chimie et la biochimie des sucres. Elles intéressent également des domaines de la biologie tels que le stockage du calcium ou l'adhésion des cellules.

Les travaux de S. J. Angyal (1, 2) ont d'abord montré le rôle joué par la présence des séquences d'hydroxyles *axial–équatorial–axial* dans les cycles à 6 atomes, et *cis–cis–cis* dans les cycles à 5 atomes des molécules de sucres, de leurs dérivés ou des composés cycliques polyhydroxylés. Des études quantitatives ont permis de préciser l'ordre de grandeur des constantes d'association entre certaines cations et certains sucres. Le D-(−)-ribose, en particulier, a fait l'objet de plusieurs études; il s'agit en effet d'un des rares sucres simples qui présente des structures favorables à la complexation: les deux conformères $^4C_1$ et $^1C_4$ de la forme α-pyranose et le conformère $^1C_4$ du β-pyranose présentent une séquence *ax–eq–ax* alors que la forme α-furanose présente une séquence *cis–cis–cis* d'hydroxyles. Les études en rmn de Lenkinski et Reuben (3) et de Symons *et al.* (4) ont permis de proposer des valeurs de constante d'association pour les différentes formes ci-dessus avec l'ion Ca^{2+}. Des méthodes potentiométriques ont également été appliquées à l'étude de ce couple (5, 6).

Si la rmn est une méthode de choix qui permet de distinguer les différents isomères présents à l'équilibre, elle nécessite l'étude de solutions où le sucre est souvent présent à des concentrations de l'ordre de 1 *M* alors que la concentration du sel de calcium peut varier jusqu'à 2 *M*. Dans ces conditions, les constantes obtenues sont apparentes et comparatives mais sans nul doute assez éloignées des valeurs thermodynamiques; de plus, aux fortes concentrations en sel, l'effet des anions peut fausser notablement l'interprétation des résultats.

L'étude thermodynamique des interactions sucre–cation n'a pas été réalisée de façon approfondie. Si la première étape d'une telle étude est logiquement la détermination des paramètres d'enthalpie libre, on peut penser que la connaissance d'autres grandeurs thermodynamiques (en particulier l'enthalpie et l'entropie d'interaction) seraient également très utile à la compréhension du phénomène. Nous nous proposons d'aborder ces problèmes par une interprétation de résultats expérimentaux obtenus en potentiométrie. Les électrodes à membrane liquide sélectives à l'ion Ca^{2+} permettent des mesures très précises de l'activité de cet ion en solution aqueuse. Dans les cellules galvaniques mettant en oeuvre une telle électrode, le D-(−)-ribose sera comparé au D-(−)-arabinose, pentose isomère dont les formes pyraniques présentes à l'équilibre ne comportent aucune séquence d'hydroxyle favorable à la complexation.

[1]Auteur à qui adresser toute correspondance.

Théorie

La première cellule galvanique étudiée est:

[1] Electrode à Ca $|CaCl_2(m)$, sucre $(m_s)|AgCl|Ag$

où m est la molalité de $CaCl_2$ et m_s celle du sucre, ribose (m_R) ou arabinose (m_A). La réaction de cellule s'écrit:

[2] $Ca \text{ (électrode)} + 2\ AgCl = Ca^{2+} + 2Cl^- + Ag$

Une étude préliminaire, pour laquelle $m_s = 0$, nous permet de vérifier la réversibilité de cette cellule dont la tension s'écrit, à T et P constantes,

[3] $U(m) = U^{\ominus} + 3k/2 \log m\gamma_{\pm}$

où $U^{\ominus}$ est la tension standard dans l'échelle des molalités,

$$k = \ln 10\ RT/F = 0{,}05916 \text{ V à } 25°\text{C}$$

En utilisant les valeurs de $\gamma_{\pm}$ ($CaCl_2$) données par Robinson et Stokes (7) et les valeurs expérimentales de U, on peut calculer une pente de 88,8 mV en excellent accord avec la valeur thermodynamique.

Le principe de la mesure consiste à ajouter une solution concentrée de sucre contenant $CaCl_2$ à la molalité m par rapport au solvant (eau + sucre) dans une solution aqueuse initiale de même molalité m en $CaCl_2$ contenue dans la cellule (8). On explore ainsi une gamme de concentration en sucre variant par exemple de $m_s = 0$ à $m_s = 0{,}4$ en maintenant m constant. Les tensions de cellule s'expriment en utilisant l'état standard correspondant à $CaCl_2$ infiniment dilué dans l'eau d'une part et dans la solution sucrée d'autre part.

$$[4] \quad U(m) = U^{\ominus} + 3k/2 \log m\, \gamma_{\pm}(m)$$

$$[5] \quad U(m, m_s) = U^{\ominus}(m_s) + 3k/2 \log m\, \gamma_{\pm}(m, m_s)$$

où les $\gamma_{\pm}$ tendent vers 1 dans les deux cas lorsque $m \rightarrow 0$. On voit que:

$$U(m, m_s) - U(m) = [U^{\ominus}(m_s) - U^{\ominus}] + 3k/2 \log \frac{\gamma_{\pm}(m, m_s)}{\gamma_{\pm}(m)}$$

et lorsque $m \rightarrow 0$

$$[U(m, m_s) - U(m)] \rightarrow [U^{\ominus}(m_s) - U^{\ominus}]$$

L'expérience montre que pour des concentrations en $CaCl_2$ $m = 5 \times 10^{-3}$ et $m = 1 \times 10^{-1}$, la différence des tensions ne dépend que de m_s et représente la différence des tensions standard, c'est-à-dire qu'on peut considérer que

$$\gamma(m, m_s)/\gamma(m) \sim 1$$

Cette expérience permet donc d'accéder à l'enthalpie libre standard de transfert de l'électrolyte $CaCl_2$ de l'eau pure à la solution sucrée de molalité m_s (8).

$$[6] \quad \Delta G_t^{\ominus} = 2\, F[U^{\ominus}(m_s) - U^{\ominus}]$$

où F est le Faraday. Cette grandeur standard de transfert peut s'interpréter en terme de paramètre d'interaction par paires, triplets etc ... (9) sous la forme

$$[7] \quad \Delta G_t^{\ominus} = 2\nu\, g_{ES}\, m_s + 3\, \nu\, g_{ESS}\, m_s^2 + \ldots$$

où ν est le nombre d'ions de l'électrolyte E, c'est-à-dire, ici, $\nu = 3$ pour $CaCl_2$. Ce formalisme fait apparaître le paramètre d'enthalpie libre de la paire électrolyte–sucre, g_{ES}, qui est la moyenne des paramètres d'interaction des paires cation–sucre et anion–sucre de telle façon que

$$[8] \quad g_{ES} = (g_{Ca^{2+}s} + 2\, g_{Cl^-s})/3$$

Dans cette étude, le sucre étudié sera successivement le D-(−)-ribose et le D-(−)-arabinose. Si l'on admet que les interactions non spécifiques de ces deux sucres avec les cations et anions sont identiques, la différence $g_{ER} - g_{EA}$ sera caractéristique de l'interaction spécifique entre le D-(−)-ribose et le cation Ca^{2+} par l'intermédiaire des séquences d'hydroxyles favorables à la complexation.

Une deuxième interprétation des résultats expérimentaux donnés par cette cellule consiste à exprimer une constante d'association spécifique entre le ribose et Ca^{2+}. On utilise, dans ce cas, une expression de la tension de cellule qui se réfère à l'état infiniment dilué dans l'eau pour $CaCl_2$ et pour le sucre.

$$[9] \quad U(m, m_R) = U^{\ominus} + k/2 \log [Ca]_R\, m_{Cl}^2\, \gamma_{\pm}^3(m, m_R)$$

$$[10] \quad U(m, m_A) = U^{\ominus} + k/2 \log m_{Ca}\, m_{Cl}^2\, \gamma_{\pm}^3(m, m_A)$$

pour respectivement le ribose et l'arabinose. Si dans l'expression [10], m_{Ca} est toujours la molalité analytique en Ca^{2+}, dans [9], la concentration en ions libres est $[Ca]_R$, une fraction de ceux-ci étant associée avec le ribose. En faisant l'hypothèse que pour $m_A = m_R$, $\gamma_{\pm}(m, m_A) = \gamma_{\pm}(m, m_R)$, on tire

$$[11] \quad U(m, m_R) - U(m, m_A) = k/2 \log \frac{[Ca]_R}{m}$$

Comme nous l'avons dit plus haut, cette différence ne dépend pratiquement pas de m. La méthode de Leden (10) nous permet d'écrire la fonction

$$[12] \quad F(R) = \frac{m - [Ca]_R}{[Ca]_R[R]} = \beta_1 + \beta_2\, [R]$$

où

$$[13] \quad \beta_1 = \frac{[CaR]}{[Ca][R]} \qquad \beta_2 = \frac{[CaR_2]}{[Ca][R]^2}$$

Puisque nous opérons avec un excès de ribose et que le taux d'association est faible, il est normal d'observer que

$$[14] \quad \frac{m}{[Ca]_R} = 1 + \beta_1[R] + \beta_2[R]^2 \sim \text{constante}$$

quel que soit m si $[R] \sim m_R$. De toute façon, cette méthode consistera à calculer $F(R)$ connaissant $m/[Ca]_R$, c'est-à-dire

$$[Ca]_R \text{ et } [R] = m_R - m + [Ca]_R$$

L'étude d'une deuxième cellule galvanique comportant une jonction liquide va nous permettre d'accéder aux mêmes grandeurs que ci-dessus moyennant des hypothèses différentes. La cohérence des résultats obtenus par les deux méthodes pourra être considérée comme un critère de leurs validités respectives. La cellule

$$[15] \quad \text{Electrode à Ca}|CaCl_2(m), \text{ sucre } (m_s) \left\| \begin{matrix} KNO_3 \\ \text{Sat.} \end{matrix} \right\| \begin{matrix} KCl \\ \text{Sat.} \end{matrix} \left| Hg_2Cl_2 \right| Hg$$

possède une double jonction liquide qui permet d'éviter la jonction directe de la solution étudiée avec l'électrode au calomel (l'expérience montre, dans ce cas, une grande instabilité des tensions mesurées due probablement à la présence des ions mercureux). Avec ce montage, les tensions sont parfaitement stables et reproductibles. La tension de cette cellule s'écrit:

$$[16] \quad U(m, m_s) = (U_{Ca}^{\ominus} - U_R) + U_j(m, m_s) + k/2 \log m\, \gamma_{Ca}(m, m_s)$$

où $U_{Ca}^{\ominus}$ est la tension standard de l'électrode à calcium, U_R la tension de l'électrode de référence et U_j la tension de la première jonction liquide. Les hypothèses de travail sont ici

$$U_j(m, m_A) = U_j(m, m_R) \text{ si } m_A = m_R$$

c'est-à-dire que la valeur de la tension de jonction ne dépend pas de la nature du sucre. De plus, comme plus haut,

$$\gamma_{Ca}(m, m_A) = \gamma_{Ca}(m, m_R)$$

Expérimentalement, on constate que la différence $U(m, m_s) - U(m)$dépend de la concentration m en électrolyte, contrairement à ce que nous avions constaté avec la cellule sans jonction (ceci traduit très probablement la variation de U_j avec m). Par contre, la différence $U(m, m_R) - U(m, m_A)$ est sensiblement indépendante de m. On pourra donc, comme plus haut, accéder à la grandeur $m/[Ca]_R$ et calculer la constante d'association spécifique Ca^{2+}–ribose.

Partie expérimentale

L'électrode sélective aux ions Ca^{2+} est une Orion 93-20, l'électrode AgCl|Ag une Tacussel et l'électrode au calomel à double jonction une Tacussel RDJ 17. Le millivoltmètre électronique Tacussel ISIS 20000

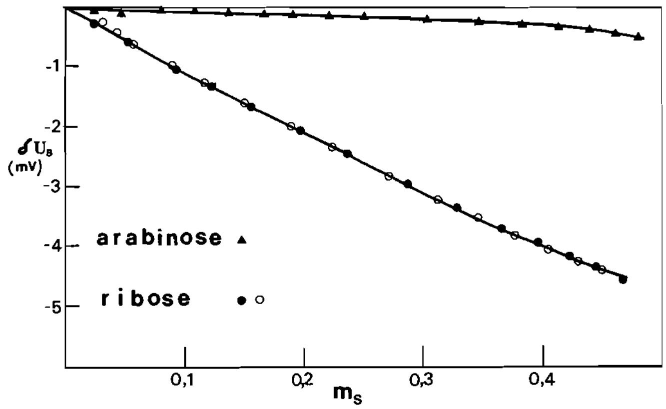

FIG. 1. Variation de tension δU_s de la cellule électrochimique [1] avec la molalité en sucre m_s. ●▲ m_{CaCl_2} = 0,1; ○ m_{CaCl_2} = 5×10^{-3} (molalités en Ca^{2+} par rapport à l'eau).

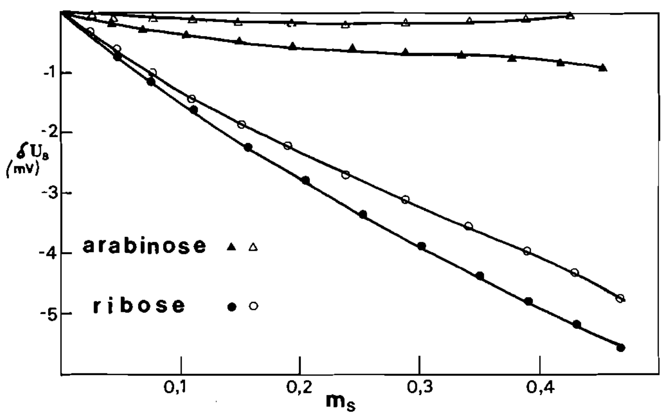

FIG. 2. Variation de tension δU_s de la cellule électrochimique [15] avec la molalité en sucre m_s. ○△ $m_{CaCl_2} = 5 \times 10^{-3}$; ●▲ m_{CaCl_2} = 2×10^{-2} (molalités en Ca^{2+} par rapport à l'eau).

permet de lire le 1/100^e de mV.

L'eau est tridistillée et dégazée avant usage.

Les sucres sont des produits Fluka Puriss pour analyse utilisés comme tel; le chlorure de calcium un produit Merck Pro Analysi.

Toutes les solutions sont réalisées par pesée et l'addition de la solution concentrée en sucre se fait à l'aide d'une burette gravimètrique Mettler P 160 N. La cellule de mesure est thermorégulée par circulation d'eau, la stabilité en température étant de l'ordre de 1/100^e de degré.

Résultats

Les figures 1 et 2 montrent, respectivement, les variations de la tension des deux cellules galvaniques étudiées, soit $\delta U_s = U(m, m_s) - U(m)$ en fonction de la concentration en sucre de la solution. Notons que malgré le faible domaine de variation des tensions mesurées (au maximum 5 mV), celles-ci sont connues avec une précision remarquable (la reproductibilité des mesures et de l'ordre de ±0,02 mV). Pour la cellule [1] (fig. 1), on voit que δU_s est identique pour $m = 5 \times 10^{-3}$ et $m = 1 \times 10^{-1}$ en $CaCl_2$, ce qui justifie notre précédente hypothèse. Au contraire, pour la cellule à jonction liquide [15] (fig. 2), δU_s dépend de la concentration en $CaCl_2$.

Les résultats des calculs sont regroupés dans le tableau 1. Les enthalpies libres standard de transfert de $CaCl_2$ de l'eau aux solutions de ribose ($\Delta G^{\ominus}_{tR}$) et aux solutions d'arabinose ($\Delta G^{\ominus}_{tA}$) sont calculées grâce à la relation [6]. En portant $\Delta G^{\ominus}_t/m_s$ en fonction de m_s (relation [7]), une extrapolation linéaire permet d'obtenir les paramètres d'interaction. Un tel traitement graphique donne ici:

$$2\nu g_{ER} = -1160 \text{ J mol}^{-2} \text{ kg} \quad 3\nu g_{ERR} = +750 \text{ J mol}^{-3} \text{ kg}^2$$

$$2\nu g_{EA} = +950 \text{ J mol}^{-2} \text{ kg} \quad 3\nu g_{EAA} = -100 \text{ J mol}^{-3} \text{ kg}^2$$

Les valeurs de $\Delta U(R - A) = \delta U_R - \delta U_A$ permettent de calculer (relations [11] et [12]) la fonction de Leden $F(R)$. Pour la cellule [1], les valeurs de ΔU correspondent aux interpolations effectuées sur la courbe moyenne de 3 essais à des molalités différentes en $CaCl_2$ (0,005, 0,02, 0,1). La fonction $F(R)$ décroit de façon significative quand m_s croît; cette variation ne met donc pas en évidence la formation du complexe CaR_2, puisque la pente β_2 devrait alors être positive. L'extrapolation à concentration nulle en sucre conduit à $\beta_1 = 0,89 \pm 0,10$ environ. Pour la cellule [15], les calculs de $F(R)$ sont effectués pour deux concentrations en $CaCl_2$ (m = 0,005 et 0,02) et l'on voit que ΔU dépend peu de cette concentration. Les valeurs de $F(R)$ sont pratiquement indépendantes de m_s, concentration en sucre, et le complexe CaR_2 n'est pas mis en évidence dans le domaine étudié; on admettra donc que $F(R) = \beta_1$. Pour m = 0,005 on trouve une valeur moyenne $\beta_1 = 0,93 \pm 0,07$ et pour m = 0,02, $\beta_1 = 0,93 \pm 0,16$.

Discussion

L'enthalpie libre standard de transfert de $CaCl_2$ de l'eau aux solutions de ribose est négative alors que la grandeur de transfert de l'eau aux solutions d'arabinose est positive. C'est la manifestation immédiate de l'interaction spécifique du premier de ces deux pentoses isomères avec l'ion Ca^{2+}. Quantitativement, cette interaction spécifique est caractérisée par la différence

$$2\nu(g_{ER} - g_{EA}) = 2g_{CaR} = -2110 \text{ J mol}^{-1} \text{ (voir relation [8])}$$

si l'on fait l'hypothèse de l'identité des interactions non spécifiques entre $CaCl_2$ d'une part, et ribose ou arabinose d'autre part. Nous n'interpréterons pas ici les paramètres g relatifs aux triplets, mais remarquons cependant que g_{ERR} est positif, ce qui ne plaide pas pour l'existence du complexe CaR_2.

Les calculs de la constante d'association conduisent à β_1 = 0,89 avec la cellule [1] et β_1 = 0,93 avec la cellule [15]. Compte tenu des incertitudes évaluées, la bonne concordance de ces deux résultats montre que les hypothèses formulées sont satisfaisantes en première approximation. Ces calculs ne conduisent pas, eux non plus, à la prise en compte d'un complexe du type CaR_2.

Les résultats obtenus précédemment par des méthodes potentiométriques sont: d'une part (5), β_1 = 1,6 par une méthode de compétition entre Ca^{2+} et Pb^{2+} en présence de $NaClO_4$ 1 M, la concentration en ribose étant 0,1 M et celle en ion Ca^{2+} variant jusqu'à 0,15 M; d'autre part (6), β_1 = 1,1 et β_2 = 8,5 avec une solution 0,1 M en ribose et des concentrations en Ca^{2+} allant jusqu'à 0,16 M. Au contraire des expériences réalisées ci-dessus, les méthodes que nous présentons consistent à faire varier la concentration en sucre alors que celle de $CaCl_2$ reste constante. Compte tenu de l'importance des facteurs d'activité dans l'expression de la constante thermodynamique d'équilibre, il est important de prouver, comme nous l'avons fait, que les résultats obtenus ne dépendent pas de la concentration en $CaCl_2$. On s'affranchit également de la présence de tout sel de fond dont on ne peut, à priori, négliger les interactions des ions avec la molécule de sucre.

La valeur que nous obtenons pour β_1, soit environ 0,9, est en

TABLEAU 1. Enthalpies libres standard de transfert de $CaCl_2$ de l'eau aux solutions d'arabinose et de ribose de molalité m_s (cellule [1]) et fonctions de Leden F(R) de la complexation du calcium par le ribose (cellule [1] et cellule [15])

	Cellule [1]				Cellule [15]			
					m_{CaCl_2} = 0,005		m_{CaCl_2} = 0,02	
m_s (mol kg^{-1})	$-\Delta G^{\ominus}_{tR}$ (J mol^{-1})	$\Delta G^{\ominus}_{tA}$ (J mol^{-1})	$-\Delta U$ (mV)	F(R)	$-\Delta U$ (mV)	F(R)	$-\Delta U$ (mV)	F(R)
0,05	55	45	0,55	0,890	0,55	0,879	0,58	0,940
0,10	108	95	1,06	0,874	1,13	0,923	1,14	0,944
0,15	160	145	1,52	0,850	1,65	0,917	1,70	0,959
0,20	205	195	1,98	0,845	2,20	0,938	2,16	0,930
0,25	245	240	2,44	0,848	2,70	0,939	2,61	0,915
0,30	280	285	2,86	0,842	3,16	0,933	3,06	0,909
0,35	315	335	3,27	0,839	3,62	0,933	3,53	0,916
0,40	340	380	3,66	0,834	4,06	0,932	4,01	0,928
0,45	370	430	3,98	0,817	4,47	0,928	4,51	0,947

accord passable avec la moyenne que l'on peut calculer en considérant, qu'à l'équilibre, la solution de ribose contient environ: 35% (soit 60% de 59%) de β-pyranose $^1C_4$ (β = 0,8), 21% de α-pyranose (β = 3,4) et 6,5% de α-furanose (β = 5,3) (1). Avec ces valeurs données à 31°C par Angyal, le calcul conduit en effet à une valeur moyenne pour β_1 égale à 1,3. Les deux expressions de l'enthalpie libre d'interaction spécifique entre le calcium et le ribose, d'une part g_{CaR} et d'autre part β_1, sont naturellement reliées. La relation qui existe entre deuxième coefficient du viriel et constante d'association en phase gazeuse peut être établie de façon très simple (11). Pour ce qui concerne la thermodynamique statistique des solutions, Wood *et al.* (12) ont comparé les développements possibles du coefficient osmotique d'une solution, ϕ_{MM}, exprimé dans les conditions de McMillan-Mayer (T, π, c): d'une part le développement en série des activités où interviennent les constantes de "Sociation", d'autre part le développement en série des concentrations molaires avec les coefficients du viriel. On peut montrer que les coefficients d'interaction par paires de type g_{ij} de la relation [7] interviennent dans le développement du coefficient osmotique ϕ_{LR} (conditions de Lewis et Randall qui sont celles de nos mesures, soit T, P, m) sous la forme

$$[17] \quad \phi_{LR} = 1 + B_{LR}m = 1 + \frac{g_{ij}}{RT}m$$

si on se limite au coefficient d'interaction par paires d'espèces différentes dans le cas $m_i = m_j = m$, pour simplifier la présentation. Dans les conditions de McMillan-Mayer, le développement du coefficient osmotique s'écrit

$$[18] \quad \phi_{MM} = 1 + B_{MM}\, c$$

et l'on peut montrer (13) que

$$[19] \quad B_{MM} = B_{LR}/\rho^0 + \frac{1}{2}\bar{V}_i^{\ominus} + \frac{1}{2}\bar{V}_j^{\ominus} - \frac{1}{2}RT\beta^0$$

où ρ^0 est la masse volumique et β^0 le coefficient de compressibilité isotherme du solvant, $\bar{V}_i^{\ominus}$ et $\bar{V}_j^{\ominus}$ les volumes molaires partiels à dilution infinie des espèces i et j en interaction. Ici, $\bar{V}_R^{\ominus}$ = 0,095 L mol^{-1} (14) et $\bar{V}_{Ca^{2+}}^{\ominus}$ = −0,029 L mol^{-1} (15). Le dernier terme de [19] étant négligeable, on trouve

$$B_{MM} = -0{,}41 \text{ L mol}^{-1}$$

Compte tenu de la forme des développements en fonction des concentrations que nous avons utilisés ici, on peut montrer que la relation fondamentale évoquée plus haut s'écrit

$$[20] \quad \beta_1 = -2\, B_{MM}$$

où, en toute rigueur, β_1 est la constante thermodynamique d'association dans l'échelle des molarités. Celle-ci, dans l'eau, est naturellement très voisine de celle que nous avons calculée plus haut dans l'échelle des molalités. Comme on voit, cette relation est vérifiée de façon très satisfaisante dans le cas que nous venons d'examiner. Notons que la relation [20] peut s'écrire avec une approximation en général acceptable

$$[21] \quad \beta_1 = -2g_{ij}/RT$$

Cet exemple nous permet d'apprécier la cohérence des deux différents langages utilisés pour exprimer l'interaction entre deux espèces en solution. En thermodynamique statistique, c'est B_{MM}, grandeur directement liée au potentiel de force moyenne (12), qui caractérise fondamentalement cette interaction.

On peut s'interroger sur les causes de la petite différence observée sur les valeurs de β_1 obtenues respectivement avec les cellules [1] et [15], soit 0,89 et 0,93. La première cellule fait intervenir les interactions des anions chlorures avec le sucre, interactions qui sont éliminées en supposant que

$$g_{Cl^-R} = g_{Cl^-A}$$

Si l'on considère les valeurs des termes triplet g_{ERR} et g_{EAA}, on voit qu'elles sont de signes opposés; on peut en conclure que les interactions non spécifiques avec les deux pentoses isomères peuvent être notoirement différentes.

Il est tout à fait probable que les interactions impliquant les ions Cl^- contribuent à cette différence et que l'hypothèse ci-dessus n'est pas rigoureusement exacte. Ainsi, les résultats obtenus en étudiant la cellule [15], et dont on a vérifié qu'ils ne dépendaient pas de la concentration en $CaCl_2$, peuvent être considérés comme plus satisfaisants.

Conclusion

Nous avons utilisé et discuté deux méthodes potentiométriques qui permettent de mesurer de façon satisfaisante l'interaction spécifique entre le cation Ca^{2+} et les séquences d'hydroxyles favorables à la "complexation" d'un sucre. Ces méthodes consistent à comparer le sucre en question avec un isomère dont la structure ne permet pas d'interaction spécifique avec le cation.

Nous proposons pour l'interaction spécifique Ca^{2+} – D-(–)-ribose dans l'eau, à 25°C, une valeur de la constante d'association égale à 0,93. Le complexe comportant deux sucres pour un calcium n'a pas été mis en évidence.

Cette étude nous a permis de comparer les deux langages possibles pour caractériser le phénomène de "complexation", celui de l'interaction par paire et celui de la constante d'association.

1. S. J. ANGYAL. Aust. J. Chem. **25**, 1957 (1972).
2. S. J. ANGYAL. Carbohydrates in solution. Advances in Chemistry Séries 117, American Chem. Soc., Washington, D.C. 1973.
3. R. E. LENKINSKI et J. REUBEN. J. Am. Chem. Soc. **98**, 3089 (1976).
4. M. C. R. SYMONS, J. A. BENBOW et H. PELMORE. J. Chem. Soc. Faraday Trans. 1, **78**, 3671 (1982).
5. L. G. EKSTRÖM et A. OLIN. Acta Chem. Scand. Ser. A, **31**, 838 (1977).
6. M. TOMAŠKOVIČ, Z. CIMERMAN, Z. ŠTEFANAC, E. PRETSCH et J. BENDL. Microchem. J. **27**, 372 (1982).
7. R. A. ROBINSON et R. M. STOKES. Electrolyte solutions. 2ème éd. Butterworths, London. 1959. p. 481.
8. Y. POINTUD, J. JUILLARD, J.-P. MOREL et L. AVEDIKIAN. Electrochim. Acta, **19**, 229 (1974).
9. G. PERRON, D. JOLY, J. E. DESNOYERS, L. AVEDIKIAN et J.-P. MOREL. Can. J. Chem. **56**, 552 (1978).
10. F. R. HARTLEY, C. BURGESS et R. ALCOCK. *Dans* Solution equilibria. *Édité par* Ellis Horwood. Chichester, U.K. 1980. p. 67.
11. K. S. PITZER. *Dans* Activity coefficients in electrolyte solutions. Vol. I. *Édité par* R. M. Pytkowicz. CRC Press, Boca Raton, U.S.A. 1979.
12. R. H. WOOD, T. H. LILLEY et P. T. THOMPSON. J. Chem. Soc. Faraday Trans. 1, **74**, 1301 (1978).
13. H. L. FRIEDMAN. J. Solution Chem. **1**, 387 (1972).
14. F. FRANKS. *Dans* Biochemical Thermodynamics. *Édité par* M. N. Jones. Elsevier Scientific Publishing Company, New York. 1979. p. 64.
15. F. J. MILLERO. *Dans* Water and aqueous solutions. *Edité par* R. A. Horne. Wiley–Interscience, New York. 1972. p. 545.

Molecular recognition. II.[1] The binding of the Lewis b and Y human blood group determinants by the lectin IV of *Griffonia simplicifolia*

ULRIKE SPOHR,[2] OLE HINDSGAUL,[3] AND RAYMOND U. LEMIEUX[4]
Department of Chemistry, University of Alberta, Edmonton, Alta., Canada T6G 2G2

Received December 21, 1984

ULRIKE SPOHR, OLE HINDSGAUL, and RAYMOND U. LEMIEUX. Can. J. Chem. **63**, 2644 (1985).

Using a radioimmunoassay to measure the relative potencies as inhibitors of a wide number of chemically modified structures related to the Lewis b human blood group determinant, it was found that derivatives of the Lewis b (αLFuc(1→2)βDGal(1→3)[αLFuc(1→4)]βDGlcNAc) and the Y (αLFuc(1→2)βDGal(1→4)[αLFuc(1→3)]βDGlcNAc) determinants are complexed by the lectin IV of *Griffonia simplicifolia* through the recognition of a topographical feature that is common to both the tetrasaccharides. This surface provides a nonpolar region formed by the two methyl groups of the fucose units and extends along the C-1—O-5—C-5 side of the αLFuc(1→2) unit and terminates at one end by a polar grouping which is formed by OH-3 and OH-4 of the βDGal unit and OH-4 of the αLFuc(1→4) unit. Association constants were determined from changes in ultraviolet absorption that occur as the result of complex formation. For the reaction of the Lewis b-OCH_3 tetrasaccharide, the thermodynamic parameters were found to be $\Delta H = -13$ kcal/mol and $\Delta S = -22$ cal/mol/K. The inhibition data for the relevant monodeoxy derivatives indicated that OH-2 and OH-3 of both of the αLFuc units are not directly involved in the binding reaction. The basis for drawing these conclusions was strengthened by finding that the reaction of the simple Lewis b analog, methoxymethyl (1→2)βDGal(1→3)[αLFuc(1→4)]βDGlcNAcOCH_3 displayed very similar thermodynamic values; namely, $\Delta H = -14$ kcal/mol and $\Delta S = -26$ cal/mol/K, to those mentioned above for the Le^b-OCH_3 tetrasaccharide. The OH-4 of the αLFuc(1→2) unit may be bound in an intramolecularly hydrogen bonded form.

ULRIKE SPOHR, OLE HINDSGAUL et RAYMOND U. LEMIEUX. Can. J. Chem. **63**, 2644 (1985).

Utilisant un essai radioimmunologique pour mesurer les pouvoirs inhibiteurs relatifs d'un grand nombre de structures modifiées chimiquement et qui sont reliées au déterminant du groupe sanguin humain de type Lewis b, on a trouvé que les dérivés des déterminants du type Lewis b (αLFuc(1→2)βDGal(1→3)[αLFuc(1→4)]βDGlcNAc) et Y (αLFuc(1→2)βDGal(1→4)[αLFuc(1→3)]βDGlcNAc) sont complexés par la lectine IV de la *Griffonia simplicifolia* par le biais d'une reconnaissance d'une caractéristique topographique qui est commune aux deux tétrasaccharides. Cette surface fournit une région non polaire formée par les deux groupes méthyles des unités fucose; elle s'étend le long du côté C-1—O-5—C-5 de l'unité αLFuc(1→2) et se termine à l'une des extrémités par un groupement polaire qui est formé par les OH-3 et OH-4 de l'unité βDGal et par le OH-4 de l'unité αLFuc(1→4). On a déterminé les constantes d'association à partir des changements d'absorption dans l'ultraviolet qui sont associés à la formation du complexe. Pour la réaction du tétrasaccharide-OCH_3 du type Lewis-b, on a trouvé que les paramètres thermodynamiques sont les suivants: $\Delta H = -13$ kcal/mol et $\Delta S = -22$ cal/mol/K. Les données relatives au pouvoir inhibiteur des dérivés monodéoxy correspondants indiquent que les fonctions OH-2 et OH-3 des deux unités αLFuc ne sont pas directement impliquées dans la réaction de liaison. Ces conclusions sont confirmées par le fait que les valeurs thermodynamiques de la réaction de l'analogue simple de type Lewis b, le méthoxyméthyl (1→2)βDGal(1→3)[αLFuc(1→4)]βDGlcNAcOCH_3, soit un $\Delta H = -14$ kcal/mol et un $\Delta S = -26$ cal/mol/K, sont très semblables à celles mentionnées plus haut pour le tétrasaccharide Lewis-b-OCH_3. Le groupe OH-4 de l'unité αLFuc(1→2) pourrait être lié par des liaisons hydrogènes intramoléculaires.

[Traduit par le journal]

Introduction

The [1]H nmr investigation (1) of the synthetic Y hapten (αLFuc(1→2)βDGal(1→4)[αLFuc(1→3)]βDGlcNAcO$(CH_2)_8$-$COOCH_3$) (**5**) (2) required that this compound possess a topography about the fucose units and the terminal end of the galactose virtually identical to that present in the Lewis b (Le^b) blood group determinant (αLFuc(1→2)βDGal(1→3)[αLFuc-(1→4)]βDGlcNAcO$(CH_2)_8COOCH_3$) (**2**) (3). It was therefore considered (4) that a polyclonal population of anti-Le^b antibodies raised in rabbits and collected by affinity chromatography on a commercial Le^b-immunoadsorbent (Synsorb Le^b) (5) might contain antibodies that would cross-react with the Y determinant. In fact, an immunoadsorbent prepared from **5** was found (4) to bind nearly half the antibodies present in the anti-Le^b antibody preparation. In view of this observation, Dr. D. A. Baker (Chembiomed Ltd.) examined whether or not the then recently isolated fourth lectin of *Griffonia simplicifolia* seeds (6) which was known to be Le^b active would also be Y active. Indeed, the lectin was found to recognize both the Le^b and Y determinants (6).

A wide range of Le^b-related structures have now been synthesized (7) to serve as inhibitors in a systematic probing of the combining site of the lectin. It is recognized that differences in the amounts of inhibitors that provide 50% inhibition at a given temperature are only related to the differences of the binding free energies ($\Delta\Delta G^0 = -RT \ln K$). Since these $\Delta\Delta G^0$ values may arise, as demonstrated by Neurohr *et al.* (8), from major differences in both the enthalpies and entropies for the various complexation reactions, interpretations of 50% inhibition data may be misleading in the sense that structurally quite different complexes may exhibit the same thermodynamic stabilities. Nevertheless, we suggest that serious misconceptions in this regard are not likely to arise in the context of the present study, which involves measuring relative 50% inhibitions for a wide range of structures that represent the reference oligosaccharide with, in each case, only a minor change in structure. This

[1] The first paper in this series is ref. 9.
[2] University of Alberta postdoctoral fellow, since 1982.
[3] Alberta Heritage Foundation for Medical Research Scholar, since 1981.
[4] Author to whom correspondence may be addressed.

opinion is supported by the discovery that all of the data obtained to date have consistently allowed appraisals of the combining sites of lectins (10) and antibodies (9, 11, 12) based on sound chemical principles. The first paper in this series (9) demonstrated that the monoclonal anti-I Ma antibody interacts with a large weakly polar and wedge-shaped portion of the trisaccharide βDGal(1→4)βDGlcNAc(1→6)α,βDGal and that only OH-4 and OH-6 of the terminal βDGal unit are involved in a strong polar interaction with the protein. The arguments, based on inhibition data, to reach this conclusion are strongly supported by results obtained in this present study.

The following discussion of results employs a number of widely used terms which, however, require special definition in the context of this presentation. For example, the term "amphiphilic" normally is used to refer to a molecule or ion which has a polar (hydrophilic) end attached to a hydrocarbon-like (hydrophobic) end. In this paper, amphiphilic is used in the same way but with reference to only a portion of the surface of a molecule. The term "polar interaction" means an interaction between two polar groupings. Since these interactions are directional in nature, the result can be either attractive or repulsive. In this paper, all considerations of polar interactions are necessarily restricted to intermolecular hydrogen bonding. The term "lipophilic" will mean a structure (surface) that is either nonpolar (hydrocarbon-like) or weakly polar.

Reference will be made to "nonpolar interactions". The strengths of these interactions (dispersion forces of attraction) are distance dependent, are always attractive, and occur between all types of surfaces. Salem (13) has pointed out that these forces can cause large forces of attraction between large molecules if the complex involves a substantial number of appropriate distances between atoms in both molecules. Being nondirectional in character, nonpolar interactions increase in strength with increasing complementarity between the interacting surfaces.

It is to be expected, when water is the solvent, that the nonpolar interactions will be less effective in keeping polar and nonpolar surfaces together than in keeping two nonpolar surfaces together. The contribution of the nonpolar interactions to the stability of the complex will, of course, increase as one or both of the surfaces become less polar in character and, therefore, interact more weakly with the surrounding water molecules. An outstanding feature of the results obtained in this and related investigations is that, in all likelihood, nonpolar interactions between polar and nonpolar groups contribute importantly to the stability of certain of the complexes formed between oligosaccharides and antibodies or lectins. A strongly polar group such as a free hydroxyl group is not expected to be sufficiently compatible with a hydrophobic environment to become importantly involved in a totally nonpolar interaction. However, it is well known that the involvement of a hydroxyl group in intramolecular hydrogen bond formation can increase the lipophilicity of the grouping and thereby render it more acceptable for nonpolar interaction. Intramolecular hydrogen bonding effects on the binding of a saccharide by antibodies were discussed in a paper (14) in which a number of concepts related to molecular recognition were reviewed. In this present paper, intramolecular hydrogen bonding will be invoked only when the steric relationship between the proton donor and proton acceptor atoms is known to be appropriate.

The use of the terms "specific" and "nonspecific" can also be troublesome. A specific interaction will mean an interaction between an inhibitor and a protein binding site of the limited

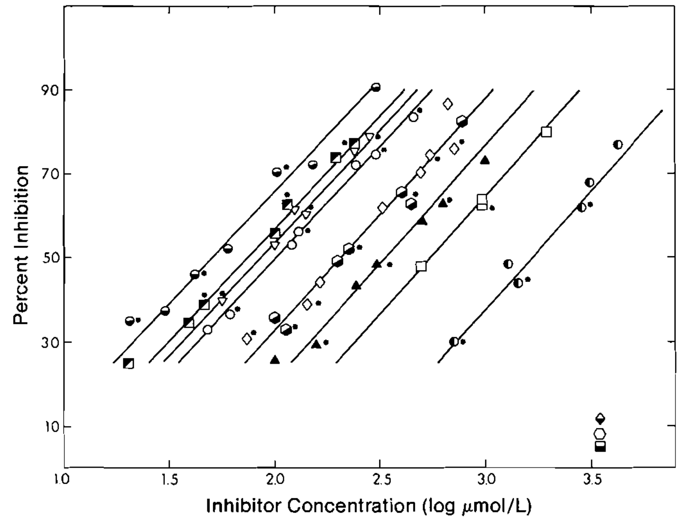

FIG. 1. Inhibition of the lectin IV of *Griffonia simplicifolia* by a selected group of compounds related to the Lewis-b human blood group determinant. The reproducibility of the data from run to run in the solid-phase radioimmunoassay is indicated by the points with an asterisk. 4^{d}-deoxy-4^{d}-fluoro-Le^{b}-OCH_3 (**22**); Le^{b}-$O(CH_2)_8$-$COOCH_3$ (**2**); ▽ 4^{d}-deoxy-Le^{b}-OCH_3 (**21**); ○ Le^{b}-OCH_3 (**1**); Y-$O(CH_2)_8COOCH_3$ (**5**); ◇ 2^{d}-methoxymethyl-Le^{a}-OCH_3 (**13**); ▲ 2^{d}-deoxy-Le^{b}-OCH_3 (**19**); □ c-nor-Le^{b}-OCH_3 (**17**); ◐ Le^{a}-OCH_3 (**10**); 4^{c}-deoxy-Le^{b}-OCH_3 (**25**); ⬡ 4^{b}-deoxy-Le^{b}-OCH_3 (**28**); 3^{b}-deoxy-Le^{b}-OCH_3 (**27**).

size defined by the reference oligosaccharide. Fortuitous interactions of the inhibitor with protein structure outside this recognition site are described as nonspecific. Differences of binding free energies ($\Delta\Delta G^0$ values) are calculated from the inhibition data and possible reasons for the occurrence of these differences are offered. These conclusions, especially when the $\Delta\Delta G^0$ values are small, are, of course, tentative and presented primarily for heuristic purposes. It is to be noted that the inhibition data presented in this and the following papers are interpreted in terms of the binding of the minimum energy conformer, as derived by HSEA calculation (1) and supported by nmr evidence.

Results and discussion

The inhibition data for the various structures listed in Tables 1–3 and 5, 6 were obtained using a previously reported solid-phase radioimmunoassay (15). In this present study, the reaction between a ^{125}I-labelled (Le^{b})$_{19}$-BSA artificial antigen and the immobilized lectin was examined. Throughout the tables, the amount of the Le^{b}-OCH_3 compound (**1**) in μmol/L required to provide 50% inhibition, under standardized experimental conditions, was used to calculate relative inhibition potencies. The 50% inhibitions were reproducible to within ±5% of the amounts reported. Typical inhibition curves are presented in Fig. 1. A compound was declared inactive when it became apparent that 50% inhibition would not be reached using 50 times the amount of the reference inhibitor (**1**) that provided 50% inhibition under the same experimental conditions. The phosphate buffer used in the radioimmunoassay contained calcium and manganese ions. An attempt to establish that the binding is dependent on these ions failed, in the sense that no detectable amount of activity was lost when the lectin was dialyzed, first against salt-free water, then against phosphate buffer 0.01 M in ethylenediamine tetraacetate, and finally with

TABLE 1. Noninvolvement of the βDGlcNAc unit

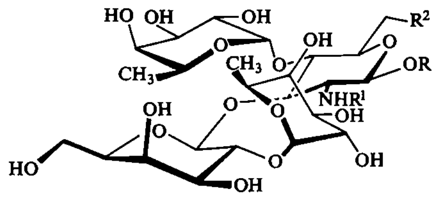

Le^b

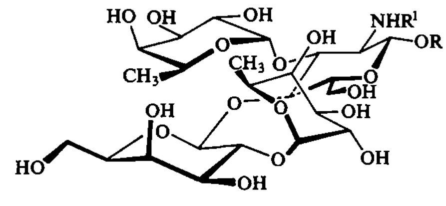

Y

Compound	Substituent R	R^1	R^2	50% Inhibition μmol/L	Relative potency	$\Delta\Delta G^0$ kcal/mol
Lewis b-related						
1	CH_3	Ac	OH	100	100	0
2	$(CH_2)_8COOCH_3$	Ac	OH	73	137	−0.2
3	$(CH_2)_8COOH$	H	OH	116	86	0.09
4	CH_3	Ac	H	106	94	0.03
Y-related						
5	$(CH_2)_8COOCH_3$	Ac	—	195	51	0.4
6	$(CH_2)_8COOH$	H	—	340	29	0.7

calcium-free (Chelex 100 (Bio-Rad) treated) phosphate buffer. Thus, the lectin may be neither calcium nor manganese ion dependent. Nevertheless, these ions were added to the buffered solution of the lectin that was used to coat the tubes and in the binding studies based on ultraviolet absorption.

Shibata *et al.* (6) reported that the Le^b-$O(CH_2)_8COOCH_3$ hapten (**2**) was somewhat less strongly bound ($\Delta\Delta G^0 = 0.3$ kcal/mol) by the lectin than was the hexasaccharide Le^b(1→3)βDGal(1→4)DGlc. This increase in binding must arise from nonspecific interactions since our inhibition data (Table 1) infer noninvolvement of the βDGlcNAc unit in the binding reaction. This condition, presumably, would extend to include the aglycon. In fact, as seen in Table 1, change of the aglycon from CH_3 (**1**) to $(CH_2)_8COOCH_3$ (**2**) provided an insignificant change in the inhibitor potency. De-*N*-acetylation of **2** and **5** to form **3** and **6** also produced only minor effects on the inhibitor potencies, as did deoxygenation at the 6-position of the βDGlcNAc residue of **1** to form **4**. These findings are in accord with the expectation, based on molecular modelling of the ^1H nmr conformers for the Le^b and Y structures (1, 16), that the binding of these structures by the lectin should occur on the other end of the molecule where a topography common to both the Le^b and Y structures can be recognized (4).

Involvement of the fucosyl units in the binding reaction was established by the inhibition studies reported by Shibata *et al.* (6). The inhibitions (Table 2) provided by compounds **7**, **8**, **9**, and **10** substantiate these observations and, furthermore, confirm that the αLFuc(1→4) unit (unit c[5]) present in compounds **8** and **10** is more importantly involved in the binding reaction than is the αLFuc(1→2) unit (unit d) which is present in the virtually inactive compounds **7** and **9**. As will be seen below, the αLFuc(1→4) unit provides one of the hydroxyl groups (OH-4^c) to the key polar grouping which is presented to the lectin by both the Le^b and Y tetrasaccharides. The inactivities of **7** and **9**, therefore, result from the absence of this specific grouping in these compounds. In contrast, the complete "key" polar grouping is presented by the trisaccharides **8** and **10**, and these compounds do show residual activities.

As seen from the data presented in Table 2, replacement of the αLFuc(1→2) unit of **1** by hydrogen to form **10** decreased the stability of the complex by 1.7 kcal/mol, and a greater decrease (by 2.1 kcal/mol) occurred when the substitution was by a methyl group to form **11**. Thus it was tempting to surmise that the binding of the αLFuc(1→2) unit was polar in character. However, it is seen that replacement of this group by the *n*-propyl group to form **12** led to a decrease in the stability of the complex of only 1.2 kcal/mol. This observation is made primarily to underline the hazards involved in drawing conclusions from limited data.

A change in the structure of a hapten must be expected to cause a change in the total energy (enthalpy) of the system since the chemical change is bound to influence the hydration of both the free oligosaccharide and the complex that is formed. Thus, even the replacement of an hydroxyl group that is not involved in the complexing reaction by hydrogen may somewhat influence the energetics of the reaction. In order to assess this situation, the 2^b-alkoxymethyl derivatives **13**, **14**, and **15** were examined. It was expected for reasons of the anomeric effect that these substituents would better imitate the αLFuc(1→2) unit of the Le^b structure than would the *n*-propyl group present in **12**. Indeed, as seen in Table 2, the three alkoxymethyl compounds were better inhibitors than the *n*-propyl derivative **12**, but only barely so for the ethoxymethyl (**14**) and isopropoxymethyl (**15**) analogs. On the other hand, the simple methoxymethyl derivative **13** was half as strong an inhibitor as the reference Le^b compound (**1**). This result strongly suggested that the hydroxyl groups of the αLFuc(1→2) unit of **1** are not involved in polar interactions within the complex. That this is, in fact, the case for OH-2^d and OH-3^d, as will be discussed below, is supported by the inhibition data presented in Table 3 for the deoxy compounds **19** and **20**. The relatively lower activities displayed by the ethoxy (**14**) and isopropoxy

[5] As previously done (3), the βDGlcNAc, βDGal, αLFuc(1→4), and αLFuc(1→2) units of the Le^b determinant are designated as the a, b, c, and d units, respectively.

TABLE 2. Involvement of the αLFuc units

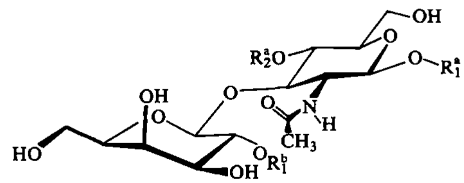

Compound	Substituent R_2^a	R_1^b	50% Inhibition μmol/L	Relative potency	$\Delta\Delta G^0$ kcal/mol
$R_1^a = (CH_2)_8COOCH_3$					
2 (Le^b)	αLFuc	αLFuc	73	137	−0.2
7 (Le^d)	H	αLFuc	Inactive*	—	—
8 (Le^a)	αLFuc	H	1263	8	1.5
$R_1^a = CH_3$					
1 (Le^b)	αLFuc	αLFuc	100	100	0
9 (Le^d)	H	αLFuc	Inactive†	—	—
10 (Le^a)	αLFuc	H	1724	6	1.7
11	αLFuc	CH_3	3571	3	2.1
12	αLFuc	$CH_2CH_2CH_3$	833	12	1.2
13	αLFuc	CH_2OCH_3	197	51	0.4
14	αLFuc	$CH_2OCH_2CH_3$	667	15	1.1
15	αLFuc	$CH_2OCH(CH_3)_2$	556	18	1.0

* 12% at 3340.
† 21% at 4290.

TABLE 3. Involvement of the αLFuc(1→2^b) unit

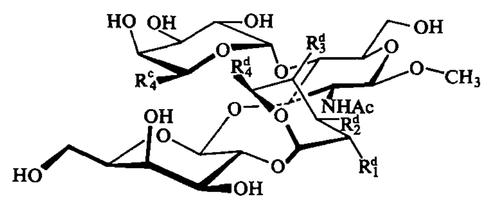

Compound	Substituent R_1^d	R_2^d	R_3^d	R_4^d	R_4^c	50% Inhibition μmol/L	Relative potency	$\Delta\Delta G^0$ kcal/mol
1 (Le^b)	OH	OH	OH	CH_3	CH_3	100	100	0
16	OH	OH	OH	H	CH_3	125	80	0.1
17	OH	OH	OH	CH_3	H	530	19	1.0
18	OH	OH	OH	H	H	1130	9	1.4
19	H	OH	OH	CH_3	CH_3	333	30	0.7
20	OH	H	OH	CH_3	CH_3	267	38	0.6
21	OH	OH	H	CH_3	CH_3	87	115	−0.08
22	OH	OH	F	CH_3	CH_3	50	200	−0.4

(**15**) compounds as compared to **13** can be attributed to steric hindrance to these groups adopting the required orientation for the presentation of a surface similar to that presented by the CH-1^d—O-5^d—CH-6^d region of the Le^b tetrasaccharide.

The inhibition data provided by the βDAra(1→2) compound **16** (Table 3) indicate that the CH_3-6 group of the αLFuc(1→2) unit is only marginally involved in the binding reaction. This result is in accord with the high activity possessed by the methoxymethyl compound **13**, especially when it is considered that the methoxymethyl group is conformationally labile whereas the ^{1}H nmr evidence requires the αLFuc(1→2) unit to be held rigidly in place (3). In contrast, replacement of the CH_3-6 group of the αLFuc(1→4) unit by hydrogen to form the βDAra(1→4) compound (**17**) provided a much weaker inhibitor, with the stability of the complex decreasing by 1.0 kcal/mol. The effect of replacing both the CH_3-6 methyl groups by hydrogen produced a compound (**18**) with a potency in line with the potencies displayed by **16** and **17**. Thus, these data indicate that the binding of the Le^b tetrasaccharide involves strong interaction with H-1 and O-5 of the αLFuc(1→2) unit, the CH_3-6 group of the αLFuc(1→4) unit, and likely H-2 of the αLFuc(1→2) unit as well, because of its close proximity to the H-1 and O-5 atoms of the same unit. The possibility of marginal involvement of the CH_3-6^d group suggests that OH-4^d of the αLFuc(1→2) unit may also be involved since it is very close to the O-5^d and H-2^d atoms of the same unit which, as

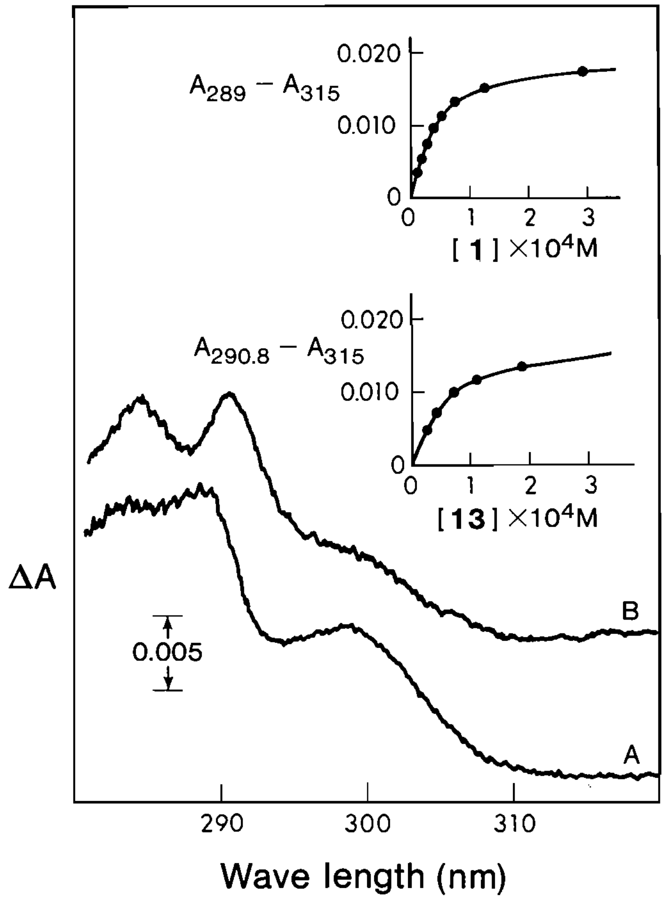

FIG. 2. Ultraviolet difference spectra of the lectin IV of *Griffonia simplicifolia*, at 25°C, complexed with αLFuc(1→2)βDGal(1→3)[αLFuc(1→4)]βDGlcNAc-OCH_3 (**1**, spectrum A) and methoxymethyl(1→2)βDGal(1→3)[αLFuc(1→4)]βDGlcNAc-OCH_3 (**13**, spectrum B). The insets show the variation of the maximum absorbance change as a function of the concentration of both **1** and **13**. The concentration of lectin binding sites was near 2×10^{-5} *M*.

discussed above, appear to be involved in the complexation. This possibility was tested by synthesis of the 4-deoxy compound **21**. In fact, **21** proved to be slightly superior to **1** as an inhibitor. This enhancement suggests that if OH-4^d is indeed involved it is by way of a nonpolar interaction. This must surely be the case since the 4^d-deoxy-4^d-fluoro derivative of **1**, namely, **22**, proved to be twice as potent an inhibitor as is **1**. Therefore, the Le^b tetrasaccharide appears to be accepted by the lectin with OH-4^d hydrogen bonded either to the neighboring *cis*-OH-3^d (or *cis*-O-5^d) or to water but, in whatever the manner, to become engaged in the formation of the complex by way of a nonpolar interaction. It is unlikely that the fluorine atom of **22** acts as a proton acceptor in the complex formation since the 4^d-deoxy compound **21** would then surely have been a much poorer inhibitor.

As seen in Table 3, replacement of either OH-2^d or OH-3^d of the αLFuc(1→2) unit to produce structures **19** and **20**, respectively, led to inhibitors with about one-third the potency of **1**. As mentioned above with reference to **13**, these hydroxyl groups are not required for the formation of a highly stable complex and, therefore, do not appear to be directly involved in the complexation reaction. However, as mentioned above, the deoxygenation of an oligosaccharide must have an influence on the hydration shell of the compound and thereby,

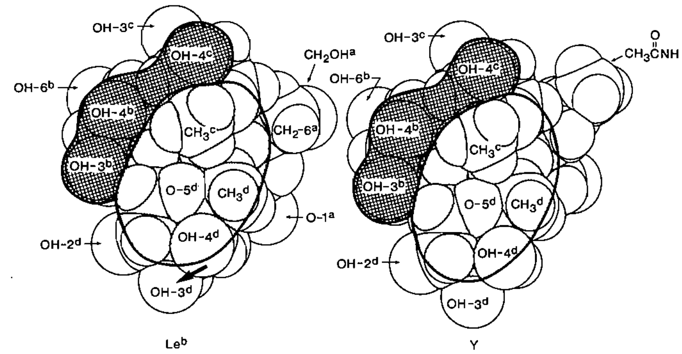

FIG. 3. Computer drawn projections (HSEA calculation) of CPK models for the Lewis b (Le^b) and Y determinants in their preferred conformations. The a, b, c, and d superscripts refer to atoms on the βDGlcNAc, βDGal, αLFuc(1→4), and αLFuc(1→2) units, respectively. The shaded areas represent regions that are bound by the lectin IV of *Griffonia simplicifolia*. Note that these surfaces are present in both the structures, which react almost equally well with the lectin. The heavily shaded surface represents the cluster of hydroxyl groups that become involved in the key polar interaction. The lightly shaded area displays the surface that becomes engaged in nonpolar interactions. It is possible that hydrogen atoms on the β-side of the βDGal unit also become involved through nonpolar interactions that stabilize the complex. These atoms are not shown but reside just below the OH-4^b and OH-3^b groups.

indirectly, on the stability of the complex that is formed. On the other hand, it seems reasonable to expect that such a change may not affect the thermodynamics of the reaction in a dramatic fashion since the change in structure that results from a simple monodeoxy substitution is very small. To test this hypothesis, the thermodynamic parameters for the methoxymethyl(1→2)βDGal(1→3)[αLFuc(1→4)]βDGlcNAcOCH$_3$ (**13**) analog of Le^b-OCH_3 (**1**) were determined. These data were obtained by measuring the effect of temperature on the association constants as determined by ultraviolet difference spectroscopy (Fig. 3). As seen from Fig. 2, the difference spectra are not the same. The complex formed with **1** showed a maximum absorbance at 289 nm in comparison to a maximum absorbance at 290.8 nm for **13**. Also, the shapes of the difference absorption spectra are different. This difference need not be taken as evidence that the conformation of the protein is importantly different for the complexes that are formed, since the difference in the structures complexed involves a change in the hydrophobicity of a major substituent. Indeed, taken together with the thermodynamic data presented in Table 4, this difference in spectral change suggests that the ultraviolet absorption involves amino acid residues that are directly involved in forming the combining site. As seen from Table 4, the ΔH and ΔS terms for the binding of **13**, where the αLFuc(1→2) unit of **1** has been replaced by the simple CH_3OCH_2 group, are very similar to those measured for **1**. Therefore it seems reasonable to conclude that the structures of the complexes are very similar and that these results lend support to our contention that the influences on complex stability of 0.6–0.7 kcal/mol observed on deoxygenation at positions 2^d or 3^d to form **19** and **20** (structural changes that are smaller than that between **1** and **13**) result only from indirect effects, and that OH-2^d and OH-3^d remain in contact with water. Therefore, in the interpretation of the effect of a deoxygenation on binding, we tentatively assign influences on the $\Delta\Delta G^0$ value of 0.4 ± 0.4 kcal/mol to indirect marginal effects on complex stability. As discussed above with reference

TABLE 4. Thermodynamic parameters for specific binding by the lectin IV of *Griffonia simplicifolia**

K_{Assoc}†	ΔH kcal/mol	ΔS cal/mol/K	$T\Delta S$† kcal/mol	ΔG^0† kcal/mol
αLFuc(1→2)βDGal(1→3)[αLFuc(1→4)]βDGlcNAc-OCH_3 (**1**, Lewis b-OCH_3)				
$4.4 \pm 0.3 \times 10^4$	−13	−22	−6.6	−6.4
CH_3OCH_2(1→2)βDGal(1→3)[αLFuc(1→4)]βDGlcNAc-OCH_3 (**13**)				
$2.9 \pm 0.3 \times 10^4$	−14	−26	−7.8	−6.2

*Determined from the change in ultraviolet absorption at 25°, 35°, and 45°C for both compounds, and also at 15°C for **1**.
† At 298 K.

TABLE 5. Involvement of the αLFuc(1→4[a]) unit

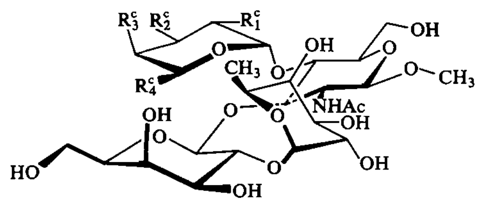

Compound	Substituent R_1^c	R_2^c	R_3^c	R_4^c	50% Inhibition μmol/L	Relative potency	$\Delta\Delta G^0$ kcal/mol
1 (Le[b])	OH	OH	OH	CH_3	100	100	0
17	OH	OH	OH	H	530	19	1.0
23	H	OH	OH	CH_3	331	30	0.7
24	OH	H	OH	CH_3	390	26	0.8
25	OH	OH	H	CH_3	Inactive*	—	—
26	OH	OH	F	CH_3	5555†	2	2.4

* 13% at 3460.
† By extrapolation.

to **7** and **9** (Table 2), a deoxygenation which results in an essentially inactive compound ($\Delta\Delta G^0 > 2.3$ kcal/mol compared with the parent tetrasaccharide) is interpreted as meaning that the hydroxyl group which was replaced becomes directly involved in a key polar interaction for complex formation. Deoxygenations which provide compounds with $\Delta\Delta G^0$ values in the range 0.8–2.3 kcal/mol are then interpreted as being engaged in the complexation reaction through polar interactions that are not of crucial importance to the formation of a complex.

In certain cases, deoxygenation leads to a superior inhibitor. This has been demonstrated for the lectin I of *Ulex europaeus* (2, 10) and the monoclonal anti-I Ma antibody (9), and now observed for **21**. In such cases, the hydroxyl group that was replaced by hydrogen must become involved in nonpolar interactions with its environment in the complex. In the case of the binding by the anti-I Ma antibody (9), the trisaccharide is undoubtedly accepted with the hydroxyl group at the 3-position of the βDGlcNAc unit intramolecularly hydrogen bonded. In the case of the *Ulex* lectin, the circumstantial evidence for intramolecular hydrogen bonding appears convincing. Therefore, whenever enhancements in binding are observed as the result of a specific monodeoxygenation of an oligosaccharide, it is expected that the hydroxyl group acts as a proton donor to hydrogen bond formation either with the aqueous environment for the resulting complex or intramolecularly with a suitable proton acceptor but not with a proton acceptor that is provided by the protein. To date, whenever such enhancements have been observed, the hydroxyl group has been either sterically well disposed for intramolecular hydrogen bonding with a neighboring atom that can serve as a proton acceptor or can assume an orientation that provides the necessary (about 2.7–3.0 Å) oxygen-to-oxygen internuclear distance by way of a low-energy conformational change (11). Whether or not intramolecular hydrogen bond formation actually occurs may be tested in a number of ways. In the instance of a rigidly held *cis*-glycol grouping, replacement by hydrogen of the hydroxyl group that serves as the proton acceptor should have a deleterious effect on binding and this has been observed (11). In contrast, replacement by fluorine should have little if any effect but this remains to be examined. On the other hand, both the replacement of the hydroxyl group that serves as proton donor by hydrogen or fluorine should lead to a relatively stronger inhibition and this has been observed not only for compounds **21** and **22** but also in another similar situation (11). A consideration of a situation wherein intramolecular hydrogen bond formation appears to involve important conformational changes is reserved for the discussion of the binding of the Le[b] tetrasaccharide (**1**) by a monoclonal anti-Lewis b antibody (11).

The effects of changes in the structure of the αLFuc(1→4) unit of **1** are presented in Table 5. The evidence for important involvement of the CH_3-6 group was presented in connection with Table 3. The hydroxyl groups at positions 2 and 3 appear

TABLE 6. Involvement of the βDGal unit

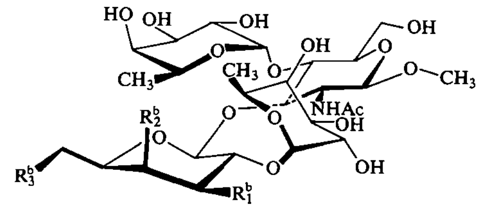

Compound	Substituent R_1^b	R_2^b	R_3^b	50% Inhibition μmol/L	Relative potency	$\Delta\Delta G^0$ kcal/mol
1 (Le[b])	OH	OH	OH	100	100	0
27	H	OH	OH	Inactive*	—	—
28	OH	H	OH	Inactive†	—	—
29	OH	OH	H	110	91	0.06

*5% at 3460.
†8% at 3460.

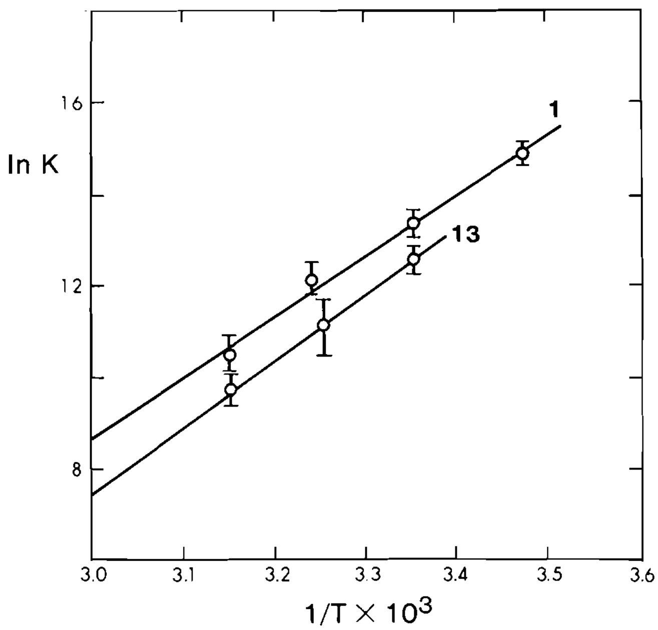

FIG. 4. The van't Hoff plot of the effect of temperature on the association constants for the binding by the lectin IV of *Griffonia simplicifolia* with αLFuc(1→2)βDGal(1→3)[αLFuc(1→4)]βDGlcNAc-OMe (**1**) and methoxymethyl(1→2)βDGal(1→3)[αLFuc(1→4)]-βDGlcNAc-OMe (**13**). The equilibria were determined at near 25°C, 35°C, and 45°C for both compounds and also at 15°C for **1**.

not to be directly involved in the binding reaction since their replacement by hydrogen to form **23** and **24** provided compounds that still retained a third of the inhibitory potency of **1**. In contrast, replacement of OH-4[c] by hydrogen led to the virtually inactive compound **25**. Therefore, OH-4[c] is considered to be involved in a key polar interaction. This involvement may be as a proton donor to complex formation since the 4[c]-deoxy-4[c]-fluoro compound **26** is also essentially inactive. Thus, the data indicate that only the CHOH-4[c] – CH_3-6[c] portion of the αLFuc(1→4) unit of **1** becomes directly involved in the binding reaction.

The manner in which the βDGal unit of **1** becomes involved in the complex is at once apparent from the data presented in Table 6. Obviously, both OH-3[b] and OH-4[b] contribute to the key polar interaction since both **27** and **28** are inactive. In contrast, replacement of the OH-6[b] group by hydrogen to form **29** had little influence on the stability of the complex and, therefore, this hydroxyl group appears to remain in contact with the aqueous phase.

The conclusions reached in this study are summarized in Fig. 4, where the 3-dimensional models for the Le[b] and Y tetrasaccharides are projected. Our nmr studies (1, 3, 16) require that these structures be rigidly held in the conformations shown, which were produced by HSEA calculation (1). It is seen that the topography of the Le[b] determinant, which our interpretation of the inhibition data indicates to be directly involved in interaction with the protein to stabilize the complex, is also present in the Y determinant. This correspondence lends strong support to the interpretations of the inhibition data that led to these conclusions.

It is to be noted that the topography that is recognized by the lectin is amphiphilic in character in that it possesses a polar cluster formed by OH-3[b], OH-4[b], and OH-4[c] adjacent to a relatively large lipophilic surface that is essentially nonpolar except for OH-4[d]. However, OH-4[d] was found to become engaged with the protein by way of a nonpolar interaction and perhaps intramolecularly hydrogen bonded to OH-3[d] (or O-5[d]). Thus, it appears that the Le[b] determinant is accepted by a shallow amphiphilic combining site at the surface of the lectin. Judging from the large decrease in entropy (Table 4) which occurs, considerable organization of the system is required to form the complex. The freeing of water from the nonpolar regions of the amphiphilic surfaces that interact to form the complex should lead to an increase, not a decrease, in entropy. Perhaps the organization of a conformationally highly labile protein into a specific conformer may be all that is needed to account for most of the decreases in entropy that are observed in these complexation reactions (10). It is important to note in this regard that complex formation results in response to a demand made on the system by an essentially rigid oligosaccharide.

The relative contributions to the stability of the complex made by the polar and nonpolar interactions are not known although there can be no doubt that the nonpolar contribution is most important (10). Nevertheless, it seems definitely established (9–12) that the integrity of the polar interaction is of crucial importance to complex formation. This situation need not mean that the polar interaction contributes importantly to the stability of the complex. Indeed, it would be exceedingly surprising if it did, unless both prior to and after binding the polar grouping provided by the protein was imbedded in a hydrophobic well at the surface of the protein (17). However, this does not appear to be the case since neighboring hydroxyl groups (OH-6^b, OH-2^d, and OH-3^c) appear to remain in contact with the aqueous phase after the complex has formed. On the other hand, the polar complex after it has formed could be inside a *narrow* hydrophobic cleft presented by the protein should the nonpolar β-side of the βDGal unit also become involved in the formation of the complex. Compounds designed to test this possibility were not synthesized. Nevertheless, this possibility does not appear attractive, primarily because the bringing of the polar complex into a hydrophobic pocket must be expected to be highly demanding in energy and this energy would have to be compensated by the additional nonpolar interactions gained through interaction with the relatively small nonpolar surface that is present on the β-side of the βDGal unit. As previously suggested (2, 14, 16), it is considered that the main source of the stability of the complex derives from changes in dispersion forces of attraction. The "hydrated polar group gate effect" (18) proposes that the sum of these forces of attraction between the complementary surfaces that interact to form the complex is greater than the sum of the dispersion forces between the separated surfaces and the surrounding water molecules. This condition is expected to arise from water seeking its own structure when interacting with amphiphilic surfaces (19).

Experimental

The syntheses and characterization of the compounds used in the inhibition studies will be reported separately (7).

Buffers

All at pH 7.2 adjusted either with HCl or NaOH.

I. 0.08 *M* in Na_2HPO_4, 0.02 *M* in KH_2PO_4, 0.15 *M* in NaCl, 0.015 *M* in NaN_3, 0.5 m*M* in $Na_2S_2O_4$, and 0.14 m*M* in $CaCl_2$.

II. 0.072 *M* in Na_2HPO_4, 0.028 *M* in NaH_2PO_4, 0.15 *M* in NaCl, 3 m*M* in NaN_3, 0.1 m*M* in $CaCl_2$, and 0.1 m*M* in $MnCl_2$.

III. 7.8 m*M* in Na_2HPO_4, 2.2 m*M* in KH_2PO_4, 15 m*M* in NaN_3, and 0.15 *M* in NaCl.

Lectin IV of Griffonia simplicifolia

The lectin was prepared in a manner closely analogous to that reported by Shibata *et al.* (6). Finely ground seeds (500 g) were stirred at room temperature for 15 min with 1 L of methanol and recovered by filtration. This extraction was repeated 6 times and then the residue was extracted 3 times with dichloromethane (3 × 1 L). After drying, the grey meal (280 g) was stirred for 2 h at 4°C with 2 L of buffer I solution. The solids were collected by centrifugation and extracted a second time under the same conditions with buffer I (1.5 L). The aqueous extracts were combined and 170 g/L of solid $(NH_4)_2SO_4$ were added, always keeping the solution at 4°C. The solids that precipitated were removed by centrifugation and more solid $(NH_4)_2SO_4$ (130 g/L) was added. After standing at 4°C for 16 h, the precipitate which had formed was collected by centrifugation, dissolved in buffer I (70 mL), and this solution was dialyzed against two changes of the buffer (4 L) each for 24 h using dialysis tubing (Fisher Scientific seamless cellulose with a 12 000 m.wt. cutoff). The resulting solution (225 mL) was then absorbed using Synsorb-Le^b (Chembiomed Ltd., University of Alberta) in the following manner. Always at 4°C in the cold room, an aliquot (50 mL) was passed down a column of the immunoadsorbent (25 g) in 1 h and the column was washed with 1.4 L of buffer I. At this point the eluate showed an absorbance at 280 nm of less than 0.03. A solution 0.1 *N* in acetic acid and 0.015 *N* in NaCl was then passed down the column while collecting 13-mL fractions of the eluate. The fractions which showed absorbance at 280 nm greater than 0.1 were combined and brought to pH 7.0 using 1 *N* NaOH. The solutions from the various chromatograms were combined (750 mL) and dialyzed using an ultrafiltration membrane (Diaflo PM10, Amicon) against phosphate buffer II to provide 400 mL of a solution which showed absorbance of 1.15 at 280 nm. The solution was then passed through a column of Synsorb A (30 g) followed by a column of Synsorb B (30 g) using buffer II as eluent. The protein-containing fraction was then concentrated by ultrafiltration to an absorbance of 2.0 (175 mL). The behavior of the protein on polyacrylamide gel electrophoresis was identical to that published (6) for the lectin IV of *Griffonia simplicifolia* and showed no evidence of other proteins.

Solid-phase radioimmunoassay

The procedure was essentially that briefly reported by Young *et al.* (15). The 2-mL polystyrene vials (Simport Plastics, Montreal) were coated using 0.15 milliliters per tube of a solution of the lectin in buffer II, which showed an absorbance of 0.1 at 280 nm and which corresponds to about 60 μg/mL of the lectin. The incubation was overnight at 4°C. The coating of the tubes was then completed by incubation at room temperature for 2 h with 0.2 mL of a 15% solution of BSA in buffer II. The tubes were then washed by the addition of a 1% solution of BSA in the same buffer, followed by aspiration, and air dried for 30 min prior to use. The ^{125}I-labelled $(Le^b)_{19}$-BSA artificial antigen (54 ng/mL in buffer III prepared by the iodogen procedure (20)) was purchased from Chembiomed Ltd. and usually produced near 200 000 cpm/100 μL. It was not used after the radioactivity had diminished to less than 160 000 cpm. The radioactivity of a coated tube after incubation at room temperature (23°C) and washing with buffer II was about 120 000 cpm. The solution of the inhibitor in buffer II (50 μL) was added to the tube and this was immediately followed by addition of 100 μL of the labelled antigen. All runs were done in triplicate and the measured radioactivities (Beckman 4400 gamma counter) were averaged for calculation of the % inhibition obtained in a given run. The 50% inhibitions were estimated using plots as shown in Fig. 1. Whenever 50% inhibition was achieved, the value obtained was checked in at least one separate similar run using concentrations of the inhibitor near the amounts required for 50% inhibition. In the case of separate runs, the amount of the reference inhibitor required to provide 50% inhibition was divided by the amount of the inhibitor that also provided 50% inhibition in order to obtain the relative potency under the prevailing experimental conditions. These relative potencies agreed well from run to run, as can be gauged from the data plotted in Fig. 1. To arrive at the points marked with an asterisk, the amounts of **1** required to reach 50% inhibition in separate runs were brought to a common value. It is noteworthy that the $\Delta\Delta G^0$ value of 0.4 kcal/mol calculated for the 50% inhibition data for compounds **1** and **13** (Table 2) is in good agreement with the value of 0.2 kcal/mol determined in the solution binding studies at 25°C (Table 4).

Ultraviolet difference spectroscopy (ref. 21)

The spectra were recorded on a Cary-210 spectrophotometer with both the sample and the reference base thermostated by circulating water. A solution of the lectin (750 μL in buffer II) having A_{280} near 1.0 was placed in both sample and reference semi-micro cells and a baseline was recorded into the instrument memory for automatic digital subtraction from subsequent spectra. The experiment was then initiated by addition of an aliquot (1–16 μL) of a solution of the oligosaccharide (5 × 10^{-3} *M* in buffer II) to the sample cell and the addition of an identical volume of buffer to the reference cell. The contents of the cells were then briefly mixed with a Teflon rod and the solutions were allowed to equilibriate until a stable difference spectrum was obtained, usually within 20–30 min. Spectra were then recorded at a scan rate of 3 nm/min. In a typical titration experiment, sequential additions of 1, 1, 2, 4, 8, and 16 μL of the oligosaccharide solution were made with the oligosaccharide concentrations, and addition volumes, selected to provide difference spectra where the percentage of the lectin bound ranged from 20% to 80%. The temperature was recorded at several places along the titration curve using a thermistor probe inserted directly into the sample cell and was found to be constant to within ±0.1°C. The difference spectra obtained in the above experiments were corrected for absorption due to the oligosaccharide alone, values which were determined in separate experiments and which, in all cases, amounted to less than 10% of the observed difference spectrum. Each titration experiment was repeated at least once.

The difference spectra were positive (Fig. 2) with the maximum absorbance changes occurring at 289.0 nm for binding with the Le^b tetrasaccharide (**1**) ($\epsilon = 1800\ M^{-1}\ cm^{-1}$) and 290.8 nm for its analog (**13**) ($\epsilon = 1680\ M^{-1}\ cm^{-1}$). The values of the equilibrium binding constants were determined from the slope and intercept of a Scatchard plot (22) and based on the assumption that the two lectin subunits bind independently. Since the Scatchard plots were linear, this assumption seems justified.

The extinction coefficient of the lectin was estimated by weighing a lyophilized sample of the affinity purified protein, which had been exhaustively dialyzed against distilled water. This method gave $E^{1\%}_{280} = 17$, which corresponds, based on a molecular weight of 58 000 for the lectin (6), to $\epsilon^{280} = 1 \times 10^5\ M^{-1}\ cm^{-1}$.

Acknowledgements

This research was supported by the Natural Sciences and Engineering Research Council of Canada (Grant A-172 to R.U.L.) and the Alberta Heritage Foundation for Medical Research.

1. H. THØGERSEN, R. U. LEMIEUX, K. BOCK, and B. MEYER. Can. J. Chem. **60**, 44 (1982).
2. O. HINDSGAUL, T. NORBERG, J. LE PENDU, and R. U. LEMIEUX. Carbohydr. Res. **109**, 109 (1982).
3. R. U. LEMIEUX, K. BOCK, L. T. J. DELBAERE, S. KOTO, and V. S. RAO. Can. J. Chem. **58**, 631 (1980).
4. R. U. LEMIEUX, J. LE PENDU, and T. NORBERG. Joint Congress of the International Society of Hematology and the International Society of Blood Transfusion, Montreal, Canada. August 16–22, 1980. Abstracts of Papers, No. 261.
5. R. U. LEMIEUX, D. A. BAKER, W. M. WEINSTEIN, and C. M. SWITZER. Biochemistry, **20**, 199 (1981).
6. S. SHIBATA, I. J. GOLDSTEIN, and D. A. BAKER. J. Biol. Chem. **25**, 9324 (1982).
7. U. SPOHR, O. HINDSGAUL, and R. U. LEMIEUX. In preparation.
8. K. J. NEUROHR, H. H. MANTSCH, N. M. YOUNG, and D. R. BUNDLE. Biochemistry, **21**, 498 (1982).
9. R. U. LEMIEUX, T. C. WONG, J. LIAO, and E. A. KABAT. Mol. Immunol. **21**, 751 (1984).
10. O. HINDSGAUL, D. P. KHARE, M. BACH, and R. U. LEMIEUX. Can. J. Chem. **63**, 2653 (1985).
11. U. SPOHR, N. MORISHIMA, O. HINDSGAUL, and R. U. LEMIEUX. Can. J. Chem. **63**, 2659 (1985).
12. R. U. LEMIEUX, A. P. VENOT, U. SPOHR, P. BIRD, G. MANDAL, N. MORISHIMA, O. HINDSGAUL, and D. R. BUNDLE. Can. J. Chem. **63**, 2664 (1985).
13. L. SALEM. *In* Electronic aspects of biochemistry. *Edited by* B. Pullman. Academic Press, New York. 1964. pp. 293–299.
14. R. U. LEMIEUX, P. H. BOULLANGER, D. R. BUNDLE, D. A. BAKER, A. NAGPURKAR, and A. P. VENOT. Nouv. J. Chim. **2**, 321 (1978).
15. W. W. YOUNG, JR., H. S. JOHNSON, Y. TAMURA, K. A. KARLSSON, G. LARSON, J. M. R. PARKER, D. P. KHARE, U. SPOHR, D. A. BAKER, O. HINDSGAUL, and R. U. LEMIEUX. J. Biol. Chem. **258**, 4890 (1983).
16. R. U. LEMIEUX and K. BOCK. Arch. Biochem. Biophys. **220**, 125 (1983).
17. J.-P. BEHR, J.-M. LEHN, and P. VIERLING. Helv. Chim. Acta, **65**, 1853 (1982).
18. R. U. LEMIEUX. 187th ACS National Meeting. St. Louis, Mo. April 8–13, 1984. Abstracts of Papers, CARB 5.
19. R. U. LEMIEUX. Proceedings of the VIIIth International Symposium on Medicinal Chemistry, Uppsala, Sweden. August 27–31, 1984.
20. P. SALACINSKY, J. HOPE, C. MCLEAN, V. CLEMENT-JONES, J. PRICE, and P. J. LOWRY. J. Endocrinol. **81**, 131P (1979).
21. K. J. NEUROHR, N. M. YOUNG, and H. H. MANTSCH. J. Biol. Chem. **255**, 9205 (1980).
22. G. SCATCHARD. Ann. N.Y. Acad. Sci. **51**, 660 (1949).

Molecular recognition. III. The binding of the H-type 2 human blood group determinant by the lectin I of *Ulex europaeus*

OLE HINDSGAUL,[1] DEVESHWARI P. KHARE,[2] MIMI BACH, AND RAYMOND U. LEMIEUX[3]

Department of Chemistry, University of Alberta, Edmonton, Alta., Canada T6G 2G2

Received December 21, 1984

OLE HINDSGAUL, DEVESHWARI P. KHARE, MIMI BACH, and RAYMOND U. LEMIEUX. Can. J. Chem. **63**, 2653 (1985).

Using a radioimmunoassay to measure the relative potencies of a wide range of chemically modified structures related to the H-type 2 human blood group determinant, evidence was accumulated that the binding of αLFuc(1→2)βDGal(1→4)-βDGlcNAc-OMe by the lectin I of *Ulex europaeus* involves a wedge-shaped amphiphilic surface which extends on one side of the molecule from the methoxy aglycon to OH-3 of the βDGal unit. A cluster which involves OH-3, OH-4, and OH-2 of the αLFuc unit along with OH-3 of the βDGal unit provides the polar interactions with the lectin. However, only OH-3 and OH-4 of the αLFuc are indispensable to complex formation and are regarded as providing the key polar interaction. The binding reaction involves both a decrease in enthalpy of 29 kcal/mol and a decrease of 68 cal/mol/K in entropy. It is submitted that the main source of the decrease in enthalpy is the establishment of nonpolar interactions that extend from the aglycon over the nonpolar portion of the β-side of the βDGlcNAc unit and on to include a major portion of the α-side of the αLFuc unit. The binding of the βDGlcNAc unit includes OH-6 intramolecularly hydrogen bonded to O-5 in order to extend the nonpolar interactions to the α-side of this unit and perhaps beyond. The decreases in enthalpy (6.0 kcal/mol) and entropy (2.7 cal/mol/K) which occur on the binding of methyl α-L-fucopyranoside are much smaller than for the H-type 2 trisaccharide and are compatible with the much smaller surface that interacts to form the complex. The inhibition data obtained using a range of structures related to methyl α-L-fucopyranoside are in general accord with expectations based on the results obtained with the more complex structures.

OLE HINDSGAUL, DEVESHWARI P. KHARE, MIMI BACH et RAYMOND U. LEMIEUX. Can. J. Chem. **63**, 2653 (1985).

Utilisant un essai radioimmunologique pour mesurer la puissance relative d'un grand nombre de composés chimiquement modifiés et apparentés au déterminant du groupe sanguin humain de type H-2, on a accumulé des données suggérant que la liaison du αLFuc(1→2)βDGal(1→4)βDGlcNAc-OMe avec la lectine I de l'*Ulex europaeus* implique une surface amphiphile en forme de coin qui s'étend sur un côté de la molécule du groupement méthoxyle de l'aglycone jusqu'au groupement OH-3 de l'unité βDGal. Un aggrégat impliquant les groupements OH-3, OH-4 et OH-2 de l'unité αLFuc ainsi que le groupement OH-3 de l'unité βDGal est responsable des interactions polaires avec la lectine. Toutefois, seuls les groupements OH-3 et OH-4 de l'unité αLFuc sont indispensables à la formation d'un complexe et on les considère comme les éléments clés des interactions polaires. La réaction de liaison implique à la fois une diminution d'enthalpie de 29 kcal/mol et une diminution d'entropie de 68 cal/mol/K. On pense que la diminution d'enthalpie est due principalement à l'existence d'interactions non polaires qui vont de l'aglycone qui se trouve au-dessus de la portion non polaire de la face β de l'unité βDGlcNAc et qui incluent aussi une partie importante de la face α de l'unité αLFuc. La liaison de l'unité βDGlcNAc comprend le groupement OH-6 qui est lié par des liaisons hydrogènes intramoléculaires au O-5 de façon à étendre les interactions non polaires à la face α de cette unité et peut être même au-delà. Les diminutions d'enthalpie (6 kcal/mol) et d'entropie (2,7 cal/mol/K) qui sont observées lorsqu'il se produit une liaison de l'α-L-fucopyrannoside de méthyle sont plus faibles que celles qui sont observées avec le trisaccharide de type H-2; ces valeurs sont compatibles avec le fait que la surface impliquée pour former des complexes est beaucoup plus petite. Les données concernant le pouvoir inhibiteur qui ont été obtenues en utilisant une grande variété de structures apparentées au α-L-fucopyrannoside de méthyle sont en général en accord avec les hypothèses fondées sur les résultats obtenus avec des structures plus complexes.

[Traduit par le journal]

Introduction

The lectin I of *Ulex europaeus* (common gorse) was found (1) to agglutinate O human red cells and proved to be a useful reagent for the classification of people of the O blood group as secretors or nonsecretors (2). This proved to be a fortunate circumstance, which is now known to arise because the lectin has a strong affinity for the H-type 2 determinant (αLFuc(1→2)βDGal(1→4)βDGlcNAc--) but does not recognize the H-type 1 determinant (αLFuc(1→2)βDGal(1→3)βDGlcNAc--) (3). The lectin is available commercially and its binding characteristics have received major previous attention (4). Our recent studies (5–7) of the binding of oligosaccharides by lectins and antibodies have shown that complex formation may require a polar interaction involving hydroxyl groups that are present in different sugar units. In such cases, the protein binds neither the simple sugars that make up the oligosaccharides nor their methyl glycosides. Thus, binding of the H-type 2 determinant by the lectin I of *Ulex europaeus* was of special interest since it was known (4) that both fucose and methyl α-L-fucopyranoside are effective as inhibitors of the agglutination of O red cells by the lectin.

Recently, we reported on the ability of a number of modified H-type 2 structures to inhibit the agglutination of O red cells (8). This study confirmed that the acetamido group is not involved in the binding reaction (4). Also, it became apparent that neither OH-3 of the βDGlcNAc unit nor OH-4 of the βDGal unit interact with the protein. Structural changes involving the αLFuc were not extended beyond replacement of its CH_3-6 group by hydrogen. It was concluded that the binding involves the recognition by the lectin of a wedge-shaped lipophilic surface which includes OH-6 of the βDGlcNAc unit intramolecularly hydrogen bonded to O-5. We now wish to report

[1] Alberta Heritage Foundation for Medical Research Scholar, since 1981.

[2] Alberta Heritage Foundation for Medical Research Postdoctoral Fellow, 1982–1984.

[3] Author to whom correspondence may be addressed.

TABLE 1. Inhibition of the binding of an H-type 2 artificial antigen by the Lectin I of *Ulex europaeus*. Involvement of the βDGlcNAc-OR portion of **1**

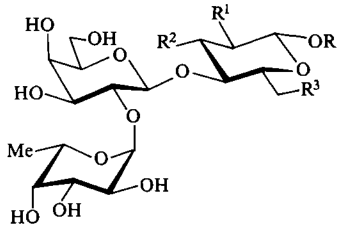

Compound	Substituent R	R^1	R^2	R^3	50% Inhibition μmol/L	Relative potency	$\Delta\Delta G^0$ kcal/mol at 23°C
1	CH_3	NHAc	OH	OH	9	67	0.24
2	$(CH_2)_8COOCH_3$	NHAc	OH	OH	6	100	0
3	$(CH_2)_8COOH$	NH_2	OH	OH	6*	—	—
4	$(CH_2)_8COOCH_3$	NHAc	H	OH	13	46	0.46
5	$(CH_2)_8COOCH_3$	NHAc	αLFucO	OH	23	26	0.79
6	$(CH_2)_8COOCH_3$	NHAc	OH	H	1.7	352	−0.75
7	αLFuc(1→2)βDGal-O$(CH_2)_8COOCH_3$				290	2	2.3
8	αLFuc(1→2)α,βDGalOH				730	0.8	2.8

* Based on the previous observation (8).

a continuation of these studies but using a solid-phase radioimmunoassay to determine relative inhibition potencies. This paper includes the examination of the eight possible monodeoxy derivatives of the H-type 2 determinant αLFuc(1→2)-βDGal(1→4)βDGlcNAc (9). Also, a wide number of derivatives of methyl α-L-fucopyranoside were examined.

In our previous study (8), the inhibitors were synthesized with $(CH_2)_8COOCH_3$ as aglycon. A number of these compounds were used in this investigation but most of the structures are new (9) and contain the simple methyl group as aglycon. In Tables 2 and 3, the reference inhibitor for the expression of relative potencies is the methyl glycoside (**1**) of the H-type 2 trisaccharide and the sugar units are labelled a, b, and c, as shown. The formula for **1** is drawn as a projection that

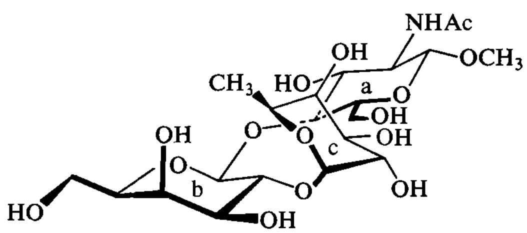

1

imitates the conformational preference suggested by HSEA calculation and supported by ^{1}H nmr (10, 11). It is noteworthy in this regard that the lectin IV of *Griffonia simplicifolia* binds the Lewis b and Y determinants nearly equally well and that this finding is in agreement with the conformational analyses, based on ^{1}H nmr, for these two structures (5). We therefore have confidence that the conformer for **1** with ϕ^b/ψ^b = 55°/0° and ϕ^c/ψ^c = 50°/15° (11) well represents the compound in aqueous solution. Furthermore, the ^{1}H and ^{13}C nmr parameters found (9) for the various modifications of **1** used in this study indicate that this conformational preference is maintained. The specific deshielding of H-5 of the αLFuc unit by O-4 of the βDGlcNAc unit (8, 11) supports our contention that these are rigidly held conformers.

Results and discussion

The radioimmunoassay used to determine the inhibition data presented in Tables 1–4 was described in detail in paper II of this series (5) and the 50% inhibitions proved reproducible to within ±5% of the values listed.

The results presented in Table 1 confirm the conclusions reached in our previous publication (8). Previously, the activity of the Y determinant (**5**) was taken as evidence that OH-3^a is not involved in the binding reaction. On the basis of the criteria set for noninvolvement of a hydroxyl group (5), this conclusion is now confirmed by the high potency displayed by the 3^a-deoxy derivative **4**. The fact that **2** is only slightly more active than **1** suggests that binding of the aglycon does not extend importantly beyond the aglyconic carbon grouping, as was found, for example, for the anti-I Ma antibody (12). In contrast, in the case of a monoclonal anti-Lewis b antibody (6), the change in aglycon from CH_3 to $(CH_2)_8COOCH_3$ increased the potency by a factor of 6.5. As previously reported (8), deoxygenation of the CH_2OH^a group importantly increased the potency. On the basis of the presently used radioimmunoassay, elimination of the requirement of OH-6^a to become intramolecularly hydrogen bonded to O-5^a increases the potency by a factor of 3.5 and, therefore, appears to increase the driving force for reaction by about 0.75 kcal/mol. Replacement of the βDGlcNAc-O$(CH_2)_8COOCH_3$ portion of **2** by the $O(CH_2)_8$-$COOCH_3$ group led to the much less potent inhibitor **7**. However, replacement by an hydroxyl group provided an even weaker inhibitor (**8**). These results were not surprising since it had become evident that binding about the aglycon of the βDGal unit of **1** is extensive and nonpolar in nature (8). Evidently, the $(CH_2)_8COOCH_3$ group of **7** does not well provide a conformation that is complementary to the hydrophobic cleft of the lectin which binds the βDGlcNAc unit of **1**.

As seen from Table 2 and as previously noted (8), the 4^b-epimer of **2**, namely, **10**, is only about twice less active than **2**. This observation was interpreted as noninvolvement of OH-4^b and, therefore, probably also OH-6^b. This latter prediction is now confirmed by the high potency displayed by the 6^b-deoxy

TABLE 2. Inhibition of the binding of an H-type 2 artificial antigen by the lectin I of *Ulex europaeus*. Involvement of the βDGal unit of **1**

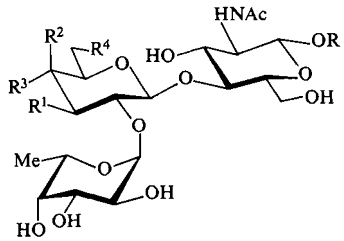

Compound	Substituent R	R^1	R^2	R^3	R^4	50% Inhibition μmol/L	Relative potency	$\Delta\Delta G^0$ kcal/mol at 23°C
1	CH_3	OH	OH	H	OH	9	100	0
9	CH_3	H	OH	H	OH	360	2.5	2.2
10	$(CH_2)_8COOCH_3$	OH	H	OH	OH	15	40*	0.5
11	CH_3	OH	OH	H	H	15	60	0.3

*Relative to **2** (Table 1).

TABLE 3. Inhibition of the binding of an H-type 2 artificial antigen by the lectin I of *Ulex europaeus*. Involvement of the αLFuc unit of **1**

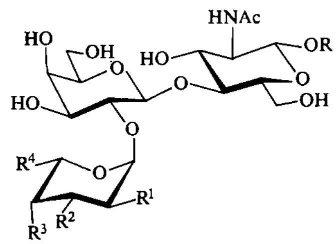

Compound	Substituent R	R^1	R^2	R^3	R^4	50% Inhibition μmol/L	Relative potency	$\Delta\Delta G^0$ kcal/mol at 23°C
1	CH_3	OH	OH	OH	CH_3	9	100	0
12	CH_3	H	OH	OH	CH_3	1420	0.63	3.0
13	CH_3	OH	H	OH	CH_3	16000*	0.06	4.4
14	CH_3	OH	OH	H	CH_3	Inactive†	—	—
15	$(CH_2)_8COOCH_3$	OH	OH	OH	H	160	3.8‡	1.9
16	αLFuc-OCH_3					950	0.95	2.7
17	βDAra-OCH_3					42000	0.02	5.0

*Extrapolated from 20% inhibition at 4400 and classified as inactive.
†8% Inhibition at 4400.
‡Relative to **2** (Table 1).

compound (**11**). On the other hand, deoxygenation of the OH-3^b position of **1** to form **9** decreased the potency by a factor of 40. Thus, OH-3^b is importantly involved in a polar interaction with the combining site. For reasons previously discussed (5), a polar interaction that is not essential to complex formation is not included in the so-called key polar interaction. As will be seen below, OH-2^c, which projects in space close to OH-3^b, is also involved in an important but not essential interaction with the lectin.

The effects on binding that arose from modifications of the αLFuc unit are reported in Table 3. It is seen at once that all three hydroxyl groups become involved in polar interactions with the lectin. However, only deoxygenation at positions 3^c and 4^c yielded essentially inactive compounds, namely, **13** and **14**. In contrast, replacement of OH-2^c of **1** by hydrogen to produce **12** caused a marked decrease in potency but the compound retained an activity near that of methyl α-L-fucopyranoside (**16**). Judging from the $\Delta\Delta G^0$ values, this complex is nearly 3 kcal/mol less stable than that formed from **1**. As will be discussed in more detail below, OH-2^c projects close to OH-3^b and these two hydroxyl groups appear to form a polar grouping adjacent to the key polar grouping provided by OH-3^c and OH-4^c. Important involvement of the CH_3-6^c group is indicated by the large decrease in potency that results from the replacement of this group in the inhibitor **2** (Table 1) by hydrogen to form **15**. This observation is confirmed by the large difference in the inhibitions provided by methyl α-L-fucopyranoside (**16**) and methyl β-D-arabinopyranoside (**17**), the latter compound being essentially inactive.

The results obtained using a variety of derivatives of methyl α-L-fucopyranoside (**16**) are reported in Table 4. As was to be expected from the results obtained using the 3^c- and 4^c-deoxy

TABLE 4. Inhibition by L-fucose and derivatives of the binding of an H-type 2 artificial antigen by the lectin I of *Ulex europaeus*

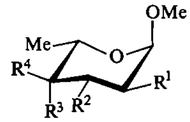

Compound	Substituent R1	R2	R3	R4	50% Inhibition μmol/L	Relative potency	$\Delta\Delta G^0$ kcal/mol at 23°C
16	OH	OH	OH	H	950	100	0
18	H	OH	OH	H	7300	13	1.2
19	OH	H	OH	H	Inactive*	—	—
20	OH	F	OH	H	31000	3	2.1
21	OH	OH	H	H	Inactive*	—	—
22	OH	OH	F	H	Inactive*	—	—
23	OH	OH	OH	CH_3	Inactive†	—	—
24	βLFuc-OCH_3				11500	8.3	1.5
25	α,βLFuc-OH				4300	22	0.9

* Inactive at 55 000.
† Inactive at 35 000.

TABLE 5. Thermodynamic parameters for binding by the lectin I of *Ulex europaeus*

	$K_{\mathrm{Assoc.}}$*	ΔH kcal/mol	ΔS cal/mol/K	ΔG^0* kcal/mol
αLFuc-OCH_3 (**16**)	$6.4 \pm 0.2 \times 10^3\ M^{-1}$	−6.0	−2.7	−5.2
H-type 2-OCH_3 (**1**)	$1.8 \pm 0.8 \times 10^6\ M^{-1}$	−29	−68	−8.5

* At 298 K.

derivatives of **1**, namely, **13** and **14** (Table 3), the 3-deoxy (**19**) and 4-deoxy (**21**) derivatives of **16** proved inactive. In the case of the 2-deoxy derivative (**18**) of **16**, substantial residual activity (13% of **16**) was found. This decrease in activity is much less than that observed on deoxygenation of **1** to form the 2^c-deoxy derivative **12** where the decrease in potency was to less than 1% that of **1**. It appears, therefore, that the combining site formed to accept **1** with the establishment of a polar interaction with the OH-3^b–OH-2^c grouping is not completed for the acceptance of the simple methyl α-L-fucopyranoside (**16**). In fact, the thermodynamic data presented in Table 5 strongly support this indication that the extent of the organization of the lectin to accept **1** is much greater than that for the acceptance of **16**. It is seen that the decrease in entropy to form the complex with the trisaccharide **1** involves 68 entropy units in contrast to only 2.7 entropy units for the simple methyl α-L-fucopyranoside. These thermodynamic parameters were determined by measuring the change in ultraviolet absorption (A_{286}–A_{290} nm) under the same experimental conditions described in our study of the lectin IV of *Griffonia simplicifolia* (5). In contrast to the experience with this lectin, the difference ultraviolet spectra for the binding of **1** and **16** by the *Ulex* lectin were very similar. Experimental details and the discussion of the results obtained using **1**, **16**, and a number of other structures that are bound by *Ulex* are reserved for a separate communication (13).

It is considered interesting to note that the thermodynamic parameters for the binding of oligosaccharides by a variety of lectins have recently appeared in the literature. Some of the findings are summarized in Fig. 1 where it is seen that a fairly linear relationship exists between the ΔH and $T\Delta S$ terms. It appears, therefore, that any gain in complex stability resulting from a decrease in enthalpy is always accompanied by some cancelling from a decrease in entropy. Thus, it can be expected that the larger the combining site, the greater the effort may be for organization as reflected by a greater decrease in entropy. The thermodynamic parameters reported herein for the *Ulex* lectin and those previously reported (5) for the lectin IV of *Griffonia simplicifolia* appear in accord with this observation. The findings for **1** (Table 5) are the highest values reported to date ($\Delta H = -29$ and $T\Delta S = -20$ kcal/mol at 25°C).

Returning to Table 4, it is seen that replacement of either OH-3 or OH-4 of **16** by fluorine, to form **20** and **22**, led to essentially inactive compounds. It is likely, therefore, that these key hydroxyl groups act as proton donors in the complex formation.

As previously mentioned (8), the α-side of an α-L-fucopyranosyl group presents substantial nonpolar surface to its environment. As noted above, the CH_3-6 group of both **1** and **16** appears involved in the binding reaction and this result would be in keeping with the *Ulex* lectin recognizing the nonpolar α-side of the αLFuc unit. That this is the case is supported by the fact (Table 4) that αLFuc-OCH_3 (**16**) is much more strongly bound than its β-anomer (**24**). In fact, even free L-fucose (**25**) is more strongly bound than is **24**. Evidently O-1 of L-fucose becomes involved in the binding reaction but this must surely be by way of a nonpolar interaction since **16** is about 5 times more potent than **25** as an inhibitor. It is apparent, therefore, that the binding of **16** involves a polar interaction between OH-3 and OH-4 with a polar grouping provided by the lectin and which allows the establishment of nonpolar interactions between a complementary surface provided by the protein and the surface of **16** defined by H-3, H-4, H-5, CH_3-6, O-1, and the methyl aglycon. In order to test this hypothesis,

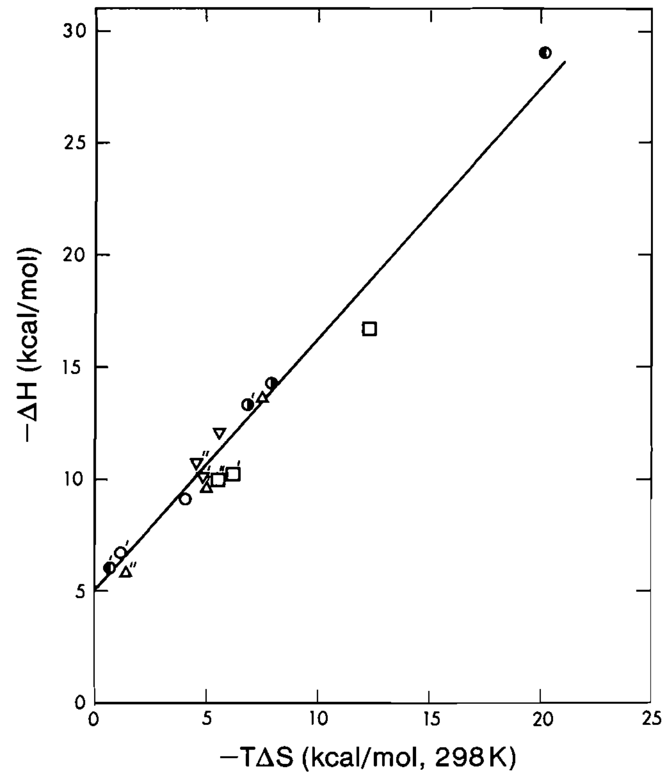

FIG. 1. A plot of selected literature values for the changes in enthalpy and entropy at 25°C which occur on the binding of a variety of carbohydrates by a variety of plant lectins. Lectin I of *Ulex europaeus:* ◐ αLFuc(1→2)βDGal(1→4)βDGlcNAc-OMe (this work); ◐′ αLFuc-OMe (this work). Lectin IV of *Griffonia simplicifolia:* ◑ αLFuc-(1→2)βDGal(1→3)[αLFuc(1→4)]βDGlcNAc-OMe (5); ◑′ Methoxymethyl(1→2)βDGal(1→3)[αLFuc(1→4)]βDGlcNAc-OMe (5). Peanut agglutinin: □ βDGal(1→4)βDGlc-OMe (14); □′ βDGal-OMe (15, 16); □″ αDGal-OMe (15, 16). *Erythrina cristagalli* agglutinin: △ βDGal(1→4)βDGlcNAc(1→2)DMan (17); △′ βDGal(1→4)DGlc (17); △″ α,βDGalNAc (17). Soybean agglutinin: ▽ βDGalNAc-OPh-*p*-NO_2 (18); ▽′ αDGal-OMe (18); ▽″ αDGalNAc-OMe (18). Concanavalin A: ○ αDMan-OMe (19); ○′ αDMan-OPh-*p*-NO_2 (20).

the 4-*C*-methyl derivative of **16**, namely, **23**, was synthesized.[4] It is seen that the simple substitution of H-4 by CH_3 led to an inactive compound. It is possible that the substitution interferes with the polar interaction and that this is the main reason why **23** is inactive. On the other hand, this inactivity could result from the methyl group preventing the establishment of a proper interfacing of complementary nonpolar surfaces. We submit that the latter is the case since the small decrease in entropy (2.7 entropy units) that accompanies the binding of **16** suggests that the combining site is virtually already present in the lectin. Thus, the formation of the complex must be highly dependent on the complementarity of the interacting surfaces. Only a slight change in the topography of one of these surfaces may so weaken a complex, which is formed through a decrease in enthalpy of only 6 kcal/mol, that complex formation is not observed.

The results of this study are summarized in Fig. 2 where the H-type 2-OCH_3 compound (**1**) is presented in the conformer indicated by ^1H nmr (11) and produced by HSEA calculation. It is seen that the polar interactions involve OH-4^c, OH-3^c, OH-2^c, and OH-3^b and that these groups form a polar cluster at one end of the molecule. The OH-4^c and OH-3^c groups provide the key polar interaction which is indispensible to complex formation. In contrast, the OH-2^c and OH-3^b region, while providing important stability to the complex, are not essential. The lightly shaded area, part of which is expected to extend behind the CH_3-6^c group, represents the lipophilic surface which appears to make the major contribution to the stability of the complex. This surface may well extend to include more of the β-side of the βDGlcNAc unit and the α-side of the βDGal unit than is indicated. In order to extend the nonpolar interactions to this side of the structure, OH-6^a forms an intramolecular hydrogen bond with O-5^a. Although not reexamined in this present study, it was previously established (8) that the H-type 1 determinant (αLFuc(1→2)βDGal(1→3)βDGlcNAc-$O(CH_2)_8COOH$) is not bound but that the free amine form (αLFuc(1→2)βDGal(1→3)βDGlcNH$_2$-$O(CH_2)_8COOH$) interacts quite strongly with the lectin. This observation was taken as evidence that the de-*N*-acetylation exposed the α-side of the αLFuc unit for binding by the lectin while providing a lipophilic surface very similar in topography to that provided by **2**. Thus, the evidence appears convincing that the surface of **1** that is recognized by the lectin is amphiphilic in character, as represented in Fig. 2. There can be no doubt that the NHAc-2^a, OH-3^a, OH-4^b, and OH-6^b groups remain in contact with the aqueous phase. The nonpolar interactions may involve a greater surface than that shown but no evidence in this regard was obtained in this present study.

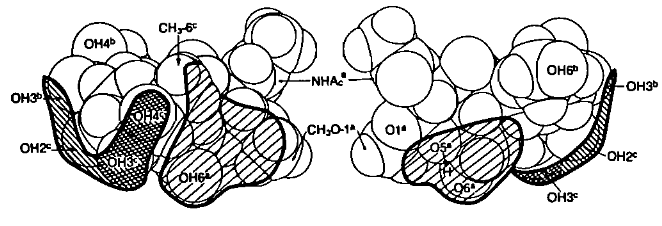

FIG. 2. The HSEA molecular model for αLFuc(1→2)βDGal(1→4)βDGlcNAc-OMe (**1**) (H-type 2). Opposite sides of the model are shown and the hatched areas display the surface which comes into interaction for complex formation with the lectin I of *Ulex europaeus*. The cross-hatched key polar interaction involving OH-4^c and OH-3^c of the fucose unit is seen to occur adjacent to the lipophilic region (lightly hatched). The OH-3^b and OH-2^c groups are seen to be adjacent to the key polar group. These hydroxyl groups also become involved in important polar interactions with the lectin but this involvement appears to arise from a conformative response that is not essential for the formation of a complex.

Experimental

Inhibitors

The various compounds used as inhibitors were synthesized following well-established procedures (8, 9). The structures and their purity were confirmed by appropriate ^1H nmr (400 MHz) and ^{13}C nmr (100 MHz) studies.

Lectin I of Ulex europaeus was purchased from Sigma Chemical Company.

Radioimmunoassay

The procedure followed was that previously reported (5) using an ^{125}I-labelled (αLFuc(1→2)βDGal(1→4)βDGlcNAc-$O(CH_2)_8CO$-$NH)_{11}$BSA antigen purchased from Chembiomed Ltd. (University of Alberta, Edmonton, Alberta, T6G 2G2). The solution provided nearly 200 000 cpm/100 μL and the tubes were incubated at room temperature (23°C). In the absence of the inhibition, about 65% of the radioactivity was bound.

[4] G. Deslongchamps, unpublished.

Acknowledgements

This research was supported by the Natural Sciences and Engineering Research Council of Canada (Grant A-172 to R.U.L.) and the Alberta Heritage Foundation for Medical Research (O.H. and D.P.K.).

1. P. CAZAL and M. LALAURIE. Acta Haematol. **8**, 73 (1952).
2. W. C. BOYD and E. SHAPLEIGH. Blood, **9**, 1195 (1954).
3. R. U. LEMIEUX, D. A. BAKER, W. M. WEINSTEIN, and C. M. SWITZER. Biochemistry, **20**, 199 (1981).
4. M. E. A. PEREIRA, E. C. KISAILUS, F. GRUEZO, and E. A. KABAT. Arch. Biochem. Biophys. **185**, 108 (1978).
5. U. SPOHR, O. HINDSGAUL, and R. U. LEMIEUX. Can. J. Chem. **63**, 2644 (1985).
6. U. SPOHR, N. MORISHIMA, O. HINDSGAUL, and R. U. LEMIEUX. Can. J. Chem. **63**, 2659 (1985).
7. R. U. LEMIEUX, A. P. VENOT, U. SPOHR, P. BIRD, G. MANDAL, N. MORISHIMA, O. HINDSGAUL, and D. R. BUNDLE. Can. J. Chem. **63**, 2664 (1985).
8. O. HINDSGAUL, T. NORBERG, J. LEPENDU, and R. U. LEMIEUX. Carbohydr. Res. **109**, 109 (1982).
9. D. P. KHARE, O. HINDSGAUL, and R. U. LEMIEUX. Carbohydr. Res. **136**, 285 (1985).
10. R. U. LEMIEUX, K. BOCK, L. T. J. DELBAERE, S. KOTO, and V. S. RAO. Can. J. Chem. **58**, 631 (1980).
11. H. THØGERSEN, R. U. LEMIEUX, K. BOCK, and B. MEYER. Can. J. Chem. **60**, 44 (1982).
12. R. U. LEMIEUX, T. C. WONG, J. LIAO, and E. A. KABAT. Mol. Immunol. **21**, 751 (1984).
13. N. MORISHIMA, M. BACH, O. HINDSGAUL, and R. U. LEMIEUX. In preparation.
14. K. J. NEUROHR, H. H. MANTSCH, N. M. MARTIN, and D. R. BUNDLE. Biochemistry, **21**, 498 (1982).
15. K. J. NEUROHR, N. M. YOUNG, and H. H. MANTSCH. J. Biol. Chem. **255**, 9205 (1980).
16. K. J. NEUROHR, N. M. MARTIN, I. C. P. SMITH, and H. H. MANTSCH. Biochemistry, **20**, 3499 (1981).
17. H. DE BOECK, F. G. LOONTIENS, H. LIS, and N. SHARON. Arch. Biochem. Biophys. **234**, 297 (1984).
18. H. DE BOECK, H. LIS, H. VAN TILBEURGH, N. SHARON, and F. G. LOONTIENS. J. Biol. Chem. **259**, 7067 (1984).
19. A. VAN LANDSCHOOT, F. G. LOONTIENS, and C. K. DE BRUYNE. Eur. J. Biochem. **103**, 307 (1980).
20. F. G. LOONTIENS, R. M. GREGG, and T. M. JOVIN. Biochemistry, **16**, 159 (1977).

Molecular recognition. IV. The binding of the Lewis b human blood group determinant by a hybridoma monoclonal antibody

ULRIKE SPOHR,[1] NAOHIKO MORISHIMA,[2] OLE HINDSGAUL,[3] AND RAYMOND U. LEMIEUX[4]
Department of Chemistry, University of Alberta, Edmonton, Alta., Canada T6G 2G2

Received December 21, 1984

ULRIKE SPOHR, NAOHIKO MORISHIMA, OLE HINDSGAUL, and RAYMOND U. LEMIEUX. Can. J. Chem. **63**, 2659 (1985).

A commercial hybridoma monoclonal anti-Lewis b antibody appears to accept the Lewis b human blood group determinant (αLFuc(1→2)βDGal(1→3)[αLFuc(1→4)]βDGlcNAc--) by involving OH-3 of the βDGal unit and OH-2 of the αLFuc(1→2) unit in a key polar interaction at the periphery of a large wedge-shaped lipophilic surface that extends about the tetrasaccharide and essentially leaves 5 of the 8 other hydroxyl groups in contact with the aqueous phase. It is proposed that the three remaining hydroxyl groups, namely, OH-4 of the βDGal unit, OH-3 of the αLFuc(1→4) unit, and OH-4 of the αLFuc(1→2) unit, become intramolecularly hydrogen bonded for acceptance into a hydrophobic environment. The results are taken as further circumstantial evidence that the stability of the complex is mainly related to the establishment of dispersion forces of attraction between complementary lipophilic surfaces provided by the oligosaccharide and the protein. These forces are expected to be stronger than those prior to binding between the amphiphilic surfaces that are involved and water.

ULRIKE SPOHR, NAOHIKO MORISHIMA, OLE HINDSGAUL et RAYMOND U. LEMIEUX. Can. J. Chem. **63**, 2659 (1985).

Un anticorps monoclonal hybride, de type anti-Lewis b et disponible commercialement, semble accepter le déterminant du groupe sanguin humain de type Lewis b, le (αLFuc(1→2)βDGal(1→3)[αLFuc(1→4)]βDGlcNAc--), en faisant intervenir le groupe OH-3 de l'unité βDGal et le groupe OH-2 de l'unité αLFuc(1→2) dans une interaction polaire clé à la périphérie d'une grande surface lipophile en forme de coin qui s'étend autour de tétrasaccharide et qui laisse essentiellement 5 des 8 autres groupes hydroxyles en contact avec la phase aqueuse. On propose que ce sont les trois groupes hydroxyles qui restent, soit le OH-4 de l'unité βDGal, le OH-3 de l'unité αLFuc(1→4) et le OH-4 de l'unité αLFuc(1→2), qui établissent des liaisons hydrogènes intramoléculaires qui permettent d'être accepté dans un environnement hydrophobe. On considère que les résultats fournissent une preuve circonstancielle additionnelle du fait que la stabilité du complexe est liée principalement à l'existence de forces de dispersion et d'attraction entre les surfaces lipophiles complémentaires fournies par l'oligosaccharide et la protéine. On s'attend à ce que ces forces soient supérieures à celles qui existeraient avant la liaision entre les surfaces amphiphiles impliqués et l'eau.

[Traduit par le journal]

Introduction

The Lewis b (Le^b) human blood group determinant is characteristic of the epithelial cells of nearly 70% of individuals (1, 2). The purpose of this communication is to report the results obtained in a systematic probing of the combining site of a commercial (Chembiomed Ltd., Department of Chemistry, University of Alberta, Edmonton T6G 2G2) hybridoma monoclonal anti-Le^b antibody using a wide range of synthetic analogs to inhibit the reaction of the antibody with an artificial Le^b-BSA antigen (2). The experimental data obtained by way of a solid-phase radioimmunoassay (3) are in accord with the general characteristics established for protein–oligosaccharide binding reactions involving monoclonal anti-I Ma (4) and anti-B antibodies (5), the lectin I of *Ulex europaeus* (6), and the lectin IV of *Griffonia simplicifolia* (3). The outstanding feature of this communication is that the binding of the Le^b determinant appears to involve its acceptance by the antibody in the extensively intramolecularly hydrogen bonded form presented in the various tables. As previously done (3, 7), and as specified in **1**, the sugar units will be designated as units a (βDGlcNAc), b (βDGal), c (αLFuc(1→4^a), and d (αLFuc(1→2^b).

Experimental evidence now exists that intramolecular hydrogen bonds form in aqueous solution only when an appropriate internuclear distance (2.7–3.0 Å) between the proton donor

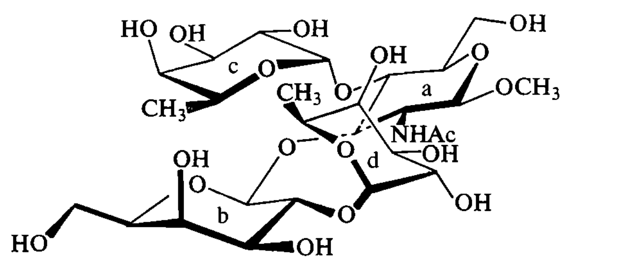

1

and the proton acceptor is enforced by the steric and stereoelectronic demands that govern the conformational preference of the oligosaccharide (8–10). Consequently, in the absence of such intramolecular enforcement, energy must be expended for the formation of intramolecular hydrogen bonds by an oligosaccharide in order that it can become bound by a protein. Since the formation of an intramolecular hydrogen bond is expected to render a polar molecule more compatible for a nonpolar interaction and since energy is required for its formation, the conclusion appears unavoidable that the stability of the complex has its origins in strong dispersion forces of attraction between the oligosaccharide and a hydrophobic binding site on the protein (11, 12).

Results and discussion

As seen from Table 1, both the αLFuc units of the Le^b determinant are involved in the binding reaction, as both the Le^d (H-type 1, **3**) and the Le^a (**4**) trisaccharides are poor inhibitors. Because **4** is essentially inactive, the compound appears not to contain intact the key polar grouping that is essen-

[1] University of Alberta postdoctoral fellow, since 1982.
[2] Alberta Heritage Foundation for Medical Research postdoctoral fellow, since 1982.
[3] Alberta Heritage Foundation for Medical Research Scholar, since 1981.
[4] Author to whom correspondence may be addressed.

TABLE 1. Involvement of the αLFuc units

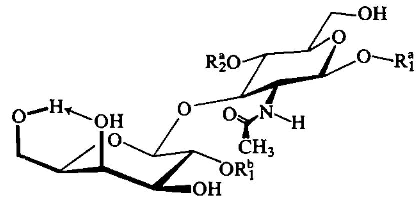

Compound	Substituent R_2^a	Substituent R_1^b	50% Inhibition μmol/L	Relative potency	$\Delta\Delta G^0$ kcal/mol
R_1^a = $(CH_2)_8COOCH_3$					
2 (Le[b])	αLFuc	αLFuc	29	650	−1.1
3 (Le[d])	H	αLFuc	4480	4	1.9
4 (Le[a])	αLFuc	H	Inactive*	—	—
R_1^a = CH_3					
1 (Le[b])	αLFuc	αLFuc	189	100	0
5	αLFuc	CH_2OCH_3	Inactive†	—	—

* 12% at 3336.
† No inhibition at 3970.

TABLE 2. Involvement of the βDGlcNAc unit

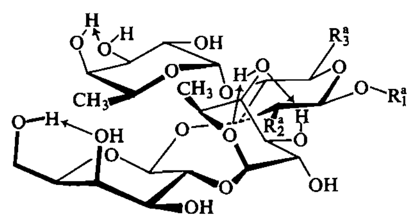

Compound	Substituent R_1^a	Substituent R_2^a	Substituent R_3^a	50% Inhibition μmol/L	Relative potency	$\Delta\Delta G^0$ kcal/mol
2 (Le[b])	$(CH_2)_8COOCH_3$	NHAc	CH_2OH	29	650	−1.1
6 (Y)*	—	—	—	Inactive†	—	—
7	$(CH_2)_8COOH$	NH_2	CH_2OH	2110‡	9	1.4
1	CH_3	NHAc	CH_2OH	189	100	0
8	CH_3	NHAc	CH_3	180	105	−0.03

* αLFuc(1→2)βDGal(1→4)[αLFuc(1→3)]βDGlcNAcO$(CH_2)_8COOCH_3$
† No inhibition at 2760.
‡ By extrapolation.

tial for binding (3). However, **3**, as a weak but still active inhibitor, is expected to possess this grouping and, in view of the inactivity of **4**, the αLFuc(1→2[b]) unit is expected to contribute to this grouping. In fact, as will be seen below (Table 5), the key polar grouping does involve OH-2[d] of **3**. This situation is in contrast to the binding of the Le[b] tetrasaccharide by the lectin IV of *Griffonia simplicifolia* (3), where it is the αLFuc(1→4[a]) residue which provides an hydroxyl group to the key polar interaction. Not surprisingly, therefore, replacement of the d-fucosyl group by a methoxymethyl group to simulate (3) the αLFuc(1→2[b]) anomeric linkage produced an inactive compound (**5**). It may be noted at this point that the substantially greater activity of **2** as compared to the simple methyl glycoside (**1**) requires that binding occurs about the aglycon (R_1^a) (Table 1) and that this region of the combining site is hydrophobic in nature. Also, it should be noted that the formulas presented in Tables 1–5 describe, in each case, the intramolecular hydrogen bonds that are present in the Le[b] determinant *after* it was bound by the antibody. These intramolecular hydrogen bonds are not expected to be abundant prior to the formation of the complex.

That the βDGlcNAc residue is involved in the binding reaction became apparent when the Y determinant (**6**) was found to be inactive (Table 2). In fact, involvement of the acetamido group is indicated by the low activity demonstrated by the amino acid (**7**). The hydroxymethyl group of the βDGlcNAc residue is definitely not involved in a polar interaction with the combining site since the 6[a]-deoxy derivative (**8**) is slightly more active than the parent structure (**1**). Possible involvement of this hydroxymethyl group must then be limited to a hydrophobic interaction, perhaps while hydrogen bonded to the ring oxygen (6). An involvement of this group may importantly contribute to the stability of the complex as, for example, does the hydroxymethyl group of the αDGal unit of the human B determinant when bound by monoclonal anti-B antibodies (5). As will be seen with reference to Fig. 1, the CH_2OH^a group is

TABLE 3. Involvement of the βDGal unit

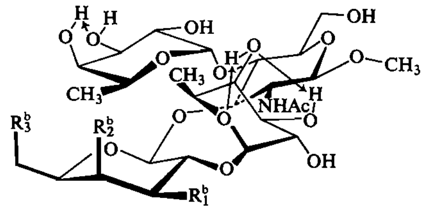

Compound	Substituent R_1^b	R_2^b	R_3^b	50% Inhibition μmol/L	Relative potency	$\Delta\Delta G^0$ kcal/mol
1 (Le[b])	OH	OH	OH	189	100	0
9	H	OH	OH	Inactive*	—	—
10	OH	H	OH	1584	12	1.3
11	OH	OH	H	10.5	1800	−1.7

*No inhibition at 3460.

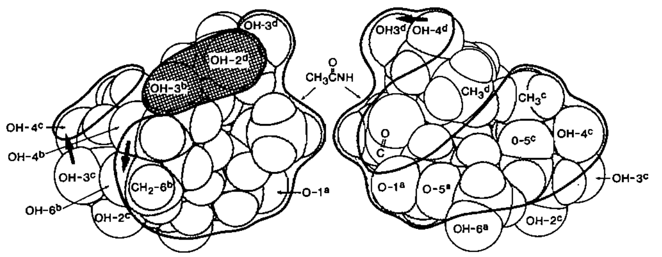

FIG. 1. The HSEA molecular model for αLFuc(1→2)βDGal(1→3)-[αLFuc(1→4)]βDGlcNAc-OMe. Opposite sides of the model are shown and the hatched areas display the surface which was identified as that which comes into interaction for complex formation with a hybridoma monoclonal anti-Lewis b antibody. The cross-hatched region involving the OH-3[b] and OH-2[d] provides the key polar interaction. The arrows indicate the location of the three intramolecular hydrogen bonds that are postulated to form in the course of complex formation. It is noteworthy that the most hydrophobic region is adjacent to the key polar grouping.

included in the topography that is bound in order to extend the lipophilic surface to both sides of the molecule. The high activity of **8** supports this contention.

The results presented in Table 3 with regard to involvement of the βDGal unit are particularly interesting. First of all, replacement of OH-3[b] by hydrogen provided an inactive product (**9**) but deoxygenation at position 4[b] to produce **10** left an active compound. Thus, OH-3[b] and OH-2[d] form the polar key and, as seen in Fig. 1, these are located in close proximity to each other. Replacement of OH-6[b] by hydrogen provided an inhibitor (**11**) that is 18 times more potent than the parent Le[b] tetrasaccharide (**1**). This truly remarkable event amounts to an increase in the stability of the complex by 1.7 kcal/mol. Angyal and McHugh (13) estimated the nonbonded interaction between *syn*-axial hydroxyl groups to be 1.8 kcal/mol. Also, the nonbonded interaction between *syn*-axial acetoxy groups was estimated to be approximately 2.1 kcal/mol (14, 15). We therefore propose that replacement of OH-6[b] by hydrogen relieves the system of the energy required to bring OH-6[b] in *syn*-axial-like relationship with OH-4[b]. In this orientation, an intramolecular hydrogen bond between OH-6[b] and O-4[b] should be enforced and it is for this reason that this bond is displayed in the formula for **1** in Table 2. The reason for the enforcement of this unfavorable orientation for OH-6[b] is clearly apparent from a consideration of Fig. 1 where it is seen that, as the result of losing the energy required to orient OH-6[b], a larger hydrophobic area is gained, stretching from the CH_2-6[b] methylene group to the methyl of the acetamido group. In the normal orientation, OH-6[b] would project largely *syn*-axial-like to H-4[b] (8, 9) and thereby disrupt the continuity of the weakly polar–nonpolar wedge-shaped topography indicated in Fig. 1 and which is expected to be complementary to the hydrophobic cleft defined by the combining site. As mentioned above, replacement of OH-4[b] by hydrogen provided a weak inhibitor. On the basis of the proposal for binding presented in Fig. 1, this result is not surprising. First of all, at least marginal involvement of OH-4[b] in the polar interaction provided by the neighboring OH-3[b] must be anticipated. Secondly, in the absence of OH-4[b], OH-6[b] must adopt the energetically less favorable orientation wherein it is *anti*-periplanar to H-5[b] in order to form a bond with O-5[b]. This latter hydrogen bond should be weaker than that when O-4[b] was available as the proton acceptor since OH-4[b] must be a proton donor (most likely to water) in the complex. The cooperativity of hydrogen bonds (16), when first observed (17), was termed hydrogen-bond conjugation.

Further rather convincing evidence for the formation of intramolecular hydrogen bonds in the course of the binding of **1** by the antibody is presented in Table 4. First of all, replacement of OH-2[c] by hydrogen to form **12** had no effect on the extent of binding and it is therefore concluded that this hydroxyl group remains in contact with water. However, replacement of OH-4[c] by hydrogen to form **14** led to a nearly two-fold increase in potency. Thus, OH-4[c] appears to become involved, through intramolecular hydrogen bonding, in a nonpolar interaction with the protein. This conclusion is supported by the fact that replacement of OH-4[c] by fluorine to provide **15** led to a nearly five-fold increase in potency. This is in accord with expectation since the engagement of a polar fluorine atom in a nonpolar interaction can be expected to resemble that of an hydroxyl group involved as the proton donor to an intramolecular hydrogen bond. On the basis that **1** is accepted with OH-4[c] hydrogen bonded to O-3[c], it is to be expected that replacement of OH-3[c] by hydrogen to form **13** would provide a weaker inhibitor. In fact, as seen in Table 4, its potency is about five times less than that of **1**. That it is not an even less active compound is not surprising, since OH-4[c] can still form an intramolecular hydrogen bond with O-5[c]. Finally, should

TABLE 4. Involvement of the αLFuc(1→4[a]) unit

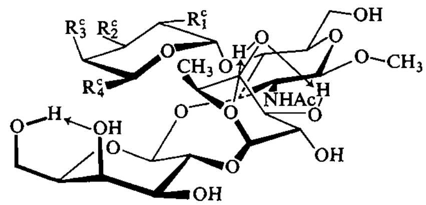

Compound	Substituent R_1^c	R_2^c	R_3^c	R_4^c	50% Inhibition μmol/L	Relative potency	$\Delta\Delta G^0$ kcal/mol
1 (Le[b])	OH	OH	OH	CH_3	189	100	0
12	H	OH	OH	CH_3	188	100	0
13	OH	H	OH	CH_3	850	22	0.9
14	OH	OH	H	CH_3	102	185	−0.4
15	OH	OH	F	CH_3	40.2	470	−0.9
16	OH	OH	OH	H	1628	12	1.3

TABLE 5. Involvement of the αLFuc(1→2[b]) unit

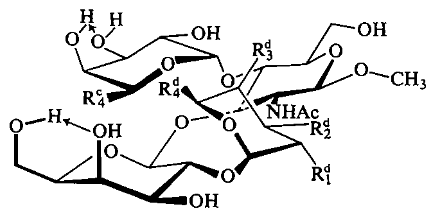

Compound	Substituent R_1^d	R_2^d	R_3^d	R_4^d	R_4^c	50% Inhibition μmol/L	Relative potency	$\Delta\Delta G^0$ kcal/mol
1 (Le[b])	OH	OH	OH	CH_3	CH_3	189	100	0
17	OH	OH	OH	H	CH_3	210	90	0.06
16	OH	OH	OH	CH_3	H	1628	12	1.3
18	OH	OH	OH	H	H	2570	7	1.5
19	H	OH	OH	CH_3	CH_3	Inactive*	—	—
20	OH	H	OH	CH_3	CH_3	82	230	−0.5
21	OH	OH	H	CH_3	CH_3	900	21	0.9
22	OH	OH	F	CH_3	CH_3	402	47	0.45

*No inhibition at 3460.

OH-4[c] become involved in a nonpolar interaction within the complex, it would be surprising indeed if the neighboring nonpolar CH_3-6[c] group was not similarly involved. In fact, as seen in Table 4, replacement of CH_3-6[c] by hydrogen to form **16** led to a nearly eight-fold reduction in potency, which amounts to a near 1.3 kcal/mol reduction in the stability of the complex. On the other hand, as seen in Table 5, replacement of CH_3^d by hydrogen to form **17** had little effect on the binding reaction. In the case of compound **18**, both the CH_3^c and CH_3^d groups of **1** are replaced by hydrogen. As expected from the potencies of **16** and **17**, **18** is only slightly less potent than **16**.

As was mentioned above, the activity displayed by the Le[d] determinant (**3**) suggested that the αLFuc(1→2[b]) unit provides an hydroxyl group to the key polar interaction. Indeed, as seen in Table 5, the 2[d]-deoxy derivative (**19**) of **1** proved to be inactive. The superiority of the 3[d]-deoxy compound (**20**) as an inhibitor suggests that OH-3[d] of **1** becomes involved, hydrogen bonded to O-4[d], as displayed in the formula for Table 4. On this basis, deoxygenation at position 4[d] should provide an inferior inhibitor. In fact, this is the case and compound **21** is only about a fifth as active as **1**. The requirement for OH-3[d] to form an intramolecular hydrogen bond should be fulfilled, although not as effectively, by a fluorine atom at position 4[d]. In fact, replacement of OH-4[d] by fluorine to provide **22** resulted in a compound that proved to be about half as potent as **1**. As to involvement of OH-4[d], it is possible that, in the complex, this hydroxyl becomes intramolecularly hydrogen bonded to O-5[d], as is displayed in Table 4. However, as seen in Fig. 1, this hydroxyl group is also well disposed for interaction with water. It is shown bonded to O-5[d] only to indicate that this possibility exists and that the lipophilic surface that becomes involved in the complexation reaction may be even more extensive than is indicated in Fig. 1.

In summary, compound **1** appears to be recognized by this particular monoclonal anti-Le[b] antibody through interaction with the wedge-shaped amphiphilic surface depicted in Fig. 1 for the tetrasaccharide in its energetically favored conformation in aqueous solution (7). In order to present this surface to the antibody, three and perhaps four intramolecular hydrogen bonds are formed. In view of the involvement of such hydrogen bonds, the surface is not strictly hydrophobic in nature. Instead, it can only, because of the intramolecular hydrogen bonds, become energetically more compatible for interaction with a nonpolar complementary surface provided by the protein. Most likely the engagement of these groupings is enforced in order for the protein to gain access to the adjacent nonpolar groupings. It seems unlikely that the intramolecularly hydrogen bonded hydroxyl groups become involved in polar interactions within the complex, since in each case the deoxygenation produced a superior inhibitor.

These observations justify the idea presented in 1978, "that carbohydrates (depending on their structure and configuration) through intramolecular hydrogen bonding can assume (depending on demand by the environment and by way of a low energy process) either hydrophilic or hydrophobic properties. . ." (11). In this context, the oligosaccharides comprise a wide range of conformationally well-defined non-surface-active structures which, because of their polar groups, are compatible with water and can serve to extend amphiphilic surfaces into the aqueous phase where these can seek receptor sites for the guidance of biological processes. To date (3–6), our experimental data indicate that these interactions comprise sterically well-directed and coordinated polar and nonpolar interactions between complementary surfaces, with the greater the complementarity presented for lipophilic interaction, the greater the stability of the complex. However, whether or not a complex is formed appears to depend on the integrity of the polar interaction. This interaction could correspond to the first step proposed by Neurohr *et al.* (18) for the binding of methyl α-D-galactopyranoside by peanut agglutinin. This step could not be followed but was considered to occur with a low equilibrium constant and probably diffusion controlled or nearly so. There then follows a mutual fitting of site and sugar which is much slower than expected for a diffusion-controlled process and which is associated with a negative entropy of activation (6). We propose that the polar interaction provides the key to the complexation reaction in that it allows the mutual fitting to begin and that its main function is to bring a nonpolar portion of the oligosaccharide into a position suitable for it to interact with the protein. On this basis, the polar grouping of the oligosaccharide serves as a key that opens a "hydrated polar gate" (12) provided by the protein which, like the key polar group, is adjacent to a nonpolar region which is complementary to the nonpolar surface of the oligosaccharide. Low energy conformational changes by the protein toward completion of the complex then occur. These changes involve both a decrease in enthalpy and decrease in entropy. On this basis, the specificity of the reaction depends on an ability of the nonpolar interaction to become established in accord with the stereochemical requirements of the key polar interaction. Important cross reactions (that is, different inhibitor potencies) occur when the requirements of the key polar interaction are met, but the extent to which complementary lipophilic surfaces can be established differs. This coordination of effort is probably basic to all *specific* processes for molecular recognition, including the organization of macromolecules and the binding of substrates by enzymes (19). It has been suggested that the main driving force for the "fitting" of a protein to an oligosaccharide is the filling of voids along amphiphilic surfaces (12).

Experimental

Inhibitors

The structures and purity of the various compounds used as inhibitors were established by appropriate ^{1}H (400 MHz) and ^{13}C (100 MHz) nuclear magnetic resonance studies (20).

Radioimmunoassay

These assays were conducted following the procedure described in the study of the lectin IV of *Griffonia simplicifolia* (3). The results were similar in quality. It was found that an antigen of the composition $(Le^{b})_{19}$-BSA-^{125}I was so strongly absorbed that prohibitively high concentrations of **1** were required to reach 50% inhibition. This problem was solved by using an antigen with a lower degree of substitution, namely, $(Le^{b})_{1-2}$-BSA-^{125}I. In the absence of an inhibitor, about 85 000 cpm (50% of that added) were bound by an antibody-coated tube. The IgM antibody (clone 96FR 2.10) can be purchased from Chembiomed Ltd. in the form of a reagent suitable for blood typing.

Acknowledgements

This research was supported by the Natural Sciences and Engineering Research Council of Canada (Grant A-172 to R.U.L.) and the Alberta Heritage Foundation for Medical Research (N.M. and O.H.). The antibody was donated by Chembiomed Ltd.

1. R. R. RACE and R. SANGER. Blood groups in man. 6th ed. Blackwell Scientific Publications, Oxford. 1975. pp. 323–349.
2. R. U. LEMIEUX, D. A. BAKER, W. M. WEINSTEIN, and C. M. SWITZER. Biochemistry, **20**, 199 (1981).
3. U. SPOHR, O. HINDSGAUL, and R. U. LEMIEUX. Can. J. Chem. **63**, 2644 (1985).
4. R. U. LEMIEUX, T. C. WONG, J. LIAO, and E. A. KABAT. Mol. Immunol. **21**, 751 (1984).
5. R. U. LEMIEUX, A. P. VENOT, U. SPOHR, P. BIRD, G. MANDAL, N. MORISHIMA, O. HINDSGAUL, and D. R. BUNDLE. Can. J. Chem. **63**, 2664 (1985).
6. O. HINDSGAUL, D. P. KHARE, M. BACH, and R. U. LEMIEUX. Can. J. Chem. **63**, 2653 (1985).
7. R. U. LEMIEUX, K. BOCK, L. T. J. DELBAERE, S. KOTO, and V. S. RAO. Can. J. Chem. **58**, 631 (1980).
8. K. BOCK and R. U. LEMIEUX. Carbohydr. Res. **100**, 63 (1982).
9. O. HINDSGAUL, T. NORBERG, J. LE PENDU, and R. U. LEMIEUX. Carbohydr. Res. **109**, 109 (1982).
10. E. ALVARADO, O. HINDSGAUL, R. U. LEMIEUX, K. BOCK, and H. PEDERSEN. Abstracts of the XIIth International Carbohydrate Symposium, Utrecht, The Netherlands, July 1–7, 1984. p. 480.
11. R. U. LEMIEUX, P. H. BOULLANGER, D. R. BUNDLE, D. A. BAKER, A. NAGPURKAR, and A. VENOT. Nouv. J. Chim. **2**, 321 (1978).
12. R. U. LEMIEUX. Proceedings of the VIIIth International Symposium on Medicinal Chemistry, August 27–31, 1984, Uppsala, Sweden. To be published by the Swedish Pharmaceutical Society.
13. S. J. ANGYAL and D. J. MCHUGH. Chem. Ind. (London), 1147 (1956).
14. R. U. LEMIEUX and N. J. CHÜ. Abstracts of Papers, Am. Chem. Soc. **133**, 31N (1958).
15. R. U. LEMIEUX. *In* Molecular rearrangements. Part 2. *Edited by* P. de Mayo. Interscience Publishers, New York. 1964. pp. 735–743.
16. J. E. DEL BENE and J. A. POPLE. J. Chem. Phys. **58**, 3605 (1973).
17. R. U. LEMIEUX and A. A. PAVIA. Can. J. Chem. **47**, 4441 (1969).
18. K. J. NEUROHR, H. H. MANTSCH, N. M. YOUNG, and D. R. BUNDLE. Biochemistry, **21**, 498 (1982).
19. D. P. KHARE, O. HINDSGAUL, and R. U. LEMIEUX. Carbohydr. Res. **136**, 285 (1985).
20. U. SPOHR, O. HINDSGAUL, and R. U. LEMIEUX. In preparation.

Molecular recognition. V. The binding of the B human blood group determinant by hybridoma monoclonal antibodies

RAYMOND U. LEMIEUX,[1] ANDRÉ P. VENOT,[2] ULRIKE SPOHR,[2] PAUL BIRD,[2] GAURHARI MANDAL,[2] NAOHIKO MORISHIMA,[3] AND OLE HINDSGAUL[4]
Department of Chemistry, University of Alberta, Edmonton, Alta., Canada T6G 2G2

AND

DAVID R. BUNDLE
Division of Biological Sciences, National Research Council of Canada, Ottawa, Ont., Canada K1A 0R6

Received December 21, 1984

RAYMOND U. LEMIEUX, ANDRÉ P. VENOT, ULRIKE SPOHR, PAUL BIRD, GAURHARI MANDAL, NAOHIKO MORISHIMA, OLE HINDSGAUL, and DAVID R. BUNDLE. Can. J. Chem. **63**, 2664 (1985).

A systematic study was made of the effect of changes in the structure of αLFuc(1→2)[αDGal(1→3)]βDGal-OMe (**1**) on the inhibition of the binding of an artificial antigen by two monoclonal anti-B antibodies. Both OH-4 of the βDGal unit and OH-2 of the αDGal unit are essential for binding by one of the antibodies. For the other antibody, OH-3 of the αDGal unit also forms part of the key polar grouping. Both the antibodies recognize a large lipophilic surface extending from the CH_3-6 group of the αLFuc unit along the α-sides of this group and the βDGal unit to include its CH_2OH-6 group, most likely intramolecularly hydrogen bonded to the neighboring O-5. The lipophilic surface then extends to include the CH_2OH-6 group of the αDGal unit intramolecularly hydrogen bonded to the O-5 atom. The stability of the complex is attributed to nonpolar interaction of this surface within a hydrophobic cleft-like combining site which offers a polar grouping at its periphery for interaction with the key polar grouping of the trisaccharide. The solution conformer for **1**, as determined by ^1H nmr, is present in its crystal structure.

RAYMOND U. LEMIEUX, ANDRÉ P. VENOT, ULRIKE SPOHR, PAUL BIRD, GAURHARI MANDAL, NAOHIKO MORISHIMA, OLE HINDSGAUL et DAVID R. BUNDLE. Can. J. Chem. **63**, 2664 (1985).

On a effectué une étude systématique sur l'effet des changements dans la structure du trisaccharide αLFuc(1→2)-[αDGal(1→3)]βDGal-OMe (**1**) sur l'inhibition de la liaison d'un antigène artificiel par deux anticorps anti-B monoclonaux. La présence tant du OH-4 de l'unité βDGal que du OH-2 de l'unité αDGal est essentielle pour qu'il se produise une liaison avec l'un des anticorps. Dans le cas de l'autre anticorps, le OH-3 de l'unité αDGal fait également partie du groupment polaire clé. Chacun des deux anticorps reconnaît une grande surface lipophile qui comprend le groupement CH_3-6 de la portion αLFuc, situé le long du côté α de cette portion, la portion βDGal ainsi que le groupement CH_2OH-6 de cette dernière qui est probablement lié à l'atome O-5 voisin par une liaison hydrogène intramoléculaire. La surface lipophile s'étend alors de façon à inclure le groupement CH_2OH-6 de l'unité αDGal qui est liée à l'atome O-5 par une liaison hydrogène intramoléculaire. On attribue la stabilité de ce complexe à une interaction non polaire de cette surface à l'intérieur d'un site de liaison hydrophobe ressemblant à une crevasse qui présente, à sa périphérie, un groupement polaire qui permet d'effectuer une interaction avec le groupe polaire principal du trisaccharide. Le conformère du composé **1** qui, d'après la rmn du ^1H, existerait en solution serait aussi présent dans la structure cristalline.

[Traduit par le journal]

Introduction

Bundle, Rahman, and co-workers (1) produced hybridoma monoclonal antibodies in mice against an artificial antigen prepared by acylation of human O red cells with the synthetic B human blood group related structure αLFuc(1→2)[αDGal-(1→3)]βDGal-$O(CH_2)_8CON_3$ (2–4). We report herein how the combining sites of the two IgM monoclonal, affinity purified, anti-B antibodies (I and II, obtained from clones 3E-7 and 1A-12, respectively) (1) recognize this trisaccharide.

The procedure, based on a solid-phase radioimmunoassay, was that used for the probing of the combining sites of the lectin IV of *Griffonia simplicifolia* (5), the lectin I of *Ulex europaeus* (6), and a hybridoma anti-Lewis b antibody (7). The conclusions are similar in kind to those reached in these previous studies in that the recognition involves an interaction of the antibody with an amphiphilic surface, a situation which was also found for the binding by the monoclonal anti-I Ma antibody where the inhibitions were determined using a quantitative precipitin assay (8).

Results and discussion

The combining sites were probed using synthetic oligosaccharides, listed in Tables 1–3, prepared, in the most part, following established procedures (2) and thoroughly characterized by high field ^1H and ^{13}C nmr studies (9). The 50% inhibitions were determined using a previously reported solid-phase radioimmunoassay (5, 10). The differences in binding free energies ($\Delta\Delta G^0$ values at 23°C) provide an assessment of how much structural changes influence the stabilities of the complexes formed as compared to that for the reference inhibitor (**1**).

In order to discover the extents of involvement of the hydroxyl groups in the binding of the reference inhibitor (**1**), the nine possible monodeoxy derivatives (**2–10**) were synthesized (11, 12) and their performances as inhibitors are reported in

[1]Author to whom correspondence may be addressed.
[2]University of Alberta postdoctoral fellows (A.P.V., 1982–1983; U.S., since 1982; P.B., 1982–1984; G.M., 1983–1984).
[3]Alberta Heritage Foundation for Medical Research postdoctoral fellow, since 1983.
[4]Alberta Heritage Foundation for Medical Research Scholar, since 1981.

TABLE 1. The effects of deoxygenation on the binding of the B determinant (**1**) by two monoclonal anti-B antibodies

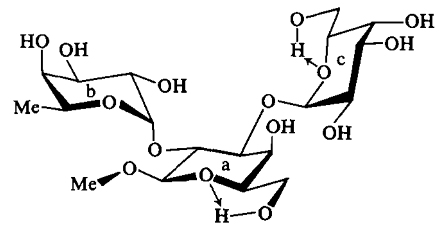

		50% Inhibition (μmol/L)		$\Delta\Delta G^0$ (kcal/mol)	
Compound	Derivative of **1**	Antibody I	Antibody II	Antibody I	Antibody II
1	—	150	150	0	0
2	2^b-Deoxy	240	290	0.28	0.39
3	3^b-Deoxy	200	170	0.17	0.07
4	4^b-Deoxy	120	210	−0.13	0.20
5	6^a-Deoxy	170	240	0.07	0.28
6	6^c-Deoxy	120	96	−0.13	−0.26
7	4^c-Deoxy	1020*	720*	1.13	0.93
8	4^a-Deoxy	Inactive†	Inactive†	—	—
9	2^c-Deoxy	Inactive†	Inactive†	—	—
10	3^c-Deoxy	2900	Inactive†	1.75	—
11	2^c-Deoxy-2^c-amino	10 000‡	3100‡	—	—
12	2^c-Deoxy-2^c-acetamido	Inactive†	Inactive†	—	—

*αLFuc(1→2)[αDGlc(1→3)]βDGalOCH_3 was inactive.
†No inhibition at 4700 μmol/L.
‡By extrapolation.

Table 1. The similarity of the results obtained for both antibodies is remarkable. These results require direct involvement of OH-4^a and OH-2^c in the binding with both the antibodies, since their removal to produce **8** and **9** resulted in complete abolishment of activity. The data for compound **10** indicate a stronger requirement of OH-3^c for antibody II than for I but important involvement occurs in both cases. In accordance with the previous proposals (5) for describing specific polar regions that are essential for binding by lectins and antibodies, OH-4^a and OH-2^c form the key polar grouping for antibody I. In the case of antibody II, this grouping also includes OH-3^c, because for this antibody compound **10** is inactive. The reduced activities that result from deoxygenation at C-4^c to form **7** may arise from changes in hydration near the strongly polar involvements of the neighboring OH-3^c. In view of these results, it was not surprising that epimerization of C-4^c to convert the αDGal unit to αDGlc provided an inactive product. These findings are in accord with the recent report by Rahuel *et al.* (13) that the 3^c-deoxy and 3^c,4^c-dideoxy derivatives of the B-trisaccharide are inactive as inhibitors of the agglutination of human B red cells. The low but detectable activity displayed by the amine **11**, as compared to the inactivity shown by the A determinant **12**, is in accord with their findings on acquired B antigens.

Change of the methyl aglycon of **1** to $(CH_2)_8COOCH_3$ to form **17** increased the binding strength by about 0.37 and 0.65 kcal/mol for antibodies I and II, respectively (Table 2). The involvement of the linking arm was not surprising (14). Indeed, antibodies from other clones showed much greater involvement of the linking arm in the immune response to the artificial antigenic determinant derived from **17** (1). The relatively low activities exhibited by the tetrasaccharide type 1 (**18**) and type 2 (**19**) B haptens are therefore understandable and establish the binding of the methoxy group of **1** in both the antibody reactions. In fact, inversion of C-1^a of **1** to form the α-anomer **13** led to substantial loss in potency. These decreases in complex stability are attributed to losses of complementarity involving both the methoxy group and the weakly polar α-side of the βDGal unit (15).

It is established (16, 17) that the preferred orientation of OH-6 of a galactopyranoside has this group *anti*-periplanar to O-5. The data in Table 1 require that neither OH-6^a nor OH-6^c are involved in polar interactions within the combining sites, since the replacement of these hydroxyls by hydrogen provided highly active compounds (**5** and **6**). Because the 6^c-deoxy derivative (**6**) is a superior inhibitor, it is anticipated that **1** is bound with OH-6^c intramolecularly hydrogen bonded to O-5^c, as is present in the crystal structure (18), a situation that was observed both for the binding of the H-type 2 determinant of *Ulex europaeus* (6, 19) and the Lewis b determinant by a hybridoma monoclonal anti-Le^b antibody (7). That binding occurs about the C-6^c grouping is required by the low activity of the βL Ara compound **24**. Since the 6^a-deoxy compound **5** is slightly less active than **1**, the evidence that OH-6^a becomes intramolecularly hydrogen bonded to O-5^a, as displayed in Table 1, is not as convincing as for the bonding of OH-6^c to O-5^c. The hydrogen bond is suggested in view of the high activity displayed by **5**, together with the fact that the L-6^a-C-methyl compound **21** is much more active than its D-isomer (**20**). In the case of **21**, OH-6^a in its preferred orientation (15) can form a hydrogen bond with O-5^a, but OH-6^a of **20** cannot.

The conformation of the trisaccharide portion of **17** in aqueous solution (9) was found to be that present in the crystal

TABLE 2. Effects of structural changes* on the binding by two monoclonal anti-B antibodies

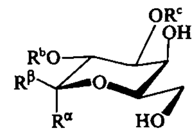

	Substituents				50% Inhibition (μmol/L)		$\Delta\Delta G^0$ (kcal/mol)	
Compound	R^{α}	R^{β}	R^b	R^c	Antibody I	Antibody II	Antibody I	Antibody II
1	H	OCH_3	αLFuc	αDGal	150	150	0	0
13	OCH_3	H	αLFuc	αDGal	450	1630	0.65	1.41
14	H	OCH_3	αLFuc	CH_3	†	†	—	—
15	H	OCH_3	H	αDGal	3000	5330	1.76	2.11
16	H	OCH_3	CH_3	αDGal	2450	3270	1.64	1.82
(**17**)	B-$(CH_2)_8COOCH_3$				80	50	−0.37	−0.65
(**18**)	B(1→3)βDGlcNAcO$(CH_2)_8COOCH_3$				700	760	0.91	0.96
(**19**)	B(1→4)βDGlcNAcO$(CH_2)_8COOCH_3$				800	2260	0.99	1.60

*The simple alkyl glycosides, methyl β-D-galactopyranoside, methyl α-L-fucopyranoside, and methyl α-D-galactopyranoside, were all inactive as inhibitors at concentrations greater than 50 000 μmol/L.
†Inactive at 4700 μmol/L.

TABLE 3. Effects of structural changes at terminal groups of the B determinant (**1**) on the binding by two monoclonal anti-B antibodies

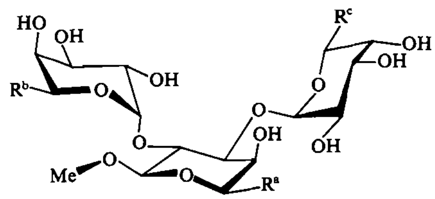

				50% Inhibition (μmol/L)		$\Delta\Delta G^0$ (kcal/mol)	
Compound	R^a	R^b	R^c	Antibody I	Antibody II	Antibody I	Antibody II
1	CH_2OH	CH_3	CH_2OH	150	150	0	0
Changes in the βDGal unit							
5	CH_3	CH_3	CH_2OH	170	240	0.07	0.28
20	D-CH_3CHOH	CH_3	CH_2OH	*	*	—	—
21	L-CH_3CHOH	CH_3	CH_2OH	1290	2030	1.27	1.54
22	$C(CH_3)_2OH$	CH_3	CH_2OH	9200	†	2.42	—
Changes in the αLFuc unit							
23	CH_2OH	H	CH_2OH	650	420	0.86	0.61
Changes in the αDGal unit							
6	CH_2OH	CH_3	CH_3	120	96	−0.13	−0.26
24	CH_2OH	CH_3	H	1910	873	1.50	1.04
25	CH_2OH	CH_3	$C(CH_3)_2OH$	690	330	0.90	0.47
26	CH_2OH	H	H	4600	1540	2.01	1.38

*30% at 4700 μmol/L.
†18% at 4700 μmol/L.

structure (18) of **1** and presented in Fig. 1. In view of the inhibition data presented in Tables 1−3 and the evidence that **1** is a conformationally rigid structure (9), we conclude that the binding reaction involves a highly directional polar interaction with the cluster of hydroxyl groups defined by OH-4^a and OH-2^c in the case of antibody I and by OH-4^a, OH-2^c, and OH-3^c in the case of antibody II. It appears that the polar interactions involving OH-3^c and OH-4^c for antibody I and that involving OH-4^c for antibody II are less demanding in terms of the structures of the complexes that are formed. For antibody II, the three hydroxyl groups of the fucosyl unit and the polar side of **1** occupied by O-5^a, O-1^a, and O-5^b appear to remain in contact with water. It is possible that OH-4^b becomes intramolecularly hydrogen bonded to OH-3^b for involvement in a nonpolar interaction with antibody I, since deoxygenation at the 4^b-position to produce **4** (Table 1) provided a superior inhibitor. Similar situations were found for the binding by the lectin IV of *Griffonia simplicifolia* (5) and a monoclonal anti-Lewis b antibody (7).

As is displayed in Fig. 1, a large lipophilic region appears to

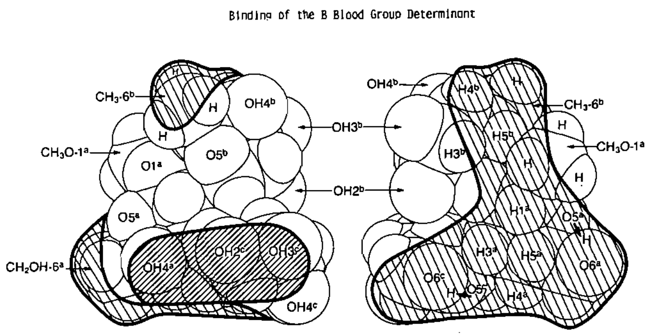

FIG. 1. Schematic representation of the combining sites for the monoclonal anti-B antibodies (I and II) to illustrate the regions of αLFuc(1→2)[αDGal(1→3)]βDGal-OMe (**1**, CPK representation of its crystal structure) that are bound. Note that the polar regions O-1^a, O-5^a, O-5^b, as well as OH-2^b and OH-3^b remain in contact with water. This condition also applies to OH-4^b in the case of antibody II. For antibody I, the lipophilic surface (lightly hatched) may extend to include OH-4^b intramolecularly hydrogen bonded to OH-3^b. The key polar grouping shown is for antibody II. For antibody I, this grouping is limited to OH-4^a and OH-2^c.

be involved, which extends from the CH_3-6^b group of the fucosyl unit to include the two hydroxymethyl groups intramolecularly hydrogen bonded to the neighboring ring oxygens (O-5^a and O-5^c). The conformation of **1** places the key polar grouping adjacent to this lipophilic surface. As in all cases so far studied (5–8), this polar grouping is well positioned to interact with a polar grouping at the periphery of the combining site and termed the polar gate (20). Prior to binding, both the polar groupings (i.e., the key and the gate) likely are strongly hydrated and their interaction may not contribute importantly to the stability of the complex. The possibility that the polar grouping provided to the complex was shielded from hydration prior to binding does not appear to be relevant. Judging from the shapes of the topographies provided by the oligosaccharide to the complex, the polar interactions within the complex occur at the interface with the aqueous environment. This matter was previously discussed in relation to the binding of the H-type 2 determinant by the lectin I of *Ulex europaeus* (6). Definitely, the interaction between the nonpolar complementary surfaces contributes importantly and, indeed, appears to be the dominating factor for complex stability (6). Considering that the polar interactions, which are directional in character, must be compatible with the required orientations for the complementary lipophilic surfaces to interact, it is evident that these interactions provide the main contribution to the specificity of the overall binding reaction. This finding is of major importance to efforts aimed at the detection of lectin and antibody specificities using partial structures as potential inhibitors (5, 7). The failure of the simple alkyl glycosides and **14** (Table 2) to display appreciable levels of activity is noteworthy in this regard. In the case of the binding of the H-type 2 determinant (αLFuc(1→2)βDGal(1→4)βDGlcNAc) by the lectin 1 of *Ulex europaeus*, the key polar grouping is provided by the 3- and 4-hydroxyl groups of the fucosyl unit and this lectin also binds methyl α-L-fucopyranoside.

The conclusions reached in this investigation regarding the nature of the combining sites for antibodies I and II are similar in kind to those reached in the case of the anti-I Ma antibody (8) and the lectin 1 of *Ulex europaeus* (6), the lectin IV of *Griffonia simplicifolia* (5), and a monoclonal anti-Lewis b antibody (7). The common feature is for the oligosaccharide to offer substantial surface which is compatible for binding by a complementary hydrophobic cleft at the surface of the antibody. In all cases, this surface terminates with a relatively much smaller cluster of hydroxyl groups that is well positioned to react with a polar grouping at a region along the periphery of the combining site. As previously noted (6, 7), the stability of the complex appears mainly derived from the extent that nonpolar interactions can be established between complementary lipophilic surfaces.

Experimental

Antibodies I and II

Commercially available (Chembiomed Ltd.) mouse hybridoma monoclonal antibody I (clone 3E-7) (ref. 1) was affinity purified by absorption on commercial B Synsorb, washing with phosphate buffer, and then isolated by desorption using 0.1 *M* aqueous acetic acid that was 0.15 *M* in sodium chloride. The solvent was then rapidly exchanged to phosphate buffer (pH 7.5) in the usual manner (14). Antibody II (clone 1A-12) (ref. 1) was similarly purified prior to use in the radioimmunoassay.

Inhibitors

The various inhibitors were obtained by chemical synthesis (11, 12) and shown to be of high purity by appropriate ^{1}H (400 MHz) and ^{13}C (100 MHz) nuclear magnetic studies.

Radioimmunoassay

The assay (5) employed a solution of (αLFuc(1→2)[αDGal(1→3)]-βDGal)$_{15}$-BSA-^{125}I which provided about 290 000 cpm/100 μL. In the absence of inhibitor, the antibody-coated tubes bound nearly 50% of these counts. The tubes were coated using solutions of antibody I (12.5 μg/mL) and antibody II (6 μg/mL) in 0.05 *N* sodium phosphate buffer (pH 7.5).

Acknowledgements

This research was supported by the Natural Sciences and Engineering Research Council of Canada (Grant A-172 to R.U.L.) and the Alberta Heritage Foundation for Medical Research. The donation of the antibody I by Chembiomed Ltd. is gratefully acknowledged.

1. D. R. BUNDLE, M. A. J. GIDNEY, N. KASSAM, and A. F. R. RAHMAN. J. Immunol. **129**, 678 (1982).
2. R. U. LEMIEUX. Chem. Soc. Rev. **7**, 423 (1978).
3. R. U. LEMIEUX, D. R. BUNDLE, and D. A. BAKER. U.S. Patent No. 4,238,473. 1980.
4. R. U. LEMIEUX, D. A. BAKER, and D. R. BUNDLE. Can. J. Biochem. **55**, 507 (1977).
5. U. SPOHR, O. HINDSGAUL, and R. U. LEMIEUX. Can. J. Chem. **63**, 2644 (1985).
6. O. HINDSGAUL, D. P. KHARE, M. BACH, and R. U. LEMIEUX. Can. J. Chem. **63**, 2653 (1985).
7. U. SPOHR, N. MORISHIMA, O. HINDSGAUL, and R. U. LEMIEUX. Can. J. Chem. **63**, 2659 (1985).
8. R. U. LEMIEUX, T. C. WONG, J. LIAO, and E. A. KABAT. Mol. Immunol. **21**, 751 (1984).
9. H. THØGERSEN, R. U. LEMIEUX, K. BOCK, and B. MEYER. Can. J. Chem. **60**, 44 (1982).
10. W. W. YOUNG, JR., H. S. JOHNSON, Y. TAMURA, K. A. KARLSSON, G. LARSON, J. M. R. PARKER, D. P. KHARE, U. SPOHR, D. A. BAKER, O. HINDSGAUL, and R. U. LEMIEUX. J. Biol. Chem. **258**, 4890 (1983).
11. A. P. VENOT and R. U. LEMIEUX. In preparation.
12. U. SPOHR, P. BIRD, G. MANDAL, N. MORISHIMA, O. HINDSGAUL, and R. U. LEMIEUX. In preparation.
13. C. RAHUEL, A. LUBINEAU, S. DAVID, C. SALMON, and J. P. CARTRON. Blood Transfus. Immunohematol. **26**, 347 (1983).

14. R. U. Lemieux, P. H. Boullanger, D. R. Bundle, D. A. Baker, A. Nagpurkar, and A. Venot. Nouv. J. Chim. **2**, 321 (1978).
15. C. Lough, O. Hindsgaul, and R. U. Lemieux. Carbohydr. Res. **120**, 43 (1983).
16. A. Maradufu, G. M. Cru, and A. S. Perlin. Can. J. Chem. **49**, 3429 (1971).
17. K. Bock and R. U. Lemieux. Carbohydr. Res. **100**, 63 (1982).
18. R. Ball, A. Venot, J. P. Praly, O. Hindsgaul, and R. U. Lemieux. In preparation.
19. O. Hindsgaul, T. Norberg, J. Lependu, and R. U. Lemieux. Carbohydr. Res. **109**, 109 (1982).
20. R. U. Lemieux. Proceedings of the VIIIth International Symposium on Medicinal Chemistry, August 27–31, 1984, Uppsala, Sweden. To be published by the Swedish Pharmaceutical Society.

The electroreduction of halogenated thiophenes

RICHARD NEVILLE GEDYE, YOGINDER NATH SADANA, AND RAYMOND LEGER
Department of Chemistry, Laurentian University, Sudbury, Ont., Canada P3E 2C6

Received June 7, 1984[1]

RICHARD NEVILLE GEDYE, YOGINDER NATH SADANA, and RAYMOND LEGER. Can. J. Chem. **63**, 2669 (1985).

Electroreduction of polyhalothiophenes results in the preferential reduction of the α-halogen atoms. Preparative electrochemical reduction of these compounds at controlled potential can be used to synthesize 2,3,4-trihalo, 3,4-dihalo, and 3-halothiophenes. Experimental conditions were developed under which these reductions could be done selectively, giving good yields of the desired products. Electroreduction of tetrabromothiophene can also lead to the formation of a polybromodithienyl mercury compound.

RICHARD NEVILLE GEDYE, YOGINDER NATH SADANA et RAYMOND LEGER. Can. J. Chem. **63**, 2669 (1985).

L'électroréduction de polyhalothiophènes conduit à la réduction des atomes d'halogènes en α. Opérant à des potentiels controlés, on peut utiliser la réduction électrochimique préparative de ces composés pour réaliser la synthèse des trihalo-2,3,4, des dihalo-3,4 et des halo-3 thiophènes. On a développé des conditions expérimentales qui permettent de réaliser de telles réduction d'une façon sélective et avec de bons rendements en produits désirés. L'électroréduction du tétrabromothiophène peut aussi conduire à la formation d'un composé polybromodithiényle mercure.

[Traduit par le journal]

Introduction

Electrophilic substitution of thiophenes occurs more rapidly in the α (2 and 5) positions than the β (3 and 4) positions. For this reason the direct synthesis of 3-halo and 3,4-dihalo derivatives from the parent heterocycles cannot be achieved. 3-Bromothiophene can be prepared by the bromination of thiophene to 2,3,5-tribromothiophene followed by reduction with zinc in acetic acid (1). This reduction results in preferential dehalogenation in the α-positions but requires a large excess of zinc and leads to large volumes of effluent containing zinc ions (2).

The electroreduction of polyhalogenated heterocycles was considered to be an attractive alternative to chemical reduction. Polarographic studies on tetrabromothiophene **1***a* (3) and tetraiodothiophene **1***b* (4) have shown that the α-halogens are reduced at a lower potential than the β-halogens and that stepwise reduction of the four halogens occurs, giving four distinct waves.

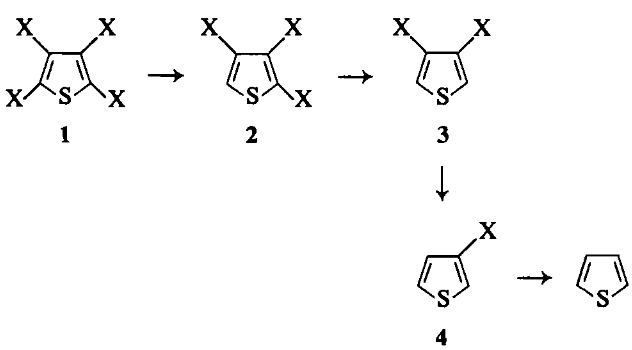

a, X = Br; *b*, X = I

Feldmann and Koberstein (5) have investigated the reduction of 2,3,5-tribromothiophene by cyclic voltammetry and confirmed the proposed pathway by preparative electrochemical reduction. Constant potential reductions at −1.2, −1.45, and −1.75 V gave 2,3-dibromothiophene, 3-bromothiophene, and thiophene, respectively. Recently the electrochemical reduction of 2,3,5-tribromothiophene to **4***a* using a lead, mercury, or graphite cathode in 70% dioxane/30% water has been reported (2). The yields, estimated by glc, were generally high at potentials (−1.5 to −1.7 V) just positive to the potential of hydrogen evolution.

This paper describes the controlled potential reduction of tetrahalothiophenes **1***a* and **1***b*, the trihalothiophene **2***a*, and the dihalothiophene **3***a*. The potentials used in these reductions were determined by polarography.

Experimental

Apparatus

Polarography was performed using a Princeton Applied Research Model 174-A polarograph, with its associated drop timer and cell, along with a Houston Instruments Omnigraph 2000 $x-y$ recorder. A 15 cm long, 0.1-mm internal diameter capillary was used and potential measurements were relative to a saturated calomel reference electrode. This calomel electrode was connected to the cell by means of a salt bridge containing a Luggin capillary tip packed tight with glass fibres. The salt bridge was filled with the same solvent and supporting electrolyte as used in the cell. When other metals were used as the working electrode, a thin polished wire of the metal was placed in the cell at a depth of about 1 mm into the solution.

Cyclic voltammetry was carried out using the same polarograph and a Princeton Applied Research Model 175 universal programmer. The results were viewed on a Tektronics model 564B storage polarograph and recorded by the same recorder used in the polarography. The x-axis signal from the polarograph was amplified using a Hewlett–Packard Harrison Model 6824A power supply/amplifier used in the amplifier mode.

A Wenking Model 66-TS10 potentiostat was used in the preparative electrolyses. Undivided cell electrolyses were carried out in a modified 400-mL beaker, the centre of the bottom of which was depressed about 5 mm to contain the mercury pool. The connection to the mercury pool was made using a short piece of platinum wire sealed into the bottom of the beaker. The beaker was covered with a rubber stopper containing holes for insertion of the salt bridge, stirrer, and anode wire, and for the introduction and removal of samples. When a solid metal electrode was used, a strip of it was suspended vertically on one side of the cell and the anode wire looped vertically on the other side.

In the divided cell electrolyses, the cathode compartment was the same beaker as described above. The anode compartment was a 12 cm long, 4.3-cm diameter glass tube containing a medium porosity glass sinter at the base. A rubber stopper covered the top of the cathode cell and held the anode compartment in place. The stopper also contained holes for the salt bridge and sample introduction/removal. The anode

[1]Revision received February 26, 1985.

TABLE 1. Undivided cell electrolysis of tetrabromothiophene **1***a* and tetraiodothiophene **1***b* in DMF, 0.1 *M* in TEAB

Substrate	Electrode	Potential	Additive	Product yield (%) 2	3	4
1*a*	Hg	−0.90	Phenol	46	0	0
1*a*	Hg	−0.88	DMA	70	10	0
1*a*	Hg	−0.88	1-Hexene	69	tr	0
1*a*	Hg	−1.20	Phenol	0	31	0
1*a*	Hg	−1.20	DMA	0	75	0
1*a*	Hg	−1.20	1-Heptene	10	73	0
1*a*	Hg	−1.20	1-Decene	0	82	0
1*a*	Cu	−1.30	1-Hexene	61	39	tr*
1*a*	Pb	−1.83	1-Hexene	34	47	11*
1*a*	Hg	−1.70	DMA	0	tr	60
1*a*	Cu	−1.92	1-Hexene	8	70	21*
1*a*	Pb	−2.00	1-Hexene	0	75	24*
1*b*	Hg	−1.30	Phenol	0	0	35

*Product not isolated—estimated by glc analysis.

TABLE 2. Divided cell electrolysis of bromo and iodothiophenes in DMF, 0.1 *M* in TEAB at a mercury electrode

Substrate	Potential	Product yield (%) 2	3	4
1*a*	−0.90	50	27	0
1*a**	−0.90	69	0	0
1*a*	−1.20	0	76	0
1*a*	−1.70	0	0	38
2*a*	−1.20	0	60	0
2*a*	−1.70	0	3	74
3*a*	−1.70	0	0	60
1*b*	−0.93	0	65	0
1*b*	−1.20	0	0	55

*Water used as the solvent in the anode compartment.

compartment was also covered with a rubber stopper that contained holes and stirrer and the anode wire. The catholyte was stirred using a small magnetic stirrer placed to one side of the mercury pool. In both types of electrolysis the anode consisted of a looped 1.1-mm diameter steel wire and the salt bridge and calomel electrode were similar to those used for polarography.

Analysis

The nmr spectra were recorded with a Varian T-60 nmr spectrometer and ir spectra with a Beckmann Acculab 1 or a Perkin–Elmer 735B spectrophotometer. Gas chromatography was performed using a Varian Aerograph 90-P gas chromatograph with a thermal conductivity detector and a 10 ft × 0.25 ft aluminum column containing 10% SE-30 on Chromosorb W. Microanalysis and mass spectrometry were carried out at the University of Alberta, Edmonton. Fast atom bombardment spectra were run on an AE1 MS9 mass spectrometer in the negative ionization mode, using a glycerol/sulfolane matrix or a pure sulfolane matrix chilled in liquid nitrogen. Chemical ionization spectra were run on an AE1 mass spectrometer in the positive ionization mode using ammonia reagent gas.

Solvents and supporting electrolytes

Dimethylformamide (DMF) and dimethylsulfoxide (DMSO) from BDH were dried by refluxing over calcium hydride and distilling at reduced pressure. Acetonitrile (Aldrich) was refluxed over P_2O_5 and distilled at atmospheric pressure. Tetraethylammonium bromide (Aldrich) was recrystallized from ethanol–ether and tetrabutylammonium iodide (Baker) from ethyl acetate. Both quaternary ammonium salts were dried *in vacuo* before use.

Electrolysis substrates

Tetrachlorothiophene (6), tetrabromothiophene (7), and tetraiodothiophene (8*a*) were prepared and purified by literature methods.

Electrolysis procedure

(a) *Undivided cell*

DMF (200 mL), which was 0.1 *M* in tetraethylammonium bromide (TEAB), was poured into the cell. This solution was pre-electrolyzed at the same potential to be used for the substrate, for about 10 min, in order to destroy trace amounts of electroactive substances and to measure the background current at that potential. The substrate (5 g) was added along with an additive to absorb bromine (approx. 2 equivalents) and a few drops of 40% HBr solution. The solution was electrolyzed until the current had decreased to a value close to the pre-electrolysis background current or when glc analysis showed that the substrate was no longer detectable. The reaction mixture was poured into cold water (1.5 L) and extracted with ether. After drying ($MgSO_4$), the ether was evaporated and the residue distilled, usually at reduced pressure. The products were identified by glc, nmr, and ir by comparing with literature data and (or) authentic samples. The results are summarized in Table 1.

(b) *Divided cell*

The sinter, dividing the cathode and anode compartments, was first impregnated with a gel of methyl cellulose. Methyl cellulose (5 g) was added to hot DMF (25 mL), which was 0.1 *M* in TEAB. The hot viscous solution was drawn through the sinter using a vacuum and then forced back using air pressure. This procedure was repeated a few times in order to remove air bubbles from the sinter. After cooling, the excess gel was scraped off the sinter.

DMF (140 mL), which was 0.1 *M* in TEAB, was introduced into the cathode compartment. Generally, 60 mL of the same solution was introduced into the anode compartment, although in one electrolysis an aqueous solution of the electrolyte (0.1 *M*) was used.[2] A slight excess of hydrazine was dissolved in the anode solution. After a pre-electrolysis, the substrate (5 g) was added to the catholyte together with a few drops of 40% HBr and the solution electrolyzed at constant potential. It was noted that the anode solution became acidic during the course of the electrolysis and was neutralized occasionally by the addition of KOH. When the electrolysis was judged over (glc analysis and (or) current monitoring), the cathode solution was worked up in the same manner as the undivided cell electrolysis. The results are given in Table 2.

3,4,5-Tribromo-2-thiophene carboxylic acid

A divided cell electrolysis was carried out as above, but in the presence of a stream of CO_2. The product was poured into water, acidified, and extracted with ether. The ether solution was extracted with aqueous NaOH and the aqueous layer acidified with HCl, giving a white precipitate of 3,4,5-tribromo-2-thiophene carboxylic acid (1.1 g, 35%), mp 258–260°C, (lit. (8*b*) mp 258–259°C; ir: 1700 (s, C═O *str*) cm^{-1}.

Di-3,4,5-tribromo-2-thienylmercury

A divided cell electrolysis of tetrabromothiophene (5 g) was carried out at −0.95 V without the addition of acid to the catholyte solution. After a few minutes the current dropped to a background level and the electrolysis was allowed to run for 3 days. On pouring the product into water a cream coloured solid, which was insoluble in ether, separated. Filtration, followed by washing with ethanol and ether, gave the crude product (1.0 g). Extraction of the filtrate with the ether gave a solid which was shown by glc to be mostly the starting material. The crude product was crystallized from DMF/ethanol giving a cream powdery solid (0.6 g, 11%), mp 295–301°C (lit. (8*c*) mp 291°C); ir (KBr):

[2]In one electrolysis water was used in the anode compartment.

TABLE 3. Polarographic half-wave potentials ($E_{\frac{1}{2}}$ values) of tetrahalothiophenes in different solvents 0.1 *M* in TEAB

Substrate	Solvents	$E_{\frac{1}{2}}$ of wave (V)			
		1	2	3	4
Tetrachlorothiophene	DMF	−1.78	−1.98	−2.28	−2.49
	DMSO	−1.69	−2.01	−2.34	
	CH_3CN	−1.74	−1.95	−2.24	
Tetrabromothiophene	DMF	−0.90	−1.22	−1.67	−2.00
	DMSO	−0.84	−1.11	−1.74	−2.00
	CH_3CN	−1.16	−1.23	−1.66	−1.98
Tetraiodothiophene	DMF	−0.67	−0.93	−1.20	−1.45
	DMSO	−0.55	−0.78	−1.22	−1.45
	CH_3CN	Insoluble			

TABLE 4. Effect of cathode material on the half-wave potentials of tetrabromothiophene in DMF, 0.1 *M* in TBAP

Electrode	$E_{\frac{1}{2}}$ for wave (V)			
	1	2	3	4
Hg	−0.84	−1.20	−1.92	−2.18
Pt	−1.50	−1.55	−1.86	
Cu	−1.83*		−1.92	−2.14
Pb	−1.83	−2.00	−2.20	−2.32
Steel	−1.90*			
Graphite	−1.30*		−2.10	

*Appears to be a combination of two waves.

1460, 1380, 1260, 1220, 960, 720, 530, 490 cm^{-1}; ^1H nmr, no signals; mass spectrum (FAB) *m/e*: 967, 921, 840 (M^+, base peak), 761 (M − Br), 681 (M − 2Br), 583, 319; mass spectrum (chem. ionization): 840 (M^+), 602, 322, 240, 161. *Anal.* calcd. for $C_8Br_6HgS_2$: C 11.43, Br 57.06, S 7.63; found: C 11.64, Br 55.10, S 7.31, H 0.14.

Results and discussion

Polarographic studies were carried out on the tetrahalothiophenes in DMF, DMSO, and acetonitrile, using TEAB as supporting electrolyte. It was noted that the polarograms of each substrate were virtually identical in the three solvents and only small differences were observed in the half-wave potentials ($E_{\frac{1}{2}}$ values) and diffusion currents (i_d). The $E_{\frac{1}{2}}$ values are listed in Table 3.

In agreement with previous polarographic studies (3, 4), both tetrabromo- **1***a* and tetraiodothiophene **1***b* showed four waves, corresponding to the successive reduction of each halogen in the molecule. Tetrachlorothiophene also showed four waves in DMF but the highest potential waves in DMSO and CH_3CN were masked by solvent decomposition. As expected, the ease of reduction for the tetrahalothiophenes was in the order I > Br > Cl.

With DMF as solvent, the effect of the presence of water and aqueous acid or base on the half-wave potentials was investigated. Up to the concentration at which their reduction waves swamped the polarograms, water, acid, and base had little or no effect on the $E_{\frac{1}{2}}$ values. It was concluded that the reduction potentials were not pH dependent.

The effect of the electrode material on the reduction potentials in DMF was investigated, with a view to the use of solid electrodes in preparative electroreductions. The results are listed in Table 4. Using solid electrodes, it was generally not found possible to obtain all four waves. It was also noted that the reduction potentials were higher and closer together than those obtained with mercury. It was confirmed later by preparative electrolyses that selective reductions were more difficult to achieve using copper and lead cathodes than with a mercury cathode.

Polarographic (3) and cyclovoltammetric studies (5) on bromothiophenes indicate that they reduce by an irreversible mechanism in which two electrons are required for reduction of each halogen atom. The resulting anion is then protonated by the autoprotolysis of DMF and (or) by water. The source of protons in aqueous media is water and it has been reported (9) that, even in reductions in DMF, water is the usual proton source since the removal of small amounts of water from the solvent using conventional drying agents is difficult.

$$RBr \xrightarrow{2e^-} R^- + Br^-$$

$$R^- \xrightarrow{SH \text{ or } H_2O} RH$$

The electroreductions of **1***a* (3) and **1***b* (4) have also been reported to be diffusion controlled.

The irreversibility of the reductions was confirmed by cyclic voltammetry of the substrates in DMF, which was 0.1 *M* in tetrabutylammonium perchlorate. The cathodic peaks in the cyclic voltammograms obtained correspond to the polarographic reduction waves of these compounds and there were no appreciable oxidation peaks associated with any of these reduction waves. Although some small anodic peaks were found in the −0.8 to +0.5-V range, these occurred in all the voltammograms and were attributed to the oxidation of the solvent decomposition products created by the high potentials used in the cathodic scans.

In our initial preparative electrolyses, **1***a* was electrolyzed in an undivided cell at a mercury electrode, using DMF as solvent and TEAB as supporting electrolyte at a potential corresponding to the $E_{\frac{1}{2}}$ value of the appropriate polarographic wave. It was found, however, that the current increased until the current limit of the potentiostat (1 amp) was reached. At this limit the cathode potential would start to decrease, preventing further reduction from occurring. Since it was believed that this problem was caused by the generation of bromine, which may react with DMF (10) or brominate the reduced bromothiophene, the effect of addition of various compounds which might trap the bromine was investigated. The most effective of these additives were found to be alkenes (such as 1-hexene, 1-heptene, and 1-decene), dimethylaniline (DMA), and phenol. It was also found necessary to add a small amount of mineral acid (HBr) in order for the electrolysis to proceed normally. In the absence of acid, it was generally observed that the currents, initially about 100 mA, decreased within minutes to a background level of about 5 mA. Acidification of the solution caused the current to increase to approximately its initial value. The addition of weaker proton donors such as acetic acid, ethanol, and water had little or no effect on the current when at the background level.

The results of these electrolyses are summarized in Table 1. In some cases good yields of the desired reduction products were obtained, but in others problems arose because of the difficulty in separating the additive or brominated additive from the product by distillation.

Preparative electrolyses were also performed using copper and lead cathodes at the potentials determined by polarography at these electrodes. The reaction products and yields are also given in Table 1. The reductions at these electrodes were not as selective as those at the mercury electrode and mixtures of reduction products were obtained.

Constant potential electrolysis using a divided cell was found to give generally good yields of the desired products and avoided the necessity for using additives to remove the bromine. Initially, satisfactory results were not obtained due to diffusion of the substrate through the sinter to the anode compartment. This problem was overcome by impregnating the sinter with a gel of methyl cellulose. The cathode compartment, in these electrolyses, contained a 0.1 *M* solution of TEAB in DMF to which the substrate was added after a short pre-electrolysis. In most experiments the same solution was used in the anode compartment, together with hydrazine as an anodic depolarizer. One preparative electrolysis was carried out using water as the anode cell solvent containing 0.1 *M* TEAB, and gave satisfactory results.

As with the undivided cell electrolysis, it was found necessary to add a small amount of acid to prevent the current dropping rapidly in the initial stages of the electrolysis. After some time the acid was depleted, causing the current to decease again even through the catholyte contained much unreacted substrate. The addition of more acid at this point restored the current to its normal value. At the end of the electrolysis, glc analysis showed that the product was present only in the catholyte. No trace of the substrate or product was found in the anolyte.

The results of the divided cell electrolyses are given in Table 2. It was observed that the electrolysis of tetrabromothiophene **1***a* at its lowest reduction potential (−0.90 V) results in the formation of **2***a*. Reduction of both **1***a* and **2***a* at the second potential (−1.20 V) yields **3***a*. Reduction of **1***a*, **2***a*, and **3***a* at the third potential (−1.70 V) yields **4***a*. Similarly, tetraiodothiophene **1***b* was reduced to **3***b* at −0.93 V and to **4***b* at −1.20 V. These results support the interpretation made by previous workers (3, 4) of their polarographic data and clearly show that each polarographic wave corresponds to the reduction of one halogen atom, and that the α-halogens of tetrahalothiophenes are reduced at lower potentials than the β-halogens.

Preliminary work on the preparative electroreductions of tetrachlorothiophene has shown that selective reductions are more difficult to achieve. It should also be noted that the pure starting material is more difficult to prepare than the tetrabromo and tetraiodo analogues.

When the electrolysis of **1***a* was allowed to run for a few days without strong acid in the catholyte solution, an organo-mercury compound identified as di-3,4,5-tribromo-2-thienylmercury, **5**, was obtained in low yield together with some unreacted starting material. This was in contrast to the stepwise replacement of bromine by hydrogen observed in the presence of acid.

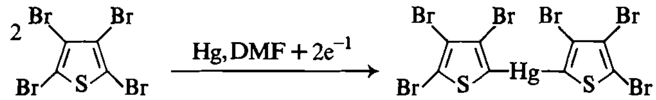

1*a* **5**

The organo-mercury compound **5** proved to be difficult to purify because of its low solubility in organic solvents. Its ir spectrum was rather similar to those of **1***a* and **2***a*, and polarography yielded three waves at essentially the same potentials as **2***a*. However, the substance had a much higher melting point than either **1***a* or **2***a* and mass spectrometry (chemical ionization and fast ion bambardment) showed a large multiple peak centred at 840 amu, which would correspond to the mass of the molecular ion of **5**. Some peaks at even higher mass numbers in the FAB spectrum indicated the presence of impurities, and multiple isotope peaks were also observed at 761 (M − Br) and 583 (M − 2Br). Computer generated isotope patterns for the peaks at 840, 761, and 583, assuming structure **5**, were in close agreement with those observed in the mass spectra. The microanalytical results for determination of C, Br, and S in the compound were consistent with structure **5** and slight differences from the calculated values could be attributed to small amounts of impurity.

It would appear that the organo-mercury compound is formed via chemisorbed radicals on the cathode surface.

$$RX + e^{-1} \rightarrow R^0 + X^-$$

$$R^0 + Hg \rightarrow RHg^0\ (\text{ads})$$

$$2RHg\ (\text{ads}) \rightarrow R_2Hg + Hg$$

In our preparative electrolyses it was observed that, in the absence of added mineral acid, the current would fall within minutes to a background level. A similar observation was made by Brown and Taylor (11) in the synthesis of mercury dialkyls from alkyl halides. These authors attributed this behaviour to the intermediate formation of adsorbed radicals, which are then converted to the product on the surface of the mercury.

1. G. GRONOWITZ and T. RAZNIKIEWICZ. Org. Synth. Coll. Vol. 5, 149 (1973).
2. D. PLETCHER and M. RAZAQ. J. Appl. Electrochem. **10**, 575 (1980).
3. S. G. MAIRANOWSKII, N. V. BARASHKOVA, and Y. B. VOL'KENSHTEIN. Electrokhimiya, **1**, 72 (1965).
4. L. W. BROWN and E. KRUPSKI. J. Pharm. Sci. **52**, 55 (1965).
5. M. FELDMANN and E. KOBERSTEIN. Chem.-Tech. (Heidelberg), **6**, 517 (1977).
6. H. L. COONRADT, H. D. HARTOUGH, and G. C. JOHNSON. J. Am. Chem. Soc. **70**, 2564 (1948).
7. S.-O. LAWESSON. Ark. Kemi, **11**, 373 (1957).
8. H. D. HARTOUGH. Thiophene and its derivatives. Interscience Publishers, New York. 501 1952. (*a*) p. 501; (*b*) p. 379; (*c*) p. 453.
9. R. A. DE LA TORRE and J. W. SEASE. J. Am. Chem. Soc. **101**, 1687 (1979).
10. H. A. TAYIM and M. ABSI. Chem. Ind. (London), 347 (1973).
11. O. R. BROWN and K. TAYLOR. J. Electroanal. Chem. Interfacial Electrochem. **50**, 211 (1974).

Reversible ring opening in the hydrolysis of spiro ortho esters

ROBERT A. MCCLELLAND

Department of Chemistry and Scarborough College, University of Toronto, Scarborough, Ont., Canada M1C 1A4

AND

CLAUDE MOREAU

Laboratoire de Chimie Organique Physique Appliquée, École Nationale Supérieure de Chimie, 8 Rue de l'École Normale, 34075 Montpellier, Cédex, France

Received February 8, 1985

ROBERT A. MCCLELLAND and CLAUDE MOREAU. Can. J. Chem. **63**, 2673 (1985).

Hydrolysis kinetics are reported for four spiro ortho esters: 3,4-dihydro-6-methoxy-1*H*-2-benzopyran-1-spiro-2′-1′,3′-dioxolane (**13**), its 1′,3′-dioxane analog (**14**), and the 6-unsubstituted versions of each (**11** and **12**). For comparison, also included are the diethoxy analogs: 1,1-diethoxy-3,4-dihydro-6-methoxy-1*H*-2-benzopyran (**10**) and the 6-unsubstituted compound (**9**). Product analysis implicates an initial opening of the dioxolane or dioxane ring in the spiro ortho esters, as expected on the basis of stereoelectronic considerations. The intermediate dialkoxycarbocations can be observed in HCl solutions. A detailed analysis has been carried out for the 6-methoxy systems to provide the rate constants k_1, the second-order rate constant for H^+-catalyzed formation of the cation from the ortho ester, k_2, the first-order rate constant for water addition to the cation, and k_{-1}, the first-order rate constant for ring closing of the cation to reform the ortho ester. The two spiro ortho esters are shown in this analysis to undergo reversible ring opening in their hydrolysis, in that values of k_{-1} are greater than k_2. The differences, however, are not large, k_{-1}/k_2 being 1.2 (dioxolane, **13**) and 3.8 (dioxane, **14**). Comparison with the diethoxy ortho ester also reveals that the ring opening process (k_1 rate constants) is inherently more difficult with the dioxolane, although not with the dioxane. An argument involving lone pair orientation is advanced to explain this.

ROBERT A. MCCLELLAND et CLAUDE MOREAU. Can. J. Chem. **63**, 2673 (1985).

On rapporte les données cinétiques relatives à l'hydrolyse que quatre spiro ortho esters: le dihydro-3,4 méthoxy-6 1*H*-benzo-2 pyrannespiro-1 dioxolane-2′-1′,3′ (**13**), son analogue dioxanne-1′,3′ (**14**) ainsi que les homologues non substitués en position 6 (**11** et **12**). Pour fins de comparaisons, on a également inclus les analogues diéthoxylés: le diéthoxy-1,1 dihydro-3,4 méthoxy-6 1*H*-benzo-2 pyranne (**10**) et le composé qui n'est pas substitué en position 6 (**9**). L'analyse des produits implique que l'ouverture initiale se fait au niveau des cycles dioxolane ou dioxanne des ortho esters spiro et ce conformément à ce que laissent prévoir les facteurs stéréoélectroniques. On peut observer les dialkoxycarbocations intermédiaires dans des solutions de HCl. On a effectué une analyse détaillée des systèmes méthoxy-6 dans le but d'obtenir: (a) les constantes de vitesse k_1, (b) la constante de vitesse d'ordre deux, k_2, relative à la formation, catalysée par H^+, du cation à partir de l'ortho ester, (c) la constante de vitesse d'ordre un relative à l'addition d'eau sur le cation et (d) k_{-1}, la constante de vitesse d'ordre un pour la cyclisation du cation qui ramène à l'ortho ester. Grâce à cette analyse on démontre que, au cours de leur hydrolyse, les deux spiro ortho esters subissent une ouverture réversible de cycle qui se traduit par le fait que la valeur de k_{-1} est supérieure à k_2. Cependant, la différence n'est pas très grande; k_{-1}/k_2 est égal à 1,2 pour le dioxolane **13** et à 3,8 pour le dioxanne **14**. Une comparaison de ces résultats avec ceux obtenus avec les diéthoxy ortho esters révèle également que l'ouverture de cycle (constante de vitesse k_1) est plus difficile dans le cas du dioxolane même si ce n'est pas le cas avec le dioxanne. On fait intervenir l'orientation du doublet libre pour expliquer ces résultats.

[Traduit par le journal]

A three-stage reaction mechanism is now commonly accepted for the hydrolysis of acetals and ortho esters (1–3): (*i*) acid-catalyzed formation of an oxocarbocation, (*ii*) hydration of this cation to produce a hemiacetal or hemiorthoester, and (*iii*) decomposition of this intermediate to products. Under the conditions normally employed for kinetic studies, namely dilute substrate in aqueous solvent, the first stage is essentially irreversible. The small amount of alcohol which is being released during the hydrolysis cannot compete with the solvent, so that the oxocarbocation once formed must go on to products. With cyclic systems where the first stage involves ring opening, reversibility is, however, a factor. Now the reverse reaction is intramolecular, and in principle it can compete even when there is a large excess of water. Cyclic acetals do undergo hydrolysis at a slower rate than their acyclic analogs, and this observation has been explained by reversibility in the cyclic cases (4). Reversibility, however, is difficult to demonstrate

[1] 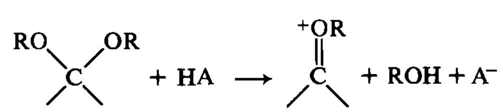

[2] 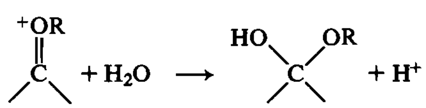

[3] 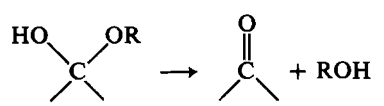

[4] 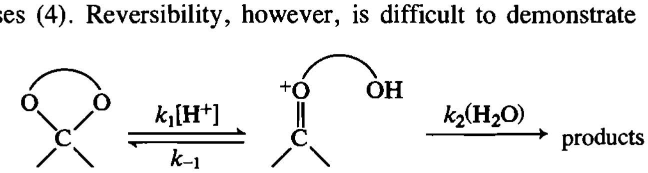

unambiguously, since the observed kinetic expression is the same regardless of the relative magnitudes of k_{-1} and k_2 (eq. [5]). Reversibility has been demonstrated unequivocally with

$$[5] \quad \text{Rate} = k_H(\text{obs})\,[\text{acetal}]\,[H^+] = \frac{k_1 k_2}{k_{-1} + k_2}\,[\text{acetal}]\,[H^+]$$

two cyclic acetals—with derivatives of *exo,exo*-norbornane-2,3-diol (**1**) where epimerization at the pro-acyl carbon is observed during hydrolysis (5), and with **2** and **3** which are

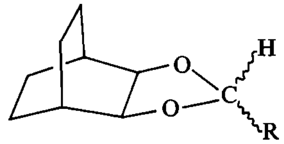

1

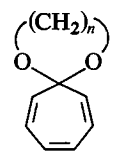

2 $n = 2$
3 $n = 3$

derivatives of tropone (6). With the latter acetals the relatively stable oxytropylium ion intermediates are observed during the hydrolysis. The kinetic behavior therefore becomes more complex than that described in eq. [5], and a kinetic analysis can furnish the exact values of the three rate constants k_1, k_{-1}, and k_2. A similar approach (7, 8) has been employed at the ortho level with trioxaadamantanes **4**, which are highly reversible in their initial ring opening (9). Results with the bicyclic ortho esters **5** (10) and **6** (11), on the other hand, are best interpreted

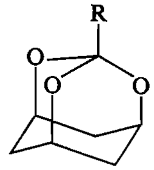

4

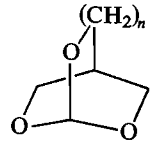

5 $n = 0$
6 $n = 1$

in terms of irreversibility. In the trioxaadamantane system the departing hydroxyl group remains directly in the face of the oxocarbocation. With **5** and **6** it appears as if strain energy in the ortho ester retards the ring closing. The ortho esters **7** (2, 11–13), **8** (14), **9** (15), and **10** (15) have a choice of endocyclic

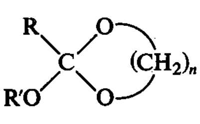

7 $n = 2$ or 3

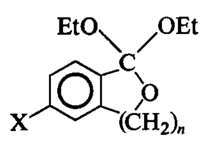

8 $n = 1$, X = H
9 $n = 2$, X = H
10 $n = 2$, X = OMe

or exocyclic bond cleavage for their oxocarbocation-forming stage, and show a strong preference for the latter. In the ortho esters **7** where the oxocarbocation can be stabilized by an adjacent phenyl (R = Ar) this tendency can be explained in terms of cation stability (16–18). This preference is also seen with **7**, R = alkyl (13, 18), where the cations derived from the two initial cleavages are expected to have similar stability. This suggests that there is an inherent difficulty in the endocyclic process.

In this paper we address the question of reversibility with the spiro ortho esters **11–14**. These combine features of both **7** and **9** or **10**, with the obvious difference that a ring must open in the first stage of the hydrolysis. We anticipated on the basis of previous results with **8** (14) that the oxocarbocation intermediate would be observed as a transient species, and that this would permit a detailed kinetic analysis similar to that carried out with the tropone acetals (6). This indeed proved to be the case.

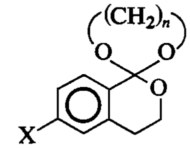

11 $n = 2$, X = H
12 $n = 3$, X = H
13 $n = 2$, X = OMe
14 $n = 3$, X = OMe

Experimental

Materials

1,1-Diethoxy-3,4-dihydro-1*H*-2-benzopyran (**9**) and 1,1-diethoxy-3,4-dihydro-6-methoxy-1*H*-2-benzopyran (**10**) were from a previous study (15). Spiro ortho esters were prepared from these by ortho ester interchange. The diethoxy ortho ester and appropriate diol were mixed in equal amounts and a crystal of 4-toluenesulfonic acid added. The flask was evacuated to 1 Torr (133.3 Pa) at room temperature to remove the ethanol product of the exchange. After complete removal of the ethanol, a small amount of triethylamine was added to neutralize the acid. The ortho ester product was then obtained by distillation under reduced pressure.

*6-Methoxy-3,4-dihydro-1*H*-2-benzopyran-1-spiro-2′-1′,3′-dioxolane* (**13**) had bp 90°C, 0.1 Torr, turning to a waxy solid on standing; ^{1}H nmr ($CDCl_3$, 200 MHz), δ: 6.97 (1H, d, J = 9 Hz, H8), 6.79 (1H, dd, J = 9 Hz and J = 3 Hz, H7), 6.66 (1H, d, J = 3 Hz, H5), 4.18 (4H, bs, H4′ and H5′), 4.07 (2H, t, J = 6 Hz, H3), 3.81 (3H, s, 6-OCH_3), 2.82 (2H, t, J = 6 Hz, H4). *Anal.* calcd. for $C_{12}H_{14}O_4$: C 64.85, H 6.35; found: C 65.03, H 6.42.

*6-Methoxy-3,4-dihydro-1*H*-2-benzopyran-1-spiro-2′-1′,3′-dioxane* (**14**) had bp 85°C, 0.05 Torr; ^{1}H nmr ($CDCl_3$, 200 MHz), δ: 6.95 (1H, d, J = 9 Hz, H8), 6.80 (1H, dd, J = 9 Hz and J = 3 Hz, H7), 6.64 (1H, d, J = 3 Hz, H5), 4.30 (2H, ddd, J = 16 Hz, 10 Hz, and 3 Hz, H4a′ and H6a′), 4.06 (2H, t, J = 6 Hz, H3), 3.81 (3H, s, 6-OCH_3), 3.78 (2H, ddd, J = 10 Hz, 5 Hz, and 1.5 Hz, H4b′ and H6b′), 2.81 (2H, t, J = 6 Hz, H4), 2.16 (1H, dtt, J = 13 Hz, 16 Hz, and 10 Hz, H5a′), 1.48 (1H, dtt, J = 13 Hz, 3 Hz, and 1.5 Hz, H5b′). *Anal.* calcd. for $C_{13}H_{16}O_4$: C 66.09, H 6.83; found: C 66.21, H 6.94.

*3,4-Dihydro-1*H*-2-benzopyran-1-spiro-2′-1′,3′-dioxolane* (**11**) had bp 70°C, 1 Torr, turning to a waxy solid on standing; ^{1}H nmr, δ: 7.5–7.2 (4H multiplet, H5, H6, H7, and H8), H3, H4, H4′ and H5′ as in **13**. *Anal.* calcd. for $C_{11}H_{12}O_3$: C 68.74, H 6.29; found: C 68.57, H 6.25.

*3,4-Dihydro-1*H*-2-benzopyran-1-spiro-2′-1′,3′-dioxane* (**12**) had bp 90°C, 1 Torr; ^{1}H nmr, δ: 7.5–7.2 (4H multiplet, H5, H6, H7, and H8), H3, H4, H4a′, H4b′, H5a′, H5b′, H6a′, H6b′ as in **14**. *Anal.* calcd. for $C_{12}H_{14}O_3$: C 69.89, H 6.84; found: C 70.03, H 6.97.

Kinetic methods

Conventional uv kinetic measurements for the hydrolysis in solutions with pH > 5 were carried out on a Unicam SP 1800 spectrophotometer. A solution of approximately 0.1 *M* concentration of the ortho ester in dry acetonitrile was prepared; 2–3 μL of this solution were added directly to the uv cuvette containing 2–3 mL of the appropriate aqueous buffer. This cuvette and solution had been previously thermostatted at 25.0°C in the uv instrument. A wavelength of 230 nm was employed for **9**, **11**, and **12** and a wavelength of 255 nm for **10**, **13**, and **14**. Kinetic plots of ln ($A_\infty - A$) versus time were excellently linear and the observed first-order rate constants were calculated as their slopes.

Stopped-flow kinetic measurements for the hydrolysis in solutions with pH < 3 were carried out with a Durrum–Gibson stopped-flow spectrophotometer thermostatted at 25.0°C. The ortho ester was dissolved in 0.002 *M* NaOH to give solutions of approximately 10^{-4} *M* and this solution mixed with excess HCl solutions. A wavelength of 300 nm (for **10**, **13**, and **14**) was chosen. The photomultiplier output of this instrument was digitized to provide 118 absorbance readings for each kinetic run. The absorbance–time values were transferred to a

[6]

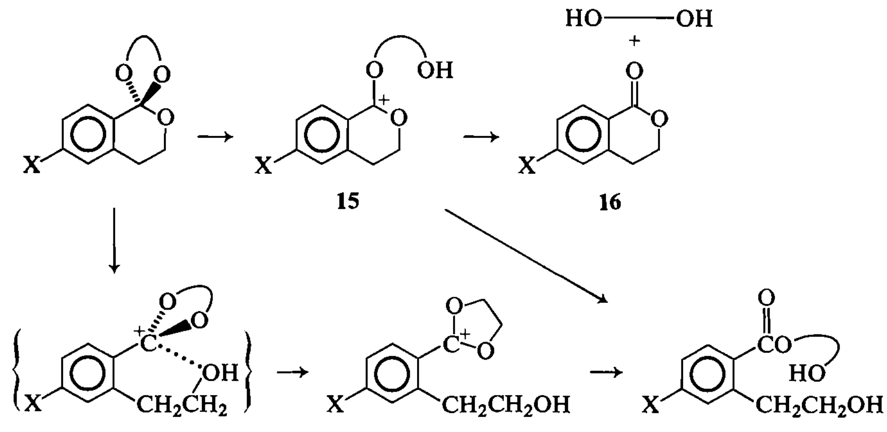

15 16 17 18 19

Tektronix 4051 microcomputer for the analysis described in the next section.

Product analysis

The pure ortho esters were injected via syringe into 0.01 M DCl in D_2O to give a solution of 0.01 M in ortho ester. The ^1H nmr spectra of these solutions were recorded on a 200-Mz nmr spectrophotometer.

Results and discussion

As summarized in eq. [6] there are two possible initial modes of cleavage producing two different dialkoxycarbocations **15** and **18**, and there are two possible types of products, the lactone **16**, which will be accompanied by diol, and the benzoate ester **19**. Products were determined in 0.01 M DCl by directly recording the nmr spectra of hydrolyzed solutions. For all four ortho esters a predominance (85–95%) of lactone plus diol is observed. The ester **19** can cyclize to the lactone but this process is slow compared to the ortho ester hydrolysis (14, 15). The nmr spectra were recorded sufficiently quickly to provide the products of kinetic control.

The lactone plus diol products obviously must arise from the cation **15**. We feel that the small amount of ester also comes from this cation. Under similar conditions the ortho ester **10** gives 85% lactone (15). This ortho ester undergoes only cleavage of the exocyclic ethoxy group (15) to produce a cation analogous to **15**. Production of the cation **15** is also expected on stereoelectronic grounds. As shown in the transition state structure **17**, the alternative cleavage to the cation **18** must proceed with the phenyl ring at right angles to the developing π system of the dialkoxycarbocation. Thus no initial stabilization associated with the aromatic ring is possible. That this conjugation is important can be seen in the faster rate of hydrolysis of 2-phenyl-2-methoxy-1,3-dioxolane compared to that of trimethyl orthobenzoate (16). Kresge and co-workers have explained this difference by a steric effect associated with the latter which prevents the phenyl ring from becoming fully conjugated with the cation center (16–18). The argument with the present system is essentially an extension of Deslongchamps antiperiplanar lone pair hypothesis (19, 20). For an efficient reaction, not only must the two remaining oxygen atoms have lone pairs antiperiplanar to the bond being broken, but also the aromatic ring should be set up with the correct orientation. The reaction forming **15** satisfies both requirements; the reaction forming **18** fails on the latter.

First-order rate constants were measured for the spiro ortho esters as well as for their diethoxy analogs in phosphate buffers of pH 5.5–7.5, following the appearance of the lactone plus benzoate ester products in the uv spectrum. As expected, these observed rate coefficients, after correction for a small contribution from the buffer by extrapolation to zero buffer concentration, are linear in H^+ concentration. Values of the H^+ catalytic coefficients are listed as k_H(obs) in Table 1. The spiro ortho esters do hydrolyze significantly more slowly than their diethoxy analogs, the difference being a factor of 60–80 for the dioxolane systems and 6 for the dioxanes.

In HCl solutions kinetic experiments were conducted using stopped-flow spectroscopy, and with all six ortho esters a transient absorbance was observed attributable to the oxocarbocation intermediate. For detailed analysis we have concentrated on the 6-methoxy compounds **10**, **13**, and **14**, where the cations are longer lived. The intermediates with these systems have uv absorbance with λ_{max} at 300 nm typical of p-methoxyphenyl dialkoxycarbocations (2, 21, 22). As shown in Fig. 1, the monitoring of this wavelength produces a rapid rise and fall in absorbance as the cation is formed and subsequently decays. The absorbance in fact starts at zero and finishes at zero since neither the ortho ester nor the product have significant extinction coefficients at this wavelength. It can also be seen from Fig. 1 that the maximum amount of the cation which is produced increases with increasing acid concentration.

For the spiro ortho esters the kinetic system has the form:

[7]

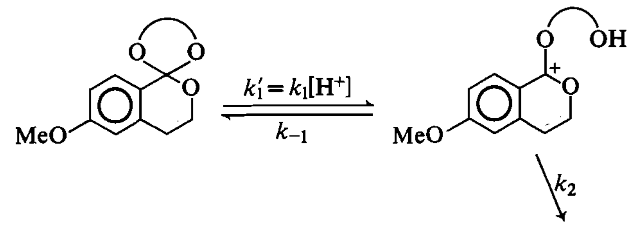

products

where k_1' is the pseudo-first-order rate constant for the ring-opening reaction at constant pH. The fraction of cation formed as a function of time is given by eq. [8] (23),

$$[8] \quad \frac{[\text{Cation}]}{A_0} = C(e^{-\lambda_2 t} - e^{-\lambda_1 t})$$

where A_0 = initial concentration of ortho ester (or total concentration of ortho ester, cation, and product), $C = k_1'/(\lambda_1 - \lambda_2)$, and $\lambda_1, \lambda_2 = (1/2)\,((k_1' + k_2 + k_{-1}) \pm ((k_1' + k_2 + k_{-1})^2 - 4k_1'k_2)^{1/2})$. In terms of absorbance this equation can be rewritten

TABLE 1. Rate constants[a] for the hydrolysis of spiro ortho esters and spiro acetals

Compound	k_H(obs), M^{-1} s^{-1}	k_1, M^{-1} s^{-1}	k_{-1}, s^{-1}	k_2, s^{-1}
9	8.4×10^3			
	(7.7×10^3)[b]			
11	1.5×10^2			
12	1.5×10^3			
10	2.9×10^4	3.4×10^4	—	23
	(1.44×10^4)[b]			
13	3.5×10^2	6.6×10^2	85	65
14	5.0×10^3	2.6×10^4	120	32
Tropone diethyl acetal[c]	2.2×10^5	2.2×10^5	—	0.017
2[c]	3.9×10^3	2.1×10^4	0.13	0.030
3[c]	6.8×10^3	1.8×10^4	0.041	0.025

[a] 25°C, ionic strength = 0.1 for **9**, **11**, **12**, tropone diethyl ketal, **2**, **3** and 1.0 for **10**, **13**, **14**.
[b] Reference 15.
[c] Reference 6.

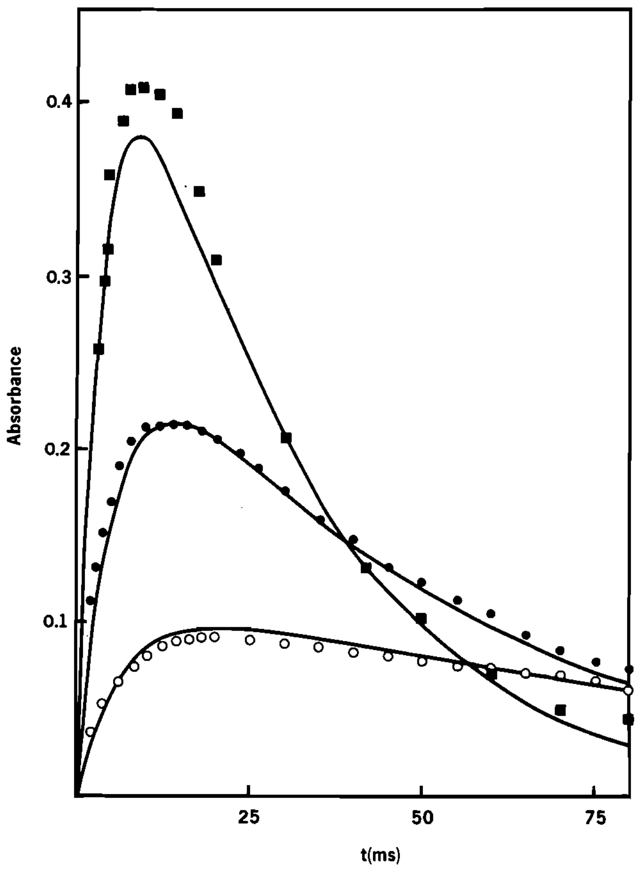

FIG. 1. Absorbance at 300 nm for the ortho ester **13** (3.5×10^{-5} M) in 0.028 M HCl (○), 0.078 M HCl (●), and 0.198 M HCl (■). The points are experimental. The curves are calculated using eq. [9] and the values of k_1, k_{-1}, and k_2 listed in Table 1. The curves have been normalized by having the maximum observed absorbance in 0.078 M HCl coincide with the calculated maximum in that acid (see text for explanation).

as follows,

$$[9] \quad \text{Absorbance} = \frac{A_0C}{\epsilon l}(e^{-\lambda_2 t} - e^{-\lambda_1 t})$$

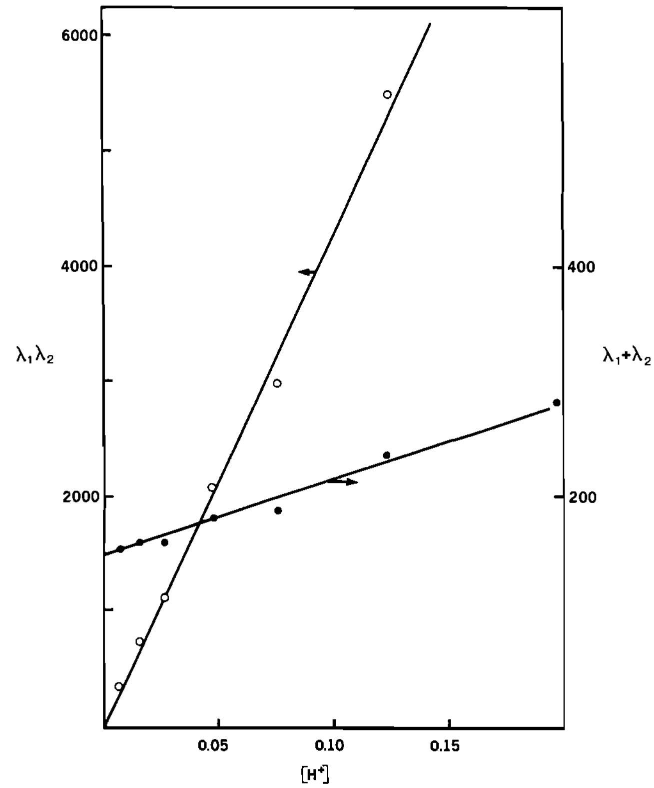

FIG. 2. Plots of the product of the relaxation coefficients $\lambda_1\lambda_2$ (○) and the sum $\lambda_1 + \lambda_2$ (●) obtained for the ortho ester **13** as a function of H^+ concentration.

where ϵ = extinction coefficient of the cation, and l = pathlength of the uv cuvette (2 cm). The stopped-flow instrument is linked to a digitization device which provides 118 absorbance–time readings per kinetic run. Using nonlinear least squares we have fit these data to eq. [9] to obtain values of λ_1 and λ_2 as a function of acidity. These are the relaxation constants (23) for this kinetic system (although this is not a relaxation process since amplitudes are large). A third parameter, $A_0C/\epsilon l$ is also provided by the curve fitting, but we have ignored these values in further calculations since the value of ϵ is unknown.

As a function of H^+ concentration the following relationships can be written for λ_1, λ_2

$$[10] \quad \lambda_1 + \lambda_2 = k_1[H^+] + (k_{-1} + k_2)$$

$$[11] \quad \lambda_1\lambda_2 = k_1k_2[H^+]$$

Both the quantities $\lambda_1 + \lambda_2$ and $\lambda_1\lambda_2$ are predicted to be linear in H^+ concentration, the latter with a zero intercept. Using data obtained with the ortho ester **13**, such plots are shown in Fig. 2, and the predicted forms are obviously obtained. The slopes and intercepts of these plots then provide the rate constants k_1, k_{-1}, and k_2. We illustrate these calculations in detail for **13** to indicate the magnitudes of the errors. The slope of the $\lambda_1 + \lambda_2$ plot gives k_1 directly, a value of $(6.6 \pm 0.6) \times 10^2 M^{-1} s^{-1}$. The slope of the $\lambda_1\lambda_2$ plot is equal to $(4.3 \pm 0.3) \times 10^4$, regardless of whether a zero intercept is enforced. This slope is equal to k_1k_2, so that by using the above value of k_1, k_2 can be calculated as 65 ± 10. The intercept in the $\lambda_1 + \lambda_2$ plot is 150 ± 10 and this is equal to $k_{-1} + k_2$. Since k_2 is now known, the value of k_{-1} can be calculated as 85 ± 14. A summary of these values along with those obtained for **14** is given in Table 1.

This analysis indicates that with both spiro ortho esters ring opening is reversible in that k_{-1} is greater than k_2. Evidence of the consistency in the analysis can be seen in Fig. 1 from the reasonable agreement between the experimental data and curves calculated on the basis of eq. [9] and the derived rate constants. One additional parameter is required in this calculation, the extinction coefficient of the cation. This has been calculated as 1.4×10^4 by forcing the maximum calculated absorbance in 0.078 M HCl to coincide with the maximum observed absorbance in that acid. All the other points in that particular curve and the two other curves then follow automatically. A second point of agreement can be seen between values of $k_1k_2/(k_{-1} + k_2)$ calculated on the basis of the HCl data and the experimental values of k_H(obs) determined at higher pH: 2.9×10^2 (calcd.) versus 3.5×10^2 for **13** and 5.5×10^3 (calcd.) versus 5.0×10^3 for **14**.

With the diethoxy ortho ester **10**, the k_{-1} process of eq. [7] can be ignored. A rise and fall in absorbance at 300 nm is observed. The rising portion of the curve can be analyzed to give a value of k_1 of 3.4×10^4 M^{-1} s^{-1}, in reasonable agreement with the k_H(obs) of 2.9×10^4 M^{-1} s^{-1} measured in phosphate buffer. The decay portion of the curves gives a value of k_2 of 23 s^{-1} for cation hydrolysis. (It can be noted that in acids more concentrated than 0.02 M HCl only the decay curve is seen, since cation formation is complete within the dead-time of the stopped-flow instrument.)

A trend can be noted in the k_2 values, namely $k_2(OCH_2CH_3) < k_2(OCH_2CH_2CH_2OH) < k_2(OCH_2CH_2OH)$. This same trend was previously observed with the tropone systems (see also Table 1). It can be explained by an electron-withdrawing inductive effect associated with the OH groups in the ring-opened cations. This destabilizes these cations, making them more reactive towards hydrolysis. The effect is more important with the ethylene compound where the hydroxyl group is closer to the cationic center, so that this is the most reactive.

With the diethoxy compound **10** as model, the decreased reactivity of the cyclic systems observed at higher pH (k_H(obs) values) can be dissected into a reversibility factor and an inherent difficulty in ring opening (see eq. [5]). The latter comes simply from a comparison of the k_1 values in the cyclic and acyclic systems. The former is measured by the extent to which $k_2/(k_{-1} + k_2)$ is less than unity. For the dioxolane system **13** the 80-fold decrease in k_H(obs) compared to **10** can be divided into a 40-fold decrease associated with k_1 and only a 2-fold decrease associated with reversibility. Thus in this system ring opening to the cation is inherently more difficult. With the dioxane system **14**, however, there is only a 6-fold decrease in reactivity compared to **10** and this is almost entirely due to reversibility since the value for k_1 for **14** is only slightly smaller than that for **10**.

It is not immediately obvious why there should be a difference between the two cyclic systems. One possible interpretation involves lone pair orientation (19). (Although this principle has been challenged recently (24), it is probably applicable to ortho esters where transition states are not well advanced towards the oxocarbocation.) As shown in structure **20**, with both spiro ortho esters a lone pair on the oxygen of the dihydrobenzopyran ring can be placed in an orientation approximately antiperiplanar to an oxygen in the dioxolane ring or dioxane ring (dashed line). In the dioxane system, there is also a lone pair on the other oxygen in the dioxane ring that is an antiperiplanar arrangement (structure **21**), so that this system is well set up for bond breaking. With the dioxolane, on the other

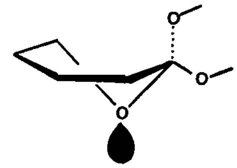

20

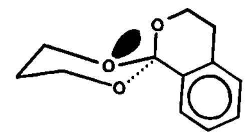

21

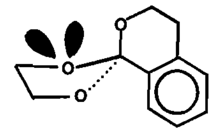

22

hand, there is distortion caused by imposing the proper ring geometry (structure **22**). In the transition state for bond breaking this may prevent 100% conjugation with the other oxygen in the dioxolane ring, making this system inherently less reactive. This argument is tantamount to a Baldwin's rule (25) application. The ring opening in the dioxolane is a disfavored 5-*endo* trig reaction with respect to the dioxolane ring.

Interestingly, the difference in ring opening reactivity between the 5-cycle and 6-cycle is not seen in the tropone system. Here the k_1 values for the two are approximately the same, each being about 10-fold smaller than the value for the diethoxy compound (see Table 1). This may be related to different geometrical features in this system where the spiro junction involves a planar 1,3,5-cycloheptatriene. This can also be looked at in terms of an argument that in the tropone system the majority of the stabilization in the cations is associated with their being tropylium ions. Although the other ring oxygen results in some additional stabilization, the effect is small so that lone pair orientation is not so important.

In summary, both the dihydrobenzopyran ortho esters and the tropone acetals exhibit the same general behavior. Ring opening is reversible. There is not a significant difference between the dioxolane (ethylene bridge) and dioxane (trimethylene bridge) with respect to relative rates of cyclization versus water addition. In no case is there an overwhelming preference for ring closure; values of k_{-1}/k_2 have now been obtained which range from 1.2 to 4.2.

Acknowledgements

The continued financial support of the Natural Sciences and Engineering Research Council of Canada is gratefully acknowledged. Support from NATO is also acknowledged.

1. E. H. Cordes and H. G. Bull. Chem. Rev. **74**, 581 (1974).
2. M. Ahmad, R. G. Bergstrom, M. J. Cashen, Y. Chiang, A. J. Kresge, R. A. McClelland, and M. F. Powell. J. Am. Chem. Soc. **101**, 2669 (1979).
3. R. A. McClelland and L. J. Santry. Acc. Chem. Res. **16**, 394 (1983).
4. A. V. Willi. *In* Comprehensive chemical kinetics. Vol. 8. *Edited by* C. H. Bamford and C. F. H. Tipper. Elsevier, New York, NY. 1979. pp. 49–50.
5. B. Capon and M. I. Page. Chem. Commun. 1443 (1970).
6. R. A. McClelland, M. Ahmad, and G. Mandrapilias. J. Am. Chem. Soc. **101**, 970 (1979).
7. R. A. McClelland and P. W. K. Lam. Can. J. Chem. **62**, 1068 (1984).
8. R. A. McClelland and P. W. K. Lam. Can. J. Chem. **62**, 1074

(1984).
9. O. BOUAB, G. LAMATY, C. MOREAU, O. POMARES, P. DESLONGCHAMPS, and L. RUEST. Can. J. Chem. **58**, 567 (1980).
10. R. A. BURT, Y. CHIANG, H. K. HALL, and A. J. KRESGE. J. Am. Chem. Soc. **104**, 3687 (1982).
11. R. A. MCCLELLAND, S. GEDGE, and J. BOHONEK. J. Org. Chem. **46**, 886 (1981).
12. R. A. BURT, Y. CHIANG, A. J. KRESGE, and M. A. MCKINNEY. J. Am. Chem. Soc. **104**, 3685 (1982).
13. Y. CHIANG, A. J. KRESGE, H. O. LAHTI, and D. P. WEEKS. J. Am. Chem. Soc. **105**, 6852 (1983).
14. R. A. MCCLELLAND and M. ALIBHAI. Can. J. Chem. **59**, 1169 (1981).
15. G. LAMATY, C. MOREAU, and Z. MOULOUNGUI. Can. J. Chem. **61**, 2463 (1983).
16. Y. CHIANG, A. J. KRESGE, P. SALOMAA, and C. I. YOUNG. J. Am. Chem. Soc. **99**, 4494 (1974).
17. Y. CHIANG, A. J. KRESGE, and C. I. YOUNG. Finn. Chem. Lett. 13 (1978).
18. R. A. BURT, C. A. CHAMBERS, Y. CHIANG, C. S. HILLOCK, A. J. KRESGE, and J. W. LARSEN. J. Org. Chem. **49**, 2622 (1984).
19. P. DESLONGCHAMPS. Heterocycles, **7**, 1271 (1977).
20. A. J. KIRBY. Acc. Chem. Res. **9**, 305 (1984).
21. R. A. MCCLELLAND and M. AHMAD. J. Am. Chem. Soc. **100**, 7027 (1978).
22. R. A. MCCLELLAND and M. AHMAD. J. Am. Chem. Soc. **100**, 7031 (1978).
23. C. F. BERNASCONI. Relaxation kinetics. Academic Press, New York. 1976.
24. L. HOSIE, P. J. MARSHALL, and M. L. SINNOTT. J. Chem. Soc. Perkin Trans. 2, 1121 (1984).
25. J. E. BALDWIN. J. Chem. Soc. Chem. Commun. 734 (1976).

Evaluation of homogeneity of marine biological tissues for lead and cadmium by GFAAS

BYRON KRATOCHVIL, RAM S. THAPA, AND NORINE MOTKOSKY
Department of Chemistry, University of Alberta, Edmonton, Alta., Canada T6G 2G2

Received February 26, 1985

BYRON KRATOCHVIL, RAM S. THAPA, and NORINE MOTKOSKY. Can. J. Chem. **63**, 2679 (1985).

Several marine biological tissues were tested for homogeneity with respect to lead and cadmium. The variance for the certified reference material TORT-1 is approximately 1 μg/g for each metal. This is of the same order as the heterogeneity of spray-dried dogfish and swordfish tissue. Scallop adductor muscle was of the same level of heterogeneity for cadmium; the lead content was below the limit of detection of the procedure used.

BYRON KRATOCHVIL, RAM S. THAPA et NORINE MOTKOSKY. Can. J. Chem. **63**, 2679 (1985).

On a fait des essais sur plusieurs types de tissus biologiques marins dans le but de déterminer leur homogénéité en plomb et en cadmium. Pour chacun des métaux présent dans l'échantillon de référence TORT-1, l'écart est d'environ 1 μg/g. Cet écart est du même ordre que l'hétérogénéité de tissus de la roussette ou de l'espadon séchés. Vis-à-vis du cadmium, le muscle de la coquille St-Jacques est du même ordre d'hétérogénéité; pour ce qui est du contenu en plomb, il est inférieur à la limite de détection de la méthode.

[Traduit par le journal]

The toxicity of heavy metals makes their determination in foodstuffs of major interest. Contamination of sea water by anthropogenic activity can cause bioaccumulations of heavy metals in marine life, particularly in economically important food species such as fish, lobster, clams, and mussels. For this reason, the accurate and precise determination of toxic elements in marine biological materials is important. To assist in the development and testing of analytical procedures for such elements a reference material, TORT-1, has been issued by the National Research Council of Canada through the Marine Analytical Chemistry Standards Program. This material was prepared from edible grade lobster tomalley (hepatopancreas) that had been spray dried and acetone extracted. The acetone extraction was performed to remove lipid components that affect stability on storage. Removal of the large amounts of lipids results in a concentration of trace elements in the material. The form in which heavy metals are present in this material is not known, but if more than one form is present distributions of the metals in the material may be affected (1). For this reason, and because many new analytical techniques require only small amounts of sample, the homogeneity of such a reference material is of interest. The concentration of lead in TORT-1 is reported to be 10.4 ± 2.0 μg/g, and that of cadmium 26.3 ± 2.0 μg/g, the uncertainties representing 95% tolerance limits for an individual subsample of 500 mg or greater. We were interested in determining the between-bottle homogeneity for lead and cadmium in samples below 50 mg (2). Single bottles of three additional spray dried marine biological materials, dogfish tissue, scallop adductor muscle, and swordfish tissue, obtained from the National Research Council of Canada, were also tested for homogeneity of lead and cadmium. The method chosen for this study was graphite furnace (electrothermal) atomic absorption spectroscopy with standard additions (3). This technique, with background correction and a L'vov platform, provides the sensitivity and selectivity required for determination of low levels of lead and cadmium in these materials.

Use of the L'vov platform (4−8) reduces matrix effects by allowing the analyte to vaporize into an atmosphere of higher temperature that favors quantitative atom formation. Addition of matrix modifiers such as $NH_4H_2PO_4$ (8) or Triton X-100 (9, 10) to digested solid samples may also reduce matrix effects by stabilizing the analyte or converting interfering sample components to volatile compounds that are removed during the ashing step.

Treatment of tissue samples before analysis ranges widely. Direct injection of freeze-dried (11), powdered (12), or untreated samples (8) has been used but problems with weighing of microgram test portions and with the ashing step make the procedure imprecise. Some of the weighing difficulties may be circumvented by injection of microliter volumes of slurries (13). Digestion of samples has been accomplished with enzymes (14), concentrated acids (7, 15−17) or dry ashing followed by dissolution in acid (18). A solvent extraction technique consisting of acid digestion followed by extraction of cadmium as dithizone complexes into an organic layer has been investigated (19). Still another separation technique involves vaporization of the sample followed by separation on a column (20). Most of these procedures give a precision for lead and cadmium of better than 10%.

For the work reported here digestion with nitric acid followed by a standard additions procedure and vaporization on a L'vov platform were found to give satisfactory results. Use of graphite furnace atomic absorption spectroscopy for the determination of lead or cadmium requires attention to numerous aspects of sample handling and furnace operation. Potential problems include memory effects in the graphite tube and platform and loss of lead or cadmium by adsorption from solution onto container walls with time or during the furnace charring step. Volatilization of lead during charring is reduced considerably by the presence of phosphate in the solution (21−24).

Experimental

Apparatus

The atomic absorption measurements were made on a Model 5000 spectrophotometer (Perkin-Elmer, Norwalk, CT) with background correction, an HGA 2200 furnace, and an AS-1 autosampler. Injected volumes were 20 μL. Pyrolytic graphite tubes with platforms (Perkin-Elmer Part No. B012-1091) were used (25). Operating conditions are given in Table 1. The argon purge gas flow was stopped during the atomization of lead, but was continued using the normal (40 cm^3/min) setting for the first 3 s during the atomization of cadmium. Peak areas were recorded on a Perkin-Elmer PRS-10 printer sequencer. Working curves were linear over the range 0 to 7.2×10^{-8} *M* lead (0 to 0.3 ng Pb per measurement) and 0 to 1.8×10^{-8} *M* cadmium (0 to 0.04 ng Cd per measurement). Blanks, carried through the same procedure as

TABLE 1. Operating conditions for graphite furnace atomic absorption measurements

Parameter	Value	
	Pb	Cd
Wavelength	283.3 nm	228.8 nm
Integration time	6 s	5 s
Spectral slit width	0.7 nm	0.7 nm
Drying temperature and time	120°C, 30 s	110°C, 30 s
Ashing temperature and time	650°C, 40 s	350°C, 40 s
Atomization temperature and time	2200°C, 5 s	2100°C, 5 s
HCL current	7 mA	8 mA

the samples, were run on the instrument after every few sample measurements and the absorbance for the appropriate blank subtracted from the sample absorbances to correct for drift and furnace deterioration. Each solution was injected at least two, and generally three, times.

Reagents

Distilled water was further purified by passage through a column of mixed strong acid and strong base ion exchange resins (Amberlite MB-3, Rohm and Haas Co.). The nitric acid for sample dissolution was either Aristar (British Drug House) or Seastar (Seastar Chemicals, Sidney, B.C. Canada). All other chemicals were either analytical or reagent grade. Certified standard solutions of lead (Fisher Scientific) and cadmium (Spex Industries) were used to prepare calibration curves and for the standard additions.

For comparison and checking purposes, a standard reference material from the U.S. National Bureau of Standards, Oyster Tissue 1566, was analyzed for lead and cadmium, and a second material, Bovine Liver 1577a, was analyzed for cadmium.

Sample preparation

Six bottles of TORT-1, obtained from Marine Standards Analytical Program, Division of Chemistry, National Research Council of Canada, Ottawa, Canada K1A 0R9, were tumbled end-over-end for 2 h. Approximately 5-g portions from each were then removed and dried in glass weighing bottles for 24 h at room temperature (23−24°C) in a vacuum oven (National Appliance Co. Model 5851-6) at approximately 0.06 mm Hg. The vacuum was produced with a pump (Welch Co.) separated from the oven by a dry ice − acetone cold trap. Previous studies had shown these drying conditions to be optimum. The dried samples were stored in closed weighing bottles in a desiccator over magnesium perchlorate.

Single bottles of spray dried scallops adductor muscle and swordfish tissue, also obtained from the National Research Council of Canada, Ottawa, were treated in the same way except that 48 h were required to bring the materials to constant weight. Dogfish tissue, obtained from the same source, was difficult to dry because the surface of the material tended to form a crust that slowed further drying. The procedure finally adopted involved recrushing of the clumps with a spatula every 6 to 8 h during the drying period. Even with intermittent crushing a total of 120 h was required to bring the material to constant weight. The total weight loss was of the order of 5%.

For the TORT-1 lead and cadmium analyses approximately 25-mg portions of the material were weighed to ±0.01 mg on a Mettler H-51 semimicro balance into 125-mL wide mouth FEB Teflon bottles (Nalgene 2100-0004). About 5 mL of 15.8 *M* nitric acid was added to each bottle, the bottle capped loosely with Tefzel closures, and the contents refluxed gently by placing the bottle in a sand bath at 130°C until dissolution was complete.

For the dogfish, sample sizes were about 0.05 g for the lead and 0.8 g for the cadmium determinations. Corresponding sample sizes were 0.8 g and 0.25 g for the swordfish, and 1.5 g and 0.125 g for the scallops. The dissolution procedure was the same as for TORT-1, except that the volume of nitric acid used for the dissolution had to be increased to as much as 15 mL for the largest samples. Other methods of sample dissolution were investigated and found to be less satisfactory (26). These included digestion at lower concentrations of nitric acid at ~180°C and digestion with various concentrations of nitric acid in a pressure cooker (27).

The digested solution was transferred to a 10-mL volumetric flask and diluted to volume. For the determination of lead, solutions for the standard additions procedure were prepared by pipetting from 0.6 to 2 mL of the sample solution, depending on the lead concentration, into each of four or five 10-mL volumetric flasks and adding from 0 to 0.15 mL of a solution containing 1 μg lead per mL with a variable micropipet (Soccorex 5-25 μL, Cat. No. 841). Next, 0.5 mL of ammonium dihydrogen orthophosphate (0.1% in 1% HNO_3) was added to each flask and the volume was made to the mark with 1% HNO_3. These solutions were then run immediately on the atomic absorption spectrophotometer. Solutions that were allowed to stand for several hours or overnight gave low and erratic results. A plot of absorbance against added lead was then drawn and the intercept on the horizontal axis used to calculate the lead present in the sample solution (28). The value of the intercept was obtained both graphically and by calculation of the least-squares intercept.

The same method was followed for cadmium except that sample volumes ranged from 0.1 to 2 mL, and the volumes of standard cadmium solution (1 μg Cd per mL) added ranged from 0 to 20 μL. Also, the addition of ammonium dihydrogen orthophosphate was omitted because its use did not improve precision or accuracy.

Results and discussion

Results for the lead study are summarized in Table 2 and those for cadmium in Table 3. The uncertainty in the measurement step can be estimated from the variance in the intercept as calculated by least squares. The overall uncertainty, which includes both the measurement and subsampling variances, can be obtained from the variance of the results for a set of measurements on individual subsamples. The difference between these two values is the subsampling variance. From the precision of the values obtained for TORT-1 on replicates from single test portions by least-squares calculations on standard additions it can be concluded that random errors in the measurement operations are sufficiently smaller than the subsampling uncertainty that the variation observed between individual test portions can be ascribed to sample variability. Results on duplicate test portions from individual bottles for TORT-1 (all bottles for Cd, one for Pb) show variations of the same magnitude as between bottles. Although more analyses would be required to establish with a high level of confidence the extent of the within-bottle variance, on the basis of results observed in studies of other elements it is likely to be of the same order as the between-bottle variance. A further conclusion is that the 95% tolerance limits (29), 4.1 μg for lead and 6.1 μg for cadmium, for individual subsamples of 30 mg are no more than two and one half times greater than those provided by NRC for 500-mg subsamples. Accordingly, for the determination of lead and cadmium in TORT-1 a subsample

TABLE 2. Lead concentrations in µg/g for marine biological tissues and reference materials

Material	Number of test portions	Graphical method[a]	Least-squares calc[b]	Certified value[c]
Dogfish	7	8.1±0.8	8.1±0.8	—
Swordfish	7	0.20±0.01	0.20±0.01	—
Lobster (TORT-1)	8	10.0±0.6	10.3±1.1	10.4±2.0[d]
Oyster tissue 1566	4	0.52±0.01	0.60±0.11	0.48±0.04[e]

[a]Values obtained from intercept of visually positioned lines; uncertainty is one standard deviation.
[b]Values obtained by least-squares calculation of intercepts on x-axis; uncertainty is one standard deviation.
[c]Uncertainties are 95% tolerance levels.
[d]Certified value from National Research Council of Canada.
[e]Certified value from U.S. National Bureau of Standards.

TABLE 3. Cadmium concentrations in µg/g for marine biological tissues and reference materials

Material	Number of test portions	Graphical method[a]	Least-squares calc[b]	Certified value[c]
Dogfish	6	0.078±0.008	0.079±0.010	—
Scallops	7	0.52±0.03	0.51±0.03	—
Swordfish	7	0.33±0.02	0.33±0.03	—
Lobster (TORT-1)	13	26.6±0.9	26.1±2.1	26.3±2.1[d]
Oyster tissue 1566	4	3.5±0.1	3.3±0.3	3.5±0.4
Bovine liver 1577a	2	0.41	0.39±0.04	0.44±0.06

[a]Values obtained from intercept of visually positioned lines; uncertainty is one standard deviation.
[b]Values obtained by least-squares calculation of intercepts on x-axis; uncertainty is one standard deviation.
[c]Uncertainties are 95% tolerance levels.
[d]Certified value from National Research Council of Canada; others from U.S. National Bureau of Standards.

size of up to a factor of 10 less than 500 mg can be taken with reasonable probability that the subsampling error will not exceed the specified tolerance limits of ±2 µg/g.

From the precision of the least-square values obtained for cadmium on individual subsamples of dogfish, scallops, and swordfish, it can be concluded that the subsampling uncertainty for these materials is of the same order or less than the measurement uncertainty. The heterogeneity of the material, therefore, does not contribute significantly to the overall analytical uncertainty. The variability in the dogfish tissue was somewhat higher for cadmium but about the same for lead as for the other materials. The dogfish tissue, unlike the finely powdered lobster, scallops, and swordfish material, contained many small clumps and some stringy material. This heterogeneity in physical properties might be expected to lead to greater variability in composition at the trace level, but evidence for this was not strong.

No lead was detected in the scallops muscle, even in samples of 1.5 g. The limit of detection for lead by the procedure used is estimated to be of the order of 0.2 ng per mL; therefore the lead content is less than 0.01 µg/g.

Acknowledgements

The assistance of E. Stubley with data treatment is gratefully acknowledged. Also, we thank S. Hrudey and W. George of the Department of Civil Engineering, University of Alberta, for the use of the atomic absorption spectrophotometer and furnace.

This research was supported by the National Research Council of Canada under Contract OSC83-00225 for the Marine Analytical Chemistry Standards Program, and by the University of Alberta.

1. Y. K. CHAU, P. T. S. WONG, G. A. BENGERT, and J. L. DUNN. Anal. Chem. **56**, 271 (1984).
2. L. FAVRETTO, G. P. MARLETTA, and L. G. FAVRETTO. Mikrochim. Acta, II, 387 (1981).
3. M. STOEPPLER, K. BRANDT, and T. C. RAINS. Analyst, **103**, 714 (1978).
4. E. PRUSZKOWSKA, G. R. CARNRICK, and W. SLAVIN. At. Spectrosc. **4**, 59 (1983).
5. F. CLAEYS-THOREAU. At. Spectrosc. **3**, 188 (1982).
6. F. J. FERNANDEZ and D. HILLIGOSS. At. Spectrosc. **3**, 130 (1982).
7. T. W. MAY and W. G. BRUMBAUGH. Anal. Chem. **54**, 1032 (1982).
8. J. F. ALDER and M. C. C. BATOREU. Anal. Chem. **155**, 199 (1983).
9. K. S. SUBRAMANIAN and J. C. MERANGER. Clin. Chem. **27**, 1866 (1981).
10. K. G. BRODIE and M. W. ROUTH. Clin. Biochem. **17**, 19 (1984).
11. T. NILSSON and P. O. BERGGREN. Anal. Chim. Acta, **159**, 381 (1984).
12. Z. GROBINSKI, R. LEHMANN, R. LAMM, and B. WELZ. Mikro-Chim. Acta, **1**, 115 (1982).
13. K. W. JACKSON and A. P. NEWMAN. Analyst, **108**, 261 (1983).
14. R. C. CARPENTER. Anal. Chim. Acta, **125**, 209 (1981).
15. V. HUDNIK, M. MAROTT-GOMISCEK, and S. GOMISCEK. Anal. Chim. Acta, **157**, 143 (1984).
16. M. BLANUSA and D. BRESKI. Talanta, **28**, 681 (1981).
17. P. A. PLEBAN, J. KERKAY, and K. H. PEARSON. Clin. Chem. **27**,

68 (1981).
18. U. KURFUERST. Fresenius' Z. Anal. Chem. **313**, 97 (1982).
19. E. KAMATA, R. NAHASHIMA, K. GOTO, M. FURUKAWA, and S. SHIBATA. Anal. Chim. Acta, **144**, 197 (1982).
20. M. YANAGISAWA, K. KITAGAWA, and S. TSUGE. Spectrochim. Acta, **37**B, 493 (1982).
21. W. SLAVIN, G. R. CARNRICK, and D. C. MANNING. Anal. Chem. **56**, 163 (1984).
22. D. C. MANNING and W. SLAVIN. Appl. Spectrosc. **37**, 1 (1983).
23. E. PRUSZKOWSKA, G. R. CARNRICK, and W. S. SLAVIN. At. Spectrosc. **4**, 59 (1983).
24. D. J. HODGES and D. SKELDING. Analyst, **108**, 813 (1983).
25. C. K. CHAKRABARTI, C. C. WAN, and W. C. LI. Spectrochim. Acta, **35**B, 547 (1980).
26. S. W. JENNISS, S. A. KATZ, and T. MOUNT. American Laboratory, Aug. 1980. pp. 18–23.
27. J. S. NIELSEN. Ph.D. Thesis, University of Alberta. 1982. pp. 99–102.
28. W. HARRIS and B. KRATOCHVIL. Introduction to chemical analysis. Saunders, Philadelphia. 1981. pp. 445–446.
29. W. J. DIXON and F. J. MASSEY, JR. Introduction to statistical analysis. 3rd ed. McGraw-Hill, New York. 1969. p. 142.

Correlations between carbon-13 nuclear magnetic resonance and X-ray crystallography for pyrroles containing electron-withdrawing groups

J. B. PAINE III, D. DOLPHIN, J. TROTTER, AND T. J. GREENHOUGH
The Department of Chemistry, University of British Columbia, 2036 Main Mall, Vancouver, B.C., Canada V6T 1Y6

Received July 24, 1984

J. B. PAINE III, D. DOLPHIN, J. TROTTER, and T. J. GREENHOUGH. Can. J. Chem. **63**, 2683 (1985).

The ^{13}C nmr chemical shifts of benzyl 4-ethyl-3,5-dimethylpyrrole-2-carboxylate (**1**), methyl *E*-3-(3-ethyl-4,5-dimethylpyrrol-2-yl)-2-cyanopropenoate (**2**), and methyl *E*-3-(5-(benzyloxy)carbonyl-3-ethyl-4-methylpyrrol-2-yl)-2-cyanopropenoate (**3**) have been compared to their X-ray crystallographic structures. The ^{13}C nmr chemical shifts were determined by direct comparison of a series of closely related homologs.

Crystal data for **1**, **2**, and **3** are as follows: **1**, monoclinic, $P2_1/c$, a = 14.934(2), b = 6.674(2), c = 15.269(2) Å, β = 101.96(1)°, Z = 4; **2**, monoclinic, $P2_1/n$, a = 7.3030(3), b = 13.478(1), c = 12.985(1) Å, β = 97.48(1)°, Z = 4; **3**, monoclinic, $P2_1/c$, a = 11.157(2), b = 13.109(2), c = 14.068(1) Å, β = 115.47(1)°, Z = 4. The structures were determined with diffractometer data by direct methods, and refined by full-matrix least-squares techniques to R = 0.052, 0.040, 0.038 for 862, 2032, 1483 reflexions, respectively. The molecules are approximately planar, except for deviations of the phenyl rings and of the terminal carbon atoms of the C_3-ethyl groups from the molecular planes. The bond lengths in the pyrrole rings differ from those in pyrrole itself, as a result of the presence of the strongly electron-withdrawing sustituents; exocyclic bond lengths also exhibit differences from normal values.

The competitive effects of the various electron withdrawing groups have been correlated to change in bond lengths, ^{13}C chemical shifts, and the chemical reactions of the pyrrolic nucleus.

J. B. PAINE III, D. DOLPHIN, J. TROTTER et T. J. GREENHOUGH. Can. J. Chem. **63**, 2683 (1985).

On a comparé les déplacements chimiques en rmn du ^{13}C de l'éthyl-4 diméthyl-3,5 pyrrolecarboxylate-2 de benzyle (**1**), de l'(éthyl-3 diméthyl-4,5 pyrrolyl-2)-3*E* cyano-2 propèonate de méthyle (**2**) et du ((benzyloxy)carbonyl-5 éthyl-3 méthyl-4 pyrrolyl-2)-3*E* cyano-2 propèonate de méthyle (**3**) avec leurs structures déterminées par cristallographie de rayons x. On a déterminé les déplacements chimiques de ces composés en rmn du ^{13}C en se basant sur une comparaison directe avec une série d'homologues très voisins.

Le composé **1** est monoclinique et il appartient au groupe d'espace $P2_1/c$ avec a = 14,934(2), b = 6,674(2), c = 15,269(2) Å, β =101,96(1)°, Z = 4; le composé **2** est monoclinique et il appartient au groupe d'espace $P2_1/n$, avec a = 7,3030(3), b = 13,478(1), c = 12,985(1) Å, β = 97,48(1)°, Z = 4; le composé **3** est monoclinique et il appartient au groupe d'espace $P2_1/c$, avec a = 11,157(2), b = 13,109(2), c = 14,068(1) Å, β = 115,47(1)°, Z = 4. On a déterminé les structures par des méthodes directes et on les a affinées par la méthode des moindres carrés (matrice entière) jusqu'à des valeurs respectives de R de 0,052, 0,040, 0,038 pour 862, 2032 et 1483 réflexions. Les molécules sont approximativement planes à l'exception des déviations, par rapport aux plans moléculaires, des cycles phényles et des atomes de carbone terminaux des groupes éthyles C_3. Les longueurs de liaison dans le cycle du pyrrole diffèrent de celles du pyrrole lui-même en raison de la présence de substituants fortement électroattracteurs. Les longueurs des liaisons exocycliques diffèrent également des valeurs normales.

On a établi une corrélation entre les effets concurrents de divers groupes électroattracteurs et les variations des longueurs de liaison, les déplacements chimiques en rmn du ^{13}C et les réactions chimiques du noyau pyrrole.

[Traduit par le journal]

Introduction

There have been few reports on the ^{13}C nmr of pyrroles even though this spectroscopic technique has been skilfully used to elucidate the biosynthesis of tetrapyrrolic macrocycles (1, 2). Lauterbur (3) was the first to show that non-alternant hydrocarbons exhibit much larger ^{13}C shieldings than alternant hydrocarbons and Grant and his colleagues (4, 5) have examined substituted and charged five-membered aromatic heterocycles. As with many homologous series a variety of empirical correlations between ^{13}C chemical shifts and substitution patterns has been made. Abraham *et al.* (6) have assigned the ^{13}C nmr of 55 variously substituted pyrroles which allowed them to describe specific substituent chemical shift effects (SCS). However, they found that the additivity of SCS effects frequently gave discrepancies of ~5 ppm. Additional allowances for steric compression shifts (7) improved their correlations. However, compounds with carbonyl groups directly attached to the pyrrolic nucleus did not give good agreement between "calculated" and observed chemical shifts. Carbonyl groups are, of course, electron-withdrawing and their anomalous behaviour coupled with the greater effects of α- compared to β-substituents led to the suggestion that resonance was involved. These authors (6) speculated as to whether this effect resulted from changes in electron densities or ring geometries. π-Charge densities were calculated using the INDO approximation, but since this assumes a fixed geometry the question as to changes in ring geometry with substitution pattern remained unanswered.

We report here the X-ray crystallographic structures of the pyrroles **1**–**3** which bear electron-withdrawing groups. Their ^{13}C nmr spectra have been assigned and correlations between ^{13}C chemical shifts, molecular structure, and chemical reactivity are presented.

Experimental methods

Benzyl 4-ethyl-3,5-dimethylpyrrole-2-carboxylate (8) (1)

Compound (**1**) was prepared by an *in-situ* diborane reduction of benzyl 4-acetyl-3,5-dimethylpyrrole-2-carboxylate (9), effected in a manner similar to the procedure of Whitlock and Hanauer (10), or via a high temperature modification (11) of the base-catalyzed transesterification (8) of ethyl 3-ethyl-4,5-dimethylpyrrole-2-carboxylate. The product crystallized from methanol as yellow plates.

Methyl E*-3-(3-ethyl-4,5-dimethylpyrrol-2-yl)-2-cyanopropenoate (2)*

3-Ethyl-4,5-dimethylpyrrole-2-carboxaldehyde (12) (3.21 g, 21.3

TABLE 1. Crystal data for **1**, **2**, and **3***

Compound	1	2	3
Formula	$C_{16}H_{19}NO_2$	$C_{13}H_{16}N_2O_2$	$C_{20}H_{20}N_2O_4$
Formula weight	257.33	232.28	352.39
Crystal system	Monoclinic	Monoclinic	Monoclinic
Space group	$P2_1/c$	$P2_1/n$	$P2_1/c$
a (Å)	14.934(2)	7.3030(3)	11.157(2)
b	6.674(2)	13.478(1)	13.109(2)
c	15.269(2)	12.985(1)	14.068(1)
β (deg)	101.96(1)	97.48(1)	115.47(1)
V (Å^3)	1488.8	1267.2	1857.6
Z	4	4	4
D_x (g cm^{-3})	1.148	1.217	1.260
Radiation	Mo	Cu	Mo
λ (Å)	0.71073	1.54188	0.71073
μ (cm^{-1})	0.8	6.8	1.0
Crystal dimensions (mm)	0.15×0.25×0.45	0.38×0.38×0.31	0.3×0.3×0.2
θ range for cell parameters (deg)	10−14	28−52	10−22
Scan	ω−2θ	ω−2θ	ω−θ
Δω (deg)	0.7 + 0.35 tan θ	0.75 + 0.15 tan θ	0.8 + 0.35 tan θ
Aperture: width (mm)	1.75 + tan θ	1.5 + 0.5 tan θ	1.5 + tan θ
height (mm)	4	4	4
Maximum scan speed (deg/min)	10.06	10.06	10.06
Maximum counting time (s)	75	120	75
Maximum θ (degrees)	25	75	25
Number of check reflexions	3	3	3
Variation of checks (%)	±2	±2	±1
Number of reflexions: total	2607	2604	3269
$I > 3\sigma(I)$	862 (33%)	2032 (78%)	1483 (45%)
Weighting scheme	$1/\sigma^2(F)$	$1/\sigma^2(F)$	$1/\sigma^2(F)$
R ($I \geq 3\sigma(I)$)	0.052	0.040	0.038
R_w	0.068	0.059	0.048
Goodness of fit	1.89	1.58	1.00
Final difference map (e Å^{-3})	±0.2	±0.1	±0.2
Extinction parameter, g	—	0.88(8)	—

***1** = Benzyl 4-ethyl-3,5-dimethylpyrrole-2-carboxylate, **2** = methyl E-3-(3-ethyl-4,5-dimethylpyrrol-2-yl)-2-cyanopropenoate, **3** = methyl E-3-(5-(benzyloxy)carbonyl)-3-ethyl-4-methylpyrrol-2-yl)-2-cyanopropenoate.

mmol) and methyl cyanoacetate (2.52 g, 25.5 mmol) were heated (steambath) in toluene (50 mL) with triethylamine (2 mL) and acetic acid (1 mL) until tlc (CH_2Cl_2, silica) showed the reaction to be nearly complete (5 h). The solvent was removed *in vacuo*, and chased with methanol. The product was stirred in methanol, filtered, washed with methanol then ether, to give after air drying 2.96 g (60%). On standing the filtrates deposited magnificent transparent golden diamonds which were used for the X-ray analysis. Mp 135.5−138.5°C. *Anal.* calcd. for $C_{13}H_{16}N_2O_2$: C 67.22, H 6.94, N 12.06; found: C 67.34, H 6.98, N 12.12.

Methyl E-*3-(5-(benzyloxy)carbonyl-3-ethyl-4-methylpyrrol-2-yl)-2-cyanopropenoate (3)*

5-Benzyloxycarbonyl-3-ethyl-4-methylpyrrole-2-carboxaldehyde (13) (20 g) in toluene (50 mL) was heated (steambath) with triethylamine (1 mL) for 1 h. The solvent was removed *in vacuo*, and the product crystallized, as golden chunks, from methanol to give, after air drying 21 g (87%). Mp 124.5−125.1°C. *Anal.* calcd. for $C_{20}H_{20}N_2O_4$: C 68.17, H 5.72, N 7.95; found: C 68.24, H 5.78, N 7.91.

X-Ray crystal analysis of ***1**, **2**, **3***

Data were measured in an Enraf-Nonius CAD4-F diffractometer, as outlined in Table 1. Additional data for all three compounds are $\sigma^2(I) = S + B + (0.05S)^2$, S = scan count, and B = normalized background count; LP but no absorption corrections. Structures were determined by direct methods, and refined by full-matrix least-squares techniques,[1] with minimization of $\Sigma w(F_o - F_c)^2$; $R = \Sigma(F_o - F_c)/\Sigma F_o$, $R_w = [\Sigma(F_o - F_c)^2/\Sigma F_o^2]^{1/2}$. Scattering factors are from refs. 14 and 15; and extinction correction as in refs. 16 and 17. Atomic positional parameters are listed in Table 2, and other material has been placed in the Depository of Unpublished Data.[2] Due to poorer crystal quality, the intensity data for **1** are less extensive than and the structural results not as accurate as for **2** and **3**, as reflected in the higher standard deviations for the parameters of **1**; comparisons involving **1** are therefore of less statistical significance.

Carbon-13 nmr spectral data were recorded on a Varian CFT-20, using saturated solutions in $CDCl_3$ and 10 mm diameter sample tubes with TMS as an internal standard.

[1]The computer programs used include locally written programs for data processing and locally modified versions of the following: MULTAN 78, direct methods by P. Main, S. E. Hull, L. Lessinger, G. Germain, J. P. Declercq, and M. M. Wolfson; TANS, direct methods by M. G. B. Drew, D. H. Templeton, and A. Zalkin; ORFLS, full-matrix least-squares, and ORFFE, function and errors, by W. R. Busing, K. O. Martin, and H. A. Levy; FORDAP, Fourier syntheses, by A. Zalkin; ORTEP II, illustrations, by C. K. Johnson.

[2]Anisotropic thermal parameters, hydrogen positional and isotropic thermal parameters, bond lengths and angles, mean planes, and structure factors may be purchased from the Depository of Unpublished Data, CISTI, National Research Council of Canada, Ottawa, Ont., Canada K1A 0S2.

TABLE 2. Final positional parameters (fractional × 10^4) for non-hydrogen atoms of **1**, **2**, and **3**, with standard deviations in parentheses

Atom	*x*	*y*	*z*	Atom	*x*	*y*	*z*	Atom	*x*	*y*	*z*
		1				**2**				**3**	
N(1)	9289(3)	−1495(7)	5913(3)	N(1)	7094(2)	4055(1)	1030(1)	N(1)	766(2)	5475(2)	4079(1)
C(2)	9203(3)	−2996(9)	6472(4)	C(2)	5704(2)	4645(1)	1333(1)	C(2)	−479(2)	5046(2)	3598(2)
C(3)	8404(4)	−2697(10)	6744(4)	C(3)	4433(2)	3998(1)	1714(1)	C(3)	−1387(2)	5847(2)	3214(2)
C(4)	7979(3)	−965(9)	6343(4)	C(4)	5085(2)	3030(1)	1632(1)	C(4)	−664(2)	6767(2)	3472(2)
C(5)	8545(3)	−228(9)	5816(3)	C(5)	6733(2)	3087(1)	1199(1)	C(5)	664(2)	6507(2)	4003(2)
C(21)	9930(4)	−4589(9)	6700(4)	C(21)	5583(2)	5682(1)	1311(1)	C(21)	−763(2)	3991(2)	3493(2)
C(31)	7921(7)	−4404(17)	7287(7)	C(6)	6723(2)	6400(1)	1022(1)	C(31)	−2860(2)	5750(2)	2609(2)
C(32)	8173(7)	−3650(16)	8094(9)	C(7)	6174(2)	7441(1)	1120(1)	C(32)	−3298(3)	5709(3)	1435(3)
C(41)	7084(4)	−87(10)	6475(4)	C(8)	6949(4)	9107(1)	879(2)	C(41)	−1221(3)	7823(2)	3247(3)
C(51)	8519(3)	1474(9)	5236(4)	C(51)	7979(3)	2280(2)	942(2)	C(51)	1843(2)	7156(2)	4489(2)
C(10)	7652(4)	4232(11)	4539(5)	C(41)	4162(3)	2097(2)	1928(2)	C(6)	65(2)	3181(2)	3828(2)
C(11)	6684(4)	4771(10)	4251(4)	C(31)	2734(2)	4303(1)	2169(1)	C(7)	−501(3)	2142(2)	3588(2)
C(12)	6370(5)	6618(13)	4418(6)	C(32)	3116(3)	4568(2)	3307(2)	C(8)	−18(4)	387(2)	3739(3)
C(13)	5458(7)	7114(17)	4134(7)	C(61)	8424(2)	6201(1)	639(1)	O(7)	−1667(2)	1960(1)	3091(2)
C(14)	4873(6)	5832(23)	3676(8)	N(61)	9798(2)	6037(1)	342(1)	O(78)	429(2)	1428(1)	3972(1)
C(15)	5148(6)	4010(19)	3479(7)	O(7)	4801(2)	7708(1)	1461(1)	C(61)	1474(2)	3287(2)	4389(2)
C(16)	6071(5)	3474(12)	3777(6)	O(78)	7388(2)	8074(1)	783(1)	N(61)	2593(2)	3409(2)	4825(2)
O(10)	7736(2)	2507(6)	5130(2)					C(10)	4164(4)	7117(5)	5620(6)
O(51)	9125(2)	1941(6)	4854(2)					C(11)	4900(2)	6519(2)	6569(3)
								C(12)	4955(3)	6813(3)	7579(5)
								C(13)	5655(5)	6214(5)	8438(4)
								C(14)	6271(4)	5366(5)	8350(5)
								C(15)	6223(3)	5078(3)	7433(5)
								C(16)	5557(3)	5645(2)	6553(3)
								O(51)	1856(2)	8065(2)	4441(2)
								O(10)	2907(2)	6583(1)	5005(2)

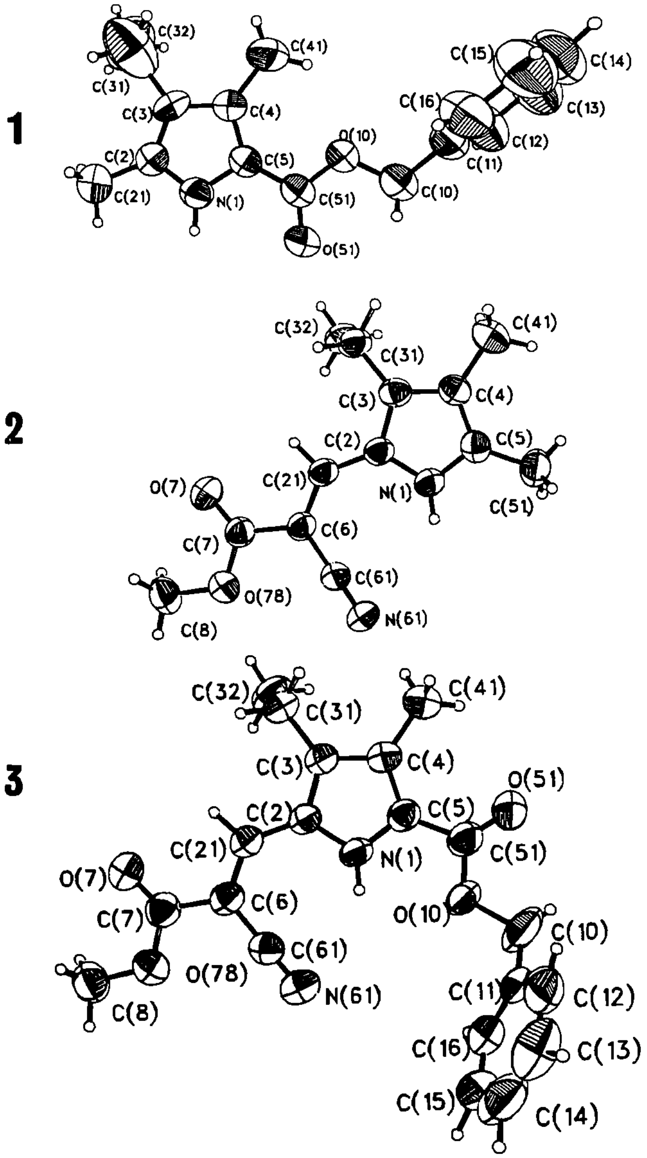

FIG. 1. ORTEP drawings of **1**, **2**, and **3**.

Results and discussion

The molecules of **1**, **2**, and **3** (Fig. 1) are approximately planar, except for the phenyl rings of the benzyloxycarbonyl substituents, which make angles of about 70° with the planes of the remainder of the molecules, and the terminal carbon atoms of the C_3-ethyl groups which are displaced by the order of 1 Å from the molecular planes. In more detail:[2] in **1** and **3** the $C—CO_2—CH_2$ planes make angles of 5.0 and 4.6°, respectively, with the planes of the pyrrole rings, and 68.4 and 74.3° with the phenyl planes; in **2** and **3**, the methoxycarbonyl groups make angles of 2.3 and 3.1°, respectively, with the pyrrole planes. The terminal ethyl C(32) atoms are displaced from the pyrrole planes by 1.0, 1.4, and 1.4 Å in **1**, **2**, and **3**, respectively.

The cyano(methoxycarbonyl)vinyl substituents in **2** and **3** are similarly oriented (Fig. 1). The cyano group is *cis* and the methoxycarbonyl group is *trans* to the pyrrole ring (with respect to the vinyl C=C bond); the vinyl C=C bond and the C(2)—N pyrrole ring bond have a *syn* conformation about C(2)—C(21), possibly because of the favourable *anti* arrange-

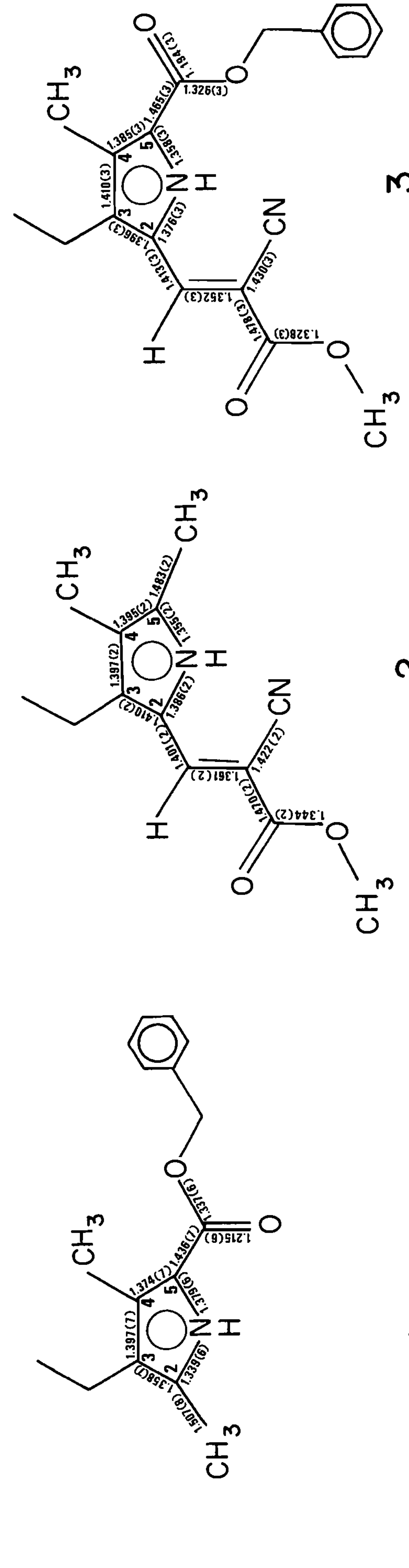

FIG. 2. Principal bond lengths for compounds **1**, **2**, and **3**.

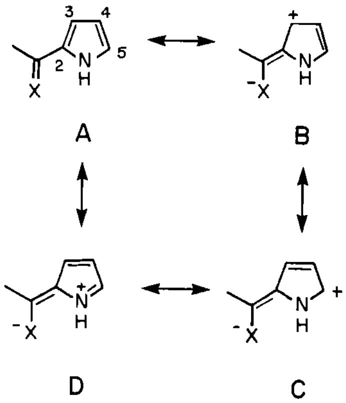

FIG. 3. Principal canonical forms for a pyrrole bearing an electron-withdrawing group in the α-position.

ment of C(21)=C(6) and C(2)=C(3). Such a conformation also minimizes steric interaction with the ethyl substituent. The benzyloxycarbonyl substituents in **1** and **3** have *different* conformational arrangements (Fig. 1); in **1** the C=O bond is *syn* to C(5)—N about C(5)—C(51). In **3** the whole group is rotated 180° about C(5)—C(51) to give an *anti* C=O/C(5)—N conformation; this may result from electrostatic repulsion between the two polar C=O and C≡N groups which would occur in a *syn* arrangement.

The chemically-interesting bond distances are illustrated in Fig. 2, and a full listing of distances and angles is given in the supplementary material.[2] The bond lengths in the pyrrole rings differ significantly from those in pyrrole itself (18), as a result of the presence of the strongly electron-withdrawing substituents. Four principal canonical structures (*A–D*, Fig. 3) may be drawn for a pyrrole α-substituted by an electron-withdrawing group capable of mesomeric interaction; these lead to an expectation of a decrease, relative to pyrrole, of the length of the C—N bond remote from the electron-withdrawing substituent, i.e., C(5)—N if the substituent is at C(2); C(2)—N should probably increase as a result of overall removal of electron-density from the ring. C(2)—C(3) should show a marked increase in length relative to pyrrole (resonance forms *B*, *C*, *D*), C(3)—C(4) a decrease (*D*, *C*), and C(4)—C(5) a smaller increase (*D*, *C*).

These differences are clearly observed in the structure of **2**. Comparison can be made with pyrrole itself whose structure has been determined by microwave spectroscopy in the gas phase (18*a*). These microwave data are quite accurate, but may suffer from vibration–rotation erros of up to 0.005 Å; taking this error estimate as 2–3σ, the N—C(2), C(2)—C(3), C(3)—C(4) distances in gaseous pyrrole are 1.370, 1.382, 1.417 (σ ~ 0.002) Å. Since spectroscopically-determined bond lengths may differ from those measured by diffraction methods in the solid state, comparison with bond lengths measured in the solid would be more appropriate. However, it is difficult to find accurate data for unsubstituted pyrrole; data for molecules in which substituents have no mesomeric interactions (18*b*, *c*) suggest lengths of 1.38, 1.37, 1.41 (σ ~ 0.003) Å for the three bonds, although these values may be slightly affected by inductive effects (18*b*).

The C(5)—N bond of 1.370 Å is gaseous pyrrole (or 1.38 Å in solid pyrroles) is shortened by 5σ (or 7σ) to 1.355(2) Å in **2**, and C(2)—N is lengthened by 6σ (or only 1.7σ) to 1.386(2) Å; the C(2)—C(3), C(3)—C(4), C(4)—C(5) distances in **2** are 1.410(2), 1.397(2), 1.395(2) Å, i.e. changes of +10, −7, +5σ, respectively, from the gaseous pyrrole distances (+11, −4, +7σ relative to solid pyrroles). Similar trends are found in **1**, although the poorer accuracy makes the differences less significant. The C—N bond remote from the benzyloxycarbonyl group (labelled C(2)—N here, since the group has been placed at position 5 to facilitate comparison with compound **3**) is shortened by 5σ (or 6σ) to 1.339(6) Å; the adjacent C—N bond at 1.379(6) Å does not differ significantly from that in pyrrole. The pyrrole C—C bond lengths in **1** are in the expected relative order, with the bond opposite the benzyloxycarbonyl substituent shorter at 1.358(7) Å than the adjacent C—C bond of 1.374(7) Å, although the difference is not statistically significant. The C(3)—C(4) bond of 1.397(7) Å is again shorter than the 1.417 (1.41) Å of pyrrole as expected, but the difference is again only 1.8σ (1.7σ).

The exocyclic bond distances add supportive evidence for contributions from canonical forms *B*, *C*, and *D* not only when compared with "normal" bond lengths, but also between themselves. In **2** the C(2)—C(21) distance is 1.401(2) Å, considerably shortened from the normal C(sp^2)—C(sp^2) single bond distance of 1.474 Å (19); the vinyl C=C bond of 1.361(2) Å shows an increase from the normal ethylenic bond distance of 1.335 Å, and the C—CN distance of 1.422(2) Å a decrease from the corresponding length of 1.46 Å in alkyl cyanides (20). In the less accurately determined **1**, the exocyclic C—C bond is again shortened, to 1.436(7) Å.

Many of these bond length variations have been observed in a few other pyrrole derivatives (21). Bond angles[2] show only minor variations from those in pyrrole.

When two electron-withdrawing groups are introduced in the C(2) and C(5) positions, as in **3**, the changes in structural effects are not additive, nor are the changes in the ^{13}C nmr parameters (see below). The electron-withdrawing power of one such group is diminished by the presence of the other, which is competing for available electron-density. As expected, the more-powerful cyano(methoxycarbonyl)vinyl group dominates, with the C(5)—N bond remote from this group shortened to 1.358(3) Å relative to pyrrole, 1.370 (1.38) Å, and to the C(2)—N bond in **3**, 1.376(3) Å; similarly the C(2)—C(3) bond adjacent to the more powerful group is lengthened, 1.396(3) Å, compared to pyrrole, 1.382 (1.37) Å, or to the C(4)—C(5) bond 1.385(3) Å. The sequence of bonds C(2)—C(3), C(3)—C(4), C(4)—C(5) at 1.396(3), 1.410(3), 1.385(3) Å, varies less from the values in pyrrole, than does the corresponding sequence in the compounds with only one electron-withdrawing substituent, **1** and **2**.

The exocyclic bond lengths in **3** are also in accord with reduced electron-withdrawing as a result of competition between the two groups. For the cyanomethoxycarbonylvinyl group, C(2)—C and C=C at 1.413(3), 1.352(3) Å show less extreme differences from normal values (1.474, 1.335 Å) than do the corresponding bonds in **2** (1.401(2), 1.361(2) Å). For the benzyloxycarbonyl group, C(5)—C at 1.465(3) Å is again much closer to 1.474 Å than the bond in **1**, 1.436(7) Å; the C=O bond of this group in **3** is situated *anti* to the C(5)—N bond and is the shortest C=O bond in all the molecules at 1.194(3) Å, again indicative of reduced electron-withdrawing properties.

Other bond lengths and angles in all the substituent groups[2] are close to normal values.

The crystal structures of **1** and **2** contain pairs of molecules joined around centres of symmetry by intermolecular hydrogen bonds. In **2** the hydrogen bonding is of the type N(pyrrole)—

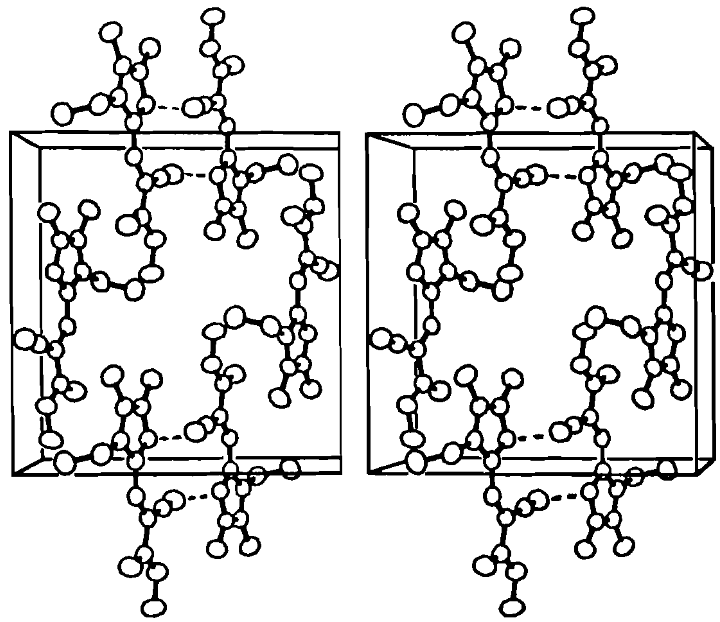

FIG. 4. Hydrogen bonding scheme for **2**; origin at upper left, x towards viewer, y down, z across.

H···N(cyano) (Fig. 4). The parameters are N···N($2 - x$, $1 - y$, $-z$) = 3.065(2), N—H = 0.85(3), H···N = 2.27(3) Å, N—H···N = 156(2)°. The N(cyano)···N(cyano) distance between two molecules is 2.960(2) Å and the intramolecular N(cyano)···H separation is 2.85(2) Å; this might indicate a very weak bifurcation of the hydrogen bond, although the distances correspond to van der Waals interactions. Other intermolecular distances in **2** are normal. The crystal of **1** contains pairs of molecules with N(pyrrole)—H···O=C type hydrogen bonds, N···O($2 - x$, $-y$, $1 - z$) = 2.868(6), N—H = 0.90(5), H···O = 1.99(5) Å, N—H···O = 164(4)°.

In **3** there is no intermolecular hydrogen bonding, forces between molecules being of van der Waals type. The disposition of the substituents results in intramolecular N(pyrrole)···N(cyano) and N(pyrrole)···O(benzyloxy) distances of 3.279(3) and 2.615(2) Å, respectively; the corresponding H(N-pyrrole)···N(cyano) and H(N-pyrrole)···O(benzyloxy) distances are 2.48(2) and 2.34(2) Å, so that weak bifurcated intramolecular hydrogen bonding is possibly present.

The assigned ^{13}C nmr chemical shifts reported for compounds **1–3** (Table 3) were determined by direct comparison of a series of closely related homologues (Table 3). Replacement of a methyl by an ethyl group, for example, deshields the pyrrolic point of attachment by ~6–7 ppm (a β-effect) and shields *adjacent* pyrrolic positions by ~0.6 ppm (a γ-effect). A judicious choice of substituents allowed all resonances for the compounds in Table 3, including compounds **1–3**, to be unambiguously assigned. Changes in shielding may result from a variety of factors including the electronegativity of substituents, field effects and strain (associated with hybridization). To a first approximation ^{13}C chemical shifts vary linearly with electron density at the carbon atom and thus this spectroscopic technique can be used to examine the nature of bonding and electronic distribution within molecules. While both inductive and mesomeric effects can affect chemical shifts the mesomeric effects are frequently more important in aromatic systems even though α-effects are larger in unsaturated compared to saturated systems.

Carbon nuclei π-conjugated to an electron-withdrawing group suffer significant deshielding by mesomeric interactions. Dipolar resonance canonical forms readily indicate which carbon atoms can be expected to experience enhanced shielding. Interacting bonds may also suffer a change in bond order as a consequence of increasing contributions from *certain canonical forms*. It is thus reasonable to expect that correlations may exist between the magnitudes of deshielding (as measured by the ^{13}C chemical shift) and the importance of such canonical forms. These will show up as changes in bond order which can be measured by changes in bond length as measured by X-ray crystallography.

In the pyrroles under discussion (**1–3**) we have chosen to examine the effects of the benzyloxycarbonyl ($-\overset{\overset{\displaystyle O}{\|}}{C}-O-CH_2OC_6H_5$) and cyano(methoxycarbonyl)vinyl ($-CH{=}C(CN)CO_2CH_3$) groups attached to the pyrrolic nucleus. It has been observed experimentally, and it is of considerable synthetic importance (22) that the latter substituent is especially strongly electron-withdrawing which affects the ease of electrophilic aromatic substitution on the pyrrolic nucleus.

From the crystallographic results it is clear that the cyano(methoxycarbonyl)vinyl group is more electron-withdrawing than a simple ester function and this is reflected in the ^{13}C nmr spectra. An electronegative substituent at C_2 acting primarily through the π-system will affect the greatest deshielding at C_3 and C_5 (canonical forms *B* and *C*). The effect at C_2 has a component of both σ- and π-withdrawal, plus an unknown and unresolvable "substituent effect." Effects at C_4 reflect a "general" deshielding of the π-system, which is appreciable, but considerably less than that at the conjugated positions. It can be seen from Table 3 that the cyano(methoxycarbonyl)vinyl group effects nearly twice as much deshielding at C_3, C_4, and C_5 than the ester, and that for a specific compound C_3 is somewhat more affected than C_5. When compounds bearing both electron withdrawing groups are compared to those bearing only one (Table 4) the cyano(methoxycarbonyl)vinyl group dominates the ^{13}C nmr just as it dominates the structural features. However, the mutual interference noted above between

TABLE 3. ^{13}C chemical shifts

				Chemical shift												
	R_1	R_2	R_3	C_2	C_3	C_4	C_5	R_1	R_2	R_3	a	b	c	d	e	$CDCl_3$
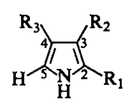	H	Me	Me	115.8	117.9	117.9	115.8	—	9.9	9.9						77.4
										14.7						
	H	Me	Et	115.9	117.3	125.2	114.6	—	10.0	18.5						77.2
									14.7	14.7						
	H	Et	Et	114.6	124.5	124.5	114.6	—	18.5	18.5						77.2
	Me	Me	Me	123.6	113.6	118.2	112.8	11.0	8.8	10.4						77.3
										14.6						
	Me	Me	Et	123.7	112.9	125.0	111.7	11.0	8.8	18.9						77.3
									15.7							
	Me	Et	Me	123.2	120.4	117.4	113.2	11.0	17.7	10.3						77.5
									15.9	14.8						
	Me	Et	Et	123.3	119.8	124.9	111.8	11.0	17.5	18.7						77.2
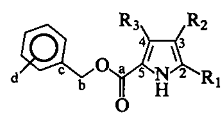														128.0		
	H	Me	Me	121.0	120.4	127.1	118.8	—	9.8	10.4	161.7	65.6	136.6	128.5		77.2
									14.6					128.0		
	H	Et	Me	120.0	127.5	126.4	119.1	—	18.3	10.4	161.9	65.6	136.8	128.5		77.4
														128.5		
	Me	Me	Me	130.5	117.1	127.8	116.3	11.2	8.7	10.8	161.9	65.3	136.8	127.8		77.2
										15.3				127.9		
	Me	Me	Et	130.5	116.4	134.6	115.7	11.3	8.5	18.7	161.6	65.5	136.8	128.5		77.2
									15.4					127.9		
	(1)Me	Et	Me	130.4	123.9	127.2	116.5	11.1	17.3	10.7	162.0	65.4	136.9	128.5		77.4
									16.0	16.1				127.9		
	Me	Et	Et	130.4	123.3	134.0	115.7	11.2	17.1	18.5	161.6	65.5	136.8	128.5		
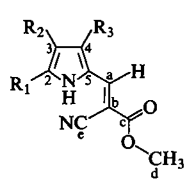	H	Me	Me	124.9	134.6	122.1	128.0	—	9.8	9.4	139.5	88.1	164.7	52.6	119.5	77.2
									14.3							
	H	Et	Me	125.0	133.7	128.9	127.5	—	18.3	9.4	139.4	88.1	164.9	52.6	119.3	77.3
										16.1						
	H	Me	Et	124.0	141.0	121.2	128.7	—	9.7	17.7	139.2	88.0	164.8	52.7	119.3	77.4
									14.6	16.7						
	H	Et	Et	124.1	140.2	128.1	127.6	—	18.0	17.6	139.2	88.1	164.7	52.6	119.2	77.4
	Me	Me	Me	123.3	136.0	119.9	139.4	12.2	8.7	9.7	137.6	84.8	165.2	52.4	120.2	77.3
									14.8							
	Me	Et	Me	123.5	135.3	126.4	139.3	12.0	17.2	9.4	137.6	84.8	165.1	52.3	119.9	77.6
										16.0						
	(2)Me	Me	Et	122.5	142.4	119.1	139.6	12.2	8.6	17.9	137.6	85.0	165.2	52.4	120.2	77.3
									15.4	17.1						
	Me	Et	Et	122.6	141.8	125.7	139.5	12.2	17.1	17.7	137.6	85.0	165.2	52.3	120.0	77.5
								12.2		16.1						
	Et	Me	Et	122.4	142.4	118.2	144.8	19.9	8.5	17.8	137.9	85.1	165.2	52.3	120.4	77.3
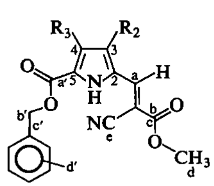	—	Me	Me	125.6	133.5	127.4	126.0	—	9.2	9.9	139.0	94.4	163.3	53.0	117.8	77.2
	—							—			a' 159.8	b' 66.6	c' 135.6	d' 128.7	d' 128.4	d' 128.1
	(3)—	Et	Me	124.9	139.9	126.7	126.2	—	16.0		138.9	94.6	163.3	53.1	117.8	—
								—	17.4	9.7	a' 159.8	b' 66.6	c' 135.6	d' 128.7	d' 128.4	d' 128.2
	—	Me	Et	125.7	132.8	133.8	125.7	—	8.9	14.7	139.2	94.4	163.4	53.0	117.9	77.2
										17.8	a' 159.7	b' 66.7	c' 135.5	d' 128.7	d' 128.4	d' 128.2
	—	Et	Et	125.0	139.2	133.2	125.7	—	17.1	15.5	138.9	94.6	163.2	53.0	117.9	77.4
	—								17.1	17.7	a' 159.4	b' 66.7	c' 135.6	d' 128.6	d' 128.4	d' 128.2

this and an ester group results in considerably smaller effects at C_2 and C_5 than at C_3 and C_4 as the charge-repulsion from the dipolar substituents removes the positive charge from the "ipso" position. Thus the marginal effect of introducing a second α-electron-withdrawing group falls mainly on the adjacent β-position. As can be seen from Table 3, addition of an ester has essentially no effect at C_4 or C_5 and is of opposite sign — slightly deshielding at C_5 and slightly shielding at C_4.

This electronic distribution is reflected not only in the pyrrole core, but in the substituents themselves. In the difunctional compound **3**, the benzyl ester carbonyl is *less* polarized, and occurs 2.26 ppm upfield from the mono-ester **1**. With the benzyl ester in opposition, the nitrile carbon occurs 2.35 ppm upfield, and the carbonyl 1.86 ppm upfield of the corresponding carbons in the mono-functional analogues. The effect is largest on the vinyl double bond itself; in the mono-substituted compound, where the cyanovinyl group has the sole access to the pyrrolic electron density, this bond is most polarized, with the negative charge shifting the 2-carbon 9.63 ppm upfield of the difunctional analog.

The competitive effects of the electron-withdrawing groups is reflected in the chemical reactivity of pyrroles bearing such groups. For example, in the synthesis of cyano(methoxycarbonyl)vinyl adducts from 2-formylpyrroles and methyl cyanoacrylate, the presence of an ester at C_5 greatly accelerates the rate of the reaction since with less electron-density available to it from the pyrrole ring, the formyl group becomes more electrophilic (22).

Acknowledgements

This work was supported by the Natural Sciences and Engineering Research Council of Canada and the United States National Institutes of Health (GM 29198). We thank the University of British Columbia Computing Centre for assistance.

1. A. R. BATTERSBY and E. MCDONALD. *In* "B_{12}". *Edited by* D. Dolphin. Wiley-Interscience, New York. 1982. pp. 107–144.
2. A. I. SCOTT. Acc. Chem. Res. **11**, 29 (1978).
3. P. C. LAUTERBUR. J. Am. Chem. Soc. **83**, 1838 (1961).
4. T. F. PAGE, T. ALGER, and D. M. GRANT. J. Am. Chem. Soc. **87**, 5333 (1965).
5. R. J. PUGMIRE and D. M. GRANT. J. Am. Chem. Soc. **90**, 4232 (1968).
6. R. J. ABRAHAM, R. D. LAPPER, K. M. SMITH, and J. F. UNSWORTH. J. Chem. Soc. Perkin II, 1004 (1974).
7. D. M. GRANT and B. V. CHENEY. J. Am. Chem. Soc. **89**, 5315 (1967).
8. A. HAYES, G. W. KENNER, and N. R. WILLIAMS. J. Chem. Soc. 3779 (1958).
9. A. W. JOHNSON, E. MARKHAM, R. PRICE, and K. B. SHAW. J. Chem. Soc. 4254 (1958).
10. H. W. WHITLOCK and R. HANAUER. J. Org. Chem. **33**, 2169 (1968).
11. J. B. PAINE. *In* The porphyrins. Vol. I. *Edited by* D. Dolphin. Academic Press, New York. 1978, pp. 101–234.
12. H. FISCHER and H. ORTH. *In* Die Chemie Des Pyrrols. Vol. I. Johnson Reprint Corporation, New York, NY. 1968. p. 157.
13. M. F. HUDSON and K. M. SMITH. Synthesis, 464 (1976).
14. D. T. CROMER and J. B. MANN. Acta Crystallogr. Sect. A **24**, 321 (1968).
15. R. F. STEWART, E. R. DAVIDSON, and W. T. SIMPSON. J. Chem. Phys. **42**, 3175 (1965).
16. P. J. BECKER and P. COPPENS. Acta Crystallogr. Sect A, **30**, 129 (1974).
17. P. J. BECKER and P. COPPENS. Acta Crystallogr. Sect A, **31**, 417 (1975).
18. (*a*) L. NYGAARD, J. T. NIELSEN, J. KIRCHHEINER, G. MALTESEN, J. RASTRUP-ANDERSEN, and G. O. SORENSEN. J. Mol. Struct. **3**, 491 (1969); (*b*) J. J. STEZOWSKI. Acta Crystallogr. Sect B, **33**, 2472 (1977); (*c*) J. V. SILVERTON and H. A. LLOYD. Acta Crystallogr. Sect B, **31**, 1576 (1975).
19. O. BASTIANSEN and M. TRAETTEBERG. Tetrahedron, **17**, 147 (1962).
20. Tables of interatomic distances and configuration in molecules and ions, Supplement 1956–1959. Special Publication No. 18, Chemical Society, London 1965.
21. (*a*) R. BONNETT, M. B. HURSTHOUSE, and S. NEIDLE. J. Chem. Soc. Perkin Trans. II, 902 (1972); 1335 (1972); (*b*) W. S. SHELDRICK, A. BORKENSTEIN, and J. ENGEL. Acta Crystallogr. Sect B, **34**, 1248 (1978).
22. J. B. PAINE, III, and D. DOLPHIN. In preparation.

Hydrodynamic studies on micellar solutions of styrene–butadiene block copolymers in selective solvents

LEVENT ORANLI, PRATAP BAHADUR,[1] AND GÉRARD RIESS
Ecole Nationale Supérieure de Chimie de Mulhouse, France

Received March 28, 1984

LEVENT ORANLI, PRATAP BAHADUR, and GÉRARD RIESS. Can. J. Chem. **63**, 2691 (1985).

Hydrodynamic radius of micelles of several block copolymers in different selective solvents (for both types of blocks) was determined from photon correlation spectroscopy. The boundaries of micellar solutions in heptane (good solvent for polybutadiene block) and dimethylformamide (good solvent for polystyrene block) were established for polymers in terms of their molecular mass and block composition. The photon correlation spectroscopy data in combination with intrinsic viscosities of block copolymers in selective solvents were used to determine micellar molecular mass and aggregation number. The influence of temperature on the micelle size was examined. The block copolymer micelles could solubilize a certain amount of insoluble homopolymer within their insoluble core. ^{1}H nmr spectra were examined to study the influence of temperature on micellar systems.

LEVENT ORANLI, PRATAP BAHADUR et GÉRARD RIESS. Can. J. Chem. **63**, 2691 (1985).

Le rayon hydrodynamique des micelles de copolymères blocs formés dans différents solvants sélectifs de l'une ou de l'autre séquence a été déterminé par spectroscopie de photocorrélation. Pour ces copolymères du type polystyrène-*block*-polybutadiène on a défini le domaine d'existence des solutions micellaires dans l'heptane (solvant sélectif de la séquence polybutadiène) et dans le diméthylformamide (solvant sélectif de la séquence polystyrène) en fonction de la masse moléculaire et de la composition. La masse moléculaire des micelles et le nombre d'agrégation ont été déterminés sur la base de la viscosité intrinsèque des copolymères et des résultats de spectroscopie de photocorrélation. On a examiné par ailleurs l'influence de la température sur la taille des micelles et la solubilisation d'homopolymères dans le coeur de celles-ci. Les caractéristiques micellaires du système ont été étudiées par spectroscopie rmn du proton à différentes températures.

Introduction

Dilute solutions of block copolymers in selective solvent (a good solvent for one sequence but a poor solvent for the other) show the existence of micelles formed through a reversible closed association process in analogy to low molecular weight surfactants (1–3). Styrene–diene block copolymers have received much attention in the study of such polymeric micelles. The micelle formation in selective solvents (pure and mixed solvents) for each block has been studied using several techniques viz. light scattering (4–14), viscosity (4, 7, 9, 13–15), osmometry (12, 15, 16), ultramicroscopy (19), electron microscopy (19–21), gel permeation chromatography (20), nmr (22, 23), small angle X-ray scattering (17, 18, 24, 25), photon correlation spectroscopy (19, 26), and sedimentation measurements (10, 15).

In most cases block copolymers in solution showed the presence of spherical micelles over a wide concentration and temperature range which had narrow size distribution and were stable for long time. However, a few studies report the formation of unusually large particles which were examined to be polydispersed and unstable.

It is realised that the micellar behaviour of block copolymers largely depends upon their molecular characteristics (type, molecular mass, and block composition), the selectivity of solvent, temperature and concentration range studied. Despite several works cited above, the authors feel scarsity of systematic data describing the domains of micellar solutions formed by different block copolymers with varying molecular characteristics in different solvents and the influence of block copolymer characteristics, nature of solvent, temperature on the micellar characteristics (size, aggregation number, critical micelle concentration, etc...).

Generally, studies on styrene–butadiene block copolymers have been carried out in solvents selectively bad for polystyrene block (e.g. *n*-alkanes). Although Tuzar and Kratochvil (1) have studied micelles with polybutadiene core but these authors have always used a mixed solvent which may cause some complexities due to preferential adsorption. In this paper, both type of solvents are used to study micelles. Further, a large number of copolymers differing in molecular weight and block composition are used to observe the domains of molecularly dissolved solutions (perhaps unimolecular micelles), true micelles (multimolecular with narrow distribution, stable over a prolonged period), and aggregates of insoluble particles in the form of coarse and unstable suspension with wide distribution. Some tapered block copolymers are also considered in order to compare tapered and pure block composition on the micelle size and aggregation number. Micellar solutions prepared using tetrahydrofuran (good solvent for both the block) to dissolve the copolymer, adding the selective solvent and subsequently removing tetrahydrofuran resulted to real micelles and the technique has proved to be better than making micellar solutions of block copolymers directly in selective solvent by simple heating, particularly with relatively high molecular mass and high percentage composition of insoluble block when it was too difficult to dissolve the block copolymer even on heating for several hours.

Micellar size and aggregation number have been estimated from the hydrodynamic properties of micellar solutions as observed from photon correlation spectroscopy, a relatively new technique for studying micellar solutions, and viscosity. Influence of temperature and solubilization of insoluble homopolymers within the cores of micelles has been examined. The temperature effect on micellar solutions affecting monomer–micelle equilibrium has also been investigated using ^{1}H nmr.

Experimental

Several two block styrene–butadiene copolymers synthesised anionically were used. Some of them were prepared in the laboratory while others were of commercial origin. All these block copolymers

[1] Present address: South Gujurat University, India.

TABLE 1. Molecular characteristics of block copolymers

Copolymer	$\bar{M}_n$ total	wt.% PS total	wt.% PS block
SB-6	72 000	52	—
SB-7	46 000	51	—
410*	68 000	48	32
TX 006*	375 000	48	—
TX 005*	320 000	28	—
TX 004*	270 000	74	—
ANIC C*	105 000	30	—
AN 28	150 000†	88	—
AN 29	130 000†	78	—
SB 308*	158 000	30	—
SB 1205*	71 000	25	18
S 317 US*	204 000	41	32
S 317 Eur*	220 000	38	27
S 314*	150 000	70	46

*Commercial samples.
†$\bar{M}_n$ from mean of bimodal distribution.

were characterised by gpc and nmr. The detailed specifications of the copolymers are shown in Table 1.

n-Alkanes (heptane, octane, decane, and dodecane), *N,N'*-dimethylformamide, *N,N'*-dimethylacetamide, and methyl ethyl ketone used as selective solvents for the block copolymers were of AnalaR grade.

The micellar solutions were prepared by using tetrahydrofuran unless stated otherwise. The block copolymers were first dissolved in small amounts of tetrahydrofuran to which the selective solvent was subsequently added. Tetrahydrofuran was then removed from the solution by distillation at 60°C. Enough care was taken in the removal of tetrahydrofuran which in turn may affect micellar characteristics of the block copolymers in selective solvents.

Stock solutions (1.5–2% by weight) of block copolymers, bluish transparent to milky opalescence in appearance (characteristics of micelles) and stable for several weeks were prepared. Dilutions were made from the stock solutions and each solution was filtered before measurements.

Photon correlation spectroscopy studies on micellar solutions of block copolymers were carried out using Coulter model N 4 to give the hydrodynamic radius of micelles.

The scattering angle was always 90°. Z-average diffusion coefficient of micelles, $\bar{D}_Z$, was calculated from the mean decay constant, $\bar{Q}$, of autocorrelation functions using the relationship

$$[1] \quad \bar{D}_Z = \frac{\bar{Q}}{2K^2}$$

where $K = (4\pi\, n \sin \theta/2)/\lambda$ is the scattering vector, θ is the scattering angle, n the refractive index of the medium, and λ the wavelength of light *in vacuo*.

The equivalent spherical hydrodynamic radius of the micelle, $R_{h,D}$ is then calculated, assuming the applicability of Stokes–Einstein equation,

$$[2] \quad R_{h,D} = kT/6\pi\eta\bar{D}_Z$$

where k is the Boltzmann constant, T, the absolute temperature, and η, the viscosity of solvent.

Measurements were generally made at 25°C at various concentrations between 0.1–1.5%. The diffusion coefficient (and thus the hydrodynamic radius) was determined by extrapolation to infinite dilution.

The viscosities were measured using Ubbelhode-type viscometer with electronic time registration. Essentially solutions were diluted till the solutions had bluish appearance. The intrinsic viscosities were calculated by extrapolating specific viscosities to zero concentrations.

The following equation relates hydrodynamic radius to the micellar weight

$$[3] \quad R^3_{h,\eta} = \frac{3[\eta]M^m}{10\pi N}$$

where M^m is the micellar weight, $[\eta]$ the intrinsic viscosity, N_A the Avogadro number, and $R_{h,\eta}$ the hydrodynamic radius of micelle obtained from viscosity.

Almost same values of hydrodynamic radii of micelles obtained from diffusion coefficient and viscosity data have been observed by various workers (27–29). We have therefore used $R_{h,D}$ instead of $R_{h,\eta}$ in eq. [3] to calculate the micellar weight and to estimate the aggregation number.

The ^{1}H nmr spectra of copolymer in heptane at various temperatures were recorded using a Bruker WP 80 CW instrument working at 80 MHz and attached to a temperature control unit (Bruker B-ST 100/700C). Enough time was provided for attaining the equilibrium of micellar solutions at different temperatures.

Results and discussion

Solutions of block copolymers in both the types of selective solvents behave in a quite peculiar way. Molecularly dispersed solutions, micellar solutions or unstable suspensions of block copolymers can be obtained depending upon the concentration and the molecular characteristics of block copolymer, solubility parameters of solvent with respect to the two blocks of the copolymer, and temperature. In general, increasing copolymer concentration, its total molecular weight, and the composition of the insoluble block favour the formation of micelles from truly molecularly dissolved solutions. Decrease in temperature and increase in precipitant nature of solvent shift the unimer $\rightleftharpoons$ micelle equilibrium to micelle side.

Micelles in each case were multimolecular, spherical in shape, and had low polydispersity. In *n*-alkanes the block copolymer micelles consisted of insoluble polystyrene core surrounded by the soluble fringes of polybutadiene. A reverse structure was observed in the other type of selective solvent. e.g., in DMF, DMA, and MEK.

(1) Micelles in various selective solvents

Micellar solutions of a few block copolymers were obtained by dissolution of the copolymers in both kinds of solvent (selectively good solvents for polybutadiene, viz. *n*-heptane, *n*-octane, *n*-decane, and *n*-dodecane as well as selectively good solvent for polystyrene viz. DMF, DMA, and MEK). Generally 1 g or less of the copolymer was dissolved in 100 mL of solvent by heating the copolymer–solvent mixture in closed tubes in a water thermostat at about ~60°C. For block copolymers in MEK the micellar solutions were obtained by heating at ~50°C.

As mentioned above, only a few copolymers formed micelles (characterised by bluish transparent tinge) whereas others were insoluble in the solvent (these showed phase separation or unstable suspension of the insoluble particles). Generally, dissolution of block copolymer above a certain critical value of insoluble block composition (which of course depends on total molecular weight and solubility parameter of the solvents) becomes difficult and results to the macro phase separation.

The size of these block copolymer micelles is shown in Table 2. Since the measurements of micelle size were carried out using photon correlation spectroscopy, the value expressed as hydrodynamic radius takes into account both the insoluble core (which depends upon the aggregation number) and soluble shell (which mainly depends upon the solubility of the soluble block in the solvent). For this reason, it is in fact usual to get different trend in R_h and N.

TABLE 2. Hydrodynamic radius, intrinsic viscosity, and aggregation number of block copolymer micelles in various selective solvents (the micellar solutions were prepared by dissolving the copolymer at ~60°C)*

	SB-7			Rh (nm)			
Solvent	Rh (nm)	[η] (cm^3 g^{-1})	N	SB-1205	SB-6	AN 28	AN 29
n-Heptane	30.5	17.1	227	41.5	i	i	i
n-Octane	28.0	14.4	209	37.0	i	i	i
n-Decane	28.2	15.9	193	38.5	i	i	i
n-Dodecane	32.9	27.3	179	43.0			
DMF	21.0	7.4	172	i	38.5	55.8	42.5
DMA	36.3	14.5	452	i	54.0	75.0	56.0
MEK	—	—	—	i	34.5	55.0	38.0

*i = insoluble.

An examination of the data on R_h for copolymers in n-alkanes, it appears that the size of micelle does not differ much. The greater size for n-dodecane may be explained on account of the fact that the soluble chain is very much extended in spite of the fact that the micelle has least aggregation number. The decreasing trend in the aggregation number of micelles of styrene–butadiene block copolymers with increasing carbon chain length in n-alkane was observed by Stacy and Kraus (5).

The hydrodynamic radius of block copolymers in DMF, DMA, and MEK are also shown in Table 2. A comparison of size of various copolymers in these three solvents shows that the values for DMF and MEK are not much different. Higher values of micelle size in DMA were observed. The high hydrodynamic radius of micelles in DMA as compared to in DMF is explained due to the higher aggregation number (which increases the core size) and more extended soluble shell (due to the difference in solubility parameter). The hydrodynamic radius of micelles in MEK, where the soluble chain seems to be most extended may result from its very low aggregation number. However, this could not be verified in case of copolymer SB-7 which at concentrations studied (even up to ~3%) contains more of unimers and such solutions were more or less clear with very faint bluish appearance.

It was observed that the size and aggregation number has no influence on heating at temperature above 60°C. Even the micellar solutions of block copolymers formed by the dissolution of copolymer at temperature just below the boiling point of the respective solvent on cooling to the measuring temperature resulted the same size. Further, that repeated heating and cooling did not affect the micelle size and aggregation number. Of course, it is to be mentioned here that enough time was given for the equilibrium of the micellar solution at the measuring temperature. The micellar solutions were generally kept for 1–2 h at the measuring temperature before the measurement.

Further studies were confined to n-heptane and DMF taken as representatives of the two types.

(2) Micelles in n*-heptane and DMF (comparison of dissolution and THF technique)*

In Table 3 are compared the hydrodynamic radii of block copolymer micelles prepared in solution by simple dissolution of the copolymer at ~60°C or using small amounts of THF as the supporting solvent, added to dissolve the copolymer and was subsequently removed. It appears that for SB-7 and SB-1205 micelles in n-heptane, the size is practically the same. Increased size for ANIC C micelles in solution prepared from simple dissolution technique may be due to large proportion of bigger particles and broader distribution in micelle size. It may be said that increasing content of insoluble block and increase in total molecular weight may result in micellar solutions (obtained by simple dissolution) which are not perfectly homogeneous and the size of the micelles is greater than that in solution prepared using THF technique.

TABLE 3. Hydrodynamic radius of block copolymer micelles in n-heptane and DMF at 25°C (micellar solutions were obtained by the dissolution of copolymer at ~60°C or using THF technique)

		Rh (nm)	
Copolymer	Solvent	Dissolution technique	THF technique
SB-7	n-Heptane	30.5	32.5
ANIC C	n-Heptane	63.6	52.5
SB-1205	n-Heptane	41.5	41.5
SB-7	DMF	21.0	14.5
AN 28	DMF	55.8	29.0
AN 29	DMF	42.0	23.0

Larger difference in the micelle size of copolymers in DMF was seen in the solutions prepared using the dissolution technique or the THF technique. This probably accounts for a rather poor solvent nature for DMF.

As a general rule, it may be said that the two techniques may result in the micellar solutions of the same size when the insoluble block % is fairly low (<30%) and total molecular weight is not too high (~50 000). The advantage of the THF technique lies in the fact that for block copolymers with high content of insoluble block and high molecular weight, micelles of lower size than obtained by simple dissolution on heating can be obtained. In addition, the critical limit of insoluble block can be extended by using the THF technique and micellar solutions of block copolymers could be prepared which were otherwise not possible by the dissolution technique where the macro phase separation resulted. However, using the THF technique also it was possible to obtain micelles of block copolymers in both the solvents up to 60 wt.% of insoluble block for copolymers with molecular mass of about 100 000.

(3) Micelles in n*-heptane and DMF (THF technique)*

Table 4 shows the hydrodynamic radius, intrinsic viscosity, micellar weight, and aggregation number of several block copolymer micelles in n-heptane and DMF. A general observable feature is that micelle size and aggregation number increase

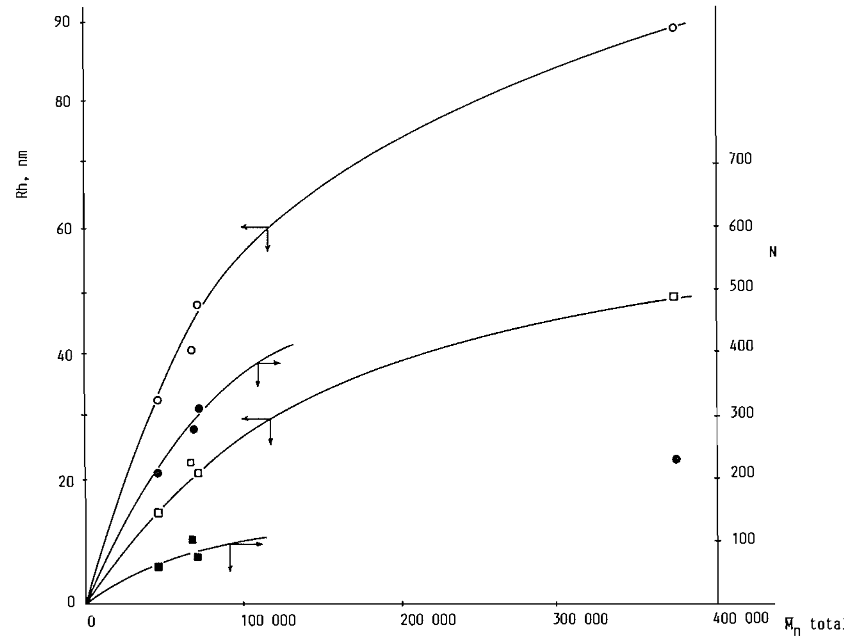

FIG. 1. Hydrodynamic radius and aggregation number of block copolymer (~50% PS) in n-heptane and DMF; ○ Rh in heptane, □ Rh in DMF, ● N in heptane, ■ N in DMF.

with increase in % insoluble block and increase in total molecular weight of copolymers. However, an additional feature is that the micelle radius as high as ~100 nm could be obtained and the aggregation number as high as ~312 was seen. Usually, the micelle size and aggregation number for the same block copolymer in n-heptane was higher compared to those in DMF. We could not observe very high micelle size and aggregation number for TX 006 (% PS 48, $\bar{M}_n$ total 375 000) in heptane as observed by Stacy and Kraus (5) and as predicted from the theoretical results of Noolandi and Hong (24). We have checked this point and results from solution of copolymers prepared at different times gave the same value.

Further experiments are necessary to check the micelle size and the aggregation number of more copolymers with high molecular weights.

Figure 1 shows R_h and N values for copolymers (~50% each of the blocks) micelles in n-heptane and DMF as a function of total molecular weight of the copolymer. A reasonably good trend in R_h and N values for the micelles in both solvents can be observed in this figure.

(4) Influence of temperature on micelles

The influence of temperature on the hydrodynamic radii of block copolymer micelles in n-heptane and DMF can be seen from Fig. 2. In both solvents, the hydrodynamic radius of micelles decreases. This decrease may be accounted for by the decrease in micellar weight or aggregation number. Similar decrease for styrene–butadiene block copolymer micelles in n-heptane has been observed by Plestil and Baldrian (17) and in tetrahydrofuran + allyl alcohol (where the micelle structure is similar to that in DMF) by Tuzar and Kratochvil (1). Of course, the relative proportion of unimers in the micellar solution increases with increasing temperature.

It was also interesting to examine the influence of temperature on ^{1}H nmr spectrum of block copolymer micelles. Spectra for SB-7 in n-heptane were recorded at different temperatures (Fig. 3). It is evident from Fig. 3 that no aromatic protons of polystyrene could be detected up to ~65°C. The

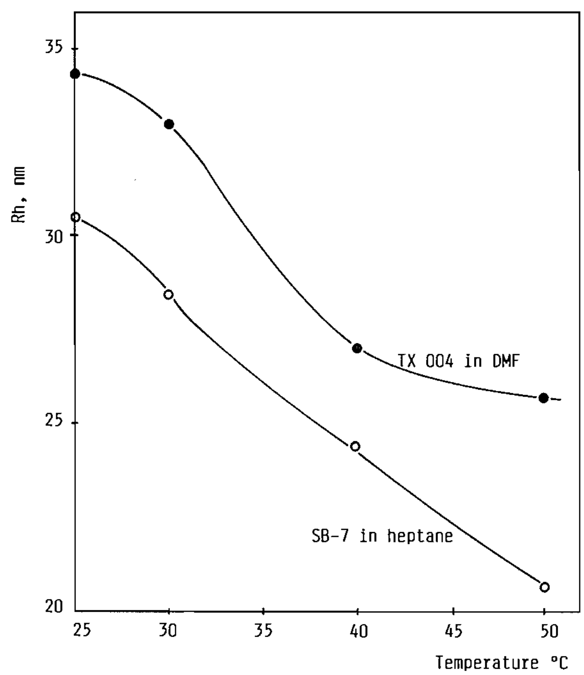

FIG. 2. Hydrodynamic radius of block copolymer micelles in heptane and DMF; ● TX 004 in DMF, ○ SB-7 in heptane.

undetectable polystyrene due to restricted motion of styrene units may account for the fact that at this temperature most of the block copolymer is in the micellar form. The small amount of unimers present may acquire the conformation similar to the so-called "unimolecular micelles", thus shielding the motion of styrene units. At the highest temperature studied i.e. 95°C, distinct peaks corresponding to polybutadiene and polystyrene were observed and calculation from integrated intensity gave the percentage composition of the two block as the actual value for the copolymer SB-7 (51% PS).

This indicates that at this temperature almost all of the co-

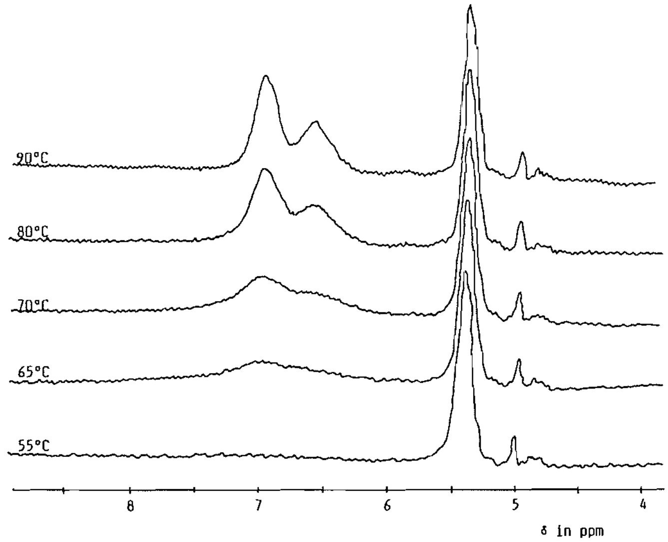

FIG. 3. ^{1}H nmr spectra of block copolymer SB-7 (concentration 5 g dL^{-1}) at different temperatures in *n*-heptane.

polymer is unimolecularly dissolved with free motion of styrene units of the polystyrene block. The nature of spectra in the intermediate temperature range is quite peculiar. On going above the temperature 65°C, broad peak of aromatic styrenic protons begins to appear, and becomes higher and narrower with a gradual increase in temperature. Several factors seem to be important here which may lead to the growth of mobility of styrene units with increase in temperature. These may be, for example, the disintegration of actual (polymolecular) micelles to unimers, the swelling of cores of micelles (both polymolecular and unimolecular), change in conformation of unimolecular micelles leading to free unimers, and the polydispersity effect in molecular weight and composition of copolymer. Different effects may be predominant in various temperature range till 95°C where the actual composition of copolymer was seen. A similar behaviour in ^{1}H nmr spectra for copolymer micelles as affected by temperature was observed by Spevacek (23).

TABLE 4. Micellar characteristics of block copolymers in *n*-heptane and DMF

Copolymer	Rh (nm)	[η] (cm^3 g^{-1})	M^m	N
		n-*Heptane*		
SB-6	48.0	30.93	2.25×10^7	312
SB-7	32.5	23.02	9.40×10^6	204
410	40.5	22.28	1.90×10^7	276
TX 006	91.0	54.30	8.70×10^7	233
ANIC C	52.5	56.50	1.61×10^7	154
SB 308	52.0	55.20	1.60×10^7	102
SB 1205	41.5	50.40	8.94×10^6	126
TX 005	95.0	—	—	—
S 317 US	53.5	63.80	1.51×10^7	74
S 317 Eur	57.0	50.90	2.29×10^7	104
		DMF		
SB-6	21.0	10.91	5.35×10^6	74
SB-7	14.5	6.80	2.80×10^6	61
410	22.5	9.68	7.42×10^6	109
TX 006	48.5	—	—	—
TX 004	34.5	39.69	6.52×10^6	24
AN 28	29.0	37.38	4.10×10^6	27
AN 29	23.0	28.47	2.70×10^6	21
S 314	29.0	20.41	7.53×10^6	50

(5) Solubilization of homopolymers

Homopolymers could be solubilized within the core of micelles of block copolymers. However, the extent of solubilization largely depended upon the molecular mass of homopolymer and of block copolymer sequence forming the insoluble core. It was only possible to solubilize homopolymer if its molecular mass did not exceed that of corresponding sequence of block copolymer. In general, lower molecular mass homopolymer enhanced the extent of solubilization. Also, it was observed that an homopolymer under certain conditions could be solubilized up to 50 wt.% of the copolymer. All the solubilized solutions had stability comparable to those of micellar solutions without any solubilized homopolymer.

Table 5 reveals some results on solubilization of polystyrene

TABLE 5. Solubilization of homopolymers within the core of micelles of block copolymers

Block Copolymer	Solvent	Homopolymer solubilized	% Homopolymer solubilized†	Rh (nm)
SB-7	Heptane	—	—	32.5
		Polystyrene $\bar{M}_n$ 9 000	5%	36.0
			10%	58.0
		Polystyrene $\bar{M}_n$ 21 000	5%	46.0
			10%	*
TX 004	DMF	—	—	34.5
		Polybutadiene $\bar{M}_n$ 20 000	20%	56.0
		Polybutadiene $\bar{M}_n$ 48 000	20%	59.0
SB-7	DMF	—	—	14.5
		Polybutadiene $\bar{M}_n$ 20 000	20%	18.4
			40%	20.9
			45%	25.0
			50%	35.4

*Could not be solubilized.
†With respect to block copolymer.

homopolymer in block copolymer micelles in *n*-heptane and polybutadiene homopolymers in block copolymer micelles in DMF. An examination of the data clearly reveals that the micelle size increases (or in fact the core size) with increased amount of homopolymer solubilized and its molecular weight. More amount of homopolymer with low molecular weight could be solubilized than of high molecular weight. The increased size in the solubilized micelles seems to be quite reasonable. More experiments on solubilized micelles are in progress and will be published later.

Acknowledgements

The authors wish to acknowledge their thanks to P. Gaillard, CdF Chimie, for supplying some of the block copolymer samples, and to H. Strub for taking the ^{1}H nmr spectra.

1. Z. TUZAR and P. KRATOCHVIL. Adv. Colloïd Interface Sci. **6**, 201 (1976).
2. C. PRICE. *In* Development of block copolymers I. *Edited by* I. Goodman. Applied Science Publishers, England. 1982. pp. 39–80.
3. G. RIESS, P. BAHADUR, and G. HURTREZ. Encyclopedia polymer science and engineering. Vol. 2. 2nd ed. John Wiley and Sons. 1985. p. 324.
4. S. KRAUSE and P. A. REISMILLER. J. Polym. Sci. Polym. Phys. Ed. **13**, 663 (1975).
5. C. J. STACY and G. KRAUS. Polym. Eng. Sci. **17**, 627 (1977).
6. M. ENYIEGBULAM and D. J. HOURSTON. Polymer, **19**, 727 (1978).
7. Z. TUZAR and P. KRATOCHVIL. Makromol. Chem. **160**, 301 (1972).
8. Z. TUZAR, P. BAHADUR, and P. KRATOCHVIL. Makromol. Chem. **182**, 1751 (1981).
9. Z. TUZAR and P. KRATOCHVIL. Makromol. Chem. **170**, 177 (1973).
10. A. PROCHAZKA, M. K. BALOCH, and Z. TUZAR. Makromol. Chem. **180**, 2521 (1979).
11. P. A. CANHAM, T. P. LALLY, C. PRICE, and R. B. STUBBERSFIELD. J. Chem. Soc. Faraday I, **74**, 1857 (1980).
12. C. PRICE. Pure Appl. Chem. **55**, 1563 (1983).
13. W. MANDEMA, H. ZELDENRUST, and C. A. EMEISS. Makromol. Chem. **180**, 1521 (1979).
14. W. MANDEMA, C. A. EMEISS, and H. ZELDENRUST. Makromol. Chem. **180**, 2163 (1979).
15. J. PERIARD and G. RIESS. Europ. Polym. J. **9**, 687 (1973).
16. A. SIKORA and Z. TUZAR. Makromol. Chem. **184**, 2049 (1983).
17. J. PLESTIL and J. BALDRIAN. Makromol. Chem. **174**, 183 (1973); **176**, 1009 (1975).
18. M. SHIBAYAMA, T. HASHIMOTO, and K. HIROMICHI. Macromolecules, **16**, 16 (1983).
19. C. PRICE, P. A. CANHAM, M. C. DUGGLEBY, T. V. NAYLOR, N. S. RAJAB, and R. B. STUBBERSFIELD. Polymer, **20**, 615 (1979).
20. C. BOOTH, T. D. NAYLOR, C. PRICE, N. S. RAJAB, and R. B. STUBBERSFIELD. J. Chem. Soc. Faraday I, **74**, 2352 (1978).
21. C. PRICE and D. WOOD. Europ. Polym. J. **9**, 827 (1973).
22. F. HEATLEY and A. BEGUM. Makromol. Chem. **178**, 1205 (1977).
23. J. SPEVACEK. Makromol. Chem., Rapid. Commun. **3**, 697 (1982).
24. J. NOOLANDI and K. M. HONG. Macromolecules, **16**, 1443 (1983).
25. T. L. BLUHM, S. L. MALHOTRA, M. HONG, and J. NOOLANDI. Am. Chem. Soc. Polym. Preprints, **24**(2), 405 (1983).
26. Z. TUZAR, B. BEDNAR, C. KONAK, M. KUBIN, S. SVOBODOVA, and K. PROCHAZKA. Makromol. Chem. **183**, 399 (1982).
27. H. K. MAHABADI and A. RUDIN. Makromol. Chem. **179**, 2977 (1978).
28. J. ROOVERS and P. M. TOPOROWSKI. J. Polym. Sci. Polym. Phys. Ed. **18**, 1907 (1980).
29. Z. TUZAR, J. PLESTIL, C. KADAK, D. HLAVATA, and A. SIKORA. Makromol. Chem. **184**, 2111 (1983).

Benzylic substitution in ring A of daunomycinone. Conversion of daunomycinone into thiodaunomycinone and related deoxy analogs[1]

MOHAMMED A. E. SALLAM[2]
Department of Chemistry, Faculty of Science, Alexandria University, Alexandria, Egypt

ROY L. WHISTLER
Department of Biochemistry, Purdue University, W. Lafayette, IN47907, U.S.A.

AND

JOHN M. CASSADY
Department of Medicinal Chemistry and Pharmacognosy, Purdue University, W. Lafayette, IN47907, U.S.A.

Received November 23, 1984

MOHAMMED A. E. SALLAM, ROY L. WHISTLER, and JOHN M. CASSADY. Can. J. Chem. **63**, 2697 (1985).

Catalytic hydrogenolysis of daunomycinone (**4**) over palladium–carbon or palladium – barium sulfate afforded a mixture of 7-deoxydaunomycinone (**5**) and 7,11-dideoxydaunomycinone (**6**). 7-Deoxy-7-thioacetyldaunomycinone (**8**) and its 7-epimer (**9**) were prepared from **5** via the intermediate 7-deoxy-7-bromo derivative **7** in 33% yield. Compound **8** was prepared from **4** in a one-step reaction by treatment with thioacetic acid (THAA) and trifluoroacetic acid (TFAA), in 13% yield. Refluxing **4** in a mixture of THAA and glacial acetic acid (GAA) increased the yield of **8** and **9** to 83%. Epimerization of **9** with TFAA afforded **8**. Hydrolysis of **8** gave a mixture of thiodaunomycinone (**10**), **5**, and bisanhydrodaunomycinone (**11**). Compound **10** converts partially into its dimeric form (**12**) on standing.

MOHAMMED A. E. SALLAM, ROY L. WHISTLER et JOHN M. CASSADY. Can. J. Chem. **63**, 2697 (1985).

L'hydrogénolyse catalytique de la daunomycinone (**4**) sur des catalyseurs de palladium/charbon ou de palladium/sulfate de baryum conduit à un mélange de déoxy-7 daunomycinone (**5**) et didéoxy-7,11 daunomycinone (**6**). On a aussi préparé la déoxy-7 thioacétyl-7 daunomycinone (**8**) et son épimère en position 7 (**9**) avec un rendement de 33% en utilisant **5** comme produit de départ et en procédant par l'intermédiaire du dérivé déoxy-7 bromo-7 (**7**). Le traitement de **4** par de l'acide thioacétique (ATHA) et de l'acide trifluoroacétique (ATFA) conduit en une étape au composé **8**, avec un rendement de 13%. Si l'on porte le composé **4** au reflux dans un mélange d'ATHA et d'acide acétique glacial (AAG), on augmente le rendement de **8** et de **9** à 83%. L'épimérisation de **9** par de l'ATFA conduit à **8**. L'hydrolyse de **8** conduit à un mélange de thiodaunomycinone (**10**), de **5** et de bisanhydrodaunomycinone (**11**). Si on le laisse à la température ambiante, le composé **10** se transforme partiellement en sa forme dimère **12**.

[Traduit par le journal]

The anthracycline antibiotics, daunorubicin (**1**, $R^1 = CH_3$, $R^2 = H$) (2, 3), doxorubicin (adriamycin; **1**, $R^1 = CH_3$, $R^2 = OH$) (3, 4), and carminomycin (**1**, $R^1 = R^2 = H$) (5) are potent and clinically useful antitumor agents, with adriamycin having an especially broad spectrum of activity, extending to certain solid tumors that are normally resistant to most modes of chemotherapy. However, the clinical use of these drugs is hampered by a number of undesirable side effects, common to many antitumor drugs, such as severe alopecia, and dose-limiting and irreversible cardiotoxicity (6) (congestive heart failure), which have limited their optimum utilization in chemotherapy. The possible covalent bindings between C-7 and various biological nucleophiles have been suggested (7) as a basis for the toxic side effects of daunorubicin and adriamycin. Major efforts have been made to modify the anthracycline molecule with the objective of developing analogs with a wider spectrum of activity and reduced toxicity (8, 9). The synthesis of anthracycline analogs with various leaving groups (10) at C-7, and displacement of the 7-OH with O- and S-nucleophiles (11), have been described.

Rapid deactivation of these useful anticancer drugs takes place by hydrolytic or reductive cleavage of the glycosidic oxygen at position 7. The *C*-glycosyl analog **2**, in which the glycosidic oxygen atom is replaced by CH_2, was suggested to be more resistant (12) to rapid metabolic deactivation than the glycosidic oxygen-linked analog **1**. It might be incapable of generating alkylating activity at the 7-position, one mechanism of action proposed (10) as following ejection of the sugar from **1**. On the other hand, **2** should retain the DNA-binding properties (13) of the anthracyclines and the free-radical generating properties from cyclic reduction and reoxidation of the quinone (14, 15). The *C*-glycosyl analog **2** might also show favored biological effect upon testing and is expected to be a superior drug. *C*-Daunosaminyl intermediates required for the elaboration of the carbon-bridged anthracyclines have been reported (12).

The sulfur-bridged glycoside **3** is also expected to be considerably more stable (16) to reductive cleavage and hydrolysis in vivo than the glycosidic oxygen bond in **1**. In addition, replacement of the glycosidic oxygen by sulfur might possibly display or exhibit biological properties markedly different from the glycosidic oxygen analog, as expected for the carbon bridged analog **2**. In this work, replacement of the oxygen atom at C-7 of daunomycinone **4** by sulfur was explored to provide the aglycon part required for the elaboration of the sulfur-bridged analog **3**.

Catalytic hydrogenolysis of daunomycinone **4** with hydrogen over palladium – barium sulfate afforded a mixture of 7-deoxydaunomycinone (**5**) and 7,11-dideoxydaunomycinone (**6**) (Scheme 1). Reported (17) catalytic hydrogenolysis of the glycoside daunomycin or the aglycone **4** afforded only com-

[1] For a preliminary account of part of this work, see ref. 1.
[2] Author to whom correspondence may be addressed.

TABLE 1. ^{1}H nuclear magnetic resonance spectra[a] of compounds **4–6** and **8–10**

Proton (coupling constant)	Compound 4	5	6	8	9	10
H-1	8.011 s	8.028 d	8.028 d	7.984 d	7.985 d	7.934 d
($J_{1,2}$)	(7.5)	(7.5)	(8.4)	(7.4)	(7.7)	(7.5)
($J_{1,3}$)	(~1)					(~1)
H-2	7.763 t	7.761 t	7.595 t	7.753 t	7.745 t	7.736 t
H-3	7.385 d	7.374 d	7.016 d	7.368 m	7.358 d	7.355 d
($J_{2,3}$)	(8.4)	(8.5)	(7.8)	(8.0)	(8.3)	(8.3)
H-7	5.306 sbs	2.951 m	2.786 m	5.447 sbs	5.077 m	5.057 bs
	$\nu_{1/2}$ 5			$\nu_{1/2}$ 4.7	$\nu_{1/2}$ 15.9	$\nu_{1/2}$ 5
9-OH	3.776 sbs	3.771s	3.813 s	3.664 s	3.586 s	3.897 s
(J)	(4.7)					
H-10e	3.160 d	3.151 dd	3.044 dd	3.114 d	3.186 d	2.940 d
H-10a	2.901 d	3.061 d	2.951 d	2.990 d	3.093 d	2.825 d
($J_{10e,10a}$)	(19.5)	(18.6)		(18.5)	(16.5)	(19.0)
H-8e	2.321 d			2.625 dd		2.694 d
($J_{8e,8a}$)	(15.3)			(14.5)		(15.3)
		2.814–	1.899–		2.431–	
H-8a	2.150 dd	2.982 m	1.942 m	2.164 d	2.540 m	2.489 dd
($J_{7,8a}$)	(3.7)					(4.8)
7-OH	4.615 s					
6-OH	13.890 s	13.844 s	13.827 s	13.889 s	13.957 s	14.096 s
11-OH	13.202 s	13.449 s	—	13.302 s	13.306 s	12.929 s
H-11	—	—	8.580 s	—	—	—
4-OMe	4.084 s	4.088 s	4.039 s	4.063 s	4.064 s	4.058 s
9-Ac	2.438 s	2.391 s	2.371 s	2.386 s	2.406 s	2.355 s
7-SAc	—	—	—	2.368 s	2.341 s	—

[a] Spectra recorded at 470 MHz in chloroform-*d*. Spin couplings (Hz) are given in parentheses. Signal multiplicities: b, broadened; d, doublet; m, multiplet; s, singlet; sbs, split broad singlet; t, triplet.

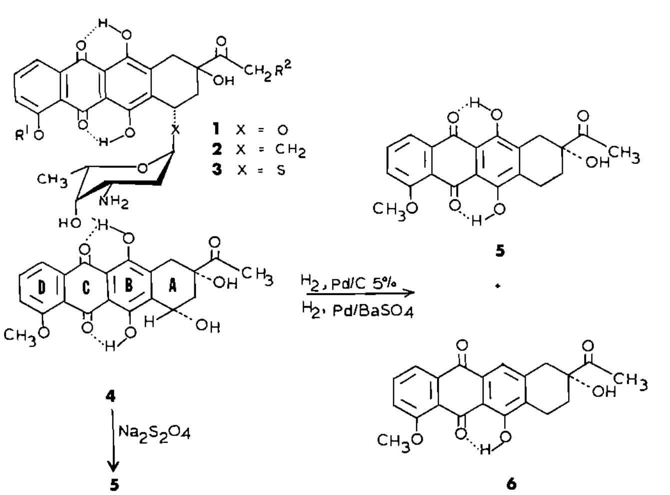

SCHEME 1

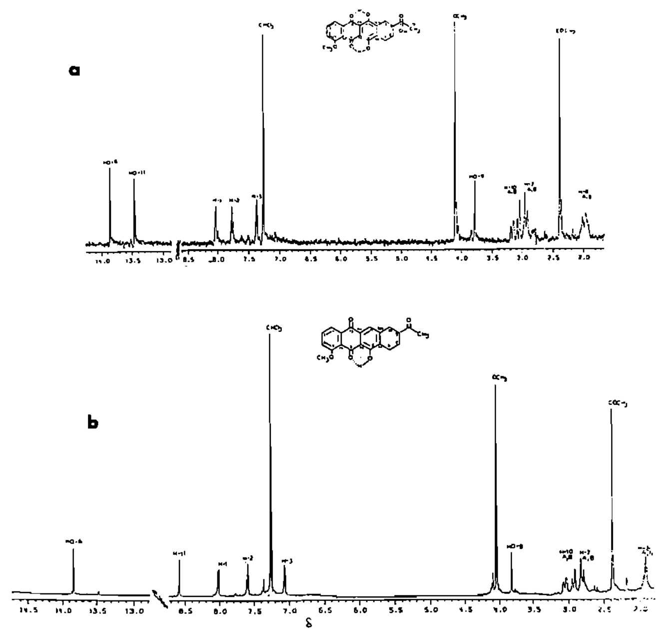

FIG. 1. The 470-MHz nmr spectra of (a) 7-deoxydaunomycinone **5** and (b) 7,11-dideoxydaunomycinone **6**.

pound **5**. The nmr spectrum of compound **6** (Fig. 1) showed the absence of the singlet corresponding to the chelated phenolic 11-OH which is present at δ 13.449 for compound **5**, and the appearance of a down-field singlet corresponding to the aromatic H-11 at δ 8.580, instead (Table 1). The further downfield shift for the chelated phenolic 6-OH at δ 13.844 and δ 13.827 for compounds **5** and **6**, respectively, can be rationalized based on extended resonance (18) with the C-4 methoxy that can occur only for the 6-OH. The nmr spectral data for compound **6** are similar to those reported for the compound obtained by catalytic hydrogenolysis of the biologically active 11-deoxydaunoribicin or 11-deoxydaunomycinone (19). Chemical reduction of compound **4** with sodium dithionite (19–21) gives compound **5**.

Several attempts were made to introduce sulfur as a thioacetyl group at the 7-position of 7-deoxydaunomycinone in a reasonable yield. Treatment of compound **5** with bromine and a catalytic amount of 2,2′-azobisisobutyronitrile (ABN) in refluxing CCl_4 gave the unstable intermediate 7-bromo-

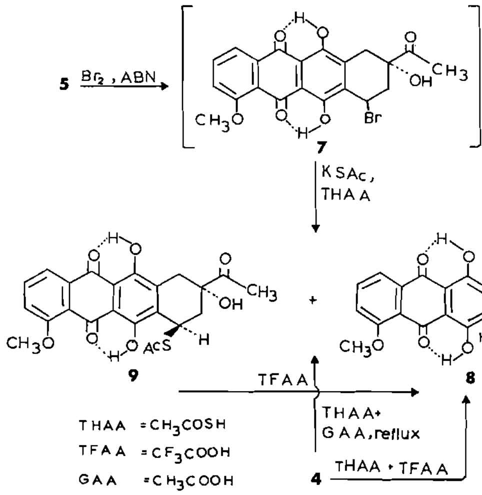

SCHEME 2

daunomycinone **7**. Wong *et al.* (22) postulated that steric hindrance about the 10-position allowed benzylic bromination to proceed regiospecifically at the 7-position. The bromine derivative **7** was treated with potassium thioacetate in a solution of thioacetic acid, giving a mixture of 7-thioacetyldaunomycinone **8** and 7-epithioacetyldaunomycinone **9** in 33% yield (Scheme 2).

In a one-step reaction, the 7-thioacetate **8** was prepared in 13% yield from **4**, by treatment with a mixture of thioacetic acid (THAA) and trifluoroacetic acid (TFAA) in the ratio of 5:2 at room temperature. This reaction mixture favors the formation of compound **8** with the stereochemistry of the natural 7,9-*cis* configuration at C-7. Replacement of TFAA with glacial acetic acid (GAA) and refluxing, gave a mixture of the thioacetate **8** and its epimer **9** in a ratio of 5:1 and in a total yield of 83%. The major isomer **8** was purified by recrystallization, and the minor isomer was separated from the mother liquor by chromatography. The reaction is assisted by the unusual reactivity of the benzylic hydroxyl group at the 7-position, which undergoes nucleophilic substitution by the thioacetate anion. The formation of two isomeric thioacetates can be explained by racemization through the formation of the carbocation at C-7 and subsequent attack of the thioacetate anion, rather than an S_N2 process which would produce the epimer. An identical benzylic carbocation was postulated (23).

The nmr spectrum of compound **8** showed two signals at δ 2.388 and δ 2.368, each of three-proton intensity corresponding to the 9-acetyl and 7-thioacetyl groups, respectively. The 7*S* configuration of **8** was determined according to a previous method of assignment (20, 21, 24–27) based on the peak widths ($\nu_{1/2}$) for the benzylic proton (H-7). Compound **8** showed H-7 as a doublet at δ 5.447 having a coupling constant of 4.7 Hz, thus assigning the natural 7*S* configuration to **8** (see Table 1).

The nmr spectrum of compound **9** also showed the three-proton signals at δ 2.406 and 2.341, characteristic for the acetyl groups. The 7*R* configuration of **9** was determined from the benzylic proton (H-7) which was shown as a multiplet at δ 5.077 having $\nu_{1/2}$ 15.9 Hz, in agreement with an axial orientation of H-7. The stereochemistry at position 7 for compounds **8** and **9** can be ascertained on the basis of the chemical shifts in pyranoid rings (28–30); equatorial protons resonate at lower field than constitutionally similar axial protons. The benzylic proton H-7 for compound **8** was shown at relatively lower field

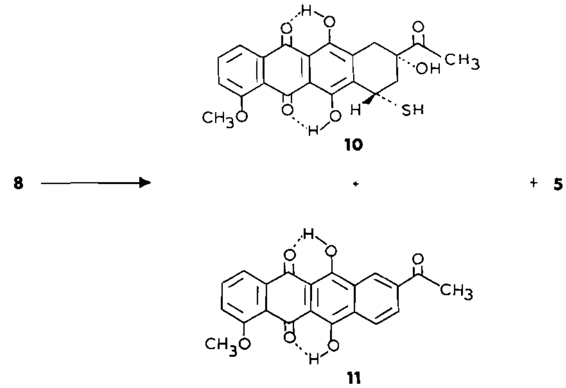

SCHEME 3

(δ 5.447) than that for compound **9** (δ 5.077). In addition, the protons associated with the methyl groups in axial acetoxy groups resonate at lower field than the corresponding protons in equatorial acetoxy groups (29). However, the appearance of the 7-thioacetyl signal at relatively lower field (δ 2.368) for compound **8** than that for compound **9** (δ 2.341) is in agreement with the axial orientation of the 7-thioacetyl group for compound **8** and the equatorial orientation for compound **9**.

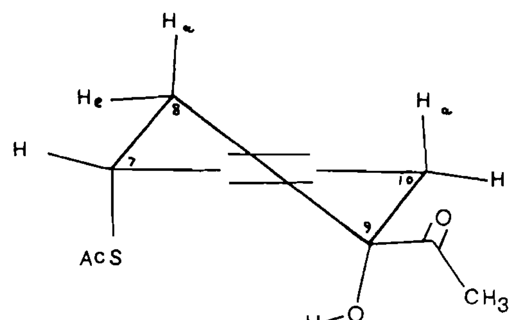

8

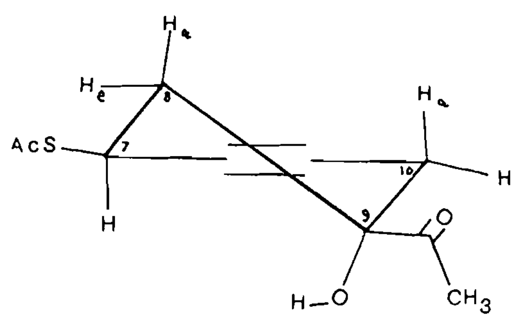

9

Half-chair conformation of ring A for compounds **8** and **9**

The mass spectrum of compound **8** showed a weak molecular ion at *m/z* 456, and a base peak at *m/z* 43 corresponding to the CH_3CO group. The mass spectrum of compound **9** did not show a molecular ion; however, its C.I. mass spectrum showed the protonated molecular ion at *m/z* 457. It showed a fragmentation pattern identical to that of compound **8**.

Anthracyclines having an axial proton at C-7 have been

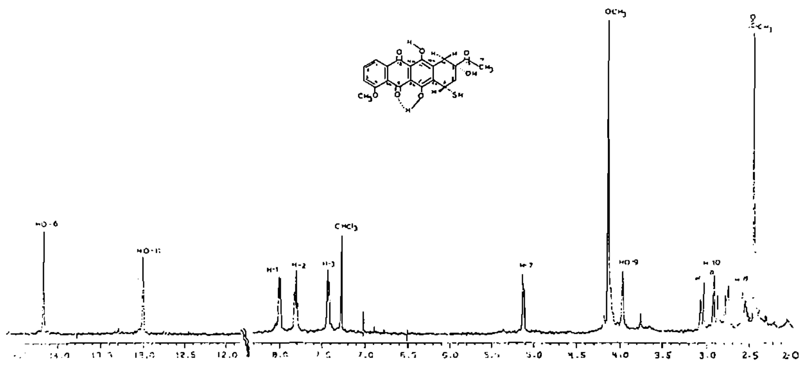

FIG. 2. The 470-MHz nmr spectrum of thiodaunomycinone **10**.

epimerized with acid (24). Treatment of compound **9** with TFAA afforded compound **8**.

Hydrolysis of compound **8** with sodium methoxide or potassium carbonate (Scheme 3) afforded a mixture of 7-deoxy-7-thiodaunomycinone **10**, **5**, and bisanhydrodaunomycinone **11** (31). The yield of **10** was low (37%) because of the concomitant formation of compound **5**, by ring-sulfur cleavage, and compound **11** by aromatization of ring A. Numerous repetitions and variation of the reaction conditions failed to give only one product. Compounds **5** and **10** were separated on preparative tlc and identified. Further purification of **11** by multiple development chromatography produced resolution into two components having very close R_f values, by partial dimerization of compound **10** into the dimer **12**.

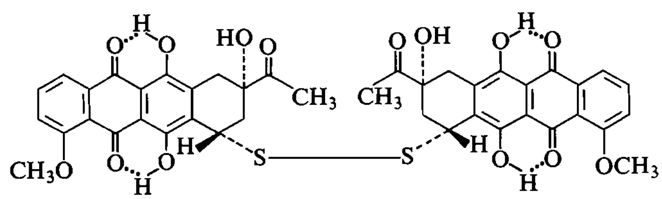

12

The nmr spectrum of compound **10** (Fig. 2) showed a singlet of three-proton intensity at δ 2.355 corresponding to the 9-acetyl group, with the disappearance of the singlet corresponding to the thioacetyl group. The signal corresponding to the 9-hydroxyl group for compound **10** was shown as a singlet shifted to lower field (δ 3.897) than that for daunomycinone (δ 3.776). In addition, the peaks corresponding to the 8-CH_2 group were shifted to lower field than that for daunomycinone (Table 1). The benzylic proton for compound **10** was shown as a broad singlet at δ 5.057, shifted to higher field than that for compound **8** (δ 5.447) due to the removal of the acetyl group, and shifted to higher field than that for compound **4** (δ 5.306) because of the shielding effect of the sulfur compared to oxygen. The shielding of the benzylic proton of **10** compared to that of **8** and **4**, confirms the substitution at position 7.

The stereochemistry at the 7-position of anthracyclines is important for the expression of biological activity (32) and of DNA binding properties (33). The signal corresponding to H-7 for compound **10** showed $\nu_{1/2}$ ($J_{7,8a} + J_{7,8e}$) = 5 Hz, indicating (20, 21, 24–27) a quasiequatorial orientation for this proton. The new substituent at C-7 for compound **10** therefore has the same 7*S* configuration as the precursor acetate **8** and the natural daunomycinone, i.e., the quasiaxial configuration.

Compound **10** was further identified by mass spectroscopy. Its C.I. or E.I. mass spectrum did not show a molecular ion. The C.I. mass spectrum showed the highest mass peak at m/z 383 corresponding to the ion ($M + 1 - S$). The base peak was shown at m/z 363 corresponding to the ion ($M + 1 - H_2S - H_2O$). The E.I. mass spectrum showed the highest mass fragment at m/z 396 corresponding to the ion ($M - H_2O$), which was followed at the lower masses by the peaks at m/z 382 corresponding to ($M - S$), and m/z 362 corresponding to the ion ($M - H_2S - H_2O$). The base peak was shown at m/z 43 corresponding to the CH_3CO group. However, the field desorption mass spectrum of compound **10** showed the molecular ion peak (M) as the most intense peak at m/z 414, followed at the lower masses by the fragments at m/z 380 ($M - H_2S$), 362 ($M - H_2S - H_2O$), and 337 ($M - H_2S - CH_3CO$). Partial dimerization of **10** into **12** was shown by the peak at m/z 826 corresponding to $M_2 - 2H$ at the high mass spectrum region.

This synthetic route represents the method for replacement of the benzylic oxygen atom of daunomycinone by a sulfur atom. The synthetic availability of the 7-thioanalog **10** provides the versatile aglycon portion required for further elaboration of the sulfur-bridged anthracyclines **3**.

Experimental

Melting points are uncorrected, infrared spectra (ir) were recorded with a Perkin Elmer 467 grating spectrometer. The ^1H nmr spectra were recorded with a Nicolet 470-MHz instrument, using internal tetramethylsilane as the reference. Mass spectra were recorded with a Finnigan 6100 Data System gas chromatograph/E.I.–C.I. spectrometer. Combustion analyses were performed in the Department of Chemistry, Purdue University.

Thin-layer chromatograms (tlc) were obtained on 200 μm silica gel G plates. Preparative layer chromatograms (plc) were obtained on 20 × 20 × 0.2 silica gel 60 F plates (E. Merck) with solvent A, 9:1 benzene–acetone and solvent B, 97:2 methylene chloride – methanol.

Reduction of daunomycinone

(a) *With hydrogen over palladium–carbon 5%*

Daunomycinone (**4**, 200 mg) was dissolved in ethanol (300 mL), and shaken under hydrogen atmosphere with palladium–carbon 5% for 3 h. Thin-layer chromatography indicated the disappearance of the starting material and formation of two more mobile spots in the ratio of 1:1; R_f 0.36 and 0.29 (solvent A). The solution was filtered off and the catalyst washed with ethanol. The filtrate and washings were combined and evaporated to dryness, yield 160 mg (83%). The solution was green in color and turned pink upon exposure to the air. The two components were separated by plc (solvent A) and recrystallized from benzene. The slower-migrating spot (orange), R_f 0.29, showed mp 234–235°C, identical to that of 7-deoxydaunomycinone **5** (lit. (17) mp 229–231°C); ir: 3480 (OH), 1720 (C═O), 1610, 1575 (H-bonded quinone) cm^{-1}; mass spectral data (E.I., selected ions): m/z 384 (1, M + 2), 383 (4, M + 1), 382 (16, M), 364 (7, M − H_2O), 340 (22), and 339 (100, M − CH_3CO). For nmr spectral data see Table 1.

The faster-migrating spot (pink), R_f 0.36, mp 190–192°C, (lit. (19) mp for 7,11-dideoxydaunomycinone **6**, 186–189°C); E.I. mass spectral data (selected ions): m/z 368 (1, M + 2), 367 (7, M + 1), 366 (28, M), 348 (23, M − H_2O), 339 (3), 324 (21), and 323 (100, M − CH_3CO). For nmr spectral data see Table 1. *Anal.* calcd. for $C_{21}H_{18}O_6$: C 68.85, H 4.95; found: C 68.66, H 5.16.

(b) *Reduction with hydrogen over palladium – barium sulfate*

Compound **4** (50 mg) was dissolved in ethanol (200 mL), treated with a catalytic amount of palladium – barium sulfate (20 mg), and shaken under hydrogen atmosphere for 2 h, and treated as above. Thin-layer chromatography indicated the disappearance of the starting material and formation of two more mobile spots at the same R_f as those of **5** and **6** (solvents A and B).

(c) *Reduction with sodium dithionite*

Compound **4** (100 mg) was dissolved in THF (50 mL), the solution was blanketed with nitrogen, and treated with dropwise addition of sodium dithionite (200 mg) in water (25 mL). After complete addition (15 min), the solution was stirred at room temperature for a further 2 h, evaporated to dryness, the residue extracted with chloroform, and the extract washed with water, dried over anhydrous sodium sulfate, filtered, and evaporated to dryness, yield 75 mg. It was recrystallized from benzene to give chromatographically (tlc) pure red needles, mp and mixture mp (with **5**) 232–233°C, having the same R_f values on tlc (solvents A and B).

7-Thioacetyldaunomycinone (8)

A solution of compound **5** (50 mg) in CCl_4 was refluxed under N_2 for 1 h. Br_2 (3 mL of 0.125 M solution in CCl_4) and ABN (4 mg) were added and refluxed for 2 h. The solvent was removed and the residue was dissolved in THAA (10 mL), then CH_3COSK (100 mg) was added and the mixture stirred under N_2 for 17 h. The mixture was evaporated to dryness, the residue extracted with $CHCl_3$, and the organic layer was then washed with water, dried over anhydrous sodium sulfate, and evaporated. The residue was recrystallized from benzene–hexane giving a red amorphous precipitate. Thin-layer chromatography (solvent B) showed two spots, R_f 0.31 and 0.21. Fractional recrystallization of the mixture from benzene gave compound **8** as orange-red needles, yield 18 mg, mp 230–232°C; R_f 0.31, solvent A; ir: 3420 (OH), 1705 (C═O), 1690 (SAc), 1610 and 1580 (chelated quinone) cm^{-1}; mass spectral data (C.I.): m/z 459 (7, M + 3), 458 (16, M + 2), 457 (83, M + 1), 425 (9), 383 (41), 363 (52), 321 (22), and 77 (100); (E.I.): m/z 456 (1, M), 438 (1, M − H_2O), 413 (1, M − CH_3CO), 382 (1, M − CH_3COSH), 362 (M − CH_3COSH − H_2O), 338 (1), 77 (2, Ph), 76 (2, CH_3COSH), 75 (1, CH_3COS), and 43 (100, CH_3CO); for nmr spectral data see Table 1. *Anal.* calcd. for $C_{23}H_{20}O_8S$: C 60.39, H 4.63, S 7.01; found: C 60.45, H 4.81, S 6.81.

7-Epithioacetyldaunomycinone (9)

The mother liquor of **8** showed two spots on tlc which were separated by plc (solvent A) and the slow migrating spot, R_f 0.21, was recrystallized from methanol giving red needles, mp 207–209°C; ir: 3440 (OH), 1705 (C═O), 1690 (SAc), 1610 and 1580 (chelated quinone) cm^{-1}; mass spectral data (C.I.): m/z 457 (1, M + 1), 385 (3), 383 (39), 363 (17), 91 (29), 85 (42), and 76 (100); (E.I.): m/z 362 (10, M − CH_3COSH − H_2O), 339 (9, M − CH_3COSH − CH_3CO), 337 (13), and 43 (100, CH_3CO). For nmr spectral data see Table 1. *Anal.* calcd. for $C_{23}H_{20}O_8S$: C 60.39, H 4.63, S 7.01; found: C 60.14, H 4.84, S 6.94.

Conversion of daunomycinone into 7-thioacetyldaunomycinone

Method "A", by treatment of 4 with a mixture of THAA and TFAA

Compound **4** (50 mg) was treated with THAA (5 mL) and TFAA (2 mL) and kept at room temperature for 6 h. Thin-layer chromatography indicated the disappearance of the starting material and formation of three spots; the slow migrating one was shown at the same R_f value as for compound **8**. It was isolated by plc and recrystallized from benzene, yield 6.5 mg, mp and mixture mp 232–234°C. Its nmr spectrum was identical to that of **8**. No spot corresponding to compound **9** was detected by tlc.

Method "B", by refluxing compound 4 with THAA and GAA

Compound **4** (100 mg) was treated with THAA (10 mL) and GAA (4 mL) and the mixture refluxed for 21 h. Monitoring of the reaction by tlc indicated disappearance of the starting material and formation of two more mobile spots at the R_f values for compounds **8** and **9**. The reaction was complete after 21 h. The mixture was evaporated to dryness and traces of acids were removed by repeated evaporation with CH_2Cl_2. The dry residue was recrystallized from benzene giving orange red needles of compound **8**, mp and mixture mp 228–230°C. The mother liquor, containing **8** and **9**, was separated with plc (solvent B); yield of **8**, 80 mg, and **9**, 15 mg; total yield 83% from **4**.

Epimerization of compound 9 into 8

Compound **9** (5 mg) was treated with TFAA (1 mL) and kept for 20 h at 20°C. The acid was removed by repeated evaporation with CH_2Cl_2. Thin-layer chromatography indicated complete conversion of **9** into **8**. Similar treatment of **8** with TFAA did not give **9** by epimerization under the same conditions.

Hydrolysis of 7-thioacetyldaunomycinone

Method "i", with 0.01 N *sodium methoxide solution*

A solution of **8** (30 mg) in THF (4 mL) was blanketed with argon and a solution of 0.01 N sodium methoxide (2 mL) was added with stirring; the blue-colored solution obtained was stirred at 20°C for 5 h. It was neutralized with glacial acetic acid which turned the solution red. Thin-layer chromatography (solvent B) showed the formation of three spots which were isolated by plc and identified. The slow migrating spot, R_f 0.47 (solvent B), was isolated, dissolved in benzene, and precipitated by hexane as an amorphous powder of thiodaunomycinone **10**; yield 10 mg, mp 195–198°C. Further purification on analytical tlc plates (solvent B) showed splitting into two non-resolvable spots, having close R_f values, probably by air oxidation and formation of the dimer **12**; ir: 3430 (OH), 1705 (C═O), and 1615 and 1580 (hydrogen bonded quinone) cm^{-1}. Mass spectral data (C.I.): m/z 383 (9, M + 1 − S), 363 (100, M + 1 − H_2S − H_2O); (E.I., selected ions): m/z 396 (1, M − H_2O), 382 (3, M − S), 362 (M − H_2S − H_2O), 344 (17), 339 (16), 337 (9, M − H_2S − CH_3CO), and 43 (100, CH_3CO). Field desorption mass spectrum (F.D.): 826 (31, M_2 − 2H), 414 (91, M), 380 (77, M − H_2S), 362 (18, M − H_2S − H_2O), 337 (18, M − H_2S − $COCH_3$). For nmr spectral data see Table 1. *Anal.* calcd. for $C_{21}H_{18}O_7S$: C 60.86, H 4.38, S 7.74; found: C 60.64, H 4.62, S 7.45.

The second hydrolysis product (orange color), R_f 0.59 (solvent B) was isolated by plc and recrystallized from benzene, mp and mixture mp (with **5**) 233–235°C (lit. (20) mp 230–232°C). The faster moving spot (violet color), R_f 0.67 (solvent B), was isolated by plc and recrystallized from benzene–methanol as brown-violet needles, yield 5 mg; mp 229–232°C (lit. (31) mp for bisanhydrodaunomycinone, 225–230°C); mass spectral data (C.I.): m/z 363 (100, M + 1), 361 (36, M + 1); (E.I., selected ions): m/z 364 (9, M + 2), 363 (40, M + 1), 361 (96, M + 1), 345 (52), 343 (38), 319 (5, M − CH_3CO), and 43 (100, CH_3CO).

Method "ii". Hydrolysis of 8 with saturated solution of potassium carbonate

A solution of compound **8** (30 mg) in THF (5 mL) was blanketed with argon, then a solution of saturated potassium carbonate (0.2 mL) was added with stirring. The solution, which turned blue, was stirred at 20°C for 2 h, then acidified with 5% oxalic acid solution which converted it into a red color; the mixture was then partitioned between water and chloroform, and the organic layer washed with water and dried. The chloroform was removed and tlc (solvent B) of the residue showed three spots at the same R_f values, for compounds **5**, **10**, and **11**, that were obtained by method i.

Acknowledgments

This work was partly supported by Adria Laboratories Inc., Columbus, Ohio, and the authors thank Dr. D. Lednicer for providing a sample of daunomycinone. The authors thank the Purdue University Biochemical Magnetic Resonance Laboratory for the 470-MHz spectral measurements, which were supported by NIH grant No. RR 01077. Thanks are also due Dr. J. L. Markley, the director of the facility, and Dr. D. Croll, Dr. R. Virudachalam, and Patricia Hoyos for recording the spectra. Finally, thanks to Dr. John L. Occolowitz, Lilly Research Laboratories, for field desorption mass spectral measurements.

1. M. A. E. SALLAM and R. L. WHISTLER. Abstracts, 184th National Meeting of the American Chemical Society, Kansas City, MO. 1982.
2. R. B. LIVINGSTON and S. K. CARTER. Daunomycin. Chemother. Fact. Sheet, National Cancer Institute, Bethesda, MD. 1970.
3. F. ARCAMONE (*Editor*). Doxorubicin. Medicinal Chemistry Series. Vol. 17. Academic Press, New York. 1981.
4. A. DIMARCO, F. ARCAMONE, and F. ZUNINO. *In* Antibiotics. Vol. 3. *Edited by* J. W. Corcoran and F. E. Hahn. Springer Verlag, New York. 1975. p. 101.
5. F. ARCAMONE, G. FRANCESCHI, S. PENCO, and A. SELVA. Tetrahedron Lett. 1007 (1969).
6. (*a*) R. H. BLUM and S. K. CARTER. Ann. Intern. Med. **80**, 249 (1974); (*b*) J. P. RINEHART, R. P. LEWIS, and S. P. BALCERCAK. Ann. Intern. Med. **81**, 475 (1974); (*c*) E. A. LEFRAK, J. PITHA, S. ROSENHEIM, and J. A. GOTTLIEB. Cancer, **32**, 302 (1973); (*d*) L. LENAZ and J. A. PAGE. Cancer Treat. Rev. **3**, 111 (1976).
7. D. Y. YESAIR, S. MCNITT, and L. BITTMAN. Microsomes Drug Oxidation. Proceeding of the 3rd International Symposium, 1976. *Edited by* V. Ullrich, I. Roots, and A. Hildebrant. Oxford. 1977. p. 688.
8. K. UMEZAWA, M. SAWAMURA, and T. SUGIMURA. Cancer Res. **38**, 1782 (1978).
9. G. L. TONG, H. Y. WU, T. H. SMITH, and D. W. HENRY. J. Med. Chem. **22**, 912 (1979).
10. H. W. MOORE. Science, **197**, 527 (1977).
11. E. M. ACTON, G. L. TONG, C. W. MOSHER, T. H. SMITH, and D. W. HENRY. J. Med. Chem. **22**, 922 (1979).
12. E. M. ACTON, K. J. RYAN, and T. H. SMITH. Carbohydr. Res. **97**, 235 (1981).
13. F. ARCAMONE. *In* Topics in antibiotic chemistry. Vol. 2. *Edited by* P. G. Sammes. John Wiley and Sons, New York. 1978. p. 99.
14. N. R. BACHUR, S. L. GORDON, M. V. GEE, and H. KQN. Proc. Natl. Acad. Sci. U.S.A. **76**, 954 (1979).
15. J. W. LOWN, S. SIM, K. C. MAJUMDAR, and R. CHANG. Biochem. Biophys. Res. Commun. **76**, 705 (1977).
16. J. M. ESSERY, T. W. DOYLE, and R. H. SCHREIBER. J. Med. Chem. **22**, 1425 (1979).
17. F. ARCAMONE, G. FRANCESCHI, P. OREZZI, G. CASSINELLI, W. BARBIERI, and R. MONDELLI. J. Am. Chem. Soc. **86**, 5334 (1964).
18. J. G. BAUMAN, R. B. BARBER, R. D. GLESS, and H. RAPOPORTS. Tetrahedron Lett. 4777 (1980).
19. F. ARCAMONE, G. GASSINELLI, F. DIMATTEO, S. FORENZA, M. C. RIPAMONTI, G. RIVOLA, A. VIGEVANTI, J. CLARDY, and T. MCCABE. J. Am. Chem. Soc. **102**, 1462 (1980).
20. T. H. SMITH, A. N. FUJIWARA, W. W. LEE, H. Y. WU, and D. W. HENRY. J. Org. Chem. **42**, 3653 (1977).
21. T. H. SMITH, A. N. FUJIWARA, W. W. LEE, and D. W. HENRY. J. Am. Chem. Soc. **98**, 1969 (1976).
22. C. M. WONG, R. SCHWENK, D. POPIEN, and T. L. HO. Can. J. Chem. **51**, 466 (1973).
23. M. J. MICHAEL, C. H. HASSALL, and G. J. THOMAS. J. Chem. Soc. Perkin Trans. 1, 2239 (1982).
24. H. BROCKMANN and J. NIEMEYER. Chem. Ber. **100**, 3587 (1967).
25. A. S. KENDE, Y. TSAY, and J. E. MILLS. J. Am. Chem. Soc. **98**, 1967 (1976).
26. P. F. WILEY, R. B. KELLY, E. L. CARON, V. H. WILEY, J. H. JOHNSON, F. A. MACKELLAR, and S. A. MIZSAK. J. Am. Chem. Soc. **99**, 542 (1977).
27. D. TRESSELT, K. ECKARDT, and J. TAX. Tetrahedron, **31**, 613 (1975).
28. R. U. LEMIEUX, R. K. KULLNIG, H. J. BERNSTEIN, and W. G. SCHNEIDER. J. Am. Chem. Soc. **80**, 6098 (1958).
29. R. U. LEMIEUX and J. D. STEVENS. Can. J. Chem. **43**, 2059 (1965).
30. R. U. LEMIEUX and J. D. STEVENS. Can. J. Chem. **44**, 249 (1966).
31. F. ARCAMONE, G. CASSINELLI, G. FRANCESCHI, R. MONDELLI, P. OREZZI, and S. PENCO. Gazz. Chim. Ital. **100**, 949 (1970).
32. R. SUPINO, A. NECCO, T. DASDIA, A. M. CASAZZA, and A. DIMARCO. Cancer Res. **37**, 4523 (1977).
33. T. W. PLUMBRIDGE and J. R. BROWN. Biochem. Biophys. Acta, **563**, 181 (1979).

Réduction photochimique des polytungstates. Mise en évidence d'un effet photogalvanique

G. FOLCHER ET J. PARIS
L.R.M.C.I. (LA 331), Département de physico-chimie, Cen-Saclay, 91191 Gif-sur-Yvette Cédex, France
AND
F. CHAUVEAU
Laboratoire de Chimie des Polymères Inorganiques, Université Pierre et Marie Curie, 75005 Paris, France

Reçu le 6 novembre 1984

G. FOLCHER, J. PARIS et F. CHAUVEAU. Can. J. Chem. **63**, 2703 (1985).

Une cellule photogalvanique est réalisée avec une solution de décatungstate ($W_{10}O_{34}^{4-}$) de tétrabutylammonium dans l'acétonitrile à la concentration 0,2 *M* en atome-gramme de tungstène. Le dispositif utilisé comporte une électrode de platine éclairée et une électrode de graphite dans l'obscurité. Les conditions d'utilisation de la pile pour obtenir le meilleur rendement électrique sont déterminées. Un mécanisme global est proposé: le décatungstate excité par la lumière est réduit reversiblement, un donneur d'électron ou l'eau est oxydée pendant la réaction. Nous montrons que le mécanisme fait vraisemblablement intervenir deux photons. La fem développée est de 650 mV et le rendement expérimental (puissance de la pile/énergie lumineuse) est voisin de 1%.

G. FOLCHER, J. PARIS, and F. CHAUVEAU. Can. J. Chem. **63**, 2703 (1985).

A photogalvanic cell which functions with an acetronitrile solution of tetrabutylammonium decatungstate ($W_{10}O_{34}^{4-}$) (0.2 *M* in gram-atoms of tungsten) has been realized. This cell utilizes an irradiated platinum electrode with a non-illuminated graphite electrode. The conditions giving the best conversion of light to electric power have been determined. An overall mechanism has been proposed. The decatungstate photooxidizes an electron donor like water. The involvement of a two-photon process has been demonstrated. The emf produced is about 650 mV, and the experimental yield is in the neighborhood of 1%.

La recherche des réactions de transfert d'électrons capables de stocker l'énergie solaire s'oriente vers des systèmes microhétérogènes (10), micelles et colloïdes. Les polyanions peuvent constituer une alternative intéressante (9): la structure déterminée à l'état solide est conservée en solution (1) et on peut faire varier dans une certaine mesure la taille et la forme des arrangements moléculaires. Ceux-ci présentent des propriétés bien spécifiques comme le montre la chimie des polytungstates (2).

Le tungstène VI engagé dans le polyanion est photosensible et joue le rôle de capteur d'électron (3). C'est précisément ce qui est observé dans le cas du décatungstate $W_{10}O_{32}^{4-}$. Celui-ci a la structure présentée sur la figure 1 (4). Une bande de transfert de charge centrée à 325 nm mais étendue dans le domaine visible peut être utilisée pour accroître son affinité électronique.

Dans le cas de l'uranium hexavalent, nous avons pu utiliser les propriétés oxydantes de l'uranyle excité pour créer un effet photogalvanique, c'est-à-dire l'apparition d'une différence de potentiel entre deux électrodes plongées dans une solution d'uranyle quand l'une d'entre elle est éclairée (5).

Le montage utilisé dans cette expérience a pu être reconduit dans le cas des solutions de polytungstates. Les premiers résultats obtenus nous ont amené à étudier ce phénomène en détail.

Partie expérimentale

Le montage de la cellule a été décrit par ailleurs (5). Nous rappelons que la lumière éclaire une électrode de platine tandis qu'une électrode de graphite reste non irradiée. La principale difficulté réside dans le réglage de la distance optimale entre la fenêtre et l'électrode. L'utilisation d'une électrode circulaire appliquée sur la paroi éclairée permet de pallier cet inconvénient (fig. 2).

Le décatungstate de tétrabutylammonium est préparé par acidification convenable d'une solution de tungstate de sodium suivant les modes opératoires déjà décrits (7, 8) (16,5 g de $WO_4Na_2 \cdot 2H_2O$ dissous à ébullition dans 100 mL d'eau, acidifiée par 90 mL de HCl normal également à la même température. La solution rapidement refroidie est précipitée par 7 g de bromure de tétrabutylammonium).

Le produit précipité est lavé successivement à l'eau, l'alcool et à l'acétone. Une fois séché, il est recristallisé dans l'acétonitrile. *Anal.* calc.: W 55,37, C 23,26, N 1,69, H 4,37%; tr.: W 55,25, C 23,1, N 2,68, H 4,33%.

La concentration adoptée dans les expériences décrites est de 0,2 *M* en atome-gramme de tungstène, 0,2 mol^{-1} dans l'acétonitrile Merck.

L'irradiation est réalisée par une lampe xénon 900 W, filtrée par une cellule de 10 cm d'une solution aqueuse de sulfate de cuivre.

Pour les mesures de rendement quantique on opère de la façon suivante:

La lumière émise par une lampe xénon est mesurée par un joulemètre, après passage dans un monochromateur, sur toute l'étendue du spectre. Le faisceau est ensuite envoyé sur une électrode de taille inférieure au diamètre du faisceau. On suppose que toute la lumière est absorbée et on mesure la puissance de la pile.

Résultats

Électrochimie

Les potentiels d'oxydoréduction de $W_{10}O_{32}^{4-}$ dans l'acétonitrile ont été déterminés en présence de perchlorate de tétrabutylammonium 0,1 *M*. On observe alors deux vagues de réduction réversibles sur le mercure (l'électrode de référence est une électrode au calomel saturé à double jonction). On sait que dans ces conditions les $E_{1/2}$ sont assimilables aux potentiels normaux d'oxydoréduction. Les deux vagues observées correspondent respectivement à 1 et 2 électrons par mole. Elles sont analogues à celles que Termes et Pope ont observées dans le carbonate de propylène (6). Les potentiels sont respectivement de $-0{,}61$ et $-1{,}08$ V par rapport à H_2 normal (6).

Dans les conditions de fonctionnement de la pile, des phénomènes différents dus aux électrodes peuvent se manifester.

Nous avons mesuré par voltamétrie cyclique sur électrodes de platine poli les potentiels de réduction d'une solution de $W_{10}O_{32}^{4-}$ dans CH_3CN, dans des conditions voisines de celles du

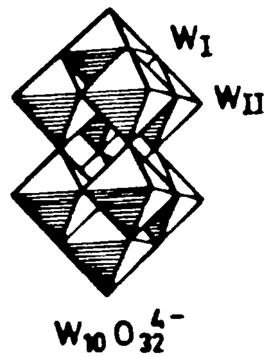

FIG. 1. Représentation polyédrique de la structure de $W_{10}O_{32}^{4-}$. Les atomes de tungstène W_I et W_{II} occupent approximativement le centre des octaèdres.

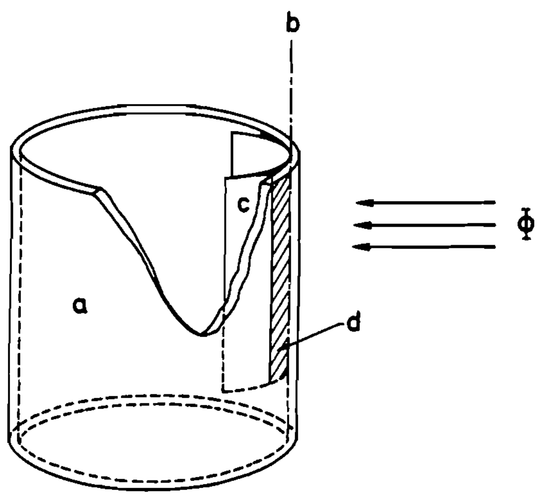

FIG. 2. Coupe schématique de la cuve avec son électrode de platine; (a) cuve en Pyrex; (b) génératrice de contact entre le platine et le verre; (c) électrode de platine; (d) localisation des espèces bleues en fonctionnement.

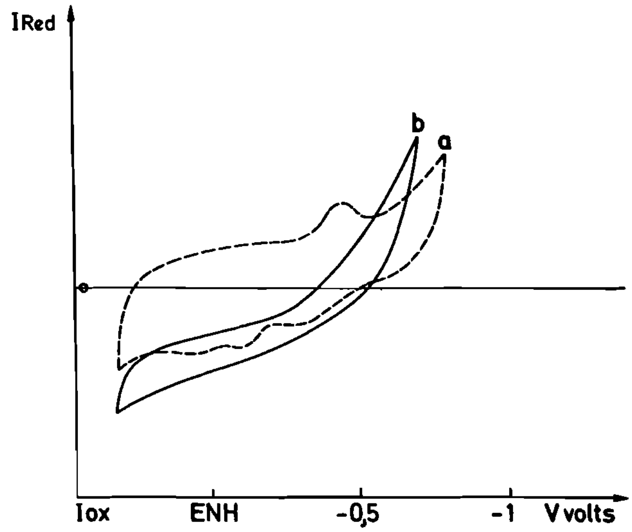

FIG. 3. Diagramme de voltamétrie cyclique obtenue dans CH_3CN, sans électrolyte support et sur électrode de platine. Vitesse de balayage 1 V/nm. L'électrode de référence est une électrode de Pleskov; (a) obscurité; (b) lumière.

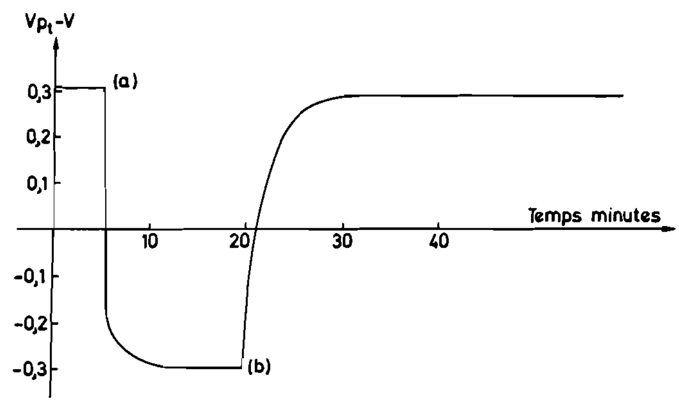

FIG. 4. Potentiel obtenu sur le platine; (a) éclairement; (b) obscurité.

fonctionnement de la pile en utilisant une électrode de Pleskov comme référence. La figure 3 présente le premier balayage qui met en évidence une réduction à −0,55 V par rapport à l'électrode de Pleskov. Pour des valeurs plus négatives, il y a formation d'un dépôt sur l'électrode qui modifie sensiblement le comportement du système. Vers les potentiels positifs, un système apparaît vers +0,20 V qui n'est pas dû à l'oxydation du solvant, observé dans ces conditions à +0,40 V. Ce système apparaît aussi comme instable dans le temps.

En présence de lumière, le voltamogramme est différent: il présente un accroissement considérable des courants d'oxydation sur le platine avant −0,5 V et une vague très intense pour les potentiels plus négatifs.

Il apparaît donc que la lumière crée des espèces réduites de polytungstate qui peuvent donc être réduites dans un deuxième temps à des potentiels inférieurs à −0,5 V.

Photochimie

Nous utilisons le montage photogalvanique (fig. 2). La différence de potentiel mesurée en circuit ouvert entre l'électrode de platine éclairée et l'électrode de graphite est de 650 mV, le platine constituant la cathode.

La coupure de l'éclairement conduit à l'annulation rapide de cette différence de potentiel. De même, en rallumant la lampe la valeur de 650 mV est atteinte en quelques secondes (fig. 4).

La figure 5 présente la courbe de la puissance fournie dans les conditions expérimentales précédentes, en fonction du potentiel entre les électrodes. Elle est obtenue en faisant varier la résistance introduite sur le circuit. En se plaçant au maximum de cette courbe, on peut faire débiter la pile pendant plusieurs heures sans observer une variation notable des constituants de la solution ni de variation importante des performances.

En fonctionnement on voit apparaître sur l'électrode éclairée deux bandes colorées en bleu, le long des génératrices du cylindre, symétriques par rapport à la génératrice de contact, entre l'électrode et la paroi (fig. 2). Nous verrons que cette coloration est due à une espèce réduite de tungstène qui est formée par action de la lumière et d'un réducteur. Cette espèce qui est réoxydée au contact du platine est donc visible en concentration stationnaire. Elle illustre le rôle critique joué par l'épaisseur de la couche de liquide entre la fenêtre d'entrée et l'électrode. En se plaçant au maximum de la courbe de la figure 5, nous avons étudié la variation de la puissance émise en fonction de la longueur d'onde. Nous interposons entre la lampe et la cellule un monochromateur dont nous ouvrons largement la fente. Le rendement est porté en fonction de la longueur d'onde (fig. 6). On constate que la courbe ne coïncide pas avec la courbe d'absorption mais est décalée vers le rouge.

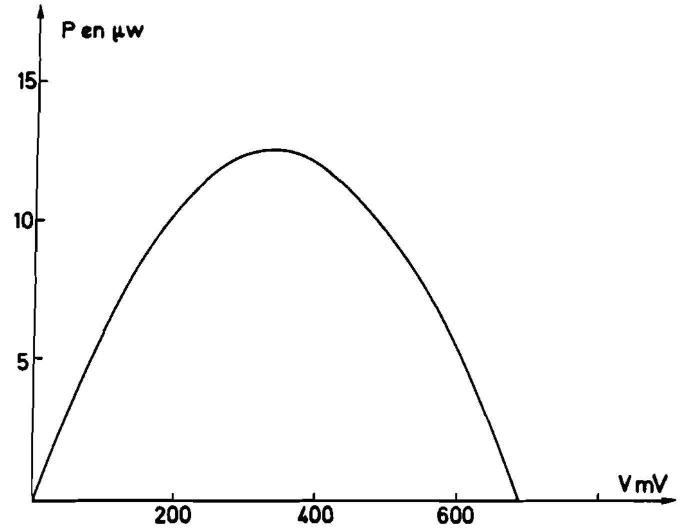

FIG. 5. Puissance électrique fournie en fonction de la tension disponible.

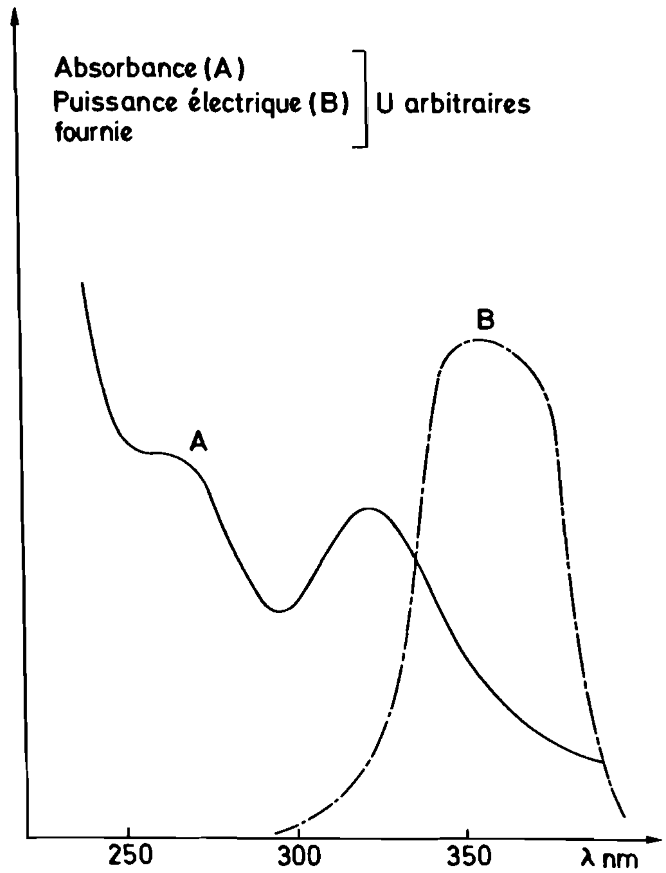

FIG. 6. (A) Spectre d'absorption électronique en fonction de la longueur d'onde. (B) Puissance électrique fournie en fonction de la longueur d'onde.

Plusieurs interprétations peuvent être données de ce phénomène parmi lesquelles un processus faisant intervenir un deuxième photon absorbé par l'espèce formée par le premier.

Si l'on porte maintenant (fig. 7) le rendement en fonction du flux lumineux, on note qu'une valeur constante n'est atteinte qu'à partir d'une valeur élevée de l'intensité incidente. Dans le cas simple de l'utilisation d'un seul photon on devrait observer

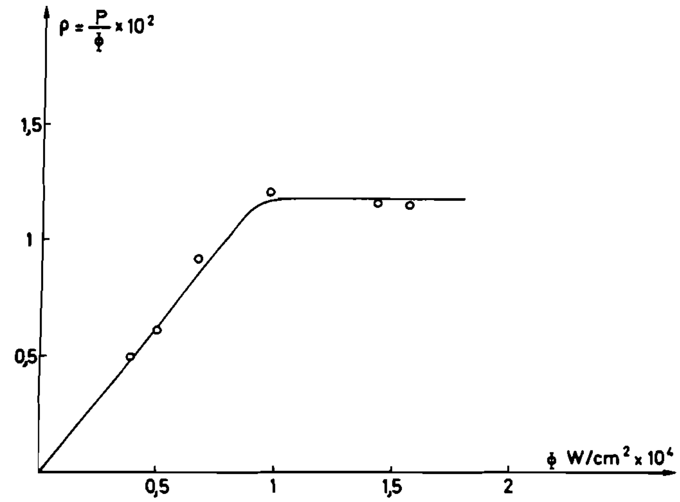

FIG. 7. Rendement en fonction du flux lumineux.

un rendement indépendant du flux lumineux au moins aussi longtemps que l'on n'a pas atteint la saturation.

Discussion

D'après les spectres uv–visibles réalisés dans l'acétonitrile la structure en solution est celle de l'état solide (fig. 1).

La molécule comporte deux entités compactes constituées de 5 octaèdres WO_6, dont le tungstène occupe le centre, et reliés entre eux par une mise en commun d'arêtes. Les deux moitiés de la molécule sont reliées entre elles par une mise en commun de sommets. Il en résulte deux variétés de tungstène W_I et W_{II} et deux types de points W_IOW_{II} et $W_{II}OW_{II}$, les derniers étant quasiment linéaires (175°) (6).

La bande à 325 nm que nous irradions serait liée à l'existence des ponts (6) et suggère que seul un type de liaison participe aux transferts de charge responsable de la photochimie.

Dans l'acétonitrile, les mesures de conductibilité ont montré que les sels du polyanion sont entièrement dissociés. Les expériences de rmn en cours confirment la présence de deux types de tungstène.

Aucune détermination des potentiels d'oxydoréduction des polyanions de tungstène n'avait été réalisée dans CH_3CN mais les travaux de Pope (2) avaient montré que la réduction électrochimique à 1 et 2 électrons était réalisée réversiblement. Nous avons pu voir dans nos conditions: CH_3CN et électrode de platine, une première réduction réversible à l'électron à 0,55 V par rapport à l'électrode de Pleskov (soit sensiblement à 0,40 V par rapport à l'électrode hydrogène. À lumière de la mise au point récente (1) sur les propriétés photochimiques des polytungstates on peut penser que l'espèce bleue dont la concentration stationnaire peut être observée au contact de l'électrode est l'espèce réduite à un électron $W_{10}O_{32}^{5-}$. Elle sera réoxydée sur le platine à un potentiel de 0,35 V en circuit ouvert. C'est l'espèce dont la quantité augmente lors de l'irradiation de la solution mais elle peut être limitée par la réaction de dismutation

$$2W^{V}W_9O_{32}^{5-} \leftrightarrows (W_2^{V}W_8^{VI}O_{32})^{6-} + (W_{10}O_{32})^{4-}$$

La réaction sur le graphite est plus difficile à caractériser. Son potentiel mesuré à +300 mV en circuit ouvert lors de l'irradiation de la solution, est aussi celui où se trouvent les deux électrodes en l'absence de lumière. Il correspond bien à la vague d'oxydation observée sur la solution de polytungstate sans que l'on puisse en définir la nature avec précision. Chemseddine *et al.* (11) ont montré que l'espèce réduite à un électron $(W_{10}O_{32})^{5-}$ présente une bande d'absorption intense à 370 nm. Il est donc possible de rendre compte du décalage vers le rouge de la courbe de rendement dont le maximum est à 350 nm en supposant qu'un deuxième photon est absorbé par l'espèce donnée par réduction à 1 électron dès sa formation. On obtiendrait alors en régime stationnaire l'espèce doublement réduite.

Nous pouvons proposer le schéma suivant:

$$(W^{VI}_{10}O_{32})^{4-} \xrightarrow{h\nu_1 = 320 \text{ nm}} (W^{VI}_{10}O_{32})^{4-*}$$

$$(W^{VI}_{10}O_{32})^{4-*} + D \rightarrow (W^{VI}_9W^{V}O_{32})^{5-} + D^+$$

$$(W^{VI}_9W^{V}O_{32})^{5-} \xrightarrow{h\nu_2 = 370 \text{ nm}} (W^{VI}_9W^{V}O_{32})^{5-*}$$

$$(W^{VI}_9W^{V}O_{32})^{5-} + (W^{VI}_9W^{V}O_{32})^{5-} \rightarrow (W^{VI}_8W^{V}_2O_{32})^{6-} + (W_{10}O_{32})^{4-}$$

$$(W^{VI}_9W^{V}O_{32})^{5-*} + D \rightarrow (W^{VI}_8W^{V}_2O_{32})^{6-} + D^+$$

et finalement

$$(W^{VI}_8W^{V}_2O_{32})^{6-} \xrightarrow{Pt} (W^{VI}_{10}O_{32})^{4-} + 2\,e^-$$

$$2\,D^+ + 2e^- \xrightarrow{\text{Graphite}} 2\,D$$

où nous appelons D l'espèce oxydable. D doit réaliser plusieurs conditions. Cette espèce doit être présente au voisinage de l'ion excité et sa forme oxydée devra pouvoir se mettre sous une forme stable qui sera réduite sur le graphite.

La cation tétrabutylammonium ne pourra pas jouer ce rôle: son potentiel d'oxydation est très élevé et nous n'avons pas mis en évidence de produits de réactions tels que le butène. On peut aussi penser à l'acétonitrile plus facilement oxydable.

On sait (12) que l'acétonitrile est oxydé en CH_2CN et que le produit final est généralement le succinonitrile en absence d'oxygène. Sinon il réagit sur l'oxygène pour donner le peroxyde O_2CH_2CN (13). Il paraît peu probable que ces produits puissent être réduits sur le graphite avec un potentiel convenable.

Yamase a montré dans le cas de polytungstate par méthode de capteur de spin que W^{VI*} était capable d'arracher un hydrogène de l'eau pour donner le radical $OH^{\bullet}$ (3). On peut donc supposer comme dans le cas de l'uranyle que ces radicaux se recombinent pour produire H_2O_2 qui serait réduit sur le graphite. Le rôle de l'électrode de platine peut être invoqué pour favoriser la réaction bimoléculaire de recombinaison des radicaux hydroxyles.

Comme dans le cas de l'uranyle, nous pensons que l'eau joue le rôle de donneur. Nous avons observé que l'addition d'une petite quantité d'eau à la solution provoquait une petite amélioration de l'effet photogalvanique.

Cependant en mesurant directement le potentiel du couple OH^-/H_2O_2 sur du platine ou du graphite on obtient une valeur voisine de 0,6 V qui ne rend pas compte des résultats obtenus dans le fonctionnement de la pile. Il est probable que le schéma proposé est approximatif.

Au plan de l'intérêt pratique du système nous soulignons le rendement relativement élevé qui a été obtenu dans des conditions non optimisées. La valeur du rendement maximale obtenue comme le rapport de la puissance de la pile à l'énergie lumineuse monochromatique incidente est de l'ordre de 1%. Cette valeur est affectée de la mauvaise utilisation de la surface de l'électrode éclairée et devrait être améliorée par un montage où l'épaisseur optimale serait réalisée sur l'ensemble de la surface éclairée. Enfin le système présente une bonne stabilité dans le temps en accord avec les hypothèses de mécanisme proposées où aucune espèce chimique n'est consommée.

Remerciement

Nous remercions M. William Mooney pour sa participation aux discussions fructueuses.

1. H. A. Levy, P. A. Agron et M. D. Danford. J. Chem. Phys. **30**, 1486 (1959).
2. M. T. Pope. Heteropoly and isopoly exometallate. Inorg. Concepts 8. Springer Verlag. 1983.
3. T. Yamase. Inorg. Chim. Acta, **76**, 425 (1983).
4. J. Fuchs, H. Harth, W. Schiller et U. Gerlach. Acta Crystallogr. Sect B, **32**, 740 (1976).
5. G. Folcher et J. Paris. Nouv. J. Chim. **5**, 149 (1981).
6. S. C. Termes et M. T. Pope. Inorg. Chem. **17**, 500 (1978).
7. F. Chauveau, M. Boyer et B. Lemcur. C.R. Acad. Sci. Ser. C, **268**, 479 (1969).
8. E. Birholz, F. Fuchs, W. Schiller et M. P. Stock. Z. Naturforsch. B, **26**, 365 (1971).
9. E. Papaconstantinou. J. Chem. Soc. Chem. Commun. 12 (1982).
10. M. S. Dc. Groot, J. M. Hendrichs et J. C. M. Brohhenzijp. Chem. Phys. Lett. **6**, 521 (1983).
11. A. Chemseddine, C. Sanchez, J. Livage, J. P. Launay et M. Fournier. Inorg. Chem. **23**, 2609 (1984).
12. D. Bradley et D. Wilkinson. J. Chem. Soc. A, 531 (1967).
13. T. Tran Thi, A. M. Koulkes Pujo et L. Gilles. Radiat. Phys. Chem. **15**, 209 (1980).

Biosynthesis of the lupine alkaloids. I. Lupinine

W. MAREK GOLEBIEWSKI[1] AND IAN D. SPENSER
Department of Chemistry, McMaster University, Hamilton, Ont., Canada L8S 4M1

Received February 5, 1985

W. MAREK GOLEBIEWSKI and IAN D. SPENSER. Can. J. Chem. **63**, 2707 (1985).

The mode of incorporation into lupinine of cadaverine, intramolecularly doubly labelled with ^{15}N and with ^{13}C at the C-atom adjacent to ^{15}N, i.e., $^{13}C,^{15}N$-"bond-labelled", was determined by ^{13}C nmr spectroscopy; lupinine is generated from two cadaverine-derived C_5-units by a route which excludes a "dimeric" intermediate with C_{2v} symmetry. The mode of incorporation of ^2H from L-(2-^{2}H)lysine, from (*R*)- and (*S*)-(1-^{2}H)cadaverine, and from (2-^{2}H)-Δ^1-piperideine into lupinine was determined by ^2H nmr spectroscopy. The results corroborate the conclusions from the $^{13}C,^{15}N$ experiment and they establish the stereochemistry of six of the steps in the biosynthetic conversion of L-lysine into lupinine.

W. MAREK GOLEBIEWSKI et IAN D. SPENSER. Can. J. Chem. **63**, 2707 (1985).

Faisant appel à la spectroscopie rmn du ^{13}C et utilisant de la cadavérine doublement marquée d'une façon intramoléculaire par du ^{15}N et du ^{13}C sur le carbone voisin du ^{15}N (liaison $^{13}C,^{15}N$ marquée), on a étudié le mode d'incorporation de la cadavérine à la lupinine. Les résultats obtenus suggèrent que la lupinine se forme à partir de deux unités en C_5 dérivées de la cadavérine par le biais d'une voie réactionnelle qui exclut la formation d'un intermédiaire "dimère" possédant une symétrie C_{2v}. Faisant appel à la rmn du ^2H, on a déterminé le mode d'incorporation du ^2H de la L-(^{2}H-2) lysine, des (^{2}H-2) cadavérines-(*R*) et -(*S*) et de la (^{2}H-2)-Δ^1-pipéridine à la lupinine. Les résultats confirment les conclusions tirées sur la base des expériences conduites avec le ^{13}C et le ^{15}N; de plus, elles permettent d'établir la stéréochimie de six des étapes conduisant à la transformation biosynthétique de la L-lysine en lupinine.

[Traduit par le journal]

Introduction

Speculations concerning the biosynthesis of the lupine alkaloids go back more than 50 years. In 1931 Schöpf suggested (1, 2) that the ring skeleton of lupinine (**20**) might be generated by condensation of two lysine (**1**) derived fragments, 5-aminopentanal (**3**) ($\rightleftharpoons$ Δ^1-piperideine (**4**) (3, 4)) and glutardialdehyde (**5**), followed by reduction (Scheme 1Bd). Schöpf later abandoned this notion in favour of the idea (3) that the iminodialdehyde (**7**) might be the intermediate between lysine and lupinine (Schemes 1Ba and 1Bb). This intermediate was favoured also by Robert Robinson (4). In a further variation of this theme it was suggested (5, 6) that lupinine arose by rearrangement of tetrahydroanabasine (**14**), a dimer of Δ^1-piperideine (**4**) (3, 5) (Scheme 1Be).

The first tracer experiments to test these ideas were carried out twenty-five years ago. Radioactivity from DL-[2-^{14}C]lysine (7) and from its decarboxylation product, [1-^{14}C]cadaverine (6, 8), was indeed incorporated into lupinine. With either substrate, approximately one quarter of the total activity of the alkaloid was present within the hydroxymethyl carbon, C-11, of lupinine. Also, the two methylene carbon atoms, C-4 and C-6, together, accounted for one half of the total alkaloid activity (7, 8). If the assumption is made that this activity is distributed equally over C-4 and C-6, and that each of these two C atoms contains one quarter of the label,[2] it follows that four sites within lupinine, C-11, C-4, C-6, and, presumably, C-10, each account for one quarter of the label of the intact alkaloid (**20**). This conclusion was substantiated by the results of a recent feeding experiment (9) with DL-(4,5-$^{13}C_2$)lysine. Enrichment was detected at four pairs of neighbouring carbon atoms of lupinine, C-1,-2, C-2,-3, C-7,-8, and C-8,-9. This labelling pattern serves as evidence that the carbon skeleton of lupinine is generated from two lysine-derived C_5-units, via an intermediate with C_{2v} symmetry (e.g., either cadaverine (**2**) or the iminodialdehyde (**7**), or both). However, since the distribution of label observed in all these experiments is that which is predicted by every one of the five hypothetical routes (Schemes 1Ba–1Be) that have been advanced to account for the derivation of lupinine from lysine, available tracer evidence cannot serve to discriminate among the biogenetic proposals.

Nor is it certain that cadaverine (**2**) is an intermediate between lysine (**1**) and lupinine (**20**): Neither the observation that incorporation of the two substrates, DL-[2-^{14}C]lysine and [1-^{14}C]cadaverine, leads to the same distribution of label within lupinine, nor the labelling pattern from DL-(4,5-$^{13}C_2$)lysine constitute conclusive evidence for the obligatory intermediacy of cadaverine. Other interpretations are possible which account for such a distribution of label (cf. ref. 10).

The tracer experiments with doubly $^{13}C,^{15}N$- and with ^2H-labelled substrates which are here reported serve as critical tests of the hypotheses that have been advanced to account for the origin of lupinine. The results, which controvert all but one of the hypothetical sequences, provide support for the tetrahydroanabasine route (Scheme 1Be). Furthermore, the results of the tracer experiments with ^2H-labelled substrates clarify stereochemical aspects of this route. Preliminary accounts of parts of this work have appeared (11, 12).

Methods and results

In six tracer experiments, compounds, specifically labelled with stable (Experiments 1–5) and with radioactive isotopes (Experiment 6), were administered by the wick method to intact plants of *Lupinus luteus* (yellow lupine) over a period of 3–6 days. Details of the experiments are summarized in Table 1.

[1] On leave from the Department of Chemistry, University of Warsaw, 02-093 Warsaw, Poland.

[2] Another possible interpretation of these results is that one of the two centres, C-4 or C-6, accounts for 50% of the activity of the intact lupinine, while the other centre is free of activity.

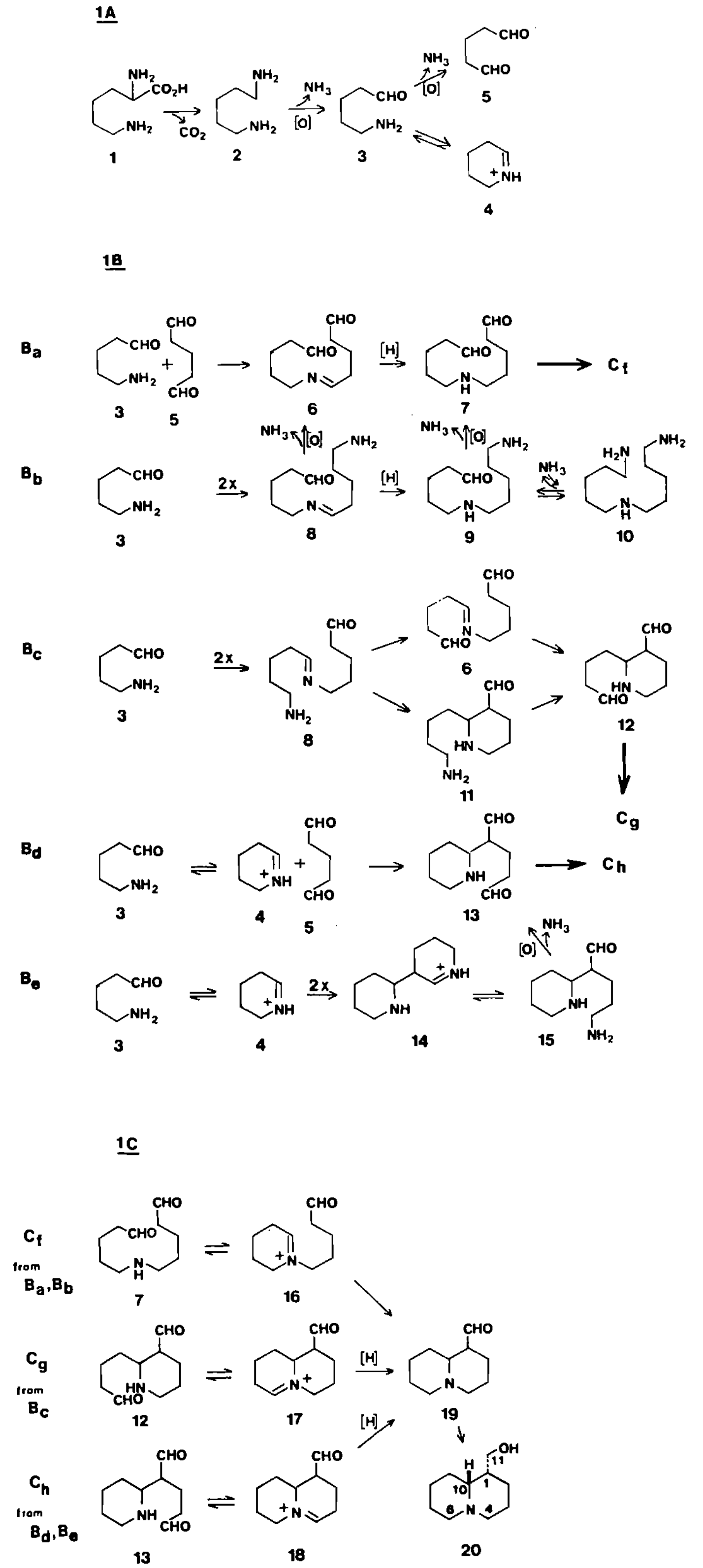

SCHEME 1. Five alternative hypothetical schemes of the biogenesis of lupinine. A. The initial steps. B_a–B_e. Variants of the intermediate steps. C_f–C_h. Variants of the final steps.

The sample of cadaverine, intramolecularly doubly labelled ("bond-labelled") with ^{13}C and ^{15}N (Experiment 5) was prepared in three steps from sodium (^{13}C,^{15}N)cyanide and 1-bromo-4-phthalimidobutane by the reaction sequence shown in Scheme 2, in analogy with the preparation of a similarly labelled sample of putrescine (10).

The samples of DL-(2-^2H)lysine (Experiment 3), (2-^2H)-Δ^1-piperideine (Experiment 4), (*S*)-(+)-(1-^2H)cadaverine dihydrochloride (Experiment 2), and (*R*)-(−)-(1-^2H)cadaverine dihydrochloride (Experiment 1) were prepared by chemical and enzymic methods, respectively, which we have previously described (13). The samples of L-[4-^3H]lysine monohydrochloride and DL-[6-^{14}C]lysine monohydrochloride (Experiment 6) were commercial products.

When the administration of tracer was complete, the plants to which labelled substrates had been administered were macerated with cold methanol in a Waring blendor and the alkaloids were isolated by methanol extraction. Lupinine and sparteine were separated by chromatography on silica gel, lupinine was converted into the hydrochloride, sparteine into the sulfate.

The present paper presents a discussion of the results obtained with lupinine. The sparteine results will be dealt with in the second paper of this series.

Lupinine hydrochloride consists of a 1.7:1 mixture of the *trans* and *cis* ring fused stereoisomers, as shown by the natural abundance ^{13}C nmr spectrum (Fig. 1B). The ^{13}C nmr spectrum (Fig. 1A) of the sample of lupinine hydrochloride from Experiment 5, in which (1-^{13}C,^{15}N)cadaverine in admixture with [1-^{14}C]cadaverine had been administered (Experiment 5), shows that four of the ten C-atoms, C-4, -6, -10, and -11, were enriched in ^{13}C, to an equal extent. The enrichment, above natural abundance, calculated for each of these four carbon atoms (Tables 2 and 3) is in agreement with the specific incorporation of ^{14}C (Table 1).

The signals in the proton noise decoupled ^{13}C nmr spectrum due to two of the ^{13}C-enriched carbon atoms, C-10 and C-11, appear as singlets, the signals due to the two others, C-6 and C-4, as multiplets (Fig. 1A). The coupling constants of the doublet component of the multiplets are different from one another ($J_{^{13}C\text{-}4,^{15}N}$: *trans* isomer 4.1 Hz, *cis* isomer 4.1 Hz; $J_{^{13}C\text{-}6,^{15}N}$: *trans* isomer 7.0 Hz, *cis* isomer 6.4 Hz; isotope shift C-4, *cis* +0.02, *trans* +0.02; C-6, *cis* −0.04, *trans*, −0.04). Each of the two sets of multiplets consists of a doublet superimposed on a singlet. The doublet (87 ± 11%) (^{13}C-6,^{15}N) in the signals due to C-6 (*trans*, δ 55.7, *cis*, δ 52.9 ppm) is much more intense than the singlet (13 ± 2%) (^{13}C-6,^{14}N) (Tables 2 and 3), so that the latter is not apparent in the unexpanded spectrum. In the signals due to C-4 (*trans*, δ 54.8, *cis*, δ 44.6 ppm) the doublet (36 ± 5% of signal area, Tables 2 and 3) (^{13}C-4,^{15}N) appears as a shoulder straddling the singlet (64 ± 8%) (^{13}C-4,^{14}N). The doublet/singlet ratios at C-6 ((87 ± 11)/(13 ± 2) = 6.7 ± 1.3) and at C-4 ((36 ± 5)/(64 ± 8) = 0.6 ± 0.1) thus differ from one another by an order of magnitude (Tables 2 and 3).

Lupinine hydrochloride obtained from the feeding experiment with [L-4-^3H/DL-6-^{14}C]lysine (Experiment 6) was converted into the methiodide and crystallized to constant radioactivity and constant tritium/^{14}C ratio. The $^3H/^{14}C$ ratio of the purified lupinine methiodide was 8.4 ± 0.1, approximately double that of the intermolecularly doubly $^3H/^{14}C$ labelled lysine that had served as the substrate ($^3H/^{14}C$ of lysine, 4.1 ± 0.1 (Table 1)).

The deuterium nmr spectra of the samples of lupinine (free base) from the experiments with deuterium labelled substrates (Experiments 1–4, Table 1) are shown in Fig. 2. The deuterium chemical shifts observed in the spectra of these four

TABLE 1. Experiments with *Lupinus luteus*

(*a*) Stable isotopes

Expt. no.	Substrate	Wt. fed (mg)	Enrichment (at.%)	Plant material: Fresh weight (g)	Plant material: No. of plants	Lupinine: Weight (mg)	Lupinine: Specific incorporation per C_5 unit (%)	Sparteine: Weight (mg)	Sparteine: Specific incorporation per C_5 unit (%)
1	(*R*)-(1-^{2}H)Cadaverine dihydrochloride[a] (March, 1983)	150	99[d]	300	40	9.5	3.0	4	8
2	(*S*)-(1-^{2}H)Cadaverine dihydrochloride[a] (Dec. 1982)	116	93[d]	211	51	13	2.3	4	2
3	DL-(2-^{2}H)Lysine monohydrochloride[a] (July, 1983)	500	95[d]	41[e]	100	5	2.3	4	3
4	(2-^{2}H)-Δ^{1}-Piperideine[a] (Nov. 1983)	300	95[d]	247	100	9	5.4	4	8
5	(1-^{13}C,1-^{15}N)Cadaverine dihydrochloride[a]	140	99,99				28		
	[1-^{14}C]Cadaverine dihydrochloride[b] (Aug. 1982)		[f]	105	50	10	[g]	5	47

(*b*) Radioactive isotopes

Expt. no.	Substrate	Nominal activity: Total (mCi)	Nominal activity: Specific (mCi/mmol)	^{3}H/^{14}C ratio	Plant material: Fresh weight (g)	Plant material: No. of plants	Lupinine (mg)	^{3}H/^{14}C ratio	Sparteine sulfate (mg)	^{3}H/^{14}C ratio
6	DL-[6-^{14}C]Lysine monohydrochloride[c]	0.20	45	4.1 ± 0.1[h]	104	36	4	8.4 ± 0.1[i]	3	6.8 ± 0.2
	L-[(*RS*)-4-^{3}H]Lysine monohydrochloride[c] (Dec. 1983)	1.0	22×10^{3}							

[a] See Experimental.
[b] New England Nuclear (nominal total and specific activities, 25 μCi, 105 mCi per mmol, respectively).
[c] CEA France.
[d] Measured by means of computer assisted peak height analysis.
[e] This experiment was done during the hot summer of 1983 when the greenhouse was very hot and dry.
[f] Net specific activity, determined for the mixture of [1,5-^{14}C]cadaverine dihydrochloride, after dilution with 140 mg (1-^{13}C,1-^{15}N)cadaverine dihydrochloride, which was fed to the plant: 5.3×10^{7} dpm per mmol.
[g] Specific acitivity of lupinine hydrochloride, after crystallization to constant specific activity: 3.0×10^{7} dpm per mmol.
[h] A 1-mL sample of the feeding solution (25 mL) containing the doubly labelled lysine, which was administered to the plants, was set aside and from it lysine hydrochloride was re-isolated by carrier dilution and purified by ion exchange chromatography and crystallization to constant ^{3}H/^{14}C ratio.
[i] Lupinine was converted into the methiodide which was crystallized to constant ^{3}H/^{14}C ratio.

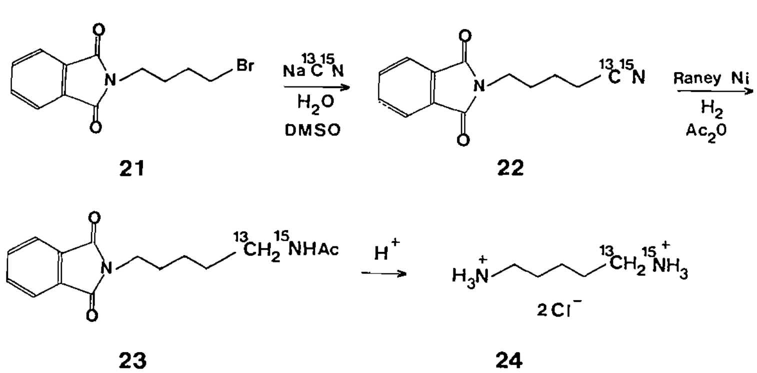

SCHEME 2. Synthesis of (1-^{13}C,1-^{15}N)cadaverine.

TABLE 2. Incorporation of (1-^{13}C,1-^{15}N)cadaverine into *trans*-lupinine hydrochloride[a]

Carbon atom	Chemical shift[b] (ppm)	Type of signal	Natural abundance ^{13}C, normalized peak area[c] (A_{NA})	Enriched in ^{13}C, normalized peak area[c] (A_E)	0.94 A_E/A_{NA}[d]	Percent enrichment above natural abundance[e,f]		Relative percent excess ^{13}C above natural abundance at individual C atoms
1	36.8	s	72	118	1.54	0.6 ± 0.2		1 ± 0.3
2	27.2	s	101	92	0.86	−0.2 ± 0.1		−0.3 ± 0.2
3	18.4	s	100	100	0.94	−0.1 ± 0.1		−0.2 ± 0.2
4	54.8	s	94	941	9.44	9.3 ± 1.3	15.2 ± 1.6	26 ± 3
		d		534	5.34	5.9 ± 0.9		
6	55.7	s	100	194	1.83	0.9 ± 0.3	13.9 ± 1.9	24 ± 4
		d		1252	11.81	13.0 ± 1.9		
7	22.7	s	112	95	0.80	−0.2 ± 0.1		−0.3 ± 0.2
8	21.7	s	121	125	0.97	−0.03 ± 0.1		−0.1 ± 0.2
9	24.8	s	118	110	0.88	−0.1 ± 0.1		−0.2 ± 0.3
10	64.7	s	78	1315	15.89	16.4 ± 2.0		28 ± 4
11	59.4	s	101	1320	12.32	12.5 ± 1.5		22 ± 3

[a]The sample in D_2O was contained in a 2-mm tube. Acquisition time 3.41 s, 0.293 Hz/data point; 1.6 μs pulses.
[b]Relative to acetone (29.8 ppm).
[c]Peak areas are normalized relative to C-3 = 100%. Estimated standard deviation ±8% for singlet signals, ±10% for composite signals.
[d]The ratio A_E/A_{NA} is normalized so that the average value for carbon atoms 1, 2, 3, 7, 8, and 9 equals 1.0.
[e]$((0.94\ A_E/A_{NA}) - 1) \times 1.1\%$ for singlets; $(0.94\ A_E/A_{NA}) \times 1.1\%$ for doublets.
[f]The average specific incorporation per C_5 unit = $1/4(15.2(\pm1.6) + 13.9(\pm1.9) + 16.4(\pm2.0) + 12.5(\pm1.5))/(99/2) \times 100\% = 29 \pm 2\%$, where 99/2 at.% ^{13}C is the average enrichment at each terminal position of cadaverine.

TABLE 3. Incorporation of (1-^{13}C,1-^{15}N)cadaverine into *cis*-lupinine hydrochloride[a]

Carbon atom	Chemical shift[b] (ppm)	Type of signal	Natural abundance ^{13}C, normalized peak area[c] (A_{NA})	Enriched in ^{13}C, normalized peak area[c] (A_E)	1.08 A_E/A_{NA}[d]	Percent enrichment above natural abundance[e,f]		Relative percent excess ^{13}C above natural abundance at individual C atoms
1	40.0	s	85	80	1.02	0.01 ± 0.1		0.02 ± 0.2
2	22.2	s	131	66	0.54	−0.5 ± 0.1		−1 ± 0.2
3	18.7	s	119	144	1.31	0.3 ± 0.2		1 ± 0.4
4	44.6	s	104	786	8.16	7.8 ± 1.1	12.7 ± 1.3	26 ± 3
		d		434	4.51	4.9 ± 0.6		
6	52.9	s	107	156	1.58	0.6 ± 0.2	12.1 ± 1.5	24 ± 3
		d		1039	10.49	11.5 ± 1.5		
7	17.1	s	131	125	1.03	0.03 ± 0.1		0.1 ± 0.3
8	21.2	s	100	100	1.08	0.08 ± 0.1		0.2 ± 0.2
9	16.3	s	119	117	1.06	0.06 ± 0.1		0.1 ± 0.2
10	58.9	s	81	1111	14.81	15.1 ± 1.8		30 ± 4
11	61.3	s	134	1238	9.98	9.9 ± 1.2		20 ± 2

[a]See footnote *a*, Table 2.
[b]See footnote *b*, Table 2.
[c]Peak areas are normalized relative to C-8 = 100%. Estimated standard deviation ±8% for singlet signals, ±10% for composite signals.
[d]The ratio A_E/A_{NA} is normalized so that the average value for carbon atoms 1, 2, 3, 7, 8, and 9 equals 1.0.
[e]$((1.08\ A_E/A_{NA}) - 1) \times 1.1\%$ for singlets; $(1.08\ A_E/A_{NA}) \times 1.1\%$ for doublets.
[f]The average specific incorporation per C_5 unit = $1/4(12.7(\pm1.3) + 12.1(\pm1.5) + 15.1(\pm1.8) + 9.9(\pm1.2))/(99/2) \times 100\% = 25 \pm 2\%$.

lupinine samples are summarized in Table 4 and are compared with the corresponding proton chemical shifts (Table 5). The ^{2}H nmr spectra of two lupinine samples, that derived from (*S*)-(1-^{2}H)cadaverine (Experiment 2) and that derived from the L-component of DL-(2-^{2}H)lysine (Experiment 3), were identical, each showing two signals, at δ 1.72 (±0.01) and 1.54 ppm. The chemical shifts of the two signals (δ 4.11 and 1.80 ppm) in the spectrum of the sample derived from (2-^{2}H)-Δ^1-piperideine (Experiment 4) corresponded to those of two of the signals (δ 4.14 and 1.77) in the spectrum of the sample from (*R*)-(1-^{2}H)cadaverine (Experiment 1). The latter spectrum showed an additional signal at δ 2.50 ppm. The assignment of these spectra will be discussed in the appropriate context of the next section.

Discussion

The results of the tracer experiments with ^{14}C-labelled lysine (7) and cadaverine (6, 8) and with DL-(4,5-$^{13}C_2$)lysine (9) do not discriminate among the various biogenetic hypotheses that have been advanced to account for the biosynthesis of lupinine (**20**) (Scheme 1A, B, C). The first task in a reexamination of the problem was to devise experiments capable of narrowing down the possibilities.

All the hypotheses that have been advanced (Scheme 1) share a common initial phase, decarboxylation of lysine (**1**) to cadaverine (**2**), followed by oxidative deamination of the latter

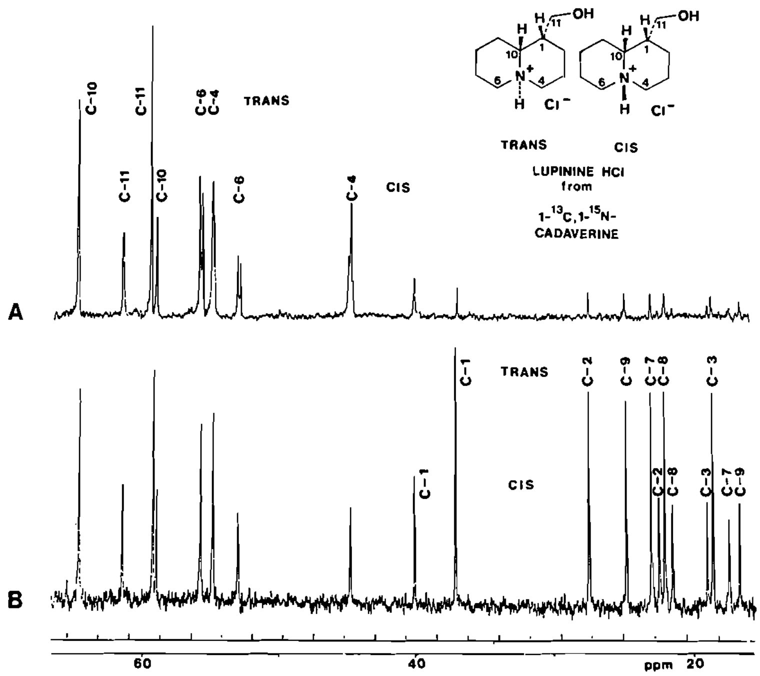

FIG. 1. ^{13}C nmr spectra (20.15 MHz) of lupinine hydrochloride. The spectra were recorded in the Fourier mode on a Bruker WP 80 spectrometer, in 2-mm tubes, with the natural abundance methyl signal of acetone (29.8 ppm) as internal reference. The acquisition time was 3.41 s. For further details see Tables 2 and 3. Top: Fig. 1A. Proton-noise decoupled (P.N.D.) spectrum (20 000 scans) of the $^{13}C,^{15}N$-enriched sample of lupinine hydrochloride (10 mg in 10 μL ^2H_2O) derived from (1-^{13}C,1-^{15}N)cadaverine (Experiment 5). Bottom: Fig. 1B. P.N.D. Spectrum (18 112 scans) of a natural abundance sample of lupinine hydrochloride (17 mg in 20 μL ^2H_2O).

TABLE 4. Incorporation of deuteriated substrates into lupinine. ^2H nmr analysis

Hydrogen atom	^1H nmr chemical shifts[a] (ppm)	^2H nmr chemical shifts[b] (ppm): Experiment 1 lupinine from *R*-(1-^2H)cadaverine (2)	Experiment 2 lupinine from *S*-(1-^2H)cadaverine (3)	Experiment 3 lupinine from DL-(2-^2H)lysine	Experiment 4 lupinine from (2-^2H)-Δ^1-piperideine
4α *si* (eq)	2.57				
4β *re* (ax)	1.75		1.73	1.71	
6α *re* (eq)	2.51	2.50			
6β *si* (ax)	1.57		1.54	1.54	
10β *R* (ax)	1.78	1.77			1.80
11 *re*	3.75				
11 *si*	4.16	4.14			4.11

[a]The ^1H nmr spectrum. Recorded in C_6D_6 at 250 MHz and 400 MHz in the Fourier mode on a Bruker WM 250 and WH 400 spectrometer, respectively. For full assignment of the proton spectrum, see Table 5.
[b]The ^2H nmr spectra. Recorded in C_6H_6 at 38.40 MHz in the Fourier mode on a Bruker WM 250 spectrometer, in 10-mm tubes with natural abundance C_6DH_5 (7.19 ppm) as internal reference. Acquisition time 2.048 s.

to 5-aminopentanal (**3**), an aminoaldehyde in equilibrium with its intramolecular Schiff base, Δ^1-piperideine (**4**) (Scheme 1A). The hypotheses also agree on the final step in the biogenetic process, reduction of lupinal (**19**) to lupinine (**20**) (Scheme 1C). The hypotheses differ in the proposed routes leading from 5-aminopentanal (**3**) ($\rightleftharpoons$ Δ^1-piperideine (**4**)) to lupinal (**19**) (Schemes 1B, 1C).

What was required for a critical examination of the biogenetic process was a method which could distinguish the different paths between 5-aminopentanal (**3**), the last early intermediate common to all the biogenetic proposals, and lupinal (**19**), the common intermediate of the final stage. One way of differentiating among the routes would be by an experiment capable of tracing the fate of the intact C—N bond of 5-aminopentanal (**3**) into the product.

A successful experiment, leading to incorporation of such a C—N bond into lupinine, can have one of three different outcomes. Two of the routes (Schemes 1Bd and 1Be) lead from **3** into **19**, via the bicyclic compound (**18**) and other intermediates, in such a way that the intact C—N bond of **3** is destined to become the C-6,N bond of lupinine (Scheme 3C). A third route (Scheme 1Bc) leads from **3** into **19**, via the bicyclic compound (**17**) and other intermediates, in such a way that the intact C—N bond of **3** is destined to become the C-4,N bond of lupinine (Scheme 3B). It can be predicted that each of these routes leads to a sample of lupinine in which only one of the three C—N bonds of the product is derived from the intact C—N bond of **3**.

The other two routes (Schemes 1Ba and 1Bb) differ from the above in that they give rise to a sample of lupinine which

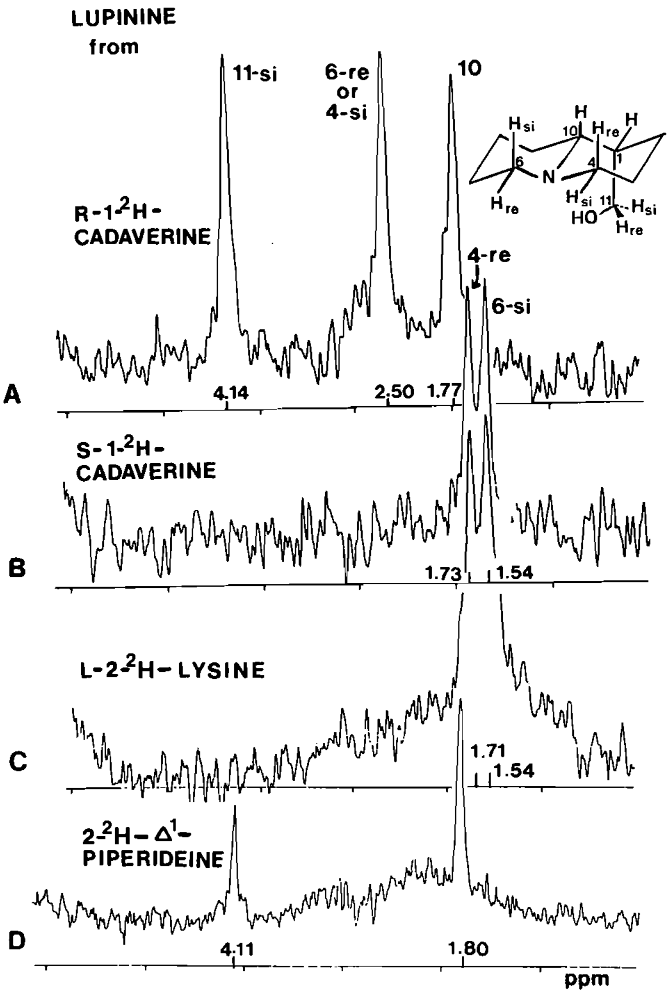

FIG. 2. ^{2}H nmr spectra (38.40 MHz) of deuterium-enriched samples of lupinine derived from deuterium labelled substrates (Experiments 1–4). The spectra were recorded in the Fourier mode on a Bruker WM 250 spectrometer, in 10-mm tubes, with natural abundance C_6DH_5 (7.19 ppm) as internal reference. The acquisition time was 2.048 s (see Table 4). 2A. Lupinine from (*R*)-(1-^{2}H)cadaverine (Experiment 1). 2B. Lupinine from (*S*)-(1-^{2}H)cadaverine (Experiment 2). 2C. Lupinine from the L-component of DL-(2-^{2}H)lysine (Experiment 3). 2D. Lupinine from (2-^{2}H)-Δ^1-piperideine (Experiment 4).

contains an equimolar mixture of two species, one of which contains the intact C—N bond of **3** at C-4,N while the other contains it at C-6,N. This is the consequence of the postulated intermediacy of the dialdehydeimine (**7**). This compound contains two C—N bonds, but only one of these is derived intact from **3**. However, the compound possesses C_{2v} symmetry. Ring closure of **7** by an intramolecular Mannich reaction to yield lupinal (**19**) can take place in two equivalent ways. The C—N bond that is derived intact from **3** has an equal chance of becoming either C-4,N or C-6,N within the product. The product will then comprise an equimolar mixture of two chemically indistinguishable species, which differ solely in the origin of the two C—N bonds, C-4,N and C-6,N (Scheme 3A).

The origin of the two C—N bonds of lupinine, C-4,N and C-6,N, can be determined by a tracer experiment with C—N "bond-labelled" 5-aminopentanal (**3**) or one of its precursors, lysine (**1**) or cadaverine (**2**). A sample of the latter, intramolecularly doubly ^{13}C,^{15}N labelled (NH_2—CH_2—CH_2—CH_2—CH_2—$^{13}CH_2$—$^{15}NH_2$), was employed to probe the incorporation of an intact C—N bond into lupinine (Experiment 5) (11). A similar experiment, with essentially identical results and conclusions, was reported in an independent investigation (14). Entry of this bond-labelled cadaverine, via 5-aminopentanal, by route Bd or Be (Scheme 1), should yield a single species of intramolecularly ^{13}C,^{15}N doubly labelled product in which the ^{13}C,^{15}N moiety is located at the C-6,N position of lupinine. Entry by Route Bc (Scheme 1) should similarly yield lupinine enriched at C-4,N. Entry via the nondissymmetric intermediate **7** (Routes Ba, Bb, Scheme 1) must yield an *equimolar mixture* of the above two enriched species (Scheme 3A). Non-equimolar enrichment at the two sites, C-4,N and C-6,N, is not consistent with the intermediacy of a "dimeric" compound with C_{2v} symmetry, such as **7**.

TABLE 5. The ^{13}C and ^{1}H nmr spectra of *trans*-lupinine (free base)

Carbon	^{13}C nmr[a] chemical shifts (ppm)[c,d]	^{1}H nmr[b] chemical shifts (ppm)[c] axial protons	equatorial protons
C-1	39.0	—	1.22(β)
C-2	31.9	1.38(β)	1.80(α)
C-3	24.4	2.37(α)	1.34(β)
C-4	57.5	1.75(β)	2.57(α)
C-6	57.4	1.57(β)	2.51(α)
C-7	26.1	1.42(α)	1.38(β)
C-8	25.1	1.05(β)	1.58(α)
C-9	30.1	1.26(α)	1.79(β)
C-10	65.4	1.78(β)	—
C-11	65.8	3.75(*re*)	4.16(*si*)

[a] Recorded in C_6D_6 (128.4 ppm) at 100.7 MHz in the Fourier mode on a Bruker WH 400 spectrometer.
[b] Recorded in C_6D_6 at 400 MHz in the Fourier mode on a Bruker WH 400 spectrometer.
[c] Reference 19.
[d] Cf. references 14–17.

The proton noise decoupled ^{13}C nmr spectrum of the sample of lupinine hydrochloride (a mixture of the *trans* and the *cis* isomers, in the ratio 1.7:1) isolated from plants to which (1-^{13}C,1-^{15}N)cadaverine dihydrochloride had been administered in admixture with [1-^{14}C]cadaverine dihydrochloride (Experiment 5, Table 1) is shown in Fig. 1A.

Lupinine hydrochloride rather than the free base was chosen as the compound for ^{13}C nmr analysis since, even though the salt consists of a mixture of the *trans* and *cis* ring fused isomers, in the ^{13}C nmr spectrum of the *cis* isomer in D_2O the signals due to C-4, -6, -10, and -11, the carbon atoms crucial for the interpretation of the biosynthetic experiment, are well resolved (15) (Δδ C-4,-6: 8.3; C-10,-11: 2.4 ppm) (Table 3). The free base, on the other hand, is *trans* ring fused, and the corresponding signals in the spectrum of the free base show poor resolution (Δδ C-4,-6: 0 (15.1 MHz (15, 16), 5.0 MHz (17)), 0.1 (22.5 MHz (18)) in $CDCl_3$; 0.1 (50.3 MHz (14)) in C_6D_6; Δδ C-10,-11: 0 (16), 0.4 (15) (15.1 MHz), 0.3 (5.0 MHz (17)), 0.9 (22.5 MHz (18)) in $CDCl_3$; 0.3 (50.3 MHz (14)) in C_6D_6).

Spectral assignments of the crucial carbon atoms, C-4, -6, -10, and -11, were made as follows: The natural abundance proton noise decoupled ^{13}C spectrum of lupinine hydrochloride (Fig. 1B) shows two sets of 10 signals, corresponding to two stereoisomers of lupinine hydrochloride that differ in the stereochemistry of the ring fusion. Since the two sets of signals show different signal areas, the two isomers are present in

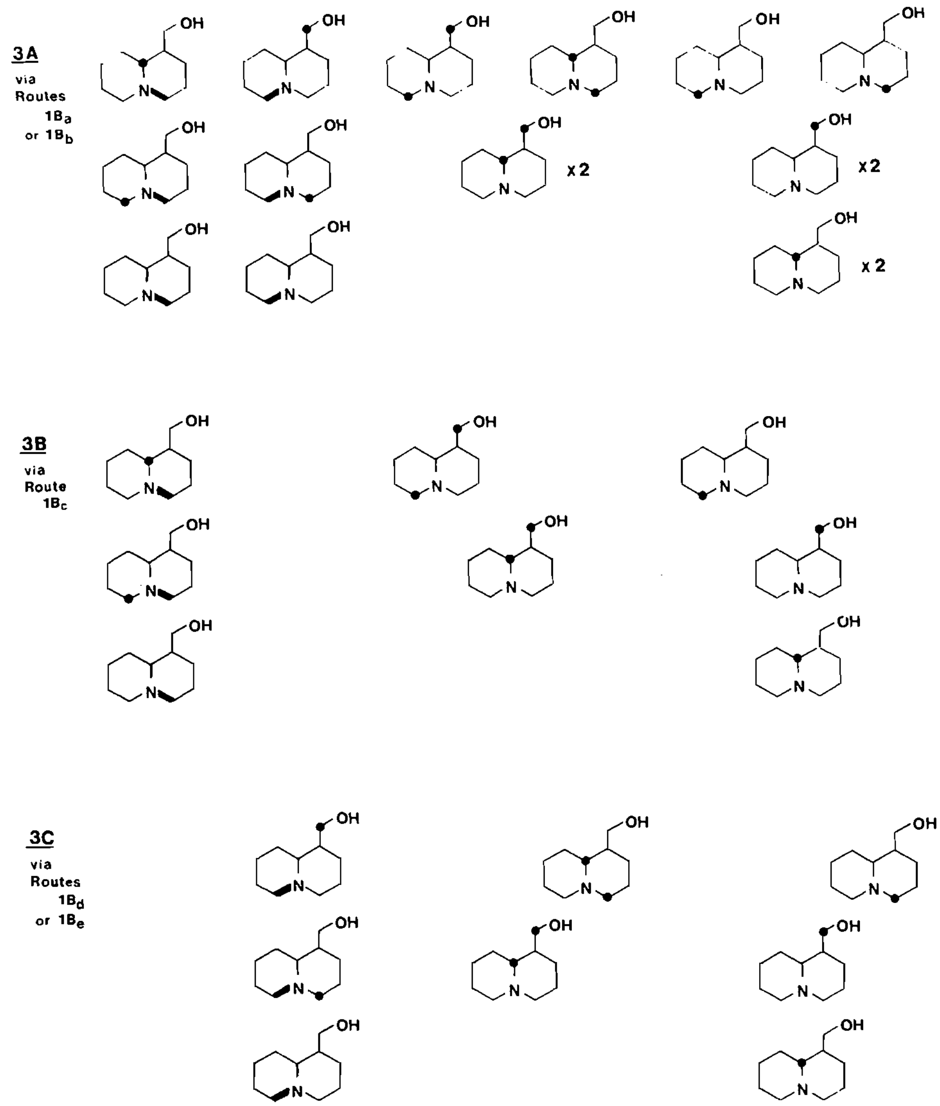

SCHEME 3. Incorporation of (1-^{13}C,1-^{15}N)cadaverine into lupinine. Labelling patterns predicted from the five biogenetic schemes outlined in Scheme 1. A. Via routes B_a or B_b, Scheme 1. B. Via route B_c, Scheme 1. C. Via routes B_d or B_e, Scheme 1. Left columns: ^{13}C,^{15}N bond-labelled species. Central columns: Doubly ^{13}C-labelled species. Right columns: Singly ^{13}C-labelled species. ● = ^{13}C; ■ = ^{13}C—^{15}N.

unequal amounts (1.7:1). The less intense set of signals shows two signals at δ 40.0 and 44.6 ppm. Signals in this spectral region are absent from the spectra of the *trans* fused free base (14–18) or the *trans* fused salt (15) but are present in the *cis* fused salt (15). The signal set of lower intensity is thus due to the *cis* fused salt, which is the less abundant (ca. 37%), and the signals at δ 40.0 and 44.6 ppm must be assigned (19) to C-1 and C-4, respectively, of this isomer. This assignment is confirmed by the off-resonance spectrum in which the signal at δ 40.0 appears as a doublet and the signal at δ 44.6 ppm as a triplet. A second signal, which in the low intensity set appears as a doublet, is that at δ 58.9 ppm, which must therefore be assigned to C-10. This leaves the downfield signal at δ 61.3 ppm to be assigned to the hydroxymethyl carbon, C-11, and the signal at δ 52.9 ppm to C-6. The corresponding resonances in the more intense signal set, due to the *trans* fused stereoisomer, which appear as doublets in the off-resonance spectrum, are those at δ 36.8 ppm (C-1) and at δ 64.7 ppm (C-10). The signal at δ 59.4 must then be assigned to C-11 and those at δ 54.8 and 55.7 ppm to the aminomethyl carbons, C-4 and C-6. Since in the spectrum of the enriched sample of lupinine hydrochloride (Fig. 1A) the high intensity signal at δ 55.7 appears as a doublet and shows a similar doublet/singlet area (1252/194 = 6.4, Table 2) as the low intensity doublet due to C-6 at δ 52.9 ppm (1039/156 = 6.7, Table 3), the signal at δ 55.7 must also be due to C-6. Similarly, the signal at δ 54.8 ppm in the high intensity set corresponds in doublet/singlet area (534/941 = 0.6, Table 2) to that at δ 44.6 ppm (434/786 = 0.6, Table 3) in the low intensity set, due to C-4.

The distribution of label within the ^{13}C,^{15}N enriched alkaloid is evident from the spectrum (Fig. 1A). As expected, only four of the ten C-atoms (C-4, C-6, C-10, C-11) are enriched in ^{13}C, to an equal extent, within experimental error (Tables 2 and 3).

The average specific incorporation of label per C_5 unit (C_5 unit A: C-6, -7, -8, -9, -10, ^{13}C enrichment in either C-6 or C-10 but not in both within the same molecule; C_5 unit B: C-11, -1, -2, -3, -4, ^{13}C enrichment in either C-11 or in C-4, but not in both), based on the ^{13}C nmr data (Tables 2 and 3), was ca. 30 at.% ^{13}C. This corresponds to an incorporation of 30/99 × 100 = 30% of cadaverine per C_5 unit, a value which is in good agreement with that obtained from ^{14}C measurements ((3.0 × 10^7)/(5.3 × 10^7)) × 100 × 1/2 = 28%, Table 1.

The signals due to C-6 and C-4 appear as multiplets. Since the coupling constants of the doublet component of these multiplets differ from one another, the multiplets do not arise from ^{13}C-6,^{13}C-4 coupling, but are due to ^{13}C,^{15}N coupling.

The intense ^{13}C-6,^{15}N doublet indicates intact incorporation of the ^{13}C—^{15}N unit of the administered cadaverine into C-6,N of lupinine. The low intensity doublet due to ^{13}C-4,^{15}N arises as a consequence of the remarkably high efficiency of incorporation, into the alkaloid, of the administered (1-^{13}C,1-^{15}N)-cadaverine. It can be calculated from the ^{13}C nmr data (Tables 2 and 3) that the enriched lupinine which was biosynthesized in the course of the experiment was diluted by natural abundance lupinine present in the plants prior to the experiment by approximately 68%. It can also be calculated that the administered doubly enriched cadaverine was diluted by no more than 25% of endogenous natural abundance cadaverine, prior to conversion into lupinine. The intensity of the ^{13}C-4,^{15}N doublet is fully accounted for by intermolecular ^{13}C,^{15}N coupling between two monomer units, derived from this highly enriched cadaverine, which are incorporated into lupinine after dimerization.

The observed difference in the doublet/singlet ratios of the signals due to C-6 and due to C-4 serves as evidence that an intermediate with C_{2v} symmetry, such as **7**, cannot be implicated in lupinine biosynthesis. The biogenetic proposals shown in Schemes 1Ba and 1Bb are thus eliminated.

Furthermore, since the intact ^{13}C—^{15}N unit of the administered cadaverine is maintained at C-6,N and not at C-4,N of lupinine, the sequence shown in Scheme 1Bc, according to which the precursor C—N bond enters C-4,N of lupinine, is no longer in contention.

The biogenetic schemes which need to be examined further are those shown in Schemes 1Bd and 1Be. These two schemes differ in the timing of the loss of the nitrogen atom of one of the two cadaverine-derived aminopentanal units. Scheme 1Bd postulates that this nitrogen atom is lost at an early stage, so that the aminopentanal-derived intermediate which serves as the precursor of the C_5 chain, C-4, -3, -2, -1, -11, of lupinine is glutardialdehyde (**5**), a compound wih C_{2v} symmetry. Scheme 1Be, on the other hand, postulates that this nitrogen atom is eliminated at a late stage of biosynthesis, following formation of the C_1 dimers, **14** and **15**.

An experiment with 5-aminopentanal or Δ^1-piperideine, labelled at the sp^2 carbon atoms with ^{13}C or ^{14}C, would serve as a critical test of these two suggested routes. In one instance (Scheme 1Bd), three of the carbon atoms of lupinine, C-10, C-11, and C-4, should carry label. In the other instance (Scheme 1Be), label should be present at two of these carbons, C-10 and C-11, but not at the third, C-4. Similarly, an experiment with 5-aminopentanal or Δ^1-piperideine labelled with deuterium at the sp^2 carbon atom would distinguish these two routes, provided that it can be demonstrated that the integrity of the C—D bond is maintained in the course of the biogenetic process. The results of an experiment with (2-^{2}H)-Δ^1-piperideine (Experiment 4) that fulfils this condition will be discussed later. On the basis of this experiment and of other experiments with deuteriated substrates (Experiments 1–3) (see later) the hypothesis based on the intermediacy of glutardialdehyde (Scheme 1Bd) can be discounted.

The biogenetic sequence shown in Scheme 1Be remains. It is consistent with all available experimental evidence.

The initial step in the biosynthetic process leading to lupinine from primary metabolites is the decarboxylation of lysine (**1**) to yield cadaverine (**2**). Two stereochemical questions concerning this step must be answered. First, it must be established whether L-(i.e., (*S*)-)lysine or D-(i.e., (*R*)-)lysine serves as the substrate. Secondly, it must be established whether the decarboxylation process which converts this lysine into cadaverine takes place with net retention of configuration or with net inversion of configuration. We have answered both these questions.

The result of the experiment with intermolecularly doubly labelled [L-^{3}H/DL-^{14}C]lysine (Experiment 6) demonstrates that L-lysine, rather than D-lysine or DL-lysine, serves as the precursor of lupinine in *L. luteus*. The ^{3}H/^{14}C ratio of the doubly labelled lysine that was administered to the plants was 4.1 ± 0.1. The ^{3}H/^{14}C ratio of the lupinine methiodide that was obtained was 8.4 ± 0.1 (Table 1). From these results it can be calculated that, within experimental error, lupinine is derived entirely (102 ± 3%) from L-lysine (% of product derived from L-substrate = 50 (^{3}H/^{14}C ratio of product)/(^{3}H/^{14}C ratio of substrate)) (20).

Demonstration that the decarboxylation of L-lysine to cadaverine takes place with net retention of configuration comes from two of the experiments with deuteriated substrates.

These experiments (Experiments 1–4), which solved not only this stereochemical problem, but which also answered all other stereochemical questions concerning the biosynthetic steps of the route from lysine into lupinine that involve transformations at those carbon atoms of lupinine which originate from the terminal carbon atoms of cadaverine, will now be discussed.

In the first two of these experiments, samples of cadaverine, chirally deuteriated at C-1, were used as substrates. The samples of lupinine obtained from these experiments were examined by ^{2}H nmr. The ^{2}H nmr spectra are shown in Figs. 2A and 2B. Chemical shifts were assigned by comparison with the corresponding ^{1}H nmr chemical shifts (Table 4).

Unambiguous assignment of the resonances due to the 19 protons of lupinine was not possible with one-dimensional nmr spectroscopy, even at 400 MHz, because of substantial overlap of some of the signals. Homo- and heteroscalar correlated two-dimensional ^{1}H and ^{1}H,^{13}C nmr spectroscopy (COSY) and *J*-resolved 2D ^{1}H nmr spectroscopy were employed for a complete assignment of the spectrum. Assignment of the downfield signals, due to the 11-*re* and 11-*si* protons, had been reported (21). A full discussion of the ^{1}H nmr spectrum of lupinine will appear elsewhere (19). Assignments of the signals due to the protons of importance in this study are given in Table 4. These assignments were originally made on the basis of a spectrum determined at 250 MHz and subsequently confirmed on the basis of 400-MHz two-dimensional spectra (Table 5). But even at this frequency the signals for two pairs of protons, 4α and 6α, and 4β and 10β, which appeared as two unresolved signals at 250 MHz, were insufficiently separated for unequivocal assignment of the deuterium signals at chemical shifts corresponding to these positions: 4α (eq) 2.57, 6α (eq) 2.51; 4β (ax) 1.75, 10β (ax) 1.78 ppm. Assignment of the other three protons of interest, 6β (ax), 1.57; 11-*re*, 3.75; 11-*si*, 4.16 ppm, did not pose a problem.

On the basis of the proton resonances, the deuterium signals in the spectrum of lupinine derived from (*R*)-(1-^{2}H)cadaverine (Fig. 2A) can be assigned as follows: δ 4.14, H-11-*si* (corresponding to the signal at δ 4.16 ppm in the ^{1}H spectrum); δ 2.50, either H-6α (2.51) or H-4α (2.57); δ 1.77, either H-4β (1.75) or H-10β (1.78 ppm). Similarly, the signals in the spectrum of lupinine from (*S*)-(1-^{2}H)cadaverine (Fig. 2B) are due to the following protons: δ 1.73, either H-4β (1.75) or H-10β (1.78); 1.54, H-6β (1.57 ppm).

These spectral assignments lead to four possible sets of deuteriated positions in the sample of lupinine from (*R*)-(1-^{2}H)-cadaverine, and to two possible sets in the sample of lupinine from (*S*)-(1-^{2}H)cadaverine, a total of eight possible combinations for the assignment of the two spectra:

	Spectrum 2A: lupinine from (*R*)-(1-^{2}H)cadaverine				Spectrum 2B: lupinine from (*S*)-(1-^{2}H)cadaverine	
	δ 4.14	δ 2.50	δ 1.77		δ 1.54	δ 1.73
1.	H-11 *si*	H-6α	H-4β	a.	H-6β	H-4β
2.	H-11 *si*	H-6α	H-10β	b.	H-6β	H-10β
3.	H-11 *si*	H-4α	H-4β			
4.	H-11 *si*	H-4α	H-10β			

A number of these combinations of assignments can be eliminated on the basis of considerations which follow from the fact that the samples of lupinine from (*R*)- and from (*S*)-(1-^{2}H)cadaverine give different ^{2}H nmr spectra and that incorporation is thus stereospecific.

Firstly, it can be assumed that, since incorporation is stereospecific, the α and β protons at any one carbon atom cannot both be deuteriated in a given lupinine sample. Thus, assignment 3 for spectrum 2A, in which H-4α and H-4β both carry deuterium, can be discounted.

Secondly, it can be assumed that since incorporation is stereospecific, the two samples of lupinine derived from the two enantiomers of (1-^{2}H)cadaverine cannot both bear deuterium at the same site. Thus, the pair (1 + a) for the assignment of the spectra of the lupinine samples derived from (*R*)- and (*S*)-(1-^{2}H)cadaverine, respectively, can be discounted, since assignment 1 and assignment a both have a resonance assigned to H-4β. Similarly, the pairs (2 + b) and (4 + b) are eliminated, since in each pair both assignments have a resonance due to H-10β.

A further restriction follows from the mode of incorporation of ^{13}C- and ^{14}C-labelled substrates into cadaverine. From these experiments it was concluded that the two C_5 chains of lupinine, C-6, -7, -8, -9, -10 and C-4, -3, -2, -1, -11, ultimately originate from one and the same C_5 precursor. The observed localization of label in all experiments with ^{14}C-labelled tracers was consistent with equimolar distribution of radioactivity between the two C_5 chains, and the mode of incorporation of ^{13}C from (1-^{13}C,1-^{15}N)cadaverine, as demonstrated by ^{13}C nmr, proved this equimolar distribution (*vide supra*). It is quite unlikely, therefore, that a sample of lupinine formed biosynthetically from a specifically deuteriated C_5-substrate would contain two deuteriated sites in one of the two C_5 units, while the other C_5 unit is free of deuterium. Yet this is the situation presented by assignment b for spectrum 2B. According to this assignment, both deuterium sites are located on the C_5-unit, C-6, -7, -8, -9, -10, while the other C_5-unit, C-4, -3, -2, -1, -11, is devoid of deuterium. In the light of the results of earlier biosynthetic experiments such a distribution is improbable.

With these restrictions, the assignment of spectrum 2B is unambiguous. The signals at δ 1.73 and 1.54 ppm can be assigned to deuterium at H-4β and H-6β, respectively. Two possible assignments remain for spectrum 2A. While the signals at δ 4.14 and 1.77 ppm can be unequivocally assigned to deuterium at H-11-*si* and H-10β, respectively, the signal at δ 2.50 ppm is due either to H-6α or to H-4α.

Notwithstanding this remaining ambiguity in the assignment of one of the ^{2}H nmr spectra of the ^{2}H-labelled samples of lupinine, the stereochemistry of every step of the biosynthetic process from cadaverine into lupinine can now be deduced from the available evidence.

As shown by the ^{13}C nmr spectrum (Fig. 1A) of lupinine derived from (1-^{13}C,1-^{15}N)cadaverine (Experiment 5), four carbon atoms of lupinine, C-6 and C-10 of one of the C_5 units and C-4 and C-11 of the other, are derived from an α-carbon atom of cadaverine. As shown further by this spectrum, only one of the three C—N bonds of lupinine, N,C-6, represents an intact C—N bond of cadaverine, whereas the three carbon atoms, C-4, C-10, and C-11, of lupinine represent cadaverine carbon atoms from which a nitrogen atom had been detached in the course of the biosynthetic process.

Biochemical separation of a primary amino group from a carbon atom is invariably accompanied by loss of hydrogen atom from the α-carbon, either by oxidation (catalyzed by a dehydrogenase, E.C.1.4.1., or by an oxidase, E.C.1.4.3.) or by transamination (catalyzed by an aminotransferase, e.g., E.C.2.6.1.). These processes are stereospecific, i.e., the α-hydrogen atom must be in the "correct" steric environment in order to be removed.

If, in the course of lupinine biosynthesis, removal of a hydrogen atom from the cadaverine carbon that is destined to become C-4, C-10, and C-11 of lupinine indeed takes place stereospecifically, then only one or the other, but not both, of the samples of lupinine derived from the two enantiomers of (1-^{2}H)cadaverine should carry deuterium at these positions. The carbon atom destined to become C-6 of lupinine, on the other hand, is shown by the experiment with ^{13}C,^{15}N-labelled cadaverine to remain attached to the original nitrogen atom throughout the biosynthetic process. Deuterium should then be found at C-6 in both samples of lupinine. It follows that the signal at δ 2.50 ppm in the spectrum of the sample of lupinine derived from (*S*)-(1-^{2}H)cadaverine (the "*S*-lupinine") is due to a 6 proton rather than to a 4 proton.

The stereospecificity of incorporation of deuterium from (*R*)- and from (*S*)-(1-^{2}H)cadaverine into the two proton sites at C-6 of lupinine serves as clear evidence that the integrity of the C—D bond of cadaverine is maintained on route into lupinine. Deuterium from (*R*)-(1-^{2}H)cadaverine enters the *re*-site (α) at C-6, whereas deuterium from (*S*)-(1-^{2}H)cadaverine enters the *si*-site (β).

With the complete assignment of the signals in the ^{2}H nmr spectra of the deuterated samples of lupinine (Figs. 2A and B), the stereochemical course of the biosynthetic steps from cadaverine into lupinine becomes clear.

The carbon atoms destined to become C-10 and C-11 of lupinine are derived, according to Schemes 1Bd and 1Be (and also 1Bc), from the aldehyde group of the intermediate 5-aminopentanal (**3**), a compound that is formed, early in the biosynthetic sequence, directly from cadaverine by loss of an amino group. Deuterium is present at C-10 and C-11 in the lupinine sample derived from (*R*)-(1-^{2}H)cadaverine ("*R*-lupinine") (Scheme 4) but not in that derived from (*S*)-(1-^{2}H)cadaverine ("*S*-lupinine") (Scheme 5). It follows that removal of the amino group in the course of conversion of cadaverine (**2**) into 5-aminopentanal (**3**) is accompanied by stereospecific loss of the *si*-proton from the α-carbon atom of cadaverine (step a, Schemes 4 and 5).

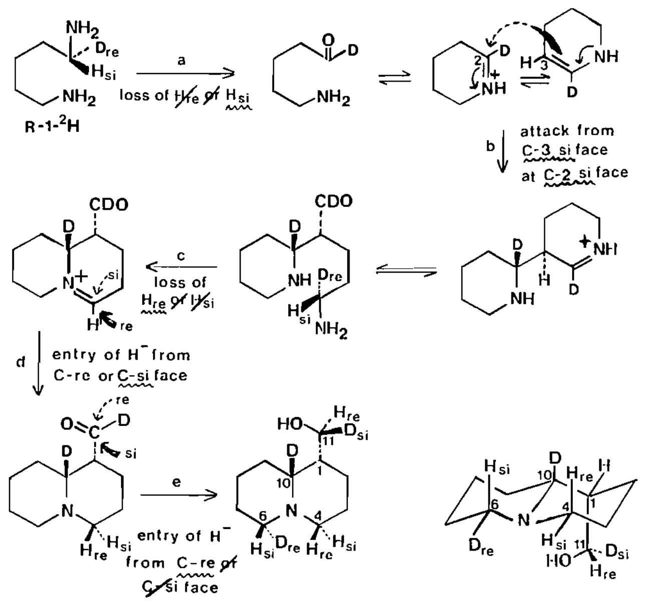

SCHEME 4. The biosynthetic route from cadaverine into lupinine and its stereochemistry: incorporation of (R)-(1-^{2}H)cadaverine.

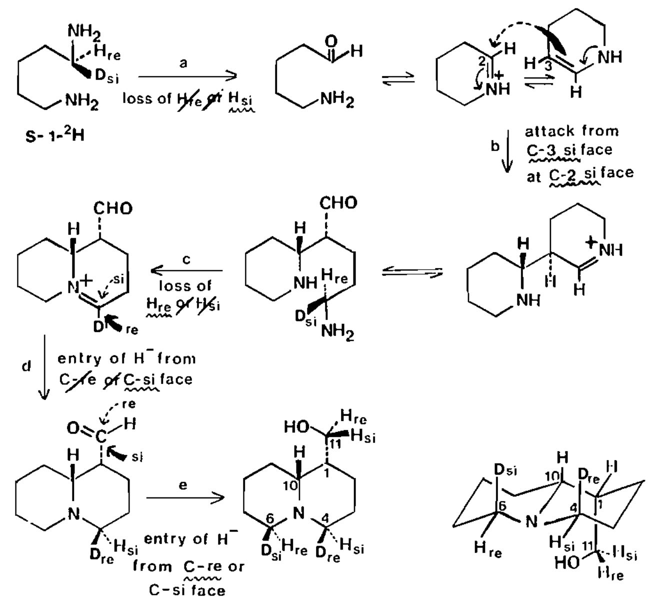

SCHEME 5. The biosynthetic route from cadaverine into lupinine and its stereochemistry: incorporation of (S)-(1-^{2}H)cadaverine.

The observation that a signal due to deuterium at C-4 is found in the spectrum of "S-lupinine" (Fig. 2B) but not in that of "R-lupinine" (Fig. 2A) proves that glutardialdehyde (**5**) (Scheme 1Bd) cannot be implicated in the biosynthetic process: Loss of the amino group of **3** to yield **5** can, in principle, be accompanied by loss of the *si* proton or the *re* proton from the carbon α to nitrogen. If the *si* proton were lost, then the sample of "S-lupinine" should show only one deuterium signal, due to deuterium at carbon-6, while the sample of "R-lupinine" should show four signals, due to deuterium at carbons 6, 10, 4, and 11. If the *re*-proton were lost then, as a consequence of the C_{2v} symmetry of glutardialdehyde, the sample of "S-lupinine" should show signals due to deuterium at carbons 6, 4, and 11, in the ratio 2:1:1, while the sample of "R-lupinine" should show signals due to deuterium at carbons 6, 10, 4, and 11, in the ratio 2:2:1:1. This is not observed. Scheme 1Bd is thereby disproven. The amino group is thus shed at a later stage of the biosynthetic process (step c, Schemes 4 and 5). Since deuterium at C-4 is preserved in "S-lupinine" (Scheme 5) and not in "R-lupinine" (Scheme 4), it is the *re*-proton which is lost, together with the amino group, in this step.

Since the deuterium at C-4 of the "S-lupinine" is found in the *re* position, reduction of the iminium bond (step d, Scheme 5) must take place by entry of the reducing hydride ion from the *si*-face at C-4. Finally, since deuterium at C-11 of the "R-lupinine" is found in the *si* position, reduction of the carbonyl carbon (step e, Scheme 4), must take place by entry of the hydride ion from the *re*-face. The two experiments with enantiotopically deuteriated (1-^{2}H)cadaverine thus clarify the hidden stereochemistry of four steps in the biosynthetic sequence. The overt stereochemistry at C-1 and C-10 of lupinine is determined in the dimerization step (step b, Schemes 4 and 5) that leads from Δ^1-piperideine (**4**) into tetrahydroanabasine (**14**).

The proposed reaction sequence (Schemes 1Be, 4, and 5) postulates that Δ^1-piperideine serves as an intermediate between cadaverine and lupinine. The validity of the proposed sequence and its stereochemistry can be further tested by means of an experiment with deuterium-labelled Δ^1-piperideine (Experiment 4). If the conclusions drawn from the experiments with chirally deuteriated cadaverine (Experiments 1 and 2) are correct, it can be predicted that deuterium from (2-^{2}H)-Δ^1-piperideine must enter at C-10 and at C-11-*si* of lupinine. The ^{2}H nmr spectrum of a sample of lupinine derived from (2-^{2}H)-Δ^1-piperideine is shown in Fig. 2D. The predictions are fully substantiated.

The final stereochemical question that was answered in this investigation concerns the prochirality of the decarboxylation of lysine in *L. luteus*. The evidence which shows that L-lysine is the precursor of lupinine in *L. luteus* (Experiment 6) has already been discussed (*vide supra*). Decarboxylation of L-lysine yields cadaverine. In principle, this decarboxylation can take place either with net retention or with net inversion of configuration. Decarboxylation of L-(i.e., (S)-)(2-^{2}H)lysine with net retention of configuration yields (S)-(1-^{2}H)cadaverine, whereas decarboxylation with net inversion yields (R)-(1-^{2}H)cadaverine. Incorporation into lupinine of the L-component of DL-(2-^{2}H)lysine yields a sample of lupinine whose ^{2}H nmr spectrum (Fig. 2C) is identical with that of the lupinine sample obtained when (S)-(1-^{2}H)cadaverine served as the substrate (Fig. 2B).

It follows that, en route to lupinine, L-(2-^{2}H)lysine is converted into (S)-(1-^{2}H)cadaverine, i.e., in the process leading from L-lysine to cadaverine the carboxyl group of lysine is replaced by a proton with net retention of configuration. This stereochemical course is consistent with the prochirality of the reactions catalyzed by other L-amino acid decarboxylases (22) (E.C.4.1.1.).

The experimental evidence here presented serves as a critical test of the biogenetic hypotheses of lupinine biosynthesis that have been proposed. All but one of the hypotheses are disproven on the basis of the results of the six biosynthetic experiments which are here reported. The remaining hypothesis (Scheme 1Be) which is presented in full detail in Schemes 4 and 5, is entirely consistent with all the experimental evidence. This evidence throws light on the steps from lysine into lupinine and on the stereochemistry of several of these steps.

Experimental

Extraction of lupinine and sparteine from Lupinus luteus

The fresh plant material was immediately ground in a blendor with methanol and extracted in a Soxhlet apparatus for 8 h. The extract was concentrated *in vacuo* and sulfuric acid (1 *M*, 1 mL) was added to the residue. The mixture was extracted with ether (4 × 10 mL) and the aqueous phase filtered through Celite and extracted with chloroform (3 × 10 mL). The aqueous phase was neutralized with solid potassium carbonate, basified with potassium hydroxide (50% w/v, 2 mL), and extracted with methylene chloride (4 × 15 mL). The solvent was evaporated *in vacuo* and the residue once again taken through an acid/base cycle (sulfuric acid, potassium hydroxide, as above), yielding a basic fraction (25 mg) which contained lupinine (**20**) and sparteine as the major components.

The alkaloid fraction (25 mg) was applied to a silica gel column (10 × 185 mm, 4 g, 230–400 mesh, BDH). The column was washed, in turn, with methylene chloride (10 mL), 3% methanol in methylene chloride/0.880 ammonia, 500:1 (20 mL) and 5% methanol in methylene chloride/0.880 ammonia, 333:1 (40 mL). The lupinine fraction was eluted with 8% methanol in methylene chloride/0.880 ammonia, 166:1 (120 mL), the sparteine fraction with 12% methanol in methylene chloride/0.880 ammonia, 100:1 (80 mL). Yield of crude alkaloids: lupinine, 10 mg; sparteine, 4.5 mg. Lupinine was dissolved in hydrochloric acid (0.1 *M*, 0.7 mL), water and excess of acid were removed *in vacuo*, and the residue dried *in vacuo*. Recrystallization from a mixture of methanol–acetone gave lupinine hydrochloride, mp 208–209°C (lit. (23) mp 207–209°C). A small sample of lupinine was converted into lupinine methiodide, lit. (23) mp 295–296°C.

Sparteine was dissolved in acetone (2 drops) and a solution of sulfuric acid in absolute ethanol (1 *M*, 60 μL freshly prepared) was added. Crystals of the sulfate derivative formed immediately, were filtered off, and washed with a mixture of acetone and absolute ethanol (3:1, 3 drops), mp 265–266°C (dec.) (lit. (24) mp 264.5–265.5°C).

Radioactive materials

DL-[6-^{14}C]Lysine and L-[4-^{3}H]lysine were obtained from commercial sources (see Table 1).

Administration of radioactive tracers to L. luteus

Plants were grown from seed and used for tracer experiments 6 weeks after germination. The experiment was carried out in the growth chambers (Experiment 6). Tracer solution was administered to 36 plants by wick in a single dose. The plants were allowed to grow 3 days in contact with tracer.

Materials labelled with stable isotopes

(1-^{13}C,1-^{15}N)Cadaverine dihydrochloride (24)

5-Phthalimidopentano(1-^{13}C,1-^{15}N)nitrile (22)

A solution of 1-bromo-4-phthalimidobutane (**21**) (0.85 g) in dimethyl sulfoxide (1.6 mL) was added dropwise over 2 min to a stirred solution of sodium (^{13}C,^{15}N)cyanide (99 at.% ^{13}C, 99 at.% ^{15}N, MSD Isotopes, Montreal) (0.15 g) in aqueous dimethyl sulfoxide (1.6 mL DMSO, 0.2 mL H_2O). The solution was stirred 4 h at 65°C and left overnight at room temperature. Water (12 mL) was added and the mixture extracted with benzene (4 × 5 mL). The benzene extract was reextracted with water, dried, and evaporated to dryness *in vacuo*, yielding crystalline product (680 mg). A small sample was recrystallized from absolute ethanol, mp 69–70°C; ^{1}H nmr ($CDCl_3$) δ: 8.13–7.87 (4H, m), 3.83 (2H, t, *J* 6 Hz, H-5) 2.65–2.35 (2H, m, H-4), 2.1–1.9 (4H, m); ^{13}C nmr ($CDCl_3$) δ: 119.2 (d, $J_{^{13}C,^{15}N}$ 16.7 Hz), 36.7 (C-5), 27.6 (C-4), 22.7 (C-3), 16.6 (d, *J* 55.2 (Hz, C-2); ms *m/z*: 230 (6.5%), 188 (31, M − (CH_2–$^{13}C^{15}N$)), 160 (100, M − (C_3H_5–$^{13}C^{15}N$)), 149 (21), 104 (98), 77 (12), 76 (13).

*1-*N*-Acetyl-5-*N*-phthaloyl-1,5-diamino(1-^{13}C,1-^{15}N) pentane (23)*

Crude 5-phthalimidopentano(1-^{13}C,1-^{15}N)nitrile (**22**) (0.67 g) in acetic anhydride (3 mL) was added to a suspension of freshly prepared Raney nickel catalyst (0.5 g) in acetic anhydride (7 mL). (The catalyst had been freshly prepared immediately before use by gradual addition of sodium hydroxide pellets to a suspension of nickel aluminum alloy (1:1 w/w, BDH) in water, without cooling. This mixture was left for 30 min and heated on the steam bath for 1 h. The solid was then washed with water, 95% alcohol, absolute alcohol, and acetic anhydride.) Hydrogenation was carried out at 80–90°C and 1 atm for 3 h. The mixture was centrifuged, the supernatant solution was decanted, and the metallic residue washed with acetic anhydride. The solvent was evaporated *in vacuo* to yield the acetyl derivative as a solid (yield 0.8 g, mp 134–136°C, after recrystallization from absolute ethanol); ^{1}H nmr ($CDCl_3$) δ: 7.9–7.7 (4H, m), 6.0 (1H, dtd, $J_{^{15}N,H}$ 89.5 Hz, $J_{CH_2\text{-}1,NH}$ 11.2 Hz, $J_{^{13}C,NH}$ 2.8 Hz), 3.67 (2H, t, *J* 6.6 Hz, H-5), 3.23 (2H, dm, $J_{^{13}C,H\text{-}1}$ 139 Hz), 1.94 (3H, d, *J* 12 Hz), 1.8–1.3 (6H, m); ^{13}C nmr ($CDCl_3$) δ: 170.2 (^{15}NCO–), 168.6 (NCO–), 134.1 (C-3′,-4′), 132.3 (C-1′,-6′), 123.3 (C-2′,-5′), 39.5 (d, $J_{^{13}C\text{-}1,^{15}N}$ 10.2 Hz, C-1), 37.7 (C-5), 29.0 (d, *J* 33 Hz, C-2), 28.2 (d, *J* 7.1 Hz, C-4), 24.1 (CH_3), 23.3 (d, *J* 8.5 Hz, C-3).

(1-^{13}C,1-^{15}N)Cadaverine dihydrochloride (24)

Hydrochloric acid (6 *M*, 14 mL) was added to the crude acetyl derivative (**23**) and the mixture was stirred for 18 h at 100°C. Crystallization of phthalic acid started on cooling and was complete after 1 h at 0°C. The phthalic acid was removed by centrifugation and the supernatant solution was extracted with ethyl acetate (3 × 10 mL). The aqueous layer was evaporated *in vacuo*. The residue was dried (0.45 g) and recrystallized from 95% ethanol. After the first crop of crystals (0.17 g), mp 255–257°C, was filtered off, the mother liquors were chromatographed on an ion exchange column (Dowex 50-X4, H^+ form, 2.1 mequiv./mL, 1.3 × 11 cm). The column was washed with water (20 mL) and the product was eluted with hydrochloric acid (1.5 *M*, 200 mL), yielding a further crop (0.13 g) of (1-^{13}C,1-^{15}N)cadaverine dihydrochloride. Total yield 57% (relative to Na^{13}C^{15}N); ^{1}H nmr (D_2O) δ: 3.76 (1H, t, *J* 7.2 Hz), 2.97 (2H, t, *J* 7.2 Hz), 2.18 (1H, t, *J* 7.2 Hz), 1.45–1.75 (6H, m); $J_{^{13}C,H\text{-}1}$ 144 Hz; the signals at δ 3.76 and 2.18 ppm are doublets of triplets, due to ^{13}C,H-1 coupling of the 1-$^{13}CH_2$ group. The signal at δ 2.97 ppm is due to the 5-CH_2 group; ^{13}C nmr (D_2O) δ: 40.0 (d, $J_{^{13}C\text{-}1,^{15}N}$ 4.4 Hz), 27.0 (s, d, $J_{^{13}C\text{-}2,^{13}C\text{-}1}$ 35.4 Hz[3]), 23.4 (s, C-3).

DL-(2-^{2}H)Lysine monohydrochloride was prepared (13) in two steps from diethyl 2-acetamidomalonate and 1-bromo-4-phthalimidobutane (**21**). Condensation yielded diethyl 2-acetamido-2-(4-phthalimidobutyl)malonate, whose hydrolysis in DCl/D_2O yielded the desired product. DL-(2-^{2}H)Lysine monohydrochloride: ^{1}H nmr (D_2O) δ: 3.7 (ca. 0.05 H, H-2), 3.05 (2H, t, *J* 7.2 Hz, H-6), 1.3–2.0 (m, 6H).

(2-^{2}H)-Δ^1-Piperideine and (*S*)-(+)-(1-^{2}H)cadaverine hydrochloride were prepared from the above DL-(2-^{2}H)lysine (*vide infra*).

(2-^{2}H)-Δ^1-Piperideine (cf. ref. 13)

Freshly crystallized *N*-bromosuccinimide (0.32 g) was added to a solution of DL-(2-^{2}H)lysine monohydrochloride (0.64 g) in water (90 mL) and the solution was heated at 50°C in a nitrogen atmosphere on a rotary evaporator under mild suction until colorless. Three more portions of *N*-bromosuccinimide (3 × 0.32 g) were added and reaction continued in the same way. The total reaction time was 55 min. The solution was used for feeding without further purification.

A small portion of the solution was concentrated and the ^{1}H and ^{2}H nmr spectra of the mixture were determined; ^{1}H nmr δ: 7.5 (s), 6.9 (s), 6.3 (s), 4.5 (H_2O), 3.5 (bm), 3.2 (s), 3.0 (m), 2.6 (s), (CH_2–$CO)_2$NH, succinimide); ^{2}H nmr δ: 8.7 (rel. area 1), 4.9 (rel. area 2.4), 4.5 (DHO, natural abundance) ppm. When the solution was evaporated and redissolved in water, the ^{2}H nmr spectrum changed considerably: ^{2}H nmr δ: 8.3 (rel. area 5.7), 8.1 (1.3), 6.7 (1.0), 4.9 (1.8), 3.8 (4.3). When the solution was basified (K_2CO_3) and extracted six times with chloroform, the chloroform evaporated, and the residue redissolved in water, a further spectral change was observed: ^{2}H nmr δ: 7.9 (rel. area 0.1), 3.1 (0.9).

(R)-(−)- and (S)-(+)-(1-^{2}H)Cadaverine hydrochloride

(R)-(−)-(1-^{2}H)Cadaverine hydrochloride was prepared by decar-

[3]The value, 18.4 Hz, for $J_{^{13}C\text{-}2,^{13}C\text{-}1}$ that was reported in our preliminary communication (11) was in error. We thank Dr. E. Leete for pointing out this mistake.

boxylation of the L-component of DL-lysine in deuterium oxide, catalyzed by L-lysine decarboxylase (13). ^{1}H nmr (D_2O) δ: 2.95 (3.01 H, t, *J* 7.2 Hz, H-1,5) 1.45–1.75 (m, 6H); ca. 1% nondeuteriated product; ms *m/z*: 89 (M' + 1, 9%) 88 (M', 100 $^+NH_3CHD(CH_2)_4$), 87 (M' − 1, 14).

(S)-(+)-(1-^{2}H)Cadaverine hydrochloride was obtained (13) by decarboxylation, catalyzed by L-lysine decarboxylase, of the L-component of DL-(2-^{2}H)lysine (95 at.% 2-^{2}H). (*S*)-(+)-(1-^{2}H)-Cadaverine dihydrochloride (93 at.% 1-^{2}H): ^{1}H nmr (D_2O) similar to that of (*R*)-(−)-(1-^{2}H)cadaverine hydrochloride, above; ms *m/z*: 89 (M' + 1, 10.6%), 88 (M', 100), 87 (M' − 1, 16), 7% non-deuteriated product, based on computer assisted peak height analysis.

Administration of enriched substrates to L. luteus

The plants used in these experiments were grown from seed and were used in feeding experiments 3–6 weeks after germination. The feeding experiments were carried out in the greenhouse (summer months, Experiments 3, 5) or in the growth chambers (winter months, Experiments 1, 2, 4). Tracer solution was administered by wick over a period of 5–6 days; the plants were then grown for a further period of 3–4 days before being harvested.

Acknowledgements

We are grateful to Professor Dr. M. Wiewiórowski, University of Poznan, for a gift of seeds of *Lupinus luteus*, to Thelma Leech, Greenhouse Supervisor, McMaster University, for providing facilities for our experiments, and to J. Ian A. Thompson and Brian G. Sayer, Department of Chemistry, for recording nmr spectra. We are greatly indebted to Dr. R. E. Lenkinski, South Western Ontario NMR Facility, University of Guelph, for determining COSY and 2-D *J* resolved spectra. This investigation was supported by a grant from the Natural Sciences and Engineering Research Council of Canada.

1. C. SCHÖPF, E. SCHMIDT, and W. BRAUN. Ber. **64**, 683 (1931).
2. C. SCHÖPF. *In* IX Congress of the International Union of Pure and Applied Chemistry, Madrid. Vol. 5. 1934. pp. 197–198.
3. C. SCHÖPF. Angew. Chem. **61**, 31 (1949).
4. R. ROBINSON. Structural relations of natural products. Oxford. 1955. p. 74.
5. C. SCHÖPF. Angew. Chem. **69**, 69 (1957).
6. H. R. SCHÜTTE. Arch. Pharm. (Weinheim), **293**, 1006 (1960).
7. H. R. SCHÜTTE and H. HINDORF. Z. Naturforsch. Teil B, **19**, 855 (1964).
8. M. SOUCEK and H. R. SCHÜTTE. Angew. Chem. Int. Ed. Engl. **1**, 597 (1962).
9. J. RANA and D. J. ROBINS. J. Chem. Research (S), 164 (1984).
10. G. GRUE-SØRENSEN and I. D. SPENSER. Can. J. Chem. **60**, 643 (1982).
11. W. M. GOLEBIEWSKI and I. D. SPENSER. J. Chem. Soc. Chem. Commun. 1509 (1983).
12. W. M. GOLEBIEWSKI and I. D. SPENSER. J. Am. Chem. Soc. **106**, 1441 (1984).
13. J. C. RICHARDS and I. D. SPENSER. Tetrahedron, **39**, 3549 (1983).
14. J. RANA and D. J. ROBINS. J. Chem. Soc. Chem. Commun. 81 (1984).
15. K. SHIMA and U. KURASHIGE. Nippon Kagaku Kaishi, 537 (1983); Chem. Abstr. **99**, 54040a (1983).
16. E. WENKERT, B. CHAUNCY, K. G. DAVE, A. R. JEFFCOAT, F. M. SCHELL, and H. P. SCHENK. J. Am. Chem. Soc. **95**, 8427 (1973).
17. F. BOHLMANN and R. ZEISBERG. Chem. Ber. **108**, 1043 (1975).
18. H. PODKOWINSKA and J. SKOLIK. Org. Magn. Reson. **22**, 379 (1984).
19. W. M. GOLEBIEWSKI. To be published.
20. E. LEISTNER, R. N. GUPTA and I. D. SPENSER. J. Am. Chem. Soc. **95**, 4040 (1973).
21. H. PODKOWINSKA. Zesz. Nauk. Akad. Ekon. Poznaniu, Ser. 1, **109**, 107 (1983); Chem. Abstr. **100**, 51872b (1984).
22. J. C. RICHARDS and I. D. SPENSER. Can. J. Chem. **60**, 2810 (1982).
23. J. F. COUCH. J. Am. Chem. Soc. **56**, 2434 (1934).
24. J. F. COUCH. J. Am. Chem. Soc. **59**, 1469 (1937).

Modification of photochemical reactivity through the use of clathrates: the Norrish type I and type II reactions in Dianin's compound

P. C. GOSWAMI, PAUL DE MAYO, AND N. RAMNATH
Department of Chemistry, University of Western Ontario, London, Ont., Canada N6A 5B7

AND

G. BERNARD, N. OMKARAM, JOHN R. SCHEFFER,[1] AND Y-F. WONG
Department of Chemistry, University of British Columbia, Vancouver, B.C. V6T 1Y6

Received December 19, 1984

P. C. GOSWAMI, PAUL DE MAYO, N. RAMNATH, G. BERNARD, N. OMKARAM, JOHN R. SCHEFFER, and Y-F. WONG. Can. J. Chem. **63**, 2719 (1985).

Dianin's compound (4-*p*-hydroxyphenyl-2,2,4-trimethylchroman) serves as host in a series of well-defined clathrate inclusion complexes with eleven linear, as well as branched chain, phenyl alkyl ketone guest molecules, chosen for their ability to undergo the Norrish type I and type II photochemical reactions in solution. The photochemical reactivity of the guest ketones within the clathrate cavity was determined by irradiation of the inclusion complexes in the solid state. The results were compared to the photoreactivity of the ketones in polar as well as nonpolar liquid media. In general, the inclusion complex medium brings about an enhancement of type I over type II reactivity and causes an increase in type II fragmentation compared to type II cyclization. This change in reactivity is interpreted as resulting from the relatively restricted environment of the clathrate cavity coupled with the greater motion required for the type II process (γ-hydrogen abstraction) compared to the type I reaction (α-cleavage), as well as from the greater steric requirements for type II cyclization (cyclobutanol formation) as compared to type II cleavage (1,4-hydroxybiradical scission).

P. C. GOSWAMI, PAUL DE MAYO, N. RAMNATH, G. BERNARD, N. OMKARAM, JOHN R. SCHEFFER et Y-F. WONG. Can. J. Chem. **63**, 2719 (1985).

Il se forme des complexes d'inclusion bien définis à l'intérieur de clathrates du composé de Dianin, le *p*-hydroxyphényl-4 triméthyl-2,2,4 chromane, avec des phényl alkyl cétones, incluant tant des composés aliphatiques en chaînes droites ou ramifiées, choisies pour leur facilité de subir des réactions photochimiques de Norrish des types I et II, en solution. On a déterminé la réactivité photochimique des molécules hôtes à l'intérieur de la cavité en procédant à l'irradiation des complexes d'inclusion à l'état solide. On compare les résultats obtenus avec les photoréactivités des cétones tant dans des milieux polaires que dans des milieux liquides non polaires. D'une façon générale, les complexes d'inclusion augmentent la réactivité du type I par rapport au type II et provoquent une augmentation de la fragmentation du type II par rapport à la cyclisation du type II. On suggère que ce changement dans la réactivité provient d'un effet combiné de l'environnement relativement restreint qui existe dans la cavité du clathrate avec le fait que, par rapport à la réaction de type I (coupure en α), le processus de type II (enlèvement d'un hydrogène en γ) nécessite de plus grands déplacements; de plus, les besoins stériques des cyclisations de type II (formation du cyclobutanol) sont plus importants que ceux requis pour les scissions du type II (scission en hydroxybiradical-1,4).

[Traduit par le journal]

Introduction

The use of organized media to modify photochemical reactivity, as compared to that observed in isotropic liquids, is a subject of considerable current interest. Media which have been investigated include crystals (1−9), liquid crystals (10−12), monolayers (13, 14), micelles (14−25), and surfaces (26−29). A major goal of such studies is to utilize the order of the medium so as to increase the rate and selectivity of the photochemical processes involved in much the same way that enzymes modify the reactivity of the substrates to which they are bound.

An additional technique which holds great promise in this regard is the use of molecular inclusion complexes. Inclusion complexes may be divided into several categories. These include the channel type (e.g., urea), the layer or intercalation type (e.g., graphite), and the true clathrate type in which the guest molecules are located in discrete closed cavities or cages of the host molecule. Examples of this last type are the cyclodextrins (30) as well as the molecule which is the subject of this paper, Dianin's compound (4-*p*-hydroxyphenyl-2,2,4-trimethylchroman), **1** (31).

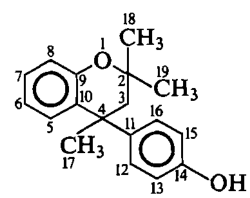

1

Compound **1** was first synthesized and its ability to retain organic solvents first noted by Dianin in 1914 (32). Subsequent work has shown that Dianin's compound is capable of including a wide variety of organic molecules, including ketones (33). X-ray crystallography (34, 35) reveals that six molecules of compound **1** form a cage and that the cages are hourglass shaped with a length of approximately 11 Å, a mid-point width of 4.2 Å, and a maximum upper and lower width of 6.3 Å. The ends of each cage have a width of 2.8 Å and are formed by six hydrogen-bonded hydroxyl groups (Fig. 1). The cages may hold two small molecules in the wide parts or one larger guest.

Some inclusion complexes, such as those formed between organic molecules and the cyclodextrins, are stable in solution, particularly in aqueous solution where the hydrophobic guest molecule seeks the cavity so as to escape from the aqueous

[1]Author to whom correspondence may be addressed.

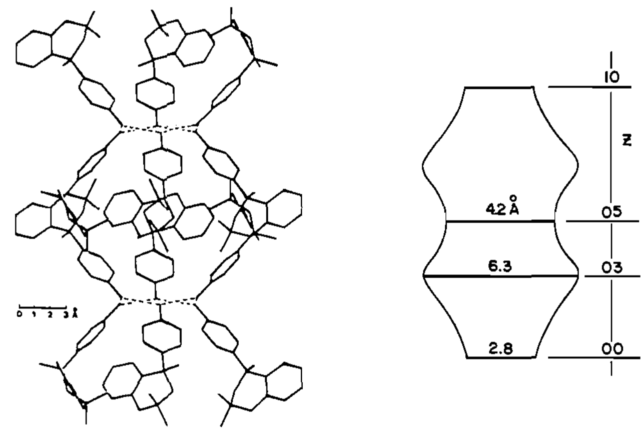

FIG. 1. The left figure is a view normal to the c-axis of unsolvated Dianin's compound (taken from ref. 31). The right figure represents the shape and size of the largest figure of revolution which can fit into the cage. The height is 11 Å (taken from ref. 34).

environment; complexes such as these are most conveniently studied in solution. On the other hand, inclusion complexes with Dianin's compound dissociate upon dissolving in organic solvents and, therefore, must be studied in the solid state. Recently there have been several reports of photochemical reactions of guest molecules in crystalline inclusion complexes of various types. These include stilbene photoisomerization in a tri-*o*-thymotide complex (36), the reactions of dialkyl and aralkyl ketones in deoxycholic acid (37−41), the photoisomerization of α-oxoamides, also in deoxycholic acid (42), the [2+2] photocycloaddition of chalcone derivatives in 1,1,6,6-tetraphenyl-2,4-hexadiyn-1,6-diol (43), the photodecomposition of alkanones in urea inclusion compounds (44), and the photochemistry of di-tert-butyl thioketone in deoxycholic acid (45). In this paper we report an investigation of the Norrish type I and type II photochemical reactions of guest aryl alkyl ketones included in Dianin's compound. These reactions were chosen because the solution state photochemistry of a wide variety of aralkyl ketones has been well established and shown to be sensitive to changes in the irradiation medium (46−51). They should, therefore, provide a sensitive probe of the environment of the Dianin complex cavity. Very recently, Turro and Wan have reported an investigation of the type I and type II reactions of aralkyl ketones adsorbed on zeolite molecular sieves (52). A comparison of our results with theirs is a further point of interest in this study.

Results

Inclusion complexes

The aryl alkyl ketones **2**−**12** (Table 1) were chosen for study. Differing only in the nature of the alkyl chain, they range from simple linear systems to moderately complex branched chain compounds. Their selection was based in part on a desire to test the limits of the size of the molecules which can be accommodated within the cavity. The solution phase photochemistry of most of these molecules has been investigated previously in some detail (53−56).

The complexes were prepared by slow crystallization from solutions of "empty" Dianin's compound dissolved in excess liquid ketone. After filtration, the crystalline complexes were dried (50−55°C, 0.05 Torr; 1 Torr = 133.3 Pa) to constant weight. The host/guest ratio in each case was determined in one or more of three ways: nmr spectroscopy, uv spectroscopy, or gas chromatography (see experimental section for details).

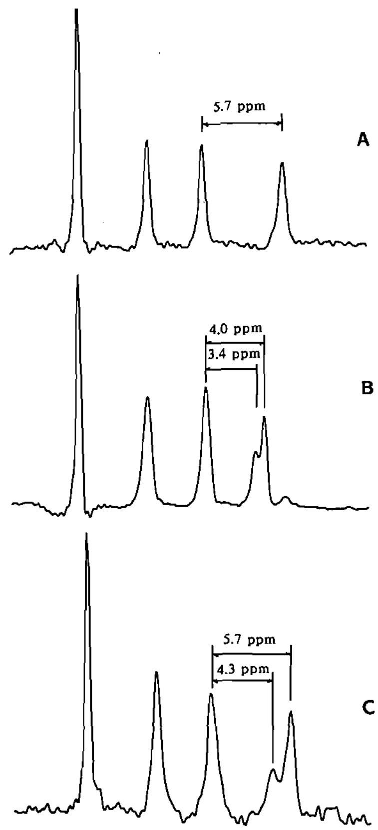

FIG. 2. Partial ^{13}C CPMAS solid state nmr spectra of Dianin's compound (A) and its inclusion complexes with ketones **7** (B) and **3** (C).

The results are summarized in Table 1. In general it was found that the host/guest ratio increased with increasing alkyl chain length and (or) methyl substitution at the α-position. Methyl substitution at the β-position (ketone **6**) also caused an increase in the host/guest ratio, but when the β-substituent is "tied back" as part of a cycloalkane ring (ketones **7** and **8**), the host/guest ratio is once again in the normal 6−9 range.

In the case of three of the complexes (those with butyrophenone (**2**), valerophenone (**3**), and α-cyclohexylacetophenone (**7**)), solid state magic angle spinning ^{13}C nmr was used to determine whether or not the guest molecules were properly included within the host cavity. These experiments were based on work by Ripmeester (57), who showed that the formation of Dianin's complexes causes certain characteristic chemical shift changes in the host spectrum compared to the uncomplexed spectrum. Specifically, the chemical shift difference between the C18 and C19 *gem*-dimethyl groups of Dianin's compound was found to decrease from 5.7 ppm in the uncomplexed form to 3.3−4.7 ppm in the complexed form, depending on the nature of the guest molecule. Figure 2 shows the spectral region in question for empty Dianin's compound as well as for its complexes with ketones **3** and **7**. We note that for both complexes there are *two* upfield methyl signals. We interpret this as indicating two nonequivalent sites for complexation. In the case of the complex with ketone **7**, the chemical shift differences are 4.0 (major) and 3.4 (minor) ppm, both consistent with full complexation. For the complex with valerophenone (**3**), the chemical shift differences are 5.7 (major) and 4.3 (minor) ppm. The closeness of the 5.7-ppm chemical shift difference to that for the unoccupied Dianin's compound may indicate that the major part of the valero-

TABLE 1. Product distribution on photolysis of ketones **2** – **12** in various media[a]

Guest ketone	Host/guest[b]	Medium	F/C[c] (Lit. value)	*t*/*c*[d] (Lit. value)	Type I/Type II[e] (Lit. value)
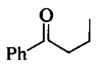 **2**	5–7	Benzene	8.0 (7.3[53], 9.0[54])		
		tert-Butyl alcohol	13.3		
		Complex	8.4		
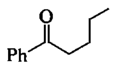 **3**	5–7	Benzene	4.0 (4.6[53], 3.6[54])	2.5 (4[53])	
		tert-Butyl alcohol	6.0 (6.5[53])	1.5 (2[53])	
		Complex	3.7	1.6	
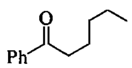 **4**	18–22	Benzene	4.9 (4.0[53])	3.4	
		tert-Butyl alcohol	7.9	1.4	
		Complex	5.3	2.8	
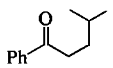 **5**	9	Benzene	7.3 (8.1[53], 5.7[54])		
		tert-Butyl alcohol	15.7 (15.7[53])		
		Complex	27.6		
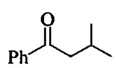 **6**	20–26	Benzene	7.3 (5.7[54])		
		tert-Butyl alcohol	9.5		
		Complex	6.1		
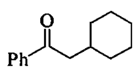 **7**	6	Benzene	0.5	2.2	
		Acetonitrile	0.5	1.3	
		Complex	0.9	1.9	
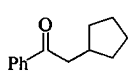 **8**	9	Benzene[f]	12.7	[h]	
		Acetonitrile	12.2		
		Complex	Large[g]		
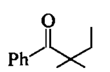 **9**	20–26	Benzene	0.1 (0.12[54])		2.3 (3.3[54])
		tert-Butyl alcohol	0.1		1.2
		Complex	0.9		1.0
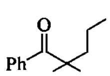 **10**	21–25	Benzene	0.2 (0.5[53], 0.4[54])	1.6 (1.3[53], 1.4[54])	0.1 (0.3[54], 0.3[55])
		tert-Butyl alcohol	0.5 (0.6[53])	1.1 (0.8[53])	<0.1 (0.03[55])
		Complex	0.9	1.7	0.6
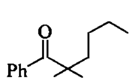 **11**	30–38	Benzene[i]	0.3	1.6	<0.1
		tert-Butyl alcohol	0.7	1.1	<0.1
		Complex	0.7	1.7	0.7
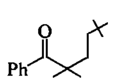 **12**	50–67	Benzene[i]	0.1	3.1	0.4
		tert-Butyl alcohol	<0.1	14.1	0.1
		Complex	1.0	3.1	1.3

[a] Conversions were generally kept below 20%. All irradiations were conducted using a 450-W Hanovia medium pressure mercury lamp except those involving ketones **7** and **8**, which utilized a pulsed nitrogen laser. The estimated error in the photoproduct ratios is 10% of the quoted values.
[b] Ratio of Dianin's compound **1** to ketone as determined by uv, nmr and (or) gc. See experimental section for details.
[c] Ratio of acetophenone **13** to cyclobutanols **14**.
[d] *trans*-Cyclobutanol to *cis*-cyclobutanol ratio.
[e] Ratio of benzaldehyde to total type II photoproducts. No entry indicates no observable benzaldehyde.
[f] Reported to give only cleavage upon irradiation in pentane or ethanol (56).
[g] Cyclobutanol photoproduct formed in trace amounts only.
[h] Not determined due to poor gc separation and small amounts.
[i] Not previously photolyzed.

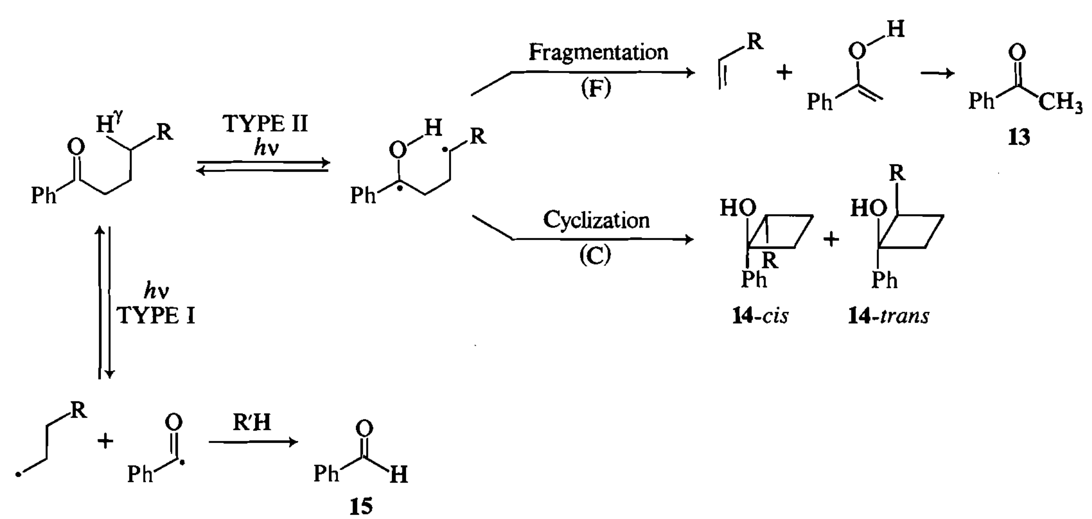

SCHEME 1

phenone is only weakly complexed. As we shall see, this may be the reason that the photochemical results with the valerophenone complex more closely resemble the solution results, whereas irradiation of the crystalline complex of ketone **7** leads to results which are more solid state-like. The solid state nmr (and photochemical) results with the butyrophenone (**2**) complex were qualitatively similar to those with the valerophenone complex, although the spectra were not as well resolved.

Photochemistry

Even though the solution phase photochemistry of most of the ketones listed in Table 1 has been reported previously (53–56), for the sake of direct comparison under a common set of reaction conditions each was re-irradiated in a nonpolar solvent (benzene) as well as in polar solution (*tert*-butyl alcohol or acetonitrile). The ketone concentration was 0.1 *M*, and the light source was a 450-W Hanovia medium pressure mercury lamp fitted with a Pyrex filter sleeve. Only in the case of ketones **7** and **8** was the light source different, consisting of the output from a Molectron UV 22 pulsed nitrogen laser (wavelength 337 nm). Irradiation of the crystalline inclusion complexes was conducted using the same light sources in sealed Pyrex sample tubes, which had been degassed by several evacuation/nitrogen purge cycles. All product ratios were determined by gas chromatography using the appropriate internal standards.

Three product ratios were determined for each compound and medium investigated. (1) F/C, the type II fragmentation to cyclization ratio. Following γ-hydrogen abstraction, the intermediate 1,4-hydroxybiradical can return to starting material, fragment to give the enol of acetophenone, or cyclize to cyclobutanol (Scheme 1) (46–51). The F/C ratio is defined as the yield of acetophenone divided by the total cyclobutanol yield, i.e., **13**/**14**. (2) *t*/*c*, the *trans*-cyclobutanol to *cis*-cyclobutanol ratio. The *trans* isomer is defined as the epimer having the phenyl and R groups *trans* to one another. (3) Type I/Type II, the ratio in which the excited ketones partition themselves between Norrish type I (α-cleavage) and Norrish type II reactivity. For the ketones **2**–**12**, type I reactivity is characterized by formation of benzaldehyde (Scheme 1), and the type I/type II ratio is defined as the yield of benzaldehyde **15** divided by the total yield of the type II products acetophenone and *cis* and *trans* cyclobutanols.

The following generalizations appear to be justified on the basis of the data collected in Table 1. (1) F/C ratio: For ketones **2**–**8**, the fragmentation/cyclization ratios obtained in the crystalline complex differ relatively little from the solution phase ratios and are closer to the benzene values than the *tert*-butyl alcohol values. An exception to this generalization is ketone **5** for which the solid state F/C ratio is some four times greater than the benzene value and approximately twice the *tert*-butyl alcohol ratio. Ketones **7** and **8** also show enhanced F/C ratios in the solid complex. For the dimethyl substituted ketones **9**–**12**, the F/C ratio is consistently higher in the complex than in solution by factors of up to 10. (2) *t*/*c* ratio: This ratio does not appear to be particularly sensitive to medium effects and consistently ranges between 1.1 and 3.4 for all ketones and media studied. A notable exception is ketone **12** with a *t*/*c* ratio in *tert*-butyl alcohol of 14.1. As was the case with the F/C ratios, the *t*/*c* ratios obtained in the solid complex more closely resemble the results found in benzene than those in *tert*-butyl alcohol or acetonitrile (3) Type I/Type II ratio: Only those ketones having *gem*-dimethyl substitution at the α-carbon atom (compounds **9**–**12**) undergo detectable Norrish type I reaction, regardless of medium. For these ketones, type I photoreaction is considerably enhanced in the solid complex compared to solution media. The exception to this rule is ketone **9** for which type I reactivity is seen to decrease somewhat in the solid complex. The type I/type II ratio in the case of ketone **9** is also noticeably greater than for ketones **10**–**12**.

Discussion

Two pieces of evidence point to the conclusion that the environment of an included guest molecule in Dianin's complex is essentially nonpolar in character. The first of these is derived from the similarity of the F/C ratios in benzene and the solid complex for ketones **2**, **3**, **4**, and **6**, and the second is based on the similarity of the *t*/*c* ratios in the same two media for ketones **4**, **7**, **10**, **11**, and **12**. This conclusion is consistent with the X-ray crystal structures of Dianin's compound and its complexes (34, 35), which show that the major portion of the cavity is bounded by hydrocarbon groups, particularly the central "hourglass" constriction which is attributable to the *gem*-dimethyl group at carbon 2. Aside from the puzzling large increase in the *trans* to *cis* cyclobutanol ratio for ketone **12** in *tert*-butyl alcohol, the relative insensitivity of the F/C and t/c ratios to changes in medium for the ketones mentioned above brings out a second conclusion from this work, which is, that, in general, inclusion of guest ketones in the host cavity of Dianin's compound does not greatly alter the chemical reactivity of the excited state and biradical intermediates produced by photolysis. Nevertheless, certain trends of a more modest nature are evident. For example, for ketones **5**, **7**, **8**, **9**, **10**, and **12**, the F/C ratio shows a definite increase in going from solution media to the environment of the solid inclusion complex. This is reasonable if we assume that the inclusion complex affords a relatively restricted environment and that cyclization is a sterically more demanding, "greater motion" process as compared to fragmentation. A similar explanation was used by one of us (58) in interpreting the increased F/C ratio that results from the irradiation of pure crystalline *p*-substituted derivatives of ketone **7** (ketone **7** itself is a liquid at room temperature). In their work on the type II photochemistry of ketones adsorbed on zeolites, Turro and Wan (52) also assumed that cyclization involves greater atomic and molecular motion than fragmentation, and used this idea to explain the greatly increased F/C ratio (>50) observed in the case of the 6 Å Silicalite molecular sieve. However, of the five zeolites tested (52), only the 6 Å pore size material gave results which differed significantly from those in solution. This was attributed to the fact that this pore size is just sufficient to accommodate the benzene ring of the aralkyl ketones investigated. Thus a "tight fit" of the guest molecule in the host cavity appears to be required to bring about increased reaction selectivity in host–guest assemblies. In analogy, it seems reasonable to suggest that those ketones which exhibit increased F/C ratios in Dianin's complex fit more snugly into the host cavity than those ketones for which the F/C ratio is medium independent. Molecular volume calculations and modeling studies may be useful in testing this idea.

With regard to the type I/type II ratios, only ketones **9–12** gave both types of reactivity, attributable of course, to the greater stability of the tertiary alkyl radicals produced by acyl–alkyl cleavage as compared to the primary alkyl radicals which would be formed in the case of ketones **2–8**. The greater type I/type II ratio in the case of ketone **9** compared to ketone **10** was shown (54) to be the result of the slower rate of primary hydrogen atom abstraction in **9** as opposed to secondary hydrogen atom abstraction in **10**. Similar low type I/type II ratios are seen for ketones **11** and **12**, which also bear secondary γ-hydrogen atoms. In three of the four cases studied, the type I/type II ratio increases significantly in proceeding from liquid media to the environment of the solid Dianin's complex. Turro and Wan (52) observed qualitatively similar, but more dramatic (type I/type II > 50) results for ketone **10** adsorbed on 6 Å Silicalite molecular sieves. An explanation similar to that used to rationalize the medium dependence of the fragmentation to cyclization ratios (above) appears reasonable, namely, that the clathrate cavity restricts the movement of its guests and that type I cleavage requires less atomic and molecular motion than the type II reaction for these compounds (γ-hydrogen abstraction).

The question arises as to the meaning of the higher host/guest ratios observed for the more substituted ketones. We presume that the host cavities are flexible and that the larger guests can occasionally be accommodated, but only at the expense of contiguous assemblies. The process then resembles the insertion of a Champagne bottle into a Bordeaux case rather than that of an egg into an egg carton. The ratio is then a measure of how much distortion can be made while maintaining a crystalline structure.

To date there have been four studies (including this one) which report the influence that immobilization within the solid state or inclusion complexes has on the Norrish type II process. These are Dianin's complexes (this study), urea inclusion complexes (44), the pure crystalline state (58), and zeolite molecular sieves (52). Of these, the zeolite environment has the greatest effect on the photoproduct ratios, but only one of the five zeolites studied, the 6 Å pore size Silicalite, was effective. In the pure, crystalline state, the F/C ratios were observed to increase by factors of 2–3 over the ratios in acetonitrile. However, the stereoselectivity of cyclobutanol formation (t/c) remained essentially constant (58). Finally, for the urea inclusion complex of 5-nonanone, the F/C ratio was actually found to decrease by a factor of 2 in going from solution (methanol) to the solid complex (44). Fascinatingly, however, only a single cyclobutanol stereoisomer (believed to be the *cis* isomer) was obtained. It is thus apparent that the ultimate goal of research of this type, to be able to direct photochemical systems completely (and in synthetically useful quantities) toward specific reaction pathways depending on the medium employed, is yet to be realized. Efforts along these lines are continuing in both our laboratories.

Experimental

Apparatus

Ultraviolet spectra were recorded on a Varian Cary 219 spectrophotometer. Proton nmr spectra were recorded on a Varian XL-200 (200 MHz) spectrophotometer using tetramethylsilane as internal standard in deuteriated methanol as solvent. The solid state ^{13}C nmr spectra were run at U.B.C. on a Bruker FT CXP-200 instrument. The ^{13}C signal of liquid benzene, lying 128.5 ppm downfield from tetramethylsilane, was used as an external reference to determine chemical shift values. Gas chromatography was carried out on Varian 3700 (5 ft × 2 mm glass column packed with 15% FFAP on 45/60 mesh Chromosorb W) and Hewlett–Packard 5890 A (12-m fused silica Carbowax 20M capillary column) instruments fitted with flame ionization detectors. Irradiations were carried out with either a 450-W Hanovia medium pressure mercury lamp housed in a Pyrex sleeve or a Molectron UV 22 pulsed nitrogen laser operating at 337 nm with an average power of 330 mW.

Materials

Baker analyzed spectrograde solvents were used for solution irradiations. Ketones **2** and **4** were obtained commercially (Aldrich). Ketones **3**, **5**, and **6** were prepared by Friedel–Crafts acylation of benzene using the appropriate acyl chloride (59). Ketones **7** and **8** were prepared according to the procedure of Wamser and Wagner (56). Ketones **9–12** were prepared from isobutyrophenone with sodium amide and the corresponding alkyl bromide (60). All ketones were purified by column chromatography and (or) vacuum distillation prior to use. Dianin's compound (**1**) was prepared and purified by the method of Baker *et al.* (33). Unsolvated Dianin's compound was obtained by sublimation of the ethanol complex at 140°C and 1 Torr (mp 166–167°C).

Preparation of inclusion complexes

The ketone inclusion complexes with Dianin's compound were prepared by slow crystallization of unsolvated Dianin's compound from the appropriate liquid ketone after dissolution at 80°C. The complexes were dried *in vacuo* (50–55°C/0.05 Torr) to constant weight. Drying was terminated when weight losses of less than 10^{-5} g/h were observed. The host/guest ratio was determined in one or more of three ways. (1) Ultraviolet spectrophotometry: methanol solutions of known concentration were made up for each complex and monitored at 330 nm. The amount of ketone incorporated was calculated by assuming that the absorption at 330 nm due to the ketone in the presence of Dianin's compound is identical to that in its absence. (2) Proton nmr spectroscopy: this method was used for ketones **2**–**6** only. The host/guest ratio was determined as the ratio of the integrated peak heights of the C3 methylene protons of Dianin's compound and the α-methylene protons of the guest ketones. (3) Gas chromatography: the amount of ketone present in a weighed sample of complex was determined by gas chromatographic integration of the ketone peak compared to that of a known amount of internal standard (heptadecane, hexadecane, or octadecane, as appropriate). Alternatively, capillary gas chromatography allowed direct integration of the peaks due to ketone and Dianin's compound. In general, agreement among the three methods was satisfactory.

Solution photolyses

Solution photolyses were carried out in Pyrex sample tubes at a concentration of 0.1 *M*. The solutions were degassed prior to irradiation by purging with nitrogen. The identity of the non-cyclobutanol-containing photoproducts was verified using authentic samples, and the product ratios were determined by gas chromatography employing the appropriate internal standards.

Photolysis of inclusion complexes

Weighed samples (10–20 mg) of the inclusion complexes (conglomerates of fibrous needles) in Pyrex sample tubes were repeatedly evacuated and purged with nitrogen before sealing the tubes under 0.05 Torr vacuum. The tubes were rotated during irradiation and, after photolysis was complete, the samples were dissolved in a methanolic solution of the appropriate internal standard of known concentration and analyzed by gas chromatography as before.

Acknowledgments

Financial support by the Natural Sciences and Engineering Research Council of Canada is gratefully acknowledged. We thank Dr. John Ripmeester for many helpful discussions, and one of us (P. de M.) is grateful to Professor J. Jacques (College de France) for advice and encouragement.

1. G. M. J. SCHMIDT. Solid state photochemistry. *Edited by* D. Ginsburg. Verlag Chemie, New York. 1976.
2. J. M. THOMAS, S. E. MORSI, and J. P. DESVERGNE. Advances in physical organic chemistry. Vol. 15. *Edited by* V. Gold and D. Bethell. Academic, New York. 1977.
3. J. M. THOMAS. Pure Appl. Chem. **51**, 1065 (1979).
4. B. S. GREEN, M. LAHAV, and D. RABINOVICH. Acc. Chem. Res. **12**, 191 (1979).
5. J. R. SCHEFFER. Acc. Chem. Res. **13**, 283 (1980).
6. L. ADDADI, S. ARIEL, M. LAHAV, L. LEISEROWITZ, R. POPOVITZ-BIRO, and C. P. TANG. Chemical physics of solids and their surfaces. Specialist periodical reports. Vol. 8. *Edited by* M. W. Roberts and J. M. Thomas. Royal Society of Chemistry, London. 1980. Chapt. 7.
7. S. R. BYRN. The solid state chemistry of drugs. Academic, New York. 1982.
8. M. HASEGAWA. Adv. Polym. Sci. **42**, 1 (1982).
9. M. HASEGAWA. Chem. Rev. **83**, 507 (1983).
10. P. DE MARIA, A. LODI, B. SAMORI, F. RUSTICHELLI, and G. TORQUATI. J. Am. Chem. Soc. **106**, 653 (1984).
11. J. M. NERBONNE and R. G. WEISS. J. Am. Chem. Soc. **101**, 402 (1979).
12. G. AVIV, J. SAGIV, and A. YOGEV. Mol. Cryst. Liq. Cryst. **36**, 349 (1976).
13. D. G. WHITTEN. Angew. Chem. Int. Ed. Engl. **18**, 440 (1979).
14. D. G. WHITTEN, J. C. RUSSELL, and R. H. SCHMEHL. Tetrahedron, **38**, 2455 (1982).
15. K-H. LEE and P. DE MAYO. J. Chem. Soc. Chem. Commun. 493 (1979).
16. N. BERENJIAN, P. DE MAYO, M-E. STURGEON, L. K. SYDNES, and A. C. WEEDON. Can. J. Chem. **60**, 425 (1982).
17. N. J. TURRO. Tetrahedron, **38**, 809 (1982).
18. N. J. TURRO and B. KRAEUTLER. Acc. Chem. Res. **13**, 369 (1980).
19. N. J. TURRO. Pure Appl. Chem. **53**, 259 (1981).
20. N. J. TURRO. Proc. Natl. Acad. Sci. **80**, 609 (1983).
21. I. R. GOULD, C-H. TUNG, N. J. TURRO, R. S. GIVENS, and B. MATUSZEWSKI. J. Am. Chem. Soc. **106**, 1789 (1984).
22. Y. NAKAMURA, T. KATO, and Y. MORITA. Tetrahedron Lett. 1025 (1981).
23. Y. NAKAMURA, Y. IMAKURA, and Y. MORITA. Chem. Lett. 965 (1978).
24. N. J. TURRO, M. GRATZEL, and A. M. BRAUN. Angew Chem. Int. Ed. Engl. **19**, 675 (1980).
25. J. C. SCAIANO, E. B. ABUIN, and L. C. STEWART. J. Am. Chem. Soc. **104**, 5673 (1982).
26. P. DE MAYO. Pure Appl. Chem. **54**, 1623 (1982).
27. P. DE MAYO, A. NAKAMURA, P. W. K. TSANG, and S. K. WONG. J. Am. Chem. Soc. **104**, 6824 (1982).
28. R. FARWAHA, P. DE MAYO, and Y. C. TOONG. J. Chem. Soc. Chem. Commun. 739 (1983).
29. M. A. FOX. Acc. Chem. Res. **16**, 314 (1983).
30. J. SZEJTLI. Cyclodextrins and their inclusion complexes. Akademiai Kiado, Budapest. 1982, and references cited therein.
31. D. D. MACNICOL, J. J. MCKENDRICK, and D. R. WILSON. Chem. Soc. Rev. **7**, 65 (1978).
32. A. P. DIANIN. J. Russ. Phys.-Chem. Soc. **46**, 1310 (1914).
33. W. BAKER, A. J. FLOYD, J. F. W. MCOMIE, G. POPE, A. S. WEAVING, and J. H. WILD. J. Chem. Soc. 2010 (1956).
34. J. L. FLIPPEN, J. KARLE, and I. L. KARLE. J. Am. Chem. Soc. **92**, 3749 (1970).
35. J. L. FLIPPEN and J. KARLE. J. Phys. Chem. **75**, 3566 (1971).
36. R. ARAD-YELLIN, S. BRUNIE, B. S. GREEN, M. KNOSSOW, and G. TSOUCARIS. J. Am. Chem. Soc. **101**, 7529 (1979).
37. R. POPOVITZ-BIRO, H. C. CHANG, C. P. TANG, N. R. SHOCHET, M. LAHAV, and L. LEISEROWITZ. Pure Appl. Chem. **52**, 2693 (1980).
38. H. C. CHANG, R. POPOVITZ-BIRO, M. LAHAV, L. LEISEROWITZ. J. Am. Chem. Soc. **104**, 614 (1982).
39. R. POPOVITZ-BIRO, C. P. TANG, H. C. CHANG, N. R. SHOCHET, M. LAHAV, and L. LEISEROWITZ. Nouv. J. Chem. **6**, 75 (1982).
40. C. P. TANG, R. POPOVITZ-BIRO, H. C. CHANG, M. LAHAV, and L. LEISEROWITZ. Nouv. J. Chem. **5**, 475 (1981).
41. M. LAHAV, L. LEISEROWITZ, R. POPOVITZ-BIRO, C. P. TANG. J. Am. Chem. Soc. **100**, 2542 (1978).
42. H. AOYAMA, K. MIYAZAKI, M. SAKAMOTO, and Y. OMOTE. J. Chem. Soc. Chem. Commun. 333 (1983).
43. K. TANAKA and F. TODA. J. Chem. Soc. Chem. Commun. 593 (1983).
44. H. L. CASAL, P. DE MAYO, J. F. MIRANDA, and J. C. SCAIANO. J. Am. Chem. Soc. **105**, 5155 (1983).
45. K. PADMANABHAN, K. VENKATESAN, and V. RAMAMURTHY. Can. J. Chem. **62**, 2025 (1984).
46. P. J. WAGNER. Acc. Chem. Res. **4**, 168 (1971).
47. P. J. WAGNER. Top. Curr. Chem. **66**, 1 (1976).
48. J. C. SCAIANO, E. A. LISSI, and M. V. ENCINA. Rev. Chem. Intermed. **2**, 139 (1978).
49. P. J. WAGNER. Molecular rearrangements in ground and excited states. *Edited by* P. de Mayo. Wiley–Interscience, New York. 1980. Chapt. 20.
50. J. C. SCAIANO. Acc. Chem. Res. **15**, 252 (1982).
51. P. J. WAGNER. Acc. Chem. Res. **16**, 461 (1983).
52. N. J. TURRO and P. WAN. Tetrahedron Lett. **25**, 3655 (1984).
53. P. J. WAGNER, P. A. KELSO, A. E. KEMPPAINEN, J. M. MCGRATH, H. N. SCHOTT, and R. G. ZEPP. J. Am. Chem. Soc. **94**, 7506 (1972).
54. F. D. LEWIS and T. A. HILLIARD. J. Am. Chem. Soc. **94**, 3852 (1972).
55. P. J. WAGNER and J. M. MCGRATH. J. Am. Chem. Soc. **94**, 3849

(1972).
56. C. C. WAMSER and W. R. WAGNER. J. Am. Chem. Soc. **103**, 7232 (1981).
57. J. A. RIPMEESTER. J. Inclusion Phenom. **1**, 87 (1983).
58. S. ARIEL, V. RAMAMURTHY, J. R. SCHEFFER, and J. TROTTER. J. Am. Chem. Soc. **105**, 6959 (1983).
59. A. J. VOGEL. A textbook of practical organic chemistry. 3rd ed. Longman, London. 1956. p. 732.
60. A. COUTURE, K. HO, M. HOSHINO, P. DE MAYO, R. SUAU, and W. R. WARE. J. Am. Chem. Soc. **98**, 6218 (1976).

Kinetics and mechanism of the oxidation of substituted benzyl alcohols by sodium *N*-bromobenzenesulfonamide

SEEMA KOTHARI AND KALYAN KUMAR BANERJI[1]
Department of Chemistry, University of Jodhpur, Jodhpur 342001, India

Received August 17, 1984[2]

SEEMA KOTHARI and KALYAN KUMAR BANERJI. Can. J. Chem. **63**, 2726 (1985).

The oxidation of substituted benzyl alcohols by sodium *N*-bromobenzenesulfonamide (BAB) in acid solution results in the formation of the corresponding benzaldehydes. The reaction is first order with respect to BAB, the alcohol, and hydrogen ions. The reaction exhibits a primary kinetic isotope effect ($k_H/k_D = 5.26$). The value of the solvent isotope effect, $k(H_2O)/k(D_2O)$, equals 0.43 at 298 K. Addition of benzenesulfonamide has no effect on the rate. Increase in amount of acetic acid in the solvent increases the rate. The reaction rate has been determined at five different temperatures and the activation parameters have been calculated. $(PhSO_2NH_2Br)^+$ has been postulated as the reactive oxidizing species. The rates of oxidation of substituted benzyl alcohols correlate very well with Brown's σ^+ constants. The value of the reaction constant is −2.84 at 298 K. A hydride transfer from the alcohol to the oxidant, in the rate-determining step, has been proposed.

SEEMA KOTHARI et KALYAN KUMAR BANERJI. Can. J. Chem. **63**, 2726 (1985).

L'oxydation d'alcools benzyliques substitués par du *N*-bromobenzènesulfonamide de sodium (BAB) en milieu acide conduit à la formation des benzaldéhydes correspondants. La réaction est du premier ordre par rapport à la concentration du BAB, de l'alcool et des ions hydrogènes. La réaction présente un effet isotopique cinétique primaire ($k_H/k_D = 5,26$). À 298 K, l'effet isotopique du solvant $k(H_2O)/k(D_2O) = 0,43$. L'addition de benzènesulfonamide n'a pas d'effet sur la vitesse. L'addition d'acide acétique dans le solvant augmente la vitesse. On a déterminé les vitesses de réactions à cinq températures différentes et on a calculé les paramètres d'activation. Il est suggéré que le $(PhSO_2NH_2Br)^+$ serait l'espèce oxydante réactive. On peut établir une bonne corrélation entre les vitesses d'oxydation des alcools benzyliques substitués et les constantes σ^+ de Brown. À 298 K, la valeur de la constante de réaction est égale à −2,84. On suggère que l'étape déterminante de la réaction impliquerait le transfert d'un hydrure de l'alcool à l'oxydant.

[Traduit par le journal]

Introduction

Recently Gunasekaran and Venkatasubramanian have reported the oxidation of diphenylmethanols (1) and fluoren-9-ols (2) by bromamine-T (BAT). Though the rate laws of oxidation of the two series of alcohols are similar, the kinetic isotope effects are different. Moreover, the authors (1) have suggested many possible mechanisms and the available data do not enable one to distinguish between them. In view of this, we have undertaken this investigation. We report in this article the kinetics of the oxidation of several monosubstituted benzyl alcohols by sodium-*N*-bromobenzenesulfonamide (bromamine-B or BAB) in aqueous acetic acid, in the presence of perchloric acid.

Experimental

The preparation and characterization of the alcohols have been described earlier (3). BAB was prepared by the bromination of benzenesulfonamide (BS) in an alkaline solution (4). It was recrystallized from hot water and the purity of the compound was found to be 99% by iodometric determination. Deuterium oxide (99.4%) was supplied by BARC, Bombay. Perchloric acid (E. Merck) was used as a source of hydrogen ions. Acetic acid (Sarabhai M) was refluxed with chromium trioxide and acetic anhydride for 3 h and then fractionated. All other chemicals were of analysed reagent grade. Double distilled water was used throughout.

Product analysis

Product analyses were carried out under kinetic conditions, i.e. with an excess of the alcohol over BAB.

In a typical experiment, benzyl alcohol (4.9 g, 0.05 mol) and BAB (2.8 g, 0.01 mol) were dissolved in 100 mL of 1:1 (v/v) acetic acid − water, in the presence of 1.0 *M* perchloric acid. The mixture was kept in the dark for ca. 10 h to ensure completion of the reaction. It was then treated overnight with an excess (250 mL) of a saturated solution of 2,4-dinitrophenylhydrazine in 2 *M* HCl. The precipitated 2,4-dinitrophenylhydrazone (DNP) was filtered off, dried, weighed, recrystallized from ethanol, and weighed again. The identity of the DNP was established by determining its mp and mixture mp with an authentic sample of DNP of benzaldehyde. The yield of DNP was 2.6 g (91%) and 2.4 g (84%) before and after recrystallization, respectively. In similar experiments with substituted benzyl alcohols, the yield of DNP, after recrystallization, was 78 to 84%.

Stoichiometry

Benzyl alcohol (1.96 g, 0.02 mol) and BAB (1.42 g, 0.005 mol) were dissolved in 100 mL of 1:1 (v/v) acetic acid − water in the presence of 0.5 *M* perchloric acid. When the reaction was complete, the reaction mixture was neutralized by Na_2CO_3 and extracted with ether (3 × 100 mL). The ether solution was dried over anhydrous magnesium sulfate and the solvent was allowed to evaporate. The residue was taken up in 3:2 (v/v) acetonitrile−water and was analysed by hplc on equipment supplied by Bioanalytical Systems, U.S.A. (LC-153), fitted with a RP-8 column and an uv detector (254 nm). The flow rate of solvent was 1.0 mL/min and operating temperature was 30°C. The concentration of residual benzyl alcohol was read from a calibration curve.

The analysis indicated a 1:1 stoichiometry for the reaction.

Kinetic measurements

The reactions were arranged to be under pseudo-first-order conditions by keeping a large excess (10-fold or greater) of the alcohol over BAB. The reactions were carried out in flasks blackened from the outside to prevent any photochemical reaction. The temperature was kept constant to ±0.1 K. The reactions were followed iodometrically for over 70% of the reaction. The pseudo-first-order rate constant, k_1, was calculated from the linear ($r > 0.98$) plots of log [BAB] against time. The specific order rate constant, k, was obtained by the relation $k = k_1/[\text{Alcohol}][H^+]$. Duplicate kinetic runs showed that the rates were reproducible to within ±4%. The solvent was 1:1 (v/v) acetic acid − water unless mentioned otherwise. Preliminary experiments showed that the reaction is not very sensitive to ionic strength, hence no attempt was made to keep it constant.

[1]Author to whom correspondence may be addressed.
[2]Revision received March 11, 1985.

TABLE 1. Rate constants for the oxidation of benzyl alcohol by BAB at 298 K

[BA] (M)	[BAB] $\times 10^3$ (M)	[H^+] (M)	$k_1 \times 10^5$ (s^{-1})
0.05	2.0	1.0	2.60
0.10	2.0	1.0	5.30
0.20	2.0	1.0	10.5
0.30	2.0	1.0	15.7
0.40	2.0	1.0	20.5
0.60	2.0	1.0	32.0
0.20	4.0	1.0	10.4
0.20	6.0	1.0	10.5
0.20	8.0	1.0	10.7
0.20	10.0	1.0	10.3
0.20	12.5	1.0	10.4
0.10	2.0	0.1	1.00
0.10	2.0	0.2	2.10
0.10	2.0	0.3	3.30
0.10	2.0	0.5	5.00
0.10	2.0	0.7	7.50
0.10	2.0	1.2	12.7
0.10	2.0	1.5	16.0
0.10	2.0	1.8	20.0
0.10	2.0	2.0	21.3

TABLE 2. Kinetic isotope effect in the oxidation of benzyl alcohol ([H^+] 1.0 M, [BAB] 0.002 M, temp. 298 K)

[BA] (M)	Type	$k_1 \times 10^6$ (s^{-1})
0.10	α,α-$^1H_2$	53.0
0.20	α,α-$^1H_2$	105
0.30	α,α-$^1H_2$	157
0.05	α,α-$^2H_2$	5.0
0.10	α,α-$^2H_2$	10.2
0.15	α,α-$^2H_2$	14.8
	$10^4 k_H = 5.26 \pm 0.04\ M^{-2}\ s^{-1}$	
	$10^4 k_D = 1.00 \pm 0.02\ M^{-2}\ s^{-1}$	
	$k_H/k_D = 5.26 \pm 0.07$	

Results

The rate laws and other experimental data were obtained for all the alcohols investigated. Since results are similar, only representative data are given here.

The analysis of product formed and determination of stoichiometry indicate the overall reaction [1].

[1] $PhCH_2OH + PhSO_2NBr^- \rightarrow PhCHO + PhSO_2NH_2 + Br^-$

Rate laws

The oxidation of benzyl alcohols by BAB is found to be clearly first order with respect to BAB both regarding time (as evidenced by good fits of log [BAB] versus time plots) and concentration (as shown by the time order rate coefficient being independent of initial [BAB]). The effect of variation in the concentration of alcohol shows a first-order dependence on the concentration of alcohol. The reaction rate increases linearly with an increase in the concentration of perchloric acid (Table 1).

Isotope effects

To ascertain the importance of the cleavage of the α-C—H bond in the rate-determining step, the oxidation of α,α-dideuteriobenzyl alcohol was studied. The results show that the primary kinetic isotope effect, k_H/k_D equals 5.26 ± 0.07 at 298 K (Table 2). This is in contrast to the absence of the kinetic isotope effect in the oxidation of diphenylmethanol (1) and the low value observed in the oxidation of fluoren-9-ol by BAT (2). This is, however, in agreement with the earlier observations of the oxidations by molecular halogens (5, 6) and other sodium N-halogeno compounds (7, 8).

The oxidation of benzyl alcohol was studied in 95% deuterium oxide. The values of rate constants at 298 K in H_2O and D_2O are $10^4 k = 1.30$ and $3.00\ L^2\ mol^{-2}\ s^{-2}$ respectively. The solvent isotope effect, $k(H_2O)/k(D_2O) = 0.43$ at 298 K. This set of experiments was carried out in the absence of acetic acid.

TABLE 3. Effect of benzenesulfonamide on the reaction rate ([BA] 0.20 M, [$HClO_4$] 1.0 M, [BAB] 0.005 M, temp. 298 K)

10^3 [BS] (M)	0.0	2.0	3.0	5.0	7.0	10.0
$10^5 k_1$ (s^{-1})	10.5	10.3	10.5	10.7	10.4	10.6

TABLE 4. Dependence of reaction rate on solvent composition ([H^+] 1.0 M, [BAB] 0.002 M, [BA] 0.2 M, temp. 298 K)

Percentage acetic acid (v/v)	0	20	30	50	60	70
$10^5 k_1$ (s^{-1})	2.60	3.70	5.20	10.5	20.0	50.2

Effect of BS

Addition of BS does not affect the rate of oxidation (Table 3).

Induced polymerization of acrylonitrile

In an atmosphere of nitrogen, the oxidation of benzyl alcohol failed to induce polymerization of acrylonitrile. Thus a radical mechanism is highly unlikely.

Effect of solvent composition

The rates of oxidation were obtained in binary solvent mixtures of acetic acid and water. The rate increases with an increase in the proportion of acetic acid in the solvent mixture (Table 4).

Effect of temperature

The rates of oxidation of eight monosubstituted benzyl alcohols were determined at five different temperatures between 298 K and 318 K (Table 5) and the activation parameters were evaluated (Table 6). The average errors in the values of ΔH^*, ΔS^*, and ΔG^* (at 298 K) are ± 2 kJ mol^{-1}, ± 5 J mol^{-1} K^{-1}, and ± 3 kJ mol^{-1} respectively.

Discussion

The enthalpy and entropy of activation of the oxidation of eight monosubstituted benzyl alcohols are linearly related (r = 0.9988, β = 508 K). The correlation was tested and found genuine by applying Exner's criterion (9). The value of isokinetic temperature, determined by Exner's method, is 509 K. Current views do not attach much physical significance to the value of isokinetic temperature (10), though a linear correlation is usually a necessary condition for the validity of linear free energy relationships. It also implies that all the alcohols are oxidized by the same mechanism and the change in rate is governed by both enthalpy and entropy of activation (11).

In an acidified solution of BAB, in aqueous acetic acid, the probable oxidizing species are BAB itself, $PhSO_2NBr_2$, Br_2, $PhSO_2NHBr$, HOBr, AcOBr, and their protonated forms.

TABLE 5. Rate constants for the oxidation of substituted benzyl alcohols by bromamine-B

	$10^6\,k\ (M^{-2}\,s^{-1})$				
Substituent	298 K	303 K	308 K	313 K	318 K
H	525	780	1150	1600	2340
m-Me	833	1200	1730	2500	3500
p-Et	3450	4790	6600	8120	11700
p-Me	6020	7950	10200	13500	18000
p-OMe	85000	100000	125000	145000	174000
m-Br	34.7	59.0	100	142	250
m-NO_2	6.75	12.1	21.3	32.0	59.2
p-NO_2	3.05	5.65	10.0	17.0	30.0

TABLE 6. Activation parameters for the oxidation of substituted benzyl alcohols by BAB

Substituent	ΔH^* (kJ mol^{-1})	ΔS^* (J mol^{-1} K^{-1})	ΔG^* (kJ mol^{-1})
H	57.3	−118	92.5
m-Me	56.9	−116	91.5
p-Et	44.7	−145	87.9
p-Me	41.5	−151	86.5
p-OMe	29.2	−170	79.9
m-Br	73.4	−86	99.0
m-NO_2	83.1	−68	103
p-NO_2	89.1	−54	105

However, no effect of BS on the reaction rate precludes a pre-equilibrium in which BS is one of the products. This in effect rules out HOBr, AcOBr, Br_2, $PhSO_2NBr_2$, and their protonated forms as reactive oxidizing species. It also rules out the formation of a hypobromite ester as an intermediate in the oxidation process. $PhSO_2NBr_2$ and molecular bromine can also be ruled out in view of the strict first-order dependence of the reaction rate on BAB. This leaves $PhSO_2NHBr$ or *N*-bromobenzenesulfonamide as the most likely oxidizing species. Gunasekaran and Venkatasubramanian (1, 2) also suggested that in the oxidation by BAT, the corresponding *N*-bromosulfonamide is the reactive species. They explained the linear dependence of rate on acidity, obtained in the oxidations by BAT, on the basis of the following equilibrium [2].

[2] $p\text{-}MeC_6H_4SO_2NBr^- + H_3O^+ \rightleftharpoons p\text{-}MeC_6H_4SO_2NHBr + H_2O$

N-Bromosulfonamides are, however, weak acids. The p*K* for $PhSO_2NHBr$ is 4.95 at 298 K in aqueous solution (12). Thus in the presence of even 0.1 *M* $HClO_4$, almost all of the BAB will be in the form of $PhSO_2NHBr$ and a further increase in the acidity of the solution will not cause any significant increase in concentration of $PhSO_2NHBr$. Therefore, the postulation of Gunasekaran and Venkatasubramanian (1, 2) and our own earlier proposal (8) that the neutral halosulfonamide is the reactive oxidizing species are in error. The linear increase in reaction rate on increasing hydrogen ion concentration can be explained by assuming a further protonation of the bromosulfonamide to give a stronger electrophile and oxidant.

[3] $PhSO_2NHBr + H_3O^+ \rightleftharpoons (PhSO_2NH_2Br)^+ + H_2O$

The rate of oxidation increases with a decrease in the polarity of the solvent. The dielectric constants of acetic acid − water mixtures have been estimated earlier (13). It is observed that a plot of log (rate) against the inverse of the dielectric constant of the solvent is linear (r = 0.9980) with a positive slope. This indicates an interaction between a dipolar molecule and a positive ion in the rate-determining step (14). This further supports the idea that the oxidizing species in this reaction is $(PhSO_2NH_2Br)^+$.

The oxidation rates of the monosubstituted benzyl alcohols correlate very well with Brown's σ^+ substituent constants (15), with large negative reaction constants (Table 7). This indicates an electron-deficient carbon centre in the rate-determining step.

D_3O^+ is a stronger acid than H_3O^+ and the rate of an acid-catalysed reaction is expected (16) to be faster in D_2O than in H_2O. Active hydrogen atoms, like those in —OH groups, undergo rapid exchange in D_2O, and if the hydroxyl group is involved in the rate-determining step or in the pre-equilibria, the k_{OH}/k_{OD} isotope effect comes into play and cancels the rate-enhancement due to D_3O^+. The oxidation of benzyl alcohol by BAB exhibits a "normal" solvent isotope effect. This makes the formation of a hypobromite ester, as suggested in the oxidation of diphenylmethanol (1), highly unlikely.

The presence of a substantial primary kinetic isotope effect confirms that the C—H bond, from the carbinol carbon, is cleaved in the rate-determining step. The deuterium isotope effect is also rather large for the non-symmetrical transition state implied in the ester mechanism.

The large negative reaction constant and the high value of the deuterium isotope effect suggest a considerable carbonium ion character in the transition state. This is in accord with the excellent correlation obtained with Brown's σ^+ values. Thus an intermolecular hydride ion transfer from the alcohol to the oxidant is strongly indicated.

[4] 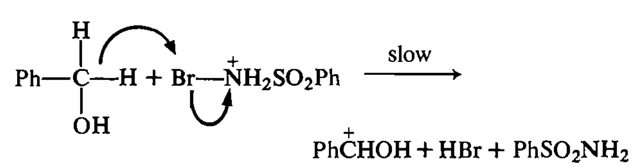

[5] $Ph\overset{+}{C}HOH \xrightarrow{\text{fast}} PhCHO + H^+$

The negative entropy of activation also supports the above mechanism. The reactions in which two molecules combine to form a single activated complex show a decrease in the entropy (17).

In the oxidation of fluoren-9-ols by BAT, Gunasekaren and Venkatasubramanian (2) have suggested synchronous removal of a hydride ion from the C—H bond, and a proton from the hydroxyl group, to account for the low value of the deuterium isotope effect (k_H/k_D = 2.2) obtained by them. Their mech-

TABLE 7. Temperature dependence of the reaction constant

Temperature (K)	298	303	308	313	318
ρ^+	−2.84	−2.71	−2.60	−2.51	−2.39
Regression coefficient	0.9976	0.9985	0.9991	0.9968	0.9993

anism is, however, inconsistent with the high magnitude of the reaction constant ($\rho = -2.8$) exhibited in the oxidation of fluoren-9-ols. In a completely synchronous process, the reaction constant is nearly zero. The oxidation of fluoren-9-ols may involve the prior formation of a hypobromite ester and its subsequent decomposition in the rate-determining step. Thus it seems that different mechanisms operate in the oxidation of fluoren-9-ol and benzyl alcohol. Many fluorene derivatives are reported to react differently from the corresponding aromatic and aliphatic compounds. For example, fluorene-9-carboxylic esters (18) are hydrolysed, in alkaline solution, by a mechanism quite different from that operative for other esters (19). This may be due to the special structural features of fluorene in which a secondary carbon is linked to two benzene rings.

Acknowledgements

Grateful thanks are due to the University Grants Commission, India, for financial support and to Dr. P. K. Sharma for help in the hplc experiments.

1. S. GUNASEKARAN and N. VENKATASUBRAMANIAN. J. Chem. Soc. Perkin Trans. 2, 949 (1983).
2. S. GUNASEKARAN and N. VENKATASUBRAMANIAN. Indian J. Chem. Sec. A, **22**, 774 (1983).
3. K. K. BANERJI. J. Chem. Soc. Perkin Trans. 2, 435 (1973).
4. E. ROBERTS. J. Chem. Soc., 2707 (1923).
5. L. KAPLAN. J. Am. Chem. Soc. **80**, 2639 (1958).
6. P. AUKETT and I. R. L. BARKER. J. Chem. Soc. Perkin Trans. 2, 568 (1972).
7. K. K. BANERJI. Bull. Chem. Soc. Jpn. **50**, 1616 (1977).
8. J. MUKHERJEE and K. K. BANERJI. J. Chem. Soc. Perkin Trans. 2, 676 (1980).
9. O. EXNER. Collect. Czech. Chem. Commun. **29**, 1094 (1964).
10. J. E. LEFFLER. J. Org. Chem. **31**, 1535 (1966).
11. J. E. LEFFLER. J. Org. Chem. **20**, 1202 (1951).
12. F. E. HARDY and J. P. JOHNSTON. J. Chem. Soc. Perkin Trans. 2, 742 (1973).
13. K. K. BANERJI. Indian J. Chem. Sec. A, **16**, 595 (1978).
14. E. S. AMIS. Solvent effect on rates and mechanism. Academic Press, New York. 1967. p. 42.
15. C. D. JOHNSON. The Hammett equation. Cambridge University Press, London. 1973.
16. F. A. CAREY and R. J. SUNDBERG. Advanced organic chemistry. Part A. Plenum Press, New York. 1983. p. 201.
17. E. S. GOULD. Mechanism and structure in organic chemistry. Holt, Rinehart and Winston, New York. 1964. p. 181.
18. M. ALBORZ and K. T. DOUGLAS. J. Chem. Soc. Perkin Trans. 2, 331 (1982).
19. M. L. BENDER. Chem. Rev. **60**, 53 (1960).

$Ni(H_2O)_2(3\text{-}CH_3C_5H_4N)_6(PF_6)_2$: a revision of the crystal data

RAYMOND M. MORRISON, ROBERT C. THOMPSON, STEPHEN V. EVANS, AND JAMES TROTTER
Department of Chemistry, University of British Columbia, Vancouver, B.C., Canada V6T 1Y6

Received October 23, 1984

RAYMOND M. MORRISON, ROBERT C. THOMPSON, STEPHEN V. EVANS, and JAMES TROTTER. Can. J. Chem. **63**, 2730 (1985).

The crystal structure of the title compound is revised and described in the orthorhombic space group *F2dd*, rather than in monoclinic *Cc*. Chemical conclusions are unchanged.

RAYMOND M. MORRISON, ROBERT C. THOMPSON, STEPHEN V. EVANS et JAMES TROTTER. Can. J. Chem. **63**, 2730 (1985).

On propose une revision de la structure cristalline du composé mentionné dans le titre et on le décrit dans le groupe d'espace orthorhombique *F2dd*, plutôt que dans le groupe monoclinique *Cc*. Les conclusions chimiques demeurent inchangées.

[Traduit par le journal]

A (100/010/102) transformation (1) of the *Cc* cell (2) and a detailed examination of the intensity data indicate that the true symmetry is orthorhombic. The revised crystal data are: Orthorhombic, *F2dd*, a = 10.497(1), b = 20.074(3), c = 42.388(10) Å, V = 8932 Å^3, Z = 8, μ(Mo) = 5.9 cm^{-1}, molecular symmetry exactly C_2 (rather than approximately (2)).

Transformation of atomic parameters [(1 0 −0.5/0 1 0/0 0 0.5) − (3/8, 1/8, 1/8)] reveals only small differences between the positions of symmetry-equivalent atoms (maximum 0.03 Å, Table 1), and averaged parameters give a reliable description of the structure, since the previous refinement (2) is still reasonably appropriate (3). The intensity data were averaged (most of the measured data are Friedel pairs, which were not averaged) and the refinement was repeated in *F2dd*; final R = 0.048 for 2483 reflections ($\geq 3\sigma(I)$, of a total

TABLE 1. Positional parameters in space group *F2dd* (the final column gives the distance in the original *Cc* determination (2) between an atom in column 1 and an atom in column 2 with transformation x, $\bar{y}$, $\bar{z}$)

Atom	Symmetry-related atom	Averaged and refined parameters 10^4x	10^4y	10^4z	Distance (Å × 10^3)
Ni	—	0	0	0	—
P(1)	P(2)	−2226.6(21)	1845.3(10)	0806.5(4)	0.7
O(1)	O(2)	−0025(4)	0965(2)	0194(1)	3
N(1)	N(2)	−1453(5)	−0317(3)	0317(1)	15
C(11)	C(21)	−2422(6)	−0686(3)	0213(1)	9
C(12)	C(22)	−3349(6)	−0945(3)	0401(2)	12
C(13)	C(23)	−3288(8)	−0811(4)	0725(2)	15
C(14)	C(24)	−2322(8)	−0417(4)	0837(1)	15
C(15)	C(25)	−1371(7)	−0175(3)	0630(1)	20
C(16)	C(26)	−4400(8)	−1373(4)	0263(2)	10
N(3)	N(4)	1433(5)	0290(3)	−0323(1)	10
C(31)	C(41)	2358(7)	−0141(3)	−0403(2)	3
C(32)	C(42)	3235(7)	−0023(4)	−0640(2)	5
C(33)	C(43)	3140(8)	0582(5)	−0801(2)	21
C(34)	C(44)	2193(7)	1043(4)	−0713(2)	11
C(35)	C(45)	1374(7)	0881(3)	−0477(1)	12
C(36)	C(46)	4244(11)	−0540(5)	−0718(3)	27
N(5)	N(6)	1864(6)	1852(3)	0317(2)	6
C(51)	C(61)	1995(8)	1982(4)	0629(2)	19
C(52)	C(62)	2951(7)	2390(4)	0749(2)	25
C(53)	C(63)	3808(8)	2649(4)	0534(2)	24
C(54)	C(64)	3683(8)	2521(4)	0216(2)	28
C(55)	C(65)	2675(8)	2117(4)	0115(2)	16
C(56)	C(66)	3033(11)	2510(7)	1096(2)	23
F(11)	F(26)	−1312(8)	2275(4)	0598(2)	32
F(12)	F(25)	−2024(7)	2346(3)	1086(1)	21
F(13)	F(24)	−2403(7)	1337(3)	0526(1)	14
F(14)	F(21)	−1015(7)	1435(3)	0903(2)	10
F(15)	F(22)	−3317(8)	2269(5)	0689(3)	23
F(16)	F(23)	−3037(11)	1400(4)	1013(2)	19

of 3686). Final positional parameters are included in Table 1, and other data have been deposited.[1]

None of the previous chemical conclusions (2) are altered significantly; Ni—N(1) = 2.130(5), Ni—N(3) = 2.114(5), Ni—O = 2.105(4) Å.

[1]Anisotropic thermal parameters, bond lengths and angles, and structure factors may be purchased from the Depository of Unpublished Data, CISTI, National Research Council of Canada, Ottawa, Ont., Canada K1A 0R6.

Acknowledgement

We thank Dr. Y. Le Page for helpful discussion.

1. Y. LE PAGE. J. Appl. Crystallogr. **15**, 225 (1982).
2. R. M. MORRISON, R. C. THOMPSON, and J. TROTTER. Can. J. Chem. **61**, 1651 (1983).
3. V. SCHOMAKER and R. E. MARSH. Acta Crystallogr. Sect. B, **35**, 1933 (1979).

Cyclic voltammetric study of acid hydrolysis of tris(bipyridine) chromium(II): a critical appraisal of CV determination of kinetic parameters[1]

SHACHAR D. NADLER, JAMES G. DICK, AND COOPER H. LANGFORD
Department of Chemistry, Concordia University, Montreal, Que., Canada H3G 1M8

Received November 13, 1984

SHACHAR D. NADLER, JAMES G. DICK, and COOPER H. LANGFORD. Can. J. Chem. **63**, 2732 (1985).

Cyclic voltammetry has been exploited to reinvestigate discrepancies in the reported rate constant for the reaction:

$$Cr(bipy)_3^{2+} + 2H_2O \xrightarrow{k_f} Cr(bipy)_2(H_2O)_2^{2+} + bipy$$

which follows electrode reduction of the substitution inert $Cr(bipy)_3^{3+}$. It is shown that the problems arise from oversimplified treatment of residual currents when estimating the anodic peak current, i_a. A "two scan" procedure for estimating the background currents is introduced which appears to resolve discrepancies. The kinetic studies were extended to a methyl-substituted bipyridine. Since ring methylation has very little effect on k_f, it appears that the aquation reaction is initiated by a rate-determining step which requires a minimum of bipyridine rearrangement.

SHACHAR D. NADLER, JAMES G. DICK et COOPER H. LANGFORD. Can. J. Chem. **63**, 2732 (1985).

Utilisant la voltamétrie cyclique, on a réexaminé les divergences rapportées au sujet de la vitesse de la réaction:

$$Cr(bipy)_3^{2+} + 2H_2O \xrightarrow{k_f} Cr(bipy)_2(H_2O)_2^{2+} + bipy$$

Cette méthode permet de suivre l'évolution de la réduction à l'électrode du $Cr(bipy)_3^{3+}$ qui est inerte à la substitution. On démontre que les problèmes proviennent d'une trop grande simplification des courants résiduels lorsqu'on évalue le courant anodique maximal, i_a. On introduit une méthode à double balayage pour évaluer les courants résiduels et cette méthode semble éliminer les irrégularités. On a étendu les études cinétiques à une bipyridine substituée par un méthyle. Puisque la méthylation du cycle n'a qu'un minime effet sur k_f, il semble que la réaction représentée par l'équation est initiée par une étape déterminant la vitesse qui nécessite un minimum de transposition de la part de la bipyridine.

[Traduit par le journal]

Introduction

The behaviour of the *tris*-(2,2-bipyridine) chromium(III) has been the subject of several electrochemical studies which have challenged the capacity of various electrochemical techniques to extract chemical kinetic information. The system has been reinvestigated in order to resolve discrepancies and refine the procedures for accurate extraction of kinetic parameters. Sato and Tanaka (1) have demonstrated that in aprotic solvents, $[Cr(bipy)_3]^{3+}$ is reduced in four, one electron steps to the $[Cr(bipy)_3]^{1-}$ anion. The aqueous behaviour of this chromium complex has been shown to be somewhat more complicated, notably because of solvolytic ligand exchange. Using conventional polarographic techniques, Tucker *et al.* (2) and Baker and Metha (3) obtained four polarographic waves for the reduction of aqueous $[Cr(bipy)_3]^{3+}$. They observed that the nature of these waves (size and shape) was a function of pH and temperature. From the behaviour of the first two polarographic waves Baker suggested the following reactions:

[1] $[Cr(bipy)_3]^{3+} + e^- \rightleftharpoons [Cr(bipy)_3]^{2+}$ $\qquad E_{1/2} = -0.89$ V

[2] $[Cr(bipy)_3]^{2+} + 2H_2O \underset{k_2}{\overset{k_1}{\rightleftharpoons}} [Cr(bipy)_2(H_2O)_2]^{2+} + bipy$

[3] $[Cr(bipy)_3]^{3+} + [Cr(bipy)_2(H_2O)_2]^{2+} \rightleftharpoons [Cr(bipy)_3]^{2+} + [Cr(bipy)_2(H_2O)_2]^{3+}$

[4] $[Cr(bipy)_2(H_2O)_2]^{3+} + e^- \rightleftharpoons [Cr(bipy)_2(H_2O)_2]^{2+}$ $\qquad E_{1/2} = -0.72$ V

In a later study, Soignet and Hargis (4, 5) suggested that the chromium(II) species undergoes further reduction and completed the cycle as shown below:

[4] $[Cr(bipy)_2(H_2O)_2]^{3+} + e^- \rightleftharpoons [Cr(bipy)_2(H_2O)_2]^{2+}$ $\qquad E_{1/2} = -0.72$ V

[5] $[Cr(bipy)_2(H_2O)_2]^{2+} + 2H_2O \rightleftharpoons [Cr(bipy)(H_2O)_4]^{2+} + bipy$

[6] $[Cr(bipy)_2(H_2O)_2]^{2+} + bipy \underset{k_1}{\overset{k_2}{\rightleftharpoons}} [Cr(bipy)_3]^{2+} + 2H_2O$

The ligand exchange in reaction [2] does not affect the electron transfer in reaction [1]. Hence, the reactions described by [1] and [2] are by themselves reversible. However, when a rapid scan technique such as cyclic voltammetry is employed, it becomes evident that in the presence of $[Cr(bipy)_3]^{3+}$ the diaquo complex formed in reaction [2] is rapidly removed in a manner described in reaction [3]. Under these conditions reactions [1] and [2] describe an electron exchange followed by an irreversible chemical reaction following the well known pattern

[7] $O + e \rightleftharpoons R$

[8] $R \xrightarrow{k_f} Z$

Hence, the rate of reaction/dissociation of the complex, K_f, can be evaluated electrochemically.

In their classical paper on stationary electrode kinetics, Nicholson and Shain (6) described a technique for cyclic voltammetry (CV) by which K_f may be evaluated from a working curve from i_a/i_c versus $K_f\tau$, where i_a/i_c is the ratio of the anodic and cathodic waves obtained by CV for reaction [7] and τ is the elapsed time between the potential at which the scan is reversed (E_{sw}) and the $E_{1/2}$ of the cathodic wave.

The only difficulty with this technique lies in the evaluation of i_a/i_c. While i_c can be easily measured from a well-defined base line (the residual current), the anodic peak i_a is quite difficult to measure since the voltammograms do not show a base line at all for the oxidation portion of the scan. In order to obtain a clear (horizontal) base line, one would have to scan

[1]We thank NSERC, Canada, and FCAC, Québec, for financial support for part of this work.

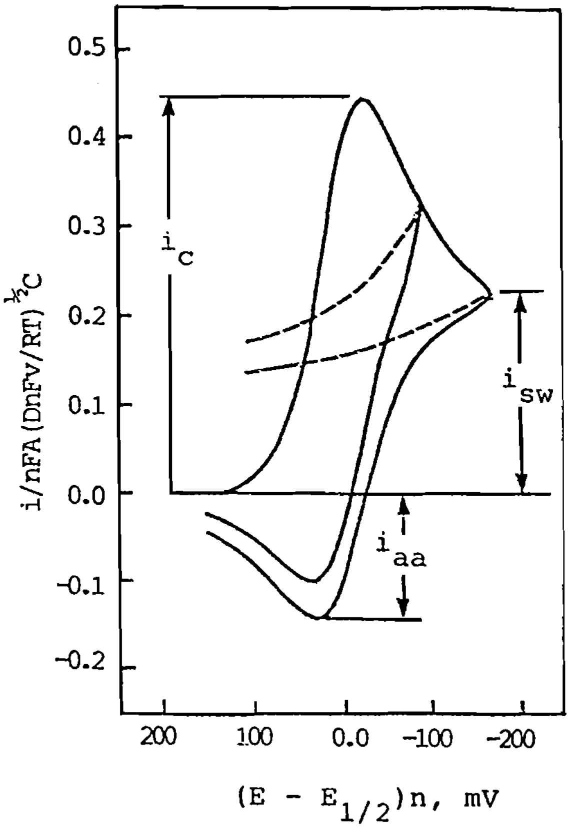

FIG. 1. Nicholson's easy-to-measure parameters from cyclic voltammograms.

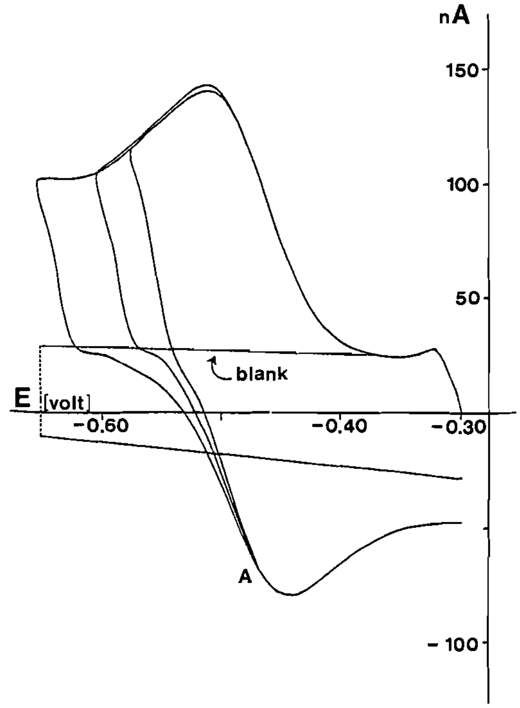

FIG. 2. Aqueous $Cr(bipy)_3$; three polarograms having different switching potentials. From these polarograms it can be seen that E_{switch} does not affect the anodic peak "A". Conditions: 5.5×10^{-5} *M* $[Cr(bipy)_3]^{3+}$ in 0.1 *M* KCl, pH 3.5, 25°C; WE: HMDE $r =$ 0.265 mm; Ref.: SCE (saturated KCl); AUX: Pt; CV: 0.10 V/s.

well past the cathodic peak. However, due to the nature of the chemical process, this will allow reaction [8] to dominate, resulting in an excellent base line but a poor anodic peak. To overcome this problem, Nicholson (7) has developed a semi-empirical procedure which permits the computation of the i_a/i_c ratio from a single-cycle voltammogram. The technique involves three easy-to-measure quantities; the cathodic current (i_c), the apparent anodic current, i_{aa}, and the current at the switching potential, i_{sw}, all measured from the cathodic base line as can be seen in Fig. 1. Using these parameters the true peak ratio was found to be:

$$\frac{i_a}{i_c} = \frac{i_{aa}}{i_c} + \frac{0.485 i_{sw}}{i_c} + 0.086$$

A striking feature of this technique is that the ratio of peak height is independent of such experimental parameters as diffusion coefficients and electrode size and surface area.

From initial CV scans on the chromium complexes it became evident, however, that Nicholson's method could not be applied in a simple fashion. The resulting voltammograms suggested the presence of multiple complicating factors, of which the most outstanding was a large residual current (capacitance). This made it impossible to measure i_{sw} and i_{aa}. Hence a different method had to be developed. The technique involves two CV runs: one of which is stopped at the switching potential and consequently provides an electrochemical equilibrium point from which the anodic current i_a is measured in the second run. Since the problems encountered with Nicholson's technique are not unique to $[Cr(bipy)_3]^{3+}$ systems, the modifications developed for the present problem may be of more general use.

Experimental

Apparatus

Electrochemical measurements were made with a Metrohm Model E-612 VA-Scanner function generator.

The cell used in the CV study consisted of 50 mL water jacketed sealed beaker fitted to hold three electrodes and fitted with an inlet and outlet for purge gas. All currents were measured at the hanging-mercury-drop-electrode (HMDE) using the Metrohm EA-290 capillary equipped with a micrometer drum allowing manual selection of drop size. Unless otherwise specified, all potentials were recorded versus a standard calomel (saturated KCl) electrode. A platinum microelectrode was used as auxiliary. Prepurified nitrogen was used for deoxygenation and subsequently blanketing the solution under studies.

All chemicals used were reagent grade. The pH was adjusted using ultrapure HCl and NaOH. All solutions of $[Cr(2,2'\text{-bipyridine})_3](ClO_4)_3 \cdot H_2O$ and $[Cr(4,4'\text{-}Me_2\text{-}2,2'\text{-bipyridine})_3](ClO_4)_3 \cdot H_2O$ were prepared to yield 5.5×10^{-5} *M* complex in 0.1 *M* KCl adjusted to pH 3.5. Measurements were taken at an ambient temperature of 24 ± 1°C or, when needed, at elevated temperature of up to 35°C, controlled by passing hot water through the built-in glass jacket of the cell.

The samples of the two complexes were a gift from Drs. N. Serpone and M. A. Jamieson. Their preparation has been described (3, 11).

Results and discussion

Initial cyclic voltammograms of $[Cr(bipy)_3]^{3+}$ indicated that in order to proceed with the determination of K_f, two major complicating factors had to be minimized. These were the size of the charging current and the presence of intermediate species at the outset. The latter caused ill-defined anodic cathodic peaks occurring at potentials significantly more anodic than those reported in the literature.

TABLE 1. Computed rate of reaction (K_f) using different scan rates for $Cr(bipy)_3$ at 23 and 25°C

Scan rate (V/s)	E_{start} (V)	E_{switch} (V)	Cathodic peak (V)	$E_{1/2}$* (V)	i_a/i_c	$K_f\tau$	τ (s)	$K_f \pm \sigma$ (s^{-1})
				(*a*) Determined at 23°C				
0.040	−0.300	−0.575	−0.503	−0.478	0.574	0.700±0.046	2.49	0.282±0.017
0.050	−0.300	−0.575	−0.502	−0.476	0.617	0.579±0.028	1.97	0.295±0.014
0.070	−0.300	−0.580	−0.500	−0.475	0.673	0.448±0.023	1.50	0.298±0.015
0.090	−0.300	−0.600	−0.524	−0.495	0.740	0.328±0.044	1.16	0.293±0.035
0.100	−0.300	−0.580	−0.508	−0.487	0.745	0.321±0.012	1.04	0.310±0.012
				(*b*) Determined at 25°C				
0.060	−0.300	−0.575	−0.502	−0.475	0.632	0.542±0.037	1.67	0.324±0.022
0.070	−0.300	−0.577	−0.502	−0.475	0.647	0.507±0.025	1.44	0.352±0.018
0.100	−0.300	−0.595	−0.520	−0.497	0.721	0.359±0.046	1.03	0.348±0.348

*Measured vs. SCE saturated KCl.

The effect of the charging current was greatly reduced by decreasing the size of the HMDE, from 0.423 to 0.265 mm in radius. This action was decided upon after it was observed that the size of the working electrode had a greater effect on the charging current than on the faradaic current.

The second problem was solved by the use of prolonged electrolysis at the HMDE. This technique involved multicycle scanning between 0 and +0.3 V vs. SCE. The positive potential electrolysis insured that most of the analyte was in primary form, $[Cr(bipy)_3]^{3+}$.

Although the electrolyzed sample gave large and well-defined peaks, the residual currents were not completely eliminated, and their effect was noted both at the beginning of the cycle and more importantly at the switching point (E_{sw}). Figure 2 shows that the potential at which the scan was reversed had little or no effect on the anodic peak. Hence, a technique was developed to create a proper base line from which the true anodic peak current (i_a) can be measured.

Earlier techniques for the establishment of anodic base lines in CV (8, 9) involved stopping the scan for several minutes upon completion of the cathodic portion and allowing the current to decay to a point of electrochemical equilibrium at the switching potential. A horizontal line passing through this point becomes the anodic base line. However, in complex reaction systems, as in the case of $[Cr(bipy)_3]^{3+}$, this technique cannot be applied directly. Stopping the scan will permit the irreversible process (reaction [8]) to dominate and consequently distort the size and shape of the anodic peak. This, however, does not affect the current equilibrium at the switching potential, since reaction [8] does not involve electron transfer (i.e. the catalytic reaction is not detected by the electrode system). Consequently the following procedure was adopted. Each determination involved two scans. The first produced the full redox cycle, and the second scan was carried out only cathodically and yielded the equilibrium point which was used in the measurement of the true anodic peak. The procedure can be seen in Fig. 3.

The results obtained from duplicate samples of $Cr(bipy)_3$ at 23 and 25°C are summarized in Table 1. The K_f values tabulated at each scan rate are averages obtained from a minimum of four determinations. Averaging all reaction rates (K_f) at all the scan rates yielded the final values for $Cr(bipy)_3$:

$$K_f = 0.293 \pm 0.022\ s^{-1} \text{ at } 23°C$$

$$K_f = 0.343 \pm 0.028\ s^{-1} \text{ at } 25°C$$

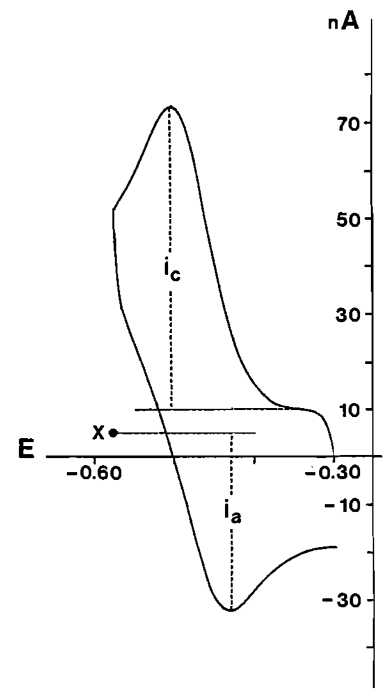

FIG. 3. Peak magnitude determinations. Reduction peak (i_c) is measured from the residual current. Oxidation peak (i_a) is measured from a point of current equilibrium (X) at half cycle. Conditions: $5.5 \times 10^{-5}\,M\,[Cr(bipy)]_3^{3+}$ in 0.1 *M* KCl, pH 3.5, 23°C; WE: HMDE, r = 0.265 mm; Ref: SCE, saturated KCl; AUX: Pt; CV: 0.05 V/s.

The results obtained at 25°C, pH 3.5, are in reasonable agreement with reported results, $K_f = 0.38\ s^{-1}$, obtained by other polarographic techniques and by direct chemical methods (3, 10). On the other hand, the value of 0.293 s^{-1} obtained at 23°C and pH 3.5 was in disagreement with 0.108 s^{-1} at pH 5 reported by Soignet and Hargis (4) and obtained by CV technique. The large difference in K_f values could not be attributed to differences in pH since K_f is pH independent in acid solutions (3). Part of the difference could be attributed to the choice of approximation for the $E_{1/2}$ value. In CV the dynamic $E_{1/2}$ occurs at a point 85.17% up the cathodic slope (5). Hence, one should not estimate $E_{1/2}$ simply by multiplying the peak potential by 0.8517 (85.17%) since this yields good results only when the cathodic slope begins at 0.00 volts.

The balance of the difference in the K_f values is probably due

TABLE 2. Computed rate of reaction (K_f) using different scan rates for $Cr(Me_2\text{-bipy})_3$ at 25°C

Scan rate (V/s)	E_{start} (V)	E_{switch} (V)	Cathodic peak (V)	$E_{1/2}$* (V)	i_a/i_c	$K_f\tau$	τ (s)	$K_f \pm \sigma$ (s^{-1})
0.040	−0.450	−0.745	−0.665	−0.645	0.533	0.846±0.040	2.50	0.339±0.015
0.060	−0.450	−0.745	−0.670	−0.642	0.599	0.637±0.048	1.80	0.355±0.027
0.080	−0.450 −0.500	−0.755	−0.677	−0.652	0.673	0.452±0.061	1.30	0.349±0.046
0.100	−0.450 −0.500	−0.755 −0.760	−0.680	−0.653	0.708	0.379±0.018	1.05	0.363±0.023

*Measured vs. SCE saturated KCl.

to the different treatment given to the residual currents. This disagreement gives a clear indication of the impact of the data treatment recommended here.

The aqueous behaviour of $[Cr(Me_2\text{-bipy})_3]^{3+}$ is similar to that of $[Cr(bipy)_3]^{3+}$ as described above. The results obtained from duplicate samples of this complex are presented in Table 2. Averaging the K_f values obtained at all scan rates yielded for 5.5×10^{-5} *M* $Cr(Me_2\text{-bipy})_3$ in 0.1 *M* KCl:

$$K_f = 0.353 \pm 0.032\ s^{-1} \text{ at 25°C, pH 3.5}$$

The present kinetic results can perhaps also add a little to the understanding of the mechanism of acid hydrolysis of $Cr(bipy)_3^{2+}$ to form $Cr(bipy)_2(H_2O)_2^{2+}$. Since the work of Baker and Metha (3) established the pH independence of this reaction between pH 1 and 9, an important contribution to understanding related mechanisms has been made by Serpone and his colleagues in a series of studies as hydrolysis of $Cr(bipy)_3^{3+}$ (11, 12). For the slower reaction of this tripositive ion, they showed pH independence in acid solution giving over to rate increasing with pH at higher pH. The interpretation suggested that acid hydrolysis is readily reversible *unless* deprotonation of a coordinated water molecule leads to coordinated —OH. The hydroxo ligand (which takes us out of the realm of acid hydrolysis) renders hydrolysis irreversible. Extending the Serpone mechanism to the Cr(II) complex explains the otherwise puzzling pH independence since a water molecule coordinated to Cr(II) will be distinctly less acidic than are coordinated to Cr(III). The low rate of the overall reaction compared to the high lability of Cr(II) complexes of monodentate ligands implies that reversal of the initial hydrolytic step is quite fast and efficient, as the Serpone mechanism suggests it would be expected to be.

The associative version of the Serpone *et al.* mechanism is shown in Scheme 1 below.

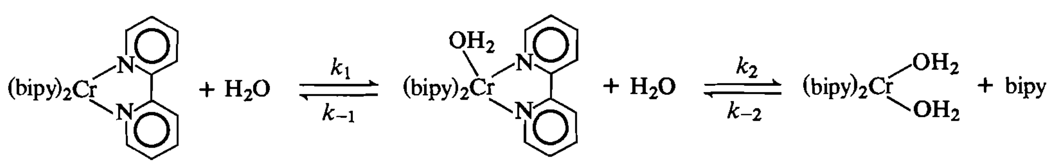

SCHEME 1

The rate-determining step for such a path is most probably k_2. The modest increase in rate for the dimethyl ligand is to be understood according to this mechanism as a consequence of the same factors which lead dimethyl bipyridine complexes of Cr(III) to exhibit longer doublet phosphorescence lifetime (II), namely, increasing rigidity. The attack by H_2O presumably goes via the "pockets" found between the ligands by X-ray (13). These appear to be rendered more accessible by the more rigid ligand, favouring attack.

1. Y. SATO and N. TANAKA. Bull. Chem. Soc. Jpn. **42**, 1021 (1969).
2. B. V. TUCKER, J. M. FITZGERALD, L. G. HARGIS, and L. B. ROGERS. J. Electroanal. Chem. **13**, 400 (1967).
3. R. B. BAKER and D. METHA. Inorg. Chem. **4**, 848 (1965).
4. D. M. SOIGNET and L. G. HARGIS. Inorg. Chem. **10**, 2349 (1972).
5. D. M. SOIGNET and L. G. HARGIS. Inorg. Chem. **4**, 877 (1973).
6. R. S. NICHOLSON and I. SHAIN. Anal. Chem. **37**, 178 (1965).
7. R. S. NICHOLSON. Anal. Chem. **38**, 1406 (1966).
8. D. HAWLEY and R. N. ADAMS. J. Electroanal. Chem. **10**, 376 (1965).
9. H. MATSUDA. Z. Electrochem. **62**, 977 (1958).
10. J. P. CANDLIN, J. HALPERN, and D. L. TRIMM. J. Am. Chem. Soc. **85**, 1019 (1964).
11. N. SERPONE, M. A. JAMIESON, M. S. HENRY, M. Z. HOFFMAN, F. BOLLETTA, and M. MAESTRI. J. Am. Chem. Soc. **101**, 2907 (1979).
12. M. MALSTRI, F. BOLLETTA, N. SERPONE, L. MOGGI, and V. BULZARI. Inorg. Chem. **15**, 2049 (1976).
13. W. A. WICKRAMASINGHE, P. H. BIRD, M. A. JAMIESON, and N. SERPONE. J. Chem. Soc. Chem. Commun. 798 (1979).

Organic reactions in liquid crystalline solvents. 2. An investigation into the use of liquid crystalline solvents to effect stereochemical control in the Diels–Alder reaction

WILLIAM J. LEIGH[1]

Department of Chemistry, McMaster University, Hamilton, Ont., Canada L8S 4M1

Received February 26, 1985

WILLIAM J. LEIGH. Can. J. Chem. **63**, 2736 (1985).

The possibility of using liquid crystalline solvents to control the stereospecificity of bimolecular reactions as a result of differences in liquid crystalline solvation of the various possible transition states has been examined. The Diels–Alder reactions of 2,5-dimethyl-3,4-diphenylcyclopentadienone with four dienophiles of varying steric size (cyclopentene, cycloheptene, indene, and acenaphthylene) have been carried out in benzene, cholesteryl nonanoate (isotropic), cholesteryl propionate (cholesteric), and 4-ethyl-4′-(4-pentylcyclohexyl)biphenyl (smectic) at 105°C. In spite of very large differences in steric solvation requirements for the *endo*- (globular in shape) and *exo*- (plate-like in shape) transition states in these reactions, no variation in product ratio with solvent phase is observed in any case.

The inability of the ordered liquid crystalline phases to differentiate between *endo*- and *exo*-transition states in the Diels–Alder reactions investigated is rationalized as being the possible result of several factors. The most important of these are believed to be free volume effects, owing to both inefficient steric solvation of the bulky diene and volume contraction in the transition states for cycloaddition.

WILLIAM J. LEIGH. Can. J. Chem. **63**, 2736 (1985).

On a étudié la possibilité d'utiliser des cristaux liquides comme solvants pour obtenir un contrôle sur la stéreospécificité de réactions bimoléculaires qui résulterait de différences de solvatation des divers états de transition possibles par les cristaux liquides. Opérant à 105°C et dans divers solvants comme le benzène, le nanoate de cholestéryle, (isotrope), le propionate de cholestéryle (cholestérique) et l'éthyl-4 (pentyl-4 cyclohexyl)-4′ biphényle (smétique), on a effectué une réaction de Diels–Alder entre la diméthyl-2,5 diphényl-3,4 cyclopentadiénone et quatre diénophiles de comportements stériques différents comme le cyclopentène, le cycloheptène, l'indène et l'acétylnaphtène). Malgré de très grandes différences dans les demandes stériques de solvatations qui proviennent d'encombrements stériques différents pour les formes *endo* (forme globulaire) et *exo* (en forme de plateau) des états de transition de ces réactions, on n'a dans aucun cas observé de variations dans les rapports de produits dans la phase solvant.

On attribue à différents facteurs cette incapacité des phases cristallines liquides ordonnées de différencier les états de transition *endo* et *exo* des réactions de Diels–Alder étudiées. On croit que les effets de volume libre sont les facteurs les plus importants et que ceci résulté à la fois d'une solvatation stérique inefficace du diène encombré et d'une contraction de volume dans les états de transition des cycloadditions.

[Traduit par le journal]

Introduction

The ability of liquid crystals to affect the rates and energetics of thermal and photochemical organic reactions is of considerable interest (1–14), both because of their considerable technological importance, as well as similarities in the microstructure of these materials to that in biological systems such as cell membranes (for comprehensive descriptions of the structure and properties of liquid crystals, see ref. 15). Their effects on chemical reactivity have been investigated primarily from the point of view of orientational effects, since it is well known that liquid crystals are able to orient dissolved solute molecules in a manner which depends primarily on steric factors, i.e., structural similarities between solute and solvent molecules (16). A rod-shaped solute is oriented in a liquid crystal so that its long molecular axis is parallel to those of the surrounding solvent molecules, and the effects of the liquid crystal on its reactivity are then the result of the solvent's ability to control this orientation. While unimolecular reactions (e.g. cyclizations) may be restricted owing to solvent-induced inhibition to achieving the optimum molecular geometry for reaction (3, 12, 17), bimolecular reactions may be inhibited or promoted depending on the relative orientation of two reactive solutes and the solvent's ability to define and hold this relative orientation (4–6, 8, 18). It would appear that there are two factors which are primarily responsible for affecting the reactivity of solutes ordered in liquid crystals: the efficiency with which the solute(s) are solvated by the liquid crystal (or, the "tightness" of the solvation shell), and the degree of distortion which the reacting system must undergo in proceeding through the transition state (19).

We have an interest in probing the possible effects of liquid crystalline solvents on the reactivity of solutes which are perhaps not highly oriented by the ordered solvent, but which undergo very large changes in molecular shape as the transition state is approached. To illustrate, consider a planar, disc-shaped solute molecule which reacts via a bulky, globular transition state in proceeding to product (Scheme 1). Such a reactant will be solvated in a liquid crystal so that its molecular plane is oriented parallel to the long axes of the surrounding solvent molecules (20). To the extent that the solute's solvation shell retains some degree of liquid crystalline order, then such a process is expected to be affected as a result of the disruption of local solvent order which may accompany formation of the globular transition state. The effect on reaction rate will then be the result of synergistic effects on the activation energy (rate retardation) and entropy (rate enhancement). That liquid crystals are indeed capable of affecting the dynamics of unimolecular reactions of this type has been demonstrated (12, 19).

If liquid crystalline solvents are capable of affecting reactivity in systems such as that depicted in Scheme 1, then it may be possible to exploit this capability to control reactivity in

[1] NSERC University Research Fellow 1983–1986.

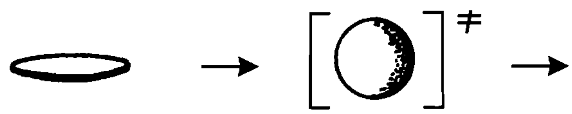

SCHEME 1

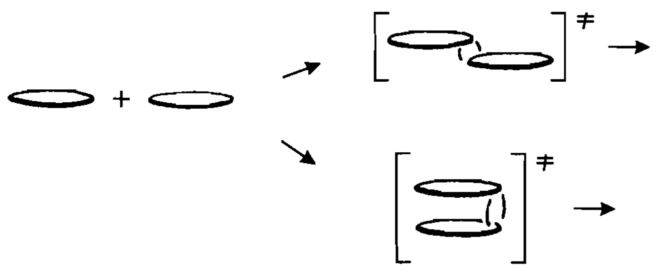

SCHEME 2

systems which normally react via a number of possible pathways through transition states which disrupt solvent order to varying extents. For example, consider two planar reactants which normally react to give two products through transition states such as those depicted in Scheme 2. By analogy with the known behaviour of liquid crystalline media with respect to the effectiveness with which they solvate planar versus globular solutes (16), it might be expected that solvent order would be more severely disrupted by the globular transition state than by the more planar one. To the extent that this difference in the solvation requirements of the two transition states is reflected in different effects on the activation parameters for the two processes, then an alteration in the product ratio may be observed in liquid crystalline solvents relative to the value in isotropic solvents.

An attractive system with which to test this hypothesis is the Diels–Alder reaction, since it proceeds to yield two adducts through transition states which differ considerably in steric shape. In choosing a substrate pair for investigation, we kept several factors in mind. For example, we endeavoured to keep the diene and dienophile as large as possible in order to maximize the difference between the shapes of the *endo*- and *exo*-transition states, without deviating too much from planarity in order to ensure that the reactants are reasonably well-solvated in a liquid crystalline solvent. Furthermore, we looked for a probe system which is known to yield both *exo*- and *endo*-adducts under ordinary conditions; when this is the case, then even small (< ca. 0.3 kcal/mol) solvent order-induced differences in the transition state energies will result in a measurable effect on the product ratio for the reaction (>20%). The Diels–Alder reaction of 2,5-dimethyl-3,4-diphenyl-cyclopentadienone (**1**) with cyclopentene (21) (reaction [1]) appeared to us to come closest to satisfying these requirements; furthermore, since dienones such as **1** are well-recognized to be rather potent dienes toward Diels–Alder addition (22), it seemed likely that other dienophiles might be used in addition to cyclopentene in order to broaden the scope of the investigation.

We wish to report the results of our investigation of the reaction of **1** with cyclopentene, cycloheptene,[2] indene, and acenaphthylene in isotropic solvents and cholesteric and smectic liquid crystalline solvents. Our results indicate that in the present cases at least, liquid crystalline solvents are incapable of distinguishing between transition states which differ in their bulk steric shape. While several possible reasons for this can be advanced, it is suggested that liquid crystalline effects of the type proposed can only be expected to occur under very special circumstances.

[2] While the reaction of **1** with cycloheptene has been reported to yield a mixture of adducts (21), their yields and characterization have apparently not been published.

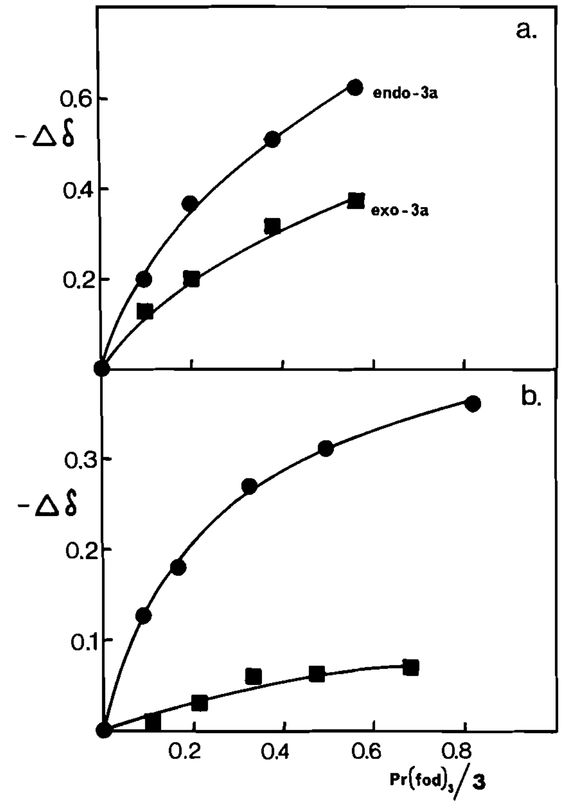

FIG. 1. Plots showing the variation in chemical shift of the 0-bridge protons versus added $Pr(fod)_3$-d_{30} for (*a*) *endo*- and *exo*-**3***a* and (*b*) *endo*- and *exo*-**3***d* in deuterochloroform solution.

Results

Reaction of 2,5-dimethyl-3,4-diphenylcyclopentadienone (**1**) with cyclopentene (**2***a*), cycloheptene (**2***b*), indene (**2***c*), and acenaphthylene (**2***d*) in benzene solution at 105°C yields mixtures of two adducts in each case (reaction [2]). The identities of *endo*- and *exo*-**3***a* were established on the basis of comparisons of their ^{1}H nmr spectra with those previously reported (21).

[1]

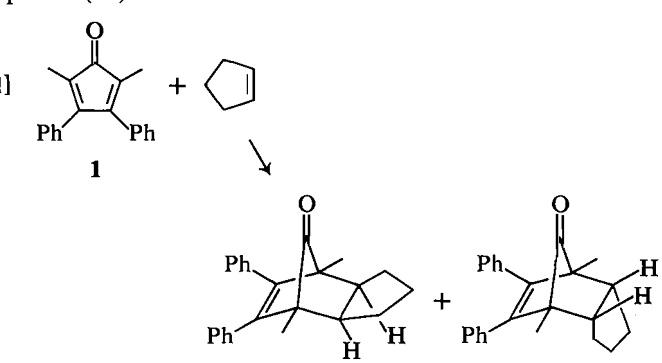

Nuclear magnetic resonance shift reagent studies, using $Pr(fod)_3$-d_{30}, were employed to assign the structures of the *endo*- and *exo*-isomers of **3***b*–*d*. While the ^{1}H nmr spectrum of

[2]

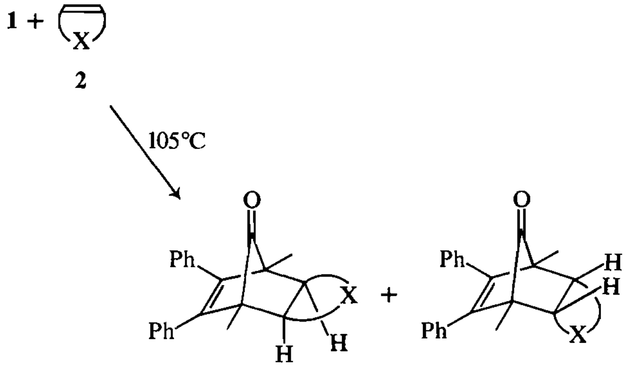

exo-3 *endo*-3

a, X = $-CH_2CH_2CH_2-$
b, X = $-CH_2(CH_2)_3CH_2-$
c, X =

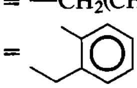

d, X =

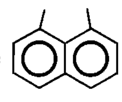

the Diels–Alder adduct of tetraphenylcyclopentadienone and styrene has been reported to be unaffected by the addition of europium shift reagents (23) we find that addition of either Eu(fod)$_3$-d_{30} or Pr(fod)$_3$-d_{30} to deuterochloroform solutions of the isomeric adducts of the comparatively less sterically hindered **1** with **2***a*–*d* results in distinct, although small, changes in the chemical shifts of the ring-juncture protons (at the 0-bridge) in each case. Plots of the change in the chemical shifts of these protons versus concentration of added shift reagent are shown in Fig. 1*a* for *endo*- and *exo*-**3***a*. As expected, the magnitude of the lanthanide-induced shift is clearly larger for *endo*-**3***a* than for the *exo*-isomer. Similar experiments conducted with the isomeric adducts **3***b*–*d* yielded similar results, and allowed structural assignments to be made. Figure 1*b* shows the plots obtained for the dienone–acenaphthylene adducts **3***d*.

That the product ratios observed for reaction of **1** and **2***a*–*d* at 105°C represent the true kinetic product ratios and not the equilibrium ratios was verified by heating samples of pure *endo*-**3***a* and *endo*-**3***d* at 105°C in benzene solution for extended periods of time. No isomerization of either adduct was apparent at this temperature under these conditions. While *endo*-**3***d* was similarly unreactive at 140°C, heating the sample of *endo*-**3***a* at this temperature did result in slow isomerization to the *exo*-isomer. At 180°C, *endo*-**3***d* was found to undergo primarily decomposition, presumably via decarbonylation (22), with minor isomerization to the *exo*-isomer.

Cholesteryl propionate (ChP) exhibits an enantiotropic cholesteric phase over the temperature range 94°C to 114.5°C (lit. 96–112°C (24)). Addition of 0.8 wt% **1** (as the Diels–Alder dimer (25)) results in a 3.5° depression in the optically-detected cholesteric-isotropic transition temperature of this compound. A similar depression (3°) is observed in the smectic–nematic transition temperature of 4-ethyl-4′-(4-pentylcyclohexyl)-biphenyl (EPCB) upon addition of 0.4 wt% **1**. Undoped EPCB exhibits an enantiotropic smectic B phase from 34–146°C, and a nematic phase from 146–164°C (8*b*, 26). Addition of 0.4 wt% **1** has no discernible effect on the nematic–isotropic transition temperature of this compound. The Diels–Alder dimer of **1** is known to be largely dissociated at 80°C (25).

TABLE 1. *Endo-/exo-* product ratios for the Diels–Alder reactions of 2,5-dimethyl-3,4-diphenylcyclopentadienone (**1**) and **2***a*–*d* in isotropic and liquid crystalline solvents at 105°C[a]

Solvent	**2***a*	**2***b*	**2***c*	**2***d*
Benzene	0.91	2.6	4.5	8.3
ChN (isotropic)	0.93	2.6	4.5	8.5
ChP (cholesteric)	0.90	2.5	4.3	7.8
EPCB (smectic)	—	—	4.6	—

[a] Average of at least two determinations. Error is estimated as ±10%.

The reactions of **1** with **2***a*–*d* were carried out in benzene, cholesteryl nonanoate (ChN, isotropic), and ChP (cholesteric), at 105°C. The reactions with **2***a*, *b* were qualitatively much slower in the steroidal solvents than was found to be the case in benzene solution. This is presumably a concentration effect, relating to the very much lower vapour pressures of the steroids compared to benzene, and hence to the fact that a considerably larger portion of available dienophile will reside in the vapour phase for the steroidal solutions relative to the benzene solutions. Regardless of differences in the absolute rates of reaction, no new products in addition to the isomeric Diels–Alder adducts **3***a*–*d* were observed in any case when the reactions were carried out in the cholesteric ester solvents. The reaction of **1** with **2***c* was also examined in the smectic phase of EPCB at 105°C. Yields of the isomeric adducts, obtained by hplc analysis of the mixtures obtained from reaction of **1** and **2***a*–*d* in these four solvents at 105°C are collected in Table 1.

Discussion

The molecular order in thermotropic liquid crystals is such that the long molecular axes of the component molecules are arranged, on the average, parallel to one another (15). In nematic phases, there is no further molecular ordering present, and these are the most fluid of liquid crystalline phases. Cholesterics are optically active nematic phases, and are characterized by a gradual twist in orientational alignment as one proceeds through the bulk of the sample. Apart from this macroscopic optical activity, there are no further differences in the bulk physical properties of nematics and cholesterics, and they are considered to belong to the same class of liquid crystalline phases (15). Smectic liquid crystals are further arranged in layers, with the long axes of the component molecules parallel to one another and perpendicular (or at some angle close to perpendicular) to the plane of the layers. As a result of this additional molecular ordering, smectics are more nearly crystalline in their appearance and bulk physical properties (15).

In liquid crystals, solutes are incorporated in the best packing arrangement based on steric factors (15, 16, 20). The structures of the reactants employed in the present study are such that they are expected to be, on the average, oriented in a liquid crystalline phase with their molecular planes held parallel to the long molecular axes of the surrounding solvent molecules (20). Indene (**2***c*) and acenaphthylene (**2***d*) are slightly elongated molecules, so there will be some preference for these two to be further oriented with their long axes parallel to those of the solvent (20). On the other hand, since the breadths of **1**, **2***a*, and **2***b* across two of their molecular axes are in each case roughly equal, their orientations within their molecular planes is expected to be random. Thus, consideration of the manner in which **1** and **2***a*–*d* will be oriented in a liquid crystal leads to the prediction that in each case, there should be an equal probability that the two reactants will approach each other in orientations favouring *endo*-product formation as those favouring *exo*-product formation. Depending on how tightly the reactants are solvated in the liquid crystalline matrix, approach to the transition states as reaction proceeds should result in some degree of disruption of local solvent order as the solvation shell reorganizes to accommodate it. If the degree of disruption is greater for one reactive pathway than the other, then that pathway should be inhibited in a liquid crystalline solvent in favour of the less disruptive one. By analogy with the solvation behaviour of liquid crystals towards differently shaped solutes (16), it is expected that a globular transition state should result in more disruption of the liquid crystalline lattice than a planar or rod-like one. These considerations lead to the prediction that the effect of a liquid crystalline phase on the Diels–Alder reaction will be to inhibit the formation of the more globular *endo*-adduct in favour of the *exo*-adduct. Furthermore, consideration of the relative sizes of **2***a*–*d* leads to the prediction that differentiation between the two transition states on the basis of their sizes and shapes should increase throughout the series **2***a* < **2***b* < **2***c* < **2***d*.

Clearly, the data in Table 1 indicate that neither cholesteric nor the more tightly ordered smectic liquid crystals are capable of distinguishing between *endo*- and *exo*-transition states in any of the Diels–Alder reactions investigated, in spite of the large differences in steric shape of the two transition states. The product ratios observed in all four of these reactions in isotropic media correspond to differences in transition state energies (*exo* relative to *endo*) of 0.2–1.3 kcal/mol, assuming identical pre-exponential factors for the two pathways. Allowing for an error of ca. 10% in our determination of product ratios, then a solvent effect of as little as 0.2 kcal/mol on the relative *exo*–*endo* transition state energies would result in a significant change in product ratio, in the absence of entropy effects. Thus, our data indicate that either there is no liquid crystalline effect on the relative energies of the *endo*- and *exo*-transition states in the systems examined, or that the effect on relative transition state energies is exactly offset by entropy effects.

The failure of liquid crystalline solvents to exert an effect on the product distributions in the Diels–Alder reactions investigated may bear some analogy to the reported effects of liquid crystalline solvents on the triplet state photodimerization of acenaphthylene (6). While the presence of cholesteric order was found to have marked effects on the overall efficiency of this process, no alteration in the *syn*-/*anti*- product ratio was observed in liquid crystalline media relative to the value in isotropic solvents. Clearly, the differences in bulk steric shape of the acenaphthylene photodimers are almost as pronounced as those of the *exo*-/*endo*- adducts in the present cases. However, the potential ability of liquid crystalline solvents to differentiate between transition states of differing steric bulk is expected to depend in large part on the degree of product character which is developed in the transition states, and this is expected to be small for fast, low activation energy processes such as triplet state olefin dimerizations. To the extent that the transition states for the present thermal cycloadditions are expected to be much more product-like in character, they should be considerably more susceptible to solvent order-induced perturbations of their relative energies.

Several factors may be contributing to the failure of these solvents toward discriminating between transition states of such grossly differing shapes. First, although the transition temperatures (as well as visual inspection) of samples of ChP and EPCB doped with **1** indicate that bulk liquid crystalline order is retained in these mixtures at the reaction temperature, it is important to note that macroscopically determined transition temperatures of solute-doped liquid crystals do not necessarily offer any indication of the effect of that solute on *local* solvent order (2*b*, *c*) (i.e., in the immediate vicinity of the solute). However, since the Ch → I and Sm → N transition temperatures of ChP and EPCB, respectively, are both substantially affected by incorporation of relatively small amounts (0.4–0.8 wt%) of **1**, it appears safe to conclude that local solvent order is probably severely disrupted. Indeed, doping of ChP at a level of 1.5 wt% **1** results in complete destruction of the bulk cholesteric phase at temperatures greater than 90°C. It may be that this solute in fact resides in an isotropic environment in at least its primary solvation shell, with the result that the disruptive effects of a bulky transition state on solvent order will be truncated (2, 19).

Second, space-filling molecular models indicate that **1** is in fact a fairly bulky, non-planar molecule, the phenyl groups being unable to achieve a coplanar arrangement owing to steric interactions. The bulkiness of this reactant is undoubtedly the cause of the large effects on the transition temperatures of ChP and EPCB discussed above, and presumably also acts to further truncate any differential solvation of the two possible transition states, especially with the relatively small dienophile **2***a*.

Third, it is well known that cycloadditions such as the Diels–Alder reaction are characterized by a substantial volume contraction in the transition states for both *endo*- and *exo*-addition (27). The occurrence of this volume contraction as the transition states are approached will further reduce the ability of an ordered environment to distinguish between the two on the basis of their sizes and shapes, since solvent reorganization in these relatively viscous media is expected to be too slow to keep up with the contracting reactive complexes.

Finally, more detailed consideration of how the reactants are expected to be oriented relative to one another in these liquid crystalline phases makes it clear that in at least some of these cases, the products may be formed in orientations which are not the favoured ones in a liquid crystalline environment, if at least one of the reactants is itself reasonably well-oriented. The best illustration of this is the reaction of **1** with **2***d*. Acenaphthylene is oriented in a cholesteric phase with its long axis preferentially parallel to those of the surrounding solvent molecules (6, 20). When reaction of **1** occurs with a **2***d* molecule which is in this solvent-preferred orientation, the product is formed in an orientation such that its long molecular axis is *perpendicular* to those of the solvent. In such a case, the reaction itself provokes additional disruption of solvent order in that the products are formed in energetically unfavourable orientations. If the extent of this disruption is similar for the two reaction pathways, then a lesser degree of discrimination between transition states can be expected. The structure and expected orientation of **2***c* indicate that products from this dienophile should be formed in their solvent-preferred orientations, while for the symmetric **2***a* and **2***b* there should be an equal probability that they will approach **1** in such orientations as to lead to products whose orientations are parallel and perpendicular to the preferred solvent alignment.

It is difficult to predict which of the above factors might be most critical in the present case, or whether they are all playing a role. Nevertheless, our observation that the stereochemical distribution of products from the Diels–Alder reaction of **1** with the four dienophiles examined in the present study is unaffected by the presence of cholesteric or smectic solvent order allows several important conclusions to be derived. It is clear that liquid crystals are not *generally* useful as solvents to affect stereochemical control on reactions in the absence of careful consideration of specific details regarding the structures of reactants, products, and transition states, their preferred orientations in a liquid crystalline environment, and the disruptive effects that each has on solvent order. Control over these factors is expected to be even more critical when the reaction in question involves overall volume contraction in the transition state, since this process will occur on a time scale which must be several orders of magnitude faster than that of solvent reorganization. It may be that effects such as that investigated here are more likely to be observed when the reactants are smaller, and hence incorporated much more efficiently in a liquid crystalline matrix. Further work in this area is in progress and will be reported in the near future.

Experimental

Melting points and transition temperatures were measured on a Reichert micro-hot stage microscope with polarizing lenses and are corrected. ^{1}H nmr spectra were recorded in deuterochloroform solution on a Varian EM390 nmr spectrometer, and are reported in parts per million downfield from TMS. Infrared spectra were recorded on a Perkin-Elmer Model 283 infrared spectrometer, and are reported in wavenumbers, calibrated against the 1601.8 cm^{-1} polystyrene absorption. Elemental analyses were performed by Guelph Chemical Laboratories, Guelph, Ontario. A Jumo-MS D.B.P. mercury thermoregulator, a Fisher Model 32 Transistor Relay, and an insulated silicon oil (Dow Corning 710) bath were used for temperature control in small scale reactions in benzene and the mesogenic solvents. Temperatures were recorded with a Leeds & Northrup Model 8692 Temperature Potentiometer and a copper–constantan thermocouple, and are considered accurate to ± 1°C.

Analyses of product mixtures were performed using a Gilson isocratic hplc system, consisting of a Model 302 pump (fitted with a 5 mL head), Model 802B manometric module, Holochrome variable wavelength detector, a Rheodyne Model 7125 loop injection valve, and a Varian Model A-6 strip chart recorder, in conjunction with a 25 $\times$ 0.46 cm Merck Hibar Si60 (10 μm) analytical column. Hexane(50%)/dichloromethane was used as eluant, with a flow rate of 0.8–1 mL/min, and an analytical wavelength of 280 nm was used for all analyses. Preparative lc was performed using the same system (50 mL pump head), in conjunction with 24 $\times$ 1.1 cm or 31 $\times$ 2.5 cm Merck Lobar Si60 (40–63 μm) glass columns, hexane(60%)/dichloromethane as eluant, and flow rates of 3.5 and 12 mL/min, respectively. For quantitative hplc analyses, the detector was interfaced to a Unitron microcomputer via an Adalab data acquisition/control card (Interactive Microware, Inc.), after amplification of the 0–10 mV signal to 0–1V with an Adaamp analog amplifier. Chromatogram acquisition, storage, and integration was performed using the Chromatochart (Interactive Microware, Inc.) software. Apparent product ratios for each product mixture so obtained were then converted to true values with working curves, constructed for each isomeric adduct pair with a few standard solutions of accurately weighed mixtures of the authentic adducts.

Benzene (BDH Reagent) was purified by repeated extraction with concentrated sulphuric acid, followed by several washings with water and saturated aqueous bicarbonate. It was dried over calcium chloride, refluxed over calcium hydride, and distilled. Dichloromethane was Caledon HPLC grade and was used as received. Hexanes (BDH Reagent) were distilled before use. Cholesteryl propionate (Sigma) was recrystallized once from *n*-pentanol (28), washed several times with aqueous ethanol, and dried in a vacuum desiccator. Cholesteryl nonanoate (Aldrich) was recrystallized once from 95% ethanol. Transition temperatures for these two compounds agreed well with published values (24). 4-Ethyl-4′-(*trans*-4-pentylcyclohexyl)biphenyl (EPCB; EM Licristal) was used as received from BDH Chemicals, Ltd. Acenaphthylene (Aldrich) was sublimed *in vacuo* and recrystallized from 95% ethanol. Indene (Aldrich) was vacuum distilled. Cyclopentene and cycloheptene were used as received from Aldrich Chemical Co. $Pr(fod)_3$-d_{30} and $Eu(fod)_3$-d_{30} were used as received from Alfa Products, Inc. The Diels–Alder dimer of 2,5-dimethyl-3,4-diphenylcyclopentadienone (**1**) was prepared according to the published procedure (26), and was purified by recrystallization from 95% ethanol to yield colourless needles (mp 185–187°C; lit. (26) 196°C). The ^{1}H nmr spectrum of this compound was consistent with its proposed structure (δ (ppm): 0.60 (s, 3H), 1.28 (s, 3H), 1.64 (s, 3H), 2.24 (s, 3H), 6.6–7.4 (cplx. mult., 20H).

*Preparation and identification of Diels–Alder adducts 3*a–d

*3*a. *Adducts of 1 and cyclopentene (2*a)

1 (0.78 g, 3 mmol) and cyclopentene (1.75 mL, 20 mmol) were dissolved in benzene (9 mL), placed in a 16 mm medium-walled Pyrex tube, degassed (3 freeze–pump–thaw cycles), and sealed. The solution was heated at 100°C for 24 h, at which time the characteristic red colour of the dissociated dienone had dissipated. The tube was opened and the solvent evaporated on the rotary evaporatory, yielding a yellow oil which solidified. Preparative lc afforded two products, which were recrystallized from ethanol. The isomer which eluted first from the column was identified as *exo-3a* (0.46 g, 47%; mp 182–182.5°C; lit. (21) 180–180.5°C. ^{1}H nmr: 1.12 (s, 6H), 1.06–1.35 (m, 2H), 1.73 (m, 4H), 2.64 (m, 2H), 7.00–7.25 (m, 10H). Ir (CCl_4): 3091 (w), 3068 (w), 3020 (w), 2960 (s), 2940 (s), 2875 (m), 1775 (s), 1499 (m), 1491 (m), 1452 (s), 1384 (m), 1174 (w), 1070 (w), 950 (w), 904 (w), 689 (s).

The second isomer to elute from the column was identified as *endo-3a* (0.43 g, 44%; mp 109–110°C; lit. (21) 109.5–110°C). ^{1}H nmr: 1.32 (s, 6H), 1.30–1.52 (m, 2H), 1.70–2.05 (m, 4H), 2.48 (m, 2H), 6.97–7.30 (m, 10H). Ir (CCl_4): 3091 (w), 3068 (w), 3020 (w), 2960 (s), 2940 (s), 2912 (m), 2878 (m), 1775 (s), 1499 (m), 1490 (m), 1450 (s), 1381 (m), 1074 (m), 957 (m), 908 (m), 690 (s).

*3*b. *Adducts of 1 and cycloheptene (2*b)

1 (0.26 g, 1 mmol) and cycloheptene (0.8 mL, 9 mmol) were dissolved in benzene (7 mL) and sealed in a 16 mm tube as described above. The solution was heated for 24 h, the tube was opened, and the solvent evaporated, yielding a colourless solid. Preparative lc afforded two products, the first of which to elute was recrystallized from ethanol, yielding colourless needles (mp 179–179.5°C), and identified as *exo-3b* (0.030 g, 10%) on the basis of nmr shift reagent studies, and comparisons of its ^{1}H nmr spectrum and hplc retention time to that of *exo-3a*. ^{1}H nmr: 1.09 (s, 6H), 0.95–1.35 (m, 4H), 1.58–2.15 (m, 6H), 2.26 (m, 2H), 7.02–7.34 (m, 10H). Ir (CCl_4): 3062 (w), 2980 (m), 2935 (s), 2860 (m), 1776 (s), 1455 (m), 1382 (w), 925 (w), 907 (w). *Anal.* calcd. for $C_{26}H_{28}O$: C 87.60, H 7.92; found: C 87.43, H 8.25.

The second isomer to elute from the column was recrystallized from ethanol to yield colourless needles (mp 173–174°C) which were identified as *endo-3b* (0.180 g, 70%). ^{1}H nmr: 1.06–1.43 (m, 4H), 1.27 (s, 6H), 1.70–2.10 (m, 6H), 2.21 (m, 2H), 7.00–7.31 (m, 10H). Ir (CCl_4): 3065 (w), 2980 (m), 2938 (s), 2862 (s), 1778 (s), 1462 (m), 1454 (m), 1443 (m), 1383 (m), 690 (s). *Anal.* calcd. for $C_{26}H_{28}O$: C 87.60, H 7.92; found: C 87.38, H 8.20.

*3*c. *Adducts of 1 and indene (2*c)

A solution of **1** (0.505 g, 1.94 mmol) and indene (0.34 mL, 3 mmol) in benzene (9 mL) were sealed in a 16 mm tube and heated at 100°C for 17 h. The tube was opened and the solvent evaporated to yield a slightly yellow oil. This was chromatographed as described above to yield two products. The first to elute was recrystallized from 95% ethanol to yield colourless needles (0.070 g, 10%, mp 209–211°C) which were identified as *exo-3c* on the basis of nmr shift reagent studies. ^{1}H nmr: 1.27 (s, 3H), 1.37 (s, 3H), 2.93–3.49 (cplx. m, 3H), 3.76 (cplx. d, 1H), 7.07–7.41 (m, 14H). Ir (CCl_4): 3080 (m), 3060 (m), 3035 (m), 2975 (m), 2935 (m), 1775 (s), 1485 (m), 1447 (m), 1384 (m), 1072 (w), 941 (w), 907 (w), 688 (s). *Anal.* calcd. for

$C_{28}H_{24}O$: C 89.33, H 6.43; found: C 89.75, H 6.57.

The second isomer to elute was recrystallized from 95% ethanol to yield colourless needles (0.49 g, 67%, mp 147–148°C), identified as *endo*-**3c** on the basis of nmr shift reagent studies. ^{1}H nmr: 1.44 (s, 6H), 3.08 (m, 3H), 3.82 (m, 1H), 6.31 (m, 2H), 6.92–7.40 (cplx. m, 12H). Ir (CCl_4): 3080 (w), 3032 (w), 2975 (m), 2935 (m), 1778 (s), 1481 (w), 1445 (w), 1379 (w), 690 (s). *Anal.* calcd. for $C_{28}H_{24}O$: C 89.33, H 6.43; found: C 89.17, H 6.60.

*3*d. *Adducts of 1 and acenaphthylene (2*d*)*

A solution of **1** (0.52 g, 2 mmol) and acenaphthylene (0.3 g, 2 mmol) in benzene (7 mL) were sealed and heated in a 16 mm tube for 5 h at 110°C. The tube was opened and the solvent evaporated to yield a slightly yellow solid which was chromatographed as described above. The first isomer to elute from the column was recrystallized from chloroform/ethanol to yield colourless needles (0.030 g, 4%, mp 225–227°C), which were identified as *exo*-**3d** on the basis of nmr shift reagent studies. ^{1}H nmr: 1.34 (s, 6H), 4.20 (s, 2H), 7.25 (m, 10H), 7.25–7.75 (m, 6H). Ir (KBr): 3050 (m), 2970 (w), 2930 (w), 1776 (s), 1600 (m), 1490 (m), 1450 (m, br), 1385 (m), 905 (m), 802 (s), 795 (s), 778 (s), 768 (m), 759 (m), 721 (w), 698 (s). *Anal.* calcd. for $C_{31}H_{24}O$: C 90.26, H 5.86; found: C 90.25, H 6.04.

The second isomer to elute yielded colourless plates upon recrystallization from chloroform/ethanol (0.40 g, 49%, mp 195–197°C), which were identified as *endo*-**3d** on the basis of nmr shift reagent studies. ^{1}H nmr: 1.60 (s, 6H), 4.12 (s, 2H), 6.06 (m, 4H), 6.93 (m, 6H), 7.30–7.80 (m, 6H). Ir (KBr): 3050 (m), 2976 (w), 2938 (w), 1770 (s), 1602 (w), 1500 (m), 1445 (m), 1382 (m), 964 (m), 797 (s), 780 (s), 760 (m), 742 (s), 704 (s), 696 (s). *Anal.* calcd. for $C_{31}H_{24}O$: C 90.26, H 5.86; found: C 90.31, H 6.30.

*Reaction of 1 with 2*a–d *in liquid crystalline solvents*

Stock solutions of **1** in ChP, ChN, and EPCB were prepared by dissolving 0.004 or 0.008 g of **1** and 1.00 g of the mesogen in 10 mL dichloromethane, distilling off the solvent on the rotary evaporator, and pumping on the resulting solids for 2–8 h under high vacuum. Accurately weighed 100 mg portions of these solutions were placed in clean 100 × 7 mm Pyrex tubes, and a slight (10%) excess of the dienophile was added using a 1-μL syringe. For **2*d*** the dienophile was added as a benzene solution to a portion of the stock dienone solution, the whole was dissolved in dichloromethane, and the volatile solvents removed as before. The tubes were degassed (two freeze–pump–thaw cycles) and sealed at 10^{-3} Torr, then placed in the insulated oil bath and heated for 12–40 h at 105°C. The tubes were then opened, and the contents were dissolved in dichloromethane and analysed by hplc; product yields are collected in Table 1.

Acknowledgments

We wish to thank Dr. H. J. Ladendorff, BDH Chemicals Canada Ltd., for a sample of EPCB. We acknowledge the Natural Sciences and Engineering Research Council of Canada for its generous financial support of this work.

1. (*a*) W. E. BACON and G. H. BROWN. Mol. Cryst. Liq. Cryst. **12**, 229 (1971); (*b*) M. J. S. DEWAR and B. D. NAHLOVSKY. J. Am. Chem. Soc. **96**, 460 (1974).
2. (*a*) V. C. ANDERSON, B. B. CRAIG, and R. G. WEISS. J. Phys. Chem. **86**, 4642 (1982); (*b*) V. C. ANDERSON, B. B. CRAIG, and R. G. WEISS. Mol. Cryst. Liq. Cryst. **97**, 351 (1983); (*c*) V. C. ANDERSON and R. G. WEISS. J. Am. Chem. Soc. **106**, 6628 (1984).
3. (*a*) J. M. NERBONNE and R. G. WEISS. Isr. J. Chem. **18**, 266 (1979); (*b*) D. A. HROVAT, J. H. LIU, N. J. TURRO, and R. G. WEISS. J. Am. Chem. Soc. **106**, 7033 (1984).
4. G. AVIV, J. SAGIV, and A. YOGEV. Mol. Cryst. Liq. Cryst. **36**, 349 (1976).
5. T. KUNIEDA, T. TAKAHASHI, and M. HIROBE. Tetrahedron Lett. **24**, 5107 (1983).
6. (*a*) J. M. NERBONNE and R. G. WEISS. J. Am. Chem. Soc. **100**, 2571 (1978); (*b*) J. M. NERBONNE and R. G. WEISS. J. Am. Chem. Soc. **101**, 402 (1979).
7. (*a*) V. C. ANDERSON, B. B. CRAIG, and R. G. WEISS. J. Am. Chem. Soc. **103**, 7169 (1981); (*b*) V. C. ANDERSON, B. B. CRAIG, and R. G. WEISS. J. Am. Chem. Soc. **104**, 2972 (1982).
8. (*a*) B. SAMORI and L. FIOCCO. J. Am. Chem. Soc. **104**, 2634 (1982); (*b*) P. DE MARIA, A. LODI, B. SAMORI, F. RUSTICHELLI, and G. TORQUATI. J. Am. Chem. Soc. **106**, 653 (1984).
9. (*a*) J. M. NERBONNE and R. G. WEISS. J. Am. Chem. Soc. **100**, 5953 (1978); (*b*) J. P. OTRUBA and R. G. WEISS. J. Org. Chem. **48**, 3448 (1983).
10. (*a*) C. ESKENAZI, J. F. NICOUD, and H. B. KAGAN. J. Org. Chem. **44**, 995 (1979), and references cited therein; (*b*) P. SEURON and G. SOLLADIE. J. Org. Chem. **45**, 715 (1980); (*c*) Y. TANAKA, T. CHIYO, S. IIJIMA, T. SHIMIZU, and T. KUSANO. Mol. Cryst. Liq. Cryst. **99**, 255 (1983).
11. E. G. CASSIS JR. and R. G. WEISS. Photochem. Photobiol. **35**, 439 (1982).
12. J. P. OTRUBA and R. G. WEISS. Mol. Cryst. Liq. Cryst. **80**, 165 (1982).
13. S. MELONE, V. MOSINI, R. NICOLETTI, B. SAMORI, and G. TORQUATI. Mol. Cryst. Liq. Cryst. **98**, 399 (1983).
14. B. M. FUNG, R. V. SIGH, and M. M. ALCOCK. J. Am. Chem. Soc. **106**, 7301 (1984).
15. (*a*) F. D. SAEVA (*Editor*). Liquid crystals. The fourth state of matter. Marcel Dekker, Inc., New York. 1979; (*b*) H. KELKER and R. HATZ. Handbook of liquid crystals. Verlag Chemie, Weinheim, Deerfield. 1980; (*c*) G. H. BROWN, J. W. DOANE, and V. D. NEFF. A review of the structure and properties of liquid crystals. Chemical Rubber Company Press, Cleveland, 1971.
16. (*a*) J. M. SCHNUR and D. E. MARTIRE. Mol. Cryst. Liq. Cryst. **26**, 213 (1974); (*b*) G. A. OWEIMREEN, G. C. LIN, and D. E. MARTIRE. J. Phys. Chem. **83**, 2111 (1979); (*c*) D. E. MARTIRE. *In* The molecular physics of liquid crystals. *Edited by* G. W. Gray and G. R. Luckhurst. Academic Press, New York. 1979. Chapt. 11; (*d*) G. A. OWEIMREEN and D. E. MARTIRE. J. Chem. Phys. **72**, 2500 (1980); (*e*) P. J. PORCARO and P. SHUBIAK. J. Chromatogr. Sci. **9**, 690 (1971).
17. W. J. LEIGH. J. Am. Chem. Soc. In press.
18. W. J. LEIGH, P. J. KLAWUNN, and D. S. MITCHELL. To be published.
19. W. J. LEIGH, D. T. FRENDO, and P. J. KLAWUNN. Can. J. Chem. In press.
20. (*a*) E. SACKMANN, P. KREBS, H. U. REGA, J. VOSS, and H. MOHWALD. Mol. Cryst. Liq. Cryst. **24**, 283 (1973); (*b*) F. D. SAEVA. Pure Appl. Chem. **38**, 25 (1974).
21. K. N. HOUK. Tetrahedron Lett. 2621 (1970).
22. C. F. H. ALLEN. Chem. Rev. **62**, 653 (1962).
23. J. K. M. SANDERS, S. W. HANSON, and D. H. WILLIAMS. J. Am. Chem. Soc. **94**, 5325 (1972).
24. P. J. SELL and A. W. NEUMANN. Z. Phys. Chem. Neue Folge, **65**, 13 (1969).
25. C. F. H. ALLEN and J. A. VANALLAN. J. Am. Chem. Soc. **72**, 5165 (1950).
26. Licristal liquid crystals. EM Chemicals, Hawthorne, New York. 1984.
27. J. R. MCCABE and C. A. ECKERT. Acc. Chem. Res. **7**, 251 (1974).
28. G. J. DAVIS and R. S. PORTER. Mol. Cryst. Liq. Cryst. **6**, 377 (1970).

Monolayers of mono- and dioxyethylene dodecyl ethers at air–water and alkane–water interfaces

ROBERT AVEYARD,[1] NEIL CARR,[2] AND HELEN SLEZOK
Department of Chemistry, The University of Hull, Hull, England HU6 7RX

Received January 14, 1985

ROBERT AVEYARD, NEIL CARR, and HELEN SLEZOK. Can. J. Chem. **63**, 2742 (1985).

Surface pressure–area isotherms have been obtained for mono- and dioxyethylene dodecyl ethers both spread at the air–water surface and adsorbed at the heptane–water interface and results are compared with those for straight chain alkanols. At the heptane–water interface it appears that the ethyleneoxy groups are disposed parallel to the interface in fairly dilute films. The dual hydrophilic/hydrophobic nature of isolated CH_2CH_2O groups is demonstrated by showing that they give a negative contribution to the standard free energy of adsorption from both water and heptane to the heptane–water interface.

ROBERT AVEYARD, NEIL CARR et HELEN SLEZOK. Can. J. Chem. **63**, 2742 (1985).

On a déterminé les isothermes de pression/surface des mono- et dioxyéthylènoxydodécanes qui ont chacun été répandus à la surface air/eau et adsorbés à la surface heptane/eau et l'on a comparé les résultats avec ceux obtenus avec des alcanols en chaînes droites. A l'interface eau/heptane et lorsque les films sont assez dilués, il semble que les groupements éthylèneoxy soient disposés parallèlement à l'interface. On démontre la nature double hydrophile/hydrophobe des groupements CH_2CH_2O isolés en se basant sur le fait que leur contribution à l'énergie libre standard d'adsorption soit de l'eau ou de l'heptane à soit l'heptane ou à l'interface heptane/eau est négative.

[Traduit par le journal]

Introduction

There has been a considerable interest over the years in the surface and micellar properties of surfactants of the type RE_n (where R is a hydrophobic moiety such as an alkyl or alkylbenzene group and E is the ethyleneoxy group CH_2CH_2O) both for mixtures with a range of n values, usually for large average n, and for pure materials with n up to about 8 (1–6). Thermodynamic studies have thrown some light onto the dual hydrophilic/hydrophobic nature of E_n groups (4–6). For example, thermodynamic parameters of micellisation have been reported, as have those for adsorption from aqueous solution to films at both high and low concentration at the air–water surface. However, the environment (and hence values of thermodynamic parameters) of individual E groups depends not only on the size of the E_n group, which is likely to become progressively more coiled as n increases, but on the environment of the E_n group as a whole. The latter can be close-packed, as at a micelle surface or in a saturated monolayer, or they may be essentially isolated in dilute solution or in a dilute monolayer.

Here we report surface pressure–area (π,A) isotherms for air–water and oil–water interfaces, and standard free energies of adsorption of mono- and dioxyethylene dodecyl ethers ($C_{12}H_{25}(OCH_2CH_2)_nOH$, denoted $C_{12}E_1$ and $C_{12}E_2$ for $n = 1$ and 2, respectively) from heptane to dilute films at the heptane–water interface. From these we have derived a free energy contribution of an E group to the adsorption of $C_{12}E_1$ and $C_{12}E_2$ from both oil and water to the oil–water interface. Since $n = 1$ or 2 we may suppose the E groups interact only with water and/or alkane in bulk and at the interface, and not with other E groups in the same E_n moiety.

Experimental

Materials

Samples of $C_{12}E_1$ and $C_{12}E_2$ were pure homogeneous samples supplied by the Nikko Chemicals Co. (Japan) and were used without further treatment. Dodecanol and octadecanol were "puriss" samples from Fluka, and pentadecanol was "purum" grade, also from Fluka. These had estimated purities (determined by glc in this laboratory) of >99.5% for "puriss" and >98.5% for "purum" samples and were used untreated. Heptane (Fisons, England) was HPLC grade and was shown by glc to be >99% pure. It was passed through chromatographic alumina immediately prior to use. It had an interfacial tension against water at 25°C of 50.78 mN m^{-1} in excellent agreement with a previous value of 50.77 mN m^{-1} obtained using a highly pure heptane sample (7). Water was distilled once, passed through an Elgastat ion exchange column and then through a Milli-Q Reagent Water System.

Techniques

Interfacial tensions between solutions of $C_{12}E_1$ and $C_{12}E_2$ and water were determined by the drop-volume technique (7). The tensions were highly reproducible (±0.05 mN m^{-1}) and showed no tendency to ageing (unlike those for aqueous solutions against air).

The π,A isotherms for materials spread from solution in heptane at the air–water surface were obtained using a Joyce-Loebl (Gateshead, England) automated recording Langmuir trough. The barrier was a constant perimeter Teflon tape, and the surface pressure was measured using the Wilhelmy plate technique. It was found that the use of filter paper as the "plate" gave very reproducible results which, in the case of octadecanol and pentadecanol were in good agreement with literature data (8). The isotherms reported here, which were very reproducible, were all obtained by compressing the film over a period of 2 min but were indistinguishable from those obtained over a 4 min period. Low temperature isotherms were obtained by circulating cold water through glass tubing immersed in the trough.

Results and discussion

Interfacial tensions γ between dilute solutions of $C_{12}E_1$ and $C_{12}E_2$ in heptane, and water are shown in Fig. 1. At the concentrations used the surfactants reside almost entirely in the alkane phase as may be deduced from the distribution data reported by Manabe *et al.* (9) As expected $C_{12}E_2$ in heptane is more surface active than $C_{12}E_1$. The tensions have been fitted to cubics in surfactant mole fraction x in overlapping concentration ranges. The fitting constants of the equations

$$[1] \quad \gamma = a + bx + cx^2 + dx^3$$

are given in Table 1. We may assume that at the high dilutions

[1] To whom all correspondence should be addressed.
[2] Present address: Plessey Research (Caswell) Ltd., Caswell, Towcester, England.

TABLE 1. Constants from eq. [1] for $C_{12}E_1$ and $C_{12}E_2$ adsorbed at the heptane–water interface at 25°C

(*a*) $C_{12}E_1$

a	$-10^{-4}\,b$	$10^{-7}\,c$	$-10^{-10}\,d$	Range of x	Number of points
50.80	5.23539	21.77382	51.03840	$0 - 15 \times 10^{-5}$	12
50.00	3.14254	4.17710	2.49578	$8 \times 10^{-5} - 51 \times 10^{-5}$	11

(*b*) $C_{12}E_2$

a	$-10^{-5}\,b$	$10^{-10}\,c$	$-10^{-14}\,d$	Range of x	Number of points
50.74	4.74867	2.17301	4.76578	$0 - 2 \times 10^{-5}$	15
50.03	2.63606	0.38145	0.19527	$0.5 \times 10^{-5} - 3.6 \times 10^{-5}$	14

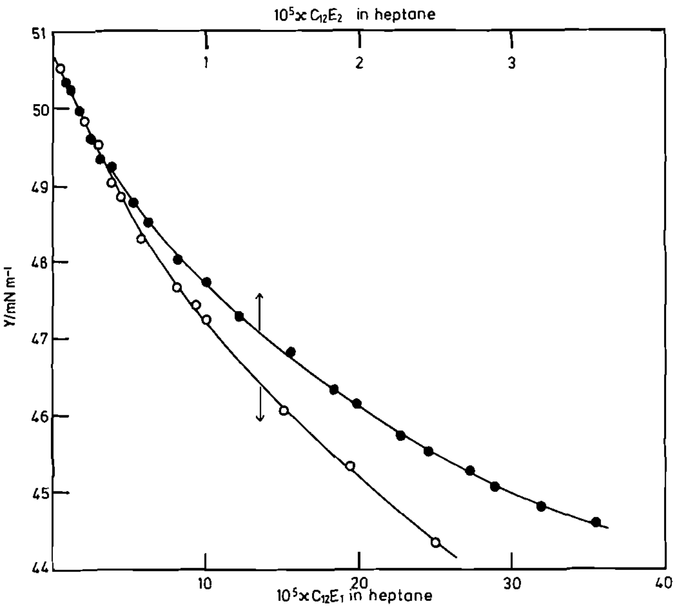

FIG. 1. Interfacial tensions between solutions of $C_{12}E_1$ and $C_{12}E_2$ in heptane and water at 25°C. Six further high concentration points ($x > 25 \times 10^{-5}$) were obtained for $C_{12}E_1$. They are not shown here but were included in the fit of data (see text).

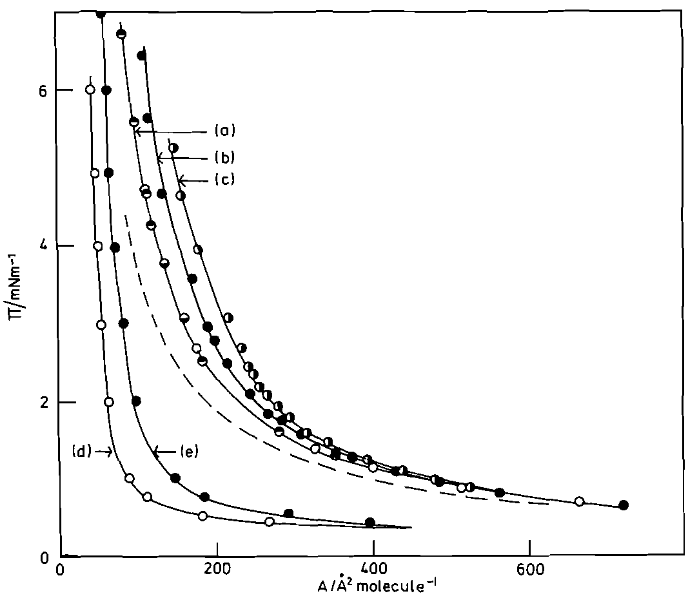

FIG. 2. π,A-isotherms at 25°C. Curves (*a*), (*b*), and (*c*) relate to alkane–water interfaces and are for, respectively, alkanols (octanol, decanol, and dodecanol — see text), $C_{12}E_1$, and $C_{12}E_2$. Curves (*d*) and (*e*) are for $C_{12}E_1$ and $C_{12}E_2$, respectively, at air–water surface.

employed ($x < 5 \times 10^{-4}$ for $C_{12}E_1$ and $x < 4 \times 10^{-5}$ for $C_{12}E_2$) surfactant activity coefficients are unity and activity may be expressed by x.

The Gibbs adsorption equation in general form is, for constant temperature,

$$[2] \quad -d\gamma = \sum_i \Gamma_i d\mu_i$$

where Γ_i are surface concentrations of species i and μ_i are chemical potentials. For low surfactant concentrations $d\mu$ for the heptane and the water may reasonably be set at zero so that from eqs. [1] and [2]

$$[3] \quad \Gamma = A^{-1} = -(x/kT)\,(b + 2cx + 3dx^2)$$

where Γ is the surface concentration of surfactant (molecules per unit area) and A is the area available per surfactant molecule in the film. We denote the surface pressure of a film, which is the lowering in γ caused by adsorption, π. The quantities π and A are related through a surface equation of state.

In addition to the study of films at the oil–water interface we have also obtained π,A data for films at the air–water surface. Adsorption of nonionic surfactants from water is not easy to study since it is time dependent and γ can change markedly over long periods of time (2). However $C_{12}E_1$ and $C_{12}E_2$ are sufficiently insoluble in water (as judged by the reproducibility of the π,A curves obtained at different rates of compression) for monolayers to be studied using the Langmuir trough.

In Fig. 2 we present (π,A) data (for π up to 6 mN m^{-1}) for $C_{12}E_1$ and $C_{12}E_2$ at both the air–water and heptane–water interfaces. Also included are data for octanol, decanol, and dodecanol adsorbed at the alkane–water interface (10). For the oil–water interface both $C_{12}E_1$ and $C_{12}E_2$ films are more expanded than the alkanol films, for which the π,A values fall on a common curve. The similarity of the π,A data for all alkanols implies that chain–chain interactions are unimportant at the oil–water interface and that the alkanol chains are oriented normal to the interface (11). It follows that the larger π (for a given A) exerted by $C_{12}E_1$ and $C_{12}E_2$ arise from the larger effective cross-sectional areas of these molecules at the interface, a point we return to shortly.

The π,A curves for the surfactants at the air–water surface fall well below those for the oil–water interface, and below the ideal curve for which $\pi A = kT$; this is a result of the lateral attractions between the hydrocarbon chains in the surface. As

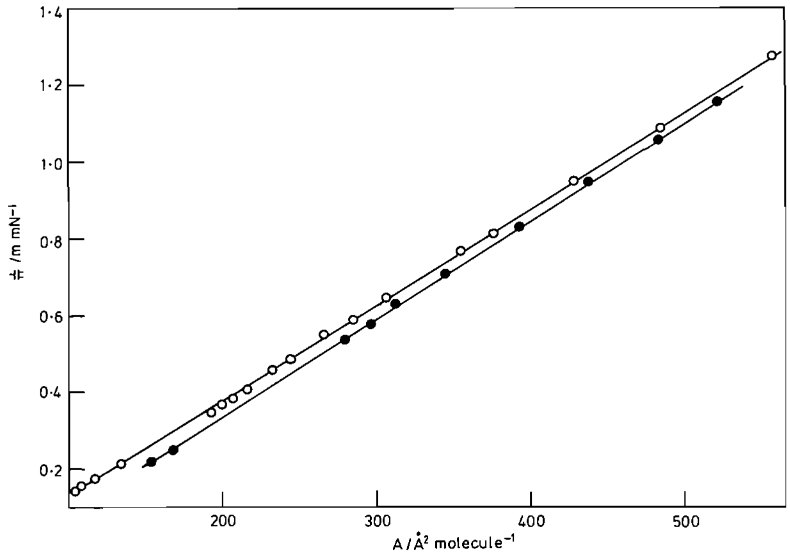

FIG. 3. Plots according to eq. [5] for $C_{12}E_1$ (upper line) and $C_{12}E_2$ at the heptane–water interface at 25°C.

for the oil–water interface, the $C_{12}E_2$ film is more expanded than that for $C_{12}E_1$ presumably due again to the greater cross-sectional area of $C_{12}E_2$. The π,A curves for $C_{12}E_1$ and $C_{12}E_2$ both at the air–water and oil–water interfaces converge at areas between 400 and 500 Å^2 molecule^{-1}.

Surface equations of state

Consideration of surface equations of state can give useful indications concerning interactions and orientations within monolayers. It is known (10) that alkanol behaviour at oil–water interfaces is well described by the Volmer equation

[4] $\quad \pi(A - A_0) = kT$ per molecule

The quantity A_0 is the molecular co-area of the adsorbate and although it is twice the area defined by closest approach of the molecules at the surface, it may be regarded as a good measure of the effective cross sectional area of the molecules (12, 13). For a series of alkanols $A_0 \simeq 27$ Å^2 molecule^{-1} (10).

In linear form eq. [4] is

[5] $\quad 1/\pi = A/kT - A_0/kT$

and plots according to this equation for $C_{12}E_1$ and $C_{12}E_2$ at the heptane–water interface are shown in Fig. 3. The plots are very linear and the values of A_0 obtained from the intercept on the A-axis are 49 and 68 Å^2 molecule^{-1} for $C_{12}E_1$ and $C_{12}E_2$, respectively. The full lines shown in Fig. 2 are those generated by eq. [4] using these A_0 values. If we suppose that the CH_2 group covers 6.5 Å^2 of surface (14) and that the CH_2 and O groups are the same size, the CH_2CH_2O is expected to cover about 20 Å^2 if disposed along the interface. Given that alkanols have $A_0 = 27$ Å molecule^{-1} we expect A_0 for $C_{12}E_1$ and $C_{12}E_2$ to be 47 and 67 Å^2 molecule^{-1} if the E groups are flat along the interfaces. The values are remarkably close to the A_0 values quoted above, and it therefore appears that both CH_2 groups and O are *at* the interface and that the E group has both hydrophilic and hydrophobic properties, a point considered further shortly.

Repulsive interactions resulting from finite size account for deviations from ideality for oil–water films as seen. Repulsive interactions also obviously occur in films at the air–water surface but here π values fall below those expected for ideal films. The difference in π (for a given A) for a film at the oil–water and the air–water surface has often been referred to as the "cohesive pressure" π_c within the air–water film and taken to be a measure of interchain cohesion (15). However, this is not a satisfactory estimate of attractive interactions between chains. At an oil–water interface the alkyl chains of adsorbate molecules are roughly normal to the surface as mentioned. At the higher area represented in Fig. 2, however, alkyl chains at an air–water surface are likely to lie along the surface in order to interact with the underlying water molecules (13). Hence at these areas, the effective A_0 will be larger than those appropriate for the oil–water interface. As the film becomes more concentrated, the alkyl chains assume more nearly vertical orientations and so A_0 changes. The cohesive pressure as defined above therefore contains (changing) repulsive contributions as well as the attractive contributions.

Data for air–water films of $C_{12}E_1$ and $C_{12}E_2$ at high surface pressures are shown in Fig. 4 where results for pentadecanol ($C_{15}OH$) are also given. The π,A curve of $C_{15}OH$ is very similar to that obtained for octadecanol ($C_{18}OH$, not shown), and these two alkanols were investigated since they have similar overall size (i.e. extended chain length) to the surfactants. Some results are also shown for dodecanol (formally $C_{12}E_0$) but these are considered to be less reliable than the others as a result of the higher solubility in water. At 25°C the films of dodecanol, $C_{12}E_1$, and $C_{12}E_2$ are all expanded up to high pressures, whereas monolayers of $C_{15}OH$ and $C_{18}OH$ are readily condensed. In the case of $C_{12}E_1$ and $C_{12}E_2$, areas are attained which are considerably less than the A_0 values obtained at the heptane–water interface and so the E groups are presumably forced out of the interface into the aqueous phase. This effect can be expected to militate against the formation of condensed films. It is interesting though that films of $C_{12}E_1$ at temperatures below 25°C do eventually become condensed at higher pressures and exhibit quite extensive expanded-condensed transition regions. Possible origins of such transition regions are discussed by Gaines (8).

Standard free energies of adsorption

We have suggested, from a consideration of an equation of state, that the E groups in $C_{12}E_1$ and $C_{12}E_2$ are disposed parallel to the oil–water interface and that they have both hydrophilic and hydrophobic character at the interface. These ideas can be

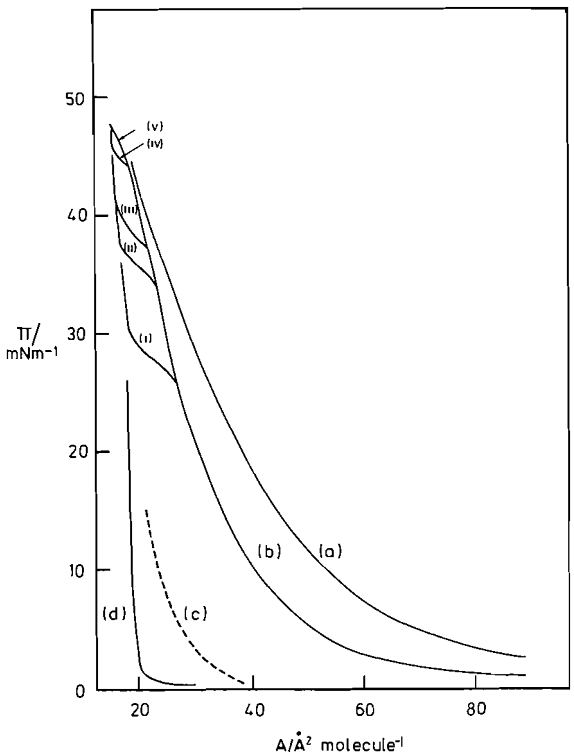

FIG. 4. π,A-isotherm for films at the air–water surface (*a*) $C_{12}E_2$ at 25°C; (*b*) $C_{12}E_1$ at (*i*) 4.6°C, (*ii*) 11.9°C; (*iii*) 15.8°C; (*iv*) 21.0°C; (*v*) 25.0°C; (*c*) dodecanol at 25°C; (*d*) pentadecanol at 25°C.

quantified in terms of standard free energies of adsorption and of transfer between aqueous and oil phases. We first consider the significance of various "adsorption free energies" which have been reported in the literature.

The adsorption isotherm equation, which contains a standard free energy of adsorption, is obtained by equating the chemical potentials of the surfactant in surface (μ^s) and bulk (μ^l) at adsorption equilibrium. For an infinitely dilute film we may write

[6] $\mu^s = \mu_\pi^{\ominus,s} + RT \ln(\pi/\pi_{st})$

[7] $\quad = \mu_\Gamma^{\ominus,s} + RT \ln(\Gamma/\Gamma_{st})$

where $\pi = \Gamma RT$, $\mu_\pi^{\ominus,s}$ and $\mu_\Gamma^{\ominus,s}$ are standard chemical potentials, and π_{st} and Γ_{st} are the standard surface pressure and standard surface concentration respectively. If, for a given temperatue, π_{st} is chosen as being equal to $\Gamma_{st}RT$ then $\mu_\pi^{\ominus,s} = \mu_\Gamma^{\ominus,s}$ for that temperature. Further, for an ideal dilute solution

[8] $\mu^l = \mu^{\ominus,l} + RT \ln(c/c_{st})$

where c_{st} is the standard concentration. It follows that for adsorption into an infinitely dilute film

[9] $\mu_\pi^{\ominus,s} - \mu^{\ominus,l} = \Delta_a\mu_\pi^\ominus = -RT \ln(\pi c_{st}/c\pi_{st})_0$

and

[10] $\mu_\Gamma^{\ominus,s} - \mu^{\ominus,l} = \Delta_a\mu_\Gamma^\ominus = -RT \ln(\Gamma c_{st}/c\Gamma_{st})_0$

where the subscript 0 denotes that the quantity in brackets is taken at infinite dilution. If we choose the same c_{st} and if $\pi_{st} = \Gamma_{st}RT$ at the given temperature T, $\Delta_a\mu_\pi^\ominus$ and $\Delta_a\mu_\Gamma^\ominus$ are equal at that temperature. If however we choose, for example, a temperature independent standard surface pressure the correspond-

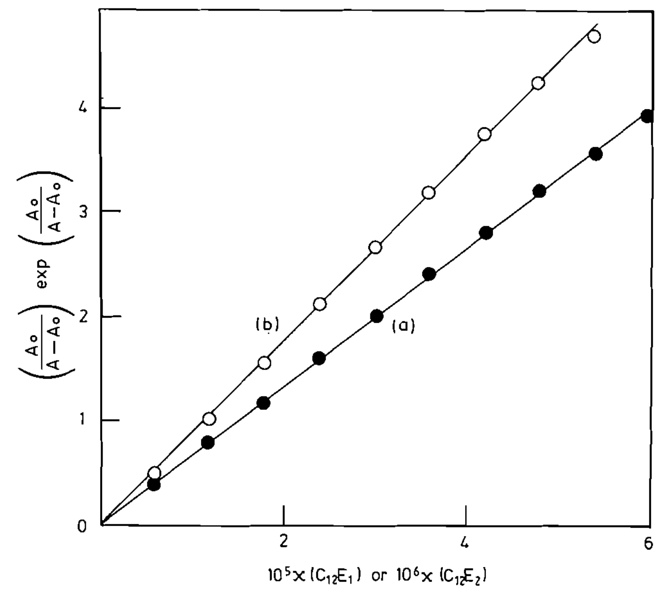

FIG. 5. Plots according to eq. [11] for (*a*) $C_{12}E_1$ and (*b*) $C_{12}E_2$ adsorbed at the heptane–water interface at 25°C.

ing Γ_{st} ($= \pi_{st}/RT$) varies with T and so the standard enthalpies and entropies obtained from the temperature variation of the two free energies will differ.

For films which are not ideally dilute, expressions [6] and [7] are no longer true, and for a film obeying the Volmer equation (eq. [4]) it can be shown that (16)

$$\Delta_a\mu_v^\ominus = RT(\ln K + 1)$$

where

[11] $K = \left\{c\Big/\left(\frac{A_0}{A - A_0}\exp\frac{A_0}{A - A_0}\right)\right\}$

and the standard state for the surface is taken as $A_{st} = 2A_0$. It can be shown that

[12] $\Delta_a\mu_v^\ominus = \Delta_a\mu_\pi^\ominus - RT\{\ln(A_0/kT) - 1\}$

where the standard state $\pi_{st} = 1$ is chosen for $\Delta_a\mu_\pi^\ominus$. We have data from which we can obtain $\Delta_a\mu_v^\ominus$ and we will wish to obtain $\Delta_a\mu_\pi^\ominus$ using eqs. [11] and [12].

Sokolowski and Burczyk (6) have obtained values of $\Delta_a\mu_\pi^\ominus$ for the adsorption of R_nE_m (where R is an alkyl group with n = 4 to 8, and m = 1 to 5) from water to the air–water surface. We will therefore be able to use their data in conjunction with our own. On the other hand, Barry and El Eini (4) and Guveli *et al.* (5) employ a free energy of adsorption defined by

[13] $\Delta_a\mu^\ominus = -RT \ln\{(\Gamma/c_0^{2/3})10^2N^{1/3}\}$

where Γ is the saturation adsorption at the cmc (c_0). The significance of $\Delta_a\mu^\ominus$ is not clear. Equation [13] implies that we may write

[14] $\mu^l = \mu^\ominus + RT \ln c^{2/3}$

Comparison of eqs. [8] and [14] (for $c_{st} = 1$) shows that $\mu^\ominus = \mu^{\ominus,l} + RT \ln c^{1/3}$ so that $\mu^\ominus$ changes with concentration. Equation [13] further implies that eq. [7] holds for a concentrated film, which it does not. This must also throw doubt upon the significance of the enthalpies and entropies obtained from $\Delta_a\mu^\ominus$.

In Fig. 5 are shown plots of $\{A_0/(A - A_0)\}\exp\{A_0/(A - A_0)\}$

TABLE 2. Standard free energies of adsorption and values of A_0

Parameter	Value		
	Dodecanol*	$C_{12}E_1$	$C_{12}E_2$
$-\Delta_a\mu_v^\ominus$/kJ mol^{-1}	14.32	19.33	25.76
$-\Delta_a\mu_\pi^\ominus$/kJ mol^{-1}	23.64	27.10	32.70
A_0/Å^2 molecule^{-1}	26	49	68

*Values for dodecanol taken from ref. 10.

($= f(A)$) against c (in mole fraction x) for $C_{12}E_1$ and $C_{12}E_2$ in the heptane–water system. Values of $f(A)$ were obtained at equal intervals of x using the constants in Table 1. The plots are very linear and values of $\Delta_a\mu_v^\ominus$ have been obtained from the slopes using eq. [11]. Since A_0 is different for $C_{12}E_1$ and $C_{12}E_2$, so are the standard states for the surface. We have therefore converted $\Delta_a\mu_v^\ominus$ to $\Delta_a\mu_\pi^\ominus$ using eq. [12] and the various free energies are given in Table 2.

For $C_{12}E_1$ and $C_{12}E_2$ in dilute solution and in dilute monolayers the E groups are probably in contact only with one or, at the interface, both of the solvents, but not in mutual contact. Manabe *et al.* (9) have shown that the standard free energy of transfer of R_nE_m (m = 1 to 4) from dilute aqueous solution to dodecane varies linearly with m (suggesting the equivalence of all E groups up to E_4), the E group contribution being within experimental error the same for n between 2 and 5. The mean standard free energy of transfer of the E group was found to be +2.74 kJ mol^{-1}. From our results, the change in $\Delta_a\mu_\pi^\ominus$ per E group (for E_1 to E_2) is −5.60 kJ mol^{-1}; in view of the transfer data we may reasonably suppose this increment holds up to E_4. It follows that the standard free energy of adsorption of the E group from water to the oil–water interface is −2.86 kJ mol^{-1}. It is seen then that the E group is surface active (i.e. has a negative standard free energy of adsorption) both from water and from alkane, but more strongly so from alkane.

Sokolowski and Burczyk (6) obtain a value for the standard free energy of adsorption of the E group from aqueous solution to infinite dilution at the air–water surface of −1.86 kJ mol^{-1}. For straight chain alkanols, the difference in $\Delta_a\mu_\pi^\ominus$ per CH_2 group for adsorption from aqueous solution to the oil–water and the air–water interfaces is 0.5 kJ mol^{-1} (16). This difference for CH_2CH_2 is thus 1.0 kJ mol^{-1}, which is the same as for the two CH_2 groups in CH_2CH_2O. Clearly, the methylene groups of the E moiety are unlikely to extend deep into the alkane phase at an alkane–water interface as do the CH_2 groups of a long chain alkanol, but it has been argued elsewhere (10, 13) that the free energy of interaction of methylene groups with interfacial water is similar to that for the corresponding interaction with alkane and that the free energies of CH_2 groups in chains normal to and parallel to the oil–water interface are essentially equal.

Included in Table 2 is a value for the standard free energy of adsorption of dodecanol from octane to the octane–water interface. The value is more negative than expected if the alcoholic OH were the same as the OH in $C_{12}E_1$ and $C_{12}E_2$. This is in accord with the findings of Manabe *et al.* (9) concerning transfer free energies.

Acknowledgements

The authors acknowledge their gratitude to the SERC for research grants, one of them a CASE award in collaboration with Unilever Research, Port Sunlight.

1. E. H. CROOK, D. B. FORDYCE, and G. F. TREBBI. J. Phys. Chem. **67**, 1987 (1963); J. Colloid Sci. **20**, 191 (1965).
2. H. LANGE. Nonionic surfactants. Vol. 1. *Edited by* M. J. Schick. Marcel Dekker. 1967. Chapt. 14.
3. M. DONBROW. J. Colloid Interface Sci. **53**, 145 (1975).
4. B. W. BARRY and D. I. D. EL EINI. J. Colloid Interface Sci. **54**, 339 (1976).
5. D. E. GUVELI, S. S. DAVIS, and J. B. KAYES. J. Colloid Interface Sci. **91**, 1 (1983).
6. A. SOKOLOWSKI and B. BURCZYK. J. Colloid Interface Sci. **94**, 369 (1983).
7. R. AVEYARD and D. A. HAYDON. Trans. Faraday Soc. **61**, 2255 (1965).
8. G. L. GAINES, JR. Insoluble monolayers at liquid–gas interfaces. Interscience. 1966.
9. M. MANABE, M. KODA, and K. SHIRAHAMA. Bull. Chem. Soc. Jpn. **48**, 3553 (1975).
10. R. AVEYARD and B. J. BRISCOE. J. Chem. Soc. Faraday I, **68**, 478 (1972).
11. R. AVEYARD. Surfactants. *Edited by* Th. F. Tadros. Academic Press. 1984.
12. J. H. DE BOER. The dynamical character of adsorption. OUP. 1953. p. 173.
13. R. AVEYARD and J. CHAPMAN. Can. J. Chem. **53**, 916 (1975).
14. L. SARAGA and I. PRIGOGINE. Mem. Serv. Chim de l'Etat **38**, 109 (1953).
15. J. T. DAVIES and E. K. RIDEAL. Interfacial phenomena. Academic Press. 1963. p. 230.
16. R. AVEYARD and D. A. HAYDON. Introduction to the principles of surface chemistry. CUP. 1973.

Novel stereochemical equilibria in crown ethers. Detection of additional conformations of *cis-syn-cis-* and *cis-anti-cis*-dicyclohexano-18-crown-6 by 100.6-MHz ^{13}C nuclear magnetic resonance at 173 K

G. W. BUCHANAN[1] AND K. BOURQUE
Ottawa–Carleton Institute for Research and Graduate Studies in Chemistry, Department of Chemistry, Carleton University, Ottawa, Ont., Canada K1S 5B6

AND

J. W. BOVENKAMP AND A. RODRIGUE
Defence Research Establishment Ottawa, Ottawa, Ont., Canada K1A 0Z4

Received January 25, 1985

G. W. BUCHANAN, K. BOURQUE, J. W. BOVENKAMP, and A. RODRIGUE. Can. J. Chem. **63**, 2747 (1985).

High field ^{13}C nmr has been utilized for the analysis of new conformational equilibria in each of the title crown ethers at low temperature. Evidence indicates that these equilibria arise from restricted rotation in the macrocyclic portions of these molecules. The conformational free energy differences between the isomers are small (0.1–0.3 kcal/mol) while barriers to their interconversion are of the order of 8.5–9.0 kcal/mol. Comparisons are made with the degenerate equilibria involving inversion of the cyclohexane rings.

G. W. BUCHANAN, K. BOURQUE, J. W. BOVENKAMP et A. RODRIGUE. Can. J. Chem. **63**, 2747 (1985).

On a fait appel à la rmn du ^{13}C à haut champ pour analyser de nouveaux équilibres conformationnels, à basse température, dans chacun des éthers couronnes mentionnés dans le titre. Les données indiquent que ces équilibres proviennent de rotations empêchées dans les portions macrocycliques de ces molécules. Les différences d'énergie libre conformationnelle entre les isomères sont petites (entre 0,1 et 0,3 kcal/mol) alors que les barrières à leur interconversion sont de l'ordre de 8,5 à 9,0 kcal/mol. On a fait des comparaisons avec les équilibres dégénérés impliquant l'inversion de cycle dans le cyclohexane.

[Traduit par le journal]

Introduction

Both the *cis-syn-cis* (**1**) and *cis-anti-cis* (**2**) isomers of dicyclohexano-18-crown-6 (below) are expected to undergo degenerate inversions of their 18-membered rings, which necessarily involve inversion of their cyclohexane rings (1).

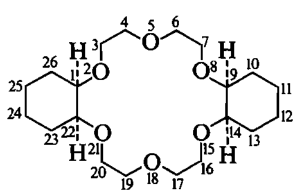

1

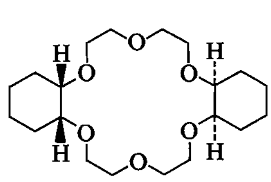

2

Recently (2) we reported determination of the ring inversion barriers for **1** and **2**, as well as their 1:1 complexes with potassium phenoxide using 50.3-MHz ^{13}C nmr at low temperature. For **1** and **2**, the magnitudes of these barriers (ca. 10.2 kcal/mol) are similar to those previously measured for *cis*-1,2-disubstituted cyclohexanes (3). Minor increases (ca. 1 kcal/mol) were observed in the barriers for the complexes with potassium phenoxide relative to the free crown ethers.

In our communication (2) it was noted that 50.3-MHz ^{13}C spectra of pure **1** and **2**, but *not* the potassium complexes, showed evidence of additional spectral features at very low temperatures. The inherent sensitivity of the instrument used, however, did not permit a clear definition of the phenomena involved.

Presently, we report the results of 100.6-MHz ^{13}C spectra of **1** and **2** at 173 K. The increased sensitivity and dispersion of these spectra have permitted the clear identification of a second conformational isomer for each of the pure crown ethers **1** and **2**. From relative intensities of the ^{13}C resonances at 173 K the conformational free energy difference between these conformers has been calculated.

[1]Author to whom correspondence should be addressed.

Results and discussion

(i) Spectra

The ^{13}C chemical shifts for **1** and **2** in two solvent media at 298 K are presented in Table 1. Assignments are consistent with those reported earlier (4). For each compound only 5 resonances appear, due to rapid ring inversion on the nmr time scale at this temperature.

As a typical example of the spectral behaviour of these materials as a function of temperature, Fig. 1 shows the 100.6-MHz ^{13}C spectra of **2** in CD_2Cl_2 between 173 and 293 K. Clearly, decoalescence phenomena are first observed for the C-1,9,14,22 site, centered at δ_C = 77.44, and the C-11,12,24,25 site at δ_C = 22.48. A slow exchange spectrum results at 198 K, where it appears that there is a simple 1:1 exchange process. The chemical shift differences at the remaining three sites appear to be too small to allow observation of resonances for separate conformers. Spectra such as this were observed at 50.3 MHz (2) and were employed in the earlier barrier calculations for pure **1** and **2**, for degenerate ring inversion.

As is evident from Fig. 1, however, further cooling to 173 K results in additional fine structure being observable at 100.6 MHz. Resolution enhanced 100.6-MHz ^{13}C spectra for the 15–30 ppm and 65–82 ppm ranges of **2** in CD_2Cl_2 are depicted in Figs. 2 and 3 respectively.

In the 15–30 ppm region (Fig. 2), the initial two resonances at 293 K have, at 173 K, split into eight resonances. These eight lines can be divided into four pairs, arising from individual non-oxygenated carbons of major and minor conformers of **2**.

TABLE 1. ^{13}C Chemical shifts for **1** and **2** at 298 K (δ_C from TMS ± 0.01)*

Compound	Solvent	C-1,9,14,22	C-3,7,16,20	C-4,6,17,19	C-10,13,23,26	C-11,12,24,25
1	CD_2Cl_2	77.59	68.43	71.20	27.92	22.47
1	CD_3OD	78.74	69.17	71.99	28.56	23.04
2	CD_2Cl_2	77.44	68.19	70.82	27.98	22.48
2	CD_3OD	78.53	69.03	71.56	28.54	23.04

*0.4 *M* solutions.

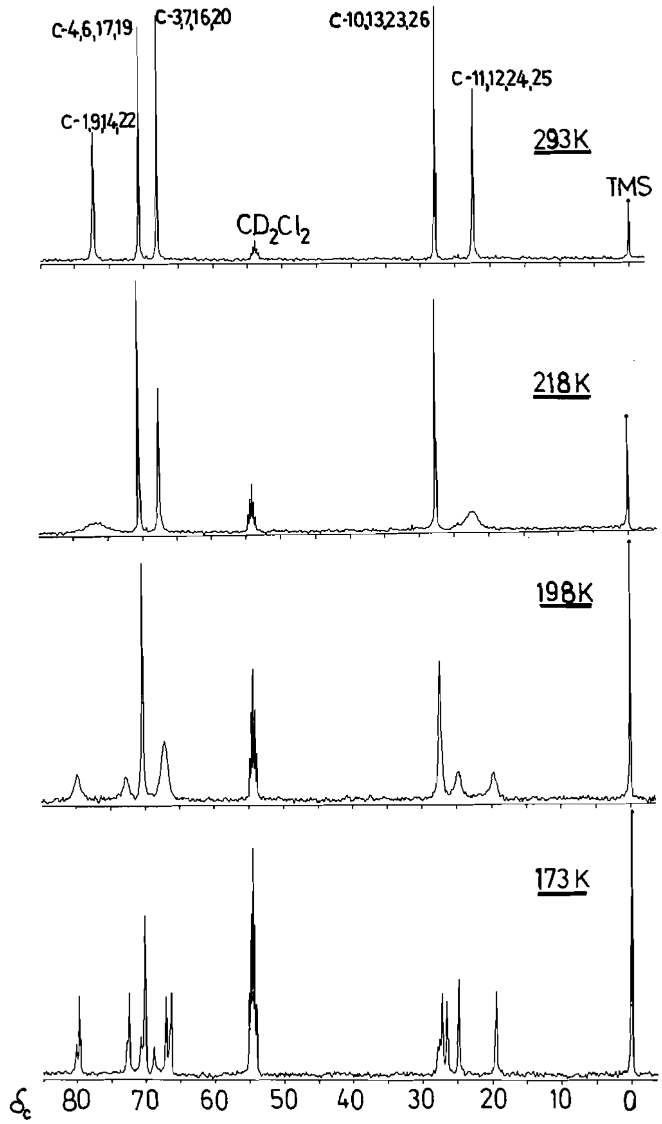

FIG. 1. The ^{13}C nmr spectra of **2** in CD_2Cl_2 as a function of temperature.

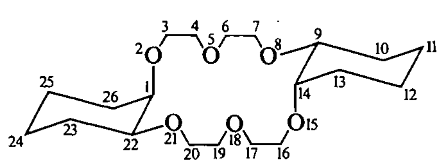

2

The highest field pair of resonances near δ_C = 19.5 arises from the symmetry equivalent C-12,25 positions in the major and minor conformations. These are the most highly shielded

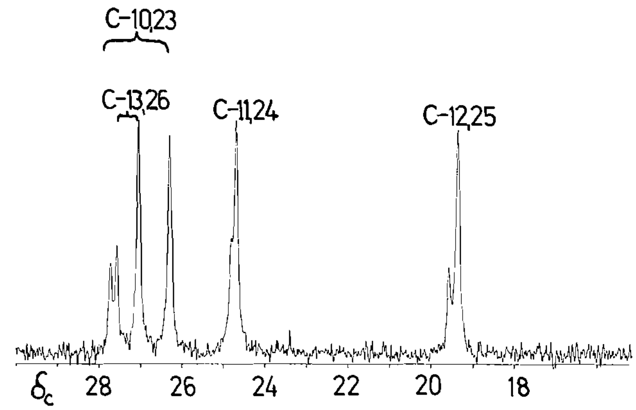

FIG. 2. The ^{13}C nmr spectrum of **2** in CD_2Cl_2 at 173 K; 15–30 ppm range, resolution enhanced.

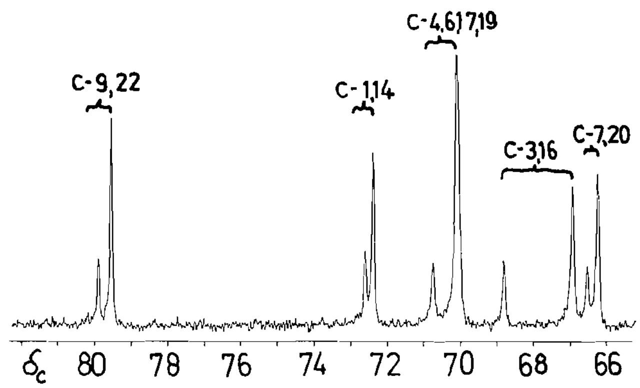

FIG. 3. The ^{13}C nmr spectrum of **2** in CD_2Cl_2 at 173 K; 65–80 ppm range, resolution enhanced.

carbons due to their *gauche* γ−relationship to the axial oxygen atoms at sites 15 and 2 respectively (5). The C-11,24 pair of carbons are deshielded by ca. 5 ppm relative to C-12,25, an observation consistent with the γ−*trans* relationship of C-11,24 to the oxygen atoms at positions 8 and 21 respectively.

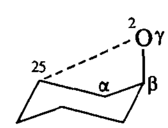

The resonance for C-10,13, 23,26 shows little broadening even at 198 K, but finally splits into 4 lines in the range of 26.30 to 27.74 ppm. Tentative signal assignments can be made from additivity using the known β and γ ^{13}C substituent effects for axial and equatorial OR groups in monosubstituted cyclohexanes at low temperature (6). This leads to the expectation that the C-10,23 site will resonate ca. 1–2 ppm upfield from the resonance for C-13,26. The observed difference is

TABLE 2. ^{13}C Chemical shifts for individual conformations of **1** (δ_C from TMS $\pm$ 0.01)* at 173 K

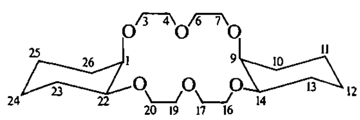

1

Conformation	Solvent	C-1,9	C-14,22	C-3,7	C-16,20	C-4,6	C-17,19	C-13,23	C-10,26	C-12,24	C-11,25
Major	CD_3OD	73.82	80.39	68.25	66.61	71.37†	71.37†	27.93†	27.93†	25.38	20.11
Minor	CD_3OD	74.45	81.42	69.17	67.93	72.64†	72.64†	28.50†	28.50†		

*0.4 *M* solutions.
†Peak overlap.

TABLE 3. ^{13}C Chemical shifts for individual conformations of **2** (δ_C from TMS $\pm$ 0.01)* at 173 K

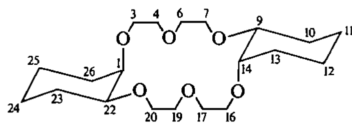

2

Conformation	Solvent	C-1,14	C-9,22	C-3,16	C-7,20	C-4,17	C-6,19	C-10,23	C-13,26	C-11,24	C-12,25
Major	CD_2Cl_2	72.38	79.55	66.94	66.24	70.11†	70.11†	26.30	27.05	24.69	19.36
Minor	CD_2Cl_2	72.60	79.90	68.81	66.52	70.74†	70.74†	27.74	27.58	24.80	19.58
Major	CD_3OD	73.23	80.34	68.78	67.18	70.61†	70.61†	27.04	27.63	25.28	20.15
Minor	CD_3OD	73.69	81.18	69.48	67.49	71.29†	71.29†	28.75	27.85		

*0.4 *M* solutions.
†Peak overlap.

0.75 ppm for the major conformations. Interestingly, in the minor conformers this difference decreases, to only 0.16 ppm.

Figure 3 shows the oxygenated carbon resonances for **2** in CD_2Cl_2 at 173 K. The lowest field pair of signals in the range 79–80 ppm arises from the C-9,22 sites of **2** in its major and minor conformations. These carbons, bearing equatorial oxygens, are expected, by analogy with cyclohexanol derivatives (7), to be substantially deshielded relative to their counterparts C-1,14 which bear axial oxygen atoms. For both the major and minor conformation, the difference is ca. 7.2 ppm.

From Fig. 3, it is evident that considerable peak overlap persists in the resonances for the C-4,6,17,19 sites of **2**, even at 100.6 MHz. Thus, instead of the 4 lines expected here, just 2 are observed. The resonance at δ_C = 70.11 represents a composite of several (probably three) signals while the intensity of the remaining signal at δ_C = 70.74 suggests that it arises from the minor conformation.

The remaining four signals are due to the C-3,16 and C-7,20 sites, as depicted in Fig. 3. Carbons directly bonded to axial oxygens (i.e. C-3,16) were found to be substantially deshielded relative to their C-7,20 counterparts, which are linked to equatorial oxygens. The result is consistent with our recent findings (8) in which axial OCH_3 carbons in vicinally di- and tri-substituted cyclohexanes are always deshielded (by ca. 0.5–1.0 ppm) relative to equatorial OCH_3 functions.

In general, similar trends were noted for **2** in CD_3OD solution, although more accidental resonance overlap was observed. Chemical shift data for individual conformers of **2** in CD_2Cl_2 and CD_3OD at 173 K are presented in Table 3.

In the case of isomer **1**, there is also clear evidence for the presence of a second conformation at 173 K. There is, however, more accidental overlap of resonances for major and minor conformers, especially in CD_2Cl_2 solution. Accordingly, only low temperature data for **1** in CD_3OD solutions are listed in Table 2.

(ii) Conformations

A considerable amount of X-ray data is available for complexes of **1** and **2** (9–11). In these cases, it is generally true that the crown ethers assume conformations in which the oxygen atoms are displaced alternately above and below the mean plane of the 18-membered ring. These conformations are referred to as the "all *gauche*-O—CH_2—CH_2—O—" or "ideal" conformations for complexation.

For the crown ethers themselves in the solid phase, however, X-ray data (12) indicate some changes from the above "ideal" complexation geometries. In fact, the results for **1** and **2** suggest that all six oxygen atoms lie approximately in a plane, with the central cavity being elliptical in shape. Of course the conformations of these molecules in solution may vary substantially from those in the crystal, but the solid state geometries can be used as a starting point for discussion.

It is important to note that the ^{13}C chemical shifts of both major and minor conformations of **1** and **2** at 173 K are, on the average, within 1 ppm of those for the potassium phenoxide complexes at comparable temperatures (2). This suggests that there are no *major* structural perturbations from the "all *gauche*-O—CH_2—CH_2—O" geometry in *either* of the conformations of free **1** and **2**. As was noted in the introduction, the ^{13}C spectra of potassium phenoxide complexes of **1** and **2** show *no* evidence of the presence of minor crown ether conformers (2) at low temperature. Presumably electrostatic interactions between the oxygen lone pairs and the cation in the cavity will stabilize the "all *gauche*-O—CH_2—CH_2—O" conformation in the complex relative to the situation for free **1** and **2**.

It has been shown (13) that for the network —O—CH_2—CH_2—O—, the conformation in which the oxygens are *gauche* is ca. 0.4 kcal/mol more stable than the conformer having *trans* oxygen atoms. With this information and the ^{13}C chemical shifts in hand, one can now speculate regarding the nature of the major and minor conformations for **1** and **2** respectively.

From relative ^{13}C peak areas at 173 K, and use of the equation $-\Delta G^0 = RT \ln K_{eq}$, the conformational free energies were determined to be as follows: for **1** in CD_3OD, 0.10 ± 0.04 kcal/mol; for **2** in CD_2Cl_2, 0.31 ± 0.05 kcal/mol; and for **2** in CD_3OD, 0.10 ± 0.04 kcal/mol.

It is of interest to note that the ^{13}C chemical shifts for minor conformers are all *downfield* relative to those for the corresponding carbons of the major isomers. In this context it is useful to recall that ^{13}C shifts for carbons involved in "γ–*gauche*" interactions are normally upfield from those for carbons experiencing more transoid-type γ steric situations (5). From Tables 2 and 3 it is also evident that the largest chemical shift differences between conformers occur at carbons in the central 18-membered ring. The smallest differences in ^{13}C shieldings between conformers are noted at the C-11,12,24,25 sites, which are the most remote from the macrocyclic cavity.

Based on the points in the preceding paragraph, we conclude that the presence of the second conformational isomer in free crown ethers **1** and **2** is a consequence of rotational isomerism in the macrocyclic ring. The more populated form, we suggest, is the one having all *gauche*-O—CH_2—CH_2—O" networks in the macrocyclic ring as depicted for **2***A* (below), with alternating g_+ and g_- arrangements. For **2***B*, the minor form, we postulate that there is ring deformation in the central region of the macrocycle leading to more transoid character in the —O—CH_2—CH_2—O networks.

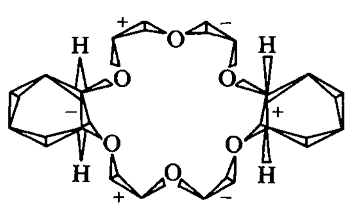

2*A*

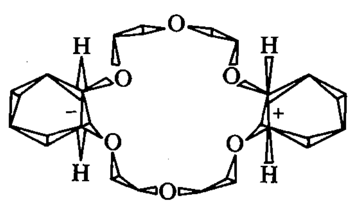

2*B*

As our results show, however, there is only a small difference in the stability of the conformational isomers, since the largest $-\Delta G^0$ value is 0.31 ± 0.05 kcal/mol for **2** in CD_2Cl_2.

The fact that the barriers to rotation in the macrocyclic rings are large enough to permit detection of conformational isomers by nmr is perhaps not surprising, in view of recent results (14) regarding rotational barriers in substituted ethane units containing vicinal heteroatoms.

The present ^{13}C data can be used to calculate $\Delta G^{\neq}$, the free energy of activation for the conformational interconversion in the macrocycle at the coalescence temperature. A modified (for unequally populated two-site exchange processes) Gutowsky–Holm equation and the Eyring equation are used. The rate constant k is calculated from the equation (15)[2]

$$K = \frac{\pi \Delta \nu}{\sqrt{2}\rho_\beta}$$

where ρ_β is the site population ratio (larger to smaller area). For **1** and **2** this calculation leads to barriers in the range of 8.5–9.0 kcal/mol. These barriers are ca. 1.5 kcal/mol lower than those for the overall ring inversion process (2) for **1** and **2**, in which cyclohexane ring inversion is necessarily involved.

An X-ray crystallographic study on complexes **1** and **2** with sodium and potassium salts involving unusual host/guest ratios has been completed recently (17). Of relevance to the present work is the finding that the macrocyclic ring of the solid complex of **1** with sodium phenoxide is in a "non-ideal" conformation, similar in nature to those postulated here for the minor isomers of **1** and **2** in solution.

Finally, it should be noted that the nature of the solvent undoubtedly plays an important role in affecting the observed conformations of the macrocyclic rings of **1** and **2**. Recently Popov and co-workers (18) have demonstrated the influence of solvent association on the ligand conformation in the cryptand C221. They classify both solvents used here, i.e. CD_2Cl_2 and methanol, as "A-class" solvents which are expected to interact with crown ethers via hydrogen bonding. We have also examined the low temperature ^{13}C spectra of **1** and **2** in a "B-class" solvent, namely toluene-d_8. In these experiments, there was again evidence for additional conformations of **1** and **2**; however, extensive peak overlap precludes a detailed discussion of results.

Experimental

(a) *Materials*

The commercial mixture of **1** and **2** was separated by published methods (16). For **1**, mp = 61–63°C and for **2**, mp = 69–70°C.

(b) *Spectra*

^{13}C Spectra were recorded at the Univesity of Guelph using a Bruker WH-400 spectrometer at 100.6 MHz. Suppressed nOe. ^1H decoupling was used. Samples were 0.4 *M*, contained in 5-mm tubes. Typical sweep width was 31 250 Hz, acquisition time 0.262 s with 56 K data points. Pulse repetition rate was 2.0 s, with 45° observe pulses. Normally 200 spectral accumulations were obtained. Temperatures are accurate to ±2.0 K. Chemical shifts are relative to internal TMS.

Acknowledgements

We thank Mr. Bill Klimpstra for expert technical aid as well as NSERC and DREO for financial assistance.

1. A. C. Coxon, D. A. Laidler, R. B. Pettman, and J. F. Stoddart. J. Am. Chem. Soc. **100**, 8260 (1978).
2. G. W. Buchanan, K. Bourque, J. W. Bovenkamp, A. Rodrigue, and R. A. B. Bannard. Tetrahedron Lett. **25**, 3963 (1984).
3. S. Wolfe and J. R. Campbell. Chem. Commun. 874 (1967).
4. M.-C. Fedarko. J. Magn. Reson. **12**, 30 (1973).

[2] Also, R. R. Fraser and J. L. Roustan, private communication.

5. N. K. WILSON and J. B. STOTHERS. Top. Stereochem. **8**, 1 (1973).
6. H.-J. SCHNEIDER and V. HOPPEN. Tetrahedron Lett. 579 (1974).
7. G. W. BUCHANAN, D. A. ROSS, and J. B. STOTHERS. J. Am. Chem. Soc. **88**, 4301 (1966).
8. G. W. BUCHANAN, J. W. BOVENKAMP, A. RODRIGUE, R. A. B. BANNARD, and R. Y. MOIR. Can. J. Chem. **63**, 000 (1985).
9. M. R. TRUTER. Struct. Bonding (Berlin), **16**, 71 (1973).
10. J. D. DUNITZ, M. DOBLER, P. SEIBER, and R. P. PHIZACKERLEY. Acta Crystallogr. Sect. B, **30**, 2733 (1974).
11. I. GOLDBERG. Acta Crystallogr. Sect. B, **31**, 754 (1975); **31**, 2592 (1975).
12. N. K. DALLEY, J. S. SMITH, S. B. LARSON, J. J. CHRISTENSEN, and R. M. IZATT. J. Chem. Soc. Chem. Commun. 43 (1975).
13. A. ABE and J. E. MARK. J. Am. Chem. Soc. **98**, 6468 (1976).
14. T. H. BRUNCK and F. WEINHOLD. J. Am. Chem. Soc. **101**, 1700 (1979).
15. G. W. BUCHANAN and B. A. DAWSON. Org. Magn. Reson. **13**, 293 (1980).
16. R. M. IZATT, B. L. HAYMORE, J. S. BRADSHAW, and J. J. CHRISTENSEN. Inorg. Chem. **14**, 3132 (1975).
17. S. FORTIER, M. E. FRASER, A. RODRIGUE, and J. W. BOVENKAMP. Manuscript in preparation.
18. E. SCHMIDT, J.-M. TREMILLON, J.-P. KINTZINGER, and A. I. POPOV. J. Am. Chem. Soc. **105**, 7563 (1983).

Structure–activity studies of β-carbolines. 3. Crystal and molecular structures of methyl β-carboline-3-carboxylate[1]

ALASTAIR K. S. MUIR AND PENELOPE W. CODDING[2]

Departments of Chemistry and Pharmacology and Therapeutics, University of Calgary, Calgary, Alta., Canada T2N 1N4

Received November 7, 1984

ALASTAIR K. S. MUIR and PENELOPE W. CODDING. Can. J. Chem. **63**, 2752 (1985).

The crystal and molecular structures of methyl β-carboline-3-carboxylate, $C_{13}H_{10}N_2O$, a high-affinity ligand for the benzodiazepine receptor, are reported. This candidate for the endogenous ligand for the receptor produces a biological response that is opposite to the anxiety-reducing effect of the usual agonists of the receptor and is, therefore, classified as an inverse-agonist. The space group is $P2_1/c$ with a = 11.4866(9), b = 5.8091(3), c = 32.417(3) Å, β = 97.111(3)°, Z = 8. In both of the unique molecules, the ester side chain has an extended conformation and is coplanar with the β-carboline moiety. The carbonyl oxygen atom and the aromatic nitrogen atom are *cis* and form a three-centre hydrogen bond to the amine nitrogen atom of the other molecule in the asymmetric unit.

ALASTAIR K. S. MUIR et PENELOPE W. CODDING. Can. J. Chem. **63**, 2752 (1985).

On rapporte les structures cristalline et moléculaire du β-carbolinecarboxylate-3 de méthyle, un ligand de grande affinité pour le récepteur benzodiazépine. Ce candidat pour le ligand endogène pour le récepteur produit une réponse biologique qui est opposée à l'effet de réduction d'anxiété des agonistes usuels du récepteur; on peut donc le classifier comme agoniste inverse. Le composé cristallise dans le groupe d'espace $P2_1/c$ avec a = 11,4866(9), b = 5,8091(3), c = 32,417(3)Å, β = 97,111(3)° et Z = 8. Dans chacune des deux molécules distinctes, la chaîne latérale de l'ester existe dans une conformation allongée et elle est coplanaire avec la β-carboline. L'atome d'oxygène du groupement carbonyle et l'atome d'azote aromatique sont *cis* et ils forment une liaison hydrogène à trois centres avec l'atome d'azote de l'amine de l'autre molécule de l'unité asymétrique.

[Traduit par le journal]

Methyl β-carboline-3-carboxylate (hereinafter CCM) is one of several β-carboline derivatives that have been studied as possible endogenous ligands for the benzodiazepine receptor (1). The identity of the natural ligand for the benzodiazepine receptor is not certain, as the isolation procedures from rat brain and from urine have been shown to chemically modify the naturally occurring β-carboline isolate to the ethyl ester. CCM binds with high affinity (2–4) to the receptor and displaces diazepam, an agonist. The β-carbolines produce three different responses when bound to the benzodiazepine receptor; the methyl ester is a convulsant (opposite to the agonists and hence labeled an inverse-agonist), the ethyl ester is a proconvulsant (potentiates the onset of convulsions), and the propyl ester acts as a weak agonist (anticonvulsant). Braestrup *et al.* (5) report that the binding of the β-carbolines and, hence, their effects are mediated by the inhibitory neurotransmitter, γ-aminobutyric acid (GABA). The sensitivity of the binding of benzodiazepine receptor ligands to the presence of GABA has suggested an allosteric regulation of the GABA receptor by benzodiazepines (6). Recent models for this mechanism propose a multiconformation receptor; the different conformations are induced by the binding of ligands of different biological effect (6, 7).

These observations indicate the importance of the β-carbolines in the development of an understanding of the benzodiazepine receptor. The shapes and receptor binding characteristics of these molecules play an integral role in the biological response that they produce. The methyl ester has the highest affinity for the receptor of any of the β-carbolines that have been structurally characterized. The X-ray structure determination of CCM is part of an ongoing study of the ligands for this receptor (8).[3]

[1]This paper has been presented in part: see Abstracts of the 13th International Congress of Crystallography, Acta Crystallogr. Sect A, **40**(S), C62 (1984).

[2]Author to whom correspondence should be addressed.

[3]As this paper was being reviewed, a communication of this structure appeared; see ref. 29.

Experimental

A sample of CCM was provided by Drs. R. Coutts and R. Micetish of the Faculty of Pharmacy, University of Alberta. CCM was recrystallized from a 3:1 ethanol–water mixture. A colourless, rectangular crystal (0.20 × 0.20 × 0.25 mm) was cut from the end of a long needle and mounted along its axis for data collection on an Enraf–Nonius CAD4F automated diffractometer.

Crystal data

Monoclinic, systematic absences ($h0l$); $l = 2n + 1$ and ($0k0$); $k = 2n + 1$, space group $P2_1/c$, a = 11.4866(9), b = 5.8091(3), c = 32.417(3) Å, β = 97.111(3)°, V = 2146.4(3)Å^3, Z = 8, D_C = 1.400 g cm^{-3}, T = 20°C, CuK_α, Ni filter, λ = 1.5418 Å, ω/2θ scan, $D_w = 1.5(0.53 + 0.14 \tan\theta)$, θ_{max} = 70°, 4043 unique reflections collected, 3290 observed ($I \geq 2.5\sigma(I)$), μ = 4.07 cm^{-1}. Three intensity standards were measured every 1800 s and showed no deterioration. Lorentz and polarization corrections were applied. E values were calculated by applying K curve.

The structure was solved using MULTAN 78 (9); all non-hydrogen atoms in the two molecules in the asymmetric unit were identified in the first E synthesis. All calculations (other than MULTAN) were done using the XRAY 76 system of programs (10) implemented on a Honeywell computer. X-ray scattering factors were those of Cromer and Mann (11) except that the scattering factor of Stewart *et al.* (12) was used for the hydrogen atom. Hydrogen atom positions were located in difference Fourier syntheses. The least-squares refinement was blocked with the anisotropic thermal parameters for the nonhydrogen atoms, the isotropic thermal parameters of the hydrogen atoms, and the positional parameters of all atoms of one unique molecule in each block. The final R value is 0.049, $R_w = ((\Sigma w|F_o| - |F_C|)^2/\Sigma w(F_o)^2)^{1/2} = 0.069$, standard deviation of an observation of unit weight is 1.36, the average shift/error = 0.10, and the maximum shift/error = 0.82. The function minimized was $w(|F_o| - |F_C|)^2$ where the weight, w, is defined as $((\sigma(F_o))^2 + 0.0015F_o^2)^{-1}$. The 3700 reflections used in the refinement were the 3290 observed reflections and only those unobserved reflections (410 data) that had $F_C^2 > 2.5\sigma(I_o)$. An isotropic extinction correction was applied (13) and refined to a value of $g = 21.9(6) \times 10^{-3}$. The peaks in the final difference Fourier synthesis had maximum/minimum values of +/− 0.33 e Å^{-3} and were associated with the C(10)—C(11) bond.

TABLE 1. Atomic coordinates ($\times 10^5$ for the non-hydrogen atoms and $\times 10^4$ for the hydrogen atoms) and equivalent isotropic thermal parameters ($\times 10$) for the two unique molecules. B_{iso} is given for the hydrogen atoms. B_{eq} = 1/3 (trace of the B_{ij} matrix)

Atom	x/a	y/b	z/c	B_{eq}
C(1)	70675(15)	71831(32)	13905(6)	46
N(2)	61866(13)	58157(27)	14558(5)	46
C(3)	64331(14)	39030(29)	16946(5)	40
C(4)	75428(14)	32983(28)	18725(5)	38
C(5)	104635(15)	32347(31)	21742(5)	41
C(6)	116379(16)	37739(35)	22453(6)	46
C(7)	120640(17)	57819(35)	20799(6)	49
C(8)	113434(16)	72933(33)	18393(6)	46
N(9)	92430(13)	79224(26)	15429(5)	42
C(10)	82188(14)	67357(28)	15626(5)	39
C(11)	84656(14)	47334(27)	18066(5)	37
C(12)	97104(14)	47274(27)	19348(5)	37
C(13)	101534(14)	67529(28)	17674(5)	39
C(31)	53952(15)	24789(32)	17542(5)	43
O(32)	56559(11)	7371(23)	20127(4)	51
C(33)	47100(19)	−8146(40)	20709(9)	60
O(34)	44093(12)	28332(33)	15988(6)	74
C(1)′	84048(16)	−22128(33)	38560(5)	47
N(2)′	95185(13)	−28011(26)	39267(4)	45
C(3)′	102505(14)	−14834(29)	41917(5)	41
C(4)′	98921(13)	4160(29)	44015(5)	40
C(5)′	82374(14)	46428(33)	47548(6)	47
C(6)′	73396(16)	61233(37)	48175(7)	56
C(7)′	62192(16)	58104(38)	46044(7)	58
C(8)′	59604(15)	40408(38)	43281(7)	54
N(9)′	68654(12)	6432(28)	40094(5)	47
C(10)′	79695(14)	−2797(32)	40472(5)	42
C(11)′	87171(14)	10255(29)	43305(5)	39
C(12)′	80102(13)	28283(30)	44752(5)	41
C(13)′	68704(14)	25248(32)	42638(5)	43
C(31)′	114957(16)	−22215(31)	42405(5)	45
O(32)′	121938(10)	−7393(23)	44708(4)	52
C(33)′	134226(18)	−13163(52)	45409(8)	60
O(34)′	118572(13)	−39148(26)	40906(5)	63
Atom	**x/a**	**y/b**	**z/c**	**B_{iso}**
H(1)	6854(17)	8597(34)	1187(6)	51(4)
H(4)	7667(15)	1912(33)	2056(6)	42(4)
H(5)	10206(17)	1850(36)	2298(6)	50(4)
H(6)	12217(18)	2803(39)	2412(7)	63(5)
H(7)	12877(19)	6185(37)	2146(6)	59(5)
H(8)	11649(15)	8647(32)	1702(5)	42(4)
H(9)	9315(16)	9168(35)	1409(6)	47(4)
H(331)	4453(25)	−1828(51)	1821(10)	91(7)
H(332)	5063(27)	−1847(59)	2304(10)	105(9)
H(333)	4054(22)	160(49)	2150(8)	91(7)
H(1)′	7859(16)	−3109(36)	3678(6)	57(5)
H(4)′	10476(15)	1261(31)	4608(6)	48(4)
H(5)′	9039(15)	4871(34)	4910(5)	50(4)
H(6)′	7473(17)	7517(41)	5012(7)	68(5)
H(7)′	5573(17)	6857(40)	4651(7)	69(5)
H(8)′	5176(18)	3920(36)	4168(6)	61(5)
H(9)′	6285(16)	155(38)	3838(6)	58(5)
H(331)′	13772(24)	−1561(54)	4300(10)	89(7)
H(332)′	13573(32)	−2936(80)	4673(12)	128(11)
H(333)′	13788(33)	−103(77)	4748(13)	138(12)

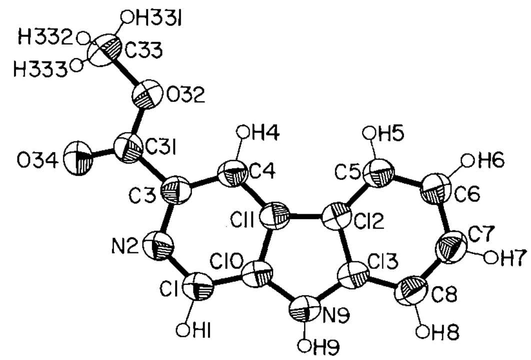

FIG. 1. The molecular conformation and the atomic labeling scheme for one of the two unique molecules of CCM. The conformation of the other unique molecule is nearly identical and the atom labels are distinguished by primes (′). The drawing was made with the program ORTEP (27).

The atomic coordinates are given in Table 1 with the atoms labeled as in Fig. 1.[4] The second molecule of the asymmetric unit is distinguished by a prime (′). The bond lengths and angles are shown in Table 2.

Discussion

The important features of this structure are the conformation of the ester side chain and the intermolecular interactions in the crystal environment. The side chain in each of the unique molecules has approximately the same orientation; the torsion angle, N(2)—C(3)—C(31)═O(34), is 3.2(1)° in one molecule and −5.3(2)° in the other. This orientation places the nitrogen atom of the pyridine fragment of the β-carboline and the carbonyl oxygen atom of the ester side chain in a *cis* configuration and is opposite to the side chain conformation observed in the carboxyamide derivative of β-carboline (8). In the carboxyamide case, all published examples of that side chain and a similar aromatic N atom were found in the *trans* configuration. Lawson *et al.* (14) have determined through structure−activity studies of β-carbolines that, for high affinity, the C(3) substituent interacts with specific sites rather than through a general electrostatic interaction. Since the methyl ester derivative has a higher affinity for the benzodiazepine receptor (1.5−19 n*M* (15, 16)) than the carboxyamide derivative (250 n*M* (17)) and has a different configuration of the side chain, the relative populations of the possible orientations of the ester group are important to the determination of the position and number of specific sites.

The Cambridge Structural Database[5] was searched for examples of the ester side chain attached to a fragment similar to the β-carboline pyridine ring; three populations of side chain orientation were found. In the cases that had a bulky substituent on the carbon atom (C(4) in this numbering scheme) that is on the opposite side of the ester bearing atom (C(3)) from the nitrogen atom (N(2)), the torsion angles (N—C—C═O) were in the range 55−127°. There were 7 examples of this steric crowding. The *trans* configuration (torsion angles from 140−180°) was observed in 8 cases. Four of these cases came from two crystal

[4]The anisotropic thermal parameters, the observed and calculated structure factors, and the REFCODES for the Database search may be purchased from the Depository of Unpublished Data, CISTI, National Research Council of Canada, Ottawa, Ont., Canada, K1A 0S2.

[5]Tables of torsion angles, ref. codes, and references are available from the authors.

TABLE 2. Bond distances (Å) and bond angles (°) for the non-hydrogen atoms of the two unique molecules. Estimated standard deviations are in parentheses

Distances (Å)	Molecule A	Molecule B*
C(01)—N(02)	1.322(3)	1.327(3)
C(01)—C(10)	1.393(4)	1.399(4)
N(02)—C(03)	1.367(3)	1.360(3)
C(03)—C(04)	1.376(3)	1.386(3)
C(03)—C(31)	1.479(3)	1.482(3)
C(04)—C(11)	1.392(3)	1.388(3)
C(05)—C(06)	1.375(3)	1.376(4)
C(05)—C(12)	1.391(3)	1.393(3)
C(06)—C(07)	1.401(4)	1.398(4)
C(06)—C(05)	1.376(4)	1.376(4)
C(07)—C(08)	1.379(4)	1.368(4)
C(08)—C(13)	1.391(3)	1.402(4)
N(09)—C(10)	1.377(3)	1.371(3)
N(09)—C(13)	1.382(3)	1.371(3)
C(10)—C(11)	1.414(3)	1.404(3)
C(11)—C(12)	1.436(3)	1.440(3)
C(12)—C(13)	1.413(3)	1.415(3)
C(31)—O(32)	1.328(3)	1.339(3)
C(31)—O(34)	1.199(3)	1.198(3)
O(32)—C(33)	1.442(4)	1.443(3)
Angles (°)	**Molecule A**	**Molecule B***
N(02)—C(01)—C(10)	122.2(2)	121.2(2)
C(01)—N(02)—C(03)	117.9(2)	118.2(2)
N(02)—C(03)—C(04)	124.1(2)	124.5(2)
N(02)—C(03)—C(31)	114.4(2)	114.4(2)
C(04)—C(03)—C(31)	121.5(2)	121.1(2)
C(03)—C(04)—C(11)	118.1(2)	117.3(2)
C(06)—C(05)—C(12)	118.8(2)	119.2(2)
C(05)—C(06)—C(07)	120.4(2)	120.2(3)
C(06)—C(07)—C(08)	122.2(2)	122.5(3)
C(07)—C(08)—C(13)	117.3(2)	117.6(2)
C(10)—N(09)—C(13)	108.7(2)	108.8(2)
C(01)—C(10)—N(09)	131.5(2)	130.3(2)
C(01)—C(10)—C(11)	119.6(2)	120.2(2)
N(09)—C(10)—C(11)	108.9(2)	109.5(2)
C(04)—C(11)—C(10)	118.0(2)	118.5(2)
C(04)—C(11)—C(12)	135.0(2)	135.0(2)
C(10)—C(11)—C(12)	106.9(2)	106.5(2)
C(05)—C(12)—C(11)	133.6(2)	134.1(2)
C(05)—C(12)—C(13)	120.2(2)	119.8(2)
C(11)—C(12)—C(13)	106.1(2)	106.1(2)
C(08)—C(12)—N(09)	129.6(2)	130.1(2)
C(08)—C(13)—C(12)	121.1(2)	120.7(2)
N(09)—C(13)—C(12)	109.3(2)	109.2(2)
C(03)—C(31)—O(32)	112.6(2)	112.2(2)
C(03)—C(31)—O(34)	125.8(2)	125.1(2)
O(32)—C(31)—O(34)	121.6(2)	122.7(2)
C(31)—O(32)—C(33)	116.2(2)	116.5(2)

*The atoms of molecules A and B have the same number except that those of molecule B are primed (see Table 1).

structures of the pyrromethane moiety; in one case the *trans* form is stabilized by an intramolecular N—H···N hydrogen bond and in the other by ion pairing with a Br^- ion. Thus these four observations are not directly comparable to the fragment contained in CCM. The *cis* configuration (torsion angles from 1–43°) was observed 10 times; in only three cases were H bonds reported. In two of these cases a three-centre H-bond involving the two *cis* electronegative atoms could be observed; in the other case the N atom is protonated and forms a hydrogen bond with a Cl^- ion. In general, these structures had few H atom donors so that the effect of stable H-bond formation on the relative populations of the configurations could not be fully assessed.

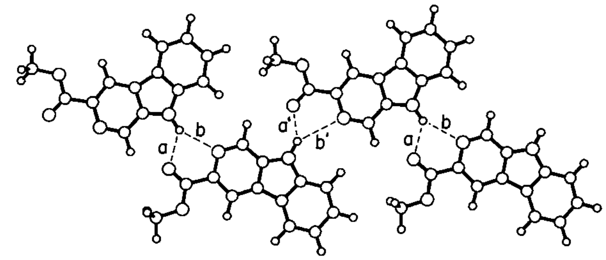

FIG. 2. A detail of the crystal packing of CCM showing the three-centre intermolecular hydrogen bonds. The labeled distances are a = 2.27(2), b = 2.54(2), a' = 2.04(2), and b' = 2.91(2) Å. The drawing was made with the computer program PLUTO (28).

The data base searches on the carboxyamide (8) and ester side chains of fragments similar to the β-carboline moiety indicate that the conformation of the side chain is dictated by π interactions that keep the side chain coplanar with the ring and by interactions with the aromatic nitrogen atom. These forces can be overcome by steric effects if there are substituents vicinal to the side chain and opposite the nitrogen atom. Bulky side chains in this position cause the rotation of the ester fragment to a position ca. 55° out of the plane.

Intermolecular contacts observed in crystals have been used as models for the types of interactions in receptor–ligand interactions (18, 19). The crystalline environment in this structure has a three-centre intermolecular hydrogen bond (see Fig. 2) formed by the interaction between the *cis* configuration of the aromatic nitrogen atom and carbonyl oxygen atom as the acceptors and the amine nitrogen atom, N(9), as the donor. The parameters describing these bonds are given in Table 3. The hydrogen-bonding distances are slightly different in the two unique interactions; the differences arise from a slip of one molecule past the other in the hydrogen-bonding plane. The distance between the two N atoms involved in the three-centre bonds is greater than the sum of the van der Waals radii for these atoms. Hamilton and Ibers (20) have noted that such a discrepancy occurs in weak hydrogen bonds and have stated that a more restrictive criterion is the separation between the H atom and the acceptor atom. To apply this criterion involving the position of the H atom, the systematic errors in X-ray determinations of bond distances involving hydrogen have to be overcome. The simplest method (21) for correcting for this error is to "normalize" the hydrogen atom position by moving the H atom along the N—H line to the average neutron-determined distance, which for N—H is 1.03 Å (22). This correction was applied; the "normalized" parameters for the hydrogen bonds are given in Table 3. All but one of the "normalized" H atom to acceptor atom distances meet the restrictive criterion of Hamilton and Ibers. The H(9)···N(2) separation is 0.2 Å longer than the sum of the van der Waals radii for the atoms; even so, this contact is still a close one and can be considered to be weakly attractive. Thus, each of the unique molecules acts as both a donor and an acceptor for these three-centre bonds.

Three-centre hydrogen bonds including the N—H···O=C functionality have been the subject of a recent analysis (22). Of 1509 hydrogen bonds with this functionality, 304 were defined as three-centre bonds. It was found that the nonbonded re-

TABLE 3. Intramolecular hydrogen bond distances and angles. The values in square brackets were obtained after the N—H distances were normalized following ref. 22

Atoms	D···A in Å	D—H in Å	H···A in Å	∠D—H···A in °
N(9)′—H(9)′···O(34)	2.819(4)	0.86(2) [1.03]	2.04(2) [1.91]	150(2) [146]
N(9)′—H(9)′···N(2)	3.637(5)	0.86(2) [1.03]	2.91(2) [2.75]	144(2) [144]
N(9)—H(9)···O(34)′	2.919(4)	0.85(2) [1.03]	2.27(2) [2.14]	134(2) [131]
N(9)—H(9)···N(2)′	3.317(3)	0.85(2) [1.03]	2.54(2) [2.38]	154(2) [151]

pulsion between the two acceptor atoms caused the hydrogen bonds to deviate considerably from linearity and made short H···O distances unfavorable. The parameters for the hydrogen bonds found in the crystal lattice of CCM are in agreement with these conclusions. In addition to the hydrogen bonds found in CCM, two examples of three-centre bonding were found in the specific Database search mentioned above. The first example has a water molecule as the donor of the shared hydrogen atom; this hydrogen bond determines the conformation of the ethyl side chain in the thiazole (23). The second example has an intramolecular three-centre bond wherein the nitrogen atom nearest the ester linkage is protonated and donates to both the carbonyl oxygen atom and a morpholino nitrogen atom (24). Together, these findings suggest that the three-centre bond is stable and can be a part of the chemistry of this molecular fragment.

Theoretical calculations (25) of the low energy conformations of the side chains in β-carbolines confirm the crystallographic observation of two equivalent conformations for the ester side chain (*cis* and *trans*) and one low energy conformation for the carboxyamide side chain (*trans*). In these calculations, the binding sites for the side chains were modeled with cationic sites on the receptor. A single cationic site would bind to the *cis* conformer of the ester side chain and another active derivative with a cyano side chain, but would not bind to the *trans* conformer of the ester or to the carboxyamide, which only exists in the *trans* conformation. Thus a single site is consistent with the high affinity of the ester and the cyano derivatives and the low affinity of the carboxyamide compound. The three-centre hydrogen bond observed in this crystal structure exemplifies the type of interaction possible with such a cationic site.

In addition, the consistent participation of the amine nitrogen atom, N(9), in hydrogen bonds in the crystal structures of β-carbolines (ref. 8 and this work) and in the naturally occurring harmaline (26) is indicative of the acidity of this atom and suggests that this interaction is also part of the receptor binding features of β-carbolines.

In summary, the crystal structures of β-carboline ligands of the benzodiazepine receptor (refs. 8, 26, and this work) have identified some possible features of their receptor site interactions. These include the formation of a three-centre hydrogen bond involving a *cis* conformation of the side chain and the participation of the acidic nitrogen atom, N(9), in a separate hydrogen bond.

Acknowledgements

This research was supported by the Alberta Heritage Foundation for Medical Research (Studentship to A.K.S.M. and Scholarship to P.W.C.) and the Medical Research Council of Canada (grant no. MA-8087 to P.W.C.). The authors wish to thank Drs. R. T. Coutts and R. Micetish for kindly supplying methyl β-carboline-3-carboxylate.

1. C. BRAESTRUP, M. NIELSON, and C. E. OLSEN. Proc. Natl. Acad. Sci. U.S.A. **77**, 2288 (1980).
2. M. SCHWERI, M. CAIN, J. COOK, S. PAUL, and P. SKOLNICK. Pharmacol. Biochem. Behav. **17**, 457 (1982).
3. L. P. DE CARVALHO, G. GRECKSCH, G. CHAPOUTHIER, and J. ROSSIER. Nature (London), **301**, 64 (1983).
4. J. H. SKERRITT and R. L. MACDONALD. Eur. J. Pharm. **101**, 135 (1984).
5. C. BRAESTRUP, R. SCHMIECHEN, G. NEFF, M. NIELSEN, and E. N. PETERSEN. Science, **216**, 1241 (1982).
6. J. F. TALLMAN. *In* Benzodiazepine recognition site ligands: biochemistry and pharmacology. *Edited by* G. Biggio and E. Costa. Raven Press, New York, 1983. p. 21.
7. P. POLC, E. P. BONETTI, R. SCHAFFNER, and W. HAEFELY. Naunyn-Schmiedeberg's Arch. Pharmacol. **321**, 260 (1982).
8. A. K. S. MUIR and P. W. CODDING. Can. J. Chem. **62**, 1803 (1984).
9. G. GERMAIN, P. MAIN, and M. M. WOOLFSON. Acta Crystallogr. Sect. A, **27**, 368 (1971).
10. J. M. STEWART. The X-ray system of crystallographic programs. Computer Science Center, University of Maryland, College Park, MD. 1976.
11. D. T. CROMER and J. B. MANN. Acta Crystallogr. Sect. A, **24**, 321 (1968).
12. R. F. STEWART, E. R. DAVIDSON, and W. T. SIMPSON. J. Chem. Phys. **42**, 3175 (1965).
13. A. C. LARSON. Acta Crystallogr. **23**, 664 (1967).
14. J. A. LAWSON, E. T. UYENO, J. R. NIENOW, G. H. LOEW, and L. TOLL. Life Sciences, **34**, 2007 (1984).
15. M. CAIN, R. W. WEBER, F. GUZMAN, J. M. COOK, S. A. BARKER, K. C. RICE, J. N. CRAWLEY, S. M. PAUL, and P. SKOLNICK. J. Med. Chem. **25**, 1081 (1982).
16. C. BRAESTRUP and M. NIELSEN. J. Neurochem. **37**, 333 (1981).
17. R. A. LOCOCK, G. B. BARKER, R. G. MICETISH, R. T. COUTTS, and A. BENDERLY. Prog. Neuro-Psychopharmacol. Biol. Psychiatry, **6**, 407 (1982).
18. G. GILLI, P. A. BOREA, V. BERTOLASI, and M. SACERDOTI. *In* Molecular structure and biological activity. *Edited by* J. F. Griffin and W. L. Duax. Elsevier Biomedical, New York. 1982. p. 259.
19. P. MURRAY-RUST and J. P. GLUSKER. J. Am. Chem. Soc. **106**, 1018 (1984).
20. W. C. HAMILTON and J. A. IBERS. *In* Hydrogen bonding in solids. W. A. Benjamin, New York. 1968. p. 15.
21. G. A. JEFFREY and L. LEWIS. Carbohydr. Res. **60**, 179 (1978).
22. R. TAYLOR, O. KENNARD, and W. VERSICHEL. J. Am. Chem. Soc. **106**, 244 (1984).
23. R. A. FLETTON, D. C. HUMBER, S. M. ROBERTS, P. G. OWSTON, and K. HENDRICK. J. Chem. Soc. Chem. Commun. 968 (1983).

24. L. Toupet and Y. Delugeard. Acta Crystallogr. Sect. B, **35**, 1935 (1979).
25. G. Loew, J. Lawson, L. Toll, E. Uyeno, C. Keys, and D. Spangler. 25th Medicinal Chemistry Symposium, SUNY Buffalo, June, 1984.
26. W. Reimers, H. Guth, and W. Zu-Tao. Acta Crystallogr. Sect. C, **40**, 977 (1984).
27. C. K. Johnson. ORTEP Report ORNL-3794. Oak Ridge National Laboratory, Oak Ridge, TN. 1965.
28. S. Motherwell. PLUTO, University Chemical Laboratory, Cambridge, England. 1979.
29. V. Bertolasi, V. Ferretti, G. Gilli, and P. A. Borea. Acta Crystallogr. Sect. C, **40**, 1981 (1984).

Synthesis and equilibration of conformationally rigid *cis* and *trans* tricyclic mono and dithioacetals. An evaluation of stereoelectronic (anomeric) effects in thioacetals[1]

PIERRE DESLONGCHAMPS AND DANIEL GUAY[2]

Laboratoire de synthèse organique, Département de Chimie, Faculté des Sciences, Université de Sherbrooke, Sherbrooke (Qué.), Canada J1K 2R1

Received December 10, 1984

PIERRE DESLONGCHAMPS and DANIEL GUAY. Can. J. Chem. **63**, 2757 (1985).

The synthesis of *cis* and *trans* tricyclic monothioacetals **5–8** and dithioacetals **9** and **10** is reported (Schemes 1 and 2). The *cis* isomers **5**, **7**, and **9** are the kinetic products of cyclization, a result which is explained on the basis of stereoelectronic principles. Equilibration studies (Table 1) led to an evaluation of the anomeric effect for sulfur; it was found to be of the same order as that for oxygen.

PIERRE DESLONGCHAMPS et DANIEL GUAY. Can. J. Chem. **63**, 2757 (1985).

La synthèse des monothioacétals **5–8** et dithioacétals tricycliques **9** et **10** est décrite (Schémas 1 et 2). Les produits cinétiques de cyclisation sont les isomères *cis* **5**, **7** et **9** tel que prédit par les principes du contrôle stéréoélectronique. Des études d'équilibration ont permis d'évaluer que l'effet anomère du soufre est du même ordre de grandeur que celui de l'oxygène.

The acetal function can take six different *gauche* conformations (3) and the relative stability of these conformers depends on stereoelectronic (anomeric (4) and *exo*-anomeric (5)) effects and standard steric interactions (1). A valuable experimental method for the determination of the relative stability of these conformers and for the evaluation of stereoelectronic effects is to construct and equilibrate stereochemical isomers which exist in different but rigid conformations.

Using this approach, Descotes *et al.* (6) carried out the acid equilibration of *cis* and *trans* bicyclic acetals **1** and **2** (Scheme 1) at 80°C and found, at equilibrium, a mixture of 57% *cis* and 43% *trans*. Since the *cis* isomer **1** has one anomeric effect (i.e., one oxygen electron pair antiperiplanar to a C—O bond) and the *trans* isomer has none, and taking into consideration steric[3] and entropic[4] factors, these authors arrived at a value of 1.4 kcal/mol for the anomeric effect in structure

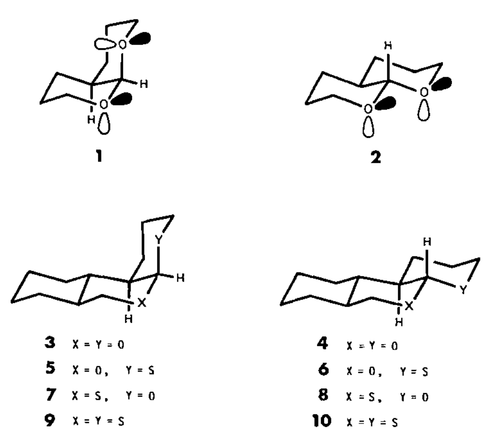

1 **2**

3 X = Y = O
5 X = O, Y = S
7 X = S, Y = O
9 X = Y = S

4 X = Y = O
6 X = O, Y = S
8 X = S, Y = O
10 X = Y = S

SCHEME 1

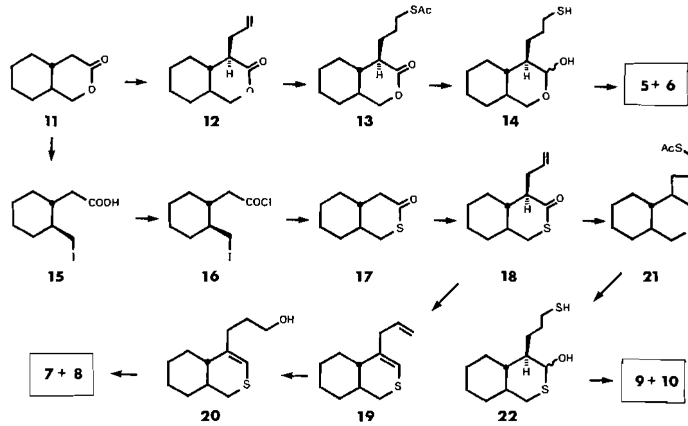

SCHEME 2

1. More recently, the equilibration of conformationally rigid *cis* and *trans* tricyclic acetals **3** and **4** was reported by our laboratory (7). The *cis* isomer **3** was found less stable (45% at equilibrium) than the *trans* isomer **4** by 0.14 kcal/mol. As a result, after taking into consideration the steric interaction of the *cis* isomer **3** (the same as in **1**, 1.65 kcal/mol),[3] the anomeric effect in structure **3** was estimated to be 1.5 kcal/mol, confirming the value of Descotes.

We wish now to report the synthesis and the acid equilibration of three pairs of *cis* and *trans* tricyclic thioacetals, namely, monothioacetals **5** and **6**, monothioacetals **7** and **8**, and dithioacetals **9** and **10**. Analysis of these results allows an evaluation of the anomeric effects of the sulfur and the oxygen atoms in the mono and the dithioacetal functions.[5]

Synthesis and equilibration studies

The syntheses of *cis* and *trans* tricyclic monothioacetals **5**, **6**, **7**, **8** and dithioacetals **9** and **10** are summarized in Scheme 2. The known bicyclic allyl lactone **12** was prepared from

[1]For general leading references on this subject, see pp. 21–26 in ref. 1 and pp. 23–26 in ref. 2.

[2]N.S.E.R.C.C. (Ottawa) and F.C.A.C. (Quebec) predoctoral fellowships 1982–1985.

[3]*Cis* isomer **1** is sterically less stable than *trans* isomer **2** by ~1.65 kcal/mol: one *gauche* form of *n*-butane, 0.85 kcal/mol and an oxygen axial to cyclohexane, 0.8 kcal/mol.

[4]Isomer **1** is a *cis* decalin which is conformationally mobile; on that basis, isomer **1** is more stable than the conformationally rigid *trans* isomer **2** by 0.42 kcal/mol at 80°C.

[5]The 1,7-dioxaspiro[5.5]undecane system and the corresponding sulfur analogs have also been extensively studied. This spiro system can theoretically take three different conformations having respectively two, one, and zero anomeric effects. This work has led to an evaluation of the anomeric and *exo*-anomeric effects in ketals, and in mono and dithioketals (8). For previous studies on 2-substituted thianes, see refs. 9 and 10.

bicyclic lactone **11** following a published procedure (7), and converted into thioacetate bicyclic lactone **13** in 91% yield via the addition of thioacetic acid (11). Reduction of **13** with diisobutylaluminium hydride (DIBAH) gave the intermediate thiol hemiacetal **14**, which on treatment with benzene containing a catalytic amount of *p*-toluenesulfonic acid (PTSA) gave a 9:1 crystalline mixture of *cis* and *trans* tricyclic monothioacetals **5** and **6** in 80% yield. A *trans* enriched mixture (ratio 85:15) was obtained after equilibration and chromatography. The complete separation of the *cis* and the *trans* isomers was not successful.

Reaction of bicyclic lactone **11** with trimethylsilyl iodide (12) gave iodo carboxylic acid **15** (97% yield), which was then converted into iodo acid chloride **16** by reaction with oxalyl chloride. The iodo acid chloride **16** was then transformed into bicyclic thiolactone **17** (87% yield) by reaction with hydrogen sulfide in dichloromethane in the presence of triethylamine. Alkylation (13) of bicyclic thiolactone **17** (LDA, THF–HMPA, −78°C) with allyl bromide gave pure allyl bicyclic thiolactone **18** in 85% yield after chromatography. Reduction of allyl bicyclic thiolactone **18** with DIBAH followed by a reflux in benzene containing PTSA gave pure allyl bicyclic thioenolether **19** in 87% yield after chromatography. Selective hydroboration–oxidation (14) (Me_2S/BH_3, cyclohexene, THF; H_2O_2, NaOH) of the terminal olefin of **19** yielded hydroxy bicyclic thioenolether **20** (82% yield), which on treatment with a mixture of benzene, methanol, trimethyl orthoformate, and PTSA at room temperature gave a 85:15 mixture of *cis* and *trans* tricyclic thioacetals **7** and **8** (88% yield). Both isomers could be obtained pure by chromatography.

Addition of thioacetic acid (11) on allyl bicyclic thiolactone **18** gave thioacetate bicyclic thiolactone **21** in 95% yield. Reduction of **21** with DIBAH followed by a reflux with PTSA in benzene gave a 95:5 mixture of *cis* and *trans* tricyclic thioacetals **9** and **10** in 93% yield. Both isomers could be separated by chromatography.

Equilibration of an 85:15 mixture of *cis* and *trans* tricyclic monothioacetals **5** and **6** (benzene, PTSA catalytic, reflux, 6 h) gave a *cis*/*trans* ratio of 47:53. Equilibration of an 88:12 mixture of *cis* and *trans* tricyclic monothioacetals **7** and **8** (methanol, benzene, trimethylorthoformate, PTSA (1 mol-equiv.), reflux, >2.5 h) gave a *cis*/*trans* ratio of 57:43. Finally, equilibration of a 95:5 mixture of *cis* and *trans* tricyclic dithioacetals **9** and **10** (PTSA (1 mol-equiv.), benzene, ≥3 days) produced a *cis*/*trans* ratio of 62:38.[6]

The following observations were also made. When the cyclization of thiol hemiacetal **14** was carried out under milder acid conditions and for a shorter time, the reaction was not completed (30–50%) but a 97:3 mixture of *cis* and *trans* tricyclic monothioacetals **5** and **6** was produced. When the cyclization reaction of **20** was quenched prior to completion, a 98:2 mixture of *cis* and *trans* tricyclic monothio acetals **7** and **8** was formed. Taking these results along with the equilibration studies just described, it appears clear that the kinetic products of the cyclization of **14**, **20**, and **22** are the *cis* isomers **5**, **7**, and **9**, respectively.

The stereochemical assignment of *cis* and *trans* tricyclic compounds **5**–**10** was made by 250-MHz nmr spectroscopy and by comparison with spectral data obtained from the *cis* and

[6]Formation of secondary products (≤20% by weight) was observed in the course of these equilibration experiments, especially under the vigorous acidic conditions.

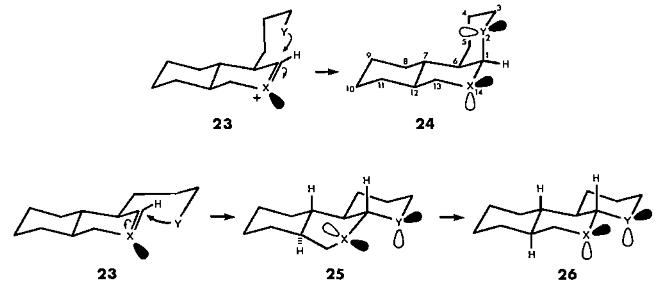

SCHEME 3

TABLE 1. Equilibration of *cis* and *trans* tricyclic mono and dithioacetals **3**–**10**

Compounds	% at equilibrium*	ΔG (kcal/mol, 80°C)	A.E.	Reference
3/4	45:55	−0.14	1.5	8
5/6	47:53	−0.08	1.6	This work
7/8	57:43	0.20	1.8	This work
9/10	62:38	0.34	2.0	This work

*Evaluated by nmr and vpc analysis (±2%).

trans bicyclic and tricyclic acetals **1**–**4**. In the *cis* series, the anomeric hydrogen appears either as a broad singlet or as a doublet ($J \cong 3$ Hz) whereas in the *trans* series, the same hydrogen shows a doublet ($J \cong 9.5$ Hz).

Discussion

The preferential formation of the *cis* tricyclic acetal **3** over the *trans* isomer **4** under kinetically controlled conditions was previously reported (7) and this selectivity was explained by a combination of steric and stereoelectronic effects which control the formation of a cyclic acetal. The preferential formation of the *cis* isomers **5**, **7**, and **9** that is similarly observed can be explained on the same basis. Indeed, between the two processes **23** → **24** and **23** → **25** → **26** (X = O or S, Y = OH or SH), which lead respectively to the *cis* and the *trans* isomer (Scheme 3), the former process, which takes place via a chair intermediate (**24**), is favored energetically over the latter, which can only occur via an intermediate having a boat conformation (**25**) because of stereoelectronic reasons. Consequently, these results demonstrate that in the cyclization of **23**, stereoelectronic effects are operative when the incoming nucleophile is either an OH or an SH group, and more interestingly, even when the heteroatom of ring B is a sulfur atom.

The equilibration study of *cis* and *trans* isomeric compounds **3**–**10** is summarized in Table 1. It can be seen that there is a small increase of the *cis* isomer when ring C contains a sulfur atom. This study also shows that the proportion of the *cis* isomer is higher when the ring B heteroatom is sulfur rather than oxygen.

The *cis* isomeric series (cf. **24**) possesses one electron pair on atom X, which is antiperiplanar to the polar C—Y bond. Such a situation is not found in the *trans* series (cf. **26**); as a result, the *cis* series should be stabilized by one anomeric effect, in contrast to the *trans* series. On the other hand, the *trans* series, by comparison with the *cis* series, is free from steric interactions. Since the difference in energy between the *cis* and the *trans* series can be established experimentally by equilibration, the stereoelectronic effects found in the *cis* series can be estimated correctly provided that the steric effects of the *cis* isomers are properly evaluated.

The *cis* isomeric series (cf. **24**) contains one *gauche* form of butane (C4—C5—C6—C7) and the two *gauche* forms of segments Y—C1—X—C13 and Y—C1—C6—C7. The *gauche* steric interactions of S—CH_2—CH_2—CH_2 and O—CH_2—CH_2—CH_2 segments can be estimated to be about 0.4 kcal/mol on the basis that steric effects due to an axial OR (15) or SR (16, 17) group in cyclohexane are approximately the same (~0.8 kcal/mol). If the assumption is made that the steric interactions of the *gauche* segment Y—C1—X—C13 will be approximately the same as those of Y—C1—C6—C7, i.e. they are of the same order (~0.4 kcal/mol), the anomeric effect for the oxygen atom of ring B in the *cis* isomer **5** must correspond to a value of 1.6 kcal/mol, whereas that for the sulfur atom in the *cis* isomers **7** and **9** must correspond to 1.8 and 2.0 kcal/mol respectively.

The first conclusion which can be reached from this analysis is that the anomeric effect of the sulfur atom is of the same order as that for the oxygen atom (Table 1). A similar conclusion was reached in our study of mono and dithio spiroketals (8–10).[5]

A second conclusion which may be reached from this analysis is that the anomeric effect of the sulfur atom in ring B would be larger than that for an oxygen, and that this stereoelectronic effect would be even larger when ring C contains a sulfur atom. We think, however, that this a priori unexpected conclusion[7] is very likely incorrect because the value taken for the steric interactions must be smaller when the heteroatom is sulfur (18–20). Indeed, with a sulfur atom, the C—X and the C—Y bonds are longer and this should lead to fewer steric interactions and, if smaller values are taken for the steric effects, the value for the anomeric effect will be diminished accordingly.[8]

It is also interesting to mention that the equilibration of the *cis* and *trans* isomers **5** and **6** requires only a catalytic amount of PTSA, whereas that of the other two series (**7**, **8**, and **9**, **10**) requires one mol of PTSA per mol of thioacetal. Furthermore, the equilibration of isomers **9** and **10** is much slower (>24 h) than that of **7** and **8** (a few hours). This order of ease of reaction (**5**, **6** > **7**, **8** > **9**, **10**) might be a reflexion of two distinct effects. First, the double bond in intermediate **23** might be more readily formed when X is an oxygen atom (22). Second, and less important, is the fact that sulfur is harder to protonate than oxygen (23). Further experimentation is, however, necessary to ascertain the rationalization of these observations.

Conclusion

The *cis* tricyclic monothio and dithioacetals **5**, **7**, and **9** are the kinetic products of cyclization and these results can be readily explained on the basis of the stereoelectronic theory. Equilibration studies carried out on the *cis* and *trans* monothio and dithioacetals **5–10** lead to an evaluation of the anomeric effect. The value obtained is of the same order of magnitude for the oxygen and the sulfur atoms (~1.5 kcal/mol). A more precise conclusion cannot be reached because of the uncertainty in the evaluation of the steric interactions.

Experimental

All reactions were conducted under an argon atmosphere. Triethylamine, methylene chloride, and benzene were distilled over calcium hydride whereas ether and tetrahydrofuran were dried by distilling over sodium benzophenone. Melting points were determined on a Büchi M-50 apparatus, and are uncorrected. Infrared (ir) spectra were taken on a Perkin–Elmer 681 spectrophotometer. Proton nuclear magnetic resonance spectra (^{1}H nmr) were recorded on a Bruker WP-60 and a Bruker WM-250 instrument. Carbon nuclear magnetic resonance spectra (^{13}C nmr) were recorded on a Bruker WM-250 instrument. Mass spectral assays and peak matching were obtained using a VG Micromass ZAB-1F spectrometer. Vapor phase chromatographic (vpc) analysis was carried out on a Hewlett–Packard 5710A gas chromatograph with a flame ionization detector (capillary column OV-101, 25 meter). For flash chromatography, Merck Kiesel gel 60 (230–400 mesh A.S.T.M.) was used.

Thioacetate bicyclic lactone 13

Allyl bicyclic lactone **12** (503 mg, 2.59 mmol) was dissolved in cyclohexane. Thiolacetic acid (5.2 mmol) was added, followed by some azobisisobutyronitrile, and the solution heated to reflux. After 30 min, the solution was cooled, diluted with ether (10 mL), and washed with saturated aqueous sodium bicarbonate (2 × 20 mL) and with brine (10 mL). The organic phase was dried over magnesium sulfate, filtered, and concentrated *in vacuo*. Flash chromatography of the crude product (35% ethyl acetate in hexane) afforded pure thioacetate lactone **13** (637 mg, 91%). An analytical sample was prepared by recrystallization from ether–pentane; mp 40–41°C; ir ($CHCl_3$): 1720, 1685, and 1170 cm^{-1}; ^{1}H nmr ($CDCl_3$) δ: 0.9–2.0 (14H), 2.17 (1H, multiplet, —CH—CO), 2.32 (3H, singlet, CH_3COS), 2.87 (2H, triplet, J = 7.1 Hz, CH_2S—), 3.85 and 4.22 (2H, AB part of an ABX system, J_{AB} = 10.9 Hz, J_{AX} = 4.4 Hz, J_{BX} = 11.1 Hz, CH_2O); ms *m/e* (70 eV): 270 (M^+). *Exact Mass* calcd.: 270.1289; found: 270.1281.

Cis *and* trans *tricyclic thioacetals 5 and 6*

To a cooled (−78°C) solution of thioacetate lactone **13** (600 mg, 2.2 mmol) in dichloromethane (20 mL) was slowly added diisobutylaluminium hydride (4.6 mmol, 1 *M* in hexane). After stirring $2\frac{1}{2}$ h at −78°C, the reaction was quenched with saturated sodium sulfate (10 mL) and dilute sulfuric acid (5%, 5 mL). The aqueous layer was decanted and extracted with dichloromethane (3 × 20 mL). The combined organic extracts were dried over magnesium sulfate, concentrated, and filtered through a pad of silica. Evaporation gave an oil (515 mg), which was dissolved in benzene (25 mL). A catalytic amount of *p*-toluenesulfonic acid monohydrate was added and the solution was refluxed with azeotropic removal of water for 1 h. Methylene chloride (15 mL) was added and the solution was washed with saturated sodium bicarbonate (5 mL). The organic phase was dried ($MgSO_4$) and evaporation of the solvents gave crude acetals (457 mg). Flash chromatography (7% ethyl acetate in hexane) afforded tricyclic thioacetals **5** and **6** (380 mg, 80%) as a mixture of *cis* and *trans* (≈9:1) isomers inseparable by chromatography. When the cyclization was conducted under milder conditions (50–60°C, trace of acid, 30 min) lower yields (30–50%) of *cis* tricyclic thioacetals could be obtained, containing only a trace (≈3%) of the *trans* isomer. On one occasion, when an equilibrated mixture (≈1:1) of isomers was chromatographed (preparative tlc, twice) a *trans* enriched mixture (≈85:15) was obtained.

Cis *tricyclic thioacetal 5*: mp (9:1): 54–55°C; ir (9:1, $CHCl_3$): 1145, 1105, and 1080 cm^{-1}; ^{1}H nmr ($CDCl_3$) δ: 0.8–2.2 (15H), 3.7 (2H, multiplet, CH_2S), 3.51 and 3.63 (2H, AB part of an ABX

[7]Recent *ab initio* calculation (STO-3G) on thiomethanol, methanedithiol, and methanediol suggests that there is a relative decrease in the anomeric effect on changing from oxygen to sulfur (21).

[8]Sources of steric energy other than the *gauche* interactions have also been neglected in our study because they are not available. More precise information on these effects is necessary to evaluate further the importance of the anomeric effect in mono and dithioacetals. Since compounds **5**, **6**, **8–10** are crystalline, X-ray structures and molecular modeling could be used to evaluate further those effects which would lead to a more precise evaluation of the anomeric effect for these compounds.

system, J_{AB} = J_{AX} = 11.1 Hz, J_{BX} = 4.6 Hz, CH_2O), 5.28 (1H, doublet, J = 3.6 Hz, O—CH—S); ^{13}C nmr ($CDCl_3$) δ: 80.6, 67.4, 42.1, 41.6, 35.1, 29.5, 27.8, 27.4, 26.5, 26.0, 25.4, 20.4; ms m/e (70 eV); 212 (M^+). *Exact Mass* calcd.: 212.1235; found: 212.1232. vpc, rt: 7.2 min (160°C).

Trans *tricyclic thioacetal* **6**: mp (4:1): 64.5–65.5°C; ir (4:1, $CHCl_3$): 1145, 1110, and 1080 cm^{-1}; ^1H nmr ($CDCl_3$) δ: 0.8–2.15 (15H), 2.7 (2H, multiplet, CH_2S), 3.20 and 3.84 (2H, AB part of an ABX system, J_{AB} = 11.1 Hz, J_{AX} = 4.1 Hz, J_{BX} = 11.0 Hz, CH_2O), 4.26 (1H, doublet, J = 9.2 Hz, O—CH—S); ^{13}C nmr ($CDCl_3$) δ: 83.9, 74.0, 48.4, 45.6, 41.8, 29.8, 28.1 (2), 27.8, 27.5, 26.1, 25.4; ms m/e (70 eV): 212 (M^+). *Exact Mass* calcd.: 212.1235; found: 212.1232; vpc, rt: 7.7 min (160°C).

Equilibration of cis *and* trans *tricyclic thioacetals 5 and 6*

A mixture of *cis* and *trans* tricyclic thioacetals **5** and **6** (310 mg, 1.46 mmol, 85:15 *cis/trans*) was dissolved in benzene (25 mL) and a few crystals of *p*-toluenesulfonic acid were added. The solution was refluxed for 6 h. Concentration and dilution with hexane was followed by filtration through silica gel and solvent evaporation. Proton nmr spectroscopy and vpc analysis of the oily residue indicated a *cis/trans* ratio of 47:53. The equilibration was repeated with the product of the first equilibration and the *cis/trans* ratio found was 48:52, indicating thermodynamic populations.

Iodo acid 15

Iodotrimethylsilane (26 mmol) was added to a solution of bicyclic lactone **11** (3.84 g, 24.9 mmol) in methylene chloride (25 mL). The reaction mixture was stirred for 5 days at room temperature. Water (20 mL) was added, the organic layer decanted, and the aqueous phase extracted with methylene chloride (4 × 10 mL). The organic extracts were washed with aqueous sodium thiosulfate (10%, 20 mL), dried over sodium sulfate, and filtered. Evaporation of the solvents afforded crude iodo acid **15** (6.82 g, 97%), which was used without further purification; ^1H nmr ($CDCl_3$) δ: 0.9–1.9 (10H), 2.15 and 2.51 (2H, AB part of an ABX system, J_{AB} = 14.4 Hz, J_{AX} = 3.6 Hz, J_{BX} = 7.0 Hz, CH_2—COO), 3.3 (2H, multiplet, CH_2I), 10.6 (1H, br singlet, COOH).

Bicyclic thiolactone 17

Oxalyl chloride (33 mmol) was added to a solution of iodo acid **15** (2.33 g, 8.27 mmol) in benzene (30 mL) and the resulting mixture was stirred at room temperature for 1 day. Evaporation to dryness afforded the crude acid chloride **16**, which could be characterized (ir (CH_2Cl_2): 1795 cm^{-1}; nmr ($CDCl_3$) δ: 0.9–2.0 (10H), 2.77 and 3.10 (2H, CH_2COCl), 3.25 (2H, CH_2I)) but was best used directly for the next step. Dissolution of this acid chloride in methylene chloride (40 mL) was followed by hydrogen sulfide bubbling. Triethylamine (25 mmol) was immediately added while continuing bubbling for 5 min. Saturated ammonium chloride (40 mL) was added. The organic layer was decanted and the aqueous layer was extracted with methylene chloride (2 × 20 mL). The combined organic extracts were dried with magnesium sulfate. Filtration, concentration, and flash chromatography (10% acetone in hexane) of the residue gave pure bicyclic thiolactone **17** (1.22 g, 87%) as an oil; ir (CH_2Cl_2): 1660, 1110 cm^{-1}; ^1H nmr ($CDCl_3$) δ: 0.95–1.9 (10H), 2.22 and 2.63 (2H, AB part of an ABX system, J_{AB} = 17.6 Hz, J_{AX} = 3.6 Hz, J_{BX} = 11.6 Hz, CH_2CO), 2.92 (2H, multiplet, CH_2S); ^{13}C nmr ($CDCl_3$) δ: 200.4, 48.7, 38.7, 38.5, 35.9, 33.8, 32.7, 25.8, 25.0; ms m/e (70 eV): 170 (M^+), 142 (M^+ – CO). *Exact Mass* calcd.: 170.0765; found: 170.0765.

Allyl bicyclic thiolactone 18

n-Butyllithium (7.8 mmol, 1.55 *M* in hexane) was added at −78°C to diisopropylamine (8.1 mmol). The resulting slurry was warmed to 0°C for 15 min. After cooling to −78°C, tetrahydrofuran (20 mL) was added, followed by bicyclic thiolactone **17** (1.26 g, 7.4 mmol) dissolved in tetrahydrofuran (10 mL). The solution was stirred $1\frac{1}{2}$ h before adding hexamethylphosphoramide (7.4 mmol) and allyl bromide (74 mmol) slowly via syringe. After 7 h at −78°C, the solution was stirred at −45°C for $1\frac{1}{2}$ h. Saturated ammonium chloride (5 mL) was added and the resulting mixture concentrated. Hexane (30 mL) and ether (15 mL) were added. The organic phase was washed with water (3 × 15 mL) and aqueous lithium chloride (14%, 15 mL), and the aqueous phases extracted with ether/hexane (1:5, 2 × 20 mL). The combined organic extracts were dried over magnesium sulfate, filtered, and evaporated *in vacuo*. Flash chromatography (10 to 20% ethyl acetate in hexane) gave pure allyl bicyclic thiolactone **18** (1.32 g, 85%) as an oil; ir (CH_2Cl_2): 1650 cm^{-1}; ^1H nmr ($CDCl_3$) δ: 0.9–2.0 (12H), 2.25 (1H, multiplet, CH—CO), 2.76 and 2.94 (2H, AB part of an ABX system, J_{AB} = 12.4 Hz, J_{AX} = 11.0 Hz, J_{BX} = 3.4 Hz, CH_2S), 5.1 (2H, multiplet, CH_2=C), 5.7 (1H, multiplet, —CH=C); ^{13}C nmr ($CDCl_3$) δ: 203.0, 134.2, 117.6, 56.4, 41.8, 38.8, 35.2, 33.8, 33.4, 32.2, 25.4, 25.1; ms m/e (70 eV): 210 (M^+), 182 (M^+ – CO). *Exact Mass* calcd.: 210.1079; found: 210.1076.

Allyl bicyclic thioenolether 19

Diisobutylaluminium hydride (4.4 mmol, 1 *M* in cyclohexane) was slowly added to a cooled (−78°C) solution of allyl bicyclic thiolactone **18** (850 mg, 4 mmol) in methylene chloride (30 mL). The resulting mixture was stirred 2 h at −78°C before being quenched with hydrochloric acid (10 mL, 1 *N*). The organic layer was decanted, and the aqueous phase was saturated with ammonium chloride and extracted with 1:1 ether–hexane (3 × 20 mL). The organic extracts were dried with magnesium sulfate, filtered, and concentrated. The crude residue was taken into benzene (20 mL) and refluxed 2 h with *p*-toluenesulfonic acid (0.5 mol) for azeotropic removal of water. Then the solution was evaporated to dryness and the residue purified by flash chromatography (5% ethyl acetate in hexane) to give pure allyl bicyclic thioenolether **19** as an oil (684 mg, 87%); ir (CH_2Cl_2): 1640 cm^{-1}; ^1H nmr ($CDCl_3$) δ: 0.8–2.2 (10H), 2.55 and 2.76 (4H, multiplets, CH_2S and =C—CH_2—C=), 5.03 (2H, multiplet, CH_2=C), 5.8 (1H, multiplet, CH=C), 5.75 (1H, broad singlet, =CH—S); ms m/e (70 eV): 194 (M^+). *Exact Mass* calcd.: 194.1129; found: 194.1131.

Hydroxy bicyclic thioenolether 20

Cyclohexene (11.3 mmol) was dissolved in ether (5 mL). The solution was cooled (−10°C) and borane/methyl sulfide complex (5.5 mmol) was added via syringe. On stirring 2 h at 0°C a white precipitate formed. The ether was partially removed by an argon stream, tetrahydrofuran (20 mL) was added, and the resulting solution cooled to −50°C. Allyl bicyclic thioenolether **19** (665 mg, 3.4 mmol) in tetrahydrofuran (5 mL) was added to the reaction mixture and the temperature was allowed to slowly (4 h) rise to 25°C. Aqueous sodium hydroxide (1 *N*, 31 mmol) and hydrogen peroxide (30%, 18 mmol) were added and the resulting mixture was vigorously stirred for 3 h. Hexane (30 mL) was added. The aqueous phase was acidified to pH 2 with dilute sulfuric acid and extracted with ether/hexane (1:1, 3 × 20 mL). The combined organic extracts were washed with brine (20 mL) and dried over magnesium sulfate, filtered, and evaporated. Flash chromatography (30% ethyl acetate in hexane) gave hydroxy bicyclic thioenolether **20** (590 mg, 82%) as an oil; ir (CH_2Cl_2): 3610, 3450, and 1060 cm^{-1}; ^1H nmr ($CDCl_3$) δ: 0.9–2.3 (15H), 2.46 (1H, split doublet, J_{AB} = 12.3 Hz, J_{BX} = 2.2 Hz, J_W = 2.2 Hz, one hydrogen of CH_2S), 2.68 (1H, A part of an ABX system, J_{AB} = 12.3 Hz, J_{AX} = 11.3 Hz, the other hydrogen of CH_2S), 3.65 (2H, doublet of triplet, J = 2 Hz, J = 6.4 Hz, CH_2O), 5.75 (1H, singlet, =CH—S); ^{13}C nmr ($CDCl_3$) δ: 134.5, 112.6, 62.3, 42.2, 40.7, 34.5, 31.9, 31.4, 30.9, 29.6, 26.9, 26.3; ms m/e (70 eV): 212 (M^+). *Exact Mass* calcd.: 212.1235; found: 212.1240.

Cis *and* trans *tricyclic thioacetals 7 and 8*

Hydroxy bicyclic thioenolether **20** (190 mg, 0.9 mmol) was dissolved in a mixture of benzene (15 mL), methanol (0.5 mL), and trimethyl orthoformate (0.2 mL). Then, *p*-toluenesulfonic acid monohydrate (1.1 mmol) was added and the solution stirred 48 h at room temperature. Ether (10 mL) and saturated sodium bicarbonate (25 mL) were added. The aqueous phase was decanted and extracted with ether (20 mL). The organic extracts were dried over magnesium sulfate, filtered, and evaporated to give crude tricyclic thioacetals **7** and **8** (167 mg, 88%) as a mixture of *cis* and *trans* isomers (85:15, nmr and vpc analysis). The *cis* isomer was most conveniently obtained by flash chromatography (10% ethyl acetate in hexane) of a reaction mixture quenched before completion, since it is the kinetic product (*cis*/*trans* ratio ≃ 98:2). Pure *trans* isomer was obtained by flash chromatography (10% ethyl acetate in hexane) of an equilibrated mixture.

Cis *tricyclic thioacetal* **7**: ir ($CHCl_3$): 1035 and 1080 cm^{-1}; ^1H nmr ($CDCl_3$) δ: 0.8–2.2 (16H), 2.75 (1H, A part of an ABX system, J_{AB} = 13.2 Hz, J_{AX} = 11.4 Hz, axial hydrogen of CH_2S), 3.59 (1H, B part of an AA'BB' system, J_{AB} = 12.0 Hz, $J_{A'B}$ = 11.5 Hz, $J_{BB'}$ = 2.6 Hz, axial hydrogen of CH_2O), 4.08 (1H, complex doublet, equatorial hydrogen of CH_2O), 4.38 (1H, br singlet, S—CH—O); ^{13}C nmr ($CDCl_3$) δ: 79.8, 70.6, 43.2, 43.0, 36.8, 33.9, 30.1, 29.3, 26.9, 26.3, 26.0, 20.1; ms *m*/*e* (70 eV): 212 (M^+). *Exact Mass* calcd.: 212.1235; found: 212.1240; vpc, rt: 9.1 min (T_1 = 140°C for 4 min, rate = 4°C/min, T_2 = 200°C).

Trans *tricyclic thioacetal* **8**: mp: 70.5–71.5°C; ir ($CHCl_3$): 1085 cm^{-1}; ^1H nmr ($CDCl_3$) δ: 0.75–2.1 (15H), 2.43 and 2.52 (2H, AB part of an ABX system, J_{AB} = 13.6 Hz, J_{AX} = 10.5 Hz, J_{BX} = 3.9 Hz, CH_2S), 3.46 (1H, B part of an AA'BB' system, J_{AB} = 11.3 Hz, $J_{A'B}$ = 11.7 Hz, $J_{BB'}$ = 3.0 Hz, axial hydrogen of CH_2O), 4.03 (1H, complex doublet, equatorial hydrogen of CH_2O), 4.26 (1H, doublet, *J* = 9.2 Hz, S—CH—O); ^{13}C nmr ($CDCl_3$) δ: 83.9, 69.1, 48.3, 45.8, 43.4, 34.8, 33.6, 28.8, 27.1, 26.2, 26.0, 25.8; ms *m*/*e* (70 eV): 212 (M^+). *Exact Mass* calcd.: 212.1235; found: 212.1240; vpc, rt: 9.9 min (T_1 = 140°C for 4 min, rate = 4°C/min, T_2 = 200°C).

Equilibration of cis *and* trans *tricyclic thioacetals 7 and 8*

A mixture of *cis* and *trans* tricyclic thioacetals **7** and **8** (150 mg, 0.71 mmol, 88:12 *cis*/*trans*) was dissolved in benzene (10 mL) containing methanol (0.5 mL) and trimethyl orthoformate (0.2 mL). The *p*-toluenesulfonic acid monohydrate (0.8 mmol) was added and the solution refluxed 1 h. Ether (10 mL) was added and the solution washed with saturated sodium bicarbonate (2 × 5 mL). Extraction of the aqueous layer with ether (10 mL) was followed by magnesium sulfate drying of the organic extracts. Concentration gave crude tricyclic thioacetals **7** and **8** (145 mg, 96%). Proton nmr spectroscopy and vpc analysis indicated a *cis*/*trans* ratio of 74:26. Further equilibrations of this crude mixture under analogous conditions (~2 h, reflux) gave a ratio of 58:42. A third equilibration gave a *cis*/*trans* ratio of 57:43.

Thioacetate bicyclic thiolactone 21

Thiolacetic acid (3.8 mmol) was added to a solution of allyl bicyclic thiolactone **18** (397 mg, 1.9 mmol) in cyclohexane (15 mL) containing some azobiisobutyronitrile. The resulting mixture was refluxed 15 min, cooled, and diluted with ether (15 mL). The solution was washed with saturated sodium bicarbonate (2 × 25 mL) and brine (10 mL) before drying with magnesium sulfate. Filtration and evaporation, followed by flash chromatography (20%, ethyl acetate in hexane) of the residue, gave the oily thioacetate bicyclic thiolactone **21** (514 mg, 95%); ir (CH_2Cl_2): 1687, 1650, 1135, and 1110 cm^{-1}; ^1H nmr ($CDCl_3$) δ: 0.9–2.05 (14H), 2.21 (1H, multiplet, CH—CO), 2.32 (3H, singlet, CH_3COS), 2.78 and 2.95 (2H, AB part of an ABX system, J_{AB} = 12.4 Hz, J_{AX} = 11.1 Hz, J_{BX} = 3.5 Hz, CH_2S of the ring), 2.85 (2H, triplet, *J* = 7.1 Hz, CH_2S of the side chain); ms *m*/*e* (70 eV): 286 (M^+), 244 (MH^+ − CH_3CO). *Exact Mass* calcd.: 286.1061; found: 286.1075.

Cis *and* trans *tricyclic dithioacetals 9 and 10*

Diisobutylaluminium hydride (3.9 mmol, 1 *M* in hexane) was slowly added to a cooled (−78°C) solution of thioacetate bicyclic thiolactone **21** (530 mg, 1.85 mmol) in methylene chloride (15 mL). After 2 h at −78°C, saturated sodium sulfate (10 mL) and dilute sulfuric acid (5%, 5 mL) were added, the organic layer decanted, and the aqueous phase was extracted with methylene chloride (3 × 20 mL). The combined organic extracts were dried over magnesium sulfate, filtered, and concentrated *in vacuo*. The oily residue was taken into benzene (20 mL). A few crystals of *p*-toluenesulfonic acid were added and the solution was refluxed 45 min with azeotropic removal of water. The resulting mixture was concentrated, diluted with methylene chloride (15 mL), and washed with saturated sodium bicarbonate (10 mL). Extraction of the aqueous phase with methylene chloride (2 × 20 mL) and magnesium sulfate drying of the organic extracts gave crude acetals. Filtration on silica gel afforded tricyclic dithioacetals **9** and **10** (393 mg, 93%) as a 95:5 *cis*/*trans* mixture of isomers (nmr and vpc analysis).

Both isomers could be separated by flash chromatography (8% ethyl acetate in hexane).

Cis *tricyclic dithioacetal* **9**: mp 125.5–127°C; ir ($CHCl_3$): 1100–1200 cm^{-1}; ^1H nmr ($CDCl_3$) δ: 0.85–2.2 (16H), 2.58 and 2.86 (3H, multiplets, three hydrogens of the two CH_2S), 4.03 (1H, doublet, *J* = 2.7 Hz, S—CH—S); ^{13}C nmr ($CDCl_3$) δ: 45.4, 44.0, 43.6, 36.5, 33.9, 31.9, 30.7, 30.1, 28.8, 26.6, 26.1, 19.6; ms *m*/*e* (70 eV): 228 (M^+). *Exact Mass* calcd.: 228.1006; found: 228.1008; vpc, rt: 9.6 min (170°C).

Trans *tricyclic dithioacetal* **10**: mp 84–85°C; ir ($CHCl_3$): 1100–1200 cm^{-1}; ^1H nmr ($CDCl_3$) δ: 0.8–2.25 (15H), 2.38 (1H, B part of an ABX system, J_{AB} = 13.3 Hz, = 3.2 Hz, equatorial hydrogen of CH_2S middle ring), 2.55 (2H, multiplet, other hydrogens of the two CH_2S), 2.79 (1H, A part of an AA'BB' system, $J_{AA'}$ = J_{AB} = 13 Hz, $J_{AB'}$ = 2.7 Hz, axial hydrogen of CH_2S outer ring), 3.74 (1H, doublet, *J* = 9.7 Hz, S—CH—S); ^{13}C nmr ($CDCl_3$) δ: 49.4, 48.0, 47.3, 44.0, 36.1, 34.4, 30.6, 29.7, 29.1, 28.3, 26.5, 25.8; ms *m*/*e* (70 eV): 228 (M^+). *Exact Mass* calcd.: 228.1006; found: 228.1008; vpc, rt: 10.9 min (170°C).

Equilibration of cis *and* trans *tricyclic dithioacetals 9 and 10*

A mixture of *cis* and *trans* tricyclic dithioacetals **9** and **10** (384 mg, 1.68 mmol, 95:5 *cis*/*trans*) was dissolved in benzene (25 mL) containing *p*-toluenesulfonic acid (1.5 mmol). The solution was refluxed 18 h and then cooled to room temperature. Ether was added (20 mL) and the solution was washed with saturated sodium bicarbonate (2 × 5 mL). The aqueous phases were extracted with ether (2 × 15 mL). The combined organic extracts were dried over magnesium sulfate, filtered, and concentrated *in vacuo*. The crude product (343 mg) was filtered through silica gel. Proton nmr spectroscopy and vpc analysis indicated a *cis*/*trans* ratio of 85:15. This crude mixture was equilibrated by refluxing 48 h with one equivalent of acid. The *cis*/*trans* ratio then obtained was 62:38. Further treatment with acid (1 equiv., 24 h) gave the same *cis*/*trans* ratio (62:38), thus determining thermodynamic populations.

Acknowledgements

Support for this work by the Natural Sciences and Engineering Research Council of Canada (NSERCC) and by the "Ministère de l'Éducation" (FCAC), Québec, is gratefully acknowledged.

1. P. DESLONGCHAMPS. *In* Stereoelectronic effects in organic chemistry. Organic Chemistry Series, Vol. 1. Pergamon Press, Oxford, England. 1983.
2. A. J. KIRBY. *In* The anomeric effect and related stereoelectronic effects at oxygen. Springer Verlag, Berlin. 1983.
3. P. DESLONGCHAMPS, C. MOREAU, D. FRÉHEL, and P. ATLANI. Can. J. Chem. **50**, 3402 (1972).
4. R. U. LEMIEUX and N. J. CHÜ. Abstracts of Papers; Am. Chem. Soc. **133**, 31N (1958).
5. R. U. LEMIEUX, A. A. PAVIA, J. C. MARTIN, and K. A. WATANABE. Can. J. Chem. **47**, 4427 (1969).
6. G. DESCOTES, M. LISSAC, J. DELMAU, and J. DUPLAN. C.R. Acad. Sci. Ser. C, **267**, 1240 (1968).
7. N. BEAULIEU, R. A. DICKINSON, and P. DESLONGCHAMPS. Can. J. Chem. **58**, 2531 (1980).
8. (*a*) P. DESLONGCHAMPS, D. D. ROWAN, N. POTHIER, G. SAUVÉ, and J. K. SAUNDERS. Can. J. Chem. **59**, 1105 (1981); (*b*) P. DESLONGCHAMPS, D. D. ROWAN, N. POTHIER, and J. K. SAUNDERS. Can. J. Chem. **59**, 1122 (1981); (*c*) N. POTHIER, D. D. ROWAN, P. DESLONGCHAMPS, and J. K. SAUNDERS. Can. J. Chem. **59**, 1132 (1981).

9. A. J. Hoog. Ph.D. Thesis (Leiden), 1971.
10. (*a*) N. S. Zefirov. Zh. Org. Khim. **1**, 594 (1971); (*b*) J. Org. Chem. USSR, **5**, 1131 (1969).
11. J. S. Showell, J. R. Russel, and D. Swern. J. Org. Chem. **27**, 2853 (1962).
12. H. R. Kricheldorf. Angew. Chem. Int. Ed. Engl. **18**, 689 (1979).
13. R. A. Gorski, G. J. Wolber, and J. Wemple. Tetrahedron Lett. 2577 (1976).
14. H. C. Brown. *In* Organic synthesis via boranes. Wiley–Interscience, New York. 1975. pp. 28–29.
15. H. J. Schneider and V. Hoppen. Tetrahedron Lett. 579 (1974).
16. E. L. Eliel and M. H. Gianni. Tetrahedron Lett. 97 (1962).
17. E. L. Eliel and B. P. Thill. Chem. Ind. 88 (1963).
18. R. W. Franck. Tetrahedron, **39**, 3251 (1983).
19. E. Kleinpeter, C. Duschek, and M. Muehlstaedt. J. Prakt. Chem. **320**, 303 (1978).
20. E. L. Eliel, K. D. Hargrave, K. M. Pietrusiewicz, and M. Manoharan. J. Am. Chem. Soc. **104**, 3635 (1982).
21. S. Vishveshwara and V. S. R. Rao. Carbohydr. Res. **104**, 21 (1982).
22. H. Böhme. Chem. Ber. **74**, 248 (1941).
23. P. Bonvicini, A. Levi, V. Lucchini, G. Modena, and G. Scorrano. J. Am. Chem. Soc. **95**, 5960 (1973).

Reactions of steroidal 5,6-epoxides and cyclohexene oxide with aluminum alkoxides

Herbert L. Holland and Saeed R. Khan
Department of Chemistry, Brock University, St. Catharines, Ont., Canada L2S 3A1

Received January 18, 1985

Herbert L. Holland and Saeed R. Khan. Can. J. Chem. **63**, 2763 (1985).

The isomeric 5,6α- and 5,6β-epoxycholestanes, in addition to an analogous series of compounds substituted at C-3 with hydroxy (α or β stereochemistry) or ethylene ketal groups, have been treated with aluminum isopropoxide or *tert*-butoxide. The latter series of reactions did not give identifiable material, but aluminum isopropoxide gave products derived from epoxide opening and rearrangement in all cases. With epoxides unsubstituted at C-3, aluminum isopropoxide functioned as a Lewis acid in promoting epoxide rearrangements. In the presence of a C-3 alcohol function, additional products were obtained arising from fragmentation of the C-4,C-5 bond, or from β-elimination of the epoxide involving the loss of a C-7 hydrogen. Meerwein–Pondorff reduction of product carbonyl groups was also observed. C-3 ketal substituted epoxides were rearranged cleanly to 6-hydroxy-Δ^4-3-ketones. Cyclohexene oxide reacted with aluminum isopropoxide (but not with *tert*-butoxide) to give two products arising from epoxide addition reactions. Structures for these products are proposed based on their ^{13}C nmr spectra, and a possible route for their formation is presented. None of the epoxides examined in this study reacted with magnesium methoxide.

Herbert L. Holland et Saeed R. Khan. Can. J. Chem. **63**, 2763 (1985).

On a fait réagir les époxy-5,6α et -5,6β cholestanes ainsi qu'une série de composés analogues substitués en C-3 par un groupement hydroxyle (de stéréochimie α ou β) ou par un groupement éthylène cétal avec l'isopropylate ou le *tert*-butylate d'aluminium. Les réactions avec le *tert*-butylate ne donnent pas de produits identifiables; toutefois, lors des réactions avec l'isopropylate d'aluminium, on obtient dans tous les cas des produits qui résultent d'une ouverture de l'époxyde suivie d'une transposition. Dans les cas des époxydes qui ne sont pas substitués en C-3, l'isopropylate d'aluminium agit comme un acide de Lewis qui favorise les transpositions de l'époxyde. En présence d'une fonction alcool en C-3, on obtient des produits additionnels provenant soit d'une fragmentation de la liaison C-4, C-5 soit d'une élimination β de l'époxyde qui implique une perte d'hydrogène en C-7. On a également observé une réduction de Meerwein–Pondorff des groupements carbonyls. Les époxydes ayant un substituant cétal en position C-3 se transposent proprement en hydroxy-6 Δ^4 cétones-3. L'époxyde du cyclohexène réagit avec l'isopropylate d'aluminium (mais non avec le *tert*-butylate) pour donner des produits découlant de réactions d'addition sur l'époxyde. À partir des spectres de rmn du ^{13}C, on propose des structures pour ces produits et l'on propose une voie possible pour leur formation. Aucun des époxydes étudiés dans ce travail ne réagit avec le méthylate de magnésium.

[Traduit par le journal]

The stereochemical control of product formation inherent in the epoxide opening reaction has ensured place for the latter in modern asymmetric synthesis (e.g. ref. 1). The opening of epoxides by nucleophiles may be assisted by Lewis acids (2); the latter reagents alone catalyse epoxide rearrangements efficiently, a reaction which has been thoroughly studied in steroidal examples (3–6). Strong Brönsted bases react with epoxides by abstracting a β-hydrogen to produce allylic alcohols (ref. 7, and references therein).

We have now studied reactions of the latter type using a reagent, aluminum isopropoxide, in which Brönsted base capability is combined with a source of potential Lewis acid activation. This reaction has been used catalytically to carry out the β-elimination reaction on several terpene epoxides (8, 9). We have now examined the reactions under both catalytic and equimolar conditions between a series of steroidal 5,6-epoxides and aluminum isopropoxide or *tert*-butoxide, in addition to magnesium methoxide. The latter reagent has proven effective in certain intramolecular fragmentations of steroidal epoxides (10).

The epoxides used in the present study, **1** and **2**, were prepared as previously outlined (7); their ^{13}C nmr spectra have been presented in an earlier publication (7). Magnesium methoxide was found not to react with the range of epoxides investigated. Reactions with aluminum alkoxides were performed in dry toluene, the choice of solvent being based on earlier studies (7, 8, 11): aluminum *tert*-butoxide gave complex, intractable reaction mixtures, and aluminum isopropoxide in catalytic amount did not promote reactions with

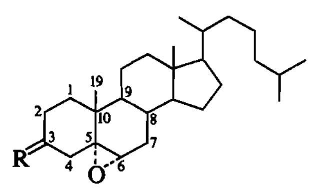

1 *a* R = H_2
b R = αH, βOH
c R = αOH, βH
d R = OCH_2CH_2O

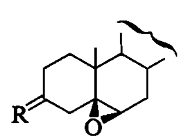

2 *a* R = H_2
b R = αH, βOH
c R = αOH, βH
d R = OCH_2CH_2O

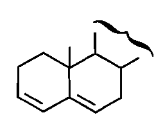

3

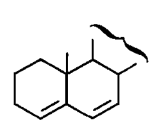

4

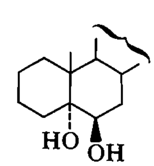

5

TABLE 1. Reactions of epoxides **1** and **2** with aluminum isopropoxide

Starting material	Products (% isolated)
1*a*	**3** + **4** (30), **5** (25), **6** (16)
1*b*	**8** (30), **9***a* (12), **9***b* (15), **10***a* (8), **10***b* (10)
1*c*	**8** (32)
1*d*	**12***a* (61)
2*a*	**3** + **4** (30), **5** (25), **7** (33)
2*b*	**8** (30), **11** (12)
2*c*	None isolated
2*d*	**12***b* (62)

TABLE 2. ^{13}C nuclear magnetic resonance spectra of products **5** and **7**–**9**

	δ (ppm)[b]						
Carbon[a]	5	7	8	9*a*	9*b*	10*a*	10*b*[c]
1	33.5	30.7	33.6	35.8*	36.2	30.1	30.1
2	20.6*	20.6*	26.6	29.4	30.2	26.2	26.3
3	20.9*	20.0*	63.5	71.7	71.3	67.8	68.1
4	31.4	26.7	102.7	30.4	34.8*	27.4	28.2
5	74.1	78.9	156.7	48.6	48.7	42.9	42.9
6	76.2	213.6	69.6	68.2	73.3	66.0	71.5
7	34.9	42.2	42.4	35.0*	34.4*	34.6	34.4
8	30.3	37.5	34.5	35.0	30.8	34.4	30.1
9	46.2	45.0	47.8	39.6	40.8	39.1	39.9
10	38.9	43.2	42.2	36.1	36.2	36.4	36.4
19	16.7	13.9	23.6	23.6	25.6	23.5	26.4

[a]Carbons 11–18 and 20–27 had chemical shifts close to those of other ring A and (or) B substituted cholestanes (13).
[b]Chemical shifts marked with asterisks may be interchanged.
[c]In $CDCl_3$/DMSO-d_6 solvent.

any of the epoxides studied. However, the latter reagent in equimolar or greater ratios gave, with one exception (reaction with **2***c*), products which were readily separated and identified.

The results of the reactions with aluminum isopropoxide are summarized in Table 1. Product identification relied heavily on ^{13}C nmr spectral data, and assignments which are hitherto unreported are listed in Table 2. The unsubstituted epoxides **1***a* and **2***a* both gave mixtures of $\Delta^{3,5}$- and $\Delta^{4,6}$-cholestadienes (**3** and **4**), which could not be separated by the chromatographic means at our disposal. The olefins **3** and **4** may be formed via β-elimination of the epoxide from C-4 or C-7, followed by dehydration. Similar reactions have been reported to occur between terpene epoxides and aluminum isopropoxide (8, 11).

Also obtained from both **1***a* and **2***a* was the 5α,6β-diol **5**. This product was produced during the hydrolytic work-up of the reaction, evidenced by its absence during the monitoring of the progress of the reaction by tlc.

In addition, the α-epoxide **1***a* gave the 5β-6-ketone **6**, one of the products of Lewis acid catalysed rearrangement (3–6), and the β-epoxide **2***a* afforded the 5α-hydroxy-6-ketone (**7**). Formation of the latter product may be rationalized as outlined in Scheme 1. Coordination of the reagent to the epoxide **2***a* can lead to formation of the 5-cation **16**; the latter cannot rearrange by transfer of the C-6 hydrogen to C-5, as happens in Lewis acid catalysed rearrangements of 5,6α-epoxides (3–6) because of the location of the hydrogen orthogonal to the empty *p* orbital on C-5. A similar phenomenon leading to abnormal rearrangement products has been reported to control the

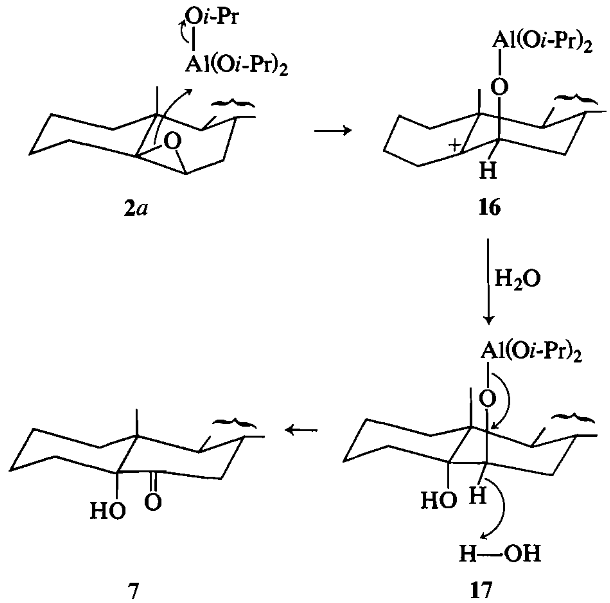

SCHEME 1. Conversion of 5,6β-epoxycholestane to 5α-hydroxycholestan-6-one by aluminum isopropoxide.

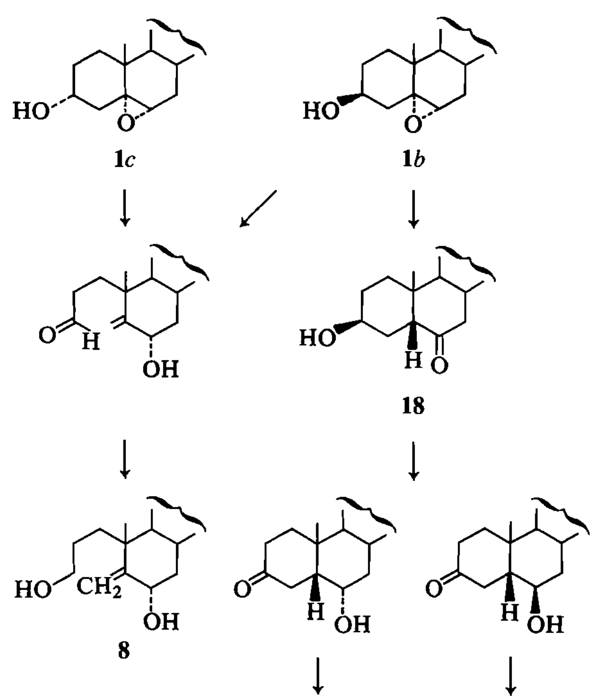

SCHEME 2. Reactions of 5,6α-epoxy-3-hydroxycholestanes with aluminum isopropoxide.

reactions of other 5,6β-epoxy cholestanes with BF_3 (12).

Capture of **16** by water (perhaps that produced by the dehydration reactions leading to **3** and **4**) can lead to **17**. The relief of strain afforded by the formation of the steroidal ketone may then lead to **7** by hydride transfer, a process analogous in mechanism to the Oppenauer oxidation. The nature of the hydride acceptor is not clear, but a possible candidate is water. The absence of **7** during the reaction (as monitored by tlc) supports its formation during the work-up.

The C-3 alcohol-substituted 5,6α-epoxides **1***b* and **1***c* both reacted with aluminum isopropoxide. The 3α-alcohol **1***c* gave

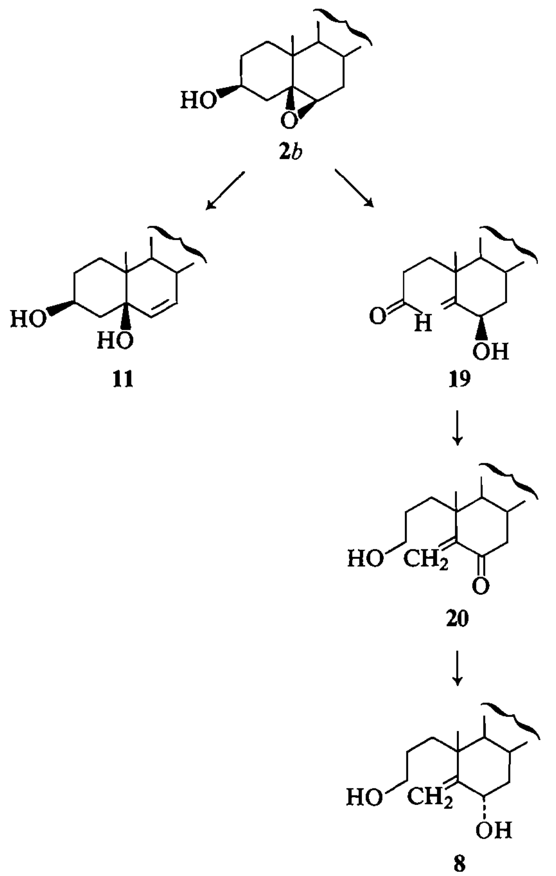

SCHEME 3. Reactions of 5,6β-epoxy-3β-hydroxycholestane with aluminum isopropoxide.

the seco-diol **8**, identified by ^{13}C nmr (Table 2) and other spectral data. The presence of the *exo*-methylene group and primary alcohol are clearly evident in the ^{13}C nmr spectrum, while the stereochemistry of substitution at C-6 follows from the resonance positions assigned to C-6 and C-8, the latter being characteristic of the stereochemistry of hydroxyl at C-6 (13). The formation of **8** is readily rationalized in terms of fragmentation followed by Meerwein–Pondorff reduction of the intermediate aldehyde (Scheme 2).

The reaction of the 3β-hydroxy-5,6α-epoxide **1***b* was complex. In addition to **8**, which can be produced as outlined above, all four isomers of 5β-cholestane-3,6-diol (**9** and **10**) were formed. These presumably arise via the 6-ketone **18** (Scheme 2) and its subsequent reduction at C-6, and oxidation and reduction at C-3. The redox reactions, the order of which is not necessarily implied in Scheme 2, may all be brought about by the metal alkoxide reagent. The structures of **9** and **10** follow from their ^{13}C nmr spectra (Table 2). Chemical shifts diagnostic of stereochemistry are those of C-19 (for 5β steroids), C-1 and C-5 (for C-3 alcohols), and C-4 and C-8 (for C-6 alcohols) (13). The ^1H nmr spectra of **9** and **10** (see Experimental), in particular the multiplicity of the signal assigned to the C-6 hydrogen, support the structural assignments.

The 5,6-epoxides **2***b* and **2***c* also reacted with aluminum isopropoxide. The C-3α alcohol epoxide **2***c* gave a complex intractable mixture: derivatives of this epoxide are prone to undergo intramolecular reactions (14), which may contribute to the complexity of the present reaction. The 3β isomer **2***b*, however, reacted cleanly to give two products. The minor product, **11**, was the result of base promoted epoxide opening

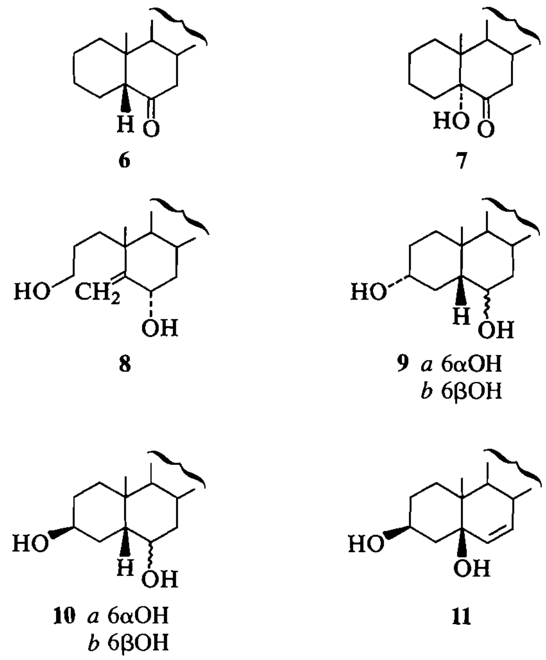

from C-7; this reaction parallels that observed with **2***b* in our earlier study (7). The major product was, surprisingly, **8**, identical with the secosteroid derived from the α epoxides **1***b* and **1***c*. This may be rationalized by the proposal of Scheme 3, in which the intermediate 6β-alcohol **19** must undergo reversible oxidation and reduction at C-6 together with reduction at C-3 (not necessarily in that order). The stereochemistry of substitution at C-6 in the product **8** appears to reflect a degree of product development control during the reaction unusual for the Meerwein–Pondorff reduction (15). However, the absence of the steric restraining influence of ring A and the presence of the sp_2 centre at C-5 in **20** contribute unknown steric influences in this particular case. The formation of **8** from **2***b* raises the possibility that undetected oxidation and reduction at C-6 may occur during the conversion of the 5,6α-epoxides **1***b* and **1***c* to **8**.

In parallel with our earlier results using LDEA as base (7), the ketal epoxides **1***d* and **2***d* react cleanly with aluminum isopropoxide to yield, following aqueous acid work-up, the corresponding Δ^4-3-keto-6-alcohols **12***a* and **12***b*. The stereochemical integrity at C-6 is maintained in these reactions as a consequence of the absence (until work-up) of a carbonyl or any other functionality in the reaction mixture capable of acting as a hydride acceptor and therefore providing the oxidizing equivalents necessary for alcohol–keto interconversion.

In view of the complexity of the reactions observed between the steroidal epoxides and aluminum isopropoxide, we decided to investigate reaction of the latter with the simple epoxide, cyclohexene oxide (**13**). Two products were isolated and identified by their spectral characteristics as isomers of a substituted dicyclohexyl ether. The ^1H nmr spectra clearly showed the presence of an isopropyl ether function and four additional protons geminal to oxygen; the ^{13}C nmr spectra confirmed these observations, and suggest the relative stereochemistry. The latter follows from a comparison of the ^{13}C nmr chemical shifts assigned to C-1, -2, -1′, and -2′ with those calculated for the possible isomeric series **14**, **15**, **21**, and **22** (Table 3).

The calculated values of Table 3 were arrived at as follows: a comparison of the spectra of isopropanol and di-isopropyl ether enable the spectrum of dicyclohexyl ether to be calculated

TABLE 3. ^{13}C nuclear magnetic resonance spectra of dicyclohexyl ethers **14**, **15**, **21**, and **22**

	δ (ppm)					
	Calculated values				Found values	
Carbon	**14**	**15**	**21**	**22**	**14**	**15**
1	82.4	80.0	82.4	80.0	84.2	78.3
2	82.8	78.3	82.8	78.3	79.6	77.6
1′	84.4	82.0	82.0	84.4	86.1	82.0
2′	77.8	73.3	73.3	77.8	75.8	72.5
Isopropyl					69.6, 24.2	70.2, 24.0
Other					33.2	32.3
					33.0	31.8
					32.3	31.5
					31.2	30.6
					25.0	24.8
					24.3	24.2
					23.6	23.1
					21.7	22.3

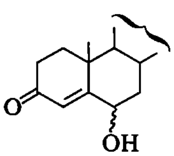

12 *a* αOH
b βOH

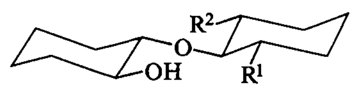

14 (*trans,trans*) *a* R¹ = OiPr, R² = H
b R¹ = H, R² = OiPr

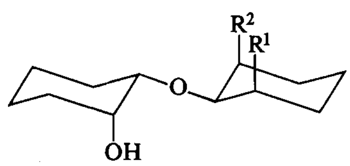

15 (*cis,cis*) *a* R¹ = OiPr, R² = H
b R¹ = H, R² = OiPr

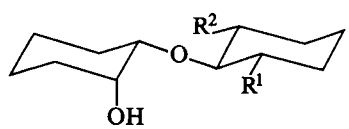

21 (*cis,trans*) *a* R¹ = OiPr, R² = H
b R¹ = H, R² = OiPr

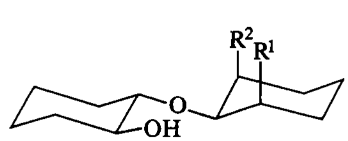

22 (*trans,cis*) *a* R¹ = OiPr, R² = H
b R¹ = H, R² = OiPr

from that of cyclohexanol to be C-1, 75.2 ppm; C-2, 33.6 ppm. The shift parameters for axial and equatorial hydroxyl (ref. 13, and references therein) can then be applied to the calculated spectrum of dicyclohexyl ether to generate predicted spectra for diols corresponding to structures **14**, **15**, **21**, and **22**. The modification of these values by the parameters for the addition of one isopropyl ether (as above) then produces the values listed in the table.

It is clear from these values that the reaction products correspond most closely to the *trans,trans* structures **14** (major product) and the *cis,cis* structures **15** (minor product). In particular, the resonance at δ 72.5 ppm in the minor product can only belong to an axial hydroxyl-substituted carbon (possible structures **15** or **21**). The absence of a series of low field resonances such as those predicted (82.0 to 82.8 ppm) for **21** now suggests structures **15***a* or **15***b* for the reaction product. The ^{13}C nmr spectrum of the major product accords most closely with that predicted for structures **14** in which the two lowest field resonances are assigned to C-1 and C-1′. An alternative calculation of the chemical shifts for **14**, **15**, **21**, and **22**, using *cis* and *trans* cyclohexane-1,2-diols as the base structures, leads to predicted chemical shifts whose relative magnitudes are identical with those listed in Table 1.

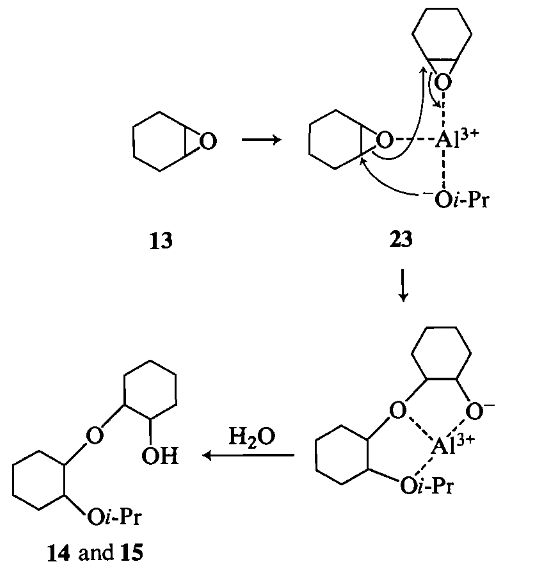

SCHEME 4. Reaction of cyclohexene oxide with aluminum isopropoxide.

A possible route for the formation of **14** and **15** is given in Scheme 4. The formation of a *trans,trans* isomer **14** as major product from a complex such as **23** accords with the expectations of sterochemistry normally associated with epoxide openings. The alumina-catalysed alcohol addition to epoxides proceeds similarly with *trans* ring opening (16). The ratio of **14** to **15** was changed from 1.6:1 to 4:1 by carrying out the reaction with 15-fold reduction in the concentration of aluminum isopropoxide relative to that of cyclohexene oxide, suggesting that the formation of a *cis,cis* isomer **15** may be due, at least in part, to an intermolecular isopropoxide transfer as opposed to the intramolecular process illustrated in Scheme 4. Alternatively, compound **15** may arise from a single complex such as **23** in which Lewis acid catalysed carbon–oxygen bond cleavage of the epoxide precedes attack by the RO^- nucleophile to such an extent that the latter reaction becomes non-stereospecific.

In either event, it is not clear why only two of the eight possible diastereomeric products are formed. An analogous result has been reported for the dimerization of **13** by activated alumina, but without elaboration of the stereochemistry involved (17). One possibility is that as the intermediate complex **23** proceeds towards a transition state, the necessity of having the three oxygens coordinated simultaneously to a single metal ion selects two of the possible geometrical combinations as belonging to pathways of lower energy. The failure of any of the steroid epoxides studied herein to react in a similar way is readily explained by their relative bulk. The formation of a complex such as **23** from steroidal epoxides would be sterically difficult.

In conclusion, the reactions between the epoxides studied and aluminum isopropoxide encompass all the possibilities of Lewis acid catalysis base catalysed fragmentation, Meerwein–Pondorff oxidation/reduction, and nucleophilic epoxide opening. Selection of the desired activities from among this range should now be possible by choosing an appropriate aluminum based reagent.

Experimental

Apparatus, materials, and methods

Melting points were determined on a Kofler heating stage and are uncorrected. Infrared spectra were recorded with an Analect 6260FX Fourier transform ir spectrometer. Proton nmr spectra were recorded at 80 MHz with a Bruker WP80CW or at 250 MHz with a WM250 spectrometer (at McMaster University), and carbon nmr spectra on a Bruker WP60 (Brock), WM250 (McMaster), or WH400 instrument (Southwestern Ontario NMR centre, University of Guelph), using $CDCl_3$ as solvent (unless otherwise stated) and TMS as internal standard. Mass spectra were obtained with an AE1 MS30 spectrometer fitted with a Kratos DS-55 data system. Thin-layer chromatography was performed on Merck silica gel 60 F-254, and column chromatography on silica gel (230–400 mesh).

Elemental analyses were performed by Guelph Chemical Laboratories, Guelph, Ontario.

Preparation of epoxides

The epoxides used in this study were all prepared as outlined earlier (5) and characterized by spectral and physical properties.

Reactions with magnesium methoxide

Magnesium methoxide solution (3.3 mL, 0.4 *M* in methanol) was added to a solution of epoxide (100 mg) in dry toluene (25 mL) and the resulting mixture refluxed for 72 h, being monitored (tlc) daily for product formation. The mixture was then cooled, diluted with water (100 mL), and neutralized (dilute HCl) prior to extraction with ether. The ether extract was dried and evaporated, yielding only starting material.

Reactions with aluminum tert*-butoxide*

Reactions of epoxides (100 mg) in dry toluene (25 mL) with aluminum *tert*-butoxide (5 molar equivalents) were monitored by tlc during treatment under reflux. The development of streaking on the plate heralded the formation of intractable products, which was confirmed by work-up as outlined above.

Reactions with aluminum isopropoxide

*5,6α-Epoxycholestane (1*a*)*

The typical reaction procedure is described as follows. A solution of aluminum isopropoxide (freshly distilled, 1.35 g) in dry toluene (25 mL) was added by syringe to a stirred solution of 5,6α-epoxycholestane (0.5 g) in dry toluene (25 mL) under a nitrogen atmosphere. The resulting mixture was refluxed for 72 h, then cooled, added to dilute HCl (100 mL, 1 *M*), and extracted with ether. The organic extract was washed with water, dried over sodium sulphate, and evaporated. The residue was chromatographed using benzene to ether elution (10% step gradient) to give, in order of elution, a mixture of cholesta-3,5-diene (**3**) and cholesta-4,6-diene (**4**) (0.145 g), mp 78–80°C, identified by ^1H and ^{13}C nmr comparison with the spectra of the authentic separated isomers (10); cholestane-5α,6β-diol (**5**) (0.135 g), mp 121–124°C (lit. (18) mp 126–128°C); ^1H nmr included signals at δ 3.45 ppm (C-6α H); ^{13}C nmr, see Table 2; ms *m/z*: 386 (67), 371 (33), 368 (29), 353 (24) relative to 55 (100); and 5β-cholestane-6-one (**6**) (0.08 g), mp 128–130°C (lit. (3) mp 131–132°C); ^{13}C nmr spectrum identical with that reported (19).

*5,6α-Epoxycholestan-3β-ol (1*b*)*

Treatment of **1***b* (0.2 g) with aluminum isopropoxide (0.52 g) as described above gave 3,4-secocholest-4-ene-3,6α-diol (**8**) (0.06 g), mp 182–183°C; ^1H nmr included signals at δ 3.45–3.70 (2H, br s, C-3 H), 4.1–4.4 (1H, dd, *J* = 4, 12 Hz, C-6β H), and 4.76 and 5.08 (each 1H, br s, C-4 H's) ppm; ^{13}C nmr, see Table 2; ms *m/z*: 404 (0.5), 386 (6), 384 (2), 371 (5), 368 (5) relative to 55 (100). *Anal.* calcd. for $C_{27}H_{48}O_2$: C 80.14, H 11.95%; found: C 80.25, H 11.62%; 5β-cholestane-3β,6β-diol (**10***b*) (0.02 g), mp 195–197°C (lit. (20) mp 198–200°C (corrected)); ^1H nmr included signals at δ 3.4–3.75 (1H, br m, C-3α H) and 3.75 (1H, br s, $W_{1/2}$ = 5 Hz, C-6α H) ppm; ^{13}C nmr, see Table 2; 5β-cholestane-3α,6β-diol (**9***b*) (0.03 g), mp 148–150°C (lit. (21) mp 142–143.5°C), ^1H nmr included signals at δ 3.4–3.85 (1H, br m, C-3β H) and 3.75 (1H, br s, $W_{1/2}$ = 5 Hz, C-6α H) ppm; ^{13}C nmr, see Table 2; 5β-cholestane-3β,6α-diol (**10***a*) (0.016 g), mp 212–215°C; ^1H nmr included signals at δ 3.35–3.75 (1H, br m, C-3α H) and 4.10 (1H, br s, $W_{1/2}$ = 12 Hz, C-6β H); ^{13}C nmr, see Table 2. *Anal.* calcd. for $C_{27}H_{48}O_2$: C 80.14, H 11.95%; found: C 80.04, H 11.74%; and 5β-cholestane-3α,6α-diol (**9***a*) (0.024 g), mp 167–170°C; ^1H nmr included signals at δ 3.4–3.9 (1H, br m, C-3β H) and 3.95 and 4.08 (1H, dd, *J* = 4, 9 Hz, C-6β H) ppm; ^{13}C nmr, see Table 2. *Anal.* calcd. for $C_{27}H_{48}O_2$: C 80.14, H 11.95%; found: C 80.17, H 11.73%.

*5,6α-Epoxycholestan-3α-ol (1*c*)*

Treatment of **1***c* (0.15 g) with aluminum isopropoxide (0.5 g) as described above gave only 3,4-secocholest-4-ene-3,6α-diol (**8**) (0.05 g), identical in all respects with the sample described above.

*5,6α-Epoxycholestan-3-one, 3-cyclic ethylene ketal (1*d*)*

Treatment of **1***d* (0.1 g) with aluminum isopropoxide (0.24 g) as described above gave cholest-4-en-6α-ol-3-one (**12***a*) (0.055 g), mp 152–153°C, identical in all respects with an authentic sample of **12***a*.

*5,6β-Epoxycholestane (2*a*)*

Treatment of **2***a* (0.1 g) with aluminum isopropoxide (0.27 g) as described above and chromatography using benzene – ethyl acetate gave a mixture of cholesta-3,5-diene (**3**) and cholesta-4,6-diene (**4**) in equal amounts (total 0.028 g) identified as described above; cholestan-5α-ol-6-one (**7**) (0.035 g), mp 150–151°C (lit. (18) mp 150–150.5°C); ^{13}C nmr, see Table 2, ms *m/z*: 402 (60), 384 (35), 369 (19), 356 (11), 341 (10), 318 (48) relative to 55 (100); and cholestane-5α,6β-diol (**5**) (0.025 g), mp 122–124°C, identical in all respects with the sample described above.

*5,6β-Epoxycholestan-3β-ol (2*b*)*

Treatment of **2***b* (0.2 g) with aluminum isopropoxide (0.52 g) gave 3,5-secocholest-4-ene-3,6α-diol (**8**) (0.06 g), identical in all respects with the samples of **8** described above; and cholest-6-ene-3β,5β-diol (**11**) (0.025 g), mp 138–140°C (lit. (22) mp 139–140°C); ^1H nmr included signals at δ 3.8–4.2 (1H, br s, C-3α H) and 5.40 (2H, s, C-6 and -7 H's) ppm; ^{13}C nmr, see ref. 5.

*5,6β-Epoxycholestan-3α-ol (2*c*)*

Treatment of **2***d* (0.1 g) with aluminum isopropoxide (0.24 g) as described above gave only an intractable mixture of products.

*5,6β-Epoxycholestan-3-one, 3-cyclic ethylene ketal (2*d*)*

Treatment of **2***d* (0.1 g) with aluminum isopropoxide (0.24 g) as described above gave, following chromatography using benzene – ethyl acetate, cholest-4-en-6β-ol-3-one (**12***b*) (0.056 g), mp 194–196°C, identical in all respects with an authentic sample.

Cyclohexene oxide

Treatment of cyclohexene oxide (0.52 g) with aluminum isopropoxide (0.55 g) as described above gave *cis,cis*-2-oxypropyl-2′-hydroxydicyclohexyl ether (**14**) (0.296 g) as an oil; ^1H nmr included signals at δ 1.18 (d, *J* = 6 Hz, isopropyl methyls), 2.8–3.6 (3H, m, C-1, -1′, and -2′ H's), and 3.75 (1H, septet, *J* = 6 Hz, isopropyl CH) ppm; ^{13}C nmr, see Table 2; ms *m/z*: 238 (M – H_2O, 0.7), 196 (0.7), 175 (1), 99 (88), 81 (100). *Anal.* calcd. for $C_{15}H_{28}O_3$: C 70.27, H 11.01%; found: C 70.41, H 11.00%; and *trans,trans*-2-oxypropyl-2′-hydroxydicyclohexyl ether (**15**) (0.186 g) as an oil; ^1H nmr included signals at δ 1.20 (d, *J* = 6 Hz, isopropyl methyls), 3.0–3.6 (3H, m, C-1, -1′, and -2′ H's) and 3.80 (1H, septet, *J* = 6 Hz, isopropyl CH) ppm; ^{13}C nmr, see Table 2; ms *m/z*: 196 (1), 175 (2.5), 99 (85), 81 (100). *Anal.* calcd. for $C_{15}H_{28}O_3$: C 70.27, H 11.01%; found: C 70.40, H 11.04%. Repetition of the reaction with 0.11 g of aluminum isopropoxide afforded only **14** and **15** in the ratio 1.5:1; repetition with 0.04 g of aluminum isopropoxide gave a 4:1 ratio of **14** to **15**.

Acknowledgements

We are grateful to Mr. T. Jones (Brock) and Mr. B. Sayer (McMaster) for their assistance in obtaining spectra, and to the Southwestern Ontario NMR Centre, Guelph, for their services. Financial support was provided by the Natural Sciences and Engineering Research Council of Canada.

1. P. G. GASSMAN and R. S. GREMBAN. Tetrahedron Lett. **25**, 3259 (1984).
2. E. W. ABAEL and D. J. WALKER. J. Chem. Soc. 2338 (1968).
3. H. B. HENBEST and T. I. WRIGLEY. J. Chem. Soc. 4596 (1957); 4765 (1957).
4. C. W. SHOPPEE, M. E. H. HOWDEN, R. W. KILLICK, and G. H. R. SUMMERS. J. Chem. Soc. 630 (1959).
5. I. G. GUEST and B. A. MARPLES. J. Chem. Soc. (C), 576 (1971).
6. J. W. BLUNT, M. P. HARTSHORN, and D. N. KIRK. Tetrahedron, **25**, 149 (1969).
7. H. L. HOLLAND and JAHANGIR. Can. J. Chem. **61**, 2165 (1983).
8. E. H. ESCHINASI. J. Org. Chem. **35**, 1598 (1970).
9. F. SCHEIDL. Synthesis, 728 (1982).
10. H. MASTALERZ and P. MORAND. J. Chem. Soc. Perkin Trans. 1, 779 (1982).
11. M. ANDO, K. TAJIMA, and K. TAKASE. Chem. Lett. 617 (1978).
12. J. W. BLUNT, M. P. HARTSHORN, and D. N. KIRK. J. Chem. Soc. (C), 635 (1968); B. N. BLACKETT, J. M. COXON, M. P. HARTSHORN, and K. E. RICHARDS. Tetrahedron, **25**, 4999 (1969).
13. J. W. BLUNT and J. B. STOTHERS. Org. Magn. Reson. **9**, 439 (1977).
14. H. L. HOLLAND and JAHANGIR. J. Org. Chem. **48**, 3134 (1983).
15. D. N. KIRK and M. P. HARTSHORN. Steroid reaction mechanisms. Elsevier, London. 1968. p. 145.
16. G. H. POSNER, D. Z. ROGERS, C. M. KINZIG, and G. M. GURRIA. Tetrahedron Lett. 3597 (1975).
17. V. S. JOSHI, N. P. DOMODARAN, and S. DEV. Tetrahedron, **27**, 459 (1971).
18. C. W. DAVEY, E. L. MCGINNIS, J. M. MCKEOWN, G. D. MEAKINS, M. W. PEMBERTON, and R. N. YOUNG. J. Chem. Soc. (C), 2674 (1968).
19. J. W. BLUNT, J. M. COXON, N. B. LINDLEY, and G. A. LANE. Aust. J. Chem. **29**, 967 (1976).
20. V. PRELOG and E. TAGMANN. Helv. Chim. Acta, **27**, 1880 (1944).
21. M. ISHIGE and M. SHIOTA. Can. J. Chem. **58**, 1061 (1980).
22. V. PRELOG, L. RUZIKA, and P. STEIN. Helv. Chim. Acta, **26**, 2222 (1943).

Synthesis of coleon C tri-*O*-methyl ether

ROBERT H. BURNELL, ANDRÉ ANDERSEN, MARTINE NÉRON, AND SYLVAIN SAVARD
Chemistry Department, Université Laval, Québec (Qué.), Canada G1K 7P4

Received February 20, 1985

ROBERT H. BURNELL, ANDRÉ ANDERSEN, MARTINE NÉRON, and SYLVAIN SAVARD. Can. J. Chem. **63**, 2769 (1985).

Starting from podocarpic acid, two model preparations are described leading to *p*-quinones suitably functionalized as intermediates in the synthesis of coleon C. The proper *p*-quinone was obtained by a regio- and stereo-selective route and, following steps previously found effective for the preparation of coleon U, a synthesis of tri-*O*-methyl coleon C has been achieved. Some of the by-products encountered have also been identified.

ROBERT H. BURNELL, ANDRÉ ANDERSEN, MARTINE NÉRON et SYLVAIN SAVARD. Can. J. Chem. **63**, 2769 (1985).

À partir de l'acide podocarpique, nous avons réalisé selon deux méthodes différentes, la préparation de modèles de *p*-quinones semblables aux intermédiaires de synthèse de la coléone C. Ensuite nous avons préparé, par une voie régio- et stéréo-sélective, une *p*-quinone possédant toutes les fonctions necessaires. Elle fut transformée en dérivés de la coléone C par une séquence réactionnelle antérieurement élaborée, lors de la synthèse de la coléone U.

The yellow pigment coleon C was isolated from *Coleus aquaticus* Gürcke by Eugster and his co-workers (1) who assigned to it the structure **1**. In unambiguous fashion they later defined the relative and absolute stereochemistry of the two chiral centres (C-10 and C-15) by X-ray diffraction (2). From the synthetic viewpoint the molecule presents the normal skeletal challenge and also the problem of obtaining selectively the *R* configuration in the side chain. Our previously reported method for elaborating the properly functionalized cyclic system (3) (such as found in coleon U) should lend itself to the synthesis of coleon C but first it would be necessary to obtain the key quinone intermediate **6***b*.

To determine the best preparation of the quinone, we chose to experiment with ester-containing analogues because these are more immediately available from podocarpic acid, allowing the saving of both time and material. Two avenues were investigated. The first started from the benzofuran **3***c* described by Cambie *et al.* (4), whose preparation involved cyclization of the acid derivative **2***b*, which was prepared from the corresponding ester **2***c*. We felt that this procedure could be streamlined in that the cyclization of the ester **2***c* could be effected during its formation, leading directly to the furan-ester **3***a*. Such was the case. In fact, we obtained both the benzofuran **3***c* and the furan-ester **3***a* which, by subsequent hydrolysis to the

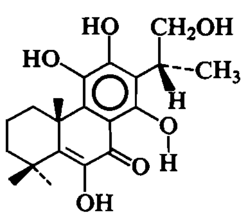

1

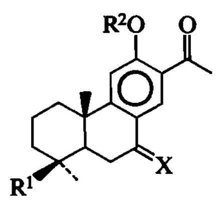

	R^1	R^2	X
2*a*	R^1 = COOMe,	R^2 = H	X = H, H
2*b*	COOMe	CH_2COOH	H, H
2*c*	COOMe	CH_2COOEt	H, H
2*d*	CH_3	H	=O

acid **3***b* and decarboxylation, gave more of the desired furan **3***c* but in unoptimized yields that fell short of Cambie's procedure. The furan double bond was then reduced catalytically to give a 4:1 mixture of C-15 epimers **4***a* (as reflected by the nmr). From examination of molecular models, it is clear that hydrogenation must be from the convex β face of the furan **3***c*, enabling us to affirm that the C-15 methyl group is α in the major product. We were unable to separate the epimers efficiently at this stage. Hence the C-7 position was oxidized to afford the epimeric ketones **5***a*. Treatment of the latter with peracetic acid (prepared *in situ*) gave two quinones **6***a* and **6***c* but in subsequent oxidations in similar ketones we were able to avoid the hydrolysis of the *O*-acetyl residue. The highly polar **6***c* was tiresome to manipulate. It was only after we had handled the epimeric quinone **10***a*, as the result of the method to be described shortly, that we were able to isolate it from the mother liquors of this reaction, thus confirming that the dihydrofuran **4***a* did contain both epimers. In a previously conceived strategy, which was abandoned after the utility of the peracid oxidation became apparent, we had reduced the ketone **5***a* to the alcohol **4***b*, which was dehydrated to the olefin **4***c*.

In our second trial quinone synthesis, the known isopropenyl derivative **7***a*, prepared by Cambie's method (5), was subjected to hydroboration/oxidation to afford the primary alcohol **8***a* in which the stereochemistry at C-15 is established. No important stereo-induction can be invoked, so the reaction must give rise to about equal amounts of the C-15 epimers. The alcohol was protected by conversion to the acetate **8***b*, which was oxidized at the benzylic position (C-7) affording the ketone **9***a*. When subjected to peracetic acid oxidation, the latter underwent, first, rupture of the C-7—C-8 bond, followed by further hydrolysis/oxidation to give the two *para*-quinones **6***a* and **10***a*. The ^{1}H nmr spectrum confirmed that the mixture contained equal quantities of the epimers. Isolation of one isomer (**6***a*) in high yield was easy, while the other proved more elusive. We felt that by using chiral boranes, this preparation could have given us the C-15 epimer of our choice.

The appropriate quinone for the coleon C synthesis, with geminal methyl groups at C-4, was prepared by both of the model sequences described. Only the more successful is detailed in the Experimental. The ^{13}C nmr data for the compounds encountered in the other approach (**7***b*, **8***c*, **8***d*, and **9***b*) are included in Table 1. The more rewarding stereoselective route involving the benzofuran afforded a 4:1 preference for the

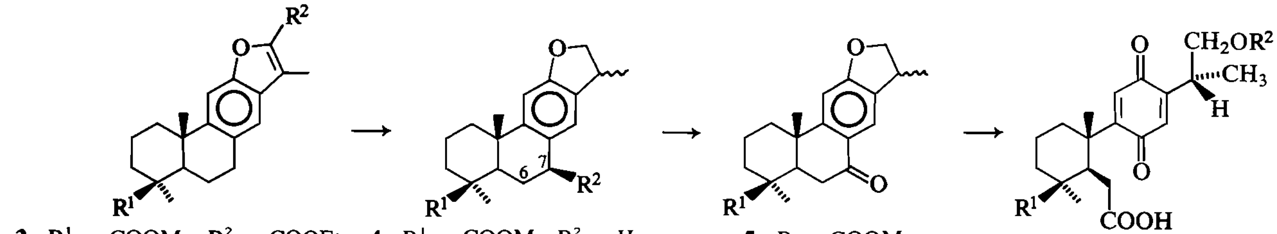

3a R^1 = COOMe R^2 = COOEt
3b COOMe COOH
3c COOMe H

4a R^1 = COOMe R^2 = H
4b COOMe OH
4c COOMe H 6,7-double bond
4d CH_3 H

5a R = COOMe
5b CH_3

6a R^1 = COOMe R^2 = Ac
6b CH_3 Ac
6c COOMe H

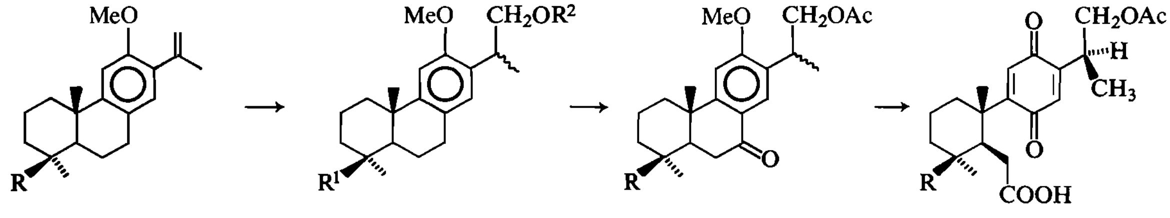

7a R = COOMe
7b CH_3

8a R^1 = COOMe R^2 = H
8b COOMe Ac
8c CH_3 H
8d CH_3 Ac

9a R = COOMe
9b CH_3

10a R = COOMe
10b CH_3

C-15(*R*) epimer, which again was the easier one to isolate. In another context (3), we had already prepared the ketone **5*b*** by oxidation of the dihydrobenzofuran **4*d***. In repeating this work we were surprised to find that the oxidation affords not only the ketone **5*b*** but also the hydroxy-acetophenone **2*d***, which we had previously isolated in small quantities and assumed to be an impurity in the starting material. As had been noticed with the ester analogs (**6*a*** and **10*a***), the two quinones **6*b*** and **10*b*** were similar in many of their physical properties but they showed marked differences in their ^{1}H nmr spectra. One peculiarity of the nmr of **10*b*** was that significant changes were noted in the spectrum on varying the concentration in $CDCl_3$. The protons in the side chain were particularly sensitive. Many of the transformations described in the following paragraphs were actually performed on both C-15 epimers, but in the text and in the drawings only the C-15(*R*) isomer will be portrayed. To not overburden the experimental section, only the C-15(*R*) experiments are described. The results for the C-15(*S*) compounds are available elsewhere (6). We should point out that at the time we were completing this synthesis, the "natural" coleon C was reputedly the C-15(*R*) epimer but, from the published nmr spectrum, we felt that it contained the C-15(*S*) isomer also (*two* methyl doublets). This turned out to be true, as Eugster and co-workers have pointed out in a recent paper (7).

The subsequent steps needed to transform the quinone **6*b*** to the coleon C derivative (**24*a***) followed methods elaborated on models and used to synthesize coleon U (3). In all previous cases, the side chain on the aromatic ring was an isopropyl residue and the steps involved were highly regioselective. In the present synthesis, however, we isolated several minor products from some of the reactions, indicating that the more substantial side chain competes more effectively with the other substituent (ring A and its appendages). In the addition of bromine to the quinone **6*b*** the major product was the dibromo derivative **12**, which almost spontaneously eliminated hydrogen bromide to afford the bromoquinone **16**. Rather than manipulate the fragile dibromo compound, we treated the crude mixture with diethylamine and in the subsequent purification we obtained the required bromoquinone **16** and only trace amounts of the isomeric bromoquinone **17**. Thus the bromination had given rise to little of the alternate dibromo derivative **13**. It is likely that the tetrabromo compound **14** was also formed and, while we could never isolate it, we did obtain substantial amounts of the dibromolactone **18** that must arise from the displacement of the relevant bromo substituent in **13**, or its equivalent, by the carboxylic function.

To replace the bromo substituent in the bromoquinone **16**, it was treated with mild aqueous base containing sufficient methanol to render the substrate soluble. The resulting hydroxyquinone **15*a*** was accompanied by minor quantities of the methoxyquinone **15*b***. The ^{13}C nmr spectra leave no doubt as to the identity of these compounds. Both quinones (**15*a*** and **15*b***) were catalytically reduced to the corresponding hydroquinones and these were *O*-methylated, while still in the hydrogenation apparatus, to avoid their re-oxidation by air during the work-up. The product was mostly the ester **19*a*** (55%) but some incompletely methylated compounds were also obtained. By further methylation of the relevant fractions, an additional quantity (22%) of the ester **19*a*** was made available to continue the synthesis. The major partially methylated intermediate, and the only one obtained pure enough to ascertain the structure, was the phenol **20** (see ^{13}C nmr, Table 1).

Some of the products from the original methylation could not be easily reintegrated into the synthesis. One compound, for instance, contained an additional *O*-methyl residue and from spectral evidence must be the product **21*a*** in which the primary alcohol function has also suffered alkylation. The final unexpected methylation by-product displayed (as seen from the nmr and other spectra) two phenolic methoxyls and the methyl ester but no primary hydroxyl nor phenol residues. The great similarity of the ^{1}H nmr spectrum to that of dihydrobenzofurans such as **4*a*** and **4*d*** showed that the product must have cyclized during the reaction. Compound **22*a***, in which the two remaining methoxyl groups were adjacent, seemed the more likely of the two possible structures, an assumption that was confirmed later.

The ester **19*a*** was hydrolysed to the corresponding acid **19*b***.

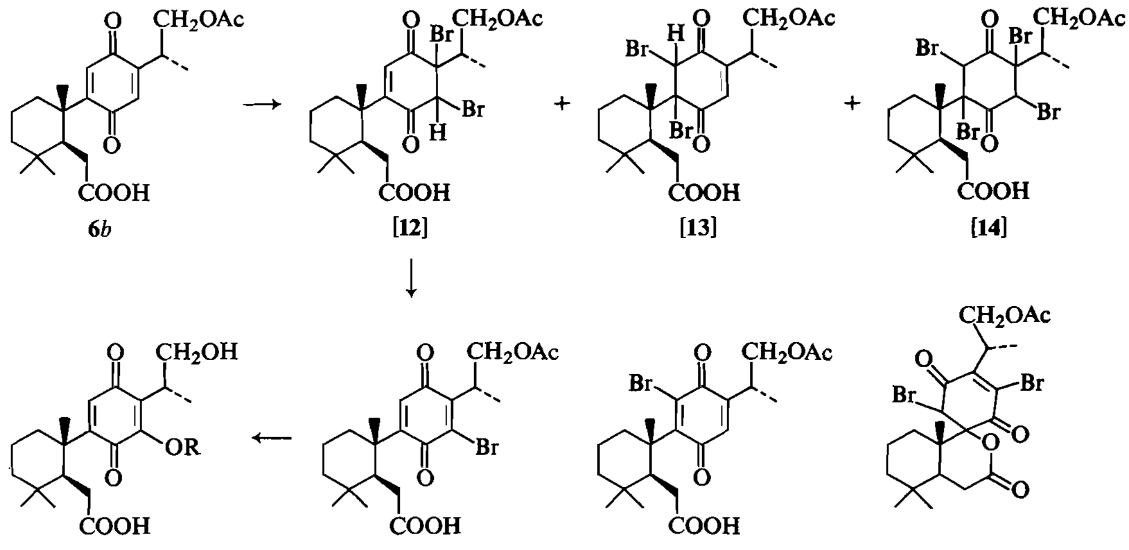

6b [12] [13] [14]

15a R = H
15b R = Me
16 17 18

The latter cyclized readily in trifluoroacetic anhydride at room temperature to the aromatic ketone **23**a. As in our previous syntheses in this field, the final oxygen was introduced by stirring the ketone **23**a in anhydrous strong base in the presence of oxygen, which afforded the coleon C tri-*O*-methyl ether **24**a in modest yield (49%). This particular derivative is not described in the literature, since in the characterization of coleon C the strongly hydrogen-bonded C-14 hydroxyl group resists methylation. Our ether was identical with the trimethyl ether obtained via coleon D, as shown by thin-layer chromatography using several different solvent systems (we are grateful to Professor C. H. Eugster, Zürich, for the sample of coleon D). The tetra-*O*-methyl coleon C derivative was also prepared. There was a second product in the oxygenation reaction, which proved to be the enolized diketone **25** that we prepared later from the cyclized ester **22**a. Repeating this part of the synthesis on a larger scale, as described in the Experimental, we were surprised that our rigorously pure ester **19**a gave rise to a significant quantity (26%) of this tetracyclic diosphenol **25**. The five-membered ring must be closed during the oxygenation in strong base.

Both of the fortuitously isolated esters, **21**a and **22**a, were hydrolysed to the acids **21**b and **22**b, respectively, and these were cyclized to the aromatic ketones **23**b and **26**. Oxygenation of the tetracyclic ketone **26** in *tert*-butanol containing potassium *tert*-butoxide gave the diosphenol **25** that had previously been isolated from the oxidation of ketone **23**a. Had the cyclization of the five-membered ring involved the C-12 hydroxyl (or methoxyl) rather than the C-14 position, the product would have been a derivative of the naturally occurring lycoxanthol (8).

During this work we found the ^{13}C nmr spectra to be of great importance in the assigning of structures to the synthetic products. These data are grouped in Table 1. The resonances were assigned by using Enzell's listing of certain diterpenoid spectra (9) and adding our own accumulated experience arising from our synthetic projects in this field (10a–c).

Experimental

Unless otherwise stated, the conditions and instruments used to characterize the products were melting points, Electrothermal, uncorrected; ultraviolet spectra, ethanol solutions (log ϵ in parentheses), Hewlett Packard 8450A; infrared spectra, solids as KBr pellets, others as carbon tetrachloride solutions, Beckman 4250 and Perkin Elmer 457; proton magnetic resonance spectra, deuteriochloroform solutions, TMS internal standard, (multiplicity, integrated peak areas—where important, coupling constants and assignments in parentheses: D_2O infers that resonances were no longer detectable after shaking the solution for a few minutes with deuterium oxide), Bruker HX 90; carbon-13 magnetic resonance spectra, deuteriochloroform solutions, TMS internal standards, Bruker WP 80; mass spectra, Hewlett Packard 5992; high resolution mass spectra were recorded on an AEI MS30. Elemental analyses were by Galbraith Laboratories, Knoxville, Tenn.

Dry column chromatography (abbreviated dry col chrom) implies that use of Merck Kieselgel 60F (70–230 mesh) in nylon foil tubing and development with either hexane – ethyl acetate or carbon tetrachloride – ethyl acetate (proportions determined by prior thin-layer chromatography using Machery–Nagel pre-coated plastic sheets).

*Benzofuran 3*c *and furan-ester 3*a

The hydroxy-acetophenone **2**a (28.3 g, prepared following Cambie *et al.* (4)) was dissolved in acetone (700 mL) to which was then added ethyl bromoacetate (43.6 mL) and anhydrous potassium carbonate (88.6 g). After 24 h the reaction appeared very slow (tlc), so the acetone was slowly distilled and the residue then heated to 140°C in an oil bath for 24 h. The mixture was then taken up in ether, which was well washed, and the residue, after drying and evaporation, was filtered through a short column of alumina (act. III) that removed much of the color, and was then chromatographed over silica gel (dry col). The benzene eluate contained the furan-ester **3**a (5.16 g: 15%), which crystallized, and the benzofuran **3**c (6.21 g: 22%) from the mother liquors. *7(β)-Methoxycarbonyl-3,7(α),10a(β)-trimethyl-5,6,6a,7,8,9,10,10a-octahydrophenanthro[3,2-*b*]furan* **3**c, mp 130–131°C (from hexane); ir: 1722, 1635, and 1580 cm^{-1}; ^{1}H nmr δ: 1.06 and 1.26 (2s, Me-C), 2.16 (d, J = 1 Hz, Me-arom), 3.64 (s, COOMe), 7.17 and 7.36 (2s, arom H), and 7.30 (d, J = 1 Hz, furan H); ^{13}Cmr, see Table 1. *Anal.* calcd. for $C_{21}H_{26}O_3$: C 77.28, H 8.03; found: C 77.28, H 8.04. *2-Ethoxycarbonyl-7(β)-methoxycarbonyl-3,7(α),10a(β)-trimethyl-5,6,6a,7,8,9,10,10a-octahydrophenanthro[3,2-*b*]furan* **3**a, mp 161–163°C (from methanol); ir: 1723, 1638, and 1600 cm^{-1}; ^{1}H nmr δ: 1.07 and 1.30 (2s, Me-C), 1.43 (t, J = 7 Hz, Me-CH_2), 2.54 (s, Me-arom), 3.67 (s, COOMe), 4.43 (q, J = 7 Hz, CH_3CH_2O—), 6.93 and 7.14 (2s, arom H); ^{13}Cmr, see Table 1. *Anal.* calcd. for $C_{24}H_{30}O_5$: C 72.33, H 7.59; found: C 72.30, H 7.80.

TABLE 1. ^{13}C nuclear

Carbon	*2c*	*3a*	*3b*	*3c*	*4a*	*4b*	*4c*	*4d*	*5a*	*5b*	*6a*	*6b*	*7a*	*7b*	*8a*	*8b*	*8c*
1	39.1	40.0	40.0	40.1	39.9	39.5	37.4	39.2	39.1	38.0	37.0	37.2	39.7	39.1	39.7	39.7	39.1
2	20.0	20.2	20.1	20.2	20.1	19.9	19.8	19.4	19.7	18.9	19.6	18.8	20.0	19.3	20.1	20.1	19.3
3	37.6	37.7	37.7	37.7	37.8	37.5	36.4	41.8	37.6	35.9	36.0	40.9	37.8	41.9	37.8	37.8	41.9
4	44.1	44.1	44.2	44.1	44.1	43.7	43.6	33.4	44.0	33.3	44.8	33.7	44.0	33.4	44.1	44.0	33.4
5	52.5	52.9	52.9	53.2	53.2	50.3	51.6	50.6	50.5	49.5	46.0	44.7	53.0	50.6	53.0	53.0	50.6
6	21.0	21.2	21.2	21.4	21.3	32.3	125.6	19.4	37.3	s[b]	33.0	31.9	21.2	19.3	21.2	21.3	19.3
7	31.0	32.3	32.3	32.3	31.9	71.5	127.0	30.2	197.6	198.1	180.4	177.1	31.2	33.5	31.4	31.4	33.4
8	129.1	127.1	127.1	127.1	127.3	130.9	126.2	127.3	125.0	125.1	188.3	187.4	127.5	127.2	127.6	127.3	127.4
9	154.3	149.6	150.5	145.3	148.2	148.4	147.7	150.3	157.3	158.9	152.9	154.8	148.1	150.3	147.1	147.2	149.2
10	39.4	39.5	40.0	39.0	38.9	39.5	38.4	38.2	38.7	38.5	43.9	43.0	38.6	38.1	38.6	38.6	38.0
11	109.7	108.7	108.9	107.8	106.1	105.6	104.5	105.1	105.1	104.2	135.3	134.6	108.4	107.8	107.9	107.8	107.1
12	155.4	153.8	154.3	154.8	158.6	159.6	159.8	158.4	165.4	165.2	188.0	187.2	155.3	155.3	155.9	155.8	155.8
13	126.7	131.0	131.4	129.7	130.2	130.8	129.5	129.7	131.6	130.9	152.9	146.4	127.5	130.4	129.7	129.0	129.4
14	131.4	120.6	120.8	118.8	124.1	122.3	122.0	124.0	123.5	123.7	133.4	135.9	130.0	129.8	128.0	128.0	128.0
15	199.2	125.2	127.9	115.0	36.4	36.4	36.4	36.5	35.7	35.9	26.3	31.8	144.0	144.1	35.3	32.1	35.3
16	31.9	9.3	9.6	7.8	19.1	19.1	19.1	75.6	19.1	79.6	21.4	66.7	114.7	114.6	67.9	68.6	68.0
17	(66.0)	141.1	140.2	141.5	78[s]	78.8	78.8	19.1	79.7	19.2	21.4	14.7	28.5	23.2	16.7	17.0	16.6
18	28.5	28.5	28.7	28.6	28.7	28.5	27.9	33.4	28.1	32.6	28.6	33.7	28.5	29.6	28.6	28.5	29.8
19	177.7	177.7	177.9	177.8	178.1	177.7	177.7	21.7	177.1	23.2	177.7	22.8	178.0	21.7	178.0	177.6	21.7
20	22.8	23.6	23.7	23.5	22.9	22.9	19.1	24.6	21.3	21.4	18.7	19.8	22.9	24.7	22.9	22.9	24.7
COOMe (C-4)	51.3	51.2	51.4	51.1	51.2	51.3	51.6	—	51.5	—	51.7	—	51.2	—	51.2	51.0	—
OMe (11)	—	—	—	—	—	—	—	—	—	—	—	—	—	—	—	—	—
OMe (12)	—	—	—	—	—	—	—	—	—	—	—	—	55.8	55.8	55.6	55.4	55.6
OMe (14)	—	—	—	—	—	—	—	—	—	—	—	—	—	—	—	—	—
Others	168.5	160.7	165.9	—	—	—	—	—	—	—	—	173.9	—	—	—	170.7	—
	61.4	60.9	—	—	—	—	—	—	—	—	—	21.3	—			20.7	
	14.2	14.4	—	—	—	—	—	—	—	—	—						

[a]In ppm from TMS.
[b]s: peak obscured by the solvent.

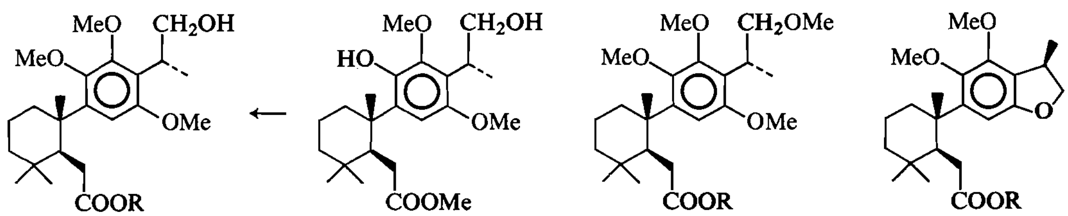

19*a* R = Me
19*b* R = H

20

21*a* R = Me
21*b* R = H

22*a* R = Me
22*b* R = H

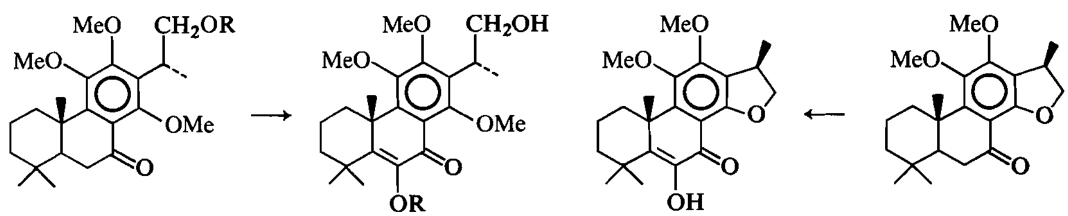

23*a* R = H
23*b* R = Me

24*a* R = H
24*b* R = Me

25

26

*Hydrolysis of the furan-ester 3*a *to the acid 3*b

To a solution of the ester **3***a* (0.475 g) in ethanol (15 mL) was added aqueous sodium hydroxide (3 mL of 10%). After refluxing for 1 h, the cooled solution was acidified (dilute hydrochloric acid) and the white precipitate was filtered, dried, and crystallized from methanol affording the *2-carboxy-7(β)-methoxycarbonyl-3,7(α),10a(β)-trimethyl-5,6,6a,7,8,9,10,10a-octahydrophenanthro[3,2-*b*]furan* **3***b*, mp 228–231°C (0.425 g: 96%); ir: 3300 (br), 1735, 1720, and 1675 cm^{-1}; ^{1}H nmr δ: 1.07, 1.30, and 2.57 (3s, Me-C), 3.68 (s, COOMe), 7.27 and 7.53 (2s, arom H), and 11.04 (br s, COOH, D_2O); ^{13}Cmr, see Table 1; mass spectra *m/e*: 370 (M^+), 355, and 327. *Anal.* calcd. for $C_{22}H_{26}O_5$: C 71.33, H 7.08; found: C 71.49, H 7.08.

*Decarboxylation of the acid 3*b

Copper powder (5 mg) was added to the acid **3***b* (112 mg) dissolved in quinoline (2 mL). The mixture was stirred for 2.5 h while the temperature was increased from 145 to 205°C. The cooled solution was treated with ice (25 g) and concentrated hydrochloric acid (20 mL) and then extracted with ether. The dark oil so obtained was chromatographed over alumina (act. III). The benzene eluate afforded the benzofuran **3***c* (70 mg: 72%), identical with that obtained earlier.

*Catalytic hydrogenation of the benzofuran 3*c

The benzofuran **3***c* (8.0 g) was dissolved in glacial acetic acid (400 mL) and 10% palladium on carbon (4.0 g) was introduced. The mixture was shaken under 3 atmospheres (1 atm = 101.3 kPa) of hydrogen for 4 h and the catalyst then filtered over Celite. The solvent was removed under vacuum and the white residue crystallized from hexane to give the dihydrofuran **4***a* (7.78 g: 97%; *7(β)-methoxycarbonyl-3,7(α),10a(β)-trimethyl-2,3,5,6,6a,7,8,9,10,10a-decahy-*

magnetic resonance data[a]

Compound																		
8*d*	**9*a***	**9*b***	**10*a***	**10*b***	**15*a***	**15*b***	**16**	**18**	**19*a***	**19*b***	**20**	**21*a***	**21*b***	**23*a***	**23*b***	**24*a***	**24*b***	**25**
39.1	37.7	38.4	36.1	36.7	36.3	36.9	38.6	40.2	37.5	37.3	36.3	37.5	37.2	37.8	38.0	28.0	29.0	28.2
19.3	19.7	18.9	18.7	18.7	18.7	18.8	18.7	18.7	19.5	19.4	19.5	19.4	19.4	19.4	19.5	18.7	18.5	18.4
41.8	38.9	41.5	37.2	40.8	41.0	41.0	40.5	40.6	41.6	41.5	41.5	41.6	41.4	41.3	41.3	36.8	37.5	37.0
33.4	44.1	33.4	44.9	34.0	34.0	34.0	34.2	33.4	34.7	34.8	34.6	34.6	34.8	33.6	33.6	36.4	36.8	36.5
50.6	50.6	49.7	46.1	44.6	44.8	44.7	44.4	44.0	46.3	46.3	45.0	46.2	46.2	49.0	49.1	140.6	145.8	141.1
19.3	37.5	36.0	32.9	32.3	32.2	32.3	32.4	29.0	33.1	33.1	32.9	33.1	33.1	37.2	37.4	143.6	150.2	143.1
33.5	197.6	198.2	178.7	179.0	178.0	178.2	178.9	168.9	175.0	179.8	175.0	174.9	180.4	198.5	198.4	178.8	179.7	178.8
127.2	124.3	124.4	187.6	187.5	183.5	183.4	179.8	185.7	107.6	107.6	108.7	107.6	107.4	122.6	122.6	117.2	130.7	108.8
149.3	155.6	157.3	153.2	154.6	153.4	153.4	154.8	90.3	147.5	147.5	142.9	147.4	147.4	147.7	147.7	147.9	153.8	147.1
38.0	38.7	38.0	43.8	43.2	43.0	43.4	44.1	43.0	43.3	43.4	43.0	43.3	43.4	41.3	41.3	41.6	42.4	42.1
106.8	105.9	104.9	135.5	134.9	136.5	134.3	134.6	52.6	140.8	140.6	133.8	140.3	140.2	148.2	148.0	147.7	147.7	144.7
155.6	162.2	162.1	187.4	187.5	187.7	188.6	184.5	188.0	153.3	153.3	147.1	153.3	153.5	157.0	157.0	156.1	155.3	155.3
128.6	130.3	129.8	147.4	147.1	150.6	159.1	146.9	153.0	124.8	124.8	123.1	125.2	125.3	130.2	130.9	131.7	130.7	124.4
128.0	127.2	127.3	136.1	136.2	124.0	130.4	140.8	140.8	153.3	153.3	151.3	153.1	153.1	157.8	157.9	157.8	156.8	157.5
32.0	32.1	32.0	34.0	33.4	31.8	32.3	36.6	35.8	33.8	33.7	33.6	31.1	31.0	34.1	31.5	30.2	30.1	34.9
68.8	68.3	68.3	67.0	67.0	65.2	65.7	66.4	66.4	66.9	66.7	66.7	76.9	76.7	67.0	77.2	66.9	66.9	80.6
17.0	16.8	16.8	15.9	15.7	14.0	14.6	15.1	15.5	16.1	16.1	16.0	16.8	16.8	16.7	17.4	16.8	16.8	19.5
29.8	28.0	29.7	28.7	33.9	33.7	33.6	33.3	32.6	33.8	33.7	34.6	33.8	33.7	33.1	33.1	34.1	34.0	32.2
21.7	177.1	21.4	177.7	22.8	22.5	22.7	22.8	21.4	23.0	23.0	22.9	22.9	23.0	21.7	21.7	27.4	29.6	27.4
24.8	21.4	23.3	19.7	20.0	19.6	20.0	20.4	13.2	21.4	21.5	20.7	21.4	21.4	19.8	19.9	32.8	32.9	29.8
—	51.5	—	51.6	—	—	—	—	—	—	—	—	—	—	—	—	—	—	—
—	—	—	—	—	—	—	—	—	59.6	59.6	—	59.5	59.7	59.9	60.1	59.8	59.8	60.3
55.5	55.6	55.5	—	—	—	—	—	—	60.1	60.0	61.9	60.0	59.9	60.1	60.1	60.2	60.2	60.7
—	—	—	—	—	—	—	—	—	56.1	56.1	56.3	56.1	56.0	62.8	62.7	62.5	62.6	—
171.0		171.1	171.9	172.1	—	—	171.2	170.3	51.0	—	51.0	51.0	—	—	—	—	58.8	—
20.9	20.8	20.9	20.9	21.0			20.9	20.8				58.5	58.5		58.7			

*drophenanthro[3,2-*b*]furan*), mp 149–150°C; ir: 1720 cm^{-1}; ^{1}H nmr δ: 1.01 and 1.24 (2s, Me-C), 1.28 (d, J = 8 Hz, Me-CH), 3.46 (m, 1H, C15-H), 3.63 (s, COOMe), 4.00 (dd, J = 8 and 9 Hz) and 4.62 (dd, J = 9 and 9 Hz, —CH_2O—), 6.68 and 6.81 (2s, arom H); ^{13}Cmr, see Table 1; mass spectra *m/e*: 328 (M^+), 313, 269, and 253. *Anal.* calcd. for $C_{21}H_{28}O_3$: C 76.79, H 8.59; found: C 76.98, H 8.76.

*Oxidation to the ketone 5*a

The dihydrofuran **4*a*** (656 mg) in glacial acetic acid (20 mL) was treated drop by drop with a solution of chromium trioxide (400 mg) in acetic acid (4 mL of 80%). After 45 min at room temperature, the solution was poured onto ice and the product obtained by ether extraction. The oil was chromatographed over alumina (act. III) affording the ketone **5*a*** as an oil which crystallized on contact with hexane (506 mg: 73%; *7(β)-methoxycarbonyl-5-oxo-3,7(α),10a(β)-trimethyl-2,3,5,6,6a,7,8,9,10,10a-decahydrophenanthro[3,2-*b*]furan*), mp 142–144°C; ir: 1720 and 1675 cm^{-1}; ^{1}H nmr δ: 1.10 and 1.27 (2s, Me-C), 1.35 (d, J = 8 Hz, Me-CH), 3.54 (m, C15-H), 3.71 (s, COOMe), 4.13 (dd, J = 8 and 9 Hz) and 4.76 (dd, J = 9 and 9 Hz, —CH_2O—), 6.78 and 7.91 (arom H at C11 and C14 resp.); ^{13}Cmr, see Table 1; mass spectra *m/e*: 342 (M^+), 327, 282, and 266. *Anal.* calcd. for $C_{21}H_{26}O_4$: C 73.66, H 7.66; found: C 73.35, H 7.36.

*Sodium borohydride reduction of ketone 5*a

To the refluxing solution of the ketone **5*a*** (0.7 g) in aqueous methanol (70 mL of 75%) containing sodium hydroxide (0.53 g) was added sodium borohydride (0.25 g) in 1 *N* aqueous sodium hydroxide (21 mL). After refluxing for 2.5 h, the cooled solution was neutralized with dilute acetic acid and the white solid alcohol **4*b*** was collected by filtration and crystallized from methanol (0.65 g: 92%; *7(β)-methoxycarbonyl-5(β)-hydroxy-3,7(α),10a(β)-trimethyl-2,3,5,6,6a,7,8,-9,10,10a-decahydrophenanthro[3,2-*b*]furan*), mp 186–190°C; ir: 3450 and 1708 cm^{-1}; ^{1}H nmr δ: 1.06 and 1.26 (2s, Me-C), 1.30 (d, J = 8 Hz, Me-CH), 2.20 (s, 1H, OH, D_2O), 3.50 (m, C15-H), 3.64 (s, COOMe), 4.02 (dd, J = 9 and 9 Hz) and 4.65 (dd, J = 9 and 9 Hz, —CH_2O—), 4.67 (dd, J = 10 and 6 Hz, *C*H—OH), 6.67 and 7.50 (2s, arom H); ^{13}Cmr, see Table 1; mass spectra *m/e*: 344 (M^+), 329, 326, 267, and 251. *Anal.* calcd. for $C_{21}H_{28}O_4$: C 73.22, H 8.19; found: C 73.47, H 8.28.

*Dehydration of alcohol 4*b

This is essentially Wenkert's method (11). The alcohol **4*b*** (250 mg) was heated to 50°C for 30 min in benzene (25 mL) containing *p*-toluene sulfonic acid monohydrate (90 mg) and anhydrous calcium chloride (150 mg). The mixture was then washed with aqueous sodium bicarbonate, dried, and evaporated. The solid was purified by dry col chrom to give the tetraene **4*c*** (220 mg: 91%; *7(β)-methoxycarbonyl-3,7(α),10a(β)-trimethyl-2,3,6a,7,8,9,10,10a-octahydrophenanthro-[3,2-*b*]furan*), mp 138–140°C (from hexane); ir: 3040 and 1720 cm^{-1}; ^{1}H nmr δ: 0.85 and 1.30 (2s, Me-C), 1.32 (d, J = 8 Hz, Me-CH), 3.48 (m, C15-H), 3.68 (s, COOMe), 4.04 (dd, J = 9 and 8 Hz) and 4.67 (dd, J = 9 and 9 Hz, —CH_2O—), 6.37 (m, 2H, C6 and C7 olefinic H), 6.71 and 6.86 (2s, arom H); ^{13}Cmr, see Table 1. *Anal.* calcd. for $C_{21}H_{26}O_3$: C 77.27, H 8.03; found: C 77.17, H 8.18.

*Peracid oxidation of ketone 5*a *(formation of quinones 6*a *and 6*c*)*

The reagent is prepared by adding hydrogen peroxide (10 mL of 30%) dropwise to a cooled solution of concentrated sulfuric acid (0.2 mL) in acetic anhydride (23 mL). After standing overnight, the peracid is slowly added to the cooled solution of the ketone **5*a*** (1.0 g) in acetic anhydride (20 mL). The mixture was allowed to warm to room temperature and stirring was continued for 7 h; it was then poured onto ice and stirred for 12 h, during which time a yellow solid precipitated. The latter was filtered and chromatographed to give the quinone **6*a*** (293 mg: 23%; *2-{2-[4-(2-acetoxy-1-methylethyl)-2,5-benzoquinone]-yl-6-methoxycarbonyl-2,6-dimethylcyclohexyl}ethanoic acid*), mp 140–141°C (from methanol): $[\alpha]_D^{20}$ −10° ($CHCl_3$); ir: 3200 (br), 1730, 1712, 1660, 1640, and 1605 cm^{-1}; ^{1}H nmr δ: 1.06 and 1.27 (2s, Me-C), 1.23 (d, J = 7 Hz, Me-CH), 2.09 (s, Me—CO—), 3.21 (m, C15-H), 3.69 (s, COOMe), 3.84 (dd, J = 11 and 4 Hz) and 4.79 (dd, J = 11 and 4 Hz, —CH_2O—Ac), 6.43 and 6.61 (2s, olefinic H), and 8.66 (br s, COOH, D_2O); ^{13}Cmr, see Table 1; mass spectra *m/e*: 434 (M^+), 374, and 330. *Anal.* calcd. for $C_{23}H_{30}O_8$: C 63.58, H 6.96; found: C 63.71, H 6.92.

The filtrate from above was extracted with methylene chloride which, after washing and drying, was evaporated to give a yellow oil (740 mg). Dry col chrom of the latter afforded more of the quinone acetate **6***a* (35 mg) and then the primary alcohol **6***c* (380 mg: 30% after recrystallization from ethyl acetate; *2-{2-[4-(2-hydroxy-1-methylethyl)-2,5-benzoquinone]yl-6-methoxycarbonyl-2,6-dimethylcyclohexyl}-ethanoic acid*), mp 191–193°C (orange needles); ir: 3300 (br), 1720, 1650, and 1595 cm^{-1}; ^{1}H nmr (DMSO-d_6) δ: 0.99 and 1.14 (2s, Me-C), 1.07 (d, J = 8 Hz, Me-CH), 3.44 (m, 3H, C15-H and —CH_2O—), 3.63 (s, COOMe), 6.49 and 6.60 (2s, olefinic H); mass spectra m/e: 392 (M$^+$), 376, 362, 348, 330, and 316. *Anal.* calcd. for $C_{21}H_{28}O_7$: C 64.27, H 7.19; found: C 64.02, H 7.11.

The alcohol **6***c* was readily acetylated by acetic anhydride/pyridine at room temperature, affording the acetoxy-quinone **6***a*.

Hydroboration/oxidation of the isopropenyl derivative **7**a

The isopropenyl compound **7***a* (3.47 g: prepared following the method of Cambie *et al.* (5)) was dissolved in THF (6 mL) and cooled to 0°C. Borane – methyl sulfide (0.97 mL of 2 *M* in THF) was added slowly and the solution then stirred at room temperature for 2 h. Aqueous sodium hydroxide (3.4 mL of 3 *N*) was introduced, followed by hydrogen peroxide (1.3 mL of 30%), which was added slowly with cooling. After 1 h at room temperature, the mixture was refluxed for 1 h and then poured into water. Ether extraction gave **8***a* as a yellowish foam that crystallized from ether–hexane as colorless prisms, mp 113–114°C (3.50 g: 96%; *methyl 12-*O*-methyl-13-(2-hydroxy-1-methylethyl)podocarpate*); ir: 1730 cm^{-1}; ^{1}H nmr δ: 1.02 and 1.25 (2s, Me-C), 1.21 (d, J = 7 Hz, Me-CH), 3.36 (m, C15-H), 3.60 (m, 2H, CH_2OH), 3.60 (s, COOMe), 3.71 (s, MeO-Ar), 6.70 and 6.79 (2s, arom H); ^{13}Cmr, see Table 1. *Anal.* calcd. for $C_{22}H_{32}O_4$: C 73.30, H 8.95; found: C 73.32, H 8.91.

Acetylation of **8**a *and oxidation of the acetate* **8**b

The primary alcohol **8***a* (3.50 g) was treated with pyridine (7 mL) and acetic anhydride (7 mL) for 40 h at room temperature. The solution was then poured into ice-water and the product obtained by ether extraction. Dry col chrom gave the acetate **8***b* as an oil which could not be crystallized (3.12 g: 92%; ir: 1735 cm^{-1}; ^{1}H nmr δ: 2.03 s, Me—CO—) and was used as such for the oxidation.

To a solution of the acetate **8***b* (3.62 g) in acetic acid (65 mL) cooled in an ice bath was added, dropwise, chromium trioxide (2.2 g) dissolved in 80% aqueous acetic acid (15 mL). Stirring was continued for 3 h and the mixture was then poured into ice-water, and the product extracted into ether and then crystallized from ether (2.62 g: 70%; *methyl 12-*O*-methyl-13-(2-acetoxy-1-methylethyl)-7-oxo-podocarpate* **9***a*), mp 145–146°C; uv: 228 (4.13) and 276 (4.06) nm; ir: 1725 and 1665 cm^{-1}; ^{1}H nmr δ: 1.12 and 1.24 (2s, Me-C), 1.27 (d, J = 7 Hz, Me-CH), 3.42 (m, C15-H), 3.65 (s, COOMe), 3.85 (s, MeO—Ar), 4.09 (dd, 2H, CH_2O—Ac), 6.74 and 7.80 (2s, arom H at C11 and C14 resp.); ^{13}Cmr, see Table 1. *Anal.* calcd. for $C_{24}H_{32}O_6$: C 69.21, H 7.74; found: C 69.33, H 7.79.

Oxidation of ketone **9**a *to quinones* **6**a *and* **10**a

The reagent was prepared by adding, slowly, hydrogen peroxide (22 mL of 30%) to acetic anhydride (51 mL) containing concentrated sulfuric acid (0.05 mL) maintained at 0°C. Stirring was continued for 24 h and the solution was then added to the cooled solution of the ketone **9***a* (2.57 g) in acetic anhydride (44 mL) over a period of 30 min. After stirring at room temperature for 20 h, the solution was poured onto ice (500 g) and one hour later the product was obtained by ether extraction as a viscous yellow oil (2.24 g). The separation of the two isomers was tedious and involved three successive silica gel columns. In this way, fractions were obtained that contained the pure quinone **6***a* (0.57 g: 19%), identical with that described earlier. The C15(*S*) epimer **10***a* (0.51 g: somewhat slower on the columns: 18%) was also isolated, mp 146–148°C (from methanol); $[\alpha]_D^{20}$ +52° ($CHCl_3$); ir: 3200 (br), 1735, and 1655 cm^{-1}; ^{1}H nmr δ: 1.04 and 1.26 (2s, Me-C), 1.21 and 1.24 (2d, J = 7 Hz, Me-CH), 2.03 (s, Me—CO—), 3.03 (m, C15-H), 3.67 (s, COOMe), 4.07 (dd, J = 11 and 6 Hz) and 4.27 (dd, J = 11 and 5 Hz, CH_2O—Ac), 6.51 and 6.56 (2s, olefinic H), and 10.1 (COOH, D_2O). *Anal.* calcd. for $C_{23}H_{30}O_8$: C 63.58, H 6.96; found: C 63.45, H 6.95.

Formation of ketone **5**b

The ketone **5***b*, prepared as described earlier (3), was identical with that obtained previously (yield 80%) but this time we were able to confirm the identity of a second product **2***d*, *7-oxo-13-acetyl-12-hydroxypodocarpa-8,11,13-triene* in 13% yield, mp 142–143°C (from hexane); uv: 248 (4.46), 279 (4.05), and 324 (3.55) nm; ir: 3400–2600 (broad OH), 1680, and 1650 cm^{-1}; ^{1}H nmr δ: 0.96, 1.01, and 1.24 (3s, Me-C), 1.82 (dd, 1H, J = 11 and 7 Hz, C5-H), 2.56 (dd, 1H, J = 18 and 11 Hz, C6-Hβ), 2.67 (s, Me—CO—), 2.79 (dd, 1H, J = 18 and 7 Hz, C6-Hα), 6.91 (s, C11-H), 8.48 (s, C14-H), and 12.36 (s, OH, D_2O); ^{13}Cmr, see Table 1; mass spectra m/e: 300 (M$^+$), 286, 285, and 217. *Anal.* calcd. for $C_{19}H_{24}O_3$: C 75.97, H 8.05; found: C 75.79, H 8.19.

Quinones **6**b *and* **10**b

A solution of peracid was prepared from hydrogen peroxide (40 mL of 30%), acetic anhydride (92 mL), and concentrated sulfuric acid (0.8 mL) as described above. This solution was stirred at room temperature for 24 h and then cautiously added dropwise to the cooled solution of the ketone **5***b* (7.5 g) in acetic anhydride (90 mL). The temperature was allowed to rise to ambiant while stirring was continued for 20 h. The mixture was poured into ice-water and, after stirring for several hours, the product was obtained by ether extraction (8 g, yellow solid) and chromatographed (silica gel, hexane – ethyl acetate, 7:3) affording some starting material **5***b* (0.51 g), the mixture of quinones **6***b* and **10***b* (5.13 g), and a mixture of the two quinones in which the primary acetate had been hydrolysed (1.63 g). The latter mixture was acetylated by dissolving in pyridine (15 mL), adding acetic anhydride (20 mL), and stirring at room temperature overnight. A normal work-up afforded the mixture of **6***b* and **10***b* (1.61 g), which was combined with the previous amount and chromatographed again to give first the major *R* component **6***b* (4.3 g: 47%), the *S* isomer **10***b* (1.5 g: 17%), and some mixed *R/S* fractions (0.9 g). Quinone **6***b* (*2-{2-[4-(2-acetoxy-1(*R*)-methylethyl)-benzoquinone-2,5]yl-2,6,6-trimethylcyclohexyl}ethanoic acid*), mp 143–145°C (from ethanol); $[\alpha]_D^{25}$ −50° ($CHCl_3$); uv: 258 (4.14) nm; ir: 3400–2400 (br OH, COOH), 1725, and 1655 cm^{-1}; ^{1}H nmr δ: 0.92, 0.98, and 1.26 (3s, Me-C), 1.21 (d, J = 7 Hz, Me-CH), 2.06 (s, Me—CO—), 2.08 (dd, 1H, J = 16 and 4.5 Hz, C6-H), 2.28 (dd, 1H, J = 16 and 8.5 Hz, C6-H), 2.73 (dd, 1H, J = 8.5 and 4.5 Hz, C5-H), 2.97–3.33 (m, C15-H), 3.79 (dd, 1H, J = 11 and 4 Hz, C16-H), 4.77 (dd, 1H, J = 11 and 3 Hz, C16-H), 6.35 (d, 1H, J = 1.5 Hz, C14-H), 6.58 (s, C11-H), and 8.94 (COOH, D_2O); ^{13}Cmr, see Table 1; mass spectra m/e: 390 (M$^+$), 374, 355, 347, 329, 313, and 285. *Anal.* calcd. for $C_{22}H_{30}O_6$: C 67.67, H 7.74; found: C 67.78, H 7.60. Quinone **10***b* (*2-{2-[4-(2-acetoxy-1(*S*)-methylethyl)-benzoquinone-2,5]yl-2,6,6-trimethylcyclohexyl}ethanoic acid*), mp 119–120°C (from ethanol); $[\alpha]_D^{25}$ −19° ($CHCl_3$); uv: 258 (4.14) nm; ir: 3400–2500 (br OH, COOH), 1730, 1705, and 1655 cm^{-1}; ^{1}H nmr (0.22 *M* in $CDCl_3$) δ: 0.89, 0.91, and 1.18 (3s, Me-C), 1.17 (d, J = 6.5 Hz, Me-CH), 1.97 (s, Me—CO—), 1.99 (dd, J = 16 and 8 Hz, C6-H), 2.28 (dd, J = 16 and 4 Hz, C6-H), 2.64 (dd, J = 8 and 4 Hz, C5-H), 2.96 (m, C15-H), 3.83 (dd, J = 11 and 5 Hz, C16-H), 4.32 (dd, J = 11 and 7 Hz, C16-H), 6.24 and 6.35 (2s, C14 and C11-H resp.); ^{13}Cmr, see Table 1; mass spectra m/e: 390 (M$^+$), 348, 330, 317, and 315. *Anal.* calcd. for $C_{22}H_{30}O_6$: C 67.67, H 7.74; found: C 67.58, H 7.78.

Bromo-quinone ***16***

This procedure is based on that described by Moore *et al.* (12). To the quinone **6***b* (3.90 g) in glacial acetic acid (50 mL) was added bromine (0.80 mL), and the mixture was stirred for 3 h and then poured into water (500 mL). The orange precipitate was filtered and well washed to afford an unstable crude product (5.03 g, after drying), which was used immediately for the next step.

The crude bromo compound was dissolved in ether and cooled to 10°C and then diethylamine (1.0 mL) in ether (10 mL) was added dropwise. After stirring for 3 h at room temperature, the mixture was poured into water and the product obtained by ether extraction. Chromatography over silica gel (hexane − ethyl acetate 4:1) afforded the *bromoquinone* **16** (3.70 g: 79%), orange solid, mp 151−153°C (dec., from ethanol); uv: 275 (3.97) and 358 (2.87) nm; ir: 1725, 1700, 1670, and 1650 cm^{-1}; ^{1}H nmr δ: 0.89 (s, 6H, 2 Me-C), 1.16 (s, Me-C), 1.19 (d, J = 7 Hz, Me-CH), 1.92 (s, Me—CO—), 1.93 (dd, J = 17 and 7 Hz, C6-H), 2.24 (dd, J = 17 and 4 Hz, C6-H), 2.60 (dd, J = 7 and 4 Hz, C5-H), 3.44 (m, C15-H), 4.21 (d, 2H, C(16)H_2—OAc), 6.31 (s, C8-H), and 9.92 (COOH, D_2O); ^{13}Cmr, see Table 1; mass spectra m/e: 470 (M^+ + 2), 468 (M^+), 454, 452, 428, 426, 410, 408, 394, and 392. *Anal.* calcd. for $C_{22}H_{29}O_6Br$: C 56.29, H 6.23, Br 17.08; found: C 56.45, H 6.43, Br 17.21.

From the mother liquors (above) a second product was obtained. Dry col chrom gave the pure *dibromo-lactone* **18** (0.45 g: 8%), mp 163−165°C (from ether); $[\alpha]_D^{25}$ −44° ($CHCl_3$); uv: 291 (3.81) and 365 (2.66) nm; ir: 1750 (br) and 1695 cm^{-1}; ^{1}H nmr δ: 0.82, 0.90, and 1.20 (3s, Me-C), 1.21 (d, J = 6.5 Hz, Me-CH), 1.91 (s, Me—CO—), 2.32 (dd, J = 16 and 10.5 Hz, C6-H), 2.69 (dd, J = 16 and 6 Hz, C6-H), 3.56 (m, C15-H), 4.22 (dd, J = 13 and 7 Hz, C16-H), 4.33 (dd, J = 13 and 7 Hz, C16-H), and 4.78 (s, CH-Br); ^{13}Cmr, see Table 1; mass spectra m/e: 550, 548, 546 (M^+), 471, 469, 467, 453, 451, 409, 407, 393, 391, and 389. *Anal.* calcd. for $C_{22}H_{28}O_6Br_2$: C 48.19, H 5.15, Br 29.15; found: C 47.95, H 5.24, Br 28.87.

Formation of the hydroxy-quinone **15**a *and the methoxy-quinone* **15**b

To a solution of the bromo-quinone **16** (2.8 g) in methanol (30 mL) was added aqueous sodium hydroxide (30 mL of 20%) and the mixture was stirred at room temperature for 15 min, after which the dark violet solution was diluted with water, acidified with 5% aqueous hydrochloric acid, and then extracted with ether. The two products (as seen by tlc) were separated by chromatography over silica gel (hexane − ethyl acetate 1:1) affording *hydroxy-quinone* **15***a* (1.41 g: 64%; *2-{2-[3-hydroxy-4-(2-hydroxy-1-methylethyl)-benzoquinone-2,5]yl-2,6,6-trimethylcyclohexyl}ethanoic acid*), orange needles, mp 168−170°C (from ethanol); uv: 273 (3.95) and 400 (2.96) nm; ir: 3600−2400 (br COOH), 3360 (OH), 1710, 1665, and 1635 cm^{-1}; ^{1}H nmr δ: 0.93, 0.98, and 1.24 (3s, Me-C), 1.13 (d, J = 7 Hz, Me-CH), 2.08 (dd, J = 16 and 9 Hz, C6-H), 2.34 (dd, J = 16 and 3.5 Hz, C6-H), 2.63 (dd, J = 9 and 3.5 Hz, C5-H), 3.10−3.44 (m, C15-H), 3.56−3.99 (m, 2H, C(16)H_2—O), 6.49 (s, C11-H), and 7.59 (m, 3H, COO*H*, CH_2O*H* and O*H*, D_2O); ^{13}Cmr, see Table 1. *Anal.* calcd. for $C_{20}H_{28}O_6$: C 65.91, H 7.74; found: 65.76, H 7.61.

The more mobile product was the *methoxy-quinone* **15***b* (0.61 g: 27%; red glass); ^{1}H nmr δ: 0.93, 0.98, and 1.24 (3s, Me-C), 1.07 (d, J = 7 Hz, Me-CH), 4.03 (s, MeO—), 6.48 (s, C11-H), and 7.76 (m, 2H, COO*H* and CH_2O*H*, D_2O); ^{13}Cmr, see Table 1; mass spectra m/e: 378 (M^+), 259, and 245.

Reduction and methylation of the hydroxy-quinone **15**a

This procedure was inspired by that of Edwards *et al.* (13). Adams' catalyst (100 mg) was hydrogenated in methanol (10 mL) at atmospheric pressure. The hydroxy-quinone **15***a* (1.80 g) was introduced dissolved in methanol (38 mL) and the mixture was stirred under hydrogen for 2 h, by which time the solution had become colorless. Then, every hour, aqueous sodium hydroxide (1.5 mL of 30%) and dimethyl sulfate (1 mL) were added, up to a total of 16.5 and 11 mL, respectively. The catalyst was removed by filtration with Celite, the solution was diluted with water (70 mL), and the bulk of the methanol was removed under vacuum. Ether extraction afforded an oily mixture which was separated by chromatography (silica gel; hexane − ethyl acetate 4:1) which gave the following.

Trimethyl ether **19***a* (1.03 g: 48%; pale oil: *methyl 2-[2,3,5-trimethoxy-4-(2-hydroxy-1(*R*)-methylethyl)-phenyl-2,6,6-trimethylcyclohexyl]ethanoate*); ir: 3500, 1730, and 1605 cm^{-1}; ^{1}H nmr δ: 0.92, 0.99, and 1.35 (3s, Me-C), 1.28 (d, J = 7 Hz, Me-CH), 2.08 (dd, J = 16 and 6 Hz, C6-H), 2.32 (dd, J = 16 and 5 Hz, C6-H), 2.48 (br s, CH_2O*H*, D_2O), 2.83 (dd, J = 6 and 5 Hz, C5-H), 3.33 (s, COOMe), 3.54 (m, C15-H), 3.61−3.89 (m, C*H*$_2$OH), 3.79 (s, 6H, OMe at C12 and C14), 3.95 (s, OMe at C11), and 6.59 (s, C8-H); ^{13}Cmr, see Table 1.

Tetramethyl ether **21***a* (352 mg: 16%; pale yellow oil); ir: 1735 cm^{-1}; ^{1}H nmr δ: 0.91, 0.97, and 1.33 (3s, Me-C), 1.29 (d, J = 7 Hz, Me-CH), 2.05 (dd, J = 15.5 and 5 Hz, C6-H), 2.28 (dd, J = 15.5 and 5 Hz, C6-H), 2.95 (dd, J = 5 and 5 Hz, C5-H), 3.29 (s, 6H, COOMe and CH_2OMe), 3.74 (s, 6H, OMe at C12 and C14), 3.91 (s, OMe at C11), and 6.55 (s, C8-H); ^{13}Cmr, see Table 1.

Dimethyl ether **20** (298 mg: 15%; pale yellow oil); ir: 3450 and 1730 cm^{-1}; ^{1}H nmr δ: 0.93, 0.97, and 1.37 (3s, Me-C), 1.31 (d, J = 7 Hz, Me-CH), 2.03 (dd, J = 15 and 6 Hz, C6-H), 2.31 (dd, J = 15 and 6 Hz, C6-H), 3.14 (dd, J = 6 and 6 Hz, C5-H), 3.28 (s, COOMe), 3.44−3.89 (m, 3H, C15-H and C*H*$_2$OH), 3.75 and 3.78 (2s, OMe at C14 and C12), 6.07 (phenolic OH, D_2O), and 6.60 (s, arom H); ^{13}Cmr, see Table 1. Further methylation of this dimethyl ether (dimethyl sulfate/sodium hydroxide) afforded the trimethyl ether **19***a* in excellent yield.

Reduction and methylation of hydroxy-quinone **15**a *(second procedure)*

The quinone **15***a* (2.02 g) in methanol (20 mL) was hydrogenated as described above (70 mg of PtO_2 in methanol). The colorless solution was then treated with aqueous sodium hydroxide (1 mL of 30%) and dimethyl sulfate (1 mL) every hour, up to a total of 12 mL of each reagent, and stirring was continued for 40 more hours. The solution had become acid during this time. Following the same work-up as in the earlier procedure afforded, as the major product, the trimethyl ether **19***a* (1.09 g: 47% after dry col chrom) but the minor product was the cyclized compound **22***a* (302 mg: 14%; colorless oil: *methyl 2-[2-(4,5-dimethoxy-3(*R*)-methyl-2,3-dihydrobenzofuran-6)yl-2,6,6-trimethyl cyclohexyl]ethanoate*); ir: 1730 cm^{-1}; ^{1}H nmr δ: 0.89, 0.97, and 1.27 (3s, Me-C), 1.34 (d, J = 6.5 Hz, Me-CH), 2.02 (dd, J = 15.5 and 5.5 Hz, C5-H), 3.38 (s, COOMe), 3.61 (m, C15-H), 3.84 and 3.94 (2s, OMe), 4.04 (dd, J = 8.5 and 6 Hz, C16-H), 4.58 (dd, J = 8.5 and 8.5 Hz, C16-H), and 6.48 (s, arom H). *Anal.* calcd. for $C_{23}H_{34}O_5$: C 70.74, H 8.78; found: C 70.48, H 8.49.

Hydrolysis of ester **19**a

Sodium hydroxide solution (40 mL of 10% aqueous) was added to the ester (1.0 g) in methanol (40 mL) and the mixture was refluxed for 20 h. After adding more water, the methanol was removed under vacuum and the product then obtained by ether extraction. The yellow oil (850 mg) was chromatographed (silica gel; hexane − ethyl acetate 7:3) to give the acid **19***b* (802 mg: 83%; *2-[2,3,5-trimethoxy-4-(2-hydroxy-1(*R*)-methylethyl)phenyl-2,6,6-trimethylcyclohexyl]ethanoic acid*), pale yellow oil; uv: 229 (sh 3.90) and 286 (3.41) nm; ir: 3600−2400 (br COOH), 3400 (OH), and 1710 cm^{-1}; ^{1}H nmr δ: 0.91, 0.98, and 1.33 (3s, Me-C), 1.23 (d, J = 7 Hz, Me-CH), 2.03 (dd, J = 16 and 5 Hz, C6-H), 2.28 (dd, J = 16 and 6 Hz, C6-H), 2.77 (dd, J = 6 and 5 Hz, C5-H), 3.51 (m, C15-H), 3.74 (s, 6H, OMe at C12 and C14), 3.89 (s, OMe at C11), 6.57 (s, arom H) and 6.67 (m, 2H, COOH and OH, D_2O); ^{13}Cmr, see Table 1; mass spectra m/e: 408 (M^+), 378, 377, 359, 235, 221, and 195. *Anal.* calcd. for $C_{23}H_{36}O_6$: C 66.62, H 8.88; found: C 66.93, H 8.67.

Cyclization of acid **19**b *(to give ketone* **23**a*)*

Following Pelletier and Ohtsuka's method (14), the acid **19***b* (850 mg) was stirred at room temperature in trifluoroacetic anhydride (7 mL) for 20 h. After pouring into water, the product was obtained by ether extraction and repeated washing. The actual product at this stage was the enol trifluoroacetate (ir 1805 cm^{-1}) but this was hydrolysed immediately by stirring in methanol (50 mL) and aqueous sodium hydroxide solution (10 mL of 10%) for 40 min. Chromatography over silica gel (hexane − ethyl acetate 7:3) of the oil obtained by extraction afforded the cyclized ketone **23***a* (820 mg: 89%; *7-oxo-11,12,14-trimethoxy-13-(2-hydroxy-1(*R*)-methylethyl)-podocarpa-8,11,13-triene*), mp 108−111°C (from ether−hexane); $[\alpha]_D^{26}$ +209° ($CHCl_3$): uv: 274 (3.92) and 314 (3.46) nm; ir: 3500 and 1680 cm^{-1}; ^{1}H nmr δ: 0.94, 0.98, and 1.33 (3s, Me-C), 1.28 (d, J = 7 Hz, Me-CH), 1.82 (dd, J = 11 and 7 Hz, C5-H), 2.32 (m, 1H, CH_2O*H*, D_2O), 2.48 (dd, J = 18 and 11 Hz, C6-H), 2.71 (dd, J = 18 and 7 Hz, C6-H), 3.56 (m, C15-H), 3.67−3.94 (m, 2H, C*H*$_2$OH), 3.75, 3.78, and 3.84 (3s, OMe at C14, 12, and 11 resp.); ^{13}Cmr, see Table 1; mass spectra m/e: 390 (M^+, very weak), 357, and 342. The molecular ion was too weak for an *Exact Mass* determination.

Oxidation to the enolic α-diketone **24**a *(coleon C trimethyl ether)*

The ketone **23***a* (400 mg) in *tert*-butanol (20 mL) was added to the solution obtained by dissolving potassium (1.5 g) in *tert*-butanol (40 mL). The mixture was stirred vigorously at room temperature in an atmosphere of oxygen for 2 h, after which water (50 mL) containing concentrated hydrochloric acid (4 mL) was added and the product extracted into chloroform. Silica gel chromatography using hexane – ethyl acetate 7:3 as eluant afforded first the enolic α-diketone **25** (130 mg: 26%; *4-oxo-5-hydroxy-1(*R*),6,6,9a(*S*)-tetramethyl-1,2,4,-6,7,8,9,9a-octahydrophenanthro[1,2-*b*]furan*), pale yellow needles, mp 180–183°C (from hexane); $[\alpha]_D^{22}$ +51° ($CHCl_3$); uv: 320 (sh 4.03), 254 (4.08), 277 (3.91), 309 (3.71), and 362 (4.00) nm; ir: 3300, 1615, and 1585 cm^{-1}; ^{1}H nmr δ: 1.35 (d, J = 7 Hz, Me-CH), 1.45 (s, 6H, Me-C at C4), 1.64 (s, Me-C at C10), 2.63–3.08 (m, 2H, C1-H), 3.66 (m, C15-H), 3.87 and 3.94 (2s, OMe), 4.34 (dd, J = 9 and 6 Hz, C16-H), 4.86 (dd, J = 9 and 8.5 Hz, C16-H), and 7.33 (OH, D_2O); ^{13}Cmr, see Table 1; mass spectra *m/e*: 372 (M^+), 357, 341, 329, and 303. *Anal.* calcd. for $C_{22}H_{28}O_5$: C 70.94, H 7.58; found: C 70.98, H 7.60. The second product was the major component, enolic α-diketone **24***a* (203 mg: 49%; *7-oxo-11,12,14-trimethoxy-6-hydroxy-13-(2-hydroxy-1(*R*)-methylethyl)podocarpa-5,8,11,13-tetraene*), pale yellow needles, mp 145–148°C (from hexane); $[\alpha]_D^{26}$ +79° ($CHCl_3$); uv: 247 (3.82), 278 (3.80), and 334 (3.79) nm; ir: 3500, 3380, 1630, and 1575 cm^{-1}; ^{1}H nmr δ: 1.32 (d, J = 7 Hz, Me-CH), 1.44, 1.47, and 1.64 (3s, Me-C), 2.67–3.06 (m, 2H, C1-H), 3.57 (m, C15-H), 3.67–4.01 (m, 2H, C*H*$_2$OH), 3.78 (s, OMe at C14), 3.88 (s, 6H, OMe at C11 and C12), and 7.42 (s, OH, D_2O); ^{13}Cmr, see Table 1; mass spectra *m/e*: 404 (M^+), 389, 374, 372, 361, 357, and 341. *Anal.* calcd. for $C_{23}H_{32}O_6$: C 68.29, H 7.97, O 23.74; found: C 67.90, H 8.11, O 24.08.

Coleon C tetramethyl ether (methylation of **24**a*)*

To the enol **24***a* (90 mg) in ethanol (15 mL) and water (15 mL) was added aqueous sodium hydroxide (10 mL of 30%). After stirring for 30 min at room temperature, dimethyl sulfate (6 mL) was introduced and the mixture was stirred for 36 h. After diluting with water and extraction, the crude material was chromatographed (silica gel; hexane – ethyl acetate 7:3) affording the crystalline tetramethyl ether **24***b* (65 mg: 70%; *7-oxo-6,11,12,14-tetramethoxy-13-(2-hydroxy-1(*R*)-methylethyl)podocarpa-5,8,11,13-tetraene*), colorless needles, mp 162–164°C (from hexane); uv: 248 (sh 3.82), 274 (3.78), 300 (3.74), and 331 (3.59) nm; ir: 3440, 1658, and 1620 cm^{-1}; ^{1}H nmr δ: 1.33 (d, J = 7 Hz, Me-CH), 1.42 (s, 6H, Me-C both at C4), 1.63 (s, Me-C at C10), 1.95 (br s, OH, D_2O), 2.61–3.01 (m, 2H, C1-H), 3.51 (m, C15-H), 3.67–3.94 (m, 2H, C*H*$_2$OH), 3.71, 3.72, 3.78, and 3.79 (4s, OMe at C6, 14, 12, and 11 resp.); mass spectra *m/e*: 418 (M^+), 404, 403, 386, 371, 355, 343, and 317. *Anal.* calcd. for $C_{24}H_{34}O_6$: C 68.87, H 8.19; found: C 69.01, H 8.14.

Ketone **23**b *(hydrolysis of ester* **21**a *and cyclization of acid* **21**b*)*

To the ester **21***a* (350 mg) in methanol (10 mL) was added aqueous sodium hydroxide (10 mL of 10%) and the mixture was refluxed for 24 h. Normal extractive isolation afforded an acid fraction (340 mg) which was chromatographed (silica gel; hexane – ethyl acetate 7:3) to give the acid **21***b* (304 mg: 89%); ir: broad acid trough, 1710 cm^{-1}; ^{1}H nmr δ: 0.89, 0.98, and 1.31 (3s, Me-C), 1.29 (d, J = 7 Hz, Me-CH), 2.03, 2.27, and 2.83 (3dd, similar to ester **21***a*, C5-H and C6-H), 3.33, 3.72 (6H), and 3.89 (3s, four OMe), 6.55 (s, arom H), and 10.03 (COOH, D_2O); ^{13}Cmr, see Table 1.

The acid **21***b* (200 mg from above without further purification) was taken up in trifluoroacetic anhydride (5 mL) and stirred at room temperature for 20 h. The enol trifluoroacetate intermediate was dissolved in methanol (40 mL) and hydrolysed by stirring for 1 h at room temperature after adding aqueous potassium hydroxide (4 mL of 10%). Dry col chrom of the extracted neutral fraction gave the ketone **23***b* (145 mg: 70%; *7-oxo-11,12,14-trimethoxy-13-(2-methoxy-1(*R*)-methylethyl)podocarpa-8,11,13-triene*), mp 72–75°C (from hexane), $[\alpha]_D^{25}$ +193° ($CHCl_3$); uv: 215 (4.25), 274 (3.91), and 314 (3.47) nm; ir: 1680 cm^{-1}; ^{1}H nmr δ: 0.93, 0.97, and 1.32 (3s, Me-C), 1.28 (d, J = 7 Hz, Me-CH), 1.81 (dd, J = 11 and 7 Hz, C5-H), 2.47 (dd, J = 18 and 11 Hz, C6-H), 2.69 (dd, J = 18 and 7 Hz, C6-H), 3.32, 3.75, 3.76, and 3.82 (4s, OMe at C16, 14, 12, and 11 resp.); ^{13}Cmr, see Table 1; mass spectra *m/e*: 404, 389, 373, 373, 359, and 344. *Exact Mass* (M^+) calcd. for $C_{24}H_{36}O_5$: 404.2564; found (high resolution ms): 404.2572.

Ketone **26** *(hydrolysis of ester* **22**a *and cyclization of acid* **22**b*)*

The ester **22***a* (70 mg) was hydrolysed by refluxing in methanol (10 mL) containing aqueous sodium hydroxide (10 mL of 10%) for 20 h. Most of the methanol was evaporated and the acid fraction obtained by extraction was purified by dry col chrom. The acid **22***b* (^{1}H nmr δ: 0.87, 0.97, and 1.24 (3s, Me-C), 1.31 (d, J = 7 Hz, Me-CH), 1.98 (dd, J = 17 and 5.5 Hz, C6-H), 2.24 (dd, J = 17 and 7 Hz, C6-H), 2.89 (dd, J = 7 and 5.5 Hz, C5-H), 3.59 (m, C15-H), 3.79 and 3.89 (2s, OMe), 4.01 (dd, J = 8.5 and 6.5 Hz, C16-H), 4.57 (dd, J = 9 and 8.5 Hz, C16-H), 6.47 (s, arom H), and 10.14 (COOH, D_2O)) was used as such for the cyclization, accomplished by stirring in trifluoroacetic anhydride (4.0 mL) for 20 h. The initial product was then hydrolysed (40 mL methanol, 4 mL aqueous potassium hydroxide 10%, 1 h) and the extracted neutral fraction was then chromatographed over silica gel (hexane – ethyl acetate 7:3) affording the glassy ketone **26** (36 mg: 54%; *4-oxo-10,11-dimethoxy-1(*R*),6,6,9a(*S*)-tetramethyl-1,2,4,5,5a(*R*),6,7,8,9,9a-decahydrophenanthro[1,2-*b*]furan*); uv: 226 (4.09), 235 (sh 4.09), 270 (3.85), and 335 (3.57) nm; ir: 1675 cm^{-1}; ^{1}H nmr δ: 0.92, 0.96, and 1.26 (3s, Me-C), 1.32 (d, J = 6.5 Hz, Me-CH), 1.79 (dd, J = 10.5 and 6.5 Hz, C5-H), 2.46 (dd, J = 17 and 10.5 Hz, C6-H), 2.67 (dd, J = 17 and 6.5 Hz, C6-H), 3.59 (m, C15-H), 3.75 and 3.90 (2s, OMe at C12 and C11 resp.), 4.24 (dd, J = 9 and 6 Hz, C16-H), and 4.79 (dd, J = 9 and 9 Hz, C16-H); mass spectra *m/e*: 358, 342, 301, 273, 261, and 247. *Exact Mass* (M^+) calcd. for $C_{22}H_{30}O_4$: 358.2145; found (high resolution ms): 358.2124.

Acknowledgments

We thank the Natural Sciences and Engineering Research Council of Canada and the Ministère de l'éducation du Québec for operating and equipment grants. A graduate bursary (N.S.E.R.C.) is also gratefully acknowledged (S.S.).

1. P. RÜEDI and C. H. EUGSTER. Helv. Chim. Acta, **54**, 1606 (1971).
2. H. P. WEBER, T. J. PETCHER, P. RÜEDI, and C. H. EUGSTER. Helv. Chim. Acta, **59**, 1221 (1976).
3. R. H. BURNELL, A. ANDERSEN, M. NÉRON-DESBIENS, and S. SAVARD. Can. J. Chem. **59**, 2820 (1981).
4. R. C. CAMBIE, G. D. BERESFORD, and K. P. MATHAI. Aust. J. Chem. **26**, 1763 (1973).
5. R. C. CAMBIE, W. A. DENNY, T. R. KLOSE, and L. N. MANDER. Aust. J. Chem. **24**, 99 (1971); W. P. CAMPBELL and D. TODD. J. Am. Chem. Soc. **64**, 928 (1942).
6. S. SAVARD. Ph.D. Thesis, Université Laval, Québec. 1983.
7. P. RÜEDI, J. M. SCHMID, and C. H. EUGSTER. Helv. Chim. Acta, **65**, 2181 (1982).
8. R. H. BURNELL, L. MO, and M. MOINAS. Phytochemistry, **11**, 2815 (1972).
9. T. NISHIDA, I. WAHLBERG, and C. R. ENZELL. Org. Magn. Reson. **9**, 203 (1977).
10. (*a*) D. POIRIER, M. JEAN, and R. H. BURNELL. Synth. Commun. **13**, 201 (1983); (*b*) R. H. BURNELL, M. JEAN, and S. SAVARD. Can. J. Chem. **61**, 2461 (1983); (*c*) R. H. BURNELL, M. JEAN, D. POIRIER, and S. SAVARD. Can. J. Chem. **62**, 2822 (1984).
11. E. WENKERT and T. STEVENS. J. Am. Chem. Soc. **78**, 2318 (1956).
12. H. W. MOORE, D. L. MAURIER, D. S. PEARCE, and M. S. LEE. J. Org. Chem. **37**, 1984 (1972).
13. O. E. EDWARDS, G. FENIAK, and M. LOS. Can. J. Chem. **40**, 1540 (1962).
14. S. W. PELLETIER and Y. OHTSUKA. Tetrahedron, 1021 (1977).

Permanganate peroxidation of cyclohexene. III. Hydroxide ion and salt effect studies

JAY E. TAYLOR AND RENÉE GREEN
Department of Chemistry, Kent State University, Kent, OH 44242, U.S.A.
Received November 24, 1984

JAY E. TAYLOR and RENÉE GREEN. Can. J. Chem. **63**, 2777 (1985).

Good yields of *cis*-1,2-cyclohexanediol were formed by the reaction of cyclohexene and aqueous potassium permanganate under turbulent stirring conditions only in the presence of low concentrations of sodium hydroxide. Larger amounts had no further benefit or were deleterious. The lack of sensitivity to low concentrations of hydroxide ion indicated that its benefit is to inhibit acid promoted oxidations. There was no indication of its participation in the mechanism of glycol formation. The addition of the neutral salts, sodium sulfate or sodium nitrate, caused a decrease in glycol yields presumably due to a positive salt effect on a secondary negative ion − negative ion reaction, which formed other oxidation products. Stoichiometric amounts of hydroxide and potassium ions were not isolated as reaction products due to interaction with the hydrated manganese dioxide in a 1:2 ratio. The mechanisms in acidic and basic solutions appear to be quite different. A mechanism for basic solutions is suggested.

JAY E. TAYLOR et RENÉE GREEN. Can. J. Chem. **63**, 2777 (1985).

Il se forme de bons rendements de cyclohexanediol-1,2-*cis* lors de la réaction du cyclohexène et du permanganate de potassium, soumis à une agitation tumultueuse et seulement en présence de faibles concentrations d'hydroxyde de sodium. Des concentrations plus fortes d'hydroxyde n'améliorent pas la réaction; elles peuvent même avoir un effet contraire. Le manque de sensibilité à la présence de faibles concentrations d'ions hydroxydes indique que ces derniers inhibent les oxydations favorisées par les milieux acides. On n'a aucune preuve de leur participtation au mécanisme de formation du glycol. L'addition de sels neutres, comme le sulfate de sodium ou le nitrate de sodium, provoque une diminution du rendement en glycol et cet effet est probablement causé par un effet de sel positif sur une réaction secondaire entre ions négatifs qui forme d'autres produits d'oxydation. À cause de l'interaction avec le dioxyde de manganèse hydraté, dans un rapport de 1:2, on n'a pas isolé des produits de la réaction des quantités stoechiométriques d'ions potassium et hydroxyde. Les mécanismes de réaction en solutions acide et basique semblent être très différents. On suggère un mécanisme pour les réactions en solutions basiques.

[Traduit par le journal]

Introduction

Aqueous potassium permanganate reacts with cyclohexene to form a variety of products including *cis*-1,2-cyclohexanediol. The yield of the latter product is markedly enhanced by turbulent stirring (1). A study has been made of conditions which influence this reaction (2). This study is continued in this paper.

Experimental

Procedure I

Potassium permanganate, 7.780 g (0.0492 *m*), was dissolved in 450 mL water, and this solution was added concurrently with 50 mL methanol over a period of 1 h to a turbulently stirred slurry (2) of 5.00 mL (0.0492 *m*) cyclohexene at 20°C, 180 mL of dilute sodium or potassium hydroxide, as indicated, and 20 mL methanol. After treatment with sulfur dioxide to remove the manganese dioxide and sodium bicarbonate (~pH 8), the glycol was extracted continuously with dichloromethane[1] for 2−3 days. This solution was concentrated to ~6 mL/g glycol and then was allowed to crystallize in an ice chest, giving the primary glycol yield. A secondary crop of crystals of lower purity was obtained by concentrating this solution. The apparatus and product isolation techniques employed have been previously described (2) as procedure A.

Procedure II

The procedure was the same as the above except that the sodium hydroxide was included with the permanganate solution instead of with the cyclohexene.

[1]After working intermittently with this solvent for several years, the major author developed, quite suddenly, a highly specific pulmonary sensitivity to the vapor of dichloromethane. No other complications have been observed. Due care in handling this solvent is therefore strongly recommended.

Hydroxide ion determination

After addition of potassium permanganate as described, the total reaction mixture was treated with Celite filter aid, filtered twice, and then titrated with 1.101 *N* sulfuric acid, phenolphthalein indicator.

Potassium ion determination

The above solution was diluted to 1 L and made slightly acidic with sulfuric acid. A 20.0-mL aliquot was removed and an excess of ammonium hydroxide added. The potassium ion was determined as potassium sulfate (3).

Manganese dioxide determination

For each determination the indicated amount of standardized potassium permanganate was added, as in Procedure I. This was followed by a weighed excess of ferrous ammonium sulfate, 10 mL of phosphoric acid, and 45 mL of 10% sulfuric acid. The excess ferrous ion was titrated with 0.1 *N* $K_2Cr_2O_7$ using barium diphenylamine sulfonate indicator. Both the $KMnO_4$ and $K_2Cr_2O_7$ solutions were standardized against the ferrous ammonium sulfate.

Results and discussion

The effects of varying hydroxide ion and inert salt concentrations upon *cis*-glycol yields have been determined for the turbulently stirred reaction of cyclohexene with potassium permanganate. Also, a disappearance of potassium and hydroxide ions from solution has been noted.

Effect of added hydroxide ion

That hydroxide ion is essential to the formation of the *cis*-glycol has been clearly demonstrated (1), and further evidence is seen in comparing experiment 1, Table 1, with the remainder of the table. Essentially no product glycol was isolated under slightly acid conditions, and it seems unlikely that it was first formed and then further oxidized since the rate of oxidation of the *cis*-glycol by permanganate is low in mildly acid solutions.

TABLE 1. Effects of varied hydroxide ion concentrations on yields of *cis*-1,2-cyclohexanediol

Expt. no.	OH^- (m)	Glycol[d] (g)	Melting point[d] (°C)	Total yield (%)
1	0[a]	>0		>0
2	0	4.275	97.5–98.5	80
		0.305	86–89	
3	0.005[b]	4.658	95–97	86
		0.267	85–87	
4	0.010[b]	4.532	96–97.5	85
		0.297	85–87	
5	0.050[b]	3.803	97–98	72
		0.321	85–87.5	
6	0.100[b]	2.938	94.5–96.5	56
		0.264	90–93.5	
7	0.005[c]	4.318	96–97.5	82
		0.393	83–86	
8	0.010[c]	4.310	97.5–98.5	80
		0.432	84–87	
9	0.050[c]	3.951	97.5–98.5	78
		0.499	92–95	
10	0.100[c]	3.867	96–97.5	72
		0.223	93.5–96	

[a]Near neutrality was maintained throughout the reaction by mixing an equimolar quantity of acetic acid with the potassium permanganate.

[b]The sodium hydroxide was mixed with the cyclohexene slurry as per Procedure I. Final volume 700 mL.

[c]The sodium hydroxide was mixed with the $KMnO_4$ solution as per Procedure II. Final volume 700 mL.

[d]The dual entries are the primary and secondary glycol yields whose relative purities are indicated by the corresponding melting points. The major impurity appeared to be *trans*-1,2-cyclohexanediol.

TABLE 2. Effects of varied inert salt concentrations on yields of *cis*-1,2-cyclohexanediol

Added salt	C_6H_{10}, $KMnO_4$ (m)	CH_3OH (%)	Glycol (g)	Melting point[b] (°C)	Total yield (%)
None	0.0492	25	4.670	97–98	85
			0.210	95–97	
Na_2SO_4	0.0492	25	4.122	97–98	76
0.5 m/L			0.242	84–87	
None	0.0985	10	7.776	97–98	73
			0.638	83–85	
Na_2SO_4	0.0985	10	7.397	94–96	68
0.05 m/L			0.391	84–87	
Na_2SO_4	0.0985	10	6.849	97–98	66
0.15 m/L			0.644	84.5–86.5	
Na_2SO_4	0.0985	10	5.979	97–98	58
0.5 m/L			0.628	85–87	
None	0.0492	10	4.130	97.5–98.5	80
			0.432	84–87	
Na_2SO_4	0.0492	10	3.998	94.5–96.5	77
0.25 m/L			0.376	85–88	
Na_2SO_4	0.0492	10	3.422	94–96.5	70
0.5 m/L			0.590	87–90	
$NaNO_3$	0.0492	10	3.751	95.5–97.5	75
0.75 m/L			0.520	85–88	
$NaNO_3$	0.0492	10	3.465	90–94	69
1.5 m/L			0.453	85–88	

[a]Procedure I was followed in all experiments. The indicated molarity of salt was maintained during the reaction by adding the appropriate amount of specified salt to both the permanganate solution and cyclohexene slurry. The methanol was included as part of the total volume. Sodium hydroxide, 0.01 m, was added in each case.

[b]The dual entries are the primary and secondary glycol yields whose relative purities are indicated by the corresponding melting points. The major impurity appeared to be *trans*-1,2-cyclohexanediol.

The effects of adding varying amounts of hydroxide ion are shown in Table 1. As seen in comparing experiments 3 with 4 or 7 with 8, doubling the hydroxide ion concentration had no significant effect on glycol yields. Even with no added hydroxide, experiment 2, the hydroxide ion which formed as a reaction product provided the needed basicity except at the start of the reaction, and, as a result, the overall yields were but slightly lowered.

For those experiments in which the sodium or potassium hydroxide was added with the potassium permanganate by Procedure II, roughly the same yields were obtained with 0, 0.005 m, or 0.010 m of hydroxide, and these yields were lower than those with 0.005 m or 0.010 m added as in Procedure I. See experiments 2, 7, 8, Table 1, and compare with experiments 3 and 4. These lowered yields again resulted from low hydroxide concentrations at the outset of the reactions.

From these observations, it is concluded that the function of added hydroxide ion was to provide a basic medium to minimize any acid promoted reactions, and that the hydroxide ion had no function in the mechanism of glycol formation, in contrast to a previous suggestion (4). Wiberg and Geer (5) had noted much earlier that these reactions are independent of concentration of base.

A large excess of hydroxide ion was deleterious to glycol formation, as seen in experiments 5 and 6, Table 1, where the yields were lowered to 72 and 56% by the presence of 0.05 m and 0.10 m, respectively, of sodium hydroxide in the reaction flask. Adding the same amount of sodium hydroxide to the potassium permanganate solution had a lesser effect since the basicity was more gradually introduced into the reaction. Compare experiments 4 and 5 with 9 and 10. The stronger base caused a decrease in yields, it appears, as a result of base promotion of the reaction, $Q^- + MnO_4^-$ or glycol + MnO_4^-. In support of the latter, it has been observed that the *cis*-glycol is more rapidly oxidized by permanganate ion in the presence of the higher hydroxide ion concentrations.

Inert salt effect

The following mechanism has been proposed for glycol formation (2):

[1] $C_6H_{10} + MnO_4^- \rightarrow Q^-$

[2] $Q^- + H_2O \rightarrow C_6H_{10}(OH)_2 + MnO_3^-$

In the presence of localized excesses of permanganate ion, adipic acid and other oxidation products may be formed.

[3] $Q^- + MnO_4^- \rightarrow$ various oxidation products $+ MnO_2$

Reaction [3] is clearly a negative ion – negative ion reaction and should show a rate increase in the presence of neutral salts, as predicted by the Bronsted, Bjerrum, Christiansen, Scatchard relationship (6). If mechanism [1]–[3] is operative, addition of inert salts should enhance reaction [3] at the expense of reaction [2] since the latter is an ion–dipole reaction with a rather small salt effect. Added salts should then cause a decrease in glycol yields. As seen in Table 2, this was definitely found to be the case, and these data thereby provide support for the above proposal. The salt effect data were repeated under the condi-

TABLE 3. Demonstration of the constancy of potassium and hydroxide ion absorption with varied potassium hydroxide additions

Column:	1	2	3	4	5
Expt. no.	Added KOH (m)	$[OH^-]$ less added KOH[d] (m)	$[K^+]$ less added KOH[d] (m)	$[OH^-]$ absorbed[e] (m)	$[K^+]$ absorbed[f] (m)
1	—[c]	0.0087	0.0256	0.0241	0.0236
2	0.00503[a,c]	0.0082	0.0241	0.0246	0.0251
3	0.01006[a,c]	0.0086	0.0260	0.0242	0.0232
4	0.00503[b,c]	0.0075	0.0261	0.0253	0.0231
5	0.01006[b,c]	0.0078	0.0262	0.0250	0.0230

[a]Procedure I.
[b]Procedure II.
[c]$KMnO_4 = C_6H_{10} = 0.0492$ m, 10% methanol, no sulfur dioxide was added, K^+ and OH^- analyses were done as described.
[d]The molarity of added KOH is subtracted from both the total K^+ and total OH^- concentrations as determined by analysis.
[e]The values in column 2 are subtracted from the predicted value of OH^- = 0.328 m.
[f]The values in column 3 are subtracted from the predicted value of K^+ = 0.0492 m.

tions 0.0492 and 0.0985 m of added permanganate using equal amounts of cyclohexene, and with 10 and 25% methanol.

It is emphasized that these salt effect studies are not an absolute proof of the existence of the mechanism because of the inherent complexity of the system. The potassium permanganate solution was added dropwise and reacted very rapidly; therefore, excess amounts of permanganate ion exist only momentarily and in localized areas. The concentration of the intermediate Q^- must have been similarly highly variant. Under turbulent stirring conditions it was obvious that reaction [2] strongly predominated over reaction [3]. Thus, a large increase in rate of reaction [3] would have had but a modest effect on the observed yields. Accordingly, the salt effect data can be interpreted only qualitatively.

Manganese dioxide analysis

Although it has been commonly assumed from earlier evidence that manganese dioxide was the final reduction product of the permanganate ion, it was decided to verify that assumption for this particular reaction. This was accomplished by titrating the total manganese oxide residue resulting from the reduction of a given volume of standardized potassium permanganate. Several methods of assay were tried. The first was sulfur dioxide using a gas buret and an oxygen-free atmosphere. The advantage was rapidity of reaction in a low acid medium. Since two products of oxidation, SO_4^{2-} and $S_2O_6^{2-}$, were formed indiscriminately, the procedure was unduly complicated and therefore rejected. Better success was obtained using the ferrous ammonium sulfate – potassium chromate procedure in the absence of methanol. An equivalent result was also obtained with an arsenic trioxide – potassium iodide procedure (not described) which was usable in the presence of methanol.

Titrations of 0.00525 m, 0.0105 m, 0.01575 m, 0.01969 m of $KMnO_4$ which had reacted in each case with 0.0263 m cyclohexene, gave respectively MnO_x analyses where x = 1.97, 1.98, 1.98, 1.99. These runs were made without added methanol using aliquot volumes of 0.0525 m/L $KMnO_4$ solution added to 200-mL volume slurries of the cyclohexene. A corresponding experiment with 0.00525 m $KMnO_4$ and 25% methanol gave x = 1.98. Thus the MnO_2 end product was substantiated with small deviations. The significance of the 0.01–0.03 unit variance from MnO_2 is not known. Note, however, that lower values were obtained with the greater C_6H_{10}/MnO_4^- ratios. The analytical procedure was accurate to ±0.2% or better. Narita and Okabe (7) have noted a similar variation in manganese dioxide analyses at pH ≥ 8.

Hydroxide ion product

The stoichiometric equations for the formation of the glycol and adipic acid are as follows.

$$[4] \quad 3C_6H_{10} + 2MnO_4^- + 4H_2O \rightarrow 2MnO_2 + 3C_6H_{10}(OH)_2 + 2OH^-$$

$$[5] \quad 3C_6H_{10} + 8MnO_4^- \rightarrow 8MnO_2 + 3C_4H_8(CO_2)_2^{2-} + 2OH^- + 2H_2O$$

Thus hydroxide ion is formed in equimolar amounts from permanganate ion with eq. [4]. In eq. [5] there is hydroxide ion formation equivalent to glycol formation (as in eq. [4]), but, beyond this, carboxyl ion is formed in place of hydroxyl ion. Along with adipic acid by eq. [5], a variety of unidentified products of intermediate oxidation states were formed, thereby complicating interpretation of the mechanism.

Let us assume a typical yield of 83% glycol. By eqs. [4] and [5], 2 m OH^- result from 3 m cyclohexene. Thus upon assuming 100% consumption of the cyclohexene with adipic acid as the exclusive by-product, $2/3 \times 0.0492 = 0.0328$ m OH^- formed. Referring to Table 3 it is seen that only about one-fourth of this amount of hydroxide ion is titrable in a filtered solution. The decrease of the hydroxide ion prompted the analyses for potassium ion. The presence or absence of potassium ion would indicate if the hydroxide was not formed or if it was initially formed and removed from solution. The potassium ion added for each experiment in Table 3 was 0.0492 m, but it is seen that only about one-half this amount is in evidence. Thus the hydroxide ions were formed and then removed along with potassium ions.

Since ideally 0.0328 m OH^- and 0.0492 m K^+ should be products, the difference is 0.0164 m. Fortuitously, this same value is approximated upon subtracting column 2 from column 3, Table 3. However, an analysis was made for adipic acid in a high yield reaction. The aqueous solution was acidified after extraction of the glycol, and this solution was extracted with ether. The adipic acid was indicated to be in the range of 6–7%. This is reasonable since other nonionic products were formed. With the low adipic acid analysis (compared to that projected above) there should be a correspondingly greater hydroxide ion analysis. That this was not the case may be attributed to incomplete reaction of the cyclohexene and formation of not otherwise identified acidic products, e.g., carbon dioxide from methanol, etc.

The disappearance of the potassium hydroxide requires special consideration. The only substance with which it can react is the hydrated manganese dioxide. The data in Table 3 show a very interesting consistency. In columns 3 and 4, Table 3, the amounts of OH^- and K^+ absorbed are listed. Allowing for experimental error and uncertainty in the 0.0328 m value projected for the hydroxide ion, the values of OH^- and K^+ absorbed are closely equal and, of even greater significance, are roughly one-half the final concentration (0.0492 m) of hydrated manganese dioxide. This 2:1 relationship holds even in the presence of excess potassium hydroxide. See experiments 2–5 as compared with 1.

An attempt was made to estimate the amount of absorbed hydroxide ion, by titrating the unfiltered slurry of product manganese dioxide with 1 *N* sulfuric acid. There was only a slight increase in titre over the filtered solution, and the pH-meter end point drifted very slowly. Thus the KOH appeared to be tightly bound.

Based on these evidences, the following is suggested.

[6] $KOH \cdot 2MnO_2 \cdot xH_2O$

The existence of a potassium manganite has been long recognized (8). A very careful structural study of the $KOH-MnO_2$ interaction has been made by Narita and Okabe (7) who have noted that at pH ≥ 8 amorphous ternary compounds of Mn(IV) oxide with an approximate composition of $K_2O \cdot 4MnO_x \cdot 4H_2O$ (x = 1.97–2.00) were formed by reduction of MnO_4^- or MnO_4^{2-}. The results in Table 3 and the manganese dioxide analyses thereby completely support the earlier conclusions of Narita and Okabe. Assuming the four H_2O molecules of their formula are chemically bound, a linear four-Mn unit is suggested. Such a structure is difficult to rationalize. With small variations in the numbers of bound water the structure could be represented with only two Mn per unit or alternatively, as more complex polymeric or cyclic units. In view of these uncertainties, formula [6] is used in the discussion to follow.

Proposed mechanism

Based on the above and earlier observations, a summarizing mechanism is proposed for the oxidation of cyclohexene by potassium permanganate.

Quite clearly, the acid and basic (OH^-) mechanisms for this reaction are quite different. There may be the common factor of an intermediate complex (4) but, beyond this stage, there appears to be no mechanistic similarity between an acidic or basic environment.

For the following mechanism, manganese dioxide is written as the potassium hydroxide adduct and 1,2-cyclohexanedione is suggested as a secondary oxidation intermediate. It has been observed that upon acidifying the post-glycol extraction solution, permanganate oxidizable substances (other than sulfur dioxide) are present in small amounts. Also the dione is base sensitive and a reaction with OH^- may account for the small amounts of unidentified neutral residues which invariably form.

The following proposal applies only in a basic medium.

[7] 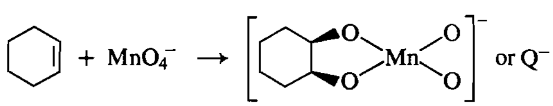

[8] 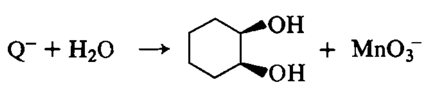

[9] $3MnO_3^- + K^+ + (x + 1)H_2O \rightarrow MnO_4^- + KOH \cdot 2MnO_2 \cdot xH_2O + OH^-$

[10] 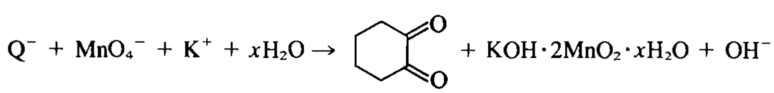

[11] 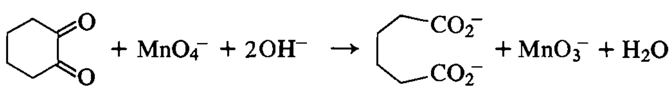

[12] 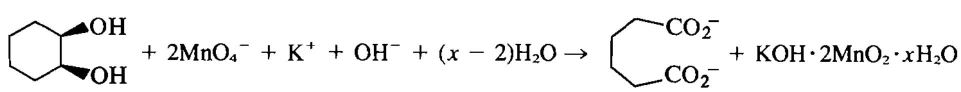

[13] 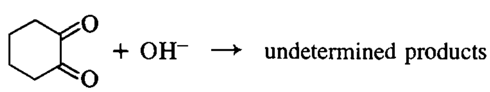

1. J. E. TAYLOR, D. WILLIAMS, K. EDWARDS, D. OTONNAA, and D. SAMANICH. Can. J. Chem. **62**, 11 (1984).
2. J. E. TAYLOR. Can. J. Chem. **62**, 2641 (1984).
3. N. H. FURMAN. Standard methods of analysis. 6th ed. Vol. 1. Van Nostrand, New York. 1962. p. 21.
4. D. G. LEE. The oxidation of organic compounds by permanganate ion and hexavalent chromium. Open Court, LaSalle, IL. 1980. p. 19.
5. K. B. WIBERG and R. D. GEER. J. Am. Chem. Soc. **88**, 5827 (1966).
6. K. J. LAIDLER. Chemical kinetics. 2nd ed. McGraw Hill, New York. 1965. pp. 219–222.
7. E. NARITA and T. OKABE. Bull. Chem. Soc. Jpn. **53**, 525 (1980).
8. G. D. PARKES. Mellor's modern inorganic chemistry. Revised edition. Wiley, New York. 1967. p. 892.

Structural determination of the group K capsular polysaccharide of *Neisseria meningitidis*: a 2D-NMR analysis[1]

FRANCIS MICHON, JEAN ROBERT BRISSON, RENÉ ROY, AND HAROLD J. JENNINGS
Division of Biological Sciences, National Research Council of Canada, Ottawa, Ont., Canada K1A 0R6

AND

FRASER E. ASHTON
Bureau of Microbiology, The Laboratory Center for Disease Control, Ottawa, Ont., Canada K1A 0L2

Received February 18, 1985

FRANCIS MICHON, JEAN ROBERT BRISSON, RENÉ ROY, HAROLD J. JENNINGS, and FRASER E. ASHTON. Can. J. Chem. **63**, 2781 (1985).

The capsular polysaccharide antigen of *Neisseria meningitidis* group K was isolated by Cetavlon precipitation and purified by ion-exchange chromatography. The structure of the K polysaccharide was determined to a large extent by comprehensive proton and carbon-13 nuclear magnetic resonance (nmr) studies. In these studies one-dimensional and two-dimensional experiments were carried out directly on the K polysaccharide. The K polysaccharide is composed of the following repeating unit: -4)β-D-Man*p*NAcA(1→3) [4-OAc]β-D-Man*p*NAcA(1→. Except for the one-bond couplings between their anomeric carbons and protons ($^1J_{^{13}\mathrm{C,H}}$), all the nmr spectroscopic evidence was consistent with both 2-acetamido-2-deoxy-D-mannopyranosyluronic acid residues adopting the $^4C_1$ (D) conformation and having the β-D-configuration. This ambiguity in $^1J_{^{13}\mathrm{C,H}}$ is probably due to through-space electronic effects generated by the presence of contiguous carboxylated sugar residues in the K polysaccharide. The *O*-acetyl substituents of the K polysaccharide are essential for its antigenicity to group K polysaccharide-specific antibodies.

FRANCIS MICHON, JEAN ROBERT BRISSON, RENÉ ROY, HAROLD J. JENNINGS et FRASER E. ASHTON. Can. J. Chem. **63**, 2781 (1985).

Faisant appel à une précipitation de Cétavlon, on a isolé le polysaccharide capsulaire antigène du groupe K du *Neisseria meningitidis* et on l'a purifié par passage sur une colonne échangeuse d'ions. En se basant principalement sur des études de rmn du ^{1}H et du ^{13}C, on a déterminé la structure du polysaccharide K. Au cours de ces études, on a réalisé des expériences en une et en deux dimensions directement sur le polysaccharide K. L'unité de base du polysaccharide K est la suivante: -4)β-D-Man*p*NAcA(1→3) [OAc-4]β-D-Man*p*NAcA(1→. À l'exception de couplages à travers une liaison entre les carbones et les protons anomères ($^1J_{^{13}\mathrm{C,H}}$), toutes les données spectroscopiques sont en accord avec le fait que les deux résidus d'acide acétamido-2 déoxy-2 D-mannopyrannosyluronique adoptent la conformation $^4C_1$ (D) et ont une configuration β-D. Cette ambiguité relative à la constante de couplage $^1J_{^{13}\mathrm{C,H}}$ est due probablement à des effets électroniques, à travers l'espace, engendrés par la présence contigue de résidus de sucres carboxylés dans le polysaccharide K. Les substituants *O*-acétylés du polysaccharide K sont indispensables pour assurer son comportement antigène envers les anticorps spécifiques du polysaccharide K.

[Traduit par le journal]

Introduction

Neisseria meningitidis is a Gram-negative organism that has been classified serologically (1–3) into groups A, B, C, D, 29E, L, W-135, X, Y, and Z. Except for group D, each group produces a unique capsular polysaccharide that is the antigen responsible for group specificity (1–3), and the structures of all the polysaccharides have been determined (2, 4). In 1981 Ding *et al.* (5) described three new meningococcal groups and designated them groups H, I, and K. The structure of the H polysaccharide has been recently reported (6, 7). As a continuation of our structural studies on the meningococcal polysaccharides we now report the structure of the K polysaccharide. The structure of the I polysaccharide has been reported elsewhere (8).

Nuclear magnetic resonance spectroscopy has played an increasingly important role in the structural elucidation of the meningococcal polysaccharides (2, 3, 6, 7), and the utility of this technique has been further demonstrated in the structural elucidation of the I (8) and K polysaccharides, where a number of one-dimensional, two-dimensional, and nuclear Overhauser enhancement (nOe) techniques were employed. Although two-dimensional techniques (9) have been used frequently on oligosaccharides since their introduction in 1982 (10–12), examples of the direct application of these techniques to polysaccharides are few (13).

Unlike the other meningococcal polysaccharides, the I (8) and K polysaccharides cross-react serologically to a certain extent. This cross-reaction is probably associated with their common 4-*O*-acetyl-2-acetamido-2-deoxy-β-D-mannopyranosyluronic acid residue.

Experimental

Materials

The *Neisseria meningitidis* strain 1811 (K) was obtained from Dr. Shao-quing Ding, National Institute for the Control of Pharmaceutical and Biological Products, Beijing, China, and was grown in a chemically defined medium (14). The capsular polysaccharide was isolated and partially purified as previously described (14) using an initial Cetavlon precipitation to obtain the crude polysaccharide. Purification of the K polysaccharide was achieved by its application to a column of DEAE-Sephadex A-25 (Cl-form, Pharmacia Fine Chemicals) in 0.01 *M* Tris–HCl buffer at pH 7.4 and the development of the column with a linear gradient of NaCl to 0.5 *M*. The polysaccharide was detected by Ouchterlony immunodiffusion using antisera to the K polysaccharide that were prepared by injecting whole group K organisms in rabbits as previously described (15). Using this assay it was shown that the K polysaccharide eluted as a single peak with approximately 0.3 *M* NaCl. The K polysaccharide had $[\alpha]_D$ −68° (*c* 0.25, in water).

[1] NRCC No. 24632.

The de-*O*-acetylated K polysaccharide was obtained by treatment of the native K polysaccharide with 0.1 *M* NaOH solution at 25°C for 16 h with subsequent neutralization, dialysis, and lyophilization of the solution. Carboxyl-reduced K polysaccharide was obtained using the method of Taylor and Conrad (16), in which sodium borohydride was added to its carbodiimide complex at pH 7.0. Two treatments were necessary in order to achieve complete reduction.

Instrumental methods

Solutions were concentrated in a rotary evaporator under reduced pressure below 40°C. Optical rotations were determined on a Perkin–Elmer 243 instrument with 1-dm semi-micro cells at 23 ± 1°C.

Gas–liquid chromatography (glc) was performed on a Hewlett–Packard 5710A instrument equipped with a flame ionization detector and a model 3380A electronic integrator using the following columns: (i) glass column (180 × 0.15 cm) containing 3% SP2340 on Supelcoport (80–100 mesh) operated at 180°C (delay 2 min) to 240°C at 4°C/min; and (ii) fused silica capillary column (0.32 mm × 25 m) containing 3% OV17 operated at 180°C to 230°C at 2°C/min and held for 10 min at 230°C. Combined gas–liquid chromatography – mass spectrometry (glc–ms) was performed on a Hewlett–Packard 5985B instrument using the above columns and an ionization potential of 70 eV.

The ^{13}C and ^{1}H nmr spectra were recorded on a Bruker AM-500 spectrometer. Acetone was used as the internal chemical shift reference for ^{1}H nmr (2.225 ppm) and dioxan was used as the external chemical shift reference for ^{13}C nmr (67.4 ppm). Polysaccharides were exchanged twice with D_2O and then run in 0.4 mL D_2O (5-mm tubes) at a concentration of 60 mg/mL.

Proton homonuclear shift correlated 2-D nmr experiments (H, H COSY) and proton dipolar correlation 2-D nmr experiments (NOESY) were performed using the standard 90–t_1–90 pulse sequence and the 90–t_1–90–τ–90 pulse sequence, respectively; a mixing time of 100 ms was used. Quadrature detection in both dimensions was employed. All phase cyclings were according to the standard software provided by Bruker (DISNMRP 840301.1). The initial (t_1, t_2) matrices were 64 × 512 data points with 4 Hz/pt digital resolution in the second domain. Data points in both dimensions were weighted by unshifted sine bell functions prior to Fourier transformation. The final (f_1, f_2) matrix was zero filled to 512 × 512 points. Magnitude spectra, which are symmetrized about the diagonal, were used to represent the data.

The ^{13}C–H shift correlation with proton decoupling in the F_1 domain was done according to Bax (17). The initial ($\mathbf{t}_1$, $\mathbf{t}_2$) matrix of 64 × 1024 points was Fourier transformed to a final matrix of 256 × 1024 points corresponding to a digital resolution of 23 Hz/pt in the F_2 domain and 15 Hz/pt in the F_1 domain. Gaussian weighting functions were used in both domains and a power spectra representation of the data points was used.

Analytical methods

Paper chromatography was carried out by the descending method using ethyl acetate – pyridine–water (5:2:5, v/v top layer) and *n*-butanol – pyridine–water (6:4:3, v/v) as eluants. Thin-layer chromatography (tlc) was performed on precoated tlc plates using ethyl acetate – pyridine – acetic acid – water (5:5:1:3, v/v) as ascending eluants. Compounds were visualized after spraying the plates with ninhydrin (amino sugars) or alkaline silver nitrate and *p*-anisidine reagents (pentoses).

Mannosamine was detected in the hydrolyzates of the carboxyl-reduced K polysaccharide either directly using a Technicon autoanalyzer, or by the identification of the products of its deamination (18) or ninhydrin degradation (19). For the purpose of deamination the K polysaccharide was first carboxyl-reduced, using sodium borodeuteride, before being hydrolyzed (2 *N* HCl for 90 min at 100°C), until complete de-*N*-acetylation had occurred. Following deamination and conversion to alditol acetates (20) the sugars were identified by glc–ms using column (i).

In preparation for ninhydrin degradation, the carboxyl-reduced K polysaccharide was first depolymerized with anhydrous HF for 16 h at 25°C and the free hexosamine generated by treating the depolymerized product with 1 *N* HCl at 100°C for 3 h. Following ninhydrin degradation of the hexosamine the derived pentose was identified by paper chromatography, and by glc–ms of its alditol acetate derivative using column (i).

Methylation analysis

The carboxyl-reduced K polysaccharide was methylated with methyl iodide in the presence of methyl sulfinyl anion according to the method of Hakomori (21). The methylated product was then purified on a small LH-20 column (10 cm × 0.5 cm) using chloroform as the eluant. The fractions were monitored by spotting the eluant on silica gel tlc plates, spraying the plates with 10% H_2SO_4 in ethanol, and charring the plates in an oven for 5 min at 130°C. The methylated polysaccharide was then hydrolyzed with 1 *M* trifluoroacetic acid for 16 h at 105°C and, following evaporation of the acid, the partially methylated monomers were reduced with $NaBH_4$, acetylated, and the products analyzed by glc–ms (22) using column (ii).

Quantitative microprecipitin experiments

Quantitative microprecipitin experiments were carried out by the method of Kabat and Mayer (23) using 0.1 mL rabbit antisera to the K polysaccharide (diluted twice in PBS at pH 7.0) and 0.1 mL of antigen solution containing from 1 to 100 μg of polysaccharide. Precipitates were dissolved in 0.1 mL of 0.1 *M* sodium hydroxide and the protein content was determined by the method of Lowry *et al.* (24).

Results and discussion

Characterization of 2-acetamido-2-deoxy-D-mannuronic acid

The presence of 2-acetamido-2-deoxy-D-mannuronic acid as a constituent of the K polysaccharide was established when 2-amino-2-deoxy-mannose was identified, by amino acid analyzer, in the hydrolyzate of the carboxyl-reduced K polysaccharide. This evidence was also consistent with the identification of arabinose, the anticipated product of the ninhydrin degradation of 2-amino-2-deoxy-mannose (19), in the ninhydrin-treated hydrolyzate. Further evidence was obtained when glucose was found to be the major product of the deamination of the de-*N*-acetylated (hydrolyzed) carboxyl-reduced K polysaccharide. The identification of glucose in the above reaction and not in the hydrolyzate of the original carboxyl-reduced K polysaccharide is indicative of its precursor being 2-amino-2-deoxy-mannose residues (25).

All the above evidence indicated that 2-acetamido-2-deoxy-mannuronic acid was probably the only sugar constituent of the K polysaccharide, and this was confirmed by treatment of the K polysaccharide with anhydrous hydrogen fluoride. Evaporation of the hydrogen fluoride yielded only 2-acetamido-2-deoxy-α- and β-D-mannofuranurono-6,3-lactone, a compound readily formed from 2-acetamido-2-deoxy-D-mannuronic acid (26). In the ^{13}C nmr spectrum of the crude depolymerization product only the signals of the lactone (26) were identified. The lactone had $[\alpha]_D$ +106° (*c* 0.35, in water), close to that reported (26) for the authentic equilibrated D-form of the lactone, which again confirmed the D-configuration of the 2-acetamido-2-deoxy-mannuronic acid residues of the K polysaccharide.

Structure of the K polysaccharide

A preliminary analysis of the ^{13}C nmr spectrum of the K polysaccharide is consistent with it being composed of a mono-*O*-acetylated disaccharide repeating unit containing only *N*-acetyl hexuronic acid residues, these residues having been previously identified as 2-acetamido-2-deoxy-D-mannuronic acid, and the structure of the repeating unit is shown in Fig. 1a. In the ^{13}C nmr spectrum of the K polysaccharide two distinct anomeric carbons at 99.20 and 96.82 ppm were observed,

TABLE 1. Chemical shifts[a] and coupling constants[b] of the signals in the ^1H nmr spectra of the K polysaccharides

	Residue A			Residue B		
Proton	Native	De-*O*-acetylated K[c]	Carboxyl-reduced K[c]	Native K	De-*O*-acetylated K[c]	Carboxyl-reduced K[c]
H1	4.96	4.91 (<3)	4.87	4.82	4.70 (<3)	4.83
H2	4.62	4.38 (<3)	4.39	4.76	4.60 (<3)	4.67
H3	na	3.86 (–)[d]	3.92	na[e]	3.93 (8.5)	3.99
H4	na	3.79 (–)[d]	3.70	4.96 (<9)	3.62 (9.5)	3.56
H5	na	3.77 (–)[d]	3.49	na	3.70	3.44
CH_3 (*N*-acetyl)	2.09	2.04	2.04	2.01	2.05	2.04
CH_3 (*O*-acetyl)	—	—	—	2.13	—	—

[a] Expressed relative to internal acetone (δ).
[b] In parentheses (Hz).
[c] Chemical shifts assigned by 2D (H, H COSY).
[d] Not resolved.
[e] na, not assigned.

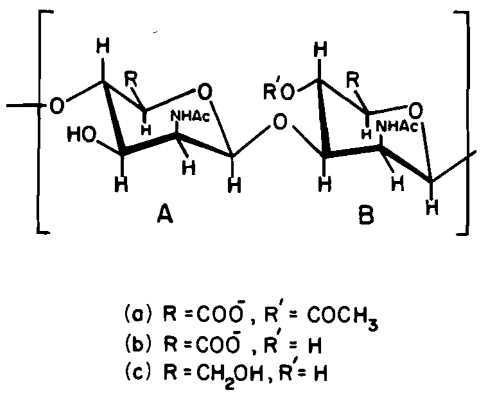

FIG. 1. The repeating units of the native, de-*O*-acetylated, and carboxyl-reduced K polysaccharide.

which were strongly indicative of a disaccharide repeating unit, and this was substantiated by the presence of only two anomeric proton signals at δ 4.91 and 4.70 in its ^1H nmr spectrum (Fig. 2). The presence of two *N*-acetyl groups could be deduced by the observation of two signals in the ^{13}C nmr spectrum of the K polysaccharide characteristic of this group at 53.50 and 51.04 ppm (C—N) and at 22.81 and 22.70 ppm (acetamido methyl groups). The signal at 21.50 ppm, which disappeared following base treatment of the K polysaccharide, could be readily assigned to the *O*-acetyl methyl groups. Consistent with the proposed repeating unit, no signals were observed in the hydroxymethyl region of the ^{13}C nmr spectrum of the K polysaccharide until, as expected, two signals at 61.4 and 61.0 ppm appeared in the ^{13}C nmr spectrum of the carboxyl-reduced K polysaccharide (Fig. 1c).

Although no monomeric *N*-acetyl-mannuronic acid units were available to assist in the assignment of the signals in the ^{13}C nmr spectrum of the de-*O*-acetylated K polysaccharide (Fig. 1b) it was possible to make an empirical assignment of the carboxyl-reduced K polysaccharide using the previously assigned (27) signals of 2-acetamido-2-deoxy-α- and β-D-mannopyranose for reference. However, due to the mixed linkages in the polysaccharide this proved to be unsatisfactory, resulting in potentially ambiguous assignments. Because these assignments were crucial to the structural elucidation of the K polysaccharide, they were made unambiguously without model compounds using a number of two-dimensional nmr techniques. This type of analysis is now routinely used for the assignment of oligosaccharide nmr signals, but only one report of its direct application to polysaccharides has so far been described (13). The method chosen was to correlate the carbon spectrum of the de-*O*-acetylated K polysaccharide with its assigned proton spectrum, thus assigning the carbon spectrum indirectly.

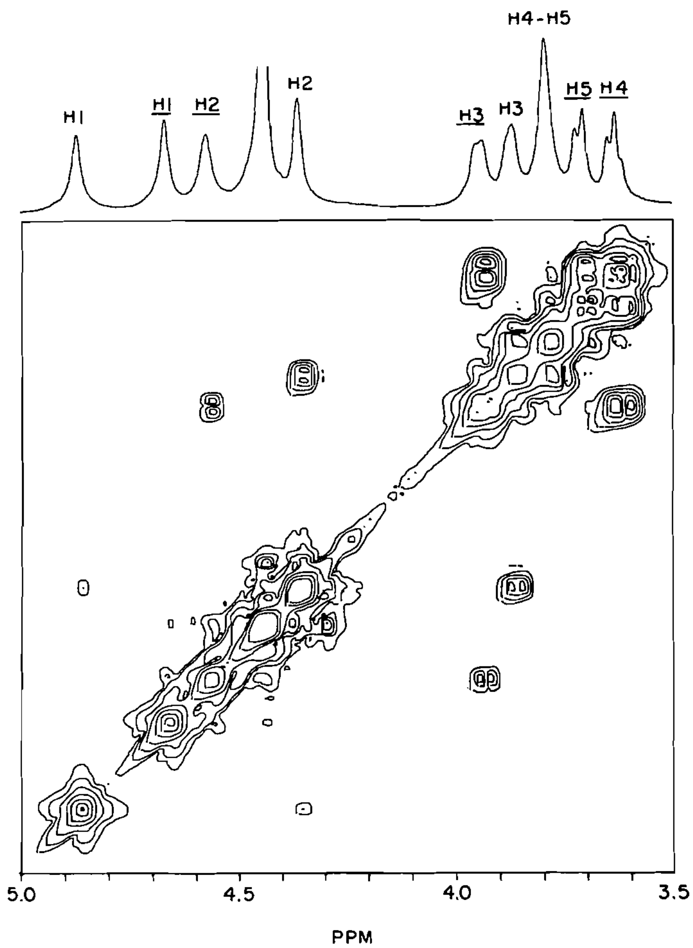

FIG. 2. Homonuclear 2-D shift correlated (H, H COSY) spectrum of the de-*O*-acetylated K polysaccharide in D_2O (330 K) with the 1-D spectrum above. The corresponding assignments for residue A and residue B (underlined) are also shown.

TABLE 2. Carbon-13 chemical shifts[a] of polysaccharides and component saccharides

Polysaccharides and component saccharides	Residue	C1	C2	C3	C4	C5	C6	CH_3 *N*-acetyl	CH_3 *O*-acetyl
Native K polysaccharide	A	96.82[b]	53.50	71.10	79.33	77.28	—	22.70[c]	—
	B	99.20[d]	51.04	76.19[c]	69.12	75.01[c]	—	22.81[c]	21.35
De-*O*-acetylated K polysaccharide[e]	A	96.82	53.50	71.45	78.99	77.09	—	22.93	—
	B	99.56	50.82	78.48	68.37	77.56	—	23.05	—
Carboxyl-reduced K polysaccharide[e]	A	97.10[f]	53.70	71.70	77.30	75.80	61.40	22.84	—
	B	100.10[g]	50.90	77.36	66.20	78.50	61.10	22.97	—
2-Acetamido-2-deoxy-β-D-mannopyranose[h]	—	94.3	55.3	73.2	67.8	77.5	61.7	23.2	—
2-Acetamido-2-deoxy-α-D-mannopyranose[h]	—	94.3	54.4	70.1	68.0	73.2	61.7	23.2	—

[a] In ppm from external dioxan.
[b] ${}^1J_{^{13}C,H}$ 168.8 Hz.
[c] Tentative assignments.
[d] ${}^1J_{^{13}C,H}$ 171.0 Hz.
[e] Assignments confirmed by 2D (^{13}C, H COSY).
[f] ${}^1J_{^{13}C,H}$ 162.7 Hz.
[g] ${}^1J_{^{13}C,H}$ 162.5 Hz.
[h] Taken from ref. 27.

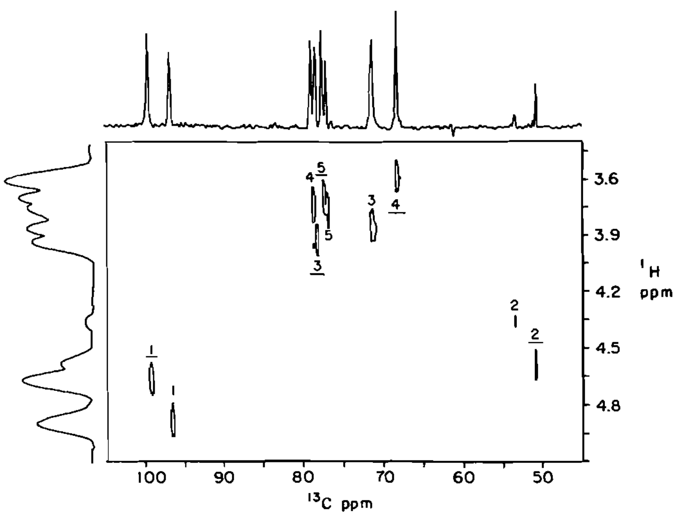

FIG. 3. Heteronuclear 2-D shift correlated (^{13}C, H COSY) spectrum of the de-*O*-acetylated K polysaccharide in D_2O (310 K) along with the f_1 and f_2 projections. The resulting assignments of the C–H correlations for residue A and residue B (underlined) are shown.

The ^{1}H nmr spectrum of the de-*O*-acetylated K polysaccharide shown in Fig. 2 was difficult to assign directly due to its complexity. Therefore a proton homonuclear shift correlated 2-D nmr (H, H COSY) experiment was performed and the spectrum is also shown in Fig. 2. As a result of this experiment it was possible to assign all the protons of both the 2-acetamido-2-deoxy-mannuronopyranosyl residues (A and B) of the repeating unit of the de-*O*-acetylated K polysaccharide (Fig. 1b). These assignments, together with some measurable coupling constants, are listed in Table 1. Using these data a heteronuclear shift correlated 2-D nmr (^{13}C, H COSY) experiment was performed and the ^{13}C–H correlation contour map is shown in Fig. 3. This experiment enabled the unambiguous assignment of all the carbons in the repeating unit of the de-*O*-acetylated K polysaccharide (Fig. 1b) to be made and they are listed in Table 2. Because of the importance of ^{13}C chemical shift data for making linkage and configurational assignments (28) on the K polysaccharide, and the lack of a suitable monomer model, the above two-dimensional experiments were also performed on the carboxyl-reduced K polysaccharide. This enabled 2-acetamido-2-deoxy-α- and β-D-mannopyranose (27) to be used as a satisfactory model for these assignments. The chemical shift data from the two-dimensional experiments are listed in Tables 1 and 2.

By studying patterns of chemical shift differences between 2-acetamido-2-deoxy-α- and β-D-mannopyranose and residues A and B of the repeating unit of the carboxyl-reduced K polysaccharide (Fig. 1c) it can be seen that regardless of anomeric configuration, although both A and B were later unambiguously assigned the β-D-configuration (*vide infra*), A is linked at *O*-4 and B at *O*-3. This is consistent with characteristic downfield displacements on C-4 of A (9.5 ppm) and C-3 of B (5.28 ppm), plus an upfield displacement on C-2 of B (4.5 ppm) (β effect), in comparison with the chemical shifts of the same carbons in the β-D-anomer of the model compound. Consistent with the above linkage assignment, both 3,6- and 4,6-di-*O*-methyl-2(*N*-methylacetamido)-2-deoxy-mannose together with their *N*-acetamido derivatives were detected (glc–ms using column (ii)) in the hydrolyzate of the methylated carboxyl-reduced K polysaccharide (Fig. 1c).

On the basis of the above chemical shift comparison it was also possible to make an assignment of the β-D-configuration to residues A and B of the carboxyl-reduced K polysaccharide (Fig. 1c), although further problems were encountered in this analysis due to substituent effects on the anomerically sensitive C5 signal of A caused by the vicinal linkage at *O*-4. However, allowing for the direction and magnitude of this effect, experience (28, 29) would indicate an approximate upfield shift of 2 ppm as a reasonable estimate, an assignment was possible. The chemical shifts of C5 of A (78.5 ppm) and B (75.8 + 2 ppm = 77.8 ppm) are more comparable to the equivalent C5 signal of 2-acetamido-2-deoxy-β-D-mannopyranose than to C5 of its α-D-anomer. The above configurational assignment was not definitive, however, as conflicting evidence was obtained using ^{1}H nmr spectroscopy.

Because residues A and B (Fig. 1a–c) are in the D-*manno* form, their anomeric configurations could not be determined with any degree of accuracy by the magnitude of their three-bond H1–H2 coupling constants (${}^3J_{H1,H2}$) (Table 1). However, in this circumstance it is common practice to use the anomeric one-bond ^{13}C–^{1}H coupling constants (${}^1J_{^{13}C,H}$) for this purpose, which have been demonstrated to be diagnostic of anomeric configuration (30–32). For example, in the case of D-glucopyranose (${}^4C_1$ (D) conformation) the α-D-anomer (equatorial H1) has ${}^1J_{^{13}C,H}$ = 169 Hz while the β-D-anomer (axial H1) has

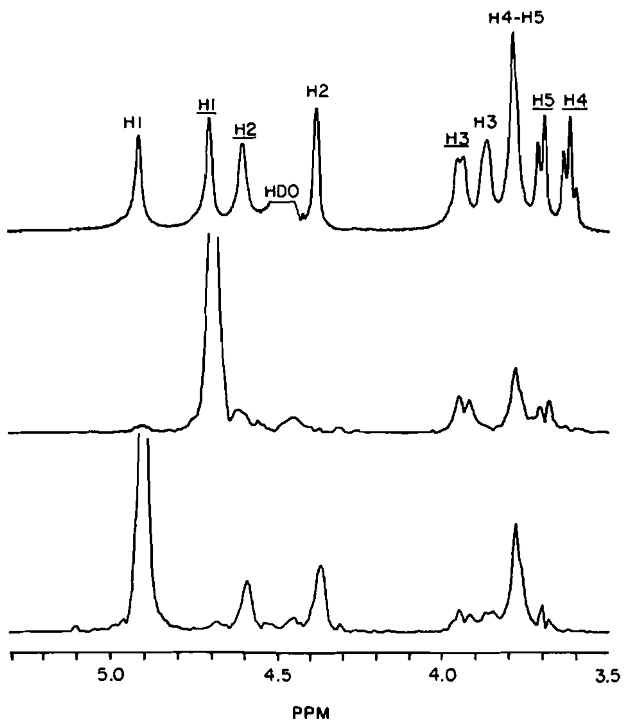

FIG. 4. The ^{1}H nmr spectrum (top) of the de-*O*-acetylated K polysaccharide in D_2O (330 K) with the assignments for residue A and residue B (underlined). Cross-sections of the 2-D NOESY contour map showing the nOe's for H1 of residue B (middle) and H1 of residue A (bottom).

$^1J_{^{13}C,H}$ = 161 Hz (31). These coupling constants and the 8–10 Hz difference between them have been found consistently in a large number of anomeric pairs of hexopyranoses (30–32) and hexopyranosyl residues in oligosaccharides and polysaccharides (33). The values of $^1J_{^{13}C,H}$ for A and B were 168.8 and 171.0 Hz, respectively, from which one could clearly deduce on the basis of the above accumulated evidence that they were both in the α-D-configuration. However, the values of $^1J_{^{13}C,H}$ for A and B of the carboxyl-reduced K polysaccharide (162.7 and 162.5 Hz) provide contradictory evidence, albeit consistent with the ^{13}C chemical shift data, that A and B of the K polysaccharide had the β-D-configuration. This latter assignment was later confirmed by nuclear Overhauser enhancement experiments (*vide infra*).

Two possible explanations for the anomalous values of $^1J_{^{13}C,H}$ for residues A and B of the K polysaccharide are that either they have equatorial anomeric protons due to their being in the $^4C_1$ (D) or twist boat conformation, or that this anomaly is associated with structural features peculiar to the K polysaccharide. In fact the latter explanation proved to be the relevant one because unambiguous assignments of the anomeric configuration (β-D) and conformation ($^4C_1$ (D)) of residues A and B of the K polysaccharide were obtained by 2-D nuclear Overhauser experiments carried out directly on the de-*O*-acetylated K polysaccharide. A number of nuclear Overhauser enhancements were observed on the resonances of protons in close proximity to the anomeric protons of residues A and B (Fig. 4). Critical to the above assignments are the intra-residue enhancements observed between H1–H3, H1–H5 of ring A and *H1–H3*, *H1–H5* of ring B which indicated that H3, H5 and *H3*, *H5* were both *cis* and 1,3-diaxially disposed to their respective anomeric protons.

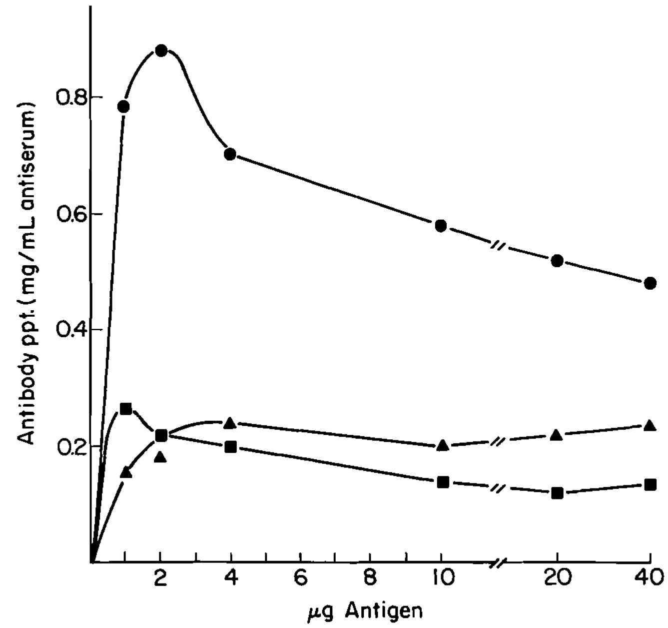

FIG. 5. Quantitative precipitin curves of the K polysaccharide (●-●), the de-*O*-acetylated K polysaccharide (■-■), and the group I meningococcal polysaccharide (△-△).

Inter-residue enhancements between H1 and H4–H5 (strongly coupled) were consistent with a β 1→4-linkage between residues B and A that would place H4 in close proximity (<2.5 Å) to *H1*. Similarly inter-residue enhancements between H1 and *H3* and between H1 and *H2* are a consequence of the β 1→3-linkage between residues A and B. Since inter-residue nOe's are dependent on the linkage conformation, the magnitude of these enhancements reflects the relative orientation of these residues with respect to each other.

The most probable explanation of the anomalous values of $^1J_{^{13}C,H}$ of residues A and B in the K polysaccharide is that they are due to electronic effects. Although this type of effect has been observed for hexopyranosyl derivatives having electronegative substituents at the anomeric center (32), no such effect has so far been observed in monomers with carboxylate groups in positions remote from the anomeric center. In fact residue B is also a constituent of the type e *H. influenzae* capsular polysaccharide and in this environment has $^1J_{^{13}C,H}$ = 164 Hz (34), a value more compatible with its β-D-configuration. Unlike the K polysaccharide, in this polysaccharide the carboxylated B residues are separated by uncharged sugar residues, which would strongly indicate that the anomalous $^1J_{^{13}C,H}$ values of the K polysaccharide are due to inter-residue through-space effects associated with the presence of contiguous carboxylated residues. This hypothesis is supported by the fact that residue B (Fig. 1b), also a constituent of the meningococcal group I polysaccharide, exhibits a similar and anomalous $^1J_{^{13}C,H}$ in this environment, where residue B alternates with a 1→4-linked 2-acetamido-2-deoxy-α-L-guluronopyranosyl residue (8). Interestingly, these latter residues (8) together with contiguous hexuronosyl residues of other glycuronans (35, 36) have been shown to have conventional values of $^1J_{^{13}C,H}$, indicating that the above phenomenon is not general.

The simple pattern of chemical shift displacement observed by comparing the ^{13}C nmr signals of the de-*O*-acetylated (Fig. 1b) with the native K polysaccharide (Fig. 1a) (Table 2) indicated that the repeating unit of the latter is specifically monosubstituted by *O*-acetyl at *O*-4 of residue B (Fig. 1a). Consistent with the above assignment, only three significant displacements were observed in the signals of the K polysaccharide: a rather small downfield displacement of 0.75 ppm on C4 of B with concomitant upfield displacements on the vicinal C3 and C5 signals of the same residue (2.29 and 2.55 ppm respectively). This assignment was also confirmed by comparing the ^{1}H nmr spectra of the de-*O*-acetylated (Fig. 1b) and native K (Fig. 1a) polysaccharide (Table 1). The only proton signal of the K polysaccharide to undergo a substantial downfield displacement, indicative of *O*-acetyl substitution, was H4 of residue B which was displaced by 1.34 ppm.

Immunological properties of the K polysaccharide

Quantitative serological precipitation experiments using the native (Fig. 1a) and de-*O*-acetylated (Fig. 1b) K polysaccharide with a meningococcal group K specific antiserum are shown in Fig. 5. These experiments demonstrate that the *O*-acetyl group is essential to the formation of the group-specific determinant. While the native K polysaccharide precipitated close to 0.9 mg of antibody from 1 mL of antiserum, the de-*O*-acetylated K polysaccharide precipitated only 0.25 mg of antibody from the same volume of antiserum. Probably due to their common 3-linked 4-*O*-acetyl 2-acetamido-2-deoxy-β-D-mannouronopyranosyl residues the meningococcal group I polysaccharide cross-reacts with the K polysaccharide-specific antiserum, although this cross-reaction is very weak.

Acknowledgement

The authors thank Fred Cooper for recording the mass spectra.

1. E. C. GOTSCHLICH, T. Y. LUI, and M. S. ARTENSTEIN. J. Exp. Med. **129**, 1349 (1969).
2. H. J. JENNINGS. Adv. Carbohydr. Chem. Biochem. **41**, 155 (1983).
3. F. E. ASHTON, A. RYAN, B. DIENA, and H. J. JENNINGS. J. Clin. Microbiol. **17**, 722 (1983).
4. H. J. JENNINGS, C. W. LUGOWSKI, F. E. ASHTON, and J. A. RYAN. Carbohydr. Res. **112**, 105 (1983).
5. S.-Q. DING, R.-B. YE, and H.-C. ZHANG. J. Biol. Stand. **9**, 307 (1981).
6. F. MICHON, R. ROY, H. J. JENNINGS, and F. E. ASHTON. Can. J. Chem. **62**, 1519 (1984).
7. A. VAN DER KAADEN, J. I. M. VAN DOORN-VAN WAKEREN, J. P. KAMERLING, J. F. G. VLIEGENTHART, and R. H. TIESJEMA. Eur. J. Biochem. **141**, 513 (1984).
8. F. MICHON, J. R. BRISSON, R. ROY, F. E. ASHTON, and H. J. JENNINGS. Biochemistry. In press.
9. S. L. PATT. J. Carbohydr. Chem. **3**, 493 (1984).
10. M. A. BERNSTEIN and L. D. HALL. J. Am. Chem. Soc. **104**, 5553 (1982).
11. J. H. PRESTEGARD, T. A. W. KOERNER, P. C. DEMON, and R. K. YU. J. Am. Chem. Soc. **104**, 4993 (1982).
12. R. C. BRUCH and M. D. BRUCH. J. Biol. Chem. **257**, 3409 (1982).
13. K. D. BARROW, J. G. COLLINS, P. L. ROGERS, and G. M. SMITH. Eur. J. Biochem. **145**, 173 (1984).
14. D. R. BUNDLE, H. J. JENNINGS, and C. P. KENNY. J. Biol. Chem. **249**, 4797 (1974).
15. F. E. ASHTON, A. RYAN, B. B. DIENA, and C. E. FRASCH. Can. J. Microbiol. **25**, 784 (1979).
16. R. L. TAYLOR and H. E. CONRAD. Biochemistry, **11**, 1383 (1972).
17. A. BAX and R. FREEMAN. J. Magn. Reson. **44**, 542 (1981).
18. B. A. DMITRIEV, L. V. BACKINOWSKY, V. L. LVOV, N. K. KOTCHETKOV, and I. L. HOFMAN. Eur. J. Biochem. **50**, 539 (1975).
19. P. J. STOFFYN and R. W. JEANLOZ. Arch. Biochem. Biophys. **52**, 373 (1954).
20. J. S. SAWARDEKER, J. H. SLONEKER, and A. R. JEANES. Anal. Chem. **37**, 1602 (1965).
21. S. HAKOMORI. J. Biochem. (Tokyo), **55**, 205 (1964).
22. B. LINDBERG. Methods Enzymol. **28**, 178 (1972).
23. E. A. KABAT and M. M. MAYER. *In* Experimental immunochemistry. Thomas, Springfield, IL. 1961. p. 241.
24. O. H. LOWRY, N. J. ROSEBROUGH, A. L. FARR, and R. J. RANDALL. J. Biol. Chem. **193**, 265 (1951).
25. J. M. WILLIAMS. Adv. Carbohydr. Chem. Biochem. **31**, 9 (1975).
26. E. DARAKAS, H. HULTBERG, K. LEONTEIN, and J. LONNGREN. Carbohydr. Res. **103**, 176 (1982).
27. D. R. BUNDLE, H. J. JENNINGS, and I. C. P. SMITH. Can. J. Chem. **51**, 3812 (1973).
28. H. J. JENNINGS and I. C. P. SMITH. Methods Enzymol. **50**, 39 (1978).
29. P. A. J. GORIN. Adv. Carbohydr. Chem. Biochem. **38**, 13 (1981).
30. A. S. PERLIN, B. CASU, and H. J. KOCH. Can. J. Chem. **48**, 2596 (1970).
31. J. A. SCHWARZ and A. S. PERLIN. Can. J. Chem. **50**, 3667 (1972).
32. K. BOCK and C. PEDERSEN. J. Chem. Soc. Perkin Trans. 2, 293 (1974).
33. G. K. HAMER and A. S. PERLIN. Carbohydr. Res. **49**, 37 (1976).
34. P. BRANEFORS-HELANDER, L. KENNE, B. LINDBERG, K. PETERSSON, and P. UNGER. Carbohydr. Res. **88**, 77 (1981).
35. H. GRASDALEN, B. LARSEN, and O. SMIDSROD. Carbohydr. Res. **56**, C11 (1977).
36. H. TSUCHIHASHI, T. YADOMAE, and T. MIYAZAKI. Carbohydr. Res. **98**, 65 (1981).

Regiospecific synthesis of cyclopentane analogs of (2′- and 3′-deoxy-*threo*-pentofuranosyl)-uracil and -2-thiouracil nucleosides

LUCJAN J. J. HRONOWSKI AND WALTER A. SZAREK
Carbohydrate Research Institute and Department of Chemistry, Queen's University, Kingston, Ont., Canada K7L 3N6

Received January 18, 1985

LUCJAN J. J. HRONOWSKI and WALTER A. SZAREK. Can. J. Chem. **63**, 2787 (1985).

Aminohydroxycyclopentanemethanols are important precursors for the synthesis of cyclopentane analogs of purine and pyrimidine nucleosides. The regiospecific synthesis of two new aminohydroxycyclopentanemethanols, **17** and **22**, is described. In these syntheses the desired configuration in the cyclopentane ring is obtained by opening the *cis*-acetoxy-1,3-cyclopentanedicarboxylic acid anhydride **3** with either ammonia or methanol. The attack by each nucleophile occurs at the carbonyl carbon farthest away from the acetoxy group to give a carbamoyl or an ester function at this position. Since the ester function is destined to become the hydroxymethyl substituent and the carbamoyl function the amino substituent, the type of nucleophile used to open the anhydride determines whether the 2-deoxy or the 3-deoxy isomer is obtained. Coupling of the aminohydroxycyclopentanemethanols with 3-ethoxypropenoyl isocyanate followed by cyclization of the acyl ureas in 2 *N* H_2SO_4 gave two new cyclopentane analogs of uracil nucleosides. Coupling of the aminohydroxycyclopentanemethanols with 3-ethoxypropenoyl isothiocyanate followed by cyclization of the acyl thioureas in 15 *N* aqueous ammonia gave two new cyclopentane analogs of 2-thiouracil nucleosides.

LUCJAN J. J. HRONOWSKI et WALTER A. SZAREK. Can. J. Chem. **63**, 2787 (1985).

Les aminohydroxycyclopentaneméthanols sont des précurseurs importants dans la synthèse des analogues cyclopentaniques des nucléosides de la pyrimidine ainsi que de la purine. On décrit des synthèses régiospécifiques des deux nouveaux aminohydroxycyclopentaneméthanols **17** et **22**. Dans ces synthèses, on obtient la configuration désirée du cyclopentane en procédant à l'ouverture de l'anhydride de l'acide acétoxy cyclopentanedicarboxylique-1,3-*cis*, **3**, à l'aide d'ammoniac ou de méthanol. Chaque nucléophile attaque le carbone du carbonyle le plus éloigné du groupe acétoxy; cette réaction donne naissance à une fonction carbamoyle ou à une fonction ester dans cette position. Puisque la fonction ester est destinée à devenir le substituant hydroxyméthyle alors que la fonction carbamoyle est destinée à devenir le substituant amino, le type de nucléophile utilisé pour ouvrir l'anhydride détermine la nature de l'isomère déoxy-2 ou déoxy-3 qui sera obtenu. Le couplage des aminohydroxycyclopentaneméthanols avec de l'isocyanate d'éthoxy-3 propénoyle, suivi d'une cyclisation des acylurées en présence de H_2SO_4 2 *N*, conduit à deux nouveaux analogues cyclopentaniques des nucléosides de l'uracile. Le couplage des aminohydroxycyclopentaneméthanols avec de l'isothioocyanate d'éthoxy-3 propénoyle, suivi d'une cyclisation des acylthiourées en présence d'ammoniaque 15 *N*, conduit à deux nouveaux analogues cyclopentaniques des nucléosides du thio-2 uracile.

[Traduit par le journal]

Introduction

The replacement of the furanose-ring oxygen by a methylene group can have a profound effect on a nucleoside's biochemical and biological activity. Guranowski *et al.* (1) showed that the cyclopentane analog of adenosine was several orders of magnitude less effective as a substrate for the beef liver enzyme *S*-adenosylhomocysteine hydrolase than adenosine and also that it is the most potent inhibitor of this enzyme with a K_i of $5 \times 10^{-9}\,M$, results which indicated the necessity of the oxygen of the ribofuranose ring for the enzymatic reaction but not for binding to the active site. A large number of cyclopentane analogs of both purine and pyrimidine nucleosides have been synthesized and many have shown antiviral and (or) anticancer activity (see, for example, refs. 2–7).

Virtually all of the syntheses of cyclopentane analogs of nucleosides described to date involve the prior preparation of an appropriately functionalized cyclopentylamine followed by the coupling of this amine with an appropriate base precursor. The central problem, therefore, in the synthesis of the cyclopentane analogs is the synthesis of a cyclopentane ring with the different substituents having the required configurations. Shealy *et al.* (8) have synthesized cyclopentane analogs of nucleosides having the "deoxy*ribo*" (8*a*) and *ribo* (8*b*) configurations by the oxidation of *exo*-5-norbornen-2-yl acetate and *exo-cis*-norbornen-2,3-diyl diacetate, respectively, with sodium permanganate. More recently, cyclopentylamines having the *ribo* (9, 10), *lyxo* (10), and *arabino* (11) configurations have been prepared from the readily available 2-azabicyclo-[2.2.1]hept-5-en-3-one (12), which is structurally analogous to norbornene. Holý (13) reported the preparation of the cyclopentane analog having the *ribo* configuration by catalytic hydrogenation of diethyl cyclopentane-2,3-dione-1,4-dicarboxylate. In the preparation of cyclopentane analogs of *C*-nucleosides, bin Sadikun *et al.* (4) achieved the *lyxo* configuration using norborn-5-ene-2-*endo*,3-*endo*-dicarboxylic acid anhydride. Just *et al.* achieved the *arabino* configuration using 5-carbomethoxy-2-*exo*,3-*endo*-dipivaloyoxybicyclo-[2.2.1]hept-5-ene (14) and the "2-deoxy*ribo*" configuration using 2-carbomethoxy-*exo*-5-*p*-nitrobenzoyloxybicyclo-[2.2.1]hept-2-ene (15). Paulsen and Maass (16) prepared cyclopentane rings having substituents in various orientations by allylhydroxylation of epoxides of cyclopentanemethanols using phenyl selenide. Shealy and O'Dell (7) obtained the cyclopentane analog of Ara-C from the cyclopentane analog of cytidine by way of the 2,2′-anhydro derivative.

In most of the above-mentioned syntheses (2–6, 8–11, 14, 15) the configurations of the cyclopentane rings are determined by the intermediacy of a bicyclo[2.2.1] derivative. The methods of Paulsen and Maass (16) and Holý (13), which do not utilize such a bicyclo[2.2.1] intermediate, give mixtures of isomers which must be resolved. Some of the methods (8*a*, 11) which utilize a bicyclo[2.2.1] intermediate also produce mixtures of isomers. The present article describes the synthesis of new aminohydroxycyclopentanemethanols, **17** and **22**,

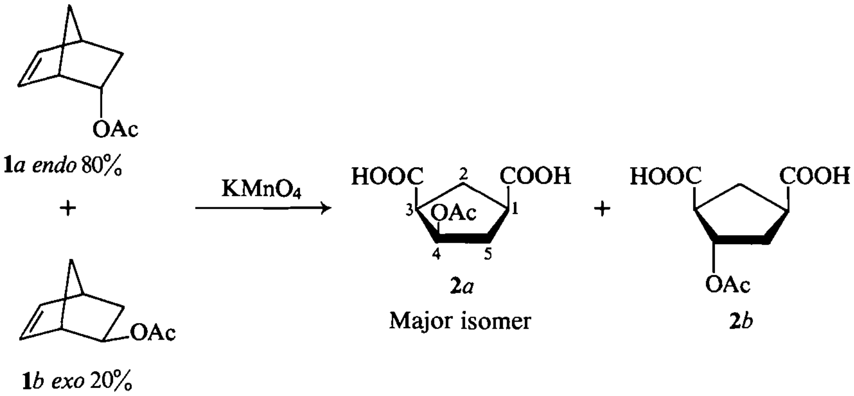

SCHEME 1

by regiospecific routes from the common precursor (±)-(1β,3β,4β)-4-acetoxy-1,3-cyclopentanedicarboxylic acid anhydride (**3**), and the conversion of each of them into uracil and 2-thiouracil nucleosides.

Results and discussion

The starting material for the synthesis of (±)-(1β,3β,-4β)-4-amino-3-hydroxycyclopentanemethanol (**17**) and (±)-(1β,2β,4β)-4-amino-2-hydroxycyclopentanemethanol (**22**) was a commercial sample (see experimental section) of 5-norbornen-2-yl acetate, which was shown to contain 80% of the *endo* (**1***a*) and 20% of the *exo* (**1***b*) isomers. An efficient method has been described by Birch *et al.* (17) for the oxidation of norbornene using $NaMnO_4$ to give cyclopentane-*cis*-1,3-dicarboxylic acid in 95% yield, and the method has been adapted for the preparation of *cis*-diacids from *exo*-5-norbornen-2-yl acetate and the *exo-cis*- and *endo-cis*-5-norbornen-2,3-diyl diacetates by Shealy *et al.* (8). In the present work the methods of the above workers (8, 17) have been utilized; however, instead of using $NaMnO_4$ as the oxidant, the more readily available $KMnO_4$ has been used to give the described diacid **2***a*[1] (Scheme 1) in 77% yield after recrystallization and a crude sample of **2** in 93%. This high yield has been consistently obtained in experiments in which the reaction temperature was maintained below 12°C; however, when the reaction temperature was allowed to rise above 40°C the yield of the desired diacid was greatly reduced.

The *cis* (**2***a*) and the *trans* (**2***b*) isomers were observed to have significantly different [1]Hmr spectra using a 200-MHz spectrometer; however, two spectral features which allow one to easily distinguish these isomers even on a 60-MHz instrument are the significantly different chemical shifts of the acetoxy methyls, which resonate at δ 1.90 in the case of the *cis* isomer (**2***a*) and at δ 2.00 in the case of the *trans* isomer (**2***b*). In addition, although the chemical shifts of the H-4 protons in the two isomers are identical at δ 5.20, the coupling patterns are quite distinct. In the *cis* isomer this proton couples with two *cis* vicinal protons and one *trans* vicinal proton to give a triplet-of-doublets coupling pattern, whereas in the *trans* isomer this proton couples with two *trans* vicinal protons and one *cis* vicinal proton to give a coupling pattern approximating an overlapping doublet of triplets.

Regiospecific opening of anhydride 3

The opening of the anhydride **3** (see Scheme 2) with anhydrous methanol followed by conversion of the carboxylic acid group into the carbamoyl function produced a single regioisomer **9**. Analysis of the [1]Hmr spectra of both the crude oily product (see experimental section) and the components separated by column chromatography on silica gel failed to reveal signals attributable to **5**. Similarily, the [1]Hmr spectrum of **4**, a compound which was produced by opening of the anhydride **3** with anhydrous ammonia, did not reveal any traces of a second regioisomer. In this second case, however, only the crystalline solid that represented a 91.3% yield was analyzed, and thus the possibility of the presence of a small amount of the other regioisomer, which may have been present in the crude mother liquor, was not eliminated. In both cases, however, the nucleophile attacks the carbonyl carbon farthest away from the acetoxy group. Compound **4** was esterified using diazomethane to give compound **5**. Therefore, since the carbamoyl function is destined to become N-1 in the pyrimidine nucleoside and the ester function the hydroxymethyl group at C-4′ in the nucleoside, it is possible to obtain the "2-deoxy*lyxo*" or the "3-deoxy*lyxo*" configuration selectively (as shown in Scheme 2). In contrast, in the case of (±)-(1β,3β,4α)-4-acetoxy-1,3-cyclopentanedicarboxylic acid anhydride, in which the acetoxy group has the *trans* configuration, Shealy and O'Dell (8*a*) obtained the two regioisomers having the 2-deoxy*ribo* and "3-deoxy*ribo*" configurations in approximately equal amounts, thus requiring the separation of the two regioisomers by column chromatography. From these observations and a consideration of a model of anhydride **3** it seems likely that the large *cis*-acetoxy group prevents facile attack by nucleophiles on the nearby carbonyl carbon by steric interactions.

The ester functions of compounds **5** and **9** were reduced using $LiBH_4$. In the case of **5** it was observed that the percentage yield of the product **6** was greatly dependent on the time of reflux during the reduction, ranging from 29% after 2 h to 81% when the time of reflux was only 20 min.

The configurations of compounds **4**–**10** (Scheme 2) have been assigned with the aid of [1]Hmr decoupling experiments. The chemical shifts of the methylene protons of the hydroxymethyl substituent in compounds **6** and **10** are of particular interest. In compound **10** these two protons are equivalent and give rise to a single multiplet (doublet of doublet due to coupling with O*H* and H-4) at δ 3.33; however, in the case of

[1] Structures **1**–**10** and **17**–**30** depict only one enantiomer of racemic mixtures. The relative configurations of substituent groups on the cyclopentane ring are specified by the α,β system used for steroids (31). Substituents which are written below the plane of the cyclopentane ring are designated α and those above the plane of the ring as β.

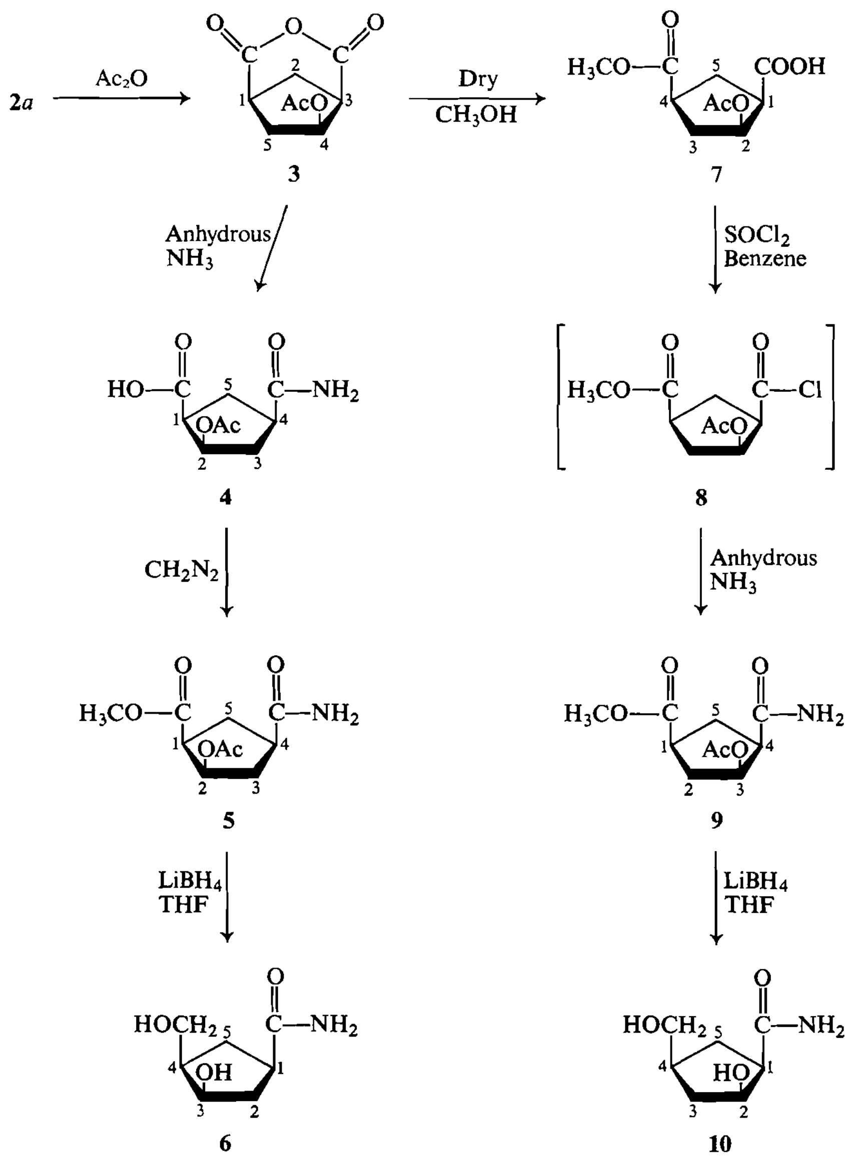

SCHEME 2

compound **6** two separate multiplets are observed for these two methylene protons, at δ 3.35 and 3.59. This non-equivalence of the hydroxymethyl methylene protons indicates that rotation of the hydroxymethyl substituent in compound **6** is restricted.

*Synthesis of the carbocyclic analogs (19 and 21) of 3-deoxy-*threo*-pentofuranosyl nucleosides*

The carbamoyl substituent in **10** was converted into the amino substituent in **17** (see Scheme 3) by the Hofmann reaction (18) using the procedure described by O'Dell and Shealy (19) for the preparation of aminohydroxycyclopentanemethanols having the "deoxy*ribo*" configurations. The amine **17** was coupled then with 3-ethoxypropenoyl isocyanate (**15**), which was prepared by previously described methods (20–23), to give compound **18**. Nucleoside analog **19** was prepared by heating **18** in 2 *N* H_2SO_4 at reflux temperature for 30 min. The ^{1}Hmr spectrum of compound **19** is very complex; however, it is different from that of the nucleoside analog having the "3-deoxy*ribo*" configuration, a sample of which had been prepared by previously described methods (22). The ^{1}Hmr signals in the spectra of these nucleosides have been assigned with the aid of spin–spin decoupling experiments.

Compound **20** was prepared by coupling **17** with 3-ethoxypropenoyl isothiocyanate (**16**) (see Scheme 3), which was prepared as described by Shaw and Warrener (21). Nucleoside analog **21** was obtained by heating **20** in 15 *N* aqueous ammonia at 100°C for 20 min. The multiplet patterns of the ^{1}Hmr spectra of nucleoside analogs **19** and **21** were observed to be very similar using a 200-MHz spectrometer; however, in general, the signals of protons in nucleoside analog **21** are found farther downfield than the signals of corresponding protons in nucleoside analog **19**. For example, the signal of H-1′ resonates at δ 4.49 in the case of **19** and at δ 5.41 in the case of **21**. The coupling constants found in the H-1′ multiplet are virtually identical for both nucleoside analogs. The largest difference in chemical shifts occurs for the H-3 proton, which in the case of **19** resonates at δ 11.20 while in the case of **21** it resonates at δ 12.59. In both of these analogs H-5 has a long-range coupling constant of 1.7–1.9 Hz to H-3 in addition to the vicinal coupling constant of 7.8–8.1 Hz to H-6.

*Synthesis of the carbocyclic analogs (24 and 26) of 2-deoxy-*threo*-pentofuranosyl nucleosides*

Two approaches have been utilized for the conversion of the

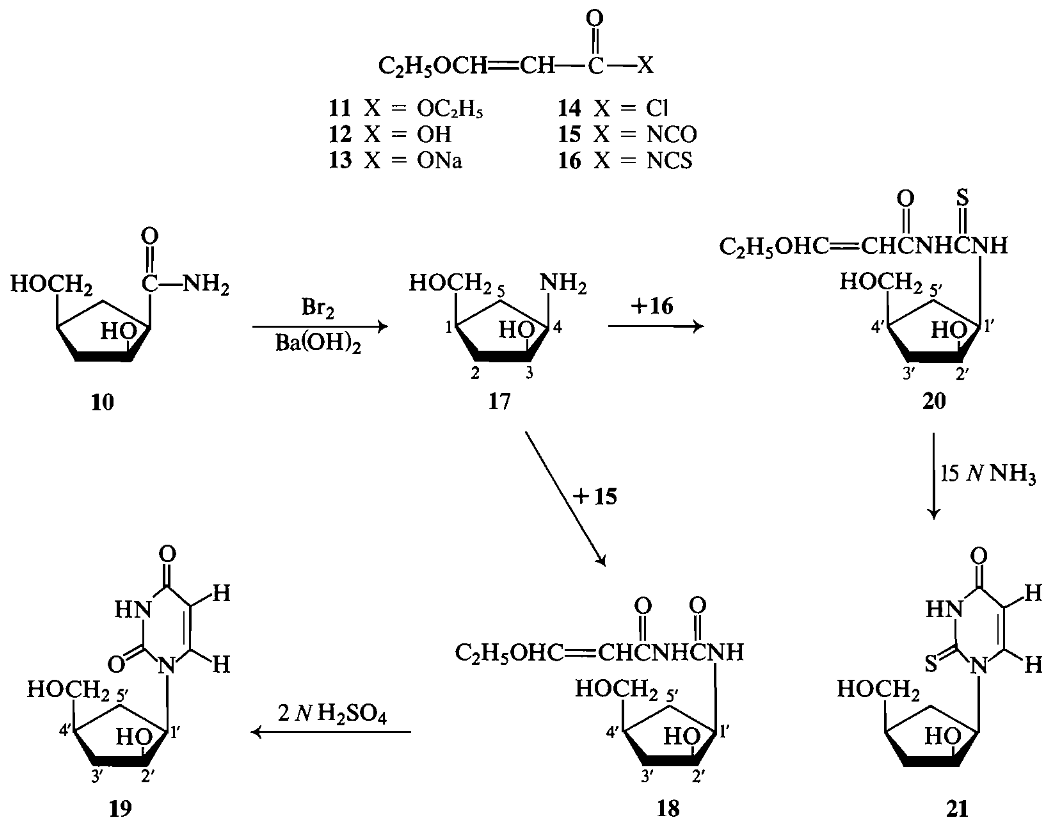

SCHEME 3

carbamoyl substituent in compound **6** to the amino substituent (see Scheme 4). In the first approach the Hofmann reaction was performed directly on **6**, which gave the amine **22** after purification on a cation-exchange resin in 27% yield. In the second approach the hydroxyls in compound **6** were protected by an isopropylidene group and the Hofmann reaction (18) was performed on **27** in methanol using sodium methoxide as the base to give the carbamate **28**. Hydrolysis of the carbamate with sodium hydroxide gave the amine **29** in 54% yield from **6**. The advantages of this latter route, despite the fact that it involves three steps instead of one, are not only the much greater overall yield but also the fact that the work-up in this latter approach is greatly simplified. In addition, the protected compound **29** gives significantly better yields in the subsequent steps leading to nucleoside analog **24** (see Scheme 4). Thus, **24** has been prepared in 26.4% yield from **6** by the latter route compared to 7.5% yield by the first route, a 3.5-fold improvement. Nucleoside analog **26** has been obtained by coupling the unprotected compound **22** with **16** to give **25**, followed by heating at 100°C in 15 *N* aqueous ammonia.

An attempt was made also to synthesize the amine **22** by first converting the carbamoyl substituent of compound **4** to an amino group by a Hofmann hypobromite reaction; however, the conditions lead to the elimination of acetic acid as shown in Scheme 5.

As was observed in the cases of the nucleoside analogs **19** and **21**, the multiplet patterns of the ^{1}Hmr spectra of analogs **24** and **26** are very similar also, with the multiplets of the 2-thiouracil-containing analog **26** occurring farther downfield than the multiplets of corresponding protons in the uracil-containing analog **24**. This difference in chemical shifts between corresponding protons in the uracil- and 2-thiouracil-containing nucleosides decreases with distance from the thio group such that the protons in the hydroxymethyl substituent resonate at virtually the same chemical shifts in the cases of both nucleoside analogs (**24** and **26**). Also, as previously observed for compound **6**, the ^{1}Hmr spectra of compounds **22**–**26** (Scheme 4) each show two well-separated multiplets for the methylene protons of the hydroxymethyl substituent. In contrast, only a single multiplet was observed for these protons in the spectra of compounds **10** and **17**–**21** (Scheme 3). The chemical shifts and the coupling constants of one of the methylene multiplets are very similar in the cases of compounds **6** and **22**–**26**; in the cases of all of these compounds this multiplet occurs in the δ 3.58–3.60 region. In the spectrum of compound **22** coupling to the hydroxyl proton is not observed. The chemical shift of the other multiplet varies over a greater range between the different compounds (**6**, **22**–**26**); in compound **6** it occurs at δ 3.35, in **22** at δ 3.37, in **23** and **25** at δ 3.40, and in the nucleoside analogs **24** and **26** at δ 3.43 and 3.44, respectively. The non-equivalence of the two methylene hydrogens in the hydroxymethyl substituent may be in part due to intramolecular hydrogen bonding between the hydroxyls. That hydrogen bonding alone may not account for these observations is indicated by the fact that, when the two hydroxyls in each of compounds **6**, **19**, and **24** are acetylated, non-equivalence is still observed to the extent of approximately 0.10 ppm for the corresponding methylene protons in the acetates of **6** and **24**, and also in the acetate of **19**; however, in this last acetate the difference in chemical shifts between these methylene protons is much smaller than in the first two.

In the ^{1}Hmr spectra of compounds **27**–**30**, in which these methylene protons are part of a heterocyclic six-membered ring, the multiplets arising from these protons are also well separated but appear farther downfield. The chemical shifts of one of the multiplets are in the δ 3.50–3.54 region and those

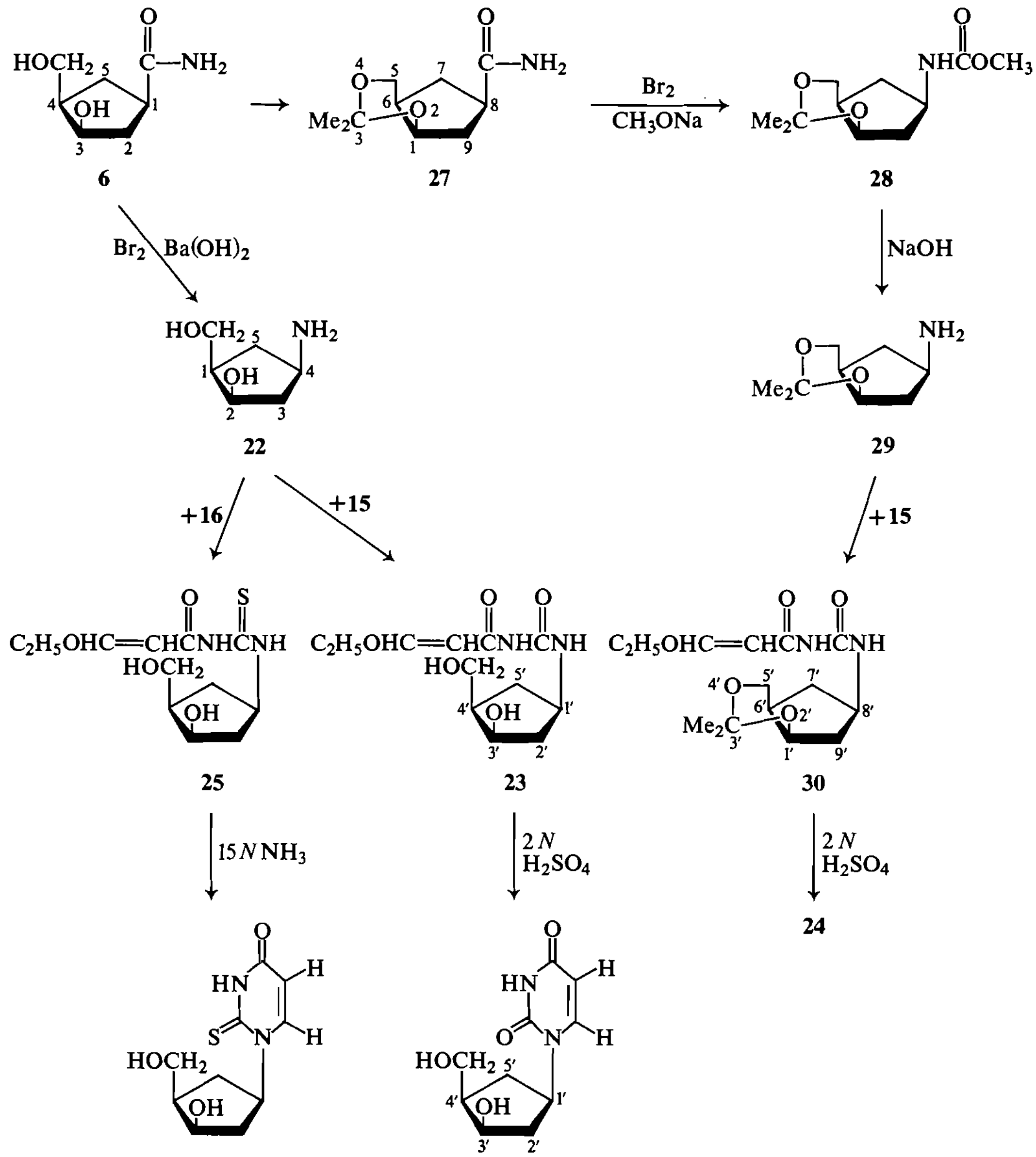

SCHEME 4

of the other in the δ 3.96–4.03 region.

Ultraviolet spectra of the nucleoside analogs

The ultraviolet spectra of the uracil-nucleoside analogs **19** and **24** exhibit virtually identical absorption maxima in both acidic and alkaline ethanol and they closely resemble the spectra of 1-methyluracil (24) at the corresponding pH's. The spectra of the 2-thiouracil-nucleoside analogs **21** and **26** are also similar in both acidic and alkaline ethanol, although quite different from those of **19** and **24**. The absorption maxima in the spectra of **21** and **26** occur at longer wavelengths and the spectra have a shoulder at approximately 290 nm in acidic and neutral ethanol. The molar absorptivities at the absorption maxima are also much greater in the cases of the 2-thiouracil-nucleoside analogs, especially in alkaline ethanol in which they are more than 2-fold greater. The ultraviolet spectra of the 2-thiouracil-nucleoside analogs **21** and **26** closely resemble those of 1-methyl-2-thiouracil (24) at the corresponding pH's.

Conclusions

Two new cyclopentane analogs of uracil nucleosides having the "2-deoxy*lyxo*" and "3-deoxy*lyxo*" configurations have been synthesized regiospecifically. In addition, the corresponding analogs of 2-thiouracil nucleosides have been synthesized; this work represents the first reported synthesis of cyclopentane analogs of nucleosides having the 2-thiouracil base. The synthetic routes also provide the possibility of regiospecific synthesis of cyclopentane analogs of nucleosides having the "deoxy*ribo*" configurations, by an inversion of configuration at C-2′ or C-3′ in the corresponding "deoxy*lyxo*" analogs. Analogs having the "2-deoxy*ribo*" configuration have been found to be biologically active in a variety of systems (2, 25).

Experimental

Melting points were determined on a Fisher–Johns apparatus and are uncorrected. The ^{1}Hmr spectra were recorded on a Bruker CXP-

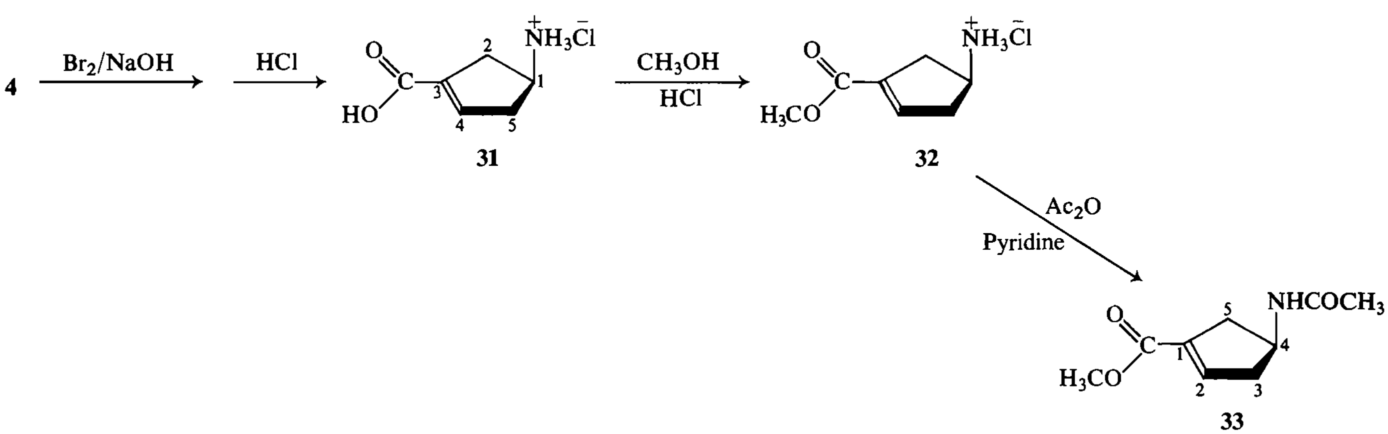

SCHEME 5

200 spectrometer at 200 MHz. Chemical shifts (δ) are given downfield from the signal of Me_4Si. Assignments of chemical shifts and coupling constants were made with the aid of spin-decoupling experiments. The following abbreviations are used in describing [1]Hmr signals: singlet (s), doublet (d), triplet (t), quartet (q), quintuplet (qu), sextuplet (se), multiplet (m), and broadened (br). Ultraviolet spectra were recorded on a Perkin–Elmer 552 spectrophotometer. Thin-layer chromatography (tlc) was performed using silica gel 60 F-254. The developed plates were dried and sprayed with a solution of ceric sulfate (1%) and molybdic acid (1.5%) in 10% aqueous sulfuric acid, and heated at ~150°C.

(±)-(1β,3β,4β)-4-Acetoxy-1,3-cyclopentanedicarboxylic acid (2a) and (±)-(1β,3β,4α)-4-acetoxy-1,3-cyclopentanedicarboxylic acid (2b)

5-Norbornen-2-yl acetate[2] (98 g, 0.64 mol) in 2,2,4-trimethylpentane (500 mL) was added to water (4 L) and the mixture was cooled to 10°C. To the stirred mixture $KMnO_4$ (325 g, 2.06 mol) in water (6 L) was added over a period of 3.5 h. During the addition of $KMnO_4$ a steady stream of CO_2 was passed through the reaction mixture and the temperature was maintained between 10 and 12°C using an ice bath. After the $KMnO_4$ had been added, SO_2 was passed through the reaction mixture until it became clear, with the temperature being maintained below 20°C. The volume of the reaction mixture was reduced to 1.6 L, and the mixture was cooled to 5°C and acidified with concentrated HCl (100 mL). It was extracted then with diethyl ether (5 × 400 mL); evaporation of the ether afforded a white solid (115.3 g). The reaction solution was reduced further to 900 mL, the solution was cooled to 5°C, and additional concentrated HCl (20 mL) was added; extraction again with ether (4 × 225 mL) gave an additional 14.3 g of solid, for a total yield of crude product of 129.6 g. The crude solid was recrystallized from ethyl acetate – hexanes and gave, in several crops, 81.3 g of a crystalline solid having mp 131–132°C and 4.0 g having mp 128–131°C, for a total yield of 85.3 g (77%) of **2***a*; [1]Hmr (200 MHz, Me_2SO-d_6) δ: 1.90 (3H, s, OAc), 1.95 (1H, m, J_{gem} = 14.7, $^3J_{5,1}$ = 6.1, $^3J_{5,4}$ = 2.7 Hz, H-5), 2.0–2.2 (2H, m, H-2 and H-2′), 2.20 (1H, m, J_{gem} = 14.7, $^3J_{5',1}$ = 10.1, $^3J_{5',4}$ = 5.2 Hz, H-5′), 2.83 (1H, m, H-1), 2.99 (1H, m, $^3J_{3,2}$ = 10.8, $^3J_{3,2'}$ = 8.4, $^3J_{3,4}$ = 5.4 Hz, H-3), 5.20 (1H, t of d, ^3J = 5.3, $^3J_{4,5}$ = 2.7 Hz, H-4), 12.31 (2H, br s, CO_2H at positions 1 and 3); spin–spin decoupled at H-4.

Two additional crops from the mother liquor of **2***a* gave 22.4 g of a white solid, mp 85–111°C, which was shown by [1]Hmr to consist primarily of **2***b*. Compound **2***b* was prepared also from *exo*-5-norbornen-2-yl acetate (**1***b*) (8*a*, 29) by the above oxidation method; mp 114–115°C (lit. (8*a*) mp 116–117°C); [1]Hmr (200 MHz, Me_2SO-d_6) δ: 1.79–1.95 (2H, m, H-2 and H-5), 2.00 (3H, s, OAc), 2.09 (1H, m, J_{gem} = 14.1, $^3J_{5',1}$ = 9.0, $^3J_{5',4}$ = 6.6 Hz, H-5′), 2.30 (1H, m, J_{gem} = 13.3, $^3J_{2',1}$ = 9.2, $^3J_{2',3}$ = 8.6 Hz, H-2′), 2.82 (1H, t of d, ^3J = 8.6, $^3J_{3,4}$ = 4.6 Hz, H-3), 2.92 (1H, qu, ^3J = 8.6 Hz, H-1), 5.20 (1H, d of t, $^3J_{4,5'}$ = 6.6, ^3J = 3.9 Hz, H-4), 12.46 (2H, br s, CO_2H at positions 1 and 3); spin–spin decoupled at H-4.

(±)-(1β,3β,4β)-4-Acetoxy-1,3-cyclopentanedicarboxylic acid anhydride (3)

A stirred mixture of **2***a* (85.1 g, 0.394 mol) in acetic anhydride (1 L) was heated at reflux temperature gently for 45 min. The reaction solution was cooled to room temperature and the solvent was removed under reduced pressure. The residual oil was shaken in the presence of diethyl ether (500 mL) and several seed crystals. The resulting white crystalline solid was collected by filtration and washed with diethyl ether to give **3** (54.6 g) having an initial mp 77–78°C which dropped to a sharp mp of 70°C overnight. The volume of the mother liquor was reduced to 200 mL and cooled in an ice bath to give an additional 4.75 g of a white crystalline solid having mp 70°C. The mother liquor was then evaporated to an oil which was heated at reflux temperature in acetic anhydride (200 mL) for 15 min to give a crystalline grey-brown solid (11.91 g), mp 69°C, for a total yield of 71.2 g (91.3%); [1]Hmr (200 MHz, $CDCl_3$) δ: 1.94 (1H, d of t, J_{gem} = 13.1, ^3J = 4.0 Hz, H-2), 2.00 (1H, m, J_{gem} = 15.3, $^3J_{5,4}$ = 3.7, $^4J_{5,2'}$ = 2.7 Hz, H-5), 2.07 (3H, s, OAc), 2.36 (1H, m, J_{gem} = 13.1, $^4J_{2',5}$ = 2.7 Hz, H-2′), 2.65 (1H, d of d of d, J_{gem} = 15.3, $^3J_{5',4}$ = 9.8, $^3J_{5',1}$ = 7.0 Hz, H-5′), 3.26 (1H, m, $^3J_{1,5'}$ = 7.0, $^3J_{1,2}$ = 4.0, $^4J_{1,3}$ = 1.5 Hz, H-1), 3.66 (1H, m, $^3J_{3,4}$ = 6.4, $^3J_{3,2}$ = 4.0, $^4J_{3,1}$ = 1.5 Hz, H-3), 5.44 (1H, d of d of d, $^3J_{4,5'}$ = 9.8, $^3J_{4,3}$ = 6.4, $^3J_{4,5}$ = 3.7 Hz, H-4). Spin–spin decoupling was performed at each of the protons. *Anal.* calcd. for $C_9H_{10}O_5$: C 54.55, H 5.09; found: C 54.22, H 5.22.

(±)-(1β,2β,4β)-2-Acetoxy-4-carbamoylcyclopentanecarboxylic acid (4)

Dry ammonia was bubbled through a stirred solution of **3** (71.2 g, 0.359 mol) in tetrahydrofuran (450 mL) which had been cooled to 5°C. The bubbling of ammonia was continued for 30 min at a rate which allowed the reaction temperature to be maintained between 10 and 12°C with an ice bath. The reaction mixture was flushed then with N_2 for 30 min. The solid was collected by filtration and dissolved in water (500 mL). The solution was then cooled to ice-bath temperature, acidified with concentrated HCl (35 mL), and left in the ice bath to crystallize. The crystalline product was collected by filtration and washed with a small amount of cold water to give a solid (57.7 g), mp 161–163°C. The volume of the mother liquor was reduced to 100 mL to give an additional 12.9 g of a light grey-brown solid, mp

[2] 5-Norbornen-2-yl acetate (bp 73–76°C/14 Torr; 1 Torr = 133.3 Pa) was purchased from the Aldrich Chemical Company and was shown to contain 80% of the *endo* (**1***a*) and 20% of the *exo* (**1***b*) isomers by integration of the well-resolved C-2 proton signals in the [1]Hmr spectrum (26). This determination is in good agreement with previous estimates of isomer composition in 5-norbornen-2-yl acetate samples prepared by the Diels–Alder reaction between vinyl acetate and cyclopentadiene (27, 28) which showed the *exo* isomer to comprise about 19% (28).

161–163°C, for a combined yield of 70.6 g (91.3%). An analytical sample was prepared by recrystallization twice from water; mp 164–165°C; [1]Hmr (200 MHz, Me_2SO-d_6) δ: 1.82 (1H, d of d of d, J_{gem} = 14.4, $^3J_{3,4}$ = 7.7, $^3J_{3,2}$ = 3.1 Hz, H-3), 1.91 (3H, s, OAc), 1.93–2.14 (2H, m, H-5 and H-5′), 2.19 (1H, m, J_{gem} = 14.4, $^3J_{3',4}$ = 9.7, $^3J_{3',2}$ = 6.0 Hz, H-3′), 2.63 (1H, qu, ^3J = 8.9 Hz, H-4), 2.95 (1H, d of d of d, $^3J_{1,5}$ = 10.8, $^3J_{1,5'}$ = 8.1, $^3J_{1,2}$ = 6.0 Hz, H-1), 5.21 (1H, t of d, $^3J_{2,1}$ = 6.0, $^3J_{2,3'}$ = 6.0, $^3J_{2,3}$ = 3.1 Hz, H-2), 6.84 (1H, br s, $CONH_2$), 7.29 (1H, br s, $CONH_2$), 12.29 (1H, br s, CO_2H); spin–spin decoupled at H-1, H-2, and H-4. D_2O exchange caused the disappearance of signals at δ 6.84, 7.29, and 12.29. *Anal.* calcd. for $C_9H_{13}O_5N$: C 50.23, H 6.09, N 6.51; found: C 49.98, H 6.14, N 6.53.

(±)-Methyl (1β,2β,4β)-2-acetoxy-4-carbamoylcyclopentane-carboxylate (5)

Diazomethane was prepared as described in Vogel (30) and was distilled into the flask containing **4** (30.8 g, 0.143 mol) in methanol (400 mL) until the reaction solution acquired a persistent bright yellow color. After several hours the yellow color faded and the product was crystallized in several crops by reducing the reaction solution's volume, diluting with ethyl acetate, and cooling to give **5** (25.94 g, 79.1%) as a crystalline solid, mp 122–124°C, and an orange oil (6.5 g) that was not examined further. An analytical sample of the solid was obtained by recrystallization from ethyl acetate; mp 123–124°C; [1]Hmr (200 MHz, Me_2SO-d_6) δ: 1.81 (1H, d of d of d, J_{gem} = 14.3, $^3J_{3,4}$ = 8.0, $^3J_{3,2}$ = 3.5 Hz, H-3), 1.90 (3H, s, OAc), 1.96–2.11 (2H, m, H-5 and H-5′), 2.21 (1H, m, J_{gem} = 14.3, $^3J_{3',4}$ = 9.6, $^3J_{3',2}$ = 6.2 Hz, H-3′), 2.64 (1H, qu, ^3J = 8.9 Hz, H-4), 3.06 (1H, m, $^3J_{1,5}$ = 11.0, $^3J_{1,5'}$ = 8.0, $^3J_{1,2}$ = 6.2 Hz, H-1), 3.58 (3H, s, OMe), 5.22 (1H, t of d, $^3J_{2,1}$ = 6.2, $^3J_{2,3'}$ = 6.2, $^3J_{2,3}$ = 3.5 Hz, H-2), 6.84 (1H, br s, $CONH_2$), 7.30 (1H, br s, $CONH_2$); spin–spin decoupled at H-1, H-2, and H-4. *Anal.* calcd. for $C_{10}H_{15}O_5N$: C 52.40, H 6.60, N 6.11; found: C 51.97, H 7.01, N 6.06.

(±)-(1β,3β,4β)-3-Hydroxy-4-(hydroxymethyl)cyclopentane-carboxamide (6)

A solution containing $LiBH_4$ (12.6 g, 0.578 mol) in tetrahydrofuran (500 mL, the Aldrich Chemical Company, 99+%) was heated at reflux temperature for 20 min and cooled to about 40°C. To this solution compound **5** (25.0 g, 0.109 mol) was added as a solid and the stirred reaction mixture was heated at reflux temperature for 20 min. The reaction mixture was cooled to ice-bath temperature, water (350 mL) was slowly added, and then Amberlite IR-120 resin (H^+ form) (350 mL). The mixture was stirred for 1.5 h, and the resin was removed by filtration and washed with water. The combined filtrate and washings were stored in the cold room overnight, the solvent was evaporated, and the residue was evaporated with methanol (4 × 100 mL) to remove boric acid. This procedure gave a viscous oil which was stirred overnight in the cold room in the presence of tetrahydrofuran (70 mL). The white solid (12.45 g) was collected by filtration; R_f 0.37 (tlc) (9:1 (v/v) acetonitrile–water). The volume of the mother liquor was reduced to about 10 mL; treatment with tetrahydrofuran (20 mL) as above gave a solid (1.56 g), R_f 0.37, and a trace of impurity having R_f 0.51, for a total yield of 14.01 g (81%). An analytical sample was prepared by recrystallization from methanol – ethyl acetate – hexanes; mp 135–136°C; [1]Hmr (200 MHz, Me_2SO-d_6) δ: 1.31–1.51 (1H, m, H-5), 1.65 (1H, d of d of d, J_{gem} = 13.6, $^3J_{2,1}$ = 5.0, $^3J_{2,3}$ = 2.7 Hz, H-2), 1.82 (1H, m, $^3J_{3,4}$ = 4.6 Hz, H-4), 1.8–2.0 (1H, m, H-5′), 1.93 (1H, m, J_{gem} = 13.6, $^3J_{2',1}$ = 9.6, $^3J_{2',3}$ = 4.9 Hz, H-2′), 2.65 (1H, m, $^3J_{1,2}$ = 5.0 Hz, H-1), 3.35 (1H, m, J_{gem} = 10.7, $^3J_{\text{to H-4}}$ = 5.9, $^3J_{\text{to OH}}$ = 5.3 Hz, C*H*$_2$OH), 3.59 (1H, m, J_{gem} = 10.7, $^3J_{\text{to H-4}}$ = 6.9, $^3J_{\text{to OH}}$ = 5.3 Hz, C*H*$_2$OH), 4.01 (1H, m, $^3J_{\text{to OH}}$ = 6.7, $^3J_{3,4}$ = 4.6, $^3J_{3,2'}$ = 4.9, $^3J_{3,2}$ = 2.7 Hz, H-3), 4.24 (1H, t, $^3J_{\text{to }CH_2OH}$ = 5.3 Hz, CH_2OH), 4.71 (1H, d, $^3J_{\text{to H-3}}$ = 6.7 Hz, OH at position 3), 6.92 (1H, br s, $CONH_2$), 7.45 (1H, br s, $CONH_2$); spin–spin decoupled at H-1, H-3, H-5, and C*H*$_2$OH. D_2O exchange caused the disappearance of signals at δ 4.24, 4.71, 6.92, and 7.45. *Anal.* calcd. for $C_7H_{13}O_3N$: C 52.82, H 8.23, N 8.80; found: C 53.00, H 8.03, N 8.91.

(±)-Methyl (1β,3β,4β)-3-acetoxy-4-carbamoylcyclopentane-carboxylate (9)

A solution of **3** (50.5 g, 0.255 mol) in anhydrous methanol (800 mL) was stirred at room temperature for 22 h. The methanol was evaporated to give **7** as an oil; [1]Hmr (200 MHz, Me_2SO-d_6) δ: 1.91 (3H, s, OAc), 1.91–2.33 (4H, m, H-3, H-3′, H-5, and H-5′), 2.87–3.08 (2H, m, H-1 and H-4), 3.62 (3H, s, OMe), 5.23 (1H, t of d, H-2), 12.33 (1H, br s, CO_2H). The oil was dissolved in benzene (950 mL) and 150 mL were distilled to remove traces of moisture. Heating was discontinued and $SOCl_2$ (85 mL) was added. The mixture was stirred for 5 min, pyridine (2 drops) was added, and stirring was continued until the vigorous evolution of gases had subsided. *N,N*-Dimethylformamide (2 drops) was then added, and the solution was heated at reflux temperature for 2 h. The solution was kept at room temperature overnight. The volatile components were evaporated to give **8** as an orange oil that was used immediately for the preparation of **9**. The oil (**8**) was dissolved in dry benzene (450 mL), and anhydrous ammonia was bubbled through the reaction solution for 30 min; there then was a 10-min purge with nitrogen. An additional 250 mL of benzene were added and the reaction mixture was heated to boiling, treated with charcoal, and filtered through a pad of Celite. The filtrate was evaporated to give an orange-brown oil (62.3 g) that was revealed by tlc (1:1 (v/v) acetone–toluene) to consist of a single major component having R_f 0.40 and several minor components. The oil was diluted with acetone (10 mL) to reduce its viscosity and resolved by liquid chromatography (Waters Associates PrepLC/System 500) to give the major component (42.2 g), mp 78–88°C, which was recrystallized from ethyl acetate – hexanes to give a white solid (35.7 g, 61.1%), mp 92–93°C. An analytical sample of **9** was prepared by a second recrystallization from ethyl acetate – hexanes, mp 93–94°C; [1]Hmr (200 MHz, Me_2SO-d_6) δ: 1.90 (3H, s, OAc), 1.90–2.27 (4H, m, H-2, H-2′, H-5, and H-5′), 2.78 (1H, d of d of d, $^3J_{4,5}$ = 11.1, $^3J_{4,5'}$ = 7.7, $^3J_{4,3}$ = 5.4 Hz, H-4), 2.91 (1H, q of d, ^3J = 9.4, ^3J = 6.5 Hz, H-1), 3.61 (3H, s, OMe), 5.24 (1H, t of d, ^3J = 5.4, $^3J_{3,2}$ = 2.9 Hz, H-3), 6.84 (1H, br s, $CONH_2$), 7.22 (1H, br s, $CONH_2$); spin–spin decoupled at H-3. *Anal.* calcd. for $C_{10}H_{15}O_5N$: C 52.40, H 6.60, N 6.11; found: C 52.15, H 6.91, N 6.05.

(±)-(1β,2β,4β)-2-Hydroxy-4-(hydroxymethyl)cyclopentane-carboxamide (10)

A solution of $LiBH_4$ (5.0 g, 228 mmol) in tetrahydrofuran (250 mL) was heated at reflux temperature for 1 h, cooled to about 40°C, **9** (13.1 g, 57 mmol) in tetrahydrofuran (60 mL) was added, and the heating was continued for 2 h. The reaction solution was then cooled to ice-bath temperature, water (200 mL) was added slowly, and then Amberlite IR-120 resin (H^+ form) (150 mL). The reaction mixture was stirred overnight, and the resin was removed by filtration and washed with water (300 mL). The pH of the combined filtrate and washings was adjusted to neutrality by treatment with Dowex 1-X8 resin (OH^- form) (~200 mL). The resin was removed by filtration and washed with water (~250 mL). The volume of the combined filtrate and washings was reduced by evaporation and the resulting oil was evaporated with methanol (3 × 50 mL). The oil was then stirred in the presence of tetrahydrofuran (45 mL). The white solid that formed (5.5 g, 60.6%) was collected by filtration; mp 113–116°C; R_f 0.44 (tlc) (3:1 (v/v) chloroform–methanol). An analytical sample was prepared by recrystallization from methanol – diethyl ether, mp 117–118°C; [1]Hmr (200 MHz, Me_2SO-d_6) δ: 1.34 (1H, d of d of d, J_{gem} = 13.4, $^3J_{3,4}$ = 5.0, $^3J_{3,2}$ = 2.6 Hz, H-3), 1.60 (1H, m, J_{gem} = 12.2, $^3J_{5,1}$ = 11.6, $^3J_{5,4}$ = 8.9 Hz, H-5), 1.75–1.89 (2H, m, H-3′ and H-5′), 2.04 (1H, m, H-4), 2.44 (1H, m, $^3J_{1,5}$ = 11.6, $^3J_{1,5'}$ = 7.0, $^3J_{1,2}$ = 4.6 Hz, H-1), 3.33 (2H, d of d, $^3J_{\text{to }CH_2OH}$ = 5.1, $^3J_{\text{to H-4}}$ = 6.6 Hz, C*H*$_2$OH), 4.18 (1H, m, $^3J_{2,3'}$ = 7.3, $^3J_{2,1}$ = 4.6, $^3J_{2,3}$ = 2.6, $^3J_{\text{to CHOH}}$ = 3.4 Hz, H-2), 4.58 (1H, t, $^3J_{\text{to }CH_2OH}$ = 5.1 Hz, CH_2OH), 4.84 (1H, d, $^3J_{\text{to H-2}}$ = 3.4 Hz, CHO*H*), 6.91 (1H, br s, $CONH_2$), 7.28 (1H, br s, $CONH_2$); spin–spin decoupled at H-1, H-2, H-3, H-4, and C*H*$_2$OH. *Anal.* calcd. for $C_7H_{13}O_3N$: C 52.82, H 8.23, N 8.80; found: C 52.90, H 8.02, N 8.85.

(±)-(1β,3β,4β)-4-Amino-3-hydroxycyclopentanemethanol (17)

A freshly prepared solution of $Ba(OH)_2 \cdot 8H_2O$ (90.9 g, 288 mmol) in water (1.85 L) was filtered to remove any $BaCO_3$ present and cooled to 5°C. To this solution was added Br_2 (3.6 mL, 70.3 mmol) and, immediately after the Br_2 had dissolved, compound **10** (10.2 g, 64 mmol) in water (50 mL) was added and the reaction solution was left to warm to room temperature during the next 2 h. The reaction solution was heated at 65–70°C for 1 h, cooled to about 10°C, acidified with 3 *M* H_2SO_4 (76 mL), and stirred for 1 h. The reaction mixture was kept in the cold room overnight and the $BaSO_4$ was removed by centrifugation. The solution was passed through Amberlite CG-120 resin (H^+ form) (150 g). The resin was then washed with water (1.1 L) and eluted with 2 *N* aqueous ammonia. Most of the product (**17**) was obtained after 1.5 L of 2 *N* ammonia solution had been used, and only traces were obtained with the next 0.5 L. The solvent was evaporated and the resulting oil was dissolved in ethanol; the solution was filtered to remove particulate matter and the filtrate was evaporated to give a pale orange oil (2.90 g, 34.5%). The ^{1}Hmr spectrum did not show any signals attributable to impurities; ^{1}Hmr (200 MHz, Me_2SO-d_6) δ: 1.08 (1H, d of t, J_{gem} = 12.5, ^3J = 7.5 Hz, H-5), 1.31 (1H, m, J_{gem} = 12.9, $^3J_{2,1}$ = 6.2, $^3J_{2,3}$ = 5.1 Hz, H-2), 1.71–1.89 (2H, m, H-2′ and H-5′), 1.85–2.08 (1H, m, H-1), 2.95 (1H, m, ^3J = 7, $^3J_{4,3}$ = 5.1 Hz, H-4), 3.29 (2H, d, $^3J_{\text{to H-1}}$ = 5.8 Hz, CH_2OH), 3.73 (1H, q, ^3J = 5.1 Hz, H-3); spin–spin decoupled at H-3, H-4, and H-5.

3-Ethoxypropenoyl chloride (14)

Ethyl 3-ethoxypropenoate (**11**) was prepared from ethyl bromoacetate and ethyl orthoformate by the Reformatsky reaction as described previously (20–22). The rate of elimination of ethanol from the crude acetal precursor was accelerated by the addition of *p*-toluenesulfonic acid or $KHSO_4$ to the refluxing solution; ^{1}Hmr (200 MHz, Me_2SO-d_6) δ: 1.20 (3H, t, ^3J = 7.1 Hz, CH_3), 1.25 (3H, t, ^3J = 7.1 Hz, CH_3), 3.97 (2H, q, ^3J = 7.1 Hz, —CH_2O—), 4.08 (2H, q, ^3J = 7.1 Hz, —CH_2O—), 5.24 (1H, d, ^3J = 12.5 Hz, H-2), 7.59 (1H, d, ^3J = 12.5 Hz, H-3); ^{1}Hmr (200 MHz, $CDCl_3$) δ: 1.28 (3H, t, ^3J = 7.2 Hz, CH_3), 1.35 (3H, t, ^3J = 7.1 Hz, CH_3), 3.91 (2H, q, ^3J = 7.1 Hz, —CH_2O—), 4.17 (2H, q, ^3J = 7.2 Hz, —CH_2O—), 5.19 (1H, d, ^3J = 12.9 Hz, H-2), 7.59 (1H, d, ^3J = 12.9 Hz, H-3).

The following compounds were prepared as described previously (21–22): 3-ethoxypropenoic acid (**12**) by alkaline hydrolysis of **11**; ^{1}Hmr (200 MHz, Me_2SO-d_6) δ: 1.24 (3H, t, ^3J = 7.1 Hz, CH_3), 3.94 (2H, q, ^3J = 7.1 Hz, —CH_2O—), 5.14 (1H, d, ^3J = 12.5 Hz, H-2), 7.52 (1H, d, ^3J = 12.5 Hz, H-3), 11.78 (1H, br s, CO_2H); ^{1}Hmr (200 MHz, $CDCl_3$) δ: 1.34 (3H, t, ^3J = 7.1 Hz, CH_3), 3.95 (2H, q, ^3J = 7.1 Hz, —CH_2O—), 5.19 (1H, d, ^3J = 12.6 Hz, H-2), 7.69 (1H, d, ^3J = 12.6 Hz, H-3), 12.15 (1H, br s, CO_2H); sodium 3-ethoxypropenoate (**13**) by neutralization of **12** with NaOH; ^{1}Hmr (200 MHz, Me_2SO-d_6 + D_2O) δ: 1.25 (3H, t, ^3J = 7.1 Hz, CH_3), 3.87 (2H, q, ^3J = 7.1 Hz, —CH_2O—), 5.16 (1H, d, ^3J = 12.7 Hz, H-2), 7.23 (1H, d, ^3J = 12.7 Hz, H-3); and 3-ethoxypropenoyl chloride (**14**) from **13**, using $SOCl_2$ in diethyl ether; ^{1}Hmr (200 MHz, $CDCl_3$) δ: 1.40 (3H, t, ^3J = 7.1 Hz, CH_3), 4.07 (2H, q, ^3J = 7.1 Hz, —CH_2O—), 5.51 (1H, d, ^3J = 12.1 Hz, H-2), 7.80 (1H, d, ^3J = 12.1 Hz, H-3).

3-Ethoxypropenoyl isocyanate (15) (refs. 22, 23)

A stirred mixture of silver cyanate (21.3 g, 142 mmol) in dry benzene (125 mL) was heated at reflux temperature for 0.5 h and 3-ethoxypropenoyl chloride (**14**) (9.57 g, 71 mmol) in benzene (25 mL) was added over a period of 10 min. The mixture was heated for an additional 0.5 h and stirred at room temperature for 2.5 h. The solid was allowed to settle and the solution of **15** was used immediately for the preparation of **18** and **23** as described below.

(±)-3-Ethoxy-N-{N′-[(1β,2β,4β)-2-hydroxy-4-(hydroxymethyl)-cyclopentyl]carbamoyl}propenamide (18)

To a dried (4 Å molecular sieves), cooled (−15°C) solution of compound **17** (2.06 g, 15.7 mmol) in *N,N*-dimethylformamide (50 mL) were added, under a nitrogen atmosphere, 40 mL of the solution of the isocyanate **15** obtained above; the reaction temperature was maintained below −10°C. After the addition of **15** was complete, the reaction solution was stirred at room temperature overnight. The solution was filtered and the solvents were removed under vacuum. The residue was evaporated with ethanol (2 × 20 mL) and fractionated by column chromatography on silica gel using toluene – ethyl acetate – 2-propanol (3:3:2, v/v/v) to give **18** (1.80 g, 42%, based on the amount of the amine) as a pale yellow solid, R_f 0.39 (tlc); ^{1}Hmr (200 MHz, Me_2SO-d_6) δ: 1.15–1.36 and 1.86–2.05 (5H, m, H-3′, H-3″, H-4′, H-5′, and H-5″), 1.25 (3H, t, ^3J = 7.1 Hz, CH_3), 3.28–3.40 (2H, m, CH_2OH), 3.76–4.08 (2H, m, H-1′ and H-2′), 3.94 (2H, q, ^3J = 7.1 Hz, CH_3CH_2O), 4.59 (1H, t, ^3J = 5.0 Hz, CH_2OH), 4.91 (1H, d, $^3J_{\text{to H-2}'}$ = 4.6 Hz, OH at position 2′), 5.51 (1H, d, $^3J_{2,3}$ = 12.3 Hz, H-2), 7.55 (1H, d, $^3J_{3,2}$ = 12.3 Hz, H-3), 8.74 (1H, br d, $^3J_{\text{to H-1}'}$ = 7.8 Hz, CONHCONH), 9.95 (1H, br s, CONHCO); spin–spin decoupled at δ 3.28–3.40, H-2 and δ 1.25.

(±)-1-[(1β,2β,4β)-2-Hydroxy-4-(hydroxymethyl)cyclopentyl]-2,4(1H,3H)-pyrimidinedione (19)

A solution of **18** (1.78 g, 6.54 mmol) in 2 *N* sulfuric acid (50 mL) was heated at reflux temperature under a nitrogen atmosphere for 30 min. The solution was cooled to room temperature, treated with charcoal, filtered, and the charcoal was washed with 10 mL of water. The combined filtrate and washings were cooled to ice-bath temperature and neutralized with 2 *N* sodium hydroxide. The solvent was evaporated and the residue was extracted with ethanol (4 × 20 mL). Evaporation of the ethanol gave an oil which was fractionated by column chromatography on silica gel to give **19** (1.00 g, 68%) as a white solid, R_f 0.34 (tlc) (1:1:1 (v/v/v) toluene – ethyl acetate – 2-propanol). An analytical sample was prepared by recrystallization from ethanol – diethyl ether, mp 158–160°C; uv λ_{max} (C_2H_5OH): 210 nm (ε 9480), 268 (11 100); λ_{max} (0.01 *N* HCl in C_2H_5OH): 210 nm (ε 9570), 268 (11 100); λ_{max} (0.01 *N* NaOH in C_2H_5OH): 220 nm (ε 9330), 265 (8310); ^{1}Hmr (200 MHz, Me_2SO-d_6) δ: 1.30 (1H, m, $^3J_{3',2'}$ = 2.0 Hz, H-3′), 1.62–1.90 (2H, m, H-4′ and H-5′), 1.96–2.16 (2H, m, H-3″ and H-5″), 3.33–3.42 (2H, m, CH_2OH), 4.02 (1H, m, H-2′), 4.49 (1H, m, $^3J_{\text{to H at 5}'}$ = 12.2, $^3J_{\text{to H at 5}'}$ = 7.1, $^3J_{1',2'}$ = 4.9 Hz, H-1′), 4.65 (1H, t, $^3J_{\text{to } CH_2OH}$ = 5.2 Hz, CH_2OH), 4.94 (1H, d, $^3J_{\text{to H-2}'}$ = 4.5 Hz, CHOH), 5.48 (1H, d of d, $^3J_{5,6}$ = 7.8, $^4J_{5,3}$ = 1.7 Hz, H-5), 7.60 (1H, d, $^3J_{6,5}$ = 7.8 Hz, H-6), 11.20 (1H, br s, H-3); spin–spin decoupled at H-3′, H-2′, and H-3. *Anal.* calcd. for $C_{10}H_{14}O_4N_2$: C 53.09, H 6.24, N 12.38; found: C 53.16, H 6.24, N 12.35.

3-Ethoxypropenoyl isothiocyanate (16)

Compound **16** was prepared from 3-ethoxypropenoyl chloride (**14**) and potassium thiocyanate as described by Shaw and Warrener (21) and was used immediately after distillation under vacuum to prepare compounds **20** and **25**.

(±)-3-Ethoxy-N-{N′-[(1β,2β,4β)-2-hydroxy-4-(hydroxymethyl)-cyclopentyl]thiocarbamoyl}propenamide (20)

To a solution of **17** (0.379 g, 2.89 mmol) in methanol (5 mL) and diethyl ether (10 mL) was added the isothiocyanate **16** (0.454 g, 2.89 mmol) at room temperature. The reaction solution was kept at room temperature overnight, filtered, and the filtrate was evaporated to give an orange oil (1.0 g) that was fractionated by column chromatography on silica gel to give **20** (0.57 g, 68%) as a pale yellow solid, R_f 0.48 (tlc) (4:4:1 (v/v/v) toluene – ethyl acetate – 2-propanol); ^{1}Hmr (200 MHz, Me_2SO-d_6) δ: 1.17–1.43 (2H, m, H-3′ and H-5′), 1.26 (3H, t, ^3J = 7.0 Hz, CH_3), 1.91–2.09 (2H, m, H-3″ and H-4′), 2.18 (1H, d of t, J_{gem} = 11.5, ^3J = 7.1 Hz, H-5″), 3.31–3.36 (2H, m, CH_2OH), 3.98 (2H, q, ^3J = 7.0 Hz, CH_3CH_2O), 3.99–4.03 (1H, m, H-2′), 4.31 (1H, m, H-1′), 4.64 (1H, t, $^3J_{\text{to } CH_2OH}$ = 5.1 Hz, CH_2OH), 5.15 (1H, d, $^3J_{\text{to H-2}'}$ = 4.9 Hz, OH at position 2′), 5.71 (1H, d, $^3J_{2,3}$ = 12.6 Hz, H-2), 7.59 (1H, d, $^3J_{3,2}$ = 12.6 Hz, H-3), 10.79 (1H, br s, CONHCS), 11.10 (1H, br d, $^3J_{\text{to H-1}'}$ = 7.7 Hz, CONHCSNH); spin–spin decoupled at H-1′, and δ 1.26 and 4.0.

(±)-2,3-Dihydro-1-[(1β,2β,4β)-2-hydroxy-4-(hydroxymethyl)-cyclopentyl]-2-thioxo-4(1H)-pyrimidinone (21)

A stirred solution of **20** (0.53 g, 1.84 mmol) in 15 *N* aqueous ammonia (20 mL) was heated in an oil bath at 100°C for 20 min. The reaction solution was cooled to room temperature and the solvent evaporated to give an oil, which was then evaporated with ethanol (3 × 10 mL). The residual oil was fractionated by column chromatography on silica gel to give **21** (0.135 g, 30%) as a white solid, R_f 0.40 (tlc) (2:2:1 (v/v/v) toluene – ethyl acetate – 2-propanol); mp 180–187°C. An analytical sample was prepared by recrystallization from methanol – diethyl ether, mp 184–186°C; uv λ_{max} (C_2H_5OH): 221 nm (ε 17 300), 274 (12 700); λ_{max} (0.01 *N* HCl in C_2H_5OH): 221 nm (ε 17 300), 274 (12 700); λ_{max} (0.01 *N* NaOH in C_2H_5OH): 241 nm (ε 21 300), 274 (15 400); ^{1}Hmr (200 MHz, Me_2SO-d_6) δ: 1.34 (1H, m, H-3′), 1.69–2.13 (4H, m, H-3″, H-4′, H-5′, and H-5″), 3.40 (2H, m, C*H*$_2$OH), 4.20 (1H, m, H-2′), 4.68 (1H, t, $^3J_{\text{to } CH_2OH}$ = 5.1 Hz, CH$_2$O*H*), 5.04 (1H, d, $^3J_{\text{to H-2}'}$ = 4.3 Hz, OH at position 2′), 5.41 (1H, m, $^3J_{1',5'}$ = 12.2, $^3J_{1',5''}$ = 6.8, $^3J_{1',2'}$ = 5.1 Hz, H-1′), 5.88 (1H, d of d, $^3J_{5,6}$ = 8.1, $^4J_{5,3}$ = 1.9 Hz, H-5), 7.75 (1H, d, $^3J_{6,5}$ = 8.1 Hz, H-6), 12.59 (1H, br s, H-3); spin–spin decoupled at δ 1.34, 4.20, 4.68, 5.04, 5.41, 5.88, and 7.75. *Anal.* calcd. for $C_{10}H_{14}O_3N_2S$: C 49.57, H 5.82, N 11.56, S 13.23; found: C 50.04, H 6.08, N 11.73, S 13.27.

(±)-(1β,2β,4β)-4-Amino-2-hydroxycyclopentanemethanol (22)

Compound **22** was prepared from **6** (9.74 g, 61.2 mmol), according to the procedure described for the preparation of **17**, to give an orange-brown oil (2.19 g, 27%). The ^{1}Hmr spectrum did not show any signals attributable to impurities; ^{1}Hmr (200 MHz, Me_2SO-d_6) δ: 1.12 (1H, m, H-5), 1.39 (1H, d of d of d, J_{gem} = 13.5, $^3J_{3,4}$ = 4.4, $^3J_{3,2}$ = 2.8 Hz, H-3), 1.71–1.97 (3H, m, H-1, H-3′, and H-5′), 3.23 (1H, m, H-4), 3.37 (1H, d of d, J_{gem} = 10.6, $^3J_{\text{to H-1}}$ = 6.2 Hz, C*H*$_2$OH), 3.59 (1H, d of d, J_{gem} = 10.6, $^3J_{\text{to H-1}}$ = 7.2 Hz, C*H*$_2$OH), 4.00 (1H, m, H-2); spin–spin decoupled at δ 1.12, 1.39, 3.59, and 4.00.

(±)-3-Ethoxy-N-{N′-[(1β,3β,4β)-3-hydroxy-4-(hydroxymethyl)-cyclopentyl]carbamoyl}propenamide (23)

Compound **23** was prepared from **22** (1.57 g, 12 mmol) and the solution of the isocyanate **15** (32 mL) according to the procedure described for the preparation of **18**. Fractionation by column chromatography on silica gel afforded a crude sample of **23** (1.5 g, 49%, based on the amount of the amine) as a pale yellow, oily solid, R_f 0.34 (tlc) (3:3:2 (v/v/v) toluene – ethyl acetate – 2-propanol). The ^{1}Hmr spectrum showed several minor signals attributable to impurities; ^{1}Hmr (200 MHz, Me_2SO-d_6) δ: 1.17–1.34 (1H, m, H-5′), 1.25 (3H, t, ^3J = 7.0 Hz, CH$_3$), 1.45 (1H, m, H-2′), 1.83 (1H, m, H-4′), 1.98–2.14 (2H, m, H-2″ and H-5″), 3.40 (1H, m, J_{gem} = 10.9, $^3J_{\text{to } CH_2OH \text{ and H-4}'}$ = 5.5 Hz, C*H*$_2$OH), 3.57 (1H, d of d of d, J_{gem} = 10.9, $^3J_{\text{to H-4}'}$ = 7.2, $^3J_{\text{to } CH_2OH}$ = 5.5 Hz, C*H*$_2$OH), 3.93 (2H, q, ^3J = 7.0 Hz, CH$_3$C*H*$_2$O), 4.03–4.22 (2H, m, H-1′ and H-3′), 4.28 (1H, t, $^3J_{\text{to } CH_2OH}$ = 5.5 Hz, CH$_2$O*H*), 4.57 (1H, d, $^3J_{\text{to H-3}'}$ = 3.8 Hz, OH at position 3′), 5.50 (1H, d, $^3J_{2,3}$ = 12.4 Hz, H-2), 7.53 (1H, d, $^3J_{3,2}$ = 12.4 Hz, H-3), 8.72 (1H, br d, $^3J_{\text{to H-1}'}$ = 8.3 Hz, CONHCON*H*), 9.92 (1H, br s, CON*H*CONH); spin–spin decoupled at δ 1.26 and 8.72.

(±)-1-[(1β,3β,4β)-3-Hydroxy-4-(hydroxymethyl)cyclopentyl]-2,4(1H,3H)-pyrimidinedione (24)

Compound **24** was prepared from **23** (1.53 g, 5.6 mmol) according to the procedure described for the preparation of **19**. Fractionation by column chromatography on silica gel afforded **24** (0.726 g, 57%) as a white solid, R_f 0.31 (tlc) (1:1:1 (v/v/v) toluene – ethyl acetate – 2-propanol). An analytical sample was prepared by recrystallization from ethanol–hexanes; mp 154–155°C; uv λ_{max} (C_2H_5OH): 209 nm (ε 9120), 268 (10 300); λ_{max} (0.01 *N* HCl in C_2H_5OH): 210 nm (ε 9140), 268 (10 300); λ_{max} (0.01 *N* NaOH in C_2H_5OH): 221 nm (ε 8310), 265 (7610); ^{1}Hmr (200 MHz, Me_2SO-d_6) δ: 1.37 (1H, t of d, J_{gem} = $^3J_{5',4'}$ = 11.8, $^3J_{5',1'}$ = 9.0 Hz, H-5′), 1.51 (1H, d of d, J_{gem} = 15.1, $^3J_{2',1'}$ = 3.9 Hz, H-2′), 1.89 (1H, m, H-4′), 2.05 (1H, m, J_{gem} = 11.8, ^3J = 7.3 Hz, H-5″), 2.30 (1H, m, J_{gem} = 15.1, $^3J_{2'',1'}$ = 11.1, $^3J_{2'',3'}$ = 4.6 Hz, H-2″), 3.43 (1H, m, J_{gem} = 10.9, $^3J_{\text{to H-4}'}$ = 6.1, $^3J_{\text{to } CH_2OH}$ = 5.3 Hz, C*H*$_2$OH), 3.60 (1H, d of d of d, J_{gem} = 10.9, $^3J_{\text{to H-4}'}$ = 7.3, $^3J_{\text{to } CH_2OH}$ = 5.3 Hz, C*H*$_2$OH), 4.11 (1H, m, H-3′), 4.39 (1H, t, $^3J_{\text{to } CH_2OH}$ = 5.3 Hz, CH$_2$O*H*), 5.03 (1H, d, $^3J_{\text{to H-3}'}$ = 3.6 Hz, OH at position 3′), 5.04 (1H, m, H-1′), 5.67 (1H, d of d, $^3J_{5,6}$ = 8.2, $^4J_{5,3}$ = 2.0 Hz, H-5), 7.90 (1H, d, $^3J_{6,5}$ = 8.2 Hz, H-6), 11.20 (1H, br s, H-3); spin–spin decoupled at δ 4.11 and 4.39. *Anal.* calcd. for $C_{10}H_{14}O_4N_2$: C 53.09, H 6.24, N 12.38; found: C 53.13, H 6.41, N 12.34.

(±)-3-Ethoxy-N-{N′-[(1β,3β,4β)-3-hydroxy-4-(hydroxymethyl)-cyclopentyl]thiocarbamoyl}propenamide (25)

Compound **25** was prepared from **22** (0.234 g, 1.78 mmol) and **16** (0.285 g, 1.81 mmol) according to the procedure described for the preparation of **20**. Fractionation by column chromatography on silica gel afforded **25** (0.275 g, 54%) as a colorless oil, R_f 0.56 (tlc) (2:2:1 (v/v/v) toluene – ethyl acetate – 2-propanol); ^{1}Hmr (200 MHz, Me_2SO-d_6) δ: 1.20–1.35 (1H, m, H-5′), 1.25 (3H, t, ^3J = 7.0 Hz, CH$_3$), 1.56 (1H, m, J_{gem} = 14.1, $^3J_{2',1'}$ = 2.3 Hz, H-2′), 1.87 (1H, m, H-4′), 2.06 (1H, m, J_{gem} = 14.1, $^3J_{2'',1'}$ = 8.5, $^3J_{2'',3'}$ = 4.7 Hz, H-2″), 2.21 (1H, d of t, J_{gem} = 13.0, ^3J = 8.2 Hz, H-5″), 3.40 (1H, m, J_{gem} = 10.7, $^3J_{\text{to } CH_2OH}$ = 5.3, $^3J_{\text{to H-4}'}$ = 5.3 Hz, C*H*$_2$OH), 3.58 (1H, d of d of d, J_{gem} = 10.7, $^3J_{\text{to H-4}'}$ = 7.2, $^3J_{\text{to } CH_2OH}$ = 5.3 Hz, C*H*$_2$OH), 3.96 (2H, q, ^3J = 7.0 Hz, CH$_3$C*H*$_2$O), 4.10 (1H, m, H-3′), 4.31 (1H, t, $^3J_{\text{to } CH_2OH}$ = 5.3 Hz, C*H*$_2$OH), 4.58–4.73 (1H, m, H-1′), 4.64 (1H, d, $^3J_{\text{to H-3}'}$ = 3.3 Hz, OH at position 3′), 5.70 (1H, d, $^3J_{2,3}$ = 12.2 Hz, H-2), 7.57 (1H, d, $^3J_{3,2}$ = 12.2 Hz, H-3), 10.73 (1H, br s, CON*H*CSNH), 11.10 (1H, br d, $^3J_{\text{to H-1}'}$ = 8.0 Hz, CONHCSN*H*); spin–spin decoupled at δ 4.10 and 4.65.

(±)-2,3-Dihydro-1-[(1β,3β,4β)-3-hydroxy-4-(hydroxymethyl)-cyclopentyl]-2-thioxo-4(1H)-pyrimidinone (26)

Compound **26** was prepared from **25** (0.27 g, 0.94 mmol) according to the procedure described for the preparation of **21**. Fractionation by column chromatography on silica gel afforded **26** (0.153 g, 67%) as a white solid, R_f 0.44 (tlc) (2:2:1 (v/v/v) toluene – ethyl acetate – 2-propanol). An analytical sample was prepared by recrystallization from ethanol–hexanes, mp 156–157°C; uv λ_{max} (C_2H_5OH): 219 nm (ε 16 600), 273 (13 700); λ_{max} (0.01 *N* HCl in C_2H_5OH): 219 nm (ε 16 600), 273 (13 800); λ_{max} (0.01 *N* NaOH in C_2H_5OH): 240 nm (ε 19 400), 272 (16 200); ^{1}Hmr (200 MHz, Me_2SO-d_6) δ: 1.35 (1H, t of d, J_{gem} = 12.3, $^3J_{5',1'}$ = 9.3 Hz, H-5′), 1.56 (1H, d of d, J_{gem} = 15.4, $^3J_{2',1'}$ = 3.7 Hz, H-2′), 1.91 (1H, m, H-4′), 2.17 (1H, m, J_{gem} = 12.3, ^3J = 7.5 Hz, H-5″), 2.36 (1H, m, J_{gem} = 15.4, $^3J_{2'',1'}$ = 11.2, $^3J_{2'',3'}$ = 4.4 Hz, H-2″), 3.44 (1H, m, J_{gem} = 10.6, $^3J_{\text{to H-4}'}$ = 6.2, $^3J_{\text{to } CH_2OH}$ = 5.2 Hz, C*H*$_2$OH), 3.60 (1H, m, J_{gem} = 10.6, $^3J_{\text{to H-4}'}$ = 7.6, $^3J_{\text{to } CH_2OH}$ = 5.2 Hz, C*H*$_2$OH), 4.14 (1H, m, H-3′), 4.40 (1H, t, $^3J_{\text{to } CH_2OH}$ = 5.2 Hz, CH$_2$O*H*), 5.15 (1H, d, $^3J_{\text{to H-3}'}$ = 3.4 Hz, OH at position 3′), 5.99 (1H, m, H-1′), 6.09 (1H, d, $^3J_{5,6}$ = 8.2 Hz, H-5), 8.11 (1H, d, $^3J_{6,5}$ = 8.2 Hz, H-6), 12.55 (1H, br s, H-3); spin–spin decoupled at δ 4.14 and 5.99. *Anal.* calcd. for $C_{10}H_{14}O_3N_2S$: C 49.57, H 5.82, N 11.56, S 13.23; found: C 49.61, H 5.97, N 11.80, S 13.25.

(±)-(1β,6β,8β)-3,3-Dimethyl-2,4-dioxabicyclo[4.3.0]nonane-8-carboxamide (27)

To a stirred mixture of **6** (14.0 g, 88 mmol) in acetone (200 mL) and 2,2-dimethoxypropane (50 mL) was added *p*-toluenesulfonic acid monohydrate (~20 mg) and the mixture was heated gently at reflux temperature for 30 min. The reaction mixture was cooled to room temperature, and the white solid was collected by filtration and washed with acetone to give **27** (10.88 g), R_f 0.31 (tlc) (2:2:1 (v/v/v) toluene – ethyl acetate – 2-propanol). The volume of the mother liquor was reduced and a second crop of **27** (2.47 g) was obtained for a total yield of 13.35 g. The volatile components were evaporated from the filtrate and the resulting oil was dissolved in acetone (30 mL) and 2,2-dimethoxypropane (10 mL). About 10 mg of the acid catalyst was added and the reaction mixture was stirred at room temperature for 30 min to give an additional 2.08 g of **27** as a white solid for a total yield of 15.43 g (88%). Thin-layer chromatography showed that this material contained trace amounts of a second component having R_f 0.08.

An analytical sample was prepared by fractionation on a column of alumina gel followed by recrystallization of the material from acetone; mp 169°C; ^{1}Hmr (200 MHz, Me_2SO-d_6) δ: 1.22 (3H, s, CH_3), 1.35 (3H, s, CH_3), 1.65–1.95 (4H, m, H-6, H-7, H-7′, and H-9), 2.07 (1H, m, J_{gem} = 14.3, $^3J_{9',8}$ = 10.1, $^3J_{9',1}$ = 5.5 Hz, H-9′), 2.56 (1H, m, H-8), 3.54 (1H, d of d, J_{gem} = 11.7, $^3J_{5,6}$ = 2.3 Hz, H-5), 3.99 (1H, d of d, J_{gem} = 11.7, $^3J_{5',6}$ = 3.7 Hz, H-5′), 4.23 (1H, m, H-1), 6.75 (1H, br s, $CONH_2$), 7.13 (1H, br s, $CONH_2$); spin–spin decoupled at δ 3.99 and 4.23. *Anal.* calcd. for $C_{10}H_{17}O_3N$: C 60.28, H 8.60, N 7.03; found: C 60.01, H 8.74, N 7.19.

(±)-Methyl [(1β,6β,8β)-3,3-dimethyl-2,4-dioxabicyclo[4.3.0]non-8-yl]carbamate (28)

A solution of sodium (1.65 g, 0.0718 g atom) in methanol (50 mL) was added to a solution of **27** (7.16 g, 35.9 mmol) in methanol (65 mL). To this solution Br_2 (1.84 mL, 35.9 mmol) was added with thorough mixing and the reaction solution was heated on a steam bath for 10 min. The solution was made just acidic with acetic acid and the solvent was evaporated. The residue was washed with water (10 mL) and the solid was collected by filtration to give **28** (6.34 g, 77%), R_f 0.72 (tlc) (2:2:1 (v/v/v) toluene – ethyl acetate – 2-propanol); tlc showed that this material contained traces of more-polar components. A small, oily sample of **28** was obtained by column chromatography on silica gel; ^{1}Hmr (200 MHz, Me_2SO-d_6) δ: 1.25 (3H, s, CH_3C), 1.34 (3H, s, CH_3C), 1.39 (1H, d of d of d, J_{gem} = 14.4, $^3J_{9,8}$ = 6.5, $^3J_{9,1}$ = 1.9 Hz, H-9), 1.65–1.93 (3H, m, H-6, H-7, and H-7′), 2.18 (1H, m, J_{gem} = 14.4, $^3J_{9',8}$ = 8.8, $^3J_{9',1}$ = 5.7 Hz, H-9′), 3.51 (3H, s, CH_3O), 3.51 (1H, d of d, J_{gem} = 11.9, $^3J_{5,6}$ = 2.1 Hz, H-5), 3.84 (1H, m, H-8), 3.98 (1H, d of d, J_{gem} = 11.9, $^3J_{5',6}$ = 3.7 Hz, H-5′), 4.20 (1H, m, H-1), 7.02 (1H, br d, $^3J_{\text{to H-8}}$ = 7.7 Hz, NH); spin–spin decoupled at δ 2.18 and 4.20.

(±)-(1β,6β,8β)-8-Amino-3,3-dimethyl-2,4-dioxabicyclo[4.3.0]-nonane (29)

A solution of **28** (6.02 g, 26.2 mmol) in 5 *N* aqueous sodium hydroxide (60 mL) and methanol (30 mL) was heated at reflux temperature for 4 h. The reaction solution was cooled to room temperature and extracted with dichloromethane (40 mL). The dichloromethane extract was evaporated under vacuum to give **29** (3.55 g, 79%) as a light yellow-green oil, R_f 0.45 (tlc) (5:1 (v/v) acetonitrile – 15 *N* aqueous ammonia). The ^{1}Hmr spectrum did not show any signals attributable to impurities; ^{1}Hmr (200 MHz, Me_2SO-d_6) δ: 1.24 (3H, s, CH_3), 1.30 (1H, m, H-9), 1.34 (3H, s, CH_3), 1.47 (1H, m, J_{gem} = 10.8, ^3J = 7.6 Hz, H-7), 1.69–1.82 (1H, m, H-6), 1.87 (1H, d of t, J_{gem} = 10.8, ^3J = 7.2 Hz, H-7′), 2.04 (1H, d of d of d, J_{gem} = 13.5, $^3J_{9',8}$ = 8.4, $^3J_{9',1}$ = 5.5 Hz, H-9′), 3.15 (1H, m, H-8), 3.50 (1H, d of d, J_{gem} = 11.6, $^3J_{5,6}$ = 3.2 Hz, H-5), 3.96 (1H, d of d, J_{gem} = 11.6, $^3J_{5',6}$ = 4.2 Hz, H-5′), 4.17 (1H, m, $^3J_{1,9'}$ = 5.5, $^3J_{1,9}$ = 2.2 Hz, H-1); spin–spin decoupled at δ 1.47, 3.15, 3.96, and 4.17.

*(±)-Ethoxy-*N*-{*N*′-[(1β,6β,8β)-3,3-dimethyl-2,4-dioxabicyclo-[4.3.0]non-8-yl]carbamoyl}propenamide (30)*

Compound **29** (1.60 g, 9.3 mmol) was dissolved in benzene (16 mL) and ~2 mL were removed by distillation. The solution was cooled to ice-bath temperature and a benzene solution (45 mL) containing **15** (13.4 mmol) was added dropwise over a period of 12 min; the reaction solution was then stirred at room temperature overnight. The solvent was evaporated and the residual oil was evaporated with ethanol (2 × 10 mL). Fractionation by column chromatography on silica gel gave **30** (2.2 g, 76%, based on the amount of the amine), R_f 0.42 (tlc) (8:8:1 (v/v/v) toluene – ethyl acetate – 2-propanol); ^{1}Hmr (200 MHz, Me_2SO-d_6) δ: 1.24 (3H, t, ^3J = 7.1 Hz, CH_3CH_2), 1.31 (3H, s, CH_3C), 1.37 (3H, s, CH_3C), 1.49 (1H, m, J_{gem} = 14.4 Hz, H-9′), 1.62 (1H, m, J_{gem} = 12.5, ^3J = 9.7, ^3J = 5.4 Hz, H-7′), 1.83 (1H, m, H-6′), 2.03 (1H, m, J_{gem} = 14.4, ^3J = 8.8, ^3J = 4.7 Hz, H-9″), 2.15 (1H, d of t, J_{gem} = 12.5, ^3J = 8.3 Hz, H-7″), 3.53 (1H, d of d, J_{gem} = 11.7, $^3J_{5',6'}$ = 2.2 Hz, H-5′), 3.94 (2H, q, ^3J = 7.1 Hz, CH_3CH_2O), 4.03 (1H, d of d, J_{gem} = 11.7, $^3J_{5'',6'}$ = 3.9 Hz, H-5″), 4.18–4.35 (2H, m, H-1′ and H-8′), 5.49 (1H, d, $^3J_{2,3}$ = 12.3 Hz, H-2), 7.52 (1H, d, $^3J_{3,2}$ = 12.3 Hz, H-3), 8.77 (1H, br d, $^3J_{\text{to H-8'}}$ = 8.6 Hz, CONHCON*H*), 9.95 (1H, br s, CON*H*CONH); spin–spin decoupled at δ 1.83 and 3.53.

*Preparation of **24** from **30***

A stirred mixture of **30** (2.2 g, 70 mmol) in 2 *N* H_2SO_4 (70 mL) was heated at reflux temperature for 20 min. The solution was cooled to ice-bath temperature and neutralized with 2 *N* NaOH. The solvent was evaporated and the residue was extracted with warm ethanol. The ethanol extract was evaporated and the residual oil was fractionated by column chromatography on silica gel to give **24** (1.034 g, 65%) as a white solid having an R_f (tlc) and ^{1}Hmr spectrum identical to those of the sample of **24** prepared from **23**.

(±)-(3-Carboxycyclopent-3-enyl)amine hydrochloride (31)

To a 1 *N* NaOH solution (1 L) at 5°C was added bromine (7.3 mL, 142 mmol); as soon as the bromine had dissolved, **4** (25.77 g, 120 mmol) in 0.7 *N* NaOH solution (175 mL) was added. The reaction solution was left at room temperature for 1 h and then heated in a water bath at 70°C for 1 h. The solution was cooled to 0°C and acidified with concentrated HCl (93 mL). The reaction solution was then passed through Amberlite CG-120 cation-exchange resin (H^+ form) (500 g), and the resin was washed with water (3.5 L) and eluted with 2 *N* HCl; the elution was monitored by tlc using *n*-butanol – water – acetic acid (5:3:2, v/v/v) as the developing solvent. The first 2.2 L contained mostly NaCl and some **31**; the solvent was evaporated and the residue was extracted with methanol (6 × 50 mL) to yield a solid (4.8 g). The next 1.3 L contained mostly **31** and gave a white solid (12.4 g) after evaporation of solvent, for a total yield of 17.2 g (88% yield) of a solid containing predominantly **31**; the sample was used directly in the next reaction; ^{1}Hmr (200 MHz, Me_2SO-d_6) δ: 2.45–2.95 (4H, m, H-2, H-2′, H-5, and H-5′), 3.87 (1H, m, H-1), 6.60 (1H, m, H-4), 8.30 (3H, br s, $\overset{+}{N}H_3$), 12.50 (1H, br s, CO_2H).

(±)-[3-(Methoxycarbonyl)cyclopent-3-enyl]amine hydrochloride (32)

Anhydrous HCl was bubbled for 1 h through a solution of compound **31** (17.0 g) in dry methanol (800 mL). The solution was stirred for an additional 1 h with cooling and then at room temperature overnight. The clear liquid was decanted from a small amount of solid and evaporated to give an orange oil of crude **32**; ^{1}Hmr (200 MHz, Me_2SO-d_6) δ: 2.56–2.94 (4H, m, H-2, H-2′, H-5, and H-5′), 3.67 (3H, s, OMe), 3.78–3.96 (1H, m, H-1), 6.67 (1H, m, H-4), 8.42 (3H, br s, $\overset{+}{N}H_3$).

(±)-Methyl 4-acetamido-1-cyclopentenecarboxylate (33)

A solution of crude **32** in pyridine (500 mL) was cooled to Dry Ice – acetone bath temperature and acetic anhydride (175 mL) was added. The reaction solution was stirred at room temperature for 18 h and then the solvent was evaporated to give a red-brown oil (48 g). This oil was mixed with crushed ice (300 g) and the mixture was extracted with methylene chloride (4 × 200 mL). The organic layer was washed sequentially with ice-cold 3 *N* HCl (2 × 30 mL), a saturated solution (30 mL) of sodium hydrogen carbonate, and a saturated solution (30 mL) of sodium chloride. The organic layer was dried over Na_2SO_4 and the solvent evaporated to give an orange-brown oil (18.7 g). This material was kept for 2 days in the cold room; a crystalline solid separated, which was collected by filtration and which, after recrystallization from diethyl ether – hexanes, gave **33** (11.63 g, 53% from **4**), mp 74–76°C. An analytical sample was obtained by recrystallization from diethyl ether; mp 75–76°C; ^{1}Hmr (200 MHz, Me_2SO-d_6) δ: 1.77 (3H, s, OAc), 2.20–2.40 and 2.68–2.87 (4H, m, H-3, H-3′, H-5, and H-5′), 3.67 (3H, s, OMe), 4.33 (1H, m, H-4), 6.68 (1H, m, H-2), 8.10 (1H, br d, $^3J_{\text{to H-4}}$ = 6.4, N*H*COMe). Spin–spin decoupling was performed at δ 4.33; ^{1}Hmr (200 MHz, $CDCl_3$) δ: 2.28–2.51 and 2.88–3.08 (4H, m, H-3, H-3′, H-5, and H-5′), 3.75 (3H, s, OMe), 4.63 (1H, m, H-4), 5.69 (1H, br m, N*H*COMe), 6.74 (1H, m, H-2). *Anal.* calcd. for $C_9H_{13}O_3N$: C 59.00, H 7.15, N 7.65; found: C 58.87, H 7.04, N 8.06.

Acknowledgement

The authors are grateful to the Natural Sciences and Engineering Research Council of Canada for its support of this work in the form of a grant (to W.A.S.).

1. A. GURANOWSKI, J. A. MONTGOMERY, G. L. CANTONI, and P. K. CHIANG. Biochemistry, **20**, 110 (1981).
2. Y. F. SHEALY, C. A. O'DELL, W. M. SHANNON, and G. ARNETT. J. Med. Chem. **26**, 156 (1983), and references therein.
3. A. K. SAKSENA. Tetrahedron Lett. **21**, 133 (1980), and references therein.
4. A. BIN SADIKUN, D. I. DAVIES, and R. F. KENYON. J. Chem. Soc. Perkin Trans. 1, 2299 (1981).
5. (*a*) R. VINCE and W. M. SHANNON. Abstracts of Papers, 185th American Chemical Society National Meeting, Seattle, Washington, CARB 26 (1983); (*b*) H. LEE and R. VINCE. J. Pharm. Sci. **69**, 1019 (1980).
6. J. A. MONTGOMERY, S. J. CLAYTON, H. J. THOMAS, W. M. SHANNON, G. ARNETT, A. J. BODNER, IN-K. KION, G. L. CANTONI, and P. K. CHIANG. J. Med. Chem. **25**, 626 (1982).
7. Y. F. SHEALY and C. A. O'DELL. J. Pharm. Sci. **68**, 668 (1979).
8. (*a*) Y. F. SHEALY and C. A. O'DELL. Tetrahedron Lett. 223 (1969); (*b*) Y. F. SHEALY and J. D. CLAYTON. J. Am. Chem. Soc. **91**, 3075 (1969).
9. R. C. CERMAK and R. VINCE. Tetrahedron Lett. **22**, 2331 (1981).
10. B. L. KAM and N. J. OPPENHEIMER. J. Org. Chem. **46**, 3268 (1981).
11. R. VINCE and S. DALUGE. J. Med. Chem. **20**, 612 (1977).
12. (*a*) J. C. JAGT and A. M. VAN LEUSEN. J. Org. Chem. **39**, 564 (1974); (*b*) S. DALUGE and R. VINCE. J. Org. Chem. **43**, 2311 (1978).
13. A. HOLÝ. Collect. Czech. Commun. **41**, 647 (1976).
14. G. JUST and R. OUELLET. Can. J. Chem. **54**, 2925 (1976).
15. G. JUST and S. KIM. Can. J. Chem. **54**, 2935 (1976).
16. H. PAULSEN and U. MAASS. Chem. Ber. **114**, 346 (1981).
17. S. F. BIRCH, W. J. OLDHAM, and E. A. JOHNSON. J. Chem. Soc. 818 (1947).
18. E. S. WALLIS and J. F. LANE. *In* Organic reactions. Vol. III. *Edited by* R. Adams. John Wiley and Sons, Inc., New York. 1946. pp. 267–306.
19. C. A. O'DELL and Y. F. SHEALY. *In* Nucleic acid chemistry. Part I. *Edited by* L. B. Townsend and R. S. Tipson. John Wiley and Sons, Inc., New York. 1978. pp. 161–167.
20. N. C. DENO. J. Am. Chem. Soc. **69**, 2233 (1947).
21. G. SHAW and R. N. WARRENER. J. Chem. Soc. 153 (1958).
22. Y. F. SHEALY and C. A. O'DELL. J. Heterocycl. Chem. **13**, 1015 (1976).
23. G. SHAW and R. N. WARRENER. J. Chem. Soc. 157 (1958).
24. M. SANO. Chem. Pharm. Bull. **10**, 320 (1962).
25. Y. F. SHEALY, J. L. FRYE, N. F. DUBOIS, S. C. SHADDIX, and R. W. BROCKMAN. J. Med. Chem. **24**, 1083 (1981).
26. W. C. WONG and C. C. LEE. Can. J. Chem. **42**, 1245 (1964).
27. (*a*) K. ALDER and H. F. RICKERT. Ann. **543**, 1 (1939); (*b*) H. L. HOLMES. *In* Organic reactions. Vol. IV. *Edited by* R. Adams. John Wiley and Sons, Inc., New York. 1948. p. 92.
28. (*a*) S. WINSTEIN and D. TRIFAN. J. Am. Chem. Soc. **74**, 1147 (1952); (*b*) J. D. ROBERTS, C. C. LEE, and W. H. SAUNDERS, JR. J. Am. Chem. Soc. **76**, 4501 (1954).
29. G. ZWEIFEL, K. NAGASE, and H. C. BROWN. J. Am. Chem. Soc. **84**, 183 (1962).
30. A. VOGEL. Vogel's textbook of practical organic chemistry. 4th ed. *Revised by* B. S. Furniss, A. J. Hannaford, V. Rogers, P. W. G. Smith, and A. R. Tatchell. Longman, London and New York. 1978. p. 291.
31. IUPAC–IUB Revised tentative rules for nomenclature of steroids. J. Org. Chem. **34**, 1517 (1969).

An *ab initio* molecular orbital theory study of the structure and stability of the hydrogen bridged radical cation molecule pairs $[CH_2CHOH—OH_2]^{+\cdot}$ and $[CH_2CHOH—OHCH_3]^{+\cdot}$

RON POSTMA, PAUL J. A. RUTTINK, AND FRANS. B. VAN DUIJNEVELDT
Theoretical Chemistry Group, University of Utrecht, Padualaan 8, 3508 TB Utrecht, The Netherlands

JOHAN K. TERLOUW
Analytical Chemistry Laboratory, University of Utrecht, Croesestraat 77a, 3522 AD Utrecht, The Netherlands

AND

JOHN L. HOLMES
Chemistry Department, University of Ottawa, Ottawa, Ont., Canada K1N 9B4

Received October 23, 1984

RON POSTMA, PAUL J. A. RUTTINK, FRANS. B. VAN DUIJNEVELDT, JOHAN K. TERLOUW, and JOHN L. HOLMES. Can. J. Chem. **63**, 2798 (1985).

Ab initio molecular orbital theory was used to determine if $C_2H_6O_2^{+\cdot}$ and $C_3H_8O_2^{+\cdot}$ radical cations represented as hydrogen bridged radical cation molecular pairs, viz. $[H_2O\text{---}H\text{---}OCHCH_2]^{+\cdot}$ and $[CH_3OH\text{---}H\text{---}OCHCH_2]^{+\cdot}$ can be expected to exist as stable species in the gas phase.

The use of several basis sets was explored at the SCF level and it was found that the above species have appreciable stabilisation energies with respect to dissociation into $CH_2{=}CHOH^{+\cdot}$ and H_2O or CH_3OH. Using a 6-31**/4-31G basis set and applying BSSE (Basis Set Superposition Error) corrections, respective stabilisation energies of 88 kJ/mol and 84 kJ/mol were calculated. Preliminary calculations further indicate that conversion barriers towards isomeric structures are high and thus ions of this type may well have been observed by experiment. Several reaction profiles have been calculated at the STO-3G level and at the 4-31G level, which show that the ions can exist in a *syn* and an *anti* conformation having comparable energies, their interconversion barrier being small.

The structure parameters and stabilisation energies for these two hydrogen bridged ions are similar to those of the well known class of even electron species, usually designated as proton bound dimers.

RON POSTMA, PAUL J. A. RUTTINK, FRANS. B. VAN DUIJNEVELDT, JOHAN K. TERLOUW et JOHN L. HOLMES. Can. J. Chem. **63**, 2798 (1985).

Utilisant la théorie *ab initio* des orbitales moléculaires on a déterminé si les cations radicalaires $C_2H_6O_2^{+\cdot}$ et $C_3H_8O_2^{+\cdot}$, représentés sous la forme de paires de cations moléculaires reliés par des ponts hydrogènes comme $[H_2O\text{---}H\text{---}OCHCH_2]^{+\cdot}$ et $[CH_3OH\text{---}H\text{---}OCHCH_2]^{+\cdot}$, peuvent exister sous forme d'espèces stables en phase gazeuse.

On a utilisé plusieurs ensembles de base en champ auto-cohérent et on a trouvé que ces espèces ont des énergies de stabilisation remarquables par rapport à la dissociation en $CH_2{=}CHOH^{+\cdot}$ et en H_2O ou en CH_3OH. On a trouvé des énergies de stabilisation de 88 kJ/mol et de 84 kJ/mol respectivement en utilisant l'ensemble de base 6-31**/4-31G et en appliquant des corrections d'ensemble de base de superposition des erreurs (EBSE). Les calculs préliminaires indiquent de plus qu'il existe des barrières élevées à la transformation en structures isomères et que par conséquent, les ions de ce type peuvent être observés expérimentalement. On a calculé plusieurs profils de réactions au niveau STO-3G et au niveau 4-31G et ces calculs montrent que les ions peuvent exister sous des conformations *syn* et *anti* ayant des énergies comparables et que la barrières à leur interconversion est faibleé.

Les paramètres de structure et les énergies de stabilisation de ces deux ions reliés par des liaisons hydrogène sont semblables à ceux de la classe bien connue des espèces à nombre pair d'électrons que l'on appelle communément des dimères liés par un proton.

[Traduit par le journal]

Introduction

A combination of mass spectrometric measurements with the results of *ab initio* calculations has recently led to the identification and the energies of small stable organic cations of unconventional structure. For example, the radical cation $CH_2OH_2^{+\cdot}$, an isomer of ionised methanol, and a wide variety of analogues $[C_nH_{2n}\cdot XH]^{+\cdot}$ (X = OH, NH_2, SH, halogen, etc.) have been both observed by experiment and calculated to be stable species in the gas phase (1).

Recently, Terlouw *et al.* (2) reported an experimental study on the structure of the $C_2H_6O_2^{+\cdot}$ and $C_3H_8O_2^{+\cdot}$ ions generated by dissociative ionisation of butan1,4-diol and 4-methoxybutan-1-ol, respectively. The ions generated were proposed to have the formal structures $[CH_2{=}CHOH/H_2O]^{+\cdot}$ and $[CH_2{=}CHOH/CH_3OH]^{+\cdot}$, having respective stabilisation energies towards dissociation into $CH_2{=}CHOH^{+\cdot} + H_2O$ or CH_3OH, of >54 kJ/mol and 88 kJ/mol. However, the experiments did not establish to which of the carbon atoms in the vinyl alcohol moiety the H_2O or CH_3OH molecule is bound, i.e. whether isomers I*a*, *b*, or *c* in Fig. 1 are present. An additional possibility is that the ions have the structure $[H_2O\text{---}H\text{---}OCHCH_2]^{+\cdot}$, I*d* in Fig. 1. Ions of type I*a* and I*b* have been shown by *ab initio* calculations to exist in potential wells, but the structure and stability of odd electron hydrogen bonded ions of type I*d* have not yet been investigated. The existence of the *even* electron analogues (proton bound dimers) is well established by both theory and experiment (3, 4).

The present paper describes the results of LCAO-MO-SCF calculations on the species $[CH_2{=}CHO\text{---}H\text{---}OH_2]^{+\cdot}$ and $[CH_2{=}CHO\text{---}H\text{---}(OH)CH_3]^{+\cdot}$, using STO-3G, 4-31G, 6-31G*, and 6-31G** basis sets and applying Basis Set Superposition Error (BSSE) corrections. For the proton bound water dimer $[H_2O\text{---}H\text{---}OH_2]^{+\cdot}$ it has been shown that SCF calculations of the stabilisation energy are sufficiently accurate for

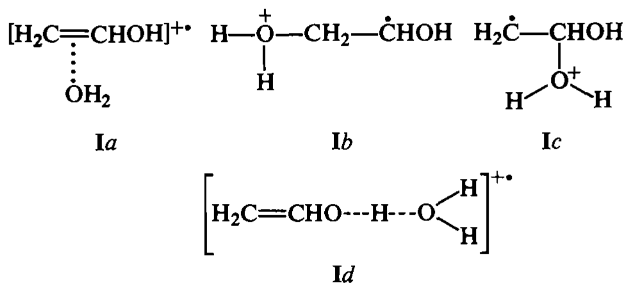

FIG. 1. Structures of $[CH_2{=}CHOH/H_2O]^{+\cdot}$ and $[CH_2{=}CHOH/CH_3OH]^{+\cdot}$ isomers.

our purpose (4). It will be shown that ions of this type are indeed stable species having two local minima corresponding to an *anti* and a *syn* conformation with comparable stabilisation energies.

Methods

Standard LCAO-MO-SCF calculations were performed using a modified version of the Gaussian 76 package (5), employing restricted (6, 7) and unrestricted (8) Hartree–Fock procedures, RHF and UHF, respectively. The basis sets used are the standard STO-3G (9), 4-31G (10), 6-31G* and 6-31G** (11) basis sets. Of these the 6-31G* and 6-31G** basis sets should give the most reliable results.

The geometries of the ions I*d* and II*d* (Fig. 1) were optimized at the STO-3G and 4-31G levels of accuracy. The results are given in Table 1 and Fig. 2, which also shows the labeling of the atoms in both species.

The stabilisation energies of the ions I*d* and II*d* were initially calculated using

$$[1] \quad E = E(\mathrm{A}) + E(\mathrm{B}) - E(\mathrm{AB})$$

where A is the vinyl alcohol radical cation and B is the water or methanol molecule. The results are given in the fourth column of Table 2 (*anti* conformation). As can be seen from Table 2 the stabilisation energy of the ions I*d* and II*d* calculated at the 4-31G level is considerably lower than that obtained with the STO-3G basis. This is consistent with the well-known tendency of small basis sets to overestimate analogous binding energies (4, 12). The difference in the stabilisation energies obtained by [1] might be accounted for by adding BSSE corrections. These were calculated using the so-called counterpoise method (13), where the dissociation energy D_e is given by

$$[2] \quad D_e = E - e(\mathrm{A}) - e(\mathrm{B})$$

with

$$[3] \quad \begin{aligned} e(\mathrm{A}) &= E(\mathrm{A}) - E_{\mathrm{AB}}(\mathrm{A}) \\ e(\mathrm{B}) &= E(\mathrm{B}) - E_{\mathrm{AB}}(\mathrm{B}) \end{aligned}$$

where $E_{\mathrm{AB}}(\mathrm{A})$ is the energy of A calculated with the basis set of the complex AB. The BSSE corrections $e(\mathrm{A})$ and $e(\mathrm{B})$ for both ions I*d* and II*d* are given in Table 3 (*anti* conformation).

Because geometry optimizations with larger basis sets are rather expensive, single point calculations were performed at the 6-31G* and 6-31G** levels, using either the STO-3G or the 4-31G optimized structures. These calculations are denoted by 6-31G*/STO-3G, etc. The results are also given in Tables 2 and 3.

In addition to the calculation of the stabilisation energies, several reaction profiles were examined for both species. Four of these are shown in Fig. 3 The reaction profiles 1 and 2 simulate the in-plane and the out-of-plane bending of the 3-center bond 01-H4-02. The reaction profiles 3 and 4 simulate the rotation of the —H—OH_2 or —H—$OHCH_3$ group around the C2—O1 bond and the variation of the C2—O1—H4 angle, respectively. A fifth reaction coordinate was selected, which lets the proton travel along the 3-center bond O1—H4—O2 at a fixed (optimized) O1—O2 distance. These reaction profiles were used to investigate the relation between the *anti* and *syn* conformations of the ions I*d* and II*d*.

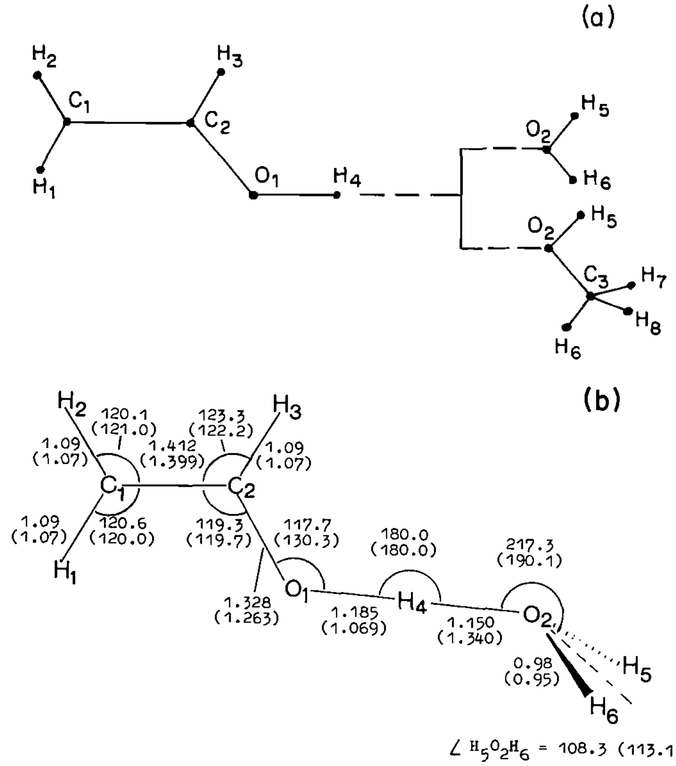

FIG. 2. (*a*) Identification of the atoms in the ions I*d* and II*d* of Fig. 1; (*b*) Optimized HF/STO-3G structure of ion I*d*, with HF/4-31G values of the structural parameters being shown in parentheses. Bond lengths are given in Å and bond angles in deg.

Results and discussion

The results obtained with the 4-31G basis and corrected for BSSE indicate that the potential energy hypersurfaces have local minima corresponding to the ions I*d* and II*d*, respectively, and that these ions are stable with respect to dissociation into the vinyl alcohol radical cation and a neutral molecule. The stabilisation energies obtained at this level of accuracy are 134 kJ/mol for I*d* and 144 kJ/mol for II*d* (BSSE corrected).

The results obtained with the polarized basis sets lead to the following conclusions: (*i*) the stabilisation energy is considerably lowered by adding polarization functions; and (*ii*) the BSSE corrections are of the same order of magnitude as in the 4-31G calculations. It may be sufficient only to optimize the geometry at the STO-3G level and to obtain the final energies by single point energy calculations at the 4-31G or 6-31G* level of accuracy. For example, Bouma, MacLeod, and Radom (1*d*) showed that the relative energy results for $C_2H_4O^{+\cdot}$ isomers calculated at the 4-31G level compare well with the

TABLE 1. Calculated total energies, interatomic distances, and interatomic angles (the 4-31G results are given in parentheses) of SCF geometry optimized structures calculated with STO-3G and 4-31G basis sets (see Fig. 3 for the atom labeling)

Molecule	Molecular energy (au)	Atoms	Interatomic distances (Å)[a]	Atoms	Interatomic angles (deg)[b]
H_2O	−74.965898(RHF) (−75.908636(RHF))	O—H	0.99(0.95)	H—O—H	99.0(111.2)
CH_3OH	−113.549073(RHF)	O2—C3	1.433(1.428)	O2—C3—H6	103.8(107.6)
	(−114.871350(RHF))	O2—H5	0.99(0.95)	O2—C3—H7	120.1(111.3)
		C3—H6	1.09(1.07)	O2—C3—H8	120.1(111.3)
		C3—H7	1.10(1.08)	C3—O2—H5	108.2(113.1)
		C3—H8	1.10(1.08)	H5—O2—C3—H6(fixed)	180.0
				H5—O2—C3—H7(fixed)	120.0
				H5—O2—C3—H8(fixed)	−120.0
$C_2H_4O^{+\cdot}$	−150.696945(UHF)	O1—C2	1.309(1.282)	O1—C2—C1	117.9(118.0)
planar	(−152.381169(UHF))	C1—C2	1.423(1.399)	C2—O1—H4	113.1(122.3)
(anti)		O1—H4	1.00(0.96)	C1—C2—H3	122.4(122.4)
		C1—H1	1.09(1.07)	C2—C1—H1	120.2(119.6)
		C1—H2	1.09(1.07)	C2—C1—H2	119.5(120.1)
		C2—H3	1.10(1.07)		
$C_2H_6O_2^{+\cdot}$	−225.753919(UHF)	O1—C2	1.328(1.263)	O1—C2—C1	119.3(119.7)
I*d*	(−228.343718(UHF))	C1—C2	1.412(1.399)	O1—H4—O2	180.0
		O1—H4	1.185(1.069)	C2—O1—H4	117.7(130.3)
		O2—H4	1.150(1.340)	C1—C2—H3	123.3(122.2)
		O2—H5	0.98(0.95)	C2—C1—H1	120.6(120.0)
		O2—H6	0.98(0.95)	C2—C1—H2	120.1(121.0)
		C1—H1	1.09(1.07)	H4—O2—H5	117.8(122.9)
		C1—H2	1.09(1.07)	H4—O2—H6	117.8(122.9)
				H5—O2—H6	108.3(113.1)
		C2—H3	1.09(1.07)	C2—O1—O2—H5	90.0(90.0)
				H1—C1—C2—H3	0.0(0.0)
$C_3H_8O_2^{+\cdot}$	−264.339918(UHF)	O1—C2	1.327(1.267)	C1—C2—O1	119.2(119.7)
II*d*	(−267.310837(UHF))	O2—C3	1.443(1.456)	O1—H4—O2	180.0
		C1—C2	1.414(1.391)	O2—C3—H6	107.7(108.2)
		O1—H4	1.180(1.298)	O2—C3—H7	109.8(122.2)
		O2—H4	1.111(1.089)	O2—C3—H8	109.8(122.2)
		O2—H5	0.98(0.99)	C2—O1—H4	117.9(126.9)
		C1—H1	1.09(1.07)	H4—O2—C3	119.2(125.9)
		C1—H2	1.09(1.07)	C2—C1—H1	120.6(120.0)
		C2—H3	1.10(1.07)	C2—C1—H2	120.1(121.0)
		C3—H6	1.09(1.09)	C1—C2—H3	123.5(122.2)
				H5—O2—C3	111.2(117.4)
		C3—H7	1.10(1.10)	H4—O2—H5	114.3(114.2)
		C3—H8	1.10(1.10)	C2—O1—O2—C3	90.0(90.0)
				H1—C1—C2—H3	0.0(0.0)

[a]Optimized C—C and C—O distances with minimum stepsize of 0.01 Å, optimized C—H and O—H distances with a minimum stepsize of 0.02 Å, O—H4 distances with a minimum stepsize of 0.01 Å.
[b]Optimized bond angles with a minimum stepsize of 0.5°.

4-31G/STO-3G results. Although it is not certain that this procedure can also be used for calculating the stabilisation energy of hydrogen bonded cations, for ion **I***d* a difference of 15 kJ/mol was found between the stabilisation energies calculated with 6-31G*/STO-3G and 6-31G*/4-31G, respectively (Table 2). Comparing the geometries used, it can be seen from Tables 1 and 2 that the O1—O2 distance and the position of the bridging hydrogen atom in the O1—H4—O2 3-center bond strongly depend on the basis set used and that the changes in the O1—O2 distance upon recombination are rather large and have opposite sign.

Because the STO-3G basis overestimates the ion-dipole interaction (see Table 2) the low value for the stabilisation energy obtained in the 6-31G*/STO-3G calculation may be explained by the artificially short O1—O2 distance in the STO-3G optimized structure. This will lead to a considerable destabilisation in the 6-31G*/STO-3G calculations. It is not clear whether STO-3G calculations yield reliable predictions for the other geometrical changes in the recombination and so this has been examined by performing a 6-31G* calculation, using the STO-3G reactant geometries together with relative orientation of the reactants as obtained in the 4-31G optimization. The resulting energy is 23 kJ/mol lower than the 6-31G*/STO-3G result. Therefore the difference between the 6-31G*/4-31G and 6-31G*/STO-3G results (15 kJ/mol) may be explained by the unsuitability of the STO-3G optimized structure for 6-31G* calculations. Consequently, the 4-31G optimized geometries will be used hereafter. Nevertheless the reliability of the 6-31G*/4-31G results should not be overestimated because the 4-31G optimized geometry may also be unreliable. This was checked by performing calculations using the 4-31G reactant geometries with the 4-31G result for the relative orientation of

TABLE 2. Stabilisation energies in kJ/mol and total energies in hartree of the proton bound dimer complexes $C_2H_6O_2^{+\bullet}$ and $C_3H_8O_2^{+\bullet}$, calculated with different basis sets

Isomer[a]	Basis set	Total energy	$E_{I,II}$[b]	
H_2O	6-31G*/STO-3G	−76.006591		
	6-31G*/4-31G	−76.009770		
	6-31G**/4-31G	−76.022689		
CH_3OH	6-31G*/STO-3G	−115.031682		
	6-31G*/4-31G	−115.034104		
	6-31G**/4-31G	−115.045358		
$CH_2CHOH^{+\bullet}$ (*anti*)	6-31G*/STO-3G	−152.603448		
	6-31G*/4-31G	−152.607096		
	6-31G**/4-31G	−152.619524		
$CH_2CHOH^{+\bullet}$ (*syn*)	6-31G**/4-31G	−152.616391		
I*d* (*anti*)	STO-3G	−225.753919	239.0	
	4-31G	−228.343718	141.6	
	6-31G*/STO-3G	−228.638468	74.6	
	6-31G*/4-31G	−228.651168	90.1	
	6-31G**/4-31G	−228.678468	95.2	99.5[c]
I*d* (*syn*)	6-31G**/4-31G	−228.676905	91.1	99.3[d]
II*d* (*anti*)	STO-3G	−264.339918	246.5	
	4-31G	−267.310837	153.1	
	6-31G*/STO-3G	−267.669023	89.0	
	6-31G*/4-31G	−267.675006	88.7	
	6-31G**/4-31G	−267.700506	93.5	84.0[c]
II*d* (*syn*)	6-31G**/4-31G	−267.696671	83.5	91.7[d]

[a]See Fig. 1 of this paper.
[b]Calculated by using eq. [1], 1 au = 2625.5 kJ/mol.
[c]Open shell RHF calculations (see text).
[d]Calculated by using eq. [1], but the vinyl alcohol radical cation *syn* conformation is used instead of the *anti* conformation (the first value given is calculated with respect to the *anti* conformation).

TABLE 3. Basis set superposition errors, *e*, calculated with different basis sets, the values are given in kJ/mol

Dimer	Basis set	$e(CH_2CHOH)$[a]	$e(H_2O)/(CH_3OH)$[b]	e(sum)
I*d*	STO-3G	2.6	51.8	54.4
(*anti*)	4-31G	1.9	5.8	7.7
	6-31G*/4-31G	1.8	3.6	5.4
	6-31G**/4-31G	0.8	4.1	4.9
II*d*	STO-3G	3.1	50.7	53.8
(*anti*)	4-31G	1.9	7.1	9.0
	6-31G*/4-31G	2.2	3.5	5.6
	6-31G**/4-31G	1.3	3.9	5.2

[a]$e(CH_2CHOH)$ is the BSSE correction obtained for the vinyl alcohol ion in the presence of the atomic orbitals on the H_2O(I*d*) or CH_3OH(II*d*) molecules.
[b]$e(H_2O/CH_3OH)$ is the BSSE correction obtained from the H_2O(I*d*) or CH_3OH(II*d*) molecules in the presence of the atomic orbitals on the [CH_2CHOH] species.

the reactants. The results are −228.3399 au (4-31G) and −228.6525 au (6-31G*). Comparing these results with those in Table 2 it can be seen that the deformation energy in the 4-31G basis equals 10 kJ/mol, whereas the 6-31G* result lies 3 kJ/mol below the value obtained with the 6-31G*/4-31G calculation. These results indicate that the error in the 6-31G*/4-31G calculations is of the order of 3−10 kJ/mol.

The results of the BSSE corrections are shown in Table 3. The reason for the substantial difference between the BSSE values for CH_2CHOH and H_2O/CH_3OH (see Table 3) is that the orbital space of a H_2O or CH_3OH molecule will be more extended by the "ghost" orbitals of vinyl alcohol than will the orbital space of vinyl alcohol be extended by the "ghost" orbitals of H_2O or CH_3OH.

Although the polarized basis sets are large, these corrections are of the same order of magnitude as in the 4-31G basis. This result has also been found by Leclerq, Allavena, and Bouteiller (14). It can be seen from Tables 2 and 3 that the differences between the 6-31G* and 6-31G** results are small, with or without BSSE corrections. We therefore conclude that the errors introduced by using non-optimal geometries is probably larger than those caused by the use of incomplete basis sets.

Finally, it should be noted that these results might be sensitive to electron correlation effects, which have been ignored in the present calculations, particularly because open shell examples are involved (15). For example, calculations including correlation may lead to non-planar $CH_2{=}CHOH$ as in the analogous $C_2H_4^{+\bullet}$ system (16). Furthermore the UHF method used is known to occasionally run into problems due to spin contamination. We therefore checked the UHF results

(6-31G**/4-31G) of I*d* and II*d* (*anti*) with open shell RHF calculations (17), giving stabilisation energies of 91.5 and 84.0 kJ/mol, respectively. The discrepancies with the UHF results for I*d* and II*d* are 3.7 and 10.5 kJ/mol, respectively. These are of the same order of magnitude as the deformation errors given previously (3−10 kJ/mol). The S^2 expectation values for the isomers I*d* and II*d* with the 6-31G**/4-31G basis set are 0.7817 and 0.8134, respectively. According to the above discussion the final result for the stabilisation energy of ion I*d* (including BSSE corrections) is 90 ± 10 kJ/mol (*anti* conformation) and for ion II*d* D_e = 88 ± 10 kJ/mol. These values compare favourably with the experimental results ($D_e \geq$ 54 kJ/mol for ion I*d*, D_e = 88 kJ/mol for ion II*d* (2) and so these structures are possible candidates for the experimentally observed isomers of $C_2H_6O_2^{+\cdot}$ and $C_3H_8O_2^{+\cdot}$, respectively. As in the vinyl alcohol radical cation, the *syn* conformations are somewhat less stable than the *anti* conformations (D_e = 85 kJ/mol and 78 kJ/mol for I*d* and II*d*, respectively).

The results may also be compared to other dimers containing hydrogen bridges. Considering $(H_2O)_2$ and $(H_3O—H_2O)^+$ as prototype systems, it should be noted that the stabilisation energies for these are widely different, viz. 20 kJ/mol for $(H_2O)_2$ and 140 kJ/mol for $H_3O^+—H_2O$ (4). Indeed, various authors (18−20) have noted that the dimerisation energy for symmetrical hydrogen bound cations is largely independent of gas phase basicity and variation in functionality (water, alcohols, ethers, aldehydes, etc.). The high stability of these complexes arises from the electrostatic attraction between the positive charge and the water molecule dipole moment. Applying this argument to the ions I*d* and II*d*, then the decrease in stability of these ions with respect to $H_3O^+—H_2O$ may be explained in terms of the charge distribution in the vinyl alcohol moiety. According to a Mulliken population analysis of the vinyl alcohol radical cation the positive charge is distributed over all atoms but with the center of charge located near to the C2 atom. This corresponds to a 30% increase in the distance between the positive charge and the water molecule compared with the $(H_3O—H_2O)^+$ system. Since according to this simple model the interaction energy varies as R^{-2}, it may be expected that the stabilisation energy for both ions I*d* and II*d* is of the order of 80 kJ, in agreement with the present results. It is also noteworthy that the hydrogen bond energies given by Bomse and Beauchamp (20) for asymmetrical hydrogen bound cations are in the same range. Their values, estimated by using an empirical method (21), lie between 105 and 85 kJ/mol for dimers of the type $[A---H---OH_2]^+$ with A = CH_3OH, C_2H_5OH, $(CH_3)_2O$, *i*-C_3H_7OH, etc. Apparently the stabilisation energy of the ions I*d* and II*d* is not affected much by the open shell character of the vinyl radical cation. This is corroborated by the agrrement of the O—O distances in the ions I*d* and II*d* (2.409 Å and 2.387 Å, respectively) with those calculated by Hagler, Karpas, and Klein (22) and by Newton and Ehrenson (23) for hydrogen bonded cations of simple carbonyl compounds with water. Using the 4-31G basis these authors found O—O distances ranging from 2.34 to 2.39 Å for these compounds.

We have also investigated the O—H—O three center bond more closely by studying several reaction coordinates. The reaction profiles 1 and 2 (Fig. 3*a*) correspond to variations of the O—H—O bond angle. The results for these profiles (not shown explicitly) indicate that reactions along these coordinates are energetically unfavourable.

Reaction coordinate 3 (Fig. 3*b*) stands for the rotation of the

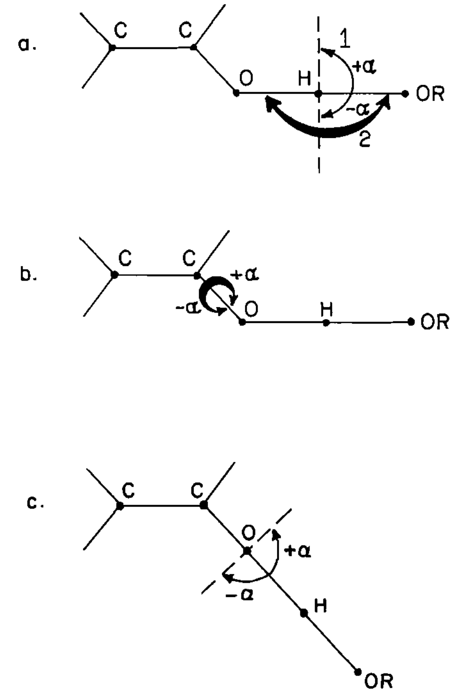

FIG. 3. R = H or CH_3. (*a*) Reaction coordinates 1 and 2, in-plane and out-of-plane bending of the O—H—O bond, respectively. (*b*) Reaction coordinate 3, rotation of the —H—OHR group around the CO bond. α = ±90° when the —H—OHR group is in the CH_2═CHO plane. α = 90° corresponds to the *anti* conformation, α = 90° to the *syn* conformation. (*c*) Reaction coordinate 4, in-plane bending of the C—O—H bond. α = 0 when the C—O—H bond is linear.

—H—OR group around the C2—O1 bond in the vinyl alcohol radical cation, whereas reaction coordinate 4 stands for a variation of the C2—O1—H4 bond angle (Fig. 3*c*). These reaction coordinates relate the *anti* conformation to the *syn* conformation. As shown in Fig. 4 *a* and *b* the corresponding STO-3G reaction profiles indicate that these conformations are separated by rather large energy barriers. However, these barriers virtually disappear with the 4-31G basis and if the position of the hydrogen atom in the O—H—O three center bond is varied. According to the STO-3G results the interconversion will take place along reaction coordinate 4, (i.e. in-plane bending) and so the 4-31G calculations were only performed for this reaction coordinate. In addition to using the optimized O1—H4 and O2—H4 distances, this reaction profile was investigated using the reversed values for these distances with respect to their optimized values. The results, shown in Fig. 5, indicate that the barrier only appears if the hydrogen atom is situated near to the CH_2CHO part of the ion. Note that the 4-31G geometry optimizations lead to opposite positions for the hydrogen atom in the ions I*d* and II*d*, respectively, cf. Table 1. Therefore the role of the curves for the two geometries used is reversed when going from ion I*d* to ion II*d*. That the energy barrier disappears when the hydrogen atom is removed from the vinyl alcohol radical cation may be explained by the absence of the energetically unfavourable distortion of the sp^2 hybridisation on O1 during the interconversion.

Finally, the O1—H4 distance was optimized for the *anti* conformations of ions I*d* and II*d* with a fixed O1—O2 distance, using the STO-3G, 4-31G, and 6-31G* basis sets. The results are shown in Fig. 6. The 6-31G* results place the

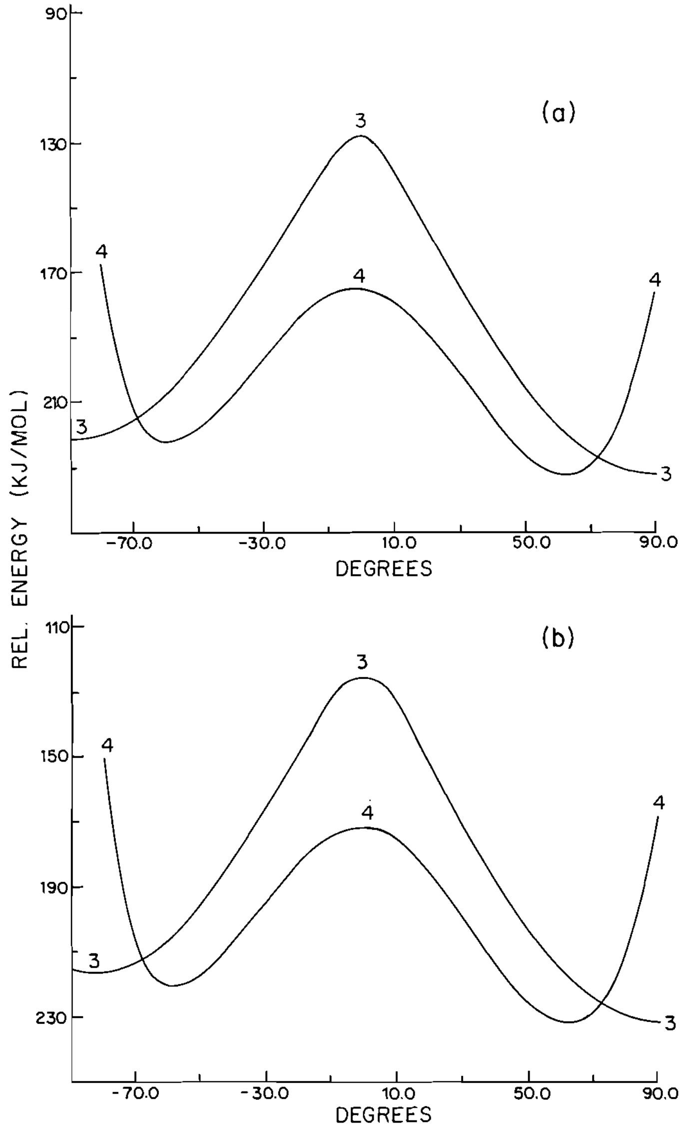

FIG. 4. (*a*) Reaction profiles 3 and 4 (see Fig. 3) for ion I*d* (STO-3G). (*b*) Reaction profiles 3 and 4 (see Fig. 3) for ion II*d* (STO-3G).

hydrogen atom near to the CH_2CHO part of the ion in both cases, and so it was concluded that the 4-31G basis is unsuitable for predicting the position of the hydrogen atom due to the flatness of the corresponding potential well, a result which has also been found in calculations on even electron proton bound dimers (24). The 6-31G* results are in agreement with the conclusions drawn by Larson and McMahon (18) from experimental data, viz. that the potential well for the bridged hydrogen atoms corresponds to a broad single minimum. The interconversion barriers separating the *anti* and *syn* conformations of the ions I*d* and II*d* were found to be small (<10 kJ/mol).

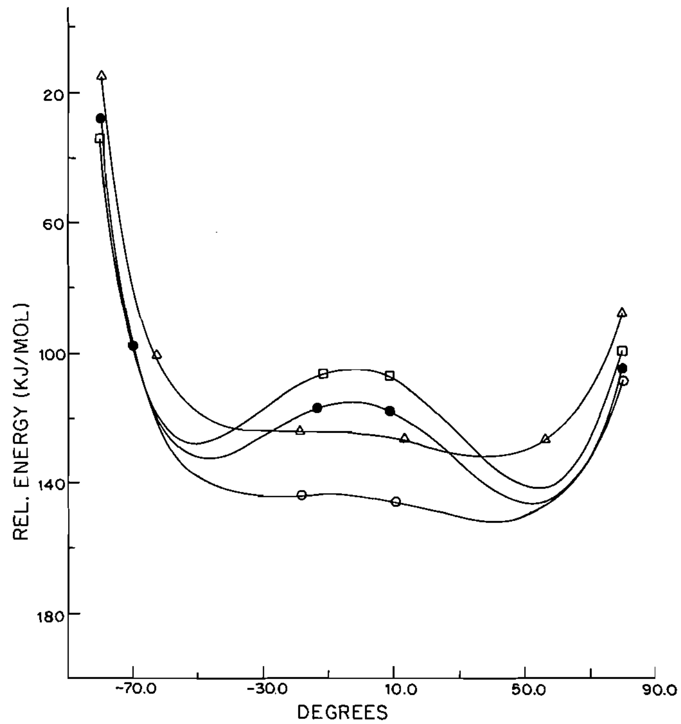

FIG. 5. Reaction profile 4 (4-31G). □ and △ for ion I*d*, ○ and ● for ion II*d*, □ and ○ for optimized O1—H4 and H4—O2 distances, △ and ● for reversed values for the O1—H4 and H4—O2 distances.

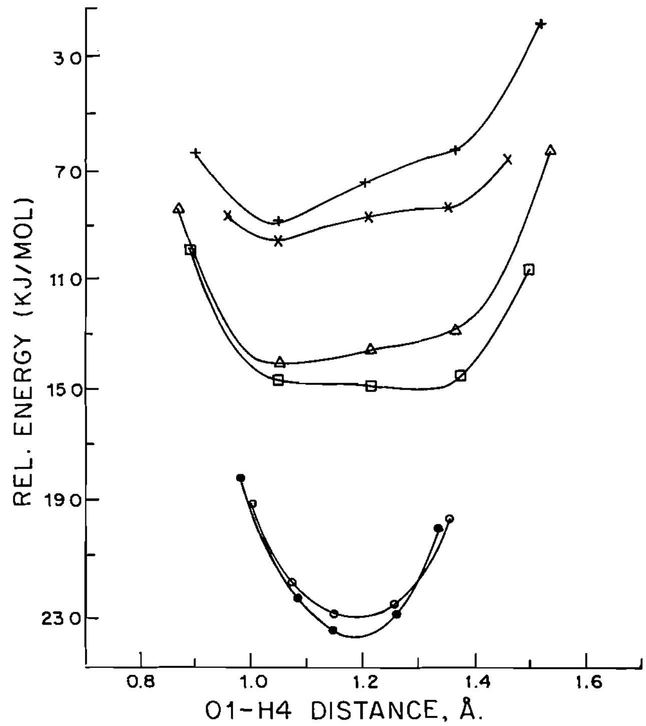

FIG. 6. Reaction profile 5, variation of the position of the bridged hydrogen atom for a fixed (optimized) O1—O2 distance. ○ and ●, STO-3G; △ and □, 4-31G; + and ×, 6-31G*/4-31G; ○, △, and + ion I*d*; ●, □, and ×, ion II*d*.

Summary

The hydrogen bonded radical cation molecule pairs $[H_2O\text{---}H\text{---}OCHCH_2]^{+\cdot}$ and $[CH_3OH\text{---}H\text{—}OCHCH_2]^{+\cdot}$ were both calculated to be stable with respect to dissociation into $CH_2CHOH^{+\cdot}$ and H_2O or CH_3OH. The *anti* and *syn* conformations have comparable energies with small interconversion barriers for both species. Thus it may be expected that both ions are observable species in gas phase ion chemistry. However, which conformation is most likely to be found cannot be predicted from the calculations. Both species have properties comparable to the well known class of even electron hydrogen bridged cations. The open shell character of the vinyl alcohol radical cation seems to have little effect on the stabilisation energy. This may be explained by the fact that the open shell electron is mainly localized away from the hydrogen bond, viz. in the $CH_2{=}CH$ part of the complex.

A comparative study with several basis sets showed that the inclusion of a polarization function is necessary for obtaining reliable results. The differences in stabilisation energy obtained by using basis sets such as STO-3G, 4-31G, 6-31G*, and 6-31G** can only partially be understood in terms of the basis set superposition errors. The remaining differences are probably due to other effects, such as the lack of short range repulsion in the STO-3G basis or an overestimation of dipole moments in the 4-31G basis. For accurate calculations on similar ions it may therefore be necessary to check the reliability of the geometries used in single point energy calculations using larger basis sets.

1. (*a*) J. L. HOLMES, F. P. LOSSING, J. K. TERLOUW, and P. C. BURGERS. J. Am. Chem. Soc. **104**, 2931 (1982); (*b*) J. L. HOLMES, F. P. LOSSING, J. K. TERLOUW, and P. C. BURGERS. Can. J. Chem. **61**, 2305 (1983); (*c*) J. K. TERLOUW, W. HEERMA, and G. DIJKSTRA. Org. Mass Spectrom. **16**, 326 (1981); (*d*) W. J. BOUMA, J. K. MACLEOD, and L. RADOM. J. Am. Chem. Soc. **101**, 5540 (1979); (*e*) W. J. BOUMA, R. H. NOBES, and L. RADOM. J. Am. Chem. Soc. **105**, 1743 (1983); (*f*) R. H. NOBES and L. RADOM. Chem. Phys. Lett. **99**, 107 (1983); (*g*) M. J. FRISCH, K. RACHAVACHARI, J. A. POPLE, W. J. BOUMA, and L. RADOM. Chem. Phys. **75**, 323 (1983).
2. J. K. TERLOUW, W. HEERMA, P. C. BURGERS, and J. L. HOLMES. Can. J. Chem. **62**, 289 (1984).
3. (*a*) I. H. WILLIAMS, G. M. MAGGIONA, and R. L. SCHOWEN. J. Am. Chem. Soc. **102**, 7831 (1980); (*b*) S. A. MCLUCKEY, D. CAMERON, and R. G. COOKS. J. Am. Chem. Soc. **103**, 1313 (1981); (*c*) W. H. JONES, R. D. MARIANI, and M. L. LIVELY. Chem. Phys. Lett. **108**, 602 (1984).
4. (*a*) S. YAMABE, T. MINATO, and K. HIRAO. J. Chem. Phys. **80**, 1576 (1984); (*b*) A. J. CUNNINGHAM, J. D. PAYZANT, and P. KEBARLE. J. Am. Chem. Soc. **94**, 7627 (1972).
5. W. J. HEHRE, W. A. LATHAN, R. DITCHFIELD, M. D. NEWTON, and J. A. POPLE. Program No. 368, QCPE, University of Indiana, Bloomington, IN, USA.
6. J. S. BINKLY, J. A. POPLE, and P. A. DOBOSH. Mol. Phys. **28**, 1423 (1974).
7. C. C. J. ROOTHAAN. Rev. Mod. Phys. **23**, 69 (1951).
8. J. A. POPLE and R. K. NESBET. J. Chem. Phys. **22**, 571 (1954).
9. W. J. HEHRE, R. F. STEWART, and J. A. POPLE. J. Chem. Phys. **51**, 2657 (1969).
10. R. DITCHFIELD, W. J. HEHRE, and J. A. POPLE. J. Chem. Phys. **54**, 724 (1971).
11. (*a*) P. C. HARIHARAN and J. A. POPLE. Chem. Phys. Lett. **16**, 217 (1972); (*b*) R. S. MULLIKEN. J. Chem. Phys. **23**, 1833, 2343 (1955).
12. (*a*) J. E. DELBENE and A. VACCARO. J. Am. Chem. Soc. **98**, 7526 (1976); (*b*) J. A. POPLE. *In*: Modern theoretical chemistry. Vol. 4. *Edited by* H. F. Schaefer III. Plenum Press, New York. 1977.
13. (*a*) H. B. JANSEN and P. ROS. Chem. Phys. Lett. **3**, 140 (1969); (*b*) S. F. BOYS and F. BERNARDI. Mol. Phys. **19**, 558 (1970).
14. J. M. LECLERQ, M. ALLAVANA, and Y. BOUTEILLER. J. Chem. Phys. **78**, 4606 (1983).
15. E. R. DAVIDSON. Int. J. Quantum Chem., Quant. Chem. Symp. **15**, 65 (1981).
16. S. D. PEYERIMHOFF and R. J. BUENKER. Chem. Phys. Lett. **11**, 65 (1971); Theoret. Chim. Acta (Berl.), **27**, 243 (1972).
17. V. R. SAUNDERS. ATMOL4: molecular integrals for contracted spherical harmonic Gaussian orbitals. 1979; V. R. SAUNDERS and M. F. GUEST. ATMOL3 SCF Programs. 1976.
18. J. W. LARSON and T. B. MCMAHON. J. Am. Chem. Soc. **104**, 6255 (1982).
19. Y. K. LAU, P. P. S. SALUJA, and P. J. KEBARLE. J. Am. Chem. Soc. **102**, 7429 (1980).
20. D. S. BOMSE and J. L. BEAUCHAMP. J. Phys. Chem. **85**, 488 (1981).
21. W. R. DAVIDSON, J. SUNNER, and P. J. KEBARLE. J. Am. Chem. Soc. **101**, 1675 (1979).
22. A. T. HAGLER, Z. KARPAS, and F. S. KLEIN. J. Am. Chem. Soc. **101**, 2191 (1979).
23. M. D. NEWTON and S. EHRENSON. J. Am. Chem. Soc. **93**, 4971 (1971).
24. G. H. F. DIERCKSEN, W. VAN NIESSEN, and W. P. KRAEMER. Theoret. Chim. Acta (Berl.), **31**, 205 (1973).

Heterogeneous reaction of nitric acid with methyl sulfide[1]

DONALD L. SINGLETON, ROBERT S. IRWIN, DONALD J. MCKENNEY,[2] AND GEORGE PARASKEVOPOULOS
Division of Chemistry, National Research Council of Canada, Ottawa, Ont., Canada K1A 0R9

Received February 21, 1985

DONALD L. SINGLETON, ROBERT S. IRWIN, DONALD J. MCKENNEY, and GEORGE PARASKEVOPOULOS. Can. J. Chem. **63**, 2805 (1985).

The reaction of gaseous mixtures of CH_3SCH_3 and HNO_3, studied by infrared spectroscopy and gas chromatography, was found to occur heterogeneously. The products detected were NO_2 and $CH_3S(O)CH_3$, and approximately one NO_2 was formed for each CH_3SCH_3 consumed. The initial rate of formation of NO_2 was first order in CH_3SCH_3 and zero order in HNO_3. The mechanism is discussed, and an upper limit is determined for the rate constant of the homogeneous reaction.

DONALD L. SINGLETON, ROBERT S. IRWIN, DONALD J. MCKENNEY et GEORGE PARASKEVOPOULOS. Can. J. Chem. **63**, 2805 (1985).

On a étudié la réaction de mélanges gazeux de CH_3SCH_3 et de HNO_3 en faisant appel à la spectroscopie infrarouge et la chromatographie en phase gazeuse et l'on a trouvé qu'elle se produit d'une façon hétérogène. Les produits que l'on a pu détecter sont le NO_2 et le $CH_3S(O)CH_3$; de plus, il se forme environ une molécule de NO_2 pour chaque molécule de CH_3SCH_3 qui est consommée. La vitesse initiale de formation du NO_2 est du premier ordre en CH_3SCH_3 et d'ordre zéro en HNO_3. On discute du mécanisme et l'on détermine une limite supérieure pour la constante de vitesse de la réaction homogène.

[Traduit par le journal]

Introduction

Nitric acid has long been known to react readily with methyl sulfide in solution to form dimethyl sulfoxide, along with lesser amounts of more highly oxidized derivatives (1). Recent studies have examined the chemically-induced dynamic nuclear polarization of the protons (2) and the catalysis of the reaction by Au^{3+} (3). Thiols and disulfides are also known to undergo oxidation by HNO_3 in solution (4). However, to our knowledge, these reactions have not been investigated in the gas phase, where they would be of interest in studies of the oxidation of reduced sulfur compounds. In the troposphere, methyl sulfide is produced by biogenic and anthropogenic processes, and efforts have been made to understand its tropospheric chemistry. Studies of the mechanism of oxidation of methyl sulfide by OH (5–7), $O(^3P)$ (8), O_3 (9), and NO_2 (10) have recently been reported and reviewed (11).

Experimental

The reaction was studied by infrared spectroscopy using a Teflon-lined absorption cell with a volume of 5.66 L and an optical path length of 20.25 m. Pressures of reactants were measured with a capacitance manometer and introduced into the cell with a vacuum system free of mercury. When very low pressures of reactants were required in the reaction cell, they were measured on a smaller calibrated volume and swept into the cell using nitrogen. The total pressure was always brought up to 1 atm using nitrogen. The temperature was 296 ± 2 K.

Spectra were obtained with a Beckman model 4030 spectrometer operated in the double beam mode. The slit width provided resolution of 4 cm^{-1} above, and about 2.5 cm^{-1} below 2000 cm^{-1}, respectively. The products and reactants were monitored at selected wavelengths as a function of time, and the amounts were determined by converting the percentage transmission to absorbance and using experimentally determined Beer's law coefficients.

The rate of formation of nitrogen dioxide was followed at 1600 cm^{-1}, and consumption of nitric acid and of methyl sulfide was monitored at 1200 and 1015 cm^{-1}, respectively. Calibration mixtures indicated that the absorbance was linear with concentration over the useful range encountered in the experiments. Although dimethyl sulfoxide was found to have a distinctive absorption at 1100 cm^{-1} in the gas phase, it was not detected, and its low volatility prevented a quantitative determination of an upper limit. Neither was NO detected at 1890 cm^{-1}, which is not surprising since, if it were formed, it would react rapidly with nitric acid. Another possible product, N_2O, could not be determined because of interference by the strong absorption bands of nitric acid.

A few experiments were done in a 155 cm^3 quartz flask which could be evacuated and filled with reactants. After a specified reaction time in the dark, the reactants and gaseous products were quickly pumped from the cell for about 20 s, followed by filling the cell with 1 atm of nitrogen and injecting 1 cm^3 of acetone. The cell was shaken to ensure that any products adhering to the walls would be dissolved. Aliquots were removed by syringe and analyzed by gas chromatography on a 1.5 m stainless steel column of Porapak P. The amount of $CH_3S(O)CH_3$ present was determined by comparing its peak area, relative to acetone, with that of standard mixtures. This procedure was followed to recover the less volatile dimethyl sulfoxide from the walls, and yet minimize any reaction between nitric acid and methyl sulfide in the solvent. However, the possibility cannot be excluded of a small amount of direct reaction in the solvent or of further reaction of an adsorbed product once it is dissolved to form dimethyl sulfoxide.

Nitric acid was prepared in vacuum by the reaction of potassium nitrate with concentrated sulfuric acid. The HNO_3 was collected in a trap at 273 K, distilled under vacuum, and stored at liquid nitrogen temperature. Gas chromatography of liquid methyl sulfide (Matheson Coleman and Bell) indicated a purity of 99.89% based on peak areas and was degassed by freeze–pump–thaw cycles. Nitrogen (99.999%) was used directly from the cylinder.

Results

Dimethyl sulfoxide was observed as a product in the experiments in which the quartz reaction cell was rinsed with acetone. After 2 h, 2% of the methyl sulfide in a reaction mixture of 1.2 Torr HNO_3 and 3.1 Torr of CH_3SCH_3 was converted to $CH_3S(O)CH_3$. Methyl sulfone was not observed (a conversion of 0.04% would have been detectable). Dimethyl sulfoxide was not detectable in a similar experiment but without nitric acid present. The only product detected by infrared spectroscopy was NO_2. In separate experiments it was found that there was no significant dark reaction between NO_2 and CH_3SCH_3 under these experimental conditions, consistent with the rate constant

[1]NRCC No. 24634.

[2]Visiting scientist. Present address: Chemistry Department, University of Windsor, Windsor, Ont., Canada N9B 3P4.

TABLE 1. Initial rates of formation of NO_2 in the reaction of HNO_3 with CH_3SCH_3[a]

$HNO_3 \times 10^{-16}$ (molecules/cm^3)	$CH_3SCH_3 \times 10^{-16}$ (molecules/cm^3)	$r(NO_2) \times 10^{-12}$ (molecules/cm^3 s)
2.1	—	0.190
2.1	0.034	0.229
2.0	0.078	0.326
2.0	0.168	0.615
2.0	0.169	0.598
2.0	0.170	0.523
2.2	0.171	0.761
2.2	0.173	0.712
2.1	0.349	1.34
2.2	0.881	2.13
0.018	1.01	1.36
0.017	—	0.224[b]
0.018	1.02	1.34
0.018	—	0.087
0.034	1.00	1.22
0.030	—	0.380[b]
0.033	1.02	1.40
0.034	—	0.098
0.077	1.01	1.55
0.079	—	0.072
0.17	1.03	1.47
0.19	—	0.096
0.17	—	0.091
0.33	0.998	1.86
0.33	—	0.148

[a]Total pressure 760 Torr, 296 K. The initial rates, $r(NO_2)$, are measured values and have not been corrected for the rate of NO_2 formation in the absence of CH_3SCH_3.

[b]This value of $r(NO_2)$ in the absence of methyl sulfide is inexplicably larger than usual.

of 9×10^{-21} cm^3/molecule s reported by Balla and Heicklen (10). Typical plots of the time dependence of the formation of NO_2 are given in Fig. 1. The initial rate of formation of NO_2, over the first 10 min or less, was used to assess which experimental parameters significantly influenced the kinetics. The rate of formation of NO_2 was typically about 30% slower in the first experiment in a day than an otherwise identical experiment performed subsequently. It was found that essentially identical values could be obtained throughout the day by introducing a small pressure of nitric acid into the reaction cell for a few minutes, followed by pumping for several minutes to a pressure less than 0.01 Torr, prior to every experiment. This procedure led to the same values as had been obtained after the first experiment of the day. Additional experiments showed that the sequence of addition of reactants to the reactor did not affect the rate of formation of NO_2. Nonetheless, in all subsequent experiments HNO_3 was added prior to CH_3SCH_3.

Nitric acid slowly decomposes to form NO_2 even in the absence of methyl sulfide. The rates of NO_2 formation in the presence of methyl sulfide could be corrected accordingly. The rate data are given in Table 1. There was no observable decay of CH_3SCH_3 with time in the absence of HNO_3. In a few experiments, the reaction cell was exposed to 0.2 Torr of water for several minutes, then briefly evacuated and treated with nitric acid in the usual manner. This procedure had no significant effect on the initial rate of NO_2 formation.

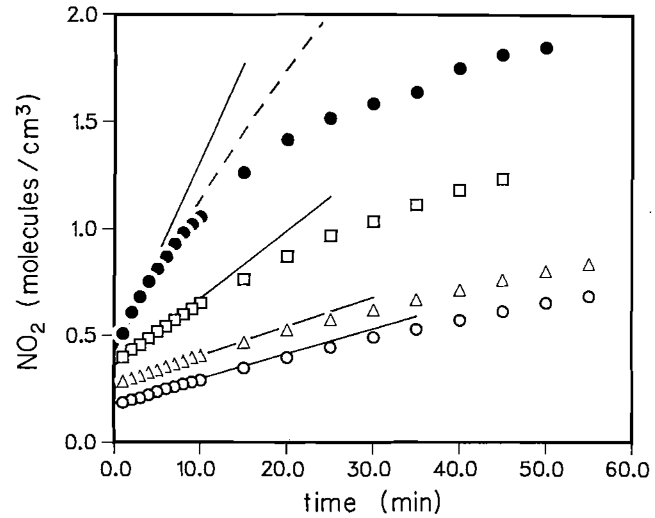

FIG. 1. Yields of NO_2 in the reaction of HNO_3 + CH_3SCH_3 as a function of time at 296 K and 760 Torr N_2. The dashed line is calculated as described in the text for the oversimplified model, $d[NO_2]/dt = k[CH_3SCH_3]$, with $[CH_3SCH_3]_0 = 0.35 \times 10^{16}$ molecules/cm^3. Initial amounts (molecules/cm^3 $\times 10^{-16}$): HNO_3, 2.0; CH_3SCH_3, ○ – 0.0, △ – 0.034, □ – 0.17, ● – 0.35.

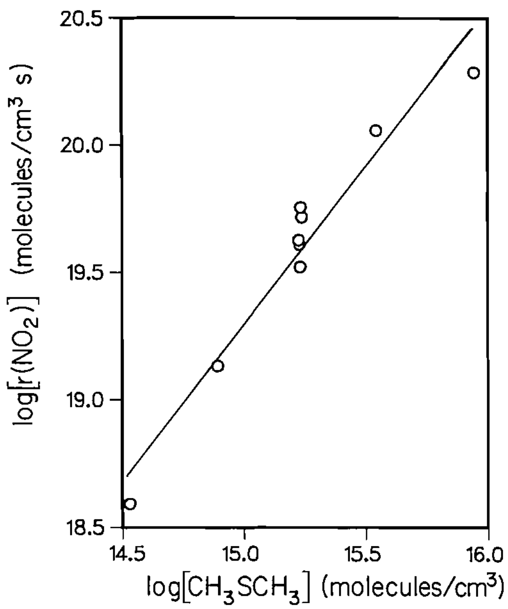

FIG. 2. Plot of the logarithm of the initial rate of NO_2 formation, $r(NO_2)$, against the logarithm of methyl sulfide concentration. Values of $r(NO_2)$ have been corrected for the rate of NO_2 formation in the absence of methyl sulfide. Total pressure, 760 Torr; 296 K.

The order of the reaction for each reactant was determined from the slopes of plots of log ($r(NO_2)$) against log $[CH_3SCH_3]$ at constant excess HNO_3 (Fig. 2), and of log ($r(NO_2)$) against log $[HNO_3]$ at constant excess CH_3SCH_3 (Fig. 3), where $r(NO_2)$ is the corrected initial rate of NO_2 formation. The slope of the former is 1.2 ± 0.3 and, the latter, 0.13 ± 0.17, where the indicated uncertainties are the 95% confidence limits. There is considerable uncertainty in the value of $r(NO_2)$ at higher pressures of CH_3SCH_3 as the initial rate approaches the time resolution of the experiment.

The stoichiometry with respect to CH_3SCH_3 and NO_2 was determined by infrared spectroscopy. The results for equal

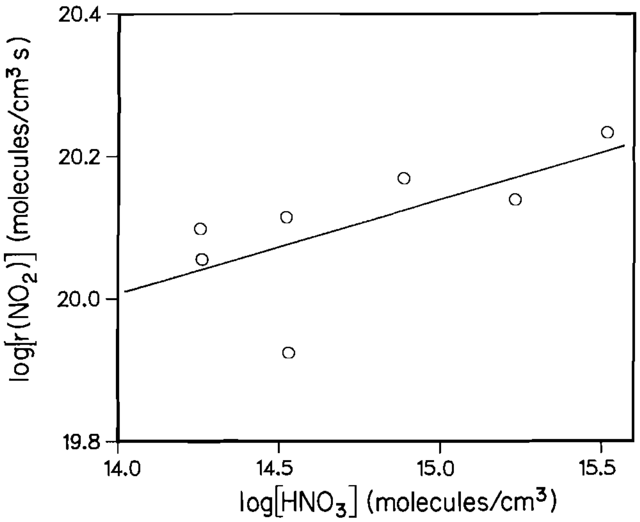

FIG. 3. Plot of the logarithm of the initial rate of NO_2 formation, $r(NO_2)$, against the logarithm of nitric acid concentration. Values of $r(NO_2)$ have been corrected for the rate of NO_2 formation in the absence of methyl sulfide. Total pressure, 760 Torr; 296 K.

initial amounts (0.1 Torr) of HNO_3 and CH_3SCH_3 were $\Delta[NO_2]/\Delta[CH_3SCH_3] = 0.89 \pm 0.09$ for reaction times of 8 to 37 min. Because the data for consumption of HNO_3 were erratic, it was not possible to obtain meaningful values of $\Delta[CH_3SCH_3]/\Delta[HNO_3]$.

Discussion

The observation that the rate of formation of NO_2 is essentially zero order in $[HNO_3]$ and that the rate increases to a reproducible value on pretreating the reaction cell with HNO_3 indicates that CH_3SCH_3 reacts with HNO_3 adsorbed on the walls of the reactor. An attempt was made to reproduce the time dependence of the observed yields of NO_2 using the integrated form of the rate law $d[NO_2]/dt = k[CH_3SCH_3]$, with the value of k obtained from the initial rate, and the time dependent value of the methyl sulfide concentration given by $[CH_3SCH_3] = [CH_3SCH_3]_0 - [NO_2]$, based on the stoichiometry measurements. Included in the calculation were the initial amount of NO_2 and the rate of NO_2 formation with HNO_3 alone in the cell. However, this model always gave NO_2 yields greater than those observed at longer times, as shown by the dashed line in Fig. 1. (Adjustment of the value of k to fit the NO_2 yields at about 50 min resulted in calculated NO_2 yields much smaller than those observed at intermediate times.) This decreasing rate of NO_2 formation may be due to the initially adsorbed HNO_3 not being replaced after reaction with methyl sulfide. The mechanism would be represented as follows, where S—HNO_3 represents nitric acid adsorbed on the wall, and the products include one molecule of NO_2 and some dimethyl sulfoxide.

[1] $HNO_3 + S \longrightarrow S\text{—}HNO_3$

[2] $S\text{—}HNO_3 + MSM \longrightarrow$ products

The rate of NO_2 formation can be represented as

$$d[NO_2]/dt = k_2[MSM][S\text{—}HNO_3]$$

where S—HNO_3 and CH_3SCH_3 are time-dependent quantities. This equation is consistent with the observation that the initial rate is proportional to the concentration of methyl sulfide and decreases as the reaction proceeds, and also with the reduction in initial rate if the reaction cell is not pre-treated with nitric acid prior to an experiment, which apparently serves to increase the initial amount of S—HNO_3 to a reproducible value. Unfortunately, there are no sufficient experimental data to allow formulation of a more detailed mechanism. In a recent study (2), the direct reaction in solution of HNO_3 with methyl sulfide was considered to be slow, with nitrous acid and dimethyl sulfoxide proposed as the products, and N_2O_4 the major oxidizing species. As mentioned above, there was no reaction between methyl sulfide and NO_2 at the concentrations encountered in the present work. However, the mechanism of the surface-catalyzed and aqueous phase reactions may be quite different.

In the discussion so far, it was assumed that reaction occurs on the Teflon-coated walls of the reactor. Although reaction could occur to some extent on the mirrors, which were nickel-plated with an aluminized reflecting surface, there was never any evidence of ir bands due to dimethyl sulfoxide.

The data indicate that any homogeneous path is very slow. If the homogeneous gas phase reaction were bimolecular, the data in Table 1 for $[HNO_3] = 2.0 \times 10^{16}$ and $[CH_3SCH_3] = 1.7 \times 10^{15}$ molecules/cm^3 would give, as a conservative upper limit, an apparent bimolecular rate constant of 1×10^{-20} cm^3/molecule s, based on NO_2 formation. This is only 10^{-8} of the rate constant of the $NO_3 + CH_3SCH_3$ reaction (12), which is indicated by recent work to dominate the nighttime chemistry of methyl sulfide in the troposphere (13). Even though the tropospheric concentration of HNO_3 (14) can be about 100 times greater than that of NO_3 (15), the $HNO_3 + CH_3SCH_3$ reaction would be insignificant.

Acknowledgement

The authors thank Dr. J. Heicklen for material prior to publication.

1. E. E. REID. Organic chemistry of bivalent sulfur. Vol. II. Chemical Publishing Co., Inc. New York, NY. 1960. p. 64.
2. E. S. RUDAKOV, V. M. MASTIKHIN, S. G. POPOV, and R. I. RUDAKOVA. Org. Magn. Reson. **5**, 343 (1973).
3. F. GASPARRINI, M. GIOVANNOLI, D. MISITI, G. NATILE, and G. PALMIERI. Tetrahedron, **39**, 3181 (1983).
4. S. OAE and T. TAKATA. Kagaku (Kyoto), **34**, 961 (1979); Chem. Abstr. **93**, 45296*n* (1980).
5. H. NIKI, P. D. MAKER, C. M. SAVAGE, and L. P. BREITENBACH. Int. J. Chem. Kinet. **15**, 647 (1983).
6. S. HATAKEYAMA and H. AKIMOTO. J. Phys. Chem. **87**, 2387 (1983).
7. D. GROSJEAN. Environ. Sci. Technol. **18**, 460 (1984).
8. R. J. CVETANOVIC, D. L. SINGLETON, and R. S. IRWIN. J. Am. Chem. Soc. **103**, 3530 (1981).
9. R. I. MARTINEZ and J. T. HERRON. Int. J. Chem. Kinet. **10**, 433 (1978).
10. R. J. BALLA and J. HEICKLEN. J. Phys. Chem. **88**, 6314 (1984).
11. J. HEICKLEN. CAES Report No. 735-85, Center for Air Environment Studies, The Pennsylvania State University.
12. R. ATKINSON, J. N. PITTS, JR., and S. M. ASCHMANN. J. Phys. Chem. **88**, 1584 (1984).
13. A. M. WINER, R. ATKINSON, and J. N. PITTS, JR. Science, **224**, 156 (1984).
14. A. L. LAZRUS, P. L. HAAGENSON, G. L. KOK, B. J. HUEBERT, C. W. KREITZBERG, G. E. LIKENS, V. A. MOHNEN, W. E. WILSON, and J. W. WINCHESTER. Atmos. Environ. **17**, 581 (1983).
15. U. F. PLATT, A. M. WINER, H. W. BIERMANN, R. ATKINSON, and J. N. PITTS, JR. Environ. Sci. Technol. **18**, 365 (1984).

Introduction of boundary conditions in the Pelton–Flengas Gibbs–Duhem integration for ternary solutions

ISHAK KARAKAYA AND WILLIAM T. THOMPSON

Department of Chemistry and Chemical Engineering, Royal Military College of Canada, Kingston, Ont., Canada K7L 2W3

Received May 13, 1985

ISHAK KARAKAYA and WILLIAM T. THOMPSON. Can. J. Chem. **63**, 2808 (1985).

A multiple linear regression technique to represent partial excess property data for one component (A) in a ternary A–B–C system is presented. The procedure, following the methodology of Pelton and Flengas, recognizes the need to satisfy Henry's law for components B and C in solutions rich in component A as well as independent experimental knowledge which may be available for the B–C binary.

ISHAK KARAKAYA et WILLIAM T. THOMPSON. Can. J. Chem. **63**, 2808 (1985).

On présente une technique de régression linéaire multiple qui permet de représenter les données relatives aux propriétés partielles en excès pour un composant (A) dans un système ternaire A–B–C. Cette technique, qui suit la méthodologie de Pelton et Flengas, reconnaît d'une part le besoin de satisfaire à la loi de Henry pour les composants B et C dans des solutions qui sont riches en A et d'autre part les connaissances expérimentales indépendantes qui peuvent être disponibles pour le mélange binaire B–C.

[Traduit par le journal]

For a ternary system A–B–C, Pelton and Flengas (1) proposed an analytical method to perform the Gibbs–Duhem integration. This is particularly well suited for use in phase diagram computations (2).

Let f_A, f_B, and f_C represent isothermal partial molar excess thermodynamic functions for components A, B, and C. The composition variation for these properties are defined by the coefficients a_{jk}, b_{jk}, and c_{jk} in the following expressions

$$[1]\quad f_A = \sum_{j=2}\sum_{k=0} a_{jk}y^j t^k$$

$$[2]\quad f_B = \sum_{j=0}\sum_{k=0} b_{jk}y^j t^k$$

$$[3]\quad f_C = \sum_{j=0}\sum_{k=0} c_{jk}y^j t^k$$

where the composition variables y and t are defined by

$$y = 1 - X_A$$

and

$$t = \frac{X_C}{X_B + X_C}$$

This choice of composition variables is particularly convenient for experimental purposes (3, 4), where concentrations of A may be altered in solutions of fixed B-to-C ratios. Coefficients a_{jk}, b_{jk}, and c_{jk} are related by the following recursion formulae (1):

$$[4]\quad b_{jk} = a_{jk} - \left(\frac{j+1-k}{j}\right)a_{(j+1)k} \text{ for } j \geq 1$$

$$[5]\quad c_{jk} = b_{jk} - \left(\frac{k+1}{j}\right)a_{(j+1)(k+1)} \text{ for } j \geq 1$$

The suggested method of applying these equations is to establish the coefficients a_{jk} for one of the components, say A, from experimental data using multiple linear regression methods (7). An example is given in ref. 1 for Cd–Bi–Sn system. It is suggested that the boundary conditions to give the complete expressions for f_B and f_C be obtained from an independent knowledge of the thermodynamic properties of the B–C binary system. However, this procedure always leads to slight thermodynamic inconsistencies in the behaviour of the partial properties of components B and C near concentrations very rich in component A (1, 4–6). In particular, the limiting properties for f_B and f_C for $X_A = 1$ are multivalued due to the indeterminacy of the variable t at this composition. This communication shows how this problem may be circumvented.

When for a given temperature, the expansion of the power series given by eq. [1] is written as

$$\begin{aligned}[6]\quad f_A = {} & (a_{20} + a_{21}t + a_{22}t^2 + \ldots + a_{2n}t^n)y^2 \\ & + (a_{30} + a_{31}t + a_{32}t^2 + \ldots + a_{3n}t^n)y^3 \\ & \cdot \\ & \cdot \\ & \cdot \\ & + (a_{m0} + a_{m1}t + a_{m2}t^2 + \ldots + a_{mn}t^n)y^m\end{aligned}$$

it follows that the series expansion of eq. [2] for the partial excess property of B must (to satisfy the Gibbs–Duhem equation) be given (1) by

$$\begin{aligned}[7]\quad f_B = {} & [(b_{00}) + (b_{01})t + (b_{02})t^2 + \ldots + (b_{0n})t^n] \\ & + \left[(-2a_{20}) + (-a_{21})t + 0 + \ldots + \left(-\frac{2-n}{1}a_{2n}\right)t^n\right]y \\ & + \left[\left(a_{20} - \frac{3}{2}a_{30}\right) + (a_{21} - a_{31})t + \left(a_{22} - \frac{1}{2}a_{32}\right)t^2 + \ldots + \left(a_{2n} - \frac{3-n}{2}a_{3n}\right)t^n\right]y^2 \\ & + \left[\left(a_{30} - \frac{4}{3}a_{40}\right) + (a_{31} - a_{41})t + \left(a_{32} - \frac{2}{3}a_{42}\right)t^2 + \ldots + \left(a_{3n} - \frac{4-n}{3}a_{4n}\right)t^n\right]y^3 \\ & \cdot \\ & \cdot \\ & + \left[(a_{m0}) + (a_{m1})t + (a_{m2})t^2 + \ldots + (a_{mn})t^n\right]y^m\end{aligned}$$

In eq. [7], coefficients b_{0k} are zero for $k \geq 1$. This simply recognizes that f_B has a fixed value in solutions approaching pure A in composition and is therefore necessarily independent of the value of the variable t which becomes indeterminate at $y = 0$ (pure A). In principle, the constant b_{00} can be determined from a knowledge of f_B at any composition (1). However, when this is done, it fixes the variation of f_B in the B−C binary where $y = 1$. Such a data treatment gives excess partial molar properties for B that are almost always inconsistent with independent experimental measurements of f_B in the B−C binary. The heart of this dilemma is the very sensitive nature of the coefficients in parentheses (eg. $(a_{21} - a_{31})$) in eq. [7] to the constants involved in eq. [6]. In other words, differences in the regression of f_A (due to very small experimental error, different number of data points etc.) which yield the coefficients a_{jk} can result in substantially different coefficients in eq. [7]. These in turn have a large effect on the calculated partial excess properties of B in the B−C binary. This difficulty may be overcome by introducing appropriate constraints into the statistical evaluation of coefficients a_{jk} so as to require behaviour in the B−C binary that is in agreement with direct experimental studies of this system.

If independently established integral excess properties in the B−C binary, f, are expressed in the form

$$[8] \quad f = p_1t + p_2t^2 + \ldots + p_nt^n$$

the partial excess thermodynamic property of B in this binary must be given by

$$[9] \quad f_B = -p_2t^2 - 2p_3t^3 + \ldots + (1 - n)p_nt^n$$

Equation [9] is eq. [7] for the case where $y = 1$. Noting that the parameter b_{01} automatically becomes zero by virtue of the Pelton−Flengas recursion relationships (1), it follows that

$$[10] \quad a_{22} = -p_2 - \frac{1}{2}a_{32} - \frac{1}{3}a_{42} - \ldots - \frac{1}{m-1}a_{m2}$$

$$\vdots$$

$$a_{2n} = -(n-1)p_n - \frac{1}{2}a_{3n} - \frac{1}{3}a_{4n} - \ldots - \frac{1}{m-1}a_{mn}$$

Incorporation of these relationships into eq. [6] gives, upon rearrangement,

$$\begin{aligned}
[11] \quad & [f_A + p_2t^2 + 2p_3t^3 + \ldots + (n-1)p_nt^n] \\
&= [a_{20}y^2 + a_{21}y^2t] \\
&+ \left[a_{30}y^3 + a_{31}y^3t + a_{32}t^2\left(y^3 - \frac{1}{2}y^2\right) + \ldots + a_{3n}t^n\left(y^3 - \frac{1}{2}y^2\right)\right] \\
&\vdots \\
&+ \left[a_{m0}y^m + a_{m1}y^mt + a_{m2}t^2\left(y^m - \frac{1}{m-1}y^2\right) + \ldots + a_{mn}t^n\left(y^m - \frac{1}{m-1}y^2\right)\right]
\end{aligned}$$

Since f_A is regarded as the measured partial excess property of A in the ternary system and the parameters p_i, we are supposing, can be obtained from an independent study of the B−C binary, the left hand side of the eq. [11] is known. The coefficients a_{jk} (other than a_{2k} for $k > 1$) can now be established by multiple linear regression in which the left hand side of eq. [11] is the dependent variable and the functions of t and y next to each coefficient are the independent variables. The procedure is completed by using eq. [10] to establish the coefficients a_{2k} for $k > 1$. In this way, it is possible to observe the constancy of the activity coefficient of B (and C at the same time) at virtually pure A as well as to incorporate independently established thermodynamic properties for the B−C binary.

The foregoing procedure has been applied to ternary salt systems investigated in this laboratory. It has been found that placing the suggested interrelationships on the coefficients does not reduce the quality of the analytical representation of the excess partial molar properties of component A.

1. A. D. PELTON and S. N. FLENGAS. Can. J. Chem. **47**, 2283 (1969).
2. P.-L. LIN, A. D. PELTON, C. W. BALE, and W. T. THOMPSON. Calphad, **4**, 47 (1980).
3. T. OSTVOLD. Acta Chem. Scand. **26**, 1751 (1972).
4. W. T. THOMPSON, A. LEUNG, and D. G. HURKOT. Can. Met. Quart. **12**, 421 (1973).
5. A. D. PELTON and W. T. THOMPSON. Prog. Solid State Chem. **10**, 119 (1975).
6. A. D. PELTON and C. W. BALE. Calphad, **1**, 253 (1977).
7. C. A. BENNETT and N. L. FRANKLIN. Statistical analysis in chemistry and chemical industries. John Wiley and Sons Inc. 1961.

Formal total synthesis of erythromycin A. Part I. Total synthesis of a 1,7-dioxaspiro[5.5]undecane derivative of erythronolide A

BRUNO BERNET, PAUL M. BISHOP, MAURICE CARON, TAKESHI KAWAMATA, BERNARD L. ROY, LUC RUEST, GILLES SAUVÉ, PIERRE SOUCY, AND PIERRE DESLONGCHAMPS[1]

Laboratoire de synthèse organique, Département de Chimie, Faculté des Sciences, Université de Sherbrooke, Sherbrooke (Qué.), Canada J1K 2R1

Received June 24, 1985

BRUNO BERNET, PAUL M. BISHOP, MAURICE CARON, TAKESHI KAWAMATA, BERNARD L. ROY, LUC RUEST, GILLES SAUVÉ, PIERRE SOUCY, and PIERRE DESLONGCHAMPS. Can. J. Chem. **63**, 2810 (1985).

The total synthesis of compound **1**, a 1,7-dioxaspiro[5.5]undecane derivative of the seco acid methyl ester of erythronolide A, is reported.

BRUNO BERNET, PAUL M. BISHOP, MAURICE CARON, TAKESHI KAWAMATA, BERNARD L. ROY, LUC RUEST, GILLES SAUVÉ, PIERRE SOUCY et PIERRE DESLONGCHAMPS. Can. J. Chem. **63**, 2810 (1985).

La synthèse totale du composé **1**, un dérivé dioxa-1,7 spiro[5.5]undécane de l'ester méthylique de l'acide seco de l'érythronolide A, est rapportée.

We wish to report the stereocontrolled synthesis of the carbamate derivative **2** (Scheme 1) of erythronolide A seco acid methyl ester. Compound **2** is a key intermediate in the synthesis of erythromycin A reported by Woodward *et al.* (1). This work therefore formally constitutes a total synthesis of erythromycin A. Part I (this communication) describes the total synthesis of the 1,7-dioxaspiro[5.5]undecane derivative **1** of erythronolide A seco acid methyl ester. Part II reports the degradation of erythromycin A into the spiro derivative **1**, whereas Part III (see following communications) discloses the conversion of the spiro derivative **1** into Woodward's key intermediate carbamate **2**.[2]

Our synthetic strategy, which is based on the fact (3) that stereoelectronic effects control the conformation of the 1,7-dioxaspiro[5.5]undecane system, has been reported elsewhere (4, 5).[3]

The two starting materials used for the construction of the 1,7-dioxaspiro[5.5]undecane derivative **1** were 4-(biscarbomethoxy)-2-methyl-δ-valerolactone **3** (Scheme 2) and optically active R-5-hexyn-3-ol (**4**, R = H). The lactone **3**[4] was prepared from the Michael reaction of dimethyl malonate with methyl methacrylate followed by an aldol condensation with formaldehyde. Optically active R-5-hexyn-3-ol (**4**, R = H) was obtained by resolution (6) (chromatography of the *O*-methyl mandelic esters).

Condensation (7) of lactone **3** with the lithium acetylide of optically active **4** (R = $(CH_3)_3Si$) gave, after treatment with trimethylsilyl chloride, the adduct **5**.[5] Controlled catalytic hydrogenation (**5** → **6**) followed by cyclization catalyzed with trimethylsilyl triflate (9) gave the optically active spiro diesters **7*A*** and **7*B*** in a ~1:1 ratio. Equilibration (3) of this C-8 epimeric mixture (erythronolide numbering system) with pyridinium tosylate (10) gave solely the spiroisomer **7*B***, which has an absolute (and relative) configuration at C-8 and C-13 corresponding to that of **1** derived from erythromycin A.[6,7]

Allylic oxidation (SeO_2, PCC (11)) of isomer **7*B*** provided spiroenone **8** with a carbonyl group at C-12. Lithium dimethylcuprate 1,4-addition (12) on spiroenone **8** and reaction of the resulting enolate with dibenzoyl peroxide (13) gave compound **9** in 75% yield (Scheme 3). Reaction of **9** with methylmagnesium iodide at low temperature (14) gave stereospecifically compound **10** having the desired stereochemistry at C-8, C-10, C-11, C-12, and C-13.

The benzoate group was removed (**10** → **11**) under mild basic conditions and decarbalkoxylation gave a C-6 epimeric mixture in which the axial ester isomer **12*A*** predominates (15). The ester enolate derived from the epimeric mixture **12** was reacted with phenylselenyl bromide (16) to give predominantly the stereoisomer **13** having the axial carbomethoxy group.[8] Oxidation of **13** gave a ~1:1 mixture of spiro olefins **14*A*** and **14*B***. On heating the mixture **14*A*** and **14*B*** at 138°C in the presence of palladium–charcoal, spiro olefin **14*A*** underwent complete isomerization into the more conjugated spiro olefin **14*B***.

Reduction of **14*B*** with lithium aluminum hydride (LAH) gave the triol **15**, which was then esterified to give the bispropionate **16** in which the tertiary alcohol was protected by a methoxymethyl group (→ **17**) (17). Claisen rearrangement

---

[1]NSERCC and FCAC predoctoral fellowships: M. Caron (1979–1982), B. L. Roy (1980–1984), and G. Sauvé (1978–1981); postdoctoral collaborators: B. Bernet (1979–1980), P. M. Bishop (1981–1983), T. Kawamata (1979–1981); Université de Sherbrooke: "titulaire de recherche" (L. Ruest) et "adjoint de recherche" (P. Soucy).

[2]For total synthesis of erythronolides reported by other groups, see ref. 2.

[3]Portions of this work have been presented at several international conferences, the first two being the "8th Natural Products Symposium", University of West Indies, Jamaica (January 1980) and the "International Symposium on Stereoelectronic Effects in Organic Chemistry", University of St. Andrews, Scotland (July 1980).

[4]For all new substances, the spectra (ir, 250-MHz and 60-MHz ^1H nmr, and high resolution mass spectra) were in complete agreement with the assigned structures. The ^{13}C nmr spectra were also recorded when necessary for structural assignment.

[5]One isomer is produced and tentatively assigned the stereostructure **5** on the basis of stereoelectronic control (see Chapt. 3 in ref. 4, and ref. 8 for a related example).

[6]Equilibration takes place via acetal cleavage, enol ether formation, and acetal reclosure, which allows epimerization at C-8. The equatorial isomer **7*B***, which exists in the conformation shown on the basis of stereoelectronic effects (3), is sterically less hindered than the axial isomer **7*A***.

[7]At the beginning of our investigation, racemic 5-hexyn-3-ol (±*4*, R = H) was used to develop the synthetic route and this led to the production of racemic intermediates (up to compound **20**).

[8]This selective reaction can be explained on the basis of stereoelectronic effects, see pp. 283–284 in ref. 4.

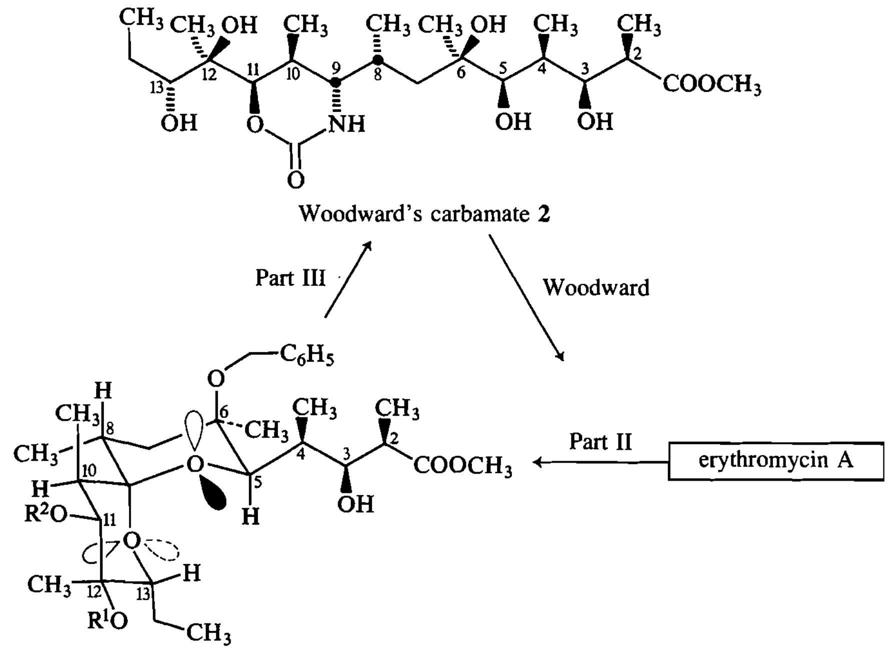

1 R¹ = R² = H
27A R¹ = CH_3OCH_2, R² = C_6H_5CO
28 R¹ = H, R² = C_6H_5CO

SCHEME 1

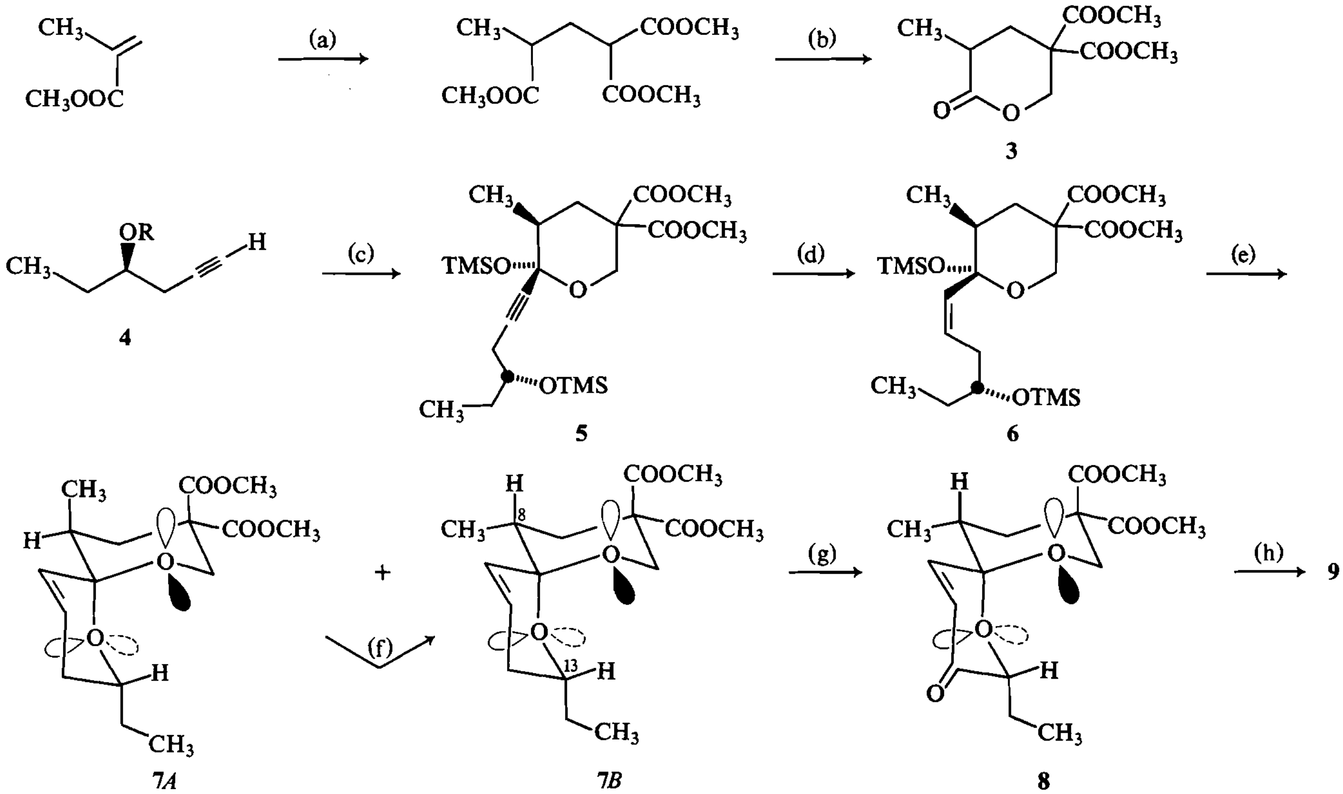

(a) $CH_2(COOCH_3)_2$, CH_3ONa, CH_3OH, reflux, 9 h, 76%
(b) NaH, benzene, $(CH_2O)_3$, r.t., 3 h, 62%
(c) *n*-BuLi, compound **3**, TMSCl, THF, −78°C → 0°C, 4 h, 80%, ref. 7
(d) Lindlar catalyst, H_2, cyclohexane, 15°C, 30 h, ~100%
(e) $(CH_3)_3SiOSO_2CF_3$, CH_2Cl_2, −78°C, 5 h, 84%, ref. 9
(f) Pyridinium *p*-toluenesulfonate, CH_2Cl_2, reflux, 40 h, 84%, ref. 10
(g) SeO_2 (2 equiv.), pyridine (4 equiv.), xylene, 140°C, 5 h; PCC, molecular sieve 3 Å, CH_2Cl_2, 25°C, 60% yield, ref. 11
(h) CuBr, CH_3Li, ether, 0–5°C, 15 min, ref. 12; $(C_6H_5CO_2)_2$, −78°C → 25°C, 30 min, 75%, ref. 13.

SCHEME 2

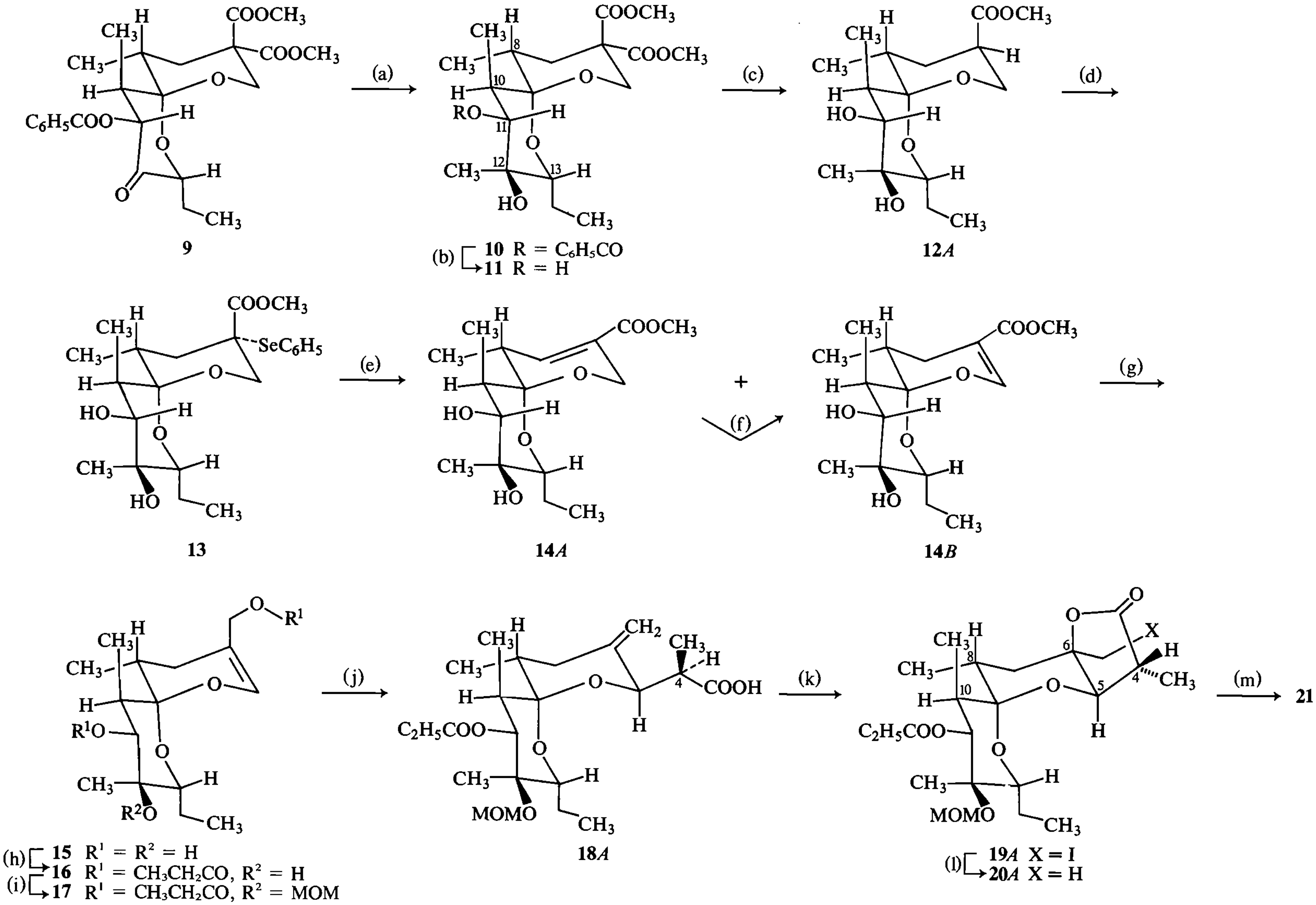

(a) CH_3MgBr, ether, −78°C, 1 h, 63%, ref. 14
(b) K_2CO_3, CH_3OH, 25°C, 1 h, 94%
(c) LiCl, DMSO−H_2O, 165−170°C, 70 min, 83%, ref. 15
(d) Lithium isopropylcyclohexylamide (LiCA), C_6H_5SeBr, DME, −78°C, 90 min, 89%, ref. 16
(e) H_2O_2, pyridine, CH_2Cl_2, 25°C (30 min) and 45°C (30 min), 86%
(f) Pd/C—10%, H_2, xylene, 138°C, 2 h, ~100%
(g) LAH, THF, 0°C → 25°C, 2 h, 90%
(h) $(C_2H_5)_3N$, $(CH_3CH_2CO)_2O$, DMAP, 25°C, 1 h, 99%
(i) Diisopropylethylamine, CH_3OCH_2Cl, CH_2Cl_2, 50°C, 4 h, 90%, ref. 17
(j) LDA, *tert*-butyldimethylsilyl chloride (TBSCl), THF, HMPA (10%), −78°C, 145 min, ref. 18
(k) $KHCO_3$, KI, I_2, H_2O−CH_3OH, 0°C (30 min) and 25°C (15 h), 65% yield from **17**, ref. 19
(l) Ra−Ni, $NaHCO_3$, H_2 (50 psi), C_2H_5OH, 25°C, 24 h, 85% yield of **20***A* and **20***B* (ratio 70:30)
(m) LAH, THF, 0°C (5 min) and 25°C (1 h), 90%

SCHEME 3

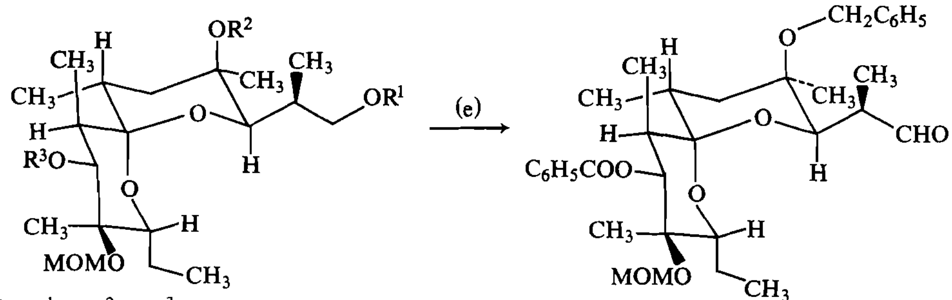

(a) → **21** $R^1 = R^2 = R^3 = H$
(b) → **22** $R^1 = SitBu(C_6H_5)_2$, $R^2 = R^3 = H$
(c) → **23** $R^1 = SitBu(C_6H_5)_2$, $R^2 = H$, $R^3 = C_6H_5CO$
(d) → **24** $R^1 = SitBu(C_6H_5)_2$, $R^2 = C_6H_5CH_2$, $R^3 = C_6H_5CO$
25 $R^1 = H$, $R^2 = C_6H_5CH_2$, $R^3 = C_6H_5CO$

(f) → **26**
(g) → **27A** + **27B** (Scheme 1)
28
(h) ↓
1

(a) TBDPSCl, imidazole, DMF, 25°C, 60 min, 95%, ref. 20
(b) C_6H_5COCl, pyridine, 70°C, 24 h, 78%
(c) $((CH_3)_3Si)_2NK$, $C_6H_5CH_2Br$, THF, 0°C → 25°C, 20 min, 92%
(d) $(n\text{-}Bu)_4NF$, THF, 65–70°C, 2 h, 95%
(e) PCC, molecular sieve 3 Å, AcONa, CH_2Cl_2, 30 min, 85%, ref. 11
(f) Methyl propionate, zirconocene dichloride, LDA, THF, −78°C (40 min), −78°C → 25°C (30 min), and −50°C (1 h), 60% yield of **27A** and **27B** (96:4), ref. 21
(g) HCl 1 *N*, CH_3OH, 25°C, 8 h, 93%
(h) K_2CO_3, CH_3OH, 25°C, 2 h, 95%

SCHEME 4

(18) of **17** gave exomethylene-carboxylic acid **18*A*** and its C-4 epimer (**18*B***, not shown) in a 4:1 ratio respectively. Iodolactonization (19) of the epimeric mixture **18** (→ **19**) followed by hydrogenolysis with Raney nickel gave an epimeric mixture at C-4 of lactones (ratio 7:3) from which the desired lactone **20*A*** was obtained pure by chromatography.

The above sequence has allowed the stereocontrolled introduction of the desired substituents at C-4, C-5, and C-6, and it remains to add a second propionic acid unit and to control the stereochemistry at C-2 and C-3 in order to complete the construction of the spiro derivative **1** of erythronolide A.

Reduction of **20*A*** with LAH gave triol **21** (Scheme 4) from which the primary and the secondary alcohols were respectively protected with a *tert*-butyldiphenylsilyl group (20) (→ **22**) and a benzoate (→ **23**). The remaining unprotected tertiary alcohol was converted into a benzyl ether (→ **24**), the silyl protecting group was then removed (→ **25**), and the primary alcohol was oxidized (11) to give the spiro aldehyde **26**.

Using the method of Evans and McGee (21), aldol condensation of **26** with the zirconium enolate of methyl propionate gave the adduct **27*A*** (Scheme 1) and its C-2 epimer (**27*B***, not shown), in a 20:1 ratio, which were separated by chromatography. The methoxymethyl protecting group of **27*A*** was removed under acid hydrolysis, and treatment of the resulting product **28** with potassium carbonate in methanol produced the 1,7-dioxaspiro[5.5]undecane derivative **1** of erythronolide A seco acid methyl ester. This compound was found to be identical (including optical rotation) with a sample of **1** prepared by degradation of erythromycin A as described in the next communication (Part II).

Acknowledgements

This work was financially supported by the Natural Sciences and Engineering Research Council of Canada (NSERCC) and by the "Gouvernement du Québec: Science et Technologie" (FCAR). An unrestricted grant from Merck Frosst Canada Inc. was also used to support this work.

1. R. B. Woodward, E. Logusch, K. P. Nambiar, K. Sakan, D. E. Ward, B.-W. Au-Yeung, P. Balaram, L. J. Browne, P. J. Card, C. H. Chen, R. B. Chênevert, A. Fliri, K. Frobel, H.-J. Gais, D. G. Garratt, K. Hayakawa, W. Heggie, D. P. Hesson, D. Hoppe, I. Hoppe, J. A. Hyatt, D. Ikeda, P. A. Jacobi, K. S. Kim, Y. Kobuke, K. Kojima, K. Krowicki, V. J. Lee, T. Leutert, S. Malchenko, J. Martens, R. S. Matthews, B. S. Ong, J. B. Press, T. V. Rajan Babu, G. Rousseau, H. M. Sauter, M. Suzuki, K. Tatsuta, L. M. Tolbert, E. A. Truesdale, I. Uchida, Y. Ueda, T. Uyehara, A. T. Vasella, W. C. Vladuchick, P. A. Wade, R. M. Williams, and H. N.-C. Wong. J. Am. Chem. Soc. **103**, 3210 (1981); **103**, 3213 (1981); **103**, 3215 (1981).
2. (*a*) E. J. Corey, P. B. Hopkins, S. Kim, S. Yoo, K. P. Nambiar, and J. R. Falck. J. Am. Chem. Soc. **101**, 7131 (1979); (*b*) E. J. Corey, S. Kim, S. Yoo, K. C. Nicolaou, L. S. Melvin, Jr., D. J. Brunelle, J. R. Falck, E. J. Trybulski, R. Lett, and P. W. Sheldrake. J. Am. Chem. Soc. **100**, 4618 and 4620 (1978); (*c*) S. Masamune, M. Hirama, S. Mori, Sk. Asrof Ali, and D. S. Garvey. J. Am. Chem. Soc. **103**, 1568 (1981); (*d*) G. Stork, I. Paterson, and F. K. C. Lee. J. Am. Chem. Soc. **104**, 4686 (1982).
3. (*a*) P. Deslongchamps, D. D. Rowan, N. Pothier, G. Sauvé, and J. K. Saunders. Can. J. Chem. **59**, 1105 (1981); (*b*) N. Pothier, D. D. Rowan, P. Deslongchamps, and J. K. Saunders. Can. J. Chem. **59**, 1132 (1981).
4. P. Deslongchamps. *In* Stereoelectronic effects in organic chemistry. Vol 1: Organic Chemistry Series. *Edited by* Pergamon Press, Oxford, England. 1983. pp. 330–335.
5. G. Sauvé, D. A. Schwartz, L. Ruest, and P. Deslongchamps. Can. J. Chem. **62**, 2929 (1984).

6. B. L. Roy and P. Deslongchamps. Can. J. Chem. **63**, 651 (1985).
7. (*a*) M. S. Kharash and O. Reinmuth. *In* Grignard reactions of non-metallic structures. Prentice–Hall, Englewood Cliffs, NJ. 1954. p. 574, and references quoted therein; (*b*) E. W. Colvin, R. A. Raphael, and J. S. Roberts. Chem. Commun. 858 (1971); (*c*) H. Ogura, H. Takahashi, and T. Itoh. J. Org. Chem. **37**, 72 (1972).
8. G. Stork and J. M. Stryker. Tetrahedron Lett. **24**, 4887 (1983).
9. (*a*) M. Schmeisser, P. Sartori, and B. Lippsmeir. Chem. Ber. **103**, 868 (1970); (*b*) T. Tsunoda, M. Suzuki, and R. Noyori. Tetrahedron Lett. **21**, 1357 (1980).
10. M. Miyashita, A. Yoshikoshi, and P. A. Grieco. J. Org. Chem. **42**, 3772 (1977).
11. E. J. Corey and J. W. Suggs. Tetrahedron Lett. 2647 (1975).
12. (*a*) H. O. House, W. L. Respress, and G. M. Whitesides. J. Org. Chem. **31**, 3128 (1966); (*b*) E. J. Corey and G. H. Posner. J. Am. Chem. Soc. **89**, 3911 (1967); (*c*) E. Piers and R. J. Keziere. Can. J. Chem. **47**, 137 (1969).
13. A. E. Greene, J. C. Muller, and G. Ourisson. J. Org. Chem. **39**, 186 (1974), and references quoted therein.
14. M. Miljkovic, M. Gligorijevic, T. Satoh, and D. Miljkovic. J. Org. Chem. **39**, 1379 (1974).
15. (*a*) A. P. Krapcho and J. F. Weimaster. J. Org. Chem. **45**, 4105 (1980), and references quoted therein; (*b*) H. D. Banks. J. Org. Chem. **46**, 1743 (1981).
16. (*a*) H. J. Reich, I. L. Reich, and J. M. Renga. J. Am. Chem. Soc. **95**, 5813 (1973); (*b*) K. B. Sharpless, R. F. Lauer, and A. Y. Teranishi. J. Am. Chem. Soc. **95**, 6137 (1973).
17. A. F. Kluge, K. G. Untch, and J. H. Fried. J. Am. Chem. Soc. **94**, 7827 (1972).
18. (*a*) R. E. Ireland and J.-P. Vevert. J. Org. Chem. **45**, 4259 (1980); (*b*) R. E. Ireland and J. P. Daub. J. Org. Chem. **46**, 479 (1981).
19. C. S. Rondesvedt and C. V. Der Nooy. J. Am. Chem. Soc. **77**, 4878 (1955).
20. (*a*) S. Hanessian and P. Lavallée. Can. J. Chem. **53**, 2975 (1975); (*b*) **55**, 562 (1977); (*c*) **59**, 870 (1981).
21. (*a*) D. A. Evans and L. R. McGee. Tetrahedron Lett. **21**, 3975 (1980); (*b*) J. Am. Chem. Soc. **103**, 2876 (1981).

Formal total synthesis of erythromycin A. Part II. Preparation of a 1,7-dioxaspiro[5.5]undecane derivative of erythronolide A seco acid methyl ester from erythromycin A

Bruno Bernet, Paul M. Bishop, Maurice Caron, Takeshi Kawamata, Bernard L. Roy, Luc Ruest, Gilles Sauvé, Pierre Soucy, and Pierre Deslongchamps

Laboratoire de synthèse organique, Département de Chimie, Faculté des Sciences, Université de Sherbrooke, Sherbrooke (Qué.), Canada J1K 2R1

Received June 24, 1985

Bruno Bernet, Paul M. Bishop, Maurice Caron, Takeshi Kawamata, Bernard L. Roy, Luc Ruest, Gilles Sauvé, Pierre Soucy, and Pierre Deslongchamps. Can. J. Chem. **63**, 2814 (1985).

Degradation of erythromycin A gives spirocompound **18***A*. Compound **18***A* is then converted into the spirolactone **22** via **21**. Compound **21** is then reconverted into spiro product **18***A*.

Bruno Bernet, Paul M. Bishop, Maurice Caron, Takeshi Kawamata, Bernard L. Roy, Luc Ruest, Gilles Sauvé, Pierre Soucy et Pierre Deslongchamps. Can. J. Chem. **63**, 2814 (1985).

Par dégradation, l'érythromycine A fournit le composé spiro **18***A*. Ce dernier est ensuite transformé en spirolactone **22** via **21**. Le composé **21** est ensuite reconverti en produit spiro **18***A*.

This communication describes the transformation of erythromycin A (**1**) (Scheme 1) into the 1,7-dioxaspiro[5.5]undecane derivative **18***A* (Scheme 3) of the seco acid methyl ester of erythronolide A. The degradation of the side chain of triol ester **18***A* to give spirolactone **22** via the spiroaldehyde **21** is also reported, as well as the reconstruction of triol ester **18***A* from spiroaldehyde **21**.

Erythromycin A (**1**) was first converted into dihydroerythronolide A (**2**) (1) using the four-step sequence developed by Jones and Rowley (2). In the next operation, the four secondary alcohols were protected by converting **2** into the bis-acetonide **3**, and the remaining two tertiary alcohols were then protected by benzylation (**3** → **4**). Acid hydrolysis of **4** removed both acetonide protecting groups yielding the bis-benzyl ether tetraol **5**, which was then selectively converted into the monoacetonide bis-benzyl ether 9,11-diol **6** using pyridinium tosylate (3) and 2-methoxypropene.

In the next step, pyridinium chlorochromate oxidation of **6** gave the benzylideneacetonide ketone **7**. In this reaction, in addition to the oxidation of the secondary alcohol at C-9 (4), and unexpectedly, the benzyl ether at C-12 was selectively oxidized and transformed into a C(11)—C(12) benzylidene protecting group.

Treatment of **7** with aqueous acetic acid gave 6-benzyl ether-11,12-benzylidene derivative **8** of 8-epi-erythronolide A (Scheme 2). In this reaction, the acetonide group was selectively hydrolyzed with concomitant epimerization of the C-8 methyl group.[1] The seco acid methyl ester derivative **9** of 8-epi-erythronolide was then obtained from **8** using sodium methoxide in methanol. Treatment of **9** with aqueous acetic acid gave the dioxaspiro[5.5]undecane derivative **10**.[2]

The 8-epi-spiro derivative **10** was first converted into the

[1] The epimerization at C-8 has precedent in the literature (5). It was established by the fact that **8** gives the 8-epi-spiro **10** which, when converted into 8-epi-spirocarbonate **12**, undergoes equilibration to give the more stable spirocarbonate **17** (*vide infra*).

[2] In the sequence **9** → **10**, spiroacetalization took place prior to the hydrolysis of the benzylidene protecting group because the C(11)—C(12) benzylidine derivative of **10** can be isolated as an intermediate product when the reaction is stopped before completion.

6. B. L. ROY and P. DESLONGCHAMPS. Can. J. Chem. **63**, 651 (1985).
7. (*a*) M. S. KHARASH and O. REINMUTH. *In* Grignard reactions of non-metallic structures. Prentice–Hall, Englewood Cliffs, NJ. 1954. p. 574, and references quoted therein; (*b*) E. W. COLVIN, R. A. RAPHAEL, and J. S. ROBERTS. Chem. Commun. 858 (1971); (*c*) H. OGURA, H. TAKAHASHI, and T. ITOH. J. Org. Chem. **37**, 72 (1972).
8. G. STORK and J. M. STRYKER. Tetrahedron Lett. **24**, 4887 (1983).
9. (*a*) M. SCHMEISSER, P. SARTORI, and B. LIPPSMEIR. Chem. Ber. **103**, 868 (1970); (*b*) T. TSUNODA, M. SUZUKI, and R. NOYORI. Tetrahedron Lett. **21**, 1357 (1980).
10. M. MIYASHITA, A. YOSHIKOSHI, and P. A. GRIECO. J. Org. Chem. **42**, 3772 (1977).
11. E. J. COREY and J. W. SUGGS. Tetrahedron Lett. 2647 (1975).
12. (*a*) H. O. HOUSE, W. L. RESPRESS, and G. M. WHITESIDES. J. Org. Chem. **31**, 3128 (1966); (*b*) E. J. COREY and G. H. POSNER. J. Am. Chem. Soc. **89**, 3911 (1967); (*c*) E. PIERS and R. J. KEZIERE. Can. J. Chem. **47**, 137 (1969).
13. A. E. GREENE, J. C. MULLER, and G. OURISSON. J. Org. Chem. **39**, 186 (1974), and references quoted therein.
14. M. MILJKOVIC, M. GLIGORIJEVIC, T. SATOH, and D. MILJKOVIC. J. Org. Chem. **39**, 1379 (1974).
15. (*a*) A. P. KRAPCHO and J. F. WEIMASTER. J. Org. Chem. **45**, 4105 (1980), and references quoted therein; (*b*) H. D. BANKS. J. Org. Chem. **46**, 1743 (1981).
16. (*a*) H. J. REICH, I. L. REICH, and J. M. RENGA. J. Am. Chem. Soc. **95**, 5813 (1973); (*b*) K. B. SHARPLESS, R. F. LAUER, and A. Y. TERANISHI. J. Am. Chem. Soc. **95**, 6137 (1973).
17. A. F. KLUGE, K. G. UNTCH, and J. H. FRIED. J. Am. Chem. Soc. **94**, 7827 (1972).
18. (*a*) R. E. IRELAND and J.-P. VEVERT. J. Org. Chem. **45**, 4259 (1980); (*b*) R. E. IRELAND and J. P. DAUB. J. Org. Chem. **46**, 479 (1981).
19. C. S. RONDESVEDT and C. V. DER NOOY. J. Am. Chem. Soc. **77**, 4878 (1955).
20. (*a*) S. HANESSIAN and P. LAVALLÉE. Can. J. Chem. **53**, 2975 (1975); (*b*) **55**, 562 (1977); (*c*) **59**, 870 (1981).
21. (*a*) D. A. EVANS and L. R. MCGEE. Tetrahedron Lett. **21**, 3975 (1980); (*b*) J. Am. Chem. Soc. **103**, 2876 (1981).

Formal total synthesis of erythromycin A. Part II. Preparation of a 1,7-dioxaspiro[5.5]undecane derivative of erythronolide A seco acid methyl ester from erythromycin A

BRUNO BERNET, PAUL M. BISHOP, MAURICE CARON, TAKESHI KAWAMATA, BERNARD L. ROY, LUC RUEST, GILLES SAUVÉ, PIERRE SOUCY, AND PIERRE DESLONGCHAMPS

Laboratoire de synthèse organique, Département de Chimie, Faculté des Sciences, Université de Sherbrooke, Sherbrooke (Qué.), Canada J1K 2R1

Received June 24, 1985

BRUNO BERNET, PAUL M. BISHOP, MAURICE CARON, TAKESHI KAWAMATA, BERNARD L. ROY, LUC RUEST, GILLES SAUVÉ, PIERRE SOUCY, and PIERRE DESLONGCHAMPS. Can. J. Chem. **63**, 2814 (1985).

Degradation of erythromycin A gives spirocompound **18***A*. Compound **18***A* is then converted into the spirolactone **22** via **21**. Compound **21** is then reconverted into spiro product **18***A*.

BRUNO BERNET, PAUL M. BISHOP, MAURICE CARON, TAKESHI KAWAMATA, BERNARD L. ROY, LUC RUEST, GILLES SAUVÉ, PIERRE SOUCY et PIERRE DESLONGCHAMPS. Can. J. Chem. **63**, 2814 (1985).

Par dégradation, l'érythromycine A fournit le composé spiro **18***A*. Ce dernier est ensuite transformé en spirolactone **22** via **21**. Le composé **21** est ensuite reconverti en produit spiro **18***A*.

This communication describes the transformation of erythromycin A (**1**) (Scheme 1) into the 1,7-dioxaspiro[5.5]undecane derivative **18***A* (Scheme 3) of the seco acid methyl ester of erythronolide A. The degradation of the side chain of triol ester **18***A* to give spirolactone **22** via the spiroaldehyde **21** is also reported, as well as the reconstruction of triol ester **18***A* from spiroaldehyde **21**.

Erythromycin A (**1**) was first converted into dihydroerythronolide A (**2**) (1) using the four-step sequence developed by Jones and Rowley (2). In the next operation, the four secondary alcohols were protected by converting **2** into the bis-acetonide **3**, and the remaining two tertiary alcohols were then protected by benzylation (**3** → **4**). Acid hydrolysis of **4** removed both acetonide protecting groups yielding the bis-benzyl ether tetraol **5**, which was then selectively converted into the monoacetonide bis-benzyl ether 9,11-diol **6** using pyridinium tosylate (3) and 2-methoxypropene.

In the next step, pyridinium chlorochromate oxidation of **6** gave the benzylideneacetonide ketone **7**. In this reaction, in addition to the oxidation of the secondary alcohol at C-9 (4), and unexpectedly, the benzyl ether at C-12 was selectively oxidized and transformed into a C(11)—C(12) benzylidene protecting group.

Treatment of **7** with aqueous acetic acid gave 6-benzyl ether-11,12-benzylidene derivative **8** of 8-epi-erythronolide A (Scheme 2). In this reaction, the acetonide group was selectively hydrolyzed with concomitant epimerization of the C-8 methyl group.[1] The seco acid methyl ester derivative **9** of 8-epi-erythronolide was then obtained from **8** using sodium methoxide in methanol. Treatment of **9** with aqueous acetic acid gave the dioxaspiro[5.5]undecane derivative **10**.[2]

The 8-epi-spiro derivative **10** was first converted into the

[1] The epimerization at C-8 has precedent in the literature (5). It was established by the fact that **8** gives the 8-epi-spiro **10** which, when converted into 8-epi-spirocarbonate **12**, undergoes equilibration to give the more stable spirocarbonate **17** (*vide infra*).

[2] In the sequence **9** → **10**, spiroacetalization took place prior to the hydrolysis of the benzylidene protecting group because the C(11)—C(12) benzylidine derivative of **10** can be isolated as an intermediate product when the reaction is stopped before completion.

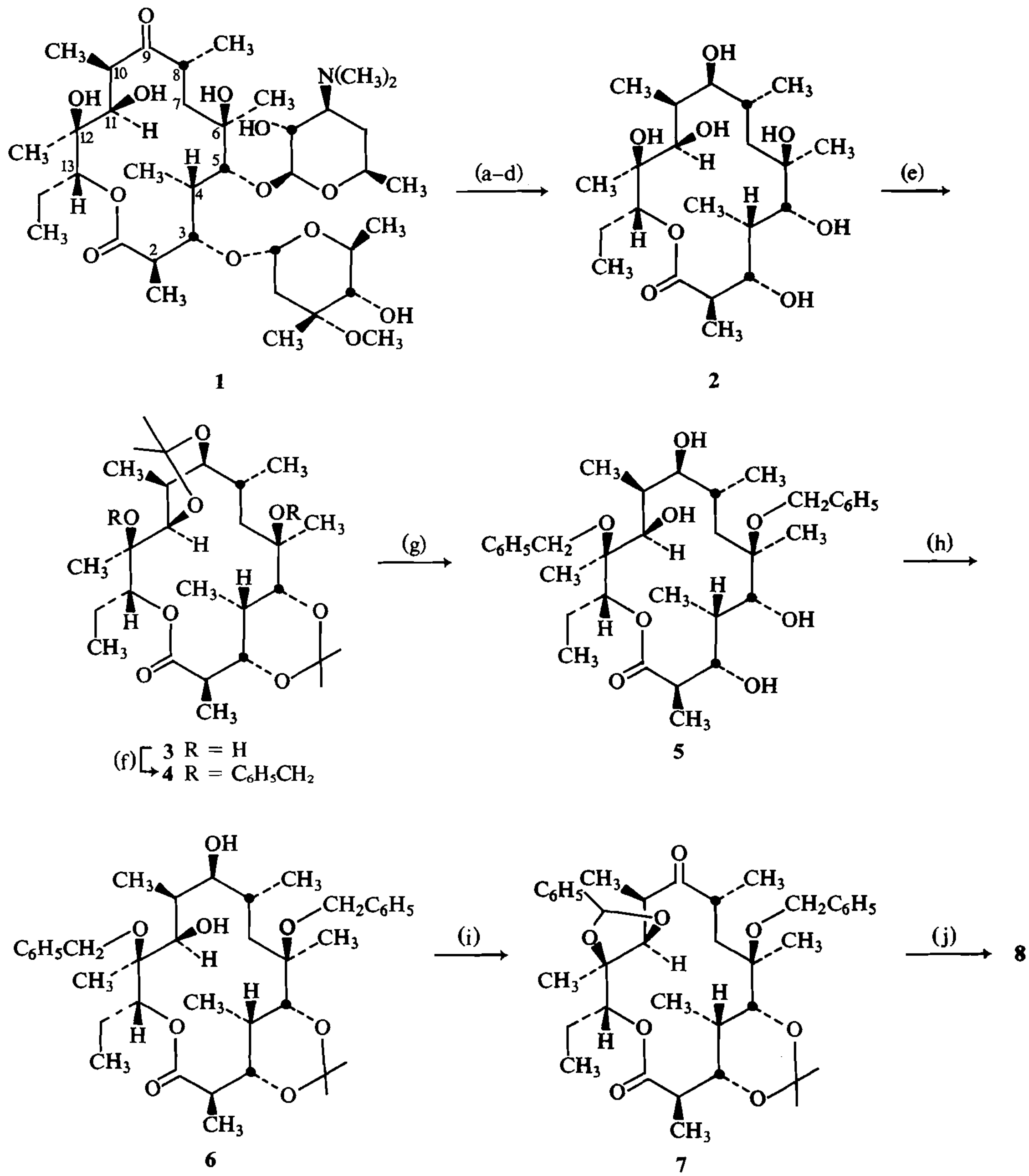

(a) H_2O_2 (3%), CH_3OH, 25°C, 24 h, 67%, ref. 2
(b) Heat at 150–155°C under vacuum, 6 h, 52%, ref. 2
(c) $NaBH_4$, isopropyl alcohol, ethyl acetate, 25°C, 2 h, 95%, ref. 2
(d) CH_3COCl (3%), CH_3OH, 25°C, 25 h, 25–65%, ref. 2
(e) 2-Methoxy propene, pyridinium tosylate, CH_2Cl_2, 25°C, 3 h, 66%, ref. 3
(f) $C_6H_5CH_2Br$, NaH, DMF, 25°C, 2.5 h, ~100%
(g) CH_3COCl (3%), CH_3OH, 25°C, 90 min, 71%
(h) HCl, acetone, Drierite, 0°C, 1 h, 95%
(i) PCC, CH_3COONa, molecular sieve 3 Å, CH_2Cl_2, 25°C, 150 min, 60%, ref. 4
(j) CH_3COOH (80%), CH_2Cl_2, ~100%

SCHEME 1

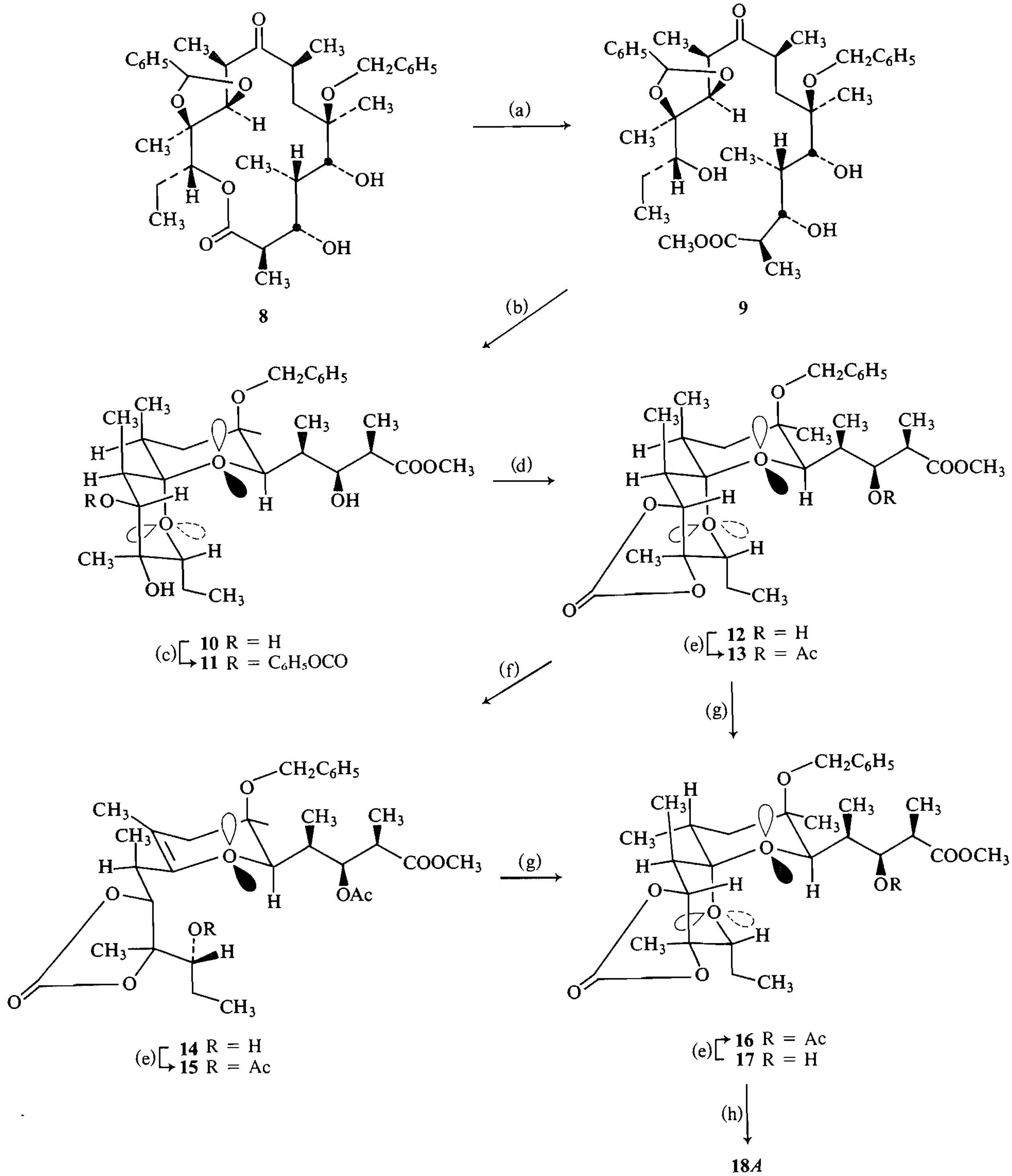

(a) CH_3ONa, CH_3OH, 25°C, 5 h, not purified
(b) CH_3COOH (80%), CH_2Cl_2, 30°C, 5 h, 70% from **8**
(c) C_6H_5OCOCl, pyridine, CH_2Cl_2, benzene, 0°C, 30 min, 82%
(d) Imidazole, toluene, 95°C → 100°C, 40 min, 98%
(e) $(CH_3CO)_2O$, $(C_2H_5)_3N$, DMAP, 25°C, 1 h, 100%
(f) $FeCl_3$, acetone, H_2O, 25°C, 15 min
(g) *p*-Toluenesulfonic acid, acetone, 25°C, 4 h, 91%
(h) K_2CO_3, CH_3OH, 25°C, 15 h, 85%

SCHEME 2

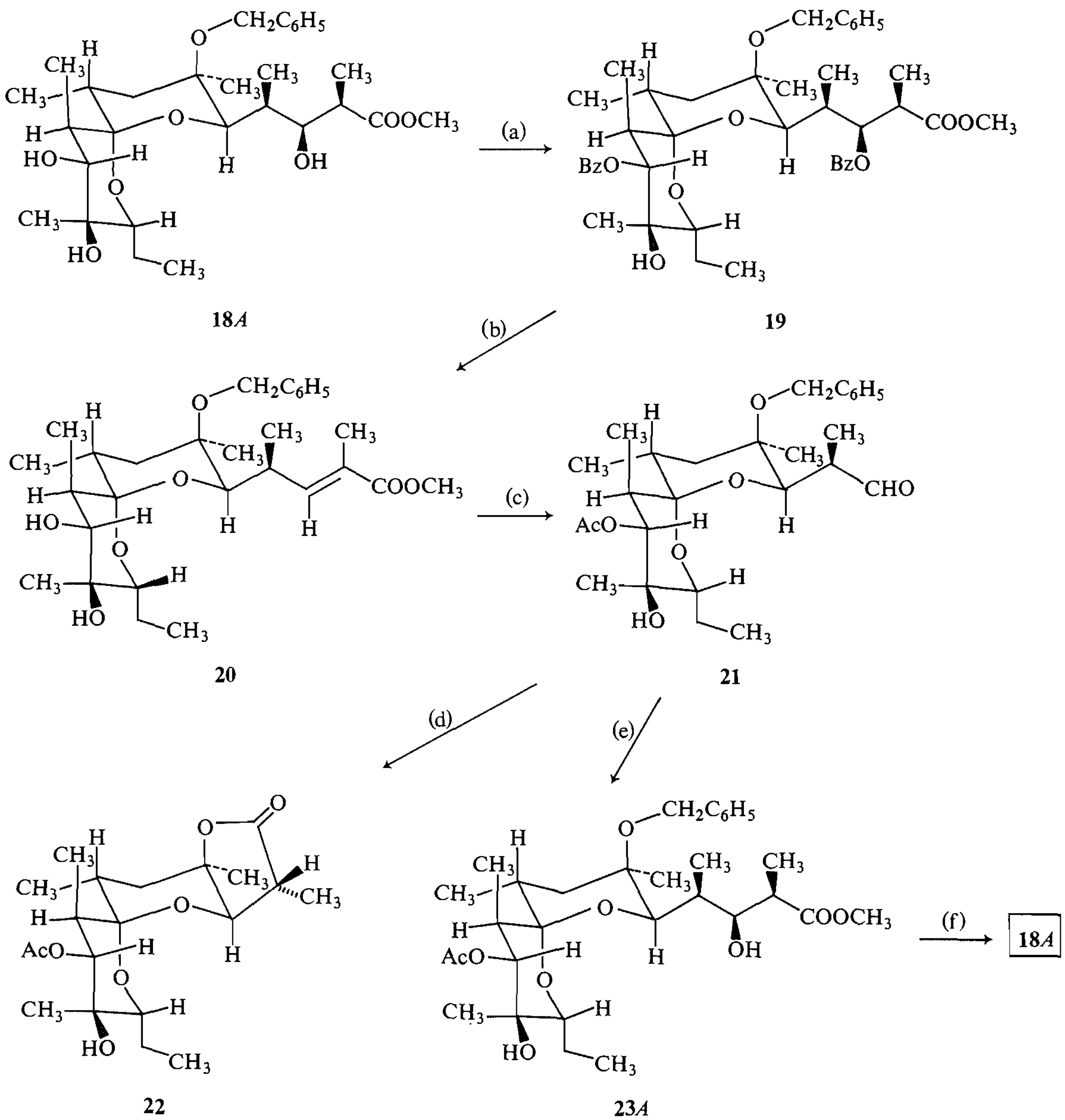

(a) C_6H_5COCl, pyridine, 70°C, 20 h, 99%
(b) CH_3ONa, CH_3OH, reflux, 2 h, 83%
(c) LAH, ether, 25°C, 90 min; $(CH_3CO)_2O$, $(C_2H_5)_3N$, DMAP, 25°C, 3 h; O_3, CH_2Cl_2, $(CH_3)_2S$, 77%
(d) Pd/C, 10%, H_2, $CH_3COOC_2H_5$, 25°C, 1 h, 100%; PCC, molecular sieve 3 Å, CH_2Cl_2, 0°C (3 min), 25°C (3 h), 100%, ref. 4
(e) $CH_3CH_2COOCH_3$, LDA, zirconocene dichloride, THF, −78°C (40 min), −78°C → −25°C (30 min), −50°C (1 h), 54%, ref. 6
(f) K_2CO_3, CH_3OH, 25°C, 1 h, 100%

SCHEME 3

C-11 phenoxycarbonate **11**, which was then transformed into the five-membered carbonate alcohol **12**. The carbonate acetate **13** obtained from **12** by acetylation yielded the substituted dihydropyran **14** on reaction with ferric chloride in wet acetone. Acetylation of **14** gave diacetate **15**. Spiroacetalization of **14** with *p*-toluenesulfonic acid in acetone gave the dioxaspiro[5.5]undecane acetate derivative **16**, having a configuration for the C-8 methyl group corresponding to that of erythromycin A. Also, on treatment with *p*-toluenesulfonic acid in acetone, 8-epi-spirocarbonate alcohol **12** can be directly converted in one step into the spirocarbonate alcohol **17**. Acetylation of **17** gave also **16**. Finally, mild basic hydrolysis of **17** with potassium carbonate in methanol provided the dioxaspiro-[5.5]undecane derivative **18***A* (Scheme 3) of the seco acid methyl ester of erythronolide A.

Degradation of the side chain of **18***A* was carried out in the following manner: **18***A* was first converted into the 3,11-dibenzoate **19**, which on treatment with sodium methoxide gave the conjugated methyl ester **20**.[3] Reduction of **20** with LAH, followed successively by acetylation and ozonolysis, gave spiro acetatealdehyde **21**. Hydrogenolysis of the benzyl ether group of **21** followed by oxidation gave spirolactone **22**. The spiro acetate-aldehyde **21** was also reacted with the zirconium enolate of methyl propionate (6, 7) to yield the adduct **23***A* and its C-2 epimer **23***B* (not shown), in a 10:1 ratio, which were separated by chromatography. Treatment of **23***A* with potassium carbonate in methanol gave spiro compound **18***A*.

Acknowledgements

This work was financially supported by the Natural Sciences and Engineering Research Council of Canada (NSERCC) and by the "Gouvernement du Québec: Science et Technologie" (FCAR). An unrestricted grant from Merck Frosst Canada Inc. was also used to support this work.

[3] A small quantity of the C-2 epimer **18***B* (not shown) of **18***A* was also isolated from this reaction.

1. M. V. SIGAL, JR., P. F. WILEY, K. GERZON, E. H. FLYNN, U. CAROL QUARCK, and O. WEAVER. J. Am. Chem. Soc. **78**, 388 (1956).
2. P. H. JONES and E. K. ROWLEY. J. Org. Chem. **33**, 665 (1968).
3. M. MIYASHITA, A. YOSHIKOSHI, and P. A. GRIECO. J. Org. Chem. **42**, 3772 (1977).
4. (*a*) E. J. COREY and J. W. SUGGS. Tetrahedron Lett. 2647 (1975); (*b*) J. HERSCOVICI and K. ANTONAKIS. J. Chem. Soc. Chem. Commun. 561 (1980).
5. (*a*) J. TADANIER, J. R. MARTIN, R. S. EGAN, A. GOLDSTEIN, R. STANASZEK, E. HIRNER, and F. FISCHER. J. Am. Chem. Soc. **95**, 593 (1973); (*b*) J. R. MARTIN, R. S. EGAN, T. J. PERUN, and A. W. GOLDSTEIN. Tetrahedron, **29**, 935 (1973).
6. (*a*) D. A. EVANS and L. R. MCGEE. Tetrahedron Lett. **21**, 3975 (1980); (*b*) J. Am. Chem. Soc. **103**, 2876 (1981).
7. G. SAUVÉ, D. A. SCHWARTZ, L. RUEST, and P. DESLONGCHAMPS. Can. J. Chem. **62**, 2929 (1984).

Formal total synthesis of erythromycin A. Part III. Synthesis of Woodward's carbamate key intermediate from a 1,7-dioxaspiro[5.5]undecane derivative of erythronolide A

BRUNO BERNET, PAUL M. BISHOP, MAURICE CARON, TAKESHI KAWAMATA, BERNARD L. ROY, LUC RUEST, GILLES SAUVÉ, PIERRE SOUCY, AND PIERRE DESLONGCHAMPS

Laboratoire de synthèse organique, Département de Chimie, Faculté des Sciences, Université de Sherbrooke, Sherbrooke (Qué.), Canada J1K 2R1

Received June 24, 1985

BRUNO BERNET, PAUL M. BISHOP, MAURICE CARON, TAKESHI KAWAMATA, BERNARD L. ROY, LUC RUEST, GILLES SAUVÉ, PIERRE SOUCY, and PIERRE DESLONGCHAMPS. Can. J. Chem. **63**, 2818 (1985).

The spirocompound **1** which was obtained by total synthesis (Part I) and by degradation from erythromycin (Part II) was converted into carbamate product **15**, a key intermediate in the Woodward's total synthesis of erythromycin A.

BRUNO BERNET, PAUL M. BISHOP, MAURICE CARON, TAKESHI KAWAMATA, BERNARD L. ROY, LUC RUEST, GILLES SAUVÉ, PIERRE SOUCY et PIERRE DESLONGCHAMPS. Can. J. Chem. **63**, 2818 (1985).

Le composé spiro **1** obtenu par synthèse totale (Partie I) et par dégradation de l'érythromycine A (Partie II) a été transformé en carbamate **15**, un intermédiaire clé de la synthèse totale de l'érythromycine A rapportée par Woodward et ses collaborateurs.

This communication describes the conversion of the dioxaspiro[5.5]undecane derivative **1** (Scheme 1) into the carbamate derivative **15** (Scheme 2) of the seco acid methyl ester of erythronolide A. Carbamate **15** is one of the key intermediates in the course of the total synthesis of erythromycin A carried out by Woodward et al. (1).

Optically active dioxaspiro[5.5]undecane derivative **1** was prepared by total synthesis and by degradation of erythromycin A (cf. preceding communications, Part I and Part II). Compound **1** was converted selectively into the 11-phenoxy-following manner: **18***A* was first converted into the 3,11-dibenzoate **19**, which on treatment with sodium methoxide gave the conjugated methyl ester **20**.[3] Reduction of **20** with LAH, followed successively by acetylation and ozonolysis, gave spiro acetatealdehyde **21**. Hydrogenolysis of the benzyl ether group of **21** followed by oxidation gave spirolactone **22**. The spiro acetate-aldehyde **21** was also reacted with the zirconium enolate of methyl propionate (6, 7) to yield the adduct **23***A* and its C-2 epimer **23***B* (not shown), in a 10:1 ratio, which were separated by chromatography. Treatment of **23***A* with potassium carbonate in methanol gave spiro compound **18***A*.

Acknowledgements

This work was financially supported by the Natural Sciences and Engineering Research Council of Canada (NSERCC) and by the "Gouvernement du Québec: Science et Technologie" (FCAR). An unrestricted grant from Merck Frosst Canada Inc. was also used to support this work.

[3] A small quantity of the C-2 epimer **18***B* (not shown) of **18***A* was also isolated from this reaction.

1. M. V. Sigal, Jr., P. F. Wiley, K. Gerzon, E. H. Flynn, U. Carol Quarck, and O. Weaver. J. Am. Chem. Soc. **78**, 388 (1956).
2. P. H. Jones and E. K. Rowley. J. Org. Chem. **33**, 665 (1968).
3. M. Miyashita, A. Yoshikoshi, and P. A. Grieco. J. Org. Chem. **42**, 3772 (1977).
4. (*a*) E. J. Corey and J. W. Suggs. Tetrahedron Lett. 2647 (1975); (*b*) J. Herscovici and K. Antonakis. J. Chem. Soc. Chem. Commun. 561 (1980).
5. (*a*) J. Tadanier, J. R. Martin, R. S. Egan, A. Goldstein, R. Stanaszek, E. Hirner, and F. Fischer. J. Am. Chem. Soc. **95**, 593 (1973); (*b*) J. R. Martin, R. S. Egan, T. J. Perun, and A. W. Goldstein. Tetrahedron, **29**, 935 (1973).
6. (*a*) D. A. Evans and L. R. McGee. Tetrahedron Lett. **21**, 3975 (1980); (*b*) J. Am. Chem. Soc. **103**, 2876 (1981).
7. G. Sauvé, D. A. Schwartz, L. Ruest, and P. Deslongchamps. Can. J. Chem. **62**, 2929 (1984).

Formal total synthesis of erythromycin A. Part III. Synthesis of Woodward's carbamate key intermediate from a 1,7-dioxaspiro[5.5]undecane derivative of erythronolide A

Bruno Bernet, Paul M. Bishop, Maurice Caron, Takeshi Kawamata, Bernard L. Roy, Luc Ruest, Gilles Sauvé, Pierre Soucy, and Pierre Deslongchamps

Laboratoire de synthèse organique, Département de Chimie, Faculté des Sciences, Université de Sherbrooke, Sherbrooke (Qué.), Canada J1K 2R1

Received June 24, 1985

Bruno Bernet, Paul M. Bishop, Maurice Caron, Takeshi Kawamata, Bernard L. Roy, Luc Ruest, Gilles Sauvé, Pierre Soucy, and Pierre Deslongchamps. Can. J. Chem. **63**, 2818 (1985).

The spirocompound **1** which was obtained by total synthesis (Part I) and by degradation from erythromycin (Part II) was converted into carbamate product **15**, a key intermediate in the Woodward's total synthesis of erythromycin A.

Bruno Bernet, Paul M. Bishop, Maurice Caron, Takeshi Kawamata, Bernard L. Roy, Luc Ruest, Gilles Sauvé, Pierre Soucy et Pierre Deslongchamps. Can. J. Chem. **63**, 2818 (1985).

Le composé spiro **1** obtenu par synthèse totale (Partie I) et par dégradation de l'érythromycine A (Partie II) a été transformé en carbamate **15**, un intermédiaire clé de la synthèse totale de l'érythromycine A rapportée par Woodward et ses collaborateurs.

This communication describes the conversion of the dioxaspiro[5.5]undecane derivative **1** (Scheme 1) into the carbamate derivative **15** (Scheme 2) of the seco acid methyl ester of erythronolide A. Carbamate **15** is one of the key intermediates in the course of the total synthesis of erythromycin A carried out by Woodward et al. (1).

Optically active dioxaspiro[5.5]undecane derivative **1** was prepared by total synthesis and by degradation of erythromycin A (cf. preceding communications, Part I and Part II). Compound **1** was converted selectively into the 11-phenoxy-

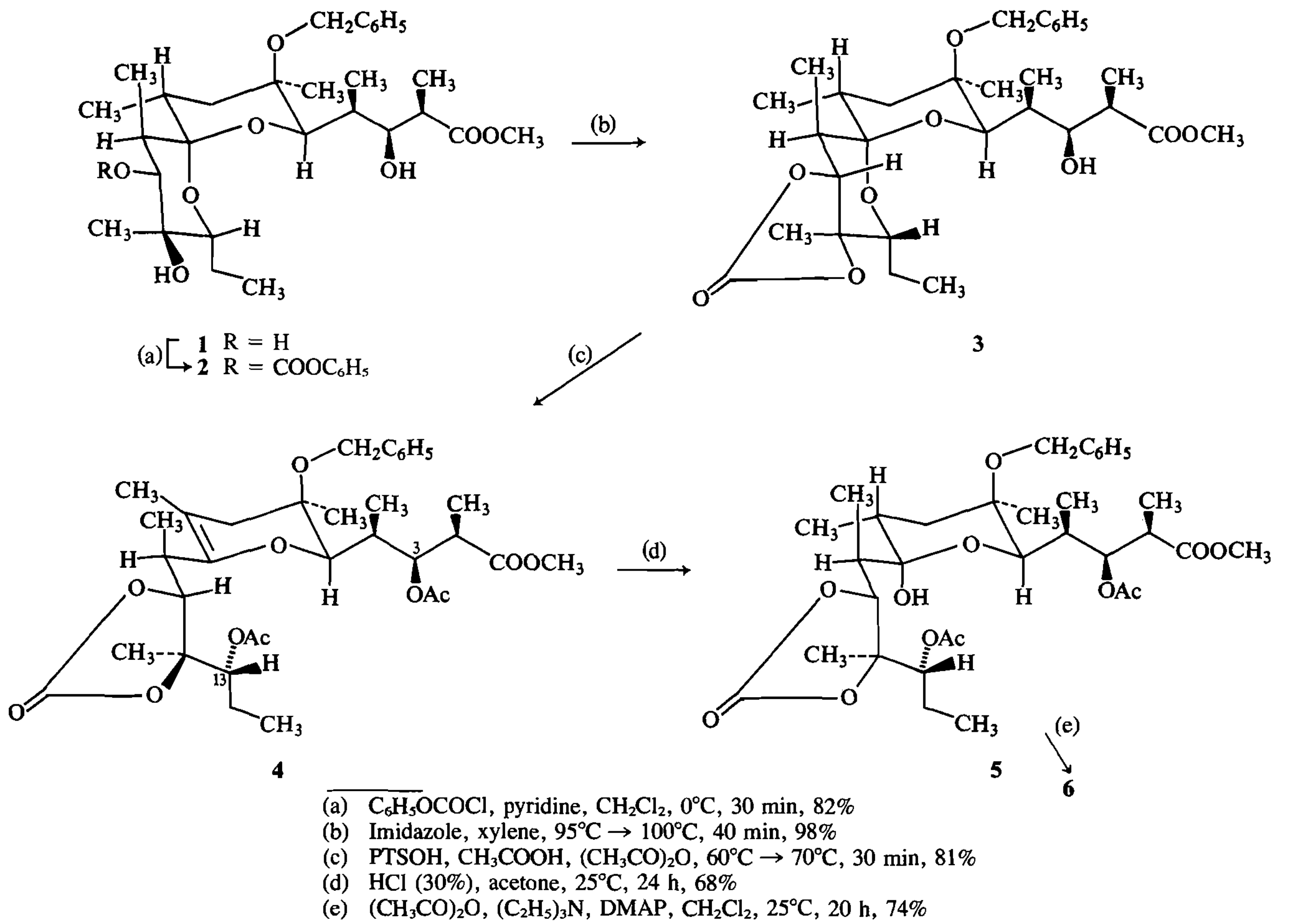

SCHEME 1

carbonate **2**, which was then transformed into the five-membered carbonate derivative **3**.[1]

On treatment of intermediate **3** with *p*-toluenesulfonic acid in a mixture of acetic acid and acetic anhydride, spiroketal ring opening and acetylation took place to yield the substituted dihydropyran 3,13-diacetate **4**.[1] On treatment with 30% hydrochloric acid in acetone, hydration of the tetrasubstituted enol ether in **4** occurred to produce the hemi-ketal **5**.[2,3] Opening of the second ring of the spiroketal was readily achieved by treating hemi-ketal **5** under acetylating conditions, which gave the 6-benzyl 11,12-carbonate 3,5,13-triacetate derivative **6** (Scheme 2) of erythronolide A seco acid methyl ester.

Reduction with sodium borohydride of the ketone function in **6** gave a mixture of 9*R* alcohol **7***A* and the epimeric 9*S* alcohol **7***B* (not shown), in a 2:1 ratio, which were separated by chromatography. The 9*R* alcohol **7***A* was then converted into the 9*S* secondary amine **10** via the intermediate formation of the mesylate **8** and the azide **9** (3). On heating compound **10** in benzene, transacylation between the secondary amino group and the carbonate took place to produce the 6-benzyl 3,5,13-triacetate carbamate derivative **11**.

The next task consisted in removing the benzyl group at C-6 and the triacetate groups at C-3, C-5, and C-13 in order to obtain the Woodward's carbamate intermediate **15**. This could not be achieved directly in two steps and it was found that the methyl ester has to be removed prior to the hydrolysis of the acetate groups. Treatment of compound **11** with lithium iodide in pyridine (4) gave the carboxylic acid **12**, which produced, on basic hydrolysis with sodium hydroxide, the corresponding tetraol carboxylic acid **13**. Esterification of **13** with diazomethane gave the methyl ester **14** which, upon hydrogenolysis with palladium/charcoal, yielded the 9,11-carbamate deriva-

[1] This compound was also prepared by a different route from erythromycin A (cf. Part II).

[2] Compound **5** was produced with totally synthetic material as well as with material obtained by degradation of erythromycin A. The remaining work (**5** → **16**) was carried out with material derived from the degradation of erythromycin A.

[3] Stereochemical assignment at C-8 and C-9 was made on the basis that the most stable isomer is expected to be produced under those conditions and by taking into account the principle of stereoelectronic control (2).

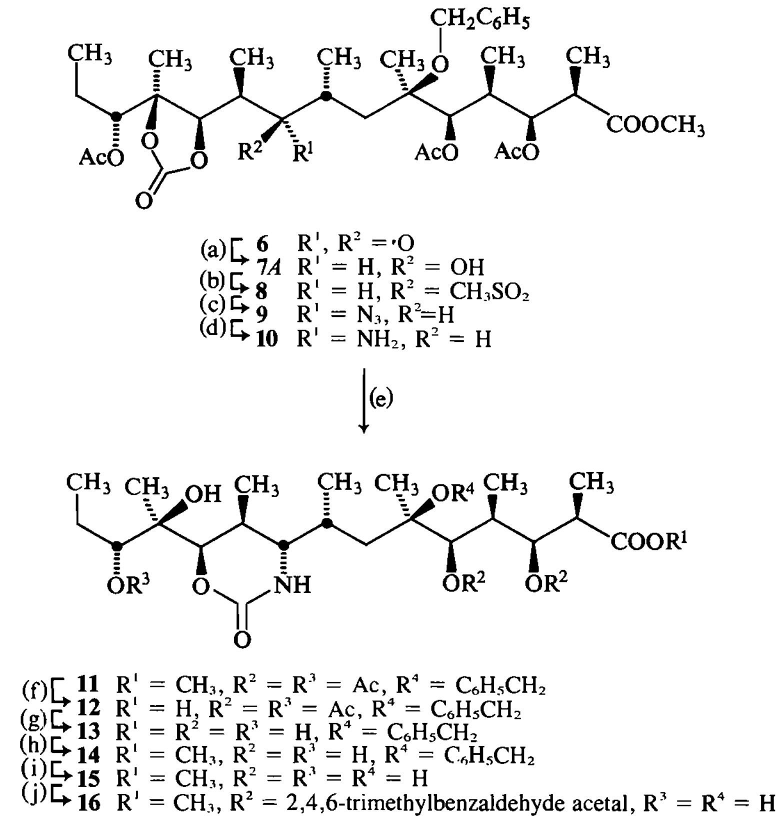

(a) $NaBH_4$, THF, CH_3OH, 25°C, 90 min, 72% yield of *7A* and *7B* (ratio 66:34)
(b) CH_3SO_2Cl, pyridine, 0°C, 20 h, 100%
(c) LiN_3, HMPA, 60°C, 1 h, 91%, ref. 3
(d) PtO_2, H_2, THF, 25°C, 3h, 100%
(e) Benzene, reflux, 120 h, 76%
(f) LiI, pyridine, reflux, 122 h, ref. 4
(g) NaOH 1 *N*, CH_3OH, 25°C, 70 h
(h) CH_2N_2, $CHCl_3$–ether, 25°C, 10 min, 60% yield from **11**
(i) Pd/C (10%), H_2, $CH_3COOC_2H_5$, 25°C, 11 h, 30 min, 85%
(j) Dimethyl acetal of mesitaldehyde, CF_3COOH (cat.), CH_2Cl_2, 0°C, 116 h, 40%, ref. 1

SCHEME 2

tive **15**. Compound **15** was found to be identical[4] with an authentic sample[5] (1) of the 9,11-carbamate derivative of 9*S*-amino-erythronolide A seco acid methyl ester. Acetalization of **15** with mesitaldehyde dimethyl acetal gave the corresponding benzylidene **16**, which was also found to be identical with an authentic sample (1).

Acknowledgements

This work was financially supported by the Natural Sciences and Engineering Research Council of Canada (NSERCC) and by the "Gouvernement du Québec: Science et Technologie" (FCAR). An unrestricted grant from Merck Frosst Canada Inc. was also used to support this work.

1. R. B. WOODWARD, E. LOGUSCH, K. P. NAMBIAR, K. SAKAN, D. E. WARD, B.-W. AU-YEUNG, P. BALARAM, L. J. BROWNE, P. J. CARD, C. H. CHEN, R. B. CHÊNEVERT, A. FLIRI, K. FROBEL, H.-J. GAIS, D. G. GARRATT, K. HAYAKAWA, W. HEGGIE, D. P. HESSON, D. HOPPE, I. HOPPE, J. A. HYATT, D. IKEDA, P. A. JACOBI, K. S. KIM, Y. KOBUKE, K. KOJIMA, K. KROWICKI, V. J. LEE, T. LEUTERT, S. MALCHENKO, J. MARTENS, R. S. MATTHEWS, B. S. ONG, J. B. PRESS, T. V. RAJAN BABU, G. ROUSSEAU, H. M. SAUTER, M. SUZUKI, K. TATSUTA, L. M. TOLBERT, E. A. TRUESDALE, I. UCHIDA, Y. UEDA, T. UYEHARA, A. T. VASELLA, W. C. VLADUCHICK, P. A. WADE, R. M. WILLIAMS, and H. N.-C. WONG. J. Am. Chem. Soc. **103**, 3210 (1981); **103**, 3213 (1981); **103**, 3215 (1981).
2. P. DESLONGCHAMPS. *In* Stereoelectronic effects in organic chemistry. Vol. 1: Organic Chemistry Series. *Edited by* Pergamon Press, Oxford, England. 1983. Chapt. 2.
3. M. C. WU, L. ANDERSON, C. W. SLIFE, and L. J. JENSEN. J. Org. Chem. **39**, 3014 (1974).
4. U. KERB, G. SCHULZ, P. HOCKS, R. WIECHERT, A. FURLENMEIER, A. FÜRST, A. LANGEMANN, and G. WALDVOGEL. Helv. Chim. Acta, **49**, 1601 (1966).

[4] Melting point 164–165°C, mixture mp 164.5–165.5°C, identical ir, 250-MHz ^{1}H nmr, and tlc.
[5] This sample was kindly provided by the late Dr. K. Sakan.

978

Disproportionation of HDS in the liquid phase[1]

JAMES D. HALLIDAY AND PATRICK E. BINDNER
Physical Chemistry Branch, Atomic Energy of Canada Limited Research Company, Chalk River Nuclear Laboratories, Chalk River, Ont., Canada K0J 1J0

Received December 12, 1984

JAMES D. HALLIDAY and PATRICK E. BINDNER. Can. J. Chem. **63**, 2821 (1985).

The deuteron–proton liquid phase isotopic disproportionation constant in hydrogen sulphide, K_l, defined for the equilibrium

$$D_2S_l + H_2S_l \overset{K_l}{\rightleftharpoons} 2HDS$$

has been measured at 25.7°C. The value of K_l was 3.99±0.11, based upon direct measurements of the concentrations of the three molecular species H_2S, HDS, and D_2S by ^1H and ^2H nuclear magnetic resonance spectroscopy (nmr) of carefully purified samples. This compares with the theoretical vapour phase isotopic distribution constant K_v = 3.92, calculated from ideal gas vapour phase isotopic partition function ratios (1, 2).

JAMES D. HALLIDAY et PATRICK E. BINDNER. Can. J. Chem. **63**, 2821 (1985).

Opérant en phase liquid et à 27,5°C, on a mesuré la constante de dismutation isotopique deutéron–proton, K_l, dans le sulfure d'hydrogène; cette constante est définie par l'équilibre suivant:

$$D_2S_l + H_2S_l \overset{K_l}{\rightleftharpoons} 2HDS$$

La valeur de K_l est égale à 3,99 ± 0,11 si l'on se base sur des mesures directes des concentrations des trois espèces moléculaires H_2S, HDS et D_2S effectuées par spectroscopie rmn du ^1H et du ^2H sur des échantillons soigneusement purifiés. Cette valeur se compare à la constante de distribution isotopique théorique en phase vapeur, K_v = 3,92, calculée (1, 2) à partir des rapports des fonctions de partition isotopique idéales en phase vapeur.

[Tradiuit par le journal]

Introduction

A literature survey showed that the isotopic disproportionation constant for liquid HDS, K_l, represented by reaction [1], has not been experimentally determined, although a value for the comparable constant for the H_2O/D_2O system has been reported (3).

$$[1] \quad H_2S_l + D_2S_l \overset{K_l}{\rightleftharpoons} 2HDS$$

where $K_l = [HDS]_l^2/[H_2S]_l[D_2S]_l$. These equilibria are of considerable interest in that they are not subject to deviation (4, 5) from the Born–Oppenheimer (B.O.) approximation (6), generally taken as the framework for calculation of partition functions. Theoretical studies using isotopic partition function ratios to determine the isotope effect on vapour phase chemical equilibria have been done by Urey, and Bigeleisen and Mayer (1) and the theory has been recently compiled in functional form by Wolfsberg (2). Deviations from the B.O. approximation tend to reduce the equilibrium constants of exchange reactions between different molecular species (by as much as 2% for exchange between H_2 and H_2O (7)). However, Wolfsberg has shown that disproportionation reactions such as [1] are not subject to this phenomenon.

Although liquid phase disproportionation constants have not been measured, an experimental determination of the vapour phase isotopic distribution constant, K_v, for H_2S/D_2S by Pyper and Newbury (8) using a pulsed molecular beam quadrupole mass filter has yielded a value of 3.88±0.03 at 24.0±0.4 °C. This is in good agreement with the calculated value of 3.919 from Wolfsberg's [2] formulations which have been used to produce the theoretical values of K_v as a function of temperature shown in Fig. 1.

Application of the rule of the mean, to convert from vapour phase to liquid phase, gives $K_l = K_v$ for this system, eq. [2].

$$[2] \quad K_l = K_v \frac{P^0_{H_2S}\, P^0_{D_2S}}{P^0_{HDS}\, P^0_{HDS}} = K_v \frac{P^0_{H_2S}}{(P^0_{H_2S}P^0_{D_2S})^{0.5}} \frac{P^0_{D_2S}}{(P^0_{H_2S}P^0_{D_2S})^{0.5}} = K_v$$

where the P^0's are the saturation vapour pressure of each species (9) indicated by the subscripts.

Although deviations from the B.O. approximation are not expected in this system, experimental values may be different owing to departures from the rule of the mean. For the H_2O/D_2O (10) system, this departure leads to the K_l being 1.5% greater than K_v for water. Hence a similar deviation may be anticipated for the H_2S/D_2S system. Any attempt to verify this hypothesis requires a direct measurement of the liquid phase isotopic distribution constant. Nuclear magnetic resonance was the obvious choice since it does not perturb the equilibrium. Gold and Tomlinson (3) used it for the H_2O/D_2O system and found K_l = 3.94±0.12. However, all published nmr spectra for isotopic mixtures of H_2S/D_2S have not shown complete resolution of the lines for the HDS component (11, 12), a triplet for ^1H and a doublet for ^2H. We have shown that chemical exchange with trace impurities determines the linewidths in these solutions and consequently highly purified H_2S/D_2S samples can be used to obtain direct measurement of the liquid phase isotopic distribution constant, K_l, by nmr.

Experimental

Care had to be exercised in handling these poisonous samples of hydrogen sulphide in glass apparatus because at 25.7°C the vapour pressure above the liquid is 2.2 MPa (21.4 atm). The commercially obtained H_2S (Air Products) and D_2S (>98 atom percent; Merck, Sharp and Dohme) were purified by distillation from their lecture bottles at dry ice temperature into glass storage flasks. Known quantities of these gases (from calibrated volumes and pressures measured

[1]AECL No. 8860.

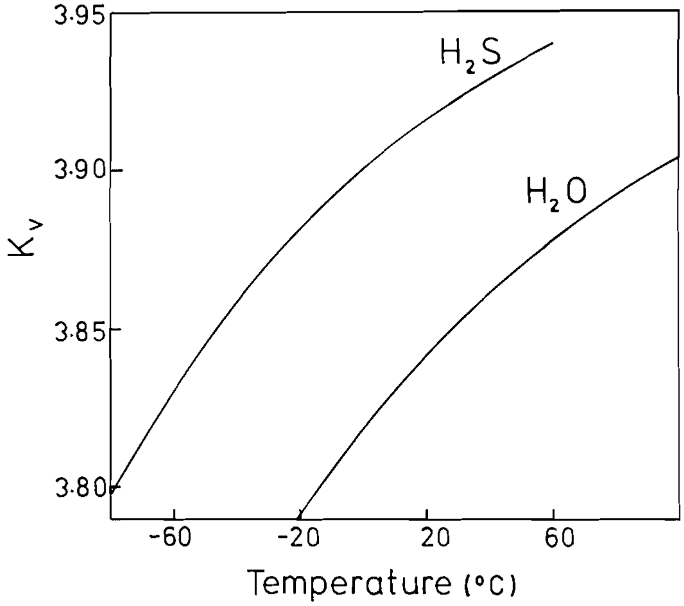

FIG. 1. Theoretical values of K_v for H_2S and H_2O calculated by Wolfsberg's isotopic partition function method (2) as a function of temperature.

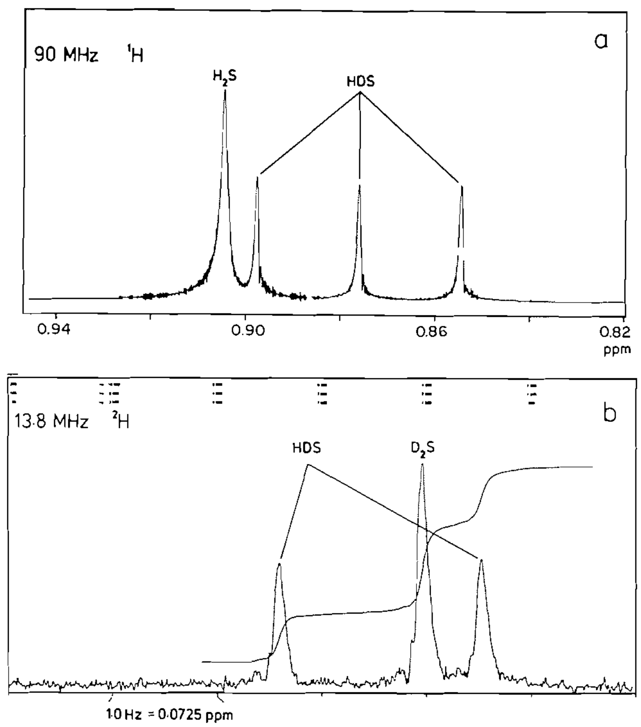

FIG. 2. (*a*) 90 MHz ^{1}H and (*b*) 13.8 MHz ^{2}H nmr spectra of a liquid phase isotopically equilibrated 1 : 1 H_2S/D_2S mixture at 25.7°C; J_{HDS} = 1.94 Hz; isotope shift (centre of HDS multiplet to H_2S singlet) = 2.56 Hz. The spectrum integral is also shown in (*b*).

with an MKS 1000 Torr electronic pressure transducer) were cryodistilled into a medium wall nmr tube (Wilmad 524) equipped with a valve. A 5 mm O-ring joint replaced the tapered one in the original design of the valved nmr tube (14). Tetramethylsilane (1%) was added to the H_2S/D_2S samples to provide a proton lock signal. All the glassware used in these experiments was pretreated by heating at 400°C for several hours to remove any exchangeable protons. This preparation technique consistently yielded nmr samples with well resolved HDS resonances (Fig. 2). Owing to the very small self-

TABLE 1. ^{1}H nmr parameters for an equilibrated 1 : 1 mixture of H_2S/D_2S (25.7°C)

Isotopic shift	2.56 Hz
Coupling constant (J_{HSD})	1.94 Hz

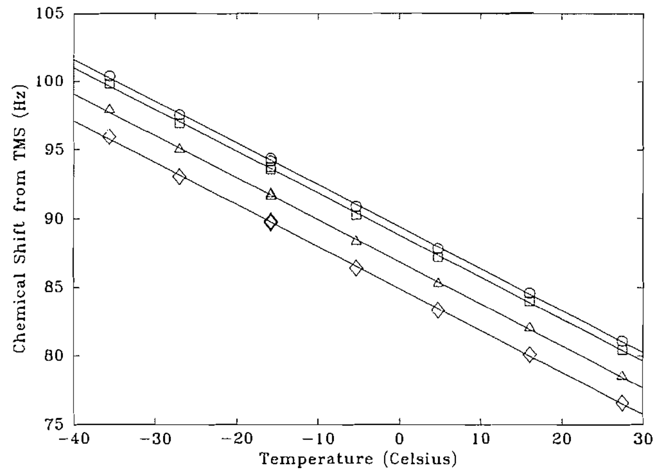

FIG. 3. Temperature dependence of the chemical shifts of the H_2S singlet and HDS triplet (Fig. 2) from TMS: ○, H_2S singlet; △, □, ⬡, HDS triplet individual lines.

protolysis constant for H_2S (2.5×10^{-33} (13)) and the removal of most exchange-causing impurities the rate of isotopic equilibration in the nmr tubes at room temperature was slow. Half-lives for equilibration in different samples were determined to be as long as 24 h.

^{1}H nmr spectra (90 MHz) were obtained on a CW Bruker HX90 spectrometer equipped with a Nicolet 1174 signal averager and a Bruker B-ST 100/700 variable temperature controller. ^{2}H nmr spectra (13.8 MHz) were also obtained on the HX90 and on a FT Bruker WH90 spectrometer in the Chemistry Department, McMaster University.

Results and discussion

(A) Temperature dependence of the hydrogen sulphide nmr spectra

The nmr parameters determined from the proton spectra in this study are summarized in Table 1. The isotopic shift was measured from the centre of the HDS multiplet (Fig. 2) to the H_2S singlet. The temperature dependence of the ^{1}H spectra was also recorded over the range 27.5 to −35.6°C. The chemical shift of the H_2S resonance with respect to TMS, Y_{H_2S}, as a function of temperature, t (°C) (Fig. 3), can be represented by

$$[3] \quad Y_{H_2S} = -0.3049t + 89.4142$$

The chemical shift of the centre line of the HDS triplet with respect to TMS, Y_{HDS}, as a function of t (°C) can be represented by

$$[4] \quad Y_{HDS} = -0.3057t + 86.8557$$

The temperature dependence of the isotopic shift, based on the slopes given in eqs. [3] and [4] is 0.0008±0.0004 Hz/°C. There was no observable temperature effect on the coupling constant J_{HSD}.

(B) Determination of the isotopic disproportionation constant

If the equation for the liquid phase isotopic disproportionation constant [1] is rearranged, i.e.,

$$[5] \quad K_l = [HDS]_l^2/[HDS]_l[D_2S]_l = \frac{[HDS]_l}{[H_2S]_l}\frac{[HDS]_l}{[D_2S]_l} = R_1R_2$$

K_l can be determined from the measurement of the two isotopic species ratios, R_1 by ^1H nmr and R_2 by ^2H nmr, independent of the starting concentrations of the protiated and deuterated species. An accurate determination of the starting concentrations for H_2S and D_2S for the small volume required for nmr measurements is difficult so this double ratio technique has a significant accuracy advantage over measuring only the protiated ratio and calculating the D_2S concentration. R_1 and R_2 for the approximately 1:1 mixture of H_2S and D_2S have been determined at 25.7°C as 1.860 ± 0.018 (26 determinations) and 2.144 ± 0.056 (14 determinations), respectively. The value calculated for K_l is 3.99 ± 0.11 (25.7°C). This measured value of K_l compares to $K_v = 3.920$ (25.7°C) calculated from Wolfsberg's isotopic partition function ratios method (2) (Fig. 1) and indicates that the deviation from the rule of the mean is as great as that found in the H_2O/D_2O system (10). However, the magnitude of the uncertainty in the measurement precludes any further discussion on deviations from the rule of the mean and the temperature dependence of K_l for comparison with that for K_v (Fig. 1).

The magnitudes of the errors in these measurements require some explanation. Firstly, on the CW HX90 spectrometer the very narrow nmr lines required long sweep times (5000 s) to avoid sweep distortions and low rf power levels to prevent saturation effects. Maintenance of a stable lock line over this time scale in these samples on our spectrometer was difficult, and spectrometer instabilities caused variations in the spectra. Secondly, on the WH90 spectrometer the internal deuterium lock saturated the deuteron signal from the D_2S and the external lock had field instabilities greater than the linewidth of the deuterons in the sample. As a result signal averaging could not be accomplished and the S/N obtainable from the Fourier transformation of a single free induction decay had to be used. The statistical error is principally due to the ^2H nmr measurements and, given a more stable spectrometer setup, could be improved upon. However, our measured K_l is comparable in accuracy to that for H_2O (3) and shows that nmr is capable of making this kind of determination in the liquid phase H_2S/D_2S system.

Acknowledgements

The authors would like to thank Dr. J. H. Rolston for helpful discussions and Mr. B. Sayer, McMaster University, for operating the WH90 spectrometer.

1. (*a*) H. C. UREY. J. Chem. Soc. 562 (1947); (*b*) J. BIGELEISEN and M. G. MAYER. J. Chem. Phys. **15**, 261 (1947).
2. J. BRON, C. F. CHANG, and M. WOLFSBERG. Z. Naturforsch. **28**A, 129 (1973).
3. V. GOLD and C. TOMLINSON. J. Chem. Soc. Chem. Commun. 472 (1970).
4. R. D. BARDO and M. WOLFSBERG. J. Chem. Phys. **62**, 4555 (1975).
5. L. I. KLEINMANN and M. WOLFSBERG. J. Chem. Phys. **59**, 2043 (1973).
6. M. BORN and R. OPPENHEIMER. Ann. Phys. Leipiz, **84**, 457 (1927).
7. J. H. ROLSTON and K. L. GALE. J. Phys. Chem. **86**, 2494 (1982).
8. J. W. PYPER and R. S. NEWBURY. J. Chem. Phys. **52**, 1966 (1970).
9. E. C. W. CLARKE and D. N. GLEW. Can. J. Chem. **48**, 764 (1970).
10. W. A. VAN HOOK. J. Chem. Soc. Chem. Commun. 479 (1972).
11. K. TAKAHASHI and G. HAZATO. Bull. Chem. Soc. Jpn. **38**, 1807 (1965).
12. H. SCHMIDBAUR and W. SIEBERT. Chem. Ber. **97**, 2090 (1964).
13. G. JANDER. Die Chemie in Wasserahnlichen Losungsmitteln. Springer Verlag, Berlin 1949. p. 102.
14. S. MOHANTY and H. J. BERNSTEIN. J. Chem. Phys. **54**, 2254 (1971).

Excess volumes and excess viscosities of binary liquid mixtures: methylisobutylketone + benzene, toluene, chlorobenzene, bromobenzene, and nitrobenzene

T. JAYALAKSHMI AND KALLURU S. REDDY
Department of Chemistry, S. V. University, Tirupati, India

Received August 15, 1984[1]

T. JAYALAKSHMI and KALLURU S. REDDY. Can. J. Chem. **63**, 2824 (1985).

Excess volumes for the binary liquid mixtures of methylisobutylketone with benzene, toluene, chlorobenzene, bromobenzene, and nitrobenzene have been measured at 303.15 and 313.15 K. Excess volumes were negative for all the systems over the entire range of composition and at both the temperatures. The behaviour of V^E as a function of composition and temperature was studied. Viscosity data have also been determined for the five systems at 303.15 K. The excess viscosity, $\Delta \ln \eta$, has been calculated and its behaviour as a function of composition was investigated. The results of V^E and $\Delta \ln \eta$ have been discussed in terms of dipole − induced dipole and dipole−dipole interactions between the components. V^E and $\Delta \ln \eta$ were analysed in the light of Prigogine−Patterson−Flory equation of state theory and Bloomfield and Dewan's viscosity relations.

T. JAYALAKSHMI et KALLURU S. REDDY. Can. J. Chem. **63**, 2824 (1985).

Opérant à 303,15, et 313,15 K, on a mesuré les volumes en excès de mélanges liquides binaires de méthylisobutylcétone avec le benzène, le toluène, le chlorobenzène, le bromobenzène et le nitrobenzène. A toutes les compositions et aux deux températures utilisées, les volumes en excès de tous les systèmes sont négatifs. On a étudié le comportement de V^E en fonction de la composition et de la température. Opérant à 303,15 K, on a également obtenu des données relatives à la viscosité des cinq systèmes. On a calculé la viscosité en excès, $\Delta \ln \eta$, et l'on a étudié son comportement en fonction de la composition du mélange. On discute des résultats relatifs à V^E et de $\Delta \ln \eta$ en fonction d'interactions dipôle − dipôle induit et dipôle−dipôle entre les composants. On a analysé les valeurs de V^E et de $\Delta \ln \eta$ à la lumière de l'équation de la théorie d'état de Prigogine−Patterson−Flory et des relations de viscosité de Bloomfield et de Dewan.

[Traduit par le journal]

Introduction

As a part of a study on thermodynamic and physical properties of binary liquid mixtures containing aliphatic ketone as one of the components (1−4), we have reported here excess volumes and viscosities for five binary liquid mixtures. Excess volumes at 303.15 and 313.15 K and viscosities at 303.15 K have been measured for methylisobutylketone (MIBK) with benzene, toluene, chlorobenzene, bromobenzene, and nitrobenzene and the molecular interactions in these systems have been investigated. The systems have been selected with a view to study the effect of molecular interactions due to substitution of different groups on the phenyl ring. Further, a literature survey revealed that the two properties have not been studied for the five systems.

Prigogine−Patterson−Flory equation of state theory developed on the basis of van der Waals model for energy (5) has been applied quite successfully to predict excess volumes (6−9). Patterson (7, 8) has stressed the importance of cohesive energy factor in the prediction of V^E. We have applied the model for the five systems in which cohesive energy difference between the components changes gradually and V^E values are calculated using pure component parameters. Further, the viscosity expressions developed by Bloomfield and Dewan (10) have been used to obtain various contributions to excess viscosity.

Experimental

Excess volumes were measured using a dilatometer described earlier (2) and were accurate to ± 0.003 cm^3 mol^{-1}. Flow times were determined for pure liquids and liquid mixtures using an Ostwald viscometer and the values were accurate to ± 0.1 s. Densities for the pure components were measured using a bicapillary pycnometer and in case of mixtures densities were obtained from excess volumes using the relation

$$[1] \quad \rho = \frac{X_1M_1 + X_2M_2}{X_1V_1 + X_2V_2 + V^E}$$

Density values obtained from both the methods were accurate to $\pm 5 \times 10^{-5}$ g cm^{-3}. Viscosities were computed by the relative method using flow times and densities. Viscosity values were accurate to 0.5%. This dynamic viscosity is defined as a product of kinematic viscosity and density. Heat of mixing data were determined using adiabatic solution calorimeter for all the systems at 0.5 mole fraction. The results were accurate to ± 1 J/mol.

Methylisobutylketone (BDH), benzene (BDH), and toluene (BDH) were purified by the methods described earlier (3, 11). Chlorobenzene (BDH), bromobenzene (E. Merck), and nitrobenzene (BDH) were dried over calcium chloride and fractionally distilled. The purity of the samples were ascertained by comparing the values of density, boiling point, and refractive index with the literature (12).

Results and discussion

Excess volume data for the five binary mixtures measured at 303.15 and 313.15 K are presented graphically in Figs. 1 to 5. Experimental excess viscosity has been calculated using the relation

$$[2] \quad \Delta \ln \eta = \ln \eta_{mix} - (X_1 \ln \eta_1 + X_2 \ln \eta_2)$$

Excess viscosity versus mole fraction profiles are shown in Fig. 6. Excess volume and excess viscosity results are represented using the empirical equations of the form

$$[3] \quad V^E = X_1X_2[a_0 + a_1(X_1 - X_2) + a_2(X_1 - X_2)^2]$$

and

$$[4] \quad \Delta \ln \eta = X_1X_2[b_0 + b_1(X_1 - X_2) + b_2(X_1 - X_2)^2]$$

The coefficients in eqs. [3] and [4] are obtained by the method of least squares and are given in Tables 1 and 2 respectively along with the standard deviation.

[1]Revision received April 16, 1985.

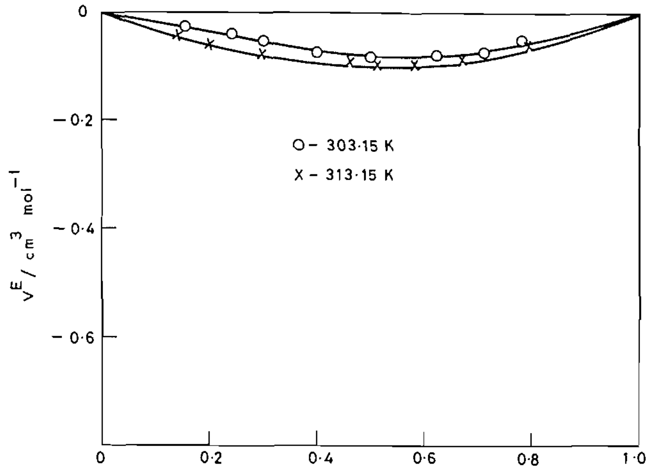

FIG. 1. Excess volume data for the methylisobutylketone and benzene binary mixture.

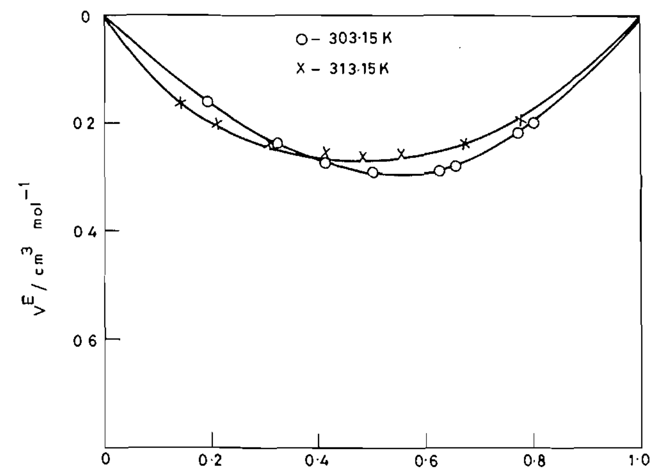

FIG. 2. Excess volume data for the methylisobutylketone and toluene binary mixture.

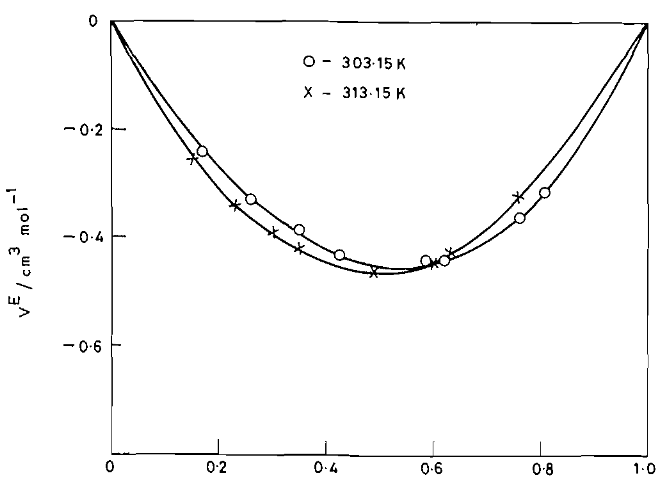

FIG. 3. Excess volume data for the methylisobutylketone and chlorobenzene binary mixture.

Excess volumes

V^E data exhibited negative deviation in all the systems over the entire range of mole fraction and at both the temperatures. The observed negative V^E values in the system methylisobutylketone with benzene may be attributed to the dominance of the interaction between ketoxy group of ketone and π-electrons of benzene over the other effects. V^E values are more negative in the system methylisobutylketone with toluene, which may be ascribed to the enhanced interaction between unlike molecules due to greater π-electron density of toluene. In the remaining systems the negative deviation in V^E is large and this behaviour may be attributed to the existence of strong dipole–dipole interaction between unlike molecules along with the n–π interaction. The algebraic values of V^E with respect to non-common component fall in the order: benzene > toluene > chlorobenzene ≈ bromobenzene > nitrobenzene. This order is similar to the order in their polarizabilities. The influence of temperature on V^E is small in the temperature interval studied: however, both positive and negative temperature coefficients are observed in these complex forming systems.

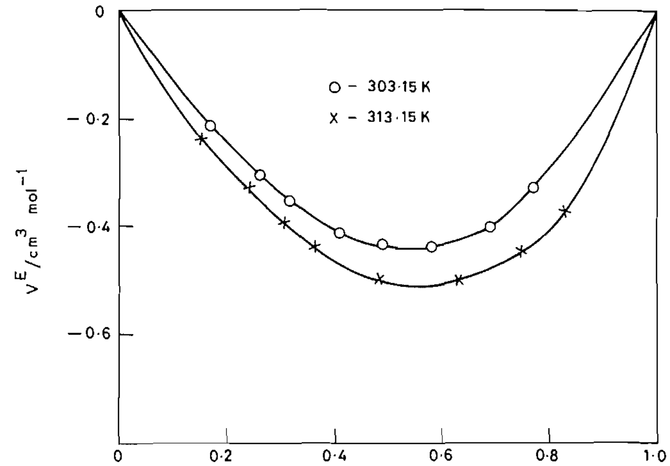

FIG. 4. Excess volume data for the methylisobutylketone and bromobenzene binary mixture.

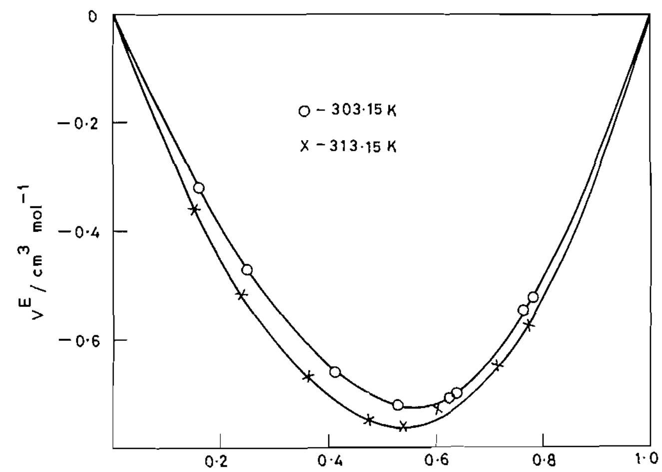

FIG. 5. Excess volume data for the methylisobutylketone and nitrobenzene binary mixture.

V^E values are predicted at 0.5 mole fraction using the following relation developed on the basis of van der Waals model [5]

$$[5]\quad \frac{V^E}{X_1V_1^* + X_2V_2^*} = \tilde{\tau}\frac{\partial\tilde{\vartheta}}{\partial\tilde{T}}\psi_1\theta_2X_{12}/P_1^* + (\tilde{\vartheta}_1 - \tilde{\vartheta}_2)(\psi_1 - \theta_1) - \frac{1}{2}\left[\frac{\tilde{\vartheta}_1 - \tilde{\vartheta}_2}{\partial\tilde{\vartheta}/\partial\tilde{T}}\right]^2\frac{\partial^2\tilde{\vartheta}}{\partial\tilde{T}^2}\{\psi_1\psi_2 + (\psi_1 - \theta_1)^2\}$$

TABLE 1. Values of the coefficients in eq. [3], number of experimental results n, and standard deviation $\sigma(V^E)$

MIBK +	T / K	n	a_0 ($cm^3\ mol^{-1}$)	a_1 ($cm^3\ mol^{-1}$)	a_2 ($cm^3\ mol^{-1}$)	$\sigma(V^E)$ ($cm^3\ mol^{-1}$)
Benzene	303.15	8	−0.3267	−0.1058	0.1571	0.003
	313.15	8	−0.4088	−0.0141	0.0584	0.002
Toluene	303.15	8	−1.1781	−0.2373	−0.0018	0.003
	313.15	8	−1.0303	0.0352	−0.5916	0.003
Chlorobenzene	303.15	8	−1.7908	−0.2707	−0.2479	0.003
	313.15	8	−1.8672	0.0901	0.0464	0.003
Bromobenzene	303.15	8	−1.7635	−0.3727	0.1438	0.003
	313.15	8	−2.0651	−0.6449	−0.3659	0.003
Nitrobenzene	303.15	8	−2.8669	−0.7289	0.0981	0.003
	313.15	8	−3.0198	−0.3811	−0.1342	0.004

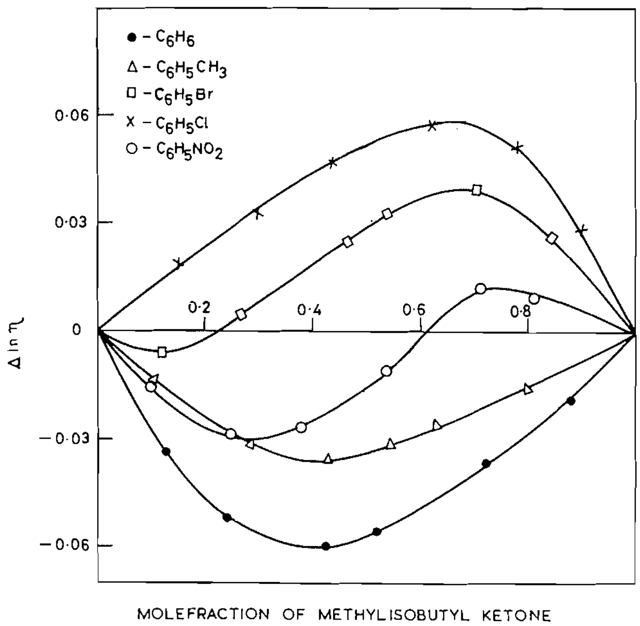

FIG. 6. Profiles of excess viscosity versus mole fraction of the binary mixtures.

The parameters in eq. [5] have their usual significance as described by Patterson and Delmas (5). The site fraction θ_2, and the interchange energy parameter X_{12} are obtained on the basis of Flory's relation (13, 14) using experimental heat of mixing data. The results of excess enthalpy are reported in Table 4. The values of the parameters of pure components are given in Table 3. The V^E value calculated from eq. [5] is a combination of three different contributions. The first term, $V^E(X_{12})$, in the equation indicates the disorder contribution to V^E due to difference in force field between unlike molecules. The contribution to V^E due to difference in internal pressure is obtained with the second term $V^E(P^*)$. The third term V^E (f.v.) is a measure of V^E contribution arises due to difference in free volume. These three contributions are given in Table 4 along with experimental and calculated V^E. The data reveal that the disorder contribution is positive in the system MIBK with nitrobenzene, this may be the reason for the negative excess viscosity observed at lower mole fraction of MIBK in this system, although its V^E values are more negative.

Excess viscosity

Excess viscosity values are negative in the systems methyl-

TABLE 2. Values of the coefficients in eq. [4], number of experimental results n, and standard deviation $\sigma(\Delta\ \ln\ \eta)$ at 303.15 K

MIBK +	n	b_0	b_1	b_2	$\sigma(\Delta\ \ln\ \eta)$
Benzene	6	−0.2309	0.0923	0.0358	0.001
Toluene	6	−0.1332	0.0467	0.0407	0.002
Chlorobenzene	6	0.2061	0.1266	0.0371	0.002
Bromobenzene	6	0.1131	0.1856	−0.0625	0.002
Nitrobenzene	6	−0.0632	0.1858	0.0648	0.003

isobutylketone with benzene and toluene and the values are positive in the system methylisobutylketone and chlorobenzene over the whole range of mole fraction. Further, excess viscosity results exhibit an inversion in sign, from negative to positive, in the systems methylisobutylketone with nitrobenzene and bromobenzene. The algebraic values of $\Delta\ \ln\ \eta$ fall in the order: benzene < toluene < nitrobenzene < bromobenzene < chlorobenzene. Negative values in excess viscosity indicate that the mixtures are more fluid than the pure components and consequently the molecular interactions between unlike molecules are weak. Positive values in excess viscosity indicate that the molecular interactions are strong. Therefore, the order in the observed excess viscosity is similar with excess volume with respect to the systems methylisobutylketone with benzene and chlorobenzene but fails in the remaining systems. The discrepancy may be explained on the basis of the significance of different contributions to $\Delta\ \ln\ \eta$ due to the difference in free volume and free energy of activation of flow (15). According to Bloomfield and Dewan (10) excess viscosity can be represented as

$$[6] \quad \Delta\ \ln\ \eta_{\text{calcd}} = \ln\ \eta_H + \ln\ \eta_S + \ln\ \eta_V$$

where

$$\ln\ \eta_H = \frac{-\Delta H}{RT}, \qquad \ln\ \eta_S = \frac{\Delta S^R}{R}$$

and

$$\ln\ \eta_V = \frac{1}{\tilde{\vartheta} - 1} - \left[\frac{X_1}{\tilde{\vartheta}_1 - 1} + \frac{X_2}{\tilde{\vartheta}_2 - 1}\right]$$

This theory is used to predict excess viscosity at 0.5 mole fraction. The reduced volume $\tilde{\vartheta}$, has been obtained from experimental V^E values. Residual entropy of mixing ΔS^R, is then calculated using $\tilde{\vartheta}$ on the basis of Flory's equations (13, 14). Experimental excess enthalpy results have been used to calculate $\ln\ \eta_H$. Experimental and calculated excess viscosity and

TABLE 3. Parameters of the pure components, coefficient of thermal expansion α, isothermal compressibility k_T, molar volume V, reduced volume $\tilde{\vartheta}$, characteristic pressure P^*, and reduced temperature $\tilde{T}$ for Flory theory

Component	T (K)	$10^3\,\alpha^a$ (deg^{-1})	k_T^b (TPa^{-1})	V (cm^3 mol^{-1})	$\tilde{\vartheta}$	V^* (cm^3 mol^{-1})	P^* (J cm^{-3})	$\tilde{T}$
MIBK	303.15	1.188	1184.9	126.59	1.289	98.22	504.9	0.06291
	313.15	1.201	1269.4	128.05	1.299	98.58	499.8	0.06426
C_6H_6	303.15	1.242	1007.0	89.81	1.299	69.12	623.4	0.06432
	313.15	1.258	1085.2	91.08	1.309	69.58	622.3	0.06557
$C_6H_5CH_3$	303.15	1.079	944.2	107.44	1.267	84.80	550.6	0.05982
	313.15	1.091	1009.8	108.61	1.277	85.05	551.6	0.06139
C_6H_5Cl	303.15	0.985	784.6	102.75	1.248	82.33	592.8	0.05704
	313.15	1.005	844.3	103.76	1.259	82.41	590.8	0.05869
C_6H_5Br	303.15	0.909	689.1	105.98	1.231	86.82	605.9	0.05436
	313.15	0.922	741.9	106.95	1.241	86.18	599.3	0.05596
$C_6H_5NO_2$	303.15	0.827	523.0	103.16	1.214	84.96	706.5	0.05155
	313.15	0.833	568.1	104.01	1.221	85.16	684.5	0.05273

[a] α values were calculated from measured density data and from literature (12, 18).
[b] k_T values were obtained from measured density, sound velocity and literature (12, 18) heat capacity data using the relation $k_T = k_S + \alpha^2 TV/C_p$ for all the components.

TABLE 4. Experimental and calculated excess volumes at 0.5 mole fraction, calculated values of the three contributions to V^E, excess enthalpy, and the interchange energy parameter

System	T (K)	V^E (cm^3 mol^{-1})	H^E (J mol^{-1})	$\theta_2 X_{12}$ (J cm^{-3})	$V^E(X_{12})$ (cm^3 mol^{-1})	$V^E(P^*)$ (cm^3 mol^{-1})	V^E (f.v.) (cm^3 mol^{-1})	V^E_{calcd} (cm^3 mol^{-1})
MIBK + C_6H_6	303.15	−0.082	−84	−1.0263	−0.042	0.042	−0.004	−0.004
	313.15	−0.102	−93	−1.1897	−0.052	0.046	−0.003	−0.009
MIBK + $C_6H_5CH_3$	303.15	−0.295	−121	−1.0549	−0.048	−0.043	−0.017	−0.108
	313.15	−0.258	−114	−1.3265	−0.054	−0.049	−0.016	−0.119
MIBK + C_6H_5Cl	303.15	−0.448	−256	−4.1411	−0.155	−0.147	−0.058	−0.360
	313.15	−0.467	−261	−4.3414	−0.174	−0.151	−0.052	−0.377
MIBK + C_6H_5Br	303.15	−0.441	−188	−3.5038	−0.122	−0.243	−0.128	−0.493
	313.15	−0.516	−202	−3.2875	−0.124	−0.242	−0.121	−0.487
MIBK + $C_6H_5NO_2$	303.15	−0.717	86	2.1182	0.064	−0.574	−0.369	−0.879
	313.15	−0.755	98	1.8574	0.062	−0.562	−0.359	−0.859

TABLE 5. Experimental and calculated excess viscosity at 0.5 mole fraction; free volume, enthalpy, entropy, and free energy contributions to excess viscosity

System	$\ln \eta_V$	$\ln \eta_H$	$\ln \eta_S$	$\ln \eta_G$	$\Delta \ln \eta_{calcd}$	$\Delta \ln \eta_{exp}$
MIBK + C_6H_6	0.021	0.033	−0.018	0.015	0.036	−0.058
MIBK + $C_6H_5CH_3$	0.026	0.048	−0.032	0.016	0.042	−0.033
MIBK + C_6H_5Cl	0.023	0.102	−0.044	0.058	0.081	0.052
MIBK + C_6H_5Br	−0.003	0.074	−0.032	0.042	0.039	0.028
MIBK + $C_6H_5NO_2$	−0.008	−0.034	−0.034	−0.064	−0.072	−0.016

the various contributions to excess viscosity are included in Table 5. An examination of the data indicates that the entropy contribution $\ln \eta_S$ is nearer to $\Delta \ln \eta_{exp}$ in the systems MIBK with benzene and toluene, $\ln \eta_V$ is close to $\Delta \ln \eta_{exp}$ in the system MIBK with nitrobenzene and the free energy contribution, $\ln \eta_G$, is close to $\Delta \ln \eta_{exp}$ in the systems MIBK with chlorobenzene and bromobenzene rather than $\Delta \ln \eta_{calcd}$ in any system. This type of behaviour is also observed in many systems earlier (4, 16, 17). The theory predicts better values in the systems studied here when considered the significance of various effects independently rather than as a combined effect.

1. K. S. REDDY, M. V. P. RAO, and P. R. NAIDU. Can. J. Chem. **54**, 2676 (1976).
2. K. S. REDDY and P. R. NAIDU. Can. J. Chem. **55**, 76 (1977).
3. K. S. REDDY and P. R. NAIDU. Aust. J. Chem. **32**, 687 (1979).
4. K. S. REDDY and P. R. NAIDU. Indian Acad. Sci. **88**A, 109 (1979).
5. D. PATTERSON and G. DELMAS. Discuss. Faraday Soc. **49**, 98 (1970).
6. G. DELMAS, P. DEST-ROMAIN, and P. PURVES. J. Chem. Soc. Faraday I, **71**, 1181 (1975).
7. D. PATTERSON and HUUTRAVAN. J. Solution Chem. **11**, 793 (1982).
8. M. COSTAS and D. PATTERSON. J. Solution Chem. **11**, 807 (1982).
9. B. RIEDL and G. DELMAS. Can. J. Chem. **61**, 1876 (1983).
10. V. A. BLOOMFIELD and R. K. DEWAN. J. Phys. Chem. **75**, 3113 (1971).
11. K. S. REDDY and P. R. NAIDU. Aust. J. Chem. **31**, 2145 (1978).
12. J. TIMMERMANS. Physico-chemical constants of pure organic

compounds. Elsevier Publishing Co., Amsterdam. 1950, 1965.
13. P. J. FLORY. J. Am. Chem. Soc. **87** 1833 (1965).
14. A. ABE and P. J. FLORY. J. Am. Chem. Soc. **87**, 1838 (1965).
15. P. B. MACEDO and T. A. LITOVITZ. J. Chem. Phys. **31**, 1164 (1965).
16. G. DELMAS, P. PURVES, and P. DEST-ROMAIN. J. Phys. Chem. **79**, 1970 (1975).
17. K. S. REDDY and P. R. NAIDU. Indian J. Chem. **20A**, 503 (1981).
18. J. A. RIDDICK and W. B. BUNGER. Organic solvents. 3rd ed. Wiley Interscience, New York. 1970.

A multinuclear (^{1}H, ^{31}P, ^{199}Hg) nuclear magnetic resonance study of some complexes of mercury(II) with ditertiary phosphines[1,2]

PHILIP A. W. DEAN[3] AND RADHEY S. SRIVASTAVA[4]
Department of Chemistry, University of Western Ontario, London, Ont., Canada N6A 5B7

Received December 6, 1984

PHILIP A. W. DEAN and RADHEY S. SRIVASTAVA. Can. J. Chem. **63**, 2829 (1985).

From $Hg(SbF_6)_2$ and an appropriate amount of the ligands $Ph_2PCHRPPh_2$ (R = H or Me), 2:2, 1:2, and 1:3 M:L complexes have been prepared in $MeNO_2$ solution and characterized by ^{1}H, ^{31}P, and ^{199}Hg nmr spectroscopy. The 2:2 complexes are ligand-bridged, as are $[Hg(Ph_2PCH_2PPh_2)(Ph_2PCHMePPh_2)Hg]^{4+}$ and $[Hg(Ph_2PCH_2PPh_2)_2Ag]^{3+}$ (prepared from $Hg(SbF_6)_2$, $Ag(AsF_6)$, or $Ag(SbF_6)$ and the ligand), examined by nmr for comparison. The complex $[Hg(\mu\text{-}Ph_2PCHMePPh_2)_2Hg]^{4+}$ exists as two isomers, which interconvert slowly on the preparative timescale. The 1:2 complexes, and the analogous mixed ligand complex are shown by their nmr spectral properties to be examples of tetrahedral bis(chelate) complexes, which are very unusual for the $Ph_2PCHRPPh_2$ ligands. In the 1:3 complexes, and the one of the two possible mixed complexes identified, both η^1- and η^2-ligands appear to be present and these undergo rapid intramolecular η^1-to-η^2 exchange. The η^1-bonding mode of $Ph_2PCH_2PPh_2$ also occurs in $[(\eta^2\text{-}Ph_2P(CH_2)_2PPh_2)Hg(\eta^1\text{-}Ph_2PCH_2PPh_2)_2]^{2+}$ and $[Hg(\eta^1\text{-}Ph_2PCH_2PPh_2)_4]^{2+}$, as evidenced by their reduced temperature ^{31}P nmr spectra in Me_2CO—$MeNO_2$.

The complex $[Hg(\eta^2\text{-}Ph_2PCH_2PPh_2)_2]^{2+}$ has ^{31}P and ^{199}Hg nmr spectral properties significantly different from those of its acyclic analog $[Hg(PMePh_2)_4]^{2+}$. To place this anomaly in perspective, the ^{31}P and ^{199}Hg nmr spectra of a much wider series of new bis(chelate) complexes $[Hg(LL)(L'L')]^{2+}$ have been obtained, with the ligand combinations LL = L'L' = $Ph_2PNPhPPh_2$; LL = dppm, L'L' = $Ph_2PNPhPPh_2$; LL = L'L' = $Ph_2P(CH_2)_nPPh_2$(n = 2−4); LL = $Ph_2P(CH_2)_mPPh_2$, L'L' = $Ph_2P(CH_2)_nPPh_2$ ($m \neq n$; m = 1−3, n = 1−5). From the data for the last two series, it is found that only the bis(chelate) complex of $Ph_2PCH_2PPh_2$ shows a large anomaly in its ^{199}Hg chemical shift (anomalously high shielding), and that in $[Hg(LL)(L'L')]^{2+}$ values of ^2J(PP), ^1J(HgP), and ^{31}P chemical shifts vary systematically with the ligand combination; of particular note, ^1J(HgP) to LL decreases as the chelate ring size of L'L' increases. These observations are discussed in terms of the variation in the intra- and inter-chelate PHgP angles expected in the complexes.

PHILIP A. W. DEAN et RADHEY S. SRIVASTAVA. Can. J. Chem. **63**, 2829 (1985).

Opérant dans le $MeNO_2$ comme solvant et utilisant du $Hg(SbF_6)_2$ et des quantités appropriées de ligands $Ph_2PCHRPPh_2$ (R = H ou Me), on a préparé des complexes 2:2, 1:2 et 1:3 M:L et on les a caractérisés par la rmn du ^{1}H, du ^{31}P et du ^{199}Hg. Les complexes 2:2 sont reliés par un ligand, comme c'est le cas avec le $[Hg(Ph_2PCH_2PPh_2)(Ph_2PCH_2PPh_2)Hg]^{4+}$ et le $[Hg(Ph_2PCH_2PPh_2)_2Ag]^{3+}$ (préparés par réaction du $Hg(SbF_6)_2$, du $Ag(AsF_6)$ ou $Ag(SbF_6)$ avec le ligand) que l'on a aussi étudiés par rmn pour fins de comparaison. Le complexe de $[Hg(\mu\text{-}Ph_2PCHMePPh_2)_2Hg]^{4+}$ existe sous la forme de deux isomères qui, à l'échelle préparative, se transforment lentement l'un dans l'autre. Les propriétés spectrales en rmn des complexes 1:2 et des complexes analogues de ligands mixtes sont des exemples de complexes bis(chélatés) tétraédriques qui sont très inusités dans le cas des ligands $Ph_2PCHRPPh_2$. Dans les complexes 1:3 et dans l'un des deux complexes mixtes possibles identifiés, il semble que des ligands η^1 ainsi que η^2 sont présents et qu'ils subissent un échange intramoléculaire rapide η^1 à η^2. Sur la base de leurs spectres rmn du ^{31}P, déterminés dans le couple Me_2CO—$MeNO_2$ et à basse température, on a déterminé que le mode de liaison η^1 du $Ph_2PCH_2PPh_2$ s'établit également dans les complexes $[(\eta^2\text{-}Ph_2P(CH_2)_2PPh_2)Hg\text{-}(\eta^1\text{-}Ph_2PCH_2PPH_2)_2]^{2+}$ et $[Hg(\eta^1\text{-}Ph_2PCH_2PPh_2)_4]^{2+}$.

Les spectres rmn du ^{31}P et du ^{199}Hg du complexe $[Hg(\eta^2\text{-}Ph_2PCH_2PPh_2)_2]^{2+}$ sont très différents de ceux de son analogue acyclique $[Hg(PMePh_2)_4]^{2+}$. Dans le but d'expliquer cette anomalie, on a déterminé les spectres de rmn du ^{31}P et du ^{199}Hg d'une série beaucoup plus importante de nouveaux complexes bis(chélatés) $[Hg(LL)(L'L')]^{2+}$ comportant les combinaisons de ligands LL = L'L' = $Ph_2PNPhPPh_2$; LL = dppm, L'L' = $Ph_2PNPhPP_2$; LL = L'L' = $Ph_3P(CH_2)_nPPh_2$ (n = 2−4); LL = $Ph_2P(CH_2)_nPPh_2$, L'L' = $Ph_2P(CH_2)_mPPh_2$ ($m \neq n$); m = 1−3, n = 1−5. A partir des données se rapportant aux deux dernières séries, on a trouvé que le complexe bis(chélaté) de $Ph_2PCH_2PPh_2$ est le seul à présenter une grande anomalie dans son déplacement chimique du ^{199}Hg (blindage anormalement grand); par ailleurs, on a établi que, dans le complexe de $[Hg(LL)(L'L')]^{2+}$, les valeurs de ^2J(PP), de ^1J(HgP) ainsi que les déplacements chimiques du ^{31}P varient d'une façon systématique avec la combinaison de ligand alors qu'il faut particulièrement noter que la valeur de ^1J de HgP à LL diminue lorsque la taille du cycle du chélate L'L' augmente. On discute de ces observations en fonction de la variation que l'on peut prévoir pour les angles PHgP internes et entre les chélates dans les complexes.

[Traduit par le journal]

Introduction

Mercury(II)−phosphine complexes have been a subject of intense interest for many years; reviews of various aspects of mercury chemistry include discussion of these species (e.g. refs. 1−4). Likewise, complexes of bis(diphenylphosphino)-methane (dppm[5]) have been widely studied (5). However, to our knowledge there has been no detailed nmr spectroscopic study of the system Hg^{2+}−dppm. We felt that such a study would be illuminating in terms of both the nmr spectroscopic and the chemical properties of the complexes formed, as there is evidence for bridging, chelating and monodentate behaviour of dppm bound to mercury(II): $X_2Hg(\mu\text{-dppm})HgX_2$ (X = Cl, Br or I), $HgX_2(\eta^2\text{-dppm})$ (X = Cl or Br) and $HgI_2(\eta^1\text{-dppm})_2$ have been detected by titration calorimetry of dilute solutions in benzene (6), and, recently, heterobimetallic dppm-bridged

[1]Dedicated to Dr. K. McL. Mitchell on the occasion of his retirement.

[2]Presented in part at the 67th Canadian Chemical Conference, Montreal, June 1984.

[3]To whom all correspondence should be addressed.

[4]On leave from Department of Chemistry, M.G. Degree College, Gorakhpur 273001, India.

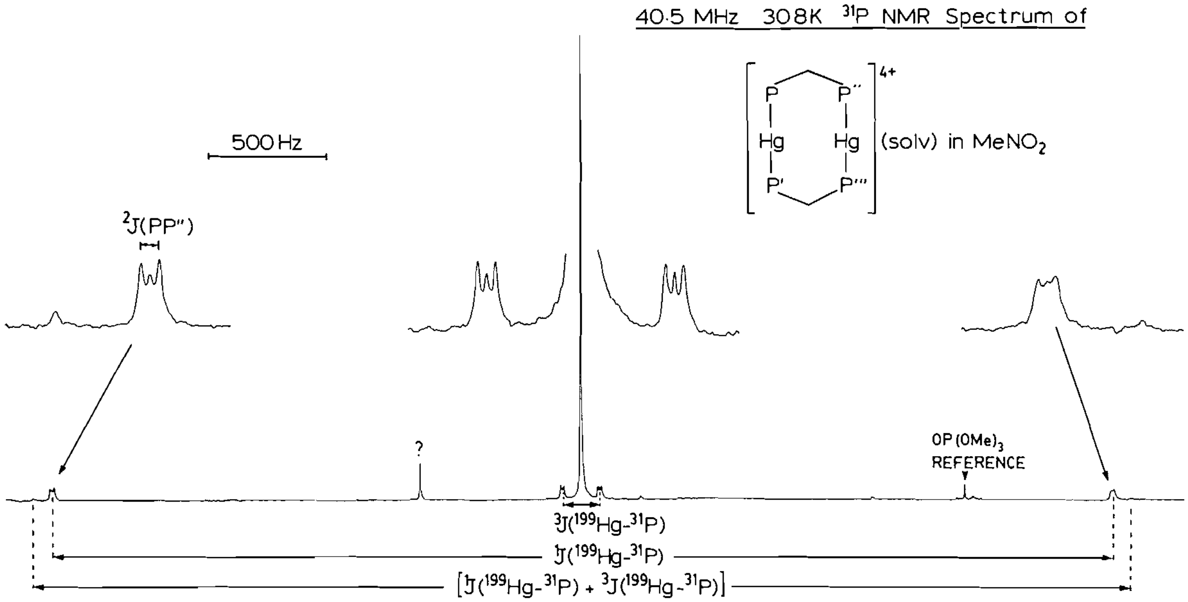

FIG. 1. The 40.54 MHz $^{31}P-\{^1H\}$ nmr spectrum of $[Hg(\mu\text{-dppm})_2Hg]^{4+}$ as the SbF_6^- salt in an $MeNO_2$ solution with 0.3 mol Hg/L of $MeNO_2$ at 308 K.

complexes of Pt(II) centres and mercuric halides have been synthesized and characterized in solution using ^{31}P nmr spectroscopy (7).

Tetrahedral complexes containing chelating dppm are rare (5), and even in square-planar complexes of η^2-dppm the metal and/or ^{31}P nmr parameters differ considerably from those found for complexes of longer-chain chelating diphosphines (e.g. refs. 8, 9). Therefore we anticipated (and indeed found) anomalous nmr spectroscopic behaviour for η^2-dppm complexes of mercury(II). To help quantify the extent of anomaly, we have obtained nmr spectra for a wide range of other bis(chelate) complexes $[Hg(LL)(L'L')]^{2+}$ with most possible combinations of the ligands[5] dppm, dppe, dppp, dppb, and dpppe and the possible combinations of dppa–dppm and dppm–mdppm. Although a variety of nmr data is available for complexes of the types $[Hg(PR_3)_4]^{2+}$ (e.g. refs. 10 and 11 and references therein) and $X_2Hg(LL)$(LL = ditertiary phosphine, X = various anions) (e.g. refs. 12 and 13), no such data seem to be available for the related bis(chelate)mercury(II) complexes; in fact few complexes of this type have been described (1–4).

In previous work from these laboratories (14) it was found that the combination of nitromethane, a weak donor solvent (15), and metal salts of the very weakly coordinating SbF_6^- anion promotes high denticity in Sn(II)– and Pb(II)–poly(tertiaryphosphine) complexes. By analogy, in the present work we have used $Hg(SbF_6)_2$ (16) as the acceptor and $MeNO_2$ (or, in a few cases, $MeNO_2$—Me_2CO) as solvent. In contrast, the $[Hg(PR_3)_4]^{2+}$ cations have usually been prepared with the ClO_4^- counterion and studied in CH_2Cl_2 solution (10, 11).

Results and discussion

Complexes of dppm, mdppm, and dppa

The ligand dppm is poorly soluble in $MeNO_2$ but dissolves in the presence of $Hg(SbF_6)_2$ if L/Hg $\lesssim$ 3.5, giving clear yellow solutions.

When dppm/$Hg(SbF_6)_2 \leq 1$, the $MeNO_2$ solutions contain a single species that is characterized by the ^{31}P and ^{199}Hg nmr[6] spectra shown in Figs. 1 and 2, respectively. These spectra demonstrate unambiguously the formation of the homobimetallic species[7] $[Hg(\mu\text{-dppm})_2Hg]^{4+}$, **1**, which, with ^{199}Hg present in natural abundance, exists as the three isotopomers **1***a–c* with populations of 69.2, 28.0, and 2.8%, respectively (17).

For **1***a*, a strong central singlet (an A_4 spectrum) is found in the ^{31}P nmr spectrum. Isotopomer **1***b* should have an AA′A″A‴X spectrum, where X = ^{199}Hg, assuming a negligible mercury isotope effect. The analysis of a spectrum of this type is well known (18, 19); the four triplets observed in the ^{31}P nmr spectrum are the components of the expected two four-spin subspectra, the shape of the triplets being consistent with the conditions $N \approx L$ where $N = J(AA'') + J(AA''')$ and $L = J(AA'') - J(AA''')$, i.e. $N \approx L \approx J(AA'')$, and $2J(AA') = 2J(A''A''') >> L$. The magnitudes of $J(AX)$ and $J(A''X)$ are given by the separations of the outer and inner pairs of triplets as shown in Fig. 1; these couplings are shown to be of the same sign by the small outermost satellite splitting shown in Fig. 1, which is due to **1**c and which gives $N' = J(AX) + J(A''X)$ for this AA′A″A‴XX′ spin system (20). The $^{199}Hg-\{^1H\}$ nmr spectrum of **1**, shown in Fig. 2, has as its major component a triplet of triplets which is the X part of the AA′A″A‴X spectrum of **1***b*; minor resonances, starred in Fig. 2, comprise part of the X part of the AA′A″A‴XX′ spectrum of **1***c* (there is considerable overlap with the spectrum of **1***b*). The proton nmr spectrum of **1** shows, in the methylene region, a quintet from

[5]Abbreviations used in this paper: $Ph_2PCH_2PPh_2$ = dppm; $Ph_2PCHMePPh_2$ = mdppm; $PhN(PPh_2)_2$ = dppa; $Ph_2P(CH_2)_2PPh_2$ = dppe; $Ph_2P(CH_2)_3PPh_2$ = dppp; $Ph_2P(CH_2)_4PPh_2$ = dppb; $Ph_2P(CH_2)_5PPh_2$ = dpppe; $Ph_2P(CH_2)_6PPh_2$ = dpph; $MePPh_2$ = dpmp.

[6] ^{31}P, 100% natural abundance, spin $I = 1/2$; ^{199}Hg, 16.84% natural abundance, spin $I = 1/2$; ^{107}Ag, 51.82% natural abundance, spin $I = 1/2$, $\mu = -0.11301\mu_N$; ^{109}Ag, 48.18% natural abundance, spin $I = 1/2$, $\mu = -0.12992\mu_N$.

[7]The extent of solvent and/or counteranion coordination in **1** and related species was not investigated, but the very large concentration dependence of ^1J(Hg—P) may indicate an appreciable equilibrium concentration of (labile) coordinated SbF_6^-.

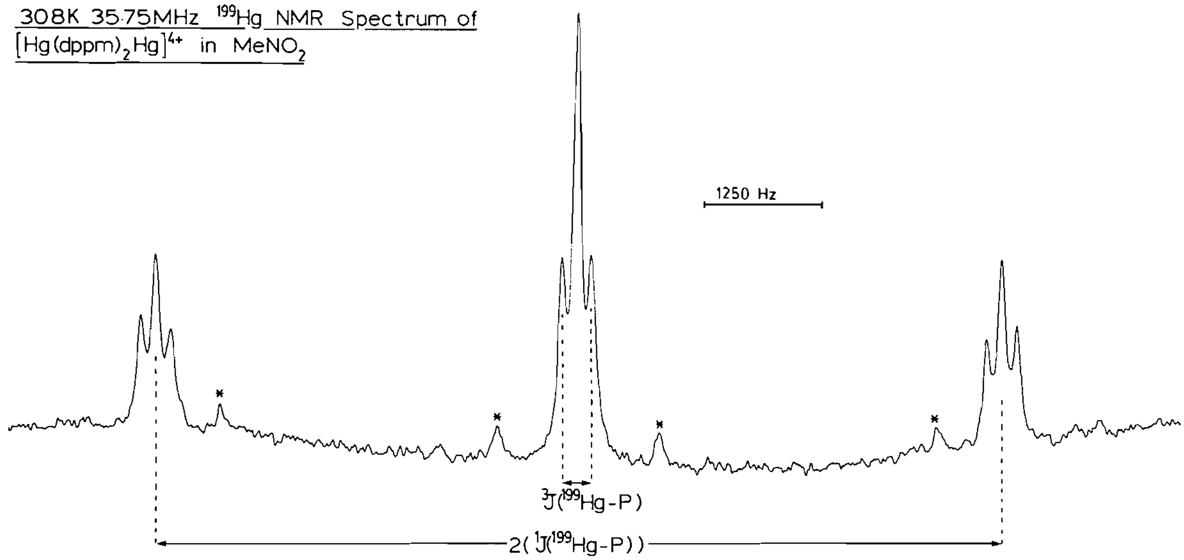

FIG. 2. The 35.75 MHz ^{199}Hg-{^{1}H} nmr spectrum of $[Hg(\mu\text{-dppm})_2Hg]^{4+}$ at 308 K in the same solution used to obtain the ^{31}P nmr spectrum of Fig. 1. Starred resonances are due to $[^{199}Hg(\mu\text{-dppm})_2{}^{199}Hg]^{4+}$. This spectrum was obtained using 61500 15μs (77°) pulses applied at $1\,s^{-1}$ with a spectral window of 25 kHz and an acquisition time of 0.64 s; an exponential factor equivalent to 20 Hz line broadening was applied to the FID.

isotopomer **1***a* (which, to give rise to the observed splitting pattern, must have $^{2}J(PHgP) \gg {}^{2}J(PCH)$), symmetrically flanked by the ^{199}Hg satellites that are the spectrum of **1***b*.[8]

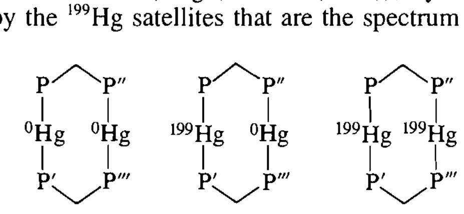

1*a* **1***b* **1***c*

Spectral parameters derived from the ^{1}H, ^{31}P, and ^{199}Hg nmr spectra of **1** are given in Table 1. The values of $^{1}J(HgP)$, 4496 Hz, and δ_{Hg}, 1250 ppm, for **1** are similar to those found for $Hg(PR_3)_2X_2$ in cases where R is an electron-donating group and X a weakly-coordinating anion (10, 11),[9] and probably signifies a near-linear PHgP skeleton as found, for instance, in $Hg(PCy_3)_2(ClO_4)_2$ (23). On the other hand, $^{1}J(HgP)$ is somewhat less than the values of 5495 and 5258 Hz reported for $[(p\text{-tolyl-C}{\equiv}C)_2Pt(\mu\text{-dppm})_2HgCl_2]$ (7*a*) and $[(NC)_2Pt(\mu\text{-dppm})_2HgCl_2]$ (7*b*), respectively, the difference presumably reflecting the relatively strong coordination of chloride to mercury in the Pt—Hg complexes.

The $^{199}Hg-{}^{199}Hg$ coupling found for $[^{199}Hg(\mu\text{-dppm})_2{}^{199}Hg]^{4+}$ found from the positions of the starred resonances in Fig. 2, is one of few such coupling reported (24, 25). The one-bond coupling in $[Hg—Hg—Hg]^{2+}$ has the remarkable value of 139.6 kHz (24*a*), so the ca. 1725 Hz coupling found in the present case need not imply significant Hg . . . Hg bonding, though the mercury atoms are undoubtedly in close proximity. (In $[(PhC{\equiv}C)_2Pt(\mu\text{-dppm})_2AgI]$, where no formal Pt—Ag bond exists, the Pt—Ag distance is 314.6(3) pm (7*a*).) As expected then, $^{4}J(^{199}Hg^{199}Hg)$ in **1** is less than the values of 2435−2959 Hz obtained for $^{2}J(^{199}HgP^{199}Hg)$ in ref. 25.

The value of $^{2}J(PHgP)$ could not be found from the various spectra of **1**. To obtain values for this coupling, as well as to support our assignments for **1** more generally, we have examined the nmr spectra of $[Hg(\mu\text{-dppm})_2Ag]^{3+}$, **2**, and $[Hg(\mu\text{-dppm})(\mu\text{-mdppm})Hg]^{4+}$, **3**, as well as the parent $[Hg(\mu\text{-mdppm})_2Hg]^{4+}$, **4**. The ^{1}H and ^{31}P nmr spectra of $[Ag(\mu\text{-dppm})_2Ag]^{2+}$ have been reported by others (26).

When equimolar amounts of $Hg(SbF_6)_2$ and $Ag(SbF_6)$ (or $AgAsF_6$) are mixed with two equivalents of dppm in $MeNO_2$, the ligand dissolves and the predominant species[7,10] is **2**, which, at 260 K gives the ^{31}P nmr spectrum shown in Fig. 3. As both silver and mercury have magnetically active nuclei,[6] this spectrum is a composite of the spectra of isotopomers **2***a*−*d* with populations of 43.1, 40.1, 8.7, and 8.1%, respectively (17). The species **2***a* and **2***b* both give rise to AA′FF′M spectra (M = $^{107/109}Ag$). These are superimposed in the higher frequency P-on-Hg region, where separate ^{107}Ag− and ^{109}Ag−P couplings could not be resolved, and overlap in the lower frequency P-on-Ag region, in both cases because the two silver

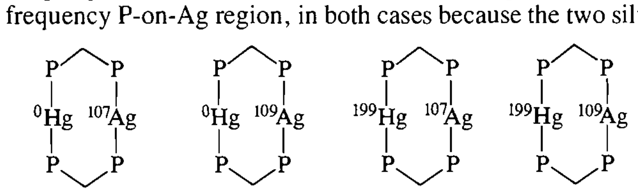

2*a* **2***b* **2***c* **2***d*

[8]These satellites are less well resolved than the centreband resonance, almost certainly as a result of relaxation of the linearly-coordinated ^{199}Hg via CSA (21). We also found (see Fig. 1) consistently poorer resolution of the lowest frequency satellite in the ^{31}P nmr spectrum of **1**; at present we have no explanation for this observation.

[9]When the ^{199}Hg nmr data of refs. 10 and 11, for example, are converted to $Hg(ClO_4)_2(aq)$ as reference, using $\delta_{Hg}(Hg(ClO_4)_2(aq), ext.) = \delta_{Hg}(HgMe_2, ext.) + 2253$ ppm $= \delta_{Hg}(1\,M$ PhHg(OAc), ext.) + 816 ppm (22), the shifts of the various $[Hg(PR_3)_2](ClO_4)_2$ reported therein cover the range 939−1297 ppm; $^{1}J(HgP)$ for these complexes covers the range 3174−5340 Hz.

[10]It is possible to prepare solutions of **2** containing no detectable amount of **1** or $[Ag(\mu\text{-dppm})_2Ag]^{2+}$ (identifiable by its reported (26) ^{31}P nmr spectrum); the redistribution $2\mathbf{2} \rightleftharpoons \mathbf{1} + [Ag(\mu\text{-dppm})_2Ag]^{2+}$ does not occur to a significant extent.

TABLE 1. Nuclear magnetic resonance spectral parameters of some ligand-bridged complexes of mercury(II) in nitromethane[a]

Complex	T (K)	δ_H[b] (ppm)	δ_P[c] (ppm)	δ_{Hg}[d] (ppm)	^1J(MP)[e] (Hz)	^3J(MP) (Hz)	^2J(PCP) (Hz)	^2J(PMP) (Hz)
$[Hg(dppm)_2Hg]^{4+}$	308	5.39(q)[f]	40.8	1250[g]	4496[h,i,j]	160±2[h,i]	15±1[k]	
$[Hg(mdppm)_2Hg]^{4+}$	308	1.63(dq),[l,m] 4.77[m]	54.2[l]	1239[n]	4343[h,i]	130±2[h,i]	34±2[k]	
			55.3[o]		~4165[h]			
$[Hg(dppm)(mdppm)Hg]^{4+}$[p]	308		41.1[q]		[r]			}~206
			53.1[s]		[r]			}
$[Hg(dppm)_2Ag]^{3+}$	260	4.74(dq)[t]	3.7[u]	1247[v]	548[w]	12±1[x]	86±1	~130[u,y]
			46.8[z]		4796[h,v]	[r]		~200[y,z]

[a] $[complex]_{total}$ = 0.15 mol/L of $MeNO_2$; abbreviations are as given in footnote 5 of the text. Phosphorus-31 and ^{199}Hg nmr spectra were measured with broadband proton decoupling. All chemical shifts are given using the convention that shifts to higher frequency than the reference are positive.

[b] Aliphatic protons, with observed splitting patterns parenthesized: q = quintet; dq = doublet of quintets; m = multiplet; at ambient probe temperature (18−23°C) unless noted otherwise.

[c] Measured relative to external 2% (v/v) $OP(OMe)_3$ in D_2O and corrected for sample-reference volume susceptibility difference (see Experimental Section); an approximate conversion to external 85% H_3PO_4 as reference, with susceptibility correction, is $\delta_P(H_3PO_4, ext) = \delta_P(OP(OMe)_3/D_2O, ext) + 3.8$ ppm; estimated error ±0.1 ppm(max); at 308 K, δ_P (uncorr) = −25.8 and −9.7 ppm for CH_2Cl_2 solutions of dppm and mdppm, respectively, from the 40.54 MHz ^{31}P nmr spectra.

[d] Measured relative to external 0.1 M $Hg(ClO_4)_2$ (aq) at 296 K; an approximate conversion to external $HgMe_2$ as reference is $\delta_{Hg}(HgMe_2, ext) = \delta_{Hg}$ (0.1 M $Hg(ClO_4)_2$(aq), ext) − 2253 ppm (22b); estimated error ±1 ppm.

[e] Estimated error in measurement ±5 Hz, except where noted; however, $^1J(^{199}Hg—^{31}P)$ are temperature and concentration dependent, and reproducibility is poorer than ±5 Hz.

[f] $|1/2(^4J(PH)) + 1/2(^2J(PH))| = 5.1 \pm 0.1$ Hz (= quintet splitting); ^3J(HgH) = 99 ± 1 Hz (broad satellites; see footnote 7 of the text).

[g] Resolved fine structure; see Fig. 2.

[h] M = ^{199}Hg.

[i] ^1J(HgP) and ^3J(HgP) have the same sign.

[j] $^4J(^{199}Hg—^{199}Hg) \approx 1725$ Hz in **1**c; see text and Fig. 2.

[k] $|^2J(PCP) + {}^4J(PMPCP)|$.

[l] Major isomer (see text).

[m] ^3J(HH) = 7.3 ± 0.1 Hz; $|1/2(^3J(PH)) + 1/2(^5J(PH))| = 8.2 \pm 0.1$ Hz.

[n] Incompletely resolved fine structure.

[o] Minor isomer (see text).

[p] In an equilibrated mixture of $[Hg(dppm)_2Hg]^{4+}$ and $[Hg(mdppm)_2Hg]^{4+}$.

[q] dppm resonance.

[r] Could not be observed with certainty.

[s] mdppm resonance.

[t] At 260 K; $|1/2(^2J(PH)) + 1/2(^4J(PH))| \approx 4.4$ Hz (the couplings from the chemically different ends of the complex appear to be equal); $^3J(^{107/109}AgP)$(ave) = 4.4 Hz; ^3J(HgP) ≈ 92 Hz (broad satellites; see footnote 8 of the text).

[u] P-on-Ag.

[v] No observable fine structure; at 308 K, δ_{Hg} and ^1J(HgP) are 1243 ppm and ~4723 Hz from the ^{199}Hg nmr spectrum.

[w] M = ^{109}Ag; $^1J(^{107}AgP)$ = 474 Hz; estimated errors ± 2 Hz.

[x] $^3J(^{107/109}AgP)$(ave).

[y] Most probable assignment (see text).

[z] P-on-Hg.

isotopes have similar magnetic moments.[6] Nevertheless the spectra can be analyzed straightforwardly, as can the AA′FF′MX spectra (M = $^{107/109}$Ag, X = ^{199}Hg) of **2**c and **2**d which result in the ^{199}Hg satellites of the P-on-Hg region.[11] (The P-on-Ag region of **2**c and **2**d is obscured by the more intense spectra of **2**a and **2**b).

The reduced temperature ^{199}Hg nmr spectrum of **2** shows only a triplet with splitting of ^1J(HgP); the linewidth of ca. 125 Hz at 260 K must obscure any $^{107/109}$Ag−^{199}Hg or longer-range Hg−P coupling. The ^{31}P nmr spectrum of **2** is less well resolved at 308 K than at 260 K, but not collapsed; in accord with this observation, the triplet ^{199}Hg nmr spectrum persists at 308 K, as do the ^{199}Hg satellites[6] in the methylene region of the proton spectrum, where the centreband is a doublet (from $^{107/109}$Ag−H coupling) of quintets (from virtual coupling to four phosphorus atoms).

The nmr spectral parameters of **2** are included in Table 1. It can be seen that the values of ^1J(HgP), δ_P (P-on-Hg region) and δ_{Hg} for **2** resemble those for **1** quite closely. Likewise, $^1J(^{107/109}AgP)$ and δ_P (in the P-on-Ag region) are similar to those of the structurally characterized (27) $[Ag(\mu\text{-}dppm)_2Ag]^{2+}$ ion ($^1J(^{109}AgP)$ = 583 Hz; δ_P (rel. 85% H_3PO_4(ext)) = 11.5 ppm, for the BF_4-salt in CD_2Cl_2 (26)). The two ^2J(PMP) (M = Ag or Hg) couplings found from the ^{31}P spectrum of **2** cannot be assigned unambiguously, but the larger coupling of ca. 200 Hz is close to the unambiguous value of ca. 206 Hz found for **3** (see below) and is presumably ^2J(PHgP). This can be compared with a zero or near-zero coupling in $HgCl_2(PBu_3)(PR_3)$ (R = 4-$MeOC_6H_4$) (28), 43 — ca. 74 Hz couplings in mixed ligand bis(chelate) complexes of mercury (Table 2 and see below), and a 567 Hz coupling in $[Hg\{P(OMe)_3\}\{P(OEt)_3\}]^{2+}$ (29), for instance.

When L/Hg < 1, fresh $MeNO_2$ solutions of mdppm and $Hg(SbF_6)_2$ give, at 308 K, ^{31}P nmr spectra showing *two* AA′A″A‴X spectra (X = ^{199}Hg) with approximately equal initial intensities. These we attribute to the isomers of **4** with

[11] As δ_P(P-on-Hg) − δ_P(P-on-Ag) is large relative to the various coupling constants, the AA′FF′ subspectra of the AA′FF′M spectra of **2**a and **2**b approach the limiting AA′XX′ case. Thus the ^{31}P nmr spectrum of **2**a, for instance, consists of a near-AA′XX′ spectrum doubled by the relatively large and relatively small couplings to ^{107}Ag in the P-on-Ag and P-on-Hg regions, respectively. In the complexes **2**c and **2**d, further observable doubling occurs in the P-on-Hg region from coupling to ^{199}Hg, giving rise to the ^{199}Hg satellites.

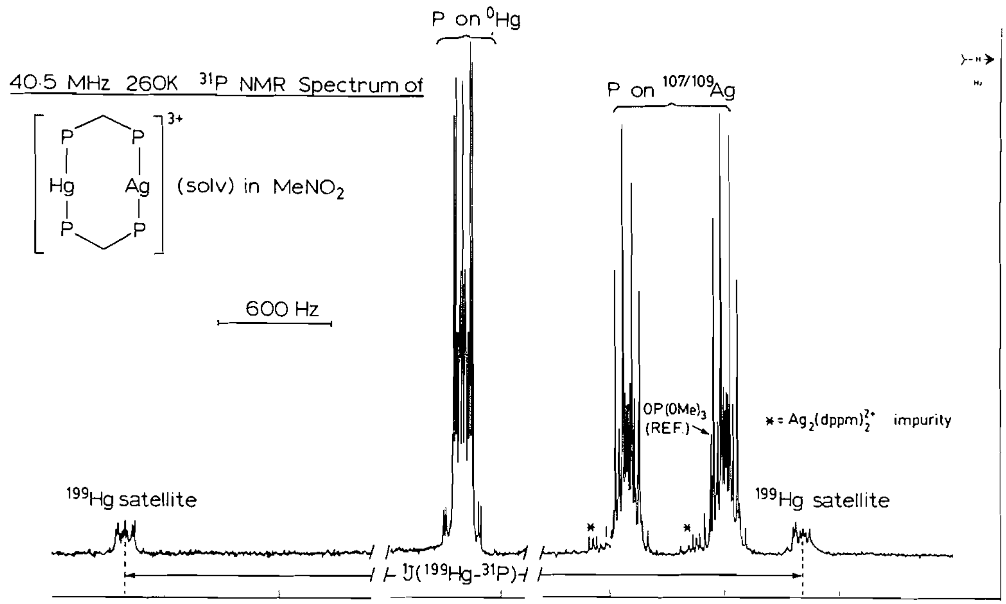

FIG. 3. The 40.54 MHz $^{31}P-\{^1H\}$ nmr spectrum of $[Hg(\mu\text{-dppm})_3Ag]^{3+}$ as the SbF_6^- salt in an $MeNO_2$ solution with 0.15 mol Hg/L of $MeNO_2$ at 260 K. Starred resonances are due to $[Ag(\mu\text{-dppm})_2Ag]^{2+}$ present as an impurity.

syn and *anti* arrangements of the methyl groups, though we cannot tell which spectrum should be assigned to which isomer. In the spectrometer probe at 308 K, the spectrum slowly changes, with the more shielded AA′A″A‴X spectrum growing at the expense of the less shielded until, at equilibrium after ca. 1.5 h [major isomer]/[minor isomer] > 10. Clearly intermolecular ligand exchange between the isomers is slow on both nmr and preparative timescales; our results for **1**–**4** mixtures (see below) suggest that intermolecular ligand exchange in **1** alone may also be slow on both timescales, but labelling studies would be needed to confirm this.

The ^{199}Hg nmr spectrum of an equilibrated solution of **4** consists of a triplet, each component of which appears to have further incompletely resolved fine structure. The poorer resolution found in the ^{199}Hg nmr spectrum of **4** compared with the corresponding spectrum of **1** (Fig. 2) is probably a result of the larger value of ^2J(PCP) in **4**.

The various nmr parameters of **4** are included in Table 1. The values of $\Delta\delta_P$, ^1J(HgP) and δ_{Hg}, particularly, are very similar to those of **1**. The ethylidene signals observed in the proton nmr spectrum confirm that there has been no loss of the methine proton(s) of the ligand(s); acid ionization did not seem an impossibility for **1**, **3**, and **4**, nominally 4+ ions.

When $MeNO_2$ solutions of **1** and **4** are mixed, the ^{31}P nmr spectrum at 308 K shows, initially, just the presence of **1** and **4**. However, equilibration occurs slowly over a period of ca. 2 h, and an apparent AB spectrum grows which we assign to **3**[12] on the basis of the chemical shifts. The apparent J(AB) of ca. 206 Hz is evidently ^2J(PHgP).[12]

[12]The centreband spectrum of **3** should be an AA′BB′ spectrum which can approximate an AB spectrum in the case that $J(AB) \gg J(AA'), J(BB')\, J(AB')$. The ^{199}Hg satellite spectrum of **3** should be an AA′BB′X spectrum (X = ^{199}Hg). Better resolution of the ^{31}P spectrum of **3** occurs at 260 K than at 308 K and further fine structure is evident. However, the spectrum is still basically of the AB type. Overlap of the centreband and satellite spectra of **3** with those of **1** and **4** in the equilibrium mixture unfortunately preclude a detailed analysis. $K = [\mathbf{3}]^2/[\mathbf{1}][\mathbf{4}] \approx 2$; this is the value expected for statistical scrambling of the ligands (17).

When additional dppm is added to an $MeNO_2$ solution of **1**, the 308 K ^{31}P nmr spectrum shows the formation of a new species, giving a singlet spectrum with ^{199}Hg satellites, that coexists with **1** when $1 < L/Hg < 2$ but is the only detectable species at L/Hg = 2. The system **4**-mdppm behaves in an analogous manner. Several lines of evidence confirm the formation of the 2:1 L:M complexes, $[Hg(dppm)_2]^{2+}$, **5**, and $[Hg(mdppm)_2]^{2+}$, **6**; these include the quartet pattern, from ^{199}Hg–P coupling, of their ^{199}Hg nmr spectra, and the formation of the single mixed complex $[Hg(mdppm)\,(dppm)]^{2+}$, **7**, when solutions of **5** and **6** are mixed. The mixed complex, formed rapidly on the preparative timescale, is characterized by a ^{31}P nmr spectrum of the A_2X_2 type (with ^{199}Hg satellites) and a ^{199}Hg nmr spectrum that is a triplet of triplets.

The nmr spectral parameters of **5**–**7** are included in Table 2. Alone they do not *prove* that in the 1:2 complexes the dppm and mdppm behave in a chelating manner, and such proof seems desirable, as tetrahedral complexes of chelating dppm are not well characterized (5). In support of our belief that dppm and mdppm *do* behave in a chelating manner, we can cite the similarity of their ^{199}Hg–P couplings to those of complexes such as $[Hg(dppe)_2]^{2+}$ and $[Hg(dppp)_2]^{2+}$ (Table 2) in which chelation is less contentious, as well as the systematic variation of ^{199}Hg–P coupling (to dppm) in the complexes $[Hg(dppm)(L'L')]^{2+}$, which parallels changes found in other mixed ligand complexes (Tables 2 and 4 and see also below). Thus **5**–**7** appear to be tetrahedral bis(chelate) complexes. However, this description of their geometry is perhaps misleading: Grdenić *et al.* have shown that in the compounds $Hg(phen)_2(NO_3)_2$ (30*a*) and $Hg(bipy)_2(NO_3)_2\cdot 2H_2O$ (30*b*), where the ligand bite angle is small, the geometry of the HgN_4 kernel is closer to square planar than to tetrahedral. We can expect similar distortion in the η^2-dppm/mdppm complexes and a structural study of **5** or **7** would be of some interest.

As shown by the data in Table 2, the ^{199}Hg nmr chemical shifts of **5**–**7** show significant shielding relative to the shifts found for bis(chelate) complexes of $Ph_2P(CH_2)_nPPh_2$ (n = 2–4). Detailed discussion of the trends found in Table 2 is given separately below, but we note here that the ^{199}Hg signal

TABLE 2. Nuclear magnetic resonance spectral parameters of some bis(ditertiaryphosphine) complexes of mercury(II), $[Hg(LL)(L'L')]^{2+}$, in nitromethane[a]

LL	LL	T (K)	δ_P[b,c] ($\Delta\delta_P$)[d] (ppm)	δ_{Hg}[e] (ppm)	$^2J(^{31}P—^{31}P)$[f] (Hz)	$^1J(^{199}Hg—^{31}P)$[c,g] (Hz)
dppm	dppm	308[h]	36.7(62.5)	1364		2104
		260[i]	31.4(57.2)	1311		2180
mdppm	mdppm	308	57.7(67.4)	1688		1945
dppm	mdppm	308	37.2(63.0); 58.5(68.3)	1523	44	~2108; 1944
dppa	dppa	308	119.1(53.7)	1839		2204
		260	120.7(55.3)			2237
dppm	dppa	260[j]	36.1(61.9); 124.2(58.8)		46	~2275; 2060
dppm	dppe	260[j]	34.1(59.9); 28.0(44.0)	1946	46	1980; 2217
dppm	dppp	260	25.8(51.6); 30.4(51.2)	2025	43	~1810; 2213
dppm	dppb	308	23.8(49.6); 33.4(52.8)	1938	59	1504; 2600
dppm	dpppe	308	22.0(47.8); 30.9(50.6)	2060	66	1219; 2844
dppe	dppe	308	18.5(34.5)	1965		2172
		260	19.3(35.3)	1963		2188
dppe	dppp	308	16.8(32.8); 12.3(33.1)	1992	50	1899; 2198
dppe	dppb	308	14.9(30.9); 22.5(41.9)	1965	65	1642; 2572
dppe	dpppe	308[k]	13.0(29.0); 20.4(40.1)	1921	~74	~1425; 2797
dppp	dppp	308	10.5(31.3)	2003		1979
		260	9.8(30.6)	2021		1972
dppp	dppb	308	9.6(30.4); 18.8(38.2)	1968	60	1769; 2287
dppp	dpppe	308	9.7(30.5); 20.2(39.9)	1886	73	1625; ~2420
dppb	dppb	308[l]	19.5(38.9)	1914		2073
$(dpmp)_4$		240[j]	5.0(35.1)	1951[m]		2143

[a]$[complex]_{total}$ = 0.15 mol/L of $MeNO_2$; abbreviations are as given in footnote 5 of the text; ^{31}P and ^{199}Hg nmr spectra were measured with broadband proton decoupling.

[b]Measured relative to 2% (v/v) $OP(OMe)_3$ in D_2O and corrected for sample-reference susceptibility difference (see Experimental section); an approximate conversion to external 85% H_3PO_4 as reference, with susceptibility correction, is $\delta_P(H_3PO_4, ext) = \delta_P(OP(OMe)_3/D_2O, ext) + 3.8$ ppm; estimated error ±0.1 ppm or less.

[c]Data for LL given first.

[d]$\Delta\delta_P = \delta_P(\text{complex}) - \delta_P(\text{free ligand})$. Values of δ_P(free ligand) were measured at 308 K using CH_2Cl_2 as solvent (this work and ref. 32); the data from Table 4 of ref. 32 were converted to $OP(OMe)_3/D_2O$ as reference using $\delta(OP(OMe)_3/D_2O) = \delta_P(OP(OMe)_3/(CD_3)_2CO) - 1.4$ ppm, but are otherwise uncorrected.

[e]Relative to external 0.1 M $Hg(ClO_4)_2$(aq) at 296 K; an approximate conversion to external $HgMe_2$ as reference is $\delta_{Hg}(HgMe_2, ext) = \delta_{Hg}(0.1\ M\ Hg(ClO_4)_2(aq), ext) - 2253$ ppm (22b); estimated error ± 1 ppm.

[f]Estimated error ±2 Hz, except where noted otherwise.

[g]Estimated error ±5 Hz, except where noted; these values are temperature and concentration dependent.

[h]In $(CD_3)_2CO$ at ambient probe temperature (18–23°C), $\delta_H(CH_2) = 4.41$ ppm, $^3J(^{199}HgH) \approx 103$ Hz, $^2J(PH)$ is not resolved. (The CH_2 resonance overlaps the proton resonance of CHD_2NO_2.)

[i]In CD_3NO_2 at ambient probe temperature (18–23°C), $\delta_H(C\mathit{H}Me) = 4.77$ ppm (incompletely resolved multiplet), $\delta_H(CH\mathit{Me}) = 1.63$ ppm (doublet of quintets: $^3J(HH) \approx |1/2(^3J(PH)) + 1/2(^5J(PH))| \approx 6.5$ Hz).

[j]Exchange-broadened lines are observed at 308 K.

[k]Complicated behaviour at 260 K (see text).

[l]Saturated solution.

[m]At 260 K.

of $[Hg(dppa)_2]^{2+}$ does not have a strongly anomalous chemical shift, pointing to a difference between dppa and dppm/mdppm as chelators. Perhaps significantly, we found no evidence for $[Hg(\mu\text{-dppa})_2Hg]^{4+}$; only $[Hg(dppa)_2]^{2+}$ is produced in $MeNO_2$ solutions where dppa/Hg = 1.

When further dppm is added to an $MeNO_2$ solution of **5**, a third Hg:dppm complex is formed which coexists with **5** when 2 < Hg < 3 and replaces the bis(chelate) complex completely at L/Hg = 3. Parallel behaviour is found for **7** with additional mdppm. The nmr spectral parameters of $[Hg(dppm)_3]^{2+}$, **8**, and $[Hg(mdppm)_3]^{2+}$, **9**, at 260 K, the temperature of best resolution, are included in Table 3. Both complexes show a singlet ^{31}P nmr spectrum, with ^{199}Hg satellites, down to the lowest accessible temperature (ca. −90°C, using $MeNO_2$–Me_2CO as solvent), with similar values of $\Delta\delta_P$ (= δ_P(complex) − δ_P(free ligand)) and J(HgP), the latter much smaller than found in **5**–**7**. Also, most notably, they both have ^{199}Hg resonances that are *septets*.[13]

When solutions of **8** and **9** are mixed, a new species is formed with its highest concentration at **8**:**9** ≈ 2:1. The ^{31}P nmr spectrum of this species consists of a triplet resonance (relative intensity 2) in the dppm region and a quintet resonance (relative intensity 1) in the mdppm region, both with ^{199}Hg satellites. Evidently $[Hg(dppm)_2(mdppm)]^{2+}$, **10** , is formed; we could find no definitive evidence for the other possible mixed complex. The nmr data for **10** are given in Table 3; the values of J(HgP) for this species are comparable to those of **8** and **9**, but the value of J(PP) in it is smaller than in any of the mixed-ligand bis(chelate) complexes studied (Table 2).

We discard the possibility that the septet ^{199}Hg nmr spectra of **8** and **9** indicate a static HgP_6 kernel; HgP_4 is the most

[13]To observe the full septet spectrum we used solutions of **8** and **9** with concentrations ca. 0.3 mol/L of $MeNO_2$.

TABLE 3. Nuclear magnetic resonance spectral parameters for some mercury(II) complexes of η^1-dppm and -mdppm[a,b]

Complex	Solvent	T (K)	δ_H[c] (ppm)	δ_P[d] (ppm)	δ_{Hg}[e] (ppm)	J(Hg—P)[f] (Hz)	J(P—P)[g] (Hz)
$[Hg(\eta^2\text{-dppe})(\eta^1\text{-dppm})_2]^{2+}$	$MeNO_2$—Me_2CO 1/2 (v/v)	198		−33.4[h] 12.5[j] 20.5[k]	[i]	— ~1430 ~2930	 73[l]
$[Hg(dppm)_3]^{2+}$	$MeNO_2$	260	3.80[m]	8.8[n]	1924[o]	1390[f]	
$[Hg(mdppm)_3]^{2+}$	$MeNO_2$	260	3.93,[m,p] 1.27[m,q]	29.6[n]	1688[o]	~1390[f]	
$[Hg(dppm)_2(mdppm)]^{+}$	$MeNO_2$	260		2.0[n] 39.8[n]	[i]	~1417[f] ~1301[f]	37[n]
$[Hg(\eta^1\text{-dppm})_4]^{2+}$	$MeNO_2-Me_2CO$ 1/2 (v/v)	198		−35.1[h] 21.1[k]	[i]	— 3172	

[a]See text for further discussion of these species; abbreviations used are those given in footnote 5 of the text.

[b]$[Hg]_{total}$ = 0.15 and 0.05 mol/L of solvent for $MeNO_2$ and $MeNO_2-Me_2CO$ solutions, respectively; ^{31}P and ^{199}Hg nmr spectra were measured with broadband proton decoupling.

[c]Aliphatic protons.

[d]Measured relative to 2% (v/v) $OP(OMe)_3$ in D_2O and corrected for sample − reference susceptibility difference (see Experimental section); an approximate conversion to external 85% H_3PO_4 as reference, with susceptibility correction, is $\delta_P(H_3PO_4, \text{ext}) = \delta_P(OP(OMe)_3/D_2O, \text{ext}) + 3.8$ ppm; estimated error ±0.1 ppm or less. From the 40.54 MHz ^{31}P nmr spectra of CH_2Cl_2 solutions δ_P (relative to external $OP(OMe)_3/D_2O$; uncorrected) = −25.8, −9.7, and −16.0 ppm for dppm, mdppm, and dppe, respectively (ref. 32 and this work) (see also footnote *d* of Table 2).

[e]Relative to 0.1 *M* $Hg(ClO_4)_2$(aq) at 296 K; an approximate conversion to external $HgMe_2$ as reference is $\delta_{Hg}(HgMe_2, \text{ext}) = \delta_{Hg}(0.1\ M\ Hg(ClO_4)_2(aq), \text{ext}) - 2253$ ppm (22*b*); estimated error ± 1 ppm.

[f]Estimated error ±5 Hz, except where noted otherwise.

[g]Estimated error ± 2 Hz.

[h]Unresolved multiplet from unbound end of η^1-dppm, P_B (see text).

[i]Insufficient concentration for measurement.

[j]Triplet from chelating dppe, P_C, of **12** (see text).

[k]Multiplet from bound end of η^1-dppm, P_A (see text).

[l]$^2J(P_A—P_C)$ in **12** (see text).

[m]No fine structure resolved.

[n]Value averaged by intramolecular exchange (see text).

[o]Septet.

[p]C*H*Me.

[q]CH*Me*.

heavily coordinated kernel found for Hg(II) with phosphorus donors (see, for examples, refs. 10 and 29). Therefore we suggest that 8 and 9 should be formulated $Hg(\eta^2\text{-LL})\ (\eta^1\text{-LL})_2$ and that rapid intramolecular exchange of coordinated and uncoordinated phosphorus atoms occurs as in [1].

[1] 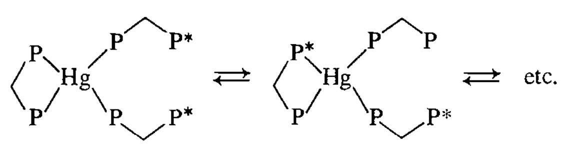

Such an exchange process requires only an HgP_4 kernel, and in addition accounts for the observation of septet ^{199}Hg nmr spectra and small values of J(HgP) (now an average, $(1/3) \times J(HgP)_{chelate} + (1/3)J(HgP)_{\eta^1\text{-bound}} + (1/3)\ J(HgP)_{\eta^1\text{-unbound}}$, with the last term small) for **8** and **9**. Similarly, the values of J(HgP) found for **10** are weighted averages, as is J(PP).

Intramolecular exchange of η^2-and η^1-dppm, at one metal centre, as in [1], does not seem to have been described previously, though possible examples of intramolecular exchange of free and bound ends of η^1-dppm have been reported (31).

Addition of dppm to $MeNO_2$ solutions of **8** causes broadening of the ^{31}P nmr spectra of both **8** and the free dppm, pointing to intermolecular exchange of dppm in a second order process. The species $[Hg(\eta^1\text{-dppm})_4]^{2+}$, **11**, is implicated as an intermediate or transition state. We have unambiguously identified the unusual species **11**; it is present at low concentration in $MeNO_2/Me_2CO$ (1/2 v/v) solutions[14] of **8** saturated with dppm, and can be detected by its low temperature ^{31}P nmr spectrum. At −75°C,[15] the spectrum consists of two approximately equally intense quintets, one somewhat broad and shielded relative to the free dppm signal (which has δ_P = −28.1 ppm in this solution), the other sharper, having ^{199}Hg satellites, and in the region expected for phosphorus bound to Hg(II). These are assigned to P_B and P_A, respectively of **11**, which should give an AA′A″A‴MM′M″M‴ spectrum (AA′A″A‴MM′M″M‴X (X = ^{199}Hg) for the ^{199}Hg satellites) if $^2J(PMP \gg |^2J(PCP) - {}^4J(PCPMP)|$ (20*b*), though the broadness of the P_B quintet suggests that the limiting spectrum may not quite have been reached. (P_B should be the resonance most affected by slow dppm exchange, as the free dppm resonance is nearby.) Coordination of one phosphorus of dppm is known to cause both shielding of the ^{31}P resonance of the uncoordinated phosphorus atom and an increase in $|^2J(PCP)|$ relative to the values for dppm (e.g. refs. 31−34). Still the value of 75 Hz calculated for $|(1/4)\ (^2J(PCP)) + (3/4)\ (^4J(PCPMP))|$ from the quintet splitting of the coordinated dppm resonance of **11** seems remarkably large.

With dppe as a ligand we could find no evidence for $[Hg(dppe)_3]^{2+}$; $[Hg(dppe)_2]^{2+}$ and excess dppe co-exist in $MeNO_2$ solutions where dppe/Hg > 2. Therefore we sought to take advantage of the stability of chelating dppe to synthesize $[(\eta^2\text{-dppe})Hg(\eta^1\text{-dppm})_2]^{2+}$, **12**, in solution. Characterization of this η^1-dppm complex would support our formulation of **8** and **9**, thus providing further (indirect) evidence for the existence of process [1], as well as help confirm our assignments

[14][complex] = 0.05 mol/L of solvent in $MeNO_2$—Me_2CO.

[15]The spectrum collapses at higher temperatures.

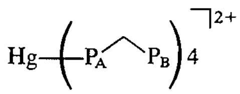

11

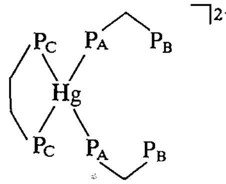

12

for **11**. Accordingly we used ^{31}P nmr to follow the addition of solid dppe to a solution of **5** in $MeNO_2$ (for our first attempt) or $MeNO_2/Me_2CO$ (1/2 v/v)[13] (for subsequent attempts).

At least the equilibria [2]–[5] are involved in **5**:dppe mixtures:

[2] $3[Hg(dppm)_2]^{2+} + 2dppe \rightleftarrows [Hg(dppe)_2]^{2+} + 2[Hg(dppm)_3]^{2+}$

[3] $[Hg(dppm)_3]^{2+} + dppe \rightleftarrows [Hg(dppe)(dppm)_2]^{2+} + dppm$

[4] $2[Hg(dppe)(dppm)_2]^{2+} \rightleftarrows [Hg(dppe)_2]^{2+} + [Hg(dppm)_4]^{2+}$

[5] $[Hg(dppe)(dppm)_2]^{2+} + dppe \rightleftarrows [Hg(dppe)_2]^{2+} + 2dppm$

However, we have already measured the ^{31}P nmr spectra of all the species except **12** and hence the spectral features due to this complex can be identified. The spectrum consists of three approximately equally intense resonances: a broad signal, probably an incompletely-resolved multiplet, at −33.4 ppm, shielded relative to free dppm; a triplet at 12.5 ppm; and a symmetrical multiplet at 20.5 ppm, overlapping the centreband of the $[Hg(dppe)_2]^{2+}$ spectrum, and close to the resonance position of P_A in **11**. The two less-shielded resonances each have ^{199}Hg satellites. We attribute these signals to P_A, P_B, and P_C, respectively of **12**, and the triplet splitting of P_C to P_AP_C coupling. The overlap of the P_A signal with the spectra of **11** and $[Hg(dppe)_2]^{2+}$, and the broadness of the P_B resonance, preclude complete analysis of the six-spin spectrum of **12**, but there can be no doubt about the existence of the species. By analogy, our formulations of **8** and **9** and the suggestion of rapid intramolecular η^1-LL-to-η^2-LL exchange in these (eq. [1]) are supported, as are our assignments for the spectrum of **11**.

The proton nmr data for **1**, **2**, **5**, and **8**, and **4**, **6**, and **9**, included in Tables 1–3, together with the data given in ref. 26, show that the $\delta(CH_2)$ for the dppm complexes is **1** > **5** > **8** and **1** > **2** > $[Ag(\mu\text{-dppm})_2Ag]^{2+}$, while $\delta(CH\text{Me})$ for the mdppm complexes is **4** > **6** > **9** and **4** > $[Ag(\mu\text{-mdppm})_2Ag]^{2+}$. These findings are in concert with the suggestion of Grim and Walton (34) that in dppm complexes increasing positive charge on the phosphorus atoms leads to decreased shielding of the CH_2 group. It is noteworthy that $\delta(CH_2)$ for **1** is very similar to that for $Ph_2P^+(Me)CH_2P^+(Me)Ph_2$ ($\delta(CH_2)$ = 5.55 ppm (34)), emphasizing the very strong electrophilic character of mercury (II) in the phosphine complexes.

Other bis(ditertiaryphosphine)mercury(II) complexes; correlations in the nmr spectral parameters of $[Hg(LL)(L'L')]^{2+}$

We have measured the ^{31}P and ^{199}Hg nmr spectra of $[Hg(dpmp)_4]^{2+}$, **13** an acyclic analog of **5**,[16] to quantify any nmr spectral anomalies caused by the presence of chelating dppm in the latter. The results are given in Table 2. Comparison of the data for **5** and the dpmp complex shows that there are large differences between $\Delta\delta_P$ (**5** > **13**) and δ_{Hg} (**13** > **5**) for the two complexes, but that their values of ^1J(HgP) are similar. This is unlike the situation for $L_2Pt(dppm)$ versus *cis*-$L_2Pt(dpmp)_2$ (8, 9) where $\Delta\delta_P$, δ_{Pt}, *and* ^1J(PtP) differ, the differences in $\Delta\delta_P$ and δ_M being the reverse of the results for the Hg(II) complexes, viz. $\Delta\delta_P(L_2Pt(dppm)) < \Delta\delta_P(L_2Pt(dpmp)_2)$ ($\Delta\delta_P$ $L_2Pt(dppm)$ *negative*[17]), $\delta_{Pt}(L_2Pt(dppm)) > \delta_{Pt}(L_2Pt(dmpm)_2$; also ^1J(PtP) $(L_2Pt(dppm)) < {}^1J$(PtP) $(L_2Pt(dpmp)_2)$. Therefore we thought it would be instructive to study the nmr spectra of a wider range of complexes $[Hg(LL)(L'L')]^{2+}$ in which LL and L′L′ are selected from the series $Ph_2P(CH_2)_nPPh_2$ (n = 1–5). The nmr spectra of the species studied are included in Table 2.

The ligands dppe, dppp, and dppb are soluble in $MeNO_2$ when $L/Hg(SbF_6)_2 \leq 2$. At L/M = 2, the ^{31}P nmr spectrum in each case consists of a singlet with ^{199}Hg satellites, while the ^{199}Hg spectrum is a quintet with splitting ^1J(HgP). Evidently the bis(chelate) complexes $[Hg(dppe)_2]^{2+}$, $[Hg(dppp)_2]^{2+}$, and $[Hg(dppb)_2]^{2+}$ are formed. We found no evidence for formation of $[Hg(dpppe)_2]^{2+}$ under the same circumstances.[18]

When mixtures of $Hg(SbF_6)_2$ and the ligands $Ph_2P(CH_2)_mPPh_2$ and $Ph_2P(CH_2)_nPPh_2$ ($m \neq n$; m = 1–3, n = 1–5) or dppm–dppa or (see above) dppm—mdppm with $L_{total}/Hg(SbF_6)_2 \approx 2$ in $MeNO_2$ solution, are studied by ^{31}P nmr spectroscopy, unambiguous evidence for the formation of mixed ligand bis(chelate) complexes is found:[19] new A_2X_2 or A_2B_2 spectra with the appropriate ^{199}Hg satellites can be seen. These four-spin spectra are quite clean, pointing to monomeric structures, except in the case of $[Hg(dppe)(dpppe)]^{2+}$. At reduced temperatures this complex gives a first-order AFMX centreband spectrum consisting of four triplets, overlapping in pairs; incomplete collapse towards an A_2X_2 spectrum occurs at 308 K. Possibly $[Hg(dppe)(dpppe)]^{2+}$ exists in a fixed conformation at low temperature or is aggregated. Wherever the concentration of the mixed species was sufficient, the ^{199}Hg nmr spectrum was measured, and showed the triplet of triplets expected for $[Hg(LL)(L'L')]^{2+}$, together with the quintet spectra of the parents complexes if present in the equilibrium mixture; again no spectrum attributable to $[Hg(dpppe)_2]^{2+}$ was ever observed.

In the cases of $[Hg(dppm)(dppa)]^{2+}$ and $[Hg(dppm)(mdppm)]^{2+}$ the assignment of the A_2X_2 ^{31}P nmr spectra can be made in a straightforward manner based on the proximity of the A and X resonances to those of the parent complexes. Assignments made in the same manner seem reasonable for $[Hg(dppe)(L'L')]^{2+}$ (L′L′ = dppp or dppb) and $[Hg(dppp)(dppb)]^{2+}$ also, in which case we observe for the limited series $[Hg(LL)(L'L')]^{2+}$ (LL = dppe, L′L′ = dppe, dppp, or dppb; LL = dppp, L′L′ = dppp or dppb), that *one-bond ^{199}Hg–P coupling to LL decreases as that to L′L′ increases and vice-*

[16]References 10 and 11 contain data for other, less comparable, $[Hg(PR_3)_4]^{2+}$ complexes.

[17]To be consistent with our data, ref. 8 and the IUPAC Convention, we have reversed the signs of δ_P in ref. 9.

[18]The ligands dppe, dppp, dppb, and dpppe also form 1:1 complexes with $Hg(SbF_6)_2$ in $MeNO_2$. We have not studied these in detail but from their nmr spectra, e.g. $Hg(dppb)^{2+}$: δ_P = 47.9 ppm, ^1J(HgP) = 4356 Hz, δ_{Hg} = 968 ppm; Hg(dpppe): δ_P = 49.6 ppm, ^1J(HgP) = 4388, δ_{Hg} = 1020 ppm, all at 308 K, they apparently have linear or near-linear PHgP skeletons and are presumably aggregated.

[19]Chelation by dpppe, which does not form $[Hg(dpppe)_2]^{2+}$ under the same conditions, is worthy of note; however, we could find no evidence for chelation by dpph in any of our experiments.

TABLE 4. Differential changes in ^{31}P nmr chemical shifts and values of ^1J(Hg—P) for LL in the complexes $[Hg(LL)(L'L')]^{2+}$ in nitromethane[a,b]

		L′L′									
		dppm		dppe		dppp		dppb		dppe	
LL	T (K)	$\delta\delta_P$[c] (ppm)	ΔJ[d] (Hz)	$\delta\delta_P$[c] (ppm)	ΔJ[d] (Hz)	$\delta\delta_P$[c] (ppm)	ΔJ[d] (Hz)	$\delta\delta_P$[c] (ppm)	ΔJ[d] (Hz)	$\delta\delta_P$[c] (ppm)	ΔJ[d] (Hz)
dppm	308	0	0					−12.9	−600	−14.7	−895
	260	0	0	2.7	−200	−5.6	−370				
dppe	308			0	0	−1.7	−273	−3.6	−530	−5.5	−747
	260	8.7	29	0	0						
dppp	308					0	0	−0.9	−210	−0.8	−354
	260	20.6	241	1.8	219	0	0				
dppb	308	13.9	527	3.0	499	−0.7	214	0	0		

[a]Abbreviations are those given in footnote 5 of the text.
[b]Values derived from the data in Table 2.
[c]$\delta\delta_P$ = (δ_P of LL in $[Hg(LL)(L'L')]^{2+}$) − $\delta_P[Hg(LL)_2]^{2+}$.
[d]ΔJ = (^1J(HgP) to LL in $[Hg(LL)(L'L')]^{2+}$) − (^1J(HgP) in $[Hg(LL)_2]^{2+}$).

versa. We have taken advantage of this empiricism to make the other assignments in Table 2. Assignments made this way show systematic variation in both ^1J(HgP) and δ_P. Variation relative to the values for the parent $[Hg(LL)_2]^{2+}$ can be quantified as ΔJ(= (^1J(HgP) to LL in $[Hg(LL)(L'L')]^{2+}$) − (^1J(HgP) in $[Hg(LL)_2]^{2+}$)) and $\delta\delta_P$ (= (δ_P for LL in $[Hg(LL)(L'L')]^{2+}$) − (δ_P for $[Hg(LL)_2]^{2+}$)); values of ΔJ and $\delta\delta_P$ are given in Table 4.

From the data in Table 4 it is evident that in $[Hg(LL)(L'L')]^{2+}$ ΔJ decreases by $2-3 \times 10^2$ Hz for each additional backbone carbon atom in the ligand L′L′, except that changing L′L′ from dppm to dppe produces an anomalously small decrease when LL = dppe, dppp, or dppb. Buergi, Pregosin, and co-workers (12) have demonstrated that in X_2HgP_2 ($P_2 = (PR_3)_2$ or various chelating diphosphines; X = various anions) J(HgP) can be expressed as $J(HgP) = a + b\theta(P, Hg, P) + c\theta(X, Hg, X)$ where θ(P, Hg, P) and θ(X, Hg, X) are the PHgP and XHgX bond angles, respectively, and the empirical coefficients a, b, and c have the values 5851 Hz, 25.1 Hz/deg, and −48.7 Hz/deg, respectively, for the range of compounds studied. Accordingly, the explanation we favour for the variation in ΔJ is based on systematic changes in PHgP angles[20]: in $[Hg(LL)(L'L')]^{2+}$ an increase in the chain length of L′L′ should open up the PHgP angle involving L′L′ (equivalent to θ(X, Hg, X) of ref. 12) at the expense of θ(P, Hg, P) in LL, and thus J (and ΔJ) (to LL) should decrease while J (and ΔJ) (to L′L′) should increase. The anomalous behaviour of the complexes $[Hg(LL)(L'L')]^{2+}$ (LL = dppe, dppp, or dppb, L′L′ = dppm or dppe) may reflect a saturation effect, with the intrachelate PHgP angles of LL having already reached a near maximum when combined with the relatively small dppe chelate.

The ^{31}P nmr chemical shifts of phosphorus chelate complexes frequently include a ring contribution, ΔR, where $\Delta R = \Delta\delta_P$ (chelate) − $\Delta\delta_P$ (analogous monodentate complex) (35). Comparison of $\Delta\delta_P$ for $[Hg(dpmp)_4]^{2+}$, $[Hg(dppe)_2]^{2+}$, $[Hg(dppp)_2]^{2+}$, and $[Hg(dppb)_2]^{2+}$ (Table 2) shows that ΔR for the three chelate complexes is very small. On the other hand ΔR for $[Hg(dppm)_2]^{2+}$ is substantial at ca. 25 ppm (and opposite in sign to that found for X_2Pt(dppm), as we have noted above). It seems likely that this sizeable ΔR should be associated with the small intra-chelate PHgP angle of dppm and the resulting chelate ring strain and/or geometry distortion. Significantly, it is only for dppm-containing complexes that large values of $\delta\delta_P$ are observed (Table 4): the overall trend in $\delta\delta_P$ for $[Hg(LL)(L'L')]^{2+}$ is that the LL resonance becomes shielded and the L′L′ resonance deshielded as the difference between the L′L′ and LL chelate ring sizes increases, and this effect is largest for the dppm-containing species. Thus in $[Hg(dppm)(L'L')]^{2+}$ the dppm resonance moves towads the "normal" ^{31}P chemical shift range and the L′L′ resonance away from that range as the ring size of L′L′ increases. Most likely this indicates a lessening of strain in the dppm at the expense of increasing strain in L′L′ as the two chelate ring sizes become more disparate.

The ^{199}Hg resonances of **3** and **5** are significantly shielded relative to the ^{199}Hg signals of $[Hg(LL)_2]^{2+}$ (LL = dppe, dppp, or dppb) (Table 2). It is interesting, however, that the ^{199}Hg resonances of $[Hg(LL)(L'L')]^{2+}$ (LL = dppm, L′L′ = dppe, dppp, dppb, or dpppe) fall in the same general region as the parent complexes of dppe, dppp, or dppb (and also, presumably, the hypothetical $[Hg(dpppe)_2]^{2+}$). A plausible rationalization of these observations is that coordination of *two* dppm ligands to Hg involves extensive strain/distortion, resulting in an anomalous ^{199}Hg chemical shift, whereas coordination of dppm to Hg along with a larger chelate allows a redistribution of PHgP angles (as discussed above) and to a reduction in overall strain/distortion and a more normal chemical shift.[21] Again it is worth noting that coordination of one dppm in L_2Pt(LL) causes *deshielding* of the ^{195}Pt resonance relative to those of complexes with LL = dppe, dppp, or dppb (9); this is the opposite of what we observe for the mercury complexes. At present we have no explanation for the difference.

From the ^{31}P nmr spectra of the mixed ligand complexes $[Hg(LL)(L'L')]^{2+}$, values of ^2J(PHgP) could be obtained. These are included in Table 2. For LL = dppm, dppe, or dppp, ^2J(PHgP) increases as the length of the —$(CH_2)_n$— backbone

[20]An alternative explanation, taking into account the expected increase in the basicity of $Ph_2P(CH_2)_nPPh_2$ with increase in n predicts the *reverse* of the observed trends, as J(HgP) is known to decrease with increasing basicity in $[Hg(PR_3)_4]^{2+}$ (11).

[21]We note, though, that $[Hg(dppm)(dppp)]^{2+}$ and $[Hg(dppm)(dppb)]^{2+}$ have the unusual (36) property of having δ_{Hg} outside the range of the parent complexes.

of the ligand L'L' is increased, the only discrepancy occurring between $[Hg(dppm)(dppe)]^{2+}$ and $[Hg(dppm)(dppp)]^{2+}$. However, the same trend is not observed in the fewer data available for LL = dppb or dpppe. We tentatively suggest that the results for LL = dppm, dppe, or dppp are a reflection of a decrease in the interchelate PHgP angle as n is increased in L'L', and that changes in this angle with n are less pronounced when LL = dppb or dpppe.

Experimental

Materials

Methyldiphenylphosphine and *N*,*N*-bis(diphenylphosphino)aniline (both from Aldrich Chemical Co., Inc.), α,ω-bis(diphenylphosphino)-ethane, -butane, -pentane, and -hexane (all from Strem Chemicals, Inc.), 1,3-bis(diphenylphosphino)propane (Pressure Chemical Co.), and 1,1-bis(diphenylphosphino)methane (Strem or Alfa Products) showed no significant impurities by ^{31}P nmr and were used as received. Nitromethane (Fisher Spectranalyzed) and acetone (Baker Analyzed) were freshly distilled on to 3A Molecular Sieves, and CD_3NO_2 (MSD Isotopes) dried using 3A Molecular Sieves; the solvents were deoxygenated with N_2 or Ar before use.

Literature methods were used to prepare $Hg(SbF_6)_2$ (16) and $AgSbF_6$ and $AgAsF_6$ (37). A small yield (ca. 10%) of 1,1-bis-(diphenylphosphino)ethane was obtained by route (*a*) of Sommer (38), and its authenticity confirmed by comparison of ^1H and ^{31}P-$\{^1H\}$ nmr spectra with those reported (26); at 308 K in CH_2Cl_2 solution, the 40.54 MHz ^{31}P-$\{^1H\}$ spectrum gives δ_P (rel. ext. $OP(OMe)_3/D_2O$) = −9.7 ppm.

Manipulations

All transfers of moisture-sensitive $Hg(SbF_6)_2$ and $AgSbF_6$ or $AgAsF_6$ and involatile air-sensitive ligands were carried out in an N_2-filled glove box in which the atmosphere was maintained by circulation through liquid nitrogen-filled traps. The more volatile $PMePh_2$ was handled in an N_2- or Ar-filled polyethylene glove bag. Glove bag or standard N_2-vacuum techniques were used in the preparation of Hg(II)- and Ag(I)-containing samples; here a freshly-prepared solution of the metal salt(s) was added to a slurry (solution for $PMePh_2$) of the ligand(s), causing dissolution, as described earlier for Sn(II) and Pb(II) complexes (14).

Bis[bis(diphenylphosphino)methane]mercury(II) silver(I)hexafluoroantimonate, $[Hg(dppm)_2Ag](SbF_6)_3$

Nitromethane solutions of $Hg(SbF_6)_2$ (0.336 g, 0.500 mmol) and $AgSbF_6$ (0.172 g, 0.501 mmol) were mixed and added to a slurry of dppm (0.460 g, 1.20 mmol), causing the dissolution of the ligand and production of a yellow solution. Removal of the $MeNO_2$ *in vacuo* left a yellowish-white solid. This was dissolved in CH_2Cl_2 containing a small amount of MeCN and cooled to −78°C, whereupon white crystals formed; these were filtered off at −78°C, washed with cold CH_2Cl_2 and a little MeCN, and dried *in vacuo*. The ^{31}P-$\{^1H\}$ nmr spectrum of this material showed the only phosphorus-containing impurity to be a trace of $[Ag_2(dppm)_2]^{2+}$, detected by its known (26) spectrum (see text). *Anal.* calcd. for $C_{50}H_{44}AgF_{18}HgP_4Sb_3$: C 33.65, H 2.48; found: C 33.76, H 1.53.

Nuclear magnetic resonance spectra

Samples for ^{31}P and ^{199}Hg nmr spectroscopy were prepared in 10 mm od nmr tubes under an atmosphere of N_2 or Ar. Because of the expected (see, for example, refs. 11 and 39) concentration dependence of, especially, $^1J(^{199}Hg—^{31}P)$, samples were normally prepared to have a total mercury concentration of 0.15 mol/L of solvent (0.30 mol/L for $[Hg(dppm)_2Hg]^{4+}$). Samples for ^1H nmr spectroscopy were made up in standard 5 mm od nmr tubes.

All nmr data are reported using the IUPAC convention: chemical shifts to higher frequency than the reference are taken as positive. Broad-band proton decoupling was used in obtaining all ^{31}P and ^{199}Hg nmr spectra.

Proton nmr spectra were measured using a Varian XL-200 or XL-300 spectrometer. Samples of ligands only were referenced to internal TMS in the usual manner, but for metal-containing solutions, spectra were referenced to the solvent resonance, for which the chemical shift relative to TMS under identical conditions was found separately.

Most of the ^{31}P-$\{^1H\}$ nmr spectra were measured at 40.54 MHz using a Varian XL-100 spectrometer; operating conditions, referencing to external $OP(OMe)_3$ in D_2O, and temperature measurements were made as described in earlier work from these laboratories (32). For these conditions, an approximate conversion to H_3PO_4 reference is $\delta_P(H_3PO_4, ext) = \delta_P(OP(OMe)_3/D_2O, ext) + 3.1$ ppm (before correction for susceptibility differences). Later ^{31}P nmr spectra were obtained at 80.94 MHz using a Varian XL-200 spectrometer operating unlocked (field drift ≪ 1 Hz/day). Also a few ligand spectra were measured at 121.4 MHz using a Varian XL-300 spectrometer. The temperatures of the XL-100 and XL-200 under conditions of broad-band proton decoupling were matched using the sharp, temperature-dependent ^{199}Hg satellite splitting of the spectrum of $[Hg(dppe)_2]^{2+}$ (see Table 2) and should agree within ±3°C. Using the XL-200, ^{31}P chemical shifts were measured by sample interchange with a 2% (v/v) solution of $OP(OMe)_3$ in D_2O. The different geometries of the superconducting solenoid of the XL-200 and the iron electromagnet of the XL-100 lead to different chemical shifts relative to the external reference (40). Therefore for convenience of comparison, all ^{31}P nmr chemical shift data have been corrected for sample-reference susceptibility difference using the expressions of ref. 40 and the volume susceptibility data of Gutmann and co-workers (41).

For ^{199}Hg nmr, 0.1 *M* $Hg(ClO_4)_2$ in 5% (v/v) $HClO_4$ solution was used as an external reference, with referencing made by sample interchange. An approximate conversion to $HgMe_2$ reference is $\delta_{Hg}(HgMe_2, ext) = \delta_{Hg}(Hg(ClO_4)_2, ext) - 2253$ ppm (22*b*). A few initial ^{199}Hg-$\{^1H\}$ nmr spectra were measured at 71.51 MHz using the Bruker WH-400 spectrometer of the S. W. Ontario NMR Centre in Guelph, but all of the ^{199}Hg-$\{^1H\}$ nmr data reported here were measured at 35.75 MHz using the Varian XL-200 spectrometer in this Dept., running without field/frequency lock. To obtain the spectra, typically 66° (11.5 μs) pulses were applid at 1 s^{-1} with a 0.64 s acquisition time and a 25 kHz spectral window; to reach satisfactory S/N required collection of $5-10 \times 10^3$ transients for a single species and $10-20 \times 10^3$ transients for a mixture of species. Linewidths at half height varied with sample and temperature, but were 40 Hz or more.

Simulation of nmr spectra

The ^{199}Hg nmr spectrum of $[^{199}Hg(dppm)_2\,^{199}Hg]^{4+}$ was simulated using the program LAOCN3 (42), with values of $^4J(^{199}Hg—^{199}Hg)$ selected by trial and error.

Chemical analysis

Carbon and hydrogen microanalyses were made by Guelph Chemical Laboratories Ltd.

Acknowledgments

This work was made possible by an Operating Grant to P.A.W.D. from the Natural Sciences and Engineering Research Council of Canada. Some initial high field nmr spectra were obtained at the Southwestern Ontario NMR Centre at Guelph which was funded by a Major Installation Grant from NSERC.

1. W. LEVASON and C. A. MCAULIFFE. *In* The chemistry of mercury. *Edited by* C. A. McAuliffe. Macmillan, London. 1977. Chapt. 15.
2. P. A. W. DEAN. Prog. Inorg. Chem. **24**, 109 (1978).
3. P. S. PREGOSIN and R. W. KUNZ. NMR, basic principles and progress. Vol. 16. 1979.
4. K. BRODERSEN and H.-U. HUMMEL. *In* Comprehensive coordination chemistry. *Edited by* G. Wilkinson, R. D. Gillard, and J. A. McCleverty. Pergamon, Oxford. To be published. Chapt. 56, Part 3.
5. R. J. PUDDEPHATT. Chem. Soc. Rev. **12**, 199 (1983), and refer-

ences therein.
6. M. J. GALLAGHER, D. P. GRADDON, and A. R. SHEIKH. Aust. J. Chem. **29**, 759 (1976).
7. (*a*) W. S. MCDONALD, P. G. PRINGLE, and B. L. SHAW. J. Chem. Soc. Chem. Commun. 861 (1982); (*b*) P. G. PRINGLE and B. L. SHAW. J. Chem. Soc. Chem. Commun. 956 (1982).
8. T. G. APPLETON, M. A. BENNETT, and I. B. TOMKINS. J. Chem. Soc. Dalton Trans. 439 (1976).
9. S. HEITKAMP, D. J. STUFKENS, and K. VRIEZE. J. Organomet. Chem. **169**, 107 (1979).
10. R. COLTON and D. DAKTERNIEKS. Aust. J. Chem. **34**, 323 (1981).
11. T. ALLMAN and R. G. GOEL. Can. J. Chem. **62**, 621 (1984).
12. H. B. BUERGI, E. FISCHER, R. W. KUNZ, M. PARVEZ, and P. S. PREGOSIN. Inorg. Chem. **21**, 1246 (1982).
13. R. W. KUNZ, P. S. PREGOSIN, M. CAMALLI, F. CARUSO, and L. ZAMBONELLI. Helv. Chim. Acta, **66**, 1661 (1983).
14. P. A. W. DEAN, D. D. PHILLIPS, and L. POLENSEK. Can. J. Chem. **59**, 50 (1980); P. A. W. DEAN. Can. J. Chem. **61**, 1795 (1983).
15. V. GUTMANN and E. WYCHERA. Inorg. Nucl. Chem. Lett. **2**, 257 (1966); V. GUTMANN. Coordination chemistry in non-aqueous solvents. Springer Verlag, Vienna. 1968. Chapt. 2.
16. L. C. DAMUDE and P. A. DEAN. J. Organomet. Chem. **181**, 1 (1979).
17. G. CALINGAERT and H. A. BEATTY. J. Am. Chem. Soc. **61**, 2748 (1939).
18. N. SHEPPARD and J. J. TURNER. Proc. R. Soc. **252**, 506 (1959).
19. M. P. BROWN, R. J. PUDDEPHATT, M. RASHIDI, and K. R. SEDDON. J. Chem. Soc. Dalton Trans. 951 (1977).
20. (*a*) R. K. HARRIS. Can. J. Chem. **42**, 2275 (1964); (*b*) R. K. HARRIS. Inorg. Chem. **5**, 701 (1966).
21. R. BENN, H. GÜNTHER, A. MAERCKER, V. MENGER, and P. SCHMITT. Angew. Chem. Int. Ed. Engl. **21**, 295 (1982); R. E. WASYLISHEN, R. E. LENKINSKI, and C. RODGER. Can. J. Chem. **60**, 2113 (1982).
22. (*a*) M. A. SENS, N. K. WILSON, P. D. ELLIS, and J. D. ODOM. J. Magn. Reson. **19**, 323 (1975); (*b*) R. G. KIDD and R. J. GOODFELLOW. *In* NMR and the Periodic Table. *Edited by* R. K. Harris and B. E. Mann. Academic Press, London. 1978. Chapt. 8, Table 8.31.
23. E. C. ALYEA, S. A. DIAS, G. FERGUSON, and M. A. KHAN. J. Chem. Res. (S). 360 (1979); J. Chem. Res. (M). 4101 (1979).
24. (*a*) R. J. GILLESPIE, P. GRANGER, K. R. MORGAN, and G. J. SCHROBILGEN. Inorg. Chem. **23**, 887 (1984); (*b*) G. B. DEACON, G. N. STRETTON, and M. J. O'CONNOR. J. Organomet. Chem. **227**, C1 (1984).
25. J. EICHBICHLER and P. PERINGER. Chem. Ber. **117**, 1215 (1984).
26. A. F. M. J. VAN DER PLOEG and G. VAN KOTEN. Inorg. Chim. Acta, **51**, 225 (1981).
27. D. M. HO and R. BAU. Inorg. Chem. **22**, 4073 (1983).
28. R. COLTON and D. DAKTERNIEKS. Aust. J. Chem. **33**, 1463 (1980).
29. P. PERINGER and D. OBENDORF. Inorg. Chim. Acta Lett. **77**, L147 (1983).
30. (*a*) D. GRDENIĆ, B. KAMENAR, and A. HERGOLD-BRUNDIĆ. Cryst. Struct. Commun. **7**, 245 (1978); (*b*) D. GRDENIĆ, B. KAMENAR, and A. HERGOLD-BRUNDIĆ. Croat. Chem. Acta, **52**, 339 (1979).
31. M. P. BROWN, J. R. FISHER, R. H. HILL, R. J. PUDDEPHATT, and K. R. SEDDON. Inorg. Chem. **20**, 3516 (1981). C. R. LANGRICK, D. M. MCEWAN, P. G. PRINGLE, and B. L. SHAW. J. Chem. Soc. Dalton Trans. 2487 (1983).
32. P. A. W. DEAN. Can. J. Chem. **57**, 754 (1979).
33. S. W. CARR and R. COLTON. Aust. J. Chem. **34**, 35 (1981).
34. S. O. GRIM and E. D. WALTON. Inorg. Chem. **19**, 1982 (1980).
35. P. E. GARROU. Chem. Rev. **81**, 229 (1981).
36. P. PERINGER. Inorg. Nucl. Chem. Lett. **16**, 461 (1980).
37. P. A. W. DEAN, D. G. IBBOTT, and J. B. STOTHERS. Can. J. Chem. **54**, 166 (1976); **54**, 1493 (1976).
38. K. SOMMER. Z. Anorg. Chem. **376**, 37 (1970).
39. T. ALLMAN and R. G. GOEL. Can. J. Chem. **62**, 615 (1984).
40. E. D. BECKER. High resolution NMR. 2nd ed. Academic, New York. 1980, p. 59.
41. W. GERGER, U. MAYER, and V. GUTMANN. Monatsch. Chem. **108**, 417 (1977).
42. A. A. BOTHNER-BY and S. M. CASTELLANO. LAOCN3. The Mellon Institute, Pittsburgh.

Investigation of the constituents of *Ryania Speciosa*

LUC RUEST, DAVID R. TAYLOR, AND PIERRE DESLONGCHAMPS
Laboratoire de synthèse organique, Département de chimie, Faculté des Sciences, Université de Sherbrooke, Sherbrooke (Qué.), Canada J1K 2R1

Received March 20, 1985

LUC RUEST, DAVID R. TAYLOR, and PIERRE DESLONGCHAMPS. Can. J. Chem. **63**, 2840 (1985).

Six new metabolites (**2**, **5–9**) were isolated from the extracts of *Ryania Speciosa* Vahl. These compounds are closely related to ryanodine, the known insecticidal toxic alkaloid from this plant.

LUC RUEST, DAVID R. TAYLOR et PIERRE DESLONGCHAMPS. Can. J. Chem. **63**, 2840 (1985).

Six nouveaux métabolites (**2**, **5–9**) ont été isolés des extraits de la plante *Ryania Speciosa* Vahl. Ces composés sont étroitement reliés à la ryanodine, un alcaloïde toxique connu provenant de cette plante.

Although the insecticidal diterpene ester ryanodine (**1**) (1) has been isolated from *Ryania Speciosa* since 1948 (2), to our knowledge no other diterpene had been reported from this genus prior to 1984. Very recently Waterhouse, Holden, and Casida (3) reported the isolation and characterization of dehydroryanodine (**2**), the second most abundant toxic (3) alkaloid (besides ryanodine) from *Ryania Speciosa*. Ryanodine (**1**) is a complex, highly oxygenated diterpene in which the unrearranged geranyl–geraniol (**3**) unit is easily discerned as proposed by Wiesner (1). An examination of the constituents of *Ryania Speciosa* was undertaken to seek compounds related to ryanodine as (i) alternate synthetic targets;[1] (ii) possible precursors on the biogenetic pathway to ryanodine. The actual growing interest[2] in the toxic constituents of *Ryania Speciosa* prompted us to publish some results obtained some years ago in our laboratory.

This report describes the isolation and identification of six diterpene esters of α-pyrrole carboxylic acid closely related to ryanodine (**1**): the already known (3) dehydroryanodine (**2**), diterpene esters A (**5**), B (**6**), C_1 (**7**), C_2 (**8**), and D (**9**).

The structure of dehydroryanodine (**2**), the major new diterpene slightly more polar than ryanodine (see Experimental), was proven by spectral analysis and by catalytic hydrogenation to a mixture of ryanodine (**1**) and 9-epiryanodine (**10**). We will not discuss further the structure of this compound (cf. Experimental for details) since it has been at least partly described in ref. 3.

Compounds A, B, C_1, C_2, and D were isolated by chromatography of the crude extracts of powdered stems of *Ryania Speciosa* (2). Their R_f values are all greater than that of ryanodine and they are listed in order of increasing polarity, A being the least polar (see Experimental).

Spectral data of diterpene ester A (**5**) are in agreement in all respects with the proposed structure. The mass spectrum indicates a formula of $C_{26}H_{37}O_{10}N$, which is equivalent to the addition of CH_2O to ryanodine, suggesting that ester A has one more hydroxyl group than ryanodine and that one of the hydroxyl groups has been methylated. The structure is supported by nmr spectral analysis: it shows three multiplets from 6.2 to 7.1 δ (for the pyrrole-α-carboxylate moiety), a sharp singlet at 5.68 δ (3-H), a methoxy at 3.56 δ, an AB pattern at 2.62 and 1.83 δ (for 14-H_2 on the heterocyclic ring), two tertiary and three secondary methyl groups. In addition, after D_2O exchange (6 hydroxyls), a narrow multiplet at 4.01 δ (narrow doublet of triplets) and a doublet (J = 3.3 Hz) at 3.49 δ account for two hydrogens α to the secondary alcohols in positions 8 and 10, respectively. The magnitude of the coupling constants of these hydrogens suggests in each case an equatorial position.

Spectral analysis of diterpene ester D suggests that it is dehydroester A, $C_{26}H_{35}O_{10}N$. The major differences in the nmr spectra of esters A and D are (i) a secondary methyl signal (1.23 δ) in ester A has been replaced by two one-proton doublets (J = 1.32 Hz) at 5.24 and 5.43 δ in easter D; (ii) the doublet at 3.49 δ in A has become a singlet at 3.97 δ in D, and (iii) the multiplet at 4.01 δ in A has changed to a multiplet at 4.54 δ in D. The location and stereochemistry of the two secondary alcohols in ester D follow from the lack of allylic coupling between the vinylic proton of the exocyclic methylene (21-H_2) and the hydrogens in positions 8 and 10, indicating the coplanarity of the allylic protons with the double bond. In contrast, both vinylic protons in dehydroryanodine (**2**) occur as multiplets because of allylic coupling. Furthermore, in ester D there is an evident *W* coupling between the equatorial hydrogens 8-H and 10-H. This *W* coupling is also present in ester A. Being present in A, this coupling confirms the equatorial stereochemistry for 8-H and 10-H and suggests that the secondary methyl of position 9 is equatorial.

The location of the methoxyl in esters A and D follows from a consideration of the ir and nmr spectra and chemical data. The inertness of esters A and D to treatment with periodate shows that the α-glycol system present in ryanodine is blocked in A and D. Whereas the singlets for 3-H in ryanodine (**1**) and dehydroryanodine (**2**) appear at 5.35 and 5.38 δ respectively ($CDCl_3$), those for the same proton in esters A and D occur at 5.68 δ and 5.64 δ respectively. This indicates a difference in structure of these latter compounds, close to the ester function. In infrared ($CHCl_3$), the carboxylic ester absorbs at 1675 cm^{-1} in ryanodine and dehydroryanodine and at 1701 and 1703 cm^{-1} for esters A and D respectively. These data indicate that hydrogen bonding of the ester can take place in ryanodine and dehydroryanodine but not in A and D. Hence the location of the methoxyl is at the site of the hydroxyl (position 4), which is close enough to hydrogen bond with the ester carbonyl in ryanodine.

The mass spectrum of diterpene ester B (Δ^{9-10} 8-oxo ryanodine) is consistent with the formula $C_{25}H_{31}O_9N$. The nmr spectrum is similar to that of ryanodine except that the signals for 9-CH_3 and 10-H have been replaced by that for a vinyl methyl (d, 1.5 Hz) at 1.92 δ coupled to a vinylic proton (q, 1.5 Hz) at 6.70 δ. Ester B has a new AB pattern (additional to

[1] For a total synthesis of ryanodol (**4**) see ref. 4.
[2] At submicromolar concentrations, ryanodine interferes specifically with the relaxing mechanism of mammalian muscle (6).

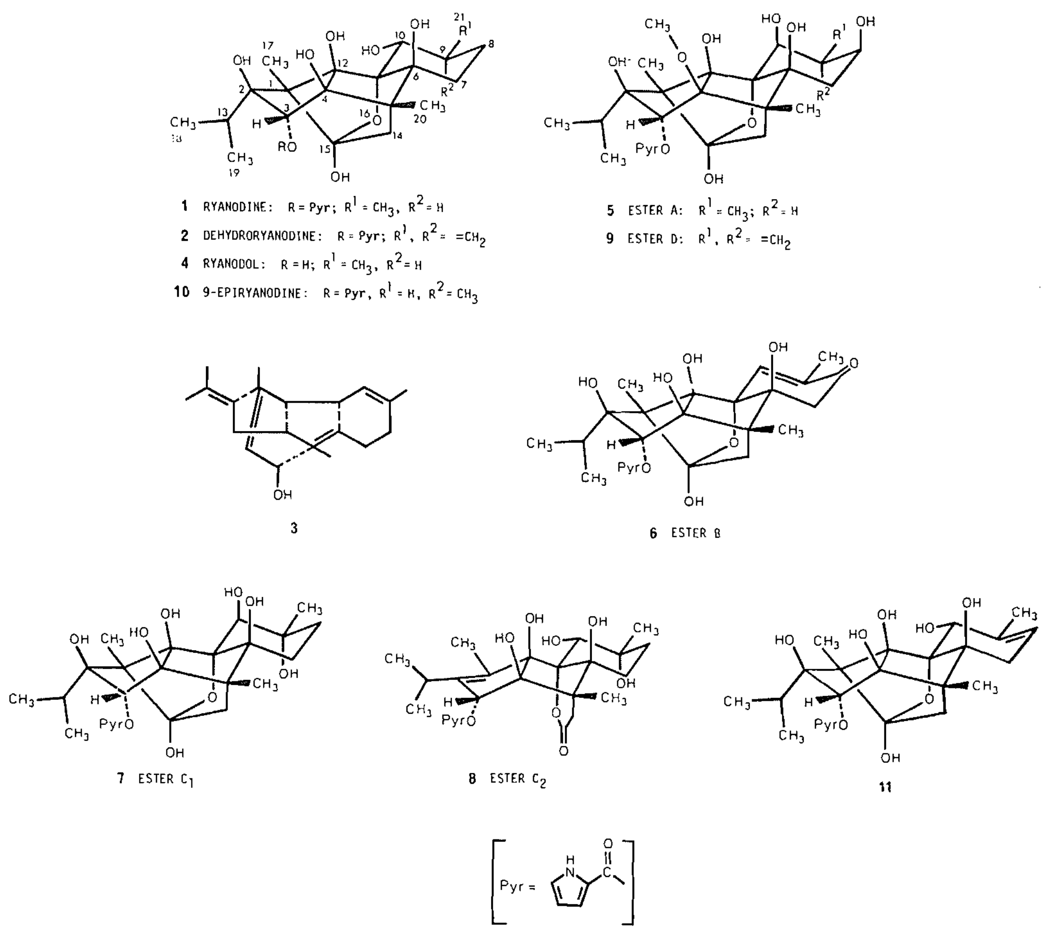

SCHEME 1

14-H$_2$) at 3.12 and 2.35 δ for 7-H$_2$. These data, in agreement with a uv absorption at 232 nm and the infrared spectrum (1681 cm^{-1}), are consistent with the proposed structure for ester B.

The mass spectrum of ester C$_1$ (9*R*-hydroxy 10*S*-ryanodine) is consistent with the molecular formula $C_{25}H_{35}O_{10}N$, equivalent to the addition of one oxygen to ryanodine. The nmr spectrum shows that the secondary methyl at C-9 (1.05 δ, d) in ryanodine has been replaced by a singlet at 1.21 δ and that the 10.1-Hz doublet at 3.94 δ for the 10-H in ryanodine has now become a broad singlet at 3.75 δ (which sharpens by irradiation at 1.53 δ (8-H$_{eq}$), *W* coupling). These data are in agreement with the structure given for ester C$_1$.

Diterpene ester C$_2$ (9*R*-hydroxy anhydroryanodine) shows a mass spectrum consistent with the formula $C_{25}H_{33}O_9N$. The nmr spectrum shows in particular an AB pattern (J = 19.5 Hz) at 3.27 and 2.28 δ for the methylenic 14-H$_2$, α to the lactone carbonyl (1745 cm^{-1}), and a vinylic methyl doublet (1.78 δ, 2.3 Hz) coupled to a one-proton signal (3-H) (q, J = 2.3 Hz) at 5.96 δ. In addition, the nmr spectrum shows a signal for a tertiary methyl at 1.16 δ (9-CH$_3$) and a very sharp singlet at 4.23 δ (no *W* coupling with the equatorial 8-H) for the axial proton at position 10. Since C$_2$ has a lower R_f than C$_1$, it is unlikely to be the anhydro C$_1$ because anhydro derivatives have R_f values always greater than those of ryanodine, dehydroryanodine, and ryanodol. In agreement, acid catalysed dehydration of C$_1$ gave anhydro C$_1$ of much higher R_f than C$_2$. Structures given to diterpene esters C$_1$ and C$_2$ account for their spectral as well as their chemical properties. In these two compounds, the equatorial stereochemistry of the 9-CH$_3$ follows the nuclear Overhauser effect (nOe) analysis of that methyl group versus the axial hydrogen at position 7. In the course of the catalytic hydrogenation of dehydroryanodine (**2**), which yields **1** and **10**, an isomer of dehydroryanodine was also observed and isolated. Its structure was shown, by spectroscopic analysis, to be **11**. Reduction of **11** gives mainly ryanodine (**1**) containing a small proportion (3:1) of 9-epiryanodine (**10**).

Biological activity: biological activities of these new metabolites (esters A, B, C$_1$, C$_2$, and D) are currently under investigation.[3]

Experimental

The infrared (ir) spectra were taken on a Perkin–Elmer 257 spectrophotometer. The ultraviolet (uv) spectra were registered on a Varian Techtron 635 spectrophotometer. Proton nmr spectra were recorded on a Bruker WM-250 instrument: chemical shifts are reported in δ values relative to chloroform (7.26 δ) or methanol (3.35 δ) as internal standard. The mass spectra (ms) were registered on a ZAB-1F mass spectrometer. The melting points were taken on a Büchi or a Reichert melting point instrument and are not corrected.

General

The crude extracts of *Ryania Speciosa* Vahl were obtained mainly as indicated by Folkers and co-workers (2). Following these authors, the moist powder (500 g, 800 mL H$_2$O) was extracted continuously with chloroform (1.5 L) during 30 h. The volume of the solvent was reduced to ~200 mL and extracted with water (4 × 300 mL). The

[3] Dr. J. L. Sutko, Department of Physiology, University of Texas Health Science at Dallas, Dallas, Texas 75235, USA.

combined aqueous layers were saturated with NaCl and extracted with amyl acetate or ethyl acetate (5×200 mL). Removal of the solvent furnished a crude extract corresponding to ~0.25% (w/w) of the dry powdered *Ryania Speciosa* wood. The greatest part of ryanodine (**1**) and dehydroryanodine (Δ^{9-21} ryanodine) (**2**) cocrystallized (acetone) from this crude extract. Classical chromatography on silica column ($CHCl_3/CH_3OH$ 95:5) of the mother liquors led to a mixture of the minor metabolites A, B, C_1, C_2, and D, plus the same mixture of ryanodine and dehydroryanodine.

Separation of ryanodine (1) and dehydroryanodine (2)

A sample of the mixture was separated by preparative thin-layer chromatography (Merck, pre-coated tlc plates, silica gel 60F-254) by multiple elution technique ($CHCl_3$/MeOH/40% aqueous CH_3NH_2 85:15:2) or by flash chromatography (5) (same solvents respectively, 90:10:1.5). The less polar compound, forming a brown chromophore when heated on tlc plates (H_2SO_4 sprayed), was shown to be pure ryanodine (**1**) (mp 234–236°C) (lit. (3) mp 235–237°C; (*1b*) mp 228–229°C); ir ($CHCl_3$): 3580, 3500, 3450, 3330, 1676, and 1550 cm^{-1}; nmr ($CDCl_3$, after exchange with D_2O); 7.07, 6.97, and 6.32 (three double doublets for pyrrole ring hydrogens), 5.35 (s, 3-H), 3.94 (d, 10.1 Hz, 10-H), 2.38 (d, 13.8 Hz) and 1.93 (d, 13.8 Hz) (AB pattern, 14-H_2), 2.33 (m, 13-H), 2.04 (m, 7-H_{ax}), 1.85 (m, 9-H_{ax}), 1.58 (m, 8-H_{ax} and 7-H_{eq}), 1.44 (s, 17-H_3), 1.27 (m, 8-H_{eq}), 1.14 and 0.94 (two d, 6.7 Hz and 6.5 Hz, 18-H_3 and 19-H_3), 1.05 (d, 6.5 Hz, 21-H_3), 0.84 (s, 20-H_3) (were exchanged by D_2O, peaks at 10.2, 5.92, 5.59, 3.95, 3.78, 2.92, 2.86, and 1.99); *m/e*: M^+ 493. The more polar compound, forming a typical red chromophore when heated on tlc (H_2SO_4 sprayed), was shown to be dehydroryanodine (Δ^{9-21} ryanodine); mp 252–254°C (crystallized from acetone, lit. (3) mp 175–179°C); ir ($CHCl_3$): 3580, 3500, 3450, 3330, 1675, and 1547 cm^{-1}; nmr ($CDCl_3$, after exchange with D_2O): 7.07, 6.97, and 6.32 (three double doublets for pyrrole ring hydrogens), 5.38 (s, 3-H), 5.09 and 4.99 (two multiplets, 21-H_2) 4.87 (m, 10-H_{ax}), 2.62 (m, 8-H_{ax}), 2.38 (d, 13.8 Hz) and 1.92 (d, 13.8 Hz) (AB pattern, 14-H_2), 2.35 (m, 8-H_{eq} and 13-H), 2.05 (m, 7-H_{ax}), 1.44 (s, 17-H_3), 1.36 (m, 7-H_{eq}), 1.14 and 0.95 (two d, 6.7 and 6.4 Hz, 18-H_3 and 19-H_3), 0.89 (s, 20-H_3) (were exchanged by D_2O, peaks at 10.4, 5.74, 5.46, 3.73, 2.87, 2.82, and 2.13). *Exact Mass* (ms *m/e*) calcd.: 473.2049 ($M^+ - H_2O$); found: 473.2044.

Minor metabolites from Ryania Speciosa

The main constituents less polar than ryanodine were separated by preparative tlc ($CHCl_3$/MeOH/40% aqueous $MeNH_2$ 85:15:3). Each one represents ≈1–2% (w/w) of the crude extract. A first separation led to two fractions, the more polar of which contained esters B, C_1, C_2, and D. The less polar fraction was resubjected to preparative tlc (petroleum ether/acetone/acetic acid 50:50:3) to yield pure Ryania diterpene A. The more polar fraction was separated on tlc (petroleum ether/acetone/acetic acid 50:50:3) to give diterpene ester B (the top band), diterpene ester C_1 (second band), and ester C_2 (fourth band). The third band was rechromatographed ($CHCl_3$/MeOH/aqueous NH_3 90:10:1): the top band was ester C_2 and the bottom band was diterpene ester D.

Ryania diterpene ester A: ir ($CHCl_3$): 3590, 3510, 3455, 3310, 1701, and 1498 cm^{-1}; nmr ($CDCl_3$, after exchange with D_2O): 7.03, 6.88, and 6.28 (three double doublets for pyrrole ring hydrogens), 5.68 (s, 3-H), 4.02 (m, sharpens by irradiation at 3.49, 8-H_{eq}), 3.56 (s, 4-OCH_3), 3.49 (d, 3.3 Hz, 10-H_{eq}), 2.62 (d, 13.7 Hz) and 1.83 (d, 13.7 Hz) (AB pattern, 14-H_2), 2.24 (dd, 13.8, 3.8 Hz, 7-H_{ax}) and 1.82 (dd, 13.8, 2.9 Hz, 7-H_{eq}) (AB pattern), 2.23 (m, 9-H), 2.20 (m, 13-H), 1.40 (s, 17-H_3), 1.23 (d, 7.3 Hz, 21-H_3), 1.07 and 0.81 (two d, 6.7 and 6.4 Hz, 18-H_3 and 19-H_3), 0.97 (s, 20-H_3) (were exchanged by D_2O, peaks at 10.2, 5.85, 5.52, 3.61, 3.26, 2.78, and 2.50). *Exact Mass* (ms *m/e*) calcd.: 505.2311 ($M^+ - H_2O$); found: 505.2320.

Ryania diterpene ester B: ir ($CHCl_3$): 3580, 3510, 3450, 3300, 1681, and 1547 cm^{-1}; uv λ_{max}: 268 and 232 nm; nmr ($CDCl_3$, after exchange with D_2O): 7.11, 6.98, and 6.31 (three double doublets for pyrrole ring hydrogens), 6.70 (q, 1.6 Hz, 10-H), 5.27 (s, 3-H), 3.12 (d, 16 Hz) and 2.35 (d, 16 Hz) (AB pattern, 7-H_2), 2.53 (d, 13.9 Hz) and 1.93 (d, 13.9 Hz) (AB pattern, 14-H_2), 2.31 (m, 13-H), 1.89 (d, 1.6 Hz, 21-H_3), 1.41 (s, 17-H_3), 1.11 and 0.92 (two d, 6.7 and 6.4 Hz, 18-H_3 and 19-H_3), 0.87 (s, 20-H_3) (were exchanged by D_2O, peaks at 10.3, 6.13, 5.85, 3.71, 3.17, and 3.00). *Exact Mass* (ms *m/e*) calcd.: 489.1998 (M^+); found: 489.1992.

Ryania diterpene ester C_1: mp 188–190°C ($CHCl_3$); ir (Nujol): 3590, 3440, 3280, 1688, 1666, and 1548 cm^{-1}; nmr ($CDCl_3$, 10% pyridine-d_5, after exchange with D_2O): 6.96, 6.84, and 6.19 (three double doublets for pyrrole ring hydrogens), 5.73 (s, 3-H), 3.75 (broad singlet, sharpens by irradiating at 1.53, 10-H), 2.60 (d, 13.9 Hz) and 1.96 (d, 13.9 Hz) (AB pattern, 14-H_2), 2.25 (m, 13-H), 2.04 (m, 7-H_{ax}), 1.96 (m, 8-H_{ax}), 1.53 (m, 8-H_{eq}), 1.43 (s, 17-H_3), 1.32 (m, 7-H_{eq}), 1.21 (s, 21-H_3), 1.10 and 0.77 (two d, 6.7 and 6.4 Hz, 18-H_3 and 19-H_3), 0.90 (s, 20-H_3) (were exchanged by D_2O, peaks at 11.5, 8.39, 4.31, 3.40, and 3.18. *Exact Mass* (ms *m/e*) calcd.: 509.2260 (M^+); found: 509.2249.

Ryania diterpene ester C_2: mp 274–275°C ($CHCl_3$); ir (Nujol) 3590, 3450, 3390, 1745, 1705, 1687 (shoulder), 1577, and 1540 cm^{-1}; nmr ($CDCl_3$, 10% pyridine-d_5, after exchange with D_2O): 6.83, 6.73, and 6.04 (three double doublets for pyrrole ring hydrogens), 5.96 (q, 2.3 Hz, 3-H), 4.23 (s, 10-H_{ax}), 3.28 (d, 19.6 Hz) and 2.28 (d, 19.6 Hz) (AB pattern, 14-H_2), 2.47 (m, 13-H), 1.96 (m, 7-H_{ax}), 1.78 (d, 2.3 Hz, 17-H_3), 1.60 (m, 8-H_{ax} and 7-H_{eq}), 1.28 (m, 8-H_{eq}), 1.16 (s, 21-H_3), 0.87 and 0.59 (two d, 7.0 Hz, 18-H_3 and 19-H_3), 0.86 (s, 20-H_3) (were exchanged by D_2O, peaks at 11.5, 6.37, 6.14, 5.86, 4.63, 3.70, and 3.34). *Exact Mass* (ms *m/e*) calcd. for $C_{25}H_{33}O_9N - H_2O$: 473.2049; found: 473.2049 ($M^+ - H_2O$).

Ryania diterpene ester D: ir ($CHCl_3$): 3590, 3510, 3455, 3365, 1703, and 1548 cm^{-1}; nmr ($CDCl_3$, after exchange with D_2O): 7.04, 6.89, and 6.29 (three double doublets for pyrrole ring hydrogens), 5.64 (s, 3-H), 5.43 (d, 1.3 Hz) and 5.24 (d, 1.3 Hz) (21-H_2), 4.54 (m, 8-H_{eq}), 3.97 (broad s, sharpens by irradiation at 4.54, 10-H_{eq}), 3.34 (s, 4-OCH_3), 2.58 (d, 13.9 Hz) and 1.82 (two d, 13.9 Hz) (AB pattern, 14-H_2), 2.33 (dd, 13.9 and 4.2 Hz, 7-H_{ax}) and 1.88 (dd, 13.9 and 2.0 Hz, 7-H_{eq}) (AB pattern), 2.22 (m, 6.5 Hz, 13-H), 1.40 (s, 17-H_3), 1.08 and 0.84 (two d, 6.7 and 6.4 Hz, 18-H_3 and 19-H_3), 0.99 (s, 20-H_3) (were exchanged by D_2O, peaks at 11.4, 5.67, 5.61, 3.97, 3.17, 2.89, and 1.62). *Exact Mass* (ms *m/e*) calcd. for $C_{26}H_{35}O_{10}N$: 521.2260; found: 521.2260 (M^+).

Hydrogenation of dehydroryanodine (Δ^{9-20} ryanodine) (2)

Dehydroryanodine (27 mg) in ethanol (15 mL) was stirred under hydrogen in the presence of palladium 10% on carbon (40 mg) for 1.1 h at room temperature. The crude material (27 mg) isolated by filtration contained three compounds, which were separated by preparative thin-layer chromatography ($CHCl_3$/MeOH/40% aqueous CH_3NH_2 85:15:1.5). The least polar compound was ryanodine (**1**) (4.7 mg), the second one was epiryanodine (**10**) (9.7 mg), and the more polar one was isodehydroryanodine (**11**) (4.4 mg) (Δ^8-ryanodine).

9-Epiryanodine: nmr (CD_3OD): 7.08, 6.93, and 6.28 (three double doublets for pyrrole ring hydrogens), 5.67 (s, 3-H), 4.35 (d, 6.3 Hz, 10-H), 2.61 (d, 13.7 Hz) and 1.96 (d, 13.7 Hz) (AB pattern, 14-H_2), 2.31 (m, 13-H), 2.20 (m, 7-H_{ax}), 2.21, 2.05, and 1.46 (three multiplets, 9-H, 8-H_{ax}, and 8-H_{eq}), 1.44 (s, 17-H_3), 1.22 (m, 7-H_{eq}), 1.16 and 0.79 (two d, 6.7 and 6.4 Hz, 18-H_3 and 19-H_3), 1.16 (d, 7.3 Hz, 21-H_3), 0.94 (s, 20-H_3).

Isodehydroryanodine (Δ^8-ryanodine) (11): nmr (CD_3OD): 7.08, 6.93, and 6.29 (three double doublets for pyrrole ring hydrogens), 5.69 (s, 3-H), 5.39 (m, 8-H), 4.42 (m, 10-H), 2.69 (d, 14 Hz) and 2.04 (d, 14 Hz) (AB pattern, 14-H_2), 2.63 (m, 7-H_{ax}), 2.33 (m, 13-H), 1.83 (m, 21-H_3), 1.81 (m, 7-H_{eq}), 1.45 (s, 17-H_3), 1.16 and 0.80 (two d, 6.8 and 6.4 Hz, 18-H_3 and 19-H_3), 0.95 (s, 20-H_3); ms *m/e*: 491.

Hydrogenation of isodehydroryanodine (Δ^8-ryanodine) (11): pure isodehydroryanodine **11** was submitted to hydrogenation as above during 4 h. The crude product was shown (nmr) to be a mixture of ryanodine and epiryanodine (3:1, integration of 10-H doublets). The same result was obtained when Δ^{9-21}-ryanodine (**2**) was first submitted to the same catalyst in ethanol under argon (3 h), then hydrogenated.

Acknowledgements

This research was supported by the Natural Sciences and Engineering Research Council of Canada and by the "Ministère de l'Éducation" of Québec.

1. (*a*) K. WIESNER. *In* Advances in organic chemistry. Vol. 8. *Edited by* E. C. Taylor. Wiley–Interscience Publishers, New York, NY. 1972. p. 295; (*b*) R. B. KELLY, D. J. WHITTINGHAM, and K. WIESNER. Can. J. Chem. **29**, 905 (1951).
2. E. F. ROGERS, F. R. KONIUSZY, J. SHAVEL, and K. FOLKERS. J. Am. Chem. Soc. **70**, 3086 (1948).
3. A. L. WATERHOUSE, I. HOLDEN, and J. E. CASIDA. J. Chem. Soc. Chem. Commun. 1265 (1984).
4. A. BÉLANGER, D. J. F. BERNEY, H.-J. BORSCHBERG, R. BROUSSEAU, A. DOUTHEAU, R. DURAND, H. KATAYAMA, R. LAPALME, D. M. LETURC, C. C. LIAO, F. N. MACLACHLAN, J. P. MAFFRAND, F. MARAZZA, R. MARTINO, C. MOREAU, L. SAINT-LAURENT, R. SAINTONGE, P. SOUCY, L. RUEST, and P. DESLONGCHAMPS. Can. J. Chem. **57**, 3348 (1979).
5. W. C. STILL, M. KAHN, and A. MITRA. J. Org. Chem. **43**, 2923 (1978).
6. D. J. JENDEN and A. S. FAIRHURST. Pharmacol. Rev. **21**, 1 (1969), and references therein; Z. J. PENEFSKY. Pfluegers Arch. 185 (1974); J. L. SUTKO and J. L. KENYON. J. Gen. Physiol. **82**, 385 (1983); M. R. MITCHELL, T. POWELL, D. A. TERRAR, and V. W. TWIST. Br. J. Pharmacol. **81**, 543 (1984).

Asymmetric synthesis towards (3*Z*,6*R*)-3-methyl-6-isopropenyl-3,9-decadien-1-yl acetate, a component of the California red scale pheromone

MARK WHITTAKER, COLIN R. MCARTHUR,[1] AND CLIFFORD C. LEZNOFF[1]
Department of Chemistry, York University, Downsview (Toronto), Ont., Canada M3J 1P3

Received January 31, 1985

MARK WHITTAKER, COLIN R. MCARTHUR, and CLIFFORD C. LEZNOFF. Can. J. Chem. **63**, 2844 (1985).

The key chiral synthons, (*R*)-3-isopropenyl-6-heptenoic acid and (*R*)-3-isopropenyl-6-heptenal, needed for the synthesis of (3*Z*,6*R*)-3-methyl-6-isopropenyl-3,9-decadien-1-yl acetate, a component of the sex pheromone of the California red scale, *Aonidiella aurantii*, have been prepared by asymmetric synthesis. The chiral acid was synthesized in 86% ee by an asymmetric 1,4-addition of isopropenylmagnesium bromide to the *l*-ephedrine amide derived from (*E*)-2,6-heptadienoic acid, followed by base hydrolysis. Acid hydrolysis gave the chiral 3-(3-buten-1-yl)-4,4-dimethylbutyrolactone. The chiral aldehyde was prepared in greater than 99% ee by an asymmetric 1,4-addition of isopropenylmagnesium bromide to the imine derived from (*S*)-(+)-*tert*-butyl 2-amino-3,3-dimethylbutyrate and (*E*)-2,6-heptadienal. The 1,4-addition reactions of *n*-butyllithium or isopropenyllithium to (4*S*,5*S*)-(+)-2-[1-(*E*-1,5-hexadienyl)]-4-methoxymethyl-5-phenyl-2-oxazoline gave the addition products, and sequential mild hydrolysis and reduction of these adducts yielded chiral 3-*n*-butyl-6-hepten-1-ol for the former adduct but a mixture of products was obtained from the latter adduct.

MARK WHITTAKER, COLIN R. MCARTHUR et CLIFFORD C. LEZNOFF. Can. J. Chem. **63**, 2844 (1985).

Utilisant une synthèse asymétrique, on a préparé les synthons chiraux clés, acide isopropényl-3(*R*) heptène-6 oïque et isopropényl-3(*R*) heptène-6 al, nécessaires à la synthèse de l'acétate du méthyl-3(*Z*) isopropényl-6(*R*) décadiène-3,9 yle-1, une composante de la phérémone sexuelle de l'écaille rouge de la Californie *Aonidiella aurantii*. On a préparé l'acide chiral avec un ee de 86% en faisant appel à une addition asymétrique-1,4 du bromure d'isopropénylmagnésium sur l'amide de la *l*-éphédrine provenant de l'acide heptadiène-2,6(*E*) oïque, suivie d'une hydrolyse basique. L'hydrolyse acide permet d'accéder à la (butène-3 yl-1)-3 diméthyl-4,4 butyrolactone chirale. On a préparé l'aldéhyde chiral avec un ee supérieur à 99% en procédant à une addition-1,4 asymétrique du bromure d'isopénylmagnésium sur l'imide obtenu par réaction du (+)-amino-2(*S*) diméthyl-3,3 butyrate de *tert*-butyle et de l'heptadiène-2,6(*E*) al. Les réactions d'additions-1,4 du *n*-butyllithium ou de l'isopropényllithium sur la (+)-[(hexadiène-1,5(*E*) yl)-1]-2 méthoxyméthyl-4(*S*) phényl-5(*S*) oxazoline-2 conduisent aux produits d'addition et une hydrolyse douce subséquente suivie d'une réduction de ces adduits conduit au *n*-butyl-3 heptène-6 ol-1 chiral lorsqu'on part du premier adduit; toutefois, le second adduit ne conduit qu'à un mélange de produits.

[Traduit par le journal]

The sex pheromones of the California red scale, *Aonidiella aurantii* (Maskell), an insect which is a severe pest of citrus in California, Australia, and the Mediterranean countries, were identified as a mixture of (3*Z*,6*R*)-3-methyl-6-isopropenyl-3,9-decadien-1-yl acetate (**1**) and (3*S*,6*R*)-3-methyl-6-isopropenyl-9-decen-1-yl acetate (**2**) (1–4). Each of these compounds exhibits equal independent ability to attract the male insects (4).

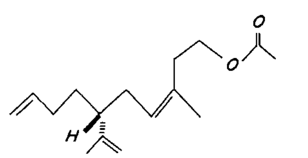

1

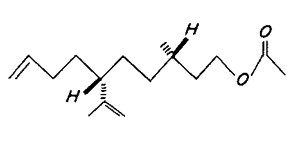

2

Our related interests in the synthesis of insect sex attractants on insoluble polymer supports (5) and the use of solid phases in asymmetric syntheses (6) have naturally led us to consider the possibilities of asymmetric synthesis of chiral sex pheromones on solid phases. Our attention focussed on compound **1** containing a single chiral centre. Component **1** was first synthesized from (*S*)-(+)-carvone in 2.6% overall yield (2). A racemic mixture of **1** and its enantiomer was subsequently synthesized in 32% (7) and 27% (8) yields, respectively. Two other preparations of **1** have been reported recently, starting from (*S*)-(+)-carvone (9). Thus, all syntheses of **1** (2, 9) started from the same naturally occurring chiral precursor. Our desire to prepare compound **1** using polymer-bound chiral auxillaries *via asymmetric synthesis* led us to examine satisfactory methods for the asymmetric synthesis of **1** in solution as a necessary prerequisite step.

A key chiral intermediate used in the synthesis of **1** was (*R*)-3-isopropenyl-6-heptenal (**3**), previously obtained by lengthy conversion of the natural product (*S*)-(+)-carvone (2, 9*a*). Compound **3** could potentially be made much more readily by asymmetric 1,4-additions to at least three different possible α,β-unsaturated functionalized precursors, and we can designate these routes as the ephedrine, the aldimine, and the oxazoline routes.

The ephedrine route

It has been shown that chiral α,β-unsaturated amides, prepared from (1*R*,2*S*)-(−)-α-(1-methylaminoethyl)benzyl alcohol (*l*-ephedrine) in 1,4-addition reactions with Grignard reagents, can give, after acid hydrolysis, chiral β-substituted carboxylic acids in greater than 95% enantiomeric excess (ee) (10). This initial report (10), however, used only simple aliphatic amides and Grignard reagents and it remained to be seen if this attractive asymmetric synthesis could be applied to the synthesis of a more complex β-substituted aldehyde such as **3**. The chiral α,β-unsaturated amide necessary for this synthesis is *N*-(*E*-2,6-heptadienoyl)-*l*-ephedrine (**4**) and is prepared as shown in Scheme 1.

[1] Authors to whom correspondence may be addressed.

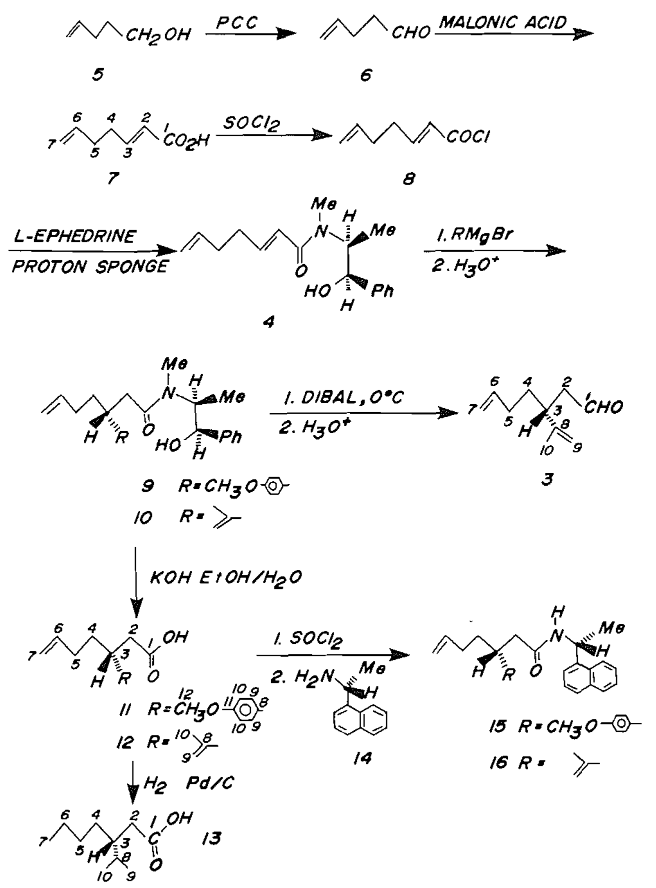

SCHEME 1

Oxidation of 4-penten-1-ol (**5**) with pyridinium chlorochromate (PCC) in methylene chloride (11) gave the volatile 4-pentenal (**6**) (12, 13) in 55% yield. Treatment of **6** with malonic acid in pyridine and pyrrolidine at 20°C overnight followed by refluxing for 5 h gives a 70–80% yield of (*E*)-2,6-heptadienoic acid (**7**) (13), contaminated by some of the *Z* isomer as shown by ^{13}C nmr. The mixture of (*E*) and (*Z*)-**7** was treated with thionyl chloride to give pure (*E*)-2,6-heptadienoyl chloride (**8**) in high yield with concomitant conversion of the minor (*Z*)-**7** isomer to the (*E*)-**7** isomer (14). Compound **8** was converted to the desired **4** by treatment with *l*-ephedrine in the presence of proton sponge (10). To test the usefulness of 1,4-addition reactions to adduct **4**, *p*-methoxyphenylmagnesium bromide in tetrahydrofuran (THF) was caused to react with **4** at 0°C for 24 h to give *N*-(3-*p*-methoxyphenyl-6-heptenoyl)-*l*-ephedrine (**9**) in 59% yield. Similarly, treatment of **4** with isopropenylmagnesium bromide in ether/THF mixtures at 0°C for 48 h gave *N*-(3-isopropenyl-6-heptenoyl)-*l*-ephedrine (**10**) in 51–69% yield. Compounds **9** and **10** were cleaved by base hydrolysis with a 10% potassium hydroxide in ethanol/water mixture to give optically active 3-*p*-methoxyphenyl-6-heptenoic acid (**11**) and 3-isopropenyl-6-heptenoic acid (**12**) in 49–57% and 63–80% yield, respectively. Hydrogenation of **12** gave the known compound (*R*)-3-isopropylheptanoic acid (**13**) (15), thus confirming the absolute configuration of **12** to be *R*, as desired. The absolute configuration of **11** has not been determined in this study, but it is considered likely that it is also *R*, since it possesses a negative optical rotation as has been reported (15) for a structurally related series of (*R*)-3-*o*-methoxyphenylalkanoic acids.

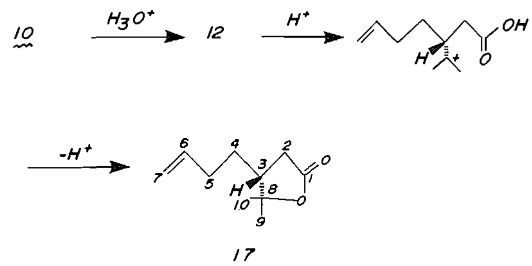

SCHEME 2

Determination of the enantiomeric excess of **12** by hydrogenation to **13** and comparison of the optical rotation with that reported in the literature was not reliable, because of some racemization occurring during the hydrogenation. Attempts to evaluate the enantiomeric excess in which acids **11** and **12** were formed, by hplc separation of the respective diastereomers of amides **9** and **10**, were not successful. Consequently, the method of Bergot *et al.* (16) was adopted. Acids **11** and **12** were converted to their acid chlorides and treated with (*R*)-(+)-1-(1-naphthyl)ethylamine (**14**) to give *N*-[(*R*)-1-(1-naphthyl)-ethyl]-3-*p*-methoxyphenyl-6-heptenamide (**15**) and (*R*)-*N*-[(*R*)-1-(1-naphthyl)ethyl]-3-isopropenyl-6-heptenamide (**16**). The chiral amides **15** and **16** were analysed by hplc (2, 16, 17) and the results indicated that the asymmetric 1,4-addition to **4** gave **9** and **10** having up to 86% ee (Table 1). In order to obtain this extent of asymmetric induction it was necessary to employ, in the 1,4-addition step, a high proportion of ether to THF. However, the use of pure ether was precluded by the instability of isopropenylmagnesium bromide in the absence of THF (18). It was found that the sluggish formation of this Grignard reagent at low THF concentrations could be ameliorated by ultrasonic irradiation (19). Compound **10** can be cleaved (20) with diisobutylaluminium hydride (DIBAL) at 0°C to **3**, albeit in low yield, and hence **3** has now been prepared via asymmetric synthesis.

Simple amides of *l*-ephedrine were cleaved under strong acid conditions (10). Acid hydrolysis of **10** did not give the free acid **12** but rather 3-(3-buten-1-yl)-4,4-dimethylbutyrolactone (**17**) in 75% yield. Compound **17** was optically active but its ee has not yet been determined. The mechanism of formation of **17** from **10** has not been explored but is likely to follow a pathway outlined in Scheme 2.

Although we had succeeded in preparing the key chiral pheromone intermediate **3** by an asymmetric synthesis route, several difficulties were still apparent. Firstly, the ee of **3**, although high, was not as high as **3** prepared via a natural product precursor such as (*S*)-(+)-carvone. Secondly, the direct cleavage of the amide **10** to **3** proceeded in low yield and hence **3** would have to be made via acid **12** which would most likely involve two more steps. Thirdly, the ephedrine route seemed less adaptable to solid phase methods than other possible routes and hence further approaches to the asymmetric synthesis of **3** were sought.

The aldimine route

The 1,4-addition of Grignard reagents to chiral α,β-unsaturated aldimines prepared from α,β-unsaturated aldehydes and chiral *tert*-butyl 2-amino-3,3-dimethylbutyrate (**26**) has been demonstrated (21) to give chiral β-substituted aldehydes in greater than 95% ee. Since the key intermediate (**3**) in the synthesis of **1** is a β-substituted aldehyde, we decided to attempt this method for the preparation of **3**. The original

TABLE 1. Results from asymmetric 1,4-addition reactions and subsequent cleavage

Entry	Substrate	Nucleophile (equivalents)	Solvent	Conditions (temp. (°C)/time (h))	Product after cleavage	Overall yield (%)	Optical rotation ($[\alpha]_D$ (c))[a]	Enantiomeric excess (%)
1	**4**	p-$CH_3OC_6H_4MgBr$ (6)	THF	0/14	**11**	25	−11.32° (3.28)	55[b]
2	**4**	p-$CH_3OC_6H_4MgBr$ (8)	THF/Et_2O(1:15)	−55/4, then −18/48	**11**	56	−16.90° (5.38)	82
3	**4**	$CH_2(CH_3)CMgBr$ (6)	THF	0/48	**12**	41	−3.13° (2.05)	46[b]
4	**4**	$CH_2(CH_3)CMgBr$ (10)	THF/Et_2O(1:19)	−50/3, then 0/48	**12**	51	−5.28° (13.67)	78[b]
5	**4**	$CH_2(CH_3)CMgBr$ (10)	THF/Et_2O(1:49)	−55/3, then −20/48	**12**	41	−5.85° (18.36)	86
6	**27**	$CH_2(CH_3)CMgBr$ (4)	THF/Et_2O(1:5)	−60/1, then −21/14	**3**	43	−0.47° (7.89)	>99
7	**30**	$CH_3(CH_2)_3Li$ (1.5)	THF	−78/3.5	**34**	40	−1.18° (2.12)	96
8	**30**	$CH_2(CH_3)CLi$ (3)	THF	−78/3	**35**	0	—	—

[a]Optical rotations measured at 21 ± 2°C using $CHCl_3$ as solvent.
[b]Enantiomeric excess determined indirectly by comparison of optical rotation with that of sample of known ee, as determined by hplc separation of diastereomeric amides.

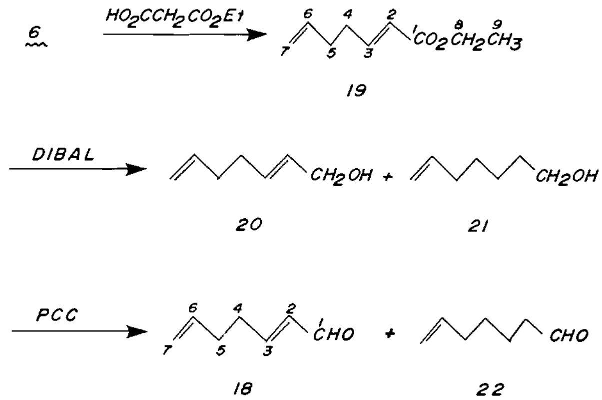

SCHEME 3

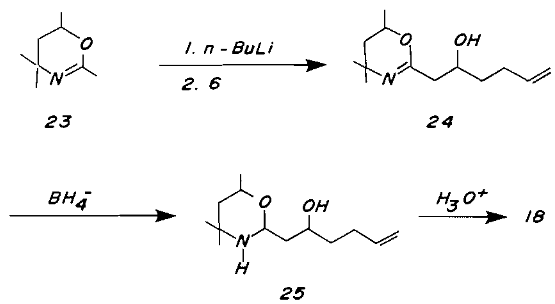

SCHEME 4

publication of this method was restricted to rather simple α,β-unsaturated aldimines, but we considered that this aldimine route would be successful even for more complicated substrates such as (E)-2,6-heptadienal (**18**) (Scheme 3).

Treatment of **6** with ethyl malonate (half-ester) in a pyridine/pyrrolidine mixture yielded ethyl 2,6-heptadienoate (**19**) in 79% yield. Reduction of **19** with two equivalents of diisobutylaluminium hydride at −25°C gave a 4:1 mixture of 2,6-heptadien-1-ol (**20**) and 6-hepten-1-ol (**21**) in 82% yield. Oxidation of this mixture by PCC yielded a mixture of 2,6-heptadienal (**18**) and 6-heptenal (**22**) as shown in Scheme 3. Compound **22** was removed from this mixture by washing with aqueous sodium bisulphite, giving pure **18** in 39% yield from **19**.

During the course of this work, Bestmann *et al.* (22) described the synthesis of **18** in 25% yield by the direct reaction of **6** with a stabilized ylide and indeed our own early synthesis by this route also gave **18** in 20% yield. The preparation of **18** according to Scheme 3 was unsatisfactory as a result of poor overall yields, contamination with **22**, and, in addition, the fact that **18** was obtained as a mixture of E and Z isomers. Many procedures described in the literature exist for the synthesis of α,β-unsaturated aldehydes from a simple aldehyde, but attempts to prepare **18** by various methods (23–25) were either unsuccessful or gave impure **18** in low yield. Finally, treatment of **6** with 2,4,4,6-tetramethyl-5,6-dihydro-1,3-oxazine (**23**) according to the procedure of Meyers *et al.* (26) gave the alcohol adduct (**24**). Reduction of **24** with sodium borohydride gave the tetrahydro-1,3-oxazine (**25**), which on mild acid hydrolysis gave **18** in 37% overall yield (Scheme 4).

Treatment of the α,β-unsaturated aldehyde **18** with racemic *tert*-butyl 2-amino-3,3-dimethylbutyrate (**26**) or (S)-(+)-**26** at 0°C in benzene overnight gave the crude α,β-unsaturated aldimine **27**. Addition of isopropenylmagnesium bromide in ether/THF (5:1) at −60°C gave, upon mild acid work-up, a

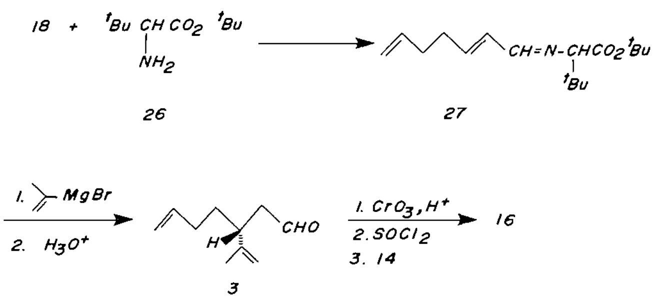

SCHEME 5

racemic mixture of **3** with its enantiomer or optically active **3** in a 43–50% yield. The enantiomeric purity of **3** was determined in a similar manner (2) to that described above for **12**. Thus oxidation of **3** gave **12**, which was converted to its acid chloride and treated with **14** to give **16**. The hplc analysis (2, 16, 17) of **16**, prepared from a racemic mixture of **3** and its enantiomer, resulted in complete resolution of the two equally abundant diastereomers, while **16** prepared from optically active **3** showed only one diastereomer and no trace of the other isomer. Furthermore, **16**, prepared from optically active **3** and (*S*)-(−)-1-(1-naphthyl)ethylamine (the enantiomer of **14**), showed only the other diastereomer by hplc analysis. The absolute configuration of pure **3** was determined to be *R*, by comparison of the hplc retention times of these diastereomeric amides (**16**) with those of **16** prepared from **12** in the ephedrine route described above. Thus, the asymmetric synthesis of **3** has been achieved in >99% ee ((*R*)-configuration), which is as high or higher than that derived from a natural product. In addition, the aldimine route lends itself particularly to development using solid-phase techniques, which would ensure ready recovery of the chiral auxiliary. The one limitation is the rather modest yield in the key coupling step. For this reason we examined even a third method for asymmetric 1,4-addition reactions.

The oxazoline route

It has been reported that nucleophilic additon of organolithium reagents to chiral α,β-unsaturated oxazolines can lead to chiral β-substituted alkanoic acids having >90% ee (15). This strategy can be readily adapted to the synthesis of the key intermediate **3** as shown in Scheme 6. Treatment of **6** with (4*S*,5*S*)-(−)-4-methoxymethyl-2-methyl-5-phenyl-2-oxazoline (**28**) (15) or (4*S*,5*S*)-(−)-2-(diethylphosphonomethyl)-4-methoxymethyl-5-phenyl-2-oxazoline (**29**) (27) by reported methods gave (4*S*,5*S*)-(+)-2-[1-(*E*-1,5-hexadienyl)]-4-methoxymethyl-5-phenyl-2-oxazoline (**30**) in 26 and 84% yield, respectively. Since the 2-substituted oxazoline **30**, containing two olefinic groups, was more elaborate than the simpler oxazolines previously described, we wished to test the reactivity of **30** with a simple alkyllithium as well as the desired isopropenyllithium. The reaction of oxazoline **30** was thus carried out with either *n*-butyllithium or isopropenyllithium in THF at −78°C to give either (4*S*,5*S*)-2-[1-(3-*n*-butyl-5-hexenyl)]-4-methoxymethyl-5-phenyl-2-oxazoline (**31**) or (4*S*,5*S*)-2-[1-(3-isopropenyl-5-hexenyl)]-4-methoxymethyl-5-phenyl-2-oxazoline (**32**) in 90% and 63% yields, respectively.

The normal strong acid hydrolysis (15) of **31** gave a complex mixture of products, from which the desired 3-*n*-butyl-6-heptenoic acid could not be separated. Consequently the similar hydrolysis of **32** was not attempted. However, this result did lead us to examine the hydrolysis of the precursor α,β-

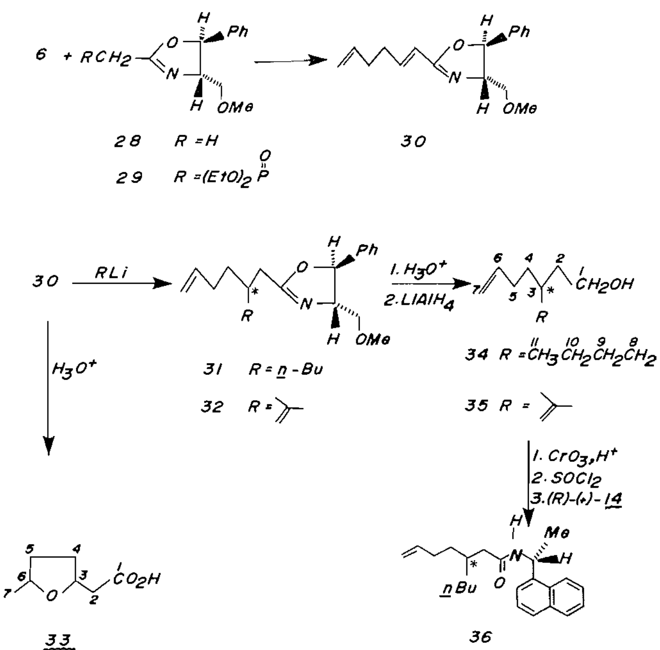

SCHEME 6

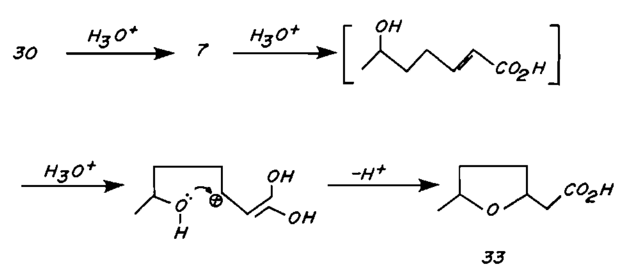

SCHEME 7

unsaturated oxazoline **30**, which we found gave 2-(5-methyltetrahydrofuranyl)acetic acid (**33**) in 62% yield, as did the strong acid treatment of **7**. Although the order and details of the mechanism of the hydrolysis of **30** have not been examined, a likely course of reaction, involving hydrolysis of the oxazoline with concomitant hydration of the terminal olefin, is outlined (Scheme 7). It is probable that hydration of the terminal olefin is also responsible for the mixture of products obtained from the hydrolysis of **31**.

The two-step procedure for the cleavage of oxazolines involving mild acid hydrolysis, followed by reduction with lithium aluminium hydride (28) of **31**, did give predominantly one enantiomer of 3-*n*-butyl-6-hepten-1-ol (**34**) in 44% yield, but an identical cleavage of **32** gave a complex mixture of products from which the desired 3-isopropenyl-6-hepten-1-ol (**35**) could not be isolated. Oxidation of **34** gave 3-*n*-butyl-6-heptenoic acid, which was converted to its acid chloride and treated with **14** to give *N*-[(*R*)-1-(1-naphthyl)ethyl]-3-*n*-butyl-6-heptenamide (**36**). Analysis of this diastereomeric amide by hplc, as described above for **15** and **16**, indicated that **34** had been formed in 96% ee. However, no attempts were made in this study to determine the absolute configuration of the enantiomer, **34**, that was formed.

Although the 1,4-addition of isopropenyllithium to the α,β-unsaturated oxazoline **30** proceeded well to give **32**, sufficiently mild methods of cleavage of **32** to give **3**, **12**, or **35** were not found. Various methods reported to cleave oxazolines

TABLE 2. ^{13}C Chemical shifts of **3**, **7**, **11**–**13**, **17**–**19**, **33**, and **34**

	δ ppm									
Carbon[a]	**3**	**7**[d]	**11**	**12**	**13**	**17**	**18**	**19**[d]	**33**[e]	**34**
1	202.3	172.3	178.6(p)	178.3(p)	180.3(p)	175.6	193.2	166.4	175.8, 175.7(p)	60.6(p)
2	47.4	121.2	41.7(p)	38.9(p)	35.9(p)	34.9	132.6	121.5	40.7, 40.4(p)	36.5(p)[b]
3	40.9	151.2	40.3(n)	42.8(n)	40.6(n)	45.1	157.1	148.1	75.7, 75.0(n)[b]	33.6(n)
4	31.1[b]	31.5[b]	31.3(p)[b]	31.2(p)[b]	30.6(p)[b]	28.2[b]	31.2	31.8[b]	33.3, 32.3(p)[c]	33.1(p)[b]
5	32.2[b]	31.9[b]	35.3(p)[b]	32.0(p)[b]	29.4(p)[b]	32.4[b]	31.2	31.3[b]	74.9, 74.5(n)[b]	32.8(p)[b]
6	138.1	137.0	138.0(n)	138.2(n)	22.9(p)	137.3	136.6	136.9	31.7, 30.9(p)[c]	139.0(n)
7	114.9[c]	115.4	114.8(p)	114.8(p)[c]	14.0(n)	115.7	115.2	115.3	21.1, 20.8(n)	114.0(p)
8	145.5	—	135.3(p)	145.6(p)	29.6(n)	86.7	—	60.0	—	30.7(p)[b]
9	112.7[c]	—	128.3(n)	112.6(p)[c]	19.3(n)[c]	27.4[c]	—	14.0	—	28.5(p)[b]
10	18.6	—	113.8(n)	18.6(n)	18.5(n)[c]	21.9[c]	—	—	—	22.9(p)
11	—	—	158.1(p)	—	—	—	—	—	—	13.9(n)
12	—	—	55.1(n)	—	—	—	—	—	—	—

[a]The numbering of the carbon atoms in the above compounds follows that given for these structures in Schemes 1, 2, 3, and 6 and does not necessarily follow from the names of these compounds. All spectra were recorded, using $CDCl_3$ as solvent, at 300 MHz except for compounds **7** and **18**, whose spectra were recorded at 400 MHz. Inversion–recovery (*J*-modulated spin-echo) spectra were recorded for **11**–**13**, **33**, and **34** (p indicates a positive signal due to C or CH_2, n indicates a negative signal due to CH or CH_3).
[b]These assignments may be interchanged.
[c]These assignments may be interchanged.
[d]Minor signals due to *Z*-isomer are not reported.
[e]*Cis* and *trans* isomers give rise to a duplication of signals.

under mild conditions (29–31) were attempted using **31** as a model. However, either no reaction or low yields of cleavage products were observed. A new procedure for the cleavage of oxazolines has not been attempted (32).

In summary, we have shown that a chiral pheromone intermediate can be prepared in a satisfactory yield having an extremely high ee (Table 1) by asymmetric synthesis, which demonstrates that asymmetric synthesis can compete effectively with the synthesis of chiral molecules from natural products, or through resolution of racemates. The elaboration of the key intermediate **3**, by reaction with a ylide, to the red scale pheromone component **1** has not been attempted in this study, since a procedure for this transformation has been previously reported (2). Although this method lacked stereoselectivity, resulting in a 1:1 mixture of (*E*)- and (*Z*)-**1**, the problem has been overcome by Heath *et al.* (17) in the synthesis of (3*Z*,6*R*)-3,9-dimethyl-6-isopropenyl-3,9-decadien-1-yl propionate (the white peach scale pheromone) from a similar chiral synthon, (*R*)-6-methyl-3-isopropenyl-6-heptenal.

Experimental

Linde argon was used to maintain inert atmosphere conditions. Solvents required for reactions were dried and distilled before use. All reaction mixtures were stirred with a magnetic stirrer. Grignard reagents were prepared by slow addition of alkenyl or aryl bromide to activated magnesium turnings in an appropriate solvent, and sonication (19) of the reaction flask and contents in a 125-W Branson B220 ultrasonic bath filled with distilled water at 20°C. Most distillations were conducted using a Kugelrohr apparatus (bulb-to-bulb) and, for these, the temperature range of the heater at which the main fraction was collected is reported. Flash chromatography (33) was carried out using 20–45 μm silica gel as supplied by Terochem Laboratories Ltd., Toronto, Ont. High-performance liquid chromatography was conducted on a Spectra Physics SP8000 fitted with an analytical column (6.3 mm × 25 cm) of 10-μm Spherisorb silica gel and a mobile phase of 5–12.5% ethyl acetate in hexane (water saturated) with uv detection (254 nm). Melting points (mp) were determined using a Kofler hot stage melting point apparatus and are uncorrected. Optical rotations were determined using a Perkin–Elmer 141 polarimeter at 21 ± 2°C. Infrared spectra (ir) were recorded on a Pye Unicam SP1000 infrared spectrophotometer as neat films between NaCl discs unless specified otherwise. Nuclear magnetic resonance spectra for protons (^1H nmr) were recorded on a Varian EM360 (60 MHz), Bruker AM300 (300 MHz), or Bruker WH400 (400 MHz) spectrometer and are expressed in ppm (δ values) relative to tetramethylsilane as internal reference in deuteriochloroform. (The splittings of the signals are described as singlets (s), broad singlets (bs), doublets (d), triplets (t), quartets (q), doublet of doublets (dd), doublet of triplets (dt), or multiplets (m).) The ^{13}C nmr spectra were recorded in $CDCl_3$ on a Bruker AM300 (300 MHz) or a Bruker WH400 (400 MHz) and have been assigned using standard correlations (34) (Table 2). Mass spectra (ms) were recorded at 70 eV on a VG Micromass 16F mass spectrometer. Microanalyses were performed by Guelph Chemical Laboratories Ltd., Guelph, Ont., Dr. C. Daessele, Montreal, P.Q., or Canadian Microanalytical Service Ltd., Vancouver, B.C.

4-Pentenal (6)

Following the method of Corey and Suggs (11) 4-penten-1-ol (**5**) (8.51 g, 99 mmol) was oxidized by pyridinium chlorochromate (PCC) (38.4 g, 178 mmol) in methylene chloride (185 mL). Distillation and careful fractionation gave the volatile **6** (4.57 g, 55% yield); bp 102–104°C (lit. (35) bp 103–104°C); liquid; ir ν: 1735 (C=O) cm^{-1}; ^1H nmr (60 MHz) δ: 9.75 (t, 1H, *J* = 2 Hz, C*H*O), 6.30–5.50 (m, 1H, =C*H*—), 5.30–4.80 (m, 2H, CH_2=), 2.80–2.00 (m, 4H, CH_2CH_2). 2,4-Dinitrophenylhydrazone derivative; mp 119–120°C (lit. (34) mp 120°C).

2,6-Heptadienoic acid (7)

A mixture of **6** (4.38 g, 52 mmol), malonic acid (6.51 g, 63 mmol), pyridine (10 mL), and pyrrolidine (2 mL) was stirred overnight under argon and subsequently heated at 90°C for 5 h. The reaction mixture was cooled, acidified with 2 *N* hydrochloric acid, and extracted with ether. The combined organic extracts were washed with water and saturated brine, then dried over magnesium sulphate ($MgSO_4$) and concentrated. The residue was distilled (bulb-to-bulb, 1.0 Torr (1 Torr = 133.3 Pa), 74–84°C) to give **7** (5.16 g, 79% yield); liquid; ir ν: 3000 (O—H), 1710 (C=O) cm^{-1}; ^1H nmr (60 MHz) δ: 12.45 (s, 1H, disappears in D_2O, O*H*), 7.45–6.85 (m, 1H, C*H*=$CHCO_2H$), 6.15–5.50 (m, 2H, CH_2=C*H* and C*H*CO_2H), 5.25–4.85 (m, 2H, CH_2=CH), 2.55–2.15 (m, 4H, CH_2CH_2). *Anal.* calcd. for $C_7H_{10}O_2$: C 66.65, H 7.99; found: C 66.66, H 8.26.

(E)-2,6-Heptadienoyl chloride (8)

Freshly distilled thionyl chloride (7 mL) was added dropwise to **7**

(1.443 g, 11.5 mmol) at 0°C with stirring. The mixture was allowed to warm to ambient temperature, and after 1 h it was heated to reflux for 0.5 h before removing excess thionyl chloride by distillation. Distillation (bulb-to-bulb, 0.075 Torr, 60–70°C) of the residue gave **8** (1.570 g, 94% yield); liquid; ir ν: 1765 (C═O) cm^{-1}; ^{1}H nmr (60 MHz) δ: 7.60–7.05 (m, 1H, *CH*═CHCOCl), 6.30–5.50 (m, 2H, CH$_2$═*CH* and *CH*COCl), 5.30–4.85 (m, 2H, *CH$_2$*═CH), 2.60–2.20 (m, 4H, *CH$_2$CH$_2$*).

N-(E-*2,6-Heptadienoyl*)-l-*ephedrine* (*4*)

Compound **8** (1.494 g, 10.3 mmol) was added in one portion to a stirred mixture of proton sponge (2.20 g, 10.3 mmol) and *l*-ephedrine (1.697 g, 10.3 mmol) in THF (25 mL) at 0°C under argon. The mixture was allowed to warm up to room temperature and then stirred overnight. Cold 1 *N* hydrochloric acid (20 mL) was added and the product extracted with ethyl acetate, dried (MgSO$_4$), and concentrated. Flash chromatography (40% ethyl acetate/hexane) of the residue gave **4** (2.456 g, 88% yield); viscous oil; $[\alpha]_D$ −129.91° (*c* 2.62, CHCl$_3$); ir ν: 3390 (O—H), 1610 (C═O) cm^{-1}; ^{1}H nmr (400 MHz) δ: 7.32–7.16 (m, 5H, C$_6$*H*$_5$), 6.76 (dt, 0.7H, *J* = 15 Hz, *CH*═CHCON of *E*-amide[2]), 6.37 (dt, 0.3H, *J* = 15 Hz, *CH*═CHCON of *Z*-amide[2]), 6.10 (d, 0.7H, *J* = 15 Hz, C*H*CON of *E*-amide), 5.84 (d, 0.3H, *J* = 15 Hz, C*H*CON of *Z*-amide), 5.80–5.60 (m, 1H, CH$_2$═C*H*), 5.04–4.86 (m, 2H, C*H$_2$*═CH), 4.76 (d, 1H, *J* = 3 Hz, C*H*OH), 4.52–4.49 (m, 0.7H, NC*H*CH$_3$ of *E*-amide), 4.05–3.99 (m, 0.3H, NC*H*CH$_3$ of *Z*-amide), 2.77 (s, 0.7H, NC*H$_3$* of *E*-amide), 2.74 (s, 0.7H, NC*H$_3$* of *Z*-amide), 2.26–2.12 (m, 4H, C*H$_2$*C*H$_2$*), 2.06 (bs, 1H, O*H*), 1.27 (d, 0.3H, *J* = 7 Hz, NCHC*H$_3$* of *Z*-amide), 1.10 (d, 0.7H, *J* = 7 Hz, NCHC*H$_3$* of *E*-amide); ms *m/z*: 274 (M$^+$ + 1, 0.3), 255 (3), 166 (81), 109 (53), 81 (35), 79 (17), 58 (100), 55 (16). *Anal.* calcd. for C$_{17}$H$_{23}$NO$_2$: C 74.69, H 8.48, N 5.12; found: C 74.32, H 8.39, N 5.08.

N-(*3*-p-*Methoxyphenyl-6-heptenoyl*)-l-*ephedrine* (*9*)

To a stirred solution of the Grignard reagent, prepared from *p*-methoxyphenyl bromide (2.75 mL, 22 mmol) and magnesium (0.53 g, 22 mmol) in THF (20 mL), was added dropwise a solution of **4** (0.990 g, 3.6 mmol) in THF (5 mL) at 0°C under argon. After 14 h at 0°C a phosphate buffer solution (pH 7, 20 mL) was added and the resulting mixture filtered through Celite. The product was extracted into ethyl acetate, dried (MgSO$_4$), and concentrated. Flash chromatography (40% ethyl acetate/hexane) of the residue gave **9** (0.812 g, 59% yield); viscous oil; ir ν: 3400 (O—H), 1625 (C═O) cm^{-1}; ^{1}H nmr (300 MHz) δ: 7.33–7.22 (m, 5H, C$_6$*H$_5$*), 7.01 (AA′XX′, 4H, CH$_3$OC$_6$*H$_4$*), 5.84–5.68 (m, 1H, CH$_2$═C*H*), 4.95–4.89 (m, 2H, C*H$_2$*═CH), 4.70 (d, 1H, *J* = 3 Hz, C*H*OH), 4.42–4.29 (m, 1H, NC*H*CH$_3$), 3.75 (s, 3H, C*H$_3$*O), 3.19–3.07 (m, 1H, CH$_3$OC$_6$H$_4$C*H*), 2.90–2.74 (m, 2H, C*H$_2$*CON), 2.54 (s, 3H, NC*H$_3$*), 2.49–2.44 (bs, 1H, O*H*), 1.89–1.56 (m, 4H, C*H$_2$*C*H$_2$*), 1.06 (d, 3H, *J* = 7 Hz, CHC*H$_3$*); ms *m/z*: 382 (M$^+$ +1, 3), 275 (32), 274 (86), 175 (65), 134 (35), 121 (100), 79 (29), 58 (99). *Anal.* calcd. for C$_{24}$H$_{31}$NO$_3$: C 75.56, H 8.19, N 3.67; found: C 75.54, H 8.19, N 3.70.

N-(*3-Isopropenyl-6-heptenoyl*)-l-*ephedrine* (*10*)

In a manner similar to that described above for **9**, **4** was converted, under the conditions listed in Table 1, to **10** (51–69% yield); viscous oil; ir ν: 3480 (O—H), 1660 (C═O) cm^{-1}; ^{1}H nmr (300 MHz) δ: 7.35–7.22 (m, 5H, C$_6$*H$_5$*), 5.83–5.73 (m, 1H, CH$_2$═C*H*), 5.01–4.70 (m, 4H, C*H$_2$*═CH and C*H$_2$*═C), 4.61–4.42 (m, 1H, NC*H*CH$_3$), 4.36 (d, 1H, *J* = 3 Hz, C*H*OH), 2.70 (s and smaller s due to *E*- and *Z*-amide isomers, 3H, NC*H$_3$*), 2.64–2.55 (m, 1H, C*H*CH$_2$CON), 2.40–2.19 (m, 2H, C*H$_2$*CON), 2.16–1.76 (m, 2H, CH$_2$═CHC*H$_2$*), 1.66 (s and smaller s due to *E*- and *Z*-amide isomers, 3H, C*H$_3$*(CH$_2$═)C), 1.55–1.29 (m, 3H, CH$_2$═CHCH$_2$C*H$_2$* and O*H*), 1.16 (d, 3H, *J* = 7 Hz, CHC*H$_3$*); ms *m/z*: 316 (M$^+$ + 1, 0.8), 3.15 (M$^+$, 0.6), 209 (23), 208 (92), 109 (22), 81 (20), 67 (23), 58 (100), 55 (23). *Anal.* calcd. for C$_{20}$H$_{29}$NO$_2$: C 76.15, H 9.27, N 4.44; found: C 76.33, H 9.37, N 4.54.

3-p-*Methoxyphenyl-6-heptenoic acid* (*11*)

A solution of **9** (0.2401 g, 0.63 mmol) in 10% NaOH (20 mL, 1 : 1 EtOH/H$_2$O) was heated at reflux for 78 h. After cooling, the mixture was acidified with 2 *N* HCl, and the product extracted into ether, dried (MgSO$_4$), and concentrated. Distillation (bulb-to-bulb, 0.05 Torr, 120–130°C) gave **11** (0.0619 g, 42% yield); liquid; $[\alpha]_D$ −11.32° (*c* 3.28, CHCl$_3$); ir ν: 3200 (O—H), 1720 (C═O) cm^{-1}; ^{1}H nmr (300 MHz) δ: 10.10 (bs, 1H, O*H*), 6.96 (AA′XX′, 4H, CH$_3$OC$_6$*H$_4$*), 5.85–5.68 (m, 1H, CH$_2$═C*H*), 4.97–4.90 (m, 2H, C*H$_2$*═CH), 3.78 (s, 3H, C*H$_3$*O), 3.10–3.01 (m, 1H, C*H*CH$_2$CO$_2$H), 2.60 (t, 2H, *J* = 7 Hz, C*H$_2$*CO$_2$H), 1.95–1.60 (m, 4H, C*H$_2$*C*H$_2$*); ms *m/z*: 234 (M$^+$, 48), 192 (49), 179 (93), 175 (89), 137 (99), 134 (26), 121 (100), 91 (20). *Anal.* calcd. for C$_{14}$H$_{18}$O$_3$: C 71.77, H 7.74; found: C 71.72, H 7.99.

(R)-*3-Isopropenyl-6-heptenoic acid* (*12*)

In a manner similar to that described above for **11**, **10** was converted to **12** (distilled bulb-to-bulb, 0.05 Torr, 95–105°C, 63–80% yield); liquid; $[\alpha]_D$ see Table 1; ir ν: 3150 (O—H), 1730 (C═O) cm^{-1}; ^{1}H nmr (300 MHz) δ: 10.60 (bs, 1H, O*H*), 5.89–5.72 (m, 1H, CH$_2$═C*H*), 5.04–4.78 (m, 4H, C*H$_2$*═CH and C*H$_2$*═C), 2.69–2.57 (m, 1H, C*H*CH$_2$CO$_2$H), 2.41 (d, 2H, *J* = 7.5 Hz, C*H$_2$*CO$_2$H), 2.10–1.93 (m, 2H, CH$_2$═CHC*H$_2$*), 1.67 (s, 3H, C*H$_3$*), 1.52–1.45 (m, 2H, CH$_2$═CHCH$_2$C*H$_2$*); ms *m/z*: 168 (M$^+$, 4), 108 (63), 93 (38), 81 (52), 69 (100), 67 (46), 55 (67), 43 (50), 41 (90). *Anal.* calcd. for C$_{10}$H$_{16}$O$_2$: C 71.39, H 9.59; found: C 71.20, H 9.99.

(R)-*3-Isopropylheptanoic acid* (*13*)

Hydrogen was passed over a stirred mixture of **12** (0.0682 g, 0.41 mmol; $[\alpha]_D$ −3.13 (*c* 2.05, CHCl$_3$)) and 10% palladium on charcoal (0.0212 g) in ethanol (15 mL) for 16 h at room temperature. The solution was filtered, the solvent removed, and the resulting oil distilled (bulb-to-bulb, 0.1 Torr, 100–110°C) to give **13** (0.0677 g, 97% yield); liquid; $[\alpha]_D$ −0.45° (*c* 2.23, CHCl$_3$) (lit. (15) $[\alpha]_D$ −0.82° (neat)); ir ν: 3050 (O—H), 1720 (C═O) cm^{-1}; ^{1}H nmr (300 MHz) δ: 10.52 (bs, 1H, O*H*), 2.37–2.14 (m, 2H, C*H$_2$*CO$_2$H), 1.84–1.72 (m, 2H, (CH$_3$)$_2$C*H*C*H*), 1.41–1.18 (m, 6H, CH$_3$C*H$_2$*C*H$_2$*C*H$_2$*), 0.98–0.84 (m, 9H, C*H$_3$*CH$_2$ and (C*H$_3$*)$_2$CH); ms *m/z*: 173 (M$^+$ + 1, 2), 129 (42), 113 (78), 112 (69), 72 (56), 70 (71), 69 (100), 60 (40), 57 (99), 56 (54), 55 (64), 43 (68), 41 (76). *Anal.* calcd. for C$_{10}$H$_{20}$O$_2$: C 69.72, H 11.70; found: C 69.66, H 11.85.

N-[(R)-*1-(Naphthyl)ethyl*]-*3*-p-*methoxyphenyl-6-heptenamide* (*15*)

To a solution of **11** (0.0677 g, 0.29 mmol; $[\alpha]_D$ −16.90 (*c* 5.38), CHCl$_3$)) in ether (3 mL) containing a catalytic amount of *N,N*-dimethylformamide (5 μL) was added thionyl chloride (63 μL, 0.87 mmol). After stirring for 4 h at room temperature, the mixture was concentrated to remove excess thionyl chloride. Ether (5 mL) was added and the resulting solution cooled to 0°C, whereupon a solution of **14** (0.0744 g, 0.44 mmol) and proton sponge (0.0932 g, 0.44 mmol) in ether (5 mL) was added dropwise. A precipitate formed, and the reaction mixture was allowed to warm to room temperature and was stirred overnight. Ice-cold 1 *N* hydrochloric acid (15 mL) was added and the product extracted into ether, washed with brine, dried (MgSO$_4$), and concentrated to give crude **15** (0.1093 g, 98% yield). Crude **15** was analysed by hplc directly, to avoid fractionation. Separation of the two diastereomers was obtained in 0.8 h by using 10% ethyl acetate in hexane at 1.0 mL/min. The predominant diastereomer, the second to elute, was collected by hplc; ir ν: 3300 (N—H), 1650 (C═O) cm^{-1}; ^{1}H nmr (300 MHz) δ: 7.94–7.10 (m, 7H, C$_{10}$*H$_7$*), 6.84 (AA′XX′, 4H, CH$_3$OC$_6$*H$_4$*), 5.85–5.65 (m, 2H, C*H*NH and CH$_2$═C*H*), 5.41 (s, 1H, N*H*), 5.96–5.89 (m, 2H, C*H$_2$*═CH), 3.75 (s, 3H, C*H$_3$*O), 3.14–3.00 (m, 1H, C*H*CH$_2$CO$_2$H), 2.24–2.14 (m, 2H, C*H$_2$*CON), 1.84–1.60 (m, 4H, C*H$_2$*C*H$_2$*), 1.54 (d, 3H, C*H$_3$*CH).

(R)-N-[(R)-*1-(1-Naphthyl)ethyl*]-*3-isopropenyl-6-heptenamide* (*16*) *via route shown in Scheme 1*

In a manner similar to that described above for **15**, **12** was converted

[2] The *E*- and *Z*-amide isomers are distinguishable on the nmr time scale (36).

to **16** (78% crude yield) and analysed directly by hplc. Separation of the two diastereomers was achieved in 0.25 h using 12.5% ethyl acetate in hexane at 1.5 mL/min. The (*R,S*)-diastereomer (11 min) eluted prior to the predominant (*R,R*)-diastereomer (13 min); the identity of these diastereomers was confirmed as described below for the aldimine route. A sample of **16** was purified by flash chromatography (25% ethyl acetate/hexane); ir ν: 3320 (N—H), 1650 (C=O) cm^{-1}; ^{1}H nmr (300 MHz) δ: 8.12–7.40 (m, 7H, $C_{10}H_7$), 6.02–5.87 (m, 2H, N*H* and C*H*NH), 5.82–5.75 (m, 1H, CH_2=C*H*), 5.11–4.72 (m, 4H, CH_2=CH and CH_2=C), 2.68–2.55 (m, 1H, C*H*CH_2CON), 2.26–2.15 (m, 2H, CH_2CON), 2.07–1.88 (m, 2H, CH_2=CHCH_2), 1.61 (s and d, 6H, CH_3=C and CH_3CH), 1.50–1.33 (m, 2H, CH_2=CHCH_2CH_2).

(R)-3-Isopropenyl-6-heptenal (3) via route shown in Scheme 1

DIBAL (5.2 mL of a 1 *M* solution in hexane, 5.2 mmol) was added dropwise over 1.5 h to a stirred solution of **10** (0.544 g, 1.7 mmol) (Entry 5 in Table 1) in THF (10 mL) at 0°C under argon. After 0.5 h the mixture was quenched by the addition of ice-cold 10% sulphuric acid (30 mL), and then stirred for 1 h. The product was extracted with ether, washed with saturated NaCl, dried ($MgSO_4$), and concentrated. The residue was distilled (bulb-to-bulb, 0.05 Torr, 55–65°C) to give **3** (0.055 g, 21% yield); liquid; $[\alpha]_D$ −0.42° (*c* 2.53, $CHCl_3$); ir ν: 1735 (C=O), 1650 (C=C) cm^{-1}; ^{1}H nmr (300 MHz) δ: 9.66 (t, 1H, *J* = 2 Hz, C*H*O), 5.87–5.72 (m, 1H, CH_2=C*H*), 5.04–4.78 (m, 4H, CH_2=CH and CH_2=C), 2.78–2.67 (m, 1H, C*H*CH_2CO_2H), 2.49–2.42 (m, 2H, CH_2CO_2H), 2.07–1.93 (m, 2H, CH_2=CHCH_2), 1.66 (d, 3H, *J* = 0.9 Hz, CH_3), 1.56–1.42 (m, 2H, CH_2=CHCH_2CH_2); ms *m/z*: 152 (M^+, 0.2), 123 (12), 108 (11), 95 (26), 81 (24), 69 (100), 67 (29), 55 (21), 41 (16). 2,4-Dinitrophenylhydrazone derivative; mp 81–83°C. *Anal.* calcd. for $C_{16}H_{20}N_4O_4$: C 57.82, H 6.07, N 16.86; found: C 57.93, H 6.24, N 16.73.

(R)-3-(3-Buten-1-yl)-4,4-dimethylbutyrolactone (17)

Compound **10** (0.1239 g, 0.39 mmol) (Entry 3 in Table 1) was dissolved in ethanolic hydrochloric acid (5 mL of a solution prepared by the addition of 35% hydrochloric acid (4 mL) and ethanol (50 mL)) and the resulting mixture was refluxed overnight. After cooling, water (10 mL) was added and the product extracted with ether. The combined organic extracts were washed with saturated brine, dried ($MgSO_4$), and concentrated. The residue was distilled (bulb-to-bulb, 0.35 Torr, 110–120°C) to give **17** (0.0496 g, 75% yield); liquid; $[\alpha]_D$ −24.85° (*c* 0.780, $CHCl_3$); ir ν: 1780 (C=O) cm^{-1}; ^{1}H nmr (300 MHz) δ: 5.86–5.70 (m, 1H, CH_2=C*H*), 5.12–5.01 (m, 2H, CH_2=CH), 2.72–2.59 (m, 1H, C*H*CH_2CO_2), 2.37–1.95 (m, 4H, CH_2CO_2 and CH_2=CHCH_2), 1.67–1.53 (m, 2H, CH_2=CHCH_2-CH_2), 1.45 (s, 3H, CH_3), 1.26 (s, 3H, CH_3); ms *m/z*: 168 (M^+, 14), 153 (100), 135 (45), 110 (35), 82 (35), 67 (65), 59 (44), 41 (62). *Anal.* calcd. for $C_{10}H_{16}O_2$: C 71.39, H 9.59; found: C 71.20, H 9.59.

Ethyl 2,6-heptadienoate (19)

Following a similar procedure to that described for the preparation of **7**, the monoethyl ester of malonic acid (37) (13.2 g, 100 mmol) was reacted with **6** (6.5 g, 77 mmol) in a mixture of pyridine (8 mL) and pyrrolidine (1.5 mL). Distillation (bulb-to-bulb, 0.05 Torr, 50–55°C) gave **19** (9.42 g, 79% yield); liquid; ir ν: 1735 (C=O) cm^{-1}; ^{1}H nmr (60 MHz) δ: 7.50–6.80 (m, 1H, C*H*=$CHCO_2$), 6.10–5.50 (m, 2H, C*H*CO_2 and CH_2=C*H*), 5.30–4.80 (m, 2H, CH_2=CH), 4.18 (q, 2H, *J* = 7 Hz, CH_2CH_3), 2.55–2.15 (m, 4H, CH_2CH_2), 1.24 (t, 3H, *J* = 7 Hz, CH_3); ms *m/z*: 154 (M^+, 1), 109 (44), 81 (100), 80 (42), 79 (28), 55 (25), 41 (59), 39 (34). *Anal.* calcd. for $C_9H_{14}O_2$: C 70.10, H 9.15; found: C 69.64, H 9.50.

2,6-Heptadienal (18) via route shown in Scheme 3

To a stirred solution of **19** (2.029 g, 13.2 mmol) in hexane (40 mL), at −20°C under argon, was added dropwise DIBAL (26.5 mL of 1 *M* solution in hexane) over 1 h. The reaction mixture after 1 h was allowed to warm to 0°C. Methanol (4 mL) was added, followed by water (1 mL) and sufficient dilute hydrochloric acid to acidify the reaction mixture. The product was extracted with ether, washed with 1 *N* hydrochloric acid, saturated sodium hydrogen carbonate, saturated brine, dried ($MgSO_4$), and concentrated. The residue (1.218 g, 82% yield) was shown by ^{1}H nmr to be a 4:1 mixture of **20** and **21**; ^{1}H nmr (60 MHz) δ: 6.35–5.30 (m, 3.3H, C*H*=CHCH_2OH, CH_2=C*H* of **20** and CH_2=C*H* of **21**), 5.25–4.85 (m, 2.5H, CH_2=CH of **20** and of **21**), 3.67 (t, 0.5H, *J* = 5.5 Hz, CH_2OH of **21**), 2.90 (bs, 1.3H, disappears in D_2O, O*H* of **20** and of **21**), 2.40–1.85 (m, 5.5H, CH_2CH_2 of **20** and CH_2CH_2CH_2CH_2 of **21**).

The crude mixture of **20** and **21** (1.218 g, 10.8 mmol) was oxidized by PCC (3.00 g, 13.9 mmol) in methylene chloride (35 mL) following the procedure of Corey and Suggs (11). The crude product oil was washed with 0.4 *M* sodium metabisulphite (10 mL), extracted with ether, dried ($MgSO_4$), and concentrated. Distillation (bulb-to-bulb, 16 Torr, 60–71°C (lit. (22) bp 16 Torr, 58–65°C)), gave **18**, contaminated by 3% of **22**, (0.566 g, 39% yield from **19**); liquid; ir ν: 1700 (C=O) cm^{-1}; ^{1}H nmr (60 MHz) δ: 9.82 (t, 0.03H, *J* = 1.5 Hz, C*H*O of **22**), 9.55 (d, 1H, *J* = 8 Hz, C*H*O), 7.35–6.60 (m, 1H, C*H*=CHCHO), 6.40–5.50 (m, 2H, C*H*CHO and CH_2=C*H*), 5.30–4.85 (m, 2H, CH_2=CH), 2.60–2.10 (m, 4H, CH_2CH_2).

(E)-2,6-Heptadienal (18) via route shown in Scheme 4

Following the general procedure of Meyers *et al.* (26), 2,4,4,6-tetramethyl-5,6-dihydro-1,3-oxazine (3.613 g, 25.6 mmol) in THF (25 mL) was lithiated by the dropwise addition of *n*-butyllithium (17.6 mL of a 1.6 *M* solution in hexane, 28.2 mmol) at −78°C under argon over 1 h. After a yellow precipitate had formed, **6** (2.368 g, 28.2 mmol) in THF (5 mL) was added dropwise over 0.5 h. The reaction mixture was allowed to warm slowly to room temperature and worked up as described by Meyers *et al.* (26) to give crude **24** (4.787 g, 83% yield); liquid; ir ν: 3360 (O—H), 1670 (C=N) cm^{-1}. Reduction of crude **24** (3.574 g, 15.9 mmol) by sodium borohydride (0.613 g, 16.1 mmol) at pH 6–8 in the manner described by Meyers *et al.* (26) gave crude **25** (3.543 g, 98% yield); liquid; ir ν: 3350 (O—H) cm^{-1}. Crude **25** (3.543 g, 15.6 mmol) was added dropwise to a boiling aqueous solution (100 mL) of oxalic acid (7 g). The water azeotrope, which distilled off, was collected and the product extracted into ether, dried ($MgSO_4$), and concentrated to give **18** (0.769 g, 44% yield from **24**); liquid; ir ν: 1700 (C=O) cm^{-1}; ^{1}H nmr (300 MHz) δ: 9.51 (d, 1H, *J* = 8 Hz, C*H*O), 6.90–6.81 (m, 1H, C*H*=CHCHO), 6.18–6.09 (m, 1H, CH=C*H*CHO), 5.88–5.74 (m, 1H, CH_2=C*H*), 5.11–5.02 (m, 2H, CH_2=CH), 2.50–2.24 (m, 4H, CH_2CH_2); ms *m/z*: 110 (M^+, 4), 109 (14), 95 (32), 81 (100), 79 (42), 41 (71).

Racemic 3-isopropenyl-6-heptenal (3) via route shown in Scheme 5

Following the general procedure described by Hashimoto *et al.* (21), **18** (0.349 g, 3.17 mmol) was condensed with racemic **26** (0.592 g, 3.16 mmol) in benzene (16 mL) to afford, after work-up, crude **27** (0.838 g, 95% yield); oil; ir ν: 1735 (C=O), 1660 (C=N) cm^{-1}; ^{1}H nmr (300 MHz) δ: 7.76 (d, 1H, *J* = 9 Hz, C*H*=N), 6.43–6.15 (m, 2H, C*H*=C*H*CH=N), 5.90–5.72 (m, 1H, CH_2=C*H*), 5.11–4.92 (m, 2H, CH_2=CH), 3.30 (s, 1H, C*H*CO_2), 2.39–2.13 (m, 4H, CH_2CH_2), 1.47 (s, 9H, $CO_2C(CH_3)_3$), 0.98 (s, 9H, $CHC(CH_3)_3$). A solution of the total crude **27** in THF (5 mL) was added dropwise to a stirred solution of isopropenylmagnesium bromide, prepared from isopropenyl bromide (1.15 g, 9.5 mmol) and magnesium (0.23 g, 9.5 mmol), in THF (20 mL) at −70°C. After 3 h the reaction mixture was allowed to warm up to −15°C and was kept at this temperature overnight. Hydrolytic work-up, as described by Hashimoto *et al.* (21), followed by flash chromatography (10% ether/hexane) and subsequent distillation (bulb-to-bulb, 0.1 Torr, 65–75°C) gave racemic **3** (0.243 g, 50%), identical to **3** prepared via Scheme 1, as described above.

(R)-3-Isopropenyl-6-heptenal (3) via route shown in Scheme 5

In a manner similar to that described above for racemic **3**, **18** was condensed with chiral **26** and converted, under the conditions reported in Table 1, to **3** (43% yield); $[\alpha]_D$ −0.47° (*c* 7.89, $CHCl_3$).

(R)-N-[(R)-1-(1-Naphthyl)ethyl]-3-isopropenyl-6-heptenamide (16) via route shown in Scheme 5

Following the procedure described by Heath *et al.* (17), **3** (0.0883 g, 0.58 mmol) in acetone (15 mL) was oxidized by Jones reagent (38)

(0.3 mL, 0.8 mmol) to give crude **12** (0.0823 g, 84% yield). This compound was converted, in a manner similar to that described above, to crude **16** (0.0959 g, 52% overall yield) and analysed directly by hplc. At identical retention times to those reported above, the (*R*,*S*)-diastereomer (11 min) eluted prior to the predominant (*R*,*R*)-diastereomer (13 min). Under identical hplc conditions, a preparation of **16** from a racemic mixture of **3** and its enantiomer gave two peaks of identical area at 11 and 13 min, whereas for a preparation of **16** from optically active **3** and (*S*)-(−)-**14** the predominant (*S*,*R*)-diastereomer (11 min) eluted prior to the (*S*,*S*)-diastereomer (13 min).

(4S,5S)-(+)-2-[1-(E-1,5-Hexadienyl)]-4-methoxymethyl-5-phenyl-2-oxazoline (30)

Method A

Following the procedure described by Meyers *et al.* (15), **28** (6.00 g, 29.3 mmol) in THF (50 mL) was lithiated at −78°C, and **6** (2.50 g, 29.8 mmol) in THF (4 mL) was added dropwise. After the appropriate work-up the product was treated with trifluoroacetic acid (6 drops) in benzene (150 mL) and the mixture refluxed overnight; a Dean–Stark trap was employed to remove water. The cooled solution was washed with 5% sodium hydrogen carbonate, dried ($MgSO_4$), and concentrated. Flash chromatography (20% ether/hexane) gave **30** (3.30 g, 26% yield); oil; $[\alpha]_D$ 50.31° (*c* 1.60, $CHCl_3$); ir ν: 1680 (C=N) cm^{-1}; ^1H nmr (60 MHz) δ: 7.32 (s, 5H, C_6H_5), 7.04–6.51 (m, 1H, C*H*=CHC=N), 6.31–5.52 (m, 2H, CH_2=C*H* and C*H*C=N), 5.32 (d, 1H, *J* = 7 Hz, OC*H*), 5.24–5.01 (m, 2H, CH_2=CH), 4.32–4.00 (m, 1H, NC*H*), 3.66–3.46 (m, 2H, CH_2O), 3.40 (s, 3H, OCH_3), 2.45–2.12 (m, 4H, CH_2CH_2); ms *m/z*: 271 (M^+, 11), 241 (6), 226 (100), 182 (28), 151 (29), 134 (32), 119 (95), 109 (44), 91 (60), 74 (37), 45 (39).

Method B

Crude **29** (8.056 g, 24.6 mmol), prepared by the method of Ziegler and Gilligan (27), and **6** (2.94 g, 35.0 mmol) were dissolved in THF (25 mL, containing two drops of water) and cooled to −78°C. Potassium *tert*-butoxide (3.4 g, 30.0 mmol) in THF (20 mL) was added slowly and the reaction conducted and worked up in the manner described by Meyers *et al.* (15) to give **30** (5.88 g, 89% yield), identical to **30** prepared by method A, described above.

(4S,5S)-2-[1-(3-n-Butyl-5-hexenyl)]-4-methoxymethyl-5-phenyl-2-oxazoline (31)

A solution of **30** (2.707 g, 9.99 mmol) in THF (30 mL) was added dropwise over 1 h to *n*-butyllithium (13.8 mL of a 1.6 *M* solution in hexane, 22.1 mmol) in THF (125 mL) at −78°C under argon, and the mixture was stirred for 2.5 h at the same temperature. The reaction was quenched at −78°C by the addition of methanol (3 mL). The reaction mixture was allowed to warm up to ambient temperature, then treated with water (100 mL) and extracted with ether. The organic extracts were washed with brine, dried ($MgSO_4$), and concentrated to give crude **31** (2.949 g, 90% yield); ir ν: 1655 (C=N) cm^{-1}; ^1H nmr (60 MHz) δ: 7.36 (s, 5H, C_6H_5), 6.27–5.52 (m, 1H, CH_2=C*H*), 5.32 (d, 1H, *J* = 7 Hz, OC*H*), 4.31–3.98 (m, 1H, NC*H*), 3.80–3.47 (m, 2H, CH_2O), 3.40 (s, 3H, OCH_3), 2.60–0.75 (m, 16H, aliphatic envelope); ms *m/z*: 321 (M^+, 2), 284 (22), 222 (100), 180 (84), 152 (41), 124 (57), 99 (46), 83 (64), 55 (62), 41 (84).

(4S,5S)-2-[1-(3-Isopropenyl-5-hexenyl)]-4-methoxymethyl-5-phenyl-2-oxazoline (32)

In a manner similar to that described above for **31**, **30** was reacted with isopropenyllithium, prepared from *tert*-butyllithium and isopropenyl bromide (39), to give after flash chromatography (40% ethyl acetate/hexane) **32** (0.680 g, 63% yield); ir ν: 1660 (C=N) cm^{-1}; ^1H nmr (60 MHz) δ: 7.33 (s, 5H, C_6H_5), 6.25–5.51 (m, 1H, CH_2=C*H*), 5.30 (d, 1H, *J* = 7 Hz, OC*H*), 5.22–4.78 (m, 4H, CH_2=CH and CH_2=C), 4.32–3.95 (m, 1H, NC*H*), 3.75–3.50 (m, 2H, CH_2O), 3.43 (s, 3H, OCH_3), 2.70–1.05 (m, 10H, aliphatic envelope); ms *m/z*: 313 (M^+, 1), 224 (18), 193 (13), 165 (13), 136 (15), 109 (24), 74 (100), 55 (22), 43 (26).

2-(5-Methyltetrahydrofuranyl)acetic acid (33)

A solution of **30** or **7** (1.73–2.57 mmol) in 4 *N* sulphuric acid (10–15 mL) was refluxed for 4 h. The reaction mixture was allowed to cool, and then was extracted with ether. The ether extracts were washed with brine, dried ($MgSO_4$), concentrated, and distilled (bulb-to-bulb, 1.20 Torr, 125–135°C) to give **33** (62% yield from either **30** or **7**); liquid n_D^{23} 1.4532 (lit. (40) n_D^{25} 1.4520); ir ν: 3100 (O—H), 1720 (C=O) cm^{-1}; ^1H nmr (60 MHz) δ: 10.31 (s, 1H, O*H*), 4.65–3.75 (m, 2H, C*H*OC*H*), 2.55 (dt, 2H, *J* = 2 and 7 Hz, CH_2CO_2), 2.40–1.35 (m, 4H, CH_2CH_2), 1.23 (dd, 3H, *J* = 1.5 and 6 Hz, CH_3); ms *m/z*: 144 (M^+, 5), 111 (30), 102 (100), 85 (87), 84 (38), 56 (82), 55 (92), 43 (89), 41 (89). *Anal.* calcd. for $C_7H_{12}O_3$: C 58.32, H 8.39; found: C 58.32, H 8.32.

3-n-Butyl-6-hepten-1-ol (34)

A solution of crude **31** (0.416 g, 1.26 mmol) in 3% ethanolic hydrochloric acid (10 mL) was refluxed overnight. After cooling, the mixture was concentrated, water (10 mL) was added, and the resulting solution was neutralized and then extracted with ether. The organic extracts were dried ($MgSO_4$) and concentrated. The resulting viscous oil was dissolved in THF (7 mL), lithium aluminum hydride (0.15 g, 3.90 mmol) added, and the reaction mixture stirred overnight at ambient temperature. The reaction mixture was cooled to 0°C and the excess hydride destroyed by the slow addition of methanol (1 mL), followed by water (10 mL). The product was extracted into ether, washed with brine, dried ($MgSO_4$), concentrated, and distilled (bulb-to-bulb, 0.1 Torr, 66–77°C) to give **34** (0.094 g, 44% yield); liquid; $[\alpha]_D$ −1.18° (*c* 2.12, $CHCl_3$); ir ν: 3475 (O—H) cm^{-1}; ^1H nmr (300 MHz) δ: 5.81–5.66 (m, 1H, CH_2=C*H*), 4.98–4.83 (m, 2H, CH_2=CH), 3.54 (t, 2H, *J* = 7 Hz, CH_2OH), 3.11 (bs, 1H, O*H*), 2.06–1.92 (m, 2H, CH_2=CHCH_2), 1.50–0.75 (m, 14H, aliphatic envelope); ms *m/z*: 137 (M^+ − CH_3 and H_2O, 0.5), 124 (M^+ − CH_2=CH_2 and H_2O, 5), 123 (13), 113 (11), 110 (10), 109 (6), 95 (47), 81 (30), 69 (53), 67 (34), 55 (100), 43 (30), 41 (60). Compound **34** was oxidized by PCC to 3-*n*-butyl-6-heptenal (81% yield); ir ν: 1740 (C=O) cm^{-1}; ms *m/z*: 168 (M^+, 0.2), 150 (2). 2,4-Dinitrophenylhydrazone derivative; mp 65–67°C. *Anal.* calcd. for $C_{17}H_{24}N_4O_4$: C 58.61, H 6.94, N 16.08; found: C 58.42, H 6.87, N 15.80.

N-[(R)-1-(Naphthyl)ethyl]-3-n-butyl-6-heptenamide (36)

Jones reagent (38) (1.18 mL, 2.26 mmol) was used to oxidize **34** (0.1285 g, 0.76 mmol), in a manner similar to that described above for **3**, to give after distillation (bulb-to-bulb, 1.5 Torr, 130–140°C) 3-*n*-butyl-6-heptenoic acid (0.0605 g, 44% yield); ir ν: 3105 (O—H), 1720 (C=O) cm^{-1}; ^1H nmr (60 MHz) δ: 11.00 (bs, 1H, O*H*), 6.10–5.43 (m, 1H, CH_2=C*H*), 5.17–4.74 (m, 2H, CH_2=CH), 2.34 (d, 2H, *J* = 6 Hz, CH_2CO_2), 2.28–0.80 (m, 14H, aliphatic envelope). Following a procedure similar to that described above for **16**, 3-*n*-butyl-6-heptenoic acid was converted to crude **36** (0.1021 g, 92% yield) and analysed directly by hplc. Separation of the two diastereomers was achieved in 0.75 h using 5% ethyl acetate in hexane at 1.0 mL/min. The predominant diastereomer eluted first. A sample of **36** was purified by flash chromatography (20% ethyl acetate/hexane); ir ν: 3320 (N—H), 1640 (C=O) cm^{-1}; ^1H nmr (300 MHz) δ: 8.13–7.38 (m, 7H, $C_{10}H_7$), 5.98–5.86 (m, 2H, N*H* and C*H*NH), 5.78–5.62 (m, 1H, CH_2=C*H*), 4.97–4.86 (m, 2H, CH_2=CH), 2.14–1.85 (m, 5H, CH_2=CHCH_2CH_2C*H*CH_2), 1.63 (d, 3H, *J* = 6 Hz, CHCH_3), 1.39–1.16 (m, 8H, $(CH_2)_3CH_3$ and CH_2=CHCH$_2$CH_2), 0.86 (t, 3H, *J* = 6.5 Hz, CH$_2$CH_3); ms *m/z*: 337 (M^+, 15), 213 (29), 170 (19), 156 (38), 155 (100), 153 (17), 55 (19).

Acknowledgements

We gratefully acknowledge the financial support of this research by the Natural Sciences and Engineering Research Council of Canda and the Faculty of Science, York University.

1. W. L. Roelofs, M. J. Gieselmann, A. M. Carde, H. Tashiro, D. S. Moreno, C. A. Henrick, and R. J. Anderson. Nature,

267, 698 (1977).

2. W. ROELOFS, M. GIESELMANN, A. CARDE, H. TASHIRO, D. S. MORENO, C. A. HENRICK, and R. J. ANDERSON. J. Chem. Ecol. **4**, 211 (1978).
3. R. J. ANDERSON, K. G. ADAMS, H. R. CHINN, and C. A. HENRICK. J. Org. Chem. **45**, 2229 (1980).
4. M. J. GIESELMANN, C. A. HENRICK, R. J. ANDERSON, D. S. MORENO, and W. L. ROELOFS. J. Insect Physiol. **26**, 179 (1980).
5. (*a*) T. M. FYLES, C. C. LEZNOFF, and J. WEATHERSTON. J. Chem. Ecol. **4**, 109 (1978); (*b*) T. M. FYLES, C. C. LEZNOFF, and J. WEATHERSTON. Can. J. Chem. **56**, 1031 (1978); (*c*) C. C. LEZNOFF. Acc. Chem. Res. **11**, 327 (1978); (*d*) P. I. SVIRSKAYA and C. C. LEZNOFF. J. Chem. Ecol. **10**, 321 (1984).
6. (*a*) P. M. WORSTER, C. R. MCARTHUR, and C. C. LEZNOFF. Angew. Chem. Int. Ed. Engl. **18**, 221 (1979); (*b*) C. R. McArthur, P. M. Worster, J.-L. Jiang, and C. C. LEZNOFF. Can. J. Chem. **60**, 1836 (1982); (*c*) C. R. MCARTHUR, J.-L. JIANG, and C. C. LEZNOFF. Can. J. Chem. **60**, 2984 (1982).
7. W. C. STILL and A. MITRA. J. Am. Chem. Soc. **100**, 1927 (1978).
8. M. P. COOKE, JR. and D. L. BURMAN. J. Org. Chem. **47**, 4955 (1982).
9. (*a*) V. R. MEYER. Chimia. **36**, 475 (1982); (*b*) D. Caine and E. CREWS. Tetrahedron Lett. **25**, 5359 (1984).
10. T. MUKAIYAMA and N. IWASAWA. Chem. Lett. 913 (1981).
11. E. J. COREY and J. W. SUGGS. Tetrahedron Lett. 2647 (1975).
12. H. J. BESTMANN, K. H. KOSCHATZKY, W. SCHATZKE, J. SUB, and O. VOSTROWSKY. Justus Liebigs Ann. Chem. 1705 (1981).
13. V. R. MAMDAPUR, C. S. SUBRAMANIAN, and M. S. CHADHA. Indian J. Chem. Sect. B, **18**, 75 (1979).
14. M. B. HOCKING. Can. J. Chem. **46**, 466 (1968).
15. A. I. MEYERS, R. K. SMITH, and C. E. WHITTEN. J. Org. Chem. **44**, 2250 (1979).
16. B. J. BERGOT, R. J. ANDERSON, D. A. SCHOOLEY, and C. A. HENRICK. J. Chromatogr. **155**, 97 (1978).
17. R. R. HEATH, R. E. DOOLITTLE, P. E. SONNET, and J. H. TUMLINSON. J. Org. Chem. **45**, 2910 (1980).
18. H. NORMANT. Adv. Org. Chem. **2**, 1 (1960).
19. J.-L. LUCHE and J.-C. DIAMIANO. J. Am. Chem. Soc. **102**, 7926 (1980).
20. K. PSOTTA and A. WIECHERS. Tetrahedron, **35**, 255 (1979).
21. S. HASHIMOTO, S. YAMADA, and K. KOGA. Chem. Pharm. Bull. **27**, 771 (1979).
22. H. J. BESTMANN, K. H. KOSCHATZKY, H. PLATZ, J. SUB, O. VOSTROWSKY, W. KNAUF, G. BURGHARDT, and I. SCHNEIDER. Justus Liebigs Ann. Chem. 1359 (1982).
23. T. M. CRESP. M. V. SARGENT, and P. VOGEL. J. Chem. Soc. Perkin Trans. 1, 37 (1974).
24. E. J. COREY, D. ENDERS, and M. G. BOCK. Tetrahedron Lett. 7 (1976).
25. A. I. MEYERS, K. TOMIOKA, and M. P. FLEMING. J. Org. Chem. **43**, 3788 (1978).
26. A. I. MEYERS, A. NABEYA, H. W. ADICKES, I. R. POLITZER, G. R. MALONE, A. C. KOVELESKY, R. L. NOLEN, and R. C. PORTNOY. J. Org. Chem. **38**, 36 (1973).
27. F. E. ZIEGLER and P. J. GILLIGAN. J. Org. Chem. **46**, 3874 (1981).
28. A. I. MEYERS and K. A. LUTOMSKI. J. Am. Chem. Soc. **104**, 879 (1982).
29. I. C. NORDIN. J. Heterocycl. Chem. **3**, 531 (1966).
30. S. R. WILSON, D. T. MAO, and H. N. KHATI. Synth. Commun. **10**, 17 (1980).
31. J. I. LEVIN and S. M. WEINREB. Tetrahedron Lett. **23**, 2347 (1982).
32. A. I. MEYERS, R. J. HIMMELSBACH, and M. REUMAN. J. Org. Chem. **48**, 4053 (1983).
33. W. C. STILL, M. KAHN, and A. MITRA. J. Org. Chem. **43**, 2923 (1978).
34. F. W. WEHRLI and T. WIRTHLIN. Interpretation of carbon-13 NMR spectra. Heyden, London. 1980.
35. C. D. Hurd and M. A. POLLACK. J. Am. Chem. Soc. **60**, 1905 (1938).
36. M. B. ROBIN, F. A. BOREY, and H. BASCH. *In* The chemistry of amides. *Edited by* J. Zabicky. Interscience, London. 1970. p. 1.
37. D. S. BRESLOW, E. BAUMGARTEN, and C. R. HAUSER. J. Am. Chem. Soc. **66**, 1286 (1944).
38. L. F. FIESER and M. FIESER. Reagents for organic synthesis. Vol. I. Wiley–Interscience, New York. 1967. p. 142.
39. B. M. TROST and J. L. STANTON. J. Am. Chem. Soc. **97**, 4018 (1975).
40. J. COLONGE and J.-P. CAYREL. Bull. Soc. Chem. Fr. 3598 (1965).

Radiolabelling with organomercury compounds. Part 1. The synthesis and structure of 6-halocholest-5-en-3β-ols

RICHARD J. FLANAGAN, F. PETER CHARLESON, AND EYVIND I. SYNNES
Merck Frosst Canada Inc., P.O. Box 1005, Pointe Claire – Dorval, P.Q. Canada H9R 4P8

LEONARD I. WIEBE AND YVON X. THERIAULT
Faculty of Pharmacy and Pharmaceutical Sciences, University of Alberta, Edmonton, Alta., Canada T6G 2N8

AND

THOMAS T. NAKASHIMA
Department of Chemistry, University of Alberta, Edmonton, Alta., Canada T6G 2N8

Received February 10, 1984

RICHARD J. FLANAGAN, F. PETER CHARLESON, EYVIND I. SYNNES, LEONARD I. WIEBE, YVON X. THERIAULT, and THOMAS T. NAKASHIMA. Can. J. Chem. **63**, 2853 (1985).

The synthetic route to 6-chloromercuricholest-5-en-3β-ol has been studied and the yield improved from 2% to 20%. The reaction of 6-chloromercuricholest-5-en-3β-ol with fluorine, chlorine, bromine, and iodine has been examined. 6-Bromocholest-5-en-3β-ol and 6-chlorocholest-5-en-3β-ol have been directly prepared from 6-iodocholest-5-en-3β-ol using cuprous halides. A new intermediate, 6-tosyloxycholest-5-en-3β-ol, has also been synthesized by the action of silver tosylate on 6-iodocholest-5-en-3β-ol. The structures of the compounds were proven by a combination of high-resolution ^{1}Hmr and ^{13}Cmr. A new crystal modification of 6-chloromercuricholest-5-en-3β-ol has been found.

RICHARD J. FLANAGAN, F. PETER CHARLESON, EYVIND I. SYNNES, LEONARD I. WIEBE, YVON X. THERIAULT et THOMAS T. NAKASHIMA. Can. J. Chem. **63**, 2853 (1985).

On a étudié la voie d'accès au chloromercuri-6 cholestène-5 ol-3β et on a amélioré le rendement de 2% à 20%. On a étudié la réaction du chloromercuri-6 cholestène-5 ol-3β avec le fluor, le chlore, le brome et l'iode. Faisant appel à la réaction des halogénures cuivreux avec l'iodo-6 cholestène-5 ol-3β, on a réalisé des synthèses directes des bromo-6 et chloro-6 cholostène-5 ols-3β. On a également synthétisé un nouvel intermédiaire, le tosyloxy-6 cholestène-5 ol-3β, en faisant réagir le tosylate d'argent sur l'iodo-6 cholestène-5 ol-3β. La rmn du ^{1}H et du ^{13}C à haute résolution a permis d'élucider les structures des composés. On a trouvé une nouvelle modification cristalline du chloromercuri-6 cholestène-5 ol-3β.

[Traduit par le journal]

Introduction

The need for high speed stereospecific methods for the introduction of radioligands into organic molecules has necessitated the development of novel synthetic methods. Some of the newer methods developed recently involve the reaction of selected organoboron (1–3), organotin (4), and organothallium compounds (5) with elemental iodine. We have chosen to examine the feasibility of using organomercury compounds for this procedure. We felt that organomercury compounds offered a number of advantages over other organometallic intermediates in that they are easily accessible from organic halides, olefins, and aromatic amines. Such is not the case for organotin and especially organoboron compounds. Furthermore, organomercury compounds are known in the three common forms required for most labelling procedures, i.e. aliphatic, vinylic, and aromatic. We chose a vinyl organomercury compound as our first compound, as it would offer the most difficulties from the point of view of competing reactions since vinyl systems have considerable reactivity with the common halogens. A useful starting point for this study was 6-chloromercuricholest-5-en-3β-ol (**1**) first prepared by Merz (6, 7) in 1926. This compound has been used recently in the preparation of 6-iodocholest-5-en-3β-ol (**2**) which is the precursor for [^{131}I]-6-iodocholest-5-en-3β-ol (8, 9). This latter compound shows great promise as an adrenal imaging agent (10). This recent interest in the use of [^{131}I]-6-iodocholest-5-en-3β-ol for adrenal imaging has required the preparation of large quantities of this compound and its precursor, 6-chloromercuricholest-5-en-3β-ol (**1**). The standard approach has been the reaction of cholesterol with mercuric acetate, a method that proceeds with low yield. This reaction was examined in order to optimize the conditions and we have improved the yield from 2% to 20%. We have also prepared 6-bromocholest-5-en-3β-ol (**3**) and 6-chlorocholest-5-en-3β-ol (**4**) directly from **1** and indirectly from **2**. A detailed structural analysis (11) of these compounds was also carried out, since it is well known that rearrangements are very common in cholesterol molecules with functionalities at the 6-position (12, 13), and as part of an ongoing program to study structure–activity relationships in steroids.[1]

Discussion and results

The reaction of cholesterol with mercuric acetate is complicated by a number of competing routes (see Scheme 1). These arise out of the decomposition of the mercurinium ion (**5**) formed when mercuric acetate adds to the 5,6 double bond of cholesterol. Two of these routes comprise the major course of the reaction and result from the loss of a proton from **5** to form either a 4,5 or a 5,6 double bond. The formation of the 4,5 double bond gives the allylic mercuriacetate (**6**) which reacts further with mercuric acetate via the Triebs reaction (14, 15) to give the vinylic acetate (**7**). The percentage yield of this compound can be estimated from the recovered mercurous acetate, which precipitates out during the course of the reaction and is about 60%. The formation of a 5,6 double bond from the decomposition of **5** gives rise to the desired vinylic mercuri-

[1]This paper is Part 1 of a series. Part 2 is "High Specific Activity Syntheses of [^{125}I] and [^{131}I]-6-Iodocholest-5-en-3β-ol" and Part 3 is "The Synthesis of [^{77}Br] and [^{82}Br]-6-Bromocholest-5-en-3-β-ol".

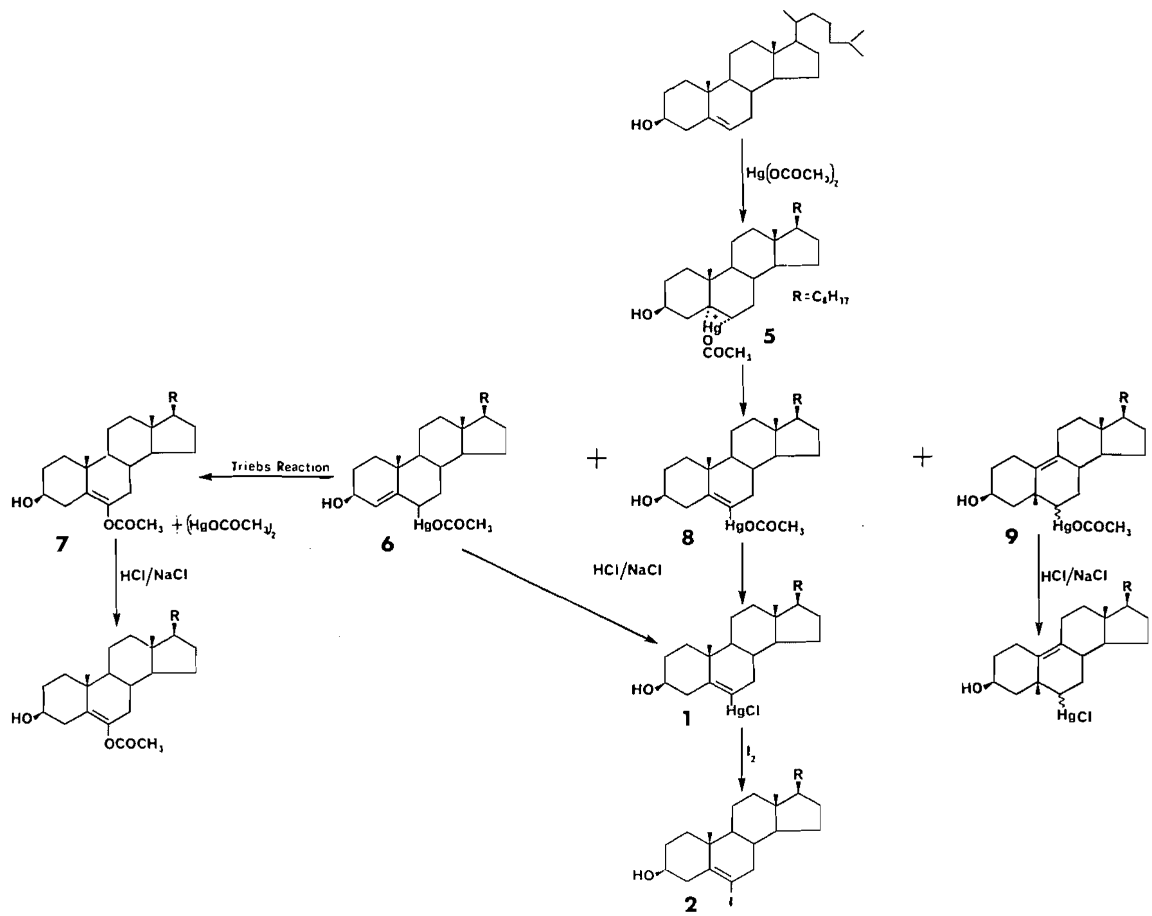

SCHEME 1

acetate (**8**). This route would appear to be an unusual one for the decomposition of mercurinium ions, and very few examples exist in which mercuric acetate addition to a double bond results in substitution for a vinylic hydrogen (16, 17). Such examples as exist all involve mercurinium ions that possess good carbonium stabilization at one of the vinyl carbons. It would appear that a carbonium ion at C-5 of the cholesterol has some of these stable properties. The complexity of the product mixture is greatly simplified on treatment with 1% HCl in aqueous sodium chloride, giving rise to a further mixture consisting mainly of 6-acetoxycholest-5-en-3ol (**7**) (60%) and the desired product, 6-chloromercuricholest-5-en-3β-ol (**1**) (40%). Since the mixture becomes simplified, it is reasonable to assume that some of the components rearrange in the presence of acid to form **1**, the most likely candidate being **6**. This mixture can be separated by preparative centrifugal chromatography on silica gel and after crystallization from acetone the 6-chloromercuricholest-5-en-3β-ol is obtained in 20% yield.

The 6-chloromercuricholest-5-en-3β-ol prepared in this fashion generally has a melting point of 208°C but sometimes material with a melting point of 154°C is obtained. The lower melting allotrope is produced from highly saturated solutions and is quite amorphous when compared to the needles of the higher melting point allotrope. Merz (6) also observed this lower melting point form but ascribed it to a double compound of 6-chloromercuricholest-5-en-3β-ol and cholesterol. We have examined this lower melting allotrope extensively and found it to be pure 6-chloromercuricholest-5-en-3β-ol by both ^{13}Cmr (11) and combustion analysis. The lower melting allotrope can be converted to the higher melting allotrope by careful recrystallization from acetic acid. The lower melting allotrope appears to be the same crystal modification as found in all other 6-halocholest-5-en-3-ols that have melting points in the range 147–154°C. Such behaviour, in which molecules of similar structure have very similar melting points, is well known for cholesterol compounds (18–20).

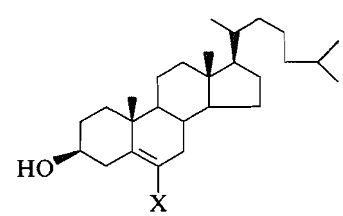

1 = HgCl
2 = I
3 = Br
4 = Cl
12 = F
13 = OTs

6-Chloromercuricholest-5-en-3β-ol reacts rapidly with elemental iodine at room temperature to give a quantitative yield of 6-iodocholest-5-en-3β-ol (**2**). We have tried this reaction in various solvents including methanol, ethanol, acetone, chloroform, and hexane and found it to proceed well in all. Shortly after the beginning of the reaction a violet precipitate of mercuric chloroiodide forms, which must be removed before the product is crystallized from the reaction solvent. A similar reaction occurs for iodine monochloride, giving only **2** and no measurable amount of 6-chlorocholest-5-en-3β-ol (**4**). This implies that the reaction of halogens with the carbon–mercury bond proceeds via a polarized intermediate state in which the more electropositive of the halide pair becomes joined to the carbon. This fact is of paramount importance for the use of these organomercury compounds as substrates for the introduction of halogen radiolabels into carbon skeletons.

The reaction of **1** with elemental bromine is quite similar to that for iodine, but is slower, and care must be taken to avoid an excess of bromine, in which case addition of bromine to the 5,6 double bond takes place. This is easily accomplished by slow addition of the bromine and by monitoring the disappearance of the yellow colour due to the excess bromine. An alternative solution to the problem of addition to the double bond is the use of *N*-bromosuccinimide. This reagent reacts smoothly with **1** to give the monobromo product **3**. This observation is particularly important for labelling applications since it allows the perparation of **3** using radiobromide. The reaction of **1** with pyridinium bromide perbromide is more controlled than that for elemental bromine but some addition to the double bond can still take place if an excess is present.

The reaction of 6-chloromercuricholest-5-en-3β-ol with chlorine gas is not successful, since the addition of chlorine to the 5,6 double bond proceeds faster than the cleavage of the carbon–mercury bond. The main product is 5,6,6-trichloro-5α-cholestan-3β-ol (**10**) resulting from addition to the double bond followed by cleavage of the carbon–mercury bond. The

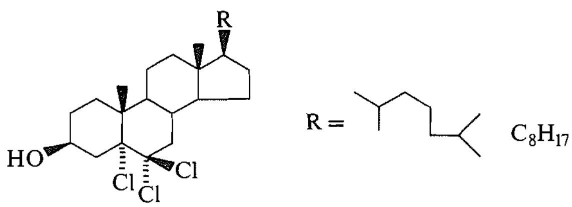

10

use of very dilute solutions of chlorine in methanol in conjunction with slow addition resulted in the formation of some 6-chlorocholest-5-en-3β-ol, but the amount was less than 10%. *N*-Chlorosuccinimide does not react with the carbon–mercury bond of **1** nor does it add to the 5,6 double bond. This a very fortunate circumstance since *N*-chloro species are commonly used for oxidizing iodide to iodine monochloride in labelling reactions. This fact also allows for some improvement in the yield of **4** by generating the Cl_2 *in situ* using chloride ion and *N*-chlorosuccinimide in ethanol/water as solvent. This results in a small steady-state concentration of Cl_2 and permits a moderate improvement in the yield of **4** to 20%. Because it would appear that *N*-chloro bonds are not sufficiently reactive to attack the carbon–mercury bond, it was of interest to see if an *O*-chloro bond might achieve this goal, since oxygen is more electronegative and the *O*-chloro bond should be more polarized. Such is indeed the case and 6-chloromercuricholest-5-en-3β-ol undergoes a rapid reaction with *tert*-butyl hypochlorite to form a complex mixture. The major component of this mixture, upon examination by mass spectroscopy, appeared to be an oxychloro derivative (tentatively assigned structure **11**) but no further structural determination was carried out.

The reaction of **1** with fluorine gas was also investigated but no direct reaction of fluorine and the carbon–mercury bond could be detected and no 6-fluorocholest-5-en-3β-ol (**12**) could

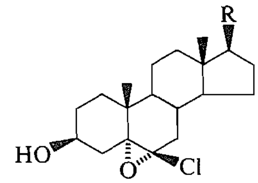

11

be found in the resulting mixture. A number of different methods of introducing the fluorine gas were examined, including 5% fluorine in neon at various temperatures from −78 to 25°C and in various solvents such as carbon tetrachloride, Freon-11, chloroform, and acetic acid. Other reactions examined included the use of acetyl hypofluorite (21) and xenon difluoride. The chemical literature contains no record of chloromercury groups reacting with fluorine to form carbon–fluorine bonds.

6-Chlorocholest-5-en-3β-ol was produced by treating 6-iodocholest-5-en-3β-ol with excess cuprous chloride in DMF at 50°C for 24 h. The nature of the carbon–iodine bond in **2** is such that it is very resistant to nucleophilic exchange (8) but, since the mechanism for halide exchange with cuprous halides is a ligand exchange process, it proceeds well in this instance. The same method also allows exchange of bromine for iodine using Cu_2Br_2 and **2**, giving a quantitative yield of **3**. Since halide exchange using cuprous halides is known to proceed with retention of configuration (22) for vinyl halides, this correlation of the structure of 6-chloromercuricholest-5-en-3β-ol with the previously known 6-chlorocholest-5-en-3β-ol (18) offers the first chemical structure proof for **1**.

Nucleophilic exchange at the 6-position of cholesterol is very difficult and proceeds only for the iodo compound **2** (8). Elevated temperatures and a large excess of nucleophile are required. We have been unable to exchange the bromine atom in **3** or the chlorine atom in **4** using even the most forcing conditions without destroying the molecule, usually by loss of the C-3 hydroxyl group and with formation of a double bond. The methods examined for exchange included the melt method with lithium, sodium, and potassium halides, dipolar aprotic methods using solvents such as DMF and DMSO, and catalytic methods with cuprous cyanide, chloride, and acetate. This unusual stability of halides attached to the 6-position of cholesterol is of course a favourable circumstance since it probably contributes to the *in vivo* stability of such molecules and accounts at least in part for the success of [^{131}I]-6-iodocholest-5-en-3β-ol as an adrenal imaging agent. Since, as we have already shown, these halides can be introduced electrophilically, the resistance to nucleophilic exchange is an added advantage. 6-Tosyloxycholest-5-en-3β-ol (**13**) can be prepared by the reaction of **2** with excess silver tosylate in DMF at 110°C. As is the case with 6-halocholest-5-en-3β-ols, however, the tosyl group in this compound is difficult to exchange.

A major concern of this work was the confirmation of the proposed structure for **1** and the corresponding halides **2**, **3**, and **4**. In particular, we wished to prove that the chloromercury function in **1** was indeed attached at the 6-position. Despite the fact that **1** has been known since 1926, no rigorous determination of its structure has yet been made. Since the synthetic route to **1** is quite unusual and involves the substitution of a vinylic hydrogen of cholesterol by an acetoxymercury group, there is some real doubt as to the position of the mercury function in the molecule. Furthermore, since the mechanism of formation of **1** must involve either a carbonium ion at C-5 or

TABLE 1.[a] ^{13}C chemical shifts of 6-substituted cholest-5-en-3β-ols

Carbon	Compound 1	2	3	4
1	37.29	37.38	37.25	37.27
2	31.44	31.56	31.21	31.15
3	71.23	70.70	70.53	70.57
4	48.87	49.06	43.46	40.49
5	147.29	143.88	138.25	135.52
6	146.35	100.67	120.61	127.21
7	41.63	47.18	40.12	36.41
8	33.85	35.55	34.17	33.14
9	49.63	49.98	49.70	49.68
10	40.76	41.27	40.47	39.26
11	21.11	21.39	21.21	21.15
12	39.64	39.67	39.55	39.54
13	42.54	42.53	42.39	42.36
14	56.62	56.22	56.27	56.31
15	24.22	24.17	24.14	24.14
16	28.25	28.21	28.19	28.18
17	56.17	56.22	56.06	56.07
18	11.89	11.89	11.83	11.83
19	20.14	19.84	19.56	19.53
20	35.80	35.79	35.77	35.75
21	18.75	18.78	18.73	18.71
22	36.24	36.27	36.18	36.18
23	23.87	23.95	23.87	23.85
24	39.58	39.60	39.56	39.54
25	28.07	28.04	28.02	28.01
26	22.58	22.57	22.57	22.55
27	22.83	22.80	22.81	22.79

[a]All values are in ppm relative to TMS in $CDCl_3$ at ambient temperature.

a mercurinium ion across the C-5,6 double bond, the possibility of a rearrangement must be taken into consideration. The homoallylic rearrangement has been found to occur for 19-iodonorcholesterol (**14**), a radiolabelled adrenal imaging agent (23).

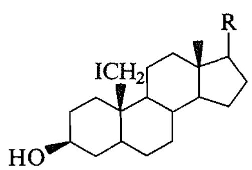

14

A further reason for confirming the structure of these compounds was provided by their apparently different physical properties when compared to cholesterol. In this sense they are much more stable towards oxidative decomposition than cholesterol. Although **2**, **3**, and **4** would not be expected to react facilely via a nucleophilic mechanism, they exhibited an extraordinary resistance to any such reaction. These properties were mirrored in the excellent in vivo stability of both **2** (8) and **3** (see footnote 1, Part 3 and ref. 24). The vinyl iodide **2**, in particular, is one of the more stable iodides that we have yet studied (25). These properties, in conjunction with the mechanistic considerations mentioned earlier, led to some serious doubts as to the correct structure of this series of compounds. Because of the difficulties involved in chemical transformations of these compounds we chose to undertake a rigorous spectroscopic study. Since a major problem in the design of radiohalogen labelled radiopharmaceuticals is the subsequent in vivo loss of the label, it was hoped that the structural information collected in this fashion would help in the design of other radiolabelled pharmaceuticals with greater in vivo stability.

The ^{13}Cmr data for **1**, **2**, **3**, and **4** are contained in Table 1. The assignments of the various carbons were made by analogy with the published spectrum of cholesterol (26) and through the use of the gated ^{1}H decoupled ^{13}C spin echo technique (GASPE) developed in these laboratories (27, 28). This technique allows the facile determination of the multiplicity of an individual carbon resonance. The assumption was made that the structures were as proposed and, therefore, that differences between the spectra of **1**, **2**, **3**, **4**, and cholesterol could be rationalized on the basis of known shift parameters. Fortunately this was the case. If one considers the non-olefinic carbons, the only major differences discernible between the ^{13}Cmr spectra of cholesterol and the compounds under consideration occur for carbons 4, 7, 8, and 10. Since carbon 10 is a singlet and carbon 8 is a doublet these resonances are easily reassigned in their shifted positions. Carbons 4 and 7 are both triplets and their assignment therefore might lead to some ambiguity. When one compares the positions for these new triplets in the spectra of **1**, **2**, **3**, and **4** there is only one rational assignment that can be made, since such an assignment must conform to the known shift parameters for halogens. This required the arrangement of the resonances for C-4 and C-7 in such a manner that they both demonstrated a decreasing pattern of shifts from I to Cl. It was also noted that, whereas the olefinic resonances for cholesterol are a doublet and a singlet, in **1**, **2**, **3**, and **4** these resonances appear as singlets, confirming the presence of a functionality at C-6. The shifts observed on the introduction of the various functionalities into the cholesterol skeleton are given in Table 2. Also included in this table are the predicted values for these shifts where such values are available (29). These shifts are best considered in terms of α, β, γ, and δ effects. The high positive value for the shift observed in **2** at C-7, which is β to the iodine at C-6, is without precedent. Such an abnormally high value must be taken in the context of the abnormal negative value for the shift of the C-6 carbon. Apparently the iodine in **2** is electropositive with respect to the double bond and, if one assumes a partial negative charge at C-5 and a corresponding positive charge at C-6, one can explain the effect. This must also be partially responsible for the absence of any *observed γ-gauche* effect at C-4. In fact C-4 shows a downfield shift. However, no γ-*gauche* effect would be expected at C-8 or C-10 since these atoms are γ-*anti* to C-6. A γ-*gauche* effect of some degree would be expected at C-4, since it is known this effect is related to the removal of 1,3-diaxial hydrogen interactions (30) such as might be expected for the C-4 equatorial hydrogen and the C-6 pseudo-equatorial hydrogen. It appears that the absence of a γ-*gauche* effect at C-4 is due to an overiding downfield inductive effect, which is in turn caused by the partial negative charge at C-5. This inductive effect should be observed at both C-4 and C-10, although not necessarily to the same degree, and C-4 should have an additional upfield component due to an expected γ-*gauche* effect. The effects observed at C-8 should be due to the corresponding partial positive charge at C-6, and C-8 does indeed show small but consistent downfield shifts in the series **4** to **2**. In summary, although the γ effects observed are probably due to a combination of inductive and steric effects, they can be rationalized to some extent. Any further analysis of these effects is hampered by the lack of available literature values for alicyclic vinylic halides. The δ effects observed are too small to be significant and, futhermore, shifts in choles-

TABLE 2.[a] ^{13}C induced chemical shifts of 6-substituted cholest-5-en-3β-ols compared to cholesterol

		Compound			
Position		1	2	3	4
Carbon 6	Measured	+25.0	−20.7	−0.8	+5.8
	Expected		−38.0	−8.0	+3.0
Carbon 5	Measured	+6.7	+3.3	−2.3	−5.1
	Expected		+7.0	−1.0	−6.0
Carbon 7	Measured	+9.9	+15.2	+8.2	+4.5
Carbon 4	Measured	+6.7	+6.8	+1.3	−1.7
Carbon 8	Measured	+1.9	+3.6	+2.2	+1.2
Carbon 10	Measured	+4.3	+4.8	+4.0	+2.8
Carbon 3	Measured	−0.4	−0.9	−1.1	−1.1
Carbon 9	Measured	−0.6	−0.2	−0.5	−0.5
Carbon 14	Measured	−0.2	−0.6	−0.5	−0.5
Carbon 19	Measured	+0.7	+0.4	+0.1	+0.1

[a]All values are in ppm and are the difference between the published values for cholesterol (25) and the various compounds measured in deuterochloroform at ambient temperature. The expected values for C-5 and C-6 are taken from ref. 10.

TABLE 3.[a] $^{13}C-^{199}H$ coupling constants

Coupling	Measured	Expected
$J(^{13}C_6-^{199}Hg)$	1079	1133
$J(^{13}C_5-^{199}Hg)$	36	38
$J(^{13}C_7-^{199}Hg)$	Not found	60
$J(^{13}C_8-^{199}Hg)$	160	157

[a]All coupling values are in hertz and were measured in deuterochloroform at ambient temperature. The expected values for C-5 and C-6 are taken from ref. 34 and the values for C-7 and C-8 are from ref. 35.

terol are known to be concentration and temperature dependent (31, 32).

Further evidence comes from the observation of the ^{199}Hg satellites in the spectrum of 6-chloromercuricholest-5-en-3β-ol (**1**). The natural abundance of ^{199}Hg is 16% and it is the only mercury isotope with a nuclear spin of 1/2. One might therefore expect to observe satellites on either side of selected carbon resonances in **1** with intensities of 8% each. In practice, the amplitude of these satellites is known to show solvent dependency (33) but is was nevertheless possible to observe three sets of such satellites. These were found for the resonances of carbons 5, 6, and 8. We also anticipated finding satellites on the resonance of C-7 but they were obscured by the close proximity of the resonances due to C-13, C-10, C-12, and C-24. It is also possible that the $^{13}C-^{199}Hg$ coupling is too small to be observed since such a coupling would be expected to be of the order of 30–50 Hz, which is close to the bandwidth at the base of the peak. The couplings observed correspond closely to those observed by other investigators (34). These coupling constants and their expected values are shown in Table 3. It was assumed, when choosing the expected values for the C-7 and C-8 coupling constants, that the B ring of the cholest-5-ene system was a quasi chair and that the expected values for the coupling constants would be intermediate between those found for boat and chair chloromercuri-cyclohexyl systems. Although a Karplus equation for the dependence of these couplings on bond angles has been developed (35), we found that the observed values bore an excellent similarity to those in conformationally mobile cyclohexyl systems and chose the latter on the assumption that those values, being an

TABLE 4.[a] ^{1}H chemical shifts of 6-substituted cholest-5-en-3β-ols

Proton	1	2*a*	2*b*	3	4
3-Axial	3.50	3.58	3.91	3.58	3.60
4-Axial	2.33	2.28	2.70	2.20	nf
4-Equatorial	2.69	3.02	3.50	3.20	3.28
7-Axial	nf	2.25	2.37	2.15	nf
7-Equatorial	2.33	2.72	2.82	2.50	2.32
8-Axial	nf	1.72	1.75	nf	nf

[a]All shifts are in ppm and were measured in $CDCl_3$ except for **2***b* which was measured in pyridine-d_5. nf = not found.

TABLE 5.[a] $^{1}H-^{1}H$ coupling constants

Coupling	1	2*a*	2*b*	3	4
J(3ax, 2ax)	nm	12	11	12	11.5
J(3ax, 2eq)	nm	5	4.5	5.2	4.5
J(3ax, 4ax)	11	12	11	12	11.5
J(3ax, 4eq)	nm	5.5	4.5	5	4.5
J(4ax, 4eq)	14	14	13.5	14.7	14
J(7ax, 7eq)	nm	20	17	18.5	17.3
J(7ax, 8ax)	nm	12	10	11	nm
J(7eq, 8ax)	nm	5.5	5	5.5	5.5

[a]All couplings are in Hertz and were measured in $CDCl_3$ except for **2***b* which was measured in pyridine-d_5. nm = not measured.

average of boat and chair values, represented a quasi chair. Since $^{13}C-^{199}Hg$ coupling constants are very sensitive to changes in bond angles, the excellent correlation between the observed and expected constants serve to confirm the quasi-chair conformation of the B ring. This fact, in conjunction with the lack of any observed steric effects in ^{13}Cmr shifts of B ring carbons, implies that the introduction of bulky functional groups such a chloromercury group into the 6-position of cholesterol causes remarkably few conformational changes in that ring.

The ^{1}Hmr spectra for these compounds also provide some structural evidence. Generally, ^{1}Hmr spectroscopy of cholesterol species is complicated by the close proximity of all the resonances (36), and all the protons of cholesterol except the olefinic protons occur in an envelope of 3 ppm. This problem is lessened in the case of the current compounds because the functionalities at C-6 serve to shift the protons at C-4 and C-7 downfield. This is fortunate since it is these protons that provide the structural information. It is possible to clearly observe the resonances of the C-3, C-4, C-6, and, sometimes, the C-7 protons and in most cases to determine their coupling constants. The observable resonances for some of the A and B ring protons of **1**, **2**, **3**, and **4** are given in Table 4 and their coupling constants are given in Table 5. In the case of **2**, the ^{1}Hmr spectrum was measured in $CDCl_3$ and also in perdeuteropyridine in order to distinguish between the resonances of the 7ax and 4ax protons, which overlap in chloroform. Decoupling experiments were carried out only on **2** and **3** and the identity of the various resonances was deciphered in this manner. This information was then applied to the spectra of **1** and **4**. No major differences in shifts or couplings between the four compounds were observed but the spectrum of **1** was complicated by the additional couplings between ^{199}Hg and the various protons. In only a few cases was it possible to determine coupling constants. In the case of **2** it was possible to observe the 8ax proton and this provided some very useful information. This proton was shown to be coupled to the 7eq proton with the

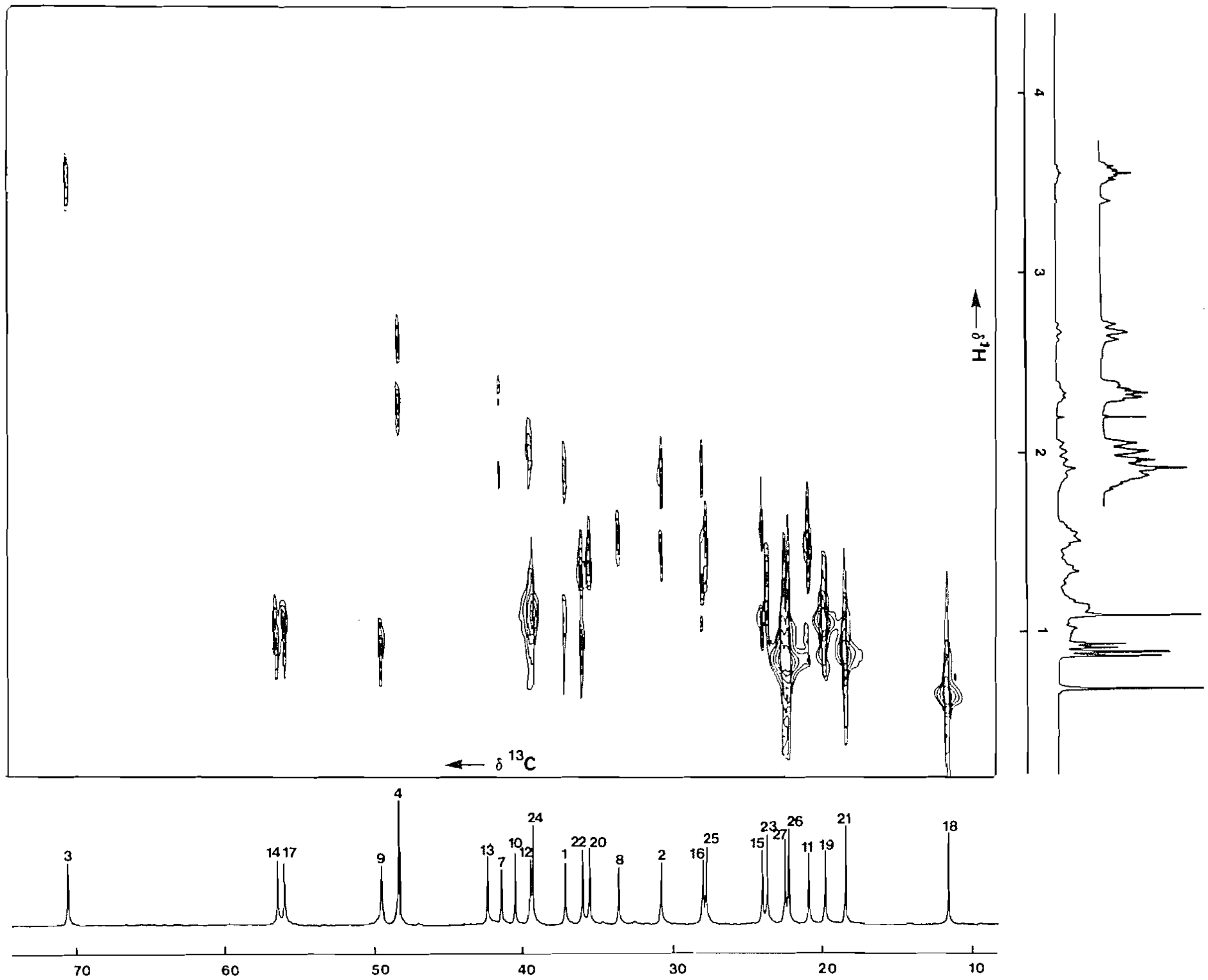

FIG. 1. Contour plot of the 2D heteronulcear $^{13}C-^{1}H$ shift correlation experiment.

expected *syn* coupling of 5.5 Hz. When 7eq was decoupled, 8ax collapsed to a symmetrical quartet with a coupling of 11 Hz. The implication of this was clear. There is only one proton in the entire ring system of cholesterol that has three *trans*-diaxial interactions, and that is the 8ax proton. This proton is also coupled in a *syn* manner to another proton that is shifted substantially downfield by the introduction of a chloromercury function or a halogen atom. Since there is only one proton that is *syn* to 8ax, and that is the 7eq proton, the introduced functionality must be at C-6. The observed proton–proton coupling constants, although less sensitive to changes in conformation than the corresponding carbon–mercury coupling constants, are in good agreement with the quasi-chair nature of the B ring.

A further experiment was undertaken to correlate the assignments of the ^{13}Cmr spectrum of **1** with that of the ^{1}Hmr spectrum. This involved a new technique developed in these laboratories (37) in which a two-dimensional spectrum is produced that shows which protons in the ^{1}Hmr spectrum are coupled to which carbons in the ^{13}Cmr spectrum. This two-dimensional spectrum is shown in Fig. 1. The vertical lines in the diagram correspond to correlations between the ^{13}Cmr and ^{1}Hmr spectra of **1**. It can be seen that the assignments for C-3, C-4, and C-7 in both spectra can be verified. The C-3 protons show as a multiplet, the C-4 protons as an AB doublet, and C-7 protons also as an AB doublet. Using this method it is possible to identify all the protons in the ^{1}Hmr spectrum and measure their shifts. As a result of this it was possible to confirm all the structural assignments made for **1** in both ^{13}Cmr and ^{1}Hmr.

The evidence presented so far serves to confirm the structural assignment made for **1**, **2**, **3**, and **4**. It was also of interest to see if this spectroscopic evidence could provide any further information to explain the unusual properties of these molecules. The first point to emerge is that there are remarkably few steric effects to be observed from the introduction of such bulky functional groups as chloromercury and iodine into the 6-position of cholesterol. This is evident from both ^{13}Cmr and ^{1}Hmr, where the observed shifts were explainable *mainly* on the basis of inductive effects. If the carbon skeleton of **1** or **2** were conformationally altered from that of cholesterol, then there would have been greater differences in the resonances of carbons outside the zone of inductive effect and this was not found.

The ^{13}Cmr data show that, compared to cholesterol, **2** demonstrates greater perturbations than **3**. This behaviour is mirrored in biological behaviour. The uptake of 6-iodocholest-5-en-3β-ol (**2**) in the adrenal glands is efficient but the evidence indicates that it becomes metabolically trapped there (10). In the case of the 6-bromocholest-5-en-3β-ol (**3**), where the ^{13}Cmr inductive effects are of a lesser degree than for **2**, both ^{13}Cmr and ^{1}Hmr indicate a remarkable similarity between this compound and cholesterol itself. The ^{13}Cmr shifts for C-5 and C-6 in **2** are practically identical to those for cholesterol and the greatest difference occurs for C-7 (+8.2 ppm). In fact **3** is taken up in the adrenals but, in addition, it passes through the metabolic chain and is released as a bromosteroid (see footnote 1, Part 3 and ref. 24).

We anticipate using nmr spectroscopy as a tool to evaluate structural activity relationships in the design of future radiopharmaceuticals. It would appear that ^{13}Cmr spectroscopy, with its wider range of resonances and its greater sensitivity to steric effects, is better suited to this task.

Experimental

All reagents and solvents were reagent grade and were used without further purification. Thin-layer chromatographic (tlc) analysis was carried out on silica gel Whatman MK6F micro plates using 7% methanol in chloroform as developing solvent. High-pressure liquid chromatographic (hplc) analysis was carried out using a Waters CN radial compression column and methanol/chloroform/hexane 10:20:70 as solvent. Preparative hplc separations were performed with a Whatman M9 10/50 PAC Partisil column and methanol/chloroform/hexane 5:20:75 as solvent. All melting points are uncorrected.

The ^{13}Cmr spectra were measured either on a Bruker WH-200 at 50.3 MHz or a Bruker AM-300 at 75.4 MHz. The ^{1}Hmr spectra were measured either on a Bruker WH-400, a Bruker WH-200, or a Bruker AM-300 at the stated frequencies. Except in the case of **2**, all spectra were measured in $CDCl_3$ at ambient temperature using tetramethylsilane as a reference. For the ^{1}H–^{13}C heteronuclear shift correlation experiment (38), the following pulse sequence was used:

$$(90x)\,{}^1\mathrm{H}-t_1/2-(180x)\,{}^{13}\mathrm{C}-t_1/2-\underbrace{\tau-(180x)\,{}^1\mathrm{H}(90\psi)\,{}^{13}\mathrm{C}-\tau-(\Theta\phi)\,{}^1\mathrm{H}(180x)\,{}^{13}\mathrm{C}}_{\text{DEPT}}-\tau-\text{acquis}\,{}^{13}\mathrm{C}$$

where $(90x)^1$H represents a 90° ^{1}H pulse directed along the x-axis. ψ and ϕ are phase cycled as follows: $\psi = x, y, -x, -y$ and $\phi = y, -x, -y, x$ to suppress the Boltzmann contribution to the ^{13}C signal and to allow quadrature detection in the f_1 domain. t_1 is incremented in the normal fashion, τ is fixed at $1/(2J_{CH})$, and the ^{13}C signal is acquired with ^{1}H broadband decoupling. Transverse ^{1}H magnetization is created by the first 90° ^{1}H pulse and is allowed to precess freely during the t_1 interval, thus labelling ^{1}H magnetization with their characteristic frequency (or chemical shift). The 180° ^{13}C pulse in the middle of this period serves to remove the large directly bonded coupling (38). Polarization transfer of the "labelled" ^{1}H magnetization to ^{13}C is accomplished by the Distortionless Enhancement by Polarization Transfer (DEPT) (39) part of the sequence. The amount of ^{1}H polarization transfer to the carbon spin is dependent upon the ϕ, the final ^{1}H pulse angle, and its functional form depends upon the number of protons directly attached to the carbon. The amplitude of the ^{13}C signals will be modulated at the chemical shift of the directly bonded ^{1}H as t_1 is incremented, and Fourier transformation along the f_1 domain will yield ^{1}H chemical shift information.

Mass spectra were measured with a Hewlett–Packard 5995 mass spectrometer and only significant peaks over 10% of the base peak are reported. Five percent fluorine in neon was supplied by Matheson Gas Products.

*6-Chloromercuricholest-5-en-3β-ol (**1**)*

Fifteen grams of cholesterol in 60 mL of boiling acetic acid was added to 36 g of mercuric acetate in 60 mL of boiling acetic acid. The mxiture was stirred vigorously while continuing to boil for another 6 min and then cooled to room temperature using an ice bath. Mercurous acetate started to precipitate at this point. The precipitate was collected and washed with 20 mL of acetic acid. The combined filtrates were then added to 800 mL of saturated NaCl solution containing 1% HCl and stirred for 2 h. The yellow precipitate was collected by filtration and air dried overnight. This precipitate was suspended in a mixture of 250 mL each of diethyl ether and water. The aqueous layer was discarded and the ether layer washed once with 1% sodium bicarbonate and twice with saturated sodium chloride solution. The ether layer was dried over calcium chloride and concentrated *in vacuo*. The yield at this point was 20 g of 50% pure material.

This crude material was chromatographed in batches of 3 g on 100 g of silica gel (tlc grade) using chloroform as solvent on a Hitachi CLC-3 centrifugal chromatograph. The 6-chloromercuricholesterol was the third fraction to exit and was 95% pure. The combined 6-chloromercuricholest-5-en-3β-ol fractions were dissolved in an excess of acetone and the solution let stand for 10 days at room temperature while the crystals of **1** slowly formed. Colourless needles (>99%) were collected; yield 5 g, 20% of theory; mp allotrope(1) 208°C, allotrope(2) 154°C; tlc, rf = 0.4; ^{1}Hmr($CDCl_3$): 3.6 (m, 1H), 2.69 (m, 1H), 2.35(m, 2H), 2.1–1.8(m, 5H), 1.6–0.65(complex); ms (DIP, EI 70 eV): 624(M$^+$, 0.2), 623(M$^+$, 0.2), 622(M$^+$, 0.5), 621(M$^+$, 0.3), 620(M$^+$, 0.4), 619(M$^+$, 0.3), 618(M$^+$, 0.2), 386(19), 385(14), 368(16), 318(10), 201(17), 159(20), 144(19), 133(30), 107(35), 105(37), 95(45), 91(43), 71(60), 57(100). *Anal.* calcd. for $C_{27}H_{45}OHgCl$: C 52.10, H 7.30, Cl 5.71; found: C 52.17, H 7.30, Cl 5.71.

*6-Iodocholest-5-en-3β-ol (**2**)*

To a solution of 30 mg of **1** in 10 mL of chloroform a saturated solution of iodine in chloroform was slowly added until the purple colour was sustained. The chloroform solution was washed with 10% sodium thiosulphate solution, dried, and concentrated *in vacuo* to yield an oil. This oil was taken up in 95% ethanol and on standing deposited colourless amorphous crystals of 6-iodocholest-5-en-3β-ol; yield 22 mg, 95% of theory; mp 157°C; tlc, rf = 0.6; ^{1}Hmr($CDCl_3$): 3.9(m, 1H), 3.5(m, 1H), 2.8(m, 1H), 2.7(m, 1H), 2.37(m, 1H), 2.15–0.7(complex); ms (DIP, EI 70 eV): 512(M$^+$, 78), 479(5), 386(15), 385(54), 159(27), 145(21), 119(46), 105(38), 93(30), 91(52), 57(100). *Anal.* calcd. for $C_{27}H_{45}OI$: C 63.20, H 8.85; found: C 63.32, H 8.92.

*6-Bromocholest-5-en-3β-ol (**3**)*

A solution of bromine in chloroform (40 mg, 0.25 mmol) was slowly added to a vigorously stirred solution of **1** (150 mg, 0.24 mmol) in chloroform. The rate of addition was such that the concentration of unreacted bromine was kept to a minimum. The chloroform solution was washed with 10% sodium thiosulphate solution, dried, and concentrated *in vacuo*. The residue was crystallized from 95% ethanol; yield 99 mg, 99% of theory; mp 155°C; tlc, rf = 0.55; ^{1}Hmr($CDCl_3$): 3.59(m, 1H), 3.2(m, 1H), 2.5(m, 1H), 2.2–0.7(complex); ms (DIP, EI 70 eV): 466(M$^+$, 9), 464(M$^+$, 9), 386(33), 385(86), 367(30), 173(27), 159(30), 135(30), 105(30), 100(50), 97(60), 95(57), 81(80), 71(82), 69(92), 57(100). *Anal.* calcd. for $C_{27}H_{45}OBr$: C 69.65, H 9.74, Br 17.16; found: C 69.61, H 9.70, Br 17.25.

*Reaction of 6-chloromercuricholest-5-en-3β-ol (**1**) with Cl_2 gas*

A solution of chlorine in methanol was slowly added to a solution of **1** (100 mg, 0.16 mmol) in chloroform. After 5 min the solution was examined by tlc, which indicated the absence of starting material and two new components. The major component (90%) appeared only on charring with H_2SO_4 and failed to quench the 254-nm fluorescence, implying that the double bond had been consumed. The smaller component did quench the uv indicator and was identified as 6-chlorocholest-5-en-3β-ol by tlc and ms. The major component was identified by its distinctive mass spectrum as 5,6,6-trichloro-5α-cholestan-3β-ol. Subsequent dechlorination experiments were carried out with this mixture since one of the components was the desired product; ms (DIP, EI 70 eV): 494(M$^+$, 8), 492(M$^+$, 23), 490(M$^+$, 25), 421(14), 420(21), 419(26), 418(28), 387(26), 386(15), 385(56), 384(27), 383(51), 159(33), 155(100). Dechlorination of this crude material with zinc in dioxane or THF was unsuccessful.

*6-Bromocholest-5-en-3β-ol (**3**) from **2** via Cu_2Br_2*

Cuprous bromide (dried at 120°C, 40 Torr; 1 Torr = 133.3 Pa) (1.44 g, 10 mmol) was added to a solution of **2** (512 mg, 1 mmol) in dry DMF (10 mL). The mixture was stirred at room temperature for 16 h and then filtered to remove solids. The solution was diluted with 5% aqueous $Na_2S_2O_3$ (100 mL) and extracted with chloroform (3 × 20 mL). The chloroform extracts were dried over $MgSO_4$ and concentrated *in vacuo* to give an off-white residue. Recrystallization from 95% ethanol gave **3** as colourless needles; yield 460 mg, 99% of theory; mp 155°C.

6-Chlorocholest-5-en-3β-ol (4) from 2 via Cu_2Cl_2

The procedure is similar to that for **3**. Cu_2Cl_2 (1.0 g, 10 mmol) was added to **2** (512 mg, 1 mmol) in DMF (20 mL) and the mixture stirred at 50°C for 24 h. Work-up as for **3** gave 6-chlorocholest-5-en-3β-ol (**4**) as colourless needles; yield 373 mg, 89% of theory; mp 156°C; tlc, rf = 0.45; ^{1}Hmr($CDCl_3$): 3.6(m, 1H), 3.28(m, 1H), 2.32(m, 1H); ms (DIP, EI 70 eV): 422(M^+, 6), 420(M^+, 18), 387(21), 386(14), 385(50), 384(26), 179(16), 177(15), 159(17), 95(36), 93(32), 57(93), 55(100).

6-Bromocholest-5-en-3β-ol (3) from 2 via N*-bromosuccinimide*

N-bromosuccinimide (150 mg, 5.2 mmol) was added to a solution of **2** (100 mg, 0.16 mmol) in chloroform (20 mL) and stirred at room temperature overnight. Analysis by tlc indicated a single product and complete consumption of starting material. The reaction mixture was washed with water, dried over $MgSO_4$, and concentrated *in vacuo* to give a residue that on crystallization from ethanol gave pure 6-bromocholest-5-en-3β-ol (**3**); yield 65 mg, 88% of theory; mp 155°C.

Attempted fluorination of 6-chloromercuricholest-5-en-3β-ol (1) using F_2 gas

A mixture of 5% fluorine in neon gas was bubbled through a solution of **1** in Freon 11 at −78°C. Examination of the reaction mixture indicated partial consumption of the starting material and the formation of a large number of new less-polar components. The same results were obtained in all other variations on this reaction.

The reaction of 1 with tert*-butyl hypochlorite*

tert-Butyl hypochlorite (40 mg, 0.37 mmol) was added to a solution of **1** (50 mg, 0.08 mmol) in chloroform (5 mL) and the solution stirred at room temperature for 30 min. Thin-layer chromatographic analysis indicated that the starting material had been consumed, with the formation of a number of products, one of which constituted the major component, 70%. The mixture was not separated but was analysed by mass spectrometry using the direct inlet probe method and a gradual increase in temperature to separate the components. In this fashion the mass spectrum of the major compound, which was tentatively assigned structure **11**, was obtained; ms (DIP, EI 70 eV): 438(M^+, 20), 436(M^+,6), 400(17), 385(20), 281(25), 161(17), 149(20), 119(23), 55(100).

6-Tosyloxycholest-5-en-3β-ol (13)

Silver tosylate (200 mg, 0.56 mmol) was added to a solution of **2** (250 mg, 0.40 mmol) in DMF (5 mL) and the mixture heated to 110°C for 30 min. By this time a grey precipitate had formed and tlc analysis of the reaction mixture indicated that all the starting material had been consumed. The solution was diluted with water (100 mL) and extracted with ether (3 × 20 mL). The extracts were dried over $MgSO_4$ and concentrated *in vacuo*. The residue was chromatographed on a Whatman PAC-Magnum 9 column and the major fraction collected. This material proved to be 6-tosyloxycholest-5-en-3β-ol (**13**) and was isolated as an oil; yield 90 mg, 40% of theory; ^{1}Hmr($CDCl_3$): 7.81(d, 2H, ArH), 7.42(d, 2H, ArH), 3.55(m, 1H, C3ax), 3.12(m, 1H, C4eq), 2.7(m, 2H, C7eq), 2.45(s, 3H), 2.30–0.7(42H); ms (DIP, EI 70 eV): 556(M^+, 2), 538(3), 402(8), 384(15), 365(10), 247(13), 185(14), 161(21), 121(44), 91(100), 57(54), 55(56).

Acknowledgments

We wish to acknowledge an NSERC/Merck Frosst Fellowship and an Alberta Heritage Foundation for Medical Research Allowance for one of us (R.J.F.). Technical assistance was provided by Mr. Brian M. McCloskey.

1. G. W. KABALKA and E. E. GOOCH. J. Org. Chem. **45**, 3578 (1980).
2. G. W. KABALKA, E. E. GOOCH, and K. A. R. SASTRY. J. Nucl. Med. **22**, 908 (1981).
3. G. W. KABALKA, K. A. R. SASTRY, H. C. HSU, and M. D. HYLARIDES. J. Org. Chem. **46**, 3113 (1981).
4. M. J. ADAM, B. D. PATE, T. J. RUTH, J. M. BERRY, and L. D. HALL. J. Chem. Soc. Chem. Commun. 733 (1981).
5. D. L. GILLIAND, G. P. BASMADJIAN, A. P. MARCHAND, G. H. HINKLE, A. EARLYWINE, and R. D. ICE. J. Radioanal. Chem. **15**, 7 (1978).
6. W. MERZ. Z. Physiol. Chem. **154**, 225 (1926).
7. R. H. LEVIN and M. A. SPIELMAN. J. Am. Chem. Soc. **62**, 920 (1940).
8. L. BO-LI, J. YU-TAI, L. ZHENGHAO, S. ZHAOXIANG, L. GONGX, and L. TAI-HUA. J. Labelled Comp. Radiopharm. **18**, 112 (1980).
9. L. BO-LI, J. YU-TAI, M. MAEDA, and M. KOJIMA. Radioisotopes, **30**, 275 (1981).
10. L. BO-LI, J. YU-TAI, L. ZHENGHAO, S. ZHAOXIANG, L. GONGX, and L. TAI-HUA. J. Nucl. Radiochem. (Beijing), **2**, 107 (1980).
11. R. J. FLANAGAN, L. I. WIEBE, F. P. CHARLESON, B. C. LENTLE, and R. CHERVU. J. Labelled Comp. Radiopharm. **19**, 1496 (1982).
12. T. WESTPHALEN. Chem. Ber. **48**, 1064 (1915).
13. D. V. KIRK and M. P. HARTSHORN. Steroid reaction mechanism. Elsevier Publishing, Amsterdam. 1968.
14. H. ARZOUMANIAN and J. METZGER. Synthesis, 527 (1971).
15. G. MASSIOT, H. HUSSON, and P. POTHIER. Synthesis, 722 (1974).
16. V. I. SOLOKOV, V. V. BASHILOV, and O. A. REUTOV. Dokl. Akad. Nauk SSR, **188**, 127 (1969).
17. J. M. COXON, M. P. HARTSHORN, and A. J. LEWIS. Tetrahedron Lett. 3521 (1969).
18. C. J. BERG and E. S. WALLIS. J. Biol. Chem. **162**, 683 (1946).
19. D. H. R. BARTON and E. MILLER. J. Am. Chem. Soc. **72**, 370 (1950).
20. D. H. R. BARTON and E. MILLER. J. Am. Chem. Soc. **72**, 1066 (1950).
21. O. LERMAN and S. ROSEN. J. Org. Chem. **48**, 724 (1983).
22. R. LAPOUYADE, M. DANEY, M. LAPENUE, and H. BONAS-LAURENT. Bull. Soc. Chim. 720 (1973).
23. M. MAEDA, M. KOJIMA, and H. OGAWA. Steroids, **26**, 241 (1980).
24. FLANAGAN *et al.* U. S. Patent No. 4,430,321. Feb. 7, 1984.
25. R. J. FLANAGAN, B. C. LENTLE, D. G. MCGOWAN, and L. I. WIEBE. J. Radioanal. Chem. **65**, 85 (1981).
26. J. W. APSIMON, H. BEIERBECK, and J. K. SAUNDERS. Can. J. Chem. **51**, 3874 (1973).
27. D. W. BROWN, T. T. NAKASHIMA, and D. L. RABENSTEIN. J. Magn. Reson. **45**, 302 (1981).
28. D. J. COOKSON and B. E. SMITH. Org. Magn. Reson. **16**, 111 (1981).
29. G. MACIEL. J. Phys. Chem. **69**, 1947 (1965).
30. H. BEIERBECK, J. K. SAUNDERS, and J. W. APSIMON. Can. J. Chem. **55**, 2813 (1977).
31. H. EGGERT and C. DJERASSI. J. Org. Chem. **38**, 3788 (1973).
32. H. J. SCHNEIDER and W. FREITAG. J. Am. Chem. Soc. **98**, 478 (1976).
33. A. J. BROWNE, O. W. HOWARTH, and P. MOORE. J. Chem. Soc. Dalton Trans. 1589 (1976).
34. V. S. PETROSYAN and O. A. REUTOV. J. Orgmetal. Chem. **76**, 123 (1974).
35. W. KITCHING, D. PRAEGER, D. DODDRELL, F. A. L. ANET, and J. KRANE. Tetrahedron Lett. **10**, 759 (1975).
36. S. P. SAWAN, T. L. JAMES, L. D. GRUENKE, and J. C. CRAIG. J. Magn. Reson. **33**, 409 (1979).
37. T. T. NAKASHIMA, B. K. JOHN, and R. E. D. MCCLUNG. J. Magn. Reson. **59**, 124 (1984).
38. R. FREEMAN and G. A. MORRIS. J. Chem. Soc. Chem. Commun. 684 (1978).
39. D. M. DODDRELL, D. T. PEGG, and M. R. BENDALL. J. Magn. Reson. **48**, 323 (1982).

Characterization of thymidine ultraviolet photoproducts. Cyclobutane dimers and 5,6-dihydrothymidines[1]

JEAN CADET, LUCIENNE VOITURIEZ, AND FRANK E. HRUSKA[2]
Laboratoires de Chimie, Département de Recherche Fondamentale, Centre d'Études Nucléaires de Grenoble, 85 X, F.38041 Grenoble Cédex, France

LOU-SING KAN
Division of Biophysics, School of Hygiene and Public Health, The Johns Hopkins University, Baltimore, MD 21205, U.S.A.

AND

FRANK A. A. M. DE LEEUW AND CORNELIS ALTONA
Gorlaeus Laboratories, Department of Chemistry, State University Leiden, P.O. Box 9502, NL-2300 RA Leiden, The Netherlands

Received February 22, 1985

JEAN CADET, LUCIENNE VOITURIEZ, FRANK E. HRUSKA, LOU-SING KAN, FRANK A. A. M. DE LEEUW, and CORNELIS ALTONA. Can. J. Chem. **63**, 2861 (1985).

We describe the preparation of the six configurationally distinct cyclobutane-type photodimers generated by the acetone-sensitized uv irradiation of thymidine in aqueous solution. Also prepared as minor photoproducts are the 5*R* and 5*S* diastereoisomers of 5,6-dihydrothymidine, and two novel molecules, the 5*R* and 5*S* diastereoisomers of 5-acetonyl-5,6-dihydrothymidine. The purification of the ten molecules by chromatographic techniques (hplc, tlc) is described, along with their extensive characterization by uv, ir, cd, FAB-ms and ^{1}H nmr. The proton chemical shifts and coupling constants are discussed in terms of the geometry of the pyrimidine, cyclobutane, and sugar rings.

JEAN CADET, LUCIENNE VOITURIEZ, FRANK E. HRUSKA, LOU-SING KAN, FRANK A. A. M. DE LEEUW et CORNELIS ALTONA. Can. J. Chem. **63**, 2861 (1985).

Les six diastéréoisomères possibles de la cyclobutidithymidine ont été préparés par photosensibilisation de la thymidine à la lumière du proche ultra-violet en utilisant l'acétone. Les diastéréoisomères 5*R* et 5*S* de la dihydro-5,6 thymidine et deux nouveaux photoproduits, les formes 5*R* et 5*S* de l'acétonyl-5 dihydro-5,6 thymidine ont aussi été isolés. L'identification de ces photoproduits a fait appel à diverses techniques spectroscopiques: uv, ir, dichroïsme circulaire, spectrométrie de masse par bombardement avec des atomes rapides et rmn ^{1}H. Les valeurs des paramètres de rmn (déplacements chimiques, constantes de couplage) sont discutées en termes de stéréochimie des cycles pyrimidiniques, cyclobutyles et osidiques.

Introduction

The cyclobutane-type of photoproduct formed from adjacent thymine bases is the most thoroughly studied of the lesions induced by uv irradiation of DNA (1). The biological significance of these thymine photodimers is evidenced by the existence of mechanisms for their removal (2). Several studies reveal that the presence of the dimers leads to distortions in nucleic acid structure (3–7) that could play a role in the recognition by the enzymes of the repair system and may account for the altered specificity of, for example, restriction enzymes which employ DNA as a substrate (8). The numerous studies of the photodimerized thymine bases, Thy⟨ ⟩Thy (R = H; Fig. 1), have provided valuable photochemical and structural information (1), but relatively fewer data are available for the corresponding thymidine derivatives, dThd⟨ ⟩dThd (R = 2-deoxy-β-D-ribose), which are the molecules of main interest in the present work. Wulff and Fraenkel (9) originally listed four isomeric forms of Thy⟨ ⟩Thy. Actually, six configurationally-distinct forms are possible, since the *trans–syn* (*ts*) and *cis–anti* (*ca*) isomers exist as enantiomeric pairs *ts*1, *ts*2 and *ca*1, *ca*2 whereas the *cis–syn* (*cs*) and *trans–anti* (*ta*) isomers exist as single (*meso*) molecules. Similarly, six dThd⟨ ⟩dThd are possible and are denoted CS, TS1, etc. according to the geometry of the Thy⟨ ⟩Thy fragment (Fig. 1). Partial characterization of the CS, TA, CA(+), and CA(−) diastereoisomers of dThd⟨ ⟩dThd has been made by Ben-Hur *et al.* (10) and Kuneida and Witkop (11).

In the present work we show that the six dThd⟨ ⟩dThd can be isolated from uv-irradiated aqueous solutions of dThd containing acetone as a photosensitizer. In addition to these dimers, which comprise 90% of the photoproduct mixture, we could isolate in smaller amounts the 5*R* and 5*S* diastereoisomers of 5,6-dihydrothymidine (DHT-*R* and DHT-*S*) and of the novel adducts 5-acetonyl-5,6-dihydrothymidine (ADT-*R*, ADT-*S*) (Fig. 2). The latter pair arise by the combination of the dihydrothymidin-5-yl and acetonyl radicals generated in the photosensitized solutions. The various products are characterized by cd, uv, ir, ^{1}H nmr, and mass spectrometric techniques.

There remains some uncertainty as to the structure of the photodimers formed in uv-irradiated DNA. Evidence has been provided (12) that the predominant product has the *cs* geometry; a minor *ts* product has also been detected (13), but its assignment to the *ts*1 or *ts*2 form was not made. Furthermore, it has been pointed out (4) that, though only a single *cs* isomer exists at the level of the photodimerized thymine bases or nucleosides, there are *two* possible diastereomers at the dinucleoside monophosphate level, d(T[p]T), each having a *cs* Thy⟨ ⟩Thy fragment but differing in the configurational relationship between the Thy⟨ ⟩Thy and sugarphosphate segments. (The two diastereomers were labelled A_1 and A_2 by Hruska *et al.* (4).) At present there is no information about the

[1]This work is dedicated to the memory of S. Y. Wang.
[2]Permanent address: Department of Chemistry, University of Manitoba, Winnipeg, Man., Canada R3T 2N2.

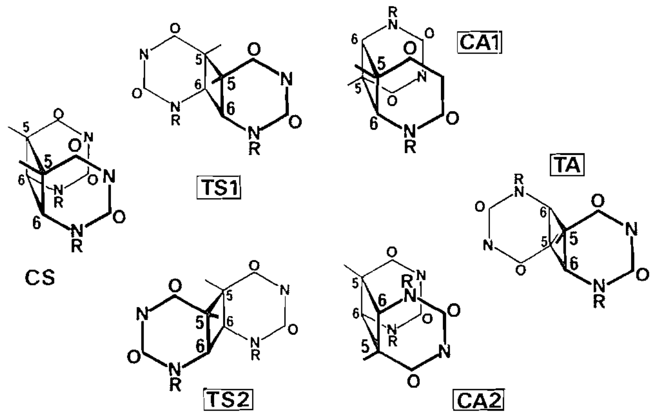

FIG. 1. Structure of the dThd⟨ ⟩dThd photodimers (R = 2-deoxy-D-ribose) with the *cis–syn* (CS), *trans–syn* (TS), *cis–anti* (CA), and *trans–anti* (TA) cyclobutane geometry. The corresponding Thy⟨ ⟩Thy (R = H) are denoted by *cs*, *ts*, *ca*, and *ta*.

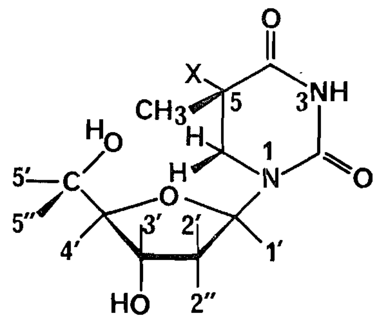

FIG. 2. Structure and atomic numbering of the 5*R* diastereoisomer of 5,6-dihydrothymidine (X = H) (DHT-*R*) and 5-acetonyl-5,6-dihydrothymidine (X = CH_3—CO—CH_2—) (ADT-*R*). Invert CH_3 and X at C5 to obtain *S* isomers, DHT-*S* and ADT-*S*.

proportion of the two isomers formed in uv-irradiated DNA, since characterization of the photodimers has been limited to the Thy⟨ ⟩Thy fragments after detachment from the sugars by acid hydrolysis of the *N*-glycosyl bonds (12). An additional question concerns the formation of the *ca* and *ta* forms. These are unlikely products of a uv-irradiated polynucleotide since geometrical constraints prevent their formation from thymines adjacent on a strand, and indeed they have not been detected above the base and nucleoside levels. However, the *ca* and *ta* forms could, in principle, result from fusion of distant bases of a properly folded strand, or from bases on separate strands.

Clearly there are important questions regarding the nature of the *cs* and *ts* products detected in DNA, and some interesting possibilities for the *ca* and *ta* forms. Our extensive data characterizing the six dThd⟨ ⟩dThd isomers could prove useful in these matters. Finally, our isolation of the novel acetonyl adducts should serve to caution those who use acetone as a uv photosensitizer to generate thymine dimers in DNA. Given the right conditions, these could be generated as minor products and would complicate the situation.

Results and discussion

Isolation of the molecules

Near uv photolysis (λ = 313 nm) of 2 m*M* dThd in acetone–water solution (35:65 v/v) gave rise to 10 photoproducts, which made up 95% of the product mixture, and a small amount of unidentified material. The 10 products were isolated by preparative thin-layer chromatography on silica gel plates and by reversed-phase hplc (14). Each showed with the cysteine – sulfuric acid reagent a pink coloration characteristic of 2′-deoxyribosides. Six of the products (**1**–**6**) constituting 90% of the mixture could be photoreversed to the starting material (dThd) by far uv light (λ > 250 nm), a feature of cyclobutadipyrimidines (15) and of the corresponding adducts formed by photocyclization of pyrimidine and psoralen ring systems (16). The other four, relatively minor products (**7**–**10**) did not undergo detectable photosplitting when exposed to far uv light. Evidence is presented below that they are the molecules represented in Fig. 2.

Structural assignments of the thymidine photodimers

Evidence of a dimeric structure for **1**–**6** is provided by their fast-atom bombardment (FAB) mass spectra. In the positive mode prominent peaks are observed at m/z 507 and m/z 485, which can be assigned, respectively, to the pseudomolecular $[M + Na]^+$ and $[M + H]^+$ ions of dThd⟨ ⟩dThd. The fragment at m/z 369 would reflect the loss of a single 2-deoxyribose unit from the dimeric species, whereas that at m/z 243 would reflect the cleavage of the cyclobutane ring to form the monomeric species $[\text{dThd} + H]^+$. In the negative FAB mode particularly prominent peaks at m/z 483 and m/z 241 would correspond to the $[M - H]^-$ and $[\text{dThd} - H]^-$ ions, respectively. The appearance of the molecular ions at high relative intensity (20–50%) demonstrates clearly the advantage of the soft-ionization FAB method for the analysis of the cyclobutane dimers. In her review, Fenselau (17) mentioned the unpublished report (S. Y. Wang, M. N. Khattak, and C. Fenselau) of molecular ions of a *fully-derivatized* Urd⟨ ⟩Urd generated at low relative intensity (ca. 2%) by electron impact ionization, but we are aware of no published report of molecular ions of an *underivatized* pyrimidine nucleoside photodimer that were generated by any of the commonly used ionization techniques. At the level of the photodimerized *bases*, Fenselau also noted (17) the unpublished report (H. Fales and S. Y. Wang) of molecular ions in the chemical ionization mass spectrum of Thy⟨ ⟩Thy (*cs*). However, this method would seem to be less useful for the corresponding nucleosides, due to their lower volatility. The absence of unambiguous molecular ion peaks in the electron impact mass spectra of cyclobutadipyrimidines has been widely reported (17), even when the bases are stabilized as their *N*-methyl derivatives. This has been attributed (17) to the facile fragmentation of the molecular ions as well as to the thermal fragmentation occurring before ionization.

Relative to dThd, photoproducts **1**–**6** show a bathochromic shift in their uv absorption maxima to about 220 nm, consistent with the saturation of their C5—C6 bonds (12). The upfield chemical shifts of 3.1–3.7 ppm in the H6 proton resonance and of 0.4 ppm in the methyl proton resonance are in line with the changes noted for thymine dimer formation in other systems (4, 9).

The configurations of **1**–**6** could be assigned following the release, by mild acid hydrolysis (12), of the corresponding Thy⟨ ⟩Thy fragment. Reasonable assignments of the *cs*, *ts*, *ca*, and *ta* isomers have been based on several X-ray crystallographic structure determinations (18), as well as on nmr (19) and ir (12) data. Thus, the major products **1** and **6**, were assigned the CS and TA configurations, respectively, by comparison of the hplc and ir characteristics of their Thy⟨ ⟩Thy fragments with those of Thy⟨ ⟩Thy prepared according to Weinblum and Johns (12). Furthermore, as expected for the *meso cs* and *ta* isomers, circular dichroic and optical rotation $[\alpha]_D$ measurements revealed no optical activity.

The acid hydrolysis of the two isomers (**4**, **5**) showing tlc behavior similar to that of **1** yielded Thy⟨ ⟩Thy which were assigned the *ca* geometry by considering their hplc and ir properties. Circular dichroic and optical rotation data identify the fragment from **4** as *ca*(+) and that from **5** as *ca*(−). The parent dThd⟨ ⟩dThd show the same sign of rotation as their Thy⟨ ⟩Thy and are denoted CA(+) and CA(−). Similarly **2** and **3** were shown to yield the fragments *ts*(+) and *ts*(−), respectively. **2** and **3** showed the same sign of rotation as their fragments and are denoted TS(+) and TS(−), respectively.

Unambiguous assignments of TS(+) and TS(−) to geometries TS1 and TS2, and of CA(+) and CA(−) to CA1 and CA2 (Fig. 1) are not possible in the absence of appropriate crystallographic data. Kuneida and Witkop (11) proposed a tentative assignment of CA(+) and CA(−) to CA2 and CA1, respectively, which was based on the assumption that the sign of the ord Cotton effect of CA2 would be the same as that of (*S*)-(−)-dihydrothymidine. (Note that these authors interchanged the CA and TS labels.) Extending their arguments to our cd spectra allows us to assign tentatively TS(+) and TS(−) to the TS1 and TS2 geometries, respectively. However, the Kuneida–Witkop reasoning seems to be based on the assumption that the sign of the Cotton effect associated with the C4 carbonyl absorption band is determined solely by the configuration of the methyl group at the contiguous C5 atom and is not inverted by the attachment of the second pyrimidine base. Examination of models of dThd⟨ ⟩dThd with reference to the octant rule (20) suggests that this assumption is open to discussion.

Structural assignment of the dihydrothymidines

Compounds **7** and **8** were assigned the structures DHT-*R* and DHT-*S*, respectively, by comparison of the ^{1}H nmr, uv, cd, and mass spectrometric properties with published data for these molecules (22). Evidence that photoproducts **9** and **10** involve the addition of an acetonyl fragment (Fig. 2) is provided by their FAB-ms spectra, which show the protonated molecular cation $(M + H)^+$ at m/z 301, the molecular anion $(M - H)^-$ at m/z 299, and the sodium adduct $(M + Na)^+$ at m/z 323. Support for the structure is provided by their 250-MHz ^{1}H nmr spectra, which show strong singlets at 1.3 ppm and 2.2 ppm that can be assigned to the C5 and acetonyl methyl groups, respectively. Furthermore, **9** and **10** show the expected AB patterns for the methylene hydrogen pairs of C6 centered at 3.4 ppm ($J(gem) = -12.5$ Hz) and of the acetonyl group centered at 3.1 ppm ($J(gem) = -18.7$ Hz). That no further splitting is seen in the AB patterns is consistent with the absence of a proton vicinal to either of these methylene groups. The diastereoisomeric relationship between **9** and **10** is indicated by the observation of a positive Cotton effect for **9** (hence ACD(+)) and a negative one for **10** (hence (ACD(−)). No absolute (*R*, *S*) assignment of **9** and **10** can be made at present.

The formation of thymine dimers via the triplet excited state is well documented (23–26). The generation of **7**–**10** via the triplet state also seems likely since we noted that it is inhibited in the presence of oxygen, a triplet state quencher (26). Analogous photoreductions and analogous photoadditions of acetonyl have been observed for olefins such as norbornene (27, 28) and dicyclopentadiene (29), with energy transfer to acetone from the triplet state of the olefin as the initial step of the process. Energy transfer to the acetone is expected to generate acetonyl radicals and hydrogen atoms (30). Addition of the hydrogen atoms to dThd (which occurs preferentially at C6 in aqueous solution and in the solid state (31, 32)) would generate the 5,6-dihydrothymidin-5-yl radical. Combination of this with an acetonyl radical could generate **9** and **10** in a process analogous to that involving the stable organic radical 2,2,6,6-tetramethyl-1,4-piperidone-*N*-oxyl, which has recently been reported (33). The competitive disproportionation involving two 5,6-dihydrothymidin-5-yl radicals would lead to **7** or **8**, and dThd (34). An additional mechanism for quenching by acetone that leads to oxetane derivatives has been noted in the near uv photolysis of uracil in aqueous solution (35). The corresponding oxetane derivatives of dThd were not noted here.

Nuclear magnetic resonance spectra of the thymidine photodimers

Additional evidence for the configurational assignments of dThd⟨ ⟩dThd follows from consideration of their symmetry properties and the appearance of the 600-MHz ^{1}H nmr spectra. The *ts* isomers of Thy⟨ ⟩Thy possess a two-fold rotation axis passing through the centres of the C5—C5 and C6—C6 bonds (Fig. 1). This axis is retained after attachment of the two deoxyribose sugars. The *ca* isomers possess a two-fold symmetry axis that is perpendicular to the cyclobutane ring at its centre and is retained after attachment of the two sugars. Thus, the two nucleoside units have "symmetrical equivalence" (36) in each of the four TS and TA isomers. This symmetry is reflected in their ^{1}H nmr spectra, which have the appearance of simple 2′-deoxyribonucleoside spectra, accountable for by a single set of chemical shifts (H6, etc.) and coupling constants ($J_{1'2'}$, etc.). In the sample spectrum of TS(+) (Fig. 3a) note in particular the single lines at 4.62 ppm and 1.37 ppm due to H6 and methyl protons, respectively.

In contrast, the *cs* isomer has a mirror plane perpendicular to the cyclobutane ring that bisects the C5—C5 and C6—C6 bonds, whereas *ta* is centrosymmetric. In neither case is the symmetry retained by the addition of the two D-sugars (it would be retained if one L-sugar replaced either of the D-sugars). Thus, the two nucleoside units are not symmetrically equivalent in CS and TA. This absence of symmetry is apparent in the ^{1}H nmr spectra of CS (Fig. 3b) and of TA, which show distinct signals from corresponding protons on the two fragments. Note in the CS spectrum the AB pattern centered at 4.32 ppm due to the nonequivalent H6 protons ($J_{66} = 5.3$ Hz) and the pair of single resonances at 1.49 ppm and 1.45 ppm due to the pair of methyl groups (Fig. 3b). By spin-decoupling experiments the sugar protons (but not H6 or the methyl group) could be associated with the "A" or "B" units of CS or of TA, but an absolute assignment of two units could not be made for either of these two isomers.

The magnitude of J_{66} in CS (5.3 Hz) is similar to that observed (19) in the ^{13}C satellite spectra of *cs* (4.8 Hz), which suggests that the extent of pucker of the cyclobutane ring is similar in the two molecules. A larger J_{66} (ca. 6.0 Hz) was noted in d(T[*p*]T) (*cs* isomer) which may be a reflection of a somewhat flatter ring in the photodimerized dinucleoside monophosphate (4). J_{66} is about 0 Hz in TA, consistent with the general attenuation of four-bond coupling constants (37). For the same reason the four-bond J_{66} in the TS and CA isomers is expected to be about zero. However, because of their equivalence in TS and CA, any coupling between the H6 protons would not be seen in their spectrum.

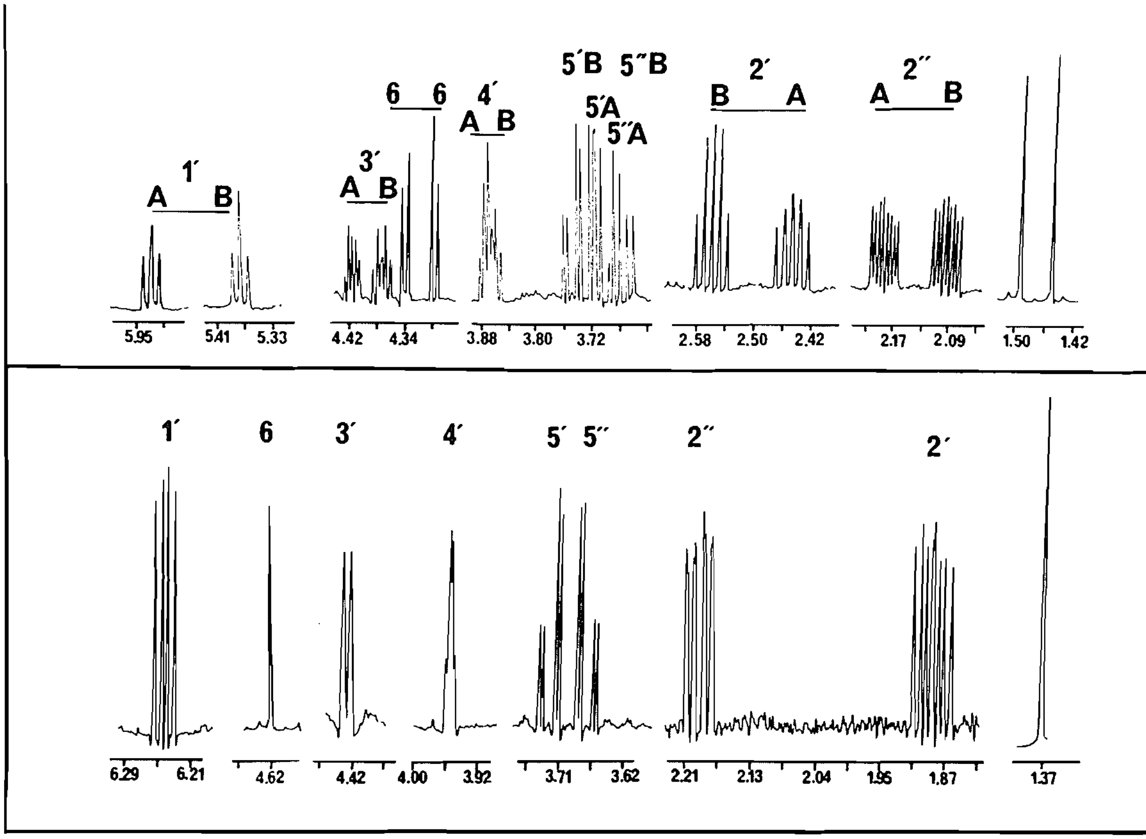

FIG. 3. The 600.1-MHz ^{1}H nmr spectra of (a) (bottom) **2**, or TS (+), and (b) (top) CS in aqueous solution relative to TSP. In b, the signals were assigned to the "A" or "B" nucleoside by homonuclear spin decoupling experiments. In a, the two units are symmetrically equivalent.

TABLE 1. ^{1}H Chemical shifts for dThd photoproducts relative to TSP[a]

Nucleoside[b]	H6	H5[c]	Me[d]	1′	2′	2″	3′	4′	5′	5″
1. CS-A	4.34	—	1.46	5.94	2.45	2.19	4.45	3.91	3.76	3.74
-B	4.30	—	1.51	5.38	2.57	2.09	4.41	3.90	3.78	3.71
2. TS(+)	4.62	—	1.37	6.24	1.89	2.19	4.42	3.95	3.72	3.67
3. TS(−)	4.44	—	1.37	5.96	2.16	2.25	4.34	3.94	3.67	3.67
4. CA(+)	4.15	—	1.54	6.30	2.20	2.29	4.44	3.94	3.76	3.75
5. CA(−)	3.97	—	1.48	6.09	2.20	2.20	4.35	3.95	3.78	3.76
6. TA-A	4.27	—	1.42	6.27	2.37	2.11	4.35	3.90	3.68	3.63
-B	4.42	—	1.44	5.85	2.38	2.16	4.34	3.88	3.74	3.71
7. DHT(+)	3.62 3.25	2.84	1.22	6.28	2.30	2.13	4.38	3.92	3.78	3.71
8. DHT(−)	3.57 3.26	2.84	1.22	6.27	2.33	2.15	4.37	3.89	3.75	3.68
9. ADT(+)	3.65 3.24	3.23 2.92	1.26 2.20*	6.28	2.21	2.11	4.34	3.90	3.74	3.69
10. ADT(−)	3.66 3.21	3.22 2.93	1.30 2.22*	6.29	2.30	2.17	4.35	3.89	3.74	3.68

[a]Aqueous solution, pH 7. **1–6**: 600.1 MHz; 293 K; **7–10**: 250 MHz.
[b]In **1** and **6** the nucleoside units (A and B) are distinguishable.
[c]Entries **9** and **10** are the methylene protons of the acetonyl group.
[d]All entries for 5-methyl except second entry of **9** and **10** (acetonyl methyl).

Sugar conformation

The ^{1}H chemical shifts and coupling constants (Tables 1, 2) reveal little conformational variation for the sugar rings of **7–10** (Table 3). The bias towards the *S*-type pucker (64–69%, estimated following de Leeuw and Altona (38)) is characteristic of 2′-deoxyribosides, but is slightly enhanced relative to 5,6-saturated pyrimidine 2′-deoxyribosides (60%) (39). The *J* data reveal no unusual behaviour in the phase angles of pseudorotation (P) or the amplitudes of pucker (τ_m). The $\Sigma(J_{4'5'} + J_{4'5''})$ values lie in the range 8.8–9.6 Hz, revealing values of 45 ± 4% for $\%g^{+}$ (C4′—C5′) which are marginally smaller than those noted for 5,6-unsaturated molecules (39). The ^{1}H chemical shifts of, in particular, H1′ and H2′ suggest no exceptional behavior in the *syn–anti* blend about the *N*-glycosyl linkage of **7–10**.

The dThd⟨ ⟩dThd show a greater variation in sugar *S*-type

TABLE 2. Coupling constants (Hz) for dThd photoproducts[a]

Nucleoside[b]	1′2′	1′2″	2′2″	2′3′	2″3′	3′4′	4′5′	4′5″	5′5″
1. CS-A	7.9	6.7	13.7	6.9	3.2	3.3	3.8	5.0	12.2
-B	7.0	7.1	13.8	6.7	4.1	3.7	3.7	5.9	12.2
2. TS(+)	9.6	5.8	13.7	5.5	1.1	1.7	2.8	2.8	12.4
3. TS(−)	7.1	6.1	14.0	6.2	3.6	3.2	4.2—	4.2	12.2
4. CA(+)	9.1	5.9	14.0	6.3	2.5	2.7	3.4	4.3	12.4
5. CA(−)	7.1—	7.1	13.5	4.8—	4.8	3.8	4.1	4.9	12.2
6. TA-A	9.0	6.1	13.9	5.8	2.4	2.6	3.6	4.6	12.4
-B	7.8	6.3	13.8	6.7	3.4	3.7	4.1	5.6	12.0
7. DHT(+)	7.9	6.5	14.1	6.7	3.6	3.6	4.0	5.2	12.1
8. DHT(−)	7.6	6.7	14.2	6.7	3.8	3.7	4.1	5.5	12.3
9. ADT(+)	7.8	6.5	14.2	6.5	3.4	3.3	4.2	5.3	12.3
10. ADT(−)	7.5	6.6	14.2	6.7	3.6	3.4	3.6	5.2	12.0

[a]See footnotes, Table 1.
[b]Due to isochronous H2′ and H2″ (or H5′ and H5″) only the sum of connected couplings is meaningful.

TABLE 3. Calculated population of the 2′-*endo* (*S*) pucker[a] and of the g^+, t, g^- rotamers around the C4′—C5′ bond

Nucleosides	*S*	g^+	t	g^-
1. CS-A	69	49	35	16
-B	59	41	44	15
2. TS(+)	96	81	13	6
3. TS(−)	66	53	c	c
4. CA(+)	83	60	28	12
5. CA(−)	66	47	34	19
6. TA-A	83	55	31	14
-B	67	40	41	19
7. DHT(+)	67	45	37	18
8. DHT(−)	64	41	40	19
9. ADT(+)	69	42	38	20
10. ADT(−)	66	49	37	14

[a]Calculated with the program PSEUROT (P_N 13°, ϕ_N 27°, P_S 159°, ϕ_S 37°, rms < 0.3 Hz).
[b]Following ref. 46.
[c]Not determined due to $\delta_{H5'} \simeq \delta_{H5''}$.

population (Table 3). Thus, on the one hand, **1** (sugar rings A and B), **3**, **5**, and **6** (sugar B) resemble **7–10** in ring pucker (%*S*: 66–67%) and in the C4′—C5′ conformer distribution (%g: 40–53%) but, on the other hand, **2**, **4**, and **6** (sugar A) show increased importance of *S* pucker and the g^+ conformer about C4′—C5′. This trend is particularly strong in **2**, or TS(+) (96% *S*; 81% g^+). This exceptional behavior in TS(+) is accompanied by an unusually large upfield shift in H2′ to 1.89 ppm. In no other molecule has the H2′ signal been noted at less than 2 ppm from the TSP reference. Thus the geometrical constraints required for the formation of a cyclobutane ring system are reflected in the sugar conformation, as has been noted in d(T⟨p⟩T) (4). Finally, it is interesting to point to the prevailing trend in **1–10** for %g^+ to increase with increasing %*S*; a similar situation has been noted for other 5,6-saturated pyrimidine nucleosides (40).

Geometry of the pyrimidine ring in 7–10

Evidence points to a distorted half-chair conformation for 5,6-saturated pyrimidines in which C5 and C6 lie on opposite sides of the plane defined by N1, C2, N3, C4, with the substituents at C5 and C6 occupying pseudo-axial and pseudo-equatorial positions (16, 41–45). In **7** and **8** the pair of vicinal H–H coupling constants involving H5 with the methylene protons at C6 provide information about this geometry. Analysis of the ABX system yields vicinal couplings of 10.6 Hz and 6.0 Hz for **7**, and 9.4 Hz and 5.5 Hz in **8**. (A geminal H6–H6 coupling of about 12.5 Hz was noted in each case.) The larger of the couplings indicates that in **7** and in **8** H5 has a *trans*, diaxial relationship with one of the H6 hydrogens, and thus the preferred conformation of **7** and **8** must be as indicated in Fig. 4. The smaller of the couplings is in line (44) with the equatorial position for the second C6 proton. In each case the 5-methyl occupies an equatorial position, a preference that is apparent in the crystal state (16). It is interesting to note that the axial H6 is less shielded, by about 0.3–0.4 ppm, than the equatorial one. A similar analysis of the ring pucker of **9** and **10** can not be made.

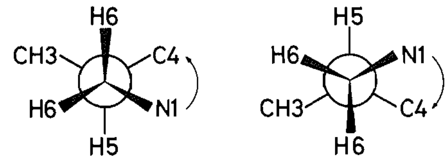

FIG. 4. Preferred conformation of DHT-*T* (left) and DHT-*S* (right) based on the magnitudes of the two vicinal H5–H6 coupling constants. View from C6 to C5.

Conclusion

We have shown that all six dThd⟨ ⟩dThd photodimers can be isolated from acetone-sensitized uv irradiation of aqueous thymidine solutions. Also produced as minor photoproducts are the 5*R* and 5*S* diastereomers of 5,6-dihydrothymidine and of the novel adduct 5-acetonyl-5,6-dihydrothymidine. Extensive spectroscopic and mass spectrometric data are provided for the ten molecules. Particularly important is the clear demonstration of the advantages of the FAB method for mass spectral analysis of thymidine photodimers.

Experimental

Spectroscopic measurements

The uv absorption spectra were recorded on a Beckman spectrophotometer (model 5230). The ir spectra (KBr micropellet method) were obtained on a Perkin–Elmer spectrophotometer (model 177). Fast atom bombardment (FAB) mass spectrometry was carried out on a Kratos spectrometer (model MS 50) equipped with a commercially available FAB gun; desorption of the molecules in a glycerol mull was effected by exposure to a 8-keV beam of xenon atoms.

Optical rotation and circular dichroism (cd) spectra were recorded in methanol or water with a Quick Jouan polarimeter and a Jobin–Yvon spectrometer respectively.

The decoupled and nondecoupled ^{1}H nmr spectra of the six dThd⟨ ⟩dThd isomers were recorded with resolution enhancement on a 600-MHz spectrometer located at the Carnegie–Mellon University (Pittsburgh, PA). The spectrometer is operated (20°C) in the fast-correlation spectrum mode using the HDO solvent resonance as the lock. 2,2-Dimethyl-2-silapentane (DSS) was used as the internal reference. Spectra for the four 5,6-dihydrothymidines and their 5-acetoxy derivatives were obtained on a 250-MHz Cameca TSN spectrometer (FT mode, 20°C). The nucleoside samples were lyophilized twice and dissolved in 99.9% D_2O to a concentration of 0.05 *M*. Metal ions were removed using Chelex-100 resin columns (Bio-Rad, Richmond, CA). Spectral analysis (LAOCOON III) and computer simulated spectra were the final test of the chemical shift (δ) and coupling constant (*J*) data listed in Tables 1 and 2. Pseudorotational parameters were calculated with the PSEUROT program (38) and are given in the relevant sections.

High performance liquid chromatography (hplc)

The high performance liquid equipment consists of a Model 6000 dual piston pump (Waters Associates, Milford, MA) and a Rheodyne Model 7100 loop injector (Berkeley, CA). The solutes were detected either by using a Model RI 401 refractometer index detector (Waters Associates) and (or) a Cecil Model CE 212 variable uv wavelength spectrophotometer (Cecil, Cambridge, U.K.) operating at 230 nm. It should be mentioned that no detectable photoreversion of any cyclobutadithymidine was observed under these detection conditions due to the very low intensity of the far uv light in the flow cell. Analytical stainless steel columns (25 × 0.47 cm id) were packed under 400 atm (1 atm = 101.3 kPa) with a Haskell pump (Chromatem, Paris, France) by using 10-μm octadecylsilyl silica gel bonded phase Lichrosorb RP-18 (Merck, Darmstadt, G.F.R.). Propan-1-ol was used as the dispersing agent for the preparation of the slurry, which was sonicated before the packing procedure.

Thin-layer chromatography

Two-dimensional thin-layer chromatography analyses were carried out on 20 × 20 cm precoated silica gel plates F_{254} (Merck). Eluent 1 was the lower phase of chloroform–methanol–water (4:2:1) v/v to which 5 mL of methanol was added for each 100 mL of the organic phase. Eluent 2 consisted of ethyl acetate – propan-2-ol – water (75:16:9).

Visualization of 2′-deoxyribonucleosides was made by spraying the chromatoplates with the cysteine – sulfuric acid reagent and subsequent heating for 5 min at 100°C. Cyclobutadithymidines were visualized by fluorescence quenching at 254 nm after photoreversal to thymidine upon exposure to wavelength lower than 230 nm.

Ultraviolet irradiation

Near uv irradiation was carried out in a Pyrex glass flask with a bank of 6 BLB lamps (λ_{max} centered about 313 nm). Thymidine (350 mg) (Sigma Chemical Co.) was dissolved in 180 mL of water and 100 mL of acetone. Prior to irradiation the solution was degassed for 30 min with a stream of nitrogen saturated with aqueous acetone. During photolysis the sample was air-cooled with a fan. The solution was irradiated for 18 h, giving over 95% decomposition of the starting material. The solution was evaporated to dryness, and the resulting yellow residue was applied to three precoated, thick-layer, preparative silica gel chromatographic plates (Merck, Darmstadt). The plates were developed with eluent system 1. Five bands could be detected by spraying the plates with a cysteine – sulfuric acid reagent, followed by heating at 100°C for 3 min.

(−) cis–anti *thymidine⟨⟩thymidine (5)*

The slowest moving zone (R_f 0.15) was scraped off and the resulting silica gel was extracted with 3 × 20 mL of water–methanol (1:1). Evaporation to dryness of the aqueous methanolic solution yielded 35 mg of an oily residue which contained two major compounds as shown by reversed-phase high performance liquid chromatography analysis. The mixture of photoproducts was dissolved in 2 mL of aqueous methanol (9:1) and 0.1 mL of the resulting solution was applied for each injection on the RP-18 octadecylsilylsilicagel column. Elution was accomplished with an aqueous solution of methanol (9:1) in an isocratic mode. The fractions containing the fastest eluting nucleoside (k' = 3.11), as monitored by its uv absorption at 230 nm, were collected. Evaporation to dryness of the resulting aqueous methanol solution afforded 14 mg of (−) *cis–anti* cyclobutadithymidine (2%) as a colorless hygroscopic solid; $[\alpha]_D^{22}$ − 45° (*c* 2.1, in H_2O); uv (λ_{max} H_2O): 220 nm; cd(*c* 2.1, H_2O): $[\theta]_{290}$ ≈0, $[\theta]_{280}$ −40, $[\theta]_{270}$ −1040, $[\theta]_{260}$ −4400, $[\theta]_{252}$ −5920, $[\theta]_{250}$ −5800, $[\theta]_{240}$ −2000, $[\theta]_{236}$ ≈0, $[\theta]_{230}$ +2800, $[\theta]_{227}$ +3200, $[\theta]_{220}$ +2160; FAB-ms, *m/e* (relative intensity), positive mode: 529 (6, M^+ + 2 Na), 507 (19, M^+ + Na), 447 (6), 391 (7, M^+ + Na − deoxyribose), 287 (15, thymidine + 2 Na), 265 (10, thymidine + Na), 150 (21), 116 (36); negative mode: 483 (19, M^- − H), 241 (24, thymidine − H), 125 (100, thymidine − H).

(+) cis–anti *thymidine⟨⟩thymidine (4)*

Evaporation to dryness of the second main hplc fractions (k' = 4.21) gave 13 mg of (+) *cis–anti* cyclobutadithymidine (1.9%) as a hygroscopic solid, which was recrystallized from aqueous methanol (95:5); mp 222–224°C (lit. (11) mp 150°C); $[\alpha]_D^{22}$ + 48.8° (*c* 1.8, in H_2O); uv (λ_{max} H_2O): 219 nm; cd (*c* 1.9, H_2O): $[\theta]_{300}$ ≈0, $[\theta]_{290}$ +80, $[\theta]_{280}$ +200, $[\theta]_{270}$ +1280, $[\theta]_{260}$ +4400, $[\theta]_{250}$ +6600, $[\theta]_{248}$ +6880, $[\theta]_{240}$ +4240, $[\theta]_{235}$ ≈0, $[\theta]_{224}$ −6360; FAB-ms, *m/e* (relative intensity), positive mode: 969 (2, $2M^+$ + H), 507 (22, M^+ + Na), 485 (17, M^+ + H), 369 (7, M^+ − deoxyribose), 335 (8, thymidine + glycerol), 243 (43, thymidine + H), 207 (84); negative mode: 967 (1, $2M^-$ − H), 483 (36, M^- − H), 241 (44, thymidine − H).

cis–syn *thymidine⟨⟩thymidine (1)*

The silica gel containing the main photoproduct **1** (R_f 0.22) was extracted with 3 × 10 mL of 50% aqueous methanol. The resulting solution was evaporated to dryness, giving 73 mg of a mixture of the three nucleosides **1**, **4**, and **5** with a preponderance of the *cis–syn* cyclobutidithymidine (**1**). The latter photoproduct was further purified by reversed-phase high performance liquid chromatography as reported above. The main uv absorbing fractions (k' = 9.50) were collected and evaporated to dryness under reduced pressure, yielding 60 mg of **1** (8.6%) as a white solid that was further recrystallized from aqueous methanol (95:5); mp 182–184°C (lit. (11) mp 184–188°C); $[\alpha]_D^{22}$ +10.2 (*c* 1.7, in H_2O); uv λ_{max} H_2O): 219 nm; cd (*c* 2.3, H_2O): $[\theta]_{280}$ ≈0, $[\theta]_{270}$ +20, $[\theta]_{260}$ +280, $[\theta]_{250}$ +800, $[\theta]_{240}$ +1500, $[\theta]_{233}$ +1720, $[\theta]_{230}$ +1340, $[\theta]_{226}$ ≈0, $[\theta]_{224}$ −1060; FAB-ms, *m/e* (relative intensity), positive mode: 507 (12, M^+ + Na), 485 (9, M^+ + H), 369 (11, M^+ − deoxyribose), 243 (9, thymidine + H), 127 (46, thymine + H), 117 (49, deoxyribose); negative mode: 483 (19, M^- − H), 367 (12, M^- − deoxyribose), 241 (10, thymidine − H), 125 (46, thymine − H).

(+) trans–syn *thymidine⟨⟩thymidine (2)*

The silica gel containing the three *trans* diastereoisomers of dThd⟨⟩dThd (R_f 0.34) was scraped off and further extracted with 3 × 20 mL of aqueous methanol (1:1). The solution was evaporated to dryness under reduced pressure. The resulting oily residue (96 mg) was shown to contain three main photoproducts, which were separated by reversed phase hplc on the RP-18 ODS column using water–methanol (9:1) as the isocratic solvent. The fastest eluting fractions (k' = 2.60) were collected and combined. Evaporation to dryness of the resulting solution afforded 8 mg of (+) *trans–syn* cyclobutadithymidine (**2**) (1.1%); $[\alpha]_D^{22}$ + 11.0 (*c* 2.2, in H_2O); uv (λ_{max} H_2O): 219 nm; cd (*c* 1.8, H_2O): $[\theta]_{290}$ ≈ 0, $[\theta]_{280}$ −290, $[\theta]_{270}$ −1680, $[\theta]_{260}$ −3920, $[\theta]_{255}$ −4400, $[\theta]_{250}$ −4000, $[\theta]_{240}$ ≈0, $[\theta]_{230}$ + 8800; FAB-ms, *m/e* (relative intensity), positive mode: 507 (10, M^+ + Na), 369 (8, M^+ − deoxyribose), 243 (20, thymidine + H), 127 (20, thymine + H); negative mode: 483 (29, M^- − H), 367 (12, M^- − deoxyribose), 241 (60, thymidine − H), 125 (100, thymine − H).

(−) trans–syn *Thymidine⟨⟩thymidine (3)*

The combined eluting fractions (k' = 3.23) containing the (−) *trans–syn* dThd⟨⟩dThd (**3**) as monitored by its uv absorption at 230 nm were evaporated to dryness under reduced pressure yielding 10 mg of **3** (1.4%) as an oily compound; $[\alpha]_D^{22}$ −38.6° (*c* 2.4, in H_2O); uv (λ_{max} H_2O): 218 nm; cd (*c* 2.0, H_2O): $[\theta]_{290}$ ≈0, $[\theta]_{280}$ +80, $[\theta]_{270}$ +1420, $[\theta]_{260}$ +5050, $[\theta]_{250}$ +7880, $[\theta]_{248}$ +8000, $[\theta]_{240}$ +5280, $[\theta]_{233}$ ≈0, $[\theta]_{230}$ −4240, $[\theta]_{227}$ −8000; FAB-ms, *m/e* (relative intensity), positive mode: 509 (2, M^+ + Na), 127 (30, thymine + H) 118 (59, deoxyribose + H); negative mode: 575 (2, M^- + glycerol), 483 (45, M^- − H), 367 (16, M^- − deoxyribose), 241 (23, thymidine − H), 219 (30), 192 (85), 152 (60), 125 (75, thymine − H).

trans–anti *Thymidine⟨⟩thymidine (6)*

Evaporation to dryness of the slowest eluting hplc fractions (k' = 11.00) gave 54 mg of *trans–anti* dThd⟨⟩dThd (9.8%) that was recrystallized from water–methanol (95:5) as a white solid; mp 170–172°C; $[\alpha]_D^{22}$ −3.0° (*c* 4.2, in H_2O); uv (λ_{max} H_2O): 219 nm; cd (*c* 2.1, H_2O): $[\theta]_{280}$ ≈0, $[\theta]_{270}$ −20, $[\theta]_{261}$ −40, $[\theta]_{260}$ −30, $[\theta]_{257}$ ≈0, $[\theta]_{250}$ +320, $[\theta]_{240}$ +1050, $[\theta]_{238}$ +1080, $[\theta]_{230}$ +40, $[\theta]_{229}$ ≈0, $[\theta]_{225}$ −1000; FAB-ms, *m/e* (relative intensity), positive mode: 507 (4, M^+ + Na), 485 (6, M^+ + H), 243 (29, thymidine + H), 127 (89, thymine + H); negative mode: 483 (4, M^- − H), 241 (5, thymidine − H), 125 (10, thymine − H).

(+) (5R)-*5,6-Dihydrothymidine (7)*

The fastest eluting tlc zone (R_f 0.53) was scraped off and the resulting silica gel was extracted with 3 × 20 mL of aqueous methanol (1:1). Evaporation to dryness of the resulting filtrate provided 33 mg of a mixture of the four dihydrothymidine derivatives **7**, **8**, **9**, and **10**, which was applied on the RP-18 ODS column. A complete separation of the four photoproducts was achieved using a mixture of methanol–water (9:1) as the solvent. Evaporation of the fastest eluting compound ($k' = 1.96$), which was detected by its uv absorption at 230 nm, yielded 6 mg of (+) (5*R*)-5,6-dihydrothymidine (1.7%) as a white solid; uv (λ_{max} H_2O) 219 nm; cd (*c* 4.7, methanol): $[\theta]_{275}$ ≈0, $[\theta]_{270}$ −40, $[\theta]_{260}$ −200, $[\theta]_{250}$ −900, $[\theta]_{240}$ −2100, $[\theta]_{239}$ −2400, $[\theta]_{230}$ −600. *Anal.* calcd. for $C_{10}H_{16}N_2O_5$: C 49.17, H 6.60, N 11.47; found: C 49.12, H 6.34, N 11.39.

(−) (5S)-*5,6-Dihydrothymidine (8)*

Evaporation to dryness under reduced pressure of the second eluting fractions ($k' = 2.24$) gave 7 mg of **8** (2%). This nucleoside was found to exhibit identical uv, ^{1}H nmr, and cd spectroscopic features to those of the authentic sample as prepared by catalytic hydrogenation of thymidine in the presence of Rhd/Al_2O_3; mp 154–155°C (lit. (21) mp 152–153°C); $[\alpha]_D^{22}$ −19.5° (*c* 1.4, in H_2O) (lit. (21) $[\alpha]_D^{22}$ = −20.5° (*c* 1.1, in H_2O); cd (*c* 5.2, methanol): $[\theta]_{275}$ ≈0, $[\theta]_{270}$ +30, $[\theta]_{260}$ +130, $[\theta]_{250}$ +660, $[\theta]_{240}$ +1750, $[\theta]_{238}$ +1800, $[\theta]_{230}$ +500. *Anal.* calcd. for $C_{10}H_{16}N_2O_5$: C 49.17, H 6.60, N 11.47; found: C 49.08, H 6.55, N 11.40.

(+) *5-Acetonyl-5,6-dihydrothymidine (9)*

The hplc fractions containing the photoproduct **9** ($k' = 2.89$) were combined and evaporated to dryness under reduced pressure. The resulting oily compound **9** (5 mg, 1.4%) was shown to be homogeneous by two-dimensional tlc analysis on precoated silica gel plates using eluents 1 and 2; uv (λ_{max} H_2O) 219 nm; cd (*c* 1.3, H_2O): $[\theta]_{280}$ ≈0, $[\theta]_{270}$ +40, $[\theta]_{250}$ +1560, $[\theta]_{240}$ +4040, $[\theta]_{238}$ + 4060, $[\theta]_{230}$ +1480, $[\theta]_{228}$ ≈0, $[\theta]_{224}$ −2920; FAB-ms, *m/e* (relative intensity), positive mode: 323 (11, M^+ + Na), 301 (10, M^+ + Na), 301 (10, M^+ + H), 117 (9, 2-deoxyribose); negative mode: 299 (5, M^- − H), 255 (5), 149 (15).

(−) *5-Acetonyl-5,6-dihydrothymidine (10)*

Evaporation to dryness of the slowest eluting hplc fraction (k' = 3.40), as detected by its absorption at 230 nm, yielded 6 mg of **10** (1.7%) as an oily homogeneous compound; uv (λ_{max} H_2O) 219 nm; cd (*c* 1.9, H_2O): $[\theta]_{290}$ ≈0, $[\theta]_{280}$ +40, $[\theta]_{270}$ ≈0, $[\theta]_{260}$ −160, $[\theta]_{250}$ −1360, $[\theta]_{240}$ −2920, $[\theta]_{239}$ −2980, $[\theta]_{230}$ −1080, $[\theta]_{228}$ ≈0, $[\theta]_{223}$ +2760; FAB-ms, *m/e* (relative intensity), positive mode: 323 (12, M^+ + Na), 301 (10, M^+ + H), 117 (11, deoxyribose); negative mode: 299 (7, M^- − H), 255 (8), 149 (18).

cis–syn *Thymine⟨⟩thymine*

A 10% HCl aqueous solution of 7 mg of the *cis–syn* cyclobutadithymidine (**1**) was heated at 90°C for 20 min. Then the aqueous solution was evaporated to dryness and the resulting residue was crystallized from water to give colorless prisms. This compound, which was found to be homogeneous by two-dimensional thin-layer chromatography, shows a similar capacity factor ($k' = 2.64$) to that of the authentic *cis–syn* cyclobutadithymine on an ODS-Nucleosil C_{18} column (14) by using water as the eluent. In addition, this compound, which does not exhibit any optical activity, has an identical ir spectrum to that of the *cis–syn* thymine cyclobutyl dimer (12).

trans–anti *Thymine⟨⟩thymine*

Acidic hydrolysis of 8 mg of *trans–anti* cyclobutadithymidine (**6**) under the above conditions yielded 3 mg of *trans–anti* cyclobutadithymine as a colorless solid, after crystallization from water. The retention times ($k' = 3.75$) and the ir spectrum were identical to those of the authentic *trans–anti* thymine dimer (12).

(+) cis–anti *Thymine⟨⟩thymine*

Acidic hydrolysis of 7 mg of the (+) *cis–anti* diastereoisomer of cyclobutadithymidine with 10% HCl for 20 min at 90°C gave quantitatively the (+) *cis–anti* enantiomer of the thymine cyclobutyl dimer. This compound, which was crystallized from water as colorless prisms (3 mg), has an identical capacity factor ($k' = 1.86$) and ir spectroscopic features to those of the racemic *cis–anti* cyclobutadithymine; cd (*c* 1.7, H_2O): $[\theta]_{280}$ ≈0, $[\theta]_{270}$ +1320, $[\theta]_{260}$ +6390, $[\theta]_{250}$ +9140, $[\theta]_{240}$ +5400, $[\theta]_{236}$ ≈0, $[\theta]_{230}$ −4070.

(−) cis–anti *Thymine⟨⟩thymine*

The levorotatory diasteroisomer (6 mg) of the *cis–anti* cyclobutadithymidine was hydrolyzed with 10% HCl at 90°C for 20 min. Evaporation of the solvent, followed by crystallization of the residue from water, gave 2.5 mg of (−) *cis–anti* cyclobutadithymine as colorless prisms. The ir spectrum and the hplc capacity factor ($k' = 1.85$) of this compound are identical to those of the *cis–anti* thymine cyclobutyl dimer; cd (*c* 1.9, H_2O): $[\theta]_{280}$ ≈0, $[\theta]_{270}$ −1350, $[\theta]_{260}$ −6400, $[\theta]_{250}$ −9150, $[\theta]_{240}$ −5400, $[\theta]_{236}$ ≈0, $[\theta]_{230}$ +4090.

Acknowledgements

We thank Dr. A. Bothner-By (Carnegie–Mellon Institute) for the 600.1-MHz spectra, H. Reutenauer (Centre Grenoblois de Résonance Magnétique) for the 250-MHz spectra, and J. Ulrich (CENG) for the FAB-ms spectra. F.E.H. acknowledges the support of the Canada–France Scientific Exchange Program, the Natural Sciences and Engineering Research Council of Canada, the Commissariat à l'Energie Atomique, and the University of Manitoba during his sabbatical leave. The authors thank Mr. A. A. van Beuzekem for carrying out the pseudorotation analysis of photoproducts **7**–**10**.

1. G. J. Fisher and H. E. Johns. *In* Photochemistry and photobiology of nucleic acids. Vol. 1. *Edited by* S. Y. Wang. Academic Press, New York. 1976. p. 225.
2. R. B. Setlow. Nature, **271**, 713 (1978).
3. F. N. Hayes, D. L. Williams, R. L. Ratcliffe, A. J. Varghese, and C. S. Rupert. J. Am. Chem. Soc. **93**, 4940 (1971).
4. F. E. Hruska, D. J. Wood, K. K. Ogilvie, and J. L. Charlton. Can. J. Chem. **53**, 1193 (1975).
5. H. Fritsche, H. Lang, and W. Pohle. Biochim. Biophys. Acta, **432**, 409 (1976).
6. S. Broyde, S. Stellman, and B. Hingerty. Biopolymers, **19**, 1695 (1980).
7. A. Ciarrochi and A. M. Pedrini. J. Mol. Biol. **155**, 177 (1982).
8. J. E. Cleaver. J. Mol. Biol. **170**, 305 (1983).
9. D. L. Wulff and G. Fraenkel. Biochim. Biophys. Acta, **51**, 332 (1961).
10. E. Ben-Hur, D. Elad, and R. Ben-Ishai. Biochim. Biophys. Acta, **149**, 355 (1967).
11. T. Kunieda and B. Witkop. J. Am. Chem. Soc. **93**, 3493 (1971).
12. D. Weinblum and H. E. Johns. Biochim. Biophys. Acta, **114**, 450 (1966).
13. E. Ben-Hur and R. Ben-Ishai. Biochim. Biophys. Acta, **166**, 9 (1968).
14. J. Cadet, L. Voituriez, B. S. Hahn, and S. Y. Wang. J. Chromatogr. **195**, 139 (1980).
15. M. N. Khattak and S. Y. Wang. Tetrahedron, **20**, 945 (1972).
16. K. Straub, D. Kanne, J. E. Hearst, and H. Rapoport. J. Am. Chem. Soc. **103**, 2347 (1981).
17. C. Fenselau. *In* Photochemistry and photobiology of nucleic acids. Vol. 1. *Edited by* S. Y. Wang. Academic Press, New York. 1976. p. 419.
18. I. L. Karle. *In* Photochemistry and photobiology of nucleic acids. Vol. 1. *Edited by* S. Y. Wang. Academic Press, New York. 1976. p. 483.
19. D. P. Hollis. *In* Photochemistry and photobiology of nucleic acids. Vol. 1. *Edited by* S. Y. Wang. Academic Press, New York. 1976. p. 447.

20. P. CRABBE. *In* Optical rotatory dispersion and circular dichroism in organic chemistry. Holden–Day, London. 1965. p. 72.
21. Y. KONDO and B. WITKOP. J. Am. Chem. Soc. **90**, 764 (1968).
22. J. CADET, A. BALLAND, and M. BERGER. Int. J. Radiat. Biol. **39**, 119 (1981).
23. C. L. GREENSTOCK and H. E. JOHNS. Biochem. Biophys. Res. Commun. **30**, 21 (1968).
24. B. H. JENNINGS, S.-C. PASTRA, and J. L. WELLINGTON. Photochem. Photobiol. **11**, 215 (1970).
25. A. A. LAMOLA, M. GUÉRON, T. YAMANE, and R. G. SHULMAN. J. Chem. Phys. **47**, 2210 (1967).
26. D. W. WHILLANS and H. E. JOHNS. Curr. Top. Radiat. Res. Q. **9**, 119 (1973).
27. H.-D. SCHARF. Tetrahedron, **23**, 3057 (1967).
28. P. D. BARTLETT, A. A. M. ROOF, and W. J. WINTER. J. Am. Chem. Soc. **103**, 6520 (1981).
29. D. R. PAULSON, A. S. MURRAY, and E. J. FORNORET. J. Org. Chem. **43**, 2010 (1978).
30. A. PADWA and W. KOEHN. J. Org. Chem. **38**, 4007 (1973).
31. L. S. MYERS and L. M. THEARD. J. Am. Chem. Soc. **92**, 2868 (1970).
32. B. PRUDEN, W. SNIPES, and W. GORDY. Proc. Natl. Acad. Sci. U.S.A. **53**, 917 (1965).
33. M. BERGER, J. ULRICH, and J. CADET. Can. J. Chem. **62**, 6 (1984).
34. G. SCHOLES. *In* Photochemistry and photobiology of nucleic acids. Vol. 1. *Edited by* S. Y. Wang. Academic Press, New York. 1976. p. 521.
35. A. J. VARGHESE. Photochem. Photobiol. **21**, 147 (1975).
36. J. W. EMSLEY, J. FEENEY, and L. H. SUTCLIFFE. High resolution nuclear magnetic resonance spectroscopy. Vol. 1. Pergamon Press, Oxford. 1965. p. 283.
37. M. BARFIELD and B. CHAKRABARTI. Chem. Rev. **69**, 757 (1969).
38. F. A. A. M. DE LEEUW and C. ALTONA. J. Comput. Chem. **4**, 428 (1983).
39. B. D. ALLORE, A. QUEEN, W. J. BLONSKI, and F. E. HRUSKA. Can. J. Chem. **61**, 2397 (1983).
40. F. E. HRUSKA, L. VOITURIEZ, J. CADET, and M. REMIN. Can. J. Chem. **62**, 15 (1984).
41. A. GRAND and J. CADET. Acta Crystallogr. Sect. B, **34**, 1524 (1978).
42. J. EMERSON and M. SUNDARALINGAM. Acta Crystallogr. Sect. B, **36**, 537 (1980).
43. A. R. KATRITZKY, M. R. NESBIT, B. J. KURTEV, M. LYAPOVA, and I. G. POJARLIEFF. Tetrahedron, **25**, 3807 (1969).
44. F. S. EZRA, M. MACCOSS, and S. S. DANYLUK. Biopolymers, **19**, 1983 (1983).
45. P. ROUILLIER, J. DELMAU, and C. NOFRE. Bull. Soc. Chim. Fr. 3515 (1966).
46. C. A. G. HAASNOOT, F. A. A. M. DE LEEUW, H. P. M. DE LEEUW, and C. ALTONA. Recl. Trav. Chim. Pays-Bas, **98**, 576 (1979).

Influence cinétique et chimique d'alcènes sur la pyrolyse d'alcanes: mise au point et nouveaux résultats

FRANCIS BILLAUD, FRANÇOIS BARONNET[1] ET MICHEL NICLAUSE
Département de chimie–physique des réactions, L.A. n° 328 C.N.R.S., I.N.P.L.–E.N.S.I.C., 1, rue Grandville, 54042 Nancy, France

Reçu le 22 novembre 1984

FRANCIS BILLAUD, FRANÇOIS BARONNET et MICHEL NICLAUSE. Can. J. Chem. **63**, 2869 (1985).

En tenant compte de résultats antérieurs et à partir de nouveaux résultats expérimentaux, nous présentons une mise au point sur l'influence cinétique et chimique d'alcènes sur la pyrolyse d'alcanes. L'ensemble de ces résultats confirme que les processus d'*addition* d'atomes libres H· sur la double liaison d'alcènes ne paraissent pas suffisants pour rendre compte de leur influence *cinétique* (inhibitrice) sur la pyrolyse d'alcanes. Nos résultats montrent en revanche que ces processus d'addition permettent d'interpréter l'effet *chimique* d'alcènes ajoutés sur la pyrolyse d'alcanes, c'est-à-dire les modifications apportées à la nature et à la répartition des produits de la réaction. La présente contribution permet de vérifier que l'addition de radicaux alcoyle sur la double liaison d'alcènes ne conduit pas à d'importants effets chimiques. Les résultats expérimentaux antérieurs (pyrolyse de l'éthane en présence d'éthylène ou de propène, pyrolyse du diméthyl-2,2 butane en présence de propène, d'isobutène ou de deux isopentènes) complétés par de nouveaux résultats (pyrolyse de l'éthane en présence d'isobutène, pyrolyse de l'isobutane en présence d'éthylène, de propène, de butène-2 *trans* ou de méthyl-2 butène-2) conduisent à proposer des règles générales relativement simples; elles permettent d'interpréter et de prévoir les modifications de la nature et de la répartition des produits de la pyrolyse d'un alcane vers 500°C (773 K) par l'addition d'un alcène. En dehors de leur aspect fondamental, ces observations et leurs conséquences mécanistiques peuvent se révéler utiles lors de la modélisation de réactions thermiques, en particulier pour la simplification de modèles complexes. Ces observations expliquent également un certain nombre d'observations effectuées sur des unités industrielles et peuvent apporter une contribution aux problèmes posés par le traitement des coupes pétrolières lourdes.

FRANCIS BILLAUD, FRANÇOIS BARONNET, and MICHEL NICLAUSE. Can. J. Chem. **63**, 2869 (1985).

On the basis of previously reported, as well as new, experimental results, a review is presented of the kinetic and chemical influences of alkenes on the pyrolysis of alkanes. The results confirm that the *addition* of free H· atoms to the double bonds of alkenes is not sufficient to explain their inhibiting influence on the pyrolysis of alkanes. On the contrary, our results show that the processes of addition can account for the *chemical* effects of added alkenes on the pyrolysis of alkanes, namely, the modifications brought to the nature and the ratio of the products formed during the reaction. The results presented here confirm that the addition of alkyl free radicals to the double bond of alkenes does not lead to important chemical effects. The previously reported experimental results (pyrolysis of ethane in the presence of ethylene or propene, the pyrolysis of 2,2-dimethylbutane in the presence of propene, isobutene, or two isopentenes), completed by our new results (pyrolysis of ethane in the presence of isobutene, pyrolysis of isobutane in the presence of ethylene, of propene, of *trans*-2-butene, or of 2-methyl-2-butene), can lead to very simple general rules, on the basis of which it is possible to explain the results and to predict the modifications (relating to the nature of the products and to their ratios) that will result from the addition of an alkene during the pyrolysis of an alkane at a temperature of 500°C (773 K). Aside from their fundamental aspects, these observations and their mechanistic consequences could be useful for the preparation of models for these thermal reactions, especially for the simplification of complex models. These observations also explain certain facts observed in industry and can help in solving some of the problems associated with the thermal cracking of heavy oils.

[Traduit par le journal]

Introduction

L'influence d'alcènes, généralement de C_2 à C_4, sur la pyrolyse d'alcanes légers (de C_2 à C_5 ou C_6) a fait l'objet de nombreux travaux. Ces recherches avaient pour but principal d'élucider l'origine de l'effet inhibiteur exercé par ces alcènes sur la pyrolyse d'alcanes. Les alcènes peuvent être ajoutés à l'instant initial ou générés au cours de la réaction donnant lieu ainsi respectivement aux phénomènes d'inhibition ou d'auto-inhibition.

De tels travaux ont été menés de façon active dans différents laboratoires, en particulier à Nancy (Niclause et coll.) et à Swansea (Purnell et coll.). Ils ont conduit à une bonne compréhension des processus à l'origine de l'inhibition et de l'auto-inhibition de la pyrolyse d'alcanes par des alcènes. Ces effets cinétiques ont été interprétés par deux types de mécanismes dont les importances relatives peuvent varier en fonction de différents facteurs: nature de l'alcène, nature des radicaux porteurs de chaînes dans la pyrolyse de l'alcane, conditions opératoires, etc...

Le premier type de mécanismes consiste en l'*arrachement* d'un atome d'hydrogène de la molécule de l'alcène par un radical porteur de chaînes de la pyrolyse de l'alcane, conduisant à un radical stabilisé par résonance, donc relativement peu réactif. C'est ainsi que ce mécanisme a permis d'interpréter l'inhibition de la pyrolyse du néopentane par le propène (1) ou l'isobutène (2) et l'auto-inhibition de cette même réaction par l'isobutène formé (2–4). Il a fait également l'objet de généralisations par Niclause et coauteurs (5, 6).

Le second type de mécanismes consiste en l'*addition* d'un atome d'hydrogène, porteur de chaînes, sur la double liaison de la molécule d'alcène pour donner un radical relativement stable thermiquement lorsqu'il ne peut se décomposer unimoléculairement que par rupture d'une liaison C—H. Ce radical intervient alors dans des processus de terminaison. C'est ainsi que Purnell et coauteurs ont interprété l'auto-inhibition de la pyrolyse du propane par le propène (7) et celle de l'isobutane par l'isobutène (8), tout au moins à relativement "basse" température (423–462°C, 696–735 K) et "haute" pression (300–550 Torr; 1 Torr = 133.3 Pa).

Certaines controverses ont parfois eu lieu pour préciser la

[1] Auteur à qui adresser la correspondance.

part de chaque type de mécanisme pour rendre compte de l'auto-inhibition observée dans des exemples où les deux mécanismes pouvaient intervenir simultanément. En effet, les modèles mathématiques des lois de vitesse ont des formes voisines avec l'un ou l'autre des deux mécanismes possibles d'auto-inhibition (9). Des études complémentaires ont été réalisées, avec pour but de résoudre cette difficulté, sur les exemples de l'isobutane (10) et du propane (11), mais elles n'ont pas permis d'éliminer un des mécanismes possibles d'inhibition.

Par conséquent, à quelques détails mécanistiques près, l'ensemble des travaux effectués sur les pyrolyses d'alcanes légers a conduit à une bonne connaissance du rôle *cinétique* des alcènes sur ces pyrolyses.

Certaines études entreprises il y a une dizaine d'années avaient conduit à penser que, non seulement l'alcène ajouté ou généré dans la réaction avait l'effet cinétique mentionné ci-dessus, mais qu'il pouvait aussi, dans certains cas, modifier la répartition des produits issus de la pyrolyse de l'alcane et faire apparaître de nouveaux produits, c'est-à-dire avoir aussi un effet *chimique*.

De telles complications avaient été observées par Scacchi et coauteurs lors de l'étude de l'influence du butène-2 *trans* sur la pyrolyse de l'éthane (12) et par Rondeau *et al.* lors de l'étude de l'inhibition de la pyrolyse de l'isobutane par des alcènes (13). Ces premières observations avaient conduit à penser qu'il se produisait en réalité une *co-réaction* entre l'alcane et l'alcène. Des travaux de Purnell et Pacey (14, 15) allaient également dans ce sens.

Il nous a donc semblé opportun, tant d'un point de vue fondamental qu'en vue d'une meilleure maîtrise des réactions de craquage des hydrocarbures (optimalisation des rendements, amélioration de la sélectivité), d'entreprendre une étude systématique de ces effets chimiques sur des exemples significatifs. Notre but était une généralisation des premières conclusions des articles précités et la formulation de règles permettant de décrire et de prévoir les modifications envisageables dans la nature et la répartition des produits formés dans la réaction thermique d'un alcane vers 500°C (773 K) lors de l'addition d'un alcène.

Nous complèterons les études déjà publiées sur la pyrolyse de l'éthane en présence d'éthylène ou de propène (16, 17) et sur celle du diméthyl-2,2 butane en présence de divers alcènes (isobutène, méthyl-2 butène-2 et propène (18, 19)) par les nouvelles investigations suivantes: pyrolyse de l'éthane en présence d'isobutène; pyrolyse de l'isobutane en présence d'éthylène, de propène, de butène-2 *trans* ou de méthyl-2 butène-2.

À partir de cet ensemble de résultats, nous en proposerons une interprétation globale et synthétique.

Résultats expérimentaux et interprétation

1. *Généralités*

Afin d'obtenir une concision suffisante, nous ne rappellerons que les résultats indispensables à la compréhension de l'article sur les réactions de référence des alcanes purs et sur l'origine de l'inhibition et de l'auto-inhibition due aux alcènes. Les effets "chimiques", c'est-à-dire les modifications observées sur la répartition des produits de la réaction (modification de l'importance relative des diverses stoechiométries, apparition de stoechiométries nouvelles), seront abordés sur les exemples les plus significatifs et les résultats globaux présentés sous forme de tableaux.

Afin que nos résultats aient une ampleur suffisante pour pouvoir en déduire des conclusions généralisables, nous avons, dans le cadre de ces études, choisi trois alcanes caractéristiques pouvant constituer des modèles intéressants:

TABLEAU 1. Mélanges binaires alcane–alcène étudiés

	Alcane		
Alcène	Éthane	Isobutane	Diméthyl-2,2 butane
Éthylène	(17)	Présent travail	
Propène	(16)	Présent travail	(18) et présent travail
Isobutène	Présent travail		(18, 19)
Butène-2 (*trans*)		Présent travail	
Méthyl-2 butène-2		Présent travail	(18, 19)
Méthyl-2 butène-1			(18)

(*i*) l'*éthane*, parce ce que se décomposant selon une seule stoechiométrie primaire principale ($C_2H_6 = C_2H_4 + H_2$), ce qui rend les co-réactions avec des alcènes a priori plus faciles à aborder du point de vue de l'analyse des produits; cette réaction est assez faiblement auto-inhibée par l'éthylène formé (20);

(*ii*) l'*isobutane* se décomposant selon deux stoechiométries primaires principales, une de perte d'hydrogène ($i\text{-}C_4H_{10} = H_2 + i\text{-}C_4H_8$), l'autre de perte de méthane ($i\text{-}C_4H_{10} = CH_4 + C_3H_6$), et correspondant à un degré de complexité supplémentaire par rapport à l'éthane; la décomposition de l'isobutane est auto-inhibée par les alcènes formés, et l'isobutène, de par son abondance relative, joue un rôle prépondérant de ce point de vue (21);

(*iii*) le *diméthyl-2,2 butane* dont la décomposition se produit selon cinq stoechiométries primaires principales, ainsi que le montre l'étude que nous avons effectuée au laboratoire (22); ici encore, la réaction est auto-inhibée par les alcènes formés.

Nous avons regroupé dans le tableau 1 les systèmes déjà étudiés et ayant fait l'objet de publications et ceux qui ont été soumis à de nouvelles investigations. Notons que les références 18 et 19 constituent en réalité des notes relativement brèves.

Les résultats seront classés par alcane étudié; nous développerons davantage les cas éthane–isobutène et isobutane–alcènes.

2. *Montage expérimental*

Nous avons utilisé un montage statique à volume constant, réalisé en verre "Pyrex" très proche de ceux déjà utilisés au laboratoire (23).

L'ensemble four–réacteur a été modifié et nous avons repris, sur un montage statique, un dispositif plus récent mis au point au laboratoire sur un montage dynamique (24). Le réacteur est constitué d'un ballon de Pyrex ayant un volume de 80 cm^3 dont le chauffage est réalisé par un élément chauffant Thermocoax sous forme de deux coquilles montées au contact direct de la paroi extérieure. Par sa construction, la résistance chauffante Thermocoax assure un parfait isolement électrique tout en gardant une excellente conductibilité thermique. L'ensemble est calorifugé avec de la laine de quartz et monté dans un boitier cubique de protection.

Un thermocouple de régulation est positionné entre les parois du réacteur et les coquilles de Thermocoax; la régulation de température est assurée par un régulateur électronique Eurotherm. La température de réaction est mesurée par un thermocouple placé dans un doigt de gant arrivant au centre du réacteur.

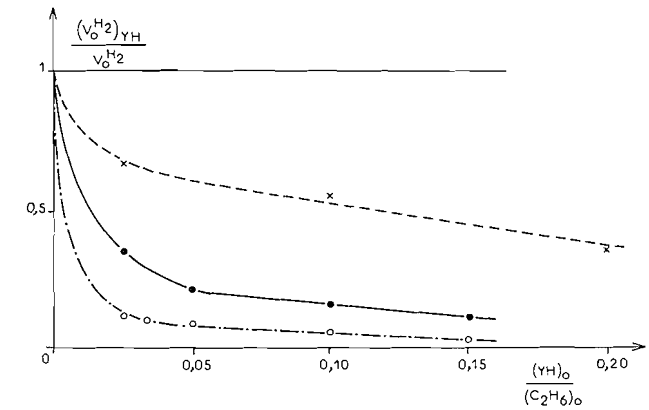

FIG. 1. Pyrolyse de l'éthane en présence d'un alcène YH vers 520°C ($P_0^{C_2H_6}$ = 100 Torr); —— YH ≡ i-C_4H_8 ●; —·— YH ≡ C_3H_6 ○ d'après réf. 16; ---- YH ≡ C_2H_4 × d'après réf. 17.

3. *Cas de l'éthane*

3.1. *Études de référence sur la pyrolyse de l'éthane pur*

Les essais de référence que nous avons effectués entre 500 et 556°C (773 et 825 K) se sont révélés en bon accord avec les résultats des autres auteurs (cf., par exemple, les références 20 et 25–27). L'ensemble des données relatives à la décomposition de l'éthane à faible avancement paraît très cohérent et cet exemple constitue ainsi une base sûre pour une étude approfondie de l'influence d'alcènes.

Rappelons que la pyrolyse de l'éthane peut être représentée, à l'instant initial, par le mécanisme radicalaire en chaînes suivant:

[1] Amorçage $C_2H_6 \rightarrow 2\ CH_3\cdot$

[2] Transfert $CH_3\cdot + C_2H_6 \rightarrow CH_4 + C_2H_5\cdot$

[3] Propagation [A] $C_2H_5\cdot \rightarrow C_2H_4 + H\cdot$
$C_2H_6 = C_2H_4 + H_2$

[4] $H\cdot + C_2H_6 \rightarrow H_2 + C_2H_5\cdot$

[μμ] Terminaison $2\ C_2H_5\cdot \rightarrow n\text{-}C_4H_{10}$; $\rightarrow C_2H_4 + C_2H_6$

La réaction étant en chaînes longues, ce mécanisme rend bien compte de l'équation stoechiométrique primaire principale [A] et du fait que CH_4 et n-C_4H_{10} se forment seulement en traces.

Le porteur de chaînes de type β (selon la terminologie de Goldfinger, Letort et Niclause (28)), c'est-à-dire réagissant bimoléculairement, est l'atome libre d'hydrogène; le porteur de chaînes de type μ, c'est-à-dire réagissant monomoléculairement, est le radical libre éthyle, $C_2H_5\cdot$; de par sa moindre réactivité, celui-ci est en concentration quasi-stationnaire nettement plus élevée que H·, $[C_2H_5\cdot]/[H\cdot] \simeq 350$, en accord avec le processus de terminaison retenu.

3.2. *Co-réaction éthane–isobutène*

3.21. *Étude cinétique*

En présence d'isobutène et vers 520°C (793 K), la vitesse initiale de formation de l'hydrogène est fortement diminuée. Cette diminution est d'autant plus grande que le mélange est riche en isobutène.

Sur la figure 1 nous avons représenté le rapport $(V_0^{H_2})_{i\text{-}C_4H_8}/V_0^{H_2}$ des vitesses initiales d'apparition d'hydrogène, en présence et en absence d'isobutène (à même concentration initiale et à 518°C, 791 K) en fonction du rapport $r = [i\text{-}C_4H_8]_0/[C_2H_6]_0$. Sur la même fig. 1 nous avons également repris des résultats sur d'autres co-réactions éthane–alcène (YH) étudiées précédemment (16, 17).

La réaction [A]: $C_2H_6 = C_2H_4 + H_2$ est donc fortement inhibée par l'isobutène. Cet effet cinétique peut s'interpréter par un mécanisme proche de celui décrit dans le cas des mélanges éthane–propène (16). Un des processus possibles à l'origine de l'inhibition est l'*arrachement* d'un atome d'hydrogène de la molécule d'isobutène par l'atome libre d'hydrogène H· (processus [5β])

[5β] $H\cdot + CH_2{=}C(CH_3)_2 \rightarrow CH_2{=}C(\dot{C}H_2)(CH_3) + H_2$

Le processus [5β] conduit au radical (i-$C_4H_7\cdot$) stabilisé par résonance et qui peut donc intervenir dans de nouveaux processus de terminaison de chaînes:

[YY] $2\ i\text{-}C_4H_7\cdot \rightarrow$ produits

[Yμ] $i\text{-}C_4H_7\cdot + C_2H_5\cdot \rightarrow$ produits

L'autre processus possible à l'origine de l'inhibition est l'*addition* de l'atome libre H· sur l'isobutène pour former un radical t-$C_4H_9\cdot$ (processus [5t] relativement stable puisqu'il ne peut se décomposer monomoléculairement que par le processus inverse de sa formation [−5t] (cf. règles de Leathard (7))[2]

[5t] et [−5t] $H\cdot + i\text{-}C_4H_8 \rightleftarrows t\text{-}C_4H_9\cdot$

Comme t-$C_4H_9\cdot$ est plus réactif que le radical stabilisé par résonance i-$C_4H_7\cdot$ nous avons également écrit le processus [6]:

[6] $t\text{-}C_4H_9\cdot + C_2H_6 \rightarrow i\text{-}C_4H_{10} + C_2H_5\cdot$

Le radical t-$C_4H_9\cdot$ peut aussi intervenir dans de nouveaux processus de terminaison de chaînes:

[tt] $2\ t\text{-}C_4H_9\cdot \rightarrow$ produits

[μt] $C_2H_5\cdot + t\text{-}C_4H_9\cdot \rightarrow$ produits

[tY] $t\text{-}C_4H_9\cdot + i\text{-}C_4H_7\cdot \rightarrow$ produits

Remarque à propos de la réactivité de t-$C_4H_9\cdot$:

Pour que les radicaux t-$C_4H_9\cdot$ puissent avoir une influence cinétique notable sur la réaction en intervenant dans les terminaisons, il faut que ces radicaux se détruisent assez facilement par combinaison et (ou) dismutation. Or, ceci est en contradiction avec les valeurs basses de la constante de combinaison et de dismutation de t-$C_4H_9\cdot$ qui avaient été avancées par certains auteurs (par exemple $10^{8,4}$ cm^3 mol^{-1} s^{-1} d'après Hiatt et Benson (29)). Dans un article paru en 1976, Parkes et Quinn (30) ont montré par une méthode de mesure directe que la valeur de la constante de recombinaison des radicaux t-$C_4H_9\cdot$ était de $10^{12,5}$ cm^3 m^{-1} s^{-1} et donc nettement plus élevée que celle admise auparavant.

Un article de Marshall *et al.* (31) a d'ailleurs confirmé ce point de vue en montrant que les valeurs basses admises pour les constantes de combinaison de certains radicaux alcoyles (dont le radical *tert*-butyle) provenaient vraisemblablement d'erreurs sur les données thermochimiques. Il semble que le travail de Parkes et Quinn (30) ait mis fin à cette controverse et que seule la valeur élevée soit à retenir, en accord avec les mécanismes que nous proposons.

3.22. *Étude chimique*

En présence d'isobutène, la pyrolyse de l'éthane n'est pas

[2] Le radical t-$C_4H_9\cdot$ ainsi formé par addition est en fait un radical vibrationnellement excité.

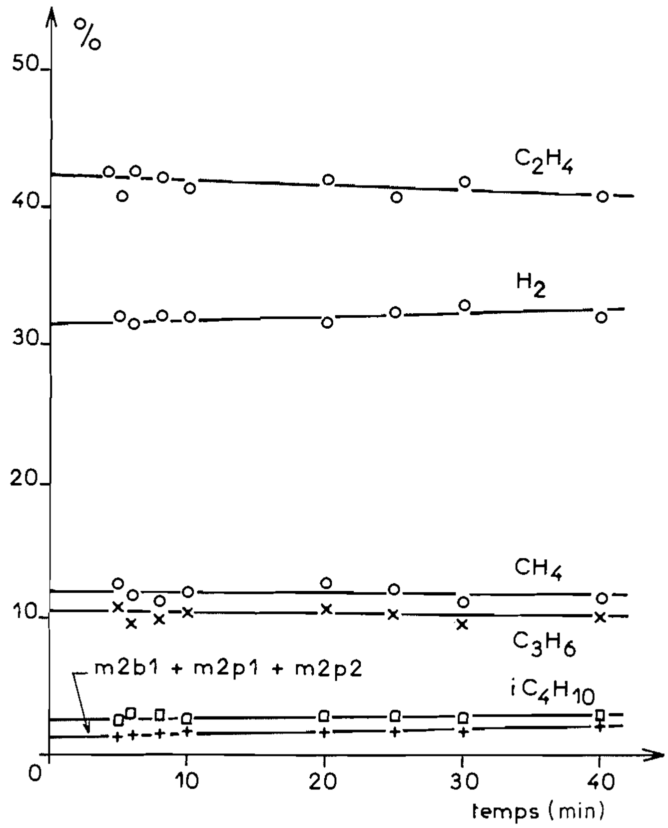

FIG. 2. Pyrolyse de l'éthane en présence d'isobutène; composition des produits primaires principaux (T = 518°C (791 K), $P_0^{C_2H_6}$ = 100 Torr, $r = [i\text{-}C_4H_8]_0/[C_2H_6]_0$ = 0,15); méthyl-2 butène-1 ≡ m2b1, méthyl-2 pentène-1 ≡ m2p1, méthyl-2 pentène-2 ≡ m2p2.

seulement inhibée mais la répartition des produits est modifiée. Il n'y a plus d'égalité entre C_2H_4 et H_2 et il se forme des quantités notables de méthane et de propène et un peu d'isobutane.

La figure 2 représente la composition des produits H_2, CH_4, C_2H_4, C_3H_6 et $i\text{-}C_4H_{10}$ en fonction du temps de pyrolyse (à 518°C, 791 K et pour une teneur en isobutène r = 0,15); il se forme aussi des traces de méthyl-2 butène-1, de méthyl-2 pentène-1 et de méthyl-2 pentène-2. Ces trois produits représentent à l'instant initial environ 1% de l'ensemble des produits mesurés.

On peut interpréter ces effets en considérant l'addition de l'atome libre H· sur la double liaison de la molécule d'isobutène. Cette addition peut conduire soit à un radical isobutyle primaire:

p-C_4H_9· 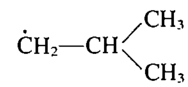

soit à un radical isobutyle tertiaire:

t-C_4H_9· 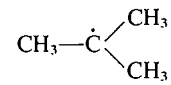

La formation de p-C_4H_9· peut effectivement interpréter la formation de méthane et de propène, si l'on considère la séquence fermée:

[5p] H· + i-C_4H_8 → p-C_4H_9·

[7] p-C_4H_9· → CH_3· + C_3H_6

[2] CH_3· + C_2H_6 → CH_4 + C_2H_5·

[3] C_2H_5· → H· + C_2H_4

correspondant à la stoechiométrie [B]

[B] C_2H_6 + i-C_4H_8 = C_2H_4 + C_3H_6 + CH_4

La formation de t-C_4H_9· en dehors de son rôle cinétique mentionné précédemment, permet d'interpréter la formation d'isobutane par la séquence fermée, où t-C_4H_9· réagit bimoléculairement avec une molécule d'éthane:

[5t] et [−5t] H· + i-C_4H_8 ⇄ t-C_4H_9·

[6] t-C_4H_9· + C_2H_6 → C_2H_5· + i-C_4H_{10}

[3] C_2H_5· → H· + C_2H_4

correspondant à la stoechiométrie [C]

[C] C_2H_6 + i-C_4H_8 = C_2H_4 + i-C_4H_{10}

Le radical tertiaire t-C_4H_9· doit être relativement moins réactif vis-à-vis d'une molécule d'éthane qu'un radical alcoyle plus léger et par conséquent la stoechiométrie [C] doit avoir une importance limitée devant [A] et [B].

Le mécanisme global de pyrolyse de l'éthane en présence d'isobutène qui permet d'interpréter les trois stoechiométries [A], [B] et [C] et donc les produits dosés en quantités les plus importantes H_2, CH_4, C_2H_4, C_3H_6 et i-C_4H_{10} peut être le suivant, en tenant compte des effets inhibiteurs et de leur interprétation, mentionnés dans ce qui précède.

Mécanisme de pyrolyse de l'éthane en présence d'isobutène (à faible avancement)

[1]	Amorçage	C_2H_6 → 2 CH_3·
[3]	Propagation [A]	C_2H_5· → H· + C_2H_4
[4]	C_2H_6 = C_2H_4 + H_2	H· + C_2H_6 → C_2H_5· + H_2
[5p]	Propagation [B]	H· + i-C_4H_8 → p-C_4H_9·
[7]		p-C_4H_9· → CH_3· + C_3H_6
[2]	C_2H_6 + i-C_4H_8 = C_2H_4 + CH_4 + C_3H_6	CH_3· + C_2H_6 → CH_4 + C_2H_5·
[5t] et [−5t]	Propagation [C]	H· + i-C_4H_8 ⇄ t-C_4H_9·
[6]	C_2H_6 + i-C_4H_8 = C_2H_4 + i-C_4H_{10}	t-C_4H_9· + C_2H_6 → C_2H_5· + i-C_4H_{10}
[5β]	Arrachement d'hydrogène	H· + i-C_4H_8 → i-C_4H_7· + H_2

[μμ]		$2\ C_2H_5\cdot \rightarrow$	
[Yμ]		$i\text{-}C_4H_7\cdot + C_2H_5\cdot \rightarrow$	
[YY]		$2\ i\text{-}C_4H_7\cdot \rightarrow$	
	Terminaison		produits
[μt]		$C_2H_5\cdot + t\text{-}C_4H_9\cdot \rightarrow$	
[tY]		$t\text{-}C_4H_9\cdot + i\text{-}C_4H_7\cdot \rightarrow$	
[tt]		$2\ t\text{-}C_4H_9\cdot \rightarrow$	

Les autres produits en quantités moins importantes sont expliqués par l'intervention de $C_2H_5\cdot$ qui peut s'additionner sur la molécule d'isobutène. Il suffit de construire des séquences fermées avec des processus du mécanisme général précédent. Les nouvelles stoechiométries obtenues rendent alors compte de la formation du méthyl-2 butène-1 (m2b1), du méthyl-2 pentène-1 (m2p1) et du méthyl-2 pentène-2 (m2p2):

1ère Possibilité: addition de $C_2H_5\cdot$ sur le carbone central:

[8A] et [−8A] 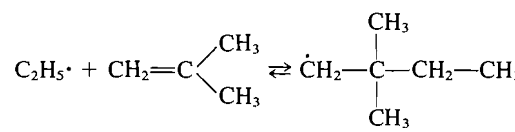

[9] 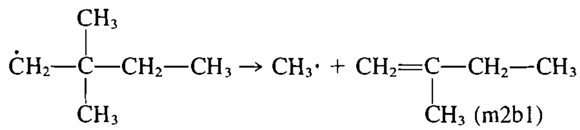

[2] $CH_3\cdot + C_2H_6 \rightarrow CH_4 + C_2H_5\cdot$

d'où:

[D] $C_2H_6 + i\text{-}C_4H_8 = CH_4 + C_5H_{10}$ (m2b1)

2ème Possibilité: addition de $C_2H_5\cdot$ sur le carbone terminal:

[8B] et [−8B] 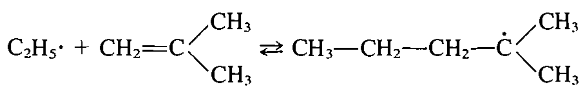

[10A] 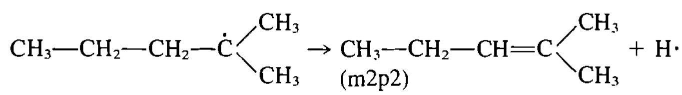

ou:

[10B] 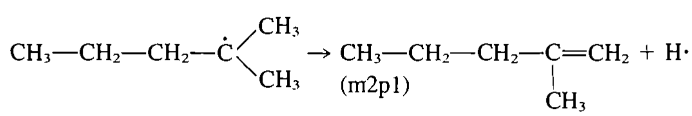

[4] $H\cdot + C_2H_6 \rightarrow H_2 + C_2H_5\cdot$

d'où:

[E] et [F] $C_2H_6 + i\text{-}C_4H_8 = H_2 + C_6H_{12}$ (m2p1 et m2p2)

Si l'on tient compte de l'ensemble des produits dosés (y compris les traces de méthyl-2 butène-1, de méthyl-2 pentène-1 et de méthyl-2 pentène-2), la décomposition thermique de l'éthane en présence d'isobutène peut être représentée par six stoechiométries primaires principales dont nous indiquons à titre d'exemple les importances relatives à l'instant initial (à 518°C, 791 K et r = 0,15):

[A]	$C_2H_6 = C_2H_4 + H_2$	66,6%
[B]	$C_2H_6 + i\text{-}C_4H_8 = CH_4 + C_2H_4 + C_3H_6$	23,6%
[C]	$C_2H_6 + i\text{-}C_4H_8 = C_2H_4 + i\text{-}C_4H_{10}$	6,4%
[D]	$C_2H_6 + i\text{-}C_4H_8 = CH_4 + C_5H_{10}$ (m2b1)	3,4%
[E]	$C_2H_6 + i\text{-}C_4H_8 = H_2 + C_6H_{12}$ (m2p1)	
[F]	$C_2H_6 + i\text{-}C_4H_8 = H_2 + C_6H_{12}$ (m2p2)	

Soit a = $(C_2H_4) - [(C_3H_6) + (i\text{-}C_4H_{10})]$, b = (C_3H_6), c = $(i\text{-}C_4H_{10})$, d = (m2b1) + (m2p1) + (m2p2). Les quantités a, b, c, d sont représentatives pour chaque temps de pyrolyse des stoechiométries [A], [B], [C] et [D] + [E] + [F]. L'extrapolation des droites obtenues (cf. figure 3) à avancement nul fournit la répartition des stoechiométries à l'instant initial.

Nous avons montré dans la partie "résultats expérimentaux" que la somme des produits caractéristiques des stoechiométries [D], [E] et [F] est de l'ordre d'un pour cent de l'ensemble des produits dosés (dans les conditions: T = 518°C, 791 K et r = 0,15). L'importance de ces stoechiométries qui résultent de l'addition du radical alcoyle $C_2H_5\cdot$ sur l'isobutène sera inférieure à un pour cent dans le cas des pyrolyses à plus haute température (540 et 556°C, 813 et 829 K). En effet, dans ces conditions, nous rappelons, comme dans le cas des mélanges C_2H_6–C_3H_6, que la vitesse des processus inverses (processus [−8A] ou [−8B]) augmente plus rapidement que celle des processus directs avec la température; l'énergie d'activation de ces processus inverses est plus grande que celle des processus directs.

Nos nouveaux résultats expérimentaux sur les mélanges éthane–isobutène peuvent donc en première approximation être correctement décrits par les seules stoechiométries [A], [B] et [C], avec [A] la stoechiométrie de l'éthane pur et [B] et [C] les stoechiométries déduites de l'addition de l'atome libre H· sur la double liaison de l'alcène ajouté.

TABLEAU 2. Pyrolyse de l'éthane en présence d'un alcène

Alcène ajouté	Radical(aux) potentiellement responsable(s) de l'inhibition	Radical(aux) responsable(s) de l'effet chimique	T (°C)	Stoechiométries		Importance relative† (%)
Isobutène	$CH_2{=}C(CH_2\cdot)CH_3$* (i-$C_4H_7\cdot$)	$\dot{C}H_2{-}CH(CH_3)_2$ (p-$C_4H_9\cdot$)	500–518	$C_2H_6 = C_2H_4 + H_2$	[A]	69,0
				$C_2H_6 + i\text{-}C_4H_8 = CH_4 + C_2H_4 + C_3H_6$	[B]	24,4
	$CH_3{-}\dot{C}(CH_3)_2$ (t-$C_4H_9\cdot$)	$CH_3{-}\dot{C}(CH_3)_2$ (t-$C_4H_9\cdot$)	540–556	$C_2H_6 + i\text{-}C_4H_8 = C_2H_4 + i\text{-}C_4H_{10}$	[C]	6,6
Propène	$\dot{C}H_2{-}CH{=}CH_2$*	$CH_3{-}CH_2{-}\dot{C}H_2$	500–520	$C_2H_6 = C_2H_4 + H_2$	[A]	59,6
				$C_2H_6 + C_3H_6 = CH_4 + 2C_2H_4$	[G]	29,0
	$CH_3{-}\dot{C}H{-}CH_3$	$CH_3{-}\dot{C}H{-}CH_3$	540–556	$C_2H_6 + C_3H_6 = C_2H_4 + C_3H_8$	[H]	11,4
Éthylène	$C_2H_5\cdot$	$C_2H_5\cdot$	500–520	$C_2H_6 = C_2H_4 + H_2$	[A]	93,2
				$C_2H_6 + C_2H_4 = 1\text{-}C_4H_8 + H_2$	[I]	3,8
			540–556	$C_2H_6 + C_2H_4 = CH_4 + C_3H_6$	[J]	3,0

*Radicaux formés par arrachement d'hydrogène sur l'alcène considéré, les autres radicaux sont formés par addition de H· sur l'alcène correspondant.
†Importances relatives des diverses stoechiométries (extrapolation à l'instant initial); T = 518°C (791 K), $P_0^{C_2H_6}$ = 100 Torr, r = [alcène]$_0$/[éthane]$_0$ = 0,15.

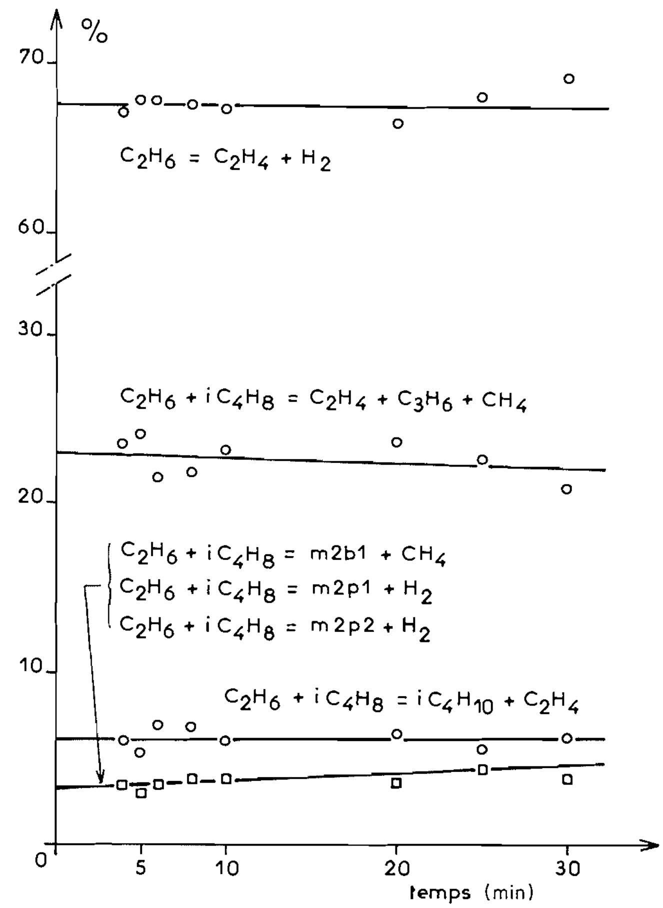

FIG. 3. Pyrolyse de l'éthane en présence d'isobutène. Répartition des stoechiométries primaires principales (T = 518°C (791 K), $P_0^{C_2H_6}$ = 100 Torr, r = [i-C_4H_8]$_0$/[C_2H_6]$_0$ = 0,15).

3.23. *Comparaison des résultats obtenus par addition d'isobutène avec ceux obtenus par addition de propène ou d'éthylène*

Nous avons regroupé l'ensemble de nos résultats et résumé leur interprétation mécanistique dans un même tableau (cf. tableau 2).

Pour les trois co-réactions éthane–alcène YH étudiées précédemment (éthylène, propène) et dans ce travail (isobutène), nous mentionnons quels sont les radicaux pouvant être à l'origine de l'auto-inhibition et les radicaux responsables des effets "chimiques" (nouvelles stoechiométries).

Sur le plan purement cinétique, la figure récapitulative (fig. 1) et la lecture du tableau 2, compte-tenu des interprétations mécanistiques proposées, permettent de penser que l'inhibition de la pyrolyse de l'éthane par un alcène sera relativement faible s'il n'y a pas, dans les radicaux potentiellement responsables de l'inhibition, un radical Y· formé par arrachement d'un atome d'hydrogène de la molécule d'alcène YH et stabilisé par résonance (radical de type allylique). Ce point de vue est corroboré par l'influence cinétique de l'éthylène sur la pyrolyse de l'éthane.

Ces résultats ne permettent pas de conclure que le mécanisme par arrachement d'hydrogène est suffisant pour rendre compte des influences inhibitrices et auto-inhibitrices d'alcènes; en effet, nous ne disposons pas, dans le cas de l'éthane, d'exemples de réactions avec un alcène YH où *seul* le mécanisme par arrachement d'hydrogène serait possible.

La lecture du tableau 2 fait apparaître que les importances relatives des nouvelles stoechiométries restent limitées dans le cas de mélanges C_2H_6–C_2H_4; rappelons que ces nouvelles stoechiométries sont attribuées à l'addition du radical libre éthyle sur la molécule d'éthylène et aux processus subséquents (17). Ceci suggère donc que, dans nos conditions expérimentales, les changements de nature et de répartition des produits lors de la pyrolyse de l'éthane en présence d'un alcène sont essentiellement dus à l'addition d'un atome libre H· sur la double liaison de la molécule d'alcène et aux processus subséquents des radicaux libres ainsi formés, s'ils réagissent par des processus élémentaires *autres* que par le processus inverse de leur formation, impliquant la rupture de liaisons carbone–carbone, plus fragiles que des liaisons carbone–hydrogène.

En revanche, lorsque l'on considère l'addition de radicaux alcoyles sur une double liaison d'un alcène, le processus inverse de la formation des nouveaux radicaux ainsi obtenus est par définition la rupture d'une liaison carbone–carbone. De par la relative fragilité de ce type de liaison, les nouvelles stoechiométries ne pourront pas prendre une importance appréciable. C'est naturellement le cas du radical éthyle dans le cas de l'éthane; comme on l'a vu précédemment, les stoechiométries nouvelles dérivées de l'addition de ce radical ne prennent pas une importance appréciable dans les co-réactions de consommation de l'éthane.

Cette analyse des schémas réactionnels a été facilitée grâce au nombre limité de produits de réaction, puisque l'éthane ne se pyrolyse que selon une seule équation stoechiométrique primaire principale.

Cependant, on peut se demander si les conclusions précédentes restent valables dans le cas beaucoup plus général d'alcanes qui se décomposent selon plusieurs équations stoechiométriques primaires principales, en particulier dans le cas où les porteurs de chaînes de type β (c'est-à-dire réagissant bimoléculairement) comprennent des espèces autres que l'atome libre d'hydrogène (radicaux alcoyles légers, en particulier $CH_3\cdot$, $C_2H_5\cdot$, ...) et dans les cas où il existe plusieurs formes isomères du radical $\mu\cdot$.

Afin d'évaluer la validité des conclusions précédentes, nous allons aborder d'autres exemples de pyrolyses d'alcanes en présence d'alcènes ajoutés; les alcanes choisis pour cette nouvelle comparaison seront l'isobutane dans une première série et le diméthyl-2,2 butane dans une seconde série.

4. *Cas de l'isobutane*

4.1. *Isobutane pur*

Nos essais de référence ont confirmé les caractéristiques déjà connues de cette pyrolyse, en particulier l'importance relative des deux stoechiométries primaires principales de décomposition déterminée par la composition des produits primaires qui d'ailleurs varie assez peu avec le temps. À titre d'exemple, nous avons mentionné la répartition des deux stoechiométries primaires principales, déterminée à 470°C (743 K) et pour une pression initiale d'isobutane de 100 Torr:

[A′] $\quad$ $i\text{-}C_4H_{10} = CH_4 + C_3H_6$ $\quad$ 25%

[B′] $\quad$ $i\text{-}C_4H_{10} = H_2 + i\text{-}C_4H_{10}$ $\quad$ 75%

Plus généralement, nos résultats de référence font apparaître un bon accord avec les études effectuées antérieurement sur cette réaction (cf., par exemple, les références 8, 10, 32, et 33).

Compte-tenu des travaux de Muller (32), de Konar *et al.* (8, 10) et des vérifications complémentaires que nous avons entreprises, le mécanisme de la pyrolyse de l'isobutane à relativement faible avancement que nous avons retenu s'écrit:

[11]	Amorçage	$i\text{-}C_4H_{10} \rightarrow$ radicaux libres
[7]	Propagation [A′]	$p\text{-}C_4H_9\cdot \rightarrow CH_3\cdot + C_3H_6$
[12p]	$i\text{-}C_4H_{10} = CH_4 + C_3H_6$	$CH_3\cdot + i\text{-}C_4H_{10} \rightarrow CH_4 + p\text{-}C_4H_9\cdot$
[12t]		$CH_3\cdot + i\text{-}C_4H_{10} \rightarrow CH_4 + t\text{-}C_4H_9\cdot$
[−5t] et [5t]	Propagation [B′]	$t\text{-}C_4H_9\cdot \rightleftarrows H\cdot + i\text{-}C_4H_8$
[13p]	$i\text{-}C_4H_{10} = H_2 + i\text{-}C_4H_8$	$H\cdot + i\text{-}C_4H_{10} \rightarrow H_2 + p\text{-}C_4H_9\cdot$
[13t]		$H\cdot + i\text{-}C_4H_{10} \rightarrow H_2 + t\text{-}C_4H_9\cdot$
[14] et [−14]	Isomérisation	$t\text{-}C_4H_9\cdot + i\text{-}C_4H_{10} \rightleftarrows p\text{-}C_4H_9\cdot + i\text{-}C_4H_{10}$
[5β]	Auto-inhibition	$H\cdot + i\text{-}C_4H_8 \rightarrow H_2 + i\text{-}C_4H_7\cdot$
	Terminaison	combinaison ou dismutation des radicaux: $CH_3\cdot$ (β·), $t\text{-}C_4H_9\cdot$ (μ·) et $i\text{-}C_4H_7\cdot$ (Y·)

La séquence fermée constituée des processus [7] et [12p] conduit à la stoechiométrie [A′]; celle constituée de [−5t] et [13p] conduit à la stoechiométrie [B′]. Il y a donc deux porteurs de chaînes de type β·, H· et $CH_3\cdot$, et deux formes isomères du radical μ·, $p\text{-}C_4H_9\cdot$ et $t\text{-}C_4H_9\cdot$, qui peuvent d'ailleurs s'isomériser également bimoléculairement par les processus [14] et [−14].

L'allure auto inhibée de la réaction (32, 8) s'explique par la formation des deux alcènes (propène et isobutène); l'isobutène joue un rôle prépondérant dans ce phénomène, parce qu'il est formé en quantités plus importantes que le propène (environ 3 fois plus); rappelons que dans nos conditions expérimentales, l'isobutène a une influence inhibitrice comparable à celle du propène (13), pour des quantités égales.

Il est admis, comme nous l'avons vu dans le cas de l'éthane, que deux types de processus peuvent être à l'origine de l'auto-inhibition d'une pyrolyse d'alcane; des processus d'arrachement d'hydrogène sur les molécules d'alcène et des processus d'addition de l'atome libre H· sur la double liaison. Si l'on admet que l'isobutène joue un rôle prépondérant dans ces phénomènes d'auto-inhibition de la pyrolyse de l'isobutane, on aura ainsi: par arrachement d'hydrogène de l'isobutène, formation de radicaux isobutényles $i\text{-}C_4H_7\cdot$ (processus [5β]), stabilisés par résonance et pouvant intervenir dans de nouveaux processus de terminaison des chaînes; par addition d'hydrogène sur l'isobutène, formation de radicaux *tert*-butyle (processus [5t]) relativement stables thermiquement parce que ne pouvant se décomposer que par rupture d'une liaison C—H et, de ce fait, intervenant également dans les processus de terminaison.

Il est difficile, dans l'état actuel de nos connaissances sur cette réaction, de préciser quelle est la part relative de chacun des mécanismes possibles dans le phénomène global d'auto-inhibition, mais il ne nous paraît pas possible de négliger a priori l'un devant l'autre. Ce point sera d'ailleurs évoqué plus loin. Ceci nous conduit donc à tenir compte, au cours du temps, de trois types de radicaux dans les processus de terminaison de la réaction: $CH_3\cdot$, $t\text{-}C_4H_9\cdot$ et $i\text{-}C_4H_7\cdot$. Les mesures d'ordre et les déterminations de vitesse initiale à partir d'un modèle de la réaction sont compatibles avec les considérations précédentes.

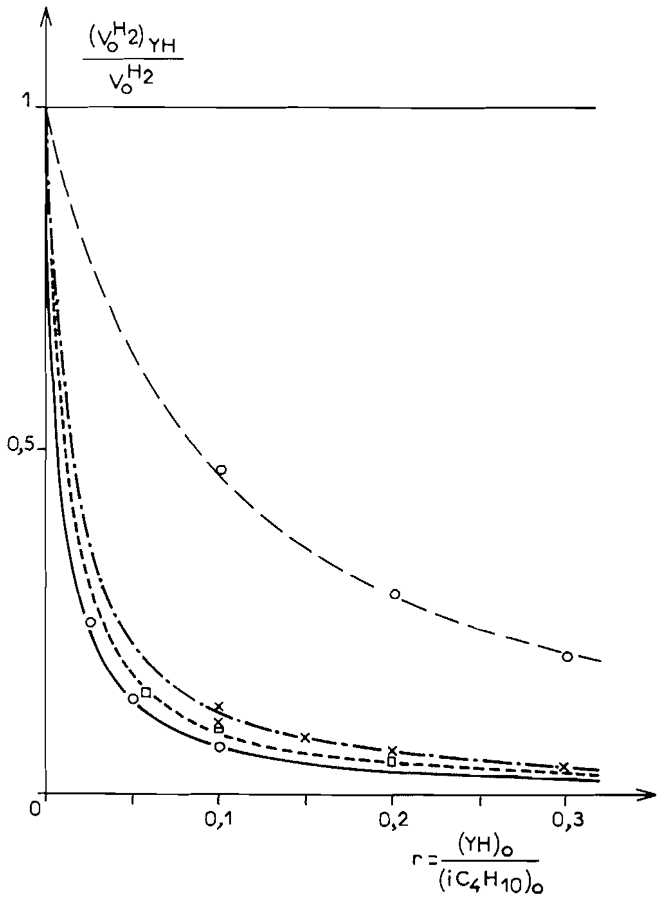

FIG. 4. Pyrolyse de l'isobutane en présence de propène et comparaison de l'effet cinétique du butène-2 *trans* et du méthyl-2 butène-2 sur la pyrolyse de l'isobutane par rapport au propène et à l'éthylène. Variation du rapport $(V_0^{H_2})_{YH}/V_0^{H_2}$ avec r = $[YH]_0/[i\text{-}C_4H_{10}]_0$; ---- YH = méthyl-2 butène-2; —— YH = butène-2 *trans*; -•-•- YH = propène; ——— YH = éthylène (T = 470°C (743 K), $P_0^{i\text{-}C_4H_{10}}$ = 100 Torr).

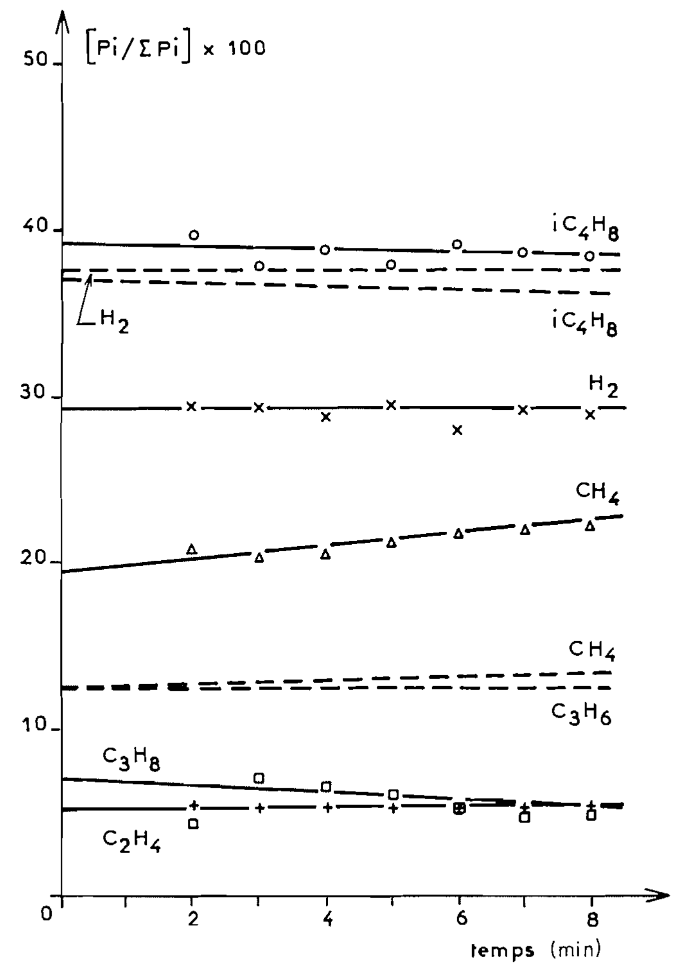

FIG. 5. Pyrolyse de l'isobutane en présence de propène. Répartition des produits primaires principaux de la réaction (T = 470°C (743 K), $P_0^{i\text{-}C_4H_{10}}$ = 100 Torr, r = $[C_3H_6]_0/[i\text{-}C_4H_{10}]_0$ = 0,10); ----- référence isobutane pur.

4.2. *Co-réaction isobutane–propène*

Nos résultats expérimentaux ont montré que l'addition de propène (10 à 30 Torr) à l'isobutane (pression initiale 100 Torr, température 470°C, 743 K) conduisait à une importante inhibition de la réaction, comparable à celle observée antérieurement dans le cas de l'éthane (16). Cette forte inhibition peut être expliquée par des processus analogues à ceux écrits dans le cas des mélanges éthane–propène, c'est-à-dire à la fois par des processus d'arrachement d'hydrogène de la molécule de propène conduisant au radical allyle stabilisé par résonance et par des processus d'addition d'hydrogène sur cette même molécule de propène et conduisant au radical isopropyle.

Sur la figure 4 nous avons représenté les effets cinétiques du propène et d'autres alcènes qui seront étudiés et comparés ensuite.

L'addition de propène exerce non seulement le fort effet cinétique mentionné ci-dessus et représenté en fig. 4, mais modifie aussi de façon importante la répartition des produits primaires principaux. Les égalités approximatives observées dans la pyrolyse de l'isobutane pur entre les concentrations des produits principaux extrapolées à l'instant initial rappelées en fig. 5 ($[H_2]_0 \simeq [i\text{-}C_4H_8]_0$ = 37,4%; $[CH_4]_0 \simeq [C_3H_6]_0 \simeq$ 12,6%) ne sont plus vérifiées et il se forme aussi primairement de l'éthylène et du propane. La figure 5 représente, en fonction du temps, à 470°C (743 K) et pour un rapport r = $[C_3H_6]_0/[i\text{-}C_4H_{10}]_0$ = 0,10, la répartition des produits exprimée en pourcentage de l'ensemble des produits dosés; les valeurs suivantes sont obtenues par extrapolation à l'instant initial: $[i\text{-}C_4H_8]_0 \simeq$ 39,2%; $[H_2]_0 \simeq$ 29,2%; $[CH_4]_0 \simeq$ 19,4%; $[C_2H_4]_0 \simeq$ 5,2%; $[C_3H_8]_0 \simeq$ 7%.

Les traces de produits plus lourds (des butènes-2 à des oléfines en C_7) sont pratiquement négligeables par rapport à ces produits (leur somme ne représente que 0,25% environ de l'ensemble des produits principaux dosés).

Nos résultats expérimentaux peuvent être décrits par quatre équations stoechiométriques primaires principales (leurs importances relatives extrapolées à l'instant initial sont données à 470°C (743 K) et pour un rapport r = 0,10).

[A′]	$i\text{-}C_4H_{10} = CH_4 + C_3H_6$	25,4%
[B′]	$i\text{-}C_4H_{10} = H_2 + i\text{-}C_4H_8$	51,7%
[C′]	$i\text{-}C_4H_{10} + C_3H_6 = C_3H_8 + i\text{-}C_4H_8$	13,7%
[D′]	$i\text{-}C_4H_{10} + C_3H_6 = CH_4 + C_2H_4 + i\text{-}C_4H_8$	9,2%

Nous avons regroupé dans ce qui suit les processus élémentaires de propagation et les séquences fermées qui conduisent aux quatre équations stoechiométriques précédentes; le mécanisme global de la pyrolyse de l'isobutane en présence de propène que nous proposons pour rendre compte de tous les effets observés s'écrit:

[11]	Amorçage	$i\text{-}C_4H_{10} \rightarrow$ radicaux libres
[7]	Propagation [A′]	$p\text{-}C_4H_9\cdot \rightarrow CH_3\cdot + C_3H_6$
[12p]	$i\text{-}C_4H_{10} = CH_4 + C_3H_6$	$CH_3\cdot + i\text{-}C_4H_{10} \rightarrow CH_4 + p\text{-}C_4H_9\cdot$
[12t]		$CH_3\cdot + i\text{-}C_4H_{10} \rightarrow CH_4 + t\text{-}C_4H_9\cdot$
[−5t]	Propagation [B′]	$t\text{-}C_4H_9\cdot \rightarrow H\cdot + i\text{-}C_4H_8$
[13p]	$i\text{-}C_4H_{10} = H_2 + i\text{-}C_4H_8$	$H\cdot + i\text{-}C_4H_{10} \rightarrow H_2 + p\text{-}C_4H_9\cdot$
[13t]		$H\cdot + i\text{-}C_4H_{10} \rightarrow H_2 + t\text{-}C_4H_9\cdot$
[15s] et [−15s]	Propagation [C′]	$H\cdot + C_3H_6 \rightleftarrows s\text{-}C_3H_7\cdot$
[16p]	$i\text{-}C_4H_{10} + C_3H_6 =$	$s\text{-}C_3H_7\cdot + i\text{-}C_4H_{10} \rightarrow C_3H_8 + p\text{-}C_4H_9\cdot$
[16t]	$C_3H_8 + i\text{-}C_4H_8$	$s\text{-}C_3H_7\cdot + i\text{-}C_4H_{10} \rightarrow C_3H_8 + t\text{-}C_4H_9\cdot$
[15p]	Propagation [D′][3] $i\text{-}C_4H_{10} + C_3H_6 =$	$H\cdot + C_3H_6 \rightarrow p\text{-}C_3H_7\cdot$
[17]	$CH_4 + C_2H_4 + i\text{-}C_4H_8$	$p\text{-}C_3H_7\cdot \rightarrow CH_3\cdot + C_2H_4$
[14] et [−14]	Isomérisation	$t\text{-}C_4H_9\cdot + i\text{-}C_4H_{10} \rightleftarrows p\text{-}C_4H_9\cdot + i\text{-}C_4H_{10}$
[18β]	Arrachement d'hydrogène	$H\cdot + C_3H_6 \rightarrow H_2 + CH_2 \overset{\cdot}{=} CH \overset{\cdot}{=} CH_2$
	Terminaison	combinaison ou dismutation impliquant les radicaux: $CH_3\cdot$, $C_3H_5\cdot$, $s\text{-}C_3H_7\cdot$, $t\text{-}C_4H_9\cdot$

Ceci montre à nouveau que l'addition de l'atome libre H· sur la double liaison du propène est susceptible d'expliquer l'essentiel des effets chimiques observés lors de la pyrolyse de l'isobutane en présence de propène. L'addition de radicaux alcoyles ($CH_3\cdot$, $s\text{-}C_3H_7\cdot$) sur la double liaison du propène est effectivement capable d'interpréter la formation de produits en traces mentionnés ci-dessus mais leur importance relative est négligeable comparée à celle des produits formés dans les stoechiométries [A′], [B′], [C′] et [D′].

Il apparaît donc que, malgré la présence d'un autre radical β· [$CH_3\cdot$] et l'existence de 2 formes isomères du radical μ· (isobutyle primaire et *tert*-butyle), l'addition de H· joue encore un rôle prépondérant dans les modifications observées dans la répartition des produits.

4.3. *Co-réaction isobutane–éthylène*

Les résultats obtenus sur cet exemple sont très proches de ceux observés dans l'étude des mélanges éthane–éthylène et décrits dans des publications antérieures (17): la réaction de décomposition de l'isobutane est inhibée par l'éthylène, mais nettement moins (environ 5 fois) que par le propène; la pyrolyse de l'isobutane est moins perturbée chimiquement par l'éthylène que par le propène; le seul produit nouveau qui apparaît est l'éthane et la répartition des produits primaires principaux peut être décrite par les trois équations stoechiométriques primaires principales suivantes:

[A′]	$i\text{-}C_4H_{10} = CH_4 + C_3H_6$	30,4%
[B′]	$i\text{-}C_4H_{10} = H_2 + i\text{-}C_4H_8$	55,8%
[E′]	$i\text{-}C_4H_{10} + C_2H_4 = C_2H_6 + i\text{-}C_4H_8$	13,8%

Les importances relatives des trois stoechiométries sont données ci-dessus à titre d'exemple, à une température de 470°C et pour un rapport $r = [C_2H_4]_0/[i\text{-}C_4H_{10}]_0$ de 0,10.

Nos résultats sont ici encore interprétables par l'addition (réversible) de l'atome libre H· sur la molécule d'éthylène, conduisant au radical libre $C_2H_5\cdot$ qui réagit bimoléculairement avec l'isobutane pour donner une molécule d'éthane et un radical *tert*-butyle, l'hydrogène tertiaire de l'isobutane étant nettement plus facile à arracher que les hydrogènes primaires; la stoechiométrie [E′] se déduit de la séquence ci-dessous:

[−3] et [3]	$H\cdot + C_2H_4 \rightleftarrows C_2H_5\cdot$
[19t]	$C_2H_5\cdot + i\text{-}C_4H_{10} \rightarrow C_2H_6 + t\text{-}C_4H_9\cdot$
[−5t]	$t\text{-}C_4H_9\cdot \rightarrow H\cdot + i\text{-}C_4H_8$

4.4. *Co-réaction de l'isobutane avec d'autres alcènes*

De la même manière et avec le même objectif, nous avons étudié l'influence du butène-2 *trans* (noté en abrégé $2\text{-}C_4H_8$) et du méthyl-2 butène-2 sur la décomposition thermique de l'isobutane. L'ensemble des cas étudiés sur l'exemple de l'isobutane est résumé dans le tableau 3, où nous avons également rappelé les résultats obtenus avec le propène et l'éthylène. Cette comparaison montre à nouveau le rôle fondamental de l'addition de l'atome libre H·.

Les études effectuées avec le butène-2 *trans* et le méthyl-2 butène-2 présentent un intérêt supplémentaire en ce qui concerne les mécanismes d'inhibition. L'effet inhibiteur du butène-2 *trans* et du méthyl-2 butène-2 sur la décomposition thermique de l'isobutane, contrairement à l'effet chimique, ne paraît pas attribuable à l'addition de l'atome libre H· sur la double liaison. En effet, les radicaux alcoyles ainsi obtenus ne possèdent pas de stabilité thermique particulière car ils peuvent se redécomposer par rupture d'une liaison carbone–carbone (radical $CH_3 \vdots CH_2—\dot{C}H—CH_3$ pour le butène-2, radicaux $CH_3—CH(\vdots CH_3)—\dot{C}H—CH_3$ et $CH_3—\dot{C}(CH_3)—CH_2 \vdots CH_3$ pour le méthyl-2 butène-2) et donc ne peuvent pas atteindre des concentrations quasi-stationnaires suffisantes pour jouer un rôle cinétique (inhibiteur) notable par leur intervention dans des processus de terminaison.

Malgré cette unicité de mécanisme d'inhibition envisageable, c'est-à-dire seulement le mécanisme par arrachement d'hydrogène conduisant à un radical allylique stabilisé par résonance, les effets inhibiteurs observés avec les deux alcènes précités sont du même ordre de grandeur, voire même supé-

[3] Complétée par [12t] et [−5t].

rieurs, à ceux obtenus en présence de propène (fig. 4); rappelons qu'avec le propène les deux mécanismes d'inhibition (addition d'un atome H· ou arrachement d'un atome d'hydrogène conduisant au radical allyle) pouvaient intervenir stimultanément.

Ces résultats tendent donc à prouver que le mécanisme par *arrachement d'hydrogène* est suffisant pour interpréter les effets inhibiteurs observés dans la pyrolyse d'alcanes en présence d'alcènes. Lorsque seul le mécanisme par addition est envisageable, comme c'est le cas en présence d'éthylène, les effets observés sont nettement moins importants (fig. 4). Ceci nous conduit à penser, de façon simplifiée, que les effets *cinétiques* (inhibition) sont attribuables essentiellement à l'*arrachement* d'un atome d'hydrogène sur la molécule d'alcène lorsque ce processus conduit à un radical libre stabilisé par résonance; les effets *chimiques*, c'est-à-dire les modifications de la répartition des produits de la réaction introduites par l'addition d'alcène, paraissent provenir essentiellement de l'*addition* de l'atome libre d'hydrogène sur la double liaison de la molécule d'oléfine et des processus subséquents des radicaux alcoyle ainsi obtenus.

En pratique, lorsqu'on s'intéresse au craquage d'alcanes liquides, on franchit encore un degré dans la complexité des schémas réactionnels. En effet, le nombre d'équations stoechiométriques décrivant la décomposition de l'alcane croît très vite avec le nombre d'atomes de carbone de celui-ci, ainsi que le nombre d'espèces radicalaires porteuses de chaînes. Pour contrôler la validité de nos observations dans un exemple se rapprochant de cette complexité, nous avons choisi comme alcane le diméthyl-2,2 butane.

5. *Cas du diméthyl-2,2 butane*

Pour la compréhension de ce mémoire et surtout dans un but de comparaison avec des résultats publiés antérieurement sur l'éthane (16, 17) ou mentionnés dans ce qui précède (réactions éthane–isobutène et réactions isobutane–alcène), il nous a paru nécessaire, compte-tenu de la relative complexité de cette réaction, de résumer les résultats obtenus sur la pyrolyse du diméthyl-2,2 butane pur (22).

5.1. *Diméthyl-2,2 butane pur*

Vers 450°C (723 K), le diméthyl-2,2 butane se décompose selon cinq stoechiométries primaires principales qui décrivent l'ensemble des produits dosés:

[A″]	C_6H_{14} (2,2 DMB) = CH_4 + C_5H_{10} (m2b1)	4,2%
[B″]	C_6H_{14} (2,2 DMB) = H_2 + C_2H_4 + i-C_4H_8	35,6%
[C″]	C_6H_{14} (2,2 DMB) = C_2H_6 + i-C_4H_8	15,0%
[D″]	C_6H_{14} (2,2 DMB) = C_2H_4 + i-C_4H_{10}	1,6%
[E″]	C_6H_{14} (2,2 DMB) = CH_4 + C_5H_{10} (m2b2)	43,6%

Les valeurs reportées ci-dessus sont les importances relatives des stoechiométries à l'instant initial à 450°C (723 K) et pour une pression initiale de diméthyl-2,2 butane de 100 Torr.

Ces cinq stoechiométries peuvent s'interpréter par un mécanisme radicalaire en chaînes comportant 6 séquences fermées (la stoechiométrie [B″] est déduite de deux séquences fermées différentes). Si l'on appelle $\mu_1\cdot$, $\mu_1'\cdot$ et $\mu_2\cdot$ les trois formes isomères du radical $\mu\cdot$ dérivé de la molécule de diméthyl-2,2 butane μH par arrachement d'un atome d'hydrogène,

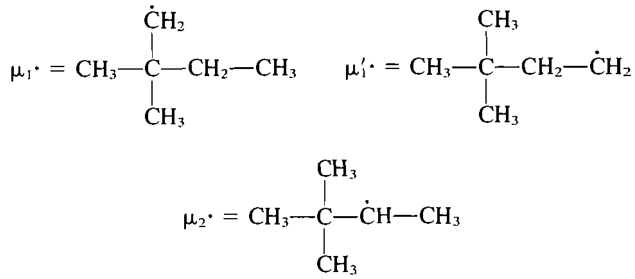

le mécanisme proposé (22) pour rendre compte de nos résultats expérimentaux est le suivant:

[20] Amorçage 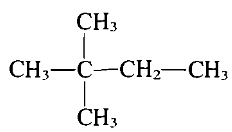 → radicaux libres

[9]	Propagation [A″]	$\mu_1\cdot \rightarrow CH_3\cdot + C_5H_{10}$ (m2b1)
[21]	$C_6H_{14} = CH_4 + C_5H_{10}$ (m2b1)	$CH_3\cdot + C_6H_{14} \rightarrow CH_4 + \mu\cdot$
[−8A]	Propagation [B″]	$\mu_1\cdot \rightarrow C_2H_5\cdot$ + i-C_4H_8
[3]	$C_6H_{14} = H_2 + C_2H_4$ + i-C_4H_8	$C_2H_5\cdot \rightarrow H\cdot + C_2H_4$
[22]		$H\cdot + C_6H_{14} \rightarrow H_2 + \mu\cdot$
[23]	Propagation [B″ bis]	$\mu_1'\cdot \rightarrow$ *t*-$C_4H_9\cdot + C_2H_4$
[−5t]	$C_6H_{14} = H_2 + C_2H_4$ + i-C_4H_8	*t*-$C_4H_9\cdot \rightarrow H\cdot$ + i-C_4H_8
[22]		$H\cdot + C_6H_{14} \rightarrow H_2 + \mu\cdot$
[−8A]	Propagation [C″]	$\mu_1\cdot \rightarrow C_2H_5\cdot$ + i-C_4H_8
[24]	$C_6H_{14} = C_2H_6$ + i-C_4H_8	$C_2H_5\cdot + C_6H_{14} \rightarrow C_2H_6 + \mu\cdot$
[23]	Propagation [D″]	$\mu_1'\cdot \rightarrow$ *t*-$C_4H_9\cdot + C_2H_4$
[25]	$C_6H_{14} = C_2H_4$ + i-C_4H_{10}	*t*-$C_4H_9\cdot + C_6H_{14} \rightarrow$ i-$C_4H_{10} + \mu\cdot$
[26]	Propagation [E″]	$\mu_2\cdot \rightarrow CH_3\cdot + C_5H_{10}$ (m2b2)
[27]	$C_6H_{14} = CH_4 + C_5H_{10}$ (m2b2)	$CH_3\cdot + C_6H_{14} \rightarrow CH_4 + \mu\cdot$

Terminaison: combinaison ou dismutation des radicaux $CH_3\cdot$, $C_2H_5\cdot$ et *t*-$C_4H_9\cdot$

L'ordre global de la réaction est proche de 1; la constante de vitesse globale déterminée expérimentalement peut se mettre sous la forme:

$$k_0 = 10^{11}\ 10^{-\frac{51\,000}{4{,}577\,T}}\ \mathrm{s}^{-1}$$

L'allure auto-inhibée des courbes de formation de produits est attribuée, en accord avec ce qui précède, à la formation au cours du temps de méthyl-2 butène-2, de méthyl-2 butène-1 et d'isobutène (22).

5.2. *Co-réaction diméthyl-2,2 butane – alcène*

Les rappels précédents montrent donc que le mécanisme de pyrolyse est assez complexe; il y a trois formes isomères du radical $\mu\cdot$ et plusieurs porteurs de chaînes, dont certains d'entre eux peuvent à la fois réagir en $\beta\cdot$ et en $\mu\cdot$ (t-$C_4H_9\cdot$, $C_2H_5\cdot$). H· intervient également comme porteur de chaînes.

Pour éviter une trop longue et fastidieuse écriture de processus élémentaires, dont le nombre augmenterait encore en présence d'alcène ajouté, et qui, par ailleurs, sont fondamentalement de même nature que ceux écrits dans le cas de l'éthane ou de l'isobutane, nous présentons nos résultats expérimentaux sous forme d'un tableau récapitulatif (tableau 4). Nous ajouterons quelques commentaires sur les aspects les plus significatifs de ces résultats.

En additionnant l'atome libre d'hydrogène formé dans des processus de propagation sur la double liaison de l'alcène ajouté et en écrivant les processus élémentaires subséquents des radicaux libres ainsi formés, on peut rendre compte des modifications apportées à la distribution des produits de réaction par des schémas proches de ceux décrits précédemment.

Dans le cas où l'alcène ajouté est le *propène*, les nouvelles stoechiométries de co-réactions aboutissent à une transformation de l'alcène en C_n ($n = 3$) en alcène en C_{n-1} ($n - 1 = 2$, C_2H_4, stoechiométrie [F″]); on observe la formation de l'alcane correspondant au nombre d'atomes de carbone de l'alcène (ici, du propane, stoechiométrie [G″]) et la diminution parallèle des quantités relatives d'hydrogène moléculaire formé; la stoechiométrie [B″] passe de 35,6% dans le cas du diméthyl-2,2 butane pur à 20,8% dans le cas de mélanges diméthyl-2,2 butane – propène (rapport $r = [C_3H_6]_0/[2{,}2\ \mathrm{DMB}]_0 = 0{,}10$. L'importance relative de la stoechiométrie de perte de méthane [E″] est peu modifiée.

Les résultats observés en présence d'*isobutène* ajouté confirment ces observations qui peuvent également être traduites en termes de processus élémentaires qui, regroupés en séquences fermées, permettent de vérifier les équations stoechiométriques déduites des résultats expérimentaux.

Lorsque l'alcène ajouté est le méthyl-2 butène-2 ou le méthyl-2 butène-1, on peut remarquer (cf. tableau 4) que, par addition d'un atome libre d'hydrogène sur une des 2 extrémités de la double liaison, on ne forme plus, contrairement au cas des 2 alcènes précédents, un radical libre ne pouvant se décomposer que par rupture d'une liaison C—H (dans le cas du propène, il s'agissait du radical isopropyle, dans le cas de l'isobutène, du radical *tert*-butyle). Cette observation présente de l'intérêt pour l'interprétation de résultats expérimentaux: (*i*) sur le plan des effets chimiques, la stoechiométrie conduisant à un alcane ayant le même nombre d'atomes de carbone que l'alcène ajouté n'apparaît plus (cf. tableau 4). Par exemple, l'addition d'un méthyl-butène ne conduit pas à la formation de quantités appréciables d'isopentane, alors que celle de propène conduit à la formation de propane (stoechiométrie [G″], tableau 4). Ce résultat est logique, puisque dans le cas des méthyl-butènes, le radical précurseur de l'isopentane n'a pas

TABLEAU 3. Pyrolyse de l'isobutane en présence d'un alcène

Alcène ajouté	Radical(aux) responsable(s) de l'inhibition	Radical(aux) responsable(s) de l'effet chimique	T (°C)	Stoechiométries		Importance relative† (%)
Propène	$\dot{C}H_2—CH{=}CH_2$*	$CH_3—CH_2—\dot{C}H_2$	470, 490	$i\text{-}C_4H_{10} = CH_4 + C_3H_6$	[A′]	25,4
	$CH_3—\dot{C}H—CH_3$	$CH_3—\dot{C}H—CH_3$	510, 520	$i\text{-}C_4H_{10} = H_2 + i\text{-}C_4H_8$	[B′]	51,7
				$i\text{-}C_4H_{10} + C_3H_6 = C_3H_8 + i\text{-}C_4H_8$	[C′]	13,7
				$i\text{-}C_4H_{10} + C_3H_6 = CH_4 + C_2H_4 + i\text{-}C_4H_8$	[D′]	9,2
Éthylène	$C_2H_5\cdot$	$C_2H_5\cdot$	470	$i\text{-}C_4H_{10} = CH_4 + C_3H_6$	[A′]	30,4
			490	$i\text{-}C_4H_{10} = H_2 + i\text{-}C_4H_8$	[B′]	55,8
			510	$i\text{-}C_4H_{10} + C_2H_4 = C_2H_6 + i\text{-}C_4H_8$	[E′]	13,8
Butène-2 *trans* ($2\text{-}C_4H_8$)	$\dot{C}H_2—CH{=}CH—CH_3$*	$CH_3—CH_2—\dot{C}H—CH_3$	470	$i\text{-}C_4H_{10} = CH_4 + C_3H_6$	[A′]	43,4
				$i\text{-}C_4H_{10} = H_2 + i\text{-}C_4H_8$	[B′]	39,4
			490	$i\text{-}C_4H_{10} + 2\text{-}C_4H_8 = CH_4 + C_3H_6 + i\text{-}C_4H_8$	[F′]	17,2
Méthyl-2 butène-2 (C_5H_{10})	$CH_3—C(CH_3){=}CH—CH_2\cdot$*	$CH_3—\dot{C}(CH_3)—CH_2—CH_3$	470	$i\text{-}C_4H_{10} = CH_4 + C_3H_6$	[A′]	28,8
	$\dot{C}H_2—C(CH_3){=}CH—CH_3$*	$CH_3—CH(CH_3)—\dot{C}H—CH_3$		$i\text{-}C_4H_{10} = H_2 + i\text{-}C_4H_8$	[B′]	40,2
				$i\text{-}C_4H_{10} + C_5H_{10}$ (m2b2) $= CH_4 + i\text{-}C_4H_8 + 2\text{-}C_4H_8$ (*cis* et *trans*)	[G′]	3,8
				$i\text{-}C_4H_{10} + C_5H_{10}$ (m2b2) $= CH_4 + 2i\text{-}C_4H_8$	[H′]	27,2

*Radicaux formés par arrachement d'hydrogène sur l'alcène considéré, les autres radicaux sont formés par addition de H· sur l'alcène correspondant.
†Importances relatives des diverses stoechiométries (extrapolation à l'instant initial); $T = 470$°C (743 K), $P_0^{i\text{-}C_4H_{10}} = 100$ Torr, $r = [\text{alcène}]_0/[\text{isobutane}]_0 = 0{,}10$.

TABLEAU 4. Pyrolyse du diméthyl-2,2 butane en présence d'un alcène

Alcène ajouté	Radical(aux) responsable(s) de l'inhibition	Radical(aux) responsable(s) de l'effet chimique	T (°C)	Nouvelle(s) stoechiométrie(s)	
Propène	$\dot{C}H_2-CH=CH_2$*	$CH_3-CH_2-CH_2\cdot$	450	C_6H_{14} (2,2 DMB) + C_3H_6 = CH_4 + $2C_2H_4$ + i-C_4H_8	[F″]
	$CH_3-\dot{C}H-CH_3$	$CH_3-\dot{C}H-CH_3$		C_6H_{14} (2,2 DMB) + C_3H_6 = C_2H_4 + C_3H_8 + i-C_4H_8	[G″]
Isobutène	$\cdot CH_2-C(CH_3)=CH_2$*	$\dot{C}H_2-CH(CH_3)_2$	450	C_6H_{14} (2,2 DMB) = CH_4 + C_2H_4 + C_3H_6	[H″]
	$CH_3-\dot{C}(CH_3)-CH_3$	$CH_3-\dot{C}(CH_3)_2$		C_6H_{14} (2,2 DMB) = C_2H_4 + i-C_4H_{10}	[D″]†
Méthyl-2 butène-2 (m2b2)	$\dot{C}H_2-C(CH_3)=CH-CH_3$*	$CH_3-CH(CH_3)-\dot{C}H-CH_3$	450	C_6H_{14} (2,2 DMB) + C_5H_{10} (m2b2) = CH_4 + C_2H_4 + i-C_4H_8 + 2-C_4H_8 (*cis* ou *trans*)	[I″]
	$CH_3-C(CH_3)=CH-CH_2\cdot$*	$CH_3-\dot{C}(CH_3)-CH_2-CH_3$		C_6H_{14} (2,2 DMB) + C_5H_{10} (m2b2) = CH_4 + C_2H_4 + 2i-C_4H_8	[J″]
Méthyl-2 butène-1 (m2b1)	$CH_3=C(CH_3)-\dot{C}H-CH_3$*	$\dot{C}H_2-CH(CH_3)-CH_2-CH_3$	450	C_5H_{10} (m2b1) = C_2H_4 + C_3H_6	[K″]
				C_6H_{14} (2,2 DMB) + C_5H_{10} (m2b1) = CH_4 + C_2H_4 + 1-C_4H_8 + i-C_4H_8	[L″]
	$CH_2=C(\dot{C}H_2)-CH_2-CH_3$*	$CH_3-\dot{C}(CH_3)-CH_2-CH_3$		C_6H_{14} (2,2 DMB) + C_5H_{10} (m2b1) = CH_4 + C_2H_4 + 2i-C_4H_8	[M″]

* Radicaux formés par arrachement d'hydrogène sur l'alcène considéré, les autres radicaux sont formés par addition de H· sur l'alcène correspondant.
† [D″] est déjà une stoechiométrie de la pyrolyse du produit pur.

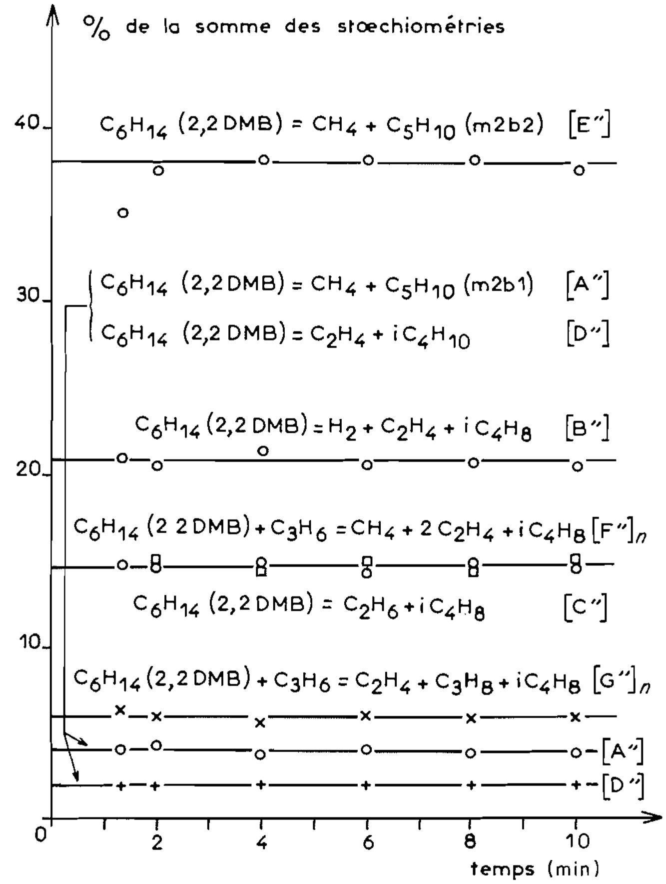

FIG. 6. Pyrolyse du diméthyl-2,2 butane en présence de propène. Répartition des stoechiométries primaires principales (T = 450°C (723 K), $P_0^{2,2\,\mathrm{DMB}}$ = 100 Torr, r = $[C_3H_6]_0/[2,2\ \mathrm{DMB}]_0$ = 0,10). L'indice n désigne les nouvelles stoechiométries qui apparaissent en présence de propène.

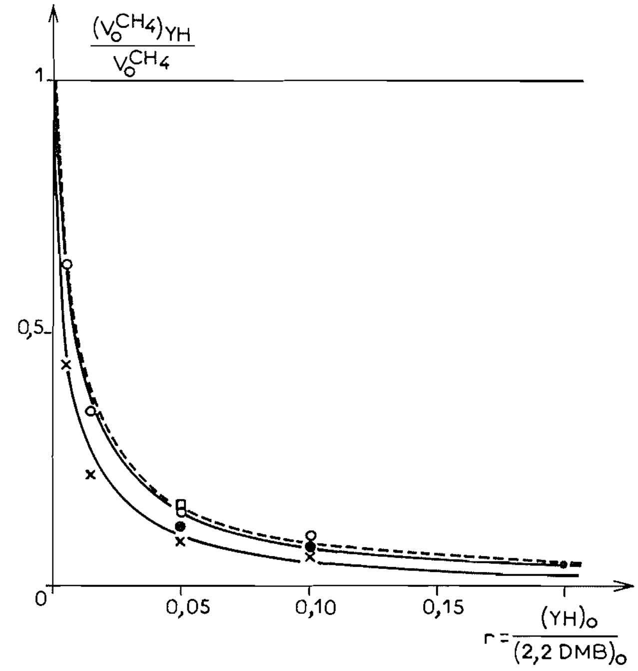

FIG. 7. Pyrolyse du diméthyl-2,2 butane en présence d'alcènes (YH) d'après Billaud *et al.* (18). Variation du rapport $(V_0^{CH_4})_{YH}/V_0^{CH_4}$ avec r = $[YH]_0/[2,2\ \mathrm{DMB}]_0$. YH = méthyl-2 butène-2 ×; YH = isobutène ●; YH = propène ○; YH = méthyl-2 butène-1 □; —— courbes calculées (T = 450°C (723 K), $P_0^{2,2\,\mathrm{DMB}}$ = 100 Torr).

une stabilité thermique suffisante pour se trouver en concentration stationnaire significative; (*ii*) sur le plan des effets cinétiques, dans le cas des méthyl-butènes, l'effet inhibiteur (ou auto-inhibiteur) ne peut pas être attribué, même partiellement, à l'addition de l'atome libre H· sur la double liaison de la molécule d'oléfine, en raison de la relativement faible stabilité thermique des radicaux alcoyle ainsi formés (décomposition unimoléculaire par rupture d'une liaison C—C, cf. ci-dessus). Cet effet inhibiteur peut être attribué *uniquement à des processus d'arrachement* d'un atome d'hydrogène conduisant à un radical de type allylique, stabilisé par résonance.

Les deux types d'effets observés sont donc très cohérents avec la stabilité thermique des radicaux.

Sur la figure 7, adaptée de la réf. 18, nous avons représenté le rapport $(V_0^{CH_4})_{YH}/V_0^{CH_4}$ des vitesses initiales de formation de méthane en présence et en absence d'alcène YH ajouté, en fonction du rapport r des concentrations initiales d'alcène $[YH]_0$ et de diméthyl-2,2 butane $[2,2\ \mathrm{DMB}]_0$; la température est de 450°C (723 K) et la pression initiale de diméthyl-2,2 butane est de 100 Torr.

Cette comparaison de l'effet inhibiteur de quatre alcènes montre à nouveau que le méthyl-2 butène-2 a un effet inhibiteur *légèrement supérieur à celui du propène*, bien que pouvant agir *uniquement par un mécanisme par arrachement d'hydrogène*. Le méthyl-2 butène-1 a un effet inhibiteur pratiquement identique à celui du propène.

Ceci paraît donc confirmer les observations faites sur l'exemple de l'isobutane.

Par conséquent, dans le cas de la pyrolyse du diméthyl-2,2 butane, dont le mécanisme est relativement complexe, nous avons encore vérifié les conclusions, tant sur le plan cinétique que sur le plan chimique, mises en évidence lors de l'étude de réactions thermiques d'alcanes plus légers (éthane et isobutane). Il faut d'ailleurs remarquer que, dans le cas du diméthyl-2,2 butane, contrairement aux cas de l'éthane et de l'isobutane, l'atome libre H· n'est pas formé par décomposition unimoléculaire d'une des formes isomères du radical μ·, mais provient de la décomposition soit du radical éthyle, soit du radical *tert*-butyle, ces radicaux étant issus de la décomposition unimoléculaire de μ·. H· n'est donc dans ce cas pas un porteur de chaînes β· "direct" comme il l'était dans les cas de l'éthane et de l'isobutane et il faut aussi noter que les radicaux dont il est issu (éthyle et *tert*-butyle) peuvent aussi agir comme porteurs de chaînes β· (stoechiométries [C″] et [D″]).

Malgré cette complexité plus grande des schémas cinétiques et des séquences de propagation, le rôle des additions de l'atome libre H· sur les alcènes ajoutés apparaît encore prépondérant pour rendre compte des modifications apportées à la répartition des produits.

L'addition d'autres porteurs de chaînes sur la double liaison des alcènes ajoutés ne permet pas de rendre compte des effets observés sur la répartition des produits; la raison fondamentale en est encore, sur cet exemple, la réversibilité du processus d'addition (rupture de la liaison C—C formée). Les additions de radicaux alcoyle permettent au plus de rendre compte de la formation d'un certain nombre de produits en traces, mais dont l'importance reste négligeable dans l'établissement d'un bilan entre réactifs consommées et produits formés.

Discussion et conclusion

Dans cette discussion, nous apporterons des éléments complémentaires sur le rôle de l'addition d'espèces radicalaires autres que H·; nous essaierons, à partir de nos résultats, de formuler des principes plus généraux régissant les modifications apportées à la répartition des produits et nous mentionnerons quelques applications envisageables de ces travaux.

1. *Rôle de l'addition d'espèces radicalaires autres que H·*

Pour corroborer les conclusions des études précédentes, nous avons recherché dans la littérature un exemple de pyrolyse d'alcane où il n'y a pas d'atomes libres d'hydrogène jouant le rôle de porteurs de chaînes β·. Le néopentane (diméthyl-2,2 propane), qui se décompose selon une seule équation stoechiométrique primaire principale:

[K] $\text{néo-}C_5H_{12} = CH_4 + \text{i-}C_4H_8$

répond à cette condition. En effet, des études détaillées effectuées par différents auteurs montrent que le seul porteur de chaînes de type β· (réagissant bimoléculairement) est le radical libre méthyle (cf., par exemple, les références 3, 4 et 34). La séquence de propagation conduisant à l'équation stoechiométrique ci-dessus s'écrit:

[28] $\text{néo-}C_5H_{11}\cdot \rightarrow \text{i-}C_4H_8 + CH_3\cdot$

[29] $CH_3\cdot + \text{néo-}C_5H_{12} \rightarrow CH_4 + \text{néo-}C_5H_{11}\cdot$

Dans le cas de la pyrolyse de mélanges néopentane–isobutène, Baronnet *et al.* (2) ont observé la formation primaire de petites quantités de méthyl-2 butène-1 et de méthyl-2 butène-2. Pour expliquer la formation de ces produits, il semble logique de considérer l'addition réversible de $CH_3\cdot$ sur la molécule d'isobutène conduisant à un radical *tert*-pentyle:

[30] $CH_3\cdot + CH_2{=}C(CH_3)_2 \rightleftarrows CH_3{-}CH_2{-}\dot{C}(CH_3)_2$

Ce radical peut aussi se décomposer, mais nettement moins facilement, par rupture d'une liaison carbone–hydrogène plus solide qu'une liaison C—C pour conduire à la formation de méthyl-butènes 1 et 2 selon:

[−10B] $CH_3{-}CH_2{-}\dot{C}(CH_3){-}CH_3 \rightarrow CH_3{-}CH_2{-}C(CH_3){=}CH_2 + H\cdot$

[−10A] $CH_3{-}CH_2{-}\dot{C}(CH_3){-}CH_3 \rightarrow CH_3{-}CH{=}C(CH_3){-}CH_3 + H\cdot$

H· réagit sur le néopentane pour former une molécule d'hydrogène et un radical néo-$C_5H_{11}\cdot$; la décomposition de celui-ci en $CH_3\cdot$ et isobutène conduit effectivement à une séquence fermée.

[31] $H\cdot + \text{néo-}C_5H_{12} \rightarrow H_2 + \text{néo-}C_5H_{11}\cdot$

[28] $\text{néo-}C_5H_{11}\cdot \rightarrow CH_3\cdot + \text{i-}C_4H_8$

Les équations stoechiométriques dérivées des séquences fermées ainsi écrites rendent compte de la formation primaire des méthyl butènes lors de la pyrolyse du néopentane en présence d'isobutène. L'importance relative des 2 équations stoechiométriques correspondantes:

[L] $\text{néo-}C_5H_{12} = H_2 + C_5H_{10}$ (méthyl-2 butène-1)

[M] $\text{néo-}C_5H_{12} = H_2 + C_5H_{10}$ (méthyl-2 butène-2)

est représentée sur la figure 8 (d'après les résultats de F. Baronnet (35)).

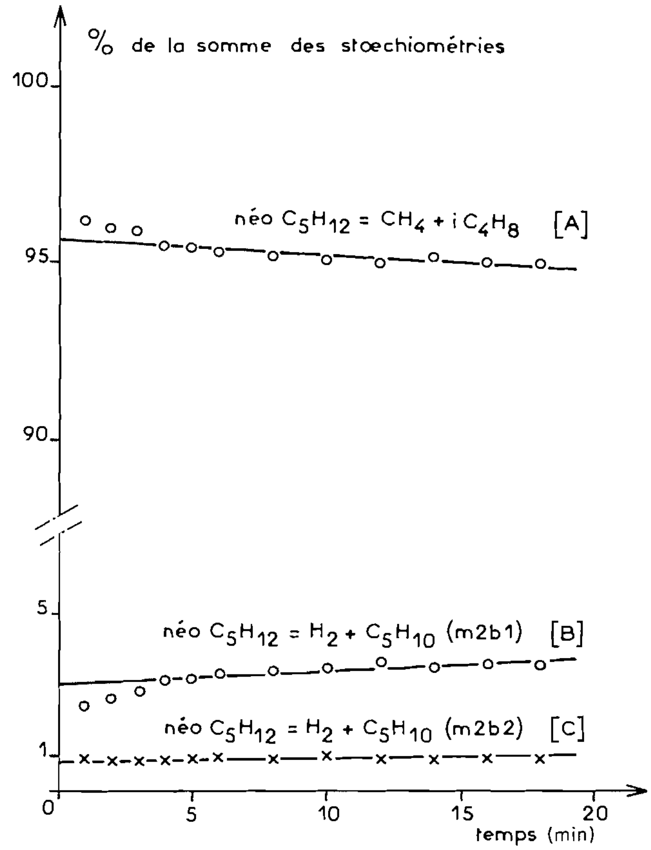

FIG. 8. Pyrolyse du néopentane en présence d'isobutène d'après les résultats de F. Baronnet (35). Répartition des stoechiométries primaires principales (T = 512°C (785 K), $P_0^{\text{néo}C_5H_{12}}$ = 100 Torr, $r = [\text{i-}C_4H_8]_0/[\text{néo }C_5H_{12}]_0 = 0{,}25$).

Ces résultats montrent qu'à 512°C (785 K), pour une pression initiale de néopentane de 100 Torr et un rapport des concentrations initiales $r = [\text{i-}C_4H_8]_0/[\text{néo-}C_5H_{12}]_0 = 0{,}25$, la répartition des stoechiométries extrapolée à l'instant initial est la suivante:

[K]	$\text{néo-}C_5H_{12} = CH_4 + \text{i-}C_4H_8$	95,7%
[L]	$\text{néo-}C_5H_{12} = H_2 + C_5H_{10}$ (m2bl)	3,0%
[M]	$\text{néo-}C_5H_{12} = H_2 + C_5H_{10}$ (m2b2)	1,3%

Ces deux nouvelles stoechiométries [L] et [M] correspondant à l'addition de $CH_3\cdot$ sur l'isobutène représentent seulement 4,3% des stoechiométries de consommation du néopentane alors que, dans des conditions comparables de température et de rapport de concentrations initiales, les stoechiométries dues à l'addition de H· sur l'isobutène lors de la pyrolyse de mélanges éthane–isobutène représentent environ 30% de l'ensemble des stoechiométries de consommation de l'éthane.

Un travail récent de P. Azay (36) sur la modélisation de réactions radicalaires complexes est en bon accord avec nos conclusions. En effet, Azay souligne que, malgré leur concentration relative généralement très faible par rapport à celle des autres radicaux libres présents dans le milieu, il faut *en premier lieu* écrire *systématiquement* les processus d'addition de H· sur les alcènes.

Pour tenir compte éventuellement de l'addition des *autres* radicaux libres, Azay estime que les concentrations relatives des espèces radicalaires considérées doivent être suffisantes. Ceci explique que, pour ses résultats, à température assez élevée, l'addition de $CH_3\cdot$ puisse être considérée, bien que jouant un rôle nettement moins important que celle de H·. L'addition d'autres espèces a un effet totalement négligeable.

2. *Essai de formulation des principes régissant les changements de stoechiométrie*

Leathard (37) a résumé en quatre règles les principes susceptibles de régir l'influence auto-inhibitrice (et donc inhibitrice) d'alcènes sur la pyrolyse d'alcanes; rappelons ces quatre règles:

(a) "De tous les radicaux alcoyle saturés qui peuvent être présents dans le milieu réactionnel, seuls les radicaux méthyle, éthyle, isopropyle et *tert*-butyle peuvent terminer les chaînes par des processus homogènes de combinaison."

(b) "L'addition de radicaux alcoyle à des oléfines ne peut pas conduire à l'apparition de l'auto-inhibition."

(c) "Les processus d'addition d'un atome libre d'hydrogène sur une oléfine peuvent conduire à des processus d'auto-inhibition lorsqu'ils forment des radicaux éthyle, isopropyle et *tert*-butyle."

(d) "L'arrachement d'hydrogène par des radicaux alcoyle sur un produit saturé, y compris l'hydrogène moléculaire, ne peut pas conduire à l'appartition d'auto-inhibition."

Ces quatre règles, initialement formulées par Leathard pour rendre compte des phénomènes d'auto-inhibition sont en très bon accord avec les observations faites dans des études d'inhibition (par des oléfines ajoutées) et avec les résultats précédents (point (b) en particulier).

Leathard ne s'est intéressé qu'à la *cinétique* des stoechiométries primaires principales et n'a pas abordé le problème des perturbations apportées à la distribution des produits. Rappelons également que de nombreux travaux du Laboratoire, confirmés d'ailleurs par des résultats décrits dans cet article, ont montré qu'il fallait également tenir compte des processus d'arrachement d'un atome d'hydrogène sur des oléfines pour décrire correctement les phénomènes d'inhibition et d'auto-inhibition; ces processus conduisent à la formation de radicaux libres stabilisés par résonance et peuvent même jouer un rôle prépondérant par rapport aux processus d'addition.

Compte-tenu des résultats précédents ainsi que de ceux de certains autres auteurs, nous pouvons compléter les règles de Leathard qui traitent de l'aspect *cinétique* par de nouvelles règles simples de formulation voisine et qui traiteront de l'aspect *chimique* des réactions de pyrolyse d'alcanes en présence d'oléfines, soit ajoutées à l'instant initial, soit formées par la réaction elle-même:

(a) Parmi tous les porteurs de chaînes de type β (réagissant bimoléculairement avec l'alcane pyrolysé), seul l'atome libre H·, par addition sur des oléfines, peut conduire à d'importants changements dans la répartition des stoechiométries de consommation de l'alcane et à l'apparition de nouvelles stoechiométries d'importance notable.

(b) L'addition de radicaux alcoyle à des oléfines ne conduit pas à d'importantes modifications de la répartition des stoechiométries.

(c) L'addition d'atomes d'hydrogène à des oléfines peut conduire à d'importants changements dans la répartition des stoechiométries lorsque le radical alcoyle ainsi formé se décompose par la rupture d'une liaison carbone—carbone.

(d) Alors que les processus d'arrachement d'hydrogène sur des oléfines ont généralement une influence cinétique (inhibitrice) importante, de tels processus n'ont pas d'influence notable sur la répartition des produits de la réaction.

Ces règles appellent un certain nombre de commentaires permettant en particulier de préciser leurs conditions d'application. Elles ont été déduites d'études de pyrolyses d'alcanes en présence de 20 à 25% d'une oléfine ajoutée, lors de réactions effectuées à relativement faible avancement, généralement inférieur à 5%. Les températures d'expérience se situent généralement dans le domaine 450—550°C (723—823 K), mais les résultats d'Azay (36) suggèrent que les conclusions obtenues demeurent valables jusque vers 700°C et pour des avancements de réaction nettement supérieurs à 5%.

Remarquons qu'un certain nombre de points développés dans ce qui précède avaient déjà été mis en évidence, plus ou moins partiellement, dans des travaux antérieurs (12—15). Nous pensons que la présentation qui en est faite ici leur donne un caractère plus complet et surtout plus synthétique.

3. *Applications possibles de ces résultats*

On pourrait se demander si de telles études nécessitant un nombre élevé d'expériences et des procédures analytiques souvent délicates et complexes restent compétitives par rapport à des approches totalement différentes, telles que celles d'Allara et Edelson (38) qui ont cherché à déterminer des mécanismes réactionnels par des méthodes informatiques. Ces auteurs ont mis au point un compilateur permettant d'écrire automatiquement l'ensemble des processus intervenant dans des réactions de pyrolyse d'alcanes linéaires légers. Les équations différentielles résultantes sont résolues par une adaptation de la méthode de Gear (39), en utilisant une évaluation des constantes de vitesse des processus élémentaires.

Le nombre de ceux-ci devient rapidement très élevé. Dans le cas du propane, il intervient 293 processus élémentaires impliquant 32 espèces de radicaux libres et 29 molécules hydrocarbonées. Ces nombres augmentent rapidement avec le nombre d'atomes de carbone de l'alcane linéaire de départ.

La complexité des mécanismes risquerait de devenir prohibitive dans le cas de molécules relativement lourdes; il se révèle indispensable de pouvoir simplifier le mécanisme en diminuant le nombre de processus à considérer, en ne tenant compte que des processus ayant de l'importance dans la formation des produits et la cinétique de la réaction.

Les considérations précédentes peuvent se révéler utiles dans de telles démarches simplificatrices. Elles montrent par exemple que, pour une description suffisamment réaliste de la réaction, il suffit, dans le cas des processus d'addition, de tenir compte seulement de l'addition de l'atome libre H· sur les oléfines, les additions des radicaux alcoyle pouvant être considérées comme négligeables.

Ces études peuvent également avoir des applications dans le craquage des alcanes légers, pour la production d'oléfines légères, en particulier de propène et d'éthylène. En effet, à la suite de la découverte de gisements de gaz en Mer du Nord, la modification de craqueurs en vue de leur alimentation à l'éthane et la construction de craqueurs nouveaux alimentés en éthane ont été entreprises.

Le présent travail montre que la présence d'atomes libres H· dans le milieu réactionnel est favorable à la transformation d'oléfines en C_n en oléfines en C_{n-1}. Par des co-réactions analogues à celles étudiées précédemment, il est possible de passer des butènes au propène et du propène à l'éthylène. Ceci laisse entrevoir des possibilités d'une meilleure adaptation des productions aux demandes du marché et de donner ainsi une certaine flexibilité aux unités de vapocraquage.

Nos résultats permettent aussi d'interpréter un certain nombre d'observations faites dans des unités industrielles. Il a été montré, par exemple, que le craquage de mélanges de propène et d'éthane donnait des rendements intéressants en éthylène, supérieurs à la somme des quantités issues des deux hydrocarbures craqués séparément. De même, il a été montré que le craquage simultané de naphta et d'éthane donnait de meilleurs rendements en éthylène que leur craquage séparé.

Ces observations s'expliquent logiquement par la génération *in situ* d'atomes libres H· par la co-pyrolyse de l'éthane. On peut estimer que la synergie est d'autant plus marquée que le rendement en hydrogène de l'alcane co-craqué est important; de ce point de vue, l'éthane est le meilleur alcane envisageable puisqu'il se craque en donnant une mole d'hydrogène (et une mole d'éthylène) pour une molécule d'éthane.

Enfin, on peut remarquer que des études analogues pourraient apporter une contribution substantielle à la connaissance des réactions thermiques de molécules hydrocarbonées relativement lourdes, ce qui présenterait un intérêt en vue de la valorisation de coupes pétrolières lourdes. Si la modification du rapport C/H est l'objectif essentiel des traitements, la génération *in situ* d'atomes libres d'hydrogène est vraisemblablement un outil plus efficace que de simples réactions en présence d'hydrogène moléculaire.

1. F. BARONNET, R. MARTIN et M. NICLAUSE. J. Chim. Phys. **69**, 236 (1972).
2. F. BARONNET, G. M. CÔME et M. NICLAUSE. J. Chim. Phys. **71**, 1214 (1974).
3. F. BARONNET, M. DZIERZYNSKI, G. M. CÔME, R. MARTIN et M. NICLAUSE. Int. J. Chem. Kinet. **3**, 197 (1971); Communication au 1er Symposium International "Gas Kinetics", Université de Szeged (Hongrie), 8–11 juillet 1969. Preprints. p. 73.
4. M. P. HALSTEAD, R. S. KONAR, D. A. LEATHARD, R. M. MARSHALL et J. H. PURNELL. Proc. R. Soc. London, Ser. A, **310**, 525 (1969).
5. M. NICLAUSE, F. BARONNET, G. SCACCHI, J. MULLER et J. Y. JEZEQUEL. Industrial and laboratory pyrolyses (sous la direction de L. F. Albright et B. L. Crynes), ACS Symposium Series, **32**, 17 (1976).
6. G. SCACCHI, F. BARONNET et M. NICLAUSE. Can. J. Chem. **60**, 249 (1982).
7. D. A. LEATHARD et J. H. PURNELL. Proc. R. Soc. London, Ser. A, **305**, 517 (1968).
8. R. S. KONAR, J. H. PURNELL et C. P. QUINN. Trans. Faraday Soc. **64**, 1319 (1968).
9. J. Y. JEZEQUEL, F. BARONNET et M. NICLAUSE. J. Chim. Phys. **71**, 1549 (1974).
10. R. S. KONAR, R. M. MARSHALL et J. H. PURNELL. Int. J. Chem. Kinet. **5**, 1007 (1973).
11. J. Y. JEZEQUEL, F. BARONNET et M. NICLAUSE. J. Chim. Phys. **80**, 455 (1983).
12. J. F. DECARREAU, B. DESCHAMPS, G. SCACCHI et M. NICLAUSE. J. Chim. Phys. **71**, 1554 (1974).
13. J. A. RONDEAU, F. BARONNET et M. NICLAUSE. C. R. Acad. Sci. Ser. C, **274**, 668 (1972); **274**, 1717 (1972).
14. J. H. PURNELL. Acta Cient. Venez. **24**, 40 (1973).
15. P. D. PACEY et J. H. PURNELL. An. Acad. Brasil. Cienc. **46**, 1 (1974).
16. F. BILLAUD, F. BARONNET et M. NICLAUSE. J. Chim. Phys. **77**, 175 (1980).
17. F. BILLAUD, F. BARONNET et M. NICLAUSE. J. Chim. Phys. **77**, 357 (1980).
18. F. BILLAUD, F. BARONNET et M. NICLAUSE. React. Kinet. Catal. Lett. **20**, 363 (1982).
19. F. BILLAUD, F. BARONNET et M. NICLAUSE. React. Kinet. Catal. Lett. **21**, 423 (1982).
20. G. SCACCHI. Thèse de Doctorat ès Sciences Physiques, Nancy. 1969; G. SCACCHI, R. MARTIN et M. NICLAUSE. Bull. Soc. Chim. Fr. 731 (1971).
21. J. A. RONDEAU, F. BARONNET et M. NICLAUSE. C. R. Acad. Sci. Ser. C, **274**, 668 (1972).
22. F. BILLAUD, F. BARONNET et M. NICLAUSE. React. Kinet. Catal. Lett. **19**, 125 (1982).
23. A. COMBES, R. MARTIN, M. DZIERZYNSKI et M. NICLAUSE. J. Chim. Phys. **64**, 869 (1967).
24. P. AZAY, P. M. MARQUAIRE, P. POMMIER et G. SCACCHI. J. Chem. Educ. **58**, 441 (1981).
25. M. C. LIN et M. H. BACK. Can. J. Chem. **44**, 505 (1966); **44**, 2357 (1966); **44**, 2369 (1966).
26. C. P. QUINN. Proc. R. Soc. London, Ser. A, **275**, 190 (1963).
27. L. F. LOUCKS et K. J. LAIDLER. Can. J. Chem. **45**, 2795 (1967).
28. P. GOLDFINGER, M. LETORT et M. NICLAUSE. Volume Commémoratif Victor Henri: Contribution à l'étude de la structure moléculaire. Desoer, Liège. 1947–1948. p. 283.
29. R. HIATT et S. W. BENSON. Int. J. Chem. Kinet. **5**, 385 (1973).
30. D. A. PARKES et C. P. QUINN. Trans. Faraday Soc. **72**, 1952 (1976).
31. R. M. MARSHALL, J. H. PURNELL et P. D. STOREY. J. Chem. Soc. Faraday Trans. 1, **72**, 85 (1976).
32. J. MULLER. Thèse de Doctorat ès Sciences physiques, Nancy. 1973.
33. J. FUSY. Thèse de Doctorat ès Sciences physiques, Nancy. 1966; J. FUSY, R. MARTIN, M. DZIERZYNSKI et M. NICLAUSE. Bull. Soc. Chim. Fr. 3783 (1966).
34. J. A. RONDEAU, J. F. LARGE et G. M. CÔME. Industrial and laboratory pyrolyses. A.C.S. Symp. Series, **32**, 131 (1976).
35. F. BARONNET. Thèse de Doctorat ès Sciences physiques, Nancy. 1970.
36. P. AZAY. Thèse de Doctorat ès Sciences, INPL, Nancy. 1981.
37. D. A. LEATHARD. Communication au 1er Symposium International "Gas Kinetics", Université de Szeged (Hongrie), 8–11 juillet 1969. Preprints. p. 263.
38. D. L. ALLARA et D. EDELSON. Int. J. Chem. Kinet. **7**, 479 (1975).
39. C. W. GEAR. Numerical initial value problems in ordinary differential equations. Prentice Hall, New York. 1971.

Tricyclic system containing large rings. The synthesis of fully-conjugated [12](1,3)[12](4,6)cyclophanpolyenepolyynes and related compounds

JURO OJIMA,[1] HIROSHI KAKUMI, KAZUTO KITATANI, KAZUYO WADA, EMIKO EJIRI, AND TETSUYA NAKADA

Department of Chemistry, Faculty of Science, Toyama University, Gofuku, Toyama 930, Japan

Received 19th December, 1984

JURO OJIMA, HIROSHI KAKUMI, KAZUTO KITATANI, KAZUYO WADA, EMIKO EJIRI, and TETSUYA NAKADA. Can. J. Chem. **63**, 2885 (1985).

For the purpose of preparing the ring-expanded analogue of anthracene, 1,2,4,5-tetrakis[(1*E*,3*Z*)-4-methylhexa-1,3-dien-5-ynyl]benzene, **8**, and 1,2,4,5-tetrakis[(*Z*)-2(2-ethnylphenyl)ethenyl]benzene, **16**, were oxidatively coupled; however, both of them afforded *m*-bridged derivatives, i.e., 1,3:4,6-bis[(1*E*,3*Z*,9*Z*,11*E*)-4,9-dimethyldodeca-1,3,9,11-tetraene-5,7-diyne-1,12-diyl]benzene, **3**, and 1,3:4,6-bis[(1*E*,11*E*)-3,4:9,10-dibenzdodeca-1,11-diene-5,7-diyne-1,12-diyl]benzene, **5**. To ascertain the structures of **3** and **5**, the related model compounds were also prepared.

JURO OJIMA, HIROSHI KAKUMI, KAZUTO KITATANI, KAZUYO WADA, EMIKO EJIRI et TETSUYA NAKADA. Can. J. Chem. **63**, 2885 (1985).

Dans le but de préparer l'analogue de l'anthracène comportant un cycle ayant subit une extension, on a procédé à un couplage oxydant du tétrakis[méthyl-4 hexadiène-1,3(1*E*,3*Z*) yne-5 yl]-1,2,4,5 benzène (**8**) et du tétrakis[(éthynyl-2 phényl)-2(*Z*) éthènyl]-1,2,4,5 (**16**); toutefois, chacun de ces produits ne conduit qu'aux dérivés pontés en position *méta*, soit les bis[diméthyl-4,9 dodécatétraène-1,3,9,11 (1*E*,3*Z*,9*Z*,11*E*) diyne-5,7 diyl-1,12]-1,3:4,6 benzène (**3**) et bis[dibenzo-3,4:9,10 dodécadiène-1,11 (1*E*,11*E*) diyne-5,7 diyl-1,12]-1,3:4,6 benzène (**5**). Dans le but de s'assurer de la structure des composés **3** et **5**, on a aussi préparé des composés modèles apparentés.

[Traduit par le journal]

Introduction

A considerable number of monocyclic annulenes annelated with benzenoid rings (1) as well as annulenoannulenes (2) have been prepared, and an extensive examination of their properties is reviewed by Mitchell (3). Among them, the dimethylbisdehydro-2,3-naphtho[14]annulene, **1**, prepared by Walsgrove and Sondheimer (4), is only one example of the ring-expanded analogue of anthracene, in which a terminal 6π-ring has been formally expanded to a 14π-ring. Since no example of a benzannelated annulene fused with two bonds of an annelated benzenoid ring had ever been reported, we attempted a synthesis of the bis(dimethylbisdehydro[14]annulene) annelated benzene, **2**, in which two terminal rings of anthracene are formally expanded to 14π-rings. We considered that an examination of the properties of **2** might give further insight toward the understanding of benzannelated annulenes. However, an intramolecular oxidative coupling of the precursor did not afford the desired **2**, but the alternative cyclic compound, **3**.

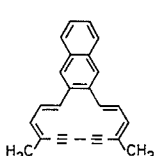

1

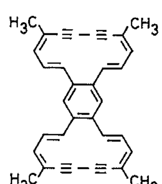

2

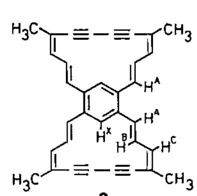

3

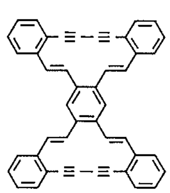

4

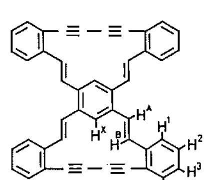

5

Since we had already reported the formation of the tetrabenzannelated derivative **4** from its precursor (5), the formation of **3** prompted us to reexamine the previous investigation. Examination of the spectral properties of the related model compounds revealed that this tetrabenzannelated derivative also had the *m*-bridged structure **5** corresponding to **3**. This paper describes these results in detail.

Results and discussion

I. *Formation of tricyclic compound, 3*

The Wittig reaction of 1,2,4,5-tetrakis(triphenylphosphoniomethyl)benzene tetrabromide, **6** (6), and 4 molar equivalents of (2*Z*)-3-methyl-2-penten-4-ynal, **7** (7), in THF with *n*-BuLi at −60°C yielded only the desired all-*trans* isomer, **8**, as crystals in 13% yield; **8** was rather unstable. Oxidative coupling of **8** was carried out with anhydrous $Cu(OAc)_2$ in pyridine and ether at 50°C (8). Column chromatography of the

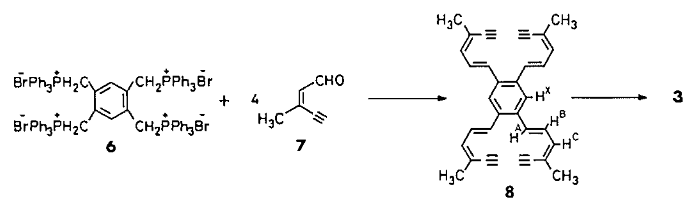

product, followed by preparative tlc gave unstable red crystals in 7% yield. The [1]Hmr spectrum of this monomeric cyclic product is illustrated in Fig. 1. We considered from the spectrum that the compound is the *m*-bridged derivative, **3**. However, to ascertain this, we attempted to prepare the related model compound, **13**.

The double Wittig reaction of 2 molar equivalents of **7** and 1 molar equivalent of *m*-bis(triphenylphosphoniomethyl)benzene dibromide, **9** (9), in DMF with ethanolic lithium ethoxide at 80°C yielded an acyclic stereoisomeric mixture in 57% yield, from which the *cis–cis* isomer, **10**, the *cis–trans* isomer, **11**, and the *trans–trans* isomer, **12**, were isolated; the structures were assigned to these compounds based on their spectral properties, mainly on [1]Hmr spectra. Oxidative coupling of each isomer was carried out as described for **8**.

[1]Author to whom correspondence may be addressed.

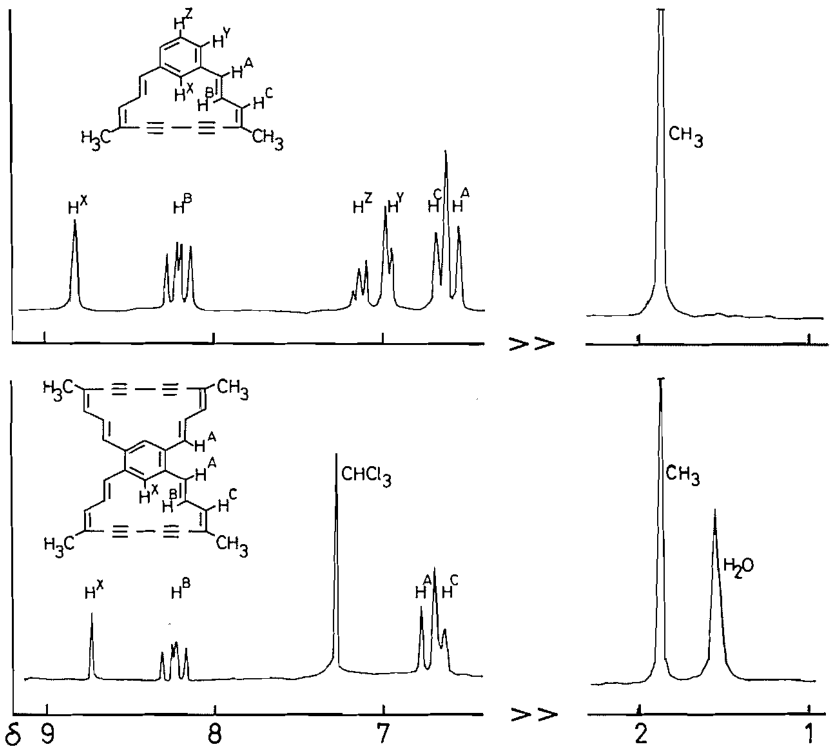

FIG. 1. Varian XL-200 [1]Hmr spectra of 3 and 13.

Although the di-*cis* isomer, **10**, gave no monomeric cyclic compound, both the mono-*cis*, **11**, and the di-*trans* isomer, **12**, gave the desired cyclic compound, **13**, in 3% and 23% yield, respectively; **13** was isolated as stable orange crystals and its [1]Hmr spectrum is also illustrated in Fig. 1. Variable-temperature [1]Hmr spectra of **13** were run at 90 MHz over the range −60 to 60°C, and the results show the spectra of **13** to be essentially temperature independent, excluding any conformational change of **13** between these temperatures. As is seen from Fig. 1, the spectra of both **3** and **13** are quite similar,

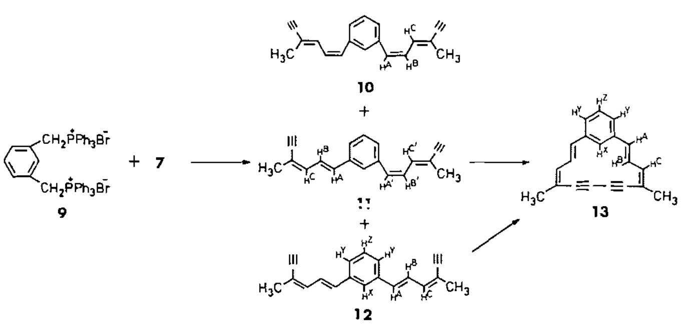

except that the H^A proton of **3** resonates at a lower field by 0.16 ppm (see Fig. 1 and Experimental) than the H^A proton of **13**, probably due to a steric compression effect between H^A and H^A protons of two large-membered rings in **3**. Thus it was confirmed that the cyclic compound from **8** has not the structure of **2**, but of **3**.

The Wittig reaction between **6** and (2*E*,4*Z*)-5-methylhepta-2,4-dien-6-ynal (10), a vinylogue of the above described aldehyde, **7**, was also attempted, but all attempts were unsuccessful.

In addition, the tetrabromide, **14**, was prepared to obtain the phenanthrene analogue corresponding to **2**. The reaction of 1,2,3,4-tetra(bromomethyl)benzene (11) with 4 molar equivalents of triphenylphosphine under reflux in acetylacetone afforded 1,2,3,4-tetrakis(triphenylphosphoniomethyl)benzene tetrabromide, **14**, in 91% yield as white crystals. The Wittig reaction between **7** and **14** under the conditions described for that between **6** and **7** was, however, unsuccessful.

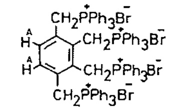

14

II. *Formation of tetrabenzannelated tricyclic compound, 5*

As described in I, it was found that the intramolecular oxidative coupling of **8** gives **3**, but not **2**. This suggested that the product from the corresponding tetrabenzannelated derivative of **8** might also be the *m*-bridged derivative, **5**, and not the *o*-bridged derivative, **4**, as we had previously reported (5).

The Wittig reaction of **6** with 4 molar equivalents of *o*-ethynylbenzaldehyde, **15** (12), yielded an acyclic stereoisomeric mixture in 27% yield, from which the all-*trans* isomer, **16**, was isolated in 6% yield as yellow crystals after chromatographic purification. The structural assignment of **16** was based on its [1]Hmr spectrum as well as elemental analysis.[2] Oxidative coupling of **16** yielded yellow crystals of **5** after

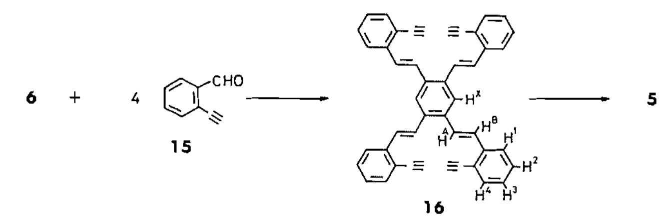

[2]In the previous study (ref. 5), we could not obtain a satisfactory elemental analysis for **16**.

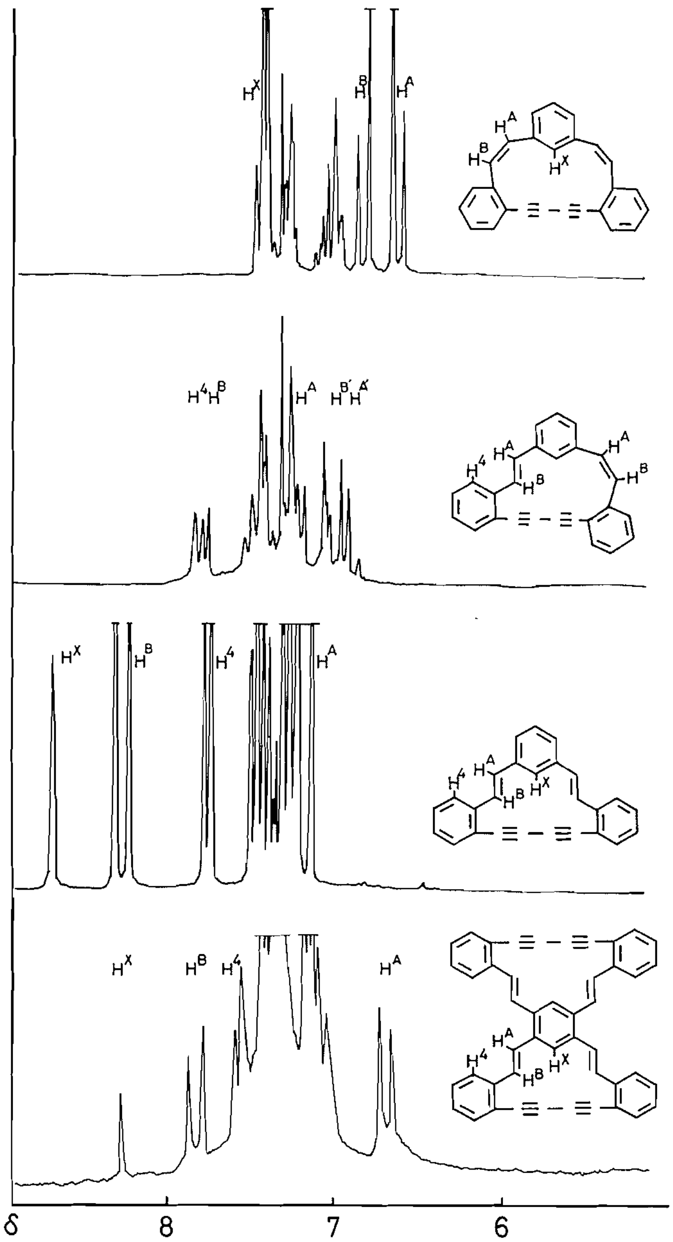

FIG. 2. Varian XL-200 ^{1}Hmr spectra of **5**, **27**, **28**, and **29**.

considerable chromatography. Its ^{1}Hmr spectrum is shown in Fig. 2. As described for the structural determination of **3**, we prepared the model compounds to determine whether structure **4** or **5** should be assigned to this product.

Firstly, the related *o*-bridged derivatives were prepared as illustrated in Scheme 1. The double Wittig reaction of 2 molar equivalents of **15** (12) and 1 molar equivalent of *o*-bis(triphenylphosphoniomethyl)benzene dibromide, **17** (13), in DMF with ethanolic lithium ethoxide at 80°C yielded an acyclic stereoisomeric mixture in 34% yield, from which the *cis–cis* isomer, **18**, the *cis–trans* isomer, **19**, and the *trans–trans* isomer, **20**, were isolated in a ratio 3:2:1 after chromatography.[3] Unexpectedly, the *trans–trans* isomer, **20**, was obtained in the smallest amount. Oxidative coupling of each isomer was performed as before. The acyclic di-*cis* isomer, **18**, gave the cyclic di-*cis*, **21**, and mono-*cis* isomer, **22**, and the acyclic mono-*cis* isomer, **19**, gave all of the three possible isomers, **21–23**. The acyclic di-*trans* isomer, **20**, gave the cyclic mono-*cis*, **22**, and di-*trans* isomer, **23**. Thus a configurational change of the double bond occurred during coupling reactions. A similar change has been observed in the formation of annulenones (14). By inspection of molecular models, the three fused benzene rings cannot lie in the same plane in the di-*cis*, **21**, and mono-*cis* isomer, **22**, but can do so in the di-*trans* isomer, **23**. This is reflected by the colours of their crystals.[3] The cyclic di-*cis*, **21**, is colourless, the mono-*cis* isomer, **22**, pale yellow, and the di-*trans* isomer, **23**, yellow.

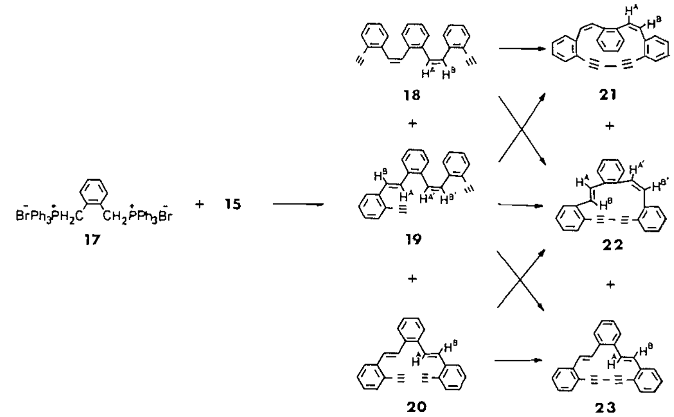

SCHEME 1

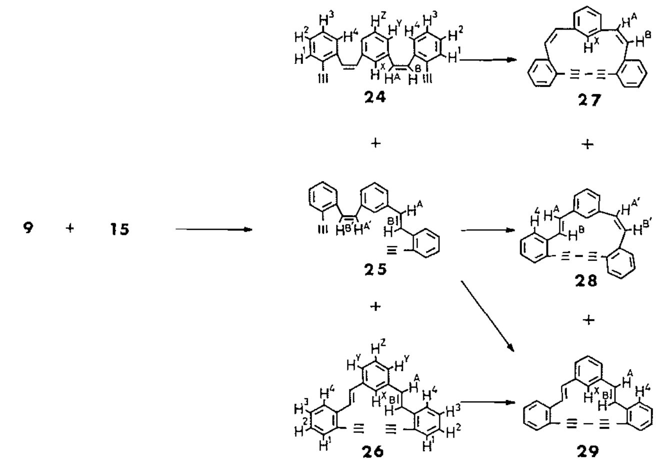

SCHEME 2

The *m*-bridged derivatives **27–29** were prepared as shown in Scheme 2. The double Wittig reaction of 2 molar equivalents of **15** (12) and 1 molar equivalent of **9** (9) gave an acyclic stereoisomeric mixture in 80% yield, from which the *cis–cis* isomer, **24**, the *cis–trans* isomer, **25**, and the *trans–trans* isomer, **26**, were isolated in a ratio of ca. 3:4:1. Again the di-*trans* isomer, **26**, was obtained in the smallest amount. Oxidative coupling of each isomer was performed as before. The acyclic di-*cis* isomer, **24**, afforded only the cyclic di-*cis* isomer, **27**, and the mono-*cis* isomer, **25**, gave the cyclic mono-*cis*, **28**, and di-*trans* isomer, **29**. The di-*trans* isomer, **26**, gave only the cyclic di-*trans* isomer, **29**.

The ^{1}Hmr spectra of the three isomers of *o*-bridged **21–23** (tribenz[14]annulene series) are illustrated in Fig. 3. As is seen

[3]In the previous study (ref. 12), we could not separate the three possible isomers completely in both the acyclic and the cyclic compounds in this system. Therefore the acyclic and cyclic di-*trans* isomers reported in ref. 12 are in error.

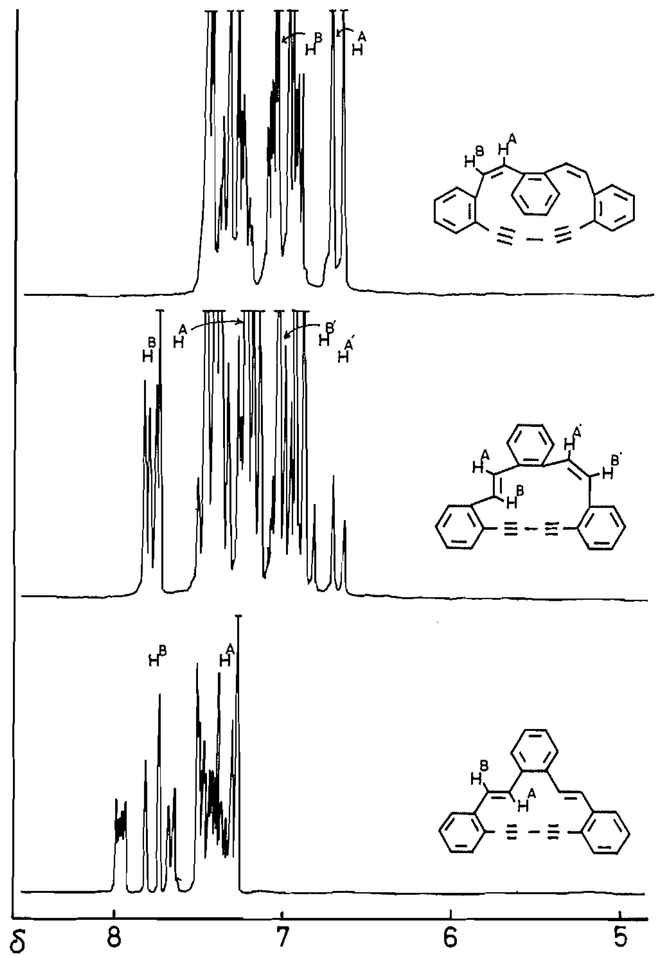

FIG. 3. Varian XL-200 ^{1}Hmr spectra of **21**, **22**, and **23**.

from Fig. 3, the resonances of the olefinic and benzenoid protons of the di-*cis*, **21**, and the mono-*cis* isomer, **22**, are at a higher field than 7δ, while the resonances of the protons of the di-*trans* isomer, **23**, are below 7δ. A similar observation is made in the ^{1}Hmr spectra of *m*-bridged model compounds, **27**–**29**, which are illustrated in Fig. 2. However, as is seen from the spectrum of the di-*trans* isomer, **29**, it is noted that the inner H^X and H^B protons of **29** resonate at considerably lower field than any proton of the other isomers, **21**–**23** and **27**–**28**.

As is shown in Fig. 2, the spectrum of the product from **16** has two doublets with the $J_{A,B}$ value of 16 Hz, indicating a *trans*–*trans* relationship of the H^A and H^B double bond, and, of the models, is most similar to that of the *m*-bridged di-*trans* isomer, **29**. This indicates that the product from **16** has the *m*-bridged structure, **5**, and not the *o*-bridged structure, **4**.

Thus it is a puzzle that neither **8** nor **16** gives an *o*-bridged tricyclic derivative.

Experimental

All melting points were determined on a hot stage apparatus and are uncorrected. The ir spectra were recorded on a Hitachi 260-50 spectrophotometer; only significant maxima are described. The uv spectra were measured for solutions in THF and run on a Hitachi 220-A spectrophotometer. Mass spectra were recorded with a JEOL JMS-200 spectrometer operating at 75 eV using a direct-inlet system, and the field desorption spectra were taken with a JEOL-OI-FG2 spectrometer. The ^{1}Hmr spectra were determined in $CDCl_3$ (unless otherwise stated) on a Varian EM-390 (90 MHz) or FX-90Q (90 MHz) or a Varian XL-200 (200 MHz) spectrometer using tetramethylsilane as internal standard. Merck alumina (activity II–III) was used for column chromatography and preparative thin-layer chromatography was carried out on 20 × 20 cm alumina plates (Merck, 0.5 or 2 mm thick). The progress of most reactions was followed by thin-layer chromatography using Merck precoated alumina. All evaporations were carried out under reduced pressure on a rotary evaporator below ca. 35°C. Extracts were dried with anhydrous sodium sulphate prior to solvent removal.

*1,2,4,5-Tetrakis[(1*E*,3*Z*)-4-methylhexa-1,3-dien-5-ynyl]benzene, 8*

To a stirred suspension of 1,2,4,5-tetrakis(triphenylphosphoniomethyl)benzene tetrabromide, **6** (6) (12.0 g, 8.0 mmol), in dry THF (60 mL) was added a solution of *n*-butyl lithium (19.4 mL, 1.85 *M*, 36 mmol) in hexane by a syringe over 10 min at −55 to −50°C under a nitrogen atmosphere. Then a solution of (2*Z*)-3-methyl-2-penten-4-ynal, **7** (7) (3.00 g, 36 mmol), in dry THF (13 mL) was added dropwise over 40 min at the same temperature. After stirring for a further 2.5 h at the same temperature, the temperature of the mixture was allowed to rise to room temperature and it was stirred for 1 h. After addition of ethyl acetate (16 mL), the mixture was poured into water and was extracted with benzene. The extracts were washed with brine, dried, and evaporated. The residual semi-solid was filtered through a short column of alumina (3.7 × 4 cm) and eluted with ether. The eluate, after solvent removal, was chromatographed on alumina (4 × 15 cm). The fractions eluted with hexane–ether (4:1) were collected and evaporated to give the desired compound, **8** (444 mg, 12.7%), as a solid. Recrystallization from hexane–benzene afforded yellow needles, mp 118°C (dec.); ir (KBr): 3290 (—C≡CH), 2090 (—C≡C—), and 965 (*trans* HC=CH) cm^{-1}; uv$_{max}$: 243 (25 000), 261 sh (21 800), 271 sh (17 100), 360 (49 000), 380 (48 100), and 404 nm sh (35 600); ^{1}Hmr (200 MHz) δ: 7.66 (s, 2H, H^X), 7.18 (dd, J = 15.5 and 11 Hz, 4H, H^B), 6.87 (d, J = 15.5 Hz, 4H, H^A), 6.51 (d, J = 11 Hz, 4H, H^C), 3.34 (s, 4H, —C≡CH), and 2.01 (s, 12H, CH_3); ms (field desorption method) *m/e*: 438, mol. wt. 438.5; *Anal.* calcd for $C_{34}H_{30}$: C 93.11, H 6.89; found: C 92.85, H 6.80.

The runs employing lithium ethoxide in DMF at 80°C or phenyllithium in THF at room temperature gave none of the desired product.

*1,3:4,6-Bis[(1*E*,3*Z*,9*Z*,11*E*)-4,9-dimethyldodeca-1,3,9,11-tetraene-5,7-diyne-1,12-diyl]benzene, 3*

A solution of **8** (2.80 g, 6.40 mmol) in pyridine (100 mL) and dry ether (33 mL) was added dropwise to a stirred solution of anhydrous $Cu(OAc)_2$ (15.9 g) in pyridine (556 mL) and dry ether (185 mL) over 5 h at 51–55°C. After stirring for 1 h at 50°C, the mixture was chilled and filtered through Hyflo Super-Cel. The precipitates formed were washed with benzene (100 mL × 3), and the filtrate was poured into water. The organic layer, combined with the benzene extracts from the aqueous layer, was washed successively with 5% HCl until it turned acidic, then with aqueous $NaHCO_3$ solution, and dried. The residual dark red liquid, after solvent removal, was chromatographed on alumina (3 × 22 cm). The fractions eluted with hexane–ether (4:1–2:3) were collected and evaporated to afford a red liquid, which was again chromatographed on alumina (3 × 22 cm). The fractions eluted with hexane–ether (1:4) were collected and evaporated to afford a partly crystallized liquid, which was further purified by preparative thin-layer chromatography. The fast-moving orange band gave the cyclic compound, **3** (193 mg, 6.95%), as a solid. It formed red microcrystals from benzene, mp 196–197°C (dec.); ir (KBr): 2160 (—C≡C—) and 960 (*trans* HC=CH) cm^{-1}; uv$_{max}$: 241 (34 300), 296 (58 800), 362 (55 400), and 421 nm sh (28 400); ^{1}Hmr (200 MHz) δ: 8.74 (s, 2H, H^X), 8.25 (dd, J = 16 and 12 Hz, 4H, H^B), 6.75 (d, J = 16 Hz, 4H, H^A), 6.68 (d, J = 12 Hz, 4H, H^C), and 1.89 (s, 12H, CH_3); see also Fig. 1; ms *m/e*: 434.2040 (M^+); calcd.: 434.2035. *Anal.* calcd. for $C_{34}H_{26}$: C 93.97, H 6.03; found: C 92.93, H 5.96. Attempts to improve the elemental analysis failed.

*The isomeric 1,3-bis(4-methylhexa-1,3-diene-5-ynyl)benzene, **10**, **11**, **12***

Lithium ethoxide prepared from lithium (740 mg, 0.106 g-atom) in absolute ethanol (280 mL) was added dropwise to a stirred solution of *m*-bis(triphenylphosphoniomethyl)benzene dibromide, **9** (9) (41.8 g, 53.0 mmol), and (2*Z*)-3-methyl-2-penten-4-ynal, **7** (7) (10.0 g, 0.106 mmol), in DMF (800 mL) over 1.5 h at 80°C under a nitrogen atmosphere. The solution was stirred for a further 0.5 h at 80°C. After being cooled, the solution was poured into water and extracted with benzene. The combined extracts were washed with brine and dried. The residual dark brown liquid, after solvent removal, was passed through a short column of alumina (4 × 9 cm). The fractions eluted with hexane–ether (1:1) were collected and evaporated to give a red liquid, which was chromatographed on alumina (4.5 × 20 cm). The initial fractions eluted with hexane were collected and evaporated to afford the *cis–cis* isomer, **10** (3.09 g, 22.5%), as a pale yellow liquid; ir (neat): 3290 (—C≡CH), 2090 (—C≡C—), and 700 (*cis* HC=CH) cm^{-1}; uv_{max}: 223 (9610), 235 (9390), and 303 nm (42 200); ^{1}Hmr (200 MHz) δ 7.34–7.16 (m, 4H, Ar-H), 6.77 (dd, J = 11 and 9.5 Hz, 2H, H^B), 6.69 (d, J = 11 Hz, 2H, H^A), 6.47 (d, J = 9.5 Hz, 2H, H^C), 3.33 (s, 2H, —C≡CH), and 1.93 (s, 6H, CH_3); ms m/e: 258 (relative intensity, M^+, 49%) and 228 (100), mol. wt. 258.3. *Anal.* calcd. for $C_{20}H_{18}$: C 92.98, H 7.02; found: C 93.23, H 7.24.

The following fractions eluted with 5–10% ether in hexane afforded the *cis–trans* isomer, **11** (1.68 g, 12.3%), as a yellow liquid. Crystallization from hexane afforded pale yellow needles, mp 41–42°C; ir (KBr): 3280 (—C≡CH), 2090 (—C≡C—), 965 (*trans* HC=CH), and 680 (*cis* HC=CH) cm^{-1}; uv_{max}: 226 (11 700), 236 sh (10 700), 305 sh (43 600), 316 (45 200), and 333 nm sh (29 300); ^{1}Hmr (200 MHz) δ: 7.36–7.20 (m, 4H, Ar-H), 7.26 (dd, J = 16 and 11 Hz, 1H, H^B), 6.79 (dd, J = 11 and 9.5 Hz, 1H, $H^{B'}$), 6.71 (d, J = 11 Hz, 1H, $H^{A'}$), 6.57 (d, J = 16 Hz, 1H, H^A), 6.50 (d, J = 9.5 Hz, 1H, $H^{C'}$), 6.43 (d, J = 11 Hz, 1H, H^C), 3.38 (s, 1H, —C≡CH), 3.36 (s, 1H, —C≡CH), and 1.96 (s, 6H, CH_3); ms m/e: 258 (M^+, 60%) and 228 (100), mol. wt. 258.3. *Anal.* calcd. for $C_{20}H_{18}$: C 92.98, H 7.02; found: C 93.22, H 6.89.

The later fractions, eluted with 15–40% ether in hexane, afforded the *trans–trans* isomer, **12** (3.05 g, 22.3%), as a solid. It formed yellow needles from hexane–benzene, mp 131–132°C; ir (KBr): 3280 (—C≡CH), 2090 (—C≡C—), 985, and 970 (*trans* HC=CH) cm^{-1}; uv_{max}: 228 (11 900), 234 sh (11 500), 306 sh (42 900), 319 (49 100), and 334 nm (39 200); ^{1}Hmr (200 MHz) δ: 7.44 (s, 1H, H^X), 7.38–7.25 (m, 3H, H^Y and H^Z), 7.25 (dd, J = 15.5 and 11 Hz, 2H, H^B), 6.58 (d, J = 15.5 Hz, 2H, H^A), 6.45 (d, J = 11 Hz, 2H, H^C), 3.35 (s, 2H, —C≡CH), and 1.97 (s, 6H, CH_3); ms m/e: 258 (M^+, 51%) and 228 (100), mol. wt. 258.3. *Anal.* calcd. for $C_{20}H_{18}$: C 92.98, H 7.02; found: C 93.23, H 6.96.

1,3-[(1E,3Z,9Z,11E)-4,9-Dimethyldodeca-1,3,9,11-tetraene-5,7-diyne-1,12-diyl]benzene, **13**

A solution of the acyclic di-*trans* isomer, **12** (2.57 g, 9.95 mmol), in pyridine – dry ether (3:1, 216 mL) was added dropwise over 4.5 h to a stirred solution of anhydrous $Cu(OAc)_2$ (12.2 g) in pyridine – dry ether (3:1, 468 mL) at 51–52°C. After stirring for 1 h at 51°C, the reaction was cooled to room temperature. After work-up as in the preparation of **3**, the residual dark brown liquid, after solvent removal, was chromatographed on alumina (5.7 × 14 cm). The fractions eluted with 5–10% ether in hexane were collected and evaporated to afford the desired cyclic compound, **13** (0.576 g, 22.6%), as a solid. It formed orange needles, mp 161–162°C; ir (KBr): 2160 (—C≡C—), and 965 (*trans* HC=CH) cm^{-1}; uv_{max}: 217 (13 900), 253 sh (14 300), 264 sh (18 400), 278 (25 400), and 306 nm (36 600); ^{1}Hmr (200 MHz) δ: 8.82 (s, 1H, H^X), 8.21 (dd, J = 16 and 12 Hz, 2H, H^B), 7.14 (t, J = 8 Hz, 1H, H^Z), 6.97 (d, J = 8 Hz, 2H, H^Y), 6.66 (d, J = 12 Hz, 1H, H^C), 6.60 (d, J = 16 Hz, 2H, H^A), and 1.88 (s, 6H, CH_3); see also Fig. 1; ms m/e: 256 (M^+, 47%) and 239 (100), mol. wt. 256.3. *Anal.* calcd. for $C_{20}H_{16}$: C 93.71, H 6.29; found: C 93.91, H 6.44.

The di-*cis* isomer, **10** (882 mg, 3.41 mmol), was also oxidatively coupled under the exactly same conditions as described for **12**, but none of monomeric cyclic product could be obtained.

The mono-*cis* isomer, **11** (730 mg, 2.82 mmol), was oxidatively coupled under the same conditions as for **12**, and only the cyclic di-*trans* isomer, **13** (17.9 mg, 3.0%), was obtained.

1,2,3,4-Tetrakis(triphenylphosphoniomethyl)benzene tetrabromide, **14**

A mixture of 1,2,3,4-tetra(bromomethyl)benzene (11) (35.8 g, 79.5 mmol) and triphenylphosphine (85.9 g, 0.327 mol) in 2,4-pentadione (240 mL) was heated under reflux for 1 h. A white, crystalline solid began to separate after 20–30 min. The mixture was allowed to cool to room temperature. The solid was collected and washed with ether to give the first crop of the desired product. The filtrate was diluted with ether and the solid formed was separated by filtration, washed with ether, and combined with the first crop to give a total of 110 g (90.7%) of tetraphosphonium salt, **14**. Recrystallization from absolute ethanol with decolourizing charcoal afforded white microcrystals, mp 307–308°C; ^{1}Hmr (90 MHz, CF_3COOD) δ: ca. 8.2–7.4 (m, 60H, Ar-H), 7.02 (d, J = 2 Hz, 2H, H^A), and 4.97–4.12 (m, 8H, —CH_2—). *Anal.* calcd. for $C_{82}H_{70}P_4Br_4$: C 65.67, H 4.71; found: C 65.35, H 4.82.

The reaction of **7** and **14** as well as that of **6** and (2*E*,4*Z*)-5-methylhepta-2,4-dien-6-ynal (10) was carried out under the same conditions as described for the reaction between **6** and **7**. However, all attempts were unsuccessful.

1,2,4,5-Tetra[(Z)-2(2-ethynylphenyl)ethenyl]benzene, **16**

Lithium ethoxide prepared from lithium (640 mg, 0.0922 g-atom) in absolute ethanol (240 mL) was added dropwise with stirring under a nitrogen atmosphere at 82–83°C over 3.5 h to *o*-ethynylbenzaldehyde, **15**, (12) (12.0 g, 0.0922 mmol), and 1,2,4,5-tetrakis-(triphenylphosphoniomethyl)benzene tetrabromide, **6** (6) (34.5 g, 0.0230 mmol), in DMF (950 mL). After completion of addition, the mixture was stirred at the same temperature for 1 h. After work-up as in the preparation of **12**, the dark brown semi-solid, after solvent removal, was passed through a short column of alumina (4 × 7.5 cm) and was eluted with ether. A red liquid, obtained on evaporation, was chromatographed on alumina (4 × 12.5 cm). The fractions eluted with 5–30% ether in hexane afforded, on evaporation, the acyclic stereoisomeric mixture (3.60 g, 26.9%) as a semi-solid, which was purified by preparative thin-layer chromatography. The fast-moving yellow band gave the desired all-*trans* isomer, **16** (0.801 g, 6.0%), as a solid. It formed yellow needles from benzene, mp 204°C (dec.); ir (KBr): 3290, 3280 (—C≡CH), 2110 (—C≡C—), and 960 (*trans* HC=CH) cm^{-1}; uv_{max}: 226 (51 800), 240 sh (46 700), 254 sh (40 900), 343 (58 300), and 377 nm sh (44 300); ^{1}Hmr (200 MHz) δ: 7.90 (s, 2H, H^X), 7.77 (d, J = 7.5 Hz, 4H, H^1), 7.67 (d, J = 16 Hz, 4H, H^A or H^B), 7.58 (d, J = 16 Hz, 4H, H^A or H^B), 7.56 (d, J = 7.5 Hz, 4H, H^4), 7.40 (t, J = 7.5 Hz, 4H, H^2), 7.26 (t, J = 7.5 Hz, 4H, H^3), and 3.28 (s, 4H, —C≡CH); ms (field desorption method) m/e: 582 (M^+), mol. wt. 582.7. *Anal.* calcd. for $C_{46}H_{30}$: C 94.81, H 5.19; found: C 94.90, H 5.11.

1,3:4,6-Bis[(1E,11E)-3,4:9,10-dibenzdodeca-1,11-diene-5,7-diyne-1,12-diyl]benzene, **5**

A solution of the acyclic all-*trans* isomer, **15** (898 mg, 1.54 mmol), in pyridine – dry ether (3:1, 34 mL) was added dropwise over 3 h to a stirred solution of anhydrous $Cu(OAc)_2$ (3.8 g) in pyridine – dry ether (3:1, 146 mL) at 50°C, and the solution was stirred for a further 1 h at the same temperature. After work-up as in the preparation of **13**, the residual brown liquid, after solvent removal, was chromatographed on alumina (3.7 × 9.0 cm). The fractions eluted with hexane–benzene (2:3) gave a yellow solid on evaporation. The solid was further purified by thin-layer chromatography. The fast-moving yellow band was collected and, on evaporation, afforded the monomeric cyclic compound, **5** (125 mg, 14%). Recrystallization from benzene afforded yellow cubes, mp 208–210°C (dec.); ir (KBr): 2200 (—C≡C—) and 970 (*trans* HC=CH) cm^{-1}; uv_{max}: 262 sh (52 700), 302 (55 400), 328 sh (42 000), 363 sh (19 400), 400 sh (9300), and 452 nm sh (2300); ^{1}Hmr (200 MHz) δ: 8.26 (s, 2H, H^X), 7.82 (d, J = 16 Hz, 4H, H^B), 7.56 (d, J = 8 Hz, 4H, H^1), 7.42–7.04 (m, 12H, H^2, H^3, and H^4), and 6.68 (d, J = 16 Hz, 4H, H^A); see also Fig. 2; ms m/e: 578 (M^+, 100%), mol. wt. 578.6. *Anal.* calcd. for

$C_{46}H_{26}$: C 95.27, H 4.53; found: C 95.47, H 4.77.

The isomeric 1,2-bis[2-(2-ethynylphenyl)ethenyl]benzene, ***18, 19, 20***

Lithium ethoxide prepared from lithium (323 mg, 0.046 g-atom) in absolute ethanol (120 mL) was added dropwise to a stirred solution of *o*-ethynylbenzaldehyde, **15** (12) (6.00 g, 0.046 mol), and 1,2-bis-(triphenylphosphoniomethyl)benzene dibromide, **17** (13) (18.6 g, 0.023 mol), in DMF (460 mL) over 1 h at 80–85°C under a nitrogen atmosphere. After completion of addition, the solution was stirred for a further 2 h at 85°C. After work-up as in the preparation of **12**, the residual dark brown liquid, after solvent removal, was passed through a short column of alumina (3.7 × 5 cm). The fractions eluted with ether were collected and on evaporation gave a red liquid, which was chromatographed on alumina (3.7 × 17 cm). The early fractions eluted with 20–30% ether in hexane afforded the *cis–cis* isomer, **18** (1.39 g, 17.6%), as a liquid. Crystallization from hexane–benzene afforded white needles, mp 92–93°C; ir (KBr): 3290 (—C≡CH), 2110 (—C≡C—), and 680 (*cis* HC=CH) cm^{-1}; uv_{max}: 218 (39 000), 249 sh (23 300), and 286 nm (17 800); ^{1}Hmr (90 MHz) δ: 7.53–7.43 (m, 2H, Ar-H), 7.16–6.89 (m, 10H, Ar-H), 6.96 (d, J = 12 Hz, 2H, H^B), 6.74 (d, J = 12 Hz, 2H, H^A), and 3.33 (s, 2H, —C≡CH); ms m/e: 330 (M^+, 100%), mol. wt. 330.4. *Anal.* calcd. for $C_{26}H_{18}$: C 94.51, H 5.49; found: C 94.68, H 5.39.

The following fractions eluted with 40–50% ether in hexane afforded the *cis–trans* isomer, **19** (0.890 g, 11.7%), as a pale yellow liquid; ir (neat): 3290 (—C≡CH), 2100 (—C≡C—), 965 (*trans* HC=CH), and 675 (*cis* HC=CH) cm^{-1}; uv_{max}: 220 (40 300), 250 (29 700), 295 (23 600), and 314 nm (23 700); ^{1}Hmr (90 MHz) δ: 7.43 (d, J = 16 Hz, 1H, H^B), 7.16 (d, J = 16 Hz, 1H, H^A), 7.70–6.95 (m, 12H, Ar-H), 6.95 (d, J = 12 Hz, 1H, $H^{B'}$), 6.74 (d, J = 12 Hz, 1H, $H^{A'}$), 3.34 (s, 1H, —C≡CH), and 3.32 (s, 1H, —C≡CH); ms m/e: 330 (M^+, 100%), mol. wt. 330.4. *Anal.* calcd. for $C_{26}H_{18}$: C 94.51, H 5.49; found: C 94.28, H 5.60.

The later fractions eluted with hexane–ether (2:3) – ether afforded the *trans–trans* isomer, **20** (0.382 g, 5.0%), as a solid. Recrystallization from hexane–benzene afforded white needles, mp 70–71°C; ir (KBr): 3300, 3290 (—C≡CH), 2100 (—C≡C—), 975, 970, and 960 (*trans* HC=CH) cm^{-1}; uv_{max}: 220 (37 600), 233 sh (32 400), 251 (32 100), 292 (29 100), and 326 nm (26 400); ^{1}Hmr (90 MHz) δ: 7.45 (d, J = 16 Hz, 2H, H^B), 7.19 (d, J = 16 Hz, 2H, H^A), 7.74–6.90 (m, 12H, Ar-H), and 3.24 (s, 2H, —C≡CH); ms m/e: 330 (M^+, 100%), mol. wt. 330.4; *Anal.* calcd. for $C_{26}H_{18}$: C 94.51, H 5.49; found: C 94.73, H 5.35.

*The isomeric 1,2-bis(3,4:9,10-dibenzdodeca-1,11-diene-5,7-diyne-1,12-diyl)benzene (tribenz[*a,e,i*]-11,13-bisdehydro[14]annulene),* ***21, 22, 23***

A solution of the acyclic di-*cis* isomer, **18** (0.995 mg, 3.01 mmol), in pyridine – dry ether (3:1, 66 mL) was added dropwise over 3 h to a stirred solution of anhydrous $Cu(OAc)_2$ (3.7 g) in pyridine – dry ether (3:1, 144 mL) at 51–53°C. The solution was stirred for 1 h at the same temperature. After work-up as in the preparation of **13**, the residual red liquid, after solvent removal, was chromatographed on alumina (3.7 × 8.5 cm). The fractions eluted with 2% ether in hexane afforded the cyclic mono-*cis* isomer, **22** (0.175 g, 17.7%), as a solid. Recrystallization from hexane–benzene afforded pale yellow cubes, mp 118°C (dec.); ir (KBr): 2110 (—C≡C—), 990, 975, 970 (*trans* HC=CH), and 710 (*cis* HC=CH) cm^{-1}; uv_{max}: 228 sh (33 600), 260 (50 800), 282 sh (28 300), 297 (27 000), and 354 nm sh (6400); ^{1}Hmr (200 MHz) δ: 7.76 (d, J = 8 Hz, 2H, Ar-H), 7.76 (d, J = 16 Hz, 1H, H^B), 7.50–6.80 (m, 14H, H^A, $H^{B'}$, and Ar-H), and 6.68 (d, J = 12.5 Hz, 1H, $H^{A'}$); see also Fig. 3; ms m/e: 328 (M^+, 66%) and 327 (100), mol. wt. 328.3. *Anal.* calcd. for $C_{26}H_{16}$: C 95.09, H 4.91; found: C 95.30, H 4.98.

The later fractions, eluted wth 3% ether in hexane, gave the cyclic di-*cis* isomer, **21** (0.0220 g, 22.3%), as a solid. Recrystallization from hexane–benzene afforded colourless cubes, mp 215–216°C; ir (KBr): 2210 (—C≡C—) and 720 (*cis* HC=CH) cm^{-1}; uv_{max}: 237 (29 700), 258 (22 900), 290 (40 500), 328 (14 500), and 355 nm (12 900); ^{1}Hmr (200 MHz) δ: 7.47–6.89 (m, 12H, Ar-H), 6.99 (d, J = 12.5 Hz, 2H, H^B), and 6.67 (d, J = 12.5 Hz, 2H, H^A); see also Fig. 3; ms m/e: 328 (M^+, 50%) and 327 (100), mol. wt. 328.3. *Anal.* calcd. for $C_{26}H_{16}$: C 95.09, H 4.91; found: C 95.22, H 4.87.

An oxidative coupling of the acyclic mono-*cis* isomer, **19** (630 mg, 1.91 mmol), was carried out under exactly the same conditions as described for **18**. The residual yellow liquid, after solvent removal, was chromatographed on alumina (3.7 × 10 cm). The early fractions eluted with 4% ether in hexane gave the cyclic mono-*cis* isomer, **22** (227 mg, 36.2%). The fractions following, eluted with 5% ether in hexane, afforded the cyclic di-*cis* isomer, **21** (87.5 mg, 14%).

The later fractions, eluted with 20% ether in hexane, afforded the cyclic di-*trans* isomer, **23** (47 mg, 7.5%), as a solid. Recrystallization from hexane–benzene afforded yellow cubes, mp 214–215°C; ir (KBr): 2200 (—C≡C—), and 965 (*trans* HC=CH) cm^{-1}; uv_{max}: 227 (20 700), 263 (19 300), 281 sh (21 800), 308 (37 200), and 360 nm (7200); ^{1}Hmr (200 MHz) δ: 7.98–7.92 (m, 2H, Ar-H), 7.77 (d, J = 16 Hz, 2H, H^B), 7.66 (d, J = 7.5 Hz, 2H, Ar-H), 7.51–7.27 (m, 8H, Ar-H), and 7.14 (d, J = 16 Hz, H^A); see also Fig. 3; ms m/e: 328 (M^+, 73%) and 327 (100), mol. wt. 328.3. *Anal.* calcd. for $C_{26}H_{16}$: C 95.09, H 4.91; found: C 95.01, H 4.67.

An oxidative coupling of the acyclic di-*trans* isomer, **20** (380 mg, 1.15 mmol), was also carried out under exactly the same conditions as described for **18**. The residual brown semi-solid, after solvent removal, was chromatographed on alumina (3.7 × 8 cm). The fractions eluted with 2–3% ether in hexane afforded the cyclic mono-*cis* isomer, **22** (59.9 mg, 15.9%). The following fractions eluted with 10–20% ether in hexane afforded the cyclic di-*trans* isomer, **23** (166 mg, 43.8%).

The isomeric 1,3-bis[2-(2-ethynylphenyl)ethenyl]benzene, ***24, 25, 26***

Lithium ethoxide prepared from lithium (270 mg, 0.039 g-atom) in absolute ethanol (100 mL) was added dropwise to a stirred solution of *o*-ethynylbenzaldehyde, **15** (12) (5.00 g, 0.038 mmol), and 1,3-bis(triphenylphosphoniomethyl)benzene dibromide, **9** (9) (15.5 g, 0.020 mol), in DMF (380 mL) over 2 h at 80–85°C under a nitrogen atmosphere. After completion of addition, the mixture was stirred for a further 2 h at the same temperature. After work-up as in the preparation of **16**, the residual red liquid, after solvent removal, was passed through a short column of alumina (3.7 × 4 cm). The fractions eluted with ether were collected and on evaporation gave a red liquid, which was chromatographed on alumina (3.7 × 10 cm). The fractions eluted with 2–3% ether in hexane afforded the acyclic *cis–cis* isomer, **24** (1.81 g, 28.8%), as a yellow liquid; ir (neat): 3290 (—C≡CH), 2110 (—C≡C—), and 700 (*cis* HC=CH) cm^{-1}; uv_{max}: 227 (25 600), 256 sh (22 800), 278 (19 200), and 314 nm sh (10 500); ^{1}Hmr (200 MHz) δ: 7.52 (d, J = 8 Hz, 2H, H^4), 7.22–6.10 (m, 10H, H^1, H^2, H^3, H^X, H^Y, H^Z), 6.81 (d, J = 12 Hz, 2H, H^B), 6.58 (d, J = 12 Hz, 2H, H^A), and 3.28 (s, 2H, —C≡CH); ms m/e: 330.1394 (M^+); calcd.: 330.1382. *Anal.* calcd. for $C_{26}H_{18}$: C 94.51, H 5.49; found: C 93.55, H 5.36. Attempts to improve the elemental analysis failed.

The following fractions eluted with 5% ether in hexane afforded the acyclic *cis–trans* isomer, **25** (2.42 g, 38.6%), as a yellow liquid; ir (neat): 3290 (—C≡CH), 2110 (—C≡C—), 965 (*trans* HC=CH), and 700 (*cis* HC=CH) cm^{-1}; uv_{max}: 228 sh (18 300), 234 sh (18 500), 252 (19 700), 260 sh (17 300), 307 (22 800), 324 sh (19 200), and 341 nm sh (9500); ^{1}Hmr (200 MHz) δ: 7.67–7.15 (m, 13H, H^B and Ar-H), 7.05 (d, J = 16.5 Hz, 1H, H^A), 6.92 (d, J = 12 Hz, 1H, $H^{B'}$), 6.74 (d, J = 12 Hz, 1H, $H^{A'}$), 3.36 (s, 1H, —C≡CH), and 3.33 (s, 1H, —C≡CH); ms m/e: 330.1376 (M^+), calcd.: 330.1346. *Anal.* calcd. for $C_{26}H_{18}$: C 94.51, H 5.49; found: C 93.07, H 5.56. Attempts to improve the elemental analysis failed.

The later fractions, eluted with 8% ether, in hexane afforded the acyclic di-*trans* isomer, **26** (0.681 g, 10.9%), as a yellow liquid; ir (neat): 3300 (—C≡CH), 2120 (—C≡C—), and 970 (*trans* HC=CH) cm^{-1}; uv_{max}: 233 (18 700), 251 (24 600), 258 sh (21 500), 308 (36 500), 318 sh (35 900), and 340 nm sh (19 200); ^{1}Hmr (200 MHz) δ: 7.71 (d, J = 8.5 Hz, 2H, H^4), 7.71 (d, J = 16.5 Hz, 2H, H^B), 7.56–7.17 (m, 10H, H^1, H^2, H^3, H^X, H^Y, H^Z), 7.18 (d, J = 16.5 Hz, 1H, H^A), and 3.39 (s, 2H, —C≡CH); ms m/e:

330.1361 (M^+); calcd.: 330.1356; *Anal.* calcd. for $C_{26}H_{18}$: C 94.51, H 5.49; found: C 93.02, H 5.59. Attempts to improve the elemental analysis failed.

The isomeric 1,3-bis(3,4:9,10-dibenzdodeca-1,11-diene-5,7-diyne-1,12-diyl)benzene, 27, 28, 29

A solution of the acyclic di-*cis* isomer, **24** (2.03 g, 6.15 mmol), in pyridine – dry ether (3:1, 134 mL) was added dropwise over 3 h to a stirred solution of anhydrous $Cu(OAc)_2$ (7.1 g) in pyridine – dry ether (3:1, 290 mL) at 50°C; the mixture was stirred for a further 1 h at the same temperature. After work-up as in the preparation of **13**, the residual red liquid, after solvent removal, was chromatographed on alumina (3.7 × 9 cm). The fractions eluted with 5–20% ether in hexane afforded the cyclic di-*cis* isomer, **27** (566 mg, 28%), as a solid. Recrystallization from hexane–benzene afforded colourless cubes, mp 225–227°C; ir (KBr): 2210 (—C≡C—) and 695 (*cis* HC=CH) cm^{-1}; uv_{max}: 223 (39 100), 232 (38 400), 273 (34 600), 288 sh (30 100), 336 (13 500), and 358 nm (11 600); ^{1}Hmr (200 MHz) δ: 7.44 (s, 1H, H^X), 7.40–6.93 (m, 11H, Ar-H), 6.80 (d, J = 13 Hz, 2H, H^B), and 6.59 (d, J = 13 Hz, 2H, H^A); see also Fig. 2; ms m/e: 328 (M^+, 53%) and 327 (100), mol. wt. 328.3. *Anal.* calcd. for $C_{26}H_{16}$: C 95.09, H 4.91; found: C 95.29, H 4.64.

An oxidative coupling of the acyclic mono-*cis* isomer, **25** (702 mg, 2.12 mmol), was carried out under exactly the same conditions as described for **24**. The dark red liquid, after solvent removal, was chromatographed on alumina (3.7 × 7.0 cm). The fractions eluted with 3% ether in hexane afforded the cyclic di-*trans* isomer, **29** (146 mg, 20.9%), as a solid. Recrystallization from benzene afforded yellow needles, mp 239–240°C; ir (KBr): 2200 (—C≡C—), 970, and 960 (*trans* HC=CH) cm^{-1}; uv_{max}: 227 (30 500), 296 (75 400), 311 sh (62 100), and 372 nm sh (4140); ^{1}Hmr (200 MHz) δ: 8.65 (s, 1H, H^X), 8.24 (d, J = 16.5 Hz, 2H, H^B), 7.73 (d, J = 8 Hz, 2H, H^4), 7.48–7.20 (m, 9H, Ar-H), and 7.10 (d, J = 16.5 Hz, 2H, H^A); see also Fig. 2; ms m/e: 328 (M^+, 56%) and 327 (100), mol. wt. 328.3. *Anal.* calcd. for $C_{26}H_{16}$: C 95.09, H 4.91; found: C 94.94, H 4.74.

The later fractions, eluted with 5% ether in hexane, afforded the cyclic mono-*cis* isomer, **28** (70.5 mg, 10.1%), as a solid. Recrystallization from hexane–benzene afforded colourless cubes, mp 228°C (dec.); ir (KBr): 2200 (—C≡C—), 960 (*trans* HC=CH), and 700 (*cis* HC=CH) cm^{-1}; uv_{max}: 222 (33 500), 268 (25 800), 285 sh (30 500), 303 sh (40 400), and 310 nm (41 200); ^{1}Hmr (200 MHz) δ: 7.76 (d, J = 16 Hz, 1H, H^B), 7.75 (d, J = 8 Hz, 1H, H^4), 7.50–7.00 (m, 11H, Ar-H), 7.18 (d, J = 16 Hz, 1H, H^A), 6.96 (d, J = 12 Hz, 1H, $H^{B'}$), and 6.85 (d, J = 12 Hz, 1H, $H^{A'}$); see also Fig. 2; ms m/e: 328 (M^+, 63%) and 327 (100), mol. wt. 328.3. *Anal.* calcd. for $C_{26}H_{16}$: C 95.09, H 4.91; found: C 94.80, H 5.19.

An oxidative coupling of the acyclic di-*trans* isomer, **26** (610 mg, 1.85 mmol), was carried out under the same conditions as described for **24**. The residual brown semi-solid, after solvent removal, was chromatographed on alumina (3.7 × 8 cm). The fractions eluted with 10–50% ether in hexane afforded only the cyclic di-*trans* isomer, **29** (472 mg, 77.9%).

Acknowledgment

Financial support by a Grant-in-Aid for Scientific Research No. 554141 from the Ministry of Education, Science and Culture, is gratefully acknowledged.

1. R. T. WEAVERS and F. SONDHEIMER. Agnew. Chem. Int. Ed. Engl. **13**, 139 (1974); A. YASUHARA, M. IYODA, T. SATAKE, and M. NAKAGAWA. Tetrahedron Lett. 3931 (1975); R. H. MITCHELL, R. V. WILLIAMS, R. MAHADEVAN, Y-H. LAI, and T. W. DINGLE. J. Am. Chem. Soc. **104**, 2571 (1982).
2. M. NAKAGAWA. Angew. Chem. Int. Ed. Engl. **18**, 202 (1979).
3. R. H. MITCHELL. Isr. J. Chem. **20**, 594 (1980).
4. T. C. WALSGROVE and F. SONDHEIMER. Tetrahedron Lett. 2719 (1978).
5. J. OJIMA, M. ENKAKU, and C. UWAI. Bull. Chem. Soc. Jpn. **50**, 933 (1977).
6. C. A. DORNFELD and L. E. THIELEN. U. S. Patent No. 2,865,964 (December, 1958); Chem. Abstr. **53**, 8073 (1959).
7. J. OJIMA, T. KATAKAMI, G. NAKAMINAMI, and M. NAKAGAWA. Bull. Chem. Soc. Jpn. **49**, 292 (1976).
8. N. DARBY, T. M. CRESP, and F. SONDHEIMER. J. Org. Chem. **42**, 1960 (1977).
9. R. H. MITCHELL, B. N. CHOSE, and M. E. WILLIAMS. Can. J. Chem. **55**, 210 (1977).
10. J. OJIMA, M. KIRITA, Y. MUROSAWA, and T. NAKADA. Bull. Chem. Soc. Jpn. **56**, 1467 (1983).
11. J. T. STAPLER and J. BORNSTEIN. J. Heterocycl. Chem. **10**, 983 (1973).
12. J. OJIMA, T. YOKOMACHI, and A. KIMURA. Bull. Chem. Soc. Jpn. **49**, 2840 (1976).
13. C. E. GRIFFIN, K. R. MARTIN, and B. E. DOUGLAS. J. Org. Chem. **27**, 1627 (1962); C. E. GRIFFIN and J. A. PETERS. J. Org. Chem. **28**, 1715 (1965).
14. P. D. HOWES, E. LEGOFF, and F. SONDHEIMER. Tetrahedron Lett. 3695 (1972).

Influence of surface micellar head group neutralized in hexadecyltrimethylammonium bromide (CTAB) and hydroxide (CTAOH) on the dehydrochlorination of 1,1,1-trichloro-2,2-bis(*p*-chlorophenyl)ethane (DDT) and 1,1-dichloro-2,2-bis(*p*-chlorophenyl)ethane (DDD)

C. OTERO AND E. RODENAS[1]
Physical Chemistry Department, Alcalá de Henares University, Alcalá de Henares, Spain

Received November 19, 1984

C. OTERO and E. RODENAS. Can. J. Chem. **63**, 2892 (1985).

The basic dehydrohalogenation reactions of 1,1,1-trichloro-2,2-bis(*p*-chlorophenyl)ethane (DDT) and 1,1-dichloro-2,2-bis(*p*-chlorophenyl)ethane (DDD) have been studied in cationic micelles of hexadecyltrimethylammonium bromide (CTAB) and hexadecyltrimethylammonium hydroxide (CTAOH). Different theoretical approaches are discussed, considering the fraction of micellar head group neutralized, β, as a constant, or supposing different kinds of variation in its value. The following two empirical expressions for β have been found: $\beta = 0.8 + 0.5$ ([NaOH] + [KBr]) for DDT, and $\beta = 0.8 + 1$ ([NaOH] + [KBr]) for DDD, and this is the best way to explain the experimental results.

C. OTERO et E. RODENAS. Can. J. Chem. **63**, 2892 (1985).

Opérant dans des micelles cationiques de bromure d'hexadécyltriméthylammonium (CTAB) et d'hydroxyde d'hexadécyltriméthylammonium (CTAOH), on a étudié la réaction de déshydrohalogénation basique du trichloro-1,1,1 bis(*p*-chlorophényl)-2,2 éthane, le DDT, et du dichloro-1,1 bis(*p*-chlorophényl)-2,2 éthane, le DDD. On discute de diverses approches théoriques en considérant la fraction du groupe micellaire neutralisé, β, comme étant égale à une constante ou en faisant diverses hypothèses relativement à sa variation. On a trouvé que les valeurs de β peuvent être exprimées par les expressions empiriques suivantes: $\beta = 0{,}8 + 0{,}5$ ([NaOH] + [KBr]) pour le DDT et $\beta = 0{,}8 + 1$ ([NaOH] + [KBr]) pour DDD; ceci correspond à la meilleure façon d'expliquer les résultats expérimentaux.

[Traduit par le journal]

Introduction

Reactions between a hydrophobic organic substrate and ions in solution are too much affected by micellar systems (1–3). Rate acceleration (4) or inhibition (5) arises from different rates of reactions of the substrates in the micellar phase and in the bulk solution, and from the distribution of the substrate between these two phases. Most of the kinetic results can be explained with the pseudophase kinetic model proposed by Menger and Portnoy (6) and developed by Bunton (7) and Romsted (8), with the restriction of considering the fraction of micellar head group neutralized, β, as a constant independent of ion and surfactant concentration, although there is strong evidence showing that addition of counterions in solution increases β, and to consider it a constant is only an approximation (9, 10). The results in the literature at high concentration of ions in solution or when the reactive ion is too hydrophilic (11) cannot be explained by means of this model, in which it is necessary to make modifications (5, 12, 13) in order to explain the experimental results.

In this paper we have studied the basic dehydrohalogenation of 1,1,1-trichloro-2,2-bis(*p*-chlorophenyl)ethane (DDT) and 1,1-dichloro-2,2-bis(*p*-chlorophenyl)ethane) (DDD) in cationic micelles of hexadecyltrimethylammonium bromide (CTAB) and hexadecyltrimethylammonium hydroxide (CTAOH). These reactions have very important biological implications (14), since micelles have also been used as single membrane models (15, 16), but also because these non-charged hydrophobic substrates are very appropriate in discussing the validity of different theoretical models in order to explain the experimental values. These reactions were first studied by Nome and co-workers in CTAB (17) and, currently, in CTAOH (18), and they found that the simple pseudophase kinetic model considering β as a constant cannot explain the results at high ion concentration.

[1] Author to whom correspondence may be addressed.

In this paper we discuss the validity of a model that considers independent distribution equilibria of ions between aqueous and micellar phases in which β varies with surfactant and ion concentrations. This model has been used, with success, to explain the basic hydrolysis of acetylsalicylate ester and homologs (19).

Theoretical description of the pseudophase kinetic model

The pseudophase kinetic model (6–8) considers the micelle as a different phase from the aqueous phase, the reaction occurring in both phases according to Scheme 1:

$$\begin{tikzcd} S_W + Dn \arrow[rr, shift left, "K_S"] \arrow[dr, "k'_W"'] & & S_M \arrow[ll, shift left] \arrow[dl, "k'_M"] \\ & \text{Products} & \end{tikzcd}$$

SCHEME 1

where the subscripts M and W denote the micellar and aqueous phases respectively, S is the substrate, Dn the micellized surfactant whose concentration is given by [Dn] = [D] − cmc, cmc is the critical micelle concentration, and K_S the binding constant of the substrate to the micelle written in terms of micellized surfactant:

$$[1] \quad K_S = \frac{[S_M]}{[S_W][Dn]}$$

k'_W and k_M are the pseudo-first-order rate constants in aqueous and micellar pseudophases respectively, given by

$$[2] \quad \begin{aligned} k'_W &= k_W\,[OH^-_W] \\ k'_M &= k_M\,[OH^-_M]/[Dn] \end{aligned}$$

where k_M is written in terms of the mole ratio of micellar OH^- bound to the micellar head groups. The pseudo-first-order rate constant can be easily derived as:

$$[3] \quad k_\psi = \frac{k_W[OH^-_T] + (k_M K_S - k_W)[OH^-_M]}{1 + K_S[Dn]}$$

where OH^-_M is the concentration of hydroxide ion bound to micelle.

For a reaction where the reactive ion OH^- is the micelle counterion, as CTAOH micelles (20), the distribution of this ion between aqueous and micellar pseudophases can be expressed by an equilibrium:

$$[4] \quad OH^-_W + Dn \overset{K'_{OH}}{\rightleftharpoons} OH^-_M$$

where

$$[5] \quad K'_{OH} = \frac{[OH^-_M]}{[OH^-_W]([Dn] - [OH^-_M])}$$

This equation reduces to:

$$[6] \quad K'_{OH}[OH^-_M]^2 - (K'_{OH}[Dn] + K'_{OH}[OH^-_T] + 1)[OH^-_M] + K'_{OH}[Dn][OH^-_T] = 0$$

with the fraction of micellar head groups neutralized, β, given by $\beta = [OH^-_M]/[Dn]$. Equation [5] predicts that β increases with surfactant concentration.

In the case of two ions competing for the micellar head groups, as CTAB micelles, Romsted (8) proposed a model considering β as a constant and that ions bind to micelles according to the exchange model developed for resins. For OH^- reactive ion and Br^- as micelle counterion the ion exchange equilibrium can be expressed by:

$$[7] \quad OH^-_M + Br^-_W \overset{K^{OH}_{Br}}{\rightleftharpoons} OH^-_W + Br^-_M$$

with an equilibrium constant:

$$[8] \quad K^{OH}_{Br} = \frac{[OH^-_W][Br^-_M]}{[OH^-_M][Br^-_W]}$$

and the fraction of micellar head groups neutralized given by:

$$[9] \quad \beta = m_{OH} + m_{Br}$$

where:

$$[10] \quad m_{OH} = [OH^-_M]/[Dn]; \qquad m_{Br} = [Br^-_M]/[Dn]$$

and

$$[11] \quad [OH^-_T] = [OH^-_W] + [OH^-_M]; \qquad [Br^-_T] = [Br^-_W] + [Br^-_M]$$

the following expression for m_{OH} can be easily deduced:

$$[12] \quad m^2_{OH} + m_{OH}\left[\frac{[OH^-_T] + K^{OH}_{Br}[Br^-_T]}{(K^{OH}_{Br} - 1)[Dn]} - \beta\right] - \frac{[OH^-_T]\,\beta}{(K^{OH}_{Br} - 1)[Dn]} = 0$$

We have developed a new approximation that considers independent distribution equilibria for each of the ions in solution, between the aqueous and micellar phase, so that for OH^- as reactive ion and Br^- as micelle counterion, the equilibrium constants K'_{OH} and K'_{Br} can be written as:

$$[13] \quad K'_{OH} = \frac{[OH^-_M]}{[OH^-_W]([Dn] - [OH^-_M] - [Br^-_M])}$$

$$[14] \quad K'_{Br} = \frac{[Br^-_M]}{[Br^-_W]([Dn] - [OH^-_M] - [Br^-_M])}$$

which reduce to:

$$[15] \quad K'_{OH}[OH^-_M]^2 - (K'_{OH}[Dn] - K'_{OH}[Br^-_M] + K'_{OH}[OH^-_T] + 1)[OH^-_M] + ([Dn] - [Br^-_M])K'_{OH}[OH^-_T] = 0$$

$$[16] \quad K'_{Br}[Br^-_M]^2 - (K'_{Br}[Dn] - K'_{Br}[OH^-_M] + K'_{Br}[Br^-_T] + 1)[Br^-_M] + ([Dn] - [OH^-_M])K'_{Br}[Br^-_T] = 0$$

This new treatment does not consider β as a constant, and its value, which depends on surfactant and ion concentrations, can be determined by solving eqs. [15] and [16] simultaneously with an iterative calculation method to give the values of $[OH^-_M]$ and $[Br^-_M]$ as a function of K'_{OH} and K'_{Br} for each surfactant and ion concentration.

Experimental

Materials

The surfactant CTAB, Merck, was recrystallized from MeOH/Et_2O. The surfactant CTAOH was prepared by ion exchange from CTAB (21) with anionic resin Amberlita 21-K. The absence of Br^- in CTAOH was tested with silver ion. This surfactant was prepared and kept under N_2 and it was used within 24 h of preparation. The pesticides DDT and DDD were purchased from U.S. Environmental Protection Agency Pesticides and Industrial Chemicals Repositori (MD-8). Other reactives, NaOH, KBr, Merck, were used without further purification.

Kinetics

All the reactions were run at 25 ± 0.1°C in the thermostated cuvettes of a Spectronic 2000 Bausch and Lomb spectrophotometer. Reactions were followed at 260 nm and 257 nm, which correspond to the absorbance products of reactions for DDT and DDD respectively. To the mixture of CTABr or CTAOH and NaOH at a given concentration in the thermostated cuvettes, 0.1 mL of DDT or DDD stock solution (10^{-3} *M* in acetonitrile) was added so that the amount of CH_3CN in the reaction mixture was 3%. The concentrations were: NaOH, 0–10^{-1} *M*; CTAB and CTAOH, 1×10^{-3} *M* to 7×10^{-2} *M*; and for both substrates, 3.3×10^{-5} *M*, in all experiments. The hydroxide ion concentration was in large excess over both substrates, and the experimental results, in both presence and absence of surfactants, fit very well the first-order rate equation:

$$[17] \quad \ln(A_\infty - A_t) = \ln(A_\infty - A_0) - kt$$

Values of pseudo-first-order rate constants were obtained by least-squares fit with correlation coefficients greater than 0.999.

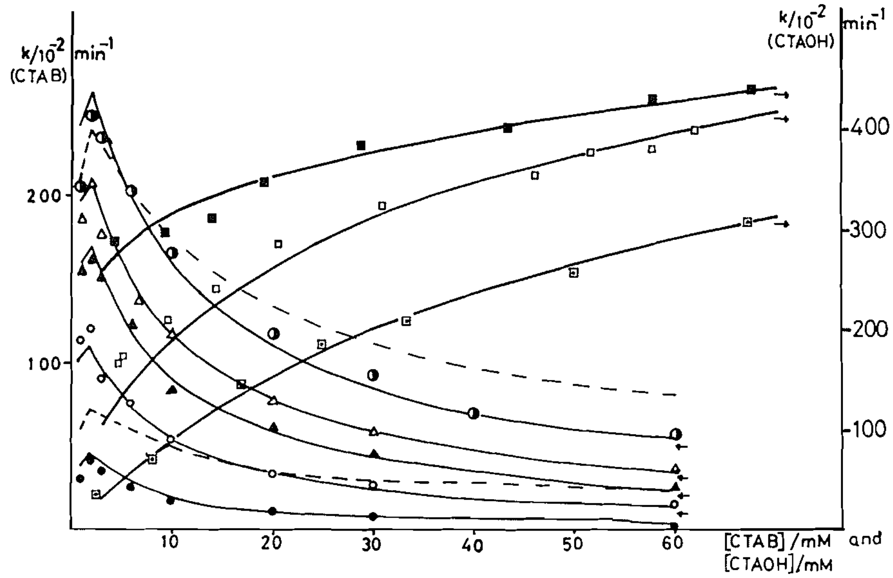

FIG. 1. Variation of the pseudo-first-order rate constant, k_ψ, for DDT in CTAOH (⊡ [NaOH] = 0 M, □ [NaOH] = 3.3 × 10^{-3} M, ■ [NaOH] = 3 × 10^{-2} M) and in CTAB (● [NaOH] = 0.33 × 10^{-2} M, ○ [NaOH] = 10^{-2} M, ▲ [NaOH] = 2 × 10^{-2} M, △ [NaOH] = 3 × 10^{-2} M, ◑ [NaOH] = 5 × 10^{-2} M). Lines are predicted values with different models.

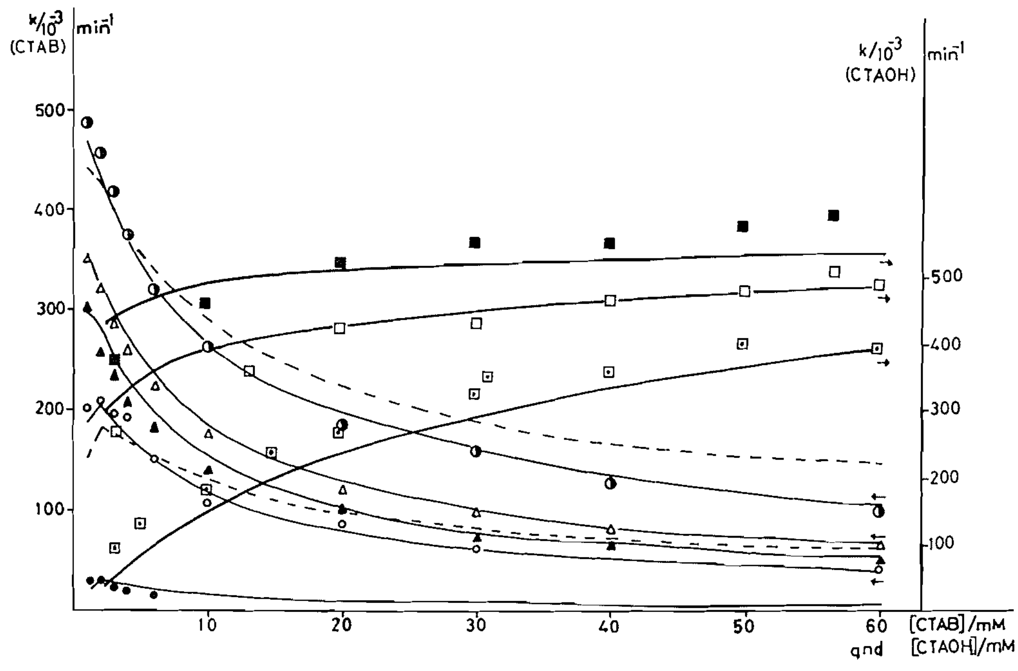

FIG. 2. Variation of the pseudo-first-order rate constant, k_ψ, for DDD in CTAOH (⊡ [NaOH] = 0 M, □ [NaOH] = 2.82 × 10^{-2} M, ■ [NaOH] = 5 × 10^{-2} M) and in CTAB (● [NaOH] = 0.27 × 10^{-2} M, ○ [NaOH] = 3 × 10^{-2} M, ▲ [NaOH] = 5 × 10^{-2} M, △ [NaOH] = 6.67 × 10^{-2} M, ◑ [NaOH] = 10^{-1} M). Lines are predicted values with different models.

TABLE 1. Values of pseudo-first-order rate constants obtained for DDT and DDD in different ethanol–water mixtures

% ETOH	30	33.3	40	50	60	70	80
k(DDT) (10^{-2} min^{-1})	3.8	4.0	—	5.8	7.8	11	13
k(DDD) (10^{-3} min^{-1})	7.3	—	8.1	13	17	25	—

Results and discussion

Both substrates DDT and DDD are very insoluble in pure aqueous solution and the second-order rate constants for the reaction in water were obtained by extrapolating the pseudo-first-order rate constant obtained in different ethanol–water mixtures to zero amount of ethanol. The experimental pseudo-first-order rate constants at OH^- concentration 10^{-1} M are given in Table 1. The values found for the second-order rate constant were 0.126 L mol^{-1} min^{-1} and 0.02844 L mol^{-1} min^{-1} for DDT and DDD respectively, which agree with the values reported in the literature (17).

The experimental pseudo-first-order rate constants for DDT in CTAB and in CTAOH micelles at different OH^- concentrations are represented by dots in Fig. 1, and the experimental pseudo-first-order rate constants for DDD in CTAB and in CTAOH micelles at different OH^- concentrations are represented by dots in Fig. 2. In Figs. 3a and 3b are represented the

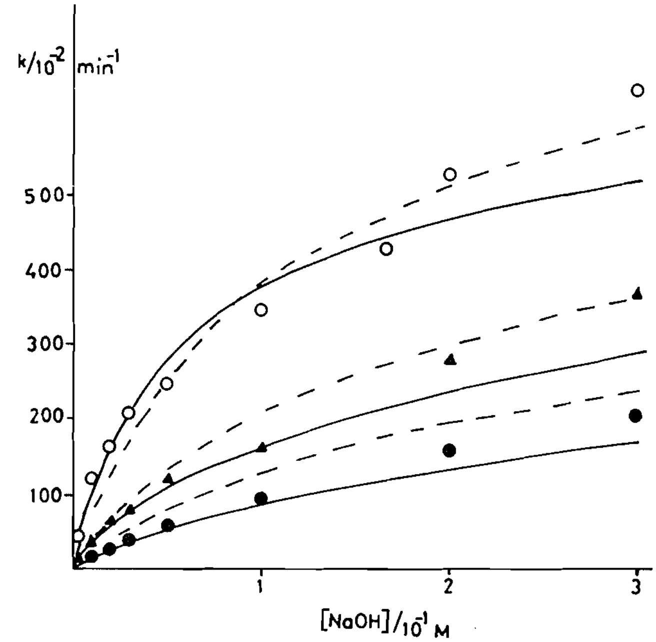

FIG. 3a. Variation of the pseudo-first-order rate constant, k_ψ, with NaOH concentration at fixed surfactant concentration for DDT (○ [CTAB] = 2 mM, ▲ [CTAB] = 20 mM, ● [CTAB] = 60 mM). Lines are predicted values with different models.

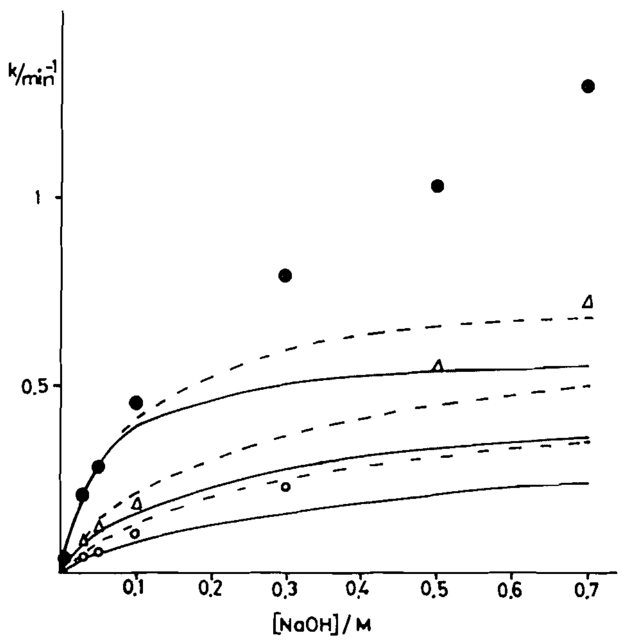

FIG. 3b. Variation of the pseudo-first-order rate constant, k_ψ, with NaOH concentration at fixed surfactant concentration for DDD (● [CTAB] = 2 mM, △ [CTAB] = 20 mM, ○ [CTAB] = 60 mM). Lines are predicted values with different models.

experimental pseudo-first-order rate constants at fixed CTAB concentration (2, 20, 60 mM) and different amounts of OH^- reactive ion, for the reactions with DDT and DDD respectively. Finally, in Figs. 4a and 4b are represented by dots the experimental pseudo-first-order rate constants for the reaction of both substrates at fixed CTAB concentration (2 and 20 mM) and different KBr concentrations.

The experimental rate constants for the reactions in CTAOH can be adapted to the pseudophase kinetic model proposed by

TABLE 2. Parameters that best fit the kinetic results for DDT and DDD in CTAOH

Substrate	[NaOH] (M)	k_M (min^{-1})	K_S (M^{-1})	K'_{OH} (M)
	0	8	2000	15
DDT	3.30×10^{-3}	8	2000	30
	3.00×10^{-2}	8	2000	20
	0	0.77	1000	35
DDD	2.82×10^{-2}	0.77	1800	35
	5.00×10^{-2}	0.77	4200	35

TABLE 3. Parameters that best fit the kinetic results for DDT and DDD in CTAB, using β as a constant

Substrate	[NaOH] (M)	k_M (min^{-1})	K_S (M^{-1})	K^{OH}_{Br}	β
	0.33×10^{-2}	8	2000	32	0.80
	1.00×10^{-2}	8	2000	32	0.80
DDT	2.00×10^{-2}	8	2000	32	0.80
	3.00×10^{-2}	8	2000	32	0.80
	5.00×10^{-2}	8	2000	32	0.80
	0.27×10^{-2}	0.77	1000	30	0.80
	3.00×10^{-2}	0.77	1800	30	0.80
DDD	5.00×10^{-2}	0.77	4200	30	0.80
	6.67×10^{-2}	0.77	5600	30	0.80
	1.00×10^{-1}	0.77	9000	30	0.88

Romsted (8) and Bunton (7), eqs. [3] and [6]. The procedure of adjusting the experimental results basically consists in calculating the value of pseudo-first-order rate constant, k_ψ, at different surfactant and ion concentrations using k_M, K_S, and K'_{OH} as arbitrary parameters. The calculated value for k_ψ does not depend on cmc value and, although the critical micellar concentration decreases slightly with electrolyte addition and with the hydrophobicity of the substrate, the value of cmc for the clear aqueous solution, cmc = 8.6×10^{-4} M, can be safely used (20). Table 2 gives the values of parameters that best fit the experimental results, and in Figs. 1 and 2 the values of k_ψ calculated with these parameters are represented by solid lines, for DDT and DDD respectively. K'_{OH} varies over a small range but, taking into account that small variations in the parameters will also fit the experimental results, K'_{OH} can be considered the same for both substrates, with an average value of $K'_{OH} \simeq 30$ M^{-1}. For DDT, small variations in the value of K_S also explain the experimental results but the K'_{OH} and k_M data are given satisfactorily in accord with the experimental error.

For the reaction in CTAB, the experimental rate constant can be adapted to the pseudophase kinetic model, proposed by Bunton (7) and Romsted (8), that considers β as a constant, eqs. [3] and [12]. In the procedure of adjusting the experimental results, k_W, cmc, and β are taken as known parameters while k_M, K_S, and K^{OH}_{Br} are taken as arbitrary ones. β can be taken as 0.8 for the case of CTAB micelles where the counterion, Br^-, binds strongly to the micelles (4, 5, 8). The calculated value of k_ψ at small surfactant concentration is too much affected by the value of critical micellar concentration and, as it decreases with electrolyte addition, the following empirical variation for cmc with ions (23) has been used in order to explain the experimental results:

$$[18] \quad \text{cmc} = 10 \times \exp(-3.7671 - 0.2133 \times \log(\text{cm} + [OH^-] + [Br^-]))$$

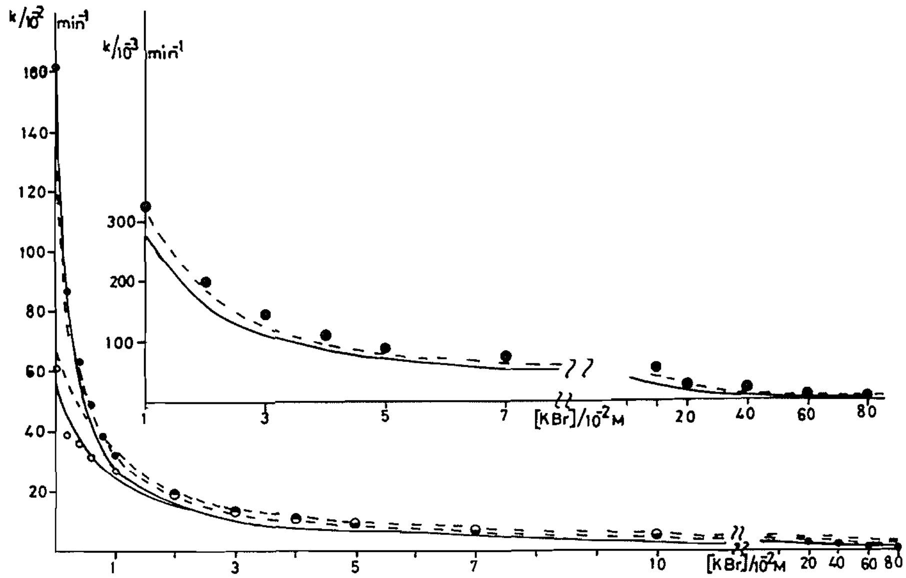

FIG. 4a. Variation of the pseudo-first-order rate constant, k_ψ, with KBr concentration at fixed surfactant and NaOH concentration for DDT (● [CTAB] = 2 mM and [NaOH] = 2 × 10^{-2} M, ○ [CTAB] = 20 mM and [NaOH] = 2 × 10^{-2} M). Lines are predicted values with different models.

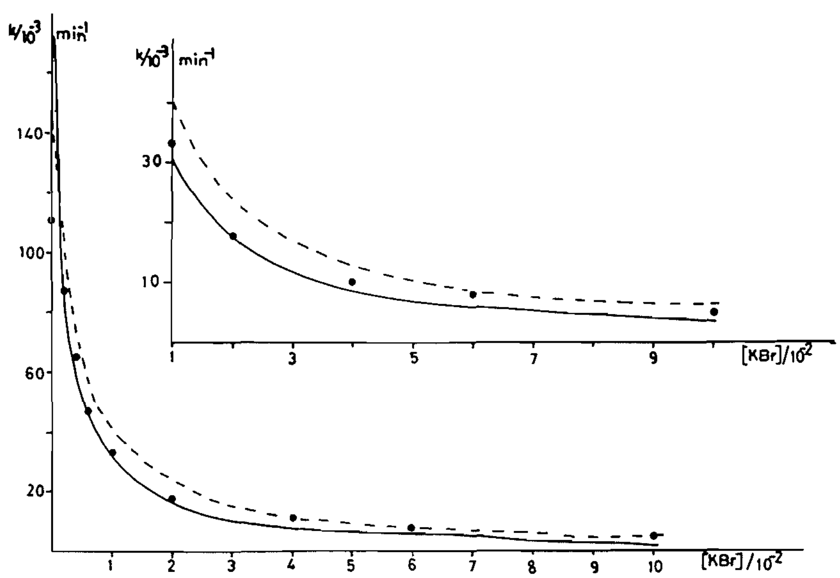

FIG. 4b. Variation of the pseudo-first-order rate constant, k_ψ, with KBr concentration at fixed surfactant and NaOH concentration for DDD (● [CTAB] = 2 mM and [NaOH] = 2 × 10^{-2} M). Lines are predicted values with different models.

where cm is the critical micellar concentration in clear aqueous solutions. Table 3 gives the values of parameters that best fit the experimental results using the above expression for cmc, and Figs. 1 and 2 show the calculated kinetic rate constant, k_ψ, with these parameters for DDT and DDD respectively (solid lines).

The values of k_M so determined are the same for the reactions in both surfactants CTAB and CTAOH, for each of the substrates. The substrate-to-micelles binding constants, K_S, for DDT are the same for the reaction in CTAOH and in CTAB, independent of ion concentration but, in the case of DDD for which higher concentrations of OH^- have been used, the value of K_S increases with increase of reactive ions in solution at these high concentrations, and this variation can be adapted to an empirical expression as:

$$[19] \quad K_S = 10^3\ (M^{-1}) + 7 \times 10^4\ (M^{-2}) \times ([\mathrm{NaOH}] + [\mathrm{KBr}])\ (M)$$

The same kind of the empirical expression for K_S can be used for DDT for the results at high OH^- concentrations.

$$[20] \quad K_S = 1500\ (M^{-1}) + 27\,000\ (M^{-2}) \times ([\mathrm{NaOH}] + [\mathrm{KBr}])\ (M)$$

This variation can be explained by the "salting-out" effect (13). These high values of K_S for both substrates agree with the results found in the literature for other hydrophobic substrates such as $(O_2NC_6H_4O)_2CO$, N—$C_{16}H_{33}$-3-CP, and PADA, with K_S values of 1000 (ref. 24), 3500 (refs. 25 and 26), and 2800 (ref. 27), respectively. The exchange constant, K_{Br}^{OH}, is the

TABLE 4. Parameters that best fit the kinetic results for DDT and DDD in CTAB, using an additional reaction step

Substrate	[CTAB] (mM)	k_M (min^{-1})	$k_{W/M}$ (min^{-1})	K_S (M^{-1})	K_{Br}^{OH}	β
	2	8	0.006	1500 + 2700 [OH$^-$]	32	0.8
DDT	20	8	0.040	1500 + 2700 [OH$^-$]	32	0.8
	60	8	0.070	1500 + 2700 [OH$^-$]	32	0.8
	2	0.77	0.002	1000 + 70000 [OH$^-$]	30	0.8
DDD	20	0.77	0.008	1000 + 70000 [OH$^-$]	30	0.8
	60	0.77	0.012	1000 + 70000 [OH$^-$]	30	0.8

TABLE 5. Parameters that best fit the kinetic results for DDT and DDD in CTAB, considering β not as a constant

Substrate	k_M (min^{-1})	K_S (M^{-1})	K'_{Br} (M^{-1})	K'_{OH} (M^{-1})
DDT	8	1500 + 2700 ([NaOH] + [KBr])	960	30
DDD	0.77	1000 + 70000 ([NaOH] + [KBr])	900	35

same for both substrates while K'_{OH} shows some variations in its value. The value of K_{Br}^{OH} is in the range of literature values for other substrates: 2, 54, and 21 for acetylsalicylate ester (28), p-nitrophenyl acetate (29), and betaine (5) respectively.

In Figs. 3a and 3b the calculated values of k_ψ at different OH^- concentrations are represented by solid lines, with the values of parameters determined before, at fixed concentrations of CTAB (2, 20, 60 mM). This model, which considers β as a constant, only explains the results up to a concentration 0.1 M of OH^-. That means that this approximation to consider β constant is valid only at low OH^- concentrations when $m_{OH} \ll m_{Br}$ and $\beta = m_{Br}$. Some of the results in the literature at high OH^- concentrations had been explained by considering an additional pathway across the micellar boundary, in which the hydroxide ion in the aqueous phase would react with the organic substrate bound to the micelle (12, 30). With this new additional reaction step with a pseudo-first-order rate constant: $k'_{W/M} = k_{W/M} \times [OH_W^-]$, it is possible to explain the experimental results over the whole range of [OH^-] used, but it is necessary to suppose that $k_{W/M}$ depends on surfactant concentration. Table 4 shows the values of parameters that best fit the experimental results with this new additional reaction step.

The experimental results at high KBr concentration, at fixed concentrations of CTAB and OH^-, can also be explained with the model that considers β as a constant, up to a value of [KBr] = 10^{-2} M, with the same values of parameters determined before (solid lines in Figs. 4a and 4b). Nevertheless, the model is not satisfactory at high KBr concentrations.

In order to explain the experimental results at high ion concentration we used the model that considers independent distribution equilibria for each of the ions in solution between aqueous and micellar pseudophases, which gives values of β depending of surfactant and ion concentrations. The values of [OH_M^-] and [Br_M^-] as a function of K'_{OH} and K'_{Br}, eqs. [15] and [16], can be obtained with an iterative calculation method setting [OH_M^-] initially as 0.000001 M and determining [OH_M^-] and [Br_M^-] as a function of K'_{OH}, K'_{Br}, [OH_T^-], and [Br_T^-]. There is no ensemble of parameters that adapts the experimental results to the whole range of surfactant and ion concentrations studied. The values of K'_{OH} and k_M should be the values obtained for the reaction in CTAOH and the values of K'_{Br} and K_S have been taken as adjustable parameters.

The best values of the parameters are given in Table 5 and the calculated values of k_ψ are represented by broken lines in Fig. 1 for DDT ([OH^-] = 10^{-2} M and [OH^-] = 5×10^{-2} M) and in Fig. 2 for DDD ([OH^-] = 3×10^{-2} M and [OH^-] = 10^{-1} M). For DDT the calculated value of k_ψ reproduces the experimental results at low surfactant concentration for [OH^-] = 0.05 M but at high surfactant concentration the calculated value of k_ψ is above the experimental results. With decreasing OH^- concentration it is necessary to increase the values of k_M and K_S in order to adapt the results at low surfactant concentration, but the calculated value at high surfactant concentration is always above the experimental result. The same effects have been found for DDD.

The values of k_ψ calculated with the parameters in Table 5 for the reaction at high OH^- concentration, using this model that considers β not a constant, are represented in Figs. 3a and 3b (broken lines). At low OH^- concentration the predicted values of k_ψ, at small surfactant concentration, 2 mM, are too low to explain the experimental results, but with increasing surfactant concentration, 20 mM and 60 mM, the calculated values are always higher than the experimental results. The values of k_ψ for the results at different KBr concentrations, calculated with the parameters in Table 5 (broken lines in Figs. 4a and 4b), are too low to explain the experimental results at small KBr concentration but, on increasing the KBr concentration, the calculated values of k_ψ become closer than the calculated values using the model that considers β as a constant. However, they are not high enough to explain these experimental results.

It can be concluded that for the reactions of these two substrates, where the determined value of K'_{OH} is as low as 30 M^{-1}, the predicted values of β at small surfactant concentration and small ion concentration are too low to explain the experimental results but that on increasing surfactant concentration the predicted values of β become too high. It is interesting to point out that this model explains very well the experimental results for the hydrolysis of acetylsalicylate ester and homologs (19) where the determined value of K'_{OH} in CTAOH is 380 M^{-1}.

It is possible to explain all of these experimental results by using an empirical variation of β with ions, as had been done by some authors (13, 31). Accordingly, for the reaction of these two substrates, the following two expressions were found: β = 0.8 + 0.5 ([NaOH] + [KBr]) for DDT and β = 0.8 + 1 ([NaOH] + [KBr]) for DDD. In Table 6 are shown the experimental and the calculated values of pseudo-first-order

TABLE 6. Experimental and calculated values of pseudo-first-order rate constants for DDT: (a) in CTAB ($[OH^-] = 5 \times 10^{-2}$, Fig 1); (b) reaction at high OH^- concentration ([CTAB] = 2 m*M*, Fig. 3a), using the three theoretical models, (1) considering β as a constant, (2) considering independent equilibria: β variable, (3) with an empirical expression for β

(a)

[CTAB]/m*M*	1	2	3	6	10	20	30	40	60
k_{exp}(min^{-1})	2.1	2.5	2.3	2.0	1.7	1.2	0.93	0.70	0.57
$k_{(1)}$(min^{-1})	2.4	2.6	2.5	2.0	1.6	1.1	0.84	0.69	0.52
$k_{(2)}$(min^{-1})	2.1	2.4	2.3	2.0	1.7	1.3	1.1	—	0.81
$k_{(3)}$(min^{-1})	2.5	2.7	2.5	2.1	1.7	1.2	0.91	0.75	0.57

(b)

$[OH^-]$/*M*	3.3×10^{-3}	10^{-2}	2×10^{-2}	3×10^{-2}	5×10^{-2}	10^{-1}	2×10^{-1}	3×10^{-1}
k_{exp}(min^{-1})	0.4	1.2	1.6	2.1	2.5	3.5	5.3	6.4
$k_{(1)}$(min^{-1})	—	1.1	1.7	2.1	2.8	3.7	4.6	5.1
$k_{(2)}$(min^{-1})	—	0.7	1.3	1.8	2.5	3.8	5.1	5.8
$k_{(3)}$(min^{-1})	—	1.1	1.7	2.2	2.9	4.0	5.2	6.0

rate constants for the reaction of DDT in CTAB ($[OH^-] = 5 \times 10^{-2}$) and the values for the reaction at high OH^- concentration ([CTAB] = 2 m*M*) using the three theoretical models:

(*1*) considering β as a constant (= 0.8)

(*2*) considering independent distribution equilibria for each of the ions in solution between the aqueous and micellar phase, with a variable β

(*3*) using the empirical expression for the value of β.
The same behavior is found for all the other results and it can be concluded that considering the empirical expression for β is the best way to explain the experimental kinetic results for the dehydrochlorination of DDT and DDD.

1. J. H. FENDLER and E. J. FENDLER. Catalysis in micellar and macromolecular systems. Academic Press, New York. 1975.
2. K. L. MITTAL and FENDLER (*Editors*). Solution behavior of surfactants. Vols. 1 and 2. Plenum Press, New York. 1982.
3. E. H. CORDES. Reactions kinetics in micelles. Plenum Press, New York. 1973.
4. C. A. BUNTON, E. RODENAS, and J. R. MOFFATT. J. Am. Chem. Soc. **102**, 2053 (1982).
5. K. AL-LOHEDAN, C. A. BUNTON, and L. S. ROMSTED. J. Phys. Chem. **85**, 2123 (1981).
6. F. M. MENGER and C. E. PORTNOY. J. Am. Chem. Soc. **89**, 4698 (1967).
7. C. A. BUNTON. Catal. Rev. Sci. Eng. **20**, 1 (1979).
8. L. S. ROMSTED. Micellization, solubilization and microemulsions. Vol. 2. *Edited by* K. L. Mittal. Plenum Press, New York. 1977. p. 509.
9. A. RHODE and E. SACKMANN. J. Phys. Chem. **84**, 1598 (1980).
10. G. GUNNARSSON, B. JONSSON, and H. WENNERSTROM. J. Phys. Chem. **84**, 3114 (1980).
11. C. A. BUNTON, J. FRANKSON, and L. S. ROMSTED. J. Phys. Chem. **84**, 2609 (1980).
12. C. A. BUNTON, L. S. ROMSTED, and G. SAVELLI. J. Am. Chem. Soc. **101**, 1253 (1979).
13. E. RODENAS. An. Quim. **79**, 638 (1983).
14. W. B. JAKOBY (*Editor*). Enzymatic basis of detoxication. Vol. 1. Academic Press, New York.
15. J. R. ESCABI-PEREZ, F. NOME, and J. H. FENDLER. J. Am. Chem. Soc. **99**, 7749 (1977).
16. Y. IHARA, M. NANGO, Y. KIMURA, and N. KUROKI. J. Am. Chem. Soc. **105**, 1252 (1983).
17. M. C. REZENDE, A. F. RUBIRA, C. FRANCO, and F. NOME. J. Chem. Soc. Perkin Trans. 2, 1075 (1983).
18. E. STADLER, D. ZANETTE, M. C. REZENDE, and F. NOME. J. Phys. Chem. **88**, 1892 (1984).
19. E. RODENAS and S. VERA. J. Phys. Chem. **89**, 513 (1985).
20. C. A. BUNTON, L. GAN, L. S. ROMSTED, and G. SAVELLI. J. Phys. Chem. **85**, 4118 (1981).
21. J. ULMIUS, B. LINDMAN, G. LINDBLOM, and T. DRAKENBERG. J. Colloid. Interface Sci. **65**, 88 (1978).
22. P. MUKERJEE and K. J. MYSELS. Critical micelle concentration of aqueous surfactant systems. NSRDS-NBS-36, Washington, D.C. 20402. 1971.
23. K. SHINODA, T. NAKAGAWA, TAMAMUSHI, and T. ISEMURA. Colloidal surfactants. Academic Press, New York. 1963. p. 58.
24. M. ALMGREN, F. GRIESER, and J. K. THOMAS. J. Am. Chem. Soc. **101**, 279 (1979).
25. E. LISSI, E. ABUIN, and A. M. ROCHA. J. Phys. Chem. **84**, 2406 (1980).
26. C. A. BUNTON, L. S. ROMSTED, and C. TAMAVIT. J. Am. Chem. Soc. **102**, 3900 (1980).
27. S. DIEKMANN and J. FRAHM. J. Chem. Soc. Faraday Trans. 1, **75**, 2199 (1979).
28. S. VERA, E. RODENAS, F. ORTEGA, and C. OTERO. J. Chim. Phys. **80**, 543 (1983).
29. F. H. QUINA, M. J. POLITI, I. M. CUCCOVIA, E. BAUMGARTEN, S. M. MARTINS-FRANCHETTI, and H. CHAIMOVICH. J. Phys. Chem. **84**, 361 (1980).
30. F. NOME, A. F. RUBIRA, C. FRANCO, and L. G. IONESCU. J. Phys. Chem. **86**, 1881 (1982).
31. A. ROHDE and E. SACKMANN. J. Colloid Interface Sci. **70**, 494 (1979).

A study of reaction mechanisms of methane in a radio-frequency glow discharge plasma using radical and ion scavengers

K. HIRAOKA,[1] K. AOYAMA, AND K. MORISE
Faculty of Engineering, Yamanashi University, Takeda-4, Kofu 400, Japan

Received February 25, 1985

K. HIRAOKA, K. AOYAMA, and K. MORISE. Can. J. Chem. **63**, 2899 (1985).

When 1 Torr of methane was decomposed in a radio-frequency glow discharge plasma, ethane, ethylene, and acetylene were produced as major products. In order to determine the relative importance of radical and ionic processes for the formation of these major products, iodine and ammonia were used as radical and ion scavengers, respectively. It was found that the major products were formed mainly by radical processes and the contribution of ionic processes is within the experimental error. The mechanisms for the formation of ethane, ethylene, acetylene, and $C_3 \sim C_4$ compounds were discussed.

K. HIRAOKA, K. AOYAMA et K. MORISE. Can. J. Chem. **63**, 2899 (1985).

Lorsqu'on décompose du méthane sous une pression de 1 torr et dans la lueur d'un plasma à décharge produit par une fréquence radio, les produits principaux sont l'éthane, l'éthylène et l'acétylène. Dans le but de déterminer l'importance relative des processus radicalaire et ionique dans la formation de ces produits principaux, on utilise respectivement l'iode et l'ammoniac comme pièges des radicaux et des ions. On a trouvé que les produits majoritaires se forment principalement par des processus radicalaires alors que la contribution des processus ioniques se situe à l'intérieur des limites des erreurs expérimentales. On discute du mécanisme de formation de l'éthane, de l'éthylène, de l'acétylène et des composés en C_3 et en C_4.

[Traduit par le journal]

Introduction

The elucidation of the reaction mechanisms of reactions in the plasma is largely impeded due to the complex nature of plasmas. The most difficult task is to determine the relative importance of ions and radicals in the reactions of plasmas. The estimation of the contribution of ions is much more difficult than that of radicals because the rates of ion–molecule reactions are too fast (often collision rate) to determine the precursor ions for the end products. The main objective of this work is to study the reaction mechanisms of methane in a glow discharge plasma in detail. In particular, we endeavored to evaluate the relative contribution of radical and ion mechanisms on the formation of reaction products.

Hiraoka and Kamada studied the reaction mechanisms of benzene in a radio-frequency glow discharge plasma using iodine as a radical scavenger (1). They found that acetylene and ethylene are produced directly from the decomposition of electronically excited benzene molecules. They claimed that radical scavengers can be used in the plasma chemistry for the study of reaction mechanisms. In this study, the reactions in the methane glow discharge plasma were investigated using iodine and ammonia as radical and ion scavengers, respectively, in order to determine the relative importance of radical and ionic processes in the glow discharge plasma of methane. Methane is the most suitable gas for the study of the reaction mechanisms because photolysis (2–5) and radiolysis (6–8) of methane were investigated in detail and the ion–molecule reactions of methane are well known (9). The use of scavengers is one method to intercept the consecutive reactions at early stage. By cooling the discharge tube at 77 K, it is also possible to avoid further decompositions and reactions of primary products in the plasma. The gaseous products condensible at 77 K are quickly trapped on the wall of the discharge tube and they escape from further decompositions in the plasmas. This method was found to give an important information about the reaction mechanisms.

[1]To whom all correspondence should be addressed.

Experimental

The pressure of methane (Taiyo Sanso, 99.9%) introduced to the vacuum line was controlled by adjusting a needle valve (Nupro SS-4BMG metering valve). The sample gas flowed continuously through the discharge tube and then passed through a trap cooled to liquid N_2 temperature and then pumped away by an oil-rotary pump with a capacity of 150 L/min. The experiments were done at three temperatures of the discharge tube, i.e. ~400, 195, and 77 K. Without cooling the discharge tube, its temperature reached to about 400 K by the inductive heating. By filling dry-ice acetone or liquid N_2 in the coaxial double cylindrical discharge tube, the temperatures of the discharge tube could be maintained at 195 and 77 K, respectively. Experiments at 77 K, all gaseous products were trapped on the wall of the discharge tube. For all experiments at ~400, 195, and 77 K, only a negligible amount of solid products was formed on the wall of the discharge tube. The sample gas was subjected to the plasma which is generated by a radio-frequency generator (Koike Engineering, 27 MHz) with a maximum power of 60 W.

For CH_4/I_2 experiments, the flow rate of iodine was controlled by dipping the iodine reservoir in a temperature-regulated water bath. Before the analysis of the gaseous products, the unreacted iodine and the hydrogen iodide produced were absorbed in the aqueous solution of sodium thiosulfate contained in the liquid N_2 trap by freeze–pump–thaw cycles.

For CH_4/NH_3 experiments, the known amounts of CH_4 and NH_3 were sampled in the 5 L flask at the total pressure of 760 Torr. The mixed gas was then flowed through the needle valve into the vacuum system. The unreacted ammonia trapped in a liquid N_2 trap was absorbed in a boric acid solution contained in the liquid N_2 trap by freeze–pump–thaw cycles.

For the analysis of gaseous products, the temperature of the trap was raised to dry-ice acetone temperature, and vaporized products were analysed by gc (Fig. 1) and gc–ms. The amounts of reaction products which are trapped at dry-ice acetone temperature were nil. The hydrogen which is one of the major gaseous products was not measured in this experiment because hydrogen cannot be trapped at 77 K.

Results and discussion

Application of scavengers in the plasma chemistry

Radical and ion scavengers have been widely used in the field of radiation chemistry. They give important information

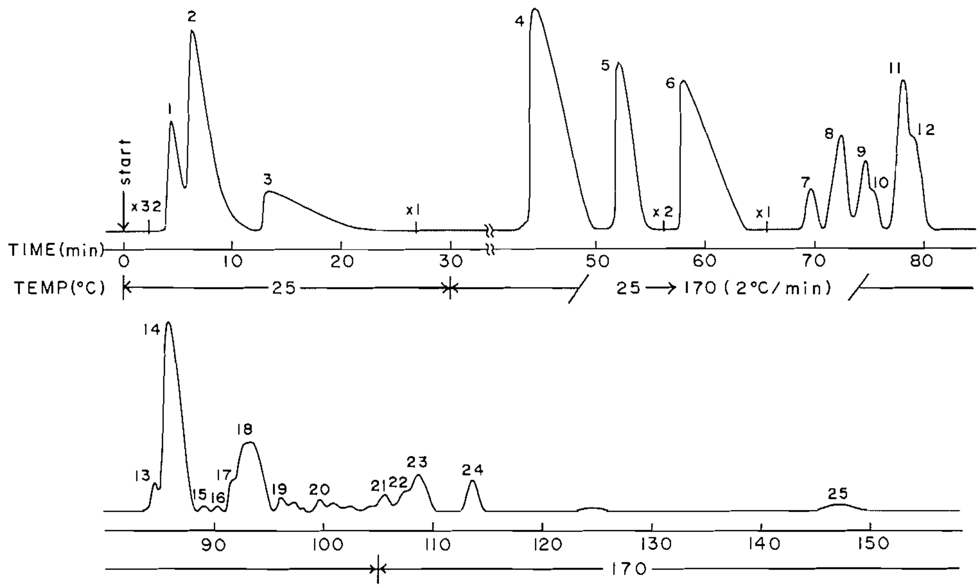

FIG. 1. Gas chromatogram of gaseous products from decomposition of 1 Torr methane in a radio-frequency glow discharge plasma at 400 K. Column: stainless steel (2 m × 3 mm id), porapak N (80–100 mesh). Detector: TCD; carrier gas: hydrogen. *1*: C=C; *2*: C—C; *3*: C≡C; *4*: C=C—C/C—C—C; *5*: C=C=C; *6*: C≡C—C; *7*: C—C—C (C); *8*: C=C—C (C); *9*: C=C—C=C/C=C—C—C; *10*: C—C=C—C; *11*: C≡C—C—C; *12*: C≡C—C=C; *13*: C—C≡C—C/C=C=C—C; *14*: C≡C—C≡C; *15*: C=C—C—C (C); *16*: C—C—C—C (C); *17*: C≡C—C—C/C=C—C—C/C=C—C—C—C (C, C); *18*: C≡C—C=C/C≡C—C—C—C/C=C=C—C—C/C—C=C—C (C, C); *20*: C≡C—C=C—C/C=C—C=C—C; *21*: C—C=C—C—C (C); *22*: C≡C—C—C—C/C=C—C=C/C—C—C—C—C (C, C C, C); *23*: C≡C—C(C)(C) /C—C=C—C/C=C—C—C (C C, C C); *24*: benzene; *25*: benzene—C.

on the mechanisms of reactions induced by the ionizing radiation. Although there seem to be no serious problems for the use of scavengers in the radiation chemistry, one should be very cautious for applications of scavengers in the plasma chemistry because plasma parameters such as electron temperature, plasma density, sheath potential, etc. are affected by the addition of scavengers in the plasma. For example, the electron temperature decreases sharply when a small amount of foreign gas is added whose ionization energy is lower than the major gas (10). It is desirable that scavengers have high ionization energies and negative electron affinities. Ironically, molecules can scavenge ions due to their low ionization energies. Besides, atoms and molecules which are used for radical scavengers generally have positive electron affinities. It seems intrinsically difficult to find "ideal" scavengers for the plasma chemistry. Thus it would be quite risky to draw out any quantitative conclusions from the results obtained by the use of scavengers in the plasma chemistry. However, if any drastic chemical changes could be observed by the addition of scavengers, we could appreciate them as important informations on the mechanisms of chemical reactions in the plasma. Because there are no other simple methods for the analysis of complicated reactions in the plasma, we dared to use ammonia and iodine as ion and radical scavengers, respectively, and see whether they are applicable in the plasma chemistry.

Use of ammonia as an ion scavenger

Although a number density of ions is generally many orders of magnitude smaller than that of free radicals in the plasma, it does not necessarily mean that the ion mechanism can be negligible compared to the free radical mechanism. This is because ions in a non-equilibrium plasma diffuse much much faster than neutral species and their lifetimes become much shorter than those of free radicals.

In a plasma, positive ions and electrons diffuse at the same rate, i.e., they diffuse by an ambipolar diffusion. The ambipolar diffusion coefficient D_a can be approximated to be (11)

$$[1]\quad D_a = \left(\frac{T_e}{T_i} + 1\right) D_i$$

where T_e is the electron temperature, T_i is the ion temperature, and D_i is the free diffusion coefficient of ions.

The characteristic diffusion length Λ for the cylindrical discharge tube can be given as (12)

$$[2]\quad \frac{1}{\Lambda^2} = \left(\frac{2.405}{r}\right)^2 + \left(\frac{\pi}{l}\right)^2$$

where r and l are radius and length of the cylinder, respectively. The value of Λ for the discharge tube used in this experiment (r = 5 mm and l = 70 mm) is calculated to be 1.7 mm. In the separate experiments (11), for the cavity with about the same value of Λ, the decay lifetime of ions in the thermal plasma ($T_e \cong T_i \cong T_{gas}$) of 1 Torr CH_4 was measured to be about 1 ms. In this case, the ambipolar diffusion coefficient D_a is larger than D_i by a factor of two, i.e. $D_a = 2D_i$ (eq. [1]).

Under the present experimental conditions where the plasma is nonthermal and $T_e \cong 100T_i$, D_a becomes about two orders of magnitude larger than D_i (eq. [1]). In such a condition, ions diffuse to the wall in ~10 μs by the ambipolar diffusion and they are neutralized there by the recombination reactions with electrons. On the other hand, free radicals are annihilated mainly by mutual recombination reactions and thus their lifetimes would be orders of magnitude longer than those of ions. Therefore, free radicals are accumulated in the plasma and their number density becomes much higher than that of ions. The large difference in the number densities between ions and free radicals in the non-thermal plasmas is mainly due to the difference in the rates of disappearance of ions and free radicals. In order to evaluate the relative importance of ion and free radical mechanisms, one should compare the *production rates* of ions and radicals instead of their densities. Numbers of ions and free radicals produced per unit time is proportional to the integral

$$\int_0^\infty Q(E)\,\sqrt{\frac{2E}{m}}\,f(E)\,\mathrm{d}E$$

where $Q(E)$ is the energy-dependent cross sections for ionization or dissociation of atoms or molecules, E is the energy of electron in the plasma, m is the mass of an electron, and $f(E)$ is the energy distribution function of electrons in a plasma. Accurate measurements of ionization and dissociation cross sections for methane are unfortunately not available. Using the available data for hydrogen (13), and assuming that the energy distribution of electrons in a plasma is Maxwellian and T_e = 5 eV, one finds that about one ionization event occurs for every ten dissociations of hydrogen molecules. This crude table calculation suggests that the relative contribution of ion mechanism is about one tenth of free radical mechanism in a hydrogen plasma. The experimental determination of the contribution of ion mechanism is very difficult because the rates of ion–molecule reactions are generally too fast to determine the precursor ions for the terminal products. Under such a situation, we think an ion–molecule reaction could be only controlled by an ion–molecule reaction itself, i.e., the use of ion scavengers.

The major ion in the methane plasma is known to be $C_2H_5^+$, the protonated ethylene (14). In order to scavenge this ion, the scavengers must have higher proton affinities than ethylene. We adopt ammonia as an ion scavenger because its proton affinity (205 kcal/mol) is much larger than those of alkanes, alkenes, and alkynes, and the protonated ammonia NH_4^+ is chemically unreactive toward hydrocarbons.

In the methane plasma, CH_3^+ and CH_4^+ are produced by the electron impact as primary product ions. They react with methane to produce $C_2H_5^+$ and CH_5^+, respectively (9).

[3] $CH_3^+ + CH_4 \rightarrow C_2H_5^+ + H_2$

[4] $CH_4^+ + CH_4 \rightarrow CH_5^+ + CH_3$

Rate constants for these reactions are of the order of 10^{-9} cm^3 molecule^{-1} s^{-1} (9). Thus lifetimes of CH_3^+ and CH_4^+ can be estimated to be ~20 ns under the present experimental conditions (1 Torr of methane). One of the main product ions CH_5^+ reacts only by a proton transfer reaction and regenerates CH_4. On the other hand, $C_2H_5^+$ has a variety of modes of reactions such as (9, 15, 16)

[5] $C_2H_5^+ + CH_4 \rightarrow C_3H_7^+ + H_2$

[6] $C_2H_5^+ + C_2H_6 \rightarrow C_4H_9^+ + H_2$

[7] $C_2H_5^+ + C_2H_4 \rightarrow C_3H_5^+ + CH_4$

[8] $C_2H_5^+ + C_2H_2 + CH_4 \rightarrow C_2H_5^+\cdot C_2H_2 + CH_4$

[9] $C_2H_5^+ + C_2H_2 \rightarrow C_3H_3^+ + CH_4$

By an addition of NH_3 in the plasma, $C_2H_5^+$ reacts with NH_3 to produce C_2H_4 by the proton transfer reaction [10],

[10] $C_2H_5^+ + NH_3 \rightarrow NH_4^+ + C_2H_4$

and reactions [5]–[9] must be suppressed. Thus, if the ion mechanism plays an important role in the methane plasma, the relative yield of C_2H_4 must be increased by an addition of NH_3.

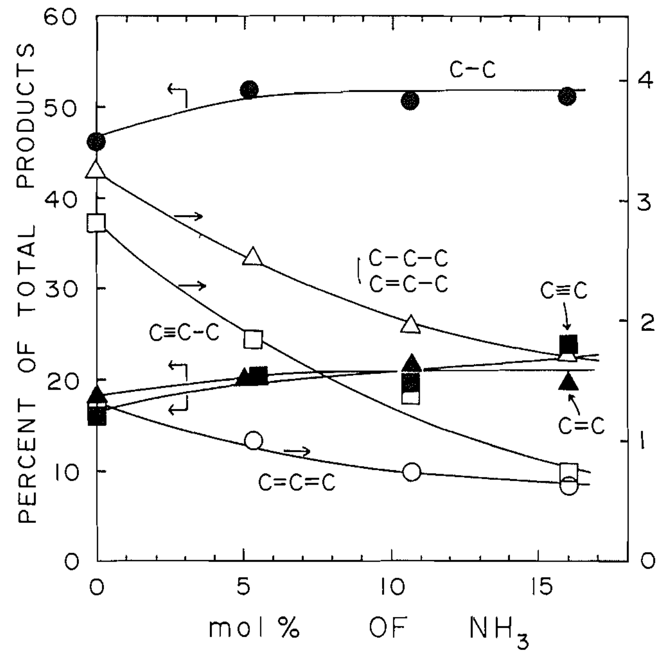

FIG. 2. The dependence of the relative yields of products on the amounts of added NH_3 in CH_4. Hydrogen is not included in the "total" products because it cannot be trapped at 77 K. The input power from the radio-frequency generator to the plasma was kept at 30 W for all measurements.

Figure 2 shows the dependence on the amount of added NH_3 of the relative yields of products. The relative yields of C_2H_6, C_2H_4, and C_2H_2 are nearly independent of the amounts of added NH_3. This result strongly suggests that the contribution of ion mechanism in the methane plasma is within the experimental error (5–10%).

Use of iodine as a radical scavenger

The results described in the previous section implicitly suggest that the free radicals play major roles in the reactions of methane plasma. To obtain further evidence, the iodine was introduced into the methane plasma as a radical scavenger. Figure 3 shows the dependence on the amounts added iodine of the relative yields of products. The yield of ethane decreases sharply with an increase of iodine, indicating that ethane is

TABLE 1. The relative yields of products from the decompositions of methane at 400, 195, and 77 K[a]

Temperature (K)	Relative yield								
	C_2H_4	C_2H_6	C_2H_2	C_3H_6 C_3H_8	C_3H_4[b]	C_3H_4[c]	C_4H_{10}	C_4H_2	C_6H_6
400	20.4	44.5	20.8	3.5	1.4	3.2	—	1.3	0.3
195	7.7	50.6	19.3	2.9	1.6	3.7	—	0.5	0.1
77	6.6	53.6	22.6	2.8	0.3	2.7	9.5	0.2	—

[a]Input power was kept at 30 W for all the measurements.
[b]Allene.
[c]Methylacetylene.

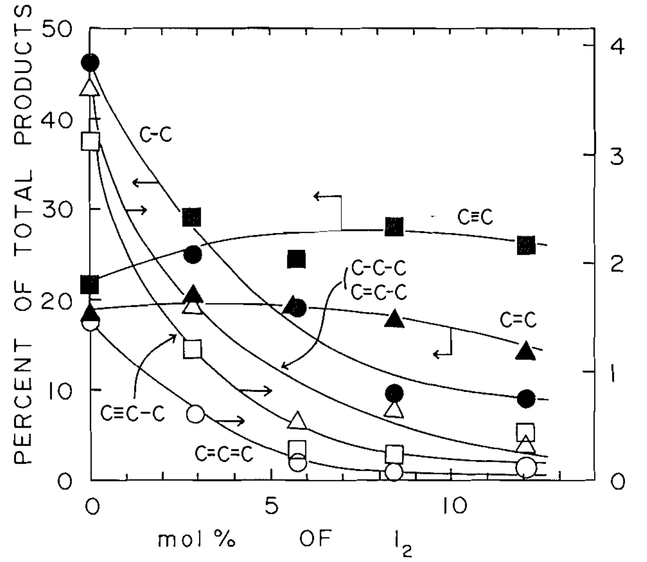

FIG. 3. The dependence of the relative yields of products on the amounts of added I_2 in CH_4. Hydrogen is not included in the "total" products because it cannot be trapped at 77 K. The input power from the radio-frequency generator to the plasma was kept at 30 W for all measurements.

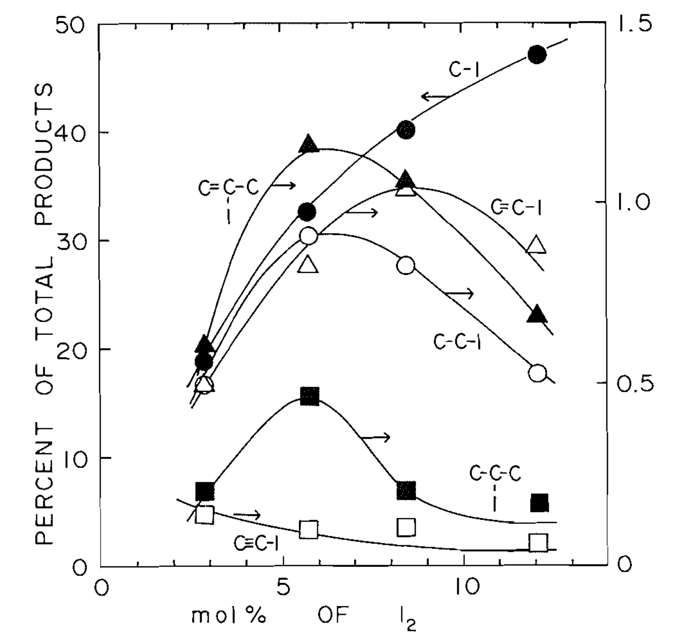

FIG. 4. The dependence of the relative yields of iodides on the amounts of added I_2 in CH_4.

produced by a radical mechanism. The yields of ethylene and acetylene are rather insensitive toward the amounts of added iodine. Iodine is considered to be less effective to scavenge precursors of ethylene and acetylene.

The benefit of using iodine as a radical scavenger is that the precursor radicals can be chemically frozen as iodides. Figure 4 shows the dependence on the amounts of added iodine of the relative yields of produced iodides. The produced CH_3I are by far the most abundant compared to other iodides and its yield shows a sharp increase with an increase of iodine. Considering results shown in Figs. 3 and 4, it can be concluded that ethane is formed by the recombination reaction of two methyl radicals,

[11] $2CH_3 \rightarrow [C_2H_6]^* \xrightarrow{M} C_2H_6$

where M represents a third body which collisionally stabilizes the intermediate complex $[C_2H_6]^*$.

Temperature effect on the relative yields of products

The lifetimes of the intermediate complexes in the radical reactions are more or less temperature dependent. The lower the temperature, the longer the lifetime of the intermediate complex. The intermediate complex has more chance to be stabilized at lower temperature. Thus the study of the temperature dependence on the plasma reactions would give some information on the reaction mechanisms. The experiment at 77 K is particularly interesting because the primary products are quickly trapped on the wall of the discharge tube and a further decomposition of primary products is expected to be greatly suppressed. In a sense, the cold wall acts as a scavenger by trapping primary products.

Table 1 summarizes the data obtained at ~400, 195, and 77 K. The relative yield of acetylene is almost independent on the temperature. The yield of ethane shows a steady increase with a decrease of temperature. Drastic decrease and increase of ethylene and *n*-butane, respectively, were observed at 77 K. This result suggests that ethylene and *n*-butane are formed from the same precursor. The detailed discussion about the reaction mechanisms will be described in the following section.

Reaction mechanisms of methane in a plasma

The major gaseous products from the decomposition of methane in a plasma were ethane, ethylene, and acetylene. The mechanisms for the formation of these products as well as C_3 and C_4 products will be considered here.

Radiolysis and photolysis of methane have been investigated in detail (2–8). The experimental evidence obtained by these investigations favors CH_2 and H_2 as the major products of the dissociation of methane. Mahan and Mandal, irradiating with a krypton resonance line (10.0 eV), found that CH_2 and H_2 were the dominant products (2). Magee (17), using a continuous hydrogen source (8.3 ~ 11.8 eV), concluded that an excited methane decomposes into CH_2 and H_2 85% of the time and into CH_3 and H 15% of the time. In a plasma, electrons have a wide range of energy and other radicals such as CH and C may also be produced as primary products. Besides, hydrogen atoms present as primary and secondary products in a methane plasma would abstract hydrogen atoms from CH_n radicals ($n \leq 3$).

[12] $CH_3 \xrightarrow{H} CH_2 \xrightarrow{H} CH \xrightarrow{H} C$

Thus the primary radicals in the methane plasma would be CH_2, CH, and C.

The CH_2 radical is known to insert into a C—H bond of methane to form internally excited $[C_2H_6]^*$ which decomposes unimolecularly into two CH_3 radicals (8, 18).

[13] $CH_2 + CH_4 \rightarrow [C_2H_6]^* \rightarrow 2CH_3$

This reaction would explain the large yield of CH_3I in the I_2 scavenger experiments (Fig. 4). Ausloos and co-worker found that $[C_2H_6]^*$ was collisionally stabilized at higher pressures (8). In the present experiments, the relative yield of ethane is increased at lower temperatures (Table 1). The lifetime of the intermediate complex $[C_2H_6]^*$ is supposed to be long enough to be collisionally stabilized in 1 Torr methane at 77 K.

Ethylene was found to be the main product from the reaction of CH with methane (3, 8).

[14] $CH + CH_4 \rightarrow [C_2H_5]^* \rightarrow C_2H_4 + H$

[15] $\xrightarrow{M} C_2H_5$

The lifetime of $[C_2H_5]^*$ was supposed to be short because the stabilization process [15] has not been observed at high pressures (8, 19). The short lifetime of $[C_2H_5]^*$ (4×10^{-13} s) has also been predicted by the theoretical RRKM calculations (19). In the present experiments at 77 K, however, the yield of C_2H_4 decreased markedly and this decrease was compensated by the increase of *n*-butane. This result suggests that there is some mechanism for the stabilization of $[C_2H_5]^*$ at 77 K which is followed by the recombination reaction [16] to form *n*-butane.

[16] $2C_2H_5 \xrightarrow{M} C_4H_{10}$

Considering that reactions [14] and [15] are 60 and 99 kcal/mol exothermic, it seems not likely that $[C_2H_5]^*$ can be stabilized even at 77 K in the gas phase. The $[C_2H_5]^*$ could be stabilized if the reaction of CH with CH_4 occurs on the cold wall. However, such an heterogeneous reaction cannot explain the large yield of *n*-butane at 77 K, and some other stabilization mechanisms might exist. For example at 77 K in the gas phase, van der Waals clusters $(CH_4)_n$ ($n \geq 2$) would be present at higher concentrations and they participate in the formation of C_2H_5 radical:

[17] $CH + (CH_4)_n \rightarrow C_2H_5 + (n - 1)CH_4$

The cluster $(CH_4)_n$ has built-in third-bodies in it and the exothermicity of the reaction could be released as kinetic energies of departing third bodies. This might explain the sudden decrease and increase of ethylene and *n*-butane, respectively, at 77 K.

If reaction [13] occurs at 77 K, the produced methyl radical would react with C_2H_5 to form C_3H_8. However, the yield of propane does not increase at 77 K (Table 1). These results suggest that a greater part of $[C_2H_6]^*$ is stabilized at 77 K.

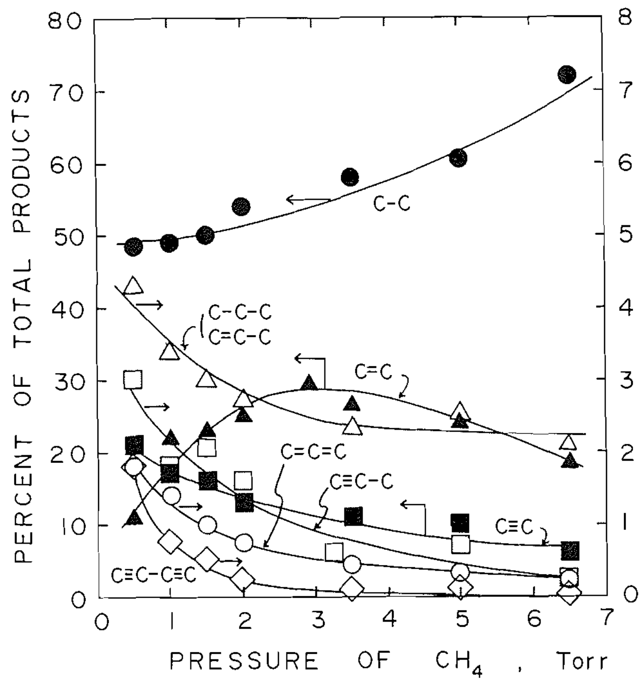

FIG. 5. The dependence of the relative yields of products on CH_4 pressure. The input power from the radio-frequency generator to the plasma was kept at 30 W for all measurements.

Braun *et al.* (20) and Husain *et al.* (21) found that acetylene is formed by the reaction of C with CH_4.

[18] $C + CH_4 \rightarrow [C_2H_4]^* \rightarrow C_2H_2 + H_2$

No evidence was obtained for the collisional stabilization of $[C_2H_4]^*$ at higher pressures (20), indicating that the lifetime of $[C_2H_4]^*$ is short.

As the pressure is decreased, the electron temperature in the plasma increases (10) and the residence time of gas molecules in a plasma gets longer because of the decrease of the linear gas velocity. Thus primary products experience more frequent secondary decompositions at lower pressures. Thus the lower the pressure becomes, the further the successive reactions [12] proceed. As shown in Fig. 5, the yield of ethane decreases steadily with decreasing pressure. The yield of ethylene increases initially, and after reaching the maximum, starts to decrease. The relative yield of acetylene is lowest at high pressures, but it increases steadily with decreasing pressure, and overcomes the yield of ethylene at low pressures. These results support the idea that CH_2, CH, and C are the precursors of ethane, ethylene, and acetylene, respectively. The power dependence on the relative yields of products as shown in Fig. 6 also supports the reaction mechanisms described above.

The ^1D state of carbon atom may be responsible for the formation of acetylene. The rate constant of the reaction of the ground state $C(^3P)$ with methane ($k < 2 \times 10^{-15}$ cm^3 molecule^{-1} s^{-1}) (22) is much smaller than that of the excited $C(^1D)$ ($k = 2 \times 10^{-10}$ cm^3 molecule^{-1} s^{-1}) (21). The energy difference between $C(^1D)$ and $C(^3P)$ is about 1 eV. The spin-forbidden excitation of $C(^3P)$ to $C(^1D)$ would occur efficiently in a nonequilibrium glow discharge plasma because electrons with energies of a few eV are abundant in a plasma (10). Recently, the diamond-like carbon films have been synthesized by radio-frequency plasma decomposition of CH_4 or mixed gases of CH_4 and H_2 (23). The hydrogen containing a small amount of CH_4 was found to be a suitable gas for the synthesis

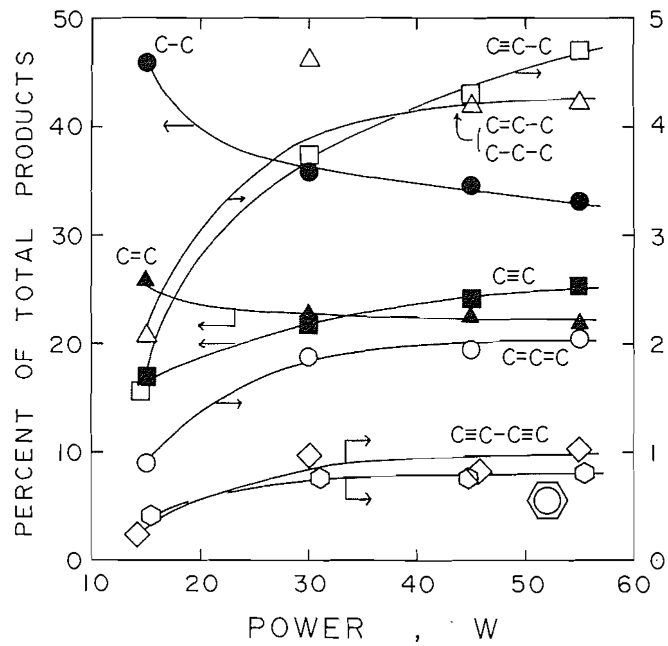

FIG. 6. The dependence of the relative yields of products on the input power to the plasma.

of diamond-like carbon film. Apparently, hydrogen atoms in a plasma play an important role to produce carbon atoms by the reactions (12). The produced $C(^1D)$ may contribute to the growth of the sp^3 skeleton of diamond-like film by the insertion reaction. The methane gas is intrinsically the best source of carbon atoms because its H/C ratio is largest in hydrocarbons and the contribution of reaction [12] is most effective for the production of carbon atoms.

Propane and propylene may be formed by reactions [19]–[22].

[19] $CH_3 + C_2H_5 \xrightarrow{M} C_3H_8$

[20] $CH_3 + C_2H_3 \xrightarrow{M} C_3H_6$

[21] $CH_2 + C_2H_6 \xrightarrow{M} C_3H_8$

[22] $CH_2 + C_2H_4 \xrightarrow{M} C_3H_6$

The formation of C_2H_5I and C_2H_3I in the I_2 scavenger experiments argues for reactions [19] and [20]. However, the possibility for reactions [21] and [22] cannot be rejected because the yields of propane and propylene do not show sharp decrease at 77 K where ethane and ethylene, which may be the precursors of C_2H_5 and C_2H_3 radicals, are trapped quickly on the wall of the discharge tube.

Baird found that allene is a principal product from the reaction of C with ethylene (24).

[23] $C + C_2H_4 \xrightarrow{M} C_3H_4$

If the precursor of allene produced in this experiment is ethylene, the yield of allene should decrease at 77 K because the yield of ethylene showed a sudden decrease at the same temperature. Table 1 shows that both yields of ethylene and allene drop sharply at 77 K. This result is a strong support for the occurrence of reaction [23] in the methane plasma.

The formation mechanism of methylacetylene seems somewhat different from that of allene, because the decrease in methylacetylene yield is not so drastic as allene at 77 K. Besides, with an increase of an input power, the yield of methylacetylene shows a steady increase but that of allene reaches a plateau (Fig. 6). Canosa-mas *et al.* found that the main product from the reaction of $CH_2(^1A_1)$ with acetylene is methylacetylene (25).

[24] $CH_2(^1A_1) + C_2H_2 \rightarrow C{\equiv}C{-}C$

All the results shown in Table 1 and Figs. 5 and 6 support the idea that the precursor of methylacetylene is acetylen (reaction [24]).

Important progress has been made by Lange and Wagner in understanding acetylene photochemistry (26). They have obtained the rate constant of the reaction,

[25] $C_2H + C_2H_2 \rightarrow C_4H_2 + H$

by measuring with the mass spectrometer the decay of C_2H and have obtained $k = 5 \times 10^{-11}$ cm^3 molecule^{-1} s^{-1}. They have also found the product to be mainly diacetylene. The very low yield of diacetylene at higher methane pressures (Fig. 5) may be due to the consumption of C_2H radical by reaction [26] (27).

[26] $C_2H + CH_4 \rightarrow C_2H_2 + CH_3$

Conclusion

Much information about the reaction mechanisms of reactions in the methane glow discharge plasma could be gained by the experiments using ammonia and iodine as ion and radical scavengers, respectively. It was found that the major products were formed mainly by radical processes and the contribution of ionic processes is within the experimental error. It is concluded that reactions of CH_2, CH, and C with methane produce ethane, ethylene, and acetylene, respectively, as major products in the methane glow discharge plasma.

1. K. HIRAOKA and H. KAMADA. Nippon Kagaku Kaishi, **90**, 1239 (1969); **90**, 1242 (1969).
2. B. H. MAHAN and R. MANDAL. J. Chem. Phys. **37**, 207 (1962).
3. W. BRAUN, K. H. WELGE, and J. R. MCNESBY. J. Chem. Phys. **45**, 2650 (1966).
4. A. H. LAUFER and J. R. MCNESBY. J. Chem. Phys. **49**, 2272 (1968).
5. S. KARPLUS and R. BERSOHN. J. Chem. Phys. **51**, 2040 (1969).
6. P. AUSLOOS, R. GORDEN, JR., and S. G. LIAS. J. Chem. Phys. **40**, 1854 (1964).
7. P. AUSLOOS, R. E. REBBERT, and S. G. LIAS. J. Chem. Phys. **42**, 540 (1965).
8. R. GORDEN, JR., and P. AUSLOOS. J. Chem. Phys. **46**, 4823 (1967).
9. K. HIRAOKA and P. KEBARLE. J. Chem. Phys. **63**, 394 (1975).
10. K. HIRAOKA and H. KAMADA. Jpn. J. Appl. Phys. **10**, 339 (1971).
11. K. HIRAOKA, M. MORISE, and T. SHODA. Int. J. Mass Spectrom. Ion Process. In press.
12. M. A. BIONDI and S. C. BROWN. Phys. Rev. **75**, 1700 (1949).
13. L. J. KIEFFER. Atom. Data, **1**(1), Pt. 1, 19 (1969).
14. M. J. VASILE and G. SMOLINSKI. Int. J. Mass Spectrom. Ion Phys. **18**, 179 (1975).
15. K. HIRAOKA and P. KEBARLE. Can. J. Chem. **58**, 2262 (1980).
16. J. A. BURT, L. J. DUNN, M. J. MCEWEN, M. M. SUTTON, A. E. ROCHE, and H. I. SCHIFF. J. Chem. Phys. **52**, 6062 (1970).
17. E. M. MAGEE. J. Chem. Phys. **39**, 855 (1963).
18. W. BRAUN, A. M. BASS, and M. PILLING. J. Chem. Phys. **52**, 5131 (1970).
19. M. R. BERMAN and M. C. LIN. Chem. Phys. **82**, 435 (1983).
20. W. BRAUN, A. M. BASS, D. D. DAVIS, and J. D. SIMMONS. Proc. R. Soc. A**312**, 417 (1969).
21. D. HUSAIN and L. J. KIRSCH. Trans. Faraday Soc. **67**, 3166 (1971).

22. D. HUSAIN and L. J. KIRSCH. Trans. Faraday Soc. **67**, 2025 (1971).
23. H. VORA and T. J. MORAVEC. J. Appl. Phys. **52**, 6151 (1981).
24. J. C. BAIRD. J. Chem. Phys. **37**, 1879 (1962).
25. C. E. CANOSA-MAS, M. ELLIS, M. FREY, and R. WALSH. Int. J. Chem. Kinet. **16**, 1103 (1984).
26. W. LANGE and H. GG. WAGNER. Ber. Bunsenges. Physik. Chem. **79**, 165 (1975).
27. D. F. STROBEL. Planet. Space Sci. **30**, 839 (1982).

The two liquid phase system $NaAl(ethyl)_4$ – benzene–HMPA

JAMES H. MEDLEY, NASEER AHMAD, AND MARION C. DAY[1]
Department of Chemistry, Louisiana State University, Baton Rouge, LA 70803, U.S.A.
Received July 24, 1984

JAMES H. MEDLEY, NASEER AHMAD, and MARION C. DAY. Can. J. Chem. **63**, 2906 (1985).

A detailed study of complexation of the sodium ion by HMPA[2] has been made using the system

$NaAlEt_4$ – benzene – HMPA

where HMPA is observed to be a strong donor towards Na^+ but does not complex $AlEt_4^-$. This system forms two liquid phases at low HMPA:Na^+ molar ratios with the salt and the HMPA, up to a 4:1 HMPA:Na^+ ratio, occurring only in the lower phase. Based on a variety of experimental techniques, reasonable proposals of the solute species in the lower phase as a function of HMPA:Na^+ ratio are presented. A 2.5:1 ratio of HMPA:Na^+ is observed to be particularly significant. This ratio is rationalized in terms of a bridging HMPA molecule resulting in a cationic species with the stoichiometry $[2Na\cdot5HMPA]^{2+}$. It is found that the ^{27}Al and ^{1}H nmr spectra are determined primarily by quadrupole relaxation of the ^{27}Al nucleus rather than by exchange.

JAMES H. MEDLEY, NASEER AHMAD et MARION C. DAY. Can. J. Chem. **63**, 2906 (1985).

On étudié d'une façon systématique la complexation de l'ion sodium par le HMPA (hexaméthylphosphoramide) dans le système

$NaAlEt_4$ – benzène – HMPA

dans lequel il a été observé que le HMPA est un puissant donneur pour le Na^+ alors qu'il ne complexe pas l'ion $AlEt_4^-$. À des rapports molaires de HMPA:Na^+ qui sont faibles, c'est-à-dire à des rapports HMPA:Na^+ allant jusqu'à 4:1, ce système forme deux phases liquides et l'on ne retrouve le sel et le HMPA que dans la phase inférieure. En se basant sur plusieurs techniques expérimentales, on présente un certain nombre de propositions raisonnables pour expliquer la présence des espèces solutés dans la phase inférieure en fonction du rapport HMPA:Na^+. Un rapport de HMPA:Na^+ de 2,5:1 semble être important. On explique ce rapport en fonction de l'action d'une molécule de HMPA qui agit comme pont et qui conduit à l'existence d'une espèce cationique de stoichiométrie $[2Na\cdot5HMPA]^{2+}$. On a établi que les spectres rmn du ^{27}Al et du ^{1}H sont déterminés essentiellement par la relaxation quadrupolaire du noyau de ^{27}Al et non par un échange.

[Traduit par le journal]

Introduction

Because of their unique property of solubility in nonpolar solvents such as hexane and benzene, the sodium tetraalkylaluminate salts have proven to be particularly useful in the study of ion–ion and ion–solvent interactions (1). Thus, for instance, a solution of $NaAl(n\text{-butyl})_4$ dissolved in hexane permits one to observe specific interactions between the ions of the salt rather than between the solvated ions which would exist in conventional solvent systems. Further, using a system of the type

$NaAl(alkyl)_4$ – inert solvent – donor

where controlled amounts of the donor are added, one can observe the effects of specific solvation on the behavior of the solution. The first reported such system was (2)

$NaAl(n\text{-butyl})_4$ – cyclohexane – $(ethyl)_2O$

Since that first study, a number of examples of the use of this type of system have been reported.

One of the most unusual properties of this system is its tendency to form two liquid phases at relatively low ratios of donor:Na^+ with strong donors such as HMPA (3). The salt, $NaAlEt_4$, shows considerable solubility in hot benzene, but it is essentially insoluble in benzene at room temperature. The addition of stoichiometric amounts of HMPA to $NaAlEt_4$, up to a ratio of 4:1 HMPA:Na^+, in the absence of benzene results in crystalline solids. However, when HMPA is added to $NaAlEt_4$ in the presence of benzene, two liquid phases are formed. The lower phase contains the salt, HMPA, and some benzene whereas, at lower ratios of HMPA:Na^+, the upper phase contains only benzene.[3] As the ratio of HMPA:Na^+ is increased, there is an increase in the volume of the lower phase (*vide infra*). After an HMPA:Na^+ ratio of 4:1, HMPA appears in the upper phase. If large quantities of benzene are added to a system containing HMPA:Na^+ ratios greater than 4:1, excess HMPA can be extracted from the lower phase but always leaving a lower phase with an HMPA:Na^+ ratio of 4:1 and with the volume characteristic of that ratio. We have never observed any salt in the upper phase. It is interesting that two liquid phases are not generally formed when the donor is a weaker donor towards the Na^+ such as pyridine or tetrahydrofuran (3).

Here we wish to report on our studies of the two liquid phase system

$NaAlEt_4$ – benzene – HMPA

We have carried out an extensive study of this system with the intent of determining the structures of the solute species and, where possible, their chemical behavior.

Experimental procedures

Because of the pyrophoric nature of aluminum alkyls and their compounds, all manipulations involving preparation of solutions and loading nmr tubes, viscometers, and conductance cells were performed under an argon atmosphere in a stainless steel, inert atmosphere box of our own design.

[1]To whom all correspondence should be addressed.
[2]HMPA = hexamethylphosphoramide.
[3]Trace amounts of HMPA can be detected.

Preparation of sodium tetraalkylaluminates

Sodium tetraethylaluminate and sodium tetrabutylaluminate were prepared by the methods of Frey *et al.* (4*a*) and of Schaschel and Day (4*b*), respectively.

Purification of solvents

All hydrocarbon solvents were refluxed over calcium hydride under N_2 for at least 8 h prior to distillation. Hexamethylphosphoramide (HMPA) was refluxed for 24–48 h over CaH_2 in a one piece 30 cm path vacuum distillation apparatus at 0.5 Torr. Fresh HMPA was prepared at 2 week intervals throughout the study. Deuterated benzene, obtained as 99+ atom% from Aldrich Chemical Co., was checked for reactivity with the salt and used without further purification.

Lower phase volume

The volume of the lower phase as a function of mole ratio HMPA:salt was determined by HMPA titrations of salt solutions in benzene. The titrations were carried out on the pan of a top loading balance in the dry box using 0.500 g of $NaAlEt_4$ in 25 mL of benzene. After phase separation, the volume of the lower phase was determined with an estimated precision of ±0.05 mL, using a calibration curve for the volume of the container plus the stirrer.

The data were treated by a General Linear Model Procedure in SAS on an IBM 365/3033.

HMPA:Na^+ ratio	R^2	F	p
<1.5	0.94	199.48	0.0001
1.5–2.2	0.72	31.10	0.0001
2.2–2.8	0.87	110.60	0.0001
2.8–4.2	0.99	1552.02	0.0001

Conductivity measurements

Conductivity measurements were made in conductance cells of conventional design using methods described earlier (5). Concentrations were determined using the volume dependence curve for the lower phase.

Viscosity measurements

The viscosity of the lower phase was determined using Canon-Fenske viscometers modified for operation under an inert atmosphere.

Nuclear magnetic resonance measurements

Aluminum-27 nmr spectra were obtained at 52.148 MHz on a Bruker WP-200 spectrometer.

Proton nmr spectra were obtained on a Varian Associates A-60A, and a Varian HA-100 spectrometer. Aluminum-27 decoupled proton spectra were obtained on the HA-100 using a home-built heteronuclear decoupler. The decoupling scheme was based on the method of Burton and Hall (6).

X-ray measurements

Data collection was performed by ω–2θ scans on an Enraf–Nonius CAD 4 diffractometer equipped with CuKα radiation (λ = 1.54184 Å) and a graphite monochromator. The crystal was sealed in a thin-walled glass capillary. Positions of Na, Al, O, and some N atoms were deduced by heavy atom methods. R = 0.34 based on 672 observed reflections ($I > 1\sigma(I)$) of the 1881 unique data having $\sin\theta/\lambda <$ 0.421. Further elucidation was not possible because of low resolution, high thermal motion, and possible disorder.

The crystals were prepared by sealing a mixture of HMPA and $NaAlEt_4$ (4:1) in a glass container. The mixture was heated to its melting temperature and then slowly cooled to room temperature.

Discussion

Crystal structure of $NaAlEt_4 \cdot 4HMPA$

We have attempted to grow satisfactory crystals of $NaAlEt_4 \cdot x$HMPA where x = 1, 2, 3, 4. The results were generally unsuccessful, but a limited study of $NaAlEt_4 \cdot 4$HMPA was carried out. The following can be stated.

The crystals are orthorhombic, with space group *Pnma*, Z = 4, a = 21.355(3) Å, b = 14.717(5) Å, c = 18.649(4) Å, v = 5861(4) Å^3. The density ≃ 1.00 g cm^{-3}. Thermal motion in the crystal is very high, and resolution is low (worse than 1.5 Å). Unfortunately, the crystals fracture on cooling to 150 K. In addition to the above, it is strongly suspected that the Na^+ is approximately tetrahedrally coordinated by oxygen atoms of HMPA with the symmetry of Na(HMPA)$^+$ being $m(C_s)$ in the crystal. The coordination appears to be nearly linear (Na—O—P angles 150°–180°) with the minimum Na—Al distance of ~9.0 Å.

Solvation by HMPA

It is generally considered that HMPA is an especially strong complexing species and, in fact, it has the highest donor number (38.8) in the original Gutmann listing of solvent donicities (7). This position has recently been substantiated with respect to Na^+ (8).

Solvation number

In earlier studies on this system it has been shown that a 4:1 ratio of HMPA:Na^+ is sufficient to convert contact ion-pairs to solvent separated ion-pairs (9). This implies that the solvation number of HMPA towards Na^+ is four and, further, that the equilibrium

$$[Na \cdot 4HMPA]^+ \rightleftharpoons [Na \cdot 3HMPA]^+ + HMPA$$

lies predominantly to the left. The proposal of a Na^+ solvation number of four is also supported by ^{23}Na nmr studies (10).

Both of the above arguments, the conversion from contact to solvent separated ion-pairs and the solvation number of four as determined from the ^{23}Na nmr, are dependent on the symmetry which determines the quadrupolar relaxation rates of ^{27}Al and ^{23}Na, respectively. With respect to the distinction between contact and solvent separated ion-pairs, one can examine the spin–spin interactions between ^{27}Al and ^1H as reflected in the methylene group proton resonance patterns in $AlEt_4^-$ (11). In a solvent separated ion-pair or free anion where t_d symmetry is expected for the $AlEt_4^-$, a nine line pattern is obtained. On the other hand, a quartet signifies a highly distorted anion such as would be expected for a contact ion-pair. Lesser distortions are indicated by line broadening of various extents (*vide infra*).

Our ^{23}Na studies are based on the line widths, and these are determined by the magnitude of the electric field gradient at the sodium nucleus and the rotational correlation time, τ_c. These are discussed in detail elsewhere (10), but the conclusion is that the average lifetime of a solvated species is much longer than the correlation time. This implies that the solvation of the sodium ion by HMPA does not involve rapid exchange of HMPA molecules between solvated cations. A model for the solvation may then be proposed whereby a series of stable stepwise solvated species such as $[Na^+ \cdot 1HMPA|AlEt_4^-]_n^0$, $[Na^+ \cdot 2HMPA|AlEt_4^-]_n^0$, and $[Na^+ \cdot 3HMPA|AlEt_4^-]^0$ are formed. Here the subscript n symbolizes aggregation.

An argument against a maximum solvation number for the sodium ion with HMPA that is greater than four can be made from the ^{23}Na nmr studies. If a 5:1 solvate of the Na^+ exists with HMPA, the loss of t_d symmetry would result in a line broadening of the ^{23}Na resonance, and this should be observed at a 5:1 HMPA:Na^+ ratio relative to that of the 4:1 solvate. Such is not the case, as can be seen in Fig. 1.

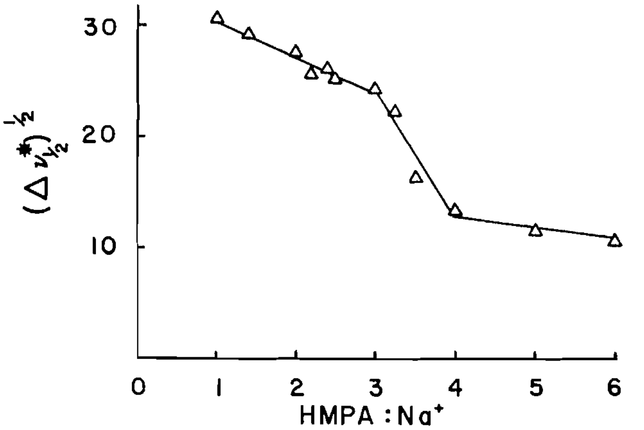

FIG. 1. Viscosity corrected linewidth measurements of ^{23}Na nmr spectra vs. HMPA:Na^+ ratio of 303 K (10).

Solution of $AlEt_4^-$

We can also utilize a symmetry argument to show that HMPA does not solvate the $AlEt_4^-$ anion. After a 4:1 ratio of HMPA:Na^+, the excess HMPA is available to solvate the anion. Such solvation, however, will destroy the cubic symmetry about the ^{27}Al nucleus and, correspondingly, result in the loss of the nine line pattern of the methylene proton resonances. This is not observed to occur even in pure HMPA as a solvent. In fact, a large variety of donors have been studied (8, 9), and we have never seen any indication of solvation of the anion. The ^{27}Al nmr studies reported later in this paper also support this view.

Kinetics

Using a system of the type

$NaAlR_4 - NaAlR'_4$ – benzene – HMPA

we have reported elsewhere (12) that exchange of alkyl groups occurs resulting in a statistical distribution of the various possible alkylaluminate ions. Of interest here is the fact that the rate of exchange is critically dependent on the HMPA:Na^+ ratio; effectively ceasing at an HMPA:Na^+ ratio of 2.5:1. The exchange reactions are interpreted as occurring within contact ion-pairs in which two or more aluminate anions occupy coordination sites on the same Na^+. The cessation of exchange at the HMPA:Na^+ ratio of 2.5:1 is attributed to the formation of solvent bridged species of stoichiometry $[2Na\cdot 5HMPA]^{2+}$. Thus, the mechanism involves mediation by the Na^+ whereby two anions are in contact as

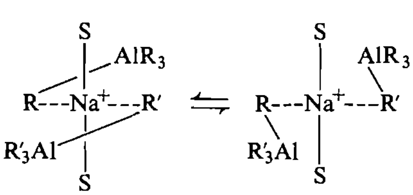

S = HMPA

From the structure

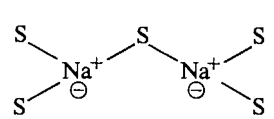

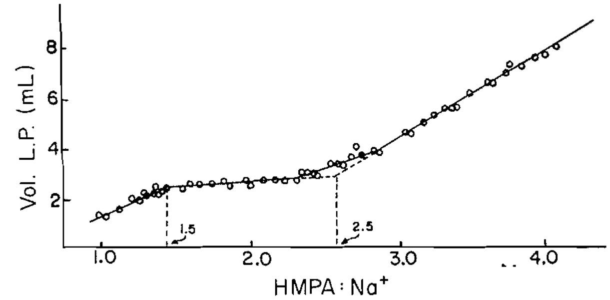

FIG. 2. Volume of the lower phase in mL as a function of mole ratio HMPA:Na^+ at ambient temperature (0.500 g $NaAlEt_4$ used).

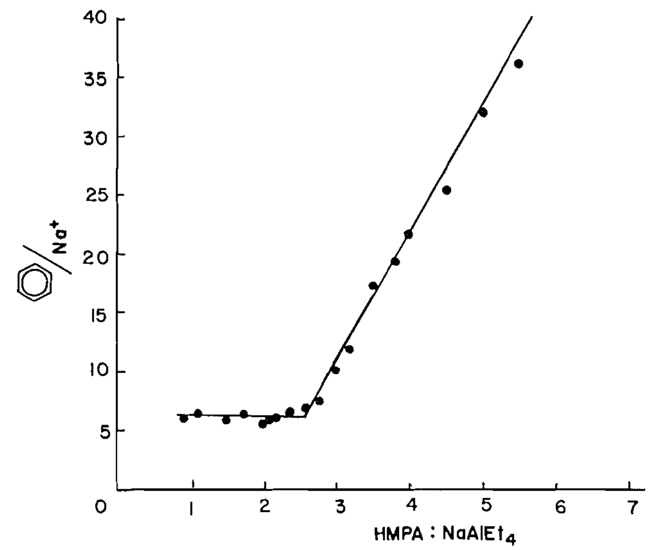

FIG. 3. Ratio of benzene:Na^+ as a function of mole ratio of HMPA:Na^+ at 303 K.

where we see a bridging HMPA molecule, it is apparent that at a HMPA:Na^+ ratio of 2.5:1 it is no longer possible to have two anions coordinated to a given Na^+ and still maintain a sodium ion coordination number of four.

Volume of the lower phase

In Fig. 2, a plot of the volume of the lower phase as a function of the molar HMPA:Na^+ ratio is shown. The curve is most conveniently treated as a collection of linear sections implying the existence of specific solute species at given HMPA:Na^+ ratios. Since there is some benzene in the lower phase, one would tend to attribute the volume increase with increasing HMPA:Na^+ ratio to an increase in the amount of benzene in that phase. However, it can be seen from Fig. 3, that this is not the case. Here the relative amount of benzene as a function of the HMPA:Na^+ ratio is presented. This was determined by integration of proton nmr peaks of benzene and $AlEt_4^-$. Up to an HMPA:Na^+ ratio of 2.5:1, the amount of benzene is seen to remain constant at approximately 6.2 times the salt concentration. Thus, since the quantity of salt (0.500 g) is constant and the HMPA is complexed to Na^+, the volume increase prior to an HMPA:Na^+ ratio of 2.5:1 as shown in Fig. 2, must be totally attributed to the HMPA–$NaAlEt_4$ structure.

Considering only the lower phase volume as a function of mole ratio, it can be noted that: (*1*) The salt concentration in this system is fixed for any given HMPA:Na^+ molar ratio. That is, a lower phase is formed having a particular volume. At a given temperature, this volume is determined only by the HMPA:Na^+ ratio. The relationship between the HMPA:Na^+ ratio and the lower phase volume is given in Table 1. (*2*) Recalling that a fixed quantity of $NaAlEt_4$ (0.500 g) is used and assuming that the HMPA is part of the salt since it is complexed to the Na^+, up to an HMPA:Na^+ ratio of 2.5:1; the weight percent of salt is roughly 50 (ranging from ~42 at an HMPA:Na^+ ratio of 1:1 to ~56 at an HMPA:Na^+ ratio of 2.5:1) but varies with the HMPA:Na^+ ratio. In contrast, the mole percent of salt is constant at ~14. (*3*) The volume increase with an increasing HMPA:Na^+ ratio cannot be attributed simply to the volume of the added HMPA. This is apparent from the relationships taken from Table 1.

HMPA:Na^+ ratio	Δ ratio	Δ volume
1.0:1 → 1.5:1	0.5	1.3 mL
1.5:1 → 2.5:1	1.0	0.7 mL

Here we see that an HMPA:Na^+ ratio change of 0.5 results in a volume change of 1.3 mL, whereas a ratio change of 1.0 (twice as large) results in a volume change of only 0.7 mL.

Solute structures in the lower phase

In attempting to rationalize these data, based on earlier studies, we can say with some confidence that in the system

$NaAlEt_4$ – benzene – HMPA

the following species are predominant in the solution at the indicated HMPA:Na^+ ratios.

Ratio HMPA:Na^+	Species	Reference
0:1	$[\oplus\ominus]_n^0$	13
1:1	$[\mathrm{S}—\oplus\ominus]_n^0$	10, 13
3:1	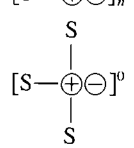	9, 10
4:1	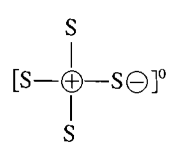	9, 10

The structural identity of the 1.5:1 and 2.5:1 HMPA:Na^+ solvates is more complicated. If, however, we make the following assumptions, we can propose reasonable structures: (*a*) HMPA molecules can bridge between two sodium ions as indicated from the kinetic studies. (*b*) The maximum solvation number of Na^+ with HMPA is four. (*c*) HMPA is a better base towards Na^+ than is $AlEt_4^-$. (*d*) All Na^+ will be equivalent when possible.

Using these assumptions we can propose structures for the intermediate ratios of the general types, but not specifically

HMPA:Na^+ ratio	Structure
1:1	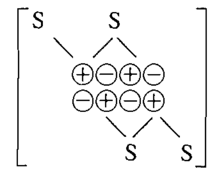
1.5:1	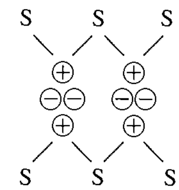
2.5:1	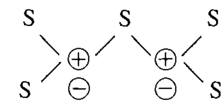

The large increase in volume prior to a 1.5:1 HMPA:Na^+ ratio correlates with the change in structure from aggregates to the more open structure of the proposed 1.5:1 species. It can also be noted that the structural difference between the proposed 1.5:1 and 2.5:1 species is relatively small which corresponds to the relatively small volume change in this region. Finally the large change in volume that occurs after the 2.5:1 HMPA:Na^+ ratio is due to the take-up of benzene in the lower phase.

Two liquid phase systems

The observed benzene:Na^+ molar ratio shown in Fig. 3 is quite confusing. It is of the type found for the liquid clathrate behavior proposed by Atwood for somewhat similar systems (14). It is not at all obvious from structural considerations why this should occur.

The formation of two liquid phases is not particularly rare in non-aqueous solution chemistry. For example, Fuoss and Kraus (15) observed that $(i\text{-amyl})_4$Npicrate forms two liquid phases in benzene above a concentration of 0.1 *M*. Other examples are $HFeCl_4$ (16) and NH_4FeCl_4 (17) in diethylether and similarly Ga_2Cl_4 (17) and $(Bu)_4NAlBu_4$ (18) in benzene. In all of these cases the two phases occur only within a certain range referred to as the miscibility gap. A yet different type of two phase system has been reported by Atwood and co-workers (14) as well as this research group (3). Atwood attributes the two liquid phasing to the formation of liquid clathrates. The unique feature of the liquid clathrates is the apparent inclusion of a fixed number of aromatic molecules per ionic unit in the salt-containing phase. In contrast, Friedman and co-worker (17, 19) have proposed a thermodynamic theory of two phasing based on the effect of an ion-pair dipole on the solution dielectric constant. The dielectric constant of a solution containing predominantly ion-pairs would be expected to increase drastically as the concentration of ion-pairs increases. Ultimately this results in a separation into two phases with different concentrations. The liquid clathrate systems on the other hand

TABLE 1. Dependence of salt concentration on selected mole ratios at ambient temperature (0.500 g $NaAlEt_4$)

Ratio HMPA:$NaAlEt_4$	Lower phase volume (mL)	Salt conc. (mol/L)	Ratio HMPA:$NaAlEt_4$	Lower phase volume (mL)	Salt conc. (mol/L)
0.91	1.02	2.95	2.79	4.30	0.70
1.04	1.32	2.28	2.82	4.40	0.68
1.09	1.74	1.73	3.14	5.17	0.58
1.18	1.97	1.53	3.24	5.43	0.55
1.29	2.20	1.37	3.37	5.88	0.51
1.47	2.49	1.21	3.47	6.23	0.48
1.65	2.76	1.09	3.53	6.33	0.47
1.77	2.75	1.09	3.66	6.91	0.44
1.82	2.90	1.04	3.78	7.29	0.41
1.90	2.95	1.02	4.02	8.03	0.37
2.06	3.00	1.00	4.11	8.48	0.35
2.14	3.05	0.99	4.70	9.49	0.32
2.22	3.07	0.98	4.86	10.20	0.30
2.29	3.26	0.92	4.94	10.34	0.29
2.38	3.40	0.89	5.06	10.58	0.28
2.43	3.42	0.88	5.48	12.74	0.24
2.48	3.59	0.84	5.70	14.54	0.21
2.54	3.82	0.80	5.91	15.36	0.20
2.63	3.88	0.78	6.50	15.40	0.19
2.66	4.19	0.73	7.00	15.50	0.19

appear to contain no electrolyte in the upper phase. In this respect the two phase system

$NaAlEt_4$ – benzene – HMPA

does appear to resemble the liquid clathrate systems.

A third explanation is based upon the extent of solute aggregation. Myers and Metzler (20) observed two phases in the isopropylether extracts of aqueous solutions of HCl and $FeCl_3$. They were able to show that the two phasing results from an aggregation of the ion-pair species. In a system of the type used in the present study, Muller and Day (13) showed that aggregation does occur with the sodium tetraalkylaluminate salts, and that the extent of aggregation decreases with increasing ion–solvent interactions. It can be proposed then that the formation of two liquid phases is related to the extent of aggregation. This does not, however, explain the break in the benzene:Na^+ curve at 2.5:1 as shown in Fig. 3. In fact, none of the three theories is consistent with the observations of this system over the range of HMPA:Na^+ ratios studied, but the behavior up to a 2.5:1 HMPA:Na^+ ratio most closely correlates with the experimental observations of Atwood.

Equivalent conductance and viscosity

The temperature dependence of both the conductance and the viscosity of the system

$NaAlEt_4$ – benzene – HMPA

has been determined as a function of the HMPA:Na^+ ratio. Because of the unique character of this system, interpretations are not straightforward. It was mentioned earlier, for example, that up to an HMPA:Na^+ ratio of 2.5:1, the weight percent of the salt is roughly 50. Further, it can reasonably be assumed that the solute species change with a change in HMPA:Na^+ ratio. Nevertheless, there are some observations that correlate with our solute proposals.

The equivalent conductances of the salt as a function of temperature and HMPA:Na^+ ratio are presented in Fig. 4. If these data are fitted to the Arrhenius equation

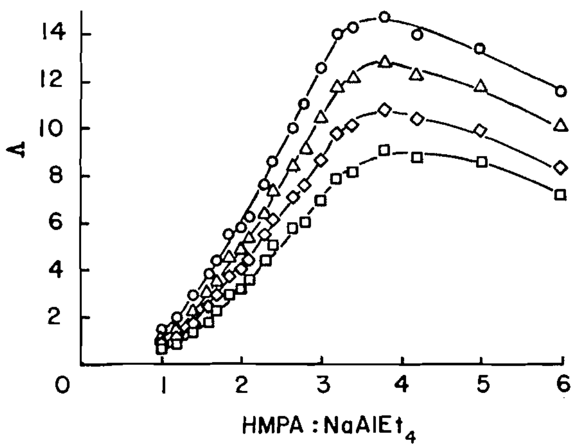

FIG. 4. Equivalent conductance as a function of HMPA:Na^+ ratio: ○, 60°C; △, 50°C; ◇, 40°C; □, 30°C.

$$\ln \Lambda = A - \frac{\Delta E_n^*}{RT}$$

we can obtain the activation energies for ionic mobility as a function of HMPA:Na^+ as shown in Fig. 5. The rapid drop in ΔE_n at a 1.5:1 ratio, a minimum at a 2.5:1 ratio, a leveling off at the 4.0:1 ratio, and a maximum at a 3.0:1 ratio all correlate qualitatively with the proposed structures.

The viscosity, as shown in Fig. 6, is of particular interest. Here we see a strong peak at an HMPA:Na^+ ratio of 2.5:1. The drop off after this maximum can readily be attributed to the increase in the amount of benzene in the lower phase. What is not obvious is the reason for the increase in viscosity prior to the 2.5:1 ratio. Note that in this region, the volume is actually increasing in spite of the fact that the number of moles of both benzene and salt remain constant. Thus, the increase in volume is apparently due to structural changes occurring in the salt on the addition of HMPA. These same structural changes must result in the observed viscosity increase. Qualitatively, this

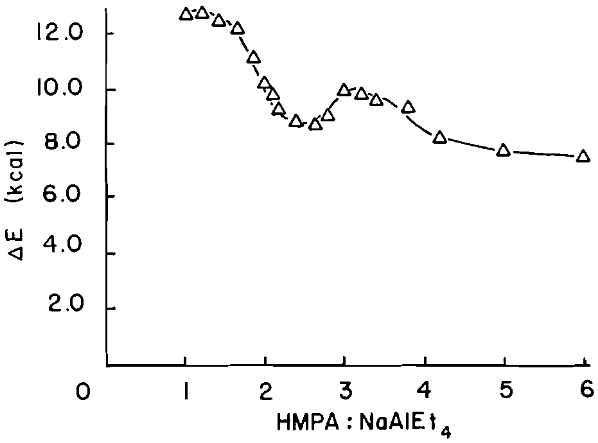

FIG. 5. Activation energy for ionic mobility as a function of HMPA:Na^+ ratio.

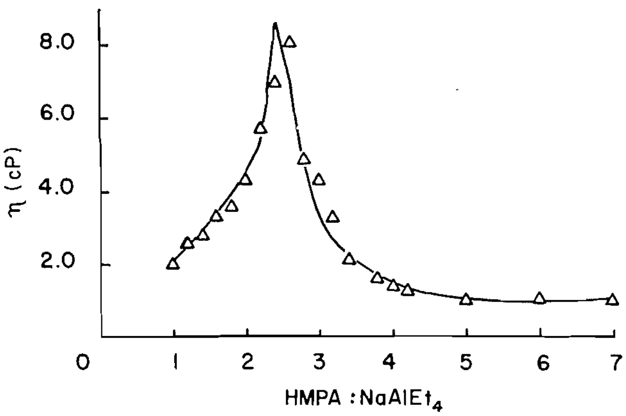

FIG. 6. Viscosity as a function of HMPA:Na^+ ratio at 30°C.

correlates well with the proposed change from a compact aggregate structure at lower HMPA:Na^+ ratios to more open chain-like structures in the 1.5:1 to 2.5:1 ratio range.

Nuclear magnetic resonance studies

The ^{23}Na nmr studies of the system

$NaAlEt_4$ – benzene – HMPA

have been discussed elsewhere (10). Here we will focus on the ^{27}Al and ^{1}H nmr studies of this system.

Aluminum nmr

The ^{27}Al linewidths are a full order of magnitude less than the corresponding sodium linewidths. There are several reasons for this. First, since the linewidth is proportional to the term $(2I + 3)/I^2(2I - 1)$, the spin 5/2 ^{27}Al nucleus has an intrinsically narrower linewidth than the spin 3/2 ^{23}Na nucleus. In addition, the quadrupole coupling constant (e^2qQ/h) for the aluminum nucleus must be significantly different from that for the sodium nucleus to give rise to such a great disparity in the linewidths. Since ^{27}Al and ^{23}Na have very similar quadrupole moments, $Q = 0.15$ and 0.14 Barnes, respectively, there must then be a much larger electric field gradient, q, produced at the sodium ion. This is certainly not unreasonable. It has been shown that the electric field gradient at the sodium ion is affected by both the number of HMPA molecules in the complex and by the proximity of the anion (10). On the other hand, since in this system solvation occurs only at the cation, the electric field gradient at the aluminum nucleus can, therefore,

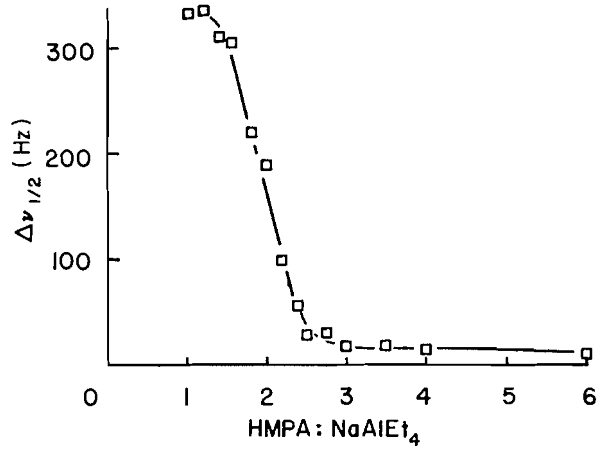

FIG. 7. ^{27}Al linewidth at half height (proton noise decoupled) vs. HMPA:Na^+ ratio at ambient temperature.

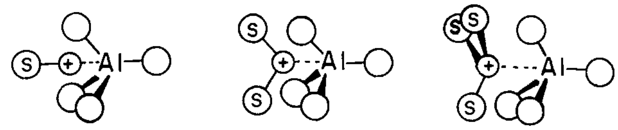

FIG. 8. Proposed effect of donor molecules on the proximity of a Na^+ to an $AlEt_4^-$ ion.

be affected only by the proximity of the cation. Because of the high molecular symmetry possessed by the unperturbed tetraalkylaluminate anion, the electric field gradient at the ^{27}Al nucleus should be particularly sensitive to interaction with the cation and, due to the spherical symmetry of the sodium ion, the interaction should depend only on the cation–anion distance and not the orientation.

The dependence of the proton-decoupled ^{27}Al linewidth on the mole ratio is given in Fig. 7. The important feature here is the sharp decrease in linewidth from a maximum at a 1:1 ratio with a leveling off at a 2.5:1 ratio of HMPA:Na^+. This implies that there is a significant decrease in the electric field gradient at a 2.5:1 ratio relative to that at a 1:1 ratio. The leveling off of the curve well before the formation of solvent separated ion-pairs implies that the electric field gradient relaxation broadening is less than the intrinsic linewidth of the ^{27}Al nucleus.

An explanation for this result is that there is an increase in the cation size upon successive complexation. This then imposes a steric restriction on the approach of the cation to the anion. Because of the stability of the $Na^+\cdot$HMPA complexes up to a 4:1 HMPA:Na^+ ratio and the greater basicity of HMPA than $AlEt_4^-$ towards the Na^+, qualitatively the expected effect might be as seen in Fig. 8. A minimum linewidth would be expected at a 4:1 ratio of HMPA:Na^+ and, in light of the structures proposed in Fig. 8, it would not be unexpected to see it approached at a 3:1 ratio. In addition, from the proposed bridged structure for the 2.5:1 HMPA:Na^+ ratio, it can be seen that the proximity of the cation to the anion is essentially the same as it is for the 3:1 complex. Consequently the approximately zero slope of the curve in this region (2.5–4.0) can be rationalized.

Further, the correlation time for the ^{27}Al resonance is not the same as for the ^{23}Na resonance. This is apparent from the lack of any viscosity dependence of the ^{27}Al linewidth as can be seen in Fig. 7, thereby ruling out the simple rotational diffusion model which adequately describes the ^{23}Na correlation time. If the same ion–ion interactions were responsible for the electric field gradient at the sodium nucleus and the aluminum nucleus, then the correlation function for both nuclei should be similar. This is apparently not the case.

This can be rationalized by again noting that solvation by HMPA occurs only at the cation. Therefore any electric field gradient produced by the presence of the HMPA will be directly affective only at the sodium ion. The electric field gradient at the sodium ion then depends on both ion–solvent and ion–ion interactions. In contrast, since there are no specific ion–solvent interactions at the anion, the electric field gradient at the aluminum nucleus will be dependent only on the ion–ion interactions. Thus, two separate correlation functions relating to the electric field gradient at the sodium ion and at the aluminum nucleus can be proposed. For the sodium ion, it has been shown that the rotational diffusion model is sufficient (10). However, for the aluminum nucleus, the fluctuating electric field gradient must be produced by a change in the ion–ion interactions. Such a change could result from either a rapid equilibrium between ion-pairs and free ions or a vibration of the ion-pair species. Ion-pair vibrations are well known and have been observed by Tsatsas and Risen (21) for $NaAlBu_4$. Therefore, it seems reasonable to attribute the fluctuating electric field gradient at the aluminum nucleus to an ion-pair vibrational motion.

Proton nmr

The scalar coupling between the proton resonance and the quadrupolar ^{27}Al nucleus renders the proton nmr spectra an excellent probe of ion–ion interactions. As was pointed out earlier, Ahmad and Day (9) used this to differentiate between contact and solvent separated ion-pairs in this system. For the donor, HMPA, it was shown that a well-defined quartet attributed to contact ion-pairs is observed at a 1:1 ratio of HMPA:Na^+ while a nine-line pattern attributed to solvent separated ion-pairs is observed at a 4:1 ratio. The exact mechanism for the transition between the two ion-pair types was not discussed. There are two possible mechanisms for such a transition. In the first mechanism, the complexed species can be considered to exist in only two forms, contact and solvent separated ion-pairs. All intermediate spectra would correspond to equilibrium distributions between the two ion-pair types. However, it has been shown by ^{23}Na nmr (10) that the complexation occurs via the formation of a series of stable complexes, and one can posit a characteristic ^1H nmr spectrum for each of these. This gradual transition via sequential complexes forms the second mechanism.

It is well recognized that the nmr signals arising from spin 1/2 nuclei which are scalar coupled to nuclei of spin greater than 1/2 are broadened by the rapid quadrupole-electric field gradient relaxation undergone by the latter. With respect to the scalar relaxation process responsible for the proton lineshape, Abragam (22) has defined two distinct processes: scalar relaxation of the first kind resulting from chemical exchange processes and scalar relaxation of the second kind resulting from scalar coupling to a rapidly relaxing nucleus. A significant result of Abragam's discussion is that the lineshape equation has the same functional form for both processes. Consequently, it is not a trivial problem to distinguish between chemical exchange broadening and quadrupole broadening.

The proton nmr spectrum of $NaAlEt_4$ may be viewed as a simple A_2M_3X system. Since the AM coupling is not affected

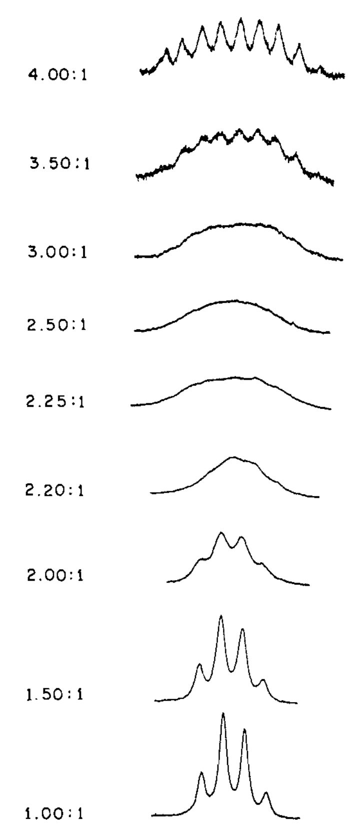

FIG. 9. ^1H nmr spectra of —CH_2— in $NaAlEt_4$ at different HMPA:Na^+ ratios at ambient temperature.

to any large extent by the quadrupole relaxation of X, the limiting spectra are a quartet resulting from J_{AM} and a multiplet resulting from both J_{AM} and J_{AX}. In the tetraethylaluminate anion, the values of J_{AM} and J_{AX} are such that, instead of the expected 24 lines, there are only nine lines (11*b*). Since J_{AM} can be determined from the quartet splitting, there is only one value of J_{AX} which will give rise to a symmetrical nine-line pattern. It is then possible to compare the quadrupole relaxation time with the value of J_{AX} and gain some insight into the expected lineshapes based upon a pure scalar relaxation process of the second kind.

The methylene resonance of the anion as a function of the mole ratio HMPA:$NaAlEt_4$ is shown in Fig. 9. It can be noted that the resolution of the quartet becomes lost completely at a ratio of 2.20:1. Additionally, the spectrum rapidly becomes a broad featureless hump showing no fine structure until approximately 3.5:1. Re-examining Fig. 7, it can be seen that the ^{27}Al relaxation time is undergoing a drastic increase in this region (1.5–2.5). According to Abragram's theoretical treatment of the A_3X case, the value of the relaxation time must drop to approximately $1/(10\pi J_{AX})$ in order to yield a sharp spectrum in which the AX coupling is not observed. Since the $^3J_{H-H}$ coupling constant is 7.5 Hz, the value of $^2J_{Al-H}$ can be calculated by a spectrum simulation program (PANIC.81 on the ASPECT 2000 computer) and is found to be 8.5 Hz. Therefore, by the relation $\Delta\nu_{1/2} = 1/\pi T_2$, and Abragam's relationship the linewidth of the ^{27}Al resonance should be in the vicinity of 85 Hz. The measured ^{27}Al linewidth at a ratio 2.2:1 is 99 Hz, thus providing a very strong indication that the proton lineshape is the result of a pure quadrupole broadening effect.

For scalar relaxation of the second kind, the effect of tem-

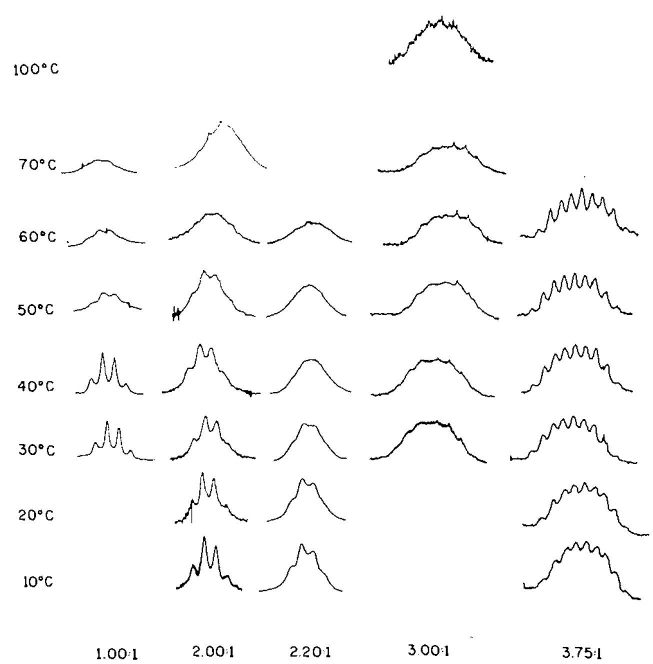

FIG. 10. Temperature dependence of ^{1}H nmr spectra of —CH_2— in $NaAlEt_4$ at different HMPA:Na^+ ratios.

perature should be to decrease the correlation time, τ_c, and increase the relaxation time by the equation

$$\frac{1}{T_1} = \frac{1}{T_2} = \frac{3}{40}\frac{2I+3}{I^2(2I-1)}\left(1+\frac{\sigma^2}{3}\right)\left(\frac{e^2Qq_{zz}}{\hbar}\right)^2\tau_c$$

Therefore, the ^{1}H spectra corresponding to longer relaxation times should be expected at higher temperatures. In Fig. 10, the temperature dependence of the ^{1}H spectra is shown for several ratios. It can be seen that the quartet becomes broadened at higher temperatures while the nine-line multiplet becomes better resolved, exactly as expected for a quadrupole broadening. However, it can also be argued that an exchange mechanism between ion-pairs and free ions would yield similar results. At high temperatures free ions would be more favored than at low temperatures.

In order to distinguish between a pure quadrupole mechanism and the equilibrium process, the ^{27}Al decoupled proton nmr spectrum was recorded for a 2.50:1 HMPA:Na^+ ratio. At this ratio, the proton line is extensively broadened. If the line broadening is the result of such an equilibrium then the chemical shift difference between contact ion-pairs and free ions should cause an extensive broadening to remain even in the complete absence of the aluminum-proton coupling. In Fig. 11, the ^{27}Al decoupled proton nmr spectra of a 2.5:1 ratio in toluene is shown as a function of temperature. There is no indication of any significant line broadening over the range of temperatures studied. On this basis, it can be concluded that the proton nmr lineshape does not result from any equilibrium process between ion-pair types. Rather, the lineshape is determined solely by the scalar coupling constants and the ^{27}Al spin–lattice relaxation time.

Summary

Of particular interest in this study is the fact that the HMPA:Na^+ ratio of 2.5:1 is a unique number for this system. A logical interpretation of the origin of this ratio is a bridging donor molecule between two Na^+ with the strongest support for

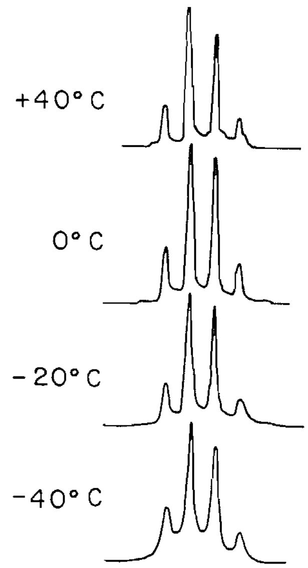

FIG. 11. Temperature dependence of ^{27}Al decoupled ^{1}H nmr spectra of —CH_2— in $NaAlEt_4$ for a 2.5:1 HMPA:$NaAlEt_4$ ratio in toluene.

this argument being found in the kinetic studies. It, however, is also observed in the viscosity, ^{27}Al nmr, transport activation energy, and both the volume of the lower phase and the benzene:Na^+ ratio as a function of HMPA:Na^+ ratio.

If previously determined solute structures are utilized along with the assumptions (*a*) HMPA molecules can bridge between two sodium ions as indicated from the kinetic studies; (*b*) the maximum solvation number of Na^+ is four towards HMPA; (*c*) HMPA is a better base towards Na^+ than is $AlEt_4^-$; (*d*) all Na^+ will be equivalent when possible reasonable solute structures can be proposed for HMPA:Na^+ ratios between 1:1 and 4:1.

A number of additional conclusions are supported by this study. These are (*1*) HMPA is a strong donor towards Na^+; (*2*) successive solvates (1:1, 2:1, 3:1, 4:1) of lifetimes that are long relative to the nmr time scale are formed; (*3*) the maximum solvation number of Na^+ by HMPA is four; (*4*) the $AlEt_4^-$ ion is not solvated by HMPA; (*5*) liquid clathrate type behavior is observed in this system up to an HMPA:Na^+ ratio of 2.5:1; (*6*) the viscosity change up to an HMPA:Na^+ ratio of 2.5:1 is dependent on structural changes of the solute; and (*7*) the ^{1}H and ^{27}Al nmr spectra are determined predominantly by quadrupole relaxation of the ^{27}Al nucleus rather than by exchange.

Acknowledgements

The authors wish to express their appreciation for the support of this work by the National Science Foundation through NSF grant CHE-8004473 and to the Ethyl Corporation for the aluminum alkyls. We wish to thank Dr. F. R. Fronczek for the X-ray measurements and Professor George S. Tracy of the Department of Experimental Statistics for the treatment of the data for the HMPA:Na^+ dependence of the volume of the lower phase.

1. (*a*) M. C. DAY. Pure Appl. Chem. **49**, 75 (1977); (*b*) J. L. GRAY and G. E. MACIEL. J. Phys. Chem. **87**, 5290 (1983); (*c*) J. L. GRAY and G. E. MACIEL. J. Phys. Chem. **87**, 5418 (1983).
2. M. C. DAY, H. M. BARNES, and A. J. COX. J. Phys. Chem. **68**, 2595 (1964).
3. N. AHMAD and M. C. DAY. J. Inorg. Nucl. Chem. **40**, 1383 (1978).

4. (*a*) F. W. FREY, JR., P. KOBETZ, G. C. ROBINSON, and T. O. SISTRUCK. J. Org. Chem. **26**, 2950 (1961); (*b*) E. SCHASCHEL and M. C. DAY. J. Am. Chem. Soc. **90**, 503 (1968).
5. T. D. WESTMORELAND, JR., N. AHMAD, and M. C. DAY. J. Organomet. Chem. **25**, 329 (1970).
6. R. BURTON and L. D. HALL. Can. J. Chem. **48**, 59 (1970).
7. V. GUTMANN. Coordination chemistry in nonaqueous solvents. Springer Verlag, Vienna, 1968.
8. M. C. DAY, J. H. MEDLEY, and N. AHMAD. Can. J. Chem. **61**, 1719 (1983).
9. N. AHMAD and M. C. DAY. J. Am. Chem. Soc. **99**, 941 (1977).
10. J. H. MEDLEY, E. S. MOOBERRY, and M. C. DAY. Can. J. Chem. **61**, 558 (1983).
11. (*a*) E. S. GORE and H. S. GUTOWSKY. J. Phys. Chem. **73**, 2515 (1969); (*b*) T. D. WESTMORELAND, N. S. BHACCA, J. D. WANDER, and M. C. DAY. J. Organomet. Chem. **38**, 1 (1972).
12. N. AHMAD, F. K. CARTLEDGE, M. C. DAY, and J. H. MEDLEY. Organometallics, **3**, 389 (1984).
13. J. H. MULLER and M. C. DAY. J. Phys. Chem. **76**, 3472 (1972).
14. (*a*) J. L. ATWOOD and J. D. ATWOOD. Adv. Chem. Ser. **150**, 112 (1976); (*b*) J. L. ATWOOD and W. R. NEWBERRY, III. J. Organomet. Chem. **65**, 145 (1974).
15. R. M. FUOSS and C. A. KRAUS. J. Am. Chem. Soc. **55**, 3617 (1933).
16. J. HOUBON and W. FISCHER. J. Prakt. Chem. **123**, 89 (1929).
17. H. L. FRIEDMAN. J. Phys. Chem. **66**, 1595 (1962).
18. J. IMHOF, T. D. WESTMORELAND, and M. C. DAY. J. Soln. Chem. **3**, 83 (1974).
19. H. L. FRIEDMAN and B. LARSEN. J. Chem. Phys. **70**, 92 (1979).
20. R. J. MYERS and D. E. METZLER. J. Am. Chem. Soc. **72**, 3772 (1950).
21. A. T. TSATSAS and W. M. RISEN. J. Am. Chem. Soc. **92**, 1789 (1970).
22. A. ABRAGAM. Principles of nuclear magnetism. Clarendon Press, Oxford. 1961.

Configurational and conformational studies on condensation products of biogenic amines with 2,5-anhydro-D-mannose

IAN M. PIPER, DAVID B. MACLEAN,[1] ROMOLO FAGGIANI, AND COLIN J. L. LOCK
Department of Chemistry, McMaster University, Hamilton, Ont., Canada L8S 4M1

AND

WALTER A. SZAREK[1]
Department of Chemistry, Queen's University, Kingston, Ont., Canada K7L 3N6

Received December 19, 1984

IAN M. PIPER, DAVID B. MACLEAN, ROMOLO FAGGIANI, COLIN J. L. LOCK, and WALTER A. SZAREK. Can. J. Chem. **63**, 2915 (1985).

The products of a Pictet–Spengler condensation of tryptamine and of histamine with 2,5-anhydro-D-mannose have been studied by X-ray crystallography to establish their absolute configuration. 1(*S*)-(α-D-Arabinofuranosyl)-1,2,3,4-tetrahydro-β-carboline (**1**), $C_{16}H_{20}N_2O_4$, is monoclinic, $P2_1$ (No. 4), with cell dimensions a = 13.091(4), b = 5.365(1), c = 11.323(3) Å, β = 115.78(2)°, and Z = 2. 4-(α-D-Arabinofuranosyl)imidazo[4,5-*c*]-4,5,6,7-tetrahydropyridine (**3**), $C_{11}H_{17}N_3O_4$, is orthorhombic, $P2_12_12_1$ (No. 19), with cell dimensions a = 8.118(2), b = 13.715(4), c = 10.963(3) Å, and Z = 4. The structures were determined by direct methods and refined to R_1 = 0.0514, R_2 = 0.0642 for 3210 reflections in the case of **1**, and to R_1 = 0.0312, R_2 = 0.0335 for 1569 reflections in the case of **3**. Bond lengths and angles within both molecules are normal and agree well with those observed in related structures. In **3** the base and sugar adopt a *syn* arrangement, which is maintained by an internal hydrogen bond between O(2′) and N(3). The sugar adopts a normal $^2T_3$ twist conformation. The sugar has the opposite *anti* arrangement in the β-carboline **1** and the conformation of the sugar is unusual; it is close to an envelope conformation with O(4′) being the atom out of the plane. This conformation is caused by a strong intermolecular hydrogen bond from O(5′) in a symmetry-related molecule to O(4′). Both compounds are held together in the crystal by extensive hydrogen-bonding networks. The conformations of the compounds in solution have been investigated by ^{1}H nmr spectroscopy, and the results obtained were compared with those obtained by X-ray crystallography for **1** and **3**.

IAN M. PIPER, DAVID B. MACLEAN, ROMOLO FAGGIANI, COLIN J. L. LOCK et WALTER A. SZAREK. Can. J. Chem. **63**, 2915 (1985).

Faisant appel à la diffraction des rayons X, on a étudié la nature des produits de condensation du type Pictet–Spengler de la triptamine et de l'histamine avec l'anhydro-2,5 D-mannose et on a établi leur configuration absolue. Le composé (α-D-arabinofurannosyl)-1(*S*) tétrahydro-1,2,3,4 β-carboline (**1**), $C_{16}H_{20}N_2O_4$, appartient au groupe d'espace monoclinique $P2_1$ (No. 4), avec a = 13,091(4), b = 5,365(1), c = 11,323(3) Å, β = 115,78(2)° et Z = 2. Le composé (α-D-arabinofurannosyl)-4 imidazo[4,5-*c*] tétrahydro-4,5,6,7 pyridine (**3**), $C_{11}H_{17}N_3O_4$, appartient au groupe d'espace orthorhombique $P2_12_12_1$ (No. 19) avec a = 8,118(2), b = 13,715(4), c = 10,963(3) Å et Z = 4. On a déterminé les structures par des méthodes directes et on les a affinées jusqu'à des valeurs de R_1 = 0,0514 et de R_2 = 0,0642 pour 3210 réflexions dans le cas du composé **1** et à des valeurs de R_1 = 0,0312 et de R_2 = 0,0335 pour 1569 réflexions dans le cas du composé **3**. Les deux molécules ont des longueurs de liaisons et des angles normaux qui s'accordent bien avec ceux observés dans des structures apparentées. Dans le cas du composé **3**, l'unité de sucre et celle de la base adoptent un arrangement *syn* que des liaisons hydrogènes internes entre le O(2′) et le N(3) maintiennent en place. L'unité de sucre adopte une conformation croisée $^2T_3$ qui est normale. L'unité de sucre du composé β-carbolino **1** adopte l'arrangement opposé, *anti*, et sa conformation est inhabituelle. Elle se rapproche d'une conformation enveloppe avec l'atome O(4′) hors du plan. Cette conformation est due à une forte liaison hydrogène intermoléculaire entre le O(5′) d'une molécule apparemment symétrique et le O(4′). Les deux composés sont reliés dans le cristal par un réseau intense de liaisons hydrogènes. Faisant appel à la spectroscopie de rmn, on a étudié les conformations des composés **1** et **3** en solution et on a comparé les résultats à ceux obtenus par diffraction des rayons X sur les mêmes composés.

[Traduit par le journal]

Introduction

In a recent paper (1), the synthesis was reported of a number of novel *C*-nucleosides arising from the Pictet–Spengler condensation of biogenic amines with 2,5-anhydro-D-mannose. The compounds so obtained have in common an α-D-arabinofuranosyl moiety attached to a ring-fused tetrahydropyridine nucleus. We report here an X-ray crystallographic study of two of these compounds, **1** and **3**, which has established their absolute configuration, and hence that of the epimer (**2**) of **1**, at the carbon center at which the sugar unit is attached. Information about the conformations of the compounds in solution has been deduced from an ^{1}H nmr spectroscopic examination. The results obtained have been compared with those obtained by X-ray crystallography for the solid state.

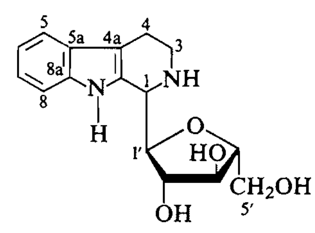

1 1(*S*)-isomer
2 1(*R*)-isomer

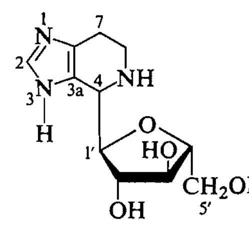

3 4(*S*)-isomer

Results and discussion

The reaction of tryptamine hydrochloride and 2,5-anhydro-D-mannose was reported (1) to yield a mixture of two isomers, namely 1(*R*)- and 1(*S*)-(α-D-arabinofuranosyl)-1,2,3,4-

[1]Authors to whom correspondence may be addressed.

tetrahydro-β-carboline, in the approximate ratio of 40:60. Each of these was obtained pure; however, the configuration at C(1) was not determined. This information now has been obtained by an X-ray crystallographic structure determination. The structure of the major isomer **1** is illustrated in Fig. 1, from which it is evident that the configuration at C(1) is *S*; the minor isomer **2** then must have the *R* configuration at C(1).

In Table 1 are listed selected interatomic distances and angles for **1**. For the most part, the values obtained for bond lengths and angles within the β-carboline moiety agree well with those found for 1,2,3,4-tetrahydroharman-3-carboxylic acid (**4**) (2); the exceptions are the values obtained for the lengths of the C(1)–N(2) (1.475(5) Å) and N(2)–C(3) (1.487(4) Å) bonds, which are 0.047 Å and 0.030 Å shorter, respectively, in **1** than in the harman derivative. This difference is attributable presumably to the fact that the nitrogen atom in **4** is protonated. As a consequence of the shorter distances, the internal ring angles at C(1) and C(3) are slightly larger in **1** than in **4**. The values obtained for the bond lengths and angles in the sugar moiety are in good agreement with those for 9-α-D-

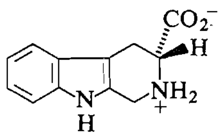

4

arabinofuranosyladenine (3) and the more accurate values for 9-β-D-arabinofuranosyladenine (4). The χ torsion angle, N(2)C(1)C(1′)O(4′), is −66(1)°, a value in the *anti* range, namely −30° to −72°, observed (5) for α-nucleosides.[2] The conformation at the exocyclic C(4′)—C(5′) bond is *gauche–trans*. The conformation of the furanoid ring is unusual and can be regarded as an envelope having O(4′) 0.544(4) Å out of the plane of the other four atoms. This unusual conformation is caused by a very strong intermolecular hydrogen bond (see below).

The packing of **1** is shown in Fig. 2. The important feature of the structure is the spiral chain of molecules up the *b* axis related by the 2_1 axis at $x = 1/2$, $z = 1/2$. A molecule in the chain is bound to the next by the N(9)—H(9)...O(5′) and O(5′)—H(5″)...O(4′) hydrogen bonds. These intermolecular hydrogen bonds determine the conformation of the molecule. The latter bond is particularly strong (O(1)...O(4′) 2.757(4) Å); in addition, there is a further hydrogen bond near the *c* face, O(3′)—H(3″)...O(2′), between translationally equivalent molecules along *c*. Interactions between these chains in the *a* and *c* directions are almost entirely van der Waals, the exception being an O(2′)—H(2′)...N(2) hydrogen bond in the *c* face.

The molecular structure of **3** is shown in Fig. 3 and selected interatomic distances and angles are given in Table 2. Bond lengths and angles in the nitrogen-containing moiety agree well with those found in histamine (6). The C(2)—N(3) distance (1.323(3) Å) is longer by 0.02 Å than the corresponding bond in histamine, and the C(6)—N(5) distance (1.483(3) Å) is longer by 0.035 Å. The bond angles N(1)—C(7a)—C(7) (125.6(2)), C(3a)—C(7a)—C(7) (125.6(2)), C(7a)—C(7)—C(6) (107.2(2)), and C(7)—C(6)—N(5) (110.3(2)°) are

[2]The values for the glycosyl torsion angle, χ(C(8)N(9)C(1′)O(4′)), in two crystallographically-independent molecules of 9-α-D-arabinofuranosyladenine have been found to be −64(2)° and −73(2)° (3).

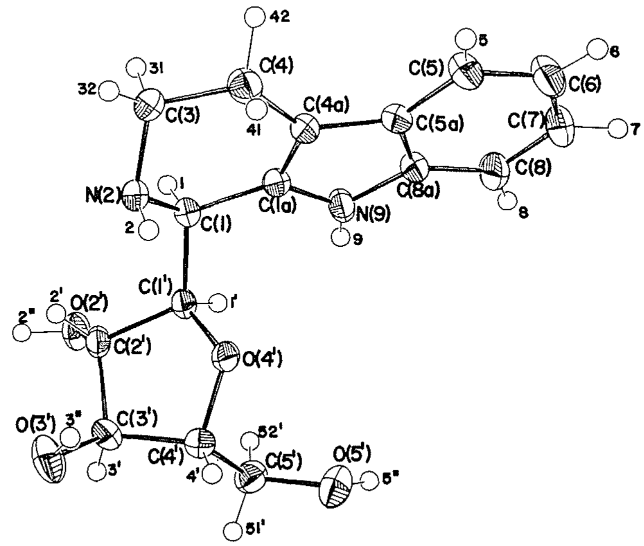

FIG. 1. The molecular structure of 1(*S*)-(α-D-arabinofuranosyl)-1,2,3,4-tetrahydro-β-carboline (**1**).

smaller by 2.9°, 5.8°, 7.6°, and 4.5°, respectively, than the corresponding angles in histamine. The changes in the bond angles and that in the distance of the C(6)—N(5) bond are a consequence of the differences in structure. The values obtained for the bond lengths and angles in the sugar moiety again agree well with those previously determined (3, 4). The χ torsion angle, N(5)C(4)C(1′)O(4′), is 73.7(2)°, a value consistent with a *syn* arrangement of the sugar moiety with respect to the base. The conformation of the furanoid ring is $^3T_2$ and the conformation at the exocyclic C(4′)—C(5′) bond is *gauche–trans*.

The packing of **3** is shown in Fig. 4 in which it is apparent that a strong three-dimensional hydrogen-bonding network holds the crystal together through the bonds N(1)—H(1)...O(5′), O(3′)—H(3″)...N(5), and O(5′)—H(5″)...O(3′).

Conformations in solution of the α-D-arabinofuranosyl moieties by ¹H nmr spectroscopy

The conformations of the sugar rings in the solid state in **1** and **3** were discussed in the previous section and it was of interest to compare these conformations with those in solution. ¹H nuclear magnetic resonance experiments have been widely used to study the conformation of β-nucleosides in solution (7) and we have applied this method to compounds **1–3**. The method relies upon the use of the Karplus relationship in relating the dihedral angle of C—H bonds on adjacent carbon atoms to the vicinal coupling constant between the H atoms. Recently, Ekiel *et al.* (8) have reported an extension of this method to the conformational analysis of α-D-arabinofuranosyl nucleosides. A central assumption of this method is the existence predominantly in solution of a two-state equilibrium, the extreme forms of which are shown (for the case of α-D-arabinofuranosyl nucleosides) in Fig. 5 (for rules of nomenclature, see ref. 9). Using this assumption, comparison of the observed vicinal coupling constants with calculated values for the extreme conformers permits an estimate of relative populations of $^3T_2$ (Type N) and $^2T_3$ (Type S) to be made, thereby giving the average conformation in solution.

The assumption of a two-state equilibrium has been described recently (10) as an oversimplification in studies of this

TABLE 1. Selected interatomic distances (Å) and angles (deg) for **1**

Bond	Distance	Bond	Distance
C(1)—N(2)	1.475(5)	N(2)—C(3)	1.487(4)
C(3)—C(4)	1.530(4)	C(4)—C(4a)	1.488(5)
C(4a)—C(5a)	1.440(3)	C(5a)—C(5)	1.408(4)
C(5)—C(6)	1.379(4)	C(6)—C(7)	1.393(5)
C(7)—C(8)	1.392(4)	C(8)—C(8a)	1.398(4)
C(8a)—N(9)	1.391(3)	N(9)—C(1a)	1.388(4)
C(1a)—C(1)	1.506(3)	C(4a)—C(1a)	1.357(5)
C(5a)—C(8a)	1.403(5)	C(1)—C(1′)	1.528(4)
C(1′)—C(2′)	1.535(2)	C(2′)—O(2′)	1.408(5)
C(2′)—C(3′)	1.548(4)	C(3′)—O(3′)	1.417(5)
C(3′)—C(4′)	1.533(3)	C(4′)—O(4′)	1.449(3)
C(4′)—C(5′)	1.512(5)	C(5′)—O(5′)	1.424(4)
C(1′)—O(4′)	1.433(5)		

Hydrogen bonds[a]					
N(9)...O(5′)i	2.935(5)	N(9)—N(9)	0.93(5)	H(9)...O(5′)i	2.02(5)
O(2′)...N(2)ii	2.741(3)	O(2′)—H(02′)	0.91(5)	H(02′)...N(2)ii	1.86(5)
O(3′)...O(2′)iii	2.840(5)	O(3′)—H(03′)	0.86(5)	H(03′)...O(2′)iii	2.05(6)
O(5′)...O(4′)i	2.757(4)	O(5′)—H(05′)	0.92(5)	H(05′)...O(4′)i	1.86(5)

Bonds	Angle	Bonds	Angle
C(1a)—C(1)—N(2)	109.9(3)	C(1)—N(2)—C(3)	112.2(2)
N(2)—C(3)—C(4)	113.8(3)	C(3)—C(4)—C(4a)	109.6(3)
C(4)—C(4a)—C(5a)	130.0(3)	C(4)—C(4a)—C(1a)	123.1(2)
C(1a)—C(4a)—C(5a)	106.9(3)	C(4a)—C(5a)—C(5)	133.5(3)
C(4a)—C(5a)—C(8a)	107.1(2)	C(5)—C(5a)—C(8a)	119.5(2)
C(5a)—C(5)—C(6)	118.6(4)	C(5)—C(6)—C(7)	121.1(3)
C(6)—C(7)—C(8)	121.9(3)	C(7)—C(8)—C(8a)	116.8(3)
C(8)—C(8a)—C(5a)	122.2(3)	C(8)—C(8a)—N(9)	130.0(3)
C(5a)—C(8a)—N(9)	107.8(2)	C(8a)—N(9)—C(1a)	107.9(3)
N(9)—C(1a)—C(4a)	110.2(2)	N(9)—C(1a)—C(1)	125.2(3)
C(4a)—C(1a)—C(1)	124.6(3)	C(1a)—C(1)—C(1′)	111.7(2)
N(2)—C(1)—C(1′)	111.3(2)	C(1)—C(1′)—C(2′)	116.5(2)
C(1)—C(1′)—O(4′)	109.5(3)	C(1′)—C(2′)—C(3′)	104.4(2)
C(1′)—C(2′)—O(2′)	109.7(2)	O(2′)—C(2′)—C(3′)	115.5(3)
C(2′)—C(3′)—C(4′)	104.3(2)	C(2′)—C(3′)—O(3′)	112.8(3)
C(4′)—C(3′)—O(3′)	112.3(3)	C(3′)—C(4′)—O(4′)	104.3(2)
C(3′)—C(4′)—C(5′)	112.7(3)	C(5′)—C(4′)—O(4′)	111.9(2)
C(4′)—C(5′)—O(4′)	109.2(3)	C(4′)—O(4′)—C(1′)	106.5(3)
O(4′)—C(1′)—C(2′)	105.0(2)		

[a] i–iii, Atoms are related to those given in Table 5 by the transformations i, $1 - x, y - 1/2, 1 - z$; ii, $1 - x, y - 1/2, -z$; iii, $x, 1 + y, z$.

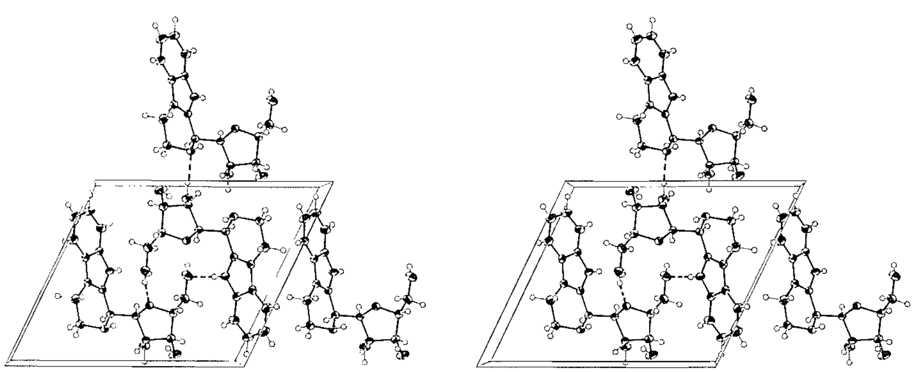

FIG. 2. The packing of **1** within the unit cell; ***a*** and ***c*** are parallel to the bottom and sides of the page, respectively, and the view is down ***b***.

type, better results being obtained in several cases by invoking a three-state equilibrium involving $^3T_2$, $^2T_3$, and the conformation in the crystal (when the latter is neither $^3T_2$ nor $^2T_3$). However, Ekiel *et al.* (8) report in one case a close correlation between the crystal conformation and the observed conformation in solution.

In the present study, it is clear that the conformation in solution need not be related to the crystal conformation, be-

TABLE 2. Selected interatomic distances (Å) and angles (deg) for **3**

Bond	Distance	Bond	Distance
N(1)—C(2)	1.346(3)	C(2)—N(3)	1.323(3)
N(3)—C(3a)	1.383(2)	C(3a)—C(7a)	1.358(3)
C(7a)—N(1)	1.368(3)	C(3a)—C(4)	1.502(3)
C(4)—N(5)	1.486(2)	N(5)—C(6)	1.483(3)
C(6)—C(7)	1.525(3)	C(7)—C(7a)	1.489(3)
C(4)—C(1′)	1.517(3)	C(1′)—C(2′)	1.539(3)
C(2′)—C(3′)	1.520(3)	C(2′)—O(2′)	1.413(2)
C(3′)—C(4′)	1.510(3)	C(3′)—O(3′)	1.424(2)
C(4′)—O(4′)	1.434(2)	C(4′)—C(5′)	1.491(3)
C(5′)—O(5′)	1.425(2)	O(4′)—C(1′)	1.434(2)

Hydrogen bonds

N(3)...O(2′)	2.714(2)	O(2′)—H(2′)	1.00	H(2′)...N(3)	1.77
O(5′)...O(3′)	2.735(2)	O(5′)—H(5′)	0.95	H(5′)...O(3′)	1.79
O(3′)...N(5)	2.752(2)	O(3′)—H(3′)	0.85	H(3′)...N(5)	1.91
N(1)...O(5′)	2.797(2)	N(1)—H(1)	0.95	H(1)...O(5′)	1.85

Bonds	Angle	Bonds	Angle
C(7a)—N(1)—C(2)	107.1(2)	N(1)—C(2)—N(3)	112.3(2)
C(2)—N(3)—C(3a)	104.2(2)	N(3)—C(3a)—C(4)	126.6(2)
N(3)—C(3a)—C(7a)	110.5(2)	C(7a)—C(3a)—C(4)	122.9(2)
C(3a)—C(4)—N(5)	105.5(1)	C(3a)—C(4)—C(1′)	113.8(1)
C(1′)—C(4)—N(5)	110.8(2)	C(4)—N(5)—C(6)	111.2(2)
N(5)—C(6)—C(7)	110.3(2)	C(6)—C(7)—C(7a)	107.2(2)
C(7)—C(7a)—N(1)	128.5(2)	C(7)—C(7a)—C(3a)	125.6(2)
C(3a)—C(7a)—N(1)	105.9(2)	C(4)—C(1′)—C(2′)	113.9(2)
C(4)—C(1′)—O(4′)	108.8(1)	O(4′)—C(1′)—C(2′)	106.0(2)
C(1′)—C(2′)—C(3′)	102.1(2)	C(1′)—C(2′)—O(2′)	114.6(2)
O(2′)—C(2′)—C(3′)	112.2(2)	C(2′)—C(3′)—C(4′)	102.8(2)
C(2′)—C(3′)—O(3′)	114.6(2)	O(3′)—C(3′)—C(4′)	111.3(2)
C(3′)—C(4′)—C(5′)	114.4(2)	C(3′)—C(4′)—O(4′)	105.4(2)
O(4′)—C(4′)—C(5′)	109.7(2)	C(4′)—C(5′)—O(5′)	111.6(2)

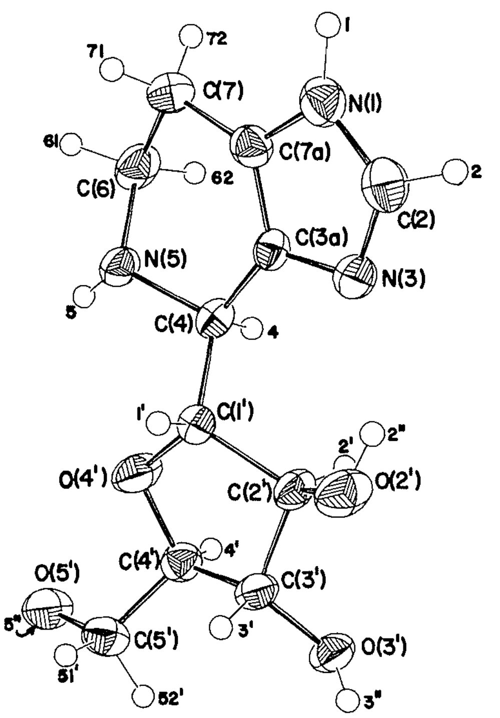

FIG. 3. The molecular structure of 4-(α-D-arabinofuranosyl)-imidazo[4,5-*c*]-4,5,6,7-tetrahydropyridine (**3**).

cause neither **1** nor **3** have strong intramolecular forces, the conformation in the solid state being determined primarily by intermolecular crystal forces. Therefore, although the compounds in the present study differ greatly in structure from other known α-D-arabinofuranosyl nucleosides (being *C*-nucleosides, and having a chiral centre in the base adjacent to C(1′) of the sugar moiety), it was thought useful to apply the procedure of Ekiel *et al.* (8) to our compounds, using the two-state equilibrium assumption.

Analysis of the 250-MHz ^{1}H nmr spectra of compounds **1**, **2**, and **3** was complicated by strongly overlapping signals, preventing direct measurement of chemical shifts and coupling constants. However, use of the nmr simulation program ITRCAL (11) enabled these values to be determined; the coupling constants are assembled in Table 3.

The coupling constants were used to obtain values for P_N (i.e. relative population of the N conformer) using eq. [1] (the mean of the three values obtained for each compound is reported in Table 3).

$$[1] \quad P_N = \frac{(J_{1',2'} - 0.5)}{7.5}; \quad P_N = \frac{J_{2',3'}}{8.3}; \quad P_N = \frac{J_{3',4'}}{10.0}$$

The values obtained for $J_{1',2'}$, $J_{2',3'}$, and $J_{3',4'}$ are in the same range as those reported for other α-D-arabinofuranosyl nucleosides, and thus lead to P_N values similar to those reported previously (8). While this indicates that the α-*C*-nucleosides in the present study behave in a fashion similar to the previously

TABLE 3. Coupling constants for the α-D-arabinofuranosyl moiety of Pictet–Spengler reaction products **1**, **2**, and **3**

Compound	$J_{1',2'}$	$J_{2',3'}$	$J_{3',4'}$	$J_{4',5'}$	$J_{4',5''}$	P_N[a]	$P_{g\text{-}g}$[b]	$P_{g\text{-}t}$[c]
1	6.6	5.6	6.6	3.3	5.3	0.71	0.44	0.38
2	4.5	5.4	5.5	3.5	6.2	0.58	0.33	0.47
3	6.8	6.5	6.6	3.2	5.2	0.76	0.46	0.37

[a]Calculated from eq. [1], as the mean of the three values obtained.
[b]Calculated from eq. [2].
[c]Calculated from eq. [3].

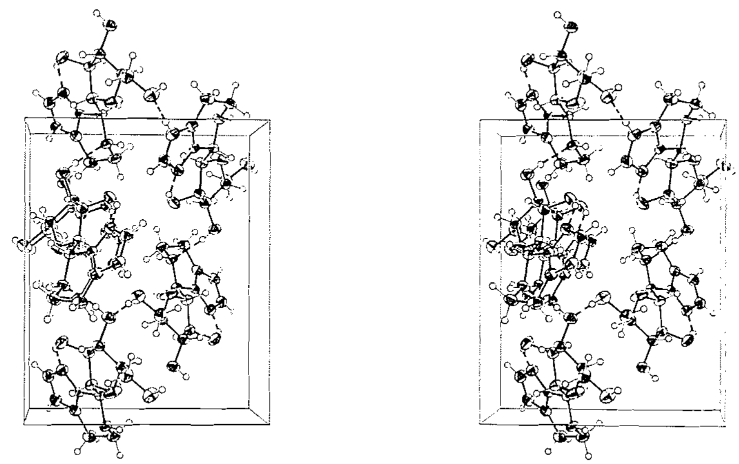

FIG. 4. The packing of **3** within the unit cell; ***b*** and ***c*** are parallel to the sides and bottom of the page, respectively, and the view is down ***a***.

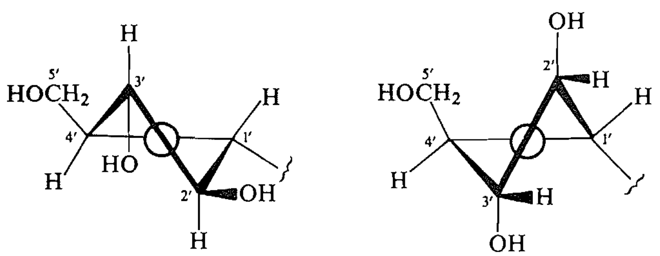

Type N, $^3T_2$ Type S, $^2T_3$

FIG. 5. Type N and Type S conformations for α-D-arabinofuranosides (see ref. 9).

reported examples (8), this may be an oversimplification, for the reasons described above. However, it seems clear that the crystal conformation of compound **1** is not present to any great extent in solution, because the all-eclipsed conformation would give much smaller vicinal coupling constants (~2–3 Hz) than those observed.

In the case of **3** the conformation of the sugar moiety in the solid is $^3T_2$, and this is also the dominant conformation calculated for this compound in solution. The calculated P_N values for **1** and **3** are very similar, as might be expected for compounds having the same sugar moiety and the same configuration at C(1) of the base, but differ from that of **2**, which has the opposite configuration at C(1). The fact that **1** has a different conformation in solution than in the solid is not surprising because the solid state conformation is a consequence of intermolecular hydrogen bonding as discussed in the preceding section. The intermolecular bonds of the solid would not be expected to survive in solution.

The C(5′) hydroxymethyl group of the arabinose unit may

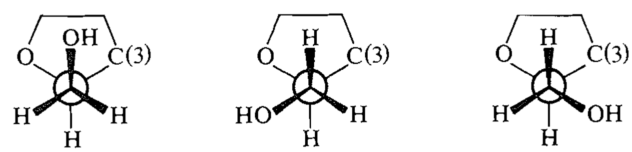

gauche–gauche (g–g) *gauche–trans* (g–t) *trans–gauche* (t–g)

FIG. 6. Conformations at the C(5′)—C(4′) bond.

adopt three extreme conformations, as shown in Fig. 6. In the case of compounds **1** and **3** the crystal structures show that this group adopts the *gauche–trans* (g–t) conformation in the solid state. Studies of the crystal structures of a large group of nucleosides have shown that there is no direct correlation between the orientation of this group and the conformation of the sugar ring in the solid state, although such a correlation does hold in solution, as evidenced by the results of ^{1}H nmr experiments (see ref. 12, and refs. therein). Ekiel *et al.* (8) have shown such a correlation in the case of α-D-arabinofuranosyl nucleosides, finding that the g–g rotamer appeared to be associated with only the Type N conformation.

The populations of the g–g and g–t rotamers of **1**, **2**, and **3** were estimated using relationships developed by Wood *et al.* (13) and applied by others (10*a*). Equation [2] was used to calculate the value of $P_{g\text{-}g}$ and the values of $P_{g\text{-}t}$ were determined using eq. [3] (10*a*).

$$[2] \quad P_{g\text{-}g} = \frac{13 - (J_{4',5'} + J_{4',5''})}{10}$$

$$[3] \quad P_{g\text{-}t} = \frac{J_{4',5''} - 1.5}{10}$$

The values of $J_{4',5'}$ are similar to those observed by Ekiel *et al.* (8), although the values for $J_{4',5''}$ are considerably higher,

TABLE 4. Crystal data

Parameters	1, $C_{16}H_{20}N_2O_4$	3, $C_{11}H_{17}N_3O_4$
Formula weight	304.3	255.3
Crystal size (mm)	0.25, 0.27, 0.38	0.27, 0.33, 0.43
Systematic absences	$0k0$, $k = 2n + 1$	$h00$, $h = 2n + 1$ $0k0$, $k = 2n + 1$ $00l$, $l = 2n + 1$
Space group (No.)	$P2_1(4)$	$P2_12_12_1(19)$
Unit cell parameters (Å and deg)	$a = 13.091(4)$ $\beta = 115.78(2)$ $b = 5.365(1)$ $c = 11.323(3)$	$a = 8.118(2)$ $b = 13.715(4)$ $c = 10.963(3)$
Volume (Å^3)	716.2(3)	1221.0(4)
Z	2	4
ρ_{obs}, ρ_{calc} (g cm^{-3})	1.411, 1.40(2)	1.389, 1.40(2)
Linear absorption coefficient, μ, (cm^{-1})	1.10	1.15
Standard reflections (esd %)	3 1 0 (1.48), 4 1 −1(1.40)	4 0 1 (1.27), 0 −7 −2 (1.39)
Temperature (°C)	22	22
No. of independent reflections	3289	1595
No. with $I > 0$	3210	1569
Final R_1, R_2[a]	0.0514, 0.0642	0.0312, 0.0335
Final shift/error, maximum, average	0.037, 0.006	0.012, 0.002
g (secondary extinction)	0.00302	0.01231
Weighting	$w = (\sigma_F^2 + 0.001381\ F_o^2)^{-1}$	$w = (\sigma_F^2 + 0.000338\ F_o^2)^{-1}$
Final difference map, peak, valley, (e Å^{-3})	+0.49, −0.39	+0.20, −0.21
Error in an observation of unit weight	1.27	1.18
$F(000)$	324	544

[a] $R_1 = \Sigma\|F_o| - |F_c\|/\Sigma|F_o|$; $R_2 = \{\Sigma w(|F_o| - |F_c|)^2/\Sigma wF_o^2\}^{1/2}$.

leading (as shown in Table 3) to a lower population of the g−g rotamer and a higher population of the g−t rotamer than that previously observed. From these data examined, it is not possible to establish a correlation between the sugar conformation and the orientation of the side chain. Probably both features are strongly affected by the configuration at C(1), an aspect which deserves exploration. However, it may be noted that compounds **1** and **3** have similar coupling constants and conformer populations but which are different from those in compound **2**.

Experimental

The ^{1}H nmr spectra were recorded on a Bruker WM250FT spectrometer (250 MHz) in D_2O – DMSO-d_6 for **1** and **2** and D_2O for **3** (see ref. 1). The nmr simulations were obtained using the ITRCAL program (11). In all cases the program was iterated to give an rms error of less than 0.5 Hz between the observed and simulated spectra.

Compounds 1, 2, and 3

The preparation of **1**, **2**, and **3** has been reported (1). Crystals of **1** and **3** for X-ray examination were obtained by crystallization from water.

Collection of X-ray data

Colorless crystals of both compounds were selected for X-ray studies, after examination for perfection under a polarizing microscope. Precession photographs revealed the symmetry of the crystals, and unit cell parameters were obtained from least-squares fit of χ, ϕ, and 2θ from 15 reflections for each compound in the range $20.3° < 2\theta < 36.0°$ for **1**, $20.2° < 2\theta < 26.3°$ for **3**, recorded on a Nicolet P3 diffractometer in the case of **1**, and a Syntex $P2_1$ diffractometer in the case of **3**, using graphite-monochromatized MoK_α radiation (0.71069 Å at 22°C). Crystal data and other numbers related to data collection are summarized in Table 4.

Densities were obtained by flotation in acetone–bromoform. Intensities were measured on the Nicolet P3, in the case of **1**, and Syntex $P2_1$, in the case of **3**, diffractometers using a coupled θ(crystal) – 2θ (counter) scan. The methods of selection of scan rates and initial data treatment have been described (14, 15). Corrections were made for Lorentz polarization effects but not for absorption. This will give a maximum error in F of <1.0% for **1** and <1.6% for **3**.

TABLE 5. Atomic positional parameters ($\times 10^4$) and temperature factors (Å^2 $\times$ 10^3) for **1**

Atom	x	y	z	U_{eq}[a]
C(1)	6586(2)	6436(8)	2667(2)	21(1)
N(2)	6549(2)	8662(7)	1882(2)	23(1)
C(3)	7702(2)	9557(8)	2139(2)	29(1)
C(4)	8414(2)	10308(8)	3554(2)	27(1)
C(4a)	8253(2)	8623(8)	4470(2)	23(1)
C(5a)	8866(2)	8397(8)	5873(2)	23(1)
C(5)	9759(2)	9761(8)	6836(3)	31(1)
C(6)	10167(2)	9015(8)	8126(3)	38(1)
C(7)	9712(2)	6951	8478(2)	40(1)
C(8)	8823(2)	5569(8)	7553(2)	24(1)
C(8a)	8413(2)	6336(8)	6247(2)	25(1)
N(9)	7529(2)	5383(7)	5125(2)	25(1)
C(1a)	7451(2)	6805(7)	4064(2)	21(1)
C(1′)	5415(2)	5832(8)	2581(2)	21(1)
C(2′)	4441(2)	5610(8)	1198(2)	22(1)
O(2′)	4318(2)	3103(7)	784(2)	30(1)
C(3′)	3406(2)	6759(8)	1321(2)	25(1)
O(3′)	2941(2)	8829(8)	477(2)	37(1)
C(4′)	3864(2)	7480(8)	2772(2)	23(1)
O(4′)	5073(1)	7778(7)	3200(2)	24(1)
C(5′)	3604(2)	5544(8)	3575(2)	27(1)
O(5′)	4017(2)	6397(8)	4893(2)	32(1)

[a] $U_{eq} = \frac{1}{3}(U_{11} + U_{22} + U_{33} + 2U_{13}\cos\beta)$.

TABLE 6. Atomic positional parameters ($\times 10^4$) and temperature factors ($\text{Å}^2 \times 10^3$) for **3**

Atom	x	y	z	U_{eq}[a]
N(1)	4101(2)	5268(1)	8803(2)	38(1)
C(2)	4634(3)	6161(2)	9126(2)	40(1)
N(3)	5951(2)	6433(1)	8502(2)	36(1)
C(3a)	6271(2)	5651(1)	7741(2)	27(1)
C(4)	7627(2)	5581(1)	6812(2)	29(1)
N(5)	7841(2)	4523(1)	6573(1)	33(1)
C(6)	6271(3)	4069(1)	6177(2)	41(1)
C(7)	5088(3)	3987(1)	7252(2)	43(1)
C(7a)	5145(2)	4932(1)	7918(2)	33(1)
C(1′)	0236(2)	6038(1)	7221(2)	33(1)
C(2′)	9165(3)	7155(1)	7341(2)	32(1)
C(3′)	10888(2)	7454(1)	6949(2)	33(1)
C(4′)	11291(2)	6721(1)	5965(2)	33(1)
C(5′)	13087(3)	6529(2)	5805(2)	39(1)
O(2′)	8771(2)	7496(1)	8522(1)	48(1)
O(3′)	11014(2	8426(1)	6504(1)	39(1)
O(4′)	10472(2)	5839(1)	4323(2)	55(1)
O(5′)	13391(2)	5889(1)	4807(1)	46(1)

[a]$U_{eq} = 1/3(U_{11} + U_{22} + U_{33})$.

Solution of the structures

For both compounds the phases were determined by direct methods using 242 reflections with $E > 1.66$ and 12 sets of starting phases. All non-hydrogen atoms were found in the subsequent E maps. The correct handedness for each structure was chosen by making the known configuration at C(1′) correct. The coordinates were refined by minimizing the function $\sum w(|F_o| - |F_c|)^2$, and subsequent difference maps revealed all of the hydrogen atoms. Further refinement using anisotropic temperature factors for all of the non-hydrogen atoms and isotropic temperature factors for the hydrogen atoms was terminated when the maximum shift/error dropped below 0.1. Scattering curves were taken from the International Tables (16). The atom parameters are listed in Tables 5 and 6.[3] Initial data treatment used programs from the X-RAY package (17). The structures were solved using programs from SHELX (18). The least-squares planes program was NRC-22 (19) and diagrams were prepared using ORTEP-II (20). All calculations were carried out on Cyber 170/730 and 170/815 computers.

Acknowledgements

We thank the Natural Sciences and Engineering Research Council of Canada for financial support of this work in the form of grants to D.B.M., C.J.L.L., and W.A.S.

[3]Tables of atomic positions for hydrogen atoms, interatomic distances and angles involving hydrogen, best planes, dihedral and torsional angles, and the moduli of F_o and F_c have been deposited and may be purchased from the Depository of Unpublished Data, CISTI, National Research Council of Canada, Ottawa, Ont., Canada K1A 0S2.

1. I. M. PIPER, D. B. MACLEAN, I. KVARNSTRÖM, and W. A. SZAREK. Can. J. Chem. **61**, 2721 (1983).
2. P. W. CODDING. Can. J. Chem. **61**, 529 (1983).
3. S. J. CLINE and D. J. HODGSON. Biochim. Biophys. Acta, **563**, 540 (1979); **610**, 20 (1980).
4. J. S. SHERFINSKI and R. S. MARSH. Acta Crystallogr. Sect. B, **29**, 192 (1973); P. TOLLIN, H. R. WILSON, and D. W. YOUNG. Acta Crystallogr. Sect. B, **29**, 1641 (1973).
5. M. SUNDARALINGAM. J. Am. Chem. Soc. **93**, 6644 (1971). See also J. DONOHUE and K. N. TRUEBLOOD. J. Mol. Biol. **2**, 363 (1960).
6. J. J. BONNET and J. A. IBERS. J. Am. Chem. Soc. **95**, 4829 (1973).
7. (*a*) C. ALTONA and M. SUNDARALINGAM. J. Am. Chem. Soc. **94**, 8205 (1972); (*b*) J. Am. Chem. Soc. **95**, 2333 (1973); (*c*) A. JAWORSKI, I. EKIEL, and D. SHUGAR. J. Am. Chem. Soc. **100**, 4357 (1978); (*d*) I. EKIEL, M. REMIN, E. DARŻYNKIEWICZ, and D. SHUGAR. Biochim. Biophys. Acta, **562**, 177 (1979).
8. I. EKIEL, E. DARŻYNKIEWICZ, and D. SHUGAR. Carbohydr. Res. **92**, 21 (1981), and references therein.
9. (*a*) Eur. J. Biochem. **111**, 295 (1980); (*b*) J. Chem. Soc. Chem. Commun. 505 (1973).
10. (*a*) G. I. BIRNBAUM, T.-S. LIN, G. T. SHIAU, and W. H. PRUSOFF. J. Am. Chem. Soc. **101**, 3353 (1979); (*b*) G. I. BIRNBAUM, R. DESLAURIERS, T.-S. LIN, G. T. SHIAU, and W. H. PRUSOFF. J. Am. Chem. Soc. **102**, 4236 (1980).
11. 1180 ITRCAL. Nicolet Instrument Corporation, 5225 Verona Road, Madison, WI. 1977.
12. G. I. BIRNBAUM, K. A. WATANABE, and J. J. FOX. Can. J. Chem. **58**, 1633 (1980).
13. D. J. WOOD, F. E. HRUSKA, and K. K. OGILVIE. Can. J. Chem. **52**, 3353 (1974).
14. R. P. HUGHES, N. KRISHNAMACHARI, C. J. L. LOCK, J. POWELL, and G. TURNER. Inorg. Chem. **16**, 314 (1977).
15. B. LIPPERT, C. J. L. LOCK, B. ROSENBERG, and M. ZVAGULIS. Inorg. Chem. **16**, 1525 (1977).
16. D. T. CROMER and J. T. WABER. *In* International tables for X-ray crystallography. Vol. IV. *Edited by* J. A. Ibers and W. C. Hamilton. Kynoch Press, Birmingham, England. 1974. Table 2.2B, pp. 99–101.
17. J. M. STEWART. The X-RAY 76 system. Technical Report TR-446. Computer Science Center, University of Maryland, College Park, MD. 1976.
18. G. M. SHELDRICK. SHELX. A program for crystal structure solution. Cambridge University, Cambridge, England. 1976.
19. F. R. AHMED and M. E. PIPPY. Mean plane and torsion angles. Program Number NRC-22. National Research Council of Canada, Ottawa, Ontario. 1978.
20. C. K. JOHNSON. ORTEP-II. Report ORNL-5138. Oak Ridge National Laboratory, Oak Ridge, TN. 1976.

Synthesis and study of new mesogen compounds: 4-alkoxy-2-hydroxy-4′-substituted-α,α′-dimethylbenzalazines. Correlation analysis between T_{N-I} transition and electronic parameters in five series of liquid crystals

MERCEDES MARCOS, ENRIQUE MELENDEZ, BLANCA ROS, AND JOSE LUIS SERRANO
Departamento de Química Orgánica, Facultad de Ciencias, Universidad de Zaragoza, 50009 Zaragoza, Spain

Received October 18, 1984

MERCEDES MARCOS, ENRIQUE MELENDEZ, BLANCA ROS, and JOSE LUIS SERRANO. Can. J. Chem. **63**, 2922 (1985).

Two new series of compounds with mesomorphic properties were synthesized: the 4-ethoxy and 4-octyloxy-4′-X-2-hydroxy-α,α′-dimethylbenzalazines (X = CN, NO_2, F, Cl, Br, CH_3, and $N(CH_3)_2$). Thermodynamic measurements were made. All the compounds gave mesogenic behaviour. Some of them exhibit polymorphism in the solid state. A study of the existent correlation between the temperatures at which the N−I transition appears in five series of mesogenic compounds and electronic parameters of the polar terminal chain was carried out. Seven terminal groups were studied: —F, —Cl, —Br, —CH_3, —OCH_3, —NO_2, and —CN. None of the electronic parameters used enabled us to obtain a good correlation with all the groups. However, when the methoxy group was omitted, the parameters that measured π electronic delocalization in the aromatic ring showed an excellent correlation with the T_{N-I}. The best correlation was obtained in all cases with Swain and Lupton's $\mathcal{R}$, which defined the resonance effect.

MERCEDES MARCOS, ENRIQUE MELENDEZ, BLANCA ROS et JOSE LUIS SERRANO. Can. J. Chem. **63**, 2922 (1985).

On a synthétisé deux nouvelles séries de composés mésomorphes, soit les éthoxy-4 et les octyloxy-4 X-4′ hydroxy-2 α,α′-diméthylbenzalazines (X = CN, NO_2, F, Cl, CH_3 et $N(CH_3)_2$). On a effectué des mesures thermodynamiques. Tous les composés ont un comportement mésogène. Certains d'entres-eux présentent du polymorphisme à l'état solide. On a effectué une étude sur les corrélations qui existent entre les températures auxquelles apparaissent les transitions N−I dans cinq séries de composés mésogènes et les paramètres électroniques de la chaîne polaire terminale. On a étudié sept groupes terminaux, soit les groupes —F, —Cl, —Br, —CH_3, —OCH_3, —NO_2 et —CN. Aucun des paramètres électroniques utilisés ne nous a permis d'obtenir une bonne corrélation avec tous les groupes. Cependant, si l'on omet le groupement méthoxy, les paramètres qui mesurent la délocalisation électronique π du noyau aromatique présentent une bonne corrélation avec le T_{N-I}. Dans tous les cas, on obtient la meilleure corrélation avec le paramètre R de Swain et Lupton qui définit l'effet de résonance.

[Traduit par le journal]

Introduction

One of the most interesting aspects of the study of liquid crystals is the relation between structure and mesogen activity.

Numerous papers of great interest have been published about this subject to date. Among them, the study of the influence of the terminal groups on the temperature at which nematic−isotropic liquid transition occurs (1, 2) is classic.

Basing themselves on the Maier−Saupe theory, Van der Veen (3, 4), Griffin (5), and others, have established the correlation between α (factor of molecular electronic polarizability) of the terminal groups and the N−I transition temperatures of nematogen compounds.

However, a thorough mathematical analysis makes it clear that these correlations, generally limited to the graphic method, are insufficient in many cases. Moreover, a large number of well-characterized empirical parameters of aromatic substituents are presently known (6), which has permitted us to study the correlation between some of these parameters and some molecular properties of the compounds that have those substituents, among them, the N−I transition temperatures in series of liquid crystals.

Unfortunately, it is not easy to find series of compounds with different terminal groups in order to make the correlation. Consequently, this study has been limited to five series of compounds which have terminal groups with different empirical parameters: —CN, —NO_2, —F, —Cl, —Br, —CH_3, —OCH_3 (see Fig. 1).

Two of these series of compounds were synthesized by us: the 4-ethoxy-(**I***a*) and 4-octyloxy-(**I***b*)-4′-substituted-2-hydroxy-α,α′-dimethylbenzalazines. In order to check the results obtained, the compounds of these series with the terminal groups X: —OC_2H_5 and —$N(CH_3)_2$ were synthesized.

The other series studied were taken from scientific literature. Two of them correspond to the compounds studied by Van der Veen (3), derivatives of *p*-*N*-alkoxybenzylidene-*p*-X-anilines (**II**) (4), and derivatives of the phenyl-*p*-benzoyloxybenzoates (**III**) described by Van Metter and Klanderman (7). The last series corresponds to derivatives of the *p*-phenylenedibenzoate compounds (**IV**) described by Schroeder and Bristol (8).

Experimental

Synthesis

While the compounds with the terminal group —OCH_3 (9) and —OC_2H_5 (9, 10) have already been described, the rest of them were synthesized for the first time for this study.

The general scheme of synthesis of the compounds studied in this paper was similar to the method described in a previous paper (10). The compounds were generally synthesized in three stages: (*1*) formation of the derivative hydrazone of 4-substituted ketone; (*2*) condensation of the preceding hydrazone and the 2,4-dihydroxyacetophenone and separation of the required product by column chromatography; and (*3*) alkylation of the OH group in position 4 of the compound obtained in the second stage.

The transition temperatures and enthalpy data of the compounds synthesized are gathered in Table 1.

Textures observed

The mesophase textures were observed with a polarizing microscope using thin films of the samples mounted between a glass slide and a cover slip.

They were identified because of their similarity to the descriptions of the textures made by Demus and Richter (11).

Techniques

The melting points, transition temperatures, and enthalpies were determined using a Perkin-Elmer DSC-2 differential scanning calorimeter. The apparatus was calibrated by measuring the known melting

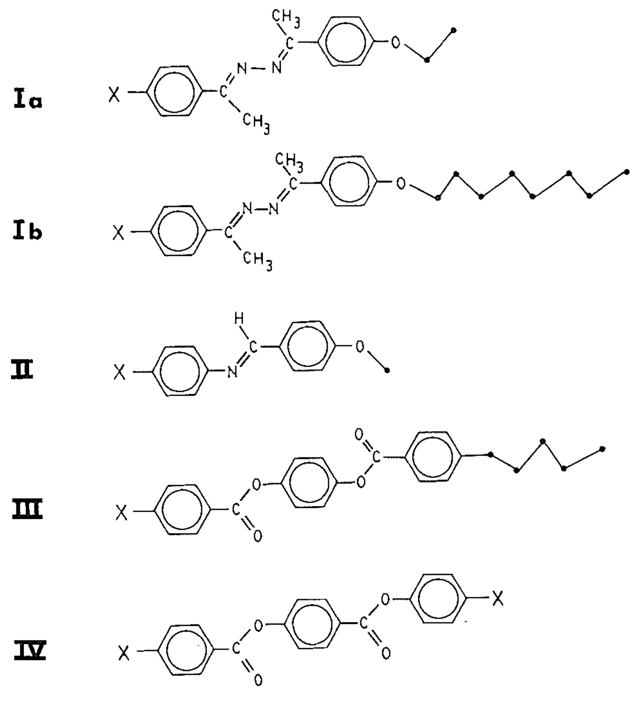

X = F, Cl, Br, CH_3, NO_2, CN, OCH_3.

FIG. 1. Structures of I*a*, I*b*, **II**, **III**, and **IV**.

points and fusion heat of benzoic acid (394.0 K, 141.7 J/g), indium (429.8 K, 28.42 J/g), and tin (505.0 K, 60.8 J/g).

The optical observations were made using a Reichert–Thermovar HT1 B11 polarizing microscope equipped with a heating stage.

The identification of the products was carried out by the usual spectroscopic methods: uv (Perkin–Elmer 200), ir (Perkin–Elmer 283), nmr (Perkin–Elmer R-12-B), and mass spectrometry (Hewett Packard 5943 A). The purity of the products was checked by the above-mentioned techniques and tlc.

The correlation analysis was carried out in a Digital VAX-11780 minicomputer using a subroutine of the SPSS programme (12): "multiple regression analysis: subprogramme regression".

Parameters of substituents used for correlation analysis

A previous study was carried out in which numerous electronic parameters of the substituents with T_{N-I} were correlated. After this preliminary study $\mathcal{R}$ and $\mathcal{F}$ (13), defined by Swain and Lupton, were selected as fundamental parameters. In order to make a comparative study the α-parameter used by Van der Veen (3) and others was also used in the study.

The values of all the parameters used for the correlation analysis are listed in Table 2.

Results and discussion

Correlation between the values of N–I transition temperatures of the five series of compounds

As can be observed in Table 3, a good correlation exists between the values of the N–I transition temperatures of the five series of the compounds studied, which confirms that the influence of the different types of substituents X, is almost the same in each of the series.

Only the slightly smaller values of the correlation found between series **II** and series I*b* and **III** (r_{II-Ib} = 0.864 and r_{II-III} = 0.884) are notable.

The compounds of these last two series have the longest molecules (Fig. 1), whereas the imino-derivatives (series **II**) have the shortest molecules. It seems, therefore, that besides the electronic influence of the common substituents X, the geometry of the molecule is also of fundamental importance.

TABLE 1. Transition temperature and enthalpies for the compounds synthesized

R	X	Transition	Temperature (K)	ΔH (kJ/mol)
OC_2H_5	F[b]	C_1-C_2	350.2	5.48
		C_3-C_2	360.1	5.81
		C_2-N	386.9	28.13
		N–I	404.5	0.88
OC_2H_5	Cl	C–N	417.2	34.03
		N–I	430.6	0.63
OC_2H_5	Br	C–I	427.9	41.47
		I–N[a]	425.1	1.13
OC_2H_5	NO_2	C–N	435.5	37.75
		N–I	459.3	0.92
OC_2H_5	CH_3	C–N	399.9	32.90
		N–I	433.0	2.05
OC_2H_5	CN	C–N	413.7	29.89
		N–I	482.2	1.00
OC_2H_5	$N(CH_3)_2$	C–I	448.1	35.45
		I–N[a]	448.1	—
OC_8H_{17}	F	C–N	370.1	39.33
		N–I	379.2	0.71
OC_8H_{17}	Cl	C–N	381.1	37.62
		N–I	407.4	1.25
OC_8H_{17}	Br	C–N	381.7	31.44
		N–I	404.4	1.63
OC_8H_{17}	NO_2	C–N	372.4	31.81
		N–I	420.2	1.17
OC_8H_{17}	CH_3	C–N	360.7	39.71
		N–I	396.5	1.34
OC_8H_{17}	CN[b]	C_1-C_2	374.2	39.75
		C_2-N	375.3	
		N–I	433.7	1.30
OC_8H_{17}	$N(CH_3)_2$	C–N	406.1	42.39
		N–I	415.8	1.59

[a]Monotropic transition.
[b]Crystal–crystal transition.

$$C_1 \rightleftharpoons \underset{\underset{\textstyle C_3}{\upharpoonleft\downharpoonright}}{C_2} \rightleftharpoons N \rightleftharpoons I\ (F),\quad C_1 \rightleftharpoons C_2 \rightleftharpoons N \rightleftharpoons I\ (CN).$$

TABLE 2. Physical parameters of every substituent and N–I transition temperatures

	Electronic parameters			T_{N-I} (K)				
X	α	$\mathcal{R}$	$\mathcal{F}$	I*a*	I*b*	II	III	IV
CN	4.4	0.19	0.51	482.2	433.7	392.2	522.2	626.7
NO_2	4.0	0.16	0.67	459.3	420.2	355.7	—	554.2
F	0.5	−0.34	0.43	404.5	370.2	297.2	453.7	472.2
Cl	2.5	−0.15	0.41	430.6	407.4	320.2	485.2	519.2
Br	3.9	−0.17	0.44	425.1	404.4	307.2	486.2	525.2
CH_3	1.2	−0.13	−0.04	433.0	396.5	311.2	472.7	509.2
OCH_3	—	−0.51	0.26	454.0	416.5	375.2	496.2	573.2
OC_2H_5	—	−0.44	0.22	469.6	428.8	—	—	—
$N(CH_3)_2$	—	−0.92	0.10	448.9	415.8	—	—	—

Correlation between T_{N-I} *transition and electronic parameters*

The following symbols are used in this paper. $\mathcal{R}$, resonance effect of Swain and Lupton (modified by Charton); $\mathcal{F}$, field effect of Swain and Lupton (modified by Charton); σ_{ORES}, σ

TABLE 3. Correlation coefficients among the values of T_{N-I} of the five series

	I*a*	I*b*	II	III	IV
I*a*	1.00	0.941	0.947	0.949	0.965
I*b*		1.00	0.864	0.983	0.934
II			1.00	0.884	0.951
III				1.00	0.975
IV					1.00

zero resonance: effect of π electron delocalization normalized; $\sigma_{B\,RES}$, σ benzoic acid resonance: π electron delocalization from benzoic acid model; $\sigma_{A\,RES}$, σ aniline resonance: π electron delocalization from aniline model; σ_{RES+}, σ resonance plus: π electron delocalization from model structure with positive charge, e.g., solv. of cumyl chlorides; σ_L, σ localized; σ_{INDQ}, σ from quinuclidines, i.e., from sp^3 carbon; σ_{PRIME}, field effect through bicyclooctane ring; and σ_P, ionization of phenols.

Correlation between T_{N-I} and some electronic parameters of the substituents (see Appendix) indicated that the methoxy group behaved differently from the other six groups studied: —CN, —NO_2, —F, —Cl, —Br, and —CH_3.

Once this group was removed, it was observed that the T_{N-I} showed a good correlation with the electronic parameters that measured the effect of π electronic delocalization in the aromatic ring: $\mathcal{R}$ (13), $\sigma_{O\,RES}$ (14), $\sigma_{B\,RES}$ (14), $\sigma_{A\,RES}$ (14), σ_{RES+} (14).

However, the other parameters that measure the field effect $\mathcal{F}$ (13), σ_L (15), σ_{INDQ} (16), σ_{PRIME} (17) and the parameters that indicate the resonance effect and field effect σ_P (18), show very little or practically no correlation with T_{N-I}.

In some cases the value of F of each correlation is also indicated. The validity of the results was checked by means of Snedecor's F defined for a percentage of distribution points α of 0.05 (12).

As can be observed from Table 4, when the methoxy group is not present, the correlation obtained between T_{N-I} and $\mathcal{R}$ is much better than the one used by Van der Veen (3) between T_{N-I} and α.

The F value for the five series of compounds studied are higher than those used as references.

The F values for the correlation T_{N-I}—α are clearly lower than those observed for the correlation T_{N-I}—$\mathcal{R}$ and in some cases even lower (see series I*a* and II, Table 4) than the F of Snedecor used as a reference.

The correlation between T_{N-I} and $\mathcal{F}$ shows lower values still, which indicates that the interrelation between both factors is practically non-existent.

Figure 2 shows a graphic representation of the relation between T_{N-I} and $\mathcal{R}$ for the five series of compounds studied. The values of the constants and slope of the straight line of lineal regression with the six groups in each series (five in the case of the series **III** because the T_{N-I} data for the nitro group are unavailable) are also shown.

As can be seen in the figure, the regression straight line corresponding to the compounds with two X groups (series **IV**) has a much greater slope than those of the other series studied.

However, when the methoxy group is present correlation between T_{N-I} and $\mathcal{R}$ is almost non-existent (see Table 4). This group, of electronic-releasing character, behaves very differently from the rest of the groups. In fact when the T_{N-I} values of the compounds with the methoxy group are introduced in the regression straight line of each of the series, it is observed that they correspond to $\mathcal{R}$ values very different from the ones experimentally obtained (see Fig. 2).

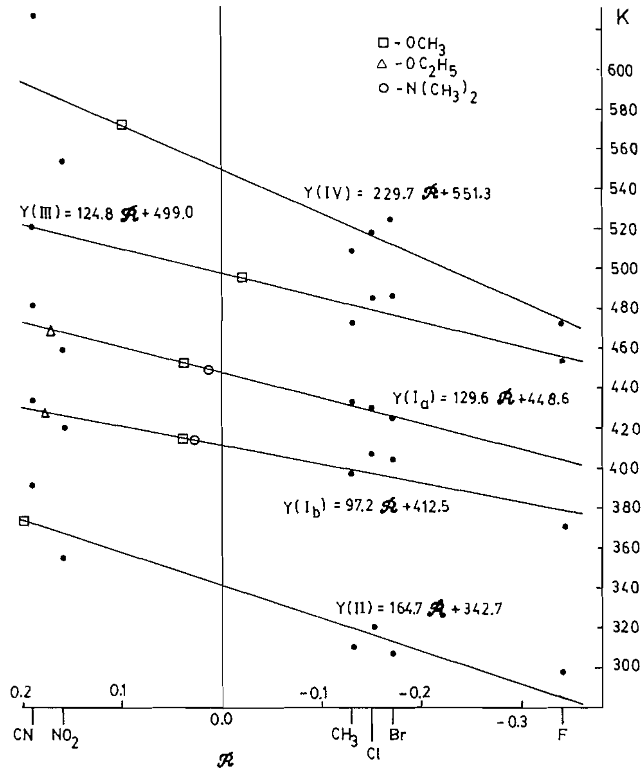

FIG. 2. Equations and graphic representation of the relation T_{N-I}—$\mathcal{R}$ for the five series of compounds studied.

In both the series of compounds synthesized by us, I*a* and I*b*, we can observe a type of behaviour in the $\mathcal{R}$ value of the methoxy group in the regression straight line similar to that defined by other six groups studied.

This effect was repeated when other compounds with strongly electron-releasing groups X: —OC_2H_5 and —$N(CH_3)_2$ were synthesized and studied. In both cases a behaviour similar to that of the methoxy group was observed.

As occurs with the methoxy group, the representation of T_{N-I} values in the regression straight line defined by other six groups, is similar in the series I*a* and I*b* (see Fig. 2).

Conclusions

The excellent correlation observed between the T_{N-I} of the five series of compounds studied confirms that the influence of the different terminal groups is similar in each of them. However, none of the electronic parameters of the terminal groups shows an excellent correlation with the T_{N-I} of all the compounds studied. Nevertheless, it is observed that the T_{N-I} of the compounds with electron-attracting or weakly electron-releasing substituents show a good correlation with the electronic parameters of the substituents which measure the π electronic delocalization in the aromatic ring, especially with Swain and Lupton's $\mathcal{R}$. In spite of the fact that the substituents with strong electron-releasing characteristics deviate from the general behaviour previously indicated, the contribution of these substituents is similar in all the cases studied.

The electronic modification introduced in the molecule by the electron-attracting or weakly electron-releasing terminal groups obviously has a considerable effect on T_{N-I}. However,

TABLE 4. Statistical data of the correlation between T_{N-I} transition and electronic parameters

Series	$r[\mathcal{R}]$	$r[\mathcal{F}]$	α^a r^b	F^c	SE^d	$\mathcal{R}^a$ r^b	F^c	SE^d	$F^e \nu_1/\nu_2$ (α:0.05)	$r[\mathcal{F}]^a$
I*a*	0.571	0.272	0.763	5.56	19.8	0.975	76.57	6.8	$F_{1/4}$ 7.70	0.344
I*b*	0.546	0.317	0.892	15.63	10.9	0.928	24.67	9.0	$F_{1/4}$ 7.70	0.389
II	0.331	0.293	0.728	4.51	27.8	0.939	29.58	14.0	$F_{1/4}$ 7.70	0.366
III[f]	0.539	0.322	0.898	12.45	12.7	0.958	33.74	8.2	$F_{1/3}$ 10.13	0.377
IV	0.459	0.290	0.822	8.36	33.3	0.905	18.16	24.9	$F_{1/4}$ 7.70	0.390

[a]Methoxy group not included.
[b]Correlation coefficient.
[c]Snedecor's F.
[d]Standard error.
[e]Relation of number of independent variables and free degrees: ν_1 number of independent variables, ν_2 free degrees.
[f]One group less as there were no data available for the compound with X: —NO_2.

the influence of some other factors is fundamental, particularly, in the case of the substituents with strong electron-releasing characteristics. Logically, the attempt to quantify the inter- and intramolecular interactions which govern T_{N-I} is very difficult and the approximation that the electronic parameters allow is insufficient to explain all the results satisfactorily.

Acknowledgments

We are grateful to Dr. J. Elguero for his kind suggestions and helpful comments and to D. E. Rivas for his help in the mathematical treatment.

1. E. SACKMAN, S. MEIBOON, and L. C. SNEYDER. J. Am. Chem. Soc. **89**, 5981 (1967).
2. G. W. GRAY. Mol. Cryst. Liq. Cryst. **7**, 127 (1969).
3. J. VAN DER VEEN. J. Phys. **36**, Q-357 (1955).
4. W. H. DE JEU and J. VAN DER VEEN. Mol. Cryst. Liq. Cryst. **40**, 1 (1977).
5. A. C. GRIFFIN. Mol. Cryst. Liq. Cryst. Lett. **34**, 111 (1976).
6. C. HANSCH and A. J. LEO. Substituent constants correlation analysis in chemistry and biology. John Wiley Sons, New York. 1979.
7. J. P. VAN METTER and B. H. KLANDERMAN. Mol. Cryst. Liq. Cryst. **22**, 1405 (1973).
8. J. P. SCHROEDER and D. W. BRISTOL. J. Org. Chem. **38**, No. 18, 3160 (1973).
9. J. BARBERÁ, M. MARCOS, E. MELÉNDEZ, and J. L. SERRANO. Mol. Cryst. Liq. Cryst. **94**, 367 (1983).
10. M. MARCOS, E. MELÉNDEZ, and J. L. SERRANO. Mol. Cryst. Liq. Cryst. **91**, 157 (1983).
11. D. DEMUS and L. RICHTER. Textures of liquid crystals. *Edited by* Verlag Chemie. Weinheim, New York. 1978.
12. M. MORRINGTON and C. M. THOMPSON. Biometrika, **33**, 73 (1943).
13. B. HANSCH and A. LEO. J. Med. Chem. **16**, 1207 (1973).
14. S. DAYAL, S. EHRENSON, and R. TAFT. J. Am. Chem. Soc. **94**, 9113 (1972).
15. M. CHARTON. Desing of Biopharm. Prop. *Edited by* E. Roche. Am. Ph. Assoc. 1977.
16. C. GROB and M. SCHLAGETER. Helv. Chim. Acta, **59**, 2064 (1976).
17. F. BACKER, P. PARISH, and L. STOCK. J. Am. Chem. Soc. **89**, 5677 (1967).
18. M. SJOSTROM and S. WOLD. Chem. Script. **9**, 200 (1976).

A multinuclear nuclear magnetic resonance study of *t*-butylthiol

SANDRA MOOIBROEK[1] AND RODERICK E. WASYLISHEN
Department of Chemistry, Dalhousie University, Halifax, N.S., Canada B3H 4J3

Received February 12, 1985

SANDRA MOOIBROEK and RODERICK E. WASYLISHEN. Can. J. Chem. **63**, 2926 (1985).

Deuterium nmr lineshapes for polycrystalline samples of $(CD_3)_3CSH$ and $(CH_3)_3CSD$ have been investigated between 110 and 200 K. Unlike *t*-butylchloride-d_9 which undergoes line narrowing in three distinctive stages, *t*-butylthiol-d_9 undergoes almost complete motional line narrowing at 120 ± 5 K. Above the solid II ↔ solid I phase transition no quadrupolar splitting is observed, consistent with rapid "isotropic" reorientation in the solid I phase.

An analysis of the ^2H and ^{13}C spin–lattice relaxation times of $(CD_3)_3CSH$, $(CH_3)_3CSD$ and unlabelled *t*-butylthiol in both liquid and solid phases is also reported. The rotational correlation time is observed to decrease by an order of magnitude at the solid II → solid I transition and to increase slightly at the melting point. Deuterium T_1s in solids III and IV of the labelled species indicate abrupt changes at the phase transitions and motion slower than ω_0^{-1} in solid IV.

SANDRA MOOIBROEK et RODERICK E. WASYLISHEN. Can. J. Chem. **63**, 2926 (1985).

Opérant à 110 et 200 K et faisant appel à la rmn du ^2H, on a étudié la forme des pics d'échantillons polycristallins de $(CD_3)_3CSH$ et $(CH_3)_3CSD$. Contrairement à ce qui est observé avec le chlorure de *tert*-butyle-d_9 alors que les pics subissent un retrécissement impliquant trois étapes distinctes, les pics du *tert*-butylthiol-d_9 subissent un retrécissement qui est pratiquement complet à 120 ± 5 K. Au-dessus de la transition de phase solide II ↔ solide I, on n'observe pas de dédoublement quadrupolaire; ce resultat est accord avec une réorientation "isotopique" rapide dans la phase solide I.

On rapporte également une analyse des temps de relaxation spin–réseau du ^2H et du ^{13}C du $(CD_3)_3CSH$, $(CH_3)_3CSD$ et du *tert*-butylthiol non marqué tant dans la phase liquide que solide. On a observé que le temps de corrélation rotationnelle diminue d'un ordre de grandeur lors de la transition solide II → solide I et qu'il augmente légèrement au voisinage du point de fusion. Les valeurs du T_1s du deutérium dans les solides III et IV des espèces marquées indiquent qu'il se produit des changements radicaux lors des transitions de phase ainsi qu'un mouvement plus faible que ω_0^{-1} dans le solide IV.

[Traduit par le journal]

Introduction

2-Methyl-2-propanethiol (*t*-butylthiol) is one of a class of approximately spherical molecules which is capable of existing in one or more solid phases that are orientationally disordered (1). At atmospheric pressure, *t*-butylthiol is known to undergo three solid–solid phase transitions at 152, 157, and 199 K, with corresponding entropy changes of 3.22, 0.50, and 0.58 R (2, 3). The entropy change at the melting point of 274 K is small (1.09 R), a characteristic of orientationally disordered molecular solids (plastic crystals).

Deuterium nmr is a very attractive technique for studying plastic crystals since it provides a selective probe for detailed studies of molecular motion. In particular, changes in the absorption lineshape of a powder sample may, in favorable cases, yield information as to the type(s) of reorientational motion occurring at rates on the order of the quadrupolar interaction, which for deuterium, is approximately 10^{-5} to 10^{-6} s. Motions occurring on the timescale of the inverse Larmor frequency (nanosecond to picosecond range) can also be monitored by relaxation measurements, and hence, a fairly wide range of motional frequencies is accessible to nmr methods.

In this paper we present the results of a detailed deuterium nmr study of $(CD_3)_3CSH$ and $(CH_3)_3CSD$ between 110 and 330 K. Natural abundance ^{13}C nmr data are also reported for the liquid and two high temperature solid phases (I and II) of the unlabelled compound. The results of these measurements, together with earlier proton nmr (4, 5) and dielectric (5, 6) studies, have enabled us to better characterize the rotations occurring in the various phases of *t*-butylthiol. Comparisons are made with the related compounds *t*-butyl-X (see Fig. 1*a*) where X = CH_3, Cl, and Br.

[1] Holder of an NSERC 1967 Science and Engineering Scholarship.

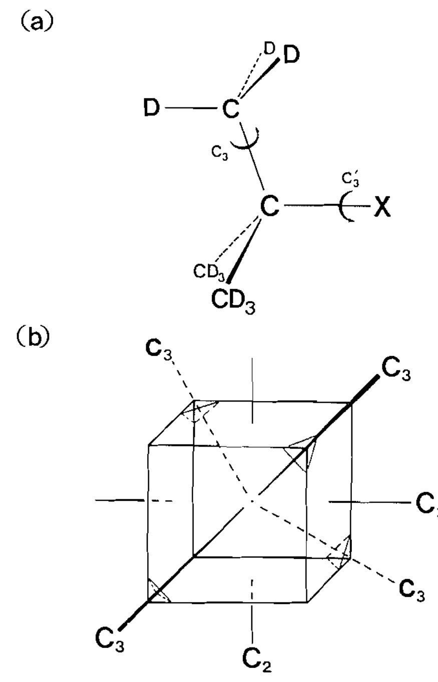

FIG. 1. (*a*) Depiction of $(CD_3)_3C$—X molecule indicating one of three C_3 axes and the C_3' axis. One D in each group is very nearly parallel to the C_3' axis, while the other two form an angle of 70.53°. (*b*) Representation of a tetrahedral molecule in a cube. Two of three orthogonal C_2 axes are indicated along with the C_3 axes.

Theory

A. Quadrupolar powder lineshapes

The ^2H nmr spectrum of labelled *t*-butylthiol is completely dominated by the electric quadrupole interaction, which in the

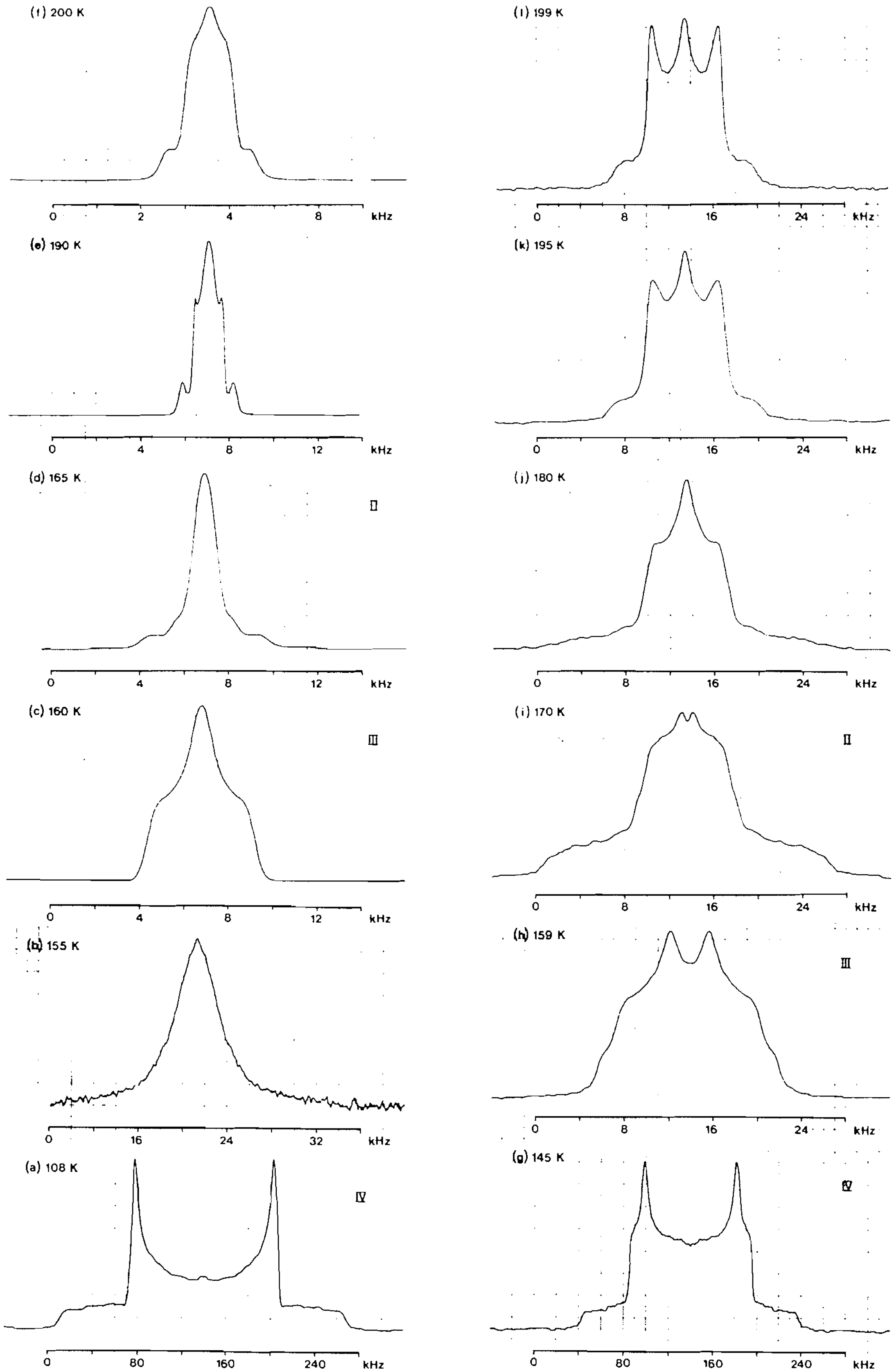

FIG. 2. Deuterium nmr powder spectra of (*a*)–(*f*) $(CD_3)_3CSH$ and (*g*)–(*l*) $(CH_3)_3CSD$ at various temperatures. Experimental conditions are described in the text.

absence of molecular motion, yields a characteristic spin $I = 1$ crystalline powder pattern (7). Figure 2*a*, the "rigid lattice" spectrum of $(CD_3)_3CSH$, is a typical powder pattern for an electric field gradient, $eq_{zz} = V_{zz}$, which is axially symmetric about the deuterium–carbon bond vector. In this case, the frequency separation between the singularities is $(3/4)\chi$ and between the edges it is $(3/2)\chi$, where χ is the quadrupolar coupling constant, $(e^2q_{zz}Q)/h$.

The field gradient of the sulfur bonded deuterium of *t*-butylthiol is not quite axially symmetric, as shown in Fig. 2*g*. Computer simulation of this powder pattern yields an asymmetry parameter $\eta = (V_{xx} - V_{yy})/V_{zz}$, $(0 \leq \eta \leq 1)$, of approximately 0.07. General expressions for the splitting between the spectral discontinuities in this case are given in refs. 8 and 9.

B. Effect of rapid molecular motion upon lineshape

For general *t*-butyl-X compounds, several different motions which influence the powder lineshape are possible: (*i*) internal rotations of the methyl groups about an approximate C_3 axis; (*ii*) internal rotations of the *t*-butyl group about the C—X axis, denoted C_3' rotations; (*iii*) general overall rotations of the molecules. For tetrahedral molecules such as neopentane, (Fig. 1*a*, X = CH_3), these latter rotations are generally regarded as consisting of motions about both the C_2 and the C_3 axes, illustrated in Fig. 1*b* (10).

Rotation about an axis may occur via continuous diffusion or by "jumps"; either will affect the powder lineshape when comparable to, or faster than (^{2}H) χ^{-1}. If motions can be treated independently, the rotationally averaged spectrum can be simulated using theoretical models (7–9, 11, 12).

The effect of rapid rotational diffusion is simply to reduce the splitting by a factor of $(1/2)\,(3\cos^2\beta - 1)$, where β is the angle between the axis of rotation and the C—D bond vector. The rotationally averaged spectrum is always axially symmetric when the motion is very rapid ($\tau \ll \Delta\nu_3^{-1}$). If perfect tetrahedral symmetry about each of the carbon sites in the *t*-butyl compounds is assumed (a good approximation in the gas phase, according to the geometry computed by ref. 13), the angles of interest are 1/2 the tetrahedral angle, or 54.74°, for C_2 rotation, and the complement to the tetrahedral angle, 70.53°, for C_3 rotations. The reduction factors for these angles are 0 and 1/3, respectively; therefore, one would expect rapid diffusion about a C_2 axis to completely collapse the quadrupolar splitting, and rapid diffusion about a C_3 axis to reduce it to one third the original value.

In the rapid motion limit, the effect of jumps between sites of three-fold or greater symmetry is exactly the same as for rotational diffusion. Once this limit is reached, one cannot distinguish, for example, between 120° jumps or continuous rotation about a C_3 axis. On the other hand, rapid jumps and diffusion about a C_2 axis yield substantially different spectra (7–9, 11, 12). Theory predicts that 180° flips about a C_2 axis in *t*-butyl compounds will result in an effective asymmetry parameter of 1, with $V_{xx} = V_{zz} = 64$ kHz for the methyl deuterons.

The situation for more complex motion — e.g. a combination of C_2 jumps and C_3 jumps about different axes — is much more complex, and will not be dealt with here.

C. Spin–lattice relaxation

The spin–lattice relaxation rate due to modulation of the electric quadrupole interaction of a spin 1 nucleus is given by

$$[1]\quad \frac{1}{T_1} = \frac{3}{20}\pi^2\chi^2(1 + \eta^2/3)\,\{J_1(\omega_0) + 4J_2(2\omega_0)\}$$

where $J_1(\omega_0)$ and $J_2(2\omega_0)$ are spectral density functions at the Larmor frequency ω_0 and at $2\omega_0$, respectively, such that $J(\omega) = 2\tau_{eff}/(1 + \omega^2\tau_{eff}^2)$. In this expression, τ_{eff} is an effective correlation time associated with the rotation of V_{zz}, and the function describing τ is assumed to have an exponential form. For $\omega_0\tau \ll 1$, the extreme narrowing condition which holds in all but the lowest solid phase of *t*-butylthiol, $J_1(\omega_0) = J_2(2\omega_0) = 2\tau_{eff}$.

In a similar manner, the relaxation rate of a proton decoupled methyl ^{13}C nucleus, in the extreme narrowing region, is given by

$$[2]\quad \frac{1}{T_1} = \frac{3\hbar^2\gamma_C^2\gamma_H^2\tau_{eff}}{r_{CH}^6}$$

where γ_C and γ_H refer to the magnetogyric ratios of ^{13}C and ^{1}H, respectively, and r_{CH} is the carbon–hydrogen internuclear separation. In this case, the carbon-13 nuclei are assumed to be relaxed solely by nearby protons via the dipole–dipole mechanism.[2]

The precise meaning of τ_{eff} in the above equations will be dependent on temperature and the particular phase of *t*-butylthiol under consideration. For the liquid phase, τ_{eff} can be related to rotational diffusion constants parallel and perpendicular to the C_3' axis illustrated in Fig. 1*a* (15). In the solid phases where the quadrupolar powder patterns are observed, i.e. II, III, and IV, τ_{eff} is related to the product of τ_2 and an order parameter (see ref. 16).

Experimental

Samples of $(CD_3)_3CSH$ and $(CH_3)_3CSD$ were purchased from Merck, Sharp, & Dohme Chemical Co.; $(CH_3)_3CSH$ (99+%) was obtained from Aldrich Chemical Co. The samples were transferred to 1 cm cylindrical microcells of 9 mm outer diameter, then de-gassed using repetitive freeze–pump–thaw cycles before sealing. Most of the experiments were performed on a Nicolet 360 narrow bore instrument, while some of the carbon-13 relaxation measurements were carried out on a Varian CFT-20. The low temperature deuterium spectra were obtained on a Bruker CXP 180 MHz instrument.

Temperature regulation is estimated to be within ±1 K. Typical $\pi/2$ pulse widths are in the range 35 to 45 μs for ^{2}H and 25 μs for ^{13}C on the Nicolet 360 and 22 μs for ^{13}C on the CFT-20. A phase-alternated quadrupole echo technique (17) was employed on the Bruker CXP spectrometer in order to obtain the spectra shown in Fig. 2. For these spectra, the echo-pulse spacing was ~40 μs with pulse widths of 3 μs. Dwell times of 0.5 μs were used to record 512 point quadrupole echoes (at very low temperatures, 1 μs dwell time and 1K points were used), which were zero-filled to 4K before Fourier transformation.

Spin–lattice relaxation times were measured by either standard inversion-recovery, or in some cases, inversion-recovery with a compensating pulse (18), using 10 or more τ values and a delay of at least 5 times T_1. Generally, only one scan was required to obtain satisfactory signal/noise ratios in the deuterium measurements; eight or more were required for the natural abundance carbon-13 study. The T_1 values were calculated using a 3-parameter-fit program in the Nicolet 1280 software package (19). Reproducibility is within 1–2%; errors are expected to be within 5%. Carbon-13 T_1s on the unlabelled compound and ^{2}H T_1s on $(CH_3)_3CSD$ were conducted over the temperature range 160 to 320 K, while ^{2}H measurements on $(CD_3)_3CSH$ were extended down to 140 K. For the low temperature phases, the T_1 data are obtained from measurement of the peak height of the central component.

[2] Within experimental error, a full nOe was observed up to ~315 K. Figure 3 does not include ^{13}C data above this temperature.

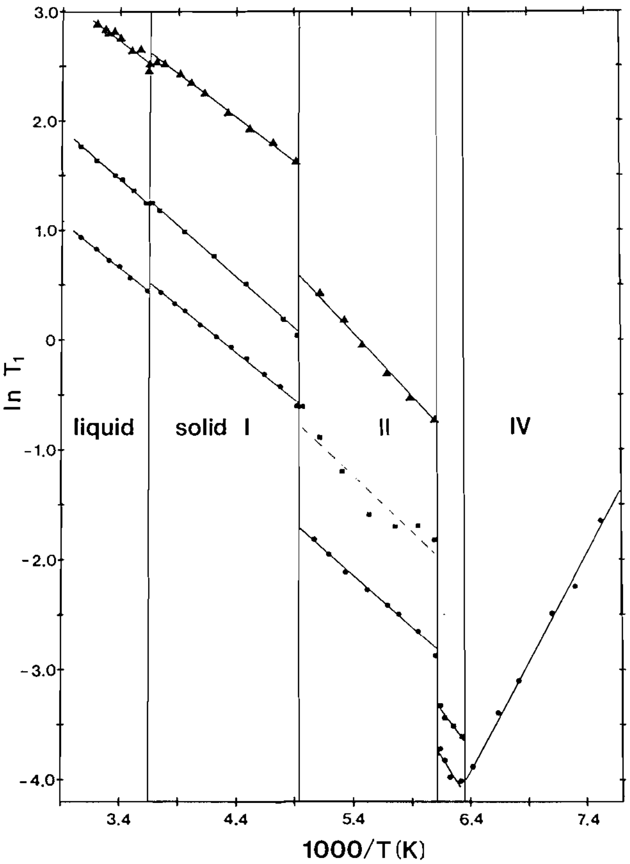

FIG. 3. Plot of ln $T_1(s)$ vs. reciprocal temperature for: (*a*) ^{13}C relaxation in unlabelled *t*-butylthiol (▲); (*b*) ^2H relaxation in $(CH_3)_3CSD$ (■); (*c*) ^2H relaxation in $(CD_3)_3CSH$ (●). The vertical lines represent the observed phase transition temperatures of 274 K (mp), 203 K (I/II), 164 K (II/III), and 158 K (III/IV).

Results and discussion

Deuterium nmr spectra of *t*-butylthiol at selected temperatures are shown in Fig. 2; spin–lattice relaxation data are summarized in Fig. 3 and Table 1.

A. Solid IV

The ^2H nmr spectrum of $(CD_3)_3CSH$ at 108 K (Fig. 2*a*), is the axially symmetric powder pattern, χ = 171 kHz, of the rigid solid. When the sample is warmed above ~120 K, the 128 kHz splitting between the singularities collapses to a broad, featureless peak of about 10 kHz in half-height width (Fig. 2*b*). We interpret this spectrum as arising from a combination of C_3 internal methyl and *t*-butyl group jumps occuring at a rate comparable to the inverse of the quadrupolar splitting (~10^{-6} s). This interpretation is based upon (*i*) comparison to the ^2H nmr spectra of other *t*-butyl-X compounds, (*ii*) the temperature dependence of the spin–lattice relaxation time, and (*iii*) the nmr powder pattern observed for $(CH_3)_3CSD$ in this phase.

The process of motional averaging of the ^2H nmr powder lineshape in several $(CD_3)C$—X compounds, including X = Cl, Br, I, and CHO, is accompanied by the observation of a spectrum similar to Fig. 2*b* upon warming the rigid solid. In *t*-butylchloride and *t*-butylbromide, however, the averaging process in the lowest temperature phase occurs stepwise (20–22). The first type of motion to become fast enough to average the quadrupolar interaction is reorientation about the C—X, or C_3' axis (21, 22). Since, in the absence of internal methyl rotation, two of the three C—D vectors in each methyl group form an angle of 70.53° with the C_3' axis, while the remaining C—D vector is parallel to this axis (Fig. 1*a*), two overlapping powder spectra are observed (21): one with the original static splitting, and one averaged to 1/3 the static value, or approximately 43 kHz. When the sample is heated another 30°, methyl rotation also becomes much faster than the inverse of the ^2H quadrupole interaction, roughly χ^{-1}, rendering the three deuterons in each methyl group equivalent. The averaged principal axes then lie along the C—C axes, 70.53° from the C—D bonds, and the quadrupolar splitting is again reduced by the 1/3 factor to ~14 kHz. Between these two steps, that is, in the approximately 20° temperature range in which C_3' rotation is relatively fast and C_3 (methyl) rotation is ~χ^{-1}, the equivalent of spectrum 2*b* is observed. *t*-Butyliodide and *t*-butylaldehyde show a similar progression in achieving the 14 kHz powder pattern, although in these compounds, as in *t*-butylthiol, averaging due to C_3' rotation is not established before C_3 rotation also affects the spectra (23).

TABLE 1. Least-squares fit parameters of the Arrhenius equation $\tau = \tau_0 \exp [E_a/Rt]$ obtained from the data in Fig. 3

	Correlation coefficient r	Activation energy E_a(kJ mol^{-1})	Pre-exponential factor $\tau_0(\times 10^{14})$
Liquid:			
^{13}C	0.948	7.03	6.0
^2H (d_9)	0.996	7.11	6.5
^2H (SD)	0.994	7.70	3.0
Solid I:			
^{13}C	0.997	6.5	6.6
^2H (d_9)	0.998	7.1	6.0
^2H (SD)	0.999	7.8	2.8
Solid II:			
^{13}C	0.996	9.8	2.6
^2H (d_9)	0.997	8.0	10
Solid III:			
^2H (d_9)	0.860	13	0.65
^2H (SD)	0.921	11	2.7

t-Butylthiol is further distinguished from the other *t*-butyl-X compounds in that it undergoes a phase change before methyl rotation becomes rapid enough for the 14 kHz splitting to appear. This is borne out by the behaviour of the spin–lattice relaxation time in solid IV: the increasing T_1 with decreasing temperature (see Fig. 3) indicates that the motion causing relaxation must be slower than ω_0^{-1}. Using eq. [1], the observed T_1s correspond to τ_{eff} values of 1×10^{-5} s at approximately 133 K, and 1.1×10^{-6} s at the solid IV → solid III phase transition (158 K), consistent with rotation rapid enough to affect the spectrum yet not rapid enough to average it to the 14 kHz powder pattern.

The possibility that the broad, single peak of Fig. 2*b* represents averaging by molecular C_2 jumps with an asymmetry parameter approaching unity, or that the entire molecule reorients under C_3' jumps can be ruled out by the ^2H nmr spectrum of $(CH_3)_3CSD$. For this isotopomer, a full powder pattern (Fig. 2*g*) was observed throughout solid IV, indicating very slow or no motion of the thiol substituent in this phase. Using the geometry shown in Fig. 1*a*, with ∠CSD = 97.5° (13), we would expect rapid C_3 jumps about the C—S axis to average the quadrupolar splitting to less than half the static value, while C_2 jumps (Fig. 1*b*) would average the splitting to an even greater extent. The only conceivable motion which would not be detected in the ^{2}H nmr spectrum of $(CH_3)_3CSD$ would be rotation about an axis parallel or nearly parallel to the S—D bond vector; but this can be ruled out by the low dielectric constant (6), indicating that the dipole moment (oriented approximately perpendicular to the S—D bond axis (13)) is not reorienting.

Internal C_3 and C_3' rotations are also consistent with the results of Smith (4), who reports a decrease in the ^{1}H second moment from about 30 G^2 to ~2.4 G^2 over the temperature range 90 to 120 K.

B. Solid III and II

Although thermodynamic data (2, 3) report phase transitions at 151.6 and 157 K, no abrupt changes are observed in the ^{2}H solid IV spectra of either of the deuterium labelled *t*-butylthiol samples until they are heated to 158 K. At this temperature, the spectrum of $(CD_3)_3CSH$, Fig. 2*c*, sharpens to a powder pattern approximately 4 kHz in width with an effective asymmetry parameter of almost 1, while that of $(CH_3)_3CSD$, Fig. 2*h*, collapses from the rigid powder lineshape of χ = 130 kHz, η = 0.07, to a lineshape of ~9 kHz in width, with $\eta_{eff} \simeq 0.5$. We associate these spectral changes with the solid IV → solid III phase transition.

The short solid III phase can be clearly distinguished from solids II and IV by the discontinuities in the ln T_1 versus reciprocal temperature plots, Fig. 3. The slope of these plots indicates motion in the extreme narrowing region, and use of eq. [1] yields τ_{eff} values of 1.2×10^{-10} s for $(CD_3)_3CSH$ and 1.3×10^{-10} s for $(CH_3)_3CSD$ at 160 K. The similarity in these two results and the relatively narrow ^{2}H powder patterns demonstrates that overall molecular reorientation is the dominant motion causing relaxation in this phase. Since neither rapid diffusion or fast C_3 jumps predict $\eta_{eff} > 0$, the highly asymmetric lineshapes observed in this phase imply that C_2 jumps must be involved in the reorientation of the molecule.

Further discontinuous changes in the deuterium nmr lineshapes do not take place until 164 K (d_9 compound) or 166 K (SD isotopomer), corresponding to the solid III → solid II phase transition. At 164 K, the $(CD_3)_3CSH$ spectrum (Fig. 2*d*) undergoes further narrowing to a featureless peak of ~1 kHz in width with low intensity shoulders. The spectrum of $(CH_3)_3CSD$, Fig. 2*i*, undergoes a very unusual change at this transition: a broad component about 25 kHz in width appears along the baseline, accompanied by an increase in η_{eff} and a slight narrowing of the central component to 8 kHz.

Discrepancies between our transition temperatures and those reported by McCullough *et al.* (2, 3) for the IV → III and III → II transitions may be due to the relatively short periods (15 to 30 min) which we could allow for thermal equilibrium to be reached. The upwards shift of approximately 6° is rather large to be considered an isotope effect, although such shifts are not unusual in solid–solid phase transitions (1).

The occurrence of the solid III phase is apparent only upon heating. Upon cooling a sample displaying a solid II spectrum, no drastic changes occur until a solid IV spectrum is attained, which is observed at ~151 K for both the d_9 and the SD samples. Kondo (6) also reported "a thermal hysteresis of phase change" for $(CH_3)_3CSH$; he observed sharp discontinuities in the dielectric constant, ϵ, at 151.6 and 161.6 K upon heating, but only the corresponding drop in ϵ at 151.6 K upon cooling. The proton nmr second moment does not appear to be sensitive to the solid III → solid II transition, showing only an abrupt change at 153 K in this temperature range (4). Again, there is considerable hysteresis in the heating/cooling data, suggesting that *t*-butylthiol is very slow to reach equilibrium.

TABLE 2. Entropy change (in units of R) at the solid–solid phase transitions in *t*-butyl compounds

	Entropy change		
Transition	$(CH_3)_3CSH$[a]	$(CH_3)_3CCl$[b]	$(CH_3)_3CBr$[b]
I → liq	1.09	0.95	0.9
II → I	0.58	3.2	0.55
III → II	0.50	1.2	3.25
IV → III	3.22		

[a]References 2, 3.
[b]Reference 14.

Upon warming through the solid II temperature range, both $(CD_3)_3CSH$ and $(CH_3)_3CSD$ deuterium spectra evolve to very complex motionally averaged powder patterns, with fairly well defined shoulders and edges but also with relatively broad central components. In *t*-butylthiol-SD, Fig. 2(*j*, *k*), the powder splitting of the outer edges is about 8 kHz; in the d_9 compound, Fig. 2*e*, it is only 1–1.5 kHz. The unusual lineshapes might be due to a purely dynamic effect, but the spectra appear to consist of two overlapping powder patterns, indicative of more than one type of molecule in the unit cell. A lattice contribution to the electric field gradient from a non-cubic crystal structure also remains a distinct possibility (24).

The spin–lattice relaxation times obtained for solid II indicate that the rate of reorientation in this phase is an order of magnitude faster than in solid III. The activation energy also appears to have decreased somewhat, as shown in Table 1. The non-Arrhenius behaviour of the thiol deuteron T_1s in this phase is likely due to differing relaxation rates in the two overlapping powder patterns; the result underlines the difficulty in interpreting the T_1s from such unusual lineshapes, especially since the spectra continue to vary with temperature throughout the phase.

Just below the transition to solid I, which occurs at 204 K, the $(CD_3)_3CSH$ spectrum becomes increasingly asymmetric (Fig. 2*f*), while one component of the $(CH_3)_3CSD$ spectrum appears to be approaching $\eta_{eff} = 0$ (Fig. 2*l*). Entrance into the solid I phase is heralded by the collapse of all quadrupolar splitting in both ^{2}H spectra. When either sample is subsequently cooled back down into solid II, small non-reproducible splittings are observed, which are interpreted as the formation of a number of monocrystalline domains in the nmr tube, rather than a purely random collection of crystallites. This observation confirms the change in crystal structure at this transition first proposed by Guthrie and McCullough (3), and supported by Smith (4).

If the sample is cooled below 150 K and then re-heated, the extra splittings in the solid II spectrum appear to be somewhat smoothed, suggesting that another change in crystal structure occurs at the solid IV boundary, cracking some of the crystalline domains. In light of the large entropy change at this transition point, a change of crystal lattice as well as the gains in orientational freedom is not surprising.

It is of interest to compare our ^{2}H nmr powder patterns with those observed for other *t*-butyl-X compounds. *t*-Butylchloride appears to be the best behaved, with the 14 kHz splitting of the lowest temperature phase, solid III, remaining up to the II → I transition, where all quadrupolar splitting collapses (20). *t*-

TABLE 3. Rotational correlation times at the melting point of various t-butyl compounds

Molecule	τ_{eff} (ps)	Reference
t-Butylthiol-d_9	1.5 (liquid) 1.3 (solid I)	This work
t-Butylbromide-d_9	2.5 (liquid) 2.2 (solid I)	16
t-Butylchloride-d_9	2.0 (liquid) 1.8 (solid I)	25
Neopentane-d_{12}	0.9	28

Butylbromide, which also has only three solid phases, undergoes an abrupt change at the III → II transition (16): the ~14 kHz splitting of solid III becomes a tiny 400 Hz splitting in solid II. The spectrum retains an axially symmetric lineshape until, as in the other t-butyl-X ^2H spectra, all splitting disappears in solid I. The unique nature of the phase II deuterium powder lineshapes in these compounds, despite the similarity in transition entropies (Table 2) and behaviour in the low and high temperature solid phases, tells us that the transition from internal C_3 and C_3' rotations to near isotropic reorientational freedom is highly substituent dependent, and cannot be described in a simple, stepwise manner.

C. Solid I and liquid

The ^2H nmr spectra of $(CD_3)_3CSH$ and $(CH_3)_3CSD$ show identical single peaks in both liquid and solid I phases, indicating that the molecule reorients through all angles at a rate much faster than ω_0^{-1}. The two phases are distinguished, however, by a slight discontinuity in the temperature dependence of the ^2H and ^{13}C spin–lattice relaxation times, shown in Fig. 3. The size of the symbols in the diagram include at least a 5% error estimate, although reproducibility of the liquid/solid I data was much better than that.

The slight discontinuity, apparent in all three plots of ln T_1 versus reciprocal temperature, represents a decrease in τ_{eff} upon freezing. A similar result was obtained for t-butylbromide (16), and although not reported in an earlier ^2H study of t-butylchloride (20), we have also found a small discontinuity in $(CD_3)_3CCl$ T_1s at the melting point (25). The possibility that this discontinuity is solely due to a change in the electric field gradient (26, 27), i.e. χ, is ruled out by the ^{13}C data, which is not affected by $\hat{V}$. The slight decrease in τ_{eff} upon freezing indicates, at least initially, greater rotational freedom in the plastic phase. This is illustrated by comparison of the τ_{eff} values obtained at this transition to those obtained in other t-butyl compounds (see Table 3). Overall rotations of t-butylthiol are comparable to those observed for the chloride; symmetric neopentane, with a methyl group on the t-butyl moiety, rotates at about twice this rate (28).

The Arrhenius parameters obtained from least-squares fitting of the data are given in Table 1. Within experimental error, the pre-exponential factors and activation energies obtained from the carbon-13 and deuterium studies on the unlabelled and the d_9 compounds are the same, as they should be since both are monitoring rotation of the same vectors. A comparison of these τ_{eff} values with those obtained from the ^2H data on $(CH_3)_3CSD$ is a measure of the isotropy of the overall reorientation of the molecule. Interestingly, τ_{eff} of the S—D vector changes very little upon freezing.

Conclusions

The deuterium nmr data on t-butylthiol lend further support to the general conclusions of Smith (4). Internal reorientation of the methyl and t-butyl groups becomes significant on the ^2H nmr timescale at 120 K in solid IV, and above the solid IV → solid III transition rapid reorientation of the dipolar axis occurs as well. Molecular rotations are relatively free in solid I, being comparable to those in the liquid. In addition, a change in crystal structure is confirmed at the solid IV/solid III and solid II/solid I transition temperatures, as is a change in the rotational correlation time of approximately one order of magnitude at the III/II and II/I boundaries. Observation of quadrupolar splittings in the solid II phase suggest that this phase is not cubic. A more detailed analysis of the nature of molecular motions in solids II and III should be possible if the powder lineshapes can be simulated and a reasonable model to interpret the T_1 data is available.

A final note: careful measurements of the spin–lattice relaxation time are required to observe a discontinuity at the melting point; it is likely a more general phenomenon among plastic crystals than has been reported to date. Theoretical or statistical mechanical models of melting should account for this.

Acknowledgements

We are grateful to Dr. John Ripmeester of National Research Council of Canada, Ottawa, for his assistance in obtaining the low temperature ^2H nmr spectra in Fig. 2. All of the ^2H and most of the ^{13}C relaxation measurements were carried out at the Atlantic Regional NMR Centre. Our thanks to NSERC for financial support in establishing and maintaining this centre, and also for an operating grant (R.E.W.).

1. N. G. PARSONAGE and L. A. K. STAVELEY. Disorder in crystals. Clarendon Press, Oxford. 1978.
2. J. P. MCCULLOUGH, D. W. SCOTT, H. L. FINKE, W. N. HUBBARD, M. GROSS, C. KATZ, R. E. PENNINGTON, J. F. MESSERLY, and G. WADDINGTON. J. Am. Chem. Soc. **75**, 1818 (1953).
3. G. B. GUTHRIE and J. P. MCCULLOUGH. J. Phys. Chem. Solids, **18**, 53 (1961).
4. G. W. SMITH. J. Chem. Phys. **51**, 3569 (1969).
5. S. L. SEGEL and A. MANSINGH. J. Chem. Phys. **51**, 4578 (1969).
6. S. KONDO. Bull. Chem. Soc. Jpn. **38**, 527 (1965).
7. M. MEHRING. Principles of high resolution NMR in solids. 2nd ed. Springer-Verlag. 1983. Chapt. 2.
8. R. G. BARNES. Advances in nuclear quadrupole resonance. Vol. 1. Heyden. 1973. pp. 335–355.
9. C. M. GALL, T. A. CROSS, J. A. DIVERDI, and S. J. OPELLA. Proc. Natl. Acad. Sci. USA, **79**, 101 (1982).
10. S. TAKEDA, G. SODA, and H. CHIHARA. Mol. Phys. **47**, 501 (1982).
11. S. ALEXANDER, A. BARAM, and Z. LUZ. Mol. Phys. **27**, 441 (1974).
12. H. W. SPIESS. NMR basic principles and progress. Vol. 15. Springer-Verlag. 1978. pp. 59–214.
13. E. VALENZUELA and R. C. WOODS. J. Chem. Phys. **61**, 4119 (1974).
14. L. M. KUSHNER, R. W. CROWE, and C. P. SMYTH. J. Am. Chem. Soc. **72**, 1091 (1950).
15. J. R. LYERLA and D. M. GRANT. J. Phys. Chem. **76**, 3213 (1972).
16. B. A. PETTITT, J. S. LEWIS, R. E. WASYLISHEN, W. DANCHURA, E. TOMCHUK, and E. BOCK. J. Magn. Reson. **44**, 508 (1981).
17. J. H. DAVIS, K. R. JEFFREY, M. BLOOM, M. I. VALIC, and T. P. HIGGS. Chem. Phys. Lett. **42**, 390 (1976).
18. R. FREEMAN, S. P. KEMPSELL, and M. H. LEVITT. J. Magn. Reson. **38**, 453 (1980).
19. G. C. LEVY and I. R. PEAT. J. Magn. Reson. **18**, 500 (1975).
20. D. E. O'REILLY, E. M. PETERSON, C. E. SCHLIE, and E. SEY-

FORTH. J. Chem. Phys. **59**, 3576 (1973).
21. J. A. RIPMEESTER and C. I. RATCLIFFE. J. Chem. Phys. **82**, 1053 (1985).
22. J. C. FROST, A. J. LEADBETTER, and R. M. RICHARDSON. Phil. Trans. R. Soc. Lond. B, **290**, 567 (1980).
23. R. E. WASYLISHEN, S. MOOIBROEK, J. B. MACDONALD, and J. RIPMEESTER. To be published.
24. T. CHIBA. J. Chem. Phys. **36**, 1122 (1962).
25. S. MOOIBROEK and R. E. WASYLISHEN. Unpublished results.
26. N. BODEN and R. FOLLAND. Chem. Phys. Lett. **32**, 127 (1975).
27. N. BODEN. The plastically crystalline state. J. N. Sherwood, John Wiley and Sons. 1979. Chapt. 5.
28. B. A. PETTITT, R. E. WASYLISHEN, R. Y. DONG, and T. P. PITNER. Can. J. Chem. **56**, 2576 (1978).

Moments analysis of restricted ternary diffusion: sodium sulfite + sodium hydroxide + water

DEREK G. LEAIST
Department of Chemistry, University of Western Ontario, London, Ont., Canada N6A 5B7

Received February 19, 1985

DEREK G. LEAIST. Can. J. Chem. **63**, 2933 (1985).

Ternary diffusion coefficients can be determined from restricted-diffusion experiments by evaluating zeroth and first time moments of the difference in a concentration-dependent property measured at two levels along the diffusion column. The method is used to determine ternary diffusion coefficients for aqueous sodium sulfite + sodium hydroxide solutions from conductance measurements. It is shown that these data can be analyzed to obtain the ternary diffusivity of sulfur dioxide in strongly alkaline solutions where sulfite is the major transporting species for the sulfur dioxide component. At high pH values, coupled flow of hydroxide ions leads to a significant increase in the diffusivity of the sulfur dioxide component relative to its diffusivity in pure water. Binary diffusion coefficients for aqueous sodium sulfite solutions are also reported.

DEREK G. LEAIST. Can. J. Chem. **63**, 2933 (1985).

On peut déterminer les coefficients de diffusion ternaire à partir d'expériences de diffusion restreinte en évaluant les moments de temps zéro et un de la différence qui existe dans une propriété qui dépend de la concentration et qui est mesurée à deux niveaux le long de la colonne de diffusion. On a utilisé la méthode pour déterminer les coefficients de diffusion ternaire de solutions aqueuses de sulfite de sodium + hydroxyde de sodium à partir de mesures de conductivité. On montre que l'on peut analyser ces données de manière à obtenir la diffusivité ternaire du dioxyde de soufre dans des solutions fortement alcalines où le sulfite est le transporteur principal du dioxyde de soufre. À des pH élevés, le flux couplé d'ions hydroxydes conduit à une augmentation marquée de la diffusivité de la composante du dioxyde de soufre par rapport à sa diffusivité dans l'eau. On rapporte également les coefficients de diffusion binaire de solutions aqueuses de sulfite de sodium.

[Traduit par le journal]

1. Introduction

The Harned restricted-diffusion method is an important technique for determining diffusion coefficients of electrolyte solutions (1–4). In this technique flows of solute are measured by following changes in electrical conductance near the ends of short diffusion columns. The concentration gradients are sufficiently small that differential diffusion coefficients are determined directly without ambiguities arising from the concentration-dependence of the diffusivity. Cell calibration with materials of known diffusivity is not required. Furthermore, diffusion can be measured conductimetrically at low concentrations of theoretical interest where other methods are unreliable.

Soon after the Harned method was developed Fujita (5) proposed moments analyses that would extend conductimetric experiments to ternary mixed electrolytes and thus enable studies of coupled diffusion. Unlike pseudo-binary treatments of restricted-diffusion (6, 7) which rely on numerical differentiation of experimental data, moments methods employ inherently more-accurate integration of conductance data. Unfortunately, Fujita's treatment applies only to symmetrically-sheared cells in which the initial diffusion boundary is formed half-way along the diffusion channel. Experience has shown that cells of this design are unreliable for studies of multicomponent diffusion owing to convection currents formed when dilute solutions are sheared (6). Consequently, moments methods, despite their promise, have not been applied to restricted-diffusion experiments. Yet integration techniques for analysis of free-diffusion experiments are well-established and accurate (8–10).

Initial concentration gradients are formed in conventional Harned cells with a needle and syringe by injecting a small volume of concentrated (i.e. dense) solution into the bottom of the solution column (3, 4). In addition to minimizing convection the injection procedure simplifies construction and operation of the cells. The purpose of this paper is to adapt Fujita's moments analysis (5) to conventional cells in which initial boundaries are formed at arbitrary levels along the diffusion channel. The difficult task of determining ternary diffusion coefficients is then reduced to simple numerical integration of conductance data. The equations that are developed can also be used to analyze optical (11) or diaphragm cell experiments (12) in which a concentration-dependent property (such as density, refractive index, or optical absorbance) is monitored at two fixed levels along the path of diffusion.

The moments procedure is used to determine diffusion coefficients for aqueous sodium sulfite + sodium hydroxide solutions. The results are analyzed to obtain the ternary diffusivity of aqueous sulfur dioxide in alkaline solutions. Data for these systems are useful in order to describe transport of SO_2 in solutions used to scrub flue gases. At high pH values coupled flow of hydroxide ions is shown to produce a sharp increase in the diffusivity of the aqueous SO_2 component (i.e. total SO_2). To aid interpretation of the results binary diffusion coefficients for aqueous Na_2SO_3 solutions are also reported.

2. Experimental

Equipment and procedure

The diffusion cells had cylindrical diffusion channels (0.03–0.05 m height, 0.0127 m diameter) machined from polypropylene or polyethylene. Pairs of circular platinum electrodes (0.001 m diameter) were set in the cell walls at levels one-sixth and five-sixths of the distance between the top and bottom of the channels. Each cell was sealed with a greased glass slide.

Initial concentration gradients were prepared by injecting 0.1–0.5 mL of electrolyte into the bottom of each diffusion chamber. The concentrations were adjusted so that the initial gradient vanished for one of the solutes. Resistances were measured with a Jones bridge. Details of the equipment and procedure can be found elsewhere (3, 4, 6, 7).

Reagent grade Na_2SO_3 was dried in a vacuum oven at 130°C and used without further purification. Stock solutions of NaOH were prepared by dilution of saturated solutions that had been filtered through sintered glass to remove insoluble carbonate.

Binary diffusion

Binary diffusion coefficients for aqueous Na_2SO_3 solutions were determined from conductance readings using the equation (2, 4)

$$[1] \quad D = -(a^2/\pi^2)\mathrm{d} \ln \Delta K(t)/\mathrm{d}t$$

in which a is the length of the diffusion channel and $\Delta K(t) = (k_B/k_T)K_B(t) - K_T(t)$ is proportional to the difference in specific conductance between the bottom (B) and top (T) electrode pairs at time t. K_B and K_T are the measured reciprocal resistances and k_B/k_T is the cell constant ratio. The slope of ln $\Delta K(t)$ against t was estimated by least squares.

Ternary diffusion

Mass transport of two solutes in one dimension under isothermal, convection-free conditions is described by ternary diffusion equations

$$[2] \quad \partial c_1/\partial t = D_{11}\partial^2 c_1/\partial x^2 + D_{12}\partial^2 c_2/\partial x^2$$

$$[3] \quad \partial c_2/\partial t = D_{21}\partial^2 c_1/\partial x^2 + D_{22}\partial^2 c_2/\partial x^2$$

in which c_i are solute concentrations in moles per unit volume, t is the time, and x is the distance coordinate. Ternary diffusion coefficients D_{ik} are treated as constants. This approximation is valid for small concentration gradients.

For restricted diffusion in a column of height a, flows of solute through the bottom ($x = 0$) and top ($x = a$) of the column vanish.

$$[4] \quad \partial c_i/\partial x = 0 \qquad (x = 0 \text{ and } x = a, t > 0)$$

At time $t = 0$ a sharp initial boundary is formed at level $x = \epsilon a$

$$[5] \quad c_i = \bar{c}_i + (1 - \epsilon)\Delta c_{i0} \qquad (0 < x < \epsilon a, t = 0)$$

$$[6] \quad c_i = \bar{c}_i - \epsilon\Delta c_{i0} \qquad (\epsilon a < x < a, t = 0)$$

where $\bar{c}_i$ is the mean cell concentration for solute i and Δc_{i0} is the difference in concentration of solute i across the initial boundary. (For a symmetrically-sheared cell: $\epsilon = 0.5$. If the boundary is formed by injecting a small amount of electrolyte into the bottom of the solution column: $\epsilon \ll 0.5$.)

Solutions $c_i(x, t)$ to eqs. [2], [3] with boundary conditions [4] and initial conditions [5], [6] have been obtained by Fourier analysis (6). The series expression for the difference in solute concentrations between reference levels $x = a/6$ and $x = 5a/6$

$$[7] \quad \Delta c_i(t) = c_i(a/6, t) - c_i(5a/6, t)$$

converges so rapidly that after a short waiting period only the first terms are significant.

$$[8] \quad \Delta c_1(t) = Q\frac{\{[(D_{11} - D_2)\Delta c_{10} + D_{12}\Delta c_{20}] \exp(-\beta D_1 t) + [(D_{22} - D_2)\Delta c_{10} - D_{12}\Delta c_{20}] \exp(-\beta D_2 t)\}}{D_1 - D_2}$$

$$[9] \quad \Delta c_2(t) = Q\frac{\{[-D_{21}\Delta c_{10} + (D_{11} - D_1)\Delta c_{20}] \exp(-\beta D_1 t) + [D_{21}\Delta c_{10} + (D_{22} - D_1)\Delta c_{20}] \exp(-\beta D_2 t)\}}{D_2 - D_1}$$

where Q and β are geometric factors

$$[10] \quad \beta = \pi^2/a^2$$

$$[11] \quad Q = (2\sqrt{3}/\pi) \sin(\pi\epsilon/a)$$

and eigenvalues D_i are defined by

$$[12] \quad D_1 = \{D_{11} + D_{22} + (D_{11} - D_{22})[1 + 4D_{12}D_{21}/(D_{11} - D_{22})^2]^{1/2}\}/2$$

$$[13] \quad D_2 = \{D_{11} + D_{22} - (D_{11} - D_{22})[1 + 4D_{12}D_{21}/(D_{11} - D_{22})^2]^{1/2}\}/2$$

Because the solute concentration differences are small the difference in specific conductance $\Delta K(t)$ between the two reference levels for a weakly associated or a strong electrolyte mixture is a linear function of the differences in solute concentration

$$[14] \quad \frac{\Delta K(t)}{\Delta K(0)} = \frac{S_1\Delta c_1(t) + S_2\Delta c_2(t)}{S_1\Delta c_1(0) + S_2\Delta c_2(0)}$$

Partial specific conductances of the components, $S_i = \partial L/\partial c_i$, are evaluated at the final composition $\bar{c}_1$, $\bar{c}_2$. Upon substitution of eqs. [8] and [9] into eq. [14], we obtain

$$[15] \quad \Delta K(t)/\Delta K(0) = A_1 \exp(-\beta D_1 t) + (1 - A_1) \exp(-\beta D_2 t)$$

for the normalized conductance difference. Constant A_1 is given by

$$[16] \quad A_1 = \frac{(S_1/S_2)D_{12} - D_{11} + D_1 + X_1[(S_2/S_1)D_{21} - (S_1/S_2)D_{12} + 2D_{11} - D_1 - D_2]}{D_1 - D_2}$$

where X_1 is the fraction of the initial conductance difference due to solute 1

$$[17] \quad X_1 = S_1\Delta c_{10}/(S_1\Delta c_{10} + S_2\Delta c_{20})$$

Moments analysis

How can ternary diffusion coefficients be evaluated from measurements of $\Delta K(t)$? Following Fujita (5), consider zeroth and first time moments of the normalized conductance difference

$$[18] \quad I_0 = \int_0^\infty [\Delta K(t)/\Delta K(0)]\mathrm{d}t$$

$$[19] \quad I_1 = \int_0^\infty t[\Delta K(t)/\Delta K(0)]\mathrm{d}t$$

Integration gives expressions for the moments as functions of X_1

$$[20] \quad I_0(X_1) = I_0(0) + [I_0(1) - I_0(0)]X_1$$

$$[21] \quad I_1(X_1) = I_1(0) + [I_1(1) - I_1(0)]X_1$$

where

$$[22] \quad I_0(0) = [D_{11} - (S_1/S_2)D_{12})/\beta D_1 D_2$$

$$[23] \quad I_0(1) = [D_{22} - (S_2/S_1)D_{21}]/\beta D_1 D_2$$

$$[24] \quad I_1(0) = [D_{11}I_0(0) - (S_1/S_2)D_{12}I_0(1)]/\beta D_1 D_2$$

$$[25] \quad I_1(1) = [D_{22}I_0(1) - (S_2/S_1)D_{21}I_0(0)]/\beta D_1 D_2$$

After some algebra it develops that the ternary diffusion coefficients are remarkably simple functions of the lower moments

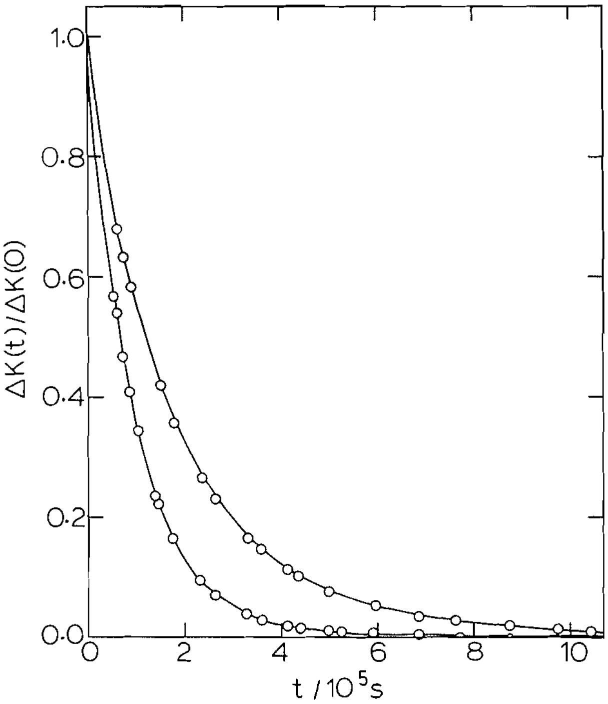

FIG. 1. Normalized conductance difference plotted against time for $c_1(Na_2SO_3) = 0.005$ mol dm^{-3} and $c_2(NaOH) = 0.035$ mol dm^{-3}. Areas under top curve (initial gradient in Na_2SO_3) and bottom curve (initial gradient in NaOH) determine moments $I_0(1)$ and $I_0(0)$, respectively.

[25] $D_{11} = [I_0(0)I_0(1) - I_1(0)]/F$

[26] $D_{12} = (S_2/S_1)[I_0(0)I_0(0) - I_1(0)]/F$

[27] $D_{21} = (S_1/S_2)[I_1(1) - I_0(1)I_0(1)]/F$

[28] $D_{22} = [I_1(1) - I_0(0)I_0(1)]/F$

[29] $F = \beta[I_0(0)I_1(1) - I_0(1)I_1(0)]$

Equations [25]–[29] reduce the difficult problem of computing ternary diffusion coefficients from conductance data to the much easier problem of determining moments. For simplicity, we chose to evaluate $I_0(0)$, $I_1(0)$, $I_0(1)$, and $I_1(1)$ by direct numerical integration of conductance vs. time data from two experiments: one with initial gradient entirely in solute 1 ($\Delta c_{20} = 0$, $X_1 = 1$), the other — performed in the same cell — with the initial gradient entirely in solute 2 ($\Delta c_{10} = 0$, $X_1 = 0$). Since I_0 and I_1 vary linearly with X_1, however, plotting measured values of I_0 and I_1 against X_1 for values of X_1 other than 0 or 1 would yield the required values of $I_0(0)$, $I_1(0)$ and $I_0(1)$, $I_1(1)$ as intercepts.

The analysis of conductimetric data is simplified by omission of higher order terms ($\sim\exp[-25\pi^2 D_i t/a^2]$) from eqs. [8], [9], and [15] (1). This approximation is valid provided conductance readings are taken for $t > a^2/50D_i$ where D_i is the smaller of the two eigenvalues. If $D_i \sim 1 \times 10^{-9}$ m^2 s^{-1} and $a \sim 0.05$ m, for example, conductance data may be analyzed for $t > 50\,000$ s, about one-half day.

By definition, moments I_0 and I_1 are obtained by integration of conductance data from $t = 0$ to infinity. When moments were evaluated from experimental data, it was necessary to estimate values of the conductance difference for values of t outside the interval of actual conductance measurements. Suppose conductance readings begin at $t = t_i$ and end at $t = t_f$. As a first approximation, values of D_{ik} were computed by integrating data available on the interval t_i to t_f. These D_{ik} values were used to estimate A_1, D_1, and D_2, and thus obtain an approximate expression for the conductance difference using eq. [15]. This expression was integrated analytically on intervals 0 to t_i and t_f to infinity to estimate contributions to I_0 and I_1 from outside the range

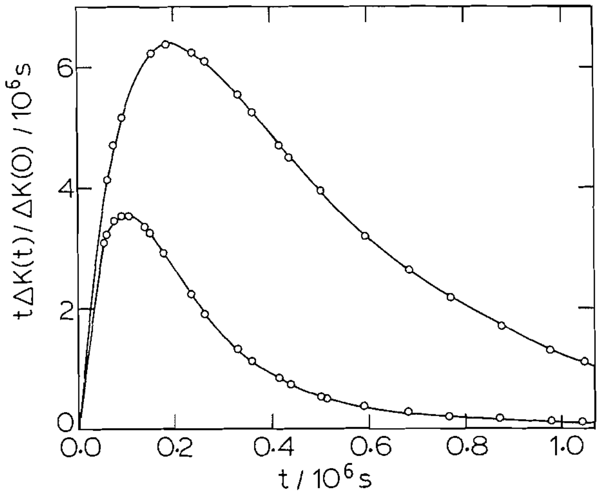

FIG. 2. $c_1(Na_2SO_3) = 0.005$ mol dm^{-3} and $c_2(NaOH) = 0.035$ mol dm^{-3}. Areas under the top curve (initial gradient in Na_2SO_3) and bottom curve (initial gradient in NaOH) determine $I_1(1)$ and $I_1(0)$.

of conductance readings. The cycle was repeated until changes in the estimates of D_{ik} were negligible. In practice only two or three iterations were required.

Unequally-spaced $\Delta K(t)/\Delta K(0)$ or $t\Delta K(t)/\Delta K(0)$ versus t data can be integrated numerically by using non-linear least-squares to fit the appropriate exponential function (eq. [15] for example) to the data, followed by analytic integration of the functions so obtained. We chose simply to fit each set of three adjacent points to a quadratic polynomial in t then integrated the polynomial, i.e. Simpson's rule on unequal intervals. Representative data are shown in Figs. 1 and 2. The excellent fits which were obtained provided a check on the internal consistency of the moments analysis procedure.

3. Results and discussion

Na_2SO_3 + H_2O

Binary diffusion coefficients for aqueous Na_2SO_3 solutions were determined at 25°C. The results of the measurements are summarized in Table 1. Uncertainties in the cell height ($\pm 2 \times 10^{-5}$ m) and cell constant ratio limit the accuracy of the data to $\pm 0.3\%$.

The limiting diffusion coefficient of the salt, D^0, was estimated from the data using the "self-consistent" equation for unsymmetrical electrolytes (13)

[30] $D(c) = (D^0 + \Delta_1)(1 + c\,d\ln y_\pm/dc)$

where Δ_1 is the first order electrophoretic correction and $y_\pm$ is the mean ionic activity coefficient on the molar-concentration scale. Thermodynamic factors $c\,d\ln y_\pm/dc$ were calculated from activities recommended by Goldberg (14). For this salt, however, accurate evaluation of D^0 was impossible because of large departures of the measured diffusion coefficients from values predicted by eq. [30]. This behavior may result from formation of ion pairs or from uncertainties in the activity coefficients, which at these low concentrations, are obtained by lengthy extrapolation of isopiestic data obtained above 0.2 mol dm^{-3} (14–16). Similar departures from predicted behavior have been observed for diffusion of aqueous Na_2SO_4 (17, 18).

In Fig. 3 diffusion coefficients for aqueous Na_2SO_3 solutions are compared with those for Na_2SO_4 obtained previously by optical (17) and conductimetric (20) methods at 25°C. D values observed for Na_2SO_3 solutions are displaced 0.04 (± 0.01) $\times 10^{-9}$ m^2 s^{-1} below those for Na_2SO_4 solutions. In order to

TABLE 1. Binary diffusion coefficients of aqueous Na_2SO_3 + H_2O at 25°C

c/mol dm^{-3}	$D/10^{-9}$ m^2 s^{-1}	$-cd \ln y_{\pm}/dc$	$-\Delta_1/10^{-9}$ m^2 s^{-1}	$D^0/10^{-9}$ m^2 s^{-1}
0.004	1.070	0.100	0.003	1.191
0.006	1.066	0.116	0.003	1.208
0.008	1.056	0.128	0.004	1.214
0.010	1.044	0.138	0.004	1.214
0.020	1.028	0.170	0.005	1.243
0.030	1.010	0.189	0.006	1.251
0.050	0.985	0.212	0.007	1.257
0.075	0.963	0.230	0.008	1.258
0.100	0.950	0.242	0.009	1.261

TABLE 2. Ternary diffusion coefficients for Na_2SO_3(1) + NaOH(2) + H_2O obtained by moments analysis[a]

$\bar{c}_1$ (mol dm^{-3})	$\bar{c}_2$ (mol dm^{-3})	D_{11} (10^{-9} m^2 s^{-1})	D_{12} (10^{-9} m^2 s^{-1})	D_{21} (10^{-9} m^2 s^{-1})	D_{22} (10^{-9} m^2 s^{-1})
0.005	0.035	0.84±0.01	−0.18±0.05	0.41±0.03	2.33±0.01
		(0.94)	(−0.16)	(0.16)	(2.40)
0.10	0.020	0.91±0.02	−0.36±0.07	0.35±0.06	2.87±0.05
		(0.93)	(−0.43)	(0.20)	(3.11)
0.015	0.005	0.97±0.02	−1.00±0.05	0.16±0.07	4.24±0.03
		(0.97)	(−0.94)	(0.11)	(4.47)
0.010	0.070	0.91±0.03	−0.16±0.04	0.24±0.03	2.24±0.01
		(0.94)	(−0.17)	(0.12)	(2.37)
0.020	0.040	0.86±0.02	−0.38±0.04	0.36±0.05	2.86±0.05
		(0.92)	(−0.43)	(0.17)	(3.09)
0.030	0.010	0.93±0.02	−0.78±0.04	0.18±0.05	4.02±0.02
		(0.95)	(−0.94)	(0.10)	(4.47)

[a]Predicted values are in parentheses.

estimate $D^0(Na_2SO_3)$ and hence $\lambda^0(SO_3^{2-})$, we will assume that $D^0(Na_2SO_4) - D^0(Na_2SO_3) = 0.04 \times 10^{-9}$ m^2 s^{-1}. The value $D^0(Na_2SO_4) = 1.231 \times 10^{-9}$ m^2 s^{-1} is accurately known from conductances of Na^+ (19, 20) and SO_4^{2-} (21). Therefore, we obtain the approximate values of $D^0(Na_2SO_3) \cong 1.19 \times 10^{-9}$ m^2 s^{-1} and $\lambda^0(SO_3^{2-}) \cong 0.00735$ m^2 S equiv.$^{-1}$. For comparison: $\lambda^0(CO_3^{2-}) = 0.00693$ (22) and $\lambda^0(SO_4^{2-}) = 0.008002$ m^2 S equiv.$^{-1}$ (21).

$Na_2SO_3(c_1)$ + NaOH(c_2) + H_2O

Ternary diffusion coefficients for Na_2SO_3 + NaOH mixtures were determined by moments analysis at six compositions. Each experiment was performed in triplicate. The results are listed in Table 2. The conductance data were also analyzed by the pseudo-binary method (7); the results are shown in Table 3. The two methods gave ternary diffusion coefficients of similar precision that agreed within the suggested uncertainties (± two standard deviations). The moments analysis, however, was more direct and computationally simpler. As an additional check, L_{ik} coefficients defined by transport equations

$$[31] \quad -J_i = \sum_{k=1}^{2} L_{ik} \nabla \mu_k$$

were obtained from experimental D_{ik} values using the relation

$$[32] \quad D_{ik} = \sum_{m=1}^{2} L_{im} \partial \mu_m / \partial c_k$$

Values of $\partial \mu_m / \partial c_k$ shown in Table 4 were obtained by differentiation of the expressions

$$[33] \quad \mu_1 = \mu_1^0 + RT \ln [(2c_1 + c_2)^2 c_1 y_{\pm 1}^3]$$

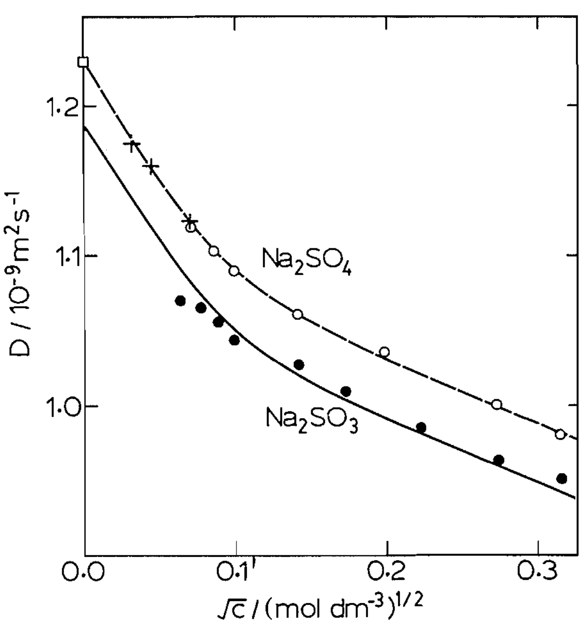

FIG. 3. Binary diffusion coefficients at 298.15 K plotted against concentration for: Na_2SO_4, top curve, + (Harned and Blake (18)), ○ (Rard and Miller (17)); Na_2SO_3, bottom curve, this work.

$$[34] \quad \mu_2 = \mu_2^0 + RT \ln [(2c_1 + c_2) c_2 y_{\pm 2}^2]$$

for the solute chemical potentials. Because the solutions were dilute (ionic strength ≤ 0.1 mol dm^{-3}), it was feasible to evaluate the activity-coefficient terms from Guggenheim

TABLE 3. Ternary diffusion coefficients for $Na_2SO_3(1) + NaOH(2) + H_2O$ determined by the pseudo-binary method

$\bar{c}_1$ (mol dm^{-3})	$\bar{c}_2$ (mol dm^{-3})	D_{11} (10^{-9} m^2 s^{-1})	D_{12} (10^{-9} m^2 s^{-1})	D_{21} (10^{-9} m^2 s^{-1})	D_{22} (10^{-9} m^2 s^{-1})
0.005	0.035	0.84±0.01	−0.18±0.04	0.44±0.04	2.34±0.01
0.010	0.020	0.93±0.02	−0.41±0.08	0.34±0.04	2.99±0.08
0.015	0.005	0.95±0.02	−0.96±0.02	0.28±0.04	4.31±0.05
0.010	0.070	0.92±0.02	−0.06±0.05	0.25±0.03	2.15±0.05
0.020	0.040	0.85±0.03	−0.37±0.04	0.36±0.06	2.76±0.06
0.030	0.010	0.90±0.05	−0.80±0.05	0.13±0.05	3.95±0.05

TABLE 4. Values of $(\partial\mu_i/\partial c_k)/RT$ for $Na_2SO_3(1) + NaOH(2) + H_2O$

c_1 (mol dm^{-3})	c_2 (mol dm^{-3})	$(\partial\mu_1/\partial c_1)/RT$ (dm^3 mol^{-1})	$(\partial\mu_1/\partial c_2)/RT$[a] (dm^3 mol^{-1})	$(\partial\mu_2/\partial c_2)/RT$ (dm^3 mol^{-1})
0.005	0.035	261.3	35.1	47.4
0.010	0.020	172.4	40.6	71.6
0.015	0.005	153.4	47.8	225.2
0.010	0.070	129.2	17.0	23.4
0.020	0.040	84.7	19.7	35.5
0.030	0.010	75.2	23.3	112.3

[a] $(\partial\mu_2/\partial c_1)/RT = (\partial\mu_1/\partial c_2)/RT$.

TABLE 5. L_{ik} coefficients for $Na_2SO_3(1) + NaOH(2) + H_2O$[a]

c_1 (mol dm^{-3})	c_2 (mol dm^{-3})	RTL_{11} (10^{-9} mol m^{-1} s^{-1})	RTL_{12} (10^{-9} mol m^{-1} s^{-1})	RTL_{21} (10^{-9} mol m^{-1} s^{-1})	RTL_{22} (10^{-9} mol m^{-1} s^{-1})
0.005	0.035	4.2±0.2	−6.3±1.2	−5.6±0.2	53.4±0.3
		(4.5)	(−6.8)	(−6.8)	(55.6)
0.010	0.020	7.4±0.4	−9.3±1.2	−8.6±0.7	45.0±1.0
		(7.9)	(−10.4)	(−10.4)	(49.3)
0.015	0.005	8.3±0.2	−6.2±0.3	−5.2±0.5	20.0±0.2
		(8.1)	(−5.9)	(−5.9)	(21.1)
0.010	0.070	8.7±0.5	−13.0±2.2	−11.8±0.4	104.3±0.8
		(9.1)	(−13.7)	(−13.7)	(111.3)
0.020	0.040	14.6±0.6	−19.0±1.4	−16.5±1.1	89.6±2.1
		(15.7)	(−20.9)	(−20.9)	(98.6)
0.030	0.010	15.5±0.4	−10.2±0.4	−9.3±0.8	37.7±0.4
		(16.3)	(−11.8)	(−11.8)	(42.2)

[a] Predicted values are in parentheses.

expressions (23)

[35] $$\ln \gamma_{\pm 1} = -[1.178\sqrt{I}/(1 + \sqrt{I})] + [(4B_1c_1 + (B_1 + 2B_2)c_2)/3]$$

[36] $$\ln \gamma_{\pm 2} = -[1.178\sqrt{I}/(1 + \sqrt{I})] + (0.5B_1 + B_2)c_1 + B_2c_2$$

The empirical ion-interaction coefficients $B_1 = 1.01$ and $B_2 = 0.08$ dm^2 mol^{-1} were determined from binary activity coefficients for each electrolyte (14, 24).

Experimental values of L_{ik} coefficients derived from the diffusion data are given in Table 5. Because it was necessary to take differences between numbers, the precision of the L_{ik} values is not as good as for the D_{ik} data. Nevertheless, the results are consistent with the Onsager reciprocal relation $L_{12} = L_{21}$ (25) which provides an independent check of the results.

Comparison of Tables 1 and 2 shows that the binary diffusivity for aqueous Na_2SO_3 solutions is similar to D_{11}, the ternary diffusivity of the salt in aqueous NaOH solutions. The mobility of Na^+ is about 35% larger than the mobility of SO_3^{2-}. When Na_2SO_3 diffuses, the induced electric field tends to slow down Na^+ and speed up SO_3^{2-} in order to keep the solution electrically neutral. If the solution contains NaOH, the electric field produces co-current flow of OH^-. Thus, values of the cross-diffusion coefficient D_{21} (which measure coupled flow of NaOH per unit gradient in concentration of Na_2SO_3) are positive. When NaOH diffuses in aqueous solutions of Na_2SO_3, highly mobile hydroxide ions ($\lambda^0(OH^-) = 0.01983$ m^2 S equiv.$^{-1}$ (26, 27)) can diffuse more rapidly than Na^+. In this case the relatively large electric field along the gradient in NaOH produces substantial counterflow of SO_3^{2-}. For this reason values of D_{12} are large and negative.

In Tables 2 and 5 experimental transport coefficients are compared with theoretical values estimated from the limiting mobilities of the diffusing ions by previously reported methods (28, 29). Though not quantitative, agreement is good. Trends in the observed transport coefficients are correctly predicted.

$SO_2(c_1') + NaOH(c_2') + H_2O$

Finally, we consider diffusion of sulfur dioxide dissolved in

TABLE 6. Ternary diffusion coefficients of $SO_2(c_1')$ + $NaOH(c_2')$ + H_2O at 298.15 K[a]

c_1' (mol dm^{-3})	c_2' (mol dm^{-3})	D_{11}' (10^{-9} m^2 s^{-1})	D_{12}' (10^{-9} m^2 s^{-1})	D_{21}' (10^{-9} m^2 s^{-1})	D_{22}' (10^{-9} m^2 s^{-1})
0.005	0.045	1.20	−0.18	−1.85	1.97
		(1.26)	(−0.16)	(−2.12)	(2.08)
0.010	0.040	1.63	−0.36	−2.13	2.15
		(1.79)	(−0.43)	(−2.44)	(2.25)
0.015	0.035	2.97	−1.00	−2.38	2.24
		(2.85)	(−0.94)	(−3.13)	(2.59)
0.010	0.090	1.23	−0.16	−1.78	1.92
		(1.28)	(−0.17)	(−2.06)	(2.03)
0.020	0.080	1.62	−0.38	−2.12	2.10
		(1.78)	(−0.43)	(−2.45)	(2.23)
0.030	0.070	2.49	−0.78	−2.88	2.46
		(2.83)	(−0.93)	(−3.18)	(2.59)

[a]Predicted values are in parentheses.

strongly alkaline solutions. If c_1', the formal concentration of the SO_2 component, is less than one-half of c_2', the formal concentration of the NaOH component, essentially all of the SO_2 component exists in solution not as molecular SO_2 but as Na_2SO_3 produced by the neutralization reaction (30)

$$SO_2(aq) + 2NaOH(aq) = Na_2SO_3(aq) + H_2O$$

$$K(298.15\ \mathrm{K}) = 1.05 \times 10^{19}\ (\mathrm{mol\ dm^{-3}})^{-2}$$

In this concentration region where SO_3^{2-} is the major transporting species for the SO_2 component the ternary diffusion coefficients D_{ik} for mixed electrolytes $Na_2SO_3(c_1)$ + $NaOH(c_2)$ are closely related to diffusion coefficients D_{ik}' for solutes $SO_2(c_1')$ + $NaOH(c_2')$.

What is the relation? Note that a solution of formal composition (c_1', c_2') is identical to one of composition (c_1, $c_2 + 2c_1$). The two sets of concentrations are related by

$$[37] \quad c_i' = \sum_{k=1}^{2} A_{ik} c_k$$

with $A_{11} = 1$, $A_{12} = 0$, $A_{21} = 2$, and $A_{22} = 1$. It is easily shown (7) that coefficients D_{ik} and D_{ik}' are related by the linear transformation

$$[38] \quad \mathbf{D}' = \mathbf{A}\mathbf{D}\mathbf{A}^{-1}$$

which gives

$$[39] \quad D_{11}' = D_{11} - 2D_{12}$$

$$[40] \quad D_{12}' = D_{12}$$

$$[41] \quad D_{21}' = 2D_{11} - 4D_{12} + D_{21} - 2D_{22}$$

$$[42] \quad D_{12}' = 2D_{12} + D_{22}$$

Table 6 gives diffusion coefficients for aqueous SO_2 + NaOH mixtures that were calculated from measurements on Na_2SO_3 + NaOH solutions.

The diffusivity of SO_2 in aqueous NaOH solutions, D_{11}', varies rapidly with composition. For solutions rich in NaOH, D_{11}' approaches the tracer diffusion coefficient of SO_3^{2-}, about 1.0×10^{-9} m^2 s^{-1} (6). But for higher proportions of SO_2, observed values of D_{11}' increase sharply and reach values significantly larger than the binary diffusivity of SO_2 at similar concentrations: 1.92×10^{-9} to 2.08×10^{-9} m^2 s^{-1} (31). The enhanced ternary diffusivity of the SO_2 component results from coupled flow of OH^-. When a gradient in concentration of the SO_2 component is formed in an aqueous solution of NaOH, the region of the system with the higher SO_2 concentration is depleted in free OH^- by formation of sulfite. As highly mobile OH^- diffuses rapidly towards this region, the induced electric field produces counterflow of SO_3^{2-} in order to maintain electroneutrality.

Acknowledgements

The author thanks Jesse Wolff and Betty Wiens for technical assistance. Financial support by the Natural Sciences and Engineering Research Council of Canada is gratefully acknowledged.

1. H. S. HARNED and R. L. NUTTALL. J. Am. Chem. Soc. **71**, 1460 (1949).
2. T. A. RENNER and P. A. LYONS. J. Phys. Chem. **78**, 1667 (1974).
3. D. G. LEAIST and P. A. LYONS. J. Solution Chem. **13**, 77 (1984).
4. D. G. LEAIST. Can. J. Chem. **62**, 1692 (1984).
5. H. FUJITA. J. Phys. Chem. **63**, 242 (1959).
6. D. G. LEAIST and P. A. LYONS. J. Phys. Chem. **86**, 564 (1982).
7. D. G. LEAIST and R. A. NOULTY. Can. J. Chem. **63**, 476 (1985).
8. H. FUJITA and L. J. GOSTING. J. Phys. Chem. **64**, 1256 (1960).
9. J. G. ALBRIGHT and D. G. MILLER. J. Phys. Chem. **76**, 1853 (1972).
10. M. NAGASAWA and H. FUJITA. J. Am. Chem. Soc. **86**, 3005 (1964).
11. M. TANIGAKI, K. KONDO, M. HARADA, and W. EGUCHI. J. Phys. Chem. **87**, 586 (1983).
12. A. F. COLLINGS, D. C. HALL, R. MILLS, and L. A. WOOLF. J. Phys. E. Sci. Instr. **4**, 425 (1971).
13. R. H. STOKES. J. Am. Chem. Soc. **75**, 4563 (1953).
14. R. N. GOLDBERG. J. Phys. Chem. Ref. Data **10**, 671 (1981).
15. I. R. LANTZKE, A. K. COVINGTON, and R. A. ROBINSON. J. Chem. Eng. Data, **18**, 421 (1973).
16. R. S. MORGAN. J. Chem. Eng. Data, **6**, 21 (1961).
17. J. A. RARD and D. G. MILLER. J. Solution Chem. **8**, 755 (1979).
18. H. S. HARNED and C. A. BLAKE. J. Am. Chem. Soc. **73**, 2448 (1951).
19. T. SHEDLOVSKY. J. Am. Chem. Soc. **54**, 1411 (1932).
20. G. C. BENSON and A. R. GORDON. J. Chem. Phys. **13**, 473 (1945).
21. I. L. JENKINS and C. B. MONK. J. Am. Chem. Soc. **72**, 2695 (1950).
22. C. B. MONK. J. Chem. Soc. 429 (1949).
23. E. A. GUGGENHEIM and J. C. TURGEON. Trans. Faraday Soc. **51**, 747 (1955).
24. R. A. NOULTY and D. G. LEAIST. J. Solution Chem. **13**, 767 (1984).
25. P. J. DUNLOP. J. Phys. Chem. **69**, 4276 (1965).

26. V. SIVERTZ, R. E. REITMEIER, and H. V. TARTAR. J. Am. Chem. Soc. **62**, 1379 (1940).
27. L. S. DARKEN and H. F. MEIER. J. Am. Chem. Soc. **64**, 621 (1942).
28. D. G. LEAIST. J. Chem. Soc. Faraday Trans. I, **78**, 3069 (1982).
29. D. G. LEAIST and R. A. NOULTY. Can. J. Chem. In press.
30. H. V. TARTAR and H. H. GARRETSON. J. Am. Chem. Soc. **63**, 808 (1941).
31. D. G. LEAIST. J. Chem. Eng. Data. **29**, 281 (1983).

Kinetics and mechanism of the oxidation of mercury by peroxidase

DONALD C. WIGFIELD AND SEASON TSE

The Ottawa-Carleton Institute for Research and Graduate Studies in Chemistry, Carleton University Campus, Ottawa, Ont., Canada K1S 5B6

Received November 28, 1984

DONALD C. WIGFIELD and SEASON TSE. Can. J. Chem. **63**, 2940 (1985).

The kinetics of oxidation of zero-valent mercury by the horseradish peroxidase system are reported. The reaction is first order in mercury and first order in peroxidase compound I, and appear to obey these kinetics to completion of the reaction. The second order rate constant is 8.58×10^5 M^{-1} min^{-1} at 23°C. The data are consistent with a simple two-electron transfer from mercury to the iron–heme system of peroxidase with the enzyme acting as a chemical oxidant that is continually being regenerated by reaction with hydrogen peroxide.

DONALD C. WIGFIELD et SEASON TSE. Can. J. Chem. **63**, 2940 (1985).

On a déterminé la cinétique de l'oxydation du mercure (étant d'oxydation égal à zéro) par le système de la peroxydase du raifort. La réaction est du premier ordre en mercure et du premier ordre en composé I de la peroxydase et il semble que la réaction obéisse à cette loi jusqu'à ce qu'elle soit complète. La constante de vitesse du deuxième ordre est 8,58 × 10^5 M^{-1} min^{-1}, à 23°C. Les données sont en accord avec un transfert simple à deux électrons, du mercure au système fer–hème de la peroxydase, au cours duquel l'enzyme agit comme un oxydant chimique qui est constamment régénéré par une réaction avec le peroxyde d'hydrogène.

[Traduit par le journal]

One of the challenges of modern chemical toxicology is the transformation of chemical-induced clinical symptoms to the identification and study of the fundamental chemical reaction underlying the symptom. In the case of elemental mercury toxicity, much of the reaction identification work is already complete. Through the elegant and wide-ranging work of Clarkson, Magos, and Nielsen-Kudsk and their co-workers it has become clear that the crucial chemical step is the oxidation of zero-valent mercury to the divalent mercuric ion and that this oxidation is caused by the enzyme catalase (1–7). It is thought that this step occurs both in blood, where it would serve as a detoxifying reaction, preventing or lessening the migration of mercury to the brain, and also in the brain where the formation of mercuric ion would have disastrous consequences.

Recently we have demonstrated the utility of the cold vapor atomic absorption method for separate analysis of zero-valent and divalent mercury (8), and also established the conditions whereby the mercury oxidation by the catalase system can be studied in homogeneous solution (9). In addition, we found that the closely related enzyme peroxidase also acted effectively as an oxidant of mercury, although somewhat more slowly than the catalase oxidation (9). Although a detailed kinetic study of the catalase system has not yet been reported, we now wish to document the kinetics of the oxidation of mercury by peroxidase. These studies provide answers to some of the key questions on the mechanism of this fascinating reaction.

Results and discussion

Peroxidase, in common with catalase, is an enzyme possessing as a prosthetic group the ferriprotoporphyrin IX nucleus shown in Fig. 1. While peroxidases are widespread in both animal and plant sources, one of the richest is horseradish roots, and this enzyme (EC 1.11.1.7) has not only been extensively studied, but is also commercially available in purified form. Particularly good summaries of the structure and function of the peroxidases have been presented by Dunford and Stillman (1976) (10), and by Dunford (1982) (11). The molecular weight of horseradish peroxidase is about 42 000; it contains about 18% carbohydrate (11), and the primary structure of the polypeptide portion has been determined (12).

In considering the possible mechanisms by which mercury might be oxidized by peroxidase, we wished to address the following questions: (*1*) Is the oxidation a two-electron, one-step process, or a sequence of two one-electron steps? (*2*) What is the role, if any, of the mercurous state in the reaction? (*3*) What is the role of hydrogen peroxide in the reaction? (*4*) What is the species of enzyme that effects the oxidation? (*5*) What is the kinetic rate law and the overall rate constant for oxidation? (*6*) What is the active site on the enzyme that is used for mercury oxidation? (*7*) Is the oxidation truly enzymatic, or is the enzyme consumed in the process?

Our earlier work had shown a distinct difference in oxidizing capability between catalase and peroxidase (9). Catalase oxidizes mercury rapidly and effectively both in the presence and in the absence of hydrogen peroxide, perhaps indicating multiple mechanisms, but peroxidase, while oxidizing mercury effectively in the presence of hydrogen peroxide, was much more sluggish at achieving oxidation in its absence. The conditions we focussed on for the present study, then, had peroxidase, hydrogen peroxide, and elemental mercury as the species present. Figure 2 shows a typical disappearance of Hg^0 under these conditions, where the main variable is hydrogen peroxide concentration. Two features are noteworthy in this figure. Firstly, the problem of mercury adsorption is under control. This is a major technical problem in handling trace quantities of metals; however, the control points on the figure show that although approximately 10% of the mercury is lost in the first few seconds of the reaction, thereafter the amount of mercury remains essentially constant. The second point is that raising the hydrogen peroxide concentration from equimolar with peroxidase concentration over three orders of magnitude makes very little difference to the rate of mercury oxidation. Clearly the reaction is not dependent on the concentration of peroxide.

This is not a surprising result. Peroxidase is known to react rapidly and essentially irreversibly ($K \simeq 10^{14}$ M^{-1}) (13) to form the so-called peroxidase compound I (HRP-I), a species that contains one, and only one, atom of oxygen from peroxide attached to iron (14).

$$\text{HRP} \xrightleftharpoons{H_2O_2} \text{HRP-I}$$

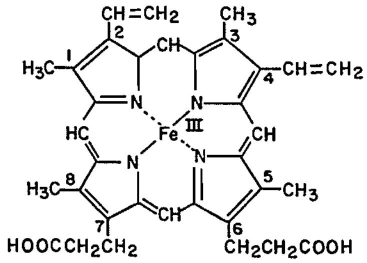

FIG. 1. The ferriprotoporphyrin IX prosthetic group of catalase and peroxidase.

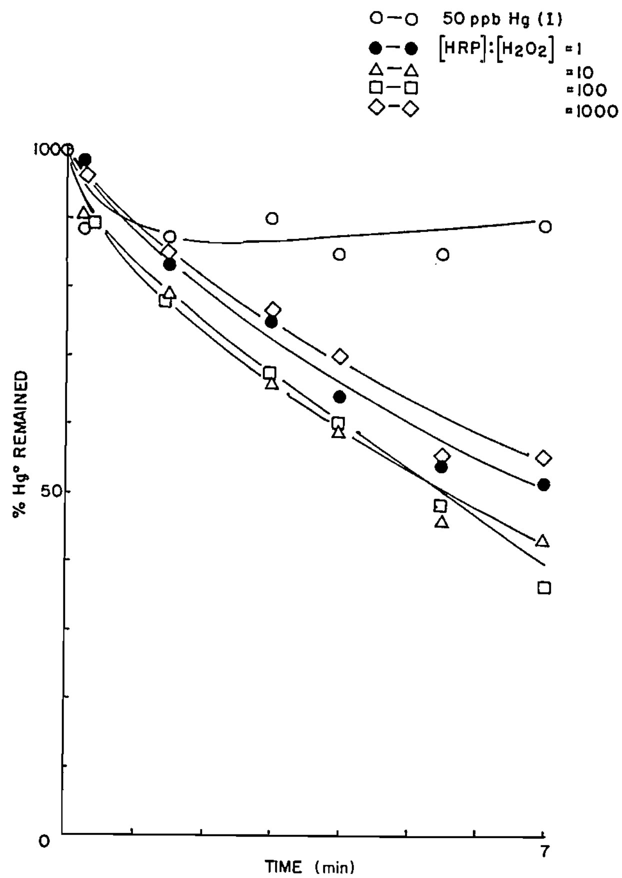

FIG. 2. Disappearance of mercury in the presence of HRP and variable concentrations of H_2O_2.

In the presence of adequate peroxide, then, the essentials of the reaction system consist only of mercury(0) and HRP-I.

Partly in order to avoid the adsorption complications that would arise from attempting to make many measurements on the initial portion of the reaction, in the classical enzyme kinetics fashion, we considered the possibility that the reaction would permit normal chemical kinetics treatment. Kinetically the reaction may be written:

$$\text{Rate} = k[\text{Hg}]^a[\text{HRP-I}]^b$$

and, if the rate law is unchanged throughout a significant portion of the reaction, the kinetic problem becomes one of determination of the powers a and b.

If hydrogen peroxide is in excess, and the consumed HRP-I can be rapidly recycled back to HRP-I by H_2O_2 (a critical assumption that is returned to later), the concentration of HRP-I throughout the reaction remains constant, and the system is set

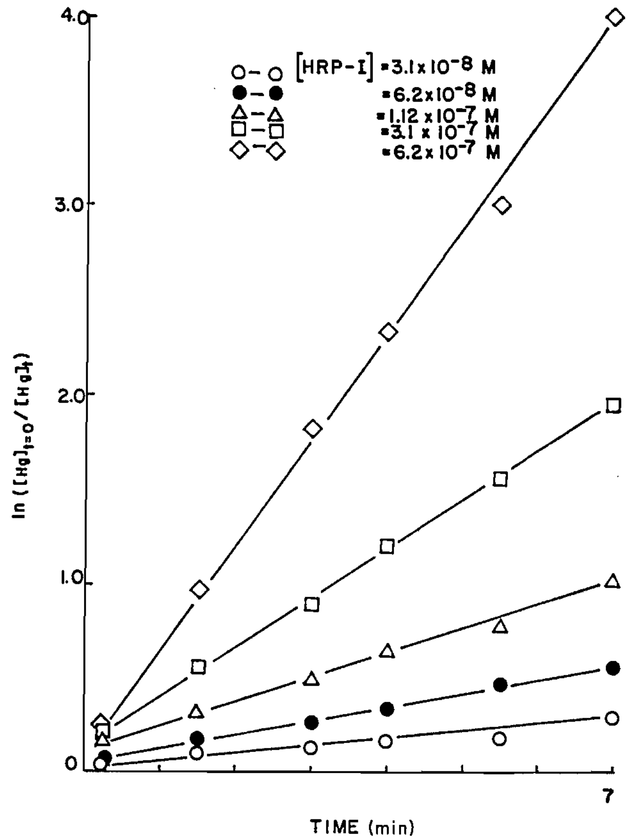

FIG. 3. First order plot of the logarithm of remaining Hg(0) as a function of time.

TABLE 1. Pseudo-first order rate constants for Hg(0) oxidation by HRP-I under homogeneous conditions; [Hg] = 1.24×10^{-7} M

[HRP] ($\times 10^8$ M)	[H_2O_2] ($\times 10^6$ M)	k (min^{-1})	Correlation coefficient
3.10	3.10	0.038±0.003	0.949
6.20	6.20	0.068±0.009	0.988
12.40	12.40	0.116±0.007	0.992
31.0	31.0	0.265±0.004	0.998
62.0	62.0	0.547±0.059	0.998

up for pseudo-order kinetics. The oxidation of mercury was therefore followed at various concentrations of HRP-I and the logarithmic first-order test of these data is shown in Fig. 3. The linearity of these plots clearly establish that the reaction is first order in mercury. It would be desirable to establish that the linearity of the first-order plots and the constancy of rate constant remain over a wide concentration range of mercury concentration. In practice, however, this cannot be done since there exists a factor of only about 20 between the maximum concentration of mercury obtainable in aqueous solution, and the minimum concentration that can reliably be analysed by cold vapor atomic absorption analysis.

The pseudo first order rate constants obtained at various concentrations of HRP-I are summarized in Table 1. To test whether the dependence on HRP-I was also first order, the plot of pseudo first order rate constant versus concentration is shown in Fig. 4 and is also linear. Thus the rate law may be written as:

$$\text{Rate} = k[\text{Hg(0)}]\,[\text{HRP-I}]$$

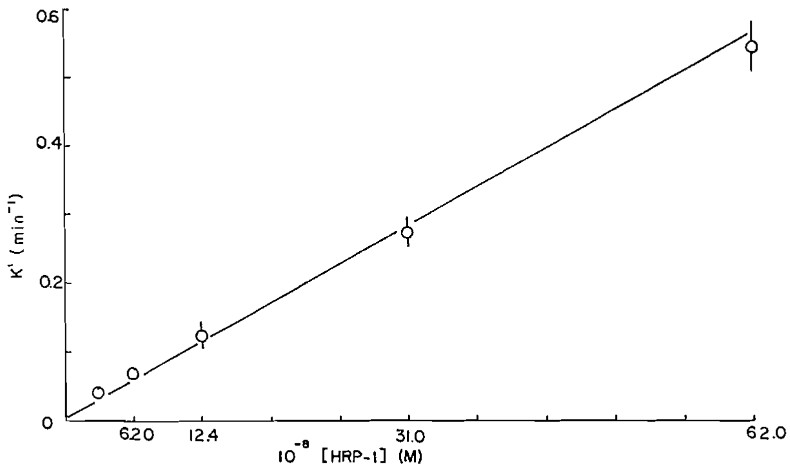

FIG. 4. Plot of pseudo first order rate constants of mercury oxidation as function of peroxidase compound I concentration.

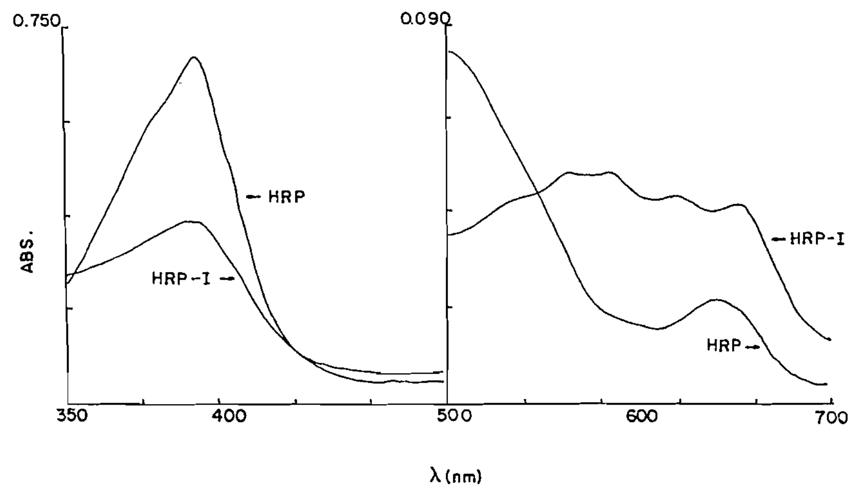

FIG. 5. Absorption spectra of HRP and HRP-I.

where $k = 8.58 \times 10^5\ M^{-1}\ \text{min}^{-1}$ at 23°C.

The fact that the reaction can be treated by this method, and in particular that pseudo-order kinetics hold, was based on the assumption of constant HRP-I concentration over a kinetic run, and this is an important finding that bears directly on the question of one- or two-electron steps in the oxidation. HRP-I is two oxidation states higher than native peroxidase. The complete oxidizing capability of hydrogen peroxide has been transferred to it. Between HRP-I and native enzyme, in terms of oxidation state, lies peroxidase compound II (HRP-II). This species is also an oxidizing agent, although less powerful than HRP-I. We have tested the oxidizing power of HRP-II to mercury and, as expected, mercury is oxidized although at a slower rate than by HRP-I. If HRP-I oxidizes mercury by a single two-electron step, then the HRP-I is reduced to native enzyme which can then be rapidly reconverted to HRP-I by hydrogen peroxide. The kinetic treatment above depends on this effective constant concentration of HRP-I, and the results are consistent with this scheme. On the other hand, if mercury were oxidized by a one-electron oxidation (initially to mercurous ion, which might then be further oxidized either directly or via disproportionation), HRP-I would be converted not to native enzyme but to HRP-II. This would severely upset the kinetics, because HRP-II can neither oxidize mercury as fast as HRP-I, nor can hydrogen peroxide rapidly convert HRP-II back to HRP-I. The only way in which the linear kinetics reported above, in which mercury and peroxidase are approximately equimolar, could be consistent with HRP-II formation would be the circumstance that HRP-II were an unusually effective oxidant of the mercurous ion, and experimentally this is not the case. It would appear, then, that the kinetic results are consistent only with a one-step two-electron oxidation of mercury directly to the mercuric ion.

Spectral confirmation of this conclusion was also obtained. The absorption spectra of HRP, HRP-I, and HRP-II are shown in Figs. 5 and 6 and are readily distinguishable. In fact most kinetic studies on peroxidase have made use of the spectral properties of the enzyme in order to follow reactions (11). Conducting the mercury oxidation by HRP-I, but not with excess hydrogen peroxide so that the enzyme cannot recycle back to HRP-I allows examination of the enzyme spectrum to see if there is any indication of HRP-II formation. In several trials, no such indication was obtained, consistent with the clean two-electron process deduced from the kinetic evidence.

Mechanistic conclusions

The questions posed at the outset of this article can now largely be answered. The species of enzyme that is the most

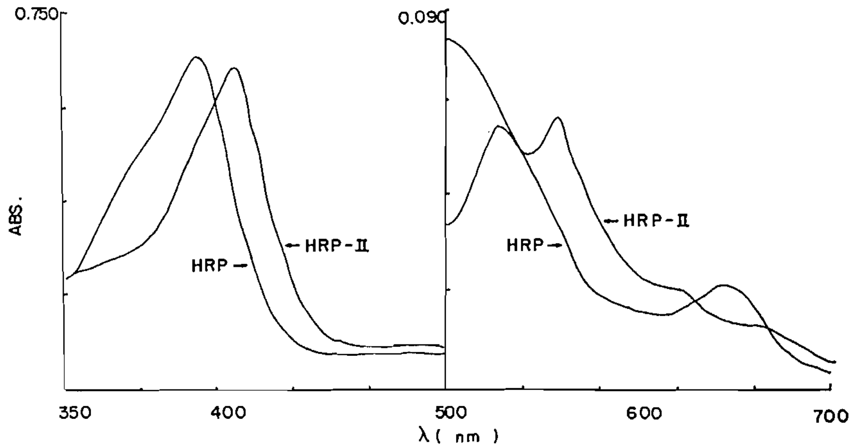

FIG. 6. Absorption spectra of HRP and HRP-II.

effective oxidant is HRP-I. This is a much more effective oxidant than native peroxidase and since the difference between these species is the addition of an oxygen atom at the iron of the heme prosthetic group, clearly, as in the case of all other reactions of peroxidase, this is the active site for the oxidation of mercury. The kinetics, supported by spectral evidence, show that the key step is a two-electron oxidation of Hg(0) to Hg(II), with HRP-I being converted back to native peroxidase in the process. The observation of linear chemical kinetics over all the observable reaction is itself of interest. On the one hand, it would appear that the reaction is a very simple one with HRP-I acting essentially as a recycling active oxidant rather than as a true enzyme; on the other hand, even in that case it is unusual that there is no evidence of product inhibition of the enzyme, since the mercuric ion would normally be expected to bind to almost any protein. This lack of product inhibition is probably a reflection of the total lack of involvement of any part of the enzyme in the reaction other than the heme prosthetic group.

The reaction may be summarized as follows:

$$\mathrm{Hg(0)} + \mathrm{HRP\text{-}I} \xrightarrow{k} \mathrm{HRP} + \mathrm{Hg(II)}$$

$$\mathrm{HRP} + \mathrm{H_2O_2} \xrightarrow{\text{fast}} \mathrm{HRP\text{-}I} + \mathrm{H_2O}$$

where $k = 8.58 \times 10^5\ M^{-1}\ \mathrm{min}^{-1}$.

The mechanism of HRP-I formation from HRP has already been extensively studied by Dunford and by others (11). The structure of HRP-I is now considered to involve the addition of a single oxygen atom to iron, with iron in the formal oxidation state of 5+. There is a great deal of evidence, however, that this oxidation state is more realistically depicted as 4+ by the transfer of an electron from the porphyrin ring system. This process may be represented as shown in Fig. 7. The crucial oxidation step following is presumably a simple two-electron transfer from mercury to oxygen, followed by cleavage of the iron-oxygen bond as shown in Fig. 7, thus producing mercury (II)[1] and iron (III).

[1]We have no further information on the subsequent fate of the Hg^{2+} formed. Although the usual form of HgO is zigzag—Hg—O—Hg— chains, it is soluble in water at the concentrations used here and is hydrolysed to form a so-called "hydroxide", actually an equilibrium mixture of several species. In the presence of other ions, other basic salts can be produced (15, 16).

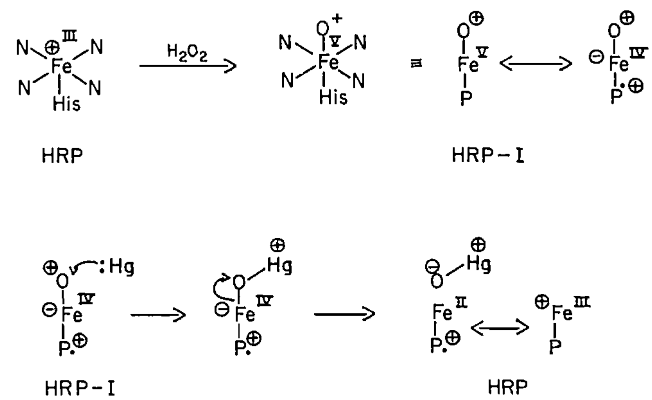

FIG. 7. Proposed mechanism of mercury oxidation.

Experimental

Reagents and solutions

Horseradish peroxidase (E.C.1.11.1.7, Type X)

Horseradish peroxidase was obtained as a $(NH_4)_2SO_4$ suspension (Sigma Chemical Co., St. Louis, MO., C-100). Solutions were freshly prepared by dissolving desired amounts of the enzyme in phosphate buffer (pH = 7.00, 0.05 M). The subsequent enzyme concentration was determined by the absorbance at 403 nm and the corresponding extinction coefficient (= $1.02 \times 10^4\ M^{-1}\ \mathrm{cm}^{-1}$). The R.I. value, an indicator of purity, was determined as the ratio of the absorbances at 403 and 280 nm.

Elemental mercury solutions

Phosphate buffer (250 mL, pH = 7.00, 0.05 M) was placed in a 500 mL two-neck round bottom flask, equipped with a septum and a side-arm. Distilled mercury (0.2 mL) was placed in the side arm and the vessel was shaken overnight, at room temperature, in a metabolic shaker.

Hydrogen peroxide

Hydrogen peroxide solutions were prepared daily from 30% stock solution (Anachemia Ltd., Montreal, Canada).

Mercury analysis

Mercury analysis by Cold Vapor Atomic Absorption, with separate determinations for elemental mercury and the mercuric ion, has been fully described previously (8).

Spectral studies

All spectral studies were performed in Beckman DU-7 U.V./Vis. Spectrophotometer. All scans were done using 1.5 mL quartz cells at a rate of 600 nm/min.

Preparation of HRP-I and HRP-II

HRP-I. Compound I was prepared by mixing (Vortex) 0.9 mL of phosphate buffer and the desired amount of HRP, and various equivalents of H_2O_2, in a 1.5 mL disposable micro test tube. Its presence was confirmed by obtaining the spectra prior to addition to mercury solutions.

HRP-II. One equivalent of HRP, H_2O_2, and ascorbic acid in phosphate buffer with a final volume of 1 mL, was mixed. The presence of HRP-II was confirmed by obtaining its absorption spectra prior to use.

Kinetic method

Into a 10 mL round bottom flask was placed 10 mL of buffered mercury solution. Initial mercury concentration was determined before the addition of any oxidants. The desired quantities of HRP and/or hydrogen peroxide were then added and mixing achieved by means of the sampling syringe for 15 s. The flask was stoppered with a glass stopper and sampling done with momentary removal of the stopper. Care was taken to ensure that the flask was neither shaken nor inverted, as these were found to contribute markedly to loss of mercury by surface adsorption. Control runs had mercury solution present, but no oxidant, and mixing and sampling were done in the same manner.

Acknowledgement

We gratefully acknowledge the continued financial support of the Natural Sciences and Engineering Research Council of Canada.

1. T. W. CLARKSON, J. GATZY, and C. DALTON. University of Rochester A.E.P. Report V.R. 582 (1961).
2. F. NIELSEN-KUDSK. Acta Pharmacol. Toxicol. **27**, 149 (1969); **27**, 161 (1969).
3. T. W. CLARKSON, S. HALBACH, L. MAGOS, and Y. SUGATA. *In* Molecular basis of environmental toxicity. Ann Arbor Science. 1980. Chapt. 18.
4. L. MAGOS, T. SUGATA, and T. W. CLARKSON. Toxicol. Appl. Pharm. **28**, 367 (1974).
5. L. MAGOS, S. HALBACH, and T. W. CLARKSON. Biochem. Pharmacol. **27**, 1373 (1978).
6. L. MAGOS, T. W. CLARKSON, and M. R. GREENWOOD. Toxicol. Appl. Pharmacol. **26**, 180 (1973).
7. I. EIDE and T. L. M. SYVERSEN. Acta Pharmacol. Toxicol. **52**, 217 (1983).
8. D. C. WIGFIELD and S. L. PERKINS. J. Anal. Toxicol. **6**, 279 (1982).
9. D. C. WIGFIELD and S. L. PERKINS. J. Appl. Toxicol. **3**, 185 (1983).
10. H. B. DUNFORD and J. S. STILLMAN. Coord. Chem. Rev. **19**, 187 (1976).
11. H. B. DUNFORD. Adv. Inorg. Biochem. **4**, 41 (1982).
12. K. G. WELINDER. Eur. J. Biochem. **96**, 483 (1979).
13. I. YAMAZAKI, M. TAMURA, and R. NAKAJIMA. Molec. Cell Biochem. **40**, 143 (1981).
14. S. A. ADEDIRAN and H. B. DUNFORD. Eur. J. Biochem. **132**, 147 (1983).
15. F. A. COTTON and G. WILKINSON. Advanced inorganic chemistry. 3rd ed. John Wiley and Sons Inc. 1972. pp. 516, 517.
16. A. G. SHARPE. Inorganic chemistry. Longman Inc., New York. 1981. pp. 640, 641.

The thermal decomposition of cyclobutane-1,2-dione[1]

J.-R. CAO[2] AND R. A. BACK

Division of Chemistry, National Research Council of Canada, 100 Sussex Drive, Ottawa, Ont., Canada K1A 0R6

Received March 1, 1985

J.-R. CAO and R. A. BACK. Can. J. Chem. **63**, 2945 (1985).

The thermal decomposition of cyclobutane-1,2-dione has been studied in the gas phase at temperatures from 120 to 250°C and pressures from 0.2 to 1.5 Torr. Products were C_2H_4 + 2CO, apparently formed in a simple unimolecular process. The first-order rate constant was strongly pressure dependent, and values of k^∞ were obtained by extrapolation of plots of $1/k$ vs. $1/p$ to $1/p = 0$. Experiments in a packed reaction vessel showed that the reaction was enhanced by surface at the lower temperatures. Arrhenius parameters for k^∞, corrected for surface reaction, were $\log A$ (s^{-1}) = 15.07 (±0.3) and E = 39.3 (±2) kcal/mol. This activation energy seems too low for a biradical mechanism, and it is suggested that the decomposition is probably a concerted process. The vapor pressure of solid cyclobutane-1,2-dione was measured at temperatures from 22 to 62°C and a heat of sublimation of 13.1 kcal/mol was estimated.

J.-R. CAO et R. A. BACK. Can. J. Chem. **63**, 2945 (1985).

Opérant à des températures allant de 120 à 250°C et dans un intervalle de pression allant de 0,2 à 1,5 Torr, on a étudié la décomposition thermique de la cyclobutanedione-1,2. Les produits de la réaction sont le C_2H_4 + 2CO qui sont apparemment formés par une réaction unimoléculaire simple. La constante de vitesse d'ordre un dépend beaucoup de la température et l'extrapolation des courbes de $1/k$ vs. $1/p$ jusqu'à $1/p = 0$ permet d'obtenir la valeur de k^∞. Des expériences conduites dans un réacteur contenant un remplissage montrent que, à basse température, la surface de contact augmente la vitesse de la réaction. Les paramètres d'Arrhénius pour k^∞, corrigées pour tenir compte de la surface de contact, sont: $\log A$ (s^{-1}) = 15,07 (±0,3) et E = 39,3 (±2) kcal/mol. Cette énergie d'activation semble être trop faible pour un mécanisme biradicalaire et on suggère que la décomposition se fait probablement selon un mécanisme concerté. On a mesuré la tension de vapeur de la cyclobutanedione-1,2 solide à des températures allant de 22 à 62°C et on a évalué que sa chaleur de sublimation est égale à 13,1 kcal/mol.

[Traduit par le journal]

Introduction

Although cyclobutane-1,2-dione (hereafter CBD) was first prepared 14 years ago (1), no studies of its thermal or photochemical decomposition have been reported. It is an interesting example of an α-dicarbonyl compound locked into the usually less stable *cis* configuration; it is also of interest in relation to other cyclic ketones, especially cyclobutanone. Both cyclobutanone (2) and several simple α-dicarbonyl compounds (3–6) have been the subjects of recent research in this laboratory, and for comparison with these systems we have undertaken studies of the spectroscopy, photochemistry, and thermal decomposition of CBD in the vapor phase. The present paper describes the thermal decomposition.

Experimental

Apparatus and techniques were similar to those used previously (3–5). The thermal decomposition was studied in a simple static system, using a cylindrical quartz reaction vessel 11.5 cm long and 3.4 cm in diameter mounted in a tube furnace. A similar vessel packed with small quartz tubing was used to test surface effects. The gas-handling manifold, quartz-spiral pressure gauge, and reagent storage trap were all enclosed in an air thermostat usually held at 40°C, which permitted operation at vapor pressures up to 2.2 Torr (1 Torr = 133.3 Pa). Small quantities of CBD, a finely-divided yellow crystalline solid, were stored in a cold finger cooled by tap water. When required, this was warmed to 35°C, and the vapor allowed to accumulate in a reservoir at 40°C until the desired pressure was attained. A pyrolysis experiment was begun by expanding this vapor through a stopcock into the reaction vessel. This procedure, used previously with oxalic acid (7), was necessary because of the rather slow sublimation from the solid.

After the experiment, reagent and products were removed through traps held first at −196°C and then at −78°C, and products were measured by gas buret and by gas chromatography. Careful blank experiments were done to correct for small amounts of decomposition during the preparation and analysis procedures. CBD is light sensitive, and light was excluded throughout the experiments.

CBD was prepared by M. Hrytsak and his colleagues at the University of Ottawa, using methods in the literature (8). No impurities were detected by nmr and mass spectrometry, and the purity would appear to be ≥99%. It was sublimed once into the storage trap after thorough degassing, and sublimed again as described before use.

Results

Vapor pressure

The vapor pressure, not previously reported, was measured and is shown in a van't Hoff plot in Fig. 1. The straight line corresponds to $\log P$ (Torr) = 9.460 − (13100/2.3 RT) from which ΔH_{sub} = 13.1 kcal/mol.

Reaction products

The thermal decomposition was studied at temperatures of 120–250°C and pressures from 0.2 to 1.5 Torr. The only significant products observed were CO and C_2H_4; traces of CH_4 and CO_2 were seen, but these were less than 0.1% of the C_2H_4. The ratio C_2H_4/CO was found to be 0.48 ± 0.05, with perhaps a slight downward trend with increasing pressure within the experimental scatter. It appears that the thermal decomposition can be described to a good approximation by the simple reaction

[1] 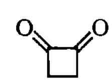 ⟶ $C_2H_4 + 2CO$

Rate measurements

First-order rate constants were calculated for reaction [1] based on formation of C_2H_4, which could be more accurately

[1] NRCC No. 24719.

[2] NRCC Research Associate, 1984–1985. Permanent address: Chemistry Department, Peking University, Peking, China.

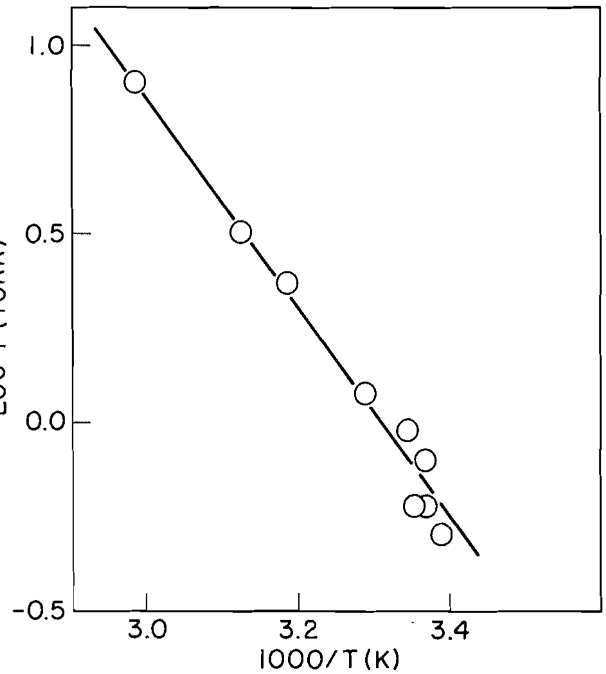

FIG. 1. The equilibrium vapor pressure of solid cyclobutane-1,2-dione.

TABLE 1. First-order rate constants for the decomposition of CBD ($s^{-1} \times 10^{-4}$)

T(°C)	k^{∞} (unpacked vessel)	k^{∞} (packed vessel)	k^0	k^{∞} (homogeneous)
175.6	1.05		0.20	0.85
181.0		4.41		
194.0	4.99		0.57	4.42
202.7		18.6		
206.4	20.1		1.2	18.9
225.9	83.3		0.04	83.8
235.9		112		
240.5	194		0.0	194

measured than CO. These were found to be independent of conversion (1–60%), confirming that no other reaction paths were important, but did show strong pressure dependence, increasing with increasing pressure (Fig. 2). Data for two temperatures are shown in a plot of $1/k$ vs. $1/p$ in Fig. 3, and from the intercepts of such plots, using least-squares analysis, values of k_1^{∞} were obtained, and are shown in Table 1.

Surface effects

Experiments in the packed vessel ($S/V = 5.6$, compared to 1.45 cm^{-1} in the unpacked vessel) showed enhanced rates of decomposition at temperatures below about 200°C. The first-order rate constants were again pressure dependent, and values of k_1^{∞} were obtained as before by extrapolation to $1/p = 0$, and are also shown in Table 1. Attempts to suppress the surface decomposition by the usual conditioning with a coating of pyrolytic carbon were unsuccessful, as this treatment had no significant effect in either reaction vessel. Surface reaction clearly makes a sizeable contribution at the lower temperatures, and initially a correction was made for this to the values of k_1^{∞} obtained in the unpacked vessel, based on the usual assumption that gas-phase and surface reactions were simply additive and that the latter was proportional to surface area. The corrected

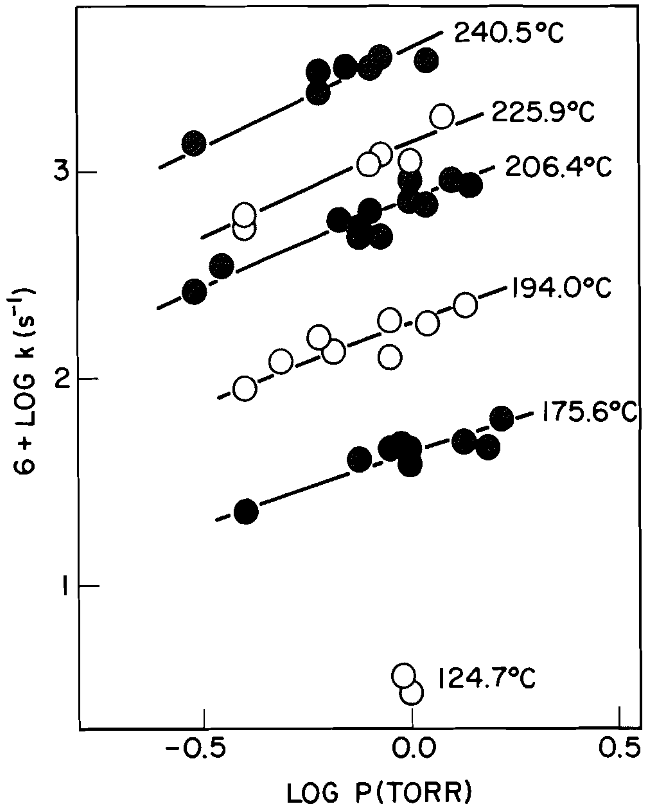

FIG. 2. The pressure dependence of the first-order rate constant, k_1, for the decomposition of cyclobutane-1,2-dione, measured in the unpacked reaction vessel and based on formation of ethylene.

values, however, led to an impossibly high frequency factor ($\sim 10^{17}$), and it appears that an overcorrection for surface reaction was made, probably through systematic differences in the extrapolation to $1/p = 0$ in the packed and unpacked vessels. Correction for surface reaction in the unpacked vessel was therefore finally made by a more direct method (suggested by a referee) in which K_1 at each temperature was extrapolated to $p = 0$ in a simple linear plot, and the intercept k^0 was taken as the first-order rate constant for the surface reaction. Values of k^0 were then simply subtracted from k^{∞} to yield corrected values of k^{∞} for the homogeneous reaction, all shown in Table 1. An Arrhenius plot of the corrected values (Fig. 4) gave $\log A$ (s^{-1}) = 15.07 (±0.3) and E = 39.3 (±2) kcal/mol.

Discussion

It seems well established that cyclobutane and most of its substituted derivatives decompose thermally by a biradical mechanism (9, 10). The case of cyclobutanone, however, most relevant to the present study, has been in some dispute. O'Neal and Benson (9, 10) calculated Arrhenius parameters for the biradical mechanism close to those observed for dissociation to $CH_2CO + C_2H_4$, with about equal rates for the two possible biradicals, $\dot{C}H_2CH_2CO\dot{C}H_2$ and $\dot{C}H_2CH_2CH_2\dot{C}O$, formed by β- and α-scission respectively. About 8 kcal/mol of resonance stabilization involving the carbonyl group appears to have been included in the calculation for both radicals, although it is not clear how this arises with $\dot{C}H_2CH_2CH_2\dot{C}O$. Subsequent measurements (11) of the heats of formation of the $\dot{C}H_2COCH_3$ and $\dot{C}H_2COC_2H_5$ radicals, however, gave estimates of the resonance stabilization of these species of 0 and 2.7 kcal/mol respectively, and it was suggested that the carbonyl group

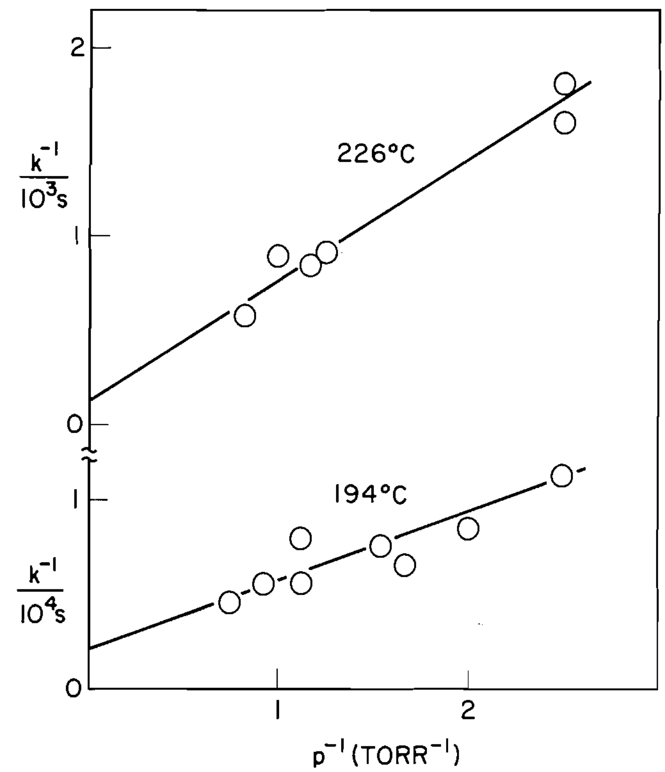

FIG. 3. Double reciprocal plots used to obtain k_1^∞.

could not develop full allylic resonance. From these data, McGee and Schleifer (12) argued that the activation energy of 52 kcal/mol for dissociation of cyclobutanone was much too low to permit a biradical mechanism, and that the reaction must be concerted. Blades disputed this (13), arguing that uncertainties in the calculations were too great to allow any firm conclusion, and to the present time these arguments do not seem to have been resolved, at least in print. They are very relevant to the present work, since the biradical likely to yield C_2H_4 from CBD could be considerably stabilized by allylic resonance of the carbonyl groups:[3]

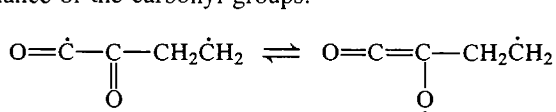

This biradical would also be stabilized relative to CBD by relief of the repulsion between the carbonyl groups, which can be taken as about 3 kcal/mol, the difference between the heats of formation of *cis-* and *trans-*glyoxal (6, 14). Taking this into account, an additional 10 kcal/mol of stabilization, persisting in the transition state, would still be needed to reach the 39.3 kcal/mol activation energy measured for CBD. All things considered, the activation energy seems much too low for a biradical mechanism, but in view of the uncertainties about the role of carbonyl groups in resonance structures, it is perhaps not impossible.

The alternative to a biradical mechanism is a concerted one, either a direct fragmentation to C_2H_4 + CO + CO, or perhaps to C_2H_4 + C_2O_2 followed by rapid dissociation of the latter, which appears to have little stability (15). It is interesting that

[3] The two other biradicals which could be formed from CBD would both tend to poduce ketene, which was not formed in the decomposition.

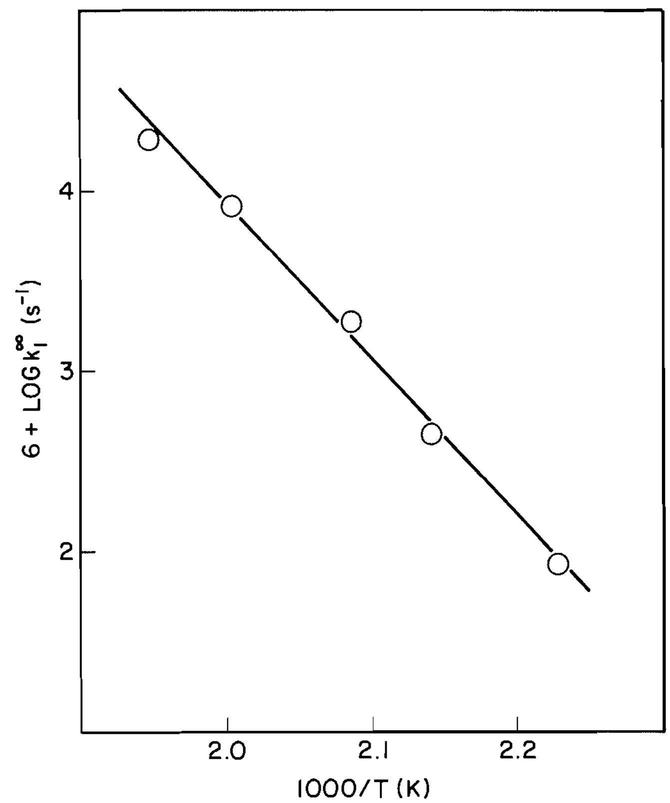

FIG. 4. Arrhenius plot of k_1^∞, corrected for surface reaction.

the analogous decomposition of *cis*-glyoxal to H_2 + 2CO is a major pathway in the thermal decomposition of glyoxal and in the dissociation of the vibrationally excited ground state excited photochemically (6, 16); Osamura *et al.* (17) have shown that the direct concerted dissociation to H_2 + CO + CO is an allowed process and appears to be the favored path of the reaction. The dissociation of CBD may be similar.

Finally, errors in the Arrhenius parameters are inherent in the need to correct simultaneously for dependence of k_1 on both pressure and surface reaction, both of which are in turn dependent on temperature. Extrapolations of k_1 to $1/p = 0$ and to $p = 0$ were relatively long and may have led to systematic errors; the confidence limits placed on the Arrhenius parameters reflect these uncertainties. Values of k^∞ at the higher temperatures, where surface effects were absent, should be fairly accurate, and since the frequency factor is relatively high when compared with those observed and calculated for many other biradical and concerted decompositions (9, 10), it seems unlikely that the activation energy can be much higher than 39 kcal/mol.

1. J. M. CONIA and J. M. DENIS. Tetrahedron Lett. 2845 (1971).
2. R. A. BACK, D. K. EVANS, and H. M. ADAMS. Can. J. Chem. **62**, 1525 (1984).
3. R. A. BACK. Can. J. Chem. **62**, 1414 (1984); R. A. BACK and S. YAMAMOTO. J. Phys. Chem. **89**, 622 (1985).
4. R. A. BACK and S. YAMAMOTO. Can. J. Chem. **63**, 542 (1985).
5. S. YAMAMOTO and R. A. BACK. Can. J. Chem. **63**, 549 (1985).
6. J. M. ROSCOE and R. A. BACK. To be published.
7. G. LAPIDUS, D. BARTON, and P. E. YANKWICH. J. Phys. Chem. **68**, 1863 (1964).
8. J. M. DENIS, J. CHAMPION, and J. M. CONIA. Org. Synth. **60**, 18 (1980).
9. H. E. O'NEAL and S. W. BENSON. J. Phys. Chem. **72**, 1866 (1968).

10. S. W. BENSON and H. E. O'NEAL. Kinetic data on gas phase unimolecular reactions. NSRDS-NBS 21, Washington. 1970.
11. R. K. SOLLY, D. M. GOLDEN, and S. W. BENSON. Int. J. Chem. Kinet. **2**, 11 (1970); **2**, 381 (1970).
12. T. H. MCGEE and A. SCHLEIFER. J. Phys. Chem. **76**, 963 (1972).
13. A. T. BLADES and S. SANDHU. J. Phys. Chem. **77**, 1316 (1973).
14. G. N. CURRIE and D. A. RAMSAY. Can. J. Phys. **49**, 317 (1971).
15. R. C. HADDON, D. POPPINGER, and L. RADOM. J. Am. Chem. Soc. **97**, 1645 (1975).
16. K. SAITO, T. KAKUMOTO, and I. MURAKAMI. J. Phys. Chem. **88**, 1182 (1984).
17. Y. OSAMURA, H. F. SCHAEFER III, M. DUPUIS, and W. A. LESTER, JR. J. Chem. Phys. **75**, 5828 (1981).

Hydrolysis of chlorophosphine ligands on platinum and palladium. ^{31}P and ^{195}Pt nmr studies and the crystal and molecular structures of *cis*-$[PtCl_2(PPh_2OH)_2].C_4H_8O$ and $[Pd_2(\mu\text{-}Cl)_2\{(P(OEt)_2O)_2H\}_2]$

DAVID ERIC BERRY, KATHRYN ANNE BEVERIDGE, GORDON WILLIAM BUSHNELL, AND KEITH ROGER DIXON
Department of Chemistry, University of Victoria, Victoria, B.C., Canada V8W 2Y2

Received December 24, 1984

DAVID ERIC BERRY, KATHRYN ANNE BEVERIDGE, GORDON WILLIAM BUSHNELL, and KEITH ROGER DIXON. Can. J. Chem. **63**, 2949 (1985).

Controlled hydrolysis of *cis*-$[PtCl_2(PPh_2Cl)_2]$ gives *cis*-$[PtCl_2(PPh_2OH)_2]$ which crystallizes as a tetrahydrofuran solvate in the monoclinic space group $P2_1/n$, with a = 14.647(3), b = 15.089(3), c = 13.107(2) Å, β = 91.22(3)°. This is the first example of a complex containing a *cis*-$M(PR_2OH)_2$ group to be structurally characterized since further reaction to P—O---H---O—P ligand systems is the more usual outcome of such hydrolyses. An example of the latter type, $[Pd_2(\mu\text{-}Cl)_2\{(P(OEt)_2O)_2H\}_2]$, crystallizes in the monoclinic space group $P2_1/c$, a = 9.674(2), b = 20.722(5), c = 8.578(2) Å, β = 92.75(3)°. Complete X-ray diffraction studies are reported for both crystals. Synthesis and $^{31}P\{^1H\}$ and $^{195}Pt\{^1H\}$ nmr studies are reported for the complexes $[PtCl_2(PEt_3)(PR_2Cl)]$, R = OEt, Ph, Cy, Et, or Bu^t, which have *cis* stereochemistry except when R = Bu^t, and for *cis*-$[PtCl_2(PR_2Cl)_2]$, R = OEt, Ph, or Et, and also for the hydrolysis products, *cis*-$[PtCl_2(PEt_3)(PR_2OH)]$, R = OEt or Ph, and *cis*-$[PtCl_2(PR_2OH)_2]$, R = OEt, Ph, or Et. Analogous products for palladium are generally less stable and more difficult to characterize. The complex of products from hydrolysis of palladium/$P(OEt)_2Cl$ compounds is discussed in detail.

DAVID ERIC BERRY, KATHRYN ANNE BEVERIDGE, GORDON WILLIAM BUSHNELL et KEITH ROGER DIXON. Can. J. Chem. **63**, 2949 (1985).

L'hydrolyse contrôlée du $[PtCl_2(PPh_2Cl)_2]$-*cis* conduit au $[PtCl_2(PPh_2OH)_2]$-*cis* qui cristallise, sous la forme d'un produit de solvatation du tétrahydrofuranne, dans le groupe d'espace monoclinique $P2_1/n$ avec a = 14,647(3), b = 15,089(3), c = 13,107(2) Å, β = 91,22(3)°. Ce composé est le premier exemple d'un complexe comportant un groupement $M(PR_2OH)_2$-*cis* qui ait pu être caractérisé du point de vue de la structure; en effet, de telles hydrolyses provoquent des réactions subséquentes qui conduisent généralement au système de ligand P—O---H---O—P. Un exemple de ce dernier type, soit le $[Pd_2(\mu\text{-}Cl)_2\{(P(OEt)_2O)_2H\}_2]$, cristallise dans le groupe d'espace monoclinique $P2_1/c$ avec a = 9,674(2), b = 20,722(5), c = 8,578(2) Å et β = 92,75(3)°. On rapporte les études complètes de diffraction de rayons X pour les deux cristaux. On rapporte également la synthèse et des études de rmn du $^{31}Pt\{^1H\}$ et du $^{195}Pt\{^1H\}$ relatives aux complexes $[PtCl_2(PEt_3)(PR_2Cl)]$, R = OEt, Ph, Cy, Et ou *tert*-Bu, qui ont une stéréochimie *cis*, sauf dans le cas où R = *tert*-Bu, ainsi que pour les complexes $[PtCl_2(PR_2Cl)_2]$-*cis* où R = OEt, Ph ou Et et leurs produits d'hydrolyse, soit le $[PtCl_2(PEt_3)(PR_2OH)]$-*cis* où R = OEt ou Ph et le $[PtCl_2(PR_2OH)_2]$-*cis* où R = OEt, Ph ou Et. Les produits analogues du palladium sont en général moins stables et plus difficile à caractériser. On discute en détail des complexes résultant de l'hydrolyse des composés du type palladium/$P(OEt)_2Cl$.

[Traduit par le journal]

Introduction

The reactivity of phosphorus–chlorine bonds is of considerable importance in phosphorus ligand chemistry, since this group is the most usual choice of reactive function for the elaboration of phosphorus ligands (1). Typical examples are reactions with ROH reagents to form phosphorus ester linkages and reactions with Grignard or organolithium reagents to form phosphorus–carbon bonds. The added groups may be introduced to achieve steric or electronic modification of the ligand or sometimes to convert the ligand into a potential chelate or bridge; either using a group containing a second electron pair donor or a reactive function such as C—Cl which can be subsequently used to form another metal–ligand bond.

The chemistry of chlorine bound to coordinated phosphorus ligands is much less studied but potentially even more interesting, offering opportunities for the *in situ* elaboration of ligands or possibly the formation of bridges to other metal centres. Moreover, if *cis* arrangements of two chlorophosphine ligands can be obtained then template syntheses become a possibility. In this connection we note the contrast between the extensive development of chemistry of nitrogen macrocycles and the situation in phosphorus chemistry where macrocyclic ligands have been prepared only very recently (2), and where template syntheses are still a rarity (3).

Knowledge of hydrolysis reactions of these ligands is fundamental to any more extensive study, both to delineate possible reaction pathways and to prepare the ground for the ready identification of adventitious products in subsequent reactions. In the particular case of systems containing *cis*-$M(PR_2Cl)_2$ fragments one might expect a simple *cis*-$M(PR_2OH)_2$ group as the first hydrolysis product but in fact more complex and unusual products involving P—O—P and P—O---H---O—P linkages are normally isolated (4–11). As detailed below, the intermediacy of the hydroxyphosphine product is not well established but we propose that the hydrolysis reaction be logically divided into the steps shown in Scheme 1. The complete scheme has not been observed for any individual example and the actual sequence may vary. For example, the order of formation of **III** and **IV** (or **V**) is likely to depend on the acidity or basicity of the reaction medium and type **IV** complexes could also be intermediates in step **4**. However, Scheme 1 is a useful framework for discussion and a primary objective of the present work is to delineate each of the possible outcomes by structural studies.

In this paper we will report the first full characterisation and X-ray structural study of a type **II** complex, namely *cis*-$[PtCl_2(PPh_2OH)_2]$, obtained as the first hydrolysis product of *cis*-$[PtCl_2(PPh_2Cl)_2]$. Synthetic and spectroscopic results related to the first two steps of Scheme 1 will also be reported together with an X-ray diffraction study of a type **III** hydrolysis product, $[Pd_2(\mu\text{-}Cl)_2\{(P(OEt)_2O)_2H\}_2]$. In subsequent papers in this series we will report the details of novel hydrolysis prod-

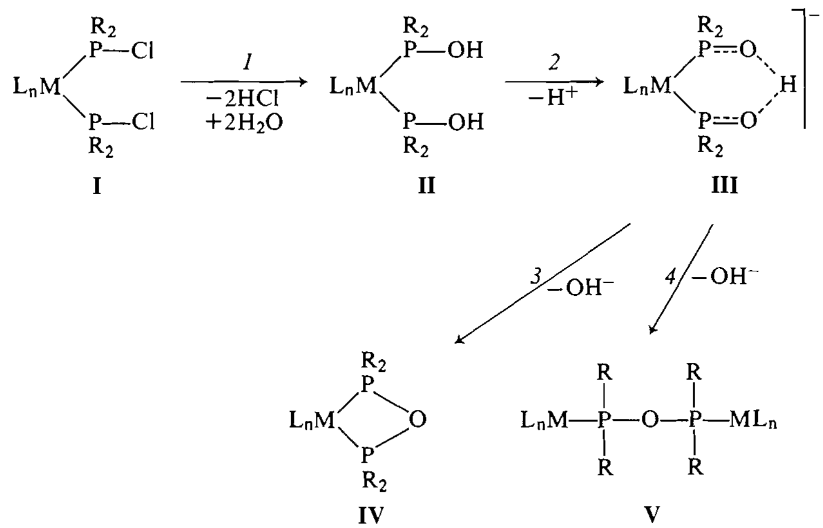

SCHEME 1

ucts obtained when R = OEt; a structural study of a type **V** product; and further results on the chemistry and structure of metal complexes derived from type **III** products by the replacement of the hydrogen bonded proton by a metal.[1] It is therefore appropriate at the present stage to briefly review the principal literature relating to each step of Scheme 1.

Formation of a hydroxyphosphine complex as the first step in hydrolysis of a coordinated chlorophosphine is well established for cases where only a single chlorophosphine ligand is present. Early work by Chatt and Heaton (14) and by Kraihanzel and Bartish (15) showed, respectively, that *cis*-$[PtCl_2(PR_3)(PR_2Cl)]$ and $[Mo(PR_2Cl)(CO)_5]$ complexes are readily converted to the corresponding hydroxyphosphine derivatives. However, verification of the first step in hydrolysis of *cis*-$M(PR_2Cl)_2$ fragments is more difficult since the reaction normally continues on to type **III** complexes. Early thesis work by Austin (16) reported the formation of *cis*-$[MCl_2(PPh_2OH)_2]$ from the corresponding chlorophosphine complexes for both M = Pt and Pd but subsequent workers have isolated only type **III** products (5, 11). Thus, reaction of $PdCl_4^{2-}$ with PPh_2Cl in aqueous acetone yielded only the chlorobridged product, $[Pd_2Cl_2\{(PPh_2O)_2H\}_2]$ (11), and a reinvestigation of the hydrolysis of *cis*-$[PdCl_2(PPh_2Cl)_2]$ also failed to isolate the simple *cis*-$[PdCl_2(PPh_2OH)_2]$ species (5). Reaction of $PtCl_4^{2-}$ with PPh_2Cl in aqueous acetone gave essentially similar results (11) but the controlled hydrolysis of *cis*-$[PtCl_2(PPh_2Cl)_2]$ has not been reinvestigated. Results on complexes of other metals also indicate type **III** products as the most common end result of hydrolysis of *cis*-$M(PR_2Cl)_2$ fragments. Basic hydrolysis of *cis*-$[Mo(CO)_4(PPh_2Cl)_2]$ gives *cis*-$[Mo(CO)_4\{(PPh_2O)_2H\}]^-$ (5, 6); $[IrCl(COD)]_2$ with PPh_2Cl in aqueous methanol gives $[IrHCl(COD)\{(PPh_2O)_2H\}]$ (9, 10); and the corresponding reaction using $[RhCl(COD)]_2$ gives a triple chloride bridged product, $[Rh_2Cl_5\{(PPh_2O)_2H\}_2]^-$ (9). In the work on rhodium complexes the authors succeeded in isolating bis(hydroxyphosphine) derivatives, $[RhL_2\{P(OMe)_2OH\}_2]^+$, by direct reaction of $(MeO)_2P(O)H$ with hydrogenated $[Rh(diene)L_2]^+$ salts but not from hydrolyses of chlorophosphines (9). These workers have also observed the reverse of step *2* in Scheme 1. Thus $[IrHCl\{Ph_2As(CH_2)_2AsPh_2\}\{(PPh_2O)_2H\}]$ may be protonated by HBF_4 to give an unstable fluoroborate salt of the $[IrHCl\{Ph_2As(CH_2)_2AsPh_2\}(PPh_2OH)_2]^+$ cation. In $CHCl_3$ solution this salt spontaneously eliminates HF to give a BF_2 capped product, $[IrHCl\{Ph_2As(CH_2)_2AsPh_2\}\{(PPh_2O)_2BF_2\}]$ (10).

Conversion of a P—O---H---O—P to a chelating P—O—P ligand system (step *3* in Scheme 1) has been achieved by treatment of *cis*-$[Mo(CO)_4\{(PPh_2O)_2H\}]^-$ with either an acid chloride/triethylamine mixture (8) or with trifluoroacetic acid/anhydride mixture (7) to form *cis*-$[Mo(CO)_4(Ph_2POPPh_2)]$. The reaction can be reversed by base hydrolysis (7). This molybdenum complex and its chromium analog are the only known examples of chelating Ph_2POPPh_2 ligands and bridging or monodentate behaviour is much more common (7). It is therefore not surprising that we have not observed any type **IV** products in our studies of platinum and palladium complexes. However, details of the formation of $[Pt_2Cl_4\{(EtO)_2POP(OEt)_2\}_2]$, a type **V** complex with a double M—P—O—P—M bridge, by hydrolysis of *cis*-$[PtCl_2\{P(OEt)_2Cl\}_2]$ will be reported in a subsequent paper.

Results and discussion

(a) Synthesis and characterisation

During their early work on the hydrolysis of *cis*-$[PtCl_2(PEt_3)(PR_2Cl)]$ complexes, Chatt and Heaton (14) had only very limited ^{31}P nmr facilities available to them. This lack of data prompted us to begin our study with a re-examination and extension of these reactions. Cleavage of the chlorobridged dimer, $[Pt_2Cl_4(PEt_3)_2]$, with the chlorophosphines, PR_2Cl, R = OEt or Ph, followed by hydrolysis of the products essentially as described by Chatt and Heaton (14) confirmed the successive formation of *cis*-$[PtCl_2(PEt_3)(PR_2Cl)]$ and *cis*-$[PtCl_2(PEt_3)(PR_2OH)]$. We also prepared $[PtCl_2(PEt_3)(PR_2Cl)]$ complexes for R = Bu^t, Cy, or Et, and were able to establish the ^{31}P nmr data given in Table 1. These results require little comment. The shifts and coupling constants follow the expected trends with substituent electronegativity and the relatively small magnitudes of $^2J(P—P)$ combined with very large values of $^1J(Pt—P)$ indicate *cis* stereochemistry for all the complexes except $[PtCl_2(PEt_3)(PBu^t_2Cl)]$. In this last complex $^2J(P—P)$ is much larger and the Pt—P couplings correspondingly reduced, a clear indication that the high *trans* influence phosphorus ligands are mutually *trans* in the square plane.

[1]Preliminary accounts of parts of this work have been published previously (12, 13).

The only unusual result encountered in this preliminay work was the occasional formation of a novel triphosphite derivative, $[Pt_2Cl_3(PEt_3)_2\{\mu\text{-}P(O)(OP(OEt)_2)_2\}]$, during hydrolysis of *cis*-$[PtCl_2(PEt_3)\{P(OEt)_2Cl\}]$. This product has been the subject of a preliminary communication (12) and full details will be published in a subsequent paper. Under most conditions the hydrolysis results in the simple *cis*-$[PtCl_2(PEt_3)\{P(OEt)_2OH\}]$ complex described here.

The experience gained during this preliminary study suggested that derivatives of PPh_2Cl and $P(OEt)_2Cl$ were the most easily handled; with the former providing the greatest stability and the latter the greatest potential for unusual reactivity. In consequence we concentrated on these two cases in most of our further studies of *cis*-$M(PR_2Cl)_2$ fragments. Complexes containing these groupings are readily synthesized by reactions of $[MCl_2(PhCN)_2]$ complexes with the appropriate chlorophosphines and use of PPh_2Cl with *cis*-$[PtCl_2(PhCN)_2]$ in this process gave *cis*-$[PtCl_2(PPh_2Cl)_2]$ in high yield. A ^{31}P spectrum of this complex in dichloromethane solution showed a single resonance at +72.2 ppm with sidebands due to coupling to ^{195}Pt (^1J(Pt—P) = 4110 Hz); the large coupling being typical of phosphorus trans to chlorine and a clear proof of *cis* stereochemistry. Addition of 2 molar equiv. of water to this complex in tetrahydrofuran solution gave small changes in the nmr parameters (+70.7 ppm and 4065 Hz) which could easily be incorrectly dismissed as solvent effects. However, crystallization at −18°C, gave white crystals showing a very strong, moderately broad infrared absorption at 900 cm^{-1} comparable with the absorptions ca. 880 cm^{-1} reported by Chatt and Heaton for ν(P—OH) in *cis*-$[PtX_2(PR_3)(PR_2OH)]$ complexes (14). Broad absorption was also observed in the 3300−3400 cm^{-1} region as expected for ν(PO—H) (14), but the position and intensity of this absorption varied greatly with sample preparation as might occur with a variation in hydrogen bonding. Microanalysis and ^1H and ^{13}C nmr spectroscopy suggested the presence in the crystals of one molecule of tetrahydrofuran of crystallization.These preliminary data strongly suggested that the product was *cis*-$[PtCl_2(PPh_2OH)_2]$ but in view of previous doubts of the isolability of such species, coupled to our own experience with related Pd and $P(OEt)_2Cl$ systems we felt that confirmation by crystal structure determination was essential. The structure was confirmed by the diffraction results described below and we were subsequently able to demonstrate by microanalysis and ^{31}P nmr spectroscopy that *cis*-$[PtCl_2(PEt_2Cl)_2]$ can be prepared and converted to *cis*-$[PtCl_2(PEt_2OH)_2]$ in a similar manner (see Table 1 and Experimental section). Moreover, *cis*-$[PtCl_2(PPh_2OH)_2]$ can also be prepared by the simpler route of reaction of $Ph_2P(O)H$ with $[PtCl_2(COD)]$.

Thus our results support the early claim by Austin (16) to have isolated *cis*-$[PtCl_2(PPh_2OH)_2]$. With regard to the stability of these compounds it is interesting to note that in the reactions of MCl_4^{2-} salts with PPh_2Cl in aqueous acetone the primary product when M = Pt can be formulated as $[PtCl(PPh_2O)(PPh_2OH)_2]$ in contrast to the immediate formation of $[Pd_2(\mu\text{-}Cl)_2\{(PPh_2O)_2H\}_2]$ for the corresponding reaction when M = Pd (11). The platinum product probably does not contain a true $M(PPh_2OH)_2$ unit since infrared spectroscopy indicated that both hydrogens are involved in very strong hydrogen bonds to the oxygens (11), but in conjunction with the failure to isolate *cis*-$[PdCl_2(PPh_2Cl)_2]$ (5) the results do support the idea that POH groupings are generally more stable on Pt than they are on Pd.

The intermediacy of the type **II** complex in the hydrolysis to type **III** was confirmed by the ready reaction of *cis*-$[PtCl_2(PPh_2OH)_2]$ with 1,8-bis(dimethylamino)naphthalene ("proton sponge") to form $[Pt_2(\mu\text{-}Cl)_2\{(PPh_2O)_2H\}_2]$ in high yield.

Turning now to studies of $P(OEt)_2Cl$ complexes, we found that the hydrolyses were considerably more complex and that intermediate products are not easily isolated. Solutions of *cis*-$[MCl_2\{P(OEt)_2Cl\}_2]$ are readily prepared and characterised by ^{31}P nmr for both M = Pd (δ = +112.1 ppm) and M = Pt (δ = +83.4 ppm, ^1J(Pt—P) = 5777 Hz) but attempts to isolate solid products under normal laboratory conditions resulted in hydrolyzed derivatives of types **IV** or **V**. For M = Pt the product was the type **V** complex, $[Pt_2Cl_4\{\mu\text{-}(EtO)_2POP(OEt)_2\}_2]$, which will be discussed more fully in a subsequent paper. The first hydrolysis product, *cis*-$[PtCl_2\{P(OEt)_2OH\}_2]$, was not isolated in this reaction but it can be prepared independently by the reaction of $[EtO)_2P(O)H$ with $[PtCl_2(COD)]$.

For M = Pd the type **III** product appears to be the most stable outcome as it was in the PPh_2Cl reactions mentioned above (11). In the present examples $[Pd_2(\mu\text{-}Cl)_2\{(P(OEt)_2O)_2H\}_2]$ is ultimately formed by hydrolysis of $P(OEt)_2Cl/[PdCl_2(PhCN)_2]$ reaction mixtures or by reaction of excess $(EtO)_2P(O)H$ with $[PdCl_2(PhCN)_2]$. The stability of the type **III** product was further illustrated by deliberate preparations of a type **V** product by reaction of $(EtO)_2POP(OEt)_2$ with $[PdCl_2(PhCN)_2]$ to give $[Pd_2Cl_4\{\mu\text{-}(EtO)_2POP(OEt)_2\}_2]$. This product hydrolyzes in moist air, even in the solid state, to give $[Pd_2(\mu\text{-}Cl)_2\{(P(OEt)_2O)_2H\}_2]$. In view of the importance and stability of $[Pd_2(\mu\text{-}Cl)_2\{(P(OEt)_2O)_2H\}_2]$ we decided to undertake a full characterization by X-ray diffraction and details of this study are presented below. The detailed course of the reactions leading to $[Pd_2(\mu\text{-}Cl)_2\{(P(OEt)_2O)_2H\}_2]$ was much more difficult to establish because the sharpness and position of the ^{31}P resonances for the intermediate products tended to vary with solution conditions, most probably with water and acid concentration. These effects are probably caused by a complex series of pH dependent equilibria, most of which are rapid on the nmr time scale. The principal species involved in these reactions are: (*1*) *cis*-$[PdCl_2\{P(OEt)_2Cl\}_2]$, δ(P) +112.1 ppm (C_6H_6), observable as the first product of reaction of $P(OEt)_2Cl$ with $[PdCl_2(PhCN)_2]$; (*2*) *cis*-$[PdCl_2\{P(OEt)_2OH\}]_2$, δ(P) +81 to +82 ppm, observable as the first product of reaction of $(EtO)_2P(O)H$ with $[PdCl_2(PhCN)_2]$; (*3*) $[Pd_2Cl_4\{\mu\text{-}(EtO)_2POP(OEt)_2\}_2]$, δ(P) +80.8 ppm ($CH_2Cl_2$), prepared by the reaction of $(EtO)_2POP(OEt)_2$ with $[PdCl_2(PhCN)_2]$ and also observed in some reactions of $P(OEt)_2Cl$; (*4*) $[Pd_2(\mu\text{-}Cl)_2\{(P(OEt)_2O)_2H\}_2]$, δ(P) +73.4 ppm ($CH_2Cl_2$), the ultimate product of most reactions under moist conditions; (*5*) A species with δ(P) +83.9 ppm (CH_2Cl_2), which results on addition of "proton sponge" to solutions of $[Pd_2(\mu\text{-}Cl)_2\{(P(OEt)_2O)_2H\}_2]$. This product is probably an anionic species resulting from proton abstraction; (*6*) a species with δ(P) +85.2 ppm, which results on addition of aqueous HCl to solutions of $[Pd_2(\mu\text{-}Cl)_2\{(P(OEt)_2O)_2H\}_2]$ in tetrahydrofuran. This product could be the result of bridge cleavage by chloride ion or possibly a dinuclear species containing *cis*-$Pd\{P(OEt)_2OH\}_2$ fragments formed by proton addition.

(b) Structures of cis-*$[PtCl_2(PPh_2OH)_2].C_4H_8O$, (I), and $[Pd_2(\mu\text{-}Cl)_2\{(P(OEt)_2O)_2H\}_2]$, (II)*

The atomic labelling schemes and the structures of single molecules of the complexes **I** and **II** are shown in Figs. 1 and 2, respectively. For **I** the associated tetrahydrofuran molecule

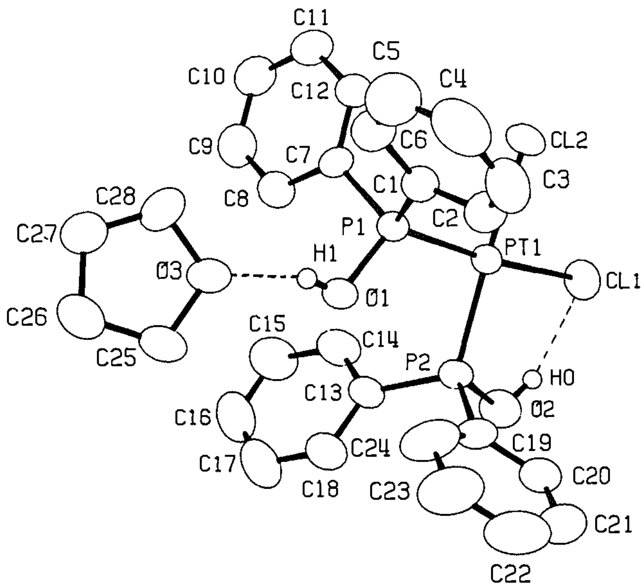

FIG. 1. ORTEP plot of compound **I**, *cis*-$[PtCl_2(PPh_2OH)_2].C_4H_8O$.

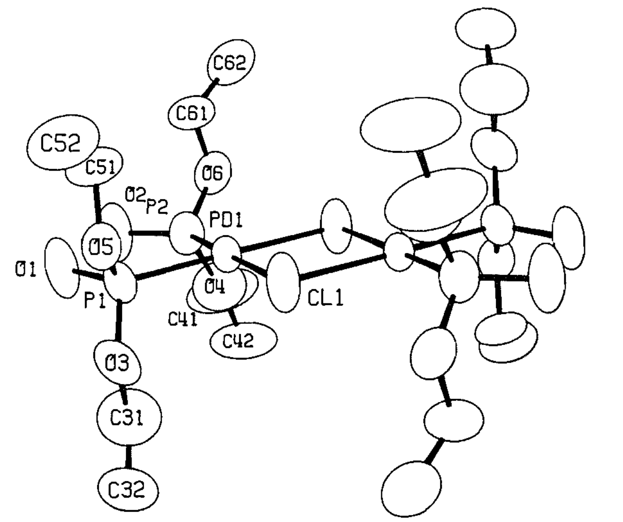

FIG. 2. ORTEP plot of compound **II**, $[Pd_2(\mu\text{-}Cl)_2\{(P(OEt)_2O)_2H\}_2]$. The unlabelled half of the molecule is related to the labelled half by a crystallographic centre of inversion.

is also shown. Fractional atomic coordinates and isotropic temperature parameters, bond lengths, and bond angles are collected in Tables 2–4 and 5–7, respectively. Further tables of atomic coordinates for the hydrogen atoms of **I**, together with anisotropic temperature factors, structure factors and selected intermolecular distances for both compounds have been deposited.[2]

The structure of **I** consists of a square planar platinum(II) centre in which the P(1)—Pt—P(2), 95.8(1)°, is slightly larger than the other three intraligand angles in order to accommodate the bulky PPh_2OH groups. The Pt—Cl lengths, average 2.364 Å, are entirely normal for chlorine *trans* to phosphorus, as are the Pt—P lengths, average 2.223 Å, for phosphorus *trans* to chlorine. For example the corresponding values in several complexes containing a *trans* Cl—Pt—P fragment ranged from 2.333 to 2.366 Å and from 2.241 to 2.262 Å, respectively (17). The angles at phosphorus which involve the platinum atom average 113°, considerably larger than the tetrahedral angle, but this is also a normal feature of tertiary phosphine complexes. The P—O bond lengths average 1.589 Å, somewhat longer than observed in the P—O---H---O—P complexes, $[Pd_2(\mu\text{-}SCN)_2\{(PPh_2O)_2H\}_2]$, 1.543 Å (18), $[Pd(S_2PMe_2)\{(PPh_2O)_2H\}]$, 1.545 Å (19), $[Mo(CO)_4\{(PPh_2O)_2H\}]^-$, 1.562 and 1.581 Å (20), and $[Mn(CO)_4\{(PPh_2O)_2H\}]$, 1.551 Å (21), but still well within the normal range of P—O single bonds (22).

The most interesting structural feature of **I** concerns the stabilization of the P—O—H groups by hydrogen bonding. This has been a consistent feature of all structures involving this group and in the present case is achieved for one ligand by intermolecular hydrogen bonding to the tetrahydrofuran of crystallization (O(1)---O(3) = 2.568(10) Å), and for the other ligand by an intramolecular hydrogen bond to a chlorine atom (O(2)---Cl(1) = 2.935(6) Å). These distances are longer than the 2.41 Å observed for intramolecular hydrogen bonds in the P—O---H---O—P complexes mentioned abvove (18–21) but, in the context of the ranges quoted by Stout and Jensen (23) for O---H---O (ca. 2.45–3.0 Å) and O---H---Cl (2.86–3.21 Å) hydrogen bonds, it is clear that all of the present values represent rather strong interactions. It is interesting that this is the second example which we have observed recently of involvement of a Pt—Cl group in an essentially ionic or electrostatic interaction to stabilize an unusual species. The other case was the Pt—Cl---Li---O—P linkage in *trans*-$[PtCl_2(PEt_3)\{CH(PPh_2O)_2Li\}]$ (24).

The structure of **II** confirms chlorine bridging rather than the alternative possibility of $P(OEt)_2O$ bridges with terminal chlorines and $P(OEt)_2OH$ groups. The two square planar palladium centres are separated by 3.488(1) Å and the Pd—Cl bonds average 2.393 Å which are normal distances for a bridged system without metal–metal interaction (25*a*). The Pd—P bonds average 2.220 Å, consistent with the low *trans* influence of chlorine (26–28) and the geometry of the P—O---H---O—P ligand is in accord with the previous studies of $[Pd_2(\mu\text{-}SCN)_2\{(PPh_2O)_2H\}_2]$ (18), $[Pd(S_2PMe_2)\{(PPh_2O)_2H\}]$ (19), $[Mo(CO)_4\{(PPh_2O)_2H\}]^-$ (20), and $[Mn(CO)_4\{(PPh_2O)_2H\}]$ (21). The intramolecular hydrogen bond, O(1)---O(2) 2.40 Å, is essentially identical in length to the previous examples (18–21) but the large temperature parameters associated with the ligand preclude any more detailed discussion of the bond lengths.

Experimental section

(a) Synthetic and spectroscopic studies

Data relating to the characterization of the complexes are given in Tables 1 to 7, the Results section, and in the preparative descriptions below. Microanalysis was by the Canadian Microanalytical Service, Vancouver, B.C., Canada. In general, the compounds tended to decompose on heating and melting points are not an especially useful method of characterization. Infrared spectra were recorded from 4000 to 200 cm^{-1} with an accuracy ±3 cm^{-1} on a Perkin–Elmer 283 spectrophotometer calibrated against polystyrene film. Solid samples were examined as Nujol mulls between caesium iodide plates.

^{31}P nmr spectra were recorded in appropriate solvents at either 24.3 MHz using a Nicolet TT14 Fourier transform spectrometer with a Varian HA60 magnet and an external C_6D_6 lock signal or at 101.3 MHz using a Bruker WP250 Fourier transform spectrometer locked to the solvent deuterium resonance. ^{195}Pt spectra were recorded at 53.5

[2]Copies of the depository material may be purchased from the Depository of Unpublished Data, CISTI, National Research Council of Canada, Ottawa, Ont., Canada K1A 0S2.

TABLE 1. Phosphorus-31 and platinum-195 nuclear magnetic resonance parameters for selected complexes[c]

Compound	Solvent	δ(*P*Et$_3$)	δ(*P*R$_2$X)	^2J(P—P)	^1J(Pt—PEt$_3$)	^1J(Pt—PR$_2$X)	δ(Pt)	Ξ(Pt)
[PtCl$_2$(PEt$_3$)(PR$_2$X)]								
X = Cl R = OEt	CH$_2$Cl$_2$	+16.0	+85.4	21	3200	6188	+184.2	21.403942
Ph	CH$_2$Cl$_2$	+14.8	+71.7	15	3312	4343	+169.4	21.403626
Bu^t	CH$_2$Cl$_2$	+12.2	+141.2	494	2515	2539	+649.6	21.413902
Cy	CH$_2$Cl$_2$	+13.8	+116.9	13	3483	4039	+167.3	21.403580
Et	CH$_2$Cl$_2$	+15.9	+105.5	15	3474	4033	+134.3	21.402873
Et	[a]	+17.5	+105.5		3454	4036		
X = OH R = OEt	CDCl$_3$	+14.9	+63.2	23	3414	5623	+46.6	21.400997
Ph	CH$_2$Cl$_2$	+10.3	+72.9	17	3497	3890	+86.6	21.401853
[PtCl$_2$(PBu$_3$)(PPh$_2$OH)]	[a]	+4.5	+70.8		3502	4172		
[PtCl$_2$(PR$_2$X)$_2$]								
X = Cl R = OEt	CH$_2$Cl$_2$		+83.4			5777	+371.7	21.407955
Ph	CH$_2$Cl$_2$		+72.2			4110	+160.5	21.403434
Et	THF		+100.9			3936	+264.1	21.405652
Et	Toluene		+100.3			3939		
X = OH R = OEt	THF		+66.6			5588	+180.6	21.403864[b]
Ph	CDCl$_3$		+71.2			4026	+163.3	21.403495
Ph	THF		+70.7			4065		
Et	CDCl$_3$		+99.2			4010	+87.5	21.401872
Et	THF		+97.8			3939		

[a]Data from ref. 14. These workers used P_4O_6 as a phosphorus reference and we have converted the shifts assuming that P_4O_6 is at +113 ppm relative to 85% H_3PO_4.

[b]In d^8 THF solution, all other platinum spectra were recorded in $CDCl_3$.

[c]Chemical shifts (δ) are quoted in ppm relative to 85% H_3PO_4 for phosphorus and relative to $\Xi(^{195}Pt)$ = 21.4 MHz for platinum (see ref. 29). For the platinum resonances the absolute values of Ξ inMHz are also quoted. Coupling constants (*J*) are in Hz. The listed solvents are for the phosphorus spectra. Data for other ligands and complexes are included in the text.

MHz using the Bruker instrument. For both nuclei protons were decoupled by broad band ("noise") irradiation at appropriate frequencies. ^{31}P chemical shifts were measured relative to external $P(OMe)_3$ and are reported in ppm relative to 85% H_3PO_4 using a conversion factor of +141 ppm. ^{195}Pt chemical shifts are reported in ppm relative to $\Xi(^{195}Pt)$ = 21.4 MHz (29). Positive values are downfield of the references. Phosphorus chemical shifts for the various ligands employed in this work were as follows: PPh_2Cl, +83.0 ppm (THF or CH_2Cl_2); PEt_2Cl, +121.0 ppm (CH_2Cl_2); PCy_2Cl, +129.6 ppm (CH_2Cl_2); $PBu^t{}_2Cl$, +148.7 ppm (CH_2Cl_2); $P(OEt)_2Cl$, +167.3 ppm (CH_2Cl_2), +166.8 ppm (C_6H_6); $(EtO)_2P(O)H$, +8.2 ppm (CH_2Cl_2), +7.4 ppm (THF), +7.2 ppm (C_6H_6); $Ph_2P(O)H$, +26.5 ppm (CH_2Cl_2), +20.6 ppm (THF); $(EtO)_2POP(OEt)_2$, +129.5 ppm (CH_2Cl_2), +128.6 ppm (C_6H_6).

Except as noted below, all operations were carried out at ambient temperature (ca. 25°C) under an atmosphere of dry nitrogen using standard Schlenk tube techniques. Solvents were dried by reflux over appropriate reagents (phosphorus pentoxide for dichloromethane and potassium/benzophenone for tetrahydrofuran, toluene, benzene, and hexane) and were distilled under nitrogen prior to use.

The chlorophosphines PR_2Cl were commercially available, R = Ph or OEt (Aldrich Chemical Co.), R = Bu^t (Strem Chemicals Inc.), R = Et or Cy (Alfa Ventron Corporation), and were used as received, as were $(EtO)_2POP(OEt)_2$, $(EtO)_2P(O)H$, 1,8-bis(dimethylamino)naphthalene ("proton sponge"), and 1,5-cyclooctadiene (COD) from the Aldrich Chemical Co. [$MCl_2(PhCN)_2$], M = Pd or Pt (25*b*), [$PtCl_2$(COD)] (31), and [$Pt_2Cl_4(PEt_3)_2$] (32), were prepared as previously described.

Recrystallizations from solvent pairs were by dissolution of the complex in the first solvent (using about double the volume required for complete solution) followed by dropwise addition of sufficient second solvent to cause turbidity at ambient temperature. Crystallization was then completed either by continued very slow dropwise addition of the second solvent or, in those cases where a temperature is indicated in the detailed descriptions below, by setting the mixture aside at a reduced temperature.

[PtCl$_2$(PEt$_3$)(PR$_2$X)], X = Cl or OH

(i) R = Ph. These complexes were prepared essentially as described by Chatt and Heaton (14).

(ii) R = OEt. A typical reaction involved dropwise addition of $P(OEt)_2Cl$ (0.1 mL, 0.7 mmol) to a stirred solution of [$Pt_2Cl_4(PEt_3)_2$] (0.25 g, 0.33 mmol) in dichloromethane (20 mL). The initial yellow colour was immediately discharged but stirring was continued for 1 h before removal of the solvent *in vacuo*. Recrystallization of the residue from dichloromethane/pentane gave *cis*-[$PtCl_2(PEt_3)\{P(OEt)_2Cl\}$] (0.20 g, 0.37 mmol) as colourless crystals. *Anal.* calcd. for $C_{10}H_{25}Cl_3O_2P_2Pt$: C 22.2, H 4.66; found: C 22.5, H 4.73. In a separate experiment hydrolysis of the crude product was achieved by heating the residue for 4 h under reflux in a mixture of aqueous HCl (5 mL, 12 *M*) and acetone (20 mL). After removal of solvent under reduced pressure the residue was extracted with dichloromethane and the extract recrystallized from dichloromethane/pentane to give *cis*-[$PtCl_2(PEt_3)\{P(OEt)_2OH\}$] as yellow crystals (0.18 g, 0.34 mmol). *Anal.* calcd. for $C_{10}H_{26}Cl_2O_3P_2Pt$: C 23.0, H 5.02; found: C 22.8, H 4.97.

(iii) R = Bu^t, Et or Cy. Preparations of [$PtCl_2(PEt_3)(PR_2Cl)$] complexes for these R groups were similar to the above procedure for R = OEt except that the crystals for R = Bu^t were yellow, consistent with the *trans* stereochemistry of this product. *Anal.* R = Bu^t, calcd. for $C_{14}H_{33}Cl_3P_2Pt$: C 29.8, H 5.89; found: C 29.5, H 5.92; R = Cy, calcd. for $C_{18}H_{37}Cl_3P_2Pt$: C 35.0, H 6.05; found: C 35.0, H 6.13. The R = Et complex was identified by ^{31}P nmr (see Table 1) but could not be obtained analytically pure. Attempts at hydrolyses of all three complexes gave generally inconsistent results and pure products were not isolated.

cis-*[PtCl$_2$(PR$_2$X)$_2$], X = Cl or OH*

(i) R = Ph. PPh_2Cl (0.152 mL, 0.847 mmol) was added to a stirred solution of [$PtCl_2(PhCN)_2$] (0.200 g, 0.424 mmol) in dichloromethane. The initial yellow colour was discharged during stirring for 15 min,

TABLE 2. Fractional atomic coordinates and temperature parameters for compound **I**, *cis*-$[PtCl_2(PPh_2OH)_2].C_4H_8O$[a]

Atom	x/a	y/b	z/c	U_{eq}
Pt(1)	33456(1)	19632(1)	81200(2)	361(1)
Cl(1)	36139(13)	18958(11)	99161(12)	566(6)
Cl(2)	17961(11)	17046(14)	84293(14)	624(6)
P(1)	29424(10)	20605(10)	64850(12)	378(4)
P(2)	48353(10)	21613(11)	78883(12)	415(5)
O(1)	3785(3)	2201(3)	5768(3)	48(1)
O(2)	5344(3)	2351(4)	8956(4)	66(2)
O(3)	−1410(3)	2478(5)	8851(4)	80(2)
C(1)	2361(4)	1079(4)	6007(5)	44(2)
C(2)	2633(5)	261(4)	6396(5)	56(2)
C(3)	2276(6)	−512(5)	5980(6)	71(3)
C(4)	1633(6)	−464(6)	5184(7)	82(3)
C(5)	1358(6)	345(6)	4797(7)	81(3)
C(6)	1738(5)	1115(5)	5199(5)	60(3)
C(7)	2206(4)	3012(4)	6239(4)	39(2)
C(8)	2614(4)	3785(4)	5878(5)	52(2)
C(9)	2096(5)	4542(5)	5751(6)	63(3)
C(10)	1180(5)	4535(4)	5972(5)	58(2)
C(11)	775(5)	3775(5)	6312(6)	59(2)
C(12)	1295(4)	3010(4)	6460(5)	52(2)
C(13)	5168(4)	3112(4)	7152(5)	44(2)
C(14)	4683(5)	3878(5)	7261(6)	62(3)
C(15)	4916(6)	4651(5)	6739(7)	79(3)
C(16)	5669(6)	4638(6)	6124(7)	80(3)
C(17)	6162(6)	3875(6)	5998(6)	77(3)
C(18)	5910(5)	3115(5)	6506(6)	64(3)
C(19)	5441(4)	1203(4)	7423(5)	52(2)
C(20)	5918(4)	685(5)	8122(6)	63(3)
C(21)	6374(6)	−67(6)	7803(10)	87(4)
C(22)	6380(6)	−282(6)	6797(10)	100(5)
C(23)	5921(6)	220(6)	6089(8)	92(4)
C(24)	5449(5)	970(6)	6387(7)	79(3)
C(25)	−578(5)	2278(7)	8343(6)	71(3)
C(26)	−874(6)	1883(6)	7334(7)	81(4)
C(27)	−1845(6)	1692(9)	7431(9)	113(5)
C(28)	−2172(7)	2155(8)	8290(7)	92(4)
H(0)	496(5)	225(6)	944(6)	8(3)′
H(1)	361(6)	230(6)	528(7)	9(3)′

[a]Estimated standard deviations are given in parentheses; coordinates $\times 10^n$ where n = 5, 5, 5, 4, 4, 3 for Pt, Cl, P, O, C, H; temperature parameters $\times 10^n$ where n = 4, 4, 4, 3, 3, 2 for Pt, Cl, P, O, C, H; U_{eq} = the equivalent isotropic temperature parameter = $(1/3)\Sigma_i\Sigma_j U_{ij} a_i^* a_j^* (\mathbf{a}_i \cdot \mathbf{a}_j)$; primed values indicate that U_{iso} is given; $T = \exp[-(8\pi^2 U_{iso} \sin^2\theta/\lambda^2)]$.

after which the solvent was removed *in vacuo* to leave *cis*-$[PtCl_2(PPh_2Cl)_2]$ as a white residue. Tetrahydrofuran (20 mL) and water (50 μL) were added and the resulting slurry stirred for 3 h. The solvent was removed *in vacuo* and the residue recrystallized from tetrahydrofuran/hexane at −20°C to give white crystals of *cis*-$[PtCl_2(PPh_2OH)_2]$.THF (0.177 g, 0.238 mmol). *Anal.* calcd. for $C_{28}H_{30}Cl_2O_3P_2Pt$: C 45.3, H 4.07; found: C 45.3, H 3.87.

In a separate experiment the intermediate *cis*-$[PtCl_2(PPh_2Cl)_2]$ complex was recrystallized from dichloromethane/pentane and characterized by ^{31}P nmr (see Table 1). *Anal.* calcd. for $C_{24}H_{20}Cl_4P_2Pt$: C 40.8, H 2.85; found: C 41.0, H 2.73.

(ii) R = Ph. Water (30 μL, 1.7 mmol) was added to a solution of PPh_2Cl (0.20 mL, 1.1 mmol) in tetrahydrofuran (2 mL). ^{31}P spectra showed complete conversion of PPh_2Cl (δ(P) +83.0 ppm) to $Ph_2P(O)H$ (δ(P) +20.6 ppm). Addition of this solution to $[PtCl_2(COD)]$ (0.186 g, 0.50 mmol) in tetrahydrofuran (10 mL) gave complete conversion to *cis*-$[PtCl_2(PPh_2OH)_2]$ as identified by ^{31}P nmr (see Table 1).

(iii) R = Ph, X = OH, reaction with 1,8-bis(dimethylamino)naphthalene. "Proton sponge" (0.043 g, 0.20 mmol) was added to a stirred solution of *cis*-$[PtCl_2(PPh_2OH)_2]$.THF (0.147 g, 0.20 mmol) in tetrahydrofuran (8 mL). After 1 h the ^{31}P spectrum showed complete conversion to $[Pt_2(\mu\text{-}Cl)_2\{(PPh_2O)_2H\}_2]$ (δ(P) +51.2 ppm, ^1J(Pt—P) 3960 Hz, Ξ(^{195}Pt) 21.385916 MHz, δ(^{195}Pt) −658 ppm in $CDCl_3$), the identity of which was confirmed by comparison with an authentic sample prepared as previously described (11).

TABLE 3. Interatomic distances (Å) for compound **I**, *cis*-$[PtCl_2(PPh_2OH)_2].C_4H_8O$[a]

Atoms	Distance	Atoms	Distance
Cl(1)—Pt(1)	2.381(2)	Cl(2)—Pt(1)	2.347(2)
P(1)—Pt(1)	2.216(2)	P(2)—Pt(1)	2.229(2)
O(1)—P(1)	1.581(4)	O(2)—P(2)	1.597(5)
H(1)—O(1)	0.70(9)	H(0)—O(2)	0.87(8)
C(1)—P(1)	1.813(6)	C(13)—P(2)	1.802(6)
C(7)—P(1)	1.821(6)	C(19)—P(2)	1.810(7)
C(2)—C(1)	1.391(9)	C(14)—C(13)	1.366(9)
C(3)—C(2)	1.385(10)	C(15)—C(14)	1.398(10)
C(4)—C(3)	1.393(11)	C(16)—C(15)	1.380(12)
C(5)—C(4)	1.380(12)	C(17)—C(16)	1.372(12)
C(6)—C(5)	1.387(10)	C(18)—C(17)	1.381(10)
C(6)—C(1)	1.385(8)	C(18)—C(13)	1.392(9)
C(8)—C(7)	1.397(8)	C(20)—C(19)	1.381(9)
C(9)—C(8)	1.379(9)	C(21)—C(20)	1.387(12)
C(10)—C(9)	1.378(10)	C(22)—C(21)	1.358(14)
C(11)—C(10)	1.371(9)	C(23)—C(22)	1.364(13)
C(12)—C(11)	1.394(9)	C(24)—C(23)	1.387(11)
C(12)—C(7)	1.372(9)	C(24)—C(19)	1.402(10)
O(1)···O(3)	2.568(10)	O(2)···Cl(1)	2.935(6)
H(1)···O(3)	1.90(9)	H(0)···Cl(1)	2.15(9)
C(25)—O(3)	1.432(8)	C(28)—O(3)	1.412(9)
C(26)—C(25)	1.506(12)	C(28)—C(27)	1.417(13)
C(27)—C(26)	1.459(12)		

[a]Estimated standard deviations are given in parentheses.

(iv) R = Et. PEt_2Cl (0.160 mL, 1.26 mmol) was added to a slurry of $[PtCl_2(PhCN)_2]$ (0.30 g, 0.64 mmol) in toluene (20 mL). Stirring was continued for 15 h but at the end of this time some yellow solid still remained and was removed by filtration. Evaporation of the supernatant *in vacuo* gave *cis*-$[PtCl_2(PEt_2Cl)_2]$ as a white residue, identified by ^{31}P nmr (see Table 1). Addition of 2 molar equiv. of water to a solution of this product in tetrahydrofuran (5 mL) gave total conversion to *cis*-$[PtCl_2(PEt_2OH)_2]$, identified by ^{31}P nmr (see Table 1). Removal of solvent *in vacuo* followed by recrystallization of the residue from tetrahydrofuran/hexane gave *cis*-$[PtCl_2(PEt_2OH)_2]$ as white crystals. *Anal.* calcd. for $C_8H_{22}Cl_2O_2P_2Pt$: C 20.1, H 4.64; found: C 20.5, H 4.53.

(v) R = OEt. $P(OEt)_2Cl$ (0.20 mL, 1.4 mmol) was added dropwise to a stirred solution of $[PtCl_2(PPhCN)_2]$ (0.30 g, 0.64 mmol) in dichloromethane (10 mL). The initial yellow colour was slowly discharged during stirring for 6 h. The solvent was removed *in vacuo* and the resulting colourless oil characterised as *cis*-$[PtCl_2\{P(OEt)_2Cl\}_2]$ by ^{31}P nmr (see Table 1). Repeated attempts at recrystallization caused conversion of the product to $[Pt_2Cl_4\{\mu\text{-}(EtO)_2POP(OEt)_2\}_2]$ which will be discussed in detail in a subsequent paper.

(vi) R = OEt. $(EtO)_2P(O)H$ (0.200 mL, 1.55 mmol) was added to a suspension of $[PtCl_2(COD)]$ (0.273 g, 0.730 mmol) in tetrahydrofuran (15 mL). After stirring for 2 h the solvent was removed *in vacuo* and the residue recrystallized from tetrahydrofuran/hexane at −20°C to yield *cis*-$[PtCl_2\{P(OEt)_2OH\}_2]$ as colourless crystals. *Anal.* calcd. for $C_8H_{22}Cl_2O_6P_2Pt$: C 17.7, H 4.09; found: C 17.9, H 4.12.

Reactions of $[PdCl_2(PhCN)_2]$

(i) With $P(OEt)_2Cl$. A solution of $P(OEt)_2Cl$ (0.10 mL, 0.70 mmol) in benzene (2 mL) gave a ^{31}P nmr resonance at +166.8 ppm. Addition of $[PdCl_2(PhCN)_2]$ (0.135 g, 0.35 mmol) caused an almost immediate change to primarily a single resonance at +112.1 ppm attributed to *cis*-$[PdCl_2\{P(OEt)_2Cl\}_2]$. Approximately 2 molar equiv. of water were

TABLE 4. Bond angles (deg) for compound **I**, *cis*-$[PtCl_2(PPh_2OH)_2].C_4H_8O$[a]

Atoms	Angle	Atoms	Angle
Cl(2) —Pt(1) —Cl(1)	87.8(1)	P(2) —Pt(1) —P(1)	95.8(1)
P(1) —Pt(1) —Cl(2)	86.5(1)	P(2) —Pt(1) —Cl(1)	89.9(1)
P(1) —Pt(1) —Cl(1)	173.9(1)	P(2) —Pt(1) —Cl(2)	177.1(1)
O(1) —P(1) —Pt(1)	112.9(2)	O(2) —P(2) —Pt(1)	110.1(2)
C(1) —P(1) —Pt(1)	113.2(2)	C(13) —P(2) —Pt(1)	117.2(2)
C(7) —P(1) —Pt(1)	111.6(2)	C(19) —P(2) —Pt(1)	115.3(2)
C(7) —P(1) —C(1)	108.1(3)	C(19) —P(2) —C(13)	108.4(3)
C(1) —P(1) —O(1)	105.7(3)	C(13) —P(2) —O(2)	101.5(3)
C(7) —P(1) —O(1)	104.9(3)	C(19) —P(2) —O(2)	102.5(3)
H(1) —O(1) —P(1)	107(7)	H(0) —O(2) —P(2)	108(5)
C(2) —C(1) —P(1)	118.0(5)	C(14) —C(13) —P(2)	118.1(5)
C(6) —C(1) —P(1)	122.0(5)	C(18) —C(13) —P(2)	123.5(5)
C(8) —C(7) —P(1)	117.5(5)	C(20) —C(19) —P(2)	118.2(6)
C(12) —C(7) —P(1)	122.4(4)	C(24) —C(19) —P(2)	122.7(6)
C(6) —C(1) —C(2)	119.6(6)	C(18) —C(13) —C(14)	118.4(6)
C(3) —C(2) —C(1)	120.0(7)	C(15) —C(14) —C(13)	121.5(7)
C(4) —C(3) —C(2)	119.7(7)	C(16) —C(15) —C(14)	118.7(8)
C(5) —C(4) —C(3)	120.6(7)	C(17) —C(16) —C(15)	120.8(8)
C(6) —C(5) —C(4)	119.4(8)	C(18) —C(17) —C(16)	119.5(8)
C(5) —C(6) —C(1)	120.7(7)	C(17) —C(18) —C(13)	121.1(7)
C(12) —C(7) —C(8)	119.9(5)	C(24) —C(19) —C(20)	119.1(7)
C(9) —C(8) —C(7)	119.6(6)	C(21) —C(20) —C(19)	120.2(9)
C(10) —C(9) —C(8)	120.2(7)	C(22) —C(21) —C(20)	120.0(9)
C(11) —C(10) —C(9)	120.3(6)	C(23) —C(22) —C(21)	121.0(9)
C(12) —C(11) —C(10)	120.0(6)	C(24) —C(23) —C(22)	120.2(9)
C(11) —C(12) —C(7)	120.0(6)	C(23) —C(24) —C(19)	119.4(8)
C(26) —C(25) —O(3)	105.1(6)	C(27) —C(28) —O(3)	107.9(8)
C(27) —C(26) —C(25)	105.3(7)	C(28) —C(27) —C(26)	108.6(8)
C(28) —O(3) —C(25)	110.9(6)		

[a]Estimated standard deviations are given in parentheses.

TABLE 5. Fractional atomic coordinates and temperature parameters for **II**, $[Pd_2(\mu\text{-}Cl)_2\{(P(OEt)_2O)_2H\}_2]$

Atom	x/a	y/b	z/c	U_e
Pd(1)	44665(5)	7388(2)	7382(6)	882(2)
Cl(1)	6567(2)	135(1)	734(3)	144(1)
P(1)	5538(3)	1528(1)	2096(3)	114(1)
P(2)	2448(2)	1234(1)	740(4)	125(1)
O(1)	4718(7)	2128(3)	2367(10)	179(4)
O(2)	2406(7)	1914(3)	1357(11)	186(4)
O(3)	6202(8)	1263(4)	3688(8)	164(4)
O(4)	1461(8)	760(5)	1745(13)	202(5)
O(5)	6951(5)	1713(3)	1378(8)	124(3)
O(6)	1673(6)	1233(3)	−849(9)	138(3)
C(31)	5448(18)	1021(10)	4869(25)	259(11)
C(32)	6360(23)	768(9)	6178(18)	250(12)
C(41)	178(17)	742(11)	1951(28)	299(14)
C(42)	−235(17)	341(12)	3022(21)	287(12)
C(51)	6999(16)	2012(6)	−131(15)	182(7)
C(52)	8359(12)	2218(8)	−407(19)	206(8)
C(61)	2225(15)	1627(6)	−2021(14)	181(6)
C(62)	1521(17)	1467(7)	−3537(21)	226(9)

[a]Estimated standard deviations are given in parentheses; coordinates $\times 10^n$ where $n = 5$ for Pd, and $n = 4$ otherwise; temperature parameters $\times 10^n$ where $n = 4$ for Pd and $n = 3$ otherwise; U_e = the equivalent isotropic temperature parameter = $(1/3)\Sigma_i\Sigma_j U_{ij}a_i^*a_j^*(a_i \cdot a_j)$; $T = \exp[-(8\pi^2 U_{iso}\sin^2\theta/\lambda^2)]$.

TABLE 6. Interatomic distances (Å) for **II**, $[Pd_2(\mu\text{-}Cl)_2\{(P(OEt)_2O)_2H\}_2]$[a]

Atoms	Distance	Atoms	Distance
Cl(1) —Pd(1)	2.387(2)	Cl(1′)—Pd(1)	2.398(2)
P(1) —Pd(1)	2.233(2)	P(2) —Pd(1)	2.207(2)
Pd(1) —Pd(1′)	3.488(1′)	Cl(1) —Cl(1′)	3.275(4)
O(1) —P(1)	1.498(6)	O(3) —P(1)	1.580(8)
O(5) —P(1)	1.573(6)	O(2) —P(2)	1.506(6)
O(4) —P(2)	1.643(9)	O(6) —P(2)	1.523(7)
C(31) —O(3)	1.372(15)	C(41)—O(4)	1.263(17)
C(51) —O(5)	1.437(11)	C(61)—O(6)	1.419(11)
C(32) —C(31)	1.489(24)	C(42)—C(41)	1.315(19)
C(52) —C(51)	1.415(16)	C(62)—C(61)	1.477(18)

[a]Estimated standard deviations are given in parentheses.

added and the resonance shifted to +87.3 ppm, consistent with the formation of $[Pd_2(\mu\text{-}Cl)_2\{(P(OEt)_2O)_2H\}_2]$ and HCl. Addition of "proton sponge" to absorb the HCl caused some precipitation but both the precipitate and the solid isolated from the supernatant showed a single ^{31}P nmr resonance at +84.3 ppm in dichloromethane. These reasonance positions may be compared with the +85.2 ppm and +83.9 ppm reported below for the respective deliberate addition of aqueous HCl or "proton sponge" to $[Pd_2(\mu\text{-}Cl)_2\{(P(OEt)_2O)_2H\}_2]$.

Attempts to employ this reaction on a preparative scale led to inconsistent results. On one occasion $[Pd_2Cl_4\{\mu\text{-}(EtO)_2POP(OEt)_2\}_2]$ was probably isolated (δ(P) +80.8 ppm, lit. +80.3 ppm (33). *Anal.* calcd. for $C_{16}H_{40}Cl_4O_{10}P_4Pd_2$: C 22.1, H 4.63; found: C 22.3, H 4.09), a further indication of the sensitivity of these reactions to the precise conditions.

(ii) with $(EtO)_2P(O)H$. Excess $(EtO)_2P(O)H$ (0.5 mL, 3.9 mmol) was added dropwise to a stirred solution of $[PdCl_2(PhCN)_2]$ (0.2 g, 0.5 mmol) in dichloromethane (20 mL). After stirring for 4 h the initially orange solution had become colourless. Solvent and excess phosphite were removed *in vacuo* and the resulting oil washed with portions of hexane and dried *in vacuo* until $[Pd_2(\mu\text{-}Cl)_2\{(P(OEt)_2O)_2H\}_2]$ (0.058 g, 0.070 mmol) was obtained as a colourless solid.

TABLE 7. Bond angles (deg) for **II**, $[Pd_2(\mu\text{-}Cl)_2\{(P(OEt)_2O)_2H\}_2]$

Atoms	Angle	Atoms	Angle
P(1) —Pd(1) —Cl(1)	90.6(1)	P(2) —Pd(1) —Cl(1)	176.1(1)
P(2) —Pd(1) —P(1)	92.7(1)	Cl(1) —Pd(1) —Cl(1′)	86.4(1)
P(1) —Pd(1) —Cl(1′)	176.9(1)	P(2) —Pd(1) —Cl(1′)	90.3(1)
Pd(1) —Cl(1) —Pd(1′)	93.6(1)		
O(1) —P(1) —Pd(1)	116.9(3)	O(2) —P(2) —Pd(1)	118.3(3)
O(3) —P(1) —Pd(1)	110.9(3)	O(4) —P(2) —Pd(1)	105.0(3)
O(3) —P(1) —O(1)	110.5(4)	O(4) —P(2) —O(2)	110.4(5)
O(5) —P(1) —Pd(1)	111.4(2)	O(6) —P(2) —Pd(1)	113.3(3)
O(5) —P(1) —O(1)	109.5(4)	O(6) —P(2) —O(2)	107.2(4)
O(5) —P(1) —O(3)	95.6(4)	O(6) —P(2) —O(4)	101.3(5)
C(31) —O(3) —P(1)	123.9(11)	C(32) —C(31) —O(3)	111.6(15)
C(41) —O(4) —P(2)	133.7(11)	C(42) —C(41) —O(4)	116.8(17)
C(51) —O(5) —P(1)	121.6(7)	C(52) —C(51) —O(5)	110.5(10)
C(61) —O(6) —P(2)	116.5(7)	C(62) —C(61) —O(6)	108.7(10)

[a]Estimated standard deviations are given in parentheses.

Anal. calcd. for $C_{16}H_{42}Cl_2O_{12}P_4Pd_2$: C 23.0, H 5.08; found: C 22.70, H 5.27. The structure of this product was confirmed by the X-ray diffraction study described below. Its ^{31}P nmr spectrum in dichloromethane showed a single resonance at +73.4 ppm shifting to +83.9 ppm on the addition of "proton sponge". Addition of a drop of aqueous HCl to a solution in tetrahydrofuran shifted the resonance to +85.2 ppm.

Other experiments showed that the use of stoichiometric quantities of $(EtO)_2P(O)H$ in the above procedure gave incomplete conversion of the starting materials and also showed the presence of an intermediate product, probably $[PdCl_2\{P(OEt)_2OH\}_2]$, with δ(P) in the range +81 to +82 ppm.

(iii) With $(EtO)_2POP(OEt)_2$. $(EtO)_2POP(OEt)_2$ (0.142 mL, 0.58 mmol) was added dropwise to a stirred solution of $[PdCl_2(PhCN)_2]$ (0.20 g, 0.52 mmol) in benzene (10 mL). An immediate colour change from orange to pale yellow was observed but stirring was continued for 30 min before removal of solvent *in vacuo*. The residue was recrystallized from dichloromethane/hexane at −20°C to give $[Pd_2Cl_4\{(\mu\text{-}(EtO)_2POP(OEt)_2\}_2]$ as colourless crystals (0.096 g, 0.11 mmol) characterised by a single ^{31}P nmr resonance at +80.8 ppm in dichloromethane solution (lit. +80.3 (33)).

One batch of crystals was exposed to moist air for several days resulting in complete conversion to a new product with δ(P) +73.1 ppm in dichloromethane or tetrahydrofuran solution. A second batch of crystals was studied by ^{31}P nmr during gradual addition of water to a solution in tetrahydrofuran. The ultimate product showed a broad resonance at +74 ppm but intermediate spectra showed a gradual shift to this position and also a weak transient intermediate resonance at +68 ppm. Addition of proton sponge to the final solution resulted in a single sharp resonance at +83.9 ppm. These results are consistent with a complex pH dependent equilibrium as discussed in the Results and Discussion section. The ultimate hydrolysis product, δ(P) +74 ppm, is $[Pd_2(\mu\text{-}Cl)_2\{(P(OEt)_2O)_2H\}_2]$.

(b) X-ray data collection

Compound **I**, *cis*-$[PtCl_2(PPh_2OH)_2]$, was prepared by the first method described above (i.e. by hydrolysis of *cis*-$[PtCl_2(PPh_2Cl)_2]$) and crystals suitable for study by X-ray diffraction were grown at −18°C from a solution of the complex in tetrahydrofuran. The crystals subsequently proved to contain 1 mol of tetrahydrofuran. Compound **II**, $[Pd_2(\mu\text{-}Cl)_2\{(P(OEt)_2O)_2H\}_2]$ was crystallized by vapour diffusion of hexane into a solution of the complex in dichloromethane. Preliminary photographic work on both compounds was carried out with Weissenberg and precession cameras using Cu K_α radiation. After establishment of symmetry and approximate unit cells the crystals were transferred to a Picker 4-circle diffractometer automated with a PDP11/10 computer and utilising Zr filtered Mo K_α radiation (λ = 0.71069 Å). The unit cells were refined by least-squares methods employing, respectively, 31 and 11 pairs of centering measurements at ±2θ in the ranges |2θ| = 17−43° (**I**) and 19−30° (**II**). The crystals were mounted approximately along the *c* axes. The crystal data at approximately 24°C were as follows:

$C_{28}H_{30}Cl_2O_3P_2Pt$ mw = 742.49
Monoclinic, space group $P2_1/n$; a = 14.647(3), b = 15.089(3), c = 13.107(2) Å; β = 91.22(3)°; V(cell) = 2896(1) Å^3; D_m = 1.692 g cm^{-3} (flotation in $CCl_4/CHBr_3$), D_c = 1.705 g cm^{-3}; Z = 4; asymmetric unit = one molecule of complex with one molecule of tetrahydrofuran.

$C_{16}H_{42}Cl_2O_{12}P_4Pd_2$ mw = 834.10
Monoclinic, space group $P2_1/c$; a = 9.674(2), b = 20.722(5), c = 8.578(2) Å; β = 92.75(3)°; V(cell) = 1717.6(6) Å^3; D_m = 1.59 g cm^{-3} (flotation in CCl_4/*m*-xylene), D_c = 1.61 g cm^{-3}; Z = 2; asymmetric unit = half molecule.

Intensity measurements for both compounds were collected for two reciprocal space octants (h unrestricted, $k \geq 0$, $l \geq 0$). For **I** measurements extended up to 2θ = 50°. A θ/2θ step scan was used with 160 steps of 0.01° in 2θ, counting for 0.25 s per step. Background measurements were for 20 s at each end of the scan. Measurements for **II** were to 2θ = 50° with 200 steps of 0.01° in 2θ, counting for 0.25 s per step and with background measurements of 25 s each. Each batch of 50 reflections was preceded by the measurement of three standard reflections (**I**: 0, 0, 6; 4, 0, 0; 0, 8, 0; and **II**: 0, 0, 4; 2, 0, 0; 0, 8, 0). The Lorentz and polarization factors were applied and each batch was scaled to maintain the sum of the standard constants. There was no evidence of sample decomposition during the data collection for **I** but there was a 5.5% decline in the intensity of the standards for **II**. Absorption corrections were applied with a numerical integration procedure utilizing Gaussian grids (**I**: 6 × 6 × 6, and **II**: 6 × 6 × 10). The crystal shapes were defined by perpendicular distances to crystal faces from a central origin as follows: **I**: ±{100}, 0.248 mm; ±{010}, 0.184 mm; ±{10$\bar{1}$}, 0.215 mm; and **II**: ±{100}, 0.143 mm; ±{010}, 0.181 mm; ±{001}, 0.411 mm. The absorption coefficients were 54.24 and 13.83 cm^{-1}, respectively, and the ranges of transmission factors were 0.13−0.23 and 0.61−0.69. For compound **I**, reflections with intensity less than 2.5σ(I) were removed from the data set to give a final file containing 4347 independent reflections. For **II** the final file contained 3014 independent reflections.

(c) Structure solution and refinement

The structures were found and refined using the SHELX-76 program package (34), and illustrations were drawn using ORTEP (35). The atomic scattering factors used were for neutral atoms, with corrections for anomalous dispersion (30). The structures were solved by direct methods, completed by standard Fourier synthesis procedures using difference maps, and refined by the method of least-squares minimising $\Sigma w\Delta^2$ where $\Delta = |F_o| - |F_c|$. The weights were obtained from counting statistics using $w = 1/(\sigma^2(F) + 0.001F^2)$. For compound **I** hydrogen atoms were included in the refinement but, with the exception of H(0) and H(1), were fixed at 1.08 Å relative to their respective carbon atoms. Hydrogen atoms were not located for **II**. All non-hydrogen atoms were treated anisotropically and convergence was obtained with maximum shift/esd ratios of 0.47 and 0.154, respectively. For compound **I** the residuals were $R = 0.0380$ and $R_w = (\Sigma w\Delta^2/\Sigma wF_o^2)^{1/2} = 0.0496$. The final difference map had a maximum of +2.3 e Å^{-3} (at 1.05 Å from Pt) and a minimum of −1.7 e Å^{-3}. Corresponding figures for **II** were $R = 0.0940$, $R_w = 0.0763$, max = +0.64 e Å^{-3} (0.96 Å from Pd), min = −0.61 e Å^{-3}. Neither difference map gave any indication that any material had been overlooked. For compound **II** the molecular symmetry was $\bar{1}$ and for the coordinates given in Table 5 the centre of inversion is located at (1/2, 0, 0).

Acknowledgements

We thank the Natural Sciences and Engineering Research Council of Canada and the University of Victoria for research grants, and Mrs. C. Greenwood for recording nmr spectra.

1. L. MAIER. Prog. Inorg. Chem. **5**, 27 (1963).
2. E. P. KYBA, R. E. DAVIS, C. W. HUDSON, A. M. JOHN, S. B. BROWN, M. J. MCPHAUL, L. K. LIU, and A. C. GLOVER. J. Am. Chem. Soc. **103**, 3868 (1981).
3. R. BARTSCH, S. HIETKAMP, S. MORTON, and O. STELZER. Angew. Chem., Int. Ed. Engl. **21**, 375 (1982).
4. D. M. ROUNDHILL, R. P. SPERLINE, and W. B. BEAULIEU. Coord. Chem. Rev. **26**, 263 (1978).
5. E. H. WONG and F. C. BRADLEY. Inorg. Chem. **20**, 2333 (1981).
6. G. M. GRAY and C. S. KRAIHANZEL. J. Organomet. Chem. **146**, 23 (1978).
7. E. H. WONG, L. PRASAD, E. J. GABE, and F. C. BRADLEY. J. Organomet. Chem. **236**, 321 (1982).
8. G. M. GRAY and C. S. KRAIHANZEL. J. Organomet. Chem. **238**, 209 (1982).
9. J. A. S. DUNCAN, D. HEDDEN, D. M. ROUNDHILL, T. A. STEPHENSON, and M. D. WALKINSHAW. Angew. Chem., Int. Ed. Engl. **21**, 452 (1982).
10. J. A. S. DUNCAN, T. A. STEPHENSON, W. B. BEAULIEU, and D. M. ROUNDHILL. J. Chem. Soc. Dalton Trans. 1755 (1983).
11. K. R. DIXON and A. D. RATTRAY. Can. J. Chem. **49**, 3997 (1971).
12. D. E. BERRY, G. W. BUSHNELL, K. R. DIXON, and A. PIDCOCK. Inorg. Chem. **22**, 1961 (1983).
13. K. R. DIXON and A. D. RATTRAY. Inorg. Chem. **16**, 209 (1977).
14. J. CHATT and B. T. HEATON. J. Chem. Soc. A, 2745 (1968).
15. C. S. KRAIHANZEL and C. M. BARTISH. J. Am. Chem. Soc. **94**, 3572 (1972).
16. T. E. AUSTIN. Ph.D. Thesis. University of North Carolina. 1966.
17. G. W. BUSHNELL, R. J. DENSMORE, K. R. DIXON, and A. C. RALFS. Can. J. Chem. **61**, 1132 (1983).
18. D. V. NAIK, G. J. PALENIK, S. JACOBSON, and A. J. CARTY. J. Am. Chem. Soc. **96**, 2286 (1974).
19. M. C. CORNOCK, R. O. GOULD, C. L. JONES, and T. A. STEPHENSON. J. Chem. Soc. Dalton Trans. 1307 (1977).
20. F. A. COTTON, L. R. FALVELLO, M. TOMAS, G. M. GRAY, and C. S. KRAIHANZEL. Inorg. Chim. Acta, **82**, 129 (1984).
21. R. FAWZI, W. HILLER, I. P. LORENZ, J. MOHYLA, and C. ZEIHER. J. Organomet. Chem. **262**, C43 (1984).
22. D. E. C. CORBRIDGE. The structural chemistry of phosphorus. Elsevier, Amsterdam. 1974.
23. G. H. STOUT and L. H. JENSEN. X-ray structure determination, a practical guide. MacMillan, New York. 1968. p. 303.
24. J. BROWNING, G. W. BUSHNELL, and K. R. DIXON. Inorg. Chem. **20**, 3912 (1981).
25. F. R. HARTLEY. The chemistry of platinum and palladium. Applied Science, London. 1973. (*a*) pp. 473–490; (*b*) p. 462.
26. R. D. WILSON, Y. KAMITORI, H. OGUSHI, Z. I. YOSHIDA, and J. A. IBERS. J. Organomet. Chem. **173**, 199 (1979).
27. W. L. STEFFEN and G. J. PALENIK. Inorg. Chem. **15**, 2432 (1976).
28. L. L. MARTIN and R. A. JACOBSON. Inorg. Chem. **10**, 1795 (1971).
29. R. G. KIDD and R. J. GOODFELLOW. *In* NMR and the Periodic Table. *Edited by* R. K. Harris and B. E. Mann. Academic Press, London. 1978. p. 249.
30. D. T. CROMER and J. T. WABER. *In* International tables for X-ray crystallography. Vol. IV. *Edited by* J. A. Ibers and W. C. Hamilton. Kynoch Press, Birmingham, England. 1974. pp. 99, 148.
31. J. X. MCDERMOTT, J. F. WHITE, and G. M. WHITESIDES. J. Am. Chem. Soc. **98**, 6521 (1976).
32. R. J. GOODFELLOW and L. M. VENANZI. J. Chem. Soc. 7533 (1965).
33. R. J. HAINES, A. PIDCOCK, and M. SAFARI. J. Chem. Soc. Dalton Trans. 830 (1977).
34. G. M. SHELDRICK. SHELX-76. A computer program for crystal structure determination. University of Cambridge, Cambridge, England. 1976.
35. C. K. JOHNSON. ORTEP: A Fortran thermal ellipsoid plot program for crystal structure illustrations. ORNL-3794, Oak Ridge National Laboratory, Oak Ridge, U.S.A. 1965.

L'*o*-nitrobenzylidènediméthylsulfuranne: synthèse, réactivité

YANNICK LE STANC ET MAURICE LE CORRE[1]
Laboratoire de Synthèse Organique, UA CNRS 415, Avenue du Général Leclerc, 35042 Rennes Cédex, France

Reçu le 9 novembre 1984

YANNICK LE STANC ET MAURICE LE CORRE. Can. J. Chem. **63**, 2958 (1985).

Le bromure d'*o*-nitrobenzyldiméthylsulfonium et l'ylure correspondant sont des composés très instables qui évoluent, en milieu aqueux, en donnant selon les conditions: l'alcool *o*-nitrobenzylique, le sulfure d'*o*-nitrobenzyle ou le sulfure de méthyle et d'*o*-hydroxyméthylbenzyle. L'accès aux *o*-nitrophényloxirannes est possible, avec les aldéhydes, dans un système biphasique soude aqueuse/dichlorométhane.

YANNICK LE STANC AND MAURICE LE CORRE. Can. J. Chem. **63**, 2958 (1985).

In aqueous solution, *o*-nitrobenzyldimethylsulfonium bromide and the corresponding ylid give, depending upon the conditions, *o*-nitrobenzyl alcohol, *o*-nitrobenzylsulfide, or methyl *o*-hydroxymethylbenzyl sulfide. The *o*-nitrophenyloxiranes may be obtained by the reaction of nitrobenzylidenedimethylsulfurane with aldehydes in a two-phase aqueous sodium hydroxide/dichloromethane system.

Bien que les *o*-nitrophényloxirannes aient été signalés à plusieurs reprises dans la littérature (1), la voie d'accès la plus générale, qui consiste à partir de l'*o*-nitrobenzylidène sulfuranne, n'a jamais été décrite. Dans le cadre de nos recherches en série indolique, nous avons été amenés à préparer et à étudier le comportement du sel de sulfonium **1** et de l'ylure correspondant.

Cette étude a révélé que le sel **1** ne conduit pas aux oxirannes dans les conditions habituelles (action d'une base puis d'un dérivé carbonylé dans un solvant anhydre) par suite notamment d'une réaction concurrente mettant en jeu le groupement NO_2. L'analyse du produit réactionnel obtenu lors des différents essais préliminaires a révélé que le sel de sulfonium **1** est susceptible d'évoluer en milieu aqueux, selon plusieurs directions que l'on peut contrôler en modifiant la concentration et le pH du milieu. L'hydrolyse du sel **1** conduit essentiellement

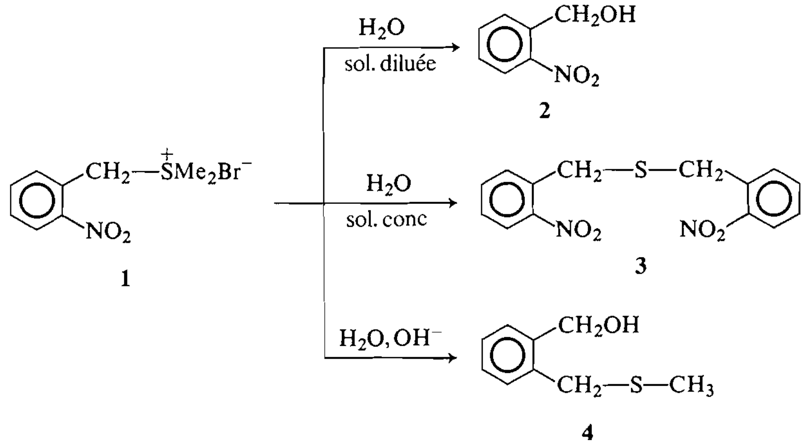

SCHÉMA 1

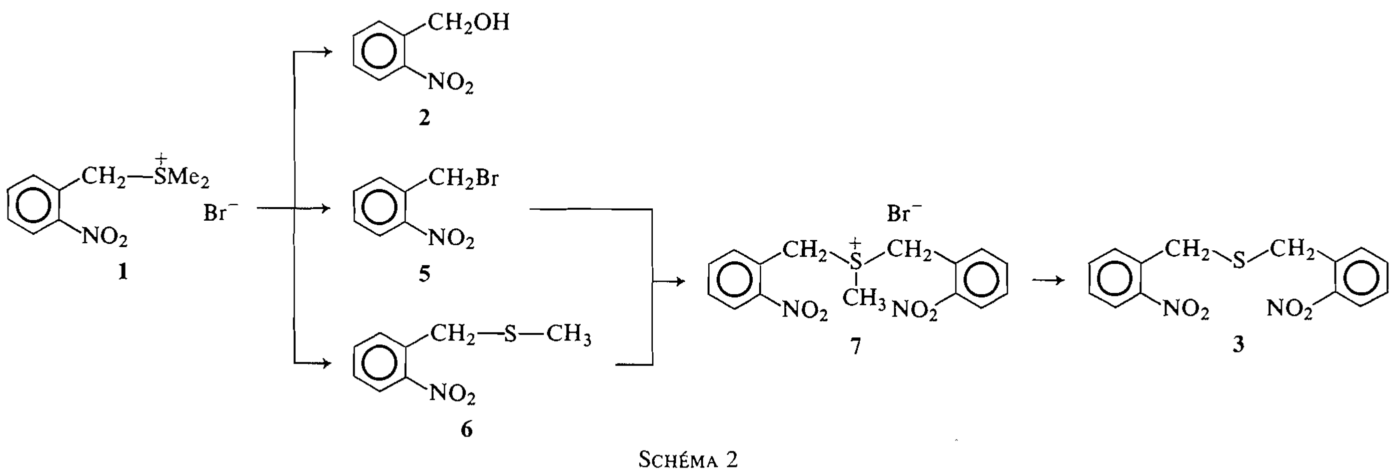

SCHÉMA 2

[1]Auteur à qui adresser la correspondance.

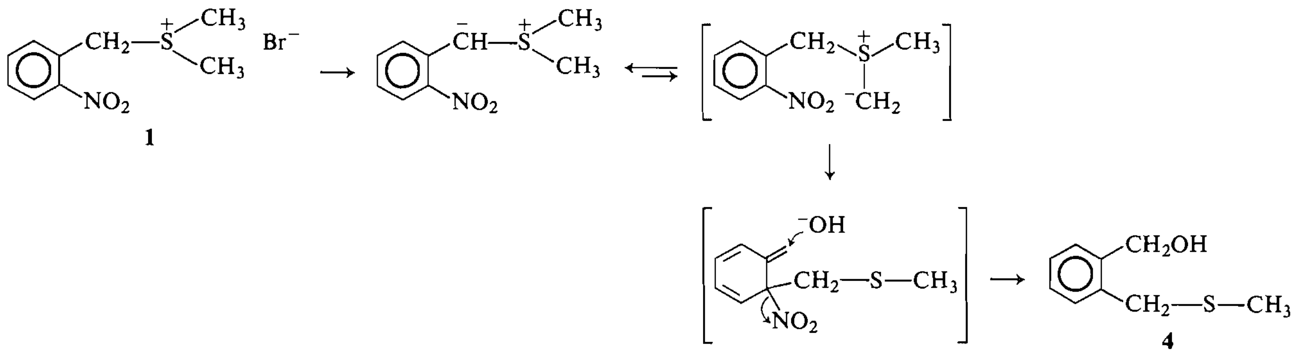

SCHÉMA 3

(schéma 1) à l'alcool *o*-nitrobenzylique **2** en solution diluée, au sulfure d'*o*-nitrobenzyle **3** en solution concentrée et au sulfure alcool **4** en milieu basique.

Interprétation

La différence d'évolution en fonction des conditions expérimentales peut s'interpréter (schéma 2) en admettant que: (*i*) en milieu dilué, la réaction principale est une hydrolyse qui conduit majoritairement à **2**; (*ii*) en milieu concentré l'attaque par les ions Br^-, présents en quantité importante, devient prépondérante et mène à un mélange des dérivés **5** et **6**.

L'hypothèse d'une hydrolyse du sulfure **6** en alcool **2** qui aurait pu expliquer la différence d'orientation de la réaction a été écartée; le sulfure **6** est en effet inattaqué après 18 h de reflux dans une solution aqueuse bromhydrique 1 *N*.

À partir de ces deux composés, la formation du sulfure **3** résulterait d'une alkylation du sulfure **6** par le dérivé bromé **5** suivie d'une hydrolyse de ce nouveau sel **7** en sulfure **3**. Il convient de remarquer que le problème de la régiosélectivité de l'hydrolyse n'intervient pas lors de cette dernière étape, puisque l'attaque du méthylène benzylique redonne les produits de départ.

La formation, tout à fait inattendue, du dérivé **4** peut s'interpréter par un réarrangement de Sommelet–Hauser au cours duquel le méthylène-cyclohexadiène intermédiaire évolue sous l'action de OH^- avec élimination du groupement NO_2 (schéma 3).

Ce résultat est à rapprocher des observations très récentes de Ta-Jyh Lee et Holts relatives aux sels de sulfonium *o*-chlorés (2) (schéma 4):

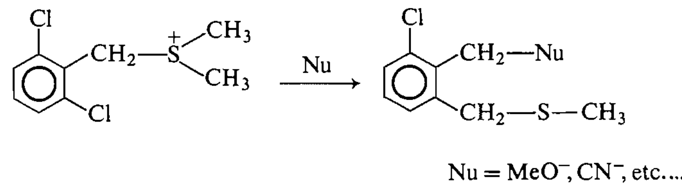

SCHÉMA 4

Il convient de noter que, dans le cas des dérivés chlorés la réaction d'élimination n'est possible que si la position *ortho* est également substituée par Cl ou SO_3R. Le résultat obtenu avec l'*o*-nitrobenzylidènesulfuranne confirme donc les excellentes propriétés nucléofuges du groupement NO_2, déjà observées dans d'autres réactions (3).

L'accès aux *o*-nitrophényloxirannes est cependant possible à partir du sel **1** si on libère l'ylure en présence du dérivé carbonylé, dans un système biphasique CH_2Cl_2/NaOH concentrée. En raison de l'instabilité de l'ylure, seuls les aldéhydes conduisent aux oxirannes (voir tableau 1). La stabilisation apportée par le groupement NO_2 est suffisante pour que, dans le cas de l'acroléine, la condensation évolue vers le formyl-cyclopropane (schéma 5):

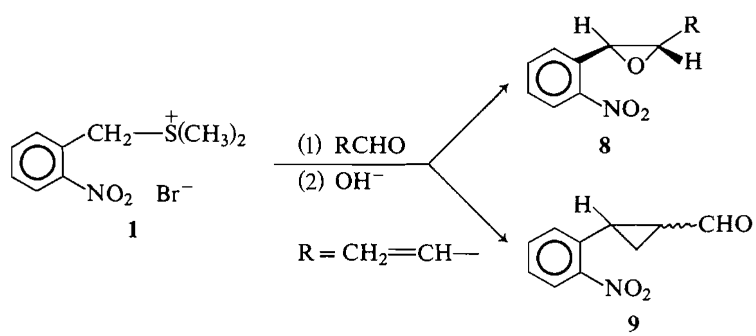

SCHÉMA 5

L'analyse par rmn ^{1}H du système époxydique (voir tableau 1) montre que la réaction est stéréospécifique et conduit exclusivement au composé *trans*.

La cyclopropanation, non stéréospécifique, conduit à un mélange *E*/*Z* dans le rapport 75:25.

Partie expérimentale

Les points de fusion ont été déterminés au banc Kofler. Sauf indication contraire, les spectres rmn ont été réalisés dans $CDCl_3$ avec comme référence le TMS. Spectres de rmn ^{1}H: Varian EM-360 L, spectres de masse: Varian MAT 311.

*Bromure d'*o*-nitrobenzyldiméthylsulfonium 1*

A 21,6 g (0,1 mol) d'α-bromo *o*-nitrotoluène dans 20 mL de chloroforme on ajoute 12,4 g (0,2 mol) de sulfure de méthyle. Après 24 h à 50°C, le sel de sulfonium, qui cristallise, est filtré, rincé avec 2 fois 5 mL de chloroforme et séché; Rtd: 96%; *F*(°C): 89–90; rmn ^{1}H

TABLEAU 1. *o*-Nitrophényl oxirannes 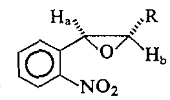

Composé	R	Rdt (%)	F(°C)	Litt.	H_a^*	H_b^*	J_{ab} (Hz)
8*a*	H	42	63−64	65(4)	4,46	2,60	2
8*b*	Phényl	92	98−100	101−102(5)	4,46	3,73	2
8*c*	Furyl-2	94	46−47	—	4,90	3,73	2
8*d*	*p*-Nitrophényl	83	165	160−162(5)	4,42	3,86	2

*δ en ppm par rapport au TMS dans $CDCl_3$.

(D_2O): CH_3 à 2,05 (s, 6H), CH_2 à 4,10 (s, 2H), protons aromatiques de 6,8−7,5 (m, 4H). *Anal.* calc. pour $C_9H_{12}BrNO_2S$: C 38,84, H 4,31, Br 28,77; tr.: C 38,61, H 4,19, Br 28,62.

Alcool o-*nitrobenzylique 2*

On porte à reflux pendant 24 h une solution de 2,78 g (0,01 mol) de sel de sulfonium dans 150 mL d'eau. Le produit brut, obtenu par extraction au dichlorométhane et évaporation du solvant, est purifié par chromatographie sur acide silicique (70−230 mesh; dichlorométhane−éther 95:5); Rdt: 77%; F(°C): 71−72 (litt. (6) F 74°C); rmn ^{1}H: O—H à 3,20 (s, 1H), CH_2 à 5,06 (s, 2H), protons aromatiques à 7,2−8,1 (m, 4H).

*Sulfure d'*o-*nitrobenzyle 3*

On porte à reflux pendant 24 h une solution de 5,56 g (0,02 mol) de sel de sulfonium **1** dans 10 mL d'eau. Le produit brut obtenu par extraction au dichlorométhane, est dissout dans 30 mL d'éthanol au reflux. Le sulfure **4** cristallise au refroidissement, il est alors filtré et séché; Rdt: 48%; F(°C): 120−122; rmn ^{1}H: CH_2 à 4,10 (s, 4H), protons aromatiques à 7,3−8,1 (m, 8H). Spectre de masse: M calculée pour $C_{14}H_{12}N_2O_4S$: 304,052; trouvée: 304,051.

*Sulfure de méthyle et d'*o-*hydroxyméthyl benzyle 4*

On porte à reflux pendant 2 h une solution de 5,56 g (0,02 mol) de sel de sulfonium **1** dans 50 mL de soude 1 N. Après extraction au dichlorométhane et évaporation du solvant, on isole, à partir du mélange obtenu, le sulfure **5** par chromatographie sur acide silicique (70−230 mesh; dichlorométhane); Rdt: 45%; $E_{0,6}$ = 114−115°C; rmn ^{1}H: CH_3 à 1,97 (s, 3H), O—H à 3,10 (s, 1H), SCH_2 à 3,73 (s, 2H), OCH_2 à 4,70 (s, 2H), protons aromatiques à 7,2−7,5 (m, 4H). Spectre de masse: M calculée pour $C_9H_{12}OS$: 168,253; trouvée: 168,252.

o-*Nitrophényl-2 oxiranne 8*a

À une suspension de 13,9 g (0,05 mol) de sel de sulfonium **1** dans 25 mL de dichlorométhane et 4 mL d'une solution aqueuse de formaldéhyde à 37%, on ajoute sous vive agitation magnétique 37,5 mL de soude 10 N; la coloration mauve d'ylure apparaît aussitôt. Après disparition de la coloration de l'ylure (10 min environ) l'ensemble est dilué par addition de 30 mL d'eau, puis extrait par 2 fois 30 mL de dichlorométhane. La phase organique décantée est concentrée à l'évaporateur rotatif et l'huile obtenue distillée sous pression réduite; Rdt: 42%; $E_{0,5}$ = 94−96°C; F(°C): 63−64 (litt. (4) F 65°C); rmn ^{1}H: protons époxydiques à 3,26 (q, 1H, J_{AM} = 6 Hz, J_{AX} = 4 Hz), 2,60 (q, 1H, J_{AM} = 6 Hz, J_{MX} = 2 Hz), 4,46 (q, 1H, J_{AX} = 4 Hz, J_{MX} = 2 Hz), protons aromatiques à 7,1−8,13 (m, 9H).

o-*Nitrophényl-2 phényl-3 oxiranne 8*b

À une suspension de 13,9 g (0,05 mol) de sel de sulfonium **1** dans 25 mL de dichlorométhane contenant 0,075 mol d'aldéhyde on ajoute, sous vive agitation magnétique 40 mL de soude 10 N. Après 2 h à température ambiante, l'ensemble est dilué par addition de 30 mL d'eau, puis extrait par 2 fois 30 mL de dichlorométhane. La phase organique obtenue après décantation est constituée presque exclusivement de l'époxyde et d'aldéhyde en excès. Après élimination de l'aldéhyde par distillation sous pression réduite l'*o*-nitrophényl-2 phényl-3 oxiranne cristallise; Rdt: 92%; F(°C) éthanol: 98−100 (litt. (5) F 101−102°C); rmn ^{1}H: protons époxydiques à 3,73 (d, 1H, ^3J = 2 Hz) et 4,46 (d, 1H, ^3J = 2 Hz), protons aromatiques à 7,1−8,13 (m, 9H).

(Furyl-2)-2 o-*nitrophényl-3 oxiranne 8*c

"Mode opératoire" identique au précédent; Rdt: 94%; F(°C) hexane: 46−47; rmn ^{1}H: protons époxydiques à 3,73 (d, 1H, ^3J = 2 Hz) et 4,9 (d, 1H, ^3J = 2 Hz), protons furyliques à 6,36−6,66 (m, 2H), protons aromatiques à 7,2−8,3 (m, 5H). *Anal.* calc. pour $C_{12}H_9NO_4$: C 62,33, H 3,89, N 6,06; tr.: C 62,15, H 3,75, N 6,01.

o-*Nitrophényl-2* p-*nitrophényl-3 oxiranne 8*d

"Mode opératoire" identique à celui utilisé pour la préparation de **8***b* et **8***c*. Le produit réactionnel brut, obtenu après évaporation du solvant, est dissout dans 30 mL d'éthanol; l'*o*-nitrophényl-1 *p*-nitrophényl-3 oxiranne cristallise au refroidissement; il est ensuite filtré et séché; Rdt: 83%; F(°C): 165 (litt. (5) F 160−162°C); rmn ^{1}H: protons époxydiques à 3,86 (d, 1H, ^3J = 2 Hz) et 4,42 (d, 1H, ^3J = 2 Hz), protons aromatiques à 7,3−8,5 (m, 8H).

Formyl-1 o-*nitrophényl-2 cyclopropane 9*

À une solution de 4,2 g d'acroléine (0,075 mol) dans 25 mL de dichlorométhane, on ajoute 13,9 g (0,05 mol) de sel de sulfonium **1**, puis sous vive agitation, 40 mL de soude 1 N.

Après disparition de la coloration de l'ylure (10 min environ), on ajoute 30 mL d'eau, décante la phase organique puis extrait deux fois la phase aqueuse au dichlorométhane (60 mL). La phase organique est concentrée à l'évaporateur rotatif et l'huile obtenue distillée sous pression réduite; Rdt 83%; $E_{0,5}$ = 134°C; rmn ^{1}H: protons cyclopropaniques de 1,3 à 3,3 (m, 4H), protons aromatiques de 7,1 à 8,1 (m, 4H), C*H*O *cis* à 9,0 (d, J = 5 Hz), C*H*O *trans* à 9,4 (d, J = 5 Hz). *Anal.* calc. pour $C_{10}H_9NO_3$: C 62,82, H 4,71, N 7,32; tr.: C 62,70, H 4,68, N 7,27.

1. T. WATANABE, F. HAMAGUCHI ET S. OHKI. Chem. Pharm. Bull. **20**, 2123 (1972); W. WIERENGA, A. W. HARRISON, B. R. EVANS et C. G. CHIDESTER. J. Org. Chem. **49**, 438 (1984).
2. TA-JYH LEE et W. J. HOLTS. Tetrahedron Lett. 2071 (1983).
3. J. R. BECK. Tetrahedron, **34**, 2057 (1978).
4. F. ARNDT et W. PARTALE. Chem. Ber. **60**, 446 (1927).
5. O. CHRZESCINSKI. Thèse, Strasbourg (1911).
6. M. P. PIERRON. Bull. Soc. Chim. Fr. 852 (1901).

^{13}C magnetic resonance studies. 119.[1] Tricyclo[3.3.0.0] and [3.2.1.0]octanones from substituted norbornenones via cyclopropanation and homoketonization

ARTHUR J. RAGAUSKAS AND J. B. STOTHERS
Department of Chemistry, University of Western Ontario, London, Ont., Canada N6A 5B7

Received February 5, 1985

ARTHUR J. RAGAUSKAS and J. B. STOTHERS. Can. J. Chem. **63**, 2961 (1985).

Simmons–Smith cyclopropanation of the trimethylsilyl enol ethers of 7-isopropylidene- and two 7-spirocyclopropyl-norbornenones leads directly to the 8-substituted 2-trimethylsilyl ethers of homoquadricyclene. Homoketonization of the unsaturated ether proceeds regiospecifically to the corresponding tricyclo[3.3.0.$0^{2,8}$]octan-4-one while the others give the tricyclo[3.2.1.$0^{2,6}$]octan-4-ones exclusively, all with high stereoselectivity favoring inversion of configuration. This difference in the regiochemistry of homoketonization can be attributed to a directive effect of β-functionalization overcoming thermodynamic control of cleavage.

ARTHUR J. RAGAUSKAS et J. B. STOTHERS. Can. J. Chem. **63**, 2961 (1985).

La réaction de cyclopropanation suivant Simmons–Smith des éthers énoliques triméthylesilyles de l'isopropylidène-7 et de deux spiro-7 cyclopropylnorbornénones conduit directement aux éthers triméthylsilyl-2 de l'homoquadricyclène substitués en position 8. L'homocétonisation de l'éther insaturé est régiospécifique et conduit à la tricyclo[3.3.0.$0^{2,8}$]octanone-4 correspondante tandis que les autres éthers conduisent exclusivement aux tricyclo[3.2.1.$0^{2,6}$]octanones-4; toutes ces réactions se produisent avec une très haute stéréosélectivité qui favorise une inversion de configuration. On attribue la différence de régiochimie dans l'homocétonisation à un effet directif de la fonction en β qui est plus puissant que le contrôle thermodynamique du clivage.

[Traduit par le journal]

Introduction

Our earlier unexpected discovery (1) of quantitative conversion of the trimethylsilyl enol ether of norbornenone (**1**) to tricyclo[3.2.1.$0^{2,7}$]octan-4-one (**2**) prompted us to examine the process in more detail. Specifically, we were interested in potential substituent effects on the course of the second step of the sequence, namely, the base-catalyzed cleavage of the homoquadricyclene addition product **3** formed by cyclopropanation of **1**. Although there are two paths for cleavage of cyclopropoxide **4** formed from **3**, its homoketonization was found to be regiospecific, yielding only **2**. If, however, one could alter the regioselectivity of cleavage to favor formation of tricyclo[3.3.0.$0^{2,8}$]octan-4-one (**5**) analogs, this would provide a new route to the latter system, examples of which have been utilized in a variety of syntheses of natural products (2).

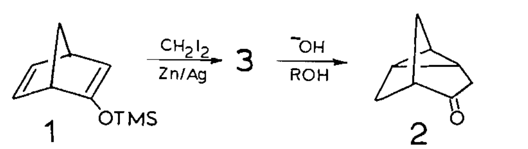

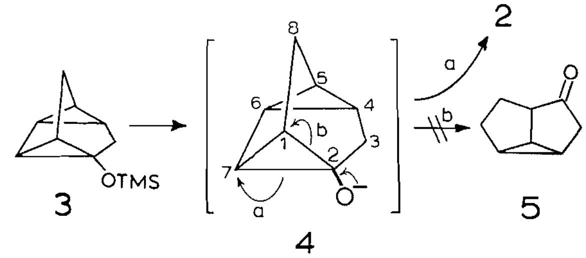

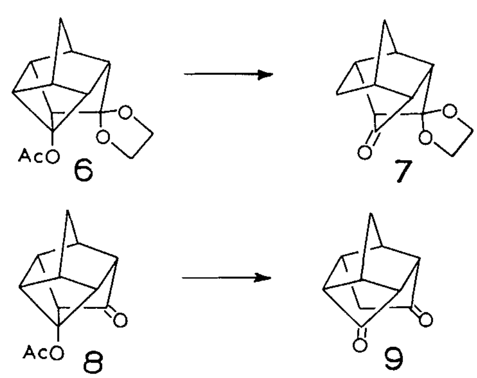

The regioselectivity of homoketonization of several β-enolates, i.e., substituted cyclopropoxides, has been established (3) and the major governing factors found to be relief of strain, product stability, and the stability of the incipient carbanion. Cleavage of β-enolate **4**, by either path a or b, will lead to a secondary carbanion but that formed via a may be stabilized by the adjacent three-membered ring. On the other hand, product stability may be responsible for the remarkable dominance of cleavage by path a. In an attempt to shed additional light on the question, the 8-spirocyclopropyl and 8-isopropylidene derivatives of **4** were selected for study. In the case of the former, the additional cyclopropyl ring could conceivably stabilize the incipient carbanion generated by cleavage analogous to path b in **4**, thereby rendering the two pathways more nearly comparable provided stabilization by the neighboring three-membered ring is a significant factor in these homoketonizations. Introduction of a double bond at C-8 in **4** could be expected to afford even greater stabilization for a developing carbanion at C-1, i.e., via cleavage b, possibly altering the regioselectivity of homoketonization in a major way. Redirection of the homoketonization process has been illustrated. Zwanenburg and co-workers (4) found that while ketal acetate **6** yields **7** exclusively, presumably by thermodynamic control, cleavage of the analog **8** leads regiospecifically to **9**, demonstrating that conjugative stabilization of one of the possible carbanionic intermediates is sufficient to

[1] For Part 118 see ref. 15; for Part 117 see ref. 16; for Part 116 see ref. 17.

alter the regiochemistry of the homoketonization.

A second feature of the homoketonization process concerns the stereoselectivity of protonation of the homoenolate which, in general, is found to be high (3). However, in the case of β-enolates, high degrees of retention and inversion of configuration have been observed and definitive interpretation in terms of the principal governing factor is difficult. Nevertheless, there is some evidence that increasing strain in polycyclic systems causes a shift from predominant inversion to dominant retention. For example, β-enolate **10** opens with >95% inversion while the more strained analog **11** exhibits

10 11

>95% retention (5). Our examination of **4** showed that ketonization proceeds with 92% inversion and, since the introduction of the spirocyclopropyl and isopropylidene substituents undoubtedly increases the strain in the corresponding β-enolates, it was of interest to establish the stereochemistry of homoketonization for the latter cases.

Results and discussion

7-Spirocyclopropylnorbornenone

In the earlier study (1), we found that cyclopropanation of **1** with methylene iodide and a zinc–silver couple led directly to **3**, presumably by facile intramolecular cycloaddition after the initial addition of the methylene group to the enolic double bond. The same treatment of the 7-spirocyclopropyl analog gives an analogous result. Reaction of **12** with lithium diisopropylamide followed by treatment with trimethylsilyl chloride and triethylamine gave the corresponding enol ether in 85% yield. Cyclopropanation afforded an addition product **13**

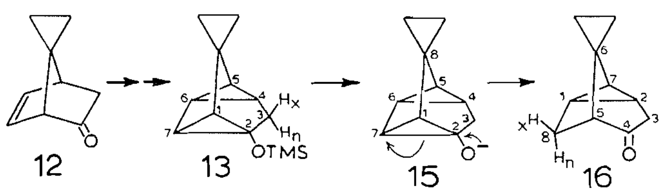

having no olefinic absorption in either the ^{1}H or ^{13}Cmr spectra, and the molecular formula $C_{13}H_{20}OSi$, by precise mass measurement, confirmed the addition of a single methylene group. The ^{13}C spectrum contained three methylene signals (δ_C 5.4, 9.9, 32.1), five methine peaks (20.6, 22.1, 28.3, 31.0, 39.6), two quaternary signals (23.1, 69.6), and trimethylsilyl absorption at δ_C 1.1. On comparison with the results for **4**, these data are consistent with the expected homoquadricyclene structure. Although specific assignments for the spirocyclopropyl methylene carbons could not be made, the signals at δ_C 5.4 and 9.9 were readily attributed to these carbons. The order of linkage of the other carbons was obtained from a double-quantum coherence (INADEQUATE) spectrum (6); these results are summarized in **14** with the J_{CC} values in parentheses.

The proton spectrum provided additional confirmation for structure **13**. The 3-methylene protons appeared at lowest field with the *exo*-proton at δ 2.27, J = 11.7 Hz and the *endo*-proton at δ 2.12, J = 1.5, 5.1, 11.7 Hz. For the latter, the small 1.5-Hz coupling was common to a pattern at δ 1.24 (dt, 1H, J

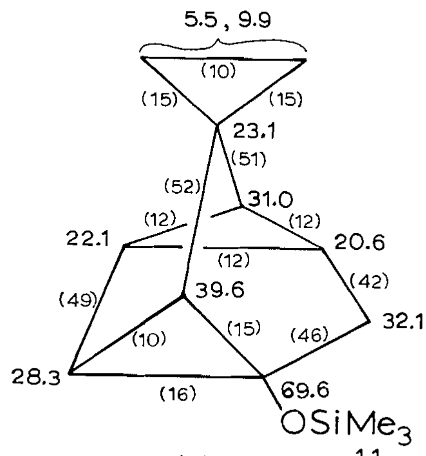

14

= 1.5, 7.3 Hz) ascribable to H-1 which was also coupled to H-7 (dd, δ 1.98, J = 4.3, 7.3 Hz). The absorption for H-6 was found at δ 1.71 (dt, J = 4.3, 6.3 Hz) with H-4 at δ 1.11 (ddd, J = 5.1, 6.3, 8.1 Hz). Irradiation of the two-proton pattern at δ 0.68 collapsed the 8.1-Hz splitting in the H-4 multiplet, a 1.5-Hz coupling for H-1, and a 6.3-Hz splitting for H-6, thereby revealing the approximate position of H-5. The spirocyclopropyl methylene protons absorb at δ 0.37 (m, 2H), 0.68 (m, 1H), and 0.76 (m, 1H) but cannot be individually identified. All of the coupling interactions were confirmed by the appropriate decoupling experiments. Thus, the generation of **13** from **12** through Simmons–Smith cyclopropanation is strictly analogous to the conversion of norbornenone to **3**.

Treatment of **13** with base gave a single ketone in 90% yield having carbonyl absorption (ir 1725 cm^{-1}, δ_C 210.2) indicative of a six-membered ring ketone. In addition to the carbonyl peak, the ^{13}Cmr spectrum contained nine signals: δ_C 4.6, 9.9, 28.0, 33.8 (4 × CH_2), 10.5, 15.9, 21.7, 55.8 (4 × CH), and 24.7 (quat C). While the quaternary and the two highest field methylene signals could be attributed to the spirocyclopropyl group, the remaining signals were in reasonable agreement with expectations for structure **16** by comparison with the data for **2**, indicating that the cleavage of **15** was regiospecific and analogous to that of **3**. Initially, a chemical proof of structure was examined since hydrogenolysis of the three-membered rings in **16** could produce 6,6-dimethylbicyclo[2.2.2]octan-2-one, a known compound. However, hydrogenation of **16** using a platinum oxide catalyst afforded an alcohol and a single new ketone having the molecular formula $C_{10}H_{14}O$, by precise mass measurement. Clearly, only one of the cyclopropyl moieties suffered cleavage. The ^{13}Cmr spectrum contained signals for two methyl (δ_C 26.0, 26.7), two methylene (26.9, 33.4), four methine (10.5, 14.4, 23.5, 58.7), one quaternary (40.8), and a carbonyl carbon (212.1). We conclude that the ketone is 6,6-dimethyltricyclo[3.2.1.0^{2,7}]octan-4-one and, on the basis of its ^{13}C spectrum, the second product appeared to be the corresponding alcohol but was not fully characterized.

Definitive structural proof for **16** was obtained by nmr. To confirm tentative assignments of the ^{13}C signals an INADEQUATE spectrum was obtained and the results are summarized in **17**. Supporting evidence was provided by the ^{1}Hmr spectrum. The 3-methylene protons absorbed at lowest field, δ 2.65 (ddd, J = 0.8, 2.6, 20.0 Hz) and 2.57 (dd, J = 2.6, 20.0 Hz), readily identified by the 20.0-Hz geminal coupling. Doublets at δ 1.87 (J = 12.6 Hz) and 1.75 (J = 5.6 Hz) were assigned to *endo*-H-8 and H-5, respectively, since both have approxi-

TABLE 1. Cyclopropanation experiments with **19**

Temperature	Expt.	Time (h)	Molar ratio (CH_2I_2)/**19**	[**19**] ($M \times 10^{-1}$)	Product composition (%)[a] **20**	**21**	**18**
Reflux (38°C)	1	21	1.2	3.4	75	25	—
	2	18	1.9	3.0	50	50	—
	3	20	2.8	3.2	15	85	—
20°C	4	22	1.2	2.6	60	—	40
	5	24	1.2	3.2	75	—	25
	6	28	1.2	4.2	33	33	33

[a]Estimated by ^{13}Cmr (±5%).

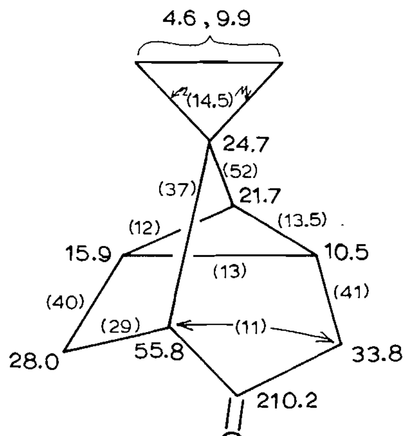

17

mately 90° dihedral angles with one of two vicinal neighbors. A multiplet at δ 2.23 containing splittings of 12.6, 5.6, 3.4, and 0.8 Hz must arise from *exo*-H-8 with the smallest coupling representing a long-range interaction with one of the 3-protons. A triplet of triplets at δ 1.11 (J = 2.6, 7.5 Hz) was readily assigned to H-2, with the larger coupling identifying the interaction with H-7, δ 0.90 (dd, J = 5.7, 7.5 Hz), and H-1, which gave rise to the remaining one-proton multiplet at δ 1.55 containing couplings of 7.5 (H-2), 5.7 (H-1), and 3.4 Hz (*exo*-H-8). A complex four-proton multiplet, δ 0.35–0.65, accounted for the four spirocyclopropyl methylene protons. Appropriate decoupling experiments confirmed each of the interactions noted.

The identification of **16** shows that the homoketonization of **13** is the same as that of **3**; clearly, the additional cyclopropyl ring does not affect the regiochemistry of cleavage.

7-Isopropylidenenorbornenone

Enol ether **19** was prepared from 7-isopropylidenenorbornenone in 80% yield and, upon reaction with methylene iodide and a zinc–silver couple under conditions similar to those employed to generate **13**, gave a 50:50 mixture of two products in >90% yield. The composition of the mixture was assessed by ^{13}Cmr spectroscopy since the product decomposed upon attempted analysis by gas–liquid chromatography (FFAP, SE-30, and Carbowax) even with the use of new columns that was essential for success with **13**. The ^{13}C spectrum of the mixture contained signals for two non-protonated olefinic carbons (δ_C 121.0, 133.3), four quaternary carbons, two of which bear oxygen (17.4, 33.6, 70.1, 70.9), and three methylene carbons (25.0, 32.8, 33.0), together with six methyl and ten methine carbon peaks. These data indicated that initial cyclopropanation of the enolic double bond followed by intramolecular cycloaddition indeed occurred, but approximately half of this product underwent a second cyclopropanation at the isopropylidene double bond, i.e. **19** → **20** → **21**.

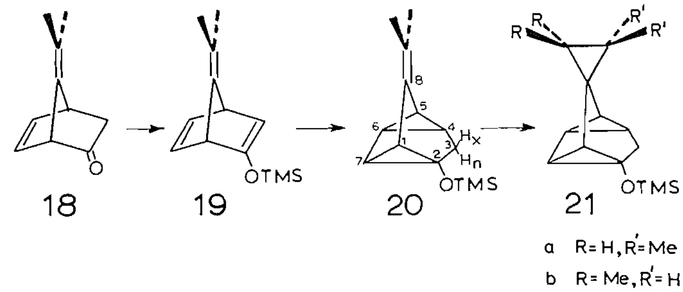

To obtain support for this suggestion, the reaction was repeated using a larger excess of methylene iodide and the resulting product gave rise to the same sets of ^{13}C signals with the important difference that the product ratio was 1:7, favoring the component lacking olefinic absorption. The ^{13}C spectrum for the major product included signals for five methyl (δ_C 1.5 (3), 24.2, 25.4), two methylene (25.0, 33.0), five methine (20.3, 22.7, 29.6, 29.9, 38.4), and three quaternary carbons (17.4, 33.6, 70.1). On comparison with the data for **13**, these results appeared to be consistent with structure **21**. Repetition of the reaction using a small excess of methylene iodide gave the same products in a 3:1 ratio favoring the unsaturated component, the ^{13}C spectrum of which included five methyl (δ_C 1.2 (3), 21.8, 22.0), one methylene (32.8), five methine (21.7, 24.9, 26.8, 30.4, 36.4), and three fully-substituted carbon signals (70.9, 121.0, 133.3). These data are consistent with structure **20** for the monocyclopropanated product. From the ratios of the products obtained with varying amounts of methylene iodide, it appeared that the second cyclopropanation was significantly slower than the initial methylene addition to the enolic double bond. Consequently, some experiments at lower temperature, varying the concentration of **19**, were carried out. Conditions were found that gave only the unsaturated addition product in 75% yield, contaminated with starting material according to the ^{13}C spectrum. The results of various trials are summarized in Table 1. Our tentative structural assignments for adducts **20** and **21** were confirmed by homoketonization experiments.

Upon treatment with base, the unsaturated adduct **20** gave rise to a single new ketone **22** whose carbonyl absorption (ir 1747 cm^{-1}, δ_C 224.1) indicated the presence of a cyclopentanone moiety. The molecular formula is $C_{11}H_{14}O$ by precise mass measurement. The ^{13}Cmr spectrum contained, in addition to the carbonyl signal, absorptions for two equivalent methyl (δ_C 21.6), two methylene (35.4, 43.1), four methine

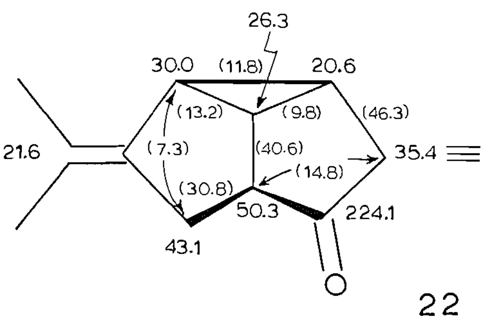

22

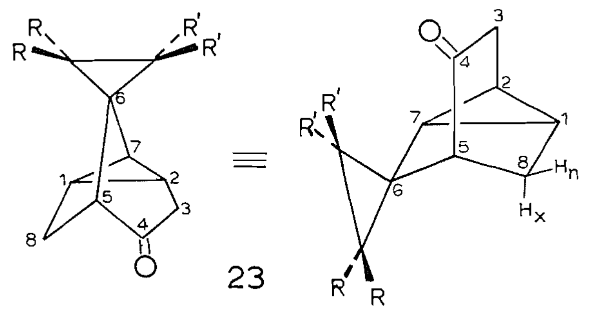

23

a R=H, R'=Me

b R=Me, R'=H

(20.6, 26.3, 30.0, 50.3), and two fully-substituted olefinic carbons (126.5, 129.8); these data are consistent with structure **22** and this was confirmed by the results of an INADEQUATE spectrum. For this purpose, the reaction was repeated on a preparative scale using 700 mg of **19**; **22** was isolated in 67% yield by flash chromatography. Although **20** was contaminated with ketone **18** because of the relatively mild conditions employed for the cyclopropanation, it was found that **18** does not survive the basic conditions required for homoketonization, as expected (7), and the purification of **22** presented no difficulty. The $^{13}C-^{13}C$ coupling constants observed for the sp^3 carbons clearly established their order of linkage and are summarized in parentheses with the formula. The geminal couplings between the carbons flanking the sp^2 centres provided additional confirmatory evidence.

From these results it became clear that the conversion of **19** → **20** by Simmons–Smith cyclopropanation is strictly analogous to that found previously for the parent system **1** → **3**. Although homoketonization of each of **3** and **20** is regiospecific with each yielding a single ketone, different bonds open in the two homoquadricyclene species. The C-2,-7 bond is cleaved exclusively in the parent β-enolate **4** but only the C-1,-2 bond is opened in the isopropylidene derivative. For the latter, a developing carbanion at C-1 can be stabilized by the neighboring double bond since it is an allylic system. Apparently this is sufficient to change the course of the cleavage to furnish the [3.3.0.0] ketone **22** exclusively. It is interesting that a single ketone is observed since, in principle, the 7-isopropyl-Δ^6-isomer of **22** could arise from the allylic carbanion. However, the isomeric structure with an endocyclic double bond may be considerably more strained than its exocyclic counterpart **22**. In any event, the marked difference in the regiochemistry of homoketonization for **4** and **20** is neatly accounted for by increased stabilization of the incipient carbanion leading to **22**.

The cyclopropanation experiments with **19** at reflux temperature (Table 1) gave a mixture of two adducts that, upon homoketonization with base, furnished a corresponding mixture of two ketones, separable by glc. One of the products was **22** while the second, **23**, appeared to contain a six-membered ring ketone (ir 1725 cm^{-1}, δ_C 210.8). The molecular formula $C_{12}H_{16}O$, by precise mass measurement, confirmed the addition of two methylene groups to **19** and its ^{13}Cmr spectrum exhibited, in addition to the carbonyl peak, two methyl (δ_C 22.7, 23.5), three methylene (22.2, 29.3, 34.2), four methine (10.4, 15.8, 20.0, 53.8), and two quaternary signals (17.0, 33.0). Many of these shieldings are remarkably similar to those found for **16**, thus leading to structure **23**. Additional support for this structural assignment was obtained from the proton spectrum. Two nearly equivalent protons δ 2.54 and 2.57, J_{AB} = 20 Hz were easily assigned to the 3-protons, each of which was coupled by 2 Hz to a proton whose absorption was part of a complex two-proton multiplet, 0.98–1.17 ppm. Clean doublets at δ 1.87 (J = 12.4 Hz) and 2.07 (J = 5.8 Hz) clearly arose from *endo*-H-8 and H-5, respectively. An eight-line pattern at δ 2.25 (J = 3.1, 5.8, 12.4 Hz) readily accounted for *exo*-H-8 which, in addition to its interactions with H-5 (5.8 Hz) and *endo*-H-8 (12.4 Hz), is coupled to H-1 (3.1 Hz). The latter nucleus gave rise to a six-line pattern at δ 1.85 (dt, J = 3.1, 6.8 Hz) with the larger splitting attributable to coupling with H-2 and -7, which appear as a multiplet near δ 1.0. Finally, the spectrum contained methyl singlets at δ 1.03 and 1.17 together with a clean AB pattern for the cyclopropyl methylene protons, δ_A 0.28, δ_B 0.42, J_{AB} = 4.6 Hz. Each of the couplings noted above was confirmed by spin-decoupling experiments. Thus, homoketonization of **21** follows the same course as that found for **3** and **13**.

From the foregoing results, it was apparent that the second cyclopropanation furnishing **21** is stereospecific and it remained to distinguish between the two possible adducts **21***a* and *b*. Molecular models indicated that methylene addition leading to **21***b* may be hindered by the *exo*-3-hydrogen of **20**. On the other hand, the well-known ability of neighboring oxygen to direct methylene transfer could facilitate the formation of **21***b* but the oxygen in **20** may be too far from the double bond to influence the reaction course. To determine the position of the geminal methyl groups in **23**, the composition of the product obtained by LAH reduction was compared with that from **16**. The ratio of epimeric alcohols produced from **23***b* and **16** would be expected to be similar and distinctly different from that formed from **23***a* in which the geminal methyls can hinder the approach of the hydride donor to the *syn* face of the carbonyl group. Upon treatment with LAH, **16** gave an 85:15 mixture of two alcohols while a 95:5 mixture of alcohols was obtained from **23**. The ^{13}Cmr spectra of the alcohols formed from **16** indicate that hydride donation occurred preferentially at the face of the carbonyl group away from the spirocyclopropyl grouping. The major alcohol **24** gave rise to four methylene carbon signals, δ_C 5.0, 7.5, 30.4$_1$, 30.3$_8$, which may be compared with the corresponding signals for the minor alcohol **25** at δ_C 4.9, 10.9, 23.2, 28.3. In each case, the two signals at highest field arise from the spirocyclopropyl methylene carbons and the 7-ppm upfield shift found for one of the remaining methylene signals in the minor isomer must be due to a shielding effect of the hydroxyl group. Hence the hydroxyl is *syn* to C-8 in the minor isomer and *anti* in the major product **24**, which is consistent with preferential hydride donation to **16** from the less hindered side. The ^{13}C spectrum of the major alcohol **26** from **23** contained methylene absorption at δ_C 24.1, 30.5, and 31.3, of which the most shielded signal arises from the spirocyclopropyl group. The near-equivalence of the remaining two methylene carbons is comparable to the situation in **24** and, therefore, we conclude that the hydroxyl group is *anti* to C-8 as shown in **26**. The difference in the ratio of the two alcohols formed from **16** and **23** indicates a greater difference in hindrance to the approach of the hydride donor in **23**, and, hence, we conclude that the geminal methyl groups are *syn* to C-4 bearing the hydroxyl group. This conclusion was supported by the results of a shift reagent study, which revealed that the quaternary carbon bearing the geminal methyls was distinctly more sensitive to added $Pr(fod)_3$ than the spirocyclopropyl methylene carbon. It was also found that the methylene carbon at δ_C 30.5 moved upfield at twice the rate of that at 31.5, confirming their assignments to C-3 and -8, respectively. The greater sensitivity of one of the methyl carbons to added shift reagent led to the methyl assignments shown in **26**.

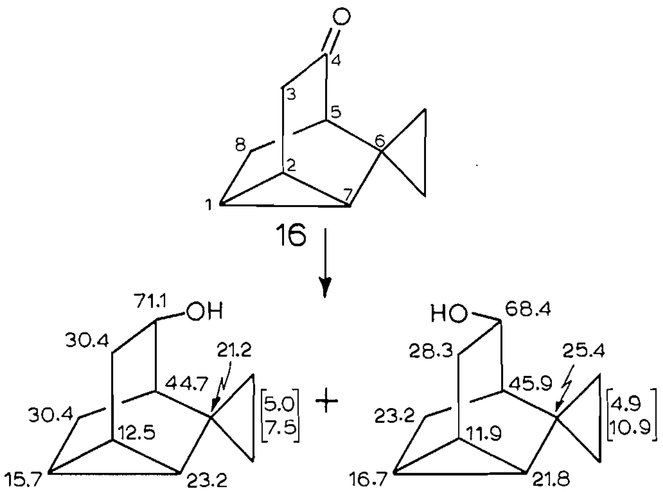

16 → **24** + **25**

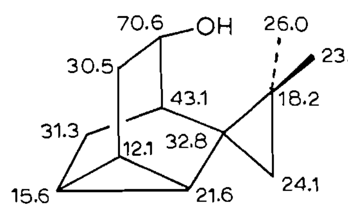

26

Stereochemistry of homoenolization

Our earlier examination of the homoketonization of **3** revealed that the resulting cyclopropoxide **4** opened with high stereoselectivity (92 ± 1%) favoring inversion of configuration at C-7. As noted in the Introduction, it was of interest to learn whether the increased strain of the spirocyclopropyl and isopropylidene analogs **13**, **21***a*, and **20**, respectively, would affect the stereochemistry of ring opening. To examine this feature, their ketonizations were carried out in deuterated media.

Treatment of **13** with KOD/*t*-BuOD at room temperature furnished **16**-d_x containing 1.80 atoms ^{2}H/molecule by mass spectrometry. The ^{2}Hmr spectrum revealed four sites of deuterium incorporation for which the relative amounts were determined by integration. The ^{2}H signals, with their ^{2}H content, were found at δ 2.64 (0.60), 2.55 (0.40), 2.24 (0.725), 1.88 (0.065), which, from the analysis of the ^{1}H spectrum, are due to deuterons at C-3 and C-8. The relative intensities of the higher field pair of signals which arise from the *exo*- and *endo*-8-deuterons show that the stereochemistry of ring opening in **15** is the same as that found for **4** (1), strongly favoring inversion of configuration at C-7 (92 ± 1%).

As a sidelight, the 3:2 intensity ratio found for the lower field pair of signals shows that α-exchange in **16**, occurring upon its formation, apparently favors the less shielded site. In the ^{1}H spectrum, described earlier, this proton exhibits a 0.8-Hz coupling with *exo*-H-8, which suggests that it is *syn* to the spirocyclopropyl group. Additional confirmation that the *exo*-8-proton is involved in this long range interaction was provided by the ^{1}H spectrum of **16**-d_x since the 0.8-Hz splitting is not observed in the multiplet for the less shielded 3-proton. The 3-methylene pattern consisted of a pair of doublets of doublets, δ 2.656, 2.569 (J = 2.6, 20.0 Hz), arising from [8-$^2H_1$]-**16** and a pair of doublets of triplets, δ 2.635, 2.548 (J = 2.6, 3.1 Hz) due to each of the [3,8-$^2H_2$]-**16** species.

The ^{13}Cmr spectrum of **16**-d_x contained the characteristic triplets, centred upfield from the normal signals, arising from one-bond ^{13}C–^{2}H coupling, for the methylene carbons at δ_C 28.0 (J_{CD} = 20.5 Hz, isotope shift (Δ) = 323 ppb) and 33.8 (J_{CD} = 19.6 Hz, Δ = 336 ppb). Two-bond isotope shifts were apparent for C-5 (δ_C 55.8, Δ = 84 ppb) and C-1 (δ_C 15.9, Δ = 98 ppb), while two isotope-shifted components accompanied the normal C-2 signal at δ 10.5 (Δ = 100 ppb/^{2}H) arising from species having one and two deuterons at C-3.

Upon treatment of **21***a* with KOD/*t*-BuOD, **23***a*-d_x containing 1.50 atoms ^{2}H/molecule was isolated and found to exhibit three signals in its ^{2}Hmr spectrum since the 3-methylene peaks are nearly equivalent and, therefore, unresolved. This product was treated with KOH/MeOH to back-exchange the α-deuterium picked up by exchange after the cleavage and its ^{2}H spectrum contained a strong signal at δ 2.25 (*exo*-^{2}H-8) and a relatively small peak at δ 1.87 (*endo*-^{2}H-8). The intensity ratio of these signals showed that the homoketonization of **21***a* proceeds with high stereoselectivity favoring inversion of configuration (93 ± 1%), strictly analogous to the results for **3** and **13**.

The ^{13}C spectra of these **23**-d_x samples confirmed the earlier assignment. The absorption for C-8, δ 29.3, contained the characteristic triplet J_{CD} = 20.4 Hz, Δ = 328 ppb and a similar pattern was observed for C-3, δ_C 34.2, J_{CD} = 19.7 Hz, Δ = 349 ppb. Two-bond isotope shifts were also apparent for C-1 (δ_C 15.8, Δ = 85 ppb), C-5 (δ_C 53.8, Δ = 85 pb), and C-2 (δ_C 10.4, Δ = 97 ppb/^{2}H).

Base-catalyzed homoketonization of **20** in KOD/*t*-BuOD furnished a sample of **22**-d_x which was found to contain 2.74 atoms ^{2}H/molecule by mass spectrometry. The ^{2}Hmr spectrum consisted of three signals at δ 1.87, 2.15, and 2.48. Treatment of this product with KOD/*t*-BuOD to back-exchange the α-deuterium picked up by exchange after the formation of **22**-d_1 furnished a sample of **22**-d_1 containing 0.96 atoms ^{2}H/molecule, whose ^{2}Hmr spectrum exhibited a major peak at δ 2.48 with very small signals at 1.87 and 2.14. Clearly homoketonization of **20** is highly stereoselective. It may be noted that the mass spectrum of this sample gave the ^{2}H content as 4.6% d_0, 94.8% d_1, and 0.6% d_2, indicating that back-exchange of the α-deuterons was not quite complete. Thus, the observation of one major signal in the ^{2}H spectrum shows that the stereoselectivity is >99%, which is significantly higher than that found for the other homoquadricyclene derivatives **3**, **13**, and **21***a*. To establish the stereochemistry of the cleavage of

20, however, analysis of the proton spectrum was required.

The ^{1}H spectrum of **22** in C_6D_6 solution exhibited two-proton multiplets near δ 2.50 and 2.18, a three-proton multiplet at 1.75–1.90, and a multiplet at 1.25 (dt, $J \approx 6.2$, 6.7 Hz, 1H) together with methyl absorptions centred at δ 1.43 and 1.58, each of which was a broadened doublet, $J = 1.5$ and 2.5 Hz, respectively. As the first step in the analysis of this spectrum, a heteronuclear correlation experiment was done since the ^{13}C spectrum had been completely assigned (see above). As a result it was found that the lowest field proton pattern was due to the bridgehead H-5 and one of the 6-methylene protons, while the absorption near δ 2.18 arose from the second 6-methylene proton and one of the 3-methylene protons. The highest field proton pattern correlated with the C-2 signal. Unfortunately, the overlap of the various multiplets precluded a definitive analysis of the ^{1}H spectrum and a shift reagent study was required to obtain suitable dispersion of the individual patterns.

In the presence of 0.1 equivalents of Eu(fod)$_3$, eight one-proton multiplets were clearly resolved, permitting complete analysis. Methylene absorption consisting of a doublet at δ 4.17 (J = 18.8 Hz) and an eight-line pattern, δ 4.70 (J = 2.5, 6.2, 18.8 Hz), was readily assigned to the *endo*- and *exo*-3-protons, respectively, exhibiting shifts (Δδ) of 2.30 and 2.56 ppm with Eu(fod)$_3$. A second methylene pattern was apparent for the 6-protons as a doublet, δ 3.70 (Δδ 1.50, J = 15.4 Hz), and a complex multiplet, δ 3.38 (Δδ 0.90). A series of spin decoupling experiments revealed that the latter multiplet contained couplings to each of the methyl groups (J = 1.5, 2.5 Hz), to H-5 (J = 8.7 Hz), and to its geminal partner (J = 15.4 Hz). An inspection of molecular models indicated that the *endo*-6-proton has a dihedral angle of ca. 90° with respect to H-5; hence the doublet was assigned to *endo*-H-6. The *exo*-6-proton is nearly perpendicular to the π-plane of the double bond, which accounts nicely for the observed homoallylic coupling to each methyl group with the larger interaction presumably involving the *transoid* methyl protons, δ 1.88 (Δδ 0.30). Thus the *cisoid* methyl appears at δ 1.72 (Δδ 0.29). The four remaining multiplets in the Eu(fod)$_3$-shifted ^{1}H spectrum were readily assigned as follows: δ 4.75 (Δδ 2.25, J = 2.5, 4.6, 8.7 Hz, H-5), 2.54 (Δδ 0.77, J = 4.6, 6.7(2) Hz, H-1), 2.32 (Δδ 0.55, J = 6.7(2), H-8), 2.01 (Δδ 0.76, J = 6.2, 6.7(2) Hz, H-2). The 2.5-Hz splitting in the absorptions for *exo*-H-3 and H-5 is a long-range interaction. All of the spin couplings noted were confirmed by the appropriate decoupling experiments.

In the presence of Eu(fod)$_3$, the three signals in the ^{2}H spectrum of **22**-d_x exhibited shifts corresponding to those found for the *exo*-6, *exo*-3, and *endo*-3 protons, thus identifying the three deuterons. The first of these is the major peak in the ^{2}H spectrum of **22**-d_1, establishing that homoketonization of **20** proceeds with highly favored inversion of configuration.

The ^{13}Cmr spectrum of **22**-d_x, the initial product of homoketonization of **20** in KOD/*t*-BuOD, indicated the presence of deuterium at C-3 and -6 and the mass spectrum showed only traces of d_4 species in the sample. Consequently it was apparent that α-exchange in **22** occurred primarily at C-3 with little ^{2}H exchange of the α-bridgehead H-5. To confirm that bridgehead exchange is much slower than exchange at C-3, a sample of **22** was heated under reflux with NaOMe/MeOD for 90 min. The recovered **22**-d_y contained 1.58 atoms ^{2}H/molecule by mass spectrometry with no detectable d_3-species and the ^{13}C spectrum indicated deuterium incorporation only at C-3. The ^{2}Hmr spectrum of **22**-d_y consisted of two equally intense signals corresponding to *exo*- and *endo*-^{2}H-3. In a second experiment, the time of reflux was increased to 9 h but a complex mixture of products resulted that was not examined. In any event, it is clear that bridgehead exchange in **22** is a relatively slow process.

Conclusions

The foregoing results show that Simmons–Smith cyclopropanation of the 7-spirocyclopropyl and 7-isopropylidene derivatives of the trimethylsilyl enol ether of norbornenone follows the same reaction course as the parent, with the formation of the corresponding 8-substituted 2-trimethylsilyl ethers of homoquadricyclene in high yield. While homoketonization of these ethers is regiospecific, the regiochemistry of cleavage for the spirocyclopropyl analogs is the same as that of the parent but differs for the isopropylidene derivative. This finding indicates that increasing the stability of the incipient carbanion formed upon cleavage of the cyclopropoxide ring can alter the course of the reaction. Thus, the ring opening can be directed by β-functionalization. In each case, the stereochemistry of homoketonization is the same, namely, strongly favoring (≤92%) inversion of configuration at the carbanionic site.

Experimental

Boiling points are uncorrected. Gas–liquid chromatography (glc) was carried out with Varian 920 or 3700 instruments using columns of 10% Carbowax, 6% FFAP, or 10% SE-30 on Chromosorb W, as indicated. Tetrahydrofuran (THF) and ether were freshly distilled before use after drying over sodium. Diisopropylamine, triethylamine, and pyridine were distilled from CaH_2 and stored over 4A molecular sieves.

Infrared spectra were recorded with a Beckman 4250 spectrophotometer and mass spectra with a Varian MAT-311A system at 70 eV (direct inlet). Routine proton spectra were obtained with Varian T-60 or EM-360 instruments while data for pure samples and for the shift reagent studies were collected with Varian XL-200 and -300 spectrometers. The latter instruments were employed for the ^{2}H and ^{13}C spectra, and comparison of the fully-decoupled ^{13}C spectra with those obtained from either APT (8) or DEPT (9) experiments served to identify the methyl, methylene, methine, and quaternary carbon signals. Correlation of the ^{1}H and ^{13}C spectra for **22** was accomplished using the HETCOR sequence of the XL software with a 2048 × 256 data matrix, 1800 (^{13}C) and 600 (^{1}H) Hz spectral widths transforming 2048 and 512 points, respectively. Double quantum coherence or INADEQUATE spectra (6) were recorded with the C13SAT sequence of the XL software using spectral widths of 3600 (**13**), 3000 (**16**), and 2500 (**22**) Hz to observe only the sp^3 carbons, with repetition rates of 15 s, 60 000 points, and 64 K transforms. To determine the ^{2}H-induced isotope shifts required for the analyses of the ^{13}C spectra of the deuterated ketones produced by homoketonization in deuterated base, spectral widths of 7500 Hz with 60 000 data points and 64 K transforms were employed at 75 MHz. The isotope shifts are given in ppb (ppm × 10^3) with an estimated precision of 5 ppb.

7-Spirocyclopropylnorbornenone (12)

Following the procedure reported by Turro and Farrington (10) a mixture of spiro[2,4]hepta-4,6-diene (13.6 g, 148 mmol), prepared from cyclopentadiene and 1,2-dibromoethane according to the method described by Alder *et al.* (11), and 2-chloroacrylonitrile (15.6 g, 178 mmol) was stirred at 105°C for 5 h. Distillation afforded 16.0 g of the Diels–Alder adduct, 15.5 g of which was added to a mixture of ethylene glycol (107 mL) and KOH (26.5 g) and stirred at 95°C for 20 h. After the addition of 380 mL of 10% aqueous NaCl solution, the product was extracted with pentane (6 × 100 mL). The combined extracts were washed with brine (2 × 70 mL) and dried over $MgSO_4$. After removal of the solvent, the residue was distilled to give **12** (7.59

g), bp 89–90°C/16 Torr (1 Torr = 133.3 Pa) (lit. (10) bp 90–92°C/21 Torr) which was >85% pure by glc analysis (FFAP). Flash chromatography (Et_2O – petroleum ether, 25:75) furnished pure **20** (5.9 g, 51% yield); ir (film): 3076, 3000, 1745, 708 cm^{-1}; ^{1}Hmr ($CDCl_3$) δ: 0.64 (bs, 4H), 1.98 (d, J = 16.2 Hz, *endo*-H-3), 2.28 (dd, J = 3.1, 16.2 Hz, *exo*-H-3), 2.50 (m, H-1 and -4), 6.20 (m, 1H), 6.62 (dd, J = 2.8, 5.6 Hz, 1H); ^{13}Cmr ($CDCl_3$) δ_C: 6.0, 7.0 (2 × CH_2), 38.3 (C-3), 46.0 (C-4), 46.1 (C-7), 60.8 (C-1), 129.4 (C-6), 142.0 (C-5), 212.7 (C-2). *Exact Mass* calcd. for $C_9H_{10}O$: 134.0732; found: 134.0729.

Trimethylsilyl enol ether of 12

This compound was prepared following the procedure reported for norbornenone (1) using diisopropylamine (0.84 mL), THF (8 mL), n-butyllithium (2.1 mL, 2.50 M in n-C_6), and **12** (0.50 g) with a quenching solution of trimethylsilyl chloride (0.76 mL), Et_3N (0.29 mL), and THF (1.5 mL). Kugelrohr distillation of the product isolated by pentane extraction gave crude enol ether (bp 102–106°C/12 Torr, 0.69 g, 90% yield) which glc analysis (Carbowax) indicated to be ~95% pure. An analytical sample was collected by preparative glc for characterization; ir (CCl_4): 3060, 2960, 1610, 1257, 839 cm^{-1}; ^{1}Hmr ($CDCl_3$) δ: 0.10 (s, 9H, $(Me)_3Si$), 0.28–0.68 (m, 4H), 2.48 (m, 1H), 2.64 (m, 1H), 5.32 (dd, J = 1.3, 3.3 Hz, H-3) 6.88 (t, J ~ 1.9 Hz, 2H), ^{13}Cmr (C_6D_6) δ_C: 0.0 (Me_3Si), 10.4, 10.6 (2 × CH_2), 53.8 (C-4), 58.8 (C-1), 67.5 (C-7), 109.3 (C-3), 141.0 (C-6), 145.4 (C-5), 172.5 (C-2). *Exact Mass* calcd. for $C_{12}H_{18}OSi$: 206.1127; found: 206.1124.

8-Spirocyclopropyl-2-trimethylsiloxyhomoquadricyclene (13)

Cyclopropanation of the silyl enol ether of **12** was carried out as previously described for the parent norbornenone derivative using a zinc–silver couple (1.26 g) and CH_2I_2 (0.85 mL) in Et_2O (2 mL) with the TMS enol ether (1.2 g) in Et_2O (15.5 mL). The usual work-up furnished an oily liquid (1.14 g) which was ca. 80% pure by glc (SE-30). Pure **13** was obtained by preparative glc; ir (CCl_4): 3078, 2975, 1250, 1154, 840 cm^{-1}; ^{1}H and ^{13}Cmr (see text). *Exact Mass* calcd. for $C_{13}H_{20}OSi$: 220.1283; found: 220.1302.

Homoketonization of 13

To 20 mL of 3 M methanolic NaOH was added **13** (485 mg) and the mixture stirred overnight at room temperature. After the addition of H_2O (20 mL), the product was extracted with n-pentane (3 × 20 mL) and the combined extracts washed with H_2O (3 × 15 mL) before drying over $MgSO_4$. Removal of the solvent gave a yellow oil (330 mg) containing one ketonic component **16** (ca. 90% yield) that was purified by preparative glc (FFAP); ir (film): 3040, 2930, 1725 cm^{-1}; ^{1}H and ^{13}Cmr (see text). *Exact Mass* calcd. for $C_{10}H_{12}O$: 148.0888; found: 148.0882.

Preparation of 16-d$_x$

A sample of **13** (90 mg) was placed in a 1.3 M solution of KOD in t-BuOD (1.6 mL) and the mixture stirred at room temperature overnight. Isolation by pentane extraction (90% yield) and purification by glc (FFAP) gave **16**-d_x; ms: 4.6% d_0, 32.6% d_1, 41.7% d_2, 21.5% d_3 (total 1.80 atoms ^{2}H/molecule).

Hydrogenation of 16

To a solution of **16** (130 mg) in glacial acetic acid (4 mL) was added 27 mg of platinum oxide catalyst and the mixture hydrogenated at 50 psi (1 psi = 6.89 kPa) in a Parr shaker for 21 h. Dilution with H_2O (15 mL) and neutralization with $NaHCO_3$ were followed by removal of the catalyst by filtration. The product was extracted with n-pentane (3 × 10 mL) and the combined extracts dried over $MgSO_4$ before removal of the solvent by evaporation to furnish 130 mg of material. Gas–liquid chromatographic analysis (FFAP) indicated the presence of two components in comparable amounts and samples were collected by preparative glc. The ^{13}Cmr spectra of the samples showed one to be a 1:2 mixture of unreacted **16** and a new compound having signals at δ_C 26.7, 29.4 (2 × CH_3), 28.8, 30.8 (2 × CH_2), 13.1, 14.7, 24.7, 46.8, 71.8 (5 × CH), and 38.3 (quat C). These data indicate that the new product is probably 6,6-dimethyltricyclo[3.2.1.0^{2,7}]octan-4-ol but the compound was not further characterized. The second component obtained by preparative glc was a single ketone identified as 6,6-dimethyltricyclo[3.2.1.0^{2,7}]octan-4-one; ir (film): 3030, 2965, 1720 cm^{-1}; ^{1}Hmr ($CDCl_3$) δ: 1.02 (s, 3H), 1.07 (s, 3H), 1.00–1.30 (m, 2H), 1.42 (dt, J = 3.4, 6.5 Hz, H-1), 1.75 (d, J = 13.3 Hz, *endo*-H-8), 2.04 (d, J = 5.5 Hz, H-5), 2.20 (ddd, J = 3.4, 5.5, 13.3 Hz, *exo*-H-8) and an AB pattern, 2.48, 2.55 (J_{AB} = 20.0 Hz, H-3) each exhibiting a 2.5-Hz splitting; ^{13}Cmr (see text). *Exact Mass* calcd. for $C_{10}H_{14}O$: 150.1044; found: 150.1041.

Reduction of 16

To a slurry of LAH (38 mg) in anhydrous Et_2O (2 mL) was added a solution of **16** (95 mg) in Et_2O (4 mL) and the mixture stirred overnight under reflux. On cooling to 0°C, excess LAH was destroyed by the cautious addition of H_2O and 10% aqueous NaOH solution (0.2 mL). After stirring, the precipitate was removed by filtration and the solvent removed after drying to furnish 75 mg of product which contained two components by glc analysis (FFAP) in a ratio of 6.5:1; both were isolated by preparative glc.

The major product, mp 67–68°C, was found to be alcohol **24**, primarily on the basis of its ^{13}C spectrum (see text); ir (CCl_4): 3630, 3040, 3000, 2940, 1055 cm^{-1}; ^{1}Hmr ($CDCl_3$) δ: 3.69 (m, 1H), 2.44 (dddd, J ≈ 0.6, 3.0, 9.8, 14.8 Hz, 1H), 1.95 (dddd, J ≈ 0.6, 3.4, 6.5, 11.6 Hz, 1H), 1.80 (ddd, J ~ 2.2, 4.6, 14.8 Hz, 1H), 1.60 (m, 1H), 1.47 (d, J = 11.6 Hz, 1H), 1.28 (m, 2H), 0.65–0.93 (m, 4H), 0.05–0.30 (m, 2H). *Exact Mass* calcd. for $C_{10}H_{14}O$: 150.1044; found: 150.1045.

The minor product **25** was identified by its ^{13}Cmr spectrum (see text); ir (CCl_4): 3620, 3040, 2925, 1060 cm^{-1}; ^{1}Hmr ($CDCl_3$) δ: 3.93 (m, 1H), 2.40 (ddd, J ≈ 3.1, 9.0, 15.0 Hz, 1H), 2.00 (d, J = 12.0 Hz, 1H), 1.75 (m, 1H), 1.65 (ddd, J ≈ 2.1, 4.2, 15.0 Hz, 1H), 1.55 (bs, OH), 1.10–1.40 (m, 3H), 0.22–0.90 (m, 5H). *Exact Mass* calcd. for $C_{10}H_{14}O$: 150.1044; found: 150.1042.

7-Isopropylidenenorbornenone (18)

A mixture of cyclopentadiene (66 g) and acetone (58 g) was cooled to 0°C before the dropwise addition of 20% ethanolic KOH solution (20 mL) with stirring (12). Stirring was continued overnight. The organic layer was separated and distilled to furnish 6,6-dimethylfulvene (32.5 g, 31%), bp 42–47°C/11 Torr (lit. (13) bp 44–46°C/10 Torr). A solution of 6,6-dimethylfulvene (3.06 g, 29 mmol) and 2-acetoxyacrylonitrile (10.00 g, 90 mmol) in dry pyridine (1.20 mL) was prepared and aliquots were transferred to six flame-dried, 5-mL thick walled Pyrex tubes under a N_2 atmosphere. The tubes were sealed under vacuum and placed in an oil bath at 90°C for 28 h (14). After cooling to room temperature, the contents of the tubes were taken up in CH_2Cl_2. The solvent was removed and the product isolated by flash chromatography using benzene as eluent to furnish an epimeric mixture (7:1) of the 2-acetoxy-2-cyano-7-isopropylidenebicyclo[2.2.1]hept-5-enes (6.0 g, 96% yield), favoring the *endo*-cyano isomer by comparison with the published data (14). This mixture was used directly for the next step.

The mixture of Diels–Alder adducts (2.0 g, 9.2 mmol) was dissolved in methanol (8.8 mL) and added, with stirring, to a 2 M solution of NaOMe in MeOH under a N_2 atmosphere. After stirring for 2.5 h, 10% aqueous NaCl solution (20 mL) was added and the product extracted with methylene chloride (4 × 20 mL). The combined extracts were washed with H_2O before drying over $MgSO_4$. Removal of the solvent gave **18** (1.0 g, 75% yield), which was >97% pure by glc (FFAP) analysis; ir (film): 3080, 2920, 1750 cm^{-1}; ^{13}Cmr ($CDCl_3$) δ: 19.4, 19.8 (2 × CH_3), 40.4 (CH_2), 42.0, 57.9, 130.9, 143.1 (4 × CH), 115.2, 146.2 (2 × olef. CH), 218.6 (C=O).

2-Trimethylsilyloxy-7-isopropylidenebicycloheptadiene (19)

Following our usual procedure, **18** (0.60 g, 4 mmol) in THF (2 mL) was added dropwise to a THF solution of LDA at −78°C. The LDA was prepared from diisopropylamine (0.92 mL, 6.6 mmol) in THF (5.5 mL) to which had been added 2.46 M n-BuLi in hexane (2.30 mL, 5.66 mmol). Quenching with chlorotrimethylsilane (0.93 mL, 7.3 mmol) and triethylamine (0.34 mL, 2.4 mmol) in THF (2 mL) and extraction with pentane as described earlier gave, after removal of the solvent, 0.71 g of oily **19** (80% yield); ir (film): 3050, 2965, 1610, 1250, 844 cm^{-1}; ^{1}Hmr (C_6D_6) δ: 0.0 (s, Me_3Si), 1.30 (s, Me), 1.33 (s, Me), 3.58 (m, 1H), 3.74 (m, 1H), 5.23 (dd, J = 1.3, 3.6 Hz, 1H), 6.78 (m, 2H); ^{13}Cmr ($CDCl_3$) δ_C: 0.1 (Me_3Si), 18.6, 18.7 (2 × CH_3), 48.9, 54.2 (2 × CH), 109.5, 141.3, 145.3 (3 × olef. CH), 93.4, 162.9, 171.8 (3 × quat C). *Exact Mass* calcd. for $C_{13}H_{20}OSi$: 220.1283; found: 220.1280.

*Cyclopropanation of **19***

Our general procedure was employed whereby a zinc–silver couple (0.53 g, 8.1 mmol) was placed in a nitrogen-purged flask and the apparatus was flame-dried. After cooling, methylene iodide in anhydrous Et_2O (2 mL) was added and the mixture warmed until refluxing occurred without external heating. Upon cessation of reflux, an ethereal solution of **19** (0.55 g, 2.4 mmol) was added and the mixture refluxed for several hours. After cooling to 0°C, a 50:50 mixture of pyridine–ether was added until no further precipitate formed. The precipitate was removed by filtration and the ether evaporated. The residue was taken up in *n*-pentane and the traces of precipitate were removed by filtration before evaporation of the solvent. The resulting oily product (0.51 g) was shown to contain a mixture of two adducts by ^{13}Cmr. All attempts to analyze the product by glc (FFAP, SE-30, Carbowax) led to decomposition even if freshly prepared glc columns were used. A series of experiments following this general procedure was carried out as summarized in Table 1.

A preparative run was carried out by reacting 710 mg of **19** in Et_2O (9.9 mL) with a zinc–silver couple (0.5 g) and CH_2I_2 (0.13 mL, 1.6 mmol) in Et_2O (3 mL) at room temperature for 5.5 h before the addition of more CH_2I_2 (0.13 mL, 1.6 mmol) and stirring for an additional 20 h. The reaction was quenched and the product isolated in the usual fashion as an oil (700 mg).

The major component in the product from Expt. 1 (Table 1) gave rise to a ^{13}C spectrum consistent with structure **20** (see text) while the major component from Expt. 3 exhibited a ^{13}C spectrum readily attributable to **21** as discussed in the text. These structural assignments were confirmed by unequivocal identification of their homoketonization products.

*Homoketonizations of **20** and **21**a*

The same procedure described above for homoketonization of **13** was employed.

Upon treatment with 3 *M* methanolic NaOH, the product from Expt. 5 (Table 1) afforded a single ketone by glc analysis (FFAP). Although the starting material was a mixture of **18** and **20**, it was apparent that **18** did not survive after several hours in base. The structure of the new ketone **22** was established by detailed analysis of its ^{13}C spectrum (see text); ir (CCl_4): 3060, 2910, 1747 cm^{-1}; ^{1}Hmr (see text). *Exact Mass* calcd. for $C_{11}H_{14}O$: 162.1045; found: 162.1039.

Homoketonization of the material from the preparative scale cyclopropanation gave 330 mg of **22**, after purification by flash chromatography (7% Et_2O – 93% petroleum ether (30–60°C), 64% overall yield from **19**).

The product from Expt. 4 (Table 1) was stirred at room temperature with 2 mL of 1 *M* KOD/*t*-BuOD overnight. The usual work-up furnished **22**-d_x containing 2.74 atoms ^{2}H/molecule; ^{13}Cmr ($CDCl_3$) δ_C (Δδ = isotope shift, ppb): 20.6 (163) C-2, 26.3 (50) C-8, 30.0 (50) C-1, 35.4 (J_{CD} = 20.4 Hz, 660) C-3, 43.4 (J = 20.2, 364) C-6, 50.3 (68) C-5, 129.8 (J_{CD} = 1.2 Hz, 23) C-7′, 26.5 (50) C-1; ms: 5.6% d_0, 1.1% d_1, 7.1% d_2, 86.0 d_3, 0.2% d_4.

A portion of **22**-d_x was treated with 3 *M* methanolic NaOH to furnish **22**-d_1 containing 0.96 atoms ^{2}H/molecule; ^{13}Cmr ($CDCl_3$) δ_C (Δδ = isotope shift, ppb): 43.4 (J = 20.2 Hz, 323) C-6, 50.3 (72) C-5, 126.5 (40) C-7, 129.8 (J_{CD} = 1.2 Hz, 50) C-7′; ms: 4.6% d_0, 94.8% d_1, 0.6% d_2.

Homoketonization of the mixture of adducts (210 mg) obtained in Expt. 3 (Table 1) gave an oily liquid (145 mg, 97% yield) shown to be a 78:12 mixture of **23** and **22** by glc (FFAP), readily separable by preparative glc. The ^{1}H and ^{13}Cmr spectra showed that **23** was a single compound; ir (CCl_4): 3050, 2925, 1725 cm^{-1}; ^{1}H and ^{13}Cmr (see text); *Exact Mass* calcd. for $C_{12}H_{16}O$: 176.1201; found: 176.1193. A second sample (130 mg) of the same starting material was treated with 1 *M* KOD/*t*-BuOD (2 mL) to furnish 85 mg (92% yield) of the mixture of **23**-d_x and **22**-d_x. After isolation by glc, ketone **23**-d_x was found to contain 1.50 atoms ^{2}H/molecule (30.0 d_0, 25.9% d_1, 34.2% d_2, 18.5% d_3). Back-exchange with 3 *M* methanolic NaOH afforded **23**-d_1; 42.0% d_0, 56.8% d_1, 1.1% d_2 (total 0.59 atoms ^{2}H/molecule).

*H/D exchange of **22***

A solution of **22** (35 mg) in 1 *M* MeONa/MeOD (2 mL) was heated under reflux for 90 min. After addition of D_2O (3 mL), the product was isolated by pentane extraction (3 × 8 mL); the combined extracts were washed with 10% aqueous NaCl solution before drying over $MgSO_4$. Evaporation of the solvent gave 30 mg of **22**-d_y and an analytical sample was obtained by glc (FFAP); ms: 6.4% d_0, 28.5% d_1, 65.4% d_2, 1.59 atoms ^{2}H/molecule. The ^{2}Hmr spectrum (C_6D_6) contained equally intense signals at δ 1.87 and 2.15 (*endo*- and *exo*-^{2}H-3, respectively).

*Reduction of **23**a*

Ketone **23** (30 mg) in Et_2O (2.2 mL) was added to a slurry of LAH (20 mg) in Et_2O (1 mL) under a N_2 atmosphere and stirred overnight. The usual work-up afforded an oil (30 mg), which by glc analysis contained two components in a ratio of 18.5:1. A sample of the major component was isolated by preparative glc and identified as **26** on the basis of its ^{13}C spectrum (see text); ir (CCl_4): 3630, 3050, 2940, 1175, 915 cm^{-1}; ^{1}Hmr ($CDCl_3$) δ: 0.25 (d, J = 3.7 Hz, 1H), 0.90 (d, J = 3.7 Hz, 1H), 0.74–0.98 (m, 2H), 1.20 (s, Me), 1.25 (s, Me), 1.29 (m, 1H), 1.50 (dd, J = 2.4, 5.8 Hz, 1H), 1.60 (d, J = 11.6 Hz, 1H), 1.67 (ddd, J = 2.0, 5.8, 13.9 Hz, 1H), 1.95 (ddd, J = 3.6, 6.0, 11.6 Hz, 1H), 2.43 (ddd, J = 3.7, 10.0, 13.9 Hz, 1H), 3.72 (m, 1H). *Exact Mass* calcd. for $C_{12}H_{18}$: 178.1358; found: 178.1357.

Acknowledgements

We are grateful for the financial support provided by the Natural Sciences and Engineering Research Council of Canada in the form of scholarships (A.J.R.) and operating grants.

1. A. J. RAGAUSKAS and J. B. STOTHERS. Can. J. Chem. **61**, 2254 (1983).
2. K. KON and S. ISOE. Tetrahedron Lett. **21**, 3399 (1980); T. TAKEMOTO and S. ISOE. Chem. Lett. 1931 (1982); M. DEMUTH and K. SCHAFFNER. Angew. Chem. Int. Ed. Engl. **21**, 205 (1983).
3. N. H. WERSTIUK. Tetrahedron, **39**, 205 (1983).
4. W. C. G. M. DE VALK, A. J. H. KLUNDER, and B. ZWANENBURG. Tetrahedron Lett. **21**, 971 (1980).
5. R. D. MILLER and D. L. DOLCE. Tetrahedron Lett. 1023 (1977).
6. A. BAX, R. FREEMAN, and S. P. KEMPSELL. J. Am. Chem. Soc. **102**, 4849 (1980).
7. A. OKU, Y. NOZAKI, H. HASEGAWA, J. NISHIMURA, and T. HARADA. J. Org. Chem. **48**, 4374 (1983).
8. S. L. PATT and J. N. SHOOLERY. J. Magn. Reson. **46**, 535 (1982).
9. D. M. DODDRELL, D. T. PEGG, and M. R. BENDALL. J. Magn. Reson. **48**, 323 (1982).
10. N. J. TURRO and G. L. FARRINGTON. J. Am. Chem. Soc. **102**, 6056 (1980).
11. K. ALDER, H. J. ACHE, and F. H. FLOCK. Chem. Ber. **93**, 1388 (1960).
12. G. CRANE, C. E. BOORD, and A. K. L. HEUNE. J. Am. Chem. Soc. **67**, 1237 (1945).
13. N. FREIESLEBEN. Ger. Patent No. 1, 146, 050 (1963); Chem. Abstr. **59**, 9914 (1963).
14. A. OKU, Y. NOZAKI, H. HASEGAWA, J. NISHIMURA, and T. HARADA. J. Org. Chem. **48**, 4374 (1983).
15. V. DAVE, R. FARWAHA, P. DE MAYO, and J. B. STOTHERS. Can. J. Chem. **63**, 0000 (1985).
16. J. L. JURLINA, A. J. RAGAUSKAS, and J. B. STOTHERS. Magn. Reson. Chem. In press.
17. A. STOESSL and J. B. STOTHERS. Can. J. Chem. **63**, 1258 (1985).

^{13}C magnetic resonance studies. 120.[1] The Simmons–Smith reaction with some silyl enol ethers. Unusual ring expansions of some norcamphors

ARTHUR J. RAGAUSKAS[2] AND J. B. STOTHERS
Department of Chemistry, University of Western Ontario, London, Ont., Canada N6A 5B7

Received March 13, 1985

ARTHUR J. RAGAUSKAS and J. B. STOTHERS. Can. J. Chem. **63**, 2969 (1985).

Unexpected difficulties with Simmons–Smith cyclopropanation of the trimethylsilyl enol ether of *exo*-tricyclo[3.2.1.0^{2,4}]-octan-6-one led to a reexamination of this reaction with the parent norcamphor derivative which under "concentrated" conditions gave ring-expanded allylic ethers in low yield. With the *tert*-butyldimethylsilyl ethers, however, the allylic product is formed in high yield in the norcamphor and *exo*-trimethylenenorcamphor (tricyclo[5.2.1.0^{2,6}]decan-8-one) systems. The *tert*-butyldimethylsilyl enol ethers of bicyclo[3.2.1]octan-6-one and nopinone do not undergo ring expansion under similar conditions but the silyl ether of 3-methylenenopinol is a major product in the latter case.

ARTHUR J. RAGAUSKAS et J. B. STOTHERS. Can. J. Chem. **63**, 2969 (1985).

Les difficultés inattendues qui se sont manifestées lors de la réaction de cyclopropanation selon Simmons–Smith de l'éther énolique triméthylsilyle de la tricyclo[3.2.1.0^{2,4}]octanone-6 *exo* nous ont incité à réétudier cette réaction avec le dérivé norcamphre apparenté qui, lorsqu'il est soumis à des conditions "concentrées", conduit avec un faible rendement aux éthers allyliques ayant subi une expansion du cycle. Toutefois, avec les éthers *tert*-butyldiméthylsilyle du norcamphre et du triméthylènenorcamphre-*exo* (tricyclo[5.2.1.0^{2,6}]décanone-8), on obtient le produit allylique avec un rendement élevé. Dans des conditions analogues, les éthers énoliques *tert*-butyldiméthylsilyles de la bicyclo[3.2.1]octanone-6 et de la nopinone ne subissent pas d'extension de cycle; toutefois, dans ce dernier cas, le produit principal est l'éther silylé du méthylène-3 nopinol.

[Traduit par le journal]

Introduction

Some years ago we described an efficient synthetic method for ring expansion of several bicyclic ketones (1). Our sequence involves generation of the trimethylsilyl enol ether followed by Simmons–Smith cyclopropanation and base-catalyzed cleavage of the cyclopropyl ether (Scheme 1). The cyclopropoxide produced by ether cleavage immediately undergoes homoketonization, which strongly favors ring expansion in [2.2.1], [2.2.2], and related systems. Subsequently this sequence was employed for ring expansion of a variety of polycyclic ketones (2–4). From these and other cases (5), we have collected more than 25 examples of the Simmons–Smith reaction with polycyclic trimethylsilyl enol ethers and, in each case, a single cyclopropanation product was obtained in good to high yield (70–95%) under a standard set of conditions ([CH_2I_2] = 0.5 *M*, [enol ether] = 0.3 *M* in ether).

In the course of a recent study (6), however, we found that, with our standard conditions, 6-trimethylsilyloxy-*exo*-tricyclo-[3.2.1.0^{2,4}]oct-6-ene (**1**) presented unexpected difficulties, such that with reflux times of 20 h or more, which are typical for good results with all other systems investigated to date (1–5), a mixture of products resulted that was too complex to warrant detailed examination. With a reflux time of 15 h, the reaction led to a product containing, by gas–liquid chromatography (glc), one major component (65%) and a minor component (~15%) together with small amounts of additional material. The ^{13}Cmr spectra of the major and minor components showed each to be a mixture of isomers. The former fraction was a 4 : 1 mixture of **2**, the expected cyclopropanation product, and an isomer that also gave rise to 10 signals in its ^{13}C spectrum, including two methylene and two monoprotonated olefinic carbon absorptions, which is consistent with structure **3**. The minor component appeared to be a 1 : 1 mixture of isomers homologous to **2** and **3**, since each exhibited signals for 11

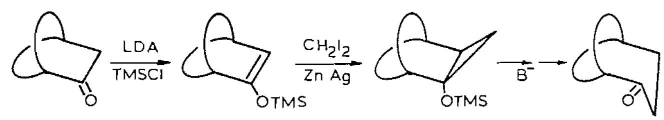

SCHEME 1

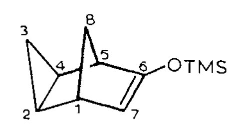

1

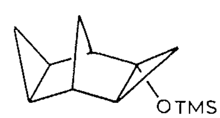

2

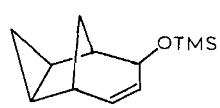

3

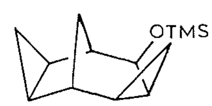

4

nonequivalent sp^3 carbons, which could be tentatively attributed to structure **4**. A further decrease in reflux time to 8 h finally accomplished the original goal, leading to the formation of **2** in 74% yield (6).

The apparent formation of the allylic ether **3** bears resemblance to the findings of Murai and co-workers (7, 8), who discovered that the concentration of the Simmons–Smith reagent is an important factor governing the ultimate product of cyclopropanation of monocyclic silyl enol ethers. Under their "diluted" conditions, which are comparable to our standard conditions, trimethylsilyl cycloalkenyl ethers **5** and **8** gave the

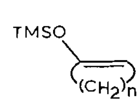

5

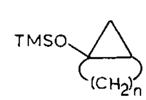

6

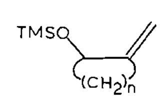

7

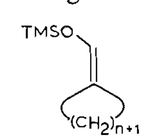

8

a n=3
b n=4

[1] For Part 119 see ref. 17.

[2] Present address: Department of Chemistry, University of Alberta, Edmonton, Alberta T6G 2E2.

expected cyclopropanated products, e.g. **6**, in good yield, whereas, under "concentrated" conditions, efficient conversion of **5** → **7** (7) and **8***a* → **9** (8) was observed. With **8***b*, only the expected cyclopropyl ether formed regardless of the conditions employed. The cleavage of the initial product under concentrated conditions was ascribed to reaction with ZnI_2, formed in the first step, leading to intermediate **10** in the isomerization to

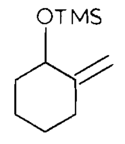

9

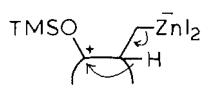

10

7. These workers showed that **6***b* was indeed isomerized to **7***b* upon refluxing with ZnI_2 in ether solution.

Our unexpected findings with **1** prompted us to examine the behavior of **1** and the parent ether **11***a* under more concentrated conditions, similar to those used by Murai and co-workers (7, 8). Results from these experiments led to the replacement of the trimethylsilyl group with the *tert*-butyldimethylsilyl moiety, and an examination of the silyl enol ethers **11***b* and **12–14** led us to examine the generality of our initial observations. We wish to describe the results of these investigations in the present paper.

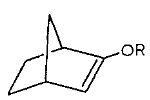

11 a R=TMS b R=t-BDMS

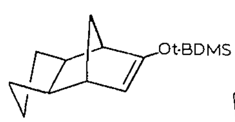

12

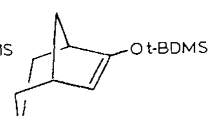

13

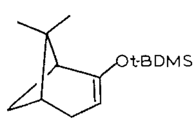

14

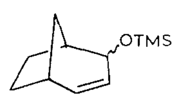

15

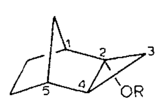

16 a R=TMS b R=t-BDMS

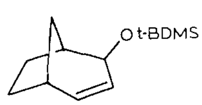

17

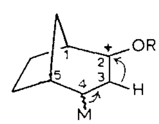

18

Results and discussion

As noted in the Introduction, Simmons–Smith cyclopropanation of the tricyclic enol ether **1** generates **2** as the initial product but it is unstable under the usual reaction conditions, in sharp contrast to the behavior of many other polycyclic analogs (1–5) for which reflux times of 20–50 h are required for optimal results. After 15 h, **2** constitutes ca. 50% of the product but was inseparable from an isomeric impurity (~15%) which was tentatively assigned structure **3**, primarily on the basis of its ^{13}Cmr spectrum, δ_C: 0.4 (Me_3Si), 10.3, 23.5 (CH_2), 15.3, 26.3, 34.6, 42.6, 71.2, 128.3, 137.9 (CH). Signals for one methylene and two methine carbons at relatively high field (10.3, 15.3, 26.3) indicated that the original three-membered ring was intact but that the cyclopropyl ring formed by methylene addition in the Simmons–Smith reaction was not, since there was only one other methylene signal together with those for a methine carbon bearing oxygen (71.2) and two monoprotonated olefinic carbons (128.3, 137.9). A minor component constituting ca. 15% of the total product was also isolated by preparative glc and found to contain two isomers in nearly equal amounts, which may be an epimeric mixture of **4** presumably arising by cyclopropanation of **3**.

In view of the results described by Murai and co-workers (7, 8), we examined the reaction of **1** under significantly more concentrated conditions,[3] $[CH_2I_2]$ = 3.1 *M*, [**1**] = 1.9 *M*, and obtained a mixture of several products in each run. However, after 25 h reflux, the product mixture contained a major component (~35% yield) which was isolated by preparative glc and found to have the molecular formula, $C_{13}H_{22}OSi$, by precise mass measurement. The ^{13}Cmr spectrum contained eleven sp^3 carbon signals, δ_C 0.4 (Me_3Si), 6.2, 7.5, 17.8 (CH_2), 13.9, 15.2, 20.9, 21.5, 32.8, 42.7, 70.7 (CH), and is identical to that exhibited by one of the isomers in the minor component isolated from the 15-h run under our standard conditions. The molecular weight clearly shows that this material arose by double cyclopropanation and the ^{13}C absorptions for three methylene and four methine carbons at relatively high field are good evidence for structure **4**. Thus, under these conditions, the sequence **1** → **2** → **3** → **4** appears to constitute a significant part of the process but **1** is also consumed in undetermined ways.

With little indication that the three-membered ring in **1** is involved directly in the reactions with the Simmons–Smith reagent, it was of interest to examine the behavior of the parent enol ether **11***a* under comparable conditions. Under our standard conditions, **11***a* gave the expected cyclopropanated TMS ether in 72% yield (1). With $[CH_2I_2]$ = 3.1 *M* and [**11***a*] = 1.3 *M*, however, **11***a* gave a mixture of several products from which one component (~15% yield) was isolated by preparative glc and found to contain a 3:2 mixture of isomers, $C_{11}H_{20}OSi$, each giving rise to a set of nine signals in the ^{13}C spectrum. The major component exhibited absorptions for three methylene (δ_C 25.0, 31.2, 31.6), five methine (35.8, 41.5, 73.0, 126.6, 136.3), and the trimethylsilyl carbons (0.4_2) similar to those for the minor isomer, δ_C 21.9, 33.1, 37.8 (CH_2), 35.6, 42.7, 74.3, 128.9, 134.9 (CH), and 0.3_5 (Me_3Si). Each of these sets of signals is very similar to those exhibited by the *exo*- and *endo*-isomers of bicyclo[3.2.1]oct-3-en-2-ol, respectively (9), which led to their assignments as the *exo* (major) and *endo* (minor) epimers of **15**. Thus we concluded that the cyclopropyl ring introduced initially by the Simmons–Smith reaction suffers cleavage leading to the allylic ether **15**, which is analogous to the observations for the tricyclic system **1**, with low yields in both cases. Specific assignments for the ^{13}C spectra of **1–4** and the epimers of **15** are given in Table 1.

Since the instability of the trimethylsilyl ethers could be a factor contributing to these low conversions, the behavior of the *tert*-butyldimethylsilyl (*t*-BDMS) counterpart **11***b* was examined. Ether **11***b* was prepared in 80% yield using the procedure (LDA, Et_3N, *t*-BDMSCl in THF) analogous to that employed previously for a variety of TMS enol ethers (1–6). Since the completion of this study, however, two, more efficient, general methods for the preparation of *t*-BDMS enol ethers have been described (10). Under dilute conditions ($[CH_2I_2]$ = 0.7 *M*, [**11***b*] = 0.35 *M*), **11***b* gave the expected single product **16***b* in 69% yield having the molecular formula

[3] In all examples with either dilute or concentrated conditions the mole ratio of Zn/Ag:CH_2I_2 was 2:1.

$C_{14}H_{26}OSi$ by precise mass measurement, confirming the addition of one methylene group. Apart from the signals for the trialkylsilyl moieties, the ^{13}C spectrum of **16***b* was virtually the same as that recorded for the normal Simmons–Smith product **16***a* from **11***a* (1); these data are listed in Table 1. However, after 33 h reflux under concentrated conditions ($[CH_2I_2] = 3.2$ *M*, $[\mathbf{11}b] = 1.3$ *M*), **11***b* was converted in 93% yield to a mixture containing three components by glc analysis. The major product **17** (80% yield) was isolated by preparative glc and its molecular formula, $C_{14}H_{26}OSi$, determined by precise mass measurement, established the addition of one methylene group. Since the ^{13}C spectrum (Table 1) contained signals for only three methylene carbons together with those for a methine carbon bearing oxygen and two monoprotonated olefinic carbons, it was apparent that the initial cyclopropanation product had undergone cleavage of the cyclopropyl ring. The shieldings for the skeletal carbons were almost identical to those found for *exo*-**15**, confirming its structural assignment as **17**. One of the minor products (8% yield) was found to be **16***b* and the second minor product (~5%) exhibited a ^{13}C spectrum consistent with that expected for the cyclopropanation product of **17**, but all samples were contaminated with **17** and the material was not fully characterized.

By analogy with earlier findings of Murai and co-workers (7, 8), cleavage of the three-membered ring in **16** may proceed via **18**, where M, the Lewis acid (presumably zinc iodide), could be *exo* or *endo* dependent upon the stereochemistry of the ring opening. Subsequent hydride migration from C-3 would lead directly to the ring-expanded allylic ether **15** (**17**). Since **17** is the major product from **16***b*, the *exo* orientation of the silyloxy group is indicative of *endo*-H-3 migration to C-2, which in turn suggests that **18** with *exo*-M is formed preferentially from **16***b*, i.e., upon cleavage with inversion of configuration. It may be recalled that Nickon *et al.* (11) have demonstrated the remarkable effect of water on the stereochemistry of acid-catalyzed ring opening of a homoenol acetate. These workers observed strongly favored inversion of configuration in the absence of water and high degrees of retention with water present. Thus their results offer a precedent for the proposed stereoselectivity. Some supporting evidence for the proposed sequence was provided by the results of a cyclopropanation experiment using CD_2I_2. After 33 h reflux under concentrated conditions, glc analysis of the product showed it to contain two components in a 4:5 ratio in 77% yield, which were isolated by preparative glc. The smaller component was shown to be **16***b*-3-d_x by its ^{13}C spectrum, in which the C-3 signal was strongly attenuated and the C-2 and -4 absorptions contained two-bond isotope-shifted components (Δ = 145 and 130 ppb/D, respectively). The major product was **17**-d_x by ^{13}Cmr, for which the spectrum indicated substantial deuteration at C-2 (~70%) and C-3 (~90%). The difference in the product composition compared to that for the same reflux time with CH_2I_2 can be attributed to a kinetic isotope effect in the cleavage of **16***b* → **17**. In any event, the labelling pattern in **17**-d_x is consistent with hydride (deuteride) shift as in **18**.

The much higher conversion of the *tert*-butyldimethylsilyl ether **11***b* to a much simpler product mixture must be due to the increased stability of this derivative relative to its trimethylsilyl analog **11***a*. Because of the much higher yield it was of interest to examine the behavior of some related polycyclic silyl enol ethers as an indication of the scope of the reaction under concentrated conditions. To this end the *tert*-butyldimethylsilyl enol ethers **12**–**14** were prepared.

TABLE 1. ^{13}C shieldings[a] for several silyl enol ethers and derivatives

Compound	C-1	C-2	C-3	C-4	C-5	C-6	C-7	C-8	C-9	C-10	C-11	TMS	*t*-BDMS
1	40.7	24.7	18.8	20.8	45.6	169.0	109.3	36.3				0.0	
2	42.2	66.9	15.6	25.8	36.6	17.9	6.7	15.9	18.4			1.0	
3	42.6	71.2	128.3	137.9	34.6	26.3	10.3	15.3	23.5			0.4	
4	42.7	70.7	21.5	7.5	20.9	32.8	15.2	6.2	13.9	17.8		0.4	
11*a*	45.9	161.5	105.0	41.4	28.2	24.8	47.2					−0.1	
11*b*	46.0	161.7	105.3	41.4	28.2	24.9	47.2						−4.2, −4.5 (Me_2), 26.1 (Me_3), 18.5
exo-**15**	41.5	73.0	126.6	136.3	35.8	(31.6)	25.0	(31.1)				0.4_2	
endo-**15**	42.7	74.3	128.9	134.9	35.6	33.1	21.9	37.8				0.3_5	
16*a*	42.5	61.0	9.8	22.2	36.6	29.1	24.7	31.2				1.0	
16*b*	42.6	61.2	10.0	22.4	36.7	29.0	24.8	31.2					−3.5, −3.7 (Me_2), 26.0 (Me_3), 18.1
17	41.5	73.2	126.6	136.3	36.0	(31.6)	25.0	(31.2)					−4.1, −4.3 (Me_2), 26.1 (Me_3), 18.4
19	51.8	72.6	125.0	137.9	49.7	45.0	(33.3)	29.2	(34.5)	40.8	26.4		−4.0, −4.2 (Me_2), 26.3 (Me_3), 18.2
20	39.3	62.6	13.7	25.5	35.0	32.3	19.6	29.2	34.4				−4.4, −4.6 (Me_2), 26.2 (Me_3), 18.3
21	47.1	60.6	19.8	16.5	28.4	42.0	40.8	26.6	21.3	26.7			−3.4, −3.5 (Me_2), 25.8 (Me_3), 17.8
22	47.5	73.4	146.7	34.3	39.8	39.8	26.0	19.7	27.1	115.0			−4.0, −4.3 (Me_2), 26.3 (Me_3), 18.6

[a]In ppm from TMS for C_6D_6 solutions, using the central solvent line as reference, δ_C 128.0; similar values in parentheses may be interchanged.

Upon reaction with CH_2I_2 (3.2 *M*) and Zn/Ag, **12** (1.2 *M*) gave, after 50 h, one major product (70% yield) having the molecular formula $C_{17}H_{30}OSi$ by precise mass measurement. The ^{13}Cmr spectrum gave no evidence of the presence of a cyclopropyl ring but rather contained signals for two monoprotonated olefinic carbons and a methine centre bearing oxygen. These and the remaining signals (Table 1) were entirely consistent with structure **19** for this product, showing that the reaction of **12** is strictly analogous to that of **11***b*. The specific assignments listed in Table 1 for **19** were aided by comparison with the results for some closely related tricyclo[5.3.1.0^{2,6}]undecane derivatives (2).

After 40 h reflux under comparable reaction conditions, **13** also gave rise to a single product having the formula $C_{15}H_{28}OSi$, by precise mass determination, showing the addition of one methylene group. In contrast to the preceding example, the ^{13}C spectrum of this product (75% yield) contained no olefinic absorption but included signals for a quaternary carbon bearing oxygen and a highly shielded methylene carbon, which is strong evidence for a cyclopropyl moiety. The spectrum is that expected for **20** arising from normal cyclopropanation. It may be noted that the shieldings (Table 1) for all skeletal carbons are very similar to those found for the cyclopropanated product obtained from the trimethylsilyl analog of **13** under our standard (dilute) conditions (1).

Under the concentrated conditions used for the Simmons–Smith reaction with **12** and **13**, **14** gave a product (80% yield) which was shown by glc analysis to contain two components in comparable amounts. Although pure samples of each could not be isolated, the ^{13}C spectra of the two components, each contaminated with ~10% of the other, readily revealed their structures as **21** and **22** (Table 1). The ^{13}C spectrum of **21** contained no olefinic absorption but exhibited highly shielded methylene (δ_C 19.8) and methine (16.5) carbons together with a quaternary signal typical of a cyclopropyl carbinyl carbon (60.6); these are entirely consistent with expectations for the compound arising from simple cyclopropanation. In addition, the shieldings for each of the skeletal carbons are very similar to those found for the product obtained by the Simmons–Smith

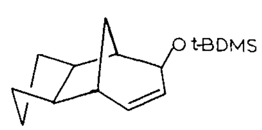

19

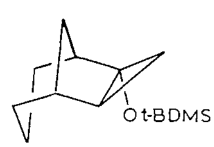

20

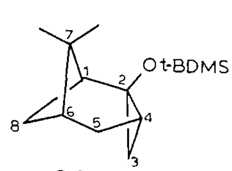

21

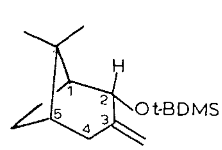

22

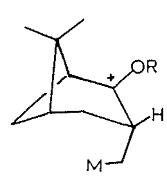

23

reaction, under dilute conditions, with the trimethylsilyl analog of **14**. The second product was identified as **22** by the appearance of olefinic signals for one fully substituted and one methylene carbon, δ_C 146.7 and 115.0, respectively, accompanied by signals for three methine carbons, one of which bears oxygen (73.4), two methyl, two methylene, and a quaternary carbon, as well as the absorptions for the *t*-BDMS grouping. An inspection of molecular models indicated that the initial cyclopropanation should favor the less hindered face of the double bond in **14** thereby generating **21**. Subsequent Lewis acid-catalyzed cleavage of the three-membered ring presumably proceeds through intermediate **23**, or equivalent, from which **22** is formed by hydride migration that dictates the orientation of the silyloxy grouping in **22**.

From these results, it is apparent that reagent concentration can be an important factor in the Simmons–Smith reaction of silyl enol ethers of polycyclic ketones. With a molar ratio of Zn/Ag:CH_2I_2:enol ether of 2:1:0:4 in Et_2O, the expected cyclopropyl silyl ether is obtained in good yield (70–90%) using dilute concentrations, typically $[CH_2I_2]$ = 0.5 *M*. Although in nearly all cases (1–8) relatively long reflux times (20–50 h) are required for optimum results, the reaction of **1** proceeds efficiently in 8 h. It may be noted that a single cyclopropanated ether has been obtained from each of the thirty polycyclic systems examined to date. Under these dilute conditions, the yields are comparable for the trimethylsilyl and *tert*-butyldimethylsilyl enol ethers. With the same molar ratio of reactants but with significantly less solvent, such that $[CH_2I_2] \geq 3$ *M*, the initial product may undergo further reaction whereby the cyclopropyl ether is cleaved to furnish an allylic ether. While the [2.2.1] derivatives **1**, **11**, and **12** yield the ring-expanded allylic ethers **3**, **15**, **17**, and **19**, the homologous [3.2.1] ether **13** gives only the expected cyclopropyl derivative **20**, indicating that the release of ring strain in species such as **2** and **16** provides the driving force for their isomerization to the ring-expanded products. The apparent instability of **21** and its isomerization to **22** can be ascribed to the relief of nonbonded interactions between the 3- and 8-methylene groups in **21**. In any event, these results clearly demonstrate two important features of the Simmons–Smith reaction with strained polycyclic silyl enol ethers. The concentrations of reactants can be a critical factor governing the composition of the reaction product, and the increased stability of the *tert*-butyldimethylsilyl derivatives relative to their trimethylsilyl counterparts leads to much more efficient conversion to allylic products arising from cleavage of the cyclopropyl ring.

Experimental

Boiling points are uncorrected. Gas–liquid chromatography (glc) was carried out on Varian 920 and 3700 instruments using columns of 10% Carbowax 20 M, 6% FFAP, or 10% SE-30 on Chromosorb W, as indicated. Tetrahydrofuran (THF) and ether were dried over sodium and freshly distilled before use. Diisopropylamine, triethylamine, and pyridine were distilled from CaH_2 and stored over 4A molecular sieves. Norcamphor and tricyclo[5.2.1.0^{2,6}]decan-8-one were available commercially and were used as purchased. Literature procedures were employed for the preparation of bicyclo[3.2.1]octan-6-one (12), 6,6-dimethylbicyclo[3.1.1]heptan-2-one (nopinone) (13), and 6-trimethylsilyloxy-*exo*-tricyclo[3.2.1.0^{2,4}]oct-6-ene (1, 6).

Infrared spectra were obtained with a Beckman 4250 spectrophotometer and mass spectra were recorded on a Varian MAT-311A instrument at 70 eV (direct inlet). Routine ^{1}Hmr spectra were obtained with either Varian T-60 or EM-360 instruments. The ^{13}Cmr spectra were obtained at 75.45 MHz with a Varian XL-300 instrument and comparison of fully decoupled ^{13}C spectra with those collected using either the APT (14) or DEPT (15) sequences identified the methyl, methylene, methine, and fully substituted carbon signals. All ^{13}C spectra were recorded for C_6D_6 solutions and the spectra calibrated using the central solvent peak (δ_C 128.0) as the reference line. Spectral widths of 200 ppm (δ_C −20 to 180) with pulse widths of 30° and 2-s repetition rates were employed for the decoupled spectra.

Preparation of silyl enol ethers

2-Trimethylsilyloxybicyclo[2.2.1]hept-2-ene (**11***a*) was prepared by the addition of norcamphor (2.0 g, 18.2 mmol) in 7 mL of THF to a stirred solution of LDA (formed from diisopropylamine (3.92 mL, 28 mmol), THF (16 mL), and *n*-BuLi (2.46 *M*, 9.74 mL) at −78°C, 30 min) under nitrogen and stirring was continued for 45 min. A quenching solution (prepared by centrifugation of a mixture of trimethylsilyl chloride (4.06 mL, 32 mmol) and Et_3N (1.40 mL, 10 mmol) in THF (7 mL) in a N_2-purged tube) was added, the mixture was allowed to warm to room temperature, and stirring continued for an additional 2.5 h. The reaction mixture was cooled to 0°C and, with vigorous stirring, a cold aqueous saturated solution of Na_2CO_3 (30 mL) was added. The product was isolated by pentane extraction (3 × 20 mL) and the combined extracts washed with saturated aqueous Na_2CO_3 solution and water before drying over $MgSO_4$. Removal of the solvent under reduced pressure gave crude **11***a*, which was purified by Kugelrohr distillation, bp 85–90°C/10 Torr (1 Torr = 133.3 Pa), 3.0 g, 84% yield, shown to be >90% pure by glc (FFAP). Preparative glc furnished an analytical sample for characterization; ir (film): 3080, 2960, 1605, 1334, 1225, 850 cm^{-1}; ^{1}Hmr ($CDCl_3$) δ: 0.37 (s, 9H, Me_3Si), 1.0–1.9 (m, 6H), 2.65 (m, 1H), 2.87 (m, 1H), and 4.80 (d, 1H, *J* = 3.8 Hz); ^{13}Cmr: Table 1.

2-tert-*Butyldimethylsilyloxybicyclo[2.2.1]hept-2-ene* (**11***b*) was prepared in a manner analogous to that described for **11***a* using diisopropylamine (2.67 mL, 19 mmol) in THF (23 mL) with *n*-Buli (16.4 mmol) in *n*-C_6H_{12} (6.5 mL) at −78°C for 30 min to generate LDA before the addition of norcamphor (1.50 g, 13.6 mmol). The quenching solution consisted of Et_3N (0.20 mL, 1.4 mmol) and *tert*-butyldimethylsilyl chloride (3.30 g, 21.9 mmol) in THF (2 mL) and, after its addition, stirring was continued for 5 h before warming to room temperature and stirring for an additional 2 h. After isolation by pentane extraction as described above, Kugelrohr distillation afforded **11***b*, bp 83–87°C/0.4 Torr, 2.57 g, 84% yield, found to be >95% pure by glc (FFAP); ir (film): 3078, 2930, 1611, 1328, 1230, 830 cm^{-1}; ^{13}Cmr: Table 1. *Exact Mass* calcd. for $C_{13}H_{24}OSi$: 224.1596; found: 224.1601.

8-tert-*Butyldimethylsilyloxytricyclo[5.2.1.0^{2,6}]dec-8-ene* (**12**) was generated from tricyclo[5.2.1.0^{2,6}]decan-8-one (1.0 g, 6.7 mmol) using the preceding procedure except that no Et_3N was required in the quenching solution. Kugelrohr distillation furnished **12**; bp 105–110°C/0.2 Torr; 1.32 g, 75% yield, which glc (FFAP) indicated to be ~95% pure; ir (film): 3080, 2940, 1625, 874 cm^{-1}; ^{13}Cmr: Table 1. *Exact Mass* calcd. for $C_{16}H_{28}OSi$: 264.1909; found 264.1912.

6-tert-*Butyldimethylsilyloxybicyclo[3.2.1]oct-6-ene* (**13**) was obtained from bicyclo[3.2.1]octan-6-one (0.50 g, 4 mmol) following the procedure described for **11***b*. Kugelrohr distillation (60–67°C/0.3 Torr) gave **13** (0.65 g, 68% yield) which was >98% pure by glc analysis (FFAP); ir (CCl_4): 3080, 2930, 1625, 1227, 875 cm^{-1}; ^{13}Cmr: Table 1. *Exact Mass* calcd. for $C_{14}H_{26}OSi$: 238.1753; found: 238.1754.

6,6-Dimethyl-2-tert-*butyldimethylsilyloxybicyclo[3.1.1]hept-2-ene* (**14**) was prepared similarly. Nopinone (0.50 g, 3.6 mmol) gave **14** (0.53 g, 58% yield) after Kugelrohr distillation (60–64°C/1 Torr) which glc (FFAP) indicated to contain 8% nopinone. Preparative glc furnished pure material; ir (CCl_4): 2930, 1650, 860 cm^{-1}; ^{13}Cmr: Table 1. *Exact Mass* calcd. for $C_{15}H_{28}OSi$: 252.1909; found: 252.1915.

Cyclopropanation reactions

General procedure

To a flask fitted with a reflux condenser, nitrogen purge, and a magnetic stirrer was added zinc–silver couple and the apparatus was flame-dried. After cooling to room temperature, a solution of CH_2I_2 in Et_2O was added and the mixture warmed until refluxing occurred without external heating. Upon the cessation of reflux, an ethereal solution of the silyl enol ether was added and the reaction mixture refluxed for several hours. At intervals small aliquots were removed by syringe and analyzed by glc to monitor the disappearance of the enol ether. After cooling to 0°C, the reaction was quenched with a 1 : 1 solution of Et_2O/pyridine and the resulting precipitate removed by filtration. After evaporation of the Et_2O, the residue was taken up in *n*-pentane, and filtered again to remove the last traces of precipitate before drying over $MgSO_4$. Upon removal of the solvent, the product was analyzed by glc and the individual components isolated by preparative glc.

In all experiments the molar ratio of zinc–silver couple: CH_2I_2 was 2:1, typically using 5 mmol of CH_2I_2. Under dilute conditions: $[CH_2I_2]$ = 0.5 *M*, $[ROSiR'_3]$ = 0.3 *M*; our concentrated conditions were $[CH_2I_2]$ = 3.0 *M*, $[ROSiR'_3]$ = 1.3 *M*.

Enol ether 1

Under dilute conditions and 15 h reflux, **1** gave a product containing by glc (SE-30) one major component (~65%) together with five minor ones, the largest of which constituted ca. 15% of the total product. Preparative glc (SE-30) furnished samples of the major and the largest minor components for ^{13}Cmr examination. The former gave rise to two sets of signals in a 4:1 ratio ascribable to **2** and **3**; as listed in Table 1, **2** had been characterized earlier (6). The ^{13}C spectrum of the second component also contained two sets of signals, one of which could be attributed tentatively to **4** (see Table 1).

Under concentrated conditions, **1** (0.45 g) gave a product mixture (0.34 g) from which the major component **4** (~35%) was isolated by preparative glc (SE-30). The ^{13}Cmr data are listed in Table 1. *Exact Mass* calcd. for $C_{13}H_{22}OSi$: 222.1440; found: 222.1429.

Enol ethers 11

After 50 h reflux under concentrated conditions, **11***a* (0.40 g) was found to give 140 mg of a mixture containing several compounds by glc from which one band was isolated by preparative glc representing ~15% of the total. The ^{13}Cmr (see Table 1) of this component indicated it to contain a 3:2 mixture of isomers **15**; ir (film): 3040, 2960, 1250, 840 cm^{-1}. *Exact Mass* calcd. for $C_{11}H_{20}OSi$: 196.1283; found: 196.1289.

Under dilute conditions, **11***b* (0.49 g) gave, after 19 h reflux, **16***b* (0.36 g, 69% yield) >98% pure by glc (FFAP); ir (CCl_4): 3015, 2960, 1340 cm^{-1}; ^{13}Cmr: Table 1. *Exact Mass* calcd. for $C_{14}H_{26}OSi$: 238.1753; found: 238.1747.

After 33 h reflux under concentrated conditions, **11***b* (0.49 g) furnished 0.50 g of product consisting of **17** (80% yield) and **16***b* (8% yield) by glc. Preparative glc furnished pure samples of **17**; ir (CCl_4): 3025, 2910, 1070 cm^{-1}; ^{13}Cmr: Table 1. *Exact Mass* calcd. for $C_{11}H_{26}OSi$: 238.1753; found: 238.1754. This experiment was repeated using CD_2I_2 (ms: 2.1% d_0, 19.4% d_1, 77.8% d_2; 1.75 atoms D/molecule), prepared according to a literature procedure (16), from which **11***b* (0.40 g) gave rise to 0.36 g of product consisting of **16***b*-d_x and **17**-d_x in a 4:5 ratio by glc, representing 90% of the total product. For **16***b*-d_x (34% yield); ms: 1.4% d_0, 10.7% d_1, 87.7% d_2; 1.87 atoms D/molecule; **17**-d_x (43% yield); ms, 3.8 d_0, 29.8% d_1, 63.5 d_2; 1.64 atoms D/molecule; ^{13}Cmr: see text.

Enol ether 12

With concentrated conditions and a 50-h reflux period, **12** (0.40 g) gave 0.37 g of product, which glc (FFAP) indicated to contain 80% of **19** (70% yield); ^{13}Cmr: Table 1. *Exact Mass* calcd. for $C_{17}H_{30}OSi$: 278.2066; found: 278.2069.

Ether 13

With 50 h reflux under concentrated conditions, **13** (0.30 g) gave a single product **20** (0.24 g, 76% yield) by glc analysis (FFAP); ir (CCl_4): 3010, 2930, 1345, 920 cm^{-1}; ^{13}Cmr: Table 1. *Exact Mass* calcd. for $C_{15}H_{28}OSi$: 252.1909; found: 252.1910.

Enol ether 14

Under concentrated conditions with 43 h reflux, **14** (0.40 g) furnished 0.34 g (80% yield) of product mixture containing approximately equal quantities of **21** and **22**. Preparative glc failed to furnish pure samples of each component but the components were identified by their ^{13}C spectra (see text and Table 1).

Acknowledgements

We wish to acknowledge the financial support provided by the Natural Sciences and Engineering Research Council of Canada in the form of scholarships (A.J.R.) and operating grants.

1. Y. HOYANO, V. PATEL, and J. B. STOTHERS. Can. J. Chem. **58**, 2730 (1980).
2. B. A. DAWSON and J. B. STOTHERS. Org. Magn. Reson. **21**, 217 (1983).
3. J. L. JURLINA, H. A. PATEL, and J. B. STOTHERS. Can. J. Chem. **62**, 1159 (1984).
4. B. A. DAWSON, A. K. GHOSH, J. L. JURLINA, A. J. RAGAUSKAS, and J. B. STOTHERS. Can. J. Chem. **62**, 2521 (1984).
5. V. PATEL and J. B. STOTHERS. Can. J. Chem. **58**, 2728 (1980).
6. A. J. RAGAUSKAS and J. B. STOTHERS. Can. J. Chem. **63**, 1250 (1985).
7. S. MURAI, T. AYA, T. RENGE, I. RYO and N. SONADA. J. Org. Chem. **39**, 858 (1974).
8. I. RYU, S. MURAI, S. OTANI, and N. SONADA. Tetrahedron Lett. 1995 (1977).
9. J. B. STOTHERS and C. T. TAN. Can. J. Chem. **55**, 841 (1977).
10. J. ORBAN, J. V. TURNER, and B. TWITCHIN. Tetrahedron Lett. **25**, 5099 (1984); L. N. MANDER and S. P. SETHI. Tetrahedron Lett. **25**, 5953 (1984).
11. A. NICKON, J. J. FRANK, D. F. COVEY, and Y.-I. LIN. J. Am. Chem. Soc. **96**, 7574 (1974).
12. K. B. WIBERG and B. A. HESS. J. Org. Chem. **31**, 2250 (1965).
13. R. CRIEGEE and P. GUNTHER. Chem. Ber. **96**, 1564 (1963).
14. S. L. PATT and J. N. SHOOLERY. J. Magn. Reson. **46**, 535 (1982).
15. D. M. DODDRELL, D. T. PEGG, and M. R. BENDALL. J. Magn. Reson. **48**, 323 (1982).
16. H. TAKAYA, T. SOZUKI, Y. KUMAGAI, M. YAMAKAWA, and K. NOYORI. J. Org. Chem. **46**, 2846 (1981).
17. A. J. RAGAUSKAS and J. B. STOTHERS. Can. J. Chem. **63**, 2961 (1985).

Quadrupolar relaxation effects in methyl-substituted ammonium ions as determined by ^1H nuclear magnetic resonance

JAMES D. HALLIDAY, PATRICK E. BINDNER, AND SHAHSULTAN PADAMSHI
Atomic Energy of Canada Limited Research Company, Chalk River Nuclear Laboratories, Chalk River, Ont., Canada K0J 1J0

Received March 14, 1985

JAMES D. HALLIDAY, PATRICK E. BINDNER, and SHAHSULTAN PADAMSHI. Can. J. Chem. **63**, 2975 (1985).

Nitrogen-14 quadrupole interactions broaden the ^1H nuclear magnetic resonances of the ammonium protons spin-coupled to ^{14}N in the methyl-substituted ammonium chlorides (methylammonium, dimethylammonium, and trimethylammonium). These proton lineshapes have been determined over the temperature range −8.3 to +93.6°C in 6 mol L^{-1} aqueous HCl solution. The ^{14}N spin-lifetimes, τ, have been calculated from the Arrhenius form equation ln τ vs. $1/T$ (K), and yield activation energies of 10.63 ± 0.92, 10.60 ± 0.52, and 11.12 ± 0.39 kJ mol^{-1} for the mono-, di-, and tri-methyl species, respectively. The ^{14}N nmr linewidths have been extracted from these data and a comparison is made with ^{14}N nmr spectra obtained by Ogg and Ray.

JAMES D. HALLIDAY, PATRICK E. BINDNER et SHAHSULTAN PADAMSHI. Can. J. Chem. **63**, 2975 (1985).

Les interactions quadrupolaires du ^{14}N élargissent les pics de rmn du ^1H des protons ammonium couplés par leurs spins au ^{14}N des chlorures d'ammonium portant des substituants méthyles (méthylammonium, diméthylammonium et triéthylammonium). On a déterminé la forme des pics de ces protons dans l'intervalle de température allant de −8,3 à +9,6°C, dans des solutions aqueuses à 6 mol L^{-1} HCl. On a calculé le temps de vie du spin du ^{14}N, τ, à partir d'une équation de type Arrhénius, ln τ vs. $1/T$ (K), et l'on en a tiré les énergies d'activation qui sont respectivement de 10,63 ± 0,92, 10,60 ± 0,52 et 11,12 ± 0,39 kJ mol^{-1} pour les espèces mono-, di- et triméthylammonium. À partir de ces données, on a déduit la largeur des pics de rmn du ^{14}N et on les a comparé avec les spectres de Ogg et Ray.

[Traduit par le journal]

Introduction

An efficient spin relaxation mechanism in compounds containing ^{14}N is provided through the interaction of the quadrupole moment of the ^{14}N nucleus with the electric field gradients present in the molecule. The spin-lifetimes and consequently the linewidths of the ^{14}N will vary with the magnitude of this interaction. Ogg and Ray (1) showed this qualitatively for the ammonium ion and a series of methyl-substituted ammonium ions. The ^{14}N linewidth in the symmetrical $\overset{+}{N}H_4$ ion is very narrow (long spin-lifetimes) and becomes much broader when one, two, or three methyl groups, which introduce increased asymmetry in the electric field gradients, are substituted (shorter spin-lifetimes). The ^{14}N spin-lifetimes may also be obtained from lineshape analysis (2, 3) of nuclei spin-coupled to the ^{14}N, i.e., ^1H for the ammonium ions. We have been able to use this latter technique to expand on the original report of Ogg and Ray (1) by determining the ^{14}N spin-lifetimes quantitatively for methyl-, dimethyl-, and trimethylammonium chlorides as a function of temperature.

Experimental

The mono-, di-, and trimethylammonium chlorides were prepared by the reaction of the corresponding free amines (Matheson, Eastman) with double distilled hydrochloric acid (Anachemia). The amines were first purified by repeated cryogenic (liquid N_2) vacuum distillation using a stainless steel and glass vacuum line. The nmr samples were 6 mol L^{-1} substituted ammonium salt in 6 mol L^{-1} aqueous HCl. A saturated solution of ammonium chloride was also prepared.

The nmr spectra of the samples in Wilmad 528 (5 mm) nmr tubes were obtained on a CW Bruker HX90 spectrometer equipped with a B-ST 100/700 variable temperature accessory (±0.5°C) and a Nicolet 1174 signal averager.

Results

The ^1H nmr spectra of the mono-, di-, and trimethylammonium chlorides and the unsubstituted ammonium chloride were recorded as a function of temperature between −8.3 and 93.6°C. Sample spectra run at 52°C are shown in Fig. 1. The coupling constants, $J_{^{14}NH}$ and $J_{HC^{14}NH}$, determined for these compounds are given in Table 1. The $J_{^{14}NH}$ were calculated from the $J_{^{15}NH}$, which are directly measurable from the spectra through the 0.37% natural abundance ^{15}N sidebands. These coupling constants are related through their gyromagnetic ratios in eq. [1].

TABLE 1. Coupling constants (^{14}N–H and H—C—^{14}N–H) in substituted ammonium ions

Compound	$J_{^{14}NH}$ (Hz)	$J_{HC^{14}NH}$ (Hz)
$\overset{+}{N}H_4$	52.5	—
NH_3[a]	43.8	—
$CH_3\overset{+}{N}H_3$	53.6	6.18
$(CH_3)_2\overset{+}{N}H_2$	54.5	5.69
$(CH_3)_3\overset{+}{N}H$	54.7	5.19

[a] Reference 4.

$$[1] \quad J_{^{14}NH} = -\frac{\gamma^{14}N}{\gamma^{15}N} \cdot J_{^{15}NH}$$

The ^{14}N spin-lifetimes found from lineshape analysis of the ^{14}N-H proton spectra are shown in Fig. 2. The method for determining these values using the theories of Sack and Pople (2, 3) has been described previously (5, 6), and is outlined briefly below for continuity.

The lineshape is given by eq. [2].

$$[2] \quad I(\nu) \propto Re(\mathbf{W} \cdot \mathbf{A}^{-1} \cdot \mathbf{1})$$

where $I(\nu)$ = line intensity at frequency ν, Re = "real part of", $\mathbf{W}$ = a vector containing the probabilities of the spin states in the ^{14}N, $\mathbf{A}$ = a lineshape matrix given by

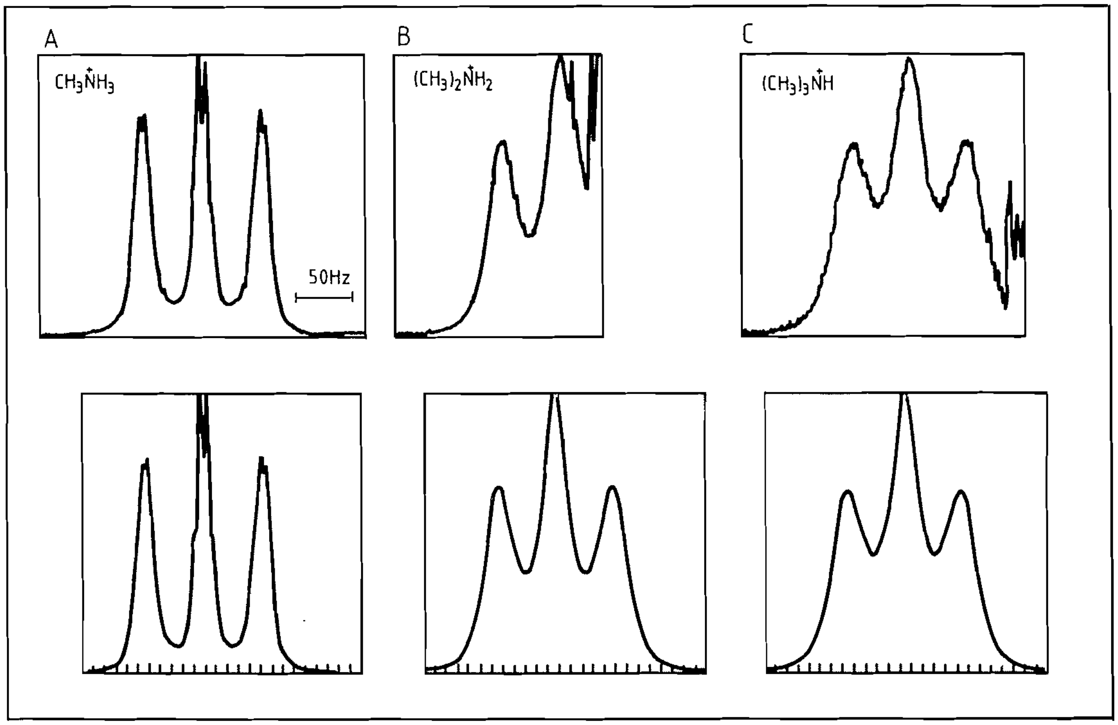

FIG. 1. Experimental methyl-substituted ammonium ion proton nmr spectra at 52°C for: (A) $CH_3\overset{+}{N}H_3$, (B) $(CH_3)_2\overset{+}{N}H_2$, and (C) $(CH_3)_3\overset{+}{N}H$, in 6 mol L^{-1} HCl. The calculated spectra are shown below each experimental one.

$$\mathbf{A} = \begin{bmatrix} \beta_1 & 1/\tau & 2/\tau \\ 1/\tau & \beta_2 & 1/\tau \\ 2/\tau & 1/\tau & \beta_3 \end{bmatrix}$$

The diagonal elements of **A** are defined by:

$$\beta_1 = i2\pi(\nu_0 - \nu + J_{^{14}NH}) - \frac{3}{\tau} - \frac{1}{T_2}$$

$$\beta_2 = i2\pi(\nu_0 - \nu) - \frac{2}{\tau} - \frac{1}{T_2}$$

$$\beta_3 = i2\pi(\nu_0 - \nu - J_{^{14}NH}) - \frac{3}{\tau} - \frac{1}{T_2}$$

with τ = ^{14}N spin-lifetime, T_2 = spin–spin relaxation time, and **1** = the unit matrix.

The fits of the simulated spectra to the experimental spectra showed small deviations at the higher temperatures and this is attributed to the onset of ammonium ion proton exchange. In these strongly acidic solutions ammonium ion proton exchange is effectively stopped on the nmr timescale at room temperature and below (7), but some exchange occurs as the temperature is raised to 93.6°C. This is consistent with some broadening of the methyl group resonances. Within the experimental error the $\ln \tau$ vs. $1/T$ plots do not show significant falloff in τ at the high temperature end and hence the effect of this exchange is considered small. Consequently no exchange parameter was included in the calculations of the lineshapes.

Discussion

The analysis of the ammonium ions' proton nmr lineshapes has enabled the extraction of the ^{14}N spin-lifetimes, τ, in solution as a function of temperature (Fig. 2). These τ may be used to calculate: (1) the ^{14}N spin lattice relaxation times, T_1; (2) the correlation times characterizing the quadrupolar or molecular reorientations in solution, τ_q; and (3) the activation parameters for the molecular reorientations.

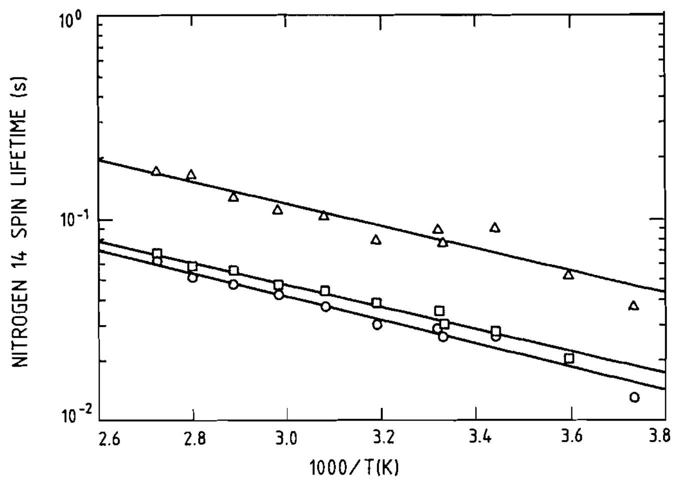

FIG. 2. Temperature dependence of the ^{14}N spin-lifetimes for the methyl-substituted ammonium ions (6 mol L^{-1} in 6 mol L^{-1} HCl): □- methyl, △- dimethyl, ○- trimethyl.

The ^{14}N T_1 are related to τ through eq. [3] (8)

[3] $\tau = 5T_1$

Since, under the conditions of observation, $T_1 = T_2$ (the spin–spin relaxation time), the ^{14}N linewidths in the absence of any spin coupling to protons may be determined by relation [4]

[4] $\Delta\nu_{1/2} = 1/\pi T_2$

Thus, the effect on the ^{14}N linewidths of substituting the ammonium ion's protons with methyl groups is shown quantitatively in Table 2.

A comparison can be made between our ^{14}N linewidth mea-

TABLE 2. Effect of methyl substitution on the ^{14}N linewidth in the ammonium ion (25°C)

Species	τ (ms)	T_1 ^{14}N (ms)	$\Delta\nu_{1/2}$ ^{14}N (Hz)	Ogg and Ray[b]
$\overset{+}{N}H_4$	>10000	>2000	<0.2	—
NH_3[a]	162.5	32.5	9.8	—
$CH_3\overset{+}{N}H_3$	49.7	9.93	32.1	32
$(CH_3)_2\overset{+}{N}H_2$	19.7	3.94	80.7	169
$(CH_3)_3\overset{+}{N}H$	16.5	3.30	96.4	146

[a]Reference 4.
[b]Reference 1.

surements obtained from proton spectra and the ^{14}N spectra measured directly by Ogg and Ray (1) on the methyl-substituted ammonium ions. The values noted in Table 2 for Ogg and Ray's results are qualitative only since they are calculated from the spectra shown in the paper. However, the differences are large enough to show that Ogg and Ray's ^{14}N linewidths for both the di- and trimethylammonium ions are much larger than the calculated ones. This is not the case for the monomethylammonium ion. Examination of Ogg and Ray's ^{14}N spectra shows a solution to this anomaly. The monomethylammonium ion has the expected quartet from coupling with the attached protons but there are no resolved couplings for either the di- or trimethylammonium ions. These unresolved proton couplings could account for the differences since the $J_{^{14}NH}$ is 54.5 Hz and 54.7 Hz respectively in these compounds, even though proton spin coupling was discounted in the original paper because no splitting was observed in the spectra. The linewidth in the unsubstituted ammonium ion is very small, indicating that the ^{14}N spin-lifetime is long. This reflects the high symmetry in the ion and the absence of any significant electric field gradients. Liquid ammonia is included in the table to show the effect of altering the symmetry by removal of a proton from the ammonium ion. The presence of the lone pair of electrons reduces by approximately two orders of magnitude the ^{14}N T_1 but, in contrast to the earlier studies (1), does not alter the electric field symmetry of the $\overset{+}{N}H_4$ as much as introducing a methyl group substituent. Table 2 also shows that there is a continued increase in the electric field asymmetry with the introduction of two and three methyl groups into the ammonium ion. Tetramethylammonium chloride does not have any ammonium protons, so a direct comparison with the ^{14}N spectrum of this compound cannot be made. However, since it is a highly symmetric species a small ^{14}N linewidth would be expected. This is confirmed through the very narrow well-resolved proton 1 : 1 : 1 triplet obtained from coupling of the ^{14}N to the methyl group protons (9); only a very long ^{14}N spin-lifetime would allow observation of this feature.

The quadrupolar (molecular reorientation) correlation time, τ_q, is related to the spin-lattice relaxation time, T_1, and the quadrupolar coupling constant, e^2qQ/h, through eq. [5] (8),

$$[5]\quad \frac{1}{T_1} = \frac{3}{40}\frac{2I+3}{I^2(2I-1)}\left(1+\frac{\eta^2}{3}\right)\left(\frac{e^2qQ}{\hbar}\right)^2\tau_q$$

For ^{14}N with $I = 1$ this equation simplifies to eq. [6] (10)

$$[6]\quad \frac{1}{T_1} = \frac{3}{8}\left(1+\frac{\eta^2}{3}\right)\chi^2\cdot 4\pi^2\cdot\tau_q$$

where η is the asymmetry parameter of the electric field gradient and $\chi = e^2qQ/h$. Unlike the methyl-substituted amines (11), values for χ in this system are not available, so τ_q cannot be calculated for these methyl-substituted ammonium ions.

TABLE 3. Activation energies for molecular reorientation of methyl-substituted ammonium chlorides

Compound	E_a (kJ mol^{-1})
NH_4Cl	—
NH_3	7.59 ± 0.23[a]
CH_3NH_3Cl	10.63 ± 0.92
$(CH_3)_2NH_2Cl$	10.60 ± 0.52
$(CH_3)_3NHCl$	11.12 ± 0.39

[a]Reference 4.

The temperature dependence of the ^{14}N spin-lifetimes (proportional to T_1) shown in Fig. 2 can be used to determine activation energies for quadrupolar (molecular reorientation) interactions in solution through the slopes of the Arrhenius plots. These are average values because the methyl-substituted ammonium ions are not spherically symmetric. The derivation of eq. [5] assumes the molecular reorientation to be isotropic with respect to the axes of the coupling tensor, and thus be described by a single τ_q. This is true only for molecule of high symmetry. The molecular reorientation energies for the methyl-substituted ammonium ions in aqueous acid solution are given in Table 3. Within the experimental error the number of methyl groups in the ammonium ion has no effect on its molecular reorientation activation energy in aqueous acid solution. However, for liquid ammonia the activation energy decreases by ~3 kJ mol^{-1}. The activation energy for the unsubstituted ammonium ion has not been determined because the spin-lifetimes of the ^{14}N are too long to measure accurately. The similarity of the activation energies for the methyl-substituted species indicates that hydrogen bonding in the aqueous phase has a more important effect than molecular geometry on molecular reorientation.

In conclusion, the nmr spectra of the protons spin-coupled to the ^{14}N of methyl-substituted ammonium ions have allowed a quantitative analysis of the ^{14}N linewidths of these ions in acid solution. Unresolved spin coupling between ^1H and ^{14}N has been shown to account for the broad lines originally observed by Ogg and Ray (1) using ^{14}N nmr. Methyl substitution in the series $\overset{+}{N}H_4 \rightarrow (CH_3)_3\overset{+}{N}H$ produced increased electric field gradients in the molecules with each additional methyl group. The similar activation energies for each methyl-substituted ammonium ion indicate that hydrogen bonding plays an important role in molecular reorientation in aqueous solution.

1. T. A. OGG and J. D. RAY. J. Chem. Phys. **26**, 1340 (1957).
2. R. A. SACK. Mol. Phys. **1**, 163 (1958).
3. J. POPLE. Mol. Phys. **1**, 168 (1958).
4. T. J. SWIFT, S. B. MARKS, and W. G. SAYRE. J. Chem. Phys. **44**, 2797 (1966).
5. J. D. HALLIDAY and P. E. BINDNER. J. Phys. Chem. **83**, 1829 (1979).
6. J. P. KINTZINGER, J. M. LEHN, and R. L. WILLIAMS. Mol. Phys. **17**, 135 (1969).
7. E. GRUNWALD, A. LOEWENSTEIN, and S. MEIBOOM. J. Chem. Phys. **27**, 630 (1957); **27**, 641 (1957).
8. A. ABRAGAM. The principles of nuclear magnetism. Oxford University Press. 1961.
9. D. W. LARSEN. J. Phys. Chem. **74**, 3380 (1970); **75**, 509 (1971).
10. W. B. MONIZ and H. S. GUTOWSKY. J. Chem. Phys. **38**, 1155 (1963).
11. J. D. HALLIDAY, P. E. BINDNER, and S. PADAMSHI. Can. J. Chem. **62**, 1258 (1984).

The X-ray crystal structure of a Corynanthé-type indole compound, $C_{22}H_{29}N_2O_4^+Br^-$, wherein an unprecedented triaxial conformation is preferred

ANGÈLE CHIARONI, CLAUDE RICHE, DAVID S. GRIERSON,[1] AND HENRI-PHILIPPE HUSSON
Institut de Chimie des Substances Naturelles, C.N.R.S., 91190 Gif s/Yvette, France

Received December 4, 1984

ANGÈLE CHIARONI, CLAUDE RICHE, DAVID S. GRIERSON, and HENRI-PHILIPPE HUSSON. Can. J. Chem. **63**, 2979 (1985).

On the basis of ^1H and ^{13}C nmr data, a conformation was proposed for the Corynanthé type indole compound **8** in which the substituents at C-3 (indole), C-14 (ethyl), and C-15 (malonyl) were all axial. An X-ray crystal study on the HBr salt of **8** confirmed that this a priori unexpected conformation is also preferred in the solid state.

ANGÈLE CHIARONI, CLAUDE RICHE, DAVID S. GRIERSON et HENRI-PHILIPPE HUSSON. Can. J. Chem. **63**, 2979 (1985).

Nous avions proposé, grâce à une étude de rmn de ^1H et de ^{13}C d'un composé **8**, analogue des alcaloïdes de type Corynanthé, une conformation pour laquelle les substituants en C-3 (noyau indole), en C-14 (chaîne éthyle) et en C-15 (groupement malonate) étaient tous axiaux. Une étude aux rayons X d'un cristal du bromhydrate de **8** a montré qu'une telle conformation a priori inattendue existe à l'état cristallin.

In a number of recent papers (1, 2) we have shown that 2-cyano Δ^3 piperideines **1** react efficiently with a wide range of nucleophiles, and that they thus represent stable "equivalent" forms of the corresponding 5,6-dihydropyridinium salts **2**.

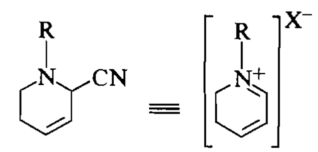

1 **2**

Taking advantage of this reactivity we demonstrated, using a model system, that the C-15 substituted indoloquinolizidine unit typical of early members of the Corynanthé type indole alkaloids could be constructed in three steps from the 2-cyano Δ^3 piperideine **3** (3) (Scheme 1). This involved (a) condensation of aminonitrile **3** with sodium dimethylmalonate in the presence of $AgBF_4$ producing the enamine **4** (90% yield); (b) cleavage of the N_a (indole)-benzene sulfonyl deactivating group (Bu^tOK, THF; 80%); and (c) cyclization of the resulting intermediate **5** in acidic media (HCl/MeOH, 3 days). The three "inside" Corynanthé compounds **6**−**8** (4) were thus obtained in a combined overall yield of 45% from **3**.

For products **6** and **7**, the relative configuration of the C-3, C-14, and C-15 centers and the preferred conformations were readily deduced from a detailed analysis of their ^1H (400 MHz) and ^{13}C nmr spectra (Fig. 1). These assignments were supported by molecular mechanics calculations using the computer program SCRIPT (ROUSSEL−UCLAF) (5), which showed that the preferred conformations for **6** and **7** were at least 3 kcal/mol more stable than the alternative conformations examined (3).

For compound **8**, however, the situation was less evident. From the downfield position of the H-3 resonance (δ 3.93, d, J = 4.5 Hz) in the ^1H nmr spectrum and the absence of Wenkert−Bohlmann bands in the ir spectrum it was deduced that the molecule adopted a *cis* C/D ring conformation. It was further deduced from the observation of a single absorption (δ 1.80, qn) for the C-19 methylene protons and a hextet resonance for H-15 with $J_{15,20ax}$ = 4.5 Hz that both the C-14 ethyl and C-15 malonyl substituents were in axial orientations. Certain aspects of the ^{13}C nmr spectrum of **8**, in particular the ~4-ppm upfield α- and γ-effect shifts of the C-15 and C-21 absorptions produced by the malonyl groups, were in agreement with these assignments.

Although several features in both the ^1H and ^{13}C spectra remained unexplainable (i.e. the unusually high field position and small coupling constant (δ 3.44, J = 9 Hz) for the H-16 absorption, and the appearance of the C-6 resonance at δ 19.0, a position intermediate between that normally attributed to the *cis* (δ 16.0) and *trans* (δ 21.0) indoloquinolizidine systems (6)) we were forced to conclude that compound **8** possessed a *cis* indoloquinolizidine structure in which the C-3 indole, C-14 ethyl, and C-15 malonyl groups were all in *axial* positions.

This result was unprecedented[2] and rather difficult to accept for two major reasons: (1) in a structure such as **8***a* (Fig. 1) a highly unfavourable 1,3-diaxial interaction between the C-3 indole and C-15 malonyl groups would be predicted, and (2) in view of this interaction one would expect that an equilibration to the a priori more stable conformer **8***a* would occur, in which the three substituents adopt an all-equatorial orientation.[3]

To lay to rest all remaining doubts concerning the structure of this unusual molecule an X-ray crystal study of a suitable derivative (HBr salt) was undertaken. It was realized that even if the solid and solution state conformations of **8** did not correspond, the relative configuration at the C-3, C-14, and C-15 centers could still be established definitively.

Experimental

Crystals of the HBr salt of **8** were obtained by slow saturation of a methanol solution of **8**·HBr with ether, mp 185−187°C (dec.). A parallelepipedic crystal of dimensions 0.35 × 0.20 × 0.15 mm was used for data collection and determination of the unit cell on a Philips PW 1100 diffractometer using graphite monochromated Cu-Kα radiation (λ = 1.5418 Å). The crystal data are:

$C_{22}H_{29}N_2O_4^+Br^-$ Mol. wt. = 465.39

Orthorhombic; space group *Pbca*; a = 11.181 (4), b = 15.130 (6), c = 26.74 (1) Å; Z = 8; V = 4523 Å^3; F_{000} = 1936, μ = 25.27 cm^{-1}.

[1]Author to whom correspondence may be addressed.

[2]Certain carbohydrates such as α-D idopyranose pentaacetate (10) also prefer a 1,2,3-triaxial conformation. This is due, however, to the strong tendency for such molecules to adopt the conformation in which the C-1 OR substituent is axial (anomeric effect) and the C-5 substituent is equatorial.

[3]The possibility that compound **8** adopts an all-equatorial conformation as in **8***a* or **8***b* was excluded on the basis of the small $J_{3,14}$ = 4.5 Hz and $J_{14,15}$ = 4.5 Hz coupling constants observed in the ^1H nmr spectrum.

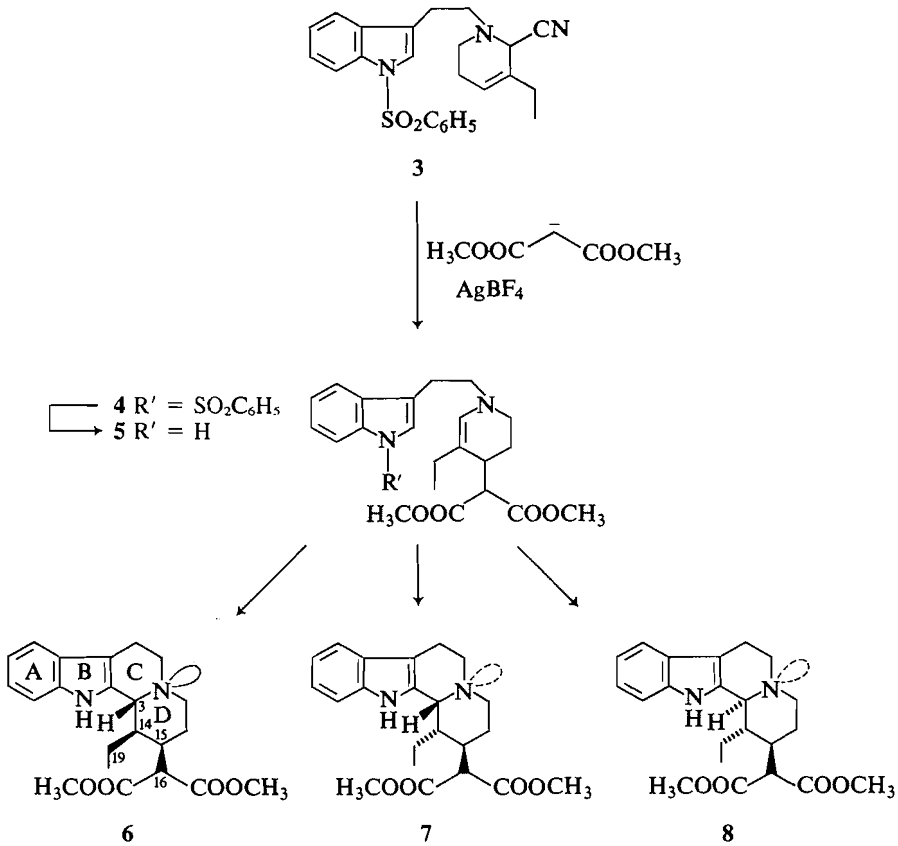

SCHEME 1

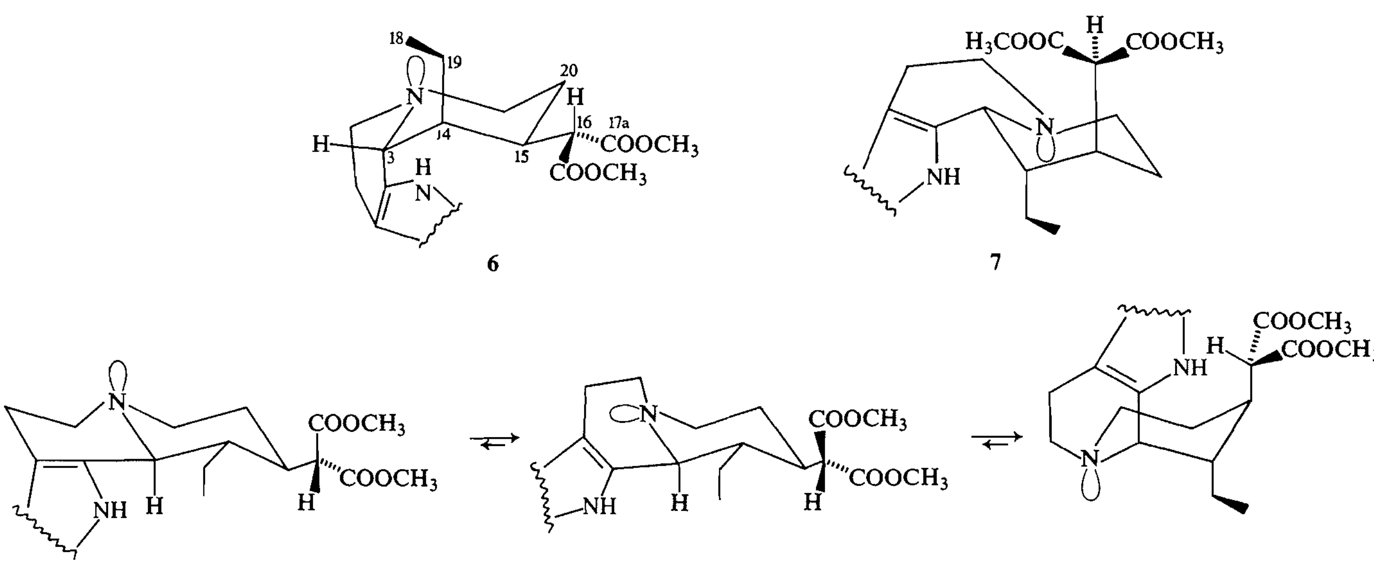

8*a* 8*b* 8*c*

FIG. 1. Three-dimensional representations of the preferred conformations of compounds **6** and **7**, and the principal conformations *a*–*c* of compound **8**.

Parameter values were obtained by the least-squares refinement of 12 well-centered reflections. The data were collected using the $\theta-2\theta$ scan technique with a speed of 0.05 deg s^{-1}, and a scan width of 1.2° + 0.2° tg θ. The three standard reflections monitored every 120 min did not show any appreciable variation in intensity during data collection. From 3360 independent intensities, 1902 with $I > 3\sigma(I)$ were considered as observed.

The structure was solved by the Patterson–Fourier method and refined by least-squares techniques which minimized the function $\Sigma w(|F_o| - |F_c|)^2$. All hydrogen atoms were located on successive difference Fourier maps and introduced in structure factor calculations in idealized positions ($d_{C—H}$ = 1.08 Å) with an isotropic temperature factor equivalent to that of the bonded atom. On the difference Fourier maps a water molecule (originating from the use of aqueous HBr to prepare the hydrogen bromide salt of **8**) displaying high thermal motion was found to be hydrogen bonded to O-22'. It was thus introduced into the refinement with an occupation factor of 0.50. This lowered the final R factor from 0.059 to 0.055 (R_w = 0.062). The weighting

TABLE 1. Fractional coordinates $\times 10^4$ for the non-hydrogen atoms

Atom	x	y	z
Br	9576(1)	7381(1)	9283(1)
N1	4944(5)	4576(3)	9239(2)
C2	5506(6)	5394(4)	9232(2)
C3	6818(6)	5511(4)	9179(2)
N4	7073(5)	6483(3)	9084(2)
C5	6364(7)	7074(4)	9442(2)
C6	5029(7)	6999(4)	9360(3)
C7	4690(6)	6039(4)	9330(2)
C8	3557(6)	5621(4)	9418(2)
C9	2426(6)	5936(4)	9548(2)
C10	1515(6)	5337(5)	9619(2)
C11	1728(7)	4425(5)	9551(2)
C12	2835(6)	4092(5)	9415(2)
C13	3745(6)	4708(4)	9357(2)
C14	7440(6)	4914(4)	8787(2)
C15	7303(5)	5232(4)	8239(2)
C16	6038(6)	5067(4)	8023(2)
C17	5780(7)	4095(5)	7965(3)
C18	9449(7)	4162(5)	8575(3)
C19	8775(6)	4789(4)	8927(3)
C20	7664(6)	6206(4)	8206(2)
C21	6920(6)	6779(4)	8552(2)
O22	6504(6)	3506(3)	7973(2)
O23	4612(6)	3984(4)	7910(3)
C24	4204(12)	3074(7)	7858(5)
C17′	5945(7)	5505(5)	7515(3)
O22′	5240(6)	6059(4)	7409(2)
O23′	6762(6)	5188(3)	7205(2)
C24′	6904(10)	5634(7)	6726(3)
W	3934(35)	7327(20)	8018(14)

scheme was $w^{-1} = (\sigma^2(F_o) + 0.007\ F_o^2)^{-1}$ where $\sigma^2(F_o)$ was based on counting statistics.

The program used was SHELX 76 (7) with coefficients for analytical approximation to the scattering factors from the International Tables for X-ray Crystallography. Final atomic coordinates with estimated standard deviations are reported in Table 1. Bond distances and angles appear in Table 2, and torsion angles in Table 3.[4]

TABLE 2. Bond lengths (Å) and bond angles (°)

Bond	Length	Bond	Angle
N1—C2	1.389(8)	C2—N1—C13	108.1(5)
N1—C13	1.391(8)	N1—C2—C3	123.7(5)
C2—C3	1.485(9)	N1—C2—C7	109.4(5)
C2—C7	1.361(9)	C3—C2—C7	126.6(6)
C3—N4	1.519(8)	C2—C3—N4	108.4(5)
C3—C14	1.549(8)	C2—C3—C14	116.0(5)
N4—C5	1.531(9)	N4—C3—C14	111.6(5)
N4—C21	1.501(8)	C3—N4—C5	111.3(5)
C5—C6	1.514(11)	C3—N4—C21	115.2(5)
C6—C7	1.504(9)	C5—N4—C21	111.1(5)
C7—C8	1.435(9)	N4—C5—C6	112.0(5)
C8—C9	1.395(9)	C5—C6—C7	109.2(6)
C8—C13	1.407(9)	C2—C7—C6	122.2(6)
C9—C10	1.376(10)	C2—C7—C8	108.0(5)
C10—C11	1.411(10)	C6—C7—C8	129.7(6)
C11—C12	1.386(10)	C7—C8—C9	133.7(6)
C12—C13	1.389(9)	C7—C8—C13	106.3(5)
C14—C15	1.550(8)	C9—C8—C13	119.9(6)
C14—C19	1.551(10)	C8—C9—C10	118.8(6)
C15—C16	1.548(9)	C9—C10—C11	120.1(6)
C15—C20	1.530(9)	C10—C11—C12	122.7(7)
C16—C17	1.507(10)	C11—C12—C13	116.1(6)
C16—C17′	1.516(10)	N1—C13—C8	108.2(5)
C17—O22	1.204(10)	N1—C13—C12	129.4(6)
C17—O23	1.324(10)	C8—C13—C12	122.5(6)
C18—C19	1.534(10)	C3—C14—C15	114.5(5)
C20—C21	1.516(9)	C3—C14—C19	109.8(5)
O23—C24	1.457(12)	C15—C14—C19	111.2(5)
C17′—O22′	1.185(10)	C14—C15—C16	113.1(5)
C17′—O23′	1.322(10)	C14—C15—C20	109.1(5)
O23′—C24′	1.457(10)	C16—C15—C20	112.0(5)
		C15—C16—C17	111.8(5)
		C15—C16—C17′	109.0(5)
		C17—C16—C17′	108.7(6)
		C16—C17—O22	126.2(7)
		C16—C17—O23	108.9(6)
		O22—C17—O23	124.8(7)
		C14—C19—C18	113.6(6)
		C15—C20—C21	111.8(5)
		N4—C21—C20	110.2(5)
		C17—O23—C24	116.1(8)
		C16—C17′—O22′	124.7(7)
		C16—C17′—O23′	110.8(6)
		O22′—C17′—O23′	124.5(7)
		C17′—O23′—C24′	117.3(7)

Results and discussion

The X-ray crystal structure determined for the HBr salt of compound **8** is illustrated in the two 3-dimensional representations in Figs. 2a and 2b. One can see that in the solid state the molecule also adopts the *cis* indoloquinolizidine conformation where the C-3, C-14, and C-15 substituents are axially oriented. From calculations of the torsion angles (Table 3) one can further see that the D-ring is in a chair conformation that is slightly flattened in the region of carbons-3, -14, and -15. This flattening effect results in an opening of the angle between the C-2—C-3 and C-15—C-16 bonds by ~27° (with respect to an idealized chair conformation), thereby increasing the separation between the indole and malonyl substituents. A clear view of the disposition of these two substituents in the molecule is presented in Fig. 2b. It can be seen that the angle between C-16—H-16 and the normal to the indole plane is 115° and that the C-17—O-22 carbonyl groups are twisted out of the normal β-dicarbonyl W conformation so as to avoid interaction with the indole nucleus. From a measurement of the interatomic distances between H-16 and C-2 (2.55 Å), N-1 (2.85 Å), and the N-1 hydrogen (3.17 Å) it is evident that the indole and malonyl groups do not crowd each other and that the 1,3-diaxial interaction between them is, in fact, minimal.

Interestingly, the flattening of the D-ring results in a short N-1 hydrogen to H-14 distance (2.12 Å), indicating that the tendency of the molecule to maximize the separation of the large C-3 and C-15 substituents is counterbalanced by the generation of an unfavourable steric interaction between these two centres.

To summarize, as a result of an almost perpendicular disposition of the C-16—H bond relative to the indole ring, and of a minor distortion in the chair conformation of the D-ring, the steric interaction between the large indole and malonyl groups

[4]Tables of the anisotropic thermal parameters, hydrogen atom coordinates, and the observed and calculated structure amplitudes are available, and may be purchased, from the Depository of Unpublished Data, CISTI, National Research Council of Canada, Ottawa, Ont., Canada K1A 0S2.

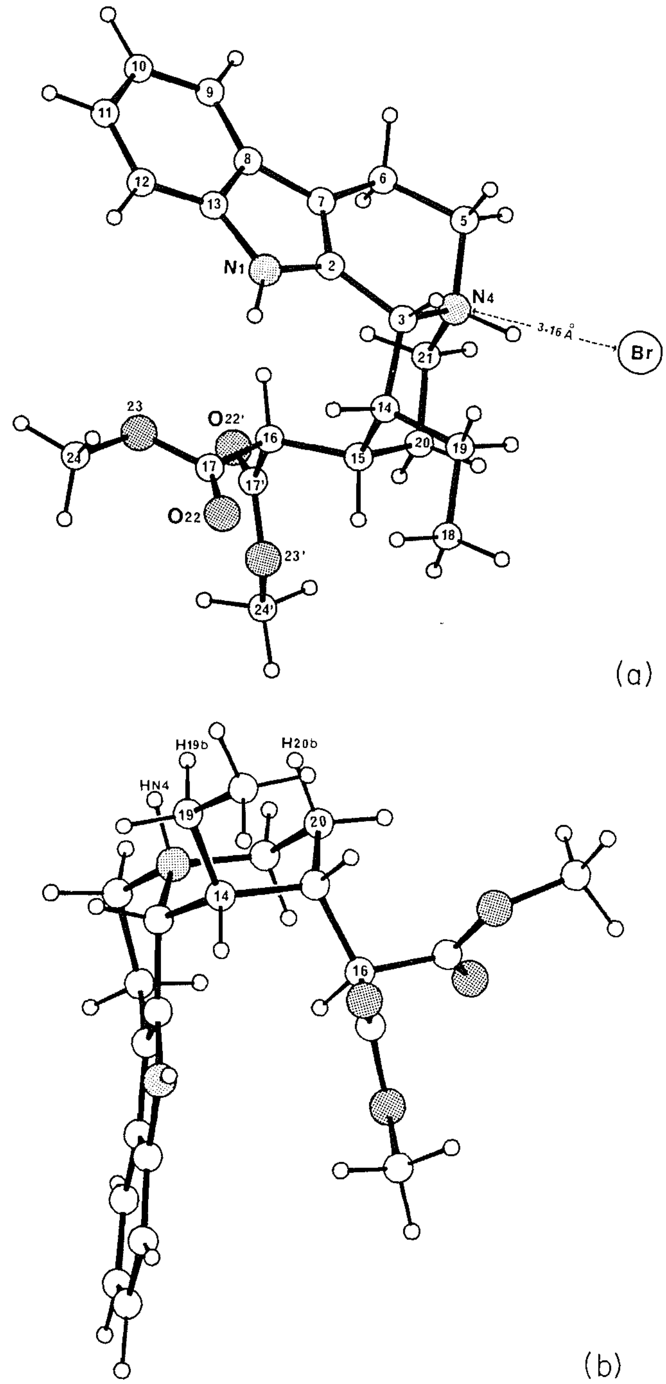

FIG. 2 a, b. An ORTEP (8) drawing of the hydrogen bromide salt of **8** with the atomic numbering.The bromide ion is hydrogen bonded to nitrogen atom N(4): distance 3.16 Å (angle $N_4—H_{N_4}\cdots Br$ of 151°).

is small. The molecule can thus accommodate their presence in axial positions, and in so doing avoid any interaction of these groups with the C-14 ethyl side chain.

This latter interaction would be particularly severe in the alternative all-equatorial conformer **8***a* (Fig. 1). In this conformation the indole ring is roughly parallel to the C-14—C-19 bond with the consequence that the N-1 hydrogen points directly at one of the C-19 methylene hydrogens ("*peri*" interaction (9)). Due to the presence of the malonyl group at C-15, release of this interaction by rotation of the ethyl side chain is not

TABLE 3. Selected torsion angles (°)

Atoms				Angle
C7	C2	C3	N4	−18.1 (5)
C2	C3	N4	C5	45.8 (5)
C3	N4	C5	C6	−64.7 (6)
N4	C5	C6	C7	47.6 (6)
C5	C6	C7	C2	−19.0 (6)
C6	C7	C2	C3	4.8 (6)
C21	N4	C3	C14	47.1 (5)
N4	C3	C14	C15	−45.6 (5)
C3	C14	C15	C20	51.1 (5)
C14	C15	C20	C21	−57.9 (6)
C15	C20	C21	N4	59.7 (6)
C20	C21	N4	C3	−54.3 (5)
C18	C19	C14	C15	−55.5 (6)
C18	C19	C14	C3	176.7 (7)
C14	C15	C16	C17	−67.1 (6)
C20	C15	C16	C17	169.1 (7)
C20	C15	C16	C17′	48.9 (6)
C14	C15	C16	C17′	172.7 (7)
C15	C16	C17	O22	−15.6 (6)
C15	C16	C17	O23	163.6 (8)
C16	C17	O23	C24	−178.8(10)
O22	C17	O23	C24	0.3 (8)
C15	C16	C17′	O22′	−120.7 (8)
C15	C16	C17′	O23′	58.9 (6)
C16	C17′	O23′	C24′	−171.1 (9)
O22′	C17′	O23′	C24′	8.5 (7)
O22	C17	C16	C17′	104.8 (8)
C17	C16	C17′	O22′	117.2 (8)

possible. In the C/D *cis* conformer **8***b* the effect of nitrogen inversion is to tilt the C-3 indole unit away from the C-14—C-19 bond, which reduces the *peri* interaction to some extent. However, this gain in stabilization is counterbalanced by the corresponding increase in energy resulting from the change to a *cis* ring junction (11).

It can thus be concluded that in the conformationally mobile "inside" Corynanthé-type indole compound **8** it is the *gauche* interactions between adjacent equatorial substituents that paradoxically render the all-equatorial conformations **8***a* and **8***b* less stable than the triaxial conformation **8***c*.

1. D. S. GRIERSON, M. HARRIS, and H.-P. HUSSON. J. Am. Chem. Soc. **102**, 1064 (1980).
2. M. BONIN, J. R. ROMERO, D. S. GRIERSON, and H.-P. HUSSON. J. Org. Chem. **49**, 2392 (1984).
3. D. S. GRIERSON, M. VUILHORGNE, G. LEMOINE, and H.-P. HUSSON. J. Org. Chem. **47**, 4439 (1982).
4. G. C. MORRISON, W. A. CETENKO, and J. SHAVEL JR. J. Org. Chem. **32**, 2768 (1967).
5. N. C. COHEN, P. COLIN, and G. LEMOINE. Tetrahedron, **37**, 1711 (1981).
6. E. WENKERT, C. J. CHANG, H. P. S. CHAWLA, D. W. COCHRAN, E. W. HAGAMAN, J. C. KING, and K. ORITO. J. Am. Chem. Soc. **98**, 3645 (1976).
7. G. M. SHELDRICK. *SHELX 76*. Program for crystal structures determination, Univ. of Cambridge, England. 1976.
8. C. K. JOHNSON. *ORTEP*. Report ORNL-5138, Oakridge National Laboratory, Tennessee. 1976.
9. E. WENKERT and B. WICKBERG. J. Am. Chem. Soc. **84**, 4914 (1962).
10. N. S. D. BHACCA, D. HORTON, and H. PAULSEN. J. Org. Chem. **33**, 2484 (1968).
11. T. A. CRABB, W. A. NEWTON, and D. JACKSON. J. Chem. Soc. Chem. Rev. **71**, 109 (1970).

Electron transfer reactions of nickel complexes of 1,4,7-triazacyclodecane

M. G. FAIRBANK, A. MCAULEY,[1] P. R. NORMAN, AND O. OLUBUYIDE[2]
Department of Chemistry, University of Victoria, Victoria, B.C., Canada V8W 2Y2

Received November 15, 1984

M. G. FAIRBANK, A. MCAULEY, P. R. NORMAN, and O. OLUBUYIDE. Can. J. Chem. **63**, 2983 (1985).

The preparation of $[Ni(1,4,7\text{-triazacyclodecane})_2]^{3+}$, $(Ni(10\text{-aneN}_3)_2{}^{3+})$ is described. The existing procedure has been modified leading to good yields of the ligand trihydrochloride. The nickel(II) analogue (reported previously) is oxidised in a facile manner, either by $Co^{3+}{}_{aq}$ in acidic aqueous media or by NO^+ in CH_3CN. Since the octahedral NiN_6 chromophore is retained upon electron transfer, outer sphere reactions both of the Ni(II) and Ni(III) species have been studied. Rates of oxidation by various nickel(III) macrocycles have been measured and details are provided. Electrochemical oxidation of the Ni(II) complex is consistent with $E^0(Ni(10\text{-aneN}_3)_2{}^{3+/2+}) = 0.997$ V (vs. NHE). The data have been used in a Marcus correlation, leading to the self-exchange rate k_{11} for the couple $(Ni(10\text{-aneN}_3)_2{}^{3+/2+}) = (2 \pm 1) \times 10^4\ M^{-1}\ s^{-1}$. This value is compared with other data derived using octahedral Ni(II)/Ni(III) centres. The oxidation of the Ni(II) complex by $Co(III)_{aq}$ has been studied in both protonated and deuterated media. There is no evidence for any proton transfer (from the N—H) being coupled to the electron transfer step. The observed rate constant for the reaction of Co^{3+} with $Ni(II)(10\text{-aneN}_3)_2{}^{2+}$ (550 M^{-1} s^{-1}) may be compared with the calculated outer sphere rate (270 M^{-1} s^{-1}). An estimate of $k_{11}(CoOH^{2+/+}) \sim 3\ M^{-1}\ s^{-1}$ for the $CoOH^{2+/+}$ exchange is discussed.

M. G. FAIRBANK, A. MCAULEY, P. R. NORMAN et O. OLUBUYIDE. Can. J. Chem. **63**, 2983 (1985).

On décrit la préparation du $[Ni(\text{triaza-}1,4,7\text{ cyclodécane})_2]^{3+}$, $(Ni(N_3\text{-}10ane)_2{}^{3+})$. La modification de la méthode existante permet d'obtenir avec un bon rendement le trichlorhydrate du ligand. On peut facilement oxyder l'analogue du nickel(II) (qui a été décrit antérieurement) soit par le Co^{3+} en milieu acide aqueux ou par le NO^+ dans le CH_3CN. Considérant que le chromophore NiN_6 octaédrique est conservé lors du transfert d'électrons, on a étudié les réactions qui se produisent dans les sphères extérieures des espèces Ni(II) et Ni(III). On a mesuré les vitesses d'oxydation par différents macrocycles de Ni(II) et on rapporte les détails. L'oxydation électrochimique du complexe de Ni(II) répond à l'équation $E^0(Ni(N_3\text{-}10ane)_2{}^{3+/2+}) = 0{,}997$ V (vs. NHE). On a utilisé les données dans une corrélation de Marcus conduisant à une vitesse d'autoéchange k_{11} pour le couple $(Ni(N_3\text{-}10ane)_2{}^{3+/2+}) = (2 \pm 1) \times 10^4\ M^{-1}\ s^{-1}$. On a comparé cette valeur avec d'autres données dérivées en utilisant des centres octaédriques Ni(II)/Ni(III). On a étudié l'oxydation du complexe de Ni(II) par le $Co(III)_{aq}$ en milieu protoné et en milieu deutéré. Il n'y a aucune preuve de transfert de proton (à partir de N—H) lors de l'étape de transfert d'électron. On peut comparer la constante de vitesse observée pour la réaction de Co^{3+} avec $Ni(II)(N_3\text{-}10ane)_2{}^{2+}$ (550 M^{-1} s^{-1}) avec la vitesse calculée pour la réaction à l'extérieur de la sphère (270 M^{-1} s^{-1}). On discute d'une évaluation de $k_{11}(CoOH^{2+/+}) \sim 3\ M^{-1}$ s^{-1} pour l'échange $CoOH^{2+/+}$.

[Traduit par le journal]

Introduction

Nickel(III) complexes stabilised by tetra-azamacrocyclic ligands (L) generally display octahedral symmetry with axial coordination of solvent or anions (1–3). In the case of $NiLCl_2{}^+$, for example (4, 5), a septet in the esr spectrum resulting from hyperfine interaction of the unpaired electron with each Cl nucleus confirms in solution what has been observed in the solid state (6). Only in relatively few instances (7) are five-coordinate species formed. In contrast, the geometry of the corresponding nickel(II) complex ions in solution is less well defined owing to the variations in extent of the square planar $\rightleftharpoons$ octahedral equilibrium. This lack of complete detail acts as a source of difficulty in the investigation of the energetics involved in reactions of $NiL^{3+/2+}$ redox couples.

Attempts have been made to address this problem using complex ions which retain the NiN_6 coordination in both oxidation states, and self exchange rate data have been determined for the tris-polypyridine (8) and bis-triazacyclononane (9) ligand systems. The use of such complexes, which show no proton equilibria in the acidity conditions used, ($[H^+] \sim 1.0$ M — pH ~ 4) also permits the assignment of reaction pathways where with the $NiL(OH_2)_2{}^{3+}$ species, ambiguities in reaction schemes deriving from proton equilibria may be envisaged.

[1] To whom all correspondence should be addressed.

[2] Present address, Chemistry Department, University of Ife, Ile-Ife, Nigeria.

The present paper describes the preparation of a nickel(III) complex incorporating the 1,4,7-triazacyclodecane ligand, $(Ni(10\text{-aneN}_3)_2{}^{3+}$. Although not quite as stable kinetically in highly acidic media with respect to decomposition as the corresponding [9]-ane N_3 ion (9), the stability is such that kinetic measurement of redox reactions may be made. The data are of interest in that they permit an evaluation of the effects on the redox process of a departure from the near octahedral symmetry of the [9]-aneN_3 ion (10) to a more distorted environment as seen from the greatly increased anisotropic esr spectrum of the [10]-aneN_3 complex.

Experimental

The nickel(II) complex, $(Ni(10\text{-aneN}_3)_2{}^{2+}$, has been prepared previously by Zompa and Margulis (10), who have shown from X-ray measurements that the octahedral field is not symmetrical. The same complex was prepared in our laboratories by a different synthesis of the ligand. This was accomplished using a modification of the method described by Atkins, which utilises the high degree of cyclisation (11, 12) achieved by the reaction of the disodium salt of *N,N′,N″*-tritosyldiethylenetriamine with the di-tosyl derivative of 1,3-propanediol (Ts = *p*-toluenesulfonyl = tosyl). A similar method has also been described by Weatherburn in the preparation of (alkyl) ring-substituted copper complexes of these ligands (13). All ligand synthesis reactions were carried out under a stream of dry N_2.

N,N′,N″-Tritosyldiethylenetriamine was prepared as described (14), and the corresponding disodium salt formed using sodium metal in absolute ethanol (15).

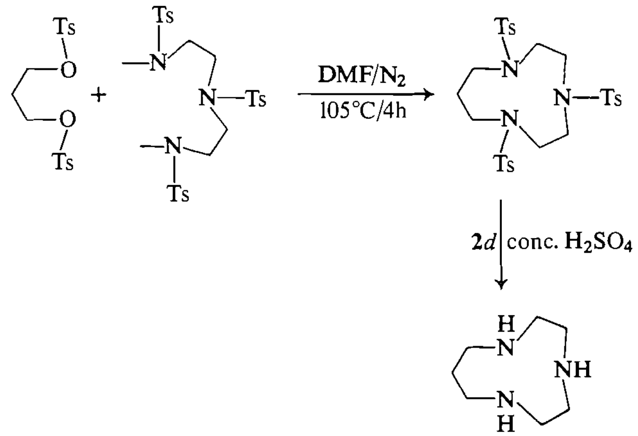

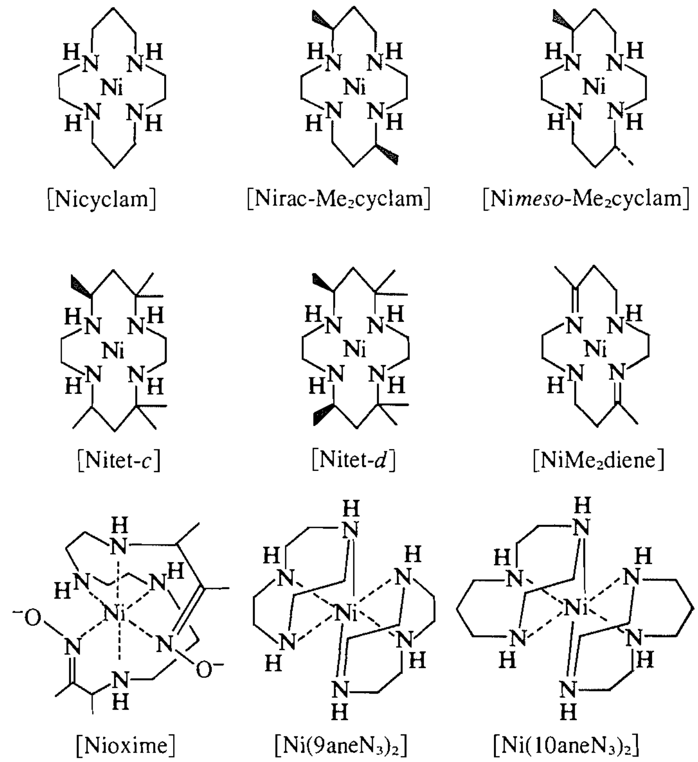

SCHEME 1. Charges omitted for clarity.

Ditosylate of 1,3-propanediol

A 7.6 g sample of 1,3-propanediol was dissolved in 500 mL dry CH_2Cl_2 in a flask (three neck). After cooling the solution to 0°C under a stream of dry N_2, 50 mL triethylamine was added. Maintaining the temperature at 0°C, a solution of 38 g of *p*-toluenesulphonyl chloride in 250 mL dry CH_2Cl_2 was added over 45 min and the mixture stirred for a further 12 h. The solid Et_3NHCl formed was filtered off and the filtrate was washed successively with 250 mL 2 *M* HCl, two, 250 mL portions of H_2O and two, 250 mL volumes of saturated Na_2CO_3 solution. After reduction in volume, a white solid crystallised which was re-crystallised from EtOH/H_2O and washed with 100% ethanol and diethyl ether. Yield 95%.

1,4,7-Tritosyl-1,4,7-triazacyclodecane

The disodium salt of diethylenetriamine (53 g) was dissolved in 350 mL dry DMF (dry N_2) in a flask equipped with a mechanical stirrer. After heating with stirring to 90°C, a solution of 35 g of 1,3-propanediol ditosylate in 180 mL DMF was added over a 45 min period. Further heating at 105°C for 4 h produced a yellow solution. The cooled DMF solution was added dropwise to 2 L of rapidly stirred water, precipitating the product which was filtered, washed with water, cold 100% ethanol, and cold diethyl ether. Yield 70%. nmr δ2.2 (CH_3), 9H; δ3.35 (NCH_2), 12H; δ7.5 (CH), 12H.

1,4,7-Triazacyclodecane trihydrochloride

The detosylation was carried out by heating a solution of the tritosyl derivative in 125 mL conc. H_2SO_4 for 48 h. After cooling and slow neutralisation using a solution of 300 g NaOH in 600 mL H_2O, further reduction of the temperature to 0°C resulted in crystallisation of Na_2SO_4. The filtrate was extracted with 600 mL $CHCl_3$ on a continuous extraction apparatus for 3 days. The solvent was removed and following addition of 25 mL ethanol and further filtration to remove any undissolved impurities, the ligand trihydrochloride was precipitated by addition of 10 mL *conc.* HCl. The product was washed with ethanol and diethyl ether. Yield 60%.

[Ni(10-aneN_3)$_2$](ClO$_4$)$_2$: NiL_2(ClO$_4$)$_2$

The ligand trihydrochloride (1 g) was dissolved in 12 mL 1 *M* NaOH and warmed on a steam bath. To this was added 0.7 g $Ni(ClO_4)_2 \cdot 6H_2O$ in 15 mL of methanol. After adjustment of the pH to ~10 a pink colour formed and lowering the pH to ~5 and cooling resulted in the precipitation of lilac crystals. These were recrystallised from methanol and dried *in vacuo*. Uv–visible: λ = 475 nm, ϵ = 30 M^{-1} cm^{-1}; λ = 302 nm, ϵ = 24 M^{-1} cm^{-1}.

The corresponding nickel(III) complex ion was formed by oxidation in 0.5 *M* $HClO_4$ using a slight deficiency of Co^{3+} aq. The 3+ species formed was less stable kinetically than the corresponding 9-aneN_3 complex and could not be isolated as a perchlorate salt. Uv: λ = 290 nm, ϵ = 11 900 M^{-1} cm^{-1}.

The complexes (Scheme 1) [Ni(cyclam)](ClO$_4$)$_2$, (16) (cyclam = 1,4,8,11-tetra-azacyclotetradecane), [Ni(*meso*-Me_2cyclam)](ClO$_4$)$_2$ (17) (Me_2cyclam = (α)-C-*meso*,-5,12-dimethyl cyclam), [Ni(tet-*c*)](ClO$_4$)$_2$ (18) and [Ni(tet-*d*)](ClO$_4$)$_2$ (18), (tet-*c* and tet-*d* = C-*rac* and C-*meso* 5,5,7,12,12,14-hexamethylcyclam), [Ni(Me_2diene)](ClO$_4$)$_2$ (17), (Me_2diene = 5,12-dimethyl-1,4,8,11-tetraazacyclotetradeca-4,11-diene) [Ni(C-*rac*-Me_2cyclam)](ClO$_4$)$_2$ (17, 19) and [Ni(IV)-oxime](ClO$_4$)$_2$ (20) (Ni(IV)-oxime = 3,4-dimethyl-4,7,10,13-tetraazahexadeca-3,13-diene-2,15-dione dioximate (2−)) were prepared as described elsewhere. Their analytical purity was confirmed (Canadian Microanalytical Services).

Solutions containing 0.01–0.04 *M* Co(ClO$_4$)$_3$ were prepared electrolytically and stored at −5°C. Lithium nitrate (Reagent grade) was used as received. Lithium perchlorate, formed on reaction of Li_2CO_3 with ~3 *M* $HClO_4$ was recrystallised three times from distilled water.

The stopped-flow and data acquisition system were described previously (21). In many instances, nickel(III) macrocyclic complexes were prepared *in situ* by oxidation of the corresponding nickel(II) species with a stoichiometric deficiency of Co(III)$_{aq}$ (22). Ionic strengths were maintained constant (1.00 *M*) using $H^+/Li^+ClO_4^-$ or where solubility factors required, $Li^+/H^+NO_3^-$. Reactions were monitored over the range 350–500 nm. Using pseudo-first-order conditions of excess reductant, rate constants derived from least-squares plots (minimum 200 points) were linear for greater than three half-lives. For several of the systems studied, e.g. (Ni(10-aneN_3)$^{2+}$ and [Ni(*meso*-Me_2cyclam)]$^{3+}$, the E^0 values of the two reactants are similar in value, leading to reaction reversibility. Under conditions of excess [(Ni(10-aneN_3)$_2$$^{2+}$] and [Ni(*meso*-$Me_2$cyclam)$^{2+}$], both the forward and reverse reactions [1] may be treated as pseudo-first order

$$[1] \quad (\mathrm{Ni(10\text{-}aneN_3)_2})^{3+} + \mathrm{Ni}(meso\text{-}\mathrm{Me_2cyclam})^{2+} \underset{k_2}{\overset{k_1}{\rightleftharpoons}} \mathrm{Ni(10\text{-}aneN_3)_2}^{2+} + \mathrm{Ni}(meso\text{-}\mathrm{Me_2cyclam})^{3+}$$

The observed first-order rate constant may thus be expressed in the form

$$[2] \quad k_{obs} = k_1[\mathrm{Ni}(meso\text{-}\mathrm{Me_2cyclam})^{2+}] + k_2[\mathrm{Ni(10\text{-}aneN_3)_2}^{2+}]$$

At constant [Ni(10-aneN_3)$_2$$^{2+}$], plots of k_{obs} against [Ni(*meso*-Me_2cyclam)$^{2+}$] should be linear (slope k_1) (Fig. 1). Also from the intercepts, k_2 may be derived by varying [Ni(10-aneN_3)$_2$$^{2+}$]. It may be seen

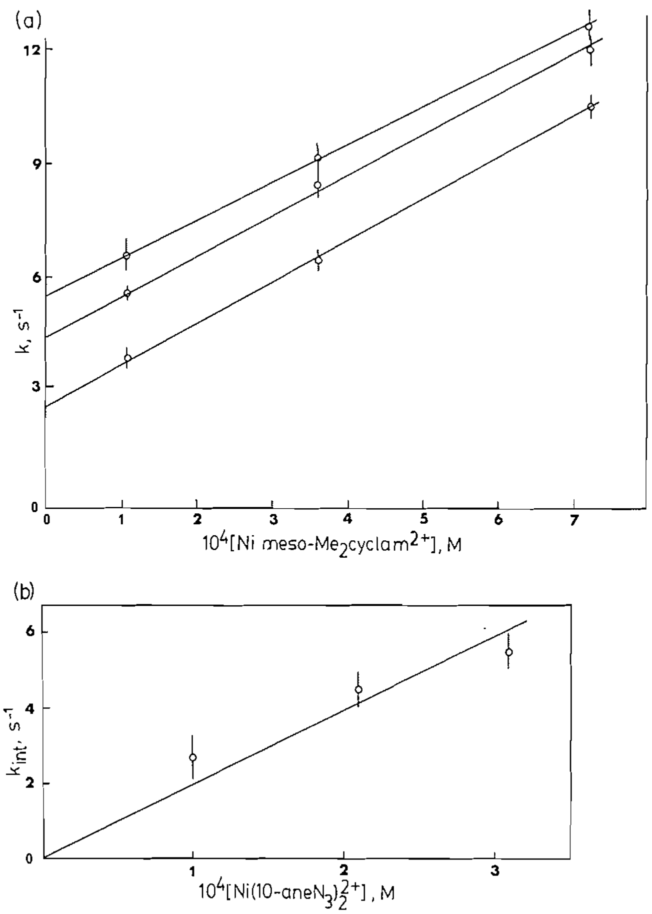

FIG. 1. (*a*) Reaction of $Ni(10\text{-}aneN_3)_2^{3+}$ with Ni(*meso*-Me_2-cyclam)$^{2+}$ (see eq. [1]). Pseudo first order behaviour observed in presence of excess $Ni(10\text{-}aneN_3)_2^{2+}$ and Ni(*meso*-Me_2cyclam)$^{2+}$ ions — see text; (*b*) k_{int} values derived graphically from plots as in (1*a*).

from Fig. 1 that $k_1 = (1.08 \pm 0.04) \times 10^4\ M^{-1}\ s^{-1}$ and $k_2 = (2.2 \pm 0.5) \times 10^4\ M^{-1}\ s^{-1}$.

Results

(a) Electron spin resonance and solution studies

The $Ni(II)(10\text{-}aneN_3)_2^{2+}$ ion may be oxidised readily to the corresponding nickel(III) species. The substantial increase in absorbance in the 300–350 nm range on reaction either in aqueous media (Co^{3+}, $S_2O_8^{2-}$) or NO^+ in CH_3CN is characteristic of the nickel(III) centre (5, 23). The low spin d^7 ion was confirmed using esr studies on the frozen aqueous solution at 77 K (Fig. 2). The $g_\perp$ and $g_\parallel$ components of the axial spectrum are identified. However, unlike the spectra for axially N-coordinated tetraazamacrocycles, where hyperfine interaction is seen in the $g_\parallel$ feature, (for N, $I = 1$) there is observed in the present system a broadening of the signal possibly owing to a smaller coupling constant. In the case of $Ni(cyclam)Cl_2^+$, $g_\perp \sim 2.18$ and $g_\parallel \sim 2.02$. For the $Ni(10\text{-}aneN_3)_2^{3+}$ species $g_\perp = 2.13$ and $g_\parallel = 2.06$ which are closer together in value. Comparison with the spectrum of the more symmetrical $Ni(9\text{-}aneN_3)_2^{3+}$ ion (15) where the extent of anisotropy is less ($g_\perp = 2.13$, $g_\parallel = 2.08$) suggests the symmetry is slightly more distorted for the 10-ane complex. This may result from the presence of an additional CH_2 group in the ligand ring. Little change is observed in the esr spectrum on the addition of high concentrations of SO_4^{2-} (3) or Cl^- (4) which are known to coordinate strongly in

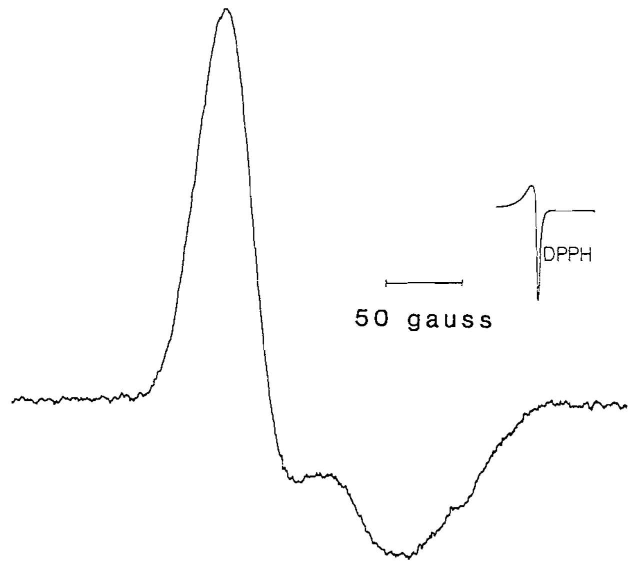

FIG. 2. Electron spin resonance spectrum of $Ni(10\text{-}aneN_3)_2^{3+}$.

the axial positions of the tetraazamacrocycles. There is thus good evidence that the octahedral NiN_6 chromophore remains intact during the redox process.

In acidic aqueous media, the $Ni(10\text{-}aneN_3)_2^{3+}$ ion is less stable kinetically than the corresponding 9-membered ring complex. (This is true also for the Ni(II) species.) In solutions of 0.1 M $HClO_4$ the half-life for the redox decomposition is ~3.5 h and at 1.0 M $[H^+]$ $t_{1/2} \sim 2.8$ h. Addition of Cl^- or SO_4^{2-} has little effect on the uv–visible spectrum. Cyclic voltammetry at 25°C (1.0 M H^+/Li^+ ClO_4^-) using a Pt electrode and calomel reference showed a 1-electron wave with quasi-reversible behaviour ($\Delta E = 78$ mV). This behaviour is typical of many Ni(III) systems (24) where deviation from the reversible 59 mV separation has been observed. The measured E^0 ($Ni(10\text{-}aneN_3)_2^{3+/2+}$) = 0.997 V vs. NHE lies in the range 0.95–1.1 V observed for most of the saturated nickel(II)/(III) macrocycles.

(b) Kinetic results

For all redox reactions studied, the stoichiometry may be represented (to ±2%) as a one-electron transfer.

$$[3] \quad Ni(II)(10\text{-}aneN_3)_2^{2+} + Ni(III)L^{3+} \rightarrow Ni(III)(10\text{-}aneN_3)_2^{3+} + Ni(II)L^{2+}$$

with the corresponding rate law

$$[4] \quad \text{Rate} = k_{12}[\text{oxidant}][\text{reductant}]$$

First order dependences of the observed rate constant (k_{obs}) were determined as is seen in Table 1. Only in the case of the Co(III) oxidation of the nickel(II) complex was a hydrogen ion dependence observed. For all other complexes, no rate variation was seen over the range $[H^+] = 0.1–1.0\ M$. Most systems were studied at 0.5 M $[H^+]$.

The rate of appearance of $Ni(10\text{-}aneN_3)_2^{3+}$ (λ 340 nm) was used to investigate the oxidation reaction involving aquocobalt(III) under conditions of excess reductant. The results are summarised in Table 1. At constant $[H^+]$ the rate law may be expressed as

$$[5] \quad d[Ni(III)]/dt = k_a[Ni(10\text{-}aneN_3)_2^{2+}][Co(III)]$$

A significant increase in k_a was observed on reducing $[H^+]$. The lack of any proton-related equilibria associated with the

TABLE 1. Kinetic results of $Ni(10\text{-aneN}_3)_2$ reactions at 25°C

(*a*) $Ni(10\text{-aneN}_3)_2^{2+}$ + Co(III)[a,b]

$[H^+]$ (M)	10^{-3} k (M^{-1} s^{-1})
1.00	1.09
0.80	1.30
0.60	1.52
0.40	2.01
0.30	2.50
0.20	3.43

[a]Observation wavelength = 340–425 nm; [Ni(III)] = $1-2 \times 10^{-5}$ M; I = 1.0 M (H^+/Li^+, ClO_4^-), except where indicated.
[b]Slope of $1/[H^+]$ plot = kK_h = 579 ± 8 s^{-1}; int = k = 550 ± 22 M^{-1} s^{-1}.

(*b*) $Ni(10\text{-aneN}_3)_2^{3+}$ + $Ni(9\text{-aneN}_3)_2^{2+}$[a]

	k, $s^{-1}/10^4[Ni(9\text{-aneN}_3)_2]^{2+}$				
$10^4[Ni(10\text{-aneN}_3)_2]^{2+}$	1.99	3.97	6.95	10^{-4} slope	Int
0.80	3.86	8.17	15.13	2.3 ± 0.1	<0.1
3.57	4.3	8.52	—	2.1	0.07
				k_1 = 2.2 × 10^4 M^{-1} s^{-1}	—

[a]A study of the rate over the range 0.1 M < $[H^+]$ < 1.0 M (5 points) showed no dependence on $[H^+]$: k_1 = (2.3 ± 0.3) × 10^4 M^{-1} s^{-1}.

(*c*) $[Ni(10\text{-aneN}_3)_2^{2+}$ + $Ni(cyclam)^{3+}$[a]

	k, $s^{-1}/10^4[Ni(10\text{-aneN}_3)_2]^{2+}$							
$10^4[Nicyclam]^{2+}$	4.46	4.85	7.81	9.38	11.16	12.14	10^{-3} slope	Int
5.00[b]	—	3.42	—	3.86	—	4.18	1.0	2.90
6.43	4.66	—	5.10	—	5.56	—	1.3	4.05
10.00[b]	—	5.95	—	6.45	—	7.00	1.4	5.23
12.86	7.56	—	7.80	—	8.40	—	1.3	6.94
15.00[b]	—	10.45	—	10.90	—	11.60	1.5	9.65

ave k_1 = (1.3 ± 0.2) × 10^3 M^{-1} s^{-1}
k_2 = (6.1 ± 0.8) × 10^3 M^{-1} s^{-1}

[a]$[H^+]$ = 0.1 M; I = 0.2 M (H^+/Li^+, ClO_4^-, or NO_3^-).
[b]NO_3^- media.

(*d*) $Ni(10\text{-aneN}_3)_2^{3+}$ + [Ni*meso*-Me_2cyclam]$^{2+}$]

	k, $s^{-1}/10^4$[Ni*meso*-Me_2cyclam^{2+}]					
$10^4[Ni(10\text{-aneN}_3)_2^{2+}$	1.09	3.62	6.88	7.24	10^{-4} slope	Int
1.00	3.97	6.55	—	10.6	1.08 ± 0.03	2.7 ± 0.1
2.10	5.66	8.6	12.1	—	1.11 ± 0.02	4.5 ± 0.1
3.10	6.7	9.2	12.7	—	1.04 ± 0.02	5.5 ± 0.1

k_1 = (1.08 ± 0.04) × 10^4 M^{-1} s^{-1}
k_2 = (2.2 ± 0.5) × 10^4 M^{-1} s^{-1}

(*e*) $Ni(10\text{-aneN}_3)_2^{2+} + Ni(Me_2diene)^{3+}$

$10^4[Ni(Me_2diene)]^{2+}$	k, $s^{-1}/10^4[Ni(10\text{-aneN}_3)_2^{2+}]$						10^{-3} slope	Int
	0.765	0.799	1.53	2.00	3.06	4.00		
1.53	—	0.443	0.75	—	1.37	—	4.09 ± 0.01	0.12 ± 0.01
4.60	0.75	—	0.97	—	1.52	—	3.4 ± 0.2	0.48 ± 0.04
9.90	1.31	—	—	1.55	—	2.21	2.8 ± 0.4	1.1 ± 0.1

$k_1 = (3.4 \pm 0.6) \times 10^3\ M^{-1}\ s^{-1}$
$k_2 = (1.13 \pm 0.04) \times 10^3\ M^{-1}\ s^{-1}$

	k_1, $M^{-1}\ s^{-1}$
$Ni(tet\text{-}c)^{3+}$	$(1.16 \pm 0.01) \times 10^5$
$Ni(tet\text{-}d)^{3+}$	$(1.38 \pm 0.02) \times 10^5$
$Ni(IV)oxime^{2+}$	23.1 ± 0.8
$Ni\,rac\text{-}Me_2cyclam^{3+}$	$(1.4 \pm 0.2) \times 10^4$

Ni(II) complex as demonstrated by the invariance of rate of the Ni(III) oxidations with changing $[H^+]$, permits attribution of the hydrogen ion dependence to hydrolysis of the aquocobalt ion

$$[6]\quad (H_2O)_5Co(OH_2)^{3+} \overset{K_h}{\rightleftharpoons} (H_2O)_5CoOH^{2+} + H^+$$

$$K_h = \frac{[CoOH^{2+}][H^+]}{[Co^{3+}]}$$

Using the mechanism in which both Co(III) species react,

$$[7]\quad Ni(10\text{-aneN}_3)_2^{2+} + Co^{3+} \xrightarrow{k_\alpha} Co^{2+} + Ni(10\text{-aneN}_3)_2^{3+}$$

$$[8]\quad Ni(10\text{-aneN}_3)_2^{2+} + CoOH^{2+} \xrightarrow{k_\beta} Co(II) + Ni(10\text{-aneN}_3)_2^{3+}$$

the overall second order rate constant k_a may be expressed in the form

$$[9]\quad k_a = k_\alpha + k_\beta K_h/[H^+]$$

From the data in Table 1, $k_\alpha = 550 \pm 22\ M^{-1}\ s^{-1}$ and $k_\beta K_h = 579 \pm 8\ s^{-1}$. Using $K_h = 2 \times 10^{-3}\ M$ (25), $k_\beta = 2.9 \times 10^5\ M^{-1}\ s^{-1}$.

In reactions where ΔE^0 for the redox process is less than 50 mV, reversibility was observed as noted previously. It is possible to calculate the equilibrium constants for these reversible reactions. In most instances, K lies in the range 1–10 and agreement with the kinetic data is considered reasonable. For example, in the reactions with the $Ni(cyclam)^{2+}$ and with $Ni(meso\text{-}Me_2cyclam)^{2+}$ the K value of unit based on equilibrium data may be compared with the kinetic values of 0.2 and 0.5, respectively. Only in the case of the reaction with $Ni(9\text{-aneN}_3)_2^{2+}$ is there an inconsistency. Predicted value of the intercepts based on reactant concentration are 0.24 and 1.1 compared with observed values essentially zero. At present, we cannot explain this anomaly.

Discussion

From the variety of systems studied, both oxidations of Ni(II) and the reductions of $Ni(III)(10\text{-aneN}_3)_2^{3+}$ may be viewed as outer-sphere processes. We have therefore used the Marcus relationship (8, 26) to determine the self-exchange rate constant for the bis(10-aneN$_3$) complex. The rate constant, k_{12}, for an outer-sphere redox reaction may be related to the individual self-exchange reactions k_{11} and k_{22} and to the overall equilibrium constant, K_{12}, by the expression [10]

$$[10]\quad k_{12} = (k_{11}k_{22}K_{12}f_{12})^{1/2}\,W'_{12}$$

$$[11]\quad \ln f_{12} = \frac{[\ln K_{12} + (W_{12} - W_{21})/RT]^2}{4\left[\dfrac{\ln(k_{11}k_{22})}{A_{11}A_{22}} + \dfrac{W_{11} + W_{22}}{RT}\right]}$$

$$[12]\quad W'_{12} = \exp\,[W_{11} + W_{22} - W_{12} - W_{21})/2RT]$$

$$[13]\quad A_{ii} = \frac{[4\pi N\sigma^2\nu\gamma]_{ii}}{1000}$$

Values of A_{11} and A_{22} were used as calculated previously for Ni(III) complexes of this type (27) $A/\sigma^2 = 3 \times 10^{10}\ M^{-1}\ s^{-1}$ Å^{-2}) for the nickel complexes, $\sigma = 3.8 \pm 0.2$ Å, $Co^{3+} = 3.0$ Å and $Fe^{2+} = 3.3$ Å, respectively. Work terms W_{ii} refer to the energies associated with bringing together the reactants to the separation distance, r, within the activated complex. In most instances, 2+ and 3+ charged reactants were involved and work terms partially cancel. A_{ii} is the diffusion rate for species ii, ν the nuclear frequency which destroys the activated complex,and γ is the thickness of the reaction layer. Assuming log $W'_{12} = 1$, eq. [10] may be expressed as

$$[14]\quad \log k_{12} = (1/2)(\log K_{12}k_{11}f_{12}) + (1/2)\log k_{22}$$

Thermodynamic and kinetic parameters used in the Marcus correlation are presented in Table 2. Using the data in Table 2, the plot (Fig. 3) is obtained where the slope 0.48 ± 0.03 (least-square analysis with correlation factor 0.97) is in excellent agreement with the value (0.5) predicted theoretically. From the intercept, k_{22}, the rate constant for the $Ni(10\text{-aneN}_3)_2^{3+/2+}$ exchange may be evaluated as $(2 \pm 1) \times 10^4\ M^{-1}\ s^{-1}$. The value is slightly higher than that for the corresponding (9-aneN$_3$)$_2$ complex, $6 \times 10^3\ M^{-1}\ s^{-1}$. The corresponding rate constant for the tris-bipyridyl complex (8) is $2 \times 10^3\ M^{-1}\ s^{-1}$. For the *trans*-Ni(cyclam)$Cl_2^{+/0}$ couple, $k_{22} = 3.4 \times 10^4\ M^{-1}\ s^{-1}$ (28). It thus appears that for these octahedrally substituted complexes, rates are within one order of magnitude suggesting similar reorganizational energies for formation of the activated complex.

The present study also provides further information on the aquo Co(II)/(III) processes. Endicott *et al.* (29) have recently provided evidence that outer sphere reactions of Co^{3+}_{aq} are consistent with a self-exchange rate $k_{11}(Co^{3+/2+}) = 10^{-12}\ M^{-1}\ s^{-1}$. Using this value, the predicted value for $k_{12}(k_\alpha)$ is 270 M^{-1}

TABLE 2. Marcus parameters for reactions of the $[Ni(10\text{-aneN}_3)_2]^{3+/2+}$ couple

No.	Complex	E^0, V vs. NHE	k_{11}, M^{-1} s^{-1}	log $(k_{11}K_{12}f_{12})$	log k_{12}
1	Co^{3+}	1.86	1×10^{-12} [a]	0.86	2.74
2	$CoOH^{2+}$	1.44	3 [b]	7.20	5.46
3	$Fe(H_2O)_6^{2+}$	0.77	0.01 [c] (0.001) [d]	1.65	3.06
4	$Ni(9\text{-aneN}_3)_2^{2+}$	0.947	6×10^3 [e]	4.61	4.32
5	$Nicyclam^{2+}$	0.99	1×10^3 [f]	3.12	3.78
6	$Nicyclam^{3+}$	0.99	1×10^3	2.88	3.11
7	Ni*meso*-$Me_2cyclam^{2+}$	0.995	7.5×10^3 [g]	3.91	4.04
8	Ni*meso*-$Me_2cyclam^{3+}$	0.995	7.5×10^3	3.84	4.23
9	Nitet-c^{3+}	1.26	31 [c]	5.65	5.06
10	Nitet-d^{3+}	1.26	60 [c]	5.94	5.14
11	$NiMe_2diene^{3+}$	1.01	6×10^2 [g]	3.00	3.53
12	$NiMe_2diene^{2+}$	1.01	6×10^2	2.56	3.05
13	$Ni(IV)oxime^{2+}$	0.65	6×10^4 [h]	−1.69	1.36
14	Ni*rac*-$Me_2cyclam^{3+}$	1.115	1.6×10^2 [g]	4.14	4.15

[a] Reference 29.
[b] See text.
[c] Derived from cross-reactions with several Ni(III) macrocyclic and Ru(II) ammine complexes (34).
[d] Reference 35.
[e] Reference 15.
[f] Reference 36.
[g] M. G. Fairbank. Unpublished results.
[h] Reference 37.

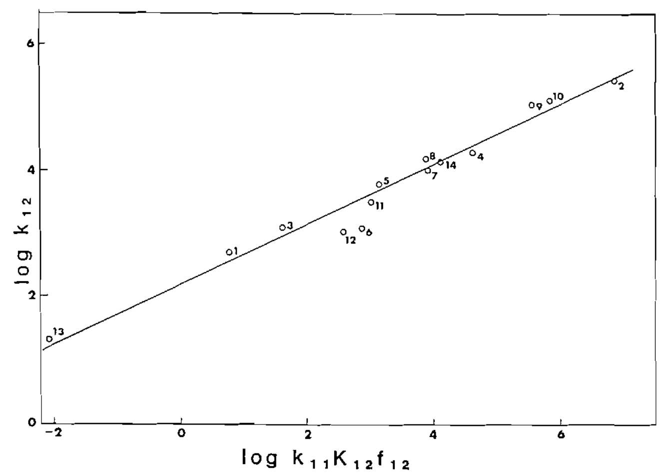

FIG. 3. Marcus plot eq. [14] used in derivation of self-exchange rate for $Ni(10\text{-aneN}_3)_2^{3+/2+}$.

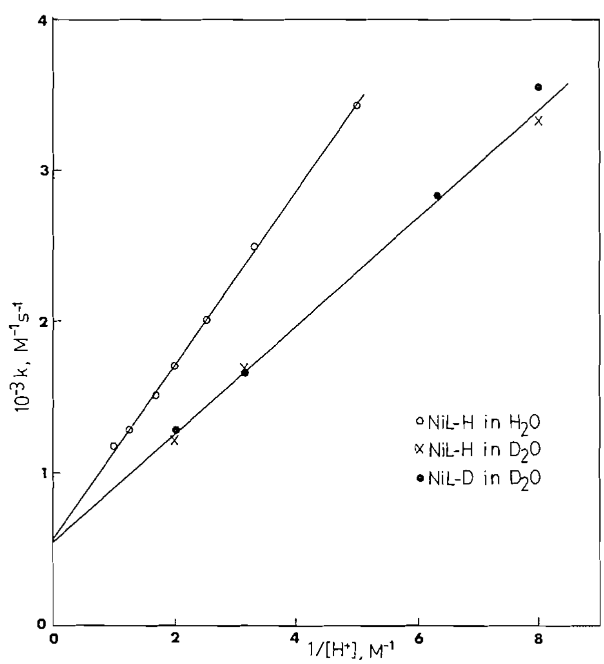

FIG. 4. Rate data for reactions of $Co(OH)^{2+}$ and $Co(OD)^{2+}$ with $Ni(10\text{-aneN}_3)_2^{2+}$ as a function of $[H^+]^{-1}$ ($[D^+]^{-1}$).

s^{-1} which compares favourably with the experimental value of 550 M^{-1} s^{-1}, given approximations made in the correlation. The question of the $CoOH^{2+/+}$ exchange is still the subject of discussion. This is in part due to the possibility of a preferred outer-sphere orientation (30) where H-bonding with the reducing substrate may be envisaged. There exists also the potential for the abstraction by $CoOH^{2+}$ of an H atom from the N—H ligand system in a "quasi inner-sphere" process. It is known that exchange of the N—H protons is a facile process in basic media (pH ~ 10) but in acidic conditions the N—H bonds are extremely inert. Using D_2O/NaOD, we have prepared the deuterated complex $Ni(10\text{-aneN}_3D_3)_2^{2+}$ and reacted this ion with both $Co(OD_2)_6^{3+}/DClO_4$ and $Co(OH_2)_6^{3+}/HClO_4$ as described above. The $[H^+]^{-1}$ ($[D^+]^{-1}$) dependences again demonstrated the existence of $Co(OH)^{2+}$ ($Co(OD)^{2+}$) reaction pathways. The kinetic data are shown in Fig. 4 where it is seen that there is a marked difference in rate between the protonated and deuterated solvent systems. In the latter, however, the complexes containing the N—H ligands react at the same rate as those containing the N—D centres. If a proton-coupled electron transfer were operative, a ratio of $k_H/k_D \sim 1.37$ would be anticipated owing to rupture of the N—D (N—H) bond. The reaction of $CoOH^{2+}$ may thus be treated as an outer-sphere process although the possibility remains of a precursor complex with OH^- located for hydroxide-mediated electron transfer. The stability constant of such a precursor would be expected to be small (there is no spectrophotometric evidence for its existence in our hands). An estimate (9) may be made of E^0 ($CoOH^{2+/+}$) = 1.44 V, and, if we treat the reaction as an outer-sphere process, the data from the cross reaction with Ni(II)-$(10\text{-aneN}_3)_2^{2+}$ may be used to obtain a value of k_{11}($CoOH^{2+/+}$)

$= 3\ M^{-1}\ s^{-1}$. This is close to that ($2\ M^{-1}\ s^{-1}$) derived (31) from the reaction of $CoOH^{2+}$ with Ni(IV)oxime^{2+}. From the corresponding reaction with Ni(9-aneN$_3$)$_2{}^{2+}$, an estimate of $k_{11} \sim 50\ M^{-1}\ s^{-1}$ may be obtained. Thus it appears that the self-exchange process for the $CoOH^{2+/+}$ couple is $\sim 10^{11}$ faster than that for the $Co^{3+/2+}$ exchange. The origin of such a large difference is not readily apparent. It is known that in most systems the contributions arising from Franck–Condon parameters outweigh any spin changes. Also significant differences (32) in rates have been identified in the exchange reactions of $Co(NH_3)_6{}^{3+/2+}$ and Co(sepulchrate)$^{3+/2+}$.

One interesting facet of the deuterium studies is that the rates of oxidation by $Co(OH_2)_6{}^{3+}$ and $Co(OD_2)_6{}^{3+}$ are indistinguishable (Fig. 4). The slopes (reactions of the hydroxo complexes), may be represented as $k_\beta K_h$ and $k_\beta K_d$. Assuming k_β constant, K_d, the dissociation constant for the deuterated ion may be evaluated. The ratio of slopes yields $K_h/K_d \approx 1.45$ and using $K_h = 2 \times 10^{-3}\ M$, $K_d = 1.4 \times 10^{-3}\ M$. As expected, the deuterated complex is less acidic, a fact noted for other aquo metal ions (33).

Acknowledgements

We thank NSERC for support. M.G.F. was the recipient of a University of Victoria fellowship. O.O. acknowledges sabbatical support from University of Ife, Ile-Ife, Nigeria. Mr. Pat O'Brien is thanked for assistance with ligand synthesis.

1. E. S. GORE and D. H. BUSCH. Inorg. Chem. **12**, 1 (1973).
2. K. NAG and A. CHAKRAVORTY. Coord. Chem. Rev. **33**, 87 (1980).
3. E. ZEIGERSON, I. BAR, J. BERNSTEIN, L. J. KIRSCHENBAUM, and D. MEYERSTEIN. Inorg. Chem. **21**, 73 (1982).
4. A. DESIDERI, J. B. RAYNOR, and C. K. POON. J. Chem. Soc. Dalton Trans, 2051 (1977).
5. R. I. HAINES and A. MCAULEY. Coord. Chem. Rev. **39**, 77 (1981).
6. T. ITO, M. SUZIMOTO, K. TORIUMI, and K. ITO. Chem. Lett. 1477 (1981).
7. L. FABBRIZZI, H. COHEN, and D. MEYERSTEIN. J. Chem. Soc. Dalton Trans. 2125 (1983); E. ZEIGERSON, G. GINSBURG, J. Y. BECKER, L. J. KIRSCHENBAUM, H. COHEN, and D. MEYERSTEIN. Inorg. Chem. **20**, 3988 (1981).
8. D. H. MACARTNEY and N. SUTIN. Inorg. Chem. **22**, 3530 (1983).
9. K. WIEGHARDT, W. SCHMIDT, W. HERRMANN, and H. J. KUEPPERS. Inorg. Chem. **22**, 2953 (1983); A. MCAULEY, P. R. NORMAN, and O. OLUBUYIDE. J. Chem. Soc. Dalton Trans. 1501 (1984).
10. L. J. ZOMPA and T. N. MARGULIS. Inorg. Chim. Acta, **45**, L263 (1980).
11. T. J. ATKINS, J. E. RICHMAN, and W. F. OETTLE. Org. Synth. **58**, 86 (1978).
12. T. J. ATKINS and J. E. RICHMAN. J. Am. Chem. Soc. **96**, 2268 (1974).
13. P. G. GRAHAM and D. C. WEATHERBURN. Austral. J. Chem. **36**, 2349 (1983).
14. R. W. HAY and P. R. NORMAN. J. Chem. Soc. Dalton trans. 1441 (1979).
15. A. MCAULEY, P. R. NORMAN, and O. OLUBUYIDE. Inorg. Chem. **23**, 1938 (1984).
16. B. BOSNICH, M. L. TOBE, and G. A. WEBB. Inorg. Chem. **4**, 1102 (1965); **4**, 1109 (1965).
17. R. A. KOLINSKI and B. KORYBUT-DASZKIEWICZ. Bull. Acad. Pol. Sci. **17**, 13 (1969).
18. N. F. CURTIS, Y. M. CURTIS, and H. K. J. POWELL. J. Chem. Soc. A, 1015 (1966).
19. M. G. FAIRBANK, A. MCAULEY, and P. R. NORMAN. Inorg. Chem. To be published.
20. J. G. MOHANTY, R. P. SINGH, and A. CHAKRAVORTY. Inorg. Chem. **14**, 2178 (1975).
21. K. J. ELLIS and A. MCAULEY. J. Chem. Soc. Dalton Trans. 1533 (1973).
22. J-C. BRODOVITCH and A. MCAULEY. Inorg. Chem. **20**, 1667 (1981).
23. A. BENCINI, L. FABBRIZZI, and A. POGGI. Inorg. Chem. **20**, 2544 (1981).
24. F. P. BOSSU and D. W. MARGERUM. Inorg. Chem. **16**, 1210 (1977); F. P. BOSSU, E. P. PANIAGO, D. W. MARGERUM, and S. T. KIRKSEY. Inorg. Chem. **17**, 1034 (1978).
25. G. DAVIES and B. WARNQVIST. Coord. Chem. Rev. **5**, 349 (1970).
26. R. A. MARCUS. Ann. Rev. Phys. Chem. **15**, 155 (1964); J. Phys. Chem. **67**, 853 (1963).
27. D. H. MACARTNEY and N. SUTIN. Inorg. Chem. **22**, 3530 (1983).
28. A. MCAULEY, O. OLUBUYIDE, L. SPENCER, and P. R. WEST. Inorg. Chem. **23**, 2594 (1984).
29. J. F. ENDICOTT, B. DURHAM, and K. KUMAR. Inorg. Chem. **21**, 2437 (1982).
30. R. A. RICKMAN, R. L. SORENSEN, K. O. WATKINS, and G. DAVIES. Inorg. Chem. **16**, 1570 (1977).
31. D. H. MACARTNEY and A. MCAULEY. Can. J. Chem. **60**, 2625 (1982).
32. I. I. CREASER, J. M. HARROWFIELD, A. J. HERLT, A. M. SARGESON, J. SPRINGBOR, R. J. GERE, and M. R. SNOW. J. Am. Chem. soc. **99**, 3181 (1977).
33. J. BURGESS. Metal ions in solution. Ellis Horwood, Chichester. 1978. p. 280.
34. D. H. MACARTNEY, A. MCAULEY, and O. OLUBUYIDE. Inorg. Chem. **24**, 307 (1985).
35. J. T. HUPP and M. J. WEAVER. Inorg. Chem. **22**, 2557 (1983).
36. A. MCAULEY, D. H. MACARTNEY, and T. OSWALD. Chem. Commun. 274 (1982).
37. D. H. MACARTNEY and A. MCAULEY. Inorg. Chem. **22**, 2062 (1983).

Substituent effects on acetylene stability. A comparison of STO-3G, 6-31G, 6-31G**, and 6-311G** calculations

PASCAL FURET, GEORGE HALLAK, ROBERT L. MATCHA, AND RICHARD FUCHS
Department of Chemistry, University of Houston, Houston, TX 77004, U.S.A.

Received March 11, 1985

PASCAL FURET, GEORGE HALLAK, ROBERT L. MATCHA, and RICHARD FUCHS. Can. J. Chem. **63**, 2990 (1985).

Ab initio calculations using STO-3G, 6-31G, 6-31G**, and 6-311G** basis sets and standard geometries, and 6-31G and 6-311G** basis sets with 6-31G optimized geometries have been performed on a series of acetylene derivatives (H—C≡C—R; –R is $—CH_3$, —Li, —C≡N, —C(=O)—H, —C(=O)—OH, $—NH_2$, —C≡CH, $—CH{=}CH_2$, and —F). Substituent effects on stability have been studied using isodesmic methyl exchange reactions (H—C≡C—R + CH_4 → H—C≡C—H + CH_3R). STO-3G and 6-31G calculations have been carried out for methyl exchange reactions involving several large substituents including phenyl, and for the *tert*-butyl exchange reactions of 10 substituents (H—C≡C—R + Me_3CH → H—C≡C—H + Me_3CR).

Geometry optimization has an appreciable effect only on the π donor substituents OCH_3 and NH_2. None of the smaller basis sets reproduces the order of stabilities or the absolute values of the 6-311G**//6-31G calculations. The latter are in satisfactory agreement with the very few experimentally based enthalpies of methyl exchange.

PASCAL FURET, GEORGE HALLAK, ROBERT L. MATCHA et RICHARD FUCHS. Can. J. Chem. **63**, 2990 (1985).

Utilisant des ensembles de base STO-3G, 6-31G, 6-31G** et 6-311G**avec des géométries normales ainsi que des ensembles de base 6-31G et 6-311G** avec des géométries optimisées à l'aide de l'ensemble 6-31G, on a effectué des calculs *ab initio* sur une série de dérivés de l'acétylène (H—C≡C—R où R est égal à $—CH_3$, —Li, —C≡N, —CHO, —COOH, $—NH_2$, —C≡CH, $—CH{=}CH_2$ et —F). Faisant appel aux réactions d'échanges de méthyles isodesmiques (H—C≡C—R + CH_4 → H—C≡C—H + CH_3R) on a étudié les effets des substituants sur la stabilité. On a réalisé des calculs aux niveaux STO-3G et 6-31G pour les réactions d'échanges de méthyles impliquant plusieurs substituants encombrants, y compris le phényle, et pour les réactions d'échange du *tert*-butyle de 10 substituants (H—C≡C—R + Me_3CH → H—C≡C—H + Me_3R).

L'optimisation de la géométrie n'a un effet appréciable que dans le cas des substituants donneurs pi, tels le OCH_3 et le NH_2. Les petits ensembles de base ne reproduisent pas l'ordre des stabilités ou les valeurs absolues des calculs faits à l'aide des ensembles 6-311G**//6-31G. Ces derniers sont en bon accord avec les quelques rares enthalpies expérimentales basées sur la réaction d'échange de méthyle.

[Traduit par le journal]

From the few available thermochemical data on gaseous heats of formation of substituted acetylene (1, 2) it appears that alkyl substituents have a stabilizing effect (in propyne, 1-butyne, 2-butyne), and cyano substituents destabilize (dicyanoacetylene). Heats of hydrogenation in solution (3) or heats of formation in the liquid state (2) have been reported for several conjugated acetylenic esters and acids, but these seriously disagree (over a 15 kcal/mol range) on the stabilizing or destabilizing effects. Furthermore, the corrections to the gaseous state (4) are unknown, and can only be crudely estimated.

Ab initio calculations at the 4-31G (5) and STO-3G (6) basis set levels have been published for some acetylene derivatives, but stabilizing or destabilizing effects have been determined mainly for small substituents.

We have carried out the present study with the objectives of (*a*) performing *ab initio* calculation using more extensive basis sets including polarization functions, (*b*) observing the effect of geometry optimization, and (*c*) examining the stabilizing or destabilizing effects of some larger common substituents.

Calculation methods

Isodesmic reactions

Stabilities of the compounds H—C≡C—R were studied using the following isodesmic reactions:

[1] H—C≡C—R + CH_4 → H—C≡C—H + CH_3R

[2] H—C≡C—R + $(CH_3)_3C$—H → H—C≡C—H + $(CH_3)_3C$—R

Reaction [1] is a simple isodesmic reaction of the type introduced by Pople and co-workers (5). In this reaction there is retention of the number of bonds of a given formal type (C≡C, C—H, C—R, etc.). Reaction [1] measures the stabilizing effect of the substituent R on acetylene, relative to the effect of R on methane. Reaction [2] has the advantage that each atom maintains both the number of bonds with each type of atom, and also equal numbers of primary, secondary, and tertiary carbon atoms on each side of the equation (6, 7). As a result, in [2] the energy changes due to factors other than electronic stabilization or destabilization should be small, and this should provide a more accurate model for the study of the stability of organic compounds.

Quantum mechanical method and geometric model

The method used was single determinant LCAO-MO-SCF theory. The calculations were made with the program GAUSSIAN 80 (8). Several basis sets were utilized, the minimum basis set STO-3G (9), the split valence set 6-31G (10), and the split valence with polarization functions basis sets 6-31G** and 6-311G** (11, 12). Where no geometry optimization was used a uniform treatment was applied to all the molecules of a given isodesmic reaction, employing a standard geometric model (13). The most stable conformation of each molecule was determined by a conformational study with the STO-3G basis set within the rigid rotor approximation. It has been established that this basis set gives reliable results in this application (14). 6-31G and 6-311G** calculations were also carried out using 6-31G geometry optimization with the con-

TABLE 1. Theoretical total energies (hartrees)

Molecule	$-E$(STO-3G)	$-E$(6-31G)	$-E$(6-31G//6-31G)	$-E$(6-31G**)	$-E$(6-311G**)	$-E$(6-311G**//6-31G)
H—C≡C—H	75.85339[a]	76.79261[b]	76.79276	76.82138[b]	76.840515	76.84092
H—C≡C—CH_3	114.44558	115.82299	115.82353	115.87055	115.89510	115.89562
H—C≡C—C≡N	166.40853	168.47859	168.47912	168.54944	168.58601	168.58789
H—C≡C—OCH_3	188.27086	190.60021	190.60610	190.69109	190.73602	190.74099
H—C≡C—C(=O)—H	187.08088	189.45788	189.45910	189.54170	189.58578	189.58744
H—C≡C—C(=O)—OH	260.93646	264.30564	264.30997	264.43093	264.49499	
H—C≡C—F			175.58320			175.69075
H—C≡C—NH_2 (planar)			131.80084			131.88489
H—C≡C—Li			83.66856			83.71759
H—C≡C—C≡C—H	150.59159	152.44811	152.44826	152.50132	152.53425	152.53467
H—C≡C—CH=CH_2			153.65522			
HC≡CCH_2OCH_3	226.85089	229.63427				
H—C≡C—C(=O)—CH_3	225.67147	228.49100		228.59293		
H—C≡C—C(=O)—OCH_3	299.51751	303.30614		303.45238		
H—C≡C—C≡C—CH_3	189.18515	191.47961				
H—C≡C—C_6H_5	302.61970	306.27266				
CH_4	39.72670	40.18038	40.18055	40.20159[b]	40.20892	40.20900
CH_3—CH_3	78.30549[a]	79.19651[b]	79.19678	79.23724[b]	79.25077	79.25093
CH_3—C≡N	130.27078	131.86449	131.86523	131.93064	131.95822	131.95995
CH_3—O—CH_3	152.13215[c]	153.99204	153.99470	154.07097	154.10546	154.10680
CH_3—C(=O)—H	150.94365	152.84164	152.84320	152.91938	152.95406	152.95606
CH_3—C(=O)—OH	224.80290	227.69616	227.70112	227.81479	227.86983	227.87451
CH_3—F			138.99438			139.07644
CH_3—NH_2			95.17090			95.23972
CH_3Li			47.00330			47.03159
CH_3—CH=CH_2			117.02828			117.10333
CH_3CH_2—O—CH_3	190.71594	193.01633				
CH_3—C(=O)—CH_3	189.53389	191.87394		191.96979		
CH_3—C(=O)—OCH_3	263.38341	266.69562		266.83542		
CH_3—C≡C—CH_3	153.03667	154.85150				
CH_3—C_6H_5	226.47382	269.64396				
Me_3C—H[d]	155.46511	157.23350				
Me_3C—CH_3	194.04502	196.25289				
Me_3C—C≡N	246.01010	248.92031				
Me_3C—OCH_3	267.86208	271.04234				
Me_3C—C(=O)—H	266.68225	269.89745				
Me_3C—C(=O)—OH	340.54140	344.75249				
Me_3C—CH_2—OCH_3	306.45529	310.07304				
Me_3C—C(=O)—CH_3	305.26888	308.92572				
Me_3C—C(=O)—OCH_3	379.12186	383.75182				

TABLE 1. (*Concluded*)

Molecule	$-E$(STO-3G)	$-E$(6-31G)	$-E$(6-31G//6-31G)	$-E$(6-31G**)	$-E$(6-311G**)	$-E$(6-311G**//6-31G)
$Me_3C—C{\equiv}C—CH_3$	268.77241	271.90452				
Me_3C— 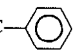	382.20294	386.68954				

[a]Reference 10.
[b]Reference 11.
[c]Reference 15.
[d]$Me_3C = (CH_3)_3C$.

TABLE 2. Energy (kcal/mol) of the methyl exchange reaction of acetylenes ($H—C{\equiv}C—R + CH_4 \rightarrow H—C{\equiv}C—H + CH_3—R$)

Molecule	ΔE STO-3G	6-31G	6-31G//6-31G	6-31G**	6-31G**	6-311G**//6-31G	DZ + P + E_{corr}[a]	ΔH (298 K) expl
$H—C{\equiv}C—CH_3$	8.4	8.9	9.1	8.5	8.0	8.0	8.1	7.6 ± 0.6[b]
$H—C{\equiv}C—Li$	48.0[c]		33.3			33.9		
$H—C{\equiv}C—C{\equiv}N$	6.9	1.2	1.1	−0.6	−2.4	−2.5		−0.5 ± 0.3[b]
$H—C{\equiv}C—OCH_3$	7.5	−2.5	−0.5	0.2	−0.6	1.4		
$H—C{\equiv}C—C({=}O)—H$	6.6	2.5	2.3	1.6	0.1	−0.3		
$H—C{\equiv}C—CH{=}CH_2$			9.2					8.1[d]
$H—C{\equiv}C—C({=}O)—OH$	4.3	−1.7	−2.1	−2.3	−4.0			
$H—C{\equiv}C—NH_2$ (planar)	6.3[c]	12.8	11.1		7.2	8.3		
$H—C{\equiv}C—C{\equiv}C—H$	12.1	8.1	7.9	6.9	4.7	4.5	7.3	3.4[d]
$H—C{\equiv}C—F$	−1.2[c]		−14.7			−11.1		

[a]Gaussian DZ + P basis set; MB-RSPT second–fourth order single–quadruple excitations + renormalization correlation energy (ref. 17).
[b]Evaluated using ΔH_f(g) from ref. 1.
[c]Reference 6.
[d]Evaluated using ΔH_f(g) from ref. 16.

straints of linearity of the four-atom system $H—C{\equiv}C—X$ and C_s symmetry.

Results and discussion

Energies of the molecules

Table 1 lists the energies of molecules used in this study, calculated with various basis sets. The most extended basis sets (6-31G** and 6-311G**) were employed only for molecules with no more than five heavy atoms. Several literature values are also tabulated.

Reaction [1]

For eight of the acetylene derivatives with small substituents in Table 2 we have studied the influence of basis sets up to 6-311G**, and of 6-31G geometry optimization, on the calculated energies of isodesmic methyl exchange reactions. All calculations indicate that lithium is the most stabilizing substituent, and fluorine is most destabilizing. For other substituents the orders of decreasing stabilizing effect (destabilizing substituents in parentheses) are

STO-3G — $C{\equiv}CH > CH_3 > OCH_3 > CN > CHO > COOH$

6-31G — $NH_2 > CH_3 > C{\equiv}CH > CHO > CN > (COOH) > (OCH_3)$

6-31G//6-31G — $NH_2 > CH_3 > C{\equiv}CH > CHO > CN > (OCH_3) > (COOH)$

6-31G** — $CH_3 > C{\equiv}CH > CHO > OCH_3 > (CN) > (COOH)$

TABLE 3. 6-311G**//6-31G population analysis of $H—C{\equiv}C—R$ with small substituents, R

—R	Total σ charge on $H—C{\equiv}C—$	Total π charge on $H—C{\equiv}C—$	Total of charge on $H—C{\equiv}C—$
$—CH_3$	9.155	4.026	13.181
$—C{\equiv}N$	8.661	3.962	12.623
$—OCH_3$	8.666	4.169	12.835
$—C({=}O)—H$	9.021	3.960	12.981
—F	8.604	4.153	12.757
$—NH_2$	8.634	4.154	12.788
—Li	9.692	3.915	13.607

6-311G** — $CH_3 > NH_2 > C{\equiv}CH > CHO > (OCH_3) > (CN) > (COOH)$

6-311G**//6-31G — $NH_2 > CH_3 > C{\equiv}CH > OCH_3 > (CHO) > (CN) > (COOH)$

The calculated energies are of hypothetical vibrationless molecules, whereas the experimental values of ΔH (Table 2) are for gaseous molecules at 298 K. While the two are not precisely comparable, differences for isodesmic reactions are not expected to be large.

The stabilizing effect of the methyl substituent varies little (8.0−9.1 kcal/mol) with basis set or geometry optimization, and all calculations are in good agreement with the experimental enthalpy of -7.6 ± 0.6 kcal/mol. If one assumes that

TABLE 4. Energy of the reaction H—C≡C—R + CH_4 → H—C≡C—H + CH_3—R for acetylene derivatives with large substituents (kcal/mol)

Molecule	ΔE(STO-3G)	ΔE(6-31G)	ΔE(6-31G**)	ΔH(298 K) expl
H—C≡C—CH_2OCH_3	5.2	3.6		
H—C≡C—C—CH_3 ‖ O	6.8	3.0	2.1	
H—C≡C—C—OCH_3 ‖ O	4.6	−1.1	−1.8	−4.1 ± 1.2[a]
H—C≡C—C≡C—CH_3	13.7	10.0		
H—C≡C—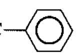	12.0	10.3		6.1 ± 1.1[b]

[a]Calculated from the heat of hydrogenation (ref. 3) and estimated ΔH_v.
[b]Calculated from ΔH_f(l) (ref. 1) and ΔH_v (ref. 20).

TABLE 5. Energies (kcal/mol) of the isodesmic reactions H—C≡C—R + $(CH_3)_3C$—H → H—C≡C—H + $(CH_3)_3C$—R

H—C≡C—R	ΔE(STO-3G)	ΔE(6-31G)	ΔH(298 K)
H—C≡C—CH_3	7.7	6.9	2.0 ± 0.6[a]
H—C≡C—C≡N	6.4	−0.5	−4.5 ± 0.4[a,b]
H—C≡C—OCH_3	12.9	−0.8	
H—C≡C—C—H ‖ O	6.5	0.8	
H—C≡C—C—OH ‖ O	4.3	−3.7	
H—C≡C—CH_2OCH_3	4.6	1.3	
H—C≡C—C—CH_3 ‖ O	9.0	3.9	
H—C≡C—C—OCH_3 ‖ O	4.6	−3.0	−8.4 ± 1.2[c]
H—C≡C—C≡C—CH_3	15.4	10.0	
H—C≡C—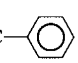	17.9	15.1	3.0 ± 1.2[d]

[a]Based on ΔH_f(g) values from ref. 1.
[b]One-half of ΔH for the reaction of dicyanoacetylene.
[c]Calculated from the heat of hydrogenation (ref. 3) and estimated ΔH_v.
[d]Calculated from ΔH_f(l) (ref. 1) and ΔH_v (ref. 20).

ΔH for the methyl exchange reaction of cyanoacetylene (H—C≡C—CN + CH_4→ H—C≡C—H + CH_3CN) is half that for dicyanoacetylene (NC—C≡C—CN + $2CH_4$ → H—C≡C—H + $2CH_3CN$), cyano is slightly destabilizing. The other experimental ΔH values (Table 2) for the ethynyl and vinyl substituents are based on heats of formation (16) of unknown uncertainty. Some additional reliable experimental values are much needed.

With the above limitations in mind we tentatively conclude that 6-311G**//6-31G calculations reproduce experimental ΔH^{298} values satisfactorily (±0.4−2.0 kcal/mol). We may draw the following conclusions concerning simpler calculations. (*a*) STO-3G calculations in this system generally grossly overestimate the stabilizing effect of substituents by more than 6 kcal/mol. The predicted order of stabilities is appreciably incorrect. (*b*) 6-31G//6-31G results appear to overestimate the stabilizing influence of CN, CHO, NH_2, and C≡CH substituents, and underestimate OCH_3, usually by 2−3 kcal/mol. 4-31G//4-31G results (A. Greenberg, private communication) are often comparable. (*c*) 6-31G geometry optimization affects 6-31G and 6-311G** results appreciably (>0.4 kcal/mol) only in the case of the π donor substituents OCH_3 and NH_2. (*d*) Addition of polarization functions for heavy atoms and hydrogen (6-31G** vs. 6-31G) decreases slightly the predicted stabilization by substituents other than OCH_3. (*e*) Increased basis set size (6-311G** vs. 6-31G**) leads to a decrease (0.5−2.2 kcal/mol) in all predicted stabilizations. In calculations on substituted acetylenes a large basis set and polarization functions have a larger and more general influence on the results than does geometry optimization. However, all three of these features should be used in such calculations.

We have not considered whether electron correlation effects might influence the above results. A small number of data have recently become available (17), calculated using a Gaussian double zeta + polarization functions basis set, and second−fourth order single−quadruple excitations + renormalization correlation energies based on the many body Rayleigh−Schrödinger perturbation theory. The correlation energy contribution for methyl exchange of 1-propyne is negligible, but for butadiyne the value is 3.2 kcal/mol. The resulting ΔE value for butadiyne (Table 2) is in poorer agreement with the experimental ΔH than is the 6-311G**//6-31G ΔE value. New experimental measurements will be needed to resolve this question.

We have carried out a Mulliken population analysis (18) at the 6-311G**//6-31G level (Table 3), and find that electron withdrawal from the triple bond tends to be associated with destabilization, whereas electron donation favors stabilization. This is in agreement with a 4-31G study of other substituents (19). Dill, Greenberg, and Liebman (6) have pointed out that σ withdrawing substituents have a particularly strong destabilizing effect in acetylenes, whereas π withdrawal stabilizes. We feel this is a more generally useful viewpoint than consideration of the total $(\sigma + \pi)$ charge on the $\mathrm{H{-}C{\equiv}C{-}}$ unit.

Table 4 gives the energies of isodesmic methyl exchange reactions involving larger substituents with 6-31G** as the most extensive basis set used. Improved basis sets lead to decreased calculated energies of the individual compounds and decreased stabilization by substituents.

Reaction [2]

The size of the *tert*-butyl reference molecules only allowed the use of the STO-3G and 6-31G basis sets. According to the results for reaction [1] (Table 2) it is doubtful that the results for reaction [2] (Table 5) will be close to the experimental values, and this is verified by the two experimental values available. However, except for R = OCH_3 the order of stabilities is expected to be correct at the 6-31G level

$$\begin{aligned}\text{Phenyl} &> \mathrm{C{\equiv}C{-}CH_3} > \mathrm{CO{-}CH_3} > \mathrm{CH_2OCH_3} > \mathrm{CHO}\\ &> (\mathrm{CN}) > (\mathrm{OCH_3}) > (\mathrm{CO{-}OCH_3}) > (\mathrm{CO{-}OH})\end{aligned}$$

This is similar to the 6-31G order for methyl exchange (reaction [1])

$$\begin{aligned}\text{Phenyl} &> \mathrm{C{\equiv}C{-}CH_3} > \mathrm{CH_3} > \mathrm{CH_2OCH_3} > \mathrm{COCH_3} > \mathrm{CHO}\\ &> \mathrm{CN} > (\mathrm{CO{-}OCH_3}) > (\mathrm{CO{-}OH}) > (\mathrm{OCH_3})\end{aligned}$$

with OCH_3 the most notable exception.

Conclusions

For the isodesmic reactions considered, STO-3G calculations do not provide useful conclusions. The 6-31G basis set is somewhat better at predicting relative stabilities of the compounds and the stabilizing or destabilizing character of substituents. 6-31G geometry optimization is significant only when π donor substituents are present. The use of extended basis sets with polarization functions seems mandatory in order to closely reproduce experimental values. Methyl and *tert*-butyl exchange reactions give approximately the same order of stability for the compounds examined, but the advantage of the latter as a better model is lost due to the difficulty of applying larger basis sets. The electron donating substituent CH_3 stabilizes the triple bond. The molecules $\mathrm{H{-}C{\equiv}C{-}C{\equiv}C{-}H}$, $\mathrm{H{-}C{\equiv}C{-}C{\equiv}C{-}CH_3}$, $\mathrm{H{-}C{\equiv}C{-}CH{=}CH_2}$, and phenylacetylene exhibit substantial stabilization, in agreement with classical resonance theory, but $\mathrm{H{-}C{\equiv}C{-}C{\equiv}N}$, $\mathrm{H{-}C{\equiv}C{-}\underset{\underset{O}{\|}}{C}{-}OH}$, and $\mathrm{H{-}C{\equiv}C{-}\underset{\underset{O}{\|}}{C}{-}OCH_3}$ show destabilization.

Acknowledgements

Acknowledgement is made to the donors of the Petroleum Research Fund, administered by the American Chemical Society, for partial support of this research, and to the Robert A. Welch Foundation (R.L.M., Grant E-397; R.F., Grant E-136) for additional support.

1. J. D. Cox and G. Pilcher. Thermochemistry of organic and organometallic compounds. Academic Press, New York, NY. 1970.
2. J. B. Pedley and J. Rylance. Sussex-N.P.L. computer analysed thermochemical data: organic and organometallic compounds. University of Sussex, Brighton, England. 1977.
3. T. L. Flitcroft and H. A. Skinner. Trans. Faraday Soc. **54**, 47 (1958); J. E. Bennett. Thesis. U. of Manchester. 1959; E. Schjanberg. Z. Phys. Chem. **42**, 317 (1938).
4. R. Fuchs and L. A. Peacock. J. Phys. Chem. **83**, 1975 (1979).
5. W. J. Hehre, R. Ditchfield, L. Radom, and J. A. Pople. J. Am. Chem. Soc. **92**, 4796 (1970); M. R. Peterson and I. G. Csizmadia. J. Mol. Struct. **92**, 323 (1983).
6. J. D. Dill, A. Greenberg, and J. F. Liebman. J. Am. Chem. Soc. **101**, 6814 (1979).
7. R. Fuchs, J. H. Hallman, and M. O. Perlman. Can. J. Chem. **60**, 1832 (1982); R. Fuchs. J. Chem. Educ. **61**, 133 (1984).
8. J. S. Binkley, R. A. Whiteside, R. Krishnan, R. Seeger, D. J. Defrees, H. B. Schlegel, S. Topiol, L. R. Kahn, and J. A. Pople. Gaussian 80, Program 437. Quantum Chemistry Program Exchange, Indiana University, Bloomington. 1980.
9. W. J. Hehre, R. F. Stewart, and J. A. Pople. J. Chem. Phys. **51**, 2657 (1969).
10. W. J. Hehre, R. Ditchfield, and J. A. Pople. J. Chem. Phys. **56**, 2257 (1972).
11. P. C. Hariharan and J. A. Pople. Theor. Chim. Acta, **28**, 213 (1973).
12. R. Krishnan, J. S. Binkley, R. Seeger, and J. A. Pople. J. Chem. Phys. **72**, 650 (1980).
13. J. A. Pople and M. Gordon. J. Am. Chem. Soc. **89**, 4253 (1967).
14. H. F. Schaefer. Methods of electronic structure theory. Plenum Press, New York, NY. 1977.
15. W. J. Hehre and J. A. Pople. Tetrahedron Lett. 2959 (1970).
16. D. R. Stull, E. F. Westrum, Jr., and G. C. Sinke. The chemical thermodynamics of organic compounds. Wiley, New York, NY. 1969.
17. V. Kello, M. Urban, J. Noga, and G. H. F. Diercksen. J. Am. Chem. Soc. **106**, 5864 (1984).
18. R. S. Mulliken. J. Chem. Phys. **23**, 1833 (1955).
19. L. Radom, W. J. Hehre, and J. A. Pople. J. Am. Chem. Soc. **93**, 289 (1971).
20. J. S. Chikos, A. S. Hyman, L. H. Ladon, and J. F. Liebman. J. Org. Chem. **46**, 4294 (1981).

Multiphoton absorption and decomposition studies of chloroform-*d* induced by a pulsed $^{13}CO_2$ laser[1]

ROBERT D. MCALPINE, J. W. GOODALE, AND D. K. EVANS

Physical Chemistry Branch, Atomic Energy of Canada Limited Research Company, Chalk River Nuclear Laboratories, Chalk River, Ont., Canada K0J 1J0

Received March 15, 1985

ROBERT D. MCALPINE, J. W. GOODALE, and D. K. EVANS. Can. J. Chem. **63**, 2995 (1985).

The multiphoton absorption (MPA) and decomposition (MPD) of chloroform-*d* induced by various $^{13}CO_2$ [00°1 → 10°0] lines were studied for pressures from 0.133 to 13.3 kPa. MPA results show a cross-section increasing with pressure up to a plateau value which is likely due to rotational hole-filling. A MPA "spectrum" of the average number of photons absorbed versus wavenumber for different $^{13}CO_2$ laser lines is shifted to lower wavenumbers compared to the small signal absorption spectrum by at least 5 cm^{-1} suggesting that a small amount of anharmonicity bottle-necking is occurring in $CDCl_3$. A comparison of the MPD probability versus fluence for $CDCl_3$ with that measured by other workers for fluoroform indicates that the $CDCl_3$ is decomposed at a slightly lower fluence by an appropriate line of a pulsed CO_2 laser.

For the pressure range (0.2 to 4.0 kPa) and laser pulse-width used, the MPD is second order in $CDCl_3$. The primary decomposition channel is elimination of DCl followed by reaction of CCl_2 to give C_2Cl_2, C_2Cl_4, and Cl_2. The DCl produced exchanges with a source of H_2O in the reaction cell to give significant quantities of HCl. A post-pulse reaction between (HCl + DCl) and C_2Cl_2. produces (C_2DCl_3 + C_2HCl_3). Significant quantities of CCl_4 are also produced by undetermined reactions.

ROBERT D. MCALPINE, J. W. GOODALE et D. K. EVANS. Can. J. Chem. **63**, 2995 (1985).

On a employé différentes raies, de la transition [00°1 → 10°0] du laser à $^{13}CO_2$ pour étudier l'absorption et la décomposition multiphotonique (AMP et DMP) de $CDCl_3$ à des pressions de $CDCl_3$ allant de 0,133 à 13,3 kPa. Les résultats AMP montrent une section efficace qui augmente jusqu'à un plateau; on peut probablement expliquer cette observation par l'effet de "rotational hole-filling". Un "spectre" AMP du nombre moyen des photons absorbés par molécule contre la longueur d'onde pour les raies diverses du laser à $^{13}CO_2$ était deplacé d'un certain nombre d'ondes plus bas que le spectre ordinaire d'au moins 5 cm^{-1}, ce qui suggère qu'une petite quantité d'"anharmonicity bottle-necking" a opéré dans le $CDCl_3$. La probabilité DMP contre fluence pour $CDCl_3$ est comparée avec celle mesurée par d'autres travailleurs pour CDF_3 et cette comparaison indique que l'on peut décomposer $CDCl_3$ un peu plus facilement que CDF_3 par la raie appropriée d'un laser à CO_2 opérant en mode pulsé.

Pour les pressions (0,2 à 4,0 kPa) et pour la durée d'impulsion constante employées, la DMP est de l'ordre de deux. Le canal primaire de la décomposition est l'élimination du DCl suivi par la réaction de CCl_2 pour donner C_2Cl_4, C_2Cl_2 et Cl_2. Le DCl produit s'échange avec une source d'H_2O dans la cellule de la réaction pour donner une quantité significative d'HCl. Une réaction, ayant lieu après l'impulsion, entre (HCl et DCl) et C_2Cl_2 produit (C_2DCl_3 et C_2HCl_3). Une quantité significative de CCl_4 est produite par des réactions actuellement indéterminées.

1. Introduction

The potential application of infrared multiphoton decomposition (MPD) processes (1) to isotope separation (2) has been the subject of many studies during the past decade (3). In particular, the separation of hydrogen isotopes, which has large scale application in the production of heavy water (deuterium from protium) for use in CANDU reactors, for the extraction of titrium from the moderator water in a CANDU reactor (tritium from deuterium), and during reprocessing of spent fuel (tritium from protium) has been pursued. In all three applications, the source of the isotope to be extracted is almost always water. However, since water does not undergo MPD efficiently (4), it is more efficient to exchange the desired isotope into a working molecule which will then undergo isotopically selective MPD (3).

Several molecules have been suggested as potentially suitable working molecules for heavy water production (3, 5). Of these, fluoroform is currently the one most promising (6–14) and may also be suitable for tritium recovery (15–18). However, there are two major obstacles to the use of fluoroform in a heavy water process: (*a*) efficient MPD of fluoroform requires fluences in excess of 20 J/cm^2, which, combined with the need to use short pulses (9) ($\Delta\tau \approx 1-2$ ns) leads to laser-induced damage of windows which complicate the design of the photolysis cell and (*b*) exchange of fluoroform with water or natural gas is too slow for a practical exchange step without the use of a catalyst (11). Consideration of a molecule which undergoes faster exchange with water would be advantageous.

As part of a search for working molecules which are improvements over fluoroform, we have considered MPD of the series CHX_3 where X = H, F, Cl, Br, and I. The enthalpies of decomposition (3) for members of this series are shown in Fig. 1.

For applications to isotope separation in a decomposition channel, such as channel 1, Fig. 1, which has the deuterium located in a stable molecule is preferred. This factor suggests the consideration of chloroform as a candidate molecule for hydrogen isotope separation. Two additional factors favour the consideration of chloroform: (*a*) The density of states increases more rapidly with excitation energy for chloroform versus fluoroform as is shown in Fig. 2. This suggests that chloroform may undergo MPD at lower fluences than fluoroform (4, 19, 20). (*b*) The isotopic exchange rate between chloroform and water is faster than between fluoroform and water (21).

In 1978, Marling and Herman (5) rejected chloroform as a potential candidate for heavy water production since $CDCl_3$ does not absorb any of the easily obtained lines of a $^{12}C^{16}O_2$ laser. However, since that time, the economic use of TEA lasers operating on $^{13}C^{16}O_2$ (producing lines which are selectively absorbed by $CDCl_3$) has been demonstrated (22). An earlier MPD study of $CDCl_3$ and $CHCl_3$ concluded that the D/H selectivity for mixtures of these isotopic species was small (23).

[1]AECL Contribution Number 8869.

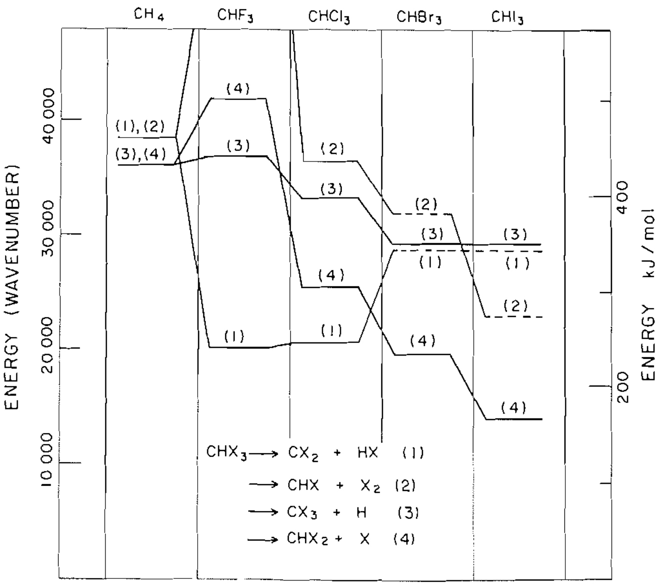

FIG. 1. Endothermicities for various decomposition channels of the haloforms CHX_3, where X = H, F, Cl, Br, and I. The sources of data are listed in ref. 3.

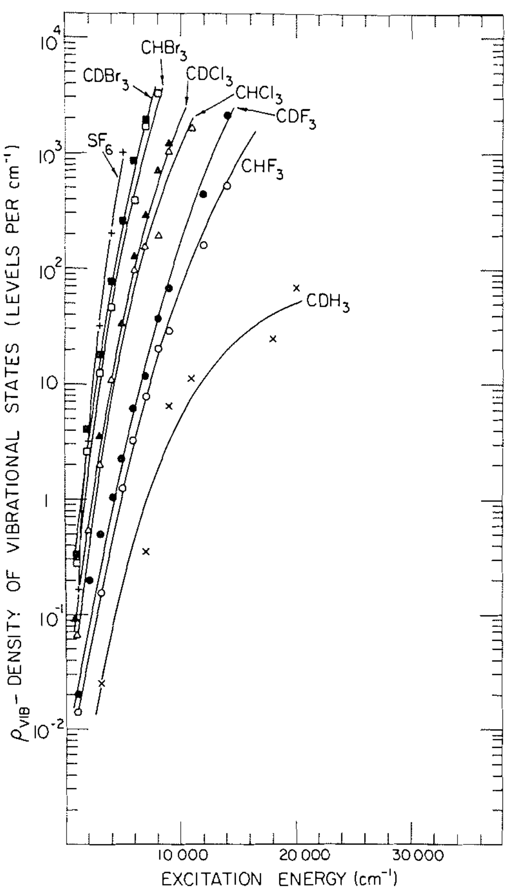

FIG. 2. The density of vibrational states as a function of excitation energy for the haloforms. The curve given for SF_6 is included for reference.

Chloroform is thought to be a suitable working molecule for tritium recovery and the selective MPD of $CDCl_3$ and $CTCl_3$ was studied using the 10P (50) line of a CO_2 laser and an NH_3 laser, respectively (24–27). Studies of the MPD of $CDCl_3$, in a molecular beam, show channel 1 of Fig. 1 to be the predominant MPD channel (25).

In this paper we report the results of a study of multiphoton absorption (MPA) and MPD of $CDCl_3$ using a $^{13}C^{16}O_2$ laser. The major stable products have been measured and a mechanism which accounts for them is discussed.

TABLE 1. MPA results for eliminate $CDCl_3$ as a function of pressure (P), pathlength (l), and fluence (Φ) for the $^{13}C^{16}O_2$ [00°1 → 10°0] P(8) line; these results were obtained by transmission techniques; for a definition of K, b, and Φ, see the text

P (kPa)	l (cm)	Range of Φ (J/cm²)	$-\log K$	b
0.133	46	0.01−0.08	19.3±0.3	0.2±0.2
0.400	46	0.003−0.07	19.58±0.03	−0.31±0.01
0.521	15	0.001−0.07	19.344±0.007	−0.264±0.003
0.667	46	0.003−0.08	19.41±0.02	−0.25±0.01
0.868	11.3	0.002−0.02	19.08±0.02	−0.19±0.01
1.080	15	0.002−0.02	19.12±0.07	−0.21±0.04
1.595	11.3	0.005−0.06	19.003±0.007	−0.191±0.004
2.000	15	0.007−0.07	18.99±0.03	−0.18±0.02
2.673	2	0.002−0.08	18.66±0.03	−0.10±0.02
3.009	2	0.002−0.08	18.67±0.4	−0.09±0.02
3.340	2	0.002−0.07	18.72±0.05	−0.13±0.03
4.290	2	0.002−0.08	18.69±0.03	−0.12±0.01
5.362	2	0.002−0.08	18.67±0.03	−0.11±0.02
5.377	1	0.001−0.05	18.40±0.02	−0.02±0.01
6.679	1	0.001−0.05	18.39±0.07	−0.01±0.03
6.697	2	0.002−0.07	18.54±0.02	−0.07±0.01
8.029	1	0.002−0.07	18.37±0.04	−0.004±0.02
9.332	1	0.001−0.04	18.44±0.02	−0.03±0.01
10.671	1	0.001−0.06	18.57±0.03	−0.06±0.02
13.252	2	0.006−0.07	18.38±0.02	−0.10±0.01
13.279	1	0.005−0.05	18.35±0.02	−0.01±0.01
6.679	1	0.001−0.05	18.39±0.07	−0.01±0.03
6.697	2	0.002−0.07	18.54±0.02	−0.07±0.01
8.209	1	0.002−0.07	18.37±0.04	−0.004±0.02
9.332	1	0.001−0.04	18.44±0.02	−0.03±0.01
10.671	1	0.001−0.06	18.57±0.03	−0.06±0.02
13.252	2	0.006−0.07	18.38±0.02	−0.10±0.01
13.279	1	0.005−0.05	18.35±0.02	−0.01±0.01

2. Experimental

2.1 $^{13}C^{16}O_2$ laser

In order to conserve the charge of $^{13}C^{16}O_2$, a Lumonics model K-920 CO_2 laser kit was modified to ensure a good gas seal during operation and to permit partial evacuation during gas fill. The gas recirculating system contained a catalytic bed to recombine the CO and O_2 formed during laser operation thus preventing the arcing that would have occurred if these gases had been permitted to build up. The laser and gas recirculating system were filled with the mixture N_2:He:$^{13}C^{16}O_2$ = 1:3:1 as follows. The system was purged of air using a N_2, He mixture in the chosen proportion; then the system was evacuated to a N_2, He mixture pressure of 80 kPa and then was filled with $^{13}C^{16}O_2$ (MSD Isotopes, lot number 1246-G, 99 atom% ^{13}C) to a pressure of ~100 kPa. A single charge of $^{13}C^{16}O_2$ lasts at least one year and can be recovered by purging the system with He or N_2 through a cold trap (77 K) if servicing is required.

The laser was equipped with a Bausch and Lomb replica grating (135 lines/mm, blazed at λ = 7.4 μm) allowing single line tuning over the 00°1 → 10°0 and 00°1 → 02°0 $^{13}C^{16}O_2$ transitions. Intracavity irises were used to force single transverse mode operation. However, many longitudinal modes were active giving a multi-mode temporal profile with a spike (~200 ns) and a tail (~1 μs) similar to that obtained with conventional $^{12}C^{16}O_2$ lasers.

For the MPA experiments, lines with $\bar{\nu}_L$ = 886.1 to 938.8 cm^{-1}

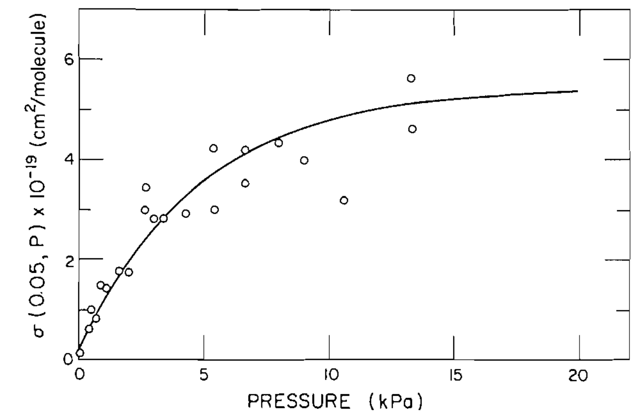

FIG. 3. The dependence of cross-section for absorption of the $^{13}CO_2$ [00°1 → 10°0] P(8) line as a function of $CDCl_3$ pressure for $\Phi = 0.05$ J/cm^2. The solid line is a plot of eq. [2] with $\sigma(0.05,0) = 2 \times 10^{-20}$, $\sigma(0.05,\infty) = 5.5 \times 10^{-19}$, and $P_0 = 5$ kPa.

were used and for MPD experiments only the P(8) line of the 00°1 → 10°0 transition ($\bar{\nu}_L = 908.4$ cm^{-1}) was used. Radiant energies were varied by use of calibrated BaF_2 attenuators.

2.2 MPA measurements

Both the automated photoacoustic data acquisition system (described in ref. 28) and transmission techniques (29) were used to obtain the results reported here. Absorption cross section, σ, and the average number of photons absorbed per molecule, $\langle n \rangle$, are expressed either as a function of fluence at beam center, ϕ, or as local fluence, Φ, as described elsewhere (9, 10, 30).

2.3. MPD measurements

MPD measurements were performed using the following two lens and cylindrical cell combinations: (*a*) a lens of focal length 55 cm and a cell of length 3.7 cm and volume 22.7 cm^3, (*b*) a lens of focal length 100 cm and a cell of length 11.0 cm and volume 53.1 cm^3. These combinations were selected to put the entire cell within the cylindrical region of the photolysis geometry.

A Finnegan model 1020B computerized gas chromatograph/mass spectrometer (equipped with a Poropak-P column) was used to identify gc peaks due to $CDCl_3$, C_2Cl_4, CCl_4, (C_2DCl_3 + C_2HCl_3), and C_2Cl_2. Quantitative analysis of these compounds was carried out on a Hewlett-Packard model 5700A gas chromatograph (3.7 m stainless steel column packed with Poropak-P, temperature 443 K, He carrier gas at a flow rate of 25 cm^3/min) equipped with a flame ionization detector. Except for C_2Cl_2, calibration curves of peak area versus concentration were obtained by injection of known amounts of authentic samples. No such curve could be obtained for C_2Cl_2 due to the problems of handling this compound; rather, stoichiometry was assumed (and is discussed in section 3.2) which provided a relationship between the C_2Cl_2 concentration and the $CDCl_3$ consumed.

A Bomem model DA3.02 Fourier Transform Infrared (FTIR) spectrometer was also used to observe $CDCl_3$ and the products DCl, HCl, C_2Cl_4, C_2Cl_2, CCl_4, C_2DCl_3, and C_2HCl_3.

3. Results and discussion

3.1. MPA measurements

The absorption as a function of pressure, P, and Φ was measured for MPA of the $^{13}CO_2$ [00°1 → 10°0] P(8) transition using transmission techniques (29). The absorption cross sections $\sigma(\Phi)$ were corrected for the Gaussian distribution of the beam and for changes in fluence along the beam as previously described (9, 10). The values of $\sigma(\Phi)$ were then found to fit well to the empirical form of (4, 9, 10, 29) of eq. [1].

$$[1] \quad \sigma(\Phi) = K\Phi^b$$

The results of these analyses are given in Table 1.

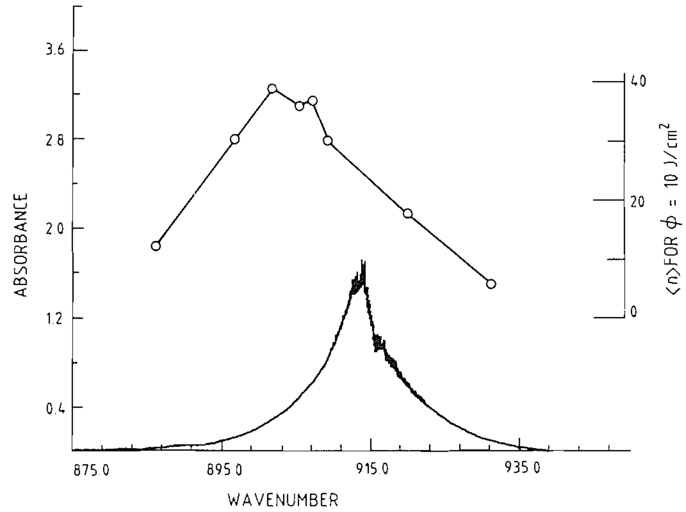

FIG. 4. The dependence of the average number of photons absorbed per molecule $\langle n \rangle$, of $CDCl_3$ on the laser wavenumber for $\phi = 10$ J/cm^2. The bottom trace is the small signal absorption spectrum of $CDCl_3$ for comparison.

The pressure dependence of σ for $\Phi = 0.05$ J/cm^2, $\sigma(0.05, P)$, calculated from the results of Table 1, is plotted in Fig. 3. These results show a behaviour similar to the $P\Delta\tau$ (where $\Delta\tau$ is laser pulse width) dependence observed for constant Φ for CDF_3 (31), CH_3OH (32), and cyclobutanone (33) and fits the empirical equation [2]

$$[2] \quad \sigma(0.05, P) = \sigma(0.05, \infty) + [\sigma(0.05, \infty) - \sigma(0.05, 0)] \times [1 - \exp(-P/P_0)]$$

A good fit to the results plotted in Fig. 3 is obtained for $\sigma(0.05, 0) = 2 \times 10^{-20}$ cm^2, $\sigma(0.05, \infty) = 5.5 \times 10^{-19}$ cm^2, $P_0 = 5$ kPa.

Due to the large σ values for low fluence (the b values in eq. [1] are negative), absorption of the laser light during transmission through the $CDCl_3$ significantly reduces ϕ in the region of the gas that the microphone samples. This, as has been discussed in ref. 32, leads to a large uncertainty in the results, and consequently we do not report σ values for the photoacoustic measurements. However, from the MPA results, $\langle n \rangle(\phi)$ for $\phi = 10$ J/cm^2 has been estimated using several laser lines. These results have an absolute accuracy of only a factor of 2 or 3 due to the absorption problem discussed above; however, the relative accuracy across the range of $\bar{\nu}_L$ is probably 20 to 30% allowing the "spectrum" of $\langle n \rangle$ (10) versus $\bar{\nu}_L$ to be qualitatively compared with the small signal spectrum. This is shown in Fig. 4. The observed peak of the large signal spectrum is shifted to lower energy by ≥ 5 cm^{-1} from that of the small signal spectrum. This is a larger shift than was observed for CDF_3 (10) and suggests that anharmonicity bottle-necking (34, 35) is more severe for $CDCl_3$ than CDF_3 (33, 36).

3.2. MPD measurements

The results of an MPD study of $CDCl_3$, as a function of pressure, fluence at beam centre, focal length, and the number of pulses are given in Table 2.

The results of Table 2 for $\phi = 18 \pm 0.5$ J/cm^2 and for focal length 55 cm are plotted as a second order plot in Fig. 5, demonstrating that the depletion of $CDCl_3$ is second order in $CDCl_3$ for the pressure range 0.2 to 4.0 kPa. Similar kinetics have been previously observed (for conditions of ≥2 collisions during the laser pulse) for HCOOH (36), CH_3OH (37, 38), and

TABLE 2. The results of a MPD study of $CDCl_3$ using the $^{13}CO_2$ $[00^{\circ}1 \rightarrow 10^{\circ}0]$ P(8) line as a function of pressure (P), fluence (ϕ), and number of laser pulses (m); the symbol N_m denotes the number of $CDCl_3$ in the cell after m pulses; the numbers in parentheses in columns 7 and 8 are respectively the quantities of C_2Cl_4* produced by reaction [6] and the quantity of C_2Cl_2 produced overall using the assumptions discussed in the text

P (kPa)	ϕ (J/cm^2)	Focal length (cm)	$m\times10^{-2}$ (pulses)	$N_0\times10^{-18}$ (molecules)	$N_m\times10^{-18}$ (molecules)	$C_2Cl_4\times10^{-18}$ (molecules)	$C_2Cl_2\times10^{-18}$ (molecules)	$C_2DCl_3\times10^{-18}$ (molecules)	$CCl_4\times10^{-18}$ (molecules)
0.198	7.7	55	70	1.097	0.58	0.02 (0.26)	(10.24)	—	—
0.268	6.3	100	10	3.467	2.86	0.01 (0.03)	(0.29)	—	—
0.268	7.5	100	42	3.465	2.97	0.06 (0.25)	(0.20)	0.038	—
0.268	9.7	100	60	3.465	2.62	0.32 (0.42)	(0.10)	0.064	—
0.268	6.4	100	180	3.469	2.88	0.14 (0.29)	(0.15)	0.051	—
0.401	18.0	55	40	2.271	1.20	0.15 (0.54)	(0.39)	0.031	—
0.431	18.2	55	40.1	2.387	1.03	0.26 (0.68)	(0.42)	0.039	0.031
0.647	18.3	55	20	3.585	1.80	0.31 (0.89)	(0.59)	0.039	0.030
1.004	18.3	55	2	5.633	4.92	0.23 (0.36)	(0.13)	0.007	0.016
1.002	17.9	55	5	5.620	3.88	0.30 (0.87)	(0.56)	0.023	0.034
1.003	18.4	55	10	5.627	3.30	0.69 (1.17)	(0.48)	0.06	0.16
1.001	18.2	55	15	5.612	2.40	0.77 (1.60)	(0.54)	0.10	0.22
1.004	17.9	55	20	5.633	2.20	1.19 (1.72)	(0.53)	0.19	0.37
1.336	2.9	100	20	17.301	16.5	0.42 (0.40)	(—)	0.052	—
1.335	3.3	55	20	7.394	7.12	0.13 (0.14)	(—)	0.016	—
1.338	4.3	100	10	17.333	12.77	1.66 (2.28)	(0.62)	0.17	0.26
1.334	6.6	100	10	17.276	11.80	2.92 (2.73)	(—)	0.31	0.43
1.335	7.6	100	5	17.295	13.69	1.49 (1.80)	(0.31)	0.14	0.069
1.335	8.6	100	10	17.291	9.11	2.55 (4.29)	(1.54)	0.28	0.19
1.336	9.5	100	10	17.300	5.37	3.78 (5.96)	(2.18)	0.33	—
1.336	13.1	55	20	7.396	2.81	0.91 (2.30)	(1.39)	0.12	0.078
1.336	18.9	55	8.6	7.398	3.14	0.79 (2.13)	(1.34)	0.063	0.045
1.335	21.1	55	10	7.394	—	1.09	—	0.086	0.15
1.335	29.2	55	5	7.395	3.39	0.72 (2.00)	(1.28)	0.047	0.13
1.335	34.3	55	5	7.393	3.08	0.76 (2.16)	(1.40)	0.047	0.12
2.000	17.9	55	5	11.073	5.34	1.23 (2.87)	(1.64)	0.078	0.33
2.672	17.6	55	1	14.794	12.03	0.58 (1.38)	(0.80)	0.023	0.23
2.684	17.8	55	3	14.861	8.05	1.41 (3.41)	(2.00)	0.10	1.21
2.670	17.5	55	5	14.787	6.22	1.63 (4.28)	(2.65)	0.10	1.21
2.784	17.9	55	7	14.861	5.93	2.41 (4.47)	(2.06)	0.15	1.43
2.669	17.3	55	10.4	14.779	3.72	2.27 (5.53)	(3.26)	0.16	0.67
4.002	17.9	55	5	22.162	8.26	2.21 (6.95)	(4.74)	0.089	1.22

CH_2O (39) and are indicative of a collisionally assisted MPD process. The decomposition probability, $f(\phi)$ (that is the fraction of the illuminated molecules which decompose) is given by

$$[3] \quad f(\phi) = \frac{k_2N_0}{(1-k_2N_0)}\frac{V_0}{V_l}$$

where k_2 is the second order rate constant, V_0 is the cell volume, and V_l is the volume of the photolysis zone given by

$$[4] \quad V_l = \frac{\pi(F\theta)^2 l}{4}$$

where F is the lens focal length, θ is the laser divergence (1.5 mrad in this case), and l is the cell length. Since the laser beam has a Gaussian rather than a "top-hat" radial distribution, the definition of the "cylindrical" photolysis zone depends on the radius chosen to define the beam width. In addition, since the MPD is second order, molecules initially outside the defined "photolysis zone" may, by collisional or diffusion processes, become excited and participate in MPD.

The following functional form for $f(\phi)$ in eq. [5] is similar to that suggested by Fuss (40), but with the addition of a scaling parameter, A.

$$[5] \quad f(\phi) = A \exp\,[-\phi_o/\phi]$$

A good fit of experimental results for MPD of 2,2,2-trifluoroethanol to the Fuss model was observed in our laboratory (20). In Fig. 6, $\log_e f(\phi)$ versus $1/\phi$ is plotted for the results of Table 1 corresponding to $P = 1.33 \pm 0.01$ kPa. From a linear least-squares fit to this plot, $A = 3.8$ and $\phi_0 = 18.0$ J/cm^2. The value $A > 1$ means that more molecules are participating in MPD than just those initially within the defined "photolysis zone". This could arise either from an underestimate of this zone for a laser beam with a Gaussian radical distribution or from the participation of molecules initially outside the photolysis zone by collisional or diffusion processes. A comparison of $CDCl_3$ results with those for CDF_3 (9) (the above results for $CDCl_3$, when analysed according to the formula used in ref. 9, give ϕ_{sat}, equal to 13.4 J/cm^2) is difficult due to the addition of buffer gases used in ref. 9; however, our results for $CDCl_3$ indicate that it undergoes MPD at slightly lower fluences than CDF_3, for comparable conditions. It would appear that the gain in ease of MPD due to a faster rising ρ_{VIB} vs excitation for $CDCl_3$ compared to CDF_3 is offset by a larger anharmonicity bottle-necking in $CDCl_3$.

3.3. Reaction mechanisms

A mechanism for the MPD of $CDCl_3$ was proposed by Herman, Magnotta, Buss, and Lee (25). Of the two likely primary steps (channels 1 and 4 of Fig. 1) they conclude that

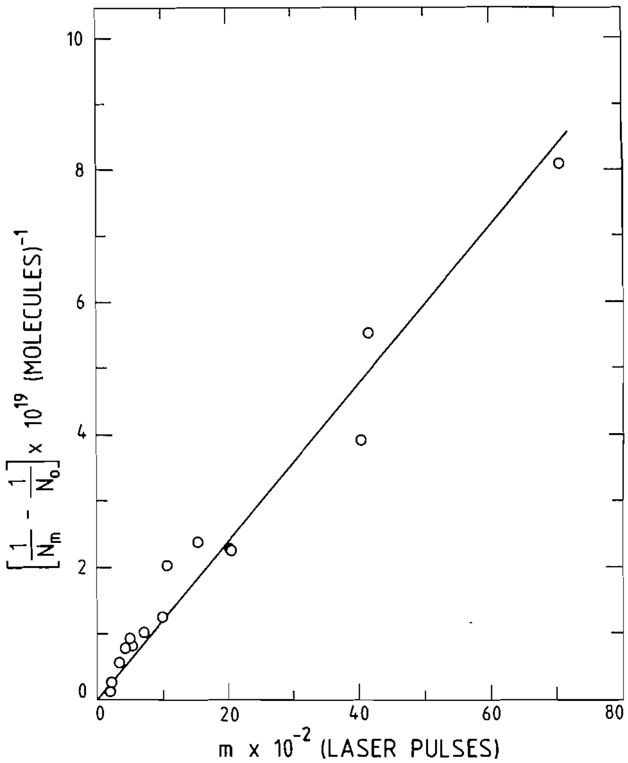

FIG. 5. Second order kinetic plot for depletion of $CDCl_3$ by $^{13}CO_2$ laser induced MPD, for ϕ = 18 J/cm^2 and F = 55 cm.

>99.1% of the decomposition occurs by channel 1 for fluence ≤35 J/cm^2.

The other major products observed by us (C_2Cl_4 and C_2Cl_2) may be accounted for as follows:

[6] $2CCl_2 \rightarrow C_2Cl_4{}^*$

[7] $C_2Cl_4{}^* \rightarrow C_2Cl_2 + Cl_2$

[8] $C_2Cl_4{}^* + M \rightarrow C_2Cl_4 + M$

[9a] $C_2Cl_4{}^* \xrightarrow{mh\nu} C_2Cl_2 + Cl_2$

[9b] $C_2Cl_4 \xrightarrow{ph\nu} C_2Cl_2 + Cl_2$

In this scheme, channel 1 is the only source of DCl and its concentration should be equal to the $CDCl_3$ depletion. To determine the relative yield of DCl by MPD, two experiments were performed. One 1.334 kPa sample and one 2.785 kPa sample were photolyzed by 2500 and 2000 laser pulses, respectively, using a 55 cm lens and appropriate cell combination. Each sample was then split into two approximately equal parts with one part being analysed by gas chromatography as for previous samples. The second part was shaken with 30 cm^3 of H_2O and the pH was measured, and from this, the number of DCl molecules produced was determined. For the 1.334 kPa sample the number of $CDCl_3$ molecules decomposed was 9.2×10^{18} and the number of C_2Cl_4 and DCl produced were 3.4×10^{18} and 1.2×10^{19}, respectively. For the 2.785 kPa sample these numbers were 3.0×10^{19}, 3.9×10^{18}, and 2.8×10^{19}, respectively. Thus, within the large error inherent in such experiments, one DCl molecule is produced for each $CDCl_3$ molecule decomposed.

As a prelude to studying the selective MPD of $CHCl_3/CDCl_3$ mixtures, a pure sample of $CDCl_3$ was photolyzed and the products were studied by observing their FTIR spectra. About 50% of the "hydrogen chloride" product consisted of HCl with the remainder as DCl. The appearance of HCl is due to exchange between DCl and a source of water in the cell.

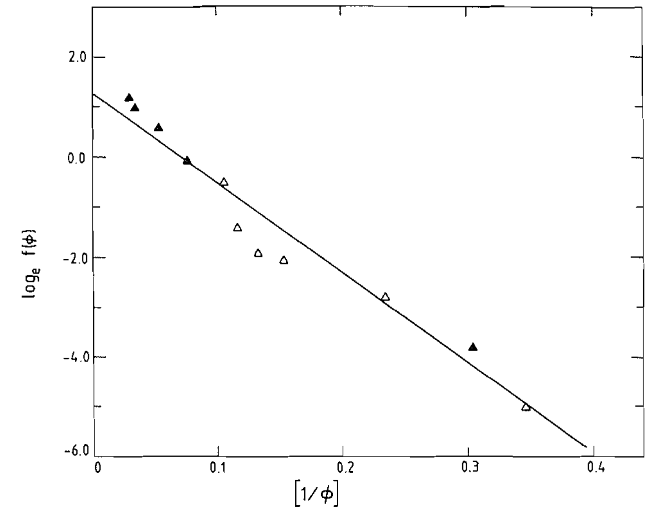

FIG. 6. A plot of $\log_e f(\phi)$ versus $1/\phi$ for MPD of $CDCl_3$ induced by a $^{13}CO_2$ laser for P = 1.33 kPa and F = 100 cm (△) and F = 55 cm (▲).

[10] $DCl + H_2O = HDO + HCl$

A similar exchange was observed for selective MPD of fluoroform (10). Attempts to study selective MPD of $CHCl_3/CDCl_3$ mixtures by observing FTIR depletion of $CHCl_3$ and $CDCl_3$ peaks was also unsuccessful since product FTIR peaks interfere with the $CDCl_3$ peaks in the spectrum.

A second order kinetic plot for C_2Cl_4, using the P = 1.0 and 2.7 kPa results, shows that the appearance of this product follows well the consumption of $CDCl_3$ with 0.24 molecule of C_2Cl_4 produced per molecule of $CDCl_3$ decomposed. If CCl_2 undergoes combination via reaction [6] followed by [8] then 0.5 molecule of C_2Cl_4 would be produced per $CDCl_3$ molecule consumed. Due to the highly reactive nature of C_2Cl_2, no absolute calibration was obtained for gas chromatography. However, if one assumes that reactions [7] and [9] are the only sources of C_2Cl_2 then the C_2Cl_2 concentrations will equal half the depletion of $CDCl_3$ minus C_2Cl_4. The numbers in parentheses in Table 2, column 8 are obtained in this way. To test the assumption that C_2Cl_2 is only formed via reactions [7] and [9] the calculated C_2Cl_2 concentrations were plotted versus the correspondingly observed gas chromatograph peak heights and this gave a straight line which passed through the origin which is consistent with the assumption. Samples of C_2Cl_4 were irradiated with the $^{13}C^{16}O_2$ [00°1 → 10°0] P(8) line; the FTIR spectrum showed that no decomposition occurred, thus reaction [9*b*] is eliminated as a source of C_2Cl_2.

Two minor products, CCl_4 and C_2DCl_3, also follow the depletion of $CDCl_3$ with 0.14 and 0.02 molecule, respectively, formed per $CDCl_3$ decomposed. The C_2DCl_3 may arise from reactions [11] (26), [12] (27), and [13].

[11] $CCl_2 + CDCl_3 \rightarrow C_2DCl_3 + Cl_2$

[12] $CDCl_2 + CDCl_3 \rightarrow C_2DCl_3 + DCl + Cl$

[13] $C_2Cl_2 + \begin{Bmatrix} DCl \\ HCl \end{Bmatrix} \rightarrow \begin{Bmatrix} C_2DCl_3 \\ C_2HCl_3 \end{Bmatrix}$

Reaction [11] represents a loss of CCl_2 and reaction [12] arises from the minor channel for MPD of $CDCl_3$ (25). Channel [13] is a reaction of products which occurs after the laser pulse, but before analysis has been performed. To determine whether [13] occurs to a significant degree, a sample of $CDCl_3$ of P = 0.54 kPa was photolyzed with 750 pulses using the [00°1 → 10°0] P(8) line, F = 55 cm, ϕ = 14 J/cm². FTIR spectra of the cell were taken of the photolyzed samples at various times up to 125 h following photolysis. Features centered near $\bar{\nu}$ = 783, 850, and 940 cm^{-1}, which are due to C_2HCl_3, were all observed to grow with time, and the 850 cm^{-1} feature was used to estimate the concentration of C_2HCl_3 as a function of time. Immediately following photolysis, the apparent C_2HCl_3 yield was 3.6×10^{16} molecules. This value became 5.4×10^{16}, 7.2×10^{16}, 1.5×10^{17}, and 2.9×10^{17} after 1 h, 2 h, 24 h, and 125 h, respectively. These results suggest that the reaction between the products of laser photolysis, reaction [13], may be the major source of C_2HCl_3 and C_2DCl_3 for MPD of $CDCl_3$.

4. Conclusions

$CDCl_3$ undergoes MPD at lower fluences than CDF_3; but the difference between the two molecules is small. This probably indicates that the small anharmonicity bottle-necking for the pumped mode of CDF_3 (9, 10, 41) compensates for the more slowly rising ρ_{VIB} versus excitation energy for CDF_3 compared to $CDCl_3$. Selective MPD measured elsewhere (23) indicates that D/H selectivity is smaller for $CDCl_3$ (with excitation at 11 μm) than for CDF_3. Thus use of $CDCl_3$ as a working molecule in an isotope enrichment process does not provide an advantage over CDF_3 from the photolysis point of view; however, redeuteration by exchange with water is easier for $CDCl_3$ than for CDF_3.

The primary decomposition channel, in agreement with other studies (24–27) is predominantly elimination of DCl followed by reactions [6]–[9*a*] but not [9*b*] with about 0.24 C_2Cl_4, 0.14 CCl_4, and 0.02 C_2DCl_3 and C_2HCl_3 molecules produced per $CDCl_3$ decomposed.

1. N. R. ISENOR and M. C. RICHARDSON. Appl. Phys. Lett. **18**, 224 (1971).
2. R. V. AMBARTZUMIAN, V. S. LETOKHOV, E. A. RYABOV, and N. V. CHECKALIN. Sov. Phys. JETP Lett. **20**, 273 (1974).
3. R. D. MCALPINE and D. K. EVANS. Adv. Chem. Phys. **60**, 31 (1985).
4. R. D. MCALPINE, D. K. EVANS, and F. K. MCCLUSKY. J. Chem. Phys. **73**, 1153 (1980).
5. J. B. MARLING and I. B. HERMAN. Presented at the Tenth International Quantum Electronics Conference, Atlanta, Georgia. May 29 – June 1, 1978.
6. I. P. HERMAN and J. B. MARLING. Chem. Phys. Lett. **64**, 75 (1979).
7. S. A. TUCCIO and A. HARTFORD. Chem. Phys. Lett. **65**, 234 (1979).
8. I. P. HERMAN and J. B. MARLING. J. Chem. Phys. **72**, 516 (1980).
9. J. B. MARLING, I. P. HERMAN, and S. J. THOMAS. J. Chem. Phys. **72**, 5603 (1980).
10. D. K. EVANS, R. D. MCALPINE, and H. M. ADAMS. J. Chem. Phys. **77**, 3551 (1982).
11. E. A. SYMONS and M. J. CLERMONT. J. Am. Chem. Soc. **103**, 3127 (1981).
12. E. A. SYMONS, J. D. BONNETT, and M. DE L. MARTINS. Can. J. Chem. **61**, 2627 (1983).
13. J. BIGELEISEN, W. B. HAMMOND, and S. TUCCIO. Nucl. Sci. Eng. **83**, 473 (1983).
14. J. A. O'NEILL and J. R. ROBINS. J. Chem. Phys. **81**, 1825 (1984).
15. Y. MAKIDE, S. HAGIWARA, O. KURIHARA, K. TAKEUCHI, Y. ISHIKAWA, S. ARAI, T. TOMINAGA, I. INOUE, and R. NAKANE. J. Nucl. Sci. Technol. **17**, 645 (1980).
16. Y. MAKIDE, S. HAGIWARA, T. TOMINAGA, O. KURIHARA, and R. NAKANE. Int. J. Appl. Rad. Isotopes, **32**, 885 (1981).
17. Y. MAKIDE, S. HAGIWARA, T. TOMINAGA, K. TAKEUCHI, and R. NAKANE. Chem. Phys. Lett. **82**, 18 (1981).
18. K. TAKEUCHI, I. INOUE, R. NAKANE, Y. MAKIDE, S. KATO, and T. TOMINAGA. J. Chem. Phys. **76**, 398 (1982).
19. D. ANDERSON, R. D. MCALPINE, D. K. EVANS, and H. M. ADAMS. Chem. Phys. Lett. **79**, 337 (1981).
20. R. D. MCALPINE, D. K. EVANS, and J. W. GOODALE. Can. J. Chem. **61**, 1481 (1983).
21. E. A. SYMONS and J. D. BONNETT. J. Catal. **93**, 209 (1985).
22. C. WILLIS and J. G. PURDON. J. Appl. Phys. **50**, 2539 (1979).
23. A. YOKOYAMA, K. SUZUKI, G. FUJISAWA, N. ISHIKAWA, and M. IWASAKI. J. Nucl. Sci. Technol. **18**, 737 (1981).
24. F. MAGNOTTA, I. P. HERMAN, and F. T. ALDRIDGE. Chem. Phys. Lett. **92**, 600 (1982).
25. I. P. HERMAN, F. MAGNOTTA, R. J. BUSS, and Y. T. LEE. J. Chem. Phys. **79**, 1789 (1983).
26. I. P. HERMAN, F. MAGNOTTA, and F. T. ALDRIDGE. Israel J. Chem. **24**, 192 (1984).
27. F. MAGNOTTA and I. P. HERMAN. J. Chem. Phys. **18**, 2363 (1984).
28. H. M. ADAMS, E. B. SELKIRK, J. W. GOODALE, D. K. EVANS, and R. D. MCALPINE. Rev. Sci. Instru. **55**, 1298 (1984).
29. S. L. CHIN, D. K. EVANS, R. D. MCALPINE, and W. N. SELANDER. Appl. Opt. **21**, 65 (1982).
30. D. K. EVANS, R. D. MCALPINE, H. M. ADAMS, and A. L. CREAGH. Chem. Phys. **80**, 379 (1983).
31. R. D. MCALPINE, D. K. EVANS, and H. M. ADAMS. J. Chem. Phys. **78**, 5990 (1983).
32. D. K. EVANS, R. D. MCALPINE, and H. M. ADAMS. Israel J. Chem. **24**, 187 (1984).
33. R. A. BACK, D. K. EVANS, and H. M. ADAMS. Can. J. Chem. **62**, 1525 (1984).
34. V. S. LETOKHOV and A. A. MAKAROV. Sov. Phys. JETP, **36**, 1091 (1973).
35. V. N. BAGRATASHVILI, I. N. KNYAZEV, V. S. LETOKHOV, and V. V. LOBKO. Opt. Commun. **18**, 525 (1976).
36. D. K. EVANS, R. D. MCALPINE, and F. K. MCCLUSKEY. Chem. Phys. **32**, 81 (1978).
37. R. D. MCALPINE, D. K. EVANS, and F. K. MCCLUSKEY. Chem. Phys. **39**, 263 (1979).
38. D. K. EVANS, R. D. MCALPINE, J. W. GOODALE, and H. M. ADAMS. To be published.
39. D. K. EVANS, R. D. MCALPINE, and F. K. MCCLUSKEY. Chem. Phys. Lett. **65**, 226 (1979).
40. W. FUSS. Chem. Phys. **36**, 135 (1979).
41. D. HARRADINE, B. FOY, L. LAUX, M. DUBS, and J. I. STEINFELD. J. Chem. Phys. **81**, 4267 (1984).

New functionalized water-soluble benzophenones: a laser flash photolysis study[1]

D. J. LOUGNOT

Laboratoire de Photochimie Générale, Equipe de Recherche Associée au CNRS n° 386, Ecole Nationale Supérieure de Chimie, 3 rue A. Werner, 68093 Mulhouse Cedex, France and Division of Chemistry, National Research Council of Canada, Ottawa, Ont., Canada K1A 0R6

P. JACQUES AND J. P. FOUASSIER

Laboratoire de Photochimie Générale, Equipe de Recherche Associée au CNRS n° 386, Ecole Nationale Supérieure de Chimie, 3 rue A. Werner, 68093 Mulhouse Cedex, France

AND

H. L. CASAL, NGUYEN KIM-THUAN, AND J. C. SCAIANO

Division of Chemistry, National Research Council of Canada, Ottawa, Ont., Canada K1A 0R6

Received October 10, 1984

D. J. LOUGNOT, P. JACQUES, J. P. FOUASSIER, H. L. CASAL, NGUYEN KIM-THUAN, and J. C. SCAIANO. Can. J. Chem. **63**, 3001 (1985).

Two water-soluble ionic benzophenones containing a quaternized amine and a sulphonate group have been investigated by laser flash photolysis. The decay kinetics and spectra of their triplet states were studied and quenching constants by triethanolamine, isopropanol, and methyl viologen determined. These data are of interest when these benzophenones are used as initiators for photo-polymerizing water-soluble acrylates in homogeneous solution or in reverse micellar assemblies. The high water solubility of these compounds allows the bimolecular deactivations due to triplet–triplet (k_{TT}) and triplet–ground state (k_{SQ}) interactions to be determined more accurately than in the case of benzophenone itself.

D. J. LOUGNOT, P. JACQUES, J. P. FOUASSIER, H. L. CASAL, NGUYEN KIM-THUAN et J. C. SCAIANO. Can. J. Chem. **63**, 3001 (1985).

Utilisant la photolyse flash au laser, on a étudié deux benzophénones ioniques, solubles dans l'eau, qui contenaient à la fois un groupement amine quaternaire et un sulfonate. On a étudié les cinétiques de disparition ainsi que les spectres de leurs états triplets; de plus, on a déterminé les constantes de piégeage par la triéthanolamine, l'isopropanol et le viologène de méthyle. Ces données présentent de l'intérêt à cause du fait que l'on utilise ces benzophénones comme initiateurs pour la polymérisation photochimique des acrylates solubles dans l'eau, tant en solution homogène que sous forme d'agrégats micellaires inversés. La grande solubilité de ces composés dans l'eau permet de déterminer, d'une façon plus précise que dans le cas de la benzophénone elle-même, les désactivations bimoléculaires dues aux interactions triplet–triplet (k_{TT}) et triplet–état fondamental (k_{SQ}).

[Traduit par le journal]

I. Introduction

A series of water-soluble carbonyl compounds have been recently introduced (1) and their activity in photopolymerizable mixtures with water soluble monomers has been demonstrated (2). The water solubility is obtained by functionalizing benzophenone with a trimethylammonium chloride or sodium sulphonate group at one of the *para* positions.

Photoactive initiators in polymerization experiments have been used in bulk as well as in homogeneous or microheterogeneous solutions (3). However, the photoinitiators generally used in these experiments are not suitable for water-soluble monomers due to their insolubility. In this work we examine two ionic, water-soluble benzophenones which can be used as photoinitiators. In addition to their use for this purpose, these molecules are of interest in other fields. Ionic benzophenones locate preferentially in water pools when dissolved in reverse micelles of AOT, and if an acrylic monomer is solubilized in the continuous oil phase, the segregation of the reactants results in a decrease of the interaction (usually quenching) between the excited state of the initiator and the monomer (3). Since the initiation quantum yield is essentially limited by this interaction (4, 5), the expected and observed consequences of compartmentalizing the reactants is a significant increase of the polymerization rate.

The same approach could be considered in the case of direct micelles. However, in this case, ionic benzophenones do not necessarily dissolve in the bulk water phase but rather locate in the immediate vicinity of the micelles, with loose interaction with the surfactant heads. Thus, the segregation between the reactants is poorly defined and as a consequence, the polymerization rates are not very affected when going from homogeneous solutions to micellar assemblies.

The study of water-soluble benzophenones yields information regarding the bimolecular interaction between two carbonyl molecules in their triplet state (i.e. annihilation) or between one excited state and one ground state molecule (i.e. self-quenching) in aqueous solution. In the case of benzophenone itself, the lifetime of the triplet state can be drastically affected by this type of deactivating interaction (6–11). However, while these processes are relatively well understood in organic solvents, the same does not hold in the case of aqueous solution (6, 7, 11), where the roles played by T–T annihilation and self-quenching are still subject to controversy. The main reason underlying this controversy is the poor solubility of benzophenone (BP) in water which limits the concentration range available and thereby the contribution of bimolecular processes relative to other modes of decay of the benzophenone triplet.

The compounds investigated here could help settle this question insofar as they behave basically as benzophenone itself. The present investigation is devoted to the study of the

[1]NRCC No. 24108.

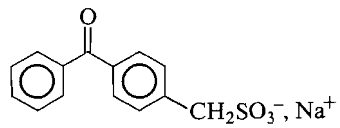

1

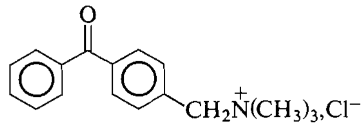

2

photophysical behaviour of **1** (*p*-(methyl sodium sulphonate)-benzophenone) and **2** (*p*-methyltrimethylammonium chloride)-benzophenone in order to rationalize their use as photoinitiators for polymerizations in aqueous homogeneous or microheterogeneous solution. Due to their water solubility, these homologues of benzophenone lend themselves to many applications involving the photoreduction of carbonyl compounds by alcohols or amines. A study of the behaviour of radical-pairs derived from reactions of these benzophenones in micellar solution has already been reported (12).

II. Experimental

The compounds studied (**1** and **2**) were synthesized and purified according to a procedure recently described by Green and co-workers (1). The crude products are washed with ether and then recrystallized from adequate mixtures of isopropanol and water.

The laser photolysis experiments have been conducted with two types of apparatus: (*i*) The first one uses the pulses from a Molectron UV-24 nitrogen laser for excitation (337 nm, ~8 ns and up to 10 mJ), associated with an R-7912 Tektronix transient digitizer and a PDP-11/23 computer which also controls the experiment and provides suitable storage and hardcopy facilities. Further details have been given elsewhere (13). (*ii*) The second one uses the pulse train from a Quantel ruby laser working in mode-locked regime (347 nm after frequency doubling, ~30 ns and up to 200 mJ) (14).

The first device induces only weak conversions to the triplet state (0.1 to 1%) and is preferably used in the case of concentrated solutions (ca. 10^{-2} *M*). The second one is better adapted to the study of more diluted solutions (ca. 10^{-3} *M*) in which high conversions to the excited triplet state can be reached (20%).

Isopropanol and triethanolamine (Janssen Chimica) were used as received. Methyl viologen (Paraquat) from K & K was purified by recrystallization from methanol/acetone mixtures. Samples were prepared by dissolving **1** and **2** in distilled water. The pH was adjusted by adding hydrochloric acid or sodium hydroxide. In some cases, kinetic experiments involving pH control, were reproduced in the presence of a chemical buffer, in order to ensure the insensitivity of the kinetics to the buffer power.

All the samples used were deaerated by nitrogen bubbling and all experiments were carried out at 300 K.

III. Results and discussion

1. The ground state of 1 and 2

The spectroscopic and photophysical features of substrates **1** and **2** are similar to those of benzophenone (BP) and 4-methylbenzophenone (4MeBP), as expected.

The uv spectra of **1** and **2** in water show an intense band around 260 nm. In the case of BP in solvents with low polarities there is a weak band corresponding to the $n\pi^*$ transition. This band is not distinguishable in the spectra of **1** and **2** in water due to the shift induced by its negative solvatochromy. The results concerning the $\pi\pi^*$ transition are reported in Table 1 along with those for 4MeBP and BP obtained under the same experimental conditions.

The uv absorption maxima are practically insensitive to ionic substitution. The same applies to the characteristic infrared frequency for the carbonyl groups; these are 1652, 1653, 1656, and 1657 cm^{-1} for BP, 4MeBP, **1**, and **2** (in KBr pellets), respectively.

TABLE 1. Absorption maxima and extinction coefficients in water

	Value			
Parameter	BP	4MeBP	**1**	**2**
$\lambda_{max}^{\pi\pi^*}$ (nm)	258	264	262	255
log ϵ^a	4.18	4.24	4.30	4.26

[a] In units of M^{-1} cm^{-1}.

TABLE 2. Unimolecular (k_0) and bimolecular (k_{SQ} and k_{TT}) rate constants of benzophenone triplet decay in aqueous solution

k_0 (s^{-1})	k_{SQ} (M^{-1} s^{-1})	k_{TT} (M^{-1} s^{-1})	Ref.
10^4	$(1.8\pm0.4)\times10^8$	[a]	6
2.5×10^4	[a]	5×10^9	11
2.2×10^4	5×10^7	5×10^9	7

[a] Not detected.

The ground state absorption spectra of **1** and **2** remain unaffected through pH changes between 2 and 12; this, together with the ^{1}H nmr spectra in neutral D_2O are consistent with **1** and **2** being present solely in the keto form.

2. Self-quenching and T—T annihilation

Table 2 summarizes the values of the self-quenching (k_{SQ}) and T—T annihilation (k_{TT}) rate constants reported in the literature for BP. The explanation for the different values in Table 2 lies in the poor accuracy of the data obtained in water solution due to the low solubility of BP. The ground state optical density of a saturated aqueous solution of BP is <0.05 per cm in the wavelength range corresponding to the $n\pi^*$ transition; this poses many difficulties in any quantitative study of T—T or self-quenching bimolecular processes using nitrogen (337 nm), frequency-doubled ruby (347 nm), or frequency-tripled neodymium (353 nm) laser excitation.

None of the spectroscopic features or the photophysical behaviour of these molecules are basically affected by the presence of the charged substituent. Therefore, these molecules can be used as adequate substitutes for BP in highly polar solvents. The only exception to this may be in the case of interactions which may be induced by, or dependent upon, the localized charge carried by these compounds.

Figure 1 shows the transient signals recorded for **1** with high ground state concentration (~10^{-2} *M*) and low excitation energy (nitrogen laser at 337 nm) and with low ground state concentration (<10^{-3} *M*) and high excitation energy (ruby laser at 347 nm), respectively. From the observed initial decay rate of the triplet state and the initial transient absorbancy (7, 11),

$$[1] \quad \frac{d[^3BP]}{dt} = -\{k_0 + k_{SQ}[BP] + k_{TT}[^3BP]\}[^3BP]$$

or

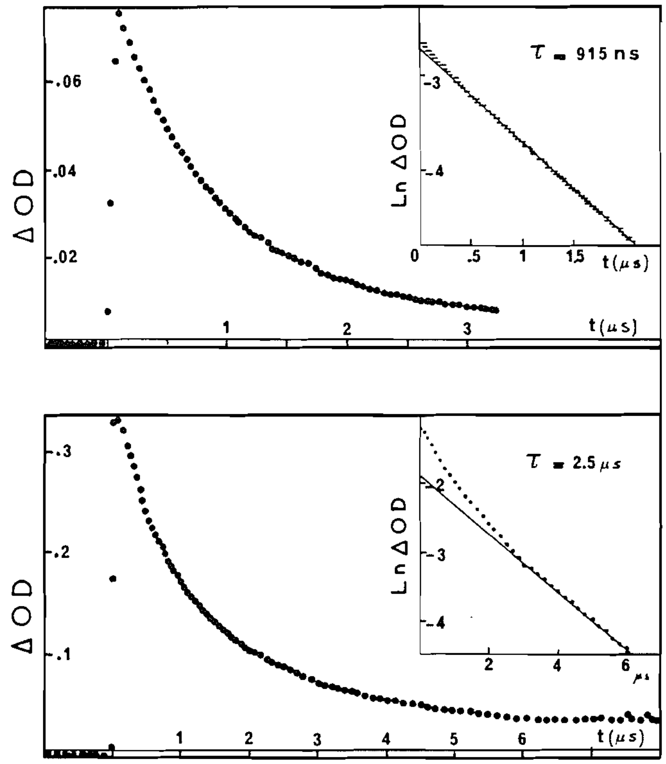

FIG. 1. Decay of the triplet state of **1**; traces obtained at λ = 525 nm. Top: λ(excitation) = 337 nm, [**1**] = 1.1×10^{-2} *M*. Bottom: λ(excitation) = 347 nm, [**1**] = 4×10^{-3} *M*.

$$[2] \quad -\frac{d}{dt} \ln [^3BP] = k_0 + k_{SQ}[BP] + k_{TT}[^3BP]$$

Thus, when the initial decay rate (at $t \rightarrow 0$) is plotted against the initial triplet concentration, the slope and intercept correspond to k_{TT} and to the pseudo first order decay rate ($k = k_0 + k_{SQ}[BP]$), respectively.

Analysis of the pseudo first order lifetimes and the initial rate constants determined from plots such as those in Fig. 1, shows that both, annihilation and self-quenching, may contribute to the decay of **1** in aqueous solution. An analysis of these bimolecular processes is possible in the case of **1** and leads to: $k_{SQ} = (7.3 \pm 0.1) \times 10^7 M^{-1} s^{-1}$ and $k_{TT} = (5.4 \pm 1.1) \times 10^9 M^{-1} s^{-1}$ (errors as two standard deviations, i.e. $\pm 2\sigma$). The same treatment is rather questionable in the case of **2**, due to traces of free amine which may originate in the poor stability of the ammonium function at neutral pH. Nonetheless, both these pathways seem active in the decay of the triplet state of **2**, in much the same way as for **1**.

This study confirms that **1** and **2** behave essentially as BP in aqueous solution, and that the rate constants corresponding to the bimolecular processes — i.e. k_{SQ} and k_{TT} — are not very sensitive to the presence of a charge. The spontaneous decay of the triplet states of **1** and **2** contributes almost insignificantly to their decay under the experimental conditions of the present study. Thus, it becomes very difficult to introduce a reliable value of k_0 which is any case lower than 10^5 s^{-1}. This is comparable in order of magnitude to the pseudo-first order decay rate expected for quenching by trace impurities.

3. T–T spectra in neutral aqueous solution

Figure 2 shows the T–T spectra of **1** and **2** recorded during the initial part of the decay, i.e. in a 200 ns time window after the laser pulse. These spectra exhibit maxima at 527 ± 3 nm (**1**) and 535 ± 3 nm (**2**) to be compared with values between 515 and 525 nm in the case of BP itself (7, 15). The small red shift observed here is probably the result of inductive effects due to the substituent, or to small changes in the dihedral angle between the rings. In the red side of these T–T absorption bands, there is a broad tail which becomes negligible only at λ > 800 nm, with two shoulders centered around 600 and 700 nm. The ratio between the extinction coefficients at the maximum and in the plateau region is in good agreement with the available data in the case of BP (15). At 800 nm, the extinction coefficients are still about 10% of the value at the corresponding maxima.

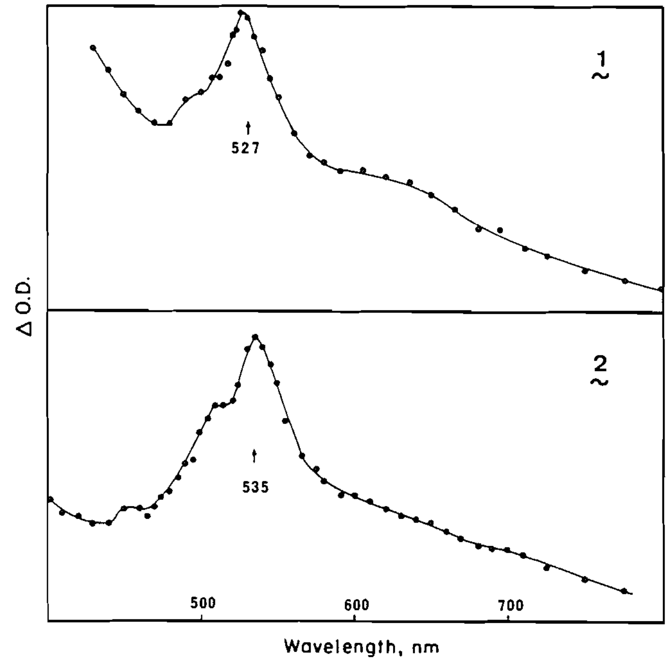

FIG. 2. T–T absorption spectra of **1** and **2** recorded at $0 < t <$ 230 ns; [**1**] = 8×10^{-3} *M*, [**2**] = 8.5×10^{-3} *M*.

The T–T spectra remain unaffected by pH changes between 3.0 and 13.0 for compound **1** and between 2.0 and 13.0 for compound **2**. In more acidic solution, the triplet lifetimes are drastically shortened due to protonation of the excited state (17). If the initial triplet intensity (ΔOD) is plotted against pH the curve obtained (Fig. 3) shows an inflexion which corresponds to p*K* (T_1). The p*K* of compound **1** is therefore estimated to be ~1.2. Owing to its poor stability, compound **2** does not lend itself easily to this kind of measurement; as a consequence, its p*K* (T) is only estimated to be lower than that for **1**.

The maximum of the T–T spectrum of protonated **1** is blue shifted by 13 nm (λ_{max} = 514 nm) with respect to the unprotonated form, and its red tail remains unaffected.

4. Interaction of 1 and 2 with water

The possibility of a direct reaction of triplet benzophenone with water to yield ketyl and OH˙ according to reaction [3] has been the subject of interest for over 10 years (6).

$$[3] \quad {}^3Ph_2CO^* + H_2O \xrightarrow{?} Ph_2\dot{C}OH + OH^{\cdot}$$

The water solubility of **1** made it possible to reexamine this question under rather favourable conditions. Our results show that photolysis of **1** in water yields ketyl radicals with yields in

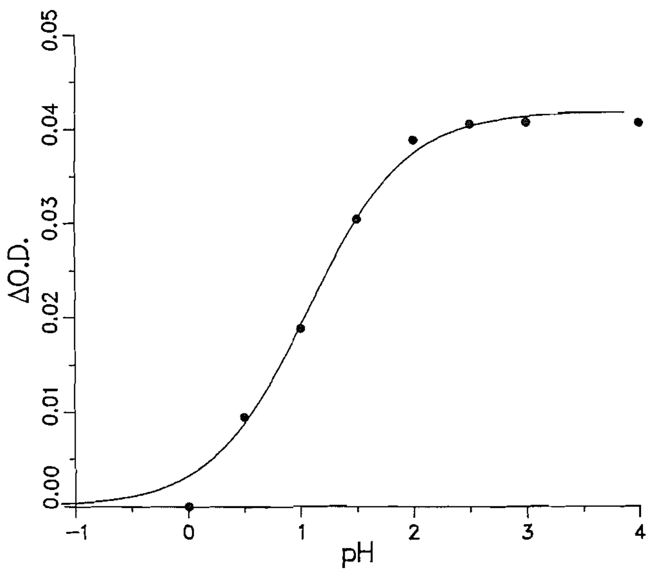

FIG. 3. Effect of pH on the changes in initial optical density at 525 nm for substrate **1**.

the 10−18% range. For example, Fig. 4 shows the decay kinetics of **1** in water at pH 6.0 observed at 625 nm (Fig. 4*A*), where the ketyl radical does not absorb and at 525 nm (T−T maximum) (Fig. 4*B*). The bottom trace (Fig. 4*C*) was obtained subtracting *a* from *b* after normalization of the initial optical density and shows that the ketyl radical is formed concurrently with triplet decay.

Time-resolved spectra showed that the weak residual absorption following triplet decay was due to the corresponding ketyl radical, with λ_{max} at 545 and 610 nm at pH 6.0 and 12.0, respectively. The band at 610 nm corresponds to the deprotonated form (15, 16, 18).

A comparison of optical densities immediately after the laser flash pulse, and after the initial triplet decay is complete leads to ketyl yields in the 10−18% range, after taking into account the known ratio of extinction coefficients for the triplet state and the ketyl radical (15, 16).

The question arises as to whether the ketyl radicals can result from reaction of the triplet state with water, or from other processes, to which impurity quenching and self-quenching could contribute.

A careful study of the laser photolysis of **1** in H_2O and D_2O, as a function of substrate concentration and laser dose leads us to the conclusion that there are no significant differences in the yield of ketyl radicals or the values of k_0, k_{SQ} or k_{TT}. Thus, we conclude that decay via triplet reaction with H_2O does not contribute significantly under our experimental conditions. This effectively puts an upper limit to the reaction of the triplet state with water of $k_H < 10^3\ M^{-1}\ s^{-1}$.

5. *Interaction of 1 and 2 with triethanolamine*

When benzophenone-based carbonyl compounds are used in photopolymerization experiments, it is necessary to incorporate a substrate capable of generating active radicals (19−22). For example, benzophenone is suitable as a photoinitiator in the presence of either:

(*a*) an amine with α-hydrogens, i.e.

$$[4] \quad \rangle C{=}O^* + \rangle N{-}CH\langle \rightarrow \rangle \dot{C}OH + \rangle N{-}\dot{C}\langle$$

(*b*) an alcohol or an ether giving direct hydrogen abstraction,

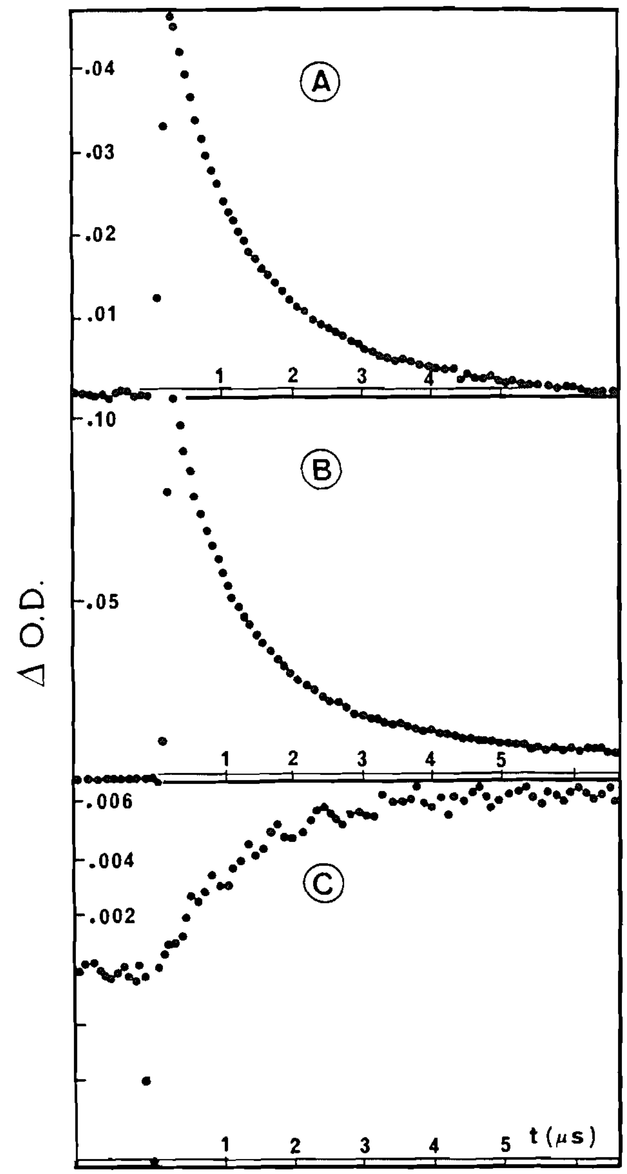

FIG. 4. Transient absorptions observed upon nitrogen laser excitation of **1**. (*A*) and (*B*): traces obtained at 625 and 525 nm, respectively. (*C*): deconvoluted trace obtained by subtracting the optical density at 625 nm from that at 525 nm after normalization at time zero ([**1**] = 0.011 *M* at pH 6.0).

e.g.

$$[5] \quad \rangle C{=}O^* + R_2CHOH \rightarrow \rangle \dot{C}OH + R_2\dot{C}OH$$

These two types of interaction were studied in the case of water-soluble benzophenones. Triethanolamine (TEA), which is water-soluble was selected to exemplify the interaction between **1** and **2** and amines. In order to eliminate any complications which could result from possible acid−base equilibrium the triplet lifetimes of **1** and **2** were measured at 525 nm. At this wavelength the extinction coefficients of the ketyl radical and of the anion radical are of the same order of magnitude (23). Thus, the total transient optical density due to ketyl radicals in neutral or anionic form is constant and the only variable component is the triplet absorption; proper kinetic analysis leads to the quenching rate constant for triethanolamine as illustrated in Fig. 5. The rate constants obtained are

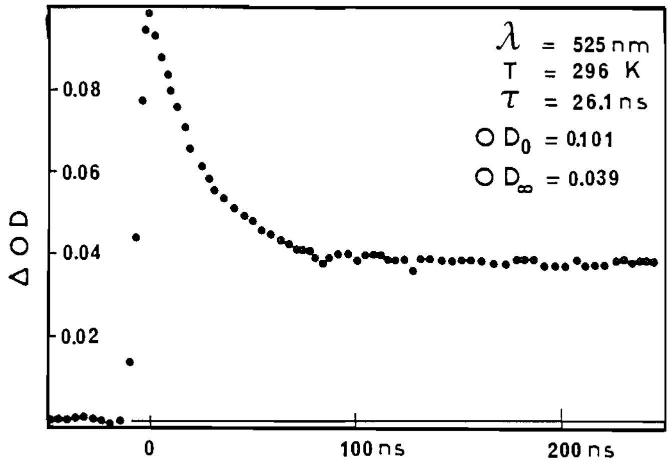

FIG. 5. Decay trace observed at 525 nm for **1** in the presence of triethanolamine; [**1**] = 8×10^{-3} *M*, [TEA] = 2.1×10^{-2} *M*.

$1.2 \times 10^9\ M^{-1}\ s^{-1}$ for **1** and $1.6 \times 10^9\ M^{-1}\ s^{-1}$ for **2**, respectively, in good agreement with the value measured for benzophenone ($1.5 \times 10^9\ M^{-1}\ s^{-1}$) under the same conditions (24).

A last point is worth mentioning: the ratio, $\Delta OD_\infty^{525}/\Delta OD_0^{525}$ between the final optical density (ΔOD_∞^{525}) which corresponds to the sum:

$$[6]\quad \Delta OD_\infty^{525} = \{\epsilon_{\text{ketyl}}^{525}[\text{ketyl}] + \epsilon_{\text{anion}}^{525}[\text{anion}]\}l$$

and the initial one ΔOD_0^{525} which is exclusively due to the triplet state, gives access to another important parameter, i.e. the relative contributions of physical and chemical quenching of **1** and **2** by TEA.

The overall process (*vide supra*) accounts for the generation of amine-derived radicals which are the main active species in the initiation of photopolymerization. The analysis of rates and quantum yields can be carried out in terms of a mechanism involving a charge transfer complex which can decay either to the ketyl and amine radicals (chemical quenching) or to BP and amine ground state (physical quenching) (25, 26).

[7]

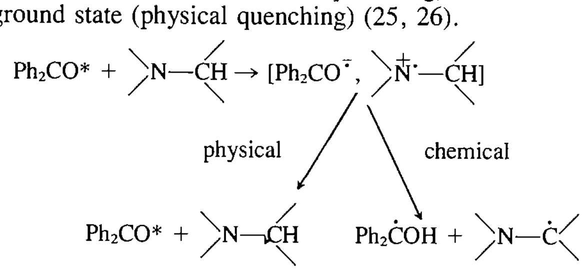

This ratio can be easily obtained from ΔOD_0 and ΔOD_∞ (see Fig. 5):

$$[8]\quad r = \frac{\text{"physical"}}{\text{"chemical"}} = \frac{\Delta OD_0 \times \left(\frac{\epsilon_K}{\epsilon_T}\right)_{525} - \Delta OD_\infty}{\Delta OD_\infty}$$

In the particular case of **1**, with $(\epsilon_K/\epsilon_T)_{525} \sim 0.37$ as mentioned before, *r* is estimated to be

$$r = \frac{0.101 \times 0.37 - 0.039}{0.039} \simeq 0$$

a result which supports an essentially quantitative chemical quenching (27).

6. Interaction of 1 and 2 with alcohols

Since compounds **1** and **2** have a lowest triplet state with $n\pi^*$ character (24), their behaviour is expected to resemble that of BP.

TABLE 3. Quenching of various benzophenones by methyl viologen in aqueous solution

Substrate	k_Q (water)	k_Q (acetate buffer, pH 4.8)
BP	$(3.7\pm0.4)\times10^9$	
	2.6×10^{9a}	
	1.03×10^{7b}	
1	$(7.8\pm0.6)\times10^9$	$(5.6\pm0.3)\times10^9$
2	$(6.5\pm0.7)\times10^8$	$(1.3\pm0.3)\times10^9$
3		$(1.7\pm0.7)\times10^9$

[a]From ref. 31.
[b]From ref. 32.

The rate constants measured in the systems **1** and **2** with isopropanol in water are $(1.5 \pm 0.2) \times 10^6$ and $(1.25 \pm 0.2) \times 10^6\ M^{-1}\ s^{-1}$, respectively; a value ca. $1.3 \times 10^6\ M^{-1}\ s^{-1}$ is generally accepted for BP (26, 28–30).

7. Interaction of 1 and 2 with methyl viologen

Das (31) has demonstrated that a number of triplet carbonyl compounds, including benzophenone, are quenched by methyl viologen (MV^{2+}), in a process that yields the readily detectable reduced form, $MV^{+\bullet}$, and presumably the ketone radical-cation, although the latter has so far escaped detection. Das's experiments for BP were carried out in 1:9 water: acetonitrile, and led to $k_Q = 2.6 \times 10^9\ M^{-1}\ s^{-1}$. Similar experiments by Chandrasekaran and Whitten (32) led to $k_Q = 1.03 \times 10^7\ M^{-1}\ s^{-1}$ in dry acetonitrile, based on phosphorescence measurements.

We have examined the electron transfer between the various benzophenones and methyl viologen in aqueous solution. The results have been summarized in Table 3, which also includes data for another ionic benzophenone, **3**.

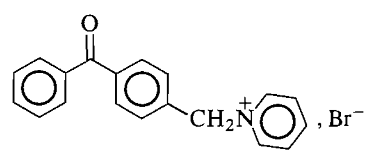

3

The data in Table 3 show that electrostatic interactions play an important role in the case of fast electron transfer processes, with ca. one order of magnitude difference between the favourable (**1**) and unfavourable (**2**) cases. The reduced form, $MV^{+\bullet}$ was detected in good yields in all these systems.

IV. Conclusion

The behaviour of the two water-soluble benzophenones, **1** and **2** closely parallels that of benzophenone itself. The effectiveness of triplet–triplet annihilation and self-quenching has been demonstrated. The reaction of **1** and **2** with neutral substrates such as amines and alcohols occur with rate constants comparable with those for BP, while in the case of electron transfer to the methyl viologen dication the rates of electron transfer reflect the role of electrostatic interactions and follow the order **1** > BP > **2** ≃ **3**.

Acknowledgements

The authors are grateful to Mr. S. E. Sugamori for his technical assistance and to Dr. P. N. Green (Ward Blenkinsop) for the gift of authentic samples of water-soluble benzophenones.

1. P. BARKER, R. A. BOTTOM, J. T. GUTHRIE, A. A. GODFREY, P. N. GREEN, and J. R. A. YOUNG. Res. Disclosure, #20221. 1981. p. 93.
2. A. BONAMY, J. P. FOUASSIER, D. J. LOUGNOT, and P. N. GREEN. J. Polym. Sci. Polym. Lett. Ed. **20**, 315 (1982).
3. D. J. LOUGNOT and J. C. SCAIANO. J. Photochem. **26**, 119 (1984).
4. R. A. CALDWELL. J. Phys. Chem. **92**, 1439 (1969).
5. G. AMIRZADEH, R. KUHLMANN, and W. SCHNABEL. J. Photochem. **10**, 133 (1979).
6. M. B. LEDGER and G. PORTER. J. Chem. Soc. Faraday I, **68**, 539 (1972).
7. D. J. LOUGNOT, P. JACQUES, and J. P. FOUASSIER. J. Photochem. **19**, 59 (1982).
8. J. P. JEANDRAN, J. C. GRAMAIN, and J. LEMAIRE. J. Chem. Res. 186 (1979).
9. D. I. SCHUSTER and T. M. WEIL. J. Am. Chem. Soc. **95**, 4091 (1973).
10. M. T. WOLF, K. D. LEGG, D. E. BROWN, L. A. SINGER, and J. M. PARKS. J. Am. Chem. Soc. **97**, 4490 (1975).
11. R. V. BENSASSON and J. C. GRAMAIN. J. Chem. Soc. Faraday I, **76**, 1801 (1980).
12. J. C. SCAIANO and D. J. LOUGNOT. J. Phys. Chem. **88**, 3379 (1984).
13. J. C. SCAIANO. J. Am. Chem. Soc. **102**, 7747 (1980).
14. D. J. LOUGNOT, J. P. FOUASSIER, and J. FAURE. J. Chim. Phys. **74**, 23 (1977).
15. M. C. DUVAL. Thesis 3rd cycle, Paris XI (1979); R. V. BENSASSON and J. C. GRAMAIN. J. Chem. Soc. Faraday I, **68**, 539 (1972).
16. M. R. TOPP. Chem. Phys. Lett. **32**, 144 (1975).
17. D. M. RAYNER and A. H. WYATT. J. Chem. Soc. Faraday II, **70**, 945 (1974).
18. E. HAYON, T. IBATA, N. N. LICHTIN, and M. SIMIC. J. Phys. Chem. **76**, 2072 (1972); N. J. TURRO. Modern molecular photochemistry. The Benjamin Cummings Publishing Co., Merlo Park. 1978. cf. pp. 374–375; E. J. LAND. Proc. R. Soc. A**277**, 549 (1964).
19. J. P. FOUASSIER, P. JACQUES, and D. J. LOUGNOT. J. Rad. Curing, **10**, 9 (1983).
20. A. MERLIN, D. J. LOUGNOT, and J. P. FOUASSIER. Polymer Bull. **2**, 847 (1980).
21. J. P. FOUASSIER. J. Chim. Phys. **80**, 339 (1983).
22. D. GRILLER, J. A. HOWARD, P. R. MARRIOTT, and J. C. SCAIANO. J. Am. Chem. Soc. **103**, 619 (1981).
23. O. BREDE, W. HELMSTREIT, and R. MEHNERT. Z. Phys. Chem. Leipzig, **256**, 513 (1975).
24. D. J. LOUGNOT, D. FLORET-DAVID, P. JACQUES, and J. P. FOUASSIER. J. Chim. Phys. In press.
25. S. G. COHEN and N. M. STEIN. J. Am. Chem. Soc. **93**, 6542 (1971) and references therein.
26. J. C. SCAIANO. J. Photochem. **2**, 81 (1973).
27. S. INBAR, H. LINSCHITZ, and S. G. COHEN. J. Am. Chem. Soc. **102**, 1419 (1980).
28. H. LUTZ, M. C. DUVAL, E. BREHERET, and L. LINDQVIST. J. Phys. Chem. **76**, 821 (1972).
29. A. BECKET and G. PORTER. Trans. Faraday Soc. **59**, 2038 (1963).
30. G. PORTER and M. R. TOPP. Proc. R. Soc. A**315**, 163 (1970).
31. P. K. DAS. Tetrahedron Lett. **22**, 1307 (1981).
32. K. CHANDRASEKARAN and D. G. WHITTEN. J. Am. Chem. Soc. **102**, 5119 (1980).

Gas-phase measurements of the influence of stepwise solvation on the kinetics of S_N2 reactions of solvated F^- with CH_3Cl and CH_3Br and of solvated Cl^- with CH_3Br

DIETHARD K. BOHME AND ASIT B. RAKSIT
Department of Chemistry and Centre for Research in Experimental Space Science, York University, Downsview, Ont., Canada M3J 1P3

Received February 14, 1985

DIETHARD K. BOHME and ASIT B. RAKSIT. Can. J. Chem. **63**, 3007 (1985).

Flowing afterglow measurements are reported which reveal the influence of stepwise solvation on the nucleophilicity of F^- and Cl^- in the gas phase at room temperature. The specific rates of nucleophilic displacement reactions with CH_3Cl and CH_3Br are followed for additions of up to three molecules of solvent for F^- solvated with D_2O, CH_3OH, and C_2H_5OH and for Cl^- solvated with CH_3OH, C_2H_5OH, CH_3COCH_3, HCOOH, and CH_3COOH. The observed precipitous response of the specific rate to solvation is attributed to intermediate features of plausible reaction energy profiles.

DIETHARD K. BOHME et ASIT B. RAKSIT. Can. J. Chem. **63**, 3007 (1985).

Les mesures des lueurs d'écoulement en phase gazeuse à la température ambiante révèlent l'influence de la solvatation graduelle sur le caractère nucléophile des ions F^- et Cl^-. On a étudié les vitesses spécifiques des réactions de déplacement nucléophile avec le CH_3Cl et le CH_3Br dans des additions impliquant jusqu'à trois molécules de solvant pour l'ion F^- solvaté avec D_2O, CH_3OH et C_2H_5OH et pour l'ion Cl^- solvaté avec CH_3OH, C_2H_5OH, CH_3COCH_3, HCOOH et CH_3COOH. On attribue la réponse en forme de pic observée pour la vitesse de solvatation, à des caractéristiques intermédiaires des profils d'énergie d'une réaction plausible.

[Traduit par le journal]

Introduction

The role of solvent in S_N2 reactions is exposed at its most fundamental level in reactions of type [1] which can now be executed and studied in the gas phase as a function of stepwise solvation of the nucleophile A^- (1, 2).

[1] $A^-\cdot S_n + CH_3B \rightarrow B^-\cdot S_m + [(n - m)S + CH_3A]$

In reactions of this type available solvent is limited to that associated directly with the reacting ion and, when the reaction proceeds in a dilute inert gas, the transport of solvent to the products must occur within the reaction complex rather than through the surrounding medium as is possible in solution. Gas-phase measurements of such reactions therefore allow the role of solvation in S_N2 displacement to be isolated and investigated at a molecular level of solvation hitherto inaccessible.

Recently we have reported measurements for reactions of type [1] between solvated *homoconjugate* anions, $A^-\cdot(AH)_n$, and the methyl halides CH_3Cl and CH_3Br with AH = H_2O, D_2O, CH_3OH, C_2H_5OH, HCOOH, CH_3COOH, and CH_3COCH_3 (1). Their specific rates were followed as a function of stepwise solvation for additions of up to three molecules of solvent and found to respond precipitously, in some instances already with the addition of just one molecule of solvent. The response appeared not to be controlled directly by the overall exothermicity of the solvated reaction but instead could be attributed to intermediate features in the appropriate potential energy profile. In this study we explore the solvent response of the specific rates of similar reactions involving solvated *heteroconjugate* anions, $A^-\cdot(BH)_n$ by subjecting CH_3Cl and CH_3Br to displacement by the halide ions F^- solvated with up to three molecules of D_2O, CH_3OH, and C_2H_5OH and Cl^- solvated with up to three molecules of CH_3OH, C_2H_5OH, HCOOH, CH_3COOH, and CH_3COCH_3.

Experimental

The measurements were taken with a flowing plasma mass spectrometer (flowing afterglow) system. Details of the instrument together with methods of operation and data analysis have been reported earlier (3, 4). Formation of solvated anions was initiated about 10 ms upstream of the reaction zone at total pressures of ca. 0.4 Torr in either a flowing helium or hydrogen buffer gas. Heteroconjugate anions were derived from solvent addition reactions of type [2].

[2] $A^-\cdot S_n + S + M = A^-\cdot S_{n+1} + M$

The parent gas of A^- was added upstream of the electron gun while the vapour of S was added just downstream in amounts of about 2×10^{18} to 2×10^{19} molecules s^{-1}. Experiments were performed with A^- = F^- derived from C_2F_6 (at about 1×10^{20} molecules s^{-1}), and Cl^- derived from CCl_4 (at about 4×10^{19} molecules s^{-1}) or CH_3Cl (at about 5×10^{20} molecules s^{-1}). The solvated ions which could be produced in this fashion were $F^-\cdot(D_2O)_n$, $F^-\cdot(CH_3COCH_3)_n$, $Cl^-\cdot(CH_3OH)_n$, $Cl^-\cdot(C_2H_5OH)_n$, $Cl^-\cdot(CH_3COCH_3)_n$, $Cl^-\cdot(HCOOH)_n$, and $Cl^-\cdot(CH_3COOH)_n$. The production of $F^-\cdot(CH_3OH)_n$ is illustrated in Fig. 1. F^- is a relatively strong base and was observed to react with CH_3COCH_3, HCOOH, and CH_3COOH primarily by proton transfer under the adopted experimental conditions. The initial relative populations of $A^-\cdot S_n$ could be varied by adjusting the amount of added vapour. As discussed previously (1, 5, 6), a wide range in the initial relative populations is desirable for the determination of rate constants because of losses associated with the depletion of the source ion, $A^-\cdot S_{n-1}$. The methyl chloride and methyl bromide used as reagents were of high purity (minimum 99.5 mol%).

Results

The results of the rate constant measurements which reveal the absolute degree to which step-wise solvation influences nucleophilicity are summarized in Table 1 *a* and *b*. The sources of uncertainty associated with the determination of rate constants have been described previously (3, 4). In deriving rate constants from the observed decays of solvated ions, account was taken of the initial decay which can arise due to the depletion of the precursor ion in the reaction region. The following section describes the results of the measurements in more detail.

$F^-\cdot(BH)_n$

F^- ions were readily solvated with up to three molecules of water and methanol and two molecules of ethanol. Figure 2 shows results of measurements taken with the addition of CH_3Cl into a $He/C_2F_6/D_2O$ plasma in which hydrated fluoride

TABLE 1

(*a*) Rate constants[a] measured for reactions of solvated fluoride ions, $F^- \cdot S_n$, with CH_3Cl at 296 ± 2 K

$F^- \cdot S_n$	Rate constant for n = 0	1	2	3
$F^- \cdot (D_2O)_n$	1.9 ± 0.4	0.015 ± 0.005	≤ 0.0003	≤ 0.003
$F^- \cdot (CH_3OH)_n$	1.9 ± 0.4	≤ 0.0006	≤ 0.0003	≤ 0.0003
$F^- \cdot (C_2H_5OH)_n$	1.9 ± 0.4	≤ 0.0003	≤ 0.0003	

[a]Rate constants and their estimated accuracies given in units of 10^{-9} cm^3 molecule^{-1} s^{-1}.

(*b*) Rate constants[a] measured for reactions of solvated anions, $A^- \cdot S_n$, with CH_3Br at 296 ± 2 K

$A^- \cdot S_n$	Rate constant for n = 0	1	2	3
$F^- \cdot (D_2O)_n$	1.2 ± 0.2	0.16 ± 0.04	≤ 0.0005	
$F^- \cdot (CH_3OH)_n$	1.2 ± 0.2	0.12 ± 0.03	≤ 0.0002	≤ 0.0002
$F^- \cdot (C_2H_5OH)_n$	1.2 ± 0.2	0.085 ± 0.020	≤ 0.0002	
$Cl^- \cdot (CH_3OH)_n$	0.017 ± 0.004	≤ 0.0004	≤ 0.0004	≤ 0.0004
$Cl^- \cdot (C_2H_5OH)_n$	0.017 ± 0.004	≤ 0.0004	≤ 0.0004	
$Cl^- \cdot (CH_3COCH_3)_n$	0.017 ± 0.004	≤ 0.0008	≤ 0.0004	
$Cl^- \cdot (HCOOH)_n$	0.017 ± 0.004	≤ 0.0002	≤ 0.0002	
$Cl^- \cdot (CH_3COOH)_n$	0.017 ± 0.004	≤ 0.0002		

[a]Rate constants and their estimated accuracies given in units of 10^{-9} cm^3 molecule^{-1} s^{-1}.

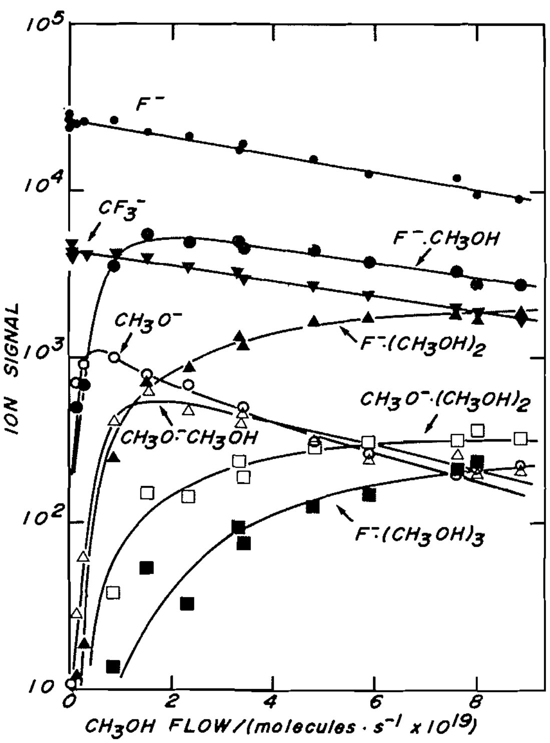

FIG. 1. The variation in dominant negative ions observed upon the addition of methanol as a 10% mixture in helium to a He/C_2F_6 plasma in which F^- and CF_3^- initially predominate. O^- and OH^- which are also present initially are not shown. T = 297 K, P = 0.320 Torr, $\bar{v}$ = 7.7 × 10^3 cm s^{-1}, L = 46 cm, flow of C_2F_6 = 2.4 × 10^{19} molecules s^{-1}.

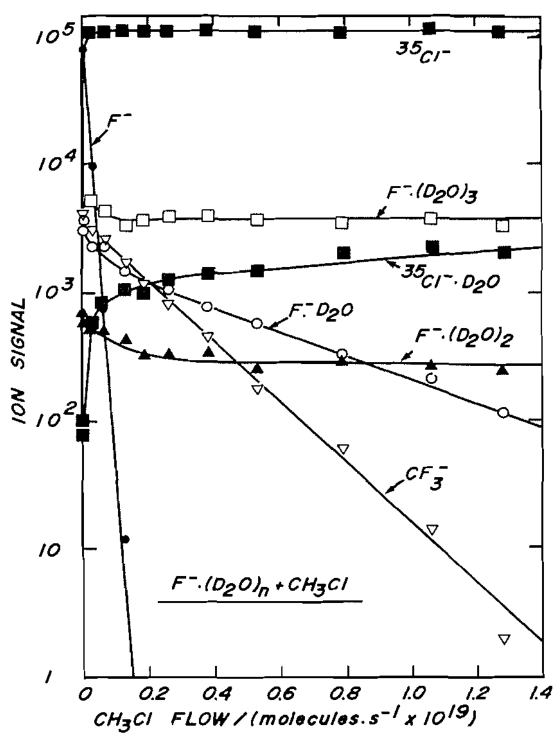

FIG. 2. Variations in ion signals recorded with the addition of CH_3Cl into a flowing $He/C_2F_6/D_2O$ plasma in which $F^- \cdot (D_2O)_n$ ions with n = 0 to 3 are initially predominant. T = 295 K, P = 0.347 Torr, $\bar{v}$ = 7.2 × 10^3 cm s^{-1}, and L = 46 cm.

ions have been established as dominant ions. Hydration is seen to reduce the reactivity of F^- already by a factor of about 100 with the addition of just one D_2O molecule. Further addition of D_2O molecules leads to immeasurably slow reactions. The slow reaction of $F^- \cdot D_2O$ with CH_3Cl appears to produce predominantly hydrated Cl^- product ions. With methanol and ethanol solvent the transition in reactivity was observed to be even more precipitous as solvation with just one solvent molecule resulted in immeasurably slow reactions.

More gradual transitions were observed with CH_3Br. The

TABLE 2. Support data and calculated values for methyl cation affinities of anions, A^-, in kcal mol^{-1}

A^-	EA(A)	Reference	$D^0(CH_3—A)^a$	Reference	$MCA(A^-)^b$
CF_3^-	42 ± 1.5	23	100	23, 24	285
F^-	78.4 ± 0.05	23	108.8	23	257
Cl^-	83.4 ± 0.07	23	82.4	23	226
Br^-	77.6 ± 0.07	23	69.1	23	218

[a] $D(CH_3—A)$ is calculated directly from the heats of formation of CH_3A, A, and CH_3.
[b] $MCA(A^-) = D(A—CH_3) - EA(A) + IP(CH_3)$ where $IP(CH_3) = 227$ kcal mol^{-1}, ref. 23.

singly solvated F^- ions were observed to react for all three solvents at a rate about 10 times less than that of the unsolvated F^- ion. There was evidence for substantial solvent retention only for the reaction of $F^- \cdot D_2O$. Figure 3 shows less than 10% solvent retention with $F^- \cdot CH_3OH$ which is similar to that observed with $F^- \cdot C_2H_5OH$. Further addition of solvent molecules resulted in a further drop in reactivity to levels which were not measurable. The reactivity of $F^- \cdot (D_2O)_3$ towards CH_3Br could not be explored because of overlap with $^{79}Br^-$ in the mass spectrum.

CF_3^-

With C_2F_6 as source gas significant amounts of CF_3^- were present initially in the flowing helium plasma. The CF_3^- was observed to react with both CH_3Cl (see Fig. 2) and CH_3Br (see Fig. 3) with rate constants of $(7 \pm 2) \times 10^{-11}$ and $(3 \pm 2) \times 10^{-10}$ cm^3 molecule^{-1} s^{-1}, respectively. The reactions are believed to proceed by nucleophilic displacement and thus contribute to the appearance of Cl^- and Br^-, respectively, whose production is dominated by the reactions with F^- present under the same operating conditions.

$Cl^- \cdot (BH)_n$

Cl^- ions were readily solvated with up to three molecules of methanol, two molecules of ethanol, acetone and formic acid, and one molecule of acetic acid. Previous measurements in our laboratory had revealed only a very slow displacement reaction between unsolvated Cl^- and CH_3Br, $k = (2.1 \pm 0.4) \times 10^{-11}$ cm^3 molecule^{-1} s^{-1} (7). This result was reproduced in the present study as k was measured to be $(1.7 \pm 0.4) \times 10^{-11}$ cm^3 molecule^{-1} s^{-1} and it was also observed that solvation with just one molecule reduced the rate of reaction by more than a factor of 20 for each of the five solvents to values corresponding to the lower limit accessible with the technique.

Discussion

Intrinsic energetics and kinetics

The reactions of F^- and CF_3^- with CH_3Cl and CH_3Br and the reaction of Cl^- with CH_3Br are all exothermic in the absence of solvent. The methyl cation affinities in Table 2 indicate a range in exothermicity for the S_N2 reactions investigated in this study from 8 to 67 kcal mol^{-1}. The reactions with CH_3Br are 8 kcal mol^{-1} more exothermic than those with CH_3Cl.

We have previously reported rate constants of (1.8 ± 0.4) and $(1.9 \pm 0.4) \times 10^{-9}$ cm^3 molecule^{-1} s^{-1} for the reaction of F^- with CH_3Cl (7, 8), $(1.2 \pm 0.2) \times 10^{-9}$ cm^3 molecule^{-1} s^{-1} for F^- with CH_3Br (7), and $(2.1 \pm 0.4) \times 10^{-11}$ cm^3 molecule^{-1} s^{-1} for Cl^- with CH_3Br (7). These earlier flowing afterglow results agree with those obtained in the present study within experimental error. Pulsed ICR measurements have led to the lower values of (8.0 ± 0.9) and $(5.8 \pm 0.3) \times 10^{-10}$ cm^3 molecule^{-1} s^{-1} for F^- reacting with CH_3Cl (9, 10), $(6.0 \pm 0.6) \times 10^{-10}$ cm^3 molecule^{-1} s^{-1} for F^- reacting with CH_3Br (9), and

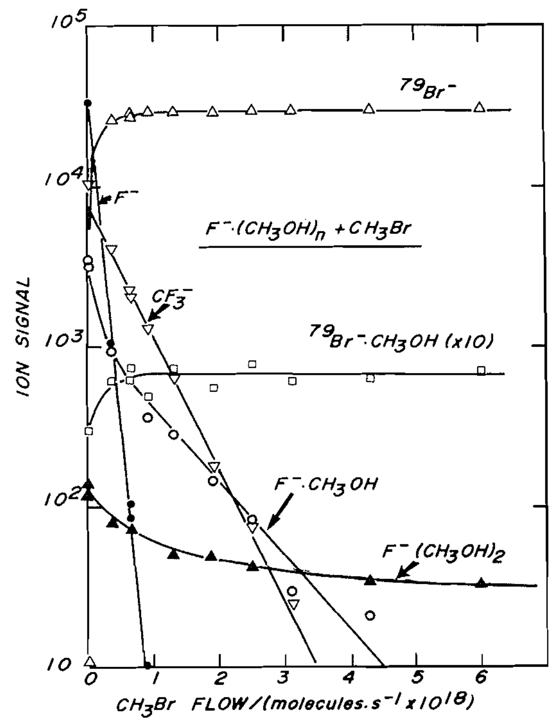

FIG. 3. Variations in ion signals recorded with the addition of CH_3Br into a flowing $He/C_2F_6/CH_3OH$ plasma in which $F^- \cdot (CH_3OH)_n$ ions with $n = 0$ to 2 are initially predominant. $T = 295$ K, $P = 0.306$ Torr, $\bar{v} = 7.7 \times 10^3$ cm s^{-1}, and $L = 46$ cm.

1.2×10^{-11} cm^3 molecule^{-1} s^{-1} for Cl^- reacting with CH_3Br (11) for which a value of $(8.0 \pm 1.0) \times 10^{-11}$ cm^3 molecule^{-1} s^{-1} had been reported earlier (9). The difference between the flowing afterglow and ICR results appears systematically to be about a factor of 2. Caldwell *et al.* have noted a similar difference for the reaction of Cl^- with CH_3Br for which they obtained a rate constant of 2.4×10^{-11} cm^3 molecule^{-1} s^{-1} at ca. 5 Torr (12) with a pulsed electron beam high pressure mass spectrometer. They have proposed that this difference can be expected as a result of the different pressures used in the different measurements. The expectation is based on a plausible "double-minimum" potential energy profile for reactions of this type. It is argued that when the energy of the central barrier in this profile lies below the initial energy of the system, as is the perception for the three reactions being considered here, collisional cooling of the excited adduct $A^- \cdot CH_3B$ will lead to an enhancement of formation of product as compared to decomposition back to reactants and so lead to an increase in the overall rate constant as the pressure is raised. Caldwell *et al.* also have provided crude model calculations which support the magnitude of the apparent pressure effect (12) but direct experimental verification has not yet been achieved so that systematic errors can not yet be ruled out to account for the disparity in

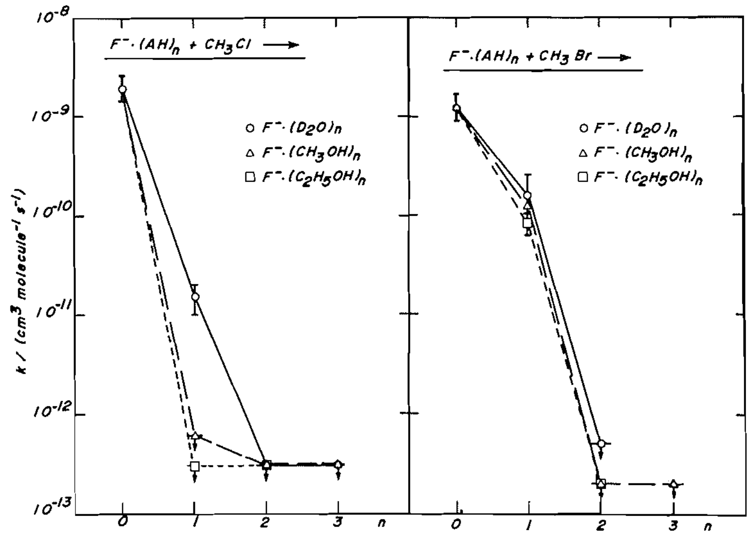

FIG. 4. Observed variations in the rate constant with the extent of solvation for gas-phase nucleophilic displacement reactions of solvated fluoride anions with methyl chloride and methyl bromide at room temperature.

results observed with the three techniques.

We have previously shown by experiment that the kinetic nucleophilicity of solvent-free S_N2 reactions in the gas phase, when expressed as a reaction probability per collision, has a dynamic range of more than 10^3. F^- exhibits nearly unit reactivity towards CH_3Cl and CH_3Br and so is among the most reactive nucleophiles in the gas phase. In comparison, the Cl^- reactivity towards CH_3Br is about 50 times smaller and puts Cl^- among anions of low nucleophilicity (7). The rate constants of $(7 \pm 2) \times 10^{-11}$ and $(3 \pm 2) \times 10^{-10}$ cm^3 molecule^{-1} s^{-1} for the reactions of CF_3^- with CH_3Cl and CH_3Br, respectively, correspond to reactivities of 0.03 and 0.2 so that this anion falls into the medium nucleophilicity range (7).

Kinetics of solvated S_N2 reactions

The results in Table 1 *a* and *b* indicate that the rate constants for the solvated reactions investigated become too small to measure with the addition of just two solvent molecules to the nucleophile or even, in some cases, just one. For the reactions of $F^- \cdot S_n$ this corresponds to a drop in the specific reaction rate in the gas phase of almost four orders of magnitude as is illustrated graphically in Fig. 4. In aqueous solution the specific rates of these S_N2 reactions are lower by another 15 to 16 orders of magnitude! The measured rate constants at 298 K for F^- reacting with CH_3Cl and CH_3Br in aqueous solution are 2.5×10^{-29} and 5.6×10^{-28} cm^3 molecule^{-1} s^{-1}, respectively (13). Also Fig. 4 shows that the rate of change of the rate constant with solvation is sensitive to the nature of both the methyl halide and the solvent. The reactions with CH_3Br show a remarkably similar decrease in specific rate with solvation for the three solvents D_2O, CH_3OH, and C_2H_5OH, but with CH_3Cl the drop in specific rate appears earlier with less solvation and is more distinct for the three solvents. A similar behaviour was evident for several of the S_N2 reactions of solvated homoconjugate anions with CH_3Cl and CH_3Br reported earlier (1). The reaction of Cl^- with CH_3Br is intrinsically about 100 times less efficient than the corresponding F^- reaction but nevertheless addition of one solvent molecule to Cl^- was observed to decrease the specific reaction rate by another factor of more than 20 for methanol, ethanol, acetone, formic acid, and acetic acid. Since the rate constant became immeasurably small for all five of these solvents with the addition of one solvent molecule, no information was available in this case on the relative sensitivity of the rate constant to the nature of the solvent. For solutions of water, methanol, and acetone, rate constants of 8.2×10^{-27}, 1.1×10^{-26}, and 5.3×10^{-21} cm^3 molecule^{-1} s^{-1}, respectively, have been reported for the S_N2 reaction of Cl^- at 298 K (13–15).

Overall energetics of solvated S_N2 reactions

The addition of solvent modifies the intrinsic exothermicity of the S_N2 reaction [1] by the solvation energies of the anions A^- and B^- entering and leaving the reaction and the neutral product D and "free" solvent S if these become solvated. A complete specification of the energetics of the solvated S_N2 reactions investigated in this study is not possible with the available data for solvation energies. Binding energies are available for additions of up to three molecules of water to F^-, Cl^-, and Br^- (16, 17). Also F^- and Cl^- affinities for single solvent molecules are available for some of the other solvents used in this study (18, 19). The available hydration energies for F^-, Cl^-, and Br^- allow the construction of the enthalpy diagrams in Fig. 5. These diagrams clearly show that hydration acts to decrease the overall exothermicities of the reactions of F^- with CH_3Cl and CH_3Br but that exothermic reaction channels remain available for additions of at least up to three water molecules, albeit, to preserve exothermicity, an increasing amount of retention of water by the product ion anion is required with increasing levels of hydration of the nucleophile. The observed kinetics for these two series of reactions therefore appear not to be controlled directly by the overall energetics, but must be attributed instead to intermediate features in the appropriate energy profiles.

Intermediate energy profiles

The intermediate features of the potential energy profiles of solvated S_N2 reactions are reasonably addressed in terms of double minima which evolve with step-wise solvation as the energy of the intermediate barrier increases relative to the initial energy of the reactants (11, 20). Morokuma has shown that several profiles are plausible at each level of solvation for the barrier itself depending on the mechanism of solvent transfer (21). For the singly solvated reactions the sequential solvate transfer and inversion mechanism indicated by reaction [3] will

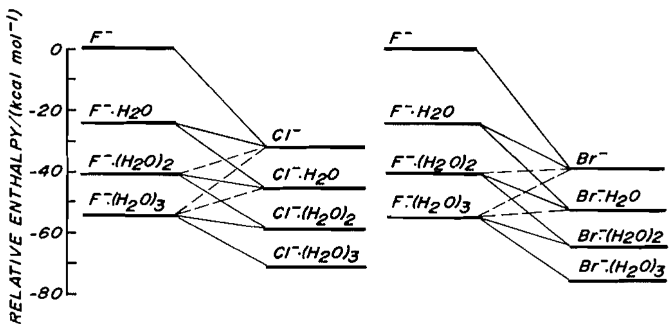

FIG. 5. Enthalpy diagrams for the gas-phase reactions of hydrated F^- with CH_3Cl and CH_3Br. The overall enthalpy changes ignore possible hydration of the neutral product CH_3F molecules. Solid diagonal lines correspond to exothermic channels while the dashed lines represent endothermic reaction channels.

be energetically unfavourable if the stability of $A^- \cdot CH_3B \cdot S$ is less than that of $A^- \cdot S + CH_3B$.

$$[3] \quad S \cdot A^- \cdot CH_3B \rightarrow A^- \cdot CH_3B \cdot S \rightarrow ACH_3 \cdot B^- \cdot S$$

Because of the substantial magnitude of fluoride and chloride solvent affinities (18, 19) this is expected to be the case for all of the singly solvated reactions in Table 1. These should therefore prefer to proceed by sequential inversion and solvate transfer as illustrated in reaction [4].

$$[4] \quad S \cdot A^- \cdot CH_3B \rightarrow S \cdot ACH_3 \cdot B^- \rightarrow ACH_3 \cdot B^- \cdot S$$

Concerted solvate transfer and inversion is expected to be less favourable on entropic grounds (22). The excess energy in the product isomer $S \cdot ACH_3 \cdot B^-$ formed in the inversion step in reaction [4] may be channeled directly into desolvation leaving unsolvated B^- as the principal product ion and so preempt the solvent transfer. Our observations are consistent with such a model. For the weakly exothermic reactions of $Cl^- \cdot S$ with CH_3Br the excess energy is insufficient to leave unsolvated Br^-. These reactions are therefore constrained to transfer solvent to the product anion but none do so with any measurably efficiency. The somewhat more exothermic reaction of $F^- \cdot D_2O$ with CH_3Cl appeared to produce $Cl^- \cdot D_2O$ exclusively but with low efficiency, while the most exothermic reactions of $F^- \cdot S$ with CH_3Br appeared to produce unsolvated Br^- preferentially.

Calculations (10, 12) suggest that the intermediate barriers for the solvent-free reactions of F^- with CH_3Cl and Cl^- with CH_3Br lie only about 1 or 2 kcal mol^{-1} below the corresponding energy of the reactants at room temperature. Consequently the intermediate barrier might be expected to emerge above the energy of the reactants already at very low levels of solvation. The results of the gas-phase measurements reported here suggest that this may indeed be the case already for the addition of one or two solvent molecules. Measurements in aqueous solution indicate that the energies of the intermediate barriers for these two reactions lie about 25 kcal mol^{-1} above the energies of the reactants (13). The observations in Fig. 4 for the reactions of $F^- \cdot S$ with CH_3Cl imply a relative enhancement of the energy of the intermediate barrier due to differential solvation by one solvent molecule which is less for D_2O than for CH_3OH and C_2H_5OH. The observations for the slightly more exothermic reactions of $F^- \cdot S$ with CH_3Br are consistent with an order of relative enhancement of $D_2O < CH_3OH < C_2H_5OH$ but the actual energies of the intermediate barriers still appear to lie below or close to the initial reactant energies since all three solvated reactions proceed with measurable efficiencies. This appears no longer to be the case at higher levels of solvation.

Acknowledgement

We thank the Natural Sciences and Engineering Research Council of Canada for financial support.

1. D. K. BOHME and A. B. RAKSIT. J. Am. Chem. Soc. **106**, 3447 (1984).
2. D. K. BOHME and G. I. MACKAY. J. Am. Chem. Soc. **103**, 978 (1981).
3. D. K. BOHME, R. S. HEMSWORTH, H. W. RUNDLE, and H. I. SCHIFF. J. Chem. Phys. **58**, 3504 (1973).
4. G. I. MACKAY, R. S. HEMSWORTH, and D. K. BOHME. Can. J. Chem. **54**, 1624 (1976).
5. G. I. MACKAY, A. B. RAKSIT, and D. K. BOHME. Can. J. Chem. **60**, 2594 (1981).
6. A. B. RAKSIT and D. K. BOHME. Can. J. Chem. **61**, 1683 (1983).
7. K. TANAKA, G. I. MACKAY, J. D. PAYZANT, and D. K. BOHME. Can. J. Chem. **54**, 1643 (1976).
8. D. K. BOHME and L. B. YOUNG. J. Am. Chem. Soc. **92**, 7354 (1970).
9. J. L. BRAUMAN, W. N. OLMSTEAD, and C. A. LIEDER. J. Am. Chem. Soc. **96**, 4030 (1974).
10. M. J. PELLERITE and J. I. BRAUMAN. J. Am. Chem. Soc. **99**, 2672 (1983).
11. W. N. OLMSTEAD and J. I. BRAUMAN. J. Am. Chem. Soc. **99**, 4219 (1977).
12. G. CALDWELL, T. F. MAGNERA, and P. KEBARLE. J. Am. Chem. Soc. **106**, 959 (1984).
13. R. H. BATHGATE and E. A. MOELWYN-HUGHES. J. Chem. Soc. 2642 (1959).
14. R. ALEXANDER, E. C. F. KO, A. J. PARKER, and T. J. BROXTON. J. Am. Chem. Soc. **90**, 5049 (1968).
15. A. J. PARKER. Chem. Rev. **69**, 1 (1969).
16. P. KEBARLE. Ann. Rev. Phys. Chem. **28**, 445 (1977).
17. R. G. KEESEE and A. W. CASTLEMAN. Chem. Phys. Lett. **74**, 139 (1980).
18. G. CALDWELL and P. KEBARLE. J. Am. Chem. Soc. **106**, 967 (1984).
19. J. W. LARSON and T. B. MCMAHON. J. Am. Chem. Soc. **105**, 2944 (1983).
20. D. K. BOHME and G. I. MACKAY. J. Am. Chem. Soc. **103**, 978 (1981).
21. K. MOROKUMA. J. Am. Chem. Soc. **104**, 3727 (1982).
22. M. HENCHMAN, J. F. PAULSON, and P. M. HIERL. J. Am. Chem. Soc. **105**, 5509 (1983).
23. H. M. ROSENSTOCK, K. DRAXL, B. W. STEINER, and J. T. HERRON. J. Phys. Chem. Ref. Data Ser. Suppl. 1, **6** (1977).
24. J. L. FRANKLIN, J. G. DILLARD, H. M. ROSENSTOCK, J. T. HERRON, K. DRAXL, and F. H. FIELD. Natl. Stand. Ref. Data Ser. **26** (1969).

Étude physico-chimique, spectres de vibration et structure du sulfaméthoxazole

Luc Maury, Joëlle Rambaud, Bernard Pauvert, Yves Lasserre, G. Berge et Michel Audran
"Groupe polymorphisme et Biodisponibilité", U.F.R. de Pharmacie, Avenue Charles Flahaut, 34060 Montpellier, France

Reçu le 22 mars 1985

Luc Maury, Joëlle Rambaud, Bernard Pauvert, Yves Lasserre, G. Berge et Michel Audran. Can. J. Chem. **63**, 3012 (1985).

Les auteurs ont identifié et caractérisé deux polymorphes et une forme solvatée pour le sulfaméthoxazole en utilisant de nombreuses méthodes thermiques et spectrales. La structure de la forme II a été résolue et comparée à celle de la forme I déjà publiée: les différences portent essentiellement sur les longueurs des liaisons hydrogène intermoléculaires. L'analyse des spectres Raman et infrarouge a permis de proposer une attribution des vibrations caractéristiques des groupements amine, amide et sulfone impliqués dans les liaisons hydrogène.

Luc Maury, Joëlle Rambaud, Bernard Pauvert, Yves Lasserre, G. Berge, and Michel Audran. Can. J. Chem. **63**, 3012 (1985).

Two polymorphic and one solvate forms of sulfamethaxozole have been identified and characterized using various thermal and spectral methods. The crystal structure of form II has been solved and compared with that of form I recently published: the lengths of the intermolecular H bonds mainly differentiate the two polymorphic forms. An assignment of the fundamental vibrations of the amine, amide, and sulfone groups involved in the H intermolecular bonds has been proposed from the analysis of the Raman and infrared spectra.

Introduction

Poursuivant nos recherches sur le polymorphisme de substances médicamenteuses, nous avons entrepris l'étude du sulfaméthoxazole ou *N*-(méthyl-5 isoxazolyl-3) sulfanilamide.

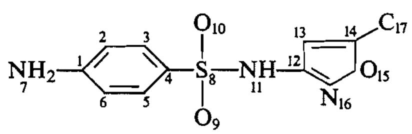

Dans un travail antérieur (1) nous avons montré que seul l'emploi simultané de nombreuses techniques peut permettre d'affirmer la présence de plusieurs formes cristallines pour un même composé; c'est pourquoi nous avons utilisé dans cette étude des méthodes thermiques et spectrales traditionnelles—thermogravimétrie, analyses thermique et calorimétrique différentielles, spectrométrie d'absorption infrarouge et diffraction des rayons X—auxquelles nous avons ajouté la diffusion Raman, notamment dans le domaine des basses fréquences. Nous avons également résolu la structure du polymorphe II afin de la comparer à celle du polymorphe I, publiée antérieurement (2).

Shiu Shiang Yang et Guillory (3), dans un travail général sur les sulfamides, ont mis en évidence pour ce composé l'existence de trois formes polymorphes, dont deux seulement caractérisées par leur spectre infrarouge. Si nous retrouvons bien les formes I et II des auteurs précités, nous n'avons pu isoler la forme III; en revanche, nous avons identifié et caractérisé une forme solvatée non signalée précédemment.

Matériel et méthode

1. *Obtention des différentes formes*

Le sulfaméthoxazole (produit Roche) a été recristallisé dans plusieurs solvants (eau, acétone, éthanol, propanol, butanol et pentanol) ainsi que dans différents mélanges: eau−éthanol et eau−acétone. Pour chaque expérience, nous avons suivi la cristallogénèse en fonction de la température. Les cristaux recueillis après filtration étaient séchés sous vide durant 48 h.

2. *Analyse thermique*

L'analyse thermogravimétrique a été effectuée avec une balance Sétaram Ugine Eyraud B60, en double version ATD−ATG, équipée d'un programmateur de température RT 64. La prise d'essai était de 50 mg et la substance de référence l'alumine.

L'analyseur enthalpique différentiel Perkin Elmer DSC 1B nous a permis de différencier les changements d'états physiques en fonction de la température et de mesurer l'énergie calorifique qui accompagne ces changements d'états. Les prises d'essai étaient de 2 à 5 mg et la montée en température de 2 ou 4°C/min.

Les phénomènes thermiques ont été vérifiés par visualisation au microscope à platine chauffante Leitz.

3. *Méthodes spectrales*

Diffraction des rayons X

Les diagrammes ont été réalisés sur un diffractomètre CGR avec tube de cuivre et monochromateur à quartz monté sur un générateur Sigma 80.

Spectrométrie infrarouge

Les spectres infrarouge ont été enregistrés à température ambiante sur un spectromètre Perkin Elmer 457. Nous avons vérifié, par enregistrement des spectres Raman de la poudre en l'état ou comprimée, que le broyage et la mise sous forme de pastilles KBr n'entraînaient aucune modification des spectres.

Spectrométrie de diffusion Raman

Les spectres Raman ont été enregistrés à température ambiante sur un spectromètre de haute résolution Jobin et Yvon "Ramanor HG 2S". La technique utilisée était celle de diffusion à 90° en incidence normale, l'excitatrice étant la radiation 514,5 nm d'un laser Spectra Physics à argon ionisé. La puissance du laser sur l'échantillon était maintenue à une valeur faible de 100 mW, pour éviter tout risque de dégradation des composés.

4. *Détermination de la structure de la forme II*

Un monocristal de 0,20 × 0,15 × 0,25 mm a été soumis au rayonnement X sur un diffractomètre automatique Syntex $P2_1$. Quinze réflexions indépendantes ont permis de définir les paramètres de la maille cristalline. Les extinctions systématiques ont donné deux groupes d'espace *Cc* et *C*2/*c*. Sur 1769 intensités mesurées, 1246 étaient considérées comme observées conformément à $I \geq 2{,}5\ \sigma\ (I)$. La longueur d'onde utilisée était celle de la raie Kα du molybdène soit λ = 0,71069 Å, l'angle de Bragg maximum étant 2 θ = 47°. La résolution a été effectuée avec le programme MULTAN 80 (4). La carte de Fourier a donné cinq atomes. Trois synthèses de Fourier ont été requises pour faire apparaître tous les atomes non hydrogène de la molécule. L'affinement a été alors poursuivi avec le programme SHELX 76 (5). Les atomes lourds ont été affinés de façon anisotrope.

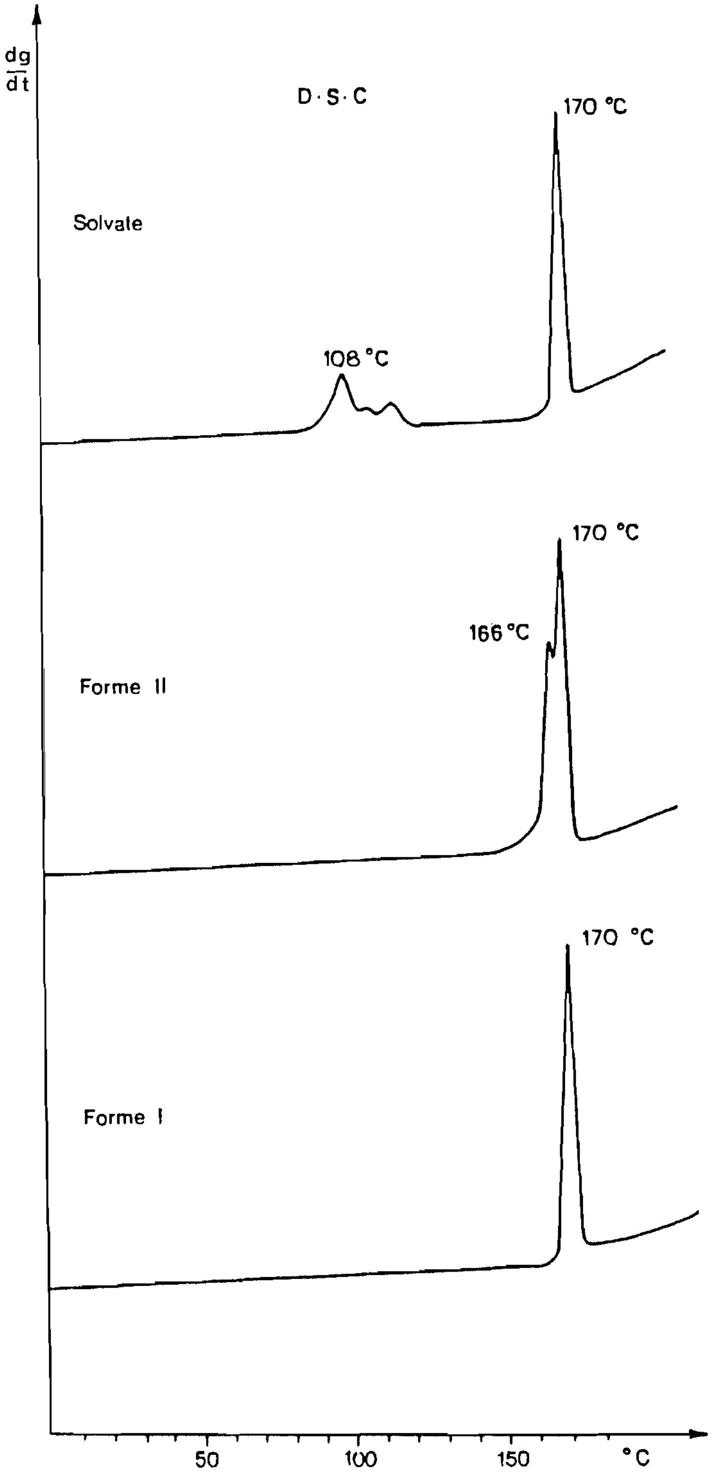

FIG. 1. Courbes d'analyse calorimétrique différentielle (vitesse 8°/min).

Les hydrogènes ont subit un affinement isotrope avec un B_{eq} de 9 Å.

Le groupe d'espace s'est avéré être $C2/c$. En fin d'affinement, le coefficient de reliabilité était R = 0,0408.

Résultats et discussion

Analyse thermique

Les courbes d'analyse calorimétrique différentielle donnent trois accidents endothermiques différents: à 108, 166 et 170°C (fig. 1).

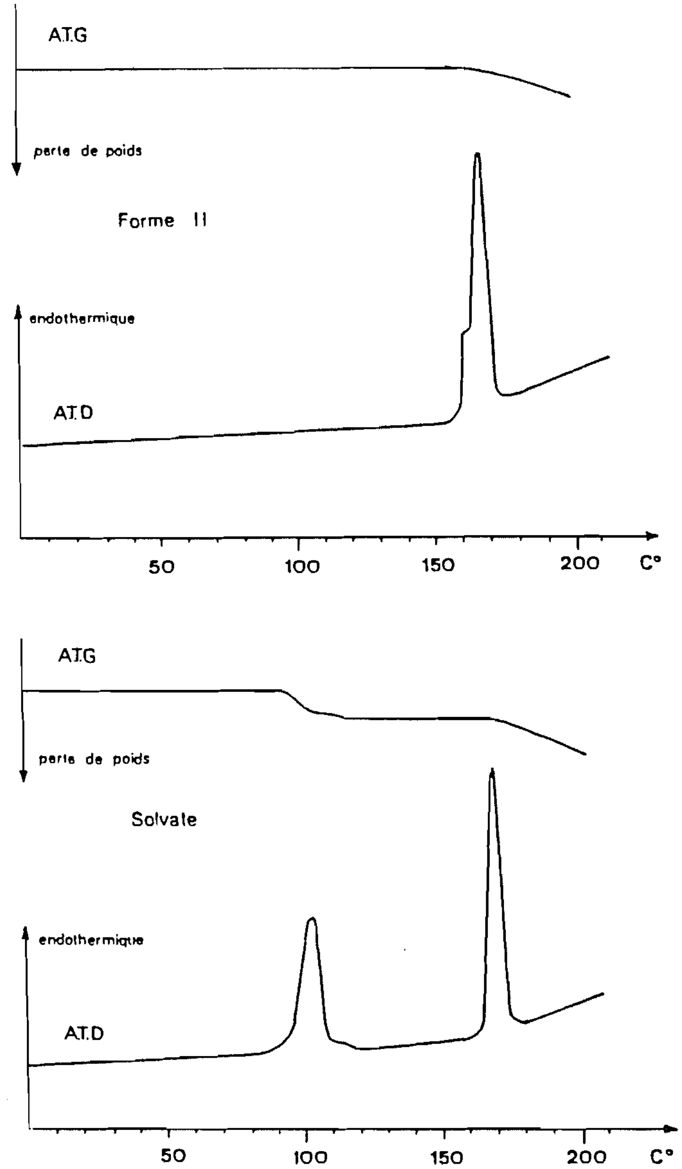

FIG. 2. Thermogrammes (ATG−ATD couplées) des trois cristallisations différentes.

Les thermogrammes obtenus pour ces trois accidents montrent que le premier s'accompagne d'une perte de poids de 3%, correspondant à la perte d'une demi-molécule d'eau (fig. 2). Les deux autres ne sont accompagnés d'aucune perte de poids. Il semble donc que l'on soit en présence de 2 polymorphes et d'un solvate. Les deux formes ont des températures de fusion très proches et il n'est possible de les séparer qu'en effectuant des mesures à une vitesse de 2°C/min.

La forme "haute température" a été obtenue dans tous les solvants. La forme solvatée est extraite par recristallisation dans un mélange eau−acétone ou dans l'eau. Il a été plus difficile d'obtenir la forme "basse température" (forme II), qui apparaît par traitement thermique de la forme I (fusion de la forme I et trempe à 0°C) ou par recristallisation dans le méthanol.

Le passage de la forme I à la forme II étant thermiquement réversible, nous en concluons que les deux formes sont énantiomorphes.

À partir des courbes d'analyse calorimétrique différentielle

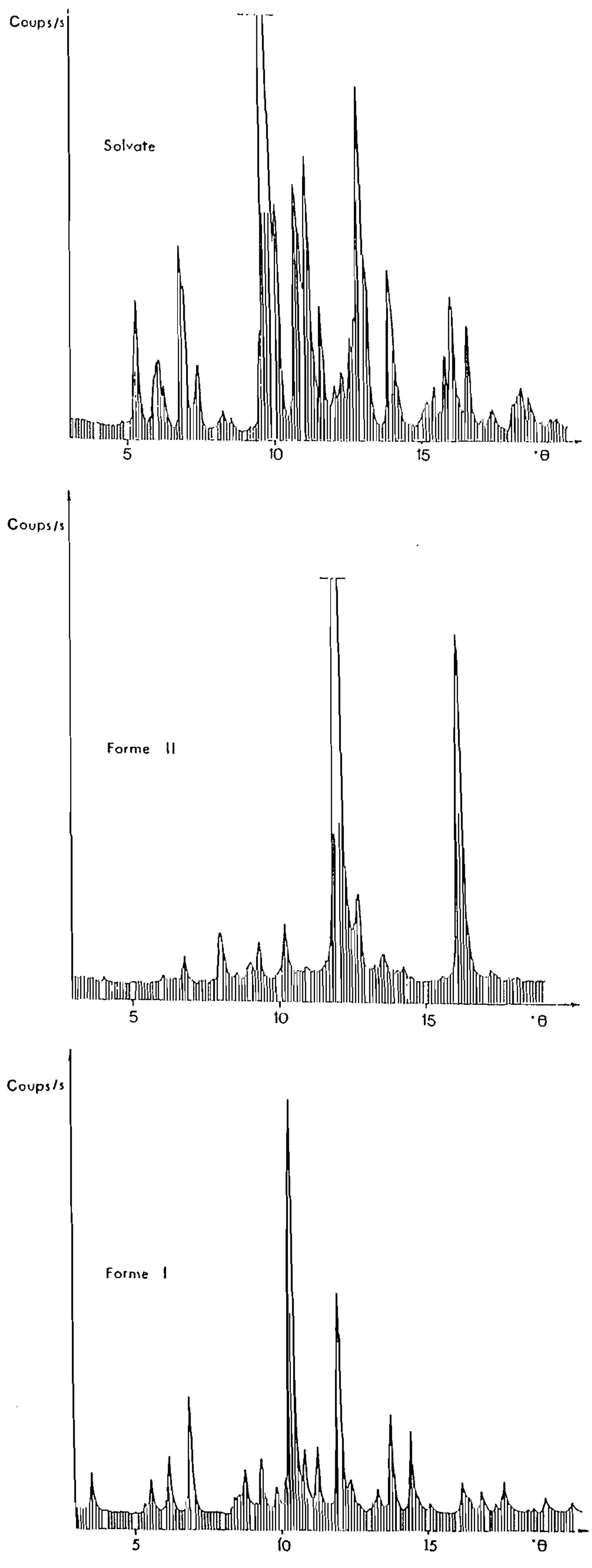

FIG. 3. Diagrammes de diffraction des rayons X.

TABLEAU 1. Distances interatomiques (Å) et angles de valence (deg) du polymorphe II

Atomes	Distance	Atomes	Angle
C1 ---C2	1,384(5)	C2 --C1 --C6	117,5(3)
C1 ---C6	1,397(5)	C2 --C1 --N7	122,6(3)
C1 ---N7	1,358(5)	C6 --C1 --N7	119,9(3)
C2 ---C3	1,355(5)	C1 --C2 --C3	122,3(4)
C3 ---C4	1,389(5)	C2 --C3 --C4	120,0(4)
C4 ---C5	1,388(5)	C3 --C4 --C5	118,8(3)
C4 ---S8	1,734(3)	C3 --C4 --S8	121,1(3)
C5 ---C6	1,370(5)	C5 --C4 --S8	120,0(3)
S8 ---O9	1,424(2)	C4 --C5 --C6	120,6(4)
S8 ---O10	1,434(2)	C1 --C6 --C5	120,7(3)
S8 ---N11	1,645(3)	C4 --S8 --O9	110,4(2)
N11---C12	1,393(4)	C4 --S8 --O10	108,0(2)
C12---C13	1,411(5)	O9 --S8 --O10	119,8(1)
C12---N16	1,302(4)	C4 --S8 --N11	107,4(1)
C13---C14	1,327(5)	O9 --S8 --N11	103,6(2)
C14---O15	1,347(4)	O10--S8 --N11	106,8(1)
C14---C17	1,481(5)	S8 --N11--C12	122,4(2)
O15---N16	1,407(3)	N11--C12--C13	129,3(3)
		N11--C12--N16	119,1(3)
		C13--C12--N16	111,6(3)
		C12--C13--C14	104,7(3)
		C13--C14--O15	110,3(3)
		C13--C14--C17	133,7(4)
		O15--C14--C17	115,9(3)
		C14--O15--N16	108,0(3)
		C12--N16--O15	105,4(3)

(fig. 1), nous avons calculé les enthalpies de fusion soit:

$$\Delta H\ (f_{\mathrm{I}}) = -26{,}200 \text{ kJ mol}^{-1}$$
$$\Delta H\ (f_{\mathrm{II}}) = -24{,}300 \text{ kJ mol}^{-1}$$

ce qui donne en première approximation une enthalpie de transformation de 2,100 kJ mol^{-1} (6).

Diffraction des rayons X

Les diagrammes de poudre (fig. 3) des trois cristallisations permettent de mettre en évidence des raies spécifiques de chaque espèce:

forme I: 7, 10,5, 12,05 θ°
forme II: 8, 11,9, 16,30 θ°
solvate: 9,7, 10,7, 11,15, 12,9 θ°

Étude comparative des structures cristallines des deux formes

Cette étude est particulièrement intéressante; en effet, les deux formes cristallisent dans le même système (monoclinique) et le même groupe d'espace ($C2/c$): un fait analogue avait déjà été observé pour d'autres sulfamides (7, 8). De plus, les paramètres (a,b,c) de la forme I sont respectivement voisins des paramètres (c,b,a) de la forme II comme le montre le tableau suivant:

	Forme I	Forme II
a (Å)	16,046(5)	25,106(2)
b (Å)	5,470(2)	7,229(3)
c (Å)	25,747(1)	14,847(9)
β (dég)	96,12 (2)	117,9 (4)
V (Å^3)	2247	2381,3
d (g cm^{-3})	1,49	1,418
z	8	8

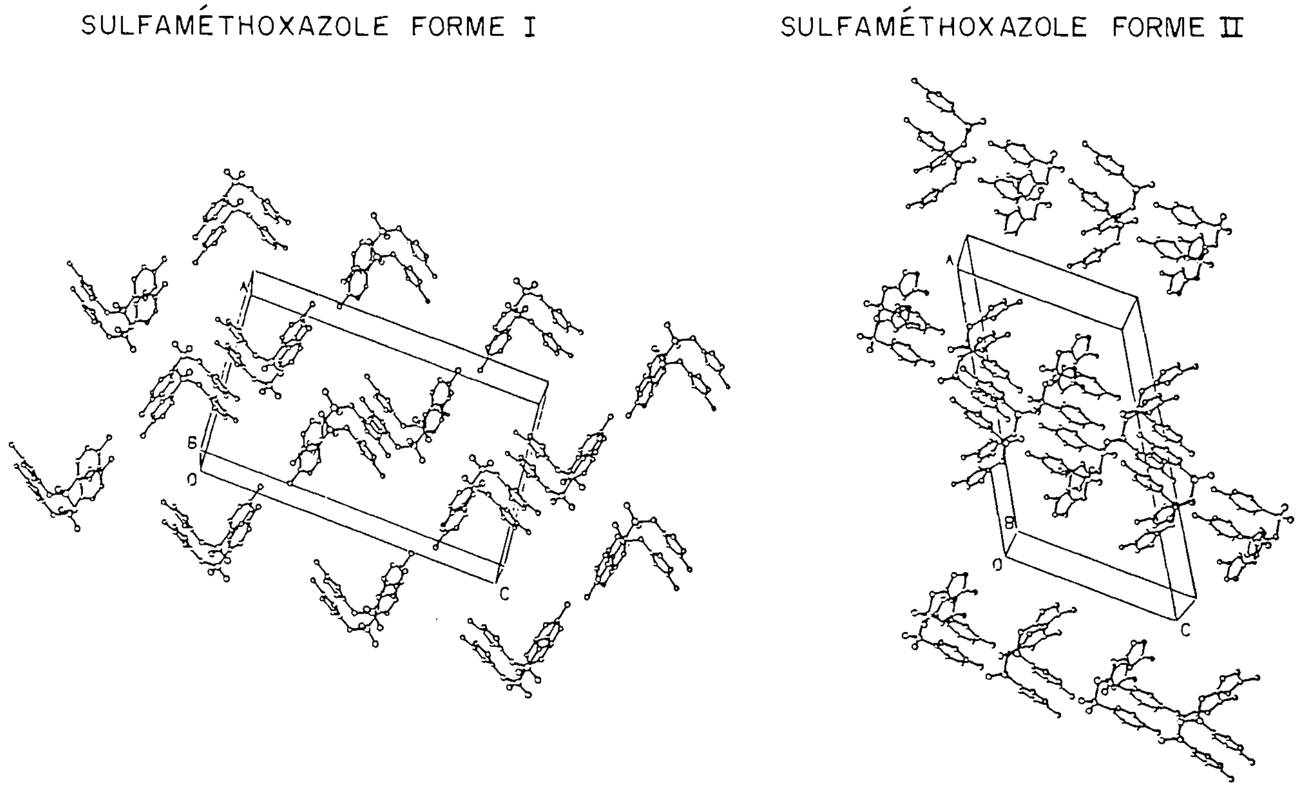

FIG. 4. Empilement moléculaire dans la maille des deux polymorphes (PLUTO (réf. 20)).

TABLEAU 2. Liaisons intermoléculaires "type hydrogène" des polymorphes I et II

Forme I		Forme II	
Code de symétrie		Code de symétrie	
I x, y, z		I x, y, z	
II $x, 1+y, z$		II $x, 1-y, -0{,}5+z$	
III $x, -1+y, z$		III $x, -y, -0{,}5+z$	
IV $0{,}5+x, 0{,}5+y, z$		IV $0{,}5-x, 0{,}5-y, z$	
N11 H11 - - - - $O9_{II}$	3,232 Å	N7 H7 - - - - $O9_{II}$	3,007 Å
C13 H13 - - - - $N16_{III}$	3,227 Å	N7 H7 - - - - $O10_{III}$	3,148 Å
N7 H7 - - - - $O10_{IV}$	3,275 Å	N11 H11 - - - - $N16_{IV}$	2,952 Å

L'ensemble des valeurs des angles de valence et des distances interatomiques de la forme II (tableau 1) fait apparaître un effet quinonique plus marqué que dans la forme I, avec des liaisons C1—N7, C2—C3 et C5—C6 plus courtes ($\Delta l = 0{,}02$ Å). Exceptées ces légères différences, les molécules I et II sont identiques et l'empilement moléculaire dans la maille (fig. 4), très semblable. Les écarts les plus marquants se situent au niveau des liaisons hydrogène (tableau 2). Les similitudes de ces deux polymorphes, tant au niveau des paramètres cristallins qu'au niveau des paramètres internes de la molécule, expliquent d'une part les points et chaleurs de fusion très voisins, d'autre part la difficulté à différencier ces deux formes.

Spectrométrie infrarouge et Raman

La spectrométrie infrarouge est une méthode utilisée depuis de nombreuses années pour mettre en évidence le polymorphisme de substances médicamenteuses, mais le domaine spectral généralement analysé s'étend seulement de 4000 à 200 cm^{-1} et ne porte donc que sur les vibrations internes de la molécule. Le polymorphisme pouvant n'influer que très peu sur les vibrations propres d'une molécule, l'absorption infrarouge—au moyen de spectromètres conventionnels—se révèle parfois insuffisante. En outre, la technique généralement adoptée de mise sous forme de pastilles KBr nécessite le broyage et la compression de la poudre, manipulations qui peuvent faire évoluer une forme instable vers une forme stable. La spectrométrie de diffusion Raman rend possible l'analyse d'un échantillon polycristallin sans lui faire subir de traitements susceptibles de le modifier. Elle permet en outre, comme l'absorption infrarouge, d'étudier le domaine des vibrations internes, mais elle trouve tout son intérêt dans l'obtention aisée du spectre des vibrations externes. Ces vibrations, qui correspondent aux mouvements de rotation et de translation des molécules au sein du réseau cristallin, sont d'un très grand intérêt pour caractériser le polymorphisme, qui se manifeste par des changements au niveau du réseau. Les raies caractéristiques apparaissent à des fréquences très basses et ne sont facilement accessibles que par diffusion Raman. Cette technique, d'application récente au médicament (9, 10), est très peu employée et nous l'avons déjà mise en oeuvre lors de l'étude de différents sulfamides (1, 11, 12, 21).

Domaine des vibrations externes

Les spectres Raman des vibrations du réseau, représentés sur la figure 5, permettent immédiatement d'identifier les deux polymorphes et le solvate. Le solvate se caractérise principalement par la raie 31 cm^{-1}, la plus intense de tout le spectre; les raies 49,5, 68 et 102 cm^{-1} peuvent également permettre de l'identifier. Les raies 41, 63, 79, 113 et 123 cm^{-1} peuvent être utilisées pour caractériser la forme II. Enfin, la forme I se reconnaît par la raie 88 cm^{-1} très intense, le massif centré à 130 cm^{-1} et le triplet 45, 37 et 31 cm^{-1}.

Domaine des vibrations internes

Les spectres Raman (fig. 6) et infrarouge (fig. 7) permettent

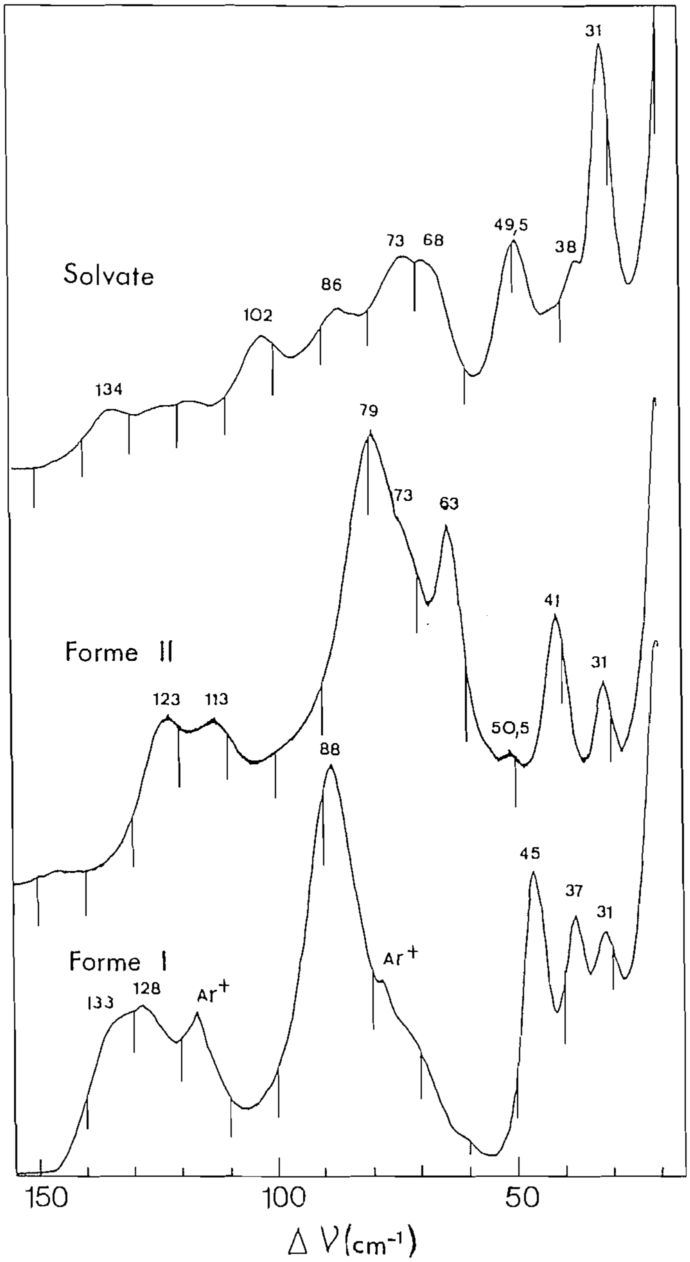

FIG. 5. Spectres Raman des vibrations du réseau du sulfaméthoxazole.

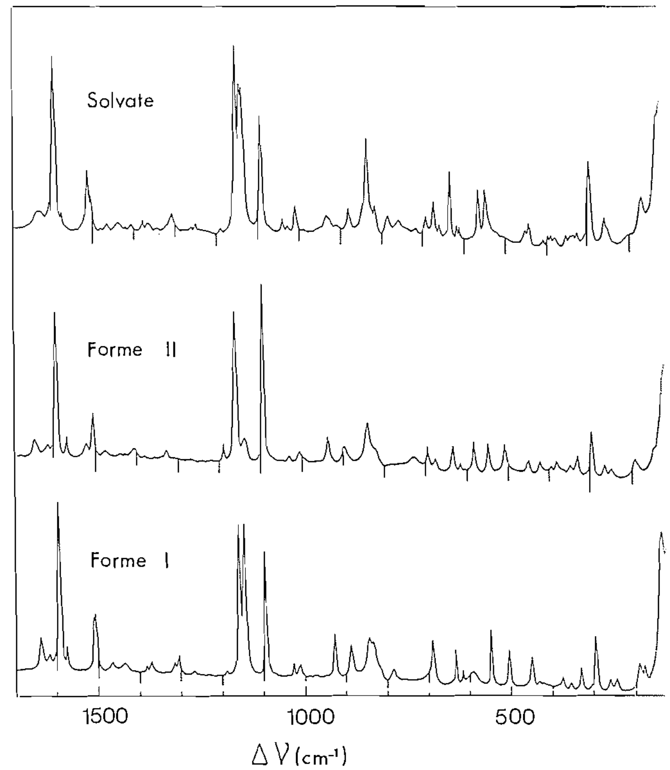

FIG. 6. Spectres Raman de trois formes de sulfaméthoxazole (1700–100 cm^{-1}).

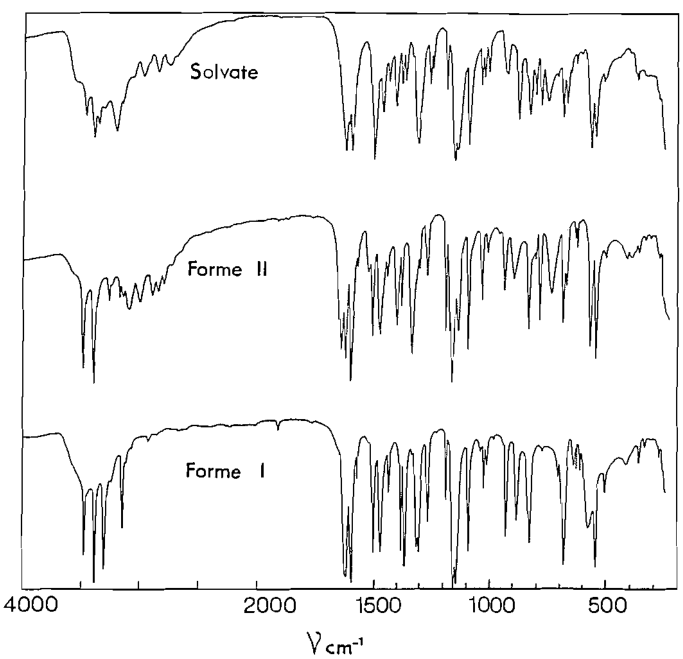

FIG. 7. Spectres infrarouge du sulfaméthoxazole.

de différencier les trois formes polymorphes bien que les différences, en particulier celles relevées sur les spectres Raman, soient moins significatives dans ce domaine que dans celui des vibrations externes.

La présence simultanée dans cette molécule d'un noyau benzénique et d'un noyau méthoxazole rend complexe l'interprétation des spectres de vibration. Nous avons signalé précédemment que les formes I et II présentent de nombreuses analogies structurales et diffèrent essentiellement par les liaisons hydrogène intermoléculaires, qui intéressent principalement les groupements amine, amide et sulfone. Par suite du nombre important de vibrations attendu et des nombreux couplages possibles nous limiterons nos propositions d'attribution à certains modes caractéristiques. Ces propositions sont basées d'une part sur les travaux antérieurs portant sur des molécules voisines, d'autre part sur la comparaison des spectres avec ceux de différents sulfamides déjà étudiés.

Région 4000–2000 cm^{-1}

Les spectres infrarouge des trois formes étudiées révèlent d'importantes modifications dans ce domaine. Les vibrations du groupement méthyle ne donnent lieu qu'à de faibles absorptions et ne seront pas discutées. En revanche, les vibrations $\nu(NH_2)$ et $\nu(NH)$ se traduisent par de fortes bandes infrarouge.

Les bandes 3475 et 3384 cm^{-1} de la forme I traduisent sans ambiguïté les modes antisymétrique et symétrique du groupement amine: ces valeurs sont en accord avec celles trouvées pour d'autres sulfamides (1, 10, 11, 12). Ces vibrations sont peu perturbées par les liaisons hydrogène dont les longueurs N—H. . .O (tableau 2) sont supérieures à 3,2 Å, ce qui confirme les conclusions de Novak et coll. (13), qui ont montré, qu'au delà d'une telle distance, l'influence de la liaison H sur la fréquence de vibration est peu importante. Dans la forme II, ces modes ν_{as} (NH_2) et ν_s (NH_2) apparaissent à des fréquences voisines de celles de la forme I, 3490 et 3400 cm^{-1}.

Si dans le solvate le mode ν_{as} (NH_2) est trouvé isolé à 3475 cm^{-1}, en revanche, le mode ν_s (NH_2) apparaît sous forme d'un doublet à 3400 et 3360 cm^{-1}: un tel dédoublement a été relié à la formation de dimères cycliques (14), comme cela a déjà été observé sur des barbituriques (15, 16) et le sulfaméthoxypyridazine (17). La détermination de la structure de ce solvate devrait nous permettre de confirmer cette hypothèse.

La fréquence ν (N—H) d'un groupement R—SO_2—NH—R′ est généralement attendue vers 3300 cm^{-1}: la raie 3305 cm^{-1} (forme I) correspond donc à cette vibration. Shiu Shiang Yang et Guillory (3) avaient attribué les raies 3300 et 3150 cm^{-1} à ce mouvement. Si l'attribution de la première fréquence nous paraît raisonnable, nous ne pensons pas que l'attribution de la seconde à ce même mode puisse être retenue; en effet, la raie 3145 cm^{-1} a été attribuée (17), dans des complexes d'aniline en particulier, au mode ν(N—H) engagé dans une liaison N—H. . .N. Or, la détermination de la structure montre qu'il n'existe pas de telle liaison dans la forme I. Nous proposons d'attribuer cette raie soit à une combinaison soit à une résonance de Fermi entre une vibration ν (CH) du noyau et l'harmonique de la raie 1592 cm^{-1}, ce qui justifierait son intensité. Sur les spectres du solvate, le mode ν(N—H) est abaissé à 3200 cm^{-1}, preuve que le vibrateur N—H est impliqué dans une liaison hydrogène.

La forme II, quant à elle, présente plusieurs bandes d'intensité moyenne entre 3300 et 2700 cm^{-1}, parmi lesquelles il est difficile de retrouver ce mode. L'étude structurale montre que dans ce polymorphe il existe une liaison N—H. . .N de longueur 2,952 Å, donc relativement forte pour une liaison de ce type (18); nous proposons d'attribuer la bande 3100 cm^{-1} au mode ν(N—H) engagé dans le pont hydrogène (18, 19).

Région 1700–200 cm^{-1}

Seules certaines vibrations caractéristiques seront discutées. Quelle que soit la forme, deux bandes intenses apparaissent vers 1600 et 1625 cm^{-1} la 1ère traduisant une vibration du noyau, la seconde le cisaillement δ (NH_2). La forme II présente en outre une bande supplémentaire à 1645 cm^{-1}, très intense, que nous proposons d'attribuer au mode δ(N—H) bien que cette fréquence soit élevée pour une telle vibration. À l'appui de cette attribution, signalons que Novak et coll. (13) ont montré que l'existence d'un pont hydrogène du type N—H. . .N abaisse la fréquence du mode ν(N—H) et déplace vers les hautes fréquences le mode δ(N—H) attendu vers 1400 cm^{-1}.

Les dernières fréquences que nous discuterons sont en rapport avec le groupement sulfone. Le mode antisymétrique ν_{as} (SO_2) apparaît très intense sur les spectres d'absorption, à 1365 cm^{-1} (forme I). La raie très fine 1383 cm^{-1} qui traduit une raie du noyau benzénique, est retrouvée à la même fréquence dans tous les composés. Cette vibration ν_{as}(SO_2) voit sa fréquence s'abaisser à 1335 cm^{-1} (forme II) et 1310 cm^{-1} (solvate). Ces abaissements de fréquence sont à mettre en relation avec l'existence des liaisons hydrogène. Cette influence se manifeste également au niveau du mode symétrique ν_s(SO_2), très intense en Raman, qui apparaît généralement sous forme d'un doublet (12). Dans la forme I, les spectres Raman et infrarouge révèlent à 1145–1160 (ir) et 1141–1156 (Raman) deux raies, d'égales intensités, attribuables à ce mode. En revanche, on observe une diminution très importante de la bande de plus basse fréquence (forme II) et un dédoublement de cette bande (solvate). Enfin, le cisaillement δ(SO_2) donne un doublet vers 545–572 cm^{-1} tant sur les spectres Raman qu'en infrarouge.

Conclusion

L'étude du sulfaméthoxazole nous a permis de mettre en évidence deux polymorphes et un solvate non répertorié dans la littérature.

Chaque forme a été identifiée et caractérisée par des méthodes thermiques et spectrales. L'analyse thermique différentielle nous a révélé l'existence du solvate qui a été caractérisé, comme les deux polymorphes, par son diagramme de rayons X et ses spectres infrarouge et Raman. La détermination de la structure cristalline de la forme II a été réalisée, ce qui nous a amené à la comparer à celle de la forme I déjà publiée. Cette comparaison révèle que les polymorphes I et II cristallisent dans le même système cristallin (monoclinique) et que l'empilement dans les mailles est très semblable. Les molécules I et II sont pratiquement identiques quant aux distances interatomiques et aux angles de valence, les différences les plus importantes se situant au niveau des liaisons hydrogène intermoléculaires.

L'existence de ces ponts hydrogène nous a conduit à réaliser une analyse, par spectrométrie d'absorption infrarouge et de diffusion Raman, des vibrations des groupements amine, amide et sulfone principalement intéressés par ces liaisons.

Nous proposons donc une attribution des modes caractéristiques de ces groupements en relation avec les longueurs des liaisons.

L'obtention de cristaux mesurables du solvate doit nous permettre de déterminer la structure de ce composé et d'effectuer une étude des cinétiques de dissolution des différentes formes.

1. J. RAMBAUD, L. MAURY, C. LEFEBVRE et R. ROQUES. Int. J. Pharm. **15**, 199 (1983).
2. J. RAMBAUD, R. ROQUES, S. ALBEROLA et F. SABON. Bul. Soc. Chim. Fr. **1**, 56 (1980).
3. SHIU SHIANG YANG et J. K. GUILLORY. J. Pharm. Sci. **61**, 26 (1972).
4. P. MAIN, S. J. FISKE, S. E. HULL, L. LESSINGER, G. GERMAIN, J. P. DECLERCQ et M. M. WOOLFSON. MULTAN 80. A system of computer programs for the automatic solution of crystal structures from X-ray diffraction data. Univs. of York, England, and Louvain-la-Neuve, Belgium. 1980.
5. G. M. SHELDRICK. SHELX 76. Program for crystal structure determination. Univ. of Cambridge, England. 1976.
6. A. BURGER et R. RAMBERGER. Mikrochim. Acta, II, 273 (1979).
7. J. RAMBAUD. Thèse Montpellier (1982).
8. G. J. KRUGER et G. GAFNER. Acta Crystallogr. Sect B, **27**, 326 (1971).
9. J. C. BELLOWS, P. C. FREEMAN et P. N. PRASAD. Drug. Dev. Ind. Pharm. **3**, 451 (1977).
10. A. BARBARA, B. A. BOLTON et P. N. PRASAD. J. Pharm. Sci. **70**, 789 (1981).
11. L. MAURY, J. RAMBAUD, B. PAUVERT, M. AUDRAN, Y. LASSERRE et G. BERGE. Pharm. Acta Helv. **59**, 112 (1984).
12. L. MAURY, J. RAMBAUD, B. PAUVERT, G. BERGE, M. AUDRAN et Y. LASSERRE. Pharm. Acta Helv. **60**, 22 (1985).
13. A. NOVAK, J. LASCOMBE et M. L. JOSIEN. J. Phys. (Paris), Colloq. **5**, 38 (1966).
14. J. BELLAMY. The infrared spectra of complex molecules. Chap-

man and Hall, London, England. 1975.
15. M. DRAGUET-BRUGHMANS, R. BOUCHE, J. P. FLANDRE et A. VAN DEN BULCKE. Pharm. Acta Helv. **54**, 140 (1979).
16. M. DRAGUET-BRUGHMANS, PH. DRAUX et R. BOUCHE. J. Pharm. Belg. **36**, 397 (1981).
17. C. ENGELTER et D. A. THORNTON. J. Mol. Struct. **33**, 119 (1976).
18. A. NOVAK. Struct. Bonding (Berlin), 18, 177 (1974).
19. A BERTOLUZZA, C. FAGNANO, P. FINELLI, M. A. MORELLI, R. SIMONI et R. TOSI. J. Raman Spectrosc. **14**, 386 (1983).
20. W. D. S. MOTHERWELL et W. CLEGG. Program for plotting molecular and crystal structures. Univ. of Cambridge, England. (1978).
21. L. MAURY, J. RAMBAUD, B. PAUVERT, Y. LASSERRE, G. BERGE et M. AUDRAN. J. Pharm. Sci. **74**, 422 (1985).

Syntheses and reactivity of square-planar Rh(I) complexes, LRh(CO) (L = unsymmetric tridentate chelating pyrazolylgallate ligand). X-ray crystal structures of $[Me_2Gapz(OCH_2CH_2NH_2)]Rh(CO)$ and $[Me_2Gapz(OCH_2CH_2NMe_2)]Rh(COMe)I$ (pz = pyrazolyl, $N_2C_3H_3$)

Brenda M. Louie, Steven J. Rettig, Alan Storr, and James Trotter

Department of Chemistry, University of British Columbia, 2036 Main Mall, Vancouver, B.C., Canada V6T 1Y6

Received January 14, 1985

Brenda M. Louie, Steven J. Rettig, Alan Storr, and James Trotter. Can. J. Chem. **63**, 3019 (1985).

The syntheses and characterization of a number of square-planar Rh(I) monocarbonyl complexes incorporating unsymmetrical, tridentate, pyrazolylgallate ligands in a meridional coordination mode are described. Oxidative addition reactions of these complexes are detailed and a facile migratory insertion reaction, following the addition of methyl iodide, has resulted in a five-coordinate square-pyramidal Rh(III) acetyl complex. Crystal structures of two compounds are presented, $[Me_2Gapz(OCH_2CH_2NH_2)]Rh(CO)$ and $[Me_2Gapz(OCH_2CH_2NMe_2)]Rh(COMe)I$, and confirm the molecular arrangements predicted on the basis of other physical measurements. Crystals of the former are monoclinic, a = 10.212(2), b = 7.8484(5), c = 16.733(2) Å, β = 105.133(6)°, z = 4, space group $P2_1/c$; and those of the latter are monoclinic, a = 10.0960(11), b = 11.5352(8), c = 15.871(2) Å, β = 105.764(6)°, z = 4, space group $P2_1/n$. Both structures were solved by conventional heavy atom methods and were refined by full-matrix least-square procedures to R = 0.026 and 0.036, respectively, for 2142 and 2941 reflections with $I \geq 3\sigma(I)$.

Brenda M. Louie, Steven J. Rettig, Alan Storr et James Trotter. Can. J. Chem. **63**, 3019 (1985).

On décrit la synthèse et la charactérisation de nombreux complexes carré-plans de Rh(I) monocarbonyle incorporant des ligands, tridentates, pyrazolylgallate dans un mode de coordination méridionale. On décrit des réactions d'addition oxydante de ces complexes et une réaction d'insertion migratoire facile suivie de l'addition de l'iodure de méthyle qui conduit à la formation d'un complexe acétylé de Rh(III) pentacoordonné et pyramidal carré. On présente les structures de ces deux composés: $[Me_2Gapz(OCH_2CH_2NH_2)]Rh(CO)$ et $[Me_2Gapz(OCH_2CH_2NMe_2)]Rh(COMe)I$, et on confirme les arrangements moléculaires prévues à partir d'autres mesures physiques. Les cristaux du premier composé appartiennent au groupe d'espace monoclinique $P2_1/c$ avec a = 10,212(2), b = 7,8484(5), c = 16,733(2) Å, β = 105,133(6)°, z = 4. Les cristaux du deuxième composé appartiennent au groupe d'espace monoclinique $P2_1/n$ avec a = 10,0960(11), b = 11,5352(8), c = 15,871(2) Å, β = 105,764(6)°, z = 4. On a résolu les deux structures par la méthode conventionnelle de l'atome lourd et on les a affinées par la méthode des moindres carrés jusqu'à des valeurs de R = 0,026 et de 0,036 respectivement pour 2142 et 2941 réflexions avec $I \geq 3\sigma(I)$.

[Traduit par le journal]

Introduction

Recently we reported the syntheses, properties, and structures of a number of Rh(I) complexes containing symmetrical bidentate pyrazolylgallate ligands (1). The novel compound, $(MeGapz_3)_2Rh_2(\mu\text{-}CO)_3$, incorporating symmetrical tridentate pyrazolylgallate ligands has also been described (2). The present paper details the synthesis of a number of square-planar Rh(I) monocarbonyl complexes, LRh(CO), containing unsymmetrical tridentate pyrazolylgallate ligands of the general formula:

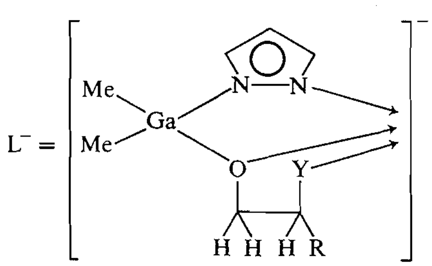

1

where R = H, Y = NH_2, NMe_2, SPh or SMe; R = Me, Y = NH_2

The reactivity of selected LRh(CO) complexes towards MeI, CO, and other small molecules is described and the crystal structures of LRh(CO) (R = H and Y = NH_2) and LRh(COMe)I (R = H and Y = NMe_2) are presented.

Experimental

Starting materials

Air-sensitive materials were handled in a nitrogen atmosphere. Tetrahydrofuran (THF), benzene, CH_2Cl_2, and hexane were dried by refluxing over Na/benzophenone, potassium, CaH_2, and $CaSO_4$, respectively, followed by distillation. $[Rh(CO)_2Cl]_2$ (Strem Chemicals) was used as supplied or alternatively prepared from $RhCl_3 \cdot 3H_2O$ following a literature method (3). MeI was distilled from P_2O_5 before use and stored over a few mercury droplets. Dihalogens (Fisher Scientific) were used as supplied. Sodium salts of the unsymmetrical tridentate pyrazolylgallate ligands were prepared as standard THF solutions as described earlier (4).

Synthesis of LRh(CO)

The following general method was used to prepare the LRh(CO) complexes listed in Table 1. Two molar equivalents of Na^+L^- were added dropwise to ~100 mg of $[Rh(CO)_2Cl]_2$ dissolved in ~75 mL THF. The resulting mixture was refluxed until ir sampling indicated complete disappearance of the starting rhodium carbonyl dimer (~3 h). The THF was removed *in vacuo* from the cooled reaction solution and the remaining residue was redissolved in ~5 mL CH_2Cl_2 and filtered. Hexane (~5 mL) was then added to the filtrate and the solvents were allowed to slowly evaporate leaving lemon yellow or yellow green powders or crystals of the desired products in approximately 50–80% yield. Elemental analyses, ^1H nmr, and ir data for the LRh(CO) complexes are collected in Table 1.

Reactions of selected LRh(CO) complexes

(a) With MeI

A slight excess of MeI (0.02 g, 0.32 mmol) was added to $[Me_2Gapz(OCH_2CH_2NMe_2)]Rh(CO)$ (0.076 g, 0.20 mmol) dissolved

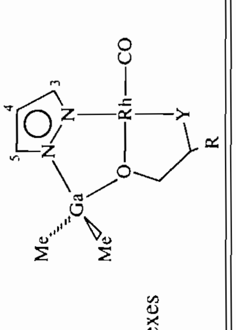

TABLE 1. Physical data for the complexes

Y	R	mp (°C)	Calcd./found C	H	N	ν_{CO} (cm^{-1}) (solvent)	^{1}H nmr in C_6D_6 ($\tau_{C_6H_6} \equiv 2.84$ ppm)† GaMe$_2$	H^3	H^4	H^5	Y	O—CH_2—	—CH_2—Y
NH_2	H	143–145d	26.85 27.05	4.22 4.22	11.74 11.55	1955 (CH_2Cl_2)	9.97s	2.39d	3.93t	2.63d	8.71m	7.03t	8.31m
NMe_2	H	101–102	31.12 31.27	4.96 5.00	10.89 11.05	1957 (hexane)	9.96s	2.44d	3.94t	2.74d	7.92s	6.74t	8.22t
SPh	H	61–62.5	37.29 37.53	4.02 4.07	6.21 6.31	1984 (hexane)	10.02s	2.26d	3.87t	2.71d	3.12m 2.14m	6.89m	7.71m
SMe	H	59–60	27.79 26.74*	4.15 3.77	7.20 7.20	1982 (hexane)	10.01s	2.31d	3.89t	2.74d	8.46m	6.84m	7.96m
NH_2	Me	97–98	29.07 29.26	4.61 4.69	11.30 11.33	1955 (CH_2Cl_2)	9.96s 9.98s	2.38d	3.92t	2.72d		7.10m	9.80d‡

* Satisfactory C analysis could not be obtained.
† s = singlet, d = doublet, t = triplet, m = multiplet; $J_{HCCH} \simeq 2$ Hz for pyrazolyl protons.
‡ R = Me.

in ~15 mL CH_2Cl_2. After stirring for 15 min the initially yellow solution gradually changed to deep orange. An ir of the solution at this stage contained two new bands at 2063 and 1720 cm^{-1}. The solvent was then removed *in vacuo* leaving an orange powder of a single product in quantitative yield. Mp 109–111°C. *Anal.* calcd. for [$Me_2Gapz(OCH_2CH_2NMe_2)$]Rh(COMe)I: C 25.03, H 4.20, N 7.96; found: C 25.75, H 4.22, N 8.23, ν_{CO}: 1720 cm^{-1} (CH_2Cl_2), 1725 cm^{-1} (hexane). ^{1}H nmr (C_6D_6, τ values refer to $\tau_{C_6H_6}$ = 2.84 ppm): —$GaMe_2$, 10.09s, 10.10s; —NMe_2, 7.50s, 8.07s; CO—Me, 7.42s; pz—H^4, 3.91t; pz—H^5, 2.80d; pz—H^3, 0.97d (J_{HCCH} = ~2 Hz for pz protons). A sample of the product was recrystallized from CH_2Cl_2 at −78°C yielding orange crystals suitable for an X-ray crystal structure determination (see below).

(b) With CO

[$Me_2Gapz(OCH_2CH_2NH_2)$]Rh(CO) (0.020 g, 0.056 mmol, ν_{CO}: 1955 cm^{-1} (CH_2Cl_2)) was dissolved in ~10 mL CH_2Cl_2 and CO was bubbled through the solution. After 5 min an ir sample indicated the presence of two new bands at 2093 and 2028 cm^{-1} (CH_2Cl_2), attributed to [$Me_2Gapz(OCH_2CH_2NH_2)$]Rh$(CO)_2$, and complete loss of the band at 1955 cm^{-1}. Attempts to isolate this dicarbonyl species by reducing the solvent and/or crystallization were not successful. The black solids recovered contained mixtures of [$Me_2Gapz(OCH_2CH_2NH_2)$]Rh$(CO)_n$ (n = 1 and 2). The ^{1}H nmr spectrum of the n = 2 species was obtained by bubbling CO through a C_6D_6 solution of [$Me_2Gapz(OCH_2CH_2NH_2)$]Rh(CO) in an nmr tube fitted with a septum cap. ^{1}H nmr (C_6D_6, τ values refer to $\tau_{C_6H_6}$ = 2.84 ppm): —$GaMe_2$, 9.77s, 10.14s; O$CH_2$$CH_2$$NH_2$, 8.5m; $OCH_2$$CH_2$$NH_2$, 6.6m; pz—H^4, 4.02t; pz—H^5, 2.72d; pz—H^3, 2.69d (J_{HCCH} = ~2 Hz for pz protons).

(c) With PPh_3

Reaction of [$Me_2Gapz(OCH_2CH_2Y)$]Rh(CO) (Y = NMe_2 or NH_2) with 1 molar equivalent of PPh_3 in THF at −78, 0°C, and reflux temperatures resulted only in the formation of the known pyrazolyl bridged Rh dimers (1) viz.

$$[Me_2Gapz(OCH_2CH_2Y)]Rh(CO) + PPh_3 \xrightarrow{THF} \tfrac{1}{2}\,[(\mu\text{-pz})Rh(CO)(PPh_3)]_2 + \tfrac{1}{2}\,[Me_2Ga(OCH_2CH_2Y)]_2$$

The volatile gallium dimers also formed in this reaction have been previously characterized (5).

(d) With dihalogens, X_2 (X_2 = Br_2 or I_2)

A slight excess of the dihalogen dissolved in THF was added dropwise to ~50 mg of LRh(CO) (R = H, Y = NH_2 or NMe_2 in **1**) prepared *in situ* in THF as described above. In all cases addition of the oxidant caused an immediate colour change in the solution and a change in the ν_{CO} region of the ir spectrum. The ν_{CO} band attributable to the LRh(CO) starting material was completely gone after a few hours stirring at room temperature, being replaced by a single ν_{CO} band (CH_2Cl_2 solution) at 2081 cm^{-1} (Y = NH_2, X_2 = I_2), 2088 cm^{-1} (Y = NMe_2, X_2 = I_2), and 2100 cm^{-1} (Y = NMe_2, X_2 = Br_2). Although these spectra of the products suggested the presence of LRh(CO)X_2 species in solution, isolation of analytically pure compounds proved impossible.

(e) With H_2

The LRh(CO) complexes were recovered unchanged when dissolved in C_6H_6 or THF and exposed to an atmosphere of H_2 for 48 h. Furthermore no reaction was observed when H_2 was bubbled through a refluxing THF solution of [$Me_2Gapz(OCH_2CH_2NH_2)$]Rh(CO) for 28 h. In addition the LRh(CO) complexes did not catalyze the hydrogenation of 1-hexene in benzene at 30°C.

X-ray crystallographic analyses

*[Dimethyl(1-pyrazolyl)(2-aminoethoxy)gallato-*N,N,O*]carbonylrhodium(I)*

A crystal bounded by the six faces (followed by their distances in mm from a common origin): ±(1 0 0), 0.063, ±(0 0 1), 0.113, ±(0 2 −1), 0.295 was mounted in a general orientation. Unit-cell parameters were refined by least-squares on 2 sin θ/λ values for 25 reflections ($2\theta = 35-42°$) measured on a diffractometer with Mo-$K\alpha$ radiation ($\lambda(K\alpha_1) = 0.70930$, $\lambda(K\alpha_2) = 0.71359$ Å). Crystal data at 22°C are:

$C_8H_{15}GaN_3O_2Rh$ fw = 357.85

Monoclinic, $a = 10.212(2)$, $b = 7.8484(5)$, $c = 16.733(2)$ Å, $\beta = 105.133(6)°$, $V = 1294.6(3)$ Å^3, $Z = 4$, $\rho_c = 1.836$ Mg m^{-3}, $F(000) = 704$, μ(Mo-$K\alpha$) = 33.2 cm^{-1}. Absent reflections: $h0l$, l odd, and $0k0$, k odd, uniquely indicate the space group $P2_1/c$ (C^5_{2h}, No. 14).

Intensities were measured with graphite-monochromated Mo-$K\alpha$ radiation on an Enraf-Nonius CAD4-F diffractometer. An $\omega-2\theta$ scan at 0.91–10.06° min^{-1} over a range of ($0.60 + 0.35 \tan\theta$) degrees in ω (extended by 25% on both sides for background measurement) was employed. Data were measured to $2\theta = 55°$. The intensities of three check reflections, measured every 3600 s throughout the data collection, remained constant to within 3%. After data reduction,[1] an absorption correction was applied using the analytical method (6, 7). Transmission factors ranged from 0.449 to 0.667. Of the 2967 independent reflections measured, 2142 (72.2%) had intensities greater than or equal to $3\sigma(I)$ above background where $\sigma^2(I) = S + 2B + (0.04\,(S - B))^2$ with S = scan count and B = normalized background count.

The structure was solved by conventional heavy atom methods, the coordinates of the Rh and Ga atoms being determined from the Patterson function and those of the remaining non-hydrogen atoms from a subsequent difference map. After full-matrix least-squares refinement of the non-hydrogen atoms with anisotropic thermal parameters to $R = 0.037$, a difference map gave the positions of all 15 hydrogen atoms. Hydrogen parameters were idealized (N—H = 0.94, C(sp^3)—H = 0.98, C(sp^2)—H = 0.97 Å, methyl positions based on observed peaks) and included in the refinement as fixed contributors. The scattering factors of ref. 8 were used for non-hydrogen atoms and those of ref. 9 for hydrogen atoms. Anomalous scattering factors from ref. 10 were used for the Rh and Ga atoms. The weighting scheme $w = 1/\sigma^2(F)$, where $\sigma^2(F)$ is derived from the previously defined $\sigma^2(I)$, gave uniform average values of $w(|F_o| - |F_c|)^2$ over ranges of both $|F_o|$ and $\sin\theta/\lambda$ and was employed in the final stages of full-matrix refinement of 137 variables. Reflections with $I < 3\sigma(I)$ were not included in the refinement. An isotropic Type I extinction correction (Thornley–Nelmes definition of mosaic anisotropy with a Lorentzian distribution) was applied (11–13). The final value of g was $1.35(21) \times 10^4$. Convergence was reached at $R = 0.026$ and $R_w = 0.032$ for 2142 reflections with $I \geq 3\sigma(I)$. For all 2967 reflections $R = 0.055$. The function minimized was $\Sigma w(|F_o| - |F_c|)^2$, $R = \Sigma||F_o| - |F_c||/\Sigma|F_o|$ and $R_w = (\Sigma w(|F_o| - |F_c|)^2/\Sigma w|F_o|^2)^{1/2}$.

On the final cycle of refinement the mean and maximum parameter shifts corresponded to 0.02 and 0.18σ, respectively. The mean error in an observation of unit weight was 1.486. A final difference map showed maximum fluctuations of −0.55 to +0.73 e Å^{-3}, 0.6 and 0.9 Å from Rh, respectively, and was essentially featureless away from the heavy atoms. The final positional and thermal parameters appear in Tables 2 and 7,[2] respectively. Measured and calculated structure factors have been placed in the Depository of Unpublished Data.[2]

*Acetyl(iodo)[dimethyl(1-pyrazolyl)(2-*N,N*-dimethylaminoethoxy)-gallato-*N,N,O*]rhodium(III)*

Experimental details are as above except where noted. The bounding planes of the crystal were: ±(1 0 −1), 0.050, ±(1 0 2), 0.107, ±(1 1 0), 0.263 mm (from a common origin). Reflections employed in the refinement of unit-cell parameters had $2\theta = 35-40°$. Crystal data are

$C_{11}H_{22}GaIN_3O_2RH$ fw = 527.84

Monoclinic, $a = 10.0960(11)$, $b = 11.5352(8)$, $c = 15.871(2)$ Å, $\beta = 105.764(6)°$, $V = 1778.8(3)$ Å^3, $Z = 4$, $\rho_c = 1.971$ Mg m^{-3}, $F(000) = 1016$, μ(Mo-$K\alpha$) = 41.4 cm^{-1}. Absent reflections: $h0l$, $h + l$ odd, and $0k0$, k odd, uniquely indicate the space group $P2_1/n$ (non-standard setting of $P2_1/c$ with equivalent positions: $\pm(x, y, z; 1/2 - x, 1/2 + y, 1/2 - z)$ chosen to give β nearer to 90°).

An $\omega-2\theta$ scan at 0.96–10.06° min^{-1} over a range of ($0.65 + 0.35 \tan\theta$)° in ω was employed. Of 5169 independent reflections measured (to $2\theta = 60°$), 2941 had intensities greater than $3\sigma(I)$ above background. The intensities of the standard reflections remained constant to within 3%. Data were corrected for absorption, transmission factors ranging from 0.410 to 0.680.

The I, Rh, and Ga coordinates were determined from the Patterson function and those of the remaining non-hydrogen atoms from a subsequent difference map. Refinement of the non-hydrogen atoms with anisotropic thermal parameters reduced R to 0.042. In the final stages of refinement the hydrogen atoms were included as fixed contributors in idealized positions. Convergence was reached at $R = 0.036$ and $R_w = 0.040$ for 2941 reflections and 172 variables, for all 5169 reflections $R = 0.084$. The mean and maximum parameter shifts on the final

TABLE 2. Final positional (fractional × 10^4; I, Rh, and Ga × 10^5) and isotropic thermal parameters ($U \times 10^3$ Å^2) with estimated standard deviations in parentheses

Atom	x	y	z	U_{iso}*
		[$Me_2Gapz(OCH_2CH_2NH_2)$]Rh(CO)		
Rh	40544(3)	41269(4)	28839(2)	45
Ga	22521(5)	44290(6)	9075(3)	51
O(1)	4030(3)	4621(3)	1672(2)	47
O(2)	4198(6)	3164(8)	4596(3)	151
N(1)	2109(3)	4989(4)	2611(2)	50
N(2)	1463(3)	5297(4)	1800(2)	54
N(3)	6043(3)	3466(4)	2950(2)	58
C(1)	4125(6)	3594(7)	3926(3)	80
C(2)	2091(6)	6206(7)	58(3)	78
C(3)	1819(5)	2002(6)	712(3)	72
C(4)	5208(5)	3959(5)	1475(3)	60
C(5)	6394(4)	4215(5)	2217(3)	61
C(6)	1317(5)	5636(6)	3068(3)	64
C(7)	191(5)	6373(7)	2562(4)	79
C(8)	310(5)	6152(6)	1786(3)	69
		[$Me_2Gapz(OCH_2CH_2NMe_2)$]Rh(COMe)I		
I	56097(4)	20424(3)	41517(3)	71
Rh	31035(3)	27697(3)	33831(2)	39
Ga	−3446(6)	29971(5)	31724(4)	60
O(1)	1175(3)	3152(4)	2677(2)	70
O(2)	3338(4)	5115(3)	3677(2)	83
N(1)	2238(4)	1915(3)	4221(2)	45
N(2)	866(4)	2070(3)	4141(3)	54
N(3)	3612(4)	3424(3)	2268(2)	53
C(1)	3319(4)	4216(4)	4048(3)	53
C(2)	−1734(5)	2004(5)	2422(4)	76
C(3)	−703(8)	4483(6)	3647(5)	108
C(4)	1083(6)	3483(6)	1800(3)	79
C(5)	2372(6)	4098(5)	1784(3)	72
C(6)	2736(5)	1222(4)	4918(3)	59
C(7)	1713(7)	924(5)	5287(3)	76
C(8)	575(6)	1467(6)	4786(4)	75
C(9)	4846(6)	4178(6)	2370(4)	81
C(10)	3798(7)	2392(5)	1753(3)	78
C(11)	3384(6)	4152(5)	5002(3)	72

* U_{iso} = average of the three principal axes.

[1] The computer programs used include locally written programs for data processing and locally modified versions of the following: ORFLS, full-matrix least-squares, and ORFFE, function and errors, by W. R. Busing, K. O. Martin and H. A. Levy; FORDAP, Patterson and Fourier syntheses, by A. Zalkin; ORTEP II, illustrations, by C. K. Johnson.

[2] The structure factor table, Table 7 (anisotropic thermal parameters), and other material mentioned in the text may be purchased from the Depository of Unpublished Data, CISTI, National Research Council of Canada, Ottawa, Canada K1A 0S2.

TABLE 3. Bond lengths (Å) with estimated standard deviations in parentheses

Bond	Length (Å)	Bond	Length (Å)
	$[Me_2Gapz(OCH_2CH_2NH_2)]Rh(CO)$		
Rh —O(1)	2.058(2)	O(2)—C(1)	1.154(6)
Rh —N(1)	2.035(3)	N(1)—N(2)	1.366(5)
Rh —N(3)	2.070(3)	N(1)—C(6)	1.349(5)
Rh —C(1)	1.776(5)	N(2)—C(8)	1.351(6)
Ga —O(1)	1.934(3)	N(3)—C(5)	1.485(6)
Ga —N(2)	1.993(3)	C(4)—C(5)	1.504(7)
Ga —C(2)	1.967(5)	C(6)—C(7)	1.365(8)
Ga —C(3)	1.963(5)	C(7)—C(8)	1.347(7)
O(1)—C(4)	1.426(5)		
	$[Me_2Gapz(OCH_2CH_2NMe_2)]Rh(COMe)I$		
I —Rh	2.6300(5)	N(1)—N(2)	1.368(5)
Rh —O(1)	2.014(3)	N(1)—C(6)	1.346(5)
Rh —N(1)	2.033(4)	N(2)—C(8)	1.335(6)
Rh —N(3)	2.111(3)	N(3)—C(5)	1.496(7)
Rh —C(1)	1.955(5)	N(3)—C(9)	1.492(6)
Ga —O(1)	1.913(3)	N(3)—C(10)	1.484(7)
Ga —N(2)	1.994(4)	C(1)—C(11)	1.499(7)
Ga —C(2)	1.947(6)	C(4)—C(5)	1.489(8)
Ga —C(3)	1.946(6)	C(6)—C(7)	1.363(7)
O(1)—C(4)	1.422(6)	C(7)—C(8)	1.360(8)
O(2)—C(1)	1.195(6)		

cycle of refinement corresponded to 0.01 and 0.08σ and the mean error in an observation of unit weight was 1.577. Anomalous scattering corrections were applied for I, Rh, and Ga atoms. A final difference map showed maximum fluctuations of -3.9 to $+1.4$ e Å^{-3} within 1.0 Å of I and was featureless away from the heavy atoms.

Bond lengths, bond angles, and intra-annular torsion angles for the two compounds appear in Tables 3–5, respectively. Calculated hydrogen coordinates and isotropic thermal parameters (Table 6) and complete listings of torsion angles (Table 8) are also included as deposited material.[2]

Physical measurements

Infrared spectra were recorded on a Perkin Elmer 598 spectrometer. ^{1}H nmr spectra were obtained on a Bruker WP 80 instrument using FT techniques. Mass spectra were recorded on either a Varian MAT CH4B or AES MS 50 spectrometer operating at 70 eV. Melting points were measured on a Gallenkamp apparatus in sealed capillary tubes and are uncorrected. Elemental analyses were performed by Mr. P. Borda of the U.B.C. Microanalytical Laboratory.

Results and discussion

Numerous carbonyl compounds incorporating tridentate pyrazolylgallate ligands of the type **1** have been reported for Cr, Mo, W, Mn, and Re (4, 14–18). In each of these complexes the pyrazolylgallate anions were found to coordinate exclusively in a *fac* mode, even though the chelating ligands are capable of meridional coordination. For example both the *fac* and *mer* isomers have been structurally characterized for the coordination compound $[Me_2Gapz(OCH_2CH_2NH_2)]_2Ni$ (19) and a meridional arrangement is observed in the novel five-coordinate iron dinitrosyl complex $[Me_2Gapz''(OCH_2CH_2NMe_2)]Fe(NO)_2$ (pz″ = 3,5-dimethylpyrazolyl, $N_2C_5H_7$) (20).

In previous publications we have often made comparisons between related transition metal complexes incorporating tridentate pyrazolylgallate, trispyrazolylborate, or cyclopentadienyl type ligands (e.g. ref. 21). Several directly analogous compounds have been prepared containing these ligands — not surprisingly since all three types of ligands are uninegative,

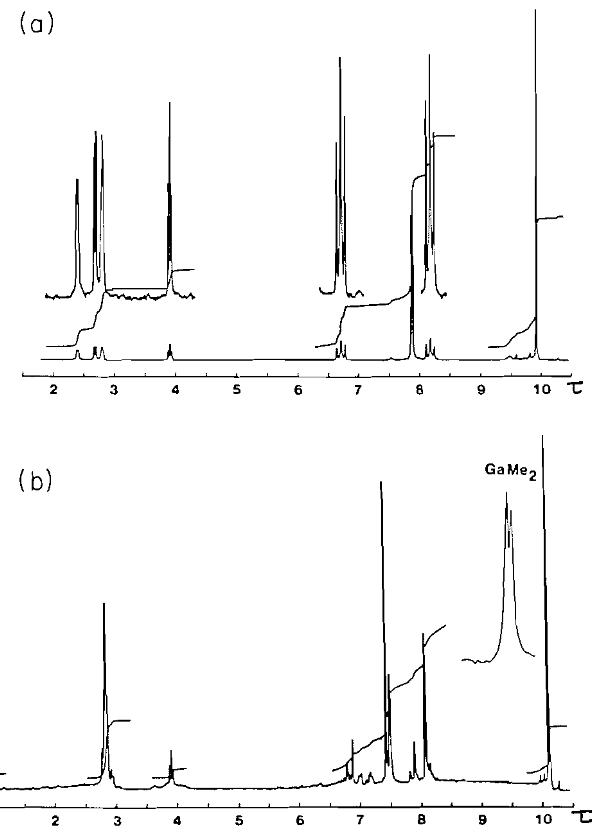

FIG. 1. Room temperature 80 MHz ^{1}H nmr spectra of (*a*) $[Me_2Gapz(OCH_2CH_2NMe_2)]Rh(CO)$ in C_6D_6; (*b*) $[Me_2Gapz(OCH_2CH_2NMe_2)]Rh(COMe)I$ in C_6D_6.

"tridentate", six-electron donors. However, the capability of the present unsymmetric pyrazolylgallate ligands to coordinate meridionally leads to markedly different behaviour when these anions are reacted with $[Rh(CO)_2Cl]_2$. For example, the preparation of $(\eta^5\text{-}C_5H_5)Rh(CO)_2$ from $[Rh(CO)_2Cl]_2$ and $Na^+(C_5H_5)^-$ has been known for some time (22). Similarly $[HB(pz'')_3]Rh(CO)_2$ can be prepared as stable yellow crystals in high yield (23, 24), although it is interesting that the ligands $MeGapz_3^-$ and $HBpz_3^-$ lead to the dinuclear rhodium species $(MeGapz_3)_2Rh_2(\mu\text{-}CO)_3$ (2) and $(HBpz_3)_2Rh_2(\mu\text{-}CO)_3$ (25). Our attempts to synthesize the analogous dicarbonyl rhodium species incorporating the "L" ligands **1** resulted instead in the isolation of stable, square-planar, 16-electron monocarbonyl complexes. The meridional configuration of the pyrazolylgallate ligand was clearly established by the presence of two triplets in the ^{1}H nmr spectrum for the O*CH*$_2$*CH*$_2$NMe$_2$ protons ($J \sim 5.5$ Hz) in the complex LRh(CO) (where R = H, Y = NMe_2) (see Fig. 1(*a*)). In addition the singlets observed for the NMe_2 and $GaMe_2$ groupings in this complex further substantiate this *mer* configuration of the "L" ligand. The remaining LRh(CO) complexes in Table 1 also display $GaMe_2$ singlets suggesting a similar planar Rh(I) species in all cases.

The mass spectra obtained for each of the LRh(CO) compounds displayed prominent signals due to the monomeric parent ion, P^+. In each case the highest intensity signals in the spectra were attributable to the $P - Me^+$ ion, with prominent signals due to the $P - CO^+$ and $P - Me - CO^+$ ions being observed.

Confirmation of a square-planar Rh(I) environment in the complex $[Me_2Gapz(OCH_2CH_2NH_2)]Rh(CO)$ has been established by an X-ray structure determination. The molecular ar-

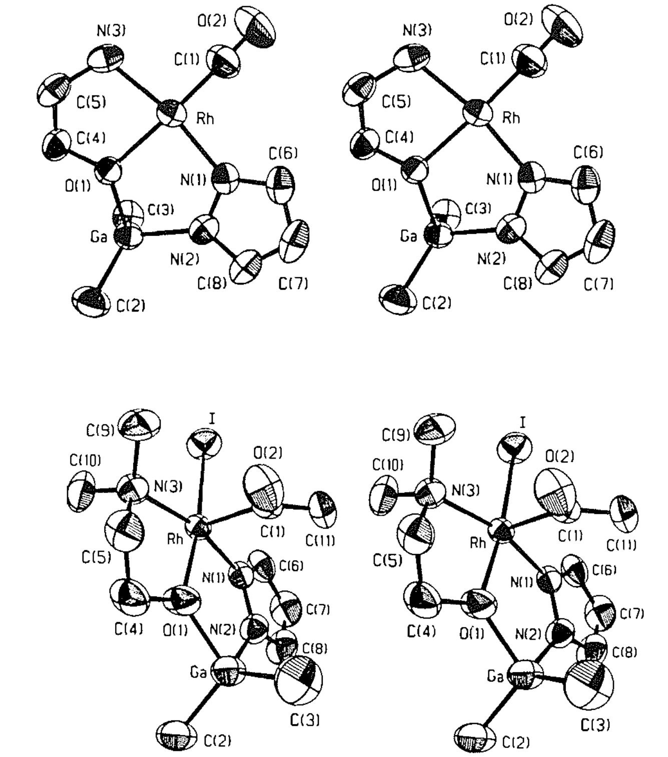

FIG. 2. Stereoscopic views of (*a*) $[Me_2Gapz(OCH_2CH_2NH_2)]$-Rh(CO) and (*b*) $[Me_2Gapz(OCH_2CH_2NMe_2)]$Rh(COMe)I. 50% probability thermal ellipsoids are shown. Hydrogen atoms have been omitted for clarity.

rangement is shown in Fig. 2(*a*). As expected the pyrazolylgallate ligand is meridionally disposed about the Rh(I) centre, with the CO ligand occupying the fourth coordination site in the square planar complex. The coordination group (RhN_2OC) is significantly non-planar (χ^2 = 541) although all five atoms lie within 0.055(6) Å of the mean plane. Bond distances involving Rh are Rh—O = 2.058(2), Rh—N(pz) = 2.035(3), Rh—N(amino) = 2.070(3), and Rh—CO = 1.776(5) Å. The carbonyl group is nearly linear, Rh—C—O = 176.8(2)°.

The pyrazolyl ring is planar to within experimental error (χ^2 = 6.5, maximum deviation from the mean plane = 0.006(5) Å) while the two five-membered chelate rings are both significantly non-planar, having irregular "puckered" conformations (see Table 5 for torsion angles). In the solid state molecules are linked by intermolecular N—H···O hydrogen bonds (N(3)—H(Nb)···O(1) ($1 - x$, $y - 1/2$, $1/2 - z$); H···O = 2.20, N···O = 3.088(4) Å, N—H···O = 158°) to form continuous spirals about the twofold screw axes along *b*. All other intermolecular distances correspond to normal van der Waals interactions.

The reaction between $[Me_2Gapz(OCH_2CH_2NMe_2)]$Rh(CO) and MeI in CH_2Cl_2 initially yielded solution ir evidence for a six-coordinate oxidative addition product. Thus the ν_{CO} band of the starting monocarbonyl species at 1958 cm^{-1} was replaced by two bands on addition of MeI at 2063 and 1720 cm^{-1}, the latter gaining in intensity with time. Attempts to isolate the species responsible for the 2063 cm^{-1} band resulted instead in crystals of a new Rh(III) compound containing a terminal acetyl group. Thus migratory insertion, as shown below, takes place readily at room temperature:

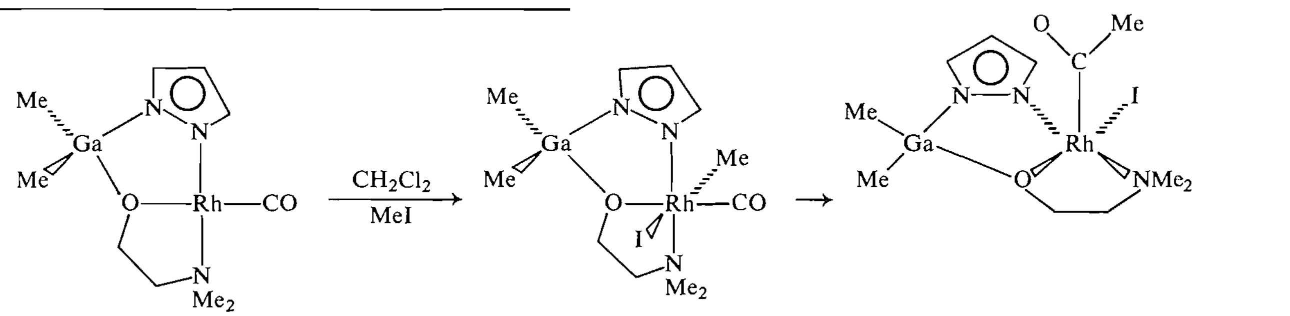

ν_{CO}: 1958 cm^{-1} (CH_2Cl_2) ν_{CO}: 2063 cm^{-1} (CH_2Cl_2) ν_{CO}: 1720 cm^{-1} (CH_2Cl_2)

The carbonyl stretching frequency for the proposed intermediate is similar to that reported for a related complex, (η^5-C_5Me_5)Ir(CO)(Me)I (ν_{CO}: 2002 cm^{-1} (CH_2Cl_2)) (26). Methyl migration does not take place with this stable Ir(III) compound, possibly due to the greater stability of Ir—C bonds compared to analogous Rh—C bonds. Interestingly related rhodium complexes containing σ-bonded methyl groups have not been observed during the reaction of MeI with cyclopentadienyl rhodium carbonyls. For example, the reaction of MeI with (η^5-C_5Me_5)$Rh(CO)_2$ proceeds directly to the (η^5-C_5Me_5)Rh(CO)(COMe)I complex at 50°C (27).

In addition to the diagnostic ν_{CO} band at 2063 cm^{-1} supportive evidence for the intermediate six-coordinate Rh(III) species emanates from the ^{1}H nmr spectra run on samples soon after the introduction of MeI to $[Me_2Gapz(OCH_2CH_2NMe_2)]$-Rh(CO) dissolved in C_6D_6. These show, in addition to peaks assignable to the five-coordinate product, patterns expected for the proposed intermediate, including a broad Rh—Me resonance at ~9 τ. With time these peaks due to the intermediate gradually disappear to leave a clean spectrum of the five-coordinate Rh(III) acetyl derivative.

The mass spectrum of $[Me_2Gapz(OCH_2CH_2NMe_2)]$Rh-(COMe)I indirectly supports the presence of an acetyl ligand. Signals corresponding to the ions P^+, $P - Me^+$, $P - Me - I^+$, and $P - 2Me - I^+$ ions are observed in the spectrum, but no evidence for the presence of the $P - Me - CO^+$ or $P - CO^+$ ions was obtained. Signals arising from these latter two ions are generally observed in the mass spectra of pyrazolylgallate transition metal complexes containing terminal carbonyl groups.

The absence of two well-defined triplets attributable to the methylene protons in the ^{1}H nmr spectrum of $[Me_2Gapz$-$(OCH_2CH_2NMe_2)]$Rh(COMe)I (Fig. 1(*b*)) is expected since

TABLE 4. Bond angles (deg) with estimated standard deviations in parentheses

Bonds	Angle (deg)	Bonds	Angle (deg)
	$[Me_2Gapz(OCH_2CH_2NH_2)]Rh(CO)$		
O(1)—Rh —N(1)	87.48(11)	Ga —O(1)—C(4)	121.4(2)
O(1)—Rh —N(3)	81.91(12)	Rh —N(1)—N(2)	118.1(2)
O(1)—Rh —C(1)	176.8(2)	Rh —N(1)—C(6)	133.8(3)
N(1)—Rh —N(3)	169.04(13)	N(2)—N(1)—C(6)	106.9(4)
N(1)—Rh —C(1)	94.9(2)	Ga —N(2)—N(1)	119.9(2)
N(3)—Rh —C(1)	95.8(2)	Ga —N(2)—C(8)	132.7(3)
O(1)—Ga —N(2)	88.32(12)	N(1)—N(2)—C(8)	107.4(3)
O(1)—Ga —C(2)	108.0(2)	Rh —N(3)—C(5)	107.6(2)
O(1)—Ga —C(3)	108.5(2)	Rh —C(1)—O(2)	176.4(6)
N(2)—Ga —C(2)	109.0(2)	O(1)—C(4)—C(5)	107.9(3)
N(2)—Ga —C(3)	109.8(2)	N(3)—C(5)—C(4)	108.2(4)
C(2)—Ga —C(3)	126.5(2)	N(1)—C(6)—C(7)	109.9(4)
Rh —O(1)—Ga	113.89(13)	C(6)—C(7)—C(8)	105.7(4)
Rh —O(1)—C(4)	111.4(2)	N(2)—C(8)—C(7)	110.1(4)
	$[Me_2Gapz(OCH_2CH_2NMe_2)]Rh(COMe)I$		
I —Rh —O(1)	172.23(12)	Rh —N(1)—C(6)	134.0(3)
I —Rh —N(1)	94.13(11)	N(2)—N(1)—C(6)	107.3(4)
I —Rh —N(3)	94.60(11)	Ga —N(2)—N(1)	122.4(3)
I —Rh —C(1)	94.00(13)	Ga —N(2)—C(8)	130.8(4)
O(1)—Rh —N(1)	87.01(14)	N(1)—N(2)—C(8)	106.8(4)
O(1)—Rh —N(3)	82.76(14)	Rh —N(3)—C(5)	104.8(3)
O(1)—Rh —C(1)	93.6(2)	Rh —N(3)—C(9)	120.3(3)
N(1)—Rh —N(3)	165.21(14)	Rh —N(3)—C(10)	105.7(3)
N(1)—Rh —C(1)	93.8(2)	C(5)—N(3)—C(9)	108.0(4)
N(3)—Rh —C(1)	97.5(2)	C(5)—N(3)—C(10)	110.3(4)
O(1)—Ga —N(2)	88.54(15)	C(9)—N(3)—C(10)	107.5(4)
O(1)—Ga —C(2)	109.2(2)	Rh —C(1)—O(2)	119.3(4)
O(1)—Ga —C(3)	109.3(3)	Rh —C(1)—C(11)	118.1(4)
N(2)—Ga —C(2)	110.2(2)	O(2)—C(1)—C(11)	122.6(5)
N(2)—Ga —C(3)	108.3(2)	O(1)—C(4)—C(5)	108.7(4)
C(2)—Ga —C(3)	125.2(3)	N(3)—C(5)—C(4)	110.9(4)
Rh —O(1)—Ga	120.9(2)	N(1)—C(6)—C(7)	110.3(5)
Rh —O(1)—C(4)	113.5(3)	C(6)—C(7)—C(8)	104.5(5)
Ga —O(1)—C(4)	125.6(3)	N(2)—C(8)—C(7)	111.3(5)
Rh —N(1)—N(2)	118.6(3)		

unlike the four-coordinate Rh(I) species, $[Me_2Gapz(OCH_2CH_2NMe_2)]Rh(CO)$ (Fig. 1(*a*)), this molecule does not possess a plane of symmetry. Thus the four methylene protons become individually unique and exhibit complex spin–spin interactions. A number of molecular arrangements are possible for the five-coordinate Rh(III) species, some of them necessarily involving concomitant meridional–facial rearrangement of the pyrazolylgallate ligand during the oxidative addition and migratory insertion reaction sequence. A definitive X-ray crystal structure of the complex $[Me_2Gapz(OCH_2CH_2NMe_2)]Rh(COMe)I$ (Fig. 2(*b*)) has shown that the pyrazolylgallate ligand in fact remains meridional, that the iodine atom replaces the CO ligand in the original square-planar arrangement, and the CO group becomes part of the acetyl moiety occupying the apical position in the observed square-pyramidal structure. The basal group (N_2OI) is planar to within 0.037(4) Å, the Rh atom being displaced from the mean plane by 0.1709(3) Å toward the apical carbon atom. Bond lengths involving Rh are Rh—I = 2.6300(5), Rh—O = 2.014(3), Rh—N(pz) = 2.033(4), Rh—N(amino) = 2.111(3), and Rh—C = 1.955(5) Å. The Rh—I distance is slightly shorter than the range of 2.65–2.69 Å observed for most Rh(III)—I distances, e.g. 2.643(3) Å in $RhI_2Me(PPh_3)_2$ (28) and 2.653(3) Å in $(\eta^5\text{-}C_5H_5)Rh(CO)(C_2F_5)I$ (29).

The pyrazolyl group is planar within experimental error (χ^2 = 0.2, maximum deviation = 0.001(5) Å) while the RhC(O)C group is slightly but significantly non-planar (χ^2 = 17.6, maximum deviation 0.018(5) Å). Both five-membered chelate rings are significantly non-planar and have "puckered" conformations. The RhNNGaO ring, however, is much more planar than that in LRh(CO) (see Table 5). In addition, the coordination about O(1) is planar compared with pyramidal in LRh(CO), the sum of angles about O(1) being 360.0° vs. 346.7° in LRh(CO).

In the solid state molecules are linked by weak C—H···O interactions (C(10)—H(10a)···O(2) (1/2 − *x*, *y* − 1/2, 1/2 − *z*); H···O = 2.42, C···O = 3.349(7) Å, C—H···O = 158°) to form continuous spirals about the twofold screw axes. The orientation of the acetyl group is determined by three weak anchoring interactions: C(5)—H(5b)···O(2), C(9)—H(9c)···O(2), and C(11)—H(11a)···N(1) (H···(O/N) = 2.50, 2.38, 2.55; C···(O/N) = 3.215(7), 3.084(8), 2.958(6) Å; C—H···(O/N) = 121, 128, 105°).

The observed reluctance of the square-pyramidal molecule, LRh(COMe)I, to accept a sixth ligand (CO or PPh_3) may result from the *trans* influence of the acetyl grouping. Cheng *et al.* have earlier described a number of 5-coordinate Rh(III) acyl derivatives in which the absence of a sixth ligand in the coordi-

TABLE 5. Intra-annular torsion angles (deg) standard deviations in parentheses

Atoms	Value (deg)
$[Me_2Gapz(OCH_2CH_2NH_2)]Rh(CO)$	
N(1)—Rh —O(1)—Ga	−29.18(15)
N(2)—Ga —O(1)—Rh	33.89(15)
O(1)—Ga —N(2)—N(1)	−29.4(3)
Rh —N(1)—N(2)—Ga	13.6(4)
O(1)—Rh —N(1)—N(2)	9.2(3)
N(3)—Rh —O(1)—C(4)	11.7(3)
Rh —O(1)—C(4)—C(5)	−37.9(4)
O(1)—C(4)—C(5)—N(3)	53.2(4)
Rh —N(3)—C(5)—C(4)	−42.1(4)
O(1)—Rh —N(3)—C(5)	17.2(3)
$[Me_2Gapz(OCH_2CH_2NMe_2)]Rh(COMe)I$	
N(1)—Rh —O(1)—Ga	16.4(2)
N(2)—Ga —O(1)—Rh	−14.5(2)
O(1)—Ga —N(2)—N(1)	5.3(3)
Rh —N(1)—N(2)—Ga	5.2(4)
O(1)—Rh —N(1)—N(2)	−12.0(3)
N(3)—Rh —O(1)—C(4)	8.2(4)
Rh —O(1)—C(4)—C(5)	−32.6(6)
O(1)—C(4)—C(5)—N(3)	49.1(7)
Rh —N(3)—C(5)—C(4)	−40.3(5)
O(1)—Rh —N(3)—C(5)	17.5(3)

nation sphere of the metal was attributed to the discouragement of any possible *trans* ligation by the presence of the apical acyl ligand (30, 31). The structural influence of the acetyl grouping in the six-coordinate Rh(III) dimer species $[Rh_2I_4(CO)_2(\mu\text{-}I)_2(COMe)_2]^{2-}$, where the Rh—I *trans* to the acetyl group is 0.322(3) Å longer than the *cis* Rh—I distance, has also been documented (32). The Rh—COMe distance of 1.955(5) Å in the present complex is significantly shorter than those of 2.062(23) Å reported for the above dimer species and the Rh(III) – acyl carbon distances reported by Cheng *et al.* of 2.002(7) Å for $(AsPh_4)[RhI(COEt)(PPh_3)(mnt)]$ and 2.006(14) Å for $[RhI(CO^nPr)(PEt_3)_2(mnt)]$ (where mnt = maleonitriledithiolate). Three of these distances are considerably shorter than the Rh(III)—C σ-bond distances compiled by Collman *et al.* which cover a range of 2.05–2.26 Å (33). The shorter Rh(III) — acyl carbon bond distances may be attributed, in part, to the smaller covalent radius of sp^2 carbon versus sp^3 carbon and, in addition, to a certain degree of back-bonding from filled d_π orbitals on the Rh(III) centre to the π^* orbitals of the acyl ligand. The occurrence of the acyl grouping in the apical position in the present five-coordinate Rh(III) species is somewhat surprising since one might expect the migratory insertion reaction to position this ligand adjacent to a vacant coordination site.

The addition of bromine or iodine to a CH_2Cl_2 solution of LRh(CO) (R = H, Y = NH_2 or NMe_2) resulted in the immediate appearance of a new single carbonyl band at ~2090 cm^{-1} with concomitant total loss of the CO stretching frequency attributable to the starting LRh(CO) species. This new band has been assigned to $LRh(CO)X_2$ (X = Br or I) and is ~30–50 cm^{-1} higher than those reported for related cyclopentadienyl compounds (e.g., ref. 34) but is very similar to frequencies reported for related pyrazolylgallate (35) and -borate (24, 25) complexes. These higher wave numbers are unusual as they oppose the trend previously observed for other related com-

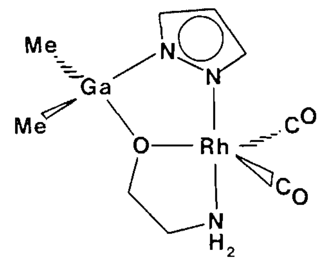

(a)

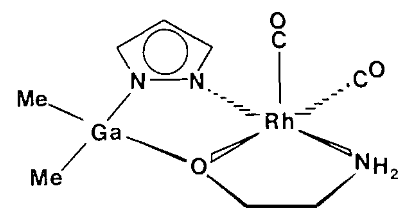

(b)

FIG. 3. (*a*) Trigonal bipyramidal and (*b*) square pyramidal structure.

plexes incorporating either cyclopentadienyl type or pyrazolylgallate anions (e.g., ref. 21). That is, pyrazolylgallate tridentate ligands, and the related isoelectronic tris(pyrazolyl)-borate anions, are generally regarded to be better electron-donating groups compared to the cyclopentadienyl ligand resulting in lower ν_{CO} values in analogous transition metal carbonyl complexes. Analytically pure samples of the $LRh(CO)X_2$ compounds could not be obtained, presumably due to the presence of trace amounts of dihalogens which could not be successfully removed. Difficulties in obtaining satisfactory elemental analyses for related pyrazolylborate dihalogen monocarbonyl species have been previously noted (24, 25). The mass spectra of the pyrazolylgallate dihalogen compounds, $LRh(CO)X_2$, exhibited the expected monomeric parent ion signals (~0.5%), in addition to signals attributable to ions arising from predictable fragmentation patterns of the parent species.

It has already been mentioned that 18-electron dicarbonyl Rh(I) complexes form with both the cyclopentadienyl and tris(3,5-dimethylpyrazolyl)borate anions. Monocarbonyl species are not observed with these ligand systems since the *pseudo* facial configuration geometrically imposed on these tridentate ligands would force an unfavourable tetrahedral symmetry around the Rh(I) centre. However, with the present unsymmetric pyrazolylgallate ligands square planar, 16-electron monocarbonyl products are isolated. These LRh(CO) complexes undergo reversible CO addition in solution. Thus bubbling CO through a hexane solution of $[Me_2Gapz(OCH_2CH_2NH_2)]Rh(CO)$ resulted in the appearance of two new bands in the carbonyl region of the ir spectrum at wavenumbers again ~50 cm^{-1} and ~90 cm^{-1} higher than those reported for the isoelectronic compounds $(\eta^5\text{-}C_5H_5)Rh(CO)_2$ (36) and $(\eta^5\text{-}C_5Me_5)Rh(CO)_2$ (27), respectively. $[Me_2Gapz(OCH_2CH_2NH_2)]Rh(CO)_2$ was unstable in solution, both in air and under a nitrogen atmosphere. With air exposure extensive sample decomposition was signaled by the precipitation of black insoluble materials. The solution, on standing under a nitrogen atmosphere, lost carbon monoxide slowly to give solutions containing both the mono- and dicarbonyl species. Complete conversion to the monocarbonyl could be effected by gently refluxing the solution.

The ^{1}H nmr of $[Me_2Gapz(OCH_2CH_2NH_2)]Rh(CO)_2$ was obtained by bubbling CO through a C_6D_6 solution of the monocarbonyl in an nmr tube. The most notable feature of this nmr spectrum was the loss of the triplets attributable to the methylene protons of the amino alcohol moiety of the pyrazolylgallate ligand, indicating that the symmetry of the starting LRh(CO) complex was lost. Therefore, the dicarbonyl is not a trigonal bipyramid as shown in Fig. 3(*a*) (as this configuration still possesses a mirror plane containing the three donor sites of L) but is more likely square pyramidal, as shown in Fig. 3(*b*). Furthermore, the two gallium methyl groups are inequivalent in the ^{1}H nmr spectrum of this complex, lending additional support for this square-pyramidal structure. Unfortunately the dicarbonyl could not be isolated as a crystalline sample and thus confirmation of this molecular arrangement was not possible via X-ray structure analysis. However, by comparison with the five-coordinate acetyl structure already discussed it seems most likely that in this molecule the pyrazolylgallate ligand again occupies three basal sites of a square pyramid.

The reaction of PPh_3 with the LRh(CO) complexes resulted in disproportionation of the rhodium complexes and the formation of the stable dimer species $[(\mu\text{-pz})Rh(CO)(PPh_3)]_2$.

The LRh(CO) complexes did not catalyze the hydrogenation of 1-hexene at 30°C, a lack of activity arising, no doubt, from the surprising indifference of these square planar Rh(I) species to the presence of molecular hydrogen under a variety of conditions. This observed nonreactivity can be compared with that of isosteric 16-electron square planar complexes containing meridional hybrid tridentate ligands $[Rh(L^\dagger)N(SiMe_2CH_2PPh_2)_2]$ ($L^\dagger$ = cyclooctene, PPh_3, or CO). When $L^\dagger$ = cyclooctene or PPh_3 this system is a catalyst precursor for the efficient hydrogenation of 1-hexene under mild reaction conditions (37). However, when $L^\dagger$ = CO no hydrogenation of olefins occurs (38). Assuming that for catalysis to take place a dihydride mechanism similar to that proposed by Halpern for Wilkinson's catalyst (39–41) most likely is operative, the presence of CO may discourage the formation of a six-coordinate "$LRh(H)_2(CO)$" intermediate. Alternatively, if the CO must dissociate before oxidative addition of H_2 will occur, the reluctance of the Rh—CO bond to break would account for the non-catalytic behaviour of the carbonyl complexes.

We are currently probing the reactions of tridentate pyrazolylgallate ligands with various rhodium phosphine and olefin complexes.

Acknowledgements

We thank the Natural Sciences and Engineering Research Council of Canada for financial support, and the University of British Columbia Computing Centre for assistance.

1. B. M. Louie, S. J. Rettig, A. Storr, and J. Trotter. Can. J. Chem. **62**, 1057 (1984).
2. B. M. Louie, S. J. Rettig, A. Storr, and J. Trotter. Can. J. Chem. **62**, 633 (1984).
3. J. A. McCleverty and G. Wilkinson. Inorg. Synth. **8**, 211 (1966).
4. B. M. Louie, S. J. Rettig, A. Storr, and J. Trotter. Can. J. Chem. **63**, 2261 (1985).
5. S. J. Rettig, A. Storr, and J. Trotter. Can. J. Chem. **53**, 58 (1975).
6. P. Coppens, L. Leiserowitz, and D. Rabinovich. Acta Crystallogr. **18**, 1035 (1965).
7. J. De Meulenaer and H. Tompa. Acta Crystallogr. **19**, 1014 (1965).
8. D. T. Cromer and J. B. Mann. Acta Crystallogr. Sect. A, **24**, 321 (1968).
9. R. F. Stewart, E. R. Davidson, and W. T. Simpson. J. Chem. Phys. **42**, 3175 (1965).
10. D. T. Cromer and D. Liberman. J. Chem. Phys. **53**, 1891 (1970).
11. P. J. Becker and P. Coppens. Acta Crystallogr. Sect. A, **30**, 129 (1974); **30**, 148 (1974); **31**, 417 (1975).
12. P. Coppens and W. C. Hamilton. Acta Crystallogr. Sect. A, **26**, 71 (1970).
13. F. A. Thornley and R. J. Nelmes. Acta Crystallogr. Sect. A, **30**, 748 (1974).
14. K. S. Chong and A. Storr. Can. J. Chem. **57**, 167 (1979).
15. K. S. Chong, S. J. Rettig, A. Storr, and J. Trotter. Can. J. Chem. **57**, 1335 (1979).
16. K. S. Chong and A. Storr. Can. J. Chem. **59**, 1331 (1981).
17. K. S. Chong, S. J. Rettig, A. Storr, and J. Trotter. Can. J. Chem. **59**, 1665 (1981).
18. S. J. Rettig, A. Storr, and J. Trotter. Can. J. Chem. **59**, 2391 (1981).
19. K. S. Chong, S. J. Rettig, A. Storr, and J. Trotter. Can. J. Chem. **56**, 1212 (1978).
20. K. S. Chong, S. J. Rettig, A. Storr, and J. Trotter. Can. J. Chem. **57**, 3113 (1979).
21. K. R. Breakell, S. J. Rettig, D. L. Singbeil, A. Storr, and J. Trotter. Can. J. Chem. **56**, 2099 (1978).
22. E. O. Fischer and K. Bittler. Z. Naturforsch. **16**b, 225 (1961).
23. S. Trofimenko. Inorg. Chem. **10**, 1372 (1971).
24. S. May, P. Reinsalu, and J. Powell. Inorg. Chem. **19**, 1582 (1980).
25. M. Cocivera, T. J. Desmond, G. Ferguson, B. Kaitner, F. T. Lalor, and D. J. O'Sullivan. Organometallics, **1**, 1125 (1982).
26. R. B. King and A. Efraty. J. Organomet. Chem. **27**, 409 (1971).
27. J. W. Kang and P. M. Maitlis. J. Organomet. Chem. **26**, 393 (1971).
28. P. G. H. Troughton and A. C. Skapski. J. Chem. Soc. Chem. Commun. 575 (1968).
29. M. R. Churchill. Inorg. Chem. **4**, 1734 (1965).
30. C. Cheng, B. D. Spivack, and R. Eisenberg. J. Am. Chem. Soc. **99**, 3003 (1977).
31. C. Cheng and R. Eisenberg. Inorg. Chem. **18**, 1418 (1979).
32. G. W. Adamson, J. J. Daly, and D. Forster. J. Organomet. Chem. **71**, C17 (1974).
33. J. P. Collman, P. A. Christian, S. Current, P. Denisevich, T. R. Halbert, E. Schmittou, and K. O. Hodgson. Inorg. Chem. **15**, 223 (1976).
34. R. B. King. Inorg. Chem. **5**, 82 (1966).
35. B. M. Louie. Ph.D. Thesis, University of British Columbia. 1984.
36. E. O. Fischer and K. Bittler. Z. Naturforsch. **16**b, 835 (1961).
37. M. D. Fryzuk and P. A. MacNeil. Organometallics, **2**, 355 (1983).
38. P. A. MacNeil. Ph.D. Thesis, University of British Columbia. 1983.
39. J. Halpern. Trans. Am. Crystallogr. Assoc. **14**, 59 (1978).
40. J. Halpern, T. Okamoto, and A. Zakhariev. J. Mol. Cat. **2**, 65 (1976).
41. J. P. Collman and L. S. Hegedus. Principles and applications of organotransition metal chemistry. University Science, Mill Valley, CA. 1980. Chapt. 6. p. 335.

Antiferromagnetic super exchange and spectral studies on dimeric 8-quinolinolato complexes of copper(II) imides

C. L. SHARMA[1] AND V. MISHRA
Chemistry Department, University of Roorkee, Roorkee (U.P.), India – 247 667

Received January 7, 1985

C. L. SHARMA and V. MISHRA. Can. J. Chem. **63**, 3027 (1985).

The complexes of the type $[Cu(Q)(P)]_2$ and $[Cu(Q)(S)]_2$ where HQ = 8-hydroxyquinoline and P and S are deprotonated phthalimide and succinimide, respectively, were prepared and characterized on the basis of molecular mass determination, elemental analysis, X-ray diffraction, ir, electronic spectra, conductance, thermal analysis, and magnetic measurements. They were of tetrahedrally distorted square planar structure. The susceptibility data at different temperatures were fitted to the Bleaney–Bowers equation which indicated medium antiferromagnetic super exchange interaction within one dimeric unit. The values of exchange integral and g were found to be $-136\ cm^{-1}$ and 2.18, respectively, for the phthalimide complex and $-128\ cm^{-1}$ and 2.16, respectively, for the succinimide complex.

C. L. SHARMA et V. MISHRA. Can. J. Chem. **63**, 3027 (1985).

On a préparé des complexes du type $[Cu(Q)(P)]_2$ et $[Cu(Q)(S)]_2$, dans lesquels HQ = hydroxy-8 quinoline et P et S = les formes déprotonées de la phtalimide et de la succinimide, et on les a caractérisés en se basant sur la détermination de la masse moléculaire, de l'analyse élémentaire, de la diffraction des rayons X, de l'ir et de la spectroscopie électronique, de la conductance, de l'analyse thermique et de mesures magnétiques. Ces complexes ont une structure plan carré déformée d'une façon tétraédrique. On peut établir une corrélation des données de susceptibilité à différentes températures grâce à l'équation de Bleaney–Bowers et ceci suggère l'existence d'une interaction de superéchange antiferromagnétique moyenne à l'intérieur d'une unité dimère. Les valeurs d'intégrale d'échange et de g sont respectivement $-136\ cm^{-1}$ et 2,18 pour le complexe de la phtalimide et $-128\ cm^{-1}$ et 2,16 pour le complexe de la succinimide.

[Traduit par le journal]

Introduction

Studies on homodinuclear complexes have been of great importance because of their interesting magnetic and spectral properties of these materials (1–3). These complexes also serve as models for certain metalloproteins and metalloenzymes, particularly for those containing copper(II) where the biological functions are related to the metal centres in pairs (4–6). Recently, the structures and magnetic properties of a number of phenoxo-, alkoxo-, and hydroxo-bridged copper(II) dimers have been studied and some interesting correlations have been developed (7–12). The present article deals with the preparation and characterization of binuclear 8-hydroxyquinolinato complexes of copper(II) phthalimide and succinimide on the basis of molecular mass determinations, elemental analysis, thermal analysis, X-ray, ir, electronic spectra, conductance and magnetic measurements.

Experimental

Physical measurements

The magnetic measurements were carried out in the temperature range 70–300 K on a PARC digital vibrating sample magnetometer model VSM-155 under two different magnetic fields 5500 and 7000 G produced by a polytronic electromagnet type H.E.M.-200. The constancy of the magnetic field was maintained by a constant current regulator Polytronic type ccP-200. The temperature of the sample chamber was regulated by filling it with liquid nitrogen and then heating it using the automatic heating assembly provided within the instrument. The cryogenic temperature controller EG & G PARC model 152 which was attached with the magnetometer regulated the heating up to desired temperatures. The magnetometer was calibrated with ultrapure nickel metal and $[HgCo(NCS)_4]$ (13). The calibration was then cross-checked at cryogenic temperatures with hydrated cupric(II) acetate (14). The three calibrations agreed well and it was estimated that the limits of error in the susceptibility values were not more than ±1%. The data were corrected for diamagnetism of the lucite sample holder and of constituent atoms with the use of Pascal's constants (15). A value of 60×10^{-6} cgsu was assumed for the temperature independent paramagnetism of copper(II) (16).

Powder X-ray patterns of the complexes were recorded on a Philips X-ray diffractometer model PW-1140/90 attached with digital, graphical, and photographic assemblies using Cu Kα radiations at 12-mA current, 32-kV voltage.

Thermal studies were done on a Stanton Redcraft TG model-770 and Fisher Differential Thermoanalyzer model 260 P at a heating rate of 8°C/min and chart speed 6 in./h in a platinum crucible in the atmosphere of air using anhydrous alumina as a reference material.

All other physical methods were the same as reported earlier (17).

Copper was estimated by atomic absorption technique, nitrogen by Kjeldhal method, and carbon and hydrogen by Pregl method on a Hosli's micro-combustion apparatus type CHA-2. Molecular masses were determined cryoscopically in dioxane.

The computational work was performed on a DEC-2050 version 4 computer system.

Reagents

Phthalimide was obtained from Fluka A.G. Buchs SG (Switzerland) and succinimide and cupric chloride of AR (B.D.H.) grade from England were used. The solvents supplied by E. Merck India Ltd. were redistilled before use.

Preparation of the complexes

Copper(II) phthalimide $[Cu(C_8H_4NO_2)_2(H_2O)_4]$ and copper(II) succinimide $[Cu(C_4H_4NO_2)_2(H_2O)_4]$ were prepared by the same method as reported earlier (18). The 0.05 M methanolic solutions of copper(II) imide and 8-hydroxyquinoline were mixed in the ratio of 1 : 1 and then refluxed on a water bath for about half an hour which gave the crystals a yellowish-green colour. They were filtered, washed several times with methanol, and then dried in a desiccator over anhydrous silica gel. These complexes were found soluble in 1,4-dioxane and dimethylsulfoxide. They were analysed for the metal, carbon, hydrogen, and nitrogen.

Anal. calcd. for **I**, $[Cu(C_9H_6NO)(C_8H_4NO_2)]_2$: Cu 17.97, C 57.69, H 2.83, N 7.92; found: Cu 17.23, C 57.80, H 2.80, N 7.92.

Anal. calcd. for **II**, $[Cu(C_9H_6NO)(C_4H_4NO_2)]_2$: Cu 20.80, C 51.06, H 3.27, N 9.17; found: Cu 20.15, C 51.46, H 3.30, N 9.20.

[1]To whom all correspondence should be addressed.

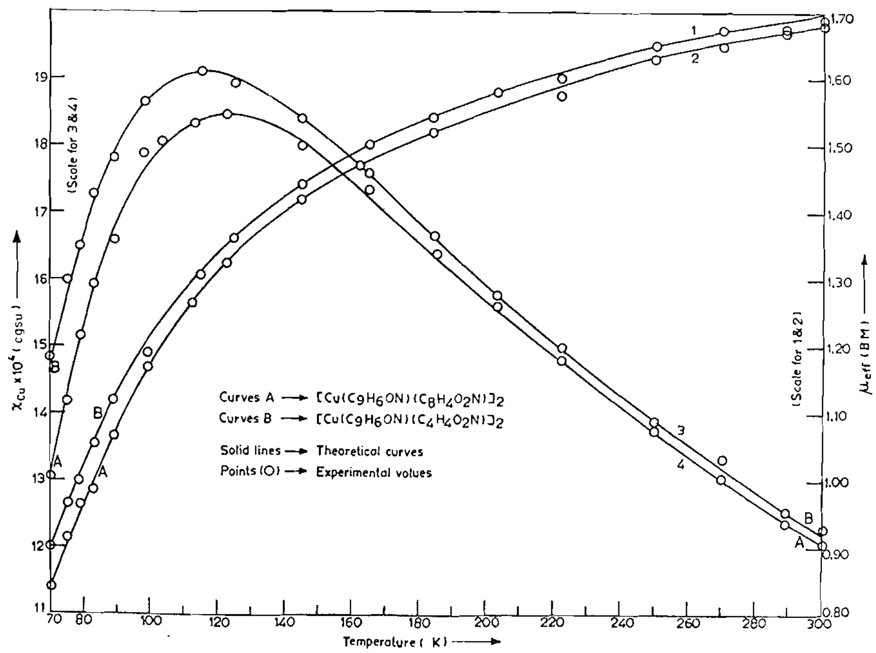

FIG. 1. Plot of χ_{Cu} and μ_{eff} vs. T for $[Cu(C_9H_6ON)(C_8H_4O_2N)]_2$ and $[Cu(C_9H_6ON)(C_4H_4O_2N)]_2$.

Results and discussion

The values of molar conductances in dioxane, i.e., 5 and 10 ohm^{-1} cm^2 mol^{-1} in the case of the first and second complexes, respectively, indicated their nonelectrolytic nature. The molecular masses in dioxane were found to be 719 and 602 which corresponded to their dimeric forms. Thermogravimetry and differential-thermal-analysis curves were similar to those of other copper(II) complexes of 8-hydroxyquinoline (19). Analysis of these curves indicated the absence of any type of water (crystalline or coordinated).

Infrared studies

The imide molecule has two interesting, NH and CO stretching, frequency regions. The ir spectra of the complexes show the shifting of the CO stretching frequency from 1750 to 1700 cm^{-1} which could be the result of an electron withdrawal effect from the CO group as a result of nitrogen coordination (20, 21). The slight increase of ν_{CN} from 1480 to 1500 cm^{-1} supports this (22). On the basis of Lewis-acid concept, the negatively charged imide nitrogen will have better possibilities of being coordinated than oxygen (23). There will be steric hindrance also if the coordination is through oxygen. A strong band due to ν_{NH} observed at 3300 cm^{-1} in the spectrum of imide disappeared in the spectra of complexes indicating thereby the deprotonation of —NH and the coordination through nitrogen. The band obtained at 3100 cm^{-1} due to ν_{OH} in the spectrum of 8-hydroxyquinoline disappeared in the spectra of the complexes. The peak at 1090 cm^{-1} due to aryl oxygen vibration of the ligand was observed at higher position ≈1110 cm^{-1} confirming the coordination of metal ion with aryl oxygen of the 8-quinolinol. The upward shifts from 740 to 750 cm^{-1} due to out-of-plane ring deformation and from 480 to 500 cm^{-1} due to in-plane ring deformation modes indicated the coordination of the metal ion through oxygen and nitrogen of 8-hydroxyquinoline (24). The bands due to $\nu_{M—O}$ and $\nu_{M—N}$ were observed at 400 and 375 cm^{-1} respectively (25).

Electronic spectra

The spectra of complexes in dioxan gave a strong band of high intensity at 25 000 cm^{-1} ($\epsilon \approx 8800$). The imide ligands and their monomeric complexes prepared by the reported methods (26–28) do not absorb in this region. However, the monomeric copper(II) complexes of 8-hydroxyquinoline gave a band of low intensity and at lower energy, i.e., 23 200 cm^{-1} ($\epsilon \approx 7000$). The presence of this band and its shift to higher energy with increased intensity in the dimeric complexes may be attributed to the combined effect of intra-ligand transition and L → M charge transfer transitions, a characteristic feature of oxo-bridged copper(II) complexes (29, 30) and hence a diagnostic feature of a dimeric structure (31). Another band was observed at ≈14 000 cm^{-1} ($\epsilon \approx 150$) while the planar monomeric copper(II) complexes of 8-quinolinol (α) (27), succinimide, and phthalimide (28), gave the bands at 15 000 ($\epsilon \approx 110$), 15 000 ($\epsilon \approx 100$), and 14 900 cm^{-1} ($\epsilon \approx 110$), respectively. The bis(8-quinolinolato)copper(II) (β) which has a $T_d \leftrightarrow$ planar structure gave this band at 13 300 cm^{-1} ($\epsilon \approx 70$) (26). The absence of any new band in the dimeric derivatives of the above monomeric species indicated an identical ligand field environment around both the metal centres (32) and hence a *trans* structure of the dimeric complexes. Since the ligands do not show any band in the visible region, the above band was definitely a $d-d$ band of copper(II). Again, there was a red shift in this energy band from mono- to dimeric complexes which may be due to the combined effects of the changes in the stereochemistry and the ligand field energy indicating thereby the difference in the steric environment around the metal centre in these two types of complexes. Since the monomeric complexes are square planar, it appears that the present dimers are tetrahedrally distorted planar complexes. This is supported by the fact that the introduction of tetrahedral distortion in the planar complexes causes a shift in the absorption band to the lower energy side (33).

X-ray diffraction

The powder X-ray diffraction patterns were analysed by modified Lipson's (34) method. The patterns of both the complexes were successfully indexed for the tetragonal crystal

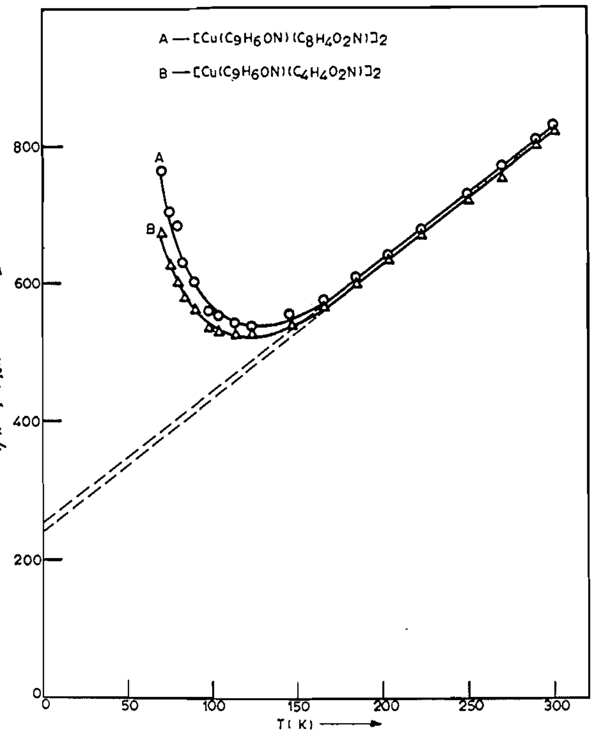

FIG. 2. Plot of $1/\chi$ vs. T for $[Cu(C_9H_6ON)(C_8H_4O_2N)]_2$ and $[Cu(C_9H_6ON)(C_4H_4O_2N)]_2$.

system (Table 1, supplementary material[2]). The observed densities, i.e., 2.10 and 1.05, in the case of complexes **I** and **II** respectively, indicated the presence of four molecules per unit cell. The lattice parameters were found to be a = 13.165 Å, c = 12.709 Å for complex **I** and a = 15.061 Å, c = 16.990 Å for complex **II**.

On the basis of the above information the following structure was proposed

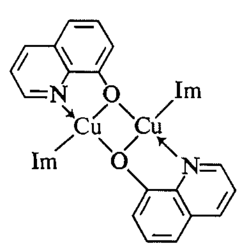

Im = deprotonated imide molecule

Magnetic studies

The magnetic properties of exchange-coupled copper(II) complexes have been studied using isotropic HDVV model (35) as simplified to the isotropic Hamiltonian in the case of dimers

$$\mathcal{H} = -2J\mathbf{S}_1 \cdot \mathbf{S}_2$$

The susceptibility per copper(II) ion was obtained from the Van Vleck's equation (36) as simplified by Bleaney and Bowers (37)

$$\chi_{Cu^{2+}} = \frac{Ng^2\beta^2}{3kT}\left[1 + \frac{1}{3}\exp\left(\frac{-2J}{kT}\right)\right]^{-1} + N\alpha$$

[2]Supplementary material is available and may be purchased from the Depository of Unpublished Data, CISTI, National Research Council of Canada, Ottawa, Ont., Canada K1A 0S2.

The exchange parameters were then evaluated by least square method. The value of the exchange integral $2J$ and g were found to be -136 cm^{-1} and 2.18 respectively in the case of complex **I** and -128 cm^{-1} and 2.16 respectively in the case of complex **II**. The curves (Fig. 1) obtained from experimental and calculated values of susceptibilities and magnetic moments at different temperatures are in good agreement with each other. The susceptibilities of both complexes at 5500 and 7000 G were nearly the same and hence anisotropy and field dependence were negligible. The values of magnetic moments at room temperature were 1.66 and 1.67 BM, i.e., sufficiently less than the spin-only value required for one unpaired electron indicating thereby the dimeric form of the complexes. The value of susceptibility increases with decreasing temperature, reaches a maximum, and beyond which it decreases while the values of magnetic moment decrease monotonically with decreasing temperature (Fig. 1). The complexes obey the Curie–Weiss law, $\chi = C/(T + \theta)$, in the temperature ranges of approximately 165–300 K for complex **I** and 145–300 K for complex **II**. For $[Cu(Q)(P)]_2$, C = 0.525, θ = 134°, while for $[Cu(Q)(S)]_2$, C = 0.515, θ = 126° (Fig. 2). In both compounds, however, the Curie–Weiss law is not obeyed at lower temperatures. This indicated the medium antiferromagnetic interaction within one dimeric unit (38, 39). The agreement between the calculated and experimental values (Fig. 1) ruled out any possibility of inter-dimer interactions. The electron exchange demagnetization in the dimers was considered to occur between pairs of oxygen-bridged copper(II) atoms (40). The antiferromagnetic interaction was therefore operative via super exchange pathway involving $d_{x^2-y^2}$ orbitals of Cu(II) and s and p orbitals of diamagnetic oxygen anion (41). The 90° cation–anion–cation exchange interaction mechanism (42) could successfully be applied to the present systems. Cu—O—Cu bridge angles, Cu—O bond lengths, the solid angle at the oxygen bridge, and the metal ion ground state, etc. may be the major contributing factors to the super-exchange.

Acknowledgements

Acknowledgements are due to Professor K. Chandra, Director, USIC, University of Roorkee, Roorkee, for providing necessary instrumental facilities. One of the authors (V.M.) is thankful to U.G.C., New Delhi, for granting a Teacher Fellowship under Faculty Improvement Programme.

1. L. ANTOLINI, L. MENABUE, P. PRAMPOLINI, and M. SALADINI. J. Chem. Soc. Dalton Trans. 2109 (1982).
2. B. G. MALMSTROM. New trends in bio-inorganic chemistry. *Edited by* R. J. P. Williams and J. R. R. F. DaSilva. Academic Press, London. 1980.
3. W. MUZUREK, K. J. BERRY, K. S. MURRAY, M. J. O'CONNOR, M. R. SNOW, and A. G. WEDD. Inorg. Chem. **21**, 3071 (1982).
4. M. KATO, K. IMAI, Y. MUTO, T. KOBII, and H. B. JONASSEN. J. Inorg. Nucl. Chem. **35**, 109 (1973).
5. D. M. DOOLEY, R. A. SCOTT, J. ELLINGHAUS, E. I. SOLOMON, and H. B. GRAY. Proc. Natl. Acad. Sci. U.S.A. **75**, 3019 (1978).
6. E. SINN and C. M. HARRIS. Coord. Chem. Rev. **4**, 391 (1969).
7. R. D. WILLET and G. L. BRENEMAN. Inorg. Chem. **22**, 326 (1983).
8. L. MERZ and W. HEASE. J. Chem. Soc. Dalton Trans. 875 (1980).
9. B. JEZOWSKA-TREZEBIATOWSKA, Z. OLEJINIK, and T. LIS. J. Chem. Soc. Dalton Trans. 251 (1981).
10. V. H. CRAWFORD, H. W. RICHARDSON, J. R. WASSON, D. J. HODGSON, and W. E. HATFIELD. Inorg. Chem. **15**, 210 (1976).

11. M. MELNIK. Coord. Chem. Rev. **42**, 259 (1982).
12. S. K. MANDAL and K. NAG. J. Chem. Soc. Dalton Trans. 2429 (1983).
13. D. B. BROWN, V. H. CRAWFORD, J. W. HALL, and W. E. HATFIELD. J. Phys. Chem. **81**, 1303 (1977).
14. B. N. FIGGIS and R. L. MARTIN. J. Chem. Soc. 3837 (1956).
15. G. FOEX, C. J. GORTER, and L. J. SMITS. Constanteo selectionnees diamagneticsme et paramagneticsme. Masson et Cie, Paris. 1957.
16. N. J. HILL. J. Chem. Soc. Faraday Trans. 2, **72**, 631 (1976).
17. C. L. SHARMA and V. MISHRA. Acta Chim. Hung. **115**, 325 (1984).
18. C. L. SHARMA and V. MISHRA. Acta Chim. Hung. **114**, 3 (1983).
19. R. G. CHARLES. Anal. Chim. Acta, **27**, 474 (1962).
20. S. SRIMN. J. Chem. Phys. **23**, 1371 (1955).
21. G. F. SVATOS, C. CURRAN, and J. V. QUAGLIANO. J. Am. Chem. Soc. **77**, 6159 (1955).
22. P. C. H. MITCHELL. J. Inorg. Nucl. Chem. **25**, 967 (1963).
23. J. C. BAILAR, JR. The chemistry of coordination compounds. Reinhold, New York. 1956. p. 180.
24. R. C. PAUL, M. HARMEET, and S. L. CHADHA. Indian J. Chem. **13**, 1180 (1975).
25. N. R. RAO, D. S. RAO, and M. C. GANORKAR. Indian J. Chem. **21**A, 839 (1982).
26. J. C. FANNING and H. B. JONASSEN. J. Inorg. Nucl. Chem. **25**, 29 (1963).
27. F. KAMAMARU, K. OGAWA, and I. NITTA. Bull. Chem. Soc. Jpn. **36**, 422 (1963).
28. S. MIKI and S. YAMADA. Bull. Chem. Soc. Jpn. **37**, 1044 (1964).
29. J. J. GRZYBOWSKI and F. L. URBACH. Inorg. Chem. **19**, 2604 (1980).
30. S. K. MANDAL and K. NAG. J. Chem. Soc. Dalton Trans. 2141 (1984).
31. L. ANTOLINI, L. MENABUE, G. C. PELLACANI, M. SALADINI, L. P. BATTUGLIA, A. B. CORRADI, and G. MARCOTRIGIANO. J. Chem. Soc. Dalton Trans. 2325 (1984).
32. P. K. BHATTACHARYA. Indian J. Chem. **59**A, 505 (1982).
33. S. H. LIU and C.-S. CHUNG. Polyhedron, **3**, 559 (1984).
34. H. LIPSON and H. STEEPLE. Interpretation of X-ray powder diffraction patterns. McMillan, London. 1970.
35. W. E. HATFIELD. Theory and applications of molecular paramagnetism. *Edited by* E. A. Bondreaux and L. N. Mulay. Wiley Interscience, New York. 1976. p. 349.
36. J. H. VAN VLECK. The theory of electric and magnetic susceptibilities. Oxford University Press, London. 1932. p. 182.
37. B. BLEANEY and K. D. BOWERS. Proc. R. Soc. London, A, **214**, 451 (1952).
38. E. UHLIG and K. STAIGER. Z. Anorg. Chem. **380**, 39 (1968).
39. Y. NISHIDA and S. KIDA. J. Inorg. Nucl. Chem. **38**, 451 (1976).
40. C. M. HARRIS, K. KOKOT, and S. L. LENZER. Nature (London), **196**, 471 (1962).
41. O. A. KAHN. Inorg. Chim. Acta, **62**, 3 (1982).
42. J. B. GOODENOUGH. Magnetism and chemical bond. Interscience, New York. 1963. p. 180.

Réaction de quelques pyrazolines substituées par deux groupes électroattracteurs géminés avec $Ce(NH_4)_2(NO_3)_6$: nouvelle synthèse de pyrones-2 électrophiles

HASSAN ABDALLAH,[1] RENÉ GRÉE ET ROBERT CARRIÉ

Groupe de Recherches de Physicochimie Structurale, U.A. n° 704 au C.N.R.S., laboratoire n° 3, Université de Rennes, 35042 Rennes Cédex, France

Reçu le 4 janvier 1985

HASSAN ABDALLAH, RENÉ GRÉE et ROBERT CARRIÉ. Can. J. Chem. **63**, 3031 (1985).

La réaction des pyrazolines acétals de formule générale **3** avec $Ce(NH_4)_2(NO_3)_6$ est étudiée. Elle conduit généralement aux oléfines **4** qui sont de bons substrats de départ pour la synthèse de pyrones électrophiles **5**. Dans deux cas une autre voie d'évolution, conduisant à des cyclobutanes, est observée.

HASSAN ABDALLAH, RENÉ GRÉE, and ROBERT CARRIÉ. Can. J. Chem. **63**, 3031 (1985).

Reaction of type **3** ketal pyrazolines with $Ce(NH_4)_2(NO_3)_6$ is studied. This leads generally to olefins **4**, which are good starting materials for the synthesis of electrophilic pyrones **5**. In two cases, another pathway leading to cyclobutanes is observed.

Les pyrazolines-1 portant en position géminée deux groupes électroattracteurs, peuvent en principe évoluer avec élimination d'azote selon trois voies: formation de cyclopropanes (voie A), migration de R (voie B) ou de H (voie C) conduisant dans les deux derniers cas à des oléfines (schéma 1).

Dans le cadre des travaux entrepris au laboratoire concernant l'utilisation en synthèse de la cycloaddition-1,3 dipolaire, nous avons montré précédemment l'intérêt synthétique du diazoacétal **1**, R′ = $(CH_3O)_2CH$, la photolyse des pyrazolines **3** correspondantes permettant l'obtention de cyclopropanes électrophiles à fonction aldéhyde libre ou masquée (1).

Le présent mémoire décrit l'évolution de ces mêmes pyrazolines **3** lorsqu'elles sont traitées par une petite quantité de $Ce(NH_4)_2(NO_3)_6$ (2). En général elles donnent avec de bons rendements les oléfines **4**, lesquelles traitées par HCO_2H conduisent à des pyrones-2 électrophiles régiospécifiquement substituées en 5 ouvrant ainsi une voie d'accès originale à ces composés (schéma 2). À notre connaissance, deux composés de ce type ont été décrits jusqu'à présent (3, 4). Les pyrones-2 électrophiles sont en outre des produits de départ intéressants en synthèse organique comme: (*i*) diènes (5–7) lors de réactions de Diels–Alder impliquées dans différentes synthèses de produits naturels; (*ii*) précurseurs de complexes cyclobutadiène – fer tricarbonyle (8).

Dans deux cas une voie d'évolution différente avec formation de dérivés cyclobutaniques est observée. Ces résultats apportent de nouveaux éléments sur le mécanisme d'évolution des pyrazolines en présence de Ce^{4+}.

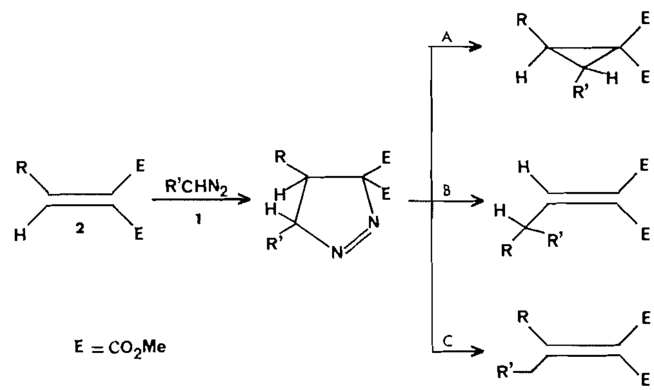

SCHÉMA 1

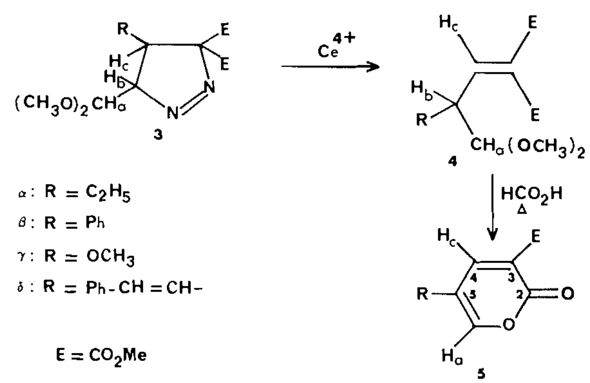

SCHÉMA 2

1. Synthèse de pyrones-2 électrophiles

Le principe de ces synthèses est résumé dans le schéma 2. Les pyrazolines **3**, traitées par $Ce(NH_4)_2(NO_3)_6$ (0,06–0,12 équiv.) dans l'acétone à 30°C pendant 3–25 h suivant la nature de R, conduisent aux oléfines **4** (Rdt 50–80% après distillation).

L'analyse (rmn ^1H) du produit brut de la réaction montre la formation exclusive des oléfines **4**. Les conditions expérimentales et les rendements sont indiqués dans le tableau 1.

Les caractéristiques de rmn[2] de ces oléfines (tableau 2) confirment leur structure. On note, en particulier, la présence de protons vinyliques H_c vers 7 ppm couplés avec le proton H_b vicinal.

Traités par HCO_2H en excès (10–20 équiv.) à chaud les composés **4** donnent les pyrones-2 électrophiles **5** (Rdt 47–83%, tableau 1). Les caractéristiques de rmn (tableau 3) confirment leur structure; elles sont en bon accord avec les données de la littérature concernant la pyrone-2 non substituée en position 5 (R = H) (6, 9).

Le mécanisme de la réaction de formation des pyrones n'a pas été établi; on notera seulement les points suivants:

Si on traite les oléfines **4** par HCO_2H pur sans solvant à la température ambiante, la formation des aldéhydes **6** (schéma 3), intermédiaires vraisemblables de la réaction, est observée.

[1]Boursier du Conseil National de la Recherche Scientifique libanais.

[2]Les notations des hydrogènes H_a, H_b, H_c qui facilitent la présentation des résultats de la rmn sont propres à chaque structure. Dans toute la mesure du possible une cohérence de notation a été maintenue pour les différentes structures.

TABLEAU 1. Conditions expérimentales de préparation des composés **4** et **5**

Composés	Equiv. de Ce^{4+} (durée 4 h)	Composés (Rdt %)	Equiv. de HCO_2H Température (°C) (durée, h)	Composés (Rdt %)*
3α	0,06	**4α** (78)	11 80 (2)	**5α** (71)
3β	0,06	**4β** (77)	20† 105–110 (2)	**5β** (83)
3γ	0,12	**4γ** (50)	20 100 (1)	**5γ** (71)
3δ	0,11	**4δ** (75)	16 50 (5)	**5δ** (47)

*Rendement par rapport à **4**.
†La réaction est effectuée dans le toluène (23 équivalents).

TABLEAU 2. Caractéristiques de rmn ^1H ($CDCl_3$) des composés **4**

Composés	$\delta(H_a)$	$\delta(H_b)$	$\delta(H_c)$	$\delta(OCH_3)$	δ(R) et (J)	J_{ab}	J_{bc}
4α	4,23	2,79	6,87	3,80 3,32 (6H) 3,76	CH_2: 1,49 (m) CH_3: 0,84 (t)	5,6	10,8
4β	4,60	4,17	7,38	3,74 3,35 3,72 3,28	Ph: 7,5–7,2 (5H, m)	5,5	10,0
4γ	4,35	4,11	6,88	3,82 3,44 3,80 3,41 3,36		5,3	7,1
4δ	4,33	3,70	7,02	3,76 3,35 (6H) 3,74	Ph: 7,4–7,1 (5H, m) PhC*H*=: 6,43 (d) PhCH=C*H*: 6,10 (dd) (J = 16,0 et 6,8)	5,3	9,7

TABLEAU 3. Caractéristiques de rmn ^1H* des pyrones **5**

Composés	$\delta(H_a)$	$\delta(H_c)$	$\delta(OCH_3)$	δ(R) et (J)	J_{ab}
5α	8,12	7,47	3,85	CH_2: 2,37 (q) CH_3: 1,13 (t) (J = 7,6 et 1,0)	2,7
5β	8,49	7,89	3,85	Ph: 7,41 (s, 5H)	2,8
5γ	8,01	7,42	3,87	OCH_3: 3,72	3,2
5δ	8,42	7,70	3,88	Ph: 7,6–7,1 (m, 5H) PhC*H*=C*H*: 6,88 (d), 6,66 (d) (J = 16,8)	2,6

*Solvant $CDCl_3$ sauf **8** ($(CD_3)_2CO$ + $CDCl_3$, 2:1).

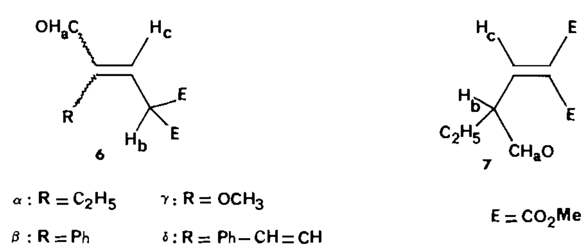

SCHÉMA 3

Placés dans les mêmes conditions (HCO_2H à chaud) ces aldéhydes conduisent également aux pyrones **5**.

Les caractéristiques de rmn des aldéhydes **6**, dont la stéréochimie n'est pas établie, sont en accord avec les structures indiquées (tableau 4).

Lors de l'évolution de **4α** en présence de HCO_2H (à la température ambiante) on observe d'abord la formation d'un composé auquel nous avons attribué la structure **7** sur la base de ses caractéristiques de rmn (tableau 4; on note en particulier un couplage J_{ab} de 1,5 Hz). Le composé **7** évolue ensuite (toujours à température ambiante) vers **6α** lequel chauffé dans HCO_2H conduit à la pyrone **5α**.

II. Réactions des pyrazolines 8 et 13. Formation de cyclobutanes

(a) *Pyrazoline 8*

Dans les mêmes conditions que précédemment, elle donne avec Ce^{4+} une réaction tout à fait différente (schéma 4). La rmn montre que le dérivé cyclobutanique **9** est le produit majoritaire de la réaction (63%). Il est accompagné du cyclopropane **10** (18%) et de l'oléfine **11** (19%). Ces trois produits sont séparés par chromatographie sur gel de silice. Les composés **10** et **11** ont été caractérisés antérieurement (1). La structure du cyclobutane **9** (un seul isomère est obtenu) est établie à l'aide de ses caractéristiques de rmn (tableaux 5 et 6): on note en particulier en rmn ^{13}C l'existence de trois atomes de carbone

TABLEAU 4. Caractéristiques de rmn ^1H* des composés **6** et **7**

Composés	δ(H_a)	δ(H_b)	δ(H_c)	δ(OCH_3)	δ(R)	J_{bc}
6α	9,51	4,57	6,67	3,82 (6H)	CH_2: 2,35 (q) CH_3: 1,01 (t)	10,0
6β	9,67	4,42	6,89	3,71 (6H)	Ph: 7,5–7,05 (m, 5H)	10,0
6γ	9,36	4,70	6,20	3,81 (6H)	CH_3O: 3,86	8,7
6δ	9,57†	4,77	6,68	3,75 (6H)	Ph: 7,6–7,0 (5H) PhC*H*=C*H*: 6,95–6,50 (2H) (m) non analysé	9,7
7	9,57‡	3,10–2,50(m)	7,01	3,80 3,77	CH_2: 2,0–1,12 (m) CH_3: 0,92 (t)	10,2

*Solvant $CDCl_3$ sauf **7** ($CDCl_3$ + HCO_2H).
†J = 2,6.
‡J_{ab} = 1,5.

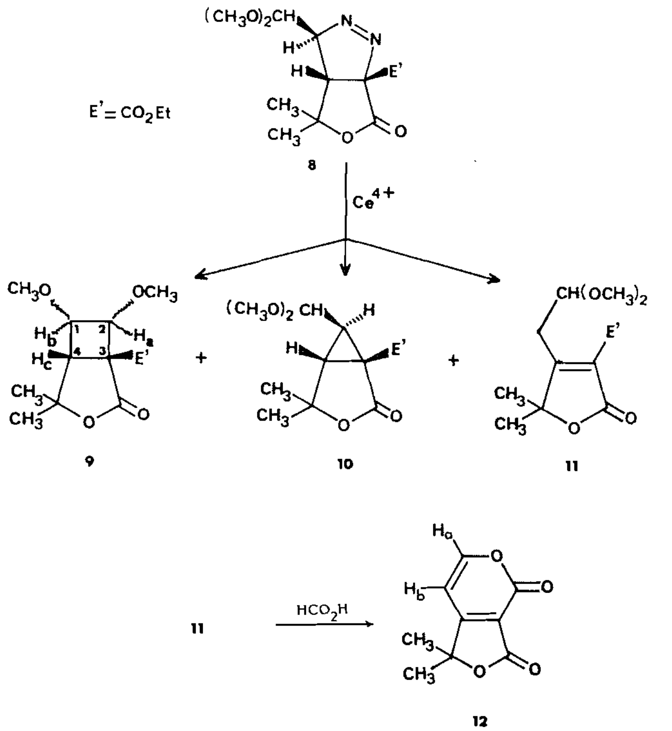

SCHÉMA 4

TABLEAU 5. Caractéristiques de rmn ^1H ($CDCl_3$) des composés **9** et **14**

Composés	δ(H_a)	δ(H_b)	δ(H_c)	δ(OCH_3)		$^3J_{ab}$	$^3J_{bc}$	$^4J_{ac}$
9*	4,22	3,79	2,56	3,50	3,39	5,3	5,0	1,0
14	4,07	4,23	2,88	3,84 3,76 3,75	3,48 3,46	6,4	7,4	1,0

*4,29 (q, OCH_2), 1,32 (t, OCH_2CH_3), 1,52 et 1,49 (2s, $C(CH_3)_2$).

présentant des couplages $^1J_{CH}$ de 150 Hz environ; *deux* de ces carbones ont des déplacements chimiques de 78,5 et 81,5 ppm et sont donc vraisemblablement en α d'un hétéroatome.

Les caractéristiques de rmn ^1H sont également en accord avec les données de la littérature (10) mais ne permettent pas d'attribuer la configuration relative des carbones cyclobutaniques, les constantes de couplage des protons vicinaux et les constantes ^4J n'étant pas caractéristiques (10).

Remarque: Le traitement du produit **11** avec HCO_2H à reflux permet d'obtenir la pyrone **12** avec un rendement de 79% (schéma 4). Ses caractéristiques spectroscopiques (cf. partie expérimentale) sont en accord avec la structure indiquée; on note, en particulier, les signaux rmn ^1H des protons H_a à 7,97 et H_b à 6,68 ppm (J = 5,2 Hz).

(b) *Pyrazolines **13***

La pyrazoline **13** donne dans les mêmes conditions un mélange complexe de sept produits (schéma 5): le cyclobutane **14** (38%), le cyclopropane **15** (7%), les oléfines **16** (34%) et **17** (6%), le dérivé **18** (5%) ainsi que deux autres produits (7% et 3%) dont la structure n'a pas été déterminée.

Les pourcentages des différents constituants sont déterminés à l'aide de la rmn et de la chromatographie de partage gaz–liquide. L'oléfine **17**, instable, a été caractérisé uniquement à l'aide de la rmn, par comparaison avec un échantillon authentique préparé au laboratoire (1); les autres composés ont été isolés par chromatographie sur colonne de SiO_2 et de partage gaz–liquide.

Les caractéristiques spectroscopiques du cyclobutane **14** (tableaux 5 et 6) sont très proches de celles trouvées pour **9**. On note également la présence de deux carbones ayant un couplage $^1J_{CH}$ de 155 Hz environ à 82,6 et 79,1 ppm et d'un troisième carbone à 45,8 ppm ($^1J_{CH}$ = 135 Hz).

Pour l'oléfine **16** on observe en rmn ^1H (cf. partie expérimentale) un triplet à 4,56 ppm couplé avec un CH_2 (doublet) à 2,96 ppm. Le traitement à HCO_2H de cette oléfine permet d'obtenir la pyrone **19**. Ce composé, fragile, a été caractérisé uniquement à l'aide de la rmn (protons H_a et H_b à 7,58 et 6,60 ppm respectivement (J = 5,4 Hz)). En ce qui concerne le composé **18** l'ensemble des caractéristiques spectroscopiques (cf. partie expérimentale) et la spectrométrie de masse (fragment m/z = 291, $C_{12}H_{19}O_8$, $[M - CH_3O]^+$ sont en accord avec la structure. Dans le spectre de rmn ^{13}C on observe un signal dû au carbone acétalique à 105,3 ppm et un signal à 80,5 ppm correspondant au carbone CH_b—OCH_3.

III. Essai de rationalisation des résultats

Les travaux antérieurs du laboratoire (2) nous ont conduit à proposer pour cette réaction de pyrazolines *gem* disubstituées par des groupements électroattracteurs avec Ce^{4+} le passage par un intermédiaire biradicalaire **20** (schéma 6).

Au vu des résultats précédents, deux points nous semblent particulièrement intéressants à noter:

1. La présence du groupe acétal en position 5 modifie sensiblement le cours de la réaction en favorisant la migration de R: ainsi dans le cas des pyrazolines avec R = Ph ou PhCH=CH pour R′ = H, on obtient environ 50% de cyclo-

TABLEAU 6. Caractéristiques de rmn ^{13}C ($CDCl_3$) des composés **9** et **14**

Composés	$\delta(C_1)$ et $\delta(C_2)(^1J)$	$\delta(C_3)$	$\delta(C_4)(^1J)$	$\delta(OCH_3)(^1J)$	$\delta(CO_2CH_2CH_3)$ ou $\delta(CO_2CH_3)(^1J)$	C=O
9*	81,5 (155)	55,7	56,4 (147)	57,7 (143)	CH_2 62,4 (148)	169,6
	78,5 (147)			56,8 (142)	CH_3 14,0 (127)	168,2
14	82,6 (154)	57,6	45,8 (135)	58,5 (144)	53,1 (148)	170,3
	79,1 (157)			57,7 (143)	52,9 (148)	170,0
					52,3 (147)	167,3

*84,5 ($(CH_3)_2C$), 27,8 et 22,2 ($(CH_3)_2C$, ^1J = 128 et 127).

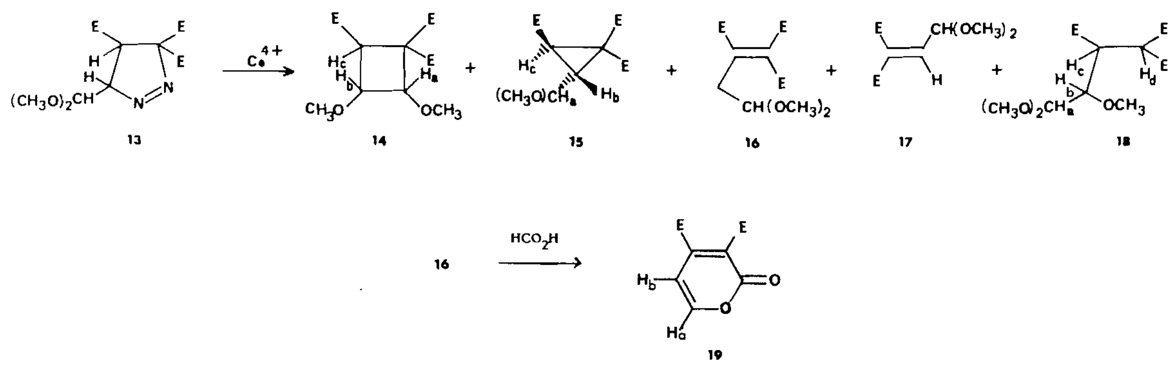

SCHÉMA 5

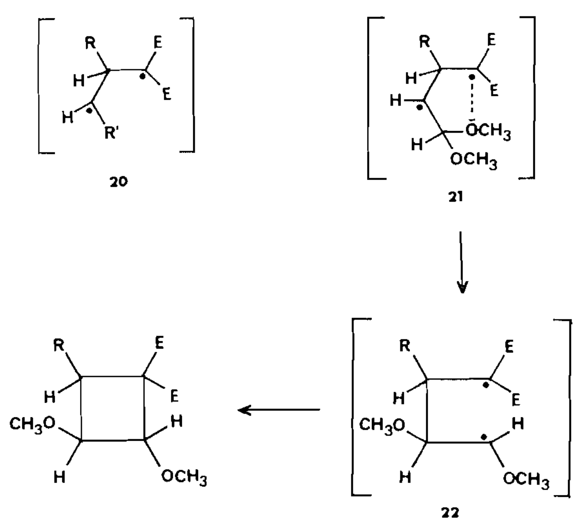

SCHÉMA 6

propanes (2) alors que pour R' = $CH(OCH_3)_2$, la migration exclusive de R est observée. On peut envisager dans ce dernier cas, une interaction entre le doublet de l'un des atomes d'oxygène acétalique et le site radicalaire à caractère électrophile que constitue le carbone portant les deux groupes esters (intermédiaire **21**). Il n'est pas surprenant dans ces conditions d'observer des réactions différentes.

2. Lorsque pour des raisons électroniques (dans le cas du produit **13** (R = CO_2Me) ou stériques (vraisemblablement dans le cas du produit **8**) le groupement R ne peut plus migrer, on observe une nouvelle voie d'évolution avec formation de cyclobutanes, évolution pour laquelle nous proposons le mécanisme suivant: une migration-1,2 d'un OCH_3 au niveau du biradical-1,3 intermédiaire **21** conduirait au biradical-1,4 **22** et serait suivie d'une fermeture en dérivé cyclobutanique (schéma 6).

Remarque: Le composé **18** correspond à l'addition (au moins formelle) de méthanol sur le biradical **21**. L'origine de **17** n'a pu être expliquée jusqu'à présent.[3]

En conclusion, les résultats précédents montrent que l'on peut moduler l'évolution des pyrazolines dérivées du diazoacétal. Si la photolyse conduit généralement aux cyclopropanes correspondants, les réactions avec Ce^{4+} donnent des produits de structure différente. Elles ouvrent ainsi une nouvelle voie d'accès à des pyrones électrophiles, composés dont l'intérêt en synthèse a été mentionné à diverses reprises dans la littérature. Une voie d'évolution originale conduisant à des dérivés cyclobutaniques a par ailleurs été mise en évidence.

Partie expérimentale

Les indications générales sont identiques à celles données précédemment (1).

1. *Pyrazolines-1*

(a) *Les pyrazolines 3α, 3β, 8 et 13* ont été décrites précédemment (1). La pyrazoline **3γ** est préparée par réaction du diazoacétal avec le méthoxyéthylidène malonate de méthyle (11).

(b) *Pyrazoline 3δ*

À 1 g ($4,1 \times 10^{-3}$ mol) de cinnamylidène malonate de méthyle (12), on ajoute sans solvant 1,1 équiv. de diazoacétal; le mélange est abandonné pendant 24 h à la température ambiante. La transformation du cinnamylidène malonate de méthyle est quantitative; **3δ** (huile jaune pâle) est caractérisée uniquement à l'aide de la rmn. **3δ**: rmn (C_6D_6) δ: 7,25–6,95 (m, aromatique), 6,70 (dd, PhC*H*=, *J* = 15,8 et 0,7), 5,97 (dd, PhCH=C*H*, *J* = 8,6), 4,95 (dd, H_b, J_{bc} = 7,4), 4,79 (d, H_a, J_{ab} = 3,8), 3,97 (m, H_c), 3,55 (3H), 3,25 (3H), 3,20 (3H) et 3,18 (3H)(OCH_3).

La présence de signaux à 6,37 ppm (d, *J* = 15,8 Hz) et à 5,92 (dd,

[3]Lors de la synthèse de la pyrazoline **13** (1) le spectre de rmn ^1H (80 MHz) du produit brut ne permet pas d'exclure la présence en faible quantité (~5%) d'un autre isomère résultant de l'orientation inverse de la cycloaddition. La rétrocycloaddition du diazoacétal pourrait alors expliquer la formation de **17**.

J = 10,6 et 15,8 Hz) indique vraisemblablement l'existence d'un second diastéréoisomère en faible quantité (<10%).

2. *Oléfines 4*

4α: À une solution de 850 mg (2,95 × 10^{-3} mol) de la pyrazoline **3**α dans 5 cm^3 d'acétone, on ajoute 100 mg (1,8 × 10^{-4} mol; 0,06 équiv.) de $Ce(NH_4)_2(NO_3)_6$. Maintenu 3 h à 30°C, le mélange est repris avec 75 cm^3 d'éther et lavé à l'eau (2 fois 50 cm^3) puis séché sur Na_2SO_4.

Après distillation du solvant, le mélange réactionnel est purifié d'abord sur une courte colonne de chromatographie (SiO_2, éluant éther – éther de pétrole 1:1) puis par distillation au four tubulaire: 95°C (3 × 10^{-3} Torr; 1 Torr = 133,3 Pa). On obtient 600 mg de **4**α (Rdt = 78%); ir (film liquide) ν: 1724 (C=O), 1640 (C=C). *Anal.* calc. pour $C_{12}H_{20}O_6$: % C 55,38, H 7,69; tr.: C 55,3, H 7,7.

De la même manière (voir tableau 1) nous avons préparé les oléfines:

4β: 135°C (4 × 10^{-3} Torr); Rdt = 77%; ir (film liquide) ν: 1720 (C=O), 1642 (C=C). *Anal.* calc. pour $C_{16}H_{20}O_6$: % C 62,34, H 6,49; tr.: C 62,2, H 6,6.

4γ: 110°C (8 × 10^{-4} Torr); Rdt = 50%; ir (film liquide) ν: 1728 (C=O), 1648 (C=C). *Anal.* calc. pour $C_{11}H_{18}O_7$: % C 50,38, H 6,87; tr.: C 50,1, H 7,1.

4δ: 195°C (3 × 10^{-3} Torr); Rdt = 75%; ir (film liquide) ν: 1722 (C=O), 1676 et 1636 (C=C). Spectre de masse: masse moléculaire calculée pour $C_{18}H_{22}O_6$: 334,142; trouvée: 334,140.

3. *Pyrones 5*

5α: À 600 mg (2,3 × 10^{-3} mol) de l'oléfine **4**α, on ajoute 1,2 g (2,61 × 10^{-2} mol) de HCO_2H pur, le mélange est maintenu à 80°C pendant 2 h. Après distillation de HCO_2Me et de HCO_2H, le produit solide obtenu est recristallisé dans l'éther, F = 74–75°C. On obtient 300 mg de **5**α (Rdt = 71%). ir (Nujol) ν: 1736 (large, C=O) et 1696 (large, C=O et C=C). *Anal.* calc. pour $C_9H_{10}O_4$: % C 59,34, H 5,49; tr.: C 59,3, H 5,3.

De la même manière (voir tableau 1) nous avons préparé les pyrones:

5β: F = 94–95°C (éther); Rdt = 83%; ir (Nujol) ν: 1780, 1762 (C=O) et 1704 (large, C=O et C=C). *Anal.* calc. pour $C_{13}H_{10}O_4$: % C 67,83, H 4,35; tr.: C 67,7, H 4,4.

5γ: F = 149–150°C (méthanol); Rdt = 71%; ir (Nujol) ν: 1736 (large) et 1704 (C=O) et 1630 (C=C). *Anal.* calc. pour $C_8H_8O_5$: % C 52,17, H 4,35; tr.: C 51,9, H 4,3.

5δ: F = 109°C (méthanol–éther 1:1); Rdt = 47%; ir (Nujol) ν: 1756 et 1704 (C=O) et 1640 (C=C). *Anal.* calc. pour $C_{15}H_{12}O_4$: % C 70,3, H 4,69; tr.: C 70,0, H 4,8.

4. *Composés **9**, **10** et **11***

À 1,6 g (5,3 × 10^{-3} mol) de la pyrazoline **8** en solution dans 7 cm^3 d'acétone, on ajoute 300 mg (5,4 × 10^{-4} mol; 0,1 équiv.) de $Ce(NH_4)_2(NO_3)_6$. Après 20 h à température ambiante, on ajoute 100 cm^3 d'éther. La phase organique est lavée à l'eau (2 fois 50 cm^3) puis séchée sur Na_2SO_4. Après élimination de l'éther on obtient 1,40 g d'un mélange dont les constituants sont séparés à l'aide de la chromatographie sur couche mince (SiO_2, mélange éluant: éther – éther de pétrole 1:1, 2 élutions).

9: R_f = 0,50; F = 74–75°C (éther); Rdt = 49%; ir (Nujol) ν: 1760 et 1712 (C=O). *Anal.* calc.: % C 57,35, H 7,35; tr.: C 57,1, H 7,5.

10: R_f = 0,30, 125°C (0,05 Torr) (l); Rdt = 15%.

11: R_f = 0,25, 130°C (0,004 Torr) (l); Rdt = 13%.

5. *Pyrone **12***

Une solution de 400 mg (1,5 × 10^{-3} mol) de la lactone **11** dans 5 g (0,11 mol) de HCO_2H est maintenue à reflux pendant 5 h. Après distillation de HCO_2H en excès et de HCO_2Me, le solide obtenu est recristallisé dans un mélange acétone–éther. On obtient 210 mg de la pyrone **12**; F = 220°C; Rdt = 79%; ir (Nujol) ν: 1794, 1772 et 1720 (C=O); rmn ($CDCl_3$ + CF_3CO_2H) δ: 7,97 (d, H_a, J_{ab} = 5,2), 6,68 (d, H_b), 1,69 (s, 6H, C(CH_3)$_2$). Spectre de masse: masse moléculaire calculée pour $C_9H_8O_4$: 180,042; trouvée: 180,043.

6. *Composés **14–18***

À 2,8 g (8,8 × 10^{-3} mol) de **13** dissous dans 7 cm^3 d'acétone, on ajoute 400 mg (0,08 équiv.) de $Ce(NH_4)_2(NO_3)_6$; le mélange réactionnel est abandonné à 30°C. Après 8 h, on ajoute 200 cm^3 d'éther, on lave à l'eau (2 fois 75 cm^3) et on sèche sur Na_2SO_4. Après élimination de l'éther et distillation au four tubulaire 125–130°C (3 × 10^{-3} Torr), on obtient 2,35 g d'un mélange des composés **14–18** formés (Rdt = 92%).

Les différents composés ont été séparés à l'aide de la chromatographie sur colonne suivie d'une chromatographie de partage gaz liquide.

La chromatographie sur colonne (70 g de SiO_2, mélange éluant: éther – éther de pétrole 1:2) de 2,50 g du produit brut de la réaction donne 110 mg de **15** (l); 200 mg d'un mélange des composés **15** et **16**; 350 mg de **16** contenant encore un peu de **15**; 250 mg d'un mélange de **15**, **17** et d'un produit **A** qui n'a pas été identifié; 400 mg d'un mélange de **14**, **15**, **17** et **A**; 340 mg d'un mélange de **14**, **16**, **17** (l) et **18** et enfin 270 mg d'un mélange de **14** et **18.**

La chromatographie de partage gaz–liquide des fractions précédentes est effectuée sur une colonne OV 225 (5% sur gas Chrom. Q 80–100 mesh), longueur 5 pieds, diamètre 1/4 pouce. Conditions de la chromatographie: T (injection) = 190°C, T(colonne) = 158°C, T (détecteur) = 200°C, T (collecteur) = 180°C, débit d'H_2 = 125 cm^3/min.

14: temps de rétention = 9 min; ir (film liquide) ν: 1728 (C=O). Spectre de masse: le pic de l'ion moléculaire est trop faible pour que la masse exacte puisse être mesurée. Masse calculée pour $[M - CH_3O]^+$, $C_{11}H_{15}O_7$ 259,082; trouvée: 259,082; pour $[M - CH_3OH]^{+\cdot}$, $C_{11}H_{14}O_7$ 258,074; trouvée: 258,074.

15: temps de rétention = 10,5 min; 105°C (0,01 Torr) (l).

16: temps de rétention = 15 min; ir (film liquide) ν: 1728 (C=O); rmn ($CDCl_3$) δ: 4,56 (t, $CH(OCH_3)_2$, J = 5,6), 3,84 (3H), 3,80 (6H) et 3,35 (6H) (3s, OCH_3), 2,96 (d, 2H, CH_2—C=). Spectre de masse: masse moléculaire calculée pour $C_{12}H_{18}O_8$: 290,100; masse trouvée: 290,100.

18: temps de rétention = 16,7 min; ir (film liquide) ν: 1734 (C=O); rmn ^1H (C_6D_6) δ: 4,63 (d, H_a, J_{ab} = 7,1), 4,35 (d, H_d, J_{cd} = 11,0), 4,00 (dd, H_c, J_{bc} = 2,7), 3,67 (dd, H_b), 3,44 (3H), 3,41 (3H), 3,36 (6H) et 3,24 (6H) (4s, OCH_3); rmn ^{13}C ($CDCl_3$) δ: 171,0, 168,9 et 168,5 (C=O), 105,3 ($CH(OCH_3)_2$), 80,5 ($CHOCH_3$), 60,0, 55,5, 52,8 et 52,1 (OCH_3), 50,8 ($CH(CO_2Me)_2$), 45,8 ($CHCO_2Me$). Spectre de masse: le pic de l'ion moléculaire est trop faible pour que la masse exacte puisse être mesurée. Masse calculée pour $[M - CH_3O]^+$ $C_{12}H_{19}O_8$: 291,108; trouvée 291,110.

Remarque: Le produit **A** de structure inconnue a un temps de rétention de 11,7 min; il représente environ 7% (intégration en chromatographie phase vapeur) du produit brut de la réaction. Un autre produit de structure inconnue (temps de rétention 29 min, abondance environ 3%) est mis en évidence dans le chromatogramme.

7. *Pyrone **19***

À 200 mg (6,9 × 10^{-4} mol) de l'oléfine **16** on ajoute 1 g (32 équiv.) de HCO_2H, le mélange est abandonné à 60°C pendant 6 h. La pyrone **19** est caractérisé uniquement à l'aide de la rmn. Ce composé est instable, il évolue lentement dans le milieu réactionnel et les essais de purification n'ont pas abouti. rmn ($CDCl_3$) δ: 7,60 (d, H_a, J_{ab} = 5,4), 6,62 (d, H_b), 3,92 (s, OCH_3, 6H).

1. H. ABDALLAH, R. GRÉE et R. CARRIÉ. Can. J. Chem. **61**, 217 (1983).
2. J. MARTELLI et R. GRÉE. J. Chem. Soc. Commun. 355 (1980).
3. C. R. ENGEL et G. DIONNE. Can. J. Chem. **56**, 424 (1978).
4. M. IHARA, K. NOGUCHI, T. OHSAWA et K. FUKUMOTO. Heterocycles, **19**, 1829 (1982).
5. D. L. BOGER et M. L. MULLICAN. Tetrahedron, **23**, 4551 (1982).
6. D. S. WATT et E. J. COREY. Tetrahedron Lett. 4651 (1972); E. J. COREY et D. S. WATT. J. Am. Chem. Soc. **95**, 2303 (1973).
7. R. E. IRELAND, R. C. ANDERSON, R. BADOUD, B. J. FITZSIMMONS, G. J. MCGARNEY, S. THAISRIVONGS et C. S. WILCOX.

J. Am. Chem. Soc. **105**, 1988 (1983).
8. J. AGAR, F. KAPLAN et B. W. ROBERTS. J. Org. Chem. **39**, 3451 (1974).
9. H. PLIENINGER et H. DUCKMAN. Chem. Ber. **105**, 2766 (1972).
10. I. FLEMING et D. H. WILLIAMS. Tetrahedron, **23**, 2747 (1967).
11. H. ABDALLAH. Thèse de Doctorat, Rennes (1983); Bull. Soc. Chim. Fr. À paraître.
12. J. THIELE et J. MEISENHEIMER. Ann. Chem. **306**, 253 (1898).

Regioselective fluoroalkoxylation and polyfluoroalkoxylation of aromatic and heteroaromatic polyhalides[1]

JOHN T. GUPTON,[2] GEORGE HERTEL, GARY DECRESCENZO, CESAR COLON, DONNA BARAN, DAN DUKESHERER, AND STEVE NOVICK
Department of Chemistry, University of Central Florida, Orlando, FL 32816, U.S.A.

DENNIS LIOTTA[2]
Department of Chemistry, Emory University, Atlanta, GA 30322, U.S.A.

AND

JOHN P. IDOUX[2]
Department of Chemistry, Lamar University, Beaumont, TX 77710, U.S.A.

Received December 13, 1984

JOHN T. GUPTON, GEORGE HERTEL, GARY DECRESCENZO, CESAR COLON, DONNA BARAN, DAN DUKESHERER, STEVE NOVICK, DENNIS LIOTTA, and JOHN P. IDOUX. Can. J. Chem. **63**, 3037 (1985).

A series of activated polyhalobenzenes and polyhaloheteroaromatic compounds have been reacted with a variety of fluoroalkoxide anions. In most cases, regioselective monosubstitution or polysubstitution was observed. The nature of these monosubstitution and polysubstitution reactions is described.

JOHN T. GUPTON, GEORGE HERTEL, GARY DECRESCENZO, CESAR COLON, DONNA BARAN, DAN DUKESHERER, STEVE NOVICK, DENNIS LIOTTA, et JOHN P. IDOUX. Can. J. Chem. **63**, 3037 (1985).

On a fait réagir une série de polyhalobenzènes et de composés polyhalohétéroaromatiques activés avec divers anions fluoroalcoolates. On observe, dans la plupart des cas, une mono ou une polysubstitution régiosélective. On décrit la nature de ces réactions de mono ou de polysubstitution.

[Traduit par le journal]

In a previous paper (1) we reported that activated monohalobenzenes and monohaloheterocycles could be reacted with fluoroalkoxide anions to produce the corresponding fluoroalkyl ethers. Such factors as the effect of solvent, time, temperature, nature of the leaving group, nature of the nucleophile, and nature of the activating group were discussed. Because of the diverse and important properties of organofluorine compounds (2) and since some of our previously reported fluoroalkyl ethers had been converted into "biologically active" derivatives,[3] we thought it would be useful to define further and delineate the scope of this reaction with regard to polyhalogenated substrates.

In related work, Tiecco *et al.* (3) have recently studied the reaction of polyhalogenated, non-activated benzenes with large excesses of alkanethiol anions in HMPA. In most of the examples reported, polysubstitution was obtained.

Because of our interest in this area we decided to examine the following factors with regard to polyhalocompounds: 1. the feasibility of polysubstitution; 2. the nature of the regiochemistry of a complete isomeric series (six isomers) of activated dihalobenzenes; 3. the halogen selectivity in the reaction; 4. the use of heteroaromatic substrates in the reaction; 5. the effect of the nucleophile in such reactions. The results of this study are reported in the subsequent sections.

Results and discussion

Reactions of activated dihalobenzenes with sodium 2,2,2-trifluoroethoxide

Our previous studies (1) involving the reaction of *o*-, *m*-, and *p*-chlorobenzonitriles and chloronitrobenzenes with sodium 2,2,2-trifluoroethoxide indicated that reaction at all three positions was possible. One would expect, however, that the relative order of reactivity might be *ortho* > *para* > *meta*. In fact, if one examines the reaction of 2,3-dichloronitrobenzene with one equivalent of 2,2,2-trifluoroethoxide (Table 1), the primary product results from substitution at the 2-position. In a like manner, 3,4-dichloronitrobenzene (**1***g*) gives mono substitution at the 4-position, and 2,5-dichloronitrobenzene (**1***d*) monosubstitutes at the 2-position. When the potential reaction sites were chemically equivalent, such as for 2,6-dichlorobenzonitrile (**1***e*) and 3,5-dichlorobenzonitrile (**1***i*), monosubstitution was also observed. When 2,4-dichloronitrobenzene (**1***b*) was examined under these conditions, a mixture of *ortho* and *para* substitution products was obtained in a ratio of 75:25, respectively. In order to make unambiguous structural assignments in these cases, the mono(trifluoroalkoxylated) substances (compounds **2***a*, **2***c*, **2***c'*, **2***f*, **2***g*, **2***i*, **2***j*, and **2***k*) were subjected to catalytic hydrogenolysis (4) to give the non-halogenated derivatives (Scheme 1).

Compounds such as **9** had been previously prepared (1) from the corresponding monohalo compounds and, therefore, a comparison by tlc and nmr of the various hydrogenolysis products enabled a straightforward structural assignment. 2-Chloro-6-fluorobenzonitrile (**1***f*) represented an interesting substrate in that it underwent regioselective reaction at the fluorine bearing carbon which provided a useful application of our previously reported (1) leaving-group reactivity study (NO_2, F > Cl > Br > I). Such a result, therefore, demonstrates the feasibility of selectively displacing one halogen in the presence of a second but different halogen.

The isomeric, activated dihalobenzenes were subsequently subjected to reaction with excess sodium 2,2,2-trifluoroethoxide. 2,6-Dichlorobenzonitrile (**1***e*), and 2,4-dichloronitrobenzene (**1***b*) underwent polysubstitution cleanly to give

[1] This work has been presented in part at the Seventh Gulf Coast Chemistry Conference, Pensacola Beach, Florida, September 20–22, 1984. Our preliminary findings were published in ref. 5.

[2] Authors to whom correspondence may be addressed.

[3] G. Cunningham, University of Central Florida, unpublished results.

TABLE 1. Reaction of activated dihalobenzenes with $NaOCH_2CF_3$

Entry	Starting material			Product	Yield[a] (%)
1	**1***a*	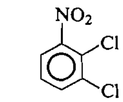	**2***a*	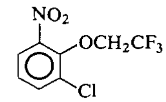	86(56)
2	**1***a*	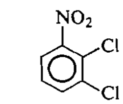	**2***b*	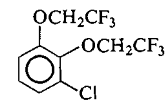	(31)
3	**1***b*	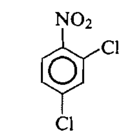	**2***c'* + **2***c*	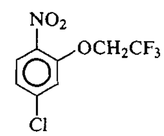 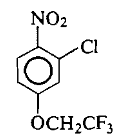	(45)
4	**1***b*	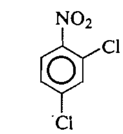	**2***d*	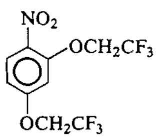	(63)
5	**1***c*	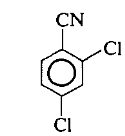	**2***e*	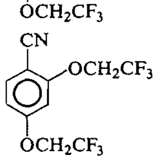	(85)
6	**1***d*	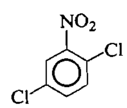	**2***f*	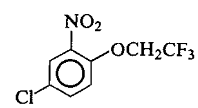	(63)
7	**1***e*	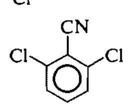	**2***g*	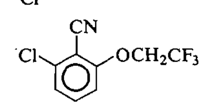	(97)
8	**1***e*	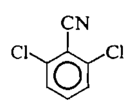	**2***h*	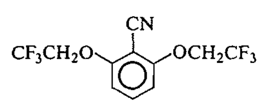	(54)
9	**1***f*	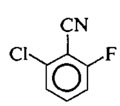	**2***g*	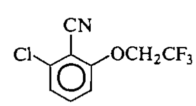	(77)
10	**1***g*	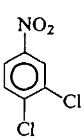	**2***i*	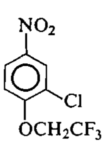	(58)
11	**1***h*	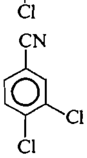	**2***j*	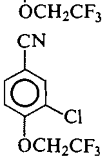	(63)
12	**1***i*	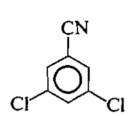	**2***k*	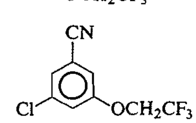	(47)

[a] All reactions were run for 15 h in DMF or HMPA at 150°C under nitrogen. These solvents (DMF and HMPA) are, for all practical purposes, interchangeable. The yields in parentheses refer to purified products. All products were subjected to gc analysis on a Shimadzu GC-7A gas chromatograph with a 1/8 in. × 6 ft 3% SB-2401 column at 100–200°C. Under these conditions, the products of the reactions were found to be greater than 90% pure. The only significant impurity which was found in some of the crude reaction mixtures was the respective starting material. When polyfluoroalkoxylation was desired, 2.2–3.0 equivalents of sodium hydride and 2,2,2-trifluoroethanol were used relative to the amount of the dihalobenzene or dihaloheteroaromatic substrate.

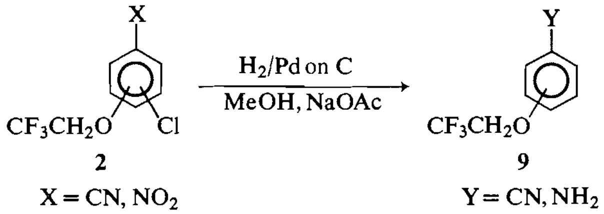

SCHEME 1

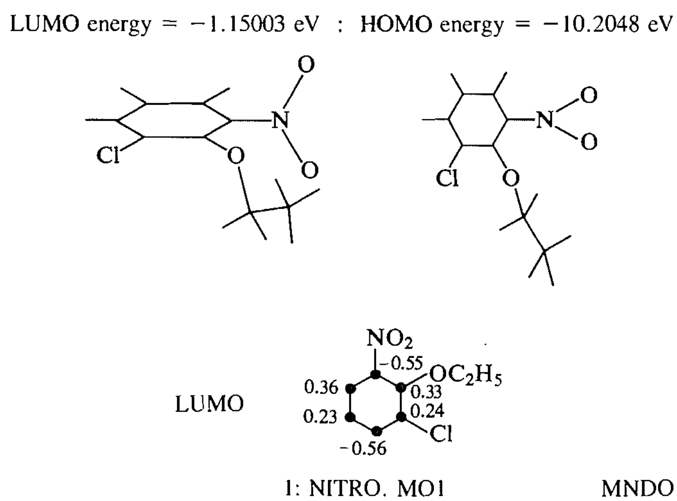

FIG. 1. 1-Chloro-2-ethoxy-3-nitrobenzene.

the respective di(trifluoroalkoxylated) derivatives. 3,4-Dichloronitrobenzene (**1***g*) was found to undergo only monosubstitution which indicated that the trifluoroalkoxy group at the 4-position was having a deactivating effect with regard to further reaction. 3,5-Dichlorobenzonitrile (**1***i*) gave monosubstitution also. Perhaps the most interesting and unusual substrate studied was 2,3-dichloronitrobenzene. This material produced 2,3-di(2,2,2-trifluoroethoxy)chlorobenzene (**2***b*) upon reaction with excess trifluoroethoxide ion. This structural assignment was based on nmr, ir, ms, and combustion analysis data. As a consequence, molecular orbital calculations with full geometric optimization, which indicate that the nitro group is distorted out of the plane of the benzene ring by 87 degrees, have been carried out on 3-chloro-2-ethoxynitrobenzene (Fig. 1). Based on the magnitude of the LUMO coefficients, these calculations further indicate that the preferred site of nucleophilic attack is the carbon bearing the nitro group. Presumably, the chlorine atom exhibits a buttressing effect on the alkoxy group and prohibits it from moving away from the nitro group; as a result, the nitro group must be non-planar with the ring in order to reduce steric repulsions. Work is now in progress to determine if this is a normal reaction for this system with other nucleophiles. 2,5-Dichloronitrobenzene (**1***d*) reacted with excess trifluoroalkoxide to give a gross mixture of products and this transformation was determined to be of little synthetic use.

Reaction of polychloroheterocycles with $NaOCH_2CF_3$

The purpose of this study was to examine the nature of mono(trifluoroalkoxylation) and poly(trifluoroalkoxylation) reactions of polyhaloheterocycles and the substrates studied are reported in Table 2. 3,6-Dichloropyridazine (**3***a*) was found to undergo cleanly both monosubstitution and disubstitution, depending on the amount of trifluoroalkoxide used. The nmr spectrum of the monosubstituted compound was easily differentiated from that of the disubstituted derivative since the monosubstituted pyridazine had two doublets in the aromatic region due to two, non-equivalent, adjacent, heteroaromatic hydrogens. The disubstituted compound was symmetric and, therefore, a singlet integrating for two hydrogens was observed in the aromatic region of the nmr spectrum. 2,4-Dichloropyrimidine (**3***b*) was also found to undergo polysubstitution cleanly but apparently this substance was too reactive to give a single monosubstitution product. 4,7-Dichloroquinoline (**3***c*) underwent selective monosubstitution at the 4-position. This was verified by catalytic hydrogenolysis of the monosubstitution product and subsequent nmr comparison of the material with the 7-chloro-4-(2,2,2-trifluoroethoxy) quinoline (**4***d*). Analysis of the nmr splitting patterns for hydrogens at positions two and three indicated no change from the set of doublets observed in the starting material. The 4,7-dichloroquinoline (**3***c*) was found to be unreactive with regard to further substitution at the 7-position when subjected to reaction with excess trifluoroalkoxide ion. 2,4,6-Trichloropyrimidine (**3***d*) represented an interesting example in that it was found to undergo substitution at all three positions to give a tris(trifluoroalkoxylated) derivative. The final example studied was 2,3-dichloro-5-trifluoromethylpyridine (**3***e*) which was found to react selectively at the 2-position.

Reaction of 3,4-dichloronitrobenzene and 3,6-dichloropyridazine with various sodium fluoroalkoxides

We had previously found (1) that fluoroalkoxide anions possessing more than four fluorines were relatively unreactive toward 4-chlorobenzonitrile. We decided to extend this study to 3,4-dichloronitrobenzene in order to determine the effect of additional halogens on the aromatic substrate. As indicated in Table 3, 1,1,1-trifluoroisopropoxide and 2,2,3,3-tetrafluoropropoxide reacted cleanly with 3,4-dichloronitrobenzene at the 4-position at room temperature in HMPA. Presumably the increased activating effect of the nitro group over the nitrile and the presence of an *ortho* chlorine allows this transformation to take place at room temperature. Perhaps even more interesting, 2,2,3,3,3-pentafluoropropoxide and 2,2,3,3,4,4,4-heptafluorobutoxide reacted with 3,4-dichloronitrobenzene at the 4-position also, albeit at a significantly higher temperature. Both of these alkoxide ions were found to be unreactive with 4-chlorobenzonitrile in our previous study. The significance of the reaction of the latter two nucleophiles is that more highly fluorinated alkoxide anions should also undergo such reactions since inductive effects would be expected to be negligible over a five-atom distance. Therefore, there should in principle be no limitation on this reaction based on the number of fluorines on the nucleophile if one chooses a sufficiently reactive aryl halide.

In order to determine the nature of polysubstitution reactions for such nucleophiles, the reaction of 3,6-dichloropyridazine with excess fluoroalkoxide anion was studied. As indicated in Table 4, 1,1,1-trifluoroisopropoxide and 2,2,3,3-tetrafluoropropoxide were found to give polysubstitution in DMF at 150°C. When dioxane was used as the solvent, both 2,2,3,3,3-pentafluoropropoxide and 2,2,3,3,4,4,4-heptafluorobutoxide were also found to undergo successful polysubstitution reactions. These latter two reactions proved to be of particular significance since they demonstrated that lower reaction temperatures (100°C) and less polar solvents could be successfully

TABLE 2. Reactions of polychloroheterocycles with $NaOCH_2CF_3$

	Substrate		Product	Yield[a] (%)
3*a*	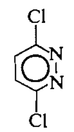	4*a*	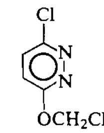	93 (62)
3*a*	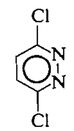	4*b*	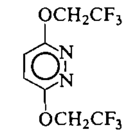	57
3*b*	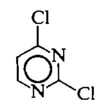	4*c*	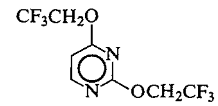	(54)
3*c*	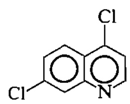	4*d*	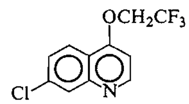	81
3*d*	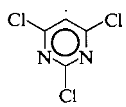	4*e*	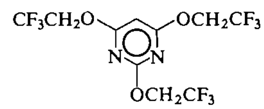	55 (37)[b]
3*e*	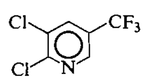	4*f*	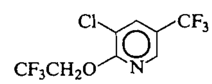	100 (42)

[a]See footnote *a*, Table 1.
[b]The reactants were mixed at 0–10°C in order to minimize any undesirable side reactions. After stirring for approximately 30 min at room temperature, the mixture was heated at *150°C for 15 h*.

TABLE 3. Reaction of 3,4-dichloronitrobenzene with various sodium fluoroalkoxides

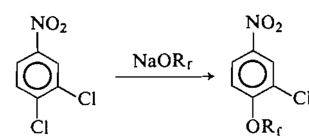

5 6

Entry	R_f	Product	Reaction temp. (°C)	Reaction time (h)	Yield[a] (%)
1	$—CH(CH_3)CF_3$	6*a*	25	24	100(70)[b]
2	$—CH_2CF_2CF_2H$	6*b*	25	24	67(50)[b]
3	$—CH_2CF_2CF_3$	6*c*	140	24	71(30)[b]
4	$—CH_2CF_2CF_2CF_3$	6*d*	140	24	80(35)[b]

[a]See footnote *a*, Table 1.
[b]HMPA was used as the solvent in these reactions.

used if one chooses a reasonably reactive heteroaromatic halide as the substrate.

In conclusion, regioselective fluoroalkoxylation and polyfluoroalkoxylation have been achieved with a variety of polyhalogenated aromatic and heteroaromatic systems. Halogen selectivity has also been observed and the presence of additional fluorines in the nucleophile does not seem to affect adversely the nature of such substitution reactions.

Experimental

The following procedure is typical of the experimental conditions used for the reaction of activated aromatic and heteroaromatic compounds with fluorinated alkoxide anions. Infrared spectra were recorded on either a Perkin Elmer Model 1420 infrared spectrometer or a Nicolet MXS FT IR as thin films or Nujol mulls. The nmr spectra were obtained in CCl_4, $DCCl_3$, or Me_2SO-d_6 solutions ($(CH_3)_4Si$ internal standard) at 60 MHz with a Varian EM-360 spectrometer. All boiling points and melting points are uncorrected and melting points were recorded on a Fisher–Johns melting-point apparatus. With regard to the characterization of the reaction products, combustion analyses were carried out on representative samples (2*b*, 2*e*, 2*g*, 2*j*, 4*b*, and 4*c*). Compounds 2*a*, 2*c*, 2*c*′, 2*f*, 2*i*, 2*j*, and 2*k* were converted to substances that we have previously reported (1). Compounds 6*a*, 6*b*, 6*c*, and 6*d* were simple analogs of 2*i* and had the appropriate, and analogous, nmr absorptions. Compounds 8*a*, 8*b*, 8*c*, and 8*d* were simple analogs of 4*b* and had the appropriate, and analogous, nmr absorptions. Compounds 2*d*, 2*h*, 4*a*, 4*d*, 4*e*, and 4*f* had relatively

TABLE 4. Reaction of 3,6-dichloropyridazine with various sodium fluoroalkoxides

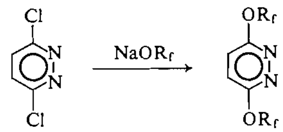

7 8

Entry	R_f	Product	Reaction temp. (°C)	Reaction time (h)	Yield[a] (%)
1	$—CH(CH_3)CF_3$	**8***a*	150	24	100(53)
2	$—CH_2CF_2CF_2H$	**8***b*	150	24	64(57)
3	$—CH_2CF_2CF_3$	**8***c*	101	24	(78)[b]
4	$—CH_2CF_2CF_2CF_3$	**8***d*	101	24	54(24)[b]

[a] See footnote *a* Table 1.
[b] These reactions were run in dioxane, *for 15 h at 101°C.*

uncomplicated and unambiguous nmr spectral properties. All reaction products gave nmr, ir, and ms spectra consistent with their assigned structure and their homogeneity was determined by the use of glc or tlc techniques.

3-Chloro-4(2,2,2-trifluoroethoxy)nitrobenzene, **2**i

A dry, three-necked round-bottomed flask equipped with a condenser, thermometer, rubber septum, and magnetic stirrer was placed under a nitrogen atmosphere. Into the flask was placed 1.37 g (0.0286 mol) of a 50% sodium hydride – mineral oil mixture which was subsequently washed with hexane. To the sodium hydride was added 125 mL of DMF (dried over 4A molecular sieves) and 2.86 g (0.0286 mol) of 2,2,2-trifluoroethanol, respectively. The mixture was allowed to stir for 20 min and 5.00 g (0.0260 mol) of 3,4-dichloronitrobenzene was added in one portion. The resulting mixture was heated at reflux (150°C) for 18 h, cooled to room temperature, and the solvent was removed *in vacuo*. The residue was carefully diluted with 100 mL of ice water, extracted with ether (3 × 100 mL), and the combined extracts were washed with water (3 × 30 mL) and dried over anhydrous magnesium sulfate. After removing the drying agents, the organic phase was concentrated *in vacuo* to yield 5.30 g of a dark liquid. This material was distilled (Kugelrohr) to give 3.25 g (58% yield) of a solid, bp 77–78°C at 0.4 Torr (1 Torr = 133.3 Pa) and mp 48–49°C.

3-Chloro-2-(2,2,2-trifluoroethoxy)nitrobenzene, **2**a: bp 60–62°C (0.1 Torr); ir (thin film): 1595, 1535, 1460, 1360, 1290, 1250, 1170, 1080, 1045, 965, 870, 800, 860, 840, and 675 cm^{-1}; nmr ($CDCl_3$) δ: 4.55 (q, J = 8 Hz, 2H), 7.31 (t, J = 8 Hz, 1H), and 7.60–7.97 (m, 2H); mass spectrum, *m/e*: 255, 257 (M^+).

2,3-Di-(2,2,2-trifluoroethoxy)chlorobenzene, **2**b: bp 60°C (0.1 Torr); ir (thin film): 1585, 1480, 1455, 1285, 1265, 1165, 1080, 1050, 965, 895, 865, 770, 735, and 705 cm^{-1}; nmr ($CDCl_3$) δ: 4.40 (q, J = 8 Hz, 4H) and 6.78–7.30 (m, 3H); mass spectrum, *m/e*: 308, 310 (M^+). *Anal.* calcd. for $C_{10}H_7O_2ClF_6$: C 38.92, H 2.29, F 36.94; found: C 39.11, H 2.50, F 37.13.

*2-Chloro-4-(2,2,2-trifluoroethoxy)nitrobenzene (***2**c*) and 4-chloro-2-(2,2,2-trifluoroethoxy)nitrobenzene,* **2**c′

This reaction produced a mixture of *para* (**2**c) and *ortho* (**2**c′) substitution products as determined by glpc analysis. The relative composition was determined to be 75% of the *ortho* substitution product (**2**c′) and 25% of the *para* substitution product (**2**c): bp (mixture) 68–72°C (0.3 Torr); ir (thin film): 1605, 1580, 1530, 1350, 1295, 1250, 1175, 1090, 1060, 980, 970, 915, 840, and 660 cm^{-1}; nmr ($CDCl_3$, mixture of isomers, *ortho* substitution absorptions) δ: 4.53 (q, J = 8 Hz, 2H), 7.08–7.33 (m, 2H), and 7.91 (d, J = 10 Hz, 1H); nmr ($CDCl_3$, mixture of isomers, *para* substitution absorptions) δ: 4.48 (q, J = 8 Hz, 2H), 7.08–7.33 (m, 2H), and 8.05 (d, J = 10 Hz, 1H); mass spectrum, *m/e*: 255, 257 (M^+). The mixture of isomers was further characterized by catalytic hydrogenolysis with Pd on carbon in methanol with sodium acetate. This mixture of *ortho*- and *para*-(2,2,2-trifluoroethoxy) anilines was compared by nmr and tlc to the catalytic hydrogenation products obtained from reduction of the known (1) *o*-(2,2,2-trifluoroethoxy)nitrobenzene and *p*-(2,2,2-trifluoroethoxy)nitrobenzene.

2,4-Di-(2,2,2-trifluoroethoxy)nitrobenzene, **2**d: mp 110–113°C (recrystallized from iPrOH/H_2O); ir (Nujol): 1620, 1520, 1365, 1280, 1185, 970, 860, 840, 815, and 750 cm^{-1}; nmr ($CDCl_3$/acetone-d_6) δ: 4.70 (q, J = 8 Hz, 2H), 4.74 (q, J = 8 Hz, 2H), 6.88 (d of d, J = 8 Hz, J = 2 Hz, 1H), 7.03 (d, J = 2 Hz, 1H), and 8.06 (d, J = 8 Hz, 1H); mass spectrum, *m/e*: 319 (M^+).

2,4-Di-(2,2,2-trifluoroethoxy)benzonitrile, **2**e: mp 109–110°C (recrystallized from iPrOH/H_2O); ir (Nujol): 2240, 1620, 1285, 1180, 1070, 860, 845, 830, and 750 cm^{-1}; nmr ($CDCl_3$/Me_2SO-d_6) δ: 4.70 (q, J = 8 Hz, 2H), 4.78 (q, J = 8 Hz, 2H), 6.83 (d of d, J = 8 Hz, J = 2 Hz, 1H), 7.04 (d, J = 2 Hz, 1H), and 7.64 (d, J = 8 Hz, 1H); mass spectrum, *m/e*: 299 (M^+). *Anal.* calcd. for $C_{11}H_7NO_2F_6$: C 44.16, H 2.36, N 4.68; found: C 44.88, H 2.84, N 4.34.

5-Chloro-2-(2,2,2-trifluoroethoxy)nitrobenzene, **2**f: bp 60°C (0.3 Torr); ir ($CHCl_3$): 1610, 1535, 1485, 1350, 1295, 1260, 1170, 1120, 970, 960, 890, 865, 810, and 660 cm^{-1}; nmr ($CDCl_3$) δ: 4.52 (q, J = 8 Hz, 2H), 7.18 (d, J = 9 Hz, 1H), 7.64 (d of d, J = 2 Hz, J = 9 Hz, 1H), and 7.94 (d, J = 2 Hz, 1H); mass spectrum, *m/e*: 255, 257 (M^+).

2-Chloro-6-(2,2,2-trifluoroethoxy)benzonitrile, **2**g: mp 110–113°C (recrystallized from iPrOH/H_2O); ir (Nujol): 2235, 1590, 1580, 1470, 1270, 1170, 1075, 970, 900, 860, 780, and 710 cm^{-1}; nmr ($CDCl_3$) δ: 4.53 (q, J = 8 Hz, 2H), 6.96 (d of d, J = 1 Hz, J = 8 Hz, 1H), 7.19 (d of d, J = 1 Hz, J = 8 Hz, 1H), and 7.55 (t, J = 8 Hz, 1H); mass spectrum, *m/e*: 237, 235 (M^+). This reaction was run at 90°C as opposed to the normal reaction temperature of 150°C. *Anal.* calcd. for $C_9H_5NOClF_3$: C 45.88, H 2.14, N 5.95; found: C 45.88, H 2.37, N 5.78.

2,6-Di-(2,2,2-trifluoroethoxy)benzonitrile, **2**h: mp 86–90°C (recrystallized from iPrOH/H_2O); ir ($CHCl_3$): 2240, 1600, 1590, 1290, 1260, 1240, 1170, 1130, 715, and 685 cm^{-1}; nmr ($CDCl_3$) δ: 4.53 (q, J = 8 Hz, 4H), 6.88 (d, J = 8 Hz, 2H), and 7.63 (t, J = 8 Hz, 1H); mass spectrum, *m/e*: 299 (M^+).

3-Chloro-4-(2,2,2-trifluoroethoxy)nitrobenzene, **2**i: bp 77–78°C (0.4 Torr); mp 48–49°C; ir (CCl_4): 1590, 1525, 1490, 1345, 1290, 1250, 1170, 1075, 970, 900, and 860 cm^{-1}; nmr ($CDCl_3$) δ: 4.58 (q, J = 8 Hz, 2H), 7.10 (d, J = 8 Hz, 1H), 8.30 (d of d, J = 8 Hz, J = 2 Hz, 1H), and 8.40 (d, J = 2 Hz, 1H); mass spectrum, *m/e*: 257, 255 (M^+).

3-Chloro-4-(2,2,2-trifluoroethoxy)benzonitrile, **2**j: mp 74–75°C (recrystallized from MeOH/H_2O); ir (Nujol): 2230, 1595, 1495, 1310, 1295, 1255, 1180, 1085, 975, 900, 860, and 810 cm^{-1}; nmr ($CDCl_3$) δ: 4.52 (q, J = 8 Hz, 2H), 7.08 (d, J = 8 Hz, 1H), and 7.48–7.90 (m, 2H); mass spectrum, *m/e*: 237, 235 (M^+). *Anal.* calcd. for $C_9H_5NOF_3Cl$: C 45.88, H 2.14, N 5.95; found: C 46.06, H 2.30, N 5.89.

3-Chloro-5-(2,2,2-trifluoroethoxy)benzonitrile, **2**k: bp 62–64°C

(0.1 Torr); ir (Nujol): 2215, 1590, 1430, 1290, 1260, 1160, 1080, 970, 860, 695, and 670 cm^{-1}; nmr ($CDCl_3$) δ: 4.42 (q, J = 8 Hz, 2H) and 7.07–7.44 (m, 3H); mass spectrum, m/e: 235, 237 (M^+).

3-Chloro-6-(2,2,2-trifluoroethoxy)pyridazine, 4a: bp 62–65°C (0.3 Torr) ir (Nujol): 1585, 1410, 1265, 1165, 1050, 960, 860, 835, and 720 cm^{-1}; nmr ($CDCl_3$) δ: 4.96 (q, J = 8 Hz, 2H), 7.20 (d, J = 10 Hz, 1H), and 7.58 (d, J = 10 Hz, 1H); mass spectrum, m/e: 212, 214 (M^+).

3,6-Di-(2,2,2-trifluoroethoxy)pyridazine, 4b: mp 79–83°C; ir (Nujol): 1470, 1370, 1280, 1250, 1175, 1055, 960, 870, 840, 690, 655, and 630 cm^{-1}; nmr ($CDCl_3$) δ: 4.90 (q, J = 8 Hz, 4H) and 7.18 (s, 2H); mass spectrum, m/e: 276 (M^+). *Anal.* calcd. for $C_8H_6N_2O_2F_6$: C 34.79, H 2.19, N 10.15; found: C 35.59, H 2.58, N 9.89.

2,4-Di-(2,2,2-trifluoroethoxy)pyrimidine, 4c: bp 53°C (0.3 Torr); ir (thin film): 1590, 1465, 1450, 1420, 1380, 1270, 1170, 1110, 1060, 985, 960, 855, 820, 695, and 670 cm^{-1}; nmr ($CDCl_3$) δ: 4.82 (q, J = 8 Hz, 4H), 6.53 (d, J = 6 Hz, 1H), and 8.35 (d, J = 6 Hz, 1H); mass spectrum, m/e: 276 (M^+). *Anal.* calcd. for $C_8H_6N_2O_2F_6$: C 34.79, H 2.19, N 10.15; found: C 35.10, H 2.29, N 9.53.

7-Chloro-4-(2,2,2-trifluoroethoxy)quinoline, 4d: mp 93–97°C; ir (Nujol): 1620, 1590, 1565, 1505, 1380, 1120, 1295, 1265, 1165, 1130, 970, 905, 870, 860, 850, 825, 760, and 680 cm^{-1}; nmr ($CDCl_3$) δ: 4.60 (q, J = 8 Hz, 2H), 6.70 (d, J = 5 Hz, 1H), 7.55 (d of d, J = 2 Hz, J = 5 Hz, 1H), 8.02–8.40 (m, 2H), and 9.80 (d, J = 5 Hz, 1H); mass spectrum, m/e: 261, 263 (M^+).

2,4,6-Tri-(2,2,2-trifluoroethoxy)pyrimidine, 4e: bp 60–63°C (0.07 Torr); ir (thin film): 1610, 1585, 1440, 1420, 1380, 1270, 1175, 1125, 1080, 960, 860, 825, 695, and 665 cm^{-1}; nmr ($CDCl_3$) δ: 4.80 (q, J = 8 Hz, 2H), 4.84 (q, J = 8 Hz, 4H), and 6.13 (s, 1H); mass spectrum, m/e: 374 (M^+).

3-Chloro-5-trifluoromethyl-2-(2,2,2-trifluoroethoxy)pyridine, 4f: bp 35–37°C (0.8 Torr); ir (thin film): 1605, 1480, 1450, 1415, 1340, 1280, 1260, 1170, 1140, 1085, 1055, 965, 920, 860, 760, 720, and 660 cm^{-1}; nmr ($CDCl_3$) δ: 4.92 (q, J = 8 Hz, 2H), 8.01 (d, J = 2 Hz, 1H), and 8.44 (d, J = 2 Hz, 1H); mass spectrum, m/e: 279, 281 (M^+).

3-Chloro-4-(1,1,1-trifluoroisopropoxy)nitrobenzene, 6a: bp 70–82°C (0.15 Torr); ir (thin film): 1585, 1525, 1485, 1350, 1270, 1185, 1165, 1090, 1055, 1020, 940, 900, 755, and 670 cm^{-1}; nmr ($CDCl_3$) δ: 1.65 (d, J = 7 Hz, 3H), 4.90 (hept, J = 7 Hz, 1H), 7.17 (d, J = 9 Hz, 1H), 8.23 (d of d, J = 3 Hz, J = 9 Hz, 1H), and 8.38 (d, J = 3 Hz, 1H); mass spectrum, m/e: 269, 271 (M^+).

3-Chloro-4-(2,2,3,3-n-tetrafluoropropoxy)nitrobenzene, 6b: bp 77–87°C (0.15 Torr); ir (thin film): 1585, 1525, 1490, 1350, 1285, 1205, 1125, 1070, 900, 840, 820, 745, and 645 cm^{-1}; nmr ($CDCl_3$) δ: 4.57 (t, J = 12 Hz, 2H), 6.20 (t of t, J = 5 Hz, J = 53 Hz, 1H), 7.10 (d, J = 8 Hz, 1H), and 8.10–8.33 (m, 2H); mass spectrum, m/e: 287, 289 (M^+).

3-Chloro-4-(2,2,3,3,3-n-pentafluoropropoxy)nitrobenzene, 6c: bp 80–92°C (0.2 Torr); ir (thin film): 1585, 1570, 1490, 1350, 1285, 1200, 1150, 1100, 1075, 1015, 900, 820, 740, and 665 cm^{-1}; nmr ($CDCl_3$) δ: 4.60 (t, J = 12 Hz, 2H), 7.05 (d, J = 9 Hz, 1H), 8.18 (d of d, J = 2 Hz, J = 9 Hz, 1H), and 8.30 (d, J = 2 Hz, 1H); mass spectrum, m/e: 305, 307 (M^+).

3-Chloro-4-(2,2,3,3,4,4,4-n-heptafluorobutoxy)nitrobenzene, 6d: bp 60–80°C (0.1 Torr); ir (thin film): 1585, 1520, 1490, 1350, 1335, 1275, 1185, 1125, 1075, 1020, 920, 900, 740, and 650 cm^{-1}; nmr ($CDCl_3$) δ: 4.72 (t, J =12 Hz, 2H), 7.17 (d, J = 9 Hz, 1H), 8.30 (d of d, J = 9 Hz, J = 2 Hz, 1H), and 8.42 (d, J = 2 Hz, 1H); mass spectrum, m/e: 355, 357 (M^+).

3,6-Di-(1,1,1-trifluoroisopropoxy)pyridazine, 8a: bp 72–75°C (0.1 Torr); ir (thin film): 1440, 1380, 1360, 1265, 1180, 1160, 1110, 1090, 1020, 935, 840, 670, and 635 cm^{-1}; nmr ($CDCl_3$) δ: 1.45 (d, J = 7 Hz, 6H), 5.82 (hept, J = 7 Hz, 2H), and 7.08 (s, 2H); mass spectrum, m/e: 304 (M^+).

3,6-Di-(2,2,3,3-n-tetrafluoropropoxy)pyridazine, 8b: bp 55–75°C (0.1 Torr); ir (thin film): 1460, 1440, 1400, 1270, 1200, 1110, 1050, 945, 835, and 680 cm^{-1}; nmr ($CDCl_3$) δ: 4.83 (t, J = 12 Hz, 4H), 6.00 (t of t, J = 5 Hz, J = 53 Hz, 2H), and 7.13 (s, 2H); mass spectrum, m/e: 340 (M^+).

3,6-Di-(2,2,3,3,3-n-pentafluoropropoxy)pyridazine, 8c: bp 70–75°C (0.5 Torr); ir (thin film): 1470, 1445, 1400, 1365, 1350, 1280, 1200, 1150, 1110, 1060, 1015, 940, 840, 725, 670, and 640 cm^{-1}; nmr ($CDCl_3$) δ: 4.97 (t, J = 12 Hz, 4H) and 7.20 (s, 2H); mass spectrum, m/e: 376 (M^+).

3,6-Di-(2,2,3,3,4,4,4-n-heptafluorobutoxy)pyridazine, 8d: bp 74–80°C (1 Torr); ir (thin film): 1470, 1450, 1350, 1280, 1230, 1185, 1130, 1060, 1020, 965, 920, 840, 760, 740, and 650 cm^{-1}; nmr ($CDCl_3$) δ: 5.02 (t, J = 12 Hz, 4H) and 7.20 (s, 2H); mass spectrum, m/e: 476 (M^+).

Catalytic hydrogenolysis of 3-chloro-4-(2,2,2-trifluoroethoxy)benzonitrile, 2j

Into a Parr, low pressure, hydrogenation bottle was placed 0.300 g of 3-chloro-4-(2,2,2-trifluoroethoxy) benzonitrile, 100 mL of anhydrous methanol, 0.585 g of anhydrous sodium acetate, and 0.200 g of 5% Pd on carbon. This mixture was then placed in a Parr hydrogenation apparatus and evacuated several times to remove any traces of oxygen. Hydrogen was introduced into the reaction vessel until a pressure of 55 psi (1 psi = 6.89 kPa) was reached. The resulting mixture was shaken for 4 h, at which point a constant pressure was obtained. The system was then evacuated for 15 min to remove hydrogen and the Pd on carbon was removed by filtration. The filtrate was concentrated *in vacuo* and the residue was partitioned between water (50 mL) and chloroform (50 mL). The chloroform phase was dried over anhydrous magnesium sulfate, filtered, and concentrated *in vacuo*. The residue was subjected to nmr, ir, and tlc analysis (50% ethyl acetate, 50% chloroform on Silica gel 7GF) and subsequently compared with an authentic sample (1) of 4-(2,2,2-trifluoroethoxy) benzonitrile. The crude residue was found to correspond to the authentic sample under these conditions of analysis. Compounds **2***a*, **2***c*, **2***c'*, **2***f*, **2***g*, and **2***k* were treated in a similar fashion and compared with the appropriate authentic samples (1). In cases where the authentic samples were nitro compounds, these standards were also subjected to hydrogenolysis under the above conditions in order that direct comparisons (nmr, ir, and tlc) could be made. In all of the examples studied, the hydrogenolysis products and the respective authentic samples were found to be identical. Compound **4***d*, Table 2, was also subjected to analogous hydrogenolysis conditions.

Acknowledgements

We thank the National Science Foundation for equipment grants (CDP-7922930 and RII-8304384), which were used for the purchase of a Varian EM-360 nmr spectrometer and a Perkin Elmer 1420 ir spectrometer. In addition, acknowledgement is made to the Donors of the Petroleum Research Fund, administered by the American Chemical Society, for partial support of this work. We also sincerely appreciate the assistance of Dr. Leon Zalkow, Dr. Robert Pierotti, and the mass spectrometry facility at the Georgia Institute of Technology for providing us with mass spectral data on our compounds.

1. J. IDOUX, J. GUPTON, C. MCCURRY, A. CREWS, C. JURSS, C. COLON, and R. RAMPI. J. Org. Chem. **48**, 3771 (1983).
2. M. GERSTENBERGER and A. HAAS. Angew. Chem. Int. Ed. Engl. **20**, 647 (1981).
3. M. TIECCO, P. COGOLLI, F. MAIOLO, L. TESTAFERRI, and M. TINGOLI. J. Org. Chem. **44**, 2642 (1979); M. TIECCO, M. TESTAFERRI, and M. TINGOLI. J. Org. Chem. **45**, 4736 (1980).
4. J. BOBBITT and D. SCOLA. J. Org. Chem. **25**, 560 (1960).
5. J. GUPTON, G. DECRESCENZO, and C. COLON. Synth. Commun. **14**, 621 (1984).

Stereochemical dependence of the mechanism of deoxygenation, with lithium triethylborohydride, in 4,6-*O*-benzylidenehexopyranoside *p*-toluenesulfonates

HANS H. BAER AND MIROSLAWA MEKARSKA-FALICKI

Ottawa–Carleton Institute for Research and Graduate Studies in Chemistry, Department of Chemistry, University of Ottawa, Ottawa, Ont., Canada K1N 9B4

Received February 14, 1985

HANS H. BAER and MIROSLAWA MEKARSKA-FALICKI. Can. J. Chem. **63**, 3043 (1985).

Lithium triethylborohydride was shown to react with methyl 4,6-*O*-benzylidene-α-D-hexopyranoside 2- and 3-tosylates, and 2,3-ditosylates, in the *manno*, *allo*, and *altro* configurational series both by O—S fission (*O*-desulfonylation) and by C—O fission (*C*-desulfonyloxylation), to produce carbinol and deoxy functions, respectively. The results were compared with those previously obtained with the corresponding *gluco* and *galacto* isomers, and the degree of facility of the cleavage reactions was seen to depend on the position of the sulfonic ester groups and the overall configuration of the molecules. The mechanism of reductive desulfonyloxylation also depended on configuration and was demonstrated to involve intermediary epoxide formation or displacement by internal hydride shift as the principal paths; competing elimination and direct nucleophilic displacement were found to occur in the *allo* series, whereas reduction accompanied by ring contraction has thus far been encountered only in the conformationally less constrained, *cis*-fused acetal system of the *galacto* series. Like the borohydride reagent, lithium aluminum hydride was found to react (though much more slowly) with the *altro* 2,3-ditosylate by the epoxide-mediated mechanism, although the latter hydride is known to desulfonyloxylate the α-D-*gluco*-isomer by a different, intramolecular reduction mechanism.

HANS H. BAER et MIROSLAWA MEKARSKA-FALICKI. Can. J. Chem. **63**, 3043 (1985).

Le borohydrure de triéthyllithium réagit avec les tosylates-2 et -3 et avec les ditosylates-2,3 du *O*-benzylidène-4,6 α-D-hexopyranosides de méthyle de configurations *manno*, *allo* et *altro* pour conduire, par fission de la liaison O—S (*O*-désulfonylation) et par fission de la liaison C—O (*C*-désulfonyloxylation), à des fonctions carbinol et désoxy respectivement. On a comparé les résultats à ceux obtenus antérieurement pour les isomères *gluco* et *galacto* correspondants et on a remarqué que le degré de facilité de les réactions de clivage dépend de la position des groupes esters sulfoniques et de la configuration générale des molécules. Le mécanisme principal de la désulfonyloxylation réductrice dépend également de la configuration et on démontre qu'il implique la formation intermédiaire d'un époxyde ou un déplacement par glissement interne d'hydrure. Dans la série *allo*, on note la présence d'une réaction compétitive d'élimination ainsi que celle d'un déplacement nucléophile direct; par ailleurs, une réduction accompagnée d'une contraction de cycle ne se produit que dans la série *galacto* contenant un système acétal *cis*-condensé ayant moins de contrainte conformationnelle. L'alanate de lithium, à l'instar du borohydrure, réagit (bien que beaucoup plus lentement) avec le ditosylate-2,3 *altro* selon un mécanisme impliquant un époxyde intermédiaire en dépit du fait qu'il est connu que ce dernier hydrure conduit à une désulfonyloxylation de l'isomère α-D-*gluco* selon un mécanisme de réduction intramoléculaire différent.

[Traduit par le journal]

Introduction

Lithium triethylborohydride (LTBH, Super Hydride®) is a powerful reagent for the deoxygenation of alcohols by reduction of their *p*-toluenesulfonic esters. It has been reported to react smoothly, not only with unhindered, primary tosylates but also with hindered ones as well as with secondary, cycloalkanol tosylates (1). Competing *O*-desulfonylation and (or) eliminative alkene formation are normally negligible or, at least, strongly curtailed in comparison to similar reduction with lithium aluminum hydride. An early application in carbohydrate chemistry (2) demonstrated the ready reduction of 1,2:3,5-di-*O*-methylidene-α-D-glucofuranose 6-tosylate to the corresponding 6-deoxy derivative; however, the secondary esters 6-deoxy-2,3-*O*-isopropylidene-5-*O*-*p*-tolylsulfonyl-α-L-manno- and -α-D-allofuranoside failed to give the desired 5,6-dideoxy derivatives (2). By contrast, we have successfully detosyloxylated secondary tosylates derived from methyl 4,6-*O*-benzylidene-α- and -β-D-glucopyranoside, achieving high yields (>90%) of 2- and 3-deoxyhexopyranosides (3). Our studies were recently extended (4) to several tosylates of a disaccharidic analog, namely, the 4,6:4′,6′-bisbenzylidene-acetal of α,α-trehalose (α-D-glucopyranosyl α-D-glucopyranoside). The results were quite similar in principle, although yields were not as high in these more complex systems. It appeared that the key to straightforward desulfonyloxylation in pyranosidic, secondary tosylates (which obviously are more hindered than cycloalkanol tosylates) is the presence of a free, or potentially free, hydroxyl group adjacent to the sulfonic ester function: When the alcohol was blocked as the methyl ether, C—O fission became very sluggish and S—O fission prevailed. In view of the hydroxy–tosyloxy *trans* relationship that exists in the glucopyranosides referred to, it could reasonably be assumed that desulfonyloxylation occurs by internal displacement via intermediary epoxides that are then reductively cleaved to give deoxyglycosides, and operation of this mechanism could in fact be proved by the isolation of such epoxides (3,4) (Scheme 1(a)). An intermediacy of epoxides has also been invoked recently to explain a number of products observed in the reductive dehalogenation of certain fluorohydrins by LTBH (5), and it is in harmony with studies (6) illustrating the general reactivity of epoxides towards that reagent. It was therefore rather surprising that various hexopyranoside tosylates which possessed a *trans*-vicinal hydroxyl group, but *lacked* the cyclic 4,6-acetal structure, were found to be desulfonyloxylated by LTBH in an entirely different way (7): The predominant course of events led to ring contraction, giving deoxy-*C*-hydroxymethylpentofuranosides (Scheme 1(b)). Although all details of the mechanism are not yet clear, it was shown that epoxides are not implicated in the formation of the rearranged products, and epoxides found in some of the reaction mixtures evidently were precursors for minor proportions of unrearranged deoxyhexopyranosides that arose in some in-

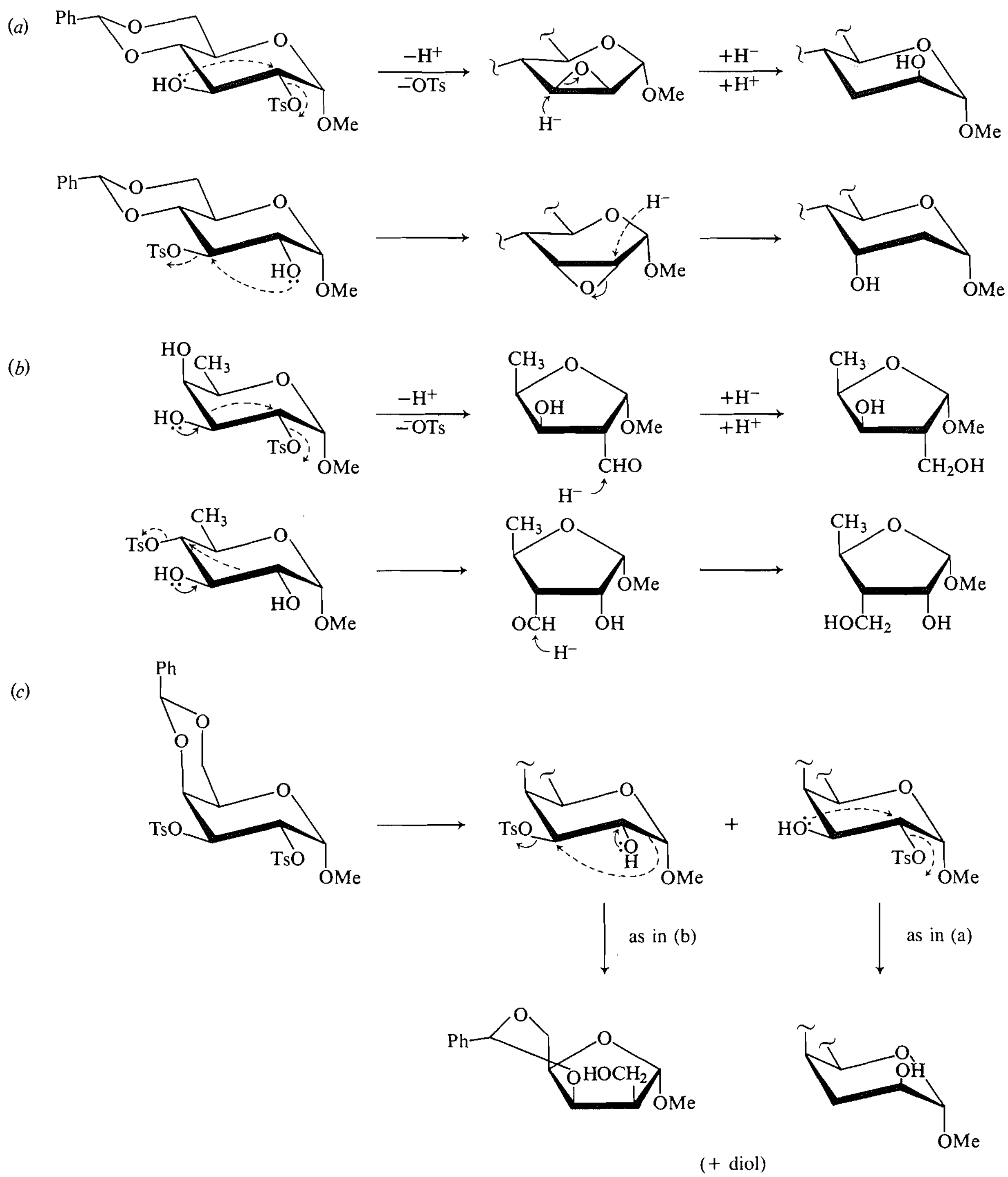

SCHEME 1

stances (7,8). The conclusion must be drawn that, under the conditions of the reaction with LTBH, carbon bond migration in the sense of Scheme 1(b) is favored over epoxide-forming internal displacement, even though the tosylates in question do produce epoxides readily when treated with such bases as sodium alkoxides (9). In view of this, it may be suggested for the case of the aforementioned glucopyranoside 4,6-acetals (Scheme 1(a)) that an intrinsically less-favored epoxide path is taken as an alternative to LTBH-induced ring contraction that, in these structures, woud lead to a highly strained, *trans*-fused bicyclo[4.3.0] system. This notion received support from the behavior of methyl 4,6-*O*-benzylidene-α-D-galactopyranoside 2,3-ditosylate, a less rigid, *cis*-fused bicyclic structure, which gave with LTBH a ring-contracted and an unrearranged product in the ratio 1.7:1 (7) (Scheme 1(c)).

Our interest was thus generated in examining the action of LTBH upon stereoisomeric glycoside tosylates in which no ring contraction should be predicted to occur because of the presence of a *trans*-fused acetal ring, and in which the epoxide option is also absent, owing to a vicinal *cis*-hydroxy – tosyloxy arrangement. Compounds meeting this description are the tosylates of methyl 4,6-*O*-benzylidenehexopyranosides having the *manno* or *allo* configuration, and the question to be answered was whether these would suffer simple and exclusive

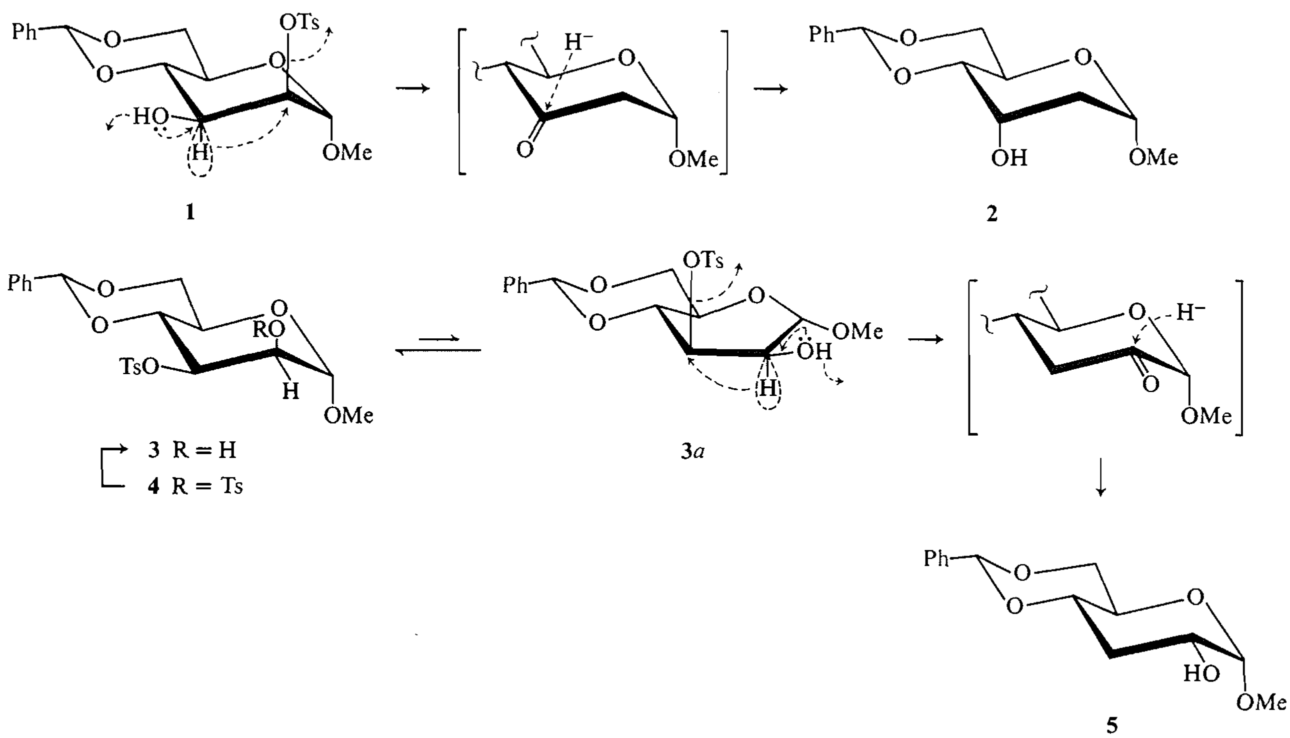

SCHEME 2

O-desulfonylation, the *C*-desulfonyloxylation pathways just mentioned being barred, or whether they would be desulfonyloxylated by some other mechanism. Normal S_N2 displacement, known to be facile for cycloalkanol tosylates (1) and shown to be possible, if difficult, for *gluco* analogs (3), might become competitive; alternatively, displacement with involvement of an internal hydride shift might take place, as was recently demonstrated (10) for LTBH-induced deoxygenations of ribonucleoside 2- and 3-monotosylates.

Results and discussion

Methyl 4,6-*O*-benzylidene-2-*O*-*p*-tolysulfonyl-α-D-mannopyranoside (**1**) reacted with excess LTBH in boiling oxolane to give, within 30 min, the known 2-deoxy-α-D-*ribo*-hexopyranoside **2**, isolated crystalline in 66% yield. The isomeric 3-tosylate **3** similarly gave, after 90 min, a 77% yield of crystalline 3-deoxy-α-D-*ribo*-hexopyranoside **5**. A 56% yield of the same product was obtained from the 2,3-ditosylate **4** after a reaction time of 2 h. Evidently, *O*-desulfonylation at the more susceptible 2-position was the primary event in the latter case, converting **4** into **3**, which was then desulfonyloxylated as before. The initiating step was familiar from the behavior of α- and β-D-*gluco* analogs (3). The inversion of carbinol configuration in the reactions **1** → **2** and **3** → **5** clearly indicates that the tosyloxy displacement cannot have occurred by external hydride attack, in S_N2 fashion, but must have involved hydride shifts as shown in Scheme 2. The *trans*-diaxially disposed migrating hydrogen atom and leaving group in **1** are particularly conducive to such a process. In **3**, the migration presumably requires the molecule to assume a transition state conformation close to the skew form (**3***a*) shown, but this factor is not a serious impediment and it also applies to the facile epoxide formations represented in Scheme 1(a). On the other hand, S_N2 displacements at the 2- and 3-positions of α-D-mannopyranosides are known to be difficult, which can be explained (11) by considering dipolar and steric interactions that develop in the transition state. The results obtained with the mannosides are thus entirely plausible.[1]

In remarkable contrast to the mannose counterparts, the α-D-*allo* 2-tosylate **6** under the same reaction conditions underwent seemingly complete *O*-desulfonylation, producing within 75 min the parent diol **7**, which was isolated crystalline in 87% yield. No deoxyglycoside was detected. In order to incur a hydride shift with concomitant *C*-desulfonyloxylation, **6** would presumably have to attain the skew boat conformation **6***a*, which is the same as **3***a* but, in the present case, would appear to be strongly disfavored as the large 2-tosyloxy substituent is pointing "inwards" at a flagstaff position. This circumstance, coupled with the general ease of S—O fission at the 2-position, may explain the observed result.

To be studied next were the α-D-*allo* 3-tosylate **10** and the 2,3-ditosylate **11**. To prepare these heretofore unknown derivatives, methyl 2-*O*-benzoyl-4,6-*O*-benzylidene-α-D-allopyranoside (**8**) was tosylated to give compound **9**. Methanolysis of **9** in the presence of barium methoxide afforded **10**, which was tosylated to produce **11**.

The alloside esters **10** and **11** proved considerably less reactive toward LTBH than their stereoisomers **3** and **4**, respectively. Treatment of the benzoate **9** with an excess of reductant in boiling oxolane caused rapid removal of the benzoyl group, as was expected, but only traces of products other than **10** were seen, in tlc, after a reaction time of 20 min. Processing at this point gave **10**, isolated crystalline (73% yield) and identical with the product from methanolysis. Prolonged reaction of **10** under the same conditions gave increased amounts of chromatographically visible products, although a substantial proportion of **10** was still recoverable crystalline after 90 min, the

[1] In their article (5) on reduction of organofluorine compounds with LTBH, the authors remarked in passing, with reference to unpublished results, that a hydride shift occurs in the reduction of **1**. No details were provided.

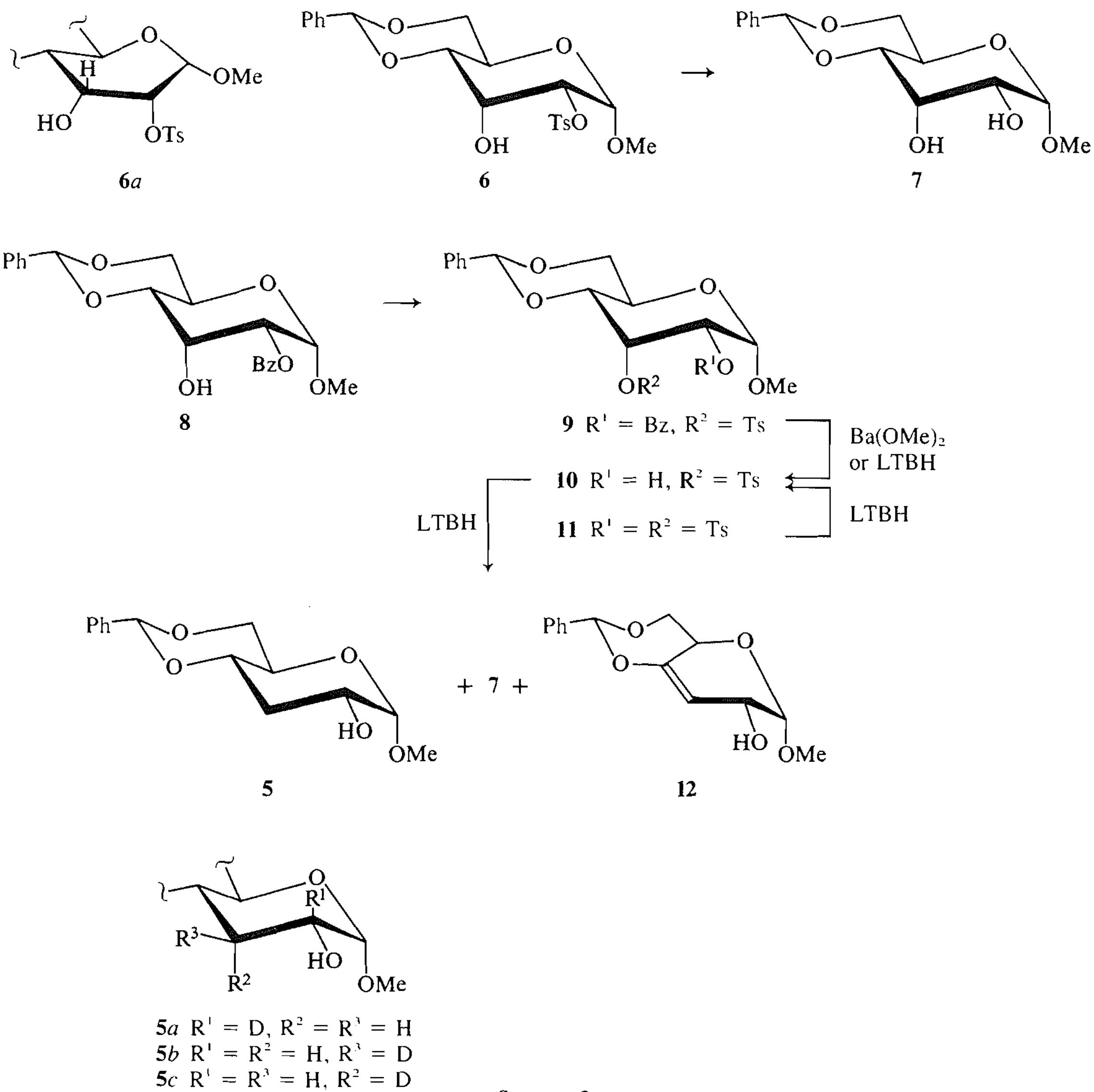

SCHEME 3

period after which the isomer **3** had been practically completely consumed. The tlc revealed formation of slow-moving diol **7** and smaller proportions of two faster-moving components. The same pattern emerged when the ditosylate **11** was used instead of **10** and, upon processing after 24 h, **7** was isolated crystalline in 36% yield, and the other products in yields of 20 and 28%. The first of the latter was identified as the 3-deoxyglycoside **5**, and the second was assigned the 3-enoside structure **12** on the basis of elemental analysis, mass spectrum, and nmr data.

The occurrence of a certain amount of elimination from **10** (or **11**), generating the enoside **12**, was not unexpected. Eliminations in 4,6-*O*-benzylidene-α-D-hexopyranosides bearing an axial 3-sulfonate group, to give such 3-enosides, have been observed previously, as reactions competing with S_N2 displacements (12); a related precedent was the formation of the β-anomer of **12**, which took place with 85% yield on treatment of the β-anomeric, 3-chloro-3-deoxy analog of **10** with sodium benzoate in boiling oxolane for 2 h (13). More surprising were the slow rate at which **5** was formed, and its modest yield, together with a relatively high proportion of diol **7**. One might have anticipated a facile desulfonyloxylation with hydride shift, as the mutual geometric dispositions of the migrating hydrogen atom and the leaving group are the same as those in **1** (but directionally inverse). In order to elucidate the mechanism operating in this case, **10** was reduced with lithium triethylborodeuteride, under otherwise unchanged conditions. The isolated 3-deoxyglycoside was revealed by nmr spectroscopy to be a ~7:3 mixture of the 2-deuterio compound **5***a* and the 3_{eq}-deuterio compound **5***b*, the former originating from reduction of the 2-ulose intermediate that is formed in the expected, hydride shift process, and the latter evidently arising through alternative S_N2 displacement, which was thus shown to compete to a considerable extent in this instance.[2] The formation of diol **7** will receive further comment below.

Finally, the action of LTBH upon methyl 4,6-*O*-benzylidene-2,3-di-*O*-*p*-tolylsulfonyl-α-D-altropyranoside (**13**) was examined. The compound was completely consumed within 1 h at 65°C, and tlc indicated the formation of two less-mobile

[2]Compounds **5***a* and **5***b* are readily distinguishable from their 3_{ax}-deuterio isomer **5***c*, for which proton nmr data have been recorded (14). Compound **5***c* arose from methyl 4,6-*O*-benzylidene-3-*O*-*p*-tolylsulfonyl-α-D-glucopyranoside as the chief product of deoxygenation with *lithium aluminum deuteride* (14); this reductant complexes with O-2 and then delivers a deuteride ion intramolecularly for displacement of the *trans*-oriented, adjacent tosyloxy group, in contradistinction to the action of LTBH (3) that is depicted in Scheme 1(a).

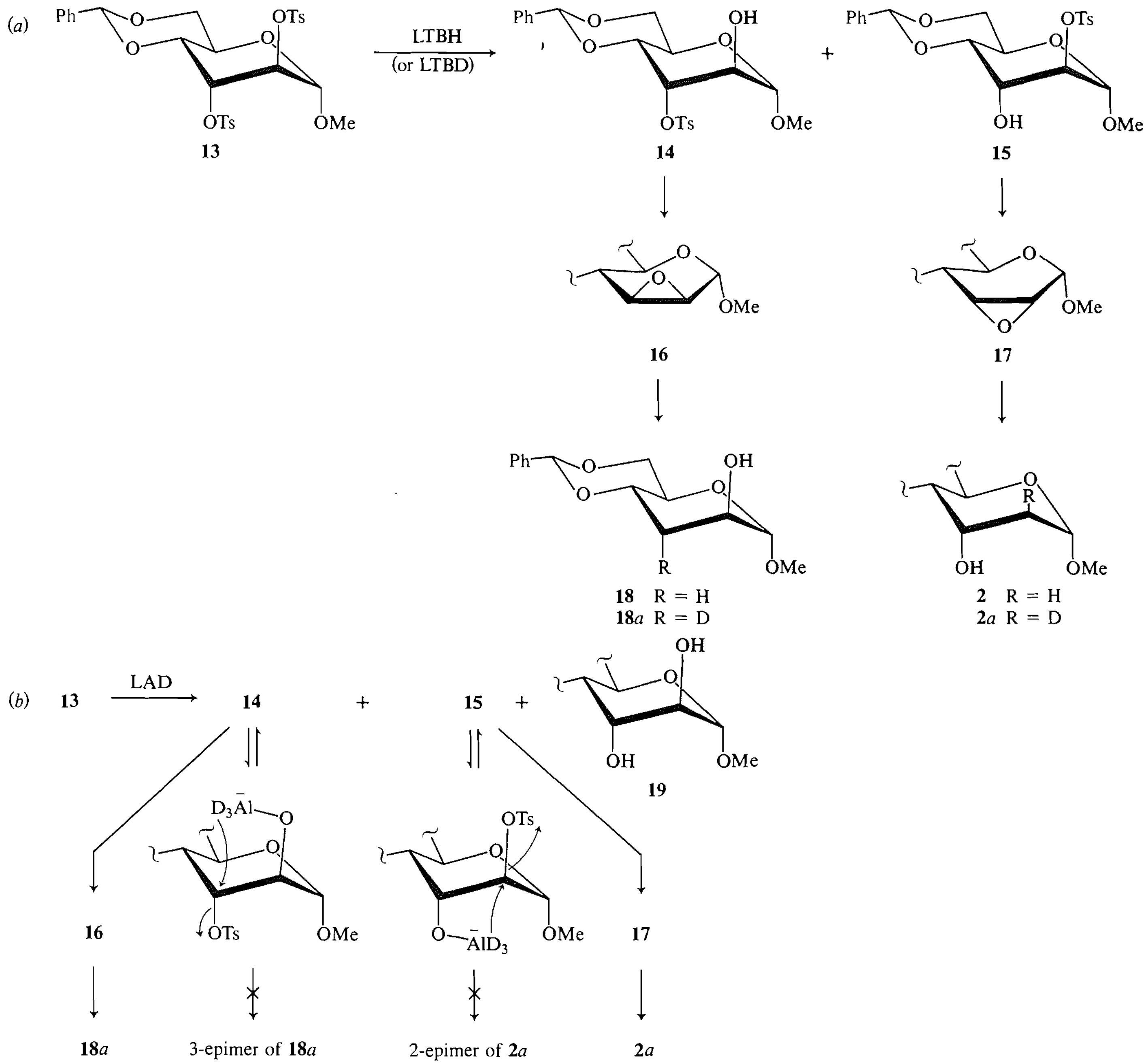

SCHEME 4

products showing roughly comparable spot intensities. The nmr spectra taken after chromatographic separation revealed the slightly preponderant product to be methyl 4,6-*O*-benzylidene-3-deoxy-α-D-*arabino*-hexopyranoside (**18**), and the less abundant product to be the 2-deoxy-α-D-*ribo* isomer **2**. Unlike **11**, **13** did not give its parent diol, nor a product of 3,4-elimination, in detectable amounts. Evidently, facile S—O fission takes place in **13** partly (and somewhat preferentially) on the 2-sulfonate, and partly on the 3-sulfonate group, and it is assumed that the two regioisomeric monoesters (**14** and **15**) so engendered undergo rapid, reductive desulfonyloxylation via the corresponding epoxides (**16** and **17**) to give the deoxyglycosides (Scheme 4(a)) in a manner analogous to the *gluco* isomers (compare Scheme 1(a)). This mechanism was proved by performance of the reaction with lithium triethylborodeuteride, which gave the axially deuterated products **18***a* and **2***a*.

Jarý and his co-workers (15) had previously reported the formation of **18** and **2**, isolated in yields of 60 and 12%, respectively, by reaction of **13** with lithium aluminum hydride (LAH) in boiling oxolane. The reaction was rather sluggish (incomplete after 18 h) and produced a significant proportion (11%) of the parent diol[3] **19**. The authors concluded that O—S fission of the 2-*O*-tosyl group was the prevalent, primary event,

[3]Significant double *O*-desulfonylation giving the diol was in line with the propensity of LAH for this mode of action, noted also in other configurational series (14–17) and confirmed by us (3) in comparison with the action of LTBH. For instance, the mannoside ditosylate **4** was desulfonylated by LAH without accompanying deoxygenation (16), in sharp contrast to its reduction by LTBH reported here.

which was then followed by tosyloxy displacement to give the main product **18**, and they recognized no immediate decision was possible as to whether the reduction proceeded through an intermediary epoxide or, alternatively, by intramolecular hydride transfer in the trihydridioaluminate complex of the carbinol as had been shown to occur (14, 16) in the α-D-*gluco* series (cf. footnote 2), because both mechanisms would in the *altro* series lead to the same products. The latter mechanism was considered "only probable", no epoxide products having been uncovered in the reaction mixture. We repeated the reaction of **13** with LAH as specified (15) and, in addition to confirming the formation of **18**, **2**, and **19**, found direct evidence by tlc and nmr spectroscopy for the intermediacy of the monotosylate **14** and the epoxide **16**. (The presumptive precursors **15** and **17** for the minor product **2** were not detected.) Upon performance of the reaction with lithium aluminum deuteride (LAD), **14** and **16** as well as the axially deuterated deoxyglycoside **18***a* could be isolated and firmly characterized by their 300-MHz ^{1}H nmr spectra. Clearly, the reaction takes place along the epoxide path; the internal displacement mechanism would have given the equatorially deuterated *epimers* of **18***a* and **2***a*, and these were not encountered (Scheme 4(b)).

The comparison that can now be made of the behavior of various methyl 4,6-*O*-benzylidenehexopyranoside 2,3-ditosylates toward LTBH not only illustrates how the different modes of *C*-desulfonyloxylation (via epoxide, by hydride shift, by direct displacement, or with ring contraction) depend on configuration, but it also invites comment upon the regioselectivity of O—S fission which precedes these processes. The *manno* 2,3-ditosylate **4** (Scheme 2) and its *gluco* isomer (3) were *O*-desulfonylated exclusively, or nearly so, at position 2, whereas selectivity was lower in the other series. Thus, the *allo* ditosylate **11** gave a large proportion (36%) of diol **7**, although desulfonylation in the 2-monotosylate **6** was faster than in the 3-monotosylate **10**, with the latter partially undergoing reductive desulfonyloxylation. Similarly, the *altro* isomer **13** must have suffered partial O—S fission in both positions, accounting for the observed products **18** and **2**. Whereas the greater lability of the 2-*O*-tosyl group found in all the series can be explained by an inductive effect of the anomeric center, the decreased stability of the 3-*O*-tosyl group in **11** and **13**, as compared to **4** and the *gluco* isomer, must be attributed to some other cause. It cannot be due solely to the axial disposition since the *galacto* isomer (Scheme 1 (C)) also exhibited diminished selectivity. Rather, there appears to be a correlation between the reactivity at O-3 and the total, non-bonded interactions present in the molecules as determined by their overall configurations. The conformational free energies in α-D-hexopyranosides increase in the order *gluco* < *manno* < *galacto* < *allo* < *altro* and are known to affect the rate of such reactions as, for example, acid hydrolysis (18). They may similarly account for the reactivity differences here discussed.

Experimental

General

General preparative methods and instrumental techniques used for performing reactions with LTBH (purchased from Aldrich Chemical Co. as a 1 *M* solution in oxolane), processing of reaction mixtures, and separation and identification of the products were the same as those previously employed (3, 4, 7). Unless indicated otherwise, optical rotations were measured at 25°C for chloroform solutions, and the ^{1}H nmr data refer to 300-MHz spectra obtained for solutions in $CDCl_3$ with a Varian XL-300 instrument. Column chromatography and tlc were performed with the following solvent systems (v/v): A, ethyl acetate −hexane, 1:2; B, the same solvents, but 2:3; C, the same, but 1:1; D, the same, but 4:1; E, the same, but 1:5; F, ethyl acetate − chloroform, 1:9; G, the same solvents, but 1:19; and H, the same, but 1:49.

Preparation of the starting glycoside p-*toluenesulfonates*

Authenticity and purity of the starting compounds were ascertained by nmr spectroscopy; see the data in Table 1.

(a) *Known compounds 1, 3, 4, 6, and 13*

Methyl 4,6-*O*-benzylidene-α-D-mannopyranoside (19) was monotosylated by the phase-transfer method (20) to give the *2-tosylate* **1** as a white, amorphous substance showing $[\alpha]_D$ +1.9° (*c* 1.1) in agreement with ref. 20 (+2°), but at variance with the value (−25°) recorded earlier (21).

Monotosylation of the above benzylidenemannoside in homogeneous phase at 0−20°C as directed (22) furnished the *3-tosylate* **3**, mp 149−150°C, $[\alpha]_D$ +19.0° (*c* 5.9) (lit. (22) mp 151−153°C, $[\alpha]_D$ +21°).

Complete tosylation (22) of the same acetal provided the *2,3-ditosylate* **4**, mp 166−168°C, $[\alpha]_D$ −5.7° (*c* 1.8) (lit. (22) mp 163−164°C, $[\alpha]_D$ −5.3°).

The α-D-*allo 2-tosylate* **6** was prepared from the parent methyl 4,6-*O*-benzylidene-α-D-allopyranoside **7** which, in turn, was obtained by reduction and deacylation, with sodium borohydride, of known (23) methyl 2-*O*-benzoyl-4,6-*O*-benzylidene-α-D-*ribo*-hexopyranosid-3-ulose according to the published procedure (24, 25). Compound **7**, obtained as anhydrous crystals from hot abolute ethanol, had mp 176−178°C, $[\alpha]_D$ +126.3° (*c* 1) (lit. (25) mp 173−177°C, $[\alpha]_D$ +117°; lit. (26) mp 167−168°C (from benzene), $[\alpha]_D$ +128°; and lit. (27) mp 175−177°C, $[\alpha]_D$ +117° (in DMF)). Compound **7** is also known as a dihydrate (24, 26). A solution of anhydrous **7** (400 mg), *p*-toluenesulfonyl chloride (300 mg), and *p*-dimethylaminopyridine (12 mg) in dry pyridine (2 mL) was allowed to stand at 0°C for 24 h and for 3 days at 25°C, with further tosyl chloride (500 mg) being added after the second day. Almost complete consumption of **7** (R_f 0.1) and the presence of **6** (R_f 0.5) and **11** (R_f 0.7) was then revealed by tlc (solvent B). The crude material (558 mg) obtained after conventional processing was dissolved in hot ethyl acetate −hexane (1:1), from which the *2-tosylate* **6** (385 mg) crystallized on cooling and addition of the some hexane; yield, 59%; mp 164−165°C, $[\alpha]_D$ +59° (*c* 0.8) (lit. (27) mp 166−167°C, $[\alpha]_D$ +35.6° (in DMF), for **6** prepared in a different way). We also obtained **6**, albeit in lower yield (39%), by applying the phase-transfer procedure for tosylation (20).

The α-D-*altro 2,3-ditosylate* **13** was prepared (28) from its parent diol by conventional tosylation. Recrystallized from ethyl acetate, it showed mp 182−183°C, $[\alpha]_D$ +44° (*c* 0.8) (lit. (28) mp 179°C, $[\alpha]_D$ +46.9° and lit. (15) mp 181−182°C, $[\alpha]_D$ +46.5°).

(b) *Methyl 2-*O*-benzoyl-4,6-*O*-benzylidene-3-*O*-p-tolylsulfonyl-α-D-allopyranoside (9)*

Methyl 2-*O*-benzoyl-4,6-*O*-benzylidene-α-D-*ribo*-hexopyranosid-3-ulose (23) was reduced with sodium borohydride at pH 6−7, to provide (25) methyl 2-*O*-benzoyl-4,6-*O*-benzylidene-α-D-allopyranoside (**8**), mp 105−107°C, $[\alpha]_D$ +73.3° (*c* 0.7) (lit. (25) mp 110−115°C, $[\alpha]_D$ +74°).

A solution of **8** (1.40 g) and *p*-toluenesulfonyl chloride (1.60 g) in chilled pyridine (7.5 mL) was stored at 0°C for 24 h and then at room temperature for 5 days, after which a strong spot for **9** (R_f 0.78) and a weak spot for remnant **8** (R_f 0.67) were seen in tlc (solvent F). Conventional processing of the mixture by treatment with ice water and extraction of the product with chloroform, followed by washing (water), drying, and evaporation of the extract, gave the crude reaction product (1.84 g). This was dissolved in hot ethanol and the solution cooled, whereby a semicrystalline gel separated. Trituration of the gel with ethanol−benzene and processing of the mother liquors gave chromatographically pure **9** (1.45 g, 74%) in several crops, which were washed with small amounts of cold ethanol followed by methanol; mp 165−166°C, $[\alpha]_D$ +67.8° (*c* 0.9). *Anal.* calcd. for $C_{28}H_{28}O_9S$ (540.6): C 62.21, H 5.22, S 5.93; found: C 62.07, H 5.36, S 5.74.

TABLE 1. Proton magnetic resonance parameters, at 300 MHz, for glycosides used as starting compounds

	Chemical shifts (δ)[b]												
Compound[a]	2-Tosyl[c]	3-Tosyl[c]	*Ph*-CH	H-1	H-2	H-3	H-4	H-5	H-6a	H-6e	*O*-Me	*Aryl*-Me	OH
1	7.81, 7.31		5.50	4.77d	4.71dd	4.07m	3.76m (3H)			4.19m	3.36	2.40	2.06d
3		7.70, 7.03	5.37	4.76d	4.30dt	4.74dd	4.04m	3.8m (2H)		4.19dd	3.35	2.18	2.61d
4[d]	7.93, 7.41	7.66, 7.21	5.63	4.94m (2H)		4.76dd	3.99dd	3.71sx	3.86t	4.21dd	3.44	2.50, 2.36	
6	7.83, 7.33		5.50	4.80d	4.49t	4.16m	3.44dd	4.11sx	3.69t	4.32dd	3.37	2.40	2.97d
7[e]			5.64	4.62d	3.59m	4.01m[f]	3.56dd	3.95sx	3.68t	4.26dd	3.32		4.62d, 4.43d
8			5.61	5.02dd	5.07t	4.46dt[f]	3.64dd	4.21sx	3.79t	4.39dd	3.44		3.20d
9		7.67, 6.90	5.44	4.95d	5.13t	5.43t	3.70dd	4.18sx	3.66t	4.28dd	3.40	2.20	
10		7.72, 7.01	5.45	4.72d	3.82dt[f]	5.28t	3.60dd	4.00sx	3.63t	4.27dd	3.42	2.31	2.89d
11	7.79, 7.32	7.71, 7.02	5.44	4.73d	4.53t	5.25t	3.57dd	4.10sx	3.63t	4.25dd	3.29	2.43, 2.31	
13	7.85, 7.4[g]	7.58, 7.01	5.38	4.54[h]	4.71dd	4.48t	3.80dd	4.14sx	3.65t	4.22dd	3.31	2.47, 2.29	
14		7.42, 6.98	5.60	4.61[h]	3.67t	4.32nm	4.25m (2H)		3.80m	4.25m	3.43	2.26	1.7br

	Coupling constants (Hz)							
Compound	$J_{1,2}$	$J_{2,3}$	$J_{3,4}$	$J_{4,5}$	$J_{5,6a}$	$J_{5,6e}$	$J_{6a,6e}$	$J_{H,OH}$
1	1.5	3.5	9	[i]	[i]	[i]	[i]	6
3	1.8	3.4	~10	~9	[i]	[i]	[i]	3.4
4	[i]	3.2	10.3	9.2	10	4.8	10	
6	4	3.5	2.5	10	10.5	5	10.5	7.5
7	4.8	2.7	2.7	9.6	10.4	5	10.4	9.6, 5.0
8[j]	4	~2.5	3	10	10	5	10	7
9	4.3	2.9	2.9	9.6	10.2	5.2	10.2	
10	4.3	3.5	2.7	9.6	10.5	5.2	10.3	12
11	4.2	3.3	2.8	9.6	10.5	5.2	10.3	
13	~1.2	3.2	2.9	9.6	10	5	10	
14	<1	3	Small	[i]	[i]	[i]	[i]	3

[a]In $CDCl_3$ solution unless otherwise indicated.
[b]Signal multiplicities are indicated as d (doublet), m (multiplet), sx (dt or ddd, appearing as a sextet), and t (triplet). The data refer to first-order analysis. The signals for *Ph*-CH, *O*-Me, and *aryl*-Me were singlets.
[c]Midpoints of the A and B parts (2 protons each) of the aromatic AB system.
[d]In acetone-d_6.
[e]In dimethyl sulfoxide-d_6.
[f]Triplet after D_2O exchange.
[g]Not determined accurately because of crowding with phenyl signals.
[h]Slightly broadened singlet representing a very narrow doublet.
[i]Not determined because of second-order effects.
[j]$J_{1,3} \approx 1$ Hz.

(c) *Methyl 4,6-*O*-benzylidene-3-*O*-*p*-tolylsulfonyl-α-D-allopyranoside (**10**)*

A suspension of **9** (2.6 g) and barium oxide (0.35 g) in dry methanol (130 mL) was boiled under reflux for 30 min, which converted **9** (R_f 0.75) into **10** (R_f 0.45, tlc with solvent C). The solvent was evaporated and the dry residue distributed between water and chloroform, with addition of brine to destabilize the emulsion that tended to form. The organic phase was dried (Na_2SO_4), and concentrated, and the product was recrystallized from methanol or ethanol, to give long needles (1.43 g, 68%), mp 198–199°C (dec.), $[\alpha]_D$ +110.8° (*c* 1). *Anal.* calcd. for $C_{21}H_{24}O_8S$ (436.5): C 57.79, H 5.53, S 7.35; found: C 57.71, H 5.69, S 7.53.

(d) *Methyl 4,6-*O*-benzylidene-2,3-di-*O*-*p*-tolylsulfonyl-α-D-allopyranoside (**11**)*

The monotosylate **10** (0.95 g) in pyridine (11 mL) was treated with *p*-toluenesulfonyl chloride (0.45 g), first at 0°C overnight and then at room temperature for 2 days. Processing with ice water, extraction of the product with chloroform, and evaporation of the washed and dried extract gave crude, crystalline **11** (1.50 g), from which pure **11** (1.05 g, 82%) was obtained by recrystallization from chloroform–ethanol; mp 195–197°C, $[\alpha]_D$ +48.7° (*c* 1.5). *Anal.* calcd. for $C_{28}H_{30}O_{10}S_2$ (590.6): C 56.93, H 5.12, S 10.86; found: C 56.87, H 5.14, S. 11.02.

Reactions of the glycoside p*-toluenesulfonates with LTBH*

(a) *General procedure*

The glycoside tosylate (0.5–2.5 mmol) was dissolved in dry (3,7) oxolane (1 mL per 100 mg of substrate), and 1 *M* LTBH solution was added by syringe, with exclusion of moisture in a reflux apparatus containing an atmosphere of dry nitrogen. The mixture was gently boiled under reflux and progress of the reaction was monitored by tlc on silica gel plates. Amounts of reactants and reaction times are stated in the individual sections, and R_f values refer to tlc using the solvent systems indicated. After completion of the reaction the mixture was allowed to cool, a few milliliters of methanol were carefully introduced to decompose the excess of hydride (until hydrogen evolution ceased), and refluxing was resumed for 10 min. The solution was cooled again, poured with stirring into ice water (50–150 mL), and neutralized against indicator paper with a solution of sodium hydrogen sulfate. (Care was taken not to render the solution acidic.) The mixture was stirred at ambient temperature for several hours (or overnight) and then concentrated under reduced pressure to a small volume, to remove the organic solvent and a large part of the water. The residue was extracted with dichloromethane (3 × 50 mL) or occasionally with chloroform, and the extract washed with water, dried (Na_2SO_4), and evaporated to give the product, which was then purified by crystallization or chromatography as indicated.

(b) *Reaction of 1*

The 2-tosylate **1** (200 mg, 0.46 mmol; R_f 0.7 with solvent C) was converted by LTBH (2 mL) into methyl 4,6-*O*-benzylidene-2-deoxy-α-D-*ribo*-hexopyranoside (**2**) (R_f 0.4) during a reaction period of 30 min. The white solid (120 mg) obtained upon work-up was recrystallized from ethyl acetate to give **2** (98 mg, 80.3%), mp 126–128°C, raised to 128–130°C by another recrystallization; $[\alpha]_D$ +140° (*c* 0.5) (lit. (3) mp 130–131°C, $[\alpha]_D$ +140°); ^{1}H nmr, δ : 7.5 (m, 5H, Ph), 5.61 (s, *Ph*-CH), 4.77 (nm, H-1), 4.31 (dd, $J_{5,6e}$ = 5.0, $J_{6a,6e}$ = 10.1 Hz, H-6e), 4.22 (sx, H-5), 4.17 (m, narrowed after D_2O exchange, H-3), 3.76 (t, $J_{5,6a}$ = $J_{6a,6e}$ = 10.1 Hz, H-6a), 3.59 (dd, $J_{3,4}$ = 2.8, $J_{4,5}$ = 9.5 Hz, H-4), 3.40 (s, 3H, OMe), 3.01 (d, J = 6.7 Hz, removed by D_2O, OH-3), 2.18 (ddd, $J_{1,2e}$ ~ 1, $J_{2e,3}$ = 3.1, $J_{2a,2e}$ = 15 Hz, H-2e), and 1.98 (dt, $J_{1,2a}$ = $J_{2a,3}$ = 3.7, $J_{2a,2e}$ = 15 Hz, H-2a).

(c) *Reaction of 3*

The 3-tosylate **3** (1.13 g, 2.59 mmol; R_f 0.6 with solvent C) was allowed to react with LTBH (12 mL) for 45 min, and for a further 45 min after addition of another 3 mL of reductant. Crude methyl 4,6-*O*-benzylidene-3-deoxy-α-D-*ribo*-hexopyranoside (**5**) (R_f 0.45) was obtained as a white solid (0.70 g), which by recrystallization from ethyl acetate gave pure **5** (531 mg, 77%), mp 189–190°C, $[\alpha]_D$ +121.6° (*c* 0.7) (lit. (3) mp 187°C, $[\alpha]_D$ + 119.5°, and closely similar values (14, 16, 29)). The ^{1}H nmr spectrum confirmed the identity with **5** obtained previously (3); see also section (g).

(d) *Reaction of 4*

The 2,3-ditosylate **4** (1.44 g, 2.44 mmol) was allowed to react with LTBH (20 mL) for 1 h, after which traces of **4** (R_f 0.57, solvent A) were still visible in tlc. Boiling was continued for 50 min with added LTBH (5 mL), and processing then gave **5** (341 mg, 52.5%, after recrystallization from ethyl acetate) whose ^{1}H nmr spectrum was identical with that mentioned under (c); mp 172–173°C, raised to 185–186°C by further recrystallization; $[\alpha]_D$ +119.2° (*c* 0.75). The identity was confirmed, moreover, by ir spectra.

(e) *Reaction of 6*

The 2-tosylate **6** (250 mg, 0.57 mmol; R_f 0.85 with solvent D) was completely consumed after 75 min by reaction with LTBH (3 mL). The product was less polar (R_f 0.2 with solvent C) than the deoxyglycosides **2** and **5**; it was obtained as a white solid (158 mg) following its extraction with chloroform, and was recrystallized from ethanol to give the diol **7** (140 mg, 87%), mp 175–177°C, $[\alpha]_D$ +125.7° (*c* 0.8), with an ir spectrum superposable on that of **7** described in a preceding section.

(f) *Reaction of 9*

The 2-*O*-benzoyl 3-tosylate **9** (500 mg, 0.93 mmol) was treated with LTBH (6 mL) for 20 min, after which tlc (solvent C) indicated complete absence of **9** (R_f 0.8) and showed a strong spot for the 3-tosylate **10** (R_f 0.45), accompanied by weak spots for other products (R_f ~ 0.7 and 0.2). Processing furnished 296 mg (73.3%) of **10** (recrystallized from ethanol), mp 195–196°C (dec.), $[\alpha]_D$ +106° (*c* 0.5). Its ir and ^{1}H nmr spectra were identical with those of the product obtained from **9** by methanolysis.

(g) *Reaction of 10*

The 3-tosylate **10** (400 mg, 0.92 mmol) was allowed to react with LTBH (7 mL) during the course of 1.5 h. The tlc pattern then was similar as under (f). Processing gave a solid mixture of products (286 mg), which by recrystallization from ethanol gave a first crop of crystals, mp 195–196°C (dec.) that proved identical (ir) with starting **10** (109 mg, 27%). A second crop of crystals was a mixture of **10** and the deoxyglycosides **5** and **12**, as judged by comparison of its ir spectrum with the spectra of the pure components. (It was noted that **5** and **10** have similar R_f values of ~0.5 in tlc with solvent C.) The mother liquor showed a spot having R_f 0.2 (**7**).

In a similar experiment, **10** (307 mg, 0.7 mmol) was treated with a 1 *M* solution of lithium triethylborodeuteride (5.6 mL) in oxolane for an extended period of time (8 h). The crude product showed 3 well-separated spots in tlc (solvent C), having R_f 0.6, 0.45, and ~0.2, and the components of the mixture were isolated by column chromatography (10 g of silica gel) using 1:5 ethyl acetate – hexane as the eluant. The fast-moving product was identified by its ir and 300-MHz ^{1}H nmr spectra as **12** (38 mg); compare section (h). The material (47 mg) of intermediate mobility was a mixture of the deuterated analogs **5*a*** and **5*b*** of **5** (approximate ratio, 7:3), as was revealed by the following data.

The 500-MHz ^{1}H nmr data for **5** (in $CDCl_3$), δ: 7.47–7.45 and 7.34–7.32 (m, 2 + 3H, Ph), 5.50 (s, *Ph*-CH), 4.67 (d, $J_{1,2}$ = 3.7 Hz, H-1), 4.25 (dd, splittings[4] 10.3 and 15.9 Hz, H-6e), 3.77 (tdd, collapsing to ddd on D_2O exchange, $J_{1,2}$ = 3.8, $J_{2,3e}$ = 4.8, $J_{2,3a}$ ≈ $J_{2,OH}$ ≈ 11.5 Hz, H-2), 3.70–3.66 (m, 2H, H-5,6a), 3.52 (m, H-4), 3.46 (s, 3H, OMe), 2.29 (dt, $J_{2,3e}$ = $J_{3e,4}$ 4.6, $J_{3a,3e}$ = 11 Hz, H-3e), 2.03 (d, removed by D_2O, $J_{2,OH}$ = 11.3 Hz, OH), and 1.84 (q, $J_{2,3a}$ = $J_{3a,3e}$ = $J_{3a,4}$ = 11.6 Hz, H-3a). For the mixture of **5*a*** and **5*b*** (500 MHz, $CDCl_3$), δ: 4.67 (s for **5*a***, superposed on d, J = 3.5 Hz, for **5*b***, intensity ratio 7:3, H-1), 3.77 (m, ~0.3H, H-2 of **5*b***), 2.28 (dd, ~0.7H, $J_{3e,4}$ = 4.1, $J_{3a,3e}$ = 11.2 Hz, H-3e of **5*a***), 1.84 (t, ~0.7H, $J_{3a,3e}$ = 11.4 Hz, H-3a of **5*a***), and 1.83 (t, ~0.3H, $J_{2,3a}$ = $J_{3a,4}$ = 11.7 Hz, H-3a of **5*b***). The remaining signals were as for **5**.

The 125-MHz ^{13}C nmr data for **5** (in $CDCl_3$), δ: 128.97, 128.19, 126.05 (Ph), 101.64 (*Ph*-C), 98.96 (C-1), 76.19 (C-4), 69.21 (C-6), 67.53 (C-2), 63.81 (C-5), 55.15 (*O*-Me), and 33.68 (C-3). The mixture **5*a*** + **5*b*** showed the same, single peaks for the substituent carbon atoms and C-6, and two sets of signals in ~7:3 ratios for the sugar-ring carbons. Signals for **5*a***: 98.93 (C-1), 76.19 (C-4), 63.80 (C-5), and 33.57 (C-3), with the C-2 signal being absent; note the isotope effects of ^{2}H-2 on C-1 and C-3 (−0.03 and −0.09 ppm). Signals for **5*b***: 98.95 (C-1), 76.12 (C-4), 67.45 (C-2), and 63.78 (C-5); a C-3 signal was not observed. Note the isotope effects of ^{2}H-3 on C-2 and C-4 (−0.08 and −0.07 ppm).

(h) *Reaction of 11*

LTBH (15 mL) was added to a suspension of the 2,3-ditosylate **11** (0.99 g, 1.68 mmol) in oxolane (10 mL), and the mixture was heated to reflux, with magnetic stirring, for 24 h. It then showed 3 strong spots in tlc (solvent C), representing **7** (R_f 0.2), **5** (R_f 0.5), and **12** (R_f 0.65). The latter was a double spot having a violet front part; very faint, more-mobile traces were seen additionally. The product mixture obtained upon processing was chromatographed on a column of silica gel (25 g) by use of solvent E as the eluant. The following fractions (10 mL) were collected: 4–5 (impurities, 3 mg, discarded), 6–13 (**12** with satellite, 110 mg), 14–28 (pure **12**, 30 mg), 29–53 (pure **5**, 89 mg), and, by elution with pure ethyl acetate, a final fraction (large) that contained pure **7** (170 mg).

Fractions 6–13 were crystallized from ethyl acetate – hexane to give pure **12** (92 mg, free from the satellite component), for a total yield of 122 mg (27.5%); mp 150–151°C (151–153°C after recrystallization from ethanol), $[\alpha]_D$ +137.4° (*c* 0.8). The spectral data agreed with the structure of methyl 4,6-*O*-benzylidene-3-deoxy-α-D-*erythro*-hex-3-enopyranoside: ν_{max} (Nujol): 3300 (broad, OH) and 1700 cm^{-1} (C=C fused to acetal ring); ^{1}H nmr, δ: 7.5 and 7.4 (m, 2 + 3H, Ph), 5.56 (s, *Ph*-CH), 5.28 (nm, W_H = 4.8 Hz, H-3), 4.81 (d with broadened lines, $J_{1,2}$ = 4.7, $J_{1,3}$ ~ −0.8 Hz, H-1), 4.43 (broad m: quintet after D_2O exchange, $J_{1,2}$ = 4.7, $J_{2,3}$ ≈ $J_{2,5}$ ≈ 2 Hz, H-2), 4.31 (m, 2H, H-5,6e), 3.73 (dd, J = 12.2 and 12.6 Hz, H-6a), 3.53 (s, 3H, OMe), and 2.23 (br, removed by D_2O, OH); m/z (CI, ether): 265 (M^+ + 1), 247 (M^+ + 1 − H_2O), 233 (M^+ − MeOH). *Anal.* calcd. for $C_{14}H_{16}O_5$ (264.3): C 63.62, H 6.10; found: C 63.62, H 6.07.

The aforementioned, chromatographically homogeneous fractions 29–53 gave crystalline **5** (89 mg, 19.9%), showing up 191–192°C after recrysallization from ethanol; the ir spectrum was congruent with those of the products obtained from **3** and **4** (sections c and d). The crystalline diol **7** (170 mg, 35.9%) gave an ir spectrum superposable on those of an authentic sample and of the product obtained from **6** (section e). It is to be noted that the glycosides **2**, **5**, **7**, and **12** are readily distinguishable by the shape of their hydroxyl absorption bands

[4]Not true coupling constants because of second-order effect due to the near equality of chemical shifts for H-5 and H-6a. In acetone-d_6 at 300 MHz, the signal appeared as a dd with splittings of 4 and 10 Hz.

and by very detailed and characteristic band patterns in the region of 600–900 cm^{-1}.

(i) *Reaction of 13*

The 2,3-ditosylate **13** (1.06 g, 1.8 mmol) was allowed to react with LTBH (16 mL). After 30 min, a small proportion of **13** (R_f 0.68) had remained, but the reaction was complete after 1 h, having given two products, R_f 0.37 (black spot) and R_f 0.47 (brown spot) in tlc with solvent C. With solvent G, the relative mobilities were reversed (R_f 0.33 and 0.23), and in that order, too, the products were eluted by solvent H in column chromatography (15 g of SiO_2) to which the processed, crude mixture (0.45 g, 94%; syrup) was subjected. The first few, chromatographically homogeneous fractions yielded crystals (120 mg, mp 126°C), identified as the 2-deoxyglycoside **2** by comparison with **2** previously obtained from **1** (ir and 300-MHz nmr spectra, and tlc).

Subsequent, mixed fractions contained mainly the second product, and these were followed by nearly pure fractions (170 mg) of the same. After a further, chromatographic purification the material (130 mg) was identified as methyl 4,6-*O*-benzylidene-3-deoxy-α-D-*arabino*-hexopyranoside (**18**) by its 300-MHz ^{1}H nmr spectrum (in $CDCl_3$), δ: 7.5 and 7.35 (m, 2 and 3H, Ph), 5.55 (s, *Ph*-CH), 4.55 (broadened s, H-1), 4.23 (distorted dd, H-6e), 3.99 (narrow m, H-2), 3.95 (td, partially overlapped by the H-2 signal, H-4), 3.8 (m, 2H, consisting of a dt for H-5 and a t with 10-Hz splitting for H-6a), 3.40 (s, 3H, OMe), 2.09 (narrow m, H-3e), and 2.05 (dd, $J_{2,3a}$ = 3.2, $J_{3a,4}$ ~11 Hz, H-3a; geminal coupling was not observed). The data agreed with the 100-MHz data recorded (3)[5] for **18**.

Performance of the same reaction, but with *lithium triethylborodeuteride*, gave the 2-deoxy-2-deuterio- and 3-deoxy-3-deuterio-α-D-*altro* analogs **2*a*** and **18*a***, which were isolated chromatographically in the same way. In comparison with the ^{1}H nmr spectrum of **2** (section b), that of **2*a*** lacked the H-2a signal, the H-2e signal was reduced to a narrow dd, H-3 gave a t with $J_{2e,3} = J_{3,4}$ = 2.8 Hz (after D_2O exchange), and H-1 gave a slightly broadened s, whereas the resonances for H-4,5,6a,6e and the substituents were identical in **2** and **2*a***. The spectrum of **18*a*** was identical with that of **18** except that the characteristic dd for H-3a was lacking and the H-4 and partially overlapping H-2 signals were reduced in multiplicity.

*Reactions of **13** with lithium aluminum hydride and lithium aluminum deuteride*

Altroside ditosylate **13** (300 mg) was reduced with LAH (80 mg) in dry, boiling oxolane (4 mL) according to Jarý's procedure (15), but with a reaction time of 25 instead of 18 h. A small proportion of **13** (R_f 0.63) remained unconsumed even then; the main products gave a single spot having R_f 0.43 and an elongated double spot, R_f 0.37–0.17, that was colored reddish-brown in the front and brownish-black in the rear part. In addition, a trace product having R_f 0.75 was detected, migrating like an authentic sample (29) of the *manno* 2,3-epoxide **16** (tlc with solvent B). Processing of the reaction mixture as described (15), followed by multiple chromatography on silica gel using solvent E and similar solvent combinations (1:4 and 1:6), resulted in partial separation of the products. Part of the most abundant product (R_f 0.37; brown spot) was isolated pure and identified as **18** by its 300-MHz ^{1}H nmr spectrum. The minor product **2** (R_f 0.27, blackish spot) was obtained in a 2:3 mixture with **18**, but its presence was clearly indicated by its distinctive nmr signals. The compound having R_f 0.43 was isolated pure in a small amount and determined to be the 3-monotosylate **14** on account of its nmr spectrum (see Table 1).

When an identical experiment was performed, but with LAD, the chromatographic pattern was similar except that a somewhat larger proportion of starting **13** appeared to have remained (after 28 h), and the fast-moving spot attributed to **16** was slightly stronger than previously. Isolated chromatographically, **16** gave a 300-MHz ^{1}H nmr spectrum ($CDCl_3$) identical in every respect with that of an authentic sample and essentially agreeing with reported (30) data; δ: 7.46 and 7.37 (m, 2 and 3H, Ph), 5.54 (s, *Ph*-CH), 4.87b (s, $J_{1,2}$ = 0 Hz, H-1), 4.23 (q, splittings of 10 and 16 Hz, H-6e; compare footnote 4; misassigned as H-4 in ref. 30), 3.7–3.6 (m, 3H, H-4,5,6a), 3.45 (d, H-2 or H-3), 3.44 (s, 3H, OMe), and 3.14 (d, $J_{2,3}$ = 3.7 Hz, H-3 or H-2; note that $J_{3,4}$ = 0 Hz).

In an attempt to effect more complete reaction, **13** (300 mg) in oxolane (7 mL) was reduced with LAD (80 mg) as before, further LAD (80 mg) was added after 22 h, and boiling continued for another 24 h, whereafter **13** was no longer detectable by tlc. However, it was found upon processing (15) that the reaction had still not been entirely complete. The syrupy mixture of products (120 mg) was subjected to a single chromatography on a silica gel column (6 g) with 1:3 ethyl acetate – hexane. Various pure and mixed fractions of products totalling 70 mg were eluted. One small, mixed fraction (~8 mg) contained mainly **13**, and another small fraction (12 mg, crystalline) consisted of **14** (nmr). The fractions which contained the main product in more or less pure form amounted to 30 mg, and the 300-MHz ^{1}H nmr spectrum of a pure fraction was superposable on that of **18*a*** obtained in the LTBD reduction. Slow-moving material eluted from the column represented mixtures in which diol **19** appeared to be present.

[5]The dd observed at δ 4.23 was erroneously assigned to H-6a. It actually belonged to H-6e, and the recorded *J* values were not true coupling constants but splittings arising from second-order effects due to a near coincidence of the H-5 and H-6a chemical shifts. Compare also footnote 4.

Acknowledgement

This work was supported by the Natural Sciences and Engineering Research Council of Canada.

1. S. KRISHNAMURTHY and H. C. BROWN. J. Org. Chem. **41**, 3064 (1976).
2. V. K. SRIVASTAVA and L. M. LERNER. Carbohydr. Res. **64**, 263 (1978).
3. H. H. BAER and H. R. HANNA. Carbohydr. Res. **110**, 19 (1982).
4. H. H. BAER, M. MEKARSKA, and F. BOUCHARD. Carbohydr. Res. **136**, 335 (1985).
5. S. BRANDÄNGE, O. DAHLMAN, and J. ÖLUND. Acta Chem. Scand. Ser. B, **37**, 141 (1983).
6. H. C. BROWN, S. C. KIM, and S. KRISHNAMURTHY. J. Org. Chem. **45**, 1 (1980); H. C. BROWN, S. NARASIMHAN, and V. SOMAYAJI. J. Org. Chem. **48**, 3091 (1983).
7. H. H. BAER, D. J. ASTLES, H.-C. CHIN, and L. SIEMSEN. Can. J. Chem. **63**, 432 (1985).
8. H. H. BAER, and D. J. ASTLES. Carbohydr. Res. **126**, 343 (1984).
9. N. R. WILLIAMS. Adv. Carbohydr. Chem. Biochem. **25**, 109 (1970).
10. F. HANSSKE and M. J. ROBINS. J. Am. Chem. Soc. **105**, 6736 (1983).
11. A. C. RICHARDSON. Carbohydr. Res. **10**, 395 (1969).
12. H. H. BAER, and A. J. BELL. Carbohydr. Res. **75**, 175 (1979); H. H. BAER, B. RADATUS, and J. DEFAYE. Can. J. Chem. **63**, 440 (1985).
13. E. H. WILLIAMS, W. A. SZAREK, and J. K. N. JONES. Carbohydr. Res. **20**, 49 (1971).
14. S. UMEZAWA, T. TSUCHIYA, and H. HINENO. Bull. Chem. Soc. Jpn. **43**, 1212 (1970).
15. A. ZOBÁČOVÁ, V. HEŘMÁNKOVÁ, and J. JARÝ. Collect. Czech. Chem. Commun. **36**, 1860 (1971).
16. A. ZOBÁČOVÁ, V. HEŘMÁNKOVÁ, and J. JARÝ. Collect. Czech. Chem. Commun. **35**, 327 (1970).
17. V. HEŘMÁNKOVÁ, A. ZOBÁČOVÁ, and J. JARÝ. Collect. Czech. Chem. Commun. **36**, 303 (1971).
18. E. L. ELIEL, N. L. ALLINGER, S. J. ANGYAL, and G. A. MORRISON. Conformational analysis. Interscience Publishers, New York. 1965. pp. 370–378, 417–421.
19. J. DEFAYE, A. GADELLE, and C. C. WONG. Carbohydr. Res. **94**, 131 (1981).

20. P. J. GAREGG, T. IVERSEN, and S. OSCARSON. Carbohydr. Res. **53**, c5 (1977).
21. F. R. SEYMOUR. Carbohydr. Res. **34**, 65 (1974).
22. J. G. BUCHANAN and J. C. P. SCHWARZ. J. Chem. Soc. 4770 (1962).
23. F. A. CAREY and K. O. HODGSON. Carbohydr. Res. **12**, 463 (1970).
24. Y. KONDO. Carbohydr. Res. **30**, 386 (1973).
25. H. HÖNIG and H. WEIDMANN. Carbohydr. Res. **39**, 374 (1975).
26. D. C. BAKER, C. BOEDER, J. DEFAYE, A. GADELLE, and D. HORTON. Carbohydr. Res. **40**, c6 (1975).
27. B. R. BAKER and D. H. BUSS. J. Org. Chem. **30**, 2304 (1965).
28. G. J. ROBERTSON and W. WHITEHEAD. J. Chem. Soc. 319 (1940).
29. D. R. HICKS and B. FRASER-REID. Synthesis, 203 (1974).
30. D. H. BUSS, L. HOUGH, L. D. HALL, and J. F. MANVILLE. Tetrahedron, **21**, 69 (1965).

Protonation of hypoxanthine, guanine, xanthine, and caffeine

ROBERT L. BENOIT AND MONIQUE FRÉCHETTE
Département de Chimie, Université de Montréal, Montréal (Qué.), Canada H3C 3V1

Received May 1, 1985

ROBERT L. BENOIT and MONIQUE FRÉCHETTE. Can. J. Chem. **63**, 3053 (1985).

The protonation equilibria of three hydroxypurines, hypoxanthine, guanine, and xanthine, and of related caffeine have been studied by ^{1}H and ^{13}C nmr and uv spectroscopies in aqueous sulfuric or perchloric acids. The results have been interpreted on the basis of the excess acidity method. The $pK_{BH_n^{n+}}$ values and the protonation sites are discussed and comparisons are made with results of recent theoretical calculations.

ROBERT L. BENOIT et MONIQUE FRÉCHETTE. Can. J. Chem. **63**, 3053 (1985).

Les équilibres de protonation de trois hydroxypurines, l'hypoxanthine, la guanine, la xanthine, et du composé voisin la caféine ont été étudiés par les spectroscopies rmn du ^{1}H et du ^{13}C et uv dans les acides sulfurique et perchlorique aqueux. On a interprété les résultats sur la base de la méthode dite "d'acidité en excès". Les valeurs des $pK_{BH_n^{n+}}$ et les sites de protonation sont examinés et des comparaisons sont faites avec les résultats de calculs théoriques récents.

In addition to their importance in biological systems, purines offer a challenging thermodynamic and structural problem specifically in the determination of the reactivity of their many basic sites. Establishing correlations between the reactivity of the purines basic sites with the proton and other electrophiles such as metal ions also presents an interesting challenge. We recently reported results of a study of the first protonation step of some purines and of the second and third protonation steps of purine and adenine in more acidic media (1). We have now extended our study to the protonation of 3 hydroxypurines,

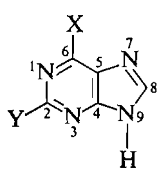

X-6	Y-2	
OH*	H	hypoxanthine (Hyp)
OH*	NH_2	guanine (Gua)
OH*	OH*	xanthine (Xan)

*tautomerization to 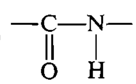

hypoxanthine (6-hydroxypurine), guanine (2-amino-6-hydroxypurine), and xanthine (2,6-dihydroxypurine), and of related caffeine (1,3,7-trimethylxanthine). For this work we abandoned the calorimetric method because a strong medium effect at high acidity interfered with the interpretation of the results, and we used, instead, uv spectroscopy. Adding uv spectroscopy to ^{13}C and ^{1}H nmr spectroscopies makes it also possible to compare data at widely different concentrations (10^{-4} M vs. 0.2 M).

The known pK_{BH^+} values for the first protonation step of hypoxanthine and guanine, which occur in dilute acid media, are respectively 1.9 (2) and 3.3 (2), while for xanthine the values quoted are 0.8 (3) and 1.2 (4) and for caffeine 0.5 (4). As for $pK_{BH_2^{2+}}$, the only value reported is −1.05 for guanine (5); $GuaH_2^{2+}$ has also been identified in both trifluoroacetic acid (TFA) and HSO_3F (6).

We present here the results of our study of the protonation reactions of the three hydroxypurines and caffeine between 0.05 and 18 M H_2SO_4. Our pK values as well as the protonation sites are discussed, and comparisons are made with results of recent theoretical calculations.

Experimental

Hypoxanthine (L. Light), guanine (L. Light), xanthine (L. Light and Aldrich), and caffeine (Baker) were used as received. Our uv spectra of $HypH^+$ and $GuaH^+$ were in agreement with those published (7). The spectra of Xan for both xanthine samples were similar to those reported (7, 8). Previous values of ϵ, the molar absorptivity, are somewhat lower than ours. We suspect that this was so because some decomposition of Xan takes place on standing. Sulfuric acid, H_2SO_4 fuming (15% SO_3) (Fisher) and 70% $HClO_4$ (Biopharm) were reagent grade. Triple-distilled HSO_3F (Aldrich) was used.

The uv spectra were recorded within 10 min of preparing the solutions on a 545 Perkin−Elmer spectrophotometer and absorbancies at a fixed wavelength were measured on a PMQ II Zeiss spectrophotometer. The ^{13}C nmr spectra were acquired at 28°C on a Bruker WP-80 spectrometer operating at 20.2 MHz. Data acquisition and Fourier transformation were performed with 8K data points. Proton decoupled spectra were recorded when needed to assist signal assignments. Carbon-13 chemical shifts were measured relative to external dioxane in D_2O (coaxial tube) and converted to the Me_4Si scale using the relationship $\delta_{Me_4Si} = \delta_{dioxane} + 67.40$ ppm. The ^{1}H nmr spectra were obtained on a Bruker WH-90 spectrometer operating at 90.0 MHz. The ^{1}H chemical shifts were determined by using the CH_3 protons of external DSS ($(CH_3)_3Si(CH_2)_3SO_3^-Na^+$) in D_2O and taking $\delta_{Me_4Si} = \delta_{DSS}$. The nmr samples were prepared by adding weighed portions of the solid bases to known volumes of titrated H_2SO_4 or $HClO_4$ solutions. The uv samples were obtained by diluting aliquots of the bases in acid solutions to 5 mL with titrated acid solutions.

Results and discussion

Chemical shifts

The nmr spectra were recorded for Hyp, Xan, and Caf with 0.05−18 M H_2SO_4 solutions and for Gua with 4−16 M H_2SO_4. For guanine, 0.5−6 M $HClO_4$ solutions were also used because of the low solubility of the base in H_2SO_4 below 4 M. In order to interpret our ^{13}C and ^{1}H shifts, H_0 values were computed from the corrected acid concentrations and literature data (9). These corrected concentrations were obtained by subtracting from the initial acid concentrations n times the concentrations of the protonated BH_n^{n+} species formed. In turn, these latter concentrations were obtained from the total base concentrations and eq. [2] and [3] given later in this discussion. The chemical shifts of the 5 carbons of Gua, Hyp, and Xan, those of C-8 and —CH_3 of Caf, and those of the H-8 protons of Gua and Xan were plotted against H_0. Carbons were assigned by using off-resonance spectra and data in Me_2SO.

The plots of ^{13}C and ^{1}H shifts are for the most part sigmoid curves indicative of protonation reactions. According to their pK_{BH^+}, Gua, Hyp, and Xan are all present as BH^+ at the lowest $HClO_4$ and H_2SO_4 concentrations used so that the ^{13}C curves show the formation of $GuaH_2^{2+}$ and $HypH_2^{2+}$. The sigmoid ^{1}H

TABLE 1. ^{13}C and ^{1}H shift values (ppm) of protonated species

Hydroxypurine	C-2	C-4	C-5	C-6	C-8	H-8
$GuaH^+$	155.9	150.7	108.7	155.9	138.2	8.67
$GuaH_2^{2+}$	152.3	137.9	110.1	152.3	138.8	8.89
$HypH^+$	150.4	148.1	116.1	155.1	139.9	—
$HypH_2^{2+}$	152.2	135.5	117.3	149.9	141.9	—
$XanH^+$	152.4	140.5	108.8	156.1	137.2	8.88
$CafH^+$	152.3	141.0	108.8	155.8	137.8	—

plot confirms $GuaH_2^{2+}$. In the case of Xan (and Caf), there is no clear evidence for BH_2^{2+}: C-8 is the only carbon noticeably shifted, but no plateau is reached, just as an early plateau, found when raw H-8 data were plotted, disappeared after bulk susceptibility corrections (10) were made.

The first protonation of Gua, Hyp, Xan, and Caf on the imidazole ring is well established (2) so that the choice of the second protonation site is restricted to N-3 or O-6 for Gua and Hyp. The shifts to high field of δC-4 and C-2 when passing from $GuaH^+$ to $GuaH_2^{2+}$ (Table 1) favour protonation at N-3 according to the α-protonation effect found by Pugmire and Grant for five- and six-membered nitrogen heterocycles (11). This assignment is in agreement with that of Wagner and von Philipsborn (6) deduced from ^1H nmr spectra in TFA at low temperature. However, these authors assumed that $GuaH_2^{2+}$ was the protonated species in TFA, whereas by comparing our ^{13}C data in TFA and H_2SO_4 we calculated that for TFA solutions $GuaH_2^{2+}/GuaH^+ = 1:1$. In the case of Hyp, C-4 shows a large upfield shift on passing from $HypH^+$ to Hyp_2^{2+}, as expected from protonation at N-3, and C-2 is moved to lower field as was observed for the third protonation of adenine at N-3 (1).

Ultraviolet spectra

On the basis of the nmr results, H_2SO_4 concentrations were selected to ensure the formation of BH^+ and BH_2^{2+}. The corresponding uv spectra were recorded and used to determine the most suitable wavelengths for measuring the absorbancies. Table 2 shows the H_2SO_4 concentrations used for the various protonated species together with the wavelengths of maximum absorption and the logarithms of the molar absorptivities ϵ. The plots of the absorbancies measured at several wavelengths (from 6 to 12 λ values) against H_0 were sigmoid curves and confirmed the formation of $GuaH_2^{2+}$ and $HypH_2^{2+}$. It is worth noting that the second protonation causes a hypsochromic shift. For Xan, there is also a hypsochromic shift of both absorption bands above 14.5 *M* H_2SO_4, but the absorbancies did not reach a plateau at 18 *M* H_2SO_4, and increasing the acidity further by adding oleum gave background absorbancies which were too high for meaningful measurements. Previous uv studies such as that for Gua (12) have already shown that it is difficult to assign the first protonation site on the basis of observed uv spectra, so that no attempt was made in this direction.

Calculation of pK_n

The values of pK_n for BH_n^{n+} were first calculated using the equation

$$[1] \quad H_0 = pK_n - m_n \log I$$

with

$$[2] \quad I = \frac{|BH_n^{n+}|}{|BH_{n-1}^{(n-1)+}|}$$

TABLE 2. Ultraviolet spectral data of hydroxypurines

Hydroxypurine	$[H_2SO_4]$ (*M*)	λ_{max} (nm)	Log ϵ
Gua	0	(246, 275)[a]	(4.01, 3.89)[a]
$GuaH^+$	0.11	248, 271	4.03, 3.85
$GuaH_2^{2+}$	10.85	236, 252	4.01, 3.95
Hyp	0	249[a]	(4.02)[a]
$HypH^+$	1.78	247	4.02
$HypH_2^{2+}$	18.09	241	4.00
Xan	0	267	3.99, (3.90)[a]
$XanH^+$	6.03−14.5	230, 259	3.87, 3.91
Caf	0	272.5	4.02
$CafH^+$	5.74	233, 265	3.79, 3.98

[a]Data from ref. 7.

The ratio *I* was obtained from the measured shifts δ and from the estimated limit chemical shifts δ_{n+} and $\delta_{(n-1)+}$ (Table 1) according to the standard equation

$$[3] \quad I = \frac{\delta - \delta_{(n-1)+}}{\delta_{n+} - \delta}$$

for the nmr shift data and the corresponding equation for the uv absorbancies data. However, the values of m_n were consistently well above 1.00, indicating that H_0 was not a satisfactory acidity function for following the protonation of these bases, just as it was not for adenine and purine (1). Two other acidity function, H_+ and H_A, were also used instead of H_0. Although H_A proved to be more satisfactory than H_+ and H_0, since our bases are very different from the amides used for H_A, we have finally chosen the Cox and Yates approach to calculated pK_n.

The excess acidity method (9) is based on the following equation:

$$[4] \quad \log I - \log C_{H^+} = m^*X + pK_n$$

Values for $\log C_{H^+}$ and *X* are independent of the bases and are taken from literature data (13) for each corrected H_2SO_4 or $HClO_4$ concentration. The program developed by Cox was used to solve simultaneously eqs. [3] and [4]. For each selected carbon and proton (or wavelength), values of C_{H^+}, *X*, δ, and the estimated values of δ_{n+} and $\delta_{(n-1)+}$ (or of the corresponding absorbancies data) were entered in the program. Thus, values of pK_n with their standard deviations (13) and m^* were obtained, as well as refined values of δ_{n+} and $\delta_{(n-1)+}$. These latter values differed from the estimated ones by less than 0.5 ppm (^{13}C), 0.01 ppm (^1H) (or 0.02 absorbancies unit). The pK_n values for the 4 bases, as well as those for adenine (Ade) and purine (Pur) (1) are summarized in Table 3. The differences found between the successive pK_n values are large enough to justify our treating the experimental data as if the protonation steps take place stepwise. An implicit, but reasonable, assumption in our treatment is that if tautomeric protonated species are present, their proportion is independent of the acid concentration. Since the agreement between pK_n values obtained by nmr and uv methods is generally satisfactory (although less so at higher acidities), considering the very different base concentrations used, 0.2 *M* vs. 10^{-4} *M*, large medium effects in one method can be ruled out. The presence of 2 isosbestic points in the uv spectra of Hyp (246 and 268 nm) between 1.8 and 18 *M* H_2SO_4 also suggests the absence of medium effect. Furthermore, no appreciable medium effect had previously been found for the protonation of Ade and Pur (1). For $XanH_2^+$, the uv pK_2 value is -10.0 ± 0.6. Additional nmr data taken on a HSO_3F

TABLE 3. pK values and protonation sites for hydroxypurines, caffeine, purine, and adenine

Hydroxypurine	pK (nmr)	pK (uv)	pK (lit.)	Protonation sites
$GuaH^+$			3.3[a]	N-7/N-9
$GuaH_2^{2+}$	-1.01 ± 0.03 (^{1}H and ^{13}C)	-0.99 ± 0.01	-1.05[b]	N-3
$HypH^+$			1.8,[a] 2.0[h]	N-7/N-9
$HypH_2^{2+}$	-3.12 ± 0.05 (^{13}C)	-3.65 ± 0.10		N-3
$XanH^+$		0.91 ± 0.01	0.8,[c] 1.2[d]	N-7/N-9
$XanH_2^{2+}$		-10.0 ± 0.6		O-6 (?)
$CafH^+$	-0.13 ± 0.03 (^{13}C)	0.18 ± 0.01	0.5[d]	N-9
$PurH^+$			2.39[a]	N-1
$PurH_2^{2+}$	-1.66 ± 0.04[e]		-1.5[e]	N-7/N-9
$AdeH^+$			4.19[f]	N-1
$AdeH_2^{2+}$	-0.43 ± 0.02[e]	-0.47[g]	-0.35[b]	N-7/N-9
$AdeH_3^{3+}$	-4.23 ± 0.2[e]			N-3

[a]Reference 2.
[b]Reference 5.
[c]Reference 3.
[d]Reference 4.
[e]Reference 1.
[f]Data from ref. 17.
[g]R. L. Benoit and M. Fréchette. Unpublished data.
[h]Reference 7.

solution ($-H_0$ = 15) of Xan and Caf to extend our results obtained with H_2SO_4 solutions ($-H_0 < 9.5$) and confirm $XanH_2^{2+}$ were inconclusive: C-8 moved further downfield and C-6 upfield but the shifts were small and no OH signal corresponding to C=O protonation could be detected at −75°C. The substantial downfield shift for the carbonyl carbons on protonation, which might have been expected with the formation of $XanH_2^{2+}$ and $CafH_2^{2+}$, is absent. Although this absence might be caused by conjugation effects, it nevertheless makes us consider the uv pK_2 value as tentative.

The discussion of the pK_n results for the ionization of the BH_n^{n+} species (Table 3) is a matter of some difficulty since the 3 tautomerized hydroxypurines first protonate on the imidazole ring while Ade and Pur first protonate on the pyrimidine ring. However, it is worth noting that for the 4 purines with successive protonations on N belonging on different rings, the differences between pK_2 and pK_1 correspond approximately to 6 kcal/mol.

Although it is difficult, we can try to relate our findings to the results of a recent molecular orbital study by Del Bene of the protonation of four DNA bases which include Gua and Ade as well as thymine and cytosine (14). The author computed the following protonation energies from optimized structures of the neutral and monoprotonated bases: for Gua, −245 kcal/mol (N-7), −233 (O-6 on the C-5 side), −228 (N-3), −220 (O-6 on the N-1 side), and for Ade, −241 (N-1), −240 (N-3), and −232 (N-7). Del Bene pointed out that these absolute values were overestimated because correlation and zero-point vibrational energy had to be neglected. In fact, Del Bene's calculated value for Ade, −241 kcal/mol, is at complete odds with the experimental gas phase proton affinity of −255 kcal/mol reported earlier by Meot-Ner (15). Furthermore, while the calculated value for thymine is right on Meot-Ner's −211 kcal/mol, for cytosine, Del Bene found a puzzling −249 kcal/mol to be contrasted with the experimental −225 kcal/mol. Thus, it is very difficult to say whether a discrepancy between data in Table 3 and Del Bene's values is due to the fact that the data in Table 3 were obtained in solution while the calculations refer to the gas phase, or to the unreliability of the reported MO calculations. For example, Gua is calculated by Del Bene to be 4 kcal/mol more basic than Ade, while the data in Table 3 indicate the reverse, with a 1.2 kcal/mol difference. This being said, her MO calculations should at least provide reasonable estimates of the relative protonation energies for the several basic sites of a given molecule. For Gua (but with the proton on N-9 although there is a N-7/N-9 tautomeric equilibrium (4, 16)), Del Bene found N-7 (−245 kcal/mol) to be the preferred protonation site and the solution data in Table 3 indicate N-7/N-9. Her next favored site is O-6 (on the C-5 side) (−233 kcal/mol) followed by N-3 (−288 kcal/mol). In contrast, our solution data show definitely that the second protonation takes place at N-3 rather than at O-6. It may be that the 5 kcal/mol difference between the calculated protonation energies at O-6 and N-3 is not high enough to counterbalance the repulsion which would exist between the second proton on O-6 (on the C-5 side) and the first proton on N-7. We must remember, however, that our results on successive protonations of the bases reflect factors additional to the relative intrinsic basicities of the various sites of the neutral bases.

Acknowledgements

We gratefully acknowledge the support of the Natural Sciences and Engineering Research Council of Canada. We thank Professor K. Yates and Dr. R. A. Cox for their continued interest in this research. We also thank D. Lefebvre, holder of an NSERC undergraduate scholarship, for her contribution to the work on caffeine.

1. (*a*) R. L. BENOIT and M. FRÉCHETTE. Can. J. Chem. **62**, 995 (1984); (*b*) R. L. BENOIT, D. BOULET, L. SÉGUIN, and

M. FRÉCHETTE. Can. J. Chem. **63**, 1228 (1985).
2. R. M. IZATT and J. J. CHRISTENSEN. Chem. Rev. **71**, 439 (1971).
3. B. PULLMAN and A. PULLMAN. Quantum biochemistry. Interscience Publishers, New York. 1963. p. 232.
4. D. LICHTENBERG, F. BERGMANN, and Z. NEIMAN. J. Chem. Soc. (C), 1676 (1971).
5. G. BUDO and J. TOMASZ. Acta Biochem. Biophys. Acad. Sci. Hung. **9**, 217 (1974).
6. R. WAGNER and W. VON PHILIPSBORN. Helv. Chim. Acta, **54**, 1543 (1971).
7. S. F. MASON. J. Chem. Soc. 2071 (1954).
8. H. M. KALCKAR. J. Biol. Chem. **167**, 429 (1947).
9. R. A. COX, and K. YATES. Can. J. Chem. **61**, 2225 (1983), and references therein.
10. T. A. MODRO, W. F. REYNOLDS, and K. YATES. Can. J. Chem. **54**, 1439 (1976).
11. R. J. PUGMIRE and D. M. GRANT. J. Am. Chem. Soc. **93**, 1880 (1971).
12. W. HUG and I. TINOCO, JR. J. Am. Chem. Soc. **95**, 2803 (1973).
13. R. A. COX and K. YATES. J. Am. Chem. Soc. **100**, 3861 (1978).
14. J. E. DEL BENE. J. Phys. Chem. **87**, 367 (1983).
15. M. MEOT-NER. J. Am. Chem. Soc. **101**, 2396 (1979).
16. J. LIN, C. YU, S. PENG, I. AKIYAMA, K. LI, L. K. LEE, and P. R. LE BRETON. J. Phys. Chem. **84**, 1006 (1980), and references therein.
17. S. ZIMMER and R. BILTONEN. J. Solution Chem. **1**, 192 (1972).

Binuclear phthalocyanines covalently linked through two- and four-atom bridges[1]

SEBASTIAN M. MARCUCCIO, POLINA I. SVIRSKAYA, SHAFRIRA GREENBERG, A. B. P. LEVER,
AND CLIFFORD C. LEZNOFF[2]
Department of Chemistry, York University, North York (Toronto), Ont., Canada M3J 1P3

AND

KENNETH B. TOMER
Midwest Center for Mass Spectrometry, University of Nebraska–Lincoln, Lincoln, NE 68588, U.S.A.

Received March 26, 1985

SEBASTIAN M. MARCUCCIO, POLINA I. SVIRSKAYA, SHAFRIRA GREENBERG, A. B. P. LEVER, CLIFFORD C. LEZNOFF, and KENNETH B. TOMER. Can. J. Chem. **63**, 3057 (1985).

Binuclear phthalocyanines in which the two phthalocyanine nuclei are covalently linked through four-atom bridges, derived from catechol, have been prepared and characterized. Metal-free 2,9,16,23-tetra-(3,3-dimethylbutyl)phthalocyanine and 2,9,16,23-tetra-(2-trimethylsilylethyl)phthalocyanine were prepared as examples of non-oxygenated mononuclear phthalocyanines soluble in organic solvents. Catalytic hydrogenation of 1,2-bis-(3,4-dicyanophenyl)ethyne and 1,4-bis-(3,4-dicyanophenyl)buta-1,3-diyne gave 1,2-bis-(3,4-dicyanophenyl)ethane and 1,4-bis-(3,4-dicyanophenyl)butane respectively. From these precursors, metal-free phthalocyanine dimers containing ethylene and tetramethylene bridges, joining the phthalocyanine nuclei, were prepared. Two of the two-atom bridge phthalocyanine dimers represent the first characterized phthalocyanine dimers not containing alkoxy or oxygenated groups.

SEBASTIAN M. MARCUCCIO, POLINA I. SVIRSKAYA, SHAFRIRA GREENBERG, A. B. P. LEVER, CLIFFORD C. LEZNOFF et KENNETH B. TOMER. Can. J. Chem. **63**, 3057 (1985).

On a préparé et on a caractérisé deux phtalocyanines binucléaires dans lesquelles deux noyaux phtalocyanines sont liés d'une façon covalente par quatre atomes de pont, dérivés du catéchol. On a préparé la tétra(diméthyl-3,3 butyl)-2,9,16,23 phtalocyanine et la tétra(triméthylsilyle-2 éthyle)-2,9,16,23 phtalocyanine exemptes de métal à titre d'exemples de phtalocyanines mononucléaires non oxygénées solubles dans des solvants organiques. Les hydrogénations catalytiques du bis(dicyano-3,4 phényl)-1,2 éthyne et du bis(dicyano-3,4 phényl)-1,4 butadiyne-1,3 conduisent respectivement au bis(dicyano-3,4 phényl)-1,2 éthane et au bis(dicyano-3,4 phényl)-1,4 butane. À l'aide de ces précurseurs, on a préparé des phtalocyanines dimères sans métal contenant des ponts éthylènes et tétraméthylène entre les noyaux phtalocyanines. Deux de ces phtalocyanines dimères correspondent aux premières phtalocyanines ne contenant pas de groupements alkoxyles ou oxygénés à être caractérisées.

[Traduit par le journal]

The electrocatalytic properties of porphyrins and phthalocyanines have been the subject of intensive research (1). A dicobalt cofacial porphyrin dimer (2, 3) containing a four-atom covalent bridge has been prepared. The four-electron reduction of oxygen to water using this dimer has been achieved but the compound tends to lose its catalytic activity with time (2). Since the phthalocyanine nucleus is likely to be more stable (4) than the porphyrin nucleus, we have tried to synthesize the related, but hitherto unknown, phthalocyanine dimers. We have recently reported the synthesis and some properties of phthalocyanine dimers incorporating five-atom covalent bridges (5, 6). Unlike typical phthalocyanines, these dimers are very soluble in organic solvents and their great solubility facilitates their purification and characterization. Recent work on the synthesis of porphyrin dimers has shown that even dimers having one rigid covalent bridge can be held in a cofacial conformation thought to be necessary for electrocatalysis (7). Since a four-electron reduction of oxygen was not achieved using the five-atom bridge dimer (5), we wished to prepare phthalocyanine dimers separated by the key four-atom bridges (2, 3) and to provide binuclear phthalocyanines containing two-atom bridges or less as control electrocatalysts that cannot assume a cofacial conformation. In addition, we wished to study the possibility of synthesizing binuclear phthalocyanines devoid of alkoxy groups or any oxygen atoms. In this paper we describe the preparation of a partially constrained binuclear phthalocyanine, containing a four-atom covalent bridge derived from catechol units; a flexible tetramethylene four-atom bridged phthalocyanine dimer; and phthalocyanine dimers containing two-atom ethylene bridges.

Synthesis of binuclear phthalocyanines bridged covalently by catechol units

Treatment of 4-nitrophthalonitrile (**1**) with 4-*tert*-butylcatechol (**2***a*) or catechol (**2***b*) and anhydrous potassium carbonate in dry dimethylformamide (DMF) at 22°C for 36 h gave 1,2-bis-(3,4-dicyanophenoxy)-4-*tert*-butylbenzene (**3***a*)[3] and 1,2-bis-(3,4-dicyanophenoxy)benzene (**3***b*)[3] in 84 and 78% yields, respectively (9, 10). Compounds **3***a*,*b* were converted to their respective 1,3-diiminoisoindolines (**4***a*,*b*) by bubbling ammonia into a solution of **3***a* or **3***b* and sodium methoxide in dry methanol under reflux for 6 h or until an infrared spectrum of an aliquot of the reaction mixture no longer exhibited the typical nitrile absorption peak (5, 6, 11, 12). Condensation (5, 6, 11, 12) of **4***a* with 5-neopentoxy-1,3-diiminoisoindoline (**5**) in 2-*N*,*N*-dimethylaminoethanol for 60 h gave a green-black solution, which was diluted with water to give a blue coloured residue. Flash chromatography (13) of the residue taken up in toluene yielded, in the first fractions using toluene as eluant, 2,9,16,23-tetraneopentoxyphthalocyanine (**6**) (5, 6) as a mix-

[1]Presented in part at the 67th Chemical conference of the Chemical Insitute of Canada, Montreal, Quebec, June 1984, Nos. IN5-5 and IN5-6.

[2]Author to whom correspondence may be addressed.

[3]See Table 1 for ^{13}C chemical shift values. Standard correlation tables were used as an aid to assignments (8).

TABLE 1. ^{13}C nuclear magnetic resonance chemical shifts in ppm (δ) of some phthalonitriles and bis-phthalonitriles

Carbon[a]	3a[b]	3b	9	12	13	14	15	29	30	32
1	109.4	109.9	113.8	115.0	115.2	112.5	112.1	115.2	112.4	114.0
2	117.6	—	116.8	116.0	115.8	115.5	115.1	114.2	115.2	114.2
3	120.8[c]	120.8[c]	141.9	135.9	135.6	132.7	133.1	136.2	132.7	133.8
4	160.7	160.4	99.7	128.9	130.1	151.9	150.1	128.0	150.6	149.2
5	120.6[c]	120.6[c]	142.4	136.2	135.9	133.3	122.6	136.5	133.3	134.2
6	135.5	135.5	133.9	133.3	133.2	132.8	133.6	133.5	132.8	134.0
7	115.2[d]	115.1[d]	114.9[c]	114.6[c]	113.6[c]	115.5	115.2[c]	114.5[c]	115.4[c]	116.1[c]
8	114.9[d]	114.7[d]	114.9[c]	114.4[c]	114.8[c]	115.5	115.3[c]	114.8[c]	115.4[c]	116.6[c]
9	144.1	144.9	—	103.2	106.7	30.0	44.8	84.4	28.4	36.0
10	142.1	144.9	—	100.5	76.4	17.9	30.8	79.7	14.3	30.6
11	123.0	123.7	—	—	28.1	—	30.0	—	—	—
12	125.6	128.6	—	−0.6	30.4	−2.0	28.7	—	—	—
13	152.8	128.6	—	—	—	—	—	—	—	—
14	120.6[c]	123.7	—	—	—	—	—	—	—	—

[a]The numbering of the carbon atoms in the compounds listed follows that given for these structures in the schemes and does not follow from the names of the compounds.
[b]The chemical shift values for the *tert*-butyl group are 34.9 and 31.1 ppm for the quaternary and methyl groups respectively.
[c]These values may be interchanged.
[d]These values may be interchanged.

TABLE 2. Absorption spectra of mononuclear and binuclear phthalocyanines (pc) and their solubilities in CH_2Cl_2[a]

Pc	λ_{max} (nm) (ε log)						Solubility (mol/L)
7a	708 (4.88)	676 (4.92)	642 (4.84)	620 (4.75)	388 (4.63)	336 (4.98)	[b]
7b	698 (4.83)	666 (4.93)	638 (4.94)	618 (4.84)	384 (4.67)	334 (5.08)	0.1
7c		672 (4.97)		628 (4.90)	326 (4.91)	290 (5.03)	0.06
18	698 (5.25)	664 (5.19)	644 (4.81)	604 (4.59)	342 (5.02)	292 (4.76)	0.7
19	698 (5.11)	664 (5.05)	644 (4.67)	604 (4.45)	342 (4.88)	290 (4.58)	0.1
20[c]		672 (5.04)		608 (4.45)	330 (4.75)	290 (4.72)	$<10^{-5}$
25[c]	702 (4.86)	668 (4.92)	642 (4.90)	620 (4.83)	340 (5.08)	292 (4.81)	$<10^{-6}$
26[c]	702 (4.93)	666 (4.96)	644 (4.90)	618 (4.81)	340 (5.10)	292 (4.85)	$<10^{-6}$
27[d]	706 (4.98)	672 (5.03)	646 (4.96)	620 (4.86)	344 (5.05)	296 (4.79)	$<10^{-5}$
28[d]		680 (4.99)		626 (4.69)	336 (4.87)	296 (5.02)	$<10^{-5}$
34[d]	708 (4.94)	672 (5.02)	644 (4.99)	620 (4.87)	342 (5.09)	296 (5.02)	$<10^{-5}$

[a]Solubilities were determined at 24°C by visible spectroscopy of saturated solutions in CH_2Cl_2.
[b]Available small quantities of 7a were insufficient to obtain reliable data on this very soluble dimer.
[c]These absorption spectra were taken in $CHCl_3$.
[d]These absorption spectra were taken in *o*-dichlorobenzene.

ture of isomers. Further elution with toluene gave mixtures of **6** and 1,2-bis-2′-(9′,16′,23′-trineopentoxyphthalocyaninoxy)-4-*tert*-butylbenzene (**7***a*) and some later fractions of pure **7***a* as shining dark purple plates.[4] Repetitive flash chromatography of the mixed fractions **6** and **7***a* gave pure **7***a* in 13% overall yield (Scheme 1). We initially selected 4-*tert*-butylcatechol (**2***a*) as the bridging moiety of binuclear phthalocyanines so that the resultant phthalocyanine dimer would be soluble in organic solvents. This idea was realized but **7***a* was actually too mobile chromatographically so that separation from the monomer **6** was tedious. The above synthesis was subsequently repeated but using catechol (**2***b*) as the bridging group. Thus, the 1,3-di-iminoisoindoline (**4***b*) was condensed with **5** as before. Flash chromatography (13) of the resultant blue-green mixture was much more facile, as monomer **6** eluted first in toluene, followed by mixed monomer−dimer fractions using toluene and toluene/2-methoxyethanol (50:1) as eluants.[4] Rechromatography of the mixed fractions gave pure 1,2-bis-2′-(9′,16′,23′-trineopentoxyphthalocyaninoxy)benzene (**7***b*) in 10% yield. Phthalocyanine dimer **7***b* was readily converted to its di-cobalt(II) derivative **7***c* by heating **7***b* with $CoCl_2$ in toluene at 110°C for 30 h. Dimer **7***c* was purified as before by flash chromatography using toluene/2-methoxyethanol (50:1) as eluant. The structures of **3***a*,*b* and **7***a*−*c* have been fully characterized by spectroscopic data and elemental analysis (see Experimental). The absorption spectra of **7***a*−*c* are characteristic of metal-free and metallophthalocyanine dimers respectively (6) (Table 2). Most importantly, the fast atom bombardment (14) (FAB) mass spectra of the binuclear phthalocyanines **7***a*−*c* all exhibit parent ion clusters almost identical in intensity to those calculated for their respective isotopic compositions. It

[4]Continued elution with toluene and toluene/2-methoxyethanol mixtures gave an additional blue-green fraction which, by fast atom bombardment analysis (FAB) (14), was shown to have a molecular ion corresponding to a phthalocyanine trimer.

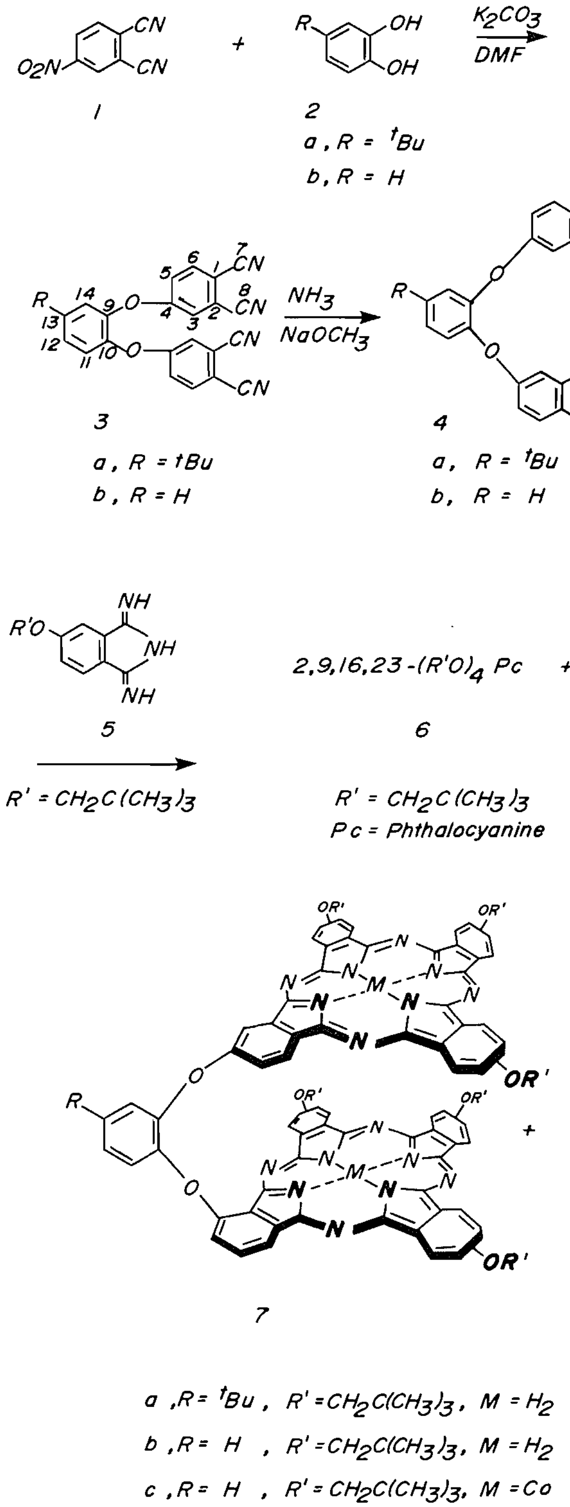

SCHEME 1

should be noted, however, that phthalocyanines 7*a* – *c* exist as a mixture of positional isomers about the phthalocyanine ring and that the depicted structure thus reflects this mixture. The broad absorbances in the ^{1}H nmr spectra of these compounds are indicative of this isomeric distribution (Table 3). On the other hand, the ^{13}C nmr spectra of 7*a* and 7*b* exhibit single resonances for the methyl and quaternary carbon groups of the neopentoxy substituents. Thus ^{13}C nmr spectra of 7*a*,*b* are diagnostic concerning their skeletal structure (Table 4), while the ^{1}H nmr spectra clearly identify the internal NH protons of 7*a*, *b* (Table 3).

Synthesis of 2,9,16,23-tetraalkylphthalocyanines

It has been shown (15, 16) that a wide variety of alkynes can couple with iodoarenes even at room temperature using cuprous iodide and bis(triphenylphosphine)palladium dichloride. We believed that this reaction could provide the basis for preparing the 4-alkylphthalonitriles and bisphthalonitriles needed for the preparation of mono and binuclear phthalocyanines containing no alkoxy substituents or oxygen atoms in the bridges of the phthalocyanines.

Catalytic hydrogenation of **1** in ethanol using 10% palladium on charcoal yielded 4-aminophthalonitrile (**8**) in 84% yield. Diazotization of **8** and subsequent reaction of the first-formed diazonium salt with potassium iodide gave 4-iodophthalonitrile (**9**)[3] in high yield. Coupling of **9** with trimethylsilylacetylene (**10**) (16) or 3,3-dimethyl-1-butyne (**11**) (15, 16) gave 4-(2-trimethylsilylethynyl)phthalonitrile (**12**)[3] or 4-(3,3-dimethyl-1-butynyl)phthalonitrile (**13**)[3] in 75% and 75% yield, respectively. Hydrogenation of **12** and **13** using palladium on charcoal as a catalyst gave the corresponding 4-alkyl derivatives, 4-(2-trimethylsilylethyl)phthalonitrile (**14**)[3] and 4-(3,3-dimethylbutyl)phthalonitrile (**15**)[3] in high yield. Conversion of **14** and **15** to their 1,3-diiminoisoindolines (**16**) and (**17**) as before (5, 6, 11, 12) and subsequent self-condensation in 2-*N*,*N*-dimethylaminoethanol gave 2,9,16,23-tetra-(2-trimethylsilylethyl)-phthalocyanine (**18**) and 2,9,16,23-tetra-(3,3-dimethylbutyl)-phthalocyanine (**19**) in 28% and 40% yields, respectively (Scheme 2). Phthalocyanine (**19**) was readily converted to its cobalt(II) derivative (**20**) as before (6, 11).

The mass spectra of **18**–**20** exhibited parent ions using the FAB technique (14). The ^{1}H nmr spectra of **18** and **19** were most informative and showed the inner NH absorptions (Table 3). In addition, the trimethylsilyl group of **18** and the *tert*-butyl group of **19** showed four and six peaks, respectively, corresponding to the eight different environments that these groups may experience in the four isomers possible for a tetrasubstituted phthalocyanine containing one substituent on each benzene ring. For 2,9,16,23-tetraneopentoxyphthalocyanine (**6**), the *tert*-butyl group gave an unresolved broad absorption peak in its ^{1}H nmr spectrum when recorded at high concentrations (6) but also exhibited 6 individual absorption peaks at lower concentrations (Table 3).

The ^{13}C nmr spectra of **18** and **19** exhibited only two peaks for the trimethyl group and the *tert*-butyl group while **6** showed only a single peak. On the other hand the —Si*C*H_2— group and —Si—CH_2*C*H_2— groups exhibited 8 and 6 peaks, respectively, indicating that all four isomers of **18** were indeed present (Table 4). Comparison of the solubilities of **18** and **19** with **6** showed that the tetraalkylphthalocyanines were less soluble than the tetraalkoxyphthalocyanine (6) (Table 2). The absorption spectra of **18** and **19** were consistent with the assigned structures (Table 2) (6).

Preparation of binuclear phthalocyanines covalently linked by dimethylene bridges

The dicoupling (15) of an acetylene to an iodoarene should provide the unknown bisphthalonitriles necessary to form binuclear phthalocyanines containing an all-carbon bridging group.

Thus treatment of 4-iodophthalonitrile (**9**) by methods previously described with acetylene (**21**) gave 1,2-bis-(3,4-dicyanophenyl)ethyne (**22**) in 90% yield. Compound **22** was very

TABLE 3. ^{1}H nuclear magnetic resonance chemical shifts in ppm (δ) of some mononuclear and binuclear phthalocyanines (Pc)

Pc	Solvent	Concentration (M)	Temperature (°C)	Proton type				
				Aromatic	CH_2X	CH_2Pc	$(CH_3)_3Z$	NH
6[a]	CD_2Cl_2	10^{-1}	22	7.6−6.0(m)	3.8(br s)	—	1.5(s)	−6.5
6[b]	CD_2Cl_2	10^{-4}	−70	[c]	4.3−3.7(br)	—	1.4(br), 1.2, 1.1, 0.9(br)	−3.1(br)
6[b,d]	$CDCl_3$	10^{-4}[d]	50	[c]	4.23, 4.22, 4.20, 4.19	—	1.09, 1.08, 0.88, 0.86, 0.85, 0.83	−1 to −3(v br)
6	C_7D_8[e]	10^{-4}	−80	[c]	4.5−3.5(br)	—	1.2(br), 0.1(br)	−0.9(br)
6	C_7D_8[e]	10^{-4}	22	[c]	3.9, 3.8	—	1.7(br), 1.3(br), 1.0(br), 0.5(br)	−2.6(v br)
6	C_7D_8[e]	10^{-4}	80	[c]	4.0, 3.9	—	1.4, 1.2, 1.1	−3.0(v br)
6Zn[a]	CD_2Cl_2	10^{-1}	22	7.7−6.1(m)	3.5(s)	—	1.3(s)	—
6Zn	$CDCl_3$	10^{-3}	22	8.2−6.4(br)	4.04, 4.01, 3.95, 3.82, 3.74, 3.72, 3.70	—	1.38, 1.37, 1.35, 1.34, 1.31, 1.25, 1.06	—
18	$CDCl_3$	2×10^{-3}	22	8.7−7.4(br)	1.25(t)	3.10(t)	0.32, 0.31, 0.30, 0.29	−2.9(br)
19	$CDCl_3$	10^{-3}	22	8.7−7.4(br)	1.88(t)	3.01(t)	1.28, 1.27, 1.24, 1.23, 1.225, 1.22	−3.2(br)
7*a*	$CDCl_3$	10^{-1}	22	[c]	4.4−3.6(br)	—	1.8−0.9(m)	−6.0(br)
7*b*	$CDCl_3$	10^{-3}	22	[c]	4.2−3.3(br)	—	1.5−0.8(m)	−3.1(br)
7*b*	$CDCl_3$	10^{-3}	50	[c]	4.4−3.3(br)	—	1.4−0.8(m)	−3.3(br)
7*b*	CD_2Cl_2	10^{-4}	−70	[c]	4.7−3.8(br)	—	1.6−0.9(m)	−3.0(br)
25	$CDCl_3$	10^{-3}	22	[c]	0.8−(−0.6)	3.5(br)	0.8−(−0.6)	−1 to −3(v br)
26	$CDCl_3$	10^{-3}	22	[c]	1.3−0.8	3.5(br)	1.3−0.8	−1 to −3(v br)
27	$CDCl_3$	10^{-3}	22	[c]	4.1−3.4(br)	—	1.3−0.7(br)	−1 to −3(v br)
34	$CDCl_3$	10^{-3}	22	[c]	4.1−3.5(br)	—	1.4−0.8(m)	−1 to −3(v br)
35	$CDCl_3$	10^{-4}	22	[c]	4.2−3.6(br)	—	1.5−0.9(m)	−1 to −3(v br)
35	$CDCl_3$	10^{-4}	50	[c]	4.2−3.2(br)	—	1.5−0.8(m)	−3.2(br)
35	CD_2Cl_2	10^{-4}	−70	[c]	3.9−3.1(br)	—	1.4−0.8(m)	−2.8(br)

[a]These data were taken from ref. 6. A Bruker WH250 instrument was used to record this spectrum.
[b]These measurements were done on a Bruker WH400 instrument.
[c]The absorptions in this region were very weak.
[d]The absorption of the NH protons was studied in $CDCl_3$ at 22°C at 10^{-1}, 10^{-2}, 10^{-3}, 10^{-4}, and 10^{-5} *M* concentrations and gave values of −5.5(br), −3.0(v br) and 4.1(br), −3.0(br), −3.0(br), and −3.0(br), respectively
[e]Toluene-d_8.

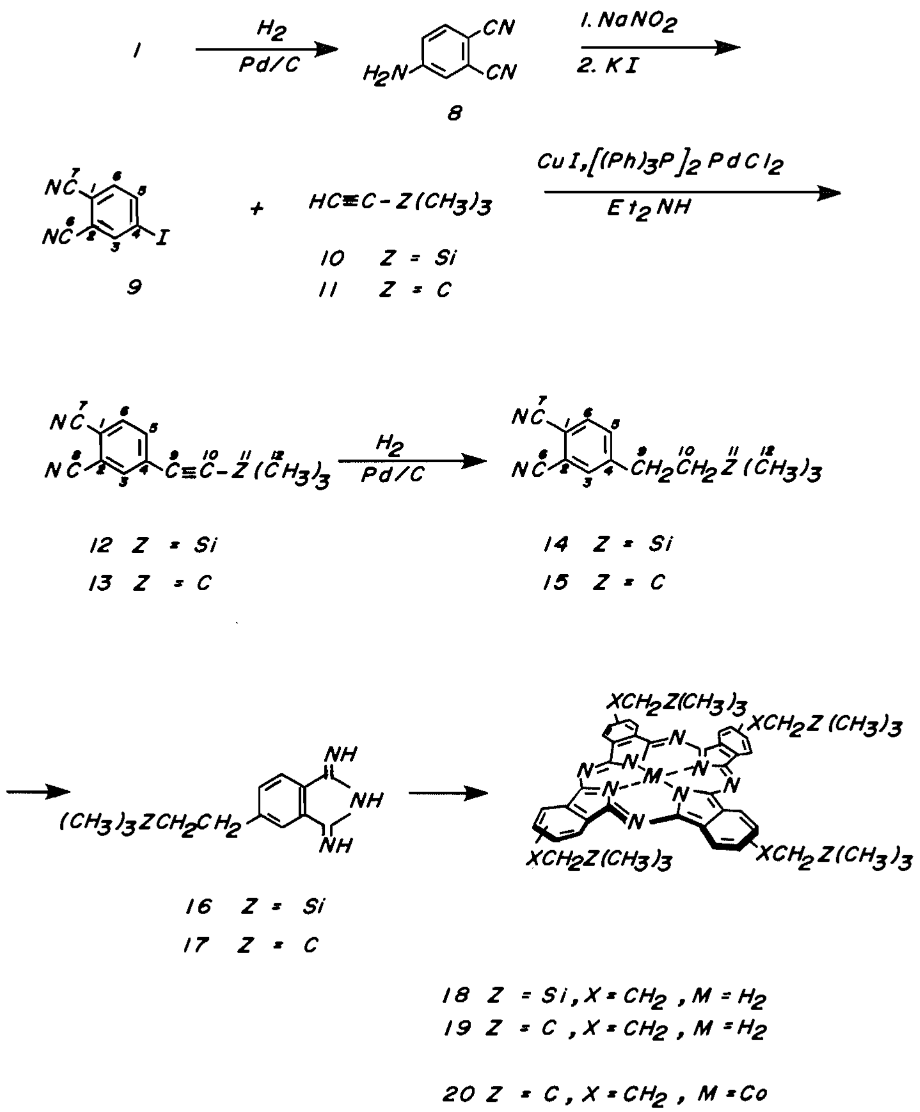

SCHEME 2

insoluble in most solvents except acetonitrile. Thus a suspension of **22** in acetonitrile was hydrogenated for 4 h at room temperature with shaking over 10% palladium on charcoal to give, in 83% yield, 1,2-bis-(3,4-dicyanophenyl)ethane (**23**). Compound **23** was converted to its 1,3-diiminoisoindoline (**24**) as before (5, 6, 11, 12) and condensed with an excess of the 1,3-diiminoisoindolines **16**, **17**, or **5** to give, after chromatographic separation, large amounts of the mononuclear phthalocyanines **18**, **19**, or **6** and 7–10% yields of 1,2-bis-2′-(9′,-16′,23′-tri-(2-trimethylsilylethyl)phthalocyaninyl)ethane (**25**), 1,2-bis-2′-(9′,16′,23′-tri-(3,3-dimethylbutyl)phthalocyaninyl) ethane (**26**) and 1,2-bis-2′-(9′,16′,23′-trineopentoxyphthalocyaninyl)ethane (**27**), respectively. Metal-free phthalocyanine **27** was readily converted to its dicobalt(II) derivative (**28**) (6, 11) (Scheme 3).

Binuclear phthalocyanines **25**–**27** exhibited the typical absorption spectra of metal-free binuclear phthalocyanines (6) while **28** exhibited the typical absorption of a metalated phthalocyanine dimer (Table 2). Compounds **25**–**28** all exhibited parent ions in their mass spectra using the FAB technique (14). Phthalocyanine dimers **25**–**28** were very much less soluble in organic solvents than the four-atom bridged catechol type dimers described above and the previously described five-atom bridged dimers (Table 2). The ^{1}H nmr of **25**–**27** were taken in dilute solutions and exhibited broad absorptions at the appropriate peak positions for the substituent groups (Table 3). The ^{1}H nmr spectra of the inner NH protons of **18**, **19**, and **6** are dependent on concentration, solvent, and temperature (Table 3). As a result of our initial examination of these effects on the ^{1}H nmr of **6** (Table 3), we generally run our samples in $CDCl_3$ or toluene-d_8 (C_7D_8) at concentrations of 10^{-3} to 10^{-4} *M* at room temperature. The effects of concentration, solvent, and temperature on porphyrin monomers and dimers have been studied and the effects noted here are consistent with those trends noted in porphyrin chemistry (17, 18).

Preparation of a binuclear phthalocyanine covalently linked by a tetramethylene bridge

As has been shown above in the preparation of **18**, 4-iodophthalonitrile (**9**) can readily couple with trimethylsilylethyne (**10**) to give **12**. Attempts to hydrolyze **12** as before (16) or by alternate procedures (19) resulted in solutions from which the desired 4-ethynylphthalonitrile (**29**)[3] could only be isolated in low yield. Hydrolysis of **12** under very mild conditions did

TABLE 4. ^{13}C nuclear magnetic resonance chemical shifts in ppm (δ) of some saturated solutions of mononuclear and binuclear phthalocyanines (Pc) in $CDCl_3$ at 22°C

	Carbon type				
Pc	Aromatic	CH_2X[a]	CH_2Pc	C^tBu	$(CH_3)_3Z$[b]
6[c]	160.6, 122.1, 117.4, 117.2	78.6, 78.4	—	32.5	27.3
6Zn[c]	160.1, 149.5, 121.7, 121.3, 116.9, 116.6, 104.2, 103.9	78.2, 78.1	—	32.2	27.1, 26.8, 26.5
18	147.4(m), 146.3(m), 132.9(m), 128.3(m), 120.4(m)	19.3, 19.2, 19.1, 19.0, 18.9, 18.8, 18.7, 18.5	31.0, 30.95, 30.8, 30.7, 30.5, 29.4	—	−1.35, −1.4
19	128.5, 120.4	30.8, 30.7	46.6	31.6, 31.5	29.7, 29.6
7*a*[d,e]	160.9	78.5	—	32.2	27.1
7*b*	[f]	78.2	—	32.1	27.1, 27.0, 26.5
25	145.5, 130.2, 120.9[f]	18.9	31.3, 29.7	—	−1.4, −1.5, −1.7
26	[f]	[f]	[f]	[f]	29.7
27	[f]	77.2	—	31.9	26.9
34[g]	—	77.8, 77.3	36.2	32.2, 32.15	27.4, 27.2
35[c,h]	[f]	78.6	[f]	32.4	27.2

[a]X = O for all compounds except **18**, **19**, **25**, and **26** where X = CH_2.
[b]Z = C for all compounds except **18** and **25** where Z = Si.
[c]These data were taken from ref. 6.
[d]Weak absorptions at 31.8 and 26.5 are likely due to the bridging *tert*-butyl group.
[e]This measurement was done on a Bruker WH400 instrument.
[f]The absorptions in this region were very weak.
[g]Weak absorptions at 26.8, 26.73, 26.7, and 26.6 are likely due to bridging carbons.
[h]Weak absorptions at 30.1 and 26.6 ppm are likely due to bridging carbons.

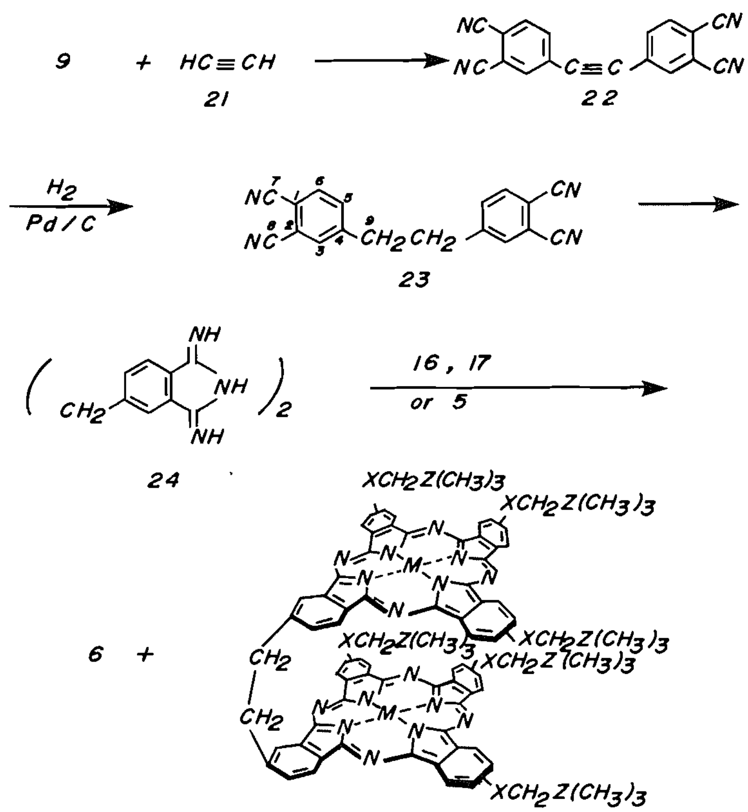

25 Z = Si , X = CH_2 , M = H_2

26 Z = C , X = CH_2 , M = H_2

27 Z = C , X = O , M = H_2

28 Z = C , X = O , M = Co

SCHEME 3

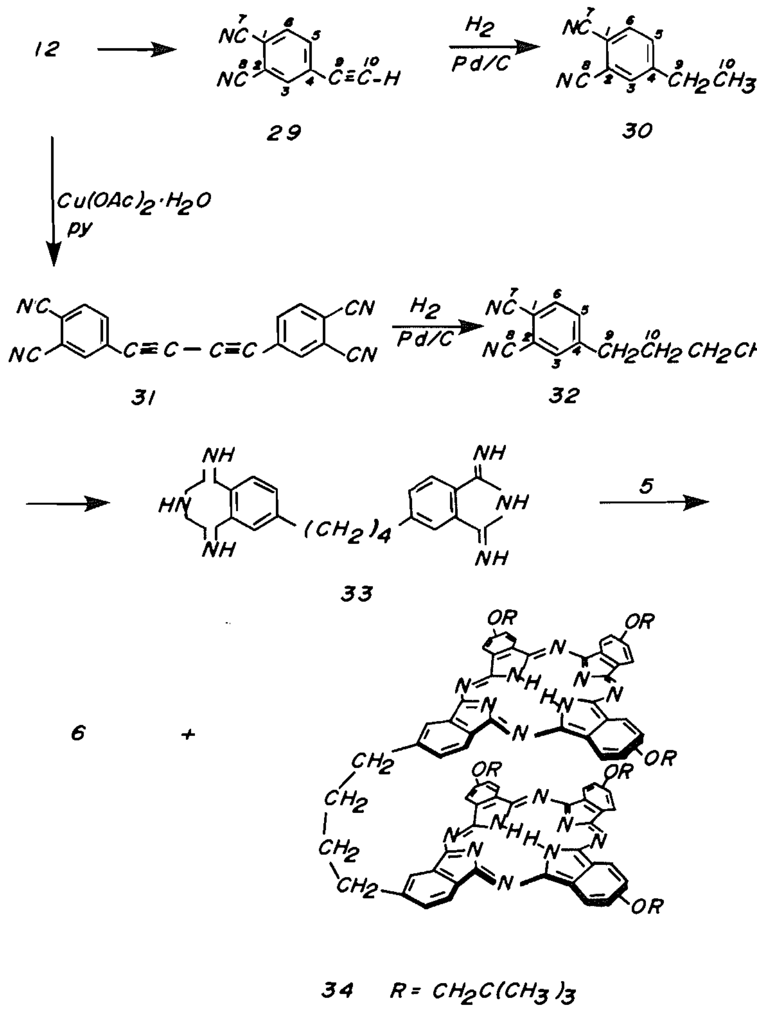

SCHEME 4

proceed in methanolic pyridine or in pyridine—$Cu(OAc)_2$ at room temperature to give **29** in high yield. Hydrogenation of **29** afforded 4-ethylphthalonitrile (**30**).[3] Since we wished to perform an oxidative dimerization (20, 21) of **29** to give 1,4-bis-(3,4-dicyanophenyl)-1,3-butadiyne (**31**) and since the conditions of this dimerization ($Cu(OAc)_2$, pyridine, methanol) are the very conditions that promote the hydrolysis of **12** to **29**, we felt that direct coupling of the precursor to **29**, i.e. **12**, should give the desired product **31**. Indeed, oxidative coupling of **12** yielded **31** in 76% yield. Catalytic hydrogenation of **31** as before gave 1,4-bis-(3,4-dicyanophenyl)butane (**32**)[3] in high yield. Conversion of **32** into its bis-1,3-diiminoisoindoline (**33**) as before (5, 6) and subsequent mixed condensation with **5** gave the undesired monomer **6** and the tetramethylene bridged dimer 1,4-bis-2′-(9′,16′,23′-trineopentoxyphthalocyaninyl)-butane (**34**) in 1.4% yield (Scheme 4).

Physical and spectroscopic properties of mononuclear and binuclear phthalocyanines

We have shown (6) that binuclear metal-free and metallophthalocyanine exhibit characteristic absorption spectra differing from each other and from the well-known absorption spectra of mononuclear metal-free and metallophthalocyanines (4). Thus, the mononuclear phthalocyanines **18**—**20** exhibit the characteristic absorptions (Table 2) of monomers, while binuclear phthalocyanines *7a*—*c*, **25**—**28**, and **34** all exhibit absorptions more typical of dimeric phthalocyanines.

The visible spectra of *7a*, *b*, **25**—**27**, and **34** show double $\pi-\pi^*$ bands near 700 and 670 nm, but the bands near 640 and 620 nm exhibit enhanced intensities compared to the model monomers **6**, **18**, and **19**. In addition, compounds **7***c* and **28** exhibit bands at 680 and 620 nm similar to the cobalt(II) derivative of **6** (5) and **20**, but the intensity of the band at 620 is greatly enhanced, typical of aggregation (22, 23). Thus, the visible spectra of *7a*—*c*, **25**—**28**, and **34** indicate substantial interaction between the phthalocyanine nuclei. This interaction is intramolecular rather than intermolecular since the blue shift is unaffected by dilutions in the range of 10^{-5}—10^{-6} M. A full description of the absorption and emission spectra of mononuclear and binuclear metal-free phthalocyanines is in progress.

As we have previously reported (6), the ^1H nmr spectra of monomeric phthalocyanines such as **6** and dimeric phthalocyanines such as 1,3-bis-2′-(9′,16′,23′-trineopentoxyphthalocyaninoxy)-2-ethyl-2-methylpropane (**35**) (Fig. 1) and, now, dimers *7a* and *7b* exhibit broad absorptions for internal NH protons in the region of −6.0 ppm when the spectra are run on samples at high concentrations (10^{-1} M) (Table 3). Although these data are consistent in general with those obtained by other workers for simple tetrasubstituted mononuclear phthalocyanines (24, 25), these workers do not record the concentrations of the phthalocyanines on which measurements were made and

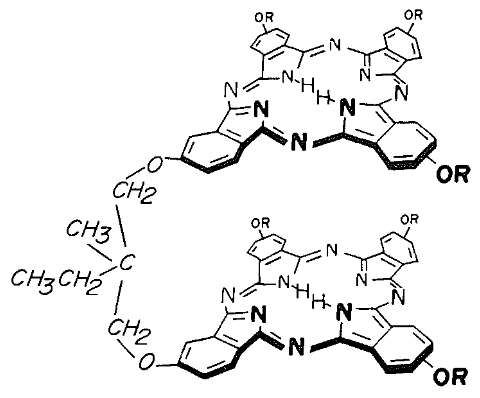

35 $R = CH_2C(CH_3)_3$

FIG. 1

the reported NH absorbances vary from −2.0 (24) to −9.0 ppm (25), an effect very concentration dependent as shown herein. The effect of concentration on the observance of the NH absorbances of **6** is described in footnote *d* to Table 3 and effectively shows that the absorption changes from −5.5 at 10^{-1} *M* to −3.0 at 10^{-3} *M* and remains constant upon further dilution. Furthermore, at intermediate concentrations (10^{-2} *M*), the observation of two NH absorbances at −4.1 and −3.0 is noted and undoubtably represents a mixture of free and aggregated phthalocyanines. The effect of temperature on the ^{1}H nmr of **6** is somewhat complicated by the concomitant effect of solvent on the internal NH absorbances. Thus in toluene-d_8 the NH absorbance (at 10^{-4} *M*) at 80°C is −3.0, at 22°C is −2.60, and at −80°C is −0.9 ppm. On the other hand, in CD_2Cl_2 the NH absorbance is invariant between −70°C and 22°C and broadens greatly in $CDCl_3$ at 50°C. Most importantly, however, the higher temperature nmr spectra do not exhibit NH absorbances at significantly lower fields, and hence 10^{-3}−10^{-4} *M* solutions most likely represent free non-aggregated phthalocyanines even at room temperature. The lack of an upfield shift of the NH absorbances at lower temperatures indicates that conformational mobility is still high enough that aggregation does not appreciably occur at −70 to −80°C. The NH absorbances of the binuclear phthalocyanines (**7*b***) and **35** at −70°C in CD_2Cl_2 and +50°C in $CDCl_3$ again do not appreciably change their value of ~−3.1 ppm, which indicates that even at low temperatures in the binuclear phthalocyanines conformational mobility is high on the nmr time scale or that intramolecular cofacial interaction is insignificant. Thus the extent of cofacial conformations of binuclear phthalocyanines **7*a***, ***b***, **25**−**27**, and **34**−**35** cannot be evaluated at present using nmr techniques. The mononuclear phthalocyanine **6** exhibits only a broad absorption peak for the CH_3 groups of the *tert*-butyl substituent in its ^{1}H nmr spectra at high concentrations (10^{-1} *M*) (Table 3) (6) but in dilute solutions (10^{-3}−10^{-4} *M*) **6**, the Zn derivative of **6** (**6**Zn) (6), **18** (26), and **19** exhibit 6, 7, 4, and 6 peaks, respectively, corresponding to this *tert*-butyl group. It should be noted that **6**, **6**Zn, **18**, and **19** each exist as a mixture of four possible positional isomers and that these isomers give rise to a total of eight possible environments for the substituent groups. For dilute solutions, up to 7 of these different absorptions are seen for the *tert*-butyl group (Table 3). In fact, for **6**Zn we can clearly see seven single absorptions for the CH_2O group of the mixture of 4 isomers. For dimers **7*a***,***b***, **25**, **26**, **27**, and **34** the ^{1}H nmr substituent absorbances of the mixtures of isomers are generally broad and not resolvable. As previously reported (6), the ^{13}C nmr of **6** at high concentrations (10^{-1} *M*) exhibited only 1 absorption peak for the CH_3 group of the *tert*-butyl group and, indeed, dimers **7*a***, **7*b***, **27**, and **34**, based on the neopentoxy substituent, all exhibited only one or two peaks for this group. On the other hand, the ^{13}C nmr of monomers **18** and **19** exhibited a multiplicity of peaks, again representing the 8 environments in which the four isomers each of **18** and **19** exist (Table 4). Indeed, **18** exhibits two absorptions for the CH_3Si carbon, all eight absorptions for the CH_2Si carbons, and six absorptions for the CH_2CH_2Si carbon (Table 4). The much greater multiplicity of isomers of the dimers and their even greater numbers of environments actually generate rather deceptively simple spectra in which single or small numbers of $(CH_3)_3Z$ absorbances are observed (Table 4). Because of this multiplicity of environments, rather poorly resolved, very weak, absorbances are observed in the aromatic region, and the bridging carbons of the dimers and these absorbances are not listed for both ^{1}H and ^{13}C nmr spectra of compounds in which these absorbances are poorly defined.

All phthalocyanines exhibited parent ions in their mass spectra (27) using the FAB system (14) and *o*-nitrophenyl octyl ether (ONPOE) as the solvent (6). The infrared spectra of all metal-free phthalocyanines exhibited characteristics NH absorptions at 3300 and 1020 cm^{-1} (28), which disappeared on formation of their cobalt derivatives.

The mononuclear phthalocyanine bearing the isohexyl substituents (**19**) was clearly less soluble than the tetraneopentoxyphthalocyanine (**6**) but the tetra-(2-trimethylsilylethyl)phthalocyanine (**18**) was almost as soluble as **6** (Table 2). Thus if one wishes to prepare soluble multinuclear phthalocyanines bearing no oxygen atoms around the periphery of the phthalocyanine nucleus, it would be possible to use isoindoline **16** as a "partner" in condensation reactions, but use of isoindoline **17** gives rather insoluble dimeric phthalocyanines (Table 2). It appears that phthalocyanine dimers containing bridges having oxygen atoms (**7*a***, ***b***, **35**) are considerably more soluble than all carbon bridge dimers such as **25**−**27** and **34**. Perhaps, not surprisingly, the more flexible tetramethylene bridged dimer **34** is more soluble than the ethylene bridged dimer **27**. Indeed, only dimers **7*a*** and **34** in this work exhibit ^{13}C nmr peaks for bridging carbons (Table 4). It was not possible to measure the solubilities of all the phthalocyanines in the same solvent, as **6** and **18** are too soluble in $CHCl_3$ or *o*-dichlorobenzene (ODCB) to conveniently obtain data while dimers **25**−**28** and **34** were generally totally insoluble in CH_2Cl_2. Using the knowledge that the phthalocyanines are generally soluble in solvents in the following order: $CDCl_3 > CHCl_3 >$ ODCB $> CH_2Cl_2$, we can generalize from the data shown in Table 2 that the order of solubility of monomeric and dimeric phthalocyanines is **6** (6) > **18** > **6**Zn (6) > **35** − **7*b*** > **19** > **20** > **34** > **27** > **25** > **26** > **28**. Thus multinuclear phthalocyanines very soluble in organic solvents are most readily made using the 5-neopentoxyisoindoline **5**, rather than the less accessible 5-alkylisoindolines **16** and **17**, as a partner in mixed condensations with bisisoindolines. In addition, multinuclear phthalocyanines bridged only by carbon atoms are less soluble than their oxygen bridged analogs. This decreased solubility may render their electrocatalytic properties less amenable to study. Further research on the synthesis of binuclear and multinuclear phthalocyanines having a fixed cofacial structure is in progress.

Experimental

Matheson high purity argon was used to maintain inert atmosphere conditions. Infrared (ir) spectra were recorded on a Pye Unicam SP1000 infrared spectrophotometer using KBr discs for solids or as neat films between NaCl discs. Nuclear magnetic resonance (nmr) spectra for protons were recorded on a Varian LM 360 spectrometer using deuterochloroform as solvent and tetramethylsilane as the internal standard. The positions of the signals are reported in δ units. (The splittings of the signals are described as singlets (s), doublets (d), triplets (t), quartets (q), or multiplets (m).) A Bruker AM300 nmr spectrometer was used for all ^{13}C nmr spectra and for ^{1}H nmr spectra of all phthalocyanines unless otherwise stated. The ^{1}H nmr spectra of 10^{-4} *M* solutions of phthalocyanines were obtained by averaging 500–1000 scans over the absorption range, while ^{13}C nmr spectra on saturated solutions of phthalocyanine were obtained by averaging 5 000–15 000 scans over the absorption range.

The visible–ultraviolet spectra (uv) were recorded on a Hewlett Packard HP8451A Diode Array spectrophotometer. Mass spectra (ms) were recorded at 70 eV on a VG Micromass 16F mass spectrometer in the EI mode.

The FAB spectra were obtained with a Kratos MS-50 triple analyzer mass spectrometer equipped with a FAB ion source of standard Kratos design and an Ion Tech atom gun. The sample was dissolved in chloroform and a microliter of the resulting solution added to a microliter of *o*-nitrophenyl octyl ether on the probe tip. The spectra of the molecular ions of the binuclear phthalocyanines were obtained by signal averaging up to 256 scans over the appropriate mass range. The number in parentheses after the indicated ion shows the percentage of the base peak represented by that ion. Melting points (mp) were determined using a Kofler hot stage melting point apparatus and are uncorrected. Thin-layer chromatography (tlc) was performed using silica gel G as the adsorbent. Flash chromatography was performed using silica gel of particle size 20–45 μm. All reactions were stirred with a magnetic stirrer. All solvents were freshly distilled before use. Microanalyses were performed by Guelph Chemical Laboratories Ltd., Guelph, Ont.

*1,2-Bis-(3,4-dicyanophenoxy)-4-*tert-*butylbenzene (3*a*) and 1,2-bis-(3,4-dicyanophenoxy)benzene (3*b*)*

A solution of 3.90 g (22.5 mmol) of **1**, 1.66 g (10 mmol) of **2***a*, and 7.0 g (50 mmol) of anhydrous potassium carbonate (K_2CO_3) in 25 mL of dry dimethylformamide (DMF) (6, 9) was stirred at room temperature for 36 h. The reaction mixture was diluted with water (150 mL), extracted with ethyl acetate, washed with saturated potassium carbonate, 4 *M* HCl, water, and saturated sodium chloride, and dried over magnesium sulphate. Evaporation of the solvent gave a brown oil, which on recrystallization from ethyl acetate – petroleum ether gave, in 84% yield, 3.51 g of **3***a*, mp 143–143.5°C; ir (cm^{-1}): 2260 (CN), 1595, 1575; ^{1}H nmr ($CDCl_3$, 60 MHz) δ: 7.85–7.05 (m, 9H, ArH), 1.35 (s, 9H, *t*Bu); ms, *m/z*: 418 (M$^+$, 21), 537 (20), 283 (10), 243 (65), 240 (100), 183 (48), 144 (19), 105 (58). *Anal.* calcd. for $C_{26}H_{18}N_4O_2$: C 74.63, H 4.34, N 13.39; found: C 74.62, H 4.33, N 13.31.

Similarly, a solution of 3.90 g (22.5 mmol) of **1**, 1.1 g (10 mmol) of **2***b*, and 7.0 g (50 mmol) of K_2CO_3 in 25 mL of DMF was stirred for 36 h at room temperature. The reaction mixture was extracted with ethyl acetate and worked up as described above to give a crude crystalline product, contaminated by a small quantity of starting material **1**. Column chromatography of this crude mixture on silica gel and elution with 1:5 ethyl acetate – petroleum ether gave **1**. Further elution with 3:2 ethyl acetate – petroleum ether gave, in 78% yield, upon evaporation of the solvent and recrystallization from ethyl acetate – petroleum ether, 2.82 g of colourless needles of **3***b*, mp 189–190°C; ir (cm^{-1}): 2260, 1595, 1572; ^{1}H nmr ($CDCl_3$, 60 MHz) δ: 7.80–7.00 (m, 10H, ArH); ms, *m/z*: 363 (31), 362 (M$^+$, 100), 219 (30). *Anal.* calcd. for $C_{22}H_{10}N_4O_2$: C 72.93, H 2.78, N 15.46; found: C 73.07, H 2.56, N 15.48.

*Preparation of isoindolines 4*a and *4*b

The bis-1,3-diiminoisoindolines **4***a* and **4***b* were prepared as previously described (6, 12). In a typical example 20 mg of sodium was added to 40 mL of dry methanol under argon to form sodium methoxide. Nitrile **3***b* (500 mg, 1.38 mmol) was added and the oil bath heated to 60°C to dissolve the nitrile. Ammonia gas was bubbled into this solution as previously described (6) and the methanol evaporated to give crude **4***b*, which was used directly in the next step. An ir spectrum of the crude isoindolines must not exhibit any residual nitrile absorption.

*1,2-Bis-2′-(9′,16′,23′-trineopentoxyphthalocyaninoxy)-4-*tert-*butylbenzene (7*a*) and 1,2-bis-2′-(9′,16′,23′-trineopentoxyphthalocyaninoxy)benzene (7*b*)*

The crude bis-1,3-diiminoisoindoline (**4***a*) and 5-neopentoxy-1,3-diiminoisoindoline (**5**) obtained from 200 mg (0.48 mmol) of **3***a* and 2.5 g (11.68 mmol) of 4-neopentoxyphthalonitrile (5, 6) respectively, were heated at 150–160°C (oil bath) in 20 mL of 2-*N*,*N*-dimethylaminoethanol for 60 h under an argon atmosphere by methods similar to those previously described (6, 12). The reaction mixture was cooled, poured into water, filtered, and washed repeatedly with water. The crude reaction mixture was dissolved in 200 mL of toluene and stirred at 70°C for 5 h with 100 mL of 1 *M* KOH. The reaction mixture was cooled; the organic layer was separated from the aqueous layer and washed with water and saturated sodium chloride, and dried over magnesium sulphate. The toluene solution containing the phthalocyanine mixture was preadsorbed onto silica gel for flash chromatography (13). Elution with 600 mL of toluene – petroleum ether (5:1) followed by elution with pure toluene gave three initial fractions (200 mL each) followed by fifteen 100-mL fractions and, finally, two 1-L fractions. The early fractions contained pure 2,9,16,23-tetraneopentoxyphthalocyanine (**6**), the middle fractions mixtures of **6** and **7***a*, and the final fractions mixtures of **7***a* and another phthalocyanine thought to be a trinuclear phthalocyanine. The middle fractions containing **6** and **7***a* were rechromatographed on fresh silica by flash chromatography using toluene as eluant. Again monomer **6** eluted first, some mixed fractions eluted next, and pure **7***a* was finally isolated. All of **7***a* was eventually recovered by rechromatography of all mixed fractions. The yield of monomer **6** recovered was 58% (1.45 g). The final fractions containing dimer **7***a* and a trimer[4] were also separated by flash chromatography to give, in total, 108 mg (13% yield) of **7***a* as a dark, blue, shining solid, mp >300°C; ir (cm^{-1}): 3310 (NH), 1620, 1245, 1100, 1020 (NH); ms *m/z*: 1707.8 (100), 1706.8 (M$^+$, 87). *Anal.* calcd. for $C_{104}H_{106}N_{16}O_8$: C 73.13, H 6.25, N 13.12; found: C 72.97, H 6.32, N 13.57.

A small fraction of the dimer–trimer mixture was chromatographed on preparative tlc plates using toluene/2-methoxyethanol (200:1) as solvent. The slower moving blue-green fraction was extracted with toluene and finally purified by flash chromatography using toluene/2-methoxyethanol (50:1) as solvent to give a very small quantity of a blue green solid. *Mol. Wt.* (FAB ms) calcd. for $C_{156}N_{154}N_{24}O_{12}$: 2556.91; found 2556.2 (100), 2555.2 (M$^+$, 76).

Similarly, the crude bis-1,3-diiminoisoindoline (**4***b*) and **5**, obtained from 500 mg (1.38 mmol) of **3***b* and 7.5 g (35.0 mmol) of 4-neopentoxyphthalonitrile (5, 6), respectively, gave monomer **6** in the toluene fractions on flash chromatography of the crude product obtained from the reaction mixture. Further elution with toluene/2-methoxyethanol (100:1) and toluene/2-methoxyethanol (200:5) gave mixed monomer–dimer fractions and pure dimer fractions. Rechromatography of the mixed fractions gave a total of 3.15 g of pure monomer **6** in 42% yield and 222 mg (10% yield) of pure dimer **7***b* as a dark, blue, shining solid, mp >300°C; ir (cm^{-1}): 3310 (NH), 1625, 1248, 1105, 1020 (NH); ms *m/z*: 1651.8 (100), 1650.8 (M$^+$, 61). *Anal.* calcd. for $C_{100}H_{98}N_{16}O_8$: C 72.71, H 5.98, N 13.57; found: C 73.24, H 5.98, N 13.19.

*1,2-Bis-2′-(9′,16′,23′-trineopentoxyphthalocyaninoxycobalt(II))benzene (7*c*)*

A solution of 100 mg (0.06 mmol) of **7***b* and 80 mg of cobalt(II) chloride in 10 mL of toluene/2-methoxyethanol (7:3) was heated at 110°C under argon for 30 h as previously described (6). Flash chromatography of the crude product using toluene/2-methoxyethanol (50:1) as eluant gave, in 69% yield, 73 mg of **7***c* as a shiny blue solid, mp >300°C; ir (cm^{-1}): 1620, 1250, 1105, 1070, 760; ms *m/z*: 1765.6

(100), 1764.6 (M^+, 62). *Anal.* calcd. for $C_{100}H_{94}N_{16}O_8Co_2$: C 68.06, H 5.37, N 12.70, Co 6.68; found: C 68.21, H 5.54, N 12.34, Co 6.44.

4-Aminophthalonitrile (8)

A suspension of 5.19 g (30 mmol) of 4-nitrophthalonitrile (**1**) (29) and 0.5–0.6 g of 10% palladium on charcoal in 150 mL of 95% ethanol was placed a 500-mL jar in a Parr hydrogenation apparatus and hydrogenated at 415 kPa according to the procedure of Rasmussen *et al.* (30). The crude product (4.2 g, mp 175–178°C) was chromatographed using normal grade silica gel. Elution with benzene – ethyl acetate (3:1) gave 3.6 g (84% yield) of pure white crystals of **8**, mp 179–180°C (lit. (30) mp 179–181°C). Compound **8** does deteriorate on standing and is usually directly converted into compound **9** described below.

4-Iodophthalonitrile (9)

A suspension of 4.29 g (30 mmol) of **8** in 60 mL of 2.5 *M* H_2SO_4 was cooled to −10°C. A solution of 2.4 g (34 mmol) of sodium nitrite in 5–8 mL of H_2O was added dropwise with stirring, while the temperature of the mixture was kept at −10 to 0°C. Stirring was continued at 0°C for 0.5 h to complete the reaction. The resulting mixture was rapidly filtered by suction filtration and the cool filtrate was added in a small portion to a cool solution of 5.4 g (32 mmol) of potassium iodide in 30 mL of water. The resulting black mixture was allowed to warm to room temperature with stirring. The precipitated black solid was collected by suction filtration, washed with cold water, and dissolved in benzene. The benzene solution was washed with cold water, 5% $NaHCO_3$, cold water, saturated $Na_2S_2O_3$, again with water, dried over $MgSO_4$, filtered, and concentrated to a small volume. Chromatography on 200 g of normal grade silica gel and elution with benzene gave, in 70% yield, 5.3 g of pure **9** as white crystals, mp 142–143°C (lit. (31) mp 141–142°C); ir (cm^{-1}): 3020–2960, 2240 (CN), 1580, 940, 850, 845; ^1H nmr ($CDCl_3$, 60 MHz) δ: 8.22–8.08 (m, 2H, ArH-3,6), 7.61–7.55 (m, 1H, ArH-5); ms m/z: 254 (M^+, 87), 127 (100), 100 (38).

4-(2-Trimethylsilylethynyl)phthalonitrile (12) and 4-(3,3-dimethyl-1-butynyl)phthalonitrile (13)

To a solution of 5.08 g (20 mmol) of **9** in 80 mL of dry, freshly distilled diethylamine was added 2.1 g (22 mmol) of triethylsilylacetylene (**10**), 38 mg (0.2 mmol) of copper(I) iodide, and 140 mg (0.2 mmol) of bis(triphenylphosphine)palladium dichloride under an argon atmosphere, using the procedure of Takahashi *et al.* (16). The reaction mixture was stirred at room temperature for 3 h, during which time a precipitate of diethylamine hydroiodide appears. The mixture was filtered to separate the precipitated salt and the filtrate was concentrated on the rotary evaporator. The residue was extracted into benzene and purified by column chromatography on neutral alumina, activity II–III, using benzene as the eluting solvent. Evaporation of the solvent gave an oil which, on distillation in a Kugelrohr apparatus at 110–120°C/0.01 Torr (1 Torr = 133.3 Pa), gave 3.4 g (75% yield) of a white solid (**12**), mp 74–75°C; ir (cm^{-1}): 3100, 2240 (CN), 1600, 1498, 1440, 1345, 1265, 1250, 860, 840; ^1H nmr (CCl_4, 60 MHz) δ: 7.65–7.52 (m, 3H, ArH), 0.05 (s, 9H, $(CH_3)_3Si$); ms m/z: 224 (M^+, 17), 209 (100), 179 (14), 73 (70), 59 (27), 43 (23). *Anal.* calcd. for $C_{13}H_{12}N_2Si$: C 69.59, H 5.39, N 12.49; found: C 69.51, H 5.53, N 12.19. Product **12** rapidly decomposed in the presence of water.

Similarly, a mixture of 2.54 g (10 mmol) of **9**, 0.82 g (10 mmol) of *tert*-butylacetylene (**11**), 20 mg (0.1 mmol) of copper(I) iodide, and 140 mg (0.2 mmol) of bis(triphenylphosphine)palladium dichloride in 50 mL of dry, freshly distilled diethylamine was stirred overnight under an argon atmosphere. Analysis by thin-layer chromatography (tlc), using ether–hexane 1:4 as eluant, showed the presence of unreacted **9**. An additional 0.16 g of **11** was added and stirring was continued for a further 12 h. A final addition of 0.16 g of **11** was added and, after stirring for a total of 72 h, the reaction was still not completed. The reaction mixture was worked up as described above. Flash chromatography of the crude product using 1:19 ether–hexane as eluant gave an oil, which on distillation in a Kugelrohr apparatus at 130–135°C/0.01 Torr yielded 1.6 g (75% yield) of pure **13**, mp 60–61°C; ir (cm^{-1}): 3100, 3000, 2250 (CN), 2235, 1600, 1490, 1370, 1320, 1275, 910, 880; ^1H nmr ($CDCl_3$, 300 MHz) δ: 7.77–7.67 (m, 3H, ArH), 1.32 (s, 9H, $(CH_3)_3C$); ms m/z: 208 (M^+, 20), 193 (100), 178 (13), 165 (18). *Anal.* calcd. for $C_{14}H_{12}N_2$: C 80.73, H 5.81, N 13.45; found: C 80.70, H 5.90, N 13.21.

4-(2-Trimethylsilylethyl)phthalonitrile (14), 4-ethylphthalonitrile (30), and 4-(3,3-dimethylbutyl)phthalonitrile (15)

A solution of 2.8 g (12.5 mmol) of **12** in 50 mL of dry ethyl acetate was hydrogenated over 10% palladium on charcoal at 275 kPa for 1 h. The catalyst was filtered and the filtrate evaporated to dryness. Column chromatography of the product on 150 g of normal grade silica gel using ethyl acetate – hexane (1:4) as eluant gave, upon evaporation of the solvent, 2.5 g (88% yield) of colourless needles. Distillation of the solid product in a Kugelrohr apparatus at 140–145°C/0.1 Torr gave pure **14**, mp 63–64°C; ir (cm^{-1}): 3090, 2970, 2240 (CN), 1605, 1498, 1345, 1265, 1250, 860, 840, 700; ^1H nmr ($CDCl_3$, 300 MHz) δ: 7.60–7.45 (m,3H, ArH), 2.71 (m, 2H, CH_2ArH), 0.84 (m, 2H, CH_2Si), 0.01 (s, 9H, $(CH_3)_3Si$); ms m/z: 228 (M^+, 41), 213 (35), 73 (100), 59 (68), 43 (17). *Anal.* calcd. for $C_{13}H_{16}N_2Si$: C 68.36, H 7.06, N 12.26; found: C 68.11, H 7.18, N 12.29.

Further elution of the silica gel gave 0.1 g of 4-ethylphthalonitrile **30**) as a white solid, mp 42–43°C; ir (cm^{-1}): 3000–2900, 2245 (CN), 1600, 1500, 1240, 1070, 870, 850; ^1H nmr ($CDCl_3$, 60 MHz) δ: 7.8–7.4 (m, 3H, ArH), 2.8 (q, J = 8 Hz, 2H, CH_2), 0.84 (t, J = 8 Hz, 3H, CH_3); ms m/z: 156 (M^+, 50), 141 (100), 114 (40). *Anal.* calcd. for $C_{10}H_8N_2$: C 76.90, H 5.16, N 17.94; found: C 77.23, H 5.33, N 17.99.

Similarly, hydrogenation of 3.6 g (17 mmol) of **13** in 100 mL of dry ethanol for 1 h as described above yielded a crude oil. Flash chromatography of this oil using ether–hexane (1:9) as eluant and distillation of product using a Kugelrohr apparatus gave 3.3 g (92% yield) of **15** as a colourless oil, bp 130–138°C/0.01 Torr; ir (neat, cm^{-1}): 2980, 2250 (CN), 1610, 1500, 1380, 1250, 850; ^1H nmr ($CDCl_3$, 300 MHz) δ: 7.80–7.78 (m, 1H, ArH), 7.65–7.58 (m, 2H, ArH), 2.74–2.68 (m, 2H, CH_2Ar), 1.54–1.48 (m, 2H, CH_2C), 1.33 (s, 9H, $(CH_3)_3C$). *Anal.* calcd. for $C_{14}H_{16}N_2$: C 79.20, H 7.59, N 13.20; found: C 79.05, H 7.49, N 13.05.

Preparation of 5-(2-trimethylsilylethyl)-1,3-diiminoisoindoline (16) and 5-(3,3-dimethylbutyl)-1,3-diiminoisoindoline (17)

All diiminoisoindolines were prepared as previously described (5, 6, 11, 12). In a typical example 115 mg (0.50 mmol) of **14** was added to a solution of 15 mg of sodium in 10 mL of dry methanol. The mixture was stirred at room temperature for 1 h and for 4 h under reflux conditions, during which ammonia gas was bubbled into the solution. Evaporation of the solvent gave crude **16**, which was used directly in condensation reactions without further purification. Compounds **16** and **17** did not exhibit nitrile absorptions in their ir spectra.

Preparation of 2,9,16,23-tetra-(2-trimethylsilylethyl)phthalocyanine (18) and 2,9,16,23-tetra-(3,3-dimethylbutyl)phthalocyanine (19)

The crude diiminoisoindoline **16**, obtained from 115 mg (0.50 mmol) of **14** in 2 mL of 2-*N*, *N*-dimethylaminoethanol, underwent self-condensation as previously described (5, 6, 11, 12) to give 60 mg of a crude reaction product. Flash chromatography of this product using toluene as eluant gave, upon evaporation of the solvent, 33 mg (28% yield) of **18** as a dark blue, shining solid; ir (cm^{-1}): 3310 (NH), 1620, 1255, 1100, 1015 (NH), 870, 840, 760; ms m/z: 915 (M^+, 100), 841 (28). *Anal.* calcd. for $C_{52}H_{66}N_8Si_4$: C 68.22, H 7.27, N 12.24; found: C 68.31, H 6.99, N 12.24.

Similarly, the crude diiminoisoindoline **17**, obtained from 118 mg (0.56 mmol) of **13** in 2 mL of 2-*N*,*N*-dimethylaminoethanol, underwent self-condensation as previously described (5, 6, 11, 12) to give 90 mg of a crude reaction product. Flash chromatography of this product using toluene as eluant gave, upon evaporation of the solvent, 48 mg (40% yield) of **19** as a dark blue, shining solid; ir (cm^{-1}): 3320 (NH), 1625, 1105, 1020 (NH), 760; ms m/z: 850 (M^+, 100), 791 (35), 424 (47). *Anal.* calcd. for $C_{56}H_{66}N_8$: C 79.02, H 7.82, N 13.16; found: C 78.71, H 7.76, N 13.09.

*2,9,16,23-Tetra-(3,3-dimethylbutyl)phthalocyaninatocobalt(II) (**20**)*

To a solution of 153 mg (0.18 mmol) of **19** in 15 mL of toluene and 5 mL of 2-methoxyethanol was added 91 mg (0.70 mmol) of anhydrous cobalt(II) chloride as previously described (6). The solution was stirred at 115°C (oil bath) under an argon atmosphere for 19 h. The crude reaction mixture was cooled to room temperature and the solvent evaporated. Flash chromatography of the residue using toluene as the eluting solvent gave, in 48% yield, 78 mg of **20** as a dark blue, shining solid; ir (cm^{-1}): 1625, 1105, 760; ms m/z: 908 (M$^+$, 75), 850 (21). *Anal.* calcd. for $C_{56}H_{64}N_8Co$: C 74.07, H 7.10, N 12.34, Co 6.49; found: C 74.50, H 7.64, N 11.58, Co 6.50.

*1,2-Bis-(3,4-dicyanophenyl)ethyne (**22**) and 1,2-bis-(3,4-dicyanophenyl)ethane (**23**)*

By the procedure described above for the preparation of **12** and **13**, 5.1 g (20 mmol) of **9**, 150 mL of dry, freshly distilled diethylamine, 38 mg (0.2 mmol) of copper(I) iodide, and 70 mg (0.1 mmol) of bis(triphenylphosphine)palladium dichloride was placed into a 250-mL two-necked flask, equipped with a magnetic stirrer, a condenser, and a gas inlet tube. The flask was flushed with argon and a moderate stream of dry acetylene was passed through the solution for 3 h at room temperature. The pale pink precipitate that was formed was collected by filtration from the brown solution. The crude product was washed with water, methanol, and ether, and air dried to give, in 90% yield, 2.5 g of **22**, mp 286–288°C. This product is sufficiently pure that it can be used directly without further purification. Two recrystallizations of a small sample of **22** from acetonitrile gave colourless crystals of pure **22**, mp 296–297°C; ir (cm^{-1}): 3090, 2240 (CN), 1600, 1500, 1260, 920, 865; ms m/z: 278 (M$^+$, 100), 251 (14), 224 (8), 149 (35), 139 (11), 85 (38), 57 (97), 43 (73). *Anal.* calcd. for $C_{18}H_6N_4$: C 77.69, H 2.17, N 20.13; found: C 77.97, H 1.96, N 20.01. Compound **22** is very insoluble in common organic solvents and is only slightly soluble in boiling acetonitrile (100 mg in 50 mL). The ^{1}H and ^{13}C nmr of **22** was not determined, as a suitable solvent was not found in which **22** was sufficiently soluble.

A suspension of 0.6 g (2.1 mmol) of **22** in 300 mL of acetonitrile, containing 100 mg of 10% palladium on charcoal, was hydrogenated at 415 kPa in a Parr hydrogenation bottle for 4 h at room temperature. The clear solution was filtered from the catalyst and concentrated. The compound was purified by flash chromatography using hot acetonitrile as eluant to give 0.5 g (83% yield) of **23** as white needles, mp 257–258°C; ir (cm^{-1}): 3100, 2980, 2240 (CN), 1600, 1490, 1390, 1240, 925, 860; ^{1}H nmr (CD_3CN, 400 MHz) δ: 7.81 (d, J = 8 Hz, 2H, ArH-5), 7.76 (s, 2H, ArH-2), 7.58 (d, J = 8 Hz, 2H, ArH-6), 3.05 (s, 4H, CH_2); ms m/z: 282 (M$^+$, 31), 141 (100), 114 (49), 57 (73), 39 (11). *Anal.* calcd. for $C_{18}H_{10}N_4$: C 76.58, H 3.57, N 19.84; found: C 76.76, H 3.47, N 19.94.

*Preparation of the bis-1,3-diiminoisoindoline (**24**)*

Compound **24** was prepared as previously described (6) for the preparation of 1,3-diiminoisoindolines derived from bisphthalonitriles only slightly soluble in methanol.

*1,2-Bis-2'-(9',16',23'-tri-(2-trimethylsilylethyl)phthalocyaninyl)ethane (**25**)*

The two crude diiminoisoindolines **16** and **24**, obtained from 4.80 g (21.1 mmol) of **14** and 203 mg (0.72 mmol) of **23**, respectively, in 30 mL of 2-N,N-dimethylaminoethanol, underwent a mixed condensation as previously described (5,6) to give 5 g of a crude reaction product. Flash chromatography on silica gel of this product on a 5-cm diameter column using toluene–hexane (1:1) as eluant gave 1.63 g of the monomeric **18** in 34% yield. Further elution with toluene gave a fraction consisting largely of dimer. This dimer fraction was purified further by flash chromatography on a 3-cm diameter column. Elution with toluene–hexane (1:1) removed all traces of monomer, as analyzed by tlc using toluene as eluant. Further elution with toluene gave a blue solid containing a trace of impurities, detected by tlc analysis and visualization with uv light. The blue solid was freed of these impurities by washing with methanol to give, in 7% yield, 83 mg of the binuclear phthalocyanine **25** as a dark blue, shining solid; ir (cm^{-1}): 3320 (NH), 1620, 1260, 1105, 1020 (NH), 870, 840, 760; ms m/z: 1659 (48), 1658 (63), 1657 (100), 1656 (91), 1655 (M$^+$, 65). *Anal.* calcd. for $C_{96}H_{110}N_{16}Si_6$: C 69.61, H 6.69, N 13.53; found: C 69.65, H 6.80, N 13.16.

*1,2-Bis-2'-(9',16',23'-tri-(3,3-dimethylbutyl)phthalocyaninyl)ethane (**26**)*

The two crude diiminoisoindolines **17** and **24**, obtained from 4.46 g (21.0 mmol) of **15** and 203 mg (0.72 mmol) of **23**, respectively, in 30 mL of 2-N,N-dimethylaminoethanol, underwent a mixed condensation as described for **7*a***, **7*b***, and **25** above and previously (5, 6) to give 5 g of a crude reaction product. Flash chromatography of this product on silica gel (5-cm diameter column) using toluene–hexane (1:1) and pure toluene gave 2.07 g of the monomeric phthalocyanine **19** containing traces of dimer, as analyzed by tlc using toluene as eluant. Further elution with 2-methoxyethanol/toluene (1:100) gave a fraction consisting largely of dimer containing traces of monomer. Finally, elution with 2-methoxyethanol/toluene (1:4) gave a green fraction consisting largely of trimer and impurities. The solid monomer fraction was placed in the thimble of a Soxhlet extractor and extracted with refluxing hexanes to give 0.52 g of pure monomer **19**. Using the Soxhlet extractor and refluxing toluene as solvent, a further 0.71 g of **19** was isolated from the extracting solvent on evaporation, leaving 0.84 g of insoluble monomer containing traces of dimer in the thimble. It is possible that some of the positional isomers of **19** are more soluble than others and that the above selective extraction has effected a partial separation of these isomers. The dimer fraction was purified by vacuum liquid chromatography (vlc) (32) using toluene–hexanes (1:1) as the eluting solvent followed by increasing amounts of 2-methoxyethanol/toluene (1:100 to 5:100). The vlc removed most of the monomer (but not all) and a final separation was achieved by flash chromatography (13) using the same eluting solvents as above to give, in 8% yield, 90 mg of the pure binuclear phthalocyanine **26** as a dark blue, shining solid; ir (cm^{-1}): 3320 (NH), 1625, 1105, 1015 (NH), 760; ms m/z: 1561 (84), 1560 (100), 1559 (M$^+$, 84). *Anal.* calcd. for $C_{102}H_{110}N_{16}$: C 78.53, H 7.11, N 14.36; found: C 79.36, H 7.62, N 13.49.

*1,2-Bis-2'-(9',16',23'-trineopentoxyphthalocyaninyl)ethane (**27**)*

The two crude diiminoisoindolines **5** and **24**, obtained from 6.0 g (28 mmol) of 4-neopentoxyphthalonitrile (5, 6) and 284 mg (1.0 mmol) of **23**, were heated to 150°C (oil bath) in 30 mL of 2-N,N-dimethylaminoethanol for 60 h under argon as previously described (5, 6). The crude product was purified by flash chromatography using a 5-cm diameter column packed with silica gel 12 cm high. The crude product was preabsorbed on silica and eluted with toluene to give 2.67 g of the monomeric **6** in 44% yield. Further elution with 2-methoxyethanol/toluene (1:100) gave a fraction consisting largely of dimer containing traces of monomer and some green material. Finally, elution with 2-methoxyethanol/toluene (1:4) gave a green fraction consisting largely of trimer and impurities. The dimer fraction was further purified by flash chromatography (3-cm diameter column). Elution with toluene removed all traces of monomer. Further elution with 2-methoxyethanol/toluene (5:200) gave a dark blue product. This product was washed with acetone to remove traces of fluorescent and light green impurities, detectable by tlc using toluene/2-methoxyethanol (200:5) as eluant, to give in 10% yield 159 mg of **27** as a dark blue, shining solid; ir (cm^{-1}): 3310 (NH), 1620, 1245, 1100, 1020 (NH), 755; ms m/z: 1574.8 (51), 1572.8 (90), 1571.8 (100), 1570.8 (M$^+$, 60). *Anal.* calcd. for $C_{96}H_{98}N_{16}O_6$: C 73.35, H 6.28, N 14.26; found: C 73.08, H 6.34, N 14.19.

The "trimer" fraction was further purified by flash chromatography (3-cm diameter column). Elution with 2-methoxyethanol/toluene (3:200) removed all traces of dimer. Further elution with 2-methoxyethanol/toluene 1:20 gave 280 mg of a dark, blue, shining solid in 25% yield. This product was not characterized.

*1,2-Bis-2'-(9',16',23'-trineopentoxyphthalocyaninyl cobalt(II))ethane (**28**)*

A mixture of 44 mg (0.028 mmol) of metal-free dimer **27** and

21 mg (0.16 mmol) of anhydrous cobalt(II) chloride in 13 mL of a 1:4 mixture of 2-methoxyethanol/toluene was heated at 120°C for 20 h under an argon atmosphere. Flash chromatography of the crude reaction mixture on a 3-cm diameter column of silica gel and elution with 2-methoxyethanol/toluene (1:20 and then 1:8) gave, in 55% yield, 26 mg of **28** as a dark blue, shining solid; ir (cm^{-1}): 1620, 1245, 1100, 760; ms *m/z*: 1687.6 (49), 1686.6 (80), 1685.6 (100), 1684.6 (M^+, 76), 1630.6 (38), 1629.6 (57), 1628.6 (72), 1627.6 (51). *Anal.* calcd. for $C_{96}H_{94}N_{16}O_6Co_2$: C 68.40, H 5.62, N 13.29, Co 6.99; found: C 68.06, H 5.75, N 12.95, Co 7.19.

4-Ethynylphthalonitrile (29)

Preliminary experiments conducted on the hydrolysis of **12** to **29** showed that hydrolysis was slow in pyridine alone, pyridine and methanol, or pyridine and copper(II) acetate, and that all three components are necessary for rapid hydrolysis. These conditions are identical with those necessary for the coupling of terminal alkynes by the Eglinton procedure (20) except that hydrolysis occurs at room temperature. A solution of 0.09 g (0.4 mmol) of **12**, 1.6 g of copper(II) acetate monohydrate, 0.8 mL of methanol, and 14 mL of pyridine was stirred for 1 h at room temperature. The reaction mixture was filtered and washed with pyridine and methanol. The filtrate was evaporated to dryness *in vacuo* and extracted with methylene chloride. The extract was washed with water, dilute hydrochloric acid, and water, and dried over $MgSO_4$. Evaporation of the solvent gave a product which was purified by flash chromatography, using ethyl acetate − hexane (1:4) as eluant. Evaporation of the eluant gave, in 82% yield, 50 mg of pure **29** as white crystals, mp 88–90°C; ir (Nujol, cm^{-1}): 3280 ($\equiv$C—H), 2250, 2135, 1600, 930, 850; ^{1}H nmr ($CDCl_3$, 60 MHz) δ: 8.0–7.8 (m, 3H, ArH), 3.45 (s, 1H, $\equiv$C—H); ms *m/z*: 152 (M^+, 100), 125 (46), 99 (28), 74 (26), 50 (37). *Anal.* calcd. for $C_{10}H_4N_2$: C 78.94, H 2.68, N 18.41; found: C 78.28, H 3.00, N 18.60.

Further elution of the silica gel gave 10 mg of **31** described below.

1,4-Bis-(3,4-dicyanophenyl)-1,3-butadiyne (31)

Using the Eglinton terminal alkyne coupling procedure (20) and recognizing that **12** gives **29** under the conditions of this reaction, 0.45 g (2.0) mmol) of **12** was mixed with 8.0 g of copper(II) acetate monohydrate in 70 mL of dry pyridine and 4 mL of dry methanol. The mixture was heated at 50–55°C for 0.75 h with stirring under argon. The reaction mixture was cooled to room temperature, filtered, and washed with pyridine and methanol. The filtrate was worked up as described for **29** above to give, in 76% yield, 0.23 g of a crude product, mp 299–302°C. Further purification by flash chromatography on silica gel using CH_2Cl_2 as eluant gave, upon evaporation of the solvent, in 70% total yield 0.21 g of pure white crystals of **31**, mp 303–304°C; ir (cm^{-1}): 3100, 2250 (CN), 2180 (C$\equiv$C), 1600, 1300, 1240, 925, 860; ^{1}H nmr (CD_2Cl_2, 60 MHz) δ: 7.9–7.7 (m, 6H, ArH); ms *m/z*: 302 (M^+, 100), 275 (7), 248 (5), 224 (8), 200 (8), 151 (8), 124 (4), 98 (4), 74 (4). *Anal.* calcd. for $C_{20}H_6N_4$: C 79.46, H 1.99, N 18.54; found: C 79.39, H 1.81, N 18.48.

1,4-Bis-(3,4-dicyanophenyl)butane (32)

A solution of 0.15 g (0.5 mmol) of **31** in 100 mL of dry tetrahydrofuran (THF) and 50 mg of 10% palladium on charcoal was hydrogenated at 275 kPa in a Parr hydrogenator for 1 h at room temperature. The catalyst was filtered over Celite and washed with THF. The filtrate was evaporated to give fine colourless crystals in quantitative yield. Further purification by flash chromatography on silica gel using CH_2Cl_2–ether (1:10) gave 0.13 g in 84% yield of pure **32**, mp 168–169°C; ir (cm^{-1}): 3100, 2950, 2240 (CN), 1600, 1500, 1250, 860, 850; ^{1}H nmr (CD_2Cl_2, 400 MHz) δ: 7.73 (d, J = 8 Hz, 2H, ArH-5), 7.62 (s, 2H, ArH-2), 7.53 (d, J = 8 Hz, ArH-6), 2.77 (t, J = 8 Hz, 4H, ArCH_2), 1.67 (m, 4H, CH_2); ms *m/z*: 310 (M^+, 39), 169 (26), 155 (58), 141 (100), 114 (41), 39 (13). *Anal.* calcd. for $C_{20}H_{14}N_4$: C 77.39, H 4.55, N 18.05; found: C 77.62, H 4.35, N 17.97.

Preparation of the bis-1,3-diiminoisoindoline (33)

Compound **33** was prepared as previously described (6) for the preparation of 1,3-diiminoisoindolines derived from bisphthalonitriles only slightly soluble in methanol.

1,4-Bis-2′-(9′,16′,23′-trineopentoxyphthalocyaninyl)butane (34)

The two crude diiminoisoindolines **5** and **33**, obtained from 6.0 g (28 mmol) of 4-neopentoxyphthalonitrile (5, 6) and 310 mg (1.0 mmol) of **32**, respectively, were heated to 150°C (oil bath) in 30 mL of 2-*N*,*N*-dimethylaminoethanol for 60 h under argon as described for the preparation of **27**. Using a work-up identical to that for **27**, purification by flash chromatography as before gave 1.64g of monomer **6** in 27% yield and, in 1.4% yield, 23 mg of dimer **34** as a dark blue, shining solid; ir (cm^{-1}): 3320 (NH), 1620, 1250, 1105, 1020 (NH), 760; ms *m/z*: 1561.8 (25), 1560.8 (85), 1599.8 (100), 1598.8 (M^+, 64). *Anal.* calcd. for $C_{98}H_{102}N_{16}O_6$: C 73.57, H 6.42, N 14.01; found: C 72.91, H 6.62, N 13.65.

Acknowledgements

We are grateful to the Natural Sciences and Engineering Research Council of Canada for financial support of this research. This work was also partially funded by the Office of Naval Research (Washington) and by the Midwest Center for Mass Spectrometry, a National Science Foundation Regional Instrumentation Facility (Grant No. CHE 8211164).

1. D. LEXA, P. MAILLARD, M. MOMENTEAU, and J.-M. SAVEANT. J. Am. Chem. Soc. **106**, 6321 (1984); P. SAYER, M. GOUTERMAN, and C. R. CONNELL. Acc. Chem. Res. **15**, 73 (1982); P. FORSWEY, T. KUWANA, N. KOBAYASHI, and T. OSA. Adv. Chem. Ser. **201**, 601 (1982); J. ZAGAL, P. BINORA, and E. YEAGER. J. Electrochem. Soc. **127**, 1506 (1980); F. VAN DEN BRINK, E. BARENDRECHT, and W. VISSCHER. Recl. Trav. Chim. Pays-Bas, **99**, 253 (1980); K. KASUEA and M. TSUTSUI. Coord. Chem. Rev. **32**, 67 (1980).
2. J. P. COLLMAN, F. C. ANSON, S. BENCOSME, A. CHONG, T. COLLINS, P. DENISEVICH, E. EVITT, T. GEIGER, J. A. IBERS, G. JAMESON, Y. KONAI, C. KOVAL, K. MEIER, P. OAKLEY, R. B. PETTMAN, E. SCHMITTOV, and J. SESSLER. *In* Organic synthesis today and tomorrow. *Edited by* B. M. Trost and C. R. Hutchinson. Pergamon, Oxford. 1981.
3. R. R. DURAND, JR., C. S. BENCOSME, J. P. COLLMAN, and F. C. ANSON. J. Am. Chem. Soc. **105**, 2710 (1983).
4. A. B. P. LEVER. Adv. Inorg. Chem. Radiochem. **7**, 27 (1965).
5. C. C. LEZNOFF, S. GREENBERG, S. M. MARCUCCIO, P. C. MINOR, P. SEYMOUR, A. B. P. LEVER, and K. B. TOMER. Inorg. Chim. Acta, **89**, 135 (1984).
6. C. C. LEZNOFF, S. M. MARCUCCIO, S. GREENBERG, A. B. P. LEVER, and K. B. TOMER. Can. J. Chem. **63**, 623 (1985).
7. C. K. CHANG, H. Y. LIU, and I. ABDALMUHDI. J. Am. Chem. Soc. **106**, 2725 (1984); C. K. CHANG and I. ABDALMUHDI. J. Org. Chem. **48**, 5388 (1983).
8. J. T. CLERC, E. PRETSCH, and J. SEIBL. Structural analysis of organic compounds. Elsevier, New York. 1981. p. 277; G. C. LEVY, D. M. WHITE, and J. D. CARGIOLI. J. Magn. Reson. **8**, 280 (1972).
9. W. O. SIEGL. J. Heterocycl. Chem. **18**, 1613 (1981).
10. T. M. KELLER, T. R. PRICE, and J. R. GRIFFITH. Synthesis, 613 (1980); T. M. KELLER and J. R. GRIFFITH. U.S. Patent No. 4,226,801 (1980); N. P. MARULLO and A. W. SNOW. ACS Symposium Series, **14**, 325 (1982).
11. G. PAWLOWSKI and M. HANACK. Synthesis, 287 (1980).
12. P. J. BRACH, S. J. GRAMMATICA, O. A. OSSANA, and L. WEINBERGER. J. Heterocycl. Chem. **7**, 1403 (1970).
13. W. C. STILL, M. KAHN, and A. MITRA. J. Org. Chem. **43**, 2923 (1978).
14. M. BARBER, R. S. BORDOLI, R. D. SEDGWICK, and A. N. TYLER. J. Chem. Soc. Chem. Commun. 325 (1981).
15. K. SONOGASHIRA, Y. TOHOA, and N. HAGIHARA. Tetrahedron Lett. 4467 (1975).
16. S. TAKAHASHI, Y. KUROYAMA, K. SONOGASHIRA, and N. HAGI-

HARA. Synthesis, 627 (1980).
17. J. P. COLLMAN, F. C. ANSON, C. E. BARNES, C. S. BENCOSME, T. GEIGER, E. R. EVITT, R. P. KREH, K. MEIER, and R. B. PETTMAN. J. Am. Chem. Soc. **105**, 2694 (1983).
18. R. J. ABRAHAM and K. M. SMITH. J. Am. Chem. Soc. **105**, 5734 (1983); K. M. SMITH, R. J. ABRAHAM, and H. PEARSON. Tetrahedron, **38**, 2441 (1982); T. R. JANSON and J. J. KATZ. *In* The porphyrins. Vol. IV. *Edited by* D. Dolphin. Academic Press, New York. 1979. p. 1.
19. C. S. KRAIHANZEL and J. E. POIST. J. Organometal. Chem. **8**, 239 (1967); C. EABORN and D. R. M. WALTON. J. Organometal. Chem. **4**, 217 (1965).
20. G. EGLINTON and A. R. GALBRAITH. Chem. Ind. 937 (1956); G. EGLINTON and A. R. GALBRAITH. J. Chem. Soc. 889 (1959).
21. H. TANI, F. TODA, and K. MATSUMIYA. Bull. Chem. Soc. Jpn. **36**, 391 (1963); S. AKIYAMA and M. NAKAGAWA. Bull. Chem. Soc. Jpn. **33**, 1291 (1960).
22. A. W. SNOW and N. L. JARVIS. J. Am. Chem. Soc. **106**, 4706 (1984); R. D. FARINA, D. J. HALKO, and J. H. SWINEHART. J. Phys. Chem. **76**, 2343 (1972).
23. H. SIGEL, P. WALDMEIER, and B. PRIJS. Inorg. Nucl. Chem. Lett. **7**, 161 (1971); K. BERNAUER and S. FALLAB. Helv. Chim. Acta, **54**, 1287 (1961).
24. M. HANACK, J. METZ, and G. PAWLOWSKI. Chem. Ber. **115**, 2836 (1982).
25. A. W. SNOW, J. R. GRIFFITH, and N. P. MARULLO. Macromolecules, **17**, 1614 (1984).
26. B. L. SHAPIRO and T. W. PROULX. Org. Magn. Reson. **8**, 40 (1976).
27. S. M. SCHILDCROUT. J. Am. Chem. Soc. **105**, 3852 (1983).
28. H. F. Shurvell and L. PINZUTI. Can. J. Chem. **44**, 125 (1966); M. P. SAMMES. J. Chem. Soc. Perkin Trans. 2, 160 (1972).
29. T. W. HALL, S. GREENBERG, C. R. MCARTHUR, B. KHOUW, and C. C. LEZNOFF. Nouv. J. Chim. **6**, 653 (1982).
30. C. R. RASMUSSEN, J. F. GARDECKI, J. N. PLAMPIN, B. L. TWARDZIK, B. E. REYNOLDS, A. J. MOLINARI, N. SCHWARTZ, W. W. BENNETTS, B. E. PRICE, and J. J. MARKOWSKI. J. Med. Chem. **21**, 1044 (1978).
31. T. M. KELLER and J. R. GRIFFITH. U.S. Pat. 4,209,458 (1980); Chem. Abstr. **93**, 221298a (1980).
32. N. M. TARGETT, J. P. KILCOYNE, and B. GREEN. J. Org. Chem. **44**, 4962 (1979).

Qinghaosu: ^{1}H and ^{13}C nuclear magnetic resonance spectral assignments and luminescence[1]

WANG ZHONGSHAN,[2] THOMAS T. NAKASHIMA, KARL R. KOPECKY,[3] AND JOSÉ MOLINA
Department of Chemistry, University of Alberta, Edmonton, Alta., Canada T6G 2G2

Received February 6, 1985

WANG ZHONGSHAN, THOMAS T. NAKASHIMA, KARL R. KOPECKY, and JOSÉ MOLINA. Can. J. Chem. **63**, 3070 (1985).

The complete assignment of the ^{1}H and ^{13}C nmr signals for Qinghaosu **1** has been made. Treatment of **1** with methoxide ion at 80°C results in bright luminescence when carried out in the presence of fluorescers. Several products are formed when methanol is present, but in toluene only one product is formed when methanol-free methoxide is used. Its structure is tentatively assigned as 1-(1-methoxycarbonylethyl)-2,6-dimethyl-2-hydroxybicyclo[3.3.1]nonan-9-one.

WANG ZHONGSHAN, THOMAS T. NAKASHIMA, KARL R. KOPECKY et JOSÉ MOLINA. Can. J. Chem. **63**, 3070 (1985).

On a complètement attribué les signaux de la rmn du ^{1}H et du ^{13}C du Qinghaosu, **1**. Le composé **1** réagit avec l'ion méthanolate à 80°C en présence de substances fluorescentes en provoquant une vive luminescence. En présence de méthanol, on obtient plusieurs produits; toutefois, dans le toluène, il ne se forme qu'un seul produit lorsqu'on utilise du méthanol exempt de méthanolate. On pense que le composé **1** est la (méthoxycarbonyl-1 éthyl)-1 diméthyl-2,6 hydroxy-2 bicyclo[3.3.1]nonanone-9.

[Traduit par le journal]

Qinghaosu **1**, isolated from *Artemisia annua* L., is the active constituent of the traditional Chinese herbal medicine Qinghao. It is a plasmocidal agent and there is intense interest in the possible use of this compound for the treatment of drug resistant malaria (1). An X-ray diffraction study of **1** shows it to be a sesquiterpene lactone containing an endoperoxide group (2). A total synthesis of **1** was reported recently (3).

The intriguing structure of **1**, one of few naturally occurring molecules containing a peroxide group, and its biological activity have led to the present nmr studies. The results should be of value for future biosynthetic studies of this molecule. Also, examination of **1** leads to the possibility that a dioxetane intermediate might be formed upon treatment with base by the sequence of reactions outlined in Chart 1.

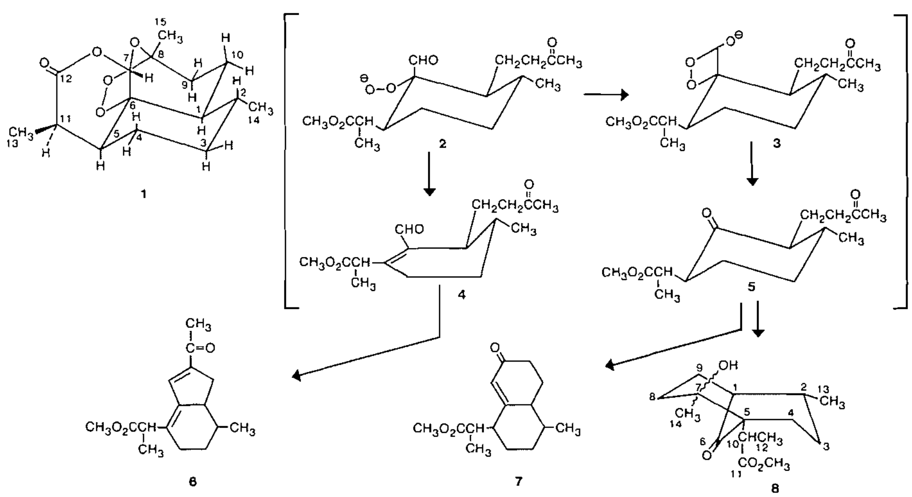

CHART 1

Decomposition of the dioxetane should be luminescent and this reaction could be the basis of a quantitative assay for **1**. In fact, a luminescent reaction does occur when **1** is treated with methoxide ion at 80°C. A tentative assignment has been made for a major product of the reaction. Consumption of the limited supply of **1** available prompts the report of the results at the present time.

Experimental

A sample of Qinghaosu was obtained from the Kunming Pharmaceutical Factory in China.

Mass spectra were taken on an AEI MS 12 (gc–ms) or MS 50 mass spectrometer using an electron impact of 70 eV.

All nmr spectra of **1** were recorded on Bruker WH200 or WH400 spectrometers in the pulsed Fourier transform mode using an Aspect 2000 computer with 16 or 32 K data points, and with sweep widths of 2500 or 5000 Hz and 12 500 or 25 000 Hz for ^{1}H and ^{13}C, respectively. The sample was dissolved in C_6D_6 or $CDCl_3$ at various concentrations to take advantage of induced solvent and concentration shifts to facilitate assignments. The chemical shifts and coupling constants were calculated to first order at 400 MHz and are reported to an accuracy of ±0.01 ppm (except as indicated), ±0.2 Hz for ^{1}H, and ±0.2 ppm and ±2 Hz for ^{13}C. The nOe (nuclear Overhauser effect) difference experiments were carried out in the standard manner (4) after removing oxygen from the solution by bubbling N_2 through it for several minutes. Multiplicities of the ^{13}C resonances were determined by the

[1] This research was supported in part by a grant from the NSERC.
[2] Visiting scholar from the People's Repulbic of China. Permanent address: Shanghai Institute for Drug Control, 46 Fuxin Silu, Shanghai, The People's Republic of China.
[3] Author to whom inquiries should be addressed.

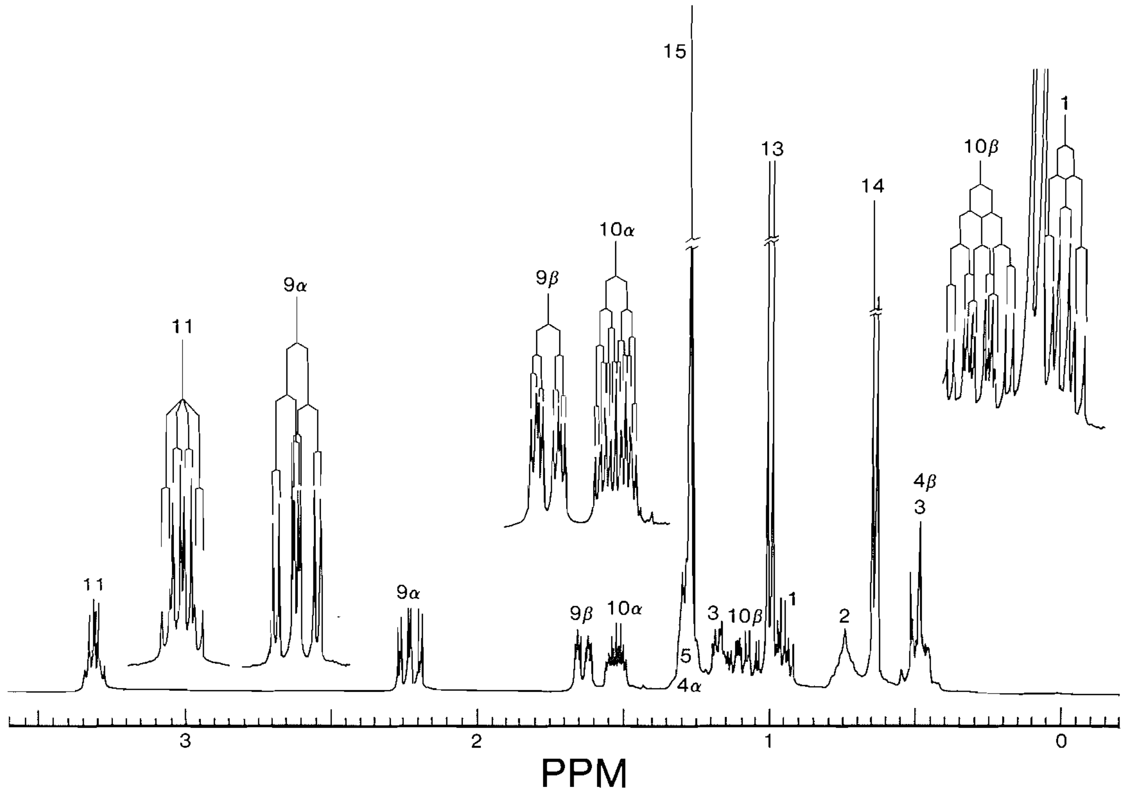

FIG. 1. The ^{1}H nmr spectrum of 0.14 *M* Qinghaosu in $CDCl_3$ at 25°C.

^{13}C spin echo technique with gated ^{1}H decoupling (5) using τ_2 = 0.0077 s, for which responses from doublets and quartets are 180° out of phase with those from singlets and triplets. The selective 2D-DEPT (6) experiment was used to correlate ^{1}H chemical shifts to ^{13}C chemical shifts. The pulse sequence used was $90_x(^1H-t_{1/2}-1/2J_{CH}-180_x(^1H)-90_y(^{13}C)-\theta_y(^1H)180_x(^1H)(^{13}C)-1/2J_{CH}$-acq. Only the θ_y = 30° 2D data set was collected, which yielded the correlation map for all $C(H)_n$ carbons. The value of $1/2(J_{CH})$ was chosen to be 0.00388.

*Reaction of **1** with methoxide ion*

A suspension of sodium methoxide in toluene was prepared by distilling a mixture of toluene and methanolic sodium methoxide until the vapor temperature reached 105°C. A solution of 0.1 g **1** in 20 mL toluene containing a suspension of two equiv. of sodium methoxide was heated at 100°C for 15 min. The cooled reaction mixture was acidified with acetic acid and evaporated to dryness. The residue was stirred with 5 mL chloroform, the resulting mixture cooled to −40°C, treated with ethereal diazomethane, and the solvent removed. Flash chromatography using ether – petroleum ether mixtures afforded 70 mg of **1** and 9 mg of **8**; ^{1}H nmr ($CDCl_3$) δ: 1.07 (3H, d, *J* = 7 Hz, H-13), 1.18 (3H, d, *J* = 7 Hz, H-12), 1.41–1.63 (3H, m), 1.66–2.09 (5H, m), 2.12 (3H, s, H-14), 2.22–2.70 (3H, m), 2.76 (1H, m, H-10), 3.67 (3H, s, O-CH_3); ms: 268 (M^+, 3), 250 ($M^+ - H_2O$, 100), 237 ($M^+ - OCH_3$, 9), 235 (8), 210 (13), 209 (21), 208 (22), 193 (17), 191 (23), 181 (15), 180 (47), 179 (34), 178 (28), 166 (14), 165 (26), 163 (41), 162 (20), 151 (42). *Exact Mass* calcd. for $C_{15}H_{24}O_4$: 268.1674; found: 268.1683. Smaller amounts of other products were formed which were not identified.

Treatment of **1** at 80°C for several min with sodium methoxide in a homogeneous toluene, benzene, or dimethoxyethane solution from which not all the methanol had been removed resulted in complete consumption of **1** and the formation of at least six products. All the four major products of this reaction were different from **8**. The products were not isolated. The most abundant ions in their mass spectra, obtained by gc–ms, are given here for the four major products, labelled A–D in the order of their elution from a SE30 gc column: A, 250 (M^+?, 30), 209 (10), 193 (10), 189 (11), 180 (21), 165 (19), 163 (21), 162 (15), 151 (23), 123 (15), 111 (17), 110 (13), 95 (21), 69 (16), 55 (22), 43 (100); B, 262 (M^+, 49), 203 (19), 175 (18), 161 (12), 131 (20), 43 (100); C, 262 (M^+, 25), 175 (40), 174 (12), 159 (13), 133 (20), 131 (35), 43 (100); D, 250 (M^+?, 38), 192 (14), 191 (100), 163 (71), 162 (25), 133 (13), 121 (20), 119 (14), 107 (21), 105 (19), 93 (16), 91 (27), 79 (19), 77 (14), 55 (26), 43 (14), 41 (21).

Formate ion was determined to be present in 30–50% yields in the aqueous extracts of these reaction mixtures. The aqueous extracts were evaporated to dryness and the formate ion was determined by a colorimetric method (7).

Results and discussion

*Nuclear magnetic resonance spectrum of **1***

The ^{1}H assignments and coupling constants for the nmr spectrum of **1**, in both $CDCl_3$, Fig. 1, and C_6D_6 are summarized in Table 1.[4,5] The assignments are based mainly on homonuclear decoupling and nOe experiments and the characteristic shifts expected for protons near certain functionalities. Assignments for H-2, H-7, H-11, H-13, H-14, and H-15 made previously (2*a*) were confirmed. Except for the resonance of H-7, the resonance of H-11, adjacent to the carbonyl group, is expected to occur at the lowest shielding. Decoupling of this resonance leads to the assignments of H-5 and H-13. The remaining methyl doublet must be H-14, irradiation of which identifies H-2. The resonance at δ 2.44 ($CDCl_3$) was assigned to H-9α because of its proximity to the endoperoxide group. The assignments of H-9β, H-10α, and H-10β were made on the basis of decoupling experiments and the values of the various coupling constants. Irradiation of H-10β and of H-2 identified H-1 and the two protons on C-3; however, the specific assignment of the

[4] The numbering is that used in the X-ray diffraction study (2).

[5] The nmr spectra of some dihydro derivatives of **1** have recently been reported (8).

TABLE 1. ^{1}H Chemical shifts and coupling constants for Qinghaosu 0.14 M in $CDCl_3$ and C_6D_6 at 25°C

Proton	δ (ppm) C_6D_6	δ (ppm) $CDCl_3$	J(Hz)	
1	0.97	1.40	$J_{1-10\alpha}$	6.9
			$J_{1-10\beta}$	11.3
			J_{1-2}	11.3
2	0.77	1.45[a]	J_{2-14}	6.0
3[b]	1.19	1.78[a]	[c]	
3[b]	0.5[a]	1.09[a]	[c]	
4α	1.30[a]	1.87	[c]	
4β	0.5[a]	1.09[a]	[c]	
5	1.30[a]	1.78[a]	J_{5-11}	5.0
7	5.52	5.86		
9α	2.22	2.44	$J_{9\alpha-9\beta}$	14.5
			$J_{9\alpha-10\alpha}$	3.9
			$J_{9\alpha-10\beta}$	13.3
9β	1.65	2.03	$J_{9\beta-10\alpha}$	3.0
			$J_{9\beta-10\beta}$	5.0
10α	1.54	2.07	$J_{10\alpha-10\beta}$	13.9
10β	1.10	1.45[a]		
11	3.29	3.40	J_{11-13}	7.2
13	0.99	1.21		
14	0.65	1.00		
15	1.27	1.45		

[a]Approximate shift corresponding to the estimated center of the signal.
[b]H-3α and H-3β could not be definitely assigned.
[c]Exact values of the coupling constant could not be determined.

TABLE 2. ^{13}Chemical shifts and coupling constants for 1 M Qinghaosu in $CDCl_3$ at 25°C

Carbon	δ (ppm)	$^{1}J_{C-H}$ (Hz)	Δδ[a] (ppm)
1	50.34 (d)	132	0.60
2	37.55 (d)	125	0.51
3	33.78 (t)	128	0.49
4	23.44 (t)	128	0.84
5	45.14 (d)	132	1.24
6	79.62 (s)		0.95
7	93.76 (d)	173 ($^{3}J_{C-H}$ = 7)	2.12
8	105.29 (s)		0.72
9	36.14 (t)	128	0.38
10	24.97 (t)	128	0.43
11	33.00 (d)	128	0.70
12	171.54 (s)	($^{3}J_{C-H}$ = 4)	5.56
13	12.52 (q)	128 ($^{3}J_{C-H}$ = 6)	1.75
14	19.76 (q)	125	0.21
15	25.22 (q)	129 ($^{3}J_{C-H}$ = 4)	1.18

[a]Downfield shift in presence of 0.55 M 2,2,6,6-tetramethylheptanedionate europium III.

signals to H-3α and H-3β could not be made. Saturation of H-7 led to the enhancement of the signal of H-2 and signals at δ 1.10 (C_6D_6), thereby confirming the assignment of H-10β, which had been made on the basis of decoupling experiments, and at δ 0.50 (C_6D_6). Inspection of molecular models shows that H-2, H-4β, and H-10β are near H-7. The signal at δ 0.50 must thus be due to H-4β. Irradiation of H-4β (and one of the protons of C-3) results in simplification of the signal of H-5, confirming that the two protons are on adjacent carbon atoms. H-4α was assigned using the ^{1}H−^{13}C shift correlation experiment.

The ^{13}C chemical shifts of **1**, Table 2, were assigned based on expected characteristic shieldings and multiplicities of signals in the fully coupled spectrum, Fig. 2, multiplicities determined from the gated decoupling ^{13}C spin echo technique, and selective ^{1}H decoupling. The ^{13}C spectrum of **1** should contain three singlets, five doublets, four triplets, and three quartets, which was confirmed using the gated spin echo technique. The three singlets and the resonance of C-7 are readily assigned. Selective ^{1}H decoupling was performed at H-1, H-2, H-3, H-5, H-11, H-14, and H-15, collapsing each doublet or quartet to a singlet and allowing the assignment of the corresponding carbon resonances. The protons associated with C-3, C-4, C-9, and C-10 give rise to nonequivalent AB pairs in the ^{1}H nmr spectrum. Thus, irradiation of the high field signal of the H-3 protons and of H-4β, H-9β, and H-10β causes the resonances at δ 33.8, 23.4, 36.1, and 25, respectively, to change from a triplet in the coupled spectrum to a doublet. Assignment of C-3 and C-4 could not be on this basis because of overlap of the corresponding proton signals. Use of the shift reagent allowed the assignments to be made. The signals at δ 23.4 and 33.8 are shifted downfield 0.49 and 0.84 ppm, respectively, in the presence of the shift reagent. The signal of C-4 would be expected to be shifted more since C-4 is closer to the carbonyl group than is C-3.

The assignments made above were confirmed by the selective 2D-DEPT ^{1}H−^{13}C shift correlation experiment, which also allowed the assignment of H-4α. Since H-4β has already been assigned, the other proton which correlates with C-4 must be H-4α.

Luminescence of 1

The functional groups of **1** are all interconnected. A reaction between base and **1** can result in an extensive structural breakdown to give **2**, when methoxide is used. Chart 1 outlines further reactions that can occur with **2**. Reaction of the hydroperoxide anion in **2** with the adjacent aldehyde function would lead to the 1,2-dioxetane **3**, and cleavage of the dioxetane ring would lead to compound **5** and formate ion, a reaction which should be luminescent (9). In fact, a brief luminescence can be observed clearly in a darkened room when solutions of **1** in benzene, toluene, or dimethoxyethane are treated with methanolic sodium methoxide at temperatures above 60–70°C in the presence of 9,10-dibromoanthracene. No luminescence was observed at lower temperatures. A competing dark reaction which would lead to **5** and formate ion, eq. [1], is also likely to occur (10).

[1]

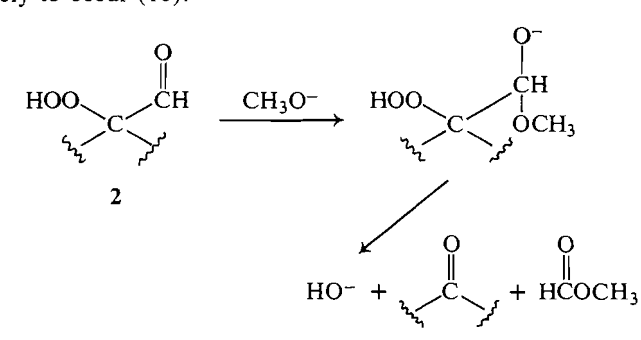

2 **5**

Exploratory experiments showed that at least six to eight products were formed and that **1** was consumed rapidly when appreciable amounts of methanol were present in the reaction

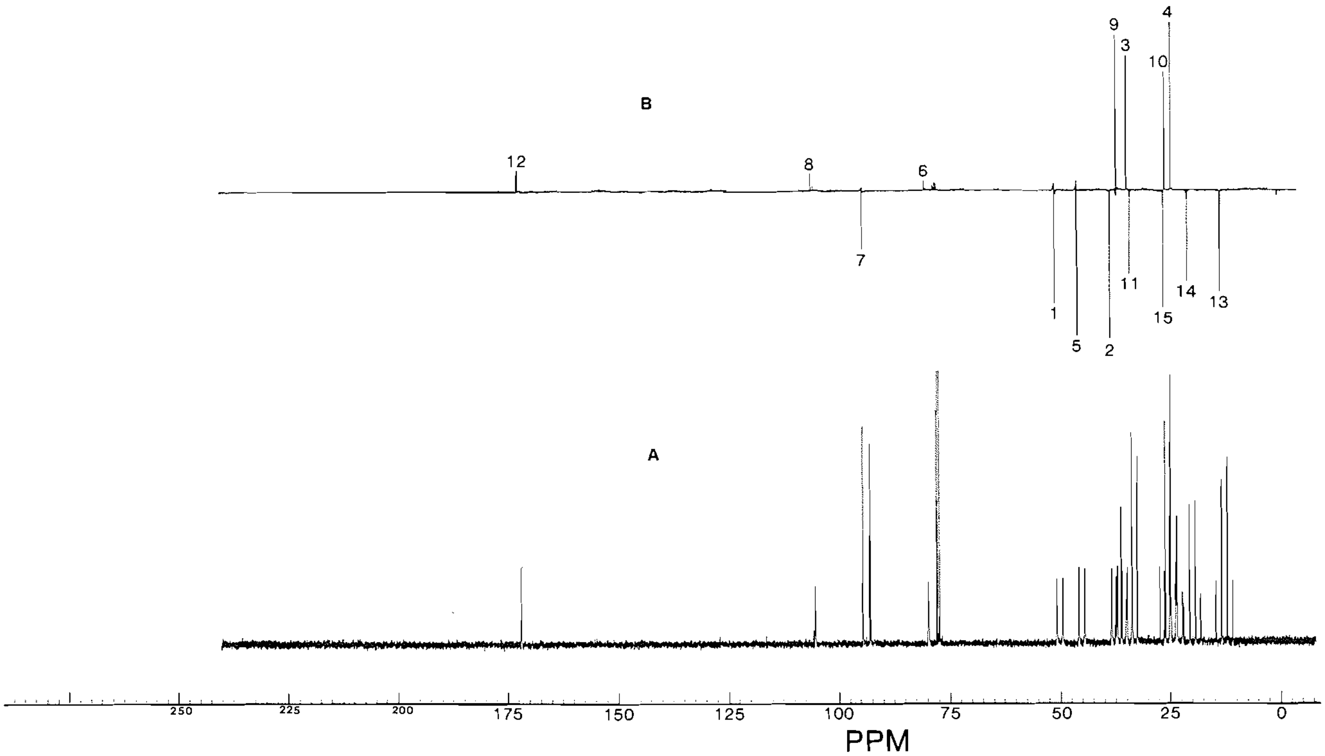

FIG. 2. Off-resonance decoupled, A, and spin echo, B, ^{13}C nmr spectrum of 1 *M* Qinghaosu in $CDCl_3$ at 25°C.

mixture. Consumption of **1** was much slower and only one main product was formed when methanol was first removed from a methanolic solution of sodium methoxide by azeotropic distillation. This product is tentatively assigned the bridged structure **8** on the basis of its mass and nmr spectra. The molecular ion, *m*/*e* 268, contains all the atoms of the presumed intermediate **5**. Loss of water gives the base peak, *m*/*e* 250. Dehydration of **8** will not occur in base, whereas intramolecular condensation of **5** to give a nonbridged ketol might lead to the formation of a dehydrated product such as **7**. The nmr spectrum contains peaks for four methyl groups: a singlet at δ 3.67 due to the methyl group of the ester, a singlet at δ 2.12, and doublets at δ 1.18 and 1.07 as required for structure **8**. The singlet at δ 2.12 is at lower field than normal for a methyl group bonded to a tertiary carbon atom. This indicates that the protons of C-14 are deshielded by one or both of the nearby carbonyl groups. The mass spectrum of the product lacked a peak at *m*/*e* 58, which should be prominent in the mass spectrum of a molecule of structure **5**. The nonbridged ketol that could be formed from **5** would have only three methyl groups.

It is interesting that little, if any, **8** was formed when the reactions with methoxide ion were carried out in the presence of methanol. There were four major products and several minor ones. Two of the products had molecular ion peaks at *m*/*e* 250, which indicates that they may be isomeric compounds of structure **7**, and two had molecular ion peaks at *m*/*e* 262 and base peaks at *m*/*e* 43. The latter peak may be $CH_3CO^{\cdot+}$, indicating that these products may be isomeric compounds of structure **6**. A compound such as **6** could result from the intramolecular condensation of **4** (or a double bond isomer), which, in turn, is a decomposition product of **2**. Such a decomposition of an α-hydroperoxy carbonyl compound does not appear to have been observed before. Previous careful studies of the base-catalyzed decompositions of these materials were carried out under much milder conditions (9, 10), but it is known that tertiary hydroperoxides are decomposed rapidly by base at elevated temperatures to give alcohols (11). Dehydration of the corresponding alcohol from **2** would produce **4**.

Other products have been isolated from the reaction between **1** and base at ambient temperatures (12). The cleavage of the intermediate **2** to give **5** as shown in Chart 1 and eq. [1] was not considered.

The luminescent reaction described here might be developed into a sensitive assay for **1**. A sensitive electrochemical assay for **1** has been described recently (13).

1. (*a*) Qinghaosu Antimalarial Coordinating Research Group. Chinese Med. J. **92**, 811 (1979); (*b*) L. J. BRUCE-CHWATT. Brit. Med. J. **284**, 767 (1982).
2. (*a*) Qinghaosu Research Group. Kexuetongbao (Science Bulletin), **22**, 142 (1977); (*b*) J.-M. LIU, M.-Y. WU, J.-F. FAN, Y.-Y. TU, Z.-H. WU, Y.-L. WU, and W.-S. CHOU. Acta Chim. Sinica, **37**, 129 (1979); (*c*) Qinghaosu Research Group. Sci. Sinica, **23**, 380 (1980).
3. G. SCHMID and W. HOFHEINZ. J. Am. Chem. Soc. **105**, 624 (1983).
4. (*a*) R. RICHARZ and K. WÜTHRICH. J. Mag. Reson. **30**, 147 (1978); (*b*) J. D. GLICKSON, S. L. GORDON, T. P. PITNER, D. G. AGRESTI, and R. WALTER. Biochemistry, **15**, 5721 (1976).
5. D. W. BROWN, T. T. NAKASHIMA, and D. L. RABENSTEIN. J. Magn. Reson. **45**, 302 (1981).
6. T. T. NAKASHIMA, R. E. D. MCCLUNG, and B. I. JOHN. J. Magn. Reson. **58**, 27 (1984).
7. F. D. SNELL and C. D. SNELL. Colorimetric methods of analysis. Vol. 2. 3rd ed. D. Van Nostrand, New York. 1948. p. 303.
8. X.-D. LUO, H. J. C. YEH, A. BROSSI, J. L. FLIPPEN-ANDERSEN, and R. GILARDI. Helv. Chim. Acta, **67**, 1515 (1984).
9. (*a*) W. H. RICHARDSON, V. F. HODGE, D. L. STIGALL, M. B. YELVINGTON, and F. C. MONTGOMERY. J. Am. Chem. Soc. **96**, 6652 (1974); (*b*) Y. SAWAKI and Y. OGATA. J. Am. Chem. Soc.

99, 6313 (1977).
10. Y. SAWAKI and Y. OGATA. J. Am. Chem. Soc. **97**, 6983 (1975).
11. N. A. MILAS and S. A. HARRIS. J. Am. Chem. Soc. **60**, 2435 (1938).
12. M.-Y. ZENG, L.-N. LI, S.-F. CHEN, G.-Y. LI, X.-T. LIANG, M. CHEN, and J. CLARDY. Tetrahedron, **39**, 2941 (1983).
13. N. ACTON, D. L. KLAYMAN, B. T. POON, A. J. LIN, and J. M. HOCH. Abstracts. 188th National Meeting of the American Chemical Society. Philadelphia, PA. August, 1984. ORGN 200.

Effects of varying solvents and of the addition of sulfur on the rate of thiohydrolysis of aromatic nitriles

KHAMIS A. ABBAS[1] AND JOHN T. EDWARD
Department of Chemistry, McGill University, 801 Sherbrooke St. W., Montreal, P.Q., Canada H3A 2K6

Received October 12, 1984[2]

KHAMIS A. ABBAS and JOHN T. EDWARD. Can. J. Chem. **63**, 3075 (1985).

Maximal rates of formation of thioamides from *m*- and *p*-substituted benzonitriles were obtained by bubbling H_2S through solutions of the nitrile in pyridine containing a 0.11 mol fraction of triethylamine or in 95% ethanol containing about 0.22 mol fraction triethylamine; at other mol fractions the rate fell off sharply. The Hammett ρ value of +2.3 in pyridine indicates that HS^- is the reactive species. The addition of enough sulfur to saturate the solution leads to about a 3-fold enhancement of rate, probably because of the formation of polysulfide ions in trace amounts.

KHAMIS A. ABBAS et JOHN T. EDWARD. Can. J. Chem. **63**, 3075 (1985).

Les vitesses de formation de thioamides à partir de benzonitriles substitués en positions *méta* et *para* sont maximales lorsqu'on fait barboter du H_2S dans des solutions de nitriles dans de la pyridine contenant 0,11 fraction molaire de triéthylamine ou dans de l'éthanol à 95% contenant environ 0,22 fraction molaire de triéthylamine; la vitesse diminue nettement si on utilise d'autres fractions molaires. La valeur ρ de Hammett est égale à +2,3 dans la pyridine et ceci indique que l'espèce réactive est le HS^-. Si on ajoute suffisamment de soufre pour saturer la solution, la vitesse de la réaction est multipliée par trois et ce résultat est du probablement à la formation de faibles quantités d'ions polysulfures.

[Traduit par le journal]

Thioamides are usually prepared from nitriles by heating the latter under pressure with an alcoholic solution of an alkali-metal hydrosulfide (1), or an ammonium (2) or substituted ammonium hydrosulfide (1). However, Fairfull, Lowe, and Peak (3) found that in pyridine solution, in the presence of a strong base such as triethylamine, addition of hydrogen sulfide to aromatic nitriles took place with remarkable ease, being complete in 2–4 h at room temperature. They made no attempt to optimize conditions, and did not specify the precise compositions of the triethylamine–pyridine solutions which they used. They noted that the role of pyridine was not purely passive; triethylamine–chloroform was much less effective than triethylamine–pyridine.

Our need for an efficient method for the thiohydrolysis of nitriles prompted us to carry out a rough kinetic study of the reaction of Fairfull *et al.*, in order to optimize conditions, and further to study the effect of different solvents and of the addition of sulfur on the rate of the reaction.

Experimental

Materials

Nitriles were used as obtained from Aldrich Chemical Company. Solvents were not purified. Hydrogen sulfide was obtained from Matheson, Coleman and Bell Company Limited.

Preparation of substituted thiobenzamides

The following procedure, modified slightly from that of Fairfull *et al.*, gave yields of more than 95% of recrystallized thiobenzamide.

Hydrogen sulfide was bubbled for 6 h through a solution of benzonitrile or substituted benzonitrile (0.02 mol) in triethylamine (50 mL) – pyridine (150 mL). The solution, which turned dark green, was left overnight, except for *p*-methoxybenzonitrile and *p*-methylbenzonitrile solutions, which were left for 40 h. Nitrogen was bubbled through the solution for 3 h to remove most of the hydrogen sulfide, and the solvent was then removed by rotary evaporation. The solid residue was twice recrystallized from ethanol–water 1:4, and the thioamides thus obtained had melting points in agreement with the literature (3–5). Ultraviolet (uv) spectral characteristics (λ_{max} (nm) and ϵ (mol^{-1} cm^{-1}) (in parentheses)) of the substituted thiobenzamides (substituent indicated) dissolved in 95% ethanol were as follows: H: 291(6850) and 242(8480); *p*-Cl: 305(5860) and 250(10 100); *m*-Cl: 296(6620) and 237(9340); *p*-Br: 300(7350) and 253(12 300); *m*-Br: 298(6340); *p*-CH_3: 300(7590), 291.5(7700), and 257(9700); *p*-CH_3O: 306(1090) and 273(11 800).

Kinetic measurements

Hydrogen sulfide was bubbled for 1 h into 200 mL of triethylamine–solvent mixture, in the case of liquid benzonitriles, or into 190 mL of triethylamine–solvent mixture in the case of solid benzonitriles, 10 mL of triethylamine–solvent being retained in the latter case to dissolve the benzonitrile. The neat liquid or dissolved solid benzonitrile (0.00687 mol) was then injected through a septum into the H_2S-saturated solvent[3] (except for *p*-methoxybenzonitrile, when 0.00500 mol was injected). Bubbling of H_2S was continued, and 1.00-mL aliquots of the reaction mixture were withdrawn with a graduated syringe at different time intervals and diluted to 25.0 mL with 5% HCl in aqueous ethanol to stop the reaction. The acidic solution was diluted tenfold with distilled water and analyzed by uv absorbance at 305 nm for substituted thiobenzamide. In experiments in which weighed amounts of sulfur were added to the triethylamine–solvent mixture before saturating with H_2S, the acidic solutions obtained after reaction were diluted tenfold with saturated sodium chloride solution and left for 2 days for sulfur to crystallize out. The clear supernatant solution could then be drawn off and analyzed as before by uv spectrophotometry. Reactions followed pseudo-first-order kinetics with a precision of about ±5%.

Results and discussion

Effect of solvent

In spite of the relative crudeness of our experiments (temperature varying between 18 and 22°C, atmospheric pressure varying between 740 and 770 Torr (1 Torr = 133.3 Pa)) we found that we could obtain reasonably reproducible reaction rates for thiohydrolyses carried out under the conditions of Fairfull *et al.* (gaseous H_2S passed continuously into a solution of nitrile in triethylamine–pyridine). Rates followed pseudo-

[1] On leave from the Department of Chemistry, Yarmouk University, Irbid, Jordan.

[2] Revision received June 20, 1985.

[3] Saturation of pyridine–triethylamine with H_2S gave a deep green solution; saturation of other solvents gave greenish-yellow solutions.

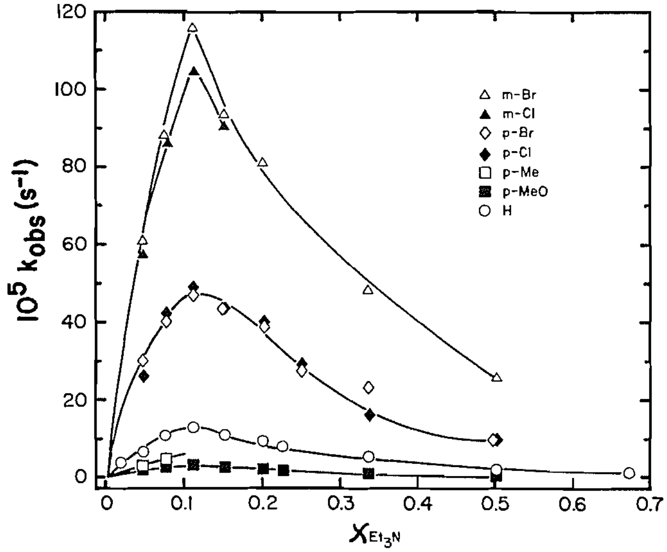

FIG. 1. Observed rate constant k_{obs} for thiohydrolysis of benzonitrile and of six *m*- and *p*-substituted benzonitriles, plotted against mol fraction χ_{Et_3N} of triethylamine in pyridine–triethylamine solvent mixtures.

first-order kinetics, and the experimental rate constants k_{obs} for seven *meta*- and *para*-substituted benzonitriles in triethylamine–pyridine mixtures of varying composition are shown in Fig. 1. Reaction was fastest for a triethylamine mol ratio χ of 0.11; triethylamine used alone as solvent was completely ineffective. In eight different triethylamine–pyridine solvent mixtures having χ varying from 0.045 to 0.499, the thiohydrolysis rate constants k_{obs} of the seven substituted benzonitriles fitted the Hammett $\rho\sigma$ relation (correlation coefficients 0.994 or better) with $\rho = 2.30 \pm 0.09$, which thus appeared unexpectedly independent of solvent composition. Kindler's results (5) for the thiohydrolysis of substituted benzonitriles by sodium hydrogen sulfide in ethanol at 61°C yield a ρ value of 2.15 (6), and hence it seems likely that in both pyridine and ethanol the bisulfide ion HS^- is the reactive entity.

Pyridine is not a uniquely effective solvent. In fact, as shown in Fig. 2, both ethanol and 95% ethanol are slightly more effective if the optimal amount of triethylamine is present. Again, beyond a certain optimal concentration, an increase in χ_{Et_3N} leads to a decrease in k_{obs}. On the other hand, toluene and thiophene proved vastly less effective than pyridine (see Fig. 2). This was not because of a greatly diminished solvent power for hydrogen sulfide, as can be seen in Table 1: the concentration of H_2S in saturated toluene–Et_3N 0.73:0.27 (mol/mol) is only 36% less than in saturated pyridine–Et_3N 0.89:0.11 (mol/mol).

No thiohydrolysis at room temperature was observed with various proportions of triethylamine in 50% aqueous ethanol, in 50% ethanol – 50% tetrahydrofuran, or in tetrahydrofuran, and with triethylamine in *tert*-butanol or n-decanol it was very slow.

Mechanistic considerations

The Hammett ρ value suggests that the rate-determining (r.d.) step in thiohydrolysis is attack of ^-SH on nitrile:

$$[1] \quad RCN + {}^-SH \xrightarrow[\text{r.d.}]{k} R{-}C{\overset{\bar{N}^-}{\underset{SH}{\lessgtr}}} \xrightarrow{\text{fast}} R{-}C{\overset{NH_2}{\underset{S}{\lessgtr}}}$$

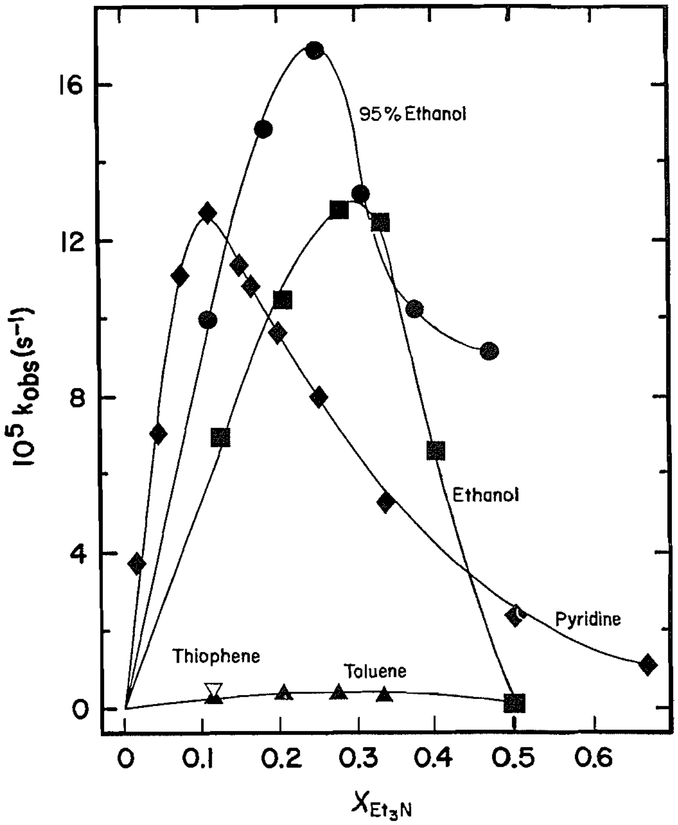

FIG. 2. Observed rate constant k_{obs} for thiohydrolysis of benzonitrile plotted against mol fraction χ_{Et_3N} of triethylamine in solvent mixtures of triethylamine–pyridine, –ethanol, – 95% ethanol, –toluene, and –thiophene.

TABLE 1. Concentrations $[S^{2-}]$ (as mg mL^{-1} of S^{2-}) of hydrogen sulfide in different solvents containing the mol fraction χ_{Et_3N} of triethylamine indicated, and saturated with H_2S at atmospheric pressure and 18–22°C

Solvent	χ_{Et_3N}	$[S^{2-}]$*
95% EtOH	0.250	34.5
EtOH	0.275	35.7
Pyridine	0.110	34.9
Toluene	0.274	22.4

* Measured by Bethge's titrimetric method (7).

The bisulfide ion ^-SH results from the equilibria:

$$[2] \quad Et_3N + H_2S \overset{K_{ion}}{\rightleftarrows} \underset{\mathbf{1}}{Et_3\overset{+}{N}{-}H\text{------}\overset{-}{S}{-}H} \overset{K_{diss}}{\rightleftarrows} Et_3\overset{+}{N}H + \overset{-}{S}H$$

In water, dissociation of the ion pair **1** will be essentially complete, and we can calculate from the pK_a values of Et_3NH^+ and H_2S (8) that in this solvent the formation of Et_3NH^+ and ^-SH will also be essentially complete, i.e. that $[^-SH] \approx [Et_3N]_{stoichiometric}$. However, in a solvent of lower dielectric constant such as ethanol, the proton transfer to form Et_3NH^+ and ^-SH will probably be incomplete (ref. 8, p. 46). Nonetheless, the lower concentration of ^-SH to be expected in absolute

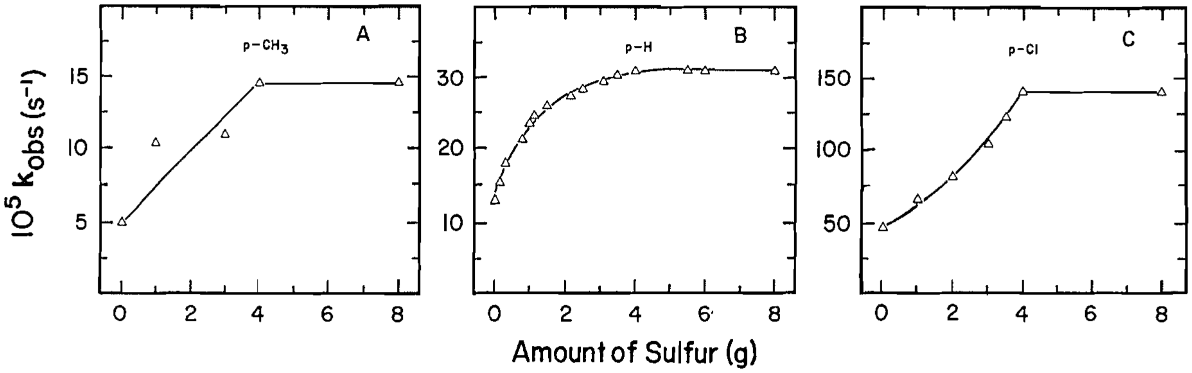

FIG. 3. Relation between k_{obs} for thiohydrolysis of benzonitrile (*p*-H), *p*-methylbenzonitrile (*p*-CH_3), and *p*-chlorobenzonitrile (*p*-Cl) and amount of sulfur added to 200 mL of pyridine–triethylamine 0.89:0.11 (mol/mol) solvent.

ethanol as compared with 50% aqueous ethanol is evidently more than compensated by the greater activity of ^{-}SH in absolute ethanol, since thiohydrolysis proceeds in the former and not in the latter solvent.

In toluene and thiophene both the extent of proton transfer (K_{ion}) and of dissociation of the ion pair (K_{diss}) should be drastically reduced, although the greater activity of ^{-}SH in these poorly-solvating media should compensate to some extent. In such non-hydrogen-bonding solvents homoconjugation often becomes of dominant importance (9):

[3] $$Et_3N + Et_3\overset{+}{N}H\text{-----}^{-}SH \rightleftarrows Et_3\overset{+}{N}H\text{-----}NEt_3 + {}^{-}SH$$
$$\mathbf{1} \qquad\qquad \mathbf{2}$$

However, in acetonitrile solution, formation of the homoconjugate ion **2** does not take place to any appreciable extent (9). In neat triethylamine the same may be true, but in toluene and thiophene a small amount may be formed, to account for the experimental results cited above. On the other hand, in pyridine solution the homoconjugate ion **3** can probably be formed more readily (cf. ref. 9):

[4] 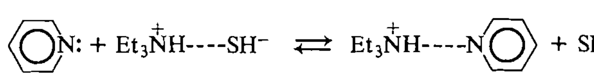

3

and the ^{-}SH ion will be very active because it will not be strongly stabilized by solvation in this aprotic solvent. This would account for the greater effectiveness of pyridine as compared with the other aprotic solvents investigated.

Effect of addition of sulfur

Sulfur dissolves in strongly alkaline aqueous solutions of sodium sulfide to form mixtures of sodium polysulfides in which the sulfur exists in chains **4** terminating with negative charges (10) (Scheme 1). Acidification of such a solution yields a mixture of hydrogen polysulfides (sulfuranes) **5**, chain compounds that, it is claimed (11–13), decompose completely to hydrogen sulfide and sulfur at normal temperatures. However, at 150°C hydrogen sulfide in molten sulfur exists in equilibrium with small amounts of hydrogen polysulfides (predominantly H_2S_n with $n \geq 6$) (14, 15), and it seems probable on thermodynamic grounds that even at 20°C the equilibrium constant for this reaction, though small, will not be zero. Furthermore it might be expected that $H—(S)_n—S^-$ would be very much more reactive than $H—S^-$ (cf. $H—O—O^-$, which is 10^4 times more effective than $H—O^-$ in the hydrolysis of benzonitrile (16)—an example of the α-effect (17)), and hence might affect the rate of thiohydrolysis even if present only in trace amounts.

$$S^{2-} + nS \xrightleftharpoons{K \gg 1} \bar{S}—(S)_{n-1}—S^- \;\; \mathbf{4}$$
$$\updownarrow H^+ \qquad\qquad \updownarrow H^+$$
$$H_2S + nS \xrightleftharpoons{K \ll 1} HS—(S)_{n-1}—SH \;\; \mathbf{5}$$

SCHEME 1

In fact, it was found that in pyridine k_{obs} for the formation of thiobenzamide and its *p*-methyl and *p*-chloro derivatives from the corresponding nitriles was increased with the addition of increasing amounts of sulfur to the reaction mixture. This is shown in Fig. 3. A limit to the rate enhancement was reached when 4 g of sulfur had been added to 200 mL of pyridine–triethylamine 0.89:0.11 (mol/mol). Beyond the limit some sulfur remained undissolved in the H_2S-saturated solvent mixture.

Sulfur is 30 times less soluble in ethanol than in pyridine at 20°C (18), and while its solubility in EtOH–Et_3N 0.725:0.275 (mol/mol) is not known, it is likely to be less than in pyridine–Et_3N 0.89:0.11 (mol/mol). Consequently, we would expect the limit to the effect of added sulfur to be reached sooner in ethanol–triethylamine than in pyridine–triethylamine. In fact, Fig. 4 shows that this limit is reached when about 1.2 g of sulfur has been added to 200 mL of ethanol–triethylamine 0.725:0.275 (mol/mol).

These kinetic results shed light on the thermodynamics of the H_2S–S_8 equilibrium at 20°C, since it is difficult to explain the enhanced rates other than by the formation of H_2S_n.[4] Previous studies (19) of the equilibrium between H_2S and molten sulfur indicated that the number-average chain length $\bar{n}$ of H_2S_n is about 27 sulfur atoms at 127°C, and increasing with temperature. In our solutions at lower temperatures and with lower concentrations of S_8, but with the possibility of preserving H_2S_n as the more stable anion $^{-}S—S_{n-2}—S^{-}$, it might be expected that $\bar{n}$ would be less than 27. Furthermore, in the various solvents saturated with H_2S and hence having $[H_2S]$ constant, $\bar{n}$ must vary with the concentration of S_8. Thus the concen-

[4] Since $[H_2S] \approx 1\ M$ in the first three solvent mixtures listed in Table 1, $[H_2S_n^-] \approx 10^{-4}\ M$ if the ion derived from it is 10^4 times more effective than ^{-}SH (see comparison of $H—O^-$ and $H—O—O^-$ above). Such a concentration might be difficult to detect by the usual spectroscopic techniques.

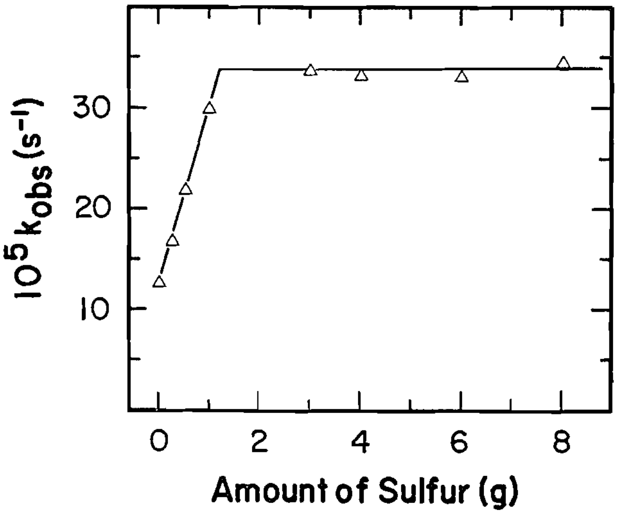

FIG. 4. Relation between k_{obs} for thiohydrolysis of benzonitrile and amount of sulfur added to 200 mL of ethanol–triethylamine 0.725:0.275 (mol/mol) solvent.

tration of H_2S_7 should follow $[S_8]^{0.75}$:

$$[5] \quad 8\,H_2S + 6\,S_8 \overset{K_7}{\rightleftarrows} 8\,H_2S_7$$

$$[6] \quad [H_2S_7] = (K_7[H_2S]^8[S_8]^6)^{1/8} = \text{const}_7\,[S_8]^{0.75}$$

and in general $[H_2S_n] = \text{const}_n[S_8]^{n-1/8}$. Hence $[H_2S_{23}]$, for example, should vary as $[S_8]^{2.75}$, and should increase more rapidly than $[H_2S_7]$ with increase in $[S_8]$. Thus $\bar{n}$ should increase with $[S_8]$.

These considerations serve to explain the effect of sulfur concentration on the rate of thiohydrolysis of the reactive nitrile, *p*-chlorobenzonitrile, if we assume that ions $^-S—S_n—S^-$ of varying lengths all have about the same reactivity. We may then write

$$[7] \quad k^S_{obs} = k_1[H_2S] + k_{\bar{n}}[H_2S_{\bar{n}}] = k^0_{obs} + k'_{\bar{n}}[S_8]^{\bar{n}-1/8}$$

where k^0_{obs} is the rate constant in the absence, and k^S_{obs} the rate constant in the presence of sulfur. From eq. [7] we obtain

$$[8] \quad \log \Delta k_{obs} = \log (k^S_{obs} - k^0_{obs}) = \log k'_{\bar{n}} + \frac{\bar{n}-1}{8} \log [S_8]$$

A plot of log Δk_{obs} of *p*-chlorobenzonitrile against log $[S_8]$ is concave upward until the plateau for the S_8-saturated solution is reached. At the lowest concentration of sulfur ($[S_8] = 0.019$ m L^{-1}), the slope of the curve is 0.73, implying (see eq. [6]) that $\bar{n} \approx 7$; at saturation ($[S_8] = 0.078$ m L^{-1}) the slope is 2.70, implying that $\bar{n} \approx 23$ (see above).

With the less reactive benzonitrile in triethylamine–pyridine or triethylamine–ethanol, the plot of log Δk_{obs} against log $[S_8]$ is concave downward, and so we can no longer assume that ions of different chain length are of equal reactivity, but rather must assume that shorter chains are more reactive. Obviously more work is required to correlate the shape of the curve with the reactivity of the nitrile.

The maximum rate enhancements caused by the addition of sulfur are modest (about threefold), presumably because of the minute amounts of H_2S_n formed, and so we made preliminary studies of the effectiveness of Na_2S_2, produced by dissolving the appropriate amount of sulfur in aqueous Na_2S (20). This proved completely ineffective in thiohydrolyzing benzonitrile at 20 ± 2°C. However, we saw above that HS^-, effective in 95% ethanol, becomes completely ineffective in 50% aqueous ethanol, and it is possible that in nonaqueous solutions Na_2S_2 might be useful.

Acknowledgements

We are grateful to the Natural Sciences and Engineering Research Council of Canada for financial support, and K. A. expresses appreciation for sabbatical leave from the Faculty of Science of Yarmouk University. We are also grateful to a referee for bringing the possible importance of homoconjugation to our attention, and for directing us to ref. 9.

1. K. KINDLER and F. BURGHARD. Ann. **431**, 201 (1923).
2. S. GABRIEL and P. HEYMANN. Ber. **23**, 157 (1890).
3. A. E. S. FAIRFULL, J. L. LOWE, and D. A. PEAK. J. Chem. Soc. 742 (1952).
4. E. C. TAYLOR and J. A. ZOLTEWICZ. J. Am. Chem. Soc. **82**, 2656 (1960).
5. K. KINDLER and A. TREY. Ann. **450**, 1 (1926).
6. K. B. WIBERG. Physical organic chemistry. John Wiley & Sons Ltd., New York. 1964. p. 404.
7. P. O. BETHGE. Anal. Chim. Acta, **10**, 310 (1954).
8. R. P. BELL. The proton in chemistry. 1st ed. Methuen, London. 1959.
9. J. F. COETZEE. *In* Progress in physical organic chemistry. Vol. 4. *Edited by* A. Streitwieser and R. W. Taft. Interscience, New York. 1967. p. 45.
10. E. MULLER and J. B. HYNE. Can. J. Chem. **46**, 2341 (1965).
11. E. FEHER and G. WINKHAUS. Z. Anorg. Allgem. Chem. **292**, 203 (1957); E. MULLER and J. B. HYNE. J. Am. Chem. Soc. **91**, 1907 (1969).
12. T. K. WIEWIOROWSKI. Endeavour, **29**, 9 (1970).
13. J. J. SMITH, D. JENSEN, and B. MEYER. J. Chem. Eng. Data, **15**, 144 (1970).
14. T. K. WIEWIOROWSKI and F. J. TOURO. J. Phys. Chem. **70**, 234 (1966); **70**, 239 (1966); **70**, 3528 (1966).
15. J. B. HYNE, E. MULLER, and T. K. WIEWIOROWSKI. J. Phys. Chem. **70**, 3733 (1966).
16. K. B. WIBERG. J. Am. Chem. Soc. **77**, 2519 (1955).
17. E. BUNCEL, H. WILSON, and C. CHUAQUI. J. Am. Chem. Soc. **104**, 4896 (1982); E. BUNCEL and S. HOZ. Tetrahedron Lett. **24**, 4777 (1983), and, references therein.
18. W. F. LINKE. Solubilities, inorganic and metal-organic compounds. 4th ed. Vol. II. American Chemical Society. pp. 1387, 1399.
19. T. K. WIEWIOROWSKI, R. F. MATSON, and C. T. HODGES. Anal. Chem. **37**, 1080 (1965).
20. K. H. BUTLER and O. MAASS. J. Am. Chem. Soc. **52**, 2184 (1930).

On the structure of poly(tetramethylene terephthalate). Structural, infrared, and Raman studies of three tetramethylene glycol dibenzoate derivatives, models for poly(tetramethylene terephthalate)

ALLAN PALMER, SUZIE POULIN-DANDURAND, AND FRANÇOIS BRISSE
Département de Chimie, Université de Montréal, C.P. 6210, Succ. A, Montréal (Qué.), Canada H3C 3V1

Received February 4, 1985

ALLAN PALMER, SUZIE POULIN-DANDURAND, and FRANÇOIS BRISSE. Can. J. Chem. **63**, 3079 (1985).

The crystal structures of tetramethylene glycol dibenzoate (**1**), tetramethylene glycol di-*para*-chlorobenzoate (**2**), and tetramethylene glycol di-*para*-nitrobenzoate (**3**) have been solved by direct methods in order to establish the possible conformations of the methylenic sequence in poly(tetramethylene terephthalate), poly(4GT). Compound **1** has a triclinic unit cell of dimensions a = 7.870(3), b = 8.574(3), c = 12.993(4) Å; α = 83.76(3), β = 89.92(3), γ = 64.68(3)°; Z = 2, space group $P\bar{1}$. For **2** the unit cell is also triclinic and has dimensions a = 5.916(3), b = 7.599(2), c = 10.404(2) Å; α = 67.81(2), β = 77.47(2), γ = 81.63(3)°; Z = 1, space group $P\bar{1}$. The unit cell dimensions of **3** are a = 6.086(1), b = 11.475(3), c = 13.162(3) Å and β = 101.93(2)°, Z = 2. The space group is $P2_1/c$. The structures were solved by direct methods using 2682, 969, and 781 observed reflections for **1**, **2**, and **3**, respectively. The refinements were concluded when R reached the values of 0.042, 0.046, and 0.045, respectively. The conformation of the methylenic sequence varies depending on the substituent on the benzoate group. The conformation observed in **1** is tg^-ttt, it is $ttttt$ for **2**, and tg^-tgt for **3** (t = *trans*, g = *gauche*). Although the equivalent fiber repeat of **3** coincides with the observed fiber repeat for α-poly(4GT), this does not imply that **3** and α-poly(4GT) have the same conformation. Compound **2** allows for the modelling of the β-form of poly(4GT). However, this does not lead to a clear choice between the two structures reported for this form. The two distinct conformations proposed for the β-form of poly(4GT) are distinguished on the basis of their ir and Raman spectra. The comparison of the spectra of the model compounds reveals that, in ir, for an all-*trans* conformation there is no absorption band at 1383 cm^{-1} but one is present at 1395 cm^{-1}. This situation that is observed in the ir spectra of β-poly(4GT) led us to propose that this form has the all-*trans* conformation as proposed by Hall and Pass. This choice is further supported by the presence of three bands at 1047, 1347, and 1405 cm^{-1} in the Raman spectra of β-poly(4GT). These three bands are only observed in the model compounds having the all-*trans* conformation.

ALLAN PALMER, SUZIE POULIN-DANDURAND et FRANÇOIS BRISSE. Can. J. Chem. **63**, 3079 (1985).

Les structures cristallines des bis(benzoate) (**1**), bis(*para*-chlorobenzoate) (**2**) et bis(*para*-nitrobenzoate (**3**) du tétraméthylène glycol ont été résolues dans le but d'établir les conformations possibles des séquences méthyléniques du poly-(téréphtalate de tétraméthylène), poly(4TG). Le composé **1** appartient au groupe d'espace triclinique $P\bar{1}$, avec a = 7,870(3), b = 8,574(3), c = 12,993(4) Å; α = 83,76(3), β = 89,92(3), γ = 64,68(3)° et Z = 2. Le composé **2** appartient également au groupe d'espace triclinique $P\bar{1}$, avec a = 5,916(3), b = 7,599(2), c = 10,404(2) Å; α = 67,81(2), β = 77,47(2), γ = 81,63(3)° et Z = 1. Le composé **3** appartient au groupe d'espace $P2_1/c$, avec a = 6,086(1), b = 11,475(3), c = 13,162(3) Å; β = 101,93(2)° et Z = 2. On a déterminé ces structures par méthodes-directes en faisant appel à 2682, 969 et 781 réflexions observées respectivement pour les composés **1**, **2**, et **3** et on les a affinées jusqu'à des valeurs respectives de R de 0,042, 0,046, et 0,045. La conformation de la séquence méthylénique dépend des substituants fixés sur le groupe benzoate. On a observé les conformations suivantes: tg^-ttt pour le composé **1**, $ttttt$ pour le composé **2** et tg^-tgt pour le composé **3** (t = *trans*, g = *gauche*). Le fait que la période de fibre équivalente du composé **3** coincide avec la période de fibre observée pour l'α-poly(4TG), n'implique pas nécessairement que ces deux composés ont la même conformation. Le composé **2** est considéré comme un modèle de la forme β du poly(4TG). Ces observations ne permettent pas d'opter clairement pour l'une ou l'autre des deux structures rapportées pour cette forme. C'est grâce aux techniques de spectroscopies infrarouge et Raman que l'on arrive à établir la conformation la plus probable de la forme β du poly(4GT). La comparaison des spectres infrarouges des composés modèles met en évidence la présence d'une bande d'absorption à 1395 cm^{-1} et l'absence de bande à 1383 cm^{-1} lorsque la conformation est entièrement *trans*. Cette situation, qui est observée sur le spectre infrarouge du poly(4GT) forme β, nous conduit à proposer que cette forme a bien la conformation entièrement *trans*, confirmant ainsi le modèle de Hall et Pass. Ce choix est renforcé par la présence de trois bandes à 1047, 1347 et 1405 cm^{-1} dans le spectre Raman du β-poly(4GT). Ces trois bandes ne sont en effet observées que dans le cas d'une conformation entièrement *trans*.

Introduction

Poly(tetramethylene terephthalate), or poly(4GT), has been shown to be dimorphic. The structures of both forms of poly(4GT) have been extensively studied in recent years. First, a model building technique allowed Joly, Nemoz, Douillard, and Vallet (1) to propose a structure for the relaxed α-form. Almost at the same time, Mencik (2) established unambiguously the structure of the α-form. The following year, Yokouchi *et al.* (3) and, independently, Hall and Pass (4) confirmed the structure of the α-form and each group proposed a structure for the newly reported stretched β-form of poly(4GT). However, the proposed conformations differ so drastically that clearly the structure of the β-form should be reinvestigated. We have recently shown (5) that the structures of well-chosen organic molecules often yield all the relevant geometrical and conformational data necessary to describe the flexible moiety of the parent polyester. Since, on the one hand, the various model compounds for a given polyester do not necessarily show the same conformation and, on the other hand, poly(4GT) is dimorphic, it was decided to synthesize and establish the crystal structure of three different model compounds of poly(4GT). The determinations of the crystal structure of tetramethylene glycol dibenzoate (**1**), tetramethylene glycol di-*para*-chlorobenzoate (**2**), and tetramethylene glycol di-*para*-nitrobenzoate (**3**) are reported here and the conformations of the methylenic sequences are compared to those of both forms of poly(4GT).

In various infrared and Raman studies of poly(2GT), poly(3GT), poly(4GT) (6, 7), and of several model compounds of

TABLE 1. Crystal data

Parameter	1	2	3
Composition	$C_{18}H_{18}O_4$	$C_{18}H_{16}O_4Cl_2$	$C_{18}H_{16}N_2O_8$
MW	298.34	366.13	388.34
$F(000)$	316	190	404
Crystal system	Triclinic	Triclinic	Monoclinic
Space group	$P\bar{1}$	$P\bar{1}$	$P2_1/c$
a, Å	7.870(3)	5.916(3)	6.086(1)
b	8.574(3)	7.599(2)	11.475(3)
c	12.993(4)	10.404(2)	13.162(3)
α, deg	83.76(3)	67.81(2)	90
β	89.92(3)	77.47(2)	101.93(2)
γ	64.68(3)	81.63(3)	90
V, Å^3	786.8	421.7	899.3
d_o, g cm^{-3}	1.28	1.43	1.44
d_c	1.259	1.445	1.434
Z	2	1	2
μ, mm^{-1} (radiation)	0.686 (Cu)	3.69 (Cu)	0.11 (Mo)
λ, Kα, Å	1.54178	1.54178	0.71069
Crystal size, mm	0.42×0.64×0.15	0.18×0.05×0.02	0.39×0.07×0.05

TABLE 2. Data collection and refinement

Parameter	1	2	3
Radiation	Cu$\bar{K\alpha}$	Cu$\bar{K\alpha}$	Mo$\bar{K\alpha}$
$2\theta_{max}$, deg	140.	140.	50.
Scan width, deg	(1.00 + 0.14 tan θ)	(1.00 + 0.14 tan θ)	(1.00 + 0.35 tan θ)
Slit width, mm	4.0	4.0	4.0
Number of measured reflections	2985	1596	1929
Acceptance level $I/\sigma(I) \geq$	2.50	2.50	1.96
Number of observed reflections	2687*	976*	781
$R = \Sigma\|\|F_o\| - \|F_c\|\|/\Sigma\|F_o\|$ observed	0.042	0.046	0.045
all	0.045	0.087	0.117
Residual fluctuations in electron density map, e Å^{-3}	±0.15	−0.27, +0.25	−0.18, +0.33
Average shift to σ ratio at the end of the refinement	0.3	0.3	0.4

*Five and seven low-order reflections suffering from extinction were given zero weights in the final cycle of the least-squares refinement.

the latter (8) the authors have attempted to establish relations between specific vibrational bands and the various conformations of the molecular chains. In their infrared spectroscopic investigation of poly(4GT) and its model compounds, Gillette *et al.* (8) concluded that the conformation of the methylenic sequence in tetramethylene glycol dibenzoate was similar to that of the β-form of poly(4GT), i.e., an all-*trans* conformation. Since in the present paper we establish that the above mentioned conformation is not all *trans* but is tg^-ttt, we decided to reexamine the infrared and Raman spectra of the model compounds of poly(4GT).

Torsion angles with values of about 180, +60, −60° are defined as having *trans, gauche*$^+$, or *gauche*$^-$ conformations which are abbreviated as t, g, and g^- respectively.

Experimental

All three compounds (abbreviated as **1** or benzoate, **2** or chlorobenzoate, and **3** or nitrobenzoate) were prepared according to the method described by Heim and Poe (9), by reacting, in pyridine, solutions of tetramethylene glycol and of benzoyl chloride or of the *para*-chloro or of the *para*-nitro substituted benzoyl chlorides. Crystals of the benzoate were obtained by slow evaporation from an ethanol solution, the chlorobenzoate was recrystallized from a carbon tetrachloride solution, and the nitrobenzoate from a DMSO solution.

X-ray diffraction

A preliminary photographic investigation followed by accurate centering of 25 reflections on the Nonius CAD-4 diffractometer provided the space group and the unit cell dimensions which are listed with other crystal data in Table 1. The intensities were collected on the Nonius diffractometer by the $\omega/2\theta$ scan technique (Table 2). The stability of the crystals during the data collection was followed by measuring the intensities of three reference reflections every hour. These did not vary by more than 3%. An absorption correction based on the crystal shape was applied in all three cases.[1] The X-ray scattering factors used were those of Cromer and Mann (10) except for H atoms for which we used the values given by Stewart, Davidson, and Simpson (11). The anomalous dispersion correction for Cl was taken from Cromer and Liberman (12).

All three structures were solved by direct methods using the MULTAN program. The set of phases with the highest combined figure of merit always yielded all the nonhydrogen atoms among the

[1]The programs used here are modified versions of NRC-2, data reduction; NRC-3, absorption correction, NRC-10, bond distances and angles and NRC-22, mean planes (13); FORDAP, Fourier and Patterson maps; NUCLS, least-squares refinement (14); MULTAN, multisolution program (15); ORTEP, stereo views (16).

highest peaks listed. The full-matrix least-squares refinement of the atomic coordinates, using anisotropic temperature factors for nonhydrogen atoms and isotropic thermal parameters for H atoms, proceeded smoothly. The various criteria confirming the correctness of the structures are assembled in Table 2.

Conformational analysis

The potential energy calculated for a given conformation included the torsion energy about the different torsion angles, the nonbonded energies, and the electrostatic interactions. Intrinsic torsional potential with a three-fold barrier was assigned to rotations about the CH_2—CH_2 bonds while the torsional barrier for the C—O bond was taken to be zero. The tilt angle between the carboxy and the phenyl planes was kept fixed, since for most benzoates and terephthalates this angle reaches at the most 8°. The van der Waals interactions between nonbonded atoms were evaluated using 6−12 potential functions. Electrostatic interactions were computed by assigning partial charges to the atoms using a Coulomb's law potential function. Energies were calculated at 2° intervals in the area of the minima and at intervals of 5° elsewhere. Isoenergy contours were drawn at 1 kcal mol^{-1} intervals with respect to the minimum energy, which was arbitrarily set at zero. The parameters selected for this calculation are given in ref. 23.

Infrared and Raman spectroscopy

The infrared and Raman spectra of compounds **1**, **2**, and **3**, as well as those of trimethylene glycol dibenzoate, di-*para*-chlorobenzoate, pentamethylene glycol di-*para*-chlorobenzoate, di-*para*-nitrobenzoate, and hexamethylene glycol dibenzoate have been recorded. The crystalline model compounds were pressed into KBr pellets and their FTIR spectra were recorded on a Nicolet 7199-FTIR spectrometer. The sample spectra were signal-averaged with 500 scans while the background noise spectra were signal-averaged with 100 scans.

The Raman spectra were recorded with the Digital SPEX Ramalog spectrometer coupled with an Innova-90-5 He−Ar laser (λ = 514.5 nm). The power of the beam at the sample was 300 mW, the time constant was 1 s, and the intensity 22 A. The solid samples were kept in a small glass tube and the spectra were recorded at a scanning rate of 2 cm^{-1} s^{-1}.

Results and discussion

Structural considerations

The final positional parameters and their standard deviations are presented in Tables 3 a, b, and c.[2] The atomic numbering is shown in Fig. 1 and the various molecular structures are presented as stereopairs in Fig. 2. The final bond distances and angles of compounds **1**, **2**, and **3** are compared in Table 4 to those of 2,5-hexanediyl dibenzoate **4**, a compound related to those studied here (17). The bond distances, angles, and torsion angles of **1** are equal, within one esd, to those reported in a paper (18) that was published shortly after our own report on this compound (19).

The benzoate groups

The $C(sp^2)$—$C(sp^2)$ bond distances in the benzene rings average 1.381, 1.383, and 1.383 Å while the C—H distances average 0.96 and 1.02 Å for **1** and **2**, respectively, and were fixed at 0.95 Å for **3**. The C═O bond distances are all within 2σ of each other. The atoms in each of the benzene rings are coplanar. However, as reported earlier (20), the chlorine atom is displaced from the benzene mean plane by 0.040(1) Å. At the same time the ring bonds adjacent to the C—Cl bond are slightly shorter than the other ring bonds (1.376 vs. 1.384 Å) while the angle at the carbon atom to which Cl is bonded, with

1

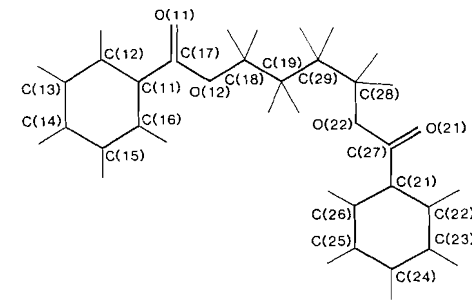

2

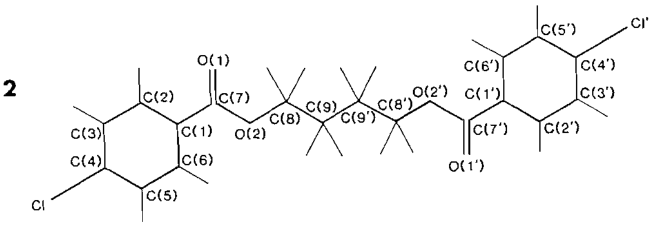

3

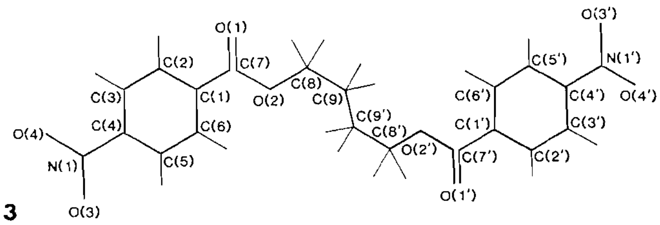

FIG. 1. Schematic representation of the molecules and atomic numbering.

a value of 122.1(4)°, is significantly larger than 120°. In the case of the nitrobenzoate, the plane of the NO_2 group is inclined by 7.4° with respect to the benzene ring mean plane. The NO_2 and carboxylate are tilted in the same way with respect to the benzene ring and are at 5.9° for each other. Finally, an important feature in a benzoate group is the dihedral angle between the benzene ring and the carboxylate group of atoms. These planes are here inclined with respect to one another by 1.2 and 6.2° for **1** and by 3.8° for both **2** and **3**. This real but limited flexibility, previously reported (21), has to be taken into account as a variable in the structural investigation of the related poly(*n*GT)'s.

The methylenic sequence

The O—$C(sp^3)$ distances ranging from 1.451(2) to 1.457(2) Å average 1.454 Å, in good agreement with published values. The $C(sp^3)$—$C(sp^3)$ distances in the three compounds studied here are as short as previously reported in hexamethylene dibenzoate (22). However, it should be noted that for **1** and **2** the middle C—C bond is longer (average 1.526 Å) than the adjacent bonds (average 1.505 Å). The C—C—C bond angles average 111.5° (range 110.3(3) to 113.0(5)°) while the O—C—C bond angles are all close to the average of 107.0°.

As can be seen in Fig. 2, the conformation of the "tetramethylene" part of the molecule is tg^-tgt in **1**, $ttttt$ in **2**, and tg^-tgt in **3**. The actual values of the conformational angles are listed in Table 5 where they are compared to the corresponding values for 2,5-hexanediyl dibenzoate **4**. One can note that among the various torsion angles describing the methylenic sequence, the angles ϕ_1 = C(7)—O(2)—C(8)—C(9) and especially ϕ_2 = O(2)—C(8)—C(9)—C(10), as well as their centrosymmetrically related counterparts, are the most flexible. That is, ϕ_1 and ϕ_2 deviate the most from 180°. It is

[2]Structure factor tables and the anisotropic thermal parameters may be purchased from the Depository of Unpublished Data, CISTI, National Research Council of Canada, Ottawa, Ont., Canada K1A 0S2.

TABLE 3a. Fractional atomic coordinates and their esd's ($\times 10^4$ for O and C; $\times 10^3$ for H atoms), U_{eq} ($\times 10^3$ for O and C) and U_{iso} ($\times 10^3$ for H atoms) for tetramethylene glycol dibenzoate

Atom	x	y	z	U_{eq}	Atom	x	y	z	U_{iso}
O(11)	−294(2)	2528(2)	−1009(1)	60	H(12)	−276(2)	500(2)	−219(1)	67
O(12)	−702(1)	3122(1)	637(1)	44	H(13)	−532(3)	767(3)	−264(1)	89
O(21)	2252(2)	−577(2)	5746(1)	63	H(14)	−705(3)	961(3)	−134(2)	98
O(22)	2653(2)	545(1)	4176(1)	48	H(15)	−589(3)	867(3)	45(2)	109
C(11)	−2771(2)	5210(2)	−640(1)	41	H(16)	−323(3)	582(2)	85(1)	81
C(12)	−3412(3)	5768(2)	−1670(1)	54	H(22)	299(2)	318(2)	417(1)	68
C(13)	−4969(3)	7359(3)	−1921(2)	64	H(23)	291(3)	571(3)	473(2)	97
C(14)	−5856(3)	8375(3)	−1163(2)	64	H(24)	205(3)	633(3)	649(2)	107
C(15)	−5220(3)	7823(2)	−142(2)	60	H(25)	144(3)	421(3)	767(2)	111
C(16)	−3677(2)	6237(2)	121(1)	49	H(26)	169(3)	159(2)	701(1)	80
C(17)	−1132(2)	3492(2)	−383(1)	42	H(181)	62(2)	49(2)	64(1)	66
C(18)	844(2)	1436(2)	976(1)	45	H(182)	211(3)	147(2)	69(1)	86
C(19)	889(2)	1179(2)	2141(1)	45	H(191)	93(2)	223(2)	241(1)	71
C(29)	2567(2)	−512(2)	2565(1)	46	H(192)	−35(3)	113(2)	238(1)	80
C(28)	2576(2)	−902(2)	3728(1)	50	H(291)	255(2)	−154(2)	224(1)	66
C(27)	2408(2)	579(2)	5195(1)	46	H(292)	382(2)	−42(2)	239(1)	69
C(26)	1897(3)	2501(3)	6566(1)	59	H(281)	139(3)	−103(2)	397(1)	81
C(25)	1812(3)	3985(3)	6919(2)	74	H(282)	371(2)	−202(2)	402(1)	69
C(24)	2185(3)	5169(3)	6270(2)	76					
C(23)	2612(3)	4880(3)	5259(2)	70					
C(22)	2686(3)	3400(2)	4889(1)	54					
C(21)	2347(2)	2186(2)	5550(1)	45					

TABLE 3b. Fractional atomic coordinates and their esd's ($\times 10^4$ for Cl, O, and C; $\times 10^3$ for H atoms), U_{eq} ($\times 10^3$ for Cl, O, and C) and U_{iso} ($\times 10^3$ for H atoms) for tetramethylene glycol di-*para*-chlorobenzoate

Atom	x	y	z	U_{eq}/U_{iso}
Cl	7771(2)	2133(2)	−1455(1)	72
O(11)	1847(4)	1496(4)	4957(3)	63
O(12)	−645(4)	3329(4)	3573(3)	53
C(11)	2876(6)	2259(5)	2472(4)	43
C(12)	5087(6)	1346(6)	2553(4)	50
C(13)	6585(6)	1291(6)	1348(4)	53
C(14)	5858(6)	2159(5)	68(4)	50
C(15)	3672(6)	3055(6)	−44(4)	54
C(16)	2188(6)	3092(6)	1173(4)	49
C(17)	1359(6)	2278(6)	3812(4)	49
C(18)	−2242(7)	3407(6)	4831(4)	56
C(19)	−4111(6)	4941(6)	4365(4)	50
H(12)	551(6)	73(5)	344(4)	61
H(13)	811(6)	55(5)	141(4)	65
H(15)	324(7)	363(6)	−96(4)	94
H(16)	71(6)	379(5)	113(3)	50
H(181)	−287(6)	212(5)	532(4)	69
H(182)	−146(6)	363(5)	545(4)	64
H(191)	−348(6)	621(5)	385(3)	52
H(192)	−474(6)	465(5)	376(4)	58

TABLE 3c. Fractional atomic coordinates and their esd's ($\times 10^4$ for O, N, and C; $\times 10^3$ for H atoms), U_{eq} ($\times 10^3$ for O, N, and C) and U_{iso} ($\times 10^2$ for H atoms) for tetramethylene glycol di-*para*-nitrobenzoate

Atom	x	y	z	U_{eq}/U_{iso}
O(1)	726(5)	3080(3)	5082(3)	61
O(2)	3680(5)	1920(2)	5651(3)	54
O(3)	10282(7)	6441(4)	7731(4)	95
O(4)	7652(7)	7676(3)	7131(3)	82
N(1)	8385(8)	6683(4)	7268(4)	66
C(1)	4141(7)	3909(3)	6040(3)	39
C(2)	3277(7)	5034(4)	6013(4)	46
C(3)	4649(8)	5950(4)	6425(4)	52
C(4)	6867(8)	5709(4)	6856(4)	48
C(5)	7761(8)	4599(4)	6908(4)	52
C(6)	6377(7)	3698(4)	6489(4)	47
C(7)	2635(7)	2951(4)	5539(4)	47
C(8)	2426(8)	923(4)	5158(4)	60
C(9)	4094(9)	−89(4)	5285(5)	68
H(2)	174	517	571	7
H(3)	408	672	641	6
H(5)	929	446	722	7
H(6)	695	293	651	5
H(81)	134	66	553	5
H(82)	180	91	443	7
H(91)	474	−18	600	9
H(92)	330	−78	503	8

therefore reasonable to expect that torsions, if they do have to take place in the polymer, will do so around the O(2)—C(8), C(8)—C(9), C(9′)—C(8′), and C(8′)—O(2′) bonds.

The three compounds seen as models for poly(4GT)

Poly(tetramethylene terephthalate) is a member of a family of aromatic polyesters, the poly(nGT)'s, where n stands for the number of methylenic groups between the terephthaloyl moieties. It has been established experimentally that all poly(nGT)'s, from $n = 2$ to 6, crystallize in triclinic unit cells, space group $P\bar{1}$, and the polymeric chains are aligned with the c-axis, the fiber axis. Furthermore, when the poly(nGT)'s have an even number of methylene groups, the center of the terephthaloyl group and the midpoint of the central CH_2—CH_2 bond coincide with the centers of symmetry at (000) and ($00\frac{1}{2}$) respectively. In a conformational analysis of a theoretical model (23) the possible conformations of the poly(nGT)'s for $n = 2$ to 6 were investigated. In the case of poly(4GT), only two conformational angles need to be varied. These are the two angles ϕ_1 and ϕ_2, found in the model compounds to be the most flexible (see Table 5). The conformational energy map as a

TABLE 4. Comparison of the bond distance and angles of the model compounds for poly(4GT)

Distances	1		2	3	4†	
σ (Å)	0.002–0.003		0.005–0.006	0.005–0.007	0.005–0.008	
C(1)—C(2)	1.390	1.391	1.392	1.392	1.377	1.382
C(2)—C(3)	1.394	1.383	1.381	1.382	1.388	1.394
C(3)—C(4)	1.371	1.378	1.376	1.380	1.354	1.355
C(4)—C(5)	1.377	1.377	1.378	1.381	1.413	1.403
C(5)—C(6)	1.389	1.374	1.383	1.375	1.396	1.367
C(6)—C(1)	1.383	1.392	1.383	1.388	1.399	1.376
C(1)—C(7)	1.488	1.482	1.489	1.494	1.487	1.482
C(7)—O(1)	1.207	1.208	1.192	1.202	1.201	1.205
C(7)—O(2)	1.338	1.338	1.345	1.337	1.333	1.337
O(2)—C(8)	1.457	1.451	1.455	1.452	1.483	1.465
C(8)—C(9)	1.505	1.511	1.499	1.529	1.498	1.523
C(9)—C(10) or C(9)—C(9*)	1.529		1.523	1.470	1.512	
C(4)—Cl or C(4)—N(1)			1.741	1.480		
N(1)—O(3)				1.221		
N(1)—O(4)				1.223		
Angles						
σ (°)	0.1–0.2		0.3–0.4	0.4–0.5	0.3–0.6	
C(1)—C(2)—C(3)	119.3	119.5	120.4	120.1	119.9	118.3
C(2)—C(3)—C(4)	120.6	120.6	118.9	118.0	121.5	121.7
C(3)—C(4)—C(5)	120.1	120.0	122.1	123.2	120.0	118.5
C(4)—C(5)—C(6)	120.1	120.1	118.4	118.1	118.5	121.1
C(5)—C(6)—C(1)	120.1	120.4	121.0	120.3	120.6	119.1
C(6)—C(1)—C(2)	119.8	119.4	119.3	120.3	119.4	121.2
C(2)—C(1)—C(7)	118.6	121.8	117.6	118.5	118.8	121.4
C(6)—C(1)—C(7)	121.5	118.8	123.2	121.1	121.7	117.4
C(1)—C(7)—O(1)	124.8	124.9	125.1	124.8	124.1	124.3
C(1)—C(7)—O(2)	111.8	112.1	111.5	111.6	112.3	112.7
O(1)—C(7)—O(2)	123.5	123.1	123.5	123.6	123.6	123.1
C(7)—O(2)—C(8)	116.1	116.8	115.0	117.0	119.9	118.8
O(2)—C(8)—C(9)	107.1	107.1	107.6	106.0	106.9	105.3
C(8)—C(9)—C(10) or C(9*)	110.5	112.3	110.3	113.0	114.0	113.3
C(3)—C(4)—Cl or N(1)			118.8	118.9		
C(5)—C(4)—Cl or N(1)			119.1	118.0		
C(4)—N(1)—O(3)				117.9		
C(4)—N(1)—O(4)				117.7		
O(3)—N(1)—O(4)				124.4		

C(9) and C(9) are centrosymmetrically related.
†Compound **4** is 2,5-hexanediyl dibenzoate (ref. 17).

TABLE 5. Torsion angles in the three tetramethylene dibenzoates compared to those of 2,5-hexanediyl dibenzoate

References	1	2	3	4
ϕ_1 = C(7)—O(2)—C(8)—C(9)	170.9(2)	168.1(3)	172.7(6)	145.4(4)
ϕ_2 = O(2)—C(8)—C(9)—C(9′)	59.6(2)	178.3(3)	−65.4(8)	−59.2(5)
ϕ_3 = C(8)—C(9)—C(9′)—C(8′)	−175.1(1)	180*	180*	−179.9(4)
ϕ_4 = C(9)—C(9′)—C(8′)—C(2′)	−176.0(1)	$-\phi_1$	$-\phi_1$	60.4(5)
ϕ_5 = C(9′)—C(8′)—O(2′)—C(7′)	−171.5(1)	$-\phi_2$	$-\phi_2$	139.2(4)
ω_1 = C(2)—C(1)—C(7)—O(2)	173.1(2)	175.1(3)	−178.3(6)	−177.7(4)
ω_2 = O(2′)—C(7′)—C(1′)—C(2′)	−178.9(2)	$-\omega_1$	$-\omega_1$	179.1(5)
τ_1 = C(1)—C(7)—O(2)—C(8)	−175.0(2)	179.4(3)	−177.4(5)	−174.3(4)
τ_2 = C(8′)—O(2′)—C(7′)—C(1′)	−177.9(2)	$-\tau_1$	$-\tau_1$	−179.9(4)
Calculated equivalent fiber repeat, Å†	11.62/13.21	13.20	11.68	11.64/11.40

*Compounds **2** and **3** have a crystallographic center of symmetry at the midpoint of the methylenic sequence.
†This is twice the distance between the center of one benzene ring to the midpoint of the methylenic sequence.

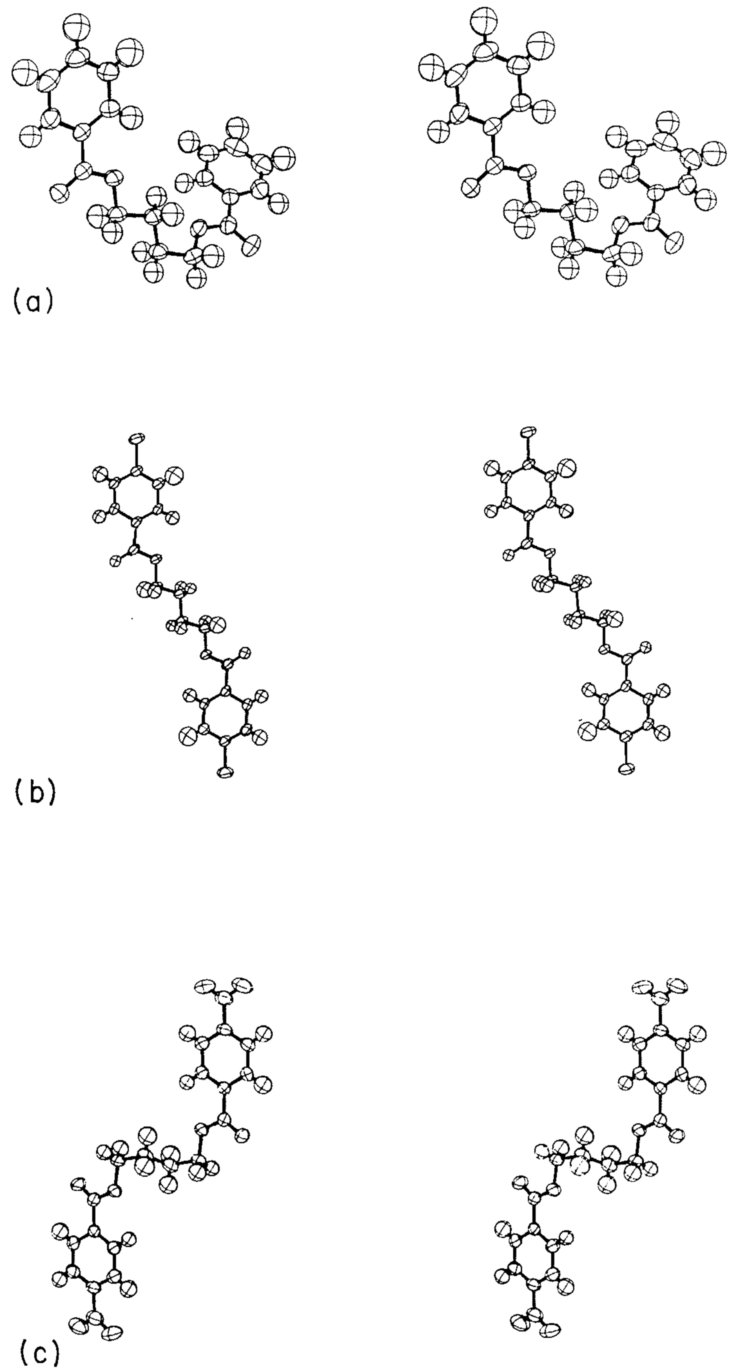

FIG. 2. Stereopairs of the three model compounds: (a) **1**, tetramethylene glycol dibenzoate; (b) **2**, tetramethylene glycol di-*para*-chlorobenzoate; (c) **3**, tetramethylene glycol di-*para*-nitrobenzoate.

function of ϕ_1 and ϕ_2, with the constraints that $\omega = \tau = 180°$, is shown in Fig. 3. The ϕ_1 and ϕ_2 combinations corresponding to the values of the fiber repeat for both the α- and the β-form of poly(4GT), which have values 11.60 and 13.00 Å respectively, have been drawn on this map. The reported conformations for the α- and β-forms of poly(4GT) have also been indicated on the conformational map. The conformations with the lowest energies are listed in Table 6.

The three model compounds studied in this work are related, as far as the conformation of the methylenic sequence is concerned, with one (or both) form(s) reported for poly(4GT).

The α-form

For instance, compound **1**, being noncentrosymmetric, may

TABLE 6. Conformational analysis of poly(4GT)

Conformation	ϕ_1*	ϕ_2	Symbol	Energy (kcal/mol)
A	180.	180.	*ttttt*	0.59
B	−80. 80.	180. 180.	$g^- tttg^+$ $g^+ tttg^-$	0.33
C	180. 180.	−60. 60.	$tg^- tg^+ t$ $tg^+ tg^- t$	0.50
D	−75. 75.	−60. 60.	$g^- g^- tg^+ g^+$ $g^+ g^+ tg^- g^-$	0.00
E	100. −100.	−65. 65.	$s^+ g^- tg^+ s^-$ $s^- g^+ tg^- s^+$	0.92

*$\phi_1' = -\phi_1$, $\phi_2' = -\phi_2$, and $\phi_3 = 180°$ while ω and τ were kept at 180°.

TABLE 7. Conformational angles of importance in the proposed models for poly(4GT)*

	Annealed form α-poly(4GT)				Stressed form β-poly(4GT)		
	1†	2	3	4	2	3	4
ω_1 = C(2)—C(1)—C(7)—O(2)	174.8	173.8	179.2	179.2	−179.	172.9	170.2
τ_1 = C(1)—C(7)—O(2)—C(8)	177.5	178.	−177.8	−177.1	179.	−178.6	−176.8
ϕ_1 = C(7)—O(2)—C(8)—C(9)	−90.6	−88.	−94.5	−92.5	−179.	−159.1	−151.5
ϕ_2 = O(2)—C(8)—C(9)—C(10)	−88.4	−68.	−79.3	−76.2	113.	162.2	146.3
ϕ_3 = C(8)—C(9)—C(10)—C(11)	180	180	180	180	180	180	180

*All these proposed structures are centrosymmetric. Hence $\phi_4 = -\phi_2$, $\phi_5 = -\phi_1$, $\omega_2 = -\omega_1$ and $\tau_2 = -\tau_1$.
† 1, ref. 2; 2, ref. 3; 3, ref. 4; 4, ref. 30.

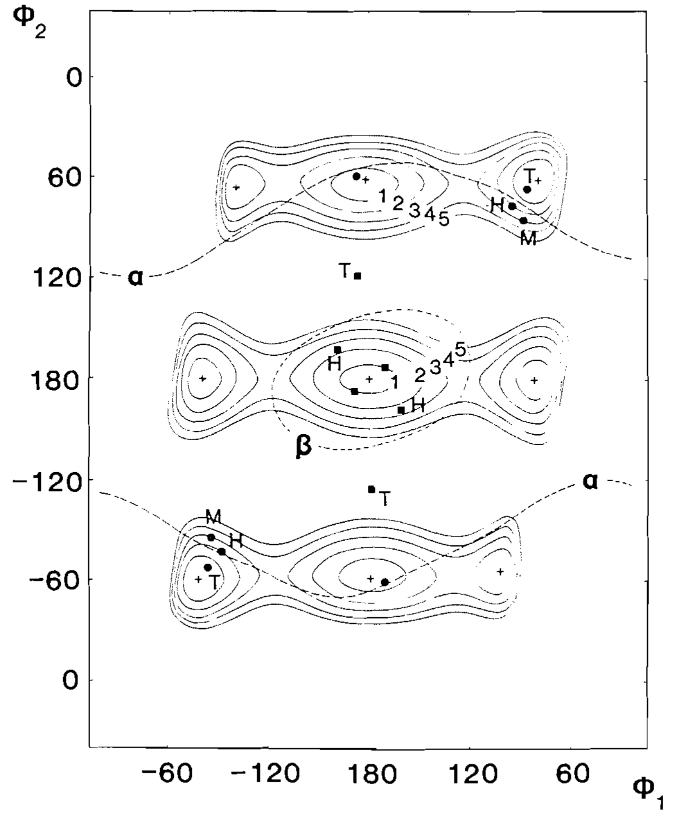

FIG. 3. Conformational energy map for poly(4GT). The energy minima are shown by (+). The black disks and squares represent the (ϕ_1, ϕ_2) combinations of the published poly(4GT) structures, α and β forms respectively. (M = ref. 2, T = ref. 3, and H = ref. 4). The unlabelled black disks correspond to the conformations found in the model compounds. The dotted lines correspond to the fiber repeat of α-poly(4GT) and β-poly(4GT).

be seen as two different half-molecules, each with a distinct conformation. Using the portion of the molecule that contains the torsion angle O(2)—C(8)—C(9)—C(10) = −59.6°, one may build a polymeric chain with a tg^-tgt conformation. In the case of compound **3**, the whole molecule with its tg^-tgt conformation has also been used as a chain generating model. These two compounds lead to calculated fiber repeat values of 11.62 Å and 11.68 Å, which are only slightly larger than the observed value of 11.60 Å for the fiber repeat of α-poly(4GT). The dot representing either of the above conformations on Fig. 3 comes close to the 11.60 Å fiber repeat as represented by the dotted line, and is also near one of the energy minima. This minimum is only 0.50 kcal mol^{-1} higher than the lowest calculated minimum that is associated with the g^-g^-tgg conformation proposed by all three authors for α-poly(4GT) (2−4). The conformational angles proposed, by various authors, for α- and β-poly(4GT) are compared in Table 7. Although energetically comparable, only one of the two conformations is acceptable. The best model can be chosen by comparing the values of the packing indexes, R_p, and the crystallographic agreement factors, $R = \Sigma||F_o| - |F_c|/\Sigma|F_o|$. The latter are obtained using our calculated structure factors, F_c, and the published F_o-values (2). The model with the tg^-tgt conformation has a packing index equal to 31.3 kcal mol^{-1} and the agreement factor between observed and calculated structure factors is R = 0.396, while these values are 13.6 kcal mol^{-1} and 0.148, respectively, when the g^-g^-tgg conformation is chosen. There is no doubt that the proposed model, with the g^-g^-tgg conformation, is the correct one. Consequently, great care should be exercised before using a model compound which seems to fit, as far as fiber repeat values and chain energy are concerned.

The β-form

Using the other half of molecule **1**, an all-*trans* conformation may be generated. A similar chain may be built using the whole methylenic sequence of the centrosymmetric molecule **2**. In both cases, the values of the conformational angles are near those proposed by Hall *et al.* (4) for β-poly(4GT). As a matter of fact, on the isoenergetic map, the values of ϕ_1 and ϕ_2 of our two model compounds are situated a little closer to the same energy minimum. The calculated fiber repeats (13.21 Å and 13.20 Å) are higher than the observed one (13.00 Å): this fact, coupled with the values of the conformational angles, seems to indicate that the polymer could adopt an even more "strained" form, if it could resist the applied tension up to that point.

Although these all-*trans* conformations, found in both model compounds, lead to calculated fiber repeats which are only slightly higher than the observed fiber repeat for β-poly(4GT), the intramolecular distances, bond and torsion angles of compound **2** (with its $ttttt$ conformation) were used to generate a model of the macromolecular chain. Since in these conditions the calculated fiber repeat is 13.24 Å, the flexible torsion angles ϕ_1 and ϕ_2 were altered so that the distance between the benzene ring centers would match the observed value (13.00 Å). The values of ϕ_1 = C(7)—O(2)—C(8)—C(9) and ϕ_2 = O(2)—C(8)—C(9)—C(10) were taken as 158.1° and 173.3°, respectively.

The resulting atomic parameters were then used to position this model chain in the observed unit cell. The chain was allowed to rotate about its axis, in order to minimize the interactions between neighboring chains, using Williams' packing program (24). A very reasonable value of the packing index

TABLE 8. FTIR bands in the regions 800–1050 cm^{-1} and 1300–1550 cm^{-1}

	Compound			α-Poly(4GT) annealed	β-Poly(4GT) stressed
	1	2	3		
Ring C—H out of plane		835(0.45)*			
	849(0.32)		843(0.65)		843
COC deformation		857(0.78)			
			875(0.54)	877	880
CH rocking	936(0.43)			917	
Glycol deformation	944(0.48)		941(0.47)		
O—CH_2 stretch	970(0.72)		965(0.73)		962
Ring C—H, in plane	1027(0.76)	1013(1.08)	1009(0.66)		
Glycol C—C stretch	1033(0.59)		1035(0.42)	1021	1020
				1030	
C—O stretch	1312(1.34)				
	1318(1.54)	1317(0.57)	1317(0.77)		
			1323(0.79)		
NO_2 stretch			1350(0.98)		
CH deformation	1366(0.62)			1350	
wagging	1388(0.42)				
	1395(0.41)	1395(0.53)			
Ring C—C stretch (disubstituted)		1404(0.51)	1411(0.33)	1408	1405
Ring C—C stretch	1450(0.88)		1447(0.36)		
CH_2 bending	1473(0.32)	1473(0.65)	1470(0.46)	1466	1470
glycol sequence	1480(0.72)	1489(0.60)			1484
NO_2 stretch				1515	1510
			1522(1.5)		

*(Absorbance), relative to that of the highest band, the C=O stretch at ~1720 cm^{-1}.

(RPACK), 15.8 kcal mol^{-1}, was reached. The atomic coordinates so obtained were introduced in a least-squares program, which compared the calculated structure factors (from the theoretical model) and those observed by Yokouchi *et al.* (3) on their X-ray fiber patterns for β-poly(4GT). In these conditions the final R factor was 0.220, a value slightly larger than the value of $R = 0.191$ reported by Yokouchi *et al.* (3). The torsion angles of the methylenic sequence published by Hall and Pass (4) are comparable to those in our own theoretical chain (see Table 9) and the values for R were either 0.218 or 0.223, depending upon which parameters were adjusted during their refinement procedure.

It is surprising to note that although different values of ϕ_2 were chosen by Yokouchi (113.0°) or by Hall (162.0°), both arrive at similar values for the calculated fiber repeat of 12.95 and 13.00 Å, and both lead to reasonable crystallographic R-factors ($R = 0.191$ and $R = 0.218$, respectively). The chain packing energies and the crystallographic R-factors for the proposed structures are indistinguishable and either may be considered an appropriate model for β-poly(4GT). Our own model compound, although it reinforces Hall's conformation, does not lead to better values of RPACK or the R-factor.

Spectroscopic study

Since our interest was in the conformation of the methylenic sequence in poly(4GT), the relevant spectral regions are 800–1050 cm^{-1} (methylene rocking) and 1300–1500 cm^{-1} (methylene bending). The FTIR and Raman bands observed in both these regions for the model compounds are compared in Tables 8 and 9 to the literature values for poly(4GT) (6). The band assignment follows the works of Snyder *et al.* (25–27) and Stokr *et al.* (28).

Infrared spectra

In FTIR, the 1300–1550 cm^{-1} region is difficult to work with because of the bands due to the mono- or di-substituted benzene rings, with their different *para*-substituents (H, Cl, or NO_2). We do, however, observe the following. There is only one very strong absorption band at 1383 cm^{-1} in the case of **3**; it is observed at 1385 cm^{-1} with a reduced intensity for **1** and it is completely absent from the spectrum of **2**. At the same time, there is no band around 1395 cm^{-1} for **3**, while **1** induces the appearance of a band of medium intensity at 1395 cm^{-1}, a band whose intensity increases significantly for compound **2**. Since we have a progression of conformations from tg^-tgt (**3**) to tg^-ttt (**1**) to $ttttt$ (**2**), the complete disappearance of the 1383 cm^{-1} band and the emergence of the 1395 cm^{-1} band are then indicative of an all-*trans* conformation, with torsion angles values near 180°, as in compound (**2**).

The 800–1050 cm^{-1} region does not reveal any significant fact such as the one above, where bands would appear or disappear according to the conformations. There is a band at 970 cm^{-1} and at 965 cm^{-1} for compounds **1** and **2**, which has been assigned to an O—CH_2 stretching mode (29), but it is not observed for compound **3**. Since all three compounds have a *trans* conformation for the C(7)—O(2)—C(8)—C(9) angle and compounds **1** and **2** have different conformations (tg^-ttt and $ttttt$), it is assumed that this particular band does not give any significant information about the overall conformation of the methylenic sequence.

The only other interesting fact is the absence of any band between 910 and 925 cm^{-1} for all three compounds, which is

TABLE 9. Raman bands in the regions 800–1050 cm^{-1} and 1300–1550 cm^{-1}

	Compound 1	Compound 2	α-Poly(4GT) annealed	β-Poly(4GT) stressed
CH rocking, glycol sequence	810(m)		808	
Ring C—C stretch	830(m)	832(w)		
Ring C—C breathing	865(m)	855(vs)	859 888	859
CH rocking glycol sequence	973(w)	973		965
Ring C—C stretch mono-substituted	1002(vs)			
Ring C—C breathing	1028(s)	1016(s)		
CH rocking, all-*trans* glycol sequence		1047(s)		1044
C—O stretch + ring CH in plane bend		1305(m)		
Ring C—C breathing	1320(m)	1320(w)		
CH deformation, all-*trans* glycol sequence		1347(m)		1348
CH wagging, glycol sequence	1388(w)		1382	
CH deformation, all-*trans* glycol sequence		1405(s)		1405
Ring C—C stretch		1408(5)	1412	1412
CH deformation, glycol	1443(m)			
		1453(s)		
	1463(m)		1460	
Ring C—C stretch	1472(w)	1480(w)		

not peculiar in itself but which will acquire important significance when compared to the ir spectrum of poly(4GT).

Raman spectra

The spectral regions considered in the Raman spectra are the same as in FTIR, the 800–1050 cm^{-1} and 1300–1550 cm^{-1} domains, which contain some CH_2 rocking and bending modes (6, 26, 27). Because compound **3** was a yellow powder, no satisfactory Raman spectrum could be obtained. Even after recrystallization and production of a yellowish-white sample, the product still showed absorption problems while its spectrum was taken. Only the results for **1** and **2** will be given here.

In the first region, compound **1** has a band at 810 cm^{-1}, while **2** does not. This band could be related to a conformation containing at least one *gauche* torsion angle, as is the case in **1** (tg^-ttt). On the other hand, only **2** exhibits a band at 1047 cm^{-1}; its presence could be indicative of an all-*trans* conformation, *ttttt* as in **2**, or at least a *ttt* conformation implicating the torsion angles between the four carbon atoms in the chain.

The spectral region where CH_2 wagging and bending modes usually appear does contain some significant changes. The spectrum of **1** shows a band between 1383 and 1388 cm^{-1}, which is absent for **2**. On the spectrum of the latter, two new bands do appear at 1347 cm^{-1} and 1405 cm^{-1}. In conclusion, the presence of the band at ~1385 cm^{-1} suggests a *gauche* torsion angle in the methylenic sequence, while the 1347 cm^{-1} and 1405 cm^{-1} bands stand for at least a *ttt* sequence or even an all-*trans* conformation.

Unfortunately, the association of bands at 1047 cm^{-1}, 1347 cm^{-1}, and 1405 cm^{-1} to an all-*trans* conformation in **2** is not verified in the case of hexamethylene glycol dibenzoate, a model compound for poly(6GT). In this product the methylenic chain has a *ttttttt* conformation but its spectrum does not show any of the above-mentioned bands. The three bands observed in **2** might then be specifically associated to the entire all-*trans* sequence (*ttttt*), including the oxygen atoms which are at both ends of the methylenic sequence.

It has already been established by FTIR that some bands are representative of a given conformation for one model compound while others, by their appearance or disappearance, can be related to an evolution of conformational sequences (from tg^-tgt to *ttttt*). These conclusions can now be extended to the different forms of poly(4GT) (6, 8) and may shed some light on the reported discrepancies in the description of the conformation of β-poly(4GT), the stressed form of the polymer.

The FTIR spectroscopic results for the three model compounds supplied two important conclusions: first, that the complete disappearance of the absorption band at 1383 cm^{-1} and the emergence of the 1395 cm^{-1} band are indicative of an all-*trans* conformation, with torsion angle values near 180°. Upon examination of the 1350–1425 cm^{-1} region of the spectra for poly(4GT), one notes an absorption band at 1386 cm^{-1} for the annealed sample and the subsequent disappearance of this band, while another one appears at 1395 cm^{-1}, in the case of the stressed sample. Consequently, the β-form of poly(4GT) possesses an all-*trans* conformation, with torsion angle values near 180°.

The second conclusion concerns the fact that there is no band around 917 cm^{-1} for all three model compounds. The very absence of any absorption band on those spectra, while there is one present, and quite important, in the spectrum of the annealed α-poly(4GT), is indicative of a peculiar conformation. It has been stated that this strong absorption is characteristic of "α crystallinity" in poly(4GT) (6, 7) and of its *sstss* conformation (where *s* is non-*trans* non-*gauche* and φ, the corresponding torsion angle, is between 90° and 120°). The absorption band at 917 cm^{-1} is not observed in either of the three model compounds with different conformations ($tg^{-}ttt$, *ttttt*, and $tg^{-}tgt$) or in the spectra of other model compounds such as pentamethylene glycol di-*para*-nitrobenzoate (*tttttt*), pentamethylene glycol di-*para*-chlorobenzoate ($g^{-}tttg^{-}$), and hexamethylene glycol dibenzoate (*ttttttt*). This absorption band is only present when there is a non-*trans* non-*gauche* conformation in the methylenic sequence. Consequently, its presence in the spectrum of the annealed polymer, α-poly-(4GT), and its absence from the spectrum of the stressed sample indicates the absence of any non-*trans* non-*gauche* conformation in β-poly(4GT). In other words, the stressed polymer has torsion angle values not too different from 180° for its all-*trans* conformation.

The Raman study of the model compounds compared to that of poly(4GT) (6) confirms the conclusion reached above. More specifically, the three bands (1047 cm^{-1}, 1347 cm^{-1}, and 1405 cm^{-1}), which are associated with the entire all-*trans* sequence (*ttttt*) of the four-carbon chain and their neighboring oxygen atoms in the model compound are also observed in the Raman spectrum of β-poly(4GT), at 1044, 1348, and 1405 cm^{-1}. Simultaneously, the band observed at 1381 cm^{-1} in the spectrum of the annealed poly(4GT) has disappeared. This last band was not present on the spectrum of compound **2** (*ttttt*). Thus it is Hall's model, with an all-*trans* conformation and torsion angle values near 180°, which describes best the β-form of poly(4GT).

Acknowledgements

We thank the Natural Sciences and Engineering Research Council of Canada for its financial support. We also thank Mr. M. J. Olivier for collecting the X-ray data.

1. A. M. JOLY, G. NEMOZ, A. DOUILLARD, and G. VALLET. Makromol. Chem. **176**, 479 (1975).
2. Z. MENCIK. J. Polym. Sci. Polym. Phys. Ed. **13**, 2173 (1975).
3. M. YOKOUCHI, Y. SAKAKIBARA, Y. CHATANI, H. TADOKORO, T. TANAKA, and K. YOKA. Macromolecules, **9**, 226 (1976).
4. I. H. HALL and M. G. PASS. Polymer, **17**, 807 (1976).
5. F. BRISSE, R. H. MARCHESSAULT, and S. PÉREZ. *In* Preparation and properties of stereoregular polymers. *Edited by* R. W. Lenz and F. Ciardelli. Reidl Publishing Co., Dordrecht, Boston, London. 1979. pp. 407–430.
6. I. M. WARD and M. A. WILDING. Polymer, **18**, 327 (1977).
7. B. STAMBAUGH, J. B. LANDO, and J. L. KOENIG. J. Polym. Sci. Polym. Phys. Ed. **17**, 1063 (1979).
8. P. C. GILLETTE, S. D. DIRLIKOV, J. L. KOENIG, and J. B. LANDO. Polymer, **23**, 1759 (1982).
9. H. C. HEIM and C. P. POE. J. Org. Chem. **9**, 299 (1944).
10. D. T. CROMER and J. B. MANN. Acta Crystallogr. Sect. A, **24**, 321 (1968).
11. R. F. STEWART, E. R. DAVIDSON, and W. T. SIMPSON. J. Chem. Phys. **42**, 3175 (1965).
12. D. T. CROMER and D. LIBERMAN. J. Chem. Phys., **53**, 1891 (1970).
13. F. R. AHMED, S. R. HALL, M. E. PIPPY, and C. P. HUBER. Accession No. 133-147 in J. Appl. Crystallogr. **6**, 309 (1973).
14. R. J. DOEDENS and J. A. IBERS. Inorg. Chem. **6**, 204 (1967).
15. P. MAIN, M. M. WOOLFSON, L. LESSINGER, G. GERMAIN, and J. P. DECLERCQ. MULTAN. A system of computer programs for the automatic solution of crystal structures from X-ray diffraction data. Univs. of York, England, and Louvain, Belgium. 1978.
16. C. K. JOHNSON. ORTEP. Report ORNL-3794. Oak Ridge National Laboratory, Tennessee. 1965.
17. G. BOCELLI and M.-F. GRENIER-LOUSTALOT. Acta Crystallogr. Sect. B, **38**, 3135 (1982).
18. G. BOCELLI and M.-F. GRENIER-LOUSTALOT. Acta Crystallogr. Sect. B, **38**, 2072 (1982).
19. A. PALMER and F. BRISSE. Acta Crystallogr. Sect. A, **37**, C243 (1981).
20. F. BRISSE and J. SYGUSCH. Acta Crystallogr. Sect. B, **30**, 480 (1974).
21. F. BRISSE and S. PÉREZ. Acta Crystallogr. Sect. B, **32**, 2110 (1976).
22. S. Pérez and F. BRISSE. Acta Crystallogr. Sect. B, **33**, 1673 (1977).
23. S. POULIN-DANDURAND. M.Sc. Thesis, Université du Québec à Montréal, 1978.
24. D. E. WILLIAMS. Acta Crystallogr. Sect. A, **25**, 464 (1969).
25. R. G. SNYDER and J. H. SCHACHTSCHNEIDER. Spectrochim. Acta, **19**, 85 (1963).
26. R. G. SNYDER. J. Mol. Spectrosc. **36**, 222 (1970).
27. R. G. SNYDER, S. L. HSU, and S. KRIMM. Spectrochim. Acta Part A, **34**, 395 (1978).
28. J. STOKR, B. SCHNEIDER, D. DOSKOEILOVA, J. LÖVG, and P. SEDLACEK. Polymer, **23**, 714 (1982).
29. F. J. BOERIO, S. K. BAHL, and G. E. MCGRAW. J. Polym. Sci. Polym. Phys. Ed. **14**, 1029 (1976).
30. I. J. DESBOROUGH and I. H. HALL. Polymer, **18**, 825 (1977).

Backbone-modified oligopeptidic bioregulators. The synthesis and configuration of thioamide, amidoxime, cyanoamidine, and amidrazone analogs of the chemotactic peptide N-formyl-methionyl-leucyl-phenylalanine (f-Met-Leu-Phe-OR)

GILLES SAUVÉ[1] AND VANGA S. RAO[1]

Département de Chimie, Faculté des Sciences, Université de Sherbrooke, Sherbrooke (Qué.), Canada J1K 2R1

AND

GILLES LAJOIE AND BERNARD BELLEAU[2]

Department of Chemistry, McGill University, Montréal (Qué.), Canada H3A 2K6

Received December 28, 1984

GILLES SAUVÉ, VANGA S. RAO, GILLES LAJOIE, and BERNARD BELLEAU. Can. J. Chem. **63**, 3089 (1985).

Reaction conditions for the synthesis of thioamide, amidoxime, and N-substituted amidine analogs of the peptide bond are described. Several new amidine analogs of the chemotactic peptide f-Met-Leu-Phe-OR were synthesized using the thioamides as precursors. The assignment of the *E*/*Z* configuration was accomplished by nuclear magnetic resonance. The biological activity of these analogs is briefly described.

GILLES SAUVÉ, VANGA S. RAO, GILLES LAJOIE et BERNARD BELLEAU. Can. J. Chem. **63**, 3089 (1985).

Des conditions de réaction pour la synthèse de thioamides, d'amidoximes et d'amidines N-substituées analogues au lien peptidique sont décrites. Plusieurs analogues du peptide chimiotactique f-Met-Leu-Phe-OR contenant une fonction amidine N-substituée furent synthétisés à partir de précurseurs thioamidés. L'attribution de la configuration *E* et *Z* est faite par analyse spectroscopique de résonance magnétique nucléaire. L'activité biologique de ces analogues est décrite brièvement.

Introduction

Until recently, studies of structure–activity relationships in the field of oligopeptidic effectors were mainly concerned with modifications of the side chains (1). However, a growing number of peptide bond analogs have been generated in an attempt to delineate the role of the backbone peptide bonds in the process of active site recognition by receptors and enzymes for biologically active oligopeptides, a question having a direct bearing on the susceptibility of such effectors to peptidases (see ref. 2 for a general review of peptide backbone modifications). We have already described appropriate methodologies (3), preferable to previous ones (4) for reasons previously outlined, for the selective incorporation of thioamide functions (5) into peptide backbones and have recently illustrated the effects of such modifications on the pharmacological properties of the endogenous opiate Leu^5-enkephalin (6). The results of a similar study by others (7) have also been divulged and are in general concordance with ours. We now wish to describe an extension of our methodology for thiopeptide formation and to illustrate the use of the thioamide function (**2**) (Scheme 1) as the precursor of novel backbone analogs where the sulfur is replaced by substituted nitrogen functions (**3**). Although similar in structure to the amide function, amidine analogs as such were not synthesized because their strongly basic properties disqualify them as relevant peptide bond analogs.

The chemotactic peptide f-Met-Leu-Phe-OH (**4**) (8) has formed the subject of considerable interest as a prototype bioregulator of immune cells such as neutrophils and monocytes and extensive structure–activity relationships have been reported (9). Nearly all of these involved side chain alterations and substituent effects at the N— and C— terminals. Some of these changes were intended to impose conformational restrictions through steric constraints about the side chains (10).

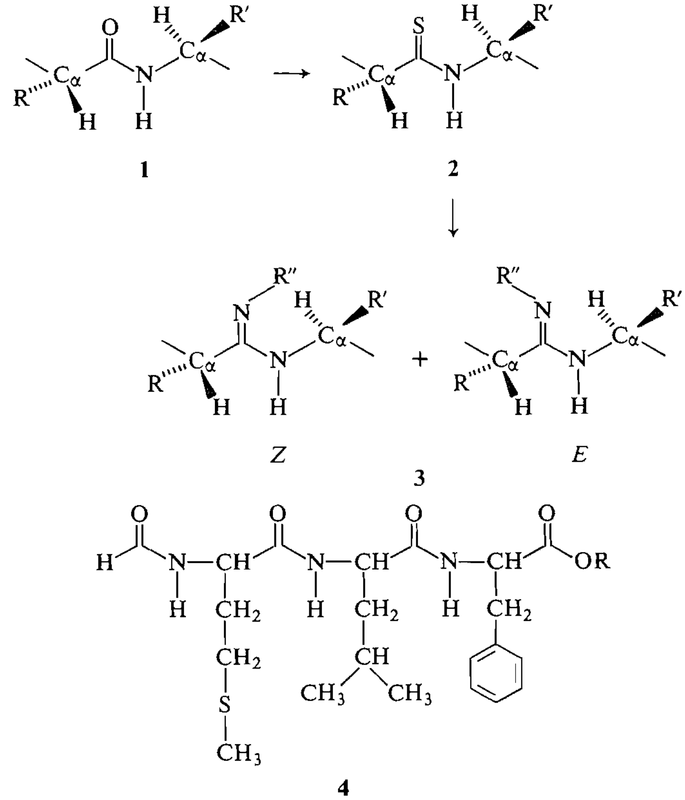

SCHEME 1

Our strategy called for backbone modifications of the chemotactic peptide through selective amide bond replacement by thioamide linkages. The resulting thiopeptides may then be used as intermediates for the synthesis of amidoxime and N-substituted amidine analogs according to literature methods (11). The conformational changes induced by such backbone modifications may then be studied by nmr and computer

[1]Present address: Department of Chemistry, McGill University, Montreal (Qué.), Canada H3A 2K6.

[2]To whom correspondence may be addressed at McGill University.

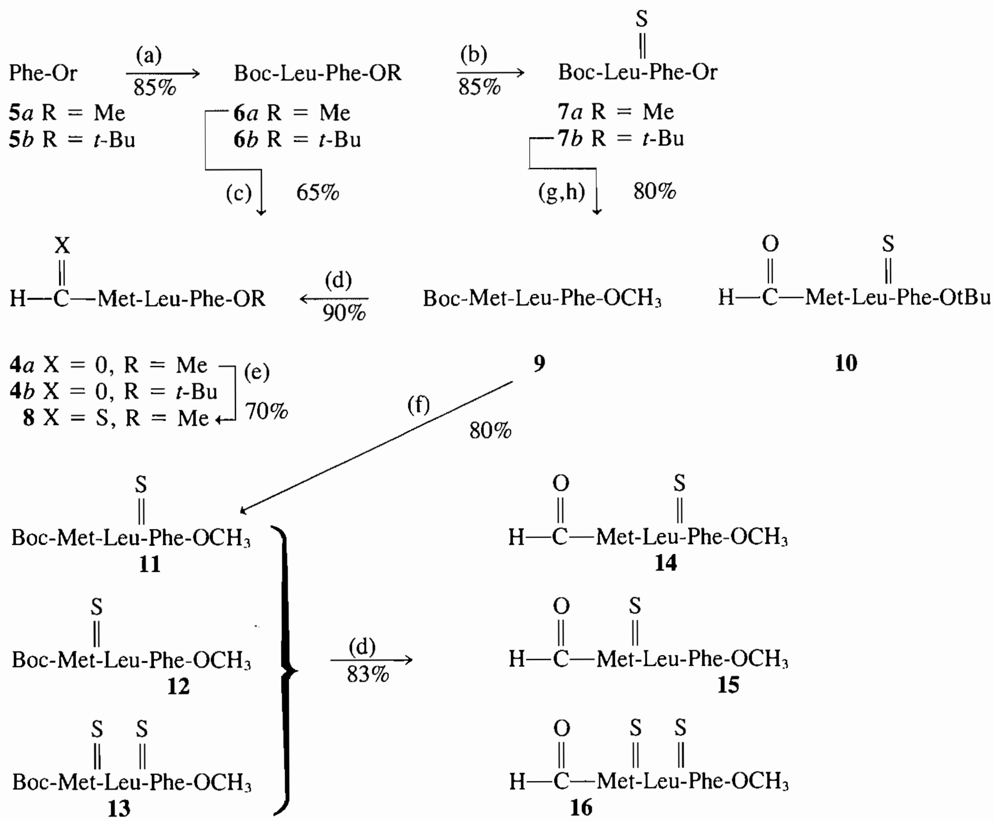

(a) Boc-Leu-OH, HOBt, DCC, CH_2Cl_2, DMF, RT, 10 h; (b) thionation reagent **17**,[3] THF, 40°C, 7 h; (c) HCO_2H, 3 h, evap.; Boc-Met-OH, HOBt, DCC, CH_2Cl_2, DMF, RT, 18 h; (d) HCO_2H, RT, 3 h, evap.; EEDQ, $CHCl_3$, RT, 5 h; (e) thionation reagent **17**, 0°C, 1 h; (f) thionation reagent **17**, 0°C, 72 h; (g) *p*TSA, MeOH, RT, 24 h; (h) OHC-Met-OH, HOBt, DCC, CH_2Cl_2, DMF, RT, 18 h.

SCHEME 2

modeling methods (V. S. Rao, G. Sauvé, G. Lajoie, and B. Belleau, to be published).

Several methods are known for the synthesis of N-substituted amidines (12, 13). However, the reaction conditions employed in most cases are unsatisfactory for our purposes because of the relative inaccessibility of the precursors and the susceptibility of peptide substrates to racemization and decomposition under the prescribed conditions. Our recently developed methodology for the selective thionation of peptide linkages (3) provided the incentive to generate thiopeptidic analogs of f-Met-Leu-Phe-OR as key intermediates and as intrinsically valuable receptor probes. Under mild, controlled conditions, our thiophosphetane reagent[3] **17** can transform regioselectively protected oligopeptides into thiopeptides, the site of transformation being determined by the relative steric bulk of the side chains adjacent to the amide bonds (3). Subsequent replacement of the sulfur atom by nitrogen functionalities would yield still other novel types of backbone analogs such as the desired N-substituted amidines.

The purpose of the present report is to describe the synthetic methodologies (as outlined in Scheme 1) and the results of nmr studies of the configurational properties of these novel backbone-modified chemotactic peptides. The detailed biological activities of the analogs will be reported elsewhere.

Results and discussion

Synthesis of mono- and di-thionated peptide analogs of f-Met-Leu-Phe-OR (Scheme 2)

The methyl ester of L-phenylalanine (**5***a*) was prepared in the conventional manner (14) by adding L-phenylalanine to a solution of thionyl chloride in methanol, whereas the *tert*-butyl ester (**5***b*) was obtained by transesterification of L-phenylalanine with *tert*-butyl acetate in the presence of catalytic amounts of perchloric acid (15). Following standard reaction conditions, **5***a* and **5***b* were then elongated to the dipeptide, Boc-Leu-Phe-OR (R = CH_3, **6***a*; R = $C(CH_3)_3$, **6***b*) by coupling with Boc-Leu-OH in the presence of DCC and HOBt (16). The amino group of **6***a* was deprotected using formic acid (17) and the resulting formate salt was treated with triethylamine followed by coupling with Boc-Met-OH under standard conditions (DCC–HOBt) to give the tripeptide Boc-Met-Leu-Phe-OCH_3 (**9**). Removal of *t*-Boc group with formic acid and subsequent addition of EEDQ (18) to the formate salt yielded the N-formyl tripeptide f-Met-Leu-Phe-OCH_3 (**4***a*).

Thionation of **4***a* with reagent **17** under controlled conditions (0°C, 1 h) gave exclusively the corresponding thioformyl derivative (**8**). Boc-Met-Leu-Phe-OCH_3 (**9**) when reacted with **17** at 0°C for 3 days gave a mixture of monothionated **11** and **12** and dithionated derivatives **13** in a 4:4:2 ratio respectively. Removal of the *t*-Boc group from these derivatives followed by N-formylation as described above, gave the corresponding for-

[3]Thionation reagent: 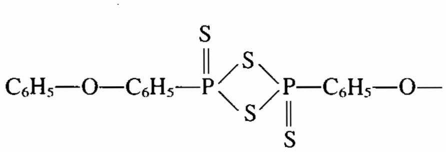
C_6H_5 (**17**) prepared from diphenyl ether and phosphorus pentasulfide.

TABLE 1. Some physical properties of some amide and thioamide derivatives related to the chemotactic peptide f-Met-Leu-Phe-OR

Peptide	Melting point[a] (°C)	$[\alpha]_D^{20°C}$ [b] (deg)	λ_{max}^{uv} [c] (log ϵ)	High resolution mass spectrum m/e M^+ calcd. (found)	^{13}C nmr chemical shifts (ppm/DMSO-d_6) (C=S)
Boc-Leu-Phe-OCH_3 **6*a***	83–85	−24.2	—	392.2311 (392.2314)	—
Boc-Leu-Phe-$OC(CH_3)_3$ **6*b***	120–122	−23.5	—	434.2781 (434.2781)	—
Boc-Leu$\overset{\text{S}}{\overset{\|}{\text{-}}}$Phe-$OCH_3$ **7*a***	73–76	+39.3	267 (4.08)	408.2083 (408.2094)	206.6
Boc-Leu$\overset{\text{S}}{\overset{\|}{\text{-}}}$Phe-$OC(CH_3)_3$ **7*b***	40–42	+2.9	267 (4.00)	450.2553 (450.2533)	206.1
CBZ-Leu$\overset{\text{S}}{\overset{\|}{\text{-}}}$Phe-$OC(CH_3)_3$ **40**	95–97	+3.5	267 (4.05)	484.2396 (484.2396)	206.1
H-$\overset{\text{O}}{\overset{\|}{\text{C}}}$-Met-Leu-Phe-$OCH_3$[e] **4*a***	136–138[d]	−39.2	—	451.2141 (451.2133)	—
H-$\overset{\text{O}}{\overset{\|}{\text{C}}}$-Met-Leu-Phe-$OC(CH_3)_3$ **4*b***	141–143	−40.6	—	493.2610 (493.2610)	—
H-$\overset{\text{S}}{\overset{\|}{\text{C}}}$-Met-Leu-Phe-$OCH_3$[f,g] **8**	158–160	−60.5	264 (4.01)	467.1913 (467.1910)	188.5
H-$\overset{\text{O}}{\overset{\|}{\text{C}}}$-Met$\overset{\text{S}}{\overset{\|}{\text{-}}}$Leu-Phe-$OCH_3$[f,h] **15**	111–112	−59.3	271 (4.05)	467.1913 (467.1913)	203.2
H-$\overset{\text{O}}{\overset{\|}{\text{C}}}$-Met-Leu$\overset{\text{S}}{\overset{\|}{\text{-}}}$Phe-$OCH_3$[f,i] **14**	142–145	−5.0	270 (4.06)	467.1913 (467.1912)	206.3
H-$\overset{\text{O}}{\overset{\|}{\text{C}}}$-Met-Leu$\overset{\text{S}}{\overset{\|}{\text{-}}}$Phe-$OC(CH_3)_3$ **10**	155–157	−32.8	270 (4.00)	509.2382 (509.2382)	206.0
H-$\overset{\text{O}}{\overset{\|}{\text{C}}}$-Met$\overset{\text{S}}{\overset{\|}{\text{-}}}Leu\overset{\text{S}}{\overset{\|}{\text{-}}}$Phe-$OCH_3$[j] **16**	103–106	+0.6	271 (4.27)	483.1684 (483.1701)	204.5 202.8

[a]Recrystallized from ethyl acetate – hexane except in the case of **4*a*** and **16** for which methanol–water was used.
[b]c = 1.0, MeOH.
[c]In EtOH at 20°C.
[d]Literature (8) mp 132–135°C.
[e]*Anal.* calcd. for $C_{22}H_{33}N_3O_5S_1$: C 58.52, H 7.37, N 9.31, S 7.08; found: C 58.41, H 7.52, N 9.29, S 6.87.
[f]*Anal.* calcd. for $C_{22}H_{33}N_3O_4S_2$: C 56.50, H 7.11, N 8.98, S 13.81.
[g]Found: C 56.87, H 7.39, N 8.84, S 13.67.
[h]Found: C 56.50, H 7.35, N 8.96, S 13.71.
[i]Found: C 56.41, H 7.31, N 8.97, S 13.47.
[j]*Anal.* calcd. for $C_{22}H_{33}N_3O_3S_3$: C 54.62, H 6.81, N 8.68, S 19.88; found: C 54.42, H 6.76, N 8.62, S 19.47.

mylated peptides **14**, **15**, and **16** which were separated on silica by flash chromatography. The *tert*-butyl ester **10** was obtained through selective removal of the N-Boc group from *7b* with *p*TSA[4] (19) followed by direct coupling with formylmethionine in the presence of DCC–HOBt. The precursor *7b* was obtained in turn by thionation of *6b* with **17**.

The structures and physical characteristics of the mono- and di-thiopeptides synthesized in this manner are assembled in Table 1. Their relevant nmr characteristics (^{1}H chemical shifts) are given in Table 3.

N-Substituted amidine backbone analogs. Syntheses and configurational determinations

The approach adopted for amidine-like analog synthesis relied on the inherent reactivity of thioamides toward nucleophiles or on electrophilic catalysis by the thiophilic mercuric ion. The high reactivity of thioamide **8** and of leucine thioamide together with the high nucleophilicity of the nucleophile hydroxylamine served to eliminate the need for electrophilic assistance in the formation of amidoximes **18** and **36** (Table 2). However, assistance by $Hg(OAc)_2$ was found necessary in all other cases, the thioamides being either less reactive or too sterically hindered for the nucleophile to react efficiently. The presence of $Hg(OAc)_2$ was even more necessary with the less nucleophilic reactant cyanamide (NH_2CN). For example, when Boc-Leu-ψ($CSNH_2$) (20) was treated with 1.1 equivalents of NH_2OH in THF at room temperature, amidoxime **18** Boc-Leu-ψ[C(=NOH)NH_2] was obtained in 62% yield. In contrast, generation of **19** and **20** from the corresponding precursor thioamides required assistance by mercuric ions in order to overcome unfavorable steric effects by the N-substituents of the substrates.

The structures of the mono-, di-, and tri-peptide N-substituted amidines synthesized in this manner, together with some relevant product characteristics, are given in Table 2, whereas their pertinent ^{1}H nmr band positions and shifts are assembled in Table 3. It is worth noting that when Boc-Leu-ψ(CSNH)-Phe-OCH_3 (*7a*) was treated with NH_2OH and $Hg(OAc)_2$ in the presence of $N(Et)_3$ in THF, the cyclic amidoxime lactone **21** was obtained in 44% yield. However, when the *tert*-butyl ester derivative of the N-CBZ protected peptide (CBZ-Leu-ψ(CSNH)-Phe-$OC(CH_3)_3$) was subjected to the same reaction conditions, the expected amidoxime analog **23** was obtained in 80% yield. Analogously, the cyclic amidrazone **22** was obtained when *7a* was reacted with NH_2—NH_2 under similar reaction conditions. This suggests that when either the amidoxime or the amidrazone derivative can adopt the *Z*- configuration, they spontaneously cyclize presumably because of favorable ϕ_3 and ψ_3 torsional angles around the Phe moiety as well as by the inherent reactivity of the terminal methyl ester function. These factors are obviously disfavored when a bulky *tert*-butyl ester function is used. To what extent the relative inductive properties of *tert*-butyl and methyl groups influence the course of the reaction is arguable (21). A similar reaction sequence led to the cyclic analogs of tripeptides **32** and **33** without interference from the terminal N-formyl groups. Some O-methyl amidoximes and N-cyanoamidines were similarly prepared using methoxamine and cyanamide as the nucleophiles and appropriate thiopeptide precursors (Table 2).[5] The O-acetyl amidoximes **29** and **42** were readily obtained by acetylation of amidoximes **28** and **36**, respectively. It is worth noting that under the adopted experimental conditions (where mercuric ions are present) the thioether functions of the methionine residues were left intact.

All the amidoxime analogs including their O-methyl derivatives (except for **36** and **38**) showed two sets of resonances (a major and a minor one) in their ^{1}H nmr spectra. With analog **30**, for example, the ratio between these two sets of signals was 63:37 in DMSO-d_6 as the solvent, and 77:23 in the less polar solvent $CDCl_3$, thus showing that these two sets of resonances originate from geometrical isomers about the amidine C=N bond and not from diastereoisomers as might have been produced through epimerization of the two α-carbons during the synthetic operations. This contention was conclusively proved by treating the geometrically inhomogeneous amidoxime **23** (Z/E = 83:17) with nitrous acid (generated *in situ* from $NaNO_2$ and *p*TSA) in methanol, which transformed the amidoxime into the parent amide function (Scheme 3). After isolation, the product was found to exhibit an ^{1}H nmr spectrum (200 MHz) and a specific rotation that were virtually identical to those of authentic CBZ-Leu-Phe-$OC(CH_3)_3$, thus confirming that no racemization occurred during the process of amidoxime **23** formation.

Interestingly, however, N-cyanoamidine derivatives **31**, **35**, and **37** (Table 2) exhibited only *one* set of relevant signals, implying in these cases the existence of either a single geometric form or the operation of a fast equilibration of two isomeric forms as depicted by the following mechanism:

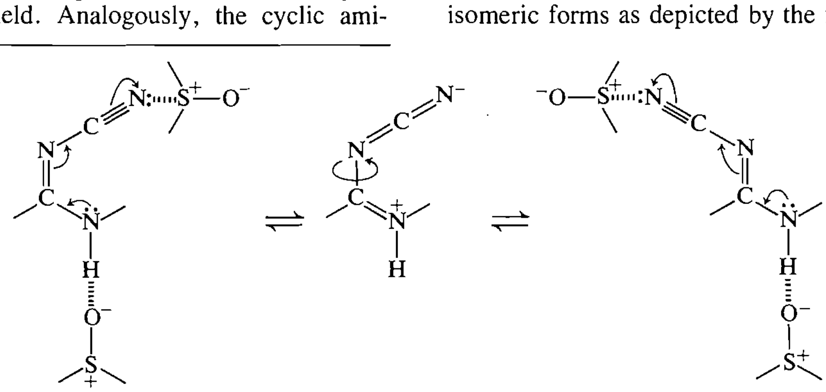

[4]The use of HCOOH also cleaved the carboxyl *tert*-butyl ester. However, as expected, the methyl ester was stable under the same conditions.

[5]All the tripeptide amidine analogs were obtained directly from the corresponding thioamides, except in the case of **30** which was obtained from **24** by cleaving the Boc-group and coupling the resulting amine **27** with formyl-methionine under the usual conditions (Scheme 3).

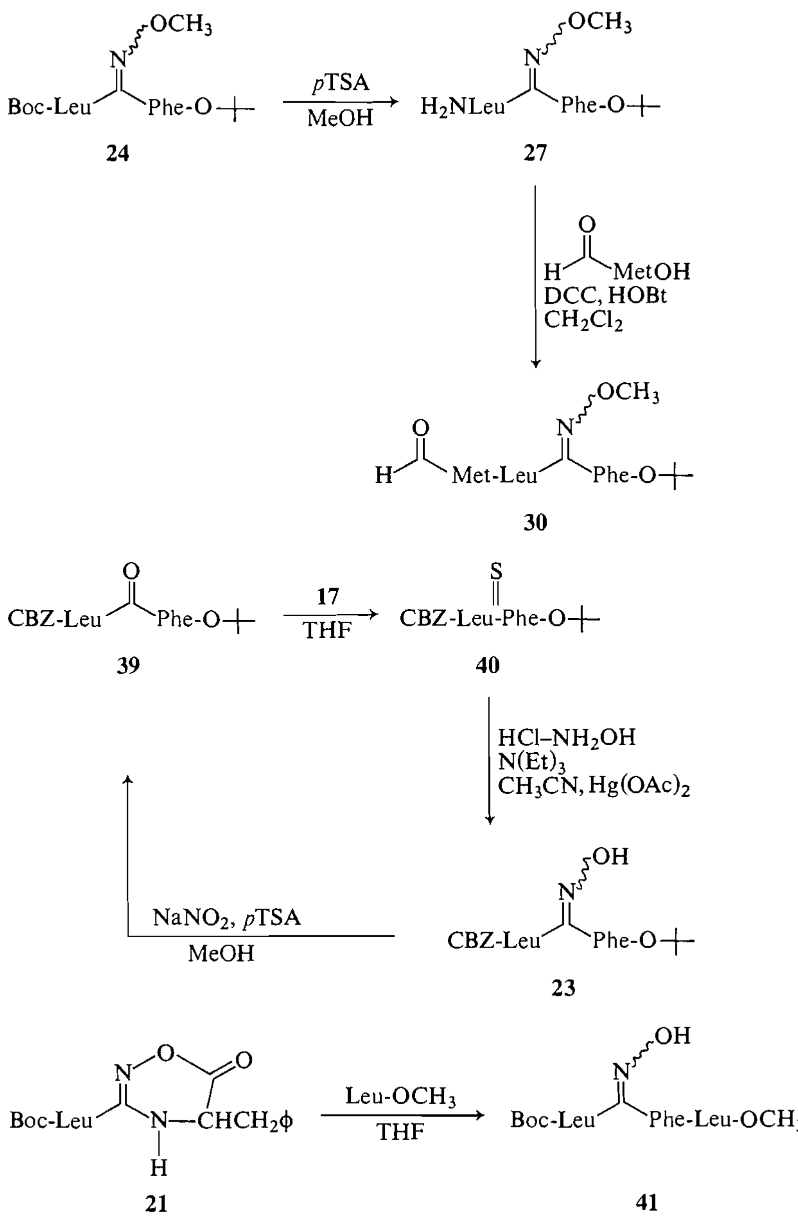

SCHEME 3

However, analog **25**, which carries a N-BOC group instead of N-formyl, exhibited two sets of signals that collapsed into a single set at 80°C in DMSO. This contrasting behavior relative to **31**, **35**, and **37** suggests that *cis–trans* isomerism about the carbamate bond of **25** may best account for the appearance of two sets of signals. Other assignments of configuration were also made on the basis of nmr evidence. For example, in compound **30**, the $C_\alpha H$ proton of Leu^2 in the predominant isomer resonates at a higher field (4.36 δ) than that of the minor isomer (5.1 δ) (13, 22). This is consistent with the parallel finding that the $C_\alpha H$ proton of Phe^3 appears at a lower field (4.25 δ) in the former whereas in the minor isomer it appears at 4.01 δ. Also, in the case of **28**, the =NOH proton resonates at a lower field (9.56 δ) in the *Z*-isomer, whereas the same proton in the minor isomer appears at 8.96 δ (13). The ^{13}C chemical shifts for the major isomer (*Z*) of **30** in $CDCl_3$ were unequivocally assigned from the *two*-dimensional (2-D) $^{13}C-^{1}H$ shift correlated spectrum (400 MHz). As compared to the parent tripeptide f-Met-Leu-Phe-OBu^t (**4***b*), the C_α-carbon of Phe^3 in **30** is shifted to a lower field by 3.00 ppm whereas the Leu^2-C_α carbon is shifted upfield by 6.29 ppm. Interestingly, the more remote Met^1-C_α carbon of **30** experiences only a small downfield shift (0.05 ppm) by comparison with the shift for the corresponding carbon in **4***b*. These relative shifts are in agreement with the configurational assignment for the major (*Z*) isomer. The downfield shift for the Phe^3-C_α carbon may arise primarily from steric compression as a result of its proximity to the oxime oxygen atom in the *Z*-isomer.

Similarly, the configuration about the C=N bond in **34** could be inferred from the relative ^1H chemical shifts pattern. As in compound **28**, the minor isomer (25%) of **34** in DMSO-d_6 could be assigned the *E*-configuration on the basis of the proton chemical shifts of both the Met^1-$C_\alpha H$ (5.08 δ) and the Leu^2-$C_\alpha H$ (3.90 δ). The major isomer can thus be automatically assigned the *Z*-configuration ($C_\alpha H$ Leu^2: 3.98 δ; $C_\alpha H$ Met^1: 4.70 δ). The ^{13}C chemical shifts for the major isomer (*Z*)

TABLE 2. Some physical properties of peptide amidine derivatives

Peptide	Yield (%)	Method	Ratio $E:Z$ from nmr $CDCl_3$ ($DMSO$-d_6)	Mass spectrum or high resolution mass spectrum M^+, m/e calcd. (found)
Monopeptide				
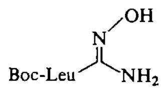 18	62	[a]	0:1	245
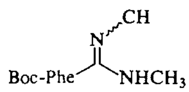 19	75	[b]	(20:80)	293.1739 (293.1739)
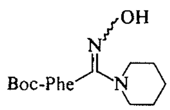 20	78	[b]	(10:90)	347.2209 (347.2208)
Dipeptide				
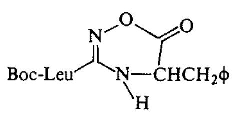 21	44	[b]	—	—
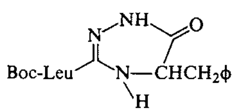 22	55	[b]	—	374.2318 (374.2318)
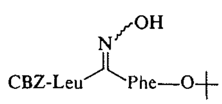 23	80	[c]	(17:83)	483.2733 (483.2733)
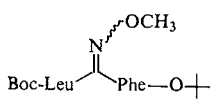 24	82	[c]	30:70 (30:70)	463.3046 (463.3046)
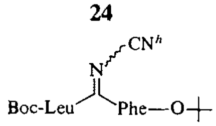 25	78	[c]	15:85[f] (40:60)[f,g]	458.2896 (458.2893)
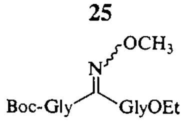 26	65	[b]	(17:83)[f]	289.1637 (289.1638)
Tripeptide chemotactic				
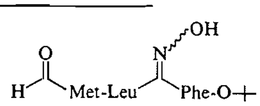 28	80	[c]	10:90 (30:70)	508.2718 (508.2718)
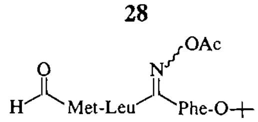 29	81	—	35:65 (50:50)	550.2823 (550.2823)

TABLE 2. (*Concluded*)

Peptide	Yield (%)	Method	Ratio $E:Z$ from nmr $CDCl_3$ ($DMSO-d_6$)	Mass spectrum or high resolution mass spectrum M^+, m/e calcd. (found)
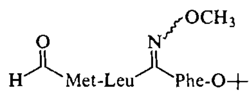 **30**	—	—	23:77 (37:63)	522.2871 (522.2871)
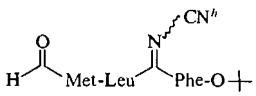 **31**	85	[c]	[e] ([e])	517.2722 (517.2722)
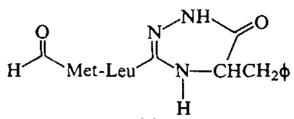 **32**	67	[c]	—	433.2149 (433.2147)
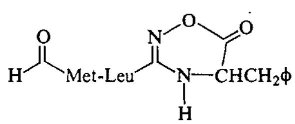 **33**	45	[b]	—	—
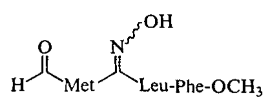 **34**	65	[c]	15:85 (25:75)	466.2250 (466.2250)
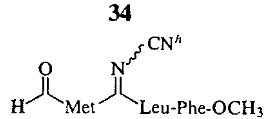 **35**	25	[c]	[e] ([e])	475.2253 (475.2253)
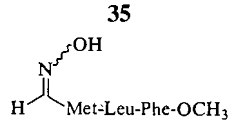 **36**	60	[d]	[e]	466.2260 (466.2250)
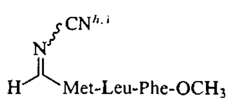 **37**	75	[c]	[e] ([e])	433.2036[j] (433.2035)
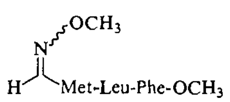 **38**	75	[c]	([e])	480.2406 (480.2406)
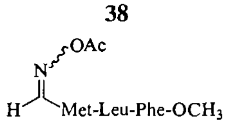 **42**	79	—	(85:15)[f]	508.2355 (508.2355)

[a]THF.
[b]Hg $(OAc)_2$, THF.
[c]$Hg(OAc)_2$, CH_3CN.
[d]CH_3CN.
[e]One isomer.
[f]The isomers are not identified.
[g]At 80°C only one set of signals was observed indicating fast equilibrium (nmr time scale) between the two geometric forms.
[h]Characteristic band in infrared spectrum at 2200 cm^{-1}.
[i]*Anal.* calcd. for $C_{24}H_{35}N_5O_4S$: C 58.90, H 7.17, N 14.31, S 6.54; found: C 57.96, H 6.55, N 14.94, S 6.64.
[j](M^+ − HNCNH).

TABLE 3. Proton chemical shifts (δ) of some amide, thioamide, and amidine derivatives

	Met					Leu				
Compound	NH	$C_{\alpha}H$	$C_{\beta}H$	$C_{\gamma}H$	CH_3	NH	$C_{\alpha}H$	$C_{\beta}H$	$C_{\gamma}H$	CH_3
18 ($CDCl_3$)						5.42	4.39 3.92	1.67 –	1.39	0.92
19 (*Z*)										
19 (*E*)										
20 (*Z*)										
20 (*E*)										
21 ($CDCl_3$)						4.81	4.26 3.98	1.77 –	1.43	0.84
22 ($CDCl_3$)						5.12	4.06			0.91 0.88
23 (*Z*)							4.12			0.75 0.72
23 (E)										0.82
6*b*						6.83	3.95	~1.36	1.52	0.84 0.81
7*b*						6.86	4.42	1.42	1.58	0.86 0.84
24 (*Z*)						6.84	~3.97			0.75 0.73
24 (*E*)						6.93	~4.91			
25 (*Z*)						7.12	~4.45			0.85
25 (*E*)										0.80 0.79
4*b*	8.26	4.40		2.39	2.00	8.04	4.33	1.41 (t)		0.86 0.82
10	8.28	4.44		2.39	1.99	8.14	4.75			0.88 0.84
28 (*Z*)	8.30	~4.40		~2.38	1.99	8.08	~4.37			0.74
28 (*E*)	8.34	~4.40		~2.38	2.02	8.15	5.15			0.85 0.79
29 (*Z*)	8.27	~4.36		~2.40	2.00	8.24	~4.36			0.73 0.70
29 (*E*)	8.38				2.02	8.20	5.04			0.87 0.82
30 (*Z*)	8.28	~4.36		2.40	2.00	8.08	~4.36			0.74 0.72
30 (*E*)	8.32	~4.36		~2.40	2.03	8.11	~5.10			0.85 0.79
31	8.36	4.45		2.44 2.40	2.02	8.40	4.61			0.89 0.81
32	8.29	4.37	~1.85 ~1.75	~2.43 ~2.37	2.01	7.93	4.26	~1.3	~1.42	0.82 0.77
33	8.33	~4.38		2.42	2.01	8.13	~4.38			0.84 0.78
15	8.29	4.78	1.9– 1.80	2.5– 2.34	1.99	10.04	4.96	1.70 –	1.50	0.88 0.83

related to the chemotactic peptide Met-Leu-Phe-OR in DMSO-d_6, unless otherwise indicated

Phe									
NH	$C_\alpha H$	$C_\beta H_A$	$C_\beta H_B$	Phenyl	OCH_3	N-Boc	O—C$(CH_3)_3$	=NO*H*	Others
						1.46		7.56	$\mathrm{N}H_2$ 4.96
6.89	4.38	2.95	2.72			1.26		9.16	$\mathrm{N}H\mathrm{CH_3}$ 9.16 $\mathrm{NHC}H_3$ 2.67
6.70	4.98							8.90	
6.77	4.70	~3.00				1.52		9.72	N(CH_2–)(CH_2–) ~3.0
6.56	~4.70	~3.00						9.53	
5.96	4.26 3.98	3.26	2.91			1.34			
5.53	4.21	3.22	2.89			1.40			=NN*H* 8.77
5.39	4.34	2.30	2.29				1.32	9.55	CBZ 5.06, 4.98 (AB)
								9.04	
8.02	4.32	2.97	2.91			1.30	1.36		
9.91	4.98	3.12				1.30	1.35		
5.43	~4.42	2.91	2.89		3.56				
5.39	~4.01				3.50				
8.50	~4.50	3.07	2.99			1.34	1.37 1.39		
8.23	4.32	2.93					1.29		C*H*O 8.00
10.30	4.95	3.16	3.07				1.29		C*H*O 8.01
5.42	4.27	2.89					1.31	9.56	C*H*O 8.00
5.02	4.03	2.94					1.29	8.96	C*H*O 7.99
6.27	~4.36	3.00					1.34		C*H*O 7.99 $\mathrm{OCOC}H_3$ 2.07
5.85	4.17						1.30		C*H*O 8.01 $\mathrm{OCOC}H_3$ 2.05
5.53	~4.25	2.91			3.61		1.32		C*H*O 7.98
5.29	4.01	2.93			3.52		1.28		C*H*O 8.01
8.84	4.42	3.03					1.30		C*H*O 8.02
6.83	4.16	2.92	2.79	*ortho* 7.15					=NNH 10.00 C*H*O 8.02
7.62	4.49	2.99	2.87	*ortho* 7.15					C*H*O 8.02
8.46	4.45	3.01	2.95		3.55				C*H*O 7.99

TABLE 3.

Compound	Met NH	Met $C_\alpha H$	Met $C_\beta H$	Met $C_\gamma H$	Met CH_3	Leu NH	Leu $C_\alpha H$	Leu $C_\beta H$	Leu $C_\gamma H$	Leu CH_3
34 (*Z*)	8.15	4.70	~1.95 ~1.70	2.41	2.01	5.42	3.98	~1.35		0.86 0.85
34 (*E*)		5.08				5.12	3.90			
35	8.60	~4.61			2.03	8.75	4.40			0.88 0.82
8 ($CDCl_3$)	8.29	5.31	2.23 2.06	2.68 2.55	2.14	6.82	4.42	1.66 –	1.48	0.91 0.89
36	5.78	3.75	1.79	2.38	2.01	7.96	4.36	1.38	1.53	0.85 0.82
36 ($CDCl_3$)	5.37	3.85	2.20 1.89	2.63 2.53	2.10	8.79	4.41	1.70 –	1.50	0.93 0.89
37	6.19	4.39		2.38	2.00	8.20	4.32			0.87 0.81
38	6.00	3.76	1.79	2.34 2.41	2.00	7.96	4.35	1.38	1.53	0.86 0.82
42		4.73– 4.63		2.60– 2.40	2.01		4.73– 4.63			0.85
	Boc-Gly[1]					Gly^2-OCH_2CH_3				
26 (Major)	7.01	3.57					5.94	3.87		
26 (Minor)							5.56			

of **34** in DMSO-d_6 were assigned from the $^1H-^{13}C$ shift correlated spectrum. The Met-C_α carbon in **34** is shifted upfield by 5.96 ppm relative to the shift for the corresponding carbon in **4***a* in $CDCl_3$.[6] The upfield shifts experienced by Met^1-C_α carbon in **34** and Leu^2-C_α in **30**, both of which have the *Z*-configuration, may be attributed to their *anti* orientation to the oxygen atom of the OH or OCH_3 group situated in the γ-position. This effect is similar to the upfield shift experienced by a carbon atom located at the γ-position and with an antiperiplanar orientation relative to an oxygen, nitrogen, or fluorine atom ("γ-*anti* effect") (23). A similar γ-*anti* upfield effect by the β-anomeric oxygen atom was also found to apply to aldopyranoses (24) despite the insertion of an O_5-ring oxygen atom. In the peptide amidoxime analogs **30** and **34** the upfield shifts experienced by the C_α carbons attached to the oxime carbon atom and in *anti* orientation relative to the OH or OCH_3 group appear to provide yet another example of this γ-*anti* effect,[7] it being transmitted not only through an intervening nitrogen atom but also incorporating a double bond where the nitrogen atom is an integral constituent. Whatever the reason for this upfield shift, it seems to be *diagnostic* of the *Z*-configuration around the C=N bond of the amidoxime moiety, an observation forming the basis of a simple method for the assignment of configuration in these peptide amidoxime analogs (25).

It is interesting to note that the *Z*-isomeric form predominates whether the *amidoxime* moiety is between Leu^2 and Phe^3 (**28**) or between Met^1 and Leu^2 (**34**). The preference for the *Z*-isomer in **28** may be rationalized on the basis that the *amidoxime* hydroxyl group avoids orienting itself towards the bulky leucine moiety. However, the preference for the same *Z* form in **34** appears contradictory in that context. In another report to be published and which centers on nmr and computer modeling studies, the *amidoxime* NH proton of **34** is shown to be involved in an intramolecular hydrogen bond with the C=O group of the N-terminal formyl group, thus favoring a $3 \rightarrow 1$ γ-turn (C_7 conformation). In the *Z*-isomer, the *amidoxime* OH group is oriented towards the leucine C_α carbon and this, in principle, may not be expected to interfere with rotation about the ψ_1 torsional angle. Such rotational freedom not only allows the molecule to adopt either of the two possible C_7 conformations ($\phi_1 = +75°$, $\psi_1 = -75°$; $\phi_1 = -75°$, $\psi_1 = +75°$) but also provides for conformational interconversion. On the other hand, in the *E*-isomer, the OH group being oriented towards the methionine C_α carbon may be expected to impose some restriction to free rotation around the ψ_1 torsional angle. In fact, in the C_7 conformation having $\phi_1 = +75°$ and $\psi_1 = -75°$ there seem to be no severe destabilizing interactions between the *amidoxime* OH group and the methionine moiety, whereas that conformation having $\phi_1 = -75°$ and $\psi_1 = +75°$ has the OH group in a destabilizing contact with the methionine

[6]The change in solvent does not preclude the comparison as the shift variation associated with it is found to be $\sim\pm 1$ ppm from similar peptide derivatives.

[7]It is difficult to estimate the magnitude of this effect because part of the upfield shift may be attributed to the apparent change involved in going from an amide to an amidoxime moiety ($C_\alpha-\overset{O}{\overset{\|}{C}}-N \rightarrow C_\alpha-\overset{NOR}{\overset{\|}{C}}-N$).

(*Concluded*)

Phe									
NH	$C_\alpha H$	$C_\beta H_A$	$C_\beta H_B$	Phenyl	OCH_3	N-Boc	$O—C(CH_3)_3$	$=NOH$	Others
8.26	4.45	2.99	2.94		3.55 3.53			9.60 8.98	C*H*O 7.87 C*H*O 8.03
8.50	4.47	~3.03	~2.94		3.56				C*H*O 8.07
6.43	4.85	3.14	3.09	*ortho* 7.11	3.72				C*H*S 9.43
8.44	4.43	3.02	2.92		3.55			9.25	*H*C=NOH 6.58
6.62	4.83	3.14	3.05		3.72			6.62	
8.37	4.44	3.02	2.92		3.55				*H*C=NCN 8.27
8.45	4.44	3.02	2.92		3.55				$HC=NOCH_3$ 6.62 $=NOCH_3$ 3.59
8.41	4.42	3.00	2.80		3.56				$=NOCOCH_3$ 2.34
					3.60	1.36			OCH_2 4.07
					3.48				OCH_2CH_3 1.17

C_β hydrogen atoms. In other words, the *E*-isomer of **34** can adopt only a single C_7 conformation with $\phi_1 = +75°$ and $\psi_1 = -75°$ whereas the *Z*-isomer can adopt, in addition, another conformation with $\phi_1 = -75°$ and $\psi_1 = +75°$. This means a loss of entropy of mixing in the *E*-isomer which may, in part, be responsible for the preference for the *Z*-isomer of **34**. However, other steric factors such as interorbital interaction between nonbonded electrons at nitrogen and oxygen, dipolar interactions, etc. (26) may also be involved but are difficult to evaluate quantitatively at this time.

Finally, the cyclic amidoxime derivative **21** was tested for its potential ability to behave as an acylating species toward aminoacids, which would allow peptide elongation from the carboxyl terminal. Accordingly, **21** was reacted with Leu-OCH_3 in THF and, after standard processing, the expected tripeptide amidoxime **41** (Scheme 3) was obtained in 72% yield. In this reaction, which may proceed under nonequilibrating conditions, the *amidoxime* moiety of tripeptide **41** would be expected to assume the *Z*-configuration characteristic of the starting cyclic material **21**. In fact, in the ^1H nmr spectrum of **41** (in $CDCl_3$) there appeared only one set of relevant signals, in agreement with expectations. However, when the ^1H spectrum was recorded in DMSO-d_6 as solvent, two sets of signals were now observed in a ratio of 67:33, thus indicating that an equilibration similar to the one proposed for the case of the cyanoamidine derivative is taking place. The major isomer was assigned the *Z*-configuration (Boc-Leu-$C_\alpha H$: 3.86 δ) and the minor one the *E*-configuration (Boc-Leu-$C_\alpha H$: 4.91 δ). Assuming that the observed single set of signals for **41** in $CDCl_3$ reflects the presence of only one isomeric form (rather than an accidental overlap with the signals for the minor isomer), this method of elongation would appear valuable for the synthesis of single geometric isomers of backbone amidoxime analogs of oligopeptides.

All the tripeptide backbone analogs listed in Tables 1 and 2 were evaluated for their ability to induce the release of lysozyme from human neutrophils, a process known to reflect chemotactic activity (8). The relative activities were computed from complete dose–response curves as recently reported for a different class of superactive releasers (27) relative to f-Met-Leu-Phe-OCH_3 as the standard. The most significant findings may be summarized as follows (details to be reported elsewhere). The presence of thioamide functions on the backbone suppresses activity except when sulfur is present as a thioformyl group, which depresses activity by 60–70%. With amidoxime functions, on the other hand, activity is restored significantly but not with cyanoamidine linkages except at the terminal formyl group level. An especially meaningful finding is the strong activity associated with cyclic structures **32** and **33**, which are completely rigid about the terminal phenylalanine residue. The significance of these observations in relation to the receptor protein topography is under scrutiny.

Experimental

Melting points were determined on a Buchi SMP-20 and are uncorrected. The ir spectra were taken with a Perkin–Elmer 257 spectrophotometer. The uv spectra were recorded on a Varian–Carey 210 spectrophotometer. The optical rotations $[\alpha]_D$ were obtained with a Perkin–Elmer 141 instrument. Proton nmr spectra were recorded with a Bruker WM-250 and (or) WH-400 instrument. Chemical shifts are given in ppm (δ) relative to $CHCl_3$ (7.24 δ) or DMSO (2.49 δ). The high resolution mass spectra (ms) were obtained with a Vg Micromass ZAB-2F spectrometer. Elemental analyses were performed by the

Guelph Laboratories, Guelph, Ont. The numbers 1, 2, and 3 used as subscripts for the ϕ and ψ torsional angles denote methionine, leucine, and phenylalanine units respectively. After conventional work-ups, all solutions were evaporated below 40°C under reduced pressure. Eastman Chromagram plates of silica gel were used for thin-layer chromatography. Anhydrous sodium sulfate was used as the drying agent for all extracts. The purity of all products and intermediates was established by thin-layer chromatography using two solvent systems (hexanes and ethyl acetate) and their compositions confirmed by ^{1}H and ^{13}C nmr spectroscopy, mass spectrometry, and in some pertinent cases by elemental analyses. The relevant data are assembled in Tables 1–3.

The following general procedures were applied where similar standard reactions are involved.

Coupling between N-protected and C-protected amino acids or peptides by the HOBt–DCC procedure

To a solution of Boc-Leucine (2.50 g, 10.8 mmol) and HOBt (1.46 g, 10.8 mmol) in methylene chloride (20 mL) and dimethylformamide (5 mL) at 0°C under N_2 was added DCC (2.22 g, 10.8 mmol). The mixture was stirred for 1 h at 0°C and then a solution of phenylalanine methyl ester hydrochloride (2.32 g, 10.8 mmol) and dry triethylamine (1.10 g, 10.8 mmol) in methylene chloride (7 mL) was added and the mixture stirred at 0°C for 1 h and at room temperature for 16 h. The solvents were evaporated, and the residue suspended in ethyl acetate followed by filtration. The filtrate was washed with aqueous citric acid (5%, 1 × 15 mL), sodium bicarbonate solution (5%, 1 × 15 mL), and brine (15 mL). The organic phase was dried, the solvent evaporated, and the resulting solid recrystallized from ethyl acetate – hexane to yield pure Boc-Leu-Phe-OMe (**6*a***) (3.60 g, 85%) as a white powder.

Cleavage of N-Boc groups with formic acid

As a typical example, Boc-Leu-Phe-OCH_3 (**6*a***) (1.5 g, 3.8 mmol) was dissolved in formic acid (98%, 30 mL) and the mixture stirred for 4 h at room temperature under N_2. The excess acid was removed *in vacuo* at 25°C and the resulting formate salt used as such either for N-formylation or for coupling in the presence of triethylamine as described below.

N-Formylation with EEDQ and formic acid

The formate salt obtained as above after cleavage of the *t*-Boc group from Boc-Met-Leu-Phe-OMe (**9**) (1.5 g, 2.9 mmol) was dissolved in dry chloroform (40 mL) followed by the addition of EEDQ (780 mg, 3.0 mmol). The mixture was stirred at room temperature for 8 h under N_2, the solvent removed *in vacuo*, and the residue was dissolved in ethyl acetate. The solution (75 mL) was washed with aqueous citric acid (5%, 2 × 20 mL), sodium bicarbonate solution (5%, 2 × 20 mL), and brine (2 × 20 mL) and then dried. Evaporation of the solvent and precipitation of the residue from methanol–water gave a white solid (**4*a***) (1.17 g, 90% from **9**).

Amide thionation

The dipeptide Boc-Leu-Phe-$OC(CH_3)_3$ (**6*b***) (2.00 g, 4.6 mmol) was dissolved in dry tetrahydrofuran (40 mL), thionation reagent **17** (2.00 g, 3.70 mmol) added, and the mixture stirred at 40°C for 10 h under N_2. The solvent was evaporated and the residue purified by flash chromatography on silica gel (hexanes – ethyl acetate (85:15)) to give pure thiodipeptide, Boc-Leu-ψ(CSNH)-Phe-$OC(CH_3)_3$ (**7*b***) (1.76 g, 85%) as a powder.

Selective cleavage of a N-Boc group with p*-toluenesulfonic acid (*p*-TSA)*

To a solution of Boc-Leu-ψ(CSNH)-Phe-$OC(CH_3)_3$ (**7*b***) (200 mg, 0.444 mmol) in methanol (7 mL) was added *p*-toluenesulfonic acid (84 mg, 0.44 mmol) under N_2 and after 24 h an additional 84 mg of *p*-toluenesulfonic acid was added, followed by standing for 18 h. Saturated aqueous sodium bicarbonate (15 mL) was added, the mixture extracted with methylene chloride (4 × 15 mL), and the extract dried and evaporated to give a crude product that was used as such in coupling reactions.

Preparation of N-substituted amidines

A solution of thiotripeptide **10** (15.0 mg, 0.029 mmol) in dry acetonitrile (2 mL) was treated with triethylamine (9.0 mg, 0.088 mmol), hydroxylamine hydrochloride (3.0 mg, 0.044 mmol), and mercuric acetate (10 mg, 0.032 mmol). The mixture was stirred under N_2 and, after 6 h, additional portions of triethylamine (9.0 mg, 0.088 mmol), hydroxylamine hydrochloride (3.0 mg, 0.044 mmol), and mercuric acetate (10 mg, 0.032 mmol) were added. The mixture was allowed to stand for 16 h, after which time saturated aqueous NH_4Cl (7 mL) was added followed by extraction with methylene chloride (4 × 10 mL). The organic phase was dried, the solvent evaporated, and the residue purified by thick-layer chromatography on silica gel (EtOAc) to give pure amidoxime **28** (12 mg, 80%).

All the other amidine derivatives were obtained from using the appropriate nucleophile by the same general procedure.

*Cyclic amidoxime (**21**)*

To a solution of thiodipeptide **7*a*** (200 mg, 0.48 mmol) in tetrahydrofuran (15 mL) was added hydroxylamine hydrochloride (40 mg, 0.58 mmol), triethylamine (146 mg, 1.46 mmol), and mercuric acetate and the mixture stirred for 2 h under N_2, then diluted with ethyl acetate (20 mL) and the suspension filtered through Celite. The filtrate was evaporated and the residue purified by flash chromatography on silica gel (hexane – ethyl acetate (6:4)) to give the pure cyclic amidoxime **21** (88 mg, 44%).

*Regeneration of parent amide from amidoxime **23**: [—C(=NOH)—N → —C(=O)—N]*

To a solution of CBZ-Leu-ψ[(C=NOH)NH]-Phe-$OC(CH_3)_3$ (**23**) (40 mg, 0.083 mmol) in methanol (4 mL) was added *p*-toluenesulfonic acid (22 mg, 0.124 mmol) and sodium nitrite (9.0 mg, 0.124 mmol). After 16 h, *p*-toluenesulfonic acid (22 mg, 0.124 mmol) and sodium nitrite (9.0 mg, 0.124 mmol) were again added and after 6 h saturated aqueous sodium bicarbonate (7 mL) was added followed by extraction with methylene chloride (4 × 10 mL). The dried organic phase was evaporated and the residue purified by column chromatography on silica gel (hexane – ethyl acetate (7:3)) to give pure CBZ-Leu-Phe-$OC(CH_3)_3$ (**39**) as an oil (27 mg, 70%); $[\alpha]_D^{30}$ +17.4° (c 0.88, $CHCl_3$); ^{1}H nmr ($CDCl_3$) δ: 7.36–7.14 (8H, phenyl), 7.12 (dd, 2H, Phe-*ortho*, J_{ortho} 7.5, J_{meta} 2.0 Hz), 6.38 (d, 1H, NH-Phe, J_{N,C_α} 8.0 Hz), 5.08 (s, 2H, OCH_2), ~5.06 (overlap, 1H, NH-Leu), 4.69 (dd, 1H, C_αH-Phe, J_{N,C_α} 8.0, J_{C_α,C_β} 6.0 Hz), 4.13 (m, 1H, C_αH-Leu), 3.06 (d, 2H, $C_\beta H_2$-Phe, J_{C_α,C_β} 6.0 Hz), 1.7–1.4 (m, 3H, $C_\beta H_2$, C_γH-Leu), 1.38 (s, 9H, $OC(CH_3)_3$), 0.89 (d, 6H, $(CH_3)_2$-Leu); high resolution ms, calcd. for $C_{27}H_{36}N_2O_5$: m/e 468.2624 (M^+); found: m/e 468.2619 (M^+).

*Reaction of cyclic amidoxime (**21**) with L-leucine methyl ester*

A solution of cyclic amidoxime **21** (9.0 mg, 0.024 mmol) in tetrahydrofuran (1 mL) was treated dropwise with a solution of L-leucine methyl ester hydrochloride (5.0 mg, 0.027 mmol) and triethylamine (3 mg, 0.028 mmol) in tetrahydrofuran (2 mL). After 16 h at room temperature under N_2, additional portions of L-leucine methyl ester hydrochloride (5.0 mg, 0.027 mmol) and triethylamine (3 mg, 0.028 mmol) were added and, after 48 h, the solvent was evaporated and the residue purified by preparative tlc (silica gel, ethyl acetate – hexane 6:4) to yield the pure tripeptide **41** (9.0 mg, 72%); ^{1}H nmr ($CDCl_3$) δ: 7.36–7.10 (m, 8H, phenyl), 6.80 (d, 1H, NH-^{3}Leu, J_{N,C_α} 6.5 Hz), 5.36 (d, 1H, NH-^{1}Leu, J_{N,C_α} 8.5 Hz), 4.95 (d, 1H, NH-^{2}Phe, J_{N,C_α} 10 Hz), 4.54 (m, 1H, C_αH-^{3}Leu), 4.27 (m, 1H, C_αH-^{2}Phe), 4.14 (m, 1H, C_αH-^{1}Leu), 3.64 (s, 3H, OCH_3), 3.11, 3.01 (AB, 2H, $C_\beta H_2$-Phe, J_{A,C_α} 6.0, J_{B,C_α} 8.0, $J_{A,B(gem)}$ 14.0 Hz), 1.34 (s, 9H, $OC(CH_3)_3$), 0.86, 0.83 (2 doublets, 6H, $(CH_3)_2$-Leu, J 6.0 Hz), 0.76, 0.75 (2 doublets, 6H, $(CH_3)_2$-Leu, J 6.0 Hz); high resolution ms, calcd. for $C_{26}H_{44}N_4O_6$: m/e 520.3261 (M^+); found: m/e 520.3261 (M^+).

*Acetylation of **28***

A solution of amidoxime **28** (20.0 mg, 0.0393 mmol) in methylene chloride (5 mL) was treated with triethylamine (22 mg, 0.22 mmol) and acetic anhydride (32 mg, 0.32 mmol) and, after 3 h at room temperature under N_2, the solvent was evaporated *in vacuo* and the residue purified by tlc (silica gel, hexane – ethyl acetate 2:8) to give acetate **29** (17 mg, 81%).

Acknowledgements

Financial support by the Natural Sciences and Engineering Research Council of Canada (NSERC) and by the Fonds F.C.A.C., Québec, is gratefully acknowledged. We are grateful to Gaston Boulay for the mass spectral analyses and Serge Bérubé for recording the nmr spectra.

1. J. RUDINGER. *In* Drug design. *Edited by* E. S. Ariens. Academic Press, New York. 1971. pp. 318–419.
2. A. SPATOLA. *In* Chemistry and biochemistry of amino acids, peptides, proteins. Vol. 7. *Edited by* B. Weinstein. Marcel Dekker, New York. 1983. pp. 267–357.
3. G. LAJOIE, F. LÉPINE, L. MAZIAK, and B. BELLEAU. Tetrahedron Lett. **24**, 3815 (1983).
4. W. REID and E. SCHMIDT. Justus Liebigs Ann. Chem. **695**, 217 (1966); W. L. MOCK, J.-T. CHEN, and J. W. TSANG. Biochem. Biophys. Res. Commun. **102**, 389 (1981); P. A. BARTLETT, K. L. SPEAR, and N. E. JACOBSEN. Biochemistry, **21**, 1608 (1982); P. CAMPBELL and N. T. NASHED. J. Am. Chem. Soc. **104**, 5221 (1982); D. W. BROWN, M. M. CAMPBELL, and C. V. WALKER. Tetrahedron, **39**, 1075 (1983); K. CLAUSEN, A. F. SPATOLA, C. LEMIEUX, P. W. SCHILLER, and S.-O. LAWESSON. Biochem. Biophys. Res. Commun. **120**, 305 (1984).
5. G. R. MARSHALL. *In* Chemical regulation of biological mechanisms. *Edited by* A. M. Creighton and S. Turner. Royal Society of Chemistry, Burlington House, London, U.K. 1982. p. 267.
6. G. LAJOIE, F. LÉPINE, S. LEMAIRE, F. JOLICOEUR, C. AUBÉ, A. TURCOTTE, and B. BELLEAU. Int. J. Pept. Protein Res. **23**, 316 (1984).
7. K. CLAUSEN, M. THORSEN, S.-O. LAWESSON, and A. F. SPATOLA. J. Chem. Soc. Perkin Trans. 1, 785 (1984).
8. H. J. SHOWELL, R. J. FREER, S. H. ZIGMOND, E. SCHIFFMANN, S. AWANIKUMAR, B. CORCORAN, and E. L. BECKER. J. Exp. Med. **143**, 1154 (1976); P. P. K. HO, A. L. YOUNG, and G. L. SOUTHARD. Arthritis Rheum. **21**, 133 (1978).
9. E. SCHIFFMANN, B. A. CORCORAN, and S. M. WAHL. Proc. Natl. Acad. Sci. U.S.A. **72**, 1059 (1975); R. J. FREER, A. R. DAY, N. MUTHUKUMARASWAMY, D. PINON, A. WU, H. J. SHOWELL, and E. L. BECKER. Biochemistry, **21**, 257 (1982).
10. M. IQBAL, P. BALARAM, H. H. SHOWELL, R. J. FREER, and E. L. BECKER. FEBS Lett. **165**, 171 (1984).
11. W. H. PRICHARD. *In* The chemistry of amidines and imidates. *Edited by* S. Patai. Interscience, London. 1975.
12. V. G. GRANIK. Russ. Chem. Rev. **52**, 377 (1983); F. ELOY and R. LENAERS. Chem. Rev. **62**, 155 (1962); R. L. SHRINER and F. W. NEWMAN. Chem. Rev. **35**, 351 (1944).
13. D. F. BUSHEY and F. C. HOOVER. J. Org. Chem. **45**, 4198 (1980).
14. M. BRENNER and W. HUBER. Helv. Chim. Acta, **36**, 1109 (1953).
15. E. TASCHNER, A. CHIMIAK, B. BATOR, and T. SOKOLOWSKA. Ann. Chem. **646**, 134 (1961).
16. W. KONING and R. GEIGER. Chem. Ber. **103**, 788 (1970); V. S. KLASNER and M. BODANSKY. Synthesis, 453 (1972).
17. D. E. NITECKI, B. HALPERN, and S. W. WESTLEY. J. Org. Chem. **33**, 864 (1968); B. HALPERN and D. E. NITECKI. Tetrahedron Lett. **31**, 3031 (1967).
18. G. LAJOIE and J. L. KRAUS. Peptides, **5**, 653 (1984).
19. J. GOODACRE, R. J. PONSFORD, and I. STIRLING. Tetrahedron Lett. 3609 (1975).
20. IUPAC–IUB RECOMMENDATIONS. Eur. J. Biochem. **138**, 9 (1984).
21. M. J. S. DEWAR. *In* Hyperconjugation. The Ronald Press Company, N.Y. 1962. p. 106.
22. H. GOZLAN, R. MICHELOT, C. RICHE, and R. RIPS. Tetrahedron, **33**, 2535 (1977); G. C. LEVY and G. L. NELSON. J. Am. Chem. Soc. **94**, 4897 (1972).
23. E. L. ELIEL, W. F. BAILEY, L. D. KOPP, R. L. WILLER, D. M. GRANT, R. BERTRAND, K. A. CHRISTENSEN, D. K. DALLING, M. W. DUCH, E. WENKERT, F. M. SCHELL, and D. W. COCHRAN. J. Am. Chem. Soc. **97**, 322 (1975).
24. V. S. RAO and A. S. PERLIN. Carbohydr. Res. **92**, 141 (1981).
25. G. E. HAWKES, K. HERWIG, and J. D. ROBERTS. J. Org. Chem. **39**, 1017 (1974); R. R. FRASER, R. CAPOOR, J. W. BOVENKAMP, B. V. LACROIX, and J. PAGOTTO. Can. J. Chem. **61**, 2616 (1984).
26. D. KEUS and J. WARKENTIN. J. Org. Chem. **49**, 3466 (1984).
27. J.-L. KRAUS, A. DIPAOLA, and B. BELLEAU. Biochem. Biophys. Res. Commun. **124**, 939 (1984).

Chemistry of 4-trimethylsilyl-3-dialkylaminocrotonate esters and the cycloaromatization reactions with enamines[1]

G. J. KANG AND T. H. CHAN[2]

Department of Chemistry, McGill University, Montreal, P.Q., Canada H3A 2K6

Received May 16, 1984[3]

G. J. KANG and T. H. CHAN. Can. J. Chem. **63**, 3102 (1985).

Methyl 4-trimethylsilyl-3-dialkylaminocrotonate is synthesized by the silylation of methyl 3-dialkylaminocrotonate. It reacts with carbonyl electrophiles at its γ-position. The unusual regiochemistry of this reaction is studied and rationalized. It reacts with enamines derived from acyclic ketones to give aromatic compounds in a 3C+3C combination and with enamines derived from cycloketones of 5- to 8-membered rings to give aromatic compounds in a 4C+2C combination. A mechanism for this cycloaromatization reaction is proposed.

G. J. KANG et T. H. CHAN. Can. J. Chem. **63**, 3102 (1985).

La silylation du dialkylamino-3 crotonate de méthyle conduit au dialkylamino-3 triméthylsilyl-4 crotonate de méthyle. Les carbonyles électrophiles réagissent en position γ de ce composé. On a étudié la régiochimie inhabituelle de cette réaction et on en fournit une explication. Ce composé réagit avec les énamines provenant des cétones acycliques pour donner des composés aromatiques dans une combinaison du type 3C+3C et avec les énamines issues des cétones cycliques comportant de 5 à 8 chaînons pour donner des composés aromatiques selon une combinaison du type 4C+2C. On propose un mécanisme réactionnel pour cette réaction de cycloaromatisation.

[Traduit par le journal]

Introduction

While tremendous progress has been made on reactions leading to the synthesis of acyclic and alicyclic compounds, less development has occurred in the domain of aromatic compounds. The problem is especially acute in the synthesis of highly substituted benzenoid compounds with multiple functional groups. The conventional approach of using electrophilic substitution reactions on simple aromatic precursors, with its tedious stepwise process and attendant problem of regioselection, has obvious limitations.

Recently, we proposed an approach for the synthesis of phenolic compounds (2, 3) by the cycloaromatization of acyclic precursors. The strategy involves the condensation of two 3-carbon units, one with two nucleophilic sites and the other containing two electrophilic sites. Compound **1** and similar bis-enol silyl ethers (2, 4) constitute the 3-carbon fragments with two nucleophilic sites. Various equivalents of β-dicarbonyl compounds (e.g. **2**) constitute the 3-carbon electrophilic components. Condensation of **1** and **2** under Lewis acid conditions (e.g. $TiCl_4$) according to eq. [1] gives the phenolic compound **3**. Furthermore, the regiochemistry of the reaction can be controlled by the differential reactivities of these sites. We have used this approach for the synthesis of sclerin (5), a plant-growth substance, and Δ^1-tetrahydrocannabinol (6), the active component of marijuana.

[1]

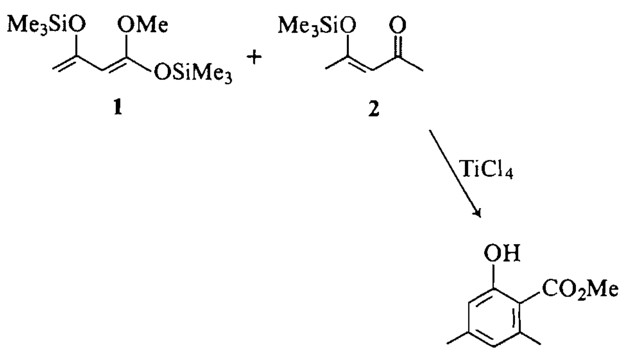

3

It is of some interest to know if this approach can be developed into a general strategy for the synthesis of all types of aromatic compounds. The possibility of a cycloaromatization reaction leading to highly substituted anilino compounds is particularly tantalizing since a number of natural products such as mitomycin and maytansine have a substituted aniline carbon skeleton.

An obvious way to modify eq. [1] for the synthesis of anilino compounds is to have an amino group in place of the 3-trimethylsiloxy group in **1**. Our first task is therefore to examine the preparation and the chemistry of 1-methoxy-1-trimethylsiloxy-3-dialkylaminobuta-1,3-dienes (**4**).

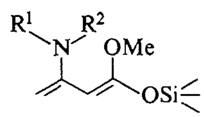

4

Chemistry of 4-trimethylsilyl-3-dialkylaminocrotonate esters

Methyl 3-dialkylaminocrotonate **5** was prepared by the usual water-separator method from the precursor methyl acetoacetate (**6**) with *p*-toluenesulfonic acid as the catalyst (7). Compound **5** was silylated by LDA in THF followed by quenching with trimethylchlorosilane. The result was, however, not the expected compound **4** but the C-silyl product, methyl 4-trimethylsilyl-3-dialkylaminocrotonate (**7**). Both **7***a* and **7***b* exist as one geometrical isomer. Sanchez and Bellanato studied a number of 3-dialkylaminocrotonate esters and concluded that all of them have *E* geometry (8). By noting the similarity of ^{1}H and ^{13}C nmr between **5** and **7**, **7** is assigned to have *E* geometry as well. The yields of the silylation reactions are greater than 90%, the products are ≥90% pure by ^{1}H nmr spectra before distillation, and **7** is thermally stable enough to be distilled under vacuum.

In the reaction of **7** with electrophiles, one would expect that

[1]For preliminary accounts of this work, see ref. 1.
[2]Author to whom correspondence may be addressed.
[3]Revision received June 4, 1985.

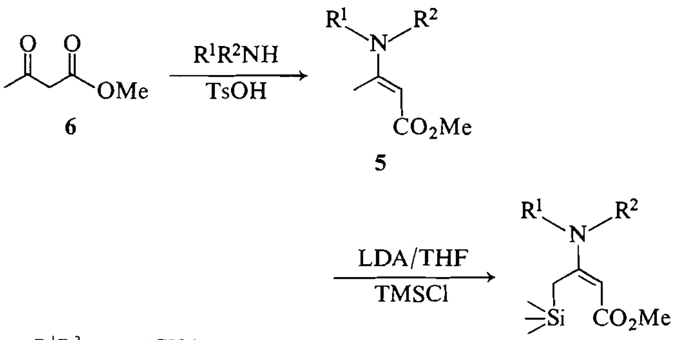

6 5 7

a: R^1R^2 = —$(CH_2)_4$—
b: R^1R^2 = $(CH_2CH_2)_2$—O

the reaction probably occurs at the α-position because of the presence of the silyl group in **7** as well as the expected reactivity of the enamine. The reactions of allylsilanes with electrophiles have been well studied and usually show high regioselectivity (9) according to eq. [2]. Therefore it was surprising

[2] 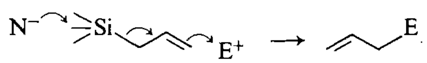

to us when we found that **7** reacted with a number of carbon electrophiles at the γ-position instead of the α-position (eq. [3]).

[3] 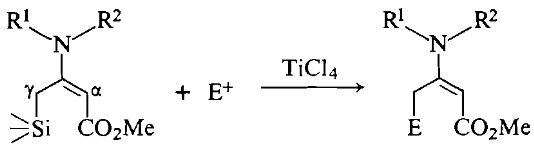

7

When compound **7** reacted with benzaldehyde in the presence of one mole of titanium tetrachloride in CH_2Cl_2, compound **8** was obtained in fairly good yield. It is clear that **8** is formed from the condensation of **7** and benzaldehyde, followed by the elimination of a molecule of water. Compound **8** has been assigned the 2*E*,4*E* geometry according to its ^{1}H nmr.

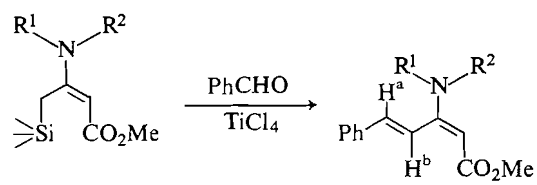

7 **8**

a: R^1, R^2 = —$(CH_2)_4$—
b: R^1, R^2 = $(CH_2CH_2)_2$—O

Condensation of **7** with cinnamaldehyde under the same condition gave the polyunsaturated ester **9** in good yield with the 2*E*,4*E*,6*E*-configuration. With butyraldehyde, condensation with **7** is followed by an intramolecular cyclization to give the δ-lactone **10**.

There are, however, differences in the reactivity between **7***a* and **7***b* (13). It seems that the morpholino compound **7***b* is more reactive than the pyrrolidino compound **7***a*. Thus with the less reactive ketone electrophiles, only **7***b* gave the corresponding products **11** and **12**. Compound **11** is the hydrolyzed product of its enamine precursor that occurs during the aqueous work-up.

When **7***a* was reacted with acetone under the same conditions, only compound **5***a* was shown in the product, apparently

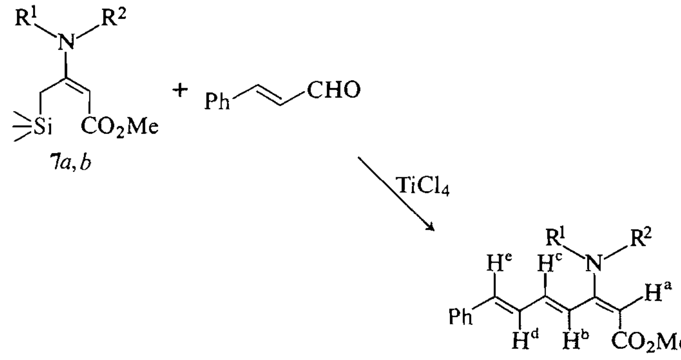

7*a*,*b* **9***a*,*b*

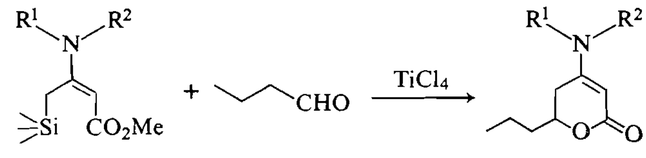

7*a*,*b* **10***a*,*b*

from the protodesilylation of the unreacted **7***a*. When cyclohexanone was used, the result was the same as the reaction of **7***a* with acetone. Even when dichloroethane was used as the solvent rather than methylene chloride, and the reaction mixture was refluxed overnight, no reaction between **7***a* and cyclohexanone was observed. With more reactive electrophiles, such as benzoyl chloride, only **7***a* gave γ-reaction product **13**, while **7***b* gave an N-substitution product, benzamide **14**.

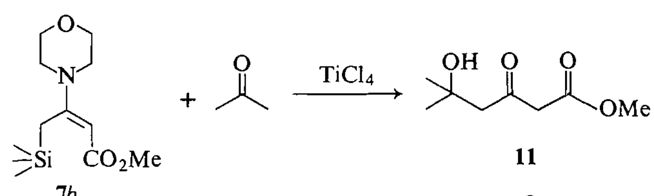

7*b* **11**

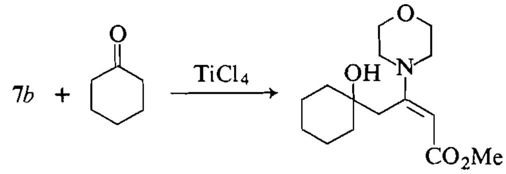

12

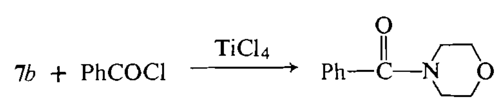

14

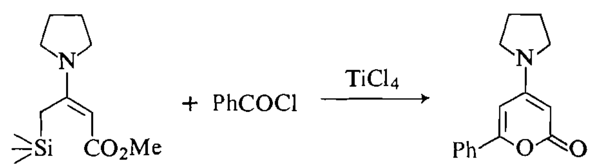

7*a* **13**

In order to explain the regiochemistry observed in the reaction of **7** with electrophiles in eq. [3], one possibility is that there is a dynamic equilibrium between **7** and **4** and it is **4** that selectively reacts with electrophiles to give the γ-products. In fact, 1,5-migration of the silyl group is well known. Diketone silyl enol ethers can exhibit silyl transmission (10). Similarly,

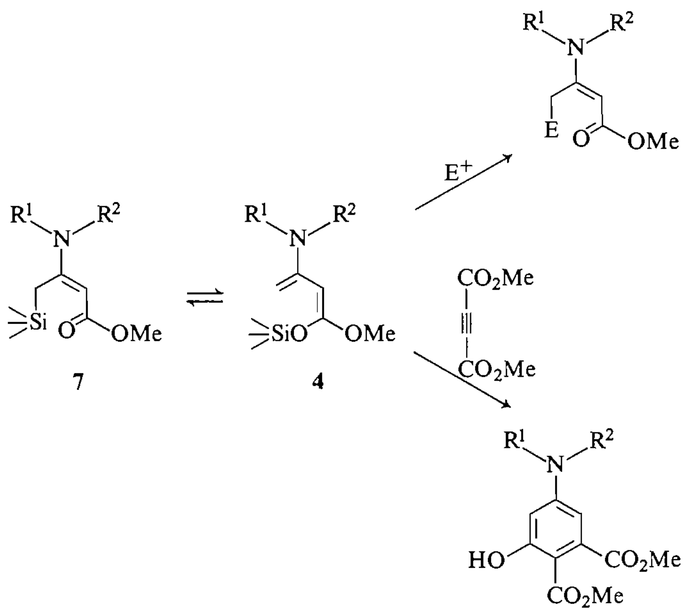

7 4 15

trimethylsilyl β-keto-esters can undergo a thermal silatropic rearrangement (11) to produce silyl enol ethers regiospecifically. The 1,5-migration of the silyl group from oxygen to carbon has also been reported (4, 12). It has been found that at room temperature compound **1** gradually rearranges to its C-silyl isomer. In our case, the *E*-geometry of compound **7** certainly renders this rearrangement process geometrically possible. In support of this explanation, when a mixture of **7***a* and dimethyl acetylenedicarboxylate was heated in benzene for 3 days, the diene **4** was indeed trapped as the Diels–Alder adduct **15**, which was isolated in 57% yield as a crystalline compound.

Self- and cross-condensations

Our initial strategy was to synthesize compound **4** and condense it with β-dielectrophiles to form aniline derivatives. Athough **4** has not been obtained directly from the silylation of methyl 3-dialkylaminocrotonate, compound **7** can be considered, in fact, as an equivalent of **4**, because we have evidence that **7** exists in a dynamic equilibrium of **7** ⇌ **4**.

We examined, therefore, the reaction of **7***b* with several β-dielectrophiles. The first β-dielectrophile used was 4-trimethylsiloxy-3-penten-2-one (**2**). The reaction was carried out under similar conditions to the cycloaromatization reactions of eq. [1] with titanium tetrachloride as catalyst and CH_2Cl_2 as solvent. Indeed an aromatic compound, **18***b*, was isolated. The

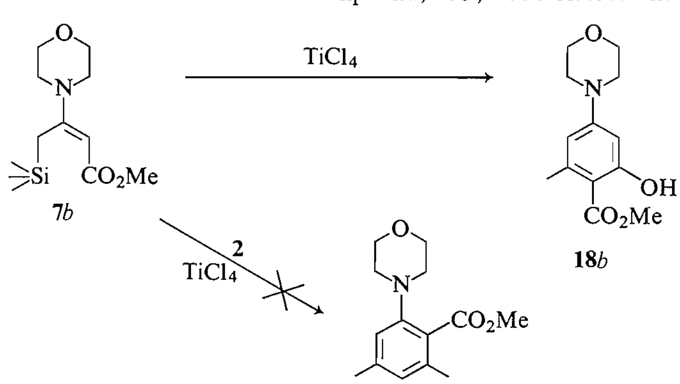

19

^{1}H nmr of **18***b* shows two aromatic protons (6.20 ppm, s, 2H), one methoxy group (3.90, s, 3H), one methyl group (2.53, s, 3H), an hydroxy group (11.7, s, 1H, D_2O exchangeable), and a morpholino group. From these data, it is definitely not the desired product **19**. Obviously **18***b* was derived from the self-condensation reaction of **7***b*. When only **7***b* was treated under the same conditions, **18***b* was obtained in 49% yield.

At this stage, it is relevant to mention the recent work by Bohme *et al.* (14), who found that 3-dialkylaminocrotonate esters (**5**) undergo self-condensation under trifluoroacetic acid conditions to give the anilino compounds **20**, sometimes in good yield. We thus repeated this reaction with **5***b* and found that the products from the two reactions, **18***b* and **20***b*, are quite different in their spectroscopic data. The two compounds are nevertheless isomeric with each other. In agreement with Bohme's observation, hydrolysis and decarboxylation of **20***b* gave **21**. It was found that the decarboxylation product of **18***b* was also **21**. From these experiments, as well as from the fact that the chemical shift of the hydroxy group in **18***b* is 11.7 ppm, which strongly suggests the existence of intramolecular hydrogen bonding, we assign structure **18***b* to the product derived from **7***b*.

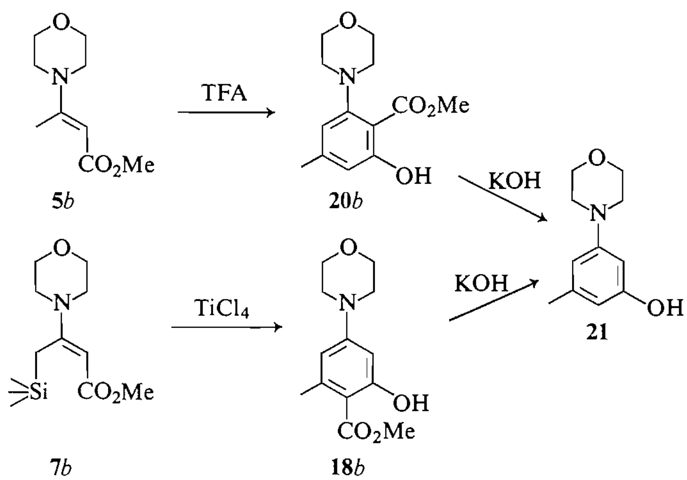

In order to understand further the self-condensation reaction both of **7** and **5**, **7***b* was allowed to react with 1 equivalent of **5***b* in the presence of titanium tetrachloride. The same compound **18***b*, which was obtained from the self-condensation of **7***b*, was isolated in 71% yield. A similar reaction between **7***a*

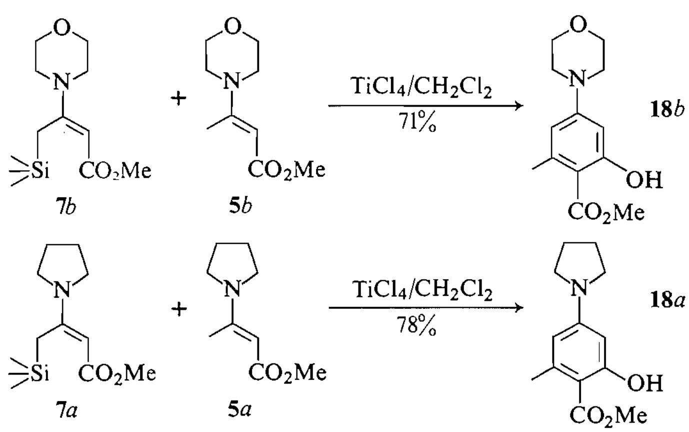

and **5***a* gave **18***a* in 78% yield. Since the yields are higher than 50%, **18***a* or **18***b* is formed from the cross-condensation between **7** and **5**. Furthermore, when **5***b* alone was treated under

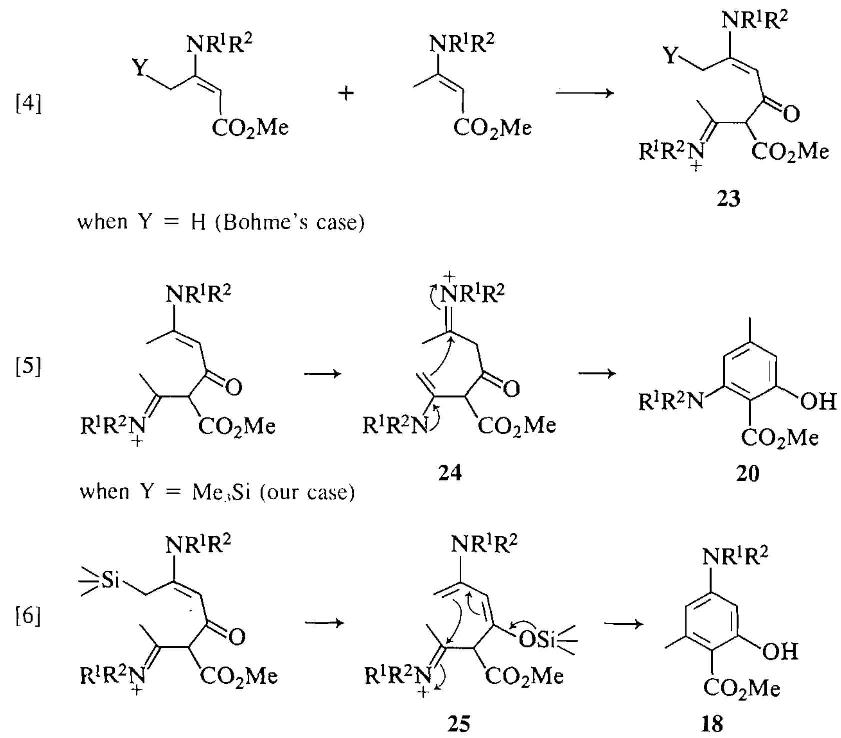

SCHEME 1

identical conditions (i.e. $TiCl_4$) the product was not **18***b* but the pyrone **22** (75% yield).

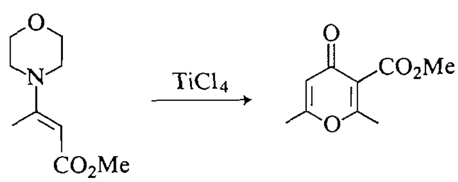

5*b* **22**

Mechanistic rationale

To facilitate subsequent discussion, we propose from the above experiments a working hypothesis to account for the cycloaromatization reactions observed in our case as well as in Bohme's case (Scheme 1).

The first step (eq. [4]) is the condensation of the enamine with the carboxyl group of another component to give the intermediate **23**. In the absence of further reaction, **23** hydrolyzes on aqueous work-up to give the pyrone **22**. In the case of Y = H (eq. [5]), TFA effects the isomerization of **23** to the deconjugated enamine **24**, which gives **20** by an intramolecular condensation in a 3C+3C combination. When Y = Me_3Si (eq. [6]), a 1,5-silyl shift causes the formation of **25**, which leads to **18** by way of an intramolecular condensation in a 4C+2C combination.

The reaction of **7***b* with **5***b* was repeated. Half of the reaction mixture was taken out of the reaction flask after 3 h at −78°C. After the usual work-up procedure, a 1 : 1 mixture of **22** and **18***b* was obtained. The other half of the reaction mixture was allowed to be stirred overnight at room temperature and then worked up. The product was found to be almost completely **18***b*, with very little **22**. This experiment supports the suggestion that **23** is indeed the intermediate in the cross-condensation reaction. Furthermore, the first step in Scheme 1 is faster than the second step.

According to the mechanism postulated in Scheme 1, in the cross-condensation between **7** and **5**, **7** acts as a four-carbon component and **5** acts as a two-carbon component. To verify this, we allowed methyl 4-trimethylsilyl-3-pyrrolidinocrotonate (**7***a*) to condense with ethyl 3-morpholinocrotonate (**26**) in the presence of $TiCl_4$. If the postulation is correct, the final product will contain pyrrolidino and ethyl groups. This was found to be the case. The product of the reaction was **27**.

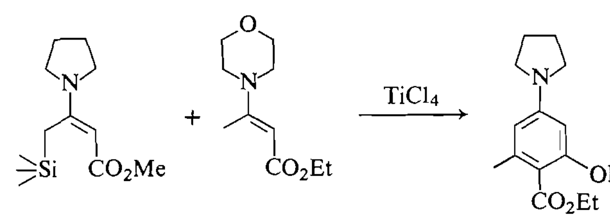

7*a* **26** **27**

One might argue that another possible pathway for the cross-condensation is the Diels−Alder reaction. For example, Diels−Alder reaction between **7***a* (by way of **4***a*) and **5***a* can lead to **18***a* if the reaction proceeds with the regiochemistry indicated. To check this possibility, a 1 : 1 mixture of **7***a* and **5***a* was refluxed in benzene for 3 days. No change was detected by ^{1}H nmr spectroscopy, showing that it was still a 1 : 1 mixture of **7***a* and **5***a*. Therefore the possibility of a Diels−Alder reaction is ruled out, at least under these thermal conditions.

Cycloaromatization reactions with enamines

At this stage, the following conclusion appears to be reasonable. The reaction between **7** and **5** is a stepwise 4C+2C cycloaddition with **7** acting as the four-carbon component and **5** as the two-carbon component. One would expect, therefore, not only compound **5** but other enamines as well to have the potential to undergo the same kind of cycloaromatization reaction with **7**. We proceeded to examine this possibility. A

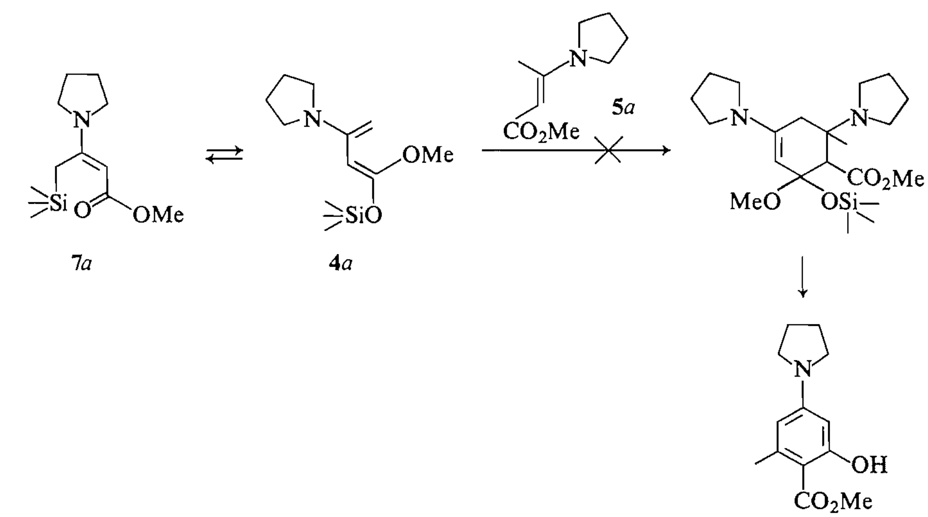

7a 4a 18a

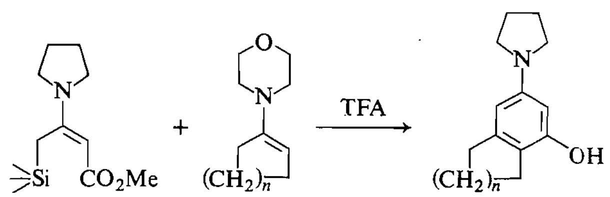

7a 28 ($n = 2$) 29 ($n = 2$)

1 : 1 mixture of 7*a* and the morpholine enamine of cyclohexanone plus two equivalents of trifluoroacetic acid was refluxed for two days in CH_2Cl_2. The reaction gave compound **29** in 63% yield.

Enamines derived from cyclopentanone, cycloheptanone, and cyclooctanone were also allowed to react with 7*a* under the same conditions except that the reaction mixtures were refluxed in dichloroethane. The yields of the corresponding cyclization products were found to be between 59 and 64% (see Table 1).

On the other hand, when the amino group in the silylcrotonate component is morpholine 7*b*, the reaction with **28** under identical conditions gave the γ-reaction product **30** instead. Since we have previously shown that 7*b* undergoes γ-reaction more readily than 7*a*, and **28** can be easily protonated to give

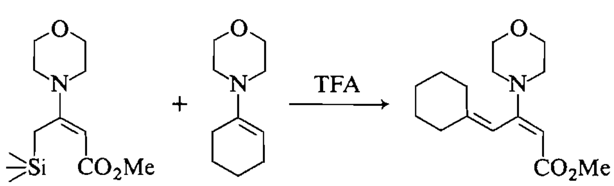

7b 28 30

the corresponding imminium cation in the presence of TFA, the observed γ-reaction between 7*b* and **28** is understandable.

There remains the 3C+3C self-condensation observed in Bohme's case. If the postulated mechanism in Scheme 1 is correct, one would expect the same pathway to proceed between **7** and an enamine of acyclic ketones. The reactions between 7*a* and enamines derived from acyclic ketones were therefore next examined. The morpholine enamine of 3-pentanone (**31**) was reacted with 7*a* in the presence of TFA. The reaction mixture was refluxed for 48 h in dichloroethane and followed by the usual work-up. Compound **32** was isolated in about 30% yield. The main reason for the low yield is the self-condensation of 7*a*. In order to improve the yield of the cross-condensation product, two equivalents of **31** were used and the yield was raised to 41%. The same reaction was also carried out by using titanium tetrachloride as the catalyst instead of TFA, and the yield of **32** was 38%.

Several similar reactions were carried out by reacting 7*a* with **33**, **34**, and **35** respectively in the presence of TFA. In all cases the 3C+3C cyclization products were observed. The yields ranged from 36 to 42% (see Table 1).

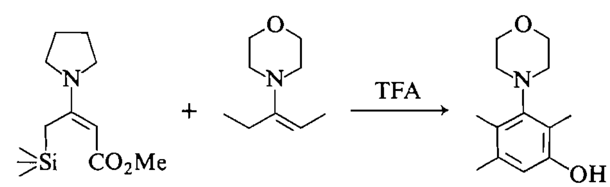

7a 31 32

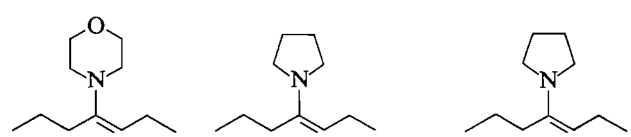

33 34 35

In summary, 4-trimethylsilyl-3-dialkylaminocrotonate esters react with enamines derived from cyclic ketones to give 4C+2C annelation with enamines acting as the 2C-component, but with enamines derived from acyclic ketones by a 3C+3C annelation. A mechanism in analogy to Scheme 1, which is consistent with the above observation, can be envisaged.

Conclusion

Even though our initial idea of a cycloaromatization reaction between **4** and various β-dicarbonyl equivalents to give anilino compounds turns out not to be feasible, reactions between 4-trimethylsilyl-3-dialkylaminocrotonate esters and enamines have been discovered. These reactions lead to the formation of highly substituted benzenoid compounds bearing an amino group.

Experimental

General

Unless otherwise stated, common reagents were commercial prod-

TABLE 1. The cycloaromatization reactions of **7** with enamines

Compound	Enamine	Reaction conditions	Product	Isolated yield%
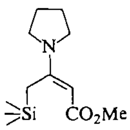	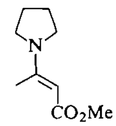	$TiCl_4/CH_2Cl_2$	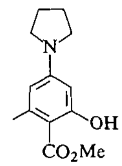	78
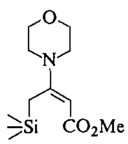	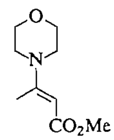	$TiCl_4/CH_2Cl_2$	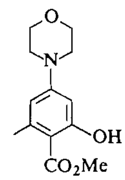	71
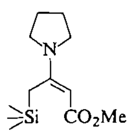	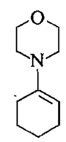	TFA/CH_2Cl_2	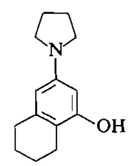	63
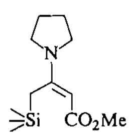	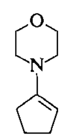	$TFA/ClCH_2CH_2Cl$	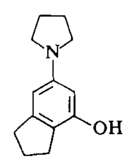	64
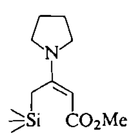	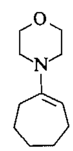	$TFA/ClCH_2CH_2Cl$	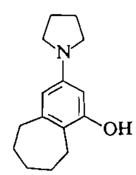	59
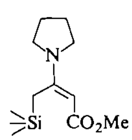	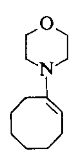	$TFA/ClCH_2CH_2Cl$	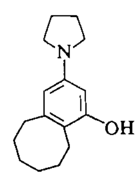	67
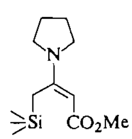	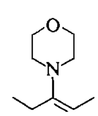	TFA/CH_2Cl_2	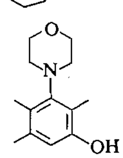	41
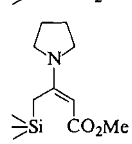	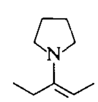	TFA/CH_2Cl_2	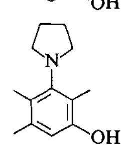	42
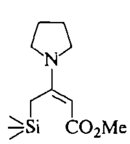	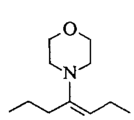	TFA/CH_2Cl_2	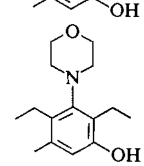	37
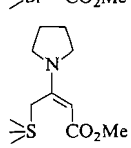	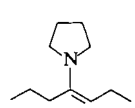	TFA/CH_2Cl_2	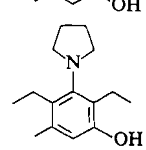	36

ucts and were reagent grade. Melting and boiling points are uncorrected. The nmr spectra were taken on a Varian T-60A nmr spectrometer or an XL-200 nmr spectrometer. All ^{1}H and ^{13}C spectra are reported in chemical shift (δ) with tetramethylsilane as the reference. Infrared spectra were taken on a Perkin–Elmer Model 257 infrared spectrophotometer and were calibrated with the 1602 cm^{-1} band of polystyrene film. Mass spectra were obtained on a Dupont 21-492B mass spectrometer. Column chromatographs were done with silica gel unless otherwise specified. Chemical analyses were performed by Guelph Chemical Laboratories Ltd. Elemental analyses or exact mass measurements were performed on most new compounds. Exceptions were made in cases where a series of compounds of similar structures, with small differences in substituent, were prepared under the same reaction conditions. If their spectral (nmr, ms, etc.) data were similar and showed no unexpected feature, then analyses were performed on representative examples of the series to establish the general structure.

Preparation of enamines

The following enamines were made by the water separator method (7). Methyl 3-pyrrolidinocrotonate (**5***a*), 88%, bp 116–118°C (2.5 Torr; 1 Torr = 133.3 Pa); methyl 3-morpholinocrotonate (**5***b*), 79%, bp 131–132°C (4 Torr); ethyl 3-morpholinocrotonate (**26**), 77%, bp 106–109°C (0.4 Torr); 1-morpholinocyclopentene, 82%, bp 108–110°C (14 Torr) (lit. (15) bp 104–106°C (12 Torr)); 1-morpholinocyclohexene (**28**), 84%, bp 112–114°C (14 Torr) (lit. (15) bp 104–106°C (12 Torr)).

The following enamines were made by the procedure of White and Weingarten (16). 1-Morpholinocycloheptene, 54%, bp 130–133°C (15 Torr) (lit. (17) bp 133–135°C (17 Torr)); 1-morpholinocyclooctene, 61%, bp 81–83°C (1 Tor) (lit. (17) bp 83–85°C (0.01 Torr)); 3-morpholino-2-pentene (**31**), 52%, bp 50–51°C (0.5 Torr) (lit. (17) bp 77–78°C (9 Torr)); 4-morpholino-3-heptene (**33**), 57%, bp 67–69°C (0.2 Torr) (lit. (17) bp 102–106°C (12 Torr)); 3-pyrrolidino-2-pentene (**34**), 57%, bp 36–38°C (0.5 Torr) (lit. (17) bp 62–67°C (8 Torr)); 4-pyrrolidino-3-heptene (**35**), 60%, bp 56–58°C (0.2 Torr).

*Methyl 4-trimethylsilyl-3-pyrrolidinocrotonate (7*a*)*

Under N_2 at 0°C, to a solution of dry diisopropylamine (3.4 mL, 24 mmol) in THF (50 mL) was added n-BuLi (16 mL of 1.5 *M* in hexane, 24 mmol), followed by TMEDA (3.2 mL). The solution was cooled to −78°C and methyl 3-pyrrolidinocrotonate (**5***a*, 3.38 g, 20 mmol) was added. The reaction mixture was stirred for 0.5 h, and then quenched with trimethylchlorosilane (4 mL). The reaction mixture was allowed to warm to 0°C and concentrated on the rotary evaporator. The residue was triturated with dry hexane (100 mL) and filtered. The filtrate was concentrated (finally under high vacuum) to give 4.43 g of **7***a* as a yellowish oil (92%), >95% pure by ^{1}H nmr; bp 132–135°C (1 Torr); ir (film): 1665, 1550, 1150 cm^{-1}; ^{1}H nmr ($CDCl_3$): 0.1 (s, 9H), 1.80–2.03 (m, 4H), 2.73 (s, 2H), 3.20–3.43 (m, 4H), 3.60 (s, 3H), 4.47 (s, 1H); ^{13}C nmr ($CDCl_3$): −1.7, 21.6, 25.0, 48.0, 49.5, 81.0, 163.0, 169.3; ms *m/z* (rel. intensity): 241 (M^+, 26), 226 (39), 210 (33), 168 (77), 138 (84), 110 (100). *Exact Mass* calcd. for $C_{12}H_{23}O_2NSi$: 241.158; found: 241.152.

*Methyl 4-trimethylsilyl-3-morpholinocrotonate (7*b*)*

Compound **7***b* was made in the same way as **7***a* from **5***b* in 90% yield (>90% pure by ^{1}H nmr); ir (film): 1680, 1560, 1145 cm^{-1}; ^{1}H nmr ($CDCl_3$): 0.1 (s, 9H), 2.73 (s, 3H), 3.10–3.33 (m, 4H), 3.60 (s, 3H), 3.55–3.80 (m, 4H), 4.73 (s, 1H); ^{13}C nmr ($CDCl_3$): −0.9, 19.5, 47.1, 50.2, 66.6, 86.2, 165.7, 169.5; ms, *m/z* (rel. intensity): 257 (M^+, 26), 242 (58), 226 (62), 184 (72), 154 (30), 126 (34).

*Methyl 5-phenyl-3-pyrrolidinopenta-2*E*,4*E*-dienoate (8*a*)*

To a mixture of benzaldehyde (1 mmol) and $TiCl_4$ (1 mmol) in 3 mL of CH_2Cl_2 at −78°C under N_2 was added **7***a* (1 mmol). The reaction mixture was stirred for 3 h at −78°C, and then overnight at room temperature. The reaction mixture was quenched with saturated sodium carbonate solution and then extracted with ether. The ether extract was dried with $MgSO_4$ and evaporated to give an oil, which was column chromatographed (ether–hexane 2:1) to give **8***a* in 68% yield as a colorless liquid; ir (film): 1680, 1550, 1140 cm^{-1}; ^{1}H nmr ($CDCl_3$): 1.95 (m, 4H), 3.33 (m, 4H), 3.60 (s, 3H), 4.60 (s, 1H), 6.66 (d, 1H, *J* = 17 Hz), 7.20–7.60 (m, 6H); ms, *m/z* (rel. intensity): 257 (M^+, 12), 226 (18), 198 (100). *Exact Mass* calcd. for $C_{16}H_{19}O_2N$: 257.139; found: 257.138.

*Methyl 5-phenyl-3-morpholinopenta-2*E*,4*E*-dienoate (8*a*)*

The reaction was performed in the same way as the reaction between **7***a* and benzaldehyde to afford **8***b* in 60% yield as a colorless liquid; ir (film): 1695, 1565, 1150 cm^{-1}; ^{1}H nmr ($CDCl_3$): 3.07 (m, 4H), 3.56 (s, 3H), 3.70 (m, 4H), 4.84 (s, 1H), 6.75 (d, 1H, *J* = 16 Hz), 7.10–7.50 (m, 6H); ms, *m/z* (rel. intensity): 273 (M^+, 9), 242 (13), 214 (100).

*Methyl 7-phenyl-3-pyrrolidinohepta-2*E*,4*E*,6*E*-trienoate (9*a*)*

To a mixture of cinnamaldehyde (0.5 mmol) and $TiCl_4$ (0.5 mmol) in 3 mL of CH_2Cl_2 at −78°C under N_2 was added **7***a* (0.5 mmol). The mixture was stirred for 3 h at −78°C, then allowed to warm to room temperature. Saturated aqueous sodium carbonate solution was added and the mixture was extracted with ether. The ether extract was dried with $MgSO_4$ and filtered. The filtrate was concentrated to give a brown oil, which was purified by alumina column chromatography (ether–hexane 2:1) to give **9***a* in 81% yield; ir (film): 1670, 1540, 1145 cm^{-1}; ^{1}H nmr ($CDCl_3$, 200 MHz): 1.93 (m, 4H), 3.33 (m, 4H), 3.60 (s, 3H), 4.57 (s, 1H), 6.54 (d, 1H, *J* = 16 Hz), 6.50 (dd, 1H, *J* = 16 and 6 Hz), 6.84 (dd, 1H, *J* = 16 and 6 Hz), 6.86 (d, 1H, *J* = 16 Hz), 7.12–7.34 (m, 5H); ms, *m/z* (rel. intensity): 283 (M^+, 24), 252 (8), 224 (100).

*Methyl 7-phenyl-3-morpholinohepta-2*E*,4*E*,6*E*-trienoate (9*b*)*

This reaction was carried out in the same manner as the reaction between **7***a* and cinnamaldehyde. Compound **9***b* was obtained in 83% yield; ir (film): 1690, 1550, 1150 cm^{-1}; ^{1}H nmr ($CDCl_3$, 200 MHz): 3.10 (m, 4H), 3.63 (s, 3H), 3.73 (m, 4H), 4.90 (s, 1H), 6.62 (d, 1H, *J* = 16 Hz), 6.63 (dd, 1H, *J* = 16 and 6 Hz), 6.90 (dd, 1H, *J* = 16 and 6 Hz), 6.97 (d, 1H, *J* = 16 Hz), 7.16–7.38 (m, 5H); ms, *m/z* (rel. intensity): 299 (M^+, 41), 268 (9), 240 (100).

*4-Pyrrolidino-6-(n-propyl)-5,6-dihydro-1,2-pyrone (10*a*)*

The reaction was done in the same manner as the reaction of **7***a* with benzaldehyde, except that a 2:1 mixture of ether and acetonitrile was used as eluant in the flash chromatography. Compound **10***a* was obtained in 53% yield; ir (film): 1660, 1570, 1240 cm^{-1}; ^{1}H nmr ($CDCl_3$): 0.73–1.77 (m, 7H), 1.93 (m, 4H), 2.40 (d, 2H, *J* = 8 Hz), 3.27 (m, 4H), 4.20 (m, 1H), 4.63 (m, 1H); ms, *m/z* (rel. intensity): 209 (M^+, 33), 166 (100), 150 (29).

*4-Morpholino-6-(n-propyl)-5,6-dihydro-1,2-pyrone (10*b*)*

The reaction was performed in the same way as the reaction of **7***a* with butanal. Compound **10***b* was obtained in 49% yield; ir (film): 1660, 1565, 1230 cm^{-1}; ^{1}H nmr ($CDCl_3$): 0.80–1.90 (m, 7H), 2.40 (d, 2H, *J* = 7 Hz), 3.23 (m, 4H), 3.77 (m, 4H), 4.33 (m, 1H), 4.87 (s, 1H); ms, *m/z* (rel. intensity): 225 (M^+, 13), 182 (100), 166 (19). *Anal.* calcd.: C 64.04, H 8.44; found: C 63.84, H 8.54%.

Methyl 5-hydroxy-5-methyl-3-oxohexanoate (11)

To a mixture of acetone (2 mmol), which was freshly distilled over anhydrous K_2CO_3, and $TiCl_4$ (1 mmol) in 3 mL of CH_2Cl_2 at −78°C under N_2 was added **7***b* (1 mmol). The reaction mixture was stirred for 3 h at −78°C, then overnight at room temperature. Saturated sodium carbonate solution was added, and the mixture was extracted with ether. The ether extract was dried with $MgSO_4$ and filtered. The filtrate was concentrated to give an oil, which was purified by flash chromatography (hexane–ether 2:1). Compound **11** was obtained in 44% yield. Its spectroscopic data are identical to those reported in the literature (18).

Methyl 4-(1′-hydroxycyclohexanyl)-3-morpholinocrotonate (12)

The reaction was done by the same procedure as the reaction between **7***b* and acetone. Compound **12** was obtained in 56% yield; ir (film): 3400, 1650, 1570, 1165 cm^{-1}; ^{1}H nmr ($CDCl_3$): 1.57 (m, 10H), 3.07 (s, 2H), 3.23 (m, 4H), 3.50 (b, 1H), 3.68 (s, 3H), 3.77 (m, 4H), 5.03 (s, 1H); ms, *m/z* (rel. intensity): 283 (M^+, 1), 265 (4), 252 (5).

4-Pyrrolidino-6-phenyl-1,2-pyrone (13)

To a mixture of **7***a* (1 mmol) and benzoyl chloride (1 mmol) in 5 mL CH_2Cl_2, was added $TiCl_4$ (1 mmol) at 0°C under N_2. The reaction mixture was stirred for 3 h at 0°C, then overnight at room temperature. Saturated sodium carbonate solution was added and the mixture was extracted with ether. The ether extract was dried with $MgSO_4$ and filtered. The filtrate was evaporated to give a yellow oil, which was purified by flash chromatography (ethyl acetate) to give compound **13** in 44% yield; ir (film): 1675, 1635, 1545 cm^{-1}; ^{1}H nmr ($CDCl_3$): 1.93 (m, 4H), 3.30 (m, 4H), 4.87 (d, 1H, J = 2 Hz), 6.20 (d, 1H, J = 2 Hz), 7.17–7.80 (m, 5H); ms, *m/z* (rel. intensity): 240 (M^+, 100), 213 (51), 77 (51). *Anal.* calcd.: C 74.69, H 6.22; found: C 74.52, H 6.39%.

Benzoyl morpholine (14)

The reaction was done in the same manner as the reaction of **7***a* with benzoyl chloride. Benzoyl morpholine (**14**) was obtained in 61% yield.

*Dimethyl 3-hydroxy-5-pyrrolidino-*o*-phthalate (15)*

A mixture of **7***a* (1 mmol) and dimethyl acetylenedicarboxylate (2 mmol) in 15 mL of dry benzene was refluxed for 3 days. The reaction mixture was cooled to room temperature. A solution of 2 mL of 1.5 *N* HCl was added and the mixture was stirred for 0.5 h. Saturated sodium bicarbonate solution was added until the mixture was basic. The mixture was extracted with ether and the ether extract was dried with $MgSO_4$ and then filtered. The filtrate was concentrated by rotary evaporator to give a brown oil, which was purified by flash chromatography to give 156 mg of **15**, mp 128–130°C. The yield was 57%; ir ($CHCl_3$); 3100, 1725, 1650 cm^{-1}; ^{1}H nmr ($CDCl_3$): 1.83–2.07 (m, 4H), 3.17–3.38 (m, 4H), 3.80 (s, 3H), 3.83 (s, 3H), 5.93 (d, 1H, J = 3 Hz), 6.03 (d, 1H, J = 3 Hz), 11.03 (s, 1H); ms, *m/z* (rel. intensity): 279 (M^+, 91), 248 (57), 189 (100). *Exact Mass* calcd. for $C_{14}H_{17}NO_4$: 279.111; found: 279.107.

Methyl 2-methyl-4-morpholino-6-hydroxybenzoate (18b)

To a solution of 257 mg of **7***b* (1 mmol) in 5 mL CH_2Cl_2 was added 0.5 mmol of $TiCl_4$ under N_2 at −78°C, the reaction mixture was stirred for 3 h at −78°C, then overnight at room temperature. It was added to a saturated sodium carbonate solution, stirred for 0.5 h, and extracted with ether. The extract was dried with $MgSO_4$, filtered, and concentrated with a rotary evaporator to give a yellow oil, which was then purified by flash chromatography (ether–hexane 1:1). Compound **18***b*, mp 108–109°C, was obtained in 49% yield; ir (KBr): 1640, 1600, 1205 cm^{-1}; ^{1}H nmr ($CDCl_3$): 2.13 (s, 3H), 3.07–3.23 (m, 4H), 3.63–3.80 (m, 4H), 3.83 (s, 3H), 6.10 (s, 2H), 11.63 (s, 1H); ms, *m/z* (rel. intensity): 251 (M^+, 76), 220 (22), 219 (50), 161 (100), 133 (28).

3-(Methoxycarbonyl)-2,6-dimethyl-1,4-pyrone (22)

The reaction was performed with **5***b* in the same manner as the self-condensation of **7***b*. 3-(Methoxycarbonyl)-2,6-dimethyl-1,4-pyrone (**22**) was obtained in 75% yield; ir (film): 1735, 1670, 1635 cm^{-1}; ^{1}H nmr ($CDCl_3$): 2.27 (s, 3H), 2.37 (s, 3H), 3.88 (s, 3H), 6.13 (s, 1H); ms, *m/z* (rel. intensity): 182 (M^+, 10), 151 (17), 124 (29), 109 (11), 67 (64), 43 (100). *Exact Mass* calcd. for $C_9H_{10}O_4$: 182.058; found: 182.058.

Compound 18b from cross-condensation of 5b and 7b

To a mixture of 257 mg of **7***b* (1 mmol) and 185 mg of **5***b* (1 mmol) in 5 mL of CH_2Cl_2 was added 1 mmol of titanium tetrachloride under N_2 at −78°C. The reaction mixture was stirred for 3 h at −78°C and then overnight at room temperature. Saturated sodium carbonate solution was added, and the mixture was extracted with ether. The ether extract was dried with $MgSO_4$, filtered, and concentrated to give a yellow solid, which was purified by flash chromatography (ether–hexane 1:1). A quantity of 203 mg of **18***b* was obtained in 71% yield.

Methyl 2-methyl-4-pyrrolidino-6-hydroxybenzoate (18a)

The reaction was performed by the reaction of **5***a* with **7***a* in the same manner as the reaction of **7***b* and **5***b*. Compound **18***a*, mp 101–102°C, was obtained in 78% yield; ir (KBr): 1630, 1615, 1320 cm^{-1}; ^{1}H nmr ($CDCl_3$): 1.80–2.03 (m, 4H), 2.40 (s, 3H), 3.13–3.33 (m, 4H), 3.80 (s, 3H), 5.83 (s, 2H), 11.80 (s, 1H); ms, *m/z* (rel. intensity): 235 (M^+, 100), 204 (33), 203 (89), 175 (17), 147 (22).

Methyl 2-morpholino-4-methyl-6-hydroxybenzoate (20b)

The reaction was performed by Bohme's procedure (14). To 740 mg of **5***b* (4 mmol) was added 432 mg of TFA (4 mmol) at 0°C. The reaction mixture was stirred for 1 h at 0°C, then overnight at 40–50°C. The reaction mixture was diluted with 50 mL of ether, and washed with saturated sodium bicarbonate. The ether phase was dried with $MgSO_4$ and filtered. The filtrate was then concentrated by rotary evaporator to give 416 mg of **20***b*, mp 115–116°C (lit. (14) mp 116°C). The yield was 83%.

3-Morpholino-5-methylphenol (21) (14, 19)

To 50 mg of **18***b* was added 5 mL of 20% KOH. The reaction mixture was refluxed overnight. It was cooled to room temperature and a solution of 1 *N* HCl was added until the solution became acidic. The mixture was extracted with ether. The ether extract was dried with $MgSO_4$, filtered, and then concentrated to give 27 mg of **21**. Compound **21** had mp 126–127°C (lit. (19) mp 126–127°C); ir ($CHCl_3$): 3600, 1610, 1590, 1120 cm^{-1}; ^{1}H nmr ($CDCl_3$): 2.30 (s, 3H), 3.03–3.20 (m, 4H), 3.78–3.95 (m, 4H), 6.17–6.30 (m, 3H).

Decarboxylation of 20b

The reaction was carried out under identical conditions as used for the decarboxylation of **18***b*. A quantity of 30 mg of **21** was obtained. It is identical in all respects with the compound obtained from the decarboxylation of **18***b*.

Ethyl 2-methyl-4-pyrrolidino-6-hydroxybenzoate (27)

To a mixture of 241 mg of **7***a* (1 mmol) and 199 mg of **26** (1 mmol) in 5 mL of CH_2Cl_2 was added 1 mmol of titanium tetrachloride under N_2 at −78°C. The reaction mixture was stirred for 6 h at −78°C, then overnight at room temperature. Saturated sodium carbonate solution was added until the mixture became basic. The mixture was extracted with ether. The ether extract was dried with $MgSO_4$, filtered, and the filtrate was concentrated to give a yellow solid, which was purified by flash chromatography (ether–hexane, 1:1). A quantity of 162 mg of **27**, mp 83–84°C, was obtained. The yield was 65%; ir (KBr): 3400, 1635, 1310 cm^{-1}; ^{1}H nmr ($CDCl_3$): 1.37 (t, 3H, J = 7 Hz), 1.83–2.07 (m, 4H), 2.50 (s, 3H), 3.17–3.40 (m, 4H), 4.33 (q, 2H, J = 7 Hz), 5.90 (s, 2H), 11.90 (s, 1H); ms, *m/z* (rel. intensity): 249 (M^+, 94), 204 (80), 203 (100), 175 (76), 147 (75). *Exact Mass* calcd. for $C_{14}H_{19}NO_3$: 249.136; found: 249.134.

*7-Hydroxy-9-pyrrolidino-[4]-*ortho*-cyclophane (29)*

To a mixture of 241 mg of **7***a* (1 mmol) and 167 mg of **28** (1 mmol) in 25 mL of CH_2Cl_2 was added 228 mg of trifluoroacetic acid at 0°C. The reaction mixture was stirred for 1 h at 0°C, then refluxed for 24 h. The reaction mixture was diluted with 50 mL of ether and washed with saturated sodium bicarbonate. The organic phase was dried with $MgSO_4$, filtered, and then concentrated with a rotary evaporator to give a yellowish solid, which was purified by flash chromatography (eluted with ethyl acetate – hexane 1:1) to give 136 mg of **29**, mp 157–159°C. The yield of **29** was 63%; ir (KBr): 3400, 1620, 1580 cm^{-1}; ^{1}H nmr ($CDCl_3$): 1.67–2.20 (m, 8H), 2.40–2.83 (m, 4H), 4.60 (b, 1H), 5.97 (s, 2H); ms, *m/z* (rel. intensity): 217 (M^+, 100), 216 (99), 189 (55), 161 (40). *Anal.* calcd.: C 77.42, H 8.76; found: C 77.48, H 8.64%.

*7-Pyrrolidino-9-hydroxy-[3]-*ortho*-cyclophane*

To a mixture of 241 mg of **7***a* (1 mmol) and 153 mg of 1-morpholinocyclopentene (1 mmol) in 25 mL of 1,2-dichloroethane was added 228 mg of TFA (2 mmol) at 0°C. The reaction mixture was stirred for 1 h at 0°C and then refluxed for 24 h. The mixture was diluted with 50 mL of ether, and washed with saturated sodium bicarbonate solution. The organic layer was dried over $MgSO_4$ and filtered. The filtrate was concentrated to give a yellow solid, which was purified by flash chromatography (eluted with petroleum ether − ethyl acetate, 5:1) to give 7-pyrrolidino-9-hydroxy-[3]-*ortho*-cyclophane, mp 166−168°C, in 64% yield; ir (KBr): 3310, 1630, 1600, 1580 cm^{-1}; ^1H nmr ($CDCl_3$): 1.90−2.20 (m, 6H), 2.80 (t, 2H), 2.93 (t, 2H), 3.17−3.37 (m, 4H), 5.92 (d, 1H, J = 2 Hz), 6.13 (d, 1H, J = 2 Hz); ms, m/z (rel. intensity): 203 (M^+, 88), 202 (100), 174 (21), 147 (32), 133 (22).

*9-Pyrrolidino-11-hydroxy-[5]-*ortho*-cyclophane*

The reaction was performed in the same manner as the reaction between **7*a*** and 1-morpholinocyclopentene. 9-Pyrrolidino-11-hydroxy-[5]-*ortho*-cyclophane, mp 149−150°C, was obtained in 59% yield; ir (KBr): 3400, 1610, 1570, 1500 cm^{-1}; ^1H nmr ($CDCl_3$): 1.53−2.12 (m, 10H), 2.67−2.87 (m, 4H), 4.80 (b, 1H), 5.88 (d, 1H, J = 2 Hz), 6.05 (d, 1H, J = 2 Hz); ms, m/z (rel. intensity): 231 (M^+, 100), 230 (82), 203 (23), 202 (44).

*10-Pyrrolidino-12-hydroxy-[6]-*ortho*-cyclophane*

The reaction of **7*a*** with 1-morpholinocyclooctene was performed in the same manner as the reaction between **7*a*** and 1-morpholinocyclopentene. 10-Pyrrolidino-12-hydroxy-[6]-*ortho*-cyclophane, mp 157−159°C, was obtained in 67% yield; ir (KBr): 3400, 1610, 1570 cm^{-1}; ^1H nmr ($CDCl_3$): 1.47 (b, 8H), 1.87−2.08 (m, 4H), 2.63−2.83 (m, 4H), 4.73 (s, 1H), 6.00 (AB quartet, 2H, J = 2 Hz); ms, m/z (rel. intensity): 245 (M^+, 100), 244 (55), 217 (41), 202 (67). *Anal.* calcd.: C 78.37, H 9.37; found: C 78.30, H 9.51%.

Methyl 3-morpholino-4-cyclohexylidenecrotonate (30)

The reaction of **7*b*** with **28** was performed in the same manner as the reaction between **7*a*** and **28**. Compound **30** was isolated in 52% yield; ir ($CHCl_3$): 1685, 1560, 1145 cm^{-1}; ^1H nmr ($CDCl_3$): 1.57 (b, 6H), 2.00−2.40 (m, 4H), 3.25−3.45 (m, 4H), 2.63−3.83 (m, 4H), 3.65 (s, 3H), 4.83 (s, 1H), 5.83 (s, 1H); ms, m/z (rel. intensity): 265 (M^+, 60), 234 (25), 222 (69), 206 (67), 122 (100).

2,4,5-Trimethyl-3-morpholinophenol (32)

To a mixture of 241 mg of **7*a*** (1 mmol) and 310 mg of **31** (2 mmol) in 25 mL of 1,2-dichloroethane was added 342 mg of TFA (3 mmol) at 0°C. The reaction mixture was stirred for 1 h at 0°C, then refluxed for 48 h. It was allowed to cool to room temperature and was diluted with 50 mL of ether. The solution was washed with saturated sodium bicarbonate solution. The organic phase was dried with $MgSO_4$ and filtered. The filtrate was concentrated to give a brown oil, which was purified by flash chromatography (eluted with hexane − ethyl acetate, 2:1) to give 92 mg of **32**, mp 163−164°C, plus 54 mg of **18*a***. The yield for **32** was 41%; ir of **32** (KBr): 3300, 1600, 1585, 1100 cm^{-1}; ^1H nmr of **32** ($CDCl_3$): 2.20 (s, 6H), 2.23 (s, 3H), 3.03−3.18 (m, 4H), 3.73−3.88 (m, 4H), 4.83 (s, 1H), 6.50 (s, 1H); ms, m/z (rel. intensity): 221 (M^+, 91), 220 (55), 206 (32), 176 (63), 163 (100). *Anal.* calcd.: C 70.59, H 8.60; found: C 70.68, H 8.77%.

Reaction of 7a *with 31 in the presence of titanium tetrachloride*

To a mixture of 241 mg of **7*a*** (1 mmol) and 310 mg of **31** (2 mmol) in 10 mL of CH_2Cl_2 was added 0.17 mL of $TiCl_4$ (1.5 mmol), at −23°C under N_2. The reaction mixture was stirred for 3 h at −23°C and then overnight at room temperature. Concentrated sodium carbonate solution was added to the mixture. It was then extracted with ether. The organic layer was dried with $MgSO_4$ and filtered. The filtrate was concentrated by rotary evaporator to give a brown oil, which was purified by flash chromatography to give **32** in 38% yield. A quantity of 62 mg of self-condensation product of **7*a*** was also isolated.

2,4,5-Trimethyl-3-pyrrolidinophenol

The reaction of **7*a*** and **34** was performed under the same conditions as the reaction of **7*a*** with **31** in the presence of TFA. 2,4,5-Trimethyl-3-pyrrolidinophenol was obtained in 42% yield; ir ($CHCl_3$): 3600, 1580, 1460, 1070 cm^{-1}; ^1H nmr ($CDCl_3$): 1.93−2.13 (m, 4H), 2.13 (s, 3H), 2.16 (s, 3H), 2.22 (s, 3H), 3.10−3.30 (m, 4H), 4.48 (s, 1H), 6.50 (s, 1H); ms, m/z (rel. intensity): 205 (M^+, 99), 204 (100), 190 (58), 176 (66), 162 (70).

5-Methyl-2,4-diethyl-3-morpholinophenol

The reaction of **7*a*** with **33** was performed under the same condition as the reaction of **7*a*** with **31** in the presence of TFA. 5-Methyl-2,4-diethyl-3-morpholinophenol, mp 185−187°C, was obtained in 37% yield; ir (KBr): 3260, 1590, 1410, 1100 cm^{-1}; ^1H nmr ($CDCl_3$): 1.15 (t, 3H, J = 7 Hz), 1.23 (t, 3H, J = 7 Hz), 2.28 (s, 3H), 2.73 (q, 2H, J = 7 Hz), 2.77 (t, 2H, J = 7 Hz), 3.13−3.30 (m, 4H), 3.77−3.93 (m, 4H), 4.83 (s, 1H), 6.53 (s, 1H); ms, m/z (rel. intensity): 249 (M^+, 95), 234 (20), 220 (66), 170 (100). *Anal.* calcd.: C 72.29, H 9.24; found: C 72.20, H 9.17%.

5-Methyl-2,4-diethyl-3-pyrrolidinophenol

The reaction of **7*a*** with **35** was performed in the same manner as the reaction between **7*a*** and **31** in the presence of TFA. 5-Methyl-2,4-diethyl-3-pyrrolidinophenol was obtained in 36% yield; ir ($CHCl_3$): 3600, 1580, 1255, 1085 cm^{-1}; ^1H nmr ($CDCl_3$): 1.13 (t, 3H, J = 7 Hz), 1.23 (t, 3H, J = 7 Hz), 1.93−3.12 (m, 4H), 2.28 (s, 3H), 2.63 (q, 4H, J = 7 Hz), 3.13−3.33 (m, 4H), 6.50 (s, 1H); ms, m/z (rel. intensity): 233 (M^+, 100), 232 (73), 218 (95), 204 (87), 160 (31).

Acknowledgement

We thank the Natural Sciences and Engineering Research Council of Canada and the "Formation de chercheurs et d'action concertée" program of Quebec for financial support and the government of the People's Republic of China for a scholarship (G.J.K.).

1. T. H. CHAN and G. J. KANG. Tetrahedron Lett. **23**, 3011 (1982); **24**, 3051 (1983).
2. T. H. CHAN and P. BROWNBRIDGE. J. Am. Chem. Soc. **102**, 3534 (1980).
3. T. H. CHAN and P. BROWNBRIDGE. Tetrahedron, **37**, 387 (1981).
4. P. BROWNBRIDGE, T. H. CHAN, M. A. BROOKE, and G. J. KANG. Can. J. Chem. **61**, 688 (1983).
5. T. H. CHAN and P. BROWNBRIDGE. J. Chem. Soc. Chem. Commun. 20 (1981).
6. T. H. CHAN and T. CHALY. Tetrahedron Lett. **23**, 2935 (1982).
7. S. HUNIG, E. BENZING, and E. LUCKE. Ber. **90**, 2833 (1957).
8. A. G. SANCHEZ and J. BELLANATO. J. Chem. Soc. Perkin Trans. 2, 1561 (1975).
9. T. H. CHAN and I. FLEMING. Synthesis, 761 (1979).
10. T. PINNAVAIA, W. T. COLLINS, and K. M. HURST. J. Am. Chem. Soc. **92**, 4544 (1970).
11. R. M. COATES, L. O. SANOLEFUR, and R. D. SMILLIE. J. Am. Chem. Soc. **97**, 1619 (1975).
12. G. ANDERSON, D. W. CAMERON, G. I. FEUTRILL, and R. W. READ. Tetrahedron Lett. 4347 (1981).
13. W. D. GUROWITZ and M. A. JOSEPH. Tetrahedron Lett. 4433 (1965).
14. H. BOHME, J. G. VONGRATZ, F. MARTIN, R. MATUSCH, and J. NEHNE. Justus Liebigs Ann. Chem. 394 (1980).
15. C. MANNICH and H. DAVIDSEN. Ber. **B69**, 2106 (1936).
16. W. A. WHITE and H. WEINGARTEN. J. Org. Chem. **32**, 213 (1967).
17. G. STORK, A. BRIZZOLARA, H. K. LANDESMAN, J. SZMUSZKOVICZ, AND R. TERRELL. J. Am. Chem. Soc. **85**, 207 (1963).
18. S. N. HUCKIN. Ph.D. thesis, University of British Columbia, April, 1973.
19. GERMAN PATENTS NO. 2,456,279 (Chem. Abstr. **85**, 142880 (1976)) and No. 2,456,280 (Chem. Abstr. **85**, 143135 (1976)).

Kinetic mechanism of copper(II) transfer between the native sequence peptide representing the copper(II)-transport site of human serum albumin and L-histidine

MASAAKI TABATA[1] AND BIBUDHENDRA SARKAR[2]

Research Institute, The Hospital for Sick Children, Toronto, Ont., Canada M5G 1X8; and Department of Biochemistry, University of Toronto, Toronto, Ont., Canada M5S 1A8

Received January 28, 1985

MASAAKI TABATA and BIBUDHENDRA SARKAR. Can. J. Chem. **63**, 3111 (1985).

The kinetics for Cu(II)-transfer reaction of the native sequence tripeptide, L-aspartyl-L-alanyl-L-histidine-*N*-methyl amide (AAHNMA), representing the Cu(II)-transport site of human serum albumin (HSA), and L-histidine (L-His) was studied in the forward and reverse reactions in a pH range 6.5–10.0 at I = 0.2 and 25°. For the Cu(II)-transfer from Cu(II)-L-His_2 to native sequence peptide, the rate-determining step is a bond formation between Cu(II) and peptide nitrogen to form $CuH_{-1}AB$ from CuAB by deprotonation of peptide nitrogen atom, where A and B denote the anionic forms of AAHNMA and L-His, respectively. For the Cu(II)-transfer reaction from Cu(II)–peptide to L-His, the rate-determining step is a bond breaking between Cu(II) and peptide nitrogen to form CuAB from $CuH_{-1}AB$ by protonation to a peptide nitrogen. The effect of carboxyl group of aspartyl residue in the native sequence peptide on the kinetic and equilibrium constants are discussed.

MASAAKI TABATA et BIBUDHENDRA SARKAR. Can. J. Chem. **63**, 3111 (1985).

Opérant à 25°C, dans un intervalle de pH allant de 6,5 à 10,0 et avec une force I = 0,2, on a étudié la cinétique des réactions directe et inverse de transfert de Cu(II) de la L-histidine (L-His) au tripeptide naturel, L-aspartyl-L-alanyl-L-histidine-*N*-méthylamide (AAHNMA) qui représente le siège du transport de Cu(II) dans l'albumine du sérum humain (ASH). Dans la réaction de transfert de Cu(II) du Cu(II)-L-His_2 au peptide de la séquence naturelle, l'étape déterminante est la formation d'une liaison entre le Cu(II) et l'azote du peptide pour former du $CuH_{-1}AB$ à partir de CuAB par déprontonation de l'azote du peptide; dans ces formules, A et B représentent respectivement les formes anioniques de AAHNMA et de la L-His. Pour la réaction de transfert du Cu(II) du Cu(II)–peptide à la L-His, l'étape déterminante est la rupture de la liaison entre le Cu(II) et l'azote du peptide pour conduire à CuAB à partir de $CuH_{-1}AB$, par protonation d'un azote du peptide. On discute de l'effet du groupement carboxylique de l'unité aspartyle du peptide naturel sur la cinétique et sur les constantes d'équilibre.

[Traduit par le journal]

Introduction

The synthesis of the native sequence peptide, L-aspartyl-L-alanyl-L-histidine-*N*-methyl amide (AAHNMA) representing the actual Cu(II)-transport site of human serum albumin (HSA) has been reported previously (1, 2). The peptide binds Cu(II) in the same manner as does albumin (3, 4). This small peptide molecule permits studies which often cannot be applied to large protein molecules. These molecules possess extensive proton binding sites which give rise to ambiguities in elucidating the role of protons. It is considered that protonation or deprotonation step has important relevance in the Cu(II)-transfer mechanism.

The equilibrium and spectroscopic studies of the ternary system: Cu(II), the native sequence tripeptide and L-histidine (L-His) show the formation of mixed ligand complexes, $CuH_{-1}AB$ and CuAB (where A and B denote the anionic forms of AAHNMA and L-His, respectively) at physiological pH (5). Furthermore, the equilibrium study reveals that the native sequence which possesses a side chain carboxyl group decreases the stability constants of the mixed ligand complexes compared to those of glycylglycyl-L-histidine (GGH) (6). We wish to report in this paper a kinetic study of the Cu(II)-transfer reaction between the native sequence peptide representing the Cu(II)-transport site of HSA and L-His. The aim of this study is to elucidate which step is rate-determining in the Cu(II)-transfer reaction and what role the mixed ligand complexes play in the kinetics of the Cu(II)-transfer mechanism.

[1] Present address: Department of Chemistry, Faculty of Science and Engineering, Saga University, 1 Hinjo-machi, Saga, 840 Japan.
[2] To whom correspondence should be addressed.

Experimental

Materials

The peptide, L-aspartyl-L-alanyl-L-histidine-*N*-methyl amide, was synthesized as described previously (1). L-Histidine-monohydrochloride ($[\alpha]_D^{20}$ + 10.0 ± 0.5) was obtained from Nutritional Biochemicals (Cleveland, OH). The purity of the peptide and the amino acid was checked by thin layer chromatography. All other reagents were of analytical grade.

Kinetic experiments

The Cu(II)-transfer reactions between AAHNMA and L-His were studied under pseudo-first order conditions. The faster reaction observed by mixing Cu(II)–L-His_2 with AAHNMA, was carried out on a Durrum–Gibson stopped-flow spectrophotometer at 25°C. The slower reaction, observed by mixing Cu(II)–AAHNMA with L-His, was carried out on a Beckman ACTA MVI spectrophotometer at 25°C. The change of absorbance was followed at both 640 nm (λ_{max} of Cu(II)–L-His_2) and 525 nm (λ_{max} of Cu(II)–AAHNMA). The values of the rate constants obtained were independent of the monitoring wave length. In all cases excellent first-order plots were obtained. The pH variation experiments were carried out by adjusting the pH of the *N*-ethylmorpholin–HCl buffer (0.1 *M*). At high pH (~9), L-His in large excess acted as its own buffer (pK_a = 9.11). All experiments were carried out at 25.0 ± 0.1°C and I = 0.2. Ionic strength was adjusted by sodium chloride and buffer.

Results

Reaction of Cu(II)-L-His_2 with AAHNMA

The reaction of Cu(II)–L-His with AAHNMA to form $CuH_{-2}A$ followed the first-order kinetic expression in eq. [1] under the large excess of CuB_2 compared to AAHNMA:

$$[1] \quad d[CuH_{-2}A]/dt = k_{obs}[A]_T$$

where k_{obs} is the conditional rate constant involving concen-

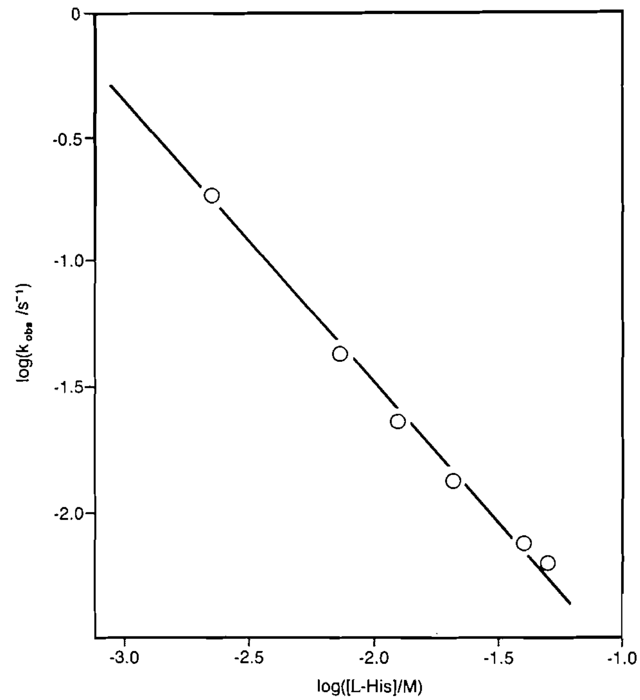

FIG. 1. Dependence of k_{obs} on L-histidine concentration for the reaction of Cu(II)–L-His$_2$ complex with the AAHNMA at 25°C. C_{Cu} = 3.90×10^{-3} M; C_{AAHNMA} = 3.00×10^{-4} M; pH = 7.50. AAHNMA = L-aspartyl-L-alanyl-L-histidine-N-methyl amide.

tration of hydrogen ion, Cu(II) and L-His. CuH$_{-2}$A is a Cu(II)-complex having two deprotonated peptide nitrogens and $[A]_T$ is the total concentration of AAHNMA. The Cu(II)-transfer reaction from Cu(II)–L-His$_2$ to AAHNMA was investigated from pH 6.5 to 10.0 in the various concentrations of L-His. The conditional rate constant (k_{obs}) is first-order in the concentration of CuB$_2$. Figure 1 shows the L-His dependence of conditional rate constant for the reaction of Cu(II)–L-His$_2$ with peptide. The rate constant decreases as the concentration of L-His increased. The slope in Fig. 1 is -1 and suggests that one molecule of L-His dissociates from CuB$_2$ before the rate-determining step as follows:

[2] $\quad \mathrm{Cu(II)\text{–}L\text{-}His_2 \rightleftharpoons Cu(II)\text{–}L\text{-}His + L\text{-}His}$

The dependence of k_{obs} upon pH is given in Fig. 2. Proceeding from pH 6.5 to 10.0, the slope increases and levels off, then again increases in higher pH region.

From the equilibrium study, the chemical species of Cu(II) under the present experimental conditions are CuB$_2$, CuH$_{-2}$A, CuAB, and CuH$_{-1}$AB. The reaction mechanism proposed to account for the observed L-His dependence and pH dependence of rate constants is given in reactions [3]–[7].

[3] $\quad \mathrm{CuB_2} + n\mathrm{H^+} \rightleftharpoons \mathrm{CuB} + \mathrm{H}_n\mathrm{B};\ K_1$

[4] $\quad \mathrm{CuB + A \rightleftharpoons CuAB};\ K_2$

[5] $\quad \mathrm{CuAB} \underset{k_{-1}}{\overset{k_1}{\rightleftharpoons}} \mathrm{CuH_{-1}AB + H^+}$

[6] $\quad \mathrm{CuAB + OH^-} \underset{k_{-2}}{\overset{k_2}{\rightleftharpoons}} \mathrm{CuH_{-1}AB}$

[7] $\quad \mathrm{CuH_{-1}AB} \xrightarrow{k_3} \mathrm{CuH_{-2}A} + \mathrm{H}_n\mathrm{B} + \mathrm{OH^-}$

SCHEME 1

Since the rate of the reaction of Cu(II)–L-His$_2$ with AAHNMA decreases with increasing L-His concentration (Fig. 1), AAHNMA cannot react directly with Cu(II)–L-His$_2$ but it reacts with the 1:1 Cu(II)–L-His complex. It is followed by the formation of the mixed ligand complex CuAB in which peptide binds through amino nitrogen and peptide oxygen atoms (λ_{max} of CuAB 595 nm; ϵ_{max} = 97 M^{-1} cm^{-1}).

Hydroxide ion assists the deprotonation of peptide to form CuH$_{-1}$AB (reaction [6]). The solvent-assisted deprotonation path is shown in reaction [5]. CuH$_{-1}$AB is the main mixed ligand complex at physiological pH. By assuming steady-state concentrations of CuH$_{-1}$AB, the above mechanism yields the rate law for the formation of CuH$_{-2}$A as given in eqs. [8] and [9].

[8] $$\frac{d[\mathrm{CuH_{-2}A}]}{dt} = \left(\frac{k_2k_3[\mathrm{OH^-}] + k_1k_3}{k_{-1}[\mathrm{H^+}] + k_{-2} + k_3}\right)[\mathrm{CuAB}]$$

[9] $$k_{obs} = \left(\frac{k_2k_3[\mathrm{OH^-}] + k_1k_3}{k_{-1}[\mathrm{H^+}] + k_{-2} + k_3}\right)\left(\frac{\alpha_{B(H)}K_1K_2[\mathrm{CuB_2}]_T}{\alpha_{A(H)}[\mathrm{B}]_T}\right)$$

where K_1 and K_2 are equilibrium constants of reactions [3] and [4], respectively. $\alpha_{A(H)}$ and $\alpha_{B(H)}$ are protonation-reaction coefficients of A and B, respectively, and defined as follows (7):

[10] $$\alpha_{A(H)} = 1 + \beta_{0110}[\mathrm{H^+}] + \beta_{0120}[\mathrm{H^+}]^2 + \beta_{0130}[\mathrm{H^+}]^3$$

[11] $$\alpha_{B(H)} = 1 + \beta_{0101}[\mathrm{H^+}] + \beta_{0102}[\mathrm{H^+}]^2 + \beta_{0103}[\mathrm{H^+}]^3$$

Values for $\alpha_{A(H)}$ and $\alpha_{B(H)}$ were calculated from eqs. [10] and [11] by using the following β values (1, 8):

$$\beta_{0110} = [\mathrm{HA}][\mathrm{H^+}]^{-1}[\mathrm{A}]^{-1} = 10^{7.73}$$
$$\beta_{0120} = [\mathrm{H_2A}][\mathrm{H^+}]^{-2}[\mathrm{A}]^{-1} = 10^{14.29}$$
$$\beta_{0130} = [\mathrm{H_3A}][\mathrm{H^+}]^{-3}[\mathrm{A}]^{-1} = 10^{17.27}$$
$$\beta_{0101} = [\mathrm{HB}][\mathrm{H^+}]^{-1}[\mathrm{B}]^{-1} = 10^{9.11}$$
$$\beta_{0102} = [\mathrm{H_2B}][\mathrm{H^+}]^{-2}[\mathrm{B}]^{-1} = 10^{15.170}$$
$$\beta_{0103} = [\mathrm{H_3B}][\mathrm{H^+}]^{-3}[\mathrm{B}]^{-1} = 10^{16.999}$$

The hydroxide ion assisted pathway is predominant above pH 9.0. As the term $k_{-1}[\mathrm{H^+}] \ll k_2 + k_3$ at higher pH, the plots of

$$k_{obs} \times \left(\frac{\alpha_{A(H)}[\mathrm{B}]_T}{\alpha_{B(H)}K_1K_2[\mathrm{CuB_2}]_T}\right) \text{ vs. } [\mathrm{OH}]$$

gives a straight line with an intercept.

Kinetic parameters of $k_2k_3/(k_{-2} + k_3)$ and $k_1k_3/(k_{-2} + k_3)$ were calculated from the slope and the intercept. The value of k_2/k_1 is 1.50×10^6 M^{-1}. At lower pH, $k_2k_3[\mathrm{OH^-}]$ is much smaller than k_1k_3 to be negligible. The values of k_{-1}/k_1k_3 and $(k_{-2} + k_3)/k_1k_3$ are obtained as a slope and an intercept of plots of

$$\left(k_{obs}\frac{\alpha_{A(H)}[\mathrm{B}]_T}{\alpha_{B(H)}K_1K_2[\mathrm{CuB_2}]_T}\right)^{-1} \text{ vs. } [\mathrm{H^+}]$$

The value of k_{-1}/k_1k_3 is 3.80×10^7 M^{-1} s. By using the value of $k_1/k_{-1} = 10^{-6.61}$ M which is determined by equilibrium study, the values of $k_3 = 0.107$ s^{-1}. The curve in Fig. 2 was calculated from eq. [9] and above values.

Reaction of Cu(II)-AAHNMA with L-His

Rate of Cu(II)-transfer reaction from Cu(II)–peptide to L-His is slower than that from Cu(II)–L-His$_2$ to peptide. The reaction of Cu(II)–AAHNMA with L-His to form CuB$_2$ followed the first-order kinetic expression in eq. [12] under the large

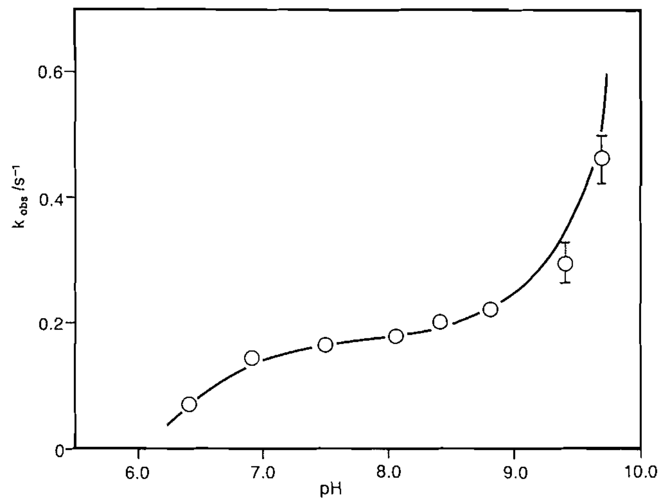

FIG. 2. Dependence of k_{obs} on pH for the reaction of Cu(II)–L-His$_2$ complex with AAHNMA at 25°C. $C_{Cu} = 3.90 \times 10^{-3}$ M; $C_{AAHNMA} = 3.00 \times 10^{-4}$ M; $C_{His} = 1.00 \times 10^{-2}$ M. AAHNMA = L-aspartyl-L-alanyl-L-histidine-N-methyl amide.

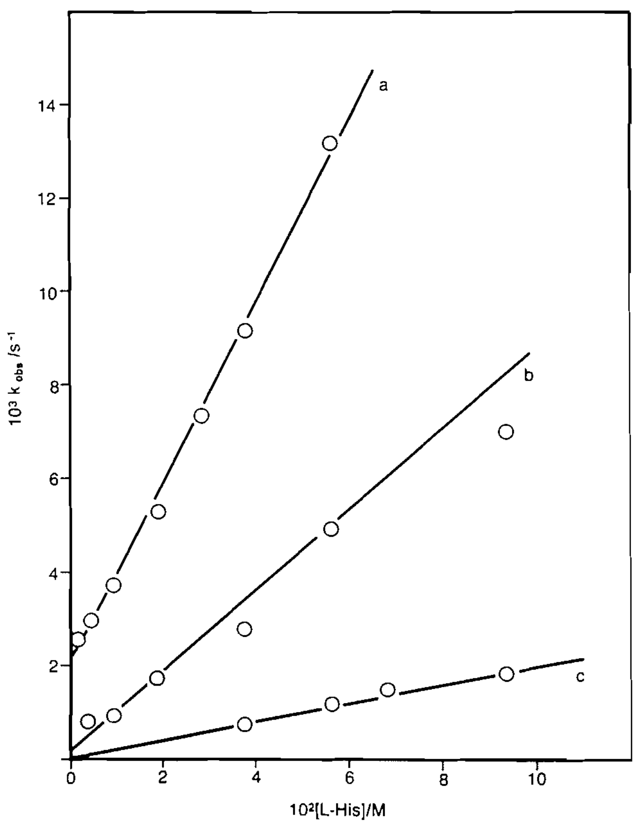

FIG. 3. Dependence of k_{obs} on L-histidine concentration for the reaction of CuH$_{-2}$A complex with L-histidine at 25°C. (a) $C_{Cu} = 6.09 \times 10^{-4}$ M, $C_A = 6.09 \times 10^{-4}$ M, pH = 7.00; (b) $C_{Cu} = 1.22 \times 10^{-4}$ M, $C_A = 1.22 \times 10^{-4}$ M, pH = 7.70; (c) $C_{Cu} = 2.44 \times 10^{-4}$ M, $C_A = 2.44 \times 10^{-4}$ M, pH = 8.50. A = L-aspartyl-L-alanyl-L-histidine-N-methyl amide.

excess of L-His compared to Cu(II)–AAHNMA:

$$[12]\quad d[CuB_2]/dt = -\,d[CuH_{-2}A]/dt = k_{obs}[CuH_{-2}A]$$

where k_{obs} is the conditional rate constant which is dependent on

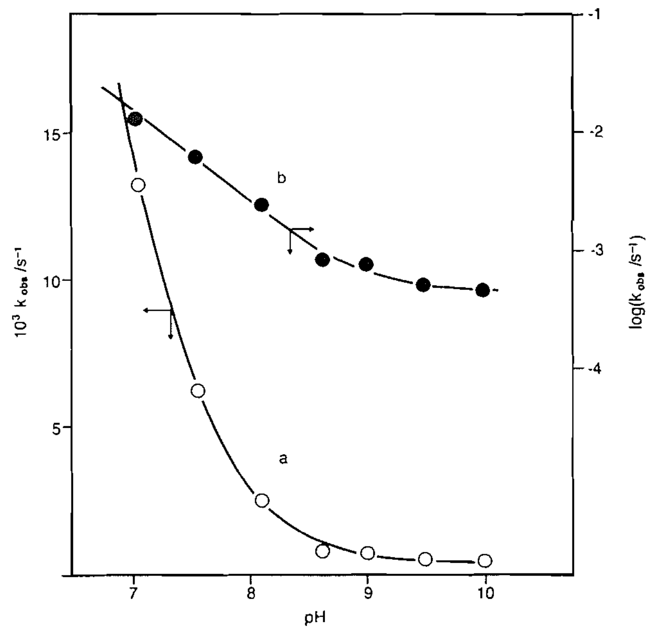

FIG. 4. Dependence of k_{obs} on pH for the reaction of Cu(H$_{-2}$A) complex with L-histidine at 25°C. $C_{Cu} = 2.44 \times 10^{-4}$ M; $C_A = 2.44 \times 10^{-4}$ M; $C_{His} = 5.63 \times 10^{-2}$ M. A = L-aspartyl-L-alanyl-L-histidine-N-methyl amide.

the concentrations of hydrogen ion and L-His. Main chemical species of Cu(II)–peptide is CuH$_{-2}$A in a pH range from 5 to 10. Figure 3 shows the effect of L-His concentration on the rate constant. The rate constant is first-order with respect to L-His. The dependence of k_{obs} on L-His becomes smaller at higher pH. Thus, the nucleophilic attack of L-His is characterized. At lower pH, there is a reaction pathway which is independent of L-His (Fig. 3a). The dependence of k_{obs} on pH is shown in Fig. 4. The observed rate constant decreases with the increasing pH and then levels off at higher pH.

The reaction mechanism proposed to account for the observed L-His dependence and pH dependence of rate constants is given in eqs. [13]–[16]:

$$[13]\quad CuH_{-2}A + HB \underset{k_{-4}}{\overset{k_4}{\rightleftharpoons}} CuH_{-1}AB$$

$$[14]\quad CuH_{-1}AB + H^+ \xrightarrow{k_5} CuAB \xrightarrow{\text{rapid, B}} CuB_2 + A$$

$$[15]\quad CuH_{-2}A + H^+ \xrightarrow{k_6} CuH_{-1}A \xrightarrow{\text{rapid, B.H}^+} CuB_2 \text{ (final product)} + HA$$

$$[16]\quad CuH_{-2}A + B \xrightarrow{k_7} CuH_{-2}AB \xrightarrow{\text{rapid, B.H}^+} CuB_2 \text{ (final product)} + A$$

SCHEME 2

As the main chemical species of L-His is HB at physiological pH, HB attacks Cu(II)–peptide to form Cu$_{-1}$AB (λ_{max} 530 nm; $\epsilon = 90$ M^{-1} cm^{-1}). In the next step, proton attacks the peptide nitrogen of CuH$_{-1}$AB to break a bonding between peptide nitrogen and Cu(II), eq. [14]).

By assuming a steady-state of CuH$_{-1}$AB, the above mechanism yields the following rate equation for the formation of

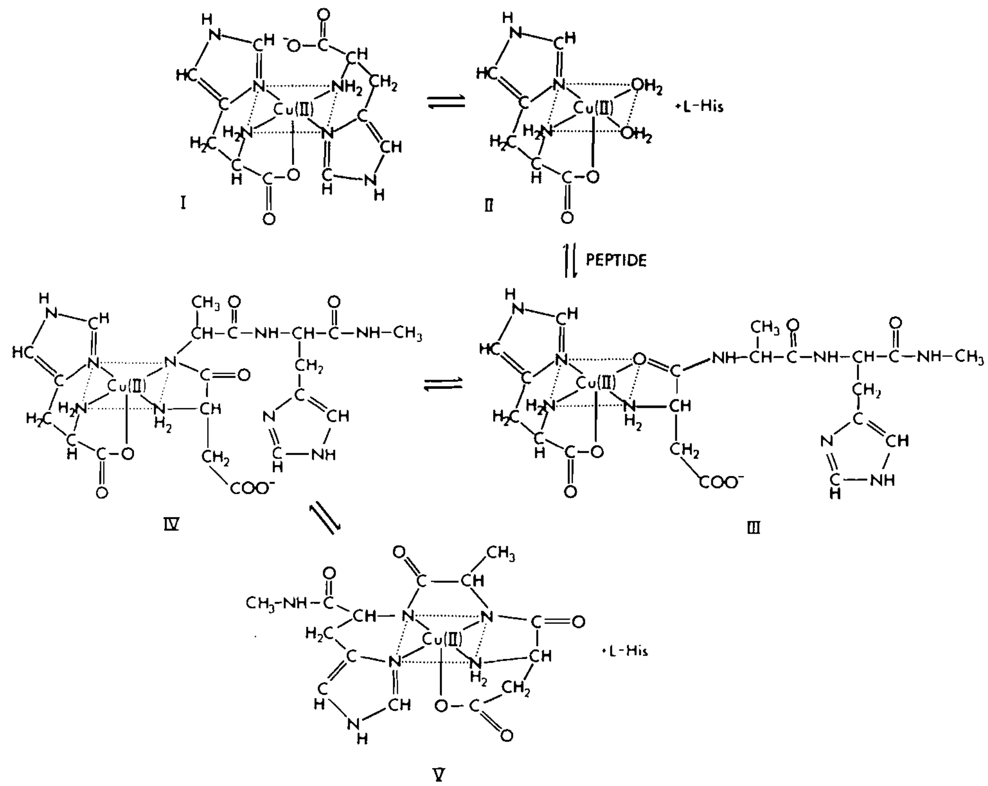

FIG. 5. Proposed reaction mechanism for the copper(II)-transfer involving Cu(II), L-aspartyl-L-alanyl-L-histidine-*N*-methyl amide (A) and L-histidine (B). **I**, CuB_2; **II**, CuB; **III**, CuAB; **IV**, $CuH_{-1}AB$; **V**, $CuH_{-2}A$.

CuB_2 as given by eq. [17]:

$$[17] \quad k_{obs} = \frac{k_4 k_5 [H^+][HB]}{k_{-4} + k_5[H^+]} + k_6[H^+] + k_7[B]$$

A plot of log k_{obs} against pH is shown in Fig. 4*b*. As pH increases from 6.5 to 8.5, the slope of the plot is -1, and then becomes less negative and levels off at high pH since L-His is converted to its free base form ($pK_a = 9.11$). Thus the rate eq. [17] is reduced to:

$$[18] \quad k_{obs} = \frac{k_4 k_5 [H^+][HB]}{k_{-4}} + k_6[H^+] + k_7[B]$$

$$[19] \quad = \frac{k_4 k_5 \beta_{0101} [H^+]^2[B]_T}{k_{-4}\,\alpha_{B(H)}} + k_6[H^+] + k_7 \frac{[B]_T}{\alpha_{B(H)}}$$

The predominant contribution to the rate at a pH lower than 8.5 is a proton and a protonated L-His pathway (eqs. [13]–[15]), and at higher pH it is a deprotonated L-His pathway (eq. [16]).

The values of k_4k_5/k_{-4}, k_6 and k_7 are $6.16 \times 10^6\ M^{-2}\ s^{-1}$, $2.06 \times 10^4\ M^{-1}\ s^{-1}$, and $1.25 \times 10^{-2}\ M^{-1}\ s^{-1}$, respectively.

Discussion

The physiological significance of the mixed ligand complex, albumin–Cu(II)–L-His in the biological transport of Cu(II) has been postulated earlier (9, 10). The preceeding equilibrium study of the ternary system containing the native sequence tripeptide (AAHNMA), Cu(II) and L-His indicates the presence of mixed ligand complexes (13% $CuH_{-1}AB$ and 3% CuAB) in addition to several binary species at physiological pH (5). The present kinetic investigation of the AAHNMA–Cu(II)–L-His ternary system shows the importance of the formation of mixed ligand complexes for the Cu(II)-transfer reaction (see Schemes 1 and 2), although the amounts of mixed ligand complexes formed are low. The combined results of the equilibrium and the kinetic studies demonstrate the mechanism and rate-controlling role played by the mixed ligand complexes in the Cu(II)-transfer reaction. A reaction scheme is derived in Fig. 5 taking into account the kinetic effect of pH, L-His, Cu(II)–L-His_2, and the distribution of chemical species in the ternary system. In this scheme, two mixed ligand complexes ($CuH_{-1}AB$, CuAB) are considered at physiological pH. In the Cu(II)-transfer from Cu(II)–L-His_2 to Cu(II)–AAHNMA, first step is the fast dissociation of one L-His molecule from Cu(II)–L-His (**I**) to form 1:1 Cu(II)–L-His complex (**II**). Two water molecules at equatorial position of 1:1 Cu(II)–L-His are substituted by the α-NH_2 nitrogen and the peptide oxygen of AAHNMA as anchoring points to form the mixed ligand complex (**III**) (CuAB, λ_{max} 595 nm). This is followed by deprotonation of the peptide nitrogen to form another mixed ligand complex (**IV**) $CuH_{-1}AB$, λ_{max} = 530 nm). Once the mixed ligand complex (**IV**) is formed, the displacement of amino and imidazole nitrogen atoms of L-His by the peptide nitrogen and imidazole nitrogen of AAHNMA would seem to be much more facilitated due to increased stability constant of tripeptide having a histidine residue (11). In the reverse reaction, the same rationale is also suggested. There is a nucleophilic attack of protonated L-His assisted by a proton to form mixed ligand complex $CuH_{-1}AB$. The mixed ligand complex $CuH_{-1}AB$ is protonated at peptide nitrogen to form another mixed ligand complex (CuAB), followed by the formation of Cu(II)–L-His.

From the kinetic data, the rate-controlling phenomenon can be determined at physiological pH. For the Cu(II)-transfer from Cu(II)–L-His_2 to native sequence peptide, the rate-determining step is a bond formation between Cu(II) and peptide nitrogen

TABLE 1. Rate and equilibrium constants for the reactions of $Cu(H_{-2}A)$ with L-histidine at 25°C (A = tripeptide; B = L-histidine)

No.	Rate and equilibrium equations	Constants	
		AAHNMA	GGH
1	$K = [Cu^{2+}][A]/[CuH_{-2}A][H^+]^2$	$3.55\ M^{-1}$†	$8.32 \times 10^1\ M^{-1}$‖
2	$K = [CuH_{-1}AB]/[CuH_{-2}A][HB]$	$1.49 \times 10^2\ M^{-1}$‡	$7.85 \times 10^3\ M^{-1}$‖
3	$K = [CuH_{-2}AB]/[CuH_{-2}A][B]$	$1.80 \times 10^2\ M^{-1}$‡	$4.16 \times 10^3\ M^{-1}$‖
4*	Rate = $k[H^+][HB][CuH_{-2}A]$	$6.16 \times 10^6\ M^{-2}\ s^{-1}$§	$4 \times 10^8\ M^{-2}\ s^{-1}$¶
5*	Rate = $k[H^+][CuH_{-2}A]$	$2.06 \times 10^4\ M^{-1}\ s^{-1}$§	$1.8 \times 10^5\ M^{-1}\ s^{-1}$¶
6*	Rate = $k[B][CuH_{-2}A]$	$1.25 \times 10^{-2}\ M^{-1}\ s^{-1}$§	$3 \times 10^{-1}\ M^{-1}\ s^{-1}$¶

*Rate = $-d[CuH_{-2}A]/dt = d[CuB_2]/dt$.
†Reference 1.
‡Reference 5.
§This work.
‖Reference 6.
¶Reference 12.

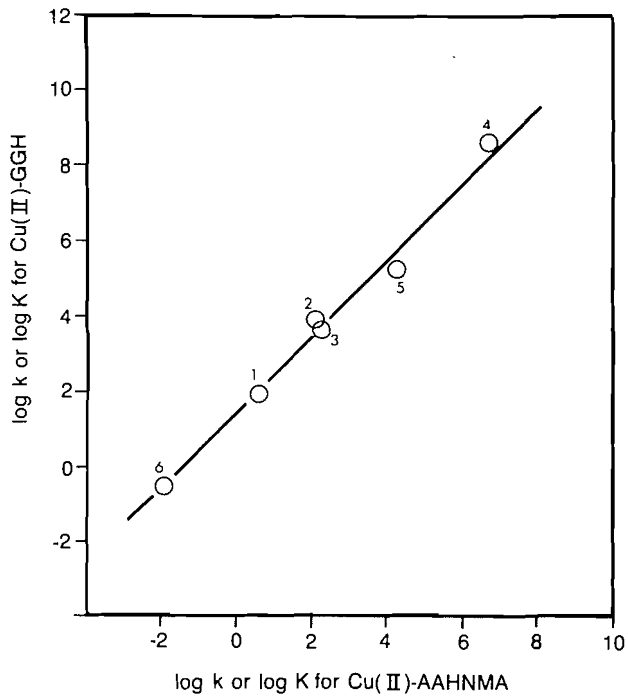

FIG. 6. Comparison of the reactivities and equilibrium constants of Cu(II)–GGH complex with those of Cu(II)–AAHNMA complex. (Refer to Table 1 for explanations of the numerical figures.) GGH = glycylglycyl-L-histidine, AAHNMA = L-aspartyl-L-alanyl-L-histidine-*N*-methyl amide.

to form $CuH_{-1}AB$ from CuAB by deprotonation of peptide nitrogen. For the Cu(II)-transfer from Cu(II)–peptide to L-His, the rate-determining step is a bond breaking between Cu(II) and peptide nitrogen to form CuAB from $CuH_{-1}AB$ by protonation to a peptide nitrogen. In both reactions, rate-determining step is a structural change of mixed ligand complex by protonation or deprotonation of peptide nitrogen.

It is interesting to compare the difference in Cu(II)-transfer reaction of peptides having different amino acid sequences. The carboxyl group of aspartyl residue of AAHNMA is bound to Cu(II) at its apical position in addition to the four nitrogen atoms in the square-plane forming a pentacoordinated structure (4, 12, 13). The ligand exchange reaction of Cu(II)–GGH complex has been reported earlier (14). The rate and equilibrium constants of reactions involving AAHNMA and GGH are shown in Table 1. The rate constants of the proton assisted nucleophilic pathway for the Cu(II)–AAHNMA complex is a factor of 65 times slower than for Cu(II)–GGH complex. Similar decreased rate constants in Cu(II)–AAHNMA are found for the nucleophilic attack pathway which is independent of L-His. Figure 6 shows a linear free energy relationship (15) between Cu(II)–AAHNMA and Cu(II)–GGH. The slope of the straight line is unity and the intercept is 1.4 (log value). This figure suggests that, in the Cu(II)-transfer reaction from Cu(II)–peptide to L-His, both peptides go through a similar activated complex in the process of bond breaking between Cu(II) and peptide. Carboxyl group of aspartyl residue in AAHNMA which coordinates to Cu(II) in an apical position (4) decreases the formation of mixed ligand complexes and makes the Cu(II)-transfer reaction from peptide to L-His difficult. Copper (II)-transfer reaction from peptide to L-His is dependent on the nature of the peptide. Hence, one should study the native sequence Cu(II)-transport site in order to delineate the kinetic mechanism of Cu(II)-transfer reaction involving albumin and L-His. The present finding suggests that the mixed ligand complexes formed by protonation or deprotonation are both kinetically and thermodynamically important intermediates in the Cu(II)-transfer reaction between albumin and L-histidine.

Acknowledgement

This investigation was supported by the Medical Research Council of Canada.

1. K. S. IYER, S. LAU, S. H. LAURIE, and B. SARKAR. Biochem. J. **169**, 61 (1978).
2. B. SARKAR. Metal ions in biological systems. *Edited by* H. Sigel. Vol. 12. 1981. pp. 233–281.
3. J-P. LAUSSAC and B. SARKAR. J. Biol. Chem. **250**, 7563 (1980).
4. J-P. LAUSSAC and B. SARKAR. Biochemistry, **23**, 2832 (1984).
5. M. TABATA and B. SARKAR. Can. J. Chem. **63**, 0000 (1985).
6. T. P. A. KRUCK and B. SARKAR. Inorg. Chem. **14**, 2383 (1975).
7. R. RINGBOM. Complexation in analytical chemistry. Interscience Publishers, New York, London. 1969. pp. 38–43.
8. T. P. A. KRUCK and B. SARKAR. Can. J. Chem. **51**, 3549 (1973).
9. B. SARKAR and Y. WIGFIELD. Can. J. Biochem. **46**, 601 (1968).
10. S. LAU and B. SARKAR. J. Biol. Chem. **246**, 5938 (1971).
11. G. F. BRYCE, R. W. ROESKE, and F. R. N. GURD. J. Biol. Chem. **240**, 2827 (1965).

12. B. SARKAR. Chem. Script. **21**, 101 (1983).
13. B. SARKAR, J-P. LAUSSAC, and S. LAU. Biological aspects of metals and metal related diseases. *Edited by* B. Sarkar. Raven Press, New York. 1983. pp. 23–40.
14. J. C. COOPER, L. F. WONG, D. L. VENEZKY, and D. W. MARGERUM. J. Am. Chem. Soc. **96**, 7560 (1974).
15. F. BASOLO and R. G. PEARSON. Mechanisms of inorganic reactions. 2nd ed. John Wiley and Sons, Inc., New York. 1968. pp. 396–400.

Equilibrium and spectroscopic studies of the ternary system: L-histidine, copper(II), and the native sequence peptide representing the copper(II)-transport site of human serum albumin

MASAAKI TABATA[1] AND BIBUDHENDRA SARKAR[2]

Research Institute, The Hospital for Sick Children, Toronto, Ont., Canada M5G 1X8; and Department of Biochemistry, University of Toronto, Toronto, Ont., Canada M5S 1A8

Received January 28, 1985

MASAAKI TABATA and BIBUDHENDRA SARKAR. Can. J. Chem. **63**, 3117 (1985).

Equilibrium and spectroscopic studies of Cu(II)-transfer of native sequence tripeptide, L-aspartyl-L-alanyl-L-histidine-*N*-methyl amide (AAHNMA), representing the Cu(II)-transport site of human serum albumin (HSA), and L-histidine (L-His) are reported. The equilibria in the ternary system, M–A–B (M = Cu(II), A = anionic form of AAHNMA, and B = anionic form of L-His) have been investigated by analytical potentiometry in I = 0.2 [(Na^+,H^+) (Cl^-,OH^-)] at 25°C. The ternary system shows the presence of five mixed ligand complexes: MH_2AB, MHAB, MAB, $MH_{-1}AB$, and $MH_{-2}AB$. The species distribution and their stability constants were evaluated by the mathematical analysis of the potentiometric data. The species were further confirmed by their individual spectra computed from the absorption measurements. At physiological pH, the equilibrium studies reveal the presence of 13% of $MH_{-1}AB$ (λ_{max} = 530 nm, ϵ = 90 M^{-1} cm^{-1}) and 3% MAB (λ_{max} = 595 nm, ϵ = 97 M^{-1} cm^{-1}). The combined results of equilibrium and spectroscopic studies indicate the mixed ligand complex $CuH_{-1}AB$ formed by deprotonation of peptide nitrogen as an important intermediate in the Cu(II)-transfer reaction. The stability constant of $CuH_{-1}AB$ is compared to those of other tripeptides which were designed to mimic the specific Cu(II)-transport site of human albumin.

MASAAKI TABATA et BIBUDHENDRA SARKAR. Can. J. Chem. **63**, 3117 (1985).

On rapporte des études spectroscopiques et d'équilibre relatives à la réaction de transfert du Cu(II) du tripeptide naturel L-aspartyl-L-alanyl-L-histidine-*N*-méthylamide (AAHNMA), qui est le siège du transport du Cu(II) dans l'albumine du sérum humain (ASH), à la L-histidine (L-His). Opérant à 25°C, avec I = 0,2 [(Na^+,H^+) (Cl^-,OH^-)] et faisant appel à la potentiométrie analytique, on a étudié l'équilibre du système ternaire M–A–B dans lequel M = Cu(II), A = forme anionique du AAHNMA et B = forme anionique de la L-His. Le système ternaire révèle la présence de cinq ligands complexes mixtes, soit MH_2AB, MHAB, MAB, $MH_{-1}AB$ et $MH_{-2}AB$. On a évalué la distribution des espèces et leur constante de stabilité en faisant appel à une analyse mathématique des données potentiométriques. Les spectres individuels calculés à partir des mesures d'absorption confirment l'existence de ces espèces. Les études d'équilibre à pH physiologique révèlent la présence de 13% de $MH_{-1}AB$ (λ_{max} = 538 nm, ϵ = 90 M^{-1} cm^{-1}) et de 3% de MAB (λ_{max} = 595 nm, ϵ = 97 M^{-1} cm^{-1}). Les résultats combinés des études d'équilibre et spectroscopiques indiquent que le complexe de ligand mixte $CuH_{-1}AB$, formé par la déprotonation de l'azote du peptide, est un intermédiaire important dans la réaction de transfert de Cu(II). On a comparé la constante de stabilité du $CuH_{-1}AB$ à celles des autres tripeptides qui ont été préparés pour reproduire le site spécifique du transport de Cu(II) dans l'albumine humaine.

[Traduit par le journal]

Introduction

Copper is an essential trace element which plays an important role in many biological systems (1). The major portion of copper (90–95%) in mammalian plasma is in the form of ceruloplasmin which is not exchangeable *in vivo* (2). However, the remainder (5–10%) is bound to albumin and amino acids which are in rapid equilibrium with copper in tissues (3). Serum albumin is the major Cu(II)-transport protein and L-histidine (L-His) is the main Cu(II)-binding amino acid in blood (4–6). At physiological pH and concentrations, there is an equilibrium between albumin–Cu(II) and L-His–Cu(II) through a ternary complex, albumin–Cu(II)–L-His (7). It has been proposed that the ternary complex plays an important role as an intermediate in the transfer of Cu(II) from albumin to an amino acid and the Cu(II) – amino acid complex in turn is readily transported across the biological membrane (7).

Earlier studies led to the proposal that the Cu(II)-binding site of albumin involves the α-amino nitrogen, two peptide nitrogens and one imidazole nitrogen (8–10). Subsequent studies in this laboratory with synthetic peptides, glycylglycyl–L-histidine (GGH) and glycylglycyl–L-histidine-*N*-methyl amide (GGHNMA) revealed very similar Cu(II)-binding properties with those of albumin–Cu(II) complex (11–16). However, the studies with NH_2-terminal native sequence tripeptide, L-aspartyl-L-alanyl-L-histidine-*N*-methyl amide (AAHNMA) showed that the native sequence peptide resembled closer to albumin as far as their Cu(II)-binding affinity and dissociation are concerned (17). The latest results of Cu(II)-binding to AAHNMA by ^{13}C-nmr experiments suggest that, in addition to the four nitrogen ligands in a square-planar coordination as suggested before, there is the involvement of the side chain carboxyl group of aspartyl residue forming a pentacoordinated structure (18). This structure is confirmed by further studies of the Cu(II)-binding to the NH_2-terminal 24-residue fragment of human serum albumin (HSA) (19, 20). Copper(II) bound to L-His is the major physiologically important Cu(II) – amino acid complex; its detailed equilibrium and structural studies have also been reported (21, 22).

The above results prompted us to study the equilibria of the ternary system containing the native sequence peptide AAHNMA, Cu(II), and L-His. In this paper, we report detailed equilibrium studies of the ternary system. The species and their stability constants in the system, AAHNMA–Cu(II)–L-His in I = 0.2 [(Na^+,H^+) (Cl^-,OH^-)] at 25°C were determined by

[1] Present address: Department of Chemistry, Faculty of Science and Engineering, Saga University, 1 Honjo-machi Saga, 840 Japan.

[2] To whom correspondence should be addressed.

TABLE 1. Sample composition of the ternary systems M–A–B (M = Cu(II), A = L-aspartyl-L-alanyl-L-histidine-*N*-methyl amide, B = L-histidine) titrated in 0.15 *M* NaCl at 25°C

	Total amount (10^{-5} mol)		
Sample No.	Metal	Ligand A	Ligand B
Metal concentration variation			
1	4.88	29.31	30.00
2	9.75	29.31	30.00
3	19.55	29.31	30.00
Ligand A concentration variation			
4	4.88	9.77	30.00
5	4.88	19.54	30.00
6	4.88	29.31	30.00
Ligand B concentration variation			
7	4.88	29.31	10.00
8	4.88	29.31	20.00
9	4.88	29.31	30.00

analytical potentiometry (23, 24). The species were further confirmed by their individual spectral characteristics.

Experiment

Materials

The peptide, L-aspartyl-L-alanyl-L-histidine-*N*-methyl amide, was synthesized according to the method described earlier (17). The purity of the peptide was checked by thin-layer chromatography. L-Histidine monohydrochloride ($[\alpha]_D^{20}$ + 10.0 ± 0.5) was obtained from Nutritional Biochemicals (Cleveland, OH). The purity was checked by thin-layer chromatography. It was dried at 110°C for 24 h and then stored over anhydrous calcium chloride at room temperature under vacuum. The peptide and L-His stock solutions were prepared in water and 40 m*M* HCl, respectively, and stored in cold and dark. All other reagents were of analytical grade.

Potentiometric titration

The potentiometric titrations were performed on a Radiometer automatic titration assembly consisting of a Radiometer PHM64 Research pH Meter, an automatic titrator, TTT60, an automatic recorder, REC61, an autoburette, ABU13, and a 50 mL titration vessel thermostated at 25.0 ± 0.1°C. The pH meter and electrodes were adjusted against standard buffers (pH 4.01, 7.00, and 9.18 at 25°C).

The 1.025 *M* sodium hydroxide was prepared carbonate-free and stored under argon atmosphere. It was standardized against phthalate (National Bureau of Standards). Analytical grade copper(II) chloride (Fisher Scientific Co.) was dissolved to give 1.0 *M* solution in 0.5 *M* HCl and standardized complexometrically with EDTA using murexide indicator. All the solutions contained 0.15 *M* NaCl and known amount of HCl to lower the starting pH. Since the stability constants of Cu(II)–L-His_2 and Cu(II)–AAHNMA complexes are very high, the formation of the chloride complex of Cu(II) is negligible. The solutions containing Cu(II), AAHNMA, and L-His were titrated with 1.025 *M* NaOH from pH 1.6 to 12.0. Ionic strength was 0.21 ± 0.01 [(Na^+,H^+) (Cl^-,OH^-)]. The slight change in ionic strength during the titration does not cause any change in the activity coefficient of hydrogen ion (25, 26). The concentrations of Cu(II) and ligands in each sample are listed in Table 1.

Spectrophotometry

The visible absorption spectra of the Cu(II)–AAHNMA–L-His ternary system were recorded on a Beckman ACTA MVI spectrophotometer as a function of pH in 0.15 *M* NaCl solution at 25°C.

Results

Determination of species distribution and stability constants

The complexation reaction in the ternary system involving metal ion M, proton H, ligands A and B can be represented as:

$$[1] \quad pM + qH + rA + sB \rightleftharpoons M_pH_qA_rB_s$$

where *p*, *q*, *r*, and *s* are the stoichiometric quantities of M, H, A, and B, respectively. A and B denote the anionic forms of AAHNMA and L-His, respectively. The stabilities of the species formed are expressed as the stoichiometric equilibrium constants β_{pqrs} in terms of concentrations at constant ionic strength, temperature, and pressure:

$$[3] \quad C_M = m + \Sigma p\beta_{pqrs}m^p h^q a^r b^s$$

$$[4] \quad C_H = h + \Sigma q\beta_{pqrs}m^p h^q a^r b^s$$

$$[5] \quad C_A = a + \Sigma r\beta_{pqrs}m^p h^q a^r b^s$$

$$[6] \quad C_B = b + \Sigma s\beta_{pqrs}m^p h^q a^r b^s$$

The experimental data and titration curves ($-\log h$ = *f*(base)) were obtained from solutions of defined concentrations of C_M, C_H, C_A, and C_B. The following relationships were used to obtain the values for the unbound portions of metal and the different ligands throughout the titration.

$$[7] \quad pM = pM_0 + \int_{pH_0}^{pH_i} \frac{\delta H_I^+}{\delta C_M} dpH$$

$$[8] \quad pA = pA_0 + \int_{pH_0}^{pH_i} \frac{\delta H_I^+}{\delta C_A} dpH$$

$$[9] \quad pB = pB_0 + \int_{pH_0}^{pH_i} \frac{\delta H_I^+}{\delta C_B} dpH$$

where pM = $-\log$ [free metal M], pA = $-\log$ [free ligand A], pH = $-\log h$, pB = $-\log$ [free ligand B], H_I^+ = moles of OH^- consumed to titrate hydrogen ions liberated through the complexation reactions. Subscript 0 denotes an initial known state of the system. The mathematical analyses of the titration data were performed by the sequential use of three computer programs, PLOT-3, GUESS-3, and LEASK-4 (written in BASIC language). The program PLOT-3 takes the numerical titration data and calculates the proton-liberation terms $\delta H_I^+/\delta C_M$, $\delta H_I^+/\delta C_A$, and $\delta H_I^+/\delta C_B$ and the amount of the free metal ion and ligands A and B at each selected pH value in eqs. [7]–[9], where H_I^+ means the released proton by complexation (24). The program GUESS-3, using data from PLOT-3, sets up a matrix of the terms $m^p h^q a^r b^s$ for each proposed species. This matrix then serves as an input to the program LEASK-4, which uses an iterative least-squares minimization procedure to calculate the stability constant β_{pqrs}. A detailed account of the data processing has been previously reported (17, 23, 24).

*Cu(II)-proton-L-aspartyl-L-alanyl-L-histidine-*N*-methyl amide-L-histidine*

In the metal-concentration variation experiments, solutions 1–3 in Table 1 were titrated, and in the ligand-concentration variation, solutions 4–6 for ligand A and solutions 7–9 for ligand B were used (Table 1). Titration curves are shown in Fig. 1. The data were processed likewise to yield $\delta H_I^+/\delta C_M$ (Fig. 2, curve *a*), $\delta H_I^+/\delta C_A$ (Fig. 2, curve *b*), and $\delta H_I^+/\delta C_B$ (Fig. 2, curve *c*) as a function of pH.

For the species selection of the complexes formed in the system, the following values for *p*, *q*, *r*, and *s* were used: *p* =

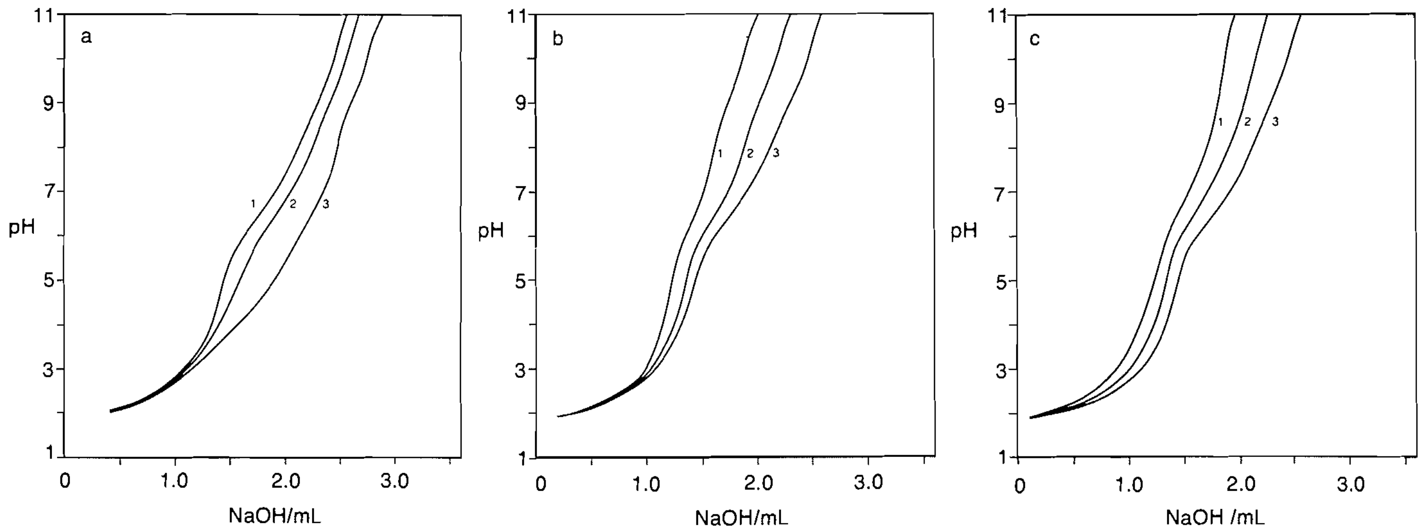

FIG. 1. Titration curves for the ternary system M–A–B (M = Cu(II), A = L-aspartyl-L-alanyl-L-histidine-*N*-methyl amide, B = L-histidine). (*a*) Metal variation: $C_A = 5.86 \times 10^{-3}$ *M*; $C_B = 6.00 \times 10^{-3}$ *M*; curve *1*, $C_M = 0.975 \times 10^{-3}$ *M*; curve *2*, $C_M = 1.950 \times 10^{-3}$ *M*; curve *3*, $C_M = 3.90 \times 10^{-3}$ *M*. (*b*) Ligand A variation: $C_M = 0.975 \times 10^{-3}$ *M*; $C_B = 6.00 \times 10^{-3}$ *M*; curve *1*, $C_A = 1.950 \times 10^{-3}$ *M*; curve *2*, $C_A = 3.91 \times 10^{-3}$ *M*; curve *3*, $C_A = 5.86 \times 10^{-3}$ *M*. (*c*) Ligand B variation: $C_M = 0.975 \times 10^{-3}$ *M*; $C_A = 5.86 \times 10^{-3}$ *M*; curve *1*, $C_B = 2.00 \times 10^{-3}$ *M*; curve *2*, $C_B = 4.00 \times 10^{-3}$ *M*; curve *3*, $C_B = 6.00 \times 10^{-3}$ *M*.

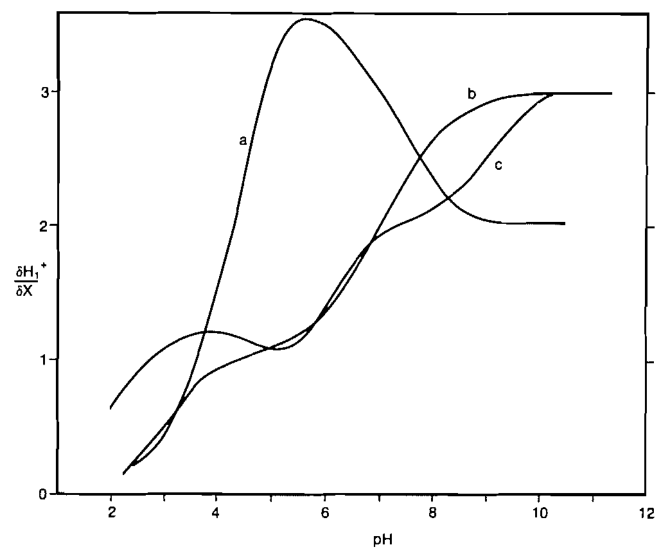

FIG. 2. Proton liberation as a function of pH for the ternary system M–A–B (M = Cu(II), A = L-aspartyl-L-alanyl-L-histidine-*N*-methyl amide, B = L-histidine). $C_M = 9.75 \times 10^{-4}$ *M*, $C_A = 5.86 \times 10^{-3}$ *M*; $C_B = 6.00 \times 10^{-3}$ *M*. Curve *a*, $\delta H_1^+/\delta C_M$; curve *b*, $\delta H_1^+/\delta C_A$; curve *3*, $\delta H_1^+/\delta C_B$.

1; $q = +2, +1, 0, -1, -2$; $r = 1, 2$; $s = 1, 2$.

To solve for the stability constants of the ternary complexes, all previously determined stability constants from the binary system (17, 21) were kept constant and only those of the ternary species $M_pH_qA_rB_s$ were treated as variables. The minimum error solution for the ternary system permitted the presence of five ternary complexes, MH_2AB, MHAB, MAB, $MH_{-1}AB$, and $MH_{-2}AB$; their stability constants are included in Table 2, and the species distribution as a function of pH is shown in Fig. 3.

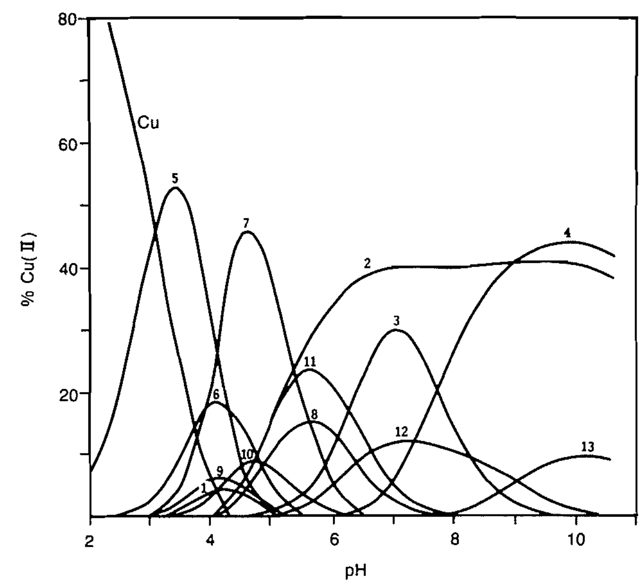

FIG. 3. Species distribution in the ternary system of M–A–B (M = Cu(II), A = L-aspartyl-L-alanyl-L-histidine-*N*-methyl amide, B = L-histidine) as a function of pH: curve *1*, CuA; curve *2*, $CuH_{-2}A$; curve *3*, $CuH_{-1}A_2$; curve *4*, $CuH_{-2}A_2$; curve *5*, CuHB; curve *6*, CuB; curve *7*, $CuHB_2$; curve *8*, CuB_2; curve *9*, $CuH_{-2}AB$; curve *10*, CuHAB; curve *11*, CuAB; curve *12*, $CuH_{-1}AB$; curve *13*, $CuH_{-2}AB$. $C_M = 9.75 \times 10^{-4}$ *M*; $C_A = 5.86 \times 10^{-3}$ *M*; $C_B = 6.00 \times 10^{-3}$ *M* at $I = 0.2$ and 25°C.

Visible absorption spectra

The spectra of a solution containing a M:A:B molar ratio of 1:6:6 and 0.15 *M* NaCl were recorded at pH 2.6–10.0 in the visible region from 400 to 800 nm. The total Cu(II) concentration was 2.925×10^{-3} *M*.

Absorbance at a fixed wavelength is correlated with the concentration of $M_pH_qA_rB_s$ as follows:

$$[10] \quad A_\lambda = \sum_{pqrs} \epsilon_{\lambda,pqrs} [M_pH_qA_rB_s]$$

where A_λ is the absorbance at wavelength λ, 1 cm light path, and ε is the molar absorbance of the species $M_pH_qA_rB_s$ at that wavelength. The mathematical analyses, of eq. [10] for the

TABLE 2. log (stability constants) (β_{pqrs}) of the complex species $M_pH_qA_rB_s$ (M = Cu(II), A = peptide, B = L-histidine) at I = 0.2 and 25°C

	log β_{pqrs}		
Chemical Species	AAHNMA[a]	GGHNMA[b]	GGH[c]
CuA	8.39		7.55
$CuH_{-2}A$	−0.55	−0.479	−1.92
$CuH_{-1}A_2$	9.78		
$CuH_{-2}A_2$	2.06		
CuH_2AB	26.29	27.75	28.83
CuHAB	22.03		23.61
CuAB	17.35		17.56
$CuH_{-1}AB$	10.74	11.31	11.05
$CuH_{-2}AB$	1.71	3.02	1.7

[a]This work.
[b]Reference 13.
[c]Reference 12.

TABLE 3. Spectral characteristics of the complex species $M_pH_qA_rB_s$ (M = Cu(II), A = L-aspartyl-L-alanyl-L-histidine-N-methyl amide, B = L-histidine) at I = 0.2 and 25°C

Species	λ_{max}/nm	ϵ/M^{-1} cm^{-1}
$CuH_{-2}A$	525	103
$CuH_{-1}A_2$	525	110
$CuH_{-2}A_2$	525	120
$CuH_{-1}AB$	530	90
$CuH_{-2}AB$	525	81
CuAB	595	97
CuB_2	640	86

spectral data at various pH's were performed by the use of computer program LEASK-2 which gave the calculated spectra for individual species $M_pH_qA_rB_s$. Their spectral parameters are included in Table 3.

Discussion

The native sequence tripeptide, AAHNMA, represents the actual Cu(II)-transport site of human albumin. The Cu(II)–tripeptide complex exists as $CuH_{-2}A$ from pH 5 to 10 (17). In the ternary system containing AAHNMA, Cu(II) and L-His, analyses of titration results indicate the presence of five ternary complexes, namely MH_2AB, MHAB, MAB, $MH_{-1}AB$, $MH_{-2}AB$, in addition to several binary species. Owing to the extensive overlap of different species, especially in low pH, it is difficult to obtain clear information about the structural features of these mixed ligand complexes from combined results of the proton displacement, the species distribution, and the computed visible absorption spectra. However, the detection of about 16% of mixed ligand complexes at physiological pH suggests the possible significance of their presence in solution.

The predominant species $MH_{-2}A$, $MH_{-2}A_2$, $MH_{-1}AB$, and $MH_{-2}AB$ all seem to have computed maximal absorption around 525 nm which indicates that four nitrogens are ligated around the central Cu(II) ion. However, MAB has calculated λ_{max} of 595 nm. Judging from its occurrence at a slightly lower pH (~4.7), an oxygen of peptide carbonyl instead of peptide nitrogen is likely to be participating in the coordination (27).

The main mixed ligand complex is in the form of $MH_{-1}AB$ at physiological pH. This is consistent with the results obtained from GGH and GGHNMA (12, 13). Distribution of the mixed ligand complex $CuH_{-1}AB$ is very dependent on the nature of the tripeptide: maximum, 35% for GGHNMA, and 13% for AAHNMA. Since the formation of a mixed ligand complex involves the making of at least one coordination bond from L-His in the coordination square-plane, it would require the removal of at least one of the Cu(II)-coordinating nitrogens of the peptide. With higher stability constant of $MH_{-2}A$ complex for the tripeptide, we would expect lesser amounts of mixed ligand complexes to be formed. Comparing the stability constants of binary and ternary systems, as shown in Table 2, two tripeptide amides, GGHNMA and AAHNMA, have comparable stability constants (β_{1-21}, $CuH_{-2}A$) whereas AAHNMA shows a lower stability constant of mixed ligand complex ($\beta_{1\text{-}111}$, $CuH_{-1}AB$) compared to the other tripeptides. Furthermore, the stability constant of Cu(II)–AAHNMA (β_{1-21}) is 23 times higher than that of Cu(II)–GGH, and the stability constant of mixed ligand complex of Cu(II)–AAHNMA–L-His (β_{1-111}) is 53 times smaller than that of Cu(II)–GGH–L-His. The difference has also been observed in the ligand-exchange rate for Cu(II)–tripeptide with L-His. The Cu(II)-exchange rate between Cu(II)–GGH and L-His is 3.5×10^{-2} s^{-1} (28), which is 5 times greater than that found for Cu(II)–AAHNMA under the same experimental conditions. The observed differences are consistent with the stability constant of mixed ligand complex ($MH_{-1}AB$). Carboxyl group of aspartyl residue in AAHNMA which coordinates to Cu(II) in apical position (18) stabilizes Cu(II)–AAHNMA complex more compared to Cu(II)–GGH. This makes the formation of mixed ligand complex and the Cu(II)-transfer reaction from peptide to L-His more difficult.

X-ray crystal structure analysis of [Cu(L-His)(L-Thr)(H_2O)]·[H_2O] shows that L-His coordinates to Cu(II) through its amino and imidazole nitrogens with the carboxylate oxygen in the apical position and that L-Thr occupies the rest of the coordination plane with a glycine-like chelation in a *cis*-configuration with respect to the amino groups (29), where L-Thr denotes L-threonine. The stability constant of the mixed ligand complex, Cu(L-His)(L-Thr), was determined in 20% v/v dioxane–water and the overall stability constant (log β_{1011}) is 17.57 (30). Yamauchi and co-workers (30) also showed that the stability constants (log β_{1011}) for a ternary system containing Cu(II), L-His, and amino acid (glycine, L-alanine, L-valine, L-asparagine, L-glutamine, L-citrulline, L-serine, L-threonine, or L-homoserine) are in the range 17.4–18.0. The stability constants of Cu(L-His) (L-amino acid) are very close to those of Cu(L-His) tripeptide: log β_{1011} is 17.35 for Cu(L-His)–AAHNMA, and 17.56 for Cu(L-His)–GGH (see Table 2). This similarity suggests that L-His in CuAB coordinates to Cu(II) through its amino and imidazole-nitrogens in the square-plane and AAHNMA or GGH binds to Cu(II) as a bidentate ligand through amino nitrogen and peptide carbonyl oxygen. The characteristic spectral property (λ_{max} 595 nm) of CuAB also supports such a structure. At a higher pH, $CuH_{-1}AB$ appears with spectral change from λ_{max} 595 to 530 nm. In $CuH_{-1}AB$, coordination takes place with the peptide amide nitrogen instead of carbonyl oxygen. The proton dissociation constants (pK_a) of CuAB to form $CuH_{-1}AB$ are 6.61 for Cu(L-His)-AAHNMA and 6.51 for Cu(L-His)GGH, respectively.

The synthetic native sequence peptide, AAHNMA represents the actual Cu(II)-transport site of human albumin. It was possible to obtain more detailed information with the synthetic peptide which one could not obtain with intact HSA because of the inherent complexity associated with a protein molecule. The present findings indicate that the mixed ligand complex formation initiated by deprotonation of peptide nitrogen ($CuH_{-1}AB$) or by protonation of peptide nitrogen (CuAB) is an important intermediate in the Cu(II)-transfer reaction (31) between human serum albumin and L-His and that the side chain-carboxyl group of aspartyl residue decreases the formation of mixed ligand complexes of CuAB and $CuH_{-1}AB$.

Acknowledgements

We wish to thank Dr. S. Lau for many helpful suggestions during these studies. This investigation was supported by the Medical Research Council of Canada.

1. B. SARKAR. Metal ions in biological systems. Vol. 12. *Edited by* H. Sigel. Marcel Dekker, New York. 1981. pp. 233–281.
2. I. STERNLIEB, A. G. MORELL, W. D. TUCKER, M. W. GREEN, and I. H. SCHEINBERG. J. Clin. Invest. **40**, 1834 (1961).
3. A. G. BEARN and H. G. KUNKEL. Proc. Soc. Exp. Biol. Med. **88**, 44 (1954).
4. B. SARKAR and T. P. A. KRUCK. Biochemistry of copper. *Edited by* Peisach, P. Aisen, and W. E. Blumberg. Academic Press, New York. 1966. pp. 183–196.
5. P. Z. NEUMANN and A. SASS-KORTSAK. J. Clin. Invest. **46**, 646 (1967).
6. B. SARKAR and Y. WIGFIELD. Can. J. Biochem. **46**, 601 (1968).
7. S. LAU and B. SARKAR. J. Biol. Chem. **246**, 5938 (1971).
8. R. B. MARTIN. Fed. Proc. Fed. Am. Soc. Exp. Biol. 20 suppl. 54 (1961).
9. E. BRESLOW. J. Biol. Chem. **239**, 3252 (1964).
10. T. PETERS, JR., and F. A. BLUMENSTOCK. J. Biol. Chem. **242**, 1574 (1967).
11. S. LAU, T. P. A. KRUCK, and B. SARKAR. J. Biol. Chem. **249**, 5878 (1974).
12. T. P. A. KRUCK and B. SARKAR. Inorg. Chem. **14**, 2383 (1975).
13. T. P. A. KRUCK, S. LAU, and B. SARKAR. Can. J. Chem. **54**, 1300 (1976).
14. N. CAMERMAN, A. CAMERMAN, and B. SARKAR. Can. J. Chem. **54**, 1309 (1976).
15. G. ARENA, E. RIZZARELLI, and B. SARKAR. Inorg. Chim. Acta, **37**, 1555 (1979).
16. S. LAU and B. SARKAR. J. Chem. Soc. Dalton, 491 (1981).
17. K. S. IYER, S. LAU, S. H. LAURIE, and B. SARKAR. Biochem. J. **169**, 61 (1978).
18. J.-P. LAUSSAC and B. SARKAR. J. Biol. Chem. **250**, 7563 (1980).
19. B. SARKAR. Chem. Script. **21**, 101 (1983).
20. J.-P. LAUSSAC and B. SARKAR. Biochemistry, **23**, 2832 (1984).
21. T. P. A. KRUCK and B. SARKAR. Can. J. Chem. **51**, 3549 (1973).
22. M. ITABISHI and K. ITOH. Bull. Chem. Soc. Jpn. **53**, 3131 (1980).
23. B. SARKAR and T. P. A. KRUCK. Can. J. Chem. **51**, 3541 (1973).
24. B. SARKAR. J. Ind. Chem. Soc. **54**, 117 (1977).
25. R. A. ROBINSON and R. H. STOKES. Electrolyte solutions. 2nd ed. Butterworth Scientific Publishing Company, London. 1959. pp. 490–503.
26. A. RINGBOM. Complexation in analytical chemistry. Vol. 24. Interscience Publishers, New York, London. 1969.
27. R.-P. MARTIN, L. MOSONI, and B. SARKAR. J. Biol. Chem. **246**, 5944 (1971).
28. S. LAU and B. SARKAR. Can. J. Chem. **53**, 710 (1975).
29. H. C. FREEMAN, J. M. GUSS, M. J. HEALY, R. P. MARTIN, C. E. NOCKOLDS, and B. SARKAR. Chem. Commun. 225 (1969).
30. O. YAMAUCHI, T. TAKABA, and T. SAKURAI. Bull. Chem. Soc. Jpn. **53**, 106 (1980).
31. M. TABATA and B. SARKAR. Can. J. Chem. **63**, 0000 (1985).

Fletcher–Powell minimization of analytical potentiometric data by microcomputer: application to the Cu(II) complexes of biological polyamines

DOUGLAS M. TEMPLETON AND BIBUDHENDRA SARKAR
Research Institute, The Hospital for Sick Children, Toronto, Ont., Canada M5G 1X8, and Department of Biochemistry, University of Toronto, Toronto, Ont., Canada M5S 1A8

Received February 8, 1985

DOUGLAS M. TEMPLETON and BIBUDHENDRA SARKAR. Can. J. Chem. **63**, 3122 (1985).

The Fletcher–Powell minimization algorithm has been successfully implemented for the extraction of metal complex stability constants from analytical potentiometric data. The procedure has been adapted to run on a microcomputer with acceptable execution times, and several strategies are employed to speed convergence and avoid false minima. This allows economical minimization for a large number of models of speciation, and improves the reliability of the proposed best fit by encouraging the checking of more models than previously possible. The Ni(II)–glycine system has been analyzed and excellent agreement with the stability constants of an earlier multi-laboratory study has been attained. The system proves useful in the evaluation of both analytical and computational methods. The procedure has also been used for speciation analysis of the Cu(II) complexes of the growth regulating polyamines, spermine, and spermidine. Both systems form fully deprotonated complexes at physiological pH, which are relevant to their biological activity.

DOUGLAS M. TEMPLETON et BIBUDHENDRA SARKAR. Can. J. Chem. **63**, 3122 (1985).

On a utilisé avec succès l'algorithme de minimisation de Fletcher–Powell dans le but d'obtenir les constantes de stabilité des complexes métalliques à partir de données potentiométriques analytiques. On a modifié la méthode de façon à utiliser un microordinateur avec des délais d'exécution acceptables et on a utilisé plusieurs approches afin d'accélérer la convergence et d'éviter les faux minima. Ceci permet de minimiser d'une façon économique pour un grand nombre de modèles de spéciation et d'améliorer l'exactitude de cette méthode en permettant l'évaluation de plus de modèles que cela n'était possible jusqu'à maintenant. On a analysé le système Ni(II)–glycine et les résultats obtenus s'accordent parfaitement avec ceux obtenus antérieurement dans une étude réalisée conjointement par plusieurs laboratoires. Le système se révèle utile pour réaliser des évaluations tant de méthodes analytiques que de méthodes de calculs à l'aide d'ordinateurs. On a également utilisé cette méthode pour l'analyse de spéciation des complexes de Cu(II) des polyamines régularisatrices de la croissance, comme la spermine et la spermidine. Les deux systèmes forment, au pH physiologique, des complexes complètement déprotonés qui sont importants à cause de leur activité biologique.

[Traduit par le journal]

Introduction

A technique for determining the free (uncomplexed) ligand concentration as a function of pH, in the presence of a metal ion, was developed by Österberg (1), based on a procedure by Lefebvre (2). Conveniently, it involved only potentiometric titration with a glass pH electrode. The method was extended by Sarkar and co-workers (3, 4) to allow both free metal and ligand concentrations to be extracted from a series of pH titrations in which both ligand and metal concentrations were systematically varied. Subsequently, this laboratory has used this technique of analytical potentiometry to study the binding of metals to a variety of ligands of biological interest (5–9), using a series of programs written for a main frame computer. A number of groups are now using variations of this technique (10–12), which we have called analytical potentiometry. This method presents the advantage over alternatives, that the free ion concentrations entering into the definition of the stability constants are calculated directly from experimental titration data in a model-independent procedure, and need not themselves be refined for each proposed speciation model.

We report here the use of the Fletcher–Powell (FP) algorithm (13) to expedite the microcomputer solution of metal complex stability constants from potentiometric data. We have tested the procedure by determining speciation of the Ni(II)–glycine system, chosen as a test system for a previous inter-laboratory procedure evaluation (14). We also report an analysis of the Cu(II) complexation of two polyamines of great biological interest (15, 16), spermidine (1,8-diamino-4-aza-octane) and spermine (1,12-diamino-4,9-diaza-dodecane).

Theory

Calculation of the free metal and ligand concentrations as a function of pH proceeds from the titration data in a straightforward manner (3). This allows direct calculation of all terms in eq. [1] except the stability constants:

$$[1] \quad \mathbf{C}\,|\beta\rangle = |m_b\rangle$$

Here $\mathbf{C}$ is a $k \times n$ coefficient matrix with terms $c_{ij} = pm^p h^q l^r$ for the jth species at the ith pH. There are k pH values and n species $M_pH_qL_r$ where p, q, r are the stoichiometric coefficients of metal (M), proton (H), and ligand (L), respectively, in the complex, and m, h, and l are the corresponding free ion concentrations. $|m_b\rangle$ is the column vector of bound metal concentrations with terms $m_{b1}, m_{b2}, \ldots m_{bk}$ calculated as $M_T - m_i$ at each pH$_i$, where M_T is the total analytical concentration of metal. $|\beta\rangle$ represents the column vector of n β values, the concentration stability constants, β_j for the jth species being defined as

$$[2] \quad \beta_j = [M_pH_qL_r]_j / m^p h^q l^r$$

The problem is then one of finding the best solution for the overdetermined ($k > n$) set of k equations in n unknowns (eq. [1]). In methods alternative to analytical potentiometry, the coefficient matrix $\mathbf{C}$ is itself modeled and refined, a computationally more demanding approach. In the most widely used of these methods, MINIQUAD (17), $\mathbf{C}$ is sparse, and some of the difficulties are overcome by factorization (18). We have sought to take advantage of our knowledge of $\mathbf{C}$ to solve eq. [1] for the least-squares solution of $|\beta\rangle$ directly by an iterative minimization technique.

The least squares solution is taken as that β which minimizes U, where

$$[3] \quad U = \sum_{i=1}^{k} \left\{ \left[\sum_{j=1}^{n} p\, (m_i^p h_i^q l_i^r)_j\, \beta_j \right] - m_{bi} \right\}^2$$

$$= \sum_{i=1}^{k} \left[\left(\sum_{j=1}^{n} c_{ij} \beta_j \right) - m_{bi} \right]^2$$

A major source of computational difficulty is presented by the preference to carry out the refinement with respect to β, and avoid a change of variables to log β values. It has been shown (19) that such a change of variables transforms the function into a highly non-linear, non-concave function which is extremely difficult to minimize by any method. The wide range of values necessitates effective scaling to achieve refinement, and also makes matrix inversion so prone to rounding errors (20) that techniques based on finding $\mathbf{C}^{-1}$ are virtually unusable. We require a method which will handle a wide range of values of C_{ij} and β (typically spanning 40 orders of magnitude), with rapid convergence and avoidance of false minima, which can be executed rapidly on a microcomputer. The FP method has been found superior to Gauss–Newton–Raphson and other gradient methods with respect to speed and reliability of convergence. It was tried with some success (18) in a forerunner of the MINIQUAD program, but was replaced by a faster, though less memory-efficient Gauss–Newton method in the final version. Because analytical potentiometric data require less computation, acceptable run times can be achieved using the FP method. Furthermore, it has allowed us to take advantage of specific strategies in solving for $|\beta\rangle$ (*vide infra*).

We define an $n \times n$ Hessian matrix $\mathbf{G}$ with terms

$$[4] \quad G_{ij} = \partial^2 U/\partial\beta_i \partial\beta_j = g_i g_j$$

where

$$[5] \quad g_x = (\partial/\partial\beta_x) \left\{ \sum_{i=1}^{k} [m_b^2 - 2m_b\,(C_{i1}\beta_1 + C_{i2}\beta_2 + \ldots + C_{ix}\beta_x + \ldots + C_{in}\beta_n) + (C_{i1}\beta_1 + C_{i2}\beta_2 + \ldots + C_{ix}\beta_x + \ldots + C_{in}\beta_n)^2] \right\}$$

$$= \sum_{i=1}^{k} \left[-2m_b C_{ix} + 2C_{ix} \left(\sum_{j=1}^{n} C_{ij}\beta_j \right) \right]$$

so that the displacement between a given point $|\beta\rangle$ and the minimum $|\beta_0\rangle$ is

$$[6] \quad |\beta_0\rangle - |\beta\rangle = -\mathbf{G}^{-1}\,|g\rangle$$

and $|g\rangle$ is the gradient vector $(g_1 \ldots, g_n)$. To avoid inverting $\mathbf{G}$, we use instead a positive definite matrix $\mathbf{H}$ and set a shift vector

$$[7] \quad |s^i\rangle = \mathbf{H}^i\,|g^i\rangle$$

at the ith iteration. We then take a step $|\sigma^i\rangle$ towards the minimum by setting

$$[8] \quad |\sigma^i\rangle = \alpha^i\,|s^i\rangle$$

and modifying $|\beta\rangle$ as

$$[9] \quad |\beta^{i+1}\rangle = |\beta^i\rangle + |\sigma^i\rangle$$

The minimization is most efficient when the scalar α^i is found to minimize $U(|\beta^i\rangle + \alpha^i\,|s^i\rangle)$ with respect to λ along $(|\beta^i\rangle + \lambda\,|s^i\rangle)$. λ is chosen and α^i found by Davidon's cubic interpolation, according to Fletcher and Powell (13).

TABLE 1. Stability constants of the Ni(II)–glycine system; entries are log β_{pqr} values for species $Ni_pH_qGly_r$[a]

pqr	A	B
011	9.65	9.653 ± 0.011
101	5.592	5.63 ± 0.071
102	10.44	10.391 ± 0.089
103	13.86	13.922 ± 0.191

[a]Column A: present work; 25°C, 0.15 M NaCl. Based on ligand variation at [Ni] = 1.08×10^{-4} M with [glycine] = 1.97×10^{-4}, 3.94×10^{-4}, 5.93×10^{-4}, 7.89×10^{-4}, 9.86×10^{-4}, and 1.18×10^{-3} M; and metal variation at [glycine] = 5.93×10^{-4} M with [Ni] = 3.60×10^{-5}, 7.20×10^{-5}, 1.08×10^{-4}, 1.44×10^{-4}, and 2.16×10^{-4} M. Standard deviation on the fit is 8.8×10^{-7}. Column B: data of ref. 14; values are mean ± SD, of the values from 7 independent laboratories; 25°C, 1 M NaCl, total concentration of reagents variable but not more than 0.1 M.

At each iterative step, $\mathbf{H}$ is also refined. We begin with $\mathbf{H}$ as a scaled unit matrix, and set

$$[10] \quad \mathbf{H}^{i+1} = \mathbf{H}^i + \frac{|\sigma^i\rangle\langle\sigma^i|}{\langle\sigma^i|y^i\rangle} - \frac{\mathbf{H}^i\,|y^i\rangle\langle y^i|\,\mathbf{H}^i}{\langle y^i|\,\mathbf{H}^i\,|y^i\rangle}$$

where $|y^i\rangle = |g^{i+1}\rangle - |g^i\rangle$, according to Fletcher and Powell. It can be shown (13) that, as the procedure converges, $\mathbf{H}$ tends to $\mathbf{G}^{-1}$.

In applying this algorithm, we use the additional strategy of initializing $\mathbf{H}$ as an $n \times n$ unit matrix, which is then scaled to ensure refinement of each β at each iteration. This is done as suggested earlier (19). An increment $\delta_i = k_\delta \beta_i$ is used to calculate

$$[11] \quad U^+ = U[\beta_1, \ldots, (\beta_i + \delta_i), \ldots, \beta_n]$$

$$U^- = U[\beta_1, \ldots, (\beta_i - \delta_i), \ldots, \beta_n]$$

where k_δ is chosen to esnure that $(U^\pm - U)$ are significant with respect to the expected precision of the final U. Then

$$[12] \quad \mathbf{H}_{ii} = \delta_i^2/|U^+ + U^- - 2U|$$

We have allowed re-initialization of $\mathbf{H}$ from partially refined solutions, retaining the current (partially refined) β values. This achieves three aims. First, it reverts to a steepest descent situation and thus speeds up convergence. Secondly, if a minimum is nearby, this steepened descent can cause wider oscillation about it, with the frequently observed result that we leap over and escape a false minimum. Finally, reinitializations allow approaching the minimum from different directions, increasing our confidence that a true minimum has been found.

Materials and methods

Chemicals

Spermidine trihydrochloride and spermine tetrahydrochloride were obtained from Sigma (St. Louis, MO) and recrystallized twice from ethanol–water. Purity was checked by high voltage paper electrophoresis at pH 5 (citrate buffer) and pH 8.9 (borate buffer), and estimated to be 99% by log K_A analysis following Motekaitis and

TABLE 2. pK's of spermidine and spermine[a]

	A	B	C	D	E	F
Spermidine	10.95 ± 0.10	10.96	11.02	11.16	11.56	10.89
	9.982 ± 0.003	9.91	10.02	10.06	10.80	9.81
	8.56 ± 0.03	8.51	8.57	8.51	9.52	8.34
Spermine	10.94 ± 0.01	—	—	10.57	11.50	10.80
	10.12 ± 0.09	—	—	10.27	10.95	10.02
	9.036 ± 0.011	—	—	9.04	9.79	8.85
	7.97 ± 0.02	—	—	8.03	8.90	7.96

Column A: this work; 25°C, 0.15 M NaCl, 2×10^{-4} M to 1×10^{-3} M polyamine. Column B: ref. 22; 25°C, 0.1 M spermidine, pH titration. Column C: ref. 22; 20°C, 0.1 M spermidine, $^{1}H-^{13}C$-correlated nmr. Column D: ref. 23; 27°C, 0.1 M NaCl, 3×10^{-3} M polyamine, potentiometric titration. Column E: ref. 23; 32°C probe temperature, no supporting electrolyte, concentrations not specified, ^{15}N-nmr pH titration. Column F: ref. 24; 25°C, 0.1 M NaCl, potentiometric titration.

Martell (21) and by the proton liberation measurements. Glycine (crystalline ammonia free; Sigma) was recrystallized twice from hot ethanol–water 1:1 (v/v). Nickel(II) and Cu(II) were obtained as their chloride salts, of Anal R grade or equivalent, and their aqueous solutions were standardized against EDTA using murexide (nickel) or fast sulphon black F (copper) as indicators. Sodium hydroxide solutions for titration were prepared carbonate free, stored under argon, and standardized against N.B.S. grade potassium hydrogen phthalate. Absorption spectra were obtained with a Cary 15 spectrophotometer with a 10 cm path length cuvette. Digitized spectra were corrected for dilution with titrant following baseline subtraction.

Potentiometric titrations

Solutions were prepared from carbonate-free deionized water kept under argon. All glassware was acid washed. Titrations were performed on solutions with starting volumes of 48.00 mL and 0.15 M in NaCl, using a Radiometer ABU13/TTT60/PHM64 titration assembly. Electrodes (Radiometer G2040C glass and K4040 calomel) were calibrated against standard N.B.S. buffers. In all cases, ligand concentrations varied between 2×10^{-4} and 1×10^{-3} M, and metal concentrations between 4×10^{-5} and 2.4×10^{-4} M (Ni(II)) or 5×10^{-5} and 5×10^{-4} M (Cu(II)). The ratio of ligand in the metal variation titrations to metal in the ligand variation titrations was always 5:1. Up to 2×10^{-4} mol standardized HCl were used to lower the starting pH, and all titrations were carried out with 0.0951 ± 0.0008 M NaOH. At the common curve conditions in the Ni(II)–glycine system, for example, ionic strength varied from 0.155 to 0.150 over the course of the titration due to addition of base. From titrations of background electrolyte, pK_W = 13.8. All titrations were performed under an argon atmosphere in vessels thermostated at 25.0 ± 0.1°C.

Data analysis

Calculations were performed by a series of programs written in Basic for an Apple Macintosh microcomputer. PKAMART calculates the stepwise ligand protonation constants by employing the algorithm of Motekaitis and Martell (21). Based on these K_a's and the experimental titration curves, FREEML calculates the free ligand and metal concentrations as functions of pH, as outlined in (3). Using the output of FREEML, GMAT constructs the coefficient matrix corresponding to a given guessed set of species. DFPMIN then uses the FP method to find the least squares set of β values corresponding to the guessed coefficient matrix. When the best set of species and the corresponding β values have been found, SPECIES calculates the species distribution as a function of pH, entailed by the set $|\beta\rangle$ and the experimental m and l, by solving eq. [2]. Program listings are available from the authors on request.

Results

The Ni(II)–glycine system was analyzed above pH 4.5, where the glycine carboxyl group is fully ionized. Below pH 10, only the species Ni-gly, $Ni(gly)_2$, and $Ni(gly)_3$ were found. Their stability constants and the amino group K_a are compared with those of an earlier study (Table 1).

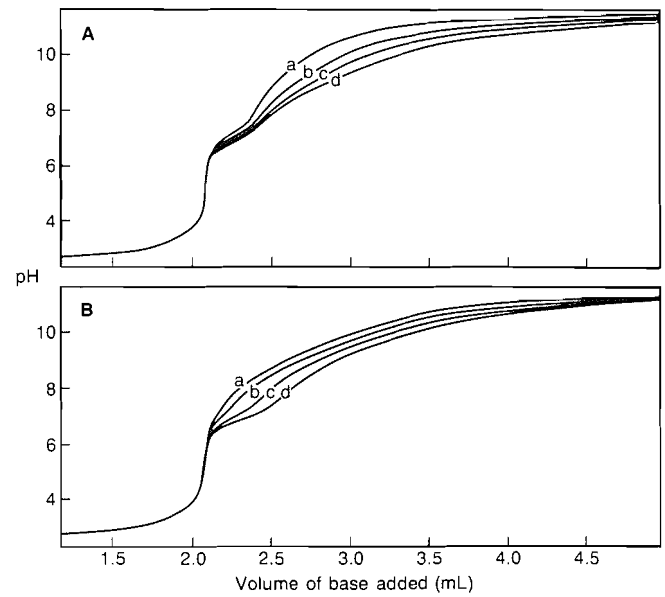

FIG. 1. Original titration data of the Cu(II)–spermidine system with 9.51×10^{-2} M NaOH. Conditions are given in the Materials and methods section. (A) Ligand variation at [Cu] = 1.964×10^{-4} M and [spermidine] = 4.252×10^{-4} M (a), 6.378×10^{-4} M (b), 8.504×10^{-4} M (c), and 1.063×10^{-3} M (d). (B) Metal variation at [spermidine] = 1.063×10^{-3} M and [Cu] = 4.910×10^{-5} M (a), 9.820×10^{-5} M (b), 1.964×10^{-4} M (c), and 2.946×10^{-4} M (d).

The three K_a's of spermidine are given in Table 2, and titration data for the Cu(II)–spermidine system are shown in Fig. 1. Complexation of Cu(II) by spermidine begins above pH 6 (Fig. 2). Complexation begins with the $CuHL^{3+}$ species, but this species deprotonates and the CuL^{2+} complex predominates over the range pH 7.5 to 9.5. At pH 8.5, this complex accounts for 90% of the total Cu(II). A variety of stable complexes are found in this system at higher pH. The data of the Cu(II)–spermidine system were re-analyzed on a GE400 series computer, using improved versions of the PLOT, GUESS, and LEASK programs reported previously (3), with consistent results. These data are summarized in Table 3.

In order to discriminate amongst the various models tested, the following statistical considerations apply. Minimization

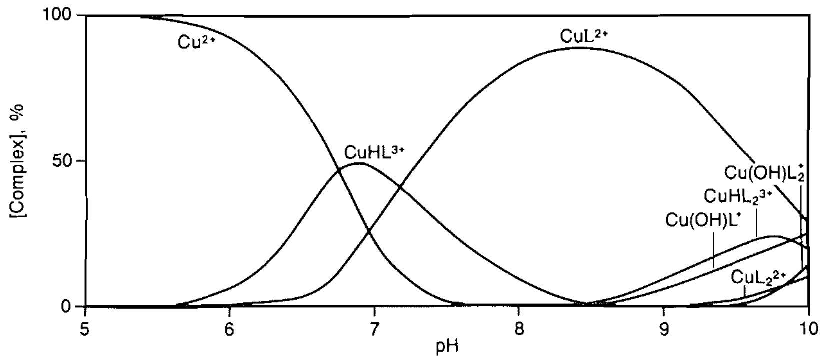

FIG. 2. Species distribution of the Cu(II)–spermidine system as a function of pH. L is spermidine. From the data of Table 3.

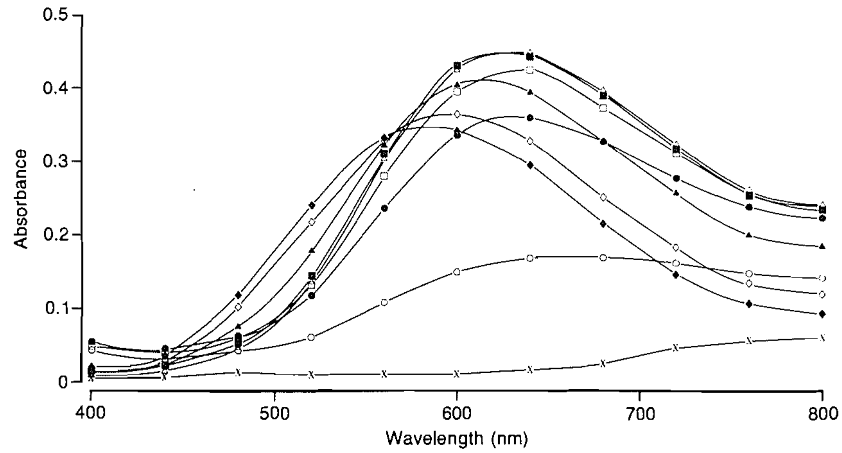

FIG. 3. Absorption spectra of the Cu(II)–spermidine system. [Cu] = 4.25×10^{-4} M, [spermidine] = 2.21×10^{-3} M. pH 2.72 ×; pH 6.51, ○; pH 6.91, ●; pH 7.24, □; pH 8.01, ■; pH 8.41, △; pH 9.26, ▲; pH 10.03 ◇; pH 10.89, ◆.

with respect to $|m_b\rangle$ gives a value of U from which the standard deviation of the overall fit can be calculated in terms of metal concentration. This may be expressed as a percentage of total metal. This does not allow the assignment of standard deviations to individual β values, which are not varied independently. These criteria, and their use in distinguishing amongst several better models, are illustrated in Table 4 for the Cu(II)–spermidine system.

The pH dependence of the absorption spectrum of the Cu(II)–spermidine system (Fig. 3) allows discernment of absorption due to the $CuHL^{3+}$ complex (λ_{max} = 655 nm, ϵ_{655} = 131 dm^3 mol^{-1} cm^{-1}) at pH 6.5 and due to the CuL^{2+} complex (λ_{max} = 626 nm, ϵ_{626} = 127 dm^3 mol^{-1} cm^{-1}) at pH 8.4. Above pH 10, where bis species are forming, the absorption shifts to higher energy ($\lambda_{max} \simeq$ 580 nm). Others have reported (25) an absorption (λ_{max} = 610 nm, ϵ_{610} = 117 dm^3 mol^{-1} cm^{-1}) in the Cu(II)–spermidine system, at unspecified pH. This was attributed to CuL^{2+}, and absorptions due to other complexes were not identified.

The Cu(II)–spermine system (Fig 4) is somewhat simpler. Complexation begins above pH 5 with the doubly protonated CuH_2L^{4+} species, but the fully deprotonated CuL^{2+} grows quickly and contains nearly 100% of the Cu(II) between pH 7 and 9. Fewer species form at high pH. Data for the Cu(II)–spermine system are summarized in Table 3 and Fig. 5. The absorption spectrum of this system (Fig. 6) is dominated by that of the CuL^{2+} complex (λ_{max} = 564 nm, ϵ_{564} = 162 dm^3 mol^{-1} cm^{-1}).

The most time consuming step in analysis is execution of the

TABLE 3. Stability constants of the Cu(II)–polyamine systems, entries are log β_{pqr} values for species $Cu_pH_qL_r$, at 25°C and 0.15 M NaCl[d]

Ligand	pqr	log β_{pqr}	log β_{pqr}[a]
Spermidine[b]	1 1 1	18.9	18.7
	1 0 1	11.7	11.7
	1-1 1	1.67	1.68
	1 1 2	26.3	26.9
	1 0 2	16.0	16.9
	1-1 2	6.18	6.43
Spermine[c]	1 2 1	27.8	
	1 0 1	14.7	
	1 1 2	29.0	
	1 0 2	18.9	

[a]Analyzed by improved versions of the PLOT, GUESS, and LEASK programs (3).

[b]Standard deviation of the fit over the range pH 5–10 is 7.0×10^{-6}.

[c]Standard deviation of the fit over the range pH 5–10 is 5.2×10^{-6}.

[d]For spermidine titrations, [Cu] = 1.964×10^{-4} M and [ligand] = 1.063×10^{-3} M. For construction of the GUESS matrices, more than 40 sets of from 3 to 10 species $M_pH_qL_r$ were considered, with p and r of 1 or 2, and q from −2 to +2. Data were minimized over the range pH 5 to 10. For spermine titrations, [Cu] = 1.008×10^{-4} M and [ligand] = 5.116×10^{-4} M. Sets of from 2 to 8 species were minimized over the range pH 5 to 10, with p and r of 1 or 2, and q from −2 to +4.

TABLE 4. Results of minimization of several of the better models of the Cu(II)–spermidine system

Model	pqr										σ(%)
	1 2 1	1 1 1	1 0 1	1-1 1	1-2 1	1 1 2	1 0 2	1-1 2	2 0 2	1-2 2	
9	—	18.8	11.8	—	—	26.0	16.7	—	—	—	6.57
10	—	19.0	11.8	1.39	—	26.0	16.7	—	—	—	4.05
11[a]	—	18.9	11.7	1.67	—	26.3	16.0	6.18	—	—	3.56
19	—	19.0	11.6	1.94	—	26.2	15.3	6.00	26.8	−5.03	8.75
20[b]	—	19.0	11.6	1.89	−9.03	26.2	15.3	5.90	26.8	−5.04	2.91
21	22.0	19.0	11.7	1.72	—	26.3	16.0	6.15	—	—	8.78

[a] Best model reported in Table 3 and Fig. 2.
[b] A slightly improved fit is obtained by inclusion of several additional minor species at higher pH, but does not significantly change the distribution of the major species. The small improvement in fit with the additional degrees of freedom provided by this model probably does not warrant inclusion of the extra minor species.

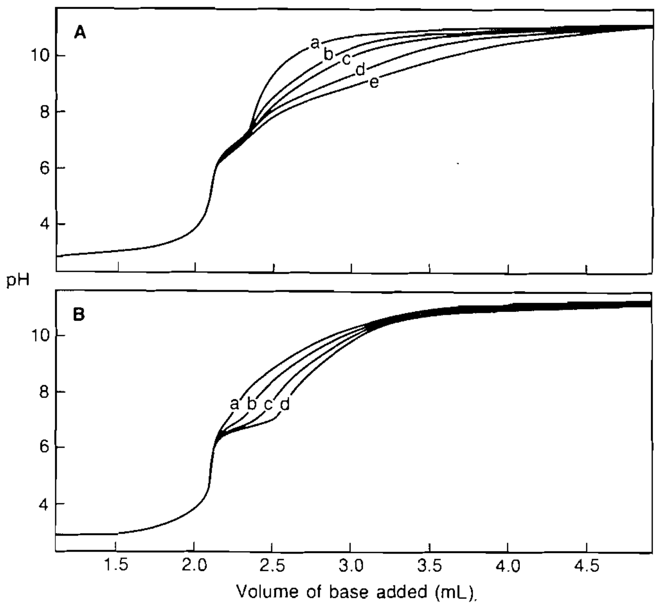

FIG. 4. Original titration data of the Cu(II)–spermine system with 9.51×10^{-2} *M* NaOH. Conditions are given in the Materials and methods section. (*A*) Ligand variation at [Cu] = 1.008×10^{-4} *M* and [spermine] = 2.046×10^{-4} *M* (*a*), 4.092×10^{-4} *M* (*b*), 5.116×10^{-4} *M* (*c*), 8.184×10^{-4} *M* (*d*), and 1.023×10^{-3} *M* (*e*). (*B*) Metal variation at [spermine] = 5.116×10^{-4} *M* and [Cu] = 5.040×10^{-5} *M* (*a*), 1.008×10^{-4} *M* (*b*), 1.512×10^{-4} *M* (*c*), and 2.016×10^{-4} *M* (*d*).

DFPMIN program. For all sets of species checked in all systems, when convergence was achieved with DFPMIN, execution times were between 1 and 5 min.

Discussion

The major polyamines of biological interest are putrescine (1,4-diaminobutane), spermine, and spermidine (15). Metal complexation by these naturally occurring polydentate ligands has not been thoroughly investigated previously, although Cu(II) complexation by spermine and spermidine has been reported (24–26). Because there has been much recent interest in determining the factors which may influence the biological activity of these entities by altering their state of protonation (23), we wished to investigate the complete species distribution of these Cu(II)–polyamine systems across a wide range of pH.

Chelation by the aliphatic polyamines has been extensively studied following Bjerrum's early work (27). The series $H_2N—(CH_2)_2—[NH—(CH_2)_2]_n—NH_2$, beginning with ethylene diamine ($n = 0$), serves as the most straightforward example of the effect of the number of chelate rings on complex stability (28), while the bidentate diamines $H_2N—(CH_2)_n—NH_2$ demonstrate the role of ring size (29). The complexes of Cu(II) and Ni(II) with 1,3-propanediamine are much less stable than those with 1,2-ethanediamine. The $-\Delta H$ values for binding are larger with propanediamine, in keeping with its stronger basicity, but the stabilities are dominated by the more favorable entropy change when the 5-membered ring is formed (29). Loss of freedom of the ligand is so great with 7-membered ring formation that 1,4-butanediamine (putrescine) does not form Cu(II), Ni(II), or Zn(II) complexes in aqueous solution (29), although these complexes can be isolated from absolute alcohol (30). It has been estimated (24) that diamine–Cu(II) chelate rings of 5, 6, and 7 members add respectively 5.3–7.0, 4.6–6.1, and 2.0–3.0 to the log K_1 value for complex formation.

These considerations suggest the following interpretation of the Cu(II)–polyamine speciation observed here. In the Cu(II)–spermidine system, the $CuHL^{3+}$ complex forms at lower pH, with the 6-membered ring as the anchor site. This allows the stabilization from a second ring to aid formation of the less favorable 7-membered ring, which must form in the CuL^{2+} complex concomitant with a lowering of the highest p*K* by about 3 units. This $CuHL^{3+}$ complex is analogous to the CuH_2L^{4+} species of spermine. Again, in the latter complex, a 6-membered ring must form the anchor site. Failure to observe a $CuHL^{3+}$ species indicates no stepwise folding of the spermine, but rather formation of a second 6-membered ring is the driving force for formation of the CuL^{2+} complex. In the latter, the obligatory 7-membered ring is stabilized by two 6-membered rings and a 3-chelate ring effect. The additional stabilization is reflected in the increased stability constant of the CuL^{2+} species of spermine (log β = 14.7) compared to that of the CuL^{2+} spermidine complex (log β = 11.7). This observation is in contrast to that of Palmer and Powell (26) who report only CuL^{2+} and $CuHL^{3+}$ species in the Cu(II)–spermine system. By pH > 9, hydroxo species $(Cu(OH)L^{+}]$ begin to form in the Cu(II)–spermidine system, while deprotonation of uncomplexed ligand at this higher pH initiates formation of bis complexes. The increased stability of the CuL^{2+} complex of spermine preserves its tetradentate structure until higher pH. No hydroxo species are seen in this system up to pH 10.

The energy of the absorption of the CuL^{2+} complex of spermine (λ_{max} = 564 nm) is consistent with tetracoordination by nitrogen. This solution structure is supported by the crystal structure of spermine Cu(II) perchlorate, which shows square

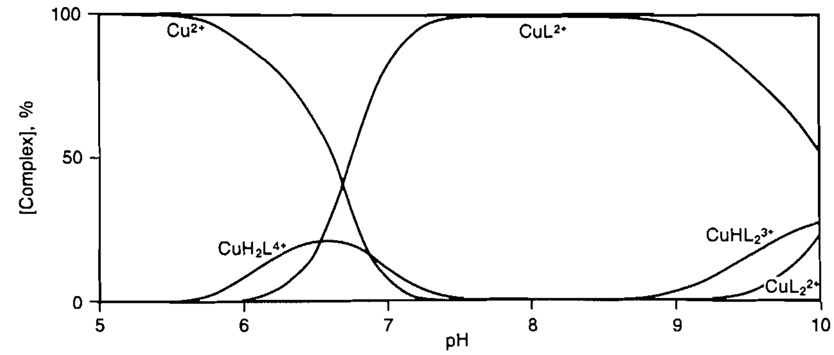

FIG. 5. Species distribution of the Cu(II)–spermine system as a function of pH. L is spermine. From the data of Table 3.

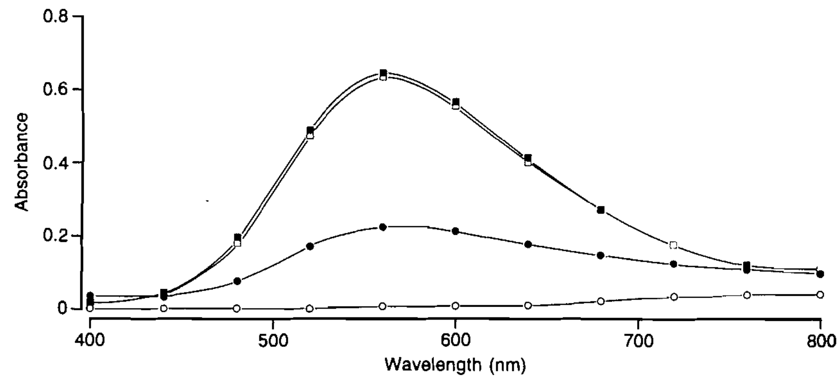

FIG. 6. Absorption spectra of the Cu(II)–spermine system. [Cu] = 4.25×10^{-4} *M*, [spermine] = 2.14×10^{-3} *M*. pH 2.65, ○; pH 6.36, ●; pH 7.36, □; pH 9.54, ■.

planar coordination of Cu by four nitrogen atoms of the same spermine molecule (31). In the Cu(II)–spermidine system, the corresponding CuL^{2+} species is tridentate. The resulting decrease in ligand field strength is reflected in the lowered energy of the transition (λ_{max} = 626 nm), which is lowered further (λ_{max} = 655 nm) when protonation of an amino group presumably removes another coordinating nitrogen atom (i.e. in the $CuHL^{3+}$ complex). The higher energy absorption (λ_{max} = 580 nm) at pH 10 supports the existence of bis complexes with 4 nitrogen ligands in a square planar geometry around Cu(II). This geometry may be more distorted than in the CuL^{2+} complex of spermine, in order to minimize intermolecular steric repulsion. In Cu(II)–spermine, geometrical requirements of accommodating the 7-membered ring are reflected in torsional strain and shortening of the C(5)—C(6) bond in the crystal (31).

The formation of stable metal complexes of spermine and spermidine *in vivo* could have profound implications for their biological function. Interaction of these polyprotonated molecules with nucleic acids at neutral pH is thought to underlie their growth regulating properties (15). Takeda *et al.* (23) have pointed out that dynamic conformational control of DNA by interaction with polyamines is likely in turn governed by the effects on protonation of small changes in the local environment, such as pH, ionic strength, and dielectric constant. To this list may now be added the more profound effect of local concentration of metal ions.

The microcomputer FP minimization of analytical potentiometric data has been applied with success to the above systems. Evaluation of both experimental and mathematical procedures has come primarily from the analysis of the Ni(II)–glycine system. This system was chosen as the subject of an interlaboratory study (14) as it provided a sufficient complexity, range of pH, and of β values, and at the same time, is a well defined system. The excellent agreement achieved by seven independent laboratories, using a variety of experimental and calculation techniques, demonstrates the variety of approaches which may be applied with success to the determination of stability constants. Interlaboratory differences in electrode type and response, liquid junction potential, electrode standardization, titration procedure, and reagent purity are clearly small. Against this yardstick, the methods reported here compare favorably.

Despite these successes, some unsolved problems remain in attempts to derive reliable stability constants of the more complicated metal complexes of biological relevance. These problems fall into two categories, the first resulting from the concentration dependence of the species distribution, the second from the poorly defined criteria for a satisfactory set of species to model the experimental data.

In a given metal : ligand system, the species distribution will depend on the ratio of the concentrations of metal-to-ligand. A more complete description, then, would be given by determining the surface in [pH, concentration, M:L ratio] space. The method of analytical potentiometry assumes that all titrations are done on a flat region of the [concentration, M:L ratio] plane, and it has been pointed out (10) that this is a potential source of experimental error. At present, there is no method for determining this surface for a sufficiently interesting system, with a manageable number of titrations.

The second type of outstanding problem has three facets. (*a*) It is never possible to know that one has found the best set of species for a given data set. It is not computationally feasible to check all combinations of possible species for any but the simplest systems, and one must always revert to some chemical intuition in deciding which combinations to minimize. The economy of microcomputer utilization encourages checking of an expanded set of possible species, however. Execution times for DFPMIN allow analysis of a large number of combinations. (*b*) The existence of false or degenerate least squares solutions could arise from systematic or random experimental errors. In light of this point, confidence in a given species distribution will increase as it is reproduced in independent studies, and ultimately corroborated by structural evidence. (*c*) Equation [1] usually represents an inconsistent set of equations. The least squares problem posed by eq. [1] is that of finding the norm $\|\mathbf{C}\beta - m_b\|$, which has an infinite number of solutions when the rank of $\mathbf{C} \neq n$, the number of species (20). This situation would be unlikely to arise unless the number of species was large or the pH range narrow, so that k approached n. Unless the rank of $\mathbf{C} = n$, there will be an infinite number of solution vectors $|\beta\rangle$, and the problem is one of finding the shortest.

Conclusions

1. A series of BASIC programs have been written which employ the Fletcher–Powell minimization method and allow metal speciation analysis to be performed on a microcomputer.

2. These programs have successfully solved the Ni(II)–glycine system. This system is one of the most carefully studied of such problems, and provides an excellent test of a given method of analysis.

3. A brief discussion has been given of some unsolved problems pertaining to the potentiometric determination of stability constants.

4. The polyamines spermidine and spermine have been shown to form complexes with Cu(II) in aqueous solution. The stability constants of these complexes have been derived by the above methods.

5. Interaction of Cu(II) with these biological polyamines causes their deprotonation at physiological pH. This could significantly influence the mechanism of dynamic control these entities exert upon DNA.

Acknowledgements

This work was supported by the Medical Research Council of Canada. DMT is the holder of a M.R.C. Postdoctoral Fellowship.

1. R. ÖSTERBERG. Acta Chem. Scand. **14**, 471 (1960).
2. J. LEFEBVRE. J. Chim. Phys. **57**, 553 (1957).
3. B. SARKAR and T. P. A. KRUCK. Can. J. Chem. **51**, 3541 (1973).
4. S. H. LAURIE, D. H. PRIME, and B. SARKAR. Can. J. Chem. **57**, 1411 (1979).
5. K. S. N. IYER, S. LAU, S. H. LAURIE, and B. SARKAR. Biochem. J. **169**, 61 (1978).
6. D. W. APPLETON, T. P. A. KRUCK, and B. SARKAR. J. Inorg. Biochem. **10**, 1 (1979).
7. S. LAU and B. SARKAR. J. Chem. Soc. Dalton, 491 (1981).
8. S. LAU and B. SARKAR. Biochem. J. **199**, 649 (1981).
9. J. D. GLENNON and B. SARKAR. Biochem. J. **203**, 25 (1982).
10. R. GUEVERMONT and D. L. RABENSTEIN. Can. J. Chem. **55**, 4211 (1977).
11. A. AVDEEF and K. N. RAYMOND. Inorg. Chem. **18**, 1605 (1979).
12. A. AVDEEF. Inorg. Chem. **19**, 3081 (1980).
13. R. FLETCHER and M. J. D. POWELL. Computer J. **6**, 163 (1963).
14. E. BOTTARI, A. BRAIBANTI, L. CIAVATTA, A. M. CORRIE, P. G. DANIELE, F. DALLAVALLE, M. GRIMALDI, A. MASTROIANNI, G. MORI, G. OSTACOLI, P. PAOLETTI, E. RIZZARELLI, S. SAMMARTANO, C. SEVERINI, A. VACCA, and D. R. WILLIAMS. Ann. Chim. **68**, 813 (1978).
15. C. W. TABOR and H. TABOR. Ann. Rev. Biochem. **53**, 749 (1984).
16. D. R. MORRIS and L. J. MARTON. Polyamines in biology and medicine. Marcel Dekker. New York. 1981.
17. A. SABATINI, A. VACCA, and P. GANS. Talanta, **21**, 53 (1974).
18. P. GANS, A. SABATINI, and A. VACCA. Inorg. Chim. Acta, **18**, 237 (1978).
19. P. GANS and A. VACCA. Talanta, **21**, 45 (1974).
20. G. E. FORSYTHE and C. B. MOLER. Computer solution of linear algebraic systems. Prentice Hall, Englewood Cliffs, NJ. 1967.
21. R. J. MOTEKAITIS and A. E. MARTELL. Can. J. Chem. **60**, 168 (1982).
22. F. ONASCH, D. AIKENS, S. BUNCE, H. SCHWARTZ, D. NAIRN, and C. HURWITZ. Biophys. Chem. **19**, 245 (1984).
23. Y. TAKEDA, K. SAMEJIMA, K. NAGANO, M. WATANABE, H. SUGETA, and Y. KYOGOKU. Eur. J. Biochem. **130**, 383 (1983).
24. B. N. PALMER and H. K. J. POWELL. J. Chem. Soc. Dalton, 2089 (1974).
25. A. ANICHINI, L. FABBRIZZI, R. BARBUCCI, and A. MASTROIANNI. J. Chem. Soc. Dalton. 2224 (1977).
26. B. N. PALMER and H. K. J. POWELL. J. Chem. Soc. Dalton, 2086 (1974).
27. J. BJERRUM. Metal ammine formation in aqueous solution. P. Haase and Son. Copenhagen. 1941.
28. K. F. PURCELL and J. C. KOTZ. Inorganic chemistry. W. B. Saunders, Philadelphia. 1977.
29. C. R. BERTSCH, W. C. FERNELIUS, and B. P. BLOCK. J. Phys. Chem. **62**, 444 (1958).
30. P. PFEIFFER. Naturwissenschaften, **35**, 190 (1948).
31. R. BOGGS and J. DONOHUE. Acta Crystallogr. **B31**, 320 (1975).

Studies of the dissociation of 2,4,6-trinitrophenol in aqueous mixtures of methanol and ethanol at 25°C

A. L. DE[1] AND A. K. ATTA

Department of Chemistry, Presidency College, Calcutta 700 073, India

Received December 7, 1984

A. L. DE and A. K. ATTA. Can. J. Chem. **63**, 3129 (1985).

Thermodynamic dissociation constants $({}_sK)_m$ of 2,4,6-trinitrophenol have been determined at 25°C in aqueous mixtures containing 30, 50, 70, and 90% by weight of methanol and 30, 50, 70, 90, and 95% by weight of ethanol by spectrophotometric method. Solvent effect on the dissociation of the acid: $\delta(\Delta G^0) = 2.303RT[p({}_sK)_N - p({}_wK)_N]$ shows an unusual behaviour, the value decreases and passes through a minimum and ultimately becomes positive as the proportion of organic component in the solvent is progressively increased. The results have been compared with those of other uncharged acids like acetic acid, benzoic acid available from literature. The difference of behaviour (minimum characteristic in $\delta(\Delta G^0)$ curve) has been attributed to very strong dispersion interaction of trinitrophenolate anion with the organic component of the solvent. The overall behaviour of this acid indicates that solvent effect is an involved process being guided by electrostatic and dispersion interactions besides relative solvent basicities.

A. L. DE et A. K. ATTA. Can. J. Chem. **63**, 3129 (1985).

Faisent appel à des méthodes spectroscopiques et opérant à 25°C, on a étudié les constantes thermodynamiques de dissociation $({}_sK)_m$ du trinitro-2,4,6 phénol dans des solutions aqueuses contenant 30, 50, 70 et 90% en poids de méthanol et 30, 50, 70, 90 et 95% en poids d'éthanol. L'effet du solvant sur la dissociation de l'acide $\delta(\Delta G^0) = 2{,}303RT[p({}_sK)_N - p({}_wK)_N]$ montre un comportement inhabituel, la valeur diminue, passe par un minimum et finalement devient positive lorsqu'on augmente progressivement la proportion de composé organique du solvant. On a comparé les résultats avec ceux d'autres acides non chargés tels l'acide acétique, l'acide benzoique, répertoriés dans la littérature. On a attribué la différence de comportement (minimum caractéristique dans la courbe de $\delta(\Delta G^0)$ à une interaction de dispersion très forte de l'anion trinitrophénolate avec la partie organique du solvant. Le comportement global de cet acide indique que la participation de l'effet du solvant est gouvernée par des interactions de dispersion et électrostatiques en plus de la basicité relative du solvant.

[Traduit par le journal]

Introduction

It is well known that the dissociation of acids is a complex phenomenon dictated by various types of interactions of the species involved in the ionization equilibrium. To understand the solvent effect on the dissociation equilibria, dissociation constants of some monopositively charged acids, nitroanilinium ions were determined earlier (1, 2) in some mixed solvents. This paper reports the dissociation constant of uncharged acid, 2,4,6-trinitrophenol, in aqueous mixtures of methanol and ethanol.

Experimental

Purification (3) of alcohols and water and the preparation (4) of mixed solvents as well as the solutions of HCl have been described. Synthetically prepared methanol (G. R., E. Merck) was refluxed with the metal magnesium and then fractionally distilled, the initial and final quarters of the distillate being rejected. The characteristic properties of methanol are density (25°C) = 0.7867 g mL^{-1}; bp (1 atm) = 64.5°C. Anhydrous ethanol prepared by fermentation (Bengal Chemicals & Pharmaceuticals Ltd., a Government of India Enterprise) was dried over freshly ignited calcium oxide for 3 days, decanted, and then distilled. The distillate was then successively refluxed (~12 h) and distilled over the metal magnesium and KOH. The finally distilled sample was preserved in a desiccator. The properties of ethanol are density (25°C) = 0.7851 g mL^{-1}; bp (1 atm) = 78.3°C. Recently Deshmukh and Coetzee (5) have shown that synthetically prepared alcohols contain 10^{-4} to 10^{-5} M alkylamine even after purification by standard methods. The maximum error introduced in the present study due to residual amine is, however, negligible being of the order of 0.001 to 0.004 pK unit depending on the proportion of alcohol in the solvent. 2,4,6-Trinitrophenol (Anal R) was used after recrystallizing twice from aqueous 95% ethanol and drying *in vacuo*. The dissociation constant in these aqueous mixtures of methanol and ethanol were determined spectrophotometrically using unbuffered solutions of HCl at different concentrations as in cases of some charged (1, 2) acids. A series of solutions were prepared in 10 cm^3 amounts by adding weighed amounts of HCl solution, indicator solution and the appropriate solvent. The spectral absorbances were determined at 25 ± 0.2°C with Carl Zeiss Jena (Germany, DDR) spectrophotometer with 1 cm cells at 355 nm where the absorbance shows a maximum for the base form. The limiting absorbances of the acid and base forms were determined in very concentrated solution of HCl (4 to 6 M) and in very dilute solution of sodium hydroxide (about 0.001 M), respectively (6), and absorbance readings were corrected, where necessary, for the identical concentration of the indicator. The indicator concentrations used in various solvent compositions were in the range 2×10^{-5} to 3×10^{-5} M.

The $p({}_sK)_m$ values in the molar scale were obtained by extrapolation of the plots of $p({}_sK)'_m$ of eq. [1] against μ to $\mu = 0$.

$$[1] \quad p({}_sK)'_m = -\log m_{SH_2^+} - \log[\alpha/(1-\alpha)] + 2S_f\sqrt{\mu}(1 + Ba_0\sqrt{\mu})^{-1} = p({}_sK)_m + f(\mu)$$

where $m_{SH_2^+}$ is the effective molality of H$^+$ in the solution, α and $1 - \alpha$ are the fractions of the indicator species present in ionic form (A$^-$) and neutral form (HA), S_f and B are Debye–Hückel constants, a_0 is the ion-size parameter, μ is the ionic strength being equal to $\mu = m_{HCl}, d_s$ where d_s is the density of the solvent. The concentration of the ionic species obtained from dissociation of acid being extremely small with respect to that of m_{HCl}, their contribution to ionic strength can be neglected. As indicator concentration is very small the value of $m_{SH_2^+}$ is practically the same as that of m_{HCl}. Density and dielectric constant values necessary for calculation of Debye–Hückel constants were available from literature (7). The values $\alpha/(1-\alpha) = (A - A_1)/(A_2 - A)$ were obtained from the absorbances A_1, A_2, and A of the completely acid form (HA), completely base form (A$^-$), and the mixture of the two forms measured at an identical concentration of the indicator in the same cell. In the calculation of $p({}_sK)'_m$, a_0 was taken to be zero, because this numerical value resulted in linear $p({}_sK)'_m$ plots.

[1]To whom all correspondence should be addressed.

TABLE 1. Data for spectrophotometric determination of $p({}_sK)_m$ of 2,4,6-trinitrophenol in methanol–water solvents at 25°C

m_{HCl}	A	$p({}_sK)'_m$	m_{HCl}	A	$p({}_sK)'_m$
Water			*70 wt% methanol*		
Completely acidic	0.160	—	Completely acidic	0.187	—
0.08396	0.306	0.985	0.09979	0.372	1.198
0.07197	0.311	0.978	0.07753	0.373	1.222
0.05997	0.312	1.022	0.06211	0.383	1.164
0.04731	0.319	1.017	0.04418	0.392	1.135
0.03154	0.331	0.993	0.02567	0.401	1.155
0.01577	0.344	1.010	0.01102	0.418	1.110
Completely basic	0.366	—	Completely basic	0.438	—
	$p({}_wK)_m = 1.01$			$p({}_sK)_m = 1.10$	
30 wt% methanol			*90 wt% methanol*		
Completely acidic	0.134	—	Completely acidic	0.120	—
0.09833	0.301	0.736	0.07985	0.202	1.955
0.07210	0.308	0.698	0.06825	0.206	1.926
0.05520	0.310	0.733	0.05621	0.215	1.857
0.04124	0.314	0.736	0.04500	0.222	1.818
0.02572	0.320	0.733	0.02277	0.238	1.785
0.01082	0.328	0.716	0.01136	0.258	1.731
Completely basic	0.336	—	Completely basic	0.301	—
	$p({}_sK)_m = 0.70$			$p({}_sK)_m = 1.69$	
50 wt% methanol					
Completely acidic	0.104	—			
0.09036	0.231	0.812			
0.07503	0.233	0.804			
0.06039	0.236	0.792			
0.04020	0.239	0.800			
0.02011	0.246	0.757			
0.01285	0.249	0.748			
Completely basic	0.256	—			
	$p({}_sK)_m = 0.74$				

TABLE 2. Data for spectrophotometric determination of $p({}_sK)_m$ of 2,4,6-trinitrophenol in ethanol–water solvents at 25°C

m_{HCl}	A	$p({}_sK)'_m$	m_{HCl}	A	$p({}_sK)'_m$
30 wt% ethanol			*70 wt% ethanol*		
Completely acidic	0.164	—	Completely acidic	0.194	—
0.1001	0.313	0.715	0.09408	0.373	1.113
0.07367	0.317	0.702	0.07803	0.375	1.084
0.05717	0.321	0.672	0.06570	0.379	1.016
0.04480	0.323	0.684	0.05236	0.383	0.950
0.02085	0.326	0.712	0.03764	0.385	0.944
0.01989	0.331	0.637	0.02099	0.391	0.870
Completely basic	0.340		Completely basic	0.403	
	$p({}_sK)_m = 0.65$			$p(sK)_m = 0.79$	
50 wt% ethanol			*90 wt% ethanol*		
Completely acidic	0.132	—	Completely acidic	0.192	—
0.08483	0.314	0.862	0.08879	0.387	1.720
0.07673	0.315	0.861	0.06738	0.388	1.663
0.06602	0.319	0.812	0.05547	0.391	1.610
0.05730	0.322	0.778	0.04561	0.399	1.496
0.03508	0.326	0.792	0.03085	0.401	1.474
0.01881	0.333	0.734	0.01832	0.411	1.357
Completely basic	0.344		Completely basic	0.435	
	$p({}_sK)_m = 0.69$			$p({}_sK)_m = 1.28$	
			95 wt% ethanol		
			Completely acidic	0.125	—
			0.08026	0.232	2.239
			0.06661	0.233	2.190
			0.05626	0.237	2.120
			0.04125	0.245	2.000
			0.02751	0.252	1.912
			0.01440	0.264	1.804
			Completely basic	0.298	
				$p({}_sK)_m = 1.71$	

Results

The values of m_{HCl}, spectral absorbances (A) and $p({}_sK)'_m$ are given in Tables 1 and 2. The $p({}_sK)_m$ values obtained in the molal scale in different solvents are given at the bottom of the column of $p({}_sK)'_m$. The uncertainty in the $p({}_sK)_m$ values is about ±0.02 unit. The literature value (8) of pK in water is 1.02 which compares favorably to our experimental value of 1.01.

Discussion

As a basis for comparison (9) in different solvents, the molal values of $p({}_sK)_m$ have been converted to the mole fraction scale $p({}_sK)_N$ by the usual relation (10) and are recorded in Table 3. The solvent effect on the dissociation of 2,4,6-trinitrophenol (HA) has been calculated (1) by using eq. [2].

$$[2]\quad \delta(\Delta G^0) = {}_s\Delta G^0 - {}_w\Delta G^0 = 2.303RT[p({}_sK)_N - p({}_wK)_N]$$

The values of $\delta(\Delta G^0)$ are recorded in Table 3.

$\delta(\Delta G^0)$ values on the mole fraction scale are plotted as a function of the mol% of nonaqueous component in Fig. 1. For comparison, the corresponding plots for acetic acid and benzoic acid are also shown. For acetic acid and benzoic acid $p({}_sK)$ values were reported in literature (11*b*) on molal scale and the values were converted to the mole fraction scale for computation of $\delta(\Delta G^0)$ values (Table 3). In case of trinitrophenol, $\delta(\Delta G^0)$ decreases when methanol or ethanol is added to a solvent that is initially pure water and passes through a minimum when mole fraction of nonaqueous component is about 0.3 and subsequently, reaches a positive value when mole fraction of water in the solvent becomes low. The $\delta(\Delta G^0)$ curve in ethanol–water lies below that in methanol–water indicating that the acid is stronger in ethanol–water for similar mol% nonaqueous component. This behaviour of trinitrophenol is in sharp contrast with those observed for uncharged acids like acetic acid, benzoic acid where no minimum in $\delta(\Delta G^0)$ curve appears and $\delta(\Delta G^0)$ rises from the very beginning (Fig. 1). In view of the fact that addition of methanol or ethanol to water produces a series of solvents of progressively decreasing dielectric constant and that the dissociation of HA is an ionogenic process, being accompanied by the creation of extra charges it is expected from electrostatic consideration that $\delta(\Delta G^0)$ will increase with increasing organic mol%. Minimum characteristic for trinitrophenol thus indicates highly specific nature of interaction of some of the species involved in the ionization process with the solvent.

TABLE 3. Values of $p({}_sK)_N$ for 2,4,6-trinitrophenol and $\delta(\Delta G^\circ)$ for 2,4,6-trinitrophenol, acetic acid, and benzoic acid in methanol–water and ethanol–water solvents at 25°C ($\delta(\Delta G^\circ)$ values are in mole fraction scale)

Organic co-solvent			$\delta(\Delta G^\circ)/(\mathrm{kJ\ mol^{-1}})$		
Wt%	Mol%	$p({}_sK)_N$	$(NO_2)_3C_6H_2(OH)$	CH_3COOH*	C_6H_5COOH*
			Methanol–water		
0	0	2.75	0	0	0
30	19.42	2.38	−2.11	2.50	3.10
50	35.99	2.38	−2.11	4.65	5.77
70	56.75	2.69	−0.34	7.50	9.16
90	83.51	3.22	2.68	13.31	15.13
			Ethanol–water		
30	14.36	2.31	−2.51	2.90	
50	28.13	2.28	−2.68	4.95	
70	47.73	2.29	−2.62	8.15	
90	77.87	2.68	−0.40	14.55	
95	88.13	3.08	1.88	17.90	

*Reference 11(*a*).

Solvent effect on the dissociation of HA is actually the resultant of the free energy transfer values of the individual species involved in the ionization and is given by (7, 12)

[3] $\delta(\Delta G^0) = \Delta G_t^0(H^+) + \Delta G_t^0(A^-) - \Delta G_t^0(HA)$

where $\Delta G_t^0(i)$ represents the free energy change accompanying the transfer of one mole of species i from the standard state in water to the standard state in the solvent concerned, both on the mole fraction scale.

Since $\Delta G_t^0(H^+)$ is common for all acids in a particular solvent system, it is evident that relative interaction of acid (HA) and its conjugate base (A^-) is very much different for 2,4,6-trinitrophenol as compared to that for acetic acid or benzoic acid. $\Delta G_t^0(H^+)$ values for methanol–water and ethanol–water solvent systems based on different extrathermodynamic assumptions are available in literature but since tetraphenyl borate assumption is most reasonable and consistent (13, 14) and is widely used (15, 16) we have utilized the $\Delta G_t^0(H^+)$ values based on *RE* (*RE* = Ph_4PBPh_4) (Ph = phenyl) based on the assumption that $\Delta G_t^0(Ph_4P^+) = \Delta G_t^0(Ph_4B^-) = \frac{1}{2}\Delta G_t^0(Ph_4PBPh_4)$ available from literature (15) to compute $\Delta G_t^0(A^-) - \Delta G_t^0(HA)$. For ethanol–water, however, reported values based on average of Ph_4PBPh_4 and Ph_4AsBPH_4 assumptions (15) have been used (results calculated via the two assumptions, however, differ by small amount which is within the range of experimental error (16).

$\Delta G_t^0(A^-) - \Delta G_t^0(HA)$ for 2,4,6-trinitrophenol, acetic acid, and benzoic acid, are reported in Table 4 which shows that for trinitrophenol it is negative in the solvent of lower mol% nonaqueous component and then becomes increasingly positive as the proportion of organic component increases in the solvent and thus passes through a minimum. Initial decrease of $\Delta G_t^0(A^-) - \Delta G_t^0(HA)$ suggests that $\Delta G_t^0(A^-) < \Delta G_t^0(HA)$; that is, trinitrophenolate anion is more stable than its conjugate acid. $\Delta G_t^0(HA)$ for trinitrophenol is likely to be negative since it contains an aromatic ring for dispersion interaction with the organic component of the solvent mixture. Thus $\Delta G_t^0(A^-)$ is appreciably large and negative and this occurs in spite of the positive contribution to the free energy transfer due to electrostatic interaction. Free energy of 2,4,6-trinitrophenolate ion which is delocalised oscillator is very much lowered by strong dispersion interaction with organic component of the solvent mixture (11, 17, 18). The very high polarisability of delocalized electrons in the trinitrophenolate ion promotes interaction with localized dispersion centre in nearby solvent molecules (11, 17, 18). The effective density of dispersion centres in the solvent molecules being found to increase in the sequence $H_2O < CH_3OH < C_2H_5OH$, dispersion interaction will be maximum in ethanol–water mixture. The minimum in $\Delta G_t^0(A^-) - \Delta G_t^0(HA)$ results from two opposing effects. $-\Delta G_t^0(HA)$ is positive and its contribution due to electrostatic

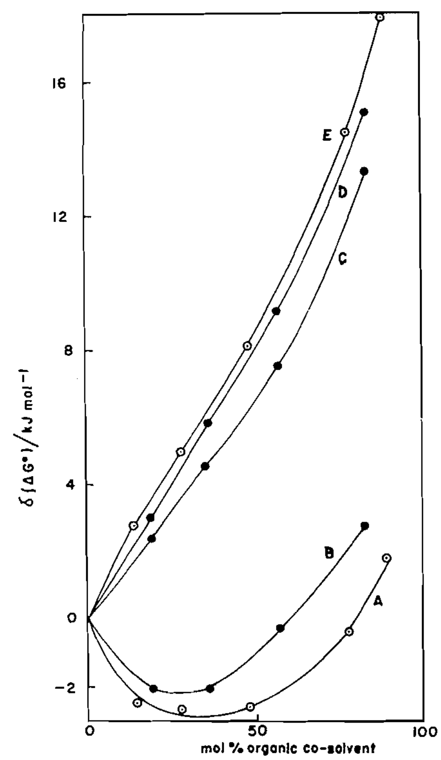

FIG. 1. Variation of $\delta(\Delta G^0)$ for different acids as a function of mol% organic co-solvent: ●, methanol + water; ⊙, ethanol + water; (*A*) and (*B*), 2,4,6-trinitrophenol; (*C*) and (*E*), acetic acid; (*D*), benzoic acid.

TABLE 4. Values of $\Delta G_t^0(H^+)$ and $\Delta G_t^0(A^-) - \Delta G_t^0(HA)$ in methanol–water and ethanol–water colvents at 25°C (ΔG^0 values in kJ mol^{-1} (mole fraction scale))

Wt% organic co-solvent	$\Delta G_t^0(H^+)$*	$\Delta G_t^0(A^-) - \Delta G_t^0(HA)$		
		$(NO_2)_3C_6H_2(OH)$	CH_3COOH	C_6H_5COOH
		Methanol–water		
30	−0.69	−1.42	3.19	3.79
50	−2.89	0.78	7.54	8.66
70	−5.87	5.53	13.37	15.03
90	−5.81	8.49	19.12	20.94
		Ethanol–water		
30	−0.84	−1.67	3.74	
50	−4.44	1.76	9.39	
70	−6.29	3.67	14.44	
90	−4.59	4.19	19.14	

*Reference 15.

interaction to $\Delta G_t^0(A^-)$ is also positive, and their combined contribution simultaneously opposes the negative contribution to $\Delta G_t^0(A^-)$ due to very strong dispersion interaction leading to a minimum in $\Delta G_t^0(A) - \Delta G_t^0(HA)$.

For acetic acid and benzoic acid, $\Delta G_t^0(A^-) - \Delta G_t^0(HA)$ is very positive (Table 4) and is probably primarily due to electrostatic interaction of A^-. Unlike delocalised oscillator trinitrophenolate ion, the localized oscillator acetate and benzoate have weaker (11) dispersion interaction with organic component of the solvent mixture. The dispersion interactions of A^- and HA are not much different as in case of nitrophenol and electrostatic contribution to $\Delta G_t^0(A^-)$ is primarily responsible for variation of $\Delta G_t^0(A^-) - \Delta G_t^0(HA)$ in the case of acetic acid and benzoic acid.

In addition to the different forms of interaction described, hydrogen bonding interaction with negative charge oxygen centres of HA and A^- also operate, but this effect is not likely to contribute much to the combined term $\Delta G_t^0(A^-) - \Delta G_t^0(HA)$ in the aqueous mixtures of ethanol or methanol and particularly it has little role in the making of large difference of dissociation behaviour between 2,4,6-trinitrophenol and acetic acid or benzoic acid. Interaction of H^+ is reflected in $\Delta G_t^0(H^+)$ which may be taken as a measure of relative solvent basicities (5, 7). The detailed interpretation of the behaviour of $\Delta G_t^0(H^+)$ in aqueous mixtures of methanol and ethanol have been presented (15). The overall dissociation behaviour of different uncharged acids in aqueous mixtures of methanol and ethanol is thus understood in terms of interactions of the species HA, A^- and H^+ reflected in $\Delta G_t^0(i)$ of eq. [3].

1. A. L. DE and T. K. DE. Can. J. Chem. (*a*) **62**, 1776 (1984); (*b*) **62**, 2245 (1984).
2. A. L. DE. Electrochim. Acta, (*a*) **28**, 1643 (1983); (*b*) **29**, 471 (1984); (*c*) **29**, 683 (1984).
3. A. WEISSBERGER (*Editor*). Technique of organic chemistry. 2nd ed. Vol. VII. Interscience, New York, NY. 1965.
4. K. K. KUNDU, A. L. DE, and M. N. DAS. J. Chem. Soc. Perkin II, 2063 (1972).
5. B. K. DESHMUKH and J. F. COETZEE. Anal. Chem. **56**, 2373 (1984).
6. D. ROSENTHAL, H. B. HETZER, and R. G. BATES. J. Am. Chem. Soc. **86**, 549 (1964).
7. R. G. BATES. Hydrogen-bonded solvent system. *Edited by* A. K. Covington and P. Jones. Taylor and Francis, London, 1968. pp. 49–86.
8. P. SYKES. A guide book of mechanism in organic chemistry. 5th ed. Orient Longman. 1981. p. 60.
9. R. A. ROBINSON and R. H. STOKES. Electrolyte solutions. 2nd ed. Butterworths, London, 1965. (*a*) p. 353; (*b*) p. 541.
10. E. J. KING. Acid–base equilibria. Pergamon Press, London, 1965. p. 17.
11. R. G. BATES. Solute solvent interaction. *Edited by* J. F. Coetzee and C. D. Ritchie, Marcel Dekker, New York, 1969. p. 75.
12. A. L. DE. Ind. J. Chem. **22A**, 932 (1983).
13. J. I. KIM. J. Phys. Chem. **82**, 191 (1978).
14. M. H. ABRAHAM and N. NASEHZADEH. Can. J. Chem. **57**, 71 (1979); **57**, 2004 (1979).
15. (*a*) O. POPOVICH, A. GIBOLSKY, and D. H. BERNE. Anal. Chem. **44**, 81 (1972); (*b*) O. Popovich. Anal. Chem. **46**, 2009 (1974).
16. B. G. COX, G. R. HEDWIG, A. J. PARKAR, and D. W. WATTS. Aust. J. Chem. **27**, 477 (1974).
17. E. GRUNWALD and E. PRICE. J. Am. Chem. Soc. **86**, 4517 (1964).
18. C. D. RITCHIE. *In* Solute solvent interaction. *Edited by* J. F. Coetzee and C. D. Ritchie. Marcel Dekker, New York, 1969. p. 225.

Assignment of the deoxyribofuranoside protons in DNA oligomers by the application of relayed coherence transfer two-dimensional nuclear magnetic resonance spectroscopy

DONALD W. HUGHES,[1,2] RUSSELL A. BELL, AND THOMAS NEILSON
Departments of Biochemistry and Chemistry, McMaster University, Hamilton, Ont., Canada L8N 3Z5

AND

ALEX D. BAIN[1]
Bruker Spectrospin (Canada) Ltd., 555 Steeles Avenue East, Milton, Ont., Canada L9T 1Y6

Received December 14, 1984

DONALD W. HUGHES, RUSSELL A. BELL, THOMAS NEILSON, and ALEX D. BAIN. Can. J. Chem. **63**, 3133 (1985).

Assignment of the deoxyribofuranose protons in short DNA oligomers by techniques such as homonuclear shift-correlated (COSY) 2-D nmr becomes difficult when there are overlapping diagonal signals. To solve this problem we have applied the method of relayed coherence transfer 2-D nmr to generate cross-peaks between protons such as 1′ and 3′, 3′ and 5′ and 5″ which are not coupled but belong to the same spin system. Plotting cross-sections through the diagonal peaks of the 3′ protons produced completely resolved spectra of the deoxyribofuranoside protons for each nucleotide. Chemical shifts were assigned by comparing each cross-section with the one-dimensional spectrum. A new phase-cycling procedure for the transmitter and receiver was determined and allowed data acquisition with suppression of p-type peaks. This technique is illustrated by the spectra of deoxycytidine and the deoxytriribonucleotide, dCpTpGp.

DONALD W. HUGHES, RUSSELL A. BELL, THOMAS NEILSON et ALEX D. BAIN. Can. J. Chem. **63**, 3133 (1985).

L'attribution des protons du déoxyfurannose des petits oligomères de l'ADN, en faisant appel à des techniques telle la spectroscopie de corrélation (COSY) en rmn 2-D, devient difficile lorsque les signaux diagonaux se recouvrent. Pour palier à cet inconvénient, nous avons utilisé la méthode du transfert de cohérence par relais en rmn 2-D pour générer des pics de référence entre les protons 1′ et 3′, 3′ et 5′ et 5″ qui ne sont pas couplés, mais qui appartiennent au même système de spin. La courbe des sections droites à travers les pics diagonaux des protons 3′ produit, pour chaque nucléotide, un spectre complètement résolu des protons du déoxyribofurannoside. On a attribué les déplacements chimiques en comparant chaque section droite avec un spectre unidimensionnel. On a déterminé une nouvelle méthode en phase cyclique pour l'émetteur et pour le récepteur. Elle permet l'acquisition de données en supprimant les pics du type p. Les spectres de la déoxycitidine et du déoxytriribonucléotide dCpTpGp illustrent cette technique.

[Traduit par le journal]

Introduction

The structure in solution of DNA oligomers is currently undergoing intensive study by nmr spectroscopy. Increased interest in this area has resulted primarily from the improved chemical synthesis of DNA oligomers and from the ability of high field ^{1}H nmr to observe the conformational changes in the deoxyribofuranoside ring and in the phosphate backbone upon the binding of various antitumor drugs (1–4). Reid *et al.* (5) have reported a difference between the solution and solid-state helical structures of a self-complementary octamer. Therefore, it may be necessary to obtain a detailed knowledge of the structure in solution of certain base-paired oligomers even though the solid-state X-ray structure may be available.

Prior to the determination of the solution structure of an oligomer by nmr, the ^{1}H resonances must be correctly assigned to a specific nucleotide in the sequence. Several methodologies are available for analyzing one-dimensional ^{1}H nmr spectra and these include incremental analysis (6, 7), chemical shift parameters (8), and a set of empirically derived rules based on observations of several DNA oligomers (9). These techniques are generally restricted to high temperature spectra (≥70°C) of single strands where base stacking and base pairing are reduced. Nuclear Overhauser effect (nOe) difference spectroscopy has been used to sequence base-paired DNA oligomers (5, 10). Considerable growth has occurred in the application of two-dimensional nmr techniques because the improved resolution and high information content facilitates the assignment of the deoxyribofuranoside protons. The connectivity and assignment of the deoxyribofuranoside protons is usually achieved by COSY (11–14) and ^{1}H–^{31}P heteronuclear shift-correlated experiments (12, 15, 16). Two-dimensional double-quantum ^{1}H spectra of DNA tetramers were recently reported (17). Information on the sequence and spatial relationship of nucleotides in base-paired duplexes can be obtained by 2-D nOe methods (11, 13, 18–20).

A two-dimensional nmr experiment that can aid in assigning the ^{1}H spectra of short DNA oligomers is relayed coherence transfer. Initially reported by Bolton and Bodenhausen (21, 22) and Eich *et al.* (23), relayed coherence transfer is a modification of the shift-correlated experiments that produced cross-peaks between nuclei which are not coupled but which belong to the same spin system. The additional cross-peaks eliminate the uncertainties encountered in the COSY experiment that arise when different spin systems have protons with identical chemical shifts on the diagonal, resulting in several indistinguishable connectivities. Recent applications of homonuclear relayed coherence transfer have dealt with the assignment of the ^{1}H spectra of proteins (24, 25). We report here the use of homonuclear relayed coherence transfer 2-D nmr in assigning the deoxyribofuranoside ^{1}H resonances of short DNA oligomers. A phase-cycling procedure for the transmitter pulses and receiver is also presented, which allows suppression of p-type signals.

Relayed coherence transfer spectra are obtained by mod-

[1] Authors to whom correspondence should be addressed.
[2] Present address: Department of Chemistry, University of Toronto, 80 St. George Street, Toronto, Ontario, Canada M5S 1A1.

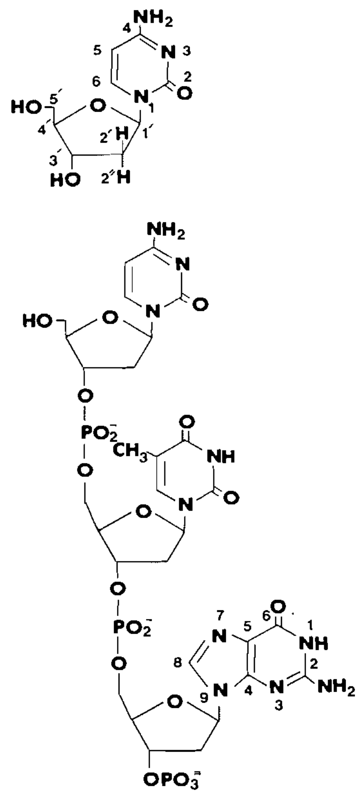

FIG. 1. Structure and numbering of deoxycytidine and the deoxytriribonucleotide triphosphate dCpTpGp.

ifying the mixing pulse of the COSY experiment as follows.

Homonuclear shift-correlated (COSY):

$$90 - t_1 - 90 - \mathrm{ACQ}$$

Relayed coherence transfer:

$$90_{\phi^1} - t_1 - 90_{\phi^2} - \tau - 180_{\phi^3} - \tau - 90_{\phi^3} - \mathrm{ACQ}_{\theta}$$

To illustrate the effect of the relayed coherence transfer pulse sequence, the example of the three-spin system formed by protons 1′, 2′, and 3′ of the deoxyribofuranoside ring (Fig. 1) will be used. Protons 1′ and 2′, and 2′ and 3′ have three-bond coupling constants, while there is no observed coupling between 1′ and 3′. The first 90° pulse in the relayed coherence transfer experiment creates transverse magnetization, which is allowed to precess during the evolution period t_1. The second 90° pulse acts in a manner similar to the COSY mixing pulse in that magnetization from the transitions of the 1′ proton is transferred to the connected transitions of 2′. A 180° pulse is inserted between the second and third 90° pulses in order to remove the effects of chemical shift modulation during this time period. The final 90° pulse transfers magnetization from the 2′ transitions, which now contain frequency information from 1′, to the 3′ proton transitions. The signal from 3′ will therefore be modulated at frequencies corresponding to both 1′ and 2′ and result after 2-D Fourier transformation in a cross-peak at $\omega_1 = \delta 1'$ and $\omega_2 = \delta 3'$. COSY cross-peaks from coupled protons are also observed because they arise from transverse magnetization components not affected by the final pulse (25).

The intensities of the relayed coherence transfer cross-peaks depend strongly on the exact nature of the spin system, since additional spin couplings can provide additional routes for the

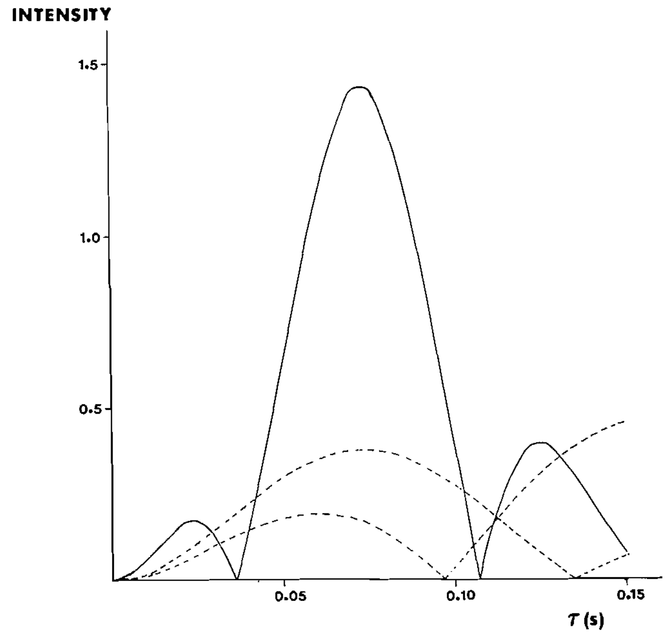

FIG. 2. Intensity of relayed cross-peaks as a function of τ for the pathway $1' \begin{smallmatrix}\nearrow 2' \searrow\\ \updownarrow\\ \searrow 2'' \nearrow\end{smallmatrix} 3'$ (solid line) and $3' \rightarrow 4' \begin{smallmatrix}\nearrow 5'\\ \searrow 5''\end{smallmatrix}$ (dashed line with higher intensity represents the 3′ to 5″ cross-peak) in deoxycytidine. Curves were calculated from eqs. [1] and [3] using an estimated T_2 value calculated from $T_2 = 1/\pi \cdot \nu_{1/2}$ with the halfwidth, $\nu_{1/2}$, of 1.0 Hz.

magnetization to follow during relayed coherence transfer (26, 27). In the present case we are interested in the relay of magnetization from A to X in an AMX spin system where $J_{AX} = 0$. If the spin M is also coupled to nuclei K, L, . . . etc. (other than A and X), then the efficiency of a relayed coherence transfer is given by (26–28)

$$[1] \quad \sin(\pi J_{AM} \tau) \sin(\pi J_{MX} \tau) \prod_{i=K,L,\ldots} \cos(\pi J_{Mi} \tau) \times \exp(-\tau/T_2(\mathrm{M}))$$

where τ is the fixed delay in the relayed coherence transfer pulse sequence and $T_2(\mathrm{M})$ is the spin–spin relaxation time of nucleus M. In particular, the intensity of the relay cross-peak between the 1′ proton and 3′ via 2′ is proportional to

$$[2] \quad \sin(\pi J_{1'2'} \tau) \sin(\pi J_{2'3'} \tau) \cos(\pi J_{2'2''} \tau) \exp(-\tau/T_2(2'))$$

There is an additional route for relaying the 1′ proton magnetization to 3′ and that is via 2″, which results in an efficiency given by an equation similar to eq. [2]. These two independent routes can be combined to provide an overall efficiency for the 1′ to 3′ relayed coherence transfer given by (27)

$$[3] \quad [\sin(\pi J_{1'2'} \tau) \sin(\pi J_{2'3'} \tau) \exp(-\tau/T_2(2')) + \sin(\pi J_{1'2''} \tau) \sin(\pi J_{2''3'} \tau) \exp(-\tau/T_2(2''))] \times \cos(\pi J_{2'2''} \tau)$$

Figure 2 shows a plot, derived from the above equations, of intensity versus τ for the 1′ to 3′ (solid line) and 3′ to 5′ and 5″ (dashed lines) relayed cross-peaks using the coupling constants for deoxycytidine (Table 1). Since the intensities of the

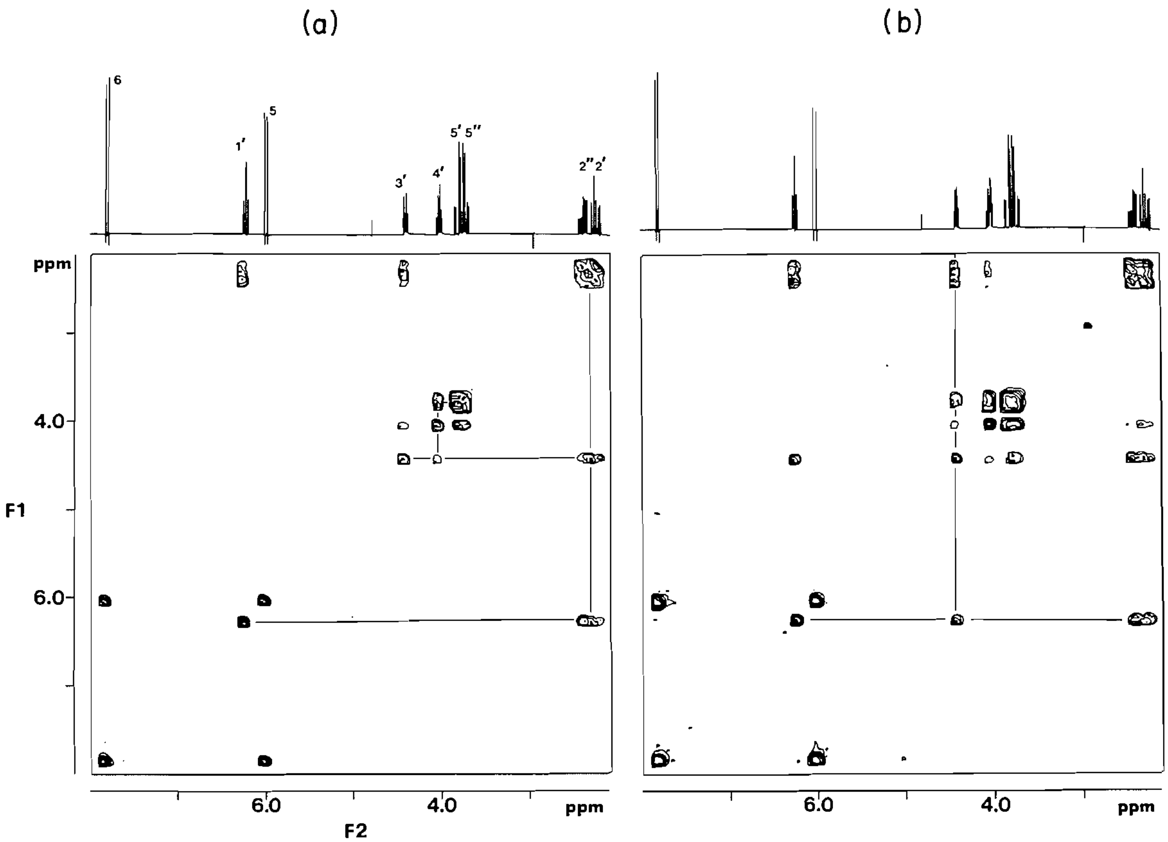

FIG. 3. (a) Contour plot of the 250-MHz ^{1}H COSY 2-D nmr spectrum of deoxycytidine in D_2O at ambient temperature. The solid line indicates the connectivity pathway starting at H-1′ through to protons 5′ and 5″. (b) Contour plot of the ^{1}H relayed coherence transfer 2-D nmr spectrum of deoxycytidine. The horizontal line indicates both the normal COSY cross-peak between H-1′ and H-2′, 2″ and the new cross-peak to H-3′. The vertical line through H-3′ shows an additional relayed coherence transfer cross-peak between H-3′ and H-5′, 5″.

TABLE 1. Proton chemical shifts and coupling constants for deoxycytidine in D_2O at 23°C

Proton	Shift	Coupling constants (Hz)	
H-6	7.829	$^3J_{1'2'}$	6.7
H-5	6.002	$^3J_{1'2''}$	6.4
		$^2J_{2'2''}$	−14.0
H-1′	6.231	$^3J_{2'3'}$	6.7
H-2′	2.257	$^3J_{2''3'}$	4.1
H-2″	2.406	$^3J_{3'4'}$	3.9
H-3′	4.410	$^3J_{4'5'}$	3.7
H-4′	4.033	$^3J_{4'5''}$	5.2
H-5′	3.817	$^2J_{5'5''}$	−12.4
H-5″	3.737	$^3J_{56}$	7.6

peaks depend on the nature of the spin system and all the coupling constants, the choice of an optimum value for τ almost requires complete knowledge of the spin system before the experiment starts. Furthermore, the range of coupling constants and spin systems in deoxyribofuranoside molecules means that an optimum τ which provides both uniform magnetization transfer and minimum effect of T_2 relaxation is impossible for the whole oligomer. The non-uniform nature of the magnetization transfer can be seen in Fig. 2 where the relayed cross-peaks reach their maximum value near $\tau = 0.07$ s; however, there is considerable variation in their relative intensities. A value of τ was therefore chosen from an average of the coupling constants, since although the functional form of eq. [1] may be complicated there are relatively few values of τ for which eq. [1] is close to zero. As in other types of two-dimensional spectroscopy, the absence of a correlation peak does not mean the absence of a correlation.

A complex pulse sequence such as this not only creates the signals needed to make the correlation, but also many artifacts. The main type of artifact that needs to be suppressed is the so-called "p-type" peaks which appear symmetrically on the other side of $F_1 = 0$ from the desired peaks. By repeating the pulse sequence with different r.f. phases it is almost always possible to suppress the undesirable peaks which could lead to spurious correlations. The concept of a coherence pathway (29, 30) was used in designating the sequence of r.f. phases for this pulse sequence.

The spectra of deoxycytidine and the deoxytriribonucleotide,[3] dCpTpGp, were used to illustrate the application of relayed coherence transfer in assigning deoxyribofuranoside resonances.

Experimental

All ^{1}H nmr spectra were recorded at 250.13 MHz on a Bruker WM-250 spectrometer. The single-pulse spectra for deoxycytidine were recorded in 16 scans over a sweep width of 1474.93 Hz (5.554

[3] Abbreviations used: 2′-Deoxyribosyl 5′-dCpTpGp-3′. The deoxyoligoribonucleotide is written in the normal 5′ → 3′ sequence, and the bases are numbered from the 5′-end: dCpTpGp.
1 2 3

TABLE 2. The phase cycling scheme for the relayed coherence transfer pulse sequence $90^\circ_{\phi_1} - t_1 - 90^\circ_{\phi_2} - \tau - 180^\circ_{\phi_3} - \tau - 90^\circ_{\phi_3} - \mathrm{ACQ}_\theta$

$90^\circ_{\phi_1}$	$90^\circ_{\phi_2}$	$180^\circ_{\phi_3}$	$90^\circ_{\phi_3}$	Receiver$_\theta$
0	0	0	0	$\pi/2$
0	0	π	π	$\pi/2$
0	π	0	0	$\pi/2$
0	π	π	π	$\pi/2$
0	0	0	0	$\pi/2$
0	0	π	π	$\pi/2$
0	π	0	0	$\pi/2$
0	π	π	π	$\pi/2$
0	$\pi/2$	$\pi/2$	$\pi/2$	$3\pi/2$
0	$\pi/2$	$3\pi/2$	$3\pi/2$	$3\pi/2$
0	$3\pi/2$	$\pi/2$	$\pi/2$	$3\pi/2$
0	$3\pi/2$	$3\pi/2$	$3\pi/2$	$3\pi/2$
0	$\pi/2$	$\pi/2$	$\pi/2$	$3\pi/2$
0	$\pi/2$	$3\pi/2$	$3\pi/2$	$3\pi/2$
0	$3\pi/2$	$\pi/2$	$\pi/2$	$3\pi/2$
0	$3\pi/2$	$3\pi/2$	$3\pi/2$	$3\pi/2$

s acquisition time) while the dCpTpGp spectra were acquired in 48 scans using a 1748.25-Hz sweep width (4.686 s acquisition time). Spectra were acquired in 16 K data points. Suppression of the HDO resonance was achieved by irradiation during the 2.0-s relaxation delay prior to acquisition. Sample temperatures were ambient temperature (23°C) for deoxycytidine and 40.3 ± 1.0°C for dCpTpGp. The latter temperature was maintained by a Bruker BVT-1000 variable temperature unit and checked by thermocouple measurement. The free induction decays were processed using Gaussian multiplication for resolution enhancement and zero-filled to 32 K before Fourier transformation.

The ^{1}H shift-correlated (COSY) 2-D nmr spectra were acquired using the pulse sequence:

$$90^\circ - t_1 - \alpha^\circ - \mathrm{ACQ}$$

where $\alpha = 90^\circ$ for the deoxycytidine experiment and $\alpha = 45^\circ$ for dCpTpGp. The 90° pulse width was 6.4 μs. Relayed coherence transfer 2-D nmr experiments used the pulse sequence:

$$90^\circ_{\phi_1} - t_1 - 90^\circ_{\phi_2} - \tau - 180^\circ_{\phi_3} - \tau - 90^\circ_{\phi_3} - \mathrm{ACQ}_\theta$$

where $\tau = 0.046$ s. The phase cycling ϕ_1, ϕ_2, ϕ_3, and θ are given in Table 2. The HDO resonance was suppressed by pre-saturation during the 2.0-s relaxation delay and the evolution and fixed delay times prior to acquisition. The 2-D spectra of deoxycytidine were obtained in 16 scans for each of the 128 FID's which contained 512 data points in F2. Zero-filling in the F1 dimension during 2-D Fourier transformation produced a 256 × 256 data matrix with a digital resolution of 5.761 Hz/point in both dimensions. The dCpTpGp 2-D spectra consisted of 256 FID's (1 K data points in F2) acquired in 48 scans each. The data were zero-filled in F1 to a 512 × 512 matrix when transformed and the resolution was 3.415 Hz/point. All spectra were transformed with the application of the squared sine-bell function in both dimensions followed by symmetrization of the transformed matrix.

Samples were lyophilized twice from 99.8% D_2O and then dissolved in 100% D_2O (MSD Isotopes) to concentrations of 0.13 *M* for deoxycytidine and 0.017 *M* for dCpTpGp. Chemical shifts are reported in ppm relative to DSS (sodium 4,4-dimethyl-4-silapentan-1-sulfonate) using *tert*-butyl alcohol-OD (1.231 ppm) as internal reference.

Results and discussion

COSY and relayed coherence transfer 2-D nmr spectra were initially recorded on deoxycytidine (Fig. 1) in D_2O. Since the relayed coherence transfer experiment creates additional cross-peaks, a mononucleoside with well-resolved riboside proton

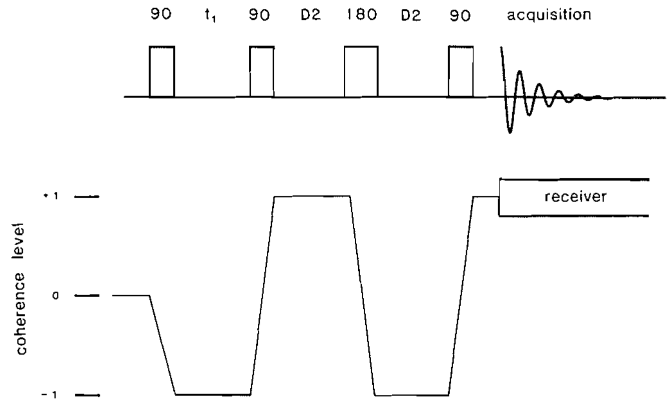

FIG. 4. Coherence pathway for the desired signals in the homonuclear relayed coherence transfer experiment. The solid line traces the changes in coherence level (see ref. 29) during the pulse sequence depicted at the top of the diagram. The phase cycling procedure in Table 2 allows this pathway to survive, but suppresses pathways that include coherence level +1 during the t_1 delay.

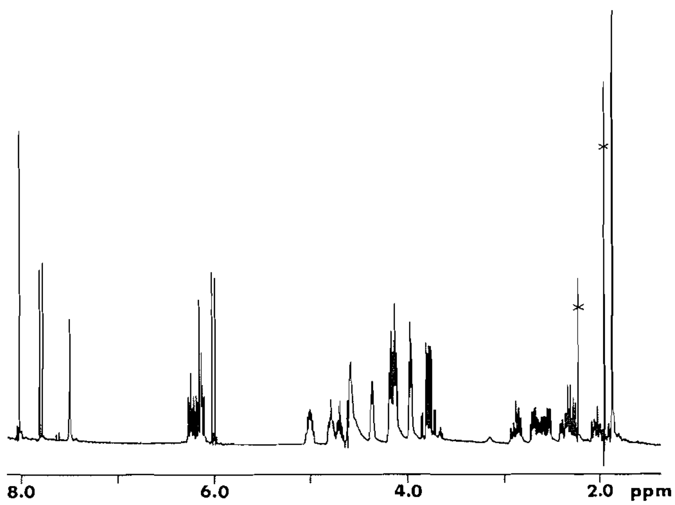

FIG. 5. The 250-MHz ^{1}H nmr spectrum of dCpTpGp in D_2O at 40.3°C. Peaks marked with (×) are impurities.

resonances was examined first in order to avoid any complications arising from overlapping multiplets. The chemical shifts and coupling constants for deoxycytidine are presented in Table 1 and the assignments are shown on the one-dimensional spectrum in Fig. 3a. Pyrimidine protons H-5 and H-6 form an AX spin system. The resonances from the seven deoxyribofuranoside protons can be grouped into three spin systems of the type ABX or ABM as follows: 1′, 2′, and 2″; 3′, 2′, and 2″; 4′, 5′, and 5″. From the contour plot of the COSY spectrum in Fig. 3a, the connectivity of the deoxycytidine riboside protons can be worked out by locating the appropriate cross-peaks indicated by the solid line. Cross-peaks of relatively high intensity were observed between 1′ and 2′, 2″ protons and similarly between 3′ and 2′, 2″. The digital resolution was insufficient to resolve the AB coupling between 2′ and 2″ protons. The connectivity pathway can be completed by following the 3′–4′ cross-peak through the 4′ diagonal peak to the cross-peak between the 4′ and 5′, 5″ protons.

With the connectivities between directly coupled riboside protons established from the COSY spectrum, the relayed coherence transfer experiment was then performed. The fixed

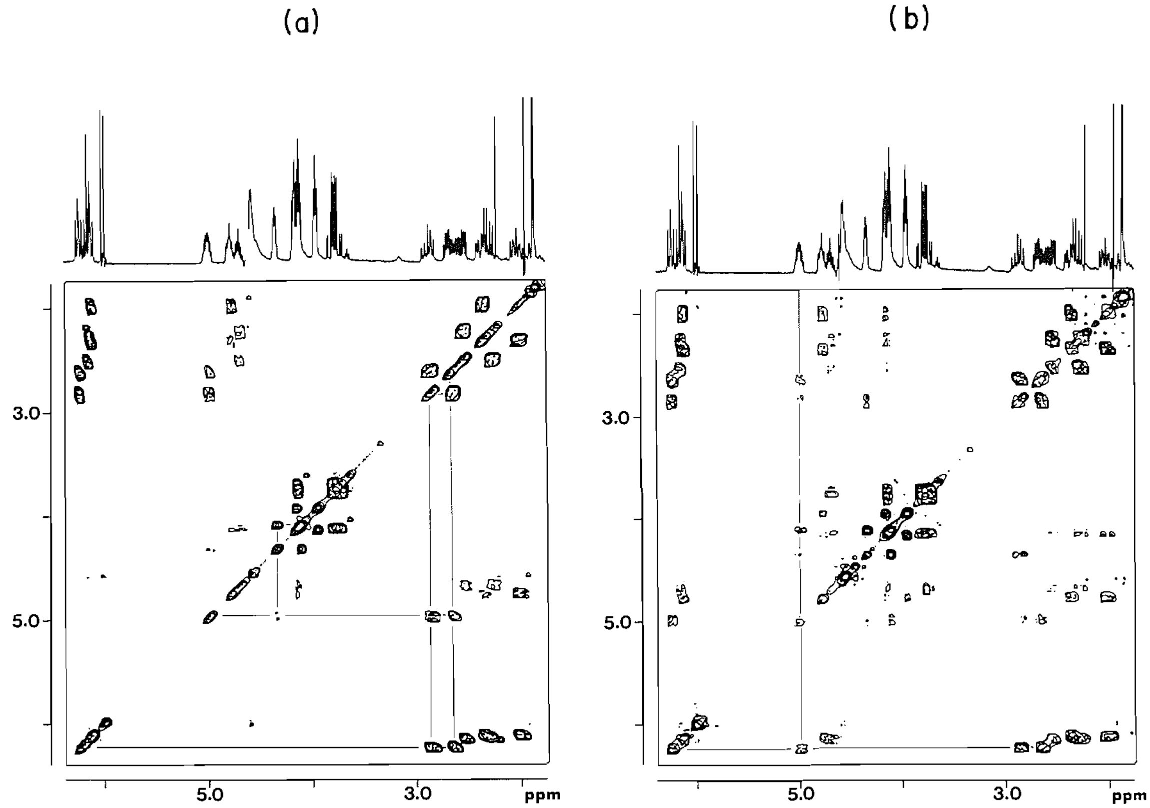

FIG. 6. (a) Contour plot of the 250-MHz ^{1}H COSY-45 2-D nmr spectrum of the deoxyribofuranoside protons of dCpTpGp in D_2O at 40.3°C. The solid line indicates the connectivity pathway through the deoxyguanosine furanoside protons. (b) Contour plot of the 250-MHz ^{1}H relayed coherence transfer 2-D nmr spectrum of dCpTpGp at 40.3°C. The vertical line indicates the COSY and relayed coherence transfer cross-peaks to the deoxyguanosine H-3′.

delay times in the pulse sequence were adjusted to produce a relayed coherence transfer cross-peak between the 1′ and 3′ protons. The advantages of a cross-peak between these protons are the large separation of the anomeric proton resonance from the other riboside proton signals and, in oligomers, the 1′ resonances are generally not overlapped. An additional advantage was that the 3′ proton chemical shift difference between phosphorylated and non-phosphorylated nucleosides could be used to identify the 3′-terminal nucleotide 1′ and 2′, 2″ protons.

The coherence pathway for the relayed transfer experiment is given in Fig. 4. The desired signals are those that are in coherence level -1 during the t_1 delay and then follow the solid line to the receiver; the p-type peaks arise from signals that are in coherence level $+1$ during t_1. There are three major routes by which the p-type signals can reach the receiver, and it can be shown by the methods in ref. 29 that the phase-cycling procedure in Table 2 eliminates all of them.

Using the phase-cycling technique in Table 2 and the fixed delay τ as 0.046 s, the relayed coherence transfer 2-D spectrum of deoxycytidine (in Fig. 3b) was acquired. The relayed coherence transfer cross-peak between 1′ and 3′ was observed along with the COSY cross-peaks. By drawing a horizontal line through the 1′–3′ cross-peak as shown in Fig. 3b, it is possible to identify four of the seven protons of the deoxyribofuranoside spin system. The particular value of τ used also gives a relatively intense cross-peak between 3′ and the 5′, 5″ protons, even though this is a different spin system (27). This additional relayed coherence transfer cross-peak arises because the 3′ proton is actually part of two magnetization transfer pathways: one from 1′ through 2′, 2″ to 3′ and the other from 3′ through 4′ to the 5′, 5″ protons. The delay τ of 0.046 s provides a balanced magnetization transfer throughout the entire deoxyriboside spin system and is derived from an average of all the deoxyriboside coupling constants of 5.5 Hz. From Fig. 2 it can be seen the $\tau = 0.046$ s results in cross-peaks that have considerably less variation in relative intensity and allow the relayed cross-peak between 3′ and the 5′ protons to be observed at a similar intensity level at the 1′ to 3′ cross-peaks. This avoids repeating the experiment with different τ values in order to obtain a specific correlation.

The significance of the 3′–5′, 5″ relayed coherence transfer cross-peak became evident when a vertical line was drawn through the H-3′ diagonal peak (Fig. 3b). It was then possible to assign all the protons that belonged to the deoxyribofuranoside ring which contained that specific 3′ proton. Extending these results to short oligomers, it should be possible to exploit the effect of phosphorylation on the 3′ chemical shifts and be able to extract all the protons for each deoxyribofuranoside ring by examining both the COSY and relayed coherence transfer cross-peaks in vertical cross-sections through the 3′ protons.

In order to evaluate the ability of the relayed coherence transfer experiment to resolve the deoxyribofuranoside proton resonances of an oligomer, the deoxytriribonucleoside triphosphate, dCpTpGp (Fig. 1) was studied. The one-dimensional spectrum of dCpTpGp (Fig. 5) was recorded in D_2O at 40.3°C. At this temperature the residual HDO signal was not overlapped with deoxyribofuranoside proton resonances. A preliminary analysis of the one-dimensional spectrum permit-

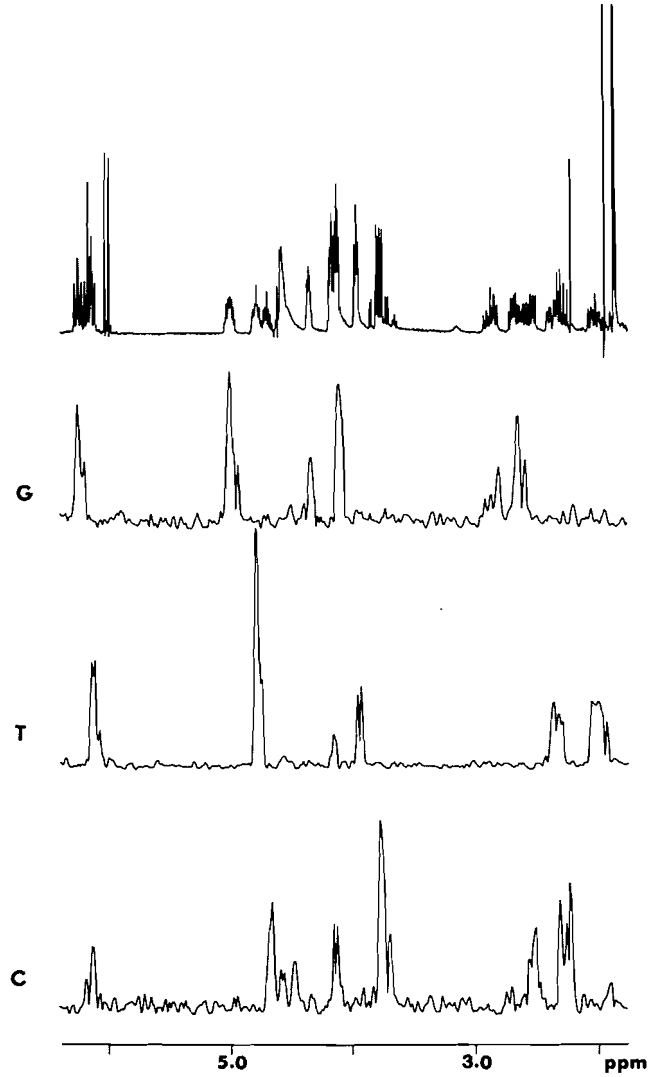

FIG. 7. Plots of the columns of the relayed coherence transfer 2-D data matrix through the H-3′ resonances showing the proton signals for each deoxyribofuranoside ring. The digital resolution of these vertical cross-sections was 3.415 Hz/point.

ted the identification of the type of deoxyribofuranose proton resonances as well as some assignments. Of the three anomeric proton signals, the H-1′ at 6.238 ppm was the only resolved multiplet, while the other H-1′ signals were overlapped. Multiplets attributed to the 3′ protons in the region of 4.7–5.0 ppm were each resolved, even though all 3′ hydroxyl groups were phosphorylated. The region from 4.0–4.4 ppm contained the 4′ protons and the 5′, 5″ protons from dT and dG. Centered near 3.9 ppm was the characteristic AB multiplet corresponding to the non-phosphorylated 5′ terminal dC 5′, 5″ protons. Between 2.0 and 3.0 ppm were the AB multiplets from the 2′, 2″ protons. Application of the rules developed by Tran-Dinh *et al.* (9) resulted in the assignment of the signals at 2.829 and 2.619 ppm to the dG H-2′ and H-2″, respectively. The highest field multiplet near 2.0 ppm had a splitting pattern characteristic of a dT H-2′ (9).

A COSY-45 spectrum (Fig. 6a) was then recorded to determine the connectivity of the deoxyribofuranoside protons. The 45° mixing pulse was used to produce a clearer representation of cross-peaks near the diagonal (31, 32). The only connectivity pathway that could be completed with reasonable certainty from Fig. 6a was that of the dG deoxyriboside protons. The dC and dT connectivities were complicated by the overlap of the H-1′ resonances and the H-4′ signals near 4.1 ppm. In the upper right corner of Fig. 6a the coupling of the dC and dT 2′ and 2″ protons could be readily observed because of the chemical shift separation of the individual AB multiplets. The chemical shift separation of the dC and dT 2′ and 2″ protons also helped to identify the coupling to the corresponding 3′ protons.

TABLE 3. ^{1}H chemical shifts for dCpTpGp at 40.3°C in D_2O

Proton	Chemical shifts C	T	G
H-6	7.792	7.491	
H-5	6.003		
H-8			8.016
H-1′	6.157	6.127	6.238
H-2′	2.272	2.015	2.829
H-2″	2.545	2.359	2.619
H-3′	4.695	4.780	4.994
H-4′	4.168	4.159	4.350
H-5′	3.803	3.954	4.116
H-5″	3.738	3.954	4.116
CH_3		1.939	

To clarify further the connectivity of the deoxyribofuranoside protons, the relayed coherence transfer spectrum of dCpTpGp was obtained with a fixed delay of 0.046 s. The contour plot of this spectrum is shown in Fig. 6b. A vertical line through the 3′ proton at 4.994 ppm identified all the deoxyriboside protons of dG. When this method was used to assign the dC and dT protons a number of problems arose in dealing with the contour plot. There was a loss of intensity of some of the 2′, 2″–3′ cross-peaks and a further reduction of the already low intensity 3′–4′ cross-peaks. The 1′–3′ relayed coherence transfer cross-peaks were reasonably intense, but those for dC and dT appeared overlapped. The intensity problems may be overcome by acquiring more scans and (or) optimizing fixed delay times for particular coupling constants. A more satisfactory approach than analyzing the contour plot was to compare the vertical cross-sections through each 3′ proton directly with the one-dimensional spectrum. This method, shown in Fig. 7, produced a spectrum for each nucleotide in the sequence without the problems of signal overlap from other deoxyribofuranoside protons. The cross-sections could be assigned to a specific nucleotide by identifying the resonances whose assignments could be made from the one-dimensional spectrum. The dC signals were determined by noting the alignment of the signal near 3.8–3.9 ppm in the bottom cross-section of Fig. 7 with the AB multiplet of the 5′, 5″ protons in the one-dimensional spectrum. As previously discussed, the dG 2′, 2″ protons generally appear at lower field than the pyrimidine 2′, 2″ protons (9). The signals in the top cross-section of Fig. 7 near 2.6–3.0 ppm correlated with the dG 2′, 2″ protons in the one-dimensional spectrum and therefore identified the dG cross-section. This confirmed the COSY-45 connectivities. The dT cross-section was assigned by elimination and confirmed by the alignment of the signal near 2.0 ppm with the multiplet attributed to the dT H-2′. The chemical shifts of dCpTpGp are presented in Table 3. These cross-sections were able to assign the dC and dT H-1′ resonances at 6.157 and

6.127 ppm, respectively. The dC and dT H-4′ signals were insufficiently resolved and the assignments given in Table 3 are tentative.

Conclusions

Relayed coherence transfer provides an effective means of assigning the deoxyribofuranoside ^{1}H resonances of each nucleotide in short DNA oligomers. The use of cross-sections through the 3′ protons avoids the ambiguities that arise during the analysis of complex shift-correlated contour plots. The ability of the cross-sections to resolve the deoxyribofuranoside protons should aid in performing other experiments such as spin decoupling and one-dimensional nOe's. It is generally recommended that the COSY spectrum also be recorded to avoid confusing the COSY and relayed coherence transfer cross-peaks in the contour plots. The successful application of this technique to DNA oligomers requires the resolution of the 3′ proton resonances and this will depend on the base composition and length of the sequence as well as the magnetic field strength.

Acknowledgements

We thank Brian D. Allore for preparing the trimer dCpTpGp used in this study. The authors acknowledge financial support from the National Cancer Institute of Canada and the Natural Sciences and Engineering Research Council of Canada.

1. J.-M. NEUMANN, S. TRAN-DINH, J.-P. GIRAULT, J.-C. CHOTTARD, T. HUYNH-DINH, and J. IGOLEN. Eur. J. Biochem. **141**, 465 (1984).
2. A. T. M. MARCELIS and J. REEDIJK. Recl. Trav. Chim. Pays-Bas, **102**, 121 (1983).
3. T. R. KRUGH. *In* Topics in nucleic acid structure. Vol. I. *Edited by* S. Neidle. MacMillan Publishers Ltd., London. 1981. pp. 197–217.
4. D. J. PATEL. Acc. Chem. Res. **12**, 118 (1979).
5. D. G. REID, S. A. SALISBURY, S. BELLARD, Z. SHAKKED, and D. H. WILLIAMS. Biochemistry, **22**, 2019 (1983).
6. P. N. BORER, L. S. KAN, and P. O. P. TS'O. Biochemistry, **14**, 4847 (1975).
7. P. O. P. TS'O, J. L. ALDERFER, P. N. BORER, and L. S. KAN. *In* Structure and conformation of nucleic acids and protein – nucleic acid interactions. *Edited by* M. Sundaralingam and S. T. Rao. University Park Press, Baltimore, MD. 1975. pp. 193–206.
8. R. A. BELL, D. ALKEMA, J. M. CODDINGTON, P. A. HADER, D. W. HUGHES, and T. NEILSON. Nucleic Acids Res. **11**, 1143 (1983).
9. S. TRAN-DINH, J.-M. NEUMANN, J. TABOURY, T. HUYNH-DINH, S. RENOUS, B. GENISSEL, and J. IGOLEN. Eur. J. Biochem. **133**, 579 (1983).
10. D. FRECHET, D. M. CHENG, L. S. KAN, and P. O. P. TS'O. Biochemistry, **22**, 5194 (1983).
11. J. FEIGON, J. M. WRIGHT, W. LEUPIN, W. A. DENNY, and D. R. KEARNS. J. Am. Chem. Soc. **104**, 5540 (1982).
12. A. PARDI, R. W. WALKER, H. RAPOPORT, G. WIDER, and K. WÜTHRICH. J. Am. Chem. Soc. **105**, 1652 (1983).
13. D. R. HARE, D. E. WEMMER, S.-H. CHOU, G. DROBNY, and B. R. REID. J. Mol. Biol. **171**, 319 (1983).
14. J. W. LOWN, C. C. HANSTOCK, R. C. BLECKLEY, J.-L. IMBACH, B. RAYER, and J. J. VASSEUR. Nucleic Acids Res. **12**, 2519 (1984).
15. K. LAI, D. O. SHAH, E. DEROSE, and D. G. GORENSTEIN. Biochem. Biophys. Res. Commun. **121**, 1021 (1984).
16. D. MARION, and G. LANCELOT. Biochem. Biophys. Res. Commun. **124**, 774 (1984).
17. C. C. HANSTOCK and J. W. LOWN. J. Magn. Reson. **58**, 167 (1984).
18. R. M. SCHEEK, N. RUSSO, R. BOELENS, R. KAPTEIN, and J. H. VAN BOOM. J. Am. Chem. Soc. **105**, 2914 (1983).
19. R. M. SCHEEK, R. BOOLENS, N. RUSSO, J. H. VAN BOOM, and R. KAPTEIN. Biochemistry, **23**, 1371 (1984).
20. D. E. WEMMER, S.-H. CHOU, D. R. HARE, and B. R. REID. Biochemistry, **23**, 2262 (1984).
21. P. H. BOLTON. J. Magn. Reson. **48**, 336 (1982).
22. P. H. BOLTON and G. BODENHAUSEN. Chem. Phys. Lett. **89**, 139 (1982).
23. G. EICH, G. BODENHAUSEN, and R. R. ERNST. J. Am. Chem. Soc. **104**, 3731 (1982).
24. G. KING, and P. E. WRIGHT. J. Magn. Reson. **54**, 328 (1983).
25. G. WAGNER. J. Magn. Reson. **55**, 151 (1983).
26. D. NEUHAUS, G. WIDER, G. WAGNER, and K. WÜTHRICH. J. Magn. Reson. **57**, 164 (1984).
27. A. BAX and G. DROBNY. J. Magn. Reson. **61**, 306 (1985).
28. O. W. SØRENSEN, G. W. EICH, M. H. LEVITT, G. BODENHAUSEN, and R. R. ERNST. Prog. Nucl. Magn. Reson. Spectrosc. **16**, 163 (1983).
29. A. D. BAIN. J. Magn. Reson. **56**, 418 (1984).
30. G. BODENHAUSEN, H. KOGLER, and R. R. ERNST. J. Magn. Reson. **58**, 370 (1984).
31. A. BAX and R. FREEMAN. J. Magn. Reson. **44**, 542 (1981).
32. A. BAX. *In* Two dimensional nuclear magnetic resonance in liquids. D. Reidel Publishing Co., Boston, MA. 1982. pp. 78–82.

Homolytic versus heterolytic cleavage for the photochemistry of 1-naphthylmethyl derivatives

B. ARNOLD, L. DONALD, A. JURGENS, AND J. A. PINCOCK[1]
Department of Chemistry, Dalhousie University, Halifax, N.S., Canada B3H 4J3

Received February 28, 1985

This paper is dedicated to Professor Gerald E. Dunn on the occasion of his 65th birthday

B. ARNOLD, L. DONALD, A. JURGENS, and J. A. PINCOCK. Can. J. Chem. **63**, 3140 (1985).

The photochemical cleavage of the 1-naphthylmethyl derivatives, **1**–**7**, has been examined in methanol solvent under both direct and sensitized conditions. The competitition between homolytic and heterolytic cleavage as a function of multiplicity and leaving group has been studied in detail. Only substrates **1**, **2**, **3**, and **7** react on sensitization with xanthone but evidence is presented that the resulting reactivity of **1**, **2**, and **3** may not be triplet energy transfer but rather exciplex formation. A semi-quantitative scale for photofugacities of the leaving groups from the excited singlet states has been established.

B. ARNOLD, L. DONALD, A. JURGENS et J. A. PINCOCK. Can. J. Chem. **63**, 3140 (1985).

Utilisant le méthanol comme solvant, on a étudié le clivage photochimique des dérivés du naphtyl-1 méthyle **1** à **7** tant dans conditions directes que sous l'influence de sensibilisateurs. On a soigneusement étudié la compétition entre les clivages homolytique et hétérolytique en fonction tant de la multiplicité que du groupe labile. Seuls les substrats **1**, **2**, **3** et **7** réagissent lorsqu'on utilise le xanthone comme sensibilateur; toutefois, on prouve que la réactivité résultante des dérivés **1**, **2** et **3** n'est pas due à un transfert d'énergie du triplet mais plutôt à la formation d'un exciplex. On a établi une échelle semi-quantitative des photofugacités des groupes labiles à partir des états singulets excités.

[Traduit par le journal]

Introduction

Since the initial reports by Zimmerman *et al.* (1, 2) on the photocleavage of benzylic derivatives ($ArCH_2$—X) in nucleophilic solvents, there has been considerable interest in this seemingly simple process. Much of the work has focused on the competition between homolytic versus heterolytic cleavage as a function of the multiplicity of the excited state (i.e. direct versus sensitized irradiations) and the nature of the photofugal group (X = Cl (3–6), Br (5, 6), I (5–7), $\overset{+}{N}R_3$ (8–10), $\overset{+}{S}R_2$ (11), $\overset{+}{P}R_3$ (12), OOCR (5, 6, 13–16), SO_2—R (17, 18), OSO_2R (19)). A partial review, including a theoretical study of spin inversion in the radical pairs generated in triplet reactions, has also appeared (20). This earlier work was mainly qualitative in that usually only product ratios were determined although in some cases quantum yields are also available. However, an understanding of multiplicity effects in these studies is complicated for two reasons. First, the high triplet energy of the benzene chromophore makes unambiguous triplet energy transfer sensitization difficult. Second, in direct irradiations, the proportion of product derived from the triplet formed via intersystem crossing from the singlet as opposed to that formed directly from the singlet is unknown since detailed quenching studies were not attempted.

Recently the Cristol group has published (3, 4) an extensive quantitative study on the photolysis of a series of substituted benzyl chlorides in *tert*-butyl alcohol. The sensitization and quenching techniques used only allowed for information about triplet state reactivity. The conclusion was that two excited triplet states are important in these reactions, a lower one of longer lifetime, which reverts only back to ground-state reactant, and an upper one of shorter lifetime that gives photosolvolysis products. The other conclusion to be reached from this study is that benzyl halides are not the ideal substrates required to do the detailed rate–structure correlations that are necessary to fully understand the factors which control homolytic versus heterolytic cleavage. This is because the high excitation energy of the benzene chromophore (110 kcal/mol (3) for the singlet and 73–74 kcal/mol (21) for the triplet) allows photochemical cleavage of the benzyl carbon – chlorine bond (bond strength, 67–69 kcal/mol (22)) to be very exothermic and consequently rapid. Cristol's (4) estimates of the lifetime of the reactive excited states of 0.4 – 1.4 ns are at, or beyond, the limit of reliable measurement by normal quenching and single-photon counting lifetime techniques.

Our interest in the synthetic utility of benzylic cleavages (23, 24) led us to examine similar substrates using the naphthalene rather than the benzene chromophore and to initiate a systematic study of homolytic versus heterolytic cleavage. As Givens *et al.* (15) have outlined previously, the naphthyl chromophore absorbs beyond 300 nm so that quenching studies free of competitive absorption problems are possible and, as well, the lower triplet energy for naphthalenes of about 60 kcal/mol is suitable for unambiguous sensitization studies. Moreover, the lower excited state energies involved make it likely that a group, X, of low enough photofugacity can be found so that reaction rates will be slow enough for convenient measurement. With this in mind, we undertook and report here a study of the photochemistry of the 1-naphthylmethyl derivatives, **1**–**7** (from here on the 1-naphthyl ring will be abbreviated as N).

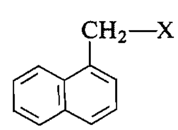

1, X = Cl; **2**, X = Br; **3**, X = $\overset{+}{S}(CH_3)_2\bar{B}F_4$;
4, X = $\overset{+}{N}(CH_3)_3Cl^-$; **5**, X = O_2CCH_3;
6, X = $O_2P(OCH_2CH_3)_2$; **7**, X = SO_2CH_3

The case for X = I was omitted because a recent study (7) indicates that this substrate reacts by a pathway quite different from that of the other X groups and involves the radical anion of molecular iodine.

Results and discussion

Direct irradiations

As expected, from the literature discussed in the Intro-

[1] Author to whom correspondence may be addressed.

TABLE 1. Product distribution[a] for the photolysis of the 1-naphthylmethyl derivatives **1–7** in methanol

X	Conditions[b]	**9**	**10**	**11**	(**9**+**10**+**11**)/**8**	R/I[c]
1, Cl	D	24	T	32	56:31[d]	52:30(3)[h]
	S	16	T	21	37:48	22:73(3)[h]
	Q[f]	20	T	29	49:27	—
2, Br	D	16	ND	T	16:74[e]	26:64(6)
	S	8	ND	T	8:79	ND:100(6)
	Q[f]	5	ND	T	5:78	—
3, $\overset{+}{S}(CH_3)_2$	D	18	T	ND	18:71	12:40(11)
BF_4^-	S	28	T	ND	28:30	—
	Q[f]	5	T	ND	5:82	—
4, $\overset{+}{N}(CH_3)_3$	D	5	21	T	26:72	27:54(9), 42:42(10)
Cl^-	S		No reaction			NR(10)
5, O_2CCH_3	D	ND	ND	ND	ND:87	10:33(6)
	S		No reaction			—
6, $O_2P(OEt)_2$	D	ND	T	ND	T:93	—
	S		No reaction			—
7, SO_2CH_3	D	68	8	ND	74:12	100:ND(24)
	S	60	10	ND	70: 5	—
	Q[g]	36	T	ND	36:19	—

[a] All values are reported as % yield; ND (none detected); T (<5%).
[b] Conditions: D, direct; S, sensitized with xanthone; Q, quenched.
[c] Product distribution for the corresponding benzyl substrate.
[d] Literature values (**9**+**10**+**11**)/**8** 61:39(23).
[e] Literature values (**9**+**10**+**11**)/**8** 12:88(23).
[f] 10^{-2} *M* in 2,5-dimethyl-2,4-hexadiene.
[g] 10^{-3} *M* in 2,5-dimethyl-2,4-hexadiene.
[h] In *tert*-butyl alcohol.

duction, direct photolysis of the derivatives **1–7** in methanol leads to the formation of several products resulting from excited state cleavage of the carbon–X bond, eq. [1].

$$[1]\quad \underset{\mathbf{1-7}}{NCH_2{-}X} \xrightarrow[CH_3OH]{h\nu} \underset{\mathbf{8}}{NCH_2{-}OCH_3} + \underset{\mathbf{9}}{NCH_2CH_2N} + \underset{\mathbf{10}}{NCH_3} + \underset{\mathbf{11}}{NCH_2CH_2OH}$$

The products are easily rationalized if both heterolytic and homolytic cleavage are involved. The ether **8** is formed by trapping of the 1-naphthylmethyl carbocation by the nucleophilic solvent, methanol. In contrast, the products, **9**, **10**, and **11**, are all formed from the 1-naphthylmethyl radical, **9** by coupling, **10** by hydrogen-atom abstraction from the solvent, and **11** by coupling with the hydroxymethyl radical formed from methanol. As will be discussed, the competition between the pathways for formation of **9**, **10**, **11** is determined by the nature of the leaving group, X, and the light intensity. However, the competition between **8** and (**9**, **10**, **11**) as a group is a reflection of the relative amounts of products derived from ionic and radical intermediates for these substrates.

The product distributions determined by calibrated hplc for the direct irradiations (Corex filter) of **1–7** are given in Table 1. As can be seen, the mass balance for the reactions is good (>85%) even with very high conversion runs, since the results reported are for complete disappearance of starting material. Because the products have essentially the same chromophore as the starting material there is an obvious internal filter effect which slows down the reactions as a function of percent conversion. However, the product ratios do not change and this was confirmed by demonstrating that all four photoproducts are stable to the reaction conditions for at least as long as any of the irradiation times. The results are best summarized by the column that gives the ratio of (**9** + **10** + **11**)/**8**; the values for the corresponding benzyl derivatives R/I, where known, are also given. Clearly, there is considerable variation in these values and this seems to be mainly a function of X, because the same trends are present for both the 1-naphthylmethyl and the benzyl derivatives. It is, of course, difficult to interpret these results for direct irradiations since, as discussed briefly in the Introduction, the multiplicity of the excited state that leads to photocleavage is unknown without results from sensitization and quenching studies. These will be presented in the next section.

The distribution of products from the radical cleavage (i.e. **9**/**10**/**11**) obviously varies with X. Normally, the 1-naphthylmethyl radical generated in methanol dimerizes to make **9** the major product rather than **10** (all substrates except **4**, X = $\overset{+}{N}(CH_3)_3Cl^-$). This is reasonable since abstraction of a hydrogen from methanol by the 1-naphthylmethyl radical will be endothermic by about 11 kcal/mol. This is based on the difference between the carbon–hydrogen bond strength in methanol (93 kcal/mol) (22) and the estimated carbon–hydrogen bond strength in 1-methylnaphthalene (82 kcal/mol, using 85 kcal/mol (22) for the bond strength in toluene and 3 kcal/mol (25) extra stabilization for the 1-naphthylmethyl radical relative to the benzyl radical). The only case, **4**, where methylnaphthalene is the major product is explained by the very favorable

$$[2]\quad NCH_2\cdot + CH_3{-}\overset{\cdot+}{N}(CH_3)_2 \rightarrow N{-}CH_3 + CH_2{=}\overset{+}{N}(CH_3)_2$$

$$[3]\quad NCH_2\cdot + CH_3{-}\overset{\cdot+}{S}CH_3 \rightarrow N{-}CH_3 + CH_2{=}\overset{+}{S}CH_3$$

step shown in eq. [2], where the radical cation of trimethylamine serves as the hydrogen atom donor. The corresponding case, eq. [3], where X is $\overset{+}{S}(CH_3)_2\bar{B}F_4$, should not be as favorable based on the known ability of nitrogen and sulfur to stabilize cations as indicated by σ^+ values of −1.7 for $-N(CH_3)_2$ and −0.6 for $-SCH_3$ (26). Finally, the only sub-

TABLE 2. Spectroscopic properties of the 1-naphthylmethyl derivatives **1–7** in methanol

Compound	E_S[a] (kcal/mol)	E_T[b] (kcal/mol)	ϕ_F[c]	$\tau_S \times 10^9$[d] (s)	$k_f \times 10^{-6}$[e] (s^{-1})	$\tau_S \times 10^9$[f] (s)
1	90.2	ND	$<4 \times 10^{-4}$	<1	1.49	<0.5
2	89.5	ND	$<8 \times 10^{-4}$	<1	—	<0.5
3	89.9	60.5	$<3 \times 10^{-4}$	<1	2.01	<0.5
4	90.2	62.0	0.056	6.9	1.87	30
5	89.3	61.3	0.14	41	1.47	95
6	90.5	61.3	0.054	13	1.46	37
7	88.5	58.8	0.14	33	1.24	112

[a] From the 0,0 band in the S_0–S_1 absorption band.
[b] From phosphorescence in 4:1 ethanol/methanol at 77 K; ND (none detected).
[c] Based on ϕ_F for naphthalene in methanol of 0.24, by comparison with naphthalene in cyclohexane as 0.23 (27).
[d] Measured by single-photon counting.
[e] Measured by the integrated absorption band for $S_0 \rightarrow S_1$.
[f] Calculated from $\tau = \phi_f/k_f$.

strate that gives significant amounts of NCH_2CH_2OH, **11**, is **1**, X = Cl. This is a result of the high value for the bond strength in hydrogen chloride (103 kcal/mol) (22) making the process, eq. [4], occur at a rate that allows competition between the dimerization of $NCH_2\cdot$ radicals and coupling of $NCH_2\cdot$ with

[4] $X\cdot + H\text{—}CH_2OH \rightarrow X\text{—}H + \cdot CH_2OH$

CH_2OH. For **2**, X = Br, the hydrogen bromide bond strength (87 kcal/mol) (22) makes the process in eq. [4] endothermic, by 16 kcal/mol, and unfavorable.

In order to sort out multiplicity effects in these reactions there are two possible approaches: (*i*) sensitization to determine the reactivity of the triplet state or (*ii*) selective quenching of the triplet state formed in a direct irradiation to determine the reactivity of the singlet state.

Sensitized irradiations

In the previous studies with benzyl derivatives, there have always been difficulties in determining the reactivity of the triplet state by sensitization techniques because there are no obvious sensitizers with triplet energies high enough to make triplet energy transfer to the benzene chromophore (~80 kcal/mol) exothermic. Acetone (E_T = 78 kcal/mol) is the logical compromise but it should only be used in non-hydrogen atom donating solvents and, therefore, if a nucleophilic alcohol is required as well, *tert*-butyl alcohol is the best choice. Concentrations of the sensitizer must be high (typically 10% or greater) to avoid competitive absorption by the benzene chromophores. The Cristol group (3) have used this method for a series of substituted benzyl chlorides and it is the observation of changes such as radical/ionic products of 60:26 in direct irradiation and 22:73 in sensitized irradiation that have attracted attention. How is the amount of ion-derived product increased if the multiplicity of the excited state changes from singlet (spin-paired) to triplet (spin-unpaired)?

Examination of this problem for the naphthyl derivatives reported here is, on the surface, more straightforward. The triplet energy of the substrates is around 60 kcal/mol (Table 2). The sensitizer chosen was xanthone, which has been shown by Scaiano (28) to have a triplet energy of 69 kcal/mol, a long wavelength absorption band with λ_{max} 338 nm (ϵ 6800), and a rate of reaction with methanol of ~$10^5\ M^{-1}\ s^{-1}$, which will not compete with the diffusion controlled quenching by the naphthalene derivatives.

The results for these sensitization experiments are given in Table 1. Three of the substrates, **4**, **5** and **6**, show no reaction on sensitization and therefore the direct irradiations must reflect singlet reactivity. The substrates **1**, X = Cl, and **2**, X = Br, have been examined in considerable detail recently by Slocum and Schuster (23) with the conclusion that this sensitization is actually exciplex formation and that the lowest triplet of these two substrates does not react. Cristol has reached the same conclusion for T_1 of benzyl chloride. Therefore the results for sensitized reactions of **1** and **2** probably have nothing to do with unimolecular excited state cleavage of the carbon–halogen bond but reflect bimolecular interactions with the sensitizer. The only questionable cases are **3** and **7**, which will be discussed in more detail in the next section on quenched irradiations.

That the sensitized photocleavage reactions do not involve complete electron transfer was confirmed by applying the Weller equation (29) to the redox potentials obtained for **1**, **7**, and xanthone, assuming the sensitizer was the donor and the substrate the acceptor. Both **1** and **7** exhibited irreversible reduction waves by cyclic voltammetry, the half-wave potentials being −2.23 and −2.05 V (vs. Ag/AgCl) respectively. Xanthone exhibits an irreversible wave on oxidation with a half-wave potential of +1.76 V. Using these redox values, singlet energy of 79 kcal/mol and triplet energy of 69 kcal/mol for xanthone and a Coulombic attraction term of 1.5 kcal/mol (ϵ of methanol = 32, encounter distance = 7 Å) in the Weller equation gives results that imply that electron transfer will be unfavorable for both **1** (ΔG singlet = 11.5 kcal/mol, ΔG triplet = 21.5 kcal/mol) and **7** (ΔG singlet = 7.3 kcal/mol, ΔG triplet = 17.3 kcal/mol).

The conclusion to reach from this section and in particular from the work of Cristol and Bindel (3, 4) and Slocum and Schuster (23) is that it will be very difficult to obtain reliable rate constants for the excited triplet states except by quenching of triplet states formed directly by intersystem crossing and applying Stern–Vollmer kinetic treatments. Even this approach is likely to be complicated because both singlet and triplet reaction may be occurring so that the quenching would have to be state selective.

Quenched irradiations

The classic method of studying the reactivity of excited singlet states is to selectively quench the triplets by taking advantage of their longer lifetime. For benzyl derivatives this is in fact quite difficult because of the very short lifetime of even the triplet states; moreover, the concentration of typical quenchers (like dienes) can not be too high because of competitive absorption problems. Again the work by the Cristol group (3, 4) for benzyl chlorides has shown the potential of these methods since a combination of sensitization and quenching techniques indicated two triplets, a long-lived one of lifetime 3–26 ns, which did not photoreact, and a short-lived one of lifetime 0.4–1.4 ns, which led to photosolvolysis products. Schuster's work (23) has resulted in a different interpretation of these experiments and, more important, demonstrated that, for the naphthyl derivatives **1**, X = Cl, and **2**, X = Br, the triplet lifetimes are much longer, 180 ns and 175 ns, respectively. Thus they are easily quenchable. However, it is well known that the excited singlet states of naphthalene derivatives are also very efficiently quenched (30) by the usual dienes that are used as triplet quenchers. This process can be easily monitored by fluorescence quenching or by direct measurement of singlet lifetimes as a function of quencher concentration.

The singlet lifetimes in methanol at 20°C measured by single-photon counting for the substrates **1–7** are shown in Table 2. Compounds **1**, X = Cl, **2**, X = Br, and **3**, X = $\overset{+}{S}(CH_3)_2\overset{-}{B}F_4$ have lifetimes too short (<1 ns) to be determined. A recent (31) value for **1** of 490 ps has been reported. The longer-lived singlet states, as expected (29), are very efficiently quenched by 2,5-dimethyl-2,4-hexadiene. For example, Stern–Volmer fluorescence intensity quenching plots for **4** and **7** gave $k_q\tau$ values of 64 and 301 M^{-1} respectively. The lifetimes in Table 2 then give k_q values of $9.3 \times 10^9\ M^{-1}\ s^{-1}$ and $9.0 \times 10^9\ M^{-1}\ s^{-1}$ respectively that are close to the calculated value (32), $1.8 \times 10^{10}\ M^{-1}\ s^{-1}$, for diffusion in methanol.

The triplet states of these naphthalene derivatives will also be quenched at the diffusion controlled rate based on their triplet energies (58.8–62.0 kcal/mol, Table 2) and the known triplet energy of 2,5-dimethyl-2,4-hexadiene (58.7 kcal/mol (33)). However, the different lifetimes of the two excited states make selective quenching of the triplet state possible. For instance, for chloromethylnaphthalene, **1**, τ_S = 490 ps (31) and τ_T = 180 ns (23). At $10^{-2}\ M$ quencher, the singlet is unquenched because it is too short-lived, but 95% of the triplets are quenched. With these conditions, irradiation of **1** does not show any significant change in rate of photodecomposition or in product ratio (Table 1) relative to direct irradiations. Substrates **2** and **3** show considerable quenching of radical products but at the expense of a good mass balance. Likely radical intermediates generated from the unquenched singlet excited state react with the diene quencher rather than dimerize. Substrates **4**, **5**, and **6** do not react from the triplet state so quenched runs were unnecessary.

The results for **7** are different. The longer singlet lifetime (33 ns, Table 2) means that, even at quencher concentrations of $10^{-3}\ M$, 25% of the singlets are quenched. The amount of the triplet state quenched is unknown because the triplet lifetime for **7** is not known. However, the extensive studies by Givens and co-workers (18) on the photochemistry of sulfones indicates that, for 1-naphthylmethyl sulfones, photocleavage on direct irradiation occurs almost exclusively from the triplet state formed by intersystem crossing from the singlet. In addition, the triplet lifetime of the sulfone, **12**, in acetonitrile is 500 ns (18*c*). Since the triplet state of **12** is of the naphthalene type this is surely a good model for **7**. At this lifetime and $10^{-3}\ M$ in the diene quencher, 80% of the triplets will be quenched. In agreement with Givens' results for **12**, the photocleavage of **7** in the presence of the quencher becomes very slow and the mass balance is low, probably because the competititive singlet quenching leads to product formation by cycloaddition of the diene to the excited naphthalene (34).

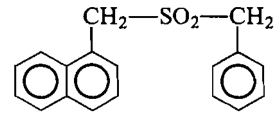

12

The conclusion from these semiquantitative studies is that reliable rate constant information on photofugacities of leaving groups can be obtained for the excited singlet states of the substrates **1–6** but that the singlet of **7** reacts too slowly to be conveniently measured.

Quantum yields and photofugacities

The measurement of rate constants of reaction for excited singlet states is, in principle, straightforward according to eq. [5] where ϕ_r is the reaction quantum yield, k_r is the rate

$$[5]\quad \phi_r = \frac{k_r}{k_d} = k_r\tau_s$$

constant in question, and k_d is the total rate of decay of the excited singlet state or the reciprocal of the lifetime τ_s. The lifetimes of the substrates **4**, **5**, **6**, and **7** are directly measurable by single-photon counting of fluorescence decay; **1**, **2**, and **3** are too short-lived.

Reliable estimates of singlet lifetimes can often be made by using the expression, eq. [6], where ϕ_f is the quantum yield

$$[6]\quad \phi_f = \frac{k_f}{k_d} = k_f\tau_s$$

of fluorescence and k_f the corresponding rate constant. Estimates of k_f can be made from the integrated absorption band for the S_0–S_1 transition according to eq. [7] (35). For these

$$[7]\quad k_f = 2.88 \times 10^{-9}\ \lambda_{max}{}^2 n^2 \int \epsilon(\nu)d\nu$$

substrates, evaluation of τ_s by these methods is not very reliable. The value for the area of the integrated absorption band is uncertain because of overlap with the S_0–S_2 band. Our best estimates are in Table 2. For the bromide **2**, the S_0–S_1 band is in fact not even observable. However, the approximate constancy of these values for the other substrates is encouraging and allows a very crude estimate of k_f for **2** as the average of the others.

According to eq. [6] the values of ϕ_f for these substrates are also necessary to evaluate τ_s. Values for **1** and **2** have been reported previously: 0.0031 and 0.0017 respectively in cyclohexane at room temperature (23) and 0.003 and 0.001 in benzene at 298 K (36). Our values (Table 2) are lower than these and force us to be very uncertain about any of these determinations. These substrates are all synthesized from naphthalene derivatives and, moreover, photoreact to produce other naphthalene compounds. Photo-unreactive naphthalene derivatives have quantum yields of fluorescence of about 0.2. Therefore impurity levels of 0.5% will give spurious fluorescence quantum yields of 10^{-3}. In fact, without great care, the intensity of fluorescence for these substrates always increased during the irradiation time of the experiment. The values for **1**, **2**, and **3** in Table 2 are therefore the maximum values possible and the true values are very likely smaller. The larger values for **4**, **5**, **6**, and **7** are presumably reliable. A value of 0.19 in cyclohexane has been reported for **6**.[2]

Using eq. [6], values of τ_s can now be calculated for **4**, **5**, **6**,

[2] R. S. Givens. Personal communication.

TABLE 3. Quantum yields and photofugacities for the singlet states of 1-naphthylmethyl derivatives **1–7** in methanol

Compound	ϕ_8	ϕ_{10}	ϕ_{11}	$k_8 \times 10^{-6}$ (s^{-1})	$k_{10+11} \times 10^{-6}$ (s^{-1})	$\Sigma\phi + \phi_f$
1	0.077	0.010	0.065	>150	>150	0.152
2	0.072	0.006	0.006	>140	>24	0.084
3	0.30	0.019	—	>600	>38	0.319
4	0.25	0.064	—	36	9.3	0.370
5	<0.005	—	—	<0.1	—	0.14
6	0.10[a]	0.003	—	7.6	0.2	0.157
7	—	0.001	0.005	—	0.2	0.14

[a] A value of 0.08 has been reported (see footnote 2).

and **7** (Table 2). They are uniformly larger than the observed values by a factor of 2 to 3. Even greater overestimations of singlet lifetimes by this method have been reported previously (37). For the cases reported here, the rigidity of the naphthalene ring will keep the geometry of the ground and excited states quite similar so the method should work well. The observed overestimations are likely due to overlap between the S_2 and S_1 absorption bands causing an overestimation of the S_0–S_1 probability. The singlet lifetimes of **1**, **2**, and **3** are then certainly below 0.5 ns.

Quantum yields for these photocleavages are reported in Table 3. All values are reported at conversions between 5 and 10% to avoid the internal filter effects that result because the products have the same chromophore as the starting materials. The dimer **9**, which is formed in the preparative scale irradiations, is now only a very minor product, presumably because of the lower light intensities on the quantum yield optical bench. Methylnaphthalene, **10**, is now a major product resulting from radical cleavage.

The rate constants for ionic cleavage, $k_8 = k_I$, radical cleavage, $k_{10+11} = k_R$, can now be calculated, but in fact only reliably for **4** (X = $\overset{+}{N}(CH_3)_3Cl^-$), **6** (X = O—$PO(OCH_2CH_3)_2$), and **7** (X = SO_2CH_3). Although a lifetime is available for the acetate **5**, the quantum yield for reaction is too small to be reliably measured. For **1** (X = Cl), **2** (X = Br), and **3** (X = $\overset{+}{S}(CH_3)_2\bar{B}F_4$) the very short lifetimes only allow lower limit estimates for these rate constants.

Although only estimates for photofugacity of most of the leaving groups studied here are available from our results, the large spread in the values is obvious, about 10^4 for the ionic and 10^3 for the radical process. Semi-quantitative trends are also obvious, so that a photofugacity order for the ionic process has $\overset{+}{S}(CH_3)_2 > Cl \simeq \overset{+}{N}(CH_3)_3 > O_2P(OEt)_2 > O_2CCH_3 > SO_2CH_3$ and for the radical process $Cl > \overset{+}{S}(CH_3)_2 \simeq Br > \overset{+}{N}(CH_3)_3 > O_2P(OEt)_2 \simeq SO_2CH_3 > O_2CCH_3$. The large range of rate constants is, in itself, somewhat surprising since from the excited singlet state of these naphthalene derivatives all of the bond cleavages are exothermic and might have been expected to be too fast for any selectivity in reaction rate. This is the observation made by Cristol (3, 4) for the excited triplets of benzylic chlorides. In fact, only two of the leaving groups, $\overset{+}{N}(CH_3)_3Cl^-$ and O—$PO(OCH_2CH_3)_2$, react with rates that are conveniently measured and create the opportunity to systematically study the effect of solvent, substituents, temperature, etc. on excited state rate constants for this simple bond cleavage process. Of these two, $\overset{+}{N}(CH_3)_3Cl^-$ is perhaps the best choice because it gives a more equal distribution of ionic and radical cleavage products, so that the effect of reaction conditions on this distribution could be studied.

Finally, we were hoping to answer questions about the two possible mechanistic pathways that have been proposed for these photocleavages. The first involves cleavage directly from the excited state to either a radical pair or an ion pair. Product distribution then reflects the partitioning of the excited state between these two pathways. The second involves initial excited state cleavage to only the radical pair and then exothermic electron transfer within the radical pair to the ion pair. Product distribution thus reflects the competition between diffusional separation of the radical pair and the rate of electron transfer.

In both of these mechanisms, the product formation and hence product distribution could be altered by return of either the ion pair or the radical pair to starting material by recombination. This is essentially a process of decay for the excited singlet, which lowers the quantum yield and rate constant for product formation. In fact, such internal return has been observed before for the photochemistry of benzylic sulfones (18*b*) in radical processes and benzylic acetates (16) in ionic processes but not for benzylic ammonium salts (38). However, even for the substrates where internal return has been observed, it is not an important enough process to change rate constants by an order of magnitude but only by at most a factor of two.

We were hopeful that some correlation between known properties of the C—X bonds in the substrates and the photochemical rates would be possible; for instance, C—X bond strength or radical cleavage and leaving group ability in solvolysis reactions for pK_a of the acid HX for ionic cleavage. We do not see trends in our results that allow correlations of this type to distinguish between the two possible mechanistic pathways.

Although bond strengths are unavailable for the leaving groups $\overset{+}{N}(CH_3)_3$ and $\overset{+}{S}(CH_3)_2$ so that a complete correlation is impossible, there are obvious discrepancies even for the known cases. Estimates[3] for the carbon–X band strength for **1** (X = Cl), 65 kcal/mol (22); **2** (X = Br), 51 kcal/mol (22); **3** (X = SO_2CH_3), 53 kcal/mol (39) predict that **7** and **2** should be similar in photolability and less reactive than **1**. As seen in Table 3, this is not true.

In terms of ionic cleavage, the order of ground state leaving group ability of X can be estimated from solvolysis data from the known logarithmic L scale for some of the leaving groups used here (40). Values for Br (1.0), Cl (−1.61), $\overset{+}{S}(CH_3)_2$ (−3.01), $\overset{+}{N}(CH_3)_3$ (−3.54), and O_2CCH_3 (−4.68) actually qualitatively follow the order in Table 3 for ionic photofugacity, but clearly not quantitatively. The sulfonium salt is

[3] The values for the corresponding benzylic cases are decreased by 3 kcal/mol (25).

closer in reactivity to the halides than it is to the ammonium salt. Similarly pK_a values for the conjugate acids H—X: Cl (−7.1) (40), Br (−7.7) (40), $\overset{+}{S}(CH_3)_2$ (−7) (41), SO_2CH_3 (−2.6) (42), $O_2P(OCH_3CH_3)_2$ (2.1) (43), O_2CCH_3 (4.7) (40), and $\overset{+}{N}(CH_3)_3$ (9.9) (40) seem to fit for the three reactive leaving groups but not at all for the four of lower reactivity.

In conclusion, we have established a qualitative scale for fugacities in photochemical benzylic cleavages from the excited singlet state. Perhaps not surprisingly, the order is not easily rationalized by comparison with related ground state reactions. More important, we have identified a leaving group $\overset{+}{N}(CH_3)_3Cl^-$ that reacts with a rate and product distribution that allows a systematic study of the variables that affect ionic versus radical cleavage. Such studies are in progress.

Experimental

Preparation and purification of 1-naphthylmethyl derivatives (NCH₂—X)

1, X = Cl: purchased from Aldrich Chemical Co. and purified by low temperature (Dry Ice) recrystallization from hexane; mp 33–34°C.

2, X = Br: 1-methylnaphthalene (3.0 g, 21 mmol), NBS (4.1 g, 23 mmol), and 40 mL of CCl_4 were irradiated with a 250-W tungsten lamp while a continuous stream of nitrogen was passed through the refluxing solution. After 4 h the mixture was cooled to 0°C and filtered. Evaporation of the solvent gave the crude bromide, which was recrystallized from pentane and sublimed to give 2.78 g (60%) of purified material; mp 54–55°C (lit (44) mp 56°C).

3, X = $\overset{+}{S}(CH_3)_2BF_4^-$: 1-mercaptomethylnaphthalene (17.4 g, 100 mmol) was added to a stirred solution of sodium methoxide (5.94 g, 150 mmol) in 150 mL of methanol. After 10 min, methyl iodide (14.2 g, 100 mmol) was added dropwise and the mixture stirred for 1 h. Addition of 100 mL of water, followed by extraction with 3 × 75 mL of CCl_4, druing with $MgSO_4$ and evaporation, gave 21 g of the crude sulfide. Vacuum distillation (bp 150–152°C at 4 Torr (1 Torr = 133.3 Pa)) gave 12.7 g (68%) of purified sulfide; nmr ($CDCl_3$) δ: 7.25–8.23 (m, 7H), 4.02 (s, 2H), 1.93 (s, 3H).

Trimethyloxonium fluoroborate (1.63 g, 11 mmol) was added to a stirred solution of the (1-naphthylmethyl) methyl sulfide (1.88 g, 10 mmol) in 20 mL of nitromethane. The resulting mixture was left at 0°C for 18 h and then filtered. The crude product was recrystallized at low temperature from 3-pentanone to give 2.17 g (75%) of purified salt: mp 150.5–151°C; ir (KBr): 950–1150 (br) cm^{-1}; nmr (acetone-d_6) δ: 7.5–8.4 (m, 7H), 5.35 (s, 2H), 3.12 (s, 6H). *Anal.* calcd. for $C_{13}H_{15}BF_4S$: C 53.82, H 5.21; found: C 53.62, H 5.17.

4, X = $\overset{+}{N}(CH_3)_3Cl^-$: trimethylamine was bubbled through a stirred solution of 1-chloromethylnaphthalene, **1** (1.88 g, 11 mmol), in 50 mL of absolute ethanol. The solvent was evaporated and the crude ammonium salt was recrystallized from acetonitrile to give 1.86 g (80%) of purified **4**; mp 231–232°C (lit. (45) mp 226–227°C); nmr (CD_3OD) δ: 7.5–8.2 (m, 7H), 5.18 (s, 2H), 3.23 (s, 9H).

5, X = O_2CCH_3. To 1-naphthylmethanol (1.6 g, 0.11 mmol) in 25 mL of dry pyridine was added, with stirring, acetyl chloride (1.0 g, 0.13 mmol). The mixture was extracted with 2 × 50 mL of 10% HCl and 50 mL of saturated aqueous NaCl. Evaporation of the solvent and distillation of the crude ester gave 1.5 g (73%) of a pale yellow oil. Two bulb-to-bulb distillations (65°C, 1 Torr; lit. (46) bp 90–92°C at 10 Torr) gave the purified ester; nmr ($CDCl_3$) δ: 7.2–8.4 (m, 7H), 5.47 (s, 2H), 2.00 (s, 3H).

6, X = $O_2P(OCH_2CH_3)_2$. This compound was supplied by Prof. R. Givens, Dept. of Chemistry, University of Kansas.

8, X = OCH_3. To a solution of sodium (0.51 g, 22 mmol) in 40 mL of absolute methanol was added 1-chloromethylnaphthalene, **1** (3.53 g, 21 mmol), and the mixture stirred for 18 h. It was then poured into 100 mL of water and extracted with 3 × 50 mL of pentane, then was combined, dried over Na_2SO_4, and concentrated to give 3.5 g (95%) of crude ether, **7**. Bulb-to-bulb distillation gave a purified sample; nmr δ: 7.2–8.4 (m, 7H), 4.90 (s, 2H), 3.43 (s, 3H).

9, 1,2-Di(1-naphthyl)ethane, X = CH_2N. This compound was isolated from photolysis mixtures of **1** and recrystallized from ethanol; mp 163–165°C (lit. (47) mp 160–161°C); nmr ($CDCl_3$) δ: 7.2–8.4 (m, 14H), 3.53 (s, 4H).

10, X = H. Purchased from Aldrich Chemical Co.

11, X = CH_2OH. Purchased from Aldrich Chemical Co.

Analytic procedure for 1-naphthylmethyl derivatives

All substrates were checked for purity by hplc (Waters) with a Brownlee 10μ RP-8 reverse phase column using 80% methanol/water as eluant and detection at 280 nm. Photolyses were monitored and products quantified by calibration of the detector with mixtures of known concentration.

Photolyses

Preparative scale irradiations were done using a 200-W medium pressure Hanovia mercury lamp in an immersion well with nitrogen purging. The following concentrations were used: direct irradiations, 200 mg of substrate, 310 mL of methanol, and a Corex filter sleeve; sensitized irradiations, 200 mg of substrate, 20 mg of xanthone, 310 mL of methanol, and a Pyrex filter sleeve; quenched irradiations were the same as direct except 2,5-dimethyl-2,5-hexadiene (Aldrich, sublimed) was added at concentrations determined by Stern–Volmer fluorescence quenching studies.

Quantum yield measurements

Quantum yields were determined using an optical bench equipped with a 450-W Hg/Xe lamp, a SPEX minimate monochromator, a beam splitter, and a reaction and reference cell. Calibration of light intensities and splitting ratios was by ferrioxalate actinometry (48). Samples were degassed by nitrogen purging, stirred, and thermostatted at 20°C during the irradiations. Quantum yields are based on appearance of products with total conversion of starting material between 5 and 10% to minimize the internal filter effects. In a typical run, a solution of **4**, X = $\overset{+}{N}(CH_3)_3Cl^-$ (2.12 × 10^{-3} M in 20 mL of CH_3OH), irradiated at 280 nm with 0.70 × 10^{-2} millieinstein gave 0.173 × 10^{-2} mmol of **8**, X = OCH_3, ϕ = 0.247, and 0.045 mmol of **10**, X = H, ϕ = 0.064, with a conversion to products of 5.8%. Values reported in Table 3 are the average of at least two runs with a mean deviation always <10%.

Fluorescence measurements

All samples for fluorescence measurements were degassed by four freeze–pump–thaw cycles and spectra obtained on an Aminco–Bowman spectrophotofluorometer. For quantum yields, naphthalene was used as a standard and concentrations used so that the absorbance at 280 nm was constant for all solutions at 0.8 (1.0 × $10^{-4}$$M$). The quantum yield of fluorescence of naphthalene is 0.24 in methanol based on a value of 0.23 (27) in cyclohexane.

Fluorescence lifetime measurements

All samples were degassed by four freeze–pump–thaw cycles and lifetimes measured by a PRA single photon counting apparatus with a hydrogen flash lamp of pulse width 0.8 ns and flash frequency of 30 kHz. The decay curves generated were deconvoluted using a program provided by Professor W. Ware, University of Western Ontario.

Acknowledgments

This work was supported by a grant from the Natural Sciences and Engineering Research Council of Canada and a Dalhousie University Faculty of Graduate Studies Award to N.M.

1. H. E. ZIMMERMAN and V. R. SANDEL. J. Am. Chem. Soc. **85**, 915 (1963).
2. H. E. ZIMMERMAN and S. SOMASEKHARA. J. Am. Chem. Soc. **85**, 922 (1963).
3. S. J. CRISTOL and T. H. BINDEL. J. Org. Chem. **45**, 951 (1980).
4. S. J. CRISTOL and T. H. BINDEL. J. Am. Chem. Soc. **103**, 7287 (1981).

5. D. C. APPLETON, B. BROCKLEHURST, J. MCKENNA, J. M. MCKENNA, M. J. SMITH, P. S. TAYLOR, S. THACKERAY, and A. R. WALLEY. Chem. Commun. 108 (1977).
6. D. C. APPLETON, B. BROCKLEHURST, J. MCKENNA, J. M. MCKENNA, S. THACKERAY, and A. R. WALLEY. J. Chem. Soc. Perkin Trans. 2, 87 (1980).
7. G. H. SLOCUM, K. KAUFMANN, and G. B. SCHUSTER. J. Am. Chem. Soc. **103**, 4625 (1981).
8. M. A. RATCLIFF and J. K. KOCHI. J. Org. Chem. **36**, 3112 (1971).
9. J. HYOMAKI and J. KOSKIKALLIO. Acta Chem. Scand. Ser. A. **31**, 321 (1977).
10. D. C. APPLETON, D. C. BULL, R. S. GIVENS, V. LILLIS, J. MCKENNA, J. M. MCKENNA, J. THACKERAY, and A. R. WALLEY. J. Chem. Soc. Perkin Trans. 2, 77 (1980).
11. A. L. MAYCOCK and G. A. BERCHTOLD. J. Org. Chem. **35**, 2532 (1970).
12. C. E. GRIFFIN and M. L. KAUFMAN. Tetrahedron Lett. 773 (1965).
13. V. L. IVANOV, V. B. IVANOV, and M. G. KUZ'MIN. J. Org. Chem. USSR (Engl.), **8**, 1263 (1972).
14. V. B. IVANOV, V. L. IVANOV, and M. G. KUZ'MIN. Mol. Photochem. **6**, 125 (1974).
15. R. S. GIVENS, B. MATUSZEWSKI, and C. V. NEYWICK. J. Am. Chem. Soc. **96**, 5547 (1974).
16. D. A. JAEGER. J. Am. Chem. Soc. **97**, 902 (1975).
17. A. S. AMIRI and J. M. MELLOR. J. Photochem. **9**, 571 (1978).
18. (*a*) R. S. GIVENS and B. MATUSZEWSKI. Tetrahedron Lett. 861 (1978); (*b*) R. S. GIVENS, B. HRINCZENKO, J. H.-S. LIU, B. MATUSZEWSKI, and J. THOLEN-COLLISON. J. Am. Chem. Soc. **106**, 1779 (1984); (*c*) I. R. GOULD, C. TUNG, N. J. TURRO, R. S. GIVENS, and B. MATUSZEWSKI. J. Am. Chem. soc. **106**, 1789 (1984).
19. D. A. JAEGER. J. Am. Chem. Soc. **98**, 6401 (1976).
20. J. R. LARSON, N. D. EPIOTIS, and L. MCMURCHIE. J. Org. Chem. **45**, 1388 (1980).
21. T. ICHIMURA, T. HIKIDA, and Y. MORI. J. Phys. Chem. **79**, 291 (1975).
22. S. W. BENSON. J. Chem. Educ. **42**, 502 (1965).
23. G. H. SLOCUM and G. B. SCHUSTER. J. Org. Chem. **49**, 2177 (1984).
24. R. F. LANGLER, Z. A. MARINI, and J. A. PINCOCK. Can. J. Chem. **56**, 903 (1978).
25. W. C. HERNDON. J. Org. Chem. **46**, 2119 (1981).
26. E. M. KOSOWER. *In* An introduction to physical organic chemistry. Wiley, New York. 1968.
27. J. BERLMAN. *In* Handbook of fluorescence spectra of aromatic molecules. 2nd ed. Academic Press, New York. 1971.
28. J. C. SCAIANO. J. Am. Chem. Soc. **102**, 7747 (1980).
29. D. REHM and A. WELLER. Isr. J. Chem. **8**, 259 (1970).
30. (*a*) L. M. STEPHENSON, D. G. WHITTEN, G. F. VESLEY, and G. S. HAMMOND. J. Am. Chem. Soc. **88**, 3665 (1966); (*b*) D. A. LABIANCA, G. N. TAYLOR, and G. S. HAMMOND. J. Am. Chem. soc. **94**, 3679 (1972).
31. D. F. KELLEY, S. V. MITTON, D. HUPPERT, and P. M. RENTZEPIS. J. Phys. Chem. **87**, 1842 (1983).
32. S. L. MUROV. *In* Handbook of photochemistry. Marcel Dekker, Inc., New York. 1973. p. 55.
33. S. L. MUROV. *In* Handbook of photochemistry. Marcel Dekker, Inc., New York. 1973. p. 4.
34. N. C. YANG, J. LIBMAN, and M. F. SAVITZKY. J. Am. Chem. Soc. **94**, 3679 (1972).
35. N. J. TURRO. *In* Modern molecular photochemistry. Benjamin/Cummongs, Menol Park, NJ. 1978. p. 87.
36. R. S. DAVIDSON, R. BONNEAU, J. JOUSSOT-DUBIEN, and K. R. TRETHEWEY. Chem. Phys. Lett. **74**, 318 (1980).
37. H. E. ZIMMERMAN, D. P. WERTHEMANN, and K. S. KAMM. J. Am. Chem. Soc. **96**, 439 (1974).
38. V. LILLIS, J. MCKENNA, J. M. MCKENNA, and I. H. WILLIAMS. Chem. Commun. 473 (1974).
39. W. K. BUSFIELD, K. J. IVIN, H. MACKLE, and P. A. G. O'HARE. Trans. Faraday Soc. **57**, 1064 (1961).
40. E. R. THORNTON. *In* Solvolysis mechanisms. Ronald Press Co., New York. 1964. p. 165.
41. E. M. ARNETT. Prog. Phys. Org. Chem. **1**, 223 (1963).
42. J. P. GUTHRIE. Can. J. Chem. **57**, 454 (1979).
43. W. D. KUMLER and J. J. EILER. J. Am. Chem. Soc. **65**, 2355 (1943).
44. N. P. BUU-HOI. Ann. **556**, 1 (1944).
45. C. P. HAUSER, D. N. VAN EENAM, and P. L. BAYLESS. J. Org. Chem. **23**, 354 (1958).
46. A. MCKILLOP and M. E. FORD. Tetrahedron, **30**, 2467 (1974).
47. A. M. KHALESTHII and Y. A. KAPLAN. Zh. Obshch. Khim. **26**, 762 (1956).
48. C. G. HATCHARD and C. A. PARKER. Proc. R. Soc. London, Ser. A, **235**, 518 (1956).

3-(η^6-Benzoyltricarbonylchromium)pyrrole. An example of how substitution isomerism in the ligand affects the type (σ or π) of complex formed

NIALL J. GOGAN, JAMES DOULL, AND JANE EVANS
Department of Chemistry, Memorial University of Newfoundland, St. John's, Nfld., Canada A1B 3X7

Received March 11, 1985

NIALL J. GOGAN, JAMES DOULL, and JANE EVANS. Can. J. Chem. **63**, 3147 (1985).

The reaction of 3-benzoylpyrrole and $Cr(CO)_6$ yields only the π-complex 3-(η^6-benzoyltricarbonylchromium)pyrrole, in contrast to the previously reported reaction of 2-benzoylpyrrole and $Cr(CO)_6$ that yielded only the σ-chelate, tris(2-benzoylpyrrolato)chromium(III). The difference in behaviour is explained by a preference for chelate formation that is allowed by the stereochemistry of 2-benzoylpyrrole but is not allowed by the stereochemistry of 3-benzoylpyrrole.

NIALL J. GOGAN, JAMES DOULL et JANE EVANS. Can. J. Chem. **63**, 3147 (1985).

La réaction du benzoyl-3 pyrrole avec le $Cr(CO)_6$ ne conduit qu'au complexe-π (η^6-benzoyltricarbonylchrome)-3 pyrrole alors qu'il a été rapporté antérieurement que la réaction du benzoyl-2 pyrrole avec le $Cr(CO)_6$ ne conduit qu'à un chélate-σ, le tris(benzoyl-2 pyrrolato)chrome(III). On explique la différence dans ces comportements par une préférence pour la formation du chélate qui est permise par la stéréochimie du benzoyl-2 pyrrole mais qui n'est pas permise par la stéréochime du benzoyl-3 pyrrole.

[Traduit par le journal]

Introduction

Benzoylpyrroles, when reacted with $Cr(CO)_6$, have the potential of forming either Cr(III) σ-coordinated complexes or π-$Cr(CO)_3$ complexes. We previously reported that 2-benzoylpyrrole forms the σ-chelate, tris(2-benzoylpyrrolato)chromium(III), when reacted with $Cr(CO)_6$ (1). No evidence of π-complexation was found. At the time of our earlier study, it was not possible to examine the effect of changing the substitution position of the benzoyl group because no readily available route to 3-benzoylpyrrole existed. Since then, Anderson, Loader and co-workers have developed successively better synthetic routes to 3-substituted pyrroles and have recently developed a good method for preparing 3-benzoylpyrroles (2). We now wish to report the result of the reaction of 3-benzoylpyrrole with $Cr(CO)_6$ and contrast the result with that obtained earlier for 2-benzoylpyrrole.

Experimental

Melting points are uncorrected. Elemental analyses were performed by Canadian Microanalytical Service, Vancouver, B.C. The ir spectra were recorded on a Perkin–Elmer 283 spectrophotometer in $CHCl_3$ solution. The ^1H nmr spectra were determined using a Bruker WP-80 instrument and are expressed in ppm (δ valves) relative to tetramethylsilane as internal reference in $CDCl_3$. Mass spectra were recorded on a VG Micromass 7070 HS spectrometer.

Reaction of hexacarbonylchromium(0) and 3-benzoylpyrrole

Hexacarbonylchromium (0.297 g; 1.30 mmol) and 3-benzoylpyrrole (0.203 g; 1.18 mmol) were allowed to react in 50 mL of di-n-butyl ether at reflux under a nitrogen atmosphere for 6 h using the general method previously described (3). The resulting orange solution was evaporated to yield an orange solid, which was recrystallized from methylene chloride/petroleum ether (60–80) to yield 0.258 g (71% yield assuming 3-benzoylpyrrole $Cr(CO)_3$) of orange crystals, mp 166–168°C. A small amount of decomposition product and some unreacted starting materials were the only other substances recovered from the reaction. *Anal.* calcd. for $C_{14}H_9O_4NCr$: C 54.72, H 2.95, N 4.56; found: C 54.57, H 2.71, N 4.58.

Results and discussion

The orange product shows two intense bands in the ir ($CHCl_3$) spectrum at 1986 and 1914 cm^{-1} characteristic of a $Cr(CO)_3$ group π-bonded to a benzene ring (4). The ketonic ν_{CO} is at 1636 cm^{-1}, virtually unchanged from the ligand (1635 cm^{-1}), and ν_{NH} is unchanged at 3470 cm^{-1}. This contrasts with tris(2-benzoylpyrrolato)chromium(III), which has no intense bands in the 1850–2100 cm^{-1} region, has the ketonic ν_{CO} shifted from 1621 cm^{-1} (ligand) to 1526 cm^{-1} (complex), and has no ν_{NH}. The product from 3-benzoylpyrrole has an ^1H nmr spectrum with benzene proton resonances (δ) at 5.36 (*meta*), 5.56 (*para*), and 6.10 (*ortho*) shifted upfield from the ligand values of 7.51, 7.39, and 7.85. These shifts are typical of a benzene ring π-bonded to a $Cr(CO)_3$ group (5). The pyrrole proton resonances are essentially unchanged. The ^1H nmr spectrum of the σ-complex from 2-benzoylpyrrole exhibits no signals, no doubt owing to its paramagnetism (μ_{eff} = 3.9 BM).

The elemental analyses agree with the values calculated for the π-complex of 3-benzoylpyrrole. The mass spectrum shows peaks at m/e: 307 (13, M^+), 279 (15), 251 (26), 223 (100), 171 (26), 94 (66), and 52 (75) corresponding to the molecular ion, successive loss of 3 COs, 3-benzoylpyrrole$^+$, $C_4H_4NCO^+$, and Cr^+.

From the above evidence, it is clear that the product from the reaction of 3-benzoylpyrrole and $Cr(CO)_6$ is 3-(η^6-benzoyltricarbonylchromium)pyrrole and has the structure shown in (a), whereas the product from the reaction of 2-benzoylpyrrole and $Cr(CO)_6$ has, in contrast, the structure shown in (b). This shows

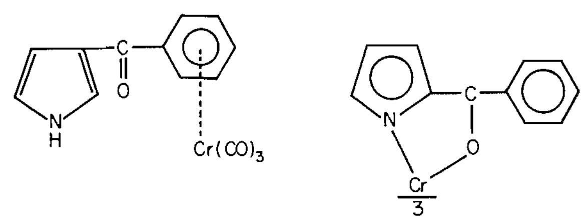

(a) (b)

a dramatic difference in complexing behaviour, under the same reaction conditions, of ligands that only differ in the substitution position of the benzoyl group on the pyrrole ring. It can be explained by a strong preference for chelation through the pyrrole N and ketonic group O. This preference is allowed by the stereochemistry of 2-benzoylpyrrole, i.e. it has the correct "bite", but it is not allowed by the stereochemistry of

3-benzoylpyrrole. Thus, in this latter case π-complexation occurs by default.

Acknowledgements

We are grateful to the Natural Sciences and Engineering Research Council of Canada for financial support and to Drs. H. J. Anderson and C. E. Loader of this department for advice and assistance in the preparation of 3-benzoylpyrrole.

1. C. S. DAVIES and N. J. GOGAN. J. Inorg. Nucl. Chem. **34**, 2791 (1972).
2. R. X. XU, H. J. ANDERSON, N. J. GOGAN, C. E. LOADER, and R. MCDONALD. Tetrahedron Lett. **22**, 4899 (1981).
3. N. J. GOGAN and C.-K. CHU. J. Organometal. Chem. **132**, 103 (1977).
4. D. A. BROWN and H. SLOAN. J. Chem. Soc. 3849 (1962).
5. E. O. FISCHER and H.-P. FRITZ. Angew. Chem. **73**, 353 (1961).

Effects of neutral and anionic substituents on the carbonyl stretching bands of ring-substituted acetophenones

IVAN G. BINEV, TSONKO M. KOLEV, and IVAN N. JUCHNOVSKI
Institute of Organic Chemistry, Bulgarian Academy of Sciences, 1113 Sofia, Bulgaria

Received December 21, 1984

IVAN G. BINEV, TSONKO M. KOLEV, and IVAN N. JUCHNOVSKI. Can. J. Chem. **63**, 3149 (1985).

Satisfactory single-parameter (σ^+) and dual-parameter (according to Yukawa–Tsuno and Taft) correlations have been found between frequencies of the title bands (ν_{CO}) and substituent constants. It has been found that use of dimethyl sulphoxide instead of carbon tetrachloride as solvent does not lower the relative accuracy of the studied correlations. The integrated intensities of the ν_{CO} bands do not correlate with any type of substituent constants. The constants σ^+, σ^0, σ_I, σ_R^+, and $\Delta\sigma_R^+$ of the anionic substituents NC—HC$^-$, O$^-$, CH_3CON^-, and CO_2^-, recently determined on the basis of cyano infrared frequencies and intensities, have proved satisfactorily reliable with respect to the ν_{CO} of acetophenones. The σ^+ constants of *m*-$CH_2CO_2^-$ (-0.22 ± 0.08) and *m*-$C_6H_5CON^-$ (-0.66 ± 0.13) have been estimated on the basis of ν_{CO} data and ν_{CO}/σ^+ correlations (solvent DMSO).

IVAN G. BINEV, TSONKO M. KOLEV et IVAN N. JUCHNOVSKI. Can. J. Chem. **63**, 3149 (1985).

On a pu établir des corrélations satisfaisantes du paramètre unique (σ^+) et du paramètre double (de Yukawa–Tsuno et Taft) entre les fréquences des bandes principales mentionnées dans le titre (ν_{CO}) et les constantes des substituants. On a trouvé que l'utilisation comme solvant du diméthylsulfoxyde au lieu du tétrachlorure de carbone ne diminue aucunement la précision relative des corrélations étudiées. On n'a pas pu établir de corrélations entre les intensités intégrées des bandes ν_{CO} et les constantes des substituants. Les constantes σ^+, σ^0, σ_I, σ_R^+ et $\Delta\sigma_R^+$ des substituants anioniques NC—HC$^-$, O$^-$, CH_3CON^- et CO_2^-, qui ont été récemment déterminés sur la base des intensités et des fréquences infrarouges du groupe cyano, s'avèrent assez fiables par rapport au ν_{CO} des acétophénones. On a évalué respectivement à $-0,22 \pm 0,03$ et à $-0,66 \pm 0,13$ les constantes σ^+ du *m*-$CH_2CO_2^-$ et du *m*-$C_6H_5CON^-$ en se basant sur les données de ν_{CO} et sur les corrélations de ν_{CO}/σ^+ (avec du DMSO comme solvant).

[Traduit par le journal]

Introduction

Correlations of ν_{CO} of ring-substituted acetophenones have been studied repeatedly (1–17); correlations satisfactory, with σ (2–7), and excellent, with σ^+ (5, 7, 10, 11, 13, 17), have been found in this series; some of the *dual*- and *multi*-parameter correlations have also proved excellent (7, 8, 13). The data obtained have been used in studies on steric and mass effects of the substituents (3, 4, 13), studies on conformational equilibria (3, 13) and intramolecular hydrogen-bond formation (13) in some *ortho*-substituted acetophenones (criticism, see ref. 17), as well as for estimation of transmission coefficients of certain bridge groups (10). Together with other spectroscopic series, ν_{CO} of acetophenones have been used to check the reliability of various types of substituent constants (5–12, 16) and to compare the fit of Hammett-type correlations with that of the correlations with certain quantum-chemical indices (14, 15). The constants for some heterocycles have been determined on the basis of acetophenone ν_{CO} data; the results have been compared with those obtained by other methods (11).

In this paper we demonstrate that the use of dimethyl sulphoxide (DMSO) instead of carbon tetrachloride as solvent does not lower the relative accuracy of the correlations of ν_{CO} of acetophenones with substituent constants. This makes it possible to use this series as a reliability test for the constants of some anionic substituents, determined recently (18) on the basis of nitrile infrared frequencies and intensities. On the other hand, collecting all the data available (both our own and literature values for 45 compounds) on ν_{CO} of ring-substituted acetophenones in CCl_4 will allow us to specify the parameters of acetophenone ν_{CO} correlations with the most common types of substituent constants.

Experimental

Acetophenones not commercially available have been prepared and purified according to the literature. Acetophenones with anionic substituents have been obtained by metalation of the corresponding conjugate acids with dry sodium methoxide in DMSO. Spectra of CCl_4 and DMSO solutions have been recorded on a UR-20 Zeiss spectrophotometer in $CaCl_2$ cells, calibration according to the H_2O–gas spectrum. A current calibration (acetophenone in CCl_4, ν_{CO} = 1691.0), has also been used. ν_{CO} were reproducible within ± 0.2 cm^{-1}; the absolute accuracy of the ν_{CO} data also seems to be high: comparison of our data for compounds **1**, **2**, **15**, **16**, **22**, **24**, **27**, **33**, **38**, and **39** with those given in ref. 17 shows a maximum deviation ± 0.5 cm^{-1}, mean deviation < 0.1 cm^{-1}. Comparison with data taken from refs. 3, 4, 7, 9, and 13 shows a similarly good agreement (cf. Table 1, data under asterisks). On the other hand, high-accuracy ν_{CO} data for a few acetophenones have been obtained recently[1] by using a Bruker-113v IR Fourier spectrophotometer, as follows (compound no., solvent, ν_{CO}): **1**, CCl_4, 1690.8; **1**, DMSO, 1682.1; **24**, DMSO, 1672.9; **39**, DMSO, 1691.3 (cf. Table 1). The integrated intensities have been determined by direct integration according to Ramsay's method (19*a*), specially adapted (19*b*) for spectrometers of the UR series. The method takes into account both the slit width effects and band wings. A_{CO} thus determined were reproducible within $\pm 3\%$.

Results and discussion

A. *Acetophenones with neutral substituents*

The frequencies and integrated intensities of the carbonyl stretching bands of a series of acetophenones with neutral substituents are listed in Table 1. Statistical treatment data of the correlations of ν_{CO} with σ and σ^+ constants (values, see refs. 22, 23) according to the equations of Hammett (σ) and Brown–Okamoto (σ^+) (eq. [1]) are given in Table 2.

$$[1] \quad \nu_{CO} = \rho\bar{\sigma} + b \; (\bar{\sigma} = \sigma \text{ or } \sigma^+)$$

It is seen in Table 2 that comparing ν_{CO} of acetophenones with σ^+ gives excellent correlations (see also Figs. 1 and 4); those

[1] R. B. Kuzmanova and J. A. Tsenov. Unpublished data.

TABLE 1. Frequencies (cm^{-1}) and integrated intensities (L mol^{-1} cm^{-2}) of the carbonyl stretching bands of acetophenones with neutral ring-substituents

No.	Substituent	Solvent CCl_4 ν_{CO}	Solvent CCl_4 $10^{-3}\cdot A_{CO}$	Solvent DMSO ν_{CO}	Solvent DMSO $10^{-3}\cdot A_{CO}$
1.	H	1691.0*	22.0[a]	1682.0	21.0
2.	3-CH_3	1689.7[b,c]	—	—	—
3.	3-C_6H_5	1691.2[c]	—	—	—
4.	3-OH	1690.6	l.s.	1681.0	21.5
5.	3-OCH_3	1689.6[b,c]	—	—	—
6.	3-O—$COCH_3$	1694.4*	s.o.	1686.0	25.0
7.	3-NH_2	1688.0*	21.5	1677.7	19.0
8.	3-$NHCOCH_3$	1691.6*	l.s.	1683 ± 1	s.o.
9.	3-$NHCOC_6H_5$	1693.1	s.o.	s.o.	s.o.
10.	3-F	1696.6[a]	16.6[a]	—	—
11.	3-Cl	1695.7[c]*	19.0[a]	—	—
12.	3-Br	1695.3[c]*	—	—	—
13.	3-I	1694.7[c]*	—	—	—
14.	3-CF_3	1698.0[c]*	—	—	—
15.	3-COOH	1696.6*	l.s.	1686.7	ca. 18
16.	3-CN	1699.9	20.0	1691.1	16.0
17.	3-NO_2	1701.2[c]*	20.2[a]	—	—
18.	3-aza	1695.7	20.0	1687.9	19.0
19.	4-CH_3	1687.1*	24.4[a]	1687.4	21.0
20.	4-C_2H_5	1687.6[c]*	—	—	—
21.	4-$C(CH_3)_3$	1687.9[c]*	—	—	—
22.	4-C_6H_5	1688.2*	24.0	1679.3	19.0
23.	4-OH	1684.2[e]*	l.s.	1670.3	24.0
24.	4-OCH_3	1682.8*	21.0	1672.7	24.0
25.	4-O-$COCH_3$	1690.6*	s.o.	1681.1	18.7
26.	4-SCH_3	1685.5[c]	—	—	—
27.	4-NH_2	1676.6*	23.8[a]	1656.1[e]	s.o.
28.	4-$N(CH_3)_3$	1672.7	20.0	1658.3	22.5
29.	4-$N(C_2H_5)_2$	1676.0[d]	—	—	—
30.	4-$NHCOCH_3$	1687 ± 1*	l.s.	1674.6	24.0
31.	4-$NHCOC_6H_5$	1687.4	s.o.	1674.3	s.o.
32.	4-F	1691.5[c]*	21.7[a]	—	—
33.	4-Cl	1692.0*	22.5[a]	1683.4	20.0
34.	4-Br	1693.3[c]*	22.4[a]	—	—
35.	4-I	1692.9[c]*	23.9[a]	—	—
36.	4-CF_3	1699.1[c]	—	—	—
37.	4-COOH	1696.4	l.s.	1686.7	ca. 18
38.	4-CN	1698.5*	22.5	1691.3	17.5
39.	4-NO_2	1700.8*	19.3	1691.5	21.0
40.	4-aza	1702.1	11.7	1694.6	17.6
41.	3,4-$(CH_3)_3$	1686.8[c]*	—	—	—
42.	3,4-$(CH)_4$	1686.4	26.0	1677.4	26.0
43.	3,4-Cl_2	1696.2[c]*	—	—	—
44.	3-NO_2—4-OCH_3	1694.3[c]	—	—	—
45.	3,4,5-$(OCH_3)_3$	1684.9[c]	—	—	—

[a] Reference 3.
[b] Reference 7.
[c] Reference 17.
[d] Reference 9.
s.o., strong overlap of bands; l.s., low solubility.
[e] Excluded from the statistical treatment.
* Other data (compound no., ν_{CO}, ref.): **1**, 1691.1 (7); 1691.2 (17); 1691–1692 (2–4, 9, 13, 15, 19); 1707 (21); **4**, 1690.9 (7); 1695 (4); **5**, 1695 (4); **6**, 1695 (4); **7**, 1688.2 (7); 1688.3 (17); 1689 (3, 20); **8**, 1694 (4); **11**, 1692–1696 (3, 4, 7, 15); **12**, 1695–1695.2 (7, 9); **15**, 1696.1 (17); **16**, 1700.4 (17); **17**, 1699–1705 (2, 3, 7, 20); **19**, 1687–1687.4 (3, 7, 17); **20**, 1687.0 (9); **21**, 1688.0 (9); **22**, 1688.6 (17); **23**, 1684.5–1684.7 (7, 17); 1680–1686 (2, 4, 9); **24**, 1683.1 (7, 17); 1683–1687 (2, 4, 9, 13); **25**, 1691–1692 (2,4); **27**, 1676.5–1677.1 (7, 17); 1675–1680 (3, 9, 15, 20); **30**, 1686 (2, 4); **32**, 1690.0 (7); **33**, 1691.6–1691.8 (7, 17); 1692–1694 (2, 3, 9); 1693–1693.2 (2, 3, 7, 9, 15); **35**, 1693.0 (7, 15); **38**, 1698.1 (17); 1697–1701 (9); **39**, 1700.5–1700.6 (7, 17); 1700–1705 (2, 3, 9, 20); **41**, 1686–1687 (9, 13); **43**, 1696.0 (13).

TABLE 2. Correlations of ν_{CO} of ring-substituted acetophenones with substituent constants, according to the equations of Hammett and Brown–Okamoto (eq. [1])

No.	Solvent	Series	$\bar{\sigma}$	ρ	b	R^a	s.d.^{b}	n^c
1	CCl_4	*m*	σ	15.7 ± 1.2	1689.8 ± 0.4	0.9544	1.2	15
2	DMSO	*m*	σ	18.6 ± 1.6	1679.9 ± 0.5	0.9795	1.0	8
3	CCl_4	*p*	σ	15.7 ± 0.6	1688.5 ± 0.3	0.9768	1.7	21
4	DMSO	*p*	σ	19.7 ± 0.9	1677.3 ± 0.5	0.9663	2.6	14
5	CCl_4	*m,p,mp*	σ	15.9 ± 0.5	1688.9 ± 0.2	0.9681	1.7	39
6	DMSO	*m,p,mp*	σ	20.0 ± 0.8	1678.0 ± 0.4	0.9587	2.4	23
7	CCl_4	*m*	σ^+	15.5 ± 1.1	1690.1 ± 0.4	0.9740	0.9	15
8	DMSO	*m*	σ^+	18.5 ± 1.3	1680.7 ± 0.4	0.9912	0.7	8
9	CCl_4	*p*	σ^+	10.8 ± 0.3	1691.6 ± 0.2	0.9887	1.2	21
10	DMSO	*p*	σ^+	13.2 ± 0.4	1682.0 ± 0.3	0.9964	0.9	14
11	CCl_4	*m,p,mp*	σ^+	11.1 ± 0.3	1691.3 ± 0.2	0.9786	1.4	39
12	DMSO	*m,p,mp*	σ^+	13.5 ± 0.4	1681.8 ± 0.2	0.9900	1.2	23

^{a}Correlation coefficient.
^{b}Standard deviation.
^{c}Number of data points.

TABLE 3. Correlations of ν_{CO} of ring-substituted acetophenones with substituent constants, according to the equations of Yukawa–Tsuno and Taft (eqs. [2] and [3])

No.	Solvent	Series	Sigma	Slope(s)	$s_\rho{}^d$	b	R^a	s.d.^{b}	n^c
13	CCl_4	*m* & *p*	σ^0, $\Delta\sigma_R^+$	ρ = 13.40, r' = 0.678	0.40	1690.6 ± 0.2	0.9877	1.1	29
14	DMSO	*m* & *p*	σ^0, $\Delta\sigma_R^+$	ρ = 14.25, r' = 0.905	0.44	1681.7 ± 0.3	0.9935	1.1	15
15	CCl_4	*m*	σ_I, σ_R^{BA}	ρ_I = 14.21, ρ_R = 6.73	0.82	1691.0 ± 0.3	0.9881	0.7	13
16	DMSO	*m*	σ_I, σ_R^{BA}	ρ_I = 17.92, ρ_R = 9.38	0.98	1680.6 ± 0.3	0.9972	0.4	7
17	CCl_4	*m*	σ_I, σ_R^+	ρ_I = 13.80, ρ_R = 3.79	0.86	1691.2 ± 0.3	0.9842	0.8	13
18	DMSO	*m*	σ_I, σ_R^+	ρ_I = 18.03, ρ_R = 3.37	1.09	1680.7 ± 0.3	0.9957	0.5	7
19	CCl_4	*p*	σ_I, σ_R^+	ρ_I = 12.99, ρ_R = 9.84	0.46	1690.5 ± 0.2	0.9897	1.0	18
20	DMSO	*p*	σ_I, σ_R^+	ρ_I = 14.40, ρ_R = 12.84	0.42	1681.4 ± 0.3	0.9965	0.8	12

^{a,b,c}See Table 2.
^{d}Slope inaccuracy or sum of slope inaccuracies.

with σ are considerably poorer. The pronounced predilection with respect to σ^+ in agreement with refs. 5, 7, 10, 11, 13, and 17 is due to the essential role of the direct resonance between electron-donating substituents and the carbonyl group. Frequencies of other electron-withdrawing groups also correlate with σ^+, as was shown in some earlier publications (5, 24, 25). It is also seen in Table 2 that use of the strongly polar DMSO instead of CCl_4 as solvent does not affect the accuracy of the correlations obtained. Similar results have been obtained in the ν_{CN} and A_{CN} series of benzonitriles (18) and ν_{CO} series of benzophenones, methylbenzoates, and ethylbenzoates (25). Correlations in the joint (*meta* and *para*) series are somewhat poorer, due to the slope differences of the *meta* and *para* series (Table 2, Fig. 1, and ref. 17). The deviation $\Delta\rho = \rho_{meta} - \rho_{para}$ of ca. 5.1 cm^{-1} found by Berthelot and Laurence remains practically the same in our correlations: 4.6 cm^{-1} (solvent CCl_4, series 7 and 9) and 5.2 cm^{-1} (solvent DMSO, series 8 and 10). We believe one should search for the origin of this kind of deviation in the different contribution of inductive and resonance effects to the total substituent effects in a given series (different, with respect to that in the standard series, in this case Brown–Okamoto's, cf. ref. 18).

It was therefore of interest to check the fit of the dual-parameter correlation equations of Yukawa–Tsuno (26) and Taft (27) (eqs. [2] and [3]) in the acetophenone ν_{CO} series.

$$[2] \quad \nu_{CO} = \rho(\sigma^0 + r'\Delta\sigma_R^+) + b$$

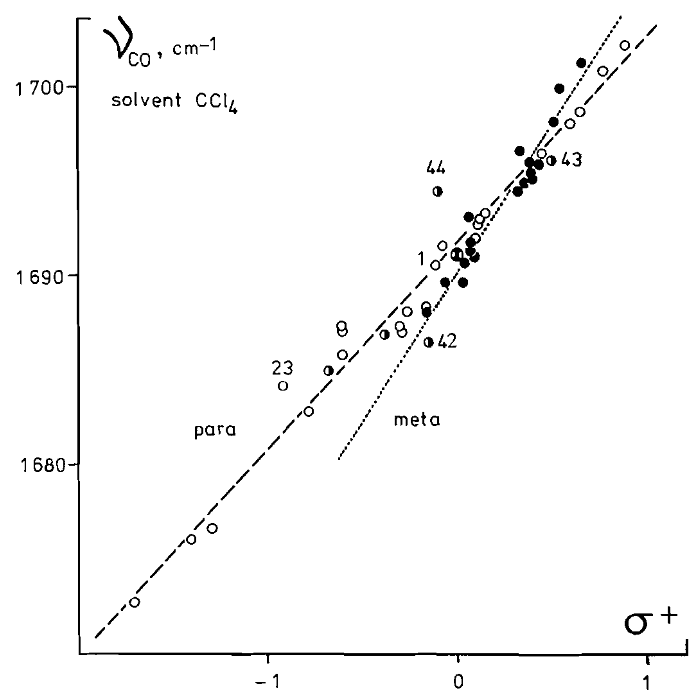

FIG. 1. Plot of ν_{CO} of ring-substituted acetophenones (solvent CCl_4) vs. σ^+ substituent constants; ●, *meta* substituted compounds; ○, *para* substituted compounds; ◑, *meta,para* di- and tri-substituted compounds.

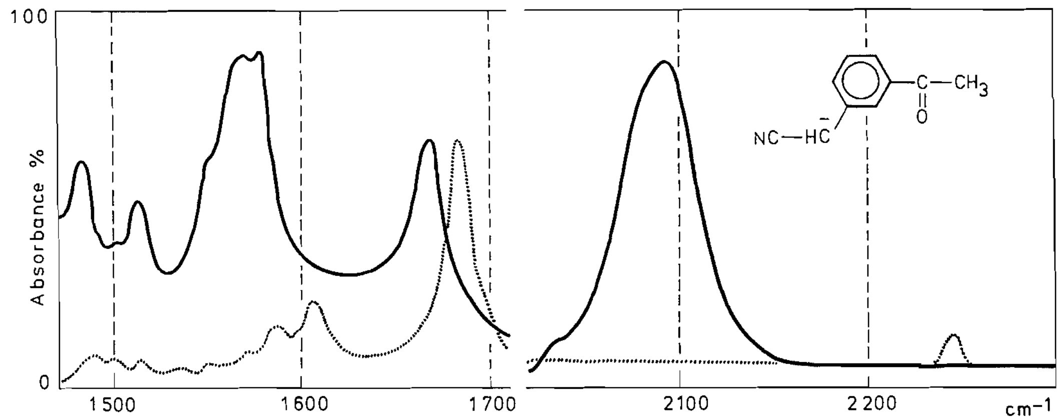

FIG. 2. Infrared spectra of the specified carbanion (solid line) and of the corresponding C—H conjugate acid (dotted line).

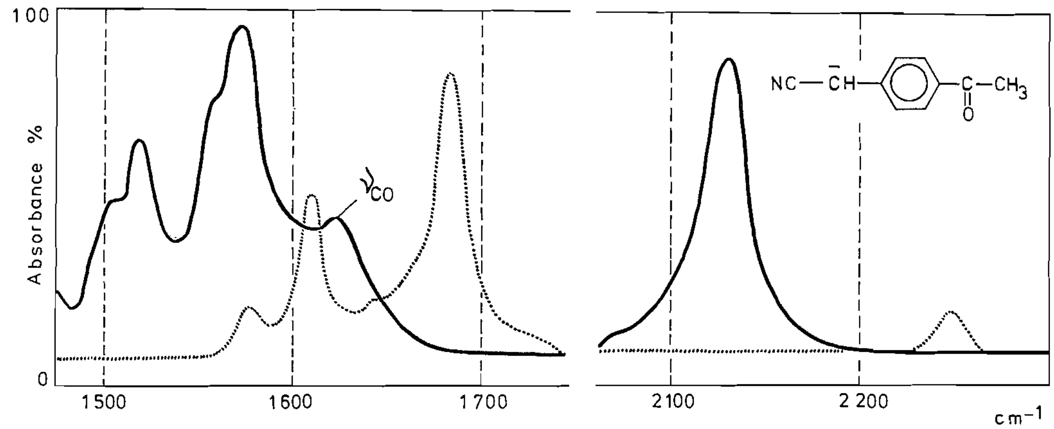

FIG. 3. Infrared spectra of the specified carbanion (solid line) and of the corresponding C—H conjugate acid (dotted line).

TABLE 4. Infrared data for acetophenones with *anionic* substituents, and constants (18) of these substituents

No.	Substituent	ν_{CO}	$10^{-3}\cdot A_{CO}$	σ^+	σ^0	$\Delta\sigma_R^+$	σ_I	σ_R^+
46.	3-CO_2^-	1680.4	12	−0.10	−0.19	0.09	−0.07	−0.32
47.	4-CO_2^-	1679.0	11	−0.41	−0.16	−0.25	−0.07	−0.32
48.	3-NC—HC^-	1668.4	7	−0.92	−0.81	−0.11	−0.54	−2.89
49.	4-NC—HC^-	1620 ± 1	Weak	−4.67	−4.16	−0.50	−0.54	−2.89
50.	3-CH_3CON^-	1671.9	23	−0.75	−0.93	0.18	−0.19	−2.66
51.	4-CH_3CON^-	1651.5	24	−2.90	−0.96	−1.92	−0.19	−2.66
52.	4-$C_6H_5CON^-$	1651.0	54	−2.77	−0.87	−1.91	−2.08	−1.08
53.	3-O^-	1666.8	26	−1.15	−1.38	0.23	−0.89	−3.17
54.	4-O^-	1630 ± 1	10	−4.27	−2.67	−1.59	−0.89	−3.17
55.	3-$CH_2CO_2^-$	1678.5	13	—	—	—	—	—
56.	3-$C_6H_5CON^-$	1672.4	25	—	—	—	—	—

[3] $\nu_{CO} = \rho_I\sigma_I + \rho_R\bar{\sigma}_R + b; \qquad \bar{\sigma}_R = \sigma_R^{BA}$ and σ_R^+

The results of the statistical treatment of ν_{CO} data according to these equations (substituent constants, see refs. 28 and 29) are listed in Table 3. Comparison of the R and s.d. parameters of the Yukawa–Tsuno-type correlations (Table 3, series 13 and 14) with those of the best-fit single-parameter correlations (Table 2, series 11 and 12) shows that use of the Yukawa–Tsuno's equation results in some improvement of the studied correlations. The r' value obtained for the carbon tetrachloride solutions (series 13) is in a good agreement with $r' = 0.612$ found earlier (7) for a series of *para*-substituted acetophenones.

The correlations according to eq. [3] (σ values from ref. 29) are also satisfactory (Table 3); their accuracy is close to that of the corresponding best-fit single-parameter correlations (Table 2, series 7–10). A direct comparison of these results with Krueger's values (13) is not possible because of the differences in the σ values used.

In agreement with ref. 3, A_{CO} of acetophenones (solvents CCl_4 and DMSO) do not correlate well with any type of substituent constants; the "correlations" obtained have R values in the 0,5–0,7 range, so they cannot be used for any practical purposes. This result could be related to the one found in the studies on A_{CO} in the substituted benzophenones series. The lack of correlation of $A_{CO}^{1/2}$ with $\bar{\sigma}$ in that case has been observed by several authors (see the references in ref. 25*a*) and then

TABLE 5. Correlations of ν_{CO} of acetophenones with *neutral* and *anionic* substituents (solvent DMSO) with substituent constants, according to eqs. [1], [2], and [3]

No.	Series	Sigma	Slope(s)	b	R^a	s.d.^{b}	n^c
8a	m	σ_m^+	14.13	1681.7	0.9902	1.2	12
10a	p	σ_p^+	12.68	1682.3	0.9951	2.2	18
12a	m & p	$\sigma_{m,p}^+$	12.69	1691.9	0.9928	2.0	30
14a	m & p	σ^0, $\Delta\sigma_R^+$	ρ = 13.32, r' = 0.79	1681.6	0.9963	1.7	24
16a	m	σ_I, σ_R^+	ρ_I = 14.40, ρ_R = 2.81	1681.6	0.9900	1.2	11
18a	p	σ_I, σ_R^+	ρ_I = 7.70, ρ_R = 13.55	1684.0	0.9879	3.3	17

^{a,b,c}See Table 2.

explained (25*a*) by the presence of a coupling between the ν_{8a} (of the benzene ring) and ν_{CO} vibrations. We assume that there is no correlation in the present case for similar reasons. This assumption finds some support in the data given in Section B, viz. data for acetophenones with extremely strong electron-releasing substituents, e.g. O^- and NC—HC^-. In these cases ν_{CO} frequencies are close to ν_{8a}, and A_{CO} intensities are the lowest ones.

B. *Acetophenones with anionic substituents*

The good fit of the correlations of ν_{CO} of acetophenones (solvent DMSO) makes it possible to use this series as a test with respect to the reliability of the constants of certain anionic substituents, determined recently (18) on the basis of nitrile infrared frequencies and intensities.

We prepared acetophenones with anionic substituents by metalation of the corresponding conjugate C—H, N—H, and O—H acids (cf. Experimental). Metalation resulted in essential changes in the infrared spectra: decrease in both ν_{CO} and ν_{CN} frequencies, strong intensification of the ν_{CN} bands and those of the aromatic skeletal vibrations, etc. (Figs. 2 and 3). ν_{CO} and A_{CO} of a series of acetophenones with anionic substituents (solvent DMSO) are listed in Table 4 together with the corresponding substituent constants.

Adding data for anions in the correlations for the neutral acetophenones gives a new set of single- and dual-parameter correlations, valid for ν_{CO} of acetophenones with both neutral and anionic substituents (Table 5). A plot of ν_{CO} vs. σ^+ for the whole series is shown in Fig. 4.

Comparison of the R values in Table 5 with those from Tables 2 and 3 (series with corresponding numbers) shows that the addition of the data for acetophenones with anionic substituents to those for neutral compounds does not change significantly the relative accuracy of both single- and dual-parameter correlations. Thus, constants σ^+, σ^0, $\Delta\sigma_R^+$, σ_I, and σ_R^+ of the anionic substituents considered, determined on the basis of nitrile frequencies and intensities in polar aprotic solvents, prove satisfactorily reliable in the ν_{CO} series of ring-substituted acetophenones. We should note that the deviation $\Delta\rho$ in the new set of correlation equations is only 1.5 cm^{-1} (cf. series 8a and 10a). This result is obviously related to the one-sided charging of the correlations with data for acetophenones with very strong donors (anionic substituents), for which the σ^+ constants have a *spectroscopic origin*.

The σ^+ constants of the anionic substituents 3-$CH_2CO_2^-$ and 3-$C_6H_5CON^-$ are not known. In principle their values can be estimated on the basis of data from Table 4 and the correlation equations for either series 8 (Table 2) by extrapolation or series 8a (Table 5) by interpolation. The latter method seems better

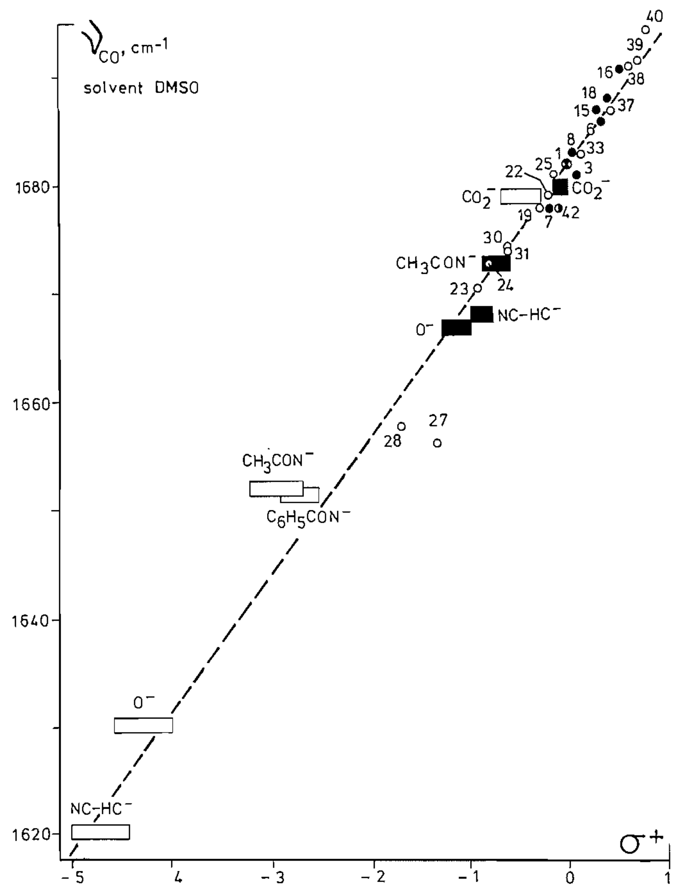

FIG. 4. Plot of ν_{CO} of acetophenones with *neutral* and *anionic* substituents (solvent DMSO) vs. σ^+ substituent constants; ●, *meta* substituted compounds; ○, *para* substituted compounds; ■ and □, compounds with *anionic* substituents. The abscissa width of the rectangular points corresponds to the inaccuracies (ref. 18) of σ^+ values of anionic substituents.

justified and it gives the following values: σ^+ (3-$CH_2CO_2^-$) = −0.22 ± 0.08; σ^+ (3-$C_6H_5CON^-$) = −0.66 ± 0.13. These values seem plausible, compared with σ^+ of other anionic substituents (18). Nevertheless, they are not of high reliability because substituent constants, determined in this way, depend strongly on the series of definition (30, 18).

Conclusion

Correlations found in this work can be used for predicting ν_{CO} of acetophenones with both neutral and anionic substituents in a wide frequency region. On the other hand, the satisfactory accuracy of these correlations could be considered as a proof of the reliability of the constants of the anionic substituents. As stated (18), further refinement of these constants could be achieved by including data for compounds with anionic substituents from other series, including ring-substituted acetophenones.

Acknowledgements

We thank Mrs. V. Radomirska, Dr. J. Kaneti, and Dr. J. Tsenov for helping us in the dual-parameter statistical treatment.

1. A. H. SOLOWAY and S. L. FRIES. J. Am. Chem. Soc. **73**, 5000 (1951).
2. M.-L. JOSIEN, N. FUSON, and P. PEARSON. C. R. Acad. Sci. **235**, 1206 (1952); N. FUSON, M.-L. JOSIEN, and E. M. SHELTON. J. Am. Chem. Soc. **76**, 2526 (1954).
3. R. N. JONES, W. F. FORBES, and W. A. MUELLER. Can. J. Chem. **35**, 504 (1957); R. N. JONES and E. SPINNER. Can. J. Chem. **36**, 1020 (1961).
4. H. H. FREEDMAN. J. Am. Chem. Soc. **82**, 2454 (1961).
5. C. N. R. RAO and R. VENKATARAGHAVAN. Can. J. Chem. **39**, 1757 (1961).
6. G. P. ROSSETI and B. P. SUSZ. Helv. Chim. Acta, **47**, 299 (1964).
7. C. LAURENCE and B. WOJTKOWIAK. Bull. Soc. Chim. Fr. 3124 (1971); 3833 (1971); 3870 (1971); 3874 (1971).
8. M. BERTHELOT, C. LAURENCE, and B. WOJTKOWIAK. Bull. Soc. Chim. Fr. 662 (1973).
9. W. A. SETH PAUL and A. VAN DUYSE. Spectrochim. Acta Part A, **28**, 211 (1972).
10. K. BOCEK, A. MANGINI, and R. ZAHRADNIK. J. Chem. Soc. 255 (1963).
11. L. I. RUDAYA, I. IA. KVITKO, and B. A. PORAY-KOSHITZ. Zh. Org. Khim. **8**, 13 (1972).
12. A. PERJESSY. Tetrahedron, **29**, 3189 (1973).
13. P. J. KRUEGER. Can. J. Chem. **51**, 1363 (1973).
14. J. TANAKA, S. NAGAKURA, and M. KOBAYASHI. J. Chem. Phys. **24**, 311 (1956).
15. Z. DINYA. Acta Chem. Acad. Sci. Hung. **72**, 323 (1972).
16. E. N. PETERS. Spectrochim. Acta Part A, **34**, 1159 (1978).
17. M. BERTHELOT and C. LAURENCE. Can. J. Chem. **53**, 993 (1975).
18. I. G. BINEV, R. B. KUZMANOVA, J. KANETI, and I. N. JUCHNOVSKI. J. Chem. Soc. Perkin Trans. 2, 1533 (1982); Izv. Khim. Bulg. Akad. Nauk, **14**, 470 (1981).
19. (*a*) D. A. RAMSAY. J. Am. Chem. Soc. **74**, 72 (1952); (*b*) K. H. SCHOWTKA and H. KRIEGSMANN. VEB Carl Zeiss Jena Nachr. **9**, 1 (1961).
20. L. J. BELLAMY. J. Chem. Soc. 4221 (1955).
21. D. COOK. J. Am. Chem. Soc. **80**, 49 (1958).
22. D. H. MCDANIEL and H. C. BROWN. J. Org. Chem. **23**, 420 (1958).
23. H. C. BROWN and Y. OKAMOTO. J. Am. Chem. Soc. **80**, 4979 (1958).
24. I. JUCHNOVSKI. Dokl. Akad. Nauk SSSR, **186**, 878 (1969); C. R. Acad. Bulg. Sci. **19**, 743 (1966); **19**, 1151 (1966); **20**, 33 (1967).
25. (*a*) I. N. JUCHNOVSKI, TS. M. KOLEV, and I. G. BINEV. Spectrosc. Lett. **14**, 763 (1981); I. G. BINEV, TS. M. KOLEV, and I. N. JUCHNOVSKI. Izv. Khim. Bulg. Akad. Nauk, **14**, 341 (1981); (*b*) P. J. VASSILEVA, I. G. BINEV, and I. N. JUCHNOVSKI. Spectrochim. Acta Part A, **39**, 709 (1983); I. G. BINEV, P. J. VASSILEVA, TS. M. KOLEV, and I. N. JUCHNOVSKI. J. Mol. Struct. **114**, 371 (1984); I. G. BINEV and P. J. VASSILEVA. J. Mol. Struct. **114**, 375 (1984).
26. Y. YUKAWA and Y. TSUNO. Bull. Chem. Soc. Jpn. **32**, 965 (1959); **32**, 971 (1959); Y. YUKAWA, Y. TSUNO, and M. SAWADA. Bull. Soc. Chem. Jpn. **45**, 1198 (1972).
27. R. W. TAFT. *In* Steric effects in organic chemistry. *Edited by* M. S. Newman. Wiley, New York. 1956. Chapt. 3; J. Am. Chem. Soc. **79**, 1045 (1957); J. Phys. Chem. **64**, 1805 (1960).
28. A. J. HOEFNAGEL and B. M. WEPSTER. J. Am. Chem. Soc. **95**, 5357 (1973); O. EXNER. *In* Advances in LFER. *Edited by* N. B. Chapman. Plenum Press, London. 1972. Chapt. 1.
29. R. T. C. BROWNLEE, S. EHRENSON, and R. W. TAFT. Prog. Phys. Org. Chem. **10**, 1 (1973).
30. YU. A. ZHDANOV and V. I. MINKIN. Correlation analysis in organic chemistry (Russ.). Rostov-na-Donu. 1966. Table 15 and pp. 110–128; A. J. HOEFNAGEL, M. A. HOEFNAGEL, and B. M. WEPSTER. J. Org. Chem. **43**, 4720 (1978).

The acid-catalyzed hydrolysis of phosphinates. IV. Pentacoordinate intermediate formation during hydrolysis of a phosphinothionate[1]

ROBERT D. COOK[2]
Department of Chemistry, Erindale College, University of Toronto, Mississauga, Ont., Canada L5L 1C6

AND

MARLENE METNI[3]
Department of Chemistry, American University of Beirut, Beirut, Lebanon

Received April 12, 1985

ROBERT D. COOK and MARLENE METNI. Can. J. Chem. **63**, 3155 (1985).

The hydrolysis of methyl dimethylphosphinothionate in D_2SO_4–D_2O solution gives as products the phosphinic acid and methyl dimethylphosphinate. The bell-shaped pH–rate profiles for both reactions as well as the values of Bunnett's w and w^* (3.31 and −0.21 respectively), Bunnett–Olsen's ϕ (0.82), and Yates–McClelland's r (6.56) support an A-2 pathway. The results are interpreted in terms of the presence of a common pentacoordinate intermediate along the reaction pathway. The pK_a of the above ester as well as that of methyl dimethylphosphinodithioate are reported (−5.53 and −5.38 respectively).

ROBERT D. COOK et MARLENE METNI. Can. J. Chem. **63**, 3155 (1985).

L'hydrolyse du diméthylphosphinothionate de méthyle dans une solution de D_2SO_4–D_2O conduit à de l'acide phosphinique et au diméthylphosphinate de méthyle. La courbe en cloche du pH en fonction de la vitesse, observée pour les deux réactions, ainsi que les valeurs w et w^* de Bunnett (3,31 et −0,21 respectivement), la valeur de ϕ (0,82) de Bunnett–Olsen ainsi que la valeur de r (6,56) de Yates–McClelland confirment l'existence d'un mécanisme du type A-2 pour les deux réactions. On interprète les résultats en fonction de la présence d'un intermédiaire commun pentacoordonné dans le processus réactionnel. On a déterminé la valeur du pK_a de l'ester ci-dessus ainsi que celle du diméthylphosphinodithioate de méthyle; ces valeurs sont respectivement −5,53 et −5,38.

[Traduit par le journal]

Introduction

From our previous studies on the acid-catalyzed hydrolysis of phosphinates we reported that methyl dialkylphosphinates hydrolyze by an A-2 process and, based on relative rate data for the esters **1**_a–d_ of 11:2.5:1.2:1, we suggested that water attacks the carbon of the protonated ester with subsequent C—O bond cleavage (2). On the other hand, McClelland has shown by O-18 studies that compounds **2**_a–c_ undergo acid-catalyzed hydrolysis with approximately 90% P—O bond cleavage (3). In the alkaline hydrolysis of phosphinates, P—O bond cleavage is the norm (4) except in the case when phosphorus is substituted with large alkyl groups like iC_3H_7 where Haake and Rahil (5) have shown that there is mixed cleavage (approximately 25% C—O cleavage). In other phosphorus esters P—O cleavage predominates in base and C—O cleavage in acid (6).

$R_2P(O)OCH_3$	R =	CH_3	C_2H_5	iC_3H_7	t-C_4H_9
		1_a_	**1**_b_	**1**_c_	**1**_d_
p-$XC_6H_4(CH_3)P(O)OCH_3$	X =		H	CH_3	Cl
			2_a_	**2**_b_	**2**_c_
$(CH_3)_2P(S)OCH_3$ **3**					

In the reactions in which nucleophilic attack on acyclic phosphorus esters takes place on phosphorus, two pathways have been suggested, one involving a direct displacement ($S_N2(P)$) (7) and the other by the formation of a pentacoordinate intermediate (4). There is, to date, only one report in the literature (8_a_) which gives direct support to intermediate formation in a displacement reaction on an acyclic phosphorus ester (phosphonate). The existence of intermediates is, however, well documented both in the displacement reactions on cyclic phosphorus esters (8_b_) as well as in the reactions of carboxylic esters (9).

Following the observations of Smith and O'Leary (10) and Edward, Wong, and Welch (11) that carboxylic thione esters undergo both hydrolysis and sulfur–oxygen exchange in acid solution and their suggestion that the reaction proceeds by a common tetrahedral intermediate, a study was undertaken on the hydrolysis in acid of a simple phosphorus analog, methyl dimethylphosphinothionate (**3**). The dimethyl ester was chosen in order to maximize the possibility of attack on phosphorus because only in this case will both hydrolysis and exchange be possible.

Results

Rate data

The hydrolysis of **3** in 25–85% D_2SO_4–D_2O solution gives not only the phosphinic acid but also methyl dimethylphosphinate (**1**_a_) (eq. [1]). The observed first-order rate constants

$$[1]\quad \mathbf{3} \xrightarrow{D_3O^+} \underset{\mathbf{4}}{(CH_3)_2P(S)OH} + \mathbf{1a} \longrightarrow \underset{\mathbf{5}}{(CH_3)_2P(O)OH}$$

for the conversion of **3** to **1**_a_ and **4** are given in Table 1. The pH–rate profiles for the above data are given in Fig. 1 and, for the sake of comparison, Fig. 2 gives the profiles for the hydrolysis reaction of **3** to **4** and of **1**_a_ to **5** (2).

Basicity data

The pK_a of **3** as well as that of another phosphinothionate,

[1] Preliminary communication of results in ref. 1.
[2] Address for the years 1984–1986 at the University of Toronto.
[3] Taken in part from the M.S. thesis of M.M., American University of Beirut, Beirut, Lebanon (1984).

TABLE 1. First-order rate constants (s^{-1}) for the hydrolysis reactions of methyl dimethylphosphinothionate[a] in D_2SO_4–D_2O solution at 75.3°C

wt.% D_2SO_4	$[D^+]$ (M)[b]	$-D_0$[c]	k_{total}[d] $\times 10^6$	k_{hyd}[e]$/k_{ex}$	$k_{hyd} \times 10^6$	$k_{ex} \times 10^6$
25.10	3.60	1.50	2.33	—	2.33	—
31.33	4.79	1.99	2.56	—	2.56	—
34.95	5.52	2.28	4.00	—	4.00	—
40.06	6.60	2.72	4.93	—	4.93	—
44.89	7.79	3.15	6.92	—	6.92	—
50.98	8.80	3.68	9.19	3.5	7.15	2.04
55.05	9.58	4.09	35.1	3.3	27.0	8.11
59.71	10.66	4.69	49.9	2.8	36.8	13.1
62.67	11.38	5.06	80.6	2.1	44.6	26.0
64.97	12.04	5.42	92.8	0.97	45.7	47.1
67.93	12.92	5.86	94.0	0.97	46.3	47.7
70.01	13.44	6.15	90.6	0.85	41.7	48.9
75.05	14.66	6.92	52.9	1.01	26.6	26.3
79.94	15.78	7.68	63.7	0.59	23.7	40.0
85.17	17.04	8.40	82.2	0.36	21.8	60.4

[a] [Ester] = 0.04–0.08 M.
[b] The molarity; determined from a calibration curve.
[c] Hammett acidity function for D_2SO_4, adjusted for temperature (refs. 12 and 13).
[d] Rate constants for the disappearance of ester **3**.
[e] Ratio of k_{hyd} (production of phosphinic acid) to k_{ex} (production of phosphinate ester **1***a*).

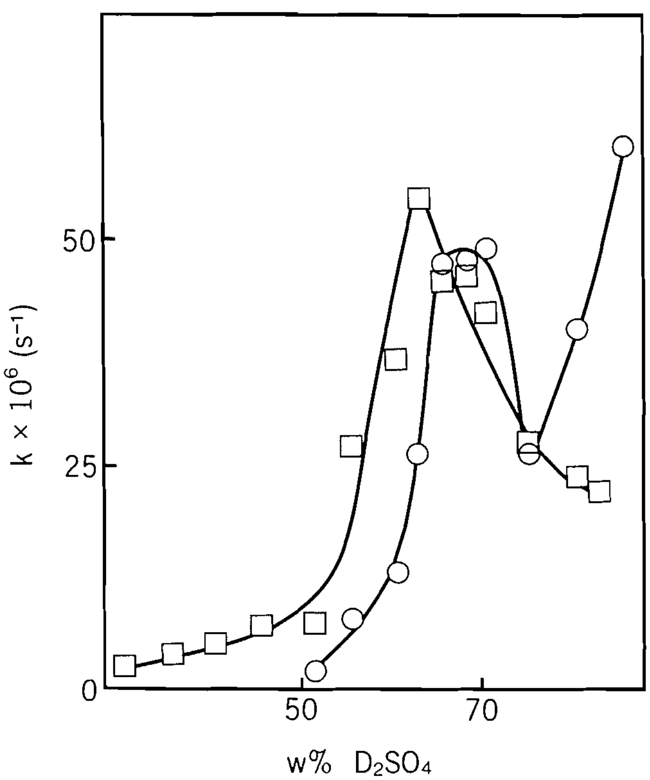

FIG. 1. Rate profiles for methyl dimethylphosphinothionate hydrolysis (□) and sulfur–oxygen exchange (○) reactions in D_2SO_4 at 75°C.

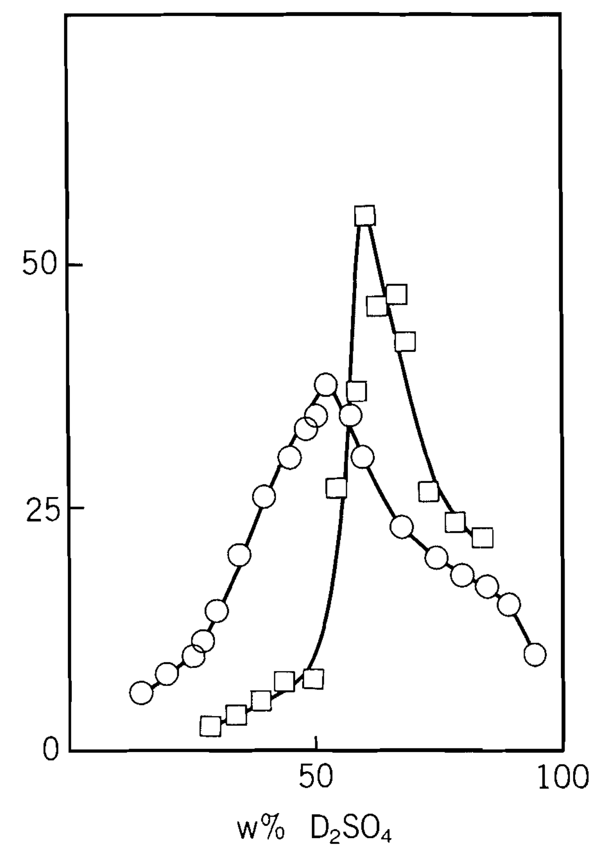

FIG. 2. Rate profiles for the hydrolysis of methyl dimethylphosphinothionate (□) and methyl dimethylphosphinate (○) in D_2SO_4 at 75°C.

methyl dimethylphosphinodithioate, were determined by the nmr method (14) and the results are given in Table 2. Included in Table 2 are the previously determined results for ester **1***a* (2). The value of m in Table 2 is the slope of the plot of $\log_{10}$ $[SD^+]/[S]$ versus $-D_0$ and its value indicates the extent of deviation of the individual substrate from Hammett basicity (anilines). Values above one are interpreted as less solvation of the substrate and values below one as more solvation of the substrate as compared to Hammett bases (14).

Treatment of the kinetic data

The rate data for the hydrolysis of **3** (k_{hyd}) were analyzed using the form of the Bunnett w and w^* equations (15), the Bunnett–Olsen ϕ equation (16), and the Yates–McClelland r

TABLE 2. Basicity of the phosphinothionates as determined by the nmr method[a]

Compound[b]	Half protonation[c]	pK_a[d]	m value[d]	r[d]
$(CH_3)_2P(S)OCH_3$	−5.53	−5.53	1.73	0.995
$(CH_3)_2P(S)SCH_3$	−5.38	−5.41	1.80	0.985
$(CH_3)_2P(O)OCH_3$[e]	−3.07	−3.14	0.49	0.993

[a]Reference 14.
[b]In D_2SO_4–D_2O solution.
[c]Taken from a plot of chemical shift versus $-D_0$.
[d]Obtained from the least-squares analysis of the plot of log $[SD^+]/[S]$ versus $-D_0$; m = slope; r = correlation coefficient.
[e]Reference 2.

TABLE 3. Results of the analyses of the kinetic data by the Bunnett, Bunnett–Olsen and Yates–McClelland equations

Compound	w[a]	w^*[a]	ϕ[b]	r[c]
$(CH_3)_2P(S)OCH_3$	3.31	−0.21	0.82	6.56
$(CH_3)_2P(O)OCH_3$[d]	2.28	−0.94	0.91	0.61

[a]Reference 15.
[b]Reference 16.
[c]Reference 17.
[d]Reference 2.

value equation (17) for a moderately basic substrate. The results for these analyses are given in Table 3 along with the results for ester **1**a (2). The r plot for **3** is given in Fig. 3.

Discussion

The bell-shaped pH–rate profiles for both reactions of **3**, indicating acid catalysis at lower acidities and acid inhibition at higher acidities, are usually interpreted in terms of an A-2 process (18). All of the other data from the treatment of the rate constants using the Bunnett, Bunnett–Olsen, and Yates–McClelland equations lend support to this conclusion. The concomitant hydrolysis of **3** to acid and exchange of oxygen for sulfur in an A-2 process can best be explained in terms of attack of water on protonated ester to give a pentacoordinate intermediate (**6**) followed by loss of either D_2S or $DOCH_3$. It can therefore be concluded that in this system there is attack on phosphorus with resultant P—O bond cleavage. There is no

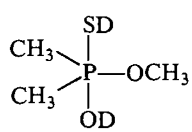

6

evidence in the acid-catalyzed hydrolysis of phosphinates of reversibility and therefore it can be ruled out that **1**a is a result of the esterification of **5** (2).

These results are analogous to those obtained on thion esters (10, 11). In these latter systems loss of H_2S is faster than loss of alcohol at the lower acidities, the opposite of what is observed for compound **3**. Since apical departure from a pentacoordinate species is favored (8), loss of D_2S should proceed from **6** and loss of $DOCH_3$ from **7**. The structures **6** and **7** are mutually interconvertible by pseudorotation and therefore the relative rates for the loss of D_2S and $DOCH_3$ are independent of the relative amounts of **6** and **7**. Since it is likely that the transition state for breakdown of the intermediate involves an

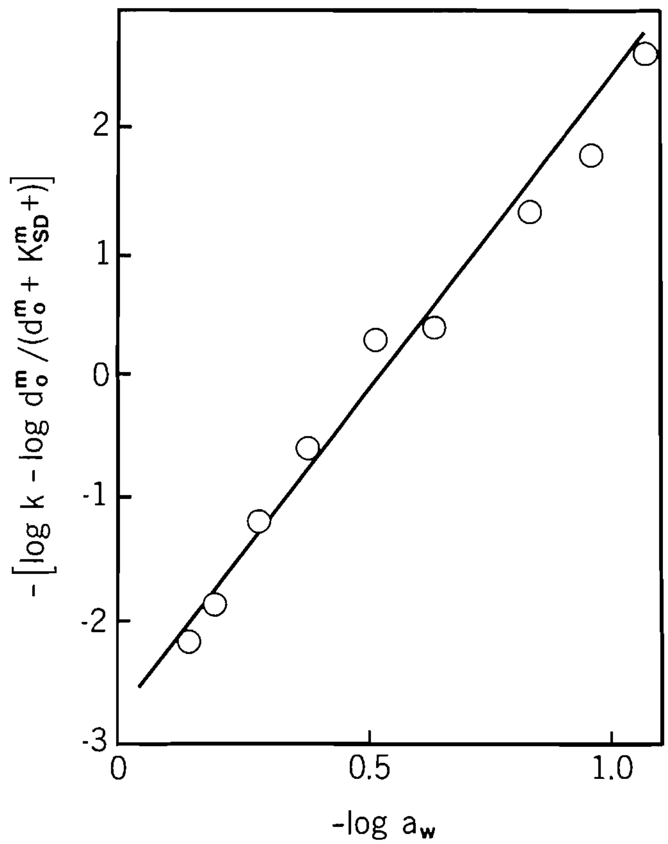

FIG. 3. Yates–McClelland r plot of the rate data obtained for methyl dimethylphosphinothionate hydrolysis.

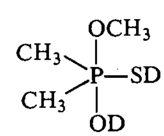

7

extra proton, the faster loss of alcohol could be due to the greater basicity of the oxygen center over the sulfur center.

The value of r of the Yates–McClelland equation is very high (it is typically 2 for carboxylic ester hydrolysis) and this is a direct result of the high m value for the ester **3**. For the five phosphinates that we have studied (ref. 2 and this work), which hydrolyze by an A-2 pathway, there is a linear relationship between r and m (using eq. [2]).

$$[2] \quad \log k_{obs} - \log \frac{h_0^m}{K_{SH^+}^m + h_0^m} = r \log a_{H_2O} + C$$

Qualitatively this is very reasonable since esters which are poorly solvated (high m values) will require more additional water in the rate-determining step (higher r value).

The sulfur exchange result is the best evidence to date in support of the formation of pentacoordinate intermediates in the displacement reactions at acyclic phosphinate esters.

The explanation proposed for these results supposes a common intermediate. We have no specific evidence on this point. It is possible that hydrolysis could proceed by a path different from sulfur to oxygen exchange, for example, by a S_N2 (P) reaction or a S_N2 process with C—O bond cleavage. The existence of an intermediate is only supported by the exchange reaction.

High acidity sulfur exchange

The upward curvature at high acidities of the pH–rate profile in hydrolysis reactions is usually associated with a change in mechanism from A-2 to A-1 (17). It is, however, difficult to contemplate the unimolecular cleavage of what is essentially a P=S double bond. This observed rate increase continues such that in 95% D_2SO_4 complete conversion of **3** to **1***a* takes only a few minutes at 75°C. Under these conditions no hydrolysis of either **3** or **1***a* is observed. If an A-1 process is not to be considered, then neither can a reaction involving water be considered, because of its vanishingly small activity at this acid concentration (18). Cox (19) has reported the changing activities of sulfuric acid related species over a large range of acid concentration. The only species with increasing activity in this high weight percent region is $D_3SO_4^+$. One possible pathway for the reaction would involve the formation of **8**, which results from the addition of **3** to $D_3SO_4^+$ (or protonated **3** to D_2SO_4) and which by loss of a proton would give a betaine similar to what is encountered in the Wittig reaction. The species **8** would then

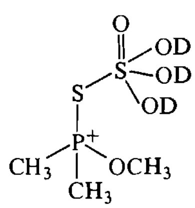

8

decompose to **1***a* and $D_2S_2O_3$, thiosulfuric acid. We have no independent evidence to support this proposal.

Basicity of the P=S system

The esters containing the P=S linkage are approximately 2.5 pK_a units less basic than those with the P=O linkage. A similar decrease in basicity is observed for thione esters with respect to their oxygen analogs (11) and dimethyl sulfide is also reported to be less basic than dimethyl ether by a similar amount (20). There is ample evidence for p–d π-bonding in the P=O system (21) but much less evidence is available in support of p–d π-bonding in the P=S linkage. The low basicity of the phosphinothionates is good evidence in support of π-bonding and the almost constant decrease in going from a oxygen base to a sulfur base in the three systems suggests that the nature of the bonding must be similar within the three pairs.

It is interesting to note that the m value is approximately the same for the thione ester and the dithio ester and both are considerably larger than the value for the P=O ester. This slope parameter, m, reflects the deviation from Hammett basicity of the substrate and values greater than 1 are considered to be less solvated than Hammett's anilines and those less than 1 more solvated (14). The almost identical values for the sulfur-containing compounds suggest that it is essentially changes in solvation of the P=X (X = O or S) part of the molecule that determine the value of m.

Experimental

Synthesis of the esters

The ester **3** was prepared by the addition of an equimolar amount of sodium methoxide in methanol to dimethylphosphinothionyl chloride in benzene. The acid chloride was prepared by treating tetramethylbiphosphine disulfide with a equimolar amount of sulfuryl chloride in benzene (22). The disulfide was synthesized by adding trichlorophosphine sulfide (1 mole) to methylmagnesium iodide (3 moles) in ether (23). The boiling point of **3** is 79–80°C/2.5 Torr (uncorrected) (1 Torr = 133.3 Pa); ir (neat): (P=S) 665, 755 cm^{-1}; ^{1}H nmr δ: 3.55 (3H, d, J = 14 Hz) and 1.87 (6H, d, J = 14 Hz).

Kinetic measurements

The hydrolysis reactions of **3** were run in different weight percent solutions of D_2SO_4 in D_2O. The molarity of the acid was determined from a calibration curve prepared by titration. All rates were followed on a Varian Model EM 360L nmr spectrometer. For acidities below 50% D_2SO_4, where no sulfur exchange was observed, the reactions were monitored in a manner similar to that of our previous report (2). At higher acidities two regions of the spectra were examined, the downfield region represented by all OCH_3 groups and the upfield region represented by all P—CH_3 groups. In the downfield region there is a doublet for **3**, a doublet for **1***a*, a singlet for methanol, and another singlet for dimethyl ether (from the dehydration of methanol). The peaks could be integrated separately and the ratio of the areas of **1***a* to methanol and ether gives the ratio of the rate constants for their production (k_{hyd}/k_{ex}). In the upfield region only 4 peaks appear, a doublet for **3** and a doublet for the other 3 compounds (**1***a*, **4**, and **5**). Integration of the two areas gives us the rate constant for loss of **3** (k_{total}). All assignments were checked at each concentration by adding authentic samples to the nmr tubes. With a few of the concentrations overlap of peaks occurs. These samples were diluted with D_2O before analysis.

Under the reaction conditions **1***a* also undergoes hydrolysis to give **5** and therefore the ratio of k_{hyd}/k_{ex} slowly increases. The values used in Table 1 are from the initial points of the reaction.

We have no evidence as to whether or not acid **4** keeps its integrity under the reaction conditions. The chemical shift of the P—CH_3 groups of the two acids **4** and **5** are the same in sulfuric acid solution.

Measurement of the pK_a

The pK_a's of the esters were measured by the nmr method of Haake *et al.* (14) in D_2SO_4–D_2O solution at room temperature.

Acknowledgement

The authors thank the Arts and Sciences Research Committee of the American University of Beirut for financial support.

1. R. D. Cook and M. Metni. J. Chem. Soc. Chem. Commun. 832 (1985).
2. K. A. Abbas and R. D. Cook. Can. J. Chem. **55**, 3740 (1977).
3. R. A. McClelland. J. Chem. Soc. Chem. Commun. 226 (1976).
4. R. D. Cook, C. E. Diebert, W. Schwarz, P. C. Turley, and P. Haake. J. Am. Chem. Soc. **95**, 8088 (1973).
5. P. Haake and J. Rahil. J. Org. Chem. **46**, 3048 (1981).
6. J. Emsley and D. Hall. The chemistry of phosphorus. John Wiley, New York. 1976. Chapt. 8.
7. A. J. Kirby and S. G. Warren. The organic chemistry of phosphorus. Elsevier, Amsterdam. 1967. Chapt. 10.
8. (*a*) I. Sigal and F. H. Westheimer. J. Am. Chem. Soc. **101**, 752 (1979); (*b*) F. H. Westheimer. Acc. Chem. Res. **1**, 70

(1968); K. MISLOW. Acc. Chem. Res. **3**, 321 (1970); D. MARQUARDING, H. KLUSACEK, P. GILLESPIE, and F. RAMIREZ. Acc. Chem. Res. **4**, 288 (1971).
9. M. L. BENDER, R. D. GINGER, and J. P. UNIK. J. Am. Chem. Soc. **80**, 1044 (1958).
10. S. SMITH and M. O'LEARY. J. Org. Chem. **28**, 2825 (1963).
11. J. T. EDWARD and S. C. WONG. J. Am. Chem. Soc. **99**, 7224 (1977); J. T. EDWARD, S. C. WONG, and G. WELCH. Can. J. Chem. **56**, 931 (1978).
12. E. HOGFELDT and J. BIGELEISEN. J. Am. Chem. Soc. **82**, 15 (1960); J. SIERRA, M. OJEDA, and P. A. H. WYATT. J. Chem. Soc. B, 1570 (1970).
13. P. TICKLE, A. G. BRIGGS, and J. M. WILSON. J. Chem. Soc. B, 65 (1970); C. D. JOHNSON, A. R. KATRITZKY, and S. A. SHAPIRO. J. Am. Chem. Soc. **91**, 6654 (1969).
14. P. HAAKE, R. D. COOK, and G. HURST. J. Am. Chem. Soc. **89**, 2650 (1967).
15. J. F. BUNNETT. J. Am. Chem. Soc. **83**, 4956 (1966); **83**, 4968 (1966); **83**, 4973 (1966); **83**, 4978 (1966).
16. J. F. BUNNETT and F. P. OLSEN. Can. J. Chem. **44**, 1899 (1966); **44**, 1917 (1966).
17. K. YATES and R. A. MCCLELLAND. J. Am. Chem. Soc. **89**, 2696 (1967); K. YATES. Acc. Chem. Res. **4**, 136 (1971).
18. M. LILER. Reaction mechanisms in sulfuric acid. Academic Press, New York. 1971. p. 183.
19. R. A. COX. J. Am. Chem. soc. **96**, 1059 (1974).
20. E. M. ARNETT. *In* Progress in physical organic chemistry. Vol. I. *Edited by* A. Streitwieser and R. W. Taft. John Wiley, New York. 1963. pp. 325, 392.
21. R. F. HUDSON. Structure and mechanism in organophosphorus chemistry. Academic Press, London. 1965. pp. 67–76; H. KWART and K. G. KING. d-Orbitals in the chemistry of silicon, phosphorus and sulfur. Springer Verlag, Germany. 1977. pp. 14–49.
22. W. KUCHEN, H. BUCHWALD, K. STROLENBERG, and J. METTER. Ann. **652**, 28 (1962).
23. K. ISSLIEB and A. TZCHACH. Chem. Ber. **92**, 704 (1959).

Proton affinities of the hydrogen, methyl, and trifluoromethyl halides from pulsed electron beam high pressure mass spectrometric equilibria measurements

T. B. McMahon[1] and P. Kebarle
Department of Chemistry, University of Alberta, Edmonton, Alta., Canada T6G 2G2

Received March 19, 1985

T. B. McMahon and P. Kebarle. Can. J. Chem. **63**, 3160 (1985).

Pulsed electron beam high pressure mass spectrometric techniques have been used to investigate proton transfer equilibria involving hydrogen and trifluoromethyl halides. Methyl cation transfer equilibria have also been used to determine methyl cation affinities of hydrogen halides. Proton affinities obtained are HCl = 137.5, HBr = 142.9, HI = 150.9, CF_3Cl = 139.0, CF_3Br = 141.3, and CF_3I = 150.4 kcal mol^{-1}. Methyl cation affinities obtained are HF = 15 ± 2, HCl = 19.8, HBr = 21.3, and HI = 31.1 kcal mol^{-1}. The values of methyl cation affinity of hydrogen halides can in turn be used to calculate proton affinities of the methyl halides of CH_3Cl = 160.8; CH_3Br = 164.8; and CH_3I = 171 kcal mol^{-1}. Linear correlations are found between proton affinities and valence ionization potentials and between proton affinities and methyl cation affinities.

T. B. McMahon et P. Kebarle. Can. J. Chem. **63**, 3160 (1985).

Faisant appel à des technique de spectrométrie de masse à haute pression utilisant un faisceau pulsé d'électron, on a étudié les réactions d'équilibre de transfert de proton impliquant des halogénures d'hydrogène et de trifluorométhyle. On a également utilisé l'équilibre de transfert du cation méthyle dans le but de déterminer les affinités du cation méthyle pour les halogénures d'hydrogène. On a obtenu les affinités suivantes pour le proton: HCl = 137,5; HBr = 142,9; HI = 150,9; CF_3Cl = 139,0; CF_3Br = 141,3 et CF_3I = 150,4 kcal mol^{-1}. Les affinités pour le cation méthyle sont les suivantes: HF = 15 ± 2; HCl = 19,8; HBr = 21,3 et HI = 31,1 kcal mol^{-1}. Par la suite, on peut utiliser les valeurs des affinités du cation méthyle pour les halogénures d'hydrogène pour calculer les affinités du proton pour les halogénures de méthyle qui sont CH_3Cl = 160,8; CH_3Br = 164,8 et CH_3I = 171 kcal mol^{-1}. On a trouvé des corrélations linéaires entre les affinités du proton et les potentiels d'ionisation de valence et entre les affinités du proton et les affinités du cation méthyle.

[Traduit par le journal]

Introduction

Investigations of gas phase proton transfer equilibria during the past decade (for extensive reviews of gas phase basicities, see ref. 1) have provided a wealth of data concerning the intrinsic basicities of molecules in the absence of solvent effects.[2] These studies have led to many insights into factors governing structure, stability, and bonding in ionic species. However, while a great deal of data exists for traditional basic functional groups such as amines, carbonyls, ethers, alcohols, mercaptans, and sulphides, there have been no accurate quantitative equilibrium proton transfer data obtained for the weakly basic halide functional groups. These particular groups of compounds are of special interest since the stability, ready availability, and ease of handling of compounds of four members of the group (F, Cl, Br, I) provide an ideal opportunity to examine periodic trends not afforded by any other group of elements.

The hydrogen halides have been examined by a number of investigators. Foster and Beauchamp (3) obtained proton transfer equilibrium between HF and N_2, eq. [1], to arrive at $\Delta H_1^0 = -1.1$ kcal mol^{-1}. However, since no accurate proton affinity

$$[1] \quad H_2F^+ + N_2 \rightleftharpoons N_2H^+ + HF$$

was available for N_2, an approximate value of proton affinity of 112 ± 2 kcal mol^{-1} was assigned to HF. No other proton transfer equilibrium measurements have previously been reported for the remaining hydrogen halides. Polley and Munson (4) have carried out a series of experiments in which a variety of proton transfer reactions to hydrogen halides, and from the protonated hydrogen halides to other species, were examined. From such observations of occurrence or non-occurrence of proton transfer (bracketing technique) to species of known basicity, approximate proton affinity values for the hydrogen halides were obtained of 135 ± 2 kcal mol^{-1} for HCl, 140 ± 1 kcal mol^{-1} for HBr, and 147 ± 2 kcal mol^{-1} for HI. It must be noted, however, that these assignments were again limited by the relatively high uncertainty in proton affinity values of the reference species involved.

In an elegant series of experiments Lee and co-workers (5, 6) have determined absolute values for proton affinities of HF, HCl, and HBr based on photoionization appearance potential measurements of the corresponding protonated hydrogen halides, H_2X^+, from the corresponding van der Waals dimers, $(HX)_2$, formed in a supersonic expansion. The value obtained for PA(HF) of 95.5 ± 1.4 kcal mol^{-1} was in poor agreement with that of Foster and Beauchamp (3); however, the values of PA(HCl) of 135 ± 1 kcal mol^{-1} and PA(HBr) of 141 ± 1 kcal mol^{-1} were in excellent agreement with those of Polley and Munson (4).

No equilibrium proton transfer measurements involving methyl halides have been possible to date due to the rapid nucleophilic displacement reactions, eq. [2], of the protonated methyl halides (7) which compete effectively with proton transfer processes, preventing attainment of equilibrium. In a

$$[2] \quad CH_3XH^+ + CH_3X \rightarrow (CH_3)_2X^+, HX$$

systematic study of the gas phase ion chemistry of methyl and ethyl halides Beauchamp *et al.* (7) were able to bracket the proton affinities of these compounds approximately. The values obtained of $PA(CH_3F)$ = 151 kcal mol^{-1}, $PA(CH_3Cl)$ = 160 kcal mol^{-1}, $PA(CH_3Br)$ = 163 kcal mol^{-1}, and $PA(CH_3I)$ = 170 kcal mol^{-1} were again limited by the uncertainties in data for the reference species used.

A number of *ab initio* quantum chemical investigations of the proton affinities of HF, HCl, CH_3F, and CH_3Cl have been

[1] Address correspondence to this author at: Department of Chemistry, University of Waterloo, Waterloo, Ont., Canada N2L 3G1.

[2] The quantitative definition of gas phase basicity of a molecule M is the proton affinity, PA(M), defined as the negative of the enthalpy change for the gas phase reaction: $M + H^+ \rightarrow MH^+$ at 298 K.

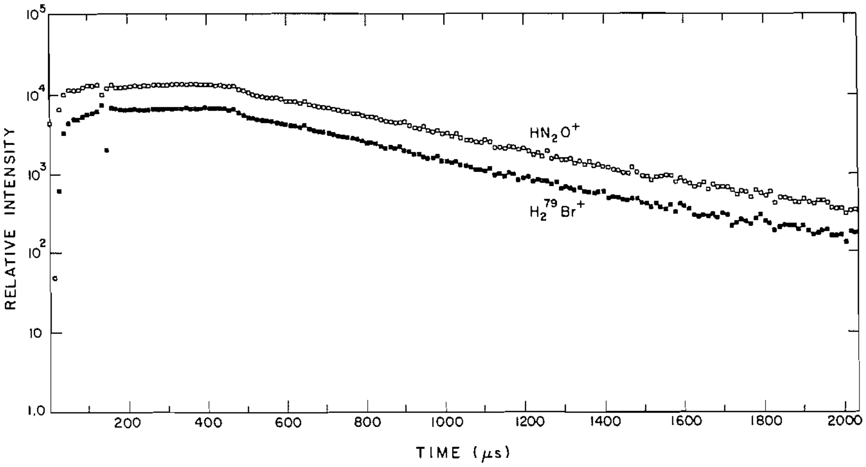

FIG. 1. Variation of relative ionic abundances as a function of time after initial ionization in a mixture of CH_4, N_2O, and HBr at a total ion source pressure of 3.0 Torr and a N_2O/HBr ratio of 2.5:1.

carried out. Diercksen *et al.* (8) carried out large basis set calculations on HF and H_2F^+ with complete geometry optimization to obtain a proton affinity of HF of 120 kcal mol^{-1}. Jorgensen and co-workers (9) have carried out calculations of each of the hydrogen and methyl fluorides and chlorides using a variety of basis sets and obtained proton affinities at the 6-31G* level of 121.4 kcal mol^{-1} for HF, 151.5 kcal mol^{-1} for CH_3F, 129.1 kcal mol^{-1} for HCl, and 151.3 kcal mol^{-1} for CH_3Cl. It should be emphasized that none of the above calculations included contributions due to zero point energy differences between ionic and neutral species or due to differences in proton affinity at 0 K and 298 K (10). Pople and co-workers (11) have carried out calculations for HF using a 6-31G** basis set incorporating fourth-order Moeller–Ploesset determinations of the correlation energies and including zero point energy differences to obtain a proton affinity of HF of 124.7 kcal mol^{-1}.

Very recently, extensive studies of proton transfer equilibria from this laboratory (12) have established a quantitative scale of gas phase basicities for the proton affinity region below water to species as weakly basic as methane. All of these data are anchored to the now well-established value for the proton affinity of ethylene (13–15). Included in this basicity scale are proton transfer equilibria involving the hydrogen halides HCl, HBr, and HI, thus establishing, for the first time, accurate values for the proton affinities of these species based on thermochemical equilibrium measurements.

As noted above, proton transfer equilibria involving methyl halides are not readily observable due to competition from nucleophilic displacement processes. However, also recently in this laboratory, we have devised techniques for the examination of methyl cation transfer equilibria, eq. [3] (16). When methyl cation transfer equilibria involving hydrogen halides

[3] $CH_3M^+ + HX \rightleftharpoons CH_3XH^+ + M$

are carried out, accurate thermochemical data for CH_3XH^+ species, i.e. protonated methyl halides, are obtained, which, when combined with known neutral thermochemistry, allow determination of accurate proton affinities of the methyl halides.

With the exception of some work on CF_4 by Bohme and co-workers (17), no information is available on protonation of any of the trifluoromethyl halides. These species are of interest because of the strongly destabilizing effect of the electronegative CF_3 substituent on basicities and because they provide another type of molecule where protonation on the halogen will occur. Fortunately, these species do not undergo nucleophilic displacement reactions and it was possible to incorporate CF_3Cl, CF_3Br, and CF_3I into the scale of proton transfer equilibrium basicity measurements.

The proton transfer equilibria involving hydrogen and trifluoromethyl halides and methyl cation transfer equilibria involving hydrogen halides provide accurate proton affinity data for HX, CH_3X, and CF_3X compounds. This makes possible an analysis of periodic trends and substituent effects in halogen basicities, described in the present study.

Experimental

All equilibrium measurements were carried out at 400 K using a pulsed electron beam high pressure mass spectrometer (hpms) described in detail previously (18), which has been recently updated incorporating a Lecroy Model 3921 Multichannel Analyzer allowing use of dwell times as short as 1 μs per channel.

For proton transfer equilibria involving HBr, HI, CF_3Cl, CF_3Br, and CF_3I the major gas used was CH_4, which was flowed through the high pressure ion source at pressures between 2 and 5 Torr (1 Torr = 133.3 Pa). Ion source pressures of the halides and reference compounds were in the range of 1–10 mTorr. Protonation of halides occurred by the well-known reaction sequence in methane, eqs. [4] and [5]. Data for a typical proton transfer equilibrium are illustrated in Fig. 1.

[4] $CH_4{}^+ + CH_4 \rightarrow CH_5{}^+ + CH_3$

[5] $CH_5{}^+ + RX \rightarrow RXH^+ + CH_4$

Proton transfer equilibria involving HCl and all methyl cation equilibria were carried out using nitrogen as the major bath gas. The use of nitrogen rather than methane for proton transfer to HCl was necessitated by the close proximity of CH_4 and HCl in proton affinity. The principle mode of formation of H_2Cl^+ is via the sequence of eqs. [6] and [7]. The use of N_2 as the major gas for methyl cation transfer equilibria arises because of the useful sequence of reactions, eqs. [8]–[11], which occurs in CH_3F–N_2 mixtures.

[6] $N_2{}^+ + HCl \rightarrow N_2H^+ + Cl$

[7] $N_2H^+ + HCl \rightarrow H_2Cl^+ + N_2$

[8] $N_2{}^+ + CH_3F \rightarrow N_2H^+ + CH_2F$

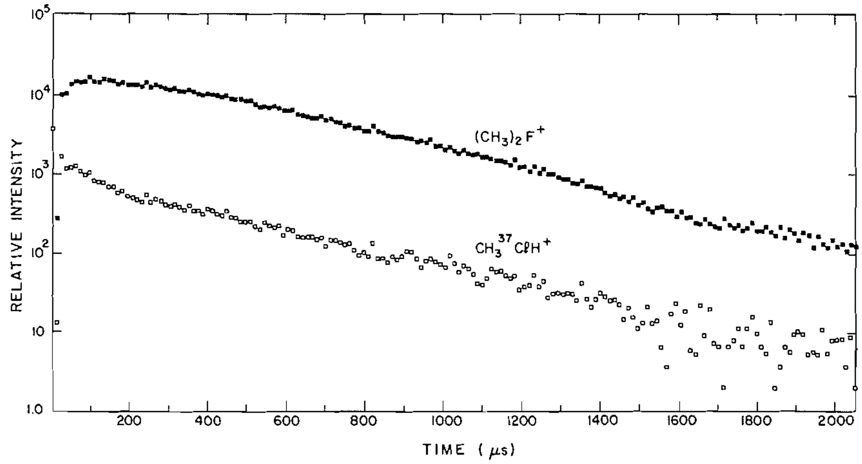

FIG. 2. Variation of relative ionic abundances as a function of time after initial ionization in a mixture of N_2, CH_3F, and HCl at a total ion source pressure of 3.8 Torr and a CH_3F/HCl ratio of 1 : 1.

TABLE 1. Proton transfer equilibria and associated thermochemical data for the reaction: $MH^+ + RX \leftrightharpoons RXH^+ + M$ used to obtain proton affinities of hydrogen and trifluoromethyl halides

RX	M	ΔG^{0a}	ΔS^{0b}	ΔH^{0a}	PA(M)[a,c]	PA(RX)[a]
HF	N_2			−1.1[d]	122.0[e]	120.9
HCl	CH_4	−2.6	−1.0	−3.0	134.7	137.7
HCl	N_2O	4.2	0.6	4.4	142.0	137.6
HBr	N_2O	−0.7	0.4	−0.5	142.0	142.5
HBr	HCl	−4.6	−0.2	−4.7	137.6	142.3
HBr	CO	1.2	3.4	2.6	145.6	143.0
HBr	SO_2F_2	5.9	2.8	7.0	150.0	143.0
HI	$(CF_3)_2CO$	1.3	4.0	2.9	153.8	150.9
CF_3Cl	CH_4	−4.3	−0.2	−4.4	134.7	139.1
CF_3Br	CH_4	−6.5	0.0	−6.5	134.7	141.2
CF_3Br	N_2O	0.3	1.6	0.9	142.0	141.1
CF_3Br	C_2H_6	4.2	3.5	5.6	146.9	141.3
CF_3I	SO_2F_2	−2.0	4.0	−0.4	150.0	150.4
CF_3I	$(CF_3)_2CO$	1.8	4.0	3.4	153.8	150.4

[a] All values in kcal mol^{-1}.
[b] All values in cal mol^{-1} K^{-1}.
[c] Reference values taken from T. B. McMahon and P. Kebarle (12).
[d] From Foster and Beauchamp (3).
[e] From $PA(CH_4)$ = 134.7 kcal mol^{-1} and Bohme (21) data.

[9] $N_2H^+ + CH_3F \rightarrow CH_3FH^+ + N_2$

[10] $CH_3FH^+ + N_2 \rightarrow CH_3N_2{}^+ + HF$

[11] $CH_3N_2{}^+ + CH_3F \rightarrow (CH_3)_2F^+ + N_2$

The $\Delta H_f^0(CH_3N_2{}^+)$ and hence the methyl cation affinity (MCA) of N_2 is known from photoionization appearance potential measurements of $CH_3N_2{}^+$ from azomethane (19). In the presence of a large excess of N_2 eq. [11] reaches equilibrium, establishing the methyl cation affinity of CH_3F. This mixture of CH_3F–N_2 can then be used as a methylating medium and, when methyl cation transfer equilibrium is observed, accurate relative methyl cation binding energies may be obtained. A typical methyl cation transfer equilibrium is illustrated in Fig. 2.

In addition to the usual procedures for carring out hpms experiments for the present studies, all gases flowing from the gas handling system to the high pressure ion source were passed through a U-trap cooled by a variety of slush baths, typically to −95 to −150°C. This procedure was necessary to remove traces of H_2O. Due to the extremely low basicities of the compounds under study, the presence of H_2O even at the part per thousand level led to production of H_3O^+ and higher proton hydrates that precluded observations of the equilibrium of interest.

$$\begin{tikzcd} CH_3^+ + HX \arrow[r, "-MCA(HX)"] \arrow[d, "PA(X^-)"] & CH_3XH^+ \arrow[d, "PA(CH_3X)"] \\ CH_3^+ + H^+ + X^- \arrow[r, "-X^-A(CH_3^+)"] & CH_3X + H^+ \end{tikzcd}$$

SCHEME 1

Results

Proton transfer equilibria between reference species, M, and the hydrogen and trifluoromethyl halides, RX, which have been used to obtain proton affinities for RX, are summarized in Table 1 together with the thermochemical data derived. Values for ΔS^0 have been estimated from experimentally known S^0 data. For ionic species these were taken from known data for isoelectronic neutral molecules (20). For example, $S^0(H_2Cl^+)$ was estimated as 49.7 cal mol^{-1} K^{-1} based on the value of $S^0(H_2S)$ of 49.2 cal mol^{-1} K^{-1} and a small correction for differences in translational entropy of H_2Cl^+ and H_2S.

Proton affinities of reference compounds CH_4, N_2O, CO, C_2H_6, SO_2F_2, and $(CF_3)_2CO$ were taken from recent data from this laboratory, in which a quantitative proton affinity scale between H_2O and CH_4 was constructed (12). Although these data did not extend to compounds as weakly basic as N_2, the values for PA(CO) and $PA(CH_4)$ may be combined with Bohme's data for compounds less basic than CH_4 (21) to yield $PA(N_2)$ = 122.0 kcal mol^{-1}. This then also permits PA(HF) to be calculated from the equilibrium data of Foster and Beauchamp (3) for eq. [7] as 120.9 kcal mol^{-1}.

Methyl cation transfer equilibria used to establish methyl cation affinities of the hydrogen halides are summarized in Table 2. The MCA scale is anchored to $MCA(N_2)$ which can be calculated from $\Delta H_f^0(CH_3N_2{}^+)$ obtained from photoionization appearance energy measurements of $CH_3N_2^+$ from $CH_3N{=}NCH_3$ (19). The $MCA(N_2)$ thus established is 51.9 kcal mol^{-1}. The thermochemical data derived from the methyl cation transfer equilibria, also summarized in Table 2, may be combined with $MCA(N_2)$ to obtain absolute methyl cation affinities of

TABLE 2. Methyl cation transfer equilibria: $CH_3M^+ + RX \rightleftharpoons CH_3XR^+ + M$ and associated thermochemical data used to obtain methyl cation affinities of hydrogen halides and proton affinities of methyl halides

M	RX	ΔG^{0a}	ΔS^{0b}	ΔH^{0a}	MCA(M)[a]	MCA(RX)	$\Delta H_f^0(RXCH_3^+)^a$	$PA(CH_3X)^a$
N_2	CH_3F	−6.2	2.7	7.3	51.9	59.2	63.7	(148 ± 2)[c]
N_2	HCl	−4.8	3.3	−3.2	51.9	55.1	184.2	160.8
CH_3F	HCl	−1.4	6.0	4.1	59.2	55.1	184.2	160.8
CH_3F	HBr	−4.2	5.5	−2.0	59.2	61.2	191.3	164.8

[a]All values in kcal mol^{-1}.
[b]All values in cal mol^{-1} K^{-1}.
[c]From T. B. McMahon and P. Kebarle (12); see reactions [13] and [14], this work.

each of the hydrogen halides as well as $\Delta H_f^0(CH_3XH^+)$ values. These latter quantities may then be used to calculate proton affinities of the methyl halides according to eq. [12], derived from the mechanism outlined in Scheme 1, where $X^-A(CH_3^+)$ represents the appropriate halide ion affinity of methyl cation.

[12] $PA(CH_3X) = MCA(HX) + PA(X^-) - X^-A(CH_3^+)$

The MCA(HX), $\Delta H_f^0(CH_3XH^+)$, and $PA(CH_3X)$ values thus obtained are also given in Table 2.

Due to difficulties in handling HF in the glass vacuum system of the hpms no experiments involving CH_3^+ transfer to HF were attempted. Based on the approximate proton affinity of CH_3F of 148 ± 2 kcal mol^{-1} (12) a value for MCA(HF) of 35 ± 2 kcal mol^{-1} is arrived at, substantially below that of N_2. This means that the MCA(HF) could not have been determined quantitatively, relative to N_2, in any case, owing to the large difference in methyl cation affinity between them. The proton affinity of CH_3F is evaluated as 148 ± 2 kcal mol^{-1}, based on the observation of reactions [13] and [14] and the recently determined values of PA(CO) = 145.6 kcal mol^{-1} and $PA(SO_2F_2)$ = 150 kcal mol^{-1} (12).

[13] $HCO^+ + CH_3F \rightarrow CH_3FH^+ + CO$

[14] $CH_3FH^+ + SO_2F_2 \rightarrow SO_2F_2H^+ + CH_3F$

Methyl cation transfer experiments with HI proceeded very slowly and equilibrium was not reached. However, the proton affinity of methyl iodide could be evaluated as 171 kcal mol^{-1}, based on the observation of reaction [15] in both forward and

[15] $H_3S^+ + CH_3I \leftrightharpoons CH_3IH^+ + H_2S$

reverse directions, with the conclusion that $PA(CH_3I) \simeq PA(H_2S)$ (7) and the known value of $PA(H_2S)$ = 169.7 kcal mol^{-1} (22). This proton affinity of CH_3I leads to a calculated methyl cation affinity for HI of 69.6 kcal mol^{-1}.

Discussion

The proton affinities of the hydrogen halides obtained in the present work are consistent with, and in basically good agreement with, previous data. The bracketing technique used by Polley and Munson (4) gave approximate values (±2 kcal mol^{-1}), which were also subject to some changes based on revisions in data for reference species used. For example, the proton affinity of HCl was bracketed as 135 ± 2 kcal mol^{-1}, based on PA(Br) < PA(HCl) < $PA(N_2O)$. In light of the recently redetermined value of $PA(N_2O)$ = 142.0 kcal mol^{-1} (12) and the established value of PA(Br) = 133 kcal mol^{-1} (22), the proton affinity of HCl based on Munson's experiment becomes 137.5 ± 4.5 kcal mol^{-1}. However, it was also observed that PA(HCl) > $PA(CH_4)$ and the value of $PA(CH_4)$ has again been recently redefined as 134.7 kcal mol^{-1} (12). Thus the bracketing experiments now define PA(HCl) as 138.5 ± 3.5 kcal mol^{-1}, which is entirely consistent with the value determined here of 137.6 kcal mol^{-1}.

Munson's bracketing data for HBr established $PA(N_2O)$ < PA(HBr) < PA(CO) with the new value of PA(CO) of 145.6 kcal mol^{-1} (12) and $PA(N_2O)$ of 142.0 kcal mol^{-1}, and defines PA(HBr) = 143.8 ± 1.8 kcal mol^{-1}, in agreement with the present determination of 142.9 kcal mol^{-1}.

The bracketing data for HI establish PA(HI) > PA(I) = 145.4 kcal mol^{-1}. The upper limit for PA(HI) was based on the observation of the dissociative hydride abstraction reaction, eq. [16]. It had been assumed that, in order for this reaction to

[16] $H_2I^+ + C_3H_8 \rightarrow s\text{-}C_3H_7^+ + H_2 + HI$

proceed, ΔH_{16}^0 must be negative; however, in reality the requirement for observation of this reaction is that ΔG_{16}^0 be negative. The entropy change for eq. [16] may be estimated fairly accurately as 20 cal mol^{-1} K^{-1}, which yields the enthalpy requirement that $\Delta H_{16}^0 \leq 6$ kcal mol^{-1}. Using recent data for $\Delta H_f^0(s\text{-}C_3H_7^+)$, the upper limit PA(HI) ≤ 156 kcal mol^{-1} is obtained, which allows assignment of PA(HI) = 151 ± 5 kcal mol^{-1}, again in agreement with the present determination of 150.9 kcal mol^{-1}.

The molecular beam photoionization data of Lee and coworkers (5, 6) potentially provide absolute values for the proton affinites of HF, HCl, and HBr based on threshold determinations for eq. [17]. These photo-ionization appearance

[17] $(HX)_2 \xrightarrow{h\nu} H_2X^+ + X$

potential measurements yield: PA(HF) = 95.5 ± 1.4 kcal mol^{-1}, PA(HCl) = 135 ± 1 kcal mol^{-1}, and PA(HBr) = 141 ± 1 kcal mol^{-1}. Previous similar studies for proton affinities of H_2O (6), H_2S (23), and NH_3 (24) have obtained agreement within ±1 kcal mol^{-1} of values arrived at by equilibrium proton transfer scales. It is immediately apparent, however, that the data for HF are in serious disagreement with the observations of proton transfer equilibrium between N_2 and HF, eq. [1], yielding PA(HF) = 120.9 kcal mol^{-1} (3). Lee and coworkers (5) have interpreted this discrepancy in terms of a non-adiabatic transition from $(HF)_2$ to $(HF)_2^+$ in which vibrationally excited $(HF)_2^+$ is produced well above the threshold for H_2F^+ formation. From an analysis of the shapes of the H_2Cl^+ and H_2Br^+ ionization efficiency curves near threshold, the authors concluded that these species are more likely to be produced in their ground states. The difference between proton affinity values for HCl and HBr determined here and in the photoionization experiment is 2.7 and 1.7 kcal mol^{-1}, with the present values both being higher. This difference could be caused by residual excitation of some 2 kcal mol^{-1} in H_2Cl^+ and H_2Br^+ produced at the observed threshold, presumably because the cross-section for production of H_2X^+ at the true adiabatic

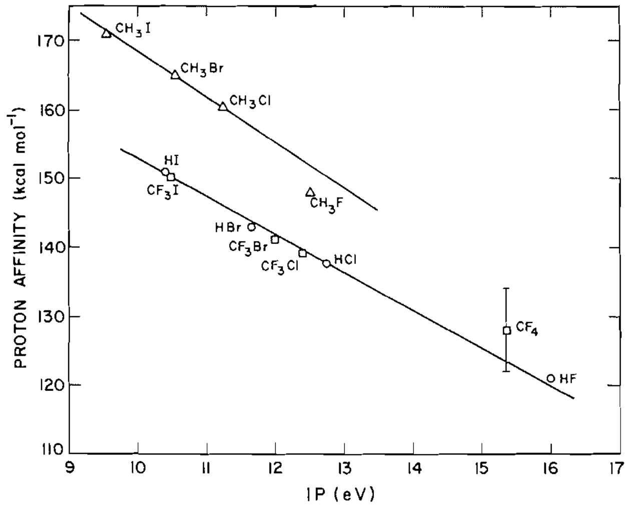

FIG. 3. Variation of proton affinities of HX, CH_3X, and CF_3X (X = F, Cl, Br, I) as a function of valence ionization potential.

limit has become sufficiently small to be beyond the detection limits of the apparatus.

Only approximate data for proton affinities of the methyl halides are available from bracketing experiments. As noted above, reactions [13] and [14] establish PA(CH_3F) as 148 ± 2 kcal mol^{-1}. Similarly, the proton affinity of CH_3Cl has previously been established (7) to be between those of C_2H_4 (162.6 kcal mol^{-1}) (9–11) and C_2H_2 (155.2 kcal mol^{-1}) (22), allowing an assignment of 159 ± 4 kcal mol^{-1}, in good agreement wih the value of 160.8 kcal mol^{-1} obtained here. The proton affinity of CH_3Br has again previously been determined to be between those of C_2H_4 and H_2O (166.4 kcal mol^{-1}) (12, 22), allowing an assignment of 164.5 ± 2 kcal mol^{-1}, again in good agreement with the value of 164.8 kcal mol^{-1} obtained here. As noted above, the proton affinity of CH_3I has been approximately determined as 171 ± 1 kcal mol^{-1} (7), based on observations of eq. [15].

No previous proton affinity measurements of any kind have been carried out for CF_3Cl, CF_3Br, or CF_3I. Bohme and coworkers (17) have bracketed the proton affinity of CF_4 by

[18] $N_2H^+ + CF_4 \rightarrow CF_4H^+ + N_2$

[19] $CF_4H^+ + CH_4 \rightarrow CH_5^+ + CF_4$

eqs. [18] and [19], allowing an assignment of PA(CF_4) = 128 ± 6 kcal mol^{-1}.

In addition to the absolute magnitudes of the proton affinities of the hydrogen, methyl, and trifluoromethyl halides, it is of interest to examine the relative changes within each group of halides, the relationships between each group, and the relationship between proton affinities and valence ionization potentials. This last relationship is illustrated in Fig. 3 in a plot of proton affinities of each of the types of halide as a function of the valence electron ionization potentials determined by either photoionization mass spectrometry or photoelectron spectroscopy. Examination of this plot reveals that there is a direct correspondence between proton affinity and ionization potential, which indicates that the factors affecting both the energy required to remove an electron from the highest occupied molecular orbital and the energy released when a proton is associated with the electrons in the highest occupied molecular orbital are similar in nature but different in magnitude. Interestingly, the points for both HX and CF_3X compounds appear to fit the

$$\begin{tikzcd} RX + H \arrow[r, "IP(H)"] \arrow[d, "IP(RX)"'] & RX + H^+ \arrow[d, "-PA(RX)"] \\ RX^+ + H \arrow[r, "-HA(RX^+)"'] & RXH^+ \end{tikzcd}$$

SCHEME 2

same line. The good proportionality between the two quantities suggests that more reliable data may be interpolated from the plot. For example, the PA(CF_4) of 128 ± 6 kcal mol^{-1} can be inferred to be at the lower end of this limit if it is assumed that CF_4 should fall on the correlation line for CF_3X compounds. If this is the case a PA(CF_4) of 123.5 kcal mol^{-1} is predicted.

The one important exception to the proton affinity – ionization potential correlation is the point for methyl fluoride. An examination of the photoelectron spectrum and molecular orbital assignments for CH_3F (24) reveals that the lowest energy ionization process does not correspond to removal of a 2p non-bonding electron, as is the case for the other CH_3X, but rather involves removal of an electron from the orbital that has primarily C—H bonding character in the methyl group. The proton affinity of CH_3F does not fall on the straight line defined by the other CH_3X for either of these ionization potentials of CH_3F. This failure to correlate with behaviour of the other methyl halides suggests that CH_3FH^+ may be structurally unlike the other CH_3XH^+ ions and may, in fact, more closely resemble CH_5^+ involving 3-centre 2-electron bond structures such as **I** or **II**.

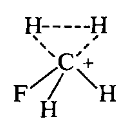

I

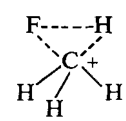

II

The accurate ionization potential and proton affinity data may also be used to calculate the homolytic bond dissociation energies of RXH^+, also called the hydrogen atom affinities (HA) of RX^+. The relationship between proton affinity, ionization potential, and hydrogen atom affinity given by eq. [20] may be derived from examination of Scheme 2. Hydrogen atom affinities, proton affinities, and ionization potential data for

[20] $HA(RX^+) = PA(RX) + IP(RX) - IP(H)$

each of the compounds examined are summarized in Table 3. Also included for comparison are the homolytic bond dissociation energies in the hydrogen halides. The D(H—X) follow the same trend as the D(H—XH^+) with the difference that the hydrogen atom affinities are all somewhat larger. This difference in magnitude should be due to the electrostatic attractive interaction between HX^+ and H, which contributes to the bond energy in H—XH^+. The value for HA(CH_3F^+) can be seen to be anomalously low compared to the relative values for HA, CH_3X, and CF_3X compounds in the other halogen series. This is again associated with the fact that the lowest energy ionization in CH_3F, and used in the calculation of HA(CH_3F^+), does not correspond to the lone pair electron of the F atom (25). This result again suggests that the bonding in CH_3FH^+ may be unusual.

It is interesting to note the order of hydrogen atom affinities for each group of halogens. In the fluorides a variation of 15

TABLE 3. Ionization potentials, proton affinities, and halogen atom affinities for the hydrogen, methyl, and trifluoromethyl halides

Species (RX)	IP(RX)[a] (eV)	PA(RX)[d] (kcal mol^{-1})	HA(RX$^+$) (kcal mol^{-1})	D(H—X)[e] (kcal mol^{-1})
HF	15.98[b]	120.9	178	136
CH_3F	12.50	148 ± 2	123	
CF_4	15.35[c]			
HCl	12.72	137.6	117	103
CH_3Cl	11.22	160.8	106	
CF_3Cl	12.39	139.0	111	
HBr	11.65	142.9	98	88
CH_3Br	10.54	164.8	94	
CF_3Br	12.0	141.3	104	
HI	10.39	150.9	77	71
CH_3I	9.54	171 ± 1	77	
CF_3I	10.45	150.4	78	

[a] Unless otherwise noted all values are taken from ref. 2.
[b] Reference 26.
[c] Reference 25.
[d] Data from ref. 12.
[e] Calculated from data from ref. 20.

kcal mol^{-1} is observed between HA(HF$^+$) and HA(CF_4^+), while for the corresponding chlorides the difference is only 6 kcal mol^{-1}; for the bromides the order actually inverts, with HA(CF_3Br^+) being larger than HA(HBr$^+$) by 6 kcal mol^{-1}, while in the iodides virtually no variation is observed. The inversion of order in the bromides and to a lesser extent the iodides can be seen, from eq. [20] and the data in Table 3, to result from the fact that IP(CF_3Br) > IP(HBr) and IP(CF_3I) > IP(HI). This may be purely a result of poor resolution in the photoelectron spectra of CF_3Br and CF_3I since only vertical rather than adiabatic ionization potentials are reported.

The magnitude of substituent effects of CH_3 and CF_3 on the proton affinities of halogen bases may be seen from the correlations shown in Fig. 4. The plot of PA(CH_3X) vs. PA(HX) gives a linear relationship with a slope of 0.74, indicating that the magnitude of the methyl substituent effect decreases in a manner proportional to the increase in basicity of the halogen, i.e. in the order X = F > Cl > Br > I. For example, replacement of hydrogen by methyl increases the basicity of F by 28 kcal mol^{-1} while only increasing that of I by 20 kcal mol^{-1}. The fact that the point for HF/CH_3F fits on the correlation line is noteworthy since it had been suggested above that the bonding in CH_3FH^+ might be fundamentally different than than in the other CH_3XH^+ species. The data of Fig. 4(a) would suggest otherwise. Evidently, the question regarding the structure of CH_3FH^+ can not be resolved on the basis of the experimental correlations considered in the present work.

The higher PA of the CH_3X relative to the HX compounds probably are largely due to stabilization of the positive charge in the CH_3XH^+ by the field effect and polarizability of the methyl group. The decreasing methyl stabilization energy with increasing size of X is then a consequence of the lengthening of the C—X bond and the resulting greater distance over which the methyl dipole and polarizability have to interact with the charge centre. The plot of PA(CF_3X) vs. PA(HX) again exhibits a good linear correlation with the exception of the point for CF_3Br. As noted above, the value for HA(CF_3Br^+) appeared anomalously high, while here the proton affinity of CF_3Br appears too low. For the present, CF_3Br must be regarded as an exceptional case.

TABLE 4. Methyl and trifluoromethyl cation affinities of the hydrogen halides

Species (HX)	D(CH_3^+—XH) (kcal mol^{-1})	D(CF_3^+—XH) (kcal mol^{-1})
HF	35 ± 2	15
HCl	55.1	19.8
HBr	61.2	21.3
HI	69.6	31.1

In all of the halogens the hydrogen halides and trifluoromethyl halides have similar basicities, indicating that the destabilizing field effect of the CF_3 group is almost exactly counterbalanced by the stabilizing through space polarization interaction of the CF_3 group.

It is also interesting to compare the methyl cation binding energies of the halogen acids to the proton affinities as shown in Fig. 4c. A good linear relationship between the two quantities is observed. The slope of 1.12 obtained indicates that methyl cation binding energies increase through the halogen series more rapidly than do proton affinities.

The proton affinity data for trifluoromethyl halides can also be used to calculate CF_3^+ binding energies for the hydrogen halides. These data are summarized in Table 4 together with the CH_3^+ binding energies. The plot of the CF_3^+ affinities of HX versus the corresponding CH_3^+ affinities, shown in Fig. 5, leads to a linear relationship with the exception of the point for HI.[3] This linear relationship, taken together with the relationship in Fig. 4c, demonstrates that the halogen acids, HX, display the same order of basicities twoards the three Lewis acids, H$^+$, CH_3^+, and CF_3^+.

[3] The deviation of the point for HI from the straight line correlation may in fact be due to a poorly defined value of D(CF_3^+—IH), arising from an uncertain value for $\Delta H_f^0(CF_3I)$.

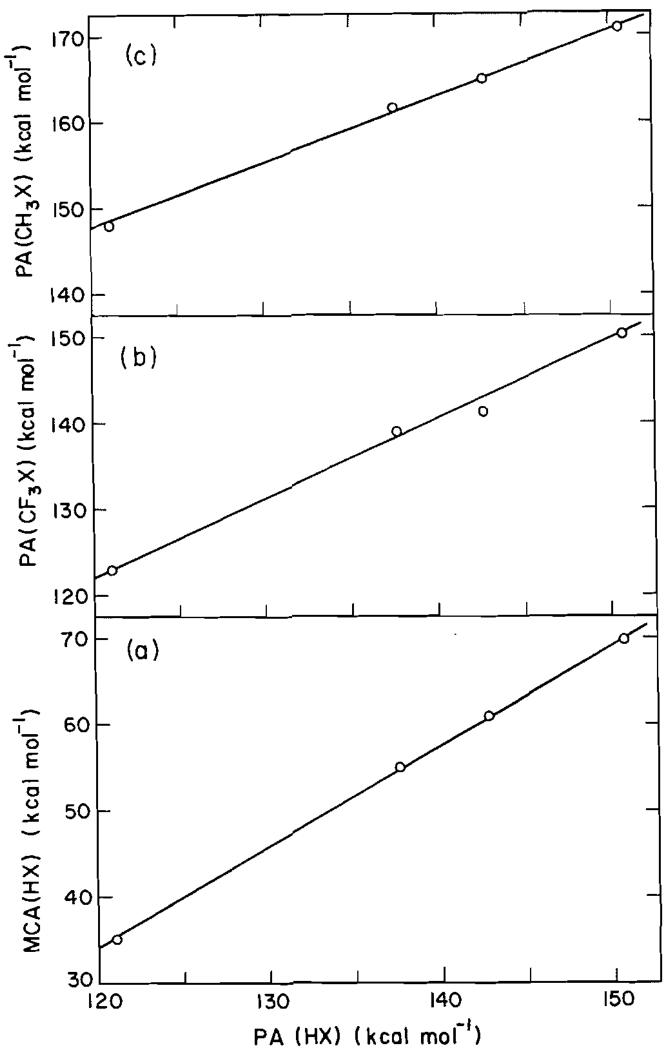

FIG. 4. Variation of (a) methyl cation affinity of HX (MCA(HX)); (b) proton affinity of CF_3X (PA(CF_3X)); (c) proton affinity of CH_3X (PA(CH_3X)) as a function of proton affinity of HX (PA(HX)); X = F, Cl, Br, I.

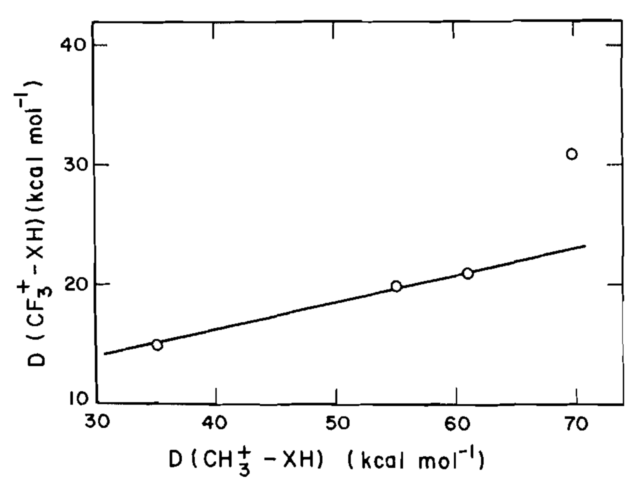

FIG. 5. Variation of CF_3^+ binding energy to HX (D(CF_3^+—XH)) as a function of CH_3^+ binding energy to HX (MCA(HX)).

The CH_3^+ affinities of HX are seen to be considerably larger than the corresponding CF_3^+ affinities (see Table 4 and Fig. 5). It is generally observed (27) that the R^+ affinities of HX, where R^+ are substituted methyl cations, decrease with increasing electronic stabilization of R^+. The present result taken in this context must mean that the CF_3^+ cation is more stable relative to CH_3^+, i.e. that stabilization by π donation from the F substituent is more important than the destabilization by the electron-withdrawing field-inductive effect of F.

Conclusion

Proton transfer and methyl cation transfer equilibrium experiments have been used to establish accurate gas phase proton affinities for hydrogen, methyl, and trifluoromethyl halides. The gas phase basicities of each series of halides are seen to correlate with valence ionization potentials and with each other. Further, the methyl cation affinities of HX correlated with the proton affinities, as do the CF_3^+ binding energies.

1. (*a*) D. H. AUE and M. T. BOWERS. *In* Gas phase ion chemistry. Vol. 2. *Edited by* M. T. Bowers. Academic Press, New York, NY. 1979; (*b*) R. WALDER and J. L. FRANKLIN. Int. J. Mass Spectrom. Ion Phys. **36**, 85 (1980); (*c*) R. W. TAFT. Prog. Phys. Org. Chem. **14**, 248 (1983); (*d*) J. I. BRAUMANN. Annu. Rev. Phys. Chem. **34**, 187 (1983).
2. R. D. LEVIN and S. G. LIAS. Ionization and appearance potential measurements, 1971–1981. NSRDS–NBS71. 1982.
3. M. S. FOSTER and J. L. BEAUCHAMP. Inorg. Chem. **14**, 1229 (1975).
4. C. W. POLLEY and M. S. B. MUNSON. Int. J. Mass Spectrom. Ion Phys. **28**, 49 (1978).
5. P. W. TIEDEMANN, S. L. ANDERSON, S. T. CEYER, T. HIROOKA, C. Y. NG, B. H. MAHAN, and Y. T. LEE. J. Chem. Phys. **71**, 1605 (1979).
6. C. Y. NG, D. J. TREVOR, P. W. TIEDEMANN, S. T. CEYER, P. L. KRONEBUSCH, B. H. MAHAN, and Y. T. LEE. J. Chem. Phys. **67**, 4235 (1977).
7. J. L. BEAUCHAMP, D. HOLTZ, S. D. WOODGATE, and S. L. PATT. J. Am. Chem. Soc. **94**, 2798 (1972).
8. G. H. F. DIERCKSEN, W. VON NIESSEN, and W. P. KRAEMER. Theor. Chim. Acta, **31**, 205 (1973).
9. S. F. SMITH, J. CHANDRASEKHAR, and W. L. JORGENSEN. J. Phys. Chem. **86**, 3308 (1982).
10. J. E. DEL BENE, H. D. METLEE, M. J. FRISCH, B. T. LUKE, and J. A. POPLE. J. Phys. Chem. **87**, 3279 (1983).
11. J. E. DEL BENE, M. J. FRISCH, K. RAGHAVACHARI, and J. A. POPLE. J. Phys. Chem. **86**, 1529 (1982).
12. T. B. MCMAHON and P. KEBARLE. J. Am. Chem. Soc. Submitted.
13. R. G. MCLOUGHLIN and J. C. TRAEGER. J. Am. Chem. Soc. **101**, 5791 (1979).
14. T. BAER. J. Am. Chem. Soc. **102**, 2482 (1980).
15. H. M. ROSENSTOCK, R. BUFF, M. A. A. FERREIRA, S. G. LIAS, A. C. PARR, R. L. STOCKBAUER, and J. L. HOLMES. J. Am. Chem. Soc. **104**, 2337 (1982).
16. T. B. MCMAHON, G. NICOL, T. HEINIS, and P. KEBARLE. To be published.
17. A. E. ROCHE, M. M. SUTTON, D. K. BOHME, and H. I. SCHIFF. J. Chem. Phys. **55**, 5480 (1971).
18. A. J. CUNNINGHAM, J. D. PAYZANT, and P. KEBARLE. J. Am. Chem. Soc. **94**, 7627 (1972).
19. M. S. FOSTER, A. D. WILLIAMSON, and J. L. BEAUCHAMP. Int. J. Mass Spectrom. Ion Phys. **15**, 429 (1974).
20. S. W. BENSON. Thermochemical kinetics. 2nd ed. J. Wiley, New York, NY. 1968.
21. D. K. BOHME, G. I. MACKAY, and H. I. SCHIFF. J. Chem. Phys. **73**, 4976 (1980).
22. S. G. LIAS, J. F. LIEBMAN, and R. D. LEVIN. J. Phys. Chem. Ref. Data. To be published.
23. H. F. PREST, W.-B. TZENG, J. M. BROM, JR., C. Y. NG. J. Am.

Chem. Soc. **105**, 7531 (1983).
24. S. T. CEYER, P. W. TIEDEMANN, B. H. MAHAN, and Y. T. LEE. J. Chem. Phys. **70**, 14 (1979).
25. C. R. BRUNDLE, M. B. ROBIN, and H. BASCH. J. Chem. Phys. **53**, 2196 (1970).
26. J. BERKOWITZ, W. A. CHUPKA, P. M. GUYON, J. H. HOLLOWAY, and R. SPOHR. J. Chem. Phys. **54**, 5165 (1971).
27. D. K. SEN SHARMA, S. MEZA DE HÖJER, and P. KEBARLE. J. Am. Chem. Soc. To be published; D. K. SEN SHARMA and P. KEBARLE. J. Am. Chem. Soc. **100**, 5826 (1978); S. P. MCMANUS. J. Org. Chem. **47**, 3070 (1982).

Isomérisation des radicaux insaturés. III. Radicaux α,α,β-, α,β,γ- et α,α,γ-triméthallyles

HÉLÈNE DESLAURIERS ET GUY J. COLLIN[1]

Département des sciences fondamentales, Université du Québec à Chicoutimi, Chicoutimi (Qué.), Canada G7H 2B1

Reçu le 21 décembre 1984

HÉLÈNE DESLAURIERS et GUY J. COLLIN. Can. J. Chem. **63**, 3168 (1985).

Nous avons généré les radicaux α,α,β-, α,β,γ- et α,α,γ-triméthallyles en photolysant à 147,0 nm les triméthyl-2,3,3 butène-1, diméthyl-3,4 pentène-2 et diméthyl-2,4 pentène-2 sous des pressions de quelques torr. Dans ces conditions, une part importante de ces radicaux ont une énergie interne suffisante pour se fragmenter en divers diènes-1,3 et un peu de diènes-1,2 et -2,3. Afin d'expliquer la formation de ces produits, on fait appel à un mécanisme d'isomérisation basé sur un transfert interne 1,4 d'un atome d'hydrogène. La fragmentation des radicaux allyles triméthylés se fait surtout par rupture d'un lien β(C—C), puis β(C—H) et, de façon beaucoup moindre, par celle d'un lien central C—CH_3.

HÉLÈNE DESLAURIERS and GUY J. COLLIN. Can. J. Chem. **63**, 3168 (1985).

α,α,β-, α,β,γ-, and α,α,γ-trimethallyl radicals have been generated in the 147.0-nm gas phase photolysis of 2,3,3-trimethyl-1-butene, 3,4-dimethyl-2-pentene, and 2,4-dimethyl-2-pentene, respectively. Under these conditions, the majority of allyl radicals have an internal energy sufficient for further decomposition: they give rise to the formation of various 1,3-dienes and small amounts of either 1,2- or 2,3-dienes. An internal sigmatropic 1,4-hydrogen atom transfer process is part of the proposed mechanism to explain such products. Moreover, the fragmentation of the trimethyl substituted allyl radicals involves the split of one β(C—C) bond, then one β(C—H), and, to a lesser extent, one central C—CH_3 bond.

Introduction

Dans de précédentes études, nous avons montré que la photolyse des alcènes entre 147,0 et 184,9 nm constitue une bonne source de radicaux allyles, puisque ceux-ci sont formés avec des rendements quantiques qui dépassent 0,5 et qui atteignent parfois 0,9 (1, 2). Ces radicaux sont cependant produits avec une énergie vibrationnelle relativement importante, de telle sorte que ces radicaux "chauds" se fragmentent pourvu que la pression soit suffisamment faible pour ne pas les stabiliser par collision (3, 4). Les précédents rapports de cette série ont de plus montré que ces réactions de fragmentation sont en compétition avec des réactions d'isomérisation. Par exemple, le radical α,β-diméthallyle s'isomérise vers la forme α,α-diméthallyle et inversement (5). Il en est de même du radical α,γ-diméthallyle qui s'isomérise vers la forme α-éthallyle et inversement (6).

Le but de ce rapport est de vérifier ces comportements sur les trois radicaux triméthallyles en scrutant leurs produits de fragmentation.

Méthode expérimentale

Les triméthyl-2,3,3 butène-1 (tM233B1), diméthyl-3,4 *cis*-pentène-2 (dM34P2) et diméthyl-2,4 pentène-2 (dM24P2) sont des produits API. Les puretés affichées de même que les analyses de ces monomères sont brièvement indiquées dans le tableau 1. L'oxygène (99,98%) et l'isobutène (99,9%) sont des produits Matheson du Canada (gaz de qualité recherche). Tous ces produits sont utilisés tels que reçus et manipulés à l'aide d'une rampe à vide en Pyrex (1–6).

Les photolyses sont effectuées à 147,0 nm en utilisant une lampe de résonance à xénon entraînée par un générateur micro-onde (7). La pureté spectrale de la lampe entre 120 et 250 nm est vérifiée à l'aide d'un monochromateur McPherson de $\frac{1}{2}$ m. L'actinométrie est réalisée en comparant les produits de décomposition à ceux obtenus dans la photolyse de l'isobutène Φ(allène) = 0,52 (8). Toutes les irradiations ont été faites à la température de la chambre ($T \simeq 20$°C). Les analyses sont faites par chromatographie en phase gazeuse en utilisant soit une colonne de squalane (9), soit une colonne de UCON (10) à la température de 50°C.

[1] Auteur à qui adresser la correspondance.

TABLEAU 1. Analyse des monomères

Monomère	Impureté affichée (%)	Impuretés visibles par chromatographie (ppm)
Isobutène	0,1	Isobutane: 920±50 Propane: 60±10
tM233B1	0,06±0,04	Diméthyl-3,3 butène-1: 15
dM34P2(*cis*)	0,11±0,08	Éthyl-2 méthyl-3 butène-1: 400±5
dM24P2	0,14±0,04	dM34P2 (*trans*): 650 Triméthyl-1,3,4 pentène-2 (?): 50

Résultats

Le tableau 2 montre les rendements quantiques des produits obtenus dans les photolyses des tM233B1, dM34P2 et dM24P2 en présence de 10% d'oxygène. On observe une formation de C_3 avec des rendements quantiques non négligeables. Par exemple, le rendement en C_3H_4 est 0,20 dans la photolyse du tM233B1. Par contre, les rendements en produits C_4 sont faibles et n'apparaissent que dans la photolyse du dM34P2. Les diènes-1,3 sont les produits majeurs dans chacun des cas. Le diméthyl-2,3 butadiène-1,3 est le produit majeur dans la photolyse du tM233B1. Dans le cas du dM34P2, l'isoprène et le méthyl-3 pentadiène-1,3 ont des rendements similaires et importants. Finalement, le dM24P2 donne lieu à la formation de méthyl-4 pentadiène-1,3, d'isoprène et de méthyl-2 pentadiène-1,3. L'effet de pression a été étudié dans le cas du mélange tM233B1–O_2 (100:10). On observe que les rendements en diméthyl-2,3 butadiène-1,3 (A) et en méthyl-3 butadiène-1,2 (B) décroissent avec l'augmentation de la pression et que $\Phi(A)/\Phi(B) = 7{,}5$ ($\sigma = 0{,}65$), quelle que soit la pression de monomère entre 2 et 50 Torr (1 Torr = 133,3 Pa). Cet effet de pression est rapporté dans la figure 1 sous la forme de courbes de type Stern–Volmer: $[\Phi(x)]^{-1} = f(P)$.

À ce point, il faut noter que les résultats semblent indiquer une certaine invariance des rendements entre 5 et 10 Torr, tout

TABLEAU 2. Photolyse d'alcènes en présence de 10% d'oxygène à 147,0 nm. Rendements quantiques des monomères

Alcène	Rendement					
	tM233B1		dM34P2		dM24P2	
	5 Torr	10 Torr	5 Torr	10 Torr	5 Torr	10 Torr
Propène	0,04	0,04	0,07	0,05	0,08	$0,05_5$
Propyne	0,15	0,15	0,07	0,08	0,04	0,03
Allène	$0,04_5$	0,05	—	—	—	—
Butadiène-1,2	—	—	$0,01_3$	0,01	—	—
Butyne-2	—	—	$0,02_5$	$0,02_5$	0,01	$0,00_7$
Méthyl-3 butadiène-1,2	0,04	$0,04_5$	—	—	—	—
Diméthyl-2,3 butadiène-1,3	$0,29_6$	0,31	—	—	—	—
Isoprène	—	—	0,26	0,20	0,18	0,09
Pentadiène-1,2 + 1,3 (*cis*)	—	—	—	—	0,03	$0,01_5$
Pentadiène-2,3	—	—	$0,03_5$	0,03	—	—
Pentadiène-1,3[a] (*trans*)	—	—	—	—	0,04	0,02
Éthyl-2 butadiène-1,3	—	—	0,02	$0,01_8$	—	—
Méthyl-3 pentadiène-1,3[b]	—	—	0,27	$0,21_6$	—	—
Méthyl-2 pentadiène-1,3[b]	—	—	—	—	0,27	0,16
Méthyl-4 pentadiène-1,3	—	—	—	—	0,12	0,06
Diméthyl-2,4 pentadiène-1,3	—	—	—	—	$0,02_5$	n.m.[c]

[a] *Trans/cis* = 1,5 ± 0,2.
[b] *Trans/cis* = 1,9 ± 0,2.
[c] n.m., non mesuré.

TABLEAU 3. Rendements quantiques observés dans la photolyse de trois heptènes ramifiés, purs, à 147 nm[a]

Produit	tM233B1[b]	dM34P2 (*cis*)	dM24P2
Méthane	n.m.	0,17	0,16
Éthane	0,29	0,51	0,46
Isobutane	0,04	0,06	0,04
Néopentane	0,04	—	—
Méthyl-2 butène-1	—	—	0,04
Diméthyl-2,3 pentène-2	0,14	—	—
Diméthyl-3,4 pentène-2 (*trans*)	—	0,11	—
Diméthyl-3,3 pentène-1	—	0,01	—
Éthyl-2 méthyl-3 butène-1	—	0,09	—
Diméthyl-4,4 pentène-2 (*trans*)	—	—	$0,01_5$
Méthyl-3 hexène-3 (*trans*) + triméthyl-2,2,4 pentane	—	—	0,11
Triméthyl-2,3,4 pentane	—	0,10	0,03
Triméthyl-2,2,3 pentane	0,02	—	—
Tétraméthyl-2,2,3,3 butane	0,07	—	—

[a] Pression de l'alcène: 5 Torr (665 N m^{-2}).
[b] 200 Torr de SF_6 ont été ajoutés.

au moins en ce qui concerne ceux obtenus dans les cas des tM233B1 et dM34P2. Précisons que sur une grande échelle de pression, il y a plutôt décroissance lente des rendements avec l'augmentation de la pression (fig. 1). Dans le cas du dM24P2, il semble au contraire y avoir une augmentation des rendements des produits avec l'augmentation de la pression (tableau 2, colonnes 6 et 7). Comme nous n'avons pas essayé d'étendre ces mesures sur une plus grande échelle de pression, et compte tenu des incertitudes expérimentales appréhendées (voir, par exemple, la distribution des résultats rapportés sur la figure 1), il semble prématuré de discuter plus à fond cette apparente augmentation des rendements.

Les dM34P2 et dM24P2 ont été photolysés sans aucun additif (tableau 3). On y a observé l'apparition d'un certain nombre de produits. L'éthane ($\Phi \simeq 0,5$) est le produit majeur. D'autres produits tels que l'isobutane, des heptanes, des heptènes et des octanes (tous ramifiés) sont aussi formés, alors qu'ils n'apparaissent pas dans les photolyses réalisées en présence d'oxygène.

Ces produits (sauf le méthane) sont formés par réactions de combinaison entre les radicaux méthyles et des radicaux allyliques C_7H_{11} ou saturés C_7H_{13}. On ne rediscutera pas plus loin de ces résultats. Il suffit ici de rappeler que ces produits (et leur mode de formation anticipée) appuient les schémas réactionnels proposés plus loin.

Discussion

Fragmentation des molécules photo-excitées

Il est maintenant bien établi que les alcènes photo-excités, électroniquement excités dans un état singulet, retournent vers

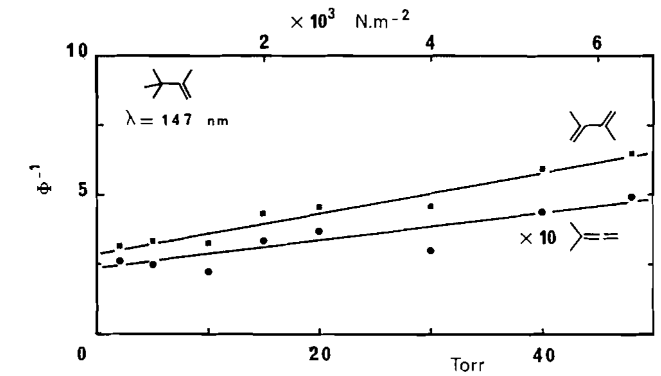

FIG. 1. Photolyse du mélange tM233B1–O_2 (100:10) à 147 nm, en fonction de la pression de l'alcène; ■: Φ(diméthyl-2,3 butadiène-1,3)$^{-1}$ (y = 2,91 + 0,072 P (Torr), r^2 = 0,97); ●: Φ(méthyl-3 butadiène-1,2)$^{-1}$.

leur état fondamental en transformant leur énergie électronique en énergie vibrationnelle, de sorte que la fragmentation observée est essentiellement le fait de la molécule vibrationnellement très chaude. Dans ces conditions, et en première approximation, la fragmentation implique la rupture du (des) lien(s) le(s) plus fragile(s). Les molécules photolysées à 147,0 nm ont toutes une liaison C—C située en position β par rapport à la double liaison. Comme ce sont des liens relativement fragiles (11–13), on ne peut que s'attendre à une scission primaire β(C—C) importante (1, 14).

[1] $CH_2{=}C(CH_3)C(CH_3)_3^{**} \rightarrow CH_3 + \overline{CH_2C(CH_3)C}(CH_3)_2^*$

[2] $CH_3CH{=}C(CH_3)CH(CH_3)_2 \rightarrow CH_3 + CH_3\overline{CHC(CH_3)CH}CH_3^*$

[3] $CH_3C(CH_3){=}CHCH(CH_3)_2 \rightarrow CH_3 + CH_3\overline{C(CH_3)CHCH}CH_3^*$

où le double astérisque dénote la molécule photo-excitée et l'astérisque simple, un radical allyle chaud. En effet, l'énergie du photon est de quelque 811 kJ einstein^{-1} auxquels il faut ajouter l'énergie thermique de la molécule à la température de la chambre, soit environ 12 kJ mol^{-1}. L'énergie du lien β(C—C) est de quelque 293 kJ mol^{-1} (11–13). L'excédent d'énergie du photon (≃530 kJ mol^{-1}) est distribué entre les tissus vibrationnels des deux fragments et leur énergie relative cinétique et rotationnelle (2–4).

D'autres réactions de fragmentation sont également possibles mais avec une probabilité beaucoup plus faible, puisque les chaleurs de liaison sont plus élevées. Des ruptures β(C—H_t) (cas des dMP2), α(C—C) et α(C—H) sont disponibles. La chaleur de liaison β(C—H_t) est d'environ 30 kJ mol^{-1} plus élevée que celle du lien β(C—C) (15). Les produits issus des fragmentations des radicaux allyles $C_7H_{13}^*$ (des C_7H_{12} et des C_6H_{10}) sont sans doute formés avec de faibles rendements et seulement certains d'entre eux peuvent interférer avec les produits mesurés ici.

Les produits en C_3, et probablement en C_4, apparaissant dans le tableau 2, sont certainement le résultat de fragmentation primaire α(C—C), avec des rendements limités. Par exemple, la formation de propyne et d'allène est raisonnablement expliquée sur la base du mécanisme impliquant la rupture primaire d'un lien α(C—C) avec fragmentation subséquente du radical propènyle-2 excité (16).

[4] $CH_3C(CH_3)_2C(CH_3){=}CH_2 \rightarrow t\text{-}C_4H_9 + CH_3\dot{C}{=}CH_2^*$

[5a] $CH_3\dot{C}{=}CH_2^* \rightarrow CH_3C{\equiv}CH + H$

[5b] $CH_3\dot{C}{=}CH_2^* \rightarrow CH_2{=}C{=}CH_2 + H$

De la même manière, le dM34P2 peut former le propyne, le propène et le butyne-2:

[6] $CH_3CH{=}C(CH_3)CH(CH_3)_2^{**} \rightarrow CH_3CH{=}\dot{C}CH_3^* + \text{iso-}C_3H_7^*$

[7] $CH_3CH{=}\dot{C}CH_3^* \rightarrow CH_3C{\equiv}CCH_3 + H$

[8] $\text{iso-}C_3H_7^* \rightarrow CH_3CH{=}CH_2 + H$

[9] $CH_3CH{=}C(CH_3)CH(CH_3)_2 \rightarrow \dot{C}H{=}C(CH_3)CH(CH_3)_2^* + CH_3$

[10] $\dot{C}H{=}C(CH_3)CH(CH_3)_2^* \rightarrow CH_3C{\equiv}CH + \text{iso-}C_3H_7 \ldots$

Compte tenu du fait que (i) le lien β(C—C) est le plus fragile, et (ii) la rupture β(C—H_t) semble moins probable, à tout le moins dans les cas du méthyl-3 butène-1 (17) et du diméthyl-2,3 butène-1 (5), l'intervention des intermédiaires résultant des fragmentations primaires β(C—H_t) peut être ignorée. Une preuve de la fragmentation de la molécule photo-excitée par rupture primaire du lien β(C—C) et de son importance peut être extraite de la lecture des rendements des produits d'origine radicalaire (tableau 3). On peut observer en effet la formation, en quantités appréciables, des radicaux méthyles (Φ ≃ 1,2 ± 0,2) à travers les formations d'éthane (CH_3 + CH_3), d'isobutane (CH_3 + iso-C_3H_7), de triméthyl pentanes (CH_3 + C_7H_{15}), de diméthylpentènes (CH_3 + C_6H_{11}), ... Il faut remarquer qu'un rendement supérieur à l'unité n'est pas anormal puisque, comme on le verra plus tard, à la rupture primaire principale, s'ajoutent des réactions secondaires libérant des radicaux méthyles avec formation concomitante de diènes en C_5. De la même manière, bien que ce soit de façon moins évidente sur le plan quantitatif, les structures des divers heptènes ramifiés formés sont compatibles avec soit le radical allyle formé dans la rupture primaire, soit les radicaux allyles issus de l'isomérisation du précédent par transfert interne d'un atome d'hydrogène entre les positions 1,4.

Radical α,α,β-*triméthallyle*

Formé dans la réaction [1], ce radical excité ne possède que des liaisons β(C—H) et une liaison centrale C—CH_3 susceptibles de se fragmenter.

[11*a*] $\overline{CH_2C(CH_3)C}(CH_3)_2^* \rightarrow H + CH_2{=}C(CH_3)C(CH_3){=}CH_2 \quad \Delta H \simeq 224\ \text{kJ mol}^{-1}$

[11*b*] $\overline{CH_2C(CH_3)C}(CH_3)_2^* \rightarrow CH_3 + CH_2{=}C{=}C(CH_3)_2 \quad \Delta H \simeq 233\ \text{kJ mol}^{-1}$

Les produits attendus sont ceux observés dans un rapport 7,5:1 à l'avantage de la formation du diméthyl-2,3 butadiène-1,3 (Φ = 0,30). Cette fragmentation est en accord avec les observations déjà réalisées dans la photochimie du tétraméthyléthylène – diméthyl-2,3 butène-2 (18). L'isomérisation du radical α,α,β-triméthallyle, par déplacement interne d'un atome d'hydrogène entre les positions 1 et 4, est triviale: elle reproduit le radical original.

Il faut noter que les réactions [11] sont endothermiques. La chaleur de formation du radical α,α,β-triméthallyle a éte mesurée: $\Delta H_f^0 \simeq 40 \pm 4$ kJ mol^{-1} (15). En admettant que l'énergie d'activation de la réaction (11*a*] est ≃5 kJ mol^{-1} (19) et celle de la réaction [11*b*], ≃ 25 kJ mol^{-1}, cela conduit à estimer les

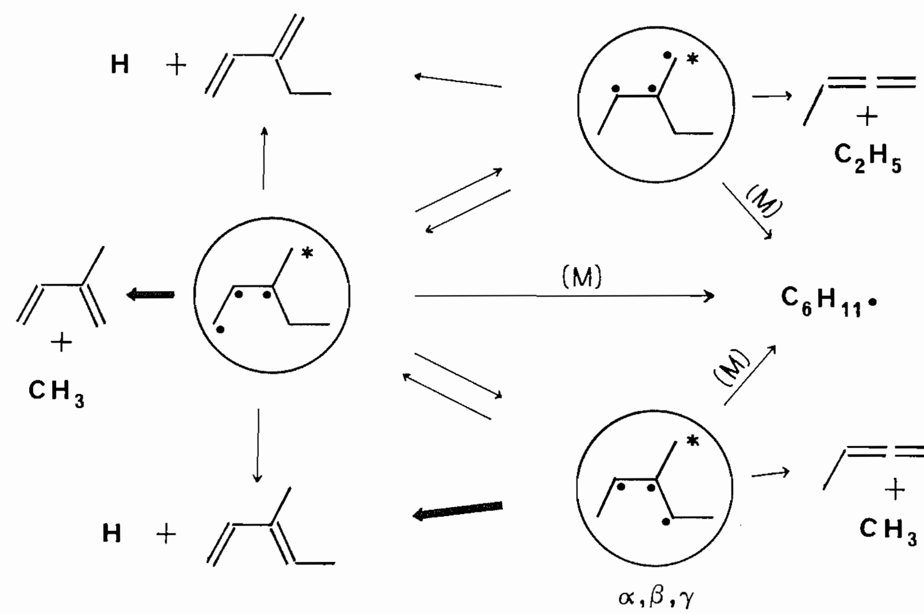

SCHÉMA 1. Évolution du radical α,β,γ-triméthallyle (cercle inférieur droit).

barrières de potentiel des réactions [11*a*] et [11*b*] à quelque 229 et 258 kJ mol^{-1}. Comme la distribution de l'excédent de l'énergie du photon dans les fragments primaires (processus [1]) se fait dans le tissu vibrationnel, il est fort probable qu'une part appréciable des radicaux $C_6H_{11}^*$ n'ont pas l'énergie interne suffisante pour passer par dessus ces barrières de potentiel ou leur vitesse de passage est si lente qu'ils sont stabilisés, refroidis par collision (fig. 1).

Radical α,β,γ-triméthallyle

Ce radical apparaît dans la photolyse du dM34P2: réaction [2]. Les réactions de fragmentation attendues impliquent à nouveau la rupture du lien β(C—H) ou du lien central C—CH_3. Les produits ainsi formés sont le méthyl-3 pentadiène (*cis* et *trans*) (Φ = 0,22) et le pentadiène-2,3 (Φ = 0,03). On remarque à nouveau que le rapport diène-1,3/diène-2,3 est de l'ordre de 7,5, en conformité avec l'observation faite précédemment sur les probabilités relatives des ruptures β(C—H) et du lien central C—CH_3 dans les radicaux allyles. On observe en outre, tableau 2, une formation importante d'isoprène (Φ = 0,20). Cette formation peut être expliquée sur la base du déplacement interne 1,4 d'un atome d'hydrogène dans le radical triméthallyle (5). Le schéma réactionnel 1 montre cette isomérisation qui produit le radical α-éthyl-α-méthallyle. Ce dernier possède une liaison β(C—C) et se fragmente en cette position avec libération concomitante d'isoprène, mais aussi d'un peu d'éthyl-2 butadiène-1,3 et de méthyl-3 pentadiène-1,3 par rupture de liens β(C—H). Par continuité, ce nouveau radical α-éthyl-α-méthallyle peut s'isomériser vers la structure α-méthyl-β-éthallyle avec les produits de fragmentation éventuels que sont le butadiène-1,2 et encore l'éthyl-2 butadiène-1,3. Si le rapport des ruptures β(C—H)/lien central C—CH_3 est encore de 7,5, et étant donné le faible rendement en éthyl-2 butadiène-1,3 le butadiène-1,2 est le résultat d'un autre processus. Peut-être est-il le résultat de la fragmentation d'un radical primaire formé dans une rupture primaire autre que β(C—C).

À ce point, il faut remarquer que le rendement en isoprène est presque égal à celui en méthyl-3 pentadiène-1,3. Ceci implique une isomérisation importante et rapide entre les deux formes α,β,γ-triméthallyles et α-éthyl-α-méthallyles. Le méthyl-3 pentadiène-1,3 est issu d'une rupture de lien β(C—H), tandis que l'isoprène est issu d'une rupture β(C—C). Ce dernier processus est probablement plus rapide que le précédent. Il s'en suit que les deux réservoirs de radicaux allyles ont chacun une grosse fuite d'inégale importance. L'équilibre est donc constamment déplacé vers la formation du radical α-éthyl-α-méthallyle. On ne peut donc avoir directement accès à la constante d'équilibre thermodynamique. Une seconde remarque concerne la somme des rendements quantiques des diènes: celle-ci est voisine de 0,46. Compte tenu du fait qu'une part des radicaux allyles sont stabilisés par collision (bien qu'on n'a pas fait ici d'études en fonction de la pression) ou n'ont pas l'énergie suffisante pour se fragmenter (voir plus haut), on obtient une preuve indirecte de l'importance de la fragmentation primaire β(C—C): processus [2].

De façon alternative, le schéma réactionnel 1 ne prévoit pas d'isomérisation directe entre les radicaux α,β,γ-triméthallyle et α-méthyl-β-éthallyle. Cette réaction commande la formation transitoire d'un intermédiaire cyclique à quatre côtés, dont la tension interne serait de l'ordre de 115 kJ mol^{-1} (20). Inversement, les transferts en 1,4 se font via la formation d'un état de transition à cinq côtés, ayant une tension interne de quelque 85 kJ mol^{-1} moins grande. Ces transferts en 1,3 d'atomes d'hydrogène sont d'ailleurs tenus pour fort rares (21) et impliquent des facteurs de fréquence plus bas que ceux des transferts en 1,4 (20).

Sur la base de la symétrie des orbitales moléculaires, ce transfert 1,3 d'un atome d'hydrogène est interdit dans la forme "supra" et extrêmement difficile dans la forme "antara" à cause de restrictions géométriques. Inversement, le transfert 1,4 a lieu par interaction entre l'orbitale 1*s* de l'atome d'hydrogène et la plus basse orbitale inoccupée du butadiène-1,3. Cette migration est permise selon les règles de conservation de la symétrie.

Radical α,α,γ-triméthallyle

La structure du dM24P2 est favorable à la formation de ce radical. Puisque ce dernier possède essentiellement des liens C—H situés en position β, le méthyl-4 pentadiène-1,3 (Φ =

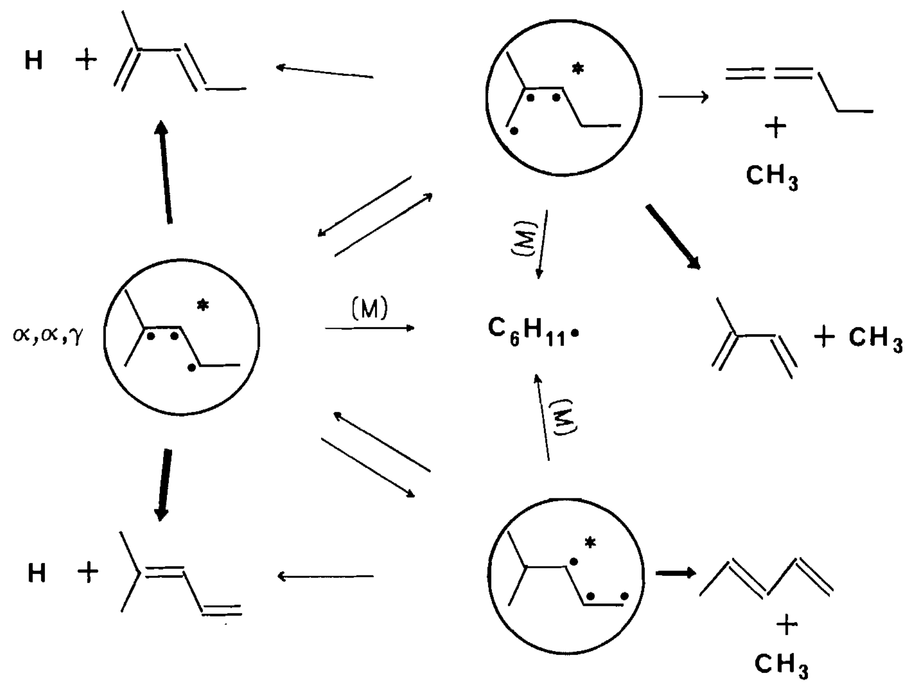

SCHÉMA 2. Évolution du radical α,α,γ-triméthallyle (cercle médian gauche).

0,13) et les méthyl-2 pentadiène-1,3 (*cis* et *trans*) (Φ = 0,06) sont les produits principaux probablement formés au prorata des atomes d'hydrogène disponibles. Le déplacement 1,4 d'un atome d'hydrogène produit les radicaux soit α-isopropyles, soit α-éthyl-β-méthallyles et on peut s'attendre à une formation subséquente de pentadiène-1,3 (*cis* et *trans*) (Φ = 0,04) et d'isoprène (Φ = 0,09).

L'importance relative de la formation de pentadiène-1,3 et d'isoprène est probablement le résultat de plusieurs facteurs. On peut cependant noter que le radical α,α,γ-triméthallyle a deux voies réactionnelles pour aller vers la forme α-éthyl-β-méthallyle et une seule vers la forme α-isopropylallyle. Cette proportion correspond au rapport Φ(pentadiène-1,3)/Φ(isoprène). Il est pertinent de revenir ici sur le mécanisme du transfert interne en 1,4 d'un atome d'hydrogène dans les radicaux méthallyles. La structure du groupe allyle est plane (22) et le radical méthyle est situé soit en position *cis*, soit en *trans* (fig. 2). Il est évident que, d'après cette figure, le déplacement 1,4 est nettement favorisé dans la structure *cis* et probablement beaucoup plus difficile dans le cas de la structure *trans*. Il faut rappeler que l'énergie interne des radicaux allyles qui se fragmentent est considérable (voir plus haut). Dans ces conditions, il est probable que les formes *cis* et *trans* sont en équilibre, en conformité avec ce qui est rapporté dans la littérature (23, 24). Une valeur ΔG comprise entre 52 et 88 kJ mol^{-1}, et probablement inférieure à 60 kJ mol^{-1}, a été estimée pour cet équilibre (24). Enfin, les schémas réactionnels 1 et 2 ne prévoient pas de transferts internes en 1,5 d'atome d'hydrogène. Ce type de transfert commande la formation transitoire d'un cycle à six côtés. On peut prévoir, dans ce cas, un facteur de fréquence plus favorable et une énergie de tension du cycle à peu près négligeable (20). Ce transfert ferait cependant disparaître l'énergie de résonance du groupe allyle, ce qui introduit une énergie d'activation de 50 kJ mol^{-1}. En outre, puisque l'atome échangé provient d'un méthyl terminal, cela ajoute quelques autres kilojoules par mole à l'énergie d'activation, puisque les liaisons C—H terminales sont plus rigides.

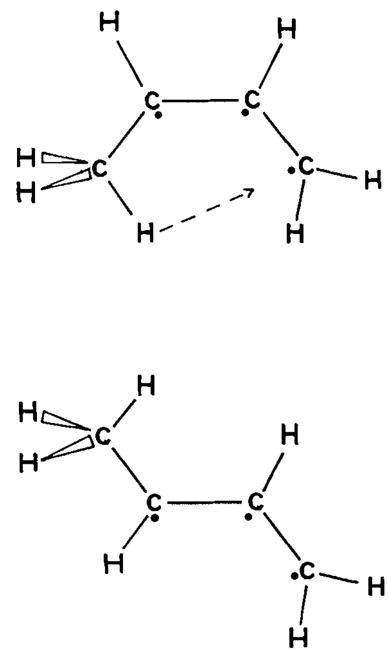

FIG. 2. Représentation schématique du transfert 1,4 de l'atome d'hydrogène dans le radical méthallyle.

Remerciements

Les auteurs remercient l'Université du Québec à Chicoutimi pour l'aide apportée sous différentes formes à la réalisation de ces travaux.

1. G. J. COLLIN, H. DESLAURIERS et S. AUCLAIR. Can. J. Chem. **57**, 863 (1979).
2. H. DESLAURIERS et G. J. COLLIN. J. Photochem. **12**, 249 (1980).
3. G. J. COLLIN et H. DESLAURIERS. Nouv. J. Chim. **3**, 701 (1979).
4. G. J. COLLIN et H. DESLAURIERS. Int. J. Chem. Kinet. **12**, 17 (1980).

5. H. DESLAURIERS et G. J. COLLIN. Can. J. Chem. **63**, 62 (1985).
6. G. J. COLLIN et H. DESLAURIERS. Can. J. Chem. **63**, 944 (1985).
7. R. GORDEN, JR., R. E. REBBERT et P. AUSLOOS. NBS-Tech. Note 496 (1969).
8. J. HERMAN, K. Herman et P. AUSLOOS. J. Chem. Phys. **52**, 28 (1970).
9. R. A. HIVELY et R. E. HIPTON. J. Gas Chromatogr. **6**, 203 (1968).
10. J. GAWLOWSKI, J. WIEDZIELSKI et A. BIERZYNSKI. Chem. Anal. (Warsaw), **15**, 721 (1970).
11. W. TSANG. Int. J. Chem. Kinet. **1**, 245 (1969); **5**, 929 (1973).
12. A. B. TRENWITH. Trans. Faraday Soc. **66**, 2805 (1970); A. B. TRENWITH et S. P. WRIGLEY. J. Chem. Soc. Faraday Trans. 1, **73**, 817 (1977).
13. K. D. KING. Int. J. Chem. Kinet. **11**, 1071 (1979).
14. N. NAKASHIMA, N. SHIMO, N. IKEDA et K. YOSHIHARA. J. Chem. Phys. **81**, 3738 (1984).
15. A. S. RODGERS et M. C. R. WU. J. Am. Chem. Soc. **95**, 6913 (1973).
16. J. NIEDZIELSKI, J. GAWLOWSKI et T. GIERCZAK. J. Photochem. **21**, 195 (1983).
17. D. HOUDE, H. DESLAURIERS et G. J. COLLIN. Can. J. Chem. **61**, 962 (1983).
18. G. J. COLLIN, H. DESLAURIERS et A. WIĘCKOWSKI. J. Phys. Chem. **85**, 944 (1981).
19. P. I. ABELL. Compr. Chem. Kinet. **18**, 111 (1976), et les références qui y sont citées.
20. S. BENSON. *Dans* Thermochemical kinetics. 2^e^ éd. J. Wiley & Sons, New York. 1976. pp. 257–258.
21. D. C. TARDY. Intern. J. Chem. Kinet. **7**, 291 (1974).
22. T. TAKADA et M. DUPUIS. J. Am. Chem. Soc. **105**, 1713 (1983).
23. N. YOKOYAMA. Bull. Chem. Soc. Jpn. **43**, 2975 (1970).
24. P. J. GORTON et R. WALSH. J. Chem. Soc. Chem. Commun. 783 (1972).

Bond dissociation energies and bond orders of diatomic alkali-earth halides

R. R. REDDY AND A. S. R. REDDY

Department of Physics, KSRM College of Engineering, Cuddapah - 516 003. India

AND

V. KRISHNA REDDY

Department of Chemistry, KSRM College of Engineering, Cuddapah - 516 003. India

Received December 5, 1984

R. R. REDDY, A. S. R. REDDY, and V. KRISHNA REDDY. Can. J. Chem. **63**, 3174 (1985).

New relations are proposed for the determination of bond dissociation energies of diatomic alkali-earth halides. The relations are

$$D_{AB} = \bar{D}_{AB} + 31.973e^{0.363\Delta x}$$

and

$$D_{AB} = \bar{D}_{AB}[1 - 0.2075(\Delta x)r_e] + 52.29\Delta x$$

where $\bar{D}_{AB} = (D_{AA}D_{BB})^{1/2}$, Δx represents Pauling's electronegativity differences $(X_A - X_B)$ and r_e is the internuclear distance. The estimated bond energies are in reasonably good agreement with the literature values. The errors calculated with our suggested relations for bond energies are 9.9% and 7.5% respectively. The corresponding errors evaluated from Matcha's and Pauling's equations are 6.1% and 48.2%, respectively. A simplified formula for the determination of bond orders of alkali-earth halides has been suggested. The formula has the form $q = 1.5783 \times 10^{-3}(\omega_e^2 r_e/B_e)^{1/2}$. The definition for bond order given by Parr and Borkman differs from that given by Politzer. Thorough investigation of the two statements reveals that the Politzer's definition is a better one.

R. R. REDDY, A. S. R. REDDY et V. KRISHNA REDDY. Can. J. Chem. **63**, 3174 (1985).

On propose de nouvelles relations pour la détermination des énergies de dissociation des liaisons des halogénures diatomiques de métaux alcalino-terreux. Ces relations sont les suivantes:

$$D_{AB} = \bar{D}_{AB} + 31{,}973e^{0.363\Delta x}$$

et

$$D_{AB} = \bar{D}_{AB}[1 - 0{,}2075(\Delta x)r_e] + 52{,}29\Delta x$$

où $\bar{D}_{AB} = (D_{AA}D_{BB})^{1/2}$ et Δx représente les différences d'électronégativité de Pauling $(X_A - X_B)$ alors que r_e représente la distance internucléaire. Les énergies de liaison évaluées sont en bon accord avec les valeurs répertoriées dans la littérature. Les erreurs calculées pour nos relations suggérées pour les énergies de liaisons sont respectivement de 9,9% et de 7,5%. Les erreurs correspondantes évaluées à partir des équations de Matcha et de Pauling sont respectivement de 6,1% et de 48,2%. On suggère une formule simplifié pour déterminer les ordres des liaisons des halogénures des métaux alcalino-terreux. La formule a la forme suivante: $q = 1{,}5783 \times 10^{-3} (\omega_e^2 r_e/B_e)^{1/2}$. La définition de l'ordre de liaison proposée par Parr et Borkman diffère de celle donnée par Politzer. Une étude soignée des deux définitions révèle que celle de Politzer est la meilleure.

[Traduit par le journal]

Introduction

The bond dissociation energy of diatomic molecules is of great importance in thermochemistry and astrophysics studies (1, 2). In molecular orbital theory, the bond order, which is referred to as the amount of bond charge located on a bond, very important in the calculation of various molecular parameters; e.g., dipole moment and oscillator strength. One procedure for the computation of the total bond order in a molecule involves the linear combination, with suitable coefficients, of atomic orbitals of the two atoms joined by the bond. This makes the computation of total bond order a tedious job. The models suggested by Parr and Borkman (3, 4) and Politzer (5, 6) are found to be suitable for those molecules in which the ionic and covalent contributions to the binding are almost comparable. This idea has been extended by the present authors to test the validity of the model for those molecules in which ionic character is predominant. Hence, it is proposed to determine the bond dissociation energies and bond orders for diatomic alkali-earth halides with the simple formulae suggested.

(i) Bond dissociation energies

In continuation of our studies on bond dissociation energy and bond order (7, 8), we have proposed new relations for the determination of bond dissociation energies based on the relation of Pauling and Matcha (9, 12). The relations are

$$[1] \quad D_{AB} = \bar{D}_{AB} + 31.973e^{0.363\Delta x}$$

$$[2] \quad D_{AB} = \bar{D}_{AB}[1 - 0.2075(\Delta x)r_e] + 52.29\Delta x$$

Where $\bar{D}_{AB} = (D_{AA}D_{BB})^{1/2}$, Δx represents Pauling's electronegativity differences $(X_A - X_B)$ and r_e is the internuclear distance. The necessary constants for the present study are taken from the literature. The bond energy value of the homonuclear molecules of alkali-earth metals and halides are given in Table 1.

Matcha (12) has pointed out that Pauling's empirical relation $D_{AB} = \bar{D}_{AB} + 30(\Delta x)^2$ works badly for ionic molecules. Keeping this point in view, it is desirable to have an accurate relationship for ionic molecules. In the present study, the bond dissociation energies are evaluated using the relations [1] and [2]. For comparison, bond dissociation energies are also computed with Pauling's relation. Matcha (12) has derived an equation relating bond energies to electronegativity differences. This equation has the form

TABLE 1. Bond energies of homonuclear molecules of alkali-earth metals and halides

Molecule	Bond energy (kcal/mol)
Be_2	51.00
Mg_2	31.00
Ca_2	25.00
Sr_2	20.00
F_2	37.00
Cl_2	58.00
Br_2	45.46
I_2	35.55

$$[3] \quad D_{AB} = \bar{D}_{AB} + N[1 - \exp[-30(\Delta x)^2/N]]$$

where $N = 103$. He has not given the electronegativity values appropriate to his relation so far. In order to test the reliability of Matcha's relation for ionic molecules, we have used Pauling's electronegativities in his formula and estimated bond energies. Some conclusions have been drawn by using Pauling's electronegativity values in Matcha's formula (P-M relation).

(2) Bond order

The Parr and Borkman (3, 4) relation of the following form for bond order has been modified by the present authors.

$$[4] \quad q = (4R_c^3K_c/7e^2)^{1/2}$$

K_c in eq. [4] can be written as $\omega_c^2/B_cr_c^2$. From these two relations, the following simplified equation has been derived.

$$[5] \quad q = 1.5783 \times 10^{-3}(\omega_c^2r_c/B_c)^{1/2}$$

Here the experimental values of ω_c, r_c, and B_c determine the bond order. The necessary constants for the present study are taken from Huber and Herzberg (10).

In the present study the definitions for bond order 'q' given by Parr and Borkman (3, 4) and Politzer (5, 6) have been studied in detail and it has been found that the interpretation given by Politzer holds.

Results and discussion

The estimated bond energies for alkali-earth halides from relations [1] and [2], the P-M relation and Pauling's expression are presented in Table 2. The average percentage deviation

$$[5] \quad \frac{(D_0)_{\text{exptl.}} - (D_0)_{\text{calcd.}}}{(D_0)_{\text{exptl.}}} \times 100$$

is also given. The bond order values calculated from relation [5] are presented in Table 3.

The results obtained from eq. [2] reveal that the bond energy values for fluoride molecules deviate from the general trend. The predicted bond energies have higher values than the experimental value by 24 kcal/mol. Similar behaviour is observed in the case of alkali halides (7). This value is deducted from the dissociation energy values obtained from eq. [2] and the modified values are presented in Table 2. It is in good agreement with Kushawaha's view (16). Several explanations have been given for the deviation of fluoride from the other halides (13−16). This may be due to the lower electronic affinity and smaller atomic size of fluorine atom as suggested by Politzer (17). The estimated bond energy values obtained from relation [2] and P-M relation are in good agreement with the experimental values (11). Since the bond energy value for Ba_2 molecule is not available, we could not calculate the bond energies for barium halides. Some of the experimental bond energy values (11) are approximate. The correct percentage deviation may be calculated if reliable experimental data are available. The estimated bond energies from Matcha's relation suggest that Matcha's electronegativities (still to be estimated) and Pauling's electronegativities for the atoms Be, Mg, Ca, Sr, F, Cl, Br, and I do not differ greatly.

TABLE 2. Comparison of experimental and predicted bond energies for alkali-earth halides

		Predicted bond energies (in kcal/mol) from			
Molecule	D_{AB} (Exptl.)	Eq. [1]	Eq. [2]	P-M relation	Pauling's relation
BeF	151±13*	122.66	118.61†	129.61	230.93
BeCl	110±15*	109.49	103.18	103.74	121.88
BeBr	89.00	99.40	91.31	88.05	98.85
BeI	69.00	88.53	76.31	68.49	72.75
MgF	123±10*	122.20	121.45†	126.25	269.06
MgCl	97.00	103.85	101.99	105.14	139.60
MgBr	81.00	94.69	92.03	91.51	114.34
MgI	63.00	84.44	78.42	73.09	83.89
CaF	132±10*	125.41	123.53†	125.83	300.41
CaCl	103±10*	104.15	103.00	108.78	158.07
CaBr	96.00	95.16	94.21	96.45	130.91
CaI	78.00	84.92	81.51	79.17	97.31
SrF	132±10*	122.20	122.82†	122.62	297.20
SrCl	112.00	100.13	100.91	104.76	154.05
SrBr	97.00	91.60	92.52	92.89	127.35
SrI	80.00	81.77	79.94	76.02	94.16
Average % deviation		9.9	7.5	6.1	48.2

*Values are approximate.
†Modifieid values — see text.

TABLE 3. Parameters q and $q/(0.5r_c)^2$ for alkali-earth halides

	q		
Molecule	Parr and Borkman	Present method	$q/(0.5r_c)^2$
BeF	1.869	1.882	4.064
BeCl	2.093	2.099	2.599
BeBr	2.130	2.134	2.238
BeI	2.190	2.194	1.848
MgF	2.059	2.062	2.693
MgCl	2.183	2.185	1.807
MgBr	2.232	2.234	1.605
SrF	2.235	2.282	2.119
BaF	2.345	2.342	2.002
CaF	2.215	2.214	2.324
CaCl	2.320	2.324	1.563
CaBr	2.362	2.363	1.405
CaI	2.405	2.407	1.203

Parr and Borkman suggested that q as defined in eq. [5], is a measure of charge located in the bond region and thus could be identified with bond order. By example, Politzer showed (5, 6) that the interpretation of q as bond order could be improved upon. According to him, a better definition of bond order is $q/(0.5r_c)^2$.

The values of q are computed for alkali-earth halides using relation [5]. It is obvious from Table 2 that if q is taken as the bond order it leads to ambiguity. As we go from F to I, the value of q increases while the binding energy decreases. According to Parr and Borkman, CaBr and CaCl; BeI, MgBr, and CaF have approximately the same values for q, 2.3 and 2.2, respectively (Table 2). It has no meaning to have the same bond order for all these molecules. The ambiguity can be removed by taking the relation $q/(0.5r_e)^2$ as the bond order given by Politzer. The present study supports the Politzer view that $q/(0.5r_e)^2$ is the correct definition for the bond order.

Acknowledgements

The authors express their sincere thanks to Professor S. V. J. Lakshman, Dr. D. V. Reddy, Dr. T. V. R. Rao, and Professor C. S. Reddy for their encouragement.

1. A. G. GAYDON. Dissociation energies. Chapman and Hall, London. 1968.
2. G. HERZBERG. Spectra of diatomic molecules. Von Nostrand, New York. 1967.
3. R. G. PARR and R. F. BORKMAN. J. Chem. Phys. **47**, 1055 (1968).
4. R. G. PARR and R. F. BORKMAN. J. Chem. Phys. **48**, 1116 (1968).
5. P. POLITZER. J. Chem. Phys. **51**, 459 (1969).
6. P. POLITZER. J. Chem. Phys. **50**, 2780 (1969).
7. R. R. REDDY, A. S. R. REDDY, and V. K. REDDY. Theor. Chim. Acta, In press.
8. R. R. REDDY and T. V. R. RAO. J. Mol. Struct., (Theor. Chem.), **90**, 49 (1982).
9. L. PAULING. The nature of the chemical bond. 3rd ed. Cornell University Press, Ithaca, New York. 1960.
10. K. P. HUBER and G. HERZBERG. Molecular spectra and molecular structure. IV. Constants of diatomic molecules. Van Nostrand Reinhold, New York. 1979.
11. J. E. HUHEEY. Inorganic chemistry. 2nd ed. Harper International Edition, New York. 1978.
12. R. L. MATCHA. J. Am. Chem. Soc. **105**, 4859 (1983).
13. R. S. MULLIKEN. J. Am. Chem. Soc. **77**, 884 (1955).
14. K. S. PITZER. Adv. Chem. Phys. **23**, 1735 (1959).
15. G. L. CALDOW and C. A. COULSON. Trans. Faraday Soc. **58**, 633 (1962).
16. V. S. KUSHAWAHA. Ind. J. Pure Appl. Phys. **11**, 63 (1973).
17. P. POLITZER. J. Am. Chem. Soc. **91**, 6235 (1969).

Stereoselective synthesis and X-ray crystallographic analysis of mixed 6,6-dihalo penicillanates

DIEGO U. BELINZONI[1] AND ORESTE A. MASCARETTI[2,5]

Departamento de Química Orgánica, Facultad de Farmacia y Bioquímica, Universidad de Buenos Aires, Junin 956, Buenos Aires, Argentina

AND

PEDRO M. ALZARI,[3] GRACIELA PUNTE,[4,5] CARLOS FAERMAN,[3] AND ALBERTO PODJARNY[4]

Departamento de Física and CINDECA, Facultad de Ciencias Exactas, Universidad Nacional de La Plata, C.C. 67, La Plata 1900, Argentina

Received May 29, 1984[6]

DIEGO U. BELINZONI, ORESTE A. MASCARETTI, PEDRO M. ALZARI, GRACIELA PUNTE, CARLOS FAERMAN, and ALBERTO PODJARNY. Can. J. Chem. **63**, 3177 (1985).

The pivaloyloxy methyl 6,6-dihalo penicillanates **1***a*, **1***b*, and **1***c* have been stereoselectively prepared from the reaction of pivaloyloxy methyl 6-diazo penicillanate **2** with either *N*-halosuccinimide/halide or the interhalogens XI (X = Cl, Br). The crystal structures of 3*S*,5*R*,6*R* pivaloyloxy methyl 6-bromo, 6-chloro penicillanate **1***a*; 3*S*,5*R*,6*R* pivaloyloxy methyl 6-iodo, 6-bromo penicillanate **1***b*, and 3S, 5R, 6R pivaloyloxymethyl 6-iodo, 6-chloro penicillanate **1***c* have been determined by X-ray single crystal analysis. The stereochemistry of the displacement reaction is discussed.

DIEGO U. BELINZONI, ORESTE A. MASCARETTI, PEDRO M. ALZARI, GRACIELA PUNTE, CARLOS FAERMAN et ALBERTO PODJARNY. Can. J. Chem. **63**, 3177 (1985).

Le diazo-6 pénicillinate de pivaloyloxyméthyle (**2**) réagit soit avec un mélange de *N*-halosuccinimide/halogénure soit avec les interhalogènes XI (X = Cl, Br) pour conduire de façon stéréosélective aux dihalo-6,6 penicillinates de pivaloyloxyméthyle **1***a*, **1***b* et **1***c*. On a déterminé, par cristallographie de rayons X sur un monocristal, la structure cristalline du bromo-6 chloro-6 pénicillinate de pivaloyloxyméthyle-3*S*,5*R*,6*R* (**1***a*); du bromo-6 iodo-6 pénicillinate de pivaloyloxyméthyle-3*S*,5*R*,6*R* (**1***b*) et du chloro-6 iodo-6 pénicillinate de pivaloyloxyméthyle-3*S*,5*R*,6*R* (**1***c*). On discute de la stéréochimie de la réaction de déplacement.

[Traduit par le journal]

Introduction

Preparation of mixed 6,6-dihalo penicillanic acids has been accomplished through the two-phase diazotization/halogenation procedure described by Volkmann *et al.* (1) or by the work of Kellogg and co-workers (2) through diazotization/halogenation in aqueous media (3). These authors did not, however, provide information regarding the stereochemistry at carbon-6.

Based on mechanistic considerations (4,5), and taking into account the peculiar structural features of the cup-shaped penicillin molecule (6, 7), one should expect to observe a noticeable control on such type of substitution.

We therefore decided to study the substitution of a diazo group on carbon-6 of the penicillanic framework by either *N*-halosuccinimide/halide or interhalogens. In order to fully characterize the resulting 6,6-dihalo penicillanates, we chose to carry out an X-ray crystallographic analysis to establish the stereochemistry.

In this paper we present the synthesis, and crystal and molecular structures of three pivaloyloxy methyl mixed 6,6-dihalo penicillanates **1***a*, **1***b*, and **1***c*.

Discussion

6-Diazo penicillanic acid and its esters have been suggested by the work of McMillan and Stoodley (5) and Clayton (3) as

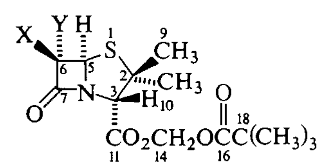

1*a* X = Br Y = Cl
1*b* X = I Y = Br
1*c* X = I Y = Cl

the key intermediates for the efficient synthesis of a wide variety of penicillin derivatives. In order to introduce two halogen atoms at C-6 we made use of the reaction of *N*-halosuccinimide/soft potassium or sodium halide[7] in the presence of a crown ether, or the interhalogens XI (X = Cl, Br) with pivaloyloxy methyl 6-diazo penicillanate **2**, in an organic medium (currently methylene dichloride or chloroform), a reaction which we found to be applicable to *N*-haloimides/soft pseudohalides. Following this procedure we were able to synthesize compounds **1***a*, **1***b*, and **1***c* (Scheme 1).

The starting intermediate **2** for these syntheses was prepared according to a known method (8, 9). Although this material can be isolated and spectroscopically characterized, it decomposes at room temperature. The yields of 6,6-dihalo derivatives obtained from the isolated diazo compound were noticeably low (ca. 20%) in comparison with those obtained when the diazo intermediate was generated *in situ* (ca. 80%), according to the procedure described by Volkmann *et al.* (1). It is important to point out that from both procedures only a single compound was detected in each case, with an R_f value within

[1]Research fellow of CONICET, Argentina.
[2]Present address: IQUIOS, Suipacha 531, 2000 Rosario, Argentina.
[3]Research fellow CICPBA, Argentina.
[4]Member of the Scientific Research Career, CONICET, Argentina.
[5]Authors to whom correspondence should be addressed.
[6]Revision received February 12, 1985.

[7]This reaction did not appear useful for the combination N-halosuccinimide/hard halides; e.g. potassium or sodium fluorides.

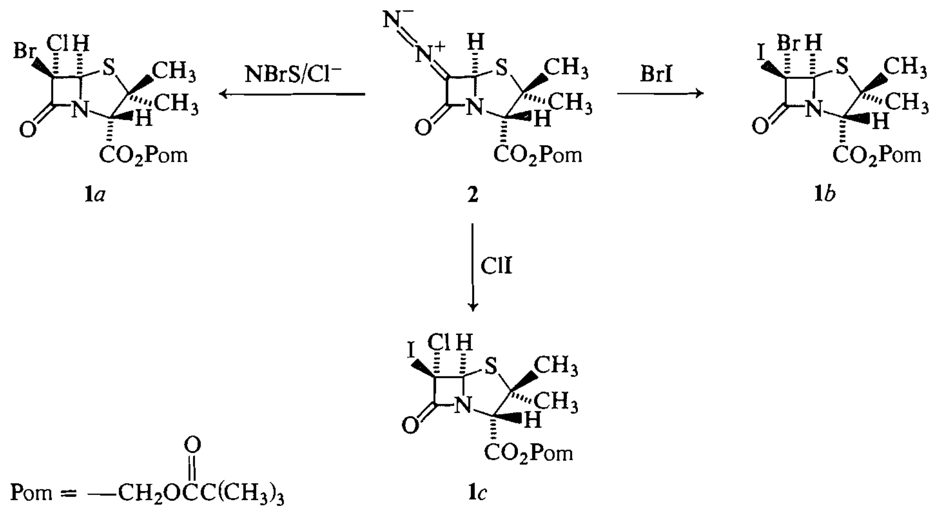

SCHEME 1

the range of the 6-6-dihalo derivatives (tlc cyclohexane–dioxane, 8:2), **1***a* R_f: 0.84; **1***b* R_f: 0.79; and **1***c* R_f: 0.82). Such noticeable stereo control could be accounted for by taking into account the peculiar structural features of the penicillin molecule, that would greatly influence the diazo group substitution.

In order to fully characterize those compounds, the ir, mass spectra, and ^{1}H and ^{13}C nmr spectra were recorded. The low resolution mass spectra of compounds **1***a*, **1***b*, and **1***c* show, in addition to the ions arising from the known fragmentation pattern (13), the prominent peaks at m/e 57 and m/e 85, characteristic of the *tert*-butyl ester moiety. The ^{1}H nmr data are in complete agreement with those reported for similar compounds (1); the assignment of the ^{13}C nmr signals was carried out by the usual techniques: chemical shift theory, signal multiplicities, the APT pulse sequence (14), correlation with related compounds (15–17), and specific decoupling experiments. The most remarkable features are the high field signal (δ 0.7 ppm) for C-6 in the diazo compound **2**, and the heavy atom effect on the same carbon for compounds **1***b* and **1***c*. Nevertheless, none of the previously mentioned spectroscopic methods gave any valid information regarding the stereochemistry at C-6; we thus undertook a single crystal X-ray study to obtain the relative configuration for all the chiral centers in the molecule. The fact that the absolute configurations at C-3 and C-5 are already known allowed us to fully characterize compounds **1***a*, **1***b*, and **1***c* as follows: 3*S*,5*R*,6*R* pivaloyloxy methyl 6-bromo, 6-chloro penicillanate, 3*S*,5*R*,6*R* pivaloyloxy methyl 6-iodo, 6-bromo penicillanate, and 3*S*,5*R*,6*R* pivaloyloxy methyl 6-iodo, 6-chloro penicillanate.

Since all the compounds synthesized are isostructural, the molecular structures of only two of them, **1***a* and **1***b*, have been solved from diffractometric data. The configuration of the asymmetric carbon-6 of the other, **1***c*, was determined from photographic studies in projection.

Details of structure solution and refinement are presented in the experimental section. Final atomic and equivalent isotropic thermal parameters for **1***a* and **1***b* are given in Tables 1 and 2 respectively.[8] A view of molecular conformation and atom labelling of **1***a* is provided in Fig. 1.

The bond lengths and angles within the nucleus (β-lactam

[8]Tables of structure factors and anisotropic thermal parameters may be purchased from the Depository of Unpublished Data, CISTI, National Research Council of Canada, Ottawa, Ont., Canada K1A 0S2.

TABLE 1. Fractional positional parameters and equivalent isotropic thermal parameter with esd's in parentheses for **1***a*

Atom	x/a	y/b	z/c	U_{eq}* (Å^2)
S(1)	−0.2229(3)	0.1282(2)	−0.0487(2)	0.041(3)
C(2)	−0.080(1)	0.2023(9)	−0.0951(9)	0.04(1)
C(3)	0.042(1)	0.133(1)	−0.0692(9)	0.03(1)
H(3)	0.110(1)	0.192(1)	−0.0466(9)	0.10(9)
N(4)	0.011(1)	0.0804(8)	0.0201(7)	0.04(1)
C(5)	−0.128(1)	0.046(1)	0.0313(9)	0.05(1)
H(5)	−0.135(1)	−0.036(1)	0.0230(9)	0.06(4)
C(6)	−0.110(1)	0.066(1)	0.1428(9)	0.05(1)
C(7)	0.026(1)	0.110(1)	0.1139(9)	0.03(1)
O(8)	0.1124(9)	0.1558(7)	0.1568(6)	0.050(9)
C(9)	−0.069(1)	0.3066(9)	−0.043(1)	0.05(1)
H(91)	−0.044(1)	0.3011(9)	0.034(1)	0.02(2)
H(92)	−0.160(1)	0.3487(9)	−0.051(1)	0.02(2)
H(93)	0.008(1)	0.3466(9)	−0.081(1)	0.02(2)
C(10)	−0.099(1)	0.219(1)	−0.2047(9)	0.05(1)
H(101)	−0.092(1)	0.146(1)	−0.2429(9)	0.07(4)
H(102)	−0.024(1)	0.271(1)	−0.2320(9)	0.07(4)
H(103)	−0.194(1)	0.252(1)	−0.2162(9)	0.07(4)
C(11)	0.078(1)	0.057(1)	−0.1456(9)	0.04(1)
O(12)	0.034(1)	−0.0275(7)	−0.1542(8)	0.07(1)
O(13)	0.1667(8)	0.0974(7)	−0.2087(7)	0.048(9)
C(14)	0.210(2)	0.040(1)	−0.290(1)	0.06(1)
H(141)	0.203(2)	−0.038(1)	−0.263(1)	0.03(3)
H(142)	0.311(2)	0.062(1)	−0.298(1)	0.03(3)
O(15)	0.123(1)	0.0537(7)	−0.3680(6)	0.06(1)
C(16)	0.133(2)	0.141(1)	−0.417(1)	0.07(2)
O(17)	0.209(1)	0.2115(9)	−0.3919(8)	0.11(1)
C(18)	0.047(1)	0.148(1)	−0.5074(9)	0.04(1)
C(19)	0.117(2)	0.084(2)	−0.585(1)	0.10(2)
H(191)	0.063(2)	0.097(2)	−0.651(1)	0.09(4)
H(192)	0.116(2)	0.003(2)	−0.567(1)	0.09(4)
H(193)	0.217(2)	0.109(2)	−0.594(1)	0.09(4)
C(20)	0.034(2)	0.261(1)	−0.539(2)	0.12(3)
H(201)	−0.015(2)	0.275(1)	−0.608(2)	0.11(5)
H(202)	0.139(2)	0.267(1)	−0.549(2)	0.11(5)
H(203)	0.002(2)	0.317(1)	−0.486(2)	0.11(5)
C(21)	−0.089(2)	0.100(1)	−0.485(1)	0.10(2)
H(211)	−0.131(2)	0.089(1)	−0.556(1)	0.13(5)
H(212)	−0.154(2)	0.146(1)	−0.441(1)	0.13(5)
H(213)	−0.075(2)	0.026(1)	−0.451(1)	0.13(5)
Cl	−0.1043(3)	−0.0475(2)	0.2174(2)	0.044(3)
Br	−0.2165(1)	0.1722(1)	0.2020(1)	0.082(2)

*Defined according to Hamilton (22).

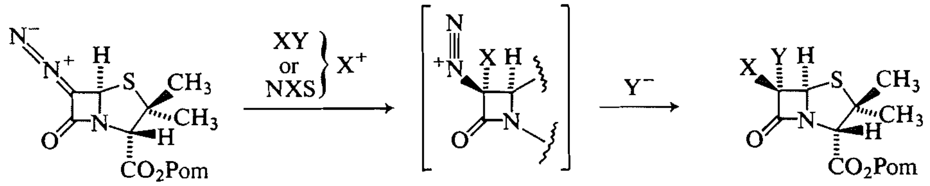

2

SCHEME 2

TABLE 2. Fractional positional parameters and equivalent isotropic thermal parameter with esd's in parentheses for **1***b*

Atom	x/a	y/b	z/c	U_{eq}* (Å^2)
S(1)	−0.2174(3)	0.1235(2)	−0.0405(2)	0.043(3)
C(2)	−0.077(1)	0.1951(8)	−0.090(1)	0.04(1)
C(3)	0.043(1)	0.129(1)	−0.0673(9)	0.03(1)
H(3)	0.133(1)	0.1694(9)	−0.0597(9)	0.03(3)
N(4)	0.014(1)	0.0748(8)	0.0213(7)	0.041(10)
C(5)	−0.120(1)	0.0429(8)	0.036(1)	0.04(1)
H(5)	−0.13(1)	−0.042(2)	0.033(8)	0.05(3)
C(6)	−0.097(1)	0.063(1)	0.1443(9)	0.05(1)
C(7)	0.033(1)	0.106(1)	0.113(1)	0.05(1)
O(8)	0.1197(9)	0.1502(7)	0.1526(7)	0.058(9)
C(9)	−0.063(1)	0.2995(8)	−0.040(1)	0.05(1)
H(91)	−0.152(1)	0.3432(8)	−0.039(1)	0.03(2)
H(92)	0.007(1)	0.3377(8)	−0.085(1)	0.03(2)
H(93)	−0.026(1)	0.294(1)	0.032(1)	0.03(2)
C(10)	−0.100(1)	0.211(1)	−0.197(1)	0.06(1)
H(101)	−0.118(1)	0.136(1)	−0.227(1)	0.01(1)
H(102)	−0.024(1)	0.249(1)	−0.236(1)	0.01(1)
H(103)	−0.188(1)	0.256(1)	−0.200(1)	0.01(1)
C(11)	0.071(1)	0.048(1)	−0.143(1)	0.06(1)
O(12)	0.027(1)	−0.0358(7)	−0.1493(8)	0.08(1)
O(13)	0.1589(9)	0.0881(5)	−0.2062(7)	0.053(9)
C(14)	0.195(2)	0.028(1)	−0.285(1)	0.07(2)
H(141)	0.153(2)	−0.029(1)	−0.236(1)	0.07(4)
H(142)	0.299(2)	0.028(1)	−0.277(1)	0.07(4)
O(15)	0.113(1)	0.0460(7)	−0.3624(7)	0.06(1)
C(16)	0.127(2)	0.135(1)	−0.410(1)	0.09(2)
O(17)	0.203(1)	0.198(1)	−0.3836(8)	0.11(1)
C(18)	0.042(1)	0.142(1)	−0.497(1)	0.05(1)
C(19)	0.114(2)	0.083(2)	−0.578(1)	0.12(2)
H(191)	0.071(4)	0.111(2)	−0.643(1)	0.05(4)
H(192)	0.136(2)	0.002(2)	−0.585(1)	0.05(4)
H(193)	0.203(2)	0.125(2)	−0.563(1)	0.05(4)
C(20)	0.028(2)	0.256(1)	−0.525(2)	0.16(3)
H(201)	−0.001(2)	0.284(1)	−0.595(2)	0.1578
H(202)	0.131(2)	0.243(1)	−0.525(2)	0.1578
H(203)	0.003(2)	0.313(1)	−0.472(2)	0.1578
C(21)	−0.090(2)	0.096(1)	−0.478(2)	0.13(2)
H(211)	−0.156(2)	0.149(1)	−0.511(2)	0.1081
H(212)	−0.071(2)	0.119(1)	−0.405(2)	0.1081
H(213)	−0.132(2)	0.020(1)	−0.478(2)	0.1081
Br	−0.0814(1)	−0.0659(3)	0.2201(1)	0.087(2)
I	−0.2099(1)	0.1725(1)	0.2168(1)	0.091(1)

*Defined according to Hamilton (22).

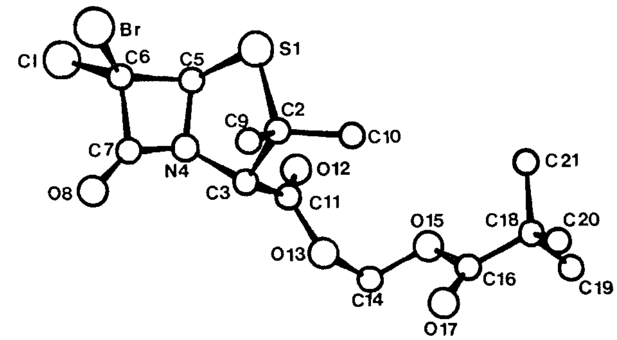

FIG. 1. Computer generated perspective drawing of **1***a* with hydrogens omitted.

TABLE 3. Main structural features of β-lactam and thiazolidine rings. Lengths in Å and angles in deg. Standard deviations in parentheses

Parameter	**1***a*	**1***b*
N4—C7	1.35(2)	1.36(2)
C7—O8	1.21(2)	1.20(2)
C5—S1—C2	95.1(5)	94.4(6)
Sum of bond angles around nitrogen	342(2)	341(3)
Distance of N4 to substituents plane	0.34(3)	0.35(2)
Distance of C3 to best least-squares plane S1,C2,N4,C5	0.49(1)	0.46(3)
Planarity of fragment C6,C7,O8,N4 (χ^2)	0.19	0.02
Distance of C5 to best least-squares plane C6,C7,O8,N4	0.19(2)	0.20(2)

TABLE 4. Side chain selected torsion angles (°). Standard deviations in parentheses

	1*a*	**1***b*
C11,O13,C14,O15	85.8(5)	84.8(5)
O13,C14,O15,C16	77.6(6)	73.9(6)
C14,O15,C16,C18	5.7(8)	5.5(7)

and thiazolidine rings) agree with those of other penicillin derivatives. The thiazolidine ring adopts the α-COOR axial, α-CH_3 equatorial, and β-CH_3 axial configuration, similar to that reported for penicillin G and V (18), carfecillin (19), and oxacillins (20). Four of its five atoms are nearly coplanar with the remaining one (C-3) out of the plane. In the β-lactam ring N-4 lies out of the plane of the substituents and shows a pyramidal arrangement, the C6,C7,O8,N4 fragment is planar within experimental accuracy. Table 3 shows the main structural features of the β-lactam and thiazolidine rings for **1***a*, and **1***b*. The pivaloyloxy methyl ester side chain exhibits an extended conformation (the torsion angles are reported in Table 4).

Conclusions

The results of X-ray analysis showed that in all reactions the positive (electrophilic) halogen atoms are placed in a β-orientation, while the nucleophilic halide atom is in the

TABLE 5. Crystal data for **1***a*, **1***b*, and **1***c*

Parameter	**1***a*	**1***b*	**1***c*
a (Å)	10.198(2)	10.337(8)	10.418(7)
b (Å)	12.956(5)	12.988(7)	13.13(1)
c (Å)	13.720(2)	13.961(3)	13.95(1)
M_r(g)	480.72	522.2	475.3
D_o(g/cm^3)	1.57	1.84	1.65
μ(cm^{-1})	24.64(MoKα)	38.31(MoKα)	44.48(CuKα)
Temperature	Liquid N	Liquid N	Room temperature

α-orientation in agreement with the proposed (4, 6, 7, 21) two-step mechanism for the displacement reaction. The fact that only one isomer was isolated in each case, with no other detected by tlc analysis of the crude reaction mixtures, strongly supports the S_N2 displacement of N_2 shown in Scheme 2, and reinforces the validity of a large number of structures for related compounds, proposed purely on the basis of mechanistic speculations.

Experimental

Apparatus and materials

Melting points were determined on a Metler FP 1 device and were corrected. The ir spectra were taken on a Perkin Elmer 700 A instrument. Mass spectra were recorded at 70 eV in a Varian-Mat CH-7 A mass spectrometer interfaced to a Varian-Mat Data System 166 computer. The ^{1}H and ^{13}C nmr spectra were taken on a Bruker WP 80SY instrument at 80.13 and 20.15 MHz, respectively, and chemical shifts are expressed in parts per million downfield from internal tetramethylsilane. The $[\alpha]_D$s were taken at 20–23°C in 0.5% chloroform solutions. Silica gel GF_{254} (Type 60 Merck) was utilized for tlc, and silica gel 60 H (Merck) for column chromatography.

Pivaloyloxy methyl 6-amino penicillanate hydrochloride

A previously described procedure (8) was used to prepare this compound.

Pivaloyloxy methyl 6-diazo penicillanate 2

This product was prepared from pivaloyloxy methyl 6-amino penicillanate hydrochloride following the method described by Wiering and Wynberg (9). Compound **2** was isolated as an amber glass (65%). This material gave essentially one spot on tlc (R_f 0.85) in benzene/acetonitrile (3:1); ir ($CHCl_3$): 2090 (N=N=C), 1760 (C=O) cm^{-1}; ^{1}Hmr ($CDCl_3$): 1.22 (s, 9H), 1.46 (s, 3H), 1.64 (s, 3H), 4.39 (s, 1H), 5.80 (d, 1H, H-C14 AB system J = 5.6 Hz), 5.85 (d, 1H, H-C14 AB system J = 5.6 Hz); ^{13}Cmr ($CDCl_3$): 176.6 (C-16), 166.7 (C-11), 166.2 (C-7), 79.7 (C-14), 70.1 (C-3), 68.5 (C-5), 63.6 (C-2), 38.7 (C-18), 33.7 (C-9), 26.8 (C-19 – C-21), 25.7 (C-10), and 0.7 (C-6).

*Pivaloyloxy methyl 6-β-bromo, 6-α-chloro penicillanate 1*a

A mixture of 18-crown-6 (2.88 g, 10.9 mmol), 50 mL of anhydrous chloroform, and potassium chloride (0.813 g, 10.9 mmol) was stirred under nitrogen at room temperature for 30 min. To the resulting solution, cooled to −30°C, was added a crude solution ($CHCl_3$) of freshly prepared compound **2**, from pivaloyloxy methyl 6-amino penicillanate hydrochloride (4.0 g, 10.9 mmol), and the mixture stirred for 10 min at −30°C, followed by the addition of *N*-bromosuccinimide (1.94 g, 10.9 mmol) in 50 mL of anhydrous chloroform, over a period of 30 min. The reaction was then allowed to reach room temperature, the mixture was washed with cold 6% sodium sulfite (50 mL) and water (2 × 50 mL), and dried (Na_2SO_4). Removal of the solvent under reduced pressure gave an oil, which was chromatographed on a column of activated charcoal (Darco) and eluted with n-hexane, affording compound **1***a* as an oil. Crystallization from methanol gave 0.844 g of white crystals (18%), mp 98.0–99.5°C; $[\alpha]_D$ +168.5°; ir (KBr): 1790 (β-lactam), 1760 and 1740 (ester) cm^{-1}; ^{1}Hmr ($CDCl_3$): 1.22 (s, 9H), 1.49 (s, 3H), 1.62 (s, 3H), 4.56 (s, 1H), 5.63 (s, 1H), 5.83 (d, 1H, H-C14 AB system J = 5.6 Hz), 5.86 (d, 1H, H-C14 AB system J = 5.6 Hz); ^{13}Cmr ($CDCl_3$): 176.6 (C-16), 165.2 (C-11), 163.5 (C-7), 80.7 (C-14), 79.6 (C-5), 74.7 (C-6), 69.1 (C-3), 64.2 (C-2), 38.6 (C-18), 33.3 (C-9), 26.7 (C-19 – C-21), 25.6 (C-10); mass spectrum, *m/e* (relative intensity): 431, 429, 427 (1:4:3, 27) M$^+$, 317, 315, 313 (1:4:3, 13), 272, 270, 268 (1:4:3, 97), 217, 215, 213 (1:4:3, 23), 115 (4), 114 (55.4), 85 (61.6), 57 (100).

*Pivaloyloxy methyl 6-β-iodo, 6-α-bromo penicillanate 1*b

To a cooled (−63°C) solution ($CHCl_3$, 50 mL) of freshly prepared compound **2**, from pivaloyloxy methyl 6-amino penicillanate hydrochloride (0.793 g, 2.16 mmol), with stirring under N_2, was added dropwise a solution of iodine monobromide (0.450 g, 2.17 mmol) in 50 mL of chloroform until a persistent brown color was present (it consumed approximately 37 mL in 15 min). The mixture was allowed to reach room temperature and was washed with cold 6% sodium sulfite (50 mL) and water (2 × 50 mL) and dried (Na_2SO_4). Removal of the solvent under reduced pressure gave an orange oil (0.462 g), which was purified by short-column chromatography on silica gel under slight pressure of N_2 and eluted with benzene/chloroform (1:1). The first eluted material furnished a light brown oil which crystallized on standing. Recrystallization from methanol yielded white crystals of compound **1***b* (0.233 g, 21%), mp 125.7°C (dec.); $[\alpha]_D$ +185.9°; ir (KBr): 1790 (β-lactam), 1770 and 1750 (ester) cm^{-1}; ^{1}Hmr ($CDCl_3$): 1.22 (s, 9H), 1.46 (s, 3H), 1.67 (s, 3H), 4.57 (s, 1H), 5.58 (s, 1H), 5.81 (d, 1H, H-C14 AB system J = 5.6 Hz), 5.84 (d, 1H, H-C14 AB system J = 5.6 Hz); ^{13}Cmr ($CDCl_3$): 176.3 (C-18), 165.2 (C-11), 164.9 (C-7), 80.9 (C-5), 79.6 (C-14), 69.5 (C-3), 65.0 (C-2), 38.6 (C-18), 33.6 (C-9), 30.6 (C-6), 26.7 (C-19 – C-21), 26.3 (C-10); ms *m/e* (relative intensity): 521, 519 (1:1, 27) M$^+$, 407, 405 (1:1, 6), 362, 360 (1:1, 8), 307, 305 (1:1, 28.1), 115 (5.4), 114 (68.8), 85 (84.3), 57 (100).

*Pivaloyloxy methyl 6-β-iodo, 6-α-chloro penicillanate 1*c

This compound was prepared as described for **1***b* (starting with 1.000 g, 2.72 mmol of pivaloyloxy methyl 6-amino penicillanate and 2.72 mmol of iodine monochloride). After removal of the solvent, recrystallization from methanol gave compound **1***c* (0.570 g, 30%), mp 118.0–120.0°C; $[\alpha]_D$ +186.0°. Compound **1***c* can be also synthesized using the procedure described for **1***a*. In this method iodine monochloride (2.72 mmol) was generated *in situ* from *N*-chlorosuccinimide and potassium iodide (10, 11) (with 21% yield); ir (KBr): 1780 (β-lactam), 1760 and 1740 (ester) cm^{-1}; ^{1}Hmr ($CDCl_3$): 1.22 (s, 9H), 1.47 (s, 3H), 1.67 (s, 3H), 4.57 (s, 1H), 5.41 (s, 1H), 5.81 (d, 1H, H-C14 AB system J = 5.6 Hz), 5.84 (d, 1H, H-C14 AB system J = 5.6 Hz); ^{13}Cmr ($CDCl_3$): 176.5 (C-16), 165.4 (C-11), 164.3 (C-7), 81.4 (C-14), 79.7 (C-5), 69.3 (C-3), 65.0 (C-2), 50.2 (C-6), 38.7 (C-18), 33.6 (C-9), 26.8 (C-19 – C-21), 26.4 (C-10); ms *m/e* (relative intensity): 477, 475 (1:3, 6.8) M$^+$, 361 (2), 318, 316 (1:3, 4.0), 263, 261 (1:3, 9.0), 115 (2), 114 (22), 85 (26), 57 (100).

Crystallographic studies

Single crystals of **1***a*, **1***b*, and **1***c* were obtained by slow crystallization from methanol. Preliminary Weissenberg photographs showed that the three compounds are isomorphous and belong to the orthorhombic system, space group $P2_12_12_1$, Z = 4. Crystal data are given in Table 5.

3S,5R,6R Pivaloyloxy methyl 6-bromo, 6-chloro penicillanate 1a and 3S,5R,6R pivaloyloxy methyl 6-iodo, 6-bromo penicillanate 1b

Intensity data were collected on an Enraf–Nonius CAD-4 diffractometer with MoK α radiation, $\lambda = 0.71069$ Å (graphite monochromated), scan mode: $\theta-2\theta$, scan range (2θ): 2-54°. Lattice parameters were refined from the setting of 25 high-angle reflections. From the 2015 reflections measured for **1***a* (2235 for **1***b*), the 1661 unique for **1***a* (2028 for **1***b*) with $I > 2.5\sigma(I)$ were considered observed. The observed intensities, corrected for Lorentz polarization and absorption effects, were used to solve the structures by Patterson and Fourier methods. The hand of the model was assigned from the known absolute configurations at C-3 and C-5. The structures were refined by the full matrix least-squares method; anisotropic thermal parameters were used for the nonhydrogen atoms. The hydrogen atoms were stereochemically positioned and allowed to refine isotropically with constraints. The final refinements converged to R factors ($R = \Sigma(|F_o| - |F_c|)/\Sigma|F_o|$) of 6.6% for both structures. The final difference maps showed some peaks of about 1 e Å^{-3} for **1***a* and 3 e Å^{-3} for **1***b* around the heaviest atoms. No attempt was made to carry out a Bijvoet analysis. All the calculations were performed on an IBM 4331 computer with the SHELX 76 system of programs (12).

3S,5R,6R Pivaloyloxy methyl 6-iodo, 6-chloro penicillanate 1c

Crystal data are given in Table 5. Accurate cell dimensions were obtained from least-squares fitting of precession film coordinates. From these data it is apparent that **1***c* is both isomorphous and isostructural with **1***a* and **1***b*. Accordingly, relative intensities for the *hk*O and *h*O*l* layers were measured on a rotating drum Optronics P1000 microdensitometer, at 100 μm scanning rasters, from precession photographic data. In order to get a qualitative R factor for the two possible configurations at the 6 position, these data were corrected for Lorentz and polarization effects and compared with the calculated ones using the structure of **1***b* as the model. Qualitative R factor values (%) for the two possible C-6 configurations of **1***c* were calculated: (1) assuming the α-chloro β-iodo configuration, $R(hk\mathrm{O}) = 18$, $R(h\mathrm{O}l) = 20$, and (2) assuming the α-iodo β-chloro configuration, $R(hk\mathrm{O}) = 60$, $R(h\mathrm{O}l) = 63$. Thus the C-6 configuration is α-chloro, β-iodo.

Acknowledgment

This research was supported in part by the Consejo Nacional de Investigaciones Científicas y Técnicas, Subsecretaría de Estado de Ciencia y Tecnología, Comisión de Investigaciones Científicas de la Provincia de Buenos Aires, and Colegio de Farmacéuticos de la Provincia de Buenos Aires. We thank Dr. M. G. Sierra at IQUIOS for recording the ^{1}H and ^{13}C nmr spectra and for helpful discussions, Dr. E. G. Gross and staff at UMYMFOR for mass spectral data, and Dr. J. G. Pecca (Laplex) and Laboratorios Bagó for a generous gift of K benzyl penicillanate and chloromethyl pivalate.

1. R. A. Volkmann, R. D. Carroll, R. B. Drolet, M. L. Elliot, and B. S. Moore. J. Org. Chem. **47**, 3344 (1982).
2. J. Aimetti, E. S. Hamanaka, D. A. Johnson, and M. S. Kellogg. Tetrahedron Lett. 4631 (1979).
3. J. P. Clayton. J. Chem. Soc. C, 2123 (1969).
4. G. A. Olah and J. Welch. Synthesis, 896 (1974).
5. I. McMillan and R. J. Stoodley. J. Chem. Soc. C, 2533 (1968).
6. J. C. Sheehan and T. J. Commons. J. Org. Chem. **43**, 2203 (1978).
7. L. D. Cama, W. J. Leanza, T. R. Beattie, and B. G. Christensen. J. Am. Chem. Soc. **94**, 1408 (1972).
8. W. J. Daehne, E. Frederiksen, E. Gundersen, F. Lund, P. Morch, H. J. Petersen, K. Roholt, L. Tybring, and W. D. Godtfredsen. J. Med. Chem. **13**, 607 (1970).
9. J. S. Wiering and H. Wynberg. J. Org. Chem. **41**, 1574 (1976).
10. D. Scott Wilbur and K. W. Anderson. J. Org. Chem. **47**, 358 (1982).
11. D. Scott Wilbur and H. A. O'Brien, Jr. J. Org. Chem. **47**, 359 (1982).
12. G. M. Sheldrick. SHELX: A program for crystal structure determination. University of Cambridge, England. (1976).
13. W. Richter and K. Biemann. Monatsh. Chem. **95**, 766 (1964).
14. M. R. Bendall, D. T. Pegg, D. M. Doddrell, and D. H. Williams. J. Org. Chem. **47**, 3023 (1982).
15. R. A. Archer, R. D. G. Cooper, and P. V. Demarco. J. Chem. Soc. Chem. Commun. 1291 (1970).
16. C. R. Harrison and P. Hodge. J. Chem. Soc. Perkin Trans. 1, 1772 (1976).
17. C. J. Chang and S. L. Hem. J. Pharm. Sci. **68**, 64 (1979).
18. R. W. Sweet. *In* Cephalosporins and penicillins, chemistry and biology. *Edited by* E. H. Flynn. Academic Press, New York. 1972. pp. 280–309.
19. P. A. C. Gane, M. D. Boles, and A. E. Bird. Acta Crystallogr. Sect. B, **38**, 399 (1980).
20. P. C. Blanpain, J. B. Nagy, G. H. Laurent, and F. V. Durant. J. Med. Chem. **23**, 1283 (1980).
21. P. J. Giddings, D. I. John, and E. J. Thomas. Tetrahedron Lett. 399 (1980).
22. W. C. Hamilton. Acta Crystallogr. **12**, 609 (1959).

A formal enantiospecific synthesis of California red scale pheromone

JOHN H. HUTCHINSON AND THOMAS MONEY
Department of Chemistry, University of British Columbia, Vancouver, B.C., Canada V6T 1Y6

Received May 15, 1985

JOHN H. HUTCHINSON and THOMAS MONEY. Can. J. Chem. **63**, 3182 (1985).

Cleavage of α,α-disubstituted β-bromoketone intermediates derived from (+)-camphor forms the basis of an alternative enantiospecific synthesis of (*Z*)-3-methyl-6-isopropenyl-3,9-decadien-1-yl acetate (**1**), one of the sex pheromones of the female California red scale, *Aonidiella aurantii* (Maskell).

JOHN H. HUTCHINSON et THOMAS MONEY. Can. J. Chem. **63**, 3182 (1985).

On a utilisé le clivage des β-bromocétones α,α-disubstituées intermédiaires qui proviennent du (+)-camphre comme base d'une nouvelle synthèse énantiospécifique de l'acétate de l'isopropényl-6 méthyl-3 décadiène-3,9 yle-(*Z*) (**1**), une des phérémones sexuelles de l'*Aonidiella aurantii* (Maskell).

[Traduit par le journal]

The isolation, structure, and enantiospecific synthesis of (*Z*)-3-methyl-6-isopropenyl-3,9-decadien-1-yl acetate (**1**), one of the sex pheromones of the female California red scale, *Aonidiella aurantii* (Maskell), has been described by Roelofs *et al.* (1). Other independent syntheses of racemic (2, 3) and optically active **1** (4) have also been reported. Diene-aldehyde **2** and trienol **3** are pentultimate intermediates in the synthetic

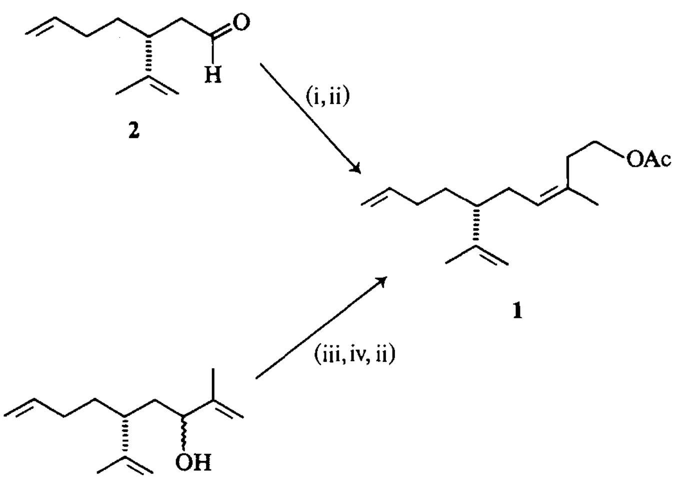

(i) $Ph_3P{=}C(CH_3)CH_2CH_2OLi$; (ii) Ac_2O/C_5H_5N; (iii) KH/Bu_3SnCH_2I; (iv) BuLi/−78°C

routes devised by Roelofs (1) and Still (2), respectively, and this report describes an alternative enantiospecific synthesis (Scheme 1) of these compounds from (+)-camphor (**4**).

Previous investigations in our laboratory have shown that (+)-camphor (**4**) can easily be converted to (+)-9,10-dibromocamphor (**6**) (5) and that the latter compound undergoes facile, efficient ring cleavage with sodium hydroxide or sodium methoxide to provide bromo-acid (**7**) or the corresponding ester in ~90% yield (6, 7). Reduction ($LiAlH_4$/THF) of acid **7** followed by ozonolysis ((*i*) O_3/MeOH, (*ii*) Me_2S) and protection of the hydroxyl group produced a cyclopentanone derivative (**10**), which, like 9,10-dibromocamphor (**6**),[1] is an α,α-disubstituted β-bromoketone and would therefore be expected to undergo Grob-type ring cleavage with base (8, 9). In the event, treatment of bromoketone **10** with sodium methoxide provided acyclic ester (9) **12** (~57%) and a ketone (~17%) which was tentatively assigned structure **13**[2] on the basis of ir (ν_{max} 1795 cm^{-1}) and nmr evidence. Attempts to reduce the proportion of bicyclic ketone **13** produced in the ring cleavage of bromoketone **10** by varying the time and temperature of the reaction did not lead to significant increases in the yield of acyclic ester **12**. Other studies in our laboratory indicated that ring cleavage of bromoketal MOM ether (**11**) can be achieved with sodium hydroxide. However, although cyclization did not seem to occur under these conditions, the product was difficult to purify and the estimated yield of acyclic acid was less than that obtained for the formation of acyclic ester **12**.

Reduction of ester **12** with $LiAlH_4$/THF followed by oxidation with PDC/CH_2Cl_2 provided an aldehyde (**17**), which on reaction wih methylenetriphenylphosphorane yielded diene **18** in ~50% overall yield from **12**. Our initial synthetic objective, diene-aldehyde **2**,[3] was then prepared from **18** by removal of the protecting group (Bu_4NF/THF) and oxidation of the alcohol **19**[4] with PDC/CH_2Cl_2. Finally, treatment of aldehyde 2 with 2-propenylmagnesium bromide provided diastereomeric trienols 3*a*, *b* (80% yield), which were easily separated by column chromatography. Since the stereoselective conversion of 3*a* and 3*b* to **1** has previously been reported (2), the sequence of reactions outlined in Scheme 1 represents a formal enantiospecific synthesis of one of the sex pheromones of California red scale[5] and also provides a further illustration of the versatility of camphor as a chiral starting material in natural product synthesis. (12).

Experimental

Melting points (mp) were determined on a Kofler micro heating stage and are uncorrected. Infrared spectra were recorded on a

[1] The yield of ~60% cited in this paper for the conversion of 3,9,10-tribromocamphor to 9,10-dibromocamphor has been increased to ~95% by using $Zn/HOAc/Et_2O$/0°C for 30 min.

[2] The structure and absolute configuration of the *p*-bromobenzoate derivative **15** derived from **13** has been confirmed by X-ray crystallographic analysis; S. J. Rettig and J. Trotter, unpublished results.

[3] We are grateful to Dr. Richard J. Anderson (Zoecon Corporation, Palo Alto, California) for providing us with comparative nmr and ir spectra for this compound.

[4] Investigations of an alternative and potentially more efficient route to dienol **19**, involving sequential treatment of bromoketal **8** with diborane and base (10), have so far been inconclusive.

[5] A total synthesis of the other pheromone of California red scale has also been described (11).

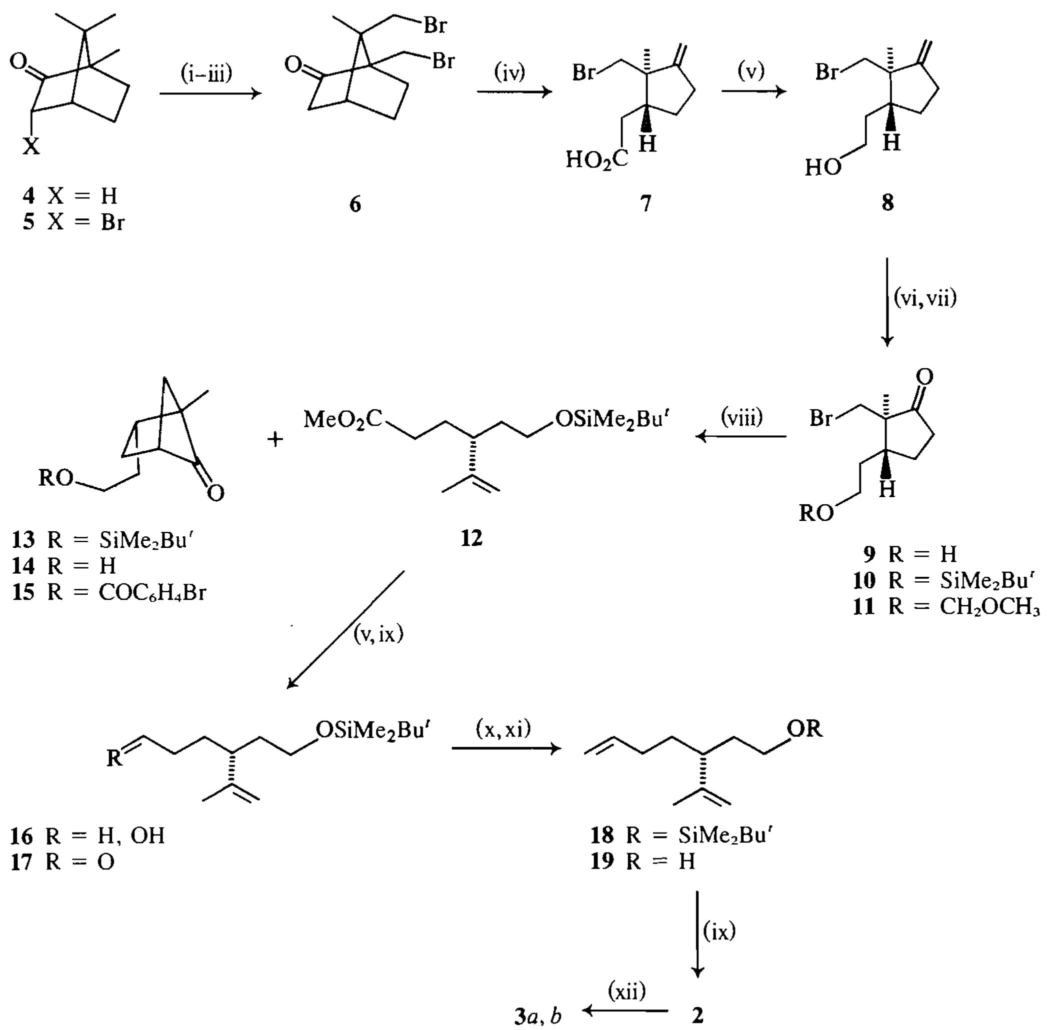

(i) $Br_2/ClSO_3H$/1 h; (ii) $Br_2/ClSO_3H$/5 days; (iii) Zn/HOAc/Et_2O/0°C; (iv) KOH/DMSO/H_2O; (v) $LiAlH_4$/THF; (vi) O_3/MeOH; Me_2S; (vii) Bu^tMe_2SiCl/DMAP/CH_2Cl_2; (viii) NaOMe/MeOH/60°C; (ix) PDC/CH_2Cl_2; (x) $CH_2{=}PPh_3$/THF; (xi) Bu_4NF/THF; (xii) $CH_2{=}C(CH_3)MgBr$/THF

SCHEME 1

Perkin–Elmer 137 spectrophotometer and optical rotations were made on a Perkin–Elmer 141 polarimeter. The ^{1}H nmr spectra were recorded on Bruker WH-400, Bruker WP-80, or Nicolet-Oxford H-270 instruments. Signal positions are given in delta (δ) with tetramethylsilane (TMS) as internal reference (except for compounds containing trialkylsilyl groups where TMS was used as an external reference). The integrated areas and signal multiplicities are indicated in parentheses. Low resolution mass spectra were determined on a MAT CH-4 spectrometer and high resolution spectra were recorded on a Kratos MS-50 spectrometer. Microanalyses were performed by Mr. P. Borda, Microanalytical Laboratory, University of British Columbia. Column chromatography was done using Merck silica gel 60 (230–400 MHz) and thin-layer chromatography (tlc) utilizing silica gel 1B2-F (Baker-flex) sheets.

Bromoacid 7

Method A

To a solution of 9,10-dibromocamphor (**6**) (5) (1.5 g, 4.8 mmol) in dimethylsulphoxide (50 mL) was added potassium hydroxide (1.35 g, 24 mmol) in water (10 mL). After 1 h, the yellow solution was poured onto water and extracted once with ether. The ether layer was washed once with water and the combined aqueous layers were then carefully acidified with 6 *N* hydrochloric acid. This was extracted with ether, the ether layers then washed with brine, dried ($MgSO_4$), and evaporated to yield bromoacid **7** (1.2 g; 98%) as a white crystalline solid, one spot on tlc. Recrystallization of a small amount of this material from petroleum ether (30–60°C) afforded an analytically pure sample of bromoacid **7**, mp 62–64°C; $[\alpha]_D$ −48.5° (*c* 0.4, MeOH); ν_{max} ($CHCl_3$): 2950, 1705, 1640, 890 cm^{-1}; δ ($CDCl_3$, 400 MHz): 1.08 (3H, s), 1.39 (1H, m), 2.01 (1H, m), 2.18 (1H, dd, *J* = 16 Hz, 10 Hz), 2.32–2.48 (2H, m), 2.55 (1H, m), 2.63 (1H, dd, *J* = 16 Hz, 4 Hz), 3.39 (d) and 3.47 (d) (2H, AB quartet, *J* = 10 Hz), 4.86 (1H, t, *J* = 2 Hz), 5.00 (1H, t, *J* = 2 Hz); *m*/*e* (relative intensity): 248/246 (M^+, 0.4/0.4), 188/186 (4/4), 167 (7), 166 (17), 153 (100), 111 (32), 107 (98). *Anal.* calcd. for $C_{10}H_{15}O_2Br$: C 48.58, H 6.12, Br 32.35; found: C 48.47, H 6.16, Br 32.20.

Method B

9,10-Dibromocamphor (**6**) (1.0 g, 3.2 mmol), 0.5 *N* potassium hydroxide (80 mL, 40 mmol), and tetrahydrofuran (80 mL) were stirred at room temperature for 4.5 h. Work-up as before gave bromo acid **7** (0.75 g; 94% yield) as a white solid.

Bromoalcohol 8

To a solution of bromoacid **7** (2.53 g, 10.2 mmol) in tetrahydrofuran (80 mL) at 0°C under argon was added lithium aluminum hydride (0.66 g, 17.4 mmol) in portions over 15 min. After a further 15 min at 0°C, the reaction was warmed to room temperature and quenched with ice 3 h later. Water and ether were added and the aqueous phase carefully acidified with 1 *N* hydrochloric acid. Extraction with ether (2×) followed by work-up in the usual way yielded a pale yellow oil (2.30 g). Flash chromatography (silica gel; petroleum ether (30–60°C)/ether 3:2) gave bromoalcohol **8** (2.25 g, 95% yield) as a colourless oil; $[\alpha]_D$ −46.2° (*c* 1.0, MeOH); ν_{max} (film): 3350, 1650, 890 cm^{-1}; δ ($CDCl_3$, 400 MHz): 1.04 (3H, s), 1.25–1.47 (2H, m), 1.62 (1H, bs, D_2O exchangeable), 1.80 (1H, m), 1.92 (1H, m), 2.16 (1H, m), 2.33 (1H, m), 2.42 (1H, m), 3.42 (d) and 3.49 (d) (2H, AB quartet, *J* = 10 Hz), 2.68 (1H, m) and 2.75 (1H, m), 4.84 (1H, t, *J* = 2 Hz), 4.98 (1H, t, *J* = 2 Hz); *m/e* (relative intensity): 217/215 (26/27), 135 (43), 121 (39), 107 (66), 95 (100), 93 (89), 91 (71), 79 (74). *Anal.* calcd. for $C_{10}H_{17}OBr$: C 51.52, H 7.35, Br 34.27; found: C 51.81, H 7.27, Br 34.09.

Bromoketal 9 and bromoketal tert-*butyldimethylsilyl ether 10*

A solution of bromoalcohol **8** (796 mg, 3.4 mmol) in dry methanol (60 mL) was cooled to −78°C and subjected to a stream of ozone. After the solution turned blue it was flushed with oxygen until colourless, dimethyl sulphide (2 mL) was added, and the mixture stirred at room temperatue for 16 h. The methanol was removed under reduced pressure and the resulting oil redissolved in ether, filtered through silica gel, and the ether evaporated to yield crude bromoketol **9** (0.77 g); ν_{max} (film): 3400, 1720; δ ($CDCl_3$, 80 MHz): 1.00 (3H, s), 1.5–2.0 (4H, m, 1 proton exchangeable with D_2O), 3.3 (d) and 3.7 (d) (2H, AB quartet, *J* = 10 Hz), 3.8 (2H, bt, *J* = 6 Hz); *m/e* (relative intensity): 236/234 (M^+, 0.5/0.6), 155 (22), 97 (100), 95 (20), 93 (19), 91 (19); *Mol. Wt.* calcd. for $C_9H_{15}O_2Br$: 236.0235/234.0255; found (high resolution mass spectrometry): 236.0233/234.0245.

The crude bromoketol **9** (0.77 g), *tert*-butyldimethylsilyl chloride (0.98 g, 6.6 mmol, freshly sublimed), and 4-(*N*,*N*-dimethylamino)-pyridine (0.8 g, 6.6 mmol) were dissolved in dry dichloromethane (40 mL) under argon. After 24 h at room temperature the reaction was partitioned between water and ether and worked up in the usual way to provide a pale yellow mobile oil (1.41 g).

Purification by flash chromatography (silica gel, petroleum ether (30–60°C)/ether 9:1) yielded **10** (0.79 g) (67% yield over 2 steps); $[\alpha]_D$ −57.6° (*c* 0.55 MeOH); ν_{max} (film): 1740 cm^{-1}; δ ($CDCl_3$, 400 MHz): 0.07 (6H, s), 0.91 (9H, s), 0.94 (3H, s), 1.40–1.54 (2H, m), 1.74 (1H, m), 2.07–2.25 (2H, m), 2.37 (1H, m), 2.62 (1H, m), 3.29 (1H, d, *J* = 10 Hz), 3.61 (1H, d, *J* = 10 Hz), 3.67–3.80 (2H, m); *m/e* (relative intensity): 293/291 (9/9), 211 (10), 169 (9), 167 (8), 137 (100), 119 (36), 109 (53), 95 (82), 93 (73). *Anal.* calcd. for $C_{15}H_{29}O_2BrSi$: C 51.57, H 8.37, Br 22.87; found: C 51.83, H 8.45, Br 22.77.

Bromoketol MOM ether 11

To a solution of bromoketol **9** (309 mg, 1.3 mmol) and methylal (5 mL, 57.5 mmol, in dry dichloromethane (9 mL) under argon was added phosphorus pentoxide (1.5 g) in three portions. After 3 h the reaction was carefully quenched with ice-cold sodium carbonate solution. Ether extraction, followed by work-up in the usual way, provided a yellow oil (297 mg) which, after flash chromatography (silica gel; petroleum ether (30–60°C)/ether 1.5:1), gave **11** (287.5 mg; 78%) as a colourless oil; ν_{max} (film): 1740 cm^{-1}; δ ($CDCl_3$, 270 MHz): 0.94 (3H, s), 1.50 (2H, m), 1.81 (1H, m), 2.17 (2H, m), 2.38 (1H, m), 2.58 (1H, m), 3.28 (1H, d, *J* = 10 Hz), 3.37 (3H, s), 3.60 (1H, d, *J* = 10 Hz), 3.64 (2H, m), 4.63 (2H, s); *m/e* (relative intensity): 280/278 (M^+, 0.1/0.2), 199 (64), 167 (100), 149 (66), 107 (62), 97 (62), 95 (61). *Exact Mass* calcd. for $C_{11}H_{19}O_3$ (M − Br): 199.1334; found (high resolution mass spectrometry): 199.1326 (M − Br).

*Ring cleavage of bromoketone 10: formation of methyl 4-isopropenyl-6-*tert-*butyldimethylsilyloxyhexanoate 12 and bicyclic ketone 13*

Sodium metal (140 mg, 6.1 mmol) was added to dry methanol (5 mL) under argon. When all the sodium had reacted, bromoketone **10** (215 mg, 0.61 mmol) in dry methanol (6 mL) was added via a cannula needle and the reaction heated to 60°C (oil bath temperature). After 3.5 h the mixture was added to saturated ammonium chloride solution and extracted (3 times) with ethyl acetate. The combined organic layers were washed with brine, dried ($MgSO_4$), and the solvent removed. The residue (193 mg) was subjected to flash chromatography (silica gel; petroleum ether (30–60°C)/ether; 50:1) to yield ester **12** (105 mg, 57% yield; 61% yield based on recovered starting material); $[\alpha]_D$ −0.45° (*c* 0.66, MeOH); ν_{max} (film): 1745, 1650, 890 cm^{-1}; δ ($CDCl_3$, 400 MHz): 0.03 (6H, s), 0.89 (9H, s), 1.53–1.77 (7H, m), 2.13–2.33 (3H, m), 3.46–3.60 (2H, m), 3.65 (3H, s), 4.69 (1H, bs), 4.78 (1H, bs); *m/e* (relative intensity): 285 (1.4), 269 (2.6), 243 (73), 211 (16), 171 (40), 157 (40), 151 (100). *Anal.* calcd. for $C_{16}H_{32}OSi$: C 63.95, H 10.73; found: C 63.79, H 10.78.

Further elution with petroleum ether/ether (10:1) provided bicyclic ketone **13** (28.4 mg; 17% yield; 19% yield based on recovered starting material); $[\alpha]_D$ +54.1° (*c* 0.29, CH_2Cl_2); ν_{max} (film): 1790 cm^{-1}; δ ($CDCl_3$, 400 MHz): 0.04 (6H, s), 0.89 (9H, s), 1.20 (3H, s), 1.46–1.62 (4H, m), 1.84 (1H, m), 2.00–2.08 (2H, m), 2.83 (1H, bs), 3.55–3.72 (2H, m); *m/e* (relative intensity): 268 (M^+, 2), 253 (4), 227 (36), 211 (71), 183 (41), 165 (33), 119 (34), 107 (32), 93 (32), 75 (100), 73 (49). *Mol. Wt.* calcd. for $C_{15}H_{28}O_2Si$: 268.1859; found (high resolution mass spectrometry): 268.1864. *Anal.* calcd. for $C_{15}H_{28}O_2Si$: C 67.11, H 10.51; found: C 67.20, H 10.44.

The final fractions from the column provided starting material **10** (11.5 mg).

p-*Bromobenzoate (15) derived from bicyclic ketone 13*

To bicyclic ketone **13** (83 mg, 0.31 mmol) was added tetrabutylammonium fluoride (3.1 mL, 3.1 mmol, 1 *M* solution in THF) and the solution stirred under argon at room temperature for 2 h. The mixture was diluted with ether, washed with brine, dried ($MgSO_4$), and the solvent removed *in vacuo* to yield a yellow oil (104 mg) which, on column chromatography (silica gel; petroleum ether (30–60°C/ether 1:2) afforded bicyclic ketoalcohol **14** (32 mg, 67% yield); ν_{max} (film): 3300, 1790 cm^{-1}; δ ($CDCl_3$, 80 MHz): 1.18 (3H, s), 2.83 (1H, bs), 3.4–3.9 (2H, m); *m/e* (relative intensity): 154 (M^+, 1), 93 (87), 81 (100).

Ketoalcohol **14** (27.4 mg, 0.17 mmol) was dissolved in dry pyridine (2 mL) and *para*-bromobenzoyl chloride (77 mg, 0.35 mmol) added. The solution was stirred under argon for 24 h, then diluted with ether and poured onto 1 *N* hydrochloric acid. The ether layer was washed twice with 2 *N* potassium hydroxide solution, then with water (3 times). The crude product, after evaporation of the solvent, was chromatographed on silica gel (petroleum ether (30–60°C)/ether 4:1) to give *para*-bromobenzoate (**15**) (44 mg, 73% yield) as an oil that crystallized on standing. Crystallization from petroleum ether (30–60°C) provided **15**, mp 47.5–48.5°C; ν_{max} (film): 1780, 1720, 1595 cm^{-1}; δ ($CDCl_3$, 80 MHz): 1.28 (3H, s), 1.30–1.85 (4H, m), 1.85–2.33 (3H, m), 2.90 (1H, bs), 4.38 (2H, t, *J* = 7 Hz), 7.50–8.00 (4H, m); *m/e* (relative intensity): 338/336 (M^+, 0.3/0.4), 297/295 (414), 185 (99), 183 (100), 108 (58), 93 (71).

*4-Isopropenyl-6-*tert-*butyldimethylsilyloxyhexanal (17)*

Lithium aluminum hydride (76 mg, 2.0 mmol) was added in 4 portions to a cooled (0°C) solution of ester **11** (400 mg, 1.33 mmol) in tetrahydrofuran (30 mL) under argon. After 1 h at 0°C and 1 h at room temperature the solution was added to ice, carefully acidified (1 *N* hydrochloric acid), and extracted with ether. Work-up in the usual way gave a pale yellow oil (380 mg) which, on flash chromatography (silica gel; petroleum ether (30–60°C)/ether 1:2), provided 3-isopropenyl-1,6-hexanediol monosilyl ether **16** (326 mg, 90%) as a colourless oil: ν_{max} (film): 3350, 1640, 880 cm^{-1}; δ ($CDCl_3$, 80 MHz): 0.08 (6H, s), 0.95 (9H, s), 1.25–1.75 (10H, m), 2.05–2.30 (1H, m), 3.40–3.80 (4H, m), 4.75 (2H, m); *m/e* (relative intensity): 257 (0.2), 213 (13), 123 (47), 105 (33), 81 (60), 75 (100). *Exact Mass* calcd. for $C_{15}H_{31}SiO_2 - C_4H_9$: 215.1474; found (high resolution mass spectrometry): 215.1467.

A solution of alcohol **16** (170 mg, 0.63 mmol) and pyridinium dichromate (1.18 g, 3.13 mmol) in dry dichloromethane (20 mL) was stirred at room temperature under an argon atmosphere for 16 h. The reaction mixture was then diluted with ether, filtered (silica gel), and the solvent evaporated under reduced pressure. The residue was purified by chromatography (silica gel; petroleum ether (30–60°C)/ether 10:1) to give aldehyde **17** (129 mg, 76% yield) as a colourless oil, $[\alpha]_D$ −3.58° (*c* 0.81, CH_2Cl_2); ν_{max} (film): 3100, 2730, 1730, 1650, 895 cm^{-1}; δ ($CDCl_3$, 80 MHz): 0.08 (6H, s), 0.92 (9H, s), 1.45–1.85 (7H, m), 2.05–2.52 (3H, m), 3.55 (2H, t, *J* = 6 Hz), 4.72 (1H, bs), 4.80 (1H, m), 9.68 (1H, t, *J* = 4 Hz); *m/e* (relative intensity): 270 (M^+, 0.1), 269 (0.4), 255 (0.5), 243 (9), 213 (27), 121 (58), 93 (59), 75 (100). *Anal.* calcd. for $C_{15}H_{30}O_2Si$: C 66.60, H 11.18; found: C 66.70, H 11.25.

3-Isopropenyl-hept-6-en-1-ol tert-*butyldimethylsilyl ether (18)*

Methyltriphenylphosphonium bromide (259 mg, 0.73 mmol) was suspended in dry tetrahydrofuran (5 mL) under an atmosphere of argon and cooled to −78°C. n-Butyllithium (0.45 mL, 0.72 mmol; 1.6 *M* solution in hexane) was added and, after 10 min at −78°C, the solution stirred for a further 40 min at room temperature. Aldehyde **17** (97 mg, 0.36 mmol) in tetrahydrofuran (5 mL) was added and the reaction mixture stirred for 1 h. After dilution with hexane (20 mL), the solution was poured onto a prepacked column of Florisil and eluted with hexane. The crude product was then chromatographed on silica gel (petroleum ether (30–60°C/ether 250:1) to provide diene **18**, 68.3 mg (71% yield); ν_{max} (film): 3100, 1640, 910, 890 cm^{-1}; δ ($CDCl_3$, 400 MHz): 0.03 (6H, s), 0.88 (9H, s), 1.42 (2H, m), 1.56 (2H, m), 1.60 (3H, bs), 1.88–2.05 (2H, m), 2.20 (1H, m), 3.46–3.60 (2H, m), 4.69 (1H, bs), 4.75 (1H, bs), 4.92 (1H, bd, *J* = 10 Hz), 4.99 (1H, bd, *J* = 17 Hz), 5.80 (1H, overlapping ddt, *J* = 17, 10, 7 Hz); *m/e* (relative intensity): 253 (0.1), 211 (20), 129 (26), 101 (39), 75 (100), 73 (27). *Exact Mass* calcd. for $C_{16}H_{31}OSi - C_4H_9$: 211.1518; found (high resolution mass spectrometry): 211.1520.

(R)*-3-isopropenyl-6-heptenal (2)*

A solution of tetrabutylammonium fluoride (2.5 mL, 2.5 mmol; 1 *M* solution in tetrahydrofuran) was added to the diene **18** (67 mg, 0.48 mmol) under argon. After 2.5 h the reaction was diluted with ether and water. The aqueous layer was extracted twice more with ether and the ether layers were combined and washed twice with brine. After drying ($MgSO_4$), the ether was removed to yield 98.6 mg of a yellow oil. Purification by column chromatography (silica gel; petroleum ether (30–60°C)/ether 6:1) provided (*R*)-3-isopropenylhex-6-en-1-ol (**19**) (38 mg); ν_{max} (film): 3320, 3080, 1640, 905, 890 cm^{-1}; δ ($CDCl_3$, 80 MHz): 1.72 (3H, dd, *J* = 1, 1 Hz), 3.65 (2H, t, *J* = 6 Hz), 4.70–5.18 (4H, m), 5.82 (1H, 10-line multiplet); *m/e* (relative intensity): 154 (M^+, 6), 41 (100).

Alcohol **19** (26 mg, 0.17 mmol) in dry dichloromethane (7 mL) was treated with pyridinium dichromate (315 mg, 0.85 mmol) and the reaction stirred under argon for 14 h. The mixture was diluted with ether and filtered through a pad of silica gel. Removal of the solvent *in vacuo* at 0°C yielded 34.8 mg of crude product. Chromatography (silica gel; petroleum ether (30–60°C)/ether 4:1) gave aldehyde **2** (16 mg, 62% over 2 steps) as an unstable volatile oil: $[\alpha]_D$ +6.1° (*c* 0.74, CH_2Cl_2); ν_{max} (film): 3080, 2740, 1730, 1640, 890 cm^{-1} (lit. (1) ν_{max} (CCl_4): 3080, 1730 cm^{-1}); δ ($CDCl_3$, 270 MHz): 1.52 (2H, m), 1.69 (3H, bs), 2.04 (2H, m), 2.46 (2H, multiplet which simplified on irradiation at δ 9.66), 2.73 (1H, 5-line multiplet), 4.79 (1H, m), 4.83 (1H, m), 4.93–5.05 (2H, m), 5.80 (1H, ddt, *J* = 17, 11, 6 Hz), 9.66 (1H, t, *J* = 2 Hz), (lit. (1) δ ($CDCl_3$): 1.67 (3H, bs), 9.75 (1H, t, *J* = 2 Hz)); *m/e* (relative intensity): 151 (M^+ − H, 0.9), 1.37 (3), 108 (17), 95 (29), 93 (29), 81 (33), 79 (29), 69 (100), 67 (53). *Exact Mass* calcd. for $C_{10}H_{16}O$ − H: 151.1123; found (high resolution mass spectrometry): 151.1129 (*M* − 1).

*(*3R,5R*)- and (*3S,5S*)-5-isopropenyl-2-methyl-1,8-nonadien-3-ol (*3a, 3b*)*

A 3-neck flask fitted with a Dry Ice condenser and a pressure equalized dropping funnel, and flushed with agron, was charged with freshly crushed magnesium turnings (300 mg, 12.5 mmol). A crystal of iodine was added, followed by 2-bromopropene (0.75 mL, 8.3 mmol) in tetrahydrofuran (20 mL, dropwise). After the addition was complete, the mixture was refluxed for 30 min and cooled to room temperature. An aliquot of this solution (4 mL, approximately 1.6 mmol) was removed by syringe and added to a solution of the aldehyde **2** (31 mg, 0.2 mmol) in tetrahydrofuran (4 mL) at −15°C. The reaction mixture was stirred at this temperature for 30 min, then allowed to warm to room temperature over a further 30 min before being added to an ice/ammonium chloride solution. Extraction with ether and work-up in the usual way provided a crude product (56 mg) which was subjected to chromatography (silica gel; petroleum ether (30–60°C)/ether 12:1) to give, in order of elution, the following.

(*i*) Least polar diastereomer (**3***a* or **3***b*) (15.5 mg), R_f 0.46 (petroleum ether (30–60°C)/ether 1:1); $[\alpha]_D$ −15.47° (*c* 1.5, CH_2Cl_2); ν_{max} (film): 3400, 3100, 1645, 890 cm^{-1}; δ ($CDCl_3$, 400 MHz): 1.38–1.60 (5H, m, one proton D_2O exchangeable), 1.63 (3H, bs), 1.72 (3H, bs), 1.98 (2H, m), 2.39 (1H, 7-line multiplet), 4.00 (1H, dd, *J* = 9, 3 Hz), 4.81 (2H, bs), 4.84 (1H, bs), 4.90–5.03 (3H, m), 5.83 (1H, ddt, *J* = 17, 10, 6.5 Hz); *m/e* (relative intensity): 194 (M^+, 0.4), 179 (7), 135 (30), 109 (35), 107 (34), 95 (34), 93 (45), 84 (47), 81 (65), 71 (86), 70 (57), 69 (100), 67 (73). *Mol. Wt.* calcd. for $C_{13}H_{22}O$: 194.1671; found (high resolution mass spectrometry): 194.1680.

(*ii*) More polar diastereomer (**3***a* or **3***b*), 15.9 mg; R_f 0.32 (petroleum ether (30–60°C)/ether 1:1); $[\alpha]_D$ +50.15°C (*c* 1.34, CH_2Cl_2); ν_{max} (film): 3380, 3100, 1645, 890 cm^{-1}; δ ($CDCl_3$, 400 MHz): 1.45 (2H, m), 1.50–1.65 (3H, m, one proton D_2O exchangeable), 1.67 (3H, bs), 1.73 (3H, bs), 1.97 (2H, m), 2.14 (1H, 7-line multiplet), 4.08 (1H, t, *J* = 6.5 Hz), 4.75 (1H, bs), 4.80 (1H, bs), 4.84 (1H, bs), 4.90–5.05 (3H, m), 5.80 (1H, ddt, *J* = 17, 10, 7 Hz); *m/e* (relative intensity): 194 (0.6), 151 (5), 139 (5), 109 (20), 107 (26), 95 (24), 94 (35), 93 (24), 81 (49), 79 (35), 71 (100), 69 (82), 68 (78). *Exact Mass* calcd. for $C_{13}H_{22}O - H_2O$: 176.1565; found (high resolution mass spectrometry): 176.1561.

Total yield of alcohols **3***a*, *b*: 31.4 mg (79%). *Anal.* (**3***a*, *b*, mixture of diastereomers) calcd. for $C_{13}H_{22}O$: C 80.35, H 11.41; found: C 80.30, H 11.47.

Acknowledgement

We thank N.S.E.R.C., Ottawa, Canada for a research grant.

1. W. Roelofs, M. Gieselmann, A. Cardé, H. Tashiro, D. S. Moreno, C. A. Henrick, and R. J. Anderson. J. Chem. Ecol. **4**, 211 (1978).
2. W. C. Still and A. Mitra. J. Am. Chem. Soc. **100**, 1927 (1978).
3. M. P. Cooke, Jr. and D. L. Burman. J. Org. Chem. **47**, 4955 (1982).
4. D. Caine and E. Crews. Tetrahedron Lett. **25**, 5359 (1984).
5. W. M. Dadson, M. Lam, T. Money, and S. E. Piper. Can. J. Chem. **61**, 343 (1983).
6. J. H. Hutchinson, T. Money, and S. E. Piper. J. Chem. Soc. Chem. Commun. 455 (1984).
7. J. H. Hutchinson and T. Money. Tetrahedron Lett. **26**, 1819 (1985).
8. (*a*) M. O. Forster. J. Chem. Soc. **81**, 264 (1902); (*b*) H. Burgess. J. Chem. Soc. **125**, 2375 (1924); (*c*) D. S. Tarbell and F. C. Loveless. J. Am. Chem. Soc. **80**, 1963 (1958); (*d*) S. A. Achmad and G. W. K. Cavill. Aust. J. Chem. **16**, 858 (1963); **18**, 1979 (1965); (*e*) J. Wolinsky and D. Chan. J. Org. Chem. **30**, 41 (1965); (*f*) J. Wolinsky and R. O. Hutchins. J. Org. Chem. **37**, 3294 (1972); (*g*) J. N. Marx and L. R. Norman. J. Org. Chem. **40**, 1602 (1975); (*h*) P. Yates, M. J. Jorgensen, and P. Singh. J. Am. Chem. Soc. **91**, 4739 (1969); (*i*) H. Rupe and K. Schafer. Helv. Chim. Acta, **11**, 463 (1928); (*j*) T. Hudlicky and R. P. Short. J. Org. Chem. **47**, 1522 (1982); (*k*) J. L. Belletire and D. R. Walley. Tetrahedron Lett. **24**, 1475 (1983); (*l*) E. Wenkert, P. Bakuzis, and R. J. Baumgarten. J. Am. Chem. Soc. **93**, 3208 (1971).
9. K. B. Becker and C. A. Grob. *In* The chemistry of double-bonded functional groups. Part 2. Suppl. A. *Edited by* S. Patai. Interscience, New York. 1977 pp. 653–723.
10. J. A. Marshall. Synthesis, 229 (1971), and references cited.
11. B. B. Snider and D. Rodini. Tetrahedron Lett. 1399 (1978).
12. T. Money. Nat. Prod. Rep. In press (1985).

Synthesis and conformational assignment of *cis*- and *trans*-2-amino-1-arylcyclohexanols[1]

ANTONIO DELGADO, RICARDO GRANADOS, DAVID MAULEON,[2] AND INMACULADA SOUCHEIRON
Departamento de Química Orgánica y Farmacéutica, Facultad de Farmacia, Universidad de Barcelona, 08028 Barcelona, Spain

AND

MIGUEL FELIZ
Departamento de Química Orgánica, Facultad de Química, Universidad de Barcelona, 08028 Barcelona, Spain

Received December 28, 1984

ANTONIO DELGADO, RICARDO GRANADOS, DAVID MAULEON, INMACULADA SOUCHEIRON, and MIGUEL FELIZ. Can. J. Chem. **63**, 3186 (1985).

The synthesis of *cis*- and *trans*-2-amino-1-arylcyclohexanols **1**–**8**, conformationally restricted analogues of the α-adrenergic drugs norephedrine **9**, methoxamine **10**, and isopropylmethoxamine **11**, is described. *trans*-Aminoalcohols were obtained through reaction of epoxides **12** or **13** with isopropylamine (to afford **4** and **8**) or with sodium azide followed by lithium aluminum hydride reduction (to afford **2** and **6**), whereas *cis*-aminoalcohols **1** and **5** were obtained by condensation of 2-aminocyclohexanone hydrobromide **26** with the appropriate organometallic reagent. Treatment of **1** and **5** with acetone followed by sodium borohydride reduction gave isopropylaminoalcohols **3** and **7**. Configurational and conformational assignments of aminoalcohols **1**–**8** have been carried out on the basis of their ^{1}H nmr and ^{13}C nmr data and by comparison with reference diols **18** and **30**. The major or exclusive chair conformation observed for all the compounds has an equatorial aryl group.

ANTONIO DELGADO, RICARDO GRANADOS, DAVID MAULEON, INMACULADA SOUCHEIRON et MIGUEL FELIZ. Can. J. Chem. **63**, 3186 (1985).

On décrit la synthèse des amino-2 aryl-1 cyclohexanols-*cis* et -*trans* (**1**–**8**) qui sont des analogues à conformation restreinte de médicaments α-adrénergiques comme la noréphédrine **9**, la méthoxamine **10** et l'isopropylméthoxamine **11**. On a obtenu les aminoalcools-*trans* en faisant réagir les époxydes **12** ou **13** soit avec de l'isopropylamine (pour obtenir les composés **4** et **8**) soit avec l'azoture de sodium, puis avec de l'alanate de lithium (pour obtenir les composés **2** et **6**). On accède aux aminoalcools-*cis* (**1** et **5**) en faisant réagir le bromhydrate de l'amino-2 cyclohexanone **26** avec un dérivé organométallique approprié. La réaction des composés **1** et **5** avec l'acétone, suivie d'une réduction par le borohydrure de sodium, conduit aux isopropylaminoalcools **3** et **7**. On a procédé aux attributions configurationnelles et conformationnelles des aminoalcools **1**–**8** en se basant sur les données rmn du ^{1}H et du ^{13}C ainsi que par une comparaison avec les diols de référence **18** et **30**. Dans tous les composés, la conformation chaise observée de façon majoritaire ou exclusive comporte un groupement aryle en position équatoriale.

[Traduit par le journal]

Introduction

In connection with our studies on adrenergic agents, we focused our attention on the synthesis, by unambiguous routes, of *cis*- and *trans*-2-amino-1-arylcyclohexanols **1**–**8**, conformationally restricted analogues of the α-adrenergic stimulants norephedrine **9**, methoxamine **10**, and of the β-adrenergic blocker isopropylmethoxamine **11**.

Although cyclic aminoalcohols **1**–**8** exhibit a higher conformational limitation than the model compounds **9**–**11**, two chair conformations are still possible for each of them. Thus, while aryl and amino groups are synclinal in both chair conformations of the *trans*-aminoalcohols, in *cis*-isomers the aryl–axial conformation has antiperiplanar aryl and nitrogen groups. Since the pharmacological activity of arylethanolamines has been related to this last disposition (1), we also wish to study the conformation in solution of compounds **1**–**8**, both in the base and hydrochloride forms.

Synthesis of trans-*aminoalcohols*[3]

Synthesis of *trans*-aminoalcohols **2**, **4**, **6**, and **8** was initially attempted through reaction of epoxides **12** or **13** with the appropriate nucleophile. The preparation of the requisite epoxides was carried out according to the synthetic sequence outlined in Scheme 2.

1-Phenylcyclohexene **16** was obtained according to described methods (2). Similarly, 2-bromo-1,4-dimethoxybenzene **15** (3) was converted into the Grignard reagent which, on condensation with cyclohexanone followed by acid dehydration, afforded 1-(2,5-dimethoxyphenyl)cyclohexene **17**. According to the literature (4), direct epoxidation of **16** with peroxybenzoic acid leads to 1-phenylcyclohexene oxide **12**. However, rearrangement products are also obtained due to the high sensitivity of aryloxiranes, such as **12**, towards acids. In order to circumvent this problem, we attempted the epoxidation reaction of **16** with *m*-chloroperbenzoic acid (MCPBA) in a two-phase system of dichloromethane and 0.5 *M* aqueous sodium bicarbonate, a process which has been successfully applied to the synthesis of acid-sensitive epoxides (5). Epoxide **12** could be obtained by this procedure but was contaminated with variable amounts of *cis*-1-phenyl-1,2-cyclohexanediol **18**. This compound was identified on the basis of its ir (4) and nmr data (6); its formation, as well as the observed stereochemistry (7), can be explained by considering the oxirane ring opening by water, catalysed by protons from the MCPBA.

The use of a complex of MCPBA and fluoride ions in di-

[1]This work was presented in a preliminary form at the XX Reunión Bienal de la Real Sociedad Española de Química, Castellón, Spain, 1984.

[2]Author to whom all correspondence should be addressed.

[3]*Cis* and *trans* refer to the hetero functions on C^1 and C^2 in all cases.

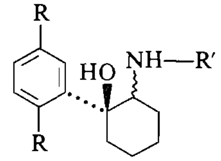

	R	R'	
1.	H	H	*cis*
2.	H	H	*trans*
3.	H	i-Pr	*cis*
4.	H	i-Pr	*trans*
5.	OCH_3	H	*cis*
6.	OCH_3	H	*trans*
7.	OCH_3	i-Pr	*cis*
8.	OCH_3	i-Pr	*trans*

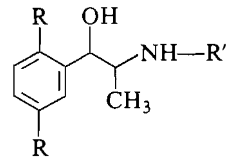

	R	R'
9.	H	H
10.	OCH_3	H
11.	OCH_3	i-Pr

SCHEME 1

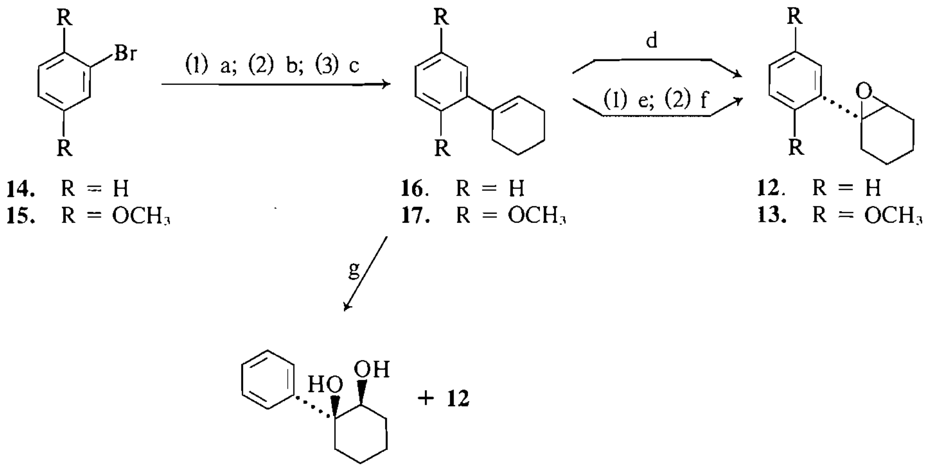

18

a: Mg/ether; b: cyclohexanone; c: $KHSO_4$/benzene or H_2SO_4/AcOH; d: MCPBA/NaF/CH_2Cl_2; e: (R = H) NBS/AcOH/dioxane–H_2O; f: (R = H) Na_2CO_3; g (R = H): MCPBA/$NaHCO_3$/CH_2Cl_2

SCHEME 2

chloromethane has recently been described for the synthesis of acid-sensitive epoxides, such as methylstyrene oxide (8). Application of this procedure to olefins **16** and **17** afforded the desired epoxides **12** and **13** in high purity and quantitative yield. Spectroscopic data of compound **12** were in agreement with those described in the literature (4). The nmr spectrum of 1-(2,5-dimethoxyphenyl)cyclohexene oxide **13** shows a multiplet at δ 2.76 due to the cyclohexane C(2)-H proton as the most characteristic signal. Epoxide **12** was also obtained from **16** in a two-step procedure via an intermediate bromohydrin which, upon treatment with excess sodium carbonate, afforded the desired epoxide in high yield. This method has been described for the preparation of sensitive epoxides, such as 2-vinylpyridine oxide (9).

trans-2-Amino-1-phenylcyclohexanol **2** and *trans*-2-amino-1-(2,5-dimethoxyphenyl)cyclohexanol **6** were obtained by reaction of the corresponding epoxides with sodium azide in *N*,*N*-dimethylformamide – water followed by reduction of the intermediate azidoalcohols with lithium aluminum hydride (Scheme 3). This procedure has been used for the synthesis of aminoalcohols related to ours (1*a*).

Reduction of the mixture of azides obtained from **12** with lithium aluminum hydride in ether afforded a mixture of two regioisomeric *trans*-aminoalcohols which were separated by column chromatography and identified as **2** and *trans*-2-amino-2-phenylcyclohexanol **23** (7:3 ratio). Similarly, *trans*-aminoalcohol **6** and *trans*-2-amino-2-(2,5-dimethoxyphenyl)cyclohexanol **24** (6:4 ratio) resulted from the starting epoxide **13**. Identification and conformational assignment of compounds **2** and **6** was carried out by ^{1}H nmr (200 MHz) and ^{13}C nmr, and will be described in the corresponding section (see below). Aminoalcohols **23** and **24** were identified in a similar way. Thus, the ^{1}H nmr spectrum (60 MHz) of **23** shows a broad singlet at δ 3.6 due to the C(1)-H proton of the cyclohexane ring, while compound **24** also shows a similar signal at δ 4.2. Equatorial disposition of this proton in both **23** and **24** was confirmed by the $W_{\frac{1}{2}}$ value near 8 Hz observed for the corresponding signal. The ^{13}C nmr spectra of these compounds (Table 2) confirmed the presence of a CH—O group (a doublet at 74.5 and 71.6 ppm in **23** and **24**, respectively). From these results it can be inferred that reaction of azide anion with epoxides **12** and **13** leads to a regioisomeric mixture of *trans*-azidoalcohols as a result of the nucleophilic attack upon C(1) and C(2) positions of the starting epoxides. While a *trans*-stereochemistry is the expected result for oxirane ring opening in alkaline conditions, the regioselectivity of the process depends on the steric hindrance around the two carbons of the ring (10), as well as on the benzylic nature of the epoxides, which can favour the attack of the nucleophile upon the more hindered benzylic carbon atom (11). The results of the overall process are similar to those described for the direct opening of epoxide **12** with ammonium hydroxyde (12).

Treatment of epoxides **12** and **13** with excess isopropylamine in ethanol (Scheme 4) afforded in each case a single product

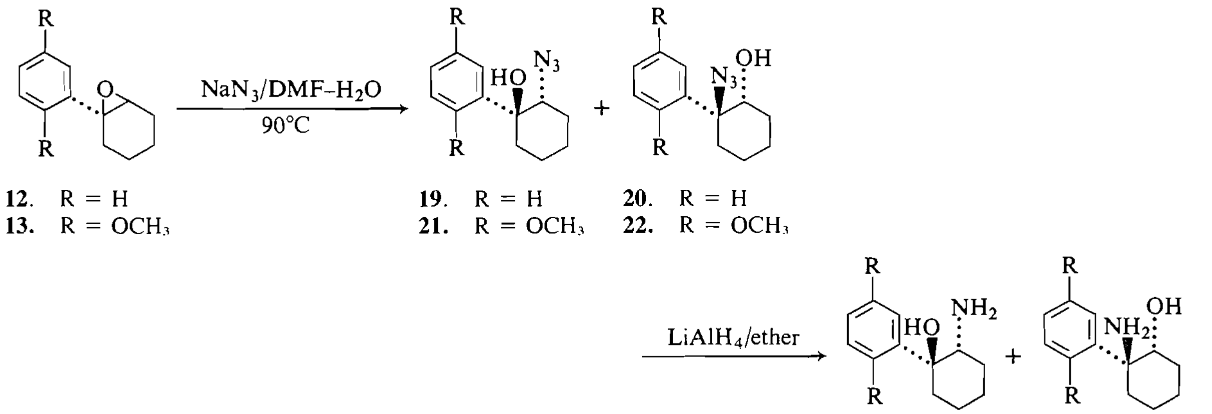

12. R = H
13. R = OCH_3

19. R = H
21. R = OCH_3

20. R = H
22. R = OCH_3

2. R = H (7:3)
4. R = OCH_3 (6:4)

23. R = H
24. R = OCH_3

SCHEME 3

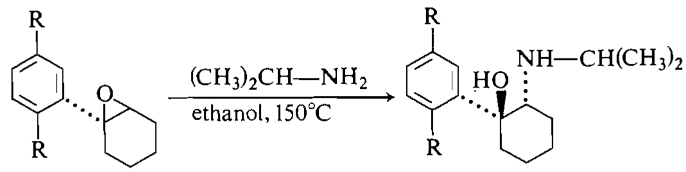

12. R = H
13. R = OCH_3

4. R = H (72%)
8. R = OCH_3 (56%)

SCHEME 4

which was identified through its ^{1}H and ^{13}C nmr spectra as *trans*-2-isopropylamino-1-phenylcyclohexanol **4** and *trans*-2-isopropylamino-1-(2,5-dimethoxyphenyl)cyclohexanol **8**, respectively (see below).

No trace of the regioisomeric 2-aryl-2-isopropylaminocyclohexanols, resulting from the attack of the amine upon the benzylic carbon atom of the starting epoxides, was detected in these reactions. This result is in agreement with the bulkier nature of isopropylamine compared to the azide anion, which prevents the former from the attack upon the more hindered position of the oxirane ring.

In an attempt to obtain *trans*-aminoalcohol **2** by an unambiguous route, we started from *cis*-diol **18**, aiming to convert its monomesylate **25** into the *trans*-azidoalcohol **19** (Scheme 5). Thus *cis*-diol **18** was treated with methanesulfonyl chloride in pyridine to afford *cis*-2-hydroxy-2-phenylcyclohexanol methanesulfonate **25**, whose ^{1}H nmr spectrum showed as characteristic signals an apparent triplet at δ 4.8 ($W_{\frac{1}{2}}$ = 18 Hz) due to the axial C(1)-H proton, as well as a singlet at δ 2.1 due to the methyl group.

Treatment of mesylate **25** with sodium azide in *N,N*-dimethylformamide – water failed to afford azidoalcohol **19**, and a mixture of nitrogen-free products was obtained instead. From this mixture, 2-phenylcyclohexanone and phenyl cyclopentyl ketone were isolated and identified by physical (12) and spectroscopic methods. These ketones are also formed when mesylate **25** is treated under the same conditions but in the absence of sodium azide, so they can result from rearrangement of the intermediate carbocation generated by loss of the mesyloxy group. S_N2 displacement of the mesyloxy group by the azide anion requires a high energy conformation in which the bulkiest groups must be axial.

Synthesis of cis-*aminoalcohols*

Condensation of organometallic compounds with suitably substituted 2-aminoketones is a general synthetic method for *cis*-aminoalcohols related to ours (13). The stereochemistry of the resulting products can be rationalized according to Cherest and Felkin (14) as well as by application of the Cram–Kopecky model (15). Thus, synthesis of *cis*-2-amino-1-phenylcyclohexanol **1** is described in the literature (12) by condensation of 2-aminocyclohexanone hydrobromide **26** with phenylmagnesium bromide (5 equivalents) in ether at reflux temperature. According to this method, we have been able to obtain *cis*-aminoalcohol **1** in substantially improved yield (64% vs. 39%). However, a small amount of *trans*-isomer **2** (ratio **1**/**2** above 9:1 based on nmr) was also obtained. This approach was also useful for the synthesis of *cis*-2-amino-1-(2,5-dimethoxyphenyl)cyclohexanol **5**, not described in the literature. In this case, the Grignard reagent from 2-bromo-1,4-dimethoxybenzene gave poor yields of **5**, so we carried out the reaction with 2,5-dimethoxyphenyllithium **27**, more reactive towards carbonyl groups than the alternative organomagnesium reagent. By this procedure, *cis*-aminoalcohol **5** was obtained in moderate yield (38%), together with small amounts of the *trans*-isomer **6** and a considerable amount of 1,4-dimethoxybenzene, arising in part from an acid–base reaction between the organometallic reagent and the NH and (or) the α-CH protons of hydrobromide **26**.

Compounds **1** and **5** were purified by column chromatography and crystallization; structural and conformational assignments were carried out by nmr spectroscopy, as described below.

Synthesis of 2-aminocyclohexanone hydrobromide **26** was effected through a combination of described procedures (12, 16). The whole synthetic pathway leading to *cis*-aminoalcohols **1** and **5** is depicted in Scheme 6.

Aiming to obtain *cis*-aminoalcohols through an unambiguous route, we tested an alternative procedure in which the key step was the S_N2 displacement of the mesyloxy group of **29** with sodium azide. Subsequent reduction of the resulting azidoalcohol should lead to the desired *cis*-aminoalcohol **1**. This two-step sequence has been successfully applied to the transformation of *cis*-2-phenylcyclohexyl tosylate into *trans*-2-phenylcyclohexylamine with 100% inversion of configuration (13). *trans*-2-Hydroxy-2-phenylcyclohexyl methanesulfonate

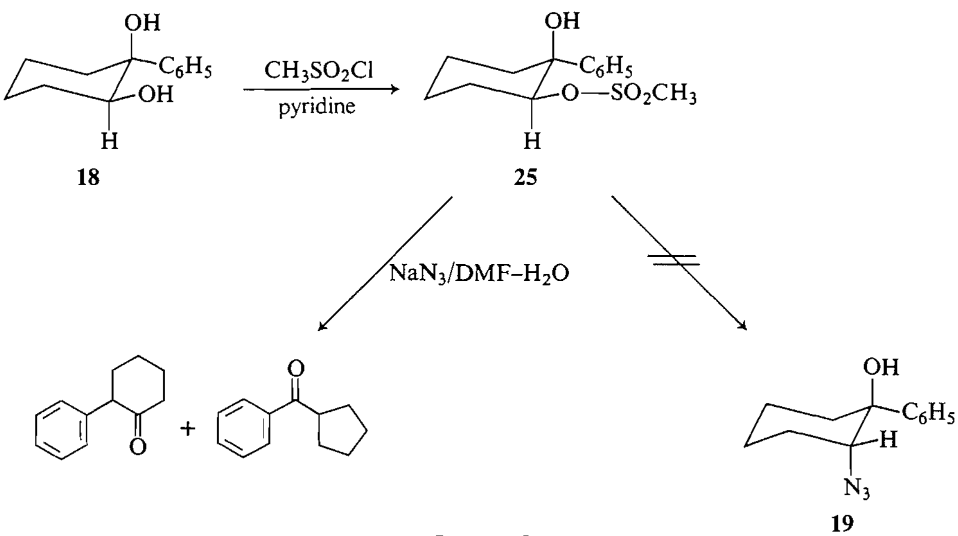

SCHEME 5

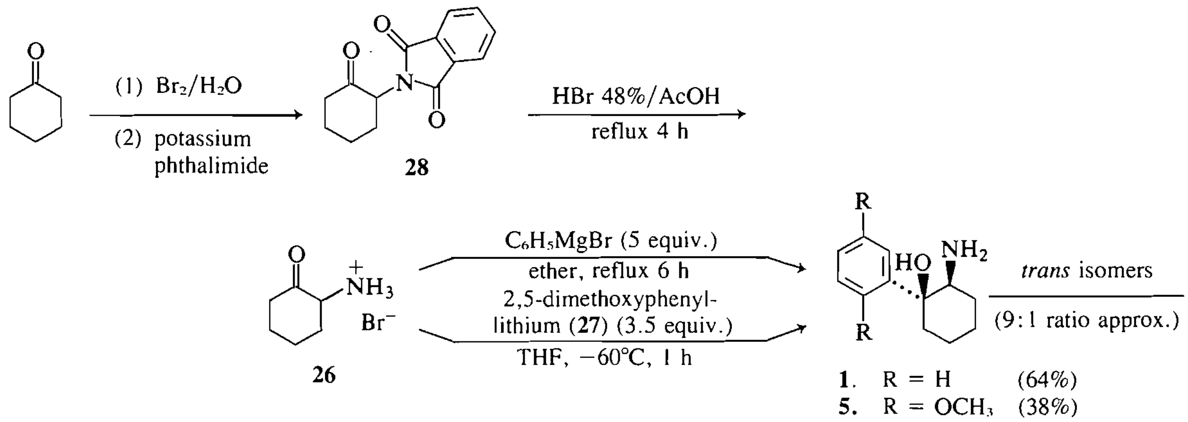

SCHEME 6

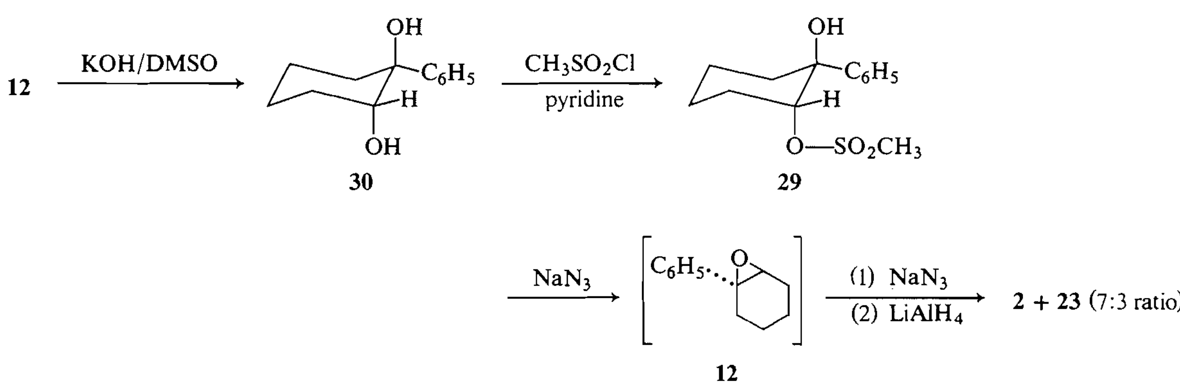

SCHEME 7

29 was obtained in good yield from *trans*-1-phenyl-1,2-cyclohexanediol **30**, synthesized from epoxide **12** according to a described procedure (17). After azide treatment of **29** and lithium aluminum hydride reduction, a 7:3 mixture of *trans*-aminoalcohol **2** and its regioisomer **23** was isolated, and no *cis* isomers were found in the reaction mixture. We have interpreted this result as a consequence of the formation of epoxide **12** through intramolecular displacement of mesyloxy group by the C(1)-hydroxyl function (Scheme 7). Epoxide **12** would then react with the azide anion in the way we have previously stated (Scheme 3). Internal displacement of the mesyloxy group is a favoured process if we take into account the *trans*-diaxial disposition of the reacting groups in the most stable conformation.

cis-2-Isopropylamino-1-phenylcyclohexanol **3** and *cis*-1-(2,5-dimethoxyphenyl)-2-isopropylaminocyclohexanol **7** were synthesized from *cis*-aminoalcohols **1** and **5**, respectively, by condensation with excess acetone in refluxing benzene and sodium borohydride reduction of the intermediate imines (Scheme 8). Their structural and conformational assignment is described in the next section.

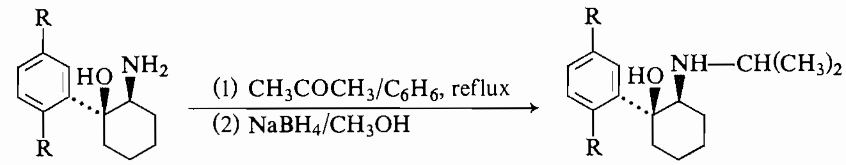

1. R = H
5. R = OCH_3

3. R = H
7. R = OCH_3

SCHEME 8

TABLE 1. ^1H nuclear magnetic resonance (200 MHz) data of aminoalcohols **1**−**8** (base and hydrochloride*) and diols **18** and **30** (in $CDCl_3$)

Compound		C(2)H				
		δ C(2)H	*J* (Hz)	$W_{\frac{1}{2}}$ (Hz)	δ C(3)H_{ax}†	δ C(6)H_{ax}†
1 (base)	*cis*	3.22	10.0/5.1	17.0	—	—
1 (HCl)	*cis*	3.59	10.8/4.2	18.2	—	—
2 (base)	*trans*	3.06	3.8/3.4	8.8	2.08	2.38
2 (HCl)	*trans*	3.56	4.0/3.6	7.8	2.19	2.40
3 (base)	*cis*	3.08	10.8/4.4	16.8	—	—
3 (HCl)	*cis*	3.69	11.5/4.5	18.4	—	—
4 (base)	*trans*	2.82	4.3/5.3	11.0	2.02	2.36
4 (HCl)	*trans*	3.50	3.8/6.6	13.0	2.18	2.38
5 (base)	*cis*	3.47	Broad signal	12.0	—	—
5 (HCl)	*cis*	4.19	11.3/4.7	18.2	—	—
6 (base)	*trans*	3.47	Broad signal	7.5	2.2−2.4	
6 (HCl)	*trans*	4.16	3.0/3.4	6.4	2.4−2.7	
7 (base)	*cis*	3.66	Broad signal	12.0	—	—
7 (HCl)	*cis*	4.34	11.5/4.8	19.2	—	—
8 (base)	*trans*	3.20	Broad signal	7.2	2.0−2.2	
8 (HCl)	*trans*	4.12	3.7/3.3	7.2	2.2−2.5	
18	*cis*	3.96	10.7/4.7	16.8	—	—
30	*trans*	3.75	2.9/3.3	7.7	2.02	2.42

*Hydrochlorides were run in D_2O.

†A lack of data means that C(3)H_a and C(6)H_a protons appear at $\delta < 1.9$, unresolved from the rest of the cyclohexane protons. A δ interval is given when C(3)H_a and C(6)H_a give rise to a single complex signal.

Conformation of aminoalcohols 1−8

As it has been stated in the introductory part of this work, aminoalcohols **1**−**8** can be considered as semirigid analogues of the open-chain drugs ephedrine **9**, methoxamine **10**, and isopropylmethoxamine **11**. Since these cyclic analogues can adopt two chair conformations (designed as aryl-equatorial and aryl-axial) it is essential from a pharmacological standpoint to determine their preferred conformation in solution, especially in the protonated form. The only reported spectroscopic data referring to molecules related to ours are the ^1H nmr spectra (60 MHz) of *cis*- and *trans*-diols **18** and **30** (6).

Although the stereochemistry of compounds **18** and **30** had previously been confirmed by chemical methods (4), our findings in relation to the reactivity of their corresponding monomesylates **25** and **29** with sodium azide in *N,N*-dimethylformamide − water are also in agreement with a *cis* stereochemistry for **18** and a *trans* one for **30**. Accordingly, we have considered these diols as suitable model compounds both for the configurational and conformational study of aminoalcohols **1**−**8**.

Configurational assignments of aminoalcohols **1**−**8** have been carried out by comparison of their C(2)-H coupling constants and (or) $W_{\frac{1}{2}}$ values with those of the corresponding reference diols **18** and **30** (see Table 1), in which the phenyl-equatorial conformation is the preferred one for both of them despite the fact that it prevents *trans*-diol **30** from the achievement of an intramolecular hydrogen bond (6). Moreover, Δδ (δ *cis* − δ *trans*) for the C(2)-H proton in each pair of molecules confirms the given assignment. Thus, contrary to the expected for cyclohexanol systems, in **1**−**8**, **18**, and **30** C(2)-H equatorial protons usually appear at higher fields than C(2)-H axial ones. This has been explained for reference diols **18** and **30** as being a consequence of a variation in the rotameric equilibrium of the phenyl ring due to the presence of the vicinal hydroxyl group (6). In our case, the presence of an amino or isopropylamino group upon the C(2) position seems to act in the same way (see Table 1).

The ^1H nmr spectra of *cis*-aminoalcohols **1**, **3**, **5**, and **7** (Table 1) indicate in all cases an axial C(2)-H proton disposition with $W_{\frac{1}{2}}$ values similar to those described for *cis*-diol **18**. In the 200-MHz spectrum of **18**, we were able to determine coupling constant values of 10.7 Hz (J_{aa}) and 4.7 Hz (J_{ae}) for the C(2)-H proton, which are in agreement with an axial disposition. *cis*-Aminoalcohols **1**, **3**, **5**, and **7** all showed coupling constants of the same range (J_{aa} between 10.0 and 11.5 Hz). In order to ascertain the conformation of these molecules in a protonated form (the expected situation at physiological pH), we have studied ^1H nmr spectra of the corresponding hydrochlorides in D_2O, recording the spectra at different temperatures, from 22 to 90°C. No variation of the coupling constants was observed within this range of temperatures. From the above results we can conclude that *cis*-aminoalcohols **1**, **3**, **5**,

TABLE 2. ^{13}C nuclear magnetic resonance spectra of aminoalcohols **1–8**, **23**, **24**, and diols **18** and **30** (in $CDCl_3$)

														Isopropyl	
Compound	C(1)	C(2)	C(3)	C(4)	C(5)	C(6)	C(1′)	C(2′)	C(3′)	C(4′)	C(5′)	C(6′)	OCH_3	NCH	CH_3
1	74.2	55.5	29.8	24.8	21.3	38.4	147.7	125.1	128.2	126.5	128.2	125.1	—	—	—
2	74.8	55.4	28.7	19.4	21.3	31.0	146.8	126.0	128.2	127.1	128.2	126.0	—	—	—
3	74.1	59.0	28.2	24.8	21.3	38.9	148.2	125.1	128.1	126.4	128.1	125.1	—	45.2	23.6/22.6
4	74.9	60.6	27.3	21.1	21.6	33.9	146.7	126.5	127.9	126.9	127.9	126.5	—	46.3	24.2/22.4
5	74.8	52.1	30.1	24.8	21.2	34.7	136.1	150.4*	114.0	112.2#	153.6*	112.4#	55.7/55.5	—	—
6	76.0	52.7	28.2	19.1	21.1	29.8	134.6	151.3*	115.2	111.9#	153.8*	111.5#	55.6/55.5	—	—
7	73.9	55.1	29.4	24.8	21.2	34.4	137.5	153.7*	113.8	111.9#	150.3*	112.3#	55.6/55.5	45.9	23.4
8	75.8	57.0	26.5	19.5	21.1	30.8	135.1	151.6*	115.3	111.7#	153.5*	111.6#	55.7/55.6	47.1	23.9/22.4
18	75.8	74.4	29.2	24.3	21.0	38.5	146.5	125.1	128.3	126.9	128.3	125.1	—	—	—
30	74.5	73.2	28.4	19.2	21.1	31.4	145.9	126.1	128.3	127.5	128.3	126.1	—	—	—
23	74.5	56.7	32.5	21.4	20.1	28.6	146.5	126.3	128.0	126.6	128.0	126.3	—	—	—
24	71.6	57.6	31.7	21.3	19.7	27.7	135.5	153.5*	115.6	112.1#	152.0*	111.5#	55.6/55.5	—	—

The superscripts * and # imply that the values may be interchanged.

and **7** adopt in solution, both in the base and hydrochloride forms, a chair conformation in which the aryl group is equatorial and, therefore, amino or isopropylamino groups are also equatorial. This conformation is favoured both for steric reasons and intramolecular NH/OH hydrogen bonding.

On the other hand, ^1H nmr spectra of *trans*-aminoalcohols **2**, **4**, **6**, and **8** (base and hydrochloride) show a signal due to the C(2)-H equatorial proton whose coupling constants and (or) $W_{\frac{1}{2}}$ values are again in agreement with those found for the reference compound *trans*-diol **30**. Thus in **2**, **6**, and **8** an apparent triplet with coupling constants between 3.0 and 4.0 Hz is observed (*trans*-diol **30**, 2.9–3.3 Hz). However, in compounds **4** and **4** · HCl, the coupling constant values are higher than those found in the above *trans*-aminoalcohols (Table 1), thus indicating an averaging of the C(2)-H equatorial and axial dispositions. Taking a J_{aa} value of 11.5 Hz (from the *cis* isomer **3** · HCl) and an approximate J_{ee} value of 3.6 Hz (from *trans* **2** · HCl), a ratio of 60:40 of phenyl-equatorial vs. phenyl-axial conformations can be calculated for compound **4** · HCl. Moreover, *trans*-aminoalcohols **2** and **4** show multiplets at about δ 2.4 and 2.0 due to the C(6)-H axial and C(3)-H axial protons, respectively. Comparable signals are also observed in the ^1H nmr spectra of the corresponding hydrochlorides as well as in that of the reference compound **30**. The assignment of these protons has been confirmed by spin-decoupling experiments and, in the case of **4**, through homonuclear chemical shift correlation $^1H-^1H$ that allowed the complete assignment of the chemical shifts of all the cyclohexane ring protons (see experimental section). The downfield chemical shift of C(6)-H and C(3)-H axial protons in the *trans* isomers (but not in the *cis* ones) can be explained by considering the anisotropic deshielding effect due to axial amino and hydroxyl groups, which confirms the preferred conformation of aminoalcohols **2** and **4**.

In the temperature range between 22 and 90°C, the ^1H nmr spectra of the hydrochlorides of aminoalcohols **2**, **4**, **6**, and **8** show a very small increment of the C(2)–H coupling constants (less than 0.5 Hz), not significant from a conformational standpoint.

Signals in the ^{13}C nmr spectra (Table 2) were assigned by their multiplicity (ADEPT program), comparison with model compounds (19), and also, in the case of **4** · HCl, through the heteronuclear chemical shift correlation $^{13}C/^1H$. *trans*-Aminoalcohols **2**, **4**, **6**, and **8**, as well as *trans*-diol **30**, showed

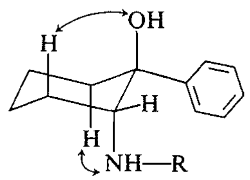

2. R = H
4. R = i-Pr

SCHEME 9

shielded C(4) and C(6) carbon atoms with respect to the corresponding C(6) and C(4) carbon atoms of *cis*-aminoalcohols **1**, **3**, **5**, and **7**, and *cis*-diol **18** (Δδ between 3.6 and 7.4 ppm). This shielding effect can be explained by considering a γ-*gauche* effect due to the axial C(2) amino (or C(2) hydroxyl) group in the *trans* isomers. On the other hand, Δδ (δ *cis* − δ *trans*) for the C(4) carbon atom in the pairs of stereoisomers **1**/**2**, **5**/**6**, and **7**/**8** is between 5.3 and 5.7 ppm, while in the pair **3**/**4** Δδ has a lower value of 3.7 ppm. This indicates again the existence in compound **4** of significant amounts of the phenyl-axial conformation, in which the C(4) position is not shielded.

Experimental

Melting points were determined in a capillary tube on a Büchi apparatus and are uncorrected. Infrared spectra were recorded on a Perkin–Elmer 577 spectrophotometer. Proton magnetic resonance were measured at 60 MHz with a Perkin–Elmer R 24B instrument or at 200 MHz with an FT Varian XL-200 spectrometer. Signal positions are reported in ppm downfield from tetramethylsilane (δ scale) as an internal standard, and $CDCl_3$ as a solvent, unless otherwise indicated; the number of protons, multiplicity, coupling constants, and proton assignments are indicated in parentheses. The ^{13}C nmr were measured at 50.3 MHz with a Varian XL-200 spectrometer, with internal tetramethylsilane as a reference. Multiplicity of the signals was determined by the ADEPT program (automatic distortionless enhancement by polarization transfer) (20). Homonuclear chemical shift correlation $^1H/^1H$ was determined by the HOMCOR program (21) and heteronuclear chemical shift correlation $^{13}C/^1H$ by the HETCOR program (22). Thin-layer chromatography and column chromatography were carried out on silica gel 60, Merck, 5–25 μm and 63–200 μm, respectively, and the spots were located with uv light or iodoplatinate reagent. All microdistillations were made on a Büchi GKR-50 Kugelrohr apparatus. Solutions in organic solvents were dried over anhydrous sodium sulfate and stripped of solvent with a Büchi rotary evaporator connected to a water aspirator. Microanalyses were performed by the Instituto de Química Bio-Orgánica, Barcelona.

trans-2-Amino-1-phenylcyclohexanol (2)

A solution of 15.6 g (0.24 mol) of sodium azide in 50 mL of water

TABLE 3. Elemental analyses and melting points

Compound	Molecular formula	Calculated C	Calculated H	Calculated N	Calculated X*	Found C	Found H	Found N	Found X*	Melting point (°C)†	Purification method‡
2 (HCl)	$C_{12}H_{18}ClNO$	63.28	7.97	6.15	15.57	63.46	7.98	6.10	15.76	212–213 (216–217)[12]	Ethanol – ethyl acetate
23 (HCl)	$C_{12}H_{18}ClNO$	63.28	7.97	6.15	15.57	63.02	7.95	5.92	15.57	195–197 (199–200)[18]	Acetone–ethanol
3 (HCl)	$C_{15}H_{24}ClNO$	66.77	8.96	5.19	13.14	66.68	8.96	5.19	13.02	217–219	Acetone–ethanol
4 (HCl)	$C_{15}H_{24}ClNO$	66.77	8.96	5.19	13.14	66.59	9.03	5.14	13.00	229–231	Acetone–ethanol
5 (HCl)	$C_{14}H_{22}ClNO_3$	58.43	7.70	4.86	12.32	58.63	7.86	4.86	12.33	256–258	Ethanol–ether
6 (HCl)	$C_{14}H_{22}ClNO_3$	58.43	7.70	4.86	12.32	58.67	7.90	4.91	12.36	211–212	Hexane – ethyl acetate
24	$C_{14}H_{21}NO_3$	66.90	8.42	5.57	—	67.08	8.61	5.71	—	115–116	Hexane–ether
7 (HCl)	$C_{17}H_{28}ClNO_3$	61.89	8.55	4.24	10.75	62.01	8.85	4.26	10.62	195–196	Ethanol–ether
8 (HCl)	$C_{17}H_{28}ClNO_3$	61.89	8.55	4.24	10.75	61.86	8.52	4.31	10.78	180–183	Ethyl acetate
13	$C_{14}H_{18}O_3$	71.77	7.74	—	—	72.01	7.92	—	—	60.5–62.5	Hexane
17	$C_{14}H_{18}O_2$	77.03	8.31	—	—	76.81	8.15	—	—	42.5–44	bp 105–107 °C (0.3 Torr)
25	$C_{13}H_{18}O_4S$	55.76	6.71	—	11.86	57.80	6.66	—	11.81	102–103	Ether
28	$C_{14}H_{13}NO_3$	69.12	5.38	5.76	—	69.06	5.39	5.83	—	169–170 (174–175)[12]	Ether–acetone
29	$C_{13}H_{18}O_4S$	57.76	6.71	—	11.86	57.95	6.84	—	11.91	96–98	Ether

*X stands for Cl or S according to the formula.
†Melting points described in the literature are indicated in brackets.
‡Crystallization, except for compound **17** (distillation).

was added to a solution of 8.8 g (0.0506 mol) of 1-phenylcyclohexene oxide **12** (4) in 350 mL of *N,N*-dimethylformamide. The reaction mixture was heated at 90°C for 14 h, then quenched with water and extracted with ether. The ethereal layers were washed thoroughly with water and saturated sodium chloride solution, dried, and evaporated to afford 9.4 g (85%) of a mixture of regioisomeric azidoalcohols **19** and **20** (ir neat: 2100 cm^{-1}, azide). A solution of the above mixture in 400 mL of dry ether was added dropwise with external cooling to a suspension of 6.8 g (0.181 mol) of lithium aluminum hydride in 400 mL of dry ether. After stirring for 2 h at room temperature, the reaction mixture was poured into 300 mL of 10 *N* sodium hydroxide solution. The ethereal layer was separated and the aqueous one was extracted with ether. The combined ethereal layers were extracted with 10% hydrochloric acid solution and the acidic aqueous phase was basified with 10 *N* sodium hydroxide solution and extracted with ether. The organic extracts were dried and evaporated to give 5.8 g of a mixture of aminoalcohols **2** and **23**, which were separated by column chromatography (eluent ether–diethylamine 97:3). Thus, 3.6 g (37%) of aminoalcohol **2** and 1.6 g (16.5%) of its regioisomer **23** were obtained (Table 3). Compound **2**, ^{1}H nmr (200 MHz) (see Table 1) δ: 1.30–2.00 (complex signal, 6H cyclohexane, 3H exchangeable), 2.08 (m, 1H, C(3)-H_a), 2.38 (m, 1H, C(6)-H_a), 3.06 (dd, 1H, C(2)-H), 7.1–7.7 (m, 5H, phenyl); ^{13}C nmr: Table 2. Compound **23**, ^{1}H nmr (60 MHz) δ: 1.2–1.9 (broad signal, 8H, cyclohexane and exchangeable), 3.6 (m, C(2)-H_e, $W_{\frac{1}{2}}$ = 8 Hz), 7.1–7.5 (m, 5H, phenyl); ^{13}C nmr: Table 2.

cis-2-Isopropylamino-1-phenylcyclohexanol (3)

A solution of 2.5 g (13.1 mmol) of *cis*-aminoalcohol **1** (12) and 3 g (51.6 mmol) of acetone in 40 mL of dry benzene was heated at reflux temperature in a Dean–Stark apparatus. After 5 h, the solvent was removed, the residue was dissolved in 40 mL of ethanol, and 0.75 g (20 mmol) of sodium borohydride was added portionwise with external cooling. After stirring for 3 h at room temperature, the reaction mixture was poured over ice-water, acidified with 2 *N* hydrochloric acid, and washed with ether. Basification of the aqueous layer with ammonium hydroxide and extraction with ether afforded, after evaporation of the dried extracts, 2.2 g (73%) of compound **3** (Table 3); ^{1}H nmr (200 MHz) (see Table 1) δ: 0.77 (d, *J* = 6.3 Hz, 3H, CH_3 isopropyl), 0.86 (d, *J* = 6.3 Hz, 3H, CH_3 isopropyl), 1.35–1.95 (complex signal, 8H cyclohexane and 2H exchangeable), 2.35 (m, 1H, CH isopropyl), 3.08 (dd, 1H, C(2)-H_a), 7.1–7.75 (m, 5H, phenyl); ^{13}C nmr: Table 2.

trans-2-Isopropylamino-1-phenylcyclohexanol (4)

A mixture of 4.2 g (24.2 mmol) of 1-phenylcyclohexene oxide **12** (4) and 8.6 g (146.3 mmol) of isopropylamine in 60 mL of absolute ethanol was heated at 120°C in a sealed tube for 15 h. After removing the solvent and the excess amine, the residue was made acidic with 2 *N* hydrochloric acid and washed with ether. The aqueous layer was basified and extracted with ether. The organic extracts were dried and evaporated to afford 4.0 g (72%) of compound **4** (Table 3); ^{1}H nmr (200 MHz, base) (see Table 1) δ: 0.72 (d, *J* = 6.2 Hz, 3H, CH_3), 0.88 (d, *J* = 6.2 Hz, 3H, CH_3), 1.45–1.67 (complex signal, 6H, cyclohexane), 2.01 (m, 1H, C(3)-H_a), 2.30–2.50 (m, 2H, CH isopropyl and C(6)-H_a), 2.82 (dd, 1H, C(2)-H_e), 7.14–7.62 (m, 5H, phenyl); homonuclear chemical shift correlation ^{1}H/^{1}H, cyclohexane protons, hydrochloride (D_2O) δ: 1.10 (CH_3), 1.19 (CH_3), 1.63 (C(4)-H_a and C(4)-H_e), 1.80 (C(5)-H_a and C(5)-H_e), 1.87 (C(3)-H_e), 1.93 (C(6)-H_e), 2.19 (C(3)-H_a), 2.35 (C(6)-H_a), 2.98 (CH isopropyl), 3.48 (C(2)-H_e); ^{13}C nmr: Table 2.

cis-2-Amino-1-(2,5-dimethoxyphenyl)cyclohexanol (5)

A solution of 6.7 g (30.9 mmol) of 2-bromo-1,4-dimethoxybenzene **15** (3) in 160 mL of dry tetrahydrofuran in a flask equipped with magnetic stirrer, gas inlet, and thermometer was treated at −70°C with 24 mL of 1.3 *N* butyllithium (31.2 mmol) in hexane. After 15 min, 1.5 g (7.7 mmol) of 2-aminocyclohexanone hydrobromide **26** (12) was added portionwise. After stirring at −60°C for 1.5 h, the mixture was poured into ice-water, acidified with 2 *N* hydrochloric acid, and extracted with ether. The organic layers were dried and evaporated to give 4.1 g of 1,4-dimethoxybenzene. The aqueous layer was made basic with concentrated ammonium hydroxide and extracted with ether to afford, after evaporation of the dried extracts, 0.75 g (38%) of *cis*-aminoalcohol **5** (Table 3); ^{1}H nmr (200 MHz) (see Table 1) δ: 1.20–2.16 (complex signal, 8H cyclohexane and 3H exchangeable), 3.47 (1H, C(2)-H_a), 3.66 (s, 6H, OCH_3), 6.54–6.76 (m, 3H, aromatic); ^{13}C nmr: Table 2.

trans-2-Amino-1-(2,5-dimethoxyphenyl)cyclohexanol (6)

A solution of 7.8 g (120 mmol) of sodium azide in 20 mL of water was added to a solution of 4.0 g (17.1 mmol) of epoxide **13** in 130 mL of *N,N*-dimethylformamide. The reaction mixture was heated at reflux temperature for 48 h and then quenched with water. Similar work-up to that described for the synthesis of **2** afforded 3.7 g (78%) of a mixture of azidoalcohols **21** and **22** (ir neat: 2100 cm^{-1}, azide). A solution of the above mixture in 150 mL of dry ether was treated with 2.0 g (53.1 mmol) of lithium aluminum hydride, under the same experimental conditions described for **2**, to afford 2.3 g of a mixture of *trans*-aminoalcohols **6** and **24**, which were separated by column chromatography. On elution with ether–diethylamine (98:2), 1.2 g (36%) of **6** was obtained (Table 3); ^{1}H nmr (200 MHz) (see Table 1) δ : 1.32–2.34 (complex signal, 8H cyclohexane and 3H exchangeable), 3.47 (1H, C(2)-H$_e$), 3.72 (s, 3H, OCH_3), 3.81 (s, 3H, OCH_3), 6.64–6.92 (m, 3H, aromatic); ^{13}C nmr: Table 2. On elution with ether–diethylamine (96:4), 1.02 g (30%) of **24** were obtained (Table 3); ^{1}H nmr (60 MHz) δ : 1.1–2.1 (complex signal, 8H cyclohexane and 3H exchangeable), 3.60 (s, 3H, OCH_3), 3.70 (s, 3H, OCH_3), 4.2 (br s, 1H, C(2)-H$_e$, $W_{\frac{1}{2}}$ = 8 Hz), 6.6 (m, 2H, aromatic), 6.8 (m, 1H, aromatic); ^{13}C nmr: Table 2.

cis-1-(2,5-Dimethoxyphenyl)-2-isopropylaminocyclohexanol (7)

By an identical procedure to that described for aminoalcohol **3**, 0.62 g (2.47 mmol) of aminoalcohol **5** afforded 0.51 g (70%) of compound **7** (Table 3); ^{1}H nmr (200 MHz) (see Table 1) δ : 0.74 (d, J = 6.3 Hz, 3H, CH_3 isopropyl), 0.86 (d, J = 6.3 Hz, 3H, CH_3 isopropyl), 1.28–1.89 (complex signal, 8H cyclohexane), 2.08 (m, 1H, CH isopropyl), 3.66 (1 H, C(2)-H$_a$), 3.79 (s, 3H, OCH_3), 3.81 (s, 3H, OCH_3), 6.76 (m, 2H, aromatic), 7.38 (m, 1H, aromatic); ^{13}C nmr: Table 2.

trans-1-(2,5-Dimethoxyphenyl)-2-isopropylaminocyclohexanol (8)

A solution of 1.5 g (6.4 mmol) of epoxide **13** and 6.0 g (100 mmol) of isopropylamine in 60 mL of absolute ethanol was heated in a sealed tube at 150°C for 72 h. Similar work-up to that described for compound **4** afforded 1.06 g (56%) of **8** (Table 3); ^{1}H nmr (200 MHz) (see Table 1) δ : 0.61 (d, J = 6.2 Hz, 3H, CH_3 isopropyl), 0.86 (d, J = 6.2 Hz, 3H, CH_3 isopropyl), 1.38–2.38 (complex signal, 8H cyclohexane and 2H exchangeable), 3.20 (1H, C(2)-H$_e$), 3.76 (s, 3H, OCH_3), 3.86 (s, 3H, OCH_3), 6.68–6.90 (m, 3H, aromatic); ^{13}C nmr: Table 2.

1-Phenylcyclohexene oxide (12)

Method A

To a stirred suspension of 1.32 g (31.4 mmol) of sodium fluoride in 200 mL of dry dichloromethane, 3.2 g (equivalent to 15.8 mmol) of 85% *m*-chloroperbenzoic acid was added. After 30 min, 1 g (6.32 mmol) of 1-phenylcyclohexene **16** (2) was added at once and the stirring was continued for 2.5 h at room temperature. The solids were removed by filtration and washed thoroughly with dichloromethane. The combined filtrates were washed with diluted sodium hydroxide solution and water and dried. Evaporation of the solvent afforded 1.07 g (97%) of epoxide **12**, which was used without further purification; ir (NaCl) (4): 1070 (C—O) cm^{-1}; ^{1}H nmr (60 MHz, CCl_4) δ : 1.1–2.3 (complex signal, 8H cyclohexane), 2.80 (m, 1H, C(2)-H), 6.9–7.3 (m, 5H, phenyl).

Method B

A solution of 10 g (63.2 mmol) of 1-phenylcyclohexene **16** (2) and 3.4 mL of acetic acid in 170 mL of dioxane–water (3:7) was treated portionwise with 12 g (67.0 mmol) of *N*-bromosuccinimide. The mixture was stirred for 1 h at room temperature, 13.3 g (125.6 mmol) of anhydrous sodium carbonate was added, and, after 12 h, the reaction mixture was poured into 300 mL of water and extracted with ether. The combined organic layers were dried and evaporated to afford 9.7 g (90%) of epoxide **12**.

1-(2,5-Dimethoxyphenyl)cyclohexene oxide (13)

To a stirred suspension of 3.0 g (13.7 mmol) of sodium fluoride in 150 mL of dry dichloromethane, 7.5 g (equivalent to 37 mmol) of 85% *m*-chloroperbenzoic acid was added. After stirring for 30 min at room temperature, the mixture was cooled to −10°C (acetone–CO_2 bath) and 3.0 g (13.7 mmol) of **17** was added in one portion. Stirring was continued at −5°C for 30 min and the reaction mixture was filtered. Solid materials were washed with small portions of dichloromethane and the combined filtrates were washed with 1 *N* sodium hydroxide solution and water and dried. Evaporation of the solvent afforded 2.8 g (87%) of epoxide **13** (Table 3); ir ($CHCl_3$): 1050 (C—O) cm^{-1}; ^{1}H nmr (60 MHz, CCl_4) δ : 1.1–2.1 (m, 8H, cyclohexane), 2.76 (m, 1H, C(2)-H), 3.56 (s, 3H, OCH_3), 3.63 (s, 3H, OCH_3), 6.43 (m, 2H, aromatic), 6.61 (m, 1H, aromatic).

1-(2,5-Dimethoxyphenyl)cyclohexene (17)

Magnesium turnings (2.75 g, 110 mmol) were placed in a three-neck flask fitted with a mechanical stirrer, a condenser, and a dropping funnel, and the entire system was flame dried. A few milliliters of a solution of bromide **15** (3) (23.5 g, 110 mmol) in 140 mL of dry ether were added to the turnings and the reaction was initiated with a small iodine crystal. The remaining solution was added dropwise over a 1-h period and the stirring was continued under reflux temperature for an additional 2 h. Cyclohexanone (10.7 g, 110 mmol) in 20 mL of dry ether was added under nitrogen to the cooled reaction mixture and the stirring was continued overnight. The reaction mixture was poured into 300 mL of saturated ammonium chloride solution, and the ethereal layer was separated, washed with water, and dried. Removal of the solvent afforded 26 g of a material which was treated with 50 mL of a freshly prepared mixture of sulfuric acid – acetic acid (1:4 by volume). The resulting mixture was swirled for 1 min and poured into ether–water (250 mL and 350 mL, respectively). The ethereal layer was washed with water and 1 *N* sodium hydroxide solution, dried, and evaporated. After distillation of the crude alkene, 9.8 g (41%) of compound **17** was obtained (Table 3); ^{1}H nmr (60 MHz, CCl_4) δ : 1.6 (m, 4H, C(4)H_2 and C(5)H_2), 2.2 (m, 4H, C(3)H_2 and C(6)H_2), 3.6 (s, 6H, OCH_3), 5.40 (m, 1H, =CH), 6.40 (s, 3H, aromatic).

cis-2-Hydroxy-2-phenylcyclohexyl methanesulfonate (25)

A solution of 4.1 g (35.7 mmol) of methanesulfonyl chloride in 25 mL of dry pyridine was added dropwise to an externally ice-cooled solution of *cis*-diol **18** (4) in 200 mL of dry pyridine. The mixture was stirred at room temperature for 24 h, poured into water, and extracted with benzene. The organic layer was washed thoroughly with 2 *N* hydrochloric acid and water, dried, and evaporated to afford 6.8 g (97%) of monomesylate **25** (Table 3); ir (KBr): 3500–3100 (OH), 1340 (SO_2) cm^{-1}; ^{1}H nmr (60 MHz) δ : 1.4–2.5 (complex signal, 8H cyclohexane and 1H exchangeable), 2.1 (s, 3H, CH_3—SO_2—), 4.8 (dd, 1H, C(1)-H$_a$, $W_{\frac{1}{2}}$ = 18 Hz), 7.1–7.6 (m, 5H, phenyl).

2-Phthalimidocyclohexanone (28)

To 24 g (129.5 mmol) of potassium phthalimide in 135 mL of *N,N*-dimethylformamide, 20 g (113 mmol) of 2-bromocyclohexanone (16) was added. After stirring at 100°C for 6 h, the mixture was poured into water and extracted with chloroform. The organic layer was washed with 2 *N* sodium hydroxide, water, and dried. Evaporation of the solvent afforded, after crystallization, 13.3 g (49%) of **28** (Table 3); ^{1}H nmr (60 MHz) δ : 1.4–2.8 (complex signal, 8H, cyclohexane), 4.6 (dd, 1H, C(2)-H), 7.2–7.6 (m, 4H, aromatic).

trans-2-Hydroxy-2-phenylcyclohexyl methanesulfonate (29)

Identical procedure to that described for mesylate **25** afforded **29** (94%, Table 3) from *trans*-diol **30** (17); ir (KBr): 3510 (OH), 1330 (SO_2) cm^{-1}; ^{1}H nmr (60 MHz, DMSO-d_6) δ : 1.2–2.4 (complex signal, 8H, cyclohexane), 2.1 (s, 3H, CH_3—SO_2—), 4.3 (br s, 1H, C(1)H$_e$, $W_{\frac{1}{2}}$ = 7 Hz), 5.2 (s, 1H, OH), 6.9–7.6 (m, 5H, phenyl).

Acknowledgements

We are grateful to the University of Barcelona for financial support of this research.

1. (*a*) D. D. Miller, J. Fowble, and P. N. Patil. J. Med. Chem. **16**, 177 (1973); (*b*) D. D. Miller, F. L. Hsu, K. N. Salman, and P. N. Patil. J. Med. Chem. **19**, 180 (1976); (*c*) H. L. Komiskey, F. L. Hsu, F. J. Bossart, J. W. Fowble, D. D. Miller, and P. N. Patil. Eur. J. Pharmacol. **52**, 37 (1978).
2. E. W. Garbisch. J. Org. Chem. **26**, 4165 (1961).
3. J. S. Swenton, D. K. Jackson, M. J. Manning, and P. W. Raynolds. J. Am. Chem. Soc. **100**, 6182 (1978).
4. G. Berti, F. Bottari, B. Macchia, and F. Macchia. Tetrahedron, **21**, 3277 (1965).

5. (*a*) W. K. ANDERSON and T. VEYSOGLU. J. Org. Chem. **38**, 2267 (1973); (*b*) M. IMUTA and H. ZIFFER. J. Org. Chem. **44**, 1351 (1979); (*c*) J. B. BUCHANAN and H. Z. SABLE. *In* Selective organic transformations. Vol. 2. *Edited by* B. S. Thyagarajan. Wiley–Interscience, New York, NY. 1972. pp. 1–95.
6. G. CECCARELLI, B. MACCHIA, F. MACCHIA, and L. MONTI. Org. Magn. Reson. **7**, 548 (1975).
7. (*a*) G. BERTI, G. CAMICI, B. MACCHIA, F. MACCHIA, and L. MONTI. Tetrahedron Lett. 2591 (1972); (*b*) C. BATTISTINI, P. CROTTI, and F. MACCHIA. Tetrahedron Lett. 2091 (1975); (*c*) C. BATTISTINI, P. CROTTI, D. DAMIANI, and F. MACCHIA. J. Org. Chem. **44**, 1643 (1979).
8. (*a*) F. CAMPS, J. COLL, A. MESSEGUER, and F. PUJOL. J. Org. Chem. **47**, 5402 (1982); (*b*) F. CAMPS, J. COLL, A. MESSEGUER, and F. PUJOL. Chem. Lett. 971 (1983).
9. R. P. HANZLIK, M. EDELMAN, W. J. MICHAELY, and G. SCOTT. J. Am. Chem. Soc. **98**, 1952 (1976).
10. R. E. PARKER. Chem. Rev. **59**, 737 (1959).
11. M. E. C. BIFFIN, J. MILLER, and D. B. PAUL. *In* The chemistry of the azido group. *Edited by* S. Patai. Interscience Publishers, London, New York. 1971. p. 95.
12. D. Y. CURTIN and S. SCHMUKLER. J. Am. Chem. Soc. **77**, 1105 (1955).
13. E. E. SMISSMAN and T. L. PAZDERNIK. J. Med. Chem. **16**, 14 (1973).
14. M. CHEREST and H. FELKIN. Tetrahedon Lett. 2205 (1968).
15. D. J. CRAM and K. R. KOPECKY. J. Am. Chem. Soc. **81**, 2748 (1959).
16. J. ALLINGER and N. L. ALLINGER. Tetrahedron, **2**, 64 (1958).
17. (*a*) G. BERTI, B. MACCHIA, and F. MACCHIA. Tetrahedron Lett. 3421 (1965); (*b*) G. BERTI, B. MACCHIA, and F. MACCHIA. Tetrahedron, **24**, 1755 (1968).
18. C. STEVENS, A. ASH, A. THUILLIER, J. AMIN, A. BALYS, W. DENNIS, J. DICKERSON, R. GLINSKY, H. HANSON, M. PILLAI, and J. STODDARD. J. Am. Chem. Soc. **88**, 2593 (1966).
19. E. BREITMAIER and W. VOELTER. *In* ^{13}C NMR spectroscopy. Methods and applications in organic chemistry. 2nd ed. Verlag Chemie, Weinheim, New York. 1978.
20. (*a*) R. RICHARG, W. AMMAN, and T. WIRTHLIN. Varian Application Note 2-15. Zug. August 1982; (*b*) D. M. DODDELL, D. T. PEGG, and M. R. BENDALL. Org. Magn. Reson. **8**, 323 (1982).
21. A. BAX, R. FREEMAN, and G. MORRIS. J. Magn. Reson. **42**, 169 (1981).
22. A. BAX and G. MORRIS. J. Magn. Reson. **42**, 501 (1981).

Selenium isotopic fractionation during SeO_3^{2-} reduction to Se^0 and H_2Se

K. RASHID[1] AND H. R. KROUSE
Department of Physics, The University of Calgary, Calgary, Alta., Canada T2N 1N4

Received March 5, 1984[2]

K. RASHID and H. R. KROUSE. Can. J. Chem. **63**, 3195 (1985).

During reduction of SeO_3^{2-} to Se^0 by $NH_2OH.HCl$, the selenium isotope selectivity fits a two step model with the second step two orders of magnitude faster than the first. The ratios of the isotopic rate constants, k_{76}/k_{82}, are 1.007 and 1.020 for the first and second steps, respectively. The corresponding k_{76}/k_{80} values are 1.004_6 and 1.013_3. During the reduction of SeO_3^{2-} to H_2Se by a $H_3PO_2-HI-HCl$ mixture, the H_2Se was initially enriched but sporadically became depleted in the heavier isotopes as the reaction progressed. This is attributed to the formation of Se^0 as an intermediate and the subsequent reaction of its surface layers to produce H_2Se.

For all data, the relation $\delta^{82}Se = (1.5_4 \pm 0.02)\delta^{80}Se$ was observed as predicted theoretically.

K. RASHID et H. R. KROUSE. Can. J. Chem. **63**, 3195 (1985).

Lors de la réduction du SeO_3^{2-}, sous l'influence du $NH_2OH.HCl$, la sélectivité isotopique du sélénium correspond à un modèle en deux étapes où la vitesse de la deuxième étape est deux ordres de grandeur supérieur à celle de la première. Les rapports des constantes des vitesses isotopiques, k_{76}/k_{82}, sont respectivement de 1,007 et de 1,020 pour la première et la deuxième étape. Les valeurs correspondantes de k_{76}/k_{80} sont de $1{,}004_6$ et de $1{,}013_3$. Lors de la réduction du SeO_3^{2-} en H_2Se sous l'influence du mélange $H_3PO_2-HI-HCl$, le H_2Se s'enrichit au début mais il s'appauvrit sporadiquement en isotopes plus lourds au cours de la réaction. On attribué ceci à la formation intermédiaire de Se^0 et à la réaction subséquente de ses couches de surface pour conduire au H_2Se.

Conformément aux hypothèses, on observe pour toutes les données la relation $\delta^{82}Se = (1{,}5_4 \pm 0{,}02)\delta^{80}Se$.

[Traduit par le journal]

1. Introduction

Relatively little has been published on selenium isotope fractionation in contrast to the many reports on the isotopes of sulfur in the same chemical group.

Krouse and Thode (1) calculated the ^{76}Se to ^{82}Se partition function ratios for several selenium compounds and predicted fractionations of up to 6% in $^{76}Se - ^{82}Se$ equilibrium exchange processes. They also studied the fractionation of selenium isotopes during the reduction of selenite to elemental selenium by hydroxylamine hydrochloride. Assuming that the rate was controlled by one step in the competitive reactions,

$$^{76}SeO_3^{2-} \xrightarrow{k_{76}} {}^{76}Se^0$$

$$^{82}SeO_3^{2-} \xrightarrow{k_{82}} {}^{82}Se^0$$

they found the ratio of the isotopic rate constants k_{76}/k_{82} to be 1.015 at room temperature. The observed fractionation was attributed to the kinetic isotope effect in the initial Se—O bond rupture.

Rees and Thode (2) conducted several experiments on selenium isotope selectivity in the reduction of selenite and selenate by $C_6H_8O_6$. They found the rate constant for the $^{76}SeO_3^{2-}$ species to be about 1.019 times that for the $^{82}SeO_3^{2-}$ species. Their data were consistent with the activated complex having an isotopic partition function ratio similar to the starting SeO_3^{2-}, but missing one frequency term. One component of the doubly-degenerate E type asymmetric stretching vibration ν_3 ($\sim$730 cm^{-1}) was omitted since it corresponds to one oxygen atom moving away from the rest of the molecule.

Webster (3) studied SeO_3^{2-} reduction by $NH_2OH.HCl$ and found k_{74}/k_{80} to be 1.010. This ratio is nearly equivalent to k_{76}/k_{82} since the mass difference is 6 in each case.

Thus in the literature, k_{76}/k_{82} values or their equivalent, range from 1.010 to 1.019 for SeO_3^{2-} reduction to Se^0 (i.e., a factor of 20 greater than the mass spectrometry errors). This could indicate that the mechanism of reduction of SeO_3^{2-} by ascorbic acid differs markedly from that by $NH_2OH.HCl$. However, the best fitting models considered only Se and O atoms in the reduced mass term and ignored the reducing agent. Further, the differences found in $NH_2OH.HCl$ experiments by different laboratories require explanation.

Because of these apparent discrepancies and the potential for SeO_3^{2-} reduction to effect isotope fractionation in the terrestrial selenium cycle, the reaction was re-examined isotopically. Since one source of disagreement among data from different laboratories might be contaminants in the prepared samples, three isotopes ^{76}Se, ^{80}Se, and ^{82}Se were employed to check the consistency of the measured isotope effects and to verify their expected mass dependence.

In addition to the conversion of SeO_3^{2-} to Se, reduction to H_2Se was investigated.

2. Theory

For a one step first order conversion, the ratio of the isotopic rate constants can be calculated from the isotopic composition of the initial reactant and accumulated product by the relation;

$$[1] \quad \frac{k_1}{k_2} = \frac{\ln (1 - f)\dfrac{1 + A_{0_2}/A_{0_1}}{1 + X_2/X_1}}{\ln (1 - rf)\dfrac{1 + A_{0_2}/A_{0_1}}{1 + X_2/X_1}}$$

where f is the fraction of reactant converted

$$r = \frac{X_2/X_1}{A_{0_2}/A_{0_1}}$$

subscripts 1 and 2 refer to the lighter and heavier isotopic species, respectively; and X and A_0 refer to accumulated product and initial reactant, respectively.

---

[1]Present address: Department of Physics, College of Science and Technology, Abu-Dis, Jerusalem.

[2]Revision received April 10, 1985.

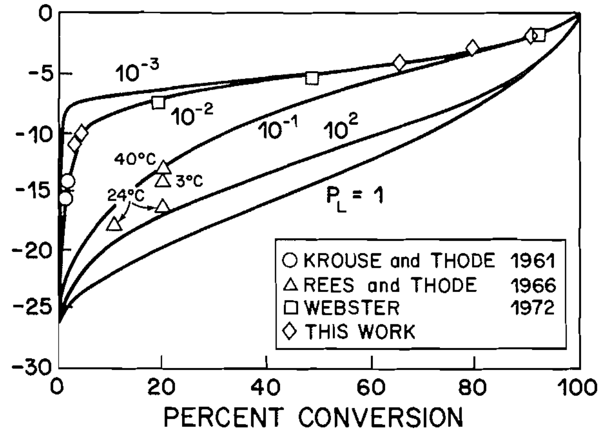

FIG. 1. Data from reduction by $NH_2OH.HCl$ (Krouse and Thode (1); Webster (3); this work), fit the plot with $P_L = 10^{-2}$, $K_1 = 1.007$, and $K_2 = 1.020$. Data from ascorbic acid reduction (Rees and Thode (2)) could fit a plot with the same K_1 and K_2 but larger P_L.

Two consecutive isotopically competitive first order irreversible reaction steps may be written:

$$[2] \quad \begin{array}{l} A_A^1 \xrightarrow{k_1} A_B^1 \xrightarrow{k_1'} A_C^1 \\ A_A^2 \xrightarrow{k_2} A_B^2 \xrightarrow{k_2'} A_C^2 \end{array}$$

where subscripts A, B, and C signify reactant, intermediate, and product, respectively. For this case, Monster (4) derived the following relation between the overall isotopic effect and the extent of reaction:

$$[3] \quad R = \left(\frac{A_C^2/A_C^1}{A_{A_0}^2/A_{A_0}^1}\right) = \frac{1 - \dfrac{K_1}{K_1 - K_2P_L}E^{1/K_1} + \dfrac{K_2P_L}{K_1 - K_2P_L}E^{1/K_2P_L}}{1 - \dfrac{E}{1 - P_L} + \dfrac{P_L}{1 - P_L}E^{1/P_L}}$$

where R = fractionation factor between the final product and the initial reactant. $(R - 1) \times 10^{-3}$ is approximately the δ value in ‰ (per mil) of the final product with respect to the initial reactant; $K_1 = k_1/k_2$ = ratio of the isotopic rate constants for the first reaction step; $K_2 = k_1'/k_2'$ = ratio of the isotopic rate constants for the second reaction step; $P_L = k_1/k_1'$ = ratio of the light isotopic rate constant for the first step over that of the second step; $E = e^{-T} = e^{-kt}$ defines the extent of the reaction.

The relation between E and the fraction of reaction f is

$$f = \frac{1 - P_L - E + P_L E^{1/P_L}}{1 - P_L}$$

A feature which emerges from Monster's derivation is that the isotopic fractionation depends on the ratios of rate constants and not their absolute values.

Figure 1 shows how the δ values of the final product behave as a function of percentage conversion. K_1 and K_2 have been chosen as 1.007 and 1.020, respectively. It is seen that isotopic effects sum for small extents of reaction. As the reaction proceeds, this summing is dependent upon the value of P_L. If $P_L = 1$, the summing effects are maximal with the δ value of the product behaving as if it were produced by a single step

TABLE 1. δ^{82}Se and δ^{80}Se values of components during a first-order one step process; $k_{76}/k_{82} = 1.018$, $k_{76}/k_{80} = 1.012$[a]

Conversion (%)	Remaining reactant δ^{82}Se	Remaining reactant δ^{80}Se	Remaining reactant R	Accumulated product δ^{82}Se	Accumulated product δ^{80}Se	Accumulated product R
10	1.90	1.27	1.50	−16.77	−11.25	1.49
20	4.03	2.69	1.50	−15.79	−10.59	1.49
30	6.45	4.29	1.50	−14.72	−9.87	1.49
40	9.24	6.15	1.50	−13.55	−9.09	1.49
50	12.56	8.36	1.50	−12.25	−8.22	1.49
60	16.63	11.06	1.50	−10.79	−7.24	1.49
70	21.91	14.56	1.50	−9.11	−6.11	1.49
80	29.40	19.51	1.51	−7.09	−4.76	1.49
90	42.32	28.02	1.51	−4.50	−3.02	1.49

[a] $R = \delta^{82}\text{Se}/\delta^{80}\text{Se}$.

conversion with $k_1/k_2 = K_1K_2$. If $P_L \ll 1$, the δ value of the product quickly approaches the behaviour of a single step with a $k_1/k_2 = 1.007$. If $P_L \gg 1$, the δ value adjusts quickly to a behaviour consistent with a single step conversion with a $k_1/k_2 = 1.020$. In summary, the δ value of the product exhibits the summing behaviour for very small conversions but adjusts to the rate controlling step as the reaction proceeds dependent upon the ratio of the slower to faster rate constants.

It follows that if one step is much slower than the other, it dominates throughout most of the reaction and the k_1/k_2 of the faster step has little influence. For example, in Fig. 1, if $P_L = 10^{-3}$, then increasing K_2 to a higher value say 1.030 means that the initial product has a δ value of about 40‰, but for most of the reaction, the product still conforms to a $k_1/k_2 = 1.007$.

For three isotopes of masses M_1, M_2, and M_3 participating in a process with rate constants k_1, k_2, and k_3, respectively, C. E. Rees (private communication, 1978) developed a power series relationship. If $\left(\dfrac{(M_2 - M_1)}{M_1}\right)^2$ and higher terms are ignored, the following approximation arises:

$$[4] \quad \frac{(k_1/k_3) - 1}{(k_1/k_2) - 1} \approx \frac{M_3 - M_1}{M_2 - M_1}$$

If the rate constant does not depend solely on M, it may not be possible to ignore higher terms in the series. For selenium, if k_{76}, k_{80}, and k_{82} depend solely on the mass of ^{76}Se, ^{80}Se, and ^{82}Se, respectively, then

$$[5] \quad (k_{76}/k_{82}) - 1 = 1.5[(k_{76}/k_{80}) - 1]$$

In stable isotope research, it is customary to use δ values by virtue of the measurements process. For the current study, two δ scales are defined:

$$[6] \quad \delta^{80}\text{Se in ‰} = \left\{\frac{[^{80}\text{Se}/^{76}\text{Se}]_{\text{sample}}}{[^{80}\text{Se}/^{76}\text{Se}]_{\text{standard}}} - 1\right\} \times 1000$$

$$[7] \quad \delta^{82}\text{Se in ‰} = \left\{\frac{[^{82}\text{Se}/^{76}\text{Se}]_{\text{sample}}}{[^{82}\text{Se}/^{76}\text{Se}]_{\text{standard}}} - 1\right\} \times 1000$$

where ‰ (per mil) is parts per thousand.

^{80}Se/^{76}Se is the ratio of the number of ^{80}Se-to-^{76}Se isotopes in the sample or standard.

TABLE 2. $\delta^{82}Se$ and $\delta^{80}Se$ values of reactant and reaction product during SeO_3^{2-} reduction to Se^0 by $NH_2OH \cdot HCl$ at room temperature

Conversion (%)	Accumulated Se^0			Remaining reactant and intermediates				
	$\delta^{82}Se$ (‰)	$\delta^{80}Se$ (‰)	R^*	$\delta^{82}Se$ (‰)	$\delta^{80}Se$ (‰)	R^*	k_{76}/k_{82}	k_{76}/k_{80}
2.5	−10.8	−7.5	1.4_4				1.011	1.007_5
3.4	−10.0	−6.4	1.5_6				1.010	1.006_5
62.7	−5.7	−3.7	1.5_4	+9.9	+6.6	1.5_0	1.010	1.007
79.5	−2.9	−1.9	1.5_3	+10.9	+7.0	1.5_6	1.007	1.004_5
90.2	−1.7	−1.2	1.4_2	+14.1	+8.8	1.6_0	1.007	1.004_5

[a]$R^* = \delta^{82}Se/\delta^{76}Se$.

The standard was the initial selenite.

In Table 1, expression [1] has been used in combination with [6] and [7] to derive the δ values of remaining reactant and accumulated product in a one step first order conversion. k_{76}/k_{82} and k_{76}/k_{80} have been chosen as 1.018 and 1.012, thus meeting the condition of eq. [5]. The results show that $\delta^{82}Se$ is also equal to $1.5\delta^{80}Se$ for both the remaining reactant and accumulated product. Such a relationship was predicted in general terms by Rees.

3. Experimental

For studies of the reduction of Se_3^{2-} to Se^0, 0.5 g of Na_2SeO_3 were dissolved in 250 mL of distilled water, and reduced by adding predetermined amounts of $NH_2OH.HCl$ in solution at room temperature. After leaving over night, Se^0 was separated by centrifuging and washing with distilled water repeatedly and drying at room temperature for several hours. An excess of $NH_2OH.HCl$ solution was then added to the supernatant to reduce all the remaining SeO_3^{2-} and any intermediate forms in solution. This Se^0 was also centrifuged, washed, and dried.

When SeO_3^{2-} was reduced using reflux apparatus and the reducing mixture $HI - H_3PO_2 - HCl$ as described by Harrison and Thode (5), a dark red color was immediately evident in the solution, characteristic of elemental selenium. Purging with N_2 revealed that hydrogen selenide was also produced and could be trapped in a cadmium acetate solution. The H_2Se production rate was slow at room temperature and evolution continued for more than a week. Precipitated CdSe was removed every 24 h and converted to Ag_2Se by adding 0.1 N $AgNO_3$ solution.

The reduction mixture (50 mL) was also added to a single commercial selenium pellet and the evolved H_2Se treated as above.

Elemental Se and Ag_2Se were fluorinated to SeF_6 by reaction with F_2 for several hours in closed nickel reaction vessels at room temperature. The reaction vessel was then immersed in a liquid air bath which was subsequently replaced by a n-pentane slush bath (−130°C) to distill off excess F_2. For environmental purposes, the excess F_2 was passed over KBr at 200°C to form KF and Br_2. The Br_2 was trapped and bottled.

The stable isotope mass spectrometry was carried out on a 90°, 30.5 cm radius magnetic deflection instrument, built "in house". Ion currents of masses 171 ($^{76}Se^{19}F_5^+$), 175 ($^{80}Se^{19}F_5^+$), and 177 ($^{82}SeF_5^+$) were collected simultaneously. The outputs of each collector amplifier were fed to a Fluke 8300A digital voltmeter which had additional circuitry for measuring the ratio of any two voltages. The analyzer tube and ion source of the mass spectrometer were baked over-night at 200°C and kept at 100°C during analysis. Without baking, the resolution of the spectra tended to deteriorate within 20 min. The baking programme in combination with the use of ion pumps made it possible to maintain the background pressure below 1×10^{-9} mm Hg.

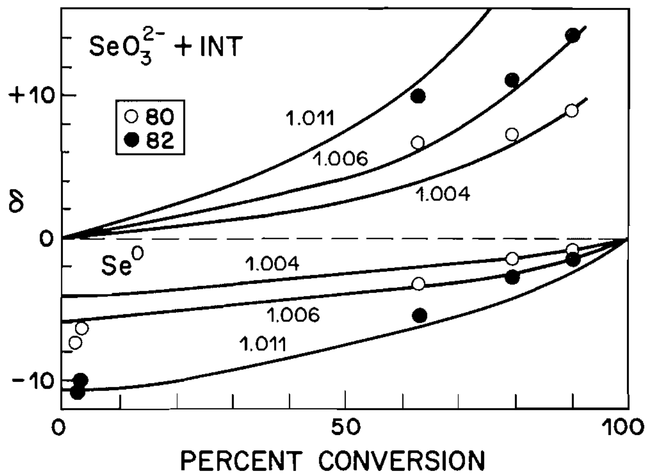

FIG. 2. $\delta^{82}Se$ and $\delta^{80}Se$ values for selenium isotope fractionation during reduction of SeO_3^{2-} by $NH_2OH.HCl$ compared to values predicted by a one step first order conversion using k_1/k_2 values of 1.004, 1.006, and 1.011. The lower curves are for the accumulated elemental selenium product while the upper curves correspond to unreacted SeO_3^{2-} plus intermediates.

4. Results

Chemical reduction of Se_3^{2-} to Se^0

$\delta^{82}Se$ and $\delta^{80}Se$ data for the reduction of SeO_3^{2-} to Se^0 using $NH_2OH.HCl$ are given in Table 2. For a given percentage reaction, k_{76}/k_{82} and k_{76}/k_{80} values are calculated from the δ values of both the accumulated product and the remaining reactant plus intermediates, using the single step approximation eq. [1]. The results from both calculations agreed to within the experimental error and hence only one entry is made in Table 2. There are no data for the remaining reactant plus possible intermediates at low conversions since the measured δ values would be smaller than the standard deviation of the measurements.

An obvious feature of Table 2 is that k_{76}/k_{82} and k_{76}/k_{80} decrease as the reaction progresses. These values represent averages for the reaction up to the percentage conversion noted. Since the k_{76}/k_{82} values are 1.011 in the initial steps but average 1.007 for all products formed up to 80% reaction, the instantaneous product formed near 80% conversion must have a k_{76}/k_{82} value considerably lower than 1.007. Alternatively, extrapolating the data back to smaller conversions gives values

TABLE 3. Selenium isotope fractionation during SeO_3^{2-} reduction to H_2Se

Trial number	Sample 1	Mass (mg) Ag_2Se	Mass (mg) Se	Conversion (%)	$\delta^{82}Se$	$\delta^{80}Se$
1	1	29	7	0.0–17.3	+4.5	+4.1
	2	8	2	17.3–22.0	+2.6	ND
	3	120	32	22.0–93.8	−1.3	−0.9
	4	10	3	93.8–100.0	+0.1	+0.3
2	1	11	3	0.0–19.0	+4.2	+2.0
	2	5	2	19.0–26.0	+9.4	+6.0
	3	7	2	26.0–33.0	−1.1	−0.2
	4	22	6	33.0–51.0	−0.2	−0.1
	5	60	16	51.0–100.0	−1.2	−0.7

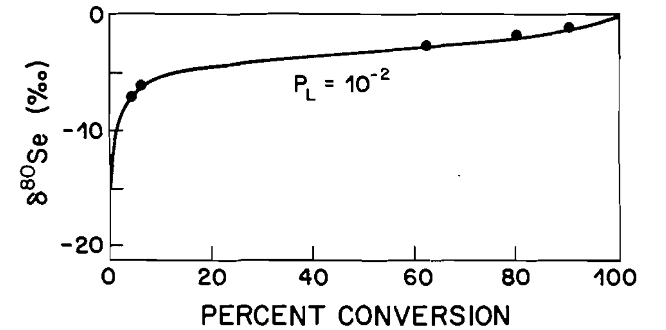

FIG. 3. $\delta^{80}Se$ data for SeO_3^{2-} reduction by $NH_2OH.HCl$ compared to a two step first order conversion with $K_1 = 1.0046$, $K_2 = 1.0133$, and $P_L = 0.01$. In comparison to Fig. 1, note that $(K_1 - 1) = 1.5(K_1' - 1)$ and $(K_2 - 1) = 1.5(K_2' - 1)$.

of k_{76}/k_{82} higher than 1.011. This inconsistency is further illustrated in Fig. 2. If one considers a k_{76}/k_{82} value of 1.006, the $\delta^{82}Se$ values at 80 and 90% reaction fall close to the curves for both the accumulated product and the remaining reactant. However, at small conversions, the $\delta^{82}Se$ values fall below the $k_{76}/k_{82} = 1.006$ curve by 5‰ or 10 times the measurement errors. Similarly, if k_{76}/k_{82} is chosen as 1.011, the data at small conversions and at 63% reaction fit well, but the data at 80 and 90% depart significantly from the curves. In the case of the remaining product curve, the departure at 90% conversion is about 20 times the measurement error. Therefore, a simple one step model is inadequate to describe the attending isotope fractionation. Accordingly, a two step model was investigated using eq. [3].

The inverse of eq. [3] has not been derived to date, i.e., one cannot obtain values for K_1, K_2, and P_L from R. Therefore, eq. [3] was programmed on an Apple II microcomputer to generate plots of δ values of product versus extent of reaction for selected values of K_1, K_2, and P_L. Experimental data were visually compared to these plots. There is considerable latitude in the choice of parameters which are consistent with the data. However, values of k_{76}/k_{82} of 1.007 and 1.020 for K_1 and K_2 and a P_L value of 10^2 give a reasonable fit (Fig. 1) which has chemical significance. 1.020 is the maximum k_{76}/k_{82} value reported for SeO_3^{2-} reduction (2) while 1.007 is the value frequently encountered during latter parts of the conversion (Table 2). It is also seen in Fig. 3 that the $\delta^{80}Se$ data fit a two-step model which is consistent with eq. [5].

Reduction of SeO_3^{2-} to H_2Se

$\delta^{82}Se$ and $\delta^{80}Se$ data for SeO_3^{2-} reduction to H_2Se by

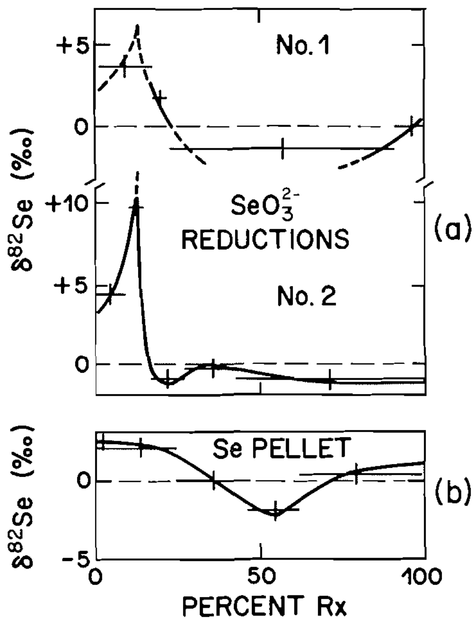

FIG. 4. (*a*) $\delta^{82}Se$ values for H_2Se evolved during reduction of SeO_3^{2-} by a $HCl-H_3PO_2-HI$ mixture at room temperature; (*b*) $\delta^{82}Se$ values for H_2Se evolved during reduction of a commercial pellet of elemental selenium at room temperature.

$HI-H_3PO_2-HCl$ are shown in Table 3, and in Fig. 4(*a*). These data differ from those for elemental selenium produced during selenite reduction. Whereas the initial Se^0 product is depleted in the heavier isotopes and its δ value increases as the reaction proceeds, the initially produced H_2Se is enriched in the heavier isotope with a tendency to become isotopically lighter in a sporadic fashion as the reaction proceeds. It is noted that in some partial runs, negative δ values ($\delta^{82}Se$ as low as −6.0‰) were obtained at earlier stages of the reaction but the usual tendency was that in Fig. 4.

Since elemental selenium precipitated during SeO_3^{2-} reduction prior to H_2Se formation, a separate experiment was conducted during which a single commercial selenium pellet was reduced by $HI-H_3PO_2-HCl$ to H_2Se. The isotopic variations were small (Table 4 and Fig. 4(*b*)).

The isotopic behaviour summarized in Table 4 and Fig. 4(*a*) is consistent with the observation that elemental selenium formation is significantly more rapid than the H_2Se generation. If the spherules of elemental selenium form and grow concentrically in the reaction medium, their centres will be depleted in the heavier isotopes, whereas the outer layers become iso-

TABLE 4. $\delta^{82}Se$ and $\delta^{80}Se$ for H_2Se evolved from one metallic selenium pellet by $HI-H_3PO_2-HCl$ reduction mixture at 100°C; original pellet mass, 54 mg

Sample number	Mass (mg) Ag_2Se	Mass (mg) Se	Conversion (%)	$\delta^{82}Se$ (%)	$\delta^{80}Se$ (%)
1	11	3	0.0−5	+1.6	+1.3
2	37	10	5−24	+1.5	+1.4
3	48	13	24−48	0.0	0.0
4	30	8	48−63	−2.7	−1.9
5	71	19	63−98	−0.4	−0.2
	Total 197	Total 53			

topically heavier with increased reduction of SeO_3^{2-}. If the production of H_2Se proceeds by peeling the Se^0 spherules layer by layer, the initially produced H_2Se is isotopically heavier. The lack of very positive $\delta^{82}Se$ values and the erratic behaviour of the isotopic release pattern possibly related to the different sizes of spherules and their different initiation times. A further complication which is difficult to demonstrate is that some H_2Se may have been produced in a parallel pathway which did not have Se^0 as an intermediate.

The small isotopic variations found with the pellet are beyond experimental uncertainties and possibly indicate isotopic partitioning between phases during manufacture. In this higher temperature process, one expects the isotopic composition of the pellet to be more uniform that that of spherules formed during the chemical reduction of SeO_3^{2-}.

5. Discussion

Selenium isotope fractionation during the chemical reduction of SeO_3^{2-} to Se^0 is more adequately described by a two step process than by the single step model which has been usually employed in similar investigations of kinetic isotope effects. The two step model derived from data of this report, is consistent with the data of Krouse and Thode (1). In addition, the $^{74}Se-^{80}Se$ data of Webster (3) which are nearly equivalent to the current $^{76}Se-^{82}Se$ data also fit the two step model (Fig. 1).

The question remains as to whether the current model is consistent with the data of Rees and Thode (2) using ascorbic acid as the reducing agent. Two points are relevant. At the same temperature (24°C), the k_{76}/k_{82} values at 10 and 20% reduction were found to be 1.020 and 1.019, respectively. Although the errors for these two determinations overlap, the trend is the same as in the current work. The second point is that different isotope selectivities have been noted in chemical reductions using different reducing agents. Whereas Harrison and Thode (5) obtained $k_{32}/k_{34} = 1.022$ for reduction of SO_4^{2-} by $HI-H_3PO_2-HCl$, Downes and Donnelly (6) obtained values as low as 1.015 using other reducing agents.

A consequence of the two-step model is that different overall isotopic fractionations result for the same K_1 and K_2 values if P_L is varied. Thus the data of Rees and Thode (2) at 24°C are consistent with the K_1 and K_2 values of the current experiments if a P_L value is chosen near 10^2 (Fig. 1). This interpretation means that the second step was more effective in rate-controlling in the reductions using $NH_2OH.HCl$. It also implies that the mass dependence of these two steps does not depend upon the reducing agent, but a particular reductant determines which step is more effective in controlling the overall rate. The relatively large variation with temperature for the $\delta^{82}Se$ values of product Se^0 (3°C, −14.6; 24°C, −16.9, −18.4; 40°C, −14.2, in ‰) during reduction by ascorbic acid could reflect variation of P_L with temperature.

The question arises as to the chemical nature of the two steps. Since the one step model was associated with the initial Se—O bond rupture, an obvious interpretation is that the two step model represents the consecutive removal of two oxygen atoms. The values of K_1 and K_2 chosen in the present work fall well within the calculated extreme values of 1.002 and 1.031 (2).

The unusual isotopic effects found during the conversion of SeO_3^{2-} to H_2Se can be attributed to the presence of Se^0 as a reaction intermediate. This has implications in natural environments where biogenic H_2Se may be formed with subsequent selenide mineral formation. During bacterial sulphate reduction, elemental sulphur is not an intermediate although it may form by subsequent reoxidation of sulphide. In these environments, significant depletions of the heavier sulphur isotopes in the sulphide phase are considered to be indicative of bacteriogenesis. In the case of sedimentary selenide deposits, the data of this report show that the analogous interpretation will be complicated if elemental selenium forms as an intermediate.

Finally, it is seen that the use of three isotopes in this investigation assures that the effects are real and not the consequence of contamination. This is particularly relevant when a sample is prepared as a fluoride since F_2 is very chemically reactive. For all data of this report, $\delta^{82}Se = (1.5_4 \pm 0.02)\delta^{80}Se$ with a multiple linear correlation coefficient of 0.998 and a probability of no correlation of less than 6×10^{-10}. Besides attesting to the experimental consistency, the data verify the relationship

$$[(k_1/k_3) - 1] = \frac{M_3 - M_1}{M_2 - M_1}.\ [(k_1/k_2) - 1]$$

as obtained by Rees (personal communication, 1978).

Acknowledgement

Financial support for this project was provided by NSERC Grant No. A 8176 to H.R.K.

1. H. R. KROUSE and H. G. THODE. Can. J. Chem. **40**, 367 (1961).
2. C. E. REES and H. G. THODE. Can. J. Chem. **44**, 419 (1966).
3. C. WEBSTER JR. Ph.D. Thesis, Colorado State University, 1972.
4. J. MONSTER. Department of Chemistry, McMaster University. Report #44.
5. A. G. HARRISON and H. G. THODE. Trans. Faraday Soc. **53**, 1648 (1957).
6. C. J. DOWNES and T. H. DONNELLY. Unpublished results.

Densities and apparent molar volumes of aqueous NaCl–KBr mixtures at 298.15 K

ANIL KUMAR[1]

Chemical Engineering Division, National Chemical Laboratory, Pune 411 008, India

Received April 1, 1985

ANIL KUMAR. Can. J. Chem. **63**, 3200 (1985).

Experimental differences in densities Δd of aqueous NaCl–KBr mixtures at $I = 1, 2, 3$, and 4 mol kg^{-1} and at 298.15 K are reported from pure NaCl to pure KBr solutions. Mean apparent molar volumes ϕ_V^* are calculated and excess volumes of mixing ΔV_m^{ex} are correlated by Friedman equation. Δd and ϕ_V^* are analysed in terms of recently developed the Pitzer formalism without and with mixing terms. Pitzer equations can estimate the densities of such mixtures with uncommon cations and anions within $\pm 0.02\%$ at the high ionic strength of 4 mol kg^{-1}.

ANIL KUMAR. Can. J. Chem. **63**, 3200 (1985).

En se basant sur les valeurs obtenues pour des solutions allant du NaCl pur au KBr pur, on a déterminé les différences expérimentales de densités, Δd, de solutions aqueuses de NaCl–KBr à $I = 1, 2, 3$, and 4 mol kg^{-1}, à 298,15 K. On a calculé les volumes molaires apparents moyens, ϕ_V^*, et on a relié les volumes de mélange en excès ΔV_m^{ex} à l'équation de Friedman. On a analysé les valeurs de Δd et de ϕ_V^* en fonction du formalisme développé récemment par Pitzer avec ou sans les termes de mélange. Les équations de Pitzer peuvent évaluer les densités de ce type de mélanges contenant des cations et dex anions qui ne sont pas communs avec une précision de $\pm 0{,}02\%$, à une grande force ionique de 4 mol kg^{-1}.

[Traduit par le journal]

Introduction

Since the development of the Pitzer formalism (1, 2) in describing the thermodynamic properties of concentrated aqueous mixed electrolyte solutions, many papers (3) have appeared dealing with activity, osmotic coefficients, and enthalpies of concentrated aqueous electrolytes. Kumar *et al.* (4) and Kumar and Atkinson (5) were the first to extend successfully the Pitzer formalism to the volume properties of aqueous $NaCl–CaCl_2$ system in the ionic strength range of 0.3 to 20 mol kg^{-1} of water and in the temperature range of 278.15 to 308.15 K. The system studied had a common anion.

In the present investigation, we report the experimental densities of the mixture composed of aqueous NaCl with KBr at the constant ionic strengths of 1, 2, 3, and 4 mol kg^{-1} at 298.15 K and analyse them in terms of the Pitzer theory. This system has two different cations and two different anions and the densities of pure electrolyte solutions are significantly different.

Experimental

NaCl and KBr (Baker Analysed) were recrystallized twice before use. The stock solutions were prepared by mass in deionized water. The molalities of stock solutions were determined by gravimetric method using $AgNO_3$.

The densities of mixtures were measured with Paar vibrating tube densitometer. The relative densities, $\Delta d = (d - d_0)$, where d_0 is the density of pure water 0.997047 g cm^{-3} at 298.15 K, were obtained as reported earlier (4). Temperature of thermostat bath was controlled to ± 0.005 K and density differences were precise to $\pm 3 \times 10^{-6}$ g cm^{-3}. Experimental method and calibration were the same as discussed earlier (4, 5). Mixtures of various compositions were prepared by appropriate combination of NaCl and KBr solutions at a particular ionic strength.

Results and discussion

Table 1 reports the differences in densities Δd of mixtures at constant ionic strengths 1, 2, 3, and 4 mol kg^{-1} as a function of ionic strength fraction of KBr (y_B). In this paper A and B refer to NaCl and KBr, respectively, and $y_A + y_B = 1$. Table 1 also reports the mean apparent molar volumes of mixture ϕ_V^*, calculated by

$$[1] \qquad \phi_V^* = \frac{1000(d_0 - d_{expt})}{\sum_J m_J d_{expt} d_0} + \frac{\sum_J m_J M_J}{\sum_J m_J d_{expt}}$$

where $\Sigma\, m_J$ is the sum over molalities of electrolytes in mixture and M_J is molecular weight of the electrolytes.

Wirth (6) reported the densities of the same system at 298.15 K, where the concentration of NaCl was kept constant while KBr was added to the total ionic strength of 1.5 mol kg^{-1}. It was difficult to compare our densities with his values as his data were neither at constant ionic strength nor at constant ionic strength fraction.

Experimental Δd and ϕ_V^* can be examined using the Pitzer equations. Details of general equations of Pitzer are given elsewhere (4, 5) but a summary of useful expressions as modified for the mixtures of 1–1 type of electrolytes mixtures is given below.

Apparent molar volume, ϕ_V, of an 1–1 electrolyte (MX) based on the Pitzer formalism is

$$[2] \qquad \phi_V = \phi_V^0 + \frac{A_V}{b} \ln(1 + bI^{1/2}) + 2RT[mB_{MX}^V + m^2 C_{MX}^V]$$

where

$$[3] \qquad B_{MX}^V = \left(\frac{\partial \beta^{(0)}}{\partial P}\right)_T + \left(\frac{\partial \beta^{(1)}}{\partial P}\right)_T (2/\alpha^2 I) [1 - (1 + \alpha I^{1/2}) \exp(-\alpha I^{1/2})]$$

and

$$[4] \qquad C_{MX}^V = (\partial C^{\phi}/\partial P)_T/2$$

In above equations, $\alpha = 2.0$ (kg/mol)$^{1/2}$ and $b = 1.2$ (kg/mol)$^{1/2}$, $R = 83.1441$ cm^3 bar mol^{-1} K^{-1} and A_V is Pitzer–Debye–Hückel slope $= 1.874$ (cm^3/mol) (kg/mol)$^{1/2}$ at 298.15 K.

The mixture under study is composed of two cations Na^+ and K^+ and two anions Cl^- and Br^-. To use the Pitzer equations,

[1] Alexander Von Humboldt Fellow. Present address: % Professor E. U. Franck, Institute of Physical Chemistry and Electrochemistry, University of Karlsruhe, 7500 Karlsruhe, West Germany.

TABLE 1. Experimental Δd, ϕ_V^*, and ΔV_m^{ex} of NaCl–KBr–H_2O at 298.15 K

y_B	$\Delta d \times 10^3$ (g cm^{-3})	ϕ_V^* (cm^3 mol^{-1})	ΔV_m^{ex} (cm^3 mol^{-1})	y_B	$\Delta d \times 10^3$ (g cm^{-3})	ϕ_V^* (cm^3 mol^{-1})	ΔV_m^{ex} (cm^3 mol^{-1})
	I = 1 mol kg^{-1}				I = 3 mol kg^{-1}		
0.0000	38.982	18.67	0.000	0.0000	108.114	20.17	0.000
0.1088	43.481	20.59	0.082	0.0856	117.793	21.75	0.141
0.2175	48.103	22.45	0.113	0.1088	120.437	22.16	0.169
0.3233	52.416	24.26	0.136	0.1596	126.198	23.07	0.221
0.4011	55.642	25.58	0.169	0.2695	138.619	25.10	0.336
0.5025	59.825	27.32	0.183	0.3721	150.223	26.81	0.393
0.5998	63.867	28.97	0.174	0.4519	159.244	28.17	0.420
0.7130	68.573	30.83	0.139	0.5613	171.685	29.98	0.407
0.8225	73.122	32.63	0.095	0.6411	180.657	31.31	0.384
0.9119	76.815	34.12	0.062	0.7651	194.708	33.04	0.295
1.0000	80.494	35.53	0.000	0.8503	204.393	34.63	0.196
				0.9601	216.792	36.34	0.064
	I = 2 mol kg^{-1}			1.0000	221.315	36.95	0.000
0.0000	75.295	19.29	0.000				
0.1152	84.304	21.40	0.136		I = 4 mol kg^{-1}		
0.2239	92.843	23.35	0.215	0.0000	138.445	20.90	0.000
0.2987	98.692	24.68	0.265	0.1251	156.636	23.18	0.211
0.4095	107.416	26.60	0.287	0.2005	167.487	24.55	0.332
0.5112	115.418	28.34	0.283	0.3110	183.687	26.49	0.427
0.6152	123.482	30.15	0.275	0.4152	198.645	28.25	0.481
0.7233	132.015	31.93	0.235	0.5081	212.055	29.81	0.502
0.8002	137.994	33.22	0.209	0.6111	227.043	31.47	0.459
0.9008	145.905	34.85	0.115	0.6918	238.692	32.77	0.420
1.0000	153.707	36.44	0.000	0.8082	255.616	34.57	0.292
				0.8825	266.320	35.71	0.205
				1.0000	283.392	37.45	0.000

TABLE 2. Pitzer coefficients for cation–anion interactions

Cation–anion	ϕ_V^0 (cm^3 mol^{-1})	$\left(\frac{\partial\beta^{(0)}}{\partial P}\right)_T \times 10^5$	$\left(\frac{\partial\beta^{(1)}}{\partial P}\right)_T \times 10^5$	$\left(\frac{\partial C^{\phi}}{\partial P}\right)_T \times 10^6$	σ (cm^3 mol^{-1})	Ref.
Na–Cl	16.58	1.14	1.15	−1.11	0.01	5
K–Br	34.08	4.93	9.18	28.15	0.03	7
Na–Br	23.59	3.49	−4.09	27.18	0.02	7
K–Cl	26.92	1.49	−0.17	2.88	0.03	8

it is essential to calculate the coefficients $(\partial\beta^{(0)}/\partial P)_T$, $(\partial\beta^{(1)}/\partial P)_T$, and $(\partial C^{\phi}/\partial P)_T$ for cation–anion pairs as Na–Cl, Na–Br, K–Br, and K–Cl. Equation [2] was used to generate these Pitzer coefficients for these pairs. Single electrolyte ϕ_V data for analysis were taken from elsewhere (5, 7, 8). Table 2 lists these coefficients along with the standard deviation of fit. As clear from this table, single salt data can be accurately fitted with Pitzer equation.

Apparent molar volume of an ion in the mixture of 1–1 electrolytes is given by

$$[5] \quad \phi_{Vi} = \phi_{Vi}^0 + \frac{A_V}{2b}\ln(1 + bI^{1/2}) + RT\sum_i B_{ij}m_j + (RT/2)\sum_i C_{ij}m_J^2$$

where the sums are over all the jth ion sof opposite charge to the ion i. In eq. [5], Pitzer coefficients listed in Table 2 are used to estimate $\phi_{Vi}\cdot\phi_{Vi}$ thus determined lead to the theoretical mean apparent molar volume (ϕ_V^*) as

$$[6] \quad \phi_{V\text{cal}}^* = \frac{\sum_J m_J\phi_{VJ}}{\sum_J m_J}$$

where $\phi_{VJ} = \sum_i \nu_i\phi_{Vi}$, and ν_i is the stoichiometric factor of the ith ion in electrolyte.

Density of mixture can then be computed by relation:

$$[7] \quad d_{\text{cal}} = \frac{1000 + \sum_J m_J M_J}{1000/d_0 + \sum_J m_J\phi_{VJ}}$$

Equations [6] and [7] calculate ϕ_V^* and the density of mixture through ϕ_{Vi} calculated by the Pitzer equation. Table 3 lists the standard deviation of fit for ϕ_V^* and Δd in mixtures using the above relations and considering that the cation–anion interactions are predominent. Examination of this table shows that one can estimate the density of such mixtures at I = 4 mol kg^{-1} to within 0.05%. Similarly ϕ_V^* can be estimated to ±0.7%.

During the above treatment, the interactions between like charges ions are neglected. Their consideration need the evalu-

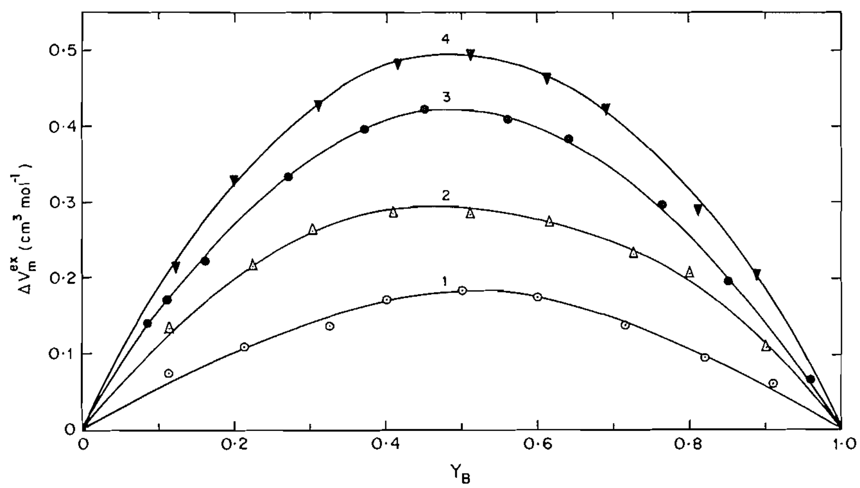

FIG. 1. ΔV_m^{ex} versus y_B for aqueous NaCl–KBr at I = 1, 2, 3, and 4 mol kg^{-1}.

TABLE 3. Standard deviation in relative densities (Δd) and ϕ_V^* of NaCl–KBr–H_2O at 298.15 K using Pitzer equations

I (mol kg^{-1})	In g cm^{-3} or cm^3 mol^{-1}	
	$\Delta d \times 10^3$	ϕ_V^*
1	0.092	0.034
	(0.061)[a]	(0.017)
2	0.255	0.056
	(0.143)	(0.023)
3	0.401	0.092
	(0.169)	(0.051)
4	0.675	0.210
	(0.254)	(0.070)

[a] Values in parentheses are the standard deviations with the use of binary mixing terms.

ation of mixing terms called as binary terms θ_{NaK} and θ_{ClBr}, and ternary terms as ψ_{NaKCl}, ψ_{NaKBr}, ψ_{NaBrCl}, and ψ_{KBrCl}. Binary interaction terms can easily be evaluated as discussed elsewhere (5). The extended Pitzer equation for evaluating ϕ_{Vi} in this mixture can be written by adding an additional term accounting for mixing as

$$[8] \quad \phi_{Vi} = \text{RHS of eq. [5]} + RT \sum_K \theta_{ik} m_k$$

where the summations are over the ions of same charge as on i.

The binary mixing terms θ_{Nak} and θ_{ClBr} calculated for these mixtures do not vary too widely with the range of I of interest. We have, therefore, used the average of the values in mixture calculations. The values of θ_{NaK} and θ_{ClBr} used are 6.31×10^{-6} and 2.83×10^{-6}, respectively. Use of these terms bring a remarkable improvement in the fit of Δd and ϕ_V^* as clear from the standard deviations listed in parentheses in Table 3. One now can estimate d and ϕ_V^* to ±0.02 and ±0.2%. The magnitude of ternary terms in this case was very small as was in NaCl–$CaCl_2$–H_2O (5).

Excess volumes of mixing ΔV_m^{ex} for this system were calculated by

$$[9] \quad \Delta V_m^{ex}/\sum_J m_J = \phi_{V\text{expt}} - \sum_J m_J \phi'_{VJ}$$

TABLE 4. Friedman parameters for correlating ΔV_m^{ex} and y_B by eq. [10]

I (mol kg^{-1})	v_0	v_1	v_2	σ (cm^3 mol^{-1})
1	0.727	−0.058	-9.019×10^{-5}	0.003
2	0.292	0.008	0.063	0.002
3	0.186	0.010	2.288×10^{-3}	0.002
4	0.124	0.003	-2.460×10^{-3}	0.002

In eq. [9], ϕ'_{VJ} indicates the ϕ_V of each electrolyte at the ionic strength of mixture. ΔV_m^{ex} thus obtained are listed in Table 1 and are fitted to Friedman equation [9],

$$[10] \quad \Delta V_m^{ex} = I^2 y_B(1 - y_B)[(v_0 + v_1(1 - 2y_B) + v_2(1 - 2y_B)^2]$$

Figure 1 presents ΔV_m^{ex} as a function of y_B and Table 4 reports the Friedman parameters along with standard deviations.

Above discussion shows that mixture density can accurately be estimated using the Pitzer equations. These equations emerge as powerful predicting tool.

Acknowledgements

I am thankful to late C.V.G. Reddy, NIO, Goa, for arranging the experimental facilities in collaboration with the Goa Government. I also thank Professor G. Atkinson of University of Oklahoma, U.S.A., for introducing me to the field of electrolytes.

1. K. S. PITZER. J. Phys. Chem. **77**, 268 (1973).
2. K. S. PITZER and J. J. KIM. J. Am. Chem. Soc. **96**, 5701 (1974).
3. K. S. PITZER. Activity coefficients in electrolyte solutions. Vol. II. *Edited by* R. M. Pytkowicz. CRC Press, Boca Raton. 1979.
4. A. KUMAR; G. ATKINSON, and R. D. HOWELL. J. Soln. Chem. **11**, 857 (1982).
5. A. KUMAR and G. ATKINSON. J. Phys. Chem. **87**, 5504 (1983).
6. H. E. WIRTH. J. Am. Chem. Soc. **59**, 2549 (1937).
7. T. ISANO. J. Chem. Eng. Data, **29**, 45 (1984).
8. L. A. ROMANKLW and I-M. CHOU. J. Chem. Eng. Data, **28**, 300 (1983).
9. H. L. FRIEDMAN. Ionic solution theory. Interscience, New York. 1962.

Ozonides de phosphite source d'oxygène singulet: rendement, mécanisme

ANNE MARIE CAMINADE, FAYEZ EL KHATIB ET MAX KOENIG[1]
U.A. 454, Université Paul Sabatier, 31062 Toulouse Cédex, France

ET

JEAN MARIE AUBRY[1]
Laboratoire de Chimie Générale, Faculté de Pharmacie, Rue du Professeur Laguesse, 59045 Lille Cédex, France

Reçu le 2 avril 1985

ANNE MARIE CAMINADE, FAYEZ EL KHATIB, MAX KOENIG et JEAN MARIE AUBRY. Can. J. Chem. **63**, 3203 (1985).

Nous avons fait réagir dans le dichlorométhane les ozonides de plusieurs phosphites sur différents capteurs d'oxygène singulet ($^1O_2$): le rubrène **2**, la tétraphénylcyclopentadienone **4** et le diphényl-9,10-anthracène **6**. Ces ozonides réagissent lors de leur décomposition ($-47°C < t < 30°C$) sur ces capteurs. Les droites de Foote obtenues en faisant varier les concentrations respectives d'ozonides et de capteurs conduisent aux mêmes paramètres que ceux obtenus lors de la photooxydation par $^1O_2$ de ces capteurs. Cela confirme l'aptitude de ces ozonides à engendrer $^1O_2$. La valeur trouvée du rendement absolu en $^1O_2$ est de 100% ($\rho = 1$). Les résultats confirment aussi la grande efficacité vis-à-vis de $^1O_2$ du rubrène ($\gamma = 1$) et la valeur moyenne de la tétraphénylcyclopentadienone ($\gamma = 0,46$). La valeur faible ($\gamma = 0,3$) de l'efficacité du diphényl-9,10-anthracène **4** est par contre inattendue.

ANNE MARIE CAMINADE, FAYEZ EL KHATIB, MAX KOENIG, and JEAN MARIE AUBRY. Can. J. Chem. **63**, 3203 (1985).

The ozonides of several phosphites in solution in dichloromethane have been reacted with some scavengers of singlet oxygen ($^1O_2$) like rubrene (**2**), tetraphenylcyclopentadienone (**4**), and 9,10-diphenylanthracene (**6**). These ozonides react on the scavengers ($-47°C < t < 30°C$) upon their decomposition. The Foote curves obtained by varying the respective concentrations of ozonides and of scavengers lead to parameters similar to those obtained upon the photooxidation of the scavengers by $^1O_2$. Results confirm that these ozonides can lead to the formation of $^1O_2$. The absolute yield of $^1O_2$ is 100% ($\rho = 1$). These results also confirm the high efficiency of the rubrene toward $^1O_2$ ($\gamma = 1$) and the lower efficiency of the tetraphenylcyclopentadienone ($\gamma = 0.46$). However, the low value ($\gamma = 0.3$) for the efficiency of the 9,10-diphenylanthracene (**4**) is unexpected.

[Journal translation]

De nombreuses sources chimiques d'oxygène singulet ($^1O_2$) sont aujourd'hui facilement utilisables en milieu aqueux ou dans des solvants organiques (1). À cet égard, les ozonides de phosphite connus depuis 1961 (2) sont de bons générateurs d'oxygène activé lors de leur décomposition thermique (3–5). De nombreuses réactions d'oxydation ont été conduites à l'aide de ces ozonides (1): elles aboutissent dans le cas des cycloadditions-1,4 ou dans les ène-réactions aux mêmes résultats que les réactions de photooxydation (6–8). Toutefois certaines réactions comme les cycloadditions-1,2 se produisent à des températures inférieures à celle qui permet de libérer $^1O_2$ (9); de plus, certaines d'entre elles présentent une stéréospécificité différente des photooxydations (10). C'est ainsi que dans la littérature les réactions observées sont attribuées soit à l'oxygène singulet libéré par l'ozonide soit à la réactivité propre de l'ozonide (schéma 1).

Afin d'éclairer les mécanismes liés à la génération chimique d'oxygène activé, des mesures des paramètres cinétiques et du rendement absolu en $^1O_2$ ont été effectuées. C'est ainsi que pour la réaction $ClO^- + H_2O_2$ la valeur du rendement est de 100% (11, 12); elle est de 70% pour la décomposition des peracides (13, 14), et varie entre 35 et 95% pour les endoperoxydes (15). Dans le cas des ozonides de phosphite, le rendement en $^1O_2$, bien que considéré comme quantitatif par certains auteurs (6, 7, 16), n'a jamais été mesuré. Nous avons mesuré, dans le cas des réactions de cycloaddition-1,4 sur différents capteurs spécifiques d'$^1O_2$ **2**, **4**, **6** le coefficient de Foote (β), l'efficacité du capteur (γ) ainsi que le rendement en oxygène singulet (ρ).

[1] Auteurs à qui adresser la correspondance.

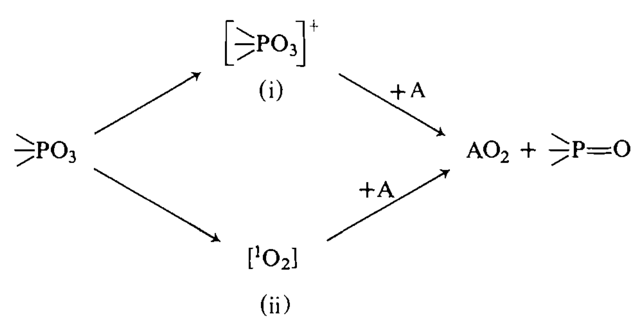

SCHÉMA 1. Chemins réactionnels (i) et (ii) conduisant au produit d'oxydation AO_2 à partir d'ozonides de phosphite.

Résultats

Nous avons fait réagir dans le dichlorométhane les différents ozonides **1***a*–*d* sur trois capteurs classiques d'oxygène singulet: le rubrène **2**, la tétraphénylcyclopentadiènone **4** et le diphényl-9,10-anthracène **6**.

Les ozonides étudiés ne réagissent pas sur ces accepteurs à basse température (−78°C) mais ceux-ci sont oxydés à des températures correspondant à la décomposition thermique des ozonides (réaction [1], tableau 1).

$$[1] \quad (RO)_3PO_3 \xrightarrow{T(°C)} RO_3P{=}O + {}^1O_2$$

Le bilan de l'action des ozonides sur ces capteurs peut s'écrire selon les réactions [2], [3] et [4]. Les concentrations des produits d'oxydation obtenus dans chaque cas (**3**, **5**, **7**) sont mesurées par clhp ou uv.

TABLEAU 1. δ ^{31}P et enthalpies libres d'activation de la réaction [1] dans CH_2Cl_2

	Ozonides	δ ^{31}P	T (°C)	ΔG^* (kcal mol^{-1})	Solvant	Références
1a	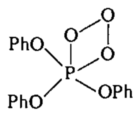	−63	−25	18	CH_2Cl_2	2, 16, 17, 18
1b	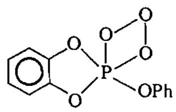	−37	+4	20,1	CH_2Cl_2	17, 19, 20
1c	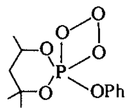	−56 −55.7	−47	16,6	Toluène-d_8/ CH_2Cl_2	19, 20
1d	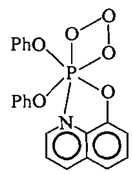	−122	+32	22,4	CH_2Cl_2	19, 20

TABLEAU 2. Comparaison des paramètres réactionnels de l'oxydation des capteurs **2**, **4**, **6** par voie photochimique et par décomposition des ozonides de phosphite **1**a–**1**d

Capteurs	Methode d'oxydation	Solvant	β 10^4 (M)	ρ	γ	k_r (M^{-1} s^{-1})	k_q (M^{-1} s^{-1})	k_d (s^{-1})	Références
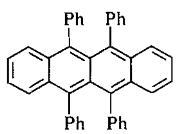 **2**	Ozonide **1**a	CH_2Cl_2	2,23	1	1	$5,4 \times 10^7$	~0	$1,2 \times 10^4$	Ce travail
	Photochim.	CH_2Cl_2	4 ± 0,8	—	1	$4,2 \pm 1,3 \times 10^7$	~0	$1,7 \times 10^4$	21, 23
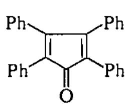 **4**	Ozonides **1**a, **1**b, **1**c	CH_2Cl_2	1	1	0,46	5×10^7	6×10^7	$1,2 \times 10^4$	Ce travail
	Photochim.	CCl_2FCClF_2	0,5	—	0,37	$3,3 \times 10^6$	$5,6 \times 10^6$	$4,7 \times 10^2$	21, 26
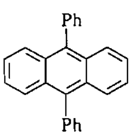 **6**	Ozonides **1**a, **1**b, **1**d	CH_2Cl_2	10	1	0,3	$4,2 \times 10^6$	8×10^6	$1,2 \times 10^4$	Ce travail
	Photochim.	CCl_4	6	—	?	$2,8 \times 10^6$	Non donnée	$1,7 \times 10^3$	21

Les paramètres cinétiques correspondant aux réactions [2], [3], [4] obtenus à partir des droites de Foote (figures 1, 2, 3) figurent dans le tableau 2.

L'oxydation du rubrène **2** par l'ozonide **1**a, pour des rapports [**1**a]/[**2**] variables, nous a permis d'obtenir une droite de Foote (fig. 1) dont la pente est $\beta = 2 \times 10^{-4}$ M et l'ordonnée à l'origine $\rho \times \gamma = 1$. Ces paramètres conduisent, à partir des valeurs de la durée de vie de $^1O_2$ dans CH_2Cl_2 (21, 22) à une constante de vitesse d'oxydation $k_r = 5,4 \times 10^7$ M^{-1} s^{-1} dont la valeur est la même (aux erreurs d'expérience près) que celle obtenue lors de la photooxydation de **2** par $^1O_2$ (23, 24). Ce résultat confirme que la voie d'oxydation la plus probable obtenue par l'ozonide **1**a est celle qui passe par la génération d'$^1O_2$ (25) (voie (ii), schéma 1).

De plus $\rho\gamma = 1$ entraîne $\rho = 1$, et $\gamma = 1$. Ces deux valeurs indiquent que le rendement absolu en $^1O_2$ de l'ozonide **1**a est de 100% et que l'efficacité du rubrène est totale puisqu'il ne désactive pas $^1O_2$ ($k_q \sim 0$).

L'oxydation de **4** par les ozonides **1**a, **1**b et **1**c conduit dans les mêmes conditions (fig. 2) aux paramètres $\beta = 1 \times 10^{-4}$ M et $\rho\gamma = 0,46$. Comme l'ozonide **1**a se trouve sur la droite de Foote, nous avons conservé sa valeur précédente $\rho = 1$ et attribué à γ la valeur 0,46. L'efficacité de la tétraphénylcyclopentadienone **4** est donc très moyenne (26). La constante de vitesse d'oxydation $k_r = 5 \times 10^7$ M^{-1} s^{-1} possède une valeur proche de celle de la constante de vitesse de désactivation k_q.

L'oxydation du diphényl-9,10-anthracène **6** par les ozonides **1**a, **1**b, **1**d (fig. 3) conduit à une valeur de la pente $\beta = 10 \times$

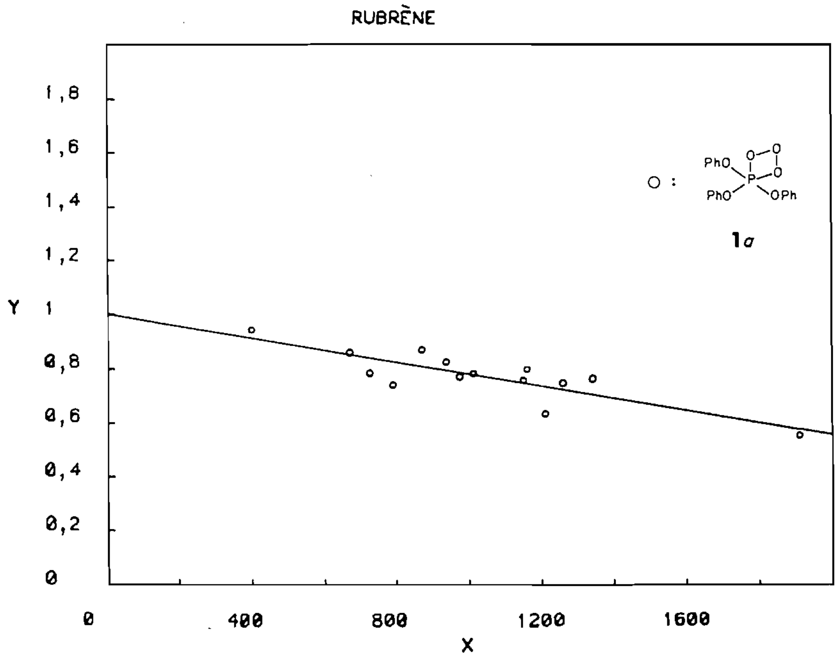

FIG. 1. Droite de Foote correspondant à l'oxydation de **2** par l'ozonide **1***a*.

[2]

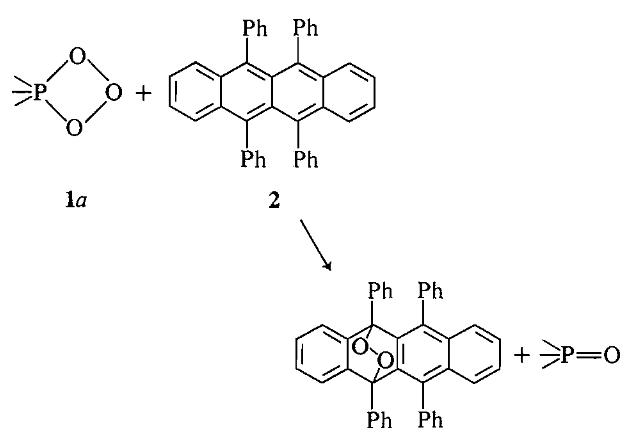

1*a* **2** **3**

[3]

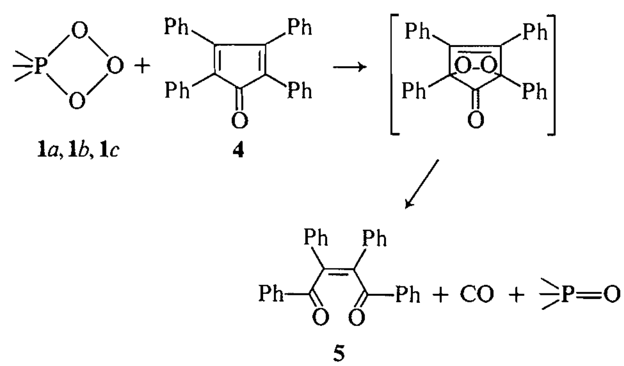

1*a*, **1***b*, **1***c* **4** **5**

[4]

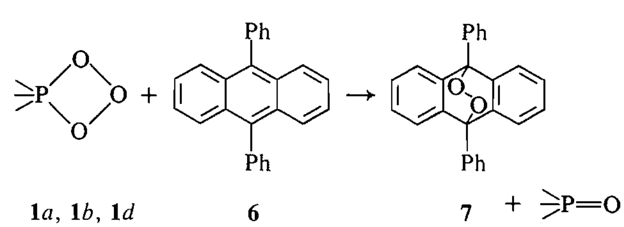

1*a*, **1***b*, **1***d* **6** **7**

10^{-4} *M*. Cette valeur élevée confirme la faible réactivité de **6** comparée à celle de **2** ($k_r = 4{,}2 \times 10^6\ s^{-1}$ et k_r (**2**)/k_r (**6**) ~ 10 (27), mais aussi sa faible efficacité puisque $\gamma = 0{,}3$.

Discussion

Comme les ozonides **1***a*–*d* ne réagissent pas sur les accepteurs **2**, **4** et **6** à basse température, nous avons écrit les réactions en considérant $^1O_2$ comme l'oxydant (nous aurions pu conduire le même calcul avec des équations similaires en considérant les ozonides et non $^1O_2$ comme l'oxydant).

Les réactions élémentaires mises en jeu peuvent s'écrire:

[5] $\quad >\!\!-PO_3 \xrightarrow{k_0} >\!\!-P{=}O + {}^1O_2$

[6] $\quad {}^1O_2 + S \xrightarrow{k_d} S + {}^3O_2$

[7] $\quad {}^1O_2 + A \xrightarrow{k_r} AO_2$

[8] $\quad {}^1O_2 + A \xrightarrow{k_q} A + {}^3O_2$

$>\!\!-PO_3$: **1***a*–*d*; A: capteurs **2**, **4**, **6**; S: solvant; AO_2: capteur oxydé.

La variation de la concentration en $^1O_2$ s'écrit alors:

$$\frac{d[{}^1O_2]}{dt} = \left(\frac{d[{}^1O_2]}{dt}\right)_f - k_d[{}^1O_2] - (k_r + k_q)[{}^1O_2][A]$$

où $(d[{}^1O_2]/dt)_f$ est la vitesse de formation de $^1O_2$ par décomposition de l'ozonide $\sim k_0[PO_3]$; en appliquant l'hypothèse des états quasi stationnaires à $^1O_2$, on obtient:

$$\frac{d[{}^1O_2]}{dt} = 0,\ [{}^1O_2] = \left(\frac{d[{}^1O_2]}{dt}\right)_f \times \frac{1}{k_d + (k_r + k_q)[A]}$$

d'autre part,

$$\frac{d[A]}{dt} = -k_r[{}^1O_2][A]$$

$$\frac{d[A]}{dt} = -\left(\frac{d[{}^1O_2]}{dt}\right)_f \times \frac{k_r[A]}{k_d + (k_r + k_q)[A]}$$

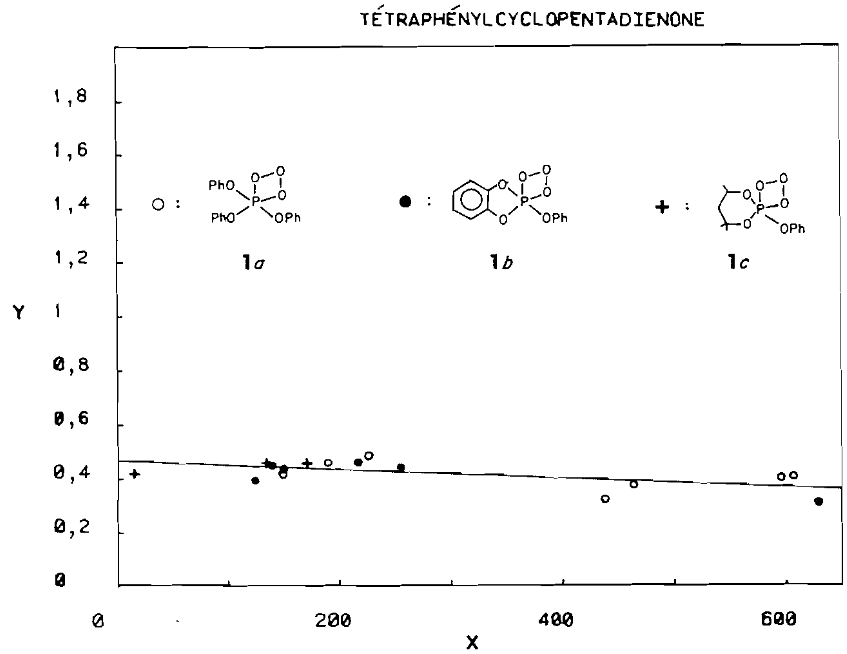

FIG. 2. Droite de Foote correspondant à l'oxydation de **4** par les ozonides **1**a, **1**b, **1**c.

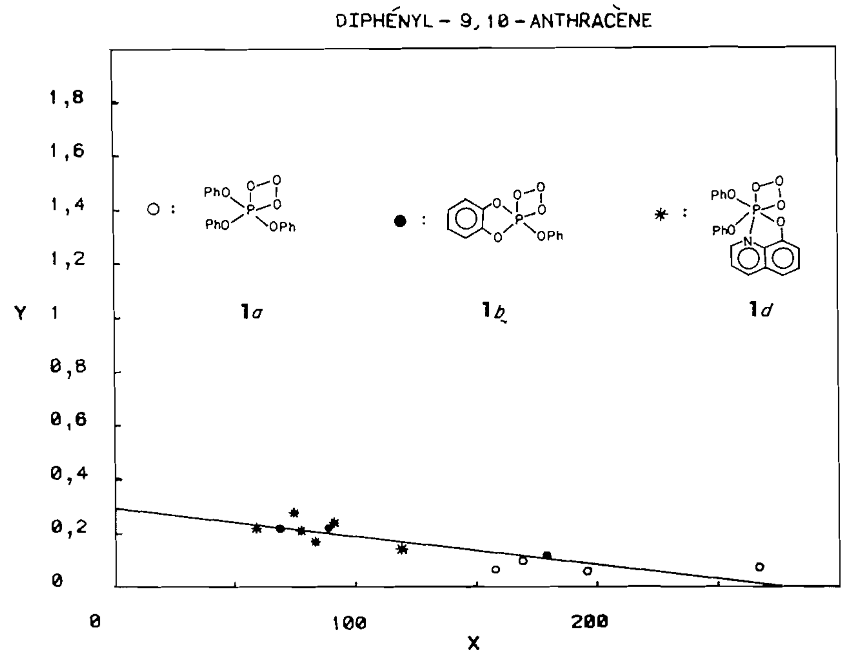

FIG. 3. Droite de Foote correspondant à l'oxydation de **6** par les ozonides **1**a, **1**b, **1**d.

L'intégration à $t \to \infty$ conduit alors à l'expression

$$\beta \ln \frac{[A]_0}{[A]_\infty} + [A]_0 - [A]_\infty = \gamma [^1O_2]_f$$

Soit en divisant par $[PO_3]_0$ concentration initiale d'ozonide

$$\gamma \frac{[^1O_2]_f}{[PO_3]_0} = \beta \frac{\ln [A]_0/[A]_\infty}{[PO_3]_0} + \frac{[A]_0 - [A]_\infty}{[PO_3]_0}$$

Avec $\beta = k_d/(k_r + k_q)$ coefficient de Foote, $\gamma = k_r/(k_r + k_q)$ efficacité du capteur et $\rho = [^1O_2]_f/[PO_3]_0$ rendement absolu en $^1O_2$, on obtient l'équation générale

$$[9] \quad \underbrace{\frac{[A]_0 - [A]_\infty}{[PO_3]_0}}_{Y} = -\beta \underbrace{\frac{\ln ([A]_0/[A]_\infty)}{[PO_3]_0}}_{X} + \rho\gamma$$

de la forme générale

$$[10] \quad Y = -\beta X + \rho\gamma$$

Cette expression est l'équation de la droite de Foote dont la pente donne β et l'ordonnée à l'origine le produit $\rho\gamma$. Dans le cas du rubrène et du diphénylanthracène, les valeurs des paramètres ainsi obtenus, en particulier k_r, sont proches de celles obtenues lors des photooxydations.

Par contre pour la tétraphénylcyclopentadienone, si la valeur de β est la même que celle obtenue par Evans et Tucker (26) la valeur de k_r diffère sensiblement. Cet écart est probablement dû aux incertitudes expérimentales mais aussi à la nature différente du solvant (CCl_2FCClF_2) et à l'estimation de la durée de vie de l'oxygène singulet dans ce solvant. Evidemment, cet écart peut aussi, dans ce cas, provenir d'un mécanisme différent.

On remarquera également que les constantes de vitesses d'oxydation k_r sont peu sensibles aux variations de température (dans le domaine $-50°C < t < +20°C$) puisque les droites de Foote contiennent des valeurs de k_r obtenues à des températures différentes pour les ozonides **1***a–d*. Ces résultats confirment la grande efficacité du rubrène ($\gamma = 1$) (21, 23) et la valeur moyenne de la tétraphénylcyclopentadiénone ($\gamma = 0{,}46$) (21, 26). Par contre malgré certaines similitudes structurales, le comportement du rubrène et du diphényl anthracène vis-à-vis de $^1O_2$ sont très différents. Pour le diphénylanthracène la constante de vitesse k_r est 10 fois inférieure à celle du rubrène et de plus sur 10 molécules d'$^1O_2$ qui réagissent 7 sont quenchées ($\gamma = 0{,}3$). La désactivation d'$^1O_2$ est même supérieure dans ce cas à celle du diméthylanthracène ($\gamma = 0{,}6$) (21, 26).

Ainsi, il nous paraît raisonnable de considérer que les résultats obtenus confirment le schéma réactionnel proposé. En effet la formation des seuls endoperoxydes de rubrène et de diphenylanthracène est caractéristique de l'oxygène singulet. La valeur de 100% du rendement obtenu pour **2** avec l'ozonide **1***a* confirme bien l'observation suivant laquelle la quantité d'endoperoxyde formé correspond strictement à la disparition du rubrène.

Comme l'ozonide **1***a* se retrouve sur les droites de Foote des autres capteurs avec les autres ozonides, nous en concluons que le rendement en $^1O_2$ des ozonides **1***b*, **1***c* et **1***d* est le même que celui de **1***a*, soit 100%. Ceci nous amène à penser que si les substituants influent sur la stabilité des ozonides c'est-à-dire sur la température de décomposition, ils n'influent pas de manière sensible sur le mécanisme de décomposition.

En effet plusieurs mécanismes sont envisageables:

(a) *Un mécanisme concerté* qui conduit directement après rupture et réarrangement à l'oxygène activé et au phosphate:

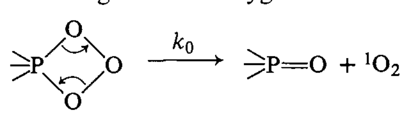

(a)

Ce mécanisme peut conduire directement à la production quantitative d'$^1O_2$. Une telle interprétation est compatible avec les résultats obtenus dans ce travail mais aussi avec le fait que les constantes de vitesse de décomposition k_0 mesurées à partir de cinétiques de dégagement d'oxygène (16–18) sont les mêmes lorsque ces cinétiques sont déterminées par rmn dans un champ magnétique de l'ordre de 23 000 gauss (19, 20).

De plus, toutes les valeurs d'entropie d'activation de la réaction [1] relevées dans la littérature, mesurées par des méthodes différentes (17–20, 28) sont négatives et comprises entre −10 et −20 u.e. Ces résultats sont en accord avec ceux obtenus par Turro *et al.* (15) dans l'étude de la thermolyse des endoperoxydes aromatiques. En effet ce dernier a établi une corrélation entre la valeur négative de l'entropie d'activation et les hauts rendements en $^1O_2$ obtenus par un mécanisme concerté de type (a).

Toutefois ce mécanisme simple ne rend pas compte de la réactivité des ozonides à basse température ou de la présence de radicaux.

(b) *Un mécanisme de type biradicalaire* (29)

L'existence de ce biradical a été confirmée en rpe par Pryor et Govindan (30) lors de l'étude de la décomposition de $(PhO)_3PO_3$ en présence de "spin trap": α-phényl-*N*-*tert*-butylnitrone (PBN).

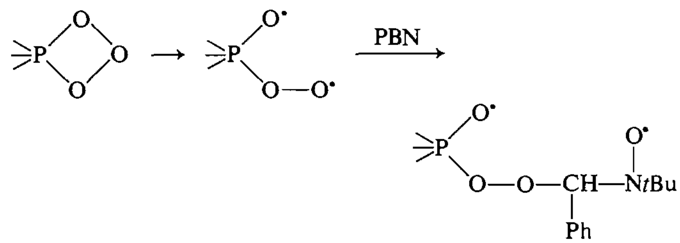

Un tel mécanisme a été envisagé dans le cas de la décomposition des endoperoxydes aromatiques par Turro *et al.* (15) et dans le cas des ozonides de phosphite par Mendenhall (16):

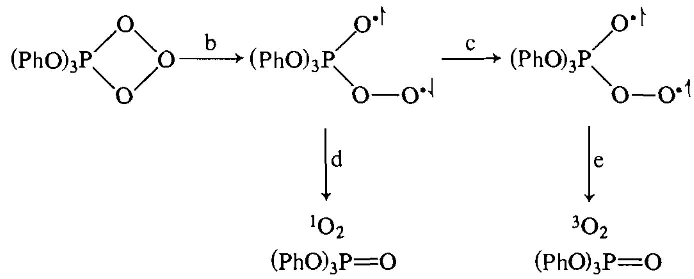

Selon ce schéma, une homolyse d'une des liaisons O—O de l'ozonide se produit (voie b) en fournissant un diradical singulet qui peut évoluer vers la formation d'oxygène singulet (voie d) ou vers un diradical triplet (voie c) par un croisement intersystème. Ce dernier peut se scinder à son tour en phosphate et en oxygène fondamental (voie e) par un processus autorisé par la règle de conservation des spins.

Les résultats de notre étude permettent d'éliminer l'hypothèse d'un intermédiaire diradicalaire à longue durée de vie qui conduirait à la formation d'une certaine proportion d'oxygène fondamental et à l'oxydation du rubrène en un produit différent de l'endoperoxyde **3**. En effet, la sensibilité aux radicaux peroxyles ROO$^\bullet$ des hydrocarbures aromatiques polycycliques en général (31) et du noyau rubrénique en particulier (12) est connue.

Toutefois nos expériences ne s'opposent pas à la proposition de Pryor (30) de l'intervention d'un diradical de faible durée de vie qui évoluerait rapidement, à température suffisante, vers la formation de $^1O_2$ (voie d) sans subir le processus relativement lent du croisement intersystème (voie c).

En conclusion, la dualité des deux processus (concerté et biradicalaire) subsiste. Cet aspect très général de nombreuses réactions est peut-être dans ce cas particulier lié à la nature complexe des états électroniques de l'oxygène singulet (1).

Partie expérimentale

1. *Oxydation du rubrène*

Les solutions d'ozonide de même concentration sont préparées à −80°C et rajoutées à cette température sur des solutions de rubrène **2** de concentrations variables. La formation d'endoperoxyde **3** est détectée par son absorption à 254 nm après séparation d'une prise d'essai du mélange réactionnel par chromatographie liquide haute performance (clhp).

(a) *Préparation des solutions*

Le solvant utilisé est du dichlorométhane 99,8% (Aldrich) conservé sur $NaHCO_3$ pour éviter l'isomérisation acido catalysée du rubrène en pseudo rubrène (32).

D'autre part le rubrène subit très facilement une photooxydation auto sensibilisée par la lumière ambiante lorsque de l'oxygène dissous est présent dans la solution (24, 33)

$$\mathbf{2} \xrightarrow{h\nu(400 < \lambda < 580 \text{ nm})} \mathbf{2}^*$$

$$\mathbf{2}^* + {}^3O_2 \rightarrow \mathbf{2} + {}^1O_2 \rightarrow \mathbf{3}$$

Il est donc nécessaire de protéger les réacteurs de la lumière et de travailler dans une pièce éclairée par une lampe émettant à $\lambda > 580$ nm. Toutes les mesures de volumes à température ambiante se font par pesée ($d_{CH_2Cl_2} = 1,326$). La concentration de la solution mère de rubrène est $[\mathbf{2}]_{\text{mère}} = 2,699 \times 10^{-3}$ M.

On fait ensuite 8 prélèvements entre 1,7 et 5 mL, de façon à obtenir 8 réacteurs contenant entre 4,52 et $13,42 \times 10^{-6}$ mol de rubrène.

On prépare également un "blanc" qui sera traité dans les mêmes conditions mais qui ne recevra pas d'ozonide, et une solution témoin contenant à la fois du rubrène et son endoperoxyde: $[\mathbf{2}] = 1,254 \times 10^{-3}$ M et $[\mathbf{3}] = 6,80 \times 10^{-4}$ M.

L'endoperoxyde **3** est préparé indépendamment en irradiant à $\lambda > 530$ nm une solution de **2** dans CH_2Cl_2 dans laquelle on fait barboter de l'oxygène jusqu'à décoloration complète. Le solvant est ensuite évaporé: le résidu est repris dans le méthanol, passé aux ultra-sons, centrifugé, repris dans l'éther, centrifugé à nouveau et séché sous vide.

(b) *Préparation de la solution d'ozonide*

La réaction d'ozonation de **1***a* ($4,98 \times 10^{-4}$ mol) se fait à -80°C (bain d'acétone/Carboglace) dans 10 mL de CH_2Cl_2. Le gaz vecteur utilisé à l'entrée de l'ozoneur est de l'oxygène, qualité aviation (concentration en eau inférieure à 20 mg/m^3). La concentration en ozone est 8×10^{-4} mol/L.

On fait passer 1,12 L de mélange O_3/O_2: l'excès d'ozone est dosé par iodométrie. Ce dosage montre que la totalité du phosphite a été oxydée avec une stoechiométrie [phosphite]/O_3 = 1:1.

La solution d'ozonide est ensuite purgée en faisant passer 8 L d'argon. Pour vérifier que cette solution ne contient plus de traces d'ozone, on fait un prélèvement maintenu à -80°C sur lequel on rajoute une solution très diluée de rubrène. On n'observe pas de décoloration de cette solution de rubrène à -80°C.

Le rendement en ozonide est déterminé par rmn ^{31}P à -80°C. En faisant varier le temps entre deux impulsions de 2,8 à 10,8 s on n'observe pas de modifications de l'intégration des pics correspondant à $(PhO)_3PO_3$ ($\delta = -62$) et $(PhO)_3P{=}O$ ($\delta = -18$). On trouve ainsi un rendement en ozonide de 85,5%. Cette solution initiale contenant 85,5% d'ozonide doit être diluée avant la réaction sur le rubrène. Pour cela on procède à des transferts dans des fioles jaugées à travers des aiguilles, par une surpression d'argon, puis on lave la fiole et l'aiguille par la quantité de CH_2Cl_2 nécessaire à la dilution.

Cette méthode est utilisée pour toutes les dilutions à -80°C. Le CH_2Cl_2 diminuant de volume à basse température, il est nécessaire de procéder à des corrections de volume. C'est ainsi que lorsqu'on passe de -80°C à la température ordinaire, on observe une augmentation de volume de 10% (mesurée par densité).

Au total, pour atteindre la concentration adéquate en ozonide, il est nécessaire de procéder à 4 transferts (2 pour une dilution et 2 pour transférer dans les solutions de rubrène). Ces transferts vont provoquer une certaine dégradation de l'ozonide. Nous avons effectué ces mêmes opérations de transfert sur une solution d'ozonide non diluée, puis nous avons mesuré par rmn de ^{31}P le pourcentage d'ozonide qui subsiste après ce traitement. On obtient alors une nouvelle valeur du rendement de 74,7% par rapport au phosphite de départ. Ce rendement servira de base aux calculs ultérieurs. Ainsi après dilution et rectifications dues à la dégradation on obtient une solution mère équivalent à $9,21 \times 10^{-4}$ M d'ozonide.

(c) *Réaction de la solution d'ozonide sur les solutions de rubrène*

On fait 8 prélèvements de 1,1 mL de la solution mère d'ozonide, dans les mêmes conditions que précédemment, que l'on transfère à -80°C sur les diverses solutions de rubrène et on complète par CH_2Cl_2 à 8,05 mL.

On laisse ensuite le mélange réactionnel remonter jusqu'à la température ambiante. On a 8 solutions de même concentration en ozonide $[\mathbf{1}a] = 1,26 \times 10^{-4}$ M et de concentration initiale en rubrène [**2**] variable:

$$5,61 \times 10^{-4}\, M < [\mathbf{2}] < 16,67 \times 10^{-4}\, M$$

(d) *Mesure de l'endoperoxyde formé par clhp*

La colonne utilisée a un diamètre de 5 mm et une longueur de 250 mm. Les particules de silice greffée phase inverse RP18 ont un diamètre de 10 μm.

Le mélange éluant est constitué par 85% d'éthanol, 15% d'eau.

Le débit est de 120 mL/h pour une pression de 200 atm. (1 atm = 101.3 kPa). La détection se fait par uv à 254 nm.

Le pic correspondant à l'endoperoxyde a un temps de rétention de 6 min, celui du rubrène de 9,4 min.

La solution témoin permet de relier la surface des pics de l'endoperoxyde (S_3) et du rubrène (S_2) ramenés à une même concentration. Pour [**2**] = [**3**] on trouve $S_3/S_2 = 2,15$.

On vérifie ensuite que le "blanc" (solution de rubrène n'ayant pas reçu d'ozonide) ne s'est pas oxydé. L'intégration des pics obtenus pour chaque solution de **1***a* + **2** permet de mesurer le pourcentage d'endoperoxyde formé

$$\% \, \mathbf{3} = S_3/(2,15\, S_2 + S_3)$$

On prend pour [**2**] une valeur moyenne

$$[\mathbf{2}] = \frac{2\,[\mathbf{2}_{\text{initial}}] - [\mathbf{3}]}{2}$$

On vérifie à $\lambda = 540$ nm que la disparition du rubrène est égale à l'apparition de son endoperoxyde.

2. *Oxydation de la tetraphénylcyclopentadienone **4** et du 9,10-diphénylanthracène **6***

(a) On prépare une solution mère de **4** ou de **6** dans CH_2Cl_2 de concentration 10^{-2} M. On prélève des quantités variables de **4** ou **6** refroidies à -80°C qui sont ajoutées sur des solutions d'ozonides **1***a*, **1***b*, **1***c*, **1***d*.

(b) *Préparation de la solution d'ozonide*

Une solution de phosphite de concentration 10^{-2} M est préparée. On prélève 1 mL de solution. Après ozonation on purge la solution avec de l'argon. Le pourcentage d'ozonide formé par rapport au phosphite de départ est obtenu par rmn ^{31}P à basse température. Il est de 80% pour les ozonides **1***a*, **1***b*, **1***c* et de 60% pour **1***d*.

(c) *Réaction de **4** et **6** sur les solutions d'ozonides*

On ajoute à -78°C des quantités croissantes de la solution mère de **4** ou **6** sur une solution d'ozonide. On laisse le mélange réactionnel revenir lentement à température ambiante. On effectue ensuite les dilutions nécessaires pour les mesures par uv des concentrations de produit non oxydée.

En effet **4** et **6** possèdent des bandes d'absorption dont les λ_{max} sont respectivement 510 nm et 370 nm. Nous avons vérifié que les esters phosphoriques correspondants et les produits d'oxydation de **4** et **6** n'absorbent pas ces longueurs d'ondes. La diminution d'absorption observée lors de la réaction par rapport à un témoin correspond à la concentration des produits oxydés.

1. H. H. WASSERMAN et R. W. MURRAY. Singlet oxygen. Organic chemistry. Vol. 40. Academic Press, New York. 1979.
2. Q. E. THOMPSON. J. Am. Chem. Soc. **83**, 845 (1961).
3. R. W. MURRAY et M. L. KAPLAN. J. Am. Chem. Soc. **90**, 537 (1968).
4. E. WASSERMAN, R. W. MURRAY, M. L. KAPLAN et W. A. YAGER. J. Am. Chem. Soc. **90**, 4160 (1968).
5. J. R. HURST, J. D. MCDONALD et G. B. SCHUSTER. J. Am. Chem. Soc. **104**, 2065 (1982).
6. R. W. MURRAY et M. L. KAPLAN. J. Am. Chem. Soc. **91**, 5358 (1969).

7. R. W. MURRAY, J. WEI-PING et M. L. KAPLAN. Ann. New York Acad. Sci. **171**, 121 (1970).
8. E. KOCH. Tetrahedron, 3503 (1970).
9. P. D. BARTLETT et G. D. MENDENHALL. J. Am. Chem. Soc. **92**, 210 (1970).
10. A. P. SCHAAP et P. D. BARTLETT. J. Am. Chem. Soc. **92**, 6055 (1970).
11. A. M. HELD, D. J. HALKO et J. K. HURST. J. Am. Chem. Soc. **100**, 5732 (1978).
12. J. M. AUBRY. Thèse Doctorat d'Etat, Paris (1982).
13. E. MCKEOWN et W. A. WATERS. J. Chem. Soc. (B), 1040 (1966).
14. M. BOTSIVALI et D. F. EVANS. J. Chem. Soc. Chem. Commun. 1114 (1979).
15. N. J. TURRO, MING-FEA CHOW et J. RIGAUDY. J. Am. Chem. Soc. **103**, 7218 (1981).
16. G. D. MENDENHALL. Ph.D. Thesis, Harvard University (1970).
17. L. M. STEPHENSON et D. E. MCCLURE. J. Am. Chem. Soc. **95**, 3074 (1973).
18. (*a*) C. M. LONZETTA. Ph.D. Thesis, Harvard University (1976); (*b*) P. D. BARTLETT et C. M. LONZETTA. J. Am. Chem. Soc. **105**, 1984 (1983).
19. (*a*) M. KOENIG, F. EL KHATIB, A. MUNOZ et R. WOLF. Tetrahedron Lett. **23**, 421 (1982); (*b*) A. M. CAMINADE, F. EL KHATIB et M. KOENIG. Phosphorus Sulfur, **18**, 97 (1983).
20. F. EL KHATIB, A. M. CAMINADE et M. KOENIG. Phosphorus Sulfur, **20**, 55 (1984).
21. F. WILKINSON et J. G. BRUMMER. J. Phys. Chem. Ref. Data, **10**, 809 (1981).
22. M. A. J. RODGERS. J. Am. Chem. Soc. **105**, 6201 (1983).
23. B. STEVENS, S. R. PEREZ et J. A. ORS. J. Am. Chem. Soc. **96**, 6846 (1974).
24. H. D. BRAUER et H. WAGENER. Ber. Bunsenges. Phys. Chem. **79**, 597 (1975).
25. (*a*) D. J. CARLSSON, G. D. MENDENHALL, T. SUPRUNCHUK et D. M. WILES. J. Am. Chem. Soc. **94**, 8960 (1972); (*b*) D. J. CARLSSON, T. SUPRUNCHUK et D. M. WILES. Can. J. Chem. **52**, 3728 (1974).
26. D. F. EVANS et J. N. TUCKER. J. Chem. Soc. Faraday Trans. 2, **72**, 1661 (1976).
27. T. WILSON. J. Am. Chem. Soc. **88**, 2898 (1966).
28. A. P. SCHAAP, K. KEES et A. L. THAYER. J. Org. Chem. **40**, 1185 (1975).
29. T. A. HINRICHS, V. RAMACHANDRAN et R. W. MURRAY. J. Am. Chem. Soc. **101**, 1282 (1979).
30. W. A. PRYOR et C. K. GOVINDAN. J. Org. Chem. **46**, 4679 (1981).
31. J. A. HOWARD et K. U. INGOLD. J. Am. Chem. Soc. **90**, 1056 (1968).
32. C. MOUREU, C. DUFRAISSE et G. BERCHET. C. R. Acad. Sci. **185**, 1085 (1927).
33. C. MOUREU, C. DUFRAISSE et P. M. DEAN. C. R. Acad. Sci. **182**, 1584 (1926).

Preparation, structure, and conformation in solution of diacetyl derivatives of 6,7-dimethyl-1,4-dihydroquinoxaline and of dihydropyridotriazines

JOSEPH ARMAND, LINE BOULARES, AND MARIE-PAULE SIMONNIN
Laboratoire de Physicochimie des Solutions, UA CNRS 403, E.N.S.C.P. 11 Rue Pierre et Marie Curie, 75231 Paris Cédex 05, France

CHRISTIAN BELLEC
Laboratoire de Chimie des Hétérocycles, Université Pierre et Marie Curie, 4, Place Jussieu, 75230 Paris Cédex 05, France

ODILE CONVERT
Laboratoire de Chimie Organique Structurale, UA CNRS 455, Université Pierre et Marie Curie, 4 Place Jussieu, 75230 Paris Cédex 05, France

AND

NELLY PLE AND GUY QUEGUINER
Laboratoire de Chimie Organique, I.N.S.C.I.R., 76130 Mont Saint Aignan, France

Received February 21, 1985

JOSEPH ARMAND, LINE BOULARES, MARIE-PAULE SIMONNIN, CHRISTIAN BELLEC, ODILE CONVERT, NELLY PLE, and GUY QUEGUINER. Can. J. Chem. **63**, 3210 (1985).

A conformational study of 1,4-diacetyl-1,4-dihydro-6,7-dimethylquinoxaline is carried out by low temperature nmr in CD_2Cl_2. Important acetyl rotation induced shifts have been observed for the *peri* and *ortho* protons. These results, together with low temperature nOe experiments, permit the determination of the structures and conformations of four diacetyl derivatives of dihydropyrido[3,4-*e*] *as*-triazines and of one diacetyl derivative of a dihydropyrido[4,3-*e*] *as*-triazine.

JOSEPH ARMAND, LINE BOULARES, MARIE-PAULE SIMONNIN, CHRISTIAN BELLEC, ODILE CONVERT, NELLY PLE et GUY QUEGUINER. Can. J. Chem. **63**, 3210 (1985).

Une étude conformationnelle de la diacétyl-1,4 dihydro-1,4 diméthyl-6,7 quinoxaline a été effectuée par rmn à basse température dans le CD_2Cl_2. La rotation d'un groupe acétyle entraîne d'importantes variations de déplacements chimiques des protons situés en *péri* et en *ortho*. Ces résultats, complétés par des mesures d'effet nucléaire Overhauser à basse température ont permis la détermination des structures et des conformations de quatre dérivés diacétylés de dihydropyrido[3,4-*e*]*as*-triazines et d'un dérivé diacétylé d'une dihydropyrido[4,3-*e*] *as*-triazine.

Introduction

N,N'-diacetyl derivatives of dihydroquinoxalines and of dihydropyrido *as*-triazines can be obtained in different ways depending on the starting materials: (*i*) from quinoxalines and pyrido *as*-triazines, by electrochemical reduction in the presence of acetic anhydride; (*ii*) from their dihydro derivatives, by action either of acetic anhydride or of a mixture of acetic acid and ethylchloroformate. Theoretically, pyrido *as*-triazines can yield four *N,N'*-diacetyl derivatives; thus starting from pyrido[3,4-*e*] *as*-triazines, structures of type I, II, III, or IV may be expected. In fact, only one or two isomers among the four possible are obtained for each compound, giving rise to the problem of elucidating their structures.

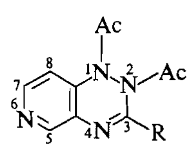

I

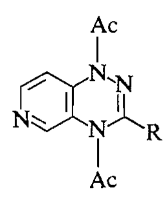

II

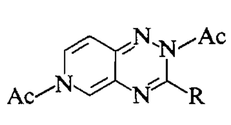

III

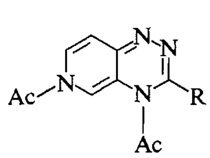

IV

^1H nuclear magnetic resonance and especially the nuclear Overhauser effect (nOe) have been shown to be the methods of choice in conformational studies of tertiary amides. This type of experiments, performed at low temperature, has been successfully used to carry out a conformational study of monacetyl derivatives of nitrogen heterocycles (1) and extended by our group (2) to the *N,N'*-diacetyl derivative **1**.

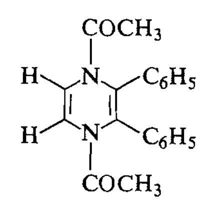

1

In the present work, we report a structural and conformational study in solution of various *N,N'*-diacetyl derivatives of nitrogen heterocycles. The conformation of 1,4-diacetyl-1,4-dihydro-6,7-dimethylquinoxaline **2** is first determined. The low temperature nmr data of **2** indicate that rotation of an acetyl group induces large changes in chemical shifts for protons located in the *peri* and *ortho* positions (the terms for the protons are according to R. H. Martin *et al.* (3)), while *meta* protons are little, or not at all, affected. The results thus obtained are applied to the determination of the structures and

TABLE 1. Room temperature ^{1}H nmr data of **5**, **6**, **9**, **10**, and **11** in CD_2Cl_2[a]

Compound	δH3	δH5	δH6	δH7	δH8	δCH_3CO	J
5	7.40 (s)	8.87 (s)	—	8.30 (d)	7.95 (d)	2.40 2.42_5	$^3J_{7-8} = 5.5$
6	7.70 (s)	6.67 (d)	—	7.17 (d × d)	5.45 (d)	2.12 2.25	$^4J_{5-7} = 2$ $^3J_{7-8} = 8$
9	—	8.72 (s)	—	8.40 (d)	8.01 (d)	2.03 2.57	$^3J_{7-8} = 5.5$
10	—	8.75 (s)	—	8.51 (d)	8.10 (d)	2.07 2.35	$^3J_{7-8} = 5.5$
11	7.36 (s)	7.66 (d)	8.33 (d)	—	9.23 (s)	2.34 2.38	$^3J_{5-6} = 5.5$

[a] δ in ppm relative to internal TMS; J in Hz.

conformations of diacetyl derivatives of dihydropyridotriazines and these are confirmed by low temperature nOe experiments.

Results

Preparations of N,N′*-diacetyl derivatives*

1,4-Diacetyl-1,4-dihydro-6,7-dimethylquinoxaline **2** is obtained by electrochemical reduction of 6,7-dimethylquinoxaline in the presence of acetic anhydride.

Heating the 1,4-dihydropyrido[3,4-*e*] *as*-triazine **4** (obtained by hydrogenation of **3** (4)) in acetic anhydride gives the 1,4-diacetyl-1,4-dihydropyrido[3,4-*e*] *as*-triazine **5**.

Heating **4** in an acetic acid – ethylchloroformate mixture leads to another derivative, the 2,6-diacetyl-2,6-dihydropyrido[3,4-*e*] *as*-triazine **6**. On heating in an excess of acetic anhydride for 15 h, compound **6** rearranges to the thermodynamically more stable derivative **5**.

Heating the 1,4-dihydro-3-phenylpyrido[3,4-*e*] *as*-triazine **8** (obtained by hydrogenation of **7** (4)) in Ac_2O yields the 1,4-diacetyl-1,4-dihydro-3-phenylpyrido[3,4-*e*] *as*-triazine **9**.

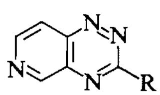

3 R = H
7 R = C_6H_5

Electrochemical reduction of **7** in the presence of Ac_2O gives the 1,2-diacetyl-1,2-dihydro-3-phenylpyrido[3,4-*e*] *as*-triazine **10**.

The reaction of acetic anhydride on 1,4-dihydropyrido[4,3-*e*] *as*-triazine gives the 1,4-diacetyl-1,4-dihydropyrido[4,3-*e*] *as*-triazine **11**.

Room temperature ^{1}H nuclear magnetic resonance spectra

The ^{1}H nmr spectra of the various *N,N′*-diacetyl derivatives, recorded at room temperature, indicate that rotation around both N—CO bonds is fast on the nmr time scale (Table 1). Due to its symmetrical structure, the spectrum of **2** displays only four singlets at 7.42, 6.41, 2.26, and 2.22 ppm, corresponding to the resonances of H5–H8, H2–H3, CH_3CO, and CH_3 respectively. The spectra of **5**, **6**, **9**, **10**, and **11** agree with the structures of these compounds and indicate the presence of two different acetyl groups.

The three protons H5, H7, and H8 (or H5, H6, and H8 in **11**) are strongly deshielded in **5**, **9**, **10**, and **11** and the same figures are observed for the vicinal coupling constant $^3J_{7-8}$ or $^3J_{5-6}$ (5.5 Hz) in these four derivatives. These δ and J values, which are close to those observed in pyridine (5), indicate that the pyridinic ring retains its aromatic character in **5**, **9**, **10**, and **11**; therefore these derivatives have structures of type I or II.

TABLE 2. Chemical shifts and relative amounts of the conformers of **2** in CD_2Cl_2 at −60°C

Conformer	%	δH2	δH3	δH5	δH8
2*a* Z_1Z_4	45	6.22		7.54	
2*b* Z_1E_4	45	6.31[a]	6.77[a]	6.85	7.59
2*c* E_1E_4	10	6.82		6.90	

[a] J_{H2-H3} = 5 Hz.

TABLE 3. Acetyl rotation induced shifts for the protons of **2**

Acetyl	Effect *peri*	*ortho*	*meta*
$CH_3CO(1)$[a]	+0.69(H8)	−0.51(H2)	−0.05(H3)
$CH_3CO(4)$[b]	+0.69(H5)	−0.55(H3)	−0.09(H2)

[a] Δδ = δ(**2***b*) − δ(**2***c*).
[b] Δδ = δ(**2***a*) − δ(**2***b*).

The resonances of H5, H7, and H8 move upfield in **6** and the vicinal coupling constant $^3J_{7-8}$ increases to 8 Hz, as previously observed in 1,4-dihydropyridines (6). Hence the pyridinic ring has lost its aromatic character in **6** and this compound has a structure of type III or IV.

The room temperature spectra give information on the nature of the pyridinic ring, but they give no indication of the location of the two acetyl groups.

Low temperature ^{1}H nuclear magnetic resonance spectra

At low temperature, if the rotation around the N—CO bonds becomes slow enough, an individual set of signals should be observed for each of the conformers. The low temperature ^{1}H spectra show the presence of the three expected conformers of **2**; the coexistence of the four possible conformers is observed only in the case of **10**, while for **5**, **6**, **9**, and **11** only two unequally populated conformers were detected within the limits of nmr detection.

Among the three conformers **2***a*, **2***b*, and **2***c* (Table 2), two (**2***a* and **2***c*) have a plane of symmetry. The signals of the methyl protons of the acetyl groups lie too close to be selectively irradiated in order to perform nOe experiments. However, the structural analogy between **1** and **2** and the similarity of their nmr data permit an unambiguous assignment of the signals due to H2 and H3, as ethylenic protons are less shielded when they are *syn* to the carbonyl oxygen (*E*) than when they are *anti* (*Z*). An identical sequence is observed for the *peri*

TABLE 4. Chemical shifts and relative amounts of conformers for **5**, **6**, **9**, and **11** in CD_2Cl_2 at low temperature

Conformer	Temperature (°C)	%	δH3	δH5	δH6	δH7	δH8	$\delta CH_3CO(1)$	$\delta CH_3CO(2)$	$\delta CH_3CO(4)$	$\delta CH_3CO(6)$	J
5*a* E_1E_4	−80	84	7.35	8.95	—	8.32	7.92	2.30	—	2.36	—	$J_{7-8} = 5.5$
5*b* E_1Z_4		16	7.87_5	8.30		8.40	7.93	2.30	—	2.37	—	
6*a* E_2E_6	−40	59	7.71	6.48	—	7.40	5.46_5	—	2.05	—	2.21	$J_{7-8} = 8$
6*b* E_2Z_6		41	7.71	6.95		6.87	5.38	—	2.05	—	2.23	$J_{5-7} = 2$
9*a* E_1E_4	−90	60	—	8.67	—	8.28_5	7.86_5	2.51	—	1.84	—	$J_{7-8} = 5.5$
9*b* E_1Z_4		40	—	8.51		8.36	7.91_5	2.51	—	2.24	—	
11*a* E_1E_4	−90	90	7.31	7.80	8.31	—	9.10	2.43	—	2.51	—	$J_{5-6} = 5.5$
11*b* E_1Z_4		10	7.83	7.02	8.38	—	9.10	2.43	—	2.53	—	

protons H5 and H8.

The differences between chemical shifts of the conformers **2***b* (Z_1E_4) and **2***c* (E_1E_4) lead to the values of Δδ related to the rotation of the 1-acetyl group for the *ortho* (H2), *meta* (H3), and *peri* (H8) protons. In the same way, Δδ values due to the rotation of the 4-acetyl group can be obtained from **2***a* (Z_1Z_4) and **2***b* (Z_1E_4). The differences Δδ = δ(**2***b*) − δ(**2***c*) and Δδ = δ(**2***a*) − δ(**2***b*), reported in Table 3, are positive for the *peri* protons and negative for the *ortho* and *meta* protons. These two series of values are very similar and mainly depend upon the

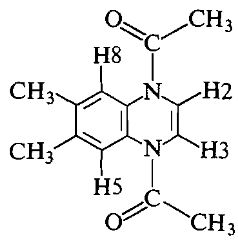

2*a*

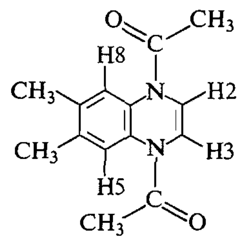

2*b*

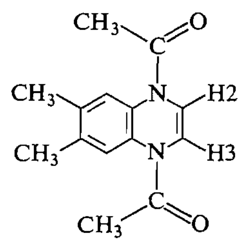

2*c*

ortho, *meta*, or *peri* position of the protons relative to the rotating acetyl group. It should be remarked that the shifts induced by an acetyl rotation are larger in *peri* than in *ortho* and that they become negligible in *meta* positions, i.e. they decrease when the distance increases. The effects at *ortho* and *meta* positions for **2** are very similar to those obtained for **1**, viz., Δδ *ortho*: −0.49 (H6) and −0.51 (H5); Δδ *meta*: −0.04 (H6) and −0.02 (H5).

The shift differences induced by the rotation of an acetyl group, applied to each pair of conformers in Table 4, allow the position of the rotating acetyl group to be determined, while nOe experiments have to be performed at low temperature to determine precisely the location of the second acetyl group; these experiments allow the position of the rotating acetyl group to be confirmed.

Structure of **5**

The differences between chemical shifts of conformers **5***a* and **5***b* are large and of opposite sign for H5 (0.65 ppm) and H3 (−0.52 ppm), but small for H7 (−0.08 ppm) and H8 (−0.01 ppm). These results, compared with those of Table 2, point to a *peri* position for H5 and to an *ortho* position for H3 with a 4-acetyl group which changes its orientation from **5***a* to **5***b*. Moreover, the low-field shift observed for H5 in the most populated conformer shows that H5 is *syn* to the carbonyl oxygen (E_4) in **5***a*.

The observation of only two conformers at −80°C, which differ in the orientation of the 4-acetyl group, does not tell anything about the position of the second acetyl group; it can be in position 1 (structure II) or in position 6 (structure IV). In both cases, either the rotation about the N′—CO bond is fast on the nmr time scale at −80°C, or the N′—$COCH_3$ adopts a

TABLE 5. ^{1}H nuclear Overhauser enhancement data (%) for the conformers of **5**, **6**, **9**, and **11** upon irradiation of the CH_3CO groups

	Proton				
Irradiated site	H3	H5	H6	H7	H8
$CH_3CO(4)$ **5**a/**5**b	16% (**5**a) 20% (**5**b)	10% (**5**a) 17% (**5**b)	—	0% (**5**a)	0%
$CH_3CO(1)$ **5**a/**5**b	0%	0%	—	0%	0%
$CH_3CO(6)$ **6**a	—	27.5% (**6**b) 24% (**6**b)	—	7% (**6**a) 12.5% (**6**b)	—
$CH_3CO(6)$ **6**b	—	25% (**6**a) 21% (**6**b)	—	7% (**6**a) 16% (**6**b)	—
$CH_3CO(2)$ **6**a/**6**b	—	0%	—	0%	—
$CH_3CO(4)$ **9**a/**9**b	—	4% (**9**a) 8% (**9**b)	—	0% (**9**a) 0% (**9**b)	—
$CH_3CO(1)$ **9**a/**9**b	—	0%	—	0%	—
$CH_3CO(4)$ **11**a/**11**b	28% (**11**a) 7% (**11**b)	5% (**11**a) 21% (**11**b)	0%	—	0%
$CH_3CO(1)$ **11**a/**11**b	0%	0%	0%	—	0%

single preferred conformation. The nOe experiments were performed at −80°C. The methyl signals of the 4-acetyl group in **5**a and **5**b are too close (2.36 and 2.37 ppm) to be selectively irradiated. The simultaneous irradiation of both signals (2.365 ppm) leads to an enhancement of the signals of H3 (**5**a), H3 (**5**b), H5 (**5**a), and H5 (**5**b) (Table 5). These results clearly

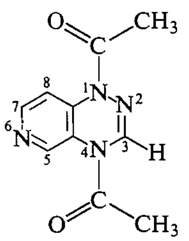

5a
84% E_1E_4

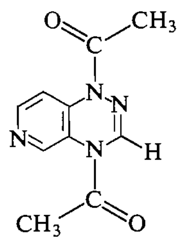

5b
16% E_1Z_4

indicate that the temperature is not low enough to avoid spin saturation transfer; however, they confirm that the rotating acetyl group is in the 4-position.

The irradiation of the methyl protons of the second acetyl group (δ = 2.30 ppm), carried out at −80°C, does not lead to any enhancement of the different signals. This absence of an nOe enhancement excludes the presence of a 6-acetyl and can only be explained by a structure in which the *peri* proton H8 is *syn* to the carbonyl oxygen of a 1-acetyl group in **5**a and **5**b. Thus, compound **5** has a structure of type II and is the 1,4-diacetyl-1,4-dihydropyrido[3,4-*e*] *as*-triazine.

Structure of 6

Due to its poor solubility at low temperature, the spectrum of **6** was recorded at −40°C. The differences Δδ between the two conformers **6**a and **6**b are large and of opposite sign for H5 (−0.47 ppm) and H7 (+0.53 ppm), very small for H8 (+0.08 ppm), and zero for H3. These Δδ values indicate the presence of a 6-acetyl group which changes its orientation from **6**a (E) to **6**b (Z), i.e. H7 is *syn* to the carbonyl oxygen in **6**a. As the structure of **6** is of type III or IV, the second acetyl group can be in a 2- or 4-position. In this case, also, one can suppose that either the rotation about the N′—CO bond is rapid at −40°C, or that the N′—$COCH_3$ adopts a single preferred conformation.

The nOe experiments performed at −40°C by successive irradiation of the methyl signals of the 6-acetyl group in **6**a and **6**b (2.21 and 2.23 ppm) confirm the position of this acetyl, although there is spin saturation transfer (Table 5). The absence of nOe enhancement upon irradiation of the 2.05-ppm signal is consistent with a 2-acetyl group, H3 being *syn* to the carbonyl oxygen in both **6**a and **6**b. Therefore **6** is the 2,6-diacetyl-2,6-dihydropyrido[3,4-*e*] *as*-triazine.

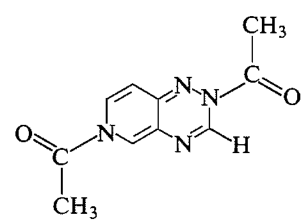

6a
59% E_2E_6

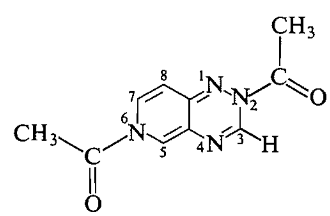

6b
41% E_2Z_6

Structure of 9

The differences between chemical shifts of conformers **9**a and **9**b are much smaller than those observed for **2**, **5**, or **6**. The largest effect is observed for H5 (Δδ = 0.16 ppm), suggesting that a 4-acetyl group changes its orientation from **9**a to **9**b. This is confirmed by the nOe experiments carried out at −90°C. The selective irradiation of the acetyl signals at 1.84 and then at 2.24 ppm leads to an enhancement of the signals of H5 in both **9**a and **9**b. This result supports the presence of a 4-acetyl group and indicates that spin saturation transfer is occurring, i.e. the 4-acetyl group changes its conformation from **9**a (E) to **9**b (Z). On the contrary, the irradiation of the signal at 2.51 ppm does not lead to any nOe enhancement, as could be expected for a 1-acetyl group with an E type conformation, in which the oxygen is *syn* to H8 in **9**a and **9**b. Thus, **9** must be the 1,4-diacetyl-1,4-dihydro-3-phenylpyrido[3,4-*e*] *as*-triazine (structure of type II).

Structure of 10

Derivative **10**, in which the pyridine ring retains its aromatic

TABLE 6. Chemical shifts and relative amounts of the conformers of **10** in CD_2Cl_2 at −70°C

Conformer	%	δH5[a]	δH7[a]	δH8[a]	δ$COCH_3$
10*a*	49	8.74	8.51_5	7.59	2.23; 2.42
10*b*	34	8.74	8.53_5	7.77	1.84; 2.33
10*c*	15	8.70	8.44	7.34	2.15; 2.25
10*d*	2	—	—	—	1.72_5; 2.29_5

[a] $^3J_{H7-H8}$ = 5.5 Hz. $^4J_{H5-H7}$ = 2 Hz.

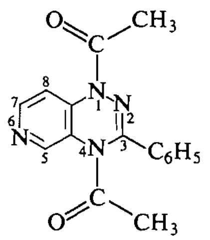

9*a*
60% E_1E_4

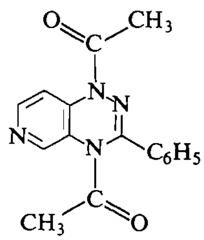

9*b*
40% E_1Z_4

character, but which is different from **9**, must have a structure of type I; i.e. it is the 1,2-diacetyl-1,2-dihydro-3-phenylpyrido-[3,4-*e*] *as*-triazine.

Among the four conformers observed at −70°C (Table 6), the population of **10***d* is so weak that the signals of H5, H7, and H8 cannot be assigned with certainty. The complexity of the spectrum and the closeness of the signals did not allow nOe experiments. However, it should be remarked that the presence of four conformers shows that rotation of the acetyl groups is not prevented, even though they are located on vicinal nitrogens.

*Structure of **11***

Results obtained with **11** at −90°C are very similar to those observed with **5**: the differences Δδ between chemical shifts of conformers **11***a* and **11***b* are large and of opposite sign for H5 (0.78 ppm) and H3 (−0.52 ppm), small for H6 (−0.07 ppm), and zero for H8, showing that a 4-acetyl group changes its orientation from **11***a* (E_4) to **11***b* (Z_4). This conclusion is supported by nOe experiments performed at −90°C. Simultaneous irradiation of both methyl signals of the 4-acetyl group in **11***a* and **11***b* (2.525 ppm) leads to an enhancement of the signals of H3 (**11***a*), H3 (**11***b*), H5 (**11***a*), and H5 (**11***b*) (Table 5).

No enhancement is observed when irradiating the methyl signal of the second acetyl group (δ = 2.43 ppm), i.e. this acetyl, located in a 1-position, adopts a single preferred conformation in which the *peri* proton H8 is *syn* to the carbonyl oxygen.

Thus compound **11** is the 1,4-diacetyl-1,4-dihydropyrido-[4,3-*e*] *as*-triazine.

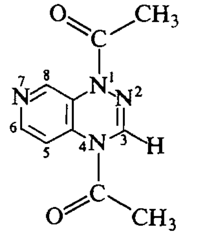

11*a*
90% E_1E_4

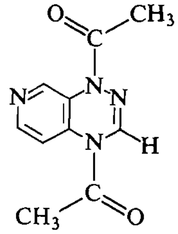

11*b*
10% E_1Z_4

Discussion

Results obtained in the course of this work indicate that low temperature ^{1}H nmr spectra are a powerful tool for determining the structure and conformation of various *N,N′*-diacetyl derivatives of dihydropyridotriazines. The location of a rotating acetyl group may be safely deduced from the difference between chemical shifts of the corresponding conformers. The shifts induced by an acetyl rotation mainly depend upon the position of a particular proton relative to the rotating acetyl group, and decrease from *peri* to *ortho* and to *meta* positions. When an acetyl group adopts a single preferred conformation, nOe experiments have to be performed at low temperature in order to indicate its precise position and its favoured conformation.

Several results deserve comment. Only two of the four possible conformers are observed in the low temperature spectra of derivatives **5**, **6**, **9**, and **11**. In each case, the acetyl group which adopts a single favoured conformation is located on a nitrogen atom next to an sp^2 hybridized nitrogen; moreover, the preferred conformation is the same in these four cases, i.e. the methyl group points towards the sp^2 nitrogen atom; the other conformation, in which the carbonyl oxygen would be *syn* to the sp^2 nitrogen, is not observed. This strongly suggests that an electrostatic repulsion between the lone pair of the sp^2 nitrogen and the negatively charged carbonyl oxygen disfavors such a conformation.

Compound **9**, which bears a phenyl in the 3-position, has a particular behavior as the shifts induced by rotation of the 4-acetyl group are much smaller than those observed for **5**, **6**, and **11**. This suggests that a steric hindrance, due to the presence of the 3-phenyl group, induces a distortion of the molecule resulting in an increased distance between H5 and the 4-acetyl group. Such a deformation would also explain that the nOe enhancements observed for **9** are smaller than those determined for the analogous structure **5**, as these effects decrease with the sixth power of the distance.

Solid-state investigations by X-ray crystallography have shown that compounds with a 1,4-diacetyl-1,4-dihydropyrazine structure (2, 7) adopt a boat conformation in which the two nitrogen atoms lie above the plane determined by the four carbon atoms. It seems likely that the triazine ring in **9** is similarly in a boat shape and that the presence of the 3-phenyl group pushes nitrogen N4 away from the mean plane formed by N2 and the three carbon atoms.

Finally, the existence of the four possible conformers **10***a*, **10***b*, **10***c*, and **10***d* implies the possibility of rotation of each of the two vicinal acetyl groups. The steric hindrance appears as rather small, which suggests that the acetyl groups are quite remote, as previously observed in the case of **12**. The solid

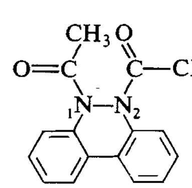

12

state structure of **12** (7) shows that the value of the dihedral angle $\widehat{C(1)N(1)C(2)N(2)}$ is 61°, and the acetyl groups are far enough apart so that they undergo no steric hindrance during their rotation.

Experimental

The ^{1}H nmr spectra were recorded on a Bruker 250 MHz spectrometer, using tetramethylsilane (TMS) as internal standard. The nOe experiments were performed using solutions carefully degassed by three freeze–pump–thaw cycles.

Preparation of 1,4-diacetyl-1,4-dihydro-6,7-dimethylquinoxaline ***2***

The compound was obtained by electrochemical reduction of 6,7-dimethylquinoxaline in acetonitrile in the presence of acetic anhydride according to the procedure used by H. Lund et J. Simonet (8) to prepare 1,4-diacetyl-1,4-dihydroquinoxaline from quinoxaline. Yield 46%; mp 246°C.

*Preparation of 1,4-diacetyl-1,4-dihydropyrido[3,4-*e*] as-triazine* ***5***

A solution of 0.5 g of 1,4-dihydropyrido[3,4-*e*] *as*-triazine (3.75×10^{-3} mol) in 20 mL of acetic anhydride was refluxed for 15 h. Acetic anhydride was evaporated under vacuum and the residue was washed with ethanol, filtered, and crystallized from ethanol–water (50:50); 350 mg (43%); mp 138°C.

*Preparation of 2,6-diacetyl-2,6-dihydropyrido[3,4-*e*] as-triazine* ***6***

To a solution of 0.18 g (3×10^{-3} mol) of acetic acid and 0.3 g (3×10^{-3} mol) of triethylamine in 20 mL of chloroform, at 0°C, was added 0.35 g (2.95×10^{-3} mol) of freshly distilled ethylchloroformate. The mixture was kept at 0°C for half an hour and then 0.3 g (2.23×10^{-3} mol) of 1,4-dihydropyrido[3,4-*e*] *as*-triazine was added. The temperature was then raised to 20°C. After being allowed to stand for $1\frac{1}{2}$ h, 150 mL of water were added. The organic layer was dried over magnesium sulfate and the solvent was evaporated. The residue was washed with ethanol, chloroform, and tetrahydrofuran to give 150 mg of **6** (31%); mp 140°C.

*Preparation of 1,4-diacetyl-1,4-dihydro-3-phenylpyrido[3,4-*e*] as-triazine* ***9***

Compound **8**, prepared according to ref. 4 (1 g), was heated under reflux for 12 h with acetic anhydride (20 mL). The excess acetic anhydride was evaporated and the residue poured into ethanol–water (50:50). The precipitate was filtered and recrystallized from ethanol–water (50:50) to give 1 g (71%) of **9**; mp 148°C.

*Preparation of 1,2-diacetyl-1,2-dihydro-3-phenylpyrido[3,4-*e*] as-triazine* ***10***

Electrolysis of **7** was carried out with the technique described previously (9) at $E = -1.4$ V (sce). The cathodic solution contained 60 mL of CH_3CN, 8 mL of acetic anhydride, 2.2 g of tetrabutylammonium iodide, and 1 g of **7**. During electrolysis a polymeric product precipitated. At the end of electrolysis (2 F/mol) the solution was filtered and the filtrate poured into 500 mL of water. The mixture was neutralized with $NaHCO_3$ and extracted with ether. The extracts were dried over Na_2SO_4 and evaporated. The residue was essentially (nmr spectrum) a mixture of **9** and **10** (25:75). Recrystallization from methanol gave 310 mg (22%) of **10**; mp 146°C.

*Preparation of 1,4-diacetyl-1,4-dihydropyrido[4,3-*e*] as-triazine* ***11***

With the same procedure as in the case of **5**, 0.5 g of 1,4-dihydropyrido[4,3-*e*] *as*-triazine gives 25 mg of **11** (3%); mp 149°C (dec.).

1. S. COMBRISSON and B. P. ROQUES. Tetrahedron, **32**, 1507 (1976), and references therein.
2. J. ARMAND, C. BOIS, M. PHILOCHE-LEVISALLES, M. J. POUET, and M. P. SIMONNIN. Can. J. Chem. **60**, 349 (1982).
3. R. H. MARTIN, N. DEFAY, and F. GEERTS-EVRARD. Tetrahedron, **20**, 1505 (1964).
4. J. ARMAND, K. CHEKIR, N. PLE, G. QUEGUINER, and M. P. SIMONNIN. J. Org. Chem. **46**, 4754 (1981).
5. W. BRUGEL. Z. Elektrochem. **66**, 159 (1962).
6. M. SAUNDERS and E. H. GOLD. J. Org. Chem. **27**, 1439 (1962).
7. J. ARMAND and M. PHILOCHE-LEVISALLES. Can. J. Chem. **60**, 2792 (1982).
8. H. LUND and J. SIMONNET. C. R. Acad. Sci. Ser. C, **277**, 1387 (1973).
9. J. ARMAND, K. CHEKIR, and J. PINSON. Can. J. Chem. **56**, 1504 (1978).

Synthèse d'une α-méthylene-γ-lactone: application des réactifs organiques du sélénium

HELENA MARIA CARVALHO FERRAZ[1] ET NICOLA PETRAGNANI
Instituto de Química, Universidade de São Paulo, C.P. 20780, São Paulo, SP., Brasil

Reçu le 10 août 1984[2]

HELENA MARIA CARVALHO FERRAZ et NICOLA PETRAGNANI. Can. J. Chem. **63**, 3216 (1985).

Nous avons développé une nouvelle synthèse de l'α-méthylène-γ-lactone **4**, qui est présente dans de nombreuses substances naturelles sesquiterpéniques.

HELENA MARIA CARVALHO FERRAZ and NICOLA PETRAGNANI. Can. J. Chem. **63**, 3216 (1985).

We have developed a new synthetic approach to the α-methylene-γ-lactone moiety **4**, which is present in numerous sesquiterpene natural products.

Introduction

Le groupement α-méthylène-γ-lactone est présent dans de nombreuses substances naturelles telles que les lactones sesquiterpéniques (1). Ce groupement est responsable de l'activité pharmacologique de ces substances (2). L'intérêt de notre groupe de recherche dans ce domaine, tout comme dans la chimie des composés organiques du sélénium, nous a amenés à développer des méthodes sélectives d'obtention d'α-méthylène-γ-lactones bicycliques à jonction *cis* ou *trans*, dont le but est l'utilisation ultérieure dans la synthèse de substances telles que le Frullanolide **1** (3) et l'Arbusculine B **2** (4). Deux synthèses des α-méthylène-γ-lactones **3** et **4** ont déjà été décrites (5) et nous voulons maintenant en présenter une troisième.

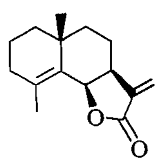

1

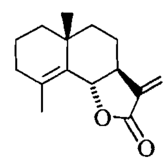

2

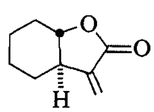

3

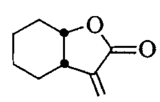

4

La formation de lactones par l'addition d'un électrophyle à des acides ou à des ésters β,γ ou γ,δ-insaturés est connue depuis longtemps et sa stéréochimie est bien établie: l'addition à la double liaison est toujours *trans* (6). Ainsi, la lactonisation de l'acide β,γ-insaturé **5**, par exemple, conduit à une jonction *cis* entre les deux cycles.

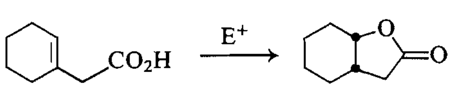

5

Cette réaction est, donc, d'une grande utilité dans la préparation stéréosélective de *cis*-lactones.

Par ailleurs, l'utilisation de réactifs organoséléniés, soit comme précurseurs de doubles liaisons, soit comme des électrophiles pour la lactonisation, a été dernièrement très explorée (7–9).

Dans un travail antérieur (5) nous avons illustré l'utilisation de l'acide 2-phénylséléno-propanoïque **6** pour la synthèse des α-méthylène-γ-lactones **3** (*trans*) et **4** (*cis*); plus récemment, nous avons employé le même acide **6** pour synthétiser le Frullanolide **1** (10).

$$H_3C—CH(SePh)—CO_2H$$

6

Nous présentons ici une nouvelle synthèse de la *cis*-lactone **4**, dont le précurseur possède le groupement sélénophényle en β du carbonyle, ce qui offre un avantage par rapport à la méthode antérieure: l'élimination du phénylsélénoxyde n'entraîne que la formation d'une double liaison exocyclique.

À partir d'une substance simple telle que la cyclohexanone, nous avons effectué la séquence réactionnelle représenteé dans le schéma 1.

Résultats et discussion

Le cyclohexylidène acétate d'éthyle **7** (11) a été obtenu par la réaction de Wittig entre la cyclohexanone et le carbéthoxyméthylènetriphénylphosphorane, avec un rendement de 80%. Ce produit a été hydrolysé en milieu basique, donnant l'acide cyclohéxylidène acétique **8** (12) avec un rendement de 81%. L'alkylation du dianion de l'acide **8** par le sélénure de bromométhylphényle a fourni 82% du produit **9**.

Nous avons éssayé d'inverser l'ordre séquentiel de ces deux dernières étapes, mais nous n'avons pas réussi à alkyler l'ester **7** par le même sélénure; le seul produit obtenu est l'ester β,γ-insaturé **11**. Le remplacement du réactif par le sélénure d'iodométhylphényle a donné l'alkylation, mais le rendement de la réaction n'a été que de 55%.

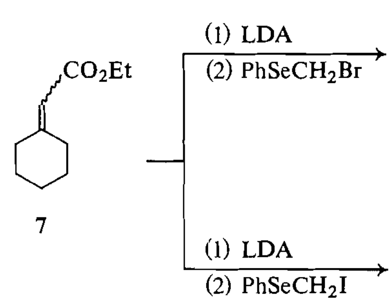

Pour l'étape suivante—lactonisation de **9** en milieu acide—plusieurs réactifs ont été employés (H_2SO_4, $HClO_4$, H_3PO_4, AcOH, acide *p*-toluènesulfonique). Dans tous les cas, nous

[1] Auteur à qui adresser la correspondance.

[2] Revision reçue le 28 mars 1985.

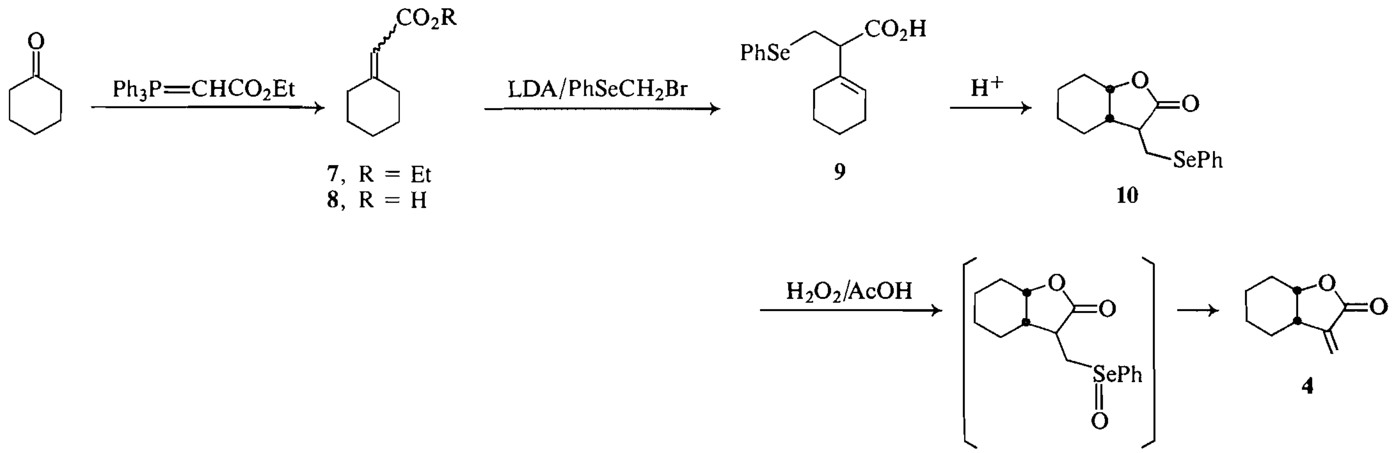

SCHEME 1

avons observé la formation d'un mélange complexe de substances, parmi lesquelles on a pu constater, outre le produit principal **10**, la présence en faible quantité de la lactone **12** (avec la double liaison endocyclique) et du disélénure de diphényle. Le meilleur résultat a été obtenu par traitement de **9** avec l'acide phosphorique, qui a produit 50% de la lactone attendue **10**.

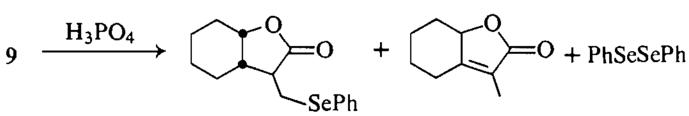

10 **12**

La formation de la lactone **12**, aussi bien que du disélénure, montre que la liaison C—Se s'est rompue; cependant, nous n'avons pas de données suffisantes pour suggérer le mécanisme de cette réaction indésirable.

Il faut bien noter que les réactions de lactonisation des acides γ,δ-insaturés portant le groupement sélénophényle n'offrent pas toujours de bons rendements (5, 13), comme on peut observer dans les exemples ci-dessous (nous n'avons trouvé dans la litérature aucun cas de lactonisation d'un acide sélénié β,γ-insaturé).

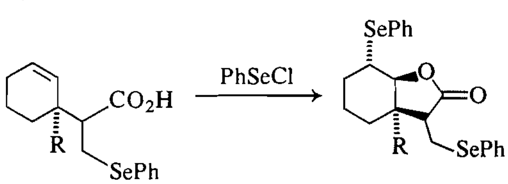

(Réf. 13)

R = H, 70%
R = Me, 61%

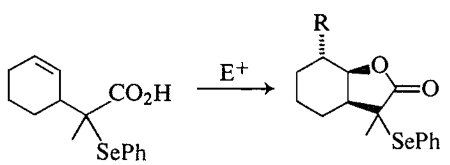

(Réf. 5)

E = I, 73%
E = H, 48%

Finalement, l'oxydation (14) de **10** a fourni l'α-méthylène-γ-lactone **4** avec un rendement de 81%.

En ce moment, nous sommes en train d'appliquer une variante de la séquence réactionnelle décrite ici aux synthèses du Frullanolide et de l'Arbusculine B.

Partie expérimentale

Les spectres ir ont été mesurés avec un spectrophotomètre Perkin–Elmer 457A. Les spectres de rmn ont été enregistrés sur un appareil Varian T-60 à 60 MHz et dans le CCl_4. Les analyses par chromatographie en phase gazeuse ont été effectuées sur un appareil Varian 2800 à ionisation de flamme; le gaz vecteur est l'azote et la colonne utilisée, la FFAP (10%) Chromosorb W 60–80 mesh. Les analyses (C, H) ont été effectuées par le Laboratoire de Microanalyse de l'Institut de Chimie de l'Université de S. Paulo.

Cyclohéxylidène acétate d'éthyle 7

Une solution de la cyclohexanone (29,4 g, 0,3 mol), du carbéthoxymethylènetriphénylphosphorane (21,0 g, 0,06 mol) et de l'acide benzoïque (2 g) dans le benzène anhydre (70 mL) est chauffée au reflux pendant 48 h, sous une atmosphère d'azote. Après la distillation du benzène, on ajoute de l'hexane et le triphenylphosphinoxide formé est filtré. La solution est lavée successivement avec une solution saturée de $NaHCO_3$, une solution dilutée de HCl et une solution saturée de NaCl. Le solvant et l'excès de la cyclohexanone sont éliminés par distillation; le résidu est distillé sous vide. Rendement: 8,1 g (80%); p.e. 116°C/30 Torr (1 Torr = 133,3 Pa).

Acide cyclohexylidène acétique 8

Une solution de l'ester **7** (5,0 g, 0,03 mol) dans l'éthanol (30 mL) est traitée par du NaOH (15 mL d'une solution à 30%). Au bout de 3 h à reflux, le mélange réactionnel est acidulé par une solution concentrée de HCl et la solution aqueuse est extraite par l'éther et sechée sur Na_2SO_4. Le résidu obtenu après l'élimination du solvant est recristallisé à partir du mélange acétate d'éthyle – hexane. Rendement: 3,4 g (81%); p.f. 90–91°C (lit. (11) p.f. 90–92°C).

Acide 3-phénylséléno-2-(1'-cyclohexényl)-propanoïque 9

À une solution de LDA (4,4 mmol) dans le THF anhydre (4,5 mL) à 0°C et sous une atmosphère d'azote, on ajoute une solution de l'acide **8** (0,28 g, 2 mmol) dans le THF (2 mL). Au bout de 1 h à 45°C, le mélange réactionnel est refroidi à 0°C et est additionné d'une solution du sélénure de bromométhylphényle (0,60 g, 2,4 mmol) dans le THF (2 mL). Après 2 h à 40°C, le mélange est acidulé par une solution concentrée de HCl, extrait par l'éther et séché sur Na_2SO_4. Le solvant est évaporé et le résidu est distillé sous vide (tube à boules). Rendement: 0,51 g (82%); p.e. 140°C/0,005 Torr; ir (Nujol) ν_{max}: 1705, 760, 730, 685 cm^{-1}; ^1H rmn (CCl_4) δ: 11,1 (s, 1H), 7,0–7,6 (m, 5H), 5,5–5,8 (m, 1H), 2,8–3,4 (m, 3H), 1,2–2,3 ppm (m, 8H). *Anal.* calc. pour $C_{15}H_{28}O_2Se$: C 58,27%, H 5,87%; trouvé: C 58,11%, H 5,78%.

*Lactone de l'acide 3-phenylséléno-2-(*cis*-2'-hydroxycyclohexyl)-propanoïque 10*

On traite l'acide **9** (0,124 g, 0,4 mmol) par de l'acide phosphorique (0,5 g) pendant 6 h à 110°C. Le mélange réactionnel est additionné d'eau (5 mL) et la solution aqueuse est extraite par $CHCl_3$. Par chromatographie sur gel de silice (par élution au mélange hexane–benzène – acétate d'éthyle, 5:3:2) on isole la lactone **10**, qui ne cristallise pas et qui est donc distillée sous vide (tube à boules). Rendement: 0,061 g (50%); p.e. 125°C/0,005 Torr; ir (film) ν_{max}: 1770, 740, 690 cm^{-1}; ^{1}H rmn (CCl_4) δ: 7,0–7,7 (m, 5H), 4,2–4,5 (m, 1H), 1,0–3,1 ppm (m, 12H). *Anal.* calc. pour $C_{15}H_{18}O_2Se$: C 58,27%, H 5,87%; trouvé: C 58,50%, H 5,69%.

*Lactone de l'acide 2-(*cis*-2'-hydroxycyclohexyl)-propénoïque 4*

Une solution de la lactone **10** (0,05 g, 0,16 mmol) et de l'acide acétique (0,03 mL) dans le THF (1 mL) est traitée par H_2O_2 à 30% (0,15 mL) pendant 30 min à 0°C. Le mélange réactionnel est additionné d'une solution saturée de $NaHCO_3$ (3 mL) et extrait par l'éther. La solution est lavée à l'eau, puis par une solution saturée de NaCl et enfin sechée sur Na_2SO_4. Le résidu obtenu après l'évaporation du solvant est chromatographié sur gel de silice (élué par le mélange hexane – acétate d'éthyle 1:1). Rendement: 0,02 g (81%). Les spectres de ^{1}H rmn et de ir sont identiques à ceux d'un échantillon preparé par une méthode différente (15).

Remerciements

Nous remercions le CNPq (Conselho Nacional de Desenvolvimento Científico e Tecnológico) et la FAPESP (Fundação de Amparo à Pesquisa do Estado de S. Paulo) de l'aide financière accordée.

1. T. K. Devon et A. I. Scott. Hand-book of naturally occurring compounds. Vol. 2. Academic Press, New York. 1972.
2. C. H. Smith et al. Biochem. Biophys. Acta, **276**, 94 (1972).
3. G. W. Perold, J. C. Muller et G. Ourisson. Tetrahedron, **28**, 5797 (1972).
4. M. A. Irwin et T. A. Geissman. Phytochemistry, **8**, 2411 (1969).
5. N. Petragnani et H. M. C. Ferraz. Synthesis, 476 (1978).
6. J. Klein. J. Am. Chem. Soc. **81**, 3611 (1959).
7. D. L. J. Clive. Tetrahedron, **34**, 1049 (1978).
8. D. Liotta. Acc. Chem. Res. **17**, 28 (1984).
9. K. C. Nicolaou et al. J. Am. Chem. Soc. **101**, 3884 (1979).
10. N. Petragnani, H. M. C. Ferraz et M. Yonashiro. Synthesis, 27 (1985).
11. W. S. Wadsworth et W. D. Emmons. J. Am. Chem. Soc. **83**, 1733 (1961).
12. E. Schwenk et D. Papa. J. Am. Chem. Soc. **67**, 1432 (1945).
13. S. Raucher, K. J. Hwang et J. E. MacDonald. Tetrahedron Lett. 3057 (1979).
14. P. A. Grieco et M. Miyashita. Tetrahedron Lett. 1869 (1974).
15. P. A. Grieco et M. Miyashita. J. Org. Chem. **39**, 120 (1974).

Solvent-induced conformational changes in benzyl fluoride. Long-range C,F; H,H; H,F spin–spin couplings

TED SCHAEFER, JAMES PEELING,[1] AND RUDY SEBASTIAN
Department of Chemistry, University of Manitoba, Winnipeg, Man., Canada R3T 2N2

Received April 15, 1985

TED SCHAEFER, JAMES PEELING, and RUDY SEBASTIAN. Can. J. Chem. **63**, 3219 (1985).

The ^{1}H and ^{19}F nmr spectra of benzyl fluoride, although very tightly coupled at 300 MHz, are analyzed for dilute CS_2 and acetone solutions. ^{13}C, ^{19}F spin–spin coupling constants for benzyl fluoride in a series of solvents are also measured. Geometry-optimized STO 3G MO computations on benzyl fluoride indicate a small twofold barrier to rotation about the exocyclic C—C bond in the gas phase. All the long-range couplings between ^{19}F and ring protons or carbon-13 nuclei and between methylene and ring protons are consistent with the conclusion that the barrier to internal rotation in benzyl fluoride is small and that the conformation in which the C—F bond lies in a plane perpendicular to the benzene plane is stabilized by 2 kJ/mol in going from CS_2 to DMSO or acetone solutions. The solvent dependence of the internal barrier may account for the diversity of conformational conclusions in the literature. Furthermore, it is clear that the internal barrier will depend on the presence of substituents at any site in the ring.

TED SCHAEFER, JAMES PEELING, and RUDY SEBASTIAN. Can. J. Chem. **63**, 3219 (1985).

Même si les spectres rmn du ^{1}H et du ^{19}F du fluorure de benzyle sont intimement couplés à 300 MHz, on a pu les analyser pour des solutions diluées dans le CS_2 ou dans l'acétone. On a aussi mesuré les constantes de couplage spin–spin ^{13}C–^{19}F dans le fluorure de benzyle en solution dans divers solvants. Des calculs d'orbitales moléculaires STO 3G, optimisés pour la géométrie, effectués sur le fluorure de benzyle indiquent que, en phase gazeuse, il existe une légère barrière binaire à la rotation autour de la liaison exocyclique C—C. Toutes les constantes de couplage à longue distance entre le ^{19}F et les protons ou les noyaux ^{13}C du cycle ainsi que entre les protons méthyléniques et ceux du cycle sont en accord avec la conclusion selon laquelle la barrière à la rotation interne, dans le fluorure de benzyle, est petite et que la conformation dans laquelle la liaison C—F se trouve dans un plan perpendiculaire à celui du benzène est stabilisée par environ 2 kJ/mol lorsqu'on passe de solutions dans le CS_2 à des solutions dans le DMSO ou dans l'acétone. L'influence du solvant sur la barrière interne explique vraisemblablement la diversité des conclusions conformationnelles que l'on retrouve dans la littérature. De plus, il est clair que la barrière interne dépendra de la présence de substituants sur divers sites du cycles.

[Traduit par le journal]

Introduction

The study of solvent effects on conformational equilibria has a long history (1, 2). The common observation that the more polar conformer becomes more stable in polar solvents is rationalized by reaction field theory (2, 3), although the model usually overestimates the degree of stabilization. Of course, the solvent is not a dielectric continuum and the origin of solvent effects must lie in the minutiae of intermolecular interactions (4), including electrostatic interactions as well as nonelectrostatic packing effects. Recent theoretical methods involving molecular dynamics and Monte Carlo statistical mechanics methods have had remarkable success in assessing the nature of the solvent-induced changes in conformational equilibria (4), although computational requirements have restricted the number of such calculations.

Experimentally, solvent effects on conformational distributions have been most often investigated by nuclear magnetic resonance, Raman, and infrared spectroscopies. These techniques suffer from various disadvantages. For example, with the latter two methods energy differences are usually obtained from the temperature dependence of equilibrium constants (assuming correct assignments of vibrational bands) under the assumption of temperature independent enthalpies. In principle, the latter assumption is surely incorrect in solution.

The nmr technique often uses angle dependent spin–spin vicinal couplings to assess energy differences between conformers, for instance in ethane derivatives (2). However, the approximation of an equilibrium between two or more rigid (*gauche* and *trans*) conformations (*n*-site model) is often made. Because conformations are not rigid, this model can lead to severe errors in the derived energy differences (5).

When the barrier to interconversion between the conformers is smaller than thermal energies, such an approach becomes useless. For example, benzyl fluoride can be thought to exist in two possible conformations, **1** and **2**. If the free energy difference between **1** and **2** were large, then a spin–spin coupling constant, J, known for **1** and **2**, could be employed as a straightforward indicator of this energy difference, that is, $\Delta G^0 = -RT \ln (p(\mathbf{1})/p(\mathbf{2}))$, and the observed J would then be given by $J(\mathbf{1})p(\mathbf{1}) + J(\mathbf{2})p(\mathbf{2})$ where $p(\mathbf{1}) + p(\mathbf{2})$ is unity.

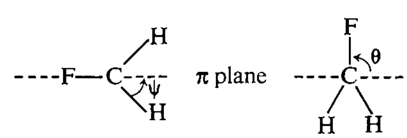

1 $\theta = 0°$, $\psi = 60°$ **2** $\theta = 90°$, $\psi = 30°$

However, if the potential hindering rotation is rather flat, then the molecule samples all θ values with comparable probability magnitudes and a 2-site treatment is invalid. It becomes necessary to know the complete θ dependence of J *and* the functional form of the potential governing the internal rotation if a satisfactory treatment of the solvent dependence of the conformational equilibrium is to be presented. A measurement of J then yields the magnitude of the potential function.

For example, for ethylbenzene derivatives (6), both ^{6}J(H,H), the coupling over six bonds between the methylene and *para* ring protons, and ^{5}J(H,C), the coupling involving the *para* ^{13}C

[1]Permanent address: University of Petroleum and Minerals, Dhahran, Saudi Arabia.

nucleus, depend on $\sin^2\psi$ (replace F with CH_3 in **1** and **2**). Both couplings, when combined with a hindered rotor model (7), demonstrate that **2** is the stable conformer in solution and that the barrier, assumed twofold, is 5.2 kJ/mol.

Returning to benzyl fluoride, a rather extensive geometry optimization procedure at the STO 3G level of *ab initio* molecular orbital theory (see Experimental) yields the twofold potential V_2 (kJ mol^{-1}) = $(1.64 \pm 0.04) \sin^2 \theta$ at the 95% confidence level. Alternatively, the computed values can be fit to a potential curve which includes a fourfold component, $V = (1.61 \pm 0.05) \sin^2 \theta + (0.05 \pm 0.04) \sin^2 2\theta$. For the isolated molecule, therefore, the computation implies a flat, essentially twofold, internal rotational potential favoring **1**. The preference of an in-plane C—F bond is possibly related to an electrostatic preference, the C^+—F^- dipole lying near the *ortho* C—H^+ dipole (calculated net charges on fluorine and the *ortho* hydrogen are +0.06 and −0.15 in units of electron charge for **1**). An analogous eclipsing conformation is found to be most stable in 3-fluoropropene (8).

Now, on the assumption that the shape of the internal potential remains twofold in solution, it seems sensible, however, that its magnitude will change in the presence of solvent molecules because of packing effects, if for no other reason, since θ can adjust easily to optimize intermolecular interactions (4). In terms of a reaction field model, **2** might well be favored over **1** in polar solvents. The dipole moment of benzyl fluoride is 1.77 ± 0.05 D in benzene at 298 K (9). CNDO MO computations give accurate dipole moments for organic fluorine compounds (10) and yield 1.73 D for **1** and 1.86 D for **2** (Experimental). In terms of the reaction field model, **1** and **2** are stabilized by 1.09 and 1.30 kJ/mol, respectively, on going from the vapor to CS_2 solution (dipole approximation). If the polarizability of the solvent is taken into account, these numbers increase by a factor of 1.25. In acetone solution, **2** is more stabilized than **1** by 0.46 kJ/mol relative to the vapor. In other words, the simplest model suggests stabilization of **2** relative to **1** by only about 0.25 kJ/mol in passing from CS_2 to acetone solution. Combined with the STO 3G MO results, one has the prediction that the twofold barrier should be as low as 1.2 kJ/mol in acetone, **1** stable.

Numerous investigations of the conformational preferences of benzyl fluoride and its derivatives vary widely in their conclusions. Confining the discussion to benzyl fluoride itself, a combined gas phase electron diffraction and molecular mechanics investigation implied a preferred conformation with θ near 50 or 60°, together with a barrier to rotation of about 1.7 kJ/mol (11). A STO 3G MO calculation was also done. The geminal proton coupling constant in $CDCl_3$ solution was interpreted to mean that either θ was 54° or that a nonplanar conformation was preferred with a small barrier to rotation (11).

CNDO/2 and PCILO computations suggest that **1** is 12.3 kJ/mol more stable than **2** (12) and extensive measurements of ^{2}H relaxation times on partially and fully deuterated benzyl fluoride by the same group (13) are interpreted to yield an internal barrier of 11.3 kJ/mol in the neat liquids. It may be relevant that the temperature dependence of the viscosity of the neat liquid indicates an activation energy of 11.3 kJ/mol. In acetone and methanol solutions (14), the internal barriers were found to be 7.6 and 10.7 kJ/mol, respectively, from ^{2}H measurements.

The temperature dependence of the ^{19}F nmr chemical shifts of benzyl fluoride and some of its derivatives in acetone solution, together with MO calculations, was taken to mean (15) that **2** is most stable, by 1.7 kJ/mol.

TABLE 1. Values of ^nJ(C,F) in Hz for benzyl fluoride in a number of solvents at 300 K

Solvent^{a,b}	$-^1J$	^2J	^3J	$\lvert ^4J \rvert$	$^5J^{b,c,d}$
CS_2 (2.3)	170.52	17.50	5.93	0.91	2.76
CCl_4 (3.4)	169.66	17.52	5.98	0.92	2.81
C_6D_6 (3.3)	167.28	17.27	5.89	1.13	2.92
$CDCl_3$ (3.0)	166.19	17.10	5.87	1.31	3.09
Neat	165.44	16.98	5.78	1.33	3.08
CD_3OD (1.0)	164.53	16.96	5.79	1.39	3.13
$(CD_3)_2$=O (2.8)	163.72	16.90	5.75	1.43	3.15
DMSO (2.5)	161.92	16.62	5.68	1.53	3.24_5

^{a}Concentrations in mol% are given in parentheses.
^{b}All couplings are reproducible to better than 0.02 Hz in all cases. For example ^5J(C,F) in DMSO solution is 3.245 ± 0.005 Hz, as judged from repeated measurements.
^{c}^2J, ^3J, and ^5J are positive; see Experimental.
^{d}For benzotrifluoride, ^3J, ^4J, and ^5J in acetone and CS_2 solutions are 3.92(5), 3.85(1); 0.0, 0.0; and 1.39(3), 1.37(1) Hz, respectively. In $CDCl_3$ and CS_2 solutions ^1J is 272.1, 272.23 Hz, respectively, and ^2J is 32.2(1), 32.28(1) Hz. These data suggest minimal intrinsic solvent perturbations of sidechain ^{19}F nuclei and aromatic ^{13}C nuclei.

An interesting application of the stereospecific coupling over five bonds betwen ^{19}F and the ^{13}C nucleus in the *para* position, ^5J(C,F), was taken to imply that, in chloroform solution, there exists essentially free rotation of the fluoromethyl group in benzyl fluoride (16).

In view of this diversity of conclusions concerning the internal rotational potential in benzyl fluoride, part of which may well be caused by solvent effects, it seems sensible to measure the solvent dependence of some molecular properties of benzyl fluoride. For this purpose ^5J(C,F) was chosen and this paper reports on its solvent dependence. Furthermore, the ^{1}H and ^{19}F nmr spectra in CS_2 and acetone solutions at 300 MHz, although extremely highly coupled, are analyzable. They yield some H,H and H,F couplings that also depend on conformation.

Experimental

Dilute solutions of benzyl fluoride from Pierce Chem. Co. were prepared in a number of solvents (see Table 1). Proton decoupled ^{13}C nmr spectra were taken on an AM300 Bruker spectrometer at a probe temperature of 300 K. Typically, 64 FIDs were accumulated for each spectral region, e.g. a width of 400 Hz into 16K, with an acquisition time of 20.48 s. Two or more sets of spectra were obtained. A dilute solution of 3,5-dichlorobenzyl fluoride was used to determine the signs of ^2J(C,F), ^3J(C,F), and ^5J(C,F) relative to ^2J(H,F) by ^{13}C{^{1}H} experiments. Decoupling (17) of the methylene protons for a given spin state of ^{19}F caused characteristic collapses in the *ipso, para*, and *ortho* ^{13}C multiplets.

A 2.3 mol% solution of benzyl fluoride in CS_2, containing 10.0 mol% of C_6D_{12}, 0.5 mol% TMS, and a drop of C_6F_6 was transferred to a 5-mm od nmr sample tube. The solution was degassed by a number of freeze−pump−thaw cycles and the tube was then flame-sealed under vacuum. A similar procedure was applied to a 2.8 mol% solution of benzy fluoride in acetone-d_6, also containing some TMS and C_6F_6.

The ^{1}H and ^{19}F nmr spectra were accumulated at a probe temperature of 300 K on the AM300 instrument. Wide sweepwidth survey spectra were obtained in order to reference the spectra with respect to TMS and C_6F_6, and to obtain the locations of the aromatic and side-chain proton peaks. Each region was examined in detail, with sweep-width and data region adjusted to give acquisition times of approximately 40 s. Four to sixteen scans were acquired. Zero filling to twice the original data region was done before transforming the FIDs using a small amount of gaussian multiplication. Line widths at half height

TABLE 2. ^1H and ^{19}F spectral parameters for benzyl fluoride in CS_2 and acetone-d_6 solutions at 300 K

Parameter	Value		Parameter	Value	
	CS_2[a]	Acetone[b]		CS_2[a]	Acetone[b]
ν_{CH}	1568.342(1)[c]	1618.561(1)[c]	$^4J(H,CH_2)$	−0.610(1)	−0.560(2)
ν_o	2170.535(1)	2226.457(2)	$^5J(H,CH_2)$	0.299(1)	0.282(2)
ν_m	2181.595(1)	2223.543(2)	$^6J(H,CH_2)$	−0.452(2)	−0.409(2)
ν_p	2170.271(2)	2212.983(1)	$^4J(H,F)$	−1.680(2)	−1.961(3)
ν_F	−12895.269(2)[d]	−12017.359(3)	$^5J(H,F)$	1.107(2)	1.164(2)
$^2J(F,CH_2)$	47.908(2)[e]	47.967(2)	$^6J(H,F)$	−1.539(2)	−1.800(2)
$^3J_{23}$	7.686(1)	7.707(1)	Calcd. transitions	833	935
$^3J_{34}$	7.492(2)	7.508(3)	Assign. transitions	662	643
$^4J_{26}$	1.876(2)	1.886(3)	Peaks observed	300	291
$^4J_{24}$	1.268(2)	1.259(3)	Largest deviation	0.041	0.039
$^4J_{35}$	1.371(1)	1.378(3)	rms deviation	0.013_7[f]	0.013_7[g]
$^5J_{25}$	0.606(1)	0.619(1)			

[a]2.3 mol% containing some internal TMS, C_6D_{12}, and C_6F_6.
[b]As in *a* but 2.8 mol% and no C_6D_{12}.
[c]The ^1H shifts are in Hz at 300.135 MHz to low field of internal tetramethylsilane, TMS.
[d]The ^{19}F shifts are in Hz at 282.363 MHz to high field of internal C_6F_6 (same probe).
[e]The numbers in parentheses are the standard deviations in the last figure from the analysis with the program NUMARIT.
[f]There are no correlations as large as 0.3, but $^4J(H,CH_2)$ and $^3J_{34}$ correlate with −0.297.
[g]There are some substantial correlations, namely, −0.576 for $^5J(H,CH_2)$ and $^4J(H,CH_2)$; −0.473 for $^4J(H,F)$ and $^5J(H,F)$. Note that the shift difference between *ortho* and *meta* protons is just under 3 Hz.

were approximately 0.04 Hz.

STO 3G MO computations (18) on benzyl fluoride employed the program MONSTERGAUSS (19) and an Amdahl V8 system. Geometry optimization of all bond angles and bond lengths was done at 15° intervals for $0 \leq \theta \leq 90°$ with the proviso that the phenyl carbon framework remain a regular hexagon. INDO MO FPT calculations (20, 21) of various coupling constants in benzyl fluoride utilized the same computer, as did CNDO/2 computations (22) of dipole moments.

Results and discussion

Spectral analyses

$^nJ(C,F)$ could be measured as splittings in the ^1H decoupled ^{13}C nmr spectra, and values appear in Table 1. Two or more sets of measurements on a given sample gave an average error of less than 0.02 Hz. The partial decoupling experiments show that $^2J(C,F)$, $^3J(C,F)$, and $^5J(C,F)$ have the same sign as $^2J(H,F)$, which is positive (23). $^5J(C,F)$ is +1.98(2) Hz and $^3J(C,F)$ is +6.86(1) Hz in 3,5-dichlorobenzyl fluoride in CS_2 solution. Comparison with the numbers in Table 1 strongly implies the same signs for benzyl fluoride.

A full analysis of the ^1H and ^{19}F nmr spectra of benzyl fluoride in CS_2 and acetone solutions was performed with the computer program NUMARIT (24). The ensuing spectral parameters are found in Table 2. Although the ring proton shift range in CS_2 solution is less than 38 ppb, the spectral parameters are known with same precision (see explanatory notes in Table 2). Figure 1 displays the observed and calculated ^1H nmr spectra of the methylene protons in acetone solution. Figure 2 shows the calculated and observed ^1H nmr spectra of the aromatic protons for the CS_2 solution.

Coupling mechanisms

INDO MO FPT computations of the contact contribution to nuclear spin–spin coupling constants, J, do not normally agree quantitatively with experiment, due to the parameterization of the semiempirical approach, to neglect of noncontact contributions, and to deviations of the assumed from the actual geometry of the molecule (25). However, often the qualitative and

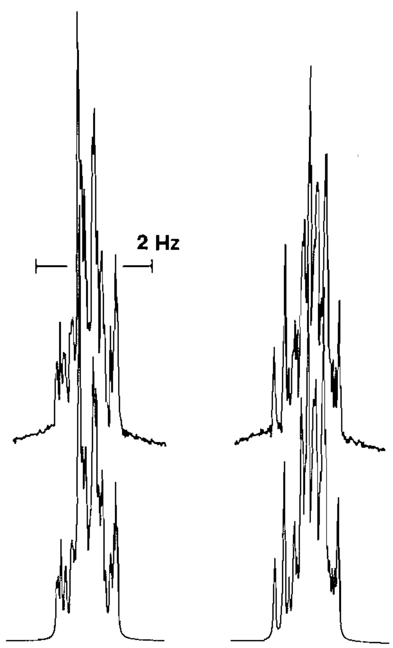

FIG. 1. The methylene proton nmr spectrum of a 2.8 mol% solution of benzyl fluoride in acetone-d_6 at 300.135 MHz and 300 K is compared to the spectrum calculated with the spectral parameters in Table 2. The computed spectrum assumes a line width at half height of 0.03 Hz.

sometimes even the quantitative conformational dependence of J is reproduced by such calculations, particularly for long-range couplings. For example, $^6J(H,H)$ in toluene depends on $\sin^2\psi$ (see **1** or **2**) and its value at $\psi = 90°$ is computed for a standard geometry as −1.22 Hz (26), in good agreement with an experimentally derived value of −1.20 Hz (27). Rather poorer agreement with experiment is obtained for $^6J(H,F)$ in *p*-fluorotoluene (28), yet its functional dependence on θ is most likely reproduced qualitatively (26, 28).

An extensive discussion of $^nJ(C,F)$ in benzotrifluoride (29)

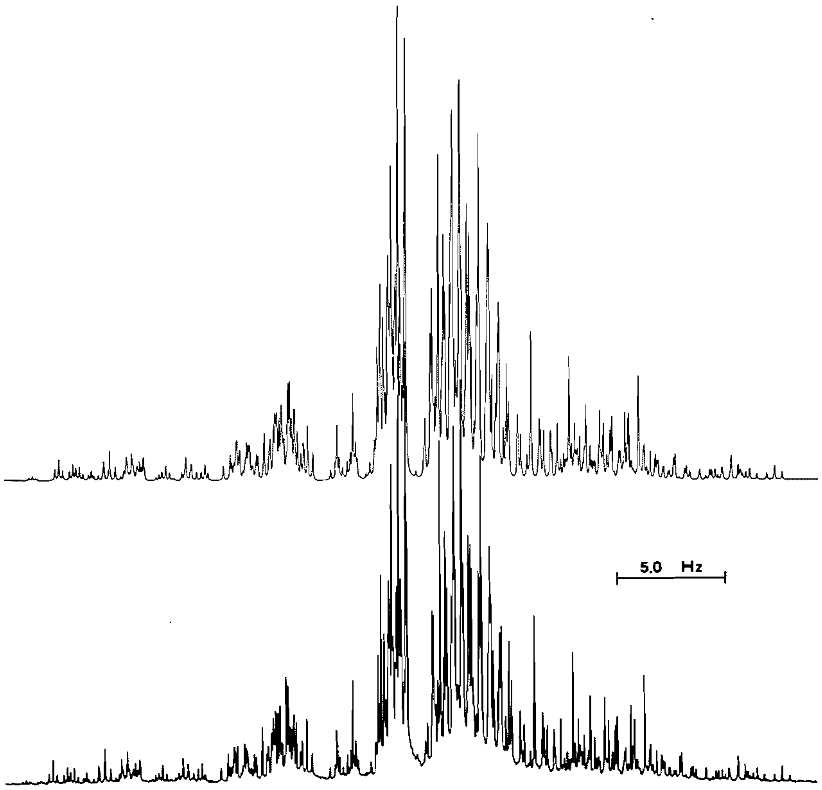

FIG. 2. The aromatic ring proton nmr spectrum of a 2.3 mol% solution of benzyl fluoride in CS_2/C_6D_{12}/TMS solution at 300.135 MHz and 300 K is compared to the spectrum calculated with the parameters in Table 2. The widths at half height of the observed peaks are about 0.04 Hz.

demonstrates the qualitative reliability of INDO MO FPT computations of many of these parameters. The calculated θ dependence of ^5J(C,F) and ^4J(C,F) can be used to rationalize the absence of ^4J(C,F), for example, as a cancellation of σ and $\sigma-\pi$ components of opposite sign; the former is dependent on $\sin^2(\theta/2)$ and the latter on $\sin^2\theta$.

In view of these remarks, computations of various couplings in benzyl fluoride were performed so as to have indications of their θ and ψ dependence. Because their absolute values are probably not very reliable, the results are not tabulated here. Their salient characteristics can be summarized as follows.

For the STO 3G MO geometry-optimized structure, in which the C—F bond length is 138.5 pm, the exocyclic C—C bond length is 154.1 pm, and the CCF bond angle is 111.9°, the θ dependence of ^6J(H,F) can be written as eq. [1]. The $\sigma-\pi$ mechanism is indicated by this equation, just as it is for ^6J(H,H)

$$[1] \quad ^6J(\mathrm{H,F})\ (\mathrm{Hz}) = -0.061 \pm 0.006 - 2.373 \pm 0.009 \sin^2\theta$$

in toluene (26). The angle-independent term may well be an artifact of the computation. As a $\sigma-\pi$ coupling, the computed ^6J(H,F) will depend strongly, probably exponentially (30), on the C—C distance. Thus, for a standard geometry (31), its computed values (32) can be written as eq. [2]. In other words, the value of ^6J(H,F) at $\theta = 90°$ cannot be certain. What is fairly

$$[2] \quad ^6J(\mathrm{H,F})\ (\mathrm{Hz}) = -0.06 \pm 0.01 - 3.12 \pm 0.01 \sin^2\theta$$

certain, however, is that the magnitude of ^6J(H,F) will increase as conformation **2** increases in stability relative to **1**. Again, because ^6J(H,H) is undoubtedly a $\sigma-\pi$ coupling (7) and because it depends on $\sin^2\psi$, its magnitude will decrease as **2** becomes more stable. It is known that the maximum magnitude of ^6J(H,H) depends on the electronegativity of the α-substituent (7), its value for benzyl fluoride not being certain. For a standard geometry, INDO methods suggest it as about -1.1 Hz (32). ^4J(H,H) and ^4J(H,F) will also contain large $\sigma-\pi$ components, whereas ^5J(H,H) and ^5J(H,F) probably consist of a $\sigma-\pi$ part together with a σ component of comparable magnitude and dependent (33) on $\sin^2(\psi/2)$ or $\sin^2(\theta/2)$.

Turning to ^nJ(C,F), the computations on the optimized geometry imply eq. [3] for ^5J(C,F) and therefore that it is a $\sigma-\pi$ coupling. The analogous ^5J(H,C) in toluene has been shown to

$$[3] \quad ^5J(\mathrm{C,F})\ (\mathrm{Hz}) = 0.26 \pm 0.04 + 7.73 \pm 0.07 \sin^2\theta$$

be a $\sigma-\pi$ coupling (6), in agreement with INDO MO FPT computations. Also, ^5J(C,F) in benzotrifluoride can be rationalized as a $\sigma-\pi$ coupling (29), although its magnitude is computed as too large. Similar remarks apply to eq. [3] but the sign agrees with that in Table 1.

^4J(C,F) in benzyl fluoride is computed as small and positive near $\theta = 0$ and 180°, becoming large and negative at 90°. In other words, it is predicted as a predominant $\sigma-\pi$ coupling. ^3J(C,F) is calculated to be large and positive at $\theta = 0$ and 180°, and decreasing for other values of θ, having a minimum near $\theta = 80°$. Its computed behavior in benzotrifluoride has been discussed in detail (29). A similar treatment could be done for ^3J(C,F) in benzyl fluoride but would not add to the present paper, except to note that its θ dependence resembles a modified Karplus behaviour. ^2J(C,F) is computed to become more negative as θ increases, as is ^1J(C,F). Both of these couplings may well contain some noncontact contributions (29).

In the next section it is pointed out that all the couplings in Tables 1 and 2 (except ^1J(C,F)), when compared with the computed trends, strongly indicate an increase in stability of **2** in the more polar solvents.

Conformational perturbations by solvent

(i) *Qualitative trends*

Qualitatively, it is clear from the long-range couplings that **2** (C—F bond in a plane perpendicular to the benzene plane) is increasingly favored over **1** as the dielectric constant of the solvent increases. Thus, ^5J(C,F) increases from 2.76 Hz in CS_2 to 3.25 Hz in DMSO solutions, as expected for a predominantly $\sigma-\pi$ coupling. If ^3J(C,F) displays a Karplus type behavior with a minimum near $\theta = 90°$ (as it apparently does in benzotrifluoride (29)), then its decrease in the polar solvents is reasonable. Again, ^6J(H,F) is larger in magnitude in acetone than in CS_2 solution, while ^6J(H,H) displays the opposite behavior (an increase in θ for the C—F bond implies a decrease in ψ). ^4J(H,F) and ^4J(H,H) display analogous trends, as expected if they are also mainly $\sigma-\pi$ couplings (26, 34).

^4J(C,F) in Table 1 increases in magnitude in the polar solvents. If it is negative as computed and is dominated by a negative $\sigma-\pi$ component, then this observation is also consistent with an increased stability of **2** in polar solvents. ^2J(C,F) decreases in magnitude in the polar solvents and is computed to decrease as **2** becomes preferred; ^2J(C,F) is large and positive in benzotrifluoride (29) and is very likely positive in benzyl fluoride.

Finally, ^1J(C,F) is no doubt negative, no positive values being known. It increases by about 9 Hz in going from CS_2 to DMSO solutions. The INDO MO FPT results suggest that ^1JC,F) *decreases* as θ increases. This single inconsistency between computation and observation may well arise from noncontact contributions to the coupling. Consequently, the theoretical result is not taken as evidence against a stabilization of **2** in the polar solvents.

(ii) *Estimates of changes in* V_2

The aim of this section is to demonstrate that the internal barrier is small in benzyl fluoride in solution and that it changes by about 2 kJ/mol in passing from CS_2 to DMSO solutions. In line with the geometry optimized STO 3G MO computations, a twofold potential barrier is assumed in the following discussion. A vanishing barrier would imply that the expectation values of $\sin^2\theta$ and θ are 0.5 and 45°, respectively.

Because of the uncertainties in the extremes of the $\sigma-\pi$ couplings, namely, their magnitudes when the C—H or C—F bonds are twisted by 90° out of the benzene plane, the following approach turns out to be useful. The various conformational conclusions in the literature are taken as reference points for V_2, the solvent-induced changes in V_2 are then deduced from ^5J(C,F), and a comparison with ^6J(H,H) and ^6J(H,F) is made in an attempt to find the most consistent set of data.

Assume that ^5J(C,F) is indeed proportional to $\sin^2\theta$ in benzyl fluoride. On the basis of ^5J(C,F) values in some model compounds (16), it is suggested that V_2 vanishes in $CDCl_3$ solution. Because ^5J(C,F) is 3.09 Hz (Table 1), $^5J_{90}$ follows as 6.18 Hz. Then $\langle\sin^2\theta\rangle$ in the other solvents follows as in Table 3. Tables (7, 35) of $\langle\sin^2\theta\rangle$ as a function of temperature and internal barrier yield the V_2 numbers in Table 3. In CS_2 solution, V_2 is 1.1 kJ/mol, **1** stable, and becomes 0.5 kJ/mol in DMSO solution, **2** preferred.

If **2** is favored by 1.7 kJ/mol in acetone solution, as deduced from ^{19}F chemical shifts (15), then $\langle\sin^2\theta\rangle$ follows as 0.585. $^5J_{90}$ becomes 5.38 Hz because ^5J(C,F) in acetone solution is 3.15 Hz (Table 1). Consequently, **2** is more stable than **1** by 0.2 kJ/mol in CS_2 solution. Increasing polarity of the solvent stabilizes **2**, until in DMSO solution **2** is more stable than **1** by 2.1 kJ/mol. V_2 has changed by about 2 kJ/mol. As usual (2), benzene behaves as a more polar solvent than its static dielectric constant would indicate.

TABLE 3. Values of the internal twofold barrier in benzyl fluoride in solution derived from different ^5J(C,F) values for $\theta = 90°$

Solvent	$\langle\sin^2\theta\rangle^a$	$V_2{}^b$	$V_2{}^c$	$V_2{}^{d,f}$	$V_2{}^e$ (kJ mol^{-1})
CS_2	0.446	1.1	0.2	0.6	0.0
CCl_4	0.455	0.9	0.4	0.8	0.2
C_6D_6	0.473	0.5	0.8	1.3	0.7
Neat	0.499	0.0	1.4	1.8	1.9
$CDCl_3$	0.500	0.0	1.4	1.8	1.9
CD_3OD	0.506	0.1	1.6	2.1	2.0
$(CD_3)_2C{=}O$	0.509	0.2	1.7	2.2	2.1
DMSO	0.525	0.5	2.1	2.6	2.5

[a]On the assumption that V_2 is zero in $CDCl_3$ solution (16). Because ^5J(C,F) is 3.09 Hz (Table 1, $^5J_{90}$ follows as 6.18 Hz because $\langle\sin^2\theta\rangle$ is 0.500 for a vanishing barrier.

[b]Following from $\langle\sin^2\theta\rangle$ in the preceding column. Values of $\langle\sin^2\theta\rangle$ less than 0.5 imply **1** as the preferred conformation. If $\langle\sin^2\theta\rangle$ is greater than 0.5, then **2** is preferred.

[c]Derived on the assumption that **2** is favored by 1.7 kJ/mol in acetone solution (15). In the latter ^5J(C,F) is 3.148(7)Hz (Table 1), so that $\langle\sin^2\theta\rangle$ becomes 0.581 and $^5J_{90}$ is 5.42 Hz. **2** is most stable in all solvents.

[d]On the assumption that ^5J(C,F) is 5,2 Hz at $\theta = 90°$, as implied by its values in 1-fluoroindan (16). **2** is most stable in all solvents.

[e]On the assumption that $^5J(C,F) = 0.3 + 4.9 \pm 0.3 \sin^2\theta$. Then **2** is the stable form in most solutions, but is of the same stability as **1** in CS_2 to within experimental error.

[f]A referee asks what consequences there are for V_2 if the extremes of 4.7 and 5.7 Hz for $^5J_{90}$(C,F) are assumed. For a value of 4.7 Hz, **2** is stable in all solvents, V_2 rising from 1.8 kJ/mol to 4.2 kJ/mol in passing from CS_2 to DMSO solution. If $^5J_{90}$ is 5.7 Hz, then **1** is stable in CS_2 solution with a V_2 of 0.3 kJ/mol and **2** is stable in DMSO solution with a V_2 of 1.4 kJ/mol.

Now, $^5J_{90}$ is computed as 5.2 ± 0.3 Hz from a value of 3.9 ± 0.2 Hz in the model compound, 1-fluoroindan, in which θ is taken as 60° (16). However, in 1-fluoro-4-methyl-1,2,3,4-tetrahydro-1,4-ethanonaphthalene, in which θ is very near 0°, ^5J(C,F) is 0.5 Hz (16). Conceivably, there exist additional coupling pathways in this bridged compound accounting for at least part of the 0.5 Hz. A similar statement would apply to the indan derivative. On the assumption that ^5J(C,F) contains an angle-independent component of 0.3 Hz, ^5J(C,F,) (Hz) = 0.3 + (4.9 ± 0.3) $\langle\sin^2\theta\rangle$. Table 3 also contains the V_2 values deduced from this equation. Then V_2 is essentially zero in CS_2 solution, becoming 2.5 kJ/mol in DMSO solution, **2** stable (uncertainties of ca. 0.5 kJ/mol).

If ^5J(C,F) (Hz) = 5.2 $\sin^2\theta$, then V_2 is 0.6 kJ/mol in CS_2 and increases to 2.6 kJ/mol in DMSO, **2** stable. These numbers are also given in Table 3. From all these comparisons, V_2 appears indeed to be small, changing by about 2 kJ/mol in passing from CS_2 to DMSO solutions.

In contrast, the relaxation data suggest an internal barrier of 11.8 kJ/mol in neat benzyl fluoride (13). If **1** is the stable form, then the value of ^5J(C,F) for $\theta = 90°$ follows as 23.4 Hz and as 15.7 Hz for a barrier of 7.6 kJ/mol deduced from relaxation data in acetone solution (14). Therefore **1** cannot be the preferred conformation if V_2 is large. If **2** is stable, then $^5J_{90}$ follows as 3.55, 3.94, and 3.65 Hz from the relaxation barriers in neat benzyl fluoride, acetone, and methanol, respectively, giving an average of 3.7 Hz. The ^5J(C,F) numbers in Table 1 then yield an internal barrier of 5.3 kJ/mol in CS_2 solution and 12.0 kJ/mol in DMSO solution. However, it is most unlikely that $^5J_{90}$ is as small as 3.7 Hz, the average of the numbers above.

This unlikelihood is emphasized by a consideration of ^6J(H,H) for benzyl fluoride in CS_2 and acetone solutions (Table 2). A relaxation barrier of 7.6 kJ/mol in acetone solution, **2** stable, implies a $\langle \sin^2 \psi \rangle$ of 0.351 (see **1** for the definition of ψ). Because ^6J(H,H) is a $\sigma-\pi$ coupling, it follows that its extreme at $\psi = 90°$ is $-0.409/0.351$ or -1.17 Hz (the barrier in CS_2 solution would then follow as 5.2 kJ/mol from the ^6J(H,H) of 0.452 Hz). This value of $^6J_{90}$ is much too large in magnitude. $^6J_{90}$ in toluene has recently been redetermined as -1.20 Hz (27) and it is known that the magnitude of $^6J_{90}$ decreases significantly as the electronegativity of the α-substituent increases (7). In particular, a detailed study of the solvent dependence of the conformational behavior of 2-hydroxybenzyl methyl ether (36) shows that $^6J_{90}$ is -1.02 Hz. Because fluorine is more electronegative than OCH_3, the magnitude of $^6J_{90}$ must be less than 1.02 Hz in benzyl fluoride. Assuming a linear dependence of $^6J_{90}$ on the electronegativity of the substituent (7, 35) and using the electronegativities deduced (37) from internal chemical shifts (see also refs. 38, 39), yields $^6J_{90}$ as -0.95 Hz in benzyl fluoride.

Concluding therefore that V_2 in benzyl fluoride in solution is indeed small, an attempt at discrimination between the V_2 sets in Table 3 essays as follows. From the relationship $\langle \sin^2 \psi \rangle = 0.75 - 0.5\langle \sin^2 \theta \rangle$, $-^6J_{90}$ for ^6J(H,H) is deduced in pairs (CS_2 and acetone): 0.878, 0.826 Hz if $V_2 = 0$ in $CDCl_3$; 0.894, 0.915 Hz if **2** is favored by 1.7 kJ/mol in acetone; and 0.964, 0.954 Hz if ^5J(C,F) is 4.9 Hz and no angle-independent contribution exists in the latter. If an angle-independent term of 0.3 Hz exists additionally, then $-^6J_{90}$ becomes 0.905, 0.891 Hz. If ^5J(C,F) (Hz) $= 5.2 \sin^2 \theta$, one has 0.933, 0.915 Hz for $-^6J_{90}$. These comparisons suggest a nonzero V_2 in $CDCl_3$ solution and that a reasonable relation is ^5J(C,F) (Hz) $= 4.9 \sin^2 \theta$. With the latter and ^6J(H,H) $= -0.959 \sin^2 \theta$, V_2 varies between 1.0 kJ/mol in CS_2 and 3.3 kJ/mol in DMSO solutions.

Similar tests for ^6J(H,F,) yield $-^6J_{90}$ as 3.45, 3.53 if V_2 vanishes in $CDCl_3$; 3.00, 3.08 if **2** is preferred by 1.7 kJ/mol in acetone; and 2.74, 2.80 Hz if ^5J(C,F) is 4.9 Hz at $\theta = 90°$ in the absence of an angle-independent component. In 2,6-dichlorobenzyl fluoride, ^6J(H,F,) is -2.43 Hz (32). Fully optimized STO 3G MO computations give V_2 (kJ/mol) $= 12.2 \cos^2 \theta - 2.0 \sin^2 2\theta$ for the internal potential. If the fourfold component is ignored, $\langle \sin^2 \theta \rangle$ is 0.879 and $^6J_{90}$ becomes -2.76 Hz. If the fourfold component is included, a classical average gives $\langle \sin^2 \theta \rangle$ as 0.844 and $^6J_{90}$ becomes -2.87 Hz. These numbers lie reasonably close to the assumption that ^5J(C,F) (Hz) $= 4.9\langle \sin^2 \theta \rangle$. Again, ^5J(C,F) is 4.0 ± 0.2 Hz in 2,6-dichlorobenzyl fluoride (16). The potential function above then implies $^5J_{90}$ as 4.7 ± 0.3 Hz for ^5J(C,F), again in reasonable agreement with the above assumption.

One further point must be made. In 2,6-dichloro-4-methylbenzyl fluoride in CS_2 solution, ^7J(F,CH_3) is 2.83 Hz (40), compared to a ^6J(H,F) of -2.43 Hz for 2,6-dichlorobenzyl fluoride in benzene solution (32). If the methyl substituent causes no change in V_2, then it follows that ^6J(H,F) contains a positive non $\sigma-\pi$ component of about 0.4 Hz, it being most unlikely that ^7J(F,CH_3) is other than a pure $\sigma-\pi$ coupling. Yet it is known that a *para* methyl group increases the stability of **2** in the absence of chlorine substituents (15, 40). Therefore part of the discrepancy above may arise in this manner. A small non $\sigma-\pi$ component of ^6J(F,H) may be present, however. The perturbation by ring substituents of the internal potential function in benzyl fluoride is significant. Thus, ^5J(C,F) is 2.0 Hz in 3,5-dichlorobenzyl fluoride in CS_2 solution (see Experimental) and, because *meta* substituents appear to cause very small changes in $\sigma-\pi$ couplings (7), it follows that V_2 is 1.9 kJ/mol with **1** as the stable form, if $^5J_{90}$ is taken as 4.9 Hz. ^6J(H,H) is $-0.537(0)$ Hz, implying **1** as more stable than **2** by 2.7 kJ/mol if $^6J_{90}$ is taken as -0.95 Hz. ^6J(H,F) is $-1.026(1)$ Hz and **1** is more stable than **2** by 2.8 kJ/mol if $^6J_{90}$ is -2.81_5 Hz, the mean of the two values above. Clearly, **1** in the 3,5-dichloro derivative is more stable than in benzyl fluoride by at least 2 kJ/mol. Our STO 3G MO calculations suggest a twofold barrier which is 0.8 kJ/mol larger than in benzyl fluoride, **1** stable. The conformational preference of a given benzyl fluoride derivative will be a function of the substituents *and* of the solvent.

In summary, there is little doubt that **2** in benzyl fluoride is stabilized relative to **1** by about 2 kJ/mol as the solvent changes from CS_2 to DMSO, in qualitative accord with simple dielectric continuum models. However, the long-range couplings used in this study, although in agreement with a rather small twofold internal barrier, leave some doubt as to the minimum in the potential function in CS_2 solution. The result most consistent with all three types of couplings is that the potential function is almost flat in this solvent, **2** being favored over **1** by perhaps as much as 1 kJ/mol.

(iii) *Conformational changes in other* ^nJ*(C,F)*

For benzotrifluoride, ^5J(C,F) was treated as a $\sigma-\pi$ coupling and the vanishing ^4J(C,F) could then be accounted for by a composite mechanism, consisting of a negative $\sigma-\pi$ component proportional to $\sin^2 \theta$ and a smaller positive σ component depending on $\sin^2 (\theta/2)$. The expectation value of $\sin^2 (\theta/2)$ is 0.5 for a twofold barrier. On the assumption that ^4J(C,F) behaves similarly in benzyl fluoride, one may write $^4J(C,F) = {}^4J_{90} \langle \sin^2 \theta \rangle + 0.5\,{}^4J_{180}$. Use of V_2 values in the last column of Table 3 for CS_2 and DMSO solutions to find $\langle \sin^2 \theta \rangle$ yields $^4J^{\pi}_{90}$ as -5.12 Hz and $^4J_{180}$ as 3.30 Hz. These numbers assume a negative ^4J in Table 1. A positive ^4J would yield a positive $^4J^{\pi}_{90}$, rather unlikely because of spin correlation (29). This parameterization can be tested for the other solvents with the result that the mean deviation between observed and calculated values for the other six solvents is 0.03 Hz, 6% of the observed change. In other words, the present formulation of the θ dependence of ^4J is consistent with an increased stability of **2** in the more polar solvents. However, the values of $^4J^{\pi}_{90}$ and $^4J^{\sigma}_{180}$ must be considered as approximate. Furthermore, ^4J(C,F) vanishes in 3,5-dichlorobenzyl fluoride, so that this coupling is strongly substituent dependent. In 4-methylbenzyl fluoride in CS_2 solution ^4J(C,F) is 1.34 ± 0.06 Hz. If negative and unperturbed by the methyl group, $\langle \sin^2 \theta \rangle$ follows as 0.58 ± 0.12 from the above parameterization, in rough agreement with the 0.64 ± 0.04 deduced (40) from ^7J(F,CH_3).

^2J(C,F) is $+18.3 \pm 0.1$ Hz in 3,5-dichlorobenzyl fluoride in CS_2 solution. In benzyl fluoride, ^2J(C,F) is therefore no doubt positive as well, decreasing from 17.5 Hz in CS_2 to 16.6 Hz in DMSO solutions. This decrease is consistent with the qualitative indications from the INDO MO FPT computations if **2** increases in stability in the polar solvents. The higher observed value in the 3,5-dichloro derivative is expected if, as deduced above, the stability of **1** is enhanced by the ring substituents.

^1J(C,F) changes from -170.5 Hz in CS_2 solution to -161.9 Hz in DMSO solution. For the sake of argument, write ^1J(C,F) as $A + B \sin^2 \theta$. Then, using the V_2 values in the last column of Table 3, one has $A = -206.4$ Hz and $B = 71.5_5$ Hz. In 3,5-dichlorobenzyl fluoride, ${}^1J(C,F)$ is -173.7 Hz, corresponding to a $\langle \sin^2 \theta \rangle$ of 0.457. Then **1** is favored by 0.9 kJ/mol for his molecule, differing by 1 kJ/mol from the value implied by ${}^5J(C,F)$ above. Any intrinsic substituent effect on ${}^1J(C,F)$ has been ignored in this comparison. Certainly, *para* and *ortho* substituents should perturb ${}^1J(C,F)$ as they do ${}^1J(H,C)$, for example (41). Therefore, further comparisons will not be done.

Conclusions

The perpendicular conformer of benzyl fluoride, in which the C—F bond lies in a plane perpendicular to the benzene plane, is stabilized by about 2 kJ/mol in passing from CS_2 to DMSO solutions. This magnitude is about equal to the error in Raman and infrared measurements of solvent effects on conformational equilibria (4). It is likely that in CS_2 solution the conformational preference is very weak at 300 K, the twofold barrier to internal rotation being very near zero. Each benzyl fluoride derivative will have its own internal barrier and this will also be solvent dependent, particularly for *meta* and *para* substituted compounds.

Acknowledgements

We are grateful to Glenn H. Penner for the molecular orbital computations and to the Natural Sciences and Engineering Research Council of Canada for financial support. Enlightening and stimulating correspondence with Ludger Ernst was important to this work. We thank the referees for cogent criticism. Grants towards the purchase of the AM300 spectrometer from the Natural Sciences and Engineering Research Council of Canada and the Manitoba Health Research Council are gratefully acknowledged.

1. S. MIZUSHIMA. Structure of molecules and internal rotation. Academic Press, New York. 1954.
2. R. J. ABRAHAM and E. BRETSCHNEIDER. *In* Internal rotation in molecules. *Edited by* W. J. Orville-Thomas. J. Wiley and Sons, New York. 1974. Chapt. 13.
3. L. ONSAGER. J. Am. Chem. Soc. **58**, 1486 (1936).
4. W. L. JORGENSEN. J. Phys. Chem. **87**, 5304 (1983).
5. V. M. S. GIL, A. J. C. VARANDAS, and J. N. MURRELL. Can. J. Chem. **61**, 163 (1983).
6. T. SCHAEFER, J. PEELING, and G. H. PENNER. Can. J. Chem. **61**, 2773 (983).
7. W. J. E. PARR and T. SCHAEFER. Acc. Chem. Res. **13**, 400 (1980).
8. J. R. DURIG, M. ZHEN, and T. S. LITTLE. J. Chem. Phys. **81**, 4259 (1984).
9. M. T. ROGERS. J. Am. Chem. Soc. **69**, 457 (1947).
10. J. A. POPLE and D. L. BEVERIDGE. Approximate molecular orbital theory. McGraw–Hill Book Co., New York. 1970. p. 119.
11. R. J. ABRAHAM, R. A. HEARMON, M. TRAETTEBERG, and P. BAKKEN. J. Mol. Struct. **57**, 149 (1979).
12. C. BÉGUIN and E. GOUT-MALLARET. J. Fluorine Chem. **8**, 279 (1976).
13. C. BÉGUIN and R. DUPEYRE. J. Magn. Reson. **44**, 294 (1981).
14. R. DUPEYRE and C. BÉGUIN. J. Chim. Phys. **78**, 363 (1981).
15. R. T. C. BROWNLEE and D. J. CRAIK. Tetrahedron Lett. **21**, 1681 (1980).
16. W. ADCOCK and A. N. ABEYWICKREMA. Aust. J. Chem. **33**, 181 (1980).
17. J. P. MAHER and D. F. EVANS. Proc. Chem. Soc. London, 208 (1961).
18. W. J. HEHRE, R. DITCHFIELD, R. F. STEWART, and J. A. POPLE. J. Chem. Phys. **52**, 2769 (1970).
19. M. R. PETERSEN and R. A. POIRIER. MONSTERGAUSS. Department of Chemistry, University of Toronto, Toronto, Ontario. 1981.
20. J. A. POPLE, J. W. MCIVER, and N. S. OSTLUND. J. Chem. Phys. **49**, 2965 (1968).
21. P. DOBOSH and N. S. OSTLUND. QCPE, **11**, 281 (1975).
22. J. A. POPLE and G. A. SEGAL. J. Chem. Phys. **44**, 3289 (1966).
23. R. A. BERNHEIM and B. J. LAVERY. J. Am. Chem. Soc. **89**, 1279 (1967).
24. A. R. QUIRT and J. S. MARTIN. J. Magn. Reson. **5**, 318 (1971); J. S. Martin, A. R. Quirt, and K. E. Worvill. The nmr program library. Daresbury Laboratory, Daresbury, U.K.
25. J. KOWALEWSKI. Annu. Rep. NMR Spectrosc. **12**, 81 (1982).
26. R. WASYLISHEN and T. SCHAEFER. Can. J. Chem. **50**, 1852 (1972).
27. T. SCHAEFER, R. SEBASTIAN, and G. H. PENNER. Can. J. Chem. **63**, 2597 (1985).
28. R. WASYLISHEN and T. SCHAEFER. Can. J. Chem. **49**, 94 (1971).
29. T. SCHAEFER, K. MARAT, J. PEELING, and R. P. VEREGIN. Can. J. Chem. **61**, 2779 (1983).
30. T. SCHAEFER, R. SEBASTIAN, and S. R. SALMAN. Can. J. Chem. **59**, 3026 (1981).
31. J. A. POPLE and M. GORDON. J. Am. Chem. Soc. **89**, 4254 (1967).
32. T. SCHAEFER, J. B. ROWBOTHAM, W. J. E. PARR, K. MARAT, and A. F. JANZEN. Can. J. Chem. **54**, 1322 (1976).
33. T. SCHAEFER and R. LAATIKAINEN. Can. J. Chem. **61**, 2785 (1983).
34. M. BARFIELD, C. J. FALLICK, K. HATA, S. STERNHELL, and P. W. WESTERMAN. J. Am. Chem. Soc. **105**, 2178 (1983).
35. W. DANCHURA. Ph.D. Thesis. University of Manitoba, Winnipeg, Manitoba. 1983.
36. R. LAATIKAINEN. Tetrahedron. In press.
37. B. P. DAILEY and J. N. SHOOLERY. J. Am. Chem. Soc. **77**, 3977 (1956).
38. J. R. CAVANAGH and B. P. DAILEY. J. Chem. Phys. **34**, 1099 (1961).
39. M. L. HUGGINS. J. Am. Chem. Soc. **75**, 4123 (1953).
40. T. SCHAEFER, W. P. NIEMCZURA, R. SEBASTIAN, L. J. KRUCZYNSKI, and W. DANCHURA. Can. J. Chem. **58**, 1178 (1980).
41. C. H. YODER, R. H. TUCK, and R. E. HESS. J. Am. Chem. Soc. **91**, 539 (1969).

Charge distributions and chemical effects. XXXVIII. Correlations between nuclear magnetic resonance shifts and electronic charges of nitrogen atoms

M. COMEAU, M.-T. BÉRALDIN, E. C. VAUTHIER, AND S. FLISZÁR[1]
Department of Chemistry, Université de Montréal, C.P. 6210, Succ. A, Montréal (Qué.), Canada H3C 3V1

Received March 22, 1985

M. COMEAU, M.-T. BÉRALDIN, E. C. VAUTHIER, and S. FLISZÁR. Can. J. Chem. **63**, 3226 (1985).

Correlations between nuclear magnetic resonance shifts and atomic charges of nitrogen in selected alkylamines, nitroalkanes, isonitriles, and azines consistently follow the general trends observed for carbon and oxygen nuclei. In azines, any increase in total electronic population on nitrogen, resulting from a gain in π charge prevailing over a concurrent loss of σ electrons, is accompanied by an upfield resonance shift—as found for aromatic and ethylenic carbon and carbonyl oxygen atoms. On the other hand, any gain in total charge dictated by that of σ populations translates into a downfield ^{15}N shift, which is the trend exhibited by alkylamines, nitroalkanes, and isonitriles—a situation encountered earlier with sp^3-hybridized carbon, carbonyl carbon, and dialkyl ether oxygen atoms.

M. COMEAU, M.-T. BÉRALDIN, E. C. VAUTHIER et S. FLISZÁR. Can. J. Chem. **63**, 3226 (1985).

Les corrélations, en rmn, entre les déplacements chimiques et les charges électroniques portées par les azotes d'alkylamines, de nitroalcanes, d'isonitriles et d'azines choisis ont le même comportement que celui précédemment établi pour les noyaux de carbone et d'oxygène. Dans le cas des azines, une augmentation de la charge électronique totale sur l'azote—qui provient d'une augmentation de la charge π au détriment de la charge σ—est accompagnée d'un déplacement chimique vers les champs forts; ce comportement est identique à celui déjà rencontré pour les ^{13}C de composés aromatiques et éthyléniques et pour les atomes d'oxygène de groupements carbonyles. Par contre, pour les alkylamines, les nitroalcanes et les isonitriles, une augmentation de la charge électronique totale sur l'azote—provenant d'un gain en électrons σ—provoque un glissement vers les champs faibles pour ce noyau; cette situation a déjà été rencontrée pour les carbones hybridés sp^3 des alcanes, pour les ^{13}C de groupements carbonyles et pour les atomes d'oxygène d'éthers dialkylés.

[Traduit par le journal]

Introduction

Correlations between atomic charges and nuclear magnetic resonance shifts have become best known for ^{13}C and ^{17}O nuclei (1, 2): in some cases they are excellent (albeit not free from conceptual difficulties) (3−5) and of considerable help in the accurate evaluation of charge effects governing molecular energies (2, 6). Unfortunately, no corresponding information is presently available for ^{15}N nuclei—a problem attacked here with a critical examination of possible charge−shift correlations for nitrogen atoms.

Indeed, a theoretical analysis of the nuclear magnetic shielding of ^{15}N in a well-diversified variety of compounds (amines, azines, etc.) reveals that the changes in total shielding are almost entirely dictated by those of the local paramagnetic contribution (i.e., $\Delta\sigma_{\text{total}} \simeq \Delta\sigma_{\text{local}}^{\text{param.}}$), in a range covering ~400 ppm (7). This result suggests possible correlations between ^{15}N nmr shifts and atomic charges which, of course, are essentially local in character. The fact, however, that $\Delta\sigma_{\text{total}} \simeq \Delta\sigma_{\text{local}}^{\text{param.}}$ holds true for different types of N atoms does not imply that all of them are covered by a single charge−shift relationship. The nature of the latter depends, indeed, on the way $\Delta\sigma_{\text{local}}^{\text{param.}}$ varies with a change in local electron density, hence the reason for distinguishing N atoms belonging to different classes of compounds.

Calculation of charges

All SCF calculations were performed by means of Pople's STO-3G method (8), using the Gaussian 76 set of programs (9). Molecular geometries and all ζ parameters were optimized in most cases, a point which is important because atomic charges are very sensitive to the molecular environment and, hence, to ζ optimization: the internally most consistent charge results are obtained when these optimizations are carried out at their best for each atom (or group of equivalent atoms) of the molecules under study, until stable charges are obtained (2). This task is practically feasible only in minimal basis set calculations, hence our choice for the fully optimized STO-3G method.

Population analyses were carried out following Mulliken (10). Of course, atomic charges deduced in this manner should *not* be taken at their face value because they are strongly basis set dependent (2, 11); *they should only be used in comparisons between like atoms* (e.g., between nitrogen atoms of primary amines, or nitrogen atoms of secondary amines, etc.), in which case the trends indicated by Mulliken's population analysis are valid (2). This restriction is important, indeed, because Mulliken's charges include, throughout, a half-and-half partitioning of overlap populations in their computation, a circumstance which may carry an error in situations involving heteronuclear atom pairs (2) (as in the NH, NC, and CH bonds, in the present case), but, as discussed below, this is not the only reason. (Typical examples illustrating the effect of lifting the equipartitioning of overlap population terms in STO-3G charge analyses based on Mulliken's scheme are found in charge − nmr shift comparisons offered for alkanes (12) and alkyl-substituted ethylenes (13).) With these reservations in mind, Mulliken charges deduced from optimized STO-3G wave functions are of undisputed value in comparative studies like the one presented below. In more realistic charge calculations, however, larger basis sets *and* inclusion of configuration interaction become a must (14).

Results

Alkylamines

Fully optimized STO-3G results obtained for selected mono-, di-, and trialkylamines are indicated in Table 1. Within each series, a comparison with known adiabatic ionization potentials (15) reveals that the latter decrease as electronic charge

[1]Author to whom correspondence may be addressed.

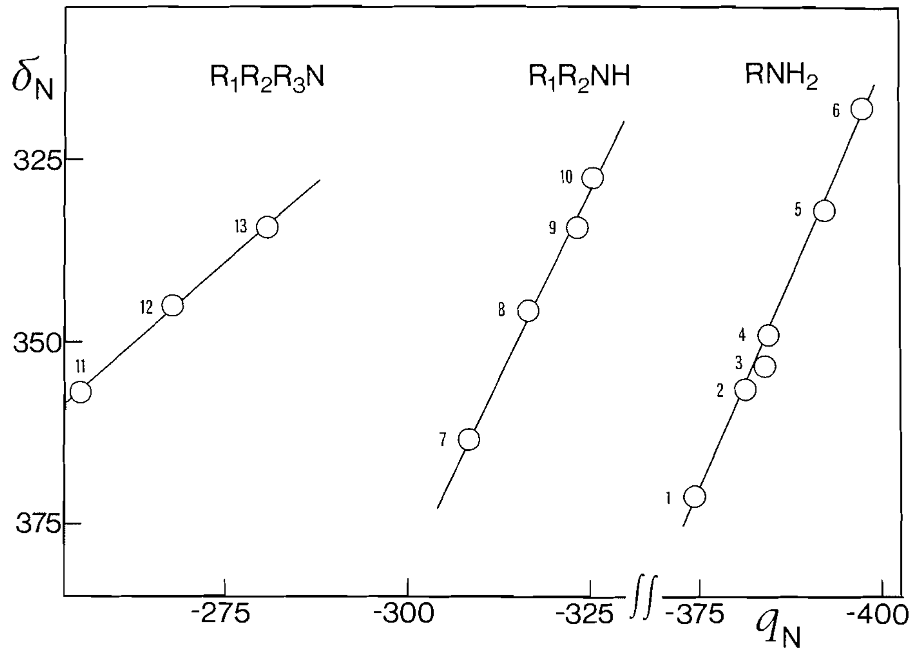

FIG. 1. Correlation between ^{15}N resonance shifts of alkylamines (ppm, upfield from HNO_3, in methanol) and nitrogen net charges (in me = 10^{-3} e units).

TABLE 1. Orbital populations N (electron), net atom charges q_N (me = 10^{-3} e), ^{15}N resonance shifts (ppm, from HNO_3, in methanol), and ionization potentials (IP) (kcal mol^{-1}) of selected alkylamines

Molecule[a]	$N(1s)$	$N(2s)$	$N(2p)$	q_N	$\delta(^{15}N)$[b]	IP
1 Methyl-NH_2	1.9949	1.5803	3.7992	−374.4	371.1	206.8
2 Isobutyl-NH_2	1.9950	1.5810	3.8055	−381.5	356.5	
3 Propyl-NH_2	1.9950	1.5831	3.8060	−384.2	353.4	202.5
4 Ethyl-NH_2	1.9950	1.5833	3.8063	−384.6	349.2	204.3
5 Isopropyl-NH_2	1.9950	1.5850	3.8122	−392.2	331.9	201.1
6 *tert*-Butyl-NH_2	1.9951	1.5874	3.8149	−397.3	318.1	199.2
7 Dimethyl-NH	1.9950	1.5784	3.7351	−308.5	363.3	190.0
8 Methyl, ethyl-NH	1.9951	1.5833	3.7382	−316.6	345.8	
9 Dipropyl-NH	1.9951	1.5856	3.7445	−323.3	334.3	
10 Diethyl-NH	1.9951	1.5840	3.7464	−325.4	327.5	184.7
11 Trimethyl-N	1.9951	1.5697	3.6903	−255.1	356.9	180.3
12 Dimethyl, ethyl-N	1.9952	1.5751	3.6977	−268.0	345.1	
13 Diethyl, methyl-N	1.9952	1.5773	3.7083	−280.8	334.3	

[a]The numbering corresponds to that of Fig. 1.
[b]In this convention, increasingly larger $\delta(^{15}N)$ values indicate upfield resonance shifts.
[c]The STO-3G Mulliken net charges (2) of carbon replacing N in the analogous hydrocarbons (see text) are, in me, −21.0 (**1**), −22.6 (**2**), −23.1 (**3**), −23.8 (**4**), −26.4 (**5**), −28.5 (**6**), 6.1 (**7**), 3.5 (**8**), 2.2 (**9**), 0.8 (**10**), 33.6 (**11**), 32.2 (**12**), and 30.2 (**13**).

tends to build up on nitrogen, as one would normally expect in a rough first approximation, thus suggesting that the charges calculated here are, indeed, in the right order. On the other hand, a gain in electronic charge also appears to be accompanied by a concurring downfield ^{15}N chemical shift (Fig. 1). This trend is similar to that encountered earlier with typical sp^3 carbon atoms (in normal and branched paraffins and in the cyclohexane series, including polycyclic hydrocarbons constructed from chair and (or) boat cyclohexane rings), with carbonyl carbon atoms, and with the oxygen atoms in dialkylethers (1, 2, 16).

Separate correlation lines are observed for mono-, di-, and trialkylamines—a fact which may *partially* be accounted for by the present use of Mulliken charges, as in the case of saturated and ethylenic hydrocarbons (2, 12, 13). Each of these charge–shift correlations can be represented by $\Delta\delta(^{15}N) = a_N \Delta q_N$. The slope, a_N, for tertiary amines would appear to differ significantly from what is found for mono- and dialkylamines. There are reasons to suspect, however, that this apparent change in a_N reflects, at least in part, a computational artefact in the evaluation of charges, rather than a genuine physical effect. Consider here the parent alkanes obtained by relacing N with CH and compare the charge of each nitrogen with that of the carbon replacing it. The slope relating the Δq_N's to the corresponding "parent" Δq_C's appears to be ~2.5 times larger for tertiary than for secondary and primary nitrogen atoms. This observation casts serious doubts concerning the balance of the present STO-3G nitrogen charges because tertiary nitrogen should not be all that exceptional as regards the regular patterns of partial charge transfers accompanying equal substitutions at N and CH. Of course, if the Δq_N's of tertiary amines were, indeed, in error by a factor ~2.5 (relative to the results deduced for the other amines), the readjusted slopes, $\Delta\delta(^{15}N)/\Delta q_N = a_N$, of Fig. 1 would be nearly the same. It must be made clear that charge analyses are plagued at the outset by an unbalance in the hydrogen basis sets currently used in *ab initio* calculations (11, 18–21), which alters significantly the description of nitrogen itself. Basis set superposition errors were evaluated (11) by replacing Pople's standard 6-31G* basis by an extended form in which the basis of the ammonia H atoms and that of the methyl groups of trimethylamine were retained in the treatment of each alkylamine (i.e., mono-, di-, and trimethylamine) and of ammonia itself: the results indicated that the quality of the treatment of amine nitrogen atoms is strongly dependent on the number of methyl groups because the replacement of alkyl groups by hydrogens greatly impoverishes the basis. On these grounds, a new, augmented basis was proposed for hydrogen, which appears to be reasonably well balanced. Comparison with familiar (e.g., 6-31G*) calculations revealed in what manner the treatment of nitrogen is worsened when even just one methyl group is replaced by hydrogen, unless the impoverishment of the basis is suitably taken care of. The effect on nitrogen atomic charges is spectacular in that only minor variations seem to occur in going from ammonia to trimethylamine (~−0.53 e for NH_3, CH_3NH_2, and $(CH_3)_2NH$; ~−0.54 e for $(CH_3)_3N$), quite unlike the trends displayed in Table 1. This and related studies (19–21) warn against reaching hasty conclusions concerning charge distributions in alkylamines, namely, as regards a direct comparison between mono-, di-, and trimethylamine. Presently we feel unable to go beyond comparisons restricted to individual series with the same number of alkyl substituents, following the approach described in the text, in which case distortions arising from superposition effects are minimized.

Adding to the theoretical difficulties, there is also the problem of assessing the appropriateness of the nmr data selected for use in comparisons like those described here, because solvent and concentration effects are often much larger for nitrogen-15 than for carbon-13 nmr spectra (22). Litchman and co-workers (23), for example, investigated in detail the effects of binding of the solvent protons to the nitrogen lone pair and (or) influences of solvent lone pairs binding with the protons on nitrogen, concluding that different solvent effects are generally to be expected for primary and tertiary amines, and probably for secondary amines as well. Besides hydrogen bonding, other possible causes for the solvent effects on ^{15}N chemical shifts include polarization of solute molecules in a very polar medium and conformational changes resulting from strong solvent–solute interactions. The large solvent effects on propylamines have been rationalized on the basis of changes in the populations of the *gauche* conformers (17, 24). The importance of these interactions is revealed by the correlations observed for the ^{15}N chemical shifts of the saturated amines with the ^{13}C shifts of the corresponding carbons in analogous hydrocarbons (17, 24–26), namely, by the very existence of separate, solvent-sensitive, linear correlations for primary, secondary, and closely related groups of tertiary amines. Results of this sort, obtained with great care for a large variety of compounds and interpreted in detail by Roberts and co-workers (17, 24–26), are instrumental in a more balanced assessment of the charge–shift correlations shown in Fig. 1. It appears, indeed, that the charges to be used in this type of correlations should not be those of the isolated amines but rather those of the (still ill-known) aggregates as they are physically present in shift measurements. However, the linearity of the $^{15}N/^{13}C$ correlations, as well as the corresponding ones between atomic charges, supports the overall validity of correlations involving observed ^{15}N shifts and nitrogen charges of model isolated amines, at least as regards general charge–shift trends within series of closely related compounds.

Hence, despite the theoretical and solvent-related difficulties outlined above, it may be concluded from the present results that any increase in electronic charge at amine nitrogen atoms translates into a downfield chemical shift. This trend is also followed by other types of nitrogen atoms.

TABLE 2. Orbital populations, N (e), net atomic charges,[a] q_N (me), and ^{14}N resonance shifts of nitroalkanes R—NO_2

R	$N(1s)$	$N(2s)$	$N(2p)$	q_N	$\delta(^{14}N)$
CH_3	1.9941	1.3513	3.1889	465.7	0
C_2H_5	1.9942	1.3535	3.1929	459.5	−12
iso-C_3H_7	1.9942	1.3555	3.1955	454.8	−24
tert-C_4H_9	1.9942	1.3570	3.1986	450.3	−30

[a]From standard STO-3G calculations using the scale factors and geometries indicated by Hehre and Pople (29), namely, those of nitromethane for N, O, C, and H in the α-position, and those determined for hydrocarbons otherwise.

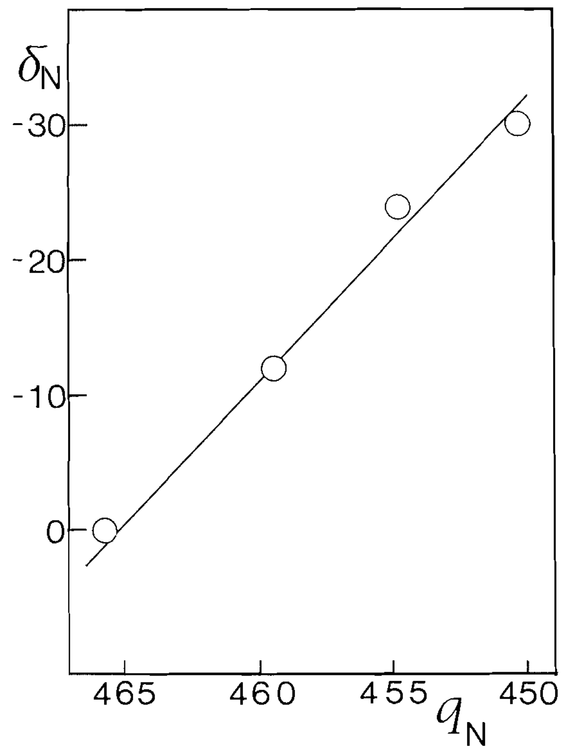

FIG. 2. Comparison between net charges and resonance shifts (ppm, downfield from CH_3NO_2) of nitrogen in selected nitroalkanes.

Nitroalkanes

In nitroalkanes, R—NO_2, a regular upfield shift of the nitrogen resonance with increasing electronegativity of R is observed and obeys simple additivity rules (27). Upon replacing hydrogen atoms in CH_3NO_2 with alkyl groups, a downfield shift of ~10 ppm takes place—a trend similar to that encoun-

TABLE 3. Orbital populations, N (e), Mulliken net charges,[a] q_N (me), and ^{14}N resonance shifts of selected isonitriles R—NC

R	$N(1s)$	$N(2s)$	$N(2p)$	q_N	$\delta(^{14}N)$
CH_3	1.9957	1.4227	3.9153	−333.8	218.0
C_2H_5	1.9958	1.4268	3.9163	−338.9	203.0
iso-C_3H_7	1.9958	1.4301	3.9170	−342.9	189.7
tert-C_4H_9	1.9958	1.4327	3.9176	−346.1	181.2

[a]From standard STO-3G calculations, using geometries defined by Pople and Gordon (31), and scale factors of ref. 8. A distance of 1.16 Å was used for NC.

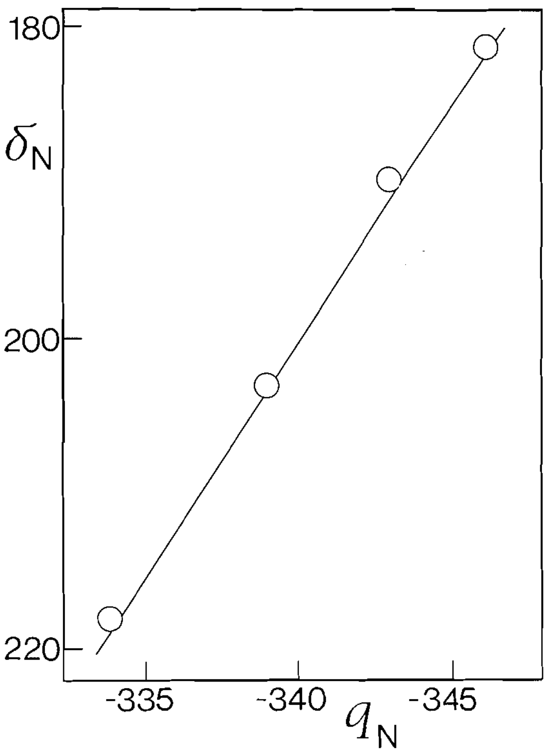

FIG. 3. Comparison between chemical shifts (ppm, upfield from NO_3^-) and atomic charges of nitrogen in selected isonitriles.

tered with amine nitrogen resonances. This trend visibly reflects the usual electron-releasing ability of alkyl groups, in the order *tert*-C_4H_9 > i-C_3H_7 > C_2H_5 > CH_3. Charge analyses at the STO-3G level, as well as the appropriate shift data (28) (downfield from nitromethane, for neat compounds) are indicated in Table 2.

Again, these are basis set dependent Mulliken charges which should not be taken at their face value. The trend indicating an electron enrichment at N for increasingly better electron-donating substituent, however, certainly corresponds to what would be expected. Figure 2 illustrates that a gain in electronic charge at nitrogen translates linearly into a downfield nmr shift in the case of nitroalkanes. Interestingly, the slope (~2 ppm/me) is similar to those found for alkylamines (2.3 ppm/me) and dialkylamines (2.1 ppm/me).

Isonitriles

The nitrogen resonance signal of isonitriles moves to higher fields (30) with increasing electronegativity of the group R in R—NC. The shift is very regular, about 15 ppm downfield for each H atom in CH_3—NC replaced with an alkyl group. This resembles the trends observed for amines and nitro groups.

TABLE 4. Nitrogen σ, π, and total (σ + π) Mulliken net charges (me) and ^{15}N resonance shifts of 4-substituted pyridines (**1–9**) and of selected azines (**10–13**)

Molecule[a]	q_σ	q_π	q_{tot}	$\delta(^{15}N)$[b]
1 HO-pyr	−175.5	−95.3	−270.8	−138
2 NH_2-pyr	−176.2	−96.6	−272.8	−42
3 OCH_3-pyr	−189.0	−69.9	−258.9	−27
4 CH_3-pyr	−190.6	−69.7	−260.3	−11
5 H-pyr	−195.5	−59.6	−255.1	0
6 CN-pyr	−200.5	−39.7	−240.2	9
7 $COCH_3$-pyr	−199.0	−51.2	−250.2	25
8 NO_2-pyr	−204.4	−28.8	−233.1	28
9 CHO-pyr	−199.4	−49.3	−248.7	29
10 1,4-Diazine	−196.0	−18.8	−214.8	46.1
11 Pyridine	−186.6	−53.8	−240.4	63.5
12 1,3-Diazine	−180.8	−84.1	−264.9	84.5
13 1,3,5-Triazine	−183.3	−101.3	−284.6	98.5

[a]Molecules **1–9** were partially optimized as described in the text; the results for **10–13** were derived with full (geometry and scale factor) optimization.

[b]In ppm from pyridine (= $\delta_{pyr} - \delta_X$) for **1–9**; ppm from external $MeNO_2$ for **10–13** (from ref. 22). In these scales, large $\delta(^{15}N)$ values indicate downfield shifts (**1–9**), viz. upfield shifts (**10–13**).

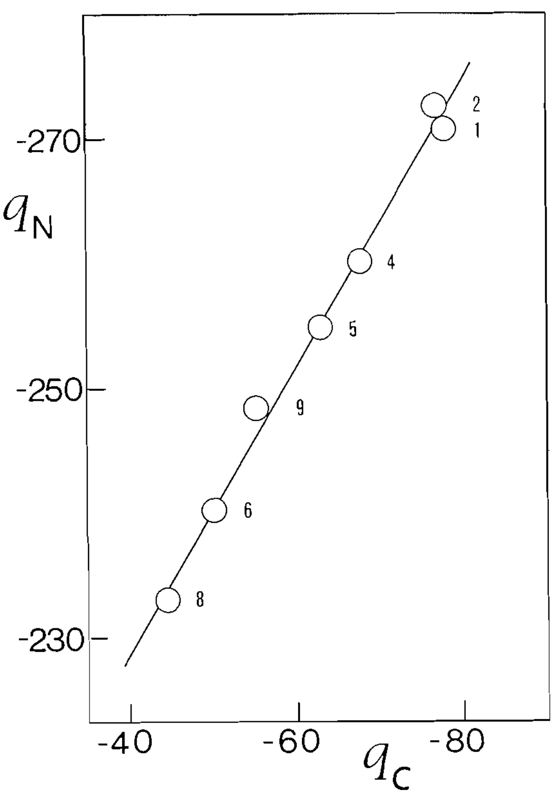

FIG. 4. Correlation between the nitrogen net charges of selected 4-R-pyridines and those of C-4 in the analogous R-substituted benzenes (5). (A similar correlation holds also for the corresponding π charges.)

STO-3G charges (Table 3) and Fig. 3 show, indeed, that the nitrogen signal (30) is farther downfield as electronic charge increases at this atom, with a slope of ~3 ppm/me.

Azines

Using the experimental geometry of pyridine (32), the STO-3G optimization of its scale factors was performed until charges

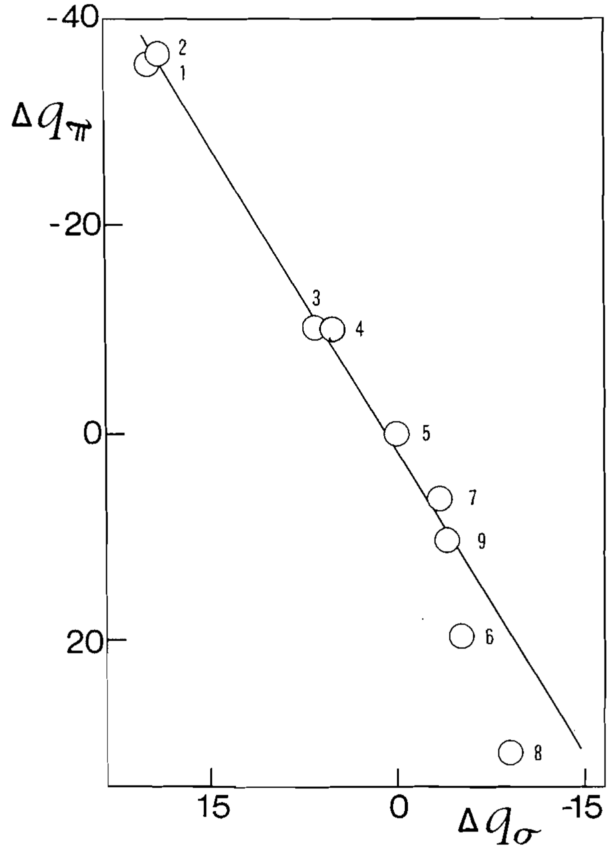

FIG. 5. Comparison between nitrogen σ and π net charges in 4-R-pyridines.

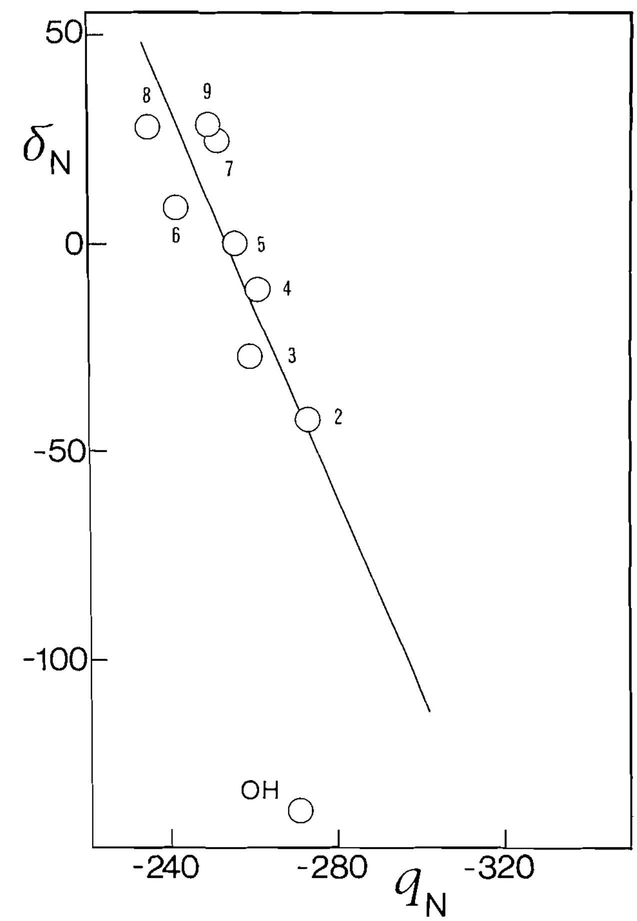

FIG. 6. Correlation between nmr shifts and net charges of nitrogen in substituted pyridines (neat for **5**, **7**, **9**; otherwise in acetone), suggesting that some scatter may be due to solvent effects and experimental uncertainties (~6 ppm for **3**, **8**, **9**; ~12 ppm for **7**).

were stable to within ~0.01 me. Taking advantage of Del Bene's work (33) showing that the pyridine ring is essentially unchanged in the equilibrium structures of 4-R-pyridines, only the geometries and scale factors of the substituents were subsequently optimized for the 4-substituted derivatives, under the appropriate symmetry constraints (C_{2v} for NO_2 and NH_2, C_s otherwise). The results are indicated in Table 4.

Electron-releasing substituents (NH_2, OH, OCH_3, CH_3) appear to increase the π (and total) charge of the ring nitrogen, whereas the opposite is true for electron-withdrawing groups (NO_2, CHO, CN, $COCH_3$), in accord with common expectation. These results match those of Hehre, Taft, and Topsom (5) showing that carbon-4 in substituted benzenes gains or loses charge depending on whether the substituent donates or withdraws electrons: earlier studies by Pople and co-workers (34) on related systems similarly concluded that theoretical charge distributions do, indeed, support many of the ideas of classical organic chemistry. The parallelism between the behavior of nitrogen in 4-substituted pyridines and that of the corresponding carbon in substituted benzenes is illustrated in Fig. 4.

The results of Table 4 reveal another important similarity between 4-pyridine nitrogens and aromatic carbons. As is the case for the latter (1, 2, 5) σ and π populations of the ring nitrogens vary in inverse manner, the changes in π charge being predominant (Fig. 5).

Finally, the correlation between resonance shifts (35) and atomic charges of the pyridine nitrogen atoms also follows the pattern which is so well known for their aromatic carbon analogs, i.e., an upfield shift accompanying a gain in total ($\sigma + \pi$) electron population (Fig. 6). 4-Hydroxypyridine is not included in this correlation because its tautomeric equilibrium is predominantly shifted in the direction of the corresponding pyridone form (36–38). Of course, because of the linear inverse relationship between σ and π charges (Fig. 5), the correlation with total charges also implies the existence of individual linear correlations with σ and π populations, namely, upfield shifts for increasing π-electron densities, just as in the case of aromatic hydrocarbons. The latter result also follows from Pariser–Parr–Pople calculations of π charge densities reported by Witanowski *et al.* (39). All the above considerations apply equally well to the series including pyridine, 1,3-diazine, 1,4- diazine, and 1,3,5-triazine (Fig. 7), as revealed by recently determined ^{15}N spectra (40).

It is clear that solvent and concentration effects should not be disregarded in the present evaluation of charge–shift correlations. Shielding solvent effects affecting the ^{15}N resonances of pyridines, and indeed more generally of sp^2-hybridized nitrogens, are associated with hydrogen bonding to the nitrogen unshared pairs. Such hydrogen bonding changes the $n \rightarrow \pi^*$ transition energies and, hence, the paramagnetic screening that appears to be the dominant influence on the chemical shifts of these compounds (41). Because of a careful selection of suitable "standard" experimental conditions, however, these solvent effects should not impair the overall validity of the present conclusions, namely, that any gain in total charge at azine nitrogens translates into an upfield shift—in sharp contrast with

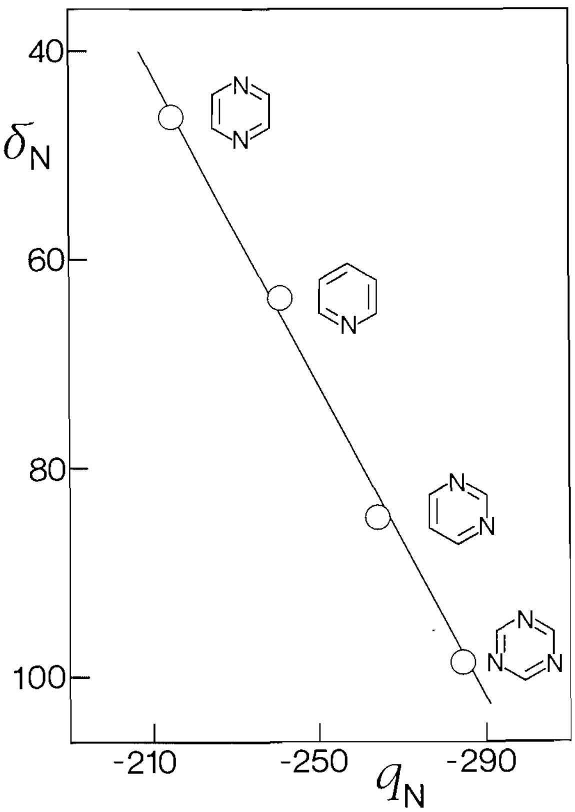

FIG. 7. Comparison between the net charges and resonance shifts of nitrogen in pyridine, 1,3-diazine, 1,4-diazine, and 1,3,5-triazine, in DMSO solution.

the results obtained for amines, nitroalkanes, and isonitriles.

Conclusions

Linear correlations between nitrogen-15 nmr shifts and atomic populations closely resemble similar empirical correlations existing for carbon-13 and oxygen-17 nuclei, namely, as regards their sign (upfield or downfield resonance shifts accompanying a gain in local charge density). Supporting evidence is offered by linear correlations involving the resonance shifts of ^{15}N nuclei and those of the corresponding carbon nuclei in analogous hydrocarbons, showing that for a large variety of substituents (i.e., over a wide chemical shift range) shielding of the ^{15}N and ^{13}C nuclei in aromatic (42) and nonaromatic (17, 24, 25, 43) systems is governed by the same electronic factors. This holds true for ^{17}O as well (44).

Nitrogen atoms contained in aromatic structures exhibit the same behavior as aromatic and ethylenic carbon atoms and carbonyl oxygen (ref. 1): an increase in total electronic population is accompanied by an upfield resonance shift when the electron enrichment results from a gain in π charge prevailing over the concurrent loss in σ electrons. On the other hand, nitrogen in alkylamines, nitroalkanes, and isonitriles behaves like typical sp^3-carbons, carbonyl carbon, and dialkyl ether oxygen atoms: any increase in total electronic population translates into a downfield resonance shift when the gain in charge is dictated by that of the σ population. For amines and nitroalkanes, STO-3G calculations indicate that charges vary in the same direction both at the 2s level (~30%) and the 2p level (~70%), whereas the 2p population remains virtually unchanged in alkylisonitriles.

Inclusion of nitrogen in a unified picture encompassing carbon and oxygen nuclei in a variety of situations hopefully paves the way to a better assessment of circumstances that may be encountered in the study of charge–shift relationships, also as regards possible drawbacks introduced by an indiscriminate use of theoretical charges. The latter, of course, depend on the basis set chosen. In addition, the inherent difficulties associated with the overlap populations of the Mulliken scheme must always be borne in mind: simply using an extended basis set is not a panacea. In our experience, the relevant trends in series of closely related compounds are, indeed, adequately described by optimized minimal basis set calculations.

In a widely accepted formulation of the local paramagnetic term (45), there are a number of variables in addition to those that may be correlated with atomic charges: thus, there is no *a priori* reason to expect good charge–shift correlations. The fact that different, but good, correlations are observed for different types of atoms is certainly of interest, moreover, as the same patterns of behavior have now been shown to exist for carbon, nitrogen, and oxygen. This observation should encourage future reexamination of the challenging question regarding the dependence of the local paramagnetic term on the local charge. In the meantime, the possibility of retrieving atomic charges from critically established empirical correlations is of interest because it opens a convenient access to the study of charge-related molecular properties, such as the energies (2).

Acknowledgements

The financial aid given by the National Research Council of Canada and the France–Quebec exchange program is gratefully acknowledged, as well as the cooperation of the Centre de Calcul de l'Université de Montréal.

1. S. FLISZÁR, G. CARDINAL, and M.-T. BÉRALDIN. J. Am. Chem. Soc. **104**, 5287 (1982), and references therein.
2. S. FLISZÁR. Charge distributions and chemical effects. Springer Verlag, New York, NY. 1983.
3. D. G. FARNUM. Adv. Phys. Org. Chem. **11**, 123 (1975); G. L. NELSON and E. A. WILLIAMS. Prog. Phys. Org. Chem. **12**, 229 (1976).
4. G. J. MARTIN, M. L. MARTIN, and S. ODIOT. Org. Magn. Reson. **7**, 2 (1975).
5. W. J. HEHRE, R. W. TAFT, and R. D. TOPSOM. Prog. Phys. Org. Chem. **12**, 159 (1976).
6. S. FLISZÁR. J. Am. Chem. Soc. **102**, 6946 (1980); S. FLISZÁR. Int. J. Quantum Chem. **24**, 743 (1984); S. FLISZÁR and G. CARDINAL. Can. J. Chem. **62**, 2748 (1984).
7. E. C. VAUTHIER, S. FLISZÁR, F. TONNARD, and S. ODIOT. Can. J. Chem. **61**, 1417 (1983).
8. W. J. HEHRE, R. F. STEWART, and J. A. POPLE. J. Chem. Phys. **51**, 2657 (1969).
9. J. S. BINKLEY, R. A. WHITESIDE, P. C. HARIHARAN, R. SEEGER, J. A. POPLE, W. J. HEHRE, and M. D. NEWTON. Program 368, Quantum Chemistry Program Exchange, University of Indiana, Chemistry Department, Bloomington, IN 47401.
10. R. S. MULLIKEN. J. Chem. Phys. **23**, 1833 (1955); **23**, 1841 (1955); **23**, 2338 (1955); **23**, 2343 (1955).
11. G. DEL RE, S. FLISZÁR, M. COMEAU, and C. MIJOULE. Can. J. Chem. **63**, 1487 (1985).
12. S. FLISZÁR, A. GOURSOT, and H. DUGAS. J. Am. Chem. Soc. **96**, 4358 (1974).
13. H. HENRY and S. FLISZÁR. J. Am. Chem. Soc. **100**, 3312 (1978).
14. C. MIJOULE, J.-M. LECLERCQ, S. ODIOT, and S. FLISZÁR. Can. J. Chem. **63**, 1741 (1985).
15. K. WATANABE, T. NAKAYAMA, and J. R. MOTTL. J. Quant. Spectrosc. Radiat. Transfer, **2**, 369 (1962).
16. M.-T. BÉRALDIN, E. C. VAUTHIER, and S. FLISZÁR. Can. J.

Chem. **60**, 106 (1982).
17. R. O. DUTHALER and J. D. ROBERTS. J. Am. Chem. Soc. **100**, 3889 (1978).
18. G. DEL RE and C. BARBIER. Croat. Chim. Acta, **57**, 787 (1984).
19. W. KOLOS. Theor. Chim. Acta, **54**, 187 (1980).
20. W. A. SOKALSKI. J. Chem. Phys. **77**, 4529 (1982).
21. J. G. M. VAN DUIJNEVELDT-VAN DE RIJDT and F. B. VAN DUIJNEVELDT. J. Mol. Struct. Theochem. **89**, 185 (1982).
22. M. WITANOWSKI, L. STEFANIAK, and H. JANUSZEWSKI. *In* Nitrogen NMR. *Edited by* M. Witanowski and G. A. Webb. Plenum Press, London, New York. 1973.
23. W. M. LITCHMAN, M. ALEI, JR., and A. E. FLORIN. J. Am. Chem. Soc. **91**, 6574 (1969); M. ALEI, JR., A. E. FLORIN, and W. M. LITCHMAN. J. Am. Chem. Soc. **92**, 4828 (1970).
24. R. O. DUTHALER and J. D. ROBERTS. J. Magn. Reson. **34**, 129 (1979).
25. R. L. LICHTER and J. D. ROBERTS. J. Am. Chem. Soc. **94**, 2495 (1972).
26. R. O. DUTHALER, K. L. WILLIAMSON, D. D. GIANNINI, W. H. BEARDEN, and J. D. ROBERTS. J. Am. Chem. Soc. **99**, 8406 (1977).
27. M. WITANOWSKI and L. STEFANIAK. J. Chem. Soc. B, 1061 (1967).
28. M. WITANOWSKI, T. URBANSKI, and L. STEFANIAK. J. Am. Chem. Soc. **86**, 2568 (1964).
29. W. J. HEHRE and J. A. POPLE. J. Am. Chem. Soc. **92**, 2191 (1970).
30. M. WITANOWSKI. Tetrahedron, **23**, 4299 (1967); E. F. MOONEY and P. H. WINSON. Ann. Rep. NMR Spectrosc. **2**, 125 (1969).
31. J. A. POPLE and M. GORDON. J. Am. Chem. Soc. **89**, 4253 (1967).
32. B. BAK, L. HANSEN-NYGAARD, and J. RASTRUP-ANDERSEN. J. Mol. Spectrosc., **2**, 361 (1958).
33. J. E. DEL BENE. J. Am. Chem. Soc. **101**, 6184 (1979).
34. W. J. HEHRE, L. RADOM, and J. A. POPLE. J. Am. Chem. Soc. **94**, 1496 (1972).
35. M. WITANOWSKI, T. SALUVERA, L. STEFANIAK, H. JANUSZEWSKI, and G. A. WEBB. Mol. Phys. **23**, 1071 (1972).
36. M. J. SCANLAN, I. H. HILLIER, and A. A. MACDOWELL. J. Am. Chem. Soc. **105**, 3568 (1983).
37. P. BEAK, F. S. FRY, JR., J. LEE, and F. STEELE. J. Am. Chem. Soc. **98**, 171 (1976).
38. M. CIGNITTI and L. PAOLONI. Gazz. Ital. **108**, 491 (1978).
39. M. WITANOWSKI, L. STEFANIAK, H. JANUSZEWSKI, and G. A. WEBB. Tetrahedron, **27**, 3129 (1971).
40. L. STEFANIAK, J. D. ROBERTS, M. WITANOWSKI, and G. A. WEBB. Org. Magn. Reson. **22**, 201 (1984).
41. R. O. DUTHALER and J. D. ROBERTS. J. Am. Chem. Soc. **100**, 4969 (1978).
42. W. STÄDELI and W. VON PHILIPSBORN. Org. Magn. Reson. **15**, 106 (1981).
43. R. O. DUTHALER and J. D. ROBERTS. J. Am. Chem. Soc. **100**, 3882 (1978).
44. C. DELSETH and J.-P. KINTZINGER. Helv. Chim. Acta, **61**, 1327 (1978); **59**, 466 (1976); **59**, 1411 (1976).
45. J. A. POPLE. J. Chem. Phys. **37**, 53 (1963).

Studies related to the synthesis of dimethyl tetracyclo[5.2.1.0^{2,6}.0^{3,8}]decane-7,8-dicarboxylate

PELAYO CAMPS[1]
Departamento de Química Orgánica, Facultad de Farmacia, Universidad de Valencia, Valencia, Spain

JOSÉ ALIAGA, MARTA FIGUEREDO, AND ROSA MARÍA ORTUÑO
Departamento de Química Orgánica, Facultad de Ciencias, Universidad Autónoma de Barcelona, Bellaterra, Barcelona, Spain

ANTONIO GIL DE GÓMEZ AND MARÍA TERESA SANTOS
Departamento de Química Orgánica, Facultad de Ciencias Químicas, Universidad del País Vasco, San Sebastián, Guipúzcoa, Spain

JOAN CASTAÑÉ
Departamento de Investigación, Menadiona S.A., Palafolls, Barcelona, Spain

AND

MIGUEL FELIZ
Departamento de Química Orgánica, Facultad de Ciencias Químicas, Universidad de Barcelona, Barcelona, Spain

Received December 4, 1984

PELAYO CAMPS, JOSÉ ALIAGA, MARTA FIGUEREDO, ROSA MARÍA ORTUÑO, ANTONIO GIL DE GÓMEZ, MARÍA TERESA SANTOS, JOAN CASTAÑÉ, and MIGUEL FELIZ. Can. J. Chem. **63**, 3233 (1985).

A synthesis of dimethyl tetracyclo[5.2.1.0^{2,6}.0^{3,8}]decane-7,8-dicarboxylate, **3**, whose key step implies the formation of the C1—C2 bond by regioselective intramolecular C—H insertion of a carbene generated from dimethyl (1*R*,2*S*,6*R*,7*S*)-10-oxotricyclo[5.2.1.0^{2,6}]decane-2,6-dicarboxylate, **1** via its tosylhydrazone, is described. Attempts to synthesize diester **3** or compounds containing its carbon skeleton, by forming the same C—C bond, starting from dimethyl (1*R*,2*R*,6*S*,7*S*)-4-oxotricyclo[5.2.1.0^{2,6}]decane-2,6-dicarboxylate, **2**, or the corresponding anhydride, **13**, are also included.

PELAYO CAMPS, JOSÉ ALIAGA, MARTA FIGUEREDO, ROSA MARÍA ORTUÑO, ANTONIO GIL DE GÓMEZ, MARÍA TERESA SANTOS, JOAN CASTAÑÉ et MIGUEL FELIZ. Can. J. Chem. **63**, 3233 (1985).

On décrit une synthèse du tétracyclo[5.2.1.0^{2,6}.0^{3,8}] décane dicarboxylate-7,8 de diméthyle (**3**) dont l'étape clé implique la formation d'une liaison C1—C2 par une insertion C—H intramoléculaire régiosélective d'un carbène généré, par le biais de sa tosylhydrazone, à partir de l'oxo-10 tricyclo[5.2.1.0^{2,6}] décane dicarboxylate de diméthyle-1*R*,2*S*,6*R*,7*S* (**1**). On a aussi inclus la description d'essais effectués dans le but de synthétiser le diester **3**, ou des composés contenant son squelette carboné, en faisant appel à la formation de la même liaison C—C à partir de l'oxo-4 tricyclo[5.2.1.0^{2,6}] décane dicarboxylate de diméthyle-1*R*,2*R*,6*S*,7*S*, **2**, ou de l'anhydride correspondant, **13**.

[Traduit par le journal]

Recently, Paquette *et al.* have published the first syntheses of dodecahedrane (1) and its methyl (2) and 1,16-dimethyl derivatives (3), the first compounds containing such a type of carbocyclic skeleton. The synthesis of dodecahedrane, however, implies 23 consecutive steps from cyclopentadiene, the overall yield being in the range of 0.1%, which limits its supply. Consequently it is still a challenge to obtain it through a shorter and higher yielding sequence (4).

As part of our contribution to polyquinane chemistry (5–7), we describe herein the studies that have led to the successful synthesis of dimethyl tetracyclo[5.2.1.0^{2,6}.0^{3,8}]decane-7,8-dicarboxylate, **3**, a possible intermediate for a convergent synthesis of dodecahedrane.

The retrosynthetic analysis of diester **3** shows that cleavage of the strategic (8) C1—C2 bond gives the well-known tricyclo[5.2.1.0^{2,6}]decane skeleton, in contrast with other cleavages, which give precursors that are not easily accessible. Since the C1 and C2 atoms and their neighbours in compound **3** have no functionality, intramolecular C—H insertion of a carbene was considered to be the reaction of choice to form the C1—C2 bond. As shown in Scheme 1, there exist two ways to carry out such a transformation, depending on the carbon atom at which the carbene is generated. In fact, Neff and Nordlander (9) had utilized the first way in order to synthesize tetracyclo[5.2.1.0^{2,6}.0^{3,8}]decane from tricyclo[5.2.1.0^{2,6}]decan-10-one.

Because the synthesis of dimethyl (1*R*,2*R*,6*S*,7*S*)-4-oxotricyclo[5.2.1.0^{2,6}]decane-2,6-dicarboxylate, **2**, appeared to be easier (5) than that of dimethyl (1*R*,2*S*,6*R*,7*S*)-10-oxotricyclo[5.2.1.0^{2,6}]decane-2,6-dicarboxylate, **1**, and because we were looking for a new entry into this carbocyclic skeleton (9, 10), we undertook the preparation of ketodiester **2** through the sequence depicted in Scheme 2.

The starting product for this synthesis was bicyclo[2.2.1]hept-2-ene-2,3-dicarboxylic anhydride, **4** (11). Reaction of anhydride **4** with excess butadiene gave (1*R*,2*R*,7*S*,8*S*)-tricyclo[6.2.1.0^{2,7}]undec-4-ene-2,7-dicarboxylic anhydride, *5*, in 81% yield. This compound had been previously prepared by Alder and Backendorf (12), but its configuration was not established. However, owing to the fact that reaction of bicyclo[2.2.1]hepta-2,5-diene-2,3-dicarboxylic anhydride with butadiene (13) gives a 1:1 mixture of the *endo* and *exo* adducts, it seems reasonable that anhydride **4**, with the C4—C5 bond

[1]Author to whom correspondence may be addressed.

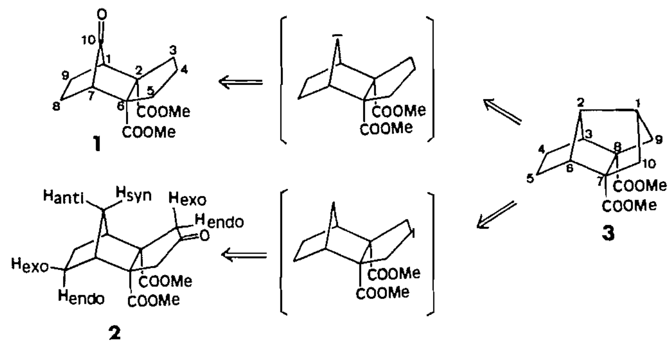

SCHEME 1

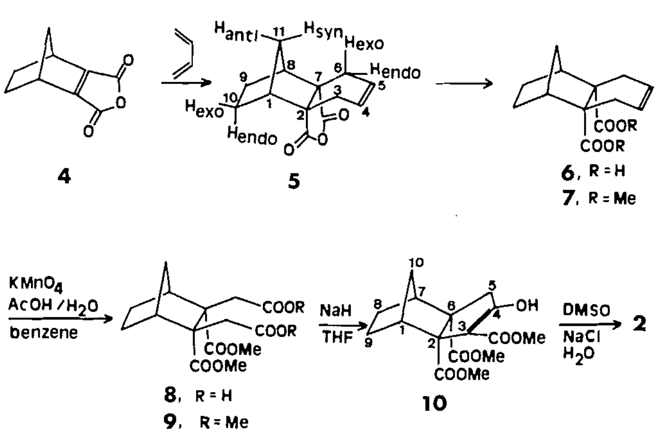

SCHEME 2

saturated, would give mainly the *exo* adduct **5** on reaction with butadiene, whether the control of the reaction is kinetic or thermodynamic. Saponification of anhydride **5** gave the corresponding diacid **6**, a compound that readily reverts to its anhydride. Thus, a solid sample of diacid **6** after several days at room temperature gave anhydride **5** nearly quantitatively, and the observed mp for diacid **6** was the same as that for anhydride **5**. For this reason, diacid **6** was esterified with an ethereal solution of diazomethane immediately after its preparation, giving rise to dimethyl (1*R*,2*R*,7*S*,8*S*)-tricyclo[6.2.1.0^{2,7}]-undec-4-ene-2,7-dicarboxylate, **7**, contaminated with a small quantity (less than 10%) of anhydride **5**. Low pressure column chromatography (14) using silica gel (230–400 mesh) and methylene chloride as eluent gave pure diester **7** (96% yield if **5** was recovered). The comparison of the 200-MHz ^{1}H nmr spectra of anhydride **5** and diester **7** showed that the H9(10)*endo* protons of **7** are deshielded by 0.45 ppm with respect to **5**. This fact is in accord with the assumed configuration of anhydride **5**, since the change of its rigid anhydride function by the freely rotating methoxycarbonyl groups of **7** must deshield the H9(10)*endo* protons, due to the contribution of conformations in which the carbonyl oxygen atoms are close to these protons (6, 15).

Oxidation of diester **7** with potassium permanganate under the phase transfer conditions described by Krapcho *et al.* (16) gave dimethyl (1*R*,2*R*,3*S*,4*S*)-2,3-bishydroxycarbonylmethylbicyclo[2.2.1]heptane-2,3-dicarboxylate, **8**, in low yield (less than 30%). The analytical sample was obtained by crystallization from ether. For preparative purposes, the crude diacid **8** was directly esterified with ethereal solution of diazomethane to give, after crystallization from methanol, pure dimethyl (1*R*,2*R*,3*S*,4*S*)-2,3-bismethoxycarbonylbicyclo[2.2.1]heptane-

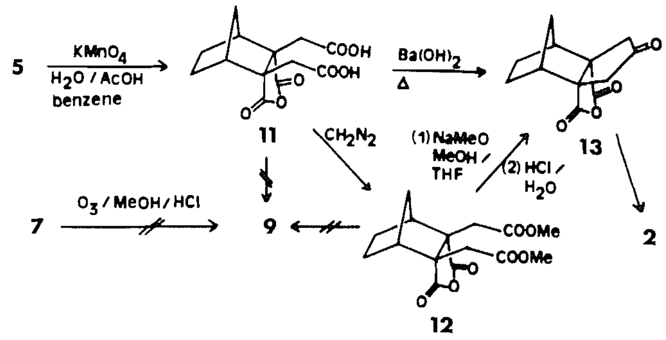

SCHEME 3

2,3-diacetate, **9**, in 13% overall yield from diester **7**. The low yield oxidation of diester **7** contrasts with the high yield (75%) oxidation of the related compound, dimethyl *cis*-bicyclo-[4.3.0]non-3-ene-1,6-dicarboxylate, under similar reaction conditions (5). However, several attempts to increase the yield of that oxidation were fruitless.

Reaction of tetraester **9** with excess sodium hydride in anhydrous tetrahydrofuran gave trimethyl (1*RS*,2*RS*,6*SR*,7*SR*)-4-hydroxytricyclo[5.2.1.0^{2,6}]dec-3-ene-2,3,6-tricarboxylate, **10**, in 99% yield. This compound exists mainly in the indicated enol form, as shown by its spectroscopic data (ir, ^{1}H and ^{13}C nmr). Decarbomethoxylation of compound **10** was easily achieved using the Krapcho and Lovey reaction conditions (17), giving rise to ketodiester **2** in 88% yield.

Since the yield of the described conversion of anhydride **5** into ketodiester **2** was very low, the transformations shown in Scheme 3 were carried out in order to increase it.

Oxidation of anhydride **5** with potassium permanganate, under the same phase transfer conditions utilized to oxidize diester **7**, gave (1*R*,2*R*,3*S*,4*S*)-2,3-bishydroxycarbonylmethylbicyclo[2.2.1]heptane-2,3-dicarboxylic anhydride, **11**, in 83% yield. This unexpected result opened the possibility of developing a higher yielding synthesis of ketodiester **2**. Conversion of compound **11** into tetraester **9** seemed the most obvious way. However, all attempts to carry out such a transformation were fruitless. Alkaline hydrolysis of **11** followed by reaction with excess dimethyl sulfate in dimethyl formamide gave, quantitatively, (1*R*,2*R*,3*S*,4*S*)-2,3-bismethoxycarbonylmethylbicyclo[2.2.1]heptane-2,3-dicarboxylic anhydride, **12**. Probably **12** is formed from the corresponding diacid during the work-up. Compound **12** was also prepared in 86% yield by esterification of **11** with an ethereal solution of diazomethane. Attempted esterification of the tetraacid corresponding to **11** with diazomethane gave, quantitatively, diester **12**. Reaction of **12** with one equivalent of sodium methoxide in methanol followed by acidification and treatment with an ethereal solution of diazomethane gave the starting product, probably reformed during acidification.

Pyrolysis of an intimate mixture of compound **11** and barium hydroxide gave (1*R*,2*R*,6*S*,7*S*)-4-oxotricyclo[5.2.1.0^{2,6}]decane-2,6-dicarboxylic anhydride, **13**, in only 25% yield. However, compound **13** could be obtained in 60% yield by reaction of compound **12** with 12 equivalents of sodium hydride in a mixture of anhydrous tetrahydrofuran and methanol, followed by heating the crude product under reflux with aqueous hydrochloric acid 1 : 1. Alkaline hydrolysis of ketoanhydride **13** gave the corresponding diacid, which was esterified with an ethereal solution of diazomethane to give ketodiester **3** in 73% yield. Thus, the overall yield for the conversion of anhydride **5** into

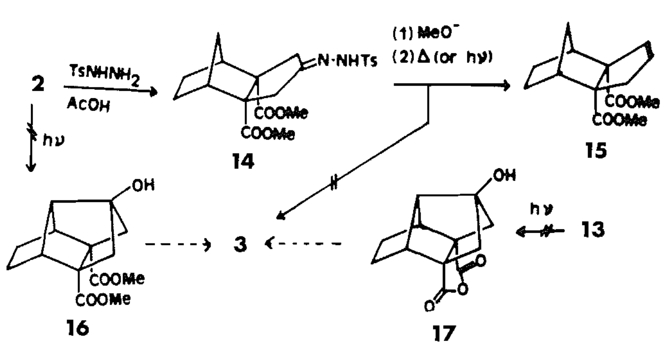

SCHEME 4

ketodiester **2** was 33%. An attempt to convert diester **7** directly into tetraester **9** by ozonolysis (18) in methanol solution containing 10% hydrogen chloride was fruitless.

According to the retrosynthetic analysis shown in Scheme 1, insertion of the intermediate carbene generated from the ketonic function of compound **2** into the C10—H_{syn} bond would give diester **3**. To carry out such a transformation, the Bamford–Stevens reaction (19) was chosen (see Scheme 4).

Reaction of ketodiester **2** with tosylhydrazide in glacial acetic acid gave the corresponding tosylhydrazone, dimethyl (1*R*,2*R*,6*S*,7*S*)-4-(*p*-toluenesulfonylhydrazono)tricyclo-[5.2.1.$0^{2,6}$]decane-2,6-dicarboxylate, **14**, in 78% yield. The sodium salt of **14** was obtained by heating under reflux a solution of **14** and a slight molar excess of sodium methoxide in anhydrous methanol. Pyrolysis of the dried sodium salt of **14** in a rotary microdistillation apparatus at 136°C/0.1 Torr (1 Torr = 133.3 Pa) gave in 93% yield a single compound, which was characterized as dimethyl (1*RS*,2*RS*,6*SR*,7*SR*)-tricyclo-[5.2.1.$0^{2,6}$]dec-3-ene-2,6-dicarboxylate, **15**. A similar result was obtained by pyrolysis of the lithium salt of **14** following the procedure described by Neff and Nordlander (9) for a related case. Photochemical decomposition of the sodium salt of **14** in a Pyrex reactor utilizing a 125-W uv lamp, in dimethoxyethane as solvent, gave a mixture of compound **15** and ketodiester **2** (probably formed by hydrolysis of the sodium salt of **14** under the reaction conditions) in the ratio 2:5, as shown by glc/ms analysis. Formation of diester **3** was not observed in all these reactions. These results must be related to the preference of the intermediate carbene, whether generated thermally or photochemically, to experience insertion at a neighbouring C—H bond rather than at the C10—H_{syn} one. Consequently, the use of other methods to generate the intermediate carbene from ketodiester **2** was not considered.

Another approach to the carbocyclic skeleton of **3** from diester **2** might be the ketone to cyclopentanol photocyclization reaction utilized three times by Paquette (1) in his synthesis of dodecahedrane (see Scheme 4). However, irradiation of ketodiester **2**, in benzene solution for 40 h utilizing a 400-W uv quartz lamp, left the starting product unchanged, while by utilizing a mixture benzene/*tert*-butyl alcohol 5:1 as solvent, the formation of a new compound, probably by addition of *tert*-butyl alcohol to **2**, was observed (glc/ms). Similar results were obtained on irradiation of ketoanhydride **13**. Formation of hydroxydiester **16** or hydroxyanhydride **17** could not be detected in all these reactions.

Just after this work had been finished, Trost and Renaut (20) published a synthesis of (±)-albene, in which the compounds **2** and **15** were prepared by an entirely different approach.

In view of the preceding results, we prepared ketodiester **1** in a non-stereoselective way from the *endo* adduct between 6,6-dimethylfulvene and cyclopent-1-ene-1,2-dicarboxylic anhydride (6). Moreover, a stereoselective synthesis of compound **1** was carried out from the Diels–Alder adduct, **18**, between 5,5-diethoxycyclopentadiene and *N*-phenylmaleimide, as shown in Scheme 5 (published as a preliminary communication (7)).

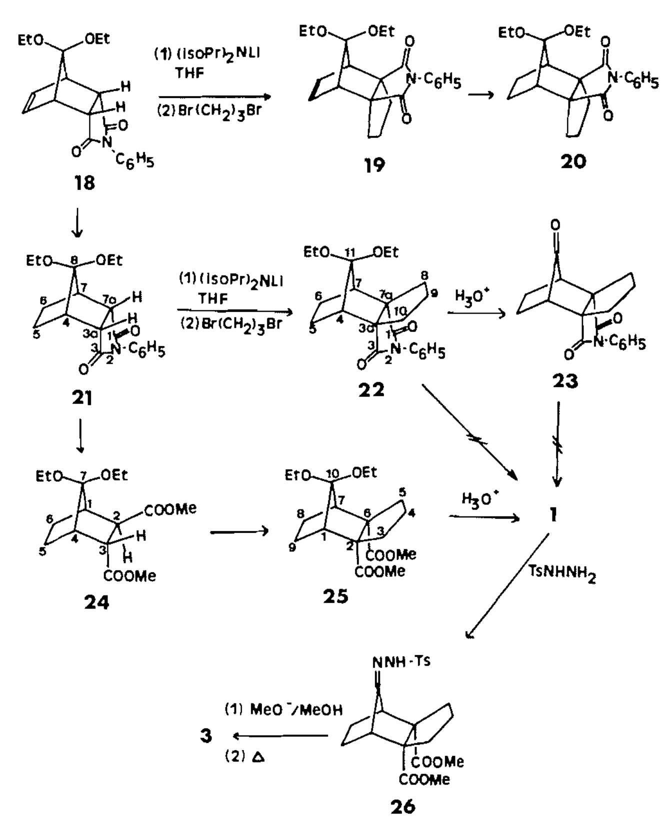

SCHEME 5

While annelation of the dianion derived from adduct **18** with 1,3-dibromopropane takes place mainly by the *endo* face (21) to give dicarboximide **19**, the corresponding reaction of the dianion derived from (3a*R*,4*S*,7*R*,7a*S*)-8,8-diethoxy-2-phenyl-3a,5,6,7a-tetrahydro-1*H*,3*H*-4,7-methanoisoindol-1,3-dione, **21**, takes place preferently by the *exo* face to give (3a*R*,4*S*,7*R*,7a*S*)-11,11-diethoxy-5,6-dihydro-2-phenyl-1*H*,3*H*-4,7-methano-3a,7a-propanoisoindol-1,3-dione, **22**. The configuration of compound **22** was clearly established (7) by comparison of its ^{13}C nmr spectrum with that of (3a*R*,4*R*,7*S*,7a*S*)-11,11-diethoxy-5,6-dihydro-2-phenyl-1*H*,3*H*-4,7-methano-3a,7a-propanoisoindol-1,3-dione, **20**, obtained by hydrogenation of compound **19**.

The conversion of dicarboximide **22** into ketodiester **1** required only two transformations: (a) hydrolysis of the acetal function, and (b) hydrolysis of the dicarboximide group followed by esterification. While the first transformation could be easily carried out by reaction of **22** with aqueous perchloric acid, giving rise to (3a*R*,4*S*,7*R*,7a*S*)-5,6-dihydro-2-phenyl-1*H*,3*H*-4,7-methano-3a,7a-propanoisoindol-1,3,11-trione, **23**, in 95% yield, we were able to hydrolyze the dicarboximide function of neither compound **22** nor **23**, under a variety of basic and acidic conditions.

The synthesis of ketodiester **1** from dicarboximide **21** was achieved by carrying out first the hydrolysis of the dicarboximide function and then the annelation with 1,3-dibromopropane. Thus, basic hydrolysis of compound **21**, followed by esterification of the corresponding diacid with an ethereal solution of diazomethane, gave dimethyl (1*RS*,2*RS*,3*RS*,4*SR*)-7,7-diethoxybicyclo[2.2.1]heptane-2,3-dicarboxylate, **24**, slightly contaminated with the *meso* stereoisomers, in 60% yield. Reaction of the dianion derived from diester **24** with 1,3-dibromopropane gave dimethyl (1*R*,2*S*,6*R*,7*S*)-10,10-diethoxytricyclo[5.2.1.$0^{2,6}$]decane-2,6-dicarboxylate, **25**, in 29% yield (22), which was easily converted into ketodiester **1** in 83% yield by reaction with aqueous perchloric acid. This compound was identical (mp, mixed mp, glc, ir, and ^{1}H nmr) to the product we had previously obtained (6), confirming the expected annelation of the dianion derived from diester **24** by the *exo* face.

Reaction of ketodiester **1** with tosylhydrazide under the conditions utilized to prepare tosylhydrazone **14** left the starting product unchanged. However, by heating under reflux for 28 h an equimolar mixture of ketodiester **1** and tosylhydrazide in isopropanol to which a catalytic amount of concentrated hydrochloric acid was added, dimethyl (1*R*,2*S*,6*R*,7*S*)-10-(*p*-toluenesulfonylhydrazono)tricyclo[5.2.1.$0^{2,6}$]decane-2,6-dicarboxylate, **26**, was obtained in 75% yield. Reaction of tosylhydrazone **26** with sodium methoxide in anhydrous methanol gave the corresponding sodium salt, which after drying was pyrolyzed at 170°C/1 Torr. The distillate was shown to be mainly a unique compound (glc, 97% relative area, 89% yield) that, crystallized from isopropanol, showed mp 62–63°C. The spectroscopic data (ir, ^{1}H and ^{13}C nmr, and ms) and elemental analysis were concordant with expectations for diester **3**. In particular, the ^{13}C nmr spectrum clearly showed its symmetry (eight carbon resonances), thus ruling out other possible products derived from the insertion of the intermediate carbene into C—H bonds different from the C4—H.

The synthesis of diester **3** opens a rapid access to complex polyquinanes, a matter that is currently being investigated.

Experimental

Infrared spectra were recorded on Perkin–Elmer model 710B, 720, or 1310 spectrometers. The ^{1}H and ^{13}C nmr spectra, unless otherwise stated, were taken at 200 MHz and 50 MHz respectively, on a Varian XL 200 spectrometer, while 80-MHz ^{1}H and 20-MHz ^{13}C nmr spectra were recorded on a Bruker model WP80SY, and 60-MHz ^{1}H nmr spectra on a Perkin–Elmer R-12A spectrometer. Chemical shifts are given in ppm relative to internal TMS (δ scale). Mass spectra and glc/ms analyses were performed on a Hewlett–Packard model 5930 mass spectrometer working at 70 eV. Gas–liquid chromatographic (glc) analyses were carried out on Perkin–Elmer models Sigma-1 and Sigma 3B and Hewlett–Packard model 5830A chromatographs. Medium pressure 125- or 400-W mercury lamps were utilized in the photochemical reactions. Melting points were determined on a Kofler hot-stage or on a Büchi SMP-20 apparatus and are uncorrected. Microanalyses were carried out at the Analytical Section of the "Instituto de Química Bio-orgánica de Barcelona (C.S.I.C.)", Spain.

Spectral data of (1R,2R,7S,8S)-tricyclo[6.2.1.$0^{2,7}$]undec-4-ene-2,7-dicarboxylic anhydride, 5

Proton nmr ($CDCl_3$)δ: 1.42 (m, 2H, H9(10)*endo*), 1.56 (br d, J = 11 Hz, 1H, H11*anti*), 1.61 (m, 2H, H9(10)*exo*), 1.96 (d, J = 15 Hz, H3(6)*exo*), 2.02 (br d, J = 11 Hz, 1H, H11*syn*), 2.43 (br s, 2H, H1(8)), 2.75 (ddd, J = 15 Hz, J' = 5 Hz, J'' = 3.5 Hz, 2H, H3(6)*endo*), 5.85 (m, 2H, H4(5)). On irradiation at δ 2.43, the absorption at δ 2.02 became a dt, J = 11 Hz, J' = 2.5 Hz; ^{13}C nmr ($CDCl_3$) δ: 25.9 (t, C9(10)), 29.5 (t, C3(6)), 39.3 (t, C11), 47.2 (d, C1(8)), 60.4 (s, C2(7)), 127.8 (d, C4(5)), 175.8 (s, —*C*OO—).

Dimethyl (1R,2R,7S,8S)-tricyclo[6.2.1.$0^{2,7}$]undec-4-ene-2,7-dicarboxylate, 7

A mixture of 6.63 g (30.4 mmol) of anhydride **5**, 3.0 g (75 mmol) NaOH, and 25 mL water was heated under reflux for 4 h. The solution was cooled in an ice bath, 10 g ice was added, and then it was acidified with 6 *N* HCl. The precipitate was filtered and the filtrate extracted with ether (2 × 20 mL). The ether extracts and the precipitate were combined and, immediately after, treated with an ethereal solution of diazomethane until the yellow colour of diazomethane persisted. Evaporation of the volatile products from the dried solution (anhydrous Na_2SO_4) gave 7.75 g of a mixture of diester **7** and starting anhydride. This mixture was chromatographed through 120 g silica gel (230–400 mesh) using a slight overpressure (14) and CH_2Cl_2 as eluent to give 7.01 g of **7** and 0.60 g of **5**. Yield of **7**, if **5** was recovered, 96%. A sample of **7** crystallized from hexane showed mp 71–73°C; ir ($CHCl_3$) ν: 1730 (s) cm^{-1}; ^{1}H nmr ($CDCl_3$) δ: 1.34 (br d, J = 10 Hz, 1H, H11*anti*), 1.48 (m, 2H, H9(10)*exo*), 1.87 (m, 2H, H9(10)*endo*), 2.03 (d, J = 15 Hz, 2H, H3(6)*exo*), 2.19 (br d, J = 10 Hz, 1H, H11*syn*), 2.27 (br s, 2H, H1(8)), 2.58 (ddd, J = 15 Hz, J' = 4 Hz, J'' = 2.5 Hz, 2H, H3(6)*endo*), 3.60 (s, 6H, —OCH_3), 5.90 (m, 2H, H4(5)). On irradiation at δ 2.27, the absorption at δ 1.34 became a sharp doublet and that at δ 2.19, a dt, J = 10 Hz, J' = 2.5 Hz. On irradiation at δ 1.48, the absorption at δ 1.87 became a doublet J = 2.5 Hz; ^{13}C nmr ($CDCl_3$) δ: 25.8 (t, C9(10)), 33.5 (t, C3(6)), 37.1 (t, C11), 49.6 (d, C1(8)), 51.4 (q, —OCH_3), 58.7 (s, C2(7)), 127.3 (d, C4(5)), 175.2 (s, —*C*OOMe). *Anal.* calcd. for $C_{15}H_{20}O_4$: C 68.16, H 7.63; found: C 68.36, H 7.79.

Dimethyl (1R,2R,3S,4S)-2,3-bishydroxycarbonylmethylbicyclo-[2.2.1]heptane-2,3-dicarboxylate, 8

To a cold (0°C) solution of 0.41 g (2.0 mmol) $KMnO_4$ in 5 mL water, 200 mg (0.76 mmol) diester **7** in 10 mL benzene, 3 mg tetra-*n*-butylammonium bromide, and 3 mL glacial acetic acid were added, and the mixture vigorously stirred magnetically at room temperature for 16 h. The mixture was cooled in an ice bath, 445 mg (3.5 mmol) Na_2SO_3 was added at once, and then, 0.9 mL 6 *N* HCl dropwise and with stirring, the final solution being slightly acidic. The organic phase was separated and the aqueous one extracted with benzene (5 × 4 mL). The organic phase and the benzene extracts were combined and washed with water (1 × 2 mL). Evaporation of the solvent from the dried extracts (anhydrous Na_2SO_4) gave 130 mg of an unidentified residue. The aqueous phase was extracted with ether (5 × 6 mL), and the combined ether extracts washed with water (1 × 2 mL) and dried over anhydrous Na_2SO_4. Evaporation of the volatile products gave 80 mg of a product consisting mainly of diacid **8**. Crystallization from ether gave pure **8**, mp 163–167°C (dec.); ir (KBr) ν: 3600–2400 (s), 1740 (s), 1710 (s) cm^{-1}; 60-MHz ^{1}H nmr (acetone-d_6) δ: 1.20–1.90 (m, 6H), 2.62 (m, 2H, H2(3)), 2.84 (s, 4H, —CH_2COOH), 3.60 (s, 6H). *Anal.* calcd. for $C_{15}H_{20}O_8$: C 54.88, H 6.14; found: C 54.94, H 6.28.

Dimethyl (1R,2R,3S,4S)-2,3-bismethoxycarbonylbicyclo[2.2.1]-heptane-2,3-diacetate, 9

An ethereal solution of diazomethane was added to 2.9 g of crude **8** (obtained from 7 g diester **7** as described before) until the yellow colour persisted. Evaporation of the dried solution (anhydrous Na_2SO_4) gave 2.6 g of a product that crystallized from methanol, yielding 1.2 g of pure **9**, bp 160–165°C (oven)/0.1 Torr, mp 109–110°C. Evaporation of the mother liquors of crystallization gave a residue whose ^{1}H nmr spectrum showed that it did not contain more **9**. Total yield of **9** from diester **7**, 13%; ir ($CHCl_3$) ν: 1750 (s), 1740 (s) cm^{-1}; ^{1}H nmr ($CDCl_3$) δ: 1.34 (dm, J = 10.8 Hz, 1H, H7*anti*), 1.42–1.56 (m, 2H, H5(6)*exo*), 1.80–1.94 (m, 3H, H5(6)*endo* and H7*syn*), 2.45 (br s, 2H, H1(4)), 2.78 (s, 4H, —CH_2COOMe), 3.67 (s, 6H), 3.69 (s, 6H); ^{13}C nmr ($CDCl_3$) δ: 24.7 (t, C5(6)), 35.7 (t, C7), 40.4 (t, —CH_2COOMe), 47.3 (d, C1(4)), 51.7 (q) and 51.9 (q) (—COOCH_3), 57.6 (s, C2(3)), 170.9 (s, —CH_2—*C*OOMe), 173.1

(s, —C—COOMe). *Anal.* calcd. for $C_{17}H_{24}O_8$: C 57.30, H 6.79; found: C 57.23, H 6.77.

Trimethyl (1RS,2RS,6SR,7SR)-4-hydroxytricyclo[5.2.1.0^{2,6}]dec-3-ene-2,3,6-tricarboxylate, ***10***

In a 50-mL flask was placed 185 mg NaH (70% in mineral oil, 5.4 mmol). After washing with anhydrous THF (3 × 10 mL), the solid was covered with a small volume of the same solvent, and the mixture cooled in an ice bath. A solution of 600 mg tetraester **9** (1.69 mmol) in 20 mL anhydrous THF was added with care, a reflux condenser with a $CaCl_2$ tube was adapted to the flask, and the reaction mixture heated under reflux for 3 h. The mixture was cooled to 0°C and treated with 6 *N* HCl until neutral pH, then made slightly acidic with 0.1 *N* HCl. The organic phase was separated and the aqueous one extracted with $CHCl_3$ (4 × 7 mL). The extracts and the organic phase were combined, washed with water (2 × 2 mL), and dried over anhydrous Na_2SO_4. Evaporation of the solvent from the extracts gave 544 mg (1.68 mmol) of **10** as a viscous liquid that solidified on standing, bp 140–145°C (oven)/0.1 Torr, mp 105–108°C (methanol), 99% yield. Gas–liquid chromatographic analysis (column SE-30, 2 m; oven temperature 180°C; injector temperature 200°C; flow 20 mL N_2/min) of this compound gave a unique signal whose rt (retention time) (4.04 min) was the same as ketodiester **2**, showing that decarbomethoxylation of **10** to **2** took place in the injection chamber. Infrared ($CHCl_3$) ν: 3600–2850 (m), 1740 (s), 1660 (s), 1620 (m) cm^{-1}; ^{1}H nmr ($CDCl_3$) δ: 1.20–1.45 (m, 3H, H8*exo*, H9*exo*, and H10*anti*), 1.50–1.80 (m, 2H, H8*endo* and H9*endo*), 2.21 (br s, 1H, H7), 2.46 (m, 1H, H10*syn*), 2.58 (d, *J* = 19 Hz, 1H) and 3.36 (d, *J* = 19 Hz, 1H) (H5*exo* and H5*endo*), 2.65 (br s, 1H, H1), 3.60 (s, 3H), 3.69 (s, 3H), 3.74 (s, 3H); ^{13}C nmr ($CDCl_3$) δ: 23.3 (t, C8), 26.4 (t, C9), 35.7 (t, C10), 42.8 (d, C7), 43.2 (t, C5), 50.6 (d, C1), 51.4 (q), 51.5 (q), and 52.0 (q) (—O—CH_3), 58.5 (s, C6), 64.3 (s, C2), 104.4 (s, C3), 168.9 (s, C4), 173.0 (s), 173.4 (s), and 176.0 (s) (—*C*OOMe). *Anal.* calcd. for $C_{16}H_{20}O_7$: C 59.25, H 6.22; found: C 59.85, H 6.41.

Dimethyl (1R,2R,6S,7S)-4-oxotricyclo[5.2.1.0^{2,6}]decane-2,6-dicarboxylate, ***2***

A mixture of 544 mg (1.68 mmol) of **10**, 100 mg NaCl (1.7 mmol), 100 mg water (5.6 mmol), and 10 mL DMSO was heated at 120°C with magnetic stirring for 2 h. To the cold (room temperature) mixture, 25 mL water was added, and then it was extracted with $CHCl_3$ (5 × 10 mL). The chloroform extracts were combined, washed with water (3 × 7 mL), and dried over anhydrous Na_2SO_4. Evaporation of the volatile products and distillation of the residue in a microdistillation apparatus gave 395 mg of **2** (1.48 mmol, 88% yield), bp 120°C (oven)/0.1 Torr, mp 84–88°C (methanol/water); ir ($CHCl_3$) ν: 1740 (s) cm^{-1}; ^{1}H nmr ($CDCl_3$) δ: 1.30–1.60 (m, 4H, H10*syn*, H10*anti*, and H8(9)*exo*), 1.68–1.82 (m, 2H, H8(9)*endo*), 2.28 (br s, 2H, H1(7)), 2.34 (d, *J* = 19.8 Hz, 2H), 2.98 (d, *J* = 19.8 Hz, 2H) (H3(5)*exo* and H3(5)*endo*), 3.62 (s, 6H); ^{13}C nmr ($CDCl_3$) δ: 25.0 (t, C8(9)), 35.5 (t, C10), 48.5 (d, C1(7)), 50.1 (t, C3(5)), 51.9 (q, —O—CH_3), 59.1 (s, C2(6)), 174.0 (s, —*C*OOMe), 214.5 (s, C4). *Anal.* calcd. for $C_{14}H_{18}O_5$: C 63.15, H 6.81; found: C 62.92, H 6.79.

(1R,2R,3S,4S)-2,3-bishydroxycarbonylmethylbicyclo[2.2.1]-heptane-2,3-dicarboxylic anhydride, ***11***

To a cold solution (0°C) of 2.48 g (15.7 mmol) $KMnO_4$ in 25 mL water, a solution of 1.0 g (4.6 mmol) anhydride **5** in 75 mL benzene, 16 mg tetra-*n*-butylammonium bromide, and 17 mL glacial acetic acid were added. The mixture was efficiently stirred magnetically at room temperature for 16 h. After cooling in an ice bath, 2.7 g (21.4 mmol) Na_2SO_3 was added at once and then, dropwise and with stirring, 5.5 mL 6 *N* HCl, the final pH being slightly acidic. The organic phase was separated and the aqueous one extracted with benzene (2 × 10 mL). The benzene extracts and the organic phase were combined, washed with water (1 × 2 mL), and dried over anhydrous Na_2SO_4. Evaporation of the solvent yielded 40 mg of an unidentified residue. The aqueous phase was extracted with ether (5 × 20 mL) and the combined ether extracts were washed with water (1 × 2 mL) and dried over anhydrous Na_2SO_4. Evaporation of the solvent left a residue that was dried in a desiccator containing KOH pellets, to give 940 mg of **11**. Continuous extraction of the aqueous phase with ether for 16 h gave 140 mg more product. Total yield 1.08 g (3.83 mmol, 83%). An analytical sample obtained by crystallization from ether showed a poorly defined mp at 240–248°C (dec.) with changes near 210°C; ir (KBr) ν: 3340–2040 (s), 1860 (m), 1780 (s), 1710 (s) cm^{-1}; 60-MHz ^{1}H nmr (acetone-d_6) δ: 1.2–1.9 (complex absorption, 6H), 2.9 (br s, 6H, H1(4)) and —CH_2COOH), 9.9 (br absorption, 2H). *Anal.* calcd. for $C_{13}H_{14}O_7$: C 55.32, H 5.00; found: C 55.57, H 5.05.

(1R,2R,6S,7S)-4-oxotricyclo[5.2.1.0^{2,6}]decane-2,6-dicarboxylic anhydride, ***13***

An intimate mixture of 930 mg (3.30 mmol) diacid **11** and 40 mg (0.20 mmol) anhydrous $Ba(OH)_2$ was heated in the oven of a rotary microdistillation apparatus at 170°C/0.05 Torr, giving rise to 185 mg (0.84 mmol) of **13**, 25% yield. Crystallized from $CHCl_3$/ether, the product showed mp 185–190°C (not well-defined); ir ($CHCl_3$) ν: 1880 (w), 1860 (w), 1780 (s), 1750 (s) cm^{-1}; ^{1}H nmr ($CDCl_3$) δ: 1.46–1.90 (m, 6H), 2.54 (d, *J* = 20.7 Hz, 2H), 2.68 (br s, 2H, H1(7)), 2.99 (d, *J* = 20.7 Hz, 2H); ^{13}C nmr ($CDCl_3$) δ: 25.3 (t, C8(9)), 38.0 (t, C10), 46.1 (t, C3(5)), 47.0 (d, C1(7)), 61.3 (s, C2(6)), 173.8 (s, —COO—), 212.5 (s, C4). *Anal.* calcd. for $C_{12}H_{12}O_4$: C 65.45, H 5.49; found: C 65.57, H 5.72.

(1R,2R,3S,4S)-2,3-bismethoxycarbonylmethylbicyclo[2.2.1]-heptane-2,3-dicarboxylic anhydride, ***12***

To a solution of 500 mg diacid **11** (1.77 mmol) in 25 mL ether was added excess ethereal solution of diazomethane. After 1 h at room temperature, the volatile material was evaporated at reduced pressure and the solid residue (600 mg) crystallized from benzene/hexane to give 470 mg of diester **12**, mp 158–160°C, 86% yield; ir ($CHCl_3$) ν: 1840 (m), 1780 (s), 1740 (s) cm^{-1}; ^{1}H nmr ($CDCl_3$) δ: 1.50–1.90 (m, 6H, H5(6)*endo*, H5(6)*exo*, H7*syn*, and H7*anti*), 2.79 (s, 4H, —CH_2COOMe), 2.83 (br s, 2H, H1(4)), 3.73 (s, 6H, —OCH_3); ^{13}C nmr ($CDCl_3$) δ: 25.3 (t, C5(6)), 36.7 (t, —CH_2COOMe), 38.2 (t, C7), 47.1 (d, C1(4)), 52.5 (q, —OCH_3), 59.2 (s, C2(3)), 171.3 (s, —*C*OOMe), 173.5 (s, —COO—). *Anal.* calcd. for $C_{15}H_{18}O_7$: C 58.06, H 5.85; found: C 57.90, H 5.88.

Attempted synthesis of dimethyl (1R,2R,3S,4S)-bismethoxycarbonylbicyclo[2.2.1]heptane-2,3-diacetate, 9 1. From (1R,2R,3S,4S)-2,3-bishydroxycarbonylmethylbicyclo[2.2.1]-heptane-2,3-dicarboxylic anhydride, ***11***. *Obtention of dimethyl (1R,2R,3S,4S)-2,3-bismethoxycarbonylmethylbicyclo[2.2.1]-heptane-2,3-dicarboxylic anhydride,* ***12***

(a) A mixture of 213 mg of compound **11** (0.76 mmol), 500 mg NaOH (12.5 mmol), and 5 mL water was heated under reflux for 4 h. The solution was evaporated to dryness *in vacuo*. The ir spectrum of the residue did not show the carbonyl anhydride absorption. This residue was dissolved in 2 mL water, 100 mg tetra-*n*-butylammonium bromide added, and the solution cooled in an ice bath. An ethereal solution of hydrogen chloride was added with vigorous stirring until the aqueous phase became slightly acidic and, immediately after, it was treated with an ethereal solution of diazomethane until a yellow colour persisted. Evaporation of the dried organic phase gave 268 mg of crude diester **12**.

(b) A mixture of 208 mg of compound **11** (0.74 mmol), 120 mg NaOH (3 mmol), and 5 mL water was heated under reflux for 4 h. The solution was evaporated to dryness *in vacuo*. Anhydrous DMF (5 mL) and 370 mg dimethyl sulfate (2.9 mmol) were added to the residue and the mixture heated under reflux for 16 h. The solvent was evaporated at reduced pressure and the solid residue washed with water and extracted with ether (5 × 10 mL). Evaporation of the solvent from the dried solution gave 260 mg of crude diester **12**.

2. *From (1R,2R,3S,4S)-2,3-bismethoxycarbonylmethylbicyclo-[2.2.1]heptane-2,3-dicarboxylic anhydride,* ***12***

A mixture of 470 mg diester **12** (1.7 mmol), 220 mg anhydrous sodium methoxide (4 mmol), and 5 mL anhydrous methanol was heated under reflux for 16 h. The mixture was cooled to 0°C and neutralized with concentrated HCl. The solvent was removed *in vacuo* without heating and the residue was treated with excess ethereal solution of diazomethane. Evaporation of the solvent left a crude mixture consisting mainly of the starting product.

Attempted conversion of (1R,2R,3S,4S)-2,3-bismethoxycarbonylmethylbicyclo[2.2.1]heptane-2,3-dicarboxylic anhydride, ***12****, into (1R,2R,3S,4S)-4-oxotricyclo[5.2.1.0^{2,6}]decane-2,6-dicarboxylic anhydride,* ***13***

A 50% dispersion of NaH in mineral oil (375 mg, 7.8 mmol) was washed with anhydrous THF (3 × 5 mL). A solution of 515 mg diester **12** (1.6 mmol) in 5 mL anhydrous THF was added and the mixture heated under reflux for 4 h. The cold mixture was acidified with aqueous 0.5 *N* HCl and extracted with ether (5 × 10 mL). After the usual work-up, a crude mixture consisting mainly of the starting product was obtained.

(1R,2R,3S,4S)-4-oxotricyclo[5.2.1.0^{2,6}]decane-2,6-dicarboxylic anhydride, ***13***

A 50% dispersion of NaH in mineral oil (600 mg, 12.5 mmol) was washed with anhydrous THF (3 × 5 mL). A solution of 211 mg of compound **12** (0.68 mmol) in 4 mL anhydrous THF and 4 mL anhydrous methanol was added and the mixture heated under reflux for 4 h. Aqueous 1 *N* HCl was added until pH 3, and the mixture extracted with $CHCl_3$. After the usual work-up a product was obtained (140 mg), which was heated under reflux with 20 mL 6 *N* HCl for 4 h. Evaporation of the volatile products *in vacuo* left a solid residue, which was washed with aqueous 7% $NaHCO_3$. The insoluble material was washed with water and dried in a desiccator to give 89.3 mg of compound **13**, 60% yield, identical (60-MHz ^{1}H nmr) to the product previously obtained.

Dimethyl (1R,2R,6S,7S)-4-oxotricyclo[5.2.1.0^{2,6}]decane-2,6-dicarboxylate, ***2***

A mixture of 91.8 mg anhydride **13** (0.42 mmol), 1.0 g NaOH, and 5 mL water was heated under reflux for 4 h. The cold solution (ice bath) was acidified with concentrated H_2SO_4. An ethereal solution of diazomethane was added with vigorous stirring until the yellow colour of diazomethane persisted. The organic layer was dried and evaporated, and the residue purified by passing it through a small column of silica gel using $CHCl_3$ as eluent, giving rise to 81.9 mg of diester **2** (0.308 mmol), 73% yield.

Dimethyl (1R,2R,6S,7S)-4-(p-toluenesulfonylhydrazono)tricyclo-[5.2.1.0^{2,6}]decane-2,6-dicarboxylate, ***14***

To a solution of 100 mg ketodiester **2** (0.376 mmol) in 3 mL glacial acetic acid, a solution of 140 mg *p*-toluenesulfonylhydrazide (0.75 mmol) in 3 mL of the same solvent was added and the reaction mixture left to stand at room temperature for 2 h. Water was added until turbidity, and the mixture allowed to stand in the refrigerator (0°C) for 16 h. The precipitate was filtered, washed with water, and dried in a desiccator containing KOH pellets, giving rise to 128 mg (0.29 mmol) of tosylhydrazone **14** (78% yield), mp 151–155°C; ir ($CHCl_3$) ν: 3325 (w), 3240 (w), 3050 (m), 1740 (s) cm^{-1}; 60-MHz ^{1}H nmr ($CDCl_3$) δ: 1.10–1.85 (m, 6H), 2.15–3.42 (complex absorption, 2.45 (s), total 9H), 3.60 (s, 6H), 7.30 (d, J = 8 Hz, 2H), 7.5–8.0 (complex absorption, 7.80 (d, J = 8 Hz), total 3H). *Anal.* calcd. for $C_{21}H_{26}N_2O_6S$: C 58.06, H 6.03, N 6.45; found: C 57.68, H 5.97, N 6.67.

Dimethyl (1RS,2RS,6SR,7SR)-tricyclo[5.2.1.0^{2,6}]dec-3-ene-2,6-dicarboxylate, ***15***

In a 10-mL flask fitted with a reflux condenser with a $CaCl_2$ tube, 64 mg (0.147 mmol) tosylhydrazone **14**, 9.7 mg (0.180 mmol) sodium methoxide, and 5 mL anhydrous methanol were placed. The mixture was heated under reflux for 2 h, the solvent was removed in a rotary evaporator without heating, and the residue dried *in vacuo* (1 Torr). The flask was connected to a microdistillation apparatus and heated progressively, the pressure in the system being 0.1 Torr. A liquid, which solidified as white crystals, distilled at 136°C/0.1 Torr, sublimed at 60–65°C/0.1 Torr, and showed mp 52–56°C. It was characterized as alkene **15**; yield, 34 mg (0.136 mmol), 93%; ir ($CHCl_3$) ν: 1740 (s), 1640 (w) cm^{-1}; ^{1}H nmr ($CDCl_3$) δ: 1.22 (br d, J = 10 Hz, 1H, H10*anti*), 1.44–1.56 (m, 2H, H8*exo* and H9*exo*), 1.66–2.00 (m, 3H, H8*endo*, H9*endo*, and H10*syn*), 2.29 (complex absorption, 3H, H1(7) and H5*endo* or H5*exo*), 2.99 (dt, J = 17.6 Hz, J' = 2.5 Hz, 1H, H5*exo* or H5*endo*), 3.63 (s, 3H), 3.66 (s, 3H), 5.64 (dt, J = 6 Hz, J' = 2.5 Hz, 1H) and 5.83 (dt, J = 6 Hz, J' = 2.5 Hz, 1H) (H3 and H4); ^{13}C nmr ($CDCl_3$) δ: 24.7 (t, C8), 25.6 (t, C9), 34.8 (t, C10), 46.6 (d, C7), 47.3 (t, C5), 47.7 (d, C1), 51.4 (q) and 51.6 (q) (—OCH_3), 60.4 (s, C6), 70.9 (s, C2), 132.0 (d) and 132.5 (d) (C3 and C4), 173.2 (s) and 175.1 (s) (—COOMe). *Anal.* calcd. for $C_{14}H_{18}O_4$: C 67.18, H 7.25; found: C 67.36, H 7.39.

Photochemical decomposition of the sodium salt of tosylhydrazone ***14***

A solution of 50 mg of the sodium salt of **14** (0.112 mmol), obtained as described before, in 15 mL anhydrous DME was placed in a Pyrex photoreactor and deoxygenated by bubbling nitrogen. The reactor was stoppered, and the mixture, magnetically stirred, was irradiated with a 125-W lamp for 16 h. The solvent was evaporated, the residue treated with 5 mL $CHCl_3$, and the suspension filtered; glc analysis of the filtrate (column, SE-30, 2 m; injector temperature 200°C; oven temperature, 160°C; flow, 20 mL N_2/min) showed it to contain mainly ketodiester **2** (rt 8.22 min, 66% relative area) and alkene **15** (rt 4.02 min, 26% relative area).

Thermal decomposition of the lithium salt of tosylhydrazone ***14***

To a cold solution (0°C) of 70 mg tosylhydrazone **14** (0.16 mmol) in 5 mL anhydrous ether, magnetically stirred under an argon atmosphere, 0.11 mL of a 1.6 *M* solution of *n*-butyllithium in hexane was added with the aid of a syringe. The mixture was stirred at room temperature for 1 h, the solvent was evaporated at reduced pressure without heating, and the residue dried *in vacuo* (1 Torr). The dry lithium salt was placed in a 10-mL flask, connected to a microdistillation apparatus, and heated gradually up to 135°C/0.2 Torr, giving rise to 25 mg of alkene **15**, 62% yield.

Attempted conversion of ketodiester ***2*** *into dimethyl 1-hydroxytetracyclo[5.2.1.0^{2,6}.0^{3,8}]decane-7,8-dicarboxylate,* ***16***

(a) *In anhydrous benzene*

A solution of 50 mg of **2** (0.188 mmol) in 5 mL benzene was placed in a quartz cell, and dry argon was bubbled through the solution for 20 min. The cell was stoppered and leaned against the refrigeration jacket of a 400-W uv lamp. The reaction was followed by glc (column SE-30, 2 m; injector temperature, 200°C; oven temperature, 180°C; flow, 20 mL N_2/min) and, after irradiating for 40 h, only the starting product (rt 3.95 min) was detected.

(b) *In benzene/*tert*-butyl alcohol*

The procedure described before, except for the use of a 5:1 benzene/*tert*-butyl alcohol mixture as solvent, was followed. After irradiating for 68 h, a new compound (rt 7.19 min) was formed, whose relative area with respect to **2** was 1.43. After irradiating for 40 h more, this ratio remained unchanged; glc/ms analysis of this mixture showed that the compound of rt 7.19 min was not the desired hydroxydiester **16**, but probably a product of addition of *tert*-butyl alcohol. Mass spectrum of the compound of rt 7.19 min: 267(5), 253(5), 252(5), 218(18), 186(20), 185(22), 153(13), 140(14), 119(14), 105(14), 91(25), 79(17), 77(18), 67(23), 59(45), 57(100).

Attempted conversion of ketoanhydride ***13*** *into 1-hydroxytetracyclo-[5.2.1.0^{2,6}.0^{3,8}]decane-7,8-dicarboxylic anhydride,* ***17***

(a) *In benzene*

The same procedure described before for compound **2** was followed, but starting with 25 mg (0.114 mmol) ketoanhydride **13**. After irradiating for 100 h, only the starting product was detected by glc analysis (rt 5.22 min, using the same conditions as before).

(b) *In benzene/*tert-*butyl alcohol*

The procedure described before was followed, using a 5:1 benzene/*tert*-butyl alcohol mixture as solvent, and starting with 20 mg of **13** (0.091 mmol). After irradiating for 90 h, the starting product had disappeared and a new compound (rt 5.90 min, 70% relative area) had been formed; glc/ms analysis showed that this compound was not the desired hydroxyanhydride **17**, but probably a product of addition of *tert*-butyl alcohol. Mass spectrum of the compound of rt 5.90 min: 279(3), 239(12), 238(10), 222(5), 221(23), 193(18), 166(28), 138(38), 91(35), 77(31), 67(34), 57(100).

*(3a*R*,4*S*,7*R*,7a*S*)-8,8-Diethoxy-2-phenyl-3a,5,6,7a-tetrahydro-1*H*,3*H*-4,7-methanoisoindol-1,3-dione,* ***21***

A mixture of 27.9 g dicarboximide **18** (85.3 mmol), 1.0 g of 10% Pd on charcoal, and 150 mL ethyl acetate was hydrogenated in a medium pressure hydrogenation apparatus at 4.2 atm for 82 h. Additional quantities of catalyst (0.5 g) were introduced after 48 and 72 h reaction. Most of the starting and reaction product remained undissolved during hydrogenation. Ethyl acetate was added to dissolve all the organic material, the mixture was filtered, and the solvent evaporated from the filtrate at reduced pressure to give 27.35 g of **21** (97% yield), mp 149–152°C (methanol); ir ($CHCl_3$) ν: 1710 (s) cm^{-1}; ^1H nmr ($CDCl_3$) δ: 1.24 (t, J = 7 Hz, 6H), 1.38–1.52 (m, 2H, H5(6)*endo*), 1.86–2.02 (m, 2H, H5(6)*exo*), 2.66–2.74 (m, 2H, H4(7)), 3.40–3.48 (m, 2H, H3a(7a)), 3.57 (q, J = 7 Hz) and 3.59 (q, J = 7 Hz) (total 4H), 7.24–7.54 (m, 5H); ^{13}C nmr ($CDCl_3$) δ: 15.40 (q) and 15.44 (q) (—OCH_2CH_3), 22.7 (t, C5(6)), 41.4 (d, C4(7)), 46.1 (d, C3a(7a)), 58.8 (t) and 59.0 (t) (—OCH_2CH_3), 115.1 (s, C8), 126.7 (d, —CH= *ortho*), 128.7 (d, —CH= *para*), 129.2 (d, —CH= *meta*), 132.0 (s, —C= *ipso*), 177.7 (s, —CO—). *Anal.* calcd. for $C_{19}H_{23}NO_4$: C 69.28, H 7.04, N 4.25; found: C 69.20, H 7.01, N 4.15.

*(3a*R*,4*S*,7*R*,7a*S*)-11,11-Diethoxy-5,6-dihydro-2-phenyl-1*H*,3*H*-4,7-methano-3a,7a-propanoisoindol-1,3-dione,* ***22***

In a one-liter three-necked flask equipped with low temperature thermometer, addition funnel, magnetic stirrer, and dry nitrogen atmosphere were placed 300 mL anhydrous THF, 4.0 g (30 mmol) naphthalene, and 2.1 g of a dispersion of lithium in solid paraffin containing 0.84 g lithium. The mixture was vigorously stirred for 10 min, taking on a dark-green colour. Diisopropylamine (18 mL, 120 mmol) was added with stirring and keeping the temperature below 30°C. The mixture was stirred until all the lithium had reacted, showing at this time an orange colour. The mixture was cooled at −78°C and 13.2 g of dicarboximide **21** (40 mmol) in 200 mL anhydrous THF was added at once. After 45 min stirring, the mixture was allowed to reach 0°C, and 4.1 mL 1,3-dibromopropane (40 mmol) was slowly added. After 1 h stirring at this temperature, most of the THF was evaporated at reduced pressure, and then 200 mL water and 200 mL $CHCl_3$ were added. The aqueous phase was acidified with dilute HCl, separated from the organic phase, and extracted with $CHCl_3$ (5 × 100 mL). The organic phase and the extracts were combined, washed with an aqueous solution of $NaHCO_3$ and water, and dried over anhydrous Na_2SO_4. Evaporation of the solvents at reduced pressure left a viscous residue that was extracted with hot hexane (5 × 50 mL), giving rise on cooling to 5.94 g of dicarboximide **22** as yellow crystals (40% yield). The product was dissolved in $CHCl_3$, decolorized with active charcoal, and crystallized from hexane, mp 132–134°C; ir ($CHCl_3$) ν: 1765 (s), 1700 (s), 1590 (w) cm^{-1}; ^1H nmr ($CDCl_3$) δ: 1.20 (t, J = 7 Hz, 3H), 1.22 (t, J = 7 Hz, 3H), 1.26–1.56 (m, 3H), 1.78–2.00 (m, 3H), 2.14–2.36 (m, 4H), 2.52–2.62 (m, 2H, H4(7)), 3.51 (q, J = 7 Hz, 2H), 3.52 (q, J = 7 Hz, 2H), 7.20–7.54 (m, 5H); ^{13}C nmr ($CDCl_3$) δ: 14.5 (q) and 15.2 (q) (—OCH_2CH_3), 23.6 (t, C5(6)), 25.4 (t, C9), 34.3 (t, C8(10)), 43.2 (d, C4(7)), 57.8 (t) and 58.4 (t) (—OCH_2CH_3), 63.1 (s, C3a(7a)), 115.4 (s, C11), 126.6 (d, —CH= *ortho*), 128.7 (d, —CH= *para*), 129.2 (d, —CH= *meta*), 132.1 (s, —C= *ipso*), 181.3 (s, —CO—). *Anal.* calcd. for $C_{22}H_{27}NO_4$: C 71.52, H 7.34, N 3.79; found: C 71.44, H 7.39, N 3.79.

*(3a*R*,4*R*,7*S*,7a*S*)-11,11-Diethoxy-2-phenyl-1*H*,3*H*-4,7-methano-3a,7a-propanoisoindol-1,3-dione,* ***19*** *(21)*

This compound was prepared, as described before for dicarboximide **21**, in 30% yield. Extraction of the crude reaction mixture with hot hexane gave, on cooling, crystalline **19**, thus avoiding the column chromatography used by Garratt and Hollowood (21) to isolate this compound; ^{13}C nmr ($CDCl_3$) δ: 15.0 (q) and 15.4 (q) (—OCH_2CH_3), 27.3 (t, C9), 34.1 (t, C8(10)), 52.1 (d, C4(7)), 58.9 (t) and 60.1 (t) (—OCH_2CH_3), 63.4 (s, C3a(7a)), 121.1 (s, C11), 125.8 (d, —CH= *ortho*), 127.8 (d, —CH= *para*), 128.7 (d, —CH= *meta*), 132.7 (s, —C = *ipso*), 135.1 (d, C5(6)), 180.6 (s, —CO—).

*(3a*R*,4*R*,7*S*,7a*S*)-11,11-Diethoxy-5,6-dihydro-2-phenyl-1*H*,3*H*-4,7-methano-3a,7a-propanoisoindol-1,3-dione,* ***20***

A mixture of 1.0 g dicarboximide **19** (2.72 mmol), 0.5 g of Pd on charcoal, and 50 mL ethyl acetate was hydrogenated in a medium pressure hydrogenation apparatus at 4.0 atm for 26 h. The mixture was filtered and the solvent evaporated from the filtrate to give 0.98 g of **20**, 98% yield, mp 136–138°C (methanol); ir ($CHCl_3$) ν: 1760 (m), 1700 (s), 1585 (w) cm^{-1}; ^1H nmr ($CDCl_3$) δ: 0.96 (t, J = 7.1 Hz, 3H), 1.20 (t, J = 7.1 Hz, 3H), 1.48–1.68 (m, 2H), 1.64–2.00 (m, 6H), 2.04–2.32 (m, 2H), 2.65 (m, 2H, H4(7)), 3.37 (q, J = 7.1 Hz, 2H), 3.50 (q, J = 7.1 Hz, 2H), 7.28–7.52 (m, 5H); ^{13}C nmr ($CDCl_3$) δ: 15.2 (q) and 15.3 (q) (—OCH_2CH_3), 21.1 (t, C5(6)), 28.7 (t, C9), 32.0 (t, C8(10)), 45.5 (d, C4(7)), 58.3 (t) and 59.1 (t) (—OCH_2CH_3), 60.4 (s, C3a(7a)), 115.3 (s, C11), 125.8 (d, —CH= *ortho*), 127.7 (d, —CH= *para*), 128.7 (d, —CH= *meta*), 132.8 (s —C= *ipso*), 181.6 (s, —CO—). *Anal.* calcd. for $C_{22}H_{27}NO_4$: C 71.52, H 7.37, N 3.79; found: C 71.44, H 7.39, N 3.79.

*(3a*R*,4*S*,7*R*,7a*S*)-5,6-Dihydro-2-phenyl-1*H*,3*H*-4,7-methano-3a,7a-propanoisoindol-1,3,11-trione,* ***23***

A mixture of 3.0 g dicarboximide **22** (8.11 mmol) and 60 mL 15% aqueous $HClO_4$ was heated under reflux for 12 h. The cold mixture was extracted with $CHCl_3$ (3 × 50 mL). The combined extracts were washed with water and dried over anhydrous Na_2SO_4. Evaporation of the solvent gave a residue that was purified by filtration through a small column of silica gel eluting with $CHCl_3$. Evaporation of the solvent gave 2.52 g of **23**, mp 118–119°C (benzene/hexane), 95% yield; ir ($CHCl_3$) ν: 1770 (s), 1710 (s), 1590 (w) cm^{-1}; ^1H nmr ($CDCl_3$) δ: 1.24–1.70 (m, 5H), 1.74–1.88 (m, 1H), 1.94–2.06 (m, 2H), 2.44–2.60 (m, 4H), 7.22–7.28 (m, 2H), 7.38–7.58 (m, 3H); ^{13}C nmr ($CDCl_3$) δ: 19.0 (t, C5(6)), 24.5 (t, C9), 35.3 (t, C8(10)), 46.5 (d, C4(7)), 56.6 (s, C3a(7a)), 126.5 (d, —CH= *ortho*), 129.1 (d, —CH= *para*), 129.4 (d, —CH= *meta*), 131.8 (s, —C= *ipso*), 178.5 (s, —CON), 208.7 (s, —CO—). *Anal.* calcd. for $C_{18}H_{17}NO_3$: C 73.20, H 5.80, N 4.87; found: C 73.28, H 5.94, N 4.74.

*Dimethyl (1*RS*,2*RS*,3*RS*,4*SR*)-7,7-diethoxybicyclo[2.2.1]heptane-2,3-dicarboxylate,* ***24***

A mixture of 11.0 g dicarboximide **21** (33.4 mmol), 11 g KOH (196 mmol), and 17 mL triethylene glycol was heated under reflux for 1h. The starting product went completely into solution and at the end of the reaction a voluminous white precipitate appeared. To the cold mixture, ice and concentrated HCl were added until the solution became acidic. The mixture was extracted with ether (3 × 50 mL) and the combined extracts were washed with water (3 × 10 mL) and dried over anhydrous Na_2SO_4. Evaporation of the solvent gave a solid residue, which was treated with an excess of an ethereal solution of diazomethane. Evaporation of the volatile material left a viscous liquid that was distilled in a rotary microdistillation apparatus, bp 165–175°C (oven)/0.2 Torr, to give 6.64 g of **24** (60% yield from **21**); ir ($CHCl_3$) ν: 1730 (s) cm^{-1}; ^1H nmr ($CDCl_3$) δ: 1.06–1.42 (m, 1.09 (t, J = 7.1 Hz), 1.19 (t, J = 7.1 Hz), total 8H, —OCH_2CH_3, H5*endo*, and H6*endo*), 1.64–1.94 (m, 2H, H5*exo* and H6*exo*), 2.47

(br t, J = 4 Hz, 1H, H4), 2.68 (br d, J = 4 Hz, 1H, H1), 2.93 (d, J = 5.5 Hz, 1H, H2), 3.38–3.67 (m, 5H, —OCH_2CH_3 and H3), 3.68 (s, 3H) and 3.72 (s, 3H) (—OCH_3); ^{13}C nmr ($CDCl_3$) δ: 15.0 (q) and 15.4 (q) (—OCH_2CH_3), 22.3 (t, C5), 26.2 (t, C6), 42.2 (d) and 42.3 (d) (C1 and C4), 46.4 (d, C2), 47.9 (d, C3), 51.8 (q) and 51.9 (q) (—OCH_3), 58.49 (t) and 58.53 (t) (—OCH_2CH_3), 112.9 (s, C7), 173.8 (s) and 174.3 (s) (—COOMe). *Anal.* calcd. for $C_{15}H_{24}O_6$: C 60.03, H 7.99; found: C 60.07, H 8.09.

*Dimethyl (1*R*,2*S*,6*R*,7*S*)-10,10-diethoxytricyclo[5.2.1.0^{2,6}]decane-2,6-dicarboxylate, 25*

In a 250-mL three-necked flask equipped with low temperature thermometer, addition funnel, magnetic stirrer, and dry nitrogen atmosphere were placed 100 mL anhydrous THF, 1.5 g (10 mmol) naphthalene, and 0.71 g of a dispersion of lithium in solid paraffin containing 0.284 g lithium. The mixture was vigorously stirred for 15 min, taking on a dark-green colour. Diisopropylamine (4.5 mL, 30 mmol) was added with stirring and keeping the temperature of the reaction mixture below 30°C. The mixture was stirred until all lithium had reacted, showing at this time an orange colour. After cooling at −78°C, 3.0 g of diester **24** (10 mmol) in 50 mL anhydrous THF was added at once. The mixture was stirred for 1h and allowed to reach 0°C. 1,3-Dibromopropane (1.1 mL, 10 mmol) was slowly added, and the mixture stirred for 75 min at this temperature. The solvent was evaporated at reduced pressure, 75 mL water and 75 mL $CHCl_3$ were added, and the aqueous phase made acidic with 25 mL dilute HCl. The organic phase was separated and the aqueous one extracted with $CHCl_3$ (3 × 30 mL). The combined organic phase and extracts were washed with water and dried over anhydrous Na_2SO_4. Evaporation of the solvent left a liquid residue that was chromatographed through silica gel, giving rise, on elution with CH_2Cl_2, to 1.7 g of a mixture of starting product and **25**, which was fractionally distilled in a rotary microdistillation apparatus. Obtained was 1.0 g of **25**, bp 200–210°C (oven)/0.2 Torr, 29% yield; ir ($CHCl_3$) ν: 1730 (s) cm^{-1}; ^{1}H nmr ($CDCl_3$) δ: 1.16 (t, J = 7.1 Hz, 3H), 1.19 (t, J = 7.1 Hz, 3H), 1.5–2.1 (m, 6H), 2.1–2.5 (m, 6H), 3.47 (q, J = 7.1 Hz, 2H), 3.49 (q, J = 7.1 Hz, 2H), 3.63 (s, 6H); ^{13}C nmr ($CDCl_3$) δ: 14.4 (q) and 15.1 (q) (—OCH_2CH_3), 22.5 (m, C8(9)), 26.1 (t, C4), 38.1 (m, C3(5)), 46.6 (d, C1(7)), 51.4 (q, —OCH_3), 57.4 (t) and 58.2 (t) (—OCH_2CH_3), 63.7 (s, C2(6)), 112.6 (s, C10), 175.2 (s, —COOMe). *Anal.* calcd. for $C_{18}H_{28}O_6$: C 63.51, H 8.29; found: C 63.93, H 8.35.

*Dimethyl (1*R*,2*S*,6*R*,7*S*)-10-oxotricyclo[5.2.1.0^{2,6}]decane-2,6-dicarboxylate, 1*

A mixture of 0.45 g diester **25** and 6.75 mL 15% aqueous $HClO_4$ was heated under reflux for 5 h. The cold mixture was extracted with $CHCl_3$ (3 × 20 mL). The combined extracts were washed with water and dried over anhydrous Na_2SO_4. Evaporation of the solvent left 0.28 g of a solid that crystallized from methanol, and showed mp 78–81°C. Ketodiester **1**, prepared by the procedure previously described (7), melts at 81–83°C. The mixture mp was 79–82°C. The spectroscopic data (ir and 60-MHz ^{1}H nmr) and glc analysis confirm the identity of both compounds.

*Dimethyl (1*R*,2*S*,6*R*,7*S*)-10-(*p*-toluenesulfonylhydrazono)tricyclo-[5.2.1.0^{2,6}]decane-2,6-dicarboxylate, 26*

A mixture of 2.66 g ketodiester **1** (10 mmol), 2.05 g tosylhydrazide (11 mmol), 16 mL isopropanol, and four drops of concentrated HCl was heated under reflux for 28 h. The mixture was cooled in the refrigerator (−10°C) for 8 days and the precipitated white crystals were filtered and dried *in vacuo* (0.05 Torr) to give 3.26 g of **26**, mp 170–172°C, 75% yield. Recrystallized from isopropanol, the mp remained unchanged; ir (KBr) ν: 3175 (m), 1732 (s), 1705 (s), 1600 (m) cm^{-1}; 80-MHz ^{1}H nmr ($CDCl_3$) δ: 0.9–2.6 (complex absorption, 14H, 2.50 (s)), 2.92 (m, 1H), 3.60 (s, 6H), 7.35 (d, J = 8 Hz, 2H), 7.85 (d, J = 8 Hz, 2H), 8.1 (br absorption, 1H); 20-MHz ^{13}C nmr ($CDCl_3$) δ: 21.2 (m) and 22.0 (m) (C8 and C9), 21.5 (q, =C—CH_3), 24.9 (t, C4), 38.5 (t) and 39.5 (t) (C3 and C5), 43.2 (d) and 49.2 (d) (C1 and C7), 51.7 (q, —OCH_3), 60.9 (s) and 61.6 (s) (C2 and C6), 127.9 (d) and 129.5 (d) (—CH=), 135.5 (s, =C—CH_3), 144.1 (s, =C—SO_2—), 167.1 (s, C10), 173.4 (s) and 173.6 (s) (—COOMe). *Anal.* calcd. for $C_{21}H_{26}N_2SO_6$: C 58.05, H 6.03, N 6.45; found: C 57.99, H 5.88, N 6.26.

Dimethyl tetracyclo[5.2.1.0^{2,6},0^{3,8}]decane-7,8-dicarboxylate, 3

In a 250-mL flask fitted with a reflux condenser with a $CaCl_2$ tube was placed a solution of 2.25 g of tosylhydrazone **26** (5.18 mmol) in 60 mL anhydrous methanol. Then a solution of 286 mg anhydrous sodium methoxide (5.3 mmol) in 40 mL anhydrous methanol was added, and the mixture heated under reflux for 2 h. The solvent was removed at reduced pressure (30 Torr) and the residue dried at 0.1 Torr for 1.5 h. The flask containing the sodium salt of **26** was connected to a rotary microdistillation apparatus and heated at 170°C/1 Torr, to give 1.14 g of a colourless viscous distillate consisting mainly of **3** (glc analysis, column OV-1, 2 m; injector temperature 250°C; oven temperature 160°C; flow, 25 mL N_2/min; rt 5.80 min; relative area 97%). Crystallization from isopropanol gave needles, mp 62–63°C, 89% yield; ir (KBr) ν: 1725 (s) cm^{-1}; ^{1}H nmr ($CDCl_3$) δ: 1.44–1.60 (m, 2H), 1.82–2.08 (m, 7H), 2.36–2.48 (m, 3H), 3.67 (s, 6H); 20-MHz ^{13}C nmr ($CDCl_3$) δ: 21.7 (t, C4(5)), 34.3 (d, C1), 49.6 (t, C9(10)), 49.9 (d, C2), 50.8 (q, —OCH_3), 57.4 (d, C3(6)), 57.8 (s, C7(8)), 172. 4 (s, —COOMe); ms: 250(M^+, 3), 219(38), 218(100), 191(11), 190(41), 159(22), 158(24), 132(16), 131(100), 130(30), 129(27), 128(14), 125(24), 124(14),119(14), 117(14), 116(16), 115(22), 93(14), 92(8), 91(38), 79(16), 78(11), 77(24), 65(11), 64(8), 63(19), 59(19). *Anal.* calcd. for $C_{14}H_{18}O_4$: C 67.18, H 7.25; found: C 67.09, H 7.31.

Acknowledgements

We gratefully thank M. Guerra from the "Instituto de Química Bio-orgánica de Barcelona, C.S.I.C." (Barcelona, Spain) for carrying out the elemental analyses and Dr. F. Sánchez-Ferrando from the Universidad Autónoma de Barcelona for running the 80-MHz ^{1}H and 20-MHz ^{13}C nmr spectra.

1. (*a*) L. A. PAQUETTE, R. J. TERNANSKY, D. W. BALOGH, and G. KENTGEN. J. Am. Chem. Soc. **105**, 5446 (1983); (*b*) R. J. TERNANSKY, D. W. BALOGH, and L. A. PAQUETTE. J. Am. Chem. Soc. **104**, 4503 (1982).
2. (*a*) L. A. PAQUETTE, R. J. TERNANSKY, D. W. BALOGH, and W. J. TAYLOR. J. Am. Chem. Soc. **105**, 5441 (1983); (*b*) L. A. PAQUETTE, R. J. TERNANSKY, and D. W. BALOGH. J. Am. Chem. Soc. **104**, 4502 (1982).
3. (*a*) L. A. PAQUETTE, D. W. BALOGH, R. USHA, D. KOUNTZ, and G. G. CHRISTOPH. Science, **211**, 575 (1981); (*b*) L. A. PAQUETTE and D. W. BALOGH. J. Am. Chem. Soc. **104**, 774 (1982); (*c*) G. G. CHRISTOPH, P. ENGEL, R. USHA, D. W. BALOGH, and L. A. PAQUETTE. J. Am. Chem. Soc. **104**, 784 (1982).
4. (*a*) P. E. EATON. Tetrahedron, **35**, 2189 (1979); (*b*) P. DESLONGHCAMPS and P. SOUCY. Tetrahedron, **37**, 4385 (1981); (*c*) P. E. EATON and W. H. BUNNELLE. Tetrahedron Lett. **25**, 23 (1984); (*d*) P. E. EATON, W. H. BUNNELLE, and P. ENGEL. Can. J. Chem. **62**, 2612 (1984).
5. P. CAMPS and M. FIGUEREDO. Can. J. Chem. **62**, 1184 (1984).
6. P. CAMPS, J. CASTAÑÉ, M. FELIZ, and M. FIGUEREDO. Tetrahedron, **40**, 5235 (1984).
7. P. CAMPS, J. CASTAÑÉ, and M. T. SANTOS. Chem. Lett. 1367 (1984).
8. (*a*) E. J. COREY, W. J. HOWE, H. W. ORF, D. A. PENSAK, and G. PETERSSON. J. Am. Chem. Soc. **97**, 6116 (1975); (*b*) F. SERRATOSA. Heuriskō, Introducción a la Síntesis Orgánica. Alhambra S.A., Madrid. 1975. p. 43.
9. J. R. NEFF and J. E. NORDLANDER. J. Org. Chem. **41**, 2590 (1976).

10. (*a*) S. GÄB, H. PARLAR, and F. KORTE. Tetrahedron, **30**, 1145 (1974); (*b*) F. I. ONUSKA and M. E. COMBA. Biomed. Mass Spectrom. **2**, 176 (1975); (*c*) E. S. LAHANIATIS, H. PARLAR, S. GÄB, and F. KORTE. Synthesis, 47 (1976); (*d*) H. PARLAR, H. MANSOUR, and S. GÄB. Tetrahedron Lett. **19**, 1597 (1978); (*e*) D. BOSSE and A. DE MEIJERE. Chem. Ber. **111**, 2223 (1978); (*f*) J. R. KNOX, C. L. RASTON, and A. H. WHITE. Aust. J. Chem. **32**, 553 (1979).
11. O. DIELS and K. ALDER. Ann. Chem. **490**, 236 (1931).
12. K. ALDER and K. H. BACKENDORF. Chem. Ber. **71**, 2199 (1938).
13. J. R. EDMAN and H. E. SIMMONS. J. Org. Chem. **33**, 3808 (1968).
14. W. CLARK STILL, M. KAHN, and A. MITRA. J. Org. Chem. **43**, 2923 (1978).
15. L. M. JACKMAN and S. STERNHELL. Applications of nuclear magnetic resonance spectroscopy in organic chemistry. 2nd ed. Pergamon Press, Germany. 1969. p. 89.
16. A. P. KRAPCHO, J. R. LARSON, and J. M. ELDRIDGE. J. Org. Chem. **42**, 3749 (1977).
17. A. P. KRAPCHO and A. J. LOVEY. Tetrahedron Lett. **14**, 957 (1973).
18. J. NEUMEISTER, H. KEUL, M. P. SAXENA, and K. GRIESBAUM. Angew. Chem. Int. Ed. Engl. **17**, 939 (1978).
19. R. H. SHAPIRO. Organic reactions. Vol. 23. John Wiley and Sons, Inc., New York. 1976. p. 405.
20. B. M. TROST and P. RENAUT. J. Am. Chem. Soc. **104**, 6668 (1982).
21. P. J. GARRATT and F. HOLLOWOOD. J. Org. Chem. **47**, 68 (1982).
22. (*a*) K. G. BILYARD, P. J. GARRATT, and R. ZAHLER. Synthesis, 389 (1980); (*b*) C. GIRARD and R. BLOCH. Tetrahedron Lett. **23**, 3683 (1982).

La liaison phosphore–azote. Étude quantochimique de modèles neutres et ioniques H_3PNH, $H_3PNH_2^+$, $H_2PNH_3^+$, H_2PNH^- et $HPNH_2^-$

DANIELLE GONBEAU ET GENEVIÈVE PFISTER-GUILLOUZO[1]

Laboratoire de physico-chimie moléculaire, UA 474, Insitut universitaire de recherche scientifique, avenue de l'Université, 64000 Pau, France

ET

MARIE-ROSE MAZIÈRES ET MICHEL SANCHEZ

Laboratoire de synthèse, structure et réactivité, UA 454 de molécules organophosphorées, Université Paul Sabatier, 31062 Toulouse Cédex, France

Reçu le 1[er] mars 1985

DANIELLE GONBEAU, GENEVIÈVE PFISTER-GUILLOUZO, MARIE-ROSE MAZIÈRES et MICHEL SANCHEZ. Can. J. Chem. **63**, 3242 (1985).

Une étude quantochimique sur le motif phosphazène a été effectuée par le biais de calculs réalisés en base *ab initio* double zeta (ζ) de valence sur des composés neutres et ioniques. La nature de la liaison P—N dans l'iminophosphane H_3PNH est à rapprocher de celle de la liaison P—C des ylures du phosphore. Les caractéristiques électroniques des formes cationiques $(H_2PNH_3)^+$, $(H_3PNH_2)^+$ et anioniques $(HPNH_2)^-$, $(H_2PNH)^-$ dérivées de l'iminophosphane et de sa forme tautomère, l'aminophosphane, ont été analysées. Les résultats obtenus permettent d'interpréter raisonnablement les données expérimentales obtenues pour ce type d'entités.

DANIELLE GONBEAU, GENEVIÈVE PFISTER-GUILLOUZO, MARIE-ROSE MAZIÈRES, and MICHEL SANCHEZ. Can. J. Chem. **63**, 3242 (1985).

Ab initio molecular orbital calculations have been performed on the phosphazene bond using a split valence basis set on neutral and ionic compounds. The nature of the P—N multiple bond in H_3PNH shows similarities with that of the P—C bond in phosphorus ylides. Electronic characteristics of cations $(H_2PNH_3)^+$, $(H_3PNH_2)^+$ and anions $(HPNH_2)^-$, $(H_2PNH)^-$ related to H_3PNH and its tautomer H_2PNH_2 were investigated. The results obtained were used to explain experimental observations for this type of compounds.

1. Introduction

L'étude quantique antérieure réalisée sur la liaison phosphazène P═N concernait l'espèce neutre à coordinence deux HP═NH (1). Nous avons étendu cette approche, d'une part, à la coordinence quatre H_3P═NH et, d'autre part, à certains modèles cationiques $(H_3PNH_2)^+$, $(H_2PNH_3)^+$ et anioniques $(HPNH_2)^-$, $(H_2PNH)^-$ correspondant pour certains à des entités récemment synthétisées; pour ces dérivés, la nature de la liaison P—N avait été établie sur la base de leur réactivité ou d'après des données spectroscopiques essentiellement de résonance magnétique nucléaire.

L'objet de ce travail est de préciser la structure électronique de ces espèces et de généraliser les degrés de polarité et de polarisabilité respectifs des atomes de phosphore et d'azote selon l'environnement.

2. Conditions de calcul

Tous les calculs ont été réalisés à l'aide du programme MONSTERGAUSS 80 (2).

Une base *ab initio* double ζ de valence 4-31G (3) avec orbitales de polarisation de type *d* sur les hétéro-atomes a été utilisée (une orbitale gaussienne de type *d*, ζ_P^d = 0,57, ζ_N^d = 0,8).

Les paramètres géométriques ont été optimisés avec la base ainsi définie, grâce à un processus de minimisation à métrique variable, avec évaluation du gradient selon l'algorithme de Broyden–Fletcher–Goldfard-Shanno.

Toutefois, afin d'obtenir une description correcte des espèces anioniques (4), nous avons ultérieurement effectué des calculs simples en introduisant, sur les deux hétéro-atomes, un jeu de fonctions diffuses de type *s* et *p* avec les exposants 0,053 pour N et 0,032 pour P, précédemment optimisés par Lohr et Ponas (4*b*).

Les calculs sur les anions $(H_2PNH)^-$ et $(HPNH_2)^-$ ont été effectués sur le Cray One du Centre de calcul vectoriel pour la recherche (École polytechnique, Palaiseau) dans le cadre de l'ATP Cray 1984.

3. Analyse des résultats

3.1 *Iminophosphane* H_3P═NH

3.1.1 *Structure géométrique, orbitales moléculaires, populations de Mulliken*

À notre connaissance, seule une approche théorique en méthode CNDO/2 a été réalisée sur ce modèle (5).

Les valeurs optimisées des paramètres géométriques pour l'iminophosphane sont présentées dans le tableau 1.

La structure énergétiquement privilégiée de cette molécule correspond à un état d'hybridation de type sp^2 de l'atome d'azote et à une position décalée de la liaison N—H vis-à-vis du groupement PH_3 tétraédrique.

La principale caractéristique concerne la longueur, particulièrement courte (1,532 Å), de la liaison P—N. Quoique très nettement différente de celle évaluée par d'autres auteurs en CNDO/2 (1,66 Å) (5), celle-ci tout à fait en accord avec les données expérimentales obtenues par ailleurs (6*a*).

De plus, une population de recouvrement de 0,51 pour la liaison P—N révèle bien une liaison à caractère multiple; pour la double liaison P═N dans HP═NH, nous avions observé une valeur de 0,45.

Par le biais d'une analyse des populations de Mulliken et des orbitales moléculaires, nous avons cherché à préciser la nature de cette liaison.

La molécule d'iminophosphane peut être considérée comme le produit de réaction d'une phosphine et d'un nitrène singulet,

[1]Auteur à qui adresser la correspondance.

TABLEAU 1. Géométries minimisées pour l'iminophosphane et l'aminophosphane[a]

Paramètre	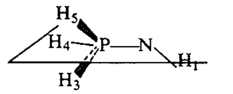	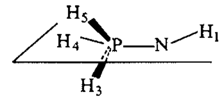	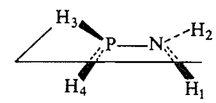
P—N	1,532	1,530	1,685
$N—H_1$	0,998	0,995	0,99
$N—H_2$			
$P—H_3$	1,405	1.396	1.435
$P—H_4$	1,383	1,402	
$P—H_5$	1,405	1,396	
$H_1\hat{N}P$	119,16	121,45	122,17
$H_2\hat{N}P$			116,84
$H_1\hat{N}H_2$			114,07
$H_3\hat{P}N$	112,88	121,52	100,26
$H_4\hat{P}N$	121,84	117,60	100,26
$H_5\hat{P}N$	121,84	117,60	
$H_3\hat{P}H_4$	99,55	98,89	94,40
$H_3\hat{P}H_5$	99,55	98,89	
H_4PNH_1	180	0	70,86
H_4PNH_2			100,72
H_3PNH_4	118,29	116,69	93,81
H_3PNH_5	123,41	121,65	
E_{el}[b]	−463,351257	−463,366160	−459,772461
E_{rep}[c] (N—N)	66,307513	66,325604	62,701753
E_t	−397,043744	−397,040556	−397,070708
ΔE_t	70,72	79,08	

[a]Longueurs, en angstroms; angles, en degrés; E, en hartrees; ΔE_t évalué vis-à-vis de la forme la plus stable, en kilojoules par mole.
[b]E_{el}: énergie d'interaction électron−noyau, électron−électron.
[c]E_{rep}: énergie de répulsion internucléaire.

l'approche de la paire libre de la phosphine n_P étant réalisée dans la direction de l'orbitale vacante du nitrène, avec les deux paires libres de cette entité dans le plan orthogonal.

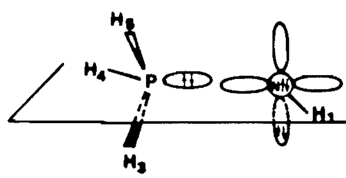

La délocalisation de la paire du phosphore vers l'orbitale vacante du nitrène assure la liaison P—N en σ. Cette liaison apparaît polarisée $P^+—N^-$, compte tenu du fort pouvoir attracteur de l'azote. On remarque toutefois un phénomène de rétrodonation selon l'axe P—N, qui aboutit à un peuplement de 0,13 e de l'orbitale d du phosphore dirigée selon cet axe.

Parallèlement, des transferts interviennent des deux paires de l'atome d'azote, que nous définissons par n_N^π (paire perpendiculaire au plan H_4PNH_1) et n_N^σ (paire dans le plan H_4PNH_1), vers les orbitales d de symétrie adaptée du phosphore, conduisant à des populations respectives de 0,17 et de 0,25 sur ces orbitales. Nous observons de plus en π une délocalisation par hyperconjugaison de la paire n_N^π vers les liaisons P—H.

Ces interactions $n_N \rightarrow d_P$ apparaissent au niveau des deux dernières orbitales occupées de l'iminophosphane à −9,79 et −10,77 eV, qui présentent de fortes localisations sur les deux paires de l'azote. La visualisation par le tracé des courbes d'isovaleurs de fonction est présentée dans la figure 1 pour l'HOMO (n_N^π).

Ainsi, les trois types de transferts analysés ($n_P \rightarrow n_N^*$, $n_N^\pi \rightarrow d_P^\pi$, $n_N^\sigma \rightarrow d_P^\sigma$) sont à l'origine de la faible longueur de liaison P—N dans l'iminophosphane, qui peut donc être considérée comme une "pseudo triple liaison".

L'ensemble des transferts en retour sur le phosphore est toutefois assez faible (population totale de 0,55 e sur les orbitales d) et, globalement, la liaison P—N apparaît comme extrêmement polaire: fort caractère positif sur le phosphore et fort caractère négatif sur l'azote (fig. 2).

Cette charge nette négative très importante sur l'atome d'azote (−1,02) est bien en accord avec les valeurs inhabituelles des déplacements chimiques δ ^{15}N observées pour ce type de systèmes (6*b*), vis-à-vis de celles caractéristiques d'un azote dicoordonné; de même la comparaison des moments dipolaires expérimental (3,1 D pour $\phi_3PN\phi$) et théorique (3,2 D pour H_3PNH) est tout à fait satisfaisante. Le caractère de ce phosphore tétracoordonné (+0,73 en charge nette totale) est nettement plus positif que celui du phosphore divalent dans HPNH (+0,49 en charge nette totale) et du phosphore trivalent dans H_2PNH_2 (+0,39 en charge nette totale). Enfin, la réactivité des iminophosphanes (6*c*) s'interprète parfaitement à partir de la polarisation $P^+—N^-$ de cette liaison.

L'analyse des facteurs géométriques et électroniques met donc en évidence le caractère particulier de la liaison P—N dans la molécule d'iminophosphane. Elle révèle une structure du type 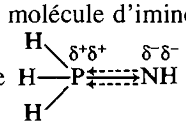 qui doit être considérée comme une simple liaison σ, issue d'un transfert en p du phosphore vers l'azote, renforcée essentiellement par les deux transferts en retour $n_N \rightarrow d_P$.

Ce caractère est à rapprocher de celui invoqué dans le cas des ylures du phosphore pour lesquels une longueur anormalement

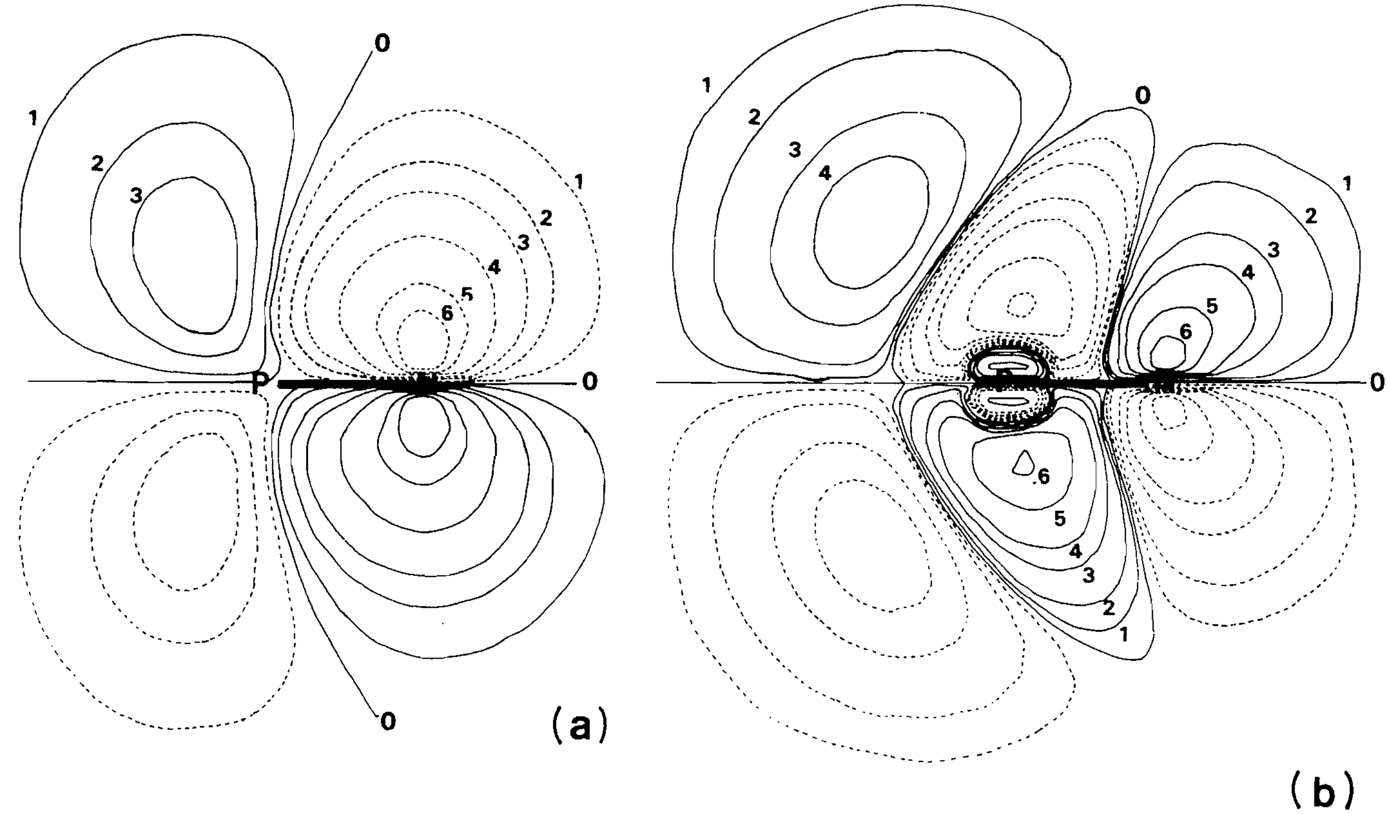

FIG. 1. H_3PNH. (*a*) HOMO (symétrie A''); (*b*) 1^re virtuelle de symétrie A''. Courbes d'isovaleurs de fonction pour les valeurs suivantes de ψ: (*a*) 0, 1: ±0,001; 2: ±0,03; 3: ±0,05; 4: ±0,1; 5: ±0,2; 6: ±0,3; (*b*) 0; 1: ±0,003; 2: ±0,01; 3: ±0,03; 4: ±0,05; 5: ±0,1; 6: ±0,15 (valeurs positives: traits pleins; valeurs négatives: traits pointillés).

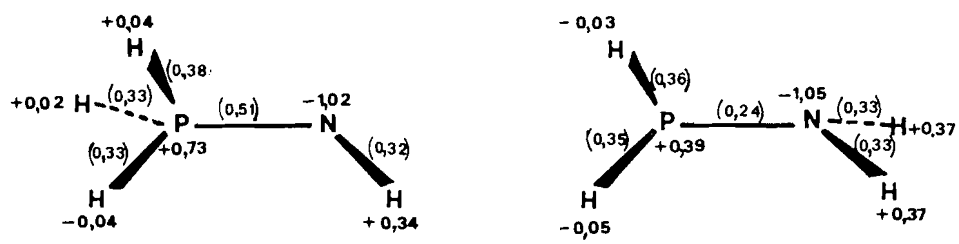

FIG. 2. $H_3PNH-H_2PNH_2$. Analyse des populations selon Mulliken. Charges nettes totales – populations de recouvrement (entre parenthèses).

courte a également été obtenue pour la liaison P—C (7) et correspond à ce qui vient d'être récemment proposé à partir d'une étude théorique pour H_3PO (8).

Cette nature particulière de la liaison P=N explique la faible barrière à la rotation calculée (de l'ordre de 8 kJ/mol) et qui n'a jamais été mise en évidence expérimentalement.

La forme mise en jeu, liaison N—H en position éclipsée vis-à-vis du groupement PH_3, présente une structure électronique très voisine de celle obtenue pour une position décalée, transferts $n_N \rightarrow d_P$ du même type et du même ordre. Ainsi, des énergies électroniques très voisines sont obtenues pour les deux entités, la forme éclipsée étant défavorisée de part des répulsions internucléaires importantes (de l'ordre de 47 kJ/mol).

Ceci conditionne l'origine de la barrière à la rotation dans l'iminophosphane, le "caractère multiple" lié à des interactions $p-d$ n'étant pas modifié par la rotation, contrairement au cas de liaisons $p^\pi-p^\pi$. En effet, pour la double liaison P—N dans l'iminophosphène, une barrière beaucoup plus élevée (environ 205 kJ/mol) avait été déterminée.

En outre, la valeur plus importante (environ 26 kJ/mol) que nous avions obtenue pour la barrière à la rotation dans l'aminophosphane avait une toute autre origine (9). Dans ce cas, c'était un facteur non pas de répulsion nucléaire mais électronique, lié aux modifications d'interactions paire P – paire N, qui gouvernait la barrière.

Pour l'iminophosphane, la rotation assez aisée autour de la liaison P—N et l'ensemble des données géométriques et électroniques favorables à une migration 1–2 sont autant de facteurs qui permettent d'interpréter l'existence de l'équilibre prototropique $H_3P{=}NH \rightleftarrows H_2P{-}NH_2$.

Cet équilibre a été mis en évidence, ces dernières années, par différentes équipes: Schmidpeter et Rossknecht (10) et Binder et Fisher (11). Ces derniers ont étudiée l'influence de la température et montré la prépondérance, dans de nombreux cas, de la forme aminophosphane.

Sur les dérivés modèles examinés (H_3PNH et H_2PNH_2), nous avons obtenu une différence énergétique de l'ordre de 71 kJ/mol en faveur de l'aminophosphane. Comme le font appa-

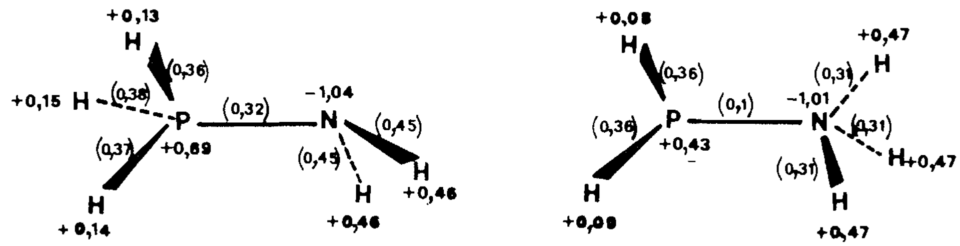

FIG. 3. $(H_3PNH_2)^+$ $(H_2PNH_3^+)$. Analyse des populations selon Mulliken. Charges nettes totales — populations de recouvrement (entre parenthèses).

raître les résultats présentés dans le tableau 1, ce sont les termes de répulsion internucléaires qui sont à l'origine de la stabilisation plus importante de l'aminophosphane.

3.1.2 *Réactivité des iminophosphanes: dimérisation*

Le phénomène de dimérisation est bien connu au niveau des liaisons phosphazènes et un grand nombre de composés diazaphosphétidines ont été synthétisés ces dernières années (12).

Lors d'une étude antérieure sur l'iminophosphène (1), l'analyse de ce phénomène a été interprétée par un mécanisme sous contrôle orbitalaire. En effet, les orbitales caractéristiques des liaisons $\pi_{P=N}$ et $\pi^*_{P=N}$ présentaient des localisations très importantes, respectivement sur l'azote et le phosphore, qui permettaient de lever les restrictions de symétrie (13) et d'envisager une addition 2+2 conduisant au dimère tête-bêche.

Pour l'iminophosphane, trois facteurs paraissent aller à l'encontre d'un mécanisme sous contrôle frontalier: (*i*) La séparation énergétique entre les deux orbitales occupée et virtuelle susceptibles d'entrer en jeu lors de la dimérisation est nettement plus importante que pour l'iminophosphène ($\simeq$ 17 eV pour l'iminophosphane, $\simeq$13 eV pour l'iminophosphène). (*ii*) L'HOMO du système présente bien un poids important sur l'atome d'azote, mais la localisation au niveau de la virtuelle est moins marquée sur le phosphore (fig. 1). (*iii*) Nous observons au niveau de cette orbitale virtuelle, une intervention des orbitales *d* du phosphore qui conduit à une diminution du recouvrement positif lors de l'approche tête-bêche.

Par contre, comme nous l'avons déjà noté, la polarité de la liaison P—N dans l'iminophosphane est très importante, avec des charges nettes de +0,73 sur P et −1,02 sur N.

Au vu de cet ensemble de résultats, nous sommes amenés à envisager une dimérisation au niveau de l'iminophosphane, mettant en jeu un mécanisme sous contrôle de charge plutôt que sous contrôle orbitalaire.

Cette conclusion se trouve confortée par les observations expérimentales selon lesquelles des substituants électrodonneurs sur l'azote ou électro-accepteurs sur le phosphore, qui tendent à accentuer la polarité de la liaison P—N, favorisent également la dimérisation (12*a*).

3.2 *Systèmes ioniques*

3.2.1 *Cations $(H_3PNH_2)^+$ et $(H_2PNH_3)^+$*

L'une des caractéristiques des iminophosphanes étant leur affinité vis-à-vis des électrophiles, nous avons entrepris l'analyse de la structure électronique du système $(H_3PNH_2)^+$ qui correspond à une protonation sur l'azote de l'iminophosphane. Cette forme peut également résulter d'une protonation sur le phosphore de l'aminophosphane.

Étant donné la prototropie $H_3PNH \rightleftarrows H_2PNH_2$, nous avons également examiné le cation $(H_2PNH_3)^+$ issu d'une protonation sur l'azote de l'aminophosphane.

L'ensemble des paramètres géométriques minimisés et la répartition des charges sur les deux cations sont présentés dans le tableau 2 et la figure 3.

TABLEAU 2. Géométries minimisées pour $(H_3PNH_2)^+$ et $(H_2PNH_3)^{+a}$

Paramètre	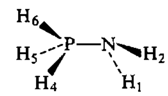	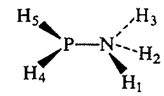
P—N	1,616	1,882
$N—H_1$	1	0,997
$N—H_2$	1	
$N—H_3$		0.996
$P—H_4$	1,405	1,412
$P—H_5$	1,405	1,412
$P—H_6$	1,405	
$H_1\widehat{N}P$	122,85	114,87
$H_2\widehat{N}P$	121,6	109,98
$H_3\widehat{N}P$		109,92
$H_1\widehat{N}H_2$	113,37	107,71
$H_1\widehat{N}H_3$		107,55
$H_4\widehat{P}N$	111,93	92,66
$H_5\widehat{P}N$	107,99	92,65
$H_6\widehat{P}N$	116,01	
$H_4\widehat{P}H_5$	108,08	94,88
$H_4\widehat{P}H_6$	105,63	
H_4PNH_1	58,76	47,43
H_5PNH_1	177,62	47,58
H_6PNH_1	62,54	
$E_{el}{}^b$	−469,851525	−464,598516
$E_{rep}{}^c$ (N—N)	72,439316	67,176273
E_t	−397,412209	−397,422143
ΔE_t	26,05	

[a]Longueurs, en angstroms; angles, en degrés; E, en hartrees; $\Delta E_t = E(H_3PNH_2^+) - E(H_2PNH_3^+)$, en kilojoules par mole.
[b]E_{el}: énergie d'interaction électron−noyau, électron−électron.
[c]E_{rep}: énergie de répulsion internucléaire.

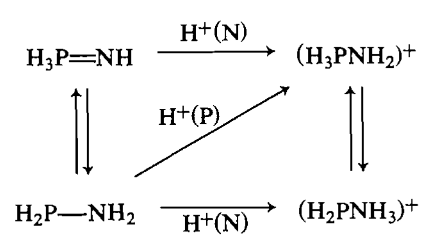

Pour le cation $(H_3PNH_2)^+$, nous observons une longueur de liaison (1,616 Å) intermédiaire entre celles de l'iminophosphane (1,532 Å) et de l'aminophosphane (1,685 Å), mais plus proche de cette dernière. De la même manière, l'indice de population obtenu pour la liaison P—N (0,32) est plus proche de celui de l'aminophosphane (0,24) que de la valeur trouvée dans le cas de l'iminophosphane (0,51).

Parallèlement, nous constatons une pyramidalisation de l'atome de phosphore plus marquée que dans l'iminophosphane. L'atome d'azote présente, quant à lui, un état d'hybridation voisin de sp^2, très proche de celui obtenu pour l'aminophosphane, la dernière orbitale occupée du système étant fortement localisée sur l'azote et correspondant à la n_N^{π}.

Au vu de sa structure géométrique, ce cation se présente plus comme le résultat d'une protonation sur le phosphore de l'aminophosphane que comme celui d'une protonation sur l'azote de l'iminophosphane.

L'analyse de population selon Mulliken fait toujours apparaître une polarité $P^+—N^-$ moins marquée que pour H_3PNH, avec un phosphore un peu moins positif et un azote légèrement plus négatif. Il faut remarquer que la charge +1 est entièrement localisée sur le groupement PH_3.

Ces résultats sont à rapprocher de ceux obtenus pour l'iminophosphène (HP=NH), à savoir que, lors d'une protonation sur l'azote, cet atome qui avait perdu des électrons en drainait toujours fortement en retour et l'espèce protonée se présentait, dans ce cas, comme un ion phosphénium $(H—P—NH_2)^+$.

De même, la structure électronique du cation $(H_3PNH_2)^+$ n'est pas celle d'un ion imminium, mais plus caractéristique d'un ion aminophosphonium du type 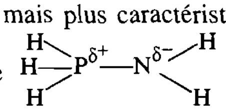 issu d'une protonation sur le phosphore de l'aminophosphane.

En ce qui concerne le cation $(H_2PNH_3)^+$ qui correspond à une protonation sur le site azote de l'aminophosphane, nous observons un allongement très important de la liaison P—N (tableau 2). Simultanément, nous notons un état d'hybridation plus nettement sp^3 au niveau de l'azote et une pyramidalisation très marquée au niveau du phosphore, l'HOMO du système étant localisée sur la paire de cet atome.

La polarité de la liaison P—N, toujours de type $P^+—N^-$, est pratiquement inchangée vis-à-vis de celle de l'aminophosphane, la charge +1 étant presque également répartie sur les deux groupements NH_3 et PH_2, avec un caractère plus positif, toutefois, chez ce dernier.

Ce cation présente donc un caractère hybride phosphane ammonium, avec une liaison P—N particulièrement longue, ce qui entraîne une importante diminution des répulsions internucléaires. Ainsi, le cation $(H_2PNH_3)^+$, en dépit du facteur électronique défavorable, apparaît comme l'espèce la plus stable énergétiquement (tableau 2).

Toutefois, la différence énergétique entre les deux formes protonées $(H_3PNH_2)^+$ et $(H_2PNH_3)^+$ est faible (de l'ordre de 26 kJ/mol), soit environ quatre fois moins importante que celle obtenue précédemment entre $(H_2PNH)^+$ et $(HPNH_2)^+$. Ceci peut expliquer la détection, par Dahl (14), des deux espèces cationiques en équilibre lors de la réaction d'aminophosphanes diversement substituées avec CF_3SO_3H.

L'atome d'azote est donc le site préférentiel de protonation dans l'aminophosphane. Il faut noter qu'une étude similaire sur l'iminosphosphène nous avait conduit à la même conclusion quant à la comparaison des sites P et N. Les affinités protoniques n'ont pas été déterminées pour les composés examinés, mais les résultats obtenus sont tout à fait cohérents avec ceux de Lohr *et al.* (15) concernant les affinités protoniques en phase gazeuse de dérivés phosphorés à liaison multiple P—C pour lesquels les comparaisons avec les analogues azotés ont toujours montré des valeurs plus importantes pour ces derniers.

L'examen comparatif, ci-dessous, des résultats obtenus pour les quatre cations provenant de la protonation de l'iminophosphène (**1** et **2**) et de l'iminophosphane (**3** et **4**), nous conduit aux remarques suivantes.

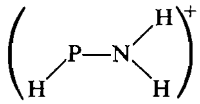

1
$d_{P—N}$ = 1,581 Å

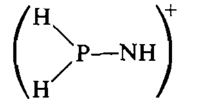

2
$d_{P—N}$ = 1,484 Å

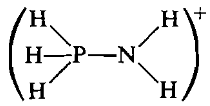

3
$d_{P—N}$ = 1,616 Å

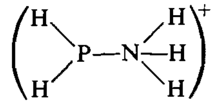

4
$d_{P—N}$ = 1,882 Å

Dans tous les cas, la polarité de la liaison P—N est du type $P^+—N^-$ et le caractère positif du phosphore va en diminuant de la structure phosphénium (**1**) au cation phospha-ammonium (**4**). Les longueurs de liaison P—N varient de 1,484 à 1,882 Å. Il est intéressant de constater que ces deux longueurs de liaison limites apparaissent dans les deux cations résultant de la protonation de l'atome d'azote d'une liaison P=N: iminophosphène pour **2** (d_{PN} = 1,481 Å), iminophosphane pour **4** (d_{PN} = 1,882 Å). Cette dernière valeur particulièrement grande est liée à la non-existence de transfert d'électrons de l'atome d'azote vers le phosphore.

3.2.2 *Anions $(H_2PNH)^-$ et $(HPNH_2)^-$*

Bien que les réactions d'abstraction d'hydrogène sur des aminophosphanes aient été fréquemment invoquées lors de synthèses de dérivés phosphorés et azotés (16), ce n'est que récemment que la structure des espèces anioniques impliquées a été discutée, par Cowley et Kemp (17), sur des bases expérimentales.

Nous avons donc entrepris l'analyse quantochimique de telles entités en examinant les deux systèmes, $(HPNH_2)^-$ et $(H_2PNH)^-$. Ils correspondent au départ d'un proton des sites P ou N de l'aminophosphane, $(H_2PNH)^-$ pouvant être aussi considéré comme issu d'une déprotonation sur le phosphore de l'iminophosphane. Il faut remarquer également que l'addition de H^- sur l'iminophosphène peut conduire formellement aux mêmes espèces.

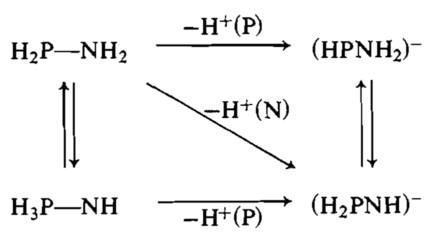

Les valeurs minimisées des paramètres géométriques et les répartitions de charge obtenues pour $(HPNH_2)^-$ et $(H_2PNH)^-$ sont présentées dans le tableau 3 et la figure 4.

Dans le cas de $(H_2PNH)^-$, c'est-à-dire lors d'un départ de H^+ du site azote de l'aminophosphane, nous constatons que l'apport électronique ne reste pas localisé sur cet atome, mais qu'un transfert vers le phosphore intervient via une interaction $p^{\pi}-d^{\pi}$; on note ainsi une population de 0,4 sur les orbitales d du phosphore et de 0,31 sur les diffuses de ce même centre. La polarité de la liaison demeure toutefois $P^+—N^-$. Ce transfert

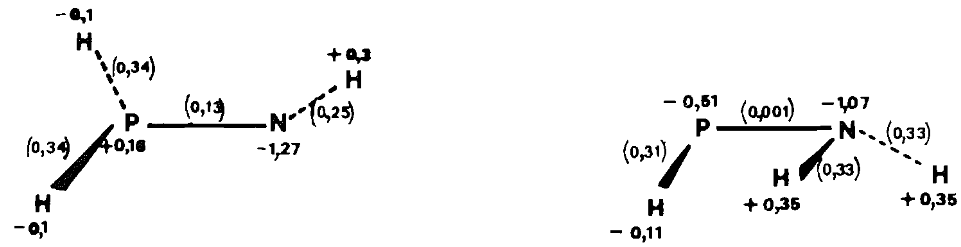

FIG. 4. $(H_2PNH)^-$ $(HPNH_2)^-$. Analyse des populations selon Mulliken. Charges nettes totales – populations de recouvrement (entre parenthèses).

TABLEAU 3. Géométries minimisées pour $(H_2PNH)^-$ et $(HPNH_2)^{-a}$

Paramètre	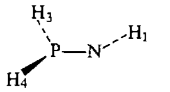	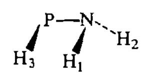
P—N	1,64	1,81
N—H₁	1	1,01
N—H₂		
P—H₃	1,39	1,42
P—H₄	105,64	113,7
$H_1\hat{N}P$		113,7
$H_2\hat{N}P$		
$H_1\hat{N}H_2$		106,2
$H_3\hat{P}N$	106,6	98,9
$H_4\hat{P}N$	106,48	
$H_3\hat{P}H_4$	89,54	
H_3PNH_1	132,32	60,62
H_4PNH_1	133,12	61,03
$E_{el}{}^{b}$	−452,8237	−448,9542
$E_{rep}{}^{c}$ (N—N)	56,37089	52,48178
E_t	−396,542795	−396,47239
ΔE_t	51,39	

[a]Longueurs, en angstroms; angles, en degrés; E, en hartrees; $\Delta E_t = E(H_2PNH^-) - E(HPNH_2^-)$, en kilojoules par mole.
[b]E_{el}: énergie d'interaction électron–noyau, électron–électron.
[c]E_{rep}: énergie de répulsion internucléaire.

est à l'origine de la diminution de la longueur de liaison P—N (1,64 Å) vis-à-vis de celle obtenue dans l'aminophosphane (1,685 Å).

On remarque également une pyramidalisation plus marquée de l'atome de phosphore et une rotation du système qui conduit à une augmentation de l'angle entre les paires du phosphore et de l'azote vis-à-vis de l'aminophosphane. L'HOMO de $(H_2PNH)^-$ résulte de l'interaction entre ces paires, l'avant dernière orbitale occupée correspondant à la paire de l'azote relocalisée par suite de la déprotonation.

En ce qui concerne l'anion $(HPNH_2)^-$, au contraire, l'apport électronique engendré par le départ de H^+, lié à P, reste localisé sur le phosphore qui présente ainsi une charge de −0,5; on remarque également, pour ce composé, une population importante de 0,77 sur les fonctions diffuses. La répartition de charge au niveau du groupement NH_2 est inchangée par rapport à celle obtenue dans l'aminophosphane; l'atome d'azote demeure néanmoins le centre porteur de la charge négative la plus importante du système.

Étant donné qu'une interaction $p_P^\pi - d_N^\pi$ ne peut intervenir, nous observons, dans ce cas, un allongement très notable de la liaison P—N (1,685 Å dans H_2PNH_2 et 1,81 Å dans $(HPNH_2)^-$), qui s'accompagne d'une nette pyramidalisation de l'atome d'azote ($\Sigma\hat{N} = 333{,}6°$).

Il est également intéressant de noter une disposition des paires du phosphore et de l'azote identique à ce qu'elle était dans H_2PNH_2, aucune rotation n'ayant eu lieu consécutivement au départ de H^+. L'interaction entre ces paires intervient au niveau de l'avant dernière orbitale occupée du système, l'HOMO étant caractéristique de la paire du phosphore relocalisée suite au départ de H^+.

Les deux anions, $(H_2PNH)^-$ et $(HPNH_2)^-$, présentent ainsi des structures bien différenciées. Dans le cas de $(H_2PNH)^-$, elle est du type $H_2\overset{\delta^-}{P}—\overset{\delta^-}{N}H$, avec une forte charge négative sur l'atome d'azote. L'anion $(HPNH_2)^-$ correspond, quant à lui, à une structure $H\overset{\delta^-}{P} — \overset{\delta^-\delta^-}{N}H_2$, simple liaison P—N avec atome d'azote porteur de la charge négative la plus importante.

Ainsi, parmi les formes limites généralement envisagées pour ces anions, les résultats obtenus mettent parfaitement en évidence une structure **6**, et non **7**, pour l'anion $(H_2PNH)^-$ qui apparaît comme un anion de type phospha-amidure.

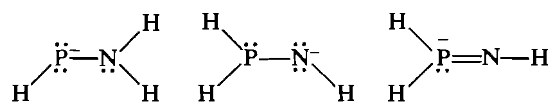

5 **6** **7**

Ceci va à l'encontre des conclusions énoncées par Cowley (17) qui, sur des bases expérimentales, proposait une structure de type **7** pour ce même anion.

En ce qui concerne les stabilités relatives des deux anions examinés, l'allongement notable de la liaison P—N dans $(HPNH_2)^-$ induit une diminution importante des répulsions internucléaires, ce qui conduit globalement, en dépit d'une énergie électronique plus basse pour $(H_2PNH)^-$, à une forme $(HPNH_2)^-$ favorisée énergétiquement. Il faut noter, toutefois, que la différence est assez faible entre les deux anions (de l'ordre de 51 kJ/mol).

L'aminophosphane peut être ainsi considérée comme un acide de site P. Ces résultats sont cohérents avec ceux obtenus par Lohr et Ponas (*4b*) lors d'une étude sur les acidités en phase gazeuse de systèmes à liaisons multiples C—N et C—P et, en particulier, de H_3CNH_2 et H_3CPH_2. Ces deux derniers composés sont apparus comme des acides de site hétéro-atome, H_3CPH_2 étant un acide plus fort que H_3CNH_2.

Si nous examinons maintenant l'addition de H^- sur l'iminophosphène, nous ne pouvons, au vu de la répartition de charge sur ce système ($Q_P = +0{,}49$; $Q_N = -0{,}81$), que conclure à un produit cinétique $(H_2PNH)^-$ de structure **6**, différent du produit thermodynamique $(HPNH_2)^-$ de structure **5**. Les dispositions relatives de la paire de l'azote et des protons du groupement PH_2 permettent d'envisager cette évolution via une migration 1,2, ce qui pourrait expliquer raisonnablement les résultats expérimentaux (17).

1. D. GONBEAU, G. PFISTER-GUILLOUZO et J. BARRANS. Can. J. Chem. **61**, 1371 (1983).
2. M. PETERSON et R. POIRIER. University of Toronto, Toronto, Ontario, Canada, W. C. Davidson, L. Nazareth, Argonne Natl. Lab. Tech. Memos, 303, 306, Argonne, Illinois, U.S.A.
3. R. DITCHFIELD, W. J. HEHRE et J. A. POPLE. J. Chem. Phys. **54**, 724 (1971).
4. (*a*) J. CHANDRASEKHAR, J. G. ANDRADE et P. v. R. SCHLEYER. J. Am. Chem. Soc. **103**, 5609 (1980), et références citées; (*b*) L. L. LOHR et S. H. PONAS. J. Phys. Chem. **88**, 2992 (1984).
5. K. A. OSTOJA STARZEWSKI et H. TOM DIECK. Inorg. Chem. **18**, 3307 (1979).
6. (*a*) M. R. MARRE, M. SANCHEZ, R. WOLF, J. JAUD et J. GALY. Can. J. Chem. **62**, 2186 (1984); (*b*) G. J. MARTIN, M. SANCHEZ et M. R. MARRE. Tetrahedron Lett. **24**, 4989 (1983); (*c*) M. R. MARRE, M. SANCHEZ, J. F. BRAZIER, R. WOLF et J. BELLAN. Can. J. Chem. **60**, 456 (1982).
7. (*a*) I. ABSAR et J. R. VAN WAZER. J. Am. Chem. Soc. **94**, 2382 (1972); (*b*) H. LISCHKA. J. Am. Chem. Soc. **99**, 353 (1977); (*c*) F. BERNARDI, H. B. SCHLEGEL, M. H. WANGBO et S. WOLFE. J. Am. Chem. Soc. **99**, 5633 (1977); (*d*) A. STRICH. Nouv. J. Chim. **3**, 105 (1979); (*e*) G. TRINQUIER et J. PL. MALRIEU. J. Am. Chem. Soc. **101**, 7169 (1979).
8. M. W. SCHMIDT, S. YABUSHITA et M. S. GORDON. J. Phys. Chem. **88**, 382 (1984).
9. D. GONBEAU, D. LIOTARD et G. PFISTER-GUILLOUZO. Nouv. J. Chim. **4**, 227 (1980).
10. A. SCHMIDPETER et J. ROSSKNECHT. Z. Naturforsch. Teil B, **26**, 81 (1971).
11. M. BINDER et R. FISHER. Chem. Ber. **107**, 205 (1974).
12. (*a*) I. N. ZHMUROVA, A. P. MARTYNYUK et A. V. KIRSANOV. Zh. Obshch. Khim. **30**, 3044 (1960); (*b*) A. F. GRAPOV, L. V. RAZVODOVSKAYA et N. N. MEL'NIKOV. Russian Chem. Rev. **50**(4), 324 (1981).
13. R. G. PEARSON. Acc. Chem. Res. **4**, 152 (1971).
14. O. DAHL. Tetrahedron Lett. **23**, 1493 (1982).
15. L. L. LOHR, H. B. SCHLEGEL et K. MOROKUMA. J. Phys. Chem. **88**, 1981 (1984).
16. (*a*) E. NIECKE et G. RINGEL. Angew Chem. Int. Ed. Engl. **16**, 486 (1977); (*b*) E. NIECKE, A. NICKLOWEIT-LUKE et R. RÜGER. Angew. Chem. Int. Ed. Engl. **20**, 385 (1981).
17. A. H. COWLEY et R. A. KEMP. J. Chem. Soc. Chem. Commun. 319 (1982).

Spectral and bonding properties of bis(*N*,*N*-disubstituted-dithiocarbamato)iron(III)dihalide complexes studied by experimental and EHMO quantum-chemical methods

GEORGE A. KATSOULOS, CONSTANTINOS A. TSIPIS,[1] AND FOTIOS D. VAKOULIS

Department of General and Inorganic Chemistry, University of Thessaloniki, Thessaloniki, Greece

Received December 20, 1984

GEORGE A. KATSOULOS, CONSTANTINOS A. TSIPIS, and FOTIOS D. VAKOULIS. Can. J. Chem. **63**, 3249 (1985).

A new series of homobinuclear iron(III) halobisdithiocarbamate complexes antiferromagnetically coupled through a molecular halogen bridging unit has been synthesised and studied. The complexes have been characterized chemically and by spectroscopic methods and magnetic susceptibility measurements. The volatility characteristics and thermogravimetric analysis data for the new compounds are also studied. Finally, quantum-chemical calculations have been used to provide a qualitative guide to the possible pathways for the superexchange processes observed in these molecular magnetic systems, as well as to interpret their electronic spectra.

GEORGE A. KATSOULOS, CONSTANTINOS A. TSIPIS et FOTIOS D. VAKOULIS. Can. J. Chem. **63**, 3249 (1985).

On a synthétisé et étudié une nouvelle série de complexes halobisdithiocarbamate de fer(III) couplés de façon antiferromagnétique à l'aide d'un halogène moléculaire en position de pont. On a fait appel à des méthodes spectroscopiques et à des mesures de susceptibilité magnétique pour caractériser chimiquement ces complexes. On a également étudié les caractéristiques de volatilité et les données d'analyse thermogravimétrique des nouveaux composés. Finalement on a fait appel à des calculs de chimie quantique pour obtenir un guide qualitatif des voies d'accès possibles au processus de superéchange observé dans ces systèmes magnétiques moléculaires, aussi bien que pour interpréter leur spectre électronique.

[Traduit par le journal]

Introduction

The rare occurrence of iron(III) in an $S = 3/2$ ground state associated with an unusual coordination of the iron atom has made the halobis(*N*,*N*-dialkyldithiocarbamato)iron(III) complexes the object of numerous experimental and theoretical investigations (1−8). In addition, the iodobisdithiocarbamate complexes, $[Fe(R_2dtc)_2I]$, were found to react with molecular iodine in aprotic solvents (9) to yield several types of products, including those with stoichiometry $Fe(R_2dtc)_2I_2$ (where R = Me or Pr^i) and $Fe(Et_2dtc)_2I_3$. The last compound has been proved to be an iron(III) complex containing coordinated triiodide, the presence of an I_3^- unit with one of the terminal iodines bonded to the metal ion of the $\{Fe(Et_2dtc)_2\}$ group being demonstrated by ^{57}Fe and ^{129}I Mössbauer spectroscopy (10, 11). For the remaining complexes it has been suggested (9) that they may be adducts of the type $2[Fe(R_2dtc)_2I]\cdot I_2$. Furthermore, Mössbauer measurements on the molecular complex $Fe(Me_2dtc)_2I_2$ have demonstrated (11) that it contains a molecular iodine (I_2) unit mediating the formation of weakly coupled dimers with antiferromagnetic interaction. These conclusions are consistent with an X-ray crystal structure determination (12) of another derivative of this series containing the pyrrolidinyldithiocarbamato ligand. Thus, an interaction between the iodine molecule and the iodide ligands of the complex was confirmed, with the overall result that there would be a loose "dimeric" association of the type $(R_2NCS_2)_2FeI\cdots I{-}I\cdots IFe(S_2CNR_2)_2$. Although a detailed study of the effect of the particular iron(III) dithiocarbamate used on the course of the aforesaid reaction has not been undertaken, it does appear that the nitrogen substituent R has an effect on the nature of the obtained products (9, 11). Moreover, a study of the role of bridging molecular halogens (X_2') in the formation of antiferromagnetically coupled dimers would be of considerable importance. In this paper we present our results on the synthesis and the characterization of some new homobinuclear iron(III) dithiocarbamate complexes of the general formula $[Fe(R_2dtc)_2X]_2(\mu - X_2')$, as well as the theoretical prediction based on EHMO quantum-chemical calculations, of the possible pathways for the superexchange processes observed in these compounds.

[1]Author to whom correspondence should be addressed.

Experimental

Physical measurements

Infrared spectra were recorded in the 4000−250 cm^{-1} region on a Perkin−Elmer 467 spectrophotometer using KBr pellets or Nujol mulls. Electronic spectra were obtained on a Cary 17DX spectrophotometer using freshly prepared methylene chloride solutions. Mössbauer spectra were obtained with a conventional constant accelerator spectrometer. The source was 25 mCi of ^{57}Co in a copper matrix. Mass spectra were measured on a RMU-6L Hitachi Perkin−Elmer mass spectrometer with ionisation source of T-2*p* type operating at 70 eV. The thermogravimetric curves were obtained on a TGS-2 Perkin−Elmer thermobalance using nitrogen furnace atmosphere. Magnetic susceptibility measurements in solid state were done by the Faraday technique at different magnetic field strengths using $Hg[Co(SCN)_4]$ as the calibrant. Diamagnetic corrections were made using Pascal's constants. Conductivity measurements were done in a Wheatstone bridge Model RC 216B$_2$ using 10^{-3} *M* solutions in acetone. Molecular weights were determined using a Perkin−Elmer molecular weight apparatus Model 115 in methylene chloride solutions. The elemental analysis of carbon, nitrogen, and hydrogen was performed on a Perkin−Elmer 240B Elemental Analyzer.

Starting materials

All solvents were of reagent grade and were used without further purification in synthetic work. Tris(*N*,*N*-disubstituted-dithiocarbamato)iron(III) complexes were prepared and recrystallised as previously reported (13). The halobis(*N*,*N*-dialkyldithiocarbamato)iron(III) complexes were obtained from the reaction between an iron(III) trisdithiocarbamate and aqueous hydrohalic acid (1, 2). All the other reagents were obtained commercially.

Preparation of the complexes

The new complexes were prepared according to the following general method. A solution of 2 mmol of the appropriate $[Fe(R_2dtc)_2X]$ complex in 50 cm^3 of methylene chloride was treated with 1 mmol of I_2 or Br_2 dissolved in the same solvent and the reaction mixture was left for 5 h at room temperature under continuous magnetic stirring.

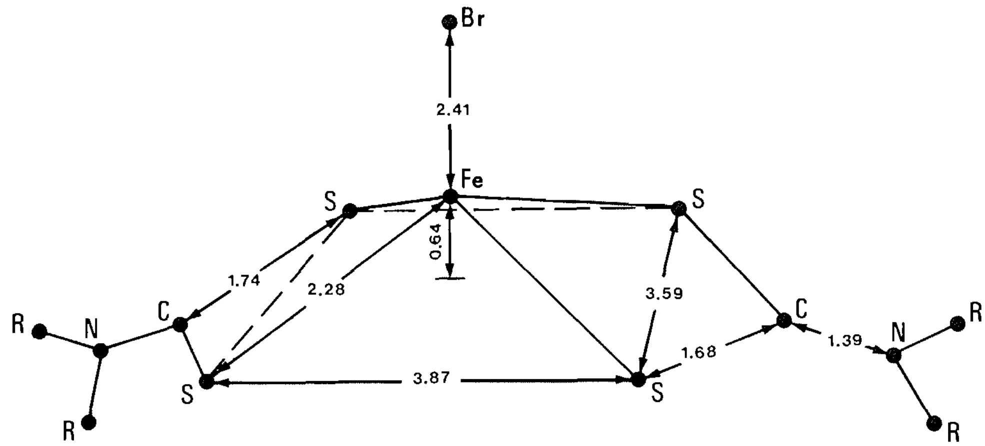

FIG. 1. Molecular structure of bromobis(*N*,*N*-diisopropyldithiocarbamato)iron(III). Distances are given in Å (8).

TABLE 1. Analytical data for the new complexes*

Compound	Yield (%)	Melting point (°C)	Analysis (%) C	N	H	Molecular weight
$2[Fe(Me_2dtc)_2Cl]\cdot I_2$	62	180–182 dec.	15.90 (15.71)	6.02 (6.11)	2.51 (2.64)	960 (917.3)
$2[Fe(Et_2dtc)_2Cl]\cdot I_2$	67	178–180 dec.	23.40 (23.33)	5.49 (5.44)	3.87 (3.92)	1050 (1029.5)
$2[Fe(Pr^i_2dtc)_2Cl]\cdot Br_2$	68	170–172 dec.	32.00 (32.10)	5.28 (5.35)	5.24 (5.39)	1100 (1047.7)
$2[Fe(Pr^i_2dtc)_2Cl]\cdot I_2$	75	212–214 dec.	29.01 (29.46)	4.71 (4.91)	4.85 (4.94)	1180 (1141.7)
$2[Fe(Pr^i_2dtc)_2Br]\cdot I_2$	77	184–186 dec.	27.62 (27.33)	4.38 (4.55)	4.61 (4.59)	1260 (1230.6)
$2[Fe(Pr^i_2dtc)_2I]\cdot Br_2$	72	210–212 dec.	27.46 (27.33)	4.67 (4.55)	4.70 (4.59)	1290 (1230.6)

*Calculated values in parentheses.

After the addition of 50 cm^3 of cyclohexane the solution was condensed to a small volume under reduced pressure, causing black crystals to separate. The resultant solid material was filtered off, washed with cyclohexane, recrystallised several times from methylene chloride–cyclohexane mixtures, and dried under vacuum.

Calculations

The quantum-chemical calculations on the $[Fe(Pr^i_2dtc)_2Br]$ complex and the linear tetratomic halogeno bridging unit were carried out by means of the LCAO-MO extended Hückel method (14). The computer program (15) used was based on the self-consistent charge method. The cartesian coordinates of the atoms were computed using a recently published (8) crystal structure of the complex which is depicted in Fig. 1. The z axis of the coordinate system has been taken along the direction of Fe—Br, and the x axis in the plane of the atoms Fe, Br, and C, and parallel to the plane of the four sulfur atoms. In order to limit the number of atomic wave functions, the isopropyl groups were replaced by hydrogen atoms, the N—H distance being 1.01 Å (16). The basis set used consisted of all the 49 valence orbitals, in which 58 electrons were placed. The radial part of the atomic wave functions were the double exponent (3*d* functions) or single exponent (all the other functions) Slater-type orbitals given in the literature (17–19).

Results and discussion

Reaction of a solution of $[Fe(R_2dtc)_2X]$ (R = Me, Et, Pr^i; X = Cl, Br, I) in methylene chloride with molecular halogens (2:1 molar ratios) rapidly gave clear solutions from which solid compounds of stoichiometry $Fe(R_2dtc)_2XX'$ (X′ = Br, I) were isolated, either by precipitation with cyclohexane or by removal of solvent under reduced pressure. The dihalide complexes crystallise as black crystals. These crystals are soluble in acetone, methylene chloride, acetonitrile, and nitromethane to give brownish solutions, and are insoluble in benzene, cyclohexane, ether, and water. The compounds are stable in the absence of moist air, while in the presence of atmospheric moisture they slowly hydrolyse. This tendency to hydrolyse increases on passing from the chloro to the iodo derivatives, perhaps because of the presence of a weak iron(III)–iodine bond. They also decompose at lower temperatures than the corresponding halobisdithiocarbamate complexes. The low values of the molar conductivity in anhydrous acetone (2–10 ohm^{-1} cm^2 mol^{-1}) indicate the non-electrolyte character of the complexes, whereas osmometric molecular-weight measurements in methylene chloride show them to be dimeric. Data from elemental analyses, decomposition temperatures, and molecular weights of the new compounds are given in Table 1.

The compounds were found to react with olefins, such as ethylene and cyclohexene, in methylene chloride solutions to afford green crystalline complexes formulated as $[Fe(R_2dtc)_2X]$ and the corresponding 1,2-addition products. The halogenation reaction were carried out at room temperature and, in the case of ethylene, under atmospheric pressure. This easy addition of halogen to an unhindered carbon–carbon double bond strongly suggests that the complexes under investigation may be adducts with molecular halogens.

The frequencies (cm^{-1}) of the most relevant absorption bands in the ir spectra of the studied compounds and their tentative assignments are presented in Table 2. The ν(C$\cdots$N)

TABLE 2. The most relevant ir frequencies (cm^{-1}) of the investigated compounds and their assignments (KBr discs)*

Compound	$\nu(\text{C}\overset{\cdot\cdot}{-}\text{N})$	$\nu(\text{C}\overset{\cdot\cdot}{-}\text{S})$	ν(Fe—S)	ν(Fe—X)
$2[Fe(Me_2dtc)_2Cl]\cdot I_2$	1540vs	992s	355vs	301m
$2[Fe(Et_2dtc)_2Cl]\cdot I_2$	1535vs	996s	355s	310m
$2[Fe(Pr^i_2dtc)_2Cl]\cdot Br_2$	1515vs	1020s	367vs	318w
$2[Fe(Pr^i_2dtc)_2Cl]\cdot I_2$	1518vs	1020s	365vs	318w
$2[Fe(Pr^i_2dtc)_2Br]\cdot I_2$	1518vs	1021s	366vs	295m
$2[Fe(Pr^i_2dtc)_2I]\cdot Br_2$	1515vs	1025m	368s	

*vs = very strong, s = strong, m = medium, w = weak.

and $\nu(\text{C}\overset{\cdot\cdot}{-}\text{S})$ stretching frequencies fall in the range 1540–1515 cm^{-1} and 1025–992 cm^{-1}, respectively. The presence of only one strong band in the region where $\nu(\text{C}\overset{\cdot\cdot}{-}\text{S})$ lies, strongly supports chelation of the dithiocarbamates, a doublet being expected in the region 1000 ± 70 cm^{-1} in the unchelated dithiocarbamates (20). However, the spectra did not show any peaks that could be ascribed to monodentate dithiocarbamato ligand or to thiuram disulfide (21). The bidentate bonding mode of the dithio-ligands was further established by the position of the $\nu(\text{C}\overset{\cdot\cdot}{-}\text{N})$ band (22). This band is shifted to somewhat higher frequencies compared to the corresponding $[Fe(R_2dtc)_2X]$ complexes (9, 23). Furthermore, single peaks have been observed in the range 370–355 cm^{-1}, which are likely to be due to metal–sulfur modes according to the observed values for the dithiocarbamates of the first-row transition metals. Finally, the bands occurring in the range 318–295 cm^{-1} were attributed to the iron–halogen stretching vibrations (24, 25) and are in good agreement with those previously reported for the five-coordinated iron(III) halobisdithiocarbamate complexes. This is an indication for the coordination of only one halogen to the metal atom, because the vibrational modes ν(Fe—X) are strongly dependent on the stereochemistry of the complex for an increasing of the coordination number results in a decrease in the M—X stretching vibrations (23, 26).

The magnetic susceptibilities corrected for diamagnetism are shown in Table 3. The room-temperature moments for all the derivatives range from 3.77 to 3.92 BM, thus approximating well the theoretical effective moment of 3.88 BM predicted for $S = 3/2$ and $g = 2.00$. The structural requirement for such behaviour can be met by a square-pyramidal symmetry around the ferric ion (27, 28).

Mössbauer spectra were recorded at liquid nitrogen temperature; the data (δ, isomer shift; Δ, quadrupole splitting) for the new complexes are listed in Table 3, and a representative spectrum is shown in Fig. 2. The spectra consisted of widely split doublets with peaks of equal area. The experimental error in the quadrupole splittings was estimated to be ± 0.03 mm s^{-1} on the bases of replicate measurements. The isomer shifts occur in the range 0.67–0.70 mm s^{-1}, relative to sodium nitroprusside. These values are comparable to the shifts expected for iron(III) dithiocarbamates (3, 29). The complexes had also quadrupole splittings in the 2.71–2.86 mm s^{-1} range similar to those of the $[Fe(R_2dtc)_2X]$ complexes (3). The similarity in magnetic susceptibility and in the Mössbauer parameters suggests a geometrical correspondence between the studied compounds and the halobisdithiocarbamates, which can be attained by the presence of a molecular halogen moiety weakly bonded to two $\{Fe(R_2dtc)_2X\}$ units as required by stoichiometry. The proposed configuration for the five-coordinated $2[Fe(R_2dtc)_2X]\cdot X'_2$ complexes is depicted in Fig. 3.

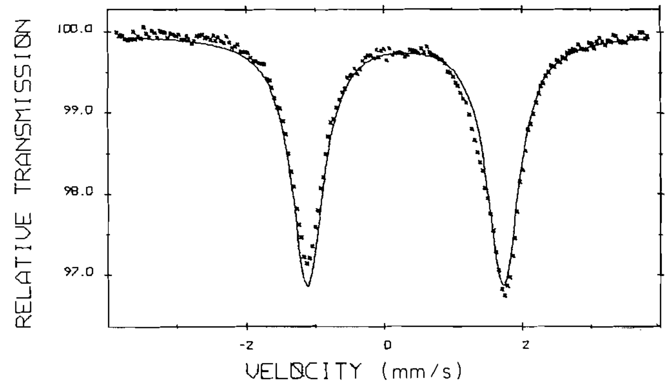

FIG. 2. Mössbauer spectrum of $[Fe(Pr^i_2dtc)_2I]_2(\mu - Br_2)$ at 77 K.

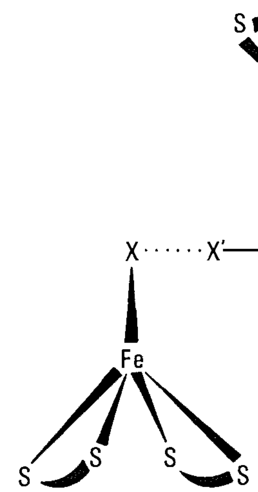

FIG. 3. Proposed structural model of the $[Fe(R_2dtc)_2X]_2(\mu - X'_2)$ complexes.

The thermogravimetric study of both the halobisdithiocarbamates and the compounds under investigation further confirms the formation of a dimeric association through a molecular halogen bridging unit. For example, the thermograms of the $[Fe(Et_2dtc)_2Cl]$ complex show three endothermic decompositions corresponding to a three-stage weight loss of 78%. A long plateau then results for which there is evidence of FeS formation. The three weight losses occur at 260, 300, and 410°C and can be attributed to the loss of $\{2Et_2NCS\}$ (found: 61.0%; calcd.: 59.9%), {Cl} (found: 9.0%; calcd.: 9.1%), and {S} (found: 8.0%; calcd.: 8.3%), respectively. On the other hand, the thermograms of $2[Fe(Et_2dtc)_2Cl]\cdot I_2$ composed of three weight losses, all of them endothermic at 110, 290, and 370°C which can be attributed to loss of $\{4Et_2NCS + 2I\}$ (found: 69.5%; calcd.: 69.8%), {2Cl} (found: 7.0%; calcd.: 6.9%), and {2S} (found: 6.5%; calcd.: 6.2%), respectively.

Finally, the mass spectra of the compounds reveal the presence of a molecular halogen moiety. The molecular ions of the dimeric species are not detected in the ms. The absence of molecular ions can be attributed either to pyrolytic decomposition, in the direct inlet, under the high temperature which was used (200–280°C), or to electron impact. However, in all spectra the ion $[Fe(R_2dtc)_2X]^+$ is present and can be regarded as direct fragment of the molecular ion upon elimination of the molecular halogen bridging unit. This is further supported by

TABLE 3. Magnetic data* and Mössbauer parameters of the complexes at 77 K

Compound	$\chi_M \times 10^6$ (cgsu)	μ_{eff}^{cor} (BM)	δ† (mm s^{-1})	Δ (mm s^{-1})
$2[Fe(Me_2dtc)_2Cl]\cdot I_2$	6149	3.88	0.68	2.72
$2[Fe(Et_2dtc)_2Cl]\cdot I_2$	5484	3.77	0.70	2.73
$2[Fe(Pr^i_2dtc)_2Cl]\cdot Br_2$	5809	3.78	0.67	2.83
$2[Fe(Pr^i_2dtc)_2Cl]\cdot I_2$	6566	3.83	0.69	2.71
$2[Fe(Pr^i_2dtc)_2Br]\cdot I_2$	6399	3.92	0.69	2.84
$2[Fe(Pr^i_2dtc)_2I]\cdot Br_2$	6755	3.89	0.69	2.86

*Temperature ≅ 22°C.
†Isomer shift relative to sodium nitroprusside.

TABLE 4. Valence molecular orbitals of the square-pyramidal (C_{2v}) $[Fe(Pr^i_2dtc)_2Br]$ complex*

		Charge distribution‡ (%)						Basis functions		
Level†	Energy (eV)	Fe	Br	4S	2N	2C	4H	Fe	Br	4S
$14b_1$	80.03	83	0	14	0	3	0	p_x		s
$10b_2$	47.95	78	0	17	0	5	0	p_y		s
$17a_1$	44.66	48	1	31	0	20	0	s		s
$16a_1$	37.99	85	13	2	0	0	0	p_z	s	
$14a_1$	13.51	24	0	25	17	13	21	s		p_x
$6a_2$	−6.99	45	0	53	0	2	0	d_{xy}		p_x
$11a_1$	−9.73	64	11	7	6	12	0	d_{z^2}	p_z	
$7b_2$	−9.87	60	5	34	0	1	0	d_{yz}	p_y	p_x
$9b_1$	−10.14	68	7	17	3	5	0	d_{xz}	p_x	p_x
$10a_1$	−10.68	98	0	1	0	1	0	$d_{x^2-y^2}$		
$6b_2$	−10.88	12	0	87	0	1	0	d_{yz}		p_y, p_z
$5a_2$	−11.06	1	0	99	0	0	0			p_x, p_z
$5b_2$	−11.64	19	0	76	4	1	0	d_{xz}		p_x, p_y
$8b_1$	−11.65	16	15	68	0	1	0	d_{yz}	p_y	p_z
$4a_2$	−11.67	28	0	66	0	6	0	d_{xy}		p_y
$9a_1$	−12.27	11	2	80	7	0	0	d_{z^2}		p_x, p_y
$8a_1$	−12.39	13	0	42	43	2	0	d_{z^2}		p_z
$6b_1$	−12.72	14	78	8	0	0	0	d_{yz}	p_y	
$4b_2$	−12.73	9	73	9	9	0	0	d_{xz}	p_x	
$7a_1$	−12.99	13	79	8	0	0	0	d_{z^2}		p_z
$3a_2$	−13.08	21	0	56	0	23	1	d_{xy}		p_x
$3b_2$	−13.77	6	3	58	0	31	2	p_y		p_x
$4b_1$	−14.56	2	1	49	17	28	3			p_y
$1b_2$	−22.72	8	0	78	0	14	0	p_y		s
$3a_1$	−24.55	10	85	3	0	2	0	p_z	s	

*The valence molecular orbitals listed are only those associated with both the central atom and ligand valence AO's.
†The highest occupied level is $11a_1$.
‡Percentage of the MO's total population located on the indicated atoms or group of atoms.

the detection of a peak with a variable relative intensity (54−100%) due to $X_2'^{+\cdot}$ ion. In the cases of $2[Fe(R_2dtc)_2X]\cdot I_2$ complexes the base peak of the spectra corresponds to the $I_2^{+\cdot}$ ion.

The electronic spectra of the studied compounds are complicated, exhibiting a number of overlapping intense bands in the ultraviolet and visible region. The complicated nature of the spectra prevents any simple classification and rationalization in terms of the ligand-field model. This is a general problem encountered in any ligand-field interpretation of the electronic spectra of many iron(III) halobisdithiocarbamate complexes (3, 7, 9, 23, 30). Therefore, an attempt was made to interpret the electronic spectra of the dimeric complexes by means of EHMO quantum-chemical calculations on a representative mononuclear complex bearing the same FeS_4X chromophore, namely, $[Fe(Pr^i_2dtc)_2Br]$.

The calculated ground state 1e energies, charge distributions and partial wave analyses for the valence molecular orbitals associated with both the central atom and the ligand valence AO's of the complex are summarized in Table 4. The energy level spacings of the predominantly 3*d*-orbital-based MO's are given in Fig. 4. This sequence of MO's is exactly the one expected on the basis of esr measurements (2). The high energy of the $6a_2$ molecular orbital accounts for the spin pairing of the fifth *d* electron. The occupied valence molecular orbitals of the complex have energies in the range −30.49 to −9.73 eV, while the energies of the virtual MO's range from −7.85 to 80.02 eV. The two-center energy terms for the Fe—Br (−7.05 eV) and Fe—S (−4.74 eV) bonds clearly show that the former is the most covalent. This is also consistent with the

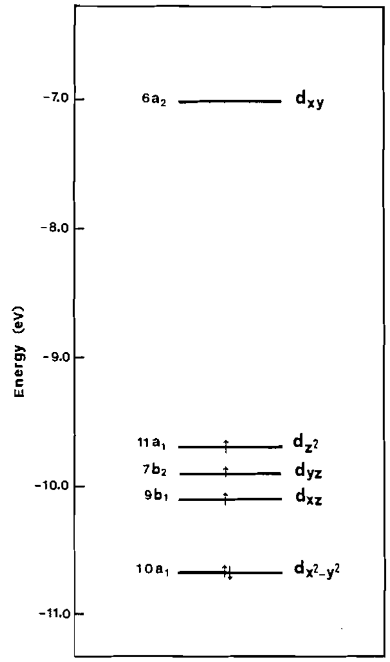

FIG. 4. Energy level spacings of the predominantly 3d-orbital-based MO's of bromobis(N,N-diisopropyldithiocarbamato)iron(III).

TABLE 5. Transitions and assignments in the electronic spectrum of the [Fe(Pr^i_2dtc)$_2$Br] complex

Observed bands kK (log ϵ_{mol})	Assignment	Calcd kK	General classification
39.7 (4.48)	$10b_1 \leftarrow 6b_1$	39.9	$L(\pi^*) \leftarrow L(\pi)$
	$12a_1 \leftarrow 6b_1$	39.3	$L(\pi^*) \leftarrow L(\pi)$
37.7sh (4.28)	$6a_2 \leftarrow 8b_1$	38.1	$M(d) \leftarrow L(\pi)$
	$11a_1 \leftarrow 6a_1$	37.8	$M(d) \leftarrow L(\pi)$
35.5sh (4.22)	$12a_1 \leftarrow 8a_1$	36.9	$L(\pi^*) \leftarrow L(\pi)$
	$10b_1 \leftarrow 9a_1$	36.8	$L(\pi^*) \leftarrow L(\pi)$
	$12a_1 \leftarrow 9a_1$	36.2	$L(\pi^*) \leftarrow L(\pi)$
	$10b_1 \leftarrow 7b_1$	35.0	$L(\pi^*) \leftarrow L(\pi)$
32.5 (4.13)	$6a_2 \leftarrow 6b_2$	31.9	$M(d) \leftarrow L(\pi)$
	$7b_2 \leftarrow 3b_2$	31.9	$M(d) \leftarrow L(\pi)$
29.9sh (4.03)	$12a_1 \leftarrow 5b_2$	31.1	$L(\pi^*) \leftarrow n(S)$
	$10b_1 \leftarrow 5a_2$	27.0	$L(\pi^*) \leftarrow n(S)$
25.8 (3.87)	$7b_2 \leftarrow 3a_2$	26.6	$M(d) \leftarrow L(\pi)$
	$11a_1 \leftarrow 7a_1$	26.5	$M(d) \leftarrow L(\pi)$
	$7b_2 \leftarrow 7a_1$	25.4	$M(d) \leftarrow L(\pi)$
	$6a_2 \leftarrow 9b_1$	25.3	$M(d) \leftarrow M(d)$
22.4 (3.88)	$6a_2 \leftarrow 7b_2$	23.0	$M(d) \leftarrow M(d)$
	$12a_1 \leftarrow 10a_1$	22.5	$L(\pi^*) \leftarrow M(d)$
20.2sh (3.66)	$10b_1 \leftarrow 9b_1$	18.9	$L(\pi^*) \leftarrow M(d)$
	$12a_1 \leftarrow 9b_1$	18.2	$L(\pi^*) \leftarrow M(d)$
16.2 (3.68)	$12a_1 \leftarrow 7b_2$	16.0	$L(\pi^*) \leftarrow M(d)$
	$10b_1 \leftarrow 11a_1$	15.6	$L(\pi^*) \leftarrow M(d)$
—	$11a_1 \leftarrow 10a_1$	7.6	$M(d) \leftarrow M(d)$
—	$7b_2 \leftarrow 10a_1$	6.5	$M(d) \leftarrow M(d)$
—	$9b_1 \leftarrow 10a_1$	4.3	$M(d) \leftarrow M(d)$

values of the overlap population which is 0.574 and 0.412, respectively. These values are characteristic for a high covalency of the two bonds which further explains the low positive charge on the central atom (Q = +0.099). Moreover, the net charges on the Br and S atoms are −0.373 and −0.039 electron units, respectively. The higher electron charge on the halogeno-ligand may also account for its weak interactions with the molecular halogen through the virtual σ^* antibonding

TABLE 6. Electronic spectral data of the new compounds for methylene chloride solutions

Observed bands, kK (log ϵ_{mol})						
2[Fe(Me_2dtc)$_2$Cl]·I_2	2[Fe(Et_2dtc)$_2$Cl]·I_2	2[Fe(Pr^i_2dtc)$_2$Cl]·Br_2	2[Fe(Pr^i_2dtc)$_2$Cl]·I_2	2[Fe(Pr^i_2dtc)$_2$Br]·I_2	2[Fe(Pr^i_2dtc)$_2$I]·Br_2	General Classification
40.2 (4.97)	40.3 (4.86)	39.2 (4.61)	39.5 (4.90)	39.7 (5.04)	39.6 (4.60)	$L(\pi^*) \leftarrow L(\pi)$
37.3sh* (4.80)	37.2sh (4.81)	37.7sh (4.55)	37.6sh (4.86)	37.6sh (4.88)	37.6sh (4.54)	$M(d) \leftarrow L(\pi)$
35.7sh (4.65)	36.4sh (4.72)	35.4sh (4.47)	35.4sh (4.70)	35.3sh (4.71)	36.0sh (4.47)	$L(\pi^*) \leftarrow L(\pi)$
32.4 (4.51)	32.8 (4.70)	32.1 (4.33)	32.5 (4.64)	32.5 (4.49)	32.9 (4.38)	$M(d) \leftarrow L(\pi)$
30.7sh (4.42)	31.1sh (4.53)	30.1sh (4.22)	30.3sh (4.46)	29.9sh (4.39)	29.9sh (4.19)	$L(\pi^*) \leftarrow n(S)$
27.0 (4.23)	27.4 (4.35)	26.0 (3.98)	27.6 (4.42)	26.1 (4.25)	26.1 (4.03)	$\{M(d) \leftarrow L(\pi)$, $M(d) \leftarrow M(d)$
22.6 (4.18)	22.7 (4.16)	22.5 (3.97)	22.7 (4.19)	22.4 (4.17)	22.3 (3.99)	$\{L(\pi^*) \leftarrow M(d)$, $M(d) \leftarrow M(d)$
20.2sh (3.97)	20.4sh (4.00)	20.5sh (3.78)	20.1sh (4.04)	20.1sh (3.98)	20.1sh (3.82)	$L(\pi^*) \leftarrow M(d)$
16.1 (3.95)	16.3 (3.84)	16.3 (3.62)	16.2 (3.88)	16.4 (3.91)	16.4 (3.70)	$L(\pi^*) \leftarrow M(d)$

*sh = shoulder.

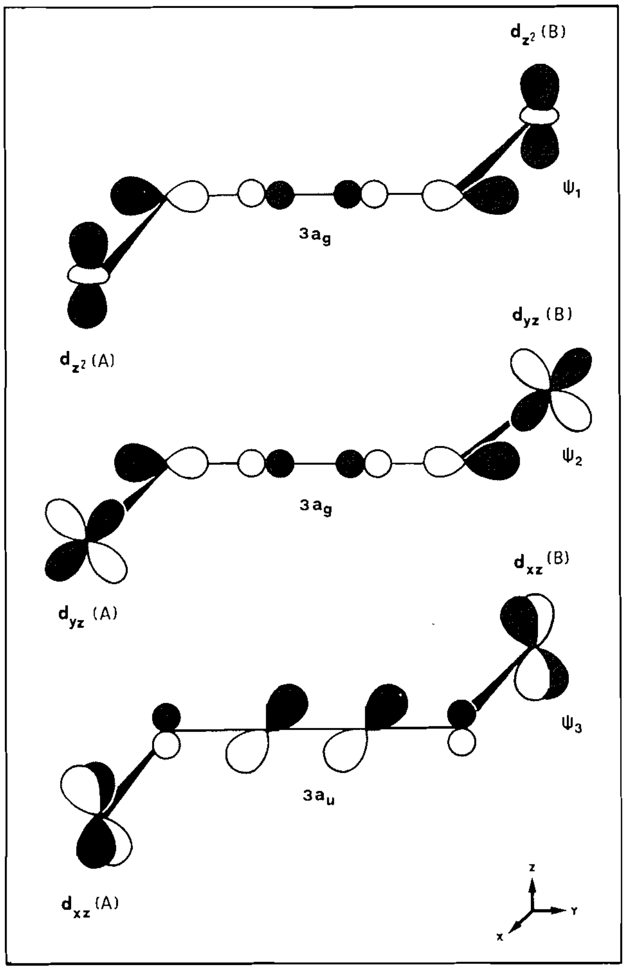

FIG. 5. The possible pairwise orbital interactions supporting the superexchange processes observed in the $[Fe(R_2dtc)_2X]_2(\mu - X_2')$ molecular magnetic systems.

MO. The accumulation of the electron density on the σ^* virtual MO of the molecular halogen due to this interaction also explains the enhancement of its reactivity towards 1,2-addition reactions to olefins.

The electronic spectral data of the complexes under investigation along with the assignments of the absorption bands are listed in Tables 5 and 6. Assignments were made by associating the observed bands with the transitions they most nearly match in energy. From these results it is evident that the electronic spectra of the $2[Fe(R_2dtc)_2X]\cdot X_2'$ complexes are similar to those of the corresponding halobisdithiocarbamates. Therefore, it is reasonable to invoke the same assignments of the bands for the dihalide complexes as well. Furthermore, the interaction between the molecular iodine and coordinated halogen in these cases persists in methylene chloride solutions since the characteristic visible peak of I_2 at 520−540 nm is missing. Unfortunately, the crystal-field bands in the electronic spectra of the compounds were impossible to observe, since the intense charge transfer bands are extended up to the ligand field part of the spectra, obscuring the weaker $d-d$ transitions. However, spectra obtained in solid state (Nujol mull) showed two distinct absorption bands at 6.9 and 8.7 kK which are in fair agreement with the spectral excitation energies derived from the quantum-chemical calculations, bearing in mind the approximate nature of the extended Hückel method.

Although facilities for low-temperature magnetic susceptibility studies were unavailable, the dependence of the room-temperature magnetic data on the magnetic field strengths strongly suggests weak magnetic exchange interactions between the two iron centers propagated probably through the linear tetratomic halogeno bridging unit (31). The low magnetic moments observed both at low and high field strengths as well as the slight decrease of the moments as the magnetic field decreases support evidence for the operation of antiferromagnetism in these compounds. The occurrence of antiferromagnetically coupled dimers and a magnetic ordering transition below 1.6 K have already been demonstrated for the $Fe(Me_2dtc)_2I_2$ complex (11) by ^{57}Fe Mössbauer spectra from 4.2 to 1.36 K and in magnetic fields up to 7.5 T. Consequently, in order to obtain additional insight on the possible pathways for the superexchange processes observed in these molecular magnetic systems, in terms of pairwise interactions of dimeric molecular orbitals (32), EHMO quantum-chemical calculations have also been used. According to these calculations the following three magnetic orbitals, depicted schematically in Fig. 5, are predicted to be the most suitable pathways for the transmission of the electronic effects over long distances:

$$\psi_1(A_g) \sim d_{z^2}(A) + 3a_g + d_{z^2}(B)$$

$$\psi_2(A_g) \sim d_{yz}(A) + 3a_g + d_{yz}(B)$$

$$\psi_3(A_u) \sim d_{xz}(A) + 3a_u - d_{xz}(B)$$

1. B. F. HOSKINS, R. L. MARTIN, and A. H. WHITE. Nature, **211**, 627 (1966).
2. R. L. MARTIN and A. H. WHITE. Inorg. Chem. **6**, 712 (1967).
3. L. M. EPSTEIN and D. K. STRAUB. Inorg. Chem. **8**, 560 (1969).
4. H. H. WICKMAN and A. M. TROZZOLO. Inorg. Chem. **7**, 63 (1968).
5. H. H. WICKMAN and A. M. TROZZOLO. Phys. Rev. Lett. **16**, 162 (1966).
6. H. H. WICKMAN and C. F. WAGNER. J. Chem. Phys. **51**, 435 (1969).
7. E. A. PASEK and D. K. STRAUB. Inorg. Chim. Acta, **21**, 29 (1977).
8. P. C. CHRISTIDIS, P. J. RENTZEPERIS, F. VAKOULIS, and C. A. TSIPIS. Inorg. Chim. Acta, **83**, 87 (1984).
9. E. A. PASEK and D. K. STRAUB. Inorg. Chim. Acta, **21**, 23 (1977).
10. C. L. RASTON, A. H. WHITE, D. PETRIDIS, and D. TAYLOR. J. Chem. Soc. Dalton, 1928 (1980).
11. D. PETRIDIS, A. KOSTIKAS, A. SIMOPOULOS, and D. NIARCHOS. Inorg. Chem. **21**, 766 (1982).
12. D. L. KEPERT, C. L. RASTON, A. H. WHITE, and D. PETRIDIS. J. Chem. Soc. Dalton, 1921 (1980).
13. E. A. PASEK and D. K. STRAUB. Inorg. Chem. **11**, 259 (1972).
14. R. HOFFMANN. J. Chem. Phys. **39**, 1397 (1963).
15. J. HOWELL, A. ROSSI, D. WALLACE, K. HARAKI, and R. HOFFMANN. Forticon 8. Q.C.P.E. No. 344, Indiana University.
16. C. P. KEIJZERS, H. J. M. DE VRIES, and A. VAN DER AVOIRD. Inorg. Chem. **11**, 1338 (1972).
17. J. W. RICHARDSON, W. C. NIEUWPOORT, R. R. POWELL, and W. F. EDGELL. J. Chem. Phys. **36**, 1057 (1962).
18. J. W. RICHARDSON, R. R. POWELL, and W. C. NIEUWPOORT. J. Chem. Phys. **38**, 796 (1963).
19. E. CLEMENTI and D. I. RAIMONDI. J. Chem. Phys. **38**, 2686 (1963).
20. F. BONATI and R. UGO. J. Oganomet. Chem. **10**, 257 (1967).
21. C. O'CONNER, J. D. CILBERT, and G. WILKINSON. J. Chem. Soc. A, 84 (1969).
22. D. A. BROWN, W. K. GLASS, and M. A. BURKE. Spectrochim. Acta, **32A**, 137 (1976).

23. C. PRETTI and G. TOSI. Z. Anorg. Allg. Chem. **418**, 188 (1975).
24. R. J. H. CLARK. Spectrochim. Acta, **21**, 955 (1965).
25. M. J. FRAZER, A. M. QURESHI, and F. B. TAYLOR. J. Chem. Soc. A. 1712 (1971).
26. R. J. H. CLARK and F. B. TAYLOR. J. Chem. Soc. A, 693 (1967).
27. H. H. WICKMAN, A. M. TROZZOLO, H. J. WILLIAMS, G. W. HULL, and F. R. MERRITT. Phys. Rev. **155**, 563 (1966).
28. B. F. HOSKINS and A. H. WHITE. J. Chem. Soc. A, 1668 (1970).
29. L. M. EPSTEIN and D. K. STRAUB. Inorg. Chem. **8**, 784 (1969).
30. J. L. K. F. DE VRIES, J. M. TROOSTER, and E. DE BOER. Inorg. Chem. **10**, 81 (1971).
31. F. D. VAKOULIS. Ph.D. Thesis, University of Thessaloniki. 1984.
32. P. J. HAY, J. C. THIBEAULT, and R. HOFFMANN. J. Am. Chem. Soc. **97**, 4884 (1975).

Analysis of solvent and substituent effects on uv and visible spectra of *N*-(α-methylarylidene)-*p*-(*N*′,*N*′-dimethylamino)-anilines

PIOTR MILART
Institute of Chemistry, Jagiellonian University, 30 060 Cracow, ul. Karasia 3, Poland

AND

TADEUSZ M. KRYGOWSKI
Department of Chemistry, Warsaw University, 02 093 Warsaw, ul. Pasteura 1, Poland

Received February 4, 1985

PIOTR MILART and TADEUSZ M. KRYGOWSKI. Can. J. Chem. **63**, 3256 (1985).

Substituent effect on the long wave band in uv/vis spectra of *p*-substituted *N*-(α-methylarylidene)-*p*-(*N*′,*N*′-dimethylamino)-anilines (X = CH_3O, CH_3, H, Cl, and NO_2) measured in eight solvents follows well the Hammett equation. Solvent effect on this band depends well on E_T only for Cl- and NO_2-substituted species. Both these findings support the conclusion that the long-wave band is in fact intramolecular charge transfer form the basicity center ($\bar{N}Me_2$ or $\bar{N}{=}C$) towards substituents.

PIOTR MILART et TADEUSZ M. KRYGOWSKI. Can. J. Chem. **63**, 3256 (1985).

Opérant dans huit solvants différents, on a mesuré l'effet des substituants sur la bande aux grandes ondes des spectres uv/vis des *N*-(α-méthylarylidènes)-*p*-(*N*′,*N*′-diméthylamino)-anilines substituées en position para par des groupements X = OCH_3, CH_3, H, Cl et NO_2; les valeurs obtenues peuvent être reliés par une équation de Hammett. L'effet du solvant sur cette bande ne dépend bien de E_T que pour les espèces substituées par les groupements Cl et NO_2. Ces deux résultats sont en accord avec la conclusion selon laquelle la bande aux grandes ondes est de fait la forme de transfert de charge intramoléculaire du centre de basicité ($\bar{N}Me_2$ ou $\bar{N}{=}C$) vers les substituants.

[Traduit par le journal]

The title compounds belong to a group of π-electron systems widely studied for their spectral properties strongly dependent on molecular geometry (1–4), which, in turn, is sometimes very complex. X-ray diffraction studies for similar systems (5, 6) corroborate this picture. In *p*- and *p*′-disubstituted benzylideneanilines with an electron donor and acceptor there occurs an intramolecular charge transfer between these substituents. Hence the title systems may bear dipoles depending on the kind of substituent at the *p*-position of the benzilidene ring. Hence it seems interesting to study solvent effect on uv/vis spectral properties of the differently *p*-substituted title compounds. For this purpose the complementary Lewis acid–base description (7) of solvent effect is applied using solvent parameters E_T (8, 9) for acidity and B_{KT} (10) for basicity. The standard Hammett rule is used to interpret the substituent effect on $\tilde{\nu}$-values.

Results and discussion

The title compounds read schematically as follows:

[1] 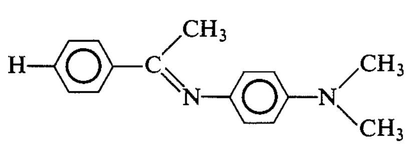

with substituents X = (*a*) OCH_3, (*b*) CH_3, (*c*) H, (*d*) Cl, and (*e*) NO_2. In these systems two uv bands are observed: the E_2 band due to local excitation in one of two rings of the molecules of **1***a*–*e*, and the K-band due to intramolecular CT transition. In the long-wave part of the spectra there exists an additional band (λ ~ 350–400 nm) strongly dependent on both, the nature of substituent X, as well as the solvent in which the measurement is carried out. Table 1 presents $\tilde{\nu}$-values of the long-wave band for **1***a*–*e* measured in eight solvents. From the scheme of canonical forms for molecules under study [2],

TABLE 1. Location of the long-wave absorption band for compounds **1***a*–*e* in eight solvents

Solvent	Location of the long-wave absorption band $\tilde{\nu}$/cm^{-1}				
	1*a*	**1***b*	**1***c*	**1***d*	**1***e*
N-Hexane	28 400	27 700	27 500	26 750	23 600
Carbon tetrachloride	29 150	28 320	27 750	26 420	23 530
1,4-Dioxane	28 090	27 700	27 620	26 880	23 980
Tetrahydrofuran	27 780	27 470	27 400	26 590	23 700
Methylene chloride	28 730	28 100	27 750	26 880	24 100
Acetonitrile	28 570	28 010	27 600	27 030	24 510
Ethanol	29 300	28 700	28 250	27 400	24 570
Methanol	28 900	28 700	28 500	27 620	24 700

[2] 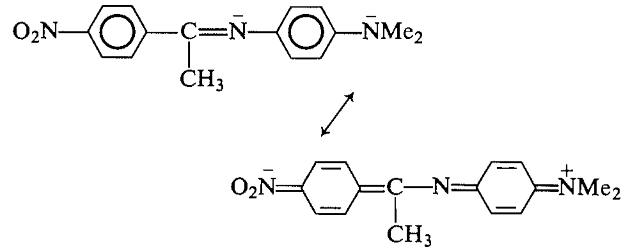

it follows that both electrical poles may be involved in specific interactions with solvent molecules. Hence, two solvent parameters, one for Lewis acidity, E_T (9, 10), and the other, B_{KT} (11, 12), for Lewis basicity of the solvent, were used to describe the dependence of $\tilde{\nu}$-values on the nature of the solvent:

[3] $\tilde{\nu} = \alpha E_T^N + \tilde{\nu}_0$

and

[4] $\tilde{\nu} = \beta B_{KT} + \tilde{\nu}'_0$

Table 2 compiles the relevent data for compounds **1***a*–*e*. It is

TABLE 2. Intercepts and slopes of eqs. [3] and [4]

Compound	α	$\tilde{\nu}_0$ (cm^{-1})	Corr. coeff. of eq. [3] R	β	$\tilde{\nu}'_0$ (cm^{-1})	Corr. coeff. of eq. [4] R
1*a*	839	28 340	0.451	230	28 543	0.140
1*b*	1217	27 690	0.732	686	27 873	0.467
1*c*	1135	27 425	0.826	811	27 542	0.668
1*d*	1312	26 522	0.925	940	26 657	0.748
1*e*	1597	23 570	0.959	997	23 774	0.678

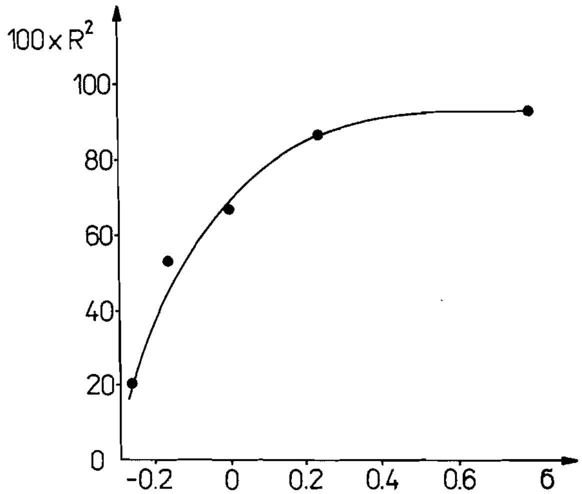

FIG. 1. Plot of the total variance explained by eq. [3], i.e. by Lewis acidity properties of solvents, against the Hammett σ_p describing an increasing dipolar character as a result of intramolecular CT of the system under study.

immediately apparent that only eq. [3] works well and only in the case when X is strongly electron accepting (Cl, NO_2). Quite unusual graph presented in Fig. 1 is obtained while plotting the squarred correlation coefficient of eq. [3] R^2 against the Hammett σ_p-constants. Its statistical meaning is that an increase of electron-accepting properties of the substituent causes an increase of percentage of the variance explained by eq. [3], i.e. by Lewis acidity of the solvents. Consequently, this means that negatively charged poles of **1***a–e* compounds are much more involved in solvent effect on electron excitation than the positively charged ones.

When we analyze the data of Table 1 by using the Hammett equation [5]

$$[5] \quad \tilde{\nu} = \rho\sigma + \tilde{\nu}''_0$$

the dependence of $\tilde{\nu}$ on the substituent effects appears to be very good (R always > 0.97). The relevant data are given in Table 3. The negative value of ρ means that an increase of electron-accepting properties of X induces a decrease of energy necessary to excite electrons involved in the transition. These electrons may come from the NMe_2— or C=$\bar{N}$-groups. This conclusion is in line with the values of the slopes in eq. [3]. For **1***d* and **1***e* the agreement of eq. [3] with experimental results ranges from good to excellent. This means that an increase of Lewis acidity of the solvents induces an increase of energy necessary to excite electrons involved in the transition. This would suggest that the transition is really an intramolecular charge transfer from most probably the $\bar{N}Me_2$-group. If the lone electron pair at the $\bar{N}$=C group had to be excited, it would need a break of near co-planarity of the whole π-electron system in **1***a–e*. However, this cannot be excluded since eq. [3]

TABLE 3. Statistical data of eq. [5]

Solvent	ρ	$\tilde{\nu}_0$ (cm^{-1})	R
n-Hexane	−4421	27 924	−0.984
Carbon tetrachloride	−5248	27 632	−0.998
1,4-Dioxane	−3886	27 297	−0.975
Tetrahydrofuran	−3901	27 032	−0.974
Methylene chloride	−4308	27 603	−0.994
Acetonitrile	−3742	27 570	−0.992
Ethanol	−4412	28 147	−0.995
Methanol	−4072	28 148	−0.979

evidently fails for $\sigma \gtrsim 0$. More detailed studies have to be undertaken in this direction.

Experimental

Compounds **1***a–e* were obtained by literature methods (13, 14) *Anal.* calcd. for **1***e*: $C_{16}H_{17}N_3O_2$ (mw 283.3); C 67.77, H 6.00, N 14.83; found: C 67.57, H 5.88, N 14.63. mp 182–183°C, ms *m/e*: 233 (M^+, 100%); 284 (M + 1, 17.7%); 268 (M − 15, 32.0%); ir (Nujol) cm^{-1}; 1590 s (C=N); 1520 s (NO_{2as}); 1345 s (NO_{2s}), ^{1}H nmr ($CDCl_3$) TMS/ppm: 8.26 (q, 4H, $J_{H,H}$ = 6 Hz); 6.90 (s, 4H); 3.08 (s, 6H); 2.40 (s, 3H).

The uv/vis spectra were recorded on a VSU-2P/Zeiss Jena, GDR/apparatus using quartz cuvettes 1.0 and 0.1 cm. The solutions were prepared directly before the measurements using solvents of spectrographic or pro analysis purity or they were purified by standard procedures (15).

1. K. EZUMI, H. NAKAI, S. SAKATA, K. NISHIKIDA, M. SHIRO, and T. KUBOTA. Chem. Lett. 1393 (1974).
2. R. PAETZOLD, M. REICHENBÄCHER, and K. APPENROTH. Zeit. Chem. **21**, 421 (1981).
3. J. M. LEHN. Fortscher. Chem. Forsch. **15**, 311 (1970).
4. R. GAWINECKI. Wiad. Chem. (Polish Chem. Rev. in Polish) **31**, 685 (1977).
5. H. H. BÜRGI and J. D. DUNITZ. Helv. Chim. Acta, **52**, 1747 (1970).
6. H. NAKAI, M. SHIRO, K. EZUMI, S. SAKATA, and T. KUBATA. Acta Crystallogr. B**32**, 1827 (1976).
7. T. M. KRYGOWSKI and W. R. FAWCETT. J. Am. Chem. Soc. **97**, 2143 (1975).
8. K. DIMROTH, C. REICHARDT, T. SIEPMANN, and F. BOHLMANN. Justus Liebig Ann. Chem. **661**, 1 (1963).
9. CH. REICHARDT. Angew Chem. Int. Ed. **18**, 98 (1979).
10. CH. REICHARDT and E. HARBUSCH-GÖRNERT. Liebigs Ann. Chem. 721 (1983).
11. M. J. KAMLET and R. W. TAFT. J. Am. Chem. Soc. **98**, 377 (1976).
12. T. M. KRYGOWSKI, E. MILCZAREK, and P. K. WRONA. J. Chem. Soc. Perkin II, 337 (1979).
13. J. MOSKAL and P. MILART. Synthesis, 128 (1984).
14. P. RAMART-LUCAS, J. HOCH, and M. MARTYNOFF. Bull. Soc. Chim. Fr. **4**, 481 (1937).
15. J. A. RIDDICH and W. B. BURGER. Organic solvents. Vol. 2. 3rd ed. *In* Techniques of chemistry. *Edited by* A. Weissenberger. Wilen, New York. 1970.

Crystal structure and infrared spectra of an inclusion compound of cyclotriveratrylene and water[1]

GEORGE I. BIRNBAUM
Division of Biological Sciences, National Research Council of Canada, Ottawa, Ont., Canada K1A 0R6

AND

DENNIS D. KLUG, JOHN A. RIPMEESTER, AND JOHN S. TSE
Division of Chemistry, National Research Council of Canada, Ottawa, Ont., Canada K1A 0R9

Received March 26, 1985

GEORGE I. BIRNBAUM, DENNIS D. KLUG, JOHN A. RIPMEESTER, and JOHN S. TSE. Can J. Chem. **63**, 3258 (1985).

A crystal grown by slow evaporation from a solution of cyclotriveratrylene (CTV) in toluene was found to be an inclusion compound with water as the only encaged guest. Its stoichiometry is $C_{27}H_{30}O_6 \cdot xH_2O$ (x = 0.16) and it belongs to the monoclinic space group $C2/c$, with a = 24.216(21), b = 9.636(2), c = 23.117(4) Å, β = 118.08(5)°, Z = 8. X-ray intensity data were measured with a diffractometer and the structure was solved by direct methods. Least-squares refinement, which included all hydrogen atoms of the host molecule, converged at R = 0.046 for 3986 observed reflections. The geometry of the host molecule is compared to that of analogous structures and to cyclononatriene. Significant differences are ascribed to the effects of homoaromaticity and steric strain. Both the X-ray analysis and an FTIR study of the OH stretching show that the water molecules are weakly bound to the methoxy oxygen atoms of CTV. The molecular packing of CTV clathrates is discussed on the basis of crystallographic and spectroscopic evidence.

GEORGE I. BIRNBAUM, DENNIS D. KLUG, JOHN A. RIPMEESTER et JOHN S. TSE. Can J. Chem. **63**, 3258 (1985).

On a trouvé que le cristal obtenu par évaporation lente d'une solution de cyclotrivératrylène (CTV) dans le toluène est un composé d'inclusion contenant uniquement l'eau comme molécule encagée. Ce composé a pour formule $C_{27}H_{30}O_6 \cdot xH_2O$ (x = 0,16) et appartient au groupe d'espace monoclinique $C2/c$, avec a = 24,216(21), b = 9,636(2), c = 23,117(4) Å, β = 118,08(5)° et Z = 8. On a utilisé un diffractomètre pour mesurer les données d'intensité de rayons X et on a résolu la structure par des méthodes directes. On l'a affinée par la méthode des moindres carrés, qui inclut tous les atomes d'hydrogènes de la molécule hôte, jusqu'à une valeur de R = 0,046 pour 3986 réflexions observées. On a comparé la géométrie de la molécule hôte à celle de structures analogues et à celle du cyclononatriène. On attribue les différences marquantes à des effets d'hétéroaromaticité et des contraintes stériques. Tant l'analyse par des rayons X que des études IR/TF de l'élongation du groupe OH montrent que les molécules d'eau sont faiblement liées à l'atome d'oxygène du groupe méthoxy du CTV. On discute de l'entassement moléculaire des clathrates de CTV en se basant sur les données cristallographiques et spectroscopiques.

[Traduit par le journal]

Introduction

Solvates of cyclotriveratrylene (2,3,7,8,12,13-hexamethoxy-5,10-dihydro-15*H*-tribenzo[*a*,*d*,*g*]cyclononene; CTV) were first reported in the literature during the fifties (1). Subsequent infrared and X-ray diffraction studies revealed that these CTV complexes belong to a special class of channel inclusion compounds. From X-ray measurements, it was found that the unit cell dimensions of the inclusion complexes depended on the size of the guest molecules (2, 3). Two monoclinic phases have been identified (3), the unique feature of each modification being the near constancy of the unit cell dimension b. The angle β and the lengths of a and c, however, vary with the nature of the encaged molecules. So far, only one complete crystal structure is available for CTV complexes, that for CTV·0.5benzene·water (CTVBW) (4). In the crystal, the host cyclotriveratrylene cyclic trimer adopts an umbrella shape with the methyl groups approximately coplanar with the benzene rings. The benzene and water molecules were trapped inside the cavities formed by the methyl groups.

Recently, CTV clathrates have been prepared by dissolving the host compound in different organic solvents (5). The crystalline solids obtained were characterized by nmr techniques. It was found that the inclusion process for CTV is quite selective and, in some instances, depends critically on the presence or absence of water. From the analysis of the solid state ^{13}C nmr splitting patterns it was established that more than one structural type of CTV inclusion can be formed (5). For example, the solid obtained by slow cooling of a solution of CTV in hot toluene gave a ^{13}C nmr splitting pattern which could only be assigned if there were two magnetically distinct CTV molecules per asymmetric unit, with toluene as the sole occupant in the cavities. This observation is at variance with the crystal structure of CTVBW where only one CTV molecule is present in each asymmetric unit. Obviously, there are fundamental structural differences between the two compounds. More intriguingly, when the toluene solution was allowed to evaporate in air, the crystal obtained showed a completely different nmr splitting pattern which was very similar to that obtained for the benzene analogue, but no toluene was found to be present. The ^{1}H nmr spectrum of the dissolved material showed a trace of water to be present, suggesting water might be the only encaged guest.

About twenty years ago, an X-ray analysis of *cis*,*cis*,*cis*-1,4,7-cyclononatriene was carried out (6) in order to resolve contradictory predictions of homoaromaticity in that molecule (7–9). The authors concluded that the $C(sp^2)$—$C(sp^3)$—$C(sp^2)$ bond angle of 108° and the $C(sp^2)\cdots C(sp^2)$ nonbonded distance of 2.46 Å in the crown-shaped triene precluded the possibility of any meaningful homoaromaticity. However, a subsequent study established a significant extent of through-space interaction between the π-orbitals by the use of photoelectron spectroscopy (10). More recently, the structure of a CTV homologue has been studied by X-ray crystallography (11) in addition to CTVBW (4) and a complex of cyclotri-

[1]NRCC No. 24723.

TABLE 1. Final atomic parameters and their standard deviations[a]

Atom	x	y	z	U_{eq}/U	Atom	x	y	z	U
O(1)	26174(6)	37512(15)	55387(6)	615	H(2)	344(1)	500(2)	662(1)	25(4)
O(2)	14706(5)	43756(14)	52254(5)	587	H(5)	138(1)	619(2)	606(1)	31(5)
O(3)	6326(6)	44327(18)	74905(6)	705	H(71)	172(1)	793(2)	685(1)	34(5)
O(4)	14500(6)	38371(17)	86893(6)	676	H(72)	245(1)	810(2)	741(1)	35(5)
O(5)	46323(6)	31391(15)	97256(5)	627	H(9)	107(1)	619(2)	693(1)	40(5)
O(6)	49502(6)	30165(15)	87997(6)	642	H(12)	253(1)	518(2)	907(1)	42(5)
C(1)	29074(7)	61336(15)	69144(7)	461	H(141)	319(1)	708(2)	906(1)	35(5)
C(2)	30220(7)	52196(16)	65136(7)	484	H(142)	306(1)	770(2)	838(1)	30(5)
C(3)	25421(7)	46478(16)	59536(7)	481	H(16)	374(1)	499(2)	949(1)	29(5)
C(4)	19230(7)	50040(16)	57806(7)	474	H(19)	433(1)	485(2)	784(1)	30(5)
C(5)	18074(7)	59250(16)	61652(7)	500	H(211)	381(1)	692(2)	739(1)	29(5)
C(6)	22947(7)	64964(15)	67399(7)	484	H(212)	336(1)	760(2)	762(1)	27(4)
C(7)	21144(8)	74098(16)	71581(8)	554	H(221)	347(1)	406(3)	570(1)	59(8)
C(8)	19720(7)	65333(15)	76165(7)	497	H(222)	344(1)	288(3)	617(1)	55(6)
C(9)	13737(7)	59366(18)	73590(7)	544	H(223)	319(1)	258(3)	539(1)	58(6)
C(10)	12070(7)	50529(18)	77153(8)	538	H(231)	84(2)	399(4)	557(2)	92(10)
C(11)	16482(7)	47328(18)	83679(7)	524	H(232)	63(1)	373(3)	482(1)	54(6)
C(12)	22329(7)	53318(17)	86253(7)	518	H(233)	65(2)	528(4)	508(2)	83(10)
C(13)	24092(7)	62232(15)	82625(7)	481	H(241)	−11(1)	382(3)	672(1)	60(8)
C(14)	30673(8)	68151(16)	85935(7)	522	H(242)	52(2)	379(4)	662(2)	77(9)
C(15)	35650(7)	58411(15)	86079(7)	452	H(243)	16(2)	518(4)	656(2)	84(10)
C(16)	38656(7)	49591(17)	91521(6)	481	H(251)	228(1)	297(2)	929(1)	43(5)
C(17)	43192(7)	40228(16)	92085(7)	478	H(252)	206(1)	421(3)	961(1)	54(6)
C(18)	44924(6)	39571(17)	87097(7)	488	H(253)	173(1)	264(3)	946(1)	65(8)
C(19)	42057(7)	48377(17)	81775(7)	481	H(261)	411(1)	299(3)	1013(1)	57(6)
C(20)	37422(7)	57820(15)	81160(6)	450	H(262)	481(2)	267(4)	1060(2)	78(9)
C(21)	34707(7)	67191(16)	75159(7)	506	H(263)	453(1)	421(3)	1041(1)	67(8)
C(22)	32350(9)	32917(25)	57206(11)	725	H(271)	527(1)	377(3)	824(1)	46(6)
C(23)	8530(9)	43435(25)	51444(11)	765	H(272)	473(1)	268(2)	789(1)	40(5)
C(24)	2674(9)	42639(27)	68064(10)	768	H(273)	544(1)	217(3)	842(2)	71(8)
C(25)	19086(11)	33768(26)	93180(9)	733					
C(26)	45098(11)	32588(26)	102606(9)	767					
C(27)	51239(9)	29155(27)	82949(2)	764					
O(W)	952(1)	853(2)	186(1)	119(8)					

[a]The nonhydrogen coordinates of CTV were multiplied by 10^5, the U_{eq} values by 10^4, and the parameters of O(W) and the hydrogen atoms by 10^3.

catechylene with 2-propanol (CTCP) (12). In all these molecules, the nine-membered ring also assumes a crown conformation, but the detailed geometry differs significantly from that of the unsubstituted cyclononatriene ring system. In order to investigate this fact, on which previous authors have not commented, as well as the guest−host interaction, we decided to carry out a precise crystallographic study. This seemed particularly desirable since in previous X-ray analyses (4, 6, 11, 12) the positions of the hydrogen atoms had not been refined. We obtained single crystals of a complex of CTV with water (CTVW) and subjected them to X-ray and FTIR analyses.

Experimental

Pale yellow prismatic crystals of cyclotriveratrylene hydrate were grown from slow evaporation of a saturated solution of CTV in toluene. Precession photographs showed systematic absences corresponding to space groups Cc and $C2/c$. A crystal fragment measuring 0.15 × 0.30 × 0.45 mm was mounted on an Enraf-Nonius CAD-4 diffractometer; it provided the following data:

$C_{27}H_{30}O_6.xH_2O$ (x = 0.16) fw = 453.39
Monoclinic, a = 24.216(21), b = 9.636(2), c = 23.117(4) Å, β = 118.08(5)°, V = 4759.30 Å^3, ρ_c = 1.26 g cm^{-3}, Z = 8 (20°C; CuKα_1, λ = 1.54056 Å); F(000) = 1931, μ(CuKα) = 6.8 cm^{-1}.

The cell dimensions were determined with high precision from angular settings of 22 high-order (2θ > 80°) reflections. However, their values, particularly that of a, were fluctuating during the data collection. The dimensions listed above represent averages of 15 determinations. Intensities were measured with Ni-filtered CuKα radiation, using ω/2θ scans with variable scan ranges and speeds. Three standard reflections were monitored at frequent intervals. Their intensities fluctuated by ±2% and decreased by 7% during the course of the data collection. There are 4905 unique reflections accessible to the diffractometer (2θ ≦ 150°), of which 900 with $I \leqq 3\sigma(I)$ were considered unobserved. The intensities were corrected for Lorentz and polarization factors; absorption corrections were considered unnecessary.

The structure was determined by direct methods with the aid of the computer program MULTAN78 (13). The E statistics clearly indicated a centrosymmetric space group, i.e. $C2/c$ rather than Cc. Of the 64 starting sets subjected to tangent refinement, the solution with the highest combined figure of merit yielded an E map on which all 33 nonhydrogen atoms of the CTV molecule were located. Atomic parameters were refined by block-diagonal least squares. All 30 hydrogen atoms were located on a difference Fourier map and refined with isotropic temperature parameters. The scattering factors were taken from the "International tables for X-ray crystallography" (14). Throughout the refinement the function $\Sigma w(|F_o| - |F_c|)^2$ was minimized and a factor of 0.8 applied to all shifts. The following weighting scheme was used during the final stages: $w = w_1 \cdot w_2$, where $w_1 = 1$ for $|F_o| \leqq 15$, $w_1 = 15/|F_o|$ for $|F_o| > 15$; and $w_2 = \sin^2\theta/0.5$ for $\sin^2\theta < 0.5$, $w_2 = 1$ for $\sin^2\theta \geqq 0.5$. This scheme made the average value of $w(\Delta F^2)$ independent of $|F_o|$ and $\sin^2\theta$. The refinement converged to a conventional residual index $R = (\Sigma|\Delta F|/\Sigma|F_o|)$ of 0.051 and a weighted index $R_w = (\Sigma w\Delta F^2/\Sigma wF_o^2)^{1/2}$ of 0.062. A difference Fourier map calculated at this stage revealed a residual peak

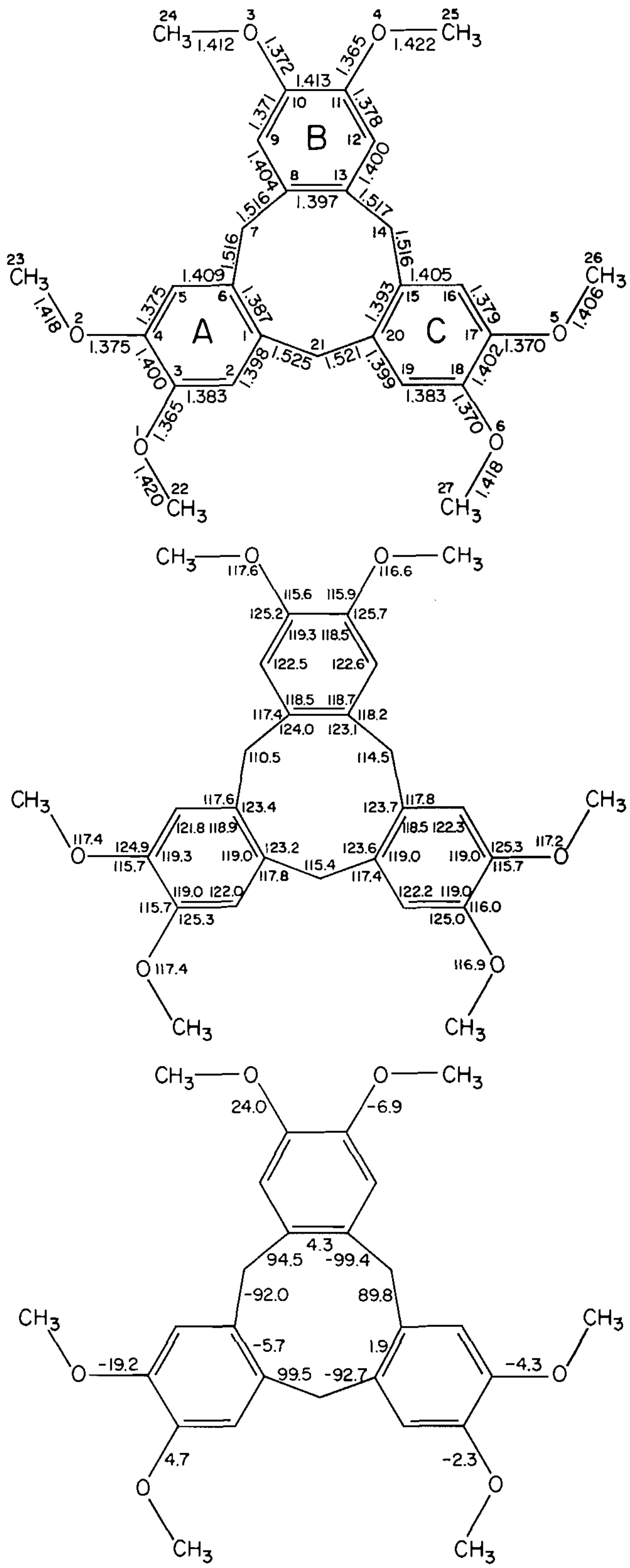

FIG. 1. Geometry of the CTV molecule. (Top) Bond distances (Å); their estimated standard deviations (esd's) are 0.002–0.003 Å. (Center) Bond angles (deg); their esd's are 0.13–0.16°. (Bottom) Torsion angles (deg); their esd's are 0.2–0.3°.

five times stronger than the background, but no other significant features. On the basis of nonbonded distances this peak was attributed to the oxygen atom of a disordered water molecule. Consequently, the refinement was resumed with the inclusion of the coordinates, an isotropic temperature parameter, and an occupancy factor for this oxygen atom. After the final cycle this occupancy factor converged to 0.16(1). The average shift for all atomic parameters equalled 0.04σ and the largest one 0.53σ. There was a significant drop of the residual indices: the final R value is 0.046 and R_w is 0.057 for 3986 observed reflections (19 low-order reflections suffered from extinction and were given zero weights). The final atomic parameters are listed in Table 1. Lists of anisotropic temperature parameters and of observed and calculated structure factors are available.[2]

The mid-infrared spectra were obtained using a Nicolet 7199 FTIR spectrometer equipped with a HgCdTe photodetector. All spectra were run with a resolution of 2 cm^{-1}. Samples (3.6 mg) were mixed with 0.40 g of KBr in a mechanical grinder and pressed into clear pellets. A KBr pellet was used as the background.

Results and discussion

The cyclononatriene ring assumes a crown conformation but certain details of its geometry (Fig. 1) are significantly different from those in unsubstituted cyclononatriene (6). We believe that this fact is due to the absence of homoaromaticity in this, as well as in related cyclic trimers. Without this stabilizing interaction, one of the aromatic rings (in the present case, ring C) is pushed away from the other two rings. Consequently, the bond angles at C(14) (114.5°) and C(21) (115.4°) and the nonbonded distances C(1)···C(20) (2.575 Å) and C(13)···C(15) (2.550 Å) are substantially increased. On the other hand, the increases of the bond angle at C(7) (110.5°) and the C(6)···C(8) distance (2.492 Å) are much smaller. Thus, instead of possessing a threefold molecular symmetry, all molecules related to CTV exhibit approximate mirror symmetry with a "mirror plane" passing through one of the methylene carbon atoms and through the midpoints of the transannular aromatic ring.

With a cyclononatriene ring in crown conformation, there are three C(sp^3)—H bonds pointed towards the center of the ring, bringing the three hydrogen atoms into close contact (Fig. 2). In the case of cyclononatriene this nonbonded distance was calculated to be 1.95 Å (6). This being the first X-ray analysis of a CTV molecule in which hydrogen parameters were refined (we normalized all C—H bond lengths to 1.09 Å), we can examine the H···H contacts in detail. It has been assumed (6, 15) that in cyclononatriene an increase of the bond angles at the trigonal carbon atoms from 120 to 124° is necessary in order to separate the intraannular hydrogen atoms. However, an increase of the C═C—C angle is normal is *cis*-substituted olefins (16). Consequently, the decrease in the tetrahedral bond angles to 108° in cyclononatriene which accompanies homoconjugation is sufficient to keep the intraannular hydrogen atoms at a distance of 1.95 Å. In CTVW, where, in the absence of homoaromaticity, two of the angles are 115.0 ± 0.5°, this separation can be achieved only by a substantial twist of the crown conformation. Thus, the endocyclic torsion angles at the aromatic bonds at rings A and B are 5.0 ± 0.7° rather than 0° (Fig. 1). Other torsion angles also differ from the values (0° and 95°) found in cyclononatriene. As a result, the intraannular H···H distances in CTVW are as follows: H(72)···H(142) 1.96 Å, H(72)···H(212) 1.96 Å, and H(142)···H(212) 2.06 Å. Similar distances are likely to occur in related molecules as well, since in all of them the crown conformation was found to be twisted (4, 11, 12).

[2]These tables may be purchased from the Depository of Unpublished Data, CISTI, National Research Council of Canada, Ottawa, Ont., Canada K1A 0S2.

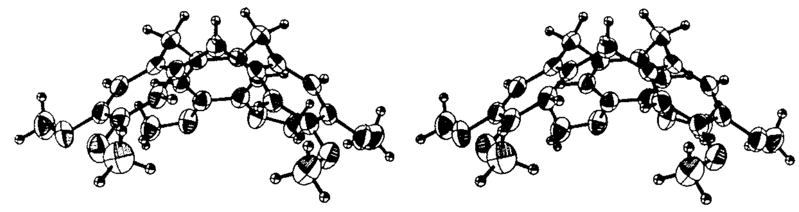

FIG. 2. Stereoscopic view of CTV. The ellipsoids correspond to 50% probability.

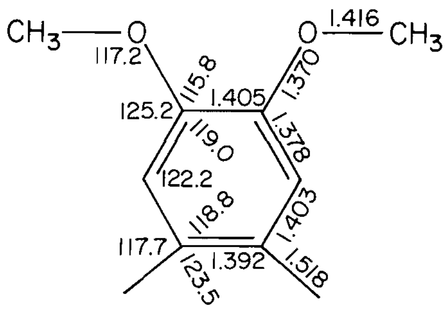

FIG. 3. Average bond lengths (Å) and bond angles (deg) in CTV.

The present X-ray analysis yielded results which are significantly more precise than those of the previously reported CTV inclusion compounds; it is the first structure determination in which the parameters of all atoms of such a host molecule were refined. Consequently, it is of interest to examine other details of the geometry of cyclotriveratrylene.

The lengths of the symmetrically disposed bonds do not deviate significantly from average values, therefore these values (shown in Fig. 3) can be used in the discussion. The bond lengths in the aromatic rings are significantly unequal: they show an alternating pattern of shorter and longer bonds which indicates partial localization of the π electrons. This is a common feature of *o*-dimethoxybenzenes (17, 18), presumably indicating some contribution of the resonance form shown below.

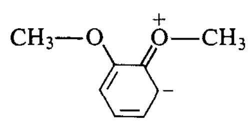

The bond angles, apart from those in the nine-membered ring, are also quite similar and can therefore be averaged. In the aromatic rings the angles deviate significantly from 120°, reflecting the effect of substitution by electron-donating groups (19). The exocyclic angles at the methoxy-bearing carbon atoms and at the oxygen atoms are in very good agreement with values obtained from a survey of crystal structures of *o*-dimethoxybenzenes (20). The survey revealed a strong preference of near-coplanarity of the methoxy groups with the aromatic rings. On the other hand, using photoelectron spectroscopy and *ab initio* STO-3G calculations, the authors found a preference for a nonplanar conformation, with one O—CH_3 bond perpendicular to the aromatic ring, both in solution and in the gas phase. In view of the contribution of the resonance form shown above (which is only one of several possible ones), this was a surprising finding which has since been disproved, at least for the solution conformation (21, 22). In the present structure the methyl groups are somewhat displaced from the ring planes in order to diminish interactions between their hydrogen atoms and those at the ortho positions. Further relief is provided by increases of the C—C—O and C—O—CH_3 bond angles.

In agreement with the nmr study (5), the X-ray analysis shows no evidence of included toluene, water being the only guest material. It is somewhat surprising that the CTV molecules preferentially occlude the water from the air rather than the more abundant toluene molecules. This suggests that polar guest molecules are preferred over nonpolar ones. The fluctuations in the length of *a* and of the intensities of the standard reflections (see above) suggest that the occupancy factor of O(W) may have varied during the period of data collection, possibly as a function of humidity. In this inclusion compound, water molecules reside in channels between CTV molecules stacked along *y* (Fig. 4). Their oxygen atoms are at a distance of 3.086 Å from the methoxy oxygen atoms O(4), indicating a weak O(W)—H···O(4) hydrogen bond. The distance to the other methoxy oxygen, O(W)···O(3) 3.330 Å, is too long for a hydrogen bond. This weak binding of water accounts for the low occupancy factor of 0.16 which means that, on average, there is approximately one water molecule per unit cell, even though there is enough space for eight molecules. If all positions were fully occupied, the shortest O(W)···O(W) distances would be 2.783 Å.

To understand the mode of hydrogen bonding in the complex, we have measured the ir spectrum of the clathrate in the OH stretching region. It is generally recognized that there are several characteristic changes in the OH stretch mode when hydrogen bonds are formed (23–25): (*a*) a decrease in the frequency of the OH stretch band; (*b*) an increase in the half-width of this band; and (*c*) an increase in the intensity of this vibrational mode. Furthermore, there have been several studies of the relationship between the hydrogen bonded O···O distance and OH stretching frequencies (26–29). It has been found that in all cases the OH frequency shifts monotonically to lower frequencies as the O···O distance is decreased. For instance, the OH stretching frequency in the matrix isolated water dimer occurs at 3691 and 3546 cm^{-1} (30, 31), and is lowered to 3150 cm^{-1} in hexagonal ice (32). These frequency shifts can be correlated with the O···O separation of 2.976 Å in the dimer (33) and 2.72 Å in the ice (23).

Two peaks can be readily identified from the ir spectrum in the OH region (Fig. 5): a strong absorption at 3520 cm^{-1} (A, ν_1) with a band width of 38 cm^{-1} and a weak but sharp band at 3660 cm^{-1} (B, ν_3) with a half-width of 20 cm^{-1}. The two bands support the conclusion that the ν_1 symmetric and the ν_3 asymmetric stretching vibrations are shifted by about 140 and 100 cm^{-1} from the gas phase values for water (34). Their splitting is increased by 40 cm^{-1} and the band at 3520 cm^{-1} has a higher intensity than the band at 3660 cm^{-1}. This is in contrast with the gas phase spectrum for an isolated water molecule, but is in qualitative agreement with the water dimer spectrum and recent theoretical calculations on the ir stretching intensities (25). It indicates that the encaged water molecule is probably weakly hydrogen-bonded to one of the methoxy oxygen atoms of CTV. From the correlation between the

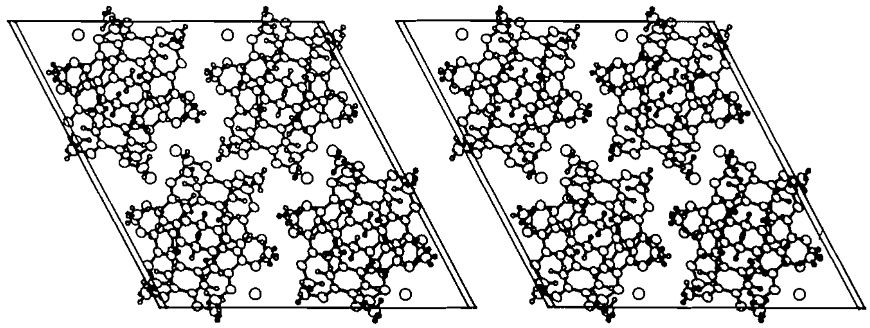

FIG. 4. Stereoscopic view along y of the molecular packing in the crystal. The isolated circles indicate possible positions of the water oxygen atoms. The directions of the axes are $x \nwarrow$ and $z \rightarrow$.

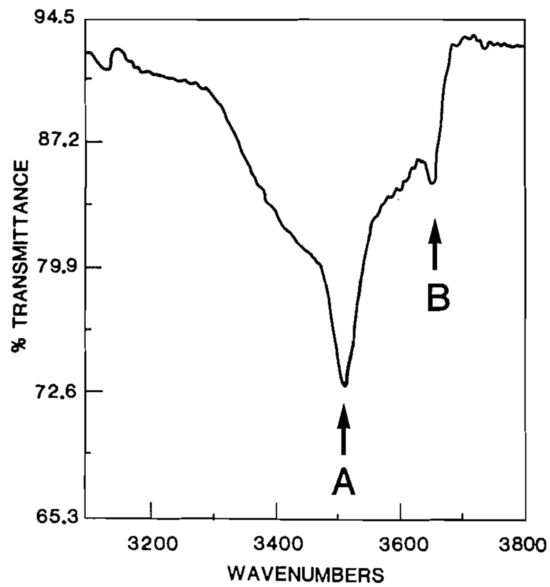

FIG. 5. Infrared spectrum of CTVW in the OH stretching region.

O···O distance and OH stretching frequencies shifts in a crystalline monohydrate (29), we estimate the O···O distance to be 2.98 Å. This value is fairly close to the O(4)···O(W) distance of 3.086 Å. Our ir data obviously do not support a water dimer structure with a short O···O distance. Therefore the water is best described as weakly bonded to the methoxy oxygen and is not tightly held. This is very similar to the situation in the CTVBW complex (4).

In several classes of organic clathrates the crystal packing of the host molecules is not affected significantly by the nature or the size of the occluded guests (35). Most notable among them are 4-*p*-hydroxyphenyl-2,2,4-trimethylchroman, widely known as Dianin's compound (36), and β-hydroquinone (37). In order to compare the packing of the CTV molecules in the present structure with that in the CTVBW crystal, we have calculated unit cell parameters for different cell choices in space group $C2/c$ (38). The parameters for CTVBW are very similar to those reported in an earlier X-ray study (3). The results, given in Table 2, show very similar cell lengths in the two crystals, but the angle β is greatly decreased in CTVBW. This gives rise to a larger unit cell (5341.0 Å^3) which can accommodate the sterically demanding benzene guest molecules.

On the basis of the ir spectra and the unit cell dimensions, it has been suggested (3) that the CTV clathrates may be classified into two monoclinic modifications. CTV clathrates of the

TABLE 2. Alternative lattice parameters for CTVBW and CTVW

Compound, space group	Lattice parameters	Transformation matrix
	$a = 22.748$ Å	0 0 1
CTVBW	$b = 9.629$ Å	0 $\bar{1}$ 0
$I2/a$	$c = 24.397$ Å	1 0 1
	$\beta = 91.91°$	
	$a = 23.117$ Å	0 0 $\bar{1}$
CTVW	$b = 9.636$ Å	0 $\bar{1}$ 0
$A2/a$	$c = 24.216$ Å	$\bar{1}$ 0 0
	$\beta = 118.08°$	

α phase have very similar a and c cell dimensions. On the other hand, the β phases have a longer c dimension (3, 4). Their ir spectra in the fingerprint region also show characteristic differences. More specifically (3), the α form shows no splitting of the ir peaks at 850, 994, and 1039 cm^{-1} and the absorption at 905 cm^{-1} is absent. We measured the ir spectrum of CTVW in this region and the positions of the peaks (in cm^{-1}) can be compared with those previously reported (3) for CTV·benzene (given in parentheses): 740 (737), 851 (850), 870 (871), 884 (882), 926 (925), 942 (942), 996 (994), 1041 (1039). Apart from a slight variation in the vibration frequencies, the two spectra are very similar. Due to better instrumental resolution, we also observed shoulders adjacent to the peaks at 851 and 1041 cm^{-1}; however, no splitting of the peaks was observed. According to the spectral features, we can identify the CTVW crystal as an α phase. The similarity in the length of the a and c cell dimensions also supports such an assignment. From limited experimental data, the α phase seems to be formed when bulky molecules are included, whereas the β phase allows the accommodation of thread-like molecules. Since water is quite small as compared with organic molecules, it is perhaps surprising that the CTVW crystal exists in the α form. Our results imply that the classification scheme may not be well founded and more structural information on this class of clathrates is needed to clarify the situation. This would be especially interesting in view of the fact that such clathrates may be used as suitable systems for photochemical reactions and as carriers of drugs.

Acknowledgments

Apart from MULTAN78 (13), all crystallographic computations were carried out with programs written by Ahmed *et al.* (39). Figures 2 and 4 were drawn with the ORTEP program of Johnson (40).

1. F. Bertinotti, V. Carelli, A. M. Liquori, and A. M. Nardi. Ric. Sci. Suppl. **22**, 65 (1952).
2. V. Caglioti, A. M. Liquori, N. Gallo, E. Giglio, and M. Scrocco. Ric. Sci. Suppl. **28**, 3 (1957).
3. V. Caglioti, A. M. Liquori, N. Gallo, E. Giglio, and M. Scrocco. J. Inorg. Nucl. Chem. **8**, 572 (1958).
4. S. Cerrini, E. Giglio, F. Mazza, and N. V. Pavel. Acta Crystallogr. Sect. B, **35**, 2605 (1979).
5. N. E. Burlinson and J. A. Ripmeester. J. Incl. Phenom. **1**, 403 (1984).
6. W. R. Roth, W. B. Bang, P. Goebel, R. L. Sass, R. B. Turner, and A. P. Yu. J. Am. Chem. Soc. **86**, 3178 (1964).
7. P. Radlick and S. Winstein. J. Am. Chem. Soc. **85**, 344 (1963).
8. K. G. Untch. J. Am. Chem. Soc. **85**, 345 (1963).
9. K. G. Untch and R. J. Kurland. J. Am. Chem. Soc. **85**, 346 (1963).
10. P. Bischof, R. Gleiter, and E. Heilbronner. Helv. Chim. Acta, **53**, 1425 (1970).
11. A. Collet, J. Gabard, J. Jacques, M. Cesario, J. Guilhem, and C. Pascard. J. Chem. Soc. Perkin Trans. 1, 1630 (1981).
12. J. A. Hyatt, E. N. Duesler, D. Y. Curtin, and I. C. Paul. J. Org. Chem. **45**, 5074 (1980).
13. P. Main, S. E. Hull, L. Lessinger, G. Germain, J.-P. Declercq, and M. M. Woolfson. MULTAN78, University of York, England, and University of Louvain, Belgium. 1978.
14. J. A. Ibers and W. C. Hamilton (*Editors*). International tables for X-ray crystallography. Vol IV. Kynoch Press, Birmingham, England.
15. R. B. Jackson and W. E. Streib. J. Am. Chem. Soc. **89**, 2539 (1967).
16. O. Ermer and S. Lifson. J. Am. Chem. Soc. **95**, 4121 (1973).
17. H. Nakamura, Y. Iitaka, Y. Kumada, T. Takeuchi, and H. Umezawa. Acta Crystallogr. Sect. B, **33**, 1260 (1977).
18. T. F. Koetzle and G. J. B. Williams. Acta Crystallogr. Sect. B, **34**, 323 (1978).
19. R. Norrestam and L. Schepper. Acta Chem. Scand. Ser. A, **35**, 91 (1981).
20. G. M. Anderson, P. A. Kollman, L. N. Domelsmith, and K. N. Houk. J. Am. Chem. Soc. **101**, 2344 (1979).
21. A. Makriyannis and S. Fesik. J. Am. Chem. Soc. **104**, 6462 (1982).
22. T. Schaefer and R. Laatikainen. Can. J. Chem. **61**, 224 (1983).
23. E. Whalley. *In* The hydrogen bond. Vol. III. *Edited by* P. Schuster, T. Zundel, and C. Sandorfy. Elsevier, New York, NY. 1976.
24. C. M. Huggins and G. C. Pimentel. J. Phys. Chem. **60**, 1615 (1956).
25. B. A. Zilles and W. B. Person. J. Chem. Phys. **79**, 65 (1983).
26. E. R. Lippincott and R. Schroeder. J. Chem. Phys. **23**, 1099 (1955).
27. H. Ratajczak and W. J. Orville-Thomas. J. Mol. Struct. **1**, 449 (1967–68).
28. L. J. Bellamy and A. J. Owen. Spectrochim. Acta, **25**A, 329 (1969).
29. J. Umemura, G. I. Birnbaum, D. R. Bundle, W. F. Murphy, H. J. Bernstein, and H. H. Mantsch. Can. J. Chem. **57**, 2640 (1979).
30. M. Van Thiel, E. D. Becker, and G. C. Pimentel. J. Chem. Phys. **27**, 486 (1957).
31. A. J. Tursi and E. R. Nixon. J. Chem. Phys. **52**, 1521 (1970).
32. J. R. Scherer and R. G. Snyder. J. Chem. Phys. **67**, 4794 (1977).
33. J. A. Odutola and T. R. Dyke. J. Chem. Phys. **72**, 5062 (1980).
34. D. F. Smith, Jr. and J. Overend. Spectrochim. Acta, **28**A, 471 (1972).
35. D. D. MacNicol, J. J. McKendrick, and D. R. Wilson. Chem. Soc. Rev. **7**, 65 (1978), and references therein.
36. (*a*) A. P. Dianin. J. Russ. Phys. Chem. Soc. **46**, 310 (1914); (*b*) H. M. Powell and B. D. P. Wetters. Chem. Ind. London 256 (1955).
37. (*a*) D. E. Palin and H. M. Powell. J. Chem. Soc. 208 (1947); (*b*) T. C. W. Mak, J. S. Tse, C. Tse, K. Lee, and Y. Chong. J. Chem. Soc. Perkin Trans. 2, 1169 (1976); (*c*) T. L. Chan and T. C. W. Mak. J. Chem. Soc. Perkin Trans. 2, 777 (1983).
38. T. Hahn (*Editor*). International tables for crystallography. Vol. A. Reidel, Dordrecht, Holland. 1983.
39. F. R. Ahmed, S. R. Hall, M. E. Pippy, and C. P. Huber. J. Appl. Crystallogr. **6**, 309 (1973).
40. C. K. Johnson. "ORTEP-II", Report ORNL-5138, Oak Ridge National Laboratory, Oak Ridge, TN. 1976.

Ab initio SCF and MRD-CI description of the $A\,^2A' - X\,^2A''$ transition of the as yet unknown HNCl molecule

BRITTA L. SCHÜRMANN AND ROBERT J. BUENKER

Lehrstuhl für Theoretische Chemie, Bergische Universität – Gesamthochschule Wuppertal, Gaußstr. 20, 5600 Wuppertal 1, West Germany

Received March 15, 1985

BRITTA L. SCHÜRMANN and ROBERT J. BUENKER. Can. J. Chem. **63**, 3264 (1985).

Ab initio potential curves of the $X\,^2A''$ ground state and the first excited $A\,^2A'$ state ($^2\Pi$ in linear geometry) of HNCl are calculated employing multi-reference single- and double-excitation configuration interaction in order to aid in the search for this system experimentally. A vibrational analysis (frequencies and Franck–Condon factors) of the $A\,^2A' - X\,^2A''$ transition is undertaken by neglecting coupling between the various modes. Diagonal and off-diagonal force constants together with the fundamental frequencies have been calculated by including mode coupling for both electronic states, and oscillator strengths and radiative lifetimes are also obtained. Comparison with theoretical and experimental results for other isovalent systems is also made in order to establish trends in this group of HAB systems.

BRITTA L. SCHÜRMANN et ROBERT J. BUENKER. Can. J. Chem. **63**, 3264 (1985).

Dans le but d'aider dans la recherche expérimentale de ce système et utilisant l'interaction de configuration à excitation simple ou double et à multi-référence, on a calculé les courbes de potentiel *ab initio* de l'état fondamental $X\,^2A''$ et du premier état excité $A\,^2A'$ ($^2\Pi$ dans la géométrie linéaire) du HNCl. On a entrepris une analyse vibrationelle (fréquences et facteurs de Franck–Condon) de la transition $A\,^2A' - X\,^2A''$ en négligeant le couplage entre les divers modes. On a calculé les constantes de force, selon la diagonale et hors de la diagonale, ainsi que les fréquences fondamentales en incluant le mode de couplage des deux états électroniques et l'on a également obtenu les forces de l'oscillateur ainsi que les temps de vie radiative. Dans le but d'établir les tendances existant dans ce groupe de systèmes de type HAB, on a également établi des comparaisons avec les résultats théoriques et expérimentaux d'autres systèmes isovalents.

[Traduit par le journal]

1. Introduction

In recent years it has been possible to predict details of the spectra of a number of small polyatomic molecules with sufficiently high accuracy to help in the subsequent identification of these systems experimentally. Several examples include the H_2CS (1, 2) and HSO (3–5) systems, for which both computed electronic transition energies and vibrational frequencies could be used effectively in confirming the successful generation of previously unknown substances. At the same time a radiative lifetime of the $^2A'$ state of HSO was predicted (3) to lie in the 40–50 μs range, and recently experimental work (6) has led to an observed value of 51 ± 5 μs. In a similar theoretical study (7) vibrational frequencies and transition energies for the related system HS_2 were obtained, which have recently aided in the detection of this molecule in chemiluminescence experiments (8); again good agreement between measured and computed vibrational frequencies was observed.

With this background it seemed promising to carry out similar calculations for a number of other HAB molecules which are as yet unobserved. Because of their isovalent relationship to the HO_2–HSO–HS_2 family, the group of molecules of HAB type in which the two non-hydrogenic atoms come from the nitrogen and halogen groups of the periodic table, respectively, is especially appropriate for such a systematic theoretical investigation. The parent system HNF is known experimentally and a theoretical study of this system has recently been reported (9), again finding good agreement with observed data. The subject of the present series of calculations is HNCl, for which no experimental information is as yet available.

The aim of this study is to predict vibrational frequencies, Franck–Condon factors and radiative lifetimes for the $A\,^2A' - X\,^2A''$ transition of HNCl, as well as the equilibrium geometries of the two participating electronic states.

2. Technical details

The cartesian gaussian AO basis set employed in this work is of double-zeta + polarization quality for the nitrogen and chlorine species. The ($4s$, $2p$) nitrogen contraction is taken from Dunning (10), augmented by a set of (six-component) d-type functions ($\alpha = 0.95$), while the chlorine set ($6s$, $5p$) is adopted from the work of McLean *et al.* (11), with the addition of a d-type set with exponent $\alpha = 0.68$. For the hydrogen atom a special ($5s$) contraction of Clementi and Lie (12) plus an s-type function ($\alpha = 1.0$) and a p-type polarization function with exponent $\alpha = 0.85$ is employed. The total AO basis thus consists of 52 contracted functions and the molecule is treated in C_s symmetry.

The *ab initio* calculations are of the standard multi-reference single- and double-excitation CI type with configuration selection, energy extrapolation (13, 14) and full-CI correction (FCI, 15); the computer programs employed make use of the Table CI method (16). A core of three MO's corresponding to the $1s$ shell of nitrogen and the $1s$ and $2s$ shells of chlorine is kept doubly occupied in all configurations, while the two virtual MO's with highest orbital energy are excluded from the excitation procedure. The single- and double-excitation space is generated from two reference configurations for each state. These correspond to $\ldots 9a'^2 10a'^2 2a''^2 3a''$ and $\ldots 9a'^2 10a'^2 2a''\, 3a''^2$ for the ground state and $\ldots 9a'^2 10a'\, 2a''^2 3a''^2$ and $\ldots 9a'\, 10a'^2 2a''^2 3a''^2$ for the $^2A'$ excited state. For geometries with large r(N—H) and r(N—Cl) nuclear distances the number of reference configurations has been increased to four. In all of these calculations the c^2 value is in the 0.89–0.90 range, which is typical for a system with 19 active electrons. The total generated (MRD-CI) configuration space has an order of approximately 200 000, and the dimension of the secular equations actually solved (the selection threshold corresponds to 10 μhartree) is in the range of 6000 – 8000. For each electronic state the parent SCF orbitals are used as MO basis for constructing the many-electron basis functions. The final (FCI) results take the energy contribution of higher-than-double-excitation-configurations into account by means of the

TABLE 1. Molecular constants computed for the HNCl molecule employing the estimated FCI data; distances are given in Å, angles in deg, force constants in mdyn/Å, mdyn/Å rad, or mdyn/rad^2, respectively, and frequencies in cm^{-1}

Parameter	$X\ ^2A''$		$A\ ^2A'$	
HN		1.026		1.046
NCl		1.714		1.626
∠HNCl		102.51		132.94
K_{11} (HN)	6.4123^a	6.6087	8.4170^a	8.7174
K_{22} (∠HNCl)	1.0789^a	1.0527	0.5364^a	0.7423
K_{33} (NCl)	3.5630^a	3.7456	4.1964^a	4.8469
K_{12}		0.1698		−0.2996
K_{13}		−0.0640		0.3755
K_{23}		0.3525		0.1046
ν_1 (HN)	3319^a	3452	3866^a	3970
ν_1 (DN)	2369^a	2522	2759^a	2904
ν_2 (∠HNCl)	1252^a	1356	922^a	1020
ν_2 (∠DNCl)	862^a	1010	672^a	734
ν_3 ($_H$NCL)	733^a	776	895^a	912
ν_3 ($_D$NCl)	702^a	760	876^a	898

^{a}These values are obtained in the independent mode approximation.

formula (15)

$$\Delta E = \left(1 - \sum_p^{\text{ref}} c_p^2\right)(E_{\text{ref}} - E_{\text{CI}})$$

3. Potential energy curves and equilibrium geometries

The first series of calculations was undertaken to determine the equilibrium geometries of both the $^2A''$ and $^2A'$ states at the estimated full CI (FCI) level. The equilibrium structural parameters (Table 1) obtained for the ground state $^2A''$ in the given basis are: H—N = 1.026 Å, N—Cl = 1.714 Å and ∠HNCl = 102.51°; for the first excited state $^2A'$ the equilibrium geometry was calculated to be: H—N = 1.046 Å, N—Cl = 1.626 Å and ∠HNCl = 132.9°. These values have been calculated by determination of the minimum of the three-dimensional hyperface polynominal fit of the FCI energy data. The resulting T_e value corresponding to the difference of the FCI energies of these two electronic states in their equilibrium geometries is 21772 cm^{-1} (2.70 eV).

It is interesting to compare these results with the corresponding data for HNF, for which experimental results are also available. The N—H bond distances for the $X\ ^2A''$ and $A\ ^2A'$ states have been computed (9) to be 1.03 and 1.02 Å, while the observed values are somewhat larger (1.06 and 1.03 Å, respectively). The N—F bond distance decreases by 0.05 Å from ground to excited state in the computations and only 0.03 Å experimentally, so the present N—Cl decrease of 0.09 Å for HNCl is relatively large. Finally the bond angle values for HNF are 101.1° ($X\ ^2A''$) and 123.2° ($A\ ^2A'$), compared with the observed values of 105 and 125°, so a definite trend toward increased bond angle upon excitation is typical for such systems. According to qualitative MO theory (Walsh's rules) this fact is understandable in terms of the fact that the $10a'$ MO favors strongly bent geometries (doubly occupied in $^2A''$ but only singly in $^2A'$) while $3a''$ shows a much weaker trend in this direction (oppositely occupied in the two states). This state of affairs is mirrored in the spectroscopic data for such systems by the occurrence of a fairly long bending progression in both absorption and emission.

Nonetheless comparison with isovalent HSO shows that such

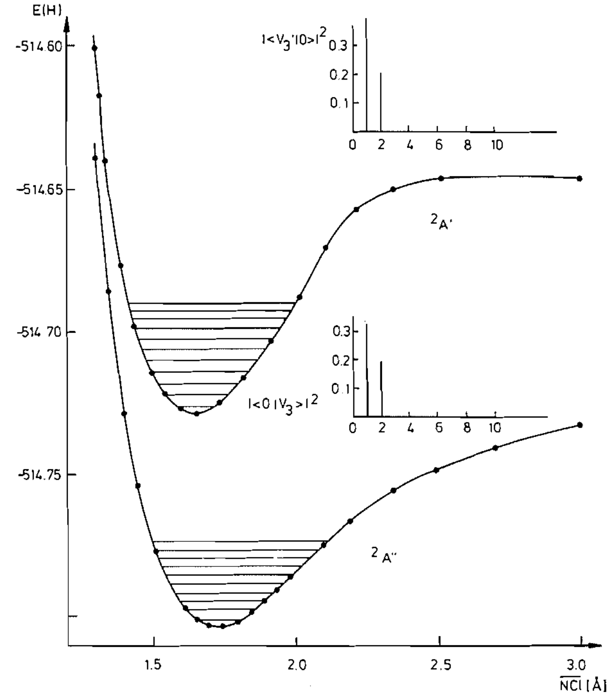

FIG. 1. Potential energy curves for the N—Cl stretching coordinate: HN = 1.026 Å, ∠HNCl = 102.51° for the ground state; HN = 1.046 Å, ∠HNCl = 132.9° for the first excited state. Franck–Condon factors for the transition from $v'' = 0$ to various v' levels and from $v_2' = 0$ to v_2'' are also given.

trends cannot be relied upon to any great degree. In this case both calculations (3) and experiment (4, 5) show that the bond angle decreases slightly upon excitation to $^2A'$, while the S—O bond length increases by 0.13 Å, in stark contrast to what is found for HNF and HNCl. At the same time the HS_2 geometrical data parallel that of HSO quite closely. Thus it is evident that there is a clear distinction between such isovalent systems, with the nitrogen–halogen HAB type showing a different pattern than their oxygen–oxygen counterparts.

The T_e value for HNF is computed at the FCI level as 2.58 eV, only 0.12 eV smaller than the present result for HNCl. These energy separations are again quite different from what is found for the HSO–HO_2–HS_2 group of isovalent species. In HO_2 the T_e value is computed (17) to be only 0.85 eV, and nearly the same result (0.86 eV) is found for HS_2 (7). The mixed system HSO has a computed T_e value of 1.56 eV (3), some 0.2 eV smaller than measured (4, 5), but its SOH isomer, not yet found experimentally, is predicted (18) to have an even smaller T_e value of only 0.65 eV.

Starting from these equilibrium geometries one-dimensional potential curves corresponding to the stretching and bending coordinates for the $^2A''$ and $^2A'$ states have been calculated without further optimization of the other structural parameters. The computations have not been extended to geometries associated with molecular fragmentation, but it is still helpful to note which asymptotes correspond to the two states under study. For N—Cl dissociation the products are in both cases Cl(^2P_u) + HN($^3\Sigma^-$). These species represent three open shells and there is therefore a change in configuration from the equilibrium structures (one open shell) in each instance; at the bond distance values treated in this work, this change in configuration has not yet occurred, so the convergence of the two N—Cl potential curves at infinite bond distance is not apparent in

TABLE 2. Franck–Condon factors $|\langle v'' | v' \rangle|^2$ for the normal modes of HNCl[a]

	H—N vibrations[a]		N—Cl vibrations		Bending vibrations	
v'	H—(NCl)	D—(NCl)	HN—Cl	DN—Cl	HNCl	DNCl
0	0.976	0.970	0.302	0.317	0.017	0.003
1	0.022	0.028	0.397	0.394	0.068	0.018
2	0.001	0.001	0.220	0.210	0.135	0.053
3	0.00001	0.0001	0.066	0.063	0.177	0.099
4			0.012	0.012	0.165	0.138

[a] In each case the fixed geometrical parameters are held equal to the respective equilibrium values of the states under consideration.

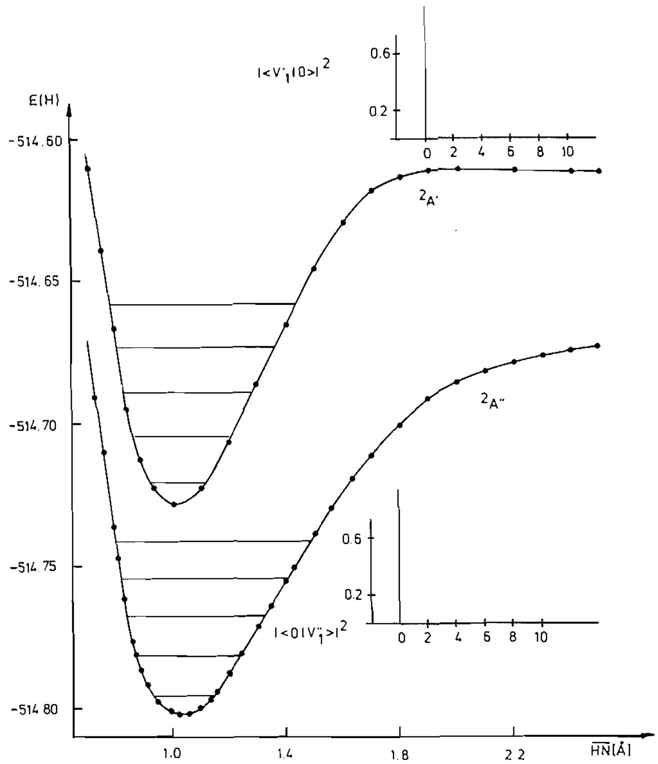

FIG. 2. Potential energy curves for the H—N stretching coordinate: NCl = 1.714 Å, ∠HNCl = 102.51° for the ground state; NCl = 1.626 Å, ∠HNCl = 132.9° for the $^2A'$ state.

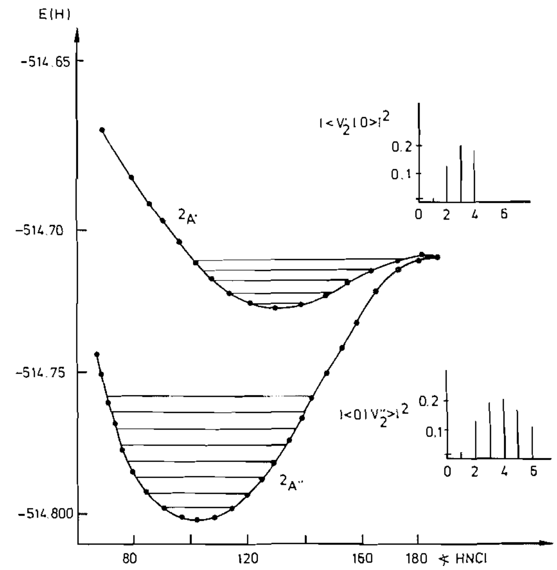

FIG. 3. Potential energy curves for the bending coordinate: NCl = 1.714 Å, HN = 1.026 Å for $^2A''$; NCl = 1.626 Å, HN = 1.046 Å for $^2A'$. Only the bound vibrational levels are calculated for the $^2A'$ state.

Fig. 1, in which the computed results are plotted. A similar situation is expected for the N—H potential curves at large distances (Fig. 2), except that in this case $X\ ^2A''$ dissociates adiabatically to H(^2S) + NCl($^3\Sigma^-$) while $A\ ^2A'$ correlates with H(^2S) + NCl ($^1\Delta$), again asymptotes with three open shells.

The corresponding bending potential curves are given in Fig. 3 and show that the two states become degenerate ($^2\pi$) in linear nuclear conformations. As a result a significant Renner–Teller interaction is expected in the region of the relatively small barrier to linearity of the upper state; an analogous situation has been found for HNF (9), for which the Renner–Teller coupling between the $X\ ^2A''$ and $A\ ^2A'$ states has been carried out explicitly.

4. Vibrational calculations and $X\ ^2A'' - A\ ^2A'$ intensity distribution

The potential curves obtained at the estimated FCI level have been fitted in terms of various polynomial expansions in order to calculate the vibrational energies within the Born–Oppenheimer approximation.

In the first approach coupling between the various modes was neglected and sixth-order polynomials were employed in each instance; standard deviations for the fits are in the order of 1×10^{-4} au. The corresponding vibrational levels and wavefunctions were then obtained in each case by diagonalizing the corresponding one-dimensional Hamiltonian matrices formed in the basis of harmonic oscillator eigenfunctions (19). These calculations were supplemented by a coupled-mode treatment employing the Wilson **F–G** matrix formalism (20), in which a strictly harmonic force field is assumed. For this purpose a three-dimensional fit to the energy hypersurface was carried out, with a root-mean-square deviation of 3×10^{-4} au being found. The resulting molecular constants and vibrational frequencies are also contained in Table 1.

The N—H stretching frequencies are 100–300 cm^{-1} higher for each electronic state than those obtained earlier for HNF (the independent-mode approximation was used exclusively for HNF (9)), but the differences are only slightly greater than the error bars expected for such calculations. In both systems it is found that the NH stretching frequency increases by 400–500 cm^{-1} upon excitation to the upper $^2A'$ electronic state. The bending frequency also shows similar behavior in HNF and HNCl upon electronic excitation, dropping in each case by roughly 300 cm^{-1}, as seems understandable on the

TABLE 3. Oscillator strengths and radiative lifetimes for the $^2A' - {}^2A''$ transition in HNCl at several nuclear geometries

Geometry NCl (au) HN = 1.939 au	∠HNCl (deg)	$f(\vec{r})$	τ (s)
3.13	102.5	0.171×10^{-2}	0.243×10^{-5}
3.23	102.5	0.183×10^{-2}	0.206×10^{-5}
3.23	107.0	0.168×10^{-2}	0.249×10^{-5}
3.33	102.5	0.190×10^{-2}	0.206×10^{-5}
3.23	97.0	0.197×10^{-2}	0.173×10^{-5}
HNF HN = 1.93 au NF = 2.56 au ∠HNF = 100°		0.396×10^{-2}	0.659×10^{-6}

basis of the potential curves of Fig. 3. In this case the computed frequencies should be accurate to 50−100 cm^{-1} according to previous experience with such calculations. Similar error limits are expected for the N—Cl frequencies, which indicate an increase of 140−160 cm^{-1} upon excitation. Not surprisingly, these results are uniformly smaller (by about 300 cm^{-1}) for the corresponding NF frequencies in HNF (9). Results for the deuterated isomer are also given in Table 2.

Previous experience with employing such *ab initio* calculations to aid in the identification of unknown substances has indicated that Franck−Condon factors are especially useful in this regard (3, 7). These results have been obtained in the independent-mode approximation (Table 2) and are also shown in Figs. 1−3 along with the corresponding potential curves; in each case results are given for both absorption and emission relative to the $v = 0$ level of the initial state. Vibrational progressions are expected in both the bending and N—Cl modes, particularly the former; only the O−O transition should be observed for N—H stretch, however. The most intense cold band should occur to the $^2A'$ (0,1,3) vibronic state with a computed transition energy of 26072 cm^{-1}.

As a further aid for the identification of the HNCl system, the dipole transition moment matrix element $\overrightarrow{R_{e'e''}}$ has been computed between the $X\ ^2A''$ and $A\ ^2A'$ states. These results are then employed to compute the oscillator strength f and radiative lifetime τ of the excited state according to the formulae (21):

$$[1]\quad f(r) = \frac{2}{3}\,|\,\overrightarrow{R_{e'e''}}\,|^2 \Delta E$$

and

$$[2]\quad \tau = 1.499/f(\vec{r})\,\bar{\nu}^2$$

where $\bar{\nu}$ is the transition energy in units of cm^{-1} and otherwise atomic units are assumed. For this purpose both electronic states have been obtained employing the ground state MO's as one-electron basis, in order to avoid the more cumbersome computations which are required when different (nonorthogonal) MO basis sets are used for each state. These results have been obtained at several N—Cl bond distances and bending angles and are shown in Table 3. The indication is that the transition moment is relatively insensitive to changes in nuclear conformation, so that the Franck−Condon approximation is quite acceptable for this system. A relatively long lifetime of 2.0 μs is indicated for this dipole-allowed transition, which is at least consistent with the fact that in the linear geometry the transition moment vanishes by symmetry. This lifetime is nonetheless some three times longer than that of HNF, which has also been computed in the present study (0.6 μs). An earlier prediction of the corresponding lifetime for HSO of 40 μs has recently been found to be of good accuracy, with an experimental value of 51 ± 5 μs having been reported (6).

TABLE 4. Dipole moment (D) calculated for the ground and first excited state of HNF and HNCl at the respective equilibrium geometries[a]

Molecule	$^2A''$ μ_x	$^2A''$ μ_y	$^2A''$ $\lvert\mu\rvert$	$^2A'$ μ_x	$^2A'$ μ_y	$^2A'$ $\lvert\mu\rvert$
HNF	−1.013	1.780	2.048	−1.203	1.213	1.708
HNCl	−0.090	1.700	1.702	−0.461	1.087	1.173

[a]The geometrical coordinates employed are HNF: $^2A''$, H (−0.336, 1.906), F (2.560, 0.0); $^2A'$, H (−1.068, 1.583), F (2.510, 0.0); HNCl: $^2A''$, H (−0.419, 1.893), Cl (3.239, 0.0); $^2A'$, H (−1.345, 1.448), Cl (3.037, 0.0).

Finally, the dipole moment matrix elements for both HNCl electronic states have also been computed, which information would also be needed in a treatment of the Renner−Teller coupling of this system. These results are presented along with the corresponding findings for HNF in Table 4; in all cases the equilibrium geometries are employed for a given state (see Table 1 and also Table 1 of ref. 9). The polarity of each molecule is seen to decrease upon $A\ ^2A' - X\ ^2A''$ excitation, with HNF being somewhat more polar than HNCl in each case.

Acknowledgements

The authors wish to thank the Deutsche Forschungsgemeinschaft for financial support in the form of the Sonderforschungsbereich 42. The computations of the study have been undertaken on the Perkin Elmer 3242 system of SFB 42 in Wuppertal and at the University of Bonn Computer Center. Special thanks are due to Bernd Hess for his help in carrying out the CI computations.

1. P. J. BRUNA, S. D. PEYERIMHOFF, R. J. BUENKER, and P. ROSMUS. Chem. Phys. **3**, 35 (1974).
2. R. H. JUDGE, C. R. DRURY-LASSARD, and D. C. MOULE. Chem. Phys. Lett. **53**, 82 (1978).
3. A. B. SANNIGRAHI, K. H. THUNEMANN, S. D. PEYERIMHOFF, and R. J. BUENKER. Chem. Phys. **20**, 25 (1977).
4. K. H. BECKER, M. A. INOCENCIO, and U. SCHURATH. Int. J. Chem. Kinet. **S1**, 205 (1975).
5. U. SCHURATH, M. WEBER, and K. H. BECKER. J. Chem. Phys. **67**, 110 (1977).
6. M. KAWASAKI, K. KASATANI, S. TANAHASHI, and H. SATO. J. Chem. Phys. **78**, 7146 (1983).
7. A. B. SANNIGRAHI, S. D. PEYERIMHOFF, and R. J. BUENKER. Chem. Phys. Lett. **46**, 415 (1977).
8. K. J. HOLSTEIN, E. H. FINK, J. WILDT, and F. ZABEL. Chem. Phys. Lett. **113**, 1 (1985).
9. M. PERIC, S. D. PEYERIMHOFF, and R. J. BUENKER. Can. J. Chem. **61**, 2500 (1983).
10. T. H. DUNNING JR. J. Chem. Phys. **53**, 2823 (1970).
11. A. D. MCLEAN and G. CHANDLER. J. Chem. Phys. **72**, 10 (1980).
12. E. CLEMENTI and G. C. LIE. J. Chem. Phys. **60**, 1275 (1974).
13. R. J. BUENKER and S. D. PEYERIMHOFF. Theor. Chim. Acta, **39**, 217 (1975); **35**, 33 (1974).
14. R. J. BUENKER, S. D. PEYERIMHOFF, and W. BUTSCHER. Mol. Phys. **35**, 771 (1978).
15. S. R. LANGHOFF and E. R. DAVIDSON. Int. J. Quant. Chem. **8**, 61 (1974).

16. R. J. BUENKER. *In* Proceedings of Workshop on Quantum Chemistry and Molecular Physics in Wollongong, Australia. February 1980; R. J. BUENKER. *In* Studies in physical and theoretical chemistry. Vol. 21. (Current Aspects of Quantum Chemistry 1981), *Edited by* R. Carbó. Elsevier Scientific Publishing Company. Amsterdam. 1982. p. 17; R. J. BUENKER and R. A. PHILLIPS. J. Mol. Struct. THEOCHEM. In press.
17. R. J. BUENKER and S. D. PEYERIMHOFF. Chem. Phys. Lett. **37**, 208 (1976).
18. A. B. SANNIGRAHI, S. D. PEYERIMHOFF, and R. J. BUENKER. Chem. Phys. **20**, 381 (1977).
19. M. PERIC, R. RUNAU, J. RÖMELT, S. D. PEYERIMHOFF, and R. J. BUENKER. J. Mol. Spectrosc. **78**, 309 (1979).
20. E. B. WILSON JR., J. C. DECIUS, and P. C. CROSS. Molecular vibrations. McGraw Hill Book Company, New York. 1955.
21. S. P. MCGLYNN, L. G. VANQUICKENBORNE, M. KINOSHITA, and D. G. CARD. Introduction to applied quantum chemistry. Holt, Rinehart and Winston, Inc., New York. 1972.

Excess volumes and excess enthalpies of acetic and its methyl-substituted acids + acetonitrile

B. S. LARK[1] AND T. S. BANIPAL

Department of Chemistry, Guru Nanak Dev University, Amritsar-143 005, India

Received October 9, 1984[2]

B. S. LARK and T. S. BANIPAL. Can. J. Chem. **63**, 3269 (1985).

Excess volumes of the systems acetonitrile (ACN) + acetic acid (AA), + propionic acid (PA) and + isobutyric acid (IBA) at 298.15 and 308.15 K and + trimethylacetic acid (TMA) at 313.15 K have been measured using dilatometric method. The observed values are found to be negative for the first three systems while the last system has sigmoid concentration dependence. Excess enthalpies for the first three systems at 308.15 K and for the last system at 313.15 K have also been determined and found to be positive. The results have been explained in terms of depolymerization of the acids, dipole–dipole interactions between heteromolecules and the steric hindrance caused by the increasing methylation.

B. S. LARK et T. S. BANIPAL. Can. J. Chem. **63**, 3269 (1985).

Utilisant une méthode dilatométrique, on a mesuré les volumes en excès de l'acétonitrile (ACN) avec les acides acétique (AA), propionique (AP) et isobutyrique (AIP) à 298,15 et 308,15 K ainsi qu'avec l'acide triméthylacétique (ATM) à 313,15 K. On a observé des valeurs négatives pour les trois premiers systèmes alors que dans le dernier cas les valeurs varient d'une façon sigmoïde avec la concentration. On a également déterminé les enthalpies en excès pour les trois premiers systèmes à 308,15 K et pour le dernier à 313,15 K et toutes ces enthalpies sont positives. On explique ces résultats en fonction d'une dépolymérisation des acides, d'interactions dipôles–dipôles entre des hétéromolécules et par des encombrements stériques provoqués par une augmentation de méthylation.

[Traduit par le journal]

Introduction

Excess thermodynamic functions of mixtures consisting of acetic and its methyl-substituted acids with variety of solvents have been reported previously from these (1–5) and other laboratories (6–12). These acids in the pure state exist mainly as cyclic dimers. However, trimers formed because of strong interactions between ring dimers and monomers do also exist (9). The mixing behaviour of these acids with various solvents is interesting: e.g., acetic and propionic acids when mixed with non-polar solvents show large positive excess free energies as compared to positive enthalpies and thus exhibit negative excess entropies (4–6). This behaviour has been attributed to the breaking up of acid dimer–monomer interactions on the addition of a non-polar solvent and to the formation of dimers from the monomers thus set free, which gives increasing proportions of dimers with the increasing mole fraction of non-polar component (6). Methanol (B) gives large negative excess volumes with these acids (1–3, 7, 8) because of the formation of hydrogen bonded AB and AB_2 type of complexes by the depolymerized acid (A) monomers, for which even the spectral evidence has been advanced by Izmailov (13) and Apelblat (14). Campbell and Gieskes (10) have shown that chloroform (μ = 1.15 D and ϵ = 4.806 at 298.15 K) with acetic acid gives positive excess volumes and negative excess enthalpies. The authors explain this phenomenon by the preferred association of ring dimers of acetic acid with chloroform molecules in an antiparallel dipole arrangement.

Acetonitrile is a purely polar unassociated solvent (μ = 3.37 D and ϵ = 36.01 at 298.15 K) which has very small tendency of H-bond formation (15). Excess functions of title acids in this solvent are unexplored and presently we report excess volumes and excess enthalpies for such mixtures and use the data to divulge qualitatively the role played by such a highly polar solvent.

[1] To whom all correspondence should be addressed.

[2] Revision received April 17, 1985.

Experimental

Acetic and propionic acids (A.R., B.D.H.) for the present work were the same as used in the earlier reports (4, 5).

Isobutyric acid (L.R., SRL) was dried by refluxing it over phosphorus pentaoxide and then fractionally distilled. Middle fraction was further refluxed over potassium permanganate and fractionally distilled. The fraction distilling at 427.5 K was collected. Trimethylacetic acid (G.R., Tokyo Kasei Kogyo Co., Ltd., Japan) was first fractionally crystallised and the liquid layer was discarded. The solid portion (mp 308.55 K) was then distilled under reduced pressure.

Acetonitrile (L.R. E. Merck) was first distilled over phosphorus pentaoxide under protection from air by a phosphorus pentaoxide tube. The same procedure was repeated until phosphorus pentaoxide no longer became coloured. This was then distilled over anhydrous potassium carbonate to remove traces of phosphorus pentaoxide and finally without a drying agent. The fraction distilling at 354.7 K was collected. The purity of the solvents was checked by determining their densities and refractive indices which have been compared with the literature (16–18) values of Table 1. The agreement is quite good. All solvents were thoroughly degassed before use.

Excess volumes have been measured by using a batch dilatometer, the design and working of which have been reported earlier (19). For measurement of excess enthalpies, adiabatic calorimeter introduced by McGlashan (20) and later modified by Nigam and Mahl (21) has been used. The two-limbed calorimeter has the advantage of the absence of the vapour phase and at the same time allows for the volume change accompanied with the mixing of the components. The presently used calorimeter had slight improvement over that of Nigam and Mahl's (21) that instead of one thermistor, two thermistors, one in its each limb were used to sense the heat changes ensuring better sensitivity. The working of this calorimeter was checked by determining H^E values for cyclohexane + benzene system at 298.15 K (Table 2). The results are fitted to the following equation by the method of least squares:

$$H^E/(\mathrm{J\ mol^{-1}}) = x(1-x)[3207.23 + 167.92(1-2x) + 86.35(1-2x)^2 + 45.07(1-2x)^3]$$

where x is the mole fraction of cyclohexane.

The differences of the presently obtained H^E values from those reported by various workers (22–28) are illustrated as a function of

TABLE 1. Physical constants of pure compounds

		Refractive index at 298.15 K		Density (g/cm^3) at 298.15 K	
Index	Compound	Obs.	Lit.	Obs.	Lit.
1	Isobutyric acid	1.3933^a	1.3930^a (16)	0.94428	0.94423 (17)
2	Trimethylacetic acid	1.3925^b	—	0.90396^b	0.90401^b (18)
3	Acetonitrile	1.3415	1.3416 (16)	0.7766	0.7768 (16)

	Dimerization constants K_d (Torr^{-1})	
T (K)	AA (9)	PA (8)
298.15	1.982	2.301
318.15	0.379	0.388

^{a}At 293.15 K.
^{b}At 313.15 K.

TABLE 2. Experimental excess enthalpies for the system $xC_6H_{12} + (1-x)C_6H_6$*

x	H^E J mol^{-1}	δH^E J mol^{-1}	x	H^E J mol^{-1}	δH^E J mol^{-1}
0.0907	283.2	0.54	0.4366	793.7	−0.82
0.1940	522.3	−1.94	0.5122	797.3	−3.02
0.2607	637.6	−0.80	0.6835	685.4	2.89
0.3225	720.9	4.30	0.8192	461.3	−1.32

*σ = 3.28.

composition in Fig. 1. It may be seen that scatter is quite random except in case of ref. 28, where H^E values are smaller throughout the composition range. Also the scatter is well within the uncertainty limit of this instrument.

The temperature of 150 L water-thermostat was controlled to ±0.01 K with the help of 0.01 K Beckmann thermometer calibrated by determining the transition temperature of Glauber's salt (305.534 K).

Results and discussion

Excess volumes as a function of mole fraction of the acid component for the systems ACN + AA, + PA, and + IBA at 298.15 and 308.15 K and for +TMA at 313.15 K have been summarized in Table 3, while H^E values for the first three systems at 308.15 K and for the last at 313.15 K appear in Table 4. The results have been fitted by the method of least squares to the equation,

$$[1] \quad X^E = x(1-x)[A + B(1-2x) + C(1-2x)^2 + \ldots]$$

where X^E may be V^E or H^E and x is the mole fraction of the acid. The values of the fitting parameters $A, B, C \ldots$ for the various systems along with the standard deviations (σ's) are summarized in Table 5. Systematic error analysis shows that for the uncertainties in (*i*) weights of the components taken in the dilatometer (*ii*) change in the level of the liquid of the capillary of the dilatometer on mixing of the components, (*iii*) the calibration of the capillary, and (*iv*) temperature variation of ±0.01 K, the total uncertainty in the final V^E values comes out to be ±0.002 cm^3 mol^{-1}. It is encouraging to note that the standard deviations as given in Table 5 are much within the uncertainty limits. In case of H^E measurements, the individual deviations of the measured values seldom exceed the standard deviations and are of the order of ±1% of the measured H^E values.

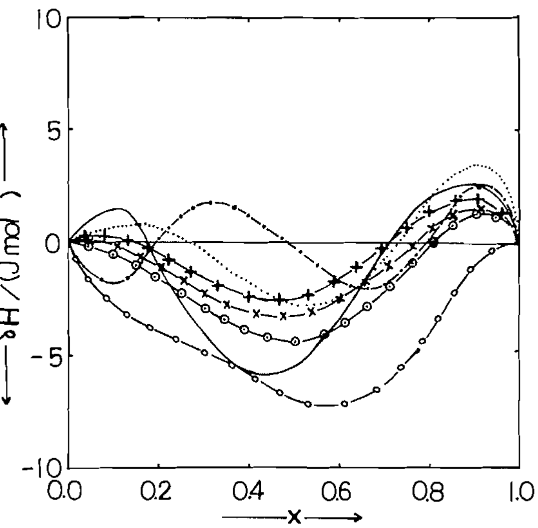

FIG. 1. Differences δH^E between the literature values and the present values as a function of x for the system $xC_6H_{12} + (1-x)C_6H_6$ at 298.15 K: -·-·- (22); -⊙- (23); -×- (24); .... (25); -+- (26) — (27); -○- (28).

V^E values as illustrated in Fig. 2 are negative for the entire concentration range at both the temperatures for all the systems except that with TMA where both positive and negative V^E values are observed. About 10% more negative V^E values at higher temperature (for first three systems only) may be explained by increased population of acid monomers to enter into hetero intermolecular interactions. It may further be seen that V^E values are most negative in case of PA and the magnitude decreases in the order:

PA > AA > IBA > TMA

The other important observation which may be made is that the minimum which in case of AA is in the acid rich region shifts slowly to the acetonitrile-rich region as the methylation of AA increases, so much so, in case of TMA sigmoid V^E dependence becomes apparent. V^E in this system is negative for x upto 0.68 and then becomes slightly positive. These observations may be explained by considering the following three

TABLE 3. Excess volumes of various carboxylic acids with acetonitrile

298.15 K			308.15 K		
x	V^E cm^3 mol^{-1}	$10^4\,\delta V^E$ cm^3 mol^{-1}	x	V^E cm^3 mol^{-1}	$10^4\,\delta V^E$ cm^3 mol^{-1}
		$x CH_3COOH + (1-x) CH_3CN$			
0.0830	−0.1005	−18	0.1037	−0.1403	−2
0.1752	−0.1838	4	0.1350	−0.1738	−9
0.2247	−0.2204	6	0.1614	−0.1985	−9
0.3065	−0.2698	−4	0.2239	−0.2461	10
0.3619	−0.2934	6	0.3001	−0.2917	9
0.4087	−0.3093	5	0.3531	−0.3154	10
0.4855	−0.3264	−6	0.4061	−0.3348	−4
0.5108	−0.3288	−5	0.4638	−0.3485	−6
0.5369	−0.3285	9	0.5217	−0.3551	−9
0.6001	−0.3258	−3	0.5982	−0.3544	−6
0.6676	−0.3109	−9	0.6756	−0.3385	−6
0.7255	−0.2875	−11	0.7518	−0.3028	15
0.7939	−0.2430	14	0.8120	−0.2629	−11
0.8372	−0.2081	9	0.8353	−0.2398	11
0.8503	−0.1971	−3	0.9043	−0.1628	−11
0.9281	−0.1087	−2	0.9712	−0.0545	14
		$x CH_3CH_2COOH + (1-x) CH_3CN$			
0.0777	−0.1459	−7	0.0258	−0.0608	−7
0.1490	−0.2522	−4	0.0748	−0.1613	−8
0.2183	−0.3323	−1	0.1231	−0.2446	−13
0.3058	−0.4017	11	0.1731	−0.3134	3
0.3827	−0.4381	1	0.2521	−0.3968	9
0.4315	−0.4482	2	0.3148	−0.4425	7
0.4858	−0.4491	1	0.3721	−0.4692	14
0.5328	−0.4418	−6	0.4374	−0.4868	0
0.5672	−0.4306	−0	0.4965	−0.4907	−20
0.6013	−0.4162	−1	0.5400	−0.4826	3
0.6078	−0.4134	−5	0.5451	−0.4824	−6
0.6870	−0.3634	−1	0.6531	−0.4396	−5
0.7301	−0.3272	12	0.7002	−0.4074	10
0.7674	−0.2947	−8	0.7857	−0.3322	3
0.8628	−0.1893	−4	0.8645	−0.2360	3
0.9422	−0.0832	−15	0.9419	−0.1138	−2
		$x (CH_3)_2CHCOOH + (1-x) CH_3CN$			
0.0613	−0.1104	−13	0.0745	−0.1481	−17
0.1176	−0.1860	−17	0.1052	−0.1942	−15
0.1915	−0.2532	−1	0.1832	−0.2778	19
0.2579	−0.2901	12	0.2476	−0.3229	11
0.3104	−0.3070	17	0.3155	−0.3494	1
0.3617	−0.3174	−5	0.3559	−0.3565	−2
0.3839	−0.3189	−7	0.4075	−0.3579	−2
0.3892	−0.3180	3	0.4672	−0.3520	−12
0.4204	−0.3164	12	0.5305	−0.3362	−8
0.4804	−0.3110	−7	0.5751	−0.3190	15
0.4814	−0.3091	10	0.6771	−0.2763	−12
0.5325	−0.2995	−8	0.7487	−0.2327	−13
0.5970	−0.2802	−15	0.8044	−0.1950	9
0.6282	−0.2675	−6	0.8772	−0.1371	−9
0.6724	−0.2485	−5	0.9286	−0.0860	−5
0.7522	−0.2058	12			
0.8496	−0.1416	13			
0.9506	−0.0552	−8			

TABLE 3. (*Concluded*)

298.15 K			308.15 K		
x	V^E cm^3 mol^{-1}	$10^4 \delta V^E$ cm^3 mol^{-1}	x	V^E cm^3 mol^{-1}	$10^4 \delta V^E$ cm^3 mol^{-1}
$x(CH_3)_3CCOOH + (1-x)CH_3CN$*					
0.0624	−0.0854	−19	0.4979	−0.0631	−18
0.1644	−0.1383	−5	0.6245	−0.0215	3
0.2294	−0.1394	3	0.7057	0.0013	12
0.2688	−0.1321	16	0.7862	0.0184	14
0.3153	−0.1204	18	0.8891	0.0245	−12
0.3538	−0.1111	−6	0.9370	0.0197	−11
0.4137	−0.0916	−13			

*At 313.15 K.

TABLE 4. Excess heats of various carboxylic acids with acetonitrile at 308.15 K

x	H^E J mol^{-1}	δH^E J mol^{-1}	x	H^E J mol^{-1}	δH^E J mol^{-1}
$xCH_3COOH + (1-x)CH_3CN$			$xCH_3CH_2COOH + (1-x)CH_3CN$		
0.0866	106.2	−1.1	0.1085	255.1	−2.9
0.1288	141.6	−1.6	0.1444	345.2	3.4
0.1572	166.0	2.1	0.1711	404.5	3.4
0.2050	192.6	−1.8	0.2273	510.8	−3.0
0.2848	241.4	2.1	0.3136	643.3	−3.0
0.3203	260.6	2.8	0.3783	708.9	0.5
0.4051	294.9	−3.1	0.4383	733.6	−2.8
0.4880	327.7	0.4	0.4676	743.8	3.7
0.5594	337.0	−1.6	0.4966	738.5	1.0
0.6063	333.7	−2.4	0.5308	729.5	2.6
0.6524	327.9	3.2	0.6366	648.5	0.5
0.7910	234.8	3.1	0.6632	614.3	−4.4
0.8559	160.3	−1.7	0.7282	533.2	−0.2
0.8852	125.8	−1.7	0.8540	323.9	1.6
$x(CH_3)_2CHCOOH + (1-x)CH_3CN$			$x(CH_3)_3CCOOH + (1-x)CH_3CN$[a]		
0.0827	225.8	3.7	0.0791	415.4	1.5
0.1765	508.0	0.2	0.1032	535.7	3.3
0.2058	589.5	2.1	0.2428	1069.6	−5.5
0.3261	859.4	−4.3	0.3162	1236.5	−4.5
0.3990	958.7	1.0	0.3546	1298.5	4.1
0.4636	998.8	4.9	0.4218	1341.0	3.6
0.4874	997.2	0.6	0.4547	1339.4	2.0
0.5901	951.4	0.5	0.5702	1248.6	−3.3
0.6531	879.9	−3.2	0.6472	1141.9	1.8
0.7242	775.6	−0.9	0.7128	1017.5	−1.7
0.8229	576.6	−1.4	0.8230	756.4	−1.2
0.8812	431.1	3.2	0.9272	393.8	3.0

[a]At 313.15 K.

equilibria accompanying the mixing process,

[2] D—M $\rightleftharpoons$ D + M

[3] D $\rightleftharpoons$ 2M

[4] M + ACN $\rightleftharpoons$ M—ACN

where D and M denote a dimer and a monomer of the acid under question. The first process is accompanied with large volume increase in the right direction, second is isochoric, i.e., the volume of the dimer is assumed to be equal to twice the volume of the monomer (9) and the third is accompanied with large contraction. The addition of acetonitrile to any one of the acids first creates monomers by the first two steps resulting in expansion and then stronger heteromolecular dipole–dipole interactions result in the observed negative V^E values. This conclusion finds sufficient support from the contractive mixing behaviour of ACN + CH_3OH and + $(CH_3)_2CO$. V^E for equimolar mixture of ACN + MeOH as reported by Cibulka *et al.* (29) is −0.131 cm^3 mol^{-1} and the corresponding value for mixture with $(CH_3)_2CO$ which we determined separately is

TABLE 5. Values of the constants in eq. [1] and standard deviations

T/K	V^E A	B	C	D	$\sigma(V^E)$ $cm^3\ mol^{-1}$
		$CH_3CN + CH_3COOH$			
298.15	−1.3098	0.1901	−0.2094		0.0009
308.15	−1.4124	0.2188	−0.4269		0.0010
		$CH_3CN + CH_3CH_2COOH$			
298.15	−1.7905	−0.2730	−0.0068		0.0007
308.15	−1.9539	−0.1514	−0.3265		0.0010
		$CH_3CN + (CH_3)_2CHCOOH$			
298.15	−1.2259	−0.4240	−0.3866		0.0012
308.15	−1.3749	−0.4912	−0.4566		0.0013
		$CH_3CN + (CH_3)_3CCOOH$			
313.15	−0.2425	−0.6728	−0.3842	−0.4502	0.0015

T/K	H^E A	B	C	D	δH^E $J\ mol^{-1}$
		$CH_3CN + CH_3COOH$			
308.15	1321.20	−461.81	−74.03	828.36	2.61
		$CH_3CN + CH_3CH_2COOH$			
308.15	2947.17	432.37	−537.50	−601.25	3.19
		$CH_3CN + (CH_3)_2CHCOOH$			
308.15	3983.69	229.01	−604.77	−1420.36	3.29
		$CH_3CN + (CH_3)_3CCOOH$			
313.15	5272.49	1295.49	619.93	−1878.21	3.96

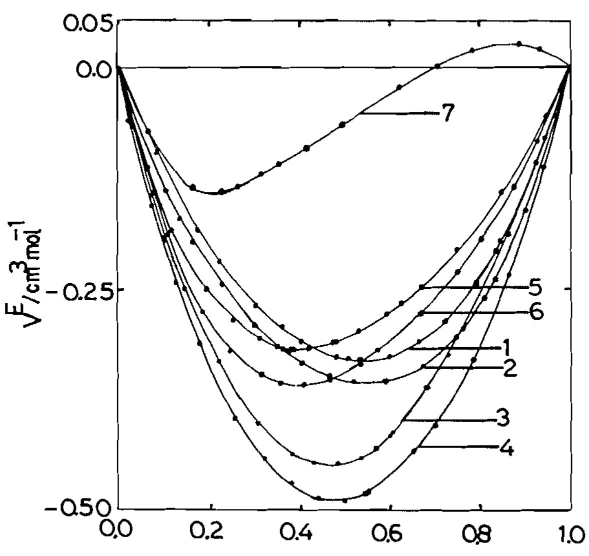

FIG. 2. Plot of V^E vs. x. *1*, *2*: AA + ACN at 298.15 K and 308.15 K; *3*, *4*: PA + ACN at 298.15 and 308.15 K; *5*, *6*: IBA + ACN at 298.15 and 308.15 K; *7*: TMA + ACN at 313.15 K.

$-0.132\ cm^3\ mol^{-1}$.

The dimerization constants (K_d's) of AA and PA are available in the vapour phase only and K_d for PA is higher than that of AA (Table 1). The increased K_d values should reduce the number of available (D—M) trimers and accordingly positive contribution to the overall V^E is diminished further. This is actually observed in case of PA but beyond that, i.e., for IBA V^E becomes less negative and in case of TMA sigmoid dependence is observed. This behaviour may be attributed to the increasing steric hindrance of methyl groups. The shifting of minimum to the acid poor region may be due to increase in both steric hindrance and dimerization constant. This is further supported by the findings of Cibulka *et al.* (29) who have shown that for the binary systems containing alkanol and ACN, V^E increases in the order

$$V^E(\text{ACN + normal alkanol}) < V^E(\text{ACN + branched alkanol}) < V^E(\text{ACN + secondary alkanol})$$

To arrive at the behaviour of individual acids and the solvent in each case, excess partial molar volumes ($\bar{V}^E$) were estimated and as a function of composition are illustrated in Fig. 3. It may be seen that in case of first three acids the behaviour is almost similar and the partial molar volume of both acid and solvent decreases as the concentration of the other component increases. In case of TMA, the excess partial molar volume is positive for $x \geq 0.27$ and then decreases very sharply. Contraction of ACN in this acid is much smaller than as observed in other acids and which becomes positive at its dilute end. To divulge the nature of interactions, the partial molar volume data in the dilute region have further been analyzed for values of $x_i \leq 0.15$ using the following equation

TABLE 6. Various quantities (in cm^3 mol^{-1}) calculated from eq. [5]

						V_{ii}		V_{iii}	
V^0_{Acid}	$\bar{V}^0_{Acid}$	$\bar{V}^0_{Acid} - V^0_{Acid}$	V^0_{ACN}	$\bar{V}^0_{ACN}$	$\bar{V}^0_{ACN} - V^0_{ACN}$	Acid	ACN	Acid	ACN
$CH_3COOH + CH_3CN$ (298.15 K)									
57.540	56.211	−1.329	52.846	51.137	−1.709	1.7868	2.9114	−1.1893	−1.8166
$CH_3CH_2COOH + CH_3CN$ (298.15 K)									
74.982	72.912	−2.070	52.846	51.322	−1.524	2.6655	1.0092	−0.8152	0.4388
$(CH_3)_2CHCOOH + CH_3CN$ (298.15 K)									
93.309	91.273	−2.026	52.846	51.658	−1.188	4.0892	1.8678	−1.6524	−1.9370
$(CH_3)_3CCOOH + CH_3CN$ (313.15 K)									
112.981	111.231	−1.750	54.009	54.505	0.496	7.2900	−2.9807	−10.8763	5.3141

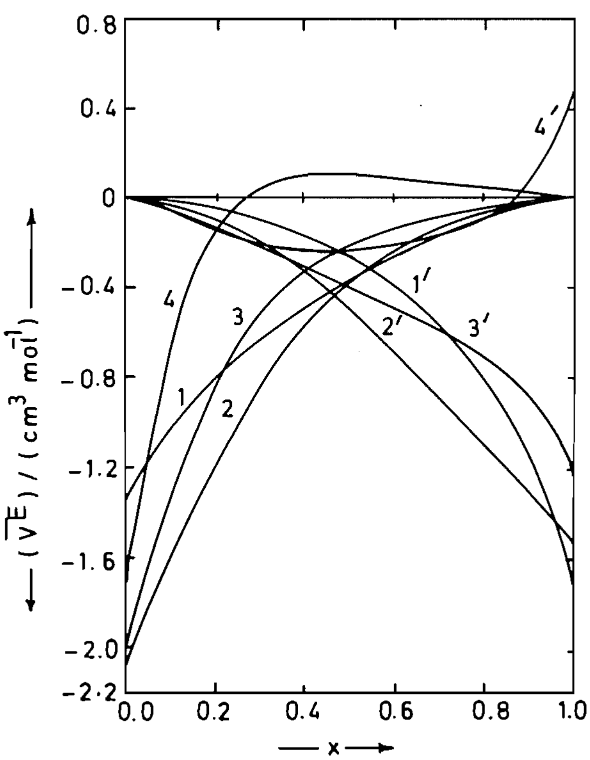

FIG. 3. Plot of $\bar{V}^E$ vs. x. *1*, *2*, *3*, *4* are the plots for AA, PA, IBA, TMA and *1′*, *2′*, *3′*, *4′* are the plots for ACN in the respective acids.

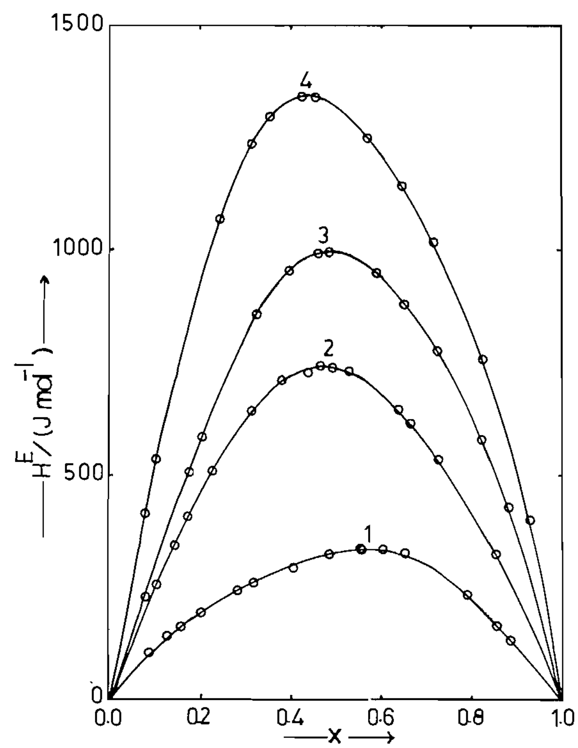

FIG. 4. Plot of H^E vs. x. *1*: AA + ACN; *2*: PA + ACN; *3*: IBA + ACN at 308.15 K; and *4*: TMA + ACN at 313.15 K.

$$[5] \quad V^E/n_i = (\bar{V}_i^0 - V_i^0) + (V_{ii}x_i + V_{iii}x_i^2 + \ldots)$$

where n_i number of moles of component i. $\bar{V}_i^0$ = molar volume of component i at infinite dilution. V_i^0 = molar volume of pure component i, V_{ii} and V_{iii} = two body and three body solute–solute interactions, i = 1,2.

The estimated values of V_i^0, $\bar{V}_i^0$, V_{ii}, and V_{iii} are summarized in Table 6. It may be seen that the values of $(\bar{V}_i^0 - V_i^0)$, i.e., volume of transfer of the solute from its pure liquid state to infinite dilution, is positive only in case of the transfer of ACN to TMA while it is negative in all other cases. The values of V_{ii} and V_{iii} show that the solute–solute interactions contribution is positive for all the acids and the values increase from AA to TMA while the acetonitrile gives negative contribution in case of TMA only. This may be due to the rebuilding of dipole–dipole interactions which at infinite dilution are torn apart by TMA molecules till when the concentration of ACN is enough to break up the acid D–M interactions.

H^E values determined for the systems under investigation are positive over the whole composition range and the magnitude decrease in the order (Fig. 4)

TMA > IBA > PA > AA

In view of the above equilibria (reactions [2]–[4]) explaining the mixing process, it may be said that endothermic contributions from the first two equilibria overweigh the possibly small exothermic contribution from the last one. The two relating evidences in support may be cited from literature. The incapability of H-bond formation between OH and CN groups result in appreciable endothermic mixing of ACN and ethanol arising mainly from depolymerization of the latter (30). H^E values in case of propionitrile + $(CH_3)_2CO$ mixtures as reported by Thacker and Rowlinson (30) do not exceed − 100 J mol^{-1} at 298.15 K. The observed trend of increasing H^E values from AA to TMA and the accompanied shift of the maximum to the acid poor region may be believed to be arising from the increasing K_d values and from steric hindrance of crowding methyl groups to dipole–dipole interactions as concluded above from the volume studies.

Acknowledgement

T.S.B. is grateful to the CSIR, New Delhi, India, for the award of Junior Research Fellowship.

1. B. S. LARK and R. C. PALTA. J. Chem. Thermodyn. **12**, 101 (1980).
2. B. S. LARK and R. C. PALTA. J. Chem. Thermodyn. **12**, 287 (1980).
3. B. S. LARK and R. C. PALTA. Malaysian J. Sci. 6(B), 159 (1980).
4. B. S. LARK, T. S. BANIPAL, S. SINGH, and R. C. PALTA. J. Chem. Eng. Data, **29**, 277 (1984).
5. B. S. LARK, T. S. BANIPAL, and S. SINGH. J. Chem. Eng. Data. In press.
6. G. MIKSCH, F. RATKOVICS, and P. KOHLER. J. Chem. Thermodyn. **1**, 257 (1969).
7. M. WAGNER, A. APELBLAT, and A. TAMIR. J. Chem. Thermodyn. **12**, 181 (1980).
8. A. APELBLAT and F. KOHLER. J. Chem. Thermodyn. **8**, 749 (1976).
9. H. E. AFFSPRUNG, G. H. FINDENEGG, and F. KOHLER. J. Chem. Soc. A, 1364 (1968).
10. A. N. CAMPBELL and J. M. T. M. GIESKES. Can. J. Chem. **43**, 1004 (1965).
11. J. M. T. M. GIESKES. Can. J. Chem. **43**, 2448 (1965).
12. F. KOHLER, R. GOPAL, G. GOTZE, H. ATROPS, M. A. DEMIRIZ, E. LIEBERMANN, E. WILHELM, F. RATKOVICS, and B. PALAGYL. J. Phys. Chem. **85**, 2524 (1981).
13. N. A. IZMAILOV. Electrochemistry of solutions. 2nd ed., Izd. Khimya, Moscow. 1966. pp. 275–284, 563–564.
14. A. J. APELBLAT. J. Phys. Chem. **74**, 2214 (1970).
15. S. N. VINOGRADOV and R. H. LINNELL. Hydrogen bonding. Van Nostrand Reinhold Co., New York. 1971. p. 15.
16. J. A. RIDDICK and E. E. TOOPS, JR. Organic solvents. Interscience Publishers Inc., New York. 1967.
17. R. C. PALTA. Ph.D. Dissertation, Guru Nanak Dev University, Amritsar, India. 1983.
18. F. KOHLER, H. ATROPS, H. KALALL, E. LIEBERMANN, E. WILHELM, F. RATKOVICS, and T. SALAMON. J. Phys. Chem. **85**, 2520 (1981).
19. B. S. LARK and R. C. PALTA. J. Indian Chem. Soc. **56**, 322 (1979).
20. J. A. LARKIN and M. L. MCGLASHAN. J. Chem. Soc. 3425 (1961).
21. R. K. NIGAM and B. S. MAHL. J. Chem. Soc. Faraday Trans. I. **68**, 1508 (1972).
22. C. YANES, J. PELLICER, E. ROJAS, and M. ZAMORA. J. Chem. Thermodyn. **11**, 177 (1979).
23. C. G. SAVINI, D. R. WINTERHALTER, L. H. KOVACH, and H. C. VAN NESS. J. Chem. Eng. Data, **11**, 40 (1966).
24. A. E. POPE, H. D. PFLUG, B. DRACE, and G. C. BENSON. Can. J. Chem. **45**, 2665 (1967).
25. G. W. LUNGBERG. J. Chem. Eng. Data. **9**, 193 (1964).
26. R. H. STOKES, K. N. MARSH, and R. P. TOMLINES. J. Chem. Thermodyn. **1**, 211 (1969).
27. H. TOUHARA, M. IKEDA, K. NAKANISHI, and N. WATANABE. J. Chem. Thermodyn. **7**, 887 (1975).
28. M. GRACIA. J. Chem. Thermodyn. **9**, 55 (1977).
29. I. CIBULKA, V. D. NGUYEN, and R. HOLUB. J. Chem. Thermodyn. **16**, 159 (1984).
30. R. THACKER and J. S. ROWLINSON. Trans. Faraday Soc. **50**, 1036 (1954).

Phase diagram measurements and thermodynamic analysis of the $PbCl_2$–NaCl, $PbCl_2$–KCl, and $PbCl_2$–KCl–NaCl systems

ARMAND GABRIEL AND ARTHUR D. PELTON
Ecole Polytechnique, Campus de l'Université de Montréal, C.P. 6079, Succ. "A", Montréal (Qué.), Canada H3C 3A7

Received July 11, 1984[1]

ARMAND GABRIEL and ARTHUR D. PELTON. Can. J. Chem. **63**, 3276 (1985).

The phase diagrams of the $PbCl_2$–NaCl and $PbCl_2$–KCl systems have been measured by the cooling curve technique. In addition, a number of measurements at compositions in the ternary system $PbCl_2$–KCl–NaCl have been made. The binary data have been analysed along with other available thermodynamic data for the binary systems in order to obtain mathematical expressions for the binary thermodynamic properties. Various estimation procedures were then used to calculate the Gibbs energy of the ternary liquid from the binary expressions, and the ternary phase diagram calculated therefrom was compared to the experimental ternary points. In the case of the Conformal Ionic Solution equation, agreement was within 3°C at all measured points. In the case of two "geometric" estimation techniques, the Kohler and Toop equations, agreement was within 10°C but could be brought to within 3°C by the addition of only one small adjustable ternary correction term. The technique of coupled thermodynamic/phase diagram analysis permits a large reduction in the amount of experimental work necessary to measure the ternary diagram. In addition, the ternary thermodynamic expressions developed can be used to calculate all thermodynamic properties of the ternary liquid.

ARMAND GABRIEL et ARTHUR D. PELTON. Can. J. Chem. **63**, 3276 (1985).

Faisant appel à la technique de la courbe de refroidissement, on a mesuré les diagrammes de phase des systèmes $PbCl_2$–NaCl et $PbCl_2$–KCl. De plus, on a fait un certain nombre de mesures à des compositions comprises dans le système ternaire $PbCl_2$–KCl–NaCl. On a analysé les données binaires de concert avec d'autres données thermodynamiques disponibles pour les systèmes binaires dans le but d'obtenir des expressions mathématiques pour les propriétés thermodynamiques binaires. On a utilisé diverses méthodes d'évaluation pour calculer l'énergie de Gibbs du liquide ternaire à partir d'expressions binaires; on a comparé les points ternaires expérimentaux avec le diagramme de phase ternaire calculé en utilisant la méthode décrite plus haut. Dans le cas de l'équation de Solution Ionique Conformale, la correspondance se situe à moins de 3°C pour chacun des points mesurés. Dans les cas des deux techniques "géométriques" d'évaluation, les équations de Kohler ou de Toop, la correspondance est meilleure que 10°C; toutefois, elle peut être ramenée à moins de 3°C par l'addition d'un seul petit terme ajustable ternaire de correction. La technique de l'analyse des diagrammes de phase couplés à la thermodynamique permet de réduire considérablement la quantité de travail expérimental nécessaire pour mesurer un diagramme ternaire. De plus, les expressions thermodynamiques ternaires développées peuvent être utilisées pour calculer toutes les propriétés thermodynamiques du liquide ternaire.

[Traduit par le journal]

Introduction

The complete measurement of the liquidus of a ternary system has usually involved the tedious determination of liquidus temperatures at a large number of compositions followed by a series of rather subjective interpolations to obtain isotherms and univariant lines.

The amount of experimental work can be greatly decreased while at the same time the accuracy of the diagram can be increased in many cases by the technique of computer-coupled thermodynamic/phase diagram analysis.

The first step in this method is the accurate determination of the phase diagrams of the three binary subsystems. These binary diagrams are then analysed along with other available binary thermodynamic data with a view to deriving equations for the Gibbs energies of all binary phases as functions of temperature and composition. In the next step, estimation formulae based upon solution models are used to calculate the Gibbs energies of the ternary phases from the previously obtained binary expressions. The ternary phase diagram is calculated from these thermodynamic expressions and compared to ternary liquidus temperatures measured at a few selected compositions. A few adjustable ternary correction terms may then be added to the expressions for the Gibbs energies in order to bring the calculated diagram into coincidence with the measured diagram. In this way, the shapes of all isotherms and univariant lines are consistent with thermodynamic principles and the number of experimental data points needed to obtain an accurate diagram is much reduced.

At the same time, a set of equations for all the thermodynamic properties of the binary and ternary systems is obtained. These equations are in a form well suited to computer storage and retrieval. They can be used along with suitable computer programs to generate, for example, ternary iso-activity, iso-vapour pressure, and iso-emf lines, as well as to generate polythermal projections or isothermal sections of the ternary phase diagram. Finally, the thermodynamic properties and the phase diagram are all rendered consistent.

The $PbCl_2$–KCl–NaCl system

The $PbCl_2$–KCl–NaCl system is of interest as a possible electrolyte in the electrowinning of lead.

The $PbCl_2$–NaCl phase diagram has been reported by a number of investigators (1–5). All are in agreement on the existence of one eutectic near 410°C. Most reported liquidus lines are in agreement with one another to within 10°C. The $PbCl_2$–KCl phase diagram has also been investigated several times (1, 6–10). A congruently melting compound $2PbCl_2 \cdot KCl$ with a melting point near 440°C and an incongruently melting compound, $PbCl_2 \cdot 2KCl$, associated with a peritectic near 490°C are reported along with two eutectics near 425°C and 410°C. Most reported diagrams are in agreement with one another to within 15°C. The melting point of pure

[1]Revision received January 11, 1985.

TABLE 1. Measured liquidus points for the $PbCl_2$–NaCl system

X_{NaCl}	Temperature (°C)
0.050	489
0.094	479
0.110	475
0.128	470
0.189	452
0.237	433
0.284	416
0.301	410.5
0.313	415.5
0.324	423
0.352	445
0.429	501
0.520	565
0.647	645
0.763	706
0.859	748
0.935	780.5

$PbCl_2$ reported by the different authors varies over a 9°C range. The $PbCl_2$–KCl–NaCl ternary phase diagram has been reported by Treis (1). Two ternary eutectics and one ternary peritectic are reported. An accuracy of about ±30°C is estimated for this ternary diagram.

In the present study, the $PbCl_2$–NaCl, $PbCl_2$–KCl, and $PbCl_2$–KCl–NaCl liquidus surfaces were studied by the method of cooling curves. The liquidus of the NaCl–KCl binary system was also measured, but is reported elsewhere (11).

Experimental

The binary and ternary liquidus curves and invariant temperatures were measured by the method of cooling curves.

Reagent grade salts were dried under vacuum and with dry HCl gas at 700°C in the case of NaCl and KCl and at 450°C in the case of $PbCl_2$. Samples of approximately 25 g were placed in sealed evacuated fused silica cells. The method of consecutive additions was not used. Samples at each composition were weighed out separately. A thermocouple was sheathed in close fitting fused silica tubes blown into the cells. The cells were placed in a grounded Inconel metal sheath and placed in a vertical electrical resistance furnace which was cooled at a rate of 1°C/min. The melt filled the cells to a depth of about 3 cm and the thermocouple sheath extended about 2 cm below the surface of the melt. Supercooling was kept to less than 2°C by attaching the cell assembly to a mechanical vibrator. A 24-gauge chromel–alumel thermocouple was used. The manufacturer's calibration was checked against the melting point of Pb, Sn, and Zn and was found to agree to within 0.5°C.

Results

Three separate measurements of the melting point of pure KCl gave 770.5, 771.2, and 771.8°C which agree well with the value of 771°C given in the most recent compilations (12). Several measurements of the melting point of pure NaCl gave values within 0.5°C of the value of 801°C given in the most recent literature (12).

Several measurements of the melting point of pure $PbCl_2$ gave 499.5 ± 1°C, in reasonable agreement with the value of 499°C given by refs. 13 and 14 and the value of 501°C given by ref. 15. Other sources, for example (12), list melting points around 495°C. Values around 495°C were also obtained in the present study unless great care was taken in drying the salt.

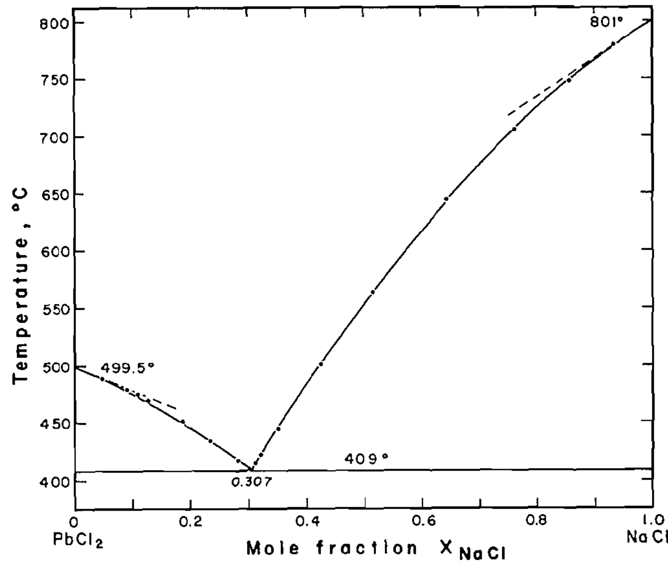

FIG. 1. The $PbCl_2$–NaCl phase diagram. Points are experimental. Lines are calculated from the thermodynamic analysis. Dashed lines are limiting liquidus slopes calculated for zero solid solubility.

TABLE 2. Measured liquidus points for the PbCl–KCl system

X_{KCl}	Temperature (°C)
0.075	479
0.129	458.5
0.198	430
0.221	421
0.251	425.5
0.288	431
0.331	434
0.345	434
0.374	433
0.432	420
0.463	413
0.474	410
0.497	423.5
0.548	453.5
0.589	474
0.616	486
0.620	488
0.629	500
0.6576	528.5
0.6582	530
0.737	615
0.792	665
0.819	686
0.928	743.5
0.943	751

$PbCl_2$–NaCl

For the $PbCl_2$–NaCl system, measured liquidus points are listed in Table 1 and are plotted in Fig. 1. Accuracy is estimated to be ±2°C.

Eutectic halts were observed in the cooling curves. Measurements at five compositions near the eutectic composition (where the eutectic halt is most pronounced) gave the temperature as 409 ± 0.5°C.

$PbCl_2$–KCl

For the $PbCl_2$–KCl system, measured liquidus points are listed in Table 2 and are plotted in Fig. 2. Accuracy is estimated

TABLE 3. Measured liquidus and invariant points for the $PbCl_2$–KCl–NaCl system

Experiment number	Mole fraction NaCl	Mole fraction KCl	Liquidus temperature (°C)	Invariant halt (°C)
1	0.168	0.119	400.5	379
2	0.178	0.192	396.5	379
3	0.070	0.251	418.5	380.5
4	0.166	0.394	441.5	385
5	0.155	0.472	447	385
6	0.119	0.567	499.5	—
7	0.102	0.616	548	—
8	0.232	0.551	558	—

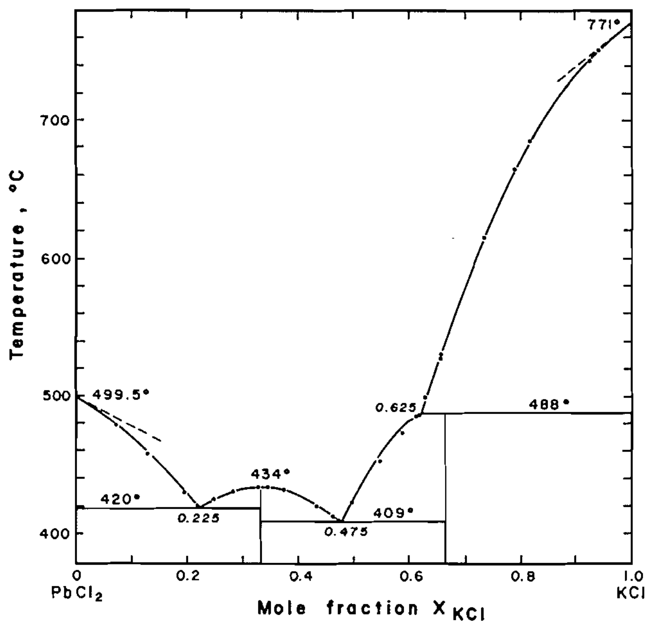

FIG. 2. The $PbCl_2$–KCl phase diagram. Points are experimental. Lines are calculated from the thermodynamic analysis. Dashed lines are limiting liquidus slopes calculated for zero solid solubility.

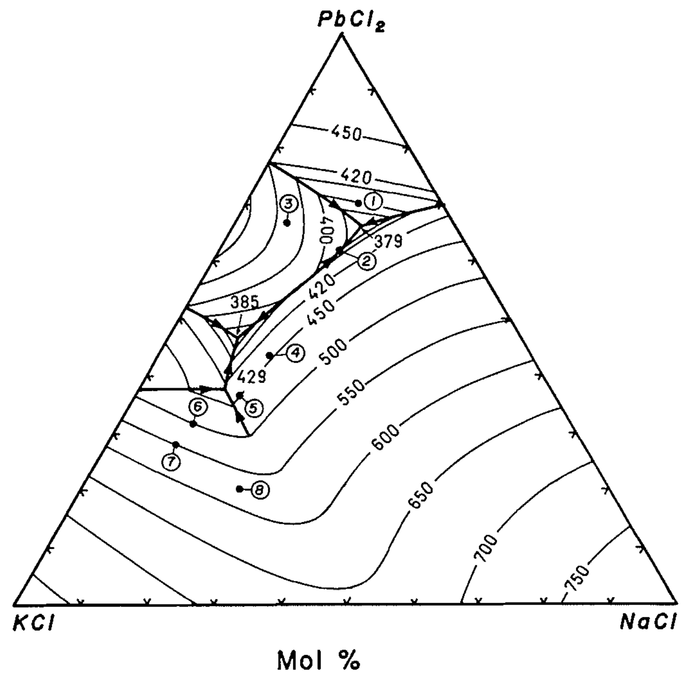

FIG. 3. The $PbCl_2$–KCl–NaCl phase diagram calculated from the thermodynamic analysis. Temperatures are in °C. Composition points indicated correspond to experimental points in Table 3.

as ±2.5°C.

Two eutectics and one peritectic were observed. Measurements of cooling curve halts at six compositions over the range $0.37 < X_{PbCl_2} < 0.55$ gave the eutectic temperature as 409 ± 0.8°C. Measurements at six compositions over the range $0.075 < X_{PbCl_2} < 0.29$ gave eutectic halts between 419 and 422°C with an average value of 420°C. Measurements at four compositions over the range $0.62 < X_{PbCl_2} < 0.66$ gave peritectic halts between 487.5 and 488°C.

$PbCl_2$–KCl–NaCl

Measurements were made at eight ternary compositions given in Table 3. These compositions are also shown on Fig. 3. Liquidus temperatures given in Table 3 are estimated to be accurate to ±3°C. Invariant halts were also observed in the cooling curves for five of the samples as indicated.

Thermodynamic analysis of binary systems

Pure components

The thermodynamic analysis of the binary systems requires a knowledge of the thermodynamic properties of the pure components. In Table 4 are listed the melting points, the enthalpies of fusion at the melting points, and the Gibbs energies of fusion of KCl, NaCl, and $PbCl_2$. The melting points are those of the present study. Enthalpies and Gibbs energies of fusion are from ref. 12. The Gibbs energies of fusion are expressed as functions of T (K) by the following expression:

$$[1] \quad \Delta G^0_{\text{fusion}} = A + BT + CT^2 + DT \ln T + ET^{-1}$$

Solid solubility – limiting slopes of liquidus curves

For a component A in a binary system A–B, the difference between the limiting slopes of the liquidus and solidus at mole fraction $X_A = 1$ is given by Raoult's law as:

$$[2] \quad (\mathrm{d}X^{\mathrm{l}}_A/\mathrm{d}T - \mathrm{d}X^{\mathrm{s}}_A/\mathrm{d}T)_{X_A=1} = \Delta H^0_{\text{fusion(A)}}/R(T^0_{\text{fusion(A)}})^2$$

where $T^0_{\text{fusion(A)}}$ and $\Delta H^0_{\text{fusion(A)}}$ are the melting point of pure A and its enthalpy of fusion at the melting point.

The liquidus curves drawn on Figs. 1 and 2 were calculated from the thermodynamic analysis discussed below under the assumption of zero solid solubility. Hence, the limiting liquidus slopes shown at compositions corresponding to pure KCl, NaCl, and $PbCl_2$ are those given by eq. [2] with $\mathrm{d}X^{\mathrm{s}}_A/\mathrm{d}T = 0$ and with values of T^0_{fusion} and $\Delta H^0_{\text{fusion}}$ from Table 4.

From the agreement with the experimental points in Figs. 1 and 2 it can be seen that solid solubility of $PbCl_2$ in NaCl and

TABLE 4. Thermodynamic properties of the pure components

	Melting point T^0_{fusion} (°C)	Enthalpy of fusion $\Delta H^0_{\text{fusion}}$ (J/mol) at T^0_{fusion}	Coefficients of eq. [1] for the Gibbs energy of fusion, $\Delta G^0_{\text{fusion}}$ (J/mol)				
			A	B	$C \times 10^3$	D	$E \times 10^{-5}$
KCl	771	26 280	4755	215.399	12.734	−33.581	1.82
NaCl	801	28 160	7735	202.091	11.925	−31.824	—
$PbCl_2$	499.5	23 850	2697	269.234	20.769	−43.426	—

KCl, or of NaCl and KCl in $PbCl_2$, is small. If error limits of ±2°C are assumed for the experimental liquidus points, then from eq [2] maximum limiting solidus slopes dX^s_A/dT of the order of 0.02 (mol% per deg) may be calculated.

In view of the low mutual solid solubility of KCl and $PbCl_2$, it is expected that the ranges of stoichiometry of the two intermediate compounds $2PbCl_2 \cdot KCl$ and $PbCl_2 \cdot 2KCl$ will be narrow. Hence, these have been indicated as stoichiometric compounds on Fig. 2.

No verification of the stoichiometry of the incongruently melting compound was made. However, the liquidus curve for this compound, when extrapolated, passes through a maximum near the composition $PbCl_2 \cdot 2KCl$.

Methodology

In the binary systems $PbCl_2$–ACl (A = Na or K), under the assumption of zero solid solubility, the following equations apply along the $PbCl_2$– and ACl–liquidus curves, respectively:

$$[3] \quad RT \ln a_{PbCl_2} = RT \ln X_{PbCl_2} + G^E_{PbCl_2} = -\Delta G^0_{\text{fusion}(PbCl_2)}$$

$$[4] \quad RT \ln a_{ACl} = RT \ln X_{ACl} + G^E_{ACl} = -\Delta G^0_{\text{fusion}(ACl)}$$

where X_i, a_i, and G^E_i are the mole fraction, activity, and excess partial molar Gibbs energy of i along the liquidus.

The excess integral molar Gibbs energy of the liquid phase may be expressed as:

$$[5] \quad G^E = \Delta H - TS^E$$

where ΔH is the molar enthalpy of mixing and S^E is the molar excess entropy. It is assumed that ΔH and S^E are independent of temperature.

For a binary system, ΔH and S^E may be conveniently expressed as polynomials in the mole fractions. In the case of molten salt solutions, it has been observed that the number of terms required in the polynomial expansions to give a satisfactory representation can sometimes be reduced if equivalent fractions rather than mole fractions are used. Furthermore, the Conformal Ionic Solution Theory discussed in the next section in relation ot the ternary calculations requires that equivalent fractions be used in the binary expansions. Since Pb^{2+} is divalent and Na^+ and K^+ are univalent, the equivalent fractions Y_i are given by:

$$[6] \quad Y_{PbCl_2} = 2X_{PbCl_2}/(2X_{PbCl_2} + X_{ACl})$$

$$[7] \quad Y_{ACl} = X_{ACl}/(2X_{PbCl_2} + X_{ACl})$$

The polynomial expansions for the molar enthalpy and excess entropy are then:

$$[8] \quad \Delta H \text{ (J/mol)} = (2X_{PbCl_2} + X_{ACl})Y_{PbCl_2}Y_{ACl}\,(h_0 + h_1Y_{ACl} + h_2Y^2_{ACl} + h_3Y^3_{ACl} + \ldots)$$

$$[9] \quad S^E \text{ (J/mol K)} = (2X_{PbCl_2} + X_{ACl})Y_{PbCl_2}Y_{ACl}\,(s_0 + s_1Y_{ACl} + s_2Y^2_{ACl} + s_3Y^3_{ACl} + \ldots)$$

where the coefficients h_i and s_i are found empirically. The number of terms in each series is chosen as the minimum required to fit the experimental data satisfactorily.

Differentiation of eqs. [8] and [9] yields the following expressions for the partial molar excess Gibbs energies of $PbCl_2$ and ACl:

$$[10] \quad G^E_{PbCl_2} = 2\sum_{j\geq 0}(h_j - Ts_j)(Y_{ACl} - jY_{PbCl_2})Y^{j+1}_{ACl}$$

$$[11] \quad G^E_{ACl} = 2\sum_{j\geq 0}(h_j - Ts_j)(j+1)Y^2_{PbCl_2}Y^j_{ACl}$$

In the case of the $PbCl_2$–NaCl and $PbCl_2$–KCl systems, ΔH has been measured by mixing calorimetry (16). These data were first fitted by a least-squares technique to obtain values of the enthalpy coefficients h_i. Next, values of the excess entropy coefficients s_i were determined in order to give the best fit to the measured $PbCl_2$– and ACl–liquidus curves in each system. To this end, a least-squares "optimisation" technique described elsewhere (17) and a computer program called FITBIN (18) were used.

Enthalpy of mixing expressions

Enthalpies of mixing in the $PbCl_2$–NaCl and $PbCl_2$–KCl systems have been measured by mixing calorimetry (16) only over the composition range $0.5 < X_{PbCl_2} < 1$. However, comparison of the experimental (16) "interaction parameter" $\lambda = \Delta H/(X_{PbCl_2}X_{ACl})$ for all the systems $PbCl_2$–ACl (A = Li, Na, K, Rb) indicates a simple dependence of λ with X_{ACl} which is not far from linearity, thereby permitting a reasonable extrapolation to be made. The following three term expressions for ΔH were thus found by least-squares regression for the $PbCl_2$–NaCl and $PbCl_2$–KCl systems, respectively:

$$[12] \quad \Delta H = (2X_{PbCl_2} + X_{NaCl})Y_{PbCl_2}Y_{NaCl}\,(-2088 + 3343Y_{NaCl} - 1937Y^2_{NaCl}) \text{ J/mol}$$

$$[13] \quad \Delta H = (2X_{PbCl_2} + X_{KCl})Y_{PbCl_2}Y_{KCl}\,(-16552 + 1167Y_{KCl} + 1046Y^2_{KCl}) \text{ J/mol}$$

The $PbCl_2$–NaCl system

With eq. [12] for ΔH, a set of coefficient s_i were found which best reproduce the measured liquidus curves. Three coefficients were found to suffice:

$$[14] \quad S^E = (2X_{PbCl_2} + X_{NaCl})Y_{PbCl_2}Y_{NaCl}\,(6.012 - 4.213Y_{NaCl} + 0.703Y^2_{NaCl}) \text{ J/mol K}$$

The phase diagram, calculated by computer with eqs. [12] and [14] for ΔH and S^E is drawn in Fig. 1. (For a description of the computer program, see ref. 18.) Agreement with the experimental points is everywhere within the experimental limits of $\pm 2°C$, and the measured and calculated eutectic agree exactly.

Furthermore, values of $G^{E}_{PbCl_2}$ calculated at 500, 600, 700, and 800°C via eqs. [10], [12], [14] agree with values measured by emf techniques (19, 20) within the experimental error limits.

The $PbCl_2$–KCl system

With eq. [13] for ΔH, the following three-term expansion for S^E was found to reproduce the measured $PbCl_2$– and KCl–liquidus curves:

$$[15] \quad S^E = (2X_{PbCl_2} + X_{KCl})Y_{PbCl_2}Y_{KCl}\,(7.950 - 14.205Y_{KCl} + 2.753Y^2_{KCl}) \text{ J/mol K}$$

Next, the following expressions for the Gibbs energies of fusion of the two intermediate compounds were determined in order to reproduce their measured liquidus curves:

$$[16] \quad \text{Compound } 2/3(PbCl_2)\cdot 1/3(KCl){:}\ \Delta G^0_{fusion} = 20700 - 29.274T \text{ J/mol}$$

$$[17] \quad \text{Compound } 1/3(PbCl_2)\cdot 2/3(KCl){:}\ \Delta G^0_{fusion} = 12107 - 15.808T \text{ J/mol}$$

The phase diagram, calculated by computer from eqs. [13], [15], [16], [17] is drawn in Fig. 2. Agreement with the experimental points is everywhere within the experimental error limits of $\pm 2.5°C$ except for two points on the $PbCl_2\cdot 2KCl$ liquidus at which the agreement is within 4°C. All measured invariant temperatures are reproduced to within 0.5°C.

Furthermore, values of $G^{E}_{PbCl_2}$ calculated at 500, 600, and 700°C via eqs. [10], [13], [15] agree with values measured by emf techniques (20) within the experimental error limits.

The NaCl–KCl system

Liquidus points in this binary system were also measured in the present study, but are reported elsewhere (11). This system exhibits complete miscibility of the solid solutions at elevated temperatures with a minimum in the solidus/liquidus at 657°C. In addition, a solid–solid miscibility gap with a consolute temperature near 500°C is observed.

A complete thermodynamic analysis of this binary system was made (11) in which measured liquidus points, miscibility gap boundaries, liquid enthalpies of mixing, and solid enthalpies of mixing at 25°C were all taken into account in order to obtain polynomial expressions for ΔH and S^E of both the liquid and solid solutions. Because of the large temperature range (25–800°C) over which data were available, a small temperature dependence was included in the expression for ΔH of the solid solution. However, the computer program TERNFIG used to calculate the ternary phase diagram as discussed below will not accept a temperature dependent ΔH. Hence, the data were re-fitted with a constant ΔH for the solid. The following expressions were obtained:

$$[18] \quad \Delta H^{liquid} = X_{NaCl}X_{KCl}\,(-2322 + 272X_{KCl}) \text{ J/mol}$$

$$[19] \quad S^{E(liquid)} = X_{NaCl}X_{KCl}\,(-1.674) \text{ J/mol K}$$

$$[20] \quad \Delta H^{solid} = X_{NaCl}X_{KCl}(27991 - 12050X_{KCl} + 7950X^2_{KCl}) \text{ J/mol}$$

$$[21] \quad S^{E(solid)} = X_{NaCl}X_{KCl}\,(12.552) \text{ J/mol K}$$

(Note that mole fractions and equivalent fractions are identical in this binary system in which both cations are univalent.)

Equations [18]–[21] differ only very slightly from those given previously (11) at temperatures above 500°C. For example, the NaCl–KCl liquidus calculated via eqs. [18]–[21] agrees everywhere within 2°C with the measured liquidus points.

Thermodynamic analysis of the ternary system

The procedure followed in the ternary analysis was as follows. First, an expression for G^E in the ternary system was calculated from the binary expressions of the preceding section by means of various estimation formulae based upon solution models. Next, the ternary phase diagram was calculated from this expression for G^E by a computer program called TERNFIG described elsewhere (18), and this calculated diagram was compared with the measured points (Table 3). If necessary, adjustable ternary correction terms were then added to the expansion of G^E in order to bring the calculated and measured diagrams into coincidence.

The Conformal Ionic Solution (CIS) Theory

The CIS theory (21–25) for an additive ternary molten salt system, which is based upon statistical mechanical perturbation theory, gives the following expression for G^E in a ternary system with components 1–2–3:

$$[22] \quad G^E \text{ (J/equivalent)} = \sum_i \sum_{j<i} a_{ij}Y_iY_j + \sum\sum_{i\neq j} b_{ij}Y_i^2Y_j + \sum\sum_{i<j} c_{ij}Y_i^2Y_j^2 + Y_1Y_2Y_3(b_{12}^{1/3} + b_{13}^{1/3})\,(b_{21}^{1/3} + b_{2/3}^{1/3}) \times (b_{23}^{1/3} + b_{13}^{1/3}) + \sum\sum_{i\neq j<k} 2(c_{ij}c_{ik})^{1/2}Y_i^2Y_jY_k$$

where, for the binary system i–j:

$$[23] \quad G^E_{ij} \text{ (J/equivalent)} = Y_iY_j(a_{ij} + b_{ij}Y_i + b_{ji}Y_j + c_{ij}Y_i^2Y_j^2)$$

Binary expressions of the type $G^E_{ij} = Y_iY_j\,(e + fY_j + gY_j^2)$ as used in eqs. [12]–[15], [18], [19] of the preceding section can easily be converted to expressions of the form of eq. [23]. (Note that as a result $b_{ij} = b_{ji}$.) Equations [22], [23] give G^E in J/equivalent. To convert to J/mol in the $PbCl_2$–KCl–NaCl system, multiply by $(2X_{PbCl_2} + X_{KCl} + X_{NaCl})$.

The ternary phase diagram calculated from eq. [22] with coefficients obtained from eqs. [12]–[15], [18], [19] is plotted in Fig. 3. As can be seen from Table 3, agreement with all experimental liquidus points is within 3°C. In addition, two ternary invariants were calculated at 379 and 385°C in agreement with the measured values. The calculations show these invariants to be ternary eutectics with compositions $X_{NaCl} = 0.20$, $X_{KCl} = 0.14$ and $X_{NaCl} = 0.11$, $X_{KCl} = 0.43$.

In addition, a ternary peritectic at 429°C is calculated at $X_{NaCl} = 0.13$, $X_{KCl} = 0.49$. Since the peritectic reaction involves the separation of the NaCl–KCl solid solution into two phases at a temperature near the consolute point where the Gibbs energy and enthalpy associated with the separation are very small, it is not surprising that this invariant was not observed in the thermal analysis experiments since the heat effect would be very small. For the same reason, the calculations are very sensitive in this area. That is, a small change in the Gibbs energy of the solid will have a large effect on the extent of solid–solid immiscibility at a given temperature. Hence, the temperature and composition of the ternary peritectic cannot be determined with accuracy.

The diagram in Fig. 3 agrees within about 25°C with that reported by Treis (1).

Because of the very good agreement of the calculations with the measurements, it was not necessary to add any adjustable ternary correction terms to eq. [22] for G^E.

Geometric estimation methods

In the "geometric" estimation formulae, G^E at a composition point in the ternary system 1–2–3 is related to G^E at one composition point in each of the three binary systems. One such formula is the Kohler equation (26):

$$[24] \quad G^E = \sum_{i \neq j < k}\sum (1 - X_i)^2 G^E_{X_j/X_k}$$

where $G^E_{X_j/X_k}$ is the value of G^E in the j–k binary at the same ratio X_j/X_k as at the ternary composition point.

Another such formula is the Toop equation (27):

$$[25] \quad G^E = \frac{X_2}{X_2 + X_3} G^E_{12} + \frac{X_3}{X_2 + X_3} G^E_{13} + (1 - X_1)^2 G^E_{23}$$

where G^E_{12} and G^E_{13} are values of G^E in the 1–2 and 1–3 binaries at the same value of X_1 as at the ternary composition point, and G^E_{23} is the value in the 2–3 binary at the same ratio X_3/X_2 as at the ternary point.

Equations [24] and [25] are exact if the solutions are regular, and may be considered as extensions of regular solution theory. The various geometrical estimation formulae have been reviewed (28).

The ternary $PbCl_2$–KCl–NaCl phase diagrams calculated from eq. [24] or from eq. [25] were very close to that shown in Fig. 3, except that the calculated ternary eutectic temperatures were 5 to 10°C too low. Consequently, one adjustable ternary correction term of the form $cX_{PbCl_2}X_{KCl}X_{NaCl}$ was added to eqs. [24] and [25], and the value of the parameter c was chosen in each case in order to best reproduce the ternary eutectic temperatures. With a value of c = 2090 J/mol in the case of the Kohler equation [24] and c = 2270 J/mol for the Toop equation [25], all three ternary invariant temperatures agreed with 1°C with those calculated by the CIS equation. Furthermore, all isotherms and univariant lines on the ternary phase diagrams calculated by the three techniques (CIS, Kohler, Toop) agreed with each other within 1 mol% everywhere.

Conclusions

Liquidus curves of the $PbCl_2$–NaCl and $PbCl_2$–KCl binary systems have been measured. A thermodynamic analysis of the measured phase diagrams, along with other available thermodynamic data for the systems, has permitted expressions for the enthalpy and entropy of the binary liquid phases to be determined which can reproduce the measured phase diagrams as well as the measured thermodynamic properties within experimental error limits.

Various estimation formulae were used to calculate the Gibbs energy of the ternary liquid from the binary data, and the ternary phase diagram calculated therefrom was compared to measured ternary liquidus and invariant temperatures. When the Conformal Ionic Solution equation was used, the calculated diagram agreed with the measured points within experimental error limits with no ternary correction terms. Similar agreement was obtained with the Kohler and Toop equations provided one small ternary correction term was added to the expression for the Gibbs energy in each case.

The ternary phase diagram resulting from this coupled thermodynamic/phase diagram analysis is estimated to be accurate to ±5° except possibily near the ternary peritectic.

The ability of a ternary Gibbs energy equation to reproduce the phase diagram is a sensitive test of its accuracy. This sensitivity has already been illustrated with regard to the aforementioned "ternary correction term". A term equal to $2720X_{PbCl_2}\cdot X_{KCl}\cdot X_{NaCl}$ J, which achieves a maximum value of only 100 J when $X_{PbCl_2} = X_{KCl} = X_{NaCl} = 1/3$, can change the ternary eutectic by 10°. Hence, eq. [22] (or eq. [24] or [25] with the one ternary correction term in each case) can be used to calculate the Gibbs energy of the ternary solution. For example, iso-activity, iso-vapour pressure, or iso-emf curves can easily be generated by computer. Separation of the Gibbs energy into enthalpy and entropy terms will be less precise. In addition, isothermal sections of the phase diagram can be computer calculated at any temperature. Hence, the storage in computer memory of a small set of coefficients along with the appropriate programs for retrieval permits the calculation of the phase diagram and all the thermodynamic properties of the ternary system.

Acknowledgement

This work was supported by the Natural Sciences and Engineering Research Council of Canada.

1. K. TREIS. Neues Jahrb. Mineral Geol. **37**, 812 (1914).
2. K. TREIS. Neues Jahrb. Mineral Geol. **37**, 772 (1914).
3. I. I. IL'YASOV and A. K. BOSTANDZHIAN. Zhur. Obshchei Khim. **26**, 2396 (1956).
4. I. I. IL'YASOV, G. G. SHCHEMELEVA, and A. G. BERGMAN. Zhur. Neorg. Khim. **2**, 2176 (1957).
5. T. N. SUMAROKOVA and T. P. MODESTOVA. Russ. J. Inorg. Chem. (Engl. Transl.), 346 (1961).
6. YA. A. UGAI and V. A. SHATILLO. J. Phys. Chem. USSR, **23**(6) 745 (1949).
7. YA. A. UGAI. Dokl. Akad. Nauk SSSR, **70**(4), 653 (1950).
8. I. I. IL'YASOV, A. K. BOSTANDZHIAN, and A. G. BERGMAN. Zhur. Neorg. Khim. **1**(11), 2549 (1956).
9. A. G. BERGMAN, YU. I. ANDRYUSHCHENKO, and R. K. BINEEVA. Russ. J. Inorg. Chem. (Engl. Transl.), 881 (1963).
10. A. G. BERGMAN and YU. I. ANDRYUSHCHENKO. Zh. Neorg. Khim. **9**(5), 1221 (1964); Russ. J. Inorg. Chem. (Engl. Transl.), 669 (1964).
11. A. GABRIEL, A. D. PELTON, and J. SANGSTER. J. Chem. Soc. Faraday Trans. 1, **81**, 1167 (1985).
12. I. BARIN, O. KNACKE, and O. KUBASCHEWSKI. Thermochemical properties of inorganic substances and Supplement, Springer-Verlag, Dusseldorf. 1973, 1977.
13. O. KUBASCHEWSKI, E. M. EVANS, and C. B. ALCOCK. Metallurgical thermodynamics. Pergamon Press, New York. 1978.
14. W. T. THOMPSON and S. N. FLENGAS. Can. J. Chem. **49**, 1550 (1971).
15. Y. UMETSU and T. EJIMA. J. Jpn. Inst. Metals, **37**, 993 (1973).
16. F. G. MCCARTY and O. J. KLEPPA. J. Phys. Chem. **68**, 3846 (1964).
17. C. W. BALE and A. D. PELTON. Met. Trans. **14**B, 77 (1983).
18. C. W. BALE, A. D. PELTON, and W. T. THOMPSON. "F*A*C*T — Facility for the Analysis of Chemical Thermodynamics", User's Guide. Edition 2. McGill University/Ecole Polytechnique, Montréal. 1985.
19. H. BLOOM, S. R. RICHARDS, and D. J. WILLIAMS. Aust. J. Chem. **25**, 2077 (1972).
20. M. F. LANTRATOV and A. F. ALABYSHEV. J. App. Chem. USSR, **26**, 235 (1953).
21. H. REISS and O. J. KLEPPA. J. Phys. Chem. **36**, 144 (1962).
22. M. BLANDER and S. J. YOSIM. J. Chem. Phys. **39**, 2610 (1963).
23. M.-L. SABOUNGI and P. CERISIER. J. Electrochem. Soc. **121**,

1258 (1974).
24. M.-L. SABOUNGI and M. BLANDER. J. Chem. Phys. **63**, 212 (1975).
25. M. BLANDER and M.-L. SABOUNGI. Molten salts. The Electrochemical Society Inc., 1976. pp. 93–106.
26. F. KOHLER. Mh. Chem. **91**, 738 (1960).
27. N. J. OLSON and G. W. TOOP. TMS-AIME, **236**, 590 (1966).
28. M. HILLERT. CALPHAD J. **4**, 1 (1980).

1,*n*-Radical ions: an *ab initio* study of racemization and isomerization of the cyclopropane radical cation

DANIAL D. M. WAYNER,[1] RUSSELL J. BOYD,[2] AND DONALD R. ARNOLD[2]
Department of Chemistry, Dalhousie University, Halifax, N.S., Canada B3H 4J3

Received April 11, 1985

DANIAL D. M. WAYNER, RUSSELL J. BOYD, and DONALD R. ARNOLD. Can. J. Chem. **63**, 3283 (1985).

The surfaces for *cis–trans* isomerization and racemization of the cyclopropane radical cation ($\mathbf{1}^+$) are determined using *ab initio* calculations. It is found that polarization functions and electron correlation have large effects on the relative energies of $\mathbf{1}^+$. Orbital symmetry arguments predict that conrotatory closure of the 0,0 conformer of $\mathbf{1}^+$ should be preferred. These predictions are supported by the calculations; however, even the conrotatory closure has a significant activation barrier. Conformational changes that accompany single methylene rotation are also discussed. The implication of these results to ion cyclotron resonance and mass spectral experiments is that isomerization of $\mathbf{1}^+$ to the 0,0 conformer can occur at energies far below the barrier required to isomerize $\mathbf{1}^+$ to the propylene radical cation. However, the 0,0 conformer of $\mathbf{1}^+$ and the propylene radical cation should display similar reactivities (e.g. deprotonation). The results also indicate that, contrary to reported esr evidence, $\mathbf{1}^+$ should not exist preferentially in the 90,0 conformation.

DANIAL D. M. WAYNER, RUSSELL J. BOYD et DONALD R. ARNOLD. Can. J. Chem. **63**, 3283 (1985).

Faisant appel à des calculs *ab initio*, on a déterminé les surfaces de l'isomérisation *cis–trans* et celle de la racémisation du cation radicalaire cyclopropane ($\mathbf{1}^+$). On a trouvé que les fonctions de polarisation ainsi que la corrélation électronique influencent beaucoup les énergies relatives du cation radicalaire $\mathbf{1}^+$. Des arguments de symétrie des orbitales permettent de prédire que la fermeture conrotatoire du conformère 0,0 du radical $\mathbf{1}^+$ est privilégiée; ces prédictions sont en accord avec des calculs qui confirment toutefois que même la fermeture conrotatoire possède une énergie d'activation assez élevée. On discute également des changements de conformations qui accompagnent la rotation d'un seul méthylène. Pour la résonance des ions dans un cyclotron et pour les expériences en spectrométrie de masse, ces résultats impliquent que l'isomérisation du radical $\mathbf{1}^+$ en son conformère 0,0 peut se produire à des énergies beaucoup plus basses que celles requises pour l'isomérisation du radical $\mathbf{1}^+$ en un cation radicalaire propylène. Cependant, le conformère 0,0 du radical $\mathbf{1}^+$ et le cation radical propylène devraient avoir des réactivités semblables (comme la déprotonation). Les résultats indiquent également que, contrairement aux résultats suggérés par la rpe, le cation $\mathbf{1}^+$ ne peut exister préférentiellement sous la conformation 90,0.

[Traduit par le journal]

Introduction

The properties of the cyclopropane radical cation $\mathbf{1}^+$ have been the subject of numerous experimental (1) and theoretical (2) investigations. Mass spectra formed by collisionally activated dissociation (CAD) of $C_3H_6{}^+$ isomers (1*a*) imply that the barrier to isomerize $\mathbf{1}^+$ to the propene radical cation $\mathbf{2}^+$ is large (35 kcal mol^{-1}) while the barrier to the formation of $\mathbf{2}^+$ from "ring-opened" cyclopropane radical cation is small. The nature of this ring-opened species, however, is unclear.

Calculations by Collins and Gallup (2*a*) did not find a minimum on the energy surface of $\mathbf{1}^+$ corresponding to a ground electronic state of the ring-opened species. Other calculations (3) have estimated the strength of the one-electron, two-center bond to be about 18 kcal mol^{-1}. In this work the energy difference between $\mathbf{1}^+$ in the 90,90 conformation (4) and the 90,0 conformation was taken as an estimate of this value. The energy barrier to the formation of the ring-opened species should be *at least* the energy required to break this one-electron, two-centre bond.

It is well known that, in cyclopropane (**1**), the barrier to double methylene rotation is less than the barrier to single methylene rotation (5). Calculations (6, 7) have shown that the energy of the 0,0 conformer of **1** (the trimethylene diradical) is lower than the 90,0 conformer (in support of the experimental evidence). Furthermore, orbital symmetry considerations suggest that conrotatory closure of the 0,0 conformer should be favoured over disrotatory closure (7). There is little experimental evidence, however, in support of this prediction (8).

There has been interest recently in the applicability of orbital symmetry rules to odd electron species (9). By analogy to studies of **1**, an investigation of the synchronous (double methylene) rotation and single methylene rotation of $\mathbf{1}^+$ will give valuable insight into the electronic nature of the one-electron, two-centre bond, and may be useful to the interpretation of mass spectral and ion cyclotron resonance (icr) experiments. Furthermore, the extent of orbital symmetry control over the synchronous rotation of the methylenes in this odd-electron species can be studied.

This paper presents the results of an *ab initio* study of the *cis–trans* isomerization (single methylene rotation) and racemization (double methylene rotation) of $\mathbf{1}^+$. Comparison with similar theoretical calculations on **1** and the cyclopropyl radical reveals some similarities as well as some interesting differences. The effects of polarization functions and electron correlation are also discussed.

Details of calculations

Standard *ab initio* self-consistent field (SCF) molecular orbital (MO) calculations were carried out with the GAUSSIAN 80 programs (10) on a Perkin Elmer 3230 minicomputer. Gradient techniques (11) were used for geometry optimizations. Calculations were performed with 4-31G and 4-31G* basis sets with valence electron correlation incorporated by using Møller–Plesset perturbation theory (12) terminated at either the second (MP2) or third (MP3) order. The energies of the radical cations were computed using the open-shell, spin-unrestricted (UHF) procedure (13). Complete geometry optimizations of **1**, and of $\mathbf{1}^+$ in the 90,90 ($^2A_1$ and $^2B_2$ states), the 90,0 and 0,0 conformers (Table 1), as well as the 90,10; 90,20;

---

[1] Present address: National Research Council of Canada, Ottawa, Ont., Canada K1A 0R6.

[2] Authors to whom correspondence should be addressed.

TABLE 1. Equilibrium geometries of **1** and **1**$^+$ (4-31G)[a]

Parameter	**1**	**1**$^+$			
		90,90 ($^2A_1$)	90,90 ($^2B_2$)	90,0 ($^2A''$)	0,0 (^2A)
r_{12}	1.503	1.941	1.400	(2.322)[b]	(2.535)[b]
r_{13}	1.503	1.483	1.720	1.434	1.430
r_{23}	1.503	1.483	1.720	1.569	1.430
r_{14}	1.072	1.072	1.072	1.076	1.072
r_{15}	1.072	1.072	1.072	1.076	1.071
r_{26}	1.072	1.072	1.072	1.071	1.072
r_{27}	1.072	1.072	1.072	1.070	1.071
r_{38}	1.072	1.075	1.069	1.080	1.119
r_{39}	1.072	1.075	1.069	1.080	1.119
∠HC(1)H	113.7	118.2	117.2	117.2	117.8
∠HC(2)H	113.7	118.2	117.2	120.9	117.8
∠HC(3)H	113.7	113.6	120.6	111.3	93.0
∠C(1)C(2)C(3)	60.0	81.7	48.0	101.2	124.8
α_1[c]	150.0	179.9	126.7	175.0	180.0
α_2[c]	150.0	179.9	126.7	179.5	180.0
α_3[c]	0.0	0.0	0.0	5.8	0.0
ω_1[d]	0.0	0.0	0.0	0.0	1.5
ω_2[d]	0.0	0.0	0.0	5.3	−1.5
ω_3[d]	0.0	0.0	0.0	0.0	0.0
θ_1[e]	90.0	90.0	90.0	90.0	0.0
θ_2[e]	90.0	90.0	90.0	0.0	0.0
θ_3[e]	90.0	90.0	90.0	90.0	90.0

[a] All bond lengths are in Å (angstrom) and all angles are in degrees.
[b] Internuclear distance.
[c] α_i is the angle representing the wagging motion of the C(i) methylene. It is the angle between the C(i)C(3) bond and the intersection of the plane of the C(i) methylene with the plane of the carbons. α_3 is measured with respect to the C(1)C(3) bond.
[d] ω_i is the angle representing the rocking motion of the C(i) methylene. It is the angle between the line which bisects the HC(i)H methylene and the line which is the intersection of the plane of the methylene and the plane of the carbons.
[e] θ_i is the angle representing the torsional motion of the C(i) methylene. It is the angle between the plane of the C(i) methylene and the plane of the carbons.

90,30; 90,60 conformers (single methylene rotation) and the 60,60; 45,45; and 30,30 conformers (conrotatory and disrotatory synchronous double methylene rotation) were carried out at the 4-31G level. Single point calculations using the 4-31G optimized structures were carried out at the MP2/4-31G, MP3/4-31G, HF/4-31G*, and MP2/4-31G* levels.[3]

Discussion

Structural and electronic aspects of **1**$^+$ in the 90,90 ($^2A_1$ and $^2B_2$ states) and the 90,0 conformations have been discussed in detail (3). The structure of the 0,0 conformer of **1**$^+$ has not been reported. It is useful, however, to review briefly some of the features of all of these structures. The Mulliken overlap between the carbons, the charge distribution, and the spin distribution in these conformers are shown in Tables 2, 3, and 4 respectively.

An interesting feature of the $^2A_1$ structure (90,90 conformer) is that the values of α_1 and α_2 indicate that C(1) and C(2) have adopted a planar geometry (i.e. C(1) and C(2) are sp^2 hybridized). This geometry allows effective bonding between C(1) and C(2) even though ∠C(1)C(3)C(2) has increased relative to

[3] The notation MP2/4-31G*//HF/4-31G indicates that a MP2 calculation with the 4-31G* basis set has been carried out at the equilibrium geometry obtained by Hartree–Fock calculations at the 4-31G level. In Table 5 the notation is simplified to MP2/4-31G*//4-31G.

TABLE 2. Mulliken overlap populations for the carbons in **1** and **1**$^+$

Molecule or ion	Basis set	Overlap		
		C_1C_2	C_1C_3	C_2C_3
1	4-31G//4-31G	0.1705	0.1705	0.1705
	4-31G*//4-31G	0.2646	0.2646	0.2646
1$^+$ ($^2A_1$)	4-31G//4-31G	0.0226	0.1922	0.1922
	4-31G*//4-31G	0.0597	0.2608	0.2608
1$^+$ ($^2B_2$)	4-31G//4-31G	0.2060	0.0883	0.0883
	4-31G*//4-31G	0.3057	0.1332	0.1332
1$^+$ (90,0)	4-31G//4-31G	−0.0326	0.2557	0.2097
	4-31G*//4-31G	−0.0169	0.3297	0.2508
1$^+$ (0,0)	4-31G//4-31G	−0.0609	0.3025	0.3025
	4-31G*//4-31G	−0.0588	0.3654	0.3654

that in **1**. The magnitude of ∠C(1)C(3)C(2) (only 81.7°) and the Mulliken overlap between C(1) and C(2) (Table 2) are an indication that there is a considerable C(1)C(2) bonding interaction in this species. This geometry is consistent with the Walsh model for bonding in cyclopropane (14) in which the electron has been removed from the e_s' orbital.

The values of α_1 and α_2 in the $^2B_2$ state (90,90 conformer) are much smaller than that in the $^2A_1$ state. This structure has been described as a π-complex between ethylene and the methylene cation. It is preferable, therefore, to consider the angle β (Fig. 1), which would have a value of 180° in the case of

TABLE 3. Atomic charge densities in **1** and **1**$^{+a}$

Molecule or ion	Atom	4-31G//4-31G	4-31G*//4-31G
1	C	6.346	6.352
	H	0.827	0.824
1$^+$ ($^2A_1$)	C(1), C(2)	6.210	6.243
	C(3)	6.393	6.359
	H(4)–H(7)	0.696	0.687
	H(8), H(9)	0.701	0.702
1$^+$ ($^2B_2$)	C(1), C(2)	6.269	6.275
	C(3)	6.316	6.327
	H(4)–H(9)	0.688	0.687
1$^+$ (90,0)	C(1)	5.946	5.992
	C(2)	6.298	6.365
	C(3)	6.512	6.477
	H(4), H(5)	0.676	0.663
	H(6)	0.772	0.710
	H(7)	0.762	0.747
	H(8), H(9)	0.703	0.706
1$^+$ (0,0)	C(1), C(2)	6.126	6.191
	C(3)	6.613	6.521
	H(4)	0.723	0.707
	H(5)	0.725	0.712
	H(6)	0.723	0.707
	H(7)	0.725	0.707
	H(8), H(9)	0.618	0.629

[a]Atomic units.

TABLE 4. Atomic spin densities and Fermi contact in **1**$^{+a}$

		4-31G//4-31G[b]		4-31G*//4-31G	
Ion	Atom	Spin density	Fermi contact	Spin density	Fermi contact
1$^+$ ($^2A_1$)	C(1), C(2)	0.677	0.106	0.652	0.080
	C(3)	−0.218	−0.057	−0.186	−0.048
	H(4)–H(7)	−0.050	−0.017	−0.043	−0.015
	H(8), H(9)	0.031	0.016	0.027	0.015
1$^+$ ($^2B_2$)	C(1), C(2)	0.112	−0.002	0.112	−0.006
	C(3)	0.923	0.152	0.902	0.117
	H(4)–H(7)	0.000	0.004	0.000	0.003
	H(8), H(9)	−0.074	−0.026	−0.063	−0.023
1$^+$ (90,0)	C(1)	−0.012	0.001	−0.027	0.002
	C(2)	1.318	0.265	1.271	0.214
	C(3)	−0.153	−0.050	−0.121	−0.040
	H(4), H(5)	0.001	0.000	0.001	0.000
	H(6)	−0.107	−0.036	−0.092	−0.032
	H(7)	−0.106	−0.036	−0.094	−0.032
	H(8), H(9)	0.036	0.020	0.031	0.018
1$^+$ (0,0)	C(1), C(2)	0.797	0.137	0.760	0.107
	C(3)	−0.187	−0.041	−0.141	−0.026
	H(4), H(6)	−0.063	−0.022	−0.054	−0.019
	H(5), H(7)	−0.058	−0.021	−0.049	−0.019
	H(8), H(9)	−0.083	−0.047	−0.086	−0.050

[a]Atomic units.
[b]The expectation value of S^2 is 0.781, 0.756, 0.766, and 0.832, for **1**$^+$ ($^2A_1$), **1**$^+$ ($^2B_2$), **1**$^+$ (90,0), and **1**$^+$ (0,0), respectively.

ethylene. For **1**$^+$ ($^2B_2$) β has a value of 167.2°. The Mulliken overlap between C(1) and C(2) has increased relative to **1**. This structure is consistent with the Walsh model in which the electron has been removed from the orbital of e'_a symmetry.

The 90,0 conformer of **1**$^+$ has approximately C_s symmetry and exists as a $^2A''$ ground state. In the 90,0 conformer of **1**$^+$ there is no evidence for bonding between C(1) and C(2). The C(1)C(3) bond has shortened while the C(2)C(3) bond (C(2) has rotated 90°) has lengthened. The interesting feature of this conformer is that while the charge density is delocalized over the three methylene groups (Table 3) the spin density is localized on C(2) (Table 4), a consequence of the orthogonality of the two methylenes. In these delocalized species, considerable spin contamination might be expected since the calculations have been carried out within the unrestricted Hartree–Fock formalism. Our results show, however, that the contamination by quartet and higher terms is substantial in the 0,0 conformer but small in the other three cases (Table 4). The application of spin annihilation methods would improve the $\langle S^2 \rangle$ values, but would not be expected to alter the basic conclusions.

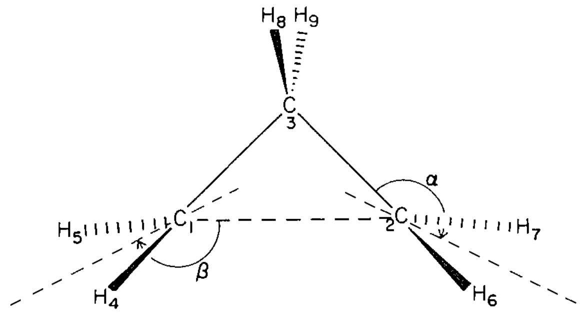

FIG. 1. Representation of bonds and angles of **1**$^+$, as defined in Table 1.

The 0,0 conformer of **1**$^+$ has C_2 symmetry and exists as a ^2A ground state. However, since the values of α_1 and α_2 in this conformer are very close to 180.0° (actually 179.95°), it could be classified in the C_{2v} point group and, as such, would have a $^2A_1$ ground state. While there is substantial overlap between C(1) and C(3) and between C(2) and C(3), there is no bond between C(1) and C(2) (Table 2). The CH bond lengths, the HCH angles, and the values of α_1 and α_2 are consistent with sp^2 hybridization at C(1) and C(2). The geometry at C(3), however, is very different. The value of ∠C(1)C(3)C(2) is anomalously large (124.8°), the C(3)H bonds are anomalously long and the HC(3)H angle is smaller than expected (Table 1). This unique geometry can be understood. The steric repulsion between the hydrogens on C(1) and C(2) must be responsible for the unusually large value of ∠C(1)C(3)C(2). The value of 124.8° is close to the value expected for a bond angle in an sp^2 hybridized carbon. If it is assumed that the hybridization at C(3) is sp^2, then each C—C bond would be formed with one of the three available sp^2 orbitals on C(3). This arrangement will leave one sp^2 and one *p*-orbital to form the two C—H bonds. Rehybridization of the sp^2 and *p*-orbitals leads to the formation of two sp^5-orbitals. The increased "*p*" character of these new orbitals leads to much longer C—H bonds (e.g. C(sp^3)—H bonds are longer than C(sp^2)—H bonds). Furthermore, the angle between two sp^5-orbitals is 101.2° (15), which is larger than the 93.0° obtained for the 0,0 conformer but, nevertheless, is in the right direction.

In the 0,0 conformer of **1**$^+$, 85% of the charge is on the C(1) and C(2) methylenes and only 15% of the charge is on the C(3) methylene. The large negative charge on C(3) is likely a result of polarization of electron density similar to that found for the 90,0 conformer (3). As expected, most of the spin density is shared between C(1) and C(2). It is found, however, that while C(3) has an excess of β-spin density, the hydrogens bonded to C(3) do *not* have, as expected, an excess of α-spin density. The reason for this unusual behaviour is not understood.

The surface for *cis–trans* isomerization and racemization of

TABLE 5. Relative energies of conformers of 1^+ (kcal mol^{-1})[a]

Conformer	4-31G//4-31G	4-31G*//4-31G	MP2/4-31G//4-31G	MP3/4-31G//4-31G	MP2/4-31G*//4-31G
90,90 ($^2A_1$)	0.00	0.00	0.00	0.00	0.00
90,90 ($^2B_2$)	6.16	4.10	2.64	3.21	1.16
90,0 ($^2A''$)	17.54	22.17	24.13	24.24	30.09
0,0 ($^2A_1$)	20.72	26.24	16.22	16.60	20.58

[a] The total energy of the 90,90 ($^2A_1$) conformer at the 4-31G//4-31G, 4-31G*//4-31G, MP2/4-31G//4-31G, MP3/4-31G//4-31G, and MP2/4-31G*//4-31G levels are −116.573588, −116.632448, −116.812395, −116.840616, and −116.979836 hartrees, respectively.

1 has been studied experimentally (5) and by molecular orbital methods (6, 7). The theoretical calculations predict that the barrier to racemization is less than the barrier to isomerization. This effect has been rationalized in terms of orbital symmetry allowed opening of the cyclopropane ring. At the transition state (the 0,0 conformer) there is "pseudo-conjugation" through the central methylene, leading to the "allowed" conrotatory closure to give **1**. The energy difference between the barriers for isomerization and racemization has been estimated to be approximately 2.5 kcal mol^{-1} (7).

It is interesting to compare the results obtained for the isomerization and racemization of $\mathbf{1}^+$ to those results for **1**. At the outset, it should be noted that the work of Collins and Gallup (2*a*) predicted the energy of the $^2A_1$ conformer to be 6.6 kcal mol^{-1} higher than that of the $^2B_2$ structure. The results obtained from this study show that at all levels of theory used, the $^2A_1$ structure is lowest in energy (Table 5). Furthermore, recent experimental results have confirmed that the unpaired electron occupies the $6a_1$ orbital (16).

The calculated barrier to *cis–trans* isomerization of **1** using a minimal basis set and configuration interaction with all single and double substitutions is 52.6 kcal mol^{-1} (6*a*). This is an underestimate of the experimental value (65 kcal mol^{-1}, 8) since CI was performed only on the 90,0 conformer. Moreover, a minimal basis set is too small for accurate CI calculations. There should be a large negative correction to the energy of **1** when CI is included. Since, for $\mathbf{1}^+$ ($^2A_1$), the electron has been removed from an orbital which is predominantly bonding between C(1) and C(2), the strength of the resulting one-electron, two-centre bond should be no more than half of the bond strength in **1**. The calculated strength of the one-electron, two-centre bond depends on the basis set used (Table 5). However, even at the MP2/4-31G* level, the bond strength is still less than half of the experimental value. It is clear that as the basis set becomes more sophisticated, the calculated bond strength increases, and that inclusion of polarization functions has as great an effect as electron correlation.

The calculated energy of the 0,0 conformer of $\mathbf{1}^+$ (Table 5) is greater than the calculated energy of the 90,0 conformer when electron correlation is *not* included. However, the effect of electron correlation is to reduce the energy of the 0,0 conformer (in contrast to the effect of electron correlation on the energy of the 90,0 conformer). The result is that the relative energy of the 0,0 conformer is much less than the energy of the 90,0 conformer when electron correlation is included. This energy difference is as much as 10 kcal mol^{-1}, far greater than the analogous energy difference calculated for racemization versus isomerization in **1**.

The conrotatory closure of the 0,0 conformer of $\mathbf{1}^+$ should be an allowed process by orbital symmetry. Since this conformer has a $^2A_1$ ground state, the singly occupied MO is symmetric with respect to rotation about the C(2) axis. Examination of the

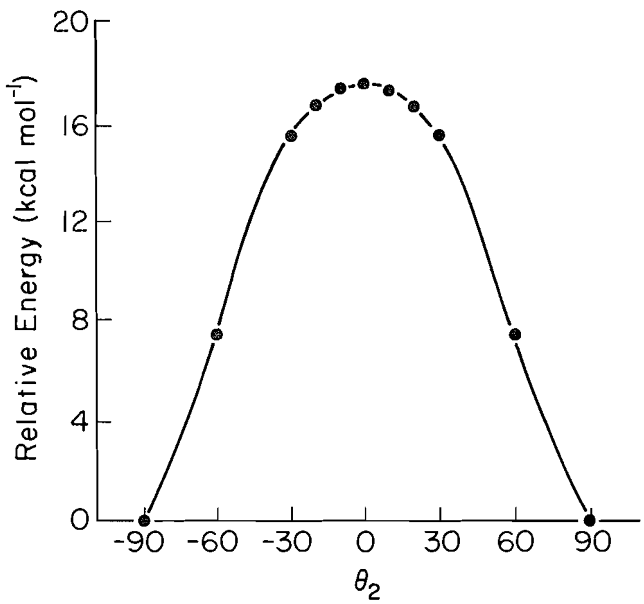

FIG. 2. Energy (relative to the 90,90 ($^2A_1$) conformer of $\mathbf{1}^+$) versus the torsional angle (θ_2) for the single methylene rotation of $\mathbf{1}^+$.

molecular orbital coefficients reveals that there is no contribution from the atomic orbitals on the C(3) methylene. This can be rationalized since the 0,0 conformer is structurally related to the allyl radical (a protonated allyl radical). The singly occupied MO of the 0,0 conformer is, in fact, electronically very similar to the singly occupied MO of the allyl radical.

The partial surface for twisting of one methylene from the $^2A_1$ state of $\mathbf{1}^+$ to the 90,0 conformer has been obtained. The fully optimized geometries of $\mathbf{1}^+$ in the 90,0; 90,10; 90,20; 90,30; 90,60; and 90,90 conformations reveal several interesting trends. The energy profile for twisting is shown in Fig. 2. It is clear that near the transition state the torsional surface is very "soft"; i.e. since there is little bonding between C(1) and C(2), rotation of C(2) has only a small effect on the relative energy. Near the $^2A_1$ structure, however, small changes in θ(2) result in larger changes in the relative energy. This is expected, since the one-electron, two-centre bond is being broken by twisting. This can be compared to twisting in the ethylene radical cation (17) where the torsional potential is much softer. At a torsional angle of 30°, the energy change is only 1.6 kcal mol^{-1} at this level of theory (compared to over 7 kcal mol^{-1} in $\mathbf{1}^+$).

The surface for synchronous conrotatory and synchronous disrotatory opening of the 90,90 conformer of $\mathbf{1}^+$ to the 0,0 conformer of $\mathbf{1}^+$ is shown in Fig. 3. The points at 90°, 60°, 45°, 30°, and 0° were obtained from the fully optimized structures in each conformation. The points at 85°, 80°, 10°, and 5° were single point calculations using the optimized structural param-

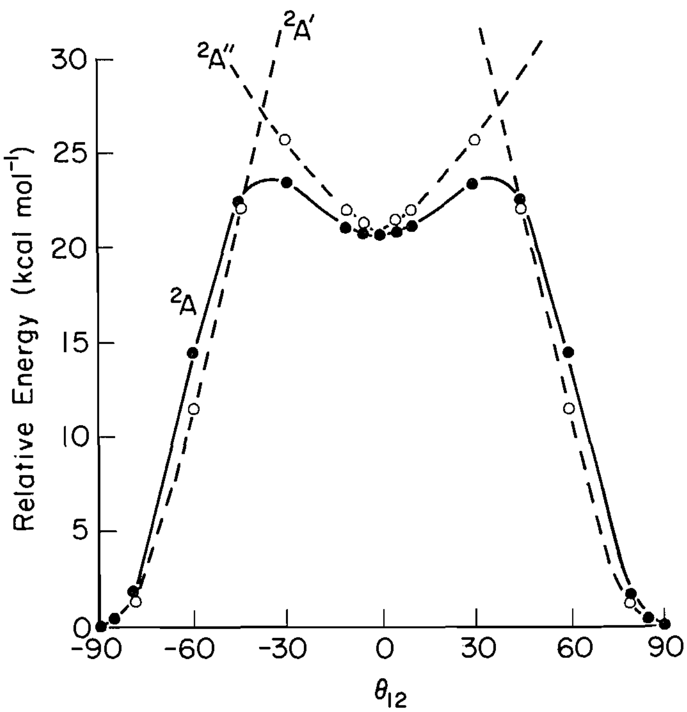

FIG. 3. Energy (relative to the 90,90 ($^2A_1$) conformer of $\mathbf{1}^+$) versus the torsional angle for (a) conrotatory double methylene rotation (●) and (b) disrotatory double methylene rotation (○) of $\mathbf{1}^+$.

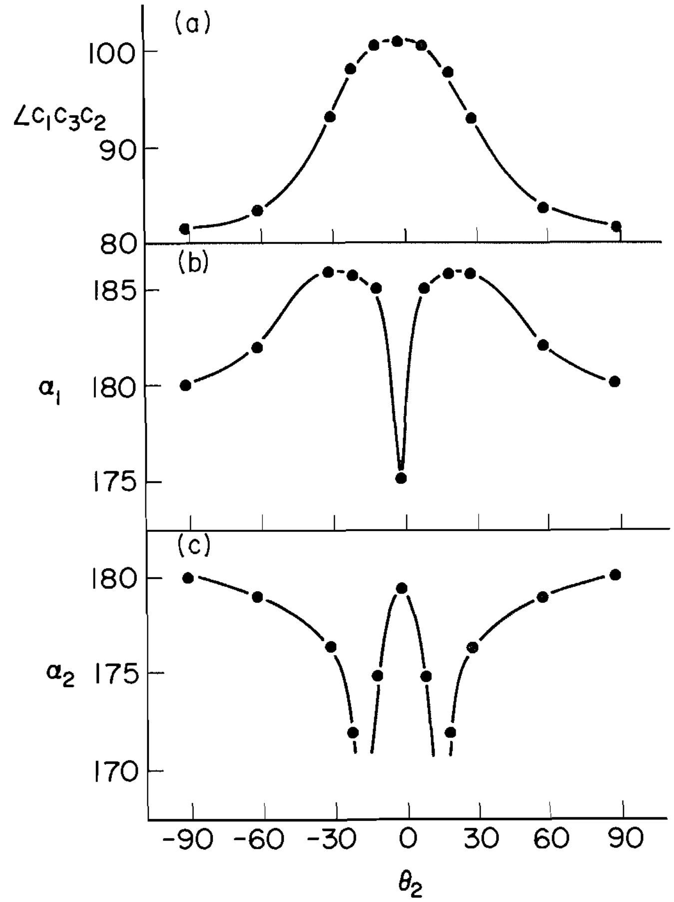

FIG. 4. (a) ∠C(1)C(3)C(2) versus torsional angle (θ_2); (b) wagging angle of the C(1) methylene (α_1, positive values are in the direction of the central methylene) versus the torsional angle (θ_2); and (c) wagging angle of the C(2) methylene (α_2, positive angles are in the direction of the central methylene) versus the torsional angle θ_2 for the single methylene rotation of $\mathbf{1}^+$.

eters from the 90,90 conformer or the 0,0 conformer.

It is found that the transformation of the 90,90 conformer ($^2A_1$) of $\mathbf{1}^+$ to the 0,0 conformer ($^2A_1$) by synchronous conrotation occurs on the ^2A surface with an activation energy of about 24 kcal mol^{-1} near a torsional angle of 40°. On the other hand, disrotation of the 90,90 conformer begins on the $^2A'$ surface while disrotation of the 0,0 conformer begins on the $^2A''$ surface. These torsional surfaces are remarkably similar to state correlation diagrams determined for disrotation and conrotation of the cyclopropyl radical (18*a*). In contrast to $\mathbf{1}^+$, however, in the case of the cyclopropyl radical the ground state orbital symmetry is not the same as the ground state orbital symmetry of the allyl radical (18*b*), so the two orbitals do not correlate with each other.

It is clear that neither disrotation nor conrotation is overwhelmingly preferred. Both modes appear to have some activation barrier. Calculations by Goddard and co-workers on the trimethylene biradical, on the other hand, suggest that disrotatory closure of the biradical is activated while conrotatary closure is activationless (7). It would appear, therefore, that the opening of $\mathbf{1}^+$ more closely parallels that of the cyclopropyl radical.

The geometric changes associated with single methylene rotation are also of interest. As the torsional angle is decreased from 90 to 0°, there is a progressive increase in the value of ∠C(1)C(3)C(2). This is expected as the extent of bonding between C(1) and C(2) decreases (Fig. 4a).

The associated wagging of the methylenes (C(1) and C(2)) is particularly intriguing. Salem and co-workers, in their study of the isomerization of **1**, found that large pyramidal distortions were associated with the trimethylene structures (6*a*). For the 90,0 conformer (of **1**) this distortion from planarity was 14° for the carbon that had twisted. At the STO-3G level, a pyramidal distortion of the C(2) methylene (in the 90,0 conformer of $\mathbf{1}^+$) of 28° is observed. However, at the 4-31G level, this distortion completely disappears.

The wagging motion of the C(1) methylene of $\mathbf{1}^+$ as the torsional angle is decreased from 90 to 0° reveals that initially there is a small pyramidal distortion away from the central methylene (Fig. 4b). This distortion reaches a minimum near $\theta_2 = 30°$ and, near the transition state, undergoes an inversion so that, at the transition state, the C(1) methylene is pyramidally distorted towards the central methylene. The inversion near the transition state is best rationalized as a result of the steric repulsion between the hydrogens of the C(1) methylene and the hydrogen of the C(2) methylene.

The C(2) methylene slowly pyramidalizes away from the C(1) methylene as the torsional angle decreases (Fig. 4c) and reaches a maximum near $\theta_2 = 15°$. At the transition state, there is no pyramidal distortion at the C(2) methylene. This motion is a response to increased steric interaction with the C(1) methylene, which moves towards one of the hydrogens bonded to C(2). The observation that the distortion of the C(2) methylene continued even after the distortion of the C(1) methylene has reached a maximum is consistent with this idea. At (or near) a torsional angle of 15°, further pyramidalization of the C(2) methylene becomes energetically less favourable than depyramidalization of the C(1) methylene. So, while the wagging motion of the C(2) methylene can be rationalized as a motion coupled to the motion of C(1), it is not immediately clear why pyramidalization of C(1) should be favourable. Goddard and co-workers (7) suggested that the pyramidal distortions in trimethylene were favourable, since this conformation avoided eclipsing of more than two bonds. This explanation is feasible in the trimethylene system where the distortions are large. For $\mathbf{1}^+$, where the distortions are much smaller, this suggestion seems less likely. However, it should be noted that this represents a non-dynamic path between the 90,90 ($^2A_1$) conformer and the 90,0 ($^2A''$) conformer, since the conformation of the C(1) methylene is fixed.

These results have some relevance to ion cyclotron resonance and mass spectral experiments reported in the literature. For example, Ausloos and co-workers reported that the proton transfer reaction between $\mathbf{1}^+$ and methanol occurred at the same rate as proton transfer from the propylene radical cation to methanol (1*c*). It was concluded that the proton transfer from $\mathbf{1}^+$ to methanol only occurred from "ring opened" $\mathbf{1}^+$ and that at an ionization voltage of 10.6 eV only 15–16% of $\mathbf{1}^+$ underwent the ring opening. It makes sense that the facile proton transfer will occur from the 0,0 conformer of $\mathbf{1}^+$, since the terminal methylenes will be in a conformation similar to the geometry of the allyl radical. The similarity of the rate coefficients to that for the propylene radical cation is expected for deprotonation from this conformation, because in both cases the proton can be lost along a line perpendicular to the developing π-system. In contrast, the "ring opened" species in the 90,90 conformation is less likely to deprotonate, since the deprotonation would either give, initially, an orthogonal π-system or synchronous rotation of two methylenes would have to occur. In neither case is the reaction expected to be even competitive with the deprotonation of the propylene radical cation.

The adiabatic ionization potential of **1** is 9.8 eV (19). It is interesting to note that, using an ionizing voltage of 10.6 eV, the initially formed ion has an excess energy of about 18 kcal mol^{-1}. That this only leads to 16% ring opening is consistent with the activation barrier of about 24 kcal mol^{-1} calculated for double methylene rotation of $\mathbf{1}^+$. An explanation of this result is important, because the barrier to isomerize $\mathbf{1}^+$ to the propylene radical cation is much larger than 20 kcal mol^{-1} (1*a*). However, it is evident from this work that isomerization of $\mathbf{1}^+$ to the propylene radical cation need not precede the deprotonation. Therefore, there is no need to invoke special conditions under which the barrier to isomerize $\mathbf{1}^+$ to the propylene radical cation would be low. The difficulty will be in distinguishing between reactions which occur from the ring opened (0,0) conformer of $\mathbf{1}^+$ and from the propylene radical cation, since their reactivities, toward deprotonation, should be similar.

Recently, Williams and co-workers have reported esr evidence for the 90,0 conformer of the cyclopropane radical cation (20) and the tetramethylcyclopropane radical cation (21). The structural assignments were based on analysis of the esr spectra that were *irreversibly* produced upon annealing a Freon matrix containing the radical cation in the 90,90 conformation. The assignments were made in part by analogy to a similar study of the oxirane radical cation (22). Clearly, these assignments cannot be correct.

In the case of oxirane, the lone pair of electrons in the 2*p* orbital will increase the bond order to the carbons. It is not surprising that the 0,0 conformer of this species is more stable than the 90,90 conformer. For $\mathbf{1}^+$, however, opening of the ring (whether by single or double methylene rotation) is endothermic. Our calculations show that the ring closure of the 90,0 conformer is activationless; therefore, if formation of this conformer were to occur, it must be reversible.

There is an alternate interpretation to the esr results of Williams and co-workers. We suggest that the irreversible reaction that occurs, upon annealing the matrix, leads to the formation of the 3-chloro-1-propyl radical, in the case of $\mathbf{1}^+$, and $C(CH_3)_2ClCH_2C(CH_3)_2\cdot$ from the tetramethylcyclopropane radical cation. The evidence in favour of this alternative is strong. Interaction of radicals and radical ions with chlorine or chloride in Freon matrices is known (23). The reported esr parameters for the 3-chloropropyl radical are very similar (within fractions of a gauss) to those parameters determined from the esr spectrum of the radical in the annealed matrix (24). In the case of the tetramethylcyclopropane radical cation (21) it was noted that the radical $CCl_3CH_2C(CH_3)_2\cdot$ has the same esr parameters as the species observed in the annealed matrix. It was suggested that the electron-withdrawing nature of $-CCl_3$ would be similar to the electron-withdrawing nature of $-C(CH_3)_2^+$ and the assignment to the perpendicular radical cations was made on this basis. However, the radical $C(CH_3)_3CH_2C(CH_3)_2\cdot$ also has a very similar spectrum (25); thus it is not unlikely that $C(CH_3)_2ClCH_2C(CH_3)_2\cdot$ also has a similar esr spectrum.

Acknowledgements

This work was supported by the Natural Sciences and Engineering Research Council of Canada, including a scholarship to D.D.M.W.

1. (*a*) F. W. McLafferty, M. P. Barbalas, and F. Turecek. J. Am. Chem. Soc. **105**, 1 (1983); (*b*) D. A. Luippold and J. L. Beauchamp. J. Phys. Chem. **80**, 795 (1976); (*c*) L. W. Sieck, R. Gorden, Jr., and P. Ausloos. J. Am. Chem. Soc. **94**, 7157 (1972); (*d*) H. D. Roth and M. L. M. Schilling. J. Am. Chem. Soc. **105**, 6805 (1983).
2. (*a*) J. R. Collins and G. A. Gallup. J. Am. Chem. Soc. **104**, 1530 (1982); (*b*) J. A. Tossell, J. H. Moore, and M. A. Coplan. Chem. Phys., Lett. **67**, 356 (1979); (*c*) C. G. Rowland. Chem. Phys. Lett. **9**, 169 (1971); (*d*) E. Haselbach. Chem. Phys. Lett. **7**, 428 (1970); (*e*) W. J. Bouma, D. Poppinger, and L. Radom. Israel J. Chem. **23**, 21 (1983); (*f*) S. Lunell, M. B. Huang, and A. Lund. Faraday Discuss. Chem. Soc. **78**, 35 (1984); (*g*) L. T. Scott, I. Edren, W. R. Brunsvold, T. H. Shultz, K. N. Houk, and M. N. Paddon-Row. J. Am. Chem. Soc. **104**, 3659 (1982).
3. D. D. M. Wayner, R. J. Boyd, and D. R. Arnold. Can. J. Chem. **61**, 2310 (1983).
4. R. Hoffmann. J. Am. Chem. soc. **90**, 1475 (1968).
5. J. A. Berson, L. D. Pederson, and B. K. Carpenter. J. Am. Chem. Soc. **98**, 122 (1976).
6. (*a*) J. A. Horsley, Y. Jean, C. Moser, L. Salem, R. M. Stevens, and J. S. Wright. J. Am. Chem. Soc. **94**, 279 (1972); (*b*) Y. Jean and L. Salem. J. Chem. Soc. Chem. Commun. 382 (1971).
7. P. J. Hay, W. J. Hunt, and W. A. Goddard III. J. Am. Chem. Soc. **94**, 638 (1972).
8. (*a*) J. A. Berson. Ann. Rev. Phys. Chem. **28**, 111 (1977); (*b*) J. E. Baldwin and T. C. Barden. J. Am. Chem. Soc. **106**, 6364 (1984).
9. (*a*) N. L. Bauld, D. J. Bellville, R. Pabon, R. Chelsky, and G. Green. J. Am. Chem. Soc. **105**, 2378 (1983); (*b*) E.

HASELBACH, T. BALLY, and Z. LANYIOVA. Helv. Chim. Acta, **62**, 577 (1979).
10. J. S. BINKLEY, R. A. WHITESIDE, R. KRISHNAN, R. SEEGER, D. J. DEFREES, H. B. SCHLEGEL, S. TOPIOL, L. R. KHAN, and J. A. POPLE. (Department of Chemistry, Carnegie–Mellon University, Pittsburgh, PA 15213.) QCPE, **13**, 406 (1981).
11. (*a*) P. PULAY. *In* Modern theoretical chemistry. Vol. 4. *Edited by* H. F. Schaefer, III. Plenum Press, New York. 1977; (*b*) H. B. SCHLEGAL, S. WOLFE, and F. BERNARDI. J. Chem. Phys. **63**, 3632 (1975).
12. C. MØLLER and M. S. PLESSET. Phys. Rev. **46**, 618 (1934).
13. J. A. POPLE and R. K. NESBET. J. Chem. Phys. **22**, 571 (1954).
14. A. D. WALSH. Trans. Faraday Soc. **45**, 179 (1949).
15. W. A. BENNETT. J. Chem. Educ. **44**, 17 (1967).
16. M. IWASAKI, K. TORIYAMA, and K. NUMONE. J. Chem. Soc. Chem. Commun. 202 (1983).
17. D. J. BELLVILLE and N. L. BAULD. J. Am. Chem. Soc. **104**, 294 (1982).
18. (*a*) H. C. LONGUET-HIGGINS and E. W. ABRAHAMSON. J. Am. Chem. Soc. **87**, 2045 (1965); (*b*) L. FARNELL and W. G. RICHARDS. J. Chem. Soc. Chem. Commun. 334 (1973); (*c*) G. SZEIMIES and G. BOCHE. Angew. Chem. Int. Ed. Engl. **10**, 912 (1971); (*d*) E. HASELBACH. Helv. Chem. Acta, **54**, 2257 (1971); (*e*) D. T. CLARK and D. B. ADAMS. Nature (London), Phys. Sci. **233**, 121 (1971); (*f*) P. MERLET, S. D. PEYERIMHOFF, R. J. BUENKER, and S. SHIH. J. Am. Chem. Soc. **96**, 959 (1974).
19. (*a*) G. BIERI, F. BURGER, E. HEILBRONNER, and J. P. MAIER. Helv. Chem. Acta, **60**, 2213 (1977); (*b*) F. P. Lossing. Can. J. Chem. **50**, 3973 (1972).
20. X. Z. QIN and F. WILLIAMS. Chem. Phys. Lett. **112**, 79 (1984).
21. X. Z. QIN, L. D. SNOW, and F. WILLIAMS. J. Am. Chem. Soc. **106**, 7640 (1984).
22. L. D. SNOW, J. T. WANG, and F. WILLIAMS. Chem. Phys. Lett. **100**, 193 (1983).
23. (*a*) D. BECKER, K. PLANTE, and M. D. SEVILLA. J. Phys. Chem. **87**, 1648 (1983); (*b*) X. Z. QIN, B. W. WALTHER, and F. WILLIAMS. J. Chem. Soc. Chem. Commun. 1667 (1984).
24. D. J. EDGE and J. K. KOCHI. J. Am. Chem. Soc. **94**, 6485 (1972).
25. J. GEROLA, B. LAMOTTE, and R. MARX. J. Chim. Phys. **66**, 216 (1969).

Synthesis, base strength, and prototropic behaviour of a number of alkyllumazines

ROSS STEWART[1] AND S. J. GUMBLEY

Department of Chemistry, University of British Columbia, Vancouver, B.C., Canada V6T 1Y6

Received May 17, 1985

ROSS STEWART and S. J. GUMBLEY. Can. J. Chem. **63**, 3290 (1985).

A number of lumazines and 5-deazalumazines containing a methyl group at C-7 have been prepared, their pK_{BH^+} values determined, and measurements made of the rates at which the hydrogen atoms of their 7-methyl groups undergo isotopic exchange in aqueous sulfuric acid. The presence of an alkyl group at N-8 in the protonated forms of these compounds activates the neighbouring methyl group at C-7; the effect is considerably larger than that previously observed for a methyl group at C-6, which is the other neighbouring position. The comparison of methyl and hydrogen at N-8 can be made only for the acid-catalyzed reaction because the structures of the neutral compounds, which take part in the base-catalyzed reaction, are not analogous.

ROSS STEWART et S. J. GUMBLEY. Can. J. Chem. **63**, 3290 (1985).

On a préparé un certain nombre de lumazines et de déaza-5 lumazines contenant un groupement méthyle en position C-7; de plus, on a déterminé les valeurs de leurs pK_{BH^+} et, opérant dans de l'acide sulfurique aqueux, on a mesuré les vitesses d'échange isotopique des atomes d'hydrogènes de leurs groupements méthyles en C-7. La présence d'un groupement alkyle dans la position N-8 des formes protonées de ces composés active le groupement méthyle voisin en C-7; cet effet est beaucoup plus important que celui observé antérieurement pour un groupement méthyle en C-6, l'autre position adjacente. On ne peut faire une comparaison entre les effets des groupements méthyles et ceux des atomes d'hydrogènes en N-8 que pour les réactions acido-catalysées puisque les structures des composés neutres, qui prennent part à la réaction catalysée par les bases, ne sont pas semblables.

[Traduit par le journal]

Introduction

In 6,7,8-trimethyllumazine, **1**, the 7-methyl group (marked by an asterisk) is reactive and undergoes rapid general base (and general acid) catalyzed exchange in protic solvents (1–6). The presence of an *N*-alkyl group (position 8) is important here, as noted by Beach and Plaut (2), since the parent ring system has the form shown in **2**, with the consequence that a 7-methyl substituent in such compounds as **2** is relatively inert to the action of base.

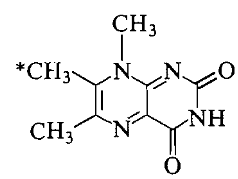

1

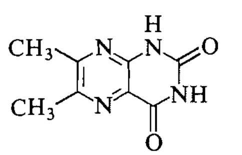

2

The kinetics and mechanism of both the general base and general acid catalyzed reactions have been thoroughly studied previously (1–6); the ease with which the two exchange processes (and other reactions) take place is a result of the stability of **3** and **4**, which are the respective intermediates in the general base and general acid catalyzed routes for **1**.

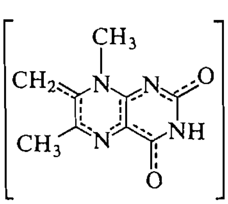

3

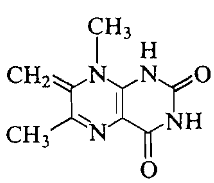

4

In the case of 5,7,8-trimethyl-5-deazalumazine **5** (R = R′ = CH_3), the methyl groups at the 5- and 7-positions both undergo isotopic exchange, although their reactivity is much less than is the case with the 7-methyl group in **1**.

We have previously observed that an alkyl group at position 6 activates the reactive methyl group at the neighbouring positions in **1** and **5**, whereas more distant methyl groups are

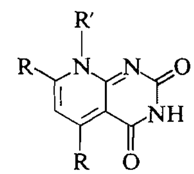

5

substantially deactivating, as shown, for example, by the mutual deactivating effects of the 5- and 7-methyl groups in **5** (R = R′ = CH_3) (6, 7).

We wished to examine the effect of a neighbouring alkyl group at nitrogen (position 8 in, for example, **1**) to see if it too activates the group at position 7. As noted earlier, the reactions of **1** and **2** with base cannot be directly compared because of structural differences. Although the general base catalyzed reaction is thus disqualified from consideration in this respect, the general acid catalyzed reaction is not. This is because protonation occurs at N-8 in **2** (7), and at N-1 in **1**,[2] which

[1] 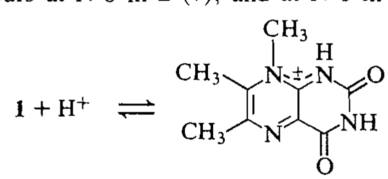

[2] 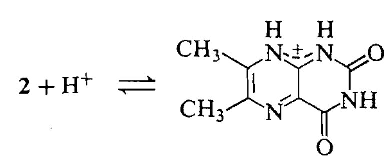

[1] Author to whom correspondence may be addressed.

[2] References 5 and 8, and references therein.

TABLE 1. Basicity constants and rates of exchange of lumazines and deazalumazines in sulfuric acid solution at 25°C

Compound	10^4 k, s^{-1}		
	25% D_2SO_4	50% D_2SO_4	pK_{BH^+}
6,7,8-Trimethyllumazine (**1**)	10.8	5.4	0.78[a]
6,7-Dimethyllumazine (**2**)	[b]	0.05	−1.55
7,8-Dimethyllumazine (**6**)	2.6	—	0.15[c]
7-Methyllumazine (**7**)	0.025	0.027	—
8-Ethyl-6,7-dimethyllumazine (**8**)	9.4	6.7	0.79
6,7,8-Trimethyl-5-deazalumazine (**9**)	0.001	0.0001	2.21[c]
6,7-Dimethyl-5-deazalumazine (**10**)	0.0002	<0.0001	0.71
5,6-Dimethyl-5-deazalumazine (**11**)	—	<0.0001	—

[a]Reference 6 gives 0.93.
[b]Insoluble.
[c]Reference 6.

produces identical cations except for the substitution of hydrogen for methyl at N-8 (eqs. [1] and [2]).

In the present work we compare the rate of exchange of deuterium for protium in the 7-methyl groups of **1** and **2** and at the 5- and 7-positions of **5** (R = CH_3, R′ = H or CH_3) under strongly acidic conditions. In addition, several other relevant lumazine derivatives have been prepared and examined.

Experimental

Synthesis

(a) *8-Alkyllumazines*

6-Chlorouracil was nitrated by the method of Cheng and Cheng (9) to give 6-chloro-5-nitrouracil, which was converted to the several 6-alkylamino-5-nitrouracils by treatment with the appropriate alkylamine. These compounds were then suspended in 50% ethanol–water and reduced with sodium dithionite. A 1,2-diketone (butane-2,3-dione or pentane-2,3-dione) was added to the warm solution of the diamine and the mixture heated for a further 15 min. The reaction solutions were then taken to dryness and separated on a silica gel column with methanol/water as the eluant. The resulting lumazines were recrystallized from ethanol–water to give yellow to orange crystals. The products were **1** (1), **6** (6), and **8**. The nmr spectra of **8** consisted of a triplet centered at δ 1.77 (3H), singlets at 2.97 (3H) and at 3.17 (3H), and a quartet centered at 4.96 (2H). *Anal.* calcd. for $C_{10}H_{12}N_4O_2$: C 54.54, H 5.49, N 25.44; found: C 54.34, H 5.57, N 25.58.

(b) *6,7-Dimethyllumazine (2) and 7-methyllumazine (7)*

These compounds were prepared in the same manner as the *N*-alkyllumazines, except that 5,6-diaminouracil and butane-2,3-dione and pyruvaldehyde were used. The latter compound gave a mixture of the 6- and 7-methyl isomers. (Sharefkin, using the same method, appeared to get only 7-methyllumazine (10).) The exchange reactions were carried out on the mixture and showed that the hydrogen atoms of the methyl group of only one of the components underwent exchange. Exchange was also observed for one of the methyl groups of **2**, presumably that at the 7-position since Beach and Plaut observed that 6-methyllumazine does not undergo exchange in D_2O (2). Compound **2** was recrystallized repeatedly from water and gave white crystals. *Anal.* calcd. for $C_8H_8N_4O_2$: C 50.00, H 4.20, N 29.15; found: C 49.75, H 4.30, N 29.05.

(c) *5-Deazalumazines*

Compound **9** was prepared as previously described (6). 6,7-Dimethyl-5-deazalumazine (**10**), which has been previously synthesized by Robins and Hitchings (11), was prepared by the following alternative procedure. 6-Aminouracil in 10% sulfuric acid was refluxed with the dimethyl acetal of 2-methyl-3-oxobutanal for 2 h. The solution was cooled and neutralized with aqueous ammonia and the precipitated solid crystallized repeatedly from water to give white crystals of **10**; nmr in trifluoroacetic acid, δ: 2.63 (3H), 2.93 (3H), and 8.94 (1H). 5,6-Dimethyl-5-deazalumazine (**11**) was prepared as described by Wood *et al.* (12), except that the mixture was refluxed for 3 h instead of being stirred at room temperature for 36 h; the product was recrystallized from water – dimethyl sulfoxide. The nmr spectrum of the product in trifluoroacetic acid agreed with that given by Wood *et al.*

pK_{BH^+} measurements

Basicity constants were determined spectrophotometrically in aqueous solution, essentially as previously described (6), except that aqueous sulfuric acid was used for the least basic compounds, with the H_0 value of the solution being used to calculate pK_{BH^+} (13).

Rate measurements

The exchange reaction was followed in D_2SO_4–D_2O mixtures by means of nmr spectroscopy, essentially as previously described (4, 14).

Results and discussion

In Table 1, the exchange kinetics for the lumazines and deazalumazines are given for two concentrations of sulfuric acid. The rates are generally smaller in the more concentrated acid, presumably as a result of the lower activity of water in this solution; incomplete protonation of some of the substrates in the 25% acid medium appears to be largely responsible for the variation in the ratios of the rates in the two media from compound to compound. (The weakest base among the compounds studied is 7-methyllumazine (**7**), for which pK_{BH^+} must be more negative than −2.0, judging from the effect of the additional 6-methyl group in **1** compared to **6**; because the H_0 scale was used in the pK determinations and the H_0 value of 25% sulfuric acid is only −1.4, the substrate will be less than 20% protonated in this medium.)

It is clear from a comparison of the reactivities of **1** and **2**, **6** and **7**, and **9** and **10** that replacing a hydrogen atom at position 8 with a methyl group has a large accelerating effect (between one and two orders of magnitude) on the exchange rate of the protons of the adjacent methyl group. This effect is in the same direction but is significantly greater than the effect of a methyl group at the other neighbouring position, that is, at position 6. It is also greater than the effect that *N*-methylation produces in pyrimidonium systems (15). There is always the possibility in reactions of the type considered herein that the reactive protonated intermediate is not the normal cationic form (eq. [2]) but a minor tautomer, which would make a simple comparison of rates invalid. This possibility seems remote in the present instance since the only stable neutral intermediate that can be

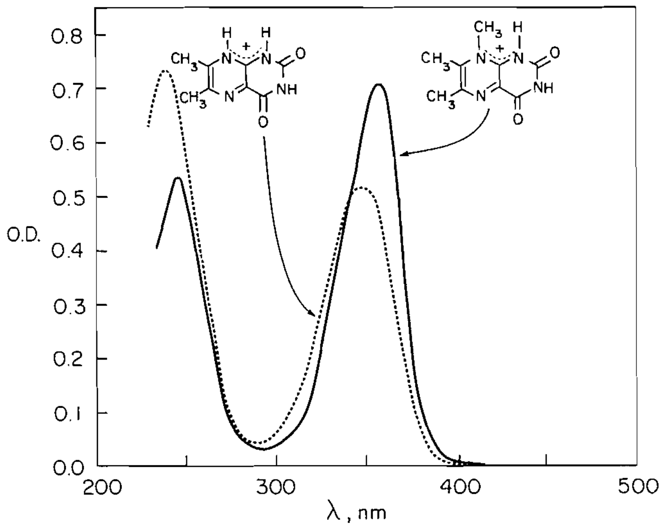

FIG. 1. Ultraviolet absorption spectra of **1** (solid line) and **2** (dotted line) in 52% aqueous sulfuric acid, $C = 5.1 \times 10^{-5}$ molar; λ_{max} and log ϵ values are, for **1**, 358 nm (4.15) and 245 nm (4.02), and for **2**, 347 nm (4.00) and 236 nm (4.15).

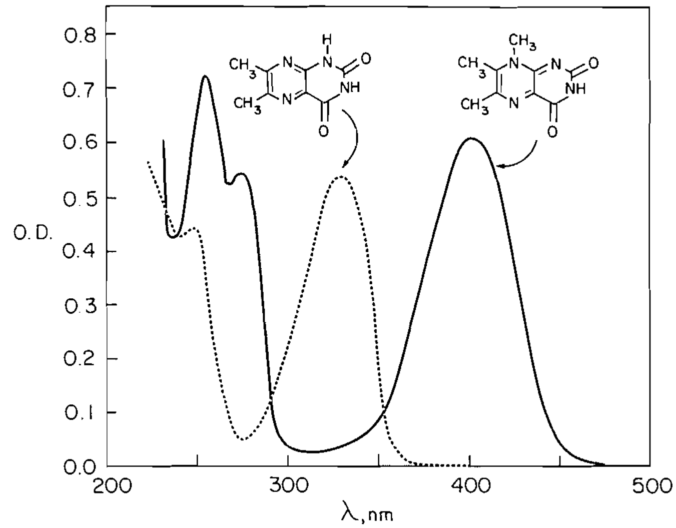

FIG. 2. Ultraviolet absorption spectra of **1** (solid line) and **2** (dotted line) in water, $C = 5.1 \times 10^{-5}$ molar; λ_{max} and log ϵ values are, for **1**, 403 nm (4.06) and 275 nm (4.02), and 255 nm (4.15), and for **2**, 328 nm (4.01) and 249 nm (3.93).

formed by deprotonating the 7-methyl group is **4**, which is derived from the predominant cation (eq. [2]). In this connection, the ultraviolet spectra of **1** and **2** are very similar in acid solution (Fig. 1), except that the 8-methyl group that is present in the conjugate acid of **1** and absent in that of **2** causes a red shift of about 10 nm in the principal absorption bands. As can be seen, the neutral forms of **1** and **2** have quite different spectra (Fig. 2). Furthermore, the nmr spectra of **1** and **2** in trifluoroacetic acid solution are very similar except for the presence of an additional methyl absorption in the conjugate acid of **1**. The 7-methyl group (that which undergoes exchange) is at δ 2.98 in **1**.H^+ and at 2.93 in **2**.H^+; the 6-methyl group is at 2.68 in **1**.H^+ and at 2.63 in **2**.H^+.

We had earlier considered the possibility that strain induced by the presence of adjacent alkyl groups might be responsible for the higher reactivity we have found to be associated with clustering of methyl groups, although it is not obvious in many cases that a partial proton loss from a C-5 or C-7 or analogous methyl group would, in fact, relieve such strain. An examination of the crystal structures of a number of alkyl substituted pyrimidonium salts that exhibit steric acceleration showed that ring strain was not the major factor in determining the reactivity of the groups in question, although it appeared to play a role in several cases (15). It is entirely possible that the lumazine system is more sensitive than the pyrimidonium system to ring strain and that this is reflected in the large effect we observe for alkylation of the nitrogen atom at position 8. At any rate, it is clear that the phenomenon of neighbouring alkyl groups increasing the prototropic reactivity of the 7-methyl group in lumazines and 5-deazalumazines applies to methyl substitution at both positions 6 and 8, with substitution at the latter position producing the larger effect. It can be seen from the results in Table 1 that the effect of ethyl at N-8 is little different from that of methyl; repeated attempts to prepare the compounds possessing an isopropyl or *tert*-butyl group at N-8 were unsuccessful.

With regard to conformational effects in the sidechains themselves, it may well be that proton loss from methyl changes the conformation from one that is gear-clashed methyl–methyl (16, 17) to one that is gear-meshed (or gear-locked) methyl– methylene. The possibility that this effect is favourable, together with a consideration of polarizability effects and hybridization changes at nitrogen, will be addressed in a subsequent publication.

Basicity constants

Lumazines that carry an 8-substituent have a ring structure of the type shown in **1** and those that lack such a group have a ring structure of the type shown in **2**. The greater stability of the latter system is reflected in the lower basicity of such compounds, the difference amounting to 1.7 p*K* units in the case of the isomeric compounds **2** and **6**. In the case of the deazalumazines the p*K* difference appears to be somewhat less, being only 1.4 units (including the inductive effect of an additional methyl group) in the cases of **9** and **10**.

Acknowledgement

The financial support of the Natural Sciences and Engineering Research Council of Canada is gratefully acknowledged.

1. J. M. McANDLESS and R. STEWART. Can. J. Chem. **48**, 263 (1970).
2. R. L. BEACH and G. W. E. PLAUT. Biochemistry, **9**, 760 (1970).
3. T. PATTERSON and H. C. S. WOOD. Chem. Commun. 290 (1969).
4. R. STEWART and J. M. McANDLESS. J. Chem. Soc. Perkin Trans. 2, 1041 (1972).
5. R. STEWART, S. J. GUMBLEY, and R. SRINIVASAN. J. Am. Chem. Soc. **102**, 6168 (1980).
6. R. STEWART, R. SRINIVASAN, and S. J. GUMBLEY. Can. J. Chem. **59**, 2755 (1981).
7. G. MÜLLER and W. VON PHILIPSBORN. Helv. Chim. Acta, **56**, 2680 (1973).
8. R. STEWART and K. OYAMA. Can. J. Chem. **52**, 3884 (1974).
9. K.-Y. Z. CHENG and C. C. CHENG. J. Med. Chem. **11**, 1107 (1968).
10. D. M. SHAREFKIN. J. Am. Chem. Soc. **24**, 345 (1959).
11. R. K. ROBINS and G. H. HITCHINGS. J. Am. Chem. Soc. **80**, 3449 (1958).

12. H. C. S. WOOD, R. WRIGGLESWORTH, D. A. YEOWELL, F. W. GURNEY, and B. S. HURLBERT. J. Chem. Soc. Perkin Trans. 1, 1225 (1974).
13. C. H. ROCHESTER. Acidity functions. Academic Press, London. 1970.
14. R. SRINIVASAN and R. STEWART. J. Chem. Soc. Perkin Trans. 2, 674 (1976).
15. T. W. S. LEE, S. J. RETTIG, R. STEWART, and J. TROTTER. Can. J. Chem. **62**, 1194 (1984).
16. U. BERG, T. LILJEFORS, C. ROUSSEL, and J. SANDSTRÖM. Acc. Chem. Res. **18**, 80 (1985), and references therein.
17. J. C. SCHUG and J. W. VIERS. Tetrahedron, **40**, 3971 (1984), and references therein.

An analysis of a second-order chemical reaction involving a single intermediate between reactants and products

MICHAEL JESSE BLANDAMER
Department of Chemistry, University of Leicester, Leicester, U.K.

JOHN MARSHALL WILLIAM SCOTT
Department of Chemistry, Memorial University of Newfoundland, St. John's, Nfld., Canada A1B 3X7

AND

DANNY SUMMERS[1]
Department of Mathematics and Statistics, Memorial University of Newfoundland, St. John's, Nfld., Canada A1C 5S7

Received February 14, 1985

MICHAEL JESSE BLANDAMER, JOHN MARSHALL WILLIAM SCOTT, and DANNY SUMMERS. Can. J. Chem. **63**, 3294 (1985).

The differential equations which describe the kinetics of the general reaction

$$\mathrm{A + B} \underset{k_2}{\overset{k_1}{\rightleftarrows}} \mathrm{C} \xrightarrow{k_3} \mathrm{D}$$

are cast in a nondimensional form and analysed. The problem reduces to two first-order nonlinear ordinary differential equations containing three nondimensional constants together with two initial conditions. Composition–time curves are deduced for the general case. For the case when $k_2/k_1\,[\mathrm{A}]_0 \ll 1$, where $[\mathrm{A}]_0$ is the initial concentration of A, simple analytical solutions are obtained. Numerical integrations of the full equations are reported and the analytical solutions are found to represent accurate solutions to the nonlinear problem for sufficiently small values of k_2.

MICHAEL JESSE BLANDAMER, JOHN MARSHALL WILLIAM SCOTT et DANNY SUMMERS. Can. J. Chem. **63**, 3294 (1985).

On a développé une forme sans dimensions et on a analysé les équations différentielles qui décrivent la réaction générale

$$\mathrm{A + B} \underset{k_2}{\overset{k_1}{\rightleftarrows}} \mathrm{C} \xrightarrow{k_3} \mathrm{D}$$

Le problème est alors réduit à deux équations différentielles ordinaires, non linéaires, du premier degré et contenant trois constantes sans dimensions et à deux conditions initiales. On a déduit, dans le cas général, les courbes de la composition en fonction du temps. On obtient des solutions analytiques simples pour le cas où $k_2/k_1\,[\mathrm{A}]_0 \ll 1$ ($[\mathrm{A}]_0$ est la concentration initiale de A). On rapporte des intégrations numériques des équations complètes et, dans les cas où les valeurs de k_2 sont suffisamment faibles, on a trouvé que les solutions analytiques représentent des solutions précises au problème nonlinéaire.

[Traduit par le journal]

Introduction

Recently we have been interested in the behaviour of the system,

$$[1] \quad \mathrm{A} \underset{k_2}{\overset{k_1}{\rightleftarrows}} \mathrm{B} \xrightarrow{k_3} \mathrm{C}$$

where k_1, k_2, and k_3 are first-order constants (1). The mathematical techniques for handling this and related systems are well developed. No analysis has been attempted in the case that k_1 is a second-order constant. The present contribution is an account of the formal treatment of the system

$$[2] \quad \mathrm{A + B} \underset{k_2}{\overset{k_1}{\rightleftarrows}} \mathrm{C} \xrightarrow{k_3} \mathrm{D}$$

where k_1 in eq. [2] is a second-order constant. It is intended to use the relationships and techniques discussed in this paper for a kinetic and thermodynamic discussion of the system

$$[2a] \quad \mathrm{A + B \rightleftarrows C \rightleftarrows D + E}$$

In the meantime the results reported in this paper would appear to be of general interest.

The general reaction, [2], is described by the following system of differential equations:

$$[3] \quad \frac{\mathrm{d[A]}}{\mathrm{d}t} = -k_1\mathrm{[A][B]} + k_2\mathrm{[C]}$$

$$[4] \quad \frac{\mathrm{d[B]}}{\mathrm{d}t} = \frac{\mathrm{d[A]}}{\mathrm{d}t}$$

$$[5] \quad \frac{\mathrm{d[C]}}{\mathrm{d}t} = k_1\mathrm{[A][B]} - (k_2 + k_3)\,\mathrm{[C]}$$

$$[6] \quad \frac{\mathrm{d[D]}}{\mathrm{d}t} = k_3\mathrm{[C]}$$

and subject to the boundary conditions,

$$[7] \quad \mathrm{[A]} = \mathrm{[A]}_0,\ \ \mathrm{[B]} = \mathrm{[B]}_0,\ \ \mathrm{[C]} = 0,\ \ \mathrm{[D]} = 0 \text{ at } t = 0$$

If the concentrations [A], [B], [C], and [D] are measured on the molar concentration scale, their second-order rate constant k_1 has the dimensions $\mathrm{dm^3\ mol^{-1}\ s^{-1}}$, and the first-order rate constants k_2 and k_3 have dimensions $\mathrm{s^{-1}}$. The system of eqs. [3]–[6] is symmetrical with respect to the interchange of [A] and [B].

Equation [4] may be readily integrated to give

$$[8] \quad \mathrm{[B]} = \mathrm{[A]} + \mathrm{[B]}_0 - \mathrm{[A]}_0$$

and from eqs. [3], [5], and [6] we may deduce that

[1] Author to whom correspondence may be addressed.

$$[9] \quad \frac{d[A]}{dt} + \frac{d[C]}{dt} + \frac{d[D]}{dt} = 0$$

from which we deduce the further integral

$$[10] \quad [A] + [C] + [D] = [A]_0$$

Equation [10] is more usually derived from the condition of mass balance for the system.

Elementary considerations of the isoclinals of the system lead to the following results:

(a) If $[A]_0 = [B]_0$, then

$$[11] \quad [A] \to 0, \ [B] \to 0, \ [C] \to 0, \ [D] \to [A]_0, \text{ as } t \to \infty$$

(b) if $[A]_0 > [B]_0$, then

$$[12] \quad [A] \to [A]_0 - [B]_0, \quad [B] \to 0, \quad [C] \to 0, \quad [D] \to [B]_0, \text{ as } t \to \infty$$

The symmetry of the problem with respect to A and B makes the case when $[A]_0 < [B]_0$ superfluous since it is equivalent to (b) above. The mathematical conclusions [11] and [12] follow the anticipated physical behaviour of the system for large times.

It is useful to define the following nondimensional variables:

$$[13] \quad y_1 = [A]/[A]_0; \quad y_2 = [C]/[A]_0; \quad y_3 = [D]/[A]_0; \quad y_4 = [B]/[A]_0 \text{ and } x = k_1[A]_0 t$$

With these variables the system [3]–[8] and [9] reduces to

$$[14] \quad \frac{dy_1}{dx} = (1 - \alpha)y_1 - y_1^2 + \beta y_2$$

$$[15] \quad \frac{dy_2}{dx} = -(1 - \alpha)y_1 + y_1^2 - (\beta + \gamma)y_2$$

$$[16] \quad y_1(0) = 1, \ y_2(0) = 0$$

$$[17] \quad y_3 = 1 - y_1 - y_2$$

$$[18] \quad y_4 = y_1 - (1 - \alpha)$$

where α, β, and γ are defined by the relationships

$$[19] \quad \alpha = [B]_0/[A]_0; \quad \beta = k_2/k_1[A]_0, \quad \text{and } \gamma = k_3/k_1[A]_0$$

The general problem is thus reduced to the solution of the nonlinear, autonomous system represented by eqs. [14] and [15], subject to the initial conditions [16], where α is a constant such that $0 < \alpha \leq 1$, and β and γ are both positive constants. Unfortunately, exact analytical solutions to eqs. [14] and [15] cannot be obtained, even in the special case when $\alpha = 1$. Nevertheless, the qualitative behaviour of the dimensionless quantities y_1, y_2, y_3, and y_4 is readily deduced, and the results are given schematically in Fig. 1.

Analysis

If we add eqs. [14] and [15] then

$$[20] \quad \frac{dy_1}{dx} + \frac{dy_2}{dx} = -\gamma y_2$$

Equation [20] may be integrated to yield

$$[21] \quad y_2(x) = e^{-\gamma x} - y_1(x) + \gamma e^{-\gamma x} \int_0^x e^{\gamma u} y_1(u) \, du$$

Solutions for the model are straightforward for cases when k_2 is small, i.e. when $0 < \beta \ll 1$. If $\beta = 0$, eq. [14] is reduced

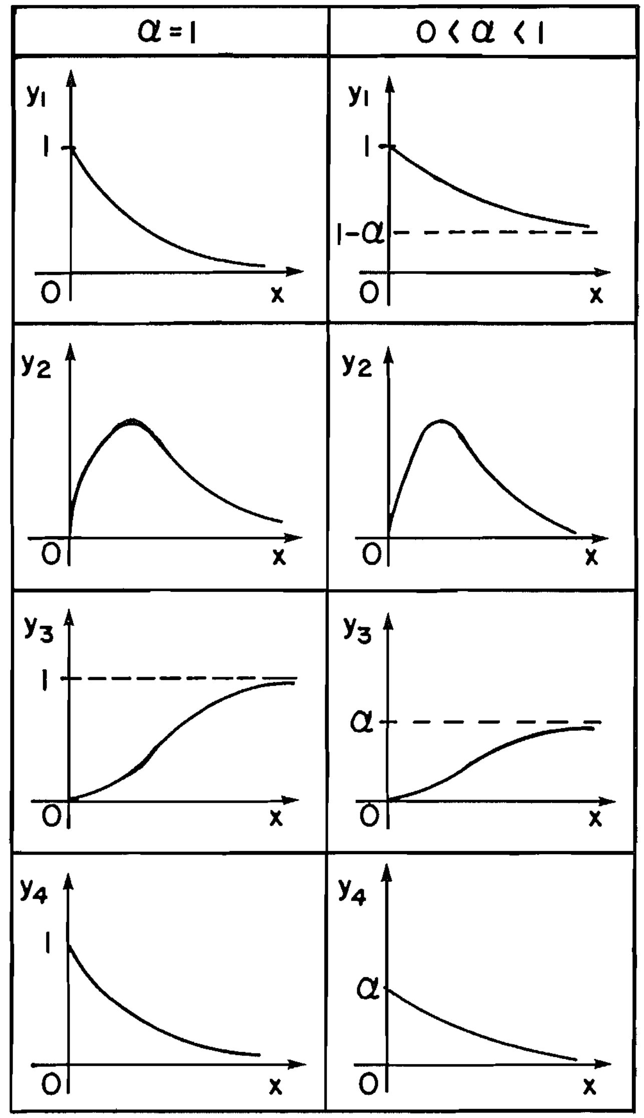

FIG. 1. Schematic solution curves of the system [14]–[18] in the cases $\alpha = 1$, and $0 < \alpha < 1$. These curves represent solutions to the reaction [2] for all possible values of the rate constants k_1, k_2, and k_3, and all initial concentrations $[A]_0$ and $[B]_0$.

to a separable equation when $\alpha = 1$, and to a Bernoulli Equation if $0 < \alpha < 1$ (e.g. see ref. 2). The appropriate solutions are given by

$$[22] \quad y_1(x) = 1/(1 + x), \quad \alpha = 1$$

$$[23] \quad y_1(x) = (1 - \alpha)/(1 - \alpha e^{-(1-\alpha)x}), \quad 0 < \alpha < 1$$

and the corresponding solutions for y_2, obtained from eq. [21], are

$$[24] \quad y_2(x) = e^{-\gamma x} - \frac{1}{x + 1} + \gamma e^{-\gamma(x+1)} I_1(x), \quad \alpha = 1$$

where

$$I_1(x) = \int_{\gamma}^{\gamma(x+1)} \frac{e^u}{u} \, du$$

$$[25] \quad y_2(x) = (1 - \alpha)\left\{1 - \frac{1}{1 - \alpha e^{-(1-\alpha)x}}\right\} + \alpha e^{-\gamma x} \times \{1 + \gamma I_2(x)\}, \quad 0 < \alpha < 1$$

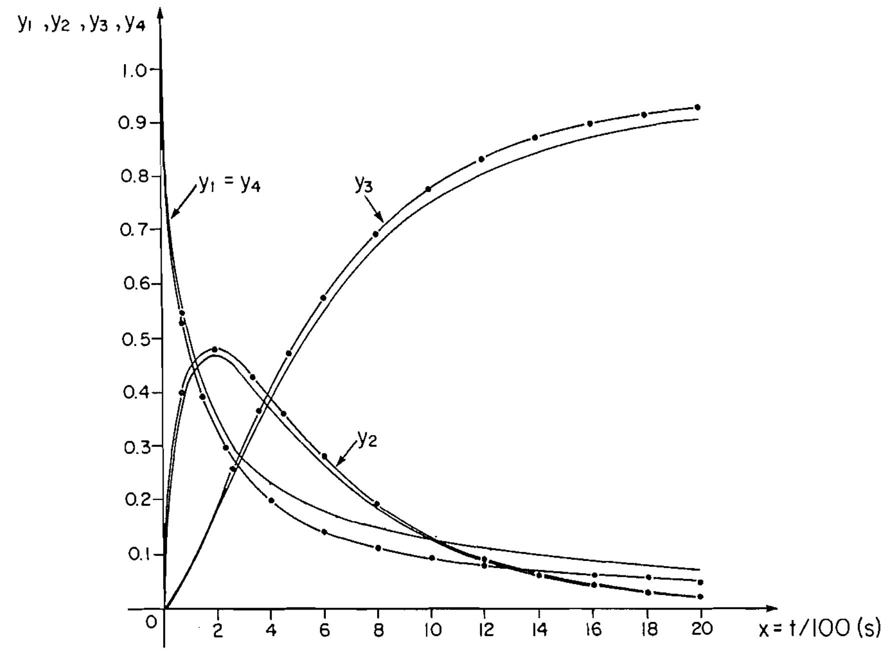

FIG. 2. Solution curves for the case k_1 = 1 $dm^3\ mol^{-1}\ s^{-1}$, $k_3 = 2.5 \times 10^{-3}\ s^{-1}$, $[A]_0 = [B]_0 = 10^{-2}$ mol dm^{-3} (i.e. $\alpha = 1$, $\gamma = 0.25$). The broken curves represent the analytical solutions [22], [24]; the full curves represent the numerical solution of the system [14]–[18] when $k_2 = 5 \times 10^{-4}\ s^{-1}$ (i.e. $\beta = 0.05$). The set of particular points shown are those of the numerical solution of [14]–[18] when $k_2 < 5 \times 10^{-5}$ s^{-1} (i.e. $\beta < 5 \times 10^{-3}$).

where

$$I_2(x) = \int_1^{e^{(1-\alpha)x}} \frac{u^{(\frac{\gamma}{1-\alpha}-1)}}{u-\alpha}\,du$$

Results [22] and [23] are well known (e.g. they appear in a slightly different form in ref. 3, pp. 335–336). The reader is also referred to the related work in refs. 6 and 7.

In general, the integrals I_1 and I_2 are not expressible in simple, closed form although they may be evaluated to any desired precision by a suitable numerical quadrature (e.g. a 5-point Newton–Cotes formula as, for instance, given in ref. 4).

The integral I_2 can be evaluated in closed form for some special cases, e.g. for $\gamma/(1-\alpha) = 1, 2, 3, \ldots,$ or for $\gamma/(1-\alpha) = 1/2$. Examples of such solutions are

$$[26] \quad I_2(x) = \ln\left\{\frac{e^{(1-\alpha)x}-\alpha}{1-\alpha}\right\}, \quad \gamma/(1-\alpha) = 1$$

$$[27] \quad I_2(x) = e^{(1-\alpha)x} - 1 + \alpha \ln\left\{\frac{e^{(1-\alpha)x}-\alpha}{1-\alpha}\right\}, \quad \gamma/(1-\alpha) = 2$$

$$[28] \quad I_2(x) = \frac{1}{\sqrt{\alpha}} \ln\left\{\left(\frac{e^{(1-\alpha)x/2}-\sqrt{\alpha}}{e^{(1-\alpha)x/2}+\sqrt{\alpha}}\right)\left(\frac{1+\sqrt{\alpha}}{1-\sqrt{\alpha}}\right)\right\}, \quad \frac{\gamma}{1-\alpha} = \frac{1}{2}$$

If desired, the solutions [21]–[24] may be extended by setting

$$[29] \quad y_1(x) = \bar{y}_1(x) + \beta Y_{11}(x) + \beta^2 Y_{12}(x) + \ldots$$

$$[30] \quad y_2(x) = \bar{y}_2(x) + \beta Y_{21}(x) + \beta^2 Y_{22}(x) + \ldots$$

where $Y_{11}(0) = Y_{12}(0) = \ldots = Y_{21}(0) = Y_{22}(0) = \ldots = 0$, and $\bar{y}_1$, $\bar{y}_2$ are the zero-order solutions given by eqs. [21]–[24]. Substitution of eqs. [29] and [30] into eqs. [13] and [10] leads to solutions for Y_{11} and Y_{21} in the form

$$[31] \quad Y_{11}(x) = \frac{1}{(x+1)^2}\int_0^x (u+1)^2 \bar{y}_2(u)\,du$$

$$[32] \quad Y_{21}(x) = -Y_{11}(x) + \gamma e^{-\gamma x}\int_0^x e^{\gamma u}\,Y_{11}(u)\,du$$

for the case $\alpha = 1$. The series solutions [29] and [30] are not considered further here. Rather, the utility of the zero-order solutions [22]–[25] is examined by comparing these with the numerical solutions of eqs. [14] and [15].

Numerical results and discussion

Figures 2 and 3 represent solutions to the model when $\alpha = 1$ and $\alpha = 0.5$, respectively. In both figures the values for k_1 and k_3 are respectively 1 $dm^3\ mol^{-1}\ s^{-1}$, $2.5 \times 10^{-3}\ s^{-1}$, and $[A]_0 = 10^{-2}$ mol dm^{-3}. In Fig. 2 we have taken $[B]_0 = 10^{-2}$ mol dm^{-3}, and in Fig. 3 we have taken $[B]_0 = 5 \times 10^{-3}$ mol dm^{-3}. Equations [14] and [15] were integrated numerically on an IBM 370 machine using an algorithm based on a modified divided-difference form of the Adams–Pece formulae and local extrapolation (see ref. 5). The algorithm adjusts the order of the interpolation scheme and the step size so as to control the local error per unit step. The analytical solutions [22]–[25] were found in general to represent accurately the numerical solutions to the full equations for sufficiently small values of the parameter β. In particular, the analytical and numerical composition–time curves are virtually coincident for values of β when $\beta < 5 \times 10^{-3}$ (or $k_2 < 5 \times 10^{-5}\ s^{-1}$) for $\alpha = 1$, and when $\beta < 0.01$ (or $k_2 < 10^{-4}\ s^{-1}$) for $\alpha = 0.5$. Numerical solutions are also given for $\beta = 0.05$ in both of the cases $\alpha = 1$ and $\alpha = 0.5$. We note that when the concentration of species B is depleted the reaction approximates a simple (first-order) reac-

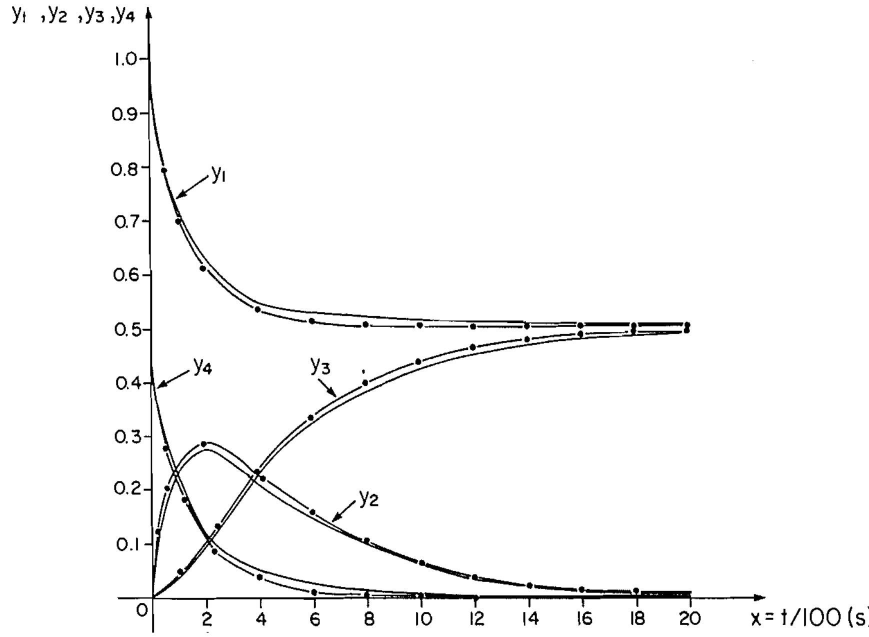

FIG. 3. Solution curves for the case k_1 = 1 dm^3 mol^{-1} s^{-1}, k_3 = 2.5 × 10^{-3} s^{-1}, [A]$_0$ = 10^{-2} mol dm^{-3}, and [B]$_0$ = 5 × 10^{-3} mol dm^{-3} (i.e. α = 0.5, γ = 0.25). The broken curves represent the analytical solutions [23], [25]; the full curves represent the numerical solution of the system [14]–[18] when k_2 = 5 × 10^{-4} s^{-1} (i.e. β = 0.05). The set of particular points shown represents those of the numerical solution of [14]–[18] when $k_2 < 10^{-4}$ s^{-1} (i.e. $\beta < 0.01$).

tion, and the model becomes virtually linear. This situation occurs in Fig. 3 for $x > 6$ (or $t > 600$ s). General solutions for [C] and [D] when [B] is negligible (or when [A] $\doteqdot$ [A]$_0$ − [B]$_0$) are given by

$$[33] \quad y_2 \doteqdot K(\alpha, \gamma)e^{-\gamma x}, \quad y_3 \doteqdot \alpha - K(\alpha, \gamma)e^{-\gamma x}$$

where K is a constant depending on the parameters α and γ. Results [33] may be deduced from the solutions [17], [18], [23], and [25] by letting $x \rightarrow \infty$.

In summary, we find that though the full nonlinear equations [13] and [14] are not amenable to analytical solutions, the simple analytical solutions [22]–[25] represent accurate, useful solutions to the nonlinear model for the case when the parameter $\beta = k_2/k_1$ [A]$_0$ is sufficiently small.

1. M. J. BLANDAMER, J. BURGESS, R. E. ROBERTSON, and J. M. W. SCOTT. Chem. Rev. **82**, 259 (1982).
2. E. L. INCE. Ordinary differential equations. Dover, New York. 1956.
3. W. J. MOORE. Physical chemistry. Prentice–Hall, New Jersey. 1972.
4. R. L. BURDEN, J. D. FAIRES, and A. C. REYNOLDS. Numerical analysis. Prindle, Weber, and Schmidt, Boston. 1981.
5. L. F. SHAMPINE and M. K. GORDON. Computer solution of ordinary differential equations. The initial value problem. Freeman, San Francisco. 1975.
6. C. H. BAMFORD and C. F. TIPPER (*Editors*). Comprehensive chemical kinetics. Vol. 2. Theory of kinetics. Elsevier, Amsterdam. 1969.
7. R. L. ANDERSON, R. S. NOHR, and L. O. SPREER. J. Chem. Educ. **52**, 437 (1975).

The crystal structure of a chiral *m*-cyclophane

T. H. CHAN[1] AND G. J. KANG
Department of Chemistry, McGill University, 801 Sherbrooke St. West, Montreal (Que.), Canada H3A 2K6

AND

F. BELANGER-GARIEPY, F. BRISSE,[1] AND K. STELIOU
Département de Chimie, Université de Montréal, C.P. 6210, Succ. A, Montréal (Qué.), Canada H3C 3V1

Received February 14, 1985

T. H. CHAN, G. J. KANG, F. BELANGER-GARIEPY, F. BRISSE, and K. STELIOU. Can. J. Chem. **63**, 3298 (1985).

The crystal structure of a chiral *m*-cyclophane, the α-isomer of (*S*)-α-methoxy-α-(trifluoromethyl)phenylacetate ester of 13-(methoxycarbonyl)-14-hydroxy-17-methyl-[11]-*m*-cyclophane ($C_{30}H_{37}O_5F_3$, FW = 534.62) has been solved by direct methods and refined by a least-squares procedure to a final R = 0.048 for 2756 independent reflections. The crystals belong to the orthorhombic system, a = 10.8077(13), b = 13.676(3), c = 19.060(4) Å, V = 2817.2 Å^3, Z = 4, and the space group is $P2_12_12_1$. The absolute configuration of the chiral plane, using the *S*-configuration of the α-methoxy-α-(trifluoromethyl)phenylacetate ester as reference, is found to be *S*, in agreement with the X-ray result. The 14-membered ring has the slightly distorted rectangular conformation that has been described by Dale as the rectangular diamond-lattice conformation [3434]. The distortions, also observed in similar 14-membered rings, have been successfully approximated by molecular mechanics calculations.

T. H. CHAN, G. J. KANG, F. BELANGER-GARIEPY, F. BRISSE et K. STELIOU. Can. J. Chem. **63**, 3298 (1985).

La structure cristalline d'un *m*-cyclophane chiral, l'isomère α de l'ester (*S*)-α-méthoxy-α-(trifluorométhyl)phénylacétate de 13-(méthoxycarbonyl)-14-hydroxy-17-méthyl-[11]-*m*-cyclophane ($C_{30}H_{37}O_5F_3$, PM = 534,62) a été déterminée par méthodes directes et affinée par moindres-carrés jusqu'à la valeur finale de R = 0,048 pour 2756 réflexions uniques. Les cristaux appartiennent au système orthorhombique, a = 10,8077(13), b = 13,676(3), c = 19,060(4) Å, V = 2817,2 Å^3, Z = 4 et le groupe d'espace est $P2_12_12_1$. En se basant sur la configuration *S* de l'ester α-methoxy-α-(trifluorométhyl) phénylacétate comme référence, la configuration absolue du plan chiral est aussi *S*, en accord avec la détermination par rayons X. Le cycle à 14 atomes a la conformation rectangulaire [3434] légèrement déformée telle que décrite à partir de la structure du diamant par Dale. Ces déformations, aussi observées dans d'autres cycles à 14 atomes, ont pu être raisonnablement reproduites par des calculs de mécanique moléculaire.

Introduction

We recently reported (1, 2) on the first successful optical resolution of a number of intraannularly substituted chiral *m*-cyclophanes such as **1** and **2**. The existence of enantiomerism in these compounds, which belong to the class of "planar"

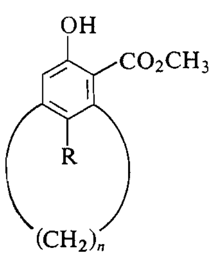

1

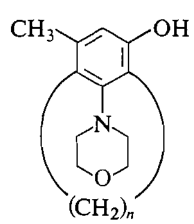

2

dissymmetric molecules, is caused by restricted rotation of the macrocyclic hydrocarbon ring. As long as the cavity of the hydrocarbon ring is not large enough to accommodate the intraannular substituent, the hydrocarbon ring and the intraannular substituent must be located on different sides of the aromatic plane. For example, since the aromatic ring in **1** is also substituted by two different groups, the compound is chiral and, in practice, resolvable if the energy barrier of the rotation is sufficiently high. This can easily be ascertained through the use of dynamic nmr studies to probe the energy barrier of the rotational process (1).

To further investigate the stereochemical properties of these chiral *m*-cyclophanes, the absolute configurations of these compounds were needed. A number of methods are available for the correlation of absolute configurations of "planar" dissymmetric molecules, provided that a configuration standard is available (3). Since these are the first optically active *m*-cyclophanes to be resolved, direct X-ray determination was used to unequivocally deduce their absolute configurations.

Experimental

Compound **3**, the (*S*)-α-methoxy-α-(trifluoromethyl)phenylacetate ester of 13-(methoxycarbonyl)-14-hydroxy-17-methyl-[11]-*m*-cyclophane, was prepared and purified by flash chromatography into two diastereoisomers (α and β) (1). The α-diastereoisomer was recrystallized from hexane to give clear, well-developed crystals. The large crystals so obtained were cut to get a fragment of 0.18 × 0.40 × 0.40 mm, suitable for X-ray diffraction. Accurate unit-cell dimensions were derived from the angular settings of 25 well-centered reflections chosen in the range $16 < 2\theta < 38°$. The space group is $P2_12_12_1$, since the only systematic absences are of the type $h00$, $h \neq 2n$; $0k0$, $k \neq 2n$; and $00l$, $l \neq 2n$. Crystal data of interest are given in Table 1. The data collection was performed by the $\omega-2\theta$ scan method with a scan width $\Delta\omega = (1.00 + 0.14 \tan\theta)°$ on a Nonius CAD-4 automatic diffractometer. The orientation and stability of the crystal were monitored using standard reflections whose intensities were measured every hour and their orientation checked every 100 reflections. Using the CuKα graphite monochromatized radiation, the intensities of 3269 reflections were measured within the sphere of reflection limited by $2\theta_{max} = 150°$ and $0 \leq h \leq 13$, $0 \leq k \leq 17$, $0 \leq l \leq 23$. The largest fluctuation of the intensities of the standards was 1.9%. The 2756 reflections satisfying $I \geq 1.96\,\sigma(I)$ were retained for the structure determination and refinement. No absorption correction was applied since the absorption coefficient was small. The structure

[1] Authors to whom correspondence may be addressed.

TABLE 1. Crystal data

$C_{30}H_{37}O_5F_3$	FW = 534.62		$F(000)$ = 1136 e
a = 10.8077(13)	b = 13.676(3)	c = 19.060(4) Å	V = 2817.2 Å^3
$P2_12_12_1$	Z = 4	d_c = 1.260 g cm^{-3}	μ(CuKα) = 0.78 mm^{-1}
λ(CuK$\bar{\alpha}$) = 1.54178 Å	T = 293 K		

TABLE 2. Fractional atomic coordinates for F, O, and C atoms ($\times 10^4$), and for H atoms ($\times 10^3$), U_{eq} (Å^2, $\times 10^4$ for F, O and C), U_{iso} (Å^2, $\times 10^3$ for H atoms). $U_{eq} = \frac{1}{3}\sum_i \sum_j U_{ij}\, a_i^* a_j^*\, a_i \cdot a_j$

Atom	x	y	z	U_{eq}	Atom	x	y	z	U_{iso}
F(1)	2888(2)	−2380(1)	8044(1)	824	H(5)	117(3)	113(2)	993(2)	63
F(2)	1636(2)	−1445(2)	7503(1)	895	H(26)	477(3)	−147(2)	907(1)	49
F(3)	1107(2)	−2067(2)	8493(1)	898	H(27)	529(4)	−194(3)	1021(2)	92
O(1)	3761(2)	−540(2)	8197(1)	594	H(28)	379(5)	−192(3)	1109(2)	116
O(2)	639(2)	−15(2)	8482(2)	749	H(29)	176(3)	−140(3)	1082(2)	81
O(3)	2325(2)	878(1)	8754(1)	424	H(30)	124(3)	−94(2)	969(2)	67
O(4)	1755(3)	1931(2)	7336(1)	918	H(101)	−102(3)	256(3)	1057(2)	73
O(5)	3197(2)	2873(2)	7797(1)	741	H(102)	−6(3)	178(3)	1074(2)	74
C(1)	2041(3)	−1674(2)	8138(2)	623	H(111)	35(3)	382(3)	1086(2)	84
C(2)	2641(3)	−806(2)	8225(1)	448	H(112)	2(3)	319(2)	1147(2)	69
C(3)	1718(3)	53(2)	8566(1)	467	H(121)	192(4)	235(3)	1145(2)	105
C(4)	1578(2)	1684(2)	8955(1)	394	H(122)	217(3)	288(2)	1072(1)	54
C(5)	1055(2)	1691(2)	9609(1)	439	H(131)	219(4)	393(3)	1204(2)	104
C(6)	343(3)	2485(2)	9817(1)	481	H(132)	337(3)	365(3)	1159(2)	80
C(7)	186(3)	3281(2)	9359(2)	502	H(141)	167(4)	505(3)	1113(2)	111
C(8)	826(2)	3309(2)	8724(1)	466	H(142)	308(3)	521(2)	1136(2)	73
C(9)	1513(2)	2479(2)	8511(1)	407	H(151)	380(3)	449(3)	1034(2)	80
C(10)	−169(3)	2482(3)	10556(2)	667	H(152)	244(3)	429(3)	1007(2)	74
C(11)	471(3)	3214(3)	11040(2)	737	H(161)	221(4)	599(3)	1002(2)	119
C(12)	1838(4)	3008(3)	11155(2)	725	H(162)	362(5)	608(3)	1030(2)	129
C(13)	2552(4)	3837(3)	11510(2)	883	H(171)	351(5)	620(3)	900(2)	130
C(14)	2546(4)	4786(3)	11109(2)	802	H(172)	447(4)	539(4)	924(2)	124
C(15)	3020(3)	4703(2)	10355(2)	674	H(181)	333(3)	480(2)	830(2)	63
C(16)	3086(4)	5661(3)	9967(2)	828	H(182)	306(3)	418(2)	895(1)	56
C(17)	3577(4)	5590(3)	9224(2)	871	H(191)	116(3)	518(2)	911(1)	56
C(18)	2925(3)	4855(2)	8737(2)	661	H(192)	149(3)	567(3)	834(2)	79
C(19)	1562(3)	5072(2)	8623(2)	643	H(201)	8(4)	442(3)	816(2)	94
C(20)	844(3)	4229(2)	8276(2)	591	H(202)	120(3)	410(2)	782(1)	48
C(21)	−719(3)	4081(3)	9543(2)	751	H(211)	−34(4)	460(3)	979(2)	106
C(22)	2129(3)	2409(2)	7814(1)	495	H(212)	−133(4)	388(3)	991(2)	100
C(23)	3850(5)	2861(4)	7137(2)	963	H(213)	−103(4)	429(3)	914(2)	114
C(24)	3697(4)	−111(3)	7508(2)	855	H(231)	336(4)	304(3)	679(2)	120
C(25)	2964(3)	−1119(2)	9271(1)	435	H(232)	409(7)	224(4)	704(3)	170
C(26)	4146(3)	−1450(2)	9426(1)	499	H(233)	458(6)	308(4)	719(3)	168
C(27)	4439(3)	−1754(2)	10103(2)	624	H(241)	451(4)	23(3)	741(3)	123
C(28)	3579(4)	−1733(2)	10617(2)	700	H(242)	294(4)	36(3)	746(3)	136
C(29)	2395(4)	−1407(3)	10472(2)	769	H(243)	377(4)	−55(3)	711(2)	85
C(30)	2088(3)	−1113(2)	9798(2)	615					

was solved by direct methods using MULTAN.[2] The least-squares refinement based on F's (by the block-diagonal approximation, anisotropic for F, O, and C and isotropic for H atoms) converged to R = 0.048, R_w = 0.058, S = 1.37. The weights were derived from the counting statistics. Maximum (Δ/σ) = 0.55 and mean (Δ/σ) = 0.09. The extreme values of the residual electron density on the final difference Fourier map were −0.21 and +0.19 e Å^{-3}. Although the anomalous dispersion contributions of O and F are very small, for the other configuration, the values of R, R_w, and S are 0.048, 0.059, and 1.38, respectively, thus indicating that the most likely absolute configuration is that which was found in the first place. The scattering curves for C, O, and F were taken from Cromer and Mann (4), and from Stewart, Davidson, and Simpson (5) for H atoms. The real and imaginary parts of the anomalous scattering for O and F were those of Cromer and Liberman (6).

Results and discussion

The final atomic coordinates and the equivalent U_{iso} values are given in Table 2.[3] For the purpose of discussion of the X-ray results the atomic numbering for compound **3** is shown

[2] The programs used here are modified versions of NRC-2, data reduction; NRC-10, bond distances and angles; and NRC-22, mean planes; FORDAP, Fourier and Patterson maps (A. Zalkin); MULTAN, multisolution program; NUCLS, least-squares refinement; and ORTEP stereodrawings (7–10).

[3] Tables of atomic positions for hydrogen atoms, least-squares planes, anisotropic temperature factors, and structure factors have been deposited and may be purchased from the Depository of Unpublished Data, CISTI, National Research Council of Canada, Ottawa, Ont., Canada K1A 0S2.

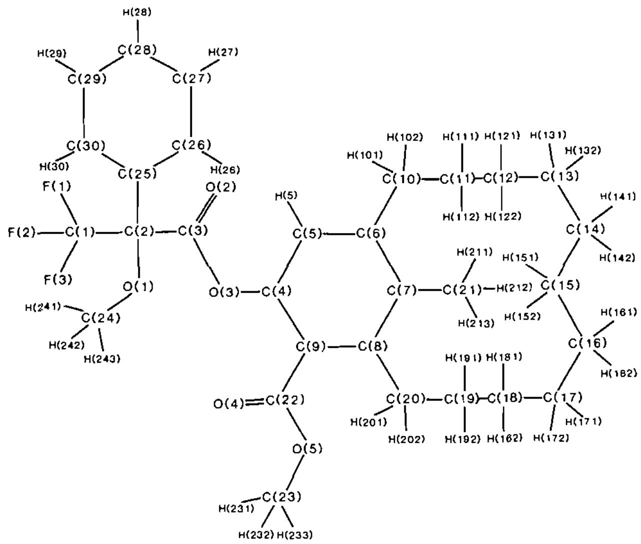

FIG. 1. Schematic view of the molecule and atomic numbering.

in Fig. 1 while a stereoview showing the molecular conformation is represented in Fig. 2. The bond distances and bond angles of the molecule are given in Table 3.

Since **3** was prepared from (*S*)-α-methoxy-α-(trifluoromethyl)phenylacetate acid, the chiral center at C(2) has the *S* configuration. This is in agreement with the absolute configuration indicated by the X-ray structure and represented in Fig. 2. One can deduce from Fig. 2 that the chiral plane in the *m*-cyclophane moiety of **3** has the *S*-configuration (11). Since **3** was reduced by lithium aluminium hydride to obtain (+)-13-hydroxymethyl-14-hydroxy-17-methyl-[11]-*m*-cyclophane (**4**), it follows that (+)-**4** has the *S*-configuration as well. Compound **4** can now serve as the configurational standard for other chiral *m*-cyclophanes.

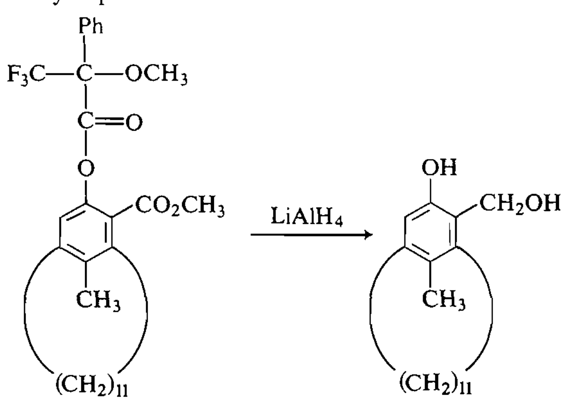

α-**3** (+)-**4**

In addition to a confirmation of the absolute configuration, the X-ray structural data yielded other information of general interest, which is discussed below.

The 14-membered ring

Previous theoretical energy minimization calculations (12–15) have led to the most likely 14-membered ring conformation, which is described by Dale in terms of a diamond lattice (14, 16). At the same time, a number of crystal structures involving 14-membered rings have been reported. These are 1,8-dihydroxy-1,8-diazacyclotetradecane (17), cyclotetradecane oxime (18), cyclotetradecane (19), and cyclotetradecanone (20). In all these compounds the "rectangular" diamond-lattice conformation [3434] is favoured (see Fig. 3). In order to describe the 14-membered ring and to compare it with the theoretical and observed conformations, the following least-squares planes of atoms characterizing the "rectangular" lattice have been defined. Plane A = [C(10), C(11), C(12), C(13)]; plane B = [C(17), C(18), C(19), C(20)]; plane C = [C(6), C(7), C(8), C(10), C(20)]; and plane D = [C(13), C(14), C(15), C(16), C(17)]. These groups of atoms are not strictly coplanar, since the extreme deviations from their respective least-squares planes[3] are 20 σ, 25 σ, 8 σ, and 8 σ, respectively. Nonetheless, the general features of the rectangular conformation are apparent from the dihedral angle values. These are compared in Table 4 to the corresponding quantities in the diamond-based rectangular conformation (4). This comparison reveals, however, one important discrepancy. The C and D planes, which should be parallel to each other, form an angle of 15° between one another. It is the presence of the C(21) methyl group that is responsible for the observed distortion. The two planes are tilted with respect to one another in order to minimize the interactions between H atoms on C(21) and those on C(10) and C(11), as well as those on C(19) and C(20). The shortest intramolecular contacts are H(211)—H(191) = 2.22(5) Å, H(211)—H(111) = 2.42(5), H(212)—H(101) = 2.23(5), H(212)—H(111) = 2.57(5), H(213)—H(191) = 2.66(5), and H(213)—H(201) = 2.23(6). Other contacts are larger than 3.00 Å. To appreciate the conformation of the 14-membered ring in greater detail, the endocyclic torsion angles of this molecule and others whose structures have already been established are compared, in Table 5, to those derived from the rectangular diamond lattice.

It is apparent that none of the crystal conformations conforms strictly to the theoretical one. Even cyclotetradecane, an unsubstituted 14-membered ring, has torsion angles in its conformation deviating by as much as 10° from predicted values. There is at least one feature common to all these structures, that is, both C(10)—C(11)—C(12)—C(13) and C(17)—C(18)—C(19)—C(20) torsion angles have values always close to 170° rather than the expected 180°. This systematic difference is

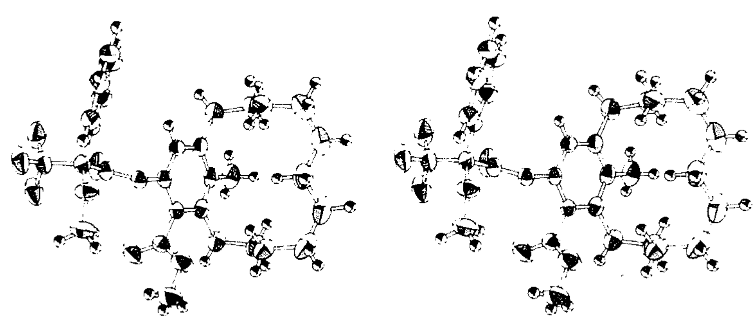

FIG. 2. Stereopair showing the molecular conformation.

TABLE 3. Bond distances (Å) and angles (degrees) calculated from the final atomic coordinates

Bond	Distance	Bond	Distance
C(1)—F(1)	1.343(4)	C(10)—C(11)	1.527(5)
C(1)—F(2)	1.325(4)	C(10)—C(16)	1.513(4)
C(1)—F(3)	1.329(4)	C(11)—C(12)	1.520(6)
C(1)—C(2)	1.541(4)	C(12)—C(13)	1.529(6)
C(1)—O(1)	1.410(4)	C(13)—C(14)	1.506(6)
C(2)—C(3)	1.543(4)	C(14)—C(15)	1.530(5)
C(2)—C(25)	1.525(4)	C(15)—C(16)	1.506(5)
C(3)—O(2)	1.181(4)	C(16)—C(17)	1.515(7)
C(3)—O(3)	1.353(3)	C(17)—C(18)	1.539(6)
C(4)—O(3)	1.419(3)	C(18)—C(19)	1.518(5)
C(7)—C(21)	1.509(5)	C(19)—C(20)	1.539(5)
C(9)—C(22)	1.489(4)	C(20)—C(8)	1.521(4)
C(22)—O(4)	1.192(4)	C(25)—C(26)	1.387(4)
C(22)—O(5)	1.318(4)	C(26)—C(27)	1.392(4)
C(23)—O(5)	1.442(5)	C(27)—C(28)	1.351(5)
C(24)—O(1)	1.440(4)	C(28)—C(29)	1.383(6)
C(4)—C(5)	1.369(4)	C(29)—C(30)	1.386(5)
C(4)—C(9)	1.380(4)	C(30)—C(25)	1.380(4)
C(5)—C(6)	1.389(4)		
C(6)—C(7)	1.406(4)		
C(7)—C(8)	1.395(4)		
C(8)—C(9)	1.416(4)		
Bond	**Angle**	**Bond**	**Angle**
F(1)—C(1)—C(2)	109.3(3)	C(5)—C(4)—C(9)	122.2(2)
F(2)—C(1)—C(2)	113.2(3)	C(4)—C(5)—C(6)	119.6(2)
F(3)—C(1)—C(2)	112.8(3)	C(5)—C(6)—C(7)	119.7(3)
F(1)—C(1)—F(2)	105.9(3)	C(6)—C(7)—C(8)	120.0(3)
F(1)—C(1)—F(3)	107.2(3)	C(7)—C(8)—C(9)	119.1(2)
F(2)—C(1)—F(3)	108.1(3)	C(8)—C(9)—C(4)	118.9(2)
C(1)—C(2)—O(1)	110.4(2)	C(5)—C(6)—C(10)	117.8(3)
C(1)—C(2)—C(3)	109.8(2)	C(7)—C(6)—C(10)	122.4(3)
C(1)—C(2)—C(25)	109.1(2)	C(7)—C(8)—C(20)	121.1(3)
O(1)—C(2)—C(3)	112.4(2)	C(6)—C(10)—C(11)	113.3(3)
O(1)—C(2)—C(25)	106.8(2)	C(9)—C(8)—C(20)	119.7(2)
C(3)—C(2)—C(25)	108.3(2)	C(10)—C(11)—C(12)	114.0(3)
C(2)—O(1)—C(24)	117.9(2)	C(11)—C(12)—C(13)	114.6(3)
C(2)—C(3)—O(2)	124.9(3)	C(12)—C(13)—C(14)	114.3(3)
C(2)—C(3)—O(3)	109.6(2)	C(14)—C(15)—C(16)	114.4(3)
O(2)—C(3)—O(3)	125.5(3)	C(15)—C(16)—C(17)	114.8(3)
C(3)—O(3)—C(4)	116.3(2)	C(16)—C(17)—C(18)	116.4(3)
O(3)—C(4)—C(5)	119.1(2)	C(17)—C(18)—C(19)	113.8(3)
O(3)—C(4)—C(9)	118.4(2)	C(18)—C(19)—C(20)	113.8(3)
C(6)—C(7)—C(21)	119.7(3)	C(19)—C(20)—C(8)	112.6(3)
C(8)—C(7)—C(21)	120.2(3)		
C(4)—C(9)—C(22)	118.3(2)		
C(8)—C(9)—C(22)	122.8(2)		
C(9)—C(22)—O(4)	124.4(3)		
C(9)—C(22)—O(5)	112.5(2)		
O(4)—C(22)—O(5)	122.9(3)		
C(22)—O(5)—C(23)	116.4(3)		
C(2)—C(25)—C(26)	120.1(2)		
C(2)—C(25)—C(30)	121.3(3)		

significant. All the other deviations are small or may be attributed to the presence of various ring substituents. For instance, in the case of the compound under study, four torsion angles differ significantly from their counterparts in other 14-membered rings. These are the torsion angles C(8)—C(7)—C(6)—C(10), C(7)—C(6)—C(10)—C(11), C(19)—C(20)—C(8)—C(7), and C(20)—C(8)—C(7)—C(6). The effect of having the 14-membered ring fused along C(6)—C(7) and C(7)—C(8) of the benzene ring in **3** should not cause the torsion angle to deviate from 180°, and yet as much as a 10° difference is observed.

The 14-membered ring has an apparent mirror plane of symmetry. The distances from equivalent atoms to the pseudo-mirror plane, defined by O(3), C(4), C(7), C(15), and C(21) are compared in Table 6. The average deviation from a perfect plane of symmetry is less than 0.02 Å.

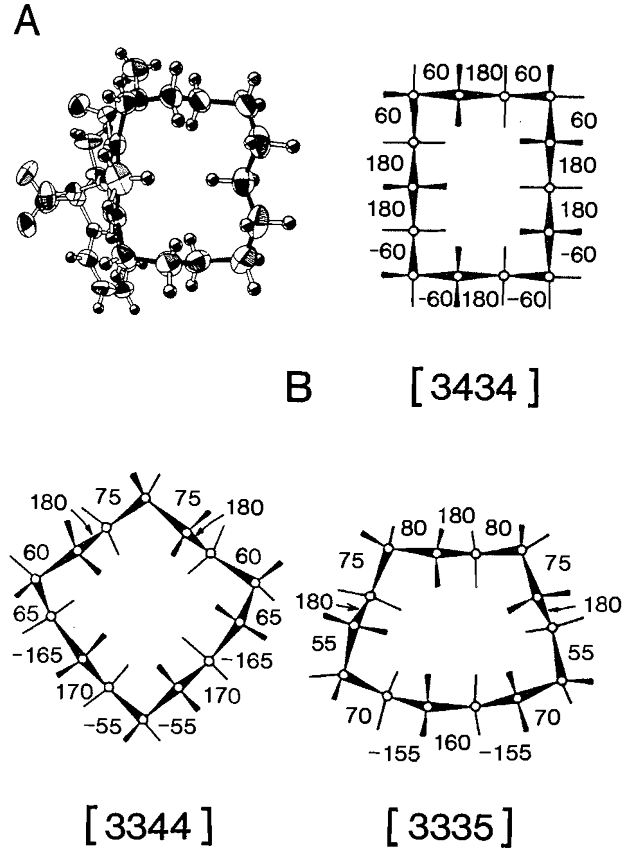

FIG. 3. (A) The conformation of the 14-membered ring of **3** shown in the same orientation. (B) The three lowest energy conformations, including the [3434] (after ref. 14) rectangular diamond conformation.

TABLE 4. Dihedral angles (degrees)

	Dihedral angles between planes					
Reference	A/B	C/D	A/C	A/D	B/C	B/D
This work	3	15	92	90	91	90
Rectangular diamond lattice (14)	0	0	90	90	90	90

The aromatic rings C(4) → C(9) and C(25) → C(30)

In the first ring, the averages of the bond distances and bond angles are 1.393 Å and 119.9°, respectively. However, the ring is very strongly distorted. When all six atoms are included in the least-squares plane calculation, C(7) is 15 σ away from the plane. Once C(7) is excluded, the five remaining atoms are closer to a plane. Then C(7) and C(21) are displaced from that plane by 0.086(3) Å and 0.318(4) Å, respectively.

This distortion is again related to the short contacts between the H atoms on C(21) and those in the 14-membered ring. The other atoms bonded to the benzene ring, C(10), C(20), and C(22), are at 0.100(3), −0.168(3), and 0.026(3) Å, respectively. There is nothing unusual in the benzene ring containing atoms C(25) → C(30); the average C(sp^2)—C(sp^2) bond distance is 1.380 Å, the six carbon atoms are coplanar, and the H atoms are all within 0.02 Å from this plane.

The trifluoro group

The three C—F distances varying between 1.325(4) and 1.343(4) Å compare well with published data. The bond angles around C(1) vary significantly, depending upon whether one or two fluorine atoms are implicated. The averages for the C—C—F and the F—C—F angles are 111.8 and 107.0°, respectively.

A view of the disposition of the various substituents at C(2) and C(3) is shown in Fig. 4 by the Newmann projection along the C(2)—C(3) bond.

There are no unduly short contacts between neighbouring molecules. The relative disposition of the molecules in their unit cell is shown in Fig. 5.

Molecular mechanics calculation

In view of some important deviations of the crystal structure of **3** and others from the "theoretical" conformation based on the diamond lattice, we have carried out a molecular mechanics calculation for **3**. Using Still's (21, 22) programs MODEL[4] (an enhanced graphics interactive version of Allinger's MM2 molecular mechanics program (23)) and RINGMAKER (a ring/chain generating program), 317 random starting conformations with torsion angle constraints of 60° resolution were generated for the 14-membered ring from an energy preminimized *m*-dimethylene substituted phenyl appendage. Multiple energy minimizations reduced these to 30 unique local energy minimized structures, 9 of which were found to be within 3.0 kcal mol^{-1} of the global energy minimum (65.2 kcal mol^{-1}) conformer. The 3.0 kcal mol^{-1} limitation was set to ignore negligibly populated conformational states.

Further minimization of the global energy minimum conformer by minor movement of the atomic coordinates of each

[4] MM2 is available from Indiana's University Quantum Chemistry Program Exchange as program number 395.

TABLE 5. Comparison of torsion angles (degrees) in 14-membered rings

Atoms	Sources[a]						
	1	2	3	4	5	6	7
C(8)—C(7)—C(6)—C(10)	180	170.6(3)[b]	176.0(2)	179.5(2)	−177.9	174.9(3)	169.4
C(7)—C(6)—C(10)—C(11)	−60	−68.1(4)	−58.0(3)	−58.0(3)	−57.9	−57.8(4)	−73.6
C(6)—C(10)—C(11)—C(12)	−60	−63.0(4)	−61.0(2)	−61.8(3)	−72.8	−60.7(4)	−63.3
C(10)—C(11)—C(12)—C(13)	180	168.1(3)[c]	170.1(3)	170.6(2)	172.8	170.4(3)	168.6
C(11)—C(12)—C(13)—C(14)	−60	−60.4(5)	−64.4(3)	−61.9(3)	−58.7	−64.8(4)	−60.2
C(12)—C(13)—C(14)—C(15)	−60	−55.4(5)	−58.6(3)	−62.7(3)	−55.6	−59.0(4)	−51.9
C(13)—C(14)—C(15)—C(16)	180	−176.6(3)	176.6(2)	173.4(2)	170.8	177.4(3)	179.9
C(14)—C(15)—C(16)—C(17)	180	178.9(3)	−176.0(2)	−172.9(2)	−177.9	−174.9(3)	177.2
C(15)—C(16)—C(17)—C(18)	60	53.8(5)	58.0(3)	63.1(3)	57.9	57.8(4)	52.3
C(16)—C(17)—C(18)—C(19)	60	61.0(5)	61.0(2)	64.8(3)	72.8	60.7(4)	62.0
C(17)—C(18)—C(19)—C(20)	180	−167.2(3)	−170.1(3)	−171.0(2)	−172.8	−170.4(3)	−170.6
C(18)—C(19)—C(20)—C(8)	60	62.9(4)	64.4(3)	59.1(3)	58.7	64.8(4)	66.1
C(19)—C(20)—C(8)—C(7)	60	67.6(4)	58.6(3)	54.4(3)	55.6	59.0(4)	66.4
C(20)—C(8)—C(7)—C(6)	180	−169.7(3)	−176.6(2)	−176.6(2)	−170.8	−177.4(3)	−165.0

[a] Numbered headings indicate the following sources: 1. Theoretical conformation based on the diamond lattice (14). 2. This work. 3. Cyclotetradecane (19). 4. Cyclotetradecane oxime (18). 5. Dihydrodiazacyclotetradecane (17). 6. Cyclotetradecanone (20). 7. MMPM calculation, this work.

[b] Values doubly underlined refer to the 14-membered ring distortions associated with the inclusion of the aromatic ring.

[c] The singly underlined values mark the systematic deviations, from an otherwise nearly perfect "rectangular" conformation, characteristic of 14-membered rings.

TABLE 6. Distances, Å, from equivalent atoms to a median plane

Atom	Distance	Atom	Distance
C(5)	−1.193(3)	C(9)	1.211(3)
C(6)	−1.205(3)	C(8)	1.220(3)
C(10)	−2.538(4)	C(20)	2.539(3)
C(11)	−2.701(4)	C(19)	2.690(4)
C(12)	−2.677(4)	C(18)	2.708(4)
C(13)	−2.549(4)	C(17)	2.545(5)
C(14)	−1.294(4)	C(16)	1.257(4)

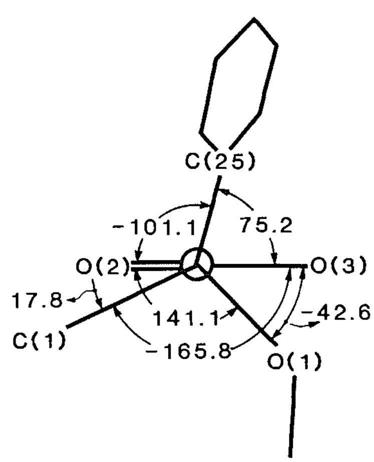

FIG. 4. Newmann projection along C(2)—C(3).

atom led to a final global energy minimum of 65.0 kcal mol^{-1}. However, since MODEL only approximates delocalized π-systems as comprisng 1,3-butadiene components, the atomic coordinates of this conformer were then used as input to

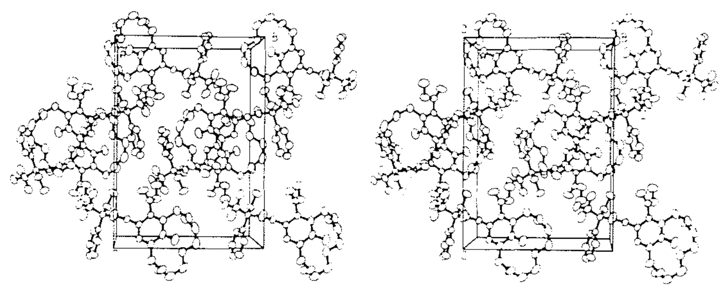

FIG. 5. Packing of the molecules in the unit cell.

MMPM,[5] a π-enhanced version of MM2 for recalculation under the π-planar non-restriction mode. This resulted in a new energy minimum of 77.8 kcal mol^{-1} and values for the torsion angles about the 14-membered ring that can be considered to be within the experimental error of the corresponding angles in the X-ray structure. For comparison, we have listed in Table 5, column 7, the torsion angles of the 14-membered ring conformer derived from the MMPM calculation. It is clear from Table 5 that, in this example, the combination of these programs has successfully approximated, within 5°, the observed deviations of the C(10)—C(11)—C(12)—C(13) and the C(17)—C(18)—C(19)—C(20) torsion angles from the ideal value of 180°. Since these deviations are also observed in all the 14-membered rings whose X-ray structures have been reported, they suggest that in the crystal structure of **3**, the deviation from the ideal diamond-lattice conformation is not due to any solid state effect in the crystal lattice, but inherent in the structure itself.

Acknowledgements

Financial support of this research by NSERC and the Pro-

[5] This program is currently under development and may be obtained from Serena Software, 489 Serena Lane, Bloomington, IN 47701.

gramme de formation de chercheurs et d'action concertée, volet "Organismes de service à la recherche" is gratefully acknowledged. We are also thankful to Mr. M. J. Olivier for the X-ray data collection and to Professor W. C. Still for making his programs (MODEL, RINGMAKER, and BAKMOD) available to us.

1. T. H. CHAN and G. J. KANG. Tetrahedron Lett. **24**, 3187 (1983); J. Org. Chem. **50**, 452 (1985).
2. P. M. KEEHN and S. M. ROSENFELD (*Editors*). Cyclophanes. Academic Press, New York. 1983.
3. G. KROW. Top. Stereochem. **5**, 31 (1970).
4. D. T. CROMER and J. B. MANN. Acta Crystallogr. Sect. A, **24**, 321 (1968).
5. R. F. STEWART, E. R. DAVIDSON, and W. T. SIMPSON. J. Chem. Phys. **42**, 3175 (1965).
6. D. T. CROMER and D. A. LIBERMAN. J. Chem. Phys. **53**, 1891 (1970).
7. F. R. AHMED, S. R. HALL, M. E. PIPPY, and C. P. HUBER. J. Appl. Crystallogr. **6**, 309 (1973). Accession Nos 133–147.
8. P. MAIN, S. E. HULL, L. LESSINGER, G. GERMAIN, J. P. DECLERCQ, and M. M. WOOLFSON. MULTAN 78. A system of computer programs for the automatic solution of crystal structures from X-ray diffraction data. Univs. of York, England and Louvain, Belgium. 1978.
9. R. J. DOEDENS and J. A. IBERS. Inorg. Chem. **6**, 204 (1967).
10. C. K. JOHNSON. ORTEP. Report ORNL-3794. Oak Ridge National Laboratory, Tennessee. 1965.
11. IUPAC tentative rules for the nomenclature of organic chemistry. J. Org. Chem. **35**, 2849 (1970).
12. J. DALE. J. Chem. Soc. 93 (1963).
13. J. DALE. Angew. Chem. Int. Ed. Engl. **5**, 1000 (1966).
14. J. DALE. Acta Chem. Scand. **27**, 1115 (1973).
15. G. BORGEN and J. DALE. Chem. Commun. 1340 (1970).
16. W. D. CELMER. Pure Appl. Chem. **28**, 413 (1971).
17. C. J. BROWN. J. Chem. Soc. C, 1108 (1966).
18. P. GROTH. Acta Chem. Scand. Ser. A, **33**, 503 (1979).
19. P. GROTH. Acta Chem. Scand. Ser. A, **30**, 155 (1976).
20. P. GROTH. Acta Chem. Scand. Ser. A, **29**, 374 (1975).
21. W. C. STILL, L. J. MACPHERSON, T. HARADA, and A. RHEINGOLD. Tetrahedron, **40**, 2275 (1984).
22. W. C. STILL and I. GALYNKER. Tetrahedron, **37**, 3981 (1981).
23. N. L. ALLINGER. J. Am. Chem. Soc. **99**, 8127 (1977).

The solvolysis of metal fluorosulfates in trifluoromethyl sulfuric acid

S. P. MALLELA, J. R. SAMS, AND F. AUBKE
Department of Chemistry, The University of British Columbia, Vancouver, B.C., Canada V6T 1Y6

Received April 2, 1985

S. P. MALLELA, J. R. SAMS, and F. AUBKE. Can. J. Chem. **63**, 3305 (1985).

The quantitative conversion of fluorosulfates into trifluoromethyl sulfates is systematically investigated. The reaction proceeds initially according to the general equation

$$E(SO_3F)_n + nHSO_3CF_3 \xrightarrow[HSO_3CF_3]{T\,=\,25-80^\circ C} E(SO_3CF_3)_n + nHSO_3F$$

where E is a coordinatively saturated metal or an organometallic moiety. However, the key to a quantitative substitution is the observed degradation of the SO_3F group by excess HSO_3CF_3 and the noted observation of various volatile by-products that do not appear to interfere in the isolation of analytically pure trifluoromethyl sulfates. The fluorosulfates selected are representatives of the most common bond and coordination types—ionic or covalent with coordination through one, two, or three oxygens of the SO_3F groups. The selected substrates display a fairly wide range of solubilities in HSO_3F. All conversion attempts are successful except for one, that of polymeric $Hg(SO_3F)_2$, and a number of new SO_3CF_3 derivatives of tin, platinum, germanium, and palladium are described. The solvolysis of tin(IV) acetate in HSO_3CF_3 is reinvestigated and the syntheses of two other trifluoromethyl sulfuric acid derivatives, $CsSO_3CF_3 \cdot HSO_3CF_3$ and $CH_3CO_2H \cdot HSO_3CF_3$, are described.

S. P. MALLELA, J. R. SAMS et F. AUBKE. Can. J. Chem. **63**, 3305 (1985).

On a étudié d'une façon systématique la conversion quantitative des fluorosulfates en sulfates de trifluorométhyles. Au départ, la réaction procède d'après l'équation générale

$$E(SO_3F)_n + nHSO_3CF_3 \xrightarrow[HSO_3CF_3]{T\,=\,25-80^\circ C} E(SO_3CF_3)_n + nHSO_3F$$

dans laquelle, E est un métal saturé par coordination ou une groupement organométallique. Toutefois, la clé à une substitution quantitative est l'observation de la dégradation du groupement SO_3F par un excès de HSO_3CF_3 ainsi que celle de la formation de divers produits secondaires volatils qui ne semblent pas interférer dans l'isolement de sulfates de trifluorométhyles qui sont analytiquement purs. Les fluorosulfates choisis sont représentatifs des types de liaisons et de coordinations les plus courantes—ionique ou covalente avec des coordinations impliquant un, deux ou trois des oxygènes des groupements SO_3F. Les solubilités, dans le HSO_3F, des diverses substantes choisies correspondent à un large éventail. Tous les essais en vue d'effectuer des conversions ont réussi, à l'exception de celui réalisé sur du $Hg(SO_3F)_2$ à l'état de polymère; on décrit les propriétés d'un certain nombre de nouveaux dérivés SO_3CF_3 de l'étain, du platine, du germanium et du palladium. On a réétudié la solvolyse de l'acétate d'étain(IV) dans le HSO_3CF_3 et on décrit les synthèses de deux autres dérivés de l'acide trifluorométhylsulfurique, $CsSO_3CF_3 \cdot HSO_3CF_3$ et $CH_3CO_2H \cdot HSO_3CF_3$.

[Traduit par le journal]

Introduction

Trifluoromethyl sulfuric acid, HSO_3CF_3, and fluorosulfuric acid, HSO_3F, have many chemical and physical properties in common (1, 2). Both rank among the strongest simple protonic acids. While the exact order of acid strength is subject to some discussion (3–5), the actual difference in acidity appears to be rather small. Both are strongly ionizing solvents, and both form the basis for superacid systems with solutes such as SbF_5 and TaF_5 (5). In addition to solvent characteristics, many physical properties are intriguingly similar for both acids (1, 2).

A large number of derivatives are known for both HSO_3CF_3 and HSO_3F. These range from ionic salts with $SO_3CF_3^-$ and SO_3F^- anions (1, 2, 6), over halogen sulfonates (7) to organic esters (1, 2, 6). When covalently bonded to metals or organometallic moieties, both sulfonate groups may coordinate through one, two, or three oxygen atoms. The resulting materials often have similar molecular structures; e.g., in organotin(IV) sulfonates of the type $R_2Sn(SO_3X)_2$, with R = CH_3, C_2H_5, n-C_3H_7, n-C_4Hg and X = F or CF_3, bidentate briding sulfonate groups produce sheet-like polymers (8) with almost identical ^{119}Sn Mössbauer parameters (9) for compounds with common R groups. Sometimes, however, possibly due to steric differences between both sulfonate groups, contrasting electronic structures of the central metal are noticed. $Ag(SO_3F)_2$ is magnetically dilute down to 80 K (10), while in $Ag(SO_3CF_3)_2$ antiferromagnetism is found in the same temperature range (11).

In respect to chemical reactivity, some important differences between HSO_3F and HSO_3CF_3 are apparent.

(*i*) Self-dissociation is found primarily for HSO_3F, reflected in the equilibrium:

[1] $HSO_3F \rightarrow HF + SO_3$

for $K_d^{25^\circ C} < 3 \times 10^{-7}\ mol^2\ kg^{-2}$. This process explains both the oxidizing ability of HSO_3F as well as its use as fluorinating agent (12).

(*ii*) The S—C linkage in HSO_3CF_3, and in its derivatives, appears to be sensitive towards oxidation. As a consequence, oxidizing agents like the peroxide $S_2O_6(CF_3)_2$ (13) or the halogen derivatives $BrSO_3CF_3$ and $ClSO_3CF_3$ (14, 15) undergo spontaneous decomposition at 25°C and are of limited use in synthesis (19, 20), quite in contrast to their fluorosulfate analogues $S_2O_6F_2$, $BrSO_3F$, and $ClSO_3F$ (7, 16). These fluorosulfate analogues dissolve readily in HSO_3CF_3, but the resulting solutions are metastable and decompose exothermically (17) at room temperature.

(*iii*) The S—F linkage in HSO_3F, as well as in most fluorosulfate derivatives, is instable towards hydrolysis, in particular in acidic or strongly basic aqueous medium. On the other hand, HSO_3CF_3 is mixable with water and forms well-defined hydrates (18). It should generally be possible to isolate trifluoromethyl sulfates in high yields, where H_2O is a by-product of the reaction.

Synthetic routes to inorganic trifluoromethyl sulfates have largely involved HSO_3CF_3 as reagent in solvolysis reactions, or, to a lesser extent, salts like $AgSO_3CF_3$ in metathetical reactions. Bis(fluorosulfuryl)peroxide, $S_2O_6F_2$, in HSO_3F as solvent, on the other hand has been widely used to prepare high valent metal fluorosulfates as well ternary fluorosulfates (21–23). Due to the unavailability of similar routes in SO_3CF_3 chemistry, solvolysis reactions of the general type:

$$[2]\quad MX_n + nHSO_3CF_3 \rightarrow M(SO_3CF_3)_n + nHX$$

with X = F, Cl, Br, H, alkyl, carboxylate, etc., have been the principal preparative method. Both the reactivity and availability of suitable precursors pose obvious limitations.

It had occurred to us some time ago (24) that extension of the solvolysis reaction to fluorosulfates according to

$$[3]\quad M(SO_3F)_n + nHSO_3CF_3 \xrightarrow{HSO_3CF_3} M(SO_3CF_3)_n + nHSO_3F$$

should be feasible, which would widen the scope of synthetic routes to trifluoromethyl sulfates considerably. Indeed a number of iodine(III)trifluoromethyl sulfates (24) and iodine oxytrifluoromethyl sulfates (25) could be obtained from their fluorosulfate precursors. The observed quantitative conversion seemed initially puzzling. A subsequent study by Olah and Ohyama (26) and a reinvestigation by Noftle (27) of the reaction of the two acids HSO_3CF_3 and HSO_3F provided a possible explanation. A degradation reaction was noted, generally formulated as:

$$[4]\quad 2HSO_3CF_3 + HSO_3F \xrightarrow{25°C} \begin{cases} COF_2,\ CO_2,\ SO_2, \\ CF_3SO_3F,\ CF_3SO_3CF_3 \\ SiF_4 + \ldots, \end{cases}$$

with SiF_4 formed as a secondary product in the interaction of HF with glass. Evidence for a similar range of volatile reaction products was later noted by us during the syntheses of $Ag(SO_3CF_3)_2$ and a number of gold(III)trifluoromethyl sulfates from the corresponding fluorosulfates (11). Mechanistic proposals (26, 27) for the acid degradation reaction had agreed on the initial step, protonation of HSO_3CF_3 by HSO_3F, but had differed in respect to reactive intermediates—$CF_3SO_2^+$ (26) or CF_3^+ (27)—and in respect to some of the final products. Our interest had focussed on the apparent similarity between the acid degradation reaction and the quantitative conversion of fluorosulfates into trifluoromethyl sulfates. It became interesting to study this conversion in a more systematic manner, in order to estimate its general usefulness.

Results and discussion

The principal bond types and coordination modes of the fluorosulfate group are illustrated in Fig. 1. Covalent bonding or coordination occurs through oxygen, with similar linkages possible also for the trifluoromethyl sulfate group. All examples of bi- or tridentate fluorosulfate groups so far studied seem to involve bridging rather than chelating configurations, resulting in polymeric structures. Hence all substrates selected are solids, and some remain solids during the conversion reaction, thus allowing easy separation from excess HSO_3CF_3. For each bonding or coordination type the following fluorosulfate substrates are selected.

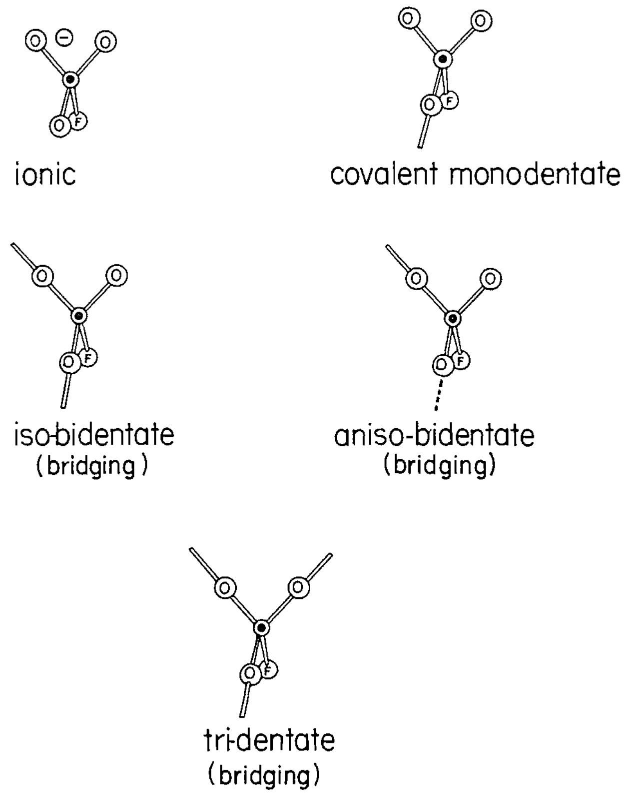

FIG. 1. The principal bonding and coordination modes of the fluorosulfate group.

(*i*) *Ionic fluorosulfates*: KSO_3F

The crystal structure of this compound is well known (28). The expected product KSO_3CF_3, like all other alkali metal trifluoromethyl sulfates, has been reported (2).

(*ii*) *Covalent monodentate*: $K_2[Sn(SO_3F)_6]$ and $Cs_2[Pt(SO_3F)_6]$

Structural studies consist of ^{119}Sn Mössbauer and vibrational spectra obtained on the solids (21, 22, 29), as well as of ^{119}Sn and ^{19}F nmr, Raman, and conductometric studies in HSO_3F solution (21, 22). Here the solvated $[M(SO_3F)_6]^{2-}$ derivatives, M = Sn or Pt, persist as integer complex ions. The corresponding $SO_3CF_3^-$ derivatives are unknown; however, the $[Sn(SO_3CF_3)_6]^{2-}$ ion appears to be present in a mixed valency tin compound formulated as $Sn(II)[Sn(SO_3CF_3)_6]$ (30).

(*iii*) *Iso-bidentate*: $(CH_3)_2Sn(SO_3F)_2$ and $GeF_2(SO_3F)_2$

Symmetrical, bridging bidentate groups are found in the polymeric, sheet-like $(CH_3)_2Sn(SO_3F)_2$ (8). The corresponding trifluoromethyl sulfate is known (31) and has, judging by the nearly identical ^{119}Sn Mössbauer spectrum, a similar molecular structure. Both sulfonates are prepared by acidolysis of either $Sn(CH_3)_4$, $(CH_3)_3SnCl$, or $(CH_3)_2SnCl_2$ in the appropriate acid, with the $(CH_3)_2Sn$ moiety resistant to further acidolysis at room temperature (31, 32). $GeF_2(SO_3F)_2$ has been obtained very recently (22) with no SO_3CF_3 analogue known. structural conclusions for $GeF_2(SO_3F)_2$ are based on vibrational spectra.

(*iv*) *Aniso-bidentate*: $Pd(II)[Pd(SO_3F)_6]$ (33) and $Mn(II)[Sn(SO_3F)_6]$ (34)

In both examples either two different metals or two different oxidation states of the same metal are encountered. The two oxidation states are +2 and +4, with the higher oxidation state implying a greater coordinating ability of the metal concerned. Structural evidence for these coordination polymers rests on

TABLE 1. Experimental details of the conversion reactions

Starting material	Substrate (mmol)	HSO_3CF_3[a] (mL)	Reaction time (h)	Reaction temp. (°C)	Method of product isolation; comments
KSO_3F	3.71	5	4.5	25	Clear solution forms, volatiles removed *in vacuo* at 50°C
$K_2[Sn(SO_3F)_6]$	1.98	5	92	25	Clear solution forms[b]
$Cs_2[Pt(SO_3F)_6]$	0.46	5	24	60	Yellow solution forms[b]
$(CH_3)_2Sn(SO_3F)_2$	2.35	5	144	25	Some solid remains throughout[b]
$GeF_2(SO_3F)_2$	1.96	5	144	60	Some solid remains throughout[c]
$Mn[Sn(SO_3F)_6]$	0.38	4	168	70	Some solid remains throughout[b]
$Pd[Pd(SO_3F)_6]$	1.27	5	96	25	Some solid remains throughout[b]
$Hg(SO_3F)_2$	0.88	5	192	85	Some solid remains throughout[b]
$Pd(SO_3F)_2$	2.34	6	122	25	Some solid remains throughout[b]
$Sn(SO_3F)_4$	2.23	10	4.5	25	Clear solution within 0.5 h[b]
$Cs[Sn(SO_3F)_5]$	1.29	5	22	25	Clear solution within 0.5 h[b]
$(CH_3)_2Sn(SO_3CF_3)_2$	1.63	5[d]	46	25	Clear solution forms immediately[b]

[a] Approximate, 5 mL HSO_3CF_3 corresponds to about 55 mmol.
[b] Isolation by removal of volatiles *in vacuo*.
[c] Isolation by filtration, washing with HSO_3CF_3.
[d] HSO_3F.

TABLE 2. ^{119}Sn Mössbauer data of tin(IV) sulfonates

Compound	Isomer shift[a] δ (mm s^{-1})	Quadrupole splitting Δ (mm s^{-1})	Line width Γ (mm s^{-1})	Temperature (K)
$Sn(SO_3CF_3)_4$	−0.213	1.18	1.037 1.085	80
$Sn(SO_3CF_3)_4$	−0.241	1.27	0.929 0.975	298
$Sn(SO_3F)_4$[b]	−0.242	1.200	1.194 1.206	80
$Cs[Sn(SO_3CF_3)_5]$	−0.208	0.499	0.918 0.833	80
$Cs[Sn(SO_3F)_5)$[b]	−0.239	0.617	1.185 1.279	80
$K_2[Sn(SO_3CF_3)_6]$	−0.305	—	0.988	80
$K_2[Sn(SO_3F)_6]$[c]	−0.260	—	1.140	80
$(CH_3CO_2H_2]_2[Sn(SO_3CF_3)_6]$	−0.231	—	1.040	80
$Mn(Sn(SO_3CF_3)_6]$	−0.257	—	1.063	80
$Mn[Sn(SO_3CF_3)_6]$	−0.281	—	1.012	298
$Mn[Sn(SO_3F)_6]$[d]	−0.271	—	1.124	80

[a] Relative to SnO_2.
[b] Reference 22.
[c] Reference 29.
[d] Reference 34.

vibrational spectra, magnetic studies down to 80 K, and, in the case of the tin compound, on ^{119}Sn Mössbauer spectra. The corresponding SO_3CF_3 complexes are unknown.

(*v*) *Tridentate*: $Hg(SO_3F)_2$ and $Pd(SO_3F)_2$

The tridentate bridging fluorosulfate group is commonly encountered in metal bis(fluorosulfates) (35). Their polymeric nature and the complete lack of solubility in HSO_3F have so far prevented an X-ray diffraction study, and indirect methods, employed to confirm the proposed structures (33, 35, 36), have provided evidence for a regular octahedral environment with a $^3A_{2g}$ groundstate for Pd^{2+} (33). Only $Hg(SO_3CF_3)_2$ has been reported previously (37). Jahn Teller distortion is expected and found for $Ag(SO_3F)_2$ (10), which had previously been converted to the trifluoromethyl sulfate.

In addition to these substrates, two materials are selected, where both bidentate bridging and monodentate fluorosulfate groups are present: $Sn(SO_3F)_4$ (38) and $Cs[Sn(SO_3F)_5]$ (22). Vibrational and ^{119}Sn Mössbauer spectra have been used to deduce the structures. Only $Sn(SO_3CF_3)_4$ has been reported before (30), obtained by acidolysis of tin(IV)tetrakis(acetate) in HSO_3CF_3.

The experimental details of the conversion reactions are summarized in Table 1. Most substrates dissolve in HSO_3CF_3 either at 25°C or, like $Cs_2[Pt(SO_3F)_6]$, after heating to 60°C, indicating instantaneous reaction. However, some, like $GeF_2(SO_3F)_2$, $Hg(SO_3F)_2$, $Pd(SO_3F)_2$, and $Pd(II)[Pd(SO_3F)_6]$, remain solids throughout. Since no dramatic color changes occur, it is difficult in these cases to monitor the conversion. Due to the rather complex mixture of volatile by-products formed, the noticeable increase in vapor pressure in the reactor provides only a rough indication. Therefore the reaction times listed constitute the upper time limits observed to achieve conversion. These times do not allow any conclusions regarding the relative rates of the various conversion reactions.

The best criterion by which to judge a successful quantitative conversion is provided by chemical analysis. In particular, the sulfur to fluorine ratio and the carbon content are useful in this regard. Analytical data are not reported here, but have been made available to the referees. ^{119}Sn Mössbauer data are listed in Table 2. Vibrational spectra, ^{19}F nmr data, obtained in some cases on solids, in some instances on solutions and other physical properties, are summarized for new compounds in the experimental section. Vibrational data are mostly used for fin-

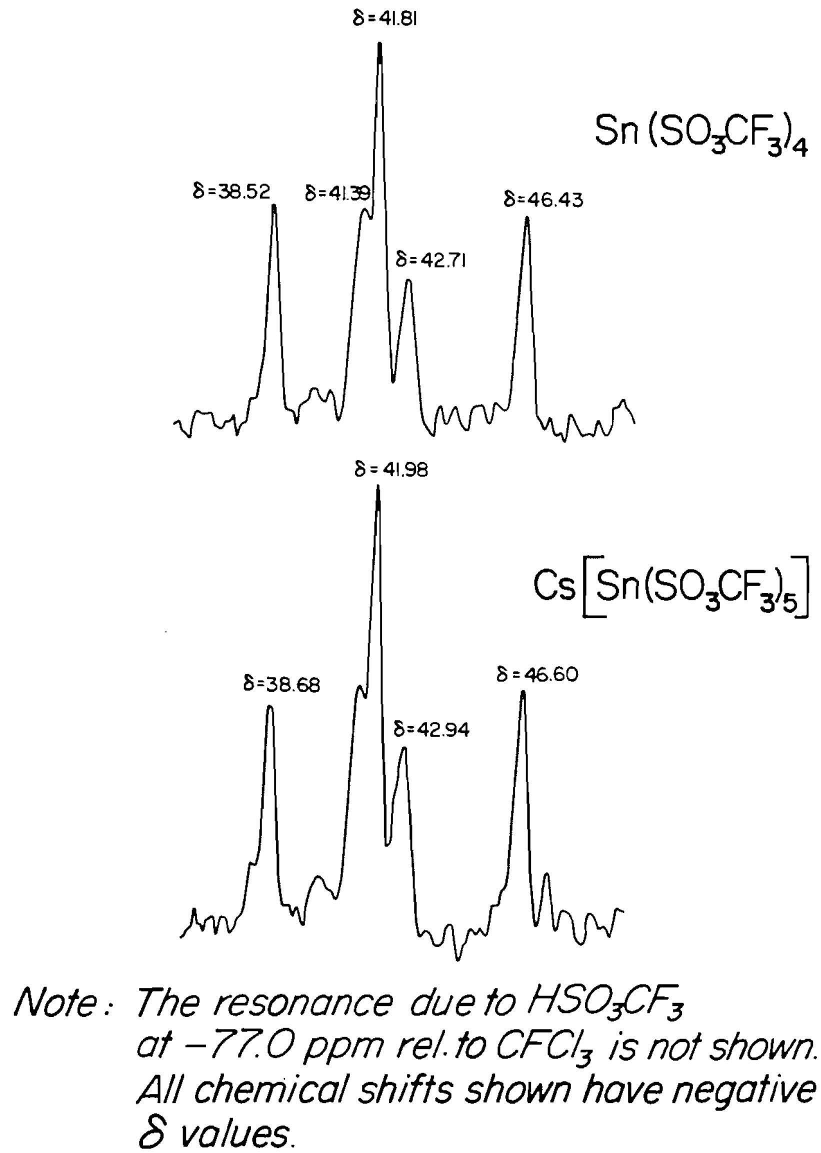

FIG. 2. The [19]F nmr spectra of $Sn(SO_3CF_3)_4$ and $Cs[Sn(SO_3CF_3)_5]$ in HSO_3CF_3 solution.

gerprinting only. Two diagnostic bands may be mentioned. Sulfur–fluorine stretching modes, usually observed between 800 and 900 cm^{-1}, should be absent in the SO_3CF_3 compounds, while a rather sharp, medium intensity ir peak with a very intense Raman counterpart is found now at ~770 cm^{-1}. In most instances strong fluorescence, found also for liquid HSO_3CF_3, prevents the acquisition of meaningful Raman data. The ^{119}Sn Mössbauer spectra for tin fluorosulfates and their SO_3CF_3 analogues differ for the most part very little. For example, the isomer shift δ and the quadrupole splitting Δ for $Cs[Sn(SO_3CF_3)_5]$, of −0.208 mm s^{-1} relative to SnO_2 and 0.499 mm s^{-1}, vary only marginally from −0.239 mm s^{-1} and 0.617 mm s^{-1}, reported previously for $Cs[Sn(SO_3F_3)_5$ (22), and a similar, possibly oligomeric, sulfonate-bridged structure is suggested for both.

A marked difference is found for the ^{19}F nmr data. Besides a rather obvious chemical shift difference (fluorosulfates have positive δ values relative to $CFCl_3$ and trifluoromethyl sulfates have negative shifts (δ between −38 and −95 ppm)), the single line resonances for $[Sn(SO_3F)_5]^-$ or $[Sn(SO_3F)_6]^{2-}$ (22, 29) are contrasted by rather broad multiplets for the triflates. A typical spectrum is shown in Fig. 2, and data for $Sn(SO_3CF_3)_4$, $Cs[Sn(SO_3CF_3)_5]$, and $K_2[Sn(SO_3CF_3)_6]$ in HSO_3CF_3 are tabulated (Table 3) and form the basis for a more detailed discussion later on.

As is apparent from Table 1 and the chemical analysis, conversions proceed quantitatively either at 25°C or, in two instances, at 60°C. There is only one exception. Highly polymeric $Hg(SO_3F)_2$ is incompletely converted even at elevated temperatures. It appears that raising the reaction temperature, first to 85°C and then to 100°C, does not increase the conversion rate but leads to rather impure materials, possibly due to side reactions with the by-products of the degradation reaction. In all other instances complete and rapid conversion is observed. A number of these conversion reactions deserve special comment.

(*i*) *Ionic salts*: The reaction of KSO_3F with an excess of HSO_3CF_3 results initially in clear solutions, from which a white, crystalline solid is obtained after removal of all volatiles *in vacuo*. Initial analysis indicates the retention of an almost equimolar amount of HSO_3CF_3. Prolonged heating to 60°C *in vacuo* produces KSO_3CF_3. A similar strong retention of excess

TABLE 3. [19]F nuclear magnetic resonance of trifluoromethane sulfonates of tin in HSO_3CF_3[a]

$Sn(SO_3CF_3)_4$ δ (ppm)[b]	$Cs[Sn(SO_3CF_3)_5]$ δ (ppm)[b]	$K_2[Sn(SO_3CF_3)_6]$ δ (ppm)[b]
−38.52 ms	−38.68 ms	−39.04 ms
−41.39 s, sh	−41.50 s, sh	−41.49 s, sh
−41.81 s	−41.98 s	−42.40 s
−46.43 ms	−46.60 ms	−46.49 ms

[a] Resonance for HSO_3CF_3 is found in all cases at −77.0 ppm relative to $CFCl_3$.
[b] Relative to $CFCl_3$.

acid is noted when alkali metal fluorosulfates are prepared from their chlorides and HSO_3F. Vast and co-workers (39) have succeeded in isolating well-defined solvates of the type $MSO_3F \cdot HSO_3F$ for M = Na and Cs only, and the crystal structure of the cesium salt (40) has suggested formulation as $Cs^+[O_2FSOHOSFO_2]^-$ with a symmetrical hydrogen bridge. Similar SO_3CF_3 salts appear to be unknown; however, the cesium salt is found to form readily via:

[5] $CsCl + 2HSO_3CF_3 \rightarrow CsSO_3CF_3 \cdot HSO_3CF_3 + HCl$

No definitive structural conclusions are possible. The [1]H nmr signal is very broad, quite unlike the sharp resonance at δ = 10.9 ppm found for $CsSO_3F \cdot HSO_3F$ (41). Two [19]F nmr signals at $\delta = -93.1$ and -78.8 ppm relative to $CFCl_3$ are found and the infrared spectrum differs only marginally from that of $CsSO_3CF_3$, similar to findings (39) for $NaSO_3F \cdot HSO_3F$ and $NaSO_3F$.

(*ii*) *Isobidentate sulfonate groups*: The conversion of $GeF_2(SO_3F)_2$ to $GeF_2(SO_3CF_3)_2$ proceeds seemingly under retention of a polymeric structure with a solid–liquid mixture present throughout the reaction. A minimum reaction temperature of 60°C and a reaction time of 6 days are required. Analysis justifies formulation as $GeF_2(SO_3CF_3)_2$, but vibrational spectroscopy, which had suggested a fluorosulfate bridged polymer with a linear GeF_2 group for $GeF_2(SO_3F)_2$ (22), is less helpful in this case. Infrared spectra compare well to those of other compounds with bidentate SO_3CF_3 groups (9, 24, 25) but the GeF_2 vibrations are not clearly identifiable, due to the observation of SO_3CF_3 vibrations in the regions expected for νGeF_2 at 770 and νGeF_2 sym. at 650 cm^{-1}. The position of a medium intensity band at 726 cm^{-1} appears to be rather low for a GeF_2 stretch. Both GeF_2-sulfonates have rather similar melting points: 150°C for $GeF_2(SO_3CF_3)_2$ and 146°C for $GeF_2(SO_3F)_2$.

The other example of an isobidentate bridging fluorosulfate group, $(CH_3)_2Sn(SO_3F)_2$ (8), can be converted smoothly at 25°C to $(CH_3)_2Sn(SO_3CF_3)_2$ within 6 days. Under the reaction conditions, some solid material persists in the reaction mixture throughout, but the conversion is quantitative. Not unexpectedly, the conversion reaction can be reversed when $(CH_3)_2Sn(SO_3CF_3)_2$ is reacted with an excess of HSO_3F. This time a clear solution forms and the reaction is complete within 2 days.

With neither reaction of any synthetic interest, three comments may be made: (a) Polymers with bridging sulfonate groups are readily susceptible to solvolysis, and complete conversion is noted. (b) The GeF_2 group in $GeF_2(SO_3F)_2$ appears to be unaffected by solvolysis. (c) With acid degradation responsible for a quantitative reaction, the fluorosulfate to trifluoromethyl sulfate conversion is expected to be reversible and more examples for reversibility should exist. However, no other attempts are made by us.

(*iii*) *Mono- and bidentate*: The successful conversion of $Sn(SO_3F)_4$ to $Sn(SO_3CF_3)_4$ presents another interesting problem. It is already surprising that $Sn(SO_3F)_4$, which is extremely sparingly soluble in HSO_3F (38), dissolves in HSO_3CF_3 at 25°C in 30 min. The resulting solution remains clear, and white, solid $Sn(SO_3CF_3)_4$ is only obtained after removal of all volatiles *in vacuo*. The very same compound has been obtained previously by us (30) when tin(IV)tetrakis(acetate), $Sn(O_2CCH_3)_4$ is solvolyzed in an excess of HSO_3CF_3. Infrared spectra for both products match fairly well, and the melting point of 235°C agrees reasonably well with the reported range of 225–227°C (30). The [119]Sn Mössbauer spectrum, observed now, differs completely from the reported (30) single line spectrum with $\delta = -0.22$ mm s^{-1} relative to SnO_2. A well-resolved doublet, with $\Delta = 1.18$ mm s^{-1} and $\delta = -0.213$ mm s^{-1} is observed at 80 K. The new data agree well with those reported for $Sn(SO_3F)_4$ (38), suggesting a similar octahedral environment for tin.

A subsequent reinvestigation of the solvolysis of $Sn(O_2CCH_3)_4$ in HSO_3CF_3 provides a plausible explanation. When the reaction is performed in a dry-box as described (30) and only a small excess of HSO_3CF_3 is used, acetic acid is formed in an exothermic reaction and $Sn(SO_3CF_3)_4$ is obtained according to:

[6] $Sn(O_2CCH_3)_4 + 4HSO_3CF_3 \rightarrow Sn(SO_3CF_3)_4 + 4CH_3CO_2H$

just as reported (30). However, where a larger excess of HSO_3CF_3 is employed and acetic acid is not immediately removed, proton transfer occurs and $CH_3CO_2H_2^+SO_3CF_3^-$ forms. This material can be obtained more directly by combining equimolar amounts of the parent acids. It is a white solid that melts at +37°C and undergoes dissociation into ions in HSO_3CF_3. The solid state structure should be similar to the one reported for $CH_3CO_2H_2^+SO_3F^-$ (42), involving extensive hydrogen bridging between the individual ions resulting in polymeric chains. The infrared spectrum of $CH_3CO_2H \cdot HSO_3CF_3$ suggests a bidentate, possibly bridging trifluoromethyl sulfate group; the single [1]H resonance in the nmr spectrum of the solid at $\delta = 11.3$ ppm is consistent with hydrogen bridging. During solvolysis of $Sn(O_2CCH_3)_4$ in excess HSO_3CF_3 the initially formed $Sn(SO_3CF_3)_4$ acts as $SO_3CF_3^-$ ion acceptor, and a solid, sparingly soluble material of the composition $[CH_3CO_2H_2]_2[Sn(SO_3CF_3)_6]$ is obtained, which melts at 255°C and gives rise to a single line in the [119]Sn Mössbauer spectrum at −0.231 mm s^{-1} relative to SnO_2. Hydrogen bridging is a plausible cause of the high melting point and the limited solubility in HSO_3CF_3. The overall reaction may be formulated as:

$$[7]\quad Sn(O_2CCH_3)_4 + 8HSO_3CF_3 \xrightarrow{HSO_3CF_3} [CH_3CO_2H_2]_2[Sn(SO_3CF_3)_6] + 2CH_3CO_2H_2^+{}_{(solv)} + 2SO_3CF_3^-{}_{(solv)}$$

It appears that the course of the $Sn(O_2CCH_3)_4$ solvolysis reaction in HSO_3CF_3 depends critically on the amount of acid used and the subsequent work-up of the reaction products. The reaction may lead to $Sn(SO_3CF_3)_4$ or to the salt $[CH_3CO_2H_2]_2[Sn(SO_3CF_3)_6]$. The use of nearly stoichiometric amounts of HSO_3CF_3 to achieve complete solvolysis and the subsequent removal of all acetic acid formed are necessary in order to obtain $Sn(SO_3CF_3)_4$, while any excess of HSO_3CF_3 will favor protonation of acetic acid and precipitation of $[CH_3CO_2H_2]_2$-$[Sn(SO_3CF_3)_6]$ while $Sn(SO_3CF_3)_4$ remains in solution. These subtleties had not been recognized in our initial preparation of $Sn(SO_3CF_3)_4$ (30) and different preparations employing different reactant ratios had apparently resulted in the formation of either $Sn(SO_3CF_3)_4$, used for chemical analysis and infrared spectroscopy, or the acetate acidium salt, evidently used to obtain the single line ^{119}Sn Mössbauer spectrum reported previously (30).

Two conclusions regarding $Sn(SO_3CF_3)_4$ may be made: (*i*) Solvolysis of $Sn(SO_3F)_4$ in an excess of HSO_3CF_3 is the better synthetic route to this compound. (*ii*) Its solubility in trifluoromethyl sulfuric acid and the existence of thermally stable salts like $Cs[Sn(SO_3CF_3)_5]$ and $K_2[Sn(SO_3CF_3)_6]$, both described in this study, together with observations made during the solvolysis of tin(IV)acetate in HSO_3CF_3, suggest a promising superacid system. The ^{19}F nmr spectra, due to the three solutes $Sn(SO_3CF_3)_4$, $Cs[Sn(SO_3CF_3)_5]$, and $K_2[Sn(SO_3CF_3)_6]$, summarized in Table 3, are intriguingly similar and point to the presence of a common species in solution. In all three cases a sharp single line resonance at $\delta = -77.0$ ppm relative to $CFCl_3^-$, attributed to HSO_3CF_3, is observed and allows the conclusion that $SO_3CF_3^-$ exchange between solvent and solute does not occur.

The irregular shapes and the spacing of the resonance lines (see Fig. 2), due to the solute in the region of $\delta = -39$ to -47 ppm relative to $CFCl_3$, suggest magnetic inequivalence of individual fluorine atoms within CF_3 groups, possibly caused by steric effects in these rather bulky solute ions, since any spin–spin coupling between fluorine in different CF_3 groups or coupling with other nuclei as causes for the observed complexity is rather improbable.

A more detailed study of the HSO_3CF_3 solvent system is required to explore the promising superacidity effects more fully. Such a study is clearly beyond the scope of the investigation described here. Similarly, the results of a magnetic susceptibility study, including $Mn[Sn(SO_3CF_3)_6]$ and the two paramagnetic palladium trifluoromethyl sulfates, is currently underway, and the results will be published later.

Summary

The strictly synthetic orientation of this study permits only a few rather general comments regarding the nature of the conversion reaction utilized extensively in this study. The quantitative conversion of fluorosulfates into trifluoromethyl sulfates is observed in all but one instance, where the polymeric nature of the substrate and the tridentate configuration of the SO_3F group appear to limit reactivity. The following conclusions can be reached:

(*i*) Complete degradation of SO_3F moieties by HSO_3CF_3 is the reason for quantitative substitution of SO_3F by SO_3CF_3.

(*ii*) Substitution does not appear to involve a change in the bond type or the denticity of the sulfonate group.

(*iii*) The volatile products formed, either initially or by reaction with the glass vessel, do not affect the conversion reaction adversely or interfere in the isolation of the trifluoromethyl sulfates. It appears unlikely that H_2SO_4, which is nonvolatile under the reaction condition, is formed, with all volatiles removable at 25°C *in vacuo*.

(*iv*) The range of volatile by-products formed, as observed by gas phase infrared spectroscopy, is the same as found during the reaction of HSO_3CF_3 and HSO_3F at a 2:1 molar ratio (27). A quantitative distribution analysis is neither intended nor meaningful. Crucial steps in the proposed reaction mechanism, initial protonation of HSO_3CF_3 by the allegedly stronger acid HSO_3F (26), or the formation of $CF_3SO_2^+$ (26) or CF_3^+ (27) in HSO_3F, are in our view unlikely in these reactions. The observed formation of CO_2 and COF_2 is not easily explained by such a previous proposal (26).

In summary, while the conversion reaction appears to be general and useful, a mechanistic understanding of the degradation reaction is still lacking.

Experimental

Chemicals

Commercially available chemicals of analytical or reagent grades were used without purification. Technical grade fluorosulfuric acid (Allied Chemicals) was doubly distilled at atmospheric pressure in a counter stream of dry nitrogen. Trifluoromethane sulfuric acid (3M Company) was distilled from concentrated H_2SO_4 in a stream of dry nitrogen. Tin(IV) acetate was synthesized by the reaction of SnI_4 with $TlCO_2CH_3$ (43). The following fluorosulfates were prepared according to literature methods: KSO_3F (44), $(CH_3)_2Sn(SO_3F)_2$ (32), $(CH_3)_2Sn(SO_3CF_3)_2$ (32), $Sn(SO_3F)_4$ (22), $K_2[Sn(SO_3F)_6]$ (22), $Cs[Sn(SO_3F)_5]$ (22), $GeF_2(SO_3F)_2$ (22), $Pd(SO_3F)_2$ (33), $Hg(SO_3F)_2$ (36), $Mn[Sn(SO_3F)_6]$ (34), $Cs_2[Pt(SO_3F)_6]$ (21), and $Pd[Pd(SO_3F)_6]$ (33).

Instrumentation

Infrared spectra were recorded on a Perkin–Elmer 598 grating spectrometer. Silver chloride and bromide (Harshaw Chemicals) were used as window materials. Samples were either mulled with Nujol or hexachlorobutadiene or used without mulling agent. The Raman and Mössbauer spectrometers have been described before (22, 29). The ^{19}F nmr spectra in HSO_3CF_3 were obtained on an XL-100 spectrometer (Varian Associates). ^{1}H and ^{19}F high resolution solid-state nmr spectra were recorded on Bruker's CXP 200 MHz spectrometer. ^{1}H and ^{19}F chemical shifts are reported with respect to TMS and $CFCl_3$, respectively, with shifts to lower fields considered positive.

All moisture-sensitive solids were handled in a Vacuum Atmospheres Corp. "Dri-Lab" Model No. HE-43-2, filled with purified dry nitrogen and equipped with a Dri-Train circulating unit. All reactions were performed in Pyrex reaction vials of about 40-mL capacity, which were fitted with Kontes Teflon stem valves and equipped with Teflon-coated spin bars. All reactions were monitored by weight. Product isolation by filtration was performed in an apparatus described by Shriver (45). Chemical analysis was carried out by the Analytische Laboratorium, Gummersbach, West Germany. The carbon and hydrogen content was determined by Mr. P. Borda of this Department.

General procedure for the conversion of fluorosulfates into trifluoromethyl sulfates

A known amount of the fluorosulfate compound was filled inside the dry-box into a pre-weighed, dried reaction vial, fitted with a Teflon-coated magnetic stirring bar and a Teflon-stem stopcock. After evacuation of the reactor an approximate volume, usually 5 mL, of freshly distilled HSO_3CF_3 was transferred on a vacuum line onto the solid substrate. The reaction mixture was allowed to warm to room temperature before stirring was commenced. Occasionally, as noted in Table 1, complete or partial dissolution of the solid substrate occurred, either at 25°C or at a slightly elevated temperature. In some instances a solid remained in the reactor throughout the reaction. Product isolation involved, in all but one instance, removal of all volatiles *in vacuo*, which permitted us to follow the reaction by weighing. The solid product was subsequently dried *in vacuo* to constant weight. A slight pressure buildup in the reaction vessel was invariably noted during the reaction, but gas evolution appeared to be too slow to allow visual detection. An identical procedure was used to convert $(CH_3)_2Sn(SO_3CF_3)_2$ back to the fluorosulfate, employing about 5 mL of HSO_3F.

Additional synthetic reactions

(a) *$[CH_3CO_2H_2]_2[Sn(SO_3CF_3)_6]$*

To a 600-mg sample of $Sn(CO_2CH_3)_4$, an excess of HSO_3CF_3 was added in the dry-box and vigorously stirred. The clear solution on slow concentration *in vacuo* produced a white, crystalline product. The compound was isolated, by vacuum filtration and subsequent washing with a small amount of HSO_3CF_3, and dried *in vacuo*.

(b) *$CH_3CO_2H \cdot HSO_3CF_3$*

Nearly equimolar quantities of HSO_3CF_3 (4.91 g, 32.72 mmol) and CH_3COOH (2.02 g, 33.5 mmol) were mixed and stirred for an hour. On cooling the solution, a crystalline product was formed. The crystals were filtered and washed with a small amount of acetic acid followed by dry carbon tetrachloride, and dried *in vacuo* at room temperatue.

(c) *$CsSO_3CF_3 \cdot HSO_3CF_3$*

About 5 mL of HSO_3CF_3 were distilled onto 554.1 mg (3.29 mmol) CsCl. In a vigorous reaction at ambivant temperature, HCl was produced and removed *in vacuo*. The mixture was vigorously stirred for 30 min. On removal of all the volatile materials, a white crystalline product, $CsSO_3CF_3 \cdot HSO_3CF_3$ (1406.1 mg, 3.25 mmol), was obtained.

Characterization of new compounds

The melting points quoted are uncorrected. the nmr data are quoted relative to TMS (^1H) or $CFCl_3$ (^{19}F). Infrared data are quoted in cm^{-1}. Relative intensities are listed using the following abbreviations: s = strong, sh = shoulder, m = medium, w = weak, v = very, b = broad.

$K_2[Sn(SO_3CF_3)_6]$: white, hygroscopic solid, does not melt below 290°C, very soluble in HSO_3CF_3; ir: 1445 m, 1427 s, 1360 vs, 1230 vs, 1195 vs, 1145 s, 1100 w, sh, 1000 w, sh, 965 s, b, 930 s, sh, 895 m, 825 m, 770 m, 730 vw, 625 vs, 606 s, sh, 572 w, 560 w, 522 m-w, 511 s, 500 msh, 425 w, sh.

$Cs_2[Pt(SO_3CF_3)_6]$: deep yellow, hygroscopic solid, which does not melt below 275°C; ir: 1445 w, 1427 m, sh, 1360 vs, b, 1230 vs b, 1195 vs, 1125 s, 1100 vw, sh, 1015 w, 965 msh, 900 s, b, 815 vw, sh, 765 ms, 685 w, 642 msh, 615 s, 606 s, 578 m, 549 vw, 518 m-s, 500 m, 418 w, 395 w, 375 m, 350 w, 340 w, 321 w, 310 m. Raman: 1381 m, 1255 s, 1235 w, 1168 s, 1020 m, 771 m, 606 s, 540 m, 372 m, 328 w, 255 s, 220 s.

$GeF_2(SO_3CF_3)_2$: white, very hygroscopic glass wool-like solid, melts at 150°C, seems insoluble in HSO_3CF_3; ir: 1409 msh, 1370 vs, 1317 vs, 1245 s, 1215 s, sh, 1201 vs, 1145 vs, 1079 s, 1035 s, 1020 s, sh, 875 vw, 782 ms, 775 ms, 726 m-w, 640 s, 612 s, 585 m, 540 m, 529 s, 433 s, 419 m, 373 s, 350 s, sh, 340 s, 320 s, sh.

$Pd[Pd(SO_3CF_3)_6]$: brown-white solid, hygroscopic, thermally stable up to 250°C; ir: 1420 w, sh, 1391 s, 1365 s, 1245 s, sh, 1208 vs, 1125 m, sh, 1035 s, 940 w, 855 vw, 771 m, 639 s, 605 w, 580 w, 529 s, 504 w, 499 m, 480 vw.

$Pd(SO_3CF_3)_2$: light purple, very hygroscopic solid, which does not melt below 250°C; ir: 1425 vw, 1392 vw, 1350 m, sh, 1220 vs, b, 1180 w, sh, 1090 s, 1050 w, sh, 1030 m, 980 vs, 852 vs, 770 vw, 720 w, 635 ms, 608 s, 595 wsh, 565 ms, 527 ms, 505 vw, 415 s, 382 w, 356 s, 340 w, 332 w, 320 w.

$Cs[Sn(SO_3CF_3)_5]$: white, hygroscopic crystalline solid, which does not melt below 280°C; ir: 1440 w, sh, 1415 s, sh, 1370 vs, 1240 s, sh, 1220 s, sh, 1195 vs, b, 1135 s, b, 1095 w, sh, 985 s, b, 930 m, sh, 920 w, sh, 830 vw, 769 ms, 730 w, 625 vs, 603 s, sh, 570 vw, 512 s, 500 m. Raman: 1390 s, 1260 s, 1240 s, 1208 m, 1173 m, 1153 w, 1081 m, 1055 s, 920 m, 775 and 772 vs, 635 w, 610 w, sh, 599 s, 569 s, 536 m, 517 w, 388 m, 343 s, 328 s, 314 s, 258 s.

$[CH_3CO_2H_2]_2[Sn(SO_3CF_3)_6]$: white, very hygroscopic crystalline solid, mp 255°C; ir: 3000 vs, b, 1610 s, 1575 w, 1555 m, 1543 m, 1360 s, 1200 vs, b, 1140 s, b, 1037 w, 980 m, 895 vw, 769 m, 755 vw, 625 vs, 602 s, 570 m, 525 m, sh, 505 s, 495 s, sh, 425 w; ^{19}F nmr, solid state: broad resonance at $\delta = -79.2$ ppm.

$Sn(SO_3CF_3)_4$: white hygroscopic solid, mp 235°C; ir: 1431 w, 1400 m, sh, 1360 s, b, 1310 vw, sh, 1256 s, sh, 1210 vs, b, 1138 m, 1060 s, 1000 vs, b, 955 vw, 915 ms, 778 m, 771 m, 635 s, 613 s, sh, 575 vw, sh, 540 w sh, 515 ms, 450 vw, sh, 410 w, 381 s, 366 s, 320 wsh.

$CH_3CO_2H \cdot HSO_3CF_3$: white crystalline hygroscopic solid, melts at +37°C, very soluble in HSO_3CF_3; ir: 2920 vs, b, 2460 s, b, 1885 m, b, 1615 s, 1545 ms, 1400 m, 1365 w, 1300 s, 1195 s, b, 1145 w, 1015 s, 930 w, 895 vw, 765 m, 634 s, 615 s, 573 mw, 515 m, 500 m, 470 w, b. Raman (strong fluorescence): 2950 wb, 1305 w, 1220 w, 1020 s, 902 m, 768 ms, 635 w, 615 w, 572 w, 498 w, 480 mb, 345 m, 319 m, 209 m.

$CsSO_3CF_3 \cdot HSO_3CF_3$: white, hygroscopic solid, mp 119°C; ir: weak, very broad band at 2800–2200 cm^{-1}, 1315 m, sh, 1285 sb, 1185 vs, b, 1145 vw, sh, 1065 w, sh, 1020 vs, 940 w, 770 m, 640 s, 611 s, 565 s, sh, 555 s, 505 s, 440 s, b; ^{19}F nmr (solid state): $\delta = -93.1$ (broad), $\delta = -78.83$.

$Mn[Sn(SO_3CF_3)_6]$: white, hygroscopic solid, does not melt below 300°C; ir: 1375 vs, 1360 s, sh, 1240 s, sh, 1200 s, b, 1125 s, 1100 w, sh, 980 m, sh, 960 vs, 870 vw, sh, 775 s, 674 m, sh, 639 s, 606 s, 585 s, 535 s, sh, 525 s, 507 m, sh, 452 w, 422 w, sh, 398 s, 361 s, 351 s, sh, 335 m.

Acknowledgements

Financial support by the Natural Sciences and Engineering Research Council of Canada is gratefully acknowledged. We are grateful to Mrs. L. Sallos for technical assistance in obtaining the ^{119}Sn Mössbauer spectra and to Paul Gehrs and Grant Wong for help in some of the preparation.

1. (*a*) R. C. THOMPSON. *In* Inorganic sulphur chemistry. *Edited by* G. Nickless. Elsevier, Amsterdam. 1968. p. 587; (*b*) A. W. JACHE. Adv. Inorg. Chem. Radiochem. **16**, 177 (1974).
2. R. D. HOWELS and J. D. MCCOWN. Chem. Rev. **77**, 69 (1977).
3. A. ENGELBRECHT and B. M. RODE. Monatsh. Chem. **103**, 1315 (1972).
4. D. G. RUSSEL and J. B. SENIOR. Can. J. Chem. **52**, 2975 (1974).
5. G. M. KRAMER. J. Org. Chem. **40**, 298 (1975); **40**, 302 (1975).
6. A. A. WOOLF. *In* New pathways in inorganic chemistry. Cambridge University Press, New York, NY. 1968. p. 327.
7. F. AUBKE and D. D. DES MARTEAU. Fluorine Chem. Rev. **8**, 73 (1974).
8. F. A. ALLEN, J. LERBSCHER, and J. TROTTER. J. Chem. Soc. A, 2507 (1971).
9. T. H. TAN, J. R. DALZIEL, P. A. YEATS, J. R. SAMS, R. C. THOMPSON, and F. AUBKE. Can. J. Chem. **50**, 1843 (1972).
10. P. C. LEUNG and F. AUBKE. Inorg. Chem. **17**, 1765 (1978).
11. P. C. LEUNG, K. C. LEE, and F. AUBKE. Can. J. Chem. **57**, 326 (1979).
12. A. ENGELBRECHT. Angew. Chem. Int. Ed. Engl. **4**, 641 (1965).
13. R. E. NOFTLE and G. H. CADY. Inorg. Chem. **4**, 1010 (1965).
14. Y. KATSUHARA, R. M. HAMMAKER, and D. D. DES MARTEAU. Inor. Chem. **19**, 607 (1980).
15. D. D. DES MARTEAU. J. Am. Chem. Soc. **100**, 340 (1978).
16. R. A. DE MARCO and J. M. SHREEVE. Adv. Inorg. Chem. Radiochem. **16**, 109 (1974).
17. J. R. DALZIEL. M.Sc. Thesis, University of British Columbia, 1975.
18. R. CORKUM and J. B. MILNE. Can. J. Chem. **56**, 1833 (1978).
19. Y. KATSUHARA and D. D. DES MARTEAU. J. Org. Chem. **45**, 2241 (1980).
20. K. K. JOHRI, Y. KATSUHARA, and D. D. DES MARTEAU. J. Fluorine Chem. **19**, 227 (1982).
21. K. C. LEE and F. AUBKE. Inorg. Chem. **23**, 2124 (1984).
22. S. P. MALLELA, K. C. LEE, and F. AUBKE. Inorg. Chem. **23**, 653 (1984).
23. P. C. LEUNG and F. AUBKE. Can. J. Chem. **62**, 2892 (1984).
24. J. R. DALZIEL and F. AUBKE. Inorg. Chem. **12**, 2707 (1973).
25. J. R. DALZIEL, H. A. CARTER, and F. AUBKE. Inorg. Chem. **15**, 1247 (1976).
26. G. A. OLAH and T. OHYAMA. Synthesis, **5**, 319 (1976).
27. R. E. NOFTLE. Inorg. Nucl. Chem. Lett. **16**, 195 (1980).
28. K. O'Sullivan, R. C. Thompson, and J. TROTTER. J. Chem. Soc. A, 2024 (1967).

29. P. A. YEATS, J. R. SAMS, and F. AUBKE. Inorg. Chem. **12**, 328 (1973).
30. R. J. BATCHELOR, J. N. R. RUDDICK, J. R. SAMS, and F. AUBKE. Inorg. Chem. **16**, 1414 (1977).
31. P. A. YEATS, B. F. E. FORD, J. R. SAMS, and F. AUBKE. Chem. Commun. 791 (1969).
32. P. A. YEATS, J. R. SAMS, and F. AUBKE. Inorg. Chem. **11**, 2634 (1972).
33. K. C. LEE and F. AUBKE. Can. J. Chem. **55**, 2473 (1977).
34. S. P. MALLELA, P. GEHRS, and F. AUBKE. To be published.
35. C. S. ALLEYNE, K. O'SULLIVAN-MAILER, and R. C. THOMPSON. Can. J. Chem. **52**, 336 (1974).
36. S. P. MALLELA and F. AUBKE. Can. J. Chem. **62**, 382 (1984).
37. M. SCHMEISSER, P. SARTORI, and B. LIPPSMEIER. Chem. Ber. **102**, 2150 (1969).
38. P. A. YEATS, B. L. POH, B. F. E. FORD, J. R. SAMS, and F. AUBKE. J. Chem. Soc. A, 2188 (1970).
39. C. JOSSON, M. DEPORCQ-STRATMAINS, and P. VAST. Bull. Soc. Chim. Fr. (9–10) 820 (1977).
40. C. BELIN, M. CHARBONNEL, and J. POTIER. J. Chem. Soc. Chem. Commun. 1036 (1981).
41. S. KARUNANITHY and F. AUBKE. Mater. Sci. Eng. **62**, 241 (1984).
42. Å. KVICK, P. G. JÖNSSON, and I. OLOVSSON. Inorg. Chem. **8**, 2775 (1969).
43. H. SCHMIDT, C. BLOHM, and G. JANDER. Angew. Chem. **59**, 233 (1947).
44. J. BARR, R. J. GILLESPIE, and R. C. THOMPSON. Inorg. Chem. **3**, 1149 (1964).
45. D. F. SHRIVER. The manipulation of air-sensitive compounds. McGraw–Hill, New York. 1969.

A brief survey of the use of the Pummerer rearrangement for the alkylation of 1,3-oxathiolan-5-ones and 1,3-thiazolidin-4-ones

JOHN M. MCINTOSH AND RANDY K. LEAVITT
Department of Chemistry, University of Windsor, Windsor, Ont., Canada N9B 3P4

Received April 24, 1985

JOHN M. MCINTOSH and RANDY K. LEAVITT. Can. J. Chem. **63**, 3313 (1985).

Oxidation of 1,3-oxathiolan-5-ones (**1**) gives acceptable yields of sulfoxides only when C4 is unsubstituted. Sulfoxides derived from 1,3-thiazolidine-4-ones (**8**) are easily prepared. Acid-catalyzed rearrangement in the presence of 1-alkenes or benzene leads to alkylation (arylation) at C5. Alkylation of **8***c* may be generally more effective than that of **1**. An aldol condensation of **8***c* shows little stereoselectivity.

JOHN M. MCINTOSH et RANDY K. LEAVITT. Can. J. Chem. **63**, 3313 (1985).

L'oxydation des oxathiolane-1,3 ones-5 (**1**) ne donne des rendements acceptables des sulfoxydes que lorsque le C4 n'est pas substitué. On peut facilement préparer les sulfoxydes qui proviennent des thiazolidine-1,3 ones-4 (**8**). La transposition acido-catalysée, en présence d'alcènes-1 ou de benzène, provoque une alkylation (ou une arylation) en position C5. L'alkylation du composé **8***c* ést généralement plus efficace que celle du composé **1**. Une condensation aldolique du composé **8***c* ne présente pas beaucoup de stéréosélectivité.

[Traduit par le journal]

Recently, we described (1) the alkylation and aldol condensation reactions of 1,3-oxathiolan-5-ones (**1**) and the use of the products in the formation of 2-mercaptoaldehydes and 2,5-dihydrothiophenes (2). In that report it was noted that the alkylation of **1***a* was unsuccessful with all alkyl halides, while alkylation of **1***b* gave acceptable yields of products only with very reactive halides. The interest in this alkylation stems from its potential to form 2-mercaptoaldehydes in a protected form from readily available starting materials. In an effort to circumvent the observed difficulties, we considered the use of the ion **3**, generated by treatment of sulfoxide **2** with acids, as the electrophilic partner in an alkylation reaction (Scheme 1). Our intent was to use olefins as the nucleophilic species, which results in an "umpolung" of the previously examined anionic alkylation. Recently disclosed examinations of closely related systems (3) prompts us to present our results at this time.

The capture of ions analogous to **3** by alkenes has been documented. In a series of papers, Tamura *et al.* (4) examined the cyclization of acyclic olefinic β-oxo-sulfoxides. The α-thiocarbocation derived formally by the elimination of OH^- from the sulfoxide was captured intramolecularly with aromatic (4*b*) and olefinic (4*a*) nucleophiles to generate 5- and 6-membered rings. Intermolecular capture (4*c*, *d*) was demonstrated with terminal alkenes. These reactions can be envisaged as proceeding either via an ene type reaction or as simple attack of the olefinic π-bond on the ion analogous to **3**. Other examples of this and related systems can also be found in the literature (5). In this report, the results of the use of **1** and the related lactams **8** in such reactions are documented.

[1]

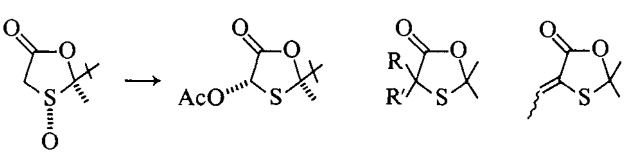

4 **5** **6***a* R = H, R′ = OTFA **7**
b R = Me, R′ = OH
c R = Ph, R′ = H

To our knowledge, only one example of the sulfoxide derived from the 1,3-oxathiolan-5-one system has been reported. Kay and co-workers reported **4** (6) and its stereospecific Pummerer rearrangement into **5**. In our hands, oxidation of **1***a* using hydrogen peroxide in acetic acid afforded **2***a* in 87% yield. Pummerer rearrangement using TFA/TFAA in benzene gave a modest yield of **6***a* with no sign of **6***c*, the product expected from capture of **3***a* by the solvent. Clearly, the intermolecular capture of **3***a* cannot compete with the intramolecular rearrangement. In view of results to be presented later, this may be ascribed to the steric hindrance imparted by the C2 *gem* substitution and (or) the instability of the lactone function to the strongly acidic conditions of the Pummerer rearrangement. Stronger acids caused immediate decomposition of **2***a* and no identifiable products could be obtained. Oxidation of **1***b* followed by aqueous work-up gave a low yield of the hydrolyzed Pummerer product **6***b*. No sulfoxide could be detected in the spectra of the crude product. When oxidation of **1***c* was attempted, an inseparable mixture of **2***c* and a compound to which the structure **7** is assigned, on the basis of the ^1H nmr of the crude mixture (quartet at $\delta = 6.8$), was formed. In addition, large amounts of **1***c* remained in the mixture. Attempted separation of **7** or **2***c* from the reaction mixture led only to severe decomposition. The use of MCPBA or TBHP as oxidants did not improve these results. The instability of **2***c*, **6***a*, and **7** precluded their purification. It is clear from these results that the sulfoxides, like **2***b* and **2***c*, that possess C4 substituents must be unusually sensitive materials whose use in synthesis would be unattractive.

Because the lactam analogs (**8** and **9**) of **1** and **2** were expected to be more stable and because the DIBAL reduction of substituted **8** to 2-mercaptoaldehydes was expected to be routine, our attention was shifted toward this heterocycle. Three examples were examined (**8***a*, *b*, *c*). In each case these were oxidized to **9** in acceptable yields and each **9** proved to be a stable material.

Treatment of **9***a* with TsOH/Ac_2O gave **10***a*, while **10***b* (the hydrolyzed Pummerer product formed from the aqueous work-up) and **10***c* were formed from **9***b* or **9***c* respectively, on treatment with TFA/TFAA. Reaction of each **9** with benzene in concentrated H_2SO_4 gave the corresponding 5-phenyl derivatives (**11**) of **8** in 75–95% yields.[1] However, these conditions

[1] Formation of **11***b* has also been observed by I. T. Kay (personal communication).

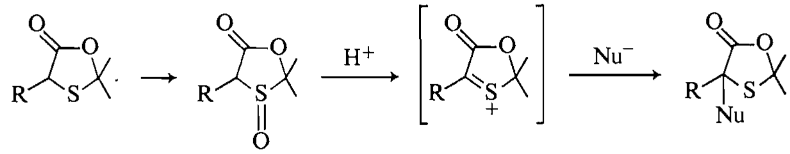

1 2 3

a R = H, *b* R = Me, *c* R = Et

SCHEME 1

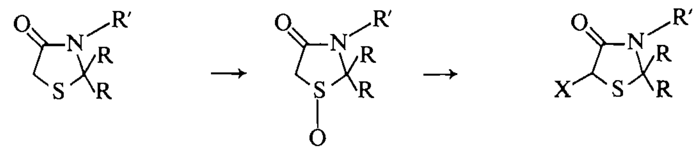

8*a* R = —$(CH_2)_5$—, R′ = Ph
b R = —$(CH_2)_5$—, R′ = Me
c R = H, R′ = Me

9

10*a* R = —$(CH_2)_5$—, R′ = Ph, X = OAc
b R = —$(CH_2)_5$—, R′ = Me, X = OH
c R = H, R′ = Me, X = OTFA

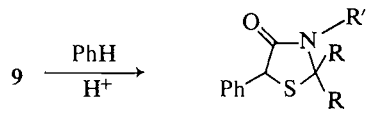

11*a* R = —$(CH_2)_5$—, R′ = Ph
b R = —$(CH_2)_5$—, R′ = Me
c R = H, R′ = Me

SCHEME 2

caused immediate decomposition of the alkenes that we hoped to use in the alkylation reaction. Attempts to use H_2SO_4 or other strong Lewis (BF_3, $SnCl_4$, $AlCl_3$) or protonic (PPA, $MeSO_3H$) acids in catalytic amounts at low temperatures in the phenylation of **9***a* or **9***b* led to low yields of complex mixtures of products. The appearance of materials whose molecular weight (mass spectra) indicated the incorporation of two heterocyclic units joined by an ether linkage suggested that the presence of water formed in the Pummerer rearrangement was interfering with the desired reaction. Presumably, when concentrated H_2SO_4 is used, the water is completely protonated and cannot react further. Incorporation of anhydrous $CuSO_4$ in the sulfuric acid catalyzed reaction did not improve the results.

Sulfoxide **9***c* did react with 1-alkenes in TFA/TFAA solution to give **12** in acceptable yields (Scheme 3). 2-Alkenes (2-hexene, cyclohexene) gave mixtures of products containing **10***c* along with a mixture of "ene" products and their addition products with TFA.

The reported (3, 4) examples of successful alkylations of β-oxo-sulfoxides by alkenes under acidic conditions all utilize compounds in which a *methyl* group is attached to sulfur. It is clear from our results that increasing the size of this group has a profoundly deleterious effect on the reaction and makes this methodology of limited applicability to **1** and **8**.

In conclusion, it is worth noting that alkylation of the anion derived from lactam **8***c* gave acceptable yields of alkylated materials (**13**), even with a halide (BuI) that was unreactive with lactones **1***a* or **1***b* (Scheme 3). Methylation afforded a 6:1 mixture of mono- and dialkylated product (**13***a*) while BuI gave only monoalkylated product (**13***b*). Again, the difference may lie in the steric effect of the *gem*-dimethyl group in **1**. Aldol reactions are also possible, as is evidenced by the reaction with benzaldehyde to afford **14** as a 3:2 mixture of diastereomers **14***a* and **14***b*. Since the C2-unsubstituted lactam **8***c* is more readily prepared than the analogous lactone, the use of this

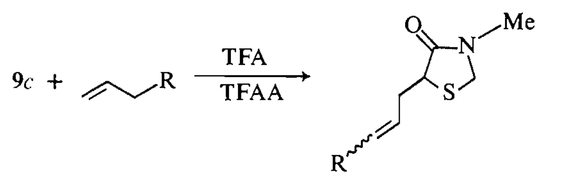

12*a* R = C_5H_{11}
b R = C_3H_7

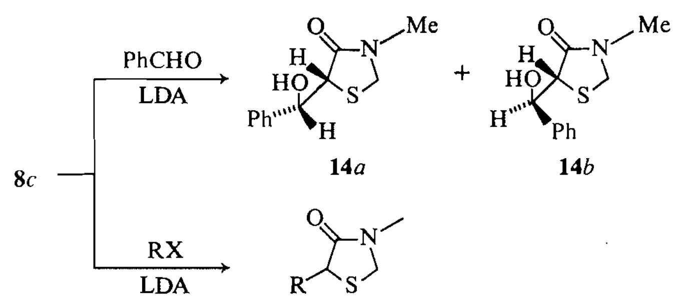

14*a* 14*b*

13*a* R = Me
b R = Bu

SCHEME 3

heterocycle may circumvent the difficulties encountered in the alkylation of **1** and permit an alkylative approach to a general synthesis of 2-mercaptoaldehydes.

This work represents the end of our investigations into the chemistry of these heterocycles.

Experimental

All infrared spectra were run in chloroform solution on either a Perkin–Elmer Model 180 instrument or on a Nicolet 5-DX instrument in the FT mode. The four strongest peaks are reported. The nmr spectra were run at 60 MHz (^{1}H nmr) or 22.64 MHz (^{13}C nmr) in $CDCl_3$ solution and are referenced to internal TMS. The data are presented in the format (multiplicity, number of hydrogens, coupling constant). Gas chromatographic analyses were performed using a 1.5 ft × 1/8 in. column packed with 5% OV-101 on Chromosorb W. Solvents were removed at reduced pressure and the drying agent was anhydrous $MgSO_4$. Column chromatography utilized silica gel 60 (Merck). Microanalyses were performed by Canadian Microanalytical Services, Vancouver; Guelph Chemical Laboratories, Guelph, Ontario; and Uniroyal Research Laboratories, Guelph, Ontario.

Materials

1,3-Oxathiolan-5-ones **1** (2) and thiazolidinone **8***c* (7) were prepared by literature procedures.

*3-Phenyl-2,2-pentamethylenethiazolidin-4-one (8*a*)*

A solution of the ketimine derived from aniline and cyclohexanone (24 g, 0.14 mol) and 15 g (0.16 mol) 2-mercaptoacetic acid was refluxed under a Dean–Stark water separator overnight (3 mL of water collected). The solvent was removed and the solid residue recrystallized to give **8***a*; 70%; mp 168°C (EtOH); ir: 2940, 1665, 1490, 1380 cm^{-1}; ^1H nmr: 7.4–6.9 (m, 5H), 3.9 (s, 2H), 2.3–0.45 (m, 10H); ^{13}C nmr: 171.7, 136.5, 130.4, 129.3, 128.6, 74.1, 39.2, 31.5, 24.2, 23.4. *Anal.* calcd. ($C_{14}H_{17}NOS$): C 67.97, H 6.92; found: C 68.08, H 6.96.

*3-Methyl-2,2-pentamethylenethiazolidin-4-one (8*b*)* (ref. 7)

A solution of methylamine in ethanol was prepared as follows. To a mixture of 27 mL of ethanol and 35 mL of 50% aqueous KOH, which was cooled in an ice bath, was added 21.9 g of methylamine hydrochloride. The solution was stirred for 1 h, filtered, and the layers separated. To the organic layer was added 2-mercaptoacetic acid (20.6 g, 0.22 mol) dropwise with stirring at 0°C. Stirring was continued for 1 h, the solvent was removed, the resulting solid dissolved in toluene, and 20 g of cyclohexanone was added. Refluxing under a Dean–Stark water separator followed by evaporation gave an oil which was distilled to give **8***b*; 64%; bp 120°C (0.1 Torr) (1 Torr = 133.3 Pa) ir: 3020, 2950, 1660, 1400 cm^{-1}; ^1H nmr: 3.50 (s, 2H), 2.87 (s, 3H), 2.35–2.07 (m, 10H); ^{13}C nmr: 170.1, 73.0, 36.9, 30.9, 26.9, 24.1, 22.8.

General oxidation procedure

In a typical experiment, 0.02 mol of sulfide was dissolved in 10 mL of glacial acetic acid and cooled to 0–5°C. To this was added 1.15 equiv. of 30% hydrogen peroxide dropwise with stirring. The mixture was allowed to come to ambient temperature overnight and diluted with 15 mL of water. Solid sodium bisulfite was added until a negative peroxide test was achieved. The organics were extracted into chloroform and washed with saturated aqueous bicarbonate until the washings were basic. The extracts were dried and the solvent removed to give the crude product, which was purified as noted below.

2*a*: (Continuous extraction ($CHCl_3$) was required for acceptable yields.) Chromatographic purification (EtOAc) gave **2***a*; 87%; mp 77°C; ir: 1799, 1780, 1236, 1070 cm^{-1}; ^1H nmr: 3.82 (ABq, 2H, J = 12 Hz), 1.75 (s, 3H), 1.60 (s, 3H); ^{13}C nmr: 169.5, 98.5, 52.7, 23.1, 20.0. *Anal.* calcd. ($C_5H_8O_3S$): C 40.53, H 5.44; found: C 40.06, H 5.31.

6*b*: Unstable oil (25% crude, not purified); ir: 3500–3300, 1750, 1450, 1375 cm^{-1}; ^1H nmr: 4.78 (bs, 1H, exchanges with D_2O), 1.90 (s, 3H), 1.88 (s, 3H), 1.76 (s, 3H); ^{13}C nmr: 174.3, 100.2, 86.6, 32.7, 30.9, 27.6.

9*a*: 86%; mp 166°C (benzene); ir: 2950, 1680, 1363, 1100 cm^{-1}; ^1H nmr: 7.7–7.0 (m, 5H), 3.65 (ABq, 2H, J = 15 Hz), 2.7–0.7 (m, 10H); ^{13}C nmr: 168.6, 135.8, 129.9, 129.5, 128.9, 83.5, 51.8, 32.7, 28.9, 24.0, 23.6, 22.3. *Anal.* calcd. ($C_{14}H_{17}NO_2S$): C 63.84, H 6.50; found: C 63.65, H 6.44.

9*b*: 57%; mp 123°C (CCl_4); ir: 3015, 2980, 1680, 1050 cm^{-1}; ^1H nmr: 3.53 (ABq, 2H, J = 9 Hz), 2.90 (s, 3H), 2.51–0.80 (m, 10H); ^{13}C nmr: 167.0, 82.12, 51.3, 29.7, 28.9, 23.7, 22.8, 21.7. *Anal.* calcd. ($C_9H_{15}NO_2S$): C 53.70, H 7.51; found: C 53.79, H 7.53.

9*c*: This very water-soluble compound was decomposed by continous extraction into $CHCl_3$. Therefore the work-up was modified as follows. After destruction of the excess peroxide, the solvents were removed at room temperature and 0.4 Torr pressure. The residue was taken up in $CHCl_3$, stirred with solid K_2CO_3, filtered, and evaporated. The product was crystallized by precipitation from acetone with petroleum ether to give **9***c*; 55%; mp 109°C (benzene); ir: 3010, 1695, 1225, 1055 cm^{-1}; ^1H nmr: 4.39 (ABq, 2H, J = 11 Hz), 3.53 (ABq, 2H, J = 3 Hz), 3.0 (s, 3H); ^{13}C nmr: 167.5, 70.2, 54.1, 31.1. *Anal.* calcd. ($C_4H_7NO_2S$): C 36.07, H 5.29; found: C 36.32, H 5.23.

Pummerer rearrangements

In a typical experiment, a solution of 0.2 mol of the heterocycle in 10–15 mL of TFA containing 2 equiv. of benzene was cooled to 0°C and 1.1 equiv. of TFAA was added dropwise. The mixture was stirred at 0°C for 3–4 h, diluted with water (10–15 mL), and extracted with chloroform. The extracts were washed with aqueous bicarbonate solution, dried, and evaporated. In the case of **10***a*, the reaction mixture consisted of CH_2Cl_2/benzene and a catalytic amount of TsOH, and the electrophile was acetic anhydride.

6*a*: 45%; bp 52°C (0.75 Torr); ir: 1800–1780, 1240, 1170, 1140 cm^{-1}; ^1H nmr: 6.58 (s, 1H), 2.15 (s, 3H), 2.10 (s, 3H); ^{13}C nmr: 166.9, 156.4 (q), 118.4 (q), 91.1, 80.5, 33.3, 30.0.

10*a*: 55%; mp 132°C (benzene or EtOH); ir: 2950, 1780, 1680, 1220 cm^{-1}; ^1H nmr: 7.75–6.90 (m, 5H), 6.28 (s, 1H), 2.65–0.85 (m, 13H); ^{13}C nmr: 168.9, 168.1, 135.9, 130.3, 129.5, 129.1, 74.9, 74.1, 40.6, 39.4, 24.1, 23.9, 23.4, 21.0. *Anal.* calcd. ($C_{16}H_{19}NO_3S$): C 62.92, H 6.27; found: C 63.16, H 6.31.

10*b*: 70%; mp 163°C (benzene); ir: 2950, 1670, 1395, 1200 cm^{-1}; ^1H nmr: 5.78 (bs, 1H), 5.57 (s, 1H), 2.86 (s, 3H), 2.43–0.67 (m, 10H).

10*c*: 100% crude (not purified); oil; ^1H nmr; 6.38 (d, 1H, J = 2 Hz), 4.56 (ABq, 2H, J = 8 Hz) (high field side further split, J = 2 Hz), 3.05 (s, 3H).

Phenylation reactions

To a vigorously stirred mixture of 5 mL of concentrated H_2SO_4 and 4 mL of benzene was added 0.5 g of the sulfoxide. Stirring was continued until the exotherm ceased (ca. 40 min). The yellow solution was poured over 10 g of ice and extracted into CH_2Cl_2. The phases were separated and the organic phase dried and evaporated to yield the crude product, which was purified by crystallization or chromatography.

11*a*: 93%; mp 119–121°C (benzene); ir: 2950, 1670, 1375, 1200 cm^{-1}; ^1H nmr: 7.82–7.05 (m, 10H), 5.08 (s, 1H), 2.35–0.47 (m, 10H); ^{13}C nmr: 172.3, 138.2, 136.8, 130.6, 129.3, 128.7, 127.9, 102.7, 72.3, 51.0, 40.2, 39.8, 24.2, 23.9, 23.6. *Anal.* calcd. ($C_{20}H_{19}NOS$): C 74.26, H 6.54; found: C 74.52, H 6.54.

11*b*: 95%; mp 163°C (benzene); ir: 2960, 1660, 1400, 1200 cm^{-1}; ^1H nmr: 7.77–7.2 (m, 5H), 5.00 (s, 1H), 2.95 (s, 3H), 2.36–0.85 (m, 10H); ^{13}C nmr: 170.8, 138.1, 128.3, 128.1, 127.5, 102.5, 71.3, 49.9, 38.0, 37.3, 27.7, 24.2, 22.9. *Anal.* calcd. ($C_{15}H_{19}NOS$): C 68.92, H 7.32; found: C 68.83, H 7.54.

11*c*: 76%; oil (chromatography 1:1 EtOAc/benzene); ir: 3015, 1670, 1390, 1230 cm^{-1}; ^1H nmr: 7.23 (m, 5H), 4.80 (s, 1H), 4.30 (s, 2H), 2.90 (s, 3H); ^{13}C nmr: 171.4, 138.3, 128.6, 128.2, 127.9, 50.6, 47.7, 31.7. *Anal.* calcd. ($C_{10}H_{11}NOS$): C 62.15, H 5.74; found: C 62.09, H 5.89.

Reaction with alkenes

To a cold solution of **9***c* in 20 mL TFA and 1.5 equiv. of the alkene (1-octene or 1-hexene) was added 1.1 equiv. of TFAA dropwise with stirring. After 1 h, the solution was diluted with 20 mL of water and extracted with chloroform. The extracts were washed with aqueous bicarbonate and water, dried, and evaporated to give **12***a* or **12***b*. *E*/*Z* ratios were determined by the relative peak intensities of the sp^2 carbons in the ^{13}C nmr spectra. When 2-alkenes (cyclohexene, 2-hexene) were used, ^1H nmr spectra and gas chromatography indicated the presence of complex mixtures.

12*a*: 62%; bp 193°C (13 Torr (E/Z = 3:1); ir: 2970, 2940, 1665, 1400 cm^{-1}; ^1H nmr: 5.78–5.03 (m, 2H), 4.22 (s, 2H), 3.92–3.55 (m, 1H), 2.92 (s, 3H), 2.85–0.55 (m, 13H); ^{13}C nmr: 172.4, 134.3, 133.4, 125.0, 124.4, 47.5, 36.9, 32.3, 31.3, 29.1, 28.8, 22.3, 18.9.

Anal. calcd. ($C_{12}H_{21}NOS$): C 63.39, H 9.30; found: C 62.78, H 9.27.

12*b*: 49%; bp 115°C (0.6 Torr) (E/Z = 2:1); ir: 2975, 1670, 1420, 1395 cm^{-1}; ^{1}H nmr: 5.65–5.05 (m, 2H), 4.25 (s, 2H), 3.95–3.60 (m, 1H), 2.92 (s, 3H), 2.90–0.80 (m, 12H); ^{13}C nmr: 172.4, 134.1, 133.3, 125.3, 124.7, 47.6, 37.0, 34.8, 34.5, 31.8, 31.6, 22.6, 22.4, 18.6. *Anal.* calcd. ($C_{10}H_{17}NOS$): C 60.26, H 8.59; found: C 59.92, H 8.58.

Alkylation reactions

All alkylation reactions were run as previously reported (1). Compound **13*a*** was obtained as a mixture of mono- and dimethylated products in a ratio of 6:1 as indicated by gas chromatographic analysis.

13*a*: bp 104°C (11 Torr); ir: 3010, 1670, 1500, 1400 cm^{-1}; ^{1}H nmr: 4.38 (s, 2H), 3.85 (q, 1H, J = 7 Hz), 2.97 (s, 3H), 1.55 (d, 3H, J = 7 Hz) [1.55 (s, 6H) for dimethyl derivative]; ^{13}C nmr: 178.2, 46.8, 40.7, 31.3, 19.3 [19.11].

13*b*: 44%; bp 95°C (0.5 Torr); ir: 2980, 2950, 1670, 1400 cm^{-1}; ^{1}H nmr: 4.3 (dd, 2H, J < 1 Hz), 4.0–3.5 (m, 1H), 2.95 (s, 3H), 2.5–0.7 (m, 9H); ^{13}C nmr: 172.9, 47.5, 47.2, 33.6, 31.2, 29.1, 22.1, 13.8. *Anal.* calcd. ($C_8H_{15}NOS$): C 55.45, H 8.72; found: C 55.44, H 8.89.

Aldol condensation

The aldol condensation was run as previously reported (1). Compound **14** was obtained as a mixture of diastereomers (**14*a*** and **14*b***) in an isolated ratio of 3:2. The total yield was 54%.

14*a*: 33%; mp 145°C (1:1 EtOAc/benzene); ir: 3650–3200 (no change upon dilution), 3010, 1670, 1400 cm^{-1}; ^{1}H nmr: 7.65–7.2 (m, 5H), 5.39 (ABq, 1H, J = 2.2 Hz), 3.60 (d, 1H, J = 2.5 Hz, exchangeable), 4.18 (d, 1H, J = 2.5 Hz), 4.16 (ABq, 2H, J = 7.0 Hz) (high field end split into doublet, J = 2.2 Hz), 2.95 (s, 3H); ^{13}C nmr: 171.4, 141.2, 128.4, 128.0, 126.0, 73.0, 55.4, 48.4, 31.6. *Anal.* calcd. ($C_{11}H_{13}NO_2S$): C 59.16, H 5.86; found: C 59.18, H 5.87.

14*b*: Oil (dec. on attempted distillation); ir: 3704–3224 (no change upon dilution), 3008, 1663, 1400 cm^{-1}; ^{1}H nmr: 7.5–7.1 (m, 5H), 5.2 (s, 1H, exchangeable), 4.90 (d, 1H, J = 8.5 Hz), 4.25 (d, 1H, J = 7 Hz), 4.15–3.95 (m, 2H), 2.75 (s, 3H); ^{13}C nmr: 172.9, 140.0, 128.7, 128.5, 127.2, 76.5, 52.2, 47.7, 31.6

Acknowledgements

The financial assistance of the Natural Sciences and Engineering Research Council of Canada in the form of operating grants made this work possible. The invaluable assistance of Dr. I. T. Kay in providing experimental details of his reactions is very gratefully acknowledged.

1. J. M. McIntosh, P. Mishra, and M. A. Siddiqui. J. Org. Chem. **49**, 1036 (1984).
2. J. M. McIntosh and M. A. Siddiqui. Can. J. Chem. **61**, 1872 (1983).
3. I. K. Stamos. Tetrahedron Lett. **26**, 477 (1985); D. K. Bates and R. T. Winters. Am. Chem. Soc. Organic Abstracts (May 1985). Abstr. #56.
4. (*a*) Y. Tamura, H. Maeda, S. Akai, K. Ishiyama, and H. Ishibashi. Tetrahedron Lett. **22**, 4301 (1981); (*b*) Y. Tamura, H-D. Choi, H. Shindo, J. Uenishi, and H. Ishibashi. Tetrahedron Lett. **22**, 81 (1981); (*c*) Y. Tamura, H-D. Choi, H. Maeda, and H. Ishibashi. Tetrahedron Lett. **22**, 1343 (1981); (*d*) Y. Tamura, H. Maeda, H-D. Choi, and H. Ishibashi. Synthesis, 56 (1982).
5. M. Lounasmaa and A. Koskinen. Heterocycles. **22**, 1591 (1984).
6. S. Glue, I. T. Kay, and M. R. Kipps. J. Chem. Soc. Chem. Commun. 1158 (1970).
7. T. Kametani, K. Kigasawa, H. Mineharu, N. Wagatsuma, T. Kohagizawa, and H. Inoue. Heterocycles, **9**, 831 (1978).

Kinetics and mechanism of oxidation of lactic acid by $KMnO_4$ in H_2SO_4 medium

M. M. Girgis, S. A. El-Shatoury, and Z. H. Khalil
Chemistry Department, Faculty of Science, Assiut University, Assiut, Egypt

Received February 6, 1985

M. M. Girgis, S. A. El-Shatoury, and Z. H. Khalil. Can. J. Chem. **63**, 3317 (1985).

The initial oxidation stages of lactic acid by acid permanganate were investigated. The rate of the induction period was slow and then gradually increased. The kinetics of oxidation were second order, first order with respect to both lactic acid and Mn(VII). The reaction was acid catalyzed. Addition of Mn(II) ions largely increased the rate of the initial stages and decreased the rate of the following stages. The oxidation rate was decreased by the addition of F^- or $P_2O_7^{4-}$ ions. The Arrhenius equation was valid for the reaction between 16.5 and 34°C. Activation parameters were evaluated and a mechanism consistent with the results obtained was proposed.

M. M. Girgis, S. A. El-Shatoury et Z. H. Khalil. Can. J. Chem. **63**, 3317 (1985).

On a étudié les étapes initiales de l'oxydation de l'acide lactique par le permanganate de potassium en milieu acide. La vitesse de la période d'induction est lente mais elle augmente graduellement. La cinétique de l'oxydation est d'ordre deux, soit d'ordre un tant par rapport à l'acide lactique que par rapport au Mn(VII). La réaction est catalysée par les acides. L'addition d'ions Mn(II) augmente grandement la vitesse des étapes initiales et diminue celle des étapes suivantes. L'addition d'ions F^- ou $P_2O_7^{4-}$ diminue la vitesse d'oxydation. L'équation d'Arrhénius s'applique à cette réaction entre 16,5 et 34°C. On a évalué les paramètres d'activation et on propose un mécanisme qui s'accorde avec les résultats obtenus.

[Traduit par le journal]

Introduction

The extent of oxidation of organic substrate by permanganate depends mainly on the acidity of the medium. In alkaline or weakly acidic solution Mn(VII) changes to Mn(IV), while in strongly acidic medium Mn(VII) is further reduced, forming ultimately Mn(II). During this valence change of manganese almost every conceivable intermediate ion was suggested as participating oxidant. But the species having the main role as potential oxidant depends on the nature of the substrate and on the pH of the medium.

Considerable kinetic data were collected on the oxidation of organic compounds by potassium permanganate. Kinetics of oxidation of some α-hydroxy carboxylic acids, e.g. tartaric acid (1–3), citric acid (4, 5), and glycolic acid (6) by acid permanganate have been reported earlier. However, the details of permanganate oxidation of lactic acid are not yet known although kinetics of oxidation of this acid by other oxidants (7–10) has been reported. We were prompted to undertake the present investigation on the oxidation of lactic acid by permanganate in acid medium with a view to having an insight into the reaction mechanism.

Materials and method

Potassium permanganate was of GR (E. Merck) grade whereas lactic and sulphuric acids were of Analar (BDH) grade. All other reagents were chemically pure. All the solutions were prepared in doubly distilled conductivity water. The solution of $KMnO_4$ was boiled and filtered into a dark glass bottle for storage. Permanganate solutions were standardized by titration against oxalate (11), whereas lactic acid solutions were standardized by titration against sodium hydroxide.

Kinetic experiments were carried out in a temperature-controlled (±0.1°C) water bath. The reaction was initiated by adding to an equilibrated mixture of lactic acid and sulphuric acid the requisite quantity of pre-equilibrated potassium permanganate solution. The course of the reaction was followed by measuring the absorbance of the remaining permanganate ions at known intervals at 545 nm on a spectromom 402 photoelectric photometer, using a 1-cm matched silica cell. Absorption spectra were recorded on a Shimadzu UV-200 S double beam spectrophotometer, using the cell of path length 1 cm. It was verified that there is no interference due to other reagents at 545 nm. The reactions were usually followed up to not less than 70% completion.

The concentration of lactic acid was always kept in large excess, and pseudo-first-order rate constants were calculated by plotting log $[MnO_4^-]$ versus time.

Results

Reaction–time curve

The log $[MnO_4^-]$ versus time plots indicate clearly that the oxidation process has an "induction period" (2, 12) followed by "autoacceleration", Fig. 1.A. It was noticed that the extent of the "induction period" depends on the reaction conditions. The rates of the initial stages of the reaction were determined from the measurements of the slopes of the lines extended over the "induction period".

Stoichiometry and identification of reaction products

A solution of potassium permanganate (0.14 *M*) was added dropwise to a warm solution (40–50°C) of lactic acid (4 mL, 0.87 *M*) containing sulphuric acid (10 mL, 2 *M*) until a permanent permanganate colour appeared. Different titrimetric experiments verified that one mole of permanganate reacts with 1.25 ± 0.02 mol of lactic acid to produce acetic acid (13) and carbon dioxide as final oxidation products according to the stoichiometric equation

$$[1] \quad 4MnO_4^- + 5C_3H_6O_3 + 12H^+ = 5C_2H_4O_2 + 5CO_2 + 11H_2O + 4Mn^{2+}$$

Acetaldehyde and carbon dioxide were detected under experimental conditions in which [lactic acid] $\gg$ $[MnO_4^-]$. These products were identified by the 2,4-DNP[1] derivative and the turbidity of the $Ca(OH)_2$ solution, respectively. Obviously acetic acid was formed by the oxidation of acetaldehyde.

To find the yield of acetaldehyde under these experimental conditions ([lactic acid] $\gg$ $[MnO_4^-]$), lactic acid (0.24 *M*) was mixed with permanganate solution (0.004–0.012 *M*) and sulphuric acid (2 *M*). After an hour, the reaction mixture was cooled in an ice bath to which an excess of 2,4-DNP solution was added and the mixture was stored overnight in the refrigerator. The precipitated 2,4-DNP product was filtered onto a weighed crucible, dried, and weighed. A blank using acetaldehyde under the same experimental conditions was also run.

[1] DNP, 2,4-dinitrophenylhydrazine.

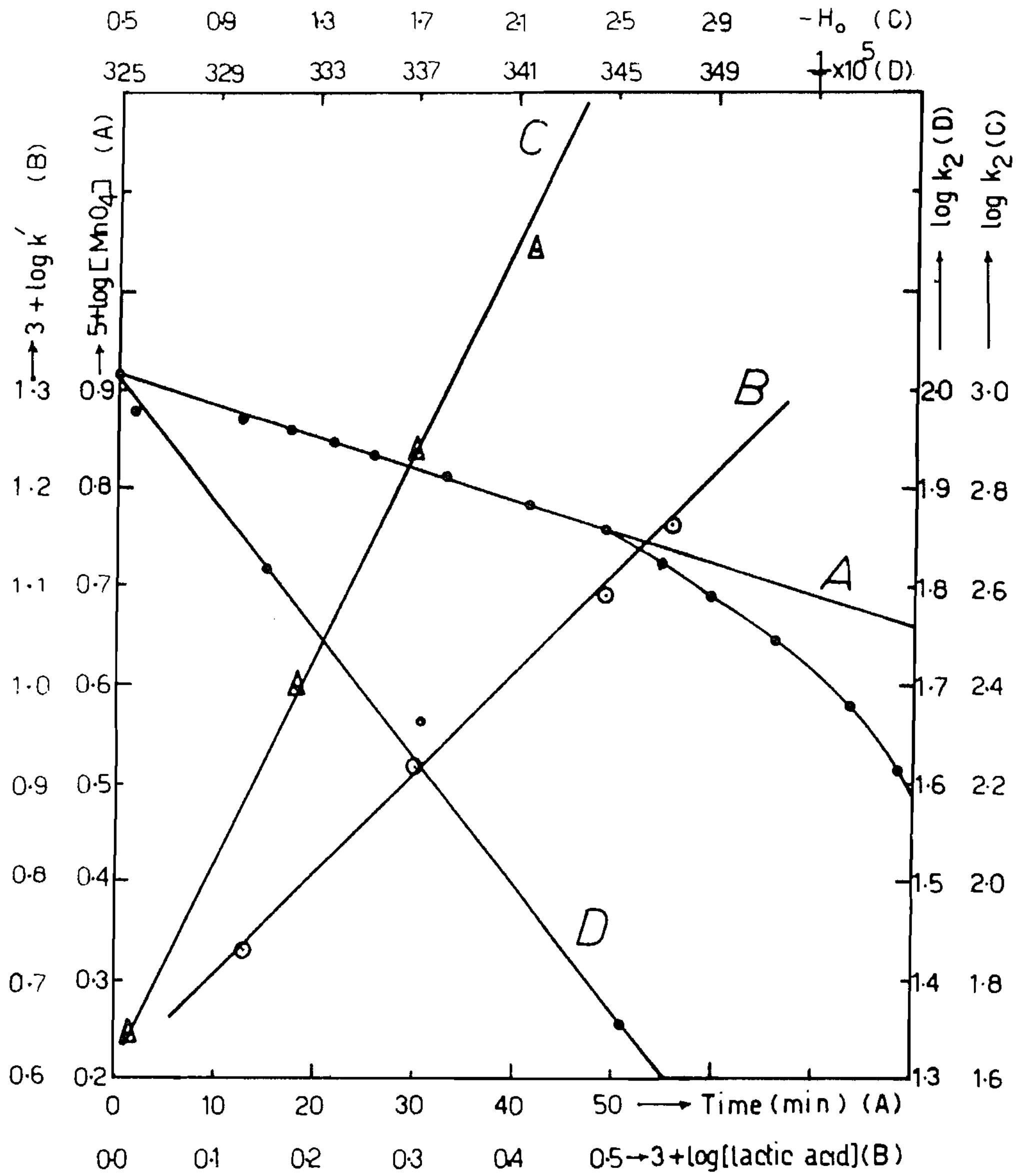

FIG. 1.A. Order with respect to [MnO_4^-]. Plot of 5 + log [MnO_4^-] versus time; [lactic acid] = 2.0 × 10^{-3} *M*; [H_2SO_4] = 2.0 *M*; temperature = 23.5°C. B. Order with respect to [lactic acid]. Plot of 3 + log *k*′ versus 3 + log [lactic acid]; [MnO_4^-] = 2.10 × 10^{-4} *M*; [H_2SO_4] = 2.0 *M*; temperature = 25°C. C. Plot of log k_2 versus $-H_0$. [MnO_4^-] = 2.11 × 10^{-4} *M*; [lactic acid] = 2.0 × 10^{-3} *M*; temperature = 23.5°C. D. The Arrhenius plot of log k_2 versus $1/T$.

It was found that the yield of 2,4-DNP derivative was 56.24% of the theoretical, according to the stoichiometric equation [2]

$$[2] \quad 2MnO_4^- + 5C_3H_6O_3 + 6H^+ = 5C_2H_4O + 5CO_2 + 8H_2O + 2Mn^{2+}$$

The precipitated 2,4-DNP derivative was recrystallized from ethanol and the product identity was established by mp and mixture mp.

Rate dependence on [permanganate]

The order with respect to permanganate was determined by studying the reaction at different initial concentrations of permanganate with fixed [lactic acid]. The [MnO_4^-] was varied in the range (0.48–10.01) × 10^{-4} *M*, [lactic acid] = 2.0 × 10^{-3} *M*, and [H_2SO_4] = 2.0 *M* at 23.5°C. Under these conditions, where [lactic acid] ≫ [MnO_4^-], the plots of log [MnO_4^-] versus time were linear, indicating the first-order dependence of rate on [$KMnO_4$] in the initial stages of the reaction, Fig. 1A. This was also confirmed by varying [$KMnO_4$], which did not show any change in pseudo-first-order rate constant (*k*′) values. The average value of *k*′ was found to be (73.6 ± 0.5) × 10^{-4} min^{-1}.

Rate dependence on [lactic acid]

The order with respect to lactic acid was deduced from the measurement of the initial rates at several lactic acid and fixed permanganate concentrations. The [lactic acid] was varied in the range (1.35–3.60) × 10^{-3} *M*, [MnO_4^-] = 2.1 × 10^{-4} *M*, and [H_2SO_4] = 2.0 *M* at 25°C. The average value of *k*′/[lactic acid] was found to be (4.03 ± 0.08) L mol^{-1} min^{-1} (Table 1). The experimental results, Fig. 1.B and Table 1, indicate that the order with respect to lactic acid is one. Thus, the reaction in the initial stages follows second-order kinetics. Our results are in good agreement with those given earlier by Sengupta *et al.* for the acid permanganate oxidation of glycolic acid (6).

TABLE 1. Effect of varying [lactic acid] on the initial rates. $[MnO_4^-]$ = 2.10 × 10^{-4} *M*; $[H_2SO_4]$ = 2.0 *M*; temperature = 25°C

[Lactic acid] × 10^3 *M*	k' × 10^3 (min^{-1})	k'/[lactic acid] (L mol^{-1} min^{-1})
1.35	5.41	4.01
2.00	8.23	4.11
3.10	12.34	3.98
3.60	14.53	4.03

TABLE 2. Effect of varying $[H_2SO_4]$ on the initial oxidation rates. $[MnO_4^-]$ = 2.11 × 10^{-4} *M*; [lactic acid] = 2.0 × 10^{-3} *M*; temperature = 25°C

$[H_2SO_4]$ *M*	k' × 10^3 (min^{-1})	$[H_2SO_4]$ *M*	k' × 10^3 (min^{-1})
2.0	8.30	4.0	83.18
3.0	31.62	5.0	173.80

Rate dependence on $[H_2SO_4]$

The reaction rates were found to increase considerably with increasing $[H_2SO_4]$, Table 2. The plot of log k_2 versus the Hammett acidity function (H_0) is linear with slope 1.04 (Fig. 1.C). Thus, an "encumbered carbonium ion" (14, 15) may be involved in the transition state involving protonation of lactic acid.

Effect of added manganous sulphate

It is reported (16) that acidified permanganate is reduced by Mn(II) to Mn(III) and Mn(IV) according to the equation:

$$[3] \quad MnO_4^- + 3Mn^{2+} + 8H^+ \rightarrow 3Mn^{3+} + Mn^{4+} + 4H_2O$$

The rate at which permanganate is reduced by Mn(II) and the effect of [Mn(II)] on the reduction rate of MnO_4^- was studied spectrophotometrically. The spectrum of acidified permanganate solution possesses absorption bands located at λ_{max} 225, 311, 490 (sh), 508, 525, 545, and 566 nm, respectively. This spectrum changes by the addition of $MnSO_4$, when the bands at 508, 525, 545, and 566 nm gradually disappear with the appearance of a single broad band of low intensity at 490 nm, and the band at 311 nm is blue-shifted to an intense shoulder located at λ_{max} 290 nm. The time needed to stabilize the new spectrum (i.e. the time required to reach a steady state of the reaction between MnO_4^- and Mn^{2+}) ranges from a few minutes to about 2 h depending on [Mn(II)]. It is worth mentioning that the new stabilized spectrum is that of Mn(III) ions (cf. Discussion).

The new oxidizing solution was prepared by adding $MnSO_4$ to an acidified permanganate solution. The mixture was kept in the dark for ~5 h before its use in lactic acid oxidation. The rate of oxidation was followed spectrophotometrically at 290 nm. The results obtained are given in Table 3 and Fig. 2. It can be noticed that the induction period disappeared completely even at low [Mn(II)] while the oxidation rates decrease gradually with increasing [Mn(II)].

Effect of added sodium pyrophosphate

It is reported that $P_2O_7^{4-}$ ions form complexes with Mn(III) and Mn(IV), while no interaction with MnO_4^- has been mentioned (17–20).[2] To substantiate the formation of Mn(III) and (or) Mn(IV) during the oxidation of lactic acid by acid permanganate and to clarify the role of these oxidizing species, different amounts of pyrophosphate were added to the reaction mixture. It was found that the oxidation rate of lactic acid is decreased by adding $P_2O_7^{4-}$ ions, while the induction period is increased with increasing $[P_2O_7^{4-}]$ (cf. Table 4). This indicates that Mn(III) and (or) Mn(IV) are the main reactive species in the autoacceleration period.

[2] See also ref. 11, p. 327.

TABLE 3. Effect of added manganous sulphate on the reaction rate. $[MnO_4^-]$ = 4.0 × 10^{-4} *M*; [lactic acid] = 2.0 × 10^{-3} *M*; $[H_2SO_4]$ = 2.0 *M*; temperature = 27°C

$[MnSO_4]$ × 10^3 *M*	k' × 10^2 (min^{-1})
0.00	1.36*
	12.49†
0.50	12.19
1.25	11.43
2.50	9.07
12.50	4.61
25.00	3.70

* In the "induction period".
† In the "autoacceleration period".

TABLE 4. Effect of added sodium pyrophosphate on the reaction rate. $[MnO_4^-]$ = 2.24 × 10^{-4} *M*; [lactic acid] = 2.0 × 10^{-3} *M*; $[H_2SO_4]$ = 2.0 *M*; temperature = 21°C

[Pyrophosphate] × 10^3 *M*	Percentage of reaction after 55 min
0.00	77.7
0.62	52.0
1.25	34.6
2.50	29.4
5.00	20.1

TABLE 5. Effect of added sodium fluoride on the reaction rate. $[MnO_4^-]$ = 2.01 × 10^{-4} *M*; [lactic acid] = 2.0 × 10^{-3} *M*; $[H_2SO_4]$ = 2.0 *M*; temperature = 24°C

[NaF] × 10^2 *M*	Percentage of reaction after 25 min
0.0	70.0
2.0	57.8
5.0	55.8
10.0	35.4
15.0	28.5

Effect of added sodium fluoride

The influence of NaF on the reaction rate parallels that observed with $Na_4P_2O_7$ (cf. Table 5). As [NaF] increases the rate decreases. This may be due to complex formation between Mn(III) and Mn(IV) and F^- ions (20).

Rate dependence on temperature

The reaction was studied at 16.5, 23.5, 29, and 34°C at [lactic acid] = 2.0 × 10^{-3} *M*, $[MnO_4^-]$ = 2.13 × 10^{-4} *M*, and $[H_2SO_4]$ = 2.0 *M*. The second-order rate constants (k_2) were calculated from rate expressions. The Arrhenius plot of log k_2 against $1/T$ was linear (Fig. 1.D). The value of activation energy was calculated from the slope of log k_2 versus $1/T$ and

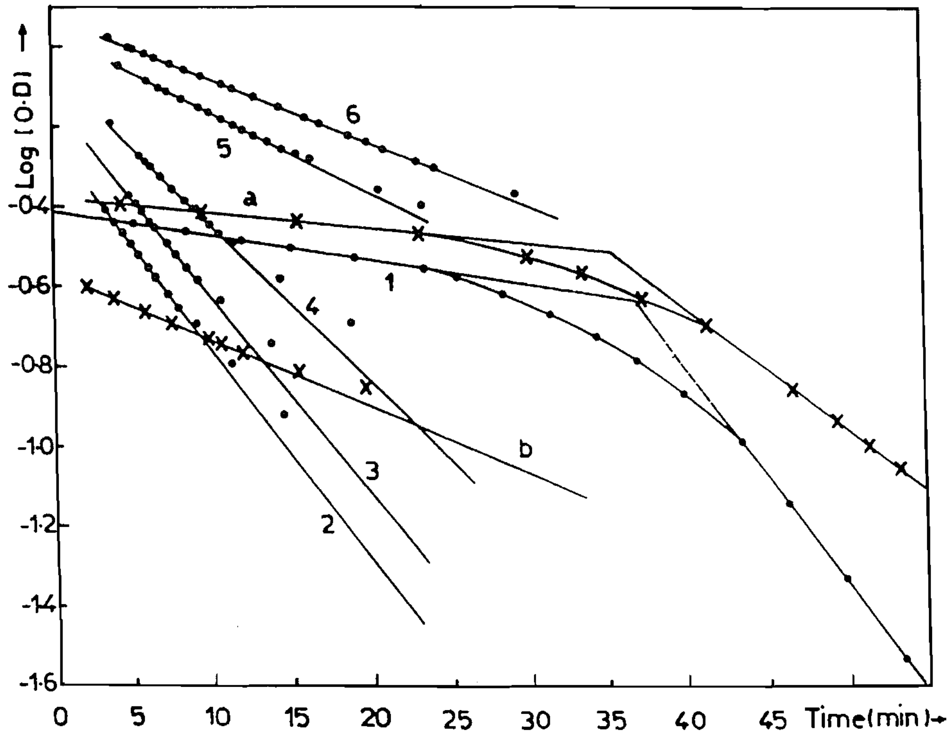

FIG. 2.A. Effect of added manganous sulphate on the reaction rate at 27°C. $[MnO_4^-] = 4.0 \times 10^{-4}$ *M*; [lactic acid] $= 2.0 \times 10^{-3}$ *M*; $[H_2SO_4] = 2.0$ *M*; $[MnSO_4] \times 10^3$ *M*: (1) 0.00, (2) 0.50, (3) 1.25, (4) 2.50, (5) 12.50, and (6) 25.00. B. Oxidation reaction of lactic acid by 2.0×10^{-3} *M* of (a) $Mn_2(SO_4)_3$; (b) $KMnO_4$ at 26°C. $[H_2SO_4] = 2.0$ *M*; [lactic acid] $= 2.0 \times 10^{-3}$ *M*; (●) = A, (×) = B.

TABLE 6. Activation parameters for the reaction between MnO_4^- and lactic acid

Parameter	Value
K* (L mol^{-1} min^{-1})	66.0
E_a (kJ mol^{-1})	61.77
$\log_{10} A$ (kJ mol^{-1})	48.13
$\Delta G_{\ddagger}$* (kJ mol^{-1})	63.44
$\Delta H_{\ddagger}$* (kJ mol^{-1})	59.26
$\Delta S_{\ddagger}$* (e.u.)	−13.84

*At 302 K.

has been recorded along with other activation parameters (Table 6).

Discussion

The first-order dependence on both MnO_4^- and lactic acid in the initial stages of the reaction leads to a simple rate expression [*i*]; assuming that MnO_4^- ion is the main oxidizing species in the induction period:

$$[i] \qquad \frac{-\mathrm{d}[\mathrm{Mn(VII)}]}{\mathrm{d}t} = k_2[\text{lactic acid}][MnO_4^-]$$

The effect of addition of Mn^{2+}, $P_2O_7^{4-}$, and F^- ions shows conclusively that MnO_4^- ion is the main reactive oxidizing species in the "induction period" whereas Mn(III) and (or) Mn(IV) are the reactive species in the "autoacceleration period".

The decrease in the oxidation rate of lactic acid with increasing amounts of manganous sulphate added (Fig. 2) indicates that Mn(IV) is involved, as the [Mn(IV)] is expected to decrease by the addition of Mn(II) ions:

$$[4] \qquad Mn^{4+} + Mn^{2+} \rightarrow 2Mn^{3+}$$

The kinetics of oxidation of lactic acid by Mn(III) (prepared as recommended by Vogel, footnote 2) were studied spectrophotometrically at 290 nm to decide whether Mn(III) and (or) Mn(IV) is the principal reactive species in the "autoacceleration period". The spectum of manganic sulphate solution shows intense bands at λ_{max} 215 (sh) and 290 (sh) nm and an absorption band of low intensity at λ_{max} 492 nm. Under identical experimental conditions, $[H_2SO_4] = 2.0$ *M*, [lactic acid] $= 2.0 \times 10^{-3}$ *M*, [Mn(III)] = [Mn(VII)] $= 4.0 \times 10^{-4}$ *M*, and temperature = 26°C, it was found that the rate of oxidation of lactic acid by acid permanganate is 6.71×10^{-2} min^{-1} in the autoacceleration period, whereas the oxidation rate using Mn(III) is 3.89×10^{-2} min^{-1}, Fig. 2. This indicates that Mn(IV) is the principal reactive species of the autoacceleration period.

From the previous results the following mechanism can be suggested, Scheme 1.
This mechanism is in agreement with the results of Sengupta *et al.* (6), Murthy and Sundaram (21), and Bakore *et al.* (22).

It is suggested that the induction period is followed by an autoacceleration between Mn(IV) and the substrate through complex formation:

$$[5] \qquad \mathrm{Mn(IV)} + \mathrm{HA} \underset{\text{fast}}{\overset{K_1}{\rightleftharpoons}} \mathrm{Mn(IV)A} + H^+$$

$$[6] \qquad \mathrm{Mn(IV)A} + \mathrm{HA} \underset{\text{fast}}{\overset{K_2}{\rightleftharpoons}} \mathrm{Mn(IV)A_2} + H^+$$

where A represents lactate species. By using the stability constants defined by eqs. [7] and [8],

$$[7] \qquad K_1 = \frac{[\mathrm{Mn(IV)A}][H^+]}{[\mathrm{Mn(IV)}][\mathrm{HA}]}$$

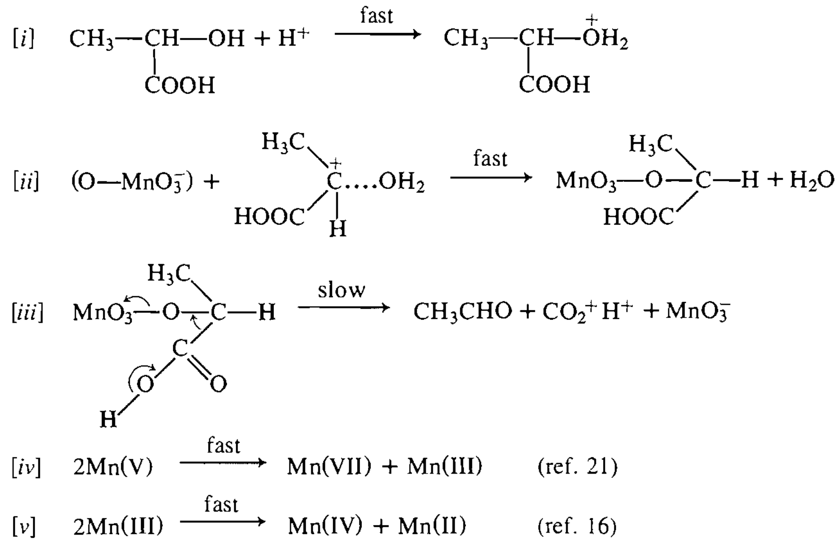

SCHEME 1

$$[8] \quad K_2 = \frac{[\mathrm{Mn(IV)A_2}][\mathrm{H^+}]}{[\mathrm{Mn(IV)A}][\mathrm{HA}]}$$

and the total concentration of Mn(IV)

$$[9] \quad [\mathrm{Mn(IV)}]_{\mathrm{total}} = [\mathrm{Mn(IV)}] + [\mathrm{Mn(IV)A}] + [\mathrm{Mn(IV)A_2}]$$

the concentrations of Mn(IV), Mn(IV)A, and Mn(IV)A_2 can be derived as

$$[10] \quad [\mathrm{Mn(IV)}] = \frac{[\mathrm{H^+}]^2[\mathrm{Mn(IV)}]_{\mathrm{total}}}{[\mathrm{H^+}]^2 + K_1[\mathrm{HA}][\mathrm{H^+}] + K_1K_2[\mathrm{HA}]^2}$$

$$[11] \quad [\mathrm{Mn(IV)A}] = \frac{K_1[\mathrm{HA}][\mathrm{H^+}][\mathrm{Mn(IV)}]_{\mathrm{total}}}{[\mathrm{H^+}]^2 + K_1[\mathrm{HA}][\mathrm{H^+}] + K_1K_2[\mathrm{HA}]^2}$$

and

$$[12] \quad [\mathrm{Mn(IV)A_2}] = \frac{K_1K_2[\mathrm{HA}]^2[\mathrm{Mn(IV)}]_{\mathrm{total}}}{[\mathrm{H^+}]^2 + K_1[\mathrm{HA}][\mathrm{H^+}] + K_1K_2[\mathrm{HA}]^2}$$

When the following competitive reactions are considered for the autoacceleration process

$$[13] \quad \mathrm{Mn(IV)A} \xrightarrow{K_a} \text{reaction products}$$

$$[14] \quad \mathrm{Mn(IV)A_2} \xrightarrow{K_b} \text{reaction products}$$

the variation of the rate of reaction with the change of substrate and hydrogen ion concentration can be expressed by the following relationship:

$$[15] \quad \text{Rate} = \frac{[K_aK_1[\mathrm{HA}][\mathrm{H^+}] + K_bK_1K_2[\mathrm{HA}]^2][\mathrm{Mn(IV)}]_{\mathrm{total}}}{[\mathrm{H^+}]^2 + K_1[\mathrm{HA}][\mathrm{H^+}] + K_1K_2[\mathrm{HA}]^2}$$

Under the experimental conditions, the factor $K_1K_2[\mathrm{HA}]^2 \ll 1$ and may be neglected. Then, eq. [15] takes the form

$$[16] \quad \text{Rate} = \frac{K'[\mathrm{HA}][\mathrm{H^+}][\mathrm{Mn(IV)}]_{\mathrm{total}}}{[\mathrm{H^+}]^2 + K_1[\mathrm{HA}][\mathrm{H^+}]}$$

where $k' = K_aK_1$. Equation [16] requires the plot of 1/rate against 1/[substrate] to be linear. The existing data satisfy this requirement. Unfortunately, the other requirement, that the plot of the reciprocal of the rate constant against the hydrogen ion concentration be linear, could not be tested because the ionic strength of the solution was not constant through the experimental conditions. Consequently, eq. [16] will no longer be expected to be valid.

1. V. M. BHALE, P. G. SANT, and S. L. BAFNA. J. Sci. Ind. Res. India, Sect. B, **15**, 45 (1956).
2. G. V. BAKORE and R. SHANKER. Indian J. Chem. **1**, 108 (1963).
3. R. PUROHIT, S. C. AMETA, and H. C. CHOWDHRY. Z. Phys. Chem. (Leipzig), **262**, 737 (1981).
4. V. M. BHALE, S. MOHAMMAD, W. V. BHAGWAT, and S. L. BAFNA. J. Sci. Ind. Res. India, Sect. B, **12**, 521 (1953).
5. G. V. BAKORE and R. SHANKER. Indian J. Chem. **1**, 286 (1963).
6. K. K. SENGUPTA, D. K. KHAMRUI, and D. C. MUKHERJEE. Indian J. Chem. **13**, 348 (1975).
7. J. SHAILENDRA, P. D. SHARMA, and Y. K. GUPTA. Inorg. Chem. **22**, 1393 (1983).
8. P. C. SAMAL, B. B. PATNAIK, S. CH. DHARMA RAO, and S. N. MAHAPATRO. Curr. Sci. **51**, 41 (1982).
9. S. C. AGARWAL and L. K. SAXENA. J. Inorg. Nucl. Chem. **42**, 932 (1980).
10. R. L. YADAV and D. P. DUBEY. J. Indian Chem. Soc. **56**, 498 (1979).
11. A. I. VOGEL. A text book of quantitative inorganic analysis. Longmans, Green, and Co., London. 1971. p. 282.
12. V. SURENDER RAO, B. SETHURAM, and T. NAVANEETH RAO. Indian J. Chem. A, **18**, 37 (1979).
13. I. L. FINAR. Organic chemistry. Longmans, Green, and Co., London, New York, Toronto. 1955. p. 344.
14. W. M. SCHUBERT, B. LAMM, and J. R. KEEFFE. J. Am. Chem. Soc. **86**, 4727 (1964).
15. R. H. BOYD, R. W. TAFT, JR., A. P. WOLF, and D. R. CHRISTMAN. J. Am. Chem. Soc. **82**, 4729 (1960).
16. P. S. RADHAKRISHNAMURTI and M. D. PRASAD RAO. Indian J. Chem. A, **15**, 524 (1977).
17. P. NATH, K. K. BANERJI, and G. V. BAKORE. Indian J. Chem. **8**, 1113 (1970).
18. R. GOPALAN and R. W. SUGUMAR. Indian J. Chem. A, **16**, 198 (1978).
19. J. S. LITTLER. J. Chem. Soc. 831 (1962).
20. H. F. LAUNER. J. Am. Chem. Soc. **54**, 2595 (1932).
21. N. S. MURTHY and E. V. SUNDARAM. Indian J. Chem. A, **16**, 806 (1978).
22. G. V. BAKORE, R. SHANKER, and U. GOYAL. Indian J. Chem. **1**, 331 (1963).

Thomsenolite, $NaCaAlF_6 \cdot H_2O$: hydrogen bonding and comparison with pachnolite

D. ADHIKESAVALU, T. STANLEY CAMERON, AND OSVALD KNOP[1]
Department of Chemistry, Dalhousie University, Halifax, N.S., Canada B3H 4J3

Received April 11, 1985

D. ADHIKESAVALU, T. STANLEY CAMERON, and OSVALD KNOP. Can. J. Chem. **63**, 3322 (1985).

The crystal structure of thomsenolite, $NaCaAlF_6 \cdot H_2O$, has been redetermined to establish the hydrogen-bonding scheme in this mineral. Both hydrogen atoms participate in branched O—H···F bonds. The hydrogen bonds link the AlF_6 octahedra to form infinite chains $\|b$, which in turn are cross-linked to form infinite double sheets $\{[AlF_6] + Ca\}$—(H_2O)—$\{[AlF_6] + Ca\}\|(001)$. The Na atoms are located exclusively in layers $\|(001)$ which separate the double sheets. A detailed comparison of thomsenolite with its dimorph, pachnolite, shows that the structure of pachnolite is obtained in essence by interchanging the positions of one half of the Na atoms and one half of the water molecules in thomsenolite. The two-dimensional, layerlike hydrogen-bonding network in thomsenolite is thereby changed to one of a three-dimensional character in pachnolite. Other features of the two structures, including the Al—F and Na···F distances, are compared and discussed in some detail.

D. ADHIKESAVALU, T. STANLEY CAMERON et OSVALD KNOP. Can. J. Chem. **63**, 3322 (1985).

On a redéterminé la structure cristalline de la thomsénolite, $NaCaAlF_6 \cdot H_2O$, dans le but d'établir la disposition des liaisons hydrogènes de ce minéral. Chacun des deux atomes d'hydrogène est impliqué dans des liaisons O—H···F ramifiées. Ces liaisons hydrogènes relient les octaèdres de AlF_6 de façon à former des chaînes infinies $\|b$ qui, à leur tour, sont réticulées pour former des doubles couches infinies $\{[AlF_6] + Ca\}$—(H_2O)—$\{[AlF_6] + Ca\}\|(001)$. Les atomes de sodium se retrouvent uniquement dans les couches $\|(001)$ qui séparent les doubles couches. Si on compare soigneusement la thomsénolite à sa forme dimorphe, la pachnolite, on s'aperçoit que, en essence, on obtient la structure de la pachnolite en interchangeant les positions de la moitié des atomes de sodium et de la moitié des molécules d'eau de la thomsénolite. Le réseau bidimensionnel des liaisons hydrogènes de la thomsénolite acquiert alors un caractère tridimensionnel dans la pachnolite. On compare d'autres caractéristiques de ces deux structures, y compris les distances Al—F et Na···F, et on les discute en détail.

[Traduit par le journal]

The hydrated fluoride mineral thomsenolite (T) has been known since 1862. Its X-ray crystal data were reported in 1946 by Ferguson (1), and its structure, with isotropic temperature factors, was determined from photographic intensities by Cocco *et al.* (2). The positions of the hydrogen atoms were not established. The absence of this detail came to our notice during our recent investigation of complex fluorides (3–5) concerned in part with hydrogen bonding, and as information on X—H···F bonds is not nearly as plentiful as that, for example, on X—H···O bonds, we set out to redetermine the structure of T with a view to completing its description.

Experimental

A small ($0.008\ mm^3$), nearly equiaxial and carefully selected crystal for this investigation was supplied by Professor H. Pauly from his comprehensive collection of fluoride minerals from Ivigtut. A CAD-4 four-circle diffractometer was used in the determination of the unit cell dimensions and in the intensity collection. The intensities were reduced by routine procedures (6). Lorentz and polarization corrections were applied, but no absorption or extinction corrections. Scattering factors were taken from ref. 7. The structure was refined using the SHELX system (8). Full-matrix least-squares ($w\Delta F^2$ = minimum) refinement was carried out with isotropic temperature factors using the positional parameters of ref. 2 as starting values. The positions, near the oxygen atom, of the maxima which were clearly visible in the difference Fourier map calculated at this stage, left no doubt that these maxima corresponded to the H atoms. The O—H bond lengths were constrained to 0.98(1) Å and the H···H distance to 1.60(2) Å, and the refinement was continued with isotropic temperature factors on the hydrogens and anisotropic on all the other atoms until $R = 4.7\%$ (Table 1). The anisotropic temperature factor is defined as $T = \exp\,[-2\pi^2(U_{11}h^2a^{*2} + U_{22}k^2b^{*2} + U_{33}l^2c^{*2} + 2U_{23}klb^*c^* + 2U_{13}hla^*c^* + 2U_{12}hka^*b^*)]$. The least-squares weights were calculated from $w^{-1} = 1.3067\sigma^2|F_o| + 0.0002F_o^2$, where σ is the weight for an individual reflection derived from the diffractometer counting statistics.

TABLE 1. Crystal data of thomsenolite

Parameter	Value: Ref. 1	Ref. 2[a]	This work
a, Å	5.57	5.583(4)	5.563(2)
b, Å	5.50	5.508(5)	5.541(2)
c, Å	16.10	16.127(6)	16.115(1)
β, deg	96.45	96.43(5)	96.35(3)
V, $Å^3$		492.8(10)	493.7(4)
ρ_o, g/cm^3	2.92–3.01	2.981	
ρ_c, g/cm^3		2.974[b]	2.986(3)
Reflections:			
Total measured		938	990
Used in refinement		735	813[c]
$100R$; $100R_w$		9.0; —	4.72; 4.58

[a]Cu Kα; isotropic temperature factors.
[b]Recalculated, 2.992.
[c]$I > 2\sigma(I)$; $\theta = 2$–$25°$.

Crystal data
$AlCaF_6H_2NaO$ fw = 221.97
Monoclinic, $P2_1/c$ (no. 14), $Z = 4$; Mo $K\alpha_1$, $\lambda = 0.70926$ Å (graphite monochromator), $\mu_{Mo} = 14.6\ cm^{-1}$, $F(000) = 432$ e. For other data see Table 1.

The structure factors are listed in Table 2,[2] the positional and thermal parameters in Table 3, interatomic distances and bond angles in Table 4, and details of the hydrogen bonding in Table 5.

Results and discussion

The positional parameters of the nonhydrogen atoms differ

[1]To whom all correspondence may be addressed.

[2]A copy of this table may be purchased from the Depository of Unpublished Data, CISTI, National Research Council of Canada, Ottawa, Ont., Canada K1A 0S2.

TABLE 3. Thomsenolite: positional and thermal parameters ($\times 10^4$)[a]

Atom	x / y / z	Δx / Δy / Δz	U_{11} / U_{22} / U_{33}	U_{12} / U_{13} / U_{23}
Na	2545(4)	−3(9)	153(10)	57(9)
	1454(4)	1(10)	193(11)	11(8)
	2484(1)	3(3)	136(10)	14(9)
Ca	1894(2)	−2(4)	42(5)	−4(3)
	6745(2)	0(4)	53(5)	−5(3)
	0990(1)	2(1)	74(5)	2(4)
Al	7177(2)	−3(6)	45(6)	1(5)
	1796(2)	−1(6)	36(7)	−14(5)
	1391(1)	−1(2)	68(7)	6(5)
F(1)	5496(5)	15(2)	79(13)	44(11)
	4643(5)	−9(13)	82(14)	−10(11)
	1267(2)	4(4)	144(15)	−3(11)
F(2)	9880(5)	7(12)	58(13)	−42(11)
	3651(5)	−2(13)	97(14)	−10(10)
	1563(2)	−1(4)	140(14)	21(12)
F(3)	4408(5)	−2(12)	84(13)	−62(11)
	0102(5)	24(13)	114(14)	14(11)
	1273(2)	8(4)	145(15)	−12(12)
F(4)	9039(5)	−2(12)	96(13)	47(11)
	−0834(5)	7(13)	76(14)	14(11)
	1576(2)	−1(4)	134(14)	8(11)
F(5)	6873(5)	−1(5)	82(13)	10(11)
	1985(5)	−2(12)	145(16)	−4(10)
	2497(2)	−2(4)	82(13)	−1(11)
F(6)	7357(5)	5(12)	121(14)	−23(11)
	1668(5)	4(14)	88(14)	3(11)
	0294(2)	7(4)	99(14)	10(11)
O	8008(6)	11(15)	94(16)	13(13)
	6599(6)	−14(16)	78(16)	2(14)
	0059(2)	6(5)	136(18)	13(14)
H(1)	7354(129)		454(205)[b]	
	6223(121)			
	0583(30)			
H(2)	7486(150)		489(257)[b]	
	8216(69)			
	−0127(46)			

[a] Δx = [x(ref. 2) − x(this work)] × 10^4, etc.; value in parentheses, esd of x in ref. 2, etc.

[b] Isotropic temperature factor U_{iso}.

only insignificantly from those of ref. 2 (Table 3), regardless of whether scattering factors for neutral or for ionized atoms were used in the refinement. For the nonhydrogen atoms the only improvement over ref. 2 is in the anisotropic refinement. The U_{ii} are small, with only a slight anisotropy. Those of Na are the largest; this agrees with ref. 2, where Na also has the largest (isotropic) temperature factor. Corrections to the Al—F distances arising from the rigid-body motion of the AlF_6 octahedron were 0.003−0.005 Å and thus comparable to 1σ for the distance; those to the FAlF angles were completely negligible.

A projection of the structure along a (Fig. 1) shows that the structure may be regarded as consisting of {[AlF_6] + Ca} layers ‖(001) which are intercalated alternately with layers of Na atoms and layers of water molecules. The coordination polyhedra of the Na and Ca atoms are irregular. Cocco *et al.* (2) describe the F_6O_2 coordination polyhedron of Ca as a distorted square antiprism and the F_8 polyhedron of Na as an augmented trigonal prism, and this description seems adequate.

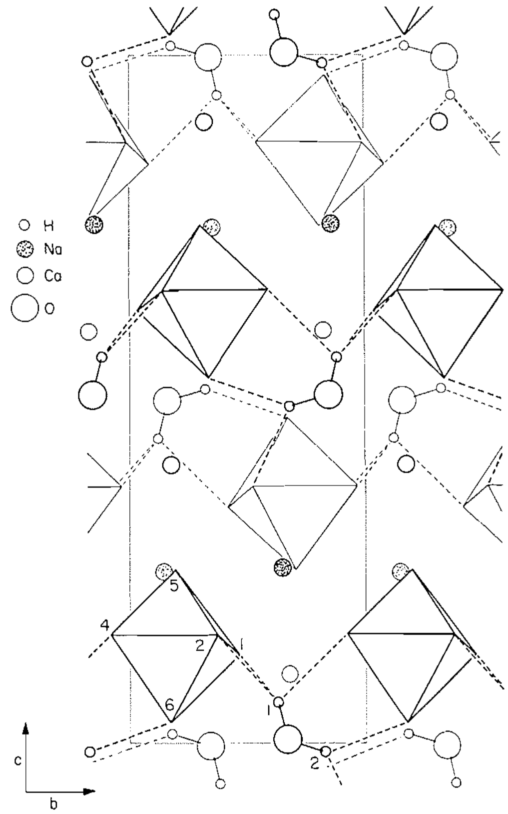

FIG. 1. Projection of the unit cell of thomsenolite along a on (100), displaying the hydrogen-bonding scheme. The hydrogen bonds are represented by broken lines; because of crowding only one of the two H···F components of the bifurcated H(2)···F bond is shown for the lower-level H(2) atoms.

The nearest cation neighbours of an oxygen atom are two almost equidistant Ca atoms (Fig. 2, top). Together with the H atoms they coordinate the oxygen atom approximately tetrahedrally. The appreciable deviations of the CaOH(1), 82(4)°, and Ca′OH(2), 120(4)°, angles from tetrahedral seem to be real, as the CaOCa′ angle is quite accurate and the dimensions to which the water molecule was constrained in the refinement represent the statistical mean for the H_2O geometry in crystalline hydrates, which is known to have only a narrow range of variation (9, 10).

Both H atoms are strongly bonded to F atoms (Table 5, Fig. 3). H(2) is involved in a fairly symmetrically bifurcated H(2)···F(6),F(3) bond, while H(1) participates in a bond to several acceptors, with O—H(1)···F(1) as the principal component. There is probably a weak participation of a more distant F neighbour in the bond to H(2). In Fig. 4 (top) OHF angles greater than 90° are plotted against their respective H···F distances. The H···F,OHF pairs are distributed fairly uniformly, with a mean of 2.31(30) Å and 123(23)°, and are strongly correlated (r = −0.93). While it is uncertain what constitutes the upper H···F limit for effective hydrogen bonding, all H···F distances corresponding to OHF ≥ 90° could in principle be viewed as involved in hydrogen-bonding interaction, especially when even the shortest H···F distances in the structure belong to bent O—H···F geometries. Without wishing to enter the "upper limit" controversy at this time,[3] we simply regard the H···F,OHF plot as a convenient description

[3] This matter will be discussed elsewhere.

TABLE 4. Thomsenolite: interatomic distances (Å) and bond angles (deg)

Atoms	Distance	Δ^a	Atoms	Angle
Al(A) —F(1A)	1.834(3)	−17(7)	F(1)—Al—F(2)	86.18(14)
—F(2A)	1.817(3)	5(7)	—F(3)	90.96(14)
—F(3A)	1.796(3)	2(7)	—F(4)	174.48(16)
—F(4A)	1.793(3)	−8(7)	—F(5)	87.44(14)
—F(5A)	1.812(3)	−1(6)	—F(6)	90.59(14)
—F(6A)	1.784(3)	−12(6)	F(2)—Al—F(3)	175.84(16)
Ca(A)···F(1A)	2.318(3)	12(7)	—F(4)	88.93(14)
···F(2Ae)	2.297(3)	−9(7)	—F(5)	89.03(14)
···F(3Aa)	2.342(3)	5(7)	—F(6)	92.13(14)
···F(4Af)	2.355(3)	0(6)	F(3)—Al—F(4)	93.79(15)
···F(5Cb)	2.461(3)	2(5)	—F(5)	87.83(14)
···F(6Bg)	2.328(3)	12(6)	—F(6)	90.91(15)
Ca(A)···O(Ae)	2.493(4)	−5(7)	F(4)—Al—F(5)	89.94(14)
···O(Bg)	2.513(4)	−5(8)	—F(6)	92.14(15)
Na(Cb)···F(1A)	2.400(4)	−11(7)	F(5)—Al—F(6)	177.64(16)
···F(2Cc)	2.323(4)	−2(8)	Symmetry code:	
···F(2A)	2.655(4)	−1(8)	A x y	z
···F(3Cb)	2.427(4)	−8(7)	B $-x$ $-y$	$-z$
···F(4Cc)	2.631(4)	0(8)	C $-x$ $\frac{1}{2}+y$	$\frac{1}{2}-z$
···F(4Aa)	2.371(4)	−4(8)	D x $\frac{1}{2}-y$	$\frac{1}{2}+z$
···F(5A)	2.497(4)	−13(8)	a X + (0, 1, 0)	
···F(5Cb)	2.424(4)	9(8)	b X + (1, 0, 0)	
			c X + (2, 0, 0)	
			d X + (0, 0, −1)	
			e X + (−1, 0, 0)	
			f X + (−1, 1, 0)	
			g X + (1, 1, 0)	

$^a\Delta = [d(\text{ref. 2}) - d(\text{this work})] \times 10^3$; value in parentheses, esd of d in ref. 2.

TABLE 5. Thomsenolite: O···F and H···F distances (Å) and OHF angles (deg) (cf. Fig. 3)^a

O	H	F	Distance O···F	Distance H···F	Angle OHF
Da	1Da	1Da	2.742(4)	1.82(6)	157(6)
		4D	2.832(4)	2.40(6)	106(4)
		2Da	3.011(4)	2.45(7)	116(5)
		6Da	2.788(4)	2.57(6)	93(4)
Da	2Da	6D	2.862(4)	2.03(7)	141(5)
		3Cb	3.019(4)	2.23(7)	137(5)
		6Cb	3.127(4)	2.68(6)	108(4)

^{a}For symmetry code see Table 4.

of the *total* (as distinct from the local) hydrogen-bonding interaction in the crystal, the standard deviations of ⟨H···F⟩ and ⟨OHF⟩ being measures of the dispersion. This plot will be found useful when comparing T with pachnolite (see below).

The shortest H···F distance, H(1)···F(1) = 1.82(6) Å, is statistically indistinguishable from 1.85(11) Å, the mean of the sample of 33 normal (i.e. to a single acceptor) H···F bond lengths in metal fluoride hydrates (X-ray data) examined in ref. 11. It is, however, appreciably longer than the H···F distances observed for H_2O coordinated to M in octahedral $[MF_5(H_2O)]^{2-}$ complexes: 1.59(6) Å in $(NH_4)_2[AlF_5(H_2O)]$ (4) and 1.61 and 1.63 Å in $Rb[VF_4(H_2O)_2]$ (11), the shortest such distances known to date. Similarly, the shortest O···F distance in T, 2.74 Å, is typical (and close to the mean) of O_w···F distances in the sample of ref. 11 and comparable to the O_w···F distances in $A_2[MF_4F_{2/2}]\cdot H_2O$, 2.73–2.75 Å (12–15), and in $A[MF_4F_{2/2}]\cdot H_2O$, 2.80–2.82 Å (16), but longer than in the

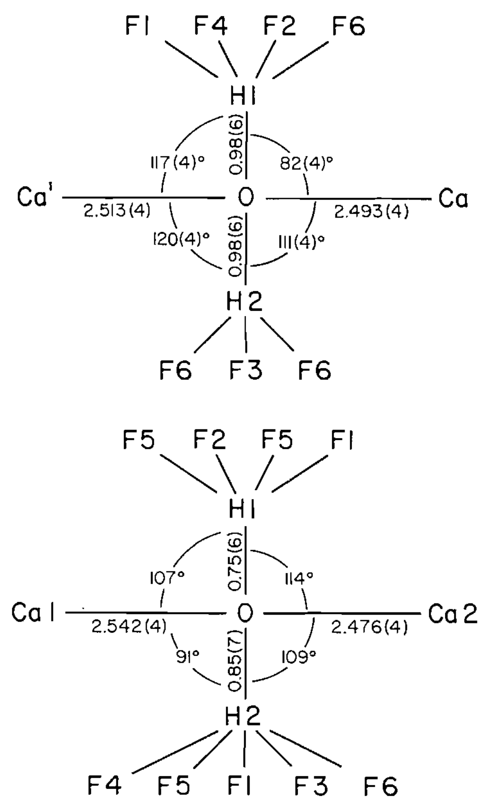

FIG. 2. Coordination of the oxygen atom in T (*top*) and P (*bottom*, after ref. 18). The CaOCa angles in T and P are 110.2(2)° and 110.5°, respectively; the HOH angles are 110(6)° and 122(6)°, respectively. Fluorine atoms at H···F distances of up to 2.9 Å are shown.

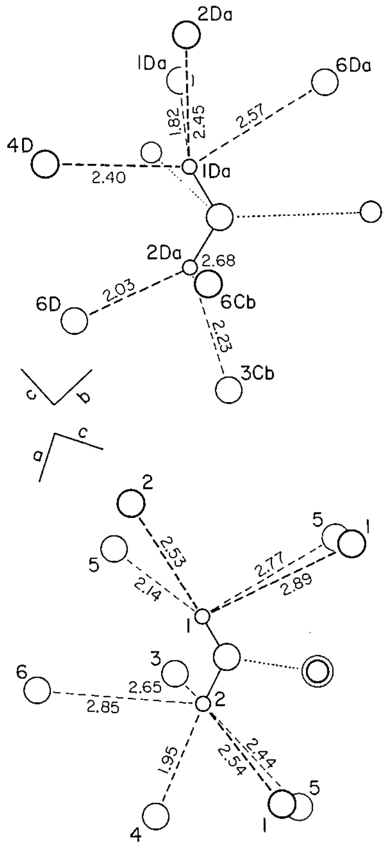

FIG. 3. Details of the hydrogen bonding in T (*top*) and P (*bottom*, after ref. 18). Projection on approximately the plane of the water molecule (on (100) in T, on (010) in P). Unlabelled circles joined to the oxygens by dotted lines are Ca atoms. For OHF angles in T see Table 5.

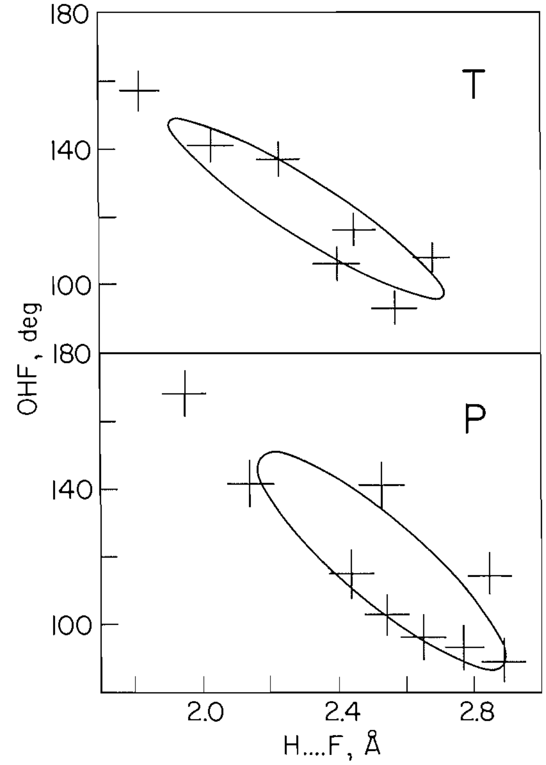

FIG. 4. Distribution of the H···F distances (≤2.9 Å) and OHF angles (≥90°) in T (*top*) and P (*bottom*, after ref. 18). The ellipses represent the normal bivariate frequency contours for half maximum frequency. Adjustment of the O—H distances in P to 0.98 Å brings the H···F, OHF distribution in P closer to that shown for T.

$A_2[MF_5(H_2O)]$ structures: 2.55 Å in $(NH_4)_2[AlF_5(H_2O)]$ (4), 2.61 Å in $Cs_2[FeF_5(H_2O)]$ (17).

The F atoms involved in the shortest H···F distances, F(1) and F(6), and the two Ca neighbours define the minimum coordination polyhedron of the water molecule. This polyhedron is, in T and $A_2[MF_4F_{2/2}]\cdot H_2O$ alike, an approximate tetrahedron. However, the AOA angle of this tetrahedron is much larger in T (and in pachnolite, see below) than in the alkali compounds, while the FOF angles are comparable:

Compound	Angle (deg) AOA	FOF
Ca_2OF_2 in T	110.2	102.3
Ca_2OF_2 in pachnolite (see below)	110.5	105.6
K_2OF_2 in $K_2MnF_5\cdot H_2O$ (12)	86.4	99.3
Rb_2OF_2 in $Rb_2MnF_5\cdot H_2O$ (14)	85.9	95.3
Cs_2OF_2 in $Cs_2MnF_5\cdot H_2O$ (13)	91.4	
Rb_2OF_2 in $Rb_2AlF_5\cdot H_2O$ (15)	86.7	83.5

Comparison with pachnolite

Pachnolite (P) is a monoclinic dimorph of T. Like the latter, it is a natural alteration product of cryolite, Na_3AlF_6. Its structure was recently reported by Hawthorne and Ferguson (18), who adopted for its description the $F2/d$ setting of $C2/c$. This setting ($\boldsymbol{a}_F = 2\boldsymbol{a}_C + \boldsymbol{c}_C$, $\boldsymbol{b}_F = \boldsymbol{b}_C$, $\boldsymbol{c}_F = \boldsymbol{c}_C$) corresponds to a very nearly orthogonal unit cell as well as to the original morphological description (1), and is retained in the following.

Hawthorne and Ferguson have pointed out that a feature common to both T and P is the presence of $[Ca_2F_{12}(H_2O)_2]^{8-}$ dimers (or, more simply, Ca_2O_2 rings), and they have shown that these dimers have, in the two structures, different orientations relative to the adopted crystallographic axes (Fig. 4 of ref. 18). Further examination brings to light an even closer similarity.

Inspection of the positional coordinates of the atoms in T (Table 3) and P (18) reveals that most of them are quite close to multiples of $\frac{1}{8}$. Furthermore, $V(P)/16 = V(T)/4$ to within 0.2%, i.e. the dimorphs are equally dense, and $a(P) \sim 2a(T)$, $b(P) \sim 2b(T)$, $c(P) \sim c(T)$, $\beta(T) - \beta(P) = 6.0°$. When the fractional coordinates are approximated by the nearest multiples of $\frac{1}{8}$ and the T cell is quadrupled by doubling a and b, the similarity of these idealized T and P structures is immediately evident (Fig. 5).

The AlF_6 octahedra in both structures are arranged in sheets ‖(010). These sheets are planar in P but undulating in T. The Ca atoms occupy analogous positions between the AlF_6 octahedra in the two structures and so do one half of the Na and one half of the O atoms, but the other half of the Na atoms in T correspond to the other half of the oxygen atoms in P, and conversely. The result of this interchange is that in T there are layers ‖(001) consisting exclusively of Na atoms; these layers alternate with similar layers consisting only of water molecules. In contrast, in P each of the corresponding layers contains both Na and O atoms in equal numbers. This has the consequence that the planes of the Ca_2O_2 rings in P are ‖(100), with the Ca atoms on C_2 axes, whereas in T the centrosymmetric rings are essentially in planes ‖(010) but tilted as a

TABLE 6. Comparison of selected interatomic distances (Å) and bond angles (deg) in T and P[a]

Distance or angle	Coordination figure	T	P
⟨Al—F⟩	AlF_6	1.806(18)	1.807(11)
⟨Na···F⟩	NaF_8 (T), NaF_9 (P)	2.47(12)	2.57(20)
⟨Ca···F⟩	CaF_6O_2	2.35(6)	2.34(4)[b]
⟨Ca···O⟩	CaF_6O_2	2.503(14)	2.509(47)
Ca···Ca	Ca_2O_2	4.108(3)	4.122(3)
O···O	Ca_2O_2	2.860(5)	2.862(6)
OCaO	Ca_2O_2	69.7(2)	69.3(18)[c]
CaOCa	Ca_2O_2	110.2(2)	110.5
⟨Al···Ca⟩	$AlCa_6$, $CaAl_6$	4.02(11)	4.02(9)
⟨Al···Na⟩	$AlNa_4$, $NaAl_4$	3.30(13)	3.30(3)[d]
⟨Ca···Na⟩	$CaNa_4$, $NaCa_4$	3.69(11)	3.68(4)

[a]For the means the value in the parentheses is the σ(mean). For other (single) values it is the esd from the structure determination.
[b]2.366 Å in CaF_2.
[c]Mean.
[d]3.39 Å in cryolithionite (22).

result of the undulation of the {$[AlF_6]$ + Ca} sheets. The rotational displacements of the AlF_6 octahedra are neglected in this idealization. However, as pointed out in ref. 18, it is these tilts that are responsible for the increase in the C.N. of Na with respect to F from eight in T to nine in P.

The geometry of the planar Ca_2O_2 rings in T and P resembles that observed with many other μ-dioxo M_2O_2 rings with M of a size comparable to Ca (19), but the dimensional similarity of these rings in the two structures (Table 6) is remarkable. The close kinship of the T and P structures is also reflected in the great similarity of the various mean interatomic distances, not only M—F and M—O, but also M—M′ (Table 6). The exception is the mean Na···F distance (2.47(12) Å in T), which is ~0.1 Å longer in P as a consequence of the increased C.N. The M—X coordination figures are AlF_6 octahedra and the less regular CaF_6O_2 and NaF_8 (or NaF_9) polyhedra.

The constancy of the mean Al—F distance in the AlF_6 octahedra is striking. The weighted mean computed from the individual Al—F means in T, P (18), α-$Li_3[AlF_6]$ (20), $Na_3[AlF_6]$ (cryolite) (21), $Na_3Li_3[AlF_6]_2$ (cryolithionite) (22), $Na_2Mg[AlF_6]F$ (weberite) (3, 23), Rb[*trans*-$AlF_2F_{4/2}$] (24), and jarlite, Na(Sr, Na, □)$_7$ (Mg, □){$[AlF_4F_{2/2}][AlF_5F_{1/2}]_2$}$_2$(OH, $H_2O)_2$ (25) — all accurately determined structures — is 1.807 Å, with a standard deviation of only 0.001 Å.[4]

The similarity of the T and P structures is also evident in the more distant coordination: in both structures the $AlCa_6$ and $CaAl_6$ coordination figures are somewhat irregular octahedra, and $NaAl_4$ and $NaCa_4$ are tetrahedra. The $AlNa_4$ and $CaNa_4$ groupings are fairly regular square pyramids (with Al or Ca at the apex) in T but highly distorted (C_2) square pyramids in P.

Hydrogen bonding in T and P

The different orientation of the Ca_2O_2 rings in the two structures results in differences in the hydrogen bonding and the

[4]In Rb_2[*trans*-$AlF_4F_{2/2}$]·H_2O (15) the unusually large elongation of the AlF_6 octahedron in the direction of the $[AlF_4F_{2/2}]_\infty^{2-}$ chain results in ⟨Al—F⟩ = 1.818(54) Å. This value has not been included in the above mean. However, the mean of the Al—F distances involving the unshared F atoms is 1.783(10) Å, i.e. identical with ⟨Al—F⟩ = 1.789(6) Å in $[AlF_5(H_2O)]^{2-}$ (4). The ⟨Al—F⟩ value in the aquo complex is smaller than in $[AlF_6]^{3-}$, which is to be expected because of the lower charge on the aquo ion.

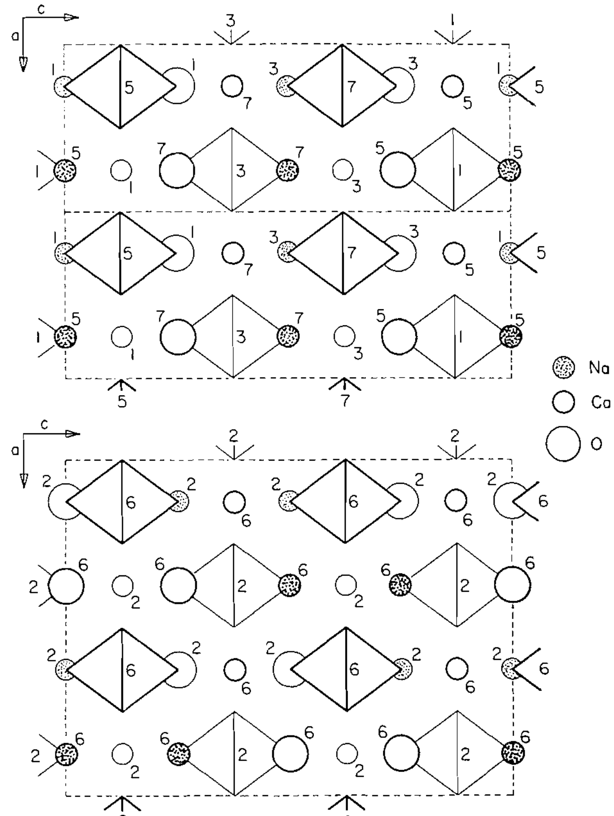

FIG. 5. Schematic representation of the relationship between the T and P structures. (*Top*) Idealized T structure. Projection of two unit cells on (010); origin shifted by (0, 0, $\frac{1}{4}$), β taken as 90°, *y* coordinates indicated in eighths of *b*(T). (*Bottom*) Idealized P structure. Projection of the lower half of the unit cell on (010); β taken as 90°, *y* coordinates indicated in sixteenths of *b*(P).

coordination of the O atom, Ca_2OH_2. A comparison can at best be approximate, given the large uncertainties in the positions of the H atoms. In the refinement of T the H_2O geometry was constrained to the mean observed in crystalline hydrates, whereas for P no constraint appears to have been applied, with the not unexpected result that O—H(1) = 0.75(6) Å, O—H(2) = 0.85(7) Å, i.e. too short, and H(1)OH(2) = 122(6)°, i.e. too large. These values, when used in the calculation of H···F distances and OHF angles, generate further uncertainties, thus affecting the comparison.

The F neighbours of a water molecule in T and P, eligible as hydrogen-bond acceptors, are shown in Fig. 3. In P the principal hydrogen bonds clearly are H(1)···F(5) and H(2)···F(4), but the bonding interaction is not necessarily restricted to these two shortest H···F distances. The OH(1)F(5) angle corresponding to H(1)···F(5) = 2.14 Å is only 142(7)° (18), and it is almost certain that the O—H(1)···F bond has a second component, with F(2) as the likely candidate. A similar, though weaker, argument can be made for H(2). Repositioning the H atoms to obtain more realistic O—H and HOH values would alter the H···F distances and OHF angles of Fig. 3: when the O—H(1) and O—H(2) distances of ref. 18 are lengthened to 0.98 Å, this adjustment alone reduces the OH(2)F(4) = 170(7)° and OH(1)F(5) = 142(7)° angles of ref. by about 20° each. The probability of the O—H···F bonds in P being nearly straight, or at least unbranched, is thus quite low, and with the H atoms properly positioned, one would expect the hydrogen-bonding situation at the water molecule in P to resemble that in T.

This expectation is supported by comparing the distributions, in T and P, of H···F distances which correspond to OHF angles favourable for O—H···F^- bonding, i.e. OHF ≥ 90° (Fig. 4). Application of a generalized *t* test (Hotelling's T^2 test) shows that the two H···F,OHF means (centres of the normal bivariate frequency contours in Fig. 4) are indistinguishable at the 0.5% significance level, i.e. there is no significant difference in the *total* hydrogen-bond engagement between T and P as measured by these distributions.[5] When the H···F and OHF values based on ref. 18 are recalculated from the lengthened O—H(1) and O—H(2) distances, the mean for P falls closer to the mean for T, so that this new mean is *a fortiori* indistinguishable from that for T. A similar result would be expected from the distribution based on more realistic (unavailable) positions of the P hydrogens.

In P the dihedral angles Ca(1)OCa(2)/F(4)OF(5) and Ca(1)-OCa(2)/H(1)OH(2) of ref. 18 are about the same, 85° and 83°, respectively, i.e. the O—H(1)···F(5) and O—H(2)···F(4) bonds are practically coplanar. In T, on the other hand, the CaOCa'/F(1)OF(6) angle, 87°, differs appreciably from the CaOCa'/H(1)OH(2) angle, 75°; this noncoincidence reflects the bifurcation of the O—H(2)···F bond.

Ultimately, a detailed comparison of the hydrogen bonds in T and P will have to await the results of a neutron-diffraction study, or at least a redetermination of both structures from low-temperature X-ray data. However, while the individual H···F and OHF values available at present suffer from large uncertainties, the overall hydrogen-bonding *schemes* can be regarded as substantially established. In T adjacent layers of AlF_6 octahedra parallel to (001) are joined by intra- and interlayer hydrogen bonds to form double layers which are separated by layers of Na atoms (Fig. 1), whereas in P the hydrogen-bond cross-linking of the AlF_6 sheets has a three-dimensional rather than a layerlike character (cf. Fig. 5).

Acknowledgments

The authors wish to thank Professor H. Pauly for selecting and supplying the thomsenolite crystal, and to the Natural Sciences and Engineering Research Council of Canada for financial support of this investigation through grants to T.S.C. and O.K.

1. R. B. FERGUSON. Trans. R. Soc. Can. **40**(IV), 11 (1946).
2. G. COCCO, P. C. CASTIGLIONE, and G. VAGLIASINDI. Acta Crystallogr. **23**, 162 (1967).
3. O. KNOP, T. S. CAMERON, and K. JOCHEM. J. Solid State Chem. **43**, 213 (1982).
4. O. KNOP, T. S. CAMERON, S. P. DERANIYAGALA, D. ADHIKESAVALU, and M. FALK. Can. J. Chem. **63**, 516 (1985).
5. O. KNOP, W. J. WESTERHAUS, M. FALK, and W. MASSA. Can. J. Chem. **63**, 3328 (1985).
6. T. S. CAMERON and R. E. CORDES. Acta Crystallogr. B, **35**, 748 (1979).
7. International tables for X-ray crystallography. Vol. IV. The Kynoch Press, Birmingham, England. 1974.
8. G. M. SHELDRICK. SHELX system report. University Chemical Laboratories, Lensfield Road, Cambridge, England. 1976.
9. M. FALK and O. KNOP. *In* Water: a comprehensive treatise. Vol. 2. *Edited by* F. Franks. Plenum Press, New York. 1973. Chapt. 2.
10. G. CHIARI and G. FERRARIS. Acta Crystallogr. B, **38**, 2331 (1982).
11. V. I. SIMONOV and B. V. BUKVETSKY. Acta Crystallogr. B, **34**, 355 (1978).
12. A. J. EDWARDS. J. Chem. Soc. A, 2653 (1971).
13. V. KAUČIČ and P. BUKOVEC. Acta Crystallogr. B, **34**, 3337 (1978).
14. P. BUKOVEC and V. KAUČIČ. Acta Crystallogr. B, **34**, 3339 (1978).
15. J.-L. FOURQUET, F. PLET, and R. DE PAPE. Rev. Chim. Miner. **18**, 19 (1981).
16. W. MASSA and V. BURK. Z. Anorg. Allg. Chem. **516**, 119 (1984).
17. N. V. BELOV, N. I. GOLOVASTIKOV, A. N. IVASHCHENKO, B. YA. KOTYUZHANSKII, O. K. MEL'NIKOV, and V. I. FILIPPOV. Kristallografiya, **27**, 511 (1982).
18. F. C. HAWTHORNE and R. B. FERGUSON. Can. Mineral. **21**, 561 (1983).
19. T. S. CAMERON, O. KNOP, and B. R. VINCENT. Can. J. Chem. **63**, 759 (1985).
20. J. H. BURNS, A. C. TENNISSEN, and G. D. BRUNTON. Acta Crystallogr. B, **24**, 225 (1968).
21. F. C. HAWTHORNE and R. B. FERGUSON. Can. Mineral. **13**, 377 (1975).
22. S. GELLER. Amer. Mineral. **56**, 18 (1971).
23. G. GIUSEPPETTI and C. TADINI. Tschermaks Mineral. Petrogr. Mitt. **25**, 57 (1978).
24. A. BULOU and J. NOUET. J. Phys. C, **15**, 183 (1982).
25. F. C. HAWTHORNE. Can. Mineral. **21**, 553 (1983).

[5] Since OHF cannot exceed 180°, the presumed normal OHF distribution is truncated. When allowance is made for the truncation, the corrected OHF mean and its σ are less than 1° smaller for both T and P.

Infrared spectra of the ammonium ion in crystals. Part XIV. Hydrogen bonding and orientation of the ammonium ion in fluorides, with observations on the transition temperatures in cubic cryolite, elpasolite, and perovskite halides[1]

OSVALD KNOP AND WOLFGANG J. WESTERHAUS[2]
Department of Chemistry, Dalhousie University, Halifax, N.S., Canada B3H 4J3

AND

MICHAEL FALK
Atlantic Research Laboratory, National Research Council of Canada,[3] Halifax, N.S., Canada B3H 3Z1

AND

WERNER MASSA
Fachbereich Chemie der Philipps-Universität Marburg, Lahnberge, D-3550 Marburg, Federal Republic of Germany

Received December 3, 1984

OSVALD KNOP, WOLFGANG J. WESTERHAUS, MICHAEL FALK, and WERNER MASSA. Can. J. Chem. **63**, 3328 (1985).

The ir spectra of the isotopic probe ion NH_3D^+ have been used to obtain information about the symmetry, orientation, and hydrogen-bonding involvement of the ammonium ion, between 10 K and room temperature, in NH_4F, NH_4HF_2, $(NH_4)_2[Cr(H_2O)_6]F_5$, NH_4PF_6, $(NH_4)_3SiF_7$, the elpasolites $(NH_4)_2BFeF_6$ (B = Na, K) and $Cs_2NH_4MF_6$ (M = Fe, Al), and the cryolites $(NH_4)_3MF_6$ (M = Al, Cr, Fe). Several of these fluorides exhibit low-temperature transitions, some of which are evident in the probe-ion spectra. It is shown that relating the isotopically isolated ND stretching and bending frequencies to the N···F distances and to the coordination numbers of the ammonium ion reveals important trends in the dependence of the behaviour of the ion on its immediate environment in the crystal. A detailed discussion is presented of the effect of ionic size and the geometric tolerance factor *t* on the transition temperatures of cubic cryolite, perovskite, and elpasolite halides, as well as on the anisotropy of the principal thermal amplitudes of the halogen atom in such compounds. The relation between T_{tr} and the frequency of the ND stretching absorption of NH_3D^+ in the ammonium representatives of these classes of halides is also explored.

OSVALD KNOP, WOLFGANG J. WESTERHAUS, MICHAEL FALK et WERNER MASSA. Can. J. Chem. **63**, 3328 (1985).

En se basant sur les spectres IR de l'ion NH_3D^+ utilisé comme sonde isotopique, on a pu obtenir des informations concernant la symétrie, l'orientation et l'implication de l'ion ammonium dans des liaisons hydrogènes dans le NH_4F, le NH_4HF_2, le $(NH_4)_2[Cr(H_2O)_6]F_5$, le NH_4PF_6, le $(NH_4)_3SiF_7$, dans les elpasolites $(NH_4)_2BFeF_6$ (B = Na, K) et $Cs_2NH_4MF_6$ (M = Fe, Al) et dans les cryolites $(NH_4)_2MF_6$ (M = Al, Cr, Fe), à des températures allant de 10 K à la température ambiante. Plusieurs de ces fluorures présentent des transitions à basses températures et certaines d'entre elles sont très évidentes dans le spectre de l'ion sonde. On montre que si l'on relie les fréquences d'élongation et de déformation de la liaison ND isotopiquement isolée aux distances N···F et au nombre de coordination de l'ion ammonium, on peut mettre en évidence des tendances importantes entre le comportement de l'ion et sont environnement immédiat dans le cristal. On discute en détail de l'effet de la dimension de l'ion et du facteur de tolérance géométrique, *t*, sur les températures de transition des halogénures cubiques de la cryolite, de la pérovskite et de l'elpasolite ainsi que sur l'anisotropie des amplitudes thermiques principales de l'atome d'halogène de ces composés. On a également étudié la relation qui existe entre le T_{tr} et la fréquence d'absorption de l'élongation de la liaison ND de l'ion NH_3D^+ de cette classe représentative d'halogénures d'ammonium.

[Traduit par le journal]

In Part VI (2) an effort was made to explore, systematically, the dependence of the strength and type of hydrogen bonding of the ammonium ion in a variety of halides on factors such as the nature of the acceptor atom X, the coordination number of the ammonium ion and the N—H···X angle. Whilst the gross features of this dependence were successfully identified, the compounds were too few to obtain a detailed picture of the overall situation. In particular, the number of fluorides included was not sufficiently large if one considers that the fluorides determine the observed trend in a greater measure than the other halides, which exhibit a relatively narrow range of behaviour and form a fairly homogeneous group.

In the present work we have supplemented these results by obtaining the ν_1 and ν_{4bc} spectra of the NH_3D^+ probe ion in additional fluorides, including some recently described (3–5) complex ammonium fluorides in which the ammonium ion has the rare C.N. of 4 and 6. Advantage has also been taken of the improved cryogenic system to reinvestigate the spectra of some of the fluorides dealt with in ref. 2, down to 10 K. These extensions have resulted, among other things, in a better understanding of some of the problems investigated by Epple (5, 6) on undeuterated samples of the $(NH_4)_3MF_6$ (M = Al, Cr, Fe) cryolites and the $(NH_4)_2BFeF_6$ (B = Na, K) and $Cs_2NH_4MF_6$ (M = Al, Cr, Fe) elpasolites.

The compounds included in the present analysis of hydrogen bonding in ammonium fluorides are listed in Table 1. The symbols, abbreviations and numbering of the compounds follow ref. 2; $\nu_1(10)$ stands for $\nu_1(NH_3D^+)$ at 10 K etc.

Experimental

Preparation of deuterated samples

High-purity NH_4F was deuterated by recrystallization from MeOH–MeOD mixtures of the requisite composition. **54** was prepared as in ref. 4 using weakly deuterated reactants throughout.

The elpasolites **57**, **58**, **63**, and **64** were prepared by reacting par-

[1] For Part XIII, see ref. 1.
[2] Present address: Max-Planck-Institut für Festkörperforschung, D-7000 Stuttgart 80, Federal Republic of Germany.
[3] NRCC No. 24746.

TABLE 1. Structural features of the ammonium fluorides discussed in this work[a]

No.	Compound	Type[b]	C.N.	S	E	T_{tr}, K	References
1	NH_4F	W	4	C_{3v}	C_{3v}		7, 8
54	$(NH_4)_2[Cr(H_2O)_6]F_5$		4	C_3	C_3		4, 9
36	NH_4SnF_3		3+3	C_3	C_3		10
53	NH_4HF_2	CsCl	4	C_2	C_2		11
40	NH_4PF_6	NaCl	?	O_h	T_d	131.3;[c] 191.8[d]	12
58	$Cs_2NH_4FeF_6$	E	6	O_h	T_d	196(3)	3, 13; this work
64	$Cs_2NH_4AlF_6$	E	6	O_h	T_d		3
39	NH_4AlF_4	CsCl	8	D_{4h}	D_{2d}		14
35	NH_4MnF_3	P	12	O_h	D_{2d}	181	15–18
50	NH_4CoF_3	P	12	O_h	D_{2d}	124.5	15
51	NH_4ZnF_3	P	12	O_h	D_{2d}	115.1	15
37	NH_4BF_4	$BaSO_4$	<12	C_s	C_s	461.9[e]	12, 19
18	$(NH_4)_2SiF_6$	A	12	T_d	T_d		2, 10
31	$(NH_4)_2SiF_6$	T	12	C_{3v}	C_{3v}	38.6[f]	20
32	$(NH_4)_2GeF_6$	T	12	C_{3v}	C_{3v}		20
20	$(NH_4)_2SnF_6$	A	12	T_d	T_d		21
34	$(NH_4)_2SnF_6$	T	12	C_{3v}	C_{3v}	~100	20, 21
33	$(NH_4)_2TiF_6$	T	12	C_{3v}	C_{3v}		20, 22
19	$(NH_4)_2PtF_6$	A	12	T_d	T_d		23
57	$(NH_4)_2NaFeF_6$	E	12	T_d	S_4	159	3, 13, 31; this work
63	$(NH_4)_2KFeF_6$	E	12	T_d	S_4	290(15)	3; this work
59	$(NH_4)_3AlF_6$	C	6; 12	O_h; T_d	T_d; D_{2d}	193.0;[g] 220.8[g]	24
60	$(NH_4)_3CrF_6$	C[h]	6; 12	O_h; T_d	T_d; D_{2d}	266	5, 13, 24
61	$(NH_4)_3FeF_6$	C[h]	6; 12	O_h; T_d	T_d; D_{2d}	267.0,[i] 264(2)	13, 25–28
62	$(NH_4)_3SiF_7$		10; 14	C_{2v}; C_{4h}	C_{2v}; S_4	?	29

[a]At room temperature. C.N., coordination number of NH_4^+; S, site symmetry; E, effective symmetry of NH_4^+; T_{tr}, transition temperature. Compounds with running numbers **44** and lower were reported in ref. 2.
[b]Cation/anion packing type. A, antifluorite; C, cryolite; E, elpasolite; P, perovskite; T, β-$(NH_4)_2SiF_6$ type; W, wurtzite.
[c]λ-point, $\Delta S_{tr}/R$ = 1.12 (30).
[d]Gradual, λ-point resembling transition; $\Delta S_{tr}/R$ = 1.24 (30).
[e]$\Delta S_{tr}/R$ = 2.3 (ref. 19, p. 340).
[f]λ-point, $\Delta S_{tr}/R$ = 0.7 (ref. 19, p. 340).
[g]λ-points, $\Delta S_{tr}/R$ = 0.5 and 2.2, respectively (24).
[h]Low-temperature phase is derived from the $Fm3m$ phase by triclinic distortion (5, 13).
[i]λ-point, $\Delta S_{tr}/R$ = 3.0 (25).

tially deuterated $(NH_4)_3MF_6$ with the appropriate anhydrous fluorides in sealed Pt capsules at 300°C. The capsules were heated in an autoclave in N_2 at 100–200 atm. The compounds **57** and **58** gave very sharp diffraction patterns; the powder patterns of **63** and **64** were less well defined. Some of the **58** preparations were slightly contaminated with Cs_2SiF_6, the silicon having been introduced through accidental contact of the reactants with silica glass. Because of this and of the variation in the detail of some of the ND absorptions in the spectra of the first two **58** preparations, a special effort was made to eliminate the contamination by modifying the conditions of the high-pressure synthesis. Altogether, three undeuterated and five deuterated samples were prepared; the last 0% D and 4% D preparations were pure elpasolite phases within the limits of detection by careful X-ray powder diffractometry (both **58** and Cs_2SiF_6 are cubic). In spite of these precautions, however, the slight variability, from sample to sample, of the ND spectra remained. The reasons for the variability have not been established, but is is possible that kinetic factors are responsible, analogous to those leading occasionally and unpredictably to the suppression of low-temperature transitions in ammonium hexabromometallates(IV) (cf. footnotes 10 and 13 below).

The cryolites **59**, **60**, and **61** were precipitated from partially deuterated hot concentrated solutions of AlF_3, CrF_3, and $Fe(NO_3)_3$, respectively, in aqueous HF with excess solid NH_4F.

To prepare **62**, solutions of $(NH_4)_2SiF_6$ and excess NH_4F in 5% D_2O were mixed and evaporated on a steam bath until crystallization began. The colourless needles were washed with ether and dried in air.

Commercial reagent-grade NH_4HF_2 and NH_4PF_6 were deuterated by recrystallization from aqueous solutions containing D_2O and acidified with HF.

Infrared spectra

Unless noted otherwise the finely ground sample powders were mulled in fluorolube and the mulls were supported between CaF_2 plates. The variable-temperature spectral runs were made in the heating mode, but thermal cycling through T_{tr} was employed where applicable. Most of the spectra were recorded on a Perkin–Elmer model 180 spectrophotometer; some were also obtained with a Fourier-transform ir spectrometer (Bomem DA3.02) which became available in the later stages of this investigation. Both instruments were fitted with a closed-cycle He refrigerator.

Results

NH_4F (1)

The site symmetry S at the N atom in this crystal is C_{3v}, hence the effective symmetry E of the NH_4^+ ion is also C_{3v}. Two bands in a 3:1 intensity ratio would therefore be expected for the ν_1 and three bands, in a 2:3:3 intensity ratio, for the ν_{4bc} fundamental of the probe ion. However, as pointed out earlier (2), the displacement between the N and F hcp sublattices of this $P6_3mc$ structure is such that each ion is equidistant, at 2.708(3) Å, from its nearest counterion neighbours (7, 8) (Fig. 1). On this evidence the symmetry of the NH_4^+ ion is indistinguishable from T_d, and one band each would be expected for the two fundamentals. A *single* ν_1 and a *single* ν_{4bc} band were indeed observed, at all temperatures between 5 and 293 K, at the levels of resolution and deuteration employed in the previous study (2). We have now reinvestigated the NH_3D^+

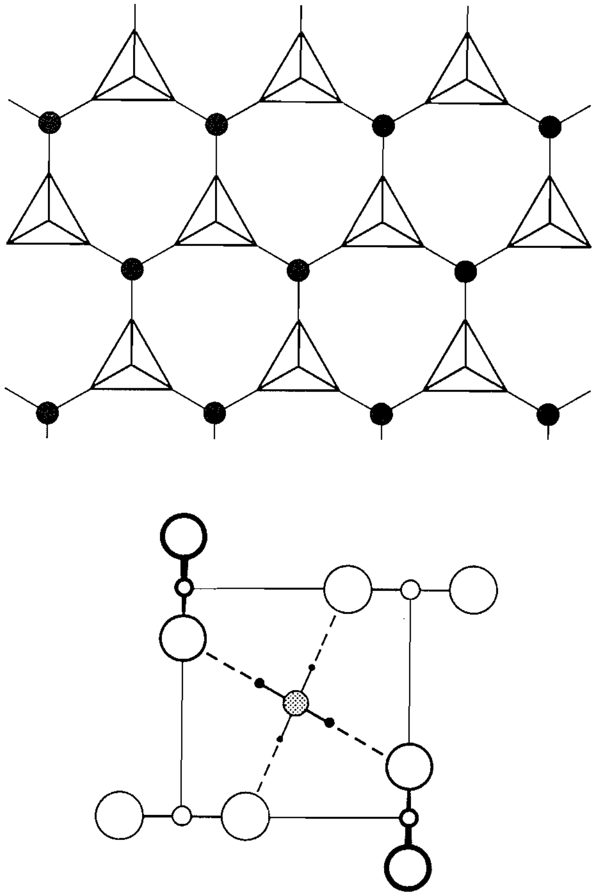

FIG. 1. Schematic representation of the hydrogen bonding in NH_4F (one layer, *top*) and NH_4HF_2 (*bottom*).

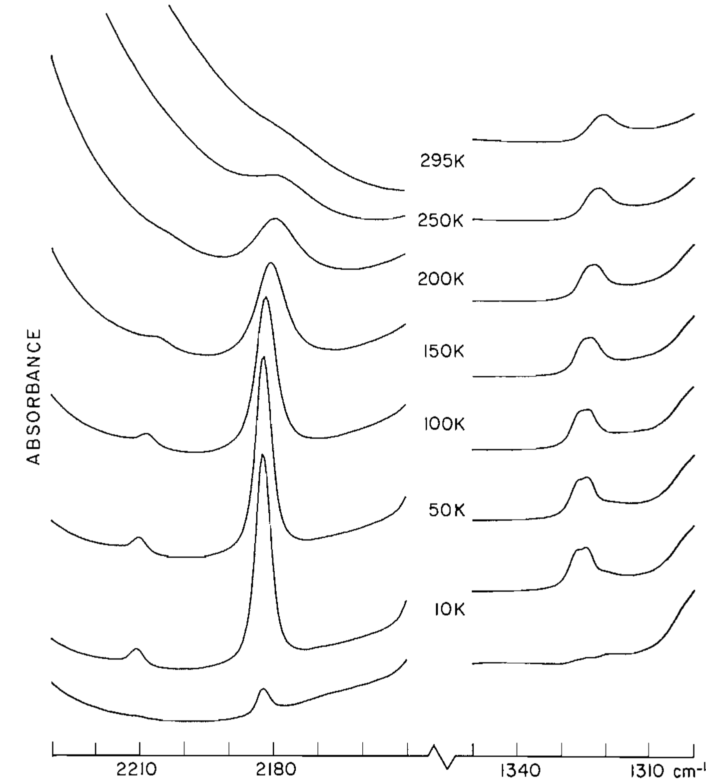

FIG. 2. Spectra of NH_4F (0.3% D) in the regions of the ND stretching fundamental ν_1 (*left*) and the ND bending fundamental ν_{4bc} (*right*) of the NH_3D^+ probe ion at different temperatures. The bottom spectrum is that of a 0.04% D sample at 10 K.

absorptions in more detail, mainly to see whether the two bands show incipient resolution under improved experimental conditions.

The ν_1 region presents a number of complications. It contains intense overtone bands of undeuterated NH_4F, so that at low deuteration the ν_1 absorption is a small band on a sloping background which changes with temperature. This and the Christiansen effect at low temperatures result in a considerable uncertainty as to the true band shape and temperature shifts. We therefore made every effort to minimize the Christiansen effect and, taking advantage of the superior sensitivity of the FT over the previously employed grating spectrometer, we were able to record very good spectra not only at ~0.3% D, but even at an estimated 0.04% D isotopic replacement, i.e. at a concentration level approaching the natural abundance of D in water.

The maximum of the ν_1 band at 10 K in these spectra (Fig. 2) was at 2182.4(2) cm^{-1}, in agreement with the previously reported value of 2182.0 cm^{-1} at 5 K (2). The small halfwidth of the band (4.0 cm^{-1} at 0.3% D and 3.3 cm^{-1} at 0.04% D), its visual symmetry, and the absence of any absorption, in the ν_1 region, responding to variable deuteration and of an intensity approximately either one-third or three times that of the 2182 cm^{-1} band, are evidence that the latter band in fact constitutes *all* of the ν_1 absorption. The two ν_1 components, if indeed distinct, cannot thus be separated by more then 2 cm^{-1}. The ν_{4bc} fundamental, on the other hand, did show structure. At 10 K it appeared as a barely resolved doublet at 1324.5 and 1326.2 cm^{-1}, with a band shape not inconsistent with the 2:3:3 triplet required by $E = C_{3v}$.

With increasing temperature both ν_1 and ν_{4bc} gradually moved to lower wavenumbers (Fig. 3). The $d\nu/dT$ coefficient was almost zero at 10 K but increased with temperature. The halfwidth of the ν_1 band changed very little with temperature up to about 100 K, after which it increased gradually. The increase was only about half that encountered with the other compounds investigated here. The integrated intensity of ν_1 decreased with increasing temperature, at first slowly and then very sharply. At room temperature the band area was only about one tenth of that at 10 K and above about 200 K the band position and halfwidth could not be measured with confidence. The halfwidth of the ν_{4bc} band remained almost stationary with temperature, while its integrated intensity decreased somewhat on warming the sample, though much less rapidly than for ν_1.

The ν_1 band was accompanied by several pairs of satellites, of which the most prominent were at 2211 and 2146 cm^{-1}, the latter enhanced by the NH_4F overtone band at 2142 cm^{-1}. The intensities of these satellites, relative to ν_1, diminished with increasing isotopic dilution and their positions shifted with temperature in the same direction though not exactly at the same rate as ν_1. The satellites appear to correspond to the in-phase and out-of-phase modes arising from pairs of adjacent NH_3D^+ ions in the crystal. Similar satellites are observed in other ammonium salts, but they are much less intense at comparable levels of deuteration. Their unusual prominence in **1** is due to the distinctive features of the NH_4F structure: the low C.N. of NH_4^+ in **1** increases the frequency of occurrence of such pairs compared with crystals of C.N. > 4, and the small

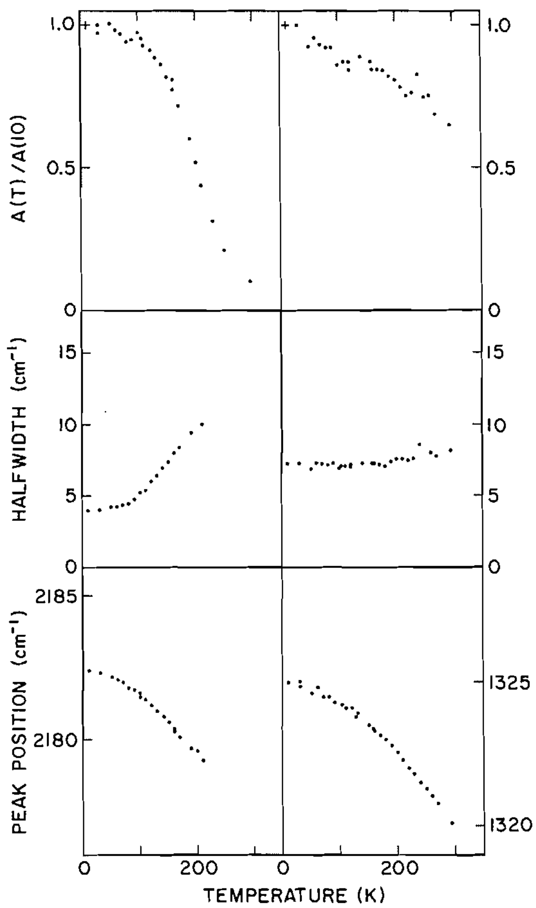

FIG. 3. Temperature variation of the peak positions, halfwidths and relative band areas $A(T)/A(10)$ for $\nu_1(NH_3D^+)$ (*left*) and ν_{4bc} (*right*) in NH_4F.

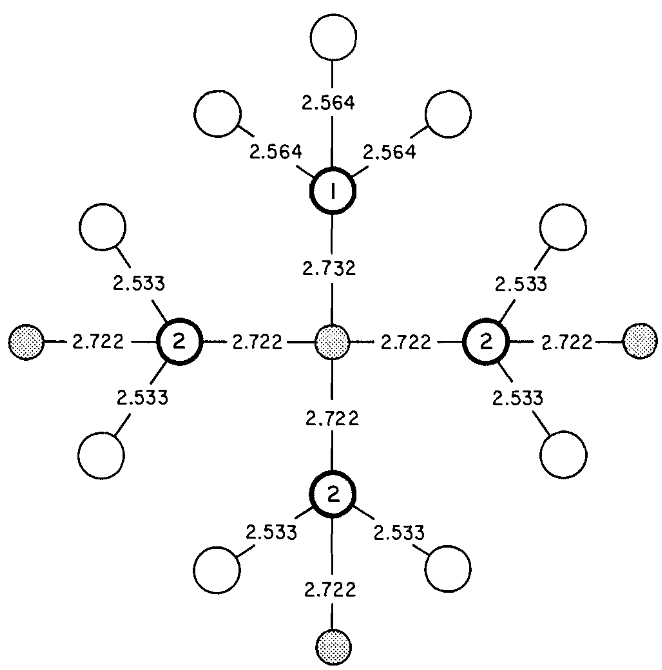

FIG. 4. Schematic representation of the hydrogen bonding of the ammonium ion in $(NH_4)_2[Cr(H_2O)_6]F_5$. Heavily outlined circles, F; open circles, O; shaded circles, N.

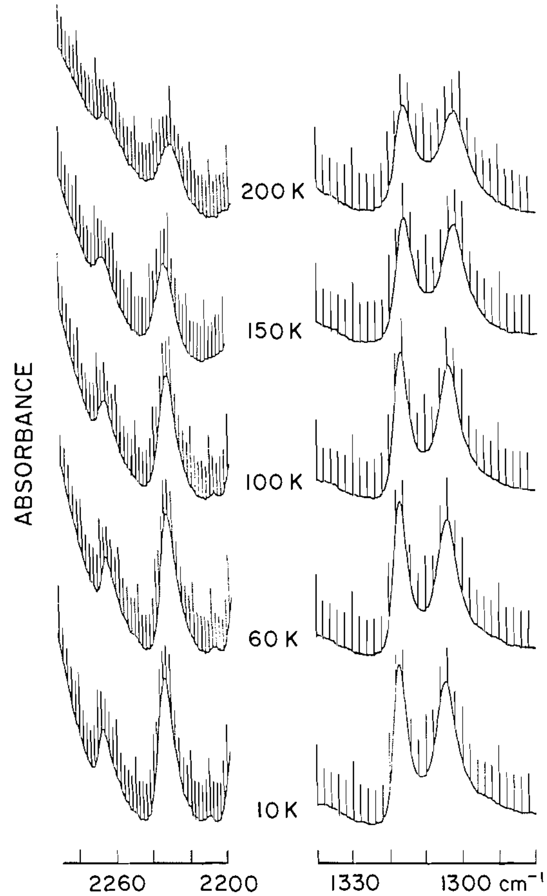

FIG. 5. Spectra of $(NH_4)_2[Cr(H_2O)_6]F_5$ (3% D) in the ν_1 (*left*) and ν_{4bc} (*right*) regions at different temperatures.

H···F separation, ~1.67 Å, which corresponds to a strong hydrogen-bonding interaction, gives rise to strong coupling of neighbouring transition dipoles.

$(NH_4)_2[Cr(H_2O)_6]F_5$ (54)

The crystal structure was originally (4) described as monoclinic ($C2/c$, no. 15; $Z = 4$) but metrically indistinguishable from orthohexagonal. It seems, however, that the true symmetry is trigonal ($P\bar{3}c1$, no. 165; $Z = 2$).[4] In the following the trigonal description has been adopted and the F and O atoms renamed accordingly (all oxygens are now equivalent; F(2) and F(3) of $C2/c$ are now F(2)).

The N atom (site symmetry C_3) is coordinated by an F(1) atom on the same threefold axis, at an N···F(1) distance of 2.732 Å, and by three nonaxial fluorines F(2) at N···F(2) = 2.722 Å. The coordination figure of N is thus an almost regular F_4 tetrahedron and resembles more closely than in any other ammonium compound the coordination of N in NH_4F. The F(1) atom in turn is coordinated by three nonaxial oxygens at 2.564 Å (Fig. 4).

For an ammonium ion of C_3 symmetry we would expect a 1:3 ν_1 doublet and a 2:3:3 ν_{4bc} triplet. Noting that in NH_4F ($E = C_{3v}$) ν_1 was a singlet and ν_{4bc} was an only partially resolved band even at 10 K, it would seem *a priori* unlikely that

[4]This has in the meantime been pointed out, independently, in a recent paper by Marsh and Herbstein (9). In $P\bar{3}c1$ the atoms would be distributed as follows: Cr in 2(b), N and F(1) in 4(d), F(2) + F(3) in 6(f), and O(1) + O(2) + O(3) in 12(g).

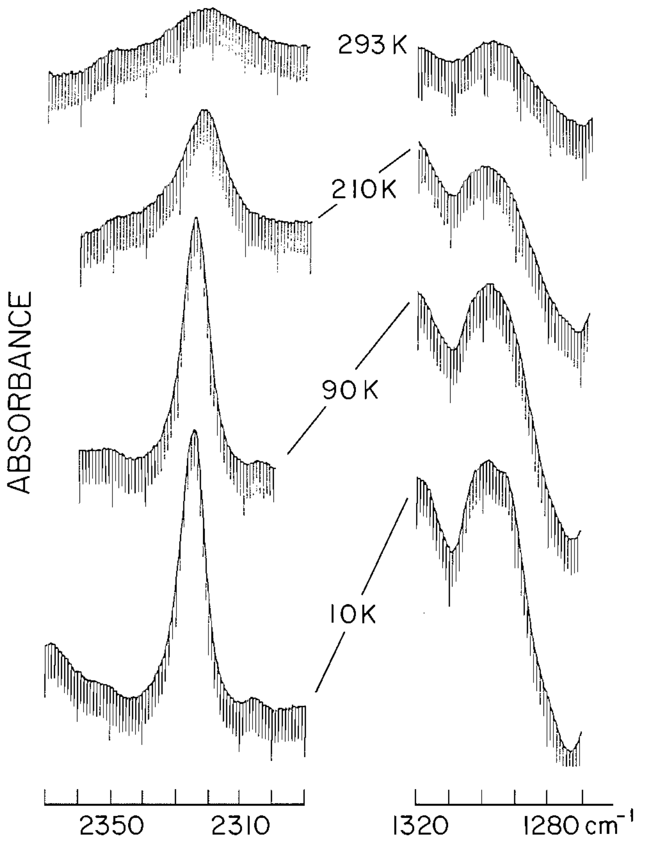

FIG. 6. Spectra of NH_4HF_2 (1.8% D) in the ν_1 (*left*) and ν_{4bc} (*right*) regions at different temperatures.

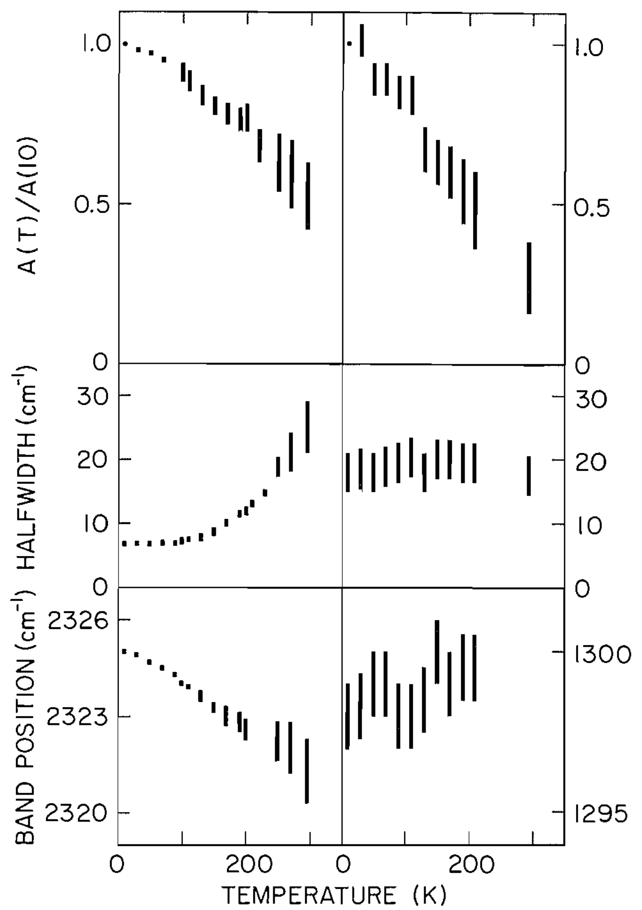

FIG. 7. Temperature variation of the ν_1 (*left*) and ν_{4bc} (*right*) peak positions, halfwidths and relative band areas $A(T)/A(10)$ in NH_4HF_2. The ν_1 band parameters have been extrapolated to 0% D; those for ν_{4bc} are for 1.8% D.

these composite absorptions would be resolved in **54**, where the N···F(1) and N···F(2) distances are practically identical and only slightly longer than the N···F distances in NH_4F.

The spectrum of the undeuterated material showed considerable complexity and was dominated by broad and very intense OH stretching bands of strongly hydrogen-bonded water of coordination. On deuteration two bands in the ND stretching region and two bands in the ND bending region appeared (Fig. 5), in positions intermediate between the corresponding respective absorptions of NH_4F and NH_4HF_2, and thus in the range expected for ν_1 and ν_{4bc}. When the lower ν_1 frequency is paired with the higher ν_{4bc} frequency, and the higher ν_1 frequency with the lower ν_{4bc} frequency, the two ν_1, ν_{4bc} points fall close to the best straight line drawn through the corresponding points for NH_4F, NH_4HF_2 and NH_4AlF_4 in the ν_1, ν_{4bc} plot of Fig. 3 of ref. 2; similarly, the two ν_1 points fall very close to the point for $\nu_1(n)$ of NH_4SnF_3 in the ν_1 vs. d(H···X) plot (Fig. 1 of ref. 2). There is thus little doubt that the observed four bands are genuine NH_3D^+ absorptions.

At 10 K the two narrow ν_1 bands, with intensities in an approximate ratio of 1:3, were at 2267(1) and 2233(1) cm^{-1}. The ν_{4bc} bands appeared at 1317 and 1304 cm^{-1}. This approximately 2:3 ν_{4bc} doublet may represent a more complex, incompletely resolved multiplet; the somewhat broader 1304 cm^{-1} feature may contain several unresolved components. The frequencies of all these bands decreased with increasing temperature by not more than 2 cm^{-1} between 10 and 200 K. The estimated halfwidths of all the ν_1 and ν_{4bc} bands at 10 K were about 9 cm^{-1}, increasing to about 14 cm^{-1} at 200 K, i.e. by an amount comparable to that observed for NH_4F.

The question arises why *two* ν_1 components, separated by 34 cm^{-1}, are observed when the N···F(1) and N···F(2) distances are practically the same. The explanation must be in the dissimilar acceptor strengths of the four nearest F neighbours of the ammonium ion. In addition to the hydrogen bond to the central nitrogen, each F(2) atom is hydrogen-bonded to another N and to two oxygens, whereas the F(1) atom is hydrogen-bonded to three oxygens (Fig. 4). This would make F(1) a weaker acceptor. The lower acceptor strength, perhaps also reflected in the marginally longer N···F(1) distance, would raise the ν_1 frequency of the axial ND bond. Explanation along these lines is consistent with the ν_1 frequency observed in NH_4F, 2183 cm^{-1} at 10 K, in which crystal the four F atoms coordinating an ammonium ion are hydrogen-bonded to three other N atoms each and thus have acceptor strength greater than any of the fluorines in **54**. From these observations it follows that for very short hydrogen-bonded N···F distances the ν_1 frequency is highly sensitive to small changes in the acceptor strength.

NH_4HF_2 (53)

This structure is a distorted version of the CsCl arrangement (*Pmna*, no. 53; Z = 4) and thus nominally it belongs to the C.N. 8 group of compounds. Although the ammonium ion in 8-coordination often is a case of 4-coordination with alternative orientations (e.g. in NH_4AlF_4), in **53** it may be considered as genuinely 4-coordinated, $E = C_2$ (Fig. 1). The N···F distances

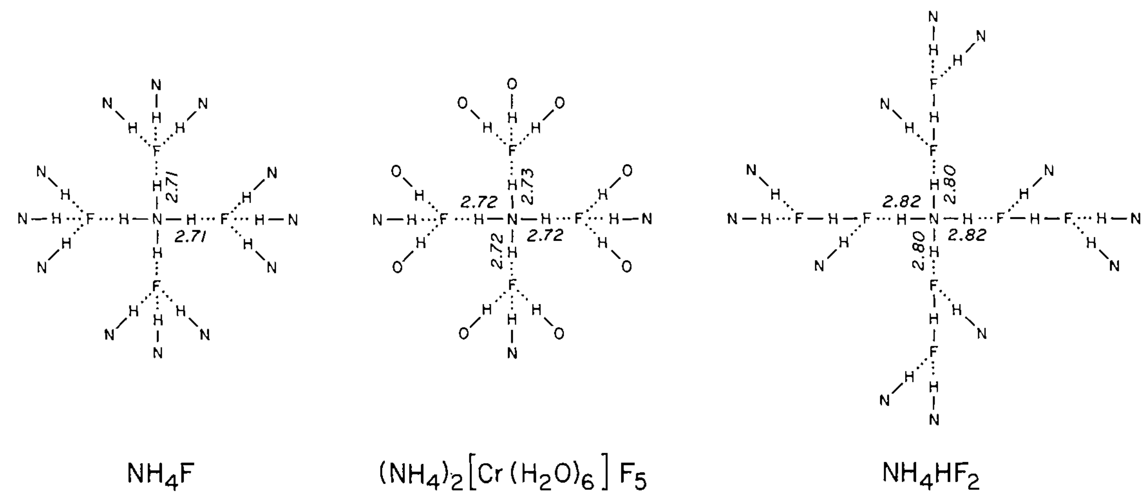

FIG. 8. Schematic representation of the environments of an ammonium ion in the 4-coordinated fluorides NH_4F, $(NH_4)_2[Cr(H_2O)_6]F_5$, and NH_4HF_2.

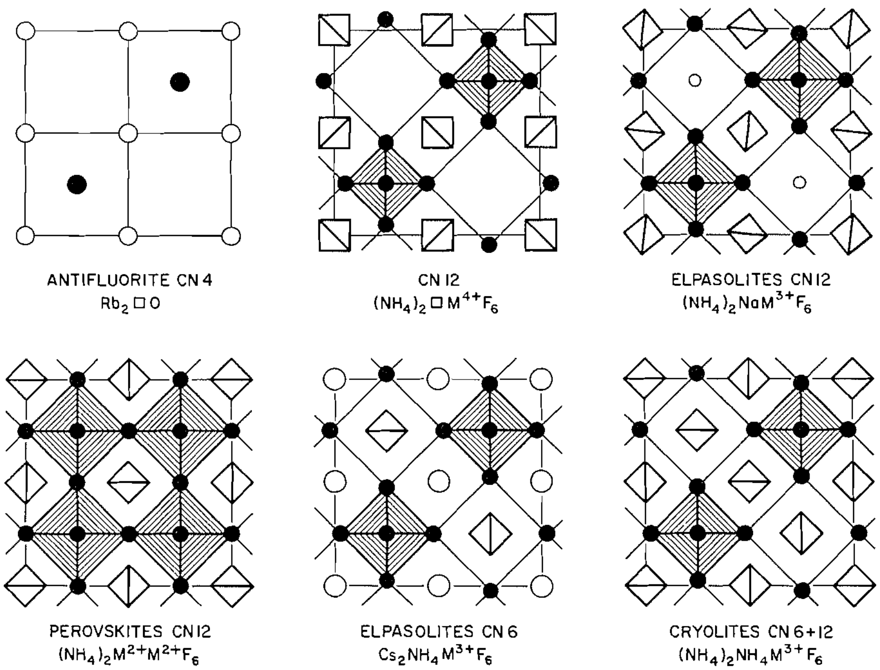

FIG. 9. Schematic representation of the relationships between the structures of complex ammonium fluorides derived from the antifluorite structure. Full circles, F; open circles, alkali ions (Na^+, Cs^+); octahedra, $[MF_6]^{2-}$ or $[MF_6]^{3-}$; tetrahedra, NH_4^+. The orientations of the ammonium ions in these room-temperature structures are well defined only in $(NH_4)_2MF_6$.

are 2.80 and 2.82 Å and the corresponding H···F distances, ~1.92 and ~1.95 Å; the N—H···F bonds are straight within the error limits of the structure determination (11). A 1 : 1 doublet would be expected for the ν_1 and a 1 : 1 : 1 : 1 quartet for the ν_{4bc} absorption.

The good quality of the spectra obtained from samples containing 0.8–3.6% D (Fig. 6) made possible extrapolation of the ν_1 band parameters to 0% D, i.e. to infinite isotopic dilution (Fig. 7). For the ν_{4bc} absorption the variation of the band parameters with the D content was insignificant.

At 10 K the ν_1 fundamental was a visually symmetric singlet at 2325 cm^{-1} which shifted gradually to 2321 cm^{-1} at room temperature (Fig. 7), i.e. in the same direction as in NH_4F and **54**. The ν_{4bc} absorption at 10 K, centred at 1298 cm^{-1}, showed evidence of at least three components; the mean position of this band remained almost stationary with temperature. The temperature variation of the ν_1 halfwidth was similar to that in NH_4F, while the width of the ν_{4bc} absorption was practically constant. The integrated intensity diminished with increasing temperature, but unlike for NH_4F the changes were more pronounced for ν_{4bc} than for ν_1.

To reconcile the probe-ion spectra with the reported crystal structure, the observed ν_1 and ν_{4bc} bands must be interpreted as an unresolved doublet and a partially resolved quartet respectively. Considering that the two nonequivalent N···F distances differ by only 0.025(4) Å (11) and that — unlike in **54** — each of the four F atoms coordinating NH_4^+ has a similar environment, it is not surprising that the presumed ν_1 doublet is unresolved.

The environments of an ammonium ion in the three fluorides

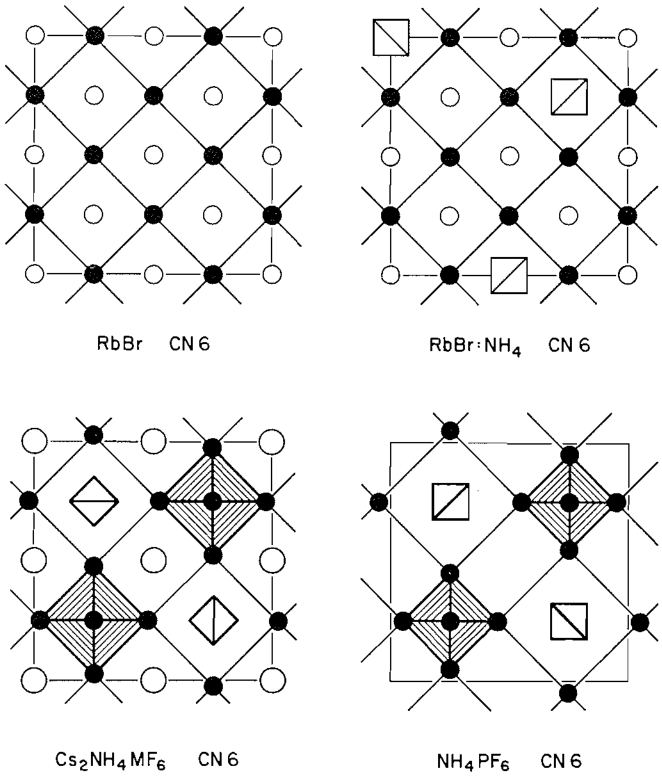

FIG. 10. Schematic representation of structures, with 6-coordinated cations, of importance for complex ammonium fluorides: NaCl type (*top left*); NaCl-type matrix containing NH_4^+ at random (*top right*). The NH_4PF_6 structure is of the NaCl type if regarded as $[NH_4^+][PF_6^-]$; for actual NH_4^+ and PF_6^- orientations see text. For symbols, see caption of Fig. 9.

with C.N. 4 (**1, 53, 54**) are compared in Fig. 8. The importance of the surrounding of the nearest-neighbour F atoms for the spectral parameters of NH_3D^+ is clearly seen.

Ammonium elpasolites and cryolites (57–61, 63, 64)

The structures of these fluorides are cubic at room temperature ($Fm3m$, no. 225; Z = 4). They are formally obtainable by filling the octahedral or the dodecahedral interstices or both in a hypothetical fcc parent structure composed of octahedral $[MF_6]$ ions:

Antifluorite type	→	Cryolites	←	NaCl type
$[(NH_4)_2]^{xii}[\square]^{vi}MF_6$		$[(NH_4)_2]^{xii}[NH_4]^{vi}MF_6$		$[\square_2]^{xii}[NH_4]^{vi}MF_6$
$(NH_4)_2SiF_6$ (**18**)		$(NH_4)_3MF_6$ (**59–61**)		NH_4PF_6 (**40**)
↓				↓
$[(NH_4)_2]^{xii}[B]^{vi}MF_6$	←	Elpasolites	→	$[A_2]^{xii}[NH_4]^{vi}MF_6$
$(NH_4)_2BFeF_6$ (**57, 63**)				$Cs_2NH_4MF_6$ (**58, 64**)

These structural relationships are represented in Figs. 9 and 10. In particular, NH_4PF_6 = $\square_2NH_4PF_6$ is to $Cs_2NH_4MF_6$ as $(NH_4)_2MF_6$ = $(NH_4)_2\square MF_6$ is to $(NH_4)_2BMF_6$, as far as interactions between adjacent cations are concerned.

The elpasolites $(NH_4)_2NaFeF_6$ (57) and $(NH_4)_2KFeF_6$ (63)

Classical description.[5] In this section it is assumed that in the $(NH_4)_2BMF_6$ structure ($Fm3m$, Z = 4) M is in 4(a) — 000 etc., B in 4(b) — $\frac{1}{2}\frac{1}{2}\frac{1}{2}$ etc., N in 8(c) — $\frac{1}{4}\frac{1}{4}\frac{1}{4}$ etc., and F in 24(e) — x00 etc. (3). The site symmetry in 8(c), T_d, is consistent with the tetrahedral symmetry of the ammonium ion. Considering that the cubic perovskites NH_4MF_3 may be represented as $(NH_4)_2BMF_6$ with B = M and x(F) = $\frac{1}{4}$, the cubic elpasolites $(NH_4)_2BMF_6$ may be regarded as ordered perovskites with B ≠ M and x(F) < $\frac{1}{4}$ (Fig. 9). The elpasolite unit cell may thus be thought of as divided into eight subcubes, each containing at its centre an ammonium ion 12-coordinated by F. This situation resembles the cubic $(NH_4)_2MF_6$ structure (Fig. 11) except that in the elpasolites *every* corner of a subcube is occupied by a metal atom, with M and B alternating. An NH_4^+ ion in its most symmetric orientation, $S \cap E = S = E = T_d$, would have the N—H vectors pointing at either the M or the B corners, unlike in $(NH_4)_2MF_6$, where these vectors point at the unoccupied corners of the subcubes. The spectroscopic expectation from this model would thus be a single ν_1 and a single ν_{4bc} absorption as long as the structure remains cubic.

[5] Objections to this classical description are briefly reviewed in Discussion.

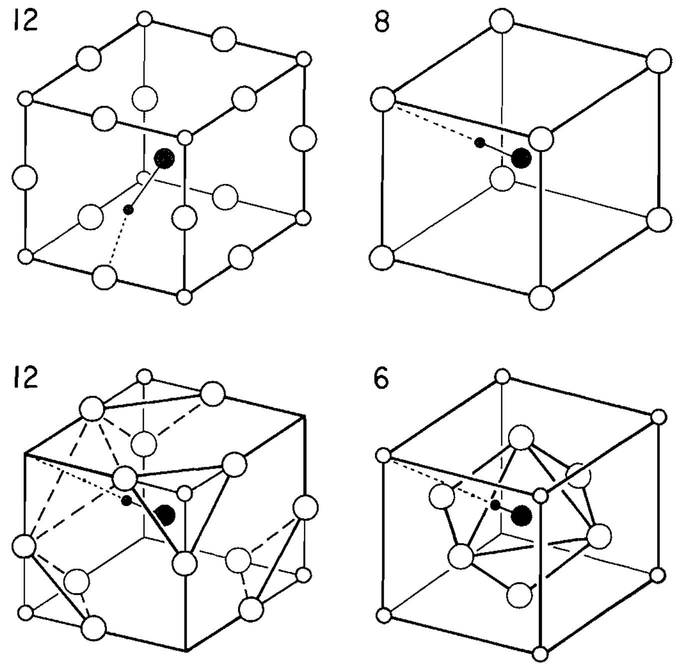

FIG. 11. Schematic representation of possible hydrogen-bonding schemes involving NH_4^+. (*Top left*) Direction of an N—H···F bond in NH_4MF_3 perovskites, C.N. 12. (*Top right*) Direction of an N—H···X bond of an ammonium ion in a CsCl-type matrix, C.N. 8. (*Bottom left*) Orientation of NH_4^+ in cubic $(NH_4)_2MX_6$, C.N. 12. (*Bottom right*) The most symmetric possible orientation of an ammonium ion in an NaCl-type matrix, C.N. 6.

Observed spectra. The spectra of **57** were of particularly good quality (Fig. 12). At 10 K a very regular 1:1:1:1 ν_1 quadruplet and an approximately 1:2:1:4 ν_{4bc} quadruplet were observed. On warming the sample the two absorptions persisted essentially unchanged until 157(1) K, when a sharp transition occurred (Fig. 13). The transition, which was reversible, manifested itself by the collapse of the ν_1 quartet to a broad singlet, while the ν_{4bc} multiplet collapsed to an asymmetric doublet. The ν_1 singlet, at 2372 at 160 K, shifted to higher wavenumbers with increasing temperature. The ν_{4bc} doublet was incompletely resolved (1283 and 1276 cm^{-1} at 160 K). The halfwidths of its components increased and the resolution decreased with increasing temperature until at ca. 200 K a single, practically symmetric band resulted. At the same time the

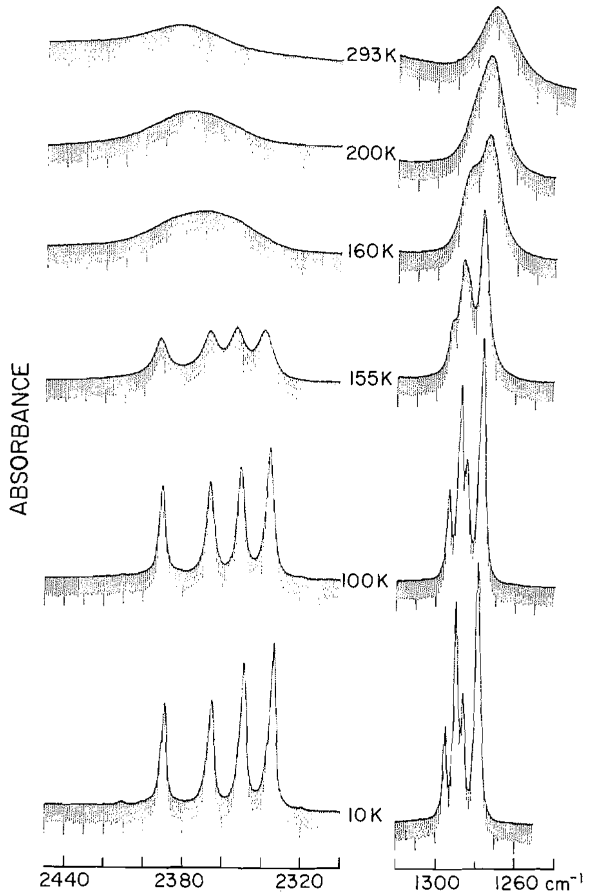

FIG. 12. Spectra of $(NH_4)_2NaFeF_6$ (4% D) in the regions of the ν_1 (*left*) and ν_{4bc} (*right*) NH_3D^+ fundamentals at different temperatures.

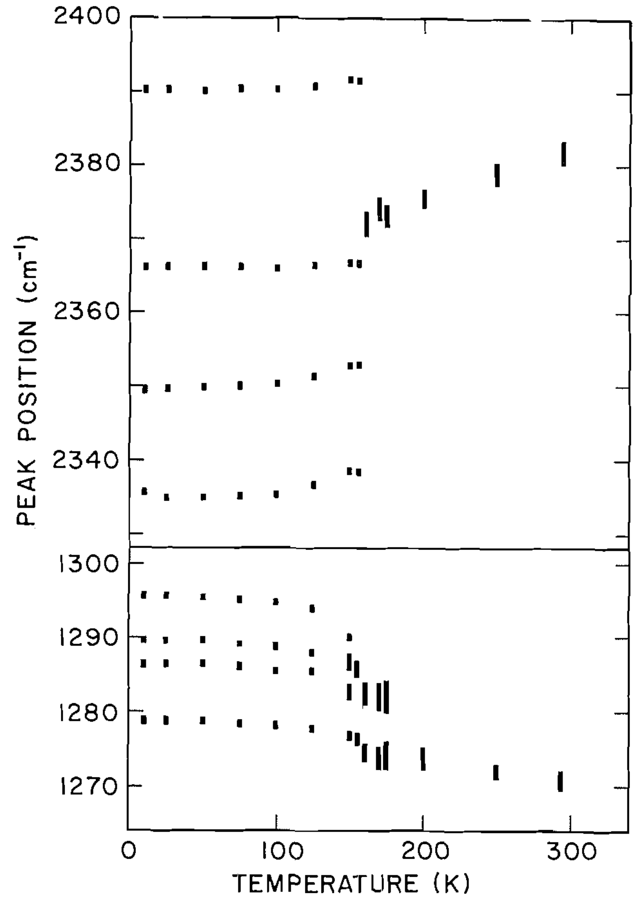

FIG. 13. Temperature variation of the peak position of the bands in Fig. 12.

bands underwent a small shift to lower wavenumbers.

The spectra of **63** resembled those of **57**, but the much higher transition temperature was difficult to estimate with any accuracy because of the considerable band breadth at sample temperatures close to room (Figs. 14 and 15). A tentative estimate of T_{tr} is 290(15) K.[6] The ν_1 component frequencies at 10 K were lower than in **57** and their spread was considerably greater, 112 cm^{-1} compared to 55 cm^{-1} in the Na compound. The ν_{4bc} absorption was again a quadruplet, but different in appearance from that in **57**. Its component intensities were estimated as 3:3:1:1. The overall frequency lowering in **63** relative to **57** is a consequence of the lattice expansion resulting from the substitution of Na (a = 8.484 Å) by K (a = 8.925 Å).

The four ν_1 components observed in the spectra of **57** (and less sharply in **63**) below T_{tr} are indicative of $E = C_1$, assuming only one type of NH_4^+ is present in the crystal. If fully resolved, the ν_{4bc} absorption for $E = C_1$ would be an octet. The observed 1:2:1:4 quadruplet is not inconsistent with this expectation. The effective symmetry $E = C_1$ corresponds to $S = C_s$ or C_1. The relative narrowness and practically no shift with temperature of the ν_1 components would indicate that the ammonium ion engages in four essentially normal hydrogen bonds, of different strength. The suddenness of the collapse of the quartet to a singlet at T_{tr} is reminiscent of the NH_4MF_3 (M = Mn, Co, Zn) perovskites (15) and points to a first-order transition.[7]

The shift of the ν_1 *singlet* to high wavenumbers with increasing temperature is characteristic of a normal rather than trifurcated hydrogen bond (15, 20). At the same time, the appearance of a ν_{4bc} *doublet* above T_{tr} instead of the singlet expected for $S = E = T_d$ of the room-temperature structure, and the gradual coalescence of this doublet to a singlet with increasing temperature are completely analogous to what is observed for the probe-ion spectra of NH_4ZnF_3 (cf. Fig. 4 of ref. 15), even to the point of similarity of the ν_1 and the ν_{4bc} frequencies at temperatures immediately above the respective T_{tr}. Referring to the argument presented for the cubic NH_4MF_3 perovskites in ref. 15, one must conclude that in **57** and **63**, too, the ammonium ions adopt, at $T > T_{tr}$, orientations of a symmetry lower than $S \cap E = T_d$, the maximum symmetry permitted by the classical structure. Similar to NH_4MF_3, the instantaneous symmetry of the ammonium ion is effectively tetragonal, with dynamic disorder over the six possible orientations relative to the directions of the crystallographic axes. The N—H···F bonds thus are not symmetrically trifurcated, with the N—H vectors pointing at Fe or Na (or K), but *normal* though bent (Fig. 11). However, unlike in NH_4MF_3, where all the corners of a subcube are occupied by the same kind of metal atom and the instantaneous symmetry is D_{2d}, in the $(NH_4)_2BMF_6$ elpasolites this symmetry can be at most S_4. This

[6] The samples prepared and studied by Massa (3) and by Epple (5) were cubic at room temperature.

[7] This agrees with the sudden disappearance of the quadrupole splitting in the Mössbauer ^{57}Fe spectrum at T_{tr} (31).

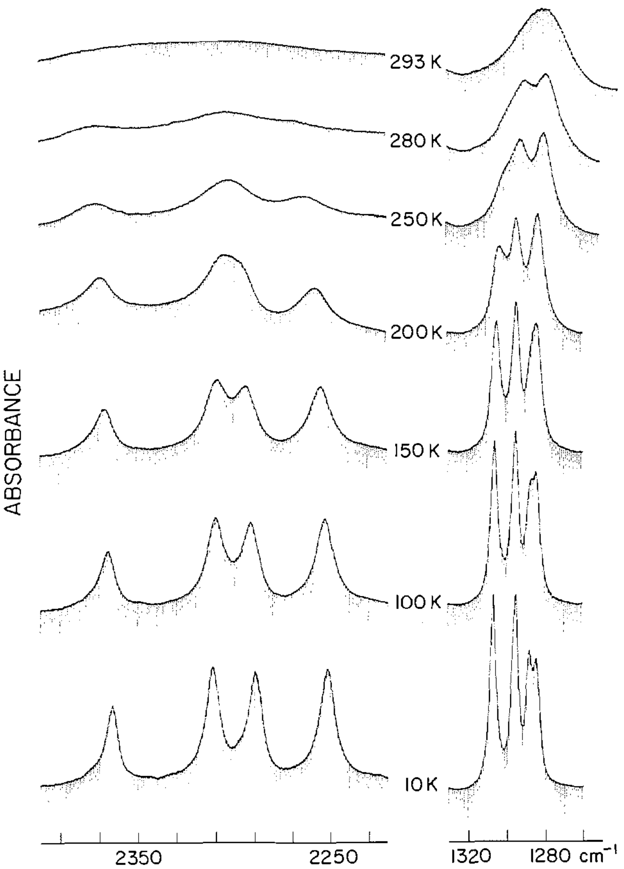

FIG. 14. Spectra of $(NH_4)_2KFeF_6$ (4% D) in the ν_1 (*left*) and ν_{4bc} (*right*) regions at different temperatures.

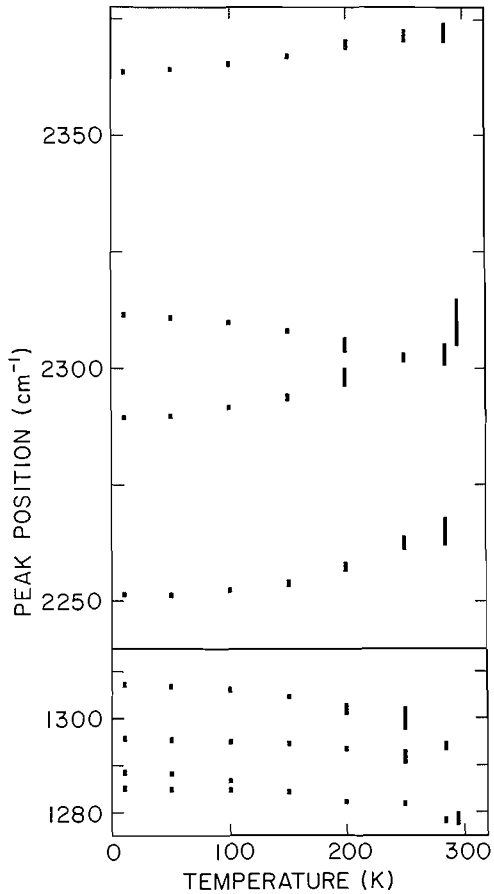

FIG. 15. Temperature variation of the peak positions of the bands in Fig. 14.

symmetry lowering would not affect the probe-ion spectrum, as a ν_1 singlet and a 1 : 1 ν_{4bc} doublet would be expected both for D_{2d} and S_4 (Table 1, ref. 15).

The difference in the corner occupancy of an elpasolite subcube and of an NH_4MF_3 unit cell is also likely the reason for the difference in the probe-ion symmetries in the respective low-temperature phases. In **57** and **63** the ν_1 absorptions are well-resolved 1 : 1 : 1 : 1 quartets, whereas in NH_4MF_3 they are 1 : 1 : 2 triplets, i.e. $E = C_1$ as against $E = C_s$. In terms of the model of ref. 15 for the perovskites, the plane of reflection of NH_4^+ in the low phase is destroyed, in the elpasolites, by the alternation of B and M at the subcube corners.

At 150 K the mean of the four ν_1 component frequencies in **57** is ~2362 cm^{-1} compared to ~2372 cm^{-1} of the singlet at 160 K, i.e. just above T_{tr} (Fig. 13). This indicates an overall strengthening of hydrogen bonding when the temperature is lowered through T_{tr}. In this respect **57** again closely resembles the NH_4MF_3 perovskites: one of the N—H···F bonds weakens on passage from the high to the low phase while the other three are strengthened, one of them appreciably (by some 35 cm^{-1}). The total high-low spread of the ν_1 component frequencies in **57** is ~55 cm^{-1} at 10 K, which compares with the corresponding spread in NH_4MnF_3, ~51 cm^{-1}; in NH_4CoF_3 and NH_4ZnF_3 the spread is only about one-half of this (15). In contrast, the spread in **63** is very large, about twice that in **57** (Fig. 15), pointing to the existence of a privileged, unusually strong N—H···F bond in the low phase. The degree of hydrogen-bond strengthening in **63** on cooling through T_{tr} could not be estimated because of the proximity of T_{tr} to room temperature (Figs. 14 and 15).

*The elpasolites $Cs_2NH_4FeF_6$ (**58**) and $Cs_2NH_4AlF_6$ (**64**)*

These elpasolites are of particular interest in that they might be expected to provide clues leading to an understanding of the vibrational behaviour of NH_4^+ in fcc alkali halide matrices, a problem which so far has eluded explanation. The ammonium ion is 6-coordinated ($S = O_h$), similar to that in KX and RbX (X = Cl, Br, I) matrices (ref. 2 and results to be published). Single ν_1 and ν_{4bc} absorptions would thus be expected, with frequencies between those in NH_4F and NH_4Cl. In **58**, for which we have low-temperature powder diffraction data, this expectation would hold down to the temperature of the reversible transition at 194(3) K.[8]

Five deuterated and three undeuterated samples of **58**, each the product of a separate high-pressure synthesis, were examined. Apart from the ND features, the intensity of which depended on the degree of deuteration, the room-temperature spectra of all eight samples were identical; those of the undeuterated samples agreed with the room-temperature spectra reported by Epple (5, 6). Some differences between samples were observed in the low-temperature spectra. The spectra shown in Fig. 16 are those of the deuterated product judged to be the purest (see Experimental).

At 10 K the ν_1 absorption consisted of a broad band centred at 2251 cm^{-1}, with a halfwidth of ~35 cm^{-1}, and a shoulder at ~2225 cm^{-1} (Fig. 16). The presence of this shoulder was

[8] At 203 K, a(cubic) = 9.196 Å; at 173 K the structure appeared to be pseudotetragonal, a = 9.118 Å, c = 9.253 Å, which would correspond to a volume reduction of about 1% on cooling through T_{tr}.

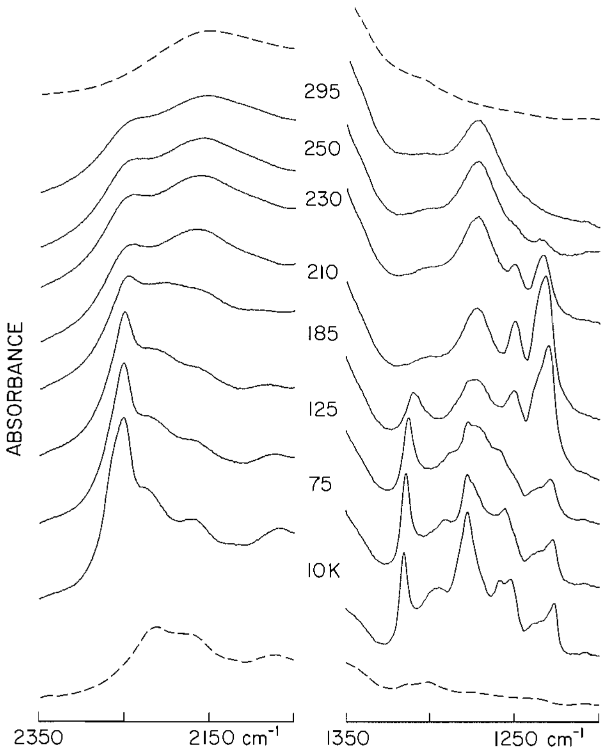

FIG. 16. FT spectra of $Cs_2NH_4FeF_6$ (4% D) in the ν_1 (*left*) and ν_{4bc} (*right*) regions at different temperatures. The spectra in broken lines are the 0% D backgrounds at 10 and 295 K, respectively.

detected only after a careful comparison with the appreciable irregular background absorption of the 0% D samples in this region. The 2251 cm^{-1} band may be considered to be an unresolved envelope of two or more features. Indeed, in the 10 K spectra of some of the samples this band was partially resolved into several components (at 2268, 2260, 2251, and 2229 cm^{-1} in the best resolved spectrum), with estimated halfwidths of ~15 cm^{-1}. This is larger than the $\nu_1(10)$ halfwidth of any of the other compounds examined in the present study and somewhat larger than for the KX and RbX matrices. Where the splitting did occur, it rapidly diminished on warming the sample and above ~70 K only a singlet was seen. With increasing temperature the 2251 cm^{-1} peak shifted to lower wavenumbers and broadened, until at room temperature only a very broad band of low peak height was visible.

The $\nu_{4bc}(10)$ absorption (Fig. 16) consisted of an unusually complex pattern of bands, with main features at 1315 and 1278 cm^{-1} and smaller bands at 1295, 1259, and 1253 cm^{-1}. An additional band at 1227 cm^{-1} was sometimes observed, as in Fig. 15. The total range of this composite absorption was at least 62 cm^{-1} (centre of gravity, ~1278 cm^{-1}). Increasing temperature caused gradual broadening and coalescence of these bands, with the outside bands moving toward the centre, as well as a sudden disappearance of the 1315 cm^{-1} peak at 195(10) K. Within the uncertainty estimate this temperature coincides with the above transition temperature established from X-ray evidence. The unusual increase of intensity of the 1227 cm^{-1} and 1253 cm^{-1} bands between 185 and 230 K (i.e. spanning the transition temperature, cf. Fig. 16) was not observed in the other samples. At room temperature only a broad singlet remained in the spectra of all the samples, consistent with the expectation from the room-temperature crystal structure.

Compared to **58**, the ND spectra of **64** were of inferior quality, owing perhaps more to poor crystallinity of the sample than to a difference between **58** and **64** *per se*. The asymmetry of the broad $\nu_1(10)$ singlet (at 2265(2) cm^{-1} and with a total halfwidth of ca. 46 cm^{-1}) decreased with increasing temperature and the peak position at 250 K was 2259(3) cm^{-1}. The $\nu_{4bc}(10)$ absorption was approximately a doublet but with clear indications of further unresolved structure. In general the ν_{4bc} absorption of **64** was reminiscent of that of **58**, with differences in the intensity distribution within the complex bands, especially at higher temperatures.

The low quality of the spectra precludes any conclusions about the possibility of existence of a structural transition in **64** between 10 and 295 K.

*The cryolites $(NH_4)_3MF_6$, M = Al (**59**), Cr (**60**), Fe (**61**)*[9]

The probe-ion spectra of the cubic phases would be expected to contain ν_1 and ν_{4bc} absorptions corresponding to those of the ammonium ion in $(NH_4)_2BMF_6$ as well as those of $Cs_2NH_4MF_6$, plus any features that might arise from the interaction of adjacent $(NH_3D^+)^{xii}$ and $(NH_3D^+)^{vi}$ ions (Fig. 8). Superposition without interaction of the $(NH_3D^+)^{xii}$ and $(NH_3D^+)^{vi}$ spectra above T_{tr} would be expected to yield two single absorptions in the ND stretching region, at ca. 2350 and 2250 cm^{-1}, respectively, and in an intensity ratio of 2:1, and a 1:1 doublet and a singlet in the ND bending region between 1280 and 1320 cm^{-1}. Unfortunately, the symmetry-lowering transitions which all three cryolites studied undergo occur above 200 K (Table 1),[10] at which temperature the appreciable broadening of the absorptions and decrease in the intensity considerably reduce the usefulness of our method for the study of the high phases, for which the structural information available is the amplest.

The X-ray powder patterns of the Cr and Fe compounds below T_{tr} could be indexed (5, 13; cf. also ref. 26) on unit cells deriving from the $Fm3m$ cell by triclinic distortions; the distortions as well as ΔV_{tr} are more appreciable for the Cr compound. A $P\bar{1}$ unit cell with $Z = 4$ would imply the existence of four nonequivalent centrosymmetric pairs of $(NH_4^+)^{xii}$ ions of $S = C_1$, and four nonequivalent types of single $(NH_4^+)^{vi}$ ions at sites of symmetry C_i. The $(NH_4^+)^{xii}$ ions would then be expected to give rise, in principle, to four ν_1 quartets and four ν_{4bc} octets. Since ammonium ions are noncentrosymmetric, the presence of the $(NH_4^+)^{vi}$ ions at sites of symmetry C_i implies twofold orientational disorder at all temperatures $T < T_{tr}$, unless a second transition is found below the lowest temperature so far investigated (i.e. below 15 K for the Fe compound, cf. ref. 22).[11] The $(NH_4^+)^{vi}$ ions, too, would then be of symmetry C_1, and four ν_1 quartets and four ν_{4bc} octets would be expected,

[9] By an oversight $(NH_4)_3FeF_6$, which was listed as **45** in ref. 2, has been renumbered here as **61**. The number **45** has been reassigned to $(NH_4)_2ReCl_6$ (cf. ref. 32).

[10] The T_{tr} obtained from C_p measurements (24, 25) and listed in Table 1 do not always agree with the estimates from X-ray powder diffraction, dta, esr, ir, and other measurements (5, 26, 27, 33, 34). A pronounced tendency to undercooling has been reported for the intermediate phase of **59** (24), and similar hysteresis phenomena known to exist in other complex fluorides (e.g. in hexafluorophosphates, cf. footnote 13) are responsible for discrepancies between different literature accounts of the same compound.

[11] Unlike **60** and **61**, the Al compound **59** has *two* low-temperature transitions (24). No information appears to be available on the crystallographic symmetry of either low-temperature phase, so we do not know whether the above arguments for **60** and **61** apply to **59**.

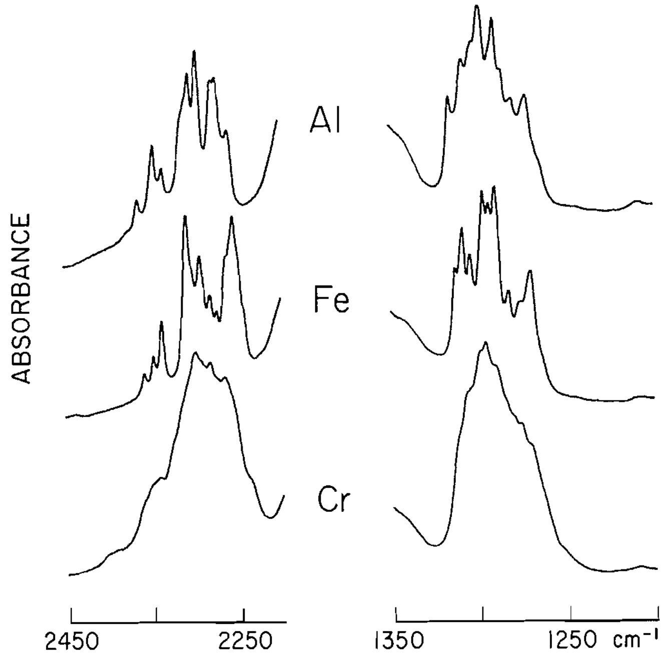

FIG. 17. Spectra of $(NH_4)_3MF_6$ (2% D) (M = Al, Cr, Fe) in the ν_1 (*left*) and ν_{4bc} (*right*) regions at 10 K. Difference FT spectra of Nujol mulls obtained by subtracting the 0% D spectra.

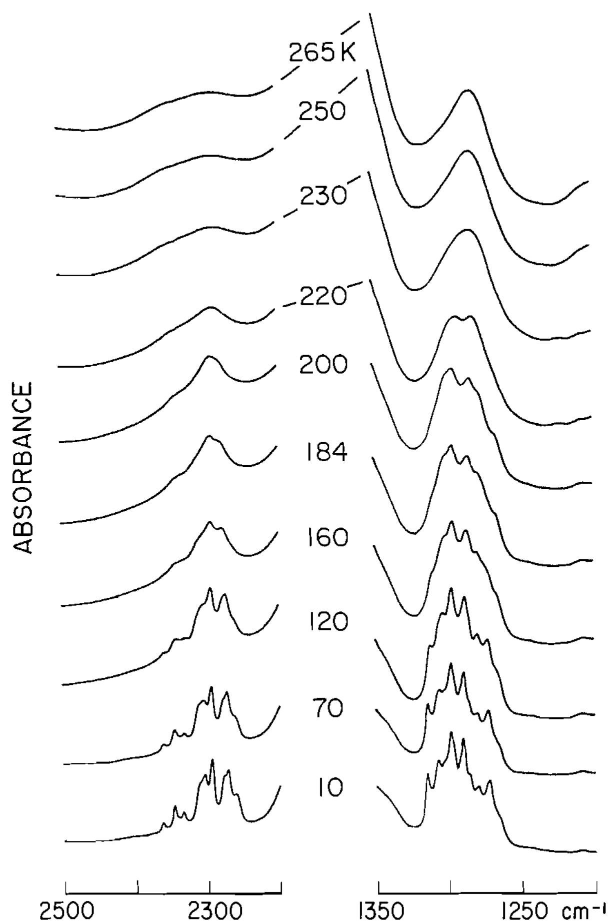

FIG. 18. Spectra of $(NH_4)_3AlF_6$ (2% D) in the ν_1 (*left*) and ν_{4bc} (*right*) regions at different temperatures.

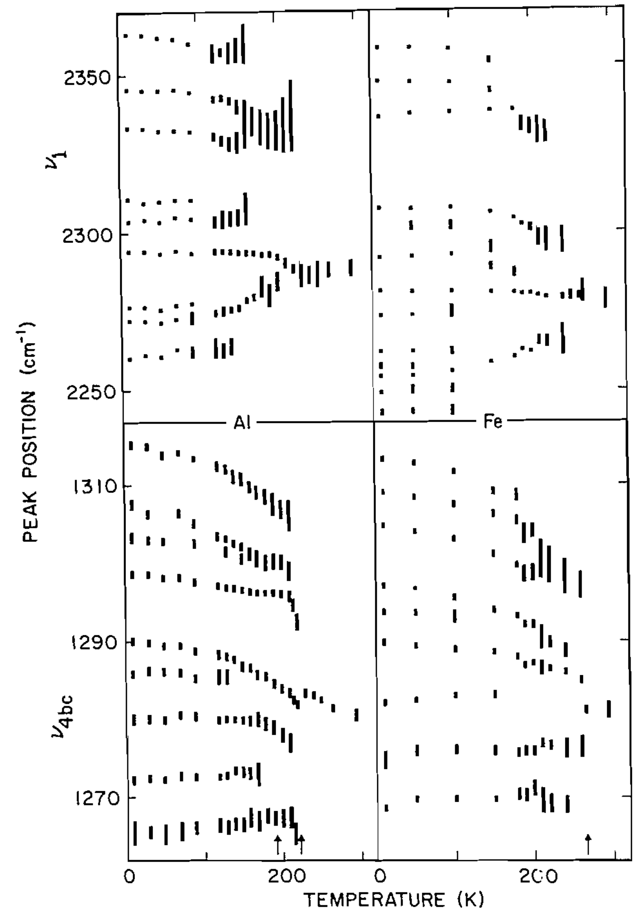

FIG. 19. Temperature variation of the peak positions of the bands in Figs. 18 and 20.

with each component in principle doubled or at least broadened in consequence of the orientational disorder.

The probe-ion spectra in the ND stretching and ND bending regions at 10 K are of the same type in all three compounds (Fig. 17). For **59** nine well-resolved ν_1 components were observed, their frequencies spanning 103 cm^{-1}, from 2260 to 2363 cm^{-1}. Shoulders and unusual breadth of the resolved features indicate the existence of an undetermined number of additional components. The highest-frequency, weak bands at 2334, 2346, and 2363 cm^{-1} (group *I*) may be assigned to the ND stretching modes of $(NH_3D^+)^{xii}$ ions, in analogy with **57** and **63**. In group *II*, of higher intensity, with bands between 2260 and 2310 cm^{-1} (centre of gravity, 2291 cm^{-1}), some of the lower-frequency bands appear to correspond to the ND stretching modes of $(NH_3D^+)^{vi}$ ions (cf. **58** and **64**), while the bands at the higher frequencies are probably a mixed set of $\nu_1(NH_3D^+)^{xii}$ and $\nu_1(NH_3D^+)^{vi}$ component bands. Detailed assignments are not possible at present.

With increasing temperature *all* the ν_1 components of **59** broadened and gradually collapsed (Figs. 18 and 19), but the collapse occurred for groups *I* and *II* separately. By 160 K region *I* showed only one broad band at 2335 cm^{-1}. By 210 K the bands of region *II* had also collapsed to a single band, at 2291 cm^{-1}. At ~225 K a large increase of width occurred, coincident with the upper transition (Fig. 18). Very little additional change was observed between 230 K and room temperature.

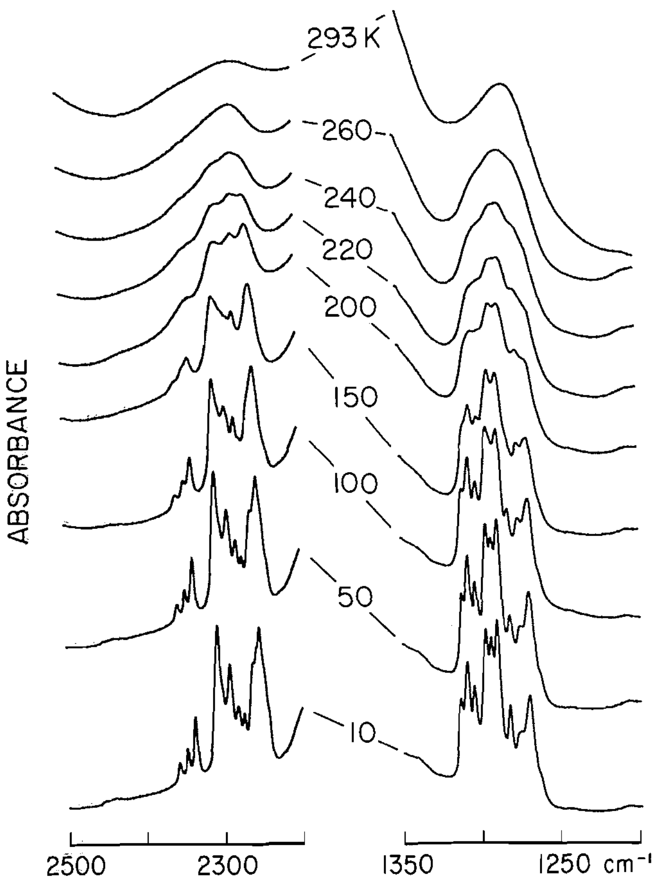

FIG. 20. Spectra of $(NH_4)_3FeF_6$ (2% D) in the ν_1 (*left*) and ν_{4bc} (*right*) regions at different temperatures.

In the ND bending region of **59** seven well-resolved components were seen, from 1266 to 1315 cm^{-1} (total range of 49 cm^{-1}), with a centre of gravity at ~1294 cm^{-1}. Comparison with the ND bending regions of **63** and **58** (Figs. 14 and 16) shows that the $(NH_3D^+)^{xii}$ and $(NH_3D^+)^{vi}$ components in the spectra of **59** almost certainly intermesh, making attempts at detailed assignment fruitless.[12] Increasing temperature caused a gradual broadening and eventual collapse of the bands until at 220 K only a broad doublet remained, at 1281 and 1292 cm^{-1}. At ~225 K a sharp change in bandwidth and band shape occurred, yielding a broad singlet at 1282 cm^{-1} (Fig. 18). Above 230 K this singlet shifted gradually to lower frequencies, ending up at 1279 cm^{-1} at room temperature.

Thus while above the upper T_{tr} the two very broad ν_1 bands are consistent in number, though not in idealized relative intensity, with the existence of $(NH_4^+)^{xii}$ and $(NH_4^+)^{vi}$ ions at sites of cubic symmetry, no structural conclusion can be made from the presence of the broad singlet in the ν_{4bc} region. Below the upper T_{tr} the ν_1 and ν_{4bc} spectra are so complex that no detailed conclusion is possible about the symmetries of the two ions, although one may reasonably assume that the respective C.N.'s are conserved, albeit in distorted environments. No evidence of the lower transition was observed in the probe-ion spectra.

The survey spectrum of **61** in the 4000–800 cm^{-1} region resembled that of **59** closely, both at room temperature and at 10 K (Fig. 20). In the $\nu_1(10)$ spectrum nine peaks were clearly resolved and the distribution of intensity approximated that for **59**. The effect of temperature also was analogous. With increasing temperature the multiplet gradually broadened and collapsed to what by 250 K was one broad asymmetric band. The large additional broadening coming into evidence between 260 and 265 K appears to be the consequence of the phase transition.

The ND bending region of **61** at 10 K, too, was very similar to that of **59** and showed a similar temperature dependence. The band resulting from the thermal collapse of the nine peaks that were clearly resolved in the 10 K spectrum (Fig. 20) still showed some structure (three residual components) at 260 K, but at 265 K only a broad singlet was observed. The same arguments are therefore applicable to the interpretation of the probe-ion spectra of **61** as advanced above for **59**.

Although the room-temperature survey spectrum of **60** resembled closely those of **59** and **61**, at 10 K the components of the probe-ion spectrum were much broader and less-well resolved. The overall pattern was clearly the same as for **59** and **61** (Fig. 17), as was also the temperature variation. However, the bands were too broad to see much change on passage through T_{tr}. It is not clear whether the less complete resolution of the probe-ion spectra is due to poor crystallinity of the material or to an intrinsic cause, e.g. fewer near-coincidences of the component frequencies, as a result of the more pronounced distortion of the structure of **60** on cooling through T_{tr}.

Considering that a typical halfwidth of $\nu_1(10)$ in ammonium halides is 5 cm^{-1}, the detail of the 10 K ND stretching absorption of **61** (Fig. 17) is reasonably well resolved, but it would be difficult to argue convincingly that the absorption contains the 12 components expected from the triclinic symmetry of the low phase. The *overall* impression, however, apart from the large variation in the intensity of the individual peaks, is that of a ν_1 spectrum arising from two nonequivalent $(NH_4^+)^{xii}$ and one $(NH_4^+)^{vi}$ ions, and this impression may well substantially correspond with the nature of the distortion of the structure below T_{tr}.

NH_4PF_6 (40)

Calorimetric and nmr (^1H, ^2H, ^{19}F) evidence indicates the existence of two transitions below room temperature (Table 1) and suggests that the upper, λ-type transition is associated with changes in the reorientational motion of the anions (30, 35, 36). The lower, "gradual" transition, at ~132 K, ought then to correspond to the onset of a cooperative process involving the ammonium ion.

The crystallography of **40** at room temperature is uncertain and nothing appears to be known about the structures of the low-temperature phases. For lack of better information we shall assume that the room-temperature phase of **40** is isostructural with the room-temperature phase *I* of KPF_6; however, even for $KPF_6(I)$ the structure cannot be regarded as completely established (cf. refs. 37 and 38). On this assumption the P and N atoms in $NH_4PF_6(I)$ are on an NaCl-type lattice ($Fm3m$, Z = 4, P in 4(a) — 000 etc., N in 4(b) — $\frac{1}{2}\frac{1}{2}\frac{1}{2}$ etc.), but for steric

[12] An unsuccessful attempt was made to identify the components by comparing the spectrum of **61** with that of $(NH_4)_{2.3}K_{0.7}FeF_6$. The latter compound was prepared especially for this purpose, in the hope that the smaller K^+ would populate exclusively the C.N. 6 sites, corresponding to $(NH_4)_2[(NH_4)_{0.3}K_{0.7}]FeF_6$ and leading to a decrease in the relative intensity of the $\nu_{4bc}(NH_4^+)^{vi}$ components. However, there was no discernible difference between the two spectra, perhaps owing to a statistical distribution of the potassium between the two types of sites.

reasons (37–39) the PF_6 octahedra cannot have the orientations shown in Fig. 10, which are the most symmetric orientations possible (F in $24(e)$ — $x00$ etc.). For the N···F distance to be reasonable, the octahedra must be rotated away from the axial directions of the unit cell. This results in a C.N. > 6 for the ammonium ion and in fractional occupancy by F of an equipoint higher than 24-fold if the diffraction symmetry is to remain $Fm3m$, i.e. that claimed for $KPF_6(I)$ (37). In the latter crystal this equipoint is taken to be $192(l)$ — xyz etc., which corresponds to 48 equivalent positions surrounding the cation in six sets of eight, one position in each set being occupied by F at any one time. The site symmetry of NH_4^+ in such a disordered structure would be *statistically* equal to O_h, with broadened ν_1 and ν_{4bc} singlets expected in the probe-ion spectrum above the upper $T_{tr} \sim 192$ K.

A preliminary account of the probe-ion spectra of **40** was given in refs. 2 and 12. Specifically, a single ν_1 and a single ν_{4bc} absorption were observed over the temperature range studied, ~90–295 K; the halfwidths at the lowest temperature were 6 and 7 cm^{-1}, respectively. The spectra did not reflect the existence of the two transitions. It is now clear from the present results for 10–293 K (Fig. 21) that in the previous experiments the lower transition had not in fact occurred.[13] Otherwise the earlier findings are confirmed.

At 10 K the ν_1 fundamental appeared to be a 1:1 doublet with components at 2441.5(3) and 2435.5(3) cm^{-1}, of about 4 cm^{-1} halfwidth. This halfwidth is quite small, comparable to that in NH_4BPh_4 (40). The ν_{4bc} fundamental at 10 K consisted of four components of about 5 cm^{-1} halfwidth, the two middle components being separated by ~1.5 cm^{-1} and hence only resolved in some of the runs (Fig. 22). With increasing temperature both the ν_1 doublet and the ν_{4bc} quartet collapsed to singlets, the collapse being complete at 120(10) K. Further increase of temperature produced a shift of ν_1 to lower and of ν_{4bc} to higher wavenumbers. There was no clear evidence of the existence of the upper transition in our spectra.

The $\nu_4 + \nu_6$ combination band of NH_4^+, which at 10 K was a narrow, clearly visible singlet at 1680 cm^{-1}, rapidly diminished with increasing temperature and by 100 K was no longer observed.

The probe-ion spectra are interpreted as follows. The collapse at 120(10) K corresponds to the lower transition. The ν_1 doublet and the ν_{4bc} quartet observed below this temperature are indicative of $E = C_2$ (consistent with the site symmetries $S = C_2$, C_{2h}, C_4) or C_{2v} ($S = C_{2v}$, D_{2h}, C_{4v}) (Table 1, ref. 15). Alternatively, though in our view less likely, there could be two crystallographically nonequivalent ammonium ions at sites of nonpolar tetragonal symmetry or D_{2h} (different orientation from that for $E = C_{2v}$) or D_2. Above ~130 K the site symmetry of the ammonium ion must be effectively cubic and $E_{eff} = T_d$ or T. The shift of ν_1 toward lower and of ν_{4bc} toward higher frequencies with increasing temperature is characteristic of weak, highly bent (bifurcated or trifurcated) N—H···F bonds (20). The ν_1 frequencies are high, between ~2432 and ~2442 cm^{-1} in the temperature range studied; values as high as these are typical of high coordination numbers and trifurcated N—H···F bonds, e.g. in $(NH_4)_2SiF_6$ or NH_4BF_4 (2), and are consistent with the observed low barrier to reorientation of the NH_4^+ ion (see Discussion).

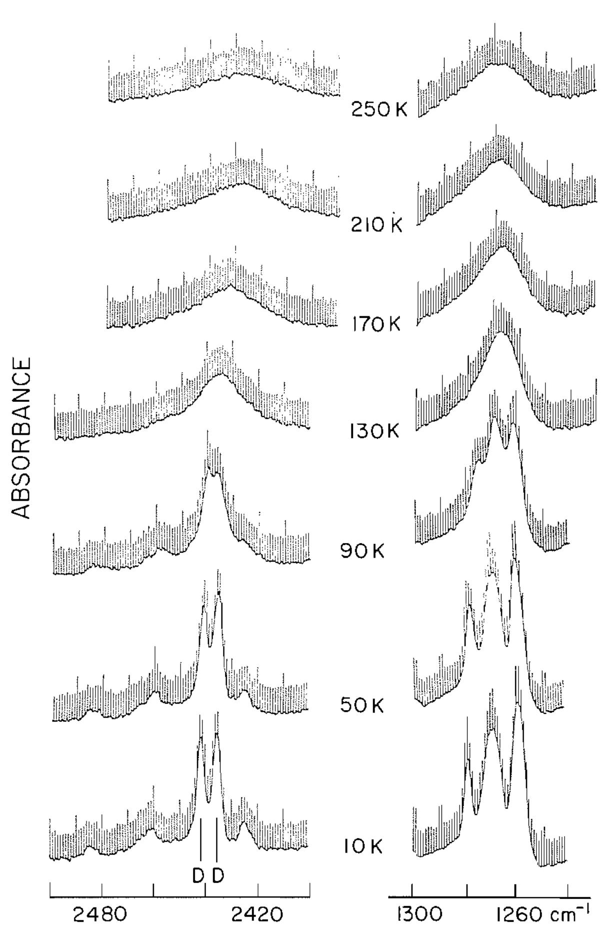

FIG. 21. Spectra of NH_4PF_6 (1% D) in the ν_1 (*left*) and ν_{4bc} (*right*) regions at different temperatures. Only the features marked D are due to the isotopically diluted NH_3D^+ ions.

$(NH_4)_3SiF_7$ (62)

The structure determination of **62** dates back to 1942 (29) and its accuracy is uncertain, but its general correctness is supported by the recent work (41) on a variety of compounds of this type ($A_2A'MF_7$: A, A' = K, Rb, Cs; M = Si, Ti, Cr, Mn, Ni). The tetragonal ($P4/mbm$, no. 127; $Z = 2$) structure is built up from SiF_6^{2-} and F^- anions and two types of NH_4^+ ions, $NH_4(1)$ in 14-coordination ($2(a)$, $S = C_{4h}$) and $NH_4(2)$ in 10-coordination ($4(h)$, $S = C_{2v}$); $NH_4(2)$ is twice as abundant as $NH_4(1)$. The approximate N···F distances for $NH_4(1)$ are 2.92 Å to F^- (2×), 3.06 Å (4×), and 3.50 Å (8×). For $NH_4(2)$ they are 2.79 Å (2×), 2.90 Å to F^- (2×), 2.98 Å (2×), and 3.09 Å (4×) (Fig. 23). A fully resolved ν_1 absorption would be expected to consist of a singlet and a doublet, and the ν_{4bc} absorption, of a doublet and a quartet, with all the component intensities ideally equal: $E = S_4$ for $NH_4(1)$ and C_{2v} for $NH_4(2)$.

At 10 K ten distinct narrow peaks were resolved in the ν_1 and no fewer than 14 in the ν_{4bc} absorption region (Fig. 24). This spectrum appears to correspond, with some unavoidable coincidences, to the 12 ν_1 and the 24 ν_{4bc} components expected for three nonequivalent, equally abundant ammonium ions of C_1 symmetry. The multiplets broadened and collapsed gradually

[13] The reason for this is difficult to establish. While the temperature control at the sample in the earlier experiments was inferior to that obtainable with the cryogenic system used at present, it is hardly likely that the actual sample temperature would have been off by more than 40 deg. Staveley *et al.* (30) experienced difficulties in obtaining reproducible C_p values with NH_4PF_6 and $RbPF_6$ as well as with $(NH_4)_2SnCl_6$ and $(NH_4)_2SnBr_6$, and suppression of low-temperature transitions in some samples of ammonium hexahalometallates(IV) was encountered in our own work (32).

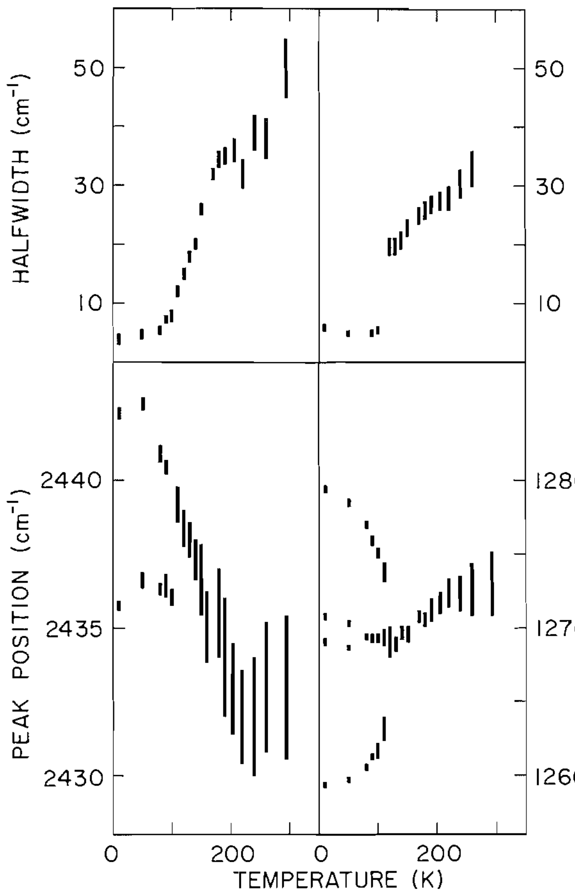

FIG. 22. Temperature variation of the peak positions of the bands in Fig. 21. The halfwidths for the lowest-temperature phase refer to the resolved single components.

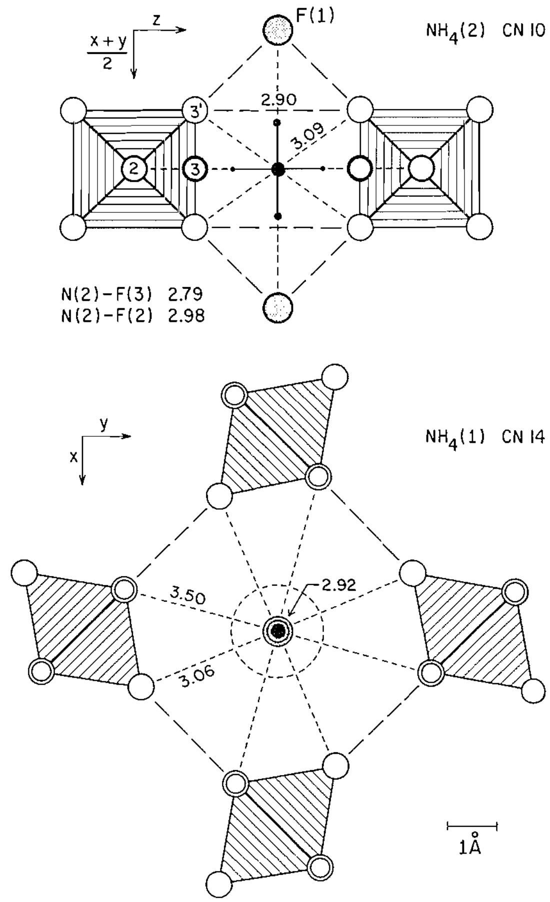

FIG. 23. Coordinations of the $NH_4(1)$ (C.N. 14, $S = C_{4h}$; *bottom*) and $NH_4(2)$ (C.N. 10, $S = C_{2v}$; *top*) ions in $(NH_4)_3SiF_7$, after ref. 29. Full circles, N; open circles, F of SiF_6^{2-}; stippled circles, F^-. In the bottom drawing the two F^- ions (on C_4) overlap in projection with N(1). The positions of the H atoms have not been determined, but if the orientation of $NH_4(2)$ matches the C_{2v} site symmetry of N(2) (as indicated in the drawing), then the hydrogen bonds are trifurcated, N—H···[F(2), 2F(3′)] for the lower and N—H···[F(1), 2F(3)] for the upper level H atoms. Assuming that the hydrogens of $NH_4(1)$ (on the dotted circle) do not point in the direction of the Si atoms, two equivalent orientations of the ammonium ion are possible; the hydrogen bonds would be asymmetrically trifurcated.

with increasing temperature. The ν_1 absorption above 100 K was on an increasingly sloping background, which made the shape and symmetry of the bands difficult to assess. At no temperature did the ν_1 and ν_{4bc} band envelopes resemble the simple bands shapes predicted for an $S = C_{4h}$ ion of single weight and an $S = C_{2v}$ ion of double weight. The possibility of existence of a transition in the 200 K region cannot be excluded.

The ν_1 frequencies are high (Fig. 25), in the range associated with NH_4PF_6 and $(NH_4)_2MF_6$. This alone would point to hydrogen bonding of the trifurcated type, in spite of the presence of F^- ions in the structure — presumably much stronger hydrogen-bond acceptors than the fluorines of the SiF_6^{2-} anions. However, the direction of the change of the ν_1 frequency with temperature could not be ascertained.

Discussion

Fluorides with C.N. 4 (1, 53, 54)

The ν_1 and ν_{4bc} frequencies in these three compounds decrease slightly with increasing temperature (Figs. 3 and 7), although in **53** the temperature variation of ν_{4bc} could not be established with certainty. Since *both* frequencies change in the same direction and the N—H···F bonds in these crystals are straight, the negative sign of the temperature coefficient $d\nu/dT$ must be attributed to the thermal variation of the lattice dimensions, i.e. expansion on heating.

The difference in the rate of decrease in the relative intensity of the ν_1 and ν_{4bc} absorption in **1** on heating (Figs. 2 and 3) is striking, as is also the constancy of the ν_{4bc} halfwidth, ~7 cm^{-1}, over the entire 10–293 K range.

NH_4PF_6 (40)

Obviously the thermal behaviour of solid **40** can be properly understood only when reliable crystallography of all three phases is available. In the interim, while attempting to secure this information, we offer the following qualitative model which permits the probe-ion spectra and other observations to be rationalized. Inasmuch as the two transitions appear to be second-order (or at least not isothermal), we assume that the basic face-centred arrangement of the P and N atoms is preserved in all the phases.

Phase I (above 192 K). The P and N atoms are in an NaCl-like cubic arrangement ($Fm3m$, $Z = 4$; cf. ref. 38). The PF_6 octahedra are rotationally displaced from their most symmetric possible orientations (i.e. those with F in $x00$ etc.) and undergo rapid reorientations as well as large-amplitude librational motions. The cation is moving in a potential field with a large number of local minima constituted by the instantaneous

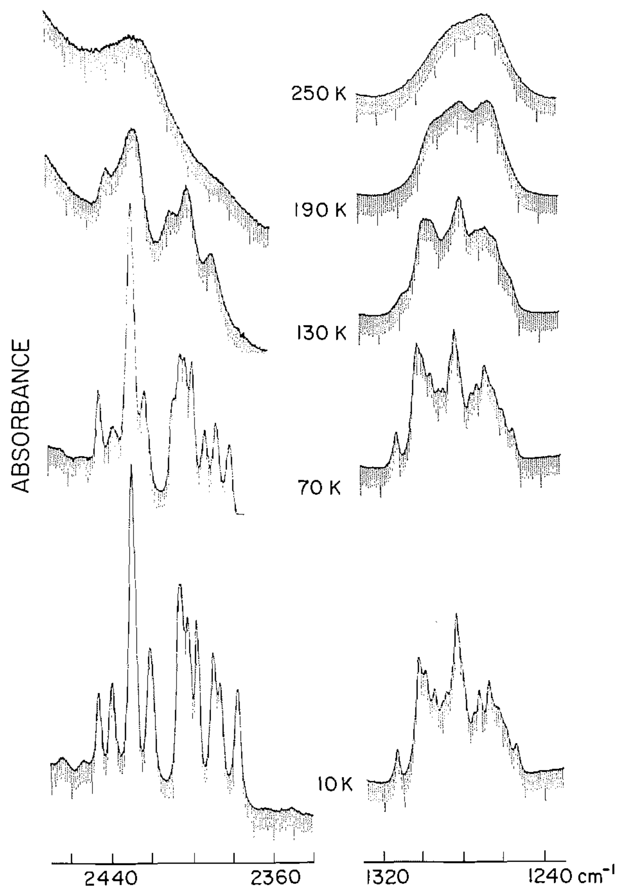

FIG. 24. Spectra of $(NH_4)_3SiF_7$ (5% D) in the ν_1 (*left*) and ν_{4bc} (*right*) regions at different temperatures.

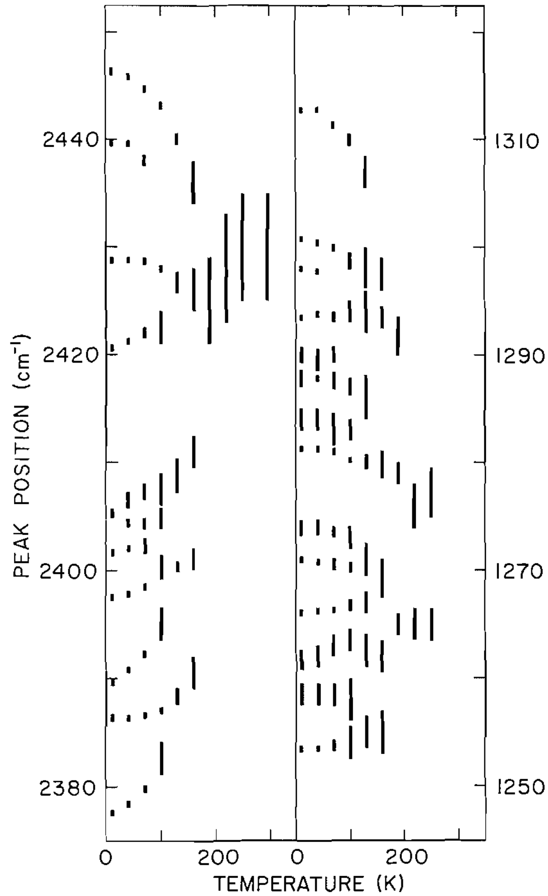

FIG. 25. Temperature variation of the peak positions of the bands in Fig. 24.

whereabouts of the F atoms (up to 48 such minima would be consistent with $Fm3m$). The *diffraction* symmetry of the crystal is thus $Fm3m$ and the effective site symmetry at N, as deduced from the probe-ion spectra, is cubic.

Phase II (132–192 K). The orientations of the rotated PF_6 octahedra are correlated, though the octahedra are still rapidly reorientating. This results in a decreased symmetry of the PF_6 sublattice, but since the ammonium ions still move in a multi-minimum, pseudospherical potential (though less "flat" than in *I*), with the F atoms at distances comparable to those in *I*, no abrupt changes are observed in the probe-ion spectra on passage through the *I* ↔ *II* transition. The effective symmetry at N is still cubic. The small but definite decrease in the ν_1 and increase in the ν_{4bc} frequency with increasing temperature (Fig. 22) indicates (20) that highly-bent hydrogen bonds are present in *II* and probably also in *I*.

Phase III (below 132 K). The PF_6 arrangement is essentially the same as in *II*, but the ammonium ions, while still reorientating rapidly, begin to respond to hydrogen-bonding interactions. Their librational motions are now increasingly restricted as the temperature decreases, with the result that the site symmetry at N is no longer cubic but C_2 or C_{2v}, and the distortion of the NH_4^+ ion (and hence the extent of the symmetry lowering of the crystal) increases smoothly with cooling. However, even at 10 K the distortion of the ammonium ion must be small, for the ν_1 absorption at this temperature is split by only about 7 cm^{-1}. The *II* → *III* transition may thus be described as a gradual change of crystallographic symmetry. The C_2 and C_{2v} site symmetries occur in a number of cubic space groups, but with $Z \neq 4$. It seems probable that the crystal symmetry of *III* is no higher than tetragonal. The increased effectivity of the hydrogen bonding in restricting the librational motion of the ammonium ion is manifested in the appearance of the $\nu_4 + \nu_6$ combination band of NH_4^+, which is absent in *II*,[14] and in the magnitude of the total splitting of ν_{4bc} at 10 K, which is about 20 cm^{-1} and thus three times that of the ν_1 splitting. It thus seems that the increased restriction of the torsional oscillation in *III* comes from a change in the coordination geometry of the ammonium ion rather than from a significant change in the H···F distance.

The ν_1 frequency in *I* and *II* differs little from the mean ν_1 frequency in *III*, and similarly for ν_{4bc}. This constancy, the negative temperature coefficient of the ν_1 and the positive temperature coefficient of the ν_{4bc} frequency all indicate that the *type* of hydrogen bonding is the same in all three phases and corresponds to highly bent, bifurcated or trifurcated N—H···F bonds. Because of the rotational displacement of the PF_6 octahedra the ammonium ion in **40** does not move inside a regular octahedron of F atoms, hence its C.N. > 6. The ν_1 and ν_{4bc} frequencies in **40** are comparable to the corresponding frequencies in cubic $(NH_4)_2MF_6$ (2, 10), but they are quite different from those for NH_4I(*I*), for NH_4^+ isolated in fcc alkali halide matrices (ref. 2 and results to be published) and, most importantly, for $Cs_2NH_4FeF_6$, the only case so far examined of

[14] The absence of this band in the room-temperature spectrum of NH_4PF_6 led Waddington (42) to conclude that the ammonium ion was free to rotate.

NH_4^+ inside a regular F_6 octahedron (cf. above and Fig. 16). The points for NH_4PF_6 (*I–III*) fall in an entirely different region of the ν_{4bc} vs. ν_1 plot (Fig. 3 of ref. 2) than the points for the C.N. 6 structures just mentioned. In fact, they fall in the extreme margin of the C.N. 12, trifurcated N—H···F bonds group. Unlike in NH_4I(*I*), the hydrogen bonding in NH_4PF_6(*I*) is not characterized by instantaneous privileged, essentially straight and strong N—H···X bonds: the ν_1 ~2250 cm^{-1} and ν_{4bc} ~1260–1320 cm^{-1} frequencies of $Cs_2NH_4FeF_6$ correspond more to the frequencies in NH_4SnF_3 (normal hydrogen bonds) and $(NH_4)_2[Cr(H_2O)_6]F_5$ than to those in **40**, even when qualitative allowance is made for the different formal charges on the F atoms in PF_6^- and FeF_6^{3-}.

Specifically, the above model is consistent with the following observations.

(*a*) The time-of-flight spectrum of slow neutrons scattered inelastically from **40** at room temperature approaches the shape expected for free rotation of NH_4^+, while the corresponding 103 K spectrum (i.e. for phase *III*) is significantly different (43).

(*b*) ^{2}H and ^{19}F nmr measurements on ND_4PF_6 (35) show that the upper transition is associated with a change in the reorientational motion of the PF_6^- ions only, while the lower transition was found to have little influence on the reorientational motions of both ions. The activation energies E_a for reorientation of the ammonium ion in *I* and *III* were found to differ only slightly: 0.71(1) kcal/mol between 170 and 300 K, and 0.83(1) kcal/mol between 20 and 71 K. The latter value is in reasonable agreement with E_a = 1.0 kcal/mol (44) and 0.90 kcal/mol (36) reported by other authors. The T_1 in *I* is long and almost temperature independent: $T_1(^1H)$ = 18 s and $T_1(^{19}F)$ = 6 s, corresponding to almost free rotation (36).

(*c*) The second moment of the ^{1}H nmr resonance, both at room temperature and at 77 K, increases by only about 50% from 1 bar to 14 kbar (45). This is consistent with the existence of a multiminimum, flat potential (i.e. C.N. > 6) and weak hydrogen bonding in all three phases.

(*d*) The upper C_p anomaly is a characteristic λ-type transition (30). In contrast, the lower transition is described as "gradual" rather than a typical λ point. This would be consistent with the postulated gradual crystallographic distortion (cf. Fig. 22) taking place simultaneously with orientational ordering of the ammonium ions (plus the attendant response from the PF_6 octahedra) on cooling below 132 K. Stated differently, the extra energy required to overcome the crystallographic distortion of the 10 K structure on heating may become significant at temperatures lower than a consideration of the C_p vs. T graph (Fig. 2 of ref. 30) alone might suggest, i.e. the ΔS_{tr} value for this transition quoted in ref. 30, 2.48 cal/deg mol, may in fact be an underestimate. Inspection of Fig. 22 and of Figs. 2 and 4 of ref. 30 would suggest 30–40 K as the temperature at which the "extra" contribution to heat capacity becomes perceptible.

(*e*) In ref. 30 the authors do not appear to exclude the possibility that the entropy change associated with the λ-transition in NH_4PF_6 and $RbPF_6$ is in fact R ln 4 = 2.75 cal/deg mol, i.e. higher than the values of 2.23 and 2.42 cal/deg mol, respectively, deduced from the experiment. The high value would be consistent with our model. If the *I* ↔ *II* transition is, for example, between $Fm3m$ (24 F in 192(*l*) — *xyz* etc.) for *I* and the subgroup $F23$ (24 F in 48(*h*) — *xyz* etc.) for *II*, the reduction in the number of possible equivalent F positions is by 192/48 = 4. Similarly, for the ammonium ion, in *III* the site symmetry S is C_2 or C_{2v}. If we assume ordering with respect to the twofold axis, $\Delta S_{tr}/R$ = 1.39 = ln 4 (1.24 measured, but see *d*), the number of equivalent NH_4^+ orientations in *II* would be 8 if $S(III) = C_2$ and 16 if $S(III) = C_{2v}$.

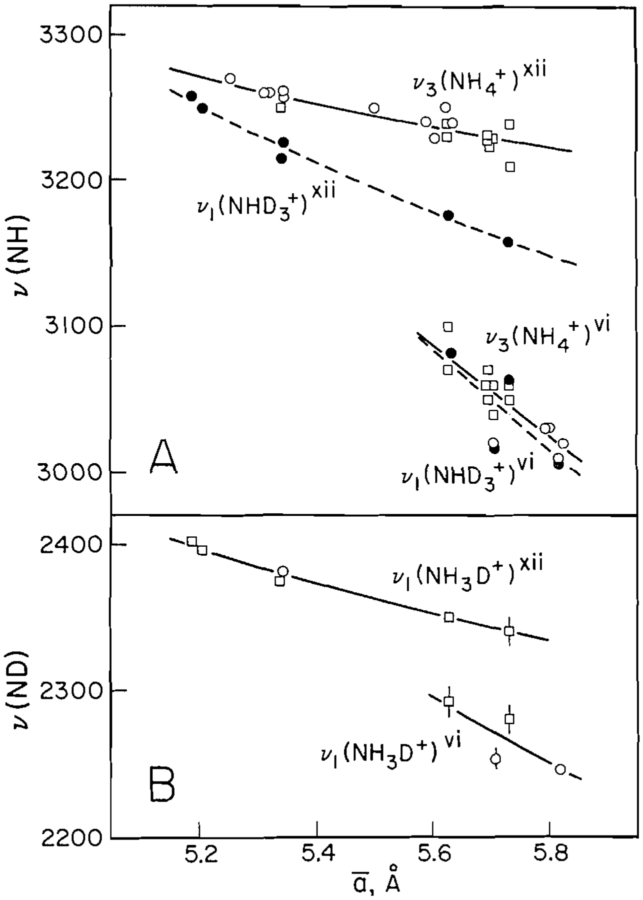

FIG. 26. Correlation of the NH stretching frequency of NH_4^+ (*A*) and the ND stretching frequency of NH_3D^+ (*B*) with $\bar{a} = (V/Z)^{1/3}$ for cubic elpasolites $(NH_4)_2BMF_6$ (B = Na, K) and $Cs_2NH_4MF_6$, cryolites $(NH_4)_3MF_6$ (squares) and perovskites NH_4MF_3. The $\nu_3(NH_4^+)$ values (room temperature) are from refs. 5, 13, and 46. The broken lines and full circles refer to the NH stretching frequencies $\nu_1(NHD_3^+)$ obtained by conversion from $\nu_1(NH_3D^+)$ (see text).

Elpasolites and cryolites: NH_4^+ vs. NH_3D^+ spectra

The effect of the C.N. (and hence of the hydrogen bonding) of the ammonium ion on the spectra of NH_4^+ in fluoride elpasolites and cryolites has been investigated by Epple and Massa (5, 6, 13) on undeuterated samples at room temperature. They were able to distinguish between the $(NH_4^+)^{vi}$ and $(NH_4^+)^{xii}$ absorptions in spite of the usual complications (broad, poorly resolved peaks, vibrational coupling and Fermi resonance) inherent in the room-temperature spectra of NH_4^+ in the NH stretching region, and they examined the implications of the coexistence of the 6- and 12-coordinated ammonium ions in the crystals as far as was possible from such spectra. It is of interest to see to what extent these NH_4^+ spectra match those of the isotopically isolated NH_3D^+ probe ion.

When Epple's $\nu_3(NH_4^+)^{xii}$ and $\nu_3(NH_4^+)^{vi}$ values for $(NH_4)_2NaMF_6$, $(NH_4)_2KMF_6$, $(NH_4)_3MF_6$, and $Cs_2NH_4MF_6$ (and also NH_4MF_3)[15] are plotted against $\bar{a}$(293) (Fig. 26*A*),

[15] Epple's $\nu_3(NH_4^+)$ values for the ammonium cryolites have been supplemented by three values estimated from the spectra shown in ref. 46.

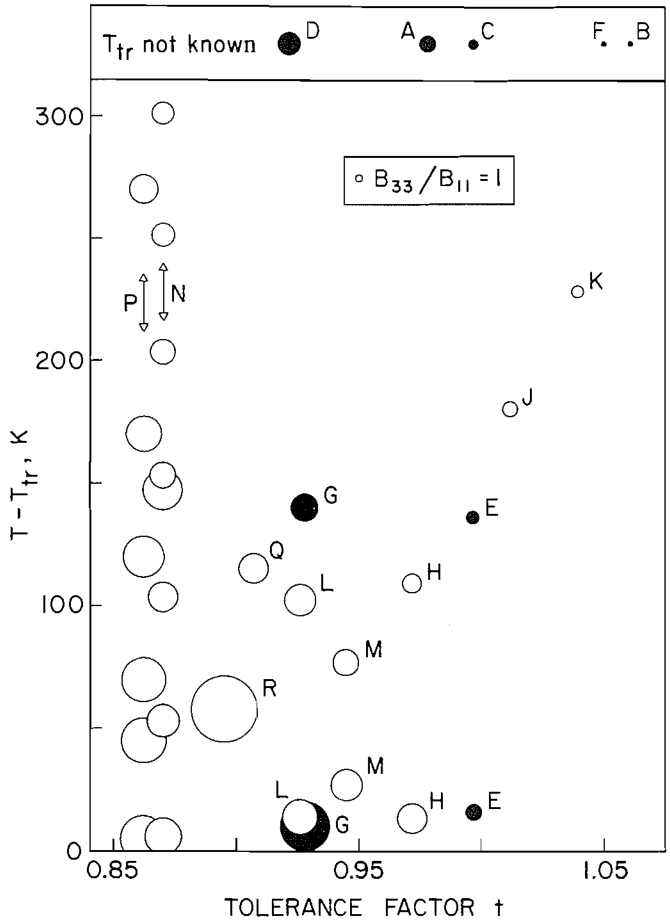

FIG. 27. Variation of the anisotropy of the principal thermal amplitudes of the X atom in cubic A_2BMX_6 elpasolites (full circles) and AMX_3 perovskites (open circles) with the tolerance factor t and the temperature difference $T - T_{tr}$. The diameters of the circles are proportional to $B_{33}/B_{11} = B_{\perp}(M - X)/B_{\parallel}(M - X)$. *A*, K_2NaCrF_6 (5); *B*, Rb_2LiFeF_6 (13); *C*, Rb_2NaFeF_6 (13, 49); *D*, Rb_2KFeF_6 (13, 49); *E*, $(NH_4)_2NaFeF_6$ (13, 31); *F*, Cs_2NaFeF_6 (13); *G*, $Cs_2NaNdCl_6$ (51); *H*, $KMnF_3$ (52–54); *J*, $KCoF_3$ (55); *K*, $KNiF_3$ (52); *L*, $RbCaF_3$ (54, 56); *M*, NH_4MnCl_3 (57); *N*, $CsPbCl_3$ (53, 58); *P*, $CsPbBr_3$ (58); *Q*, $MeNH_3PbCl_3$, and *R*, $MeNH_3PbBr_3$ (Knop, Cameron, and Adhikesavalu, to be published).

recognizable trends emerge, since the large number of compositions (M = Al, Ga, V, Cr, Fe) tends to compensate for the lack of accuracy in the indivudal estimates. The $\nu_3(NH_4^+)^{xii}$ variation with $\bar{a}$ is practically linear (r^2 = 0.82). As for $\nu_3(NH_4^+)^{vi}$, the points for $(NH_4)_3MF_6$ and $Cs_2NH_4MF_6$ have been regressed as belonging to one set, but the spread is considerable.

Regressing the available room-temperature ν_1 values linearly on $(1/\bar{a})^3$ (see below) results in a high degree of correlation for C.N. 12 ($r^2 = 0.98$) and in a poorer fit for C.N. 6 ($r^2 = 0.66$). Replotted against $\bar{a}$, the correlation lines in the observed $\bar{a}$ range are almost straight (Fig. 26*B*). When the $\nu_1(NH_3D^+)$ values for C.N. 12 are converted[16] to the corresponding $\nu_1(NHD_3^+)$ values (i.e. the isotopically isolated NH stretching frequencies), the points fall on a line which is not parallel to the $\nu_3(NH_4^+)^{xii}$ line (Fig. 26*A*). Since $\nu_1(NHD_3^+)$ is expected to vary in much the same manner as $\nu_1(NH_4^+)$, this implies that the symmetric and the antisymmetric stretching frequencies of $(NH_4^+)^{xii}$ in these fluorides converge as $\bar{a}$ decreases, i.e. increasing "chemical" lattice compression results in a significant reduction of the difference $\nu_3(NH_4^+) - \nu_1(NH_4^+)$. This convergence is analogous to that reported by Schiffer (48) for the symmetric and antisymmetric stretching modes of the H_2O molecule in crystalline hydrates.

Conversion of the $\nu_1(NH_3D^+)^{vi}$ to $\nu_1(NHD_3^+)$ frequencies for the two Cs elpasolites yields values which agree closely with Epple's $\nu_3(NH_4^+)^{vi}$ for those compounds, while the agreement is not as good for the two cryolites, **58** and **64**. It is possible that the $(NH_4^+)^{vi}$ frequencies are more sensitive to structural variation than the $(NH_4^+)^{xii}$ frequencies, and that the cryolite and the Cs elpasolite points should in fact be fitted separately. The present evidence is insufficient for resolving this problem.

The elpasolites $(NH_4)_2BFeF_6$ (57, 63)

Inadequacy of the classical model. A number of observations have been invoked in support of the suggestion (5, 13, 31, 49) that the F atoms in the cubic A_2BMF_6 elpasolites may in fact be less sharply localized than in the classical model.

(*1*) The principal thermal amplitudes B_{ii} of the F atoms show strong anisotropy. The B_{ii} in the plane perpendicular to an M—F bond (e.g. $\parallel(100)$) are several times that along the bond (refs. 13 and 49; Babel, Epple, and Massa, results to be published), and the $B_{33}/B_{11} = B\perp(M—F)/B\parallel(M—F)$ ratio increases with the decreasing tolerance factor[17] $t = (r_A^{xii} + r_F)\sqrt{2}/(r_B^{vi} + r_M^{vi} + 2r_F)$ and with decreasing temperature or, more accurately, with the decreasing difference $T - T_{tr}$. This is shown quite clearly in Fig. 27, both for cubic A_2BMX_6 elpasolites and AMX_3 (=A_2MMX_6) perovskites, in spite of the considerable dependence of the individual values of the B_{33}/B_{11} ratio on the method and accuracy of the structure refinement.

(*2*) The ^{57}Fe Mössbauer absorption of an Fe_{HS}^{3+} atom at a site of cubic symmetry (i.e. at 4(*a*) of *Fm*3*m*) should be a single, essentially unbroadened line. This is observed in $Cs_2NaFeCl_6$ both at 5 and 195 K. However, in K_2NaFeF_6, Rb_2NaFeF_6 and cubic Cs_2NaFeF_6 the linewidths of the single absorption are about twice as large at all temperatures between 5 and 600 K; even more unexpectedly, they *decrease* with increasing temperature (59). In **57**, which was investigated at our instigation by Pebler *et al.* (31), the linewidth above T_{tr} is comparable to that in the above three fluorides, but unlike in them it is practically independent of temperature.

(*3*) The absorption corresponding to the asymmetric Cr—F stretching vibration $\nu_3(F_{1u})$ in the room-temperature spectra of A_2BCrF_6 is broad and possibly asymmetric (5).

(*4*) Difference electron-density maps for K_2NaCrF_6, Rb_2NaFeF_6, and Rb_2KFeF_6 in planes perpendicualr to the M—F bond and passing through the F position of the classical model show local maxima near the F position (refs. 5 and 13; Babel, Epple, and Massa, to be published).

These observations point to displacement, static or dynamic, of the F atoms from the 24(*e*) — *x*00 etc. positions. They also raise the question of what is the proper description of the cubic elpasolite structure, and does the displacement of the F atoms from the classical position affect the conclusions from the probe-ion spectra in any significant way?

[16] The conversion is accomplished by utilizing the correlation of the isotopically isolated $\nu_1(NH_3D^+)$ and $\nu_1(NHD_3^+)$ values in $(NH_4)_2Cr_2O_7$ (47), which is linear between $\nu_1(NH_3D^+)$ = 2234 and 2392 cm^{-1} and accommodates $\nu_1(NH_3D^+)|\nu_1(NHD_3^+)$ pairs for other compounds as well (results to be published).

[17] Shannon's ionic radii (50).

The observed manifestations of the displacement would appear to be accounted for if the F atoms were placed in the equipoint 96(*j*) — *xy*0 etc. of *Fm*3*m*, with fractional occupancy (13). This would result in four symmetry-equivalent *xy*0 etc. positions, at equal distances from M, associated with each classical F position *x*00 etc., and the geometry of an individual MF_6 octahedron would depend on the (instantaneous) distribution of the six F atoms over the 24 positions, possibly subject to a minimum symmetry constraint (e.g. that MF_6 be centrosymmetric). Detailed arguments in support of this description will be reviewed elsewhere.

Effect of F displacement on probe-ion spectra. The classical description of the elpasolite structure accounts quite satisfactorily for the observed probe-ion spectra of the cubic phases. However, if the F atoms are in fact disordered over 96(*j*) — *xy*0 etc. of *Fm*3*m*, the diffraction symmetry of the crystal will remain *Fm*3*m*, but the individual MF_6 octahedra will be distorted or rotated about M. These distortions or rotations may be random or, if the disorder is dynamic, they might be correlated through a collective lattice mode. In either case the 12-coordination of NH_4^+ by F will be maintained, but the effective symmetry of an individual ion between reorientations will be $C_2 \subset S_4$ or C_1, rarely S_4. Each C_2 configuration would generate a ν_1 doublet and a ν_{4bc} quartet, and each C_1 configuration a ν_1 quartet and a ν_{4bc} octet, not necessarily resolved. The abundance-weighted superposition of all the distinct ν_1 multiplets would then result in an overall ν_1 absorption that is itself a complex multiplet or at least a broad envelope, and similarly for ν_{4bc}.

In **57** at 160 K the estimated ν_1 halfwidth was 58 cm^{-1}; in **63** an estimate is difficult because of the high T_{tr}. In NH_4MF_3 just above T_{tr} the corresponding estimated halfwidths were 60 cm^{-1} for Mn and 37 cm^{-1} for Zn (15). In the Zn compound the halfwidth was 40 cm^{-1} even at 193 K, compared with ~60 cm^{-1} for NH_4MnF_3. The ν_1 halfwidths just above T_{tr} in all three perovskites seem to mimic the magnitude of the high-low spread of the ν_1 components at 10 K in that the halfwidth is never smaller than the spread. This would seem to be the case also in **63** (Fig. 14) insofar as an estimate of the halfwidth at room temperature is possible. The symmetry of the ν_1 band shapes above T_{tr} is difficult to ascertain, given the low intensity and large width, although the bands give the general impression of being symmetric.

These halfwidths are certainly large. In the ammonium compounds we have studied to date, the $\nu_1(293)$ halfwidths rarely exceed 30–35 cm^{-1}, so the above values could be taken as evidence of the F atoms being disordered. On the other hand, it is in the cubic $(NH_4)_2BFeF_6$ and NH_4MnF_3 that the ammonium ions are librationally and reorientationally highly mobile, hence it can be argued that unusually large halfwidths are to be expected for this reason alone. As for the low-temperature phases, there is nothing in their behaviour that would suggest that ν_1 and ν_{4bc} halfwidths in these compounds should be intrinsically large. At 10 K the resolved ν_1 and ν_{4bc} bands are visually symmetric in both **57** and **63** as well as in the perovskites. The ν_1 component halfwidths were ~4 cm^{-1} in **57** and 8–10 cm^{-1} in **63**. The corresponding ν_{4bc} values were ~4 cm^{-1} in both compounds. Compared with the ν_1 and ν_{4bc} halfwidths in NH_4MF_3 at 10 K, ~11 and ~7 cm^{-1}, respectively, for NH_4MnF_3 and ~9 and ~8 cm^{-1}, respectively, for NH_4ZnF_3 (15), the elpasolite halfwidths must be regarded as narrow.

It must be concluded that the information obtainable from the probe-ion spectra neither supports nor disproves the postulated displacement of the F atoms in cubic A_2BMF_6 elpasolites and AMF_6 perovskites.

Low-temperature phases. The ν_1 and ν_{4bc} component frequencies below T_{tr} change very little with temperature (Figs. 13 and 15). This is consistent with the near constancy of the ^{57}Fe quadrupole splitting in **57** between 4.2 K and T_{tr} (31). The existence of this splitting (ca. 0.31 mm/s) indicates that the FeF_6 octahedra are not merely rotated but distorted, and this again is consistent with the low site symmetry at the NH_4^+ ion (C_1 as deduced from the probe-ion spectra) and with the nonequivalence of the N—H···F bond strengths.

Recent work (13) indicates that at 170 K the unit cell of **57** is cubic, a = 8.474 Å. Sharp Guinier patterns obtained with the sample at 150 K, i.e. just below T_{tr}, could be completely indexed on a tetragonal unit cell (a = 8.438 Å, c = 8.578 Å, c/a = 1.017, $V^{1/3}$ = 8.484 Å), but broadening of several lines suggests that the real symmetry is lower. This situation is strongly reminiscent of the NH_4MF_3 (M = Mn, Co, Zn) perovskites. Helmholdt *et al.* (16) indexed the X-ray and neutron powder patterns of the low phases of these three fluorides as tetragonal, with c/a ratios at 4.2 K between 1.014 and 1.019.[18] However, both these authors and Bartolomé *et al.* (75) adduce reasons for the actual symmetry being lower than tetragonal (cf. also ref. 15).[19]

The four ν_1 components observed in the spectra of **57** between 10 K and T_{tr} leave no doubt that the effective symmetry E of the ammonium ion is C_1 (if all the NH_4^+ ions are equivalent, i.e. the ν_1 absorption is a quartet, $S' = C_i$ or C_1) or C_{2v} or C_2 (if there are two types of NH_4^+ ions in the structure, i.e. the ν_1 absorption consists of two doublets of equal weight, $S'' = C_{4v}, C_4, D_{2h}, C_{2v}, C_{2h}, C_2$). The third possibility, $S''' = D_{2d}$, S_4, or D_2, is unlikely, as it would imply the existence of four types of ammonium ions, the four N—H···F bonds in an ion being equivalent but of different strength in each of the four types; furthermore, $E = D_{2d}$ or S_4 would imply a tetragonal unit cell. The ν_{4bc} absorption is of no help in deciding which of the three possibilities applies, as an octet would be expected in all three cases.

For the low phase to have a "zellengleiche" subgroup symmetry of *Fm*3*m* (Z = 4) and a site symmetry S' in an eightfold equipoint, or S'' in two fourfold equipoints, the cubic symmetry of the high phase would have to be reduced to no higher than monoclinic (possibly C_{2h}^3 — $F2/m$). For a "klassengleiche" subgroup symmetry the possibilities are too numerous for a conclusion to be made in the absence of further information, but even from a cursory examination of the "klassengleiche" subgroups of $F4/mmm \subset Fm3m$ it seems probable that an eligible subgroup would be no higher than orthorhombic.

It is surprising to find that pseudotetragonal distortions of the cubic cell as small as c/a ~ 1.02 should produce, in **57** and NH_4MnF_3, a high-low spread of the $\nu_1(10)$ components in excess of 50 cm^{-1}. The distortion in the low phase of **63**, where the spread is ~110 cm^{-1}, has not yet been determined. The high-low spread of ν_1 (10) (and, to a smaller extent, of ν_{4bc} (10)) appears to correlate with the tolerance factor t (Fig. 28).

The elpasolites $Cs_2NH_4MF_6$ (58, 64)

The following relates to **58**; the quality of the spectra of **64**

[18] These are the ratios from Table 3 of ref. 16. Extrapolation to 4.2 K of the a, c, and c/a curves in Figs. 2 and 3 of the same paper gives slightly different values.

[19] Tornero *et al.* (57) found single crystals of the low phase of NH_4MnCl_3 to be orthorhombic.

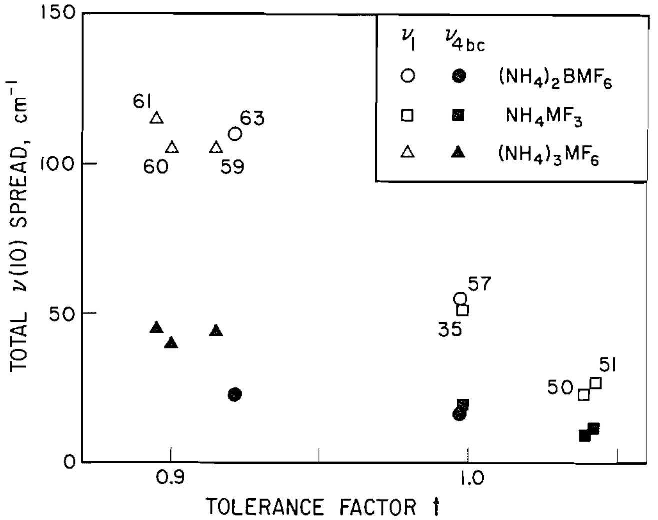

FIG. 28. Variation of the total frequency spread of the ν_1 (10) and ν_{4bc} (10) components of the $(NH_3D^+)^{xii}$ absorptions with the tolerance factor t. For the cryolites **59**–**61** the components of the $(NH_3D^+)^{xii}$ absorptions cannot be separated with confidence from those of the $(NH_3D^+)^{vi}$ absorptions; the values included in the plot represent the total range of ν_1 (10) and ν_{4bc} (10) in these fluorides.

was not good enough to provide more than a qualitative support of the results obtained with **58**.

The cubic $Cs_2NH_4MF_6$ elpasolites are at present the only known crystals that contain the ammonium ion symmetrically coordinated by six F atoms. It is therefore disappointing to find that the hoped-for opportunity for investigating the spectroscopic behaviour of the ion in **58** is frustrated by the existence of the crystallographic transition at ca. 194 K. Above T_{tr} the spectra are not well enough defined to be of much use, while below T_{tr} the NH_4^+ environment is no longer cubic and its symmetry and structure are not known.

Interpretation of the ν_1 and ν_{4bc} spectra of **58** below T_{tr} is moreover rendered uncertain by the variability of the ND absorptions from sample to sample. The ν_1 absorption observed at 10 K is a single band but not a clean singlet. The halfwidth of the main component, ca. 35 cm^{-1}, is appreciable in comparison with $\nu_1(10)$ of the probe ion in the fcc alkali halide matrices (ref. 2 and unpublished work), where the symmetric ν_1 singlet has no shoulders and a halfwidth not exceeding 12 cm^{-1}. The $\nu_1(10)$ absorption in **58** clearly is composite, but the number of components and their relative intensities cannot be established with confidence. The frequency separation of the components of this unresolved (in some spectra minimally resolved) multiplet is only about 10 cm^{-1} (ca. 20 cm^{-1} for the low-frequency shoulder). This would point to N—H···F bonds of very similar strength and thus to only a small distortion of the F_6 octahedron: in this frequency region ν_1 varies steeply with d(N···X) and thus with d(H···X) (Fig. 30), so that a large change in ν_1 corresponds to a small change in the distance. As anticipated, the peak $\nu_1(10)$ frequency is between the $\nu_1(10)$ of NH_4F and NH_4Cl, i.e. the hydrogen bonding is strong.

The surprising and entirely unexpected feature of the probe-ion spectrum of **58** is the complexity and extent of the absorption in the ND bending region (Fig. 16). The total breadth, which is at least 62 cm^{-1}, is the largest observed for ND bending in any ammonium compound to date. It is in fact larger than the total breadth of the ND bending absorption in the ammonium cryolites, which arises from both $(NH_3D^+)^{vi}$ *and* $(NH_3D^+)^{xii}$. Considering that in the fcc alkali halide matrices the halfwidth of $\nu_{4bc}(10)$ is 9–12 cm^{-1} and that, on the evidence from $\nu_1(10)$, the distortion of the F_6 coordination octahedron cannot be appreciable, this breadth is so puzzling that it invites the question, do all the components of the absorption in this region belong legitimately to ν_{4bc}? Since none of the peaks is observed in the spectra of undeuterated **58** (Fig. 16), the peaks must involve ND vibrations and thus the ammonium ion. The possibility that some of the ND absorption is due to Fermi-resonance enhanced combination or overtone bands of NH_3D^+ appears unlikely. The only bands of any intensity between 100 and 1400 cm^{-1} in Epple's spectra (6) of undeuterated $Cs_2NH_4MF_6$ are the asymmetric MF stretch $\nu_3(F_{1u})$ (at 470 cm^{-1} for Fe and 560 cm^{-1} for Al), the asymmetric MF bend $\nu_4(F_{1u})$ (at 298 cm^{-1} for Cr and 387 cm^{-1} for Al), and the $S_8(F_{1u})$ lattice mode of NH_4^+ (at 214 cm^{-1} for Cr and 215 cm^{-1} for Al). None of these fundamentals looks like a candidate for producing overtones or combinations which would give rise to absorptions of significant intensity in the 1220–1320 cm^{-1} region. It is thus concluded that the entire multiplet shown in Fig. 16 constitutes the ν_{4bc} absorption.

We can offer no explanation at present for the sample dependence of the ν_{4bc} multiplet profiles nor for the associated, seemingly erratic disappearance of the 1227 cm^{-1} component of the multiplet or for the unusual temperature variation of the intensity of the lowest-lying components (seen in Fig. 16); the same applies to the variability of the profile of the ν_1 absorption.

Variation of the ND stretching frequency

To see how the isotopically isolated ND stretching frequency varies from compound to compound, ν_1 (293) is plotted in Fig. 29 against d(N···F). This is a choice *faute de mieux*. The N···F distance may not be the most suitable parameter, but it is the best parameter available: the H···F distances are not known with sufficient accuracy (not even approximate H positions have been established in some of the structures), and the compounds included represent different structure types and C.N.'s and contain hydrogen bonds of different types. The ν_1 vs. d(N···F) plot, too, has its limitations. Some of the N···F distances are not accurately known, and for some of the compounds the room-temperature values of the ν_1 frequency are poorly defined or not available, so that estimated values had to be substituted. In **37** the F environment of the ammonium ion is quite irregular, and in **40** and in the elpasolites and cryolites the whereabouts of the F atoms are uncertain (see above).

In spite of these deficiencies Fig. 29 amply confirms, in the small, the general trends pointed out in ref. 2. The N···F distance must increase with the C.N. of the ammonium ion and hence the strength of the N—H···F bonds must decrease. This is reflected in the increase of ν_1 with d(N···F) in the sequence **1**–**54**–**53**–**39**–**50**–**18**. However, in an isostructural or quasi-isostructural series ν_1 decreases with increasing d(N···F) as a consequence of a "decompression" effect, i.e. increasing separation of the ionic charges in the structure. The perovskite and "ordered" perovskite (elpasolite and cryolite) sequence **51**–**50**–**35**–**57**–**59**–**61** is the most extended such series, but the trigonal $(NH_4)_2MF_6$ (**31**–**32**–**33**) also show this effect and the cubic $(NH_4)_2MF_6$ undoubtedly would if the d(N···F) were more accurately known.

The existence of these two trends, though clearly evident for the fluorides, is demonstrated more dramatically when other

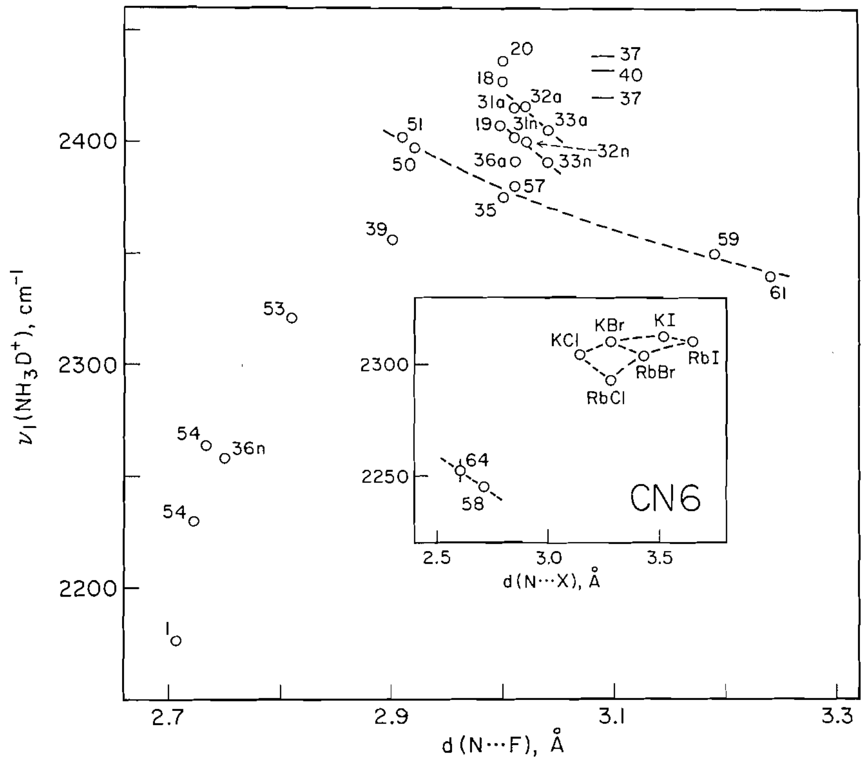

FIG. 29. Variation of the room-temperature ND stretching frequency $\nu_1 NH_3D^+$ with the N···F distance in ammonium fluorides with C.N. ≠ 6 (see text). For code numbers see Table 1; *a*, axial; *n*, nonaxial. *Inset*: the ν_1 vs. d(N···X) variation for C.N. 6, in **58** and **64** and in fcc alkali-halide matrices (ref. 2 and results to be published). Note the different *d* scales.

ammonium halides are included. In Fig. 30 and ν_1 are plotted against the inverse cube of the N···X distance. The advantage of this presentation is that it effectively linearizes the compression effect within the observed d(N···X) range.[20] The cubic $(NH_4)_2MX_6$ (X = F, Cl, Br, I) series provides a convincing illustration of the compression effect.[21] No ν_1 values are available for chloride perovskites, but if Epple's (5) $\nu_3(NH_4^+)$ = 3240 cm^{-1} for NH_4MnCl_3 is used to obtain an estimate of $\nu_1(NH_3D^+)$ (cf. Fig. 26 and footnote 16), the point for the estimate (*P* in Fig. 30) falls on an extension of the regression line for the "perovskite" fluorides.

The increase in ν_1 along the fluoride sequence **1–54–53–39–50–18** reflects the effect of decreasing acceptor strength (associated with the change in the effective ionic charge on the F atom) as well as the effect of the increasing d(N···F) and of the N—H···F bond type. In **1** and **54** the hydrogen-bond acceptors are F^- ions, whereas in the other crystals the acceptors are composite MF_n^{m-} anions of different connectivity and different formal charge on the M atom.

[20] For HF_2^- in fcc alkali halide matrices the "chemical" (i.e. not due to external pressure) compression effect appears to vary $\nu_3(HF_2^-)$ as $(1/\bar{a})^4$ (2), but this variation involves certain assumptions the validity of which is not quite clear. A plot of ν_1 against d_{NX}^{-4} is less linear than Fig. 30; we have not investigated whether the inverse cube represents the optimum power. A ν_1 vs. d_{HX}^{-3} plot is less informative than Fig. 30 owing to uncertainties in the choice and values of the H···X distances.

[21] Most of the ν_1 values in this set refer to liquid-nitrogen temperature. The consistency would improve somewhat if the actual $\nu_1(293)$ values were available: the correction would bring **20** closer to **18**, and some of the X = Cl points would be lowered by 2–5 cm^{-1}. The importance of the temperature correction decreases with increasing d(N···X).

The points for NH_4X (X ≠ F)[22] and MX:NH_4 fall in one particular region of Fig. 30. Among the conspicuous features of this group is the great similarity in the ν_1 values for NH_4Cl (**3**) and RbCl:NH_4 (**12**) (to a lesser degree also for NH_4Br (**5**) and RbBr:NH_4 (**13**)), in spite of the difference in C.N. and hence in the effective ionic radii. This observation is of fundamental importance for an understanding of the hydrogen bonding of 6-coordinated ammonium ions. We intend to discuss it elsewhere, together with two further trends in Fig. 30: (*1*) The *common-anion* tie lines for the KX:NH_4 (**9**, **12**) and RbX:NH_4 (**10**, **13**) points accommodate very well the corresponding CsX:NH_4 points **15** and **16**, respectively, again in spite of the difference in the C.N. The slopes of these straight lines are positive, i.e. they reflect a compression rather than an acceptor-strength effect. (*2*) The ν_1 values in the *common-cation* matrices (including CsX:NH_4) increase from Cl to I. In contrast, those in NH_4X (**3–5–8**) *decrease* from Cl to I, similar to $(NH_4)_2MX_6$ and probably the NH_4MF_3 perovskites.

It is not self-evident how the ν_1 frequencies in the alkali halide matrices can be related to the ν_1 frequencies in the fluorides. No instances of 4-coordinated NH_4^+ in halides are known except in fluorides, and the only fluorides in Fig. 30 that contain 6-coordinated NH_4^+ ions are **58** and **64**. However, the ν_1 frequency of an ammonium ion forming "straight" N—H···X bonds is determined principally by the N···X dis-

[22] The $\nu_1(293)$ values of NH_4Cl and NH_4Br fall in a region where ν_1 increases steeply with temperature, and $\nu_1(293)$ of NH_4I refers to the fcc phase *I*. This makes meaningful comparison at this temperature difficult. To circumvent this difficulty the $\nu_1(10)$ values are used for these halides in Fig. 30; the N···X distances are extrapolated to 10 K from literature values for different temperatures. The ν_1 values in all three halides remain practically constant up to about 150 K.

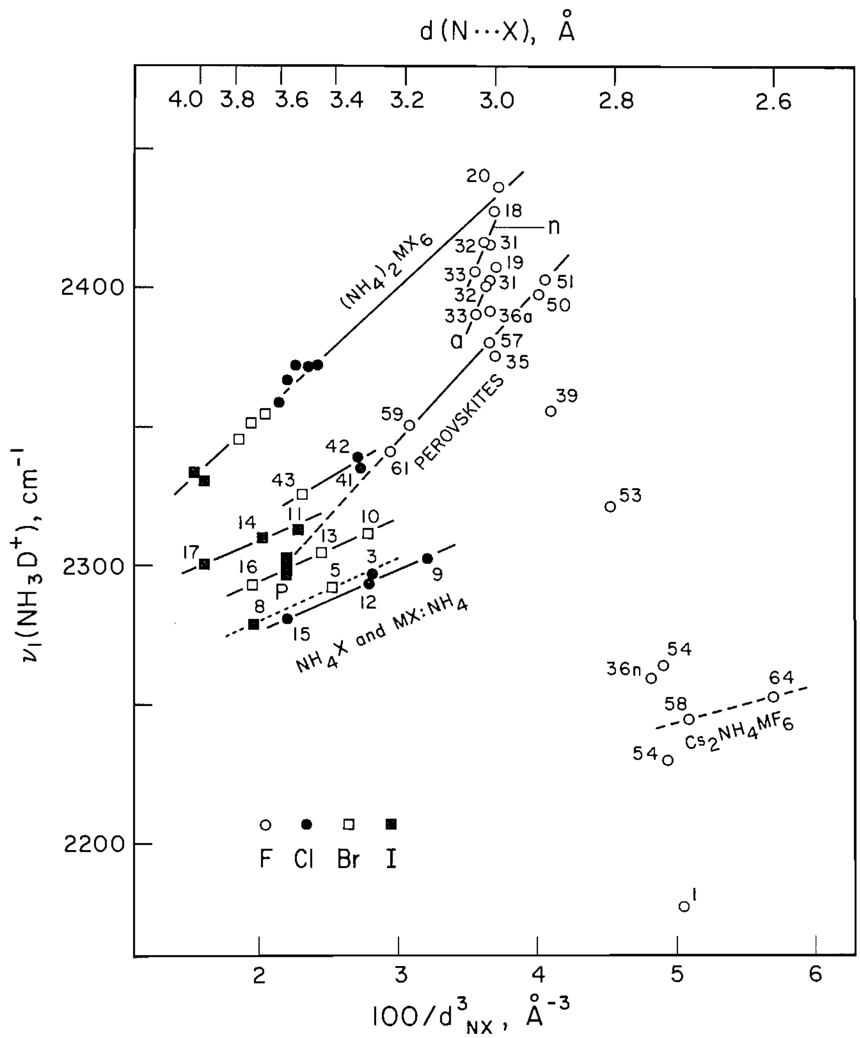

FIG. 30. Variation of the room-temperature ND stretching frequency ν_1 with the inverse cube of the N···X distance in ammonium halides. For code numbers see Table 1 and ref. 2. The two unnumbered points for $(NH_4)_2MI_6$ are for M = Pt and Te (32). For NH_4MnCl_3 (*P*) and NH_4X (**3**, **5**, **8**; 10 K values), see text. The ν_1 values are from the present work and from previous papers in this series.

tance, which in turn depends on the C.N. The orientational ambiguity which distinguishes an NH_4^+ ion in symmetric 8-coordination from that in symmetric 4-coordination is not a significant factor. A case can thus be made for comparing NH_4F with CsX:NH_4 along the sequence **1–15–16–17**, which is analogous to the fluoride sequence **1–54–53–39**. Similarly, the sequence **58–12–13–14** permits a comparison of ν_1 frequencies for 6-coordination, taking into account that the N···F distance in **58** is somewhat shorter than the nominal N···F (= Rb···F) distance would be in RbF:NH_4. An analogous sequence does not, however, obtain for NH_4F and the sc NH_4X (X = Cl, Br, I) halides (**1**, **3**, **5**, **8**) because of the decrease of ν_1 from Cl to I in the latter.

Structural transitions

Transition temperature and ionic size. Transitions from cubic to lower ("tetragonal") symmetry in A_2BMX_6 (B = A, B, M or □) halides have been shown in many cases to be the consequence of the condensation of a rotatory mode of the MX_6 octahedron on cooling. Assuming that the transition mechanism is always of this type and that comparison is thus possible, we have plotted the available T_{tr} against Shannon's r^{vi}(M) (Fig. 31) as well as against the tolerance factor *t* (Figs. 32 and 33). These plots are in many respects lacunary and the T_{tr} are often not accurately known; as well, the tolerance factor contains an accumulation of the uncertainties in the individual ionic radii as applied to the A_2BMX_6 halides. Nevertheless, examination of the plots permits the following observations.

The T_{tr} of the $(NH_4)_3MF_6$ cryolites increases with $r^{vi}(M^{3+})$ (Fig. 31). The variation can be represented, to a good approximation (r^2 = 0.96, σ = 10 deg), by a straight line. In the K_3MF_6 series the variation is, however, different: the T_{tr} *decreases* steadily at first, from Al to Ti, but then takes an upward turn with T_{tr}(In). The T_{tr} of M = Lu to Dy do not appear to be reliably known, but such as they are they provide further support for the existence of the upward turn. In fact, fitting the K_3MF_6 points of Fig. 31 to a cubic polynomial (dashed line) yields r^2 = 0.98, σ = 6.2 deg, which suggests a significant correlation. The minimum of this fit falls between Ti and Sc, but as T_{tr}(Sc) has not yet been reported, the presumed course of the variation between Ti and In cannot be verified at present.

The Rb_3MF_6 and Cs_3MF_6 series are less well defined. Apart from the T_{tr} values for Cr and Fe only upper estimates are available for some of the M = Ln compounds. When the Rb_3MF_6 points are fitted by a cubic polynomial (r^2 = 0.998, σ = 5.1 deg), the curve is quasi-parallel to the K_3MF_6 curve in

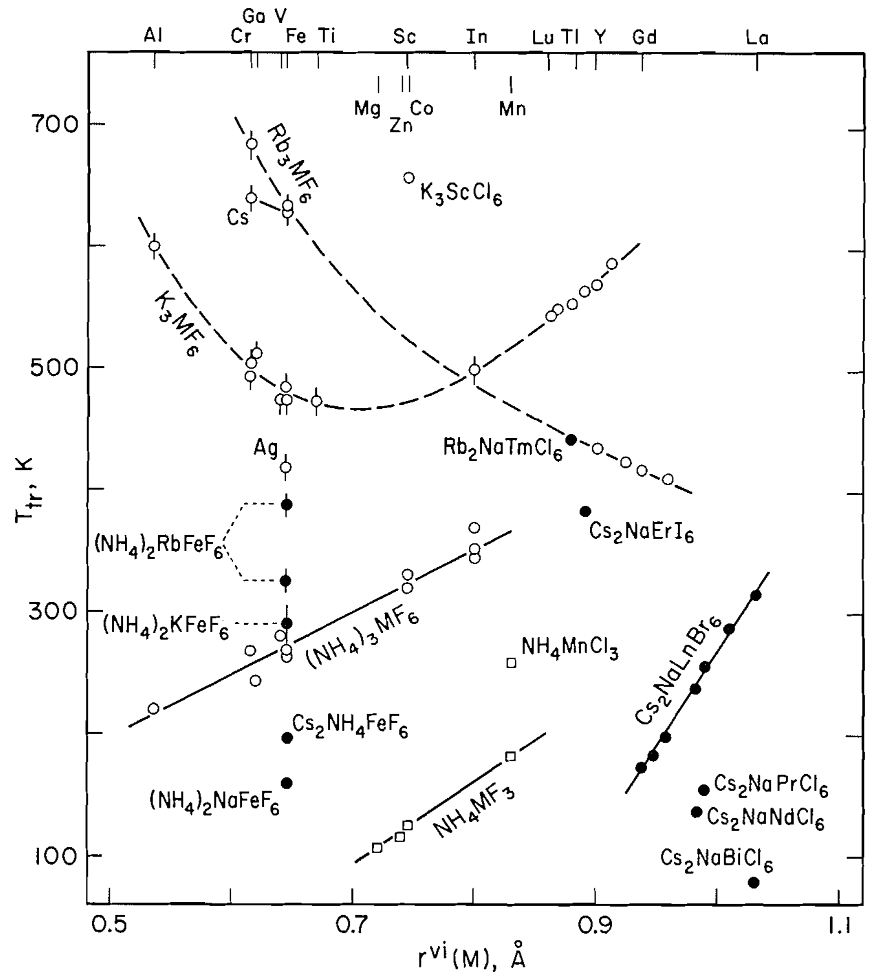

FIG. 31. Variation of T_{tr} in the cryolites A_3MF_6 (open circles), elpasolites A_2BMX_6 (full circles) and perovskites NH_4MX_3 (squares) with Shannon's effective ionic radius $r^{vi}(M)$. The T_{tr} values are from refs. 5, 13, 17, 24, 26, 34, 51, 60–74, 76–80, and from this work.

the 3*d*-element region, but it does not turn upward with increasing $r^{vi}(M)$. Instead, it keeps dropping over the entire physically possible range of $r^{vi}(M)$. The crossover of the K_3MF_6 and Rb_3MF_6 curves occurs near M = In, suggesting that the T_{tr} of the In compounds are quite similar. The set of T_{tr} values for the Cs series (not all T_{tr} shown) is of poorer quality, but the general trend appears to parallel that for Rb_3MF_6.

The T_{tr} of Rb_3MF_6 and Cs_3MF_6 (M = Cr, Fe) are higher than in the corresponding K cryolites and *some 400 deg higher* than in the corresponding $(NH_4)_3MF_6$. The essence of this observation is then that (*1*) the T_{tr} of the ammonium cryolites are much lower than the T_{tr} of any of the other cryolites studied (i.e. the presence of the NH_4^+ ion hinders the MF_6 rotatory modes from condensing), and (*2*) the increase of T_{tr} with $r^{vi}(M^{3+})$ in the $(NH_4)_3MF_6$ series is not matched by similar trends in the alkali series: for K_3MF_6 the variation is not even monotonic, and in the Rb_3MF_6 series the tend is opposite throughout, the similarity of the effective Rb^+ and NH_4^+ radii notwithstanding. Compared with Rb^+, NH_4^+ affects T_{tr} as if it were a much smaller ion.

When the cubic ($T > T_{tr}$) A_2BMX_6 (X = F, Cl, Br) elpasolites and perovskites are included in Fig. 31, it is again found that the halides containing NH_4^+ tend to have T_{tr} below ambient. The depressory effect, relative to Rb^+, of introducing a third ammonium ion into $(NH_4)_2BMF_6$ (B = Na, K, Rb), while less dramatic than for $Rb_3MF_6 \rightarrow (NH_4)_3MF_6$, still amounts to at least 60 deg (Fig. 32, inset).[23] The T_{tr} variation in the $NH_4MF_3 = (NH_4)_2MMF_6$ perovskites is roughly parallel to that for $(NH_4)_3MF_6$.

A partial rationalization of these trends in terms of a hard-sphere model is possible from the T_{tr} vs. *t* plots of Figs. 32 and 33. The ammonium compounds with the highest *t* values have the lowest T_{tr}. This is also true of most of the elpasolites and perovskites included in these plots, although for the $KMCl_3$ perovskites the trend is somewhat confused. The alkali A_3MF_6 cryolites, however, show a different behaviour.

In the elpasolites and perovskites T_{tr} is raised on replacing a smaller halogen by a larger one, i.e. on decreasing *t*: F → Cl in NH_4MX_3 and Rb_2NaTmX_6, Cl → Br → I in $CsPbX_3$ and $MeNH_3PbX_3$ (results to be published). Similarly, T_{tr} is raised by a *t*-reducing substitution of B in A_2BMF_6 and of M in AMX_3: Cs_2BHoF_6, $Cs_2NaLnBr_6$, KMF_3, $RbMX_3$, $CsMCl_3$. In contrast, *t*-reducing substitution of A in A_2BMF_6 and AMX_3 *lowers* T_{tr}:

[23] Lorient *et al.* (26) report a miscibility gap in the solid–solution system $(NH_4, Rb)_3FeF_6$ between $(NH_4)_2RbFeF_6$ (T_{tr} = 397(5) K) and $(NH_4)_{2.1}Rb_{0.9}FeF_6$. The estimated T_{tr} obtained by extrapolation from Fig. 4 of ref. 26 is 325(10) K. Since the site occupancies and the extent of order in these two limiting compositions are not known, both T_{tr} values are plotted in Figs. 31 and 32. The lower T_{tr} gives a "linear" variation of $T_{tr}[(NH_4)_2BFeF_6]$ with $r^{vi}(B)$ or *t*; the higher T_{tr} would make the depressory effect of the substitution of B by NH_4 even larger, ~130 K.

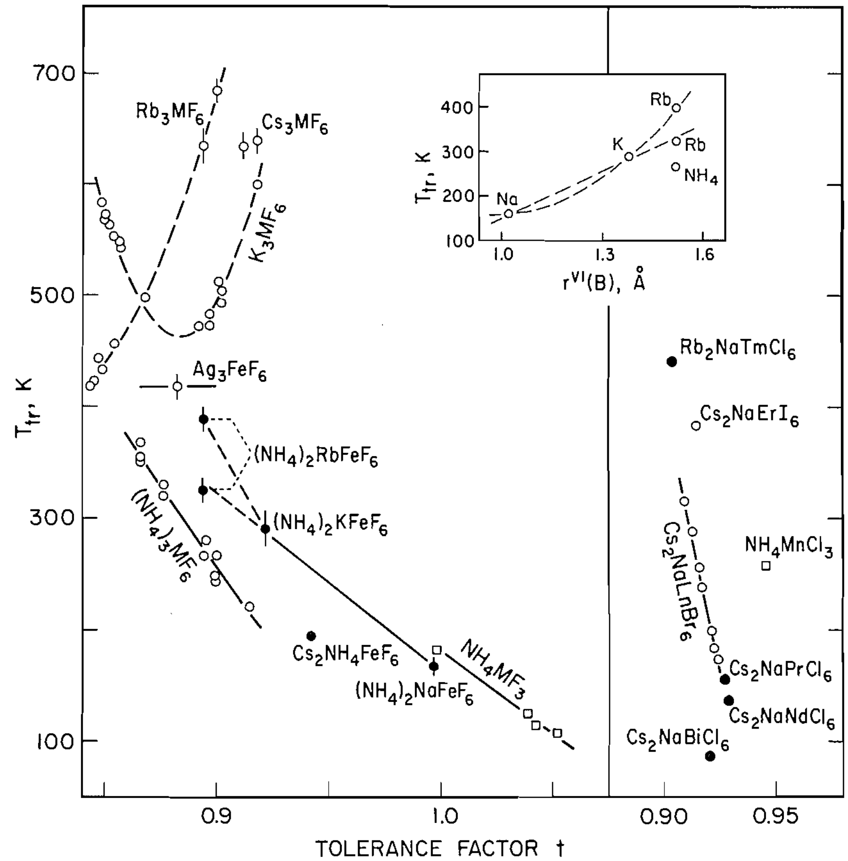

FIG. 32. (*Left*) Variation of T_{tr} in the cryolites A_3MF_6 (open circles), elpasolites A_2BMF_6 (full circles) and perovskites NH_4MF_3 (squares) with the tolerance factor *t* (see text). For sources of T_{tr} values see caption of Fig. 31; for the two T_{tr} values of $(NH_4)_2RbFeF_6$ see text. (*Right*) Variation of T_{tr} in the elpasolites A_2BLnX_6 with *t*. X = Cl (full circles), Br and I (open circles); the perovskite NH_4MnCl_3 is also included. *Inset*: Variation of T_{tr} with r^{vi} (B^+) in the series $(NH_4)_2BFeF_6$ (B = Na, K, Rb, NH_4). The lower T_{tr}(Rb) represents an estimate for $(NH_4)_{2.1}Rb_{0.9}FeF_6$; the higher T_{tr}(Rb) corresponds to $(NH_4)_2RbFeF_6$, possibly disordered (see text).

$ACaX_3$, A_2NaHoF_6.

The rate of change of T_{tr} in many of these substitution sequences is quite steep, amounting, for example, to about 100 deg per 0.01 change in *t* for the Ln substitution in $Cs_2NaLnBr_6$ and about as much for the F $\rightarrow$ Cl substitution in $RbCaX_3$. It is thus clear that T_{tr} is quite sensitive to changes in the effective ionic size and that geometry, within a given structure type, is a dominant, perhaps *the* dominant, factor affecting T_{tr}. The T_{tr}, *t* points in many of the substitution sequences can be accommodated on reasonably smooth lines. It is noteworthy that in some cases a chloride sequence is an almost smooth continuation of the corresponding fluoride sequence. Examples are $RbMF_3$ and $RbMCl_3$ (perhaps also NH_4MF_6 and NH_4MCl_3?), or the entire Cs sequence in the lower left corner of Fig. 33, and similarly for $Cs_2NaLnCl_6$ and $Cs_2NaLnBr_6$ (Fig. 32).

Figures 32 and 33 also contain material for other interesting deductions, but as these do not specifically concern ammonium compounds, they will not be discussed here. Two points may, however, be made. In some cases (e.g. $KFeF_3$) the initial lowering of the cubic symmetry is purely magnetic in origin and the T_{tr} (cubic $\rightarrow$ noncubic) cannot be compared with the transition temperatures involving condensations of rotatory modes.[24] It is conceivable, however, that a rotatory mechanism is involved in a transition occurring in such crystals at a lower temperature and that it is that T_{tr} that should appear in the T_{tr} vs. *t* plot. Secondly, if the C.N. of the B atom in cubic A_2BMX_6 elpasolites is effectively higher than six as a result of the displacement of X from the classical position, the effective ionic radius of B would be greater than the r^{vi}(B) and consequently *t* would be lower than shown in Figs. 32 and 33. The resulting change would modify, to a varying degree, the relative positions of the T_{tr}, *t* points in these figures, and there is the effect of temperature on the ionic radius as well.

The different behaviour of the alkali A_3MF_6 cryolites is at present unexplained.

Effect of T_{tr} *on the ND stretching absorption*. When considering *a* to *c* below, it must be emphasized that the volume of the available probe-ion data is limited and that the complexity (sometimes also the quality) of some of the spectra renders them intrinsically inadequate. The observations based on the present information must thus be regarded as no more than qualitative.

(*a*) The total spread of the ν_1 component frequencies in the low-temperature phases increases with the transition temperature both in the perovskite-derived and in the trigonal $(NH_4)_2MF_6$ series (Fig. 34*A*).

(*b*) The decrease $(\Delta\bar{\nu}_1)_{tr} = \bar{\nu}_1(>T_{tr}) - \bar{\nu}_1(10)$ of the mean frequency $\bar{\nu}_1$ on cooling also increases with T_{tr} (Fig. 34*B*).

(*c*) The frequency of the lowest-lying ν_1 component in the low phases decreases with increasing T_{tr}, while $(\Delta\bar{\nu}_1)_{tr}$ and the total spread increase (Fig. 35). This indicates a progressive

[24] In NH_4CoF_3 the temperatures of the crystallographic and the magnetic transition coincide (102).

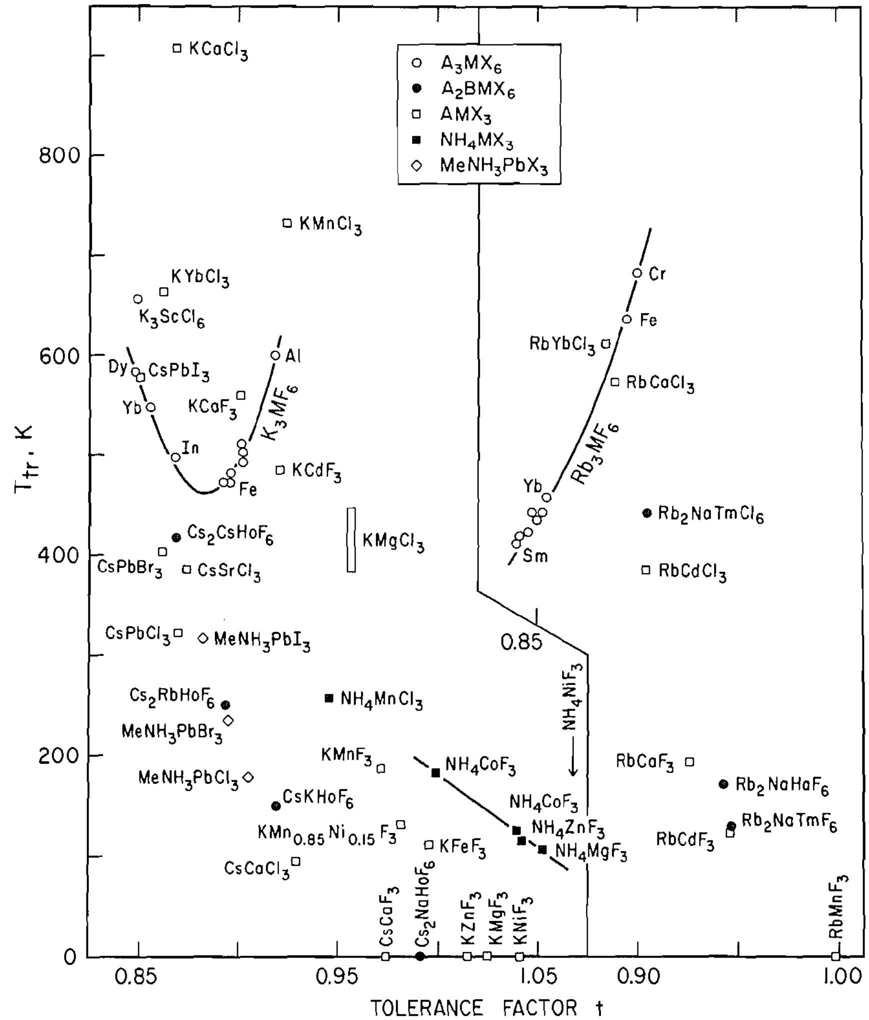

FIG. 33. Variation of T_{tr} in the cryolites A_3MX_6, elpasolites A_2BMX_6, and perovskites AMX_3 with the tolerance factor t. For sources of T_{tr} values see caption of Fig. 31 plus refs. 16, 53, 54, 58, 75, 81–102. (*Left*) K, Cs, and NH_4 compounds; (*right*) Rb compounds.

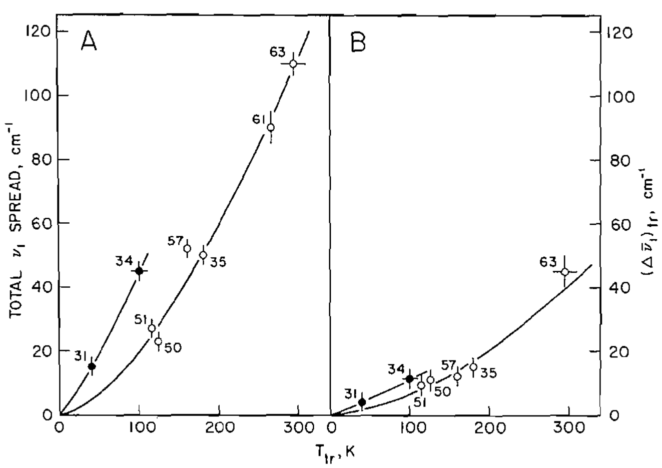

FIG. 34. (*A*) Variation of the total frequency spread, at 10 K, of the ν_1 components of the $(NH_3D^+)^{xii}$ ion with T_{tr} in perovskite-derived (open circles) and trigonal $(NH_4)_2MF_6$ (full circles) ammonium fluorides. **31**, $(NH_4)_2SiF_6$; **34**, $(NH_4)_2SnF_6$. (*B*) Variation of the ν_1 frequency decrease $(\Delta\bar{\nu}_1)_{tr}$ on cooling these fluorides through T_{tr}. In $(\Delta\bar{\nu}_1)_{tr} = \bar{\nu}_1(>T_{tr}) - \bar{\nu}_1(10)$, the first term refers to a temperature just above T_{tr} (in the cubic phases, a single frequency); the second term is the mean of the component frequencies at 10 K weighted by idealized intensity. The lines through the points are power fits cT_{tr}^{κ}.

strengthening of the strongest N—H···F bond at the expense of the others. The frequency of the highest ν_1 component approaches the limiting ν_1 value for weak N—H···F bonding modified by the compression effect.

Conclusions. While NH_4^+ and Rb^+ are dimensionally comparable, replacing Rb^+ by NH_4^+, at about the same t, has a dramatic effect on T_{tr}. In the A_3MF_6 cryolites the difference $T_{tr}(AM) - T_{tr}(NH_4M)$ amounts to as much as ~420 deg for AM = RbCr and would be expected to be even larger for RbAl.

The trends for the ammonium compounds can be rationalized, qualitatively, with recourse to the geometric meaning of the tolerance factor t. The closer t is to unity, the more complete is the contact of all the (spherical) atoms in the structure. Conversely, the more t falls below unity, the more room is there for the 12-coordinated ammonium ion, and the more opportunity for this ion to establish a strong, possibly privileged N—H···F bond at the expense of the other N—H···F bonds. This process is likely to involve a displacement of the N atom from the $\frac{1}{4}\frac{1}{4}\frac{1}{4}$ position toward the most strongly bonded F atom. The stronger this privileged bond, the lower the lowest ν_1 component frequency, the larger the spread of the ν_1 component frequencies, the larger $(\Delta\bar{\nu}_1)_{tr}$, and the greater the stability of the low phase, i.e. the higher T_{tr}. The slope of the T_{tr} vs. $r^{vi}(M)$ (Fig. 31) or the T_{tr} vs. t (Fig. 32) variation is a consequence of these trends.

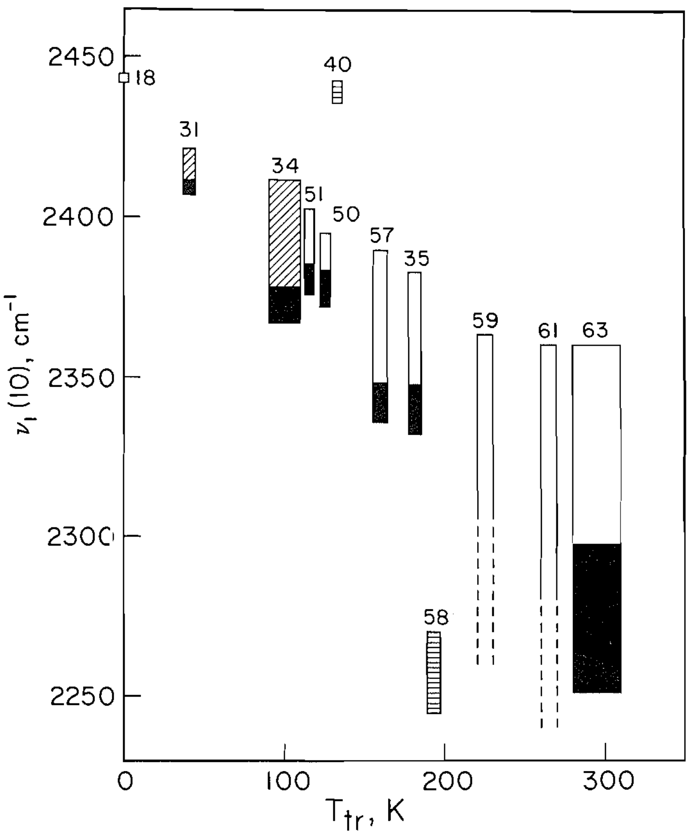

FIG. 35. Variation of the highest and the lowest ν_1 (10) component frequencies of $(NH_3D^+)^{xii}$ with T_{tr} in the perovskite-derived (open rectangles) and trigonal $(NH_4)_2MF_6$ (shaded rectangles) fluorides. The solid portion of a rectangle indicates $(\Delta\bar{\nu}_1)_{tr}$ (see caption of Fig. 34; not available for **61** and **58**; ~6 cm^{-1} for **40**).

While this rationale accounts, qualitatively, for the thermal behaviour of the above properties of the C.N.12 ammonium fluorides, it does not make clear why the large differences in T_{tr} between the ammonium and the alkali fluorides exist in the first place, i.e. what is responsible for the stability of the low phases of say K_3AlF_6 or Rb_3CrF_6 up to quite high temperatures compared with the corresponding ammonium compounds.[25] Nor does it tell us to what extent the ammonium ion is co-responsible, as a causative factor, for the occurrence of a structural transition in these compounds. It is unlikely that the marginal difference in t between Rb_3CrF_6 and K_3CrF_6, for example, would by itself produce a T_{tr} difference of 180 deg, and one has to look beyond simple packing arguments for explanations.

Acknowledgments

We thank Dr. A. Tressaud for making available unpublished results on the cryolites, and Dr. S. P. Deraniyagala for his competent assistance with the preparation of $(NH_4)_3MF_6$. This investigation was supported by a grant from the Natural Sciences and Engineering Research Council of Canada to the first-named author.

1. O. KNOP, T. S. CAMERON, S. P. DERANIYAGALA, D. ADHIKESAVALU, and M. FALK. Can. J. Chem. **63**, 516 (1985).

[25] The depressory effect on T_{tr} produced by replacing an alkali ion by NH_4^+ is noticeable even for the 6-coordinated sites: in the sequence $(NH_4)_2BFeF_6$ (B = Na, K, Rb, NH_4), the T_{tr} of the B = NH_4 member is unexpectedly low (Figs. 31 and 32).

2. O. KNOP, I. A. OXTON, and M. FALK. Can. J. Chem. **57**, 404 (1979); **57**, 2003 (1979).
3. W. MASSA. Z. Anorg. Allg. Chem. **427**, 235 (1976).
4. W. MASSA. Z. Anorg. Allg. Chem. **436**, 29 (1977).
5. M. EPPLE. Doctoral dissertation. Universität Tübingen. 1978.
6. M. EPPLE, W. RÜDORFF, and W. MASSA. Z. Anorg. Allg. Chem. **495**, 200 (1982).
7. H. W. W. ADRIAN and D. FEIL. Acta Crystallogr. A, **25**, 438 (1969).
8. B. MOROSIN. Acta Crystallogr. B, **26**, 1635 (1970).
9. R. E. MARSH and F. H. HERBSTEIN. Acta Crystallogr. B, **39**, 280 (1983).
10. O. KNOP, W. J. WESTERHAUS, and M. FALK. Can. J. Chem. **58**, 270 (1980).
11. T. R. R. MCDONALD. Acta Crystallogr. **13**, 113 (1960).
12. I. A. OXTON, O. KNOP, and M. FALK. J. Mol. Struct. **37**, 69 (1977).
13. W. MASSA. Habilitationsschrift. Philipps-Universität Marburg, 1982.
14. A. BULOU, A. LEBLÉ, A. W. HEWAT, and J. L. FOURQUET. Mater. Res. Bull. **17**, 391 (1982).
15. O. KNOP, I. A. OXTON, W. J. WESTERHAUS, and M. FALK. J. Chem. Soc. Faraday 2, **77**, 309 (1981).
16. R. B. HELMHOLDT, G. A. WIEGERS, and J. BARTOLOMÉ. J. Phys. C: Solid State Phys. **13**, 5081 (1980).
17. R. BURRIEL, J. BARTOLOMÉ, R. NAVARRO, and D. GONZÁLEZ. Recent developments in condensed matter physics. Vol. 4. *Edited by* J. T. Devreese. Plenum Press, New York. 1981. pp. 1–10.
18. R. BURRIEL. Thesis. University of Zaragoza. 1979.
19. N. G. PARSONAGE and L. A. K. STAVELEY. Disorder in crystals. Clarendon Press, Oxford. 1978.
20. O. KNOP, W. J. WESTERHAUS, and M. FALK. Can. J. Chem. **58**, 867 (1980).
21. A. LARI-LAVASSANI, G. JOURDAN, C. AVINENS, and L. COT. C.R. **279C**, 193 (1974).
22. Z. TUN and I. D. BROWN. Acta Crystallogr. B, **38**, 1792 (1982).
23. J. FAWCETT, J. H. HOLLOWAY, D. C. PUDDICK, and D. R. RUSSELL. Acta Crystallogr. B, **36**, 1921 (1980).
24. K. MORIYA, T. MATSUO, H. SUGA, and S. SEKI. Bull. Chem. Soc. Jpn. **52**, 3152 (1979).
25. K. MORIYA, T. MATSUO, H. SUGA, and S. SEKI. Bull. Chem. Soc. Jpn. **50**, 1920 (1977).
26. M. LORIENT, A. TRESSAUD, and J. RAVEZ. Rev. Chim. Min. **19**, 128 (1980).
27. M. LORIENT, R. VON DER MÜHLL, J. RAVEZ, and A. TRESSAUD. Solid State Commun. **36**, 383 (1980).
28. S. MØRUP and N. THRANE. Solid State Commun. **11**, 1319 (1972).
29. J. L. HOARD and M. B. WILLIAMS. J. Am. Chem. Soc. **64**, 633 (1942).
30. L. A. K. STAVELEY, N. R. GREY, and M. J. LAYZELL. Z. Naturforsch. **18a**, 148 (1963).
31. J. PEBLER, E. HERDTWECK, W. MASSA, and R. SCHMIDT. Studies in inorganic chemistry. Vol. 3. (1983). (Proc. 2nd Europ. Conf. Solid State Chem., Veldhoven, 7–9 June, 1982). Elsevier, Amsterdam.
32. O. KNOP, I. A. OXTON, W. J. WESTERHAUS, and M. FALK. J. Chem. Soc. Faraday 2, **77**, 811 (1981).
33. A. LEBLÉ, J.-C. FAYET, and C. JACOBONI. C.R. **277B**, 647 (1973).
34. S. SCHWARZMANN. Fortschr. Mineral. **42**, 231 (1966).
35. L. NIEMELÄ and J. TUOHI. Ann. Univ. Turku, ser. AI, no. 137 (1970).
36. I. SVARE and AIN EL HIAM ABD EL HALEEM. Phys. Scripta, **19**, 351 (1979).
37. A. M. HEYNS and C. W. F. T. PISTORIUS. Spectrochim. Acta, **30A**, 99 (1974).
38. A. M. HEYNS and G. J. VAN SCHALKWYK. Spectrochim. Acta,

29A, 1163 (1973).
39. H. BODE and H. CLAUSEN. Z. Anorg. Allg. Chem. **265**, 229 (1951).
40. W. J. WESTERHAUS, O. KNOP, and M. FALK. Can. J. Chem. **58**, 1355 (1980).
41. B. HOFMANN and R. HOPPE. Z. Anorg. Allg. Chem. **458**, 151 (1979).
42. T. C. WADDINGTON. J. Chem. Soc. 4340 (1958).
43. V. BRAJOVIĆ, H. BOUTIN, G. J. SAFFORD, and H. PALEVSKY. J. Phys. Chem. Solids, **24**, 617 (1963).
44. S. ALBERT and H. S. GUTOWSKY. J. Chem. Phys. **59**, 3585 (1973).
45. R. KALIAPERUMAL, R. SRINIVASAN, and K. V. RAMANATHAN. Chem. Phys. Lett. **102**, 29 (1983).
46. R. A. NYQUIST and R. O. KAGEL. Infrared spectra of inorganic compounds. Academic Press, New York and London. 1971.
47. G. KERESZTURY, O. KNOP, and M. FALK. Can. J. Chem. **60**, 1972 (1982).
48. J. SCHIFFER. J. Chem. Phys. **64**, 3014 (1976).
49. R. HAEGELE, W. VERSCHAREN, and D. BABEL. Z. Naturforsch. **30**b, 462 (1975).
50. R. D. SHANNON. Acta Crystallogr. A, **32**, 751 (1976).
51. I. P. MAKAROVA, S. V. MISYUL, L. A. MURADYAN, A. F. BOVINA, V. I. SIMONOV, and K. S. ALEKSANDROV. Phys. Status Solidi B, **121**, 481 (1984).
52. A. OKAZAKI and Y. SUEMUNE. J. Phys. Soc. Jpn. **17**, Suppl. B-I, 204 (1962).
53. A. A. SHEVYREV, L. A. MURADYAN, V. E. ZAVODNIK, K. S. ALEKSANDROV, and V. I. SIMONOV. Kristallogr. **25**, 555 (1980); (Engl. transl.) Sov. Phys. – Crystallogr. **25**, 319 (1980).
54. J. HUTTON and R. J. NELMES. J. Phys. C: Solid State Phys. **14**, 1713 (1981).
55. N. KIJIMA, K. TANAKA, and F. MARUMO. Acta Crystallogr. B, **37**, 545 (1981).
56. J. MAETZ, M. MÜLLNER, and H. JEX. Phys. Status Solidi A, **50**, K117 (1978).
57. J. D. TORNERO, F. H. CANO, J. FAYOS, and M. MARTÍNEZ-RIPOLL. Ferroelectrics, **19**, 123 (1978).
58. M. SAKATA, J. HARADA, M. J. COOPER, and K. D. ROUSE. Acta Crystallogr. A, **36**, 7 (1980).
59. J. PEBLER, K. SCHMIDT, R. HAEGELE, and D. BABEL. Z. Naturforsch. **31**b, 1039 (1976).
60. A. DE KOZAK. Rev. Chim. Min. **8**, 301 (1971).
61. E. G. STEWARD and H. P. ROOKSBY. Acta Crystallogr. **6**, 49 (1953).
62. A. TRESSAUD, J. PORTIER, S. SHEARER-TURRELL, J.-L. DUPIN, and P. HAGENMULLER. J. Inorg. Nucl. Chem. **32**, 2179 (1970).
63. H. BODE and E. VOSS. Z. Anorg. Allg. Chem. **290**, 1 (1957).
64. G. MEYER and H.-C. GAEBELL. Z. Naturforsch. **33**b, 1476 (1978).
65. G. E. FISH, J. J. RHYNE, J. W. LYNN, and H. H. PATTERSON. Bull. Am. Phys. Soc. **24**, 429 (1979).
66. R. NEVALD, F. W. VOSS, O. V. NIELSEN, and H. D. AMBERGER. Solid State Commun. **32**, 1223 (1979).
67. A. TRESSAUD. Personal communication.
68. R. BURRIEL, J. BARTOLOMÉ, and R. NAVARRO. Ferroelectrics, **54**, 253 (1984).
69. G. MEYER. Prog. Solid State Chem. **14**, 141 (1982).
70. O. GREIS. Rev. Inorg. Chem. **4**, 87 (1982).
71. G. MEYER. Z. Naturforsch. **35**b, 394 (1980).
72. E. PALACIOS, J. BARTOLOMÉ, R. NAVARRO, J. GARCÍA, D. GONZÁLEZ, and H. B. BROM. Ferroelectrics, **55**, 287 (1984).
73. G. MEYER and E. DIETZEL. Rev. Chim. Min. **16**, 189 (1979).
74. G. P. KNUDSEN. Solid State Commun. **49**, 1045 (1984).
75. J. BARTOLOMÉ, R. BURRIEL, F. PALACIO, D. GONZÁLEZ, R. NAVARRO, J. A. ROJO, and L. J. DE JONGH. Physica, **115**B, 190 (1983).
76. F. PELLÉ, B. CHEVALIER, and B. BLANZAT. Studies in inorganic chemistry. Vol. 3. 737 (1983). (Proc. 2nd Europ. Conf. Solid State Chem., Veldhoven, 7–9 June, 1982.) Elsevier, Amsterdam.
77. R. W. SCHWARTZ, S. F. WATKINS, C. J. O'CONNOR, and R. L. CARLIN. J. Chem. Soc. Faraday, 2, **72**, 565 (1976).
78. C. J. O'CONNOR, R. L. CARLIN, and R. W. SCHWARTZ. J. Chem. Soc. Faraday 2, **73**, 361 (1977).
79. H. B. BROM and J. BARTOLOMÉ. Physica B+C, **111**, 183 (1981).
80. M. LORIENT, R. VON DER MÜHLL, A. TRESSAUD, and J. RAVEZ. Solid State Commun. **40**, 847 (1981).
81. O. BECKMAN and K. KNOX. Phys. Rev. **121**, 376 (1961).
82. A. OKAZAKI and Y. SUEMUNE. J. Phys. Soc. Jpn. **16**, 671 (1961).
83. A. OKAZAKI, Y. SUEMUNE, and T. FUCHIKAMI. J. Phys. Soc. Jpn. **14**, 1823 (1959).
84. P. SELGERT, C. LINGNER, and B. LÜTHI. Z. Phys. B: Condens. Matter, **55**, 219 (1984).
85. M. MIDORIKAWA, Y. ISHIBASHI, and Y. TAKAGI. J. Phys. Soc. Jpn. **46**, 1240 (1979).
86. J. Y. BUZARÉ, M. FAYET-BONNEL, and J.-C. FAYET. J. Phys. C: Solid State Phys. **13**, 857 (1980).
87. D. J. LOCKWOOD and G. J. COOMBS. J. Physique, **42**, C6-761 (1981).
88. A. ITO and S. MORIMOTO. J. Phys. Soc. Jpn. **39**, 884 (1975).
89. M. HIDAKA and S. HOSOGI. J. Physique, **43**, 1227 (1982).
90. W. J. CROFT, M. KESTIGIAN, and F. D. LEIPZIGER. Inorg. Chem. **4**, 423 (1965).
91. F. PROKERT. Phys. Status Solidi B, **104**, 261 (1981).
92. S. V. MEL'NIKOVA, A. T. ANISTRATOV, and K. S. ALEKSANDROV. Fiz. Tverd. Tela, **23**, 246 (1981); (Engl. transl.) Sov. Phys. – Solid State, **23**, 138 (1981).
93. S. V. MEL'NIKOVA, I. N. FLEROV, and A. T. ANISTRATOV. Fiz. Tverd. Tela, **23**, 3570 (1981); (Engl. Transl.) Sov. Phys. – Solid State, **23**, 2074 (1981).
94. M. HIDAKA, S. YAMASHITA, and Y. OKAMOTO. Phys. Status Solidi A, **81**, 177 (1984).
95. J. IHRINGER, G. WU, R. HOPPE, and A. P. HEWAT. Z. Krist. **162**, 117 (1983).
96. J. IHRINGER, G. WU, and R. HOPPE. Z. Krist. **159**, 62 (1982).
97. J. IHRINGER. Solid State Commun. **41**, 525 (1982).
98. N. LEHNER, H. RAUH, K. STROBEL, R. GEICK, G. HEGER, J. BOUILLOT, B. RENKER, M. ROUSSEAU, and W. G. STIRLING. J. Phys. C: Solid State Phys. **15**, 6545 (1982).
99. M. SAKATA, T. NISHIWAKI, and J. HARADA. J. Phys. Soc. Jpn. **47**, 232 (1979).
100. J. BRYNESTAD, H. L. YAKEL, and G. P. SMITH. J. Chem. Phys. **45**, 4652 (1966).
101. C. K. MØLLER. Nature, **182**, 1436 (1958).
102. J. BARTOLOMÉ, R. NAVARRO, D. GONZÁLEZ, and L. J. DE JONGH. Physica, **92**B, 23, 45 (1977).

Excess molar volumes of binary mixtures of 2-hexanone with *n*-alkane at 298.15 K

J. ORTEGA

Cátedra de Termodinámica y Físicoquímica, Escuela Superior de Ingenieros Industriales, Las Palmas de Gran Canaria, Spain

AND

M. I. PAZ-ANDRADE,[1] E. RODRIGUEZ-NUÑEZ, AND E. JIMENEZ

Departamento de Física Fundamental, Facultad de Física, Universidad de Santiago, Santiago de Compostela, Spain

Received March 21, 1985

J. ORTEGA, M. I. PAZ-ANDRADE, E. RODRIGUEZ-NUÑEZ, and E. JIMENEZ. Can. J. Chem. **63**, 3354 (1985).

The excess molar volumes, V_m^E, of 2-hexanone (MBK) with *n*-hexane, *n*-heptane, *n*-octane, *n*-nonane, *n*-decane, *n*-undecane, *n*-dodecane, and *n*-tridecane have been obtained at 298.15 K from densities measured with a vibrating tube densimeter. The V_m^E are positive over the entire composition range in all mixtures, with the exception of the MBK + *n*-hexane system, where an inversion of the sign of V_m^E is observed. In other systems, V_m^E increases with increasing size of the alkyl group in *n*-alkane.

J. ORTEGA, M. I. PAZ-ANDRADE, E. RODRIGUEZ-NUÑEZ et E. JIMENEZ. Can. J. Chem. **63**, 3354 (1985).

Opérant à 298,15 K et faisant appel aux densités mesurées à l'aide d'un densimètre à tube vibrant, on a obtenu les volumes molaires en excès, V_m^E, de l'hexanone-2 (MBC) avec le *n*-hexane, le *n*-heptane, le *n*-octane, le *n*-nonane, le *n*-décane, le *n*-undécane, le *n*-dodécane et le *n*-tridécane. Les valeurs de V_m^E sont positives dans tous les domaines de composition des mélanges, à l'exception du système MBC + *n*-hexane où l'on observe une inversion du signe de V_m^E. Dans les autres systèmes, la valeur de V_m^E augmente avec la taille du groupement alkyle des *n*-alcanes.

[Traduit par le journal]

Introduction

This paper is a study of the effect of alkane chain length on the excess volumes of binary mixtures of aliphatic ketones with *n*-alkanes (1–3). We have obtained densimetrically the value at 298.15 K of the V_m^E of eight binary mixtures of 2-hexanone (MBK) with a normal alkane C_bH_{2b+2} (b = 6 to 13). The results, together with previously published findings, suggest the possibility of specific interactions between unlike molecules.

Experimental

Component liquids

The 2-hexanone (MBK) used was supplied by Aldrich Chem. Co. with a specified purity of 99+ mol%. The eight *n*-alkanes (C_6H_{14} to $C_{13}H_{28}$) were Fluka A. G. "puriss." grade and their purity was >99.5 mol%. Both 2-hexanone and *n*-alkanes were used as received, but prior to actual measurements all liquids were dried with molecular sieve (Union Carbide Type 4A, from Fluka) and were partially degassed. The purities of the liquids were tested by measuring densities at 298.15 K. Our results agree closely with the published values (Table 1).

TABLE 1. Densities ρ of component liquids at 298.15 K

Component	ρ/(kg m^{-3}) This work	ρ/(kg m^{-3}) Literature
2-Hexanone $CH_3CO(CH_2)_3CH_3$	807.25	807.96[a]
n-Hexane C_6H_{14}	654.82	654.71[b] 654.83[c]
n-Heptane C_7H_{16}	680.13	679.46[b] 679.72[d]
n-Octane C_8H_{18}	698.42	698.62[b] 698.61[d]
n-Nonane C_9H_{20}	713.85	713.75[b] 713.94[e]
n-Decane $C_{10}H_{22}$	726.63	726.35[b] 726.11[f]
n-Undecane $C_{11}H_{24}$	736.25	736.5[b] 736.49[g]
n-Dodecane $C_{12}H_{26}$	745.32	745.18[b] 745.39[f]
n-Tridecane $C_{13}H_{28}$	752.64	752.71[b]

[a]Reference 2.
[b]Reference 4.
[c]Reference 13.
[d]Reference 12.
[e]Reference 8.
[f]Reference 1.
[g]Reference 5.

Determination of excess volumes

Binary mixtures were prepared by weight (6) and the probable error in the mole fraction is less than 10^{-4}. The densities, ρ, were measured with a DMA-55 digital densimeter (Anton Paar, Graz, Austria) with a reproducibility of ±0.01 kg m^{-3}. Details of the auxiliary equipment and of the operating procedure have been described previously (7, 8).

From the densities, ρ_i, and molar masses, M_i, of the pure liquids (i = 1 for MBK, 2 for *n*-alkane) and the density ρ of the mixture, the molar excess volumes are given by

$$[1]\quad V_m^E = xM_1(\rho^{-1} - \rho_1^{-1}) + (1 - x)M_2(\rho^{-1} - \rho_2^{-1})$$

where x is the mole fraction of MBK.

The results for V_m^E are estimated to be accurate to better than ±0.002 cm^3 mol^{-1} (8). The accuracy of the technique was checked by measuring the V_m^E data for the test binary mixture benzene + cyclohexane at 298.15 K and the results agree satisfactorily with the literature (6).

[1]To whom all correspondence should be addressed.

TABLE 2. Excess molar volumes, V_m^E, for (x2-hexanone + (1 − x)n-alkane) at 298.15 K

x	V_m^E cm³ mol⁻¹	x	V_m^E cm³ mol⁻¹	x	V_m^E cm³ mol⁻¹	x	V_m^E cm³ mol⁻¹
			$x CH_3CO(CH_2)_3CH_3$ + (1 − x)C_6H_{14}				
0.0494	0.0718	0.2874	0.2121	0.5151	0.1426	0.8196	0.0060
0.0692	0.1001	0.3583	0.2053	0.5613	0.1237	0.8838	−0.0064
0.1507	0.1696	0.4021	0.1954	0.6332	0.0899	0.9298	−0.0164
0.2211	0.2054	0.4586	0.1768	0.7238	0.0505	0.9756	−0.0102
			$x CH_3CO(CH_2)_3CH_3$ + (1 − x)C_7H_{16}				
0.0599	0.1410	0.2552	0.3565	0.5196	0.3647	0.7580	0.2221
0.1013	0.2085	0.3676	0.3912	0.5563	0.3544	0.8394	0.1536
0.1402	0.2576	0.4330	0.3932	0.6067	0.3233	0.9428	0.0510
0.1931	0.3170	0.4937	0.3778	0.6746	0.2847		
			$x CH_3CO(CH_2)_3CH_3$ + (1 − x)C_8H_{18}				
0.0633	0.1731	0.3195	0.5019	0.5279	0.5098	0.7603	0.3376
0.1523	0.3464	0.3778	0.5201	0.5986	0.4757	0.8451	0.2370
0.1945	0.4064	0.4583	0.5248	0.6457	0.4417	0.9343	0.1056
0.2462	0.4548	0.5004	0.5139	0.6940	0.3997		
			$x CH_3CO(CH_2)_3CH_3$ + (1 − x)C_9H_{20}				
0.0927	0.2535	0.3156	0.5674	0.5275	0.5876	0.7767	0.3940
0.1575	0.3732	0.3755	0.5871	0.5723	0.5706	0.8755	0.2413
0.2097	0.4606	0.4546	0.6018	0.6366	0.5309	0.9564	0.0871
0.2605	0.5164	0.4943	0.5940	0.7316	0.4464		
			$x CH_3CO(CH_2)_3CH_3$ + (1 − x)$C_{10}H_{22}$				
0.0780	0.2221	0.3339	0.6085	0.5123	0.6405	0.7718	0.4541
0.1312	0.3487	0.4052	0.6386	0.5719	0.6227	0.8602	0.2978
0.2018	0.4641	0.4426	0.6420	0.6163	0.5992	0.9496	0.1187
0.2778	0.5601	0.4747	0.6437	0.6817	0.5485		
			$x CH_3CO(CH_2)_3CH_3$ + (1 − x)$C_{11}H_{24}$				
0.0535	0.1682	0.2953	0.6161	0.6021	0.6624	0.8751	0.3189
0.1173	0.3429	0.3543	0.6617	0.6695	0.6125	0.9227	0.2118
0.1641	0.4361	0.4608	0.6962	0.7595	0.5060	0.9578	0.1199
0.2384	0.5517	0.5293	0.6891	0.8149	0.4297	0.9784	0.0607
			$x CH_3CO(CH_2)_3CH_3$ + (1 − x)$C_{12}H_{26}$				
0.0969	0.2624	0.3630	0.6738	0.5578	0.7076	0.8037	0.4710
0.1330	0.3614	0.4128	0.7005	0.6022	0.6924	0.8616	0.3543
0.2123	0.5099	0.4777	0.7115	0.6691	0.6399	0.9612	0.1093
0.2731	0.5978	0.5146	0.7120	0.7395	0.5660		
			$x CH_3CO(CH_2)_3CH_3$ + (1 − x)$C_{13}H_{28}$				
0.0575	0.1726	0.2851	0.6177	0.5246	0.7398	0.7676	0.5581
0.1054	0.2973	0.3643	0.6956	0.5672	0.7304	0.8409	0.4308
0.1424	0.3820	0.4338	0.7300	0.6255	0.7069	0.9367	0.1975
0.2198	0.5307	0.4732	0.7369	0.6977	0.6464		

Results

The excess molar volumes V_m^E at 298.15 K for each of the eight binary mixtures are tabulated in Table 2 over the complete range of mole fractions x. The composition dependence of V_m^E has been calculated in accordance with the smoothing equation

$$[2] \quad V_m^E/(\mathrm{cm^3\ mol^{-1}}) = x(1-x)\sum_{i=0}^{n-1} v_i(2x-1)^i$$

where x is the mole fraction of MBK. The values of the coefficients v_i determined by the method of least squares with all points equally weighted and the standard deviations s (9) are shown in Table 3. In each case the number n of the v_i was determined by means of an F test for the validity of an additional term (10).

The experimental results for V_m^E are plotted against x in Fig. 1, together with the curves calculated in accordance with eq. [2].

Discussion

Only one of the mixtures considered here, MBK + n-heptane, appears to have been studied previously (Dusart *et al.* (2)). In general, our results for this mixture are very similar to theirs, but their V_m^E are rather higher than ours, especially $V_{m,\max}^E$ (Fig. 2); it may be pointed out that their data for the mixture MEK + n-heptane are likewise higher than those of Grolier and Benson (1).

TABLE 3. Coefficients, v_i, and standard deviations, s, for representations of $V_m^E/(cm^3\ mol^{-1})$ by eq. [2]

System	v_0	v_1	v_2	v_3	v_4	s
$xCH_3CO(CH_2)_3CH_3 + (1-x)C_6H_{14}$	0.6142	−0.8746	0.2896	−0.2018	−0.3544	0.0033
$+ (1-x)C_7H_{16}$	1.4982	−0.5694	0.1784	−0.3726	0.1363	0.0040
$+ (1-x)C_8H_{18}$	2.0658	−0.5438	0.3465	−0.1907	—	0.0022
$+ (1-x)C_9H_{20}$	2.3799	−0.3818	0.5000	−0.1823	−0.3031	0.0038
$+ (1-x)C_{10}H_{22}$	2.5726	−0.2675	0.5211	−0.1358	−0.2906	0.0039
$+ (1-x)C_{11}H_{24}$	2.7954	−0.2090	0.4551	−0.0552	—	0.0040
$+ (1-x)C_{12}H_{26}$	2.8563	−0.1089	0.7140	0.1064	−0.7250	0.0042
$+ (1-x)C_{13}H_{28}$	2.9656	0.0357	0.5418	0.0679	−0.2140	0.0016

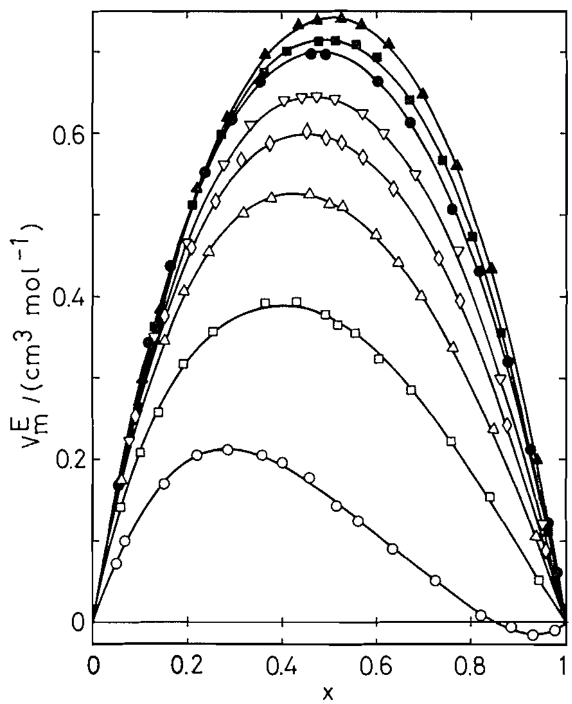

FIG. 1. Excess molar volumes, V_m^E, at 298.15 K for $\{xCH_3CO(CH_2)_3CH_3 + (1-x)C_bH_{2b+2}\}$: ○, $b = 6$; □, $b = 7$; △, $b = 8$; ◇, $b = 9$; ▽, $b = 10$; ●, $b = 11$; ■, $b = 12$; ▲, $b = 13$. The curves (—) were calculated from eq. [2] with coefficients from Table 3.

As expected, given the excess volumes (1−3) and excess enthalpies (11−14) of other 2-alkanone + n-alkane mixtures, the V_m^E are positive. This implies that the predominant effect is expansion consequent on the rupture of strong dipole−dipole interactions between ketone molecules (13). The negative values of V_m^E in the ketone-rich range of MBK + n-hexane are nevertheless indicative of important interactions between unlike molecules. The excess heat capacities, $C_{p,m}^E$ (1), and excess volumes at infinite dilution, $V_1^{E\infty}$ and $V_2^{E\infty}$ (2), show that these are probably interactions between the ketoxy group of the ketone and the alkyl group of the hydrocarbon leading to cooperative conformational arrangements such as quasi-cyclic structures (1,2).

The very steady increase in V_m^E as the size of the hydrocarbon increases suggests that with larger molecules the conformational effect is much less important. It is also interesting that the curves become more symmetrical with increasing hydrocarbon size. The V_m^E results presented in the present paper are coherent with data already published for H_m^E (11−13): for a given n-alkane mixed with different 2-alkylketones V_m^E decreases as the hydrocarbon chain of the latter lengthens (1, 2).

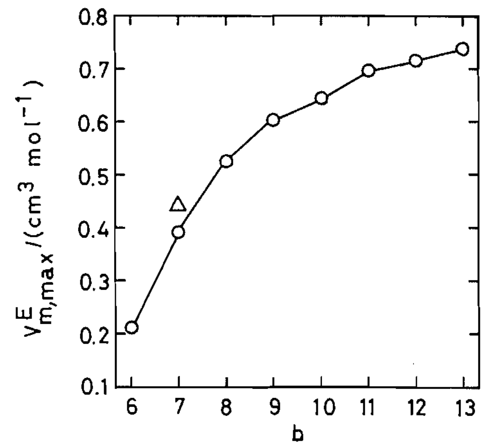

FIG. 2. Plots of $V_{m,max}^E$ at 298.15 K for $\{xCH_3CO(CH_2)_3CH_3 + (1-x)C_bH_{2b+2}\}$ against b: ○, this work; △, Dusart *et al.* (2).

1. J.-P. E. GROLIER and G. C. BENSON. Can. J. Chem. **62**, 949 (1984).
2. O. DUSART, C. PIEKARSKI, S. PIEKARSKI, and A. VIALLARD. J. Chim. Phys. **73**, 837 (1976).
3. G. R. NAIDU and P. R. NAIDU. J. Chem. Eng. Data, **26**, 197 (1981).
4. Selected Values of Properties of Hydrocarbons and Related Compounds. American Petroleum Institute Research Project 44. Thermodynamics Research Center, Texas A & M University, College Station, Texas. June 30, 1973. Table 23-2-(1.101)-d.
5. K. CHYLINSKI and R. STRYJEK. J. Chem. Thermodyn. **16**, 153 (1984).
6. M. TAKENAKA, R. TANAKA, and S. MURAKAMI. J. Chem. Thermodyn. **12**, 849 (1980).
7. J. ORTEGA and M. C. ANGULO. J. Chem. Eng. Data, **29**, 340 (1984).
8. J. R. GOATES, J. B. OTT, and R. B. GRIGG. J. Chem. Thermodyn. **11**, 497 (1979).
9. IUPAC Commission I.2 on Thermodynamics. Assignment and Presentation of Uncertainties of the Numerical Results of Thermodynamic Measurements. J. Chem. Thermodyn. **13**, 603 (1981).
10. P. BEVINGTON. Data reduction and error analysis for the physical sciences. McGraw-Hill, New York. 1969.
11. A. DE TORRE, I. VELASCO, S. OTIN, and C. GUTIERREZ LOSA. J. Chem. Thermodyn. **12**, 87 (1980).
12. O. KIYOHARA, Y. P. HANDA, and G. C. BENSON. J. Chem. Thermodyn. **11**, 453 (1979).
13. O. KIYOHARA, G. C. BENSON, and J.-P. E. GROLIER. J. Chem. Thermodyn. **9**, 315 (1977).
14. O. DUSART and S. PIEKARSKI. J. Chim. Phys. **76**, 433 (1979).

Formation constants for selected organo—metal (Al^{3+}, Fe^{3+})—phosphate complexes

PAUL A. ARP AND W. LENSE MEYER
Faculty of Forestry, University of New Brunswick, Fredericton, N.B., Canada E3B 6C2

Received April 11, 1985

PAUL A. ARP and W. LENSE MEYER. Can. J. Chem. **63**, 3357 (1985).

The possible formation of organo–metal–phosphate complexes (O–M–P) in aqueous solutions is examined by potentiometric titration analysis. The complex-forming solutions contain Al^{3+}-ions or Fe^{3+}-ions, organic acids (salicylic, phthalic, oxalic, and citric acids) and phosphate ions. The titrations are done within the precipitation-free pH-region from 2 to 4.5 (approximately) at 25°C under nitrogen at an ionic strength of 0.2 *M* KCl. The calibration of the electrode pair (glass-electrode, calomel-reference electrode) and the determination of the formation constants are facilitated by analyzing the pertinent curves with the ACBA-(Arena *et al.*) and MINIQUAD-(Gans *et al.*) computer programs. The results suggest (*i*) that O–M–P complexes are readily formed, and that the power of selected organic acids to form ternary mixed-ligand complexes with Al^{3+}-ions and phosphate ions decreases in the order salycilate > citrate > oxalate > phthalate. Also, Fe^{3+}-ions are found to be more strongly bound by salicylate and phosphate ions than Al^{3+}-ions. The effect of O–M–P formation on the chemical speciation of Al in buffered aqueous solutions containing mineral nutrients for the growth of biological organisms is demonstrated for a special case study.

PAUL A. ARP et W. LENSE MEYER. Can. J. Chem. **63**, 3357 (1985).

Faisant appel au titrate potentiométrique, on a étudié la formation possible de complexes organo–métal–phosphate (O–M–P) dans des solutions aqueuses. Les solutions qui forment ces complexes contiennent des ions Al^{3+} ou Fe^{3+}, des acides organiques (acides salicyclique, phtalique, oxalique ou citrique) et des ions phosphates. On a réalisé les titrates à 25°C, sous atmosphère d'azote, à une force ionique de 0,2 *M* de KCl et à des pH allant de 2 à 4,5 (approximativement) où il n'y a pas de précipitation. La calibration de la paire d'électrode (électrode de verre et électrode de référence ou calomel) et la détermination des constantes de formation sont facilitées par une analyse des courbes appropriées à l'aide des logiciels ACBA (Arena *et al.*) et MINIQUAD (Gans *et al.*). Les résultats suggèrent que les complexes O–M–P se forment facilement et que la facilité des acides organiques choisis à former des complexes ternaires comportant des ligands mixtes avec les ions Al^{3+} et phosphates diminue dans l'ordre suivant: salycilate > citrate > oxalate > phtalate. On a trouvé également que les ions salycilates et phosphates se lient plus fortement aux ions Fe^{3+} qu'aux ions Al^{3+}. Dans une étude d'un cas spécial, on a pu démontrer l'influence de la formation du complexe O–M–P sur la spéciation chimique de l'aluminium dans des solutions aqueuses tamponées contenant des sels minéraux facilitant la croissance d'organismes biologiques.

[Traduit par le journal]

Introduction

The objective of this paper is to provide information about the possible formation and the associated formation constants of various relevant and as yet poorly described chemical combinations of phosphate ions, metal ions (Fe^{3+} and Al^{3+}), and lower molecular weight organic acids (i.e. salicylic, phthalic, oxalic, and citric acid). Such combinations, in general, are likely found as mixed ligand complexes in aqueous environments with Al, Fe, phosphate, and organic substances as chemical components. The presence — or the formation — of such organo–metal–phosphate complexes (O–M–P) has many physiological and environmental implications be they related to Al^{3+}-, Fe^{3+}-, and phosphate-solubility, subsequent inter- and intra-cellular transport mechanisms for phosphate ions and metal ions, and metabolic processing of phosphate and metal ions via enzymatic substrate reactions (1). The particular organic acids examined here are also relevant in this respect because they are common metabolites, root exudates, microbial byproducts, and strong metal chelators (1).

Quantitative information about the formation constants of selected O–M–P complexes can be obtained by using an optimally adjusted potentiometric titration technique designed to eliminate chemical interferences from the complex-forming reactions, and from the electormotive force response of the electrode-pair used to trace the changing pH of the titrated solution ("titrand") following sequential "titrant" additions. The titration curves so generated can be analyzed with specialized computer programs (see below) which allow a complete and precise calibration of the electrode pair, a quantitative analysis of the organic reagents used, statistical refinement of the formation constants of the O–M–P complexes which are to be found in the titrated solutions with greatest likelihood, and the prediction of the chemical speciation of the O–M–P-containing titrand solutions as function of pH.

The following contains (*i*) a brief review of published results concerning O–M–P complexes, (*ii*) a description of the theoretical and experimental procedures to generate quantitative information about O–M–P complexation from potentiometric titration data, (*iii*) a summary of O–M–P complexes the formation of which is strongly suggested by the analysis, and (*iv*) a demonstration on how the presence of such complexes may affect the chemical speciation of, e.g., Al^{3+} in buffered aqueous solutions containing mineral nutrients for the growth of biological organisms. The subject of Al-speciation in aqueous solutions, in particular, is relevant towards understanding the toxic effects of solubilized Al on plant growth (2), aquatic organisms (see, e.g., (3)), and possible effects of Al-intake on human health (4).

The Al- and Fe-chelation effect of organic matter (e.g. humic substances) in aqueous solutions has been known for some time. The exact mechanism of organic metal-ion chelation probably involves several reactive groups such as carboxyl (—COOH), hydroxyl (—OH), carbonyl (—C=O), amine (—NH_2), and quinone (—R=O) groups (Mortensen (5)). Cheam (6), Stevenson (7), and VanDijk (8) suggest that salicylate-like groups occurring on, e.g., humic acids appear to bind Al^{3+}- and Fe^{3+}-ions by partial chemical bonding. Piccolo and Stevenson (9), in addition, demonstrate the participation of molecular OH- and COOH-groups in the humic binding of metal cations via phthalate- and salicylate-like groups.

There are few definite studies supporting the formation of ternary complexes having Al^{3+}- (or Fe^{3+}-) ions as central ions, and organic acids and phosphate ions as ligands. Levesque and Schnitzer (10), for example, conclude that actual organo–metal–phosphate (O–M–P) complexes will form in solutions containing low concentrations of reactive metal ions relative to the concentration of the metal-chelating groups normally found on, e.g., fulvic acid molecules. Metal phosphates may precipitate within the fulvic acid solution when the metal to reactive-group ratio (in equivalents) is large. Sinha (11) confirms the existence of O–M–P complexes in the soil and postulates metal-ion linkages between organic molecules and phosphate ions. In addition, it would appear from Sinha's work that phosphate bound as O–M–P complex tends (*i*) to be more mobile and water-soluble than the organic phosphate fraction of soil organic matter, and (*ii*) such a complex breaks apart in strong acid solution. Similar work by Bloom (12) has shown that phosphate ions may be either absorbed by an aluminum-peat complex or may precipitate as aluminum phosphate depending on the relative concentrations of peat and aluminum- and phosphate-ions. Quantitative analyses concerning the formation constants of O–M–P complexes via potentiometric titrations were done by Ramamoorthy and Manning (1, 13–18) with special emphasis on humic substances as organic ligands. Their results are summarized in Table 1 in terms of the notation of the following section.

Theory

The law of mass action for the general reaction

$$[1] \quad mM + n_1L1 + n_2L2 + pH \rightleftarrows M_mL1_{n_1}L2_{n_2}H_p$$

concerning ternary mixed-ligand complexation (with, say, M as metal ion, L1 as phosphate ligand, and L2 as organic ligand) is given by

$$[2] \quad \beta = \frac{[M_mL1_{n_1}L2_{n_2}H_p]}{[M]^m[L1]^{n_1}[L2]^{n_2}[H]^p}$$

with β as the formation constant for constant temperature and ionic strength of the complex-forming solution (19).

Empirical determinations of β-values via potentiometric analysis, in general, are facilitated by combining the law of mass action with the mass balance for each complex-forming component at each titration point of a complex-forming solution. For example, one may consider HA as the "complex" and A^- and H^+ as the complex-forming components for the reaction

$$[3] \quad A^- + H^+ \rightleftarrows HA$$

with

$$[4] \quad \beta = \frac{[HA]}{[H^+][A^-]}$$

The mass balance for each component leads to

$$[5] \quad H_T \equiv \text{total H-content of solution (equiv./L)} = [HA] + [H^+]$$

and

$$[6] \quad A_T \equiv \text{total A-content of solution (equiv./L)} = [HA] + [A^-]$$

The total concentrations (H_T and A_T) are generally known or can be determined from the "recipe" used to mix the complex-forming solution. Glass electrodes are particularly convenient for obtaining precise values for $[H^+]$ via the Nernst equation

$$[7] \quad E = E_0 + \frac{RT}{F} \ln \{H^+\}$$

which relates the activity of the H^+-ions in solution (i.e., $\{H^+\}$) to the electromotive force (E = emf) of the glass-electrode reference-electrode combination. The Nernst equation may then be used to obtain $[H^+]$ by noting that

$$[8] \quad E = E_0' + \frac{RT}{F} \ln [H^+]$$

with $E_0' = E_0 + (RT/F) \ln \gamma_H$ and γ_H as activity coefficient for $[H^+]$.

By summarizing, it is seen that there are five unknowns ($[H]^+$, [HA], $[A^-]$, β, and E_0') and four equations ([4] to [7]) for each titration point when $[H^+]$ is to be obtained by potentiometric analysis. This set of equations, therefore, cannot be solved by considering each titration point independently. Simultaneous examination of more than 1 titration point, in turn, leads to an overdetermined system of equations thereby enabling statistical procedures for obtaining best-fitted estimates for the parameters held in common across the various titration points (20).

At present there are several computer programs that facilitate the extraction of parametric information from potentiometric titration curves (Legett (21) and Nordstrom *et al.* (22). The ACBA-program developed by Arena *et al.* (23), for example, is particularly useful for the potentiometric examination of acids and bases (weak and strong). This program calculates the "best" acid/base formation constants and concentrations from glass-electrode emf-readings and added titrant volumes. It also refines E_0' simultaneously via nonlinear least-squares procedures.

The MINIQUAD-75 program by Gans *et al.* (24) yields best-fitted estimates from potentiometric titration data for the formation constants of complexes of the general type shown in eq. [2]. This program is also based on a nonlinear least-squares algorithm designed to minimize the deviations (residuals) between the actual and calculated concentrations of all complex-forming components present in the titrated solution in accordance with the mass balance for each such component, i.e.

$$\text{minimize} \sum_{i=1}^{n} \{[M_T](\text{calcd.})_i - [M_T](\text{actual})_i\}^2$$

$$\text{minimize} \sum_{i=1}^{n} \{[L_{j_T}](\text{calcd.})_i - [L_{j_T}](\text{actual})_i\}^2, \quad (j = 1, 2)$$

and

$$\text{minimize} \sum_{i=1}^{n} \{[H_T](\text{calcd.})_i - [H_T](\text{actual})_i\}^2$$

This is done iteratively starting from guess-estimates for each β for all the postulated complexes that may form in the solution during the course of the titration. The sum of all complexes or species considered constitutes the "refinement model". Several numerical checks throughout the iteration procedure may lead to the rejection of some or all of the postulated complexes from the refinement model. The "refined model", in turn, represents the best-fit of the actual component concentrations based on those chemical complexes or species that remain part of the refined model. The refined model, in turn, depends on the formulation of the original refinement model. Trial-and-error coupled with chemical thought, therefore, is required to yield successive model improvements until (*i*) all remaining species

TABLE 1. Published formation constants for organo–metal–phosphate complexes[a]

Reaction		Log β	Reaction		log β
$Al^{3+} + Cit^{3-} + HPO_4^{2-}$	$\rightleftarrows$ Cit–Al–HPO_4^{2-}	19.29(1)	Ca^{2+} + *dl*-Tar + HPO_4^{2-}	$\rightleftarrows$ *dl*-Tar–Ca–HPO_4	9.69(18)
$Al^{3+} + Cit^{3-} + HPO_4^{2-}$	$\rightleftarrows$ Cit–Al–HPO_4^{2-}	15.00[b]	Cd^{2+} + *dl*-Tar + HPO_4^{2-}	$\rightleftarrows$ *dl*-Tar–Cd–HPO_4	8.13(18)
$Fe^{3+} + Cit^{3-} + HPO_4^{2-}$	$\rightleftarrows$ Cit–Fe–HPO_4^{2-}	19.46(16)	Cu^{2+} + *dl*-Tar + HPO_4^{2-}	$\rightleftarrows$ *dl*-Tar–Cu–HPO_4	9.88(13)
$Fe^{3+} + Cit^{3-} + HPO_4^{2-}$	$\rightleftarrows$ Cit–Fe–HPO_4^{2-}	14.84[b,c]	Cu^{2+} + *meso*-Tar + HPO_4^{2-}	$\rightleftarrows$ *meso*-Tar–Cu–HPO_4	10.09(13)
$Fe^{3+} + Cit^{3-} + HPO_4^{2-}$	$\rightleftarrows$ Cit–Fe–HPO_4^{2-}	20.34[b,d]	Zn^{2+} + *dl*-Tar + HPO_4^{2-}	$\rightleftarrows$ *dl*-Tar–Zn–HPO_4	8.55(15)
$Ca^{2+} + Cit^{3-} + HPO_4^{2-}$	$\rightleftarrows$ Cit–Ca–HPO_4^{2-}	10.72(18)	Al^{3+} + Fulv + HPO_4^{2-}	$\rightleftarrows$ Fulv–Al–HPO_4	14.48(1)
$Cd^{2+} + Cit^{3-} + HPO_4^{2-}$	$\rightleftarrows$ Cit–Cd–HPO_4^{2-}	9.56(18)	Cd^{2+} + Fulv + HPO_4^{2-}	$\rightleftarrows$ Fulv–Cd–HPO_4	11.27(15)
$Cu^{2+} + Cit^{3-} + HPO_4^{2-}$	$\rightleftarrows$ Cit–Cu–HPO_4^{2-}	15.27(13)	Zn^{2+} + Fulv + HPO_4^{2-}	$\rightleftarrows$ Fulv–Zn–HPO_4	6.90(15)
$Fe^{3+} + NTA^{3-} + HPO_4^{2-}$	$\rightleftarrows$ NTA–Fe–HPO_4^{2-}	21.09(16)	$Al^{3+} + Cyst^{2-} + HPO_4^{2-}$	$\rightleftarrows$ Cyst–Al–HPO_4^{-}	15.66(1)
$Ca^{2+} + NTA^{3-} + HPO_4^{2-}$	$\rightleftarrows$ NTA–Ca–HPO_4^{3-}	14.50(18)	$Ca^{2+} + Cyst^{2-} + HPO_4^{2-}$	$\rightleftarrows$ Cyst–Ca–HPO_4^{2-}	8.49(18)
$Cd^{2+} + NTA^{3-} + HPO_4^{2-}$	$\rightleftarrows$ NTA–Cd–HPO_4^{3-}	18.35(18)	$Cd^{2+} + Cyst^{2-} + HPO_4^{2-}$	$\rightleftarrows$ Cyst–Cd–HPO_4^{2-}	11.45(18)
$Pb^{2+} + NTA^{3-} + HPO_4^{2-}$	$\rightleftarrows$ NTA–Pb–HPO_4^{3-}	13.08(15)	$Cu^{2+} + Asp^{2-} + PO_4^{3-}$	$\rightleftarrows$ Asp–Cu–PO_4^{3-}	8.28(13)
$Zn^{2+} + NTA^{3-} + HPO_4^{2-}$	$\rightleftarrows$ NTA–Zn–HPO_4^{3-}	11.55(15)	$Cu^{2+} + Gly^{-} + PO_4^{3-}$	$\rightleftarrows$ Gly–Cu–PO_4^{2-}	6.79(13)
$Cu^{2+} + HNTA^{2-} + H_2PO_4^{-}$	$\rightleftarrows$ HNTA–Cu–$H_2PO_4^{-}$	10.06(13)	HPO_4^{2-}	$\rightleftarrows H^{+} + PO_4^{3-}$	−11.83(13)
$Cu^{2+} + HNTA^{2-} + HPO_4^{2-}$	$\rightleftarrows$ HNTA–Cu–HPO_4^{2-}	13.05(13)	Pb^{2+} + Fulv + HPO_4^{2-}	$\rightleftarrows$ Fulv–Pb–HPO_4	11.27(15)
$Ca^{2+} + HNTA^{2-} + HPO_4^{2-}$	$\rightleftarrows$ HNTA–Ca–HPO_4^{2-}	9.07(13)			

[a] I = 0.1 M $NaClO_4$, T = 25.0°C; NTA = nitrilotriacetic acid, Fulv = fulvic acid, *dl*-Tar = *dl*-tartaric acid, Cyst = cysteine, *meso*-Tar = *meso*-tartaric acid, Asp = aspartic acid, Cit = citric acid.
[b] This study (I = 0.2 M KCl, T = 25.0°C).
[c] Fresh sample.
[d] Age of sample: 3 h prior to titration.

TABLE 2. Organo—metal-(Al, Fe)—phosphate test solutions

	Fe^{3+}				Al^{3+}			
Titrand name	Titrand components and molarity (M)	Titrand volume (mL)	Titrant molarity (M)	E_0' (mV)	Titrand components and molarity (M)	Titrand volume (mL)	Titrant molarity (M)	E_0' (mV)
SAL (1)	0.0010 Salicylic acid 0.005 Iron nitrate[b] 0.00105 Phosphoric acid	100	1.00 sodium hydroxide	370.9	0.005 Salicylic acid 0.001 Aluminum nitrate[c] 0.00105 Phosphoric acid	100	0.01 Sodium hydroxide	370.0
PHT (1)	0.005 Phthalic acid 0.001 Iron nitrate 0.001 Phosphoric acid	[d]	—	—	0.005 Phthalic acid 0.001 Aluminum Nitrate 0.00105 Phosphoric acid	100	0.01 Sodium hydroxide	368.6
PHT (2)	0.001 Phthalic acid 0.001 Iron nitrate 0.001 Phosphoric acid	[d]	—	—	—	—	—	—
OX (1)	0.001 Oxalic acid[e] 0.001 Iron nitrate 0.001 Phosphoric acid	[d]	—	—	0.001 Oxalic acid 0.001 Aluminum nitrate 0.00105 Phosphoric acid	100	0.01 Sodium hydroxide	370.0
OX (2)	0.001 Oxalic acid 0.005 Iron nitrate 0.001 Phosphoric acid	[d]	—	—	—	—	—	—
CIT	0.001 Citric acid 0.001 Iron nitrate 0.001 Phosphoric acid	100	0.25 sodium hydroxide	364.9	0.001 Citric acid 0.001 Aluminum nitrate 0.00105 Phosphoric acid	100	0.2 Sodium hydroxide	370.0

[a]All titrand solutions adjusted to an ionic strength of 0.2 M using potassium chloride.
[b]$Fe(NO_3)_3.9H_2O$.
[c]$Al(NO_3)_3.9H_2O$.
[d]Precipitate occurred.
[e]$(COOH)_2.12H_2O$.

are well-defined in terms of the asymptotic standard deviations associated with each β-value, and (ii) until the residuals (i.e. M_T(calcd.) − M_T(actual), L_{jT}(calcd.) − L_{jT}(actual), H_T(calcd.) − H_T(actual)] acquire a random or near random pattern about zero as function of successive titration points.

The values for the formation constants so generated may be used in conjunction with the calculation of, e.g., the chemical species distribution of aqueous solutions at given pH, temperature, ionic strength, redox potential, and imposed atmospheric conditions (e.g., total pressure and CO_2-partial pressures). This can be done with, e.g., the MINEQL computer program (Westall *et al.* (25)) which computes the concentrations (or contents) of all soluble components, soluble complexes, precipitated solids not allowed to dissolve, precipitated solids subject to dissolution, or dissolved solids subject to precipitation. In particular, the MINEQL-program contains an extensive yet readily expandable data base with an elaborate list of complexes, formation constants and solubility products. All constants (or products) are based on a temperature of $T = 25°C$ and an ionic strength of zero. All constants are recalculated with appropriate estimates for the various activity coefficients (19, 26) involved once the actual ionic strength for a given solution is specified. The input requirements of the MINEQL-program include (i) specification of the list of chemical components to be encountered (e.g., Fe, Al, H, etc.), (ii) initial estimates for the free concentrations of these components (e.g., $[Al^{3+}]$, $[Fe^{3+}]$, $[H^+]$, etc.), and (iii) the specification for all component concentrations.

Methods

Stock- and test- solutions (Table 2) were prepared with deionized water and stored (maximum 14 days) in a glove box filled with nitrogen (N_2) gas to minimize carbon dioxide contamination.

A titration cell modelled after Perrin and Sayce (27) was assembled using a flanged 200 mL Berzelius beaker and a special two-piece plexiglass seal assembly to protect the titrands from CO_2-contamination (28).

Titrant solutions were added to stirred titrand solutions with a Gilmont Precision Micrometer Buret (2.5 mL maximum capacity).

Electromotive force (emf) measurements were obtained with a glass/reference electrode pair (Orion research glass-electrode and a single-junction reference electrode Model No. 90-1) for each titration step with a precision of ±0.1 mV. The electrode pair chosen proved to be relatively free of electrode drifts with 4 N KCl as reference solution.

Titration procedures

The number of titration points and the location of these points along the pH-axis or emf-axis, in general, affects the accuracy of the titration analysis. For example, Still (29) has shown that the use of the "law of large numbers" for the determination of equivalence points and formation constants can be applied provided that each titration point carries equal weight. This diminishes the standard error of the mean by a factor of $1/\sqrt{N}$ (N = number of points). Consequently, the larger the number of observations the more confidence there is that the calculated means are good estimates of the parameters sought. About 40 to 50 equally-spaced titration points were obtained for each titration curve to comply with these observations. Furthermore, each complex-forming solution was titrated three times as a check for reproducibility.

The following solutions were tested by potentiometric titration.

(i) Solutions containing only dilute phosphoric acid (or one

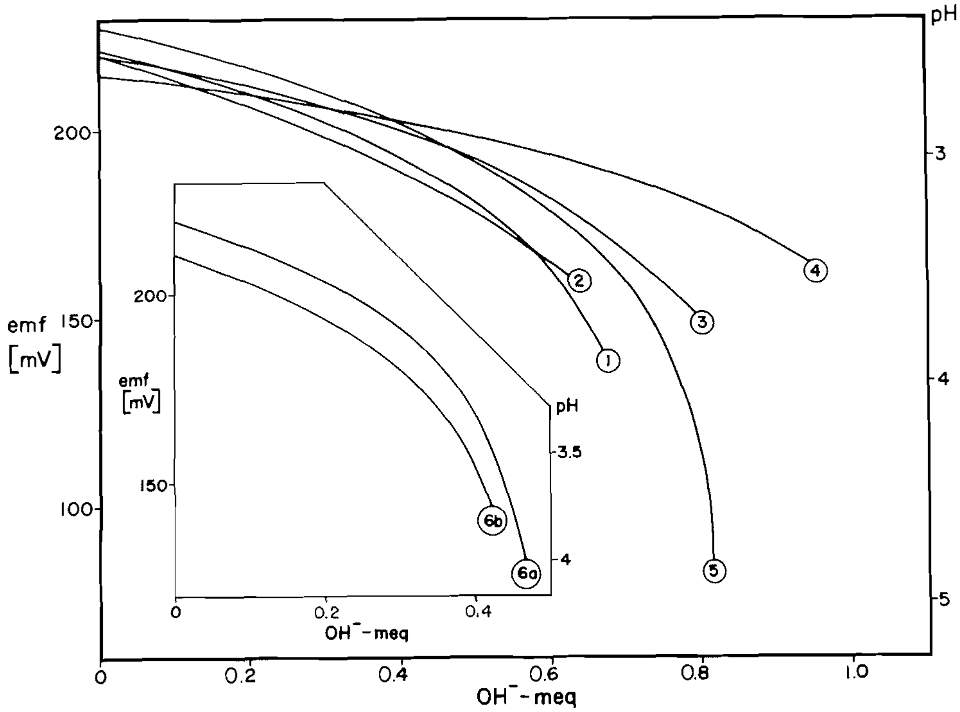

FIG. 1. Precipitation-free portions of the titration curves (emf versus mequiv. of base added) for the various complex-forming solutions in Table 2. ①: Al–Sal–PO_4, ②: Al–Pht–PO_4, ③: Al–Ox–PO_4, ④: Al–Cit–PO_4, ⑤: Fe–Sal–PO_4. The pH-scale on the right is constructed via eq. [8] with $E_0' = 370$ mV. The inset shows the titration curves for the Fe–Cit–PO_4 solutions (solution age is 3 h for (6a) and 0 for (6b).

of the organic acids listed in Table 2) were titrated and subsequently analyzed with the ACBA-program to (*a*) establish the E_0'-value in eq. [8] from time to time, and to (*b*) ascertain the precise titrand and titrant concentrations of the various stock-solutions in Table 2. The best-fitted E_0'-values so generated fluctuated drift-free between 364 and 370 mV thereby indicating that the electrode-pair employed in this study was remarkably stable for each titration and from one titration curve to another.

(*ii*) Most of the complex-forming test solution (i.e. those of Table 2) had an initial pH of $\simeq 2.5$, and were titrated with base. The resulting titration curves were subjected to analysis via the MINIQUAD program. Each titration curve was generated in the course of 2 to 3 h by adding small volume increments of titrant, one at a time. The resulting emf-response of the glass electrode as measured with a pH-meter was traced with a recorder. Digital emf-readings were taken for each volume increment once the recorder trace had stabilized. Examples of the ensuing titration curves are shown in Fig. 1 for each titration solution in Table 2.

Emf-stabilization, in general, occurred rapidly at low pH but slowed with increasing pH until complete lack of stabilization occurred on account of precipitation reactions. The first indication of such reactions terminated the titration, and only those titration points free of precipitation reactions were subjected to computer analysis. All complex-forming test solutions exhibited precipitation reactions above a certain pH-value (see Fig. 1). The Fe^{3+} solutions with oxalate and phthalate ions as ligands produced precipitation reactions soon after mixing and were, therefore, excluded from further analysis. The Fe–Cit–PO_4 solution, in contrast, remained clear initially, but yielded titration curves with increasing emf-values as function of solution age (see Fig. 1).

Results

The precipitation-free region of each titration curves for each of the stable complex-forming solutions specified in Table 2 was analyzed with the MINIQUAD program to generate information about the pH-dependent chemical species-mix for each titrated solution, and the log β-values for each ternary complex that may be present in each of these solutions in appreciable concentrations. The MINIQUAD-calculations were done in a progressive fashion starting with an initial refinement model which included all non-ternary species that may be present. The list of such species for, e.g., the Al–Ox–P mixture included Al^{3+}, $Al(OH)^{2+}$, $Al(OH)_2^+$, $AlH_2PO_4^{2+}$, HOx^-, Ox^{2-}, H_2Ox, $H_2PO_4^-$, H_3PO_4, $AlOx^+$, $Al(Ox)_2^-$, and $Al(Ox)_3^{3-}$.

All MINIQUAD-calculations based on such a list, however, led to (*i*) convergence problems, (*ii*) poor parametric estimates for the refined log β-values associated with these species, (*iii*) poor residuals for the mass-balance equations for each of the four components considered, or (*iv*) a general lack of randomness of the residual plots for each of the components as a function of successive titration points.

Adding mixed-ligand complexes of the type M–L2–L1–H with stoichiometric coefficients corresponding to 1111, 1112, or 1122 in suitable combinations strongly improved the goodness-of-fit between the MINIQUAD-calculated component concentrations and their actual counterparts as indicated in Table 3 by the "SD-values" defined as

$$SD = \left[\sum_{i=1}^{N_T} (\Delta M_i^2 + \Delta L1_i^2 + \Delta L2_i^2 + \Delta H_i^2)/DF\right]^{1/2}$$

where N_T is the number of titration points, $DF = N_T - N_\beta$ (N_β is the number of refined log β-values), and (e.g.)

$$\Delta M_i = [Al_T]_i(\text{calcd.}) - [Al_T]_i(\text{actual})$$

TABLE 3. Best-fitted log β-values for selected O–M–P complexes via the MINIQUAD computer program

Solution (M–L2–L1)[e]	Best-fitted model: stoichiometric coefficients of species: M	L1[e]	L2[e]	H	Refinement key[a]	log β[d] ± 95% CI	± Asymptotic standard deviation for log β[d]	± Standard deviation range of residuals[f] ($\times 10^{-6}$)
Al–Sal–PO_4	0	0	1	1	0	13.406[b]		
	0	0	1	2	1	15.91±0.03	0.002	0.5 to 3.0
	1	1	1	1	1	29.56±0.17	0.009	
	1	1	1	2	1	34.16±0.09	0.009	
Al–Pht–PO_4	0	0	1	1	0	4.930		
	0	0	1	2	1	7.43±0.03	0.001	1.1 to 2.2
	1	1	1	1	1	21.65±0.07	0.004	
	1	1	1	2	1	24.57±0.54	0.004	
Al–Ox–PO_4	0	0	1	1	0	3.752[b]	—	
	0	0	1	2	0	4.860[b]	—	
	1	0	1	0	0	6.100[b]	—	
	1	0	2	0	0	11.126[b]	—	0.60 to 0.67
	1	1	1	2	1	28.30±0.43	0.013	
	1	2	1	2	1	42.12±0.44	0.029	
	0	1	0	2	1	18.02±0.16	0.041	
Al–Cit–PO_4	0	0	1	1	0	5.690[b]	—	
	0	0	1	2	0	10.040[b]	—	
	0	0	1	3	0	12.910[b]	—	0.76 to 3.69
	1	1	1	1	0	26.48±0.40	0.007	
	1	1	1	2	1	30.38±0.19	0.006	
Fe–Sal–PO_4	0	0	1	1	0	13.406[b]	—	
	0	0	1	2	0	16.283[b]	—	
	1	0	1	0	0	16.300[b]	—	
	1	0	2	0	0	28.23[b]	—	0.51 to 2.4
	1	0	3	0	1	40.22±0.15	0.079	
	1	1	1	1	1	34.17±0.09	0.069	
	1	1	1	2	1	36.92±0.09	0.063	
	0	1	0	2	1	18.38±0.01	0.040	
Common to all mixtures:	0	1	0	1	0	11.538[b]	—	
	0	1	0	2	0 or 1[c]	18.174	—	
	0	1	0	3	0	21.012[b]	—	

[a]Refinement key = 1 means that β is to be refined by MINIQUAD. Refinement key = 0 means that β is to be used to refine other formation constants in the same model.
[b]Formation constants based on ACBA-analyzed titrations or obtained from Martell and Smith (30) and adjusted for ionic strength (I = 0.2 M adjusted with KCl) using the Davies formula.
[c]Refinement key = 1 for oxalate and iron-salicylate mixtures, 0 otherwise.
[d]Average values for three separate titrations for each complex-forming solution.
[e]L1 = PO_4^{3-}; L2 = Sal, Pht, Ox, or Cit.
[f]Refers to the ± SD (residuals) across M, L1, L2, and H. Temperature = 25.0°C, titrand volume = 100.0 mL.

The general SD-range for the best-fitted models in Table 3 range from ± 5 to 10^{-7} to $\pm 4 \times 10^{-6}$ M. These values are very small when compared with the actual component concentrations ranging from 0.001 to 0.005 M for H_T, L_{jT} (j = 1, 2) and M_T (see Table 2). Other mixed-ligand species with m, n_1, n_2 = 1 or 2 and $-3 \le p \le 4$ were also added to the initial refinement list either singly or in combinations. The ensuing results, however, were in each case inferior to those already obtained with the 1111-, 1112-, and 1122-combinations. In fact, the resulting SD-values rarely fell below 10^{-5} M. Also, the "residual-plot" pattern for each component was definitely not "random" as function of successive titration points.

The admission of 1111-, 1112-, and 1122-species to the original list of nonternary species led — invariably — to the mass-balance elimination of many species considered. The final MINIQUAD models are assembled in Table 3 in terms of the remaining species for each of the precipitation-free solutions in Table 2. Also indicated in Table 3 are the log β-values which were (or were not) subject to parametric refinement (refinement key = 0 or 1, respectively). Well-established values for log β pertaining to some of the species listed, in general, were accepted as such. Their inclusion as refineable parameters, however, added chemical credibility of the final solutions when the refined log β-values were in good agreement with their well-established counterparts. For example (29),

$$\log \beta_{H_2PO_4}(\text{established}) = 18.17 \text{ vs. } \log \beta_{H_2PO_4}(\text{refined}) = 18.02 \text{ and } 18.38$$

$$\log \beta_{H_2Sal}(\text{established}) = 16.28 \text{ vs. } \log \beta_{H_2Sal}(\text{refined}) = 15.91$$

and

$$\log \beta_{H_2Pht}(\text{established}) = 7.68 \text{ vs. } \log \beta_{H_2Pht}(\text{refined}) = 7.43$$

(I = 0.2 *M* in all cases).

The species list and the corresponding values for log β in Table 3, in summary, appear to represent the best possible characterization of the chemical speciation in the complex-forming solutions as affected by potentiometric titration. The actual chemical speciation pattern in the various titrated solutions is shown in Fig. 2 as function of pH. These diagrams indicated that the O–M–P complexes Ox–Al–H_2PO_4 and Sal–Fe–HPO_4 are particularly prevalent in the pH-range from 2.5 to 4.5. Other complexes such as Ox–Al–$(H_2PO_4)_2^-$ and Cit–Al–HPO_4^- appear to be prevalent at pH > 4.5; Sal–Fe–H_2PO_4 is prevalent at pH < 2.5. O–M–P complexes such as Sal–Al–H_2PO_4 and Sal–Al–HPO_4 are also present but only in minor quantities. Other O–M–P complexes may form outside the pH range considered here, but precipitation reactions above the pH cut-off levels in Fig. 1 prevent their detection by potentiometric enquiry.

Complex-forming mixtures with Fe^{3+}, in general, appear to be sensitive to precipitation reactions in the course of time as was the case for the Fe–Ox–PO_4, Fe–Pht–PO_4, and Fe–Cit–PO_4 solutions in Table 2. The Fe–Cit–PO_4 solution, as mentioned above, was originally clear, and allowed immediate titration. In fact, the MINIQUAD analysis of the resulting curve indicated the presence of mixed-ligand complexes of the types 1111- and 1112-corresponding to log β = 26.37 and 30.32, respectively. These values, however, appeared to depend on the age of the mixture, because the other titration curve in Fig. 1 generated with a 3 h-old mixture yielded (via MINIQUAD) the same complexes but with log β = 31.87 and 35.32, respectively. It is possible that these complexes continued to exist during the ensuing precipitation reaction, and that the log β-differences were caused by slow rates of reactions or, alternatively, by time-dependent structural changes within each complex so formed.

Discussion

Comparison of formation constants

The magnitude of the formation constants decreases in the order salicylate > citrate > oxalate > phthalate for the organic acid – Al – P mixtures. This sequence is probably related to the structural changes from one type of complex to the other (i.e., five- and six-membered rings being more stable than seven-membered rings) and can be compared with the chelation sequence presented by Violante and Violante (31). These authors propose that the extent of Al^{3+}-chelation (and consequent suppression of $Al(OH)_3$-precipitation) decreases in the order citric acid > salicylic acid > oxalic acid > phthalic acid. A possible reason for the salicylate–citrate reversal between this study and that of (31) may be due to the presence (or absence) of the HPO_4^{2-}-group and subsequent steric hindrance between the phosphate ion and the large citrate-ion in the formation of OM–Al–P complexes.

Oxalic acid has the smallest physical size among the acids tested which may account for the ability of the oxalate-ions to chelate Al^{3+}-ions with two HPO_4^{2-}-ions attached. The larger size of salicylic, phthalic, and citric acids, again, may cause steric hindrance thereby reducing the number of phosphate groups per O–M–P complex to one.

Compared to Al^{3+}-ions, Fe^{3+}-ions form more stable complexes with salicylate and phosphate ions. This is probably due to differences in ionic size ($r_{Al^{3+}} = 0.53$ Å, $r_{Fe^{3+}} = 0.60$ Å) and type of electronic orbital structure available for complexation (*p*-type orbitals available for Al^{3+}, and *p*- and *d*-type orbitals available for Fe^{3+}).

The values of the individual formation constants in Tables 1 and 3 suggest that Fe^{3+}- and Al^{3+}-ions form the most stable ternary complexes with phosphate ions and organic acids among all the metal ions examined. Furthermore, Fe^{3+}-ions appear to bind citrate- and phosphate-ions slightly better than Al^{3+}-ions. The values of the formation constants of the citrate mixtures (Table 3) involving iron (or aluminum) and phosphate, however, are not as small as those presented in Table 1.

In general, there are report-based differences in assessing log β depending on which species are considered for the complex-forming components. In this paper the complex-forming components are all considered to be unprotonated (see Table 3). In contrast, some complex-forming components, as defined in other papers, carry protons, e.g. HPO_4^{2-} instead of PO_4^{3-} (see Table 1). Conversions from one log β-value to the other, however, are easily done by noting that, e.g., log β(M–Cit–PO_4–H) = log β(M–Cit–HPO_4) + log β_{HPO_4} with log β_{HPO_4} = 11.53 at *I* = 0.2 *M*.

The titration results in Table 1 for the Fe–Cit–PO_4 and Al–Cit–PO_4 mixtures when referred to mixed-ligand complexes of the type M–Cit–PO_4–H yield log β = 30.8 and log β = 31.0 for the corresponding 1111-complexes, respectively. The former log β-value compares well with the corresponding 1111-value for the 3 h-old Fe–Cit–PO_4 mixture. The difference arising for the log β-value with the Al–Cit–PO_4, in contrast, is probably due to a difference with respect to the speciation assessment of the resulting titration curves. This work generated two mixed-ligand complexes, namely a 1112-complex in addition to the 1111-complex in Table 1. In fact, the former appears to be the prevalent species within the actual titration range (see Fig. 2).

Al-speciation in a buffered nutrient solution

The possible role of O–M–P complexes in buffered solutions such as those used for growing biological organisms may be examined in terms of the chemical speciation of Al in the Ingestad-solution (32) employed for growing tree seedlings. The chemical composition of this solution is shown in Table 4 with oxalic acid as the buffering agent. Added to this solution are five levels of $Al_2(SO_4)_3.6H_2O$, and two levels of oxalic acid at 6 physiologically important pH-levels. Adjustments for each pH-level can be made by adding appropriate amounts of, e.g., 1 *M* HCl or 1 *M* NaOH. Using the specifications in Table 4 as input for the MINEQL-program yields the Al-speciation pattern illustrated in Fig. 3 for the high and low oxalic acid levels when Ox–Al–P complexes are present in accordance with the results of Table 3, and when such complexes are not considered. The following can be observed.

(*i*) Consideration of Ox–Al–P complexes significantly affects the Al-speciation as function of pH, Al-content, and oxalic acid content.

(*ii*) The postulated formation of the Ox–Al–P complexes, in general, enhances the Al- and P-solubility in the buffered solutions, particularly so at low Al-levels.

(*iii*) Ox–Al–P complexation decreases with increasing Al-concentrations on account of enhanced Al–Ox-complexation and (or) enhanced $AlPO_4$- and $Al(OH)_3$-precipitation.

(*iv*) Changes in pH from 3 to 6 favors Ox–Al–2P over Ox–Al–P formation.

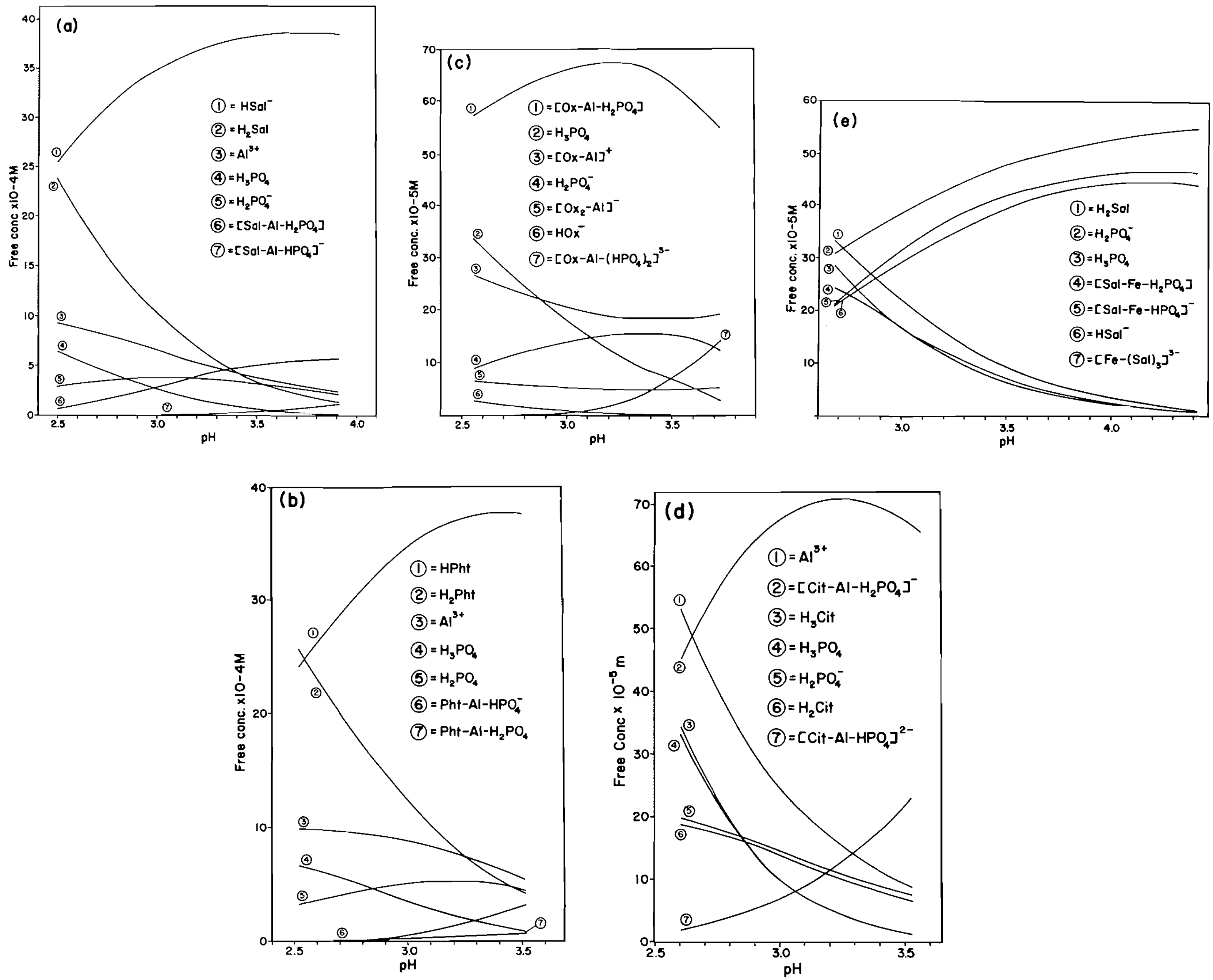

FIG. 2. Chemical speciation of the various titrand-solutions in Table 2 as function of pH. (*a*) Al–Sal–P, (*b*) Al–Pht–P, (*c*) Al–Ox–P, (*d*) Al–Cit–P, (*e*) Fe–Sal–P.

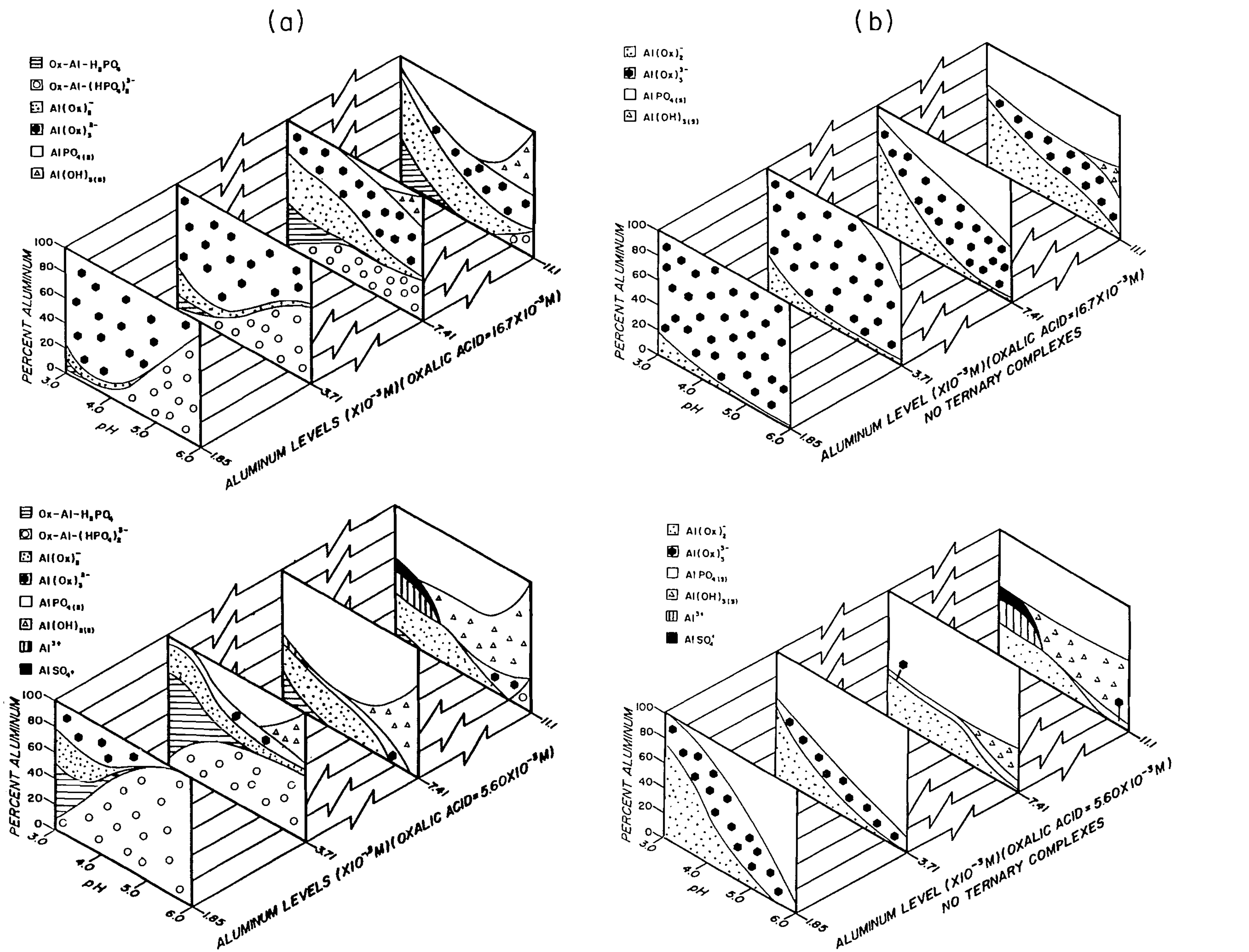

FIG. 3. Al-speciation in the buffer solutions of Table 4 as function of (*i*) pH, (*ii*) total Al- content, (*iii*) two total oxalic acid concentrations, and (*iv*) presence (*a*) or absence (*b*) of postulated Ox–Al–P complexes.

TABLE 4. Total chemical component-concentrations for the Ingestad nutrient solutions treated with 2 levels of oxalic acid, 5 levels of $Al_2(SO_4)_3$, and 6 pH-levels[a]

	Treatments		
Level	Oxalic acid (mmol/L)	Aluminum sulphate (mmol/L)	pH (adjusted with, e.g., 1 *M* HCl and 1 *M* NaOH)
1	5.6	0.00	3.0
2	16.7	1.85	3.5
3		3.71	4.0
4		7.41	4.5
5		11.10	5.0
6			6.0

[a]For all solutions: total SO_4^{2-} = 12.8 m*M*; total Ca^{2+} = 0.96 m*M*; total N = 42.84 m*M* (=$[NH_4^+]$ + $[NO_3^-]$); total Mg^{2+} = 2.10 m*M*; total PO_4^{3-} = 5.02 m*M*; total Fe^{3+} = 0.07 m*M*; total K^+ = 9.97 m*M*.

All of this suggests that O–M–P formation, in general, must be taken into account when certain growth responses of biological organisms are to be related to the chemical speciation of nutrient solutions. For example, such growth responses may be positively or negatively affected depending on the sensitivity of the growing organism with respect to, e.g., the extent of Al-solubilization, the concentration (activity) of a particular O–M-complex or O–M–P-species, or the improved availability of P and Fe due to enhanced P- and Fe-solubility.

Conclusions

The potentiometric method for extracting formation constants coupled with the ACBA and MINIQUAD data analysis proves to be a means to generate information about the chemical speciation of Al^{3+}- and Fe^{3+}-ions as affected by mixed-ligand complexation involving Al^{3+}- or Fe^{3+}-ions, phosphate ions and organic acids in aqueous solutions. This analysis indicates the presence of stable organo–metal–phosphate complexes in specifically formulated complex-forming mixtures. The magnitude of the formation constants of such complexes decreases in the order $Fe^{3+} > Al^{3+}$ and salicylate > citrate > oxalate > phthalate. Oxalic acid as a ligand yields O–M–P complexes containing two phosphate ions. The elucidation of the actual structures for the various O–M–P complexes examined in this study awaits further experimental investigations.

The potentiometric evaluations, in general, should be done repeatedly for Al^{3+}- and Fe^{3+}-complex-forming solutions of varying age to ensure that the refined log β-values are reproducible.

Acknowledgements

Financial support for this work was received from the Natural Sciences and Engineering Research of Canada (Grant #7803) and from the Canadian Forest Service (Research Contract DDS #08SC KH209-3-0136). Technical assistance from Ian Taviss, Allison Brewer, and Steve Gordon is gratefully acknowledged.

1. S. RAMAMOORTHY and P. E. MANNING. Inorg. Nucl. Chem. Lett. **10**, 623 (1974).
2. C. D. FOY, R. L. CHANEY, and M. C. WHITE. Ann. Rev. Plant. Physiol. **29**, 511 (1978).
3. I. P. MUNIZ, and H. LEIVESTAD. Toxic effects of aluminum on the brown trout, Salmo trutta L. *In* Ecological impact of acid precipitation. *Edited by* D. Drablos and A. Tollan. Sandefjord, Norway, SNSF, project. 980 p. 318.
4. TH. H. MAUGH II. Science, **226**, 1408 (1984).
5. J. L. MORTENSEN. Soil Sci. Soc. Proc. **27**, 179 (1963).
6. V. CHEAM. Can. J. Soil Sci. **53**, 377 (1973).
7. F. J. STEVENSON. Soil Sci. Soc. Am. J. **40**, 665 (1976).
8. H. VANDIJK. Geoderma, **5**, 53 (1971).
9. A. PICCOLO and F. J. STEVENSON. Geoderma, **27**, 195 (1982).
10. M. LEVESQUE and M. SCHNITZER. Soil Sci. **103**, 183 (1967).
11. M. K. SINHA. Plant Soil, **35**, 471 (1971); **35**, 485 (1971).
12. P. R. BLOOM. Soil Sci. Soc. Am. J. **45**, 267 (1981).
13. S. RAMAMOORTHY and P. G. MANNING. Inorg. Nucl. Chem. **35**, 1279 (1973).
14. S. RAMAMOORTHY and P. G. MANNING. Inorg. Nucl. Chem. **35**, 1571 (1973).
15. S. RAMAMOORTHY and P. G. MANNING. Inorg. Nucl. Chem. **36**, 695 (1974).
16. S. RAMAMOORTHY and P. G. MANNING. Inorg. Nucl. Chem. **36**, 1671 (1974).
17. S. RAMAMOORTHY and P. G. MANNING. Inorg. Nucl. Chem. **37**, 363 (1975).
18. S. RAMAMOORTHY and P. G. MANNING. Inorg. Nucl. Chem. Lett. **10**, 109 (1974).
19. W. STUMM and J. J. MORGAN. Aquatic chemistry, 2nd ed. Wiley Interscience, New York. 1981. 583 pp.
20. A. IVASKA and I. NAGYPAL. Talanta, **27**, 721 (1980).
21. D. J. LEGGETT. Am. Lab. 29 (1982).
22. D. K. NORDSTROM, L. N. PLUMMER, T. M. L. WIGLEY, T. J. WOLERY, J. W. BALL, E. A. JENNE, R. L. BASSETT, D. A. CREAR, T. M. FLORENCE, B. FRITZ, M. HOFFMAN, G. R. HOLDREN JR., G. M. LAFON, S. V. MATTIGOD, R. E. MCDUFF, F. MOREL, R. M. REDDY, G. SPOSITO, and J. THRAILKILL. Am. Chem. Soc. Symp. Ser. **93**, 857 (1979).
23. G. ARENA, E. RIZZARELLI, S. SAMMARTANO, and C. RIGANO. Talanta, **26**, 1 (1979).
24. P. GANS, A. SABATINI, and A. VACCA. Inorg. Chem. Acta **18**, 237 (1976).
25. J. C. WESTALL, J. L. ZACHARY, and F. M. M. MOREL. MINEQL, a computer program for the calculation of chemical equilibrium composition of aqueous systems. Tech. Note. 18, Dept. Civil Eng. Mass. Inst. Tech., Cambridge, MA. 1976. 91 pp.
26. J. N. BUTLER. Ionic equilibrium. A mathematical approach. Addison-Welsey, Reading Mass. 1964. 547 p.
27. D. D. PERRIN and I. G. SAYCE. Chem. Ind. **16**, 661 (1966).
28. W. L. MEYER. M.Sc.F. Thesis. University of New Brunswick. 1984. 169 pp.
29. E. R. STILL. Talanta, **27**, 573 (1980).
30. A. E. MARTELL and R. M. SMITH. Critical stability constants. Vol. 3. Other organic ligands. Plenum Press, NY. 1976. 495 pp.
31. A. VIOLANTE and P. VIOLANTE. Clays Clay Miner. **28**, 425 (1980).
32. T. INGESTAD. Medd. Stat. Skogsf. Inst. **51**, 1 (1962).

Hydrogen bonding of alcohols with AOT in carbon tetrachloride: an infrared study

PIERRE MÉNASSA AND CAMILLE SANDORFY
Département de Chimie, Université de Montréal, Montréal (Qué.), Canada H3C 3V1

Received April 5, 1985

PIERRE MÉNASSA and CAMILLE SANDORFY. Can. J. Chem. **63**, 3367 (1985).

The interaction of the inverted micelles of AOT (sodium di(2-ethylhexyl)sulfosuccinate) with different alcohols due to hydrogen bonding has been studied by means of infrared spectroscopy. Spectra of solutions of the alcohols with increasing concentrations of AOT showed a decrease in the intensity of the free OH stretching band. At the same time a new OH band due to a H-bonded alcohol-inverted micelle complex appears and its intensity increases as the intensity of the free band decreases. Calculated values of the equilibrium constants for the formation of the complexes *n*-alcohol–AOT, showed a decrease in alcohol–AOT association with the increase of the length of the aliphatic chains in the *n*-alcohols. Surprisingly, cholesterol behaved like a short chain while other cyclic alcohols like long chain alcohols.

PIERRE MÉNASSA et CAMILLE SANDORFY. Can. J. Chem. **63**, 3367 (1985).

L'interaction dans le tétrachlorure de carbone des micelles inverses du bis(éthyl-2-héxyl) sulfosuccinate de sodium (AOT) avec différents alcools a été étudiée par spectroscopie infrarouge. L'étude spectroscopique de différentes solutions d'alcool et d'AOT montrent une diminution de l'intensité de la bande OH libre alors que parallèllement l'intensité d'une bande associée alcool–AOT augmente. Les calculs des constantes d'association *n*-alcool–AOT indiquent une diminution du degré d'association avec la longueur de la chaîne hydrocarbure. Le cholestérol se comporte comme un alcool à chaîne courte tandis que d'autres alcools cycliques se comportent comme des alcools à chaîne longue.

Introduction

It has been known for a long time that *n*-alcohols have some anesthetic potency (1). Recently Pringle *et al.* (2) showed that this potency increases with the length of the hydrocarbon chain. However, a "cutoff" in this anesthetic effect occurs at C_{13}. The latter may still be considered as a very weak anesthetic but C_{14} has no anesthetic potency at all.

Recently Wilson *et al.* (3) in an attempt to explain this "cutoff" undertook a comparative study of H-bonding in *n*-alcohols from C_1 to C_{18}. The results they obtained could not explain this "cutoff". Instead, they showed that for the same solvent, the degree of association by hydrogen bonding of the dissolved *n*-alcohols did not depend on the length of their hydrocarbon chain. They also showed that the degree of association of esters with different alcohols was independent of their chain length. These results prompted us to start a series of experiments to ascertain whether this independence of chain length of the association of aliphatic alcohols was still true in membrane mimetic environments. Apart from the aformentioned considerations, the present study may be considered as a first step toward a more realistic approach to hydrogen bonded systems of biological importance.

Experimental

The method used was infrared spectroscopy. Since the region to be studied was the one between 4 000 and 3 000 cm^{-1}, carbon tetrachloride was chosen as a solvent. Sodium di(2-ethylhexyl)sulfosuccinate known under the commercial name of AOT was used as a detergent. This choice was dictated by the fact that its micellar parameters are fairly well established and its average aggregation number in CCl_4 (17 molecules of AOT per inverted micelle (4)) is relatively high for an inverted micelle in CCl_4. In order to compare different alcohols, association constants were calculated following a scheme described earlier (5).

The chemical AOT (Fluka, Switzerland) was purified from its residual organic and inorganic impurities according to the method described by El Seoud and da Silva (6). Traces of water were, however, found in the ir spectrum of dried AOT. Some authors questioned the feasability of inverted micelles without traces of water (7). Most of the alcohols (Aldrich Chemical Co. and Sigma Chemical Co.) were stated to be 99% pure or more. Nonanol 97% was distilled under vacuum and its purity confirmed by gc ms. *trans*-Decahydro-2-naphtol was a gift of International Flavour and Flagrance Inc. Spectroscopic grade carbon tetrachloride (American Chemicals Ltd.) was used without further purification. Its ir spectrum, recorded in a 5 mm cell, did not show any water or other impurity bands.

Spectra were recorded at room temperature on a Perkin Elmer model 521 spectrometer using 5 mm infrasil cells (Hellma Limited), and on a Nicolet 6000 F.T.I.R. instrument using 0.120 or 0.510 mm sodium chloride cells (Wilmad Glass Co Inc.). The spectra presented here have been recorded on the latter. Solvent and AOT absorption were compensated for on the Perkin-Elmer and were subtracted on the Nicolet F.T.I.R. instrument.

Results and discussion

n-*Alcohols*

All *n*-alcohols studied behaved the same way and presented the same spectral characteristics. The figures depicted in this work are those of n-hexanol. The dashed lines in Fig. 1 represent a part of the ir spectrum of a 0.2 *M* solution of hexanol in CCl_4. The band at 3639 cm^{-1} represents the non-bonded free OH stretching vibration. The shoulder at ca. 3498 cm^{-1} is that of the self-associated dimers H—O: . . . H—O and the broad band centered at about 3346 cm^{-1} is due to the self associated multimers. The solid line in Fig. 1 represents a part of the infrared spectrum of a mixture of alcohol (0.2 *M*) and AOT (0.02 *M*) in CCl_4. There is a decrease in the intensities of both the free and multimer bands. Note, however, that this last band shifted slightly toward higher frequencies indicating the presence of another band. It is clear from this figure that AOT dissociates a part of the H-bonded multimers and is associating with the free OH. Next a solution of 0.4 *M* of AOT and 0.2 *M* of alcohol in CCl_4 was prepared. A part of its ir spectrum is represented by the solid line of Fig. 2. There is a sharp decrease in the monomer band while the multimer band disappears almost completely. A new band located at ca. 3417 cm^{-1} is now present in the spectrum. Since the absorption due to AOT has been subtracted and since this new band appears only when AOT is added to the alcohol, it can only be attributed to the formation of a complex AOT . . . OH. The dimeric species are still seen around 3498 cm^{-1}. The broken line represents the spectrum of a solution of 0.20 *M* of alcohol in CCl_4.

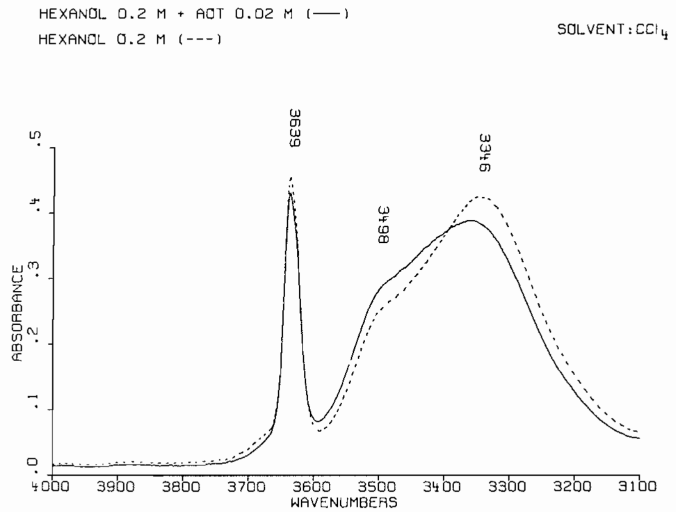

FIG. 1. Part of the infrared spectrum of (- - -) hexanol (0.2 M) and of (—) a solution of hexanol (0.2 M) and AOT (0.02 M) in CCl_4.

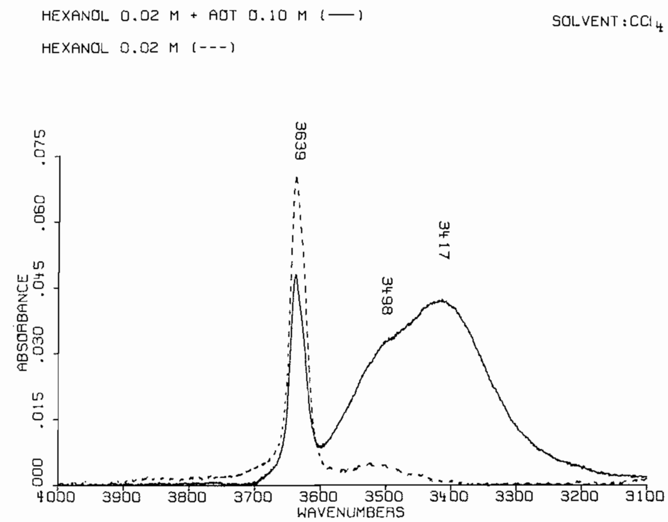

FIG. 3. Part of the infrared spectrum of 0.02 M of hexanol in CCl_4 (- - -) and a mixture of hexanol (0.02 M) and AOT (0.10 M) in CCl_4 (—).

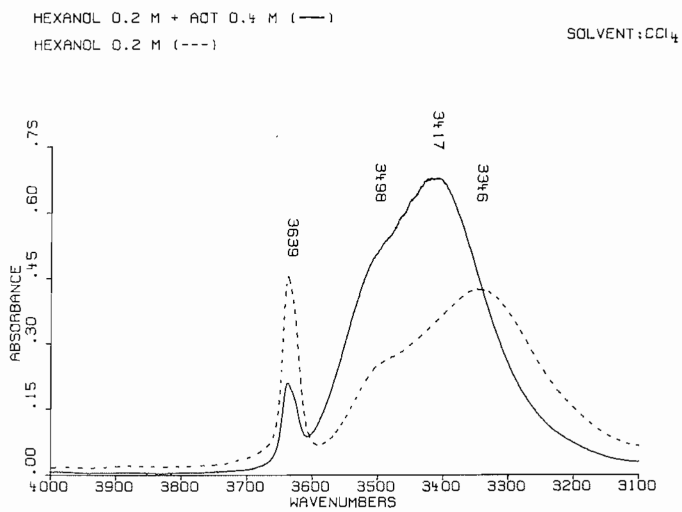

FIG. 2. Part of the infrared spectrum of (- - -) hexanol (0.2 M) and of (—) a solution containing AOT (0.4 M) and hexanol (0.2 M) in CCl_4.

TABLE 1. Formation constants, K (L mol^{-1}), of hydrogen bonded complexes between different aliphatic alcohols and AOT

n-Alcohol	Association constant K (L mol^{-1})
C_1	18.0 ± 0.7
C_3	11.0 ± 0.5
C_6	7.0 ± 0.6
C_7	9.0 ± 0.6
C_9	7.0 ± 0.3
C_{11}	6.0 ± 0.4
C_{14}	5.0 ± 0.6
C_{16}	6.0 ± 0.3

Dilute solutions of alcohols in carbon tetrachloride were then used to calculate the association constants of the complexes formed. These solutions have the advantage of containing almost exclusively monomeric species. The added AOT would have no other choice but to form a complex with the free alcohol (i.e., there is no breaking of multimers that may complicate the equilibrium). This is illustrated by Fig. 3 where the dashed line is a part of the ir spectrum of a solution of 0.02 M of hexanol in carbon tetrachloride. The intensity of the free OH band is by far stronger than that of any other band confirming that the alcohol is present almost entirely as a monomer. Adding AOT resulted in a decrease of the free band and the appearance of the 3417 cm^{-1} band. A small shoulder at ca. 3498 cm^{-1} due to the self associated dimer is also present as shown by the solid line spectrum of Fig. 3. The association constants of different alcohols were calculated by considering solutions formed from a mixture of 0.02 M of alcohol and different amounts of AOT (0.005 M to 0.150 M). The results are listed in Table 1. It is clear from this table that the association alcohol–AOT decreases with the increase of the length of the aliphatic chain of n-alcohols. This is further illustrated in Fig. 4. To understand the reason of this decrease we undertook a study of the carbonyl and sulfonate regions of the detergent. The region depicted by Fig. 5 is that of the carbonyl stretching frequency. The solid line spectrum is that of a solution of 0.010 M of AOT in CCl_4 while the broken line spectrum represents that of a mixture, in carbon tetrachloride, of 0.010 M of AOT and 0.90 M of hexanol. The intensity of the carbonyl band decreased with the addition of the alcohol. However, no shift in the band position towards lower frequencies was observed. This shift usually characterizes the C═O: . . . H—O bond. Therefore, there is no evidence that C═O groups associate with the OH of the alcohol. Figure 6 shows the asymmetric stretching vibrational region of the sulfonate group. Here again the solid line spectrum represents a solution of 0.010 M of AOT in CCl_4 while the dashed line spectrum is that of a mixture of 0.010 M of AOT and 0.90 M of hexanol in CCl_4. With the addition of hexanol, the asymmetric stretching vibration of the sulfonate located at 1250 cm^{-1} decreased in intensity and shifted to 1242 cm^{-1}. This shift and decrease in intensity of the free sulfonate band is attributable to hydrogen bonding between the sulfonate group of AOT and the hydroxyl group of the alcohol. This seems to indicate that hydrogen bonding between AOT and alcohols occurs via the sulfonate group. The latter is located deep inside the inverted micelle and is responsible for holding it together by dipole interactions (8). It seems then

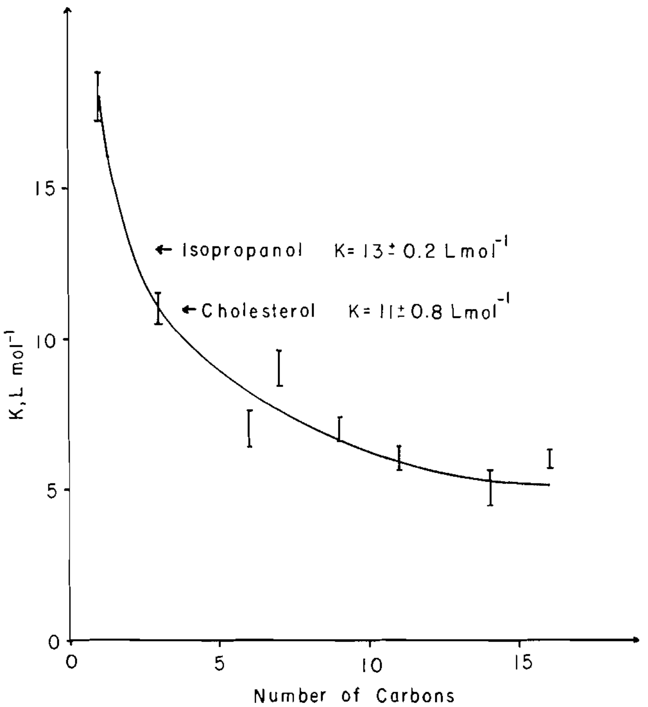

FIG. 4. Formation constants, K (L mol^{-1}), of hydrogen bonded complexes (alcohol–AOT) as a function of the number of carbons present in the aliphatic chain of the n-alcohols. The formation constants for isopropanol and cholesterol are also shown.

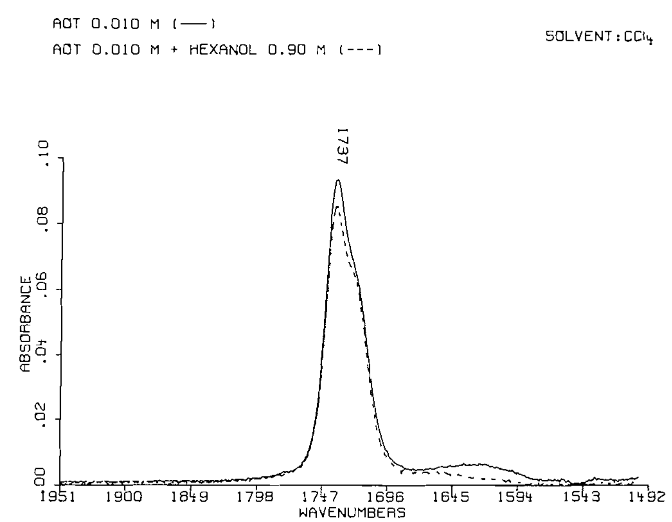

FIG. 5. Part of the infared spectrum of 0.01 M AOT (—) and a mixture of 0.01 M AOT and 0.90 M hexanol (- - -) in CCl_4.

logical that in order to reach the SO_3^- group, the OH of the alcohol must penetrate the micellar core. Thus, it appears that the longer the alcohol's paraffinic chain is, the harder it is to reach the sulfonate group and the smaller is the association constant. The association constants level off at ca. K = 6 L mol^{-1} for C ≥ 10. This shows that only a certain part of the alcohol chain is affected by the micellar core. This part can be roughly approximated by the length of a chain of 10 carbons, about 13 Å. According to the chemical structure of AOT (9), the linear length of the molecule is 12 Å. The part of the aliphatic chain laying beyond the length of an AOT molecule cannot affect the association constants since it can move freely and does not interact with the micellar tail. The association

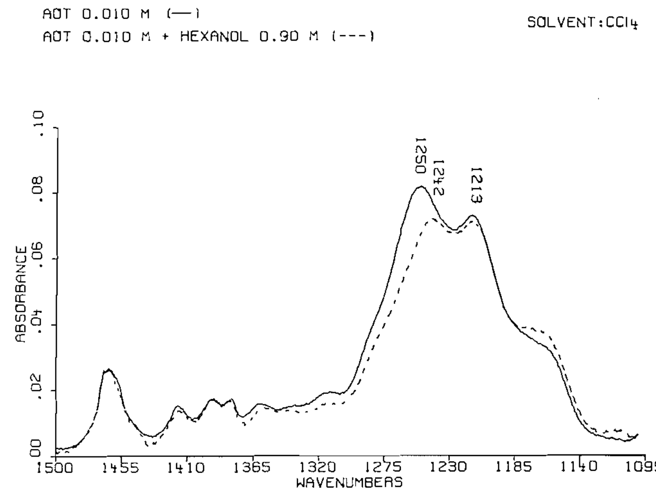

FIG. 6. Part of the infrared spectrum of (—) AOT (0.01 M) and (- - -) a solution containing AOT (0.01 M) and hexanol (0.90 M) in CCl_4.

constant of a long and branched alcohol should also be small since its OH group can hardly reach the inside of the inverted micelle. Furthermore, K of a short, branched alcohol should be large since its OH group can easily reach the inside of the inverted micelle. Moreover, the association constant of water and AOT should be extremely high since the water molecule is very small, polar and is located in the inside of the inverted micelle. The branched alcohols studied were 4-decanol and isopropanol. For isopropanol the free OH band was located at 3620 cm^{-1} and that of the OH-bonded OH . . . AOT band at ca. 3390 cm^{-1}. Although the positions of these bands are different from the respective bands of n-alcohols, upon addition of AOT the branched alcohols behaved the same way as the n-alcohols did (i.e., a decrease in the free OH band and a concomitant increase in the OH . . . AOT band). Their association constants were then calculated. As expected K of isopropanol was found to be relatively large, K = 13.0 ± 0.2 L mol^{-1} (K = 11.0 ± 0.5 L mol^{-1} for propanol), and that of 4-decanol very small, K = 2.0 ± 0.2 L mol^{-1}. The association constant of water and AOT was also calculated. Solubility considerations dictated the use of $CDCl_3$, a slightly polar solvent. The association constant of water and AOT in deuterated chloroform was found to be, as expected, extremely high, K = 57.0 ± 10.0 L mol^{-1}.

The addition of a fourth component to a three component system can alter the phase diagram of the latter (10). It is known that in the presence of small amounts of water, AOT in carbon tetrachloride forms inverted micelles. It is not known, however, to what extent these inverted micelles are affected by the presence of small amounts of cosurfactants (like alcohols). Four component systems formed of hydrocarbons, pentanol, water, and surfactants were studied by Sjöblom *et al.* (11). They showed that reversed micellar solutions were encountered only for quite high concentrations of hydrocarbons. The system we studied did not contain hydrocarbons but carbon tetrachloride which, like hydrocarbons, is an apolar solvent. In view of the results of Sjöblom *et al.* we do not have any reason to suspect major changes in the micellar form and parameters of AOT in carbon tetrachloride to which 0.02 mol of alcohol was added. Furthermore, all our experimental evidence seems to indicate the presence of inverted micelles. Therefore we feel that, in this work, the use of the words "inverted micelles" is justified.

TABLE 2. Formation constants, K (L mol^{-1}), of hydrogen bonded complexes between cyclic or branched alcohols and AOT

Alcohol	Association constant K (L mol^{-1})
Isopropanol	13.0 ± 0.2
4-Decanol	2.0 ± 0.2
Cholesterol	11.0 ± 0.8
Cyclohexylmethanol	7.0 ± 0.3
Cyclohexanol	7.0 ± 0.3
trans-Decahydro-2-naphtol	7.0 ± 0.4

Cholesterol and other cyclic alcohols

It has been recognized that excess serum cholesterol can lead to atherosclerosis (12). The latter is considered by medical authorities as a major risk factor in heart diseases. Thus the understanding of cholesterol's behaviour in membranes is important for the understanding of the way in which it interacts with the arterial wall. Parker and Bashkar (13) showed that cholesterol, like any other alcohol, self associates through hydrogen bonds. They have also shown (14) that 26-hydroxycholesterol associates with triglycerides and that this might initiate the formation of plaques causing atherosclerosis. Mercier *et al.* (15) have studied the H-bonds formed between cholesterol and ester or amide carbonyls and the way in which they are affected by various H-bond breakers. The molecule of cholesterol is known to be a planar molecule with a length of 19 Å (16). Thus according to the scheme described earlier, cholesterol should behave like a long chain alcohol with a relatively small association constant. This was not found to be the case. The association constant of cholesterol and AOT was found to be equal to $K = 11.0 \pm 0.8$ L mol^{-1}. This shows that, despite its bulky hydrocarbon radical, cholesterol behaved like a small chain alcohol (propanol). Nonetheless, a series of experiments were conducted on cyclic alcohols to see whether this "peculiar" behaviour of cholesterol is due to the interaction of the cyclic hydrocarbon radical with the inverted micelles. The cyclic alcohols studied were *trans*-decahydro-2-naphtol, cyclohexyl methanol, and cyclohexanol. The free OH band of these alochols was found between 3620 and 3640 cm^{-1} and that of the H-bonded OH . . . AOT around 3390 cm^{-1}. Their association constants with AOT were calculated. They were found equal to $K = 7.0 \pm 0.4$ L mol^{-1}, $K = 7.0 \pm 0.3$ L mol^{-1}, and $K = 7.0 \pm 0.3$ L mol^{-1} for *trans*-decahydro-2-naphtol, cyclohexyl methanol, and cyclohexanol, respectively, while as stated above, that of cholesterol is 11.0 ± 0.8 L mol^{-1}. The results are summarized in Table 2. These results are in line with the model described earlier. It clearly shows that the behaviour of cholesterol is not due to the interaction of the cycles with AOT. Fuller explanation of this behaviour will have to await further experimental work.

Conclusions

It has been shown that aliphatic alcohols and AOT form complexes in carbon tetrachloride. The degree of association of these alcohols with AOT was shown to decrease as the length of the aliphatic hydrocarbon chain increases. The association constant is probably related to the ability of the hydroxyl group of the alcohol to penetrate the inside of the inverted micelle and to bond with the sulfonate group. This was further confirmed by showing that the long branched alcohol 4-decanol has a small association constant while the association constant of the short branched alcohol isopropanol was found to be large. Cholesterol in spite of its bulky hydrocarbon radical behaved like a small chain alcohol. A study of cyclic alcohols showed that this strong association of cholesterol with AOT was not due to the interaction of the hydrocarbon cycle and AOT.

Acknowledgements

Financial help from the Natural Sciences and Engineering Research Council of Canada and Le Ministère de l'Éducation du Québec is gratefully acknowledged. Our thanks are due to Professor J. H. Fendler, Professor D. D. Patterson, Dr. M. Costas, and Mr. R. Buchet for helpful discussions and to Mr. P. Thibault for recording the gc/ms spectra.

1. J. POSTERNAK and E. ARNOLD. J. Physiol. **46**, 502 (1954).
2. M. J. PRINGLE, K. B. BROWN, and K. W. MILLER. mol. Pharmacol. **19**, 49 (1981).
3. L. WILSON, R. B. DE ALENCASTRO, and C. SANDORFY. Can. J. Chem. **63**, 40 (1985).
4. M. UENO and H. KISHIMOTO. Bull. Chem. Soc. Jpn. **50**, 1637 (1977).
5. R. BUCHET, L. BEAUVAIS, and C. SANDORFY. J. Biomol. Struct. Dyn. **2**, 221 (1984).
6. O. A. EL SEOUD and M. J. DA SILVA. J. Chem. Soc. Perkin **2**, 127 (1980).
7. H. F. EICKE and H. CHRISTEN. Helv. Chim. Acta, **61**, 2258 (1978).
8. M. UENO, H. KISHIMOTO, and Y. KYOGOKU. Bull. Chem. Soc. Jpn. **49**, 1776 (1976).
9. H. F. EICKE and V. ARNOLD. J. Colloid Interface Sci. **46**, 101 (1974).
10. J. H. FENDLER. Acc. Chem. Res. **9**, 153 (1976).
11. E. SJÖBLOM, U. HENRIKSSON, and P. STILBS. *In* Reverse micelles. *Edited by* P. L. Luisi and B. E. Straub. Plenum, New York, NY. 1984. p. 131.
12. B. LEWIS, A. CHAIT, C. M. O. OAKLEY, I. D. P. WOOTTON, D. M. A. ONITRI, G. SIGURDSSON, and A. FEBRUARY. Br. Med. J. **3**, 489 (1974).
13. F. S. PARKER and K. R. BHASKAR. Biochemistry, **7**, 1286 (1968).
14. F. S. PARKER, M. H. STRYKER, and K. R. BHASKAR. Can. J. Spectrosc. **28**, 30 (1983).
15. P. MERCIER, C. SANDORFY, and D. VOCELLE. J. Phys. Chem. **87**, 3670 (1983).
16. D. CROWFOOT. Vitam. Horm. **2**, 409 (1944).

The preparation of specifically deuterated diphenylamines[1]

WESLEY A. DOAK, CHARLES KNESSL, HENRYK LABAZIEWICZ, SALLY E. O'CONNOR, LIVIU PUP, GERARD PUTZ, MARIJO SCHRANZ, ROBERT I. WALTER,[2] AND LING YANG
Department of Chemistry, University of Illinois at Chicago, Chicago, IL 60680, U.S.A.

AND

NICK H. WERSTIUK
Department of Chemistry, McMaster University, Hamilton, Ont., Canada L8S 4M1

Received April 3, 1984[3]

WESLEY A. DOAK, CHARLES KNESSL, HENRYK LABAZIEWICZ, SALLY E. O'CONNOR, LIVIU PUP, GERARD PUTZ, MARIJO SCHRANZ, ROBERT I. WALTER, LING YANG, and NICK H. WERSTIUK. Can. J. Chem. **63**, 3371 (1985).

Procedures have been developed for the preparation, at levels of label which exceed 90%, of ring-deuterated diphenylamines (DPAs) with the label at specific ring positions. The compounds so prepared are DPA-d_{10}, DPA-2,4,6,2′,4′,6′-d_6, DPA-2,6,2′,6′-d_4, and DPA-4,4′-d_2.

WESLEY A. DOAK, CHARLES KNESSL, HENRYK LABAZIEWICZ, SALLY E. O'CONNOR, LIVIU PUP, GERARD PUTZ, MARIJO SCHRANZ, ROBERT I. WALTER, LING YANG et NICK H. WERSTIUK. Can. J. Chem. **63**, 3371 (1985).

On a développé des méthodes qui permettent de préparer des diphénylamines (DPA) marquées dans des positions spécifiques des cycles et à des niveaux de marquage qui dépassent les 90%. On a ainsi préparé les DPA-d_{10}, DPA-d_6-2,4,6,2′,4′,6′, DPA-d_4-2,6,2′,6′ et DPA-d_2-4,4′.

[Traduit par le journal]

Introduction

Only a limited number of deuterium-labelled diphenylamines (DPAs) have been described. Neugebauer and Bamberger (1) prepared DPA-d_{10} (here and subsequently we consider only deuterium on aromatic carbon, and ignore possible deuteration on the nitrogen atom, since that rapidly back exchanges in protic solvents) by synthesis from bromobenzene-d_5 and acetanilide-d_5. They subsequently converted this substance to DPA-3,5,3′,5′-d_4 by back exchange in refluxing acidified ethanol. We give here the preparations of DPAs specifically deuterated at other sets of structurally equivalent positions in the molecule. These labelled DPAs were subsequently converted to labelled 1-picryl-2,2-diphenylhydrazyl free radicals in which the labels served to identify the nmr or ENDOR (electron-nuclear double resonance) signals from various positions in this radical (2). With the modified methods described here, it is now possible to prepare even more fully labelled samples than were available for those studies.

A number of potential routes for the substitution of deuterium at specific sites were unsatisfactory in our hands. Lithiation of 4,4′-dibromodiphenylmethylamine, followed by quenching with deuterium oxide, was used by Shatenshtein *et al.* (3) to prepare the 4,4′-d_2 label on their tertiary amine. The reaction is unsuccessful with the secondary amine; the major product with a 3:1 mole ratio of butyllithium to amine probably is *N*-butyldiphenylamine (the mass spectrum (ms) gives the molecular ion at mass 225), formed by displacement of halogen from butyl bromide by the nucleophilic amide that is produced by the lithiation. The reduction of 4,4′-dihalodiphenylamines with lithium aluminum deuteride (4) is unsatisfactory because this expensive reagent is used so inefficiently: only the reaction of the first deuteride is fast, and later transfers are successively slower. Consequently it is necessary to use at least a fourfold excess of the reducing agent, even when the halogen is iodine. It is also necessary to quench the intermediate with excess deuterium oxide to avoid incorporation of protons when water is subsequently added to the reaction mixture. The procedure is viable: we used it for our first successful preparations of DPA-4,4′-d_2 and DPA-2,6,2′,6′-d_4.

We were slow to try hydrogenolysis (deuterolysis) of the aryl halide because representative procedures[4] specify excessively large amounts of the catalyst. When we did so, we found that reduction of halogen-substituted DPAs in alkaline ethanol over palladium on charcoal catalyst is fast and complete; this is our procedure of choice. Furthermore, brominated DPAs are superior to iodinated DPAs (which reduce substantially faster) whenever acid-catalyzed deuterium exchange is required, because the brominated compounds are distinctly more stable under the conditions of the exchange reaction.

Experimental

Ethanol-*d* was prepared by the method of Pasto and Meyer (6) from ethyl orthosilicate and deuterium oxide; the level of label was ca. 99%. This reaction is superior to that of Grieve and Sporek (7), which invariably gives an oily impurity that we have been unable to separate from the product. In all cases, ethanol-*d* was conserved by carrying out acid-catalyzed deuterium exchange in 3–5 stages with successively higher levels of label in the alcohol.

DPA and its labelled derivatives were purified by Soxhlet extraction into pentane, and (or) by sublimation at 45°C. With careful drying, these procedures give product DPAs which melt over 0.5–1° in the range 53–54.5°C. When sublimation is used, it is essential to remove residual acid from the amine by pouring an acetone solution into ice–bicarbonate solution. Sublimation with residual acid present gives poor recoveries and leaves a gummy residue that no longer melts at 53–55°C and is nearly insoluble in acetone and other solvents.

Levels of label in the products were checked by ms (Hewlett–Packard 5985A). Unfortunately, the ms of DPA (8) has no value because the very prominent $(M - 1)^+$ and $(M - 2)^+$ and weaker $(M$

[1] Presented in part at the ACS/CSJ Chemical Congress, Honolulu, April 1979, paper ORGN 89.

[2] Author to whom correspondence may be addressed.

[3] Revision received July 3, 1985.

[4] For example, 0.2 g halogen compound with 1 g palladium on calcium carbonate catalyst (5*a*) or 1 g catalyst with 0.5 g 7α-bromopregnenolone acetate (5*b*).

$- 3)^+$ peaks coincide with the molecular ions that arise from the most important incompletely deuterated species, and the relative intensities of these peaks vary significantly in ms runs at different times. Consequently, the quantitative determination of total label is impossible by this method, and the mass of the molecular ion M^+ is used only to confirm that the expected number of labelled positions has been reached in the major labelled product.

Positions of the labels were routinely monitored during exchange by both proton and deuterium nmr; the results obtained with the two nuclei are consistent. The proton-decoupled deuterium spectra consist of intense, somewhat broad (1–3 Hz at half-height) lines at the chemical shifts expected for the labelled sites. None of these lines display visible satellites due to introduction of label at other positions than those expected; in particular, there is no evidence for acid-catalyzed exchange in ethanol-*d* at the *meta* positions.

The 60-MHz aromatic proton spectra cannot be interpreted quantitatively; they are far from first order, and some lines are seriously broadened by unresolved structure due to coupling with other ring protons, and by the quadrupole moment of deuterium label. Better results can be obtained at 200 MHz (Bruker WP-200 SY). At this frequency, the *ortho*, *meta*, and *para* ring protons have sufficiently different chemical shifts (see discussion of DPA-d_{10}) that it is probably safe to assign all of the lines in the DPA spectrum. Duplicate spectra show scatter in the quantitative integral values from the Bruker integration routine over a range up to 7%. It is customary to assign an error of ±5% for such data (9); we believe our error may be larger. Values were confirmed by cutting out and weighing the plotted peaks; the scatter in these values was up to 10%. In these determinations, the *meta* peak was taken as an internal reference for the area due to four hydrogen atoms; this of course requires the assumption that no deuterium exchange occurs at these positions. The estimated rate ratio for electrophilic substitution at positions activated by a secondary aromatic amino group would be *ortho–para/meta* $\geq 10^6$, and this is confirmed by the absence of evidence for *meta* substitution in the deuterium nmr spectra. Our spectra were obtained with 0.10 *M* samples in DMSO-d_6 solution. The relaxation delay was set at 30 s, since our measured T_1 for the protons in DPA in DMSO solution is about 7 s. The center line of the solvent residual proton pattern was set at 2.49 ppm to establish the chemical shift scale.

Diphenylamine-d_{10}

Werstiuk's exchange procedure (10) was used to prepare this compound. DPA (17 g) and 0.5 *M* deuterium chloride in deuterium oxide (100 mL) is degassed by successive freeze–pump–thaw cycles, sealed, and heated for 30 h at 250°C. After cooling, the yellowish pellet of amine is taken up in hexane and washed with dilute potassium hydroxide solution and with water. Evaporation of the hexane gives solid, which is purified by sublimation to give 12.2 g of product; nmr indicates about 85% deuteration. A second exchange under the same conditions gives 7.4 g of sublimed product. The nmr shows weak lines due to uncoupled residual protons at 6.80 (*para*), 7.05 (*ortho*), and 7.21 ppm (*meta*) in DMSO solution. In this case, the *meta* peak is not available as an internal intensity standard; instead, the residual proton peak intensities are compared with the (possibly unreliable) N—H peak. By this standard, there are 1% residual protons at the *meta* and *para* positions, and 2% at the *ortho* positions. The mass spectrum gives the molecular ion at 179 Da (daltons). Acidification of the alkaline extracts of the crude product precipitates deuterated phenol.

Diphenylamine-2,4,6,2′,4′,6′-d_6

DPA (17 g) is refluxed for 6 h with 200 mL of ethanol-*d* which contains 0.2 *M* deuterium sulfate. (The mobile solvent deuterium is close to equilibrium with the exchangeable *ortho*, *para*, and amine H/D pool under these conditions. If 99% ethanol-*d* and D_2SO_4 are used at each stage, two exchanges to equilibrium under the conditions described would give 96% label with back exchange of the amino position assumed during work-up. However, we always used recovered ethanol-*d* at label levels in the range 75–90% for the first exchange steps, and fresh ethanol-*d* only for the last. Under these conditions, 3 or 4 exchange steps may be required to reach label levels of 95%.) After the exchange under reflux, 6 g of anhydrous Na_2CO_3 is stirred into the cold solution, the Na_2SO_4 filtered off, and solvent removed by vacuum distillation. The residue is partitioned between methylene chloride and water, the organic layer washed again, dried with anhydrous Na_2SO_4, and the solvent recovered under vacuum. The labelled product is purified by sublimation and recovered in over 90% yield. Proton nmr at 200 MHz gives line areas which show 8% residual protons at the *ortho* positions, and 4% protons at the *para* positions. These areas are measured relative to that for the *meta* proton lines; exchange is assumed to be negligible at the *meta* positions. The calculated equilibrium level is 5% residual protons after successive exchanges in 75, 90, and 99% ethanol-*d*. The mass spectrum gives the molecular ion at 175 Da.

4,4′-Dibromodiphenylamine

Three procedures for this straightforward-appearing preparation were investigated; they are listed here together with the overall yield for each. (*i*). Direct bromination of diphenylamine with bromine in acetic acid (11), 29%. (*ii*). Direct bromination with 2,4,4,6-tetrabromo-2,5-cyclohexadienone (12), 51%. (*iii*). Bromination of *N*-benzoyldiphenylamine, followed by saponification in 10% ethanolic KOH (13), 46%. The low yield in method (*i*) is due to the many (6 or 7) recrystallizations required to obtain pure product. Of the latter two methods, (*ii*) is probably better for small-scale (up to 10 g) synthesis; it would require excessive amounts of solvents on a large scale. On a mole scale, (*iii*) is best because it requires less solvent, even though there are three steps from diphenylamine. The product is pure by tlc on silica developed with cyclohexane/acetic acid (85 : 15% by volume); mp 106–107°C.

Diphenylamine-2,6,2′,6′-d_4

Much more drastic conditions are required for a reasonable exchange rate with the brominated DPA than with DPA itself. 4,4′-Dibromodiphenylamine (0.15 mol) in 225 mL of 1.7 *M* deuterium sulfate in ethanol-*d* is refluxed for 50 h, most of the solvent removed by vacuum distillation, and the liquid residue stirred into ice. The solids are then filtered, washed, and dried. After three such exchange steps the very dark and somewhat gummy residue is dissolved in methylene choride, stirred with activated silica, and the solids (which carry all of the colored impurities) filtered off. The amine can be recovered and recrystallized from heptane; the yield is 65%. Residual protons in the *ortho* positions are 6% by nmr; the calculated value after successive equilibrations with 86, 95, and 99% ethanol-*d* is 5%.

This solid is dissolved in 300 mL of 1.3 *M* ethanolic KOH, 0.5 g of 10% palladium on charcoal catalyst is added, and the mixture is reduced with hydrogen in the low pressure Parr shaker (rapid during the first hour, and complete overnight). The solution is filtered to remove spent catalyst and potassium bromide, the solvent removed under vacuum, and the amine recovered, washed thoroughly with water, dried, and purified by sublimation. The yield of purified amine exceeds 80%. Proton nmr: an A_2B pattern with the downfield (A) lines broadened by deuterium nuclear quadrupole relaxation. At 200 MHz, integration shows 8% residual *ortho* protons. Deuterium nmr shows a single line at 7.05 ppm chemical shift, and no other visible lines. The ms gives the molecular ion at 173 Da.

DPA-4,4′-d_2

4,4′-Dibromodiphenylamine (0.10 mol) is reduced in 300 mL of 1.3 *M* ethanolic KOH with deuterium gas in the presence of 0.5 g of 10% palladium on charcoal catalyst. The product is recovered and purified as described in the preceding preparation. The yields again exceed 80%. The proton nmr is an AA′BB′ pattern with the downfield lines broadened by the deuterium quadrupole relaxation. Proton nmr at 200 MHz shows 7% residual *para* protons. Deuterium nmr gives a single broadened line at 6.80 ppm, with no other visible lines. The mass spectrum gives a molecular ion at 171 Da.

Acknowledgments

We are indebted to the Research Board of the University of

Illinois at Chicago for a grant for the purchase of the deuterium probe for the WP-80 NMR, and to the U.S. Department of Energy for support during the later stages of this research. Eugene DeRose provided helpful advice on the choice of conditions for optimizing the 200-MHz nmr spectra.

1. F. A. NEUGEBAUER and S. BAMBERGER. Chem. Ber. **105**, 2065 (1972).
2. R. BIEHL, K. MÖBIUS, S. E. O'CONNOR, R. I. WALTER, and H. J. ZIMMERMANN. J. Phys. Chem. **83**, 3449 (1979).
3. A. I. SHATENSHTEIN, Y. I. RANNEVA, and T. T. KOVALENKO. J. Gen. Chem. U.S.S.R. **32**, 954 (1962).
4. H. C. BROWN and H. KRISHNAMURTHY. J. Org. Chem. **34**, 3918 (1969).
5. (*a*) M. BUSCH and H. STOVE. Ber. **49**, 1065 (1916); (*b*) H. GUT and M. OSKOKOVIC. Naturwiss. **47**, 40 (1960).
6. D. J. PASTO and G. R. MEYER. J. Org. Chem. **33**, 1257 (1968).
7. W. H. GRIEVE and K. F. SPOREK. J. Chem. Educ. **43**, 381 (1966).
8. J. H. D. ELAND and C. J. DANBY. J. Chem. Soc., 5935 (1965).
9. J. B. STOTHERS. *In* ^{13}C NMR spectroscopy. *Edited by* G. C. Levy. Wiley, New York. 1974. Chapt. 6.
10. N. H. WERSTIUK and T. KADAI. Can. J. Chem. **62**, 2169 (1974).
11. L. GALAITIS and T. MEGALOIKONOMOS. Akad. Athenon Praktika, **9**, 20 (1934); Chem. Abstr. **29**, 6886 (1935).
12. G. J. FOX, G. HALLAS, J. D. HEPWORTH, and K. N. PASKINS. Org. Synth. **55**, 20 (1976).
13. E. LELLMANN. Ber. **15**, 825 (1882).

Crystal and molecular structure of di-*o*-anisylketone

C. FAERMAN AND S. C. NYBURG[1]
Lash Miller Chemical Laboratories, University of Toronto, Toronto, Ont., Canada M5S 1A1

G. PUNTE[1,2] AND B. E. RIVERO[3]
Laboratorio de Cristalografía, Departamento de Física, Facultad de Ciencias Exactas, Universidad Nacional de La Plata, C. C. 67,1900-La Plata, Argentina

AND

A. A. VITALE AND N. S. NUDELMAN[2]
Departamento de Química Orgánica, Facultad de Ciencias Exactas y Naturales, Universidad de Buenos Aires, Ciudad Universitaria, Pab.2, Piso 3, 1428-Buenos Aires, Argentina

Received February 15, 1985

C. FAERMAN, S. C. NYBURG, G. PUNTE, B. E. RIVERO, A. A. VITALE, and N. S. NUDELMAN. Can. J. Chem. **63**, 3374 (1985).

The crystal and molecular structure of the title compound, $C_{15}H_{14}O_3$, is described. Crystals are monoclinic, space group $P2_1/n$, $a = 9.893(5)$, $b = 10.719(5)$, $c = 12.136(3)$ Å, $\beta = 90.56(3)°$. The molecule has a twist conformation and interactions between oxygen atoms of the methoxyl groups are thought to play some part in this.

C. FAERMAN, S. C. NYBURG, G. PUNTE, B. E. RIVERO, A. A. VITALE et N. S. NUDELMAN. Can. J. Chem. **63**, 3374 (1985).

On décrit la structure cristalline et moléculaire du composé mentionné dans le titre, $C_{15}H_{14}O_3$. Les cristaux sont monocliniques, groupe d'espace $P2_1/n$, $a = 9{,}893(5)$, $b = 10{,}719(5)$ et $c = 12{,}136(3)$ Å et $\beta = 90{,}56(3)°$. La molécule existe dans une conformation croisée et on croit que les interactions entre les atomes d'oxygène et les groupements méthoxyles jouent un rôle dans cette situation.

[Traduit par le journal]

Introduction

An X-ray crystal structure analysis of di-*o*-anisylketone, **1**, was undertaken as part of an investigation of the molecular conformations of bridged diphenyl compounds (1). The purpose of this investigation was to determine the influence of different bridging atoms, phenyl substituents, and lattice forces on molecular conformation.

Since the crystal structure of benzophenone, **2**, has been determined (2), showing the molecule to be in a twist conformation, an *ortho* disubstituted benzophenone, **1**, was chosen to elucidate whether its conformation is governed by the arylcarbonyl group, by steric effects of the *ortho* substituents, or by crystal environment effects.

Experimental

Compound **1** was prepared from the reaction of *o*-anisyllithium with carbon dioxide. A modification of the Glaze and Ranade (3) metal–halogen interchange method was used to prepare *o*-anisyllithium; 0.7 mL (5.6 mmol) of *o*-bromoanisole was added to 6 mmol of a 0.3 *M* ligroin solution of butyllithium prepared as previously described (4), and the reaction mixture was worked up as described for the preparation of phenyllithium (5). White crystals of *o*-anisyllithium were dissolved in THF and the solution flushed with carbon dioxide.

Recrystallization from methanol yielded white crystals of **1**, mp 104–105°C (lit. (6) mp 104°C), overall yield 70%. The compound may also be obtained from the reaction of *o*-anisyllithium with carbon monoxide (7). Infrared (KBr, cm^{-1}): 2800 (st C—H), 1620 (st C═O), 1600 (st C═C), 1450 (def C—H), 1250 (st C—O), 850 (def C—H ar); nmr (CCl_4) δ: 3.5 (s, 6H,—OCH_3), 6.84 (m, 4H, ar H3, H13 and H5, H11), 7.3 (m, 4H, ar H4, H12 and H6, H10); ms *m/e* (% rel. ab.): 242 (M, 48), 211 (12), 135 (100), 77 (40).

Structure determination and refinement

The crystal used for data collection was 0.20 × 0.08 × 0.05 mm. Preliminary data were obtained photographically. All other measurements were made on an Enraf–Nonius CAD-4 diffractometer using graphite monochromatized MoK radiation ($\lambda = 0.7107$ Å). Unit cell dimensions were based on 25 centered reflections. Intensity data were collected in the $\theta-2\theta$ scan mode in quadrants $(h,k,\pm l)$ with scan width $(0.9 + 0.35 \tan\theta)$ deg to a maximum 2θ of 50°. Three standard reflections were measured every 3 h; no significant variations were observed. Reflections were measured for intensity whenever their initial scan indicated $(\sigma(I)/I) > 0.04$. A considerable number of the 5921 measured reflections were symmetry related. Of these, 2267 were unique and, in turn, of these, 1383 significant on the criterion $I > 3\sigma(I)$. Crystal data are as follows.

$C_{15}H_{14}O_3$ $M_r = 242.28$
Monoclinic, $P2_1/n$, $a = 9.893(5)$, $b = 10.719(5)$, $c = 12.136(3)$ Å, $\beta = 90.56(3)°$, $V = 1288$ Å^3, $Z = 4$ molecules/cell, $D_c = 1.26$, D_m (not det) mg m^{-3}; $\mu(\mathrm{MoK}\alpha) = 4.8$ cm^{-1}; $t = 25°C$. No absorption corrections were applied.

The structure was solved by using MULTAN (8). All atoms were located and the positions of the non-hydrogen atoms were refined anisotropically, those of the hydrogen atoms isotropically. Full-matrix least-squares refinement minimizing $\Sigma w(|F_o - F_c|)^2$ converged (maximum shift/error = 0.05) to final agreement indices $R = 0.046$, $R_w = 0.059$. In the final cycle, weights were assigned $w = 4F^2/(\sigma(I)^2 + (0.04F^2)^2)$. The final ΔF map was featureless, the largest peak being 0.2 e A^{-3}; the goodness of fit, $s = [\Sigma w\Delta F^2/(m-n)]^2$, was 1.834. Computer programs and atomic scattering factors used were those in the Enraf–Nonius SDP package (9) on a PDP 11/23 computer.

Final positional and equivalent isotropic thermal parameters, B_{eq}, for non-hydrogen atoms are given in Table 1.

Atomic labelling and bond lengths are given in Fig. 1; bond angles in Fig. 2.[4]

Results and discussion

An ORTEP (10) stereoscopic view of the molecule is shown

[1]Authors to whom reprint requests should be addressed.
[2]Members of "Carrera del Investigador Científico," CONICET.
[3]Member of "Carrera del Investigador," CICPBA.

[4]Tables of structure factors and anisotropic thermal parameters may be purchased from the Depository of Unpublished Data, CISTI, National Research Council of Canada, Ottawa, Ont., Canada K1A 0S2.

TABLE 1. Positional parameters and their estimated standard deviations

Atom	x	y	z	B_{eq}*
C1	−0.1380(4)	0.3810(3)	0.5342(2)	8.05(9)
C2	−0.1819(2)	0.2510(2)	0.3794(2)	3.77(5)
C3	−0.3065(3)	0.2167(3)	0.4187(2)	5.13(6)
C4	−0.3816(3)	0.1275(3)	0.3654(2)	5.75(7)
C5	−0.3353(3)	0.0717(3)	0.2717(2)	5.37(7)
C6	−0.2129(3)	0.1059(3)	0.2323(2)	4.79(6)
C7	−0.1323(2)	0.1964(2)	0.2835(2)	3.83(5)
C8	−0.0049(2)	0.2300(3)	0.2286(2)	4.58(6)
C9	0.1168(2)	0.2818(2)	0.2841(2)	3.72(5)
C10	0.1906(3)	0.3724(3)	0.2285(2)	4.93(6)
C11	0.3078(3)	0.4204(3)	0.2696(3)	5.99(7)
C12	0.3552(3)	0.3772(3)	0.3691(3)	6.09(7)
C13	0.2869(3)	0.2879(3)	0.4264(2)	5.00(6)
C14	0.1676(2)	0.2398(2)	0.3846(2)	3.80(5)
C15	0.1364(4)	0.1121(3)	0.5424(2)	7.94(9)
O1	−0.1044(2)	0.3420(2)	0.4266(1)	4.82(4)
O2	0.0003(2)	0.2159(3)	0.1296(1)	9.05(7)
O3	0.0969(2)	0.1471(2)	0.4345(1)	4.83(4)

*$B_{eq} = \frac{4}{3}[a^2B(1,1) + b^2B(2,2) + c^2B(3,3) + abB(1,2) \times \cos\gamma + acB(1,3)\cos\beta + bcB(2,3)\cos\alpha]$.

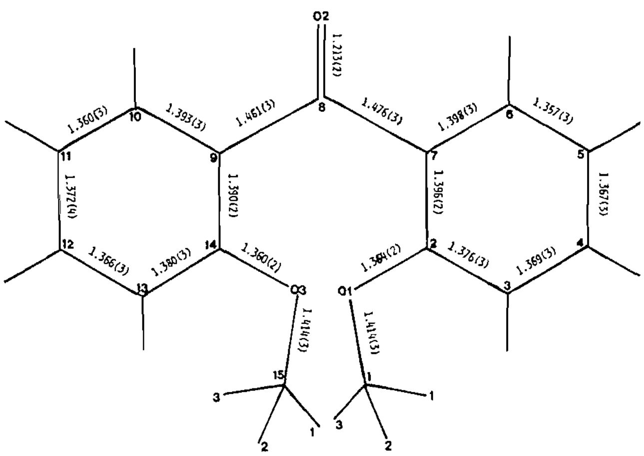

FIG. 1. Atomic labelling and intramolecular bond lengths.

in Fig. 3. The molecule has a twist conformation (11), as can be seen both from Fig. 3 and from the central torsion angles listed in Table 2. In this table are also listed the central torsion angles for three other molecules containing the benzophenone moiety, none of which, however, has any *ortho* substituents (12,13). At first sight, the conformations seem closely similar and this is suggested by an unconstrained best molecular fit (14), for example, of benzophenone (2), **2**, with **1** ($\Sigma\Delta^2$ = 0.032 Å^2). This correspondence is illustrated in Fig. 4. Nevertheless, there is some evidence that the oxygen atoms of the proximal methoxy groups have an influence on the conformation of **1**. For all the other molecules of Table 2 we have calculated what the distance between such oxygen atoms would have been had they been placed in idealized proximal *ortho* positions with the C(ar)—O bond length 1.362 Å. It can be seen that, in each case, the distance is somewhat shorter than that actually found in **1**. This suggests that the methoxy oxygen atoms in **1** are in slight steric conflict. This is also evidenced by the internal angle C7—C8—C9 of 125.4(5)° at the carbonyl group, which, as seen in Table 2, is greater than in the other three examples that lack *ortho* substituents.

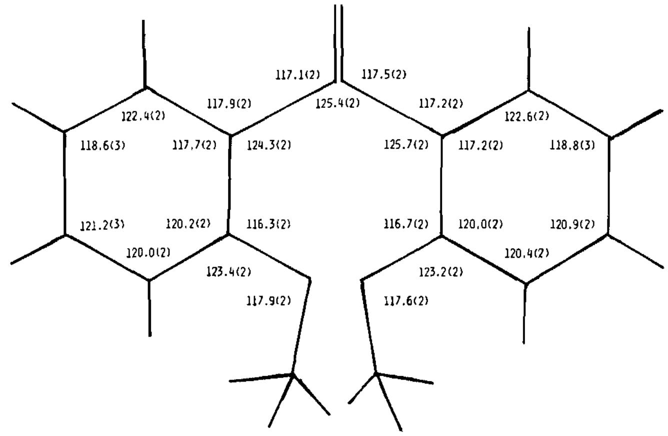

FIG. 2. Intramolecular bond angles.

It is only the oxygen atoms of the methoxyl groups that are close together; none of the hydrogen atoms of the two methyl groups are closer to each other than 3.03 Å. The bond angles at the ring carbon atoms to which the methoxyl groups are attached are of some interest. The torsion angles C1—O1—C2—C3 and C15—O3—C14—C13 are 14.0° and 8.6°, respectively. Note that angle O1—C2—C3 is larger than O1—C2—C7 (123.2° is against 116.7°) and, similarly, that O3—C14—C13 is larger than O3—C14—C9 (123.4° as against 116.3°). We have used the Cambridge Crystallographic Database (15) to retrieve all methoxy-substituted benzene rings in which the positions adjacent to methoxy are unsubstituted.[5] In every case, the exterior bond angle at the methoxy-substituted ring carbon atom was larger than 120° on the side of the smaller torsion angle and vice versa. This suggests that there is an interaction between the methyl group and the adjacent hydrogen of the benzene ring; the distances H102. . . H3 and H153 . . H13 of 2.12 and 2.31 Å, respectively, confirm this. Although there is no net force on any molecule in a crystal at equilibrium, it seems that there is a local repulsion which is forcing the methoxyl methyl groups into the plane of the benzene rings to which they are attached. Thus the methyl groups are forced up against the adjacent ring hydrogen atom and it is this interaction which opens up the exterior bond angle at the substituted ring carbon atom. There is additional supporting evidence in the present case, namely that, of the shortest ten O . . . C and C . . . C intermolecular distances, six involve the methoxy carbon atoms C1 and C15.[6] Both benzene rings are closely planar, the maximum deviation from the planes being 0.005(7) Å.[6]

An important factor governing the conformation and causing the methoxyl oxygen atoms to be in close contact is undoubtedly the need to preserve extended carbonyl resonance with the aryl rings. This will stabilize the ground state and increase the formal charge distribution on the carbonyl group. This is shown by carbonyl stretching infrared absorption frequencies. Thus, in both the crystal (16*a*) and in carbon tetrachloride solutions of dibenzophenone, **2** (16*b*), the frequency is 1670 cm^{-1} compared with a standard (unconjugated) value of 1700 cm^{-1}. One would expect the present compound to exhibit a slightly higher frequency, but it is somewhat lower, at 1620 cm^{-1}. This can

[5]The 334 REFCODES retrieved have been deposited (as in footnote 4). The results of this survey are in press (J. Mol. Struct.).

[6]Shortest non-hydrogen intermolecular contacts and least-squares planes data have been deposited (as in footnote 4).

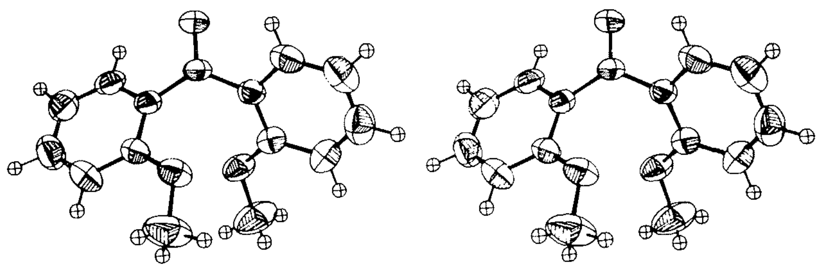

FIG. 3. ORTEP stereoscopic view of **1**.

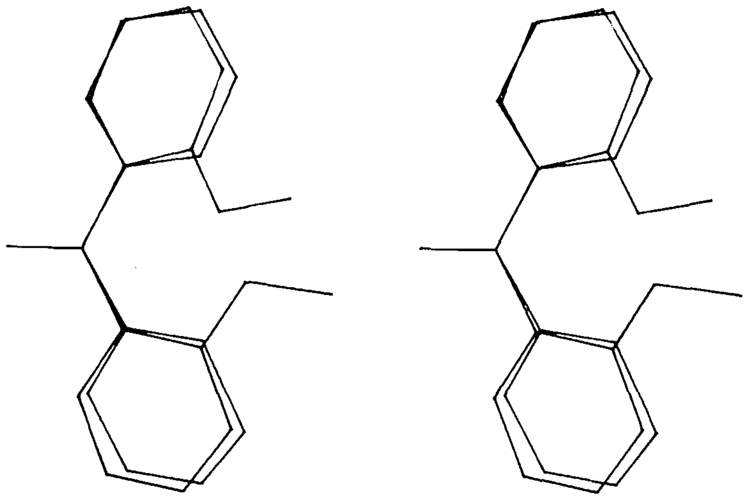

FIG. 4. Stereoscopic view of **1** and **2** superimposed by BMFIT.

TABLE 2. Conformations of benzophenones

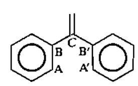

dihedral I A—B—C—B'

dihedral II A'—B'—C—B

Compound	(i)*	(ii)	(iii)	(iv)	Reference
Benzophenone	32.7	32.1	121.8	2.52	2
p,*p*-Dimethoxybenzophenone (molecule 1)	25.6	36.0	120.6	2.45	12
p,*p*-Dimethoxybenzophenone (molecule 2)	27.8	36.2	120.3	2.52	12
Bis(4-nitrophenyl)ketone	18.5	35.9	120.4	2.44	13
Di-*o*-anisylketone	42.2	28.3	125.4	2.89	This paper

*(i), (ii) are moduli (deg) of dihedral angles I, II respectively; (iii) angle at C; (iv) distance between hypothetically located (and, in the last case, actual) proximal *ortho* oxygen atoms with C(ar)—O = 1.362 Å.

be attributed to the presence of the electron-releasing methoxy groups.

In compounds where there is no conjugation through the carbonyl group, the conformation seems to be governed by other factors. In the case of unsubstituted diphenylmethane (17), the twist conformation may have been imposed by lattice forces. In di-*o*-anisylcarbinol (1), possibly both lattice forces and steric effects are responsible for the twist-skew conformation.

In summary, the results presented here are consistent with the view that the interaction between methoxy oxygen atoms brings about a slight conformational change in **1** relative to that found in *ortho*-unsubstituted molecules.

Acknowledgements

Financial assistance to C. F. and S. C. N. was provided by the Natural Sciences and Engineering Research Council of Canada. The other authors are indebted to the Consejo Nacional de Investigaciones Científicas y Técnicas and to the Comisión de Investigaciones Científicas de la Provincia de Buenos Aires for financial support.

1. C. FAERMAN, H. NEGRI, G. PUNTE, A. A. VITALE, and N. S. NUDELMAN. Can. J. Chem. **61**, 2001 (1983).
2. E. B. FLEISCHER, N. SUNG, and S. HAWKINSON. J. Phys. Chem. **72**, 4311 (1968).

3. W. H. Glaze and A. C. Ranade. J. Org. Chem. **36**, 3331 (1971).
4. N. S. Nudelman and A. A. Vitale. Org. Prep. Proced. **13**, 144 (1981).
5. N. S. Nudelman and A. A. Vitale. J. Organomet. Chem. **241**, 143 (1983).
6. C. Graebe and A. Feer. Ber. **19**, 2610 (1886).
7. A. A. Vitale, D. Perez, and N. S. Nudelman. An. Asoc. Quim. Argent. **70**, 155 (1982).
8. P. Main, S. J. Fiske, S. E. Hull, L. Lessinger, G. Germain, and M. M. Woolfson. MULTAN 80. A system of computer programs for the automatic solution of crystal structures from X-ray diffraction data. Univs. of York, England and Louvain-la-Neuve, Belgium. 1980.
9. B. A. Frenz. Enraf—Nonius structure determination package. Delft, The Netherlands. 1982.
10. C. K. Johnson. ORTEP II Report ORNL-3794. Oak Ridge National Laboratory, Tennessee. 1970.
11. S. P. N. van der Heijden, E. A. H. Griffith, W. D. Chandler, and B. E. Robertson. Can. J. Chem. **53**, 2084 (1975).
12. H. G. Norment and I. L. Karle. Acta Crystallogr. **15**, 873 (1962).
13. G. Chiari, H. C. R. Taylor, F. R. Fronzek, and G. R. Newkome. Acta Crystallogr. Sect. B, **36**, 2488 (1980).
14. P. S. Yuen and S. C. Nyburg. J. Appl. Crystallogr. **12**, 258 (1979).
15. F. H. Allen *et al.* Cambridge structural database. Acta Crystallogr. Sect. B, **35**, 2331 (1979).
16. The Sadtler standard spectra, Sadtler Research Labs., Philadelphia, 1968; (*a*) 14800; (*b*) 2494.
17. J. C. Barnes, J. D. Paton, J. R. Damewood, Jr., and K. Mislow. J. Org. Chem. **46**, 4975 (1981).

The preparation and characterization of iron trihydroxide, $Fe(OH)_3$

STEVE C. F. AU-YEUNG AND DONALD R. EATON
Department of Chemistry, McMaster University, Hamilton, Ont., Canada L8S 4M1

THOMAS BIRCHALL,[1] GEORGE DÉNÈS,[2] JOHN E. GREEDAN, AND CHRISTOPHER HALLETT
Department of Chemistry and Institute for Materials Research, McMaster University, 1280 Main Street West, Hamilton, Ont., Canada L8S 4M1

AND

KRZYSZTOF RUEBENBAUER
Department of Chemistry and Institute for Materials Research, McMaster University, 1280 Main Street West, Hamilton, Ont., Canada L8S 4M1 and Institute of Nuclear Physics, 31-342 Kraków, ul. Radzikowskiego 152, Poland

Received May 7, 1985

STEVE C. F. AU-YEUNG, DONALD R. EATON, THOMAS BIRCHALL, GEORGES DÉNÈS, JOHN E. GREEDAN, CHRISTOPHER HALLETT, and KRZYSZTOF RUEBENBAUER. Can. J. Chem. **63**, 3378 (1985).

Iron trihydroxide has been prepared by the oxidation of $FeSO_4$ with $[Co(III)(en)(dien)]_2O_2[ClO_4]_4$, $[Co(III)(tetraen)]_2O_2[ClO_4]_4$, and H_2O_2 in acid solution. These materials have been characterized by DTA, magnetic susceptibility, Mössbauer spectroscopy, X-ray powder diffraction, and electron microscopy. Particle sizes are found to be ~80 Å in diameter, but in the case of the (tetraen) preparation we find needle-like crystallites ~1200 Å × 400 Å × 50 Å in size. The magnitudes of the hyperfine fields follow the particle size variation. These materials have quite a different behaviour from the $Fe(OH)_3$ gels prepared from basic solution.

STEVE C. F. AU-YEUNG, DONALD R. EATON, THOMAS BIRCHALL, GEORGES DÉNÈS, JOHN E. GREEDAN, CHRISTOPHER HALLETT et KRZYSZTOF RUEBENBAUER. Can. J. Chem. **63**, 3378 (1985).

On a prépare du trihydroxyde de fer en procédant à l'oxydation du $FeSO_4$ par le $[Co(III)(en)(dien)]_2O_2[ClO_4]_4$, le $[Co(III)(tétraèn)]_2O_2[ClO_4]_4$ et le H_2O_2 en solution acide. On a caractérisé ces matériaux par l'analyse thermique différentielle, par les susceptibilités magnétiques, par la spectroscopie de Mössbauer, par la diffraction des rayons-X sur des poudres et par microscopie électronique. On a trouvé que le diamètre des particules est d'evniron ~80 Å; dans le cas du produit obtenu grâce à la préparation (tétraène), on trouve toutefois des aiguilles qui sont de nature cristalline et dont les dimensions sont d'environ ~1200 Å × 400 Å × 50 Å. Les amplitudes des champs hyperfins varient en fonction de la grosseur des particules. Ces matériaux ont des comportements très différents de ceux que présentent les gels de $Fe(OH)_3$, préparés en solutions basiques.

[Traduit par le journal]

Introduction

We have recently found that the oxidation of $FeSO_4 \cdot 7H_2O$ by $\{[Co(III)(en)(dien)]_2O_2\}[ClO_4]_4$ in aqueous solution results in the precipitation of iron trihydroxide, $Fe(OH)_3$ (1). This material was shown to be quite different from any other hydrated iron(III) oxide or iron(III) hydroxides that had been reported previously (2–11). It was concluded that this sample of $Fe(OH)_3$ had an average particle size of ~80 Å in diameter and that the two types of iron environment, visible in the low temperature ^{57}Fe Mössbauer spectrum, were due to surface and bulk iron; the former having a hyperfine field of 437 kOe while the latter, presumably more magnetically ordered, has a field of 486 kOe.

We have found that, by changing the reaction conditions, it is possible to obtain other varieties of $Fe(OH)_3$, some of which only appear to differ from the earlier sample (1) in particle size, while others appear to have quite different properties. In this paper we present ^{57}Fe Mössbauer, magnetization, X-ray powder diffraction, electron microscopy and therml analytical data for a number of these hydroxides. The Mössbauer data of one of these is analysed in some detail. The results are compared to those of the gels obtained by the precipitation of Fe^{3+} from aqueous solution by strong base.

[1] To whom all correspondence should be addressed.

[2] Present address: Department of Chemistry, Concordia University, 1455 De Maisonneuve Blvd. W., Montreal, P.Q., Canada H3G 1M8.

Experimental

Materials

Ferrous sulphate heptahydrate (A.C.S. spec.) and hydrogen peroxide were obtained from Baker Chemical and were used without futher purification. The Co(III) complexes were prepared according to standard literature methods (12–14).

Preparation of samples

The "powder" samples were prepared by the oxidation of Fe^{2+}, in the form of $FeSO_4 \cdot 7H_2O$, and the "gel" samples by the hydrolysis of Fe^{3+} at high pH. The majority of the samples prepared by oxidation employed peroxy cobaltate(III) complexes as the oxidant, but some samples were obtained using hydrogen peroxide as the oxidant under either acid (sample 6, Table 1), or basic (sample 8, Table 1) conditions. The peroxy complexes $\{[Co(en)(dien)]_2O_2\}^{4+}$ (en = ethylenediamine, dien = diethylenetriamine), $\{Co(tetraen)]_2O_2\}^{4+}$ (tetraen = tetraethylenepentamine), and $\{[Co(salen)]_2O_2(DMSO)_2$ (salen = bis-(salicylaldehyde)ethylinediimine, DMSO = dimethylsulfoxide) were used.

The preparation of $Fe(OH)_3$ powder samples involved dissolving stoichiometric amounts of the reactants (2:1, $FeSO_4 \cdot 7H_2O$:co-dioxygen complex) in aqueous solution under argon. In a typical preparation, 0.4654 g of the dioxygen complex was dissolved in 280 mL of argon-saturated distilled water, giving a concentration of 1.794×10^{-3} *M* in dioxygen complex. The pH of this solution was 7. $FeSO_4$, 0.2894 g, was introduced into the solution, with vigorous stirring, under a blanket of argon. Reaction started after ~10 min of stirring and was completed after 24 h, the argon atmosphere being maintained during this period. The product was collected by filtration and allowed to dry in air at room temperature until a constant weight was obtained.

TABLE 1. Chemical analysis of % wt. (Fe and Co by atomic absorption and Fe_2O_3 and H_2O by thermal decomposition)

Sample number*	wt.%				Density
	Fe	Co	Fe_2O_3	H_2O	
Calculated	52.26	0	74.71	25.29	
1	49.57	4.37			
2	54.34	0.25	74.25	25.46	3.01 ± 0.03
3	49.51	2.35			
4	50.51	0.21	72.24	24.90	2.78 ± 0.05
5	49.51	5.07			
6	49.15	0	70.02	27.27	2.60 ± 0.02
7	54.09	0	71.01	23.71	
8	52.15	0	71.07	23.26	

*1, from 5 m*M* $[Co(en)(dien)]_2O_2^{4+}$ (unwashed); 2, from 5 m*M* $[Co(en)(dien)]_2O_2^{4+}$ (washed); 3, from 1.8 m*M* $[Co(tetraen)]_2O_2^{4+}$ (unwashed); 4, from 1.8 m*M* $[Co(tetraen)]_2O_2^{4+}$ (washed); 5, from 1.8 m*M* $[Co(NH_3)_5]_2O_2^{4+}$ (unwashed pH = 8); 6, from 0.1 *M* $FeSO_4 \cdot 7H_2O + H_2O_2$ (pH = 4.5); 7, from 0.1 *M* $Fe^{3+} + OH^-$; 8, from 0.1 *M* $FeSO_4 \cdot 7H_2O + H_2O_2$ (pH = 10.86).

The yield was 90%. The pH of the filtrate was 5.83. The crude product usually contained some Co^{2+} and free amine ligands. It was essential to wash the product by completely suspending in water, stirring for 30 min and then re-filtering. The washing procedure was usually repeated three times. The weight of the product reached a limiting value after drying by standing for two days under normal atmospheric conditions.

Electron microscopy

Samples were prepared by enclosing $Fe(OH)_3$ powder in carbon by the evaporation of carbon onto a glass microscope slide which had been sparsely coated with the powder, and mounting segments of the resultant carbon film on 3 mm copper grids. Other samples were prepared by grinding $Fe(OH)_3$ powder under butanol and allowing a drop of the suspension to dry on a carbon-coated grid. The samples were examined in a "VG Microscopes" HB5 Scanning Transmission Electron Microscope (STEM) equipped with a field emission gun, and operated at an accelerating voltage of 100 kV in the STEM mode. Electron micrographs were recorded using both bright field and dark field detectors. Energy dispersive analysis of the X-rays, emitted by the specimen, was used to qualitatively distinguish the particles of $Fe(OH)_3$ examined from small numbers of contaminant particles.

Analyses

The analyses of the materials was carried out according to the procedure already reported (1). Analytical data for the various products are summarized in Table 1, together with the measured densities. Densities, thermogravimetric analyses, Mössbauer data and magnetic measurements were carried out according to the procedures already described (1). Computer fitting of the Mössbauer data were carried out using the computer program GMFP5S (15), for time independent spectra while, for time-dependent (relaxation) spectra, a simple model described below was adopted. For the latter case a newly developed GMFPSR program was used.

Results

Chemical composition

The analytical data establish that the "$Fe(OH)_3$ powders" have a composition close to that of $Fe(OH)_3$. The "$Fe(OH)_3$ gels" deviate somewhat from this stoichiometry. That the "gels" have a different structure from those of the "powders" is evident from the behaviour under controlled thermal analysis. Figure 1 shows the differential thermal analysis (DTA) curves of these compounds measured under the same conditions. The "gels" have quite a different behaviour in that they lose all of their available H_2O molecules by ~200°C, whereas the "powders" retain one molecule of H_2O up to ~600°C. At this

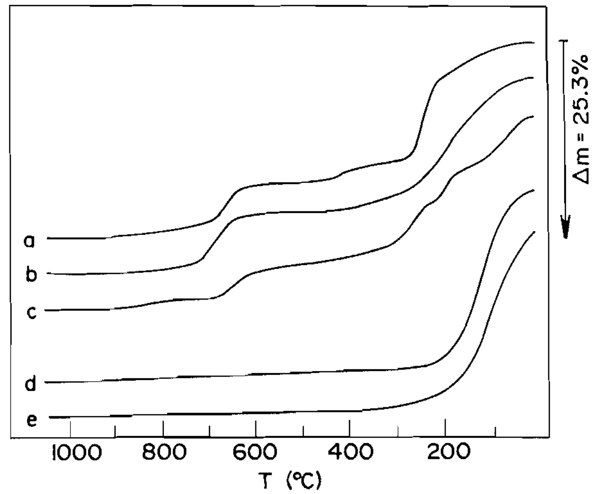

FIG. 1. Differential thermal gravimetric curves from various preparations of $Fe(OH)_3$. (*a*) Fe^{2+} + $[Co(III)(en)(dien)]_2O_2[ClO_4]_4$, 5 m*M* (powder); (*b*) $Fe^{2+} + H_2O_2$, pH = 4.5, 100 m*M* (powder); (*c*) Fe^{2+} + $[Co(III)(tetraen)]_2O_2[ClO_4]_4$, 1.8 m*M* (powder); (*d*) $Fe^{2+} + H_2O_2$, pH = 10.9, 100 m*M* (gel); (*e*) $Fe^{2+} + NH_4OH$, 100 m*M* (gel).

stage the formal composition is $Fe_2O_3 \cdot H_2O$ or FeOOH. Much stronger heating is required to remove this last water molecule and even by ~700°C a small residual amount of water (~2%) is retained. This latter stage has been characterized as "hydroxohematite", $Fe_2O_3 \cdot nH_2O$ (5).

X-ray diffraction

The X-ray powder diffraction patterns for those materials prepared from the $[Co(III)(en)(dien)]_2O_2[ClO_4]_4$ reaction both have similar powder patterns to that reported earlier (1), again with rather broad lines. The preparation using $[Co(III)(tetraen)]_2O_2[ClO_4]_4$ gives similarly broad X-ray diffraction peaks suggesting that the particle sizes are small. This broadening is illustrated in Fig. 2 which shows that part of the X-ray diffraction pattern where some of the strongest lines are observed. Those X-ray lines that could be measured were found at *d* (Å) 4.85, 4.20, 3.75, 2.70, 2.58, 2.46, 2.25, 2.19, 1.72, 1.57, 1.51, 1.46. As in our previous report on "$Fe(OH)_3$ powder" (1), the observed diffraction peaks could not be indexed to any of the known various phases of Fe_2O_3, or its hydrates, that have been published. On this figure we have indicated the positions of lines characteristic of δ'FeOOH: it is clear that none of this compound is present at room temperature.

Mössbauer spectroscopy

All of the samples examined show essentially a broadened doublet at room temperature typical of a Fe^{3+} in an oxygen ligand environment. Close examination of some of these spectra revealed that the broadened doublet was superimposed on a broad absorption indicative of the presence of a collapsed hyperfine field. This was quickly confirmed by cooling these samples to low temperature, 77 K. In addition to the paramagnetic doublet a clearly defined magnetic hyperfine spectrum was observed, but the lines were broad. Such was the case for the samples prepared using $[Co(III)(en)(dien)]_2O_2[ClO_4]_4$, 20 m*M*, or $[Co(III)(tetraen)]_2O_2[ClO_4]_4$, Fig. 3. For those preparations using lower concentrations of $[Co(III)(en)(dien)]_2O_2[ClO_4]_4$ (i.e. 5 and 8.5 m*M*), or $[Co(III)(salen)]_2O_2[DMSO]_2$ or H_2O_2 at pH 4.5, magnetic ordering only occurred below 77 K. In the case of the "$Fe(OH)_3$ gels" prepared in basic solution, magnetic ordering was only observed <77 K, that is at 4 K. At

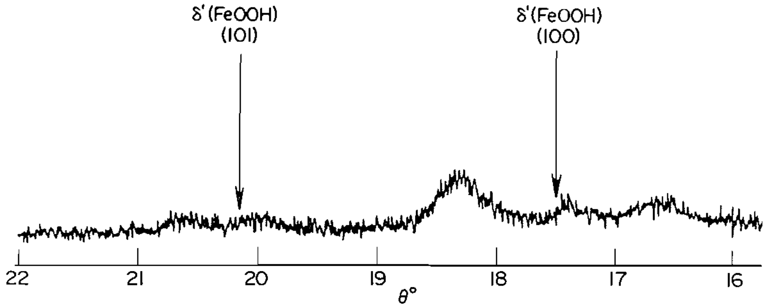

FIG. 2. X-ray powder diffraction pattern of $Fe(OH)_3$ powder prepared from Fe^{2+} and $[Co(III)(tetraen)]_2O_2[ClO_4]_4$.

TABLE 2. ^{57}Fe Mössbauer data for $Fe(OH)_3$ powders and gels

Preparation	Temperature (K)	δ*	Δ*	Γ*	H (kOe)
2	298	0.366	0.31	0.30	—
		0.365	0.85	0.47	—
	80	0.42	0.63	0.40	—
		0.49	—	0.46	430(5)
		0.49	−0.39	0.46	403(5)
	4.2	0.36	—	0.48	437(5)
		0.30	−0.38	0.42	486(5)
4	298	0.36	0.65	0.68	—
	80	0.355	0.65	0.68	
		0.49	−0.4	0.58	420(5)
	4.2	0.55	−0.25	0.58	508(5)
6	298	0.36	0.59	0.36	—
		0.37	0.82	0.52	—
	4.2	0.53	−0.4	0.60	444(5)
7	298	0.34	0.65	0.59	
	80	0.40	0.76	0.49	
	4.2	0.32	−0.46	0.55	439(5)
8	298	0.32	0.66	0.83	
	80	0.42	0.73	0.81	
	4.2	0.25	—	0.70	476(5)

* ±0.01 mm s^{-1}.

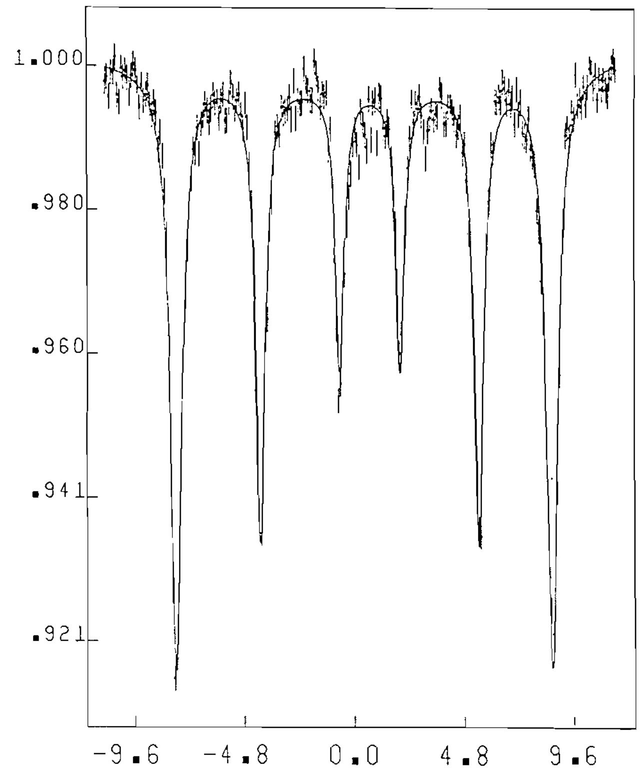

FIG. 3. ^{57}Mössbauer spectrum of $Fe(OH)_3$ gel, prepared from Fe^{2+} and H_2O_2 at pH 1.09, at 4.2 K.

room temperature and liquid nitrogen temperatures the spectra appeared as rather broad Fe^{3+} doublets suggesting that there was rather a large distribution of Fe^{3+} environments in these gels. The other paramagnetic spectra could all be fitted to overlapping doublets.

All of the data that we have obtained are summarized in Table 2. We have included data from ref. 1 pertaining to the $Fe(OH)_3$ powder preparation using a 20 m*M* solution of $[Co(III)(en)(dien)]_2O_2[ClO_4]_4$.

The behaviour of the samples which show hyperfine fields over the range of temperatures from 4.2 to 298 K is quite complex. In only one case was it possible to clearly distinguish two magnetic hyperfine sites at 4.2 K, which have been attributed as arising from bulk and surface Fe^{3+} in particles of ~80 Å diameter (1). As the temperature is raised the magnetic field collapses slowly and a paramagnetic doublet replaces the magnetic spectrum. By 298 K this conversion is virtually complete, and from this behaviour we concluded that this material was of realtively uniform particle size. None of the other samples showed more than one magnetic hyperfine component at 4.2 K (Fig. 3), but it is clear from the collapse of these spectra at higher temperature that more than one iron site is present, and at room temperature the spectra must be fitted to two quadrupole doublets. The complexity of the spectra at intermediate temperatures (see Fig. 4) for the tetraen case, and the way that the spectrum collapses, leads us to the conclusion that we are dealing here with less well ordered particles having a rather broad range of sizes. This leads to the poorly resolved spectra in the range 77–298 K (Fig. 4).

Magnetic properties

The magnetic behaviour of the powders prepared using $[Co(III)(en)(dien)]_2O_2[ClO_4]_4$ at various concentrations are very similar and the data for the sample prepared using a 20 m*M* concentration of oxidant have already been commented upon in detail (1). Similar behaviour is found for the "$Fe(OH)_3$ powder" prepared using $[Co(III)(tetraen)]_2O_2[ClO_4]_4$ (1.8 m*M*), and these data are shown in Fig. 5. At 66 K, and above, the magnetization data do not show any variation with temperature which is indicative of superparamagnetic behaviour. The data obtained in the range 66–141 K have been fitted to a Langevin function, $\sigma_g = \sigma_s \coth(mH/kT - kT/mH)$ where m is the single particle moment and σ_s the saturation moment of

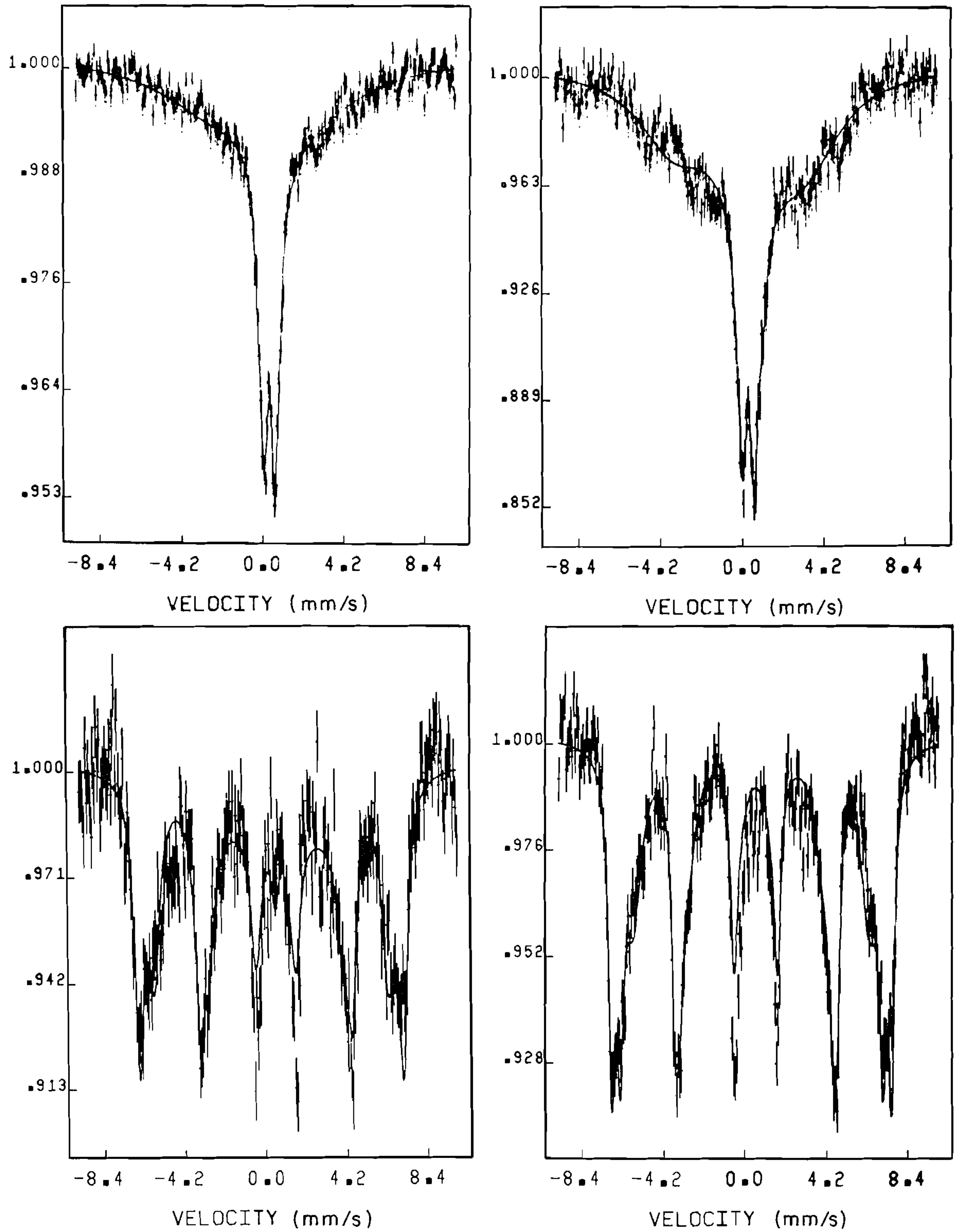

FIG. 4. ^{57}Mössbauer spectra of $Fe(OH)_3$ powder prepared from Fe^{2+} and $[Co(III)(tetraen)]_2O_2[ClO_4]_4$: sample *4*, (*a*) 298 K; (*b*) 285 K; (*c*) 150 K; (*d*) 80 K.

the bulk sample: σ_s and m were found to be 1.8 emu g^{-1} and 6.8×10^{-19} erg/Oe, respectively. These values are smaller than those obtained for the sample prepared using $[Co(III)(en)(dien)]_2O_2[ClO_4]_4$ (1). This combined with the lower density suggest that the particle size is smaller than the ~80 Å diameter found for the $[Co(III)(en)(dien)]_2O_2[ClO_4]_4$ sample.

Electron microscopy

The iron(III) hydroxide powder, prepared using the $[Co(III)(tetraen)]_2O_2[ClO_4]_4$, was investigated by electron microscopy to evaluate the morphology of the $Fe(OH)_3$ particles and the distribution of sizes of the $Fe(OH)_3$ particles.

A cursory inspection of each specimen of $Fe(OH)_3$ powder,

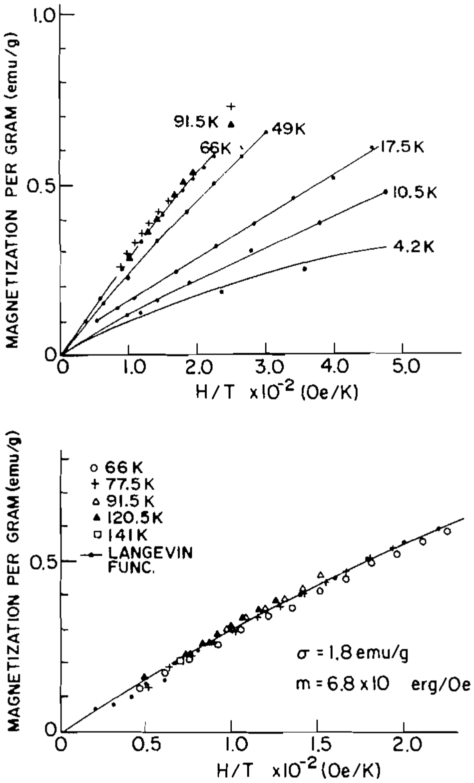

FIG. 5. Magnetization per gram versus H/T for $Fe(OH)_3$ powder prepared from Fe^{2+} and $[Co(III)(tetraen)]_2O_2[ClO_4]_4$.

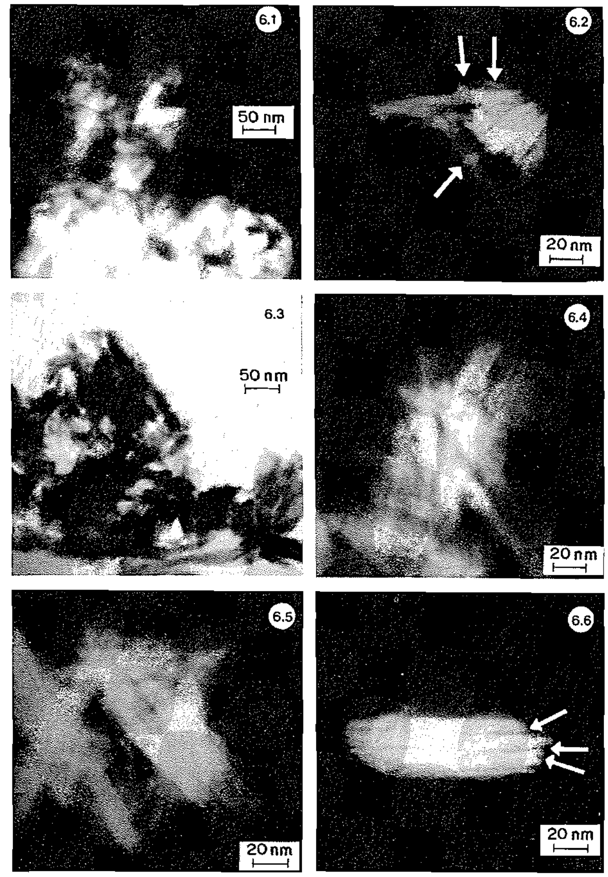

FIG. 6. Scanning transmission electron microscope photographs, *1–6*, of the $Fe(OH)_3$ powder crystallites prepared from Fe and $[Co(III)(tetraen)]_2O_2[ClO_4]_4$: *2* — arrows indicate unusually small particles, *6* — arrows indicate boundaries between different particles.

in the electron microscope, showed large areas of dark contrast which appeared to be relatively thick with regard to the penetrating power of the beam (ca. 2000 Å). Examination of these regions at higher magnification showed them to be clusters composed of large numbers of aggregated smaller particles. Some typical electron micrographs recorded from the thin areas located at, or near to, the edges of the clusters are presented in Fig. 6.

The low contrast observed in the micrographs indicates that the individual particles are thin. Indeed, the poor contrast was not significantly improved when a collector aperture was inserted into the beam to prevent scattered electrons from contributing to the bright field image. This observation reflects the limited amount of electron scattering which might be expected to be a feature of such thin particles.

It was not possible to record electron diffraction patterns which were amenable to indexing, although some weak diffraction spots were observed when the electron probe was stopped on individual particles. This observation appears to indicate that the thin particles have some degree of crystallinity and this is consistent with the regular shapes of some of the particles in Fig. 6. A future electron diffraction study might yield valuable information as to the crystallographic properties of this novel form of $Fe(OH)_3$, since powder X-ray diffraction has proved to be of limited use in the characterization of this species (1).

From Fig. 6.1 to 6.5 it appears that the $Fe(OH)_3$ powder consists of particles which take the form of needles or elongated platelets. Although the size of the microcrystals varied between 300 and 2000 Å in length and 100 and 500 Å in width, a typical microcrystal might be described as a platelet having dimensions of ca. 1200 Å by 400 Å. The precise thickness of the particles is difficult to establish in the absence of convergent beam electron diffraction patterns. However, whilst it is acknowledged that much caution must be exercised when directly interpreting contrast effects observed in electron micrographs, Fig. 6.6 shows a particle which appears to be composed of several platelets stacked "edge on" to the beam. Given this assumption the thickness of the individual microcrystals seems to be ca. 50 Å. This would be consistent with the low contrast in the images.

It is relevant to recall that attempts to determine the particle size of $Fe(OH)_3$ powder by applying the Scherrer formula to linewidths observed in the powder X-ray diffraction patterns of $Fe(OH)_3$ indicated particle sizes of ca. 80 Å. The direct measurement of particle size by electron microscopy could reasonably be expected to be more accurate than the inference of such data from X-ray diffraction pattern linewidths, which might rather reflect a low degree of crystallinity. However, it is notable that some very small particles were observed (Fig. 6.2) in the $Fe(OH)_3$ powder, of some 100 Å in length. These particles were only rarely encountered.

Iron(III) hydroxide powder might be expected (1) to undergo dehydration and recrystallization processes, to give $Fe_2O_3 \cdot 2H_2O$, FeOOH, and ultimately Fe_2O_3 if subjected to excessive heat and/or a vacuum. It is therefore pertinent to note that no recrystallization processes were observed in the electron microscope, and that the images of the $Fe(OH)_3$ crystals did not undergo change even on prolonged irradiation. Hence, although it is likely that some water was lost on exposing the powder to a vacuum and the beam, this did not appear to influence the crystal shapes and sizes.

Discussion

Mechanism of oxidation

The Co(III) peroxy complexes used as oxidants exist in a number of isomeric forms which have been distinguished by ^{59}Co nmr (16). It has also been shown (17) that the rate of the electron transfer reaction depends on the isomeric structure. It is usually considered that an inner sphere electron transfer mechanism is involved with the Fe^{2+} coordinated to the peroxy group:

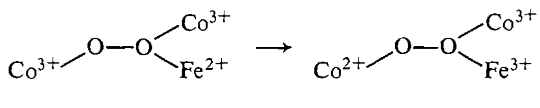

The rate depends on the nature of the ligands attached to the Co^{3+} ions. Detailed reaction schemes have been suggested by Hyde and Sykes (18) and by McLendon and Martell (19). If $Fe(OH)_3$ is produced by hydrolysis of an Fe^{3+} compound the ligand environment of the ion will be that which is most stable for an Fe^{3+} ion at that pH. If, on the other hand, $Fe(OH)_3$ is produced by an inner sphere electron transfer reaction, the Fe^{3+} will find itself in a ligand environment appropriate to Fe^{2+} at the pH of the experiment. Given that the pK_a's of water coordinated to Fe^{2+} will differ from that of water coordinated to Fe^{3+}, this effect could lead to a difference in the environment of the Fe^{3+} in the precipitated hydroxide which could, in turn, account for the differences in physical properties described above.

Mössbauer and related phenomena

It is apparent from an examination of the data for these iron(III) hydroxides that there are three different types of product. The first, characterized by preparations using low concentrations of $[Co(III)(en)(dien)]_2O_2[ClO_4]_4$ or H_2O_2 at pH 4.5, exhibits a paramagnetic ^{57}Fe Mössbauer spectrum at room temperature. At liquid nitrogen temperature a magnetic component is visible together with a paramagnetic doublet, but on cooling further to 4.2 K the sample becomes completely ordered magnetically. The second type obtained from preparations involving relatively high (20 m*M*) concentrations of $[Co(III)(en)(dien)]_2O_2[ClO_4]_4$, or $[Co(III)(tetraen)]_2O_2[ClO_4]_4$, show Mössbauer spectra which have both paramagnetic and magnetic components present, at all temperatures from liquid nitrogen to room temperature, but are magnetically ordered at 4.2 K. The $Fe(OH)_3$ gels show the third type of behaviour in that the Mössbauer spectra remain as broad doublets until below liquid nitrogen temperature and are magnetically ordered at 4.2 K. This behaviour is typical of the $Fe(OH)_3$ gels that have been reported previously.

In an earlier report (1) we presented evidence to show that the particle size of the crystallites of $Fe(OH)_3$, from the $[Co(III)(en)(dien)]_2O_2[ClO_4]_4$ preparation, was of the order of 80 Å diameter and a broad X-ray powder diffraction pattern was obtained. Of the other samples only that from the "tetraen" preparation gave an X-ray diffraction pattern, and this showed non-uniform broad Bragg peaks (Fig. 2) suggestive of a range of particle sizes. This is consistent with the electron micrographs which showed particles ranging in length from 100 to 2000 Å. The other samples gave no X-ray patterns and presumably are composed of very small particles or amorphous material. We have chosen to discuss the behaviour of the "tetraen" sample in some detail.

The magnetization measurements versus temperature and applied field, performed upon $Fe(OH)_3$ (tetraen preparation), are indicative of a complex magnetic behaviour having at least two scales of ordering. The low temperature magnetization is dominated by a kind of microscopic antiferromagnetic ordering. However, at high temperatures, the data are fitted to a Langevin function showing the presence of superparamagnetic particles with the internal coupling being largely antiferromagnetic, but with the magnetic moment per particle not being entirely compensated. At still higher temperatures the normal paramagnetic behaviour is eventually restored indicating that a phase transition to the paramagnetic state occurs at the microscopic level. Electron microscope images indicate the presence of small plate-like particles many of which are clumped into larger aggregates (see Fig. 6) and which would be expected to behave in the manner described above.

The Mössbauer spectra are relatively simple at the extreme ends of the temperature scale, but become very complex in the superparamagnetic region. The 4.2 K spectrum consists of a unique magnetically split pattern with $H_{eff} \approx 509$ kOe and $\Delta_{eff} = -0.25$ mm/s. The lines are slightly broadened, but the magnetic field distribution is not pronounced to any significant level. This finding means that the saturation value of the hyperfine magnetic field does not depend upon the particular particle size and/or location of the Fe^{3+} within a particle. This is probably due to the fact that most of the field is produced by local Fermi terms which are only spatially fixed by the interatomic interactions.

From the Mössbauer point of view at least some proportion of the material remains magnetically ordered at room temperature where the magnetization data do not show any appreciable ordering. This phenomenon could be attributed to the fact that the techniques involved have time scales which differ by several orders of magnitude, and this is indicative of relaxation phenomena within the ensemble of Neél type particles. The quadrupole splitting $|\Delta| = 0.47$ mm s^{-1} at this high temperature limit is indicative of V_{zz} being nonco-axial with the H_{eff}. However, the quadrupole interaction is small compared with the magnetic one, and therefore most of the magnetic spectra can be treated by including the quadrupole interaction as a small perturbation, so justifying the use of the first order approximation. Unfortunately, Mössbauer measurements above room temperature provide little further information, because these $Fe(OH)_3$ samples start to lose water just above this temperature. Spectra between 80 and 298 K, recorded without an external magnetic field, are composite ones showing many widely separated hyperfine fields and in addition are smeared out by magnetic relaxation occurring at different rates.

The very fact that an unique field is observed close to saturation, while many fields are present at intermediate temperatures, indicates (Fig. 4) that the magnetic transition temperature is very poorly defined. Such a poor definition of a transition point means that a significant amount of material must be composed of very fine particles. A distribution of relaxation frequencies is most likely due to the distribution of volume and shape anisotropy between the differently shaped and sized particles (Fig. 6). The clumping of the material is likely to play some secondary role in this process.

There is an obvious correlation between relaxation frequency and hyperfine field, i.e., higher frequencies are correlated with smaller fields and this corroborates the idea that these subspectra originate in smaller particles (Table 3). The complexity

TABLE 3. Hyperfine fields and relaxation frequencies as obtained from the Mössbauer data fits to the simple "Kramer's doublet" relaxation model for the $Fe(OH)_3$ powder prepared using $[Co(III)(tetraen)]_2O_2[ClO_4]_4$: sample 4

T (K)	H_1 (kOe)	H_2 (kOe)	H_3 (kOe)	W_1 (MHz)	W_2 (MHz)	W_3 (MHz)
298	24	249	—	—	36.5	—
285	35	248	—	—	23.2	—
275	162	316	—	19.2	5.3	—
262	154	323	—	17.0	5.9	—
250	141	290	350	14.9	4.2	3.1
237	170	305	365	16.0	4.2	2.6
225	173	316	373	15.2	4.4	2.7
200	201	338	391	15.0	4.1	2.3
150	195	377	424	14.3	3.1	1.7
100	375	418	450	4.4	1.5	0.3
80	379	420	447	4.9	1.2	0.8
11.4	485	—	—	0	—	—
4.2	509	—	—	0	—	—

of the magnetic behaviour prevents, in our opinion, a detailed quantitative analysis of the Mössbauer spectra unless well defined and dispersed particles, or bulk material, can be produced.

However, in order to get some idea of the system behaviour we have fitted our spectra using a very simple relaxation model as follows. Spectra were fitted, within the Lorentzian approximation, as composite ones with each component being described by the magnetic Hamiltonian, with the quadrupole interaction included as a first order approximation, and a relaxation matrix taking on the following form in the quantization coordinates,

$$\mathbf{W} = \begin{pmatrix} w & -w \\ -w & w \end{pmatrix}$$

with both states having equal probabilities at thermal equilibrium. Such a model corresponds to the exact description of the axially symmetric and isolated Kramer's doublet (20), and yields the following eigenvalues of the relaxation superoperator for the 14.4 keV of the ^{57}Fe transition

$$\lambda(m_e m_g) = iw \pm [E_M^2(m_e m_g) - w^2]^{1/2} + E_Q(m_e)$$

where

$$E_M = \pm\, g_g \mu_N H_{\text{eff}}[m_g - (g_e/g_g) m_e]$$

and

$$E_Q = \left(\frac{eQ_g V_{zz}}{4}\right)\left[m_e^2 - \frac{5}{4}\right] + S$$

All symbols have their conventional meaning with w being an average switching rate, i.e. relaxation frequency. The real (line position) and imaginary (line broadening) parts of the eigenvalue $\lambda(m_e m_g)$ are shown versus relaxation frequency w in Fig. 7. The results of the fits are summarized in Table 3, while some typical spectra are shown in Fig. 4.

No attempt was made to correct intensities (partial areas) of the "broad" and "narrow" components by using eigenvectors of the relaxation matrix **W**. However, this correction is only relevant for $w > |E_M|$ for a given pair of lines. The "broad" component is always already smeared out in this region of relaxation frequency, and therefore the correction is very small. The only parameter seriously influenced is the total area of the spectrum. This parameter can be treated, in the given context, as a phenomenological one and therefore has no special meaning. The relative contribution of different "sites" is also influenced to some extent, but they also have no special meaning for such complex spectra.

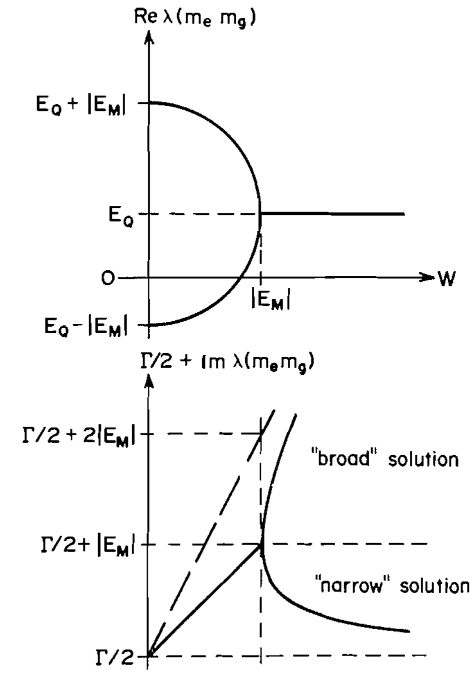

FIG. 7. The real and imaginary parts of the relaxation superoperator eigenvalues plotted versus relaxation frequency.

Conclusions

Addition of base to a solution of Fe^{3+} results in the precipitation of $Fe(OH)_3$. Oxidation of Fe^{2+} in basic solution also produces $Fe(OH)_3$. In both of these cases the precipitate is in the gelatinous form and these materials are magnetically ordered below liquid nitrogen temperature. The magnetic hyperfine fields are quite different in the two cases, being higher for the case where oxidation from Fe^{2+} to Fe^{3+} must take place. Since the DTA results show that both of these gels lose all water molecules by 250°C, we conclude that the water molecules in these two gels ($Fe_2O_3 \cdot 3H_2O$) are held in a very similar fashion in the structure. The fact that the hyperfine fields are different is perhaps due to particle size effects.

The $Fe(OH)_3$ powder, prepared by oxidation of Fe^{2+} with H_2O_2 at pH 4.5, has a similar Mössbauer behaviour to the gels. Its structure, however, must be quite different from that of the gels since the bound water molecules are lost in stages rather than all at once. The hyperfine magnetic field is smaller than for the other powders (Table 2) which we attribute to a particle size effect. No X-ray powder pattern could be observed for this material suggesting that the particle size is $\ll$80 Å in diameter. We believe that the rate of oxidation of Fe^{2+} to Fe^{3+} will govern the particle size. The "powder" preparations involving $[Co(III)(en)(dien)]_2O_2[ClO_4]_4$ and $[Co(III)(tetraen)]_2O_2[ClO_4]_4$ result in materials which have particle sizes estimated to be ~80 Å in diameter for the former case, and are ~1200 Å × 400 Å × 50 Å in the latter case (see Experimental section). As discussed above, the rate of the electron transfer reactions during these oxidations is controlled by the nature of the oxidant, and indeed the isomeric form of the Co(III) complex. Since the magnitude of the hyperfine field, in the $Fe(OH)_3$ powders, appears to follow the particle size estimates, we conclude that the oxidation of Fe^{2+} to Fe^{3+} is in the order $H_2O_2 > [Co(III)(en)(dien)]_2O_2[ClO_4]_4 > [Co(III)(tetraen)]_2O_2$-$[ClO_4]_4$.

Acknowledgements

We wish to thank the Natural Sciences and Engineering Research Council of Canada for financial support, and B. Robertson for help with the electron microscopy.

1. S. C. F. AU-YEUNG, G. DÉNÈS, J. E. GREEDAN, D. R. EATON, and T. BIRCHALL. Inorg. Chem. **23**, 1513 (1984).
2. P. PASCAL. Nouveau Traité du Chimie Minérale Masson, Paris 27. 1967. pp. 665, 677.
3. A. A. VAN DER GIESSEN. Chemical and physical properties of iron(III)-oxide hydrate. Philips Res. Ref. Suppl. **12**, 1 (1968).
4. A. L. MACKAY. Reactivity of solids. Vol. 4. *Edited by* J. H. deBoer. Elsevier, New York. 1961. p. 571.
5. E. WOLSKA. Z. Kristallogr. **154**, 69 (1981).
6. J. M. D. COEY and P. W. READMAN. Earth Planet. Sci. Lett. **21**, 45 (1973).
7. M. H. FRANCOMBE and H. P. ROOKSBY. Clay Miner Bull. **4**, 1 (1959).
8. A. A. VAN DER GIESSEN. J. Inorg. Nucl. Chem. **28**, 2155 (1966).
9. A. W. SIMPSON. J. Appl. Phys. **33**, 1203 (1962).
10. C. W. CHILDS, B. A. GOODMAN, E. PATERSON, and F. W. D. WOODHAMS. Aust. J. Chem. **33**, 15 (1980).
11. J. H. JOHNSTON, N. E. LOGAN. J. Chem. Soc. Dalton Trans. 13 (1979).
12. J. A. WEIL, D. L. DUFFY, and D. HOUSE. J. Inorg. Nucl. Chem. **31**, 2053 (1969).
13. J. CALDERAZZO and C. FLORIANI. J. Chem. Soc. A, 946 (1969).
14. M. MORI, J. A. WEIL, and M. ISHIGURO. J. Am. Chem. Soc. **90**, 615 (1968).
15. K. RUEBENBAUER and T. BIRCHALL. Hyperfine Int. **7**, 125 (1979).
16. S. C. F. AU-YEUNG and D. R. EATON. Can. J. Chem. **61**, 2431 (1983).
17. S. C. F. AU-YEUNG and D. R. EATON. Can. J. Chem. **62**, 2127 (1984).
18. M. R. HYDE and A. G. SYKES. J. Chem. Soc. Dalton Trans. 1550 (1974).
19. G. MCLENDON and A. E. MARTELL. Inorg. Chem. **15**, 2662 (1976).
20. K. RUEBENBAUER. Proc. III International Symposium on Magnetic Resonance, June 1983, Torún, Poland (Advances in Colloid and Interface Science). In press.

Reaction of 2,3-diaminonaphthalene with pyruvic acid

M. J. BERTRAND AND L. MALTAIS
Département de chimie, Université de Montréal, C.P. 6210, Succ. A, Montréal (Qué.), Canada H3C 3V1

AND

F. BRISSE[1] AND M.-J. OLIVIER
Laboratoire de diffraction des rayons X, Département de chimie, Université de Montréal, C.P. 6210, Succ. A, Montréal (Qué.), Canada H3C 3V1

Received May 14, 1985

M. J. BERTRAND, L. MALTAIS, F. BRISSE, and M.-J. OLIVIER. Can. J. Chem. **63**, 3386 (1985).

The condensation product of 1,3-diaminonaphthalene with pyruvic acid was prepared, isolated in its crystalline form, and submitted to X-ray and FT-IR analyses. Results indicate that the amide form of the derivative is predominant in the crystalline state and that nearly planar molecules form dimers through hydrogen bonding across a center of symmetry; mw = 210.24, monoclinic, $C2/c$, a = 19.834(8), b = 4.636(6), c = 22.360(2) Å, β = 96.30(9)°, V = 2043.6 Å^3, Z = 8, d_0 = 1.358, d_c = 1.366 g cm^{-3}, $\lambda(\mathrm{CuK}\bar{\alpha})$ = 1.54178 Å, $\mu(\mathrm{CuK}\bar{\alpha})$ = 6.75 mm^{-1}, $F(000)$ = 880, T = 298 K, R = 0.050 for 781 observed reflections.

M. J. BERTRAND, L. MALTAIS, F. BRISSE et M.-J. OLIVIER. Can. J. Chem. **63**, 3386 (1985).

Le produit issu de la condensation du 2,3-diaminonaphtalène avec l'acide pyruvique a été préparé, isolé sous sa forme cristalline et soumis à l'analyse par diffractions des rayons X et FT-IR. Les résultats obtenus indiquent que le dérivé existe essentiellement sous sa forme amide à l'état solide et que les molécules quasi-planaires forment, par liaisons hydrogènes, des dimères centrosymmétriques; pm 210,24, monoclinique, $C2/c$, a = 19,834(8), b = 4,636(6), c = 22,360(2) Å, β = 96,30(9)°, V = 2043,6 Å^3, Z = 8, d_0 = 1,358, d_c = 1,366 g cm^{-3}, $\lambda(\mathrm{CuK}\bar{\alpha})$ = 1,54178 Å, $\mu(\mathrm{CuK}\bar{\alpha})$ = 6,75 mm^{-1}, $F(000)$ = 880, T = 298 K, R = 0,050 pour 781 réflexions observées.

Introduction

Hinsberg was the first to report on the condensation reaction of 1,2-diaminobenzene with α-keto acids to give 3-alkyl-2-hydroxyquinoxaline (1). Later on, Morrison used this reaction as a basis for the quantitative analysis of α-keto acids from biological materials (2). The analytical advantages of this reaction reside in its rapidity and in the fact that it can be done directly in aqueous media, where under acidic conditions it yields thermally and hydrolytically stable derivatives that can readily be extracted by organic solvents.

Furthermore, the reaction is selective to α-keto acids since the formation of a six-membered ring stabilizes the derivatives, whereas other keto-containing groups form imines, which are hydrolyzed under the reaction conditions. For gas chromatographic analysis the derivatives are further converted to the trimethylsilyl ethers. This approach has been used extensively and several substituted 1,2-diaminobenzenes have been studied in order to increase the selectivity of the analysis and achieve better limits of detection (3).

In a report on the gas chromatographic analysis of quinoxalinol derivatives, Hoffman and Killinger (4) have indicated that the condensation products of the reaction of α-keto acids with 1,2-diaminobenzene existed entirely in the keto form, and not in the hydroxyquinoxaline as had been proposed previously (1, 2). They mentioned having obtained evidence from nmr and ir data that the condensation products are amides and that further silylation occurs on the nitrogen atom. Later reports by Frigerio *et al.* (5) and Langenbeck *et al.* (6) using FT-IR and mass spectrometry seem to indicate that silylation of the "quinoxalinol" derivatives takes place at the oxygen. Langenbeck suggested that an enol–keto equilibrium in solution could account for the results.

In order to eliminate the additional step of silylation necessary for the gas chromatographic analysis of the derivatives, Hayashi *et al.* (7) have used the 2,3-diaminonaphthalene derivative and hplc to analyse phenylpyruvic acid. They give the phenolic form as the reaction product but present no evidence for it. The condensation reaction of 2,3-diaminonaphthalene with pyruvic acid has also been reported by Goldstein and Streuil (8). They refer to the reaction product as 3-methyl-2-oxo-benzoquinoxaline, but do not present any structural evidence.

The use of 2,3-diaminonaphthalene to form derivatives with keto acids presents favorable conditions for their selective analysis by hplc, since the derivatives formed possess high absorbance and fluorescence properties. In seeking to use this reaction for the analysis of keto acids, we have prepared 18 derivatives (9) and have proceeded to characterize the reaction products in order to optimize the analytical method. Because some confusion remains regarding the structure of the condensation products of the reaction of 2,3-diaminonaphthalene with α-keto acids, we report here on the crystalline structure of the condensation product of 2,3-diaminonaphthalene with pyruvic acid.

Experimental

The condensation product $C_{13}H_{10}N_2O$ was prepared by reaction of pyruvic acid (Sigma Chemicals, USA) with 2,3-diaminonaphthalene hydrochloride (Aldrich Chemicals, USA) in a 2.5 *N* hydrochloric acid solution according to an existing procedure (8). The compound was isolated from the reaction media and crystals were obtained by slow vacuum sublimation. The yellow solid decomposes at 290 ± 1°C, which is in accordance with published data (8).

The mass spectrum of the compound was obtained on a Kratos MS-50 TA mass spectrometer using 70-eV electrons and a source temperature of 200°C. The molecular ion is the base peak of the spectrum and the measured monoisotopic mass at high resolution (ca. 12 000) was 210.0794, which is in accordance with the formula $C_{13}H_{10}N_2O$ (calcd. 210.0792).

FT-IR spectra were recorded on a Digilab FTS-15/C Fourier Transform Michelson interferometer, equipped with a high sensitivity

[1]Author to whom correspondence may be addressed.

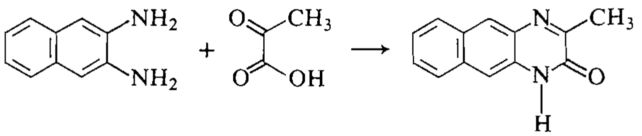

SCHEME 1

HgCdTe detector and a KBr beam splitter. The compound was introduced as KCl pellets and the resulting spectra were obtained after 1000 accumulations and subtraction of the reference material.

For the X-ray analysis, the very long flat crystalline filaments, up to 2 cm in length, were cut to an appropriate size for single crystal diffractometry. The orientation of the crystal and its unit-cell dimensions were obtained by a least-squares fit to the angular settings of 25 well-centered reflections on a Nonius CAD-4 automatic diffractometer. The crystals are monoclinic, with a unit cell of dimensions $a = 19.834(8)$, $b = 4.636(6)$, $c = 22.360(2)$ Å, $\beta = 96.30(9)°$, $V = 2043.6$ Å^3. The systematic absences of the type hkl, $h+k \neq 2n$ and $h0l$, $l \neq 2n$, are compatible with both the $C2/c$ and the Cc space groups. However, since the agreement between observed ($d_0 = 1.358$ g cm^{-3}) and calculated densities ($d_c = 1.366$ g cm^{-3}) occurs for $Z = 8$ molecules per unit cell, the most likely space group is $C2/c$. Integrated intensities were collected using Cu$K\bar{\alpha}$ ($\lambda = 1.54178$ Å) graphite-monochromatized radiation for all reflections within the hkl and $hk\bar{l}$ octants of the Ewald sphere limited by $2\theta \leq 130°$. Since the cut fragment was of dimensions 0.01 × 0.10 × 0.55 mm, the FLAT option which minimizes the absorption effects was used during the data collection. The $\omega/2\theta$ scan mode was used with a scan range defined by $\Delta\omega = (1.00 + 0.14 \tan\theta)°$. The orientation of the crystal and the intensities of three reference reflections were monitored every 100 reflections and every hour respectively. The intensity fluctuations were no higher than 2% over the duration of the measurements. The 781 reflections satisfying the criterion $I/\sigma(I) \geq 1.90$ were considered observed.

The X-ray scattering curves for C, N, and O were taken from Cromer and Mann (10) and from Stewart, Davidson and Simpson (11) for H atoms. The structure was solved by direct methods in the $C2/c$ space group using the MULTAN[2] program with all E's ≥ 1.50. The atomic coordinates and individual anisotropic temperature factors for O, N, and C atoms were refined by the block-diagonal approximation. The H atoms were found on a difference Fourier synthesis. Because of the small number of observations, the atomic coordinates and the isotropic temperature of only H(1) were refined. All the other H atoms were kept at a fixed position, 0.95 Å from their respective C atoms, and given an isotropic temperature factor B of 6.0 Å^2. At the end of the refinement, when the average (shift to σ ratio) was 0.07, $R = \Sigma\|F_o| - |F_c\|/\Sigma|F_o| = 0.050$ and $wR = [\Sigma w\Delta F^2/\Sigma wF_0^2]^{\frac{1}{2}} = 0.056$, while the goodness-of-fit, $S = [\Sigma w\Delta F^2/(m-n)]^{\frac{1}{2}} = 1.67$. The weighting scheme chosen was based on the counting statistics. The extreme fluctuations of the electron density on the final difference Fourier map were ± 0.10 e Å^{-3}.

Results and discussion

The final atomic coordinates and their standard deviations for 3-methyl-2-oxo-benzo(g)quinoxalinone are given in Table 1,[3] while the molecular structure is represented by the pair of stereoscopic drawings in Fig. 1. The molecule, which consists of a three-ring system, is best described as a naphthalene β-substituted by two amino groups taking part in a six-membered heterocycle. To that ring are attached, next to each nitrogen, a ketone and a methyl group, respectively.

TABLE 1. Fractional atomic coordinates (×10^4 for O, N, and C; ×10^3 for H atoms), U_{eq} (×10^3 for O, N, and C), and U_{iso} (× 10^3 for H atoms) for 3-methyl-2-oxo-benzo(g)quinoxalinone

Atom	x	y	z	U_{eq}/U_{iso}
O(2)	8235(1)	−3014(6)	546(1)	50
N(1)	7386(2)	240(7)	564(1)	40
N(4)	7946(2)	2016(7)	1697(1)	40
C(2)	7958(2)	−1040(9)	802(2)	37
C(3)	8240(2)	49(9)	1409(2)	39
C(5)	7341(2)	3198(9)	1439(2)	35
C(6)	7016(2)	5220(9)	1755(2)	39
C(7)	6408(2)	6456(9)	1514(2)	36
C(8)	6049(2)	8496(10)	1839(2)	47
C(9)	5459(2)	9689(11)	1596(2)	58
C(10)	5184(2)	8976(10)	1007(2)	57
C(11)	5516(2)	7035(10)	676(2)	52
C(12)	6128(2)	5697(9)	918(2)	38
C(13)	6462(2)	3627(9)	599(2)	40
C(14)	7043(2)	2373(8)	854(2)	35
C(15)	8891(2)	−1256(11)	1668(2)	57
H(1)	720(2)	−55(8)	20(2)	84
H(6)	721	578	214	76
H(8)	623	903	224	76
H(9)	523	1102	183	76
H(10)	477	983	84	76
H(11)	533	658	28	76
H(13)	628	310	20	76
H(151)	901	−54	206	76
H(152)	924	−77	143	76
H(153)	884	−329	168	76

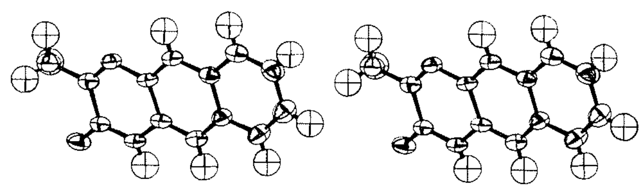

FIG. 1. Stereoscopic pair of 3-methyl-2-oxo-benzo(g)quinoxalinone.

Molecular conformation

The interatomic distances and angles are indicated on the schematic diagrams of the molecule shown in Fig. 2. In the naphthalene part of the molecule, the bond distances are alternately short and long, with values varying between 1.352(6) and 1.433(6) Å. Such an occurrence is not unusual. Indeed, it is strikingly similar to the one observed for anthracene and anthracene-like complexes with tetracyanobenzene or picric acid. The bond distances and angles from six such compounds (refs. 16−20) have been averaged and are compared in Fig. 2 to the corresponding values as found in $C_{13}H_{10}N_2O$. There are no significant differences between the two sets of bond distances and angles except for the C(13)—C(14) distance ($\Delta d = 6\sigma$) and the C(13)—C(14)—C(5) angle ($\Delta\alpha = 6\sigma$). These differences arise because of the stress imposed by N(1) being out of the molecular plane.

In the heterocycle part of the molecule, the conjugated double bonds C(2)—O(2) and C(3)—N(4), together with the

[2] The programs used here are modified versions of NRC-2, data reduction; NRC-10, bond distances and angles; NRC-22, mean planes; FORDAP, Fourier and Patterson maps (A. Zalkin); MULTAN, multisolution program; NUCLS, least-squares refinement; and ORTEP, stereodrawings (12−15).

[3] The structure factor table and the list of anisotropic temperature factors may be purchased from the Depository of Unpublished Data, CISTI, National Research Council of Canada, Ottawa, K1A 0S2.

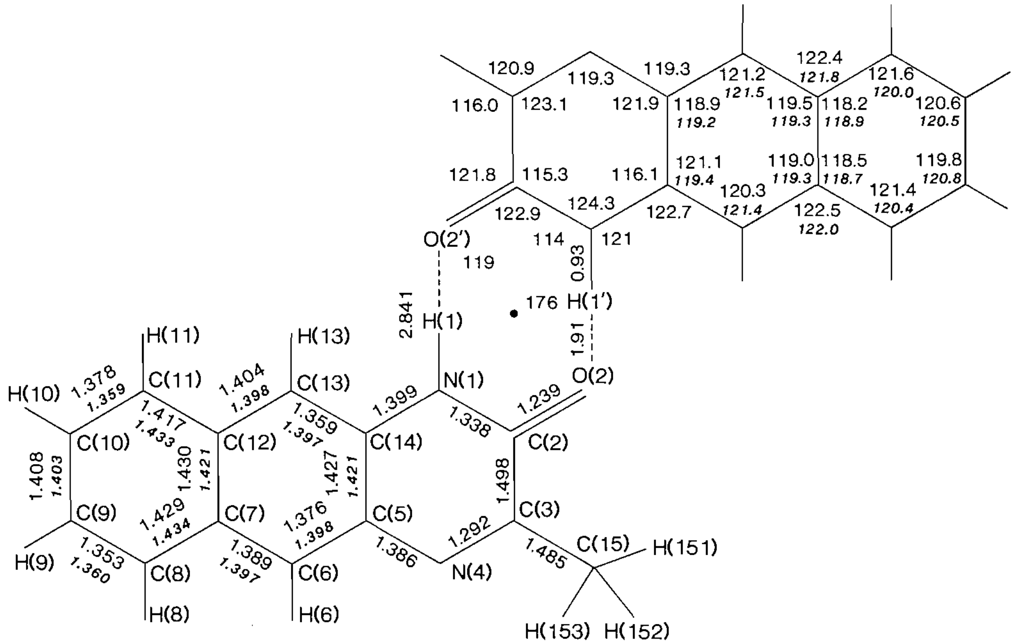

FIG. 2. Intramolecular dimensions of $C_{13}H_{10}N_2O$. The upper values are for $C_{13}H_{10}N_2O$, the values in italics refer to the corresponding distances and angles averaged from anthracene and anthracene complexes. The hydrogen bonding geometry is also included. Bond distances (Å); e.s.d. range 0.005–0.006 Å. Bond angles (°); e.s.d. range 0.3–0.4°.

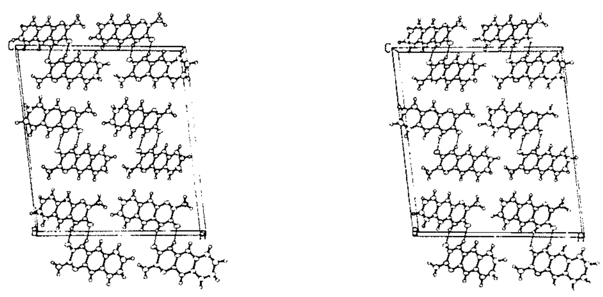

FIG. 3. Stereoscopic view of the packing of the molecules.

aromatic C(5)—C(14) bond, tend to flatten the heterocycle. Indeed, the sum of the angles in this cycle is 720.1° although there are some large deviations from 120°, especially at N(1), C(2), and C(3). The only group of atoms which is really coplanar is that constituted of C(7)−C(12), the ring farthest from the amino group. The deviations of these atoms from their mean plane ($\chi^2 = 8.9$) are of the order of 1σ. However, when the ten atoms C(5)−C(14) are included in the calculation, the deviations are more noticeable, from 5 to 10 σ. The highest deviation is noted at C(14). Of the heterocycle, C(2) and N(1) are the farthest from the above plane, at −0.101(3) and −0.133(4) Å, respectively.

Molecular packing and hydrogen bonding

H(1) is bonded to the N(1) atom at 0.94(1) Å, thus cancelling the hypothesis of enolization of the ketone at C(2). Two centrosymmetrically related molecules form a dimer through two hydrogen bonds of the type N(1)—H(1)...O(2*) where the N(1)...O(2*) distance is 2.841(5) Å. A similar situation was observed in 5-chloro-2-pyridone (21) and in 2-pyridone (22), where the N...O* distances observed in the dimers are slightly shorter, 2.796 and 2.77 Å, respectively. The characteristic geometry of the H-bonding scheme is shown schematically in Fig. 2.

The nearly planar dimers are packed in the unit cell in a herringbone manner. This arrangement is shown by the stereopair of Fig. 3.

FT-IR spectra

In order to compare these results with those that have been published in the literature on similar systems (5, 6), we have taken the FT-IR of this compound and of its deuterated analogue. The ir data are presented in Fig. 4 and are consistent with the diffraction data. The spectrum clearly indicates the presence of the carbonyl group at 1667 cm^{-1}, with additional bands at 3311, 1525, and 887 cm^{-1} that can tentatively be assigned to the NH stretching and bending modes. The 3311 band is accompanied by a series of bands in between 3233 and 3110 cm^{-1}, which can be associated with the N—H...O hydrogen bond.

The spectrum of the deuterated molecule shows that deuteration (D/H = 60:40 as measured by ms) has an effect on all the bands that are assigned to the NH group (3311, 1525, 887, and 3233−3110 cm^{-1}), thus confirming the presence of the amide form in the solid. Furthermore, in the spectrum of the partially deuterated compound, the intensity of the carbonyl band at 1667 cm^{-1} is seen to decrease by more than half and is shifted to 1652 cm^{-1}, as would be predicted by the presence of hydrogen bonding (C═O...D). A systematic study of the ir spectra of these compounds is presently being conducted on several derivatives, varying the R groups in order to confirm band assignment and the structure of the compounds in solution.

Conclusion

The results presented in this work demonstrate that the solid form of the condensation product of the reaction of 2,3-diaminonaphthalene with pyruvic acid exists predominantly in the keto form. The data obtained by both methods of analysis confirm this structure. In the X-ray analysis the compound is

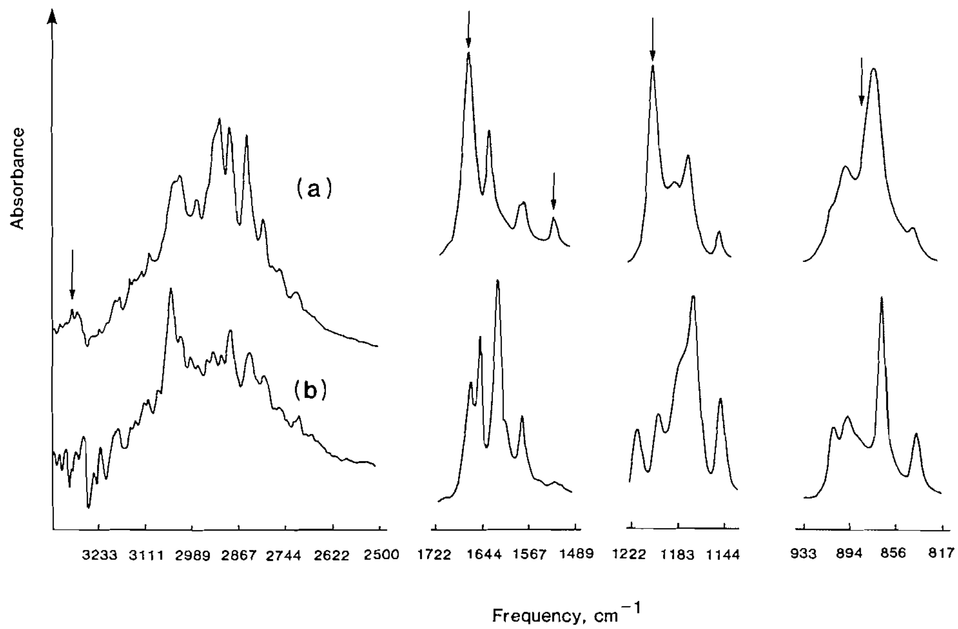

FIG. 4. FT-IR spectra of (a) 3-methyl-2-oxo-benzo(*g*)quinoxalinone; (b) D_2O exchanged as above.

found to exist solely in the amide form, the hydrogen atoms being very close to the nitrogen atoms (0.94 Å). No evidence is found for the presence of the tautomeric hydroxy form. In a similar fashion, data from the infrared analysis show the presence of the carbonyl group and also the band that can be associated to the amine at 3311, 1525, and 887 cm^{-1}. Those bands are affected by deuteration and the carbonyl band is seen as a doublet in the spectra of the partially deuterated compound, which is an indication of hydrogen bonding in the partially deuterated sample. Close examination of the ir spectra of the compound and its deuterated analogue shows a small signal at 1199 cm^{-1} that is affected by deuteration and that could possibly be related to the presence of a small amount of C—O—H. A further study on the ir spectra of several derivatives with varying R groups in the solid state and in solution is being conducted, to study the possible existence of the hydroxy compound for which there is still no evidence published.

Acknowledgements

The authors wish to thank the Fonds de Développement de la Recherche de l'Université de Montréal, and also the Fonds FCAC and NSERC for their financial support.

1. O. HINSBERG. Ann. Chim. **292**, 249 (1896).
2. D. C. MORRISON. J. Am. Chem. Soc. **769**, 4483 (1954).
3. C. F. POOLE and A. ZLATKIS. J. Chromatogr. **184**, 99 (1980).
4. N. E. HOFFMAN and T. A. KILLINGER. Anal. Chem. **41**, 162 (1969).
5. A. FRIGERIO, P. MARTELLI, and K. M. BARBER. J. Chromatogr. **81**, 141 (1973).
6. U. LANGENBECK, H. O. MOHRING, B. HINNEY, and M. SPETELLER. Biomed. Mass Spectrom. **4**, 197 (1977).
7. T. HAYASHI, T. SUGIURA, H. TERADA, S. KAWAI, and T. OHNO. J. Chromatogr. **118**, 403 (1976).
8. H. GOLDSTEIN and M. STREULI. Helv. Chim. Acta, **20**, 650 (1937).
9. M. J. BERTRAND, L. MALTAIS, and T. THEOPHANIDES. Can. J. Chem. To be published.
10. D. T. CROMER and J. B. MANN. Acta Crystallogr. Sect. A, **24**, 321 (1968).
11. R. F. STEWART, E. R. DAVIDSON, and W. T. SIMPSON. J. Chem. Phys. **42**, 3175 (1965).
12. F. R. Ahmed, S. R. Hall, M. E. Pippy, and C. P. HUBER. J. Appl. Crystallogr. **6**, 309 (1973). Accession Nos. 133–147.
13. P. MAIN, S. E. HULL, L. LESSINGER, G. GERMAIN, J. DECLERQ, and M. M. WOOLFSON. MULTAN 78. *A system of computer programs for the automatic solution of crystal structures from X-ray diffraction data*. Univs. of York, England and Louvain, Belgium. 1978.
14. R. J. DOEDENS and J. A. IBERS. Inorg. Chem. **6**, 204 (1967).
15. C. K. JOHNSON. ORTEP. Report ORNL-3794. Oak Ridge National Laboratory, Tennessee. 1965.
16. R. MASON. Acta Crystallogr. **17**, 547 (1964).
17. H. TSUCHIYA, F. MARUMO, and Y. SAITO. Acta Crystallogr. Sect. B, **28**, 1935 (1972).
18. J. J. STEZOWSKI. J. Chem. Phys. **73**, 538 (1980).
19. F. H. HERBSTEIN and M. KAFTORY. Acta Crystallogr. Sect. B, **32**, 387 (1976).
20. B. E. ROBERTSON and J. J. STEZOWSKI. Acta Crystallogr. Sect. B, **34**, 3005 (1978).
21. A. KVICK and S. S. BOOLES. Acta Crystallogr. Sect. B, **38**, 3405 (1972).
22. B. R. PENFOLD. Acta Crystallogr. **6**, 591 (1953).

Étude comparative dans la série des dibenzamido-alcanes, composés modèles des poly(oligométhylènes téréphtalamides)

JOSÉE BRISSON ET FRANÇOIS BRISSE[1]

Département de chimie, Université de Montréal, C.P. 6210, Succ. A, Montréal (Qué.), Canada H3C 3V1

Reçu le 2 avril 1985

JOSÉE BRISSON et FRANÇOIS BRISSE. Can. J. Chem. **63**, 3390 (1985).

La série des dibenzamido-alcanes (nDBN) a été synthétisée pour n = 2–10 et caractérisée par diffraction de rayons X et par spectroscopies infrarouge et Raman. L'étude par diffraction des rayons X révèle que l'angle dièdre ϵ entre le cycle aromatique et le groupement amide varie peu, étant en moyenne de 28,3°. Par contre, l'angle de torsion τ entre le groupement amide et la chaîne aliphatique prend des valeurs près de 180° pour n = 4, 6, 8 et 10, et près de 98°, pour n = 2, 3, 5 et 7. Dans ces derniers cas, le plan de la chaîne aliphatique est perpendiculaire au groupement amide. L'étude des spectres ir et Raman a permis de constater que la position de la bande amide V dépend de l'angle τ et peut servir à établir si celui-ci est près de 180° ou non.

JOSÉE BRISSON and FRANÇOIS BRISSE. Can. J. Chem. **63**, 3390 (1985).

The dibenzamido alcanes, nDBN, for n = 2–10, have been synthesized and characterized by X-ray diffraction and infrared and Raman spectroscopy. From X-ray diffraction it was observed than the dihedral angle ϵ between the aromatic ring and the amido group averaged 28.3° and did not vary significantly with n. The torsion angle τ between the amide group and the aliphatic chain was found to be near 180° for n = 4, 6, 8, and 10. However, for n = 2, 3, 5, and 7, τ averaged 98°. In this last case the plane of the aliphatic chain is nearly perpendicular to the plane of the amide group. The study of ir and Raman spectra in relation to conformation revealed that the position of the amide V band depends on the value of the τ angle and could be used to infer if the latter is close to 180° or not.

Introduction

Dans le cadre d'une étude portant sur la corrélation entre structure et propriété, nous nous sommes intéressés aux poly(oligométhylènes téréphtalamides) ou Nylons nT. Comme la structure de ces polyamides n'est pas facile à obtenir en diffraction de rayons X, en raison du faible nombre de taches de diffraction enregistrées, on fait appel à l'étude de composés modèles pour établir les conformations préférentielles de ce type de composé ainsi que les paramètres géométriques des molécules (distances et angles) et leurs modes d'assemblage par ponts hydrogène. Les composés modèles doivent avoir un motif chimique très semblable à celui des polymères apparentés, aussi avons nous choisi d'étudier les dibenzamido-alcanes (nDBN), pour n variant de 2 à 10 atomes de carbone. La relation entre l'un des composés modèles et le polymère parent est représentée en schéma 1.

Des études structurales par diffraction de rayons X et par spectroscopies infrarouge et Raman ont été effectuées sur ces produits ainsi que sur les deux séries d'analogues deutériés, les nDBN-d_2 pour lesquels les protons sur l'azote sont remplacés par des deutériums, et les nDBN-d_{10} pour lesquels les protons des cycles aromatiques sont remplacés par des deutériums.

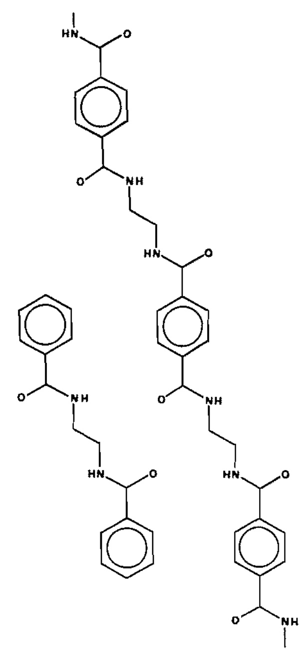

SCHÉMA 1

Partie expérimentale

Synthèse des dibenzamido-alcanes et de leurs analogues deutériés

La synthèse des dibenzamido-alcanes s'effectue par acylation de la diamine par le chlorure de benzoyle, tel que décrit par Palmer et Brisse (1). La préparation des nDBN-d_2 se fait par reflux, durant environ 6 h, des nDBN dans EtOD 95%. Les nDBN-d_{10} sont synthétisés à partir de C_6D_5COCl, de la même façon que les nDBN. Tous ont été synthétisés pour n = 2–10.

Les poly(oligométhylènes téréphtalamides) ont été synthétisés, pour n = 2–10, par polycondensation interfaciale selon la méthode de Shashoua et Eareckson (2), puis lavé avec NaOH 5%.

Les spectres infrarouges ont été enregistrés à partir de pastilles de KBr, avec un appareil IRTF Nicolet 7199 doté d'un laser HeNe de classe II. Les spectres Raman en phase solide ont été enregistrés sur un double spectromètre Spex 14018 doté d'un photomètre digital DPC-2 à partir de la raie à 514,5 nm d'un laser à argon ionisé Coherent Innova 90 série 112. Les fentes du monochromateur étaient à 100–200 μm^{-1}, ce qui correspond à une résolution de 2 cm^{-1}.

Les densités ont été mesurées par flottation dans une solution aqueuse de $ZnCl_2$. Les points de fusion ont été mesurés sur un appareil Mettler FP61 avec un taux de chauffe de 1 K min^{-1}.

Les détails des mesures de diffraction des rayons X sont rapportés dans les sections spécifiques à chacun des composés (1, 3–8).

Discussion

Les propriétés physiques des nDBN ayant un nombre pair de groupes méthyléniques sont semblables; les densités et les

[1] Auteur à qui adresser la correspondance.

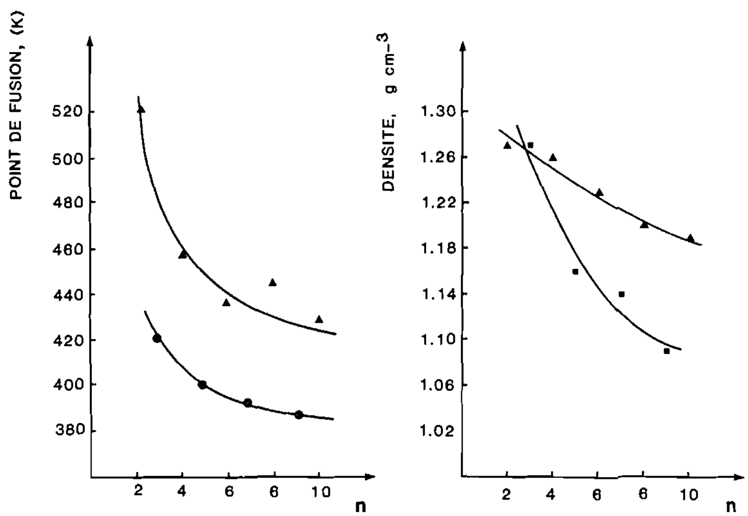

FIG. 1. Variation des points de fusion et des densités en fonction de la longueur de la chaîne.

points de fusion diminuent régulièrement lorsque le nombre d'atomes de carbone augmente en raison de la diminution relative du volume du groupement amide par rapport au restant de la molécule (fig. 1). Ces composés ont également des solubilités voisines, et l'obtention de monocristaux dans l'éthanol est rapide.

Cependant, lorsque le nombre d'unités méthyléniques de la chaîne est impair, on remarque une diminution significative des densités et des points de fusion, ce qui indique une cohésion moléculaire moins grande. Les solubilitiés sont plus élevées, et il devient plus difficile d'obtenir des monocristaux.

Les dimensions des mailles et d'autres données cristallographiques des nDBN sont présentées au tableau 1. Alors que les dimensions a et b et l'angle β varient très peu, on remarque (fig. 2) une augmentation régulière de la dimension c de la maille en fonction du nombre d'atomes de carbone de la chaîne aliphatique, pour n = 4, 6, 8 et 10. On peut exprimer cette variation linéaire des paramètres a, b et c (ângström) et du volume (ângström cube) de la maille des nDBN pairs en fonction de n par les relations:

$$a = 4{,}45 \times 10^{-3}\, n + 5{,}095$$

$$b = 8{,}70 \times 10^{-3}\, n + 5{,}291$$

$$c = 1{,}5964\, n + 21{,}976$$

$$V = 47{,}06\, n + 580{,}54$$

Il est probable qu'il en sera de même pour les autres composés pairs de cette série. Cependant, le 2DBN ne fait pas partie de cette série, et il n'existe pas de relation semblable pour les composés ayant un nombre impair de CH_2.

Les dimensions des mailles des produits deutériés ont été mesurées pour les 2DBN-d_{10}, 6DBN-d_{10}, 10DBN-d_{10}, 6DBN-d_2 et 8DBN-d_2. Les dimensions des mailles cristallines des produits deutériés sont très semblables à celles de leurs homologues non deutériés (tableau 2). Les changements sont surtout notables sur la dimension c et le volume de la maille. Toutefois, on observe que, systématiquement, les nDBN-d_{10} ont des volumes légèrement inférieurs à ceux de leurs homologues non deutériés, alors que c'est l'inverse pour les nDBN-d_2.

Les structures des dibenzamido-alcanes ont été déterminées

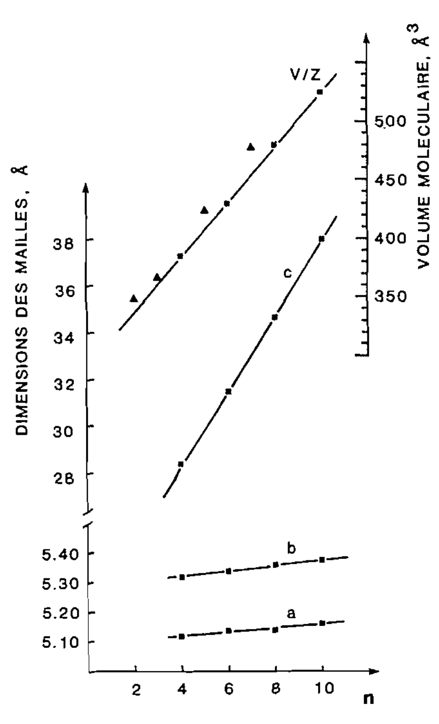

FIG. 2. Variation des paramètres de maille en fonction du nombre de méthylènes, pour n = 4, 6, 8 et 10.

pour n = 2 (1), 3 (6), 4 (4), 5 (6), 6 (5), 7 (3), 8 (7) et 10 (8). Les conformations des molécules de nDBN sont comparées à la figure 3. La structure du 5DBN présentait, à température de la pièce, un désordre évident au niveau de la chaîne aliphatique. Pour essayer d'atténuer ce désordre, nous avons effectué une seconde collection de données à T = 173 K. Effectivement, à cette température, il n'y avait plus de désordre et les distances et facteurs de température étaient alors comparables à ceux des autres dibenzamido-alcanes connus.

Distances et angles

Les distances et angles moyens des dibenzamido-alcanes sont rapportés au tableau 3, excepté pour le 10DBN, car les très faibles dimensions du cristal n'on pas permis un affinement très poussé de la structure. Les distances et angles moyens sont

TABLEAU 1. Données cristallographiques des dibenzamido-alcanes

Paramètre	2DBN	3DBN	4DBN	5DBN	6DBN	7DBN	8DBN	9DBN	10DBN
Système cristallin	Orthorhombique	Monoclinique	Monoclinique	Orthorhombique	Monoclinique	Monoclinique	Monoclinique	Monoclinique	Monoclinique
Groupe spatial	*Pbca*	$P2_1/c$	$P2_1/c$	*Pbca*	$P2_1/c$	$P2_1/n$	$P2_1/c$	—	$P2_1/n$
Maille									
a (Å)	8,982(4)	5,105(5)	5,118(3)	9,554(10)	5,136(2)	5,087(3)	5,141(3)	5,2	5,164(2)
b (Å)	9,972(4)	17,347(3)	5,324(3)	9,790(4)	5,346(1)	44,172(14)	5,361(2)	49,1	5,377(2)
c (Å)	15,579(6)	16,536(2)	28,410(5)	36,174(19)	31,497(12)	8,496(5)	34,715(12)	7,8	37,98(2)
β (°)	90,	94,75(4)	97,05(5)	90,	92,81(3)	91,08(5)	90,57(4)	91,0	94,59(4)
V (Å^3)	1395,0	1460,6	768,3	3383,3	863,7	1908,7	956,7	1976,	1051,0
ρ_o (g cm^{-3})	1,27	1,27	1,26	1,16	1,23	1,14	1,20	1,09	1,19
Z	4	4	2	8	2	4	2	4	2
ρ_c (g cm^{-3})	1,278	1,284	1,280	1,188	1,247	1,177	1,248	1,23	1,202

comparables à 2 σ près, sauf pour les angles $C(sp^3)$—$C(sp^3)$—$C(sp^3)$ dont la moyenne est de 112,4(3)° pour les 4DBN, 6DBN et 8DBN. Pour les 3DBN, 5DBN et 7DBN, cette valeur augmente légèrement avec le nombre d'atomes de carbone en chaîne: elle passe de 112,9(3)° pour le 3DBN, à 113,5(2)° pour le 5DBN et 115,3(5)° pour le 7DBN. On ne remarque pas d'effet notable sur les moyennes des distances et des angles du 5DBN dont la structure a été mesurée à basse température.

Si l'on étudie de plus près les distances et angles du cycle aromatique des composés, on remarque que l'angle α situé sur le carbone porteur du groupement amide est systématiquement inférieur de 1 à 2° à la moyenne de 120° des angles intracycliques. Domenicano et Vaciago (9) ont attribué ceci à un effet de conjugaison entre le cycle aromatique et le substituant. Ces auteurs observaient également des valeurs supérieures à 120° pour les angles β adjacents à l'angle du carbone substitué, ce qui est aussi le cas pour tous les *n*DBN, sauf pour un des angles du 6DBN.

Conformation

On peut distinguer trois éléments importants de la conformation des dibenzamido-alcanes: (*i*) l'angle dièdre ε entre les plans du cycle aromatique et du groupement amide; (*ii*) l'angle de torsion τ qui désigne l'angle entre le groupement amide et la chaîne aliphatique; (*iii*) la conformation de la chaîne aliphatique.

On remarque, pour tous les *n*DBN, une constance au niveau de la valeur de l'angle ε (fig. 4*a*). Celui-ci est de 28,3°, en moyenne, avec des valeurs extrêmes de 19,0 (2DBN) et 34,1° (3DBN). Ces valeurs concordent bien avec celles obtenues par analyse conformationnelle des benzamides par Laupètre et Monnerie (10). Ces auteurs notaient un minimum d'énergie conformationnelle pour $\epsilon = 30°$, avec une barrière d'énergie de rotation peu élevée entre 0 et 30°. La valeur de l'angle ε ne dépend pas de la longueur de la chaîne aliphatique.

Pour ce qui est de l'angle τ (fig. 4*b*), on remarque une beaucoup plus grande dispersion des résultats avec, cependant, certaines constances. Pour les *n*DBN pairs, la valeur de cet angle se situe aux alentours de 180°, sauf dans le cas du 2DBN pour lequel cet angle est de 91,5°. Dans le cas des *n*DBN impairs, on n'observe pas d'angle τ près de 180°. La valeur de cet angle se rapproche plutôt de celle observée pour le 2DBN, la moyenne de $|\tau|$ étant de 98°. Ceci, ainsi que le mode d'empilement moléculaire, nous fait inclure le 2DBN dans le groupe des *n*DBN impairs au point de vue structural.

Trois autres composés, les *N,N'*-dibenzoyl-*para*-phénylènediamine (11), *N,N'*-diéthyladipamide (12) et *N,N'*-bis(β-chloro-éthyl)pimélamide (13), présentent des angles de torsion τ différents de 180°, soient −56,3, −124 et 162°, respectivement.

La conformation de la chaîne aliphatique des *n*DBN, pour n = 4, 6, 8 et 10, est entièrement *trans* coplanaire. C'est le cas aussi du 2DBN et du 7DBN. Par ailleurs, dans les cas du 3DBN et du 5DBN, on note des conformations $a^-tg^+a^+$ et $g^+g^+tg^+ta^+$ ($t \simeq 180°$; $g \simeq 60°$; a est non *trans*, non *gauche*), soit une alternance d'angles *gauche* et *trans* si l'on fait abstraction des premiers et derniers angles de ces séquences qui sont les angles τ.

Cohésion moléculaire et ponts hydrogène

Les molécules des dibenzamido-alcanes sont maintenues entre elles par ponts hydrogène. L'empilement moléculaire reflète les disparités entre *n*DBN pairs et impairs (fig. 5). Pour n = 4, 6, 8 et 10, chaque molécule est liée par ponts hydrogène

TABLEAU 2. Comparison des dimensions des mailles cristallines des *n*DBN deutériés

Composé	*a* (Å)	*b* (Å)	*c* (Å)	β (°)	*V* (Å^3)	$\Delta V/V$ (%)
2DBN	8,982(4)	9,972(4)	15,579(6)	90	1395,5	−0,17
2DBN-d_{10}	8,982(1)	9,976(2)	15,548(1)	90	1393,1	
6DBN	5,136(2)	5,346(1)	31,497(12)	92,81(3)	863,8	−0,08
6DBN-d_{10}	5,135(2)	5,349(2)	31,463(6)	93,01(2)	863,1	
10DBN	5,164(2)	5,377(1)	37,983(23)	94,59(4)	1051,0	−0,29
10DBN-d_{10}	5,148(3)	5,379(1)	37,945(16)	94,34(4)	1047,7	
6DBN	5,136(2)	5,346(1)	31,497(12)	92,81(3)	863,8	+0,07
6DBN-d_2	5,133(7)	5,346(2)	31,542(8)	92,91(2)	864,4	
8DBN	5,141(3)	5,361(2)	34,715(12)	90,57(4)	956,7	+0,14
8DBN-d_2	5,143(4)	5,364(2)	34,734(14)	90,50(2)	958,0	

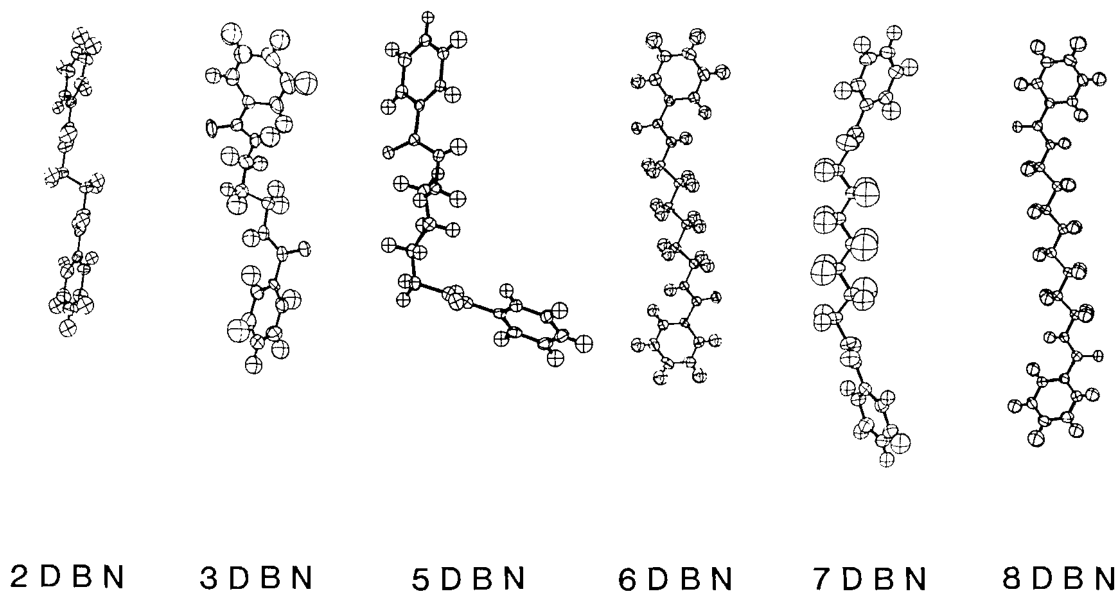

FIG. 3. Diverses conformations adoptées par les molécules de *n*DBN selon *n*.

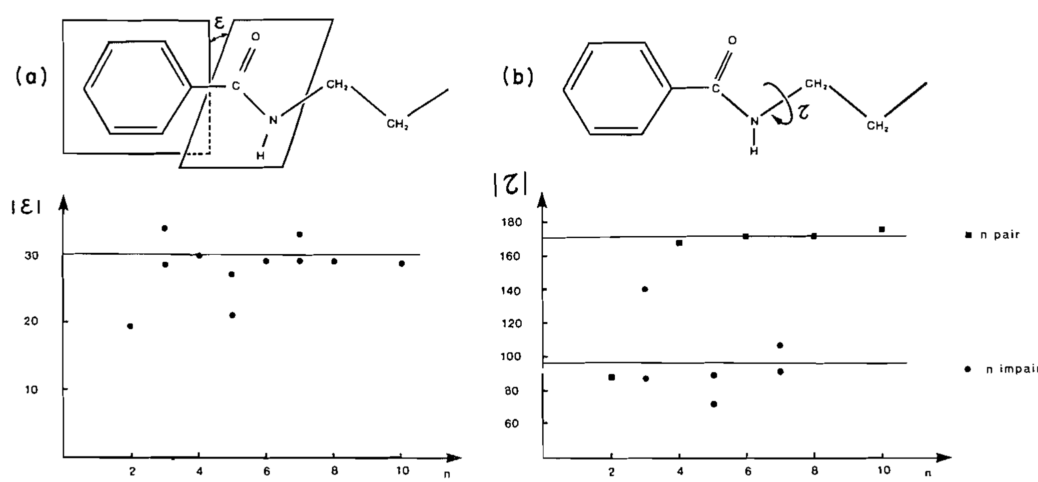

FIG. 4.(a) Variation de l'angle ϵ en fonction du nombre de méthylènes. (b) Variation de l'angle τ en fonction du nombre de méthylènes.

à deux autres, formant ainsi de longs rubans. Ces derniers sont imbriqués les uns vis-à-vis des autres par un assemblage en arête de poisson. Malgré des différences de conformation, le 3DBN adopte aussi le même arrangement. Bien que le 7DBN présente un empilement moléculaire différent, chaque molécule est liée à deux voisines par ponts hydrogène, formant aussi de longs rubans, tel que l'on peut le voir sur la figure 5.

Alors que dans les cas précédents chaque molécule était reliée à deux voisines par ponts hydrogène, dans le cas du 2DBN et du 5DBN, chaque molécule est maintenant reliée à

TABLEAU 3. Distances et angles moyens des *n*DBN et période de fibre théorique pour les polymères parents pairs

	2DBN	3DBN	4DBN	5DBN	6DBN	7DBN	8DBN
$C(sp^2)—C(sp^2)$	1,378(6)	1,378(4)	1,378(4)	1,388(3)	1,384(2)	1,382(5)	1,385(3)
$C(sp^2)—O$	1,235(6)	1,247(3)	1,238(4)	1,241(2)	1,235(2)	1,236(4)	1,239(3)
$C(sp^2)—N$	1,343(6)	1,334(3)	1,334(2)	1,333(3)	1,336(2)	1,332(4)	1,334(3)
$C(sp^3)—N$	1,445(6)	1,447(4)	1,459(3)	1,459(3)	1,457(2)	1,454(5)	1,461(4)
$C(sp^2)—C(sp^3)$	1,490(6)	1,488(4)	1,497(3)	1,498(3)	1,496(2)	1,491(5)	1,499(4)
$C(sp^3)—C(sp^3)$	1,522(6)	1,512(4)	1,513(3)	1,524(3)	1,515(2)	1,490(5)	1,522(3)
$C(sp^2)—C(sp^2)—C(sp^2)$	120,0(4)	120,0(3)	120,0(2)	120,0(2)	120,0(2)	120,0(5)	120,0(3)
α*	117,7(4)	118,4(3)	118,8(2)	119,0(2)	119,2(2)	118,6(3)	118,8(3)
β*	121,1(4)	120,7(3)	120,2(2)	120,4(2)	120,2(2)	120,8(3)	120,6(3)
$C(sp^3)—C(sp^3)—C(sp^3)$	—	112,9(3)	112,0(2)	113,5(2)	112,7(2)	115,3(5)	112,4(3)
Période de fibre théorique des polymères parents (Å)							
$\epsilon = 30°, \tau = 180°$	11,09	—	13,53	—	16,10	—	18,71
$\epsilon = 30°, \tau = 98°$	10,90	—	13,20	—	15,65	—	18,29

*α, angle intracyclique à l'atome porteur du groupement amide; β, moyenne des angles intracycliques adjacents à α.

TABLEAU 4. Géométrie des ponts hydrogène des dibenzamido-alcanes

Alcane	Distance (Å) N—H	H...O	N...O	Angles (°) N—H...O	N...O—C
3DBN					
N(1)—H(N1)...O(1)	0,80(3)	2,21(3)	3,003(3)	168(3)	125,5(2)
N(2)—H(N2)...O(2)	0,78(3)	2,22(3)	2,902(3)	147(3)	138,6(2)
5DBN					
N(1)—H(N1)...O(2)	0,80(2)	2,01(2)	2,790(2)	170(2)	151,2(1)
N(2)—H(N2)...O(2)	0,92(2)	1,92(2)	2,838(2)	170(2)	135,3(1)
7DBN					
N(1)—H(N1)...O(1)	0,91(2)	2,07(3)	2,890(3)	151(3)	151,0(8)
N(2)—H(N2)...O(2)	0,91(2)	2,03(3)	2,877(4)	153(3)	154,7(9)
2DBN					
N(1)—H(N1)...O(1)	0,89(3)	1,98(3)	2,854(4)	167(3)	156(1)
4DBN					
N(1)—H(N1)...O(1)	0,87(2)	2,13(2)	2,999(4)	165(2)	166(1)
6DBN					
N(1)—H(N1)...O(1)	0,91(2)	2,12(2)	3,012(3)	165(1)	165(1)
8DBN					
N(1)—H(N1)...O(1)	0,89(3)	2,14(3)	3,011(3)	166(2)	164(1)

quatre molécules différentes. Pour le 2DBN, ceci est dû à un glissement des molécules perpendiculairement à la direction de propagation des ponts hydrogène, et a pour effet de créer un réseau bidimensionnel de ponts hydrogène, les molécules réunies entre elles formant des feuillets. On retrouve un réseau de ponts hydrogène semblable pour le *N,N'*-bis(β-chloro-éthyl)-pimélamide (13). Le 5DBN ne peut être apparenté à aucune autre structure précédemment décrite dans cette série; celui-ci forme un réseau tridimensionnel de ponts hydrogène où le premier groupement amide de chaque molécule est perpendiculaire au second. Il s'ensuit que chaque molécule est reliée à quatre voisines selon deux directions différentes, perpendiculaires entre elles, et perpendiculaires à la direction d'élongation de la chaîne aliphatique. Si l'on compare la géométrie des ponts hydrogène des dibenzamido-alcanes (tableau 4), on remarque d'abord une déviation de la linéarité des ponts hydrogène des 2, 3, 5 et 7DBN par rapport aux 4, 6, 8 et 10DBN, car pour l'angle N...O—C, on observe une variation d'au moins 10° en passant d'un groupe à l'autre. Les distances O...N et H...O sont comparables, avec des valeurs particulièrement courtes pour le 5DBN. Même la structure mesurée à la température de la pièce donnait des distances N...O plus courtes que celles des autres *n*DBN. Leur raccourcissement n'est donc pas un effet attribuable à la température à laquelle la mesure a été prise.

Spectroscopies infrarouge et Raman

Depuis plusieurs années, on remarque la publication de nombreux articles où il est question de la détermination de la conformation de polymères à partir des spectres ir et Raman. Les Nylons aliphatiques (15–18) et, plus récemment, les poly(oligométhylènes téréphtalates) (19–21) ont ainsi été étudiés. Nous avons voulu étudier la possibilité d'appliquer l'étude des spectroscopies ir et Raman aux poly(oligométhylènes téréphtalamides). Afin d'établir une base solide pour l'étude des spectres des polymères, nous avons d'abord examiné les spectres ir et Raman des *n*DBN. Les spectres de leurs analogues N-deutériés (*n*DBN-d_2) et deutériés sur le cycle

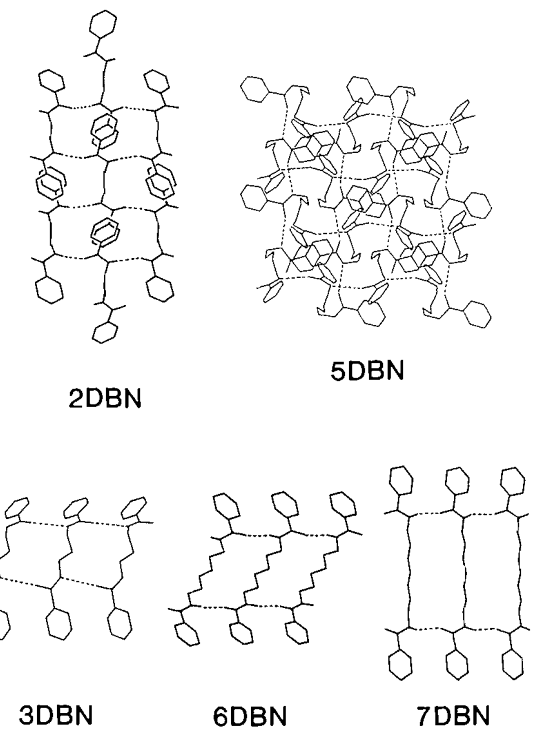

FIG. 5. Réseaux de ponts hydrogène des nDBN.

aromatique (nDBN-d_{10}) ont été utilisés pour l'attribution des bandes.[2] Les spectres ir des amides sont caractérisés par la présence de cinq bandes bien distinctes. Les bandes amide II, amide V, et la région de cisaillement des méthylènes seront surtout étudiées ici (fig. 6 et tableau 5).

(1) *Position de la bande amide II*

On observe une variation de la fréquence de la bande amide II: celle-ci passe de 1535 cm^{-1} approximativement, pour la plupart des composés, à 1562 cm^{-1} pour le 2DBN et 1553 cm^{-1} pour le 5DBN. On aurait pu attribuer cette variation aux différences de valeur de l'angle τ dans les deux formes, mais ce n'est pas le cas puisque le 3DBN et le 7DBN ne présentent pas un tel déplacement de la bande amide II. Comme ces deux composés présentent des ponts hydrogène avec quatre molécules voisines, on peut supposer que la fréquence de vibration est plus élevée, dans ce cas, en raison des contraintes accrues dans un tel réseau de ponts hydrogène.

(2) *Bande amide V*

Cette bande du spectre ir est la plus informative au point de vue conformationnel. Elle est en effet sensible à la valeur de l'angle τ. Sa valeur passe de 644–652 cm^{-1}, lorsque l'angle τ est près de 180°, à 664–673 cm^{-1}, lorsque celui-ci est différent de 180° (fig. 6 et tableau 5). Cette bande est due à la vibration de déformation hors plan δ(N—H). Lorsque l'angle τ est de 180°, la chaîne aliphatique se trouve dans le même plan que le groupement amide et la vibration hors plan peut s'effectuer sans interaction avec les méthylènes. Par ailleurs, lorsque l'angle τ est différent de 180°, les groupements méthylènes se retrouvent dans un plan perpendiculaire au groupement amide,

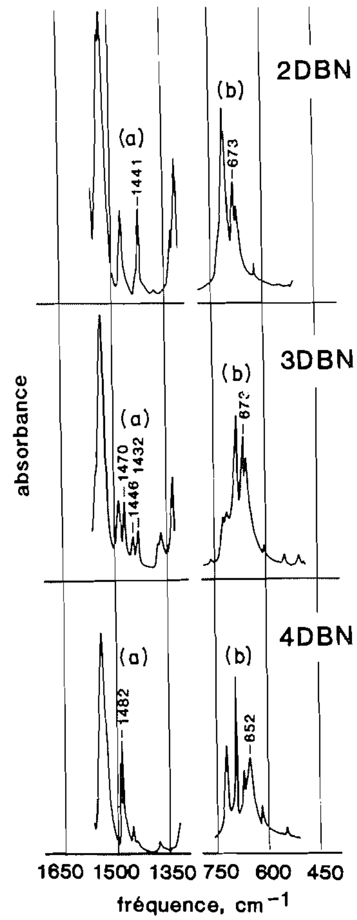

FIG. 6. Spectres infrarouges des 2DBN, 3DBN et 4DBN. (a) Région de cisaillement des méthylènes. (b) Région de la bande amide V, déformation hors plan δ(N—H).

et la vibration hors plan N—H peut être gênée par la présence des hydrogènes méthyléniques, ce qui se traduit par une augmentation de la fréquence de vibration δ(N—H).

(3) *Région de cisaillement des méthylènes*

Cette région qui s'étend de 1465 à 1431 cm^{-1} est particulièrement importante. En effet, on observe des bandes d'intensité moyenne entre 1465 et 1431 cm^{-1}, dans le cas des 2DBN, 3DBN, 5DBN et 7DBN en infrarouge, alors que celles-ci sont très faibles pour les 4DBN, 6DBN, 8DBN et 10DBN. Ces bandes sont attribuées à des vibrations de cisaillement des méthylènes. Dans les spectres Raman, par contre, les bandes entre 1465 et 1445 cm^{-1} sont d'intensité moyenne pour tous les dibenzamido-alcanes. Ceci nous mène à penser que la faible intensité de ces bandes en ir, pour les 4, 6, 8 et 10 DBN, serait due à la présence du centre de symétrie cristallographique au milieu du lien CH_2—CH_2 central de ces molécules. Les spectres du 2DBN révèlent que la bande à 1441 cm^{-1} est présente en ir, et absente en Raman. C'est l'inverse qui est observée pour les autres nDBN pairs. Ceci pourrait être dû au fait que, dans ce cas, le plan des méthylènes est perpendiculaire au plan des groupements amides. Cette vibration serait due au cisaillement des méthylènes adjacents à la fonction amide. L'intensité de ces bandes serait donc fonction de la symétrie de la chaîne et de son orientation par rapport au groupement amide.

(4) *Structure du dibenzamido-1,9 nonane (9DBN)*

Jusqu'ici, la structure du dibenzamido-1,9 nonane n'a pas pu

[2] On peut se procurer les tableaux des fréquences infrarouge et Raman des nDBN, nDBN-d_2 et nDBN-d_{10} en s'adressant au Dépôt des données non publiées, ICIST, Conseil national de recherches du Canada, Ottawa (Ont.), Canada K1A 0S2.

TABLEAU 5. Bandes caractéristiques des spectres

	4DBN		6DBN		8DBN		10DBN	
	Infrarouge	Raman	Infrarouge	Raman	Infrarouge	Raman	Infrarouge	Raman
Bande amide II	1535 TF	1540 f	1535 TF	1540 f	1530 TF	1530 tf	1534 TF	1540 tf
δ(C—H)	1482 m	1480 F	1478 m	1476 f	1476 m	1475 f	1476 m	—
Cisaillement	1456 tf	—	1461 f	1460 m	1452 f	1462 f	1465 tf	—
des méthylènes	1447 f	1447 m	1446 tf	1452 m	1447 f	1446 m	1455 tf	1445 m
			1441 tf	—	1436 f	1439 f		
Bande amide V	652 m	—	647 m	—	645 m	—	644 m	—

*TF: très forte; F: forte; m: moyenne; f: faible; tf: très faible; ep: épaulement.

être établie par diffraction de rayons X, car nous n'avons pas pu obtenir de monocristaux de taille adéquate. Cependant, nous avons pu déterminer les paramètres a, b et β de la maille par précession sur un cristal maclé. Ceci nous a permis d'indexer le diagramme de poudre du 9DBN. Les dimensions de la maille cristalline présentées au tableau 1 sont très comparables à celles du 7DBN.

L'étude des spectres ir et Raman nous permet d'affirmer que l'angle τ sera différent de 180° en raison de la position de la bande amide V qui se retrouve vers 668 cm^{-1}, comme dans le cas des 2DBN, 3DBN, 5DBN et 7DBN. On retrouve la bande amide II à 1538 cm^{-1}, comme dans le cas de la plupart des dibenzamido-alcanes, sauf du 2DBN et du 5DBN, ce qui nous fait supposer que les molécules devraient être assemblées entre elles par ponts hydrogène formant des rubans, et non par un réseau de ponts hydrogène bi- ou tri-dimensionnel. De même, les bandes à 1467 et 1431 cm^{-1} sont d'intensité moyenne en ir et en Raman, ce qui confirme la présence d'angles τ différents de 180°.

Le 9DBN aurait donc une structure comparable soit à celle du 3DBN soit à celle du 7DBN, dépendant de la conformation de la chaîne aliphatique qui n'est pas établie. On serait porté à décrire la structure du 9DBN de la même manière que celle du 7DBN, puisque leurs mailles cristallines ont de grandes analogies.

(5) *Spectroscopie des polymères*

(a) *Spectre infrarouge du Nylon 6*

Si l'on confronte les résultats obtenus par l'étude des spectres ir et Raman des dibenzamido-alcanes à ceux obtenus précédemment pour le Nylon 6 (15), on remarque une analogie évidente. Le Nylon 6 est polymorphique et l'on observe des fréquences différentes pour les bandes amide II et V des formes α et γ.

Arimoto (15) notait un déplacement de la bande amide II de 1545 pour le Nylon 6, forme α, à 1562 cm^{-1} pour le Nylon 6, forme γ. Le Nylon 6, forme α, est entièrement *trans* coplanaire, alors que dans le modèle proposé par Vogelsong (14) pour la forme γ du Nylon 6, on note un réseau de ponts hydrogène tridimensionnel, semblable à celui du 5DBN. Ceci viendrait appuyer la relation entre ce déplacement de fréquence et le type de réseau de ponts hydrogène.

D'autre part, on constate une augmentation de la fréquence de la bande amide V lorsque l'on passe de la forme α à la forme γ du Nylon 6; celle-ci varie de 692 à 708 cm^{-1} (15). Comme on observe une valeur de l'angle τ de $-93°$ (14) pour la forme γ du Nylon 6, on peut ici aussi attribuer ce déplacement à la valeur de l'angle τ, comme pour les dibenzamido-alcanes.

(b) *Structure du Nylon 6T*

La période de répétition du Nylon 6T est connue; elle est de 15,60 Å (22, 23). Si ce composé était entièrement *trans* coplanaire avec des angles ϵ de $\pm 30°$, on observerait une période de répétition de 16,10 Å. L'écart entre ces deux valeurs peut s'expliquer soit par la présence d'un angle de torsion *gauche* au sein de la chaîne aliphatique, soit par une valeur de l'angle τ de 99°. L'étude du spectre ir du Nylon 6T est en accord avec une valeur de l'angle τ différente de 180°, puisque l'on observe des bandes d'intensité moyenne entre 1450 et 1420 cm^{-1} et que la bande amide V se retrouve à une fréquence de 670 cm^{-1} comme pour les 2DBN, 3DBN, 5DBN et 7DBN.

Conclusion

L'analyse des dibenzamido-alcanes nous a permis d'établir: (*i*) que la valeur de l'angle ϵ entre le groupement aromatique et le groupement amide varie très peu et est en moyenne de 28,3°; (*ii*) que l'angle τ entre le groupement amide et la chaîne aliphatique peut varier et prend des valeurs proches de 180 ou 90°; (*iii*) que la conformation *trans* coplanaire et les conformations composées d'une alternance d'angles *gauche* et *trans* sont favorisées; (*iv*) qu'on peut, à l'aide de la spectroscopie ir, déterminer si l'angle τ est près de 180° ou non.

1. A. PALMER et F. BRISSE. Acta Crystallogr. Sect. B, **36**, 1447 (1980).
2. V. E. SHASHOUA et W. M. EARECKSON. J. Polym. Sci. **15**, 343 (1959).
3. J. BRISSON et F. BRISSE. Acta Crystallogr. Sect. B, **38**, 2663 (1982).
4. S. HARKEMA, G. J. VAN HUMMEL et R. J. GAYMANS. Acta Crystallogr. Sect. B, **36**, 3182 (1980).
5. C. PINEAULT et F. BRISSE. Acta Crystallogr. Sect. C, **39**, 1434 (1983).
6. J. BRISSON et F. BRISSE. Eur. Polym. J. Soumis.
7. C. PINEAULT et F. BRISSE. Acta Crystallogr. Sect. C, **39**, 1437 (1983).
8. C. PINEAULT. Mémoire de M.Sc., Université de Montréal. (1982).
9. A. DOMENICANO et A. VACIAGO. Acta Crystallogr. Sect. B, **31**, 221 (1965).
10. F. LAUPÈTRE et L. MONNERIE. Eur. Polym. J. **14**, 415 (1978).
11. A. FRATINI et D. R. WIFF. Acta Crystallogr. Sect. B, **34**, 954 (1978).
12. E. BENEDETTI, M. R. CIAJOLO et P. CORRADINI. Eur. Polym. J.

infrarouge et Raman des *n*DBN*

2DBN		3DBN		5DBN		7DBN		9DBN	
Infrarouge	Raman	Infrarouge	Raman	Infrarouge	Raman	Infrarouge	Raman	Infrarouge	Raman
1562 TF	1550 m	1536 TF	1536 m	1553 TF	1550 f	1534 TF	1535 f	1538 TF	1539 f
1441 m		1470 m	—	1476 m	—	1477 m	—	1480 m	
		1446 m	1449 m	1457 f	1460 m	1465 m	—	1467 m	1470 f
		1432 m	1435 m	1447 f	—	1453 tf	—	1458 f	—
				1433 f	1430 ep	1447 f	1443 f	1452 f	—
						1431 f	1437 f	1443 f	1442 m
								1431 f	1430 f
								1403 tf	
673 m	—	673 m	—	664 m	—	672 m	—	668 m	—

9, 101 (1973).
13. M. R. CIAJOLO, V. PAVONE et E. BENEDETTI. Acta Crystallogr. Sect. B, **33**, 1295 (1977).
14. D. C. VOGELSONG. J. Polym. Sci. Part A, **1**, 1055 (1963).
15. H. ARIMOTO. J. Polym. Sci. Part A, **2**, 2283 (1964).
16. I. SANDEMAN et A. KELLER. J. Polym. Sci. **XIX**, 401 (1956).
17. I. MATSUBARA et J. H. MAGILL. J. Polym. Sci. Polym. Phys. Ed. **11**, 1173 (1973).
18. B. SCHNEIDER, P. SCHMIDT et O. WICHTERLE. Collect. Czech. Chem. Commun. **27**, 1749 (1962).
19. I. M. WARD et M. A. WILDING. Polymer, **18**, 327 (1977).
20. J. L. KOENIG et S. B. LIN. J. Polym. Sci. Polym. Phys. Ed. **21**, 2067 (1983).
21. A. PALMER, S. POULIN-DANDURAND, J. F. REVOL et F. BRISSE. Eur. Polym. J. **20**, 783 (1984).
22. R. G. QUYNN. Text. Res. J. **40**, 677 (1970).
23. P. W. MORGAN et S. L. KWOLEK. Macromolecules, **8**, 104 (1975).

Adducts of diphenyllead diselenocyanate with some O- and N-donor ligands[1]

IVOR WHARF, RYSZARD WOJTOWSKI, AND MARIO ONYSZCHUK[2]
Department of Chemistry, McGill University, Montreal, P.Q., Canada H3A 2K6

Received March 22, 1985

IVOR WHARF, RYSZARD WOJTOWSKI, and MARIO ONYSZCHUK. Can. J. Chem. **63**, 3398 (1985).

The preparation and properties of $Ph_2Pb(SeCN)_2$ have been reinvestigated. Infrared spectra show that the solid is polymeric with stronger Pb—Se and weaker Pb—N bonds. In *N,N*-dimethylformamide (DMF) solution ν(CN) values are consistent with complete ionization to $NCSe^-$, but coordinated N- and Se-bound selenocyanate species are observed when DMF/CH_2Cl_2 mixtures are used as solvents. The first 1:2 adducts of $Ph_2Pb(SeCN)_2$ with hexamethylphosphoramide (HMPA), triphenylphosphine oxide (Ph_3PO), pyridine-*N*-oxide (pyO), 2,4,6-collidine-*N*-oxide (collO), and dimethyl sulphoxide (DMSO) have been prepared, while with 4-picoline-*N*-oxide (4-picO) a 1:4 adduct is obtained. Infrared data show $Ph_2Pb(SeCN)_2\cdot 2L$ (L = HMPA, Ph_3PO, collO) are in fact isoselenocyanates, but the pyO and DMSO adducts are selenocyanates. Amine adducts $Ph_2Pb(SeCN)_2\cdot 2L$ (L = morpholine (morph), quinoline (quin), piperidine (pipy)) and $Ph_2Pb(SeCN)_2\cdot 3LL$ (LL = α,α'-dipyridyl (dipy), 1,10-phenanthroline (phen)) have been prepared. Infrared data suggest that amine adducts most probably have *N*-bonded selenocyanate groups, in some cases with ionic selenocyanate also present. The adduct with 4-picO also contains ionic selenocyanate.

IVOR WHARF, RYSZARD WOJTOWSKI et MARIO ONYSZCHUK. Can. J. Chem. **63**, 3398 (1985).

On étudie de nouveau la préparation et les propriétés du $Ph_2Pb(SeCN)_2$. Les spectres infrarouges révèlent que le solide est un polymère ayant des liaisons Pb—Se plus fortes et des liaisons Pb—N plus faibles. En solution dans le *N,N*-diméthylformamide (DMF), les valeurs de ν(CN) sont en accord avec une ionisation complète donnant des ions $NCSe^-$; cependant, si on utilise des mélanges de DMF/CH_2Cl_2 comme solvants, on observe la présence d'espèces sélénocyanates N- et Se-coordonnées. On a préparé les premiers adduits-1:2 du $Ph_2Pb(SeCN)_2$ avec l'hexaméthylphosphoramide (HMPA), l'oxyde de triphénylphosphine (Ph_3PO), le *N*-oxyde de pyridine (pyO), le *N*-oxyde de collidine-2,4,6 (collO) et le diméthylsulfoxyde (DMSO) tandis qu'avec le *N*-oxyde de picoline-4 (picO-4) on obtient un adduit 1:4. Les spectres infrarouges révèlent que les complexes $Ph_2Pb(SeCN)_2\cdot 2L$ (L = HMPA, Ph_3PO, collO) sont en fait des isosélénocyanates alors que les adduits avec la pyO ou le DMSO sont des sélénocyanates. On a préparé les adduits aminés $Ph_2Pb(SeCN)_2\cdot 2L$ (L = morpholine (morph), quinoline (quin), pipéridine (pipy)) et $Ph_2Pb(SeCN)_2\cdot 3LL$ (LL = α,α'dipyridyle (dipy), phénantroline-1,10 (phen)). Les données infrarouges suggèrent que les adduits aminés sont probablement des groupes sélénocyanates liés par l'azote et que, dans certains cas, il y a aussi du sélénocyanate sous forme ionique. L'adduit avec le picO-4 contient également du sélénocyanate sous la forme ionique.

[Traduit par le journal]

Introduction

In a study of adducts formed by triphenyllead isothiocyanate and selenocyanate (1) significant changes in bonding were noticed on going from $Ph_3PbNCS\cdot L$ (all Pb—N bonded) to $Ph_3PbNCSe\cdot L$ (Pb—N or Pb—Se bonded) depending on L, with the latter systems showing linkage isomerism in solution. Therefore, we decided to study the adducts formed by diphenyllead diselenocyanate with a variety of O- and N-donor ligands for comparison with their thiocyanate analogues, $Ph_2Pb(NCS)_2\cdot 2L$, which were reported earlier (2). As before, NCSe group frequencies, particularly ν(CN) and ν(CSe), have been used to determine the selenocyanate bonding mode in these compounds.

Diphenyllead diselenocyanate was prepared earlier (3) using selenium selenocyanate and triphenyllead selenocyanate. We now report a more convenient preparation with higher yield from diphenyllead dichloride, together with a more detailed study of the selenocyanate.

Experimental

All experimental procedures were as described earlier (1, 2). Diphenyllead dichloride (Alfa) was used as received. All operations were carried out in the *absence of light*.

[1] Presented in part by I.W. at the Fourth International Conference on the Organometallic and Coordination Chemistry of Germanium, Tin and Lead, Montreal, Canada, Aug. 8–11, 1983, paper P-19.

[2] To whom correspondence should be addressed.

Preparations

Diphenyllead diselenocyanate

Diphenyllead dichloride (13.0 g) was stirred in methanol (1.0 L) at room temperature for 45 min. Potassium selenocyanate (13.0 g) was added to the well-stirred suspension and the mixture vigorously stirred for 2.5 h at room temperature. It was then poured into stirred ice-cold water (1.0 L). The resulting white solid was filtered, washed with water, and dried in a vacuum desiccator; yield, 97%, mp 179°C (dec.). *Anal.* calcd. for $(C_6H_5)_2Pb(SeCN)_2$: C 29.4, H 1.75, N 4.9; found: C 29.7, H 1.8, N 4.9.

Adducts of diphenyllead diselenocyanate

O-Donor adducts. Diphenyllead diselenocyanate (1.0 g) (**I**) was stirred at room temperature with a toluene solution containing a large excess of the ligand for 24–48 h. The white *adduct* obtained was filtered, washed with toluene, and dried in vacuum at room temperature.

Prepared in this manner from **I** were *$Ph_2Pb(SeCN)_2\cdot 2Ph_3PO$* using Ph_3PO (2.0 g) in toluene (20 mL); yield, 81%, mp 137°C. *Anal.* calcd. for $C_{50}H_{40}N_2O_2P_2PbSe_2$: C 53.2, H 3.6, N 2.5; found: C 53.1, H 3.6, N 2.35. Ir (Nujol mull): 1142 cm^{-1} (coordinated P═O); *$Ph_2Pb(SeCN)_2\cdot 2DMSO$* using DMSO (2.0 g) in toluene (10 mL); yield, 95%, mp 70°C (dec.). *Anal.* calcd. for $C_{18}H_{22}N_2O_2PbS_2Se_2$: C 29.7, H 3.0, N 3.85; found: C 29.8, H 2.9, N 3.8. Ir (Nujol mull): 950, 946 cm^{-1} (coordinated S═O); *$Ph_2Pb(SeCN)_2\cdot 2pyO$* using pyO (1.0 g) in toluene (50 mL); yield, 45%, mp 97°C. *Anal.* calcd. for $C_{24}H_{20}N_4O_2PbSe_2$: C 37.85, H 2.6, N 7.35; found: C 38.1, H 2.6, N 7.2. Ir (Nujol mull): 1206 cm^{-1} (coordinated N → O); *$Ph_2Pb(SeCN)_2\cdot 4(4\text{-}picO)$* using 4-picO (1.0 g) in toluene (100 mL); yield, 80%, mp 103°C. *Anal.* calcd. for $C_{38}H_{38}N_6O_4PbSe_2$: C 45.3, H 3.8, N 8.3%; found: C 45.1, H 3.8, N 8.1. Ir (Nujol mull): 1202 cm^{-1}

(coordinated N → O); *$Ph_2Pb(SeCN)_2 \cdot 2collO$* using collO (3.0 g) in toluene (10 mL); yield, 78%, mp 111°C. *Anal.* calcd. for $C_{30}H_{32}N_4O_2PbSe_2$: C 42.6, H 3.8, N 6.6; found: C 43.0, H 3.9, N 6.55. Ir (Nujol mull): 1199 cm^{-1} (coordinated N → O).

Diphenyllead diselenocyanate-hexamethylphosphoramide (1:2)

Pentane (50 mL) was added to a mixture of **I** (1.0 g) in HMPA (4.0 g) which had been stirred at room temperature for 24 h. Further stirring (2 h) gave the crystalline *adduct* which was filtered, washed with pentane, and dried as above; yield, 68%, mp 124°C. *Anal.* calcd. for $C_{26}H_{46}N_8O_2P_2PbSe_2$: C 33.6, H 5.0, N 12.05; found: C 33.8, H 5.1, N 12.0. Ir (Nujol mull): 1192 cm^{-1} (coordinated P=O).

N-Donor adducts. Diphenyllead diselenocyante (1.0 g) (**I**) was stirred at room temperature with a pentane, benzene, or anhydrous ether solution of a large excess of the ligand for 24–48 h. The white *adduct* (sometimes first formed as an oil) was filtered, washed with the reaction solvent, and dried in air or in vacuum at room temperature.

Prepared in this manner from **I** were *$Ph_2Pb(SeCN)_2 \cdot 2morph$* using morpholine (3.0 g) in anhydrous ether (40 mL); yield, 75%, dec. 77–83°C. *Anal.* calcd. for $C_{22}H_{28}N_4O_2PbSe_2$: C 35.4, H 3.8, N 7.5; found: C 34.9, H 3.8, N 7.2; *$Ph_2Pb(SeCN)_2 \cdot 2quin$* using quinuclidine (3.0 g) in pentane (20 mL); yield, 92%, mp 107°C. *Anal.* calcd. for $C_{28}H_{36}N_4PbSe_2$: C 42.4, H 4.6, N 7.05; found: C 42.1, H 4.5, N 7.0; *$Ph_2Pb(SeCN)_2 \cdot 3dipy$* using α,α′-dipyridyl (1.5 g) in pentane (15 mL); yield, 90%, dec. 113–123°C. *Anal.* calcd. for $C_{44}H_{34}N_8PbSe_2$: C 50.8, H 3.3, N 10.8; found: C 51.4, H 3.25, N 10.95; *$Ph_2Pb(SeCN)_2 \cdot 3phen$* using 1,10-phenanthroline (2.0 g) in benzene (20 mL); yield, 98%, mp 138°C (dec.). *Anal.* calcd. for $C_{50}H_{34}N_8PbSe_2$: C 53.95, H 3.1, N 10.1; found: C 53.2, H 3.45, N 10.1.

Diphenyllead diselenocyanate-piperidine (1:2)

A mixture of **I** (1.0 g) and piperidine (3.0 g) was stirred for 4 h at room temperature to form an oily solution. Adding pentane (15 mL) produced an oily mixture which with further stirring (24 h) gave the pale yellow *adduct*, which was isolated as above; yield, 98%, mp 36–39°C (dec.). *Anal.* calcd. for $C_{24}H_{32}N_4PbSe_2$: C 38.9, H 4.3, N 7.55; found: C 39.0, H 4.4, N 7.7.

Results and discussion

Properties

As reported earlier (3), $Ph_2Pb(SeCN)_2$ is a white powder insoluble in water and non-coordinating solvents, but soluble in strong donor organic solvents like dimethylformamide, dimethylsulphoxide, etc. However, we have found that it is light-sensitive, unlike $Ph_3PbSeCN$, turning pink on slight exposure and dark red on strong exposure to light. Presumably this reflects a stronger tendency to decompose with loss of selenium than found for $Ph_3PbSeCN$. Although apparently insoluble in weak donor solvents like acetone and tetrahydrofuran, $Ph_2Pb(SeCN)_2$ rapidly became pink when shaken with these solvents indicating sufficient solubility to promote decomposition, while $Ph_3PbSeCN$ also tends to decompose more easily in solution.

All adducts are white solids (except $Ph_2Pb(SeCN)_2 \cdot 2pipy$ which is pale yellow) with melting points (~100°C) often with decomposition, which are lower than those of their thiocyanate analogues (2). The same trend was noted earlier (1) when comparing corresponding data for $Ph_3PbX \cdot L$ (X = NCS or SeCN) pairs. All adducts decomposed when washed with organic solvents, e.g., benzene, acetone, etc., leaving behind insoluble $Ph_2Pb(SeCN)_2$, unlike those of $Ph_2Pb(NCS)_2$, including $Ph_2Pb(NCS)_2 \cdot 2HMPA$ which could be recrystallized from benzene. In this work $Ph_2Pb(NCSe)_2 \cdot 2HMPA$ could only be recrystallized by using a large excess of HMPA.

Attempts to isolate adducts of $Ph_2Pb(SeCN)_2$ with *N,N*-dimethylformamide (DMF), trimethylphosphate, triphenylphosphine sulphide, pyridine and picolines, pyrrolidine, and *N,N,N′,N′*-tetramethylethylene diamine were unsuccessful by the methods used here. Since DMF formed an adduct with $Ph_2Pb(NCS)_2$, this result could imply that the selenocyanate analogue is the weaker Lewis acid. However, when adduct formation requires the fission of chalcocyanate bridges before metal-ligand bonds can be formed, the range of adducts prepared may not reflect the relative strengths of similar Lewis acids, as was found earlier for the $Ph_3PbSeCN/Ph_3PbNCS$ pair.

Infrared spectra and selenocyanate bonding

When as in the present case substances cannot be obtained as single crystals because of the preparative methods used, or cannot be examined in solution due to their insolubility and/or decomposition, solid state infrared measurements remain as the only readily available method for studying the structures of these compounds.[3] All compounds showed the absorptions (1700–400 cm^{-1}) expected for the "Ph_2Pb" moiety as well as, for the adducts, ligand peaks, including those shifted by ligand coordination to the lead atom. In particular, ν(SO) values show the DMSO ligands are O-bonded in the adduct with this ligand, and there are no absorptions in the region for S-bonded DMSO (4). Of more significance are selenocyanate group frequencies ν(CN), ν(CSe), and ν(NCSe) as these indicate the mode of coordination. The vibrational criteria for determining NCSe bonding type used here were those proposed by Norbury (5) and have been listed elsewhere (1). Although δ(NCSe) values (or overtones) provide some useful information, in this work, we found definite identification of these weak to very weak absorptions, often overlapping with phenyl or ligand bands virtually impossible, and so only ν(CN) and ν(CSe) values have been reported in Table 1. Nearly all ν(CN) absorptions have weak shoulders 40–50 cm^{-1} to lower frequency, corresponding to the expected $\nu(^{13}CN)$ peaks.

(i) $Ph_2Pb(SeCN)_2$

Values of ν(CN) and especially ν(CSe) show $Ph_2Pb(SeCN)_2$ has bridging selenocyanate groups giving a polymeric structure similar to that proposed earlier for $Ph_2Pb(NCS)_2$ (2). The previous (3) assumption of lead–selenium bonding based on the ν(CN) value alone is inconsistent with the properties of $Ph_2Pb(SeCN)_2$, although Pb—Se bonds are probably stronger than Pb—N bonds in the suggested structure. In $Ph_2Pb(NCS)_2$ it is the Pb—N bonds which are stronger.

The infrared spectrum of a solution of $Ph_2Pb(SeCN)_2$ in dimethylformamide (0.01–0.025 *M*) has a single sharp absorption (2066 cm^{-1}; $\nu_{1/2}$ = 13–16 cm^{-1}; $A_{CN} = 2.7 \times 10^4$)[4] in the ν(CN) region characteristic of ionic selenocyanate. Thus $Ph_2Pb(SeCN)_2$ dissolves only when ionization can occur in a strong donor solvent, L.

$$Ph_2Pb(SeCN)_2(s) \overset{\text{excess L}}{\rightleftarrows} Ph_2PbL_4^{2+} + 2NCSe^-$$

To determine whether other species may exist, following our earlier work (6), the DMF was diluted with a non-coordinating solvent, CH_2Cl_2. In 50% (v/v) DMF/CH_2Cl_2 solutions of $Ph_2Pb(SeCN)_2$ (0.010–0.012 *M*) only one ν(CN) peak was observed (2067 cm^{-1}; $\nu_{1/2}$ = 17 cm^{-1}; $A = 3.0 \times 10^4$) but further dilution (20% DMF/CH_2Cl_2) caused a weak absorption

[3] Raman spectra of $Ph_2Pb(SeCN)_2$ and its adducts could not be obtained because of their ready tendency to undergo thermal- and photo-decomposition.

[4] $\nu_{1/2}$ is the width at half-peak height; A_{CN} is the integrated molar absorptivity in M^{-1} cm^{-2} $(NCSe)^{-1}$.

TABLE 1. Selenocyanate group frequencies (cm^{-1}) (ir data, Nujol mull) for $Ph_2Pb(SeCN)_2$ and adducts

Compound	ν(CN)	ν(CSe)	Bonding modes
$Ph_2Pb(SeCN)_2$	2117 vs, sp; 2072 w	5556 wm, sp	Pb-SeCN-Pb
$Ph_2Pb(NCSe)_2 \cdot 2HMPA$	2109 w; 2040 vs, br	618 w; 613 sh	Pb-NCSe
$Ph_2Pb(NCSe)_2 \cdot 2Ph_3PO$	2117 vw;[a] 2111 vw; 2033 vs, br; 1991 w	618 w; 613 w	Pb-NCSe
$Ph_2Pb(SeCN)_2 \cdot 2pyO$	2105 vs, sp; 2059 w	537 vw	Pb-SeCN
$Ph_2Pb(SeCN)_2 \cdot 4(4\text{-picO})$	2063 s; (2053 m, 2045 s) sp; 2013 w	—[b]	IONIC
$Ph_2Pb(NCSe)_2 \cdot 2collO$	2111 w; 2060 sh; 2034 vs, br; 1989 w	602 w; 565 vw	Pb-NCSe
$Ph_2Pb(SeCN)_2 \cdot 2DMSO$	2117 m, sp;[a] 2109 s; 2091 sh; 2071 sh; 2066 sh	555 w, sp[c]	Pb-SeCN
$Ph_2Pb(SeCN)_2 \cdot 2morph$	(2091, 2082) vs, br	597 w; 587 vw; 563 w	Pb-NCSe
$Ph_2Pb(SeCN)_2 \cdot 2quin$	2109 vw; 2082 sh; (2074, 2066) s, sp; 2043 sh; 2030 s; 1992 sh	618 wm, —[b]	{ Pb-NCSe +IONIC
$Ph_2Pb(SeCN)_2 \cdot 2pipy$	2144 w, m; 2107 s; 2091 vs, br; 2063 br, sh; 2045 sh	613 w	{ Pb-NCSe + Pb-NCSe-Pb
$Ph_2Pb(SeCN)_2 \cdot 3dipy$	2115 sh; 2097 s; 2034 vs, br; 1988 w	580 w	{ Pb-NCSe + Pb-NCSe-Pb
$Ph_2Pb(SeCN)_2 \cdot 3phen$	2118 w;[a] 2077 w, sp; 2059 s, sp; 2038 wm; 2016 vs, br; 1972 vw	—[b]	{ Pb-NCSe +IONIC

[a] ν(CN) for $Ph_2Pb(SeCN)_2$.
[b] Obscured by ligand bands.
[c] ν(CSe) for $Ph_2Pb(SeCN)_2$.

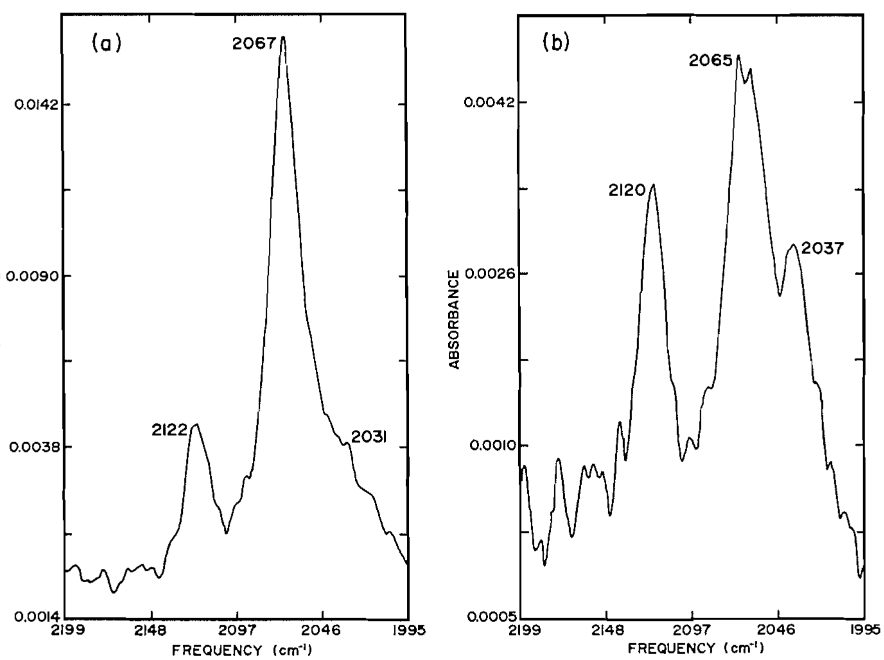

FIG. 1. Infrared spectra in the ν(CN) region of $Ph_2Pb(SeCN)_2$ in (*a*) 10% DMF/CH_2Cl_2 (0.0030 *M*), and (*b*) 5% DMF/CH_2Cl_2 (0.0021 *M*).

at 2120 cm^{-1} ($\nu_{1/2} \sim 16\ cm^{-1}$) to appear, indicative of a species containing the Pb—SeCN unit. This peak grows as more CH_2Cl_2 is added and in 10% DMF/CH_2Cl_2 the infrared spectrum (Fig. 1(*a*)) has a broad shoulder at 2031 cm^{-1} showing an N-bonded species is also present. Finally in 5% DMF/CH_2Cl_2 (Fig. 1(*b*)) two quite distinct peaks which may be assigned to Se-bonded and N-bonded selenocyanate groups were observed at 2120 and 2037 cm^{-1}, respectively. Unfortunately, as DMF is diluted with CH_2Cl_2 the solubility of $Ph_2Pb(SeCN)_2$ decreased so that in the last case (5% DMF/CH_2Cl_2), the saturated solution concentration was ≤ 0.002 *M*. With this in mind it would be unwise to attribute the splitting of the absorption at

~2065 cm^{-1} definitely to the presence of a new solute species rather than to the background "noise" expected in the spectrum of such a dilute solution. Further dilution of DMF by CH_2Cl_2 caused $Ph_2Pb(SeCN)_2$ to precipitate from even more dilute solutions, rendering solution infared studies impossible. Bearing in mind that adducts $Ph_2Pb(SeCN)_2 \cdot 2L$ do not appear to dissolve in CH_2Cl_2, it is likely that the new species which form as the DMF mixture is diluted further are still ionic, e.g., $Ph_2Pb(SeCN)L_3^+$ (L = DMF) with both Se-bonded and N-bonded isomers present. Since A_{CN}(N-bonded) $\geq 10A_{CN}$(Se-bonded) the higher intensity of the 2120 cm^{-1} absorption compared with that at 2035 cm^{-1} shows that the Se-bonded species predominates in this case, as was found also for $Ph_3PbSeCN \cdot L$ in 5% DMF/CH_2Cl_2 (6).

(ii) Adducts with O-donor ligands

Values of ν(CN) and ν(CSe) show $Ph_2Pb(SeCN)_2 \cdot 2pyO$ to be a true selenocyanate as is the DMSO adduct even though this dissociated to some extent when mulled. In contrast, adducts with HMPA and collO are N-bonded, although a weak absorption at ~2110 cm^{-1} might indicate some Pb—SeCN units are present. While there seems to be a general trend for stronger "hard" O-donor ligands to favour N-bonded species (1) this is perhaps not always the case. Thus, the triphenylphosphine oxide adduct of $Ph_2Pb(SeCN)_2$ is clearly N-bonded unlike the adduct with $Ph_3PbSeCN$ which is Se-bonded (1). While all adducts, $Ph_2Pb(SeCN)_2 \cdot 2L$, probably have linear "Ph_2Pb" units (cf. Ph_2PbCl_2 (7)), it is not possible to decide unambiguously from infrared data alone whether the ligands (and NCSe groups) are *trans* or *cis* in these compounds, although a single infrared absorption would favour the trans arrangement.

The adduct with 4-picoline-*N*-oxide is unusual not only in regard to its stoichiometry but also in its complex infrared spectrum in the ν(CN) region even though Se-bonded selenocyanate is clearly absent. Since no $\nu(N \rightarrow O)$ absorption due to free ligand is observed, the most plausible structure is ionic, probably $[Ph_2Pb(4\text{-picO})_4^{2+}]$ $[NCSe^-]_2$. However, the sharp peaks at ~2050 cm^{-1} require extensive crystal lattice effects to account for the splitting and lowering of the ν(CN) value from that found for KNCSe (2070 cm^{-1}) (8) while the broader and strong absorption at 2063 cm^{-1} could be assigned to either ionic or N-bonded selenocyanate groups.

(iii) Adducts with N-donor ligands

Adducts with monodentate N-donor ligands have the simple formula $Ph_2Pb(SeCN)_2 \cdot 2L$ but their spectra in the ν(CN) region are more complex than those for O-donor adducts with the same formula. For example, the morpholine adduct shows a doublet at ~2090 cm^{-1} which could indicate Se-bonded or N-bonded selenocyanate groups. However, the peak shape favours the latter assignment as do the ν(CSe) values observed. It is not possible to decide unequivocally whether the observed splittings in ν(CN) are due to a *cis*-$Pb(morph)_2$ arrangement in the adduct or strong crystal lattice effects. In contrast, the spectrum in the ν(CN) region of the quinoline adduct is even more complex. Sharp peaks at ~2070 cm^{-1} show the presence of ionic selenocyanate with lattice effects accounting for the splitting, while the broader ν(CN) absorption at 2030 cm^{-1} and ν(CSe) at 618 cm^{-1} are clearly due to N-bonded selenocyanate. Thus, we suggest that the bulkier quinoline ligand stabilizes the formation of 4-coordinate ions $Ph_2Pb(quin)_2^{2+}$ and adduct molecules which may have a *trans*-$Pb(quin)_2$ geometry. The similarity of ν(CN) values for this adduct and those with O-donor ligands which are also possibly trans is noteworthy.

Coordination-sensitive ring modes of the ligand show both complexed (815, 567 cm^{-1}) and "free" (800, 555 cm^{-1}) ligand molecules are present in the piperidine adduct (4). This is supported by the low melting point of this adduct and its tendency to lose piperidine readily on standing in the open. Similar intensities for equivalent "free" and complexed ligand bands suggest that only one piperidine molecule is attached to each lead with hexa-coordination maintained by equal numbers of bridging and terminal NCSe groups being present. The selenocyanate group infrared data are consistent with this picture while ν(CSe) at 613 cm^{-1} confirms that the terminal selenocyanates are N-bonded.

The $Ph_2Pb(SeCN)_2$ adducts with bidentate N-donor ligands show a quite different stoichiometry from that of their thiocyanate analogues. In the dipyridyl adduct spectrum the 2 to 1 intensity ratio of δ(CH) (out-of-plane) ligand mode absorptions at 756 cm^{-1} ("free") and 769 cm^{-1} (complexed) (4) suggests that the adduct formula is $Ph_2Pb(SeCN)_2dipy \cdot 2dipy$, i.e., only one of the three dipyridyl molecules is acting as a ligand. As with $Ph_2Pb(NCS)_2dipy$, the infrared spectrum of the selenocyanate compound can be assigned to a structure with both bridging and N-bonded selenocyanate groups. However, alternate monomeric structures containing *cis*-(SeCN—Pb—SeCN) or *cis*-$Pb(NCSe)_2$ moieties cannot be ruled out, although in the latter case strong vibrational coupling between geminal C—N bonds is required to account for the widely separated ν(CN) frequencies. The more complex pattern observed for the 1,10-phenanthroline adduct suggests at least two selenocyanate species are present, i.e., the pair of sharp peaks centered on 2068 cm^{-1} may be assigned to $NCSe^-$ with lattice effects accounting for the splitting, while the two broad absorptions at lower frequency can be assigned to N-bonded selenocyanates in a cis arrangement. Thus it is possible this adduct contains both $[Ph_2Pb(phen)_2]^{2+}[NCSe^-]_2$ and *cis*-$Ph_2Pb(NCSe)_2 \cdot phen$ species with the remaining ligands uncomplexed in the lattice as shown by absorptions at 1506, 734, 705, and 621 cm^{-1}, while bound ligands absorb at 1514, 719, and 635 cm^{-1} (4).

Conclusion

Infrared spectral data usually enable only general conclusions to be drawn regarding the chemical bonding and geometry found in complex ions and molecules, especially when complementary Raman data are not available. For the compounds studied here it was possible to suggest the type of lead–selenocyanate bonding for most adducts with O-donor ligands, but those with N-donor ligands clearly had more complex behaviour and the types of bonding proposed are very tentative. As with $Ph_2Pb(NCS)_2 \cdot 2L$ (except when L = HMPA) systems (2), the diphenyllead diselenocyanate adducts reported here were obtained as powders which could not be recrystallized without decomposition, thus rendering the necessary X-ray diffraction studies impossible at this time. Other techniques, e.g., ^{14}N nqr spectra (9) or solid state NMR measurements (10) which have been used to study thiocyanate complexes, may be required to determine better the structures of the compounds reported in this paper.

Acknowledgements

We thank le Gouvernement du Quebec, Ministère de l'Education, for financial support.

1. R. Wojtowski, I. Wharf, and M. Onyszchuk. Can. J. Chem. **61**, 743 (1983).

2. R. MAKHIJA and M. ONYSZCHUK. J. Organomet. Chem. **135**, 261 (1977).
3. E. E. AYNSLEY, N. N. GREENWOOD, G. HUNTER, and M. J. SPRAGUE. J. Chem. Soc. A, 1344 (1966).
4. I. WHARF, T. GRAMSTAD, R. MAKHIJA, and M. ONYSZCHUK. Can. J. Chem. **54**, 3430 (1976).
5. A. H. NORBURY. Adv. Inorg. Chem. Radiochem. **17**, 254 (1975).
6. M. ONYSZCHUK and I. WHARF. J. Organomet. Chem. **249**, C9 (1983).
7. M. MAMMI, V. BUSETTI, and A. DEL PRA. Inorg. Chim. Acta, **1**, 419 (1967).
8. H. W. MORGAN. J. Inorg. Nucl. Chem. **16**, 368 (1960).
9. W. C. FULTZ, J. L. BURMEISTER, C. P. CHENG, and T. L. BROWN. Inorg. Chem. **20**, 1734 (1981).
10. N. ZUMBULYADIS and H. J. GYSLING. J. Am. Chem. Soc. **104**, 3246 (1982).

Solubility of carbon dioxide in water–t-butanol solutions

PEETER KRUUS AND CATHERINE A. HAYES
Department of Chemistry, Carleton University, Ottawa, Ont., Canada K1S 5B6

Received March 19, 1985

PEETER KRUUS and CATHERINE A. HAYES. Can. J. Chem. **63**, 3403 (1985).

The solubility of carbon dioxide has been determined in tertiary butanol – water mixtures over the temperature range 1–25°C. The solubility exhibits a sharp, temperature-dependent minimum in water-rich solutions corresponding to a maximum in the activity coefficient of t-butanol, which has also been determined. The activity coefficient of t-butanol has a prominent temperature-dependent maximum ($\gamma > 7.0$) at a solution composition of about 0.06 mole fraction alcohol. Application of the scaled particle theory indicates that volume effects are a governing factor in the gas solubility, but are insufficient to explain the total effect. The pH of t-butanol–water and t-butanol–water–CO_2 mixtures reveals no major anomalous solvation effect.

PEETER KRUUS et CATHERINE A. HAYES. Can. J. Chem. **63**, 3403 (1985).

Opérant dans un intervalle de temperature aliant de 1 à 25°C, on a déterminé la solubilité du dioxyde de carbone dans des mélanges de *tert*-butanol/eau. La solubilité présente un minimum prononcé qui dépend de la température dans des solutions riches en eau qui correspondent à des maxima dans les coefficients d'activité du *tert*-butanol que l'on a aussi déterminés. A une composition de la solution correspondant à une fraction molaire en alcool d'environ 0,06, les coefficients d'activité du *tert*-butanol présentent un important maximum ($\gamma > 7,0$) qui varie avec la température. L'utilisation de la théorie des particules divisées indique que les effets de volume sont les facteurs qui influencent la solubilité du gaz; toutefois, ils ne suffisent pas pour expliquer l'effet global. Le pH de mélanges de *tert*-butanol/eau et de *tert*-butanol/eau/CO_2 ne révèle pas d'anomalies importantes dans l'effet de solvatation.

[Traduit par le journal]

1. Introduction

Carbon dioxide in its various states plays an important role in both natural and industrial processes. Recently, liquid and supercritical carbon dioxide have found wide-scale use for extractions in the food and mining industries, and are of potential use in tertiary oil recovery. Although many bulk properties of carbon dioxide solutions have been characterized, little is known of the fundamental interactions of carbon dioxide with nonelectrolyte solutes in aqueous solution. The study of simple carbon dioxide – nonelectrolyte – water systems may provide models which can be applied to more complex systems.

Tertiary butanol was chosen as a co-solute in this study for several reasons: (*i*) it is miscible with water in all proportions, (*ii*) many properties of t-butanol–water solutions have been investigated (1, 2), and (*iii*) the peculiar features of alcohol–water solutions are particularly well-developed in aqueous t-butanol due to its bulky alkyl group. Although there have been several studies of the solubility of gases in water–alcohol systems (3, 4), the combination of water (subscript 1) – t-butanol (subscript 2) – carbon dioxide (subscript 3) has not been investigated to date.

The solubility of a substance in a two-component solvent system is fundamentally related to the chemical potentials of the two solvent components. Other "continuum" properties of the solvent system are also related to the chemical potentials (or their derivatives) of the components. Kenttamaa *et al.* (2) have obtained the activities of the components of water–t-butanol at temperatures above 25°C. However, in spite of the great number of experimental studies of continuum-type properties of this system (1, 5, 6) the component activities at temperatures below 25°C have not been reported in the literature. Such activities are reported here for 1°C and 10°C.

Experimental

(a) Materials

The following chemicals were used in this study: filtered Millipore deionized water, freshly distilled Fisher Certified t-butanol, Matheson Research Grade carbon dioxide (99.95%), and helium (99.9999%). The composition of the water–t-butanol solvent mixture was determined through refractive index measurements.

(b) Apparatus

The apparatus for the measurement of gas solubility can best be described as a modified BET-type apparatus used normally to measure the adsorption of gas on a solid. It consists of a constant-volume manometer, a seven-bulb gas burette, and a solubility cell which contains the liquid sample. The volume of each bulb in the gas burette is known to ± 0.0002 cm^3 through determination of the mass of mercury it contains. The mercury level in the manometer is read with a cathetometer to ± 0.0001 cm. The solubility cell is constructed with a Teflon stopcock so that there is no contamination of the sample by vacuum grease. The sample is stirred magnetically and thermostatted to ± 0.05°C. The vacuum in the system is monitored with a thermocouple gauge (Veeco type RG-31X).

The line volume (which is all capillary tubing) and the dead volume (the volume between the first stopcock leading to the line and the liquid level in the solubility cell) were determined with research grade helium assuming He to be an ideal gas. The line volume was 15.53 ± 0.08 cm^3; the dead volume (cell empty) was 34.12 ± 0.25 cm^3. Temperatures were monitored with a five junction chromel–alumel thermocouple referenced to an ice bath.

In order to check for any adsorption of CO_2 on the glass walls of the tubing, the line volume and dead volume were also calibrated with CO_2, assuming ideal gas behaviour. The results were within 1.0% of those obtained with helium.

(c) Vapour pressure and gas solubility measurements

The procedures followed for these measurements are quite similar, and are briefly outlined here.

The sample of water–t-butanol was first degassed under vacuum by at least five freeze–pump–thaw cycles, weighed, then stirred and thermostatted to the desired temperature. The equilibrium time required before a vapour pressure measurement was typically 1 h.

For solubility measurements, the line volume was evacuated, typically to 0.0001 Torr, and then filled with CO_2 to a pressure of about 700 Torr. The number of moles of CO_2 in the line volume was determined from three volume/pressure measurements, the level of mercury in the manometer and the burette was then adjusted to give the desired pressure of CO_2, and the gas was admitted to the sample cell. When equilibrium was reached after about 1 h, the first stopcock was closed and the number of moles of CO_2 remaining in the line

TABLE 1. Experimentally measured vapour pressures of *t*-butanol–water mixtures

10.00°C		1.00°C	
X_2 ($\mp$0.0002)	P_{TOT}[a] (10^{-3} atm)	X_2 ($\mp$0.0002)	P_{TOT}[a] (10^{-3} atm)
0.0101	12.96	0.0128	6.66
0.0197	14.72	0.0295	7.68
0.0443	18.37	0.0349	8.17
0.0478	18.99	0.0409	8.46
0.0603	20.84	0.0529	9.63
0.0705	21.57	0.0657	10.88
0.0916	22.32	0.0700	11.54
0.1037	22.50	0.0756	11.64
0.1630	23.08	0.0846	11.82
0.2860	23.55	0.1228	12.25
0.4510	23.82	0.1938	12.37
0.6230	23.95	0.2246	12.41
0.7020	23.89	0.3772	12.50
0.8140	23.34	0.4347	12.50
0.8600	22.58	0.4776	12.47
		0.5797	12.63
		0.6940	12.63
		0.7898	12.29

[a]Maximum experimental error: $\pm0.07 \times 10^{-3}$ atm.

volume was measured. The number of moles of CO_2 remaining in the dead volume could be calculated from the equilibrium pressure and the known dead volume; the number of moles of CO_2 absorbed by the sample could thus be calculated.

This procedure was repeated until at least five points were obtained for a Henry's law plot of P_3 vs. X_3. At the end of the experiment the composition was determined through a measurement of the refractive index as the degassing procedure preferentially removed the alcohol and altered the initial composition. The typical time required for the complete experiment was 10 h.

In calculating the number of moles of CO_2, the pressure was corrected for the non-ideality of the gas according to the virial equation of state with values of coefficients from ref. 7. For these calculations the gas temperature was assumed to be the room temperature in the line volume and the sample temperature in the dead volume. The dead volume was corrected for the volume of the sample using densities of water–*t*-butanol solutions found in ref. 8 for 10°C and 25°C; densities at 0°C (9) were used to correct the dead volume for measurements at 1°C.

Clearly the gas contained in the dead volume consists of both carbon dioxide and sample vapour, but it can be assumed that the line volume contains only carbon dioxide since it is composed of capillary tubing, and as pressure changes from the line volume to the dead volume were always positive. The gas pressure was corrected for the presence of sample vapour in the dead volume through an iteration procedure assuming Raoult's law.

(d) Refractive index measurements

Refractive index measurements were made with an Abbe refractometer (Officione Galileo) thermostatted at 25.00 ± 0.05°C. Using solutions prepared from *t*-butanol dried over 4A molecular sieves, a calibration curve was constructed and fitted to a sixth-order polynomial. The composition of all water–*t*-butanol solutions prepared were then calculated from refractive index measurements. In the composition region of most interest ($X_2 \sim 0.1$), X_2 could be obtained to an accuracy of ±0.0001 by this method. At higher (>0.4) ranges of X_2, n is not as sensitive to X_2 and the accuracy was lower (±0.0005 to ±0.001 mole fraction alcohol).

(e) pH measurements

Measurements of pH were made with a combination glass Ag/AgCl electrode (Fisher 13-639-92) and a digital pH meter (Fisher Model 620). The pH meter calibration was checked by using buffer solutions at pH 4, 7, and 10. For the measurement of the pH of water–*t*-butanol solutions, the water was first degassed by refluxing and then sparged continuously with argon during the experiment. Solid *t*-butanol was gradually added to the solution, which was magnetically stirred and thermostatted to 25.00 ± 0.05°C.

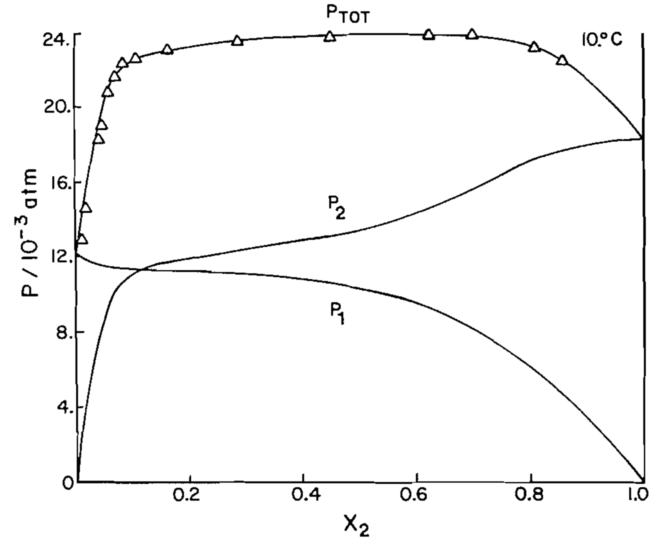

FIG. 1. Vapour pressures of *t*-butanol–water mixtures at 10.00°C: △, experimental points; —, computer-fitted curves.

For the measurement of the pH of water – *t*-butanol – carbon dioxide solutions, a water – *t*-butanol solution was first degassed under vacuum by several freeze–pump–thaw cycles. The solution was then quickly transferred to the measuring flask and carbon dioxide was bubbled continuously through the sample. The pH reading usually equilibrated within minutes. The refractive index of the solution was tested immediately after a pH reading was taken to check the solution composition.

Results

*(a) The solvent system water–*t*-butanol*

The vapour pressures of water–*t*-butanol mixtures were measured over the concentration ranges where the samples were liquid at 10.00°C and 1.00°C. The vapour pressure of pure *t*-butanol and water were taken from ref. 10 as it was difficult to reach equilibrium when the system contained only water. The vapour pressures at 25°C have been measured previously by Brown and Ives (11). The experimental vapour pressures are given in Table 1. The shapes of the total vapour pressure curves for 10°C (Fig. 1) and 1°C are similar to that reported by Brown and Ives for 25°C and by Kenttamaa *et al.* at 25, 50, and 75°C (2).

Brown and Ives used an equilibrium still to make their vapour pressure measurements and were able to determine the composition of the vapour phase with this apparatus. The partial pressure of each component was then calculated by an application of the Duhem–Margules relation. Using their data for the partial pressure of each component at 25°C, the partial pressures at other temperatures could be calculated under the assumption that the activity coefficient of the water is relatively insensitive to temperature.

The calculations were done as follows. The activity coefficient of water, γ_1, was calculated from the partial pressure of water at 25°C according to Raoult's law. It was then assumed that the activity coefficient of water changes negligibly (within experimental error) in the temperature range 1–25°C. This

TABLE 2. Vapour pressures, activity coefficients, and ΔG_M^E for water–t-butanol mixtures

	1.00°C			10.00°C			25.00°C			
X_2	P_{TOT} (10^{-3} atm)	γ_2	ΔG_M^E (kJ mol^{-1})	P_{TOT} (10^{-3} atm)	γ_2	ΔG_M^E (kJ mol^{-1})	P_{TOT} (10^{-3} atm)	γ_2	γ_1	ΔG_M^E (kJ mol^{-1})
0	6.48	—	—	12.12	—	—	31.32	—	1.000	—
0.01	6.67	3.06	0.142	13.14	6.60	0.032	34.47	6.56	0.995	0.032
0.02	7.00	3.63	0.430	14.54	7.47	0.076	38.29	7.11	0.993	0.074
0.03	7.62	4.81	0.942	16.16	8.12	0.130	43.82	8.17	0.994	0.130
0.04	8.51	6.08	0.158	17.83	8.48	0.188	49.47	8.81	0.997	0.192
0.05	9.53	7.08	0.227	19.37	8.54	0.249	53.82	8.71	1.002	0.251
0.06	10.49	7.65	0.293	20.63	8.32	0.305	56.18	8.01	1.007	0.300
0.07	11.26	7.75	0.358	21.55	7.87	0.361	56.84	7.07	1.015	0.344
0.08	11.76	7.47	0.414	22.09	7.28	0.410	57.11	6.24	1.02	0.382
0.09	11.99	6.92	0.462	22.34	6.64	0.454	57.89	5.74	1.03	0.424
0.10	12.04	6.30	0.504	22.43	6.03	0.494	58.03	5.18	1.04	0.459
0.20	12.39	3.36	0.828	23.32	3.28	0.817	60.00	2.79	1.16	0.743
0.30	12.46	2.30	0.996	23.61	2.28	0.988	60.92	1.95	1.31	0.883
0.40	12.47	1.77	1.060	23.72	1.76	1.055	61.71	1.53	1.48	0.927
0.50	12.54	1.48	1.055	23.84	1.47	1.049	62.3	1.29	1.71	0.898
0.60	12.65	1.32	1.003	23.90	1.31	0.986	62.63	1.14	1.97	0.801
0.70	12.62	1.24	0.901	23.92	1.23	0.878	62.24	1.06	2.25	0.649
0.80				23.39	1.18	0.718	60.92	1.02	2.53	0.457
0.90							58.55	0.99	2.93	0.228
1.00							55.26	1.00		

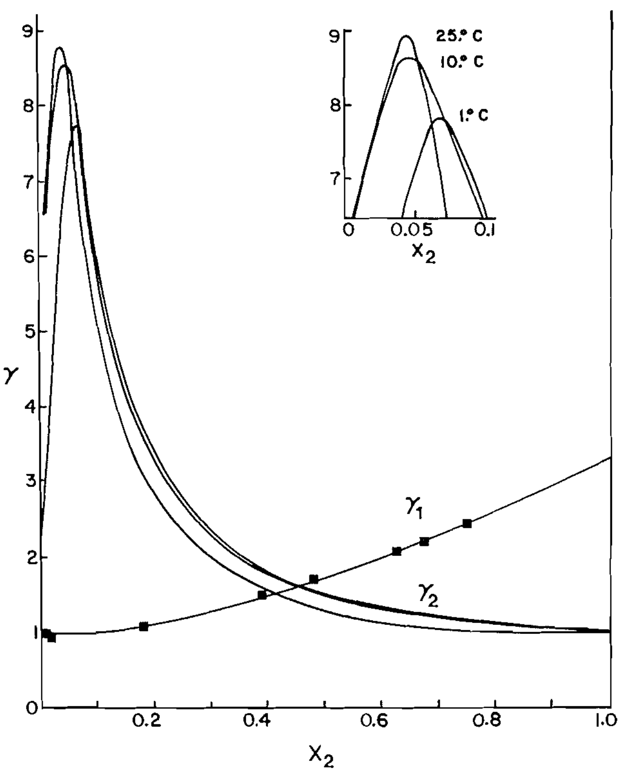

FIG. 2. Activity coefficients of t-butanol and water determined from vapour pressures. — data for γ_1 as taken from refs. 2 and 11 for 25.0°C. The γ_1 curve is assumed temperature independent. ■, data at 50.0°C from ref. 2.

assumption seems justified, as the γ_1 values at 50°C from ref. 2 are essentially the same as those at 25°C from refs. 2 and 11 (Fig. 2). The partial pressure of water at a given temperature was then calculated and the partial pressure of t-butanol determined by subtraction from the known total pressure. The activity coefficient of t-butanol is thus

$$[1] \quad \gamma_2(T) = \frac{P_{TOT}(T) - \gamma_1(25°C)X_1P_1^{\bullet}(T)}{X_2P_2^{\bullet}(T)}$$

The activity coefficients calculated in this manner were found to be consistent with the Gibbs–Duhem relation to within about 0.8%. The smoothed data for the system at 25, 10, and 1°C are tabulated in Table 2. The rms deviation for the computer fit of the total pressure curves obtained in this study ranged from (0.04 to 0.12) × 10^{-3} atm; the data of Brown and Ives were fitted with an rms deviation of about 0.24 × 10^{-3} atm. This is another indication that no great errors are introduced by assuming γ_1 to be independent of temperature from 0 to 25°C.

The large positive deviation from Raoult's law of the alcohol partial pressure is seen in Fig. 1, and more clearly in Fig. 2 where the activity coefficients of t-butanol and water as a function of solution composition are given. The activity coefficient of t-butanol exhibits a temperature-dependent maximum at a low mole fraction of alcohol (X_2 = 0.04 at 25°C, 0.05 at 10°C, and 0.07 at 1°C). The data of Kenttamaa *et al.* (2) are not detailed enough to note the value of X_2 at which γ_2 is a maximum. The magnitude of their maximum value of γ_2 does, however, also show an increase with temperature, as in Fig. 2. For 25°C they report $\gamma_{2,max}$ = 10.7 at X_2 = 0.033, for 50°C, $\gamma_{2,max}$ = 15.7 at X_2 = 0.011, and for 75°C, $\gamma_{2,max}$ = 25.5 at X_2 = 0.010.

The excess Gibb's free energy of mixing ΔG_M^E, is defined by the relation:

$$[2] \quad \Delta G_M^E = RT(X_1 \ln \gamma_1 + X_2 \ln \gamma_2)$$

The ΔG_M^E values calculated for water–t-butanol mixtures at different temperatures are illustrated in Fig. 3. The maximum ΔG_M^E values occur at $X_2 \sim 0.4$, as in the case for higher temperatures (2). It is in principle possible to calculate ΔH_M and ΔS_M^E from a knowledge of the temperature dependence of ΔG_M^E, but the data obtained here are not detailed enough for a meaningful calculation.

TABLE 3. Solubility of CO_2 in water–*t*-butanol mixtures

T = 25.00°C			T = 10.00°C			T = 1.00°C		
X_2 (∓0.0002)	k_H (atm)	ΔG^0_{sol} (kJ mol^{-1})	X_2 (∓0.0002)	k_H (atm)	ΔG^0_{sol} (kJ mol^{-1})	X_2 (∓0.0002)	k_H (atm)	ΔG^0_{sol} (kJ mol^{-1})
0	1592 ± 10	18.28 ± 0.11	0	1066 ± 7	16.41 ± 0.11	0	760 ± 2	15.12 ± 0.04
0.0163	1599 ± 20	18.29 ± 0.23	0.0094	1084 ± 8	16.45 ± 0.12	0.0192	801 ± 9	15.24 ± 0.17
0.0300	1601 ± 17	18.29 ± 0.19	0.0171	1077 ± 4	16.44 ± 0.06	0.0318	966 ± 16	15.67 ± 0.26
0.0346	1635 ± 30	18.37 ± 0.33	0.0419	1086 ± 16	16.46 ± 0.24	0.0482	987 ± 8	15.72 ± 0.13
0.0567	1635 ± 27	18.34 ± 0.30	0.0496	1234 ± 10	16.76 ± 0.14	0.0536	1049 ± 80	15.85 ± 1.21
0.0623	1514 ± 26	18.15 ± 0.31	0.0591	1360 ± 55	16.99 ± 0.69	0.0587	1059 ± 10	15.88 ± 0.15
0.0840	1294 ± 3	17.76 ± 0.04	0.0661	1205 ± 7	16.70 ± 0.10	0.0591	1011 ± 24	15.77 ± 0.37
0.1300	941 ± 34	16.97 ± 0.61	0.1024	1045 ± 21	16.37 ± 0.33	0.1576	699 ± 2	14.93 ± 0.04
0.2810	441 ± 2	15.09 ± 0.07	0.1333	874 ± 13	15.95 ± 0.24	0.2285	484 ± 5	14.09 ± 0.15
0.7752	156 ± 3	12.52 ± 0.24	0.2371	521 ± 5	14.73 ± 0.14			
			0.2883	409 ± 4	14.16 ± 0.14			

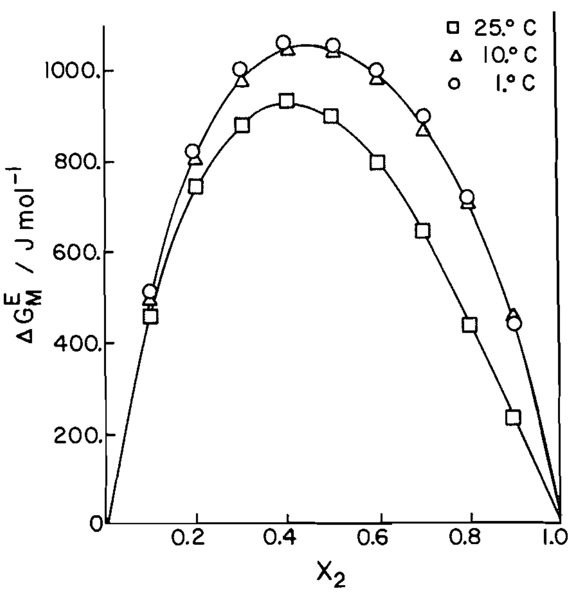

FIG. 3. Excess free energy of mixing of *t*-butanol–water mixtures.

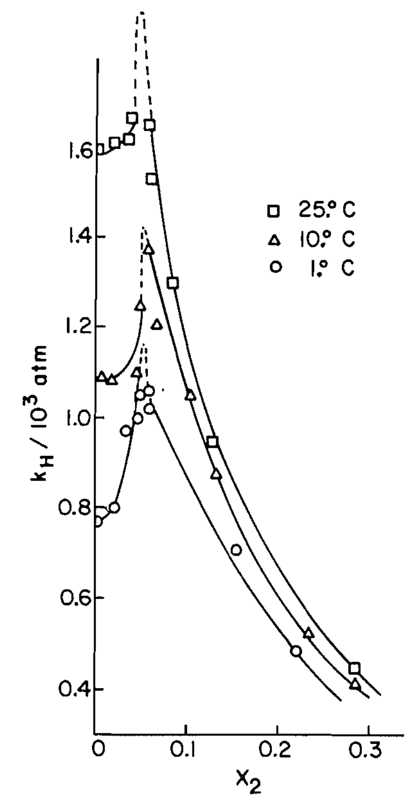

FIG. 4. Henry's law constant, k_H, as a function of *t*-butanol concentration at 25, 10, and 1°C.

(b) Solubility of carbon dioxide in t*-butanol–water mixtures*

The accuracy of the experimental method used to calculate the solubility of CO_2 can be estimated by comparing the results for the solubility of CO_2 in pure water at 25.00°C with those available in the literature (12–14). The value obtained in this study agrees with the literature values to within 3%. Some of this deviation arises from the ideal gas assumption used to convert the Henry's law constant to the Bunsen coefficient and the Ostwald solubility coefficient for comparison with the literature values. However, the main source of error in this experiment was the assumption that the gas in the dead volume is at the same temperature as the sample. It is, however, difficult to apply a correction to the thermal gradient from the sample to the room temperature. Such errors would have negligible effects in considerations of relative solubilities.

Plots (P_3 vs. X_3) for the solubility of CO_2 were linear to within an average standard deviation of 1.5% (Table 3) with no regular deviation from linearity. The pressures used were sufficiently low so that the error introduced in replacing fugacity by partial pressure is negligible (1%) and the second term in the expansion $P_3 = k_H X_3 + k' X_3^2 + \ldots$ gives a negligible contribution. The intercepts of the lines did not always pass through zero pressure as expected. The small positive intercept values noted are probably due to incomplete degassing and the assumption of uniform dead volume temperature. Figure 4 shows that there is at all three temperatures a minimum in solubility (maximum in k_H) at low X_2. It was not possible to determine the point of minimum solubility more precisely, as the solvent composition changed in the degassing procedure and could not be exactly predetermined.

The free energy change of solution, ΔG^0_{sol}, was calculated from the Henry's Law constant and is included in Table 3. The enthalpy change, ΔH^0_{sol}, and entropy change, ΔS^0_{sol} of solution at 10°C as a function of alcohol concentration are shown in Fig. 5. The shapes of these curves are similar to those for the solution of CO_2 in water–ethanol (4).

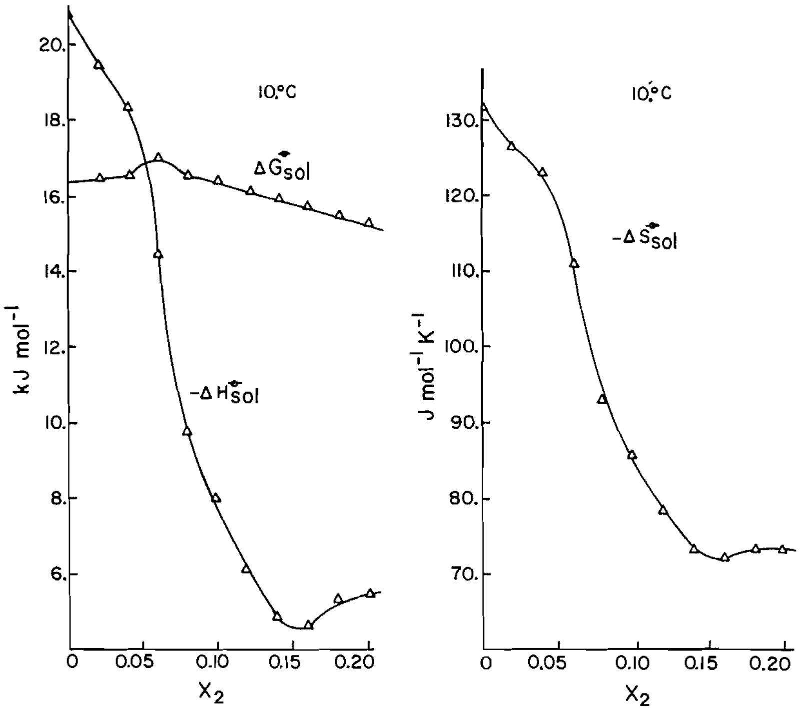

FIG. 5. Free energy, enthalpy, and entropy of solution of carbon dioxide in *t*-butanol–water mixtures at 10°C.

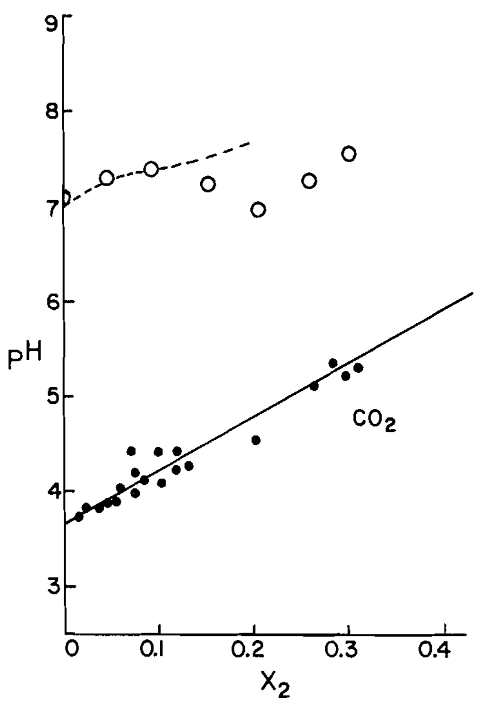

FIG. 6. pH of *t*-butanol–water and *t*-butanol–water–CO_2 mixtures at 25°C. ○, *t*-butanol–water mixtures sparged with Ar; ---, predicted pH of *t*-butanol–water mixtures from K_W values; ●, *t*-butanol–water mixtures sparged with CO_2.

(c) pH measurement

The measurements of *t*-butanol–water mixtures with an argon and a CO_2 sparge are illustrated in Fig. 6. Addition of *t*-butanol to pH 4, 7, and 10 buffers indicated a small linear increase in pH readings with addition of alcohol in all three cases. Such a change can be related to the change in the pK of the buffer due to the addition of *t*-butanol and a change in the junction potential. The latter effect is negligible as compared to experimental error.

The effect of the changing dielectric constant on the ionization constant of water must also be considered. Woolley *et al.* (15) have obtained measurements of K_W in *t*-butanol–water mixtures, from which the change in pH due to the change in K_W can be predicted. In Fig. 6, the "predicted" pH curve and the experimental pH curve obtained in this study are seen to be similar in value and in slope for dilute solutions.

In aqueous media at pH less than 7, carbon dioxide species exist as $CO_2(aq)$, $H_2CO_3(aq)$, and $HCO_3^-(aq)$. Assuming that $[CO_2(aq)] \gg [H_2CO_3(aq)]$ (16); $[HCO_3^-(aq)] \simeq [H^+(aq)] \simeq a_H$, the first dissociation constant of carbonic acid can be written as

$$[3] \quad K_1' = (a_H)^2/([CO_2(aq)] - a_H)$$

The concentration of $CO_2(aq)$ can be determined from the known solubility of CO_2 in *t*-butanol–water mixtures so that it is possible to calculate the values of pK_1' shown in Table 4. The standard state used here is that for the molarity composition scale in order to be consistent with other data (16).

The value of pK_1' in pure water calculated from the experimental pH is 5.92, as compared to Harned and Davies' (16) value of 6.352. The increase in pK_1' indicated in Table 4 is to be expected since the dielectric constant of the solvent is decreasing. The distance of closest approach, d, of the two ions formed by the dissociation of carbonic acid (H^+ and HCO_3^-) can be estimated from a plot of ln K_1' vs. $1/\epsilon$ using the Fuoss equation. The value obtained using the relative permittivity values from ref. 11 is 0.11 nm, which is of the correct order of magnitude.

Discussion

*(a) The solvent system water–*t*-butanol*

Figure 7 summarizes the behaviour of some "continuum" properties of water–*t*-butanol in the low X_2 range. Ultrasonic absorption and Rayleigh scattering are included in Fig. 7 as

TABLE 4. pK_1' of carbonic acid in *t*-butanol–water mixtures at 25°C

X_2 (±0.0002)	X_3[a] (× 10^{+4})	$[CO_2(aq)]$[b] (× 10^{+2})	pH[c] (±0.01)	a_H (× 10^{+4})	pK_1'
0	6.28	3.4	3.69	2.04	5.92
0.0163	6.25	3.26	3.78	1.66	6.07
0.0300	6.2	3.11	3.85	1.41	6.19
0.0346	6.05	2.9	3.88	1.32	6.23
0.0567	6.1	2.8	4.00	1.00	6.46
0.0623	6.6	2.96	4.03	0.933	6.53
0.0840	7.7	3.2	4.14	0.724	6.79
0.1300	10.6	3.89	4.39	0.407	7.37
0.2810	22.	5.8	5.20	0.063	9.17

[a] Calculated from k_H at 1 atm.
[b] In mol L^{-1}.
[c] Obtained by fitting experimental pH values to a straight line; standard deviation of fit = 0.09.

they involve interactions with sufficiently large wavelengths of sound and light, respectively, to be considered in terms of continuum models (5, 6).

Analyses of such data have also been carried out on the basis of molecular level models (17, 18). However, extrema in such properties are fundamentally related to extrema in the chemical potentials (or their derivatives) of the components. A desirable test of molecular-level models would be to use them to predict data for fundamental properties such as activities in addition to the more specific derived properties.

Deviations from Raoult's law for mixtures indicate non-ideal interactions between the solute and solvent molecules. The strong positive deviation of γ_2 in water-rich solution indicates that the alcohol molecules are on the average in a less favourable environment despite the possibility of formation of favourable hydrogen bonds with the water. This positive deviation arises from the strong interaction between the bulky, hydrophobic alkyl group of the alcohol and surrounding water molecules. It is interesting to note that the magnitude of this positive deviation in γ_2 becomes greater as temperature increases (Fig. 2 and ref. 2).

This phenomenon of "hydrophobic hydration" is thought to increase the water structure in the immediate vicinity of the hydrophobic residue. The sharp maximum which occurs in γ_2 at about $X_2 = 0.05$ at 25°C can be interpreted as corresponding to a maximum in the structuring effect on the surrounding water. At concentrations of alcohol greater than this maximum, the addition of further alcohol causes a rapid destruction of the water structure. The shift of the maximum to slightly lower alcohol concentrations (Fig. 2) and the increase in $\gamma_{2,\max}$ (Fig. 2, ref. 2) as the temperature is raised may be due to the smaller degree of structuring present in pure water. At higher temperatures, the structuring caused by the alcohol can be greater, but will be destroyed at lower alcohol concentrations due to greater thermal motion.

Desnoyers and colleagues (19, 20) have suggested that the sharp extrema in various thermodynamic properties of *t*-butanol–water solutions are due to transitions which resemble micellization. These "microphases" cannot be called micelles however, because alcohols do not form well-defined aggregates in water.

Mikhailov (21) has predicted the activity coefficients of ethanol and water in mixtures covering the entire concentration range based on the model he has proposed for aqueous solutions of nonelectrolytes. The predicted activity coefficient curves exhibit a sharp maximum in γ_{EtOH} in dilute solution and

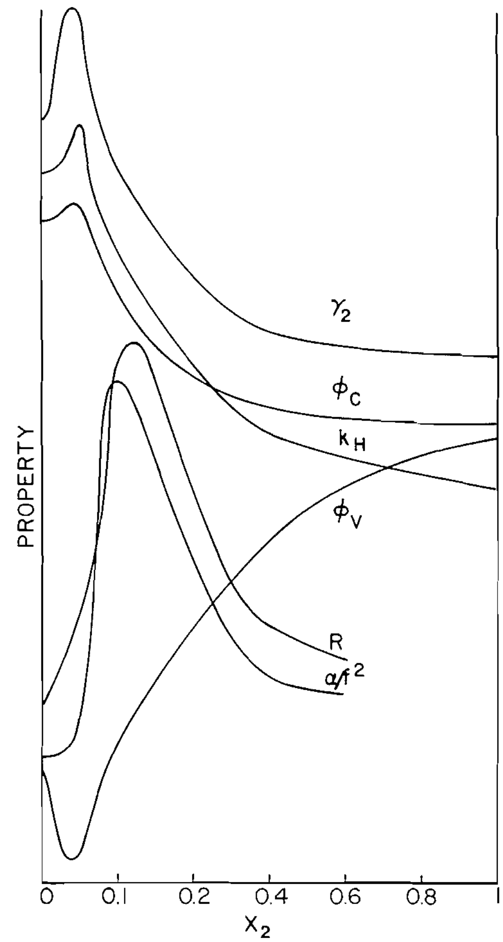

FIG. 7. Properties of *t*-butanol–water mixtures at 25°C: γ_2 activity coefficient of TBA (this work), k_H solubility of carbon dioxide (this work). ϕ_C apparent molal heat capacity of TBA (8), ϕ_V apparent molal volume of TBA (8), R, Rayleigh scattering intensity (18), α/f^2 ultrasonic absorption (26).

a positive deviation in γ_1 in more concentrated solutions. These features agree well with the curves experimentally obtained for *t*-butanol–water in this study.

The component activities in the system water–*t*-butanol obtained at three temperatures in this study are fundamental in understanding all equilibrium continuum properties. It seems desirable to check proposed models of systems against these data as well as against data derived from them.

(b) Solubility of carbon dioxide

The Henry's Law constant is related to the Gibbs free energy of solution as $\Delta G^0_{sol} = -RT \ln k_H$. The ΔG^0_{sol} for carbon dioxide in *t*-butanol–water mixtures over the entire mole fraction range at 25°C is shown in Fig. 8 as a function of both mole and volume fraction. The experimental data can be compared to an "ideal" curve where

$$[4] \quad \Delta G^{id}_{sol} = f_1 \Delta G^0_{sol,1} + f_2 \Delta G^0_{sol,2}$$

where f refers to either mole or volume fraction and $\Delta G^0_{sol,2}$ ($= -RT \ln k_{H,2}$) refers to the Gibbs free energy of solution of CO_2 in pure *t*-butanol.

When ΔG^0_{sol} is plotted as a function of the volume fraction of *t*-butanol, the curve retains the same features as the mole fraction dependent curve. The curves can be compared to the "ideal" curve by considering the excess free energy of solution, $\Delta G^E_{sol} = \Delta G^0_{sol} - \Delta G^{id}_{sol}$. For the volume fraction curve, ΔG^E_{sol}

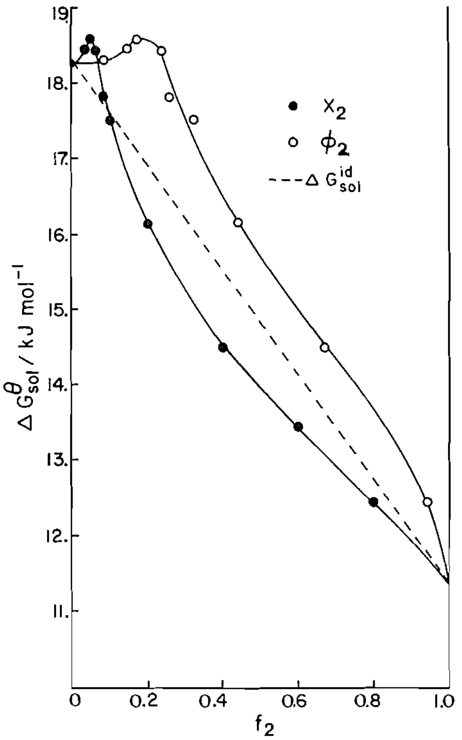

FIG. 8. — ΔG^0_{sol} for carbon dioxide solubility in *t*-butanol–water mixtures at 25.0°C as a function of mole fraction (●) and volume fraction (○) of *t*-butanol. --- ΔG^{id}_{sol} (see text for definition).

will be positive over the whole concentration range; whereas for the mole fraction curve ΔG^E_{sol} becomes negative at about $X_2 = 0.1$.

The data are analyzed in both ways, as in a study of the solubility of electrolytes in aqueous non-electrolyte solutions, the solubilities were best fitted by an expression incorporating the volume fraction rather than the mole fraction of the organic cosolute (22). When the solute molecules interact primarily with individual solvent molecules, then it is more reasonable to do the analysis using a mole fraction scale. When the interaction is primarily of a "continuium" kind, e.g. involving the dielectric constant, then a volume fraction scale is more reasonable.

The shape and temperature dependance of the ΔG^E_{sol} functions when considered on a mole fraction scale are for this system quite similar to those observed for the solubility of Ar, H_2, and He as calculated by Lucas and Cargill (23). The difference noted are that the data of Cargill shows that ΔG^E_{sol} exhibits a small negative minimum at very low mole fraction of alcohol; and the absolute magnitudes of ΔG^E_{sol} are less than in the carbon dioxide – water – *t*-butanol system.

From the ΔG^E_{sol} curves for the solubility of CO_2 in *t*-butanol–water mixtures it is possible to calculate the activity coefficient of carbon dioxide from $\mu_3^E = RT \ln \gamma_3$. Several reference states can be used to express activity coefficients, but the meaningful one here is Raoult's Law, where the reference state for the solute is unit mole fraction. When the pressure is sufficiently low to equate fugacity and partial pressure, then the solute activity is defined as

$$[5] \quad a_3 = P_3/P_3^{\bullet} = \gamma_3 X_3; \qquad \gamma_3 = k_H/P_3^{\bullet}$$

where $P_3^{\bullet}$ is the vapour pressure of the pure liquid solute. Thus the activity coefficient approaches unity as X_3 approaches the pure solute.

TABLE 5. Activity coefficient of CO_2 in CO_2–H_2O–TBA mixtures at 25.00°C

X_2	X_3 ($\times 10^{+4}$)	γ_3	μ_3^E	ΔG_t^E (kJ mol^{-1})
0	6.28	25.1	7.99	0
0.02	6.25	25.2	8.00	0.01
0.04	5.72	27.5	8.22	0.23
0.05	5.55	28.4	8.30	0.31
0.06	5.89	26.8	8.15	0.16
0.08	7.52	20.9	7.54	−0.45
0.10	8.59	18.3	7.21	−0.78
0.20	14.71	10.7	5.88	−2.11
0.40	28.82	5.5	4.23	−3.76
0.60	43.86	3.6	3.18	−4.81
0.80	65.79	2.4	2.17	−5.82
1.00	101.52	1.6	1.17	−6.82

Using the value $P_3^{\bullet} = 63.49$ atm at 25°C (10) the activity coefficients of carbon dioxide in the alcohol–water mixtures were calculated from the experimental Henry's Law constant at 25.00°C. The results (Table 5) indicate that the activity coefficient (and the excess chemical potential) of carbon dioxide in the mixture reaches a maximum at $X_2 = 0.05$. The activity coefficient of *t*-butanol in water also shows a maximum at this mole fraction (Fig. 7). The value of γ_3 in water is about 15 times that in the alcohol, where it is close to unity. This indicates that the affinity of the carbon dioxide gas for the alcohol is similar to its affinity for liquid carbon dioxide. The free energy of transfer from water to *t*-butanol (Table 3) also reflects this difference.

(c) Models for the solubility of CO_2 in water–TBA

The variation of CO_2 solubility with composition of the water–*t*-butanol mixture can involve energy, entropy, and volume effects. Scaled particle theory provides a method for estimating the importance of volume effects. Lucas and Cargill (23) have compared the experimental free energies of solubility of He, H_2, and Ar in water–ethanol and water–*t*-butanol mixtures with values predicted by the scaled particle theory (SPT). Their calculated excess free energies of solution show a similar dependence on alcohol concentration as that observed experimentally.

The expression for the free energy of solution, ΔG^0_{sol}, derived from SPT is:

$$[6] \quad \Delta G^0_{sol} = G_c + RT \ln (RT/V) + G_i$$

In [6], V is the apparent molar volume of the mixture, and G_c is the free energy of cavity formation, given by:

$$[7] \quad G_c/RT = \Big\{-\ln (1 - y) + [3X/(1 - y)] D_3 + [3Y/(1 - y)^2 + 4.5X^2/(1 - y)^3] D_3^2 + \frac{N\pi P}{6RT} D_3^3\Big\}$$

$$y, X, Y = \frac{N\pi}{6} \frac{X_1 D_1^p + X_2 D_2^p}{X_1 V_1^{\bullet} + X_2 \phi_{V,2}}$$

where p equals 3 for y, 2 for X, and 1 for Y; D_1, D_2, D_3 are the hard sphere diameters of water, alcohol, and gas, respectively; $V_1^{\bullet}$ is the molar volume of pure water and $\phi_{V,2}$ is the apparent molal volume of the alcohol in the mixture.

The contribution of the free energy of interaction, G_i, was

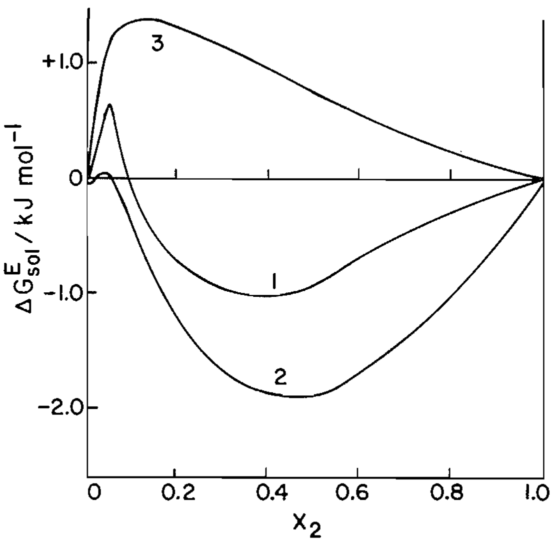

FIG. 9. Excess free energy of solution ΔG^{E}_{sol} of CO_2 in *t*-butanol–water mixtures at 25°C. Curve *1*. Experimental ΔG^{E}_{sol} (see Fig. 8). Curve *2*. Scaled particle theory. Curve *3*. Scaled particle theory, ideal volume of mixing.

neglected by Lucas and Cargill on the assumption that when a gas is transferred from water to another polar solvent, G_i is very small. The calculated and experimental free energies of transfer from alcohol to water were found to be similar, which lends some validity to this assumption.

The SPT and experimental values for the free energy of solution were compared by computing ΔG^{0}_{sol} for carbon dioxide in water–*t*-butanol mixtures at 25°C using experimental apparent molar volumes (8). The computer program was tested by calculating the free energy of transfer of argon from water to *t*-butanol at 25°C. The value of 9.21 kJ mol^{-1} computed at 25°C compares well with the value of 9.1 kJ mol^{-1} computed by Lucas and Cargill at 12°C.

The excess free energy of solution, ΔG^{E}_{sol}, for carbon dioxide is illustrated in Fig. 9. The ΔG^{E}_{sol} used in Fig. 9 are calculated using the computed values of $\Delta G^{0}_{sol,1}$ and $\Delta G^{0}_{sol,2}$; these computed values are about three times the experimental values for the case $D_3 = 0.394$ nm (24), $D_1 = 0.2733$ nm (24), and $D_2 = 0.529$ nm (25) (curve 2). The computed curve exhibits a small minimum at $X_2 = 0.015$ and a maximum at $X_2 = 0.05$. The minimum, which corresponds to a slight increase in carbon dioxide solubility, was not observed experimentally. This is possibly because the initial increase in solubility falls within the experimental error of the present study. The height of the computed maximum is much smaller than that observed experimentally.

An increase in the alcohol diameter changes the magnitude and concentrations dependence of ΔG^{0}_{sol} dramatically, but a corresponding increase in D_3 or D_1 has only a slight effect, with no change in the shape of the curve. It is of some interest to compute the solubility of carbon dioxide in "ideal" water–*t*-butanol mixtures; that is, assuming that the volume of mixing is zero rather than using experimental values of the molar volume. Curve 3 in Fig. 9 shows the value of this "excess ideal free energy" to be positive and to reach a maximum at $X_2 = 0.1$. The difference between curves 2 and 3 is an indication of the effect of the non-idealities of the system volume on the solubility of carbon dioxide. It is quite obviously a very important effect.

The variation in the chemical potential of carbon dioxide in *t*-butanol–water mixtures as a function of alcohol concentration is qualitatively the same as the variation of the chemical potentiel of the alcohol itself. The minimum in the gas solubility in very dilute alcohol solutions corresponds to the maximum in the activity coefficient curve of *t*-butanol and shows the same trends with temperature. A qualitative explanation of the variation of the solubility of carbon dioxide with concentration would be similar to the explanation of the variation of the activity coefficient of *t*-butanol with concentration given earlier.

Acknowledgements

The advice of Dr. G. C. Benson and Mr. T. Patraboy is gratefully acknowledged. We also thank Dr. J. M. Holmes for providing us with an accurately calibrated gas burette. Financial aid for this work was provided through a grant from the Natural Sciences and Engineering Research Council of Canada.

1. F. FRANKS. *In* Water, a comprehensive treatise. *Edited by* F. Franks. Plenum Press, New York. 1973. Vol. 2, chapts. 1 and 5; Vol. 4, chapt. 1.
2. J. KENTTAMAA, E. TOMMILA, and M. MARTTI. Ann. Acad. Sci. Fennicae AII, **93**, 3 (1959).
3. A. BEN-NAIM. J. Phys. Chem. **71**, 4002 (1967).
4. R. W. CARGILL and D. E. MACPHEE. J. Chem. Res. (M), 2743 (1981).
5. W. D. T. DALE, P. A. FLAVELLE, and P. KRUUS. Can. J. Chem. **54**, 355 (1976).
6. I. KATIME, L. C. CESTEROS, and C. STRAZIELLE. J. Chem. Soc. Faraday Trans. 2, **80**, 1215 (1984).
7. American Institute of Physics Handbook. 3rd ed. McGraw Hill, New York. 1972.
8. C. DE VISSER, G. PERRON, and J. E. DESNOYERS. Can. J. Chem. **55**, 856 (1977).
9. R. G. ANDERSON and M. C. R. SYMONS. Trans. Faraday Soc. **65**, 2550 (1969).
10. CRC handbook of chemistry and physics. 58th ed. CRC Press, Florida. 1979.
11. A. C. BROWN and D. J. G. IVES. J. Chem. Soc. 1608 (1962).
12. International Critical Tables. Vol. III.
13. A. E. MARKHAM and K. A. KOBE. Chem. Rev. **28**, 519 (1941).
14. J. LIVINGSTONE, R. MORGAN, and H. R. PYNE. J. Phys. Chem. **34**, 1578 (1930).
15. E. M. WOOLLEY, D. G. HURKOT, and L. G. HEPLER. J. Phys. Chem. **74**, 3908 (1970); E. M. WOOLLEY, J. TOMKINS, and L. G. HEPLER. J. Solution Chem. **1**, 341 (1972).
16. W. STUMM and J. J. MORGAN. Aquatic chemistry. Wiley Interscience, New York. 1970.
17. D. N. GLEW, H. D. MAK, and N. R. RATH. *In* Hydrogen-bonded solvent systems. *Edited by* A. K. Covington and P. Jones. Taylor and Francis, London. 1968. p. 195.
18. K. IWASAKI and T. FUJIYAMA. J. Phys. Chem. **81**, 1908 (1977).
19. J. E. DESNOYERS. Pure Appl. Chem. **54**, 1469 (1982).
20. G. ROUX, D. ROBERTS, G. PERRON, and J. E. DESNOYERS. J. Solution Chem. **9**, 629 (1980).
21. V. A. MIKHAILOV and L. I. PONOMAROVA. J. Struct. Chem. **9**, 8 (1969); V. A. MIKHAILOV. J. Struct. Chem. **9**, 332 (1968).
22. Z. B. ALFASSI and J. WEISS. Ber. Bensenges. Phys. Chem. **87**, 890 (1983).
23. M. LUCAS and R. W. CARGILL. J. Phys. Chem. **81**, 703 (1977).
24. J. O. HIRSCHFELDER, C. F. CURTISS, and R. B. BIRD. Molecular theory of gases and liquids. Wiley, New York. 1966.
25. C. L. DE LIGNY and N. G. VAN DER VEEN. Chem. Eng. Sci. **27**, 391 (1972).
26. M. J. BLANDAMER, D. E. CLARK, N. J. HIDDEN, and M. C. R. SYMONS. Chem. Commun. 341 (1966).

The dependence of the photochemically induced reduction of lumiflavin on pH, light intensity, and concentration of sulphydryl compounds

PARMINDER S. SURDHAR AND DAVID A. ARMSTRONG
Department of Chemistry, University of Calgary, Calgary, Alta., Canada T2N 1N4

Received March 19, 1985

PARMINDER S. SURDHAR and DAVID A. ARMSTRONG. Can. J. Chem. **63**, 3411 (1985).

The spectral changes which occur on photolysis of flavin solutions containing β-mercaptoethanol (RSH) and lipoamide ($L(SH)_2$) are in accord with the formation of dihydroflavin, except at pH values below 3 for RSH. Here an oxygen-stable product is formed, which has λ_{max} 360 nm and is probably a C-4a substituted dihydroflavin. The fraction of flavin present when FlH_2 reaches a photostationary state $f(FlH_2)_{ps}$ is dependent on pH and on the absorbed light intensity I_a. At certain pH values the actual photostationary concentration of FlH_2 is linear in the concentration of RSH, but for the lipoamide system shows a more complex dependence on concentration. The initial quantum yields are independent of absorbed light intensity in the pH range 7 to 10 for RSH, and increase strongly with pH in the region 7 to 9 for both sulphydryl compounds. In the pH range 5–6 they are linear in sulphydryl concentration. For RSH the results can be explained by a mechanism in which flavin triplet abstracts a hydrogen atom from RSH to form RS· and ·FlH radicals. These radicals undergo back reaction to RSH and Fl or form RSSR and FlH_2 by one of two mechanisms: (*a*) formation of $RS\dot{S}R^-$, which electron transfers to Fl or ·FlH or (*b*) reaction of RS· with ·FlH--RSH complexes. The results with $L(SH)_2$ can be explained similarly.

PARMINDER S. SURDHAR et DAVID A. ARMSTRONG. Can. J. Chem. **63**, 3411 (1985).

Les changements spectraux qui se produisent lors de la photolyse de solutions de flavines contenant du β-mercaptoéthanol (RSH) et de la lipoamide ($L(SH)_2$) pourraient être expliqués par la formation de la dihydroflavine, à l'exception des pH inférieurs à 3 dans le cas du RSH. Dans ces cas, il y a formation d'un produit qui est stable vis-à-vis de l'oxygène, qui présente un λ_{max} à 360 nm et qui est probablement une dihydroflavine substituée en position C-4a. La fraction de flavine qui est présente quand la FlH_2 atteint un état photostationnaire, $f(FlH_2)_{ps}$, qui dépend du pH et de l'intensité de la lumière absorbée, I_a. A certains pH, la concentration photostationnaire réelle de la FlH_2 varie d'une façon linéaire avec la concentration en RSH; dans le cas du système de la lipoamide, on note toutefois une relation plus complexe avec la concentration. Dans le cas du système du RSH et à des pH allant de 7 à 10, les rendements quantiques initiaux ne dépendent pas de l'intensité de la lumière absorbée; toutefois, pour chacun des composés sulfurés et à des pH allant de 7 à 9, ces rendements augmentent rapidement. Aux pH allant de 5 à 6, ils sont linéaires avec les concentrations en sulfhydryles. Pour le système RSH, les résultats peuvent être expliqués par un mécanisme dans lequel l'état triplet d'une flavine enlève une hydrogène du RSH pour former des radicaux RS· et ·FlH. Ces radicaux subissent des réactions de retour vers le RSH et la Fl ou ils forment du RSSR et de la FlH_2 par l'un des deux mécanismes suivants: (*a*) formation de $RS\dot{S}R^-$ qui donne des réactions de transferts d'électron conduisant à la Fl ou au ·FlH ou (*b*) réaction du RS· avec des complexes ·FlH--RSH. On peut expliquer de la même manière les résultats obtenus avec le $L(SH)_2$.

[Traduit par le journal]

Introduction

Flavin molecules are prosthetic groups in a large number of essential oxidation-reduction enzymes (1) and there is a strong interest in the redox chemistry of their ground and excited states (2–5). Scheme 1 depicts the sequences of reactions which have been postulated to explain products formed on photolysis with light in the wavelength range 400–500 nm. Here DH_2 represents a reductant or hydrogen donor and Fl the oxidised form of the flavin, while $Fl\cdot^-$ and $FlH\cdot$ are the anionic and neutral forms of the semiquinone free radical. Fl^1 and Fl^3 are the flavin singlet and triplet excited states. For common flavins, such as flavin mononucleotide (FMN), flavin adenine dinucleotide (FAD), and lumiflavin (LFl), the 1,5-dihydroflavin or FlH_2 form has a pK in the region of 6 to 7 (6). The

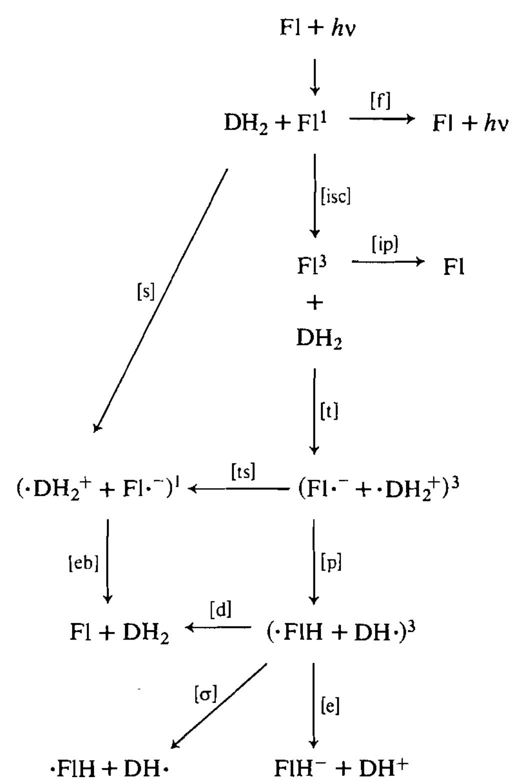

SCHEME 1. Reactions:
[f] = fluorescence,
[isc] = intersystem crossing,
[ip] = triplet decay via isc and phosphorence,
[s] = singlet quenching,
[t] = triplet quenching,
[ts] = triplet → singlet,
[p] = proton transfer,
[d] = back donation,
[eb], [e] = electron transfer,
[σ] = outward diffusion of geminate pair.

pK for the semiquinone is near 8.3 (7). The structural formulae of lumiflavin, Fl, and dihydrolumiflavin anion, FlH^-, are

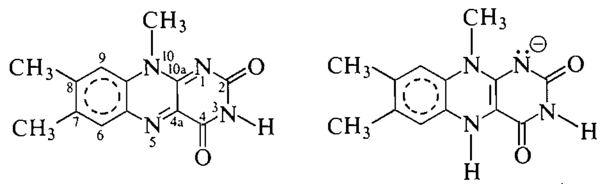

Detailed photochemical and flash photolysis experiments (2–5, 8–10) have been performed with a large variety of DH_2 species, so that values of k_t have been determined for phenols, amines, amino acids, and certain sulphur-containing compounds, as well as the photophysical constants k_f and k_{isc}.

The case of the sulphydryl-containing amino acid L-cysteine is particularly interesting. Here the value of k_t at pH 7 ($4.5 \pm 0.5 \times 10^7\ M^{-1}\ s^{-1}$) is some hundred fold or more larger than for glycine (8), implying that the sulphydryl group is involved in reaction [t]. Furthermore there are strong indications that the quenching process occurs by $\cdot H$ transfer rather than the sequence [t] and [p] as in Scheme 1. This observation is actually in line with the well-known hydrogen-donating ability of sulphydryl molecules (RSH) (11) and the reaction may be written:

[1] $\quad Fl^3 + RSH \rightarrow (\cdot FlH + RS\cdot)^3$

Ahmad and Armstrong (12) have studied the reactions of $RS\cdot$ radicals with flavin species. They pointed out that the redox potential of reaction [2] is relatively high

[2] $\quad RS\cdot + e^- \rightleftharpoons RS^-$

($E_2^0 \cong 1.0$ V), and that $RS\cdot$ would oxidise $\cdot FlH$ and FlH_2. However, at pH $\geqq$ pK_i ($\cong$8.5 for cysteine (13)), $RS\cdot$

[*i*] $\quad RSH \rightleftharpoons RS^- + H^+$

forms $RS\dot{S}R^-$

[*b*] $\quad RS^- + RS\cdot \rightleftharpoons RS\dot{S}R^-$

This species was shown to reduce Fl (12).

[3*b*] $\quad RS\dot{S}R^- + Fl \rightarrow RSSR + Fl\cdot^-$

It would also be capable of reducing $\cdot FlH$:

[3*b*′] $\quad RS\dot{S}R^- + \cdot FlH \rightarrow RSSR + FlH^-$

It follows that at pH values below pK_i the back reaction

[3] $\quad (\cdot FlH + RS\cdot)^3 \rightarrow Fl + RSH$

should be the dominant route for removal of the radical pair formed in [1]. This also should be true for radical pairs, which initially separate from each other (reaction [σ] in scheme 1) and subsequently react by random diffusion.

[3*a*] $\quad \cdot FlH + RS\cdot \rightarrow Fl + RSH$

In either event the fraction of radical pairs producing FlH^- (or FlH_2) should be small. On the other hand at pH $\geqq$ pK_i reactions [3*b*] and [3*b*′] may compete with [3*a*]. Thus the yield of dihydroflavin should rise with increasing pH in the region of pK_i, until it reaches a maximum. The surprising feature of the experiments with cysteine was the fact that a relatively large proportion of $\cdot FlH + RS\cdot$ radical pairs actually formed FlH_2 at pH 7 (3), which is well below pK_i (13). This observation suggests that there are additional reactions to those considered above.

The present study was undertaken with the objective of determining the initial quantum yields and maximum concentrations of FlH_2 formed by photolysis in the presence of sulphydryl molecules, and studying their dependence on pH, light intensity, and RSH concentration. The flavin used was lumiflavin and β-mercaptoethanol was chosen as the RSH molecule. It is simpler than cysteine in that ionisation of the —SH group is the only process which leads to changes in net charge of the molecule with pH. The pK_i and the magnitude of K_b are known to be 10.0 and $1.8 \times 10^3\ M^{-1}$, respectively (14, 15). The disulphydryl lipoamide $L(SH)_2$ was also used. It differs from monosulphydryls in that the disulphide anion ($L\dot{S}_2^-$) and its protonated form ($L\dot{S}_2H$), which has a pK of 5.5 (16–18), are both considered to exist as stable ring structures:

[*b*1] 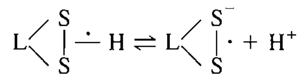

($L\dot{S}_2H$) $\qquad$ ($LS_2^-\cdot$)

Thus in this system $L\dot{S}_2H$ replaces the $RS\cdot$ species. Also the proportions of $L\dot{S}_2H$ and $LS_2^-\cdot$ are independent of $[L(SH)_2]$ and are determined only by pH, while with RSH the proportion of $RS\dot{S}R^-$ increases with [RSH].

Experimental

Materials

Lumiflavin and β-mercaptoethanol (RSH) were supplied by Sigma Chemical Co. Dihydrolipoamide ($L(SH)_2$) was prepared from lipoamide by the method of Reed *et al.* (19). All other chemicals were the purest grade available and used as supplied.

Methods

All solutions were prepared from triply distilled water and saturated with high purity N_2O (Matheson), which was first passed through a column of "ridox" (Fisher Scientific Company) to remove traces of oxygen. All solutions were buffered with phosphate buffer and protected from light as much as possible. For all solutions of $L(SH)_2$ and RSH above pH 9, the buffer and other solutes were added and the solution deareated before the addition of $L(SH)_2$ or RSH. Finally the pH was adjusted by the addition of NaOH or perchloric acid. This was done in order to minimise air oxidation of the sulphydryl. All experiments were carried out at 23 ± 2°C. Concentrations of Fl and FlH_2 were calculated with the following extinction coefficients at 44o nm — Fl: 12320 pH 4–8; 12045 pH 9–11; FlH_2/FlH^-: 1454 pH 4–6, 1488 pH 7–8, 1230 pH 9–11.

Apparatus

The photolysis lamp consisted of a 250 W Halogen Bellophot fitted with a water filter. The light was collimated through filters with maximum λ and minimum λ transmissions of 465 and 420 nm, respectively. Light intensities at various distances were determined chemically using ferrioxalate actinometry (20). The actinometer solution was 0.15 *M* potassium ferrioxalate in 0.1 *N* sulphuric acid. A molar extinction coefficient of $1.05 \times 10^4\ M^{-1}\ cm^{-1}$ at 510 nm for 1,10-phenanthroline complex was determined experimentally by the procedures of Hatchard and Parker (20).

The spectrum incident on the 1 cm square quartz photolysis cell was calculated form the emission spectrum of the lamp and the percentage transmission of the filters. The fraction of light absorbed over the band of wavelengths was calculated from the absorption spectrum of each irradiated solution.

Steady state radiolyses were performed in an AECL ^{60}Co γ cell with a steady dose rate of ~10.0 Gy min^{-1}. The dose rate was determined by ferrous sulphate dosimetry, assuming $G(Fe^{3+}) = 15.6$ molecules per 100 eV (21), and checked periodically to correct for the natural decay of the isotope. The net number of moles of radicals produced per litre of solution for a given radiation dose, e_{red}, was calculated by means of eq. [12] of ref. 22.

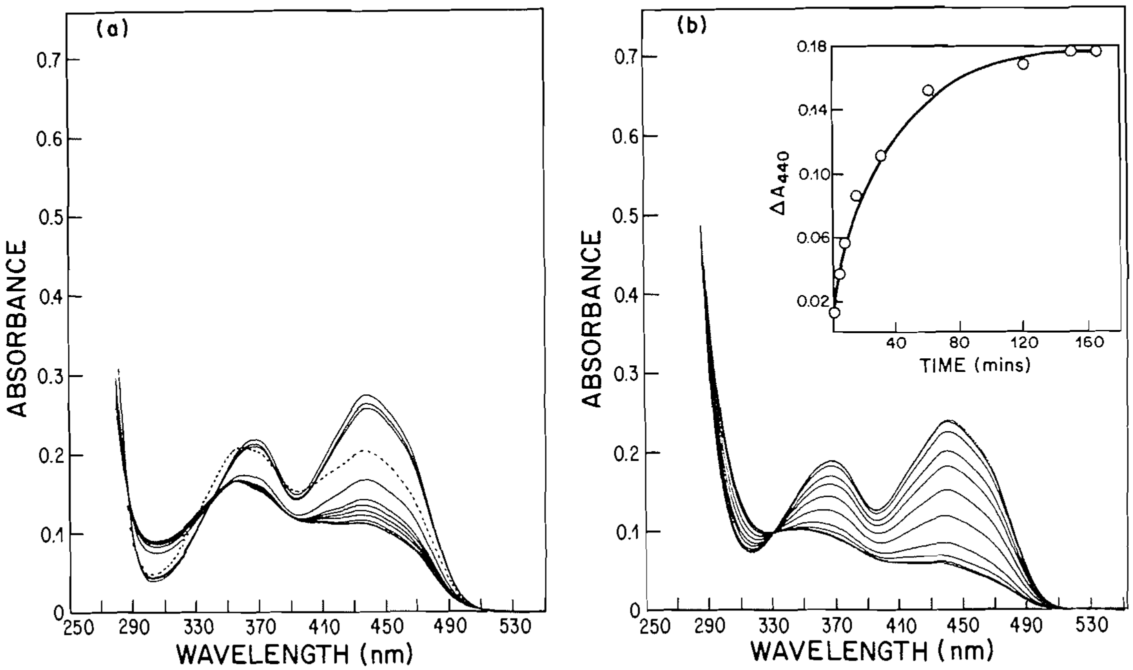

FIG. 1. Spectra obtained from N_2O-saturated solution of 20–23 μ*M* lumiflavin in 10 m*M* RSH and 10 m*M* phosphate buffer at (*a*) pH 3 and (*b*) pH 9 before and after photolysis with light intensities (I_0) of 6.82×10^{-6} and 2.09×10^{-7} einsteins cm^{-2} s^{-1}, respectively. Dashed lines (----) show spectra after aeration, the one in (*b*) coinciding with initial spectrum. Inset: Changes in ΔA_{440} versus time after photolysis.

Results

Spectral changes

The changes in absorbance which occur on photolysis of flavin solutions containing β-mercaptoethanol are illustrated in Fig. 1*a* and *b*. As shown in Fig. 1*b*, at pH 9 the flavin absorption is reduced by each successive exposure to light, until finally a photostationary state is reached. The change in absorbance at 440 nm (ΔA_{440}) has been plotted as a function of photolysis time in the inset. On addition of air the initial flavin absorbance is restored, dashed line in Fig. 1*b*. This feature, the isobestic point at 333 nm and the nature of the spectral changes are in accord with the formation of dihydroflavin, a conclusion which also conforms with the earlier study of Heelis *et al.* (3).

At pH values below 3 the changes in absorbance are different. As illustrated in Fig. 1*a* the absorbance above 330 nm is suppressed less before the stationary state is reached and there is no longer a clear cut isobestic point. In addition, on aeration the flavin absorbance is not entirely restored. The spectral changes indicate that in addition to FlH_2 an oxygen-stable product has been formed and that this has isobestic points with Fl at ~358, ~382, and ~402 nm. By estimating the concentration of FlH_2 in the mixture at the photostationary state from the change in ΔA at 440 nm on addition of air and that of residual Fl from the absorbance at 470 nm where the absorbance of reduced flavins is mall, we were able to calculate the absorbance due to Fl and FlH_2 from their known spectra. The absorbance of the other product was then obtained by subtraction from the absorbance of the mixture. This was found to have a maximum at 360 nm, which is typical of a 4*a*-substituted dihydroflavin (23, 24), such products being formed by additions of free radicals to ·FlH radicals. In the present instance the oxygen-stable product was shown to be stable under our conditions both at low and high pH. Thus there is no evidence for its reacting with RSH or RS^-. Its identification and properties were not pursued further here.

The photochemical effects observed with lipoamide as the sulphydryl were similar to those described above, except that there was no evidence for an oxygen-stable product and reversible reduction to FlH_2 was seen at all pH values.

Photostationary concentrations

The fraction of flavin present as FlH_2 in the photostationary state[1] $f(FlH_2)_{ps}$ has been plotted as a function of pH in Fig. 2*a* and *b* for solutions containing 10 m*M* β-mercaptoethanol and 1.0 m*M* lipoamide, respectively. Data are shown for different incident light intensities, I_0.

The results obtained for γ-radiolysis in the absence of light are included for comparison.[2] It is apparent that with both sulphydryl molecules $f(FlH_2)_{ps}$ is (*a*) dependent on pH, (*b*) increases with incident light intensity, (*c*) is larger for the photochemically than the radiation chemically stimulated system.

As a means of demonstrating that a true photostationary state was involved, it was shown that if after reaching a stationary state at a high intensity, the solution was subjected to a lower intensity then $f(FlH_2)_{ps}$ decreased to the value characteristic of that intensity.

The photostationary concentration of FlH_2 was measured in the presence of varying [RSH] at pH 6, where it is about half way to its maximum value at the higher intensity in Fig. 2*a*. It can be seen from Fig. 3 that $[FlH_2]_{ps}$ is linear in [RSH] and proportional to $I_a^{1/2}$. Here it should be noted that I_a, the absorbed light intensity averaged over the cell length, was calculated from the observed concentration of Fl at the stationary

[1] The formula $f(FlH_2)_{ps}$ has been used to denote reduced flavin present at the photostationary state regardless of pH.

[2] Note that in the first approximation $[FlH_2]_{ps}$ should be independent of the γ ray dose rate. Unfortunately it was not practical to check this point by altering the dose rate to give a range of radical production rates in the same range as those obtained in photolysis.

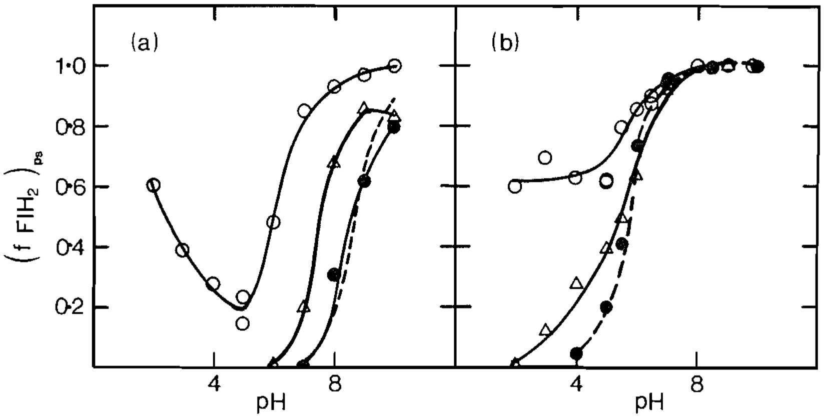

FIG. 2. Values of $f(\mathrm{FlH_2})_{ps}$ versus pH for the photoreduction of lumiflavin with 10 mM RSH (a) and 1 mM $\mathrm{L(SH)_2}$ (b) at light intensities (I_o) of (○) 6.82×10^{-6}, (△) 2.09×10^{-7} einsteins $\mathrm{cm^{-2}\ s^{-1}}$, respectively. The solid (●) points are for γ-radiolysis at a radical formation rate of 1.1×10^{-7} M $\mathrm{s^{-1}}$, and the dashed lines (----) are the calculated fraction of B· radicals.

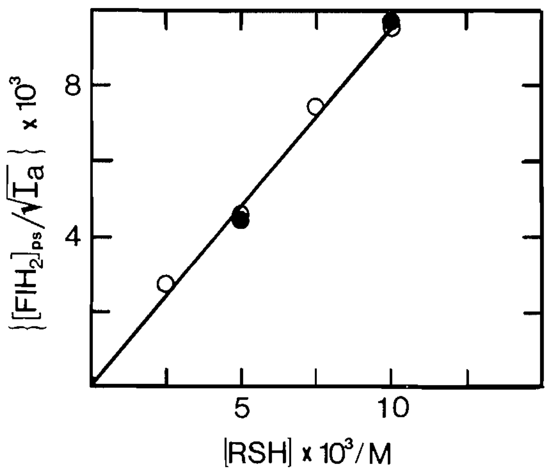

FIG. 3. Plot of $\{[\mathrm{FlH_2}]_{ps}/\sqrt{I_a}\} \times 10^3$ versus the concentration of RSH at pH 6 using light intensities (I_o) of (○) 6.82×10^{-6}, (●) 3.68×10^{-5} einsteins $\mathrm{cm^{-2}\ s^{-1}}$, respectively.

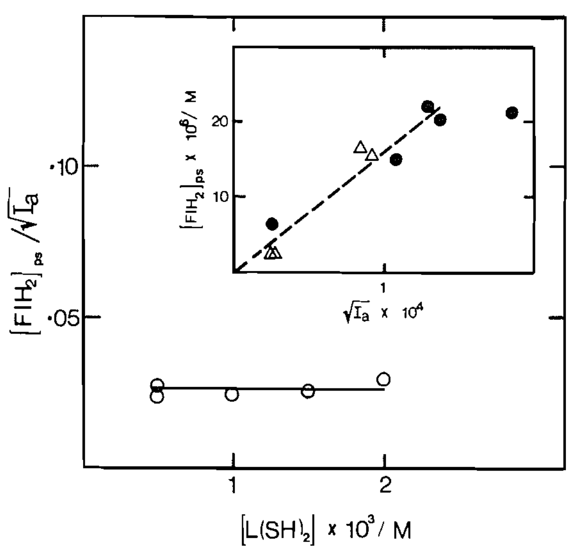

FIG. 4. Plot of $[\mathrm{FlH_2}]_{ps}/\sqrt{I_a}\}$ versus the concentration of $\mathrm{L(SH)_2}$ at pH 5 using light intensity (I_o) of 6.82×10^{-6} einsteins $\mathrm{cm^{-2}\ s^{-1}}$. Inset: plot of $[\mathrm{FlH_2}]_{ps} \times 10^6/M$ versus $\sqrt{I_a} \times 10^4$ using light intensities in the range $1-226 \times 10^{-7}$ einsteins $\mathrm{cm^{-2}\ s^{-1}}$ at pH 3 (△) and at pH 4 (●), respectively.

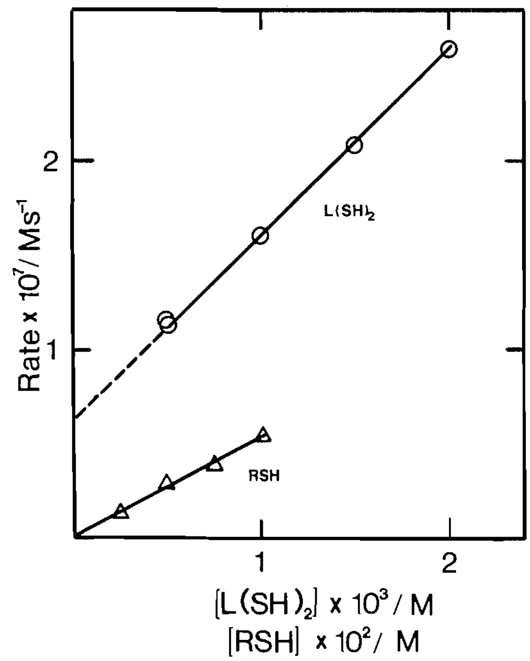

FIG. 5. Plot of initial rate versus concentration of $\mathrm{L(SH)_2}$ and RSH at pH 5 and 6, respectively, using light intensities (I_o) of 6.82×10^{-6} einsteins $\mathrm{cm^{-2}\ s^{-1}}$.

state and the incident light intensity.

For the lipoamide system in the pH range 3 to 5, where $f(\mathrm{FlH_2})_{ps}$ was rising with pH, $[\mathrm{FlH_2}]_{ps}$ is again apparently linear in $I_a^{1/2}$. However, in this instance it was independent of $[\mathrm{L(SH)_2}]$, see Fig. 4. Also the results were less reproducible.

Initial rates and quantum yields

The initial slopes of plots like the inset in Figure 1b were divided by ($\epsilon_{\mathrm{Fl}} - \epsilon_{\mathrm{FlH_2}}$) and used to calculate initial rates. The dependences of these on sulphydryl concentration were determined at pH values in the region 5 to 7, Fig. 5. For both systems they are linear in concentration. However, there is an intercept or concentration-independent component for lipoamide, which is not present for RSH.

Quantum yields, calculated by dividing the initial rates of flavin reduction by the absorbed intensity, are depicted in Fig. 6a and b for 10 mM RSH and 1 mM $\mathrm{L(SH)_2}$ respectively. A

TABLE 1. Summary of reactions for RSH*

$Fl \rightleftharpoons \cdot FlH \rightleftharpoons FlH_2$	
[1] $Fl^3 + RSH \rightarrow \cdot FlH + A\cdot$	
	[3*b*′] $\cdot FlH + B\cdot (+ H^+) \rightarrow RSSR + FlH_2$
[3*b*] $Fl + B\cdot (+ H^+) \rightarrow \cdot FlH + RSSR$	
	$2\cdot FlH \underset{[-5]}{\overset{[5]}{\rightleftharpoons}} Fl + FlH_2$
$Fl + FlH_2 \underset{[5]}{\overset{[-5]}{\rightleftharpoons}} 2\cdot FlH$	
[3*a*] $Fl + RSH \leftarrow \cdot FlH + A\cdot$	[4] $\cdot FlH + RSH \leftarrow A\cdot + FlH_2$
	[3*c*] $\cdot C + A\cdot \rightarrow RSSR + FlH_2$
[3*c*′] $Fl + 2RSH \leftarrow \cdot C + A\cdot$	
	[3*c*″] $\cdot C + A\cdot \rightarrow RSFlH + RSH$
	[3″] $\cdot FlH + A\cdot \rightarrow RSFlH$
	[6] $\cdot FlH + RSSR \leftarrow RSFlH + A\cdot$
[7] $Fl + RS\cdot + RSH \leftarrow A\cdot + RSFlH$	
	[8] $RSFlH + RS^- + H^+ \rightarrow RSSR + FlH_2$

* A few obvious alterations are needed to balance these equations for $L(SH)_2$.

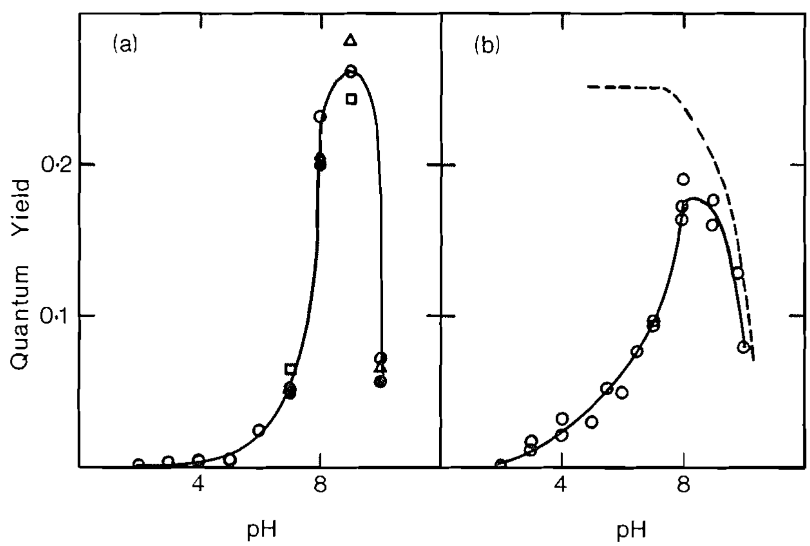

FIG. 6. Plots of quantum yield versus pH for (*a*) RSH and (*b*) $L(SH)_2$ using light intensities (I_0) of (△) 2.09×10^{-7}, (●) 3.22×10^{-7}, (○) 6.82×10^{-6}, and (□) 3.68×10^{-5} einsteins $cm^{-2}\,s^{-1}$, respectively. Dashed line (----) shows the relative quantum yields for the photoreduction of riboflavin by EDTA from Fife and Moore (4). The ordinate scale for this has been multiplied by 0.255.

strong dependence on pH is clearly evident. Also demonstrated for the RSH system is the fact that these initial yields are independent of absorbed intensity (see different sets of points) for pH in the range 7 to 10.

Discussion

The mechanism

The flavin molecule reactions considered here are summarised in Table 1. In the γ-radiolysis experiments there are the additional reactions producing the $RS\cdot$ or $L\dot{S}_2H$ radical (18):

[9] $H_2O \rightsquigarrow e^-_{aq} + \cdot H + \cdot OH + H_2O_2 + H_2$

[10] $e^-_{aq} + N_2O + H_2O \rightarrow N_2 + OH^- + \cdot OH$

[11] $\cdot OH\ (\text{or}\ \cdot H) + RSH \rightarrow H_2O\ (\text{or}\ H_2) + RS\cdot$

[11*l*] $\cdot OH\ (\text{or}\ \cdot H) + L(SH)_2 \rightarrow H_2O\ (\text{or}\ H_2) + L\dot{S}_2H$

For convenience these radicals are symbolised by $A\cdot$ in Table 1, while the $RS\dot{S}R^-$ and $LS_2^-\cdot$ radicals formed in reaction [*b*] and [*b*1], respectively (see Introduction) are referred to as $B\cdot$ radicals. Since these two reactions and the reverse processes are known to be rapid (14, 25) it is reasonable to assume as a first approximation that equilibrium is maintained between the $A\cdot$ and $B\cdot$ radicals. One then has

$$[B\cdot] = [A\cdot]\theta_B$$

where θ_B is given by

$$\theta_B = [RSH]_{total}\,K_b\{1 + [H^+]/K_i\}^{-1}$$

for RSH, and

$$\theta_B = K_{b1}[H^+]^{-1}$$

for $L(SH)_2$ respectively. It may be recalled that the $B\cdot$ radicals are reductive and the $A\cdot$ radicals oxidative towards FlH_2 and $\cdot FlH$ (ref. 12 and above).

All of the reactions down to [3*a*] and [4] in Table 1 were contained in the mechanism of Ahmad and Armstrong (12). However, those below [4] are new, and the equilibrium

[*c*] $RSH\ \text{or}\ L(SH)_2 + \cdot FlH \rightleftharpoons \cdot C$

has been assumed for $\cdot$FlH and its complex with RSH or $L(SH)_2$, $\cdot$C. The evidence for this stems from recent studies of flavin semiquinone spectra in the presence of RSH or RS^- molecules (26, 27). In the equations which follow we write $[\cdot C] = \theta_C[\cdot FlH]$, where θ_C is equal to K_c[RSH].

Given the existence of the complex $\cdot$C, it is feasible to consider the formation of FlH_2 via [3*c*]. Also the production of a C-4a adduct RSFlH could be explained through reactions [3″] and [3*c*″]. Reaction [3*c*′] is incorporated for completeness. There are then three pathways for the formation of FlH_2 from $\cdot$FlH: [3*b*′], [3*c*], and [3″] or [3*c*″] + [8]. However, as we have seen earlier, the present experiments indicate that the oxygen-stable product is stable to both RSH and RS^-. Thus there is no evidence for reaction [8] in this system. Also the C-4a adduct is not seen at pH > 3. Therefore the last pathway is not considered further here.

The photostationary state

Application of the steady state approximation now leads to the following equation for $[FlH_2]_{ps}$, in which ρ is proportional to I_a (see further below):

$$[12]\quad [FlH_2]_{ps} = \frac{\rho}{k_4[A\cdot]_{ps}} + k_{3b}\theta_B[Fl]_{ps}/k_4 + [k_{3b'}\theta_B - k_{3a} + (k_{3c} - k_{3c'})\theta_C]\,[\cdot FlH]_{ps}/k_4$$

For radiolysis the first term in ρ is zero. Furthermore, if θ_B is zero, the second term is zero and there is no process for converting Fl to $\cdot$FlH. It follows that $[FlH_2]_{ps}$ for the γ radiolysis will be near zero unless θ_B is significant (≧ 0.1). Also it will be less than $[FlH_2]_{ps}$ for photolysis under comparable conditions and should more closely depend on θ_B or more specifically the fraction of radicals present as B$\cdot$, $(\theta_B(1 + \theta_B)^{-1})$. These features are confirmed by the data in Fig. 2*a* and *b*. Note that $\theta_B(1 + \theta_B)^{-1}$, which has been plotted as a function of pH, closely parallels the points for γ-radiolysis.

Unfortunately the mechanism is too complex for exact expressions for the values of $[A\cdot]_{ps}$ and $[\cdot FlH]_{ps}$ to be derived. However, an approximate relation, which is a useful semi-quantitative quide, may be obtained, if one assumes that $k_5[\cdot FlH]^2_{ps} \cong k_{-5}[Fl]_{ps}\,[FlH_2]_{ps}$ and $[\cdot FlH]_{ps} \cong [A\cdot]_{ps}$, viz:

$$[13]\quad [FlH_2]_{ps} = \{2k_{3b'}\theta_B + 2k_{3c}\theta_C\}\rho^{1/2}k_4^{-1} \times \{k_{3b'}\theta_B + k_{3a} + \theta_C(k_{3c} + k_{3c'})\}^{-1/2}$$

The latter assumption is reasonable in the regions of low efficiency of reduction where the k_{3c} and $k_{3c'}$ terms are small and reaction [3*a*] dominates over [3*b*′]. Thus expression [13] reduces to:

$$[14]\quad [FlH_2]_{ps} = \{2k_{3b'}\theta_B + \theta_C 2k_{3c}\}\rho^{1/2}/k_4k_{3a}^{1/2}$$

This equation predicts the dependence of $[FlH_2]_{ps}$ on $\rho^{1/2}$ which is seen in Fig. 3 and the inset in Fig. 4. Basically the reason for this dependence is the competition for A$\cdot$ radicals between FlH_2 (reaction [4]) and $\cdot$C (reaction [3*c*]). At low reduction efficiencies (i.e. low pH) the concentration of $\cdot$C is controlled largely by reaction [3*a*], and is therefore approximately dependent on $\rho^{1/2}$.

One may note that we were unable to explain the dependence on $\rho^{1/2}$ on the basis of B$\cdot$ radical reactions alone. However, at high pH, where θ_B becomes > 1, reactions [3*b*] and [3*b*′] should become more important than [3*a*] and the "B$\cdot$ mechanism" takes over. The $f(FlH_2)_{ps}$ loses its intensity dependence, Fig. 2*a* and *b*.

The sulphydryl molecule concentration dependence is obtained on substituting the appropriate formulae for θ_B and θ_C. For RSH it is linear with zero intercept:

$$[15]\quad [FlH_2]_{ps} = 2\{k_{3b'}K_b/(1 + [H^+]/K_i) + k_{3c}K_C\}\,[RSH]_{total} \times (\rho^{1/2}/k_4)/k_{3a}^{1/2}$$

which is in accord with the data in Fig. 3. In the case of $L(SH)_2$ there is an $[L(SH)_2]$ independent term, arising from θ_B, viz:

$$[16]\quad [FlH_2]_{ps} = 2\{k_{3b'}K_{b1}/[H^+] + k_{3c}K_C[L(SH)_2]_{total}\} \times (\rho^{1/2}/k_4)/k_3^{1/2}$$

From the data in Fig. 5 this term seems to dominate, since there is no evidence for a strong positive slope.

Initial rates

Application of the steady state assumption to the concentrations of intermediates leads to the following expression for the initial rate of formation of FlH_2:

$$[17]\quad \frac{d[FlH_2]}{dt} = \{k_{3b'}\theta_B + k_{3c}\theta_C\}\frac{2\rho + r - 2k_5[\cdot FlH]^2}{2[k_{3b'}\theta_B + k_{3a} + \theta_C(k_{3c} + k_{3c'})]} + k_5[\cdot FlH]^2$$

Here ρ and *r* are, respectively, the rates of formation of A$\cdot$ radicals in reactions [1] and [11] or [11*l*], respectively. The former applies in photolysis and the latter in radiolysis. If the same assumptions are made for the region of low efficiency of reduction as before, then for photolysis with RSH one has:

$$[18]\quad \frac{d[FlH_2]}{dt} = \{k_{3b'}K_B/\{1 + [H^+]/K_i\} + k_{3c}K_C\}\,[RSH]_{total} \times \rho/k_{3a}$$

and with $L(SH)_2$:

$$[19]\quad \frac{d[FlH_2]}{dt} = \{k_{3b'}K_{b1}/[H^+] + k_{3c}K_C[L(SH)_2]_{total}\} \times \rho/k_{3a}$$

Again in each case there is a linear dependence on sulphydryl molecule concentration. However, for $L(SH)_2$ there is a concentration independent term containing $k_{3b'}K_{b1}$. This can explain the presence of the intercept for $L(SH)_2$ plot in Fig. 5. The linear portion of that plot is consistent with the occurrence of reaction [3*c*]. In further agreement with the mechanism there is no intercept for RSH.

Quantum yields

The maximum value of $d[FlH_2/dt$ is seen from expression [17] to occur for the condition $\{k_{3a} + \theta_C k_{3c'}\} \ll (k_{3b'}\theta_B + k_{3c}\theta_C)$. Expression [17] then reduces to:

$$\frac{d[FlH_2]}{dt} = \rho$$

for photolysis and *r*/2 for radiolysis. The efficiencies of conversion, ε, may be defined as $(d[FlH_2]/dt)/\rho$ and $2(d[FlH_2]/dt)/r$ for photolysis and radiolysis, respectively. Values of ε may be calculated from the data of Ahmad and Armstrong (12) for γ-radiolysis of the FAD–$L(SH)_2$ system at pH 7. The magnitude of ε was 1.0 ± 0.1 independent of $[L(SH)_2]$ in the range 0.5 to 1.5 m*M*. Similar results were obtained here for LFl–$L(SH)_2$. At lower pH values ε falls as expected, becoming zero at about pH 4. Values of ε for RSH are summarised in Table 2. At pH 7 and below it was immeasurably small in 10 m*M* solutions. It rises steeply at pH 8 to

TABLE 2. Values of ϵ for RSH

[LFl] μM	[RSH] mM	pH	eff., ϵ	θ_B	f_B*
22.09	10.0	8	0.83	0.18	0.15
17.90	10.0	9	0.84	1.64	0.62
22.85	10.0	10	0.75	9.00	0.90
21.50	10.0	11	1.09	16.4	0.94
24.03	5.0	10	0.56	4.50	0.82
23.66	7.5	10	0.63	6.75	0.87
22.85	10.0	10	0.75	9.00	0.90
23.13	12.5	10	0.81	11.25	0.92
22.93	15.0	10	0.88	13.50	0.93

*$f_B = \theta_B(1 + \theta_B)^{-1}$.

about 0.8 remaining at 0.75 to 1.1 up to pH 11. At pH 10 it increases with concentration of RSH.

An interesting feature is that the fraction of B· radicals $\theta_B(1 + \theta_B)^{-1}$ (see columns 4 and 6) does not correlate well with ϵ. This is probably an indication that the complex ·C is involved in the ·FlH to FlH_2 step of the γ-radiolysis mechanism, although as pointed out above the Fl to ·FlH stage is supported here only by B· radicals.

The overall quantum yields in Fig. 6*a* and *b* could be used to calculate ϵ, if the quantum yield Φ(·FlH) for eaction [1] were known. Actually this has been measured only for the cysteine–FMN system at pH 7 and 4.1, where it is 0.14 and 0.45, respectively (8). Assuming similar yields apply to the β-mercaptoethanol–LFl system, on dividing the quantum yields in Fig. 6*a* by these numbers one obtains $\epsilon = 0.41$ and 0.009 at pH 7.0 and 4.1, respectively. These results, though approximate, demonstrate clearly the pH dependence of ϵ.

The above results of Heelis *et al.* (8) demonstrate that Φ(·FlH) falls off with pH for cysteine. The reason for this is not clear. However, a dependence of Φ_{isc} on pH has been demonstrated with other hydrogen donating solutes (4). This is shown by the dashed line in Fig. 6*b*. It would be reasonable to suppose that this drop off at pH > 8 is responsible for the fall off in the overall quantum yields for FlH_2/FlH^-. More detailed conclusions cannot be drawn until further values of Φ(·FlH) have been reported.

Finally there is one published quantum yield of FlH_2 for FMN in 0.04 *M* cysteine at pH 7, with which the present results may be compared. This is the value of 0.076 ± 0.008 reported by Heelis *et al.* (3). It is in good agreement with our value of 0.050 to 0.065 for RSH in Fig. 6*a*.

To summarise, the present study has confirmed that photoreduction of Fl to FlH_2 occurs in the presence of sulphydryl molecules, and demonstrated the formation of photostationary FlH_2 concentrations and a strong dependence of the initial quantum yields on pH. The mechanism proposed rationalises these observations and the dependences of the initial rates on sulphydryl concentration. While the reactions of B· radicals undoubtedly play a dominant role at high pH, there is also evidence for reduction of ·FlH, which is precomplexed with sulphydryl, by RS· radicals in reaction [3*c*]. That process may be rewritten as

[3*ci*] $RS\cdot + RSH\text{--}\cdot FlH \rightarrow RSSR + FlH_2$

or, if the RSH in the complex is deprotonated, as

[3*cj*] $RS\cdot + RS^-\text{--}\cdot FlH \rightarrow RSSR + FlH^-$

Further studies of these reactions will be undertaken and their relevance to biological flavin systems will be examined.

Acknowledgement

This research was supported by NSERC grant A3571.

1. C. H. WILLIAM, JR. Enzyme, **13**, 89 (1976).
2. P. F. HEELIS, B. J. PARSONS, G. O. PHILLIPS, and J. F. MCKELLAR. Photochem. Photobiol. **28**, 169 (1978).
3. P. F. HEELIS, B. J. PARSONS, G. O. PHILLIPS, and J. F. MCKELLAR. Photochem. Photobiol. **30**, 343 (1979).
4. D. J. FIFE and W. M. MOORE. Photochem. Photobiol. **29**, 43 (1979).
5. J. T. SIMPSON, A. KRANTZ, F. D. LEWIS, and B. KOKEL. J. Am. Chem. Soc. **104**, 7155 (1982).
6. T. C. BRUICE. Progress in bioorganic chemistry. Vol. 4. 1979. p. 1.
7. E. J. LAND and A. J. SWALLOW. Biochemistry, **8**, 2117 (1969).
8. P. F. HEELIS, B. J. PARSONS, and G. O. PHILLIPS. Biochim. Biophys. Acta, **587**, 455 (1979).
9. M. GREEN and G. TOLLIN. Photochem. Photobiol. **7**, 129 (1968).
10. S. P. VAISH and G. TOLLIN. Bioenergetics, **2**, 61 (1971).
11. J. E. PACKER. *In* The chemistry of the thiol group. Part 2. *Edited by* S. Patai. Wiley, London. 1974. p. 481.
12. R. AHMAD and D. A. ARMSTRONG. Can. J. Chem. **62**, 171 (1984).
13. M. FRIEDMAN. The chemistry and biochemistry of the sulphydryl group in amino acids, peptides and proteins. Pergamon, New York. 1973.
14. W. KARMANN, A. GANZOW, G. MEISSNER, and A. HENGLEIN. Int. J. Radiat. Phys. Chem. **1**, 395 (1969).
15. G. G. JAYSON, D. A. STIRLING, and A. J. SWALLOW. Int. J. Radiat. Biol. **19**, 143 (1971).
16. S. W. CHAN, P. C. CHAN, and B. H. J. BIELSKI. Biochim. Biophys. Acta, **338**, 213 (1974).
17. M. FARAGGI, J. L. REDPATH, and Y. TAL. Radiation Res. **64**, 452 (1975).
18. ZHENNAN WU, R. AHMAD, D. A. ARMSTRONG. Rad. Phys. Chem. **23**, 251 (1984).
19. L. J. REED, M. KOIKE, M. E. LEVITCH, and F. R. LEACH. J. Biol. Chem. **232**, 143 (1958).
20. C. G. HATCHARD and C. A. PARKER. Proc. R. Soc. A, **235**, 518 (1956).
21. I. G. DRAGANIĆ and Z. D. DRAGANIĆ. The radiation chemistry of water. Academic Press. New York. (1971).
22. R. AHMAD and D. A. ARMSTRONG. Biochemistry, **21**, 5445 (1982).
23. W. R. KNAPPE and P. HEMMERICH. Liebigs Ann. Chem. 2037 (1976).
24. G. A. EBERLEIN and M. F. POWELL. J. Am. Chem. Soc. **106**, 3309 (1984).
25. M. Z. HOFFMAN and E. HAYON. J. Am. Chem. Soc. **94**, 7950 (1972); J. Phys. Chem. **77**, 990 (1973).
26. P. S. SURDHAR, R. AHMAD, and D. A. ARMSTRONG. Can. J. Chem. **62**, 580 (1984).
27. P. S. SURDHAR and D. A. ARMSTRONG. *In* Flavins and flavoproteins. *Edited by* R. C. Bray, P. C. Engel, and S. G. Mayhew. Walter de Gruyter and Co., Berlin. 1984.

Total synthesis of the stemodane-type diterpenoids (±)-stemodin and (±)-maritimol. Formal total synthesis of (±)-stemodinone and (±)-2-desoxystemodinone

EDWARD PIERS, BRIAN F. ABEYSEKERA, DAVID J. HERBERT, AND IAN D. SUCKLING

Department of Chemistry, University of British Columbia, 2036 Main Mall, University Campus, Vancouver, B.C., Canada V6T 1Y6

Received June 4, 1985

EDWARD PIERS, BRIAN F. ABEYSEKERA, DAVID J. HERBERT, and IAN D. SUCKLING. Can. J. Chem. **63**, 3418 (1985).

Total syntheses of the stemodane-type diterpenoids (±)-stemodin (**2**) and (±)-maritimol (**4**), as well as formal total syntheses of (±)-stemodinone (**3**) and (±)-2-desoxystemodinone (**5**), are described. The known ketol **12** was converted into the tricyclic enone **7**. Photoaddition of allene to **7** gave (96%) a mixture of the photoadducts **20**–**23** (40:51:6:3, respectively). Ozonolysis of **20**, followed by treatment of the resultant dione **24** with MeONa–MeOH (room temperature, 2.5 h), provided the keto ester **26** (94%). Subjection of **21** to an identical sequence of reactions gave (86%) the *same* product **26**. On the other hand, when the dione **25** was treated with MeONa–MeOH under much milder conditions (0°C, 5 min), the isomeric keto esters **27** (39%) and **28** (33%) were produced. Both **27** and **28**, upon reaction with MeONa–MeOH at room temperature, were converted efficiently into **26**. Reduction ($NaBH_4$ or Li*sec*-Bu_3BH) of **26** provided separable mixtures of the ester alcohol **32** and the lactone **33**, which could be transformed readily into the dimesylates **35** and **39**, respectively. Reaction of **35** and **39** with NaCN in warm hexamethylphosphoramide afforded the dinitriles **37** and **40**, both of which, upon treatment with *t*-BuOK in refluxing *t*-BuOH, produced the same enaminonitrile **41**. Acid hydrolysis of **41** provided the dione **42**. Preparatively, compound **26** could be transformed conveniently into the dione **42** (52% overall yield) without separation of mixtures of isomeric synthetic intermediates. Treatment (CH_2Cl_2, −95°C) of **42** with Me_3SiI–Et_3N, followed by oxidation of the resultant products **46** and **47** with $Pd(OAc)_2$ in acetonitrile, gave the bis enones **48** (67%) and **49** (19%). Compound **48** was converted into the dione **52** which, upon reaction with $(i\text{-PrO})_3TiMe$ in ether, provided an 86:14 mixture of the keto alcohols **53** and **54** (63% from **48**). Reduction ($NaBH_4$) of **53** afforded (±)-maritimol (**4**). On the other hand, conversion of the 86:14 mixture of **53** and **54** into the *p*-toluenesulfonylhydrazones **55** and subsequent reaction of **55** with NaH in refluxing toluene gave the alkene alcohols **56** (58%) and **57** (12%). Hydroboration–oxidation (9-BBN, refluxing tetrahydrofuran; NaOH, H_2O_2) of **56** afforded (88%) (±)-stemodin (**2**).

EDWARD PIERS, BRIAN F. ABEYSEKERA, DAVID J. HERBERT et IAN D. SUCKLING. Can. J. Chem. **63**, 3418 (1985).

On décrit des synthèses totales des diterpénoïdes, du type stémodane, (±)-stémodine (**2**) et (±)-maritimol (**4**) ainsi que des synthèses totales formelles de la (±)-stémodinone (**3**) et de la (±)-déoxy-2 stémodinone (**5**). On a transformé le cétol connu **12** en énone tricyclique **7**. La photoaddition de l'allène sur **7** conduit à un mélange (96% de rendement) des photoadduits **20**–**23** (présents respectivement dans les rapports 40:51:6:3). L'ozonolyse du composé **20**, suivie par un traitement de la dione **24** qui en résulte par du MeONa–MeOH (température ambiante, 2,5 h), conduit au céto-ester **26** (94%). Lorsqu'on soumet le composé **21** à une série identique de réactions, il y a formation du *même* composé **26** (86%). Par ailleurs, si l'on traite la dione **25** par du MeONa–MeOH, dans des conditions beaucoup plus douces (0°C, 5 min), il y a formation des céto-esters **27** (39%) et **28** (33%). Les composés **27** et **28**, par réaction avec du MeONa–MeOH à la température ambiante, sont transformés d'une façon efficace en **26**. La réduction de **26** par du $NaBH_4$ ou par du Li*sec*-Bu_3BH conduit à des mélanges de l'ester alcool **32** et de la lactone **33** qui peuvent être séparés et qui peuvent respectivement être transformés en dimésylates **35** et **39**. La réaction des composés **35** et **39** avec du NaCN dans de l'hexaméthylphosphoramide à chaud conduit aux dinitriles **37** et **40** qui, par traitement avec du *tert*-BuOK dans du *tert*-BuOH au reflux, conduisent tous les deux à la même ènaminonitrile **41**. L'hydrolyse acide de **41** conduit à la dione **42**. Sur une base préparative, on peut facilement transformer le composé **26** en dione **42** (rendement global de 52%) sans séparer les mélanges d'intermédiaires de synthèse. La réaction (CH_2Cl_2, −95°C) du composé **42** avec du Me_3SiI–Et_3N, suivie d'une oxydation des produits **46** et **47** qui en résultent par du $Pd(OAc)_2$ dans l'acétonitrile, conduit aux bis-énones **48** (67%) et **49** (19%). On peut transformer le composé **48** en dione **52** qui, par réaction avec du $(i\text{-PrO})_3TiMe$ dans de l'éther, conduit à un mélange 86:14 des céto-alcools **53** et **54** (63% à partir de **48**). La réduction ($NaBH_4$) de **53** conduit au (±)-maritimol (**4**). Par ailleurs, la transformation d'un mélange 86:14 de **53** et de **54** en *p*-toluènesulfonylhydrazones **55** et la réaction subséquente de ce dérivé avec du NaH dans du toluène au reflux conduit aux alcools oléfiniques **56** (58%) et **57** (12%). L'hydroboration suivie d'une oxydation (BBN-9, tétrahydrofuranne au reflux; NaOH, H_2O_2) du composé **56**, permet d'obtenir (88%) la (±)-stémodine (**2**).

[Traduit par le journal]

Introduction

More than a decade ago, Hesp and co-workers reported (1) the isolation and structural elucidation of (+)-aphidicolin, a diterpenoid metabolite from the fungus *Cephalosporium aphidicola* Petch.[1] This natural product was shown (1) to have the constitution and absolute stereochemistry shown in **1** and to exhibit antiviral (3) and antitumor (4) activity. These interesting physiological properties, along with the fact that aphidicolin (**1**) possesses a novel diterpenoid carbon skeleton, have prompted a considerable number of synthetic investigations. Indeed, during the past six years, several elegant, well-designed total syntheses of (±)-**1** have been completed (5) and other reports (6) have described approaches to the synthesis of this interesting substance.

Various examinations of the above-ground portion of *Stemodia maritima* L. (Scrophulariaceae), a plant used on the Caribbean island of Curacao for the treatment of venereal disease, have resulted in the isolation of a number of diterpenoids, including (−)-stemodin (**2**) (7), (+)-stemodinone (**3**) (7), (+)-maritimol (**4**) (8), and (+)-2-desoxystemodinone

[1] (+)-Aphidicolin was subsequently isolated from *Nigrosporum sphaerica* (2).

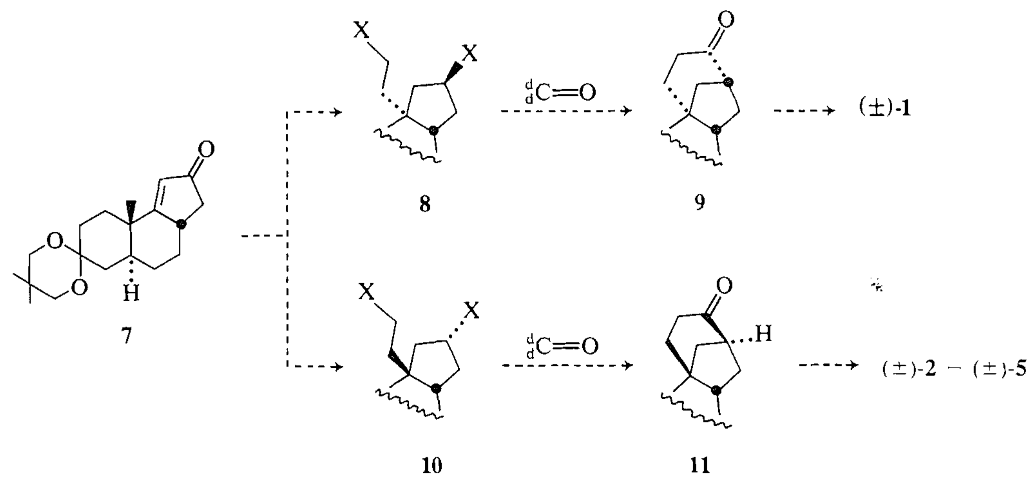

SCHEME 1

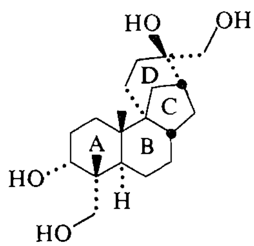

1

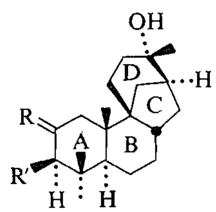

2 R = β-H, α-OH
R' = H
3 R = O, R' = H
4 R = H_2, R' = OH
5 R = H_2, R' = H

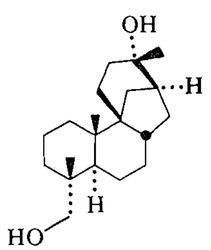

6

(5) (9).[2] Although these naturally occurring substances have structures that are quite similar to that of aphidicolin (**1**), it is evident that the aphidicolane- and stemodane-type diterpenoids differ in the stereochemical arrangement of rings C and D.

Some time ago, we initiated a program with the aim of completing the total synthesis of (±)-aphidicolin and (some of) the stemodane-type diterpenoids. We describe herein the portion of this investigation which culminated in the preparation of (±)-stemodin (**2**) and (±)-maritimol (**4**) and in the formal total synthesis of (±)-stemodinone (**3**) and (±)-2-desoxystemodinone (**5**).[3] Several other reports of the synthesis of stemodane-type diterpenoids have been published (6*g*, 9, 10, 13–16).

Results and discussion

(a) *Synthetic plan (see Scheme 1)*

An examination of the structures of **1**–**5** indicates that, although the nature, position, and arrangement of functional groups on ring A of these substances varies significantly, it should be possible to synthesize all of these diterpenoids from a common precursor. More explicitly, since the basic carbon skeleton of rings A, B, and C is common to compounds **1**–**5**, it appeared that an intermediate such as the enone ketal **7** could serve as a suitable synthetic precursor for these natural products. In our originally formulated plan, we proposed to introduce, in each of the two possible stereochemical orientations, a suitable two-carbon unit at the β-carbon of the α,β-unsaturated ketone function in **7**. Stereo- and (or) regiochemically controlled synthetic manipulations on the resultant products would, hopefully, lead to the intermediates **8** and **10** (X = leaving group). Successful reaction of each of the latter substances with a reagent synthetically equivalent to the d^1,d^1 carbonyl synthon (see ref. 17) would provide the keto ketals **9** and **11**, respectively. In order to convert compound **9** into (±)-aphidicolin (**1**), the keto group in ring D and the "hidden" carbonyl function in ring A would have to serve as handles for the introduction of the necessary appendages and functionalities. Similarly, suitable synthetic operations involving the keto and ketal groups of **11** would, presumably, provide the stemodane-type diterpenoids **2**–**5**.

(b) *Preparation of the keto ketal 7 (see Scheme 2)*

Ketalization of the known ketol **12** (18) with 2,2-dimethyl-1,3-propanediol provided the crystalline ketal alcohol **13**, which, upon oxidation with pyridinium chlorochromate in the presence of sodium acetate (19), gave the keto ketal **14** (mp 68–70°C). Conversion of the latter material into the desired enone **7** was accomplished satisfactorily via two different routes. One of these, involving a new cyclopentenone annulation method that had been developed in our laboratory, has been described (20). The other, which was somewhat more amenable to large scale reactions, was patterned on work done by Brown and Ragault (21) and was similar to the annulation method employed by McMurry *et al.* (5*b*) in their synthesis of (±)-aphidicolin (**1**). Thus, alkylation (lithium diisopropylamide, tetrahydrofuran, 0°C; excess methallyl iodide, −78°C to room temperature) of the ketone **14** gave a mixture of compounds that included the desired monoalkylation product **15**,

[2] Another diterpenoid, named stemodinol, was isolated from *S. maritima* L. and was assigned the structure represented by formula **6** (8). However, subsequent work (9, 10) showed that this substance was, in fact, identical with (+)-stemarin (11), a diterpenoid possessing a carbon skeleton different from that of compounds **2**–**5**. Apparently, **6** has not yet been obtained from natural sources.

[3] A portion of this work has been reported in preliminary form (12).

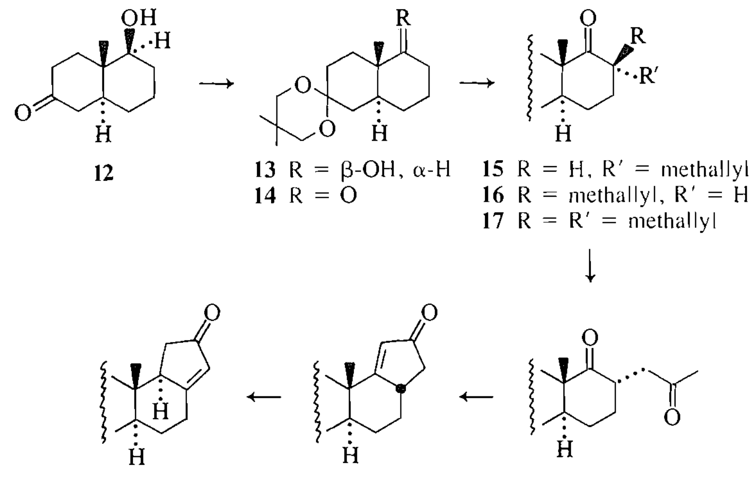

SCHEME 2

the corresponding epimer **16**,[4] and a small amount of the dialkylation product **17**. Since **16** (axial methallyl group) would be expected to be considerably less stable than **15**, the mixture was treated briefly with sodium methoxide in methanol. The resultant material consisted of a mixture of **15** and **17** in a ratio of ~95:5, respectively. Although these two substances could be separated by column chromatography and were individually characterized, the next step of the reaction sequence was typically carried out on the crude mixture. Thus, treatment of the 95:5 mixture of **15** and **17** with six equivalents of sodium metaperiodate, a catalytic amount of osmium tetroxide, and one equivalent of sodium acetate[5] in *tert*-butyl alcohol – water provided, after purification of the crude product by means of fractional crystallization and column chromatography, the crystalline (mp 90–91°C) ketal dione **18** (88% from **14**).

The synthetically crucial conversion of the dione **18** into the enone **7**, involving base-promoted intramolecular aldol condensation – dehydration, proved to be problematic. Not unexpectedly, the difficulties were associated entirely with the fact that the desired, initially formed enone **7** can, in the presence of base, isomerize to the positional isomer **19**. In fact, appropriate experiments showed that **19** is thermodynamically more stable than **7** and, thus, since **19** was of no use in our synthetic efforts, it was important to find reaction conditions under which the conversion of **18** into **7** was (considerably) faster than the transformation of **7** into **19**. Several procedures (different bases, solvents, and reaction conditions) were investigated and, eventually, it was found that the most satisfactory results were obtained employing a method (sodium hydride, catalytic amount of *tert*-amyl alcohol, benzene, reflux) similar to that used by McMurry *et al.* (5*b*) in their synthesis of (±)-aphidicolin. However, when the reaction was allowed to proceed until (nearly) all of the starting material **18** had been consumed, even this procedure produced significant amounts of the unwanted enone **19**. Therefore, the reaction mixture was monitored and work-up was carried out when traces of **19** began to appear. Chromatographic separation of the mixture thus obtained gave ~11% of the starting material **18**, 73% (83% based on consumed starting material) of the desired enone **7**, and <5% of the enone **19**.

It is pertinent to comment briefly on the stereochemistry assigned to compound **19**. This assignment was based initially on the prediction that, of the two possible epimers that could be formed from isomerization of **7**, enone **19** would be the more stable isomer. In the alternative diastereomer (β allylic bridgehead proton), ring B is required to adopt an unstable, boat-like conformation. Evidence supporting the stereochemical conclusion was obtained by examining the ^{1}H nmr spectrum of **19**. A molecular model of this compound shows that the protons of the angular methyl group are situated within the "shielding cone" (22) of the carbon–carbon double bond of the enone system, and, therefore, these protons should resonate at unusually high field. This is indeed the case, since the ^{1}H nmr spectrum of **19** exhibits a 3-proton singlet at δ 0.64. In contrast, the angular methyl group of **7** produces a singlet at δ 1.13.

(c) *Conversion of the keto ketal **7** into the keto ester **26** (see Scheme 3)*

Bearing in mind our original synthetic plan (Scheme 1), it was necessary at this stage of the synthesis to introduce a two-carbon unit to the β carbon of the α,β-unsaturated ketone function of **7**. Initial attempts in this direction, involving treatment of **7** with lithium divinylcuprate (23) under a variety of reaction conditions, failed to produce any of the desired conjugate addition product(s).[6] Therefore, an alternative method had to be adopted.

A reaction sequence involving photoaddition of allene to an enone, oxidative cleavage of the carbon–carbon double bond of the photoadduct, and subsequent ring opening of the resultant dione has been employed quite frequently as a method for the overall conjugate addition of a functionalized two-carbon side chain to an α,β-unsaturated ketone (6*d*, 9, 10, 11*b*, 15, 24). Therefore, it seemed appropriate to investigate the photochemically induced cycloaddition of allene to the enone **7**.

Irradiation of a tetrahydrofuran solution (−78°C) of allene and compound **7** provided, in 96% yield, a mixture of four isomeric products, **20–23**, in a ratio of 40:51:6:3, re-

---

[4] The relative amounts of **15** and **16** varied somewhat from experiment to experiment.

[5] In the absence of sodium acetate, a small amount of ketal hydrolysis occurred.

[6] Similar observations were recorded independently by McMurry *et al.* (5*b*), who were unsuccessful in effecting conjugate addition of various reagents (including divinylcuprate) to an enone structurally similar to **7**.

spectively (glc analysis). Subjection of the mixture to column chromatography on silica gel provided the two major products **20** (mp 134–135°C, 39% yield) and **21** (mp 132–134°C, 42% yield). On the basis of spectral data, it was clear that these two substances were isomeric and, taking into account literature precedents (6*d*, 9, 10, 11*b*, 15, 24, 25) regarding the regiochemistry of allene photoaddition to enones, the constitutions of **20** and **21** could be assigned with confidence. However, at this stage, the stereochemical designations could not be made unambiguously. Consequently, a suitable crystal of the isomer with mp 134–135°C was subjected to X-ray analysis, which showed conclusively that this substance possessed the constitution and relative stereochemistry shown in **20** (26). The isomeric photoaddition product with mp 132–134°C was, therefore, assigned the structure represented by formula **21**.[7]

In the execution of a total synthesis of a complex natural product, it is usually desirable that each (crucial) step, involving the introduction of one or more new chiral centers, be accomplished in a highly stereoselective manner. Therefore, the lack of stereoselectivity observed in the photochemically induced addition of allene to the cyclopentenone **7**[8] was initially disconcerting. On the other hand, since our original objectives included the synthesis of both aphidicolane- and stemodane-type diterpenoids and since the photoadducts **20** and **21** could be separated quite readily, it appeared that we could, in fact, take advantage of the non-stereoselective nature of the cycloaddition reaction. Thus, it seemed likely that **20** could be employed as a precursor for the stemodane natural products, while **21** could serve as an intermediate for the synthesis of (±)-aphidicolin.

Treatment (−78°C, dichloromethane containing a small amount of methanol) of the photoadduct **20** with ozone, followed by reduction of the ozonide with dimethylsulfide, gave the rather unstable dione **24**. When the latter material was allowed to react with sodium methoxide in dry methanol (room temperature, 2.5 h),[9] the keto ester **26**, mp 139–140°C, was produced in high yield.

When the photoadduct **21** was subjected to a sequence of reactions identical with that outlined above, an unexpected and initially puzzling result was obtained. Thus, the product, formed cleanly and efficiently, was not the anticipated keto ester **27** but, in fact, proved to be the same product **26** as had been obtained from the photoadduct **20**. This surprising result led to some uncertainty with respect to the stereochemistry which had been assigned to **21**. Therefore, conclusive evidence regarding this point was sought.

In contrast to **20**, the photoadduct **21** did not crystallize easily. Nevertheless, after many attempts at recrystallization, it was possible to obtain a single crystal suitable for X-ray analysis. This study (28) showed that the photoadduct in question definitely possessed the constitution and relative stereochemistry shown in formula **21**. Furthermore, reduction of **21** with sodium borohydride, followed by treatment of the resultant alcohol **29** with *p*-bromobenzoyl chloride in pyridine, provided the *p*-bromobenzoate **30**, mp 184–185°C. Recrystallization of this material from ethanol produced crystals of high quality. An X-ray crystallographic study (28) showed conclusively that this substance possessed structure **30**.

With the structures of **20** and **21** firmly established, it was of some interest to determine how the reaction sequence outlined above (O_3; Me_2S; MeONa, MeOH) converts **21** into the keto ester **26**. To obtain evidence concerning this point, the unstable diketone **25** (obtained by ozonolysis–reduction of **21**) was treated with sodium methoxide in methanol at 0°C for 5 min. The mixture of substances thus produced contained only a trace of the keto ester **26** and consisted nearly entirely of two new products. Subjection of this mixture to column chromatography provided the keto ester **27** (mp 156–157°C, 39%) and, remarkably, the cyclobutanone **28** (mp 157–158°C, 33%). Also obtained was a mixed fraction (13%) containing **26**–**28** (ratio ~1:6:4, respectively).

The spectral properties of **27**, which were similar to but clearly different from those of the previously obtained keto ester **26**, left little doubt concerning the structure of this new diastereomer. Although **27** should serve as a suitable synthetic precursor for (±)-aphidicolin (**1**), the low yield of this material from **21** (due to competitive formation of the cyclobutanone **28**) precludes the use of the route **21** → **25** → **27** as a viable pathway for the preparation of (±)-**1**. Of course, the photoadduct **21** could be used as the starting point for an alternative route to (±)-**1**, but we have not yet done any work in this direction.

Evidence for the structure of the cyclobutanone **28**, which was shown (mass spectrometry) to be isomeric with **26** and **27**, was obtained readily from spectral data. The ir spectrum of **28** shows carbonyl stretching absorptions at 1760 and 1720 cm^{-1}, while the ^1H nmr spectrum exhibits a three-proton singlet (δ 3.70, CO_2Me) and a four-proton ABMN system in the regions δ 2.57–2.78 and δ 2.91–3.08 (CH_2COCH_2). It is known (29) that protons on a cyclobutanone ring such as that present in **28** exhibit, in addition to the expected geminal couplings, long range couplings (both *cis* and *trans*) across the four-membered ring. While complete analysis of the coupling constants and chemical shifts of these four protons in **28** was not carried out, it was observed that irradiation of the higher field (δ 2.57–2.78) two-proton multiplet essentially removed the large (J = 18 Hz) geminal couplings from the δ 2.91–3.08 multiplet. This decoupling experiment indicated that the AB and MN parts of this ABMN system are, in each case, due to protons on different carbon atoms of the four-membered ring.

Treatment of the keto esters **27** and **28** with sodium methoxide in methanol (room temperature, 2.5 h) led, in each case, to the clean, efficient (91%, 81%, respectively) formation of the isomeric substance **26**. On the basis of these reactions,

[7] The structures of the two minor products, **22** and **23**, obtained from photoaddition of allene to **7** are discussed at the end of this section of the paper.

[8] Interestingly, photoaddition of allene to the enone **i** provides exclusively the ketone **ii** (27). Furthermore, a similar transformation involving a cyclohexenone **iii** structurally similar to **7** provides, highly stereoselectively, the photoadduct **iv** (11*b*). A comparison of the reactions involving substrates **7** and **iii** makes it clear that the size of the enone ring has a profound effect on the stereochemistry of the photoaddition process.

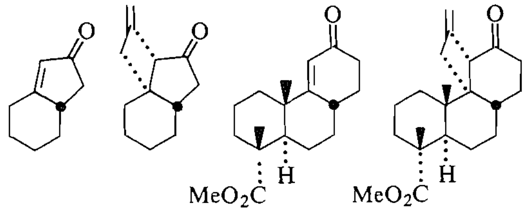

i **ii** **iii** **iv**

[9] It was shown subsequently that the conversion of **24** into **26** (with NaOMe–MeOH) was complete after the reaction mixture had been stirred for a few minutes at 0°C.

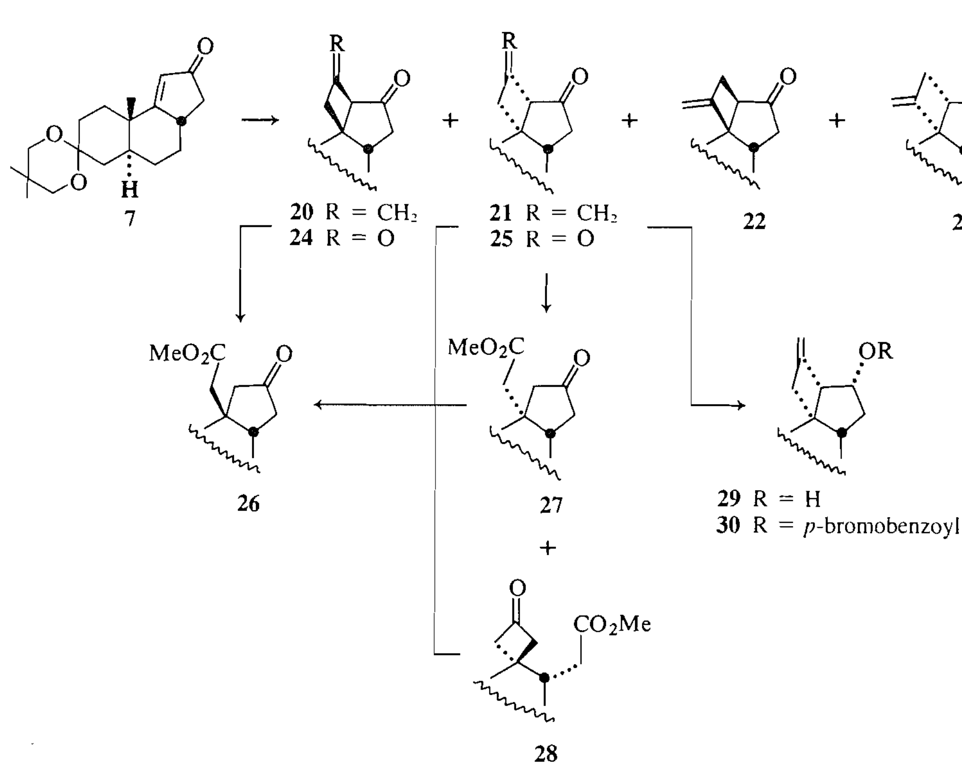

SCHEME 3

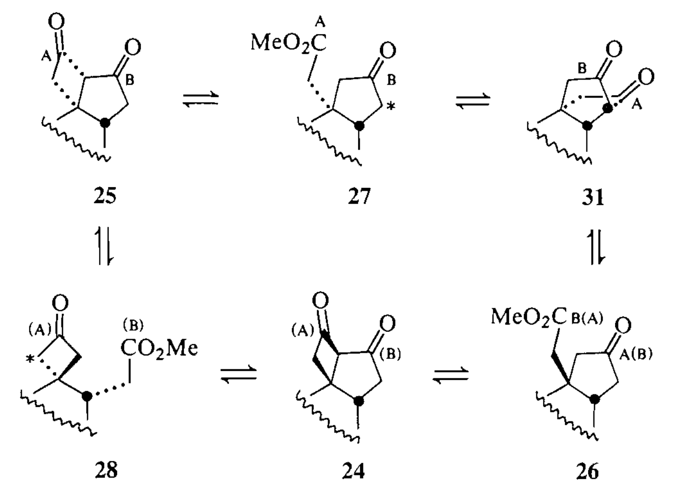

SCHEME 4

along with those summarized above, it seems reasonable to propose that the dione **25** is converted into **26** via two distinct pathways (see Scheme 4). Attack of methoxide ion on carbonyl A of **25**, followed by ring opening and protonation of the resultant enolate anion, provides the keto ester **27**, which, as noted above, can be isolated. Intramolecular condensation of **27**, involving C* and the ester carbonyl A, would lead to the dione **31** that, upon retro-condensation (attack of methoxide ion on carbonyl B), would give the final product **26**. On the other hand, the cyclobutanone **28** (also isolable) is evidently formed by initial attack of methoxide ion on carbonyl B of **25**. Subsequent condensation involving C* and the ester carbonyl (B) of **28** would produce the dione **24**. As already recorded earlier, the latter substance is rapidly transformed, presumably by methoxide ion attack on carbonyl (A), into **26**. It is interesting to note that in the first pathway, involving intermediates **27** and **31**, the ester carbonyl of **26** is ultimately derived from the cyclopentanone carbonyl of **25**, while in the second route the CO_2Me group of **26** finds its origin in the cylobutanone carbonyl of **25**.

The conversion **25** → **28** represents an unusual (probably unique) base-promoted cleavage of a bicyclo[3.2.0]heptane-2,7-dione system. Clearly, the only expected product, resulting from initial attack of methoxide ion on the strained cyclobutanone carbonyl of **25**, was the keto ester **27**. The formation of a significant quantity of **28** was, therefore, surprising and initially puzzling. However, molecular models show that the five-membered ring in **25** suffers from considerable angle strain and, consequently, one would expect the carbonyl group B of this material to be unusually susceptible to attack by nucleophilic reagents. On this basis, it is possible to rationalize, in a qualitative sense, why methoxide ion attack on carbonyl B of **25** is competitive with attack at the (probably) more strained, but quite hindered, cyclobutanone carbonyl group. In contrast, the cyclopentanone ring of **24** appears to be relatively free of angle strain and, apparently, treatment of this substance with methoxide ion leads directly and exclusively to the keto ester **26**.

If one considers the structures of compounds **24**–**28** and **31** (see Scheme 4), it is not difficult to understand why, thermodynamically speaking, the keto ester **26** is considerably more stable than each of the substances **24**, **25**, **28**, and **31**. Therefore, since all of the conversions shown in Scheme 4 are, in principle, reversible, each of the latter intermediates should eventually be transformed into **26**. However, why does the equilibrium **27** $\rightleftharpoons$ **26** favor the latter isomer? Or, in other words, why is **26** more stable than **27**? Conformational analysis indicates that the non-bonded interactions present in the two compounds are quite similar. However, molecular models indicate that angle strain in the five-membered ring of **27** (compare with **25**, see above) is considerably greater than that in the

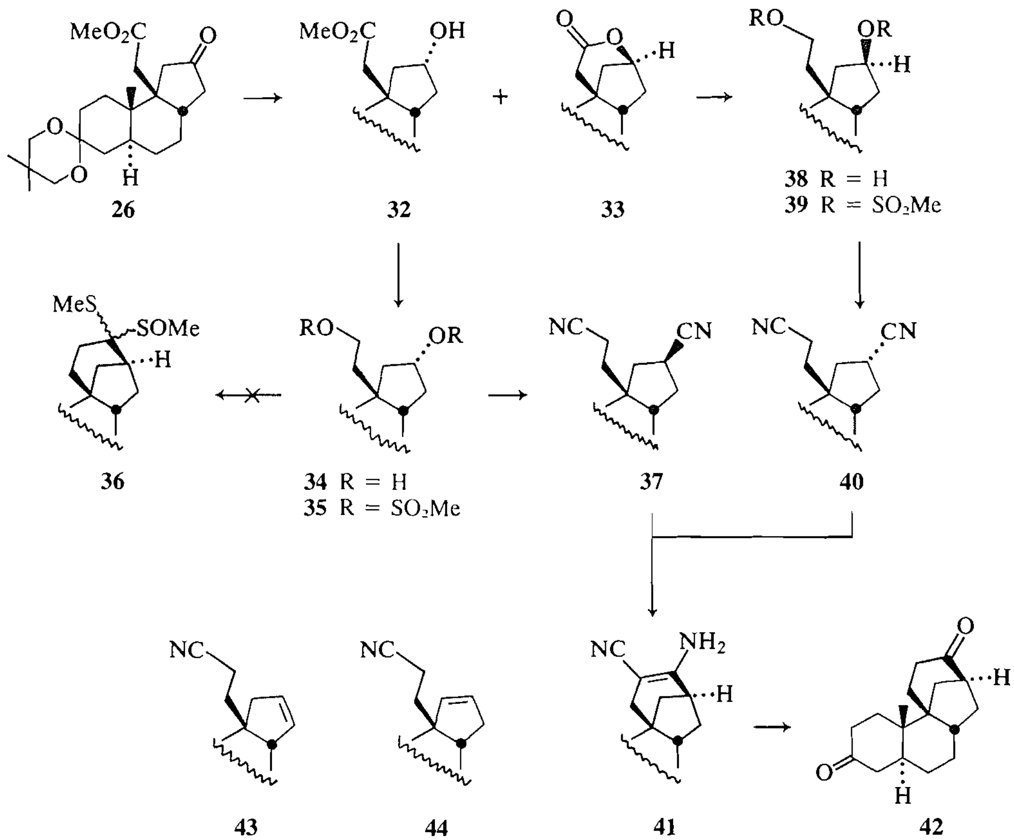

SCHEME 5

corresponding ring of **26** (compare with **24**, see above). On this basis, it is possible to rationalize, qualitatively, the fact that **27** is converted efficiently into the isomer **26**.

The results summarized above showed that, insofar as the synthesis of stemodane-type diterpenoids was concerned, the non-stereoselective nature of the photoaddition of allene to the enone **7** was of little consequence, since both of the major photoadducts **20** and **21** could be converted efficiently into the keto ester **26**, a promising stemodane precursor. Furthermore, it was obvious that chromatographic separation of **20** and **21**, although readily accomplished, was unnecessary. Thus, subjection of the mixture of photoadducts **20–23** (ratio 40:51:6:3, respectively, *vide supra*) to the sequence of reactions (O_3; Me_2S; MeONa, MeOH) developed earlier provided a mixture of compounds from which the keto ester **26** could be isolated (73% overall yield from the enone **7**) by flash column chromatography (30).

The first-eluted fractions of the above-mentioned chromatography contained a small amount of a mixture of the minor photoadducts **22** and **23**.[10] Since it seemed desirable to characterize these compounds, the mixture was resubjected to chromatography. The pure compounds **22** (mp 132–133.5°C) and **23** (mp 146–148°C) thus obtained were, on the basis of mass spectrometric measurements, isomeric with the previously isolated photoadducts **20** and **21**. The stereochemical assignments were made on the basis of the ^{1}H nmr spectra of **22** and **23**. First of all, the spectrum of **23** shows an unusually high-field (δ 0.89) one-proton multiplet. Examination of a molecular model of this material shows that the proton H* is situated directly in the "shielding cone" (22) produced by the olefinic double bond. No similarly shielded proton is found in the isomer **22**. Secondly, examination of a molecular model of **22** shows that one of the olefinic protons (H* in **22**) is very near to the angular methyl group. This close proximity was corroborated by a nuclear Overhauser effect (nOe) difference experiment (31). Thus, irradiation at δ 0.94 (the tertiary methyl groups of **22** resonate at δ 0.89, 0.94, and 0.99) caused a small enhancement of the signal (δ 5.26) due to one of the olefinic protons. No corresponding signal enhancement was observed when a similar experiment was carried out on the isomer **23**. Finally, one

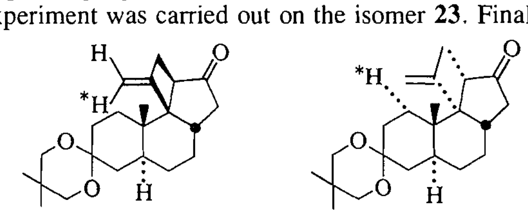

22 **23**

of the olefinic protons of the photoadduct **22** resonates (δ 5.26) significantly downfield from the olefinic protons in compounds **20**, **21**, and **23** (δ 4.80–5.02). Since steric compression is known to deshield protons (22), this evidence is also consistent with one of the olefinic protons of **22** being in close proximity to the angular methyl group. Indeed, it was the δ 5.26 signal that showed enhancement when the resonance due to the angular methyl group was irradiated.

(d) *Conversion of the keto ester **26** into the dione **42** (see Scheme 5)*

Since a suitable procedure for the efficient conversion of

[10] Probably due to the very hindered nature of the carbon–carbon double bonds in **22** and **23**, these substances, apparently, underwent ozonolysis much more slowly than the isomeric photoadducts **20** and **21**.

enone **7** into the keto ester **26** had been developed, the next stage of the original synthetic plan for the synthesis of the stemodane-type diterpenoids (see Scheme 1) could be pursued. To that end, compound **26** had to be converted into an intermediate of general structure **10** (X = leaving group), thus allowing for an investigation of the reaction of the latter substance with a d^1,d^1 carbonyl reagent (to produce **11**).

Reduction of **26** with sodium borohydride in methanol gave a 1 : 1 mixture of the alcohol **32** and the lactone **33** (mp 194°C), which could be separated readily by chromatography. In attempts to increase the relative amounts of the desired product **32**, compound **26** was reduced with lithium tri-*sec*-butylborohydride in tetrahydrofuran at −78°C. Separation of the resultant product mixture gave the alcohol **32** (74%) and the lactone **33** (23%). Treatment of **32** with lithium aluminum hydride in ether, followed by reaction of the resultant diol **34** with methanesulfonyl chloride in pyridine, gave the dimesylate **35**. The latter substance is identical with **10** (X = OMs) and, consequently, the preparation of a key, originally postulated intermediate had been achieved.

Although a number of reagents which are synthetically equivalent to the d^1,d^1 carbonyl synthon are known (32), it appears that methyl methylthiomethyl sulfoxide (**45**) (33) is particularly effective for the conversion of 1,ω-dihaloalkanes or 1,ω-di(*p*-tosyloxy)alkanes into cyclic ketones. However, when the dimesylate **35** was treated (tetrahydrofuran, −78°C to 0°C, 30 min; room temperature, 12 h) with an excess (2.5 equivalents) of the anion of **45** (prepared by reaction of **45** with *n*-butyllithium) the major substance isolated was the starting material **35**. Although the crude product contained a number of minor components, none of these had the spectral characteristics expected for the desired product **36**.

Attempts to convert **35** into **36** using modified reaction conditions (e.g. use of $[MeSCHSOMe]^-K^+$, addition of hexamethylphosphoramide to the reaction mixture, higher temperatures) also proved to be unsuccessful. Although varying amounts of starting material were consumed, careful spectroscopic examination of the product mixtures provided no evidence for the presence of compound **36**.

It seems reasonable to propose that failure to effect conversion of **35** into **36** was due primarily to steric factors. The anion of **45** is relatively bulky and molecular models indicate that both of the carbon centers bearing the mesyloxy group are quite hindered toward S_N2-type attack of a nucleophile. In any case, it was evident that our original synthetic plan had to be modified. Explicitly, it appeared that ring D of the diterpenoid skeleton would have to be formed via a route involving reaction of the dimesylate **35** with a nucleophile that is much smaller than the anion of **45**.

When compound **35** was allowed to react with excess sodium cyanide in hexamethylphosphoramide (room temperature, 3 h; 60°C, 48 h), the crystalline dinitrile **37** was produced in 60% yield. It was gratifying to find that treatment of **37** with potassium *tert*-butoxide in refluxing *tert*-butyl alcohol (34) effected smoothly a Thorpe–Ziegler condensation (35) to afford, in 90% yield,[11] the enaminonitrile **41**, mp 213–215°C.

It seemed likely that, since the secondary cyano group of the dinitrile **40** should be susceptible to base-catalyzed epimerization, this substance should also undergo a Thorpe–Ziegler cyclization. Indeed, conversion of the lactone **33**, via the intermediates **38** and **39**, into the dinitrile **40** (mp 194°C), followed by treatment of the latter material with potassium *tert*-butoxide in hot *tert*-butyl alcohol (34), provided the enaminonitrile **41** in 47% overall yield.

Although conversion of the keto ester **26** into the dinitriles **37** and **40**, along with the Thorpe–Ziegler cyclization of the latter materials, provided an efficient pathway for the construction of ring D of the stemodane carbon skeleton, it was in the next step of the synthesis that this route lost some of its attractiveness. It is known that base hydrolysis of enaminonitriles is, at best, problematic and, in fact, usually fails to provide useful quantities of ketonic products. On the other hand, while acid hydrolysis – decarboxylation is usually efficiently successful, such a procedure would, in the case of **41**, also hydrolyze the ketal group on ring A. Clearly, to make use of the resultant product **42** in subsequent steps of the synthesis, one would have to distinguish chemically between two environmentally similar carbonyl groups.

One possible way to avoid this problem would be to convert the dinitriles **37** and **40** into the corresponding di-esters and subject the latter compounds to Dieckmann condensation (35). Base hydrolysis and decarboxylation of the resultant β-keto ester could, presumably, be carried out under conditions that would not be deleterious to the ketal function on ring A. However, although both **37** and **40** could be converted by standard reactions into the corresponding di-esters, all attempts to effect Dieckmann cyclization of the latter substances, using a variety of bases, solvents, and reaction conditions, failed. These failures, although puzzling, led us back to an investigation of a synthetic route involving the enaminonitrile **41** as an intermediate.

Acid hydrolysis of **41** with phosphoric acid in refluxing aqueous acetic acid (34)[11] afforded, in 80% yield, the crystalline dione **42**, mp 132°C. At this stage, there appeared to be little doubt that this material possessed the structure implied by formula **42**. However, since the dione was formed under strongly acidic conditions and since the possibility of acid catalyzed rearrangements could not be rigorously excluded, independent structural evidence was sought. Gratifyingly, an X-ray crystallographic study (36) showed conclusively that the hydrolysis product had the constitution and relative stereochemistry shown in **42**.

The results summarized above showed clearly that, in the route eventually adopted for the transformation of the keto ester **26** into the dione **42**, the presence or absence of stereoselectivity in the reduction of the ketonic carbonyl group of **26** is irrelevant. Indeed, in preparative scale reactions, the conversion of **26** into **42** could be done without separation of isomeric compounds. Thus, reduction of **26** with excess lithium aluminum hydride, conversion of the resultant mixture of diols **34** and **38** into the corresponding dimesylates **35** and **39**, and subsequent reaction of the latter mixture with cyanide ion in warm hexamethylphosphoramide afforded, in 63% overall yield,[12] a mixture of the dinitriles **37** and **40**. Subjection of this mixture to Thorpe–Ziegler cyclization, followed by acid hy-

[11] It was found that the Thorpe–Ziegler condensation, as well as the subsequent hydrolysis–decarboxylation of the resulting enaminonitrile **41** (*vide infra*), had to be carried out with the careful exclusion of oxygen. If this was not done, significant amounts of a side product, apparently arising from oxidation of the enaminonitrile moiety, were formed.

[12] Also isolated, in 6% yield, was a 1 : 1 mixture of the two elimination products, the olefinic nitriles **43** and **44** (see Scheme 5).

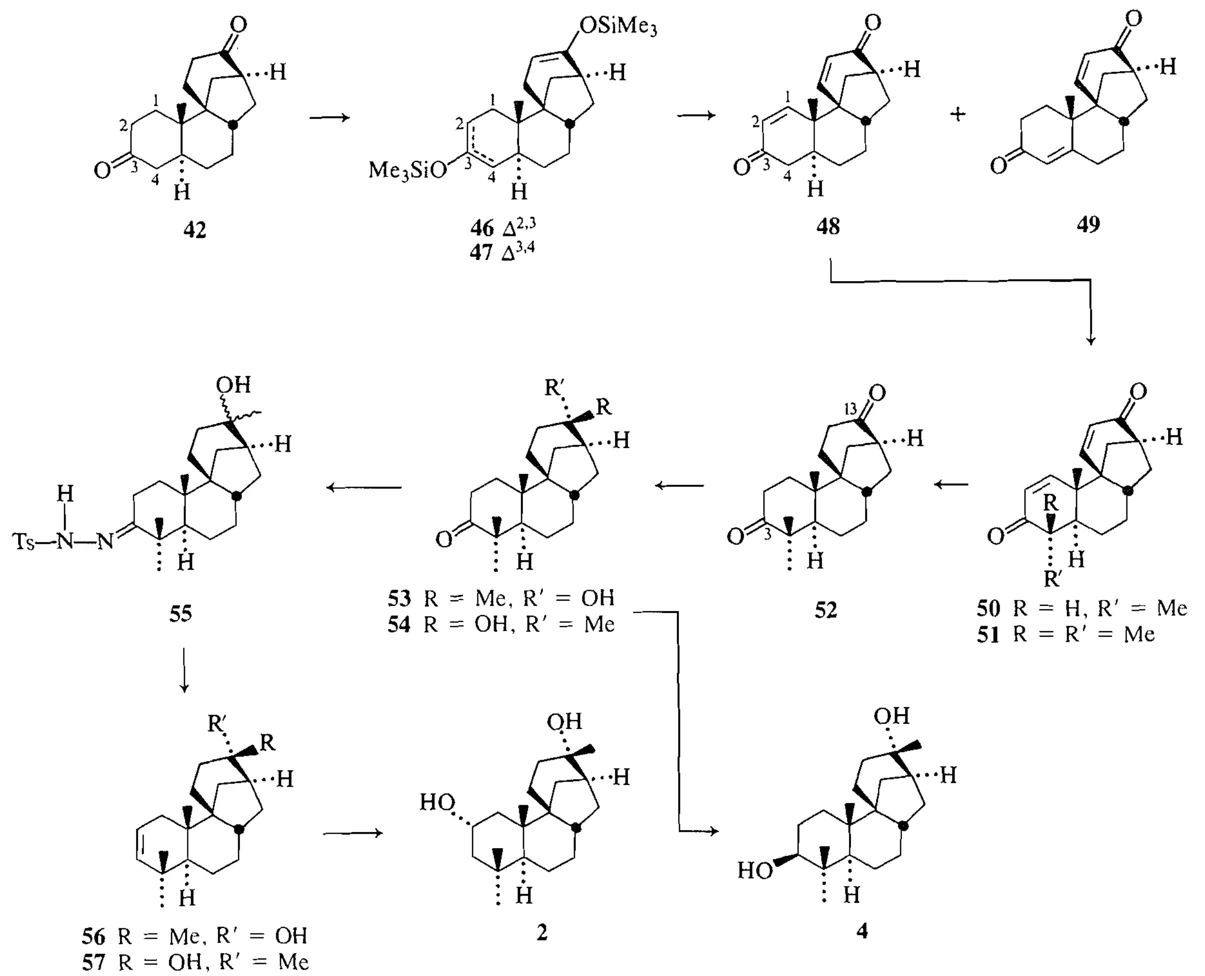

SCHEME 6

drolysis of the resultant crude enaminonitrile **41**, provided the dione **42**. In this manner, the latter substance was obtained from the keto ester **26** in 52% overall yield.

(e) *Conversion of the dione* **42** *into (±)-maritimol (4) and (±)-stemodin (2) (see Scheme 6)*

As pointed out earlier, in order to prepare stemodane-type diterpenoids from the dione **42**, it was necessary at this stage to distinguish chemically between the two carbonyl groups of the latter intermediate. In this connection, if one bears in mind that introduction of two methyl groups at C-4 of **42** is also required, it appears that conversion of **42** into the corresponding bis enone **48** would be synthetically profitable. Explicitly, it is obvious that **48** could be converted into only one enolate anion and the latter species would involve the carbon center (C-4) at which the two methyl groups have to be introduced.

Although there are many different methods via which a ketone can be converted into the corresponding enone, efficient transformation of **42** into **48** proved to be nontrivial. For example, treatment of **42** with excess lithium diisopropylamide under conditions presumed to lead to kinetically controlled deprotonation (37), followed by trapping of the bis enolate anions with *tert*-butyldimethylsilyl chloride, gave a 1:1 mixture of positionally isomeric bis enol ethers (**46**, **47**, t-BuMe$_2$Si in place of Me$_3$Si). Therefore, it was apparent that conversion of **42** into **48** had to be accomplished via a route other than that initially involving kinetically controlled deprotonation of **42**.

Eventually, after a substantial number of unsuccessful or only moderately successful experiments, it was found that treatment of **42** with an excess of freshly prepared trimethylsilyl iodide (38) in the presence of triethylamine in cold (−95°C) dichloromethane for 1 h led to a mixture of the bis enol ethers **46** and **47** in a ratio of about 4-5:1, respectively.[13] Oxidation of this mixture with palladium(II) acetate in acetonitrile (39), followed by chromatographic separation of the resultant products, gave the crystalline bis enones **48** (67%) and **49** (19%).

Dimethylation of the bis enone **48** also proved to be somewhat more difficult than anticipated. Eventually, it was found that a 2-step process gave the most satisfactory result. Rapid treatment of the enolate anion (lithium bis(trimethylsilyl)amide, dimethoxyethane, 0°C) of **48** with a large excess of methyl iodide gave nearly exclusively (95%) the monomethylated product **50**, mp 149–150°C. The stereochemistry at C-4 of this substance was shown by a ^{1}H nmr decoupling experiment. Irradiation at δ 1.17 (3-proton doublet due to C-4 methyl group) caused collapse of the doublet of quartets at δ 2.38 (C-4 proton) to a clean doublet with J = 13 Hz (geminal *trans* diaxial coupling). Subjection of **50** to a second methylation via

[13] Use of higher reaction temperatures and (or) other bases (e.g. i-Pr$_2$NEt, (Me$_3$Si)$_2$NH), as well as use of other silylating agents (e.g. Me$_3$SiCl, Me$_3$SiOSO$_2$CF$_3$) gave mixtures of **46** and **47** containing lower proportions of the desired product **46**.

a very similar procedure provided the required bis enone **51**, mp 154–156°C, in 77% yield from **48**.[14]

Catalytic hydrogenation of compound **51** proceeded smoothly to generate the crystalline dione **52** in nearly quantitative yield. Thus, the overall conversion of **42** into **52** had been accomplished quite efficiently and, importantly, had provided a synthetic intermediate in which the two carbonyl groups were now, in terms of steric hindrance, quite different.

In other reported syntheses of stemodane-type diterpenoids (9, 10, 13–15), the chiral center at C-13 was introduced in a variety of ways. However, since C-13 of **52** is, compared to C-3, relatively unhindered and since the methyl group of the desired tertiary alcohol **53** is equatorially oriented, it appeared that the desired transformation **52** → **53** might be accomplished directly by treating **52** with a bulky methyl-transfer reagent that is known to add a methyl group to the equatorial side of cyclohexanone carbonyl functions. Indeed, such a reagent, methyltriisopropoxytitanium (40, 41), is known and it was pleasing to find that when the dione **52** was allowed to react (ether, room temperature) with an excess of this reagent, the epimeric keto alcohols **53** and **54** (ratio ~86 : 14, respectively) were produced in 82% yield. Although these isomers were difficult to separate by chromatography, a pure sample of the major isomer **53**, mp 93°C, could be obtained by a combination of chromatography and fractional crystallization.

Reduction of (±)-stemodan-13α-ol-3-one (**53**) with sodium borohydride in methanol, followed by purification (chromatography, fractional crystallization) of the crude product, gave, in 73% yield, (±)-maritimol (**4**), mp 221–222°C, which showed glc and tlc behavior, as well as ^{1}H nmr and mass spectra, identical with those of an authentic sample of (+)-maritimol.[15]

Treatment of an 86 : 14 mixture of the epimeric keto alcohols **53** and **54** with 1.3 equiv. of *p*-toluenesulfonylhydrazide in hot ethanol gave a mixture of the crude *p*-toluenesulfonylhydrazones **55**. Reaction of this crude material with sodium hydride in refluxing toluene, followed by chromatographic separation of products thus obtained, gave (±)-stemod-2-en-13α-ol (**56**) (58%) and (±)-stemod-2-en-13β-ol (**57**) (12%).

Although the alkene **56** had been converted previously into (±)-stemodin (**2**) via a 4-step sequence (13), it appeared that this transformation might be accomplished more directly. To that end, a tetrahydrofuran solution of compound **56** and an excess of 9-borabicyclo[3.3.1]nonane was refluxed for 48 h. Oxidation of the resultant organoborane mixture with alkaline hydrogen peroxide provided, after purification of the crude product, (±)-stemodin (**2**), mp 220.5–222°C, in 88% yield. This material exhibited chromatographic (glc, tlc) behavior and spectra (^{1}H nmr, mass) identical with those of an authentic sample of (−)-stemodin.[16]

It should be pointed out that the racemic keto alcohol **53** has been converted into (±)-2-desoxystemodinone (**5**) (15), while the alkene **56** has been transformed into (±)-stemodinone (**3**) (13). Consequently, the work described in this paper completes another formal total synthesis of each of the stemodane diterpenoids (±)-**3** and (±)-**5**.

Experimental

General information

Melting points and distillation temperatures are uncorrected. Ultraviolet (uv) spectra were recorded on methanol solutions using a Cary model 15 spectrophotometer. Infrared (ir) spectra (liquid films, chloroform solutions, or KBr pellets) were measured using Perkin–Elmer model 710 or 710B spectrophotometers. Proton nuclear magnetic resonance (^{1}H nmr) spectra were, unless otherwise noted, recorded on deuterochloroform solutions. Signal positions are given in δ units, with tetramethylsilane as the internal standard. In the case of compounds containing one or more trimethylsilyl groups, the chemical shifts were measured relative to the chloroform signal (δ 7.25). High resolution mass spectrometric measurements were recorded with a Kratos MS-50 mass spectrometer. Gas–liquid chromatography (glc) was accomplished with Hewlett–Packard models 5832A or 5880A gas chromatographs. Microanalyses were performed in the Microanalytical Laboratory at the University of British Columbia.

Preparation of the ketal alcohol 13

A solution of the ketol **12** (18) (6.10 g, 33.5 mmol), 2,2-dimethyl-1,3-propanediol (10.4 g, 100 mmol), and *p*-toluenesulfonic acid (100 mg) in 200 mL of benzene was refluxed (nitrogen atmosphere) under a Dean–Stark water trap. After 2 h, the solution was cooled, diluted with 100 mL of ether, and then was successively washed with saturated aqueous sodium bicarbonate, water, and brine. The organic phase was dried ($MgSO_4$) and concentrated. Distillation (air-bath temperature 133–137°C/0.15 Torr (1 Torr = 133.3 Pa)) of the residual material gave 8.0 g (89%) of the ketal alcohol **13**. An analytical sample, obtained by recrystallization of a small amount of this material from pentanes, exhibited mp 80–81°C; ir ($CHCl_3$): 3480 cm^{-1}; ^{1}H nmr δ: 0.85, 0.93, 0.99 (s, s, s, 3H each), 3.30 (unresolved m, 1H), 3.40–3.60 (m, 4H). *Anal.* calcd. for $C_{16}H_{28}O_3$: C 71.60, H 10.52; found: C 71.76, H 10.44.

Preparation of the keto ketal 14

A mixture of pyridinium chlorochromate (19) (11.8 g, 55.0 mmol), sodium acetate (800 mg, 10.7 mmol), and the ketal alcohol **13** (7.2 g, 26.8 mmol) in 100 mL of dry dichloromethane was stirred for 3 h at room temperature. Ether (100 mL) was added and the resultant mixture was passed through a short column of neutral alumina. The column was washed thoroughly with ether, the combined eluate was concentrated, and the residual material was recrystallized from a mixture of ether and pentanes to give 6.30 g (88%) of the keto ketal **14**, which exhibited mp 68–70°C; ir ($CHCl_3$): 1705 cm^{-1}; ^{1}H nmr δ: 0.89, 1.02, 1.12 (s, s, s, 3H each), 3.30–3.70 (m, 4H). *Anal.* calcd. for $C_{16}H_{26}O_3$: C 72.14, H 9.84; found: C 71.95, H 9.94.

Alkylation of the keto ketal 14 with methallyl iodide

To a cold (−78°C), stirred solution of lithium diisopropylamide (22.5 mmol) in 50 mL of dry tetrahydrofuran, under an atmosphere of argon, was added dropwise (syringe) a solution of 5.0 g (18.8 mmol) of the keto ketal **14** in 10 mL of dry tetrahydrofuran. After the solution had been stirred at 0°C for 30 min, it was recooled to −78°C and 8 mL (~70 mmol) of neat methallyl iodide was added rapidly. The mixture was stirred at 0°C for 2 h and at room temperature for 1 h. The volatile materials were removed under reduced pressure, the residual viscous oil was dissolved in 50 mL of methanol containing a small amount of sodium methoxide, and the resultant solution was stirred (argon atmosphere) at room temperature for 15 min. Removal of the methanol solvent left a solid which was dissolved in ether. The solution was washed successively with aqueous ammonium chloride and brine (3 times), and dried ($MgSO_4$). Removal of the solvent afforded 6.34 g of a white solid which, on the basis of glc analysis, contained the starting material **14** (0.5%), the desired ketone **15** (94%), and the di-alkylated ketone **17** (5%). Subjection of a small amount of this mixture to flash

[14] Other procedures for the conversion of **48** into **51**, including excess potassium *tert*-butoxide and methyl iodide in refluxing *tert*-butyl alcohol, excess lithium diisopropylamide and methyl iodide in tetrahydrofuran (−78°C to room temperature), and excess potassium hydride and methyl iodide in tetrahydrofuran (room temperature), gave varying amounts of starting material and the mono- and dimethylated products **50** and **51**.

[15] We are very grateful to Professor C. D. Hufford for providing a generous sample of (+)-maritimol.

[16] We are very grateful to Dr. P. S. Manchand for providing a generous sample of (−)-stemodin.

column chromatography (30) (elution with 10% ethyl acetate in hexanes) provided samples of the products **17** (eluted first) and **15**.

Ketone **17**, a colorless, viscous oil, exhibited ^{1}H nmr (80 MHz) δ: 0.91, 1.03, 1.08 (s, s, s, 3H each), 1.61, 1.71 (br s, br s, 3H each), 3.27–3.73 (m, 4H), 4.64, 4.86 (m, m, 2H each). *Exact Mass* calcd. for $C_{24}H_{38}O_3$: 374.2821; found: 374.2821.

Ketone **15**, a white solid, was recrystallized from a mixture of ether and hexanes and exhibited mp 87°C; ir ($CHCl_3$): 1700, 1630, 1105, 1095 cm^{-1}; ^{1}H nmr (400 MHz) δ: 0.90, 1.03, 1.15 (s, s, s, 3H each), 1.69 (br s, 3H), 1.93 (d of t, 1H, J = 13, 2.5 Hz), 2.08 (m, 1H), 2.36 (d of d of d, 1H, J = 14, 6, 3 Hz), 2.54 (d of d, 1H, J = 15, 5 Hz), 2.80 (m, 1H), 3.39, 3.44 (d of d, d of d, 1H each, J = 11, 1 Hz in each case, equatorial ketal methylene protons), 3.51, 3.59 (d, d, 1H each, J = 11 Hz in each case, axial ketal methylene protons), 4.63, 4.75 (br s, br s, 1H each). *Exact Mass* calcd. for $C_{20}H_{32}O_3$: 320.2351; found: 320.2353.

Preparation of the diketone 18

To a stirred mixture (room temperature) of sodium metaperiodate (24.13 g, 112.8 mmol, freshly recrystallized from water), sodium acetate (1.54 g, 18.8 mmol), a catalytic amount of osmium tetroxide, and 200 mL of distilled water was added in one portion a solution of the mixture of ketones **15** and **17** (6.34 g, prepared as described above) in 150 mL of distilled *tert*-butyl alcohol. The mixture was stoppered and stirred for 2 h, after which time the initially formed brown color had been discharged. Distilled water (150 mL) was added, the mixture was stirred for a further 4 h, and then was extracted thoroughly with ether. The combined ethereal extract was washed with brine, dried ($MgSO_4$), and concentrated under reduced pressure. The remaining brown oil was dissolved in ether and the solution was filtered through a plug of silica gel to remove much of the colored material. Removal of the solvent, followed by crystallization of the residual oil from hexanes afforded 4.51 g (74%) of the dione **18** as off-white crystals exhibiting mp 89–91°C. Flash column chromatography (30) (elution with 20% ethyl acetate in hexanes) of the material from the mother liquor afforded a further 0.80 g of **18** (total yield = 5.31 g, 88%). Recrystallization of a small amount of this material from hexanes afforded an analytical sample of **18** as colorless needles, mp 90–91°C; ir ($CHCl_3$): 1700 cm^{-1}; ^{1}H nmr (400 MHz) δ: 0.88, 1.02, 1.17 (s, s, s, 3H each), 1.91 (d of t, 1H, J = 13, 3 Hz), 2.09 (d of d, 1H, J = 17, 5 Hz), 2.20 (s, 3H), 2.35 (d of q, 1H, J = 14, 3.5 Hz), 2.92 (d of d, 1H, J = 17, 8 Hz), 3.32 (m, 1H), 3.36–3.60 (m, 4H). *Anal.* calcd. for $C_{19}H_{30}O_4$: C 70.77, H 9.38; found: C 70.73, H 9.45.

Preparation of the enones 7 and 19

To sodium hydride (11.6 mmol, washed free of oil with ether), under an atmosphere of argon, was added dry benzene (200 mL) and dry *tert*-amyl alcohol (500 μL, 4.7 mmol). After the mixture had been stirred at room temperature for 20 min, 3.0 g (9.3 mmol) of the crystalline dione **18** was added and the resultant mixture was refluxed for 1 h. The cooled reaction mixture was treated with aqueous ammonium chloride and ether. The organic extract was washed with brine, dried ($MgSO_4$), and concentrated. Gas–liquid chromatographic analysis of the remaining yellow oil showed that it was a mixture of the starting material **18** (13%), the tricyclic enone **7** (82%), and the isomeric enone **19** (5%). Separation of this mixture by preparative hplc (silica gel, elution with 30% ethyl acetate in petroleum ether) and rechromatography of the mixed fractions by flash column chromatography (30) (solvent as above) afforded 333 mg (11%) of recovered starting material **18** as the first-eluted component, 2.08 g (73%, 83% based on consumed starting material) of the desired enone **7**, mp 115–117°C, and 139 mg (5%) of a mixture of the enones **7** and **19**.

Recrystallization (ether–hexanes) of a small sample of the major product afforded an analytical sample of the enone **7**, which exhibited mp 115–116°C; uv λ_{max}: 230 nm (ε 17 100); ir ($CHCl_3$): 1690, 1670, 1600 cm^{-1}; ^{1}H nmr (400 MHz) δ: 0.94, 1.00, 1.13 (s, s, s, 3H each), 1.18 (m, 1H), 1.39–1.67 (diffuse, 6H), 1.73 (q of d, 1H, J = 14, 4 Hz), 1.96 (d of d, 1H, J = 18, 2 Hz), 1.99 (d of t, 1H, J = 13, 3 Hz), 2.18 (m, 1H), 2.34 (d of d of d, 1H, J = 13.5, 6.5, 3 Hz), 2.57 (d of d, 1H, J = 18, 7 Hz), 2.98 (m, 1H), 3.42–3.61 (m, 4H), 5.80 (d, 1H, J = 1.5 Hz). Decoupling experiments: irradiation at δ 5.80 sharpened the multiplet at δ 2.98; irradiation at δ 2.98 caused the doublet at δ 5.80 to collapse to a singlet and the signals at δ 2.57 and δ 1.96 to collapse to doublets, J = 18 Hz; irradiation at δ 2.57 sharpened the multiplet at δ 2.98 and changed the signal at δ 1.96 to a doublet, J = 2 Hz. *Anal.* calcd. for $C_{19}H_{28}O_3$: C 74.96, H 9.27; found: C 74.76, H 9.47.

Flash column chromatography (30) (4:2:3 cyclohexane–hexanes–ethyl acetate, 3-cm column) of the mixture of **7** and **19** (see above), followed by crystallization (ether–hexanes) of the material obtained from the appropriate fractions, afforded a pure sample of the enone **19**, which exhibited mp 139–140°C; uv λ_{max}: 232 nm (ε 17 000); ir ($CHCl_3$): 1690, 1665, 1610, 1105 cm^{-1}; ^{1}H nmr (400 MHz) δ: 0.64, 0.93, 1.04 (s, s, s, 3H each), 1.31–1.49 (diffuse, 5H), 1.62 (m, 1H), 1.77 (t of t, 1H, J = 13, 3.5 Hz), 1.96 (d of t, 1H, J = 13, 3.5 Hz), 2.17 (d of d, 1H, J = 19, 2 Hz), 2.24–2.41 (m, 2H), 2.30 (d of d, 1H, J = 19, 7 Hz), 2.54 (br d, 1H, J = 7 Hz), 2.80 (br d of d, 1H, J = 15, 5 Hz), 3.45–3.65 (m, 4H), 5.90 (d of d, 1H, J = 2, 2 Hz). Decoupling experiments: irradiation at δ 5.90 sharpened the signal at δ 2.54; irradiation at δ 2.54 collapsed the signals at δ 5.90, 2.17, and 2.30 to doublets, J = 2, 19, and 19 Hz, respectively; irradiation at δ 2.17 sharpened the signal at δ 2.54. *Exact Mass* calcd. for $C_{19}H_{28}O_3$: 304.2039; found: 304.2039.

Photoaddition of allene to the enone 7. Isolation and characterization of the photoadducts 20 and 21

A cold (−78°C), stirred solution of the enone **7** (3.0 g, 9.87 mmol) and allene (5 mL) in 55 mL of dry tetrahydrofuran, contained in a Pyrex tube, was irradiated (450-W Hanovia lamp) for 7 h. During this time, a slow stream of argon was bubbled through the solution. The vigorously stirred solution was allowed to warm to room temperature and the solvent was then removed under reduced pressure. Flash column chromatography (30) (elution with 20% ethyl acetate in hexanes, 5-cm column) of the residue gave 3.25 g (96%) of a mixture (viscous oil) of the four photoadducts **20–23**, in a ratio (glc) of 40:51:6:3, respectively. Subjection of this mixture to flash column chromatography (elution with a 10:5:2 mixture of cyclohexane, hexane, and ethyl acetate) provided a white solid that, upon recrystallization from ether–hexanes, gave 1.32 g (39%) of the photoadduct **20**, which exhibited mp 134–135°C; ir ($CHCl_3$): 1725, 1670 cm^{-1}; ^{1}H nmr (400 MHz) δ: 0.87, 0.95, 0.97 (s, s, s, 3H each), 1.73 (br m, 1H), 1.89 (d of d, 1H, J = 17, 1 Hz), 1.95 (d of t, 1H, J = 14, 3 Hz), 2.12–2.27 (m, 2H), 2.66 (br d of d, 1H, J = 17, 3 Hz), 2.83 (br d of d, 2H, J = 17, 2.5 Hz), 2.93 (d of d, 1H, J = 17, 6 Hz), 3.26 (br s, 1H), 3.41–3.55 (m, 4H), 4.80 (br d, 1H, J = 2.5 Hz), 4.95 (br d, 1H, J = 2 Hz). *Anal.* calcd. for $C_{22}H_{32}O_3$: C 76.70, H 9.36; found: C 76.90, H 9.47. *Exact Mass* calcd.: 344.2351; found: 344.2349.

Further elution of the column with the same solvent mixture afforded 1.42 g (42%) of the photoadduct **21**, mp 132–134°C (recrystallization from ether–hexanes); ir ($CHCl_3$): 1725, 1670 cm^{-1}; ^{1}H nmr (400 MHz) δ: 0.90, 0.95, 1.00, (s, s, s, 3H each), 1.90 (d of t, 1H, J = 13, 3 Hz), 2.19 (d of d of d, 1H, J = 15, 6, 1 Hz), 2.23 (m, 1H), 2.38 (m, 1H), 2.45 (m, 1H), 2.68–2.83 (br AB pair of d, 2H, J = 17 Hz), 3.09 (br s, 1H), 3.43–3.58 (m, 4H), 4.78 (br d, 1H, J = 2.5 Hz), 4.92 (br d, 1H, J = 2 Hz). Decoupling experiments: irradiation at δ 3.09 simplifies the signal at δ 2.19 to a d of d, J = 15, 6 Hz; irradiation at δ 2.22 (δ 2.19 and 2.23 signals) simplifies the multiplet at δ 2.45. *Anal.* calcd. for $C_{22}H_{32}O_3$: C 76.70, H 9.36; found: C 76.99, H 9.63. *Exact Mass* calcd.: 344.2351; found: 344.2343.

Preparation of the alcohol 29 and the p*-bromobenzoate 30*

To a cold (0°C), stirred solution of the photoadduct **21** (67 mg, 0.195 mmol) in 20 mL of methanol was added an excess of sodium borohydride. The reaction mixture was allowed to warm to room temperature and was stirred for 40 min. The solvent was removed under reduced pressure and the residue was partitioned between ether and water. The organic phase was washed with brine and dried ($MgSO_4$). Removal of the solvent provided 63 mg (93%) of the alcohol **29** as a viscous colorless oil which could not be induced to crystallize. The oil exhibited ir ($CHCl_3$): 3540, 3450, 1660 cm^{-1}; ^{1}H nmr (80 MHz) δ: 0.85, 0.93, 0.98 (s, s, s, 3H each), 3.31–3.67 (m, 4H), 4.10 (br m, 1H), 4.86 (m, 2H). *Exact Mass* calcd. for $C_{22}H_{34}O_3$: 346.2508; found: 346.2509.

Treatment of the alcohol with *p*-bromobenzoyl chloride (pyridine, room temperature, 16 h) provided the *p*-bromobenzoate **30**, which was purified by preparative tlc and recrystallized from ethanol. Compound **30** exhibited mp 184–185°C; ir ($CHCl_3$): 1700, 1665, 1590 cm^{-1}; ^{1}H nmr (270 MHz) δ: 0.89, 0.92, 0.99 (s, s, s, 3H each), 2.44, 2.65 (br d, br d, 1H each, J = 19 Hz in each case), 3.29 (br d, 1H, J = 9 Hz), 3.39–3.60 (m, 4H), 4.58, 4.74 (br d, br d, 1H each, J = 2 Hz in each case), 5.15 (m, 1H), 7.54 (br d, 2H, J = 8 Hz), 7.86 (br d, 2H, J = 8 Hz). *Exact Mass* calcd. for $C_{29}H_{37}{}^{79}BrO_4$: 528.1875; found: 528.1871.

*Conversion of the photoadduct **21** into the keto esters **27** and **28***

A cold (−78°C) solution of the photoadduct **21** (88 mg, 0.255 mmol) in 15 mL of dry dichloromethane containing 16 μL (0.383 mmol) of dry methanol was treated with a stream of dry ozone in oxygen until the solution remained blue. After the solution had been flushed with a stream of dry oxygen until colorless, it was treated with 200 μL of dry dimethyl sulfide. The solution was stirred under an atmosphere of argon for 15 min at −78°C and for 2 h at room temperature. Removal of the volatile materials gave a partially crystalline viscous oil which was dissolved in 20 mL of dry methanol. The solution was cooled to 0°C and a small amount of methanolic sodium methoxide was added. After the solution had been stirred at 0°C for 5 min, 2 drops of glacial acetic acid were added and the resulting mixture was concentrated under reduced pressure. The residual material was dissolved in ether and the solution was washed successively with 10% aqueous sodium carbonate and brine, dried ($MgSO_4$), and concentrated. The remaining oil (85 mg) was subjected to flash column chromatography (30) (elution with a 4:2:3 mixture of cyclohexane, hexanes, and ethyl acetate, respectively). The first-eluted material, upon recrystallization from ether–hexanes, gave 32 mg (33%) of the cyclobutanone **28**, mp 157–158°C; ir ($CHCl_3$): 1760, 1720 cm^{-1}; ^{1}H nmr (400 MHz) δ: 0.91, 0.98, 1.00 (s, s, s, 3H each), 1.77 (d of d of d, 1H, J = 14, 7, 4 Hz), 1.89 (d of t, 1H, J = 14, 3 Hz), 2.01 (d of d, 1H, J = 15, 10 Hz), 2.26 (d of d of d, 1H, J = 13, 7, 4 Hz), 2.45 (d of d, 1H, J = 15, 3 Hz), 2.55 (m, 1H), 2.57–2.78 (AB part of ABMN system, 2H), 2.91–3.08 (MN part of ABMN system, 2H), 3.41–3.62 (m, 4H), 3.69 (s, 3H). Decoupling experiments: irradiation at δ 2.01 removes the 15-Hz coupling from the signal at δ 2.45 and simplifies the multiplet at δ 2.55; irradiation at δ 2.71 essentially removes the large (J = 18 Hz) couplings from the δ 2.91–3.08 multiplet. *Exact Mass* calcd. for $C_{22}H_{34}O_5$: 378.2406; found: 378.2410.

Further elution of the column gave 13 mg (13%) of a mixture of the keto esters **26–28** in the approximate ratio (^{1}H nmr) of 1:6:4, respectively.

Further elution of the column afforded 38 mg (39%) of the keto ester **27**, which, after recrystallization from hexanes, exhibited mp 156–157°C; ir ($CHCl_3$): 1725 (br) cm^{-1}; ^{1}H nmr (400 MHz) δ: 0.89, 1.03, 1.04 (s, s, s, 3H each), 1.65–1.75 (m, 2H), 1.84–1.96 (m, 2H), 2.03–2.21 (AB part of ABX system, 2H, J_{AB} = 18 Hz), 2.15 (d, 1H, J = 18 Hz), 2.30 (m, 1H), 2.34 (d, 1H, J = 15 Hz), 2.43 (m, 1H), 2.49 (d, 1H, J = 18 Hz), 2.73 (d of d, 1H, J = 15, 1 Hz), 3.42–3.62 (m, 4H), 3.59 (s, 3H). *Anal.* calcd. for $C_{22}H_{34}O_5$: C 69.81, H 9.05; found: C 69.84, H 8.96. *Exact Mass* calcd.: 378.2406; found: 378.2407.

*Preparation of the keto ester **26***

(a) *From the photoadduct **20***

Ozonolysis of the photoadduct **20**, followed by treatment of the resultant dione **24** with sodium methoxide in methanol, was carried out via a procedure identical with that described above (**21** → **27** + **28**). From 58 mg of compound **20** there was obtained 60 mg (94%) of the keto ester **26**, which, after recrystallization from ether–hexanes, exhibited mp 139–140°C; ir ($CHCl_3$): 1720 (br) cm^{-1}; ^{1}H nmr (400 MHz) δ: 0.92, 1.00, 1.02 (s, s, s, 3H each), 1.70–1.80 (m, 2H), 1.88 (d, 1H, J = 19 Hz), 1.93 (d of t, 1H, J = 14, 3 Hz), 2.17 (d of d of d, 1H, J = 13, 6, 3 Hz), 2.33–2.44 (m, 3H), 2.46–2.61 (m, 3H), 3.40–3.57 (m, 4H), 3.63 (s, 3H). *Anal.* calcd. for $C_{22}H_{34}O_5$: C 69.81, H 9.05; found: C 69.65, H 8.94. *Exact Mass* calcd.: 378.2406; found: 378.2410.

(b) *From the photoadduct **21***

Ozonolysis of compound **21** (295 mg, 0.86 mmol) was carried out via a procedure very similar to that described above. A solution of the resultant crude dione **25** in methanol containing a small amount of sodium methoxide was stirred at room temperature for 2.5 h. Work-up as described above, followed by recrystallization of the crude product from ether–hexanes, gave 275 mg (85%) of the keto ester **26**.

(c) *From the keto ester **27***

A solution of compound **27** (54 mg, 0.143 mmol) in 20 mL of dry methanol containing a small amount of sodium methoxide was stirred at room temperature (argon atmosphere) for 2.5 h. Most of the solvent was removed (reduced pressure) and the residue was partitioned between ether and water. The organic phase was washed with brine, dried ($MgSO_4$), and concentrated to yield 49 mg (91%) of the keto ester **26**.

(d) *From the keto ester **28***

Conversion of the cyclobutanone **28** into compound **26** was accomplished via a procedure identical with that described above (**27** → **26**). From 36 mg (0.095 mmol) of **28** there was obtained 29 mg (81%) of **26**.

(e) *From a mixture of the photoadducts **20–23***

A mixture of the photoadducts **20–23** (ratio 40:51:6:3, respectively, *vide supra*) was subjected to ozonolysis via a procedure very similar to that described previously (**21** → **27** + **28**, see above). The quantities of reagents and solvents were as follows: photoadduct mixture, 3.11 g (9.02 mmol); methanol, 550 μL (13.53 mmol); dichloromethane, 100 mL, dimethyl sulfide, 3 mL.

The semi-solid material obtained after work-up of the ozonolysis reaction was dissolved in dry methanol (80 mL) containing freshly prepared sodium methoxide and the resulting solution was stirred at room temperature for 4 h. The methanol was removed (reduced pressure) and the residual material was dissolved in ether. The solution was washed with brine, dried ($MgSO_4$), and concentrated to give a colorless solid. Flash column chromatography (30) (elution with a 2:1:1 mixture of cyclohexane, hexanes, and ethyl acetate) of this material gave initially 88 mg of a mixture of compounds that contained mainly the minor photoadducts **22** and **23** (see below).

Further elution of the column gave a white solid, which upon recrystallization from hexanes provided 2.60 (76%) of the desired keto ester **26**.

*Purification and characterization of the photoadducts **22** and **23***

Flash column chromatography (30) (elution with a 10:5:2 mixture of cyclohexane, hexanes, and ethyl acetate) of 119 mg of mixture containing mainly the minor photoadducts **22** and **23** (see previous experiment for the origin of this material) afforded, as the first-eluted compound, 62 mg of **23**. Recrystallization of this material from ether–hexanes provided pure **23**, which exhibited mp 146–148°C; ir ($CHCl_3$): 1720, 1660, 1100 cm^{-1}; ^{1}H nmr (400 MHz) δ: 0.89 (m, 1H), 0.97 (s, 6H), 1.00 (s, 3H), 1.71 (m, 1H), 1.88 (d of d, 1H, J = 17, 2 Hz), 1.98 (d of t, 1H, J = 13, 3 Hz), 2.16 (d of q, 1H, J = 13, 3 Hz), 2.26–2.35 (m, 2H), 2.67 (br d, 1H, J = 10 Hz), 2.88 (d of d, 1H, J = 17, 6 Hz), 2.90 (m, 1H), 3.47, 3.52 (s, s, 2H each), 5.00 (t, 1H, J = 2.5 Hz), 5.01 (t, 1H, J = 2 Hz). In a difference nOe experiment, irradiation at δ 0.97 gave rise to no enhancement of the signals at δ 5.00 or 5.01. *Exact Mass* calcd. for $C_{22}H_{32}O_3$: 344.2351; found: 344.2347.

Further elution of the column afforded 31 mg of the photoadduct **22**, which, after recrystallization from hexanes, exhibited mp 132–133.5°C; ir ($CHCl_3$): 1720, 1650, 1100 cm^{-1}; ^{1}H nmr (400 MHz) δ: 0.89, 0.94, 0.99 (s, s, s, 3H each), 1.85 (t of d, 1H, J = 14, 4 Hz), 1.90–2.00 (m, 2H), 1.90–2.00 (m, 2H), 2.13–2.29 (m, 4H), 2.46 (d, 1H, J = 15 Hz), 2.52 (br d, 1H, J = 10 Hz), 2.78 (d of d of t, 1H, J = 16, 11, 3 Hz), 3.43–3.58 (m, 4H), 5.11 (br s, 1H), 5.26 (t, 1H, J = 3 Hz). In a difference nOe experiment, irradiation at δ 0.94 led to enhancement of the signal at δ 5.26. *Exact Mass* calcd. for $C_{22}H_{32}O_3$: 344.2351; found: 344.2359.

Reduction of the keto ester 26. Preparation of the alcohol 32 and the lactone 33

(a) *Reduction with sodium borohydride*

A solution of the keto ester **26** (240 mg, 0.63 mmol) and sodium borohydride (190 mg, 5 mmol) in 25 mL of methanol was stirred at room temperature for 30 min, and the methanol was then removed under reduced pressure. The residual material was partitioned between ether and water. The organic phase was washed twice with water, dried (Na_2SO_4), and concentrated. The remaining oil was subjected to column chromatography on silica gel. Elution of the column with 4:1 methylene chloride – ether gave 108 mg (49%) of the lactone **33**, which, after recrystallization from methanol, exhibited mp 194°C; ir ($CHCl_3$): 1730, 1115, 1100 cm^{-1}; ^{1}H nmr δ: 0.88, 0.92, 1.00 (s, s, s, 3H each), 3.50 (m, 4H), 4.78 (m, 1H). *Anal.* calcd. for $C_{21}H_{32}O_4$: C 72.38, H 9.26; found: C 71.97, H 8.95. *Exact Mass* calcd.: 348.2301; found: 348.2304.

Further elution of the column with the same solvent mixture provided 121 mg (50%) of the alcohol **32** as a viscous, colorless oil that exhibited one spot on tlc analysis; ir ($CHCl_3$): 3400, 1725, 1115, 1095 cm^{-1}; ^{1}H nmr δ: 0.95 (s, 3H), 0.99 (s, 6H), 3.58 (m, 4H), 3.65 (s, 3H), 4.54 (m, 1H). *Exact Mass* calcd. for $C_{22}H_{36}O_5$: 380.2562; found: 380.2561.

(b) *Reduction with lithium tri-*sec*-butylborohydride*

A cold (−78°C) solution of compound **26** (25 mg, 0.066 mmol) and lithium tri-*sec*-butylborohydride (0.10 mmol) in 5 mL of dry tetrahydrofuran was stirred at −78°C for 3 h. Water (1 mL), 1 *M* aqueous sodium hydroxide (100 μL), and 30% hydrogen peroxide (25 μL) were added consecutively and the mixture was stirred at room temperature for 15 min. The mixture was extracted thoroughly with ether and the combined extract was dried (Na_2SO_4) and concentrated. Separation of the mixture of products by column chromatography as described above gave 5.3 mg (23%) of the lactone **33** and 18.6 mg (74%) of the alcohol **32**.

Preparation of the diol 34

A solution of ester alcohol **32** (57 mg, 0.15 mmol) and lithium aluminum hydride (14.4 mg, 0.38 mmol) in 6 mL of dry ether was stirred at 0°C for 15 min and at room temperature for 30 min. Excess reducing agent was destroyed by careful addition of solid sodium sulfate decahydrate. The mixture was filtered and the collected solid material was washed thoroughly with ether. Removal of the solvent from the combined filtrate gave 50 mg (94%) of the diol **34** as a colorless oil that exhibited one spot on tlc analysis; ir ($CHCl_3$): 3400 (br), 1120, 1100 cm^{-1}; ^{1}H nmr δ: 0.94 (s, 3H), 0.96 (s, 6H), 3.52 (m, 4H), 3.70 (t, 2H, J = 8 Hz), 4.54 (m, 1H). *Exact Mass* calcd. for $C_{21}H_{36}O_4$: 352.2613; found: 352.2613.

Preparation of the diol 38

A vigorously stirred solution of the lactone **33** (50 mg, 0.14 mmol) and lithium aluminum hydride (13.3 mg, 0.35 mmol) in 10 mL of dry ether was refluxed for 2.5 h. The cooled solution was subjected to a work-up procedure identical with that described above. Recrystallization of the crude product gave 48 mg (95%) of the diol **38**, mp 180–182°C; ir ($CHCl_3$): 3350 (br), 1120, 1100 cm^{-1}; ^{1}H nmr δ: 0.93 (s, 6H), 1.00 (s, 3H), 3.51 (br s, 4H), 3.80 (t, 2H, J = 7 Hz), 4.55 (m, 1H). *Exact Mass* calcd. for $C_{21}H_{36}O_4$: 352.2613; found: 352.2623.

Preparation of the dimesylate 35

A solution of the diol **34** (50 mg, 0.14 mmol) and methanesulfonyl chloride (54 μL, 0.70 mmol) in 10 mL of dry pyridine was stirred at room temperature overnight and was then poured into 10 g of crushed ice. The mixture was extracted with ether, and the combined ether extract was washed with water and dried (Na_2SO_4). Removal of the solvent, followed by column chromatography of the remaining oil on silica gel (elution with 9:1 methylene chloride – ether), provided 57.7 mg (80%) of the dimesylate **35** as a pale yellow oil which exhibited ir ($CHCl_3$): 1360, 1340, 1170 cm^{-1}; ^{1}H nmr δ: 0.93, 0.94, 1.00 (s, s, s, 3H each), 3.01, 3.04 (s, s, 3H each), 3.5 (m, 4H), 4.3 (t, 2H, J = 8 Hz), 5.28 (m, 1H). *Exact Mass* calcd. for $C_{23}H_{40}O_8S_2$: 508.2165; found: 508.2160.

Preparation of the dimesylate 39

Compound **39** was prepared from the diol **38** via a procedure identical with that used for the conversion of **34** into **35**. From 50 mg of the diol **38** there was obtained 68.5 mg (95%) of the dimesylate **39** as a pale yellow oil which showed ir ($CHCl_3$): 1350, 1330, 1175 cm^{-1}; ^{1}H nmr δ: 0.93, 0.97, 1.01 (s, s, s, 3H each), 3.02, 3.03 (s, s, 3H each), 3.5 (m, 4H), 4.4 (t, 2H, J = 8 Hz), 5.3 (m, 1H). *Exact Mass* calcd. for $C_{23}H_{40}O_8S_2$: 508.2165; found: 508.2167.

Preparation of the dinitrile 37

A stirred solution of the dimesylate **35** (30 mg, 0.059 mmol) in 3 mL of dry hexamethylphosphoramide at room temperature was treated with sodium cyanide until the solution was saturated. The mixture, under an atmosphere of argon, was stirred at room temperature for 3 h and then at 60°C for 48 h. The cooled reaction mixture was diluted with ether, washed once with water, twice with saturated aqueous copper sulfate, once with brine, and dried (Na_2SO_4). Removal of the solvent, followed by column chromatography of the residue on silica gel (elution with 3:1 hexanes – ethyl acetate) gave a white solid that, upon recrystallization from methanol, provided 13.1 mg (60%) of the dinitrile **37**, mp 159–161°C; ir ($CHCl_3$): 2240, 2230 cm^{-1}; ^{1}H nmr δ: 0.91, 0.98, 1.01 (s, s, s, 3H each), 3.03 (m, 1H), 3.5 (m, 4H). *Exact Mass* calcd. for $C_{23}H_{34}N_2O_2$: 370.2620; found: 370.2619.

Preparation of the dinitrile 40

Transformation of the dimesylate **39** into the dinitrile **40** was carried out via a procedure identical with that described above (**35** → **37**). From 30 mg of **39** there was obtained 14.2 mg (65%) of **40**, mp 194°C; ir ($CHCl_3$): 2240, 2230 cm^{-1}; ^{1}H nmr δ: 0.95 (s, 6H), 0.97 (s, 3H), 2.95 (m, 1H), 3.5 (br s, 4H). *Exact Mass* calcd. for $C_{23}H_{34}N_2O_2$: 370.2620; found: 370.2618.

Preparation of a mixture of dinitriles 37 and 40 from the keto ester 26 (preparative scale)

To a cold (0°C), stirred suspension–solution of lithium aluminum hydride (360 mg, 9.5 mmol) in 50 mL of dry ether was added, dropwise, a solution of the keto ester **26** (2.40 g, 6.33 mmol) in 100 mL of dry ether. The mixture was allowed to warm to room temperature and stirred for 4 h. The mixture was recooled to 0°C and excess reducing agent was destroyed by careful addition of solid $Na_2SO_4 \cdot 10H_2O$. The resulting mixture was filtered through a plug of Florisil and the collected solid was washed thoroughly with ethyl acetate. Concentration of the combined filtrate gave 2.17 g of a mixture (white solid) of the epimeric diols **34** and **38**.

To a cold (0°C), stirred solution of the epimeric diols and dry triethylamine (2.55 mL, 18.3 mmol) in 30 mL of dry dichloromethane was added, dropwise, 1.03 mL (13.3 mmol) of methanesulfonyl chloride. The solution was stirred at 0°C for 1 h, was diluted with dichloromethane, washed consecutively with cold water and brine, and dried ($MgSO_4$). Removal of the solvent gave a yellow residue, which was dissolved in dichloromethane. The solution was filtered through a short column of silica gel and the column was washed with ethyl acetate. Removal of the solvent from the combined eluate afforded 3.15 g of the epimeric dimesylates **35** and **39**.

The mixture of **35** and **39** was dissolved in dry hexamethylphosphoramide (25 mL) and enough sodium cyanide was added to saturate the solution. The resulting mixture was stirred, under an atmosphere of argon, at 62°C for 16 h. The cooled reaction mixture was partitioned between ether and water and the aqueous phase was extracted twice with ether. The combined organic extract was washed twice with aqueous copper sulfate, once with brine, and dried ($MgSO_4$). Removal of the solvent gave 2.48 g of a yellowish semisolid, which was subjected to flash column chromatography (30) on silica gel. Elution with a mixture of 25% ethyl acetate in hexanes provided 142 mg (6%) of a mixture (~1:1, glc analysis) of the isomeric olefinic nitriles **43** and **44** as a colorless, viscous oil which exhibited ir ($CHCl_3$): 2230, 1100 cm^{-1}; ^1H nmr (80 MHz) δ: 0.92, 0.95, 1.00 (s, s, s, 9H total), 3.34–3.70 (m, 4H), 5.43–5.93 (m, 2H). *Exact Mass* calcd. for $C_{22}H_{33}NO_2$: 343.2511; found: 343.2513.

Further elution (35% ethyl acetate in hexanes) of the column gave 1.48 g (63%) of a mixture of the epimeric dinitriles **37** and **40** (ratio ~1:2, respectively, glc analysis) as a white solid that exhibited ir (KBr): 2220, 2210 cm^{-1}; ^1H nmr (80 MHz) δ: 0.91, 0.96, 0.98, 1.00 (s, s, s, s, 9H total), 2.98 (br m, 1H), 3.35–3.68 (m, 4H). *Exact Mass* calcd. for $C_{23}H_{34}N_2O_2$: 370.2620; found: 370.2620.

*Preparation of the enaminonitrile **41***

(a) *From the dinitrile 37*

A stirred solution of the dinitrile **37** (20 mg, 0.054 mmol) in 1 mL of dry *tert*-butyl alcohol containing a small amount of freshly prepared potassium *tert*-butoxide was refluxed, under an atmosphere of argon, for 24 h. The solvent was removed (vacuum pump) and the residue was partitioned between water and ether. The organic phase was dried (Na_2SO_4) and concentrated to give a colorless oil that crystallized upon addition of a few drops of methanol. Recrystallization from methanol gave 18 mg (90%) of the enaminonitrile **41** as white needles that exhibited mp 213–215°C; ir ($CHCl_3$): 3490, 3390, 2165, 1642, 1605 cm^{-1}; ^1H nmr δ: 0.90, 0.92, 1.01 (s, s, s, 3H each), 3.52 (m, 4H), 4.23 (br s, 2H). *Exact Mass* calcd. for $C_{23}H_{34}N_2O_2$: 370.2620; found: 370.2618.

(b) *From the dinitrile 40*

The enaminonitrile **41** was obtained from the dinitrile **40** via a procedure identical with that described above. From 20 mg of **40** there was obtained 16 mg (80%) of compound **41**.

*Preparation of the dione **42***

(a) *From the enaminonitrile 41*

To a deoxygenated mixture of glacial acetic acid (1 mL), water (100 μL), and 85% phosphoric acid (400 μL) was added 18 mg (0.049 mmol) of the enaminonitrile **41** and the resulting solution was refluxed, under an atmosphere of argon, for 24 h. The cooled reaction mixture was poured onto 2 g of crushed ice and sodium bicarbonate was added until the mixture was basic. The mixture was extracted with ether and the combined extract was washed with brine and dried (Na_2SO_4). Removal of the solvent gave an oil, which was purified by column chromatography (silica gel, elution with 1:1 hexanes – ethyl acetate). The material thus obtained was recrystallized from ether–hexanes, affording 10.1 mg (80%) of the tetracyclic dione **42** as colorless cubes, mp 132°C; ir ($CHCl_3$): 1705 cm^{-1}; ^1H nmr (400 MHz) δ: 1.15 (s, 3H), 1.73 (br m, 1H), 1.85 (br m, 1H), 1.90–2.05 (m, 4H), 2.09 (br m, 1H), 2.14–2.44 (m, 7H), 2.52 (d of d of t, 1H, J = 18, 9, 1 Hz), 2.70 (br t, 1H, J = 7 Hz). *Anal.* calcd. for $C_{17}H_{24}O_2$: C 78.42, H 9.29; found: C 78.29, H 9.28. *Exact Mass* calcd.: 260.1776; found: 260.1774.

(b) *From a mixture of epimeric dinitriles 37 and 40 (preparative scale)*

A stirred solution of a mixture of the dinitriles **37** and **40** (602 mg, 1.62 mmol, *vide supra*) in 10 mL of dry *tert*-butyl alcohol containing a small amount of freshly prepared potassium *tert*-butoxide was refluxed (argon atmosphere) for 5 h, after which time the solvent was removed under reduced pressure (vacuum pump). To the residual solid was added a deoxygenated mixture of acetic acid (10 mL), water (1 mL), and 85% phosphoric acid (4 mL) and the resulting solution was refluxed with stirring (argon atmosphere) for 40 h. The cooled reaction mixture was partitioned between water and dichloromethane and the aqueous phase was extracted twice with dichloromethane. The combined organic extract was washed with brine, twice with aqueous sodium bicarbonate, and then again with brine. The solution was dried ($MgSO_4$) and the volatile materials were removed under reduced pressure to afford 444 mg of a pale brown oil. Flash column chromatography (30) of this material (elution with ether), followed by recrystallization of the solid thus obtained, gave 351 mg (83%) of the dione **42**, mp 132°C.

*Preparation of the bis enones **48** and **49***

To a cold (−95°C), stirred solution of the dione **42** (251 mg, 0.964 mmol) and triethylamine (806 μL, 5.78 mmol) in 20 mL of dry dichloromethane, under an atmosphere of argon, was added, dropwise, 686 μL (4.82 mmol) of freshly prepared trimethylsilyl iodide (38). The orange solution was stirred for 1 h at −95°C, was diluted with petroleum ether, and was then allowed to warm to room temperature. The reaction mixture was washed with cold aqueous sodium bicarbonate, dried (Na_2SO_4), and concentrated under reduced pressure. Gas–liquid chromatographic analysis of the remaining yellow oil indicated the presence of the two isomeric bis trimethylsilyl enol ethers **46** and **47**, in a ratio of 4:1. This material was dissolved in 20 mL of dry acetonitrile, 472 mg (2.12 mmol) of palladium(II) acetate was added, and the solution was stirred under an atmosphere of argon at room temperature for 14 h. The reaction mixture was filtered through a short column of silica gel and the column was washed thoroughly with ether. Removal of the solvent from the combined eluate gave a viscous brown oil, which was subjected to flash column chromatography (30) (elution with ether). Recrystallization (ether) of the first-eluted component gave 165 mg (67%) of the bis enone **48**, which exhibited mp 155–157°C; ir (KBr): 1680, 1660 cm^{-1}; ^1H nmr (400 MHz) δ: 1.34 (s, 3H), 1.70 (d, 1H, J = 12 Hz), 1.75 (d of d of d, 1H, J = 14, 8, 2 Hz), 1.84 (d of d, 1H, J = 14, 8 Hz), 1.99 (m, 1H), 2.15 (m, 1H), 2.29 (d of d of d, 1H, J = 12, 6, 2.5 Hz), 2.30–2.49 (m, 3H), 2.94 (broad t, 1H, J ~ 7 Hz), 5.89 (d, 1H, J = 10.5 Hz), 6.00 (d of d, 1H, J = 10, 2 Hz), 6.72 (d, 1H, J = 10.5 Hz), 7.33 (d of d, 1H, J = 10, 2.5 Hz). Decoupling experiment: irradiation at δ 2.94 causes (a) collapse of the signal at δ 6.00 to a doublet (J = 10 Hz), (b) collapse of the δ 2.29 signal to a d of d (J = 12, 2.5 Hz), and (c) collapse of the δ 1.75 signal to a d of d (J = 14, 2 Hz). *Anal.* calcd. for $C_{17}H_{20}O_2$: C 79.65, H 7.86; found: C 79.49, H 7.88. *Exact Mass* calcd.: 256.1464; found: 256.1463.

Further elution of the column afforded 47 mg (19%) of the bis enone **49**, which after recrystallization from ether exhibited mp 147–149°C; ir (KBr): 1680, 1665, 1650, 1605 cm^{-1}; ^1H nmr (400 MHz) δ: 1.50 (m, 1H), 1.55 (s, 3H), 1.71–1.97 (diffuse m, 4H), 2.01 (d, 1H, J = 12 Hz), 2.04–2.15 (m, 2H), 2.27–2.61 (diffuse m, 4H), 2.91 (br t, 1H, J ~ 7 Hz), 5.86 (d, 1H, J = 1.5 Hz), 5.93 (d of d, 1H, J = 10, 2 Hz), 7.26 (d of d, 1H, J = 10, 3 Hz). *Exact Mass* calcd. for $C_{17}H_{20}O_2$: 256.1463; found: 259.1459.

*Alkylation of compound **48**. Preparation of the bis enones **50** and **51***

To a cold (0°C), stirred solution of lithium bis(trimethylsilyl)amide (3.77 mmol) in 30 mL of dry dimethoxyethane, under an atmosphere of argon, was added, dropwise, a solution of the bis enone **48** (186 mg, 0.73 mmol) in 5 mL of dry dimethoxyethane. After the solution had been stirred at 0°C for 1 h, methyl iodide (15 mL) was added rapidly. The mixture was stirred at 0°C for 30 min and at room temperature for 1 h. A few drops of saturated aqueous ammonium chloride were added, the volatile materials were removed under reduced pressure, and the residual oil was partitioned between ether and aqueous ammonium chloride. The organic phase was washed with aqueous sodium thiosulfate and brine, dried (Na_2SO_4), and concentrated to afford 206 mg of a white solid. Flash column chromatography (30) (elution with 35% hexanes in ether) of a small amount of this material gave a pure sample of the bis enone **50**, which, after recrystallization from ethyl acetate – hexanes, exhibited mp 149–150.5°C; ir ($CHCl_3$): 1675, 1660 cm^{-1}; ^1H nmr (400 MHz) δ: 1.17 (d, 3H, J = 7 Hz), 1.25–1.48 (m, 2H), 1.37 (s, 3H), 1.68 (d, 1H, J = 12 Hz), 1.71 (m, 1H), 1.73 (d of d of d, 1H, J = 14, 8, 2 Hz), 1.84 (d of d, 1H, J = 14, 7 Hz), 1.91–2.07 (m, 2H), 2.15 (m, 1H), 2.27 (d of d of d, 1H, J =12, 6, 3 Hz), 2.38 (d of q, 1H, J = 13, 7 Hz), 2.91 (br t, 1H, J = 7 Hz), 5.87 (d, 1H, J = 10.5 Hz), 5.98 (d of d, 1H, J = 10.5, 2.5 Hz), 6.65 (d, 1H, J = 10.5 Hz), 7.32 (d of d, 1H, J = 10.5, 3 Hz). Decoupling experiment: irradiation at δ 1.17 caused collapse of the signal at δ 2.38 to a doublet (J = 13 Hz). *Exact Mass* calcd. for $C_{18}H_{22}O_2$: 270.1620; found: 270.1621.

The crude monomethylation product **50** (206 mg, see above) was alkylated again under identical reaction conditions, except that, after addition of the methyl iodide, the reaction mixture was stirred at room temperature for 6 h. Recrystallization (ether–hexanes) of the white solid obtained from work-up gave 126 mg of the bis enone **51**. Flash column chromatography (30) (elution with 35% hexanes in ether) of the material from the mother liquor afforded a futher 34 mg of **51**, for a total yield of 160 mg (77%). The crystalline bis enone **51** exhibited mp 154–156°C; ir ($CHCl_3$): 1660 (br) cm^{-1}; ^{1}H nmr (400 MHz) δ: 1.16, 1.20, 1.44 (s, s, s, 3H each), 1.37 (m, 1H), 1.68 (d, 1H, J = 12 Hz), 1.74 (d of d of d, 1H, J = 14, 8, 2 Hz), 1.83 (d of d, 1H, J = 14, 7.5 Hz), 2.04–2.21 (m, 3H), 2.30 (d of d of d, 1H, J = 12, 6, 3 Hz), 2.92 (br t, 1H, J ~ 7 Hz), 5.89 (d, 1H, J = 10.5 Hz), 5.99 (d of d, 1H, J = 10.5, 2.5 Hz), 6.66 (d, 1H, J = 10.5 Hz), 7.35 (d of d, 1H, J = 10.5, 3 Hz). Decoupling experiment: irradiation at δ 7.35 collapses the signal at δ 5.99 to a doublet (J = 2.5 Hz) and simplifies the signal at δ 2.30 to a d of d (J = 12, 6 Hz). *Anal.* calcd. for $C_{19}H_{24}O_2$: C 80.24, H 8.51; found: C 80.08, H 8.40. *Exact Mass* calcd.: 284.1776; found: 284.1778.

Preparation of (±)-17-nor-stemodane-3,13-dione (52)

A mixture of the bis enone **51** (77.5 mg, 0.273 mmol), dry dioxane (3 mL), and a small amount of 5% palladium-on-carbon was stirred vigorously under an atmosphere of hydrogen at room temperature and atmospheric pressure. After 2 h, tlc analysis indicated that no starting material remained. The mixture was diluted with ethyl acetate and filtered through a plug of Celite. Concentration of the filtrate afforded 77.6 mg (99%) of the dione **52** as a colorless solid. Recrystallization of a small amount of this material from ethyl acetate – hexanes provided a pure sample of **52**, which exhibited mp 151–152°C; ir ($CHCl_3$): 1700 cm^{-1}; ^{1}H nmr (400 MHz) δ: 1.10, 1.12, 1.18 (s, s, s, 3H each), 1.26 (m, 1H), 1.46–1.79 (diffuse m, 7H), 1.89–1.99 (m, 4H), 2.04 (m, 1H), 2.18–2.30 (m, 2H), 2.34 (d of d of d, 1H, J = 16, 5, 3 Hz), 2.50 (br d of d of d, 1H, J = 17, 9, 9 Hz), 2.58 (d of d of d, J = 16, 13, 6 Hz), 2.69 (br t, 1H, J ~ 7 Hz). *Anal.* calcd. for $C_{19}H_{28}O_2$: C 79.12, H 9.78; found: C 79.03, H 9.80. *Exact Mass* calcd.: 288.2089; found: 288.2086.

Preparation of a mixture of (±)-stemodan-13α-ol-3-one (53) and (±)-stemodan-13β-ol-3-one (54). Characterization of 53

To a stirred solution of the dione **52** (20.8 mg, 0.072 mmol) in 2 mL of dry ether, under an atmosphere of argon, was added 1 mL (~4 mmol) of neat methyltriisopropoxytitanium (40, 41) and the resulting solution was stirred at room temperature for 10 h. The solution was poured carefully into a well-stirred mixture of ether and 1 *N* hydrochloric acid and the aqueous phase was extracted twice more with ether. The combined organic extract was washed with aqueous sodium bicarbonate and brine, dried ($MgSO_4$), and concentrated. Flash column chromatography (30) (elution with 30% tetrahydrofuran in hexanes) of the residual material gave 18.0 mg (82%) of an 86:14 mixture (glc analysis) of the epimeric keto alcohols **53** and **54**. This oil exhibited ir ($CHCl_3$): 3580, 3400, 1690 cm^{-1}; ^{1}H nmr (80 MHz) δ: 1.09, 1.12, 1.13, 1.24 (s, s, s, s). *Exact Mass* calcd. for $C_{20}H_{32}O_2$: 304.2403; found 304.2405.

In another experiment, carried out as described above, concentration of the later fractions obtained from chromatography of the crude reaction product afforded a viscous oil containing mainly (94%) the alcohol **53**. Crystallization of this oil from hexanes provided a pure sample of (±)-stemodan-13α-ol-3-one (**53**), mp 93°C (lit. (15) mp 90–91°C); ir ($CHCl_3$): 3570, 3320, 1690, 905 cm^{-1}; ^{1}H nmr (400 MHz) δ: 1.09, 1.10, 1.12, 1.14 (s, s, s, s, 3H each), 1.91–2.03 (m, 3H), 2.29 (d of d of d, 1H, J = 16, 4.5, 3.5 Hz), 2.57 (d of d of d, 1H, J = 16, 14, 6 Hz). *Exact Mass* calcd. for $C_{20}H_{32}O_2$: 304.2402; found: 304.2404.

Preparation of (±)-maritimol (4)

A solution of the keto alcohol **53** (11.7 mg, 0.038 mmol) in 2 mL of methanol containing excess sodium borohydride was stirred at 0°C for 2 h, and the solvent was removed under reduced pressure. The residue was partitioned between ethyl acetate and brine. The organic phase was dried ($MgSO_4$) and concentrated. Crystallization of the residual oil from ethyl acetate gave 5.6 mg of (±)-maritimol (**4**). Chromatography of the material from the mother liquor on silica gel (elution with 1:1 ethyl acetate – hexanes) afforded an additional 3 mg of crystalline (±)-maritimol (**4**), for a total yield of 8.6 mg (73%). Recrystallization from ether–hexanes gave a pure sample of (±)-**4**, which exhibited mp 221–222°C (lit. (14) mp 212.5–214°C and (15) mp 211.5–212.5°C); ir (KBr): 3340 (br) cm^{-1}; ^{1}H nmr (400 MHz, $CDCl_3$–$(CD_3)_2SO$) δ: 0.84, 0.95, 1.02, 1.11 (s, s, s, s, 3H each), 1.75 (s, 1H, exchanges with D_2O), 1.83 (d, 1H, J = 12 Hz), 1.88–1.98 (m, 2H), 2.04 (d, 1H, J = 6 Hz, exchanges with D_2O), 3.18 (d of d of d, 1H, J = 13, 6, 5 Hz; on addition of D_2O, d of d, J = 13, 5 Hz). This material was identical with a sample of (+)-maritimol (8) by glc (coinjection), tlc (four solvent systems), ^{1}H nmr (400 MHz), and mass spectrometry. *Anal.* calcd. for $C_{20}H_{34}O_2$: C 78.38, H 11.18; found: C 78.26, H 11.28. *Exact Mass* calcd.: 306.2559; found: 306.2560.

Preparation of (±)-stemod-2-en-13α-ol (56) and (±)-stemod-2-en-13β-ol (57)

A stirred solution of an 86:14 mixture of the keto alcohols **53** and **54** (*vide supra*) (61.1 mg, 0.201 mmol), and *p*-toluenesulfonylhydrazide (48.6 mg, 0.261 mmol) in 1 mL of absolute ethanol was refluxed under an argon atmosphere for 3 h. A white precipitate formed. The mixture was concentrated and the residue was dried under vacuum (oil pump) for 3 h to provide the crude *p*-toluenesulfonylhydrazones **55**. A stirred suspension of this material in 15 mL of dry toluene was treated with sodium hydride (5.34 mmol, 225 mg of a 57% dispersion in mineral oil, freed of oil by washing three times with ether) and the resulting mixture was refluxed under an atmosphere of argon for 3 h. The reaction mixture was cooled to room temperature, excess base was destroyed by **cautious** addition of water, and the resulting mixture was partitioned between ether and aqueous ammonium chloride. The aqueous phase was extracted once more with ether and the combined extract was washed with brine, dried ($MgSO_4$), and concentrated. The remaining oil was subjected to column chromatography (15 g silica gel, elution with 15% ethyl acetate in hexanes) to afford 33.5 mg (58%) of (±)-stemod-2-en-13α-ol (**56**) as a white solid. Recrystallization of a small amount of this material from hexanes gave an analytical sample of **56**, which exhibited mp 129.5–131°C (lit (13) mp 119–122°C; (15) mp 128–129°C); ir ($CHCl_3$): 3600 cm^{-1}; ^{1}H nmr (400 MHz) δ: 0.92, 0.96, 0.97, 1.12 (s, s, s, s, 3H each), 2.08 (br d, 1H, J = 17 Hz), 5.32 (d of d, 1H, J = 10, 2.5 Hz), 5.50 (d of d of d, 1H, J = 10, 6.5, 2.5 Hz). *Anal.* calcd. for $C_{20}H_{32}O$: C 83.27, H 11.18; found: C 83.27, H 11.10. *Exact Mass* calcd. : 288.2453; found: 288.2455.

Further elution of the column afforded 7.0 mg (12%) of (±)-stemod-2-en-13β-ol (**57**) as a white solid that, after recrystallization from heptane, exhibited mp 153–154°C (lit. (13) mp 147–149°C); ir (KBr): 3300 cm^{-1}; ^{1}H nmr (80 MHz) δ: 0.90 (s, 3H), 0.95 (s, 6H), 1.23 (s, 3H), 5.18–5.62 (m, 2H). *Exact Mass* calcd. for $C_{20}H_{32}O$: 288.2453; found: 288.2456.

Preparation of (±)-stemodin (2)

A solution of the alkene **56** (33.3 mg, 0.116 mmol) and 9-borabicyclo[3.3.1]nonane (200 mg) in 3 mL of dry tetrahydrofuran, under an atmosphere of argon, was refluxed for 48 h. The cooled reaction mixture was treated consecutively with 3 mL of ethanol, 3 mL of 7 *M* aqueous sodium hydroxide, and 3 mL of 30% aqueous hydrogen peroxide, and was then heated at 50°C for 1 h. The cooled mixture was partitioned between ethyl acetate and aqueous sodium bicarbonate. The aqueous phase was extracted with ethyl acetate and the combined extract was washed with brine, dried ($MgSO_4$), and concentrated. Column chromatography (25 g silica gel, elution with 3:1 ethyl acetate – hexanes) of the residual oil afforded 31.3 mg (88%) of (±)-stemodin (**2**) as a white solid. Recrystallization (acetone–hexanes or ethyl acetate) of this material provided (±)-**2** as colorless plates, which exhibited mp 220.5–222°C (lit. (13) mp 218–220°C); ir (KBr): 3300 cm^{-1}; ^{1}H nmr (400 MHz, $CDCl_3$–$(CD_3)_2SO$) δ: 0.90, 0.94, 0.97, 1.08 (s, s, s, s, 3H each), 1.59–1.76 (m, 5H), 1.85–2.00 (m, 4H), 2.87, 3.41 (br s, br s, 1H each), 3.67 (m, 1H). On addition of

D_2O, the signals at δ 2.87 and 3.41 disappeared and the signal at δ 3.67 simplified. This material was identical with an authentic sample of (−)-stemodin (7) by glc (coinjection), tlc (four solvent systems), ^1H nmr (400 MHz), and mass spectrometry. *Exact Mass* calcd. for $C_{20}H_{34}O_2$: 306.2558; found: 306.2558.

Acknowledgements

We gratefully acknowledge the financial support of the Natural Sciences and Engineering Research Council of Canada, and thank the New Zealand National Research Advisory Council for a Fellowship (to I.D.S.) and the University of British Columbia for a Graduate Fellowship (to B.F.A.).

1. K. M. BRUNDRET, W. DALZIEL, B. HESP, J. A. J. JARVIS, and S. NEIDLE. J. Chem. Soc. Chem. Commun. 1027 (1972); W. DALZIEL, B. HESP, K. M. STEVENSON, and J. A. J. JARVIS. J. Chem. Soc. Perkin Trans. 1, 2841 (1973).
2. A. N. STARRAT and S. R. LOSCHIAVO. Can. J. Microbiol. **20**, 416 (1974).
3. R. A. BUCKNALL, H. MOORES, R. SIMMS, and B. HESP. Antimicrob. Agents Chemother. **4**, 294 (1973); A. ICHIKAWA, M. NEGISHI, K. TOMITA, and S. IKEGAMI. Jpn. J. Pharmacol. **30**, 301 (1980).
4. J. DOUROS and M. SUFFNESS. *In* New Anticancer drugs. *Edited by* S. K. Carter and Y. Sakurai. Springer-Verlag, Berlin. 1980. p. 29.
5. (*a*) B. M. TROST, Y. NISHIMURA, K. YAMAMOTO, and S. S. MCELVAIN. J. Am. Chem. Soc. **101**, 1328 (1979); (*b*) J. E. MCMURRY, A. ANDRUS, G. M. KSANDER, J. H. MUSSER, and M. A. JOHNSON. J. Am. Chem. Soc. **101**, 1330 (1979); Tetrahedron, **37**, Supplement No. 9, 319 (1981); (*c*) E. J. COREY, M. A. TIUS, and J. DAS. J. Am. Chem. Soc. **102**, 1742 (1980); (*d*) R. E. IRELAND, J. D. GODFREY, and S. THAISRIVONGS. J. Am. Chem. Soc. **103**, 2446 (1981); R. E. IRELAND, W. C. DOW, J. D. GODFREY, and S. THAISRIVONGS. J. Org. Chem. **49**, 1001 (1984); (*e*) E. E. VAN TAMELEN, S. R. ZAWACKY, R. K. RUSSELL, and J. G. CARLSON. J. Am. Chem. Soc. **105**, 142 (1983); (*f*) R. MARINI-BETTOLO, P. TAGLIATESTA, A. LUPI, and D. BRAVETTI. Helv. Chim. Acta, **66**, 1922 (1983).
6. (*a*) T. KAMETANI, T. HONDA, Y. SHIRATORI, and K. FUKUMOTO. Tetrahedron Lett. 1665 (1980); (*b*) K. C. NICOLAOU and R. E. ZIPKIN. Angew. Chem. Int. Ed. Engl. **20**, 785 (1981); (*c*) R. L. CARGILL, D. F. BUSHEY, J. R. DALTON, R. S. PRASAD, and R. D. DYER. J. Org. Chem. **46**, 3389 (1981); (*d*) D. BRAVETTI, R. MARINI-BETTOLO, and A. LUPI. Helv. Chim. Acta, **65**, 371 (1982); (*e*) A. J. PEARSON, G. C. HEYWOOD, and M. CHANDLER. J. Chem. Soc. Perkin Trans. 1, 2631 (1982); (*f*) R. B. KELLY, G. S. LAL, G. GOWDA, and R. N. REJ. Can. J. Chem. **62**, 1930 (1984); (*g*) C. IWATA, T. MORIE, N. MAEZAKI, H. SHIMAMURA, T. TANAKA, and T. IMANISHI. J. Chem. Soc. Chem. Commun. 930 (1984).
7. P. S. MANCHAND, J. D. WHITE, H. WRIGHT, and J. CLARDY. J. Am. Chem. Soc. **95**, 2705 (1973).
8. C. D. HUFFORD, R. O. GUERRERO, and N. J. DOORENBOS. J. Pharm. Sci. **65**, 778 (1976).
9. R. B. KELLY, M. L. HARLEY, S. J. ALWARD, R. N. REJ, G. GOWDA, A. MUKHOPADHYAY, and P. S. MANCHAND. Can. J. Chem. **61**, 269 (1983).
10. R. B. KELLY, M. L. HARLEY, S. J. ALWARD, and P. S. MANCHAND. Can. J. Chem. **60**, 675 (1982).
11. (*a*) P. S. MANCHAND and J. F. BLOUNT. J. Chem. Soc. Chem. Commun. 894 (1975); (*b*) R. B. KELLY, M. L. HARLEY, and S. J. ALWARD. Can. J. Chem. **58**, 755 (1980).
12. E. PIERS, B. F. ABEYSEKERA, D. J. HERBERT, and I. D. SUCKLING. J. Chem. Soc. Chem. Commun. 404 (1982).
13. E. J. COREY, M. A. TIUS, and J. DAS. J. Am. Chem. Soc. **102**, 7613 (1980).
14. E. E. VAN TAMELEN, J. G. CARLSON, R. K. RUSSELL, and S. R. ZAWACKY. J. Am. Chem. Soc. **103**, 4615 (1981).
15. R. MARINI-BETTOLO, P. TAGLIATESTA, A. LUPI, and D. BRAVETTI. Helv. Chim. Acta, **66**, 760 (1983).
16. P. K. GHOSAL, D. MUKHERJEE, and P. C. DUTTA. Tetrahedron Lett. 2997 (1976); S. K. MAITY, B. BASU, and D. MUKHERJEE. Tetrahedron Lett. **24**, 3921 (1983).
17. D. SEEBACH. Angew. Chem. Int. Ed. Engl. **18**, 239 (1979).
18. A. J. BIRCH, E. PRIDE, and H. SMITH. J. Chem. Soc. 4688 (1958).
19. E. J. COREY and J. W. SUGGS. Tetrahedron Lett. 2647 (1975).
20. E. PIERS and B. ABEYSEKERA. Can. J. Chem. **60**, 1114 (1982).
21. E. BROWN and M. RAGAULT. Tetrahedron, **37**, Supplement No. 9, 61 (1981).
22. L. M. JACKMAN and S. STERNHELL. Applications of nuclear magnetic resonance spectroscopy in organic chemistry. 2nd Ed. Pergamon Press, New York, NY. 1969.
23. H. O. HOUSE, C. CHU, J. M. WILKINS, and M. J. YMEN. J. Org. Chem. **40**, 1460 (1975).
24. K. WIESNER. Chem. Soc. Rev. **6**, 413 (1977).
25. P. E. EATON. Tetrahedron Lett. 3695 (1964).
26. R. A. PAUPTIT and J. TROTTER. Can. J. Chem. **59**, 524 (1981).
27. G. MARINI-BETTOLO, S. P. SAHOO, G. A. POULTON, T. Y. R. TSAI, and K. WIESNER. Tetrahedron, **36**, 719 (1980).
28. R. A. PAUPTIT and J. TROTTER. Can. J. Chem. **61**, 63 (1983).
29. I. FLEMING and D. H. WILLIAMS. Tetrahedron, **23**, 2747 (1967).
30. W. C. STILL, M. KAHN, and A. MITRA. J. Org. Chem. **43**, 2923 (1978).
31. L. D. HALL and J. K. M. SANDERS. J. Am. Chem. Soc. **102**, 5703 (1980).
32. O. W. LEVER, JR. Tetrahedron, **32**, 1943 (1976).
33. K. OGURA, M. YAMASHITA, S. FURUKAWA, M. SUZUKI, and G. TSUCHIHASHI. Tetrahedron Lett. 2767 (1975).
34. S. BALDWIN. J. Org. Chem. **26**, 3280 (1961).
35. J. P. SCHAEFER and J. J. BLOOMFIELD. Org. React. **15**, 1 (1967).
36. S. V. EVANS and J. TROTTER. Can. J. Chem. **62**, 1828 (1984).
37. H. O. HOUSE, L. J. CZUBA, M. GALL, and H. D. OLMSTEAD. J. Org. Chem. **34**, 2324 (1969).
38. D. E. SEITZ and L. FERREIRA. Synth. Commun. **9**, 931 (1979).
39. Y. ITO, T. HIRAO, and T. SAEGUSA. J. Org. Chem. **43**, 1011 (1978).
40. M. D. RAUSCH and H. B. GORDON. J. Organomet. Chem. **74**, 85 (1974).
41. B. WEIDMANN and D. SEEBACH. Helv. Chim. Acta, **63**, 2451 (1980); Angew. Chem. Int. Ed. Engl. **22**, 31 (1983).

The ion-pair mechanism and bimolecular displacement at saturated carbon. V.[1] Racemization and bromide – radio-bromide exchange for substituted 1-phenylbromoethanes in acetone

ALLAN R. STEIN[2] AND ELIZABETH A. MOFFATT

Department of Chemistry, Memorial University of Newfoundland, St. John's, Nfld., Canada A1B 3X7

Received March 29, 1985

ALLAN R. STEIN and ELIZABETH A. MOFFATT. Can. J. Chem. **63**, 3433 (1985).

Results of kinetic studies of the racemizations and *radio*-bromide exchanges with 1-arylbromoethanes in acetone with added LiBr are reported. The results are direct empirical evidence supporting the ion-pair mechanism for bimolecular nucleophilic displacement at saturated carbon. For the unsubstituted and less electron rich substrates, behaviour expected for a classical S_N2 mechanism is found, but for 1-(4-methylphenyl)bromoethane, the racemization rate is greater than twice the exchange rate, indicating internal return with racemization from a solvated ion pair. For 1-(3,4-dimethylphenyl)bromoethane, the carbocation is sufficiently stabilized that the reaction shows intermediate behaviour; the racemization rate is significantly less than twice the exchange rate, for example. Through the series from the electron withdrawer to electron donor substituted substrate, the activation parameter ΔH^{+} progressively decreases and ΔS^{+} becomes rapidly more negative.

ALLAN R. STEIN et ELIZABETH A. MOFFATT. Can. J. Chem. **63**, 3433 (1985).

On rapporte les résultats obtenus lors d'études cinétiques relatives aux racémisations et aux échanges de *radio*-bromures d'aryl-1 bromoéthanes dans de l'acétone à laquelle on a ajouté du LiBr. Les résultats obtenus correspondent à des données empiriques directes qui apportent un support au mécanisme par paire d'ions lors des réactions de substitutions nucléophiles bimoléculaires au niveau de carbones saturés. Dans les cas des substrats qui ne sont pas substitués ou qui sont moins riches en électrons, on observe le comportement attendu pour un mécanisme S_N2 classique; toutefois, avec le (méthyl-4 phényl)-1 bromoéthane, la vitesse de racémisation est au moins deux fois plus grande que la vitesse d'échange et ceci suggère la présence d'un retour interne avec racémisation dans une paire d'ions solvatés. Dans le cas du (diméthyl-3,4 phényl)-1 bromoéthane, le carbocation est suffisamment stabilisé pour que la réaction présente un comportement intermédiaire; par exemple, la vitesse de racémisation est au moins deux fois plus faible que la vitesse d'échange. Lorsque l'on passe des substrats portant des groupements électroaffinitaires à ceux portant des groupements électro-donneurs, il y a une diminution graduelle du ΔH^{+} alors que le ΔS^{+} devient rapidement plus négatif.

[Traduit par le journal]

Since Sneen and Larsen (1), in 1969, proposed an elaboration of the Winstein ion-pair scheme (2) as a "unified mechanism" for nucleophilic substitutions at saturated carbon, it has slowly been gaining respectability, so much so that the ion-pair mechanism now receives extensive discussion in undergraduate textbooks (3).

The ion-pair mechanism can perhaps best be approached by considering the process of ionization and dissociation of a substrate RX. This can be considered a stepwise process of ionization to a contact or intimate ion pair within a solvation sheath or cage followed by separation of the two ions, R^+ and X^-. The separation of the ions would occur with layer by layer of solvent inserting itself between the ions to give, progressively, the solvent-separated ion pair with one, the solvated ion pairs with two, with three, with four, and so on, layers of solvation between the ions until finally the free, independently solvated, dissociated ions are reached. In principle at least, every stage of this ionization – solvent separation – dissociation process is reversible. Introducing a nucleophile, Z^-, could, again in principle, lead to nucleophilic attack at any stage of the dissociative process as indicated in Scheme 1.

Nucleophilic attack concurrent with ionization would, of course, represent the classical Hughes–Ingold bimolecular nucleophilic substitution, the S_N2 mechanism (4), whereas attack after complete dissociation of the initially formed ion pair would represent their unimolecular reaction, the S_N1 mechanism (5).

There is much direct or empirical evidence for the involvement of ion pairs in reactions at or near the unimolecular extreme, that is for S_N1 reactions (2, 6), but while evidence is accumulating for ion-pair involvement in bimolecular displacements, it is generally indirect. Thus computer simulations of bimolecular processes may require an intermediate species, or an intermediate may be implied by various correlations (7, 8). Such intermediates *could* be ion pairs. Direct empirical evidence is, to say the least, rare. It was in hopes of finding such direct evidence that the study reported here was undertaken.

Scheme 2 contains minimal representations for the S_N2 or ion-pair bimolecular, A, and S_N1 unimolecular substitution, B. In the following discussion we will assume the substrate was optically active. If *X is identical to X, any chirality is lost by the central-intermediate or transition-state stage. If, however, *X ≠ X, be they different neutral species (e.g. H_2O vs. CH_3OH), anions (e.g. CN^- vs. Cl^-), or even isotopic (e.g. *radio*-bromide vs. bromide) as in our case, chiral differentiation remains throughout in A but not in B. Thus if return to starting material occurs with the *same* anion in an S_N2 process, i.e. Scheme 2A, chirality of the substrate is retained. There has been neither racemization nor exchange. Should substitution occur, both exchange of covalently bound X and ionic *X *and* inversion of the stereochemistry of the substrate take place. Ignoring any isotope effect on optical activity, that single substitution results in the loss of two units of optical rotation, one for the molecule of substrate inverted and, because its rotational contribution is now opposite, another to cancel that contribution. A single exchange with inversion gives two molecules as a inactive racemic mixture. In the classical S_N2 mechanism, the only route for racemization is

[1] While not sequentially numbered, refs. 22–24 and ref. 15 are considered parts I–IV of this series.

[2] Author to whom correspondence may be addressed.

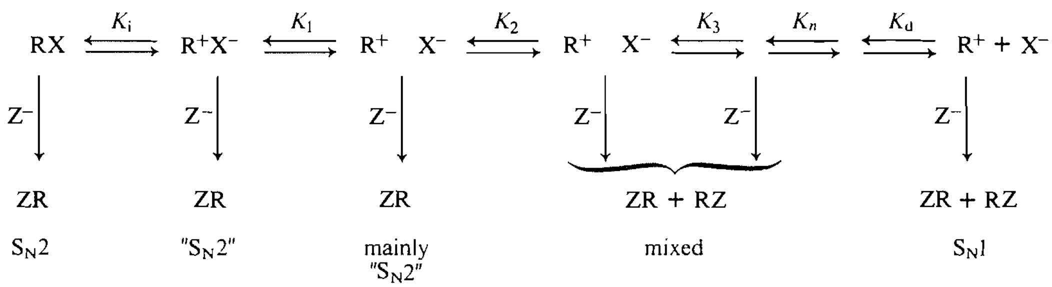

SCHEME 1. The ion-pair mechanism.

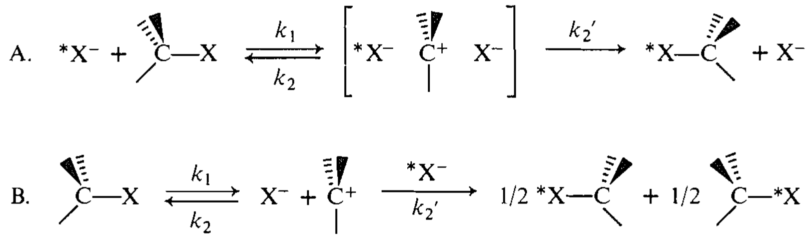

SCHEME 2. Mechanistic representations.

through nucleophilic substitution so that the racemization rate constant, k_{rac} should be precisely twice the exchange (or inversion) rate constant, k_{exch} (10).

If a bimolecular ion-pair mechanism is operating, i.e. a substitution towards the left-hand side of Scheme 1, there is another possibility. Should the ion pair become sufficiently separated for the carbocation to turn over with respect to the leaving group, internal return with inversion could occur. Such racemization without exchange would result in a racemization rate greater than twice the exchange or substitution rate. The probability that such internal return with racemization would occur should increase as the ion-pair species becomes longer lived, increasing the time available for solvent separation. Presumedly several layers of solvation would be required to "lubricate" the roll over of the carbocation.

Of course, should ion-pair separation–dissociation be favoured too much, return becomes unlikely and, in the extreme, the reaction follows the classical S_N1 mechanism indicated in Scheme 2B. Complete separation of the carbocation and the leaving group occurs before nucleophilic attack; all chiral information is lost and the leaving group enters the anion "pool". Attack by anion can occur from either side of the dissociated carbocation to give racemization with exchange; the rate constants for racemization and exchange would be equal.

The chiral 1-phenylbromoethanes, with bromide ion as the nucleophile, were selected for study. Since the leaving group and the nucleophile are the same, separation of substrate and product was unnecessary, all reactions are *pseudo*-first order, and the implied symmetry of the reaction coordinate minimizes problems associated with specific solvation effects, etc. Substitution was followed through bromide – *radio*-bromide (^{82}Br) exchange using the electrodeposition method of Beronius (9). Stereochemical inversion results in racemization of the substrate and was followed polarimetrically. There will be contributions to the observed rate of racemization from substitution and from internal return with inversion. Phenyl substituent effects on the racemization and exchange kinetics in acetone were studied initially and are reported here.

Results and discussion

The preparation of the optically active substrates is discussed in the following paper (11) and the methods employed in following the racemization and radio-bromide exchange rates have previously been presented (9, 10).

In Table 1, racemization and exchange rate constants for the various phenyl-substituted 1-phenylbromoethanes at a number of temperatures and lithium bromide concentrations in acetone are reported. The rate constants reported are usually the averages of two or three runs under the same conditions but occasionally only one (especially for the 4-nitro compound), or as many as ten, was done. In comparing the rate constants it must be kept in mind that while all but the racemization studies on 1-(4-bromophenyl)bromoethane was done by the principal investigator over a decade, racemizations were done in three different laboratories, the exchanges in two, using solvent of different origin, different equipment, different thermostat baths, and thermometers (calibrated only at 0°C). Additionally, traces of moisture greatly retard the reactions; those at the lower lithium bromide concentrations were especially sensitive. Thus exchange studies on the nitro compound with [LiBr] = 0.0005 M at 25°C gave rate constants of $10.24 \pm 0.20 \times 10^{-3}$ L mol^{-1} s^{-1} with solutions that had been stored in Parafilm-wrapped glass-stoppered volumetric flasks for 6 days and $14.67 \pm 0.16 \times 10^{-3}$ L mol^{-1} s^{-1} with freshly prepared solutions. Addition of a few microliters of water per 100 mL, a concentration of about 1×10^{-3} M water, produced similar or larger retardations. The obvious solution of using aqueous acetone was ruled out because even 0.5% water resulted in some hydrolysis of 1-phenylbromoethane, as evidenced by an accelerating rate of racemization—the bromide ion produced by hydrolysis increases the halide ion concentration and hence the reaction rate. While considerable care was taken to obtain internally consistent results, variations are greater than desirable.

Similar marked rate retardations by added water have been reported by other workers for bimolecular processes. Thus Bohme and Raksit (12*a*), in a recent study of the influence of

TABLE 1. Rate constants for racemization and bromide exchange for 1-phenylbromoethanes in acetone containing lithium bromide

T	k	Concentration of LiBr (M)				
(°C)	($\times 10^3$ L mol^{-1} s^{-1})	0.01	0.005	0.002	0.001	0.0005
1-(3,4-Dimethylphenyl)bromoethane						
25	rac	6.09 ± 0.66	6.24 ± 1.06	7.96 ± 0.57	9.10 ± 1.18	11.22 ± 0.90
	exch	—	—	5.75 ± 0.13	—	—
30	rac	9.26 ± 0.67	11.41 ± 2.09	13.70 ± 1.24	—	18.35 ± 0.35
	exch	5.03 ± 0.52	5.75 ± 0.42	7.95 ± 0.47	12.87 ± 1.09	16.61 ± 0.23
35	rac	13.39 ± 1.14	—	—	—	28.65 ± 0.41
40	rac	19.36 ± 3.38	—	26.13 ± 0.63	—	—
	exch	—	—	18.63 ± 0.12	—	—
1-(4-Methylphenyl)bromoethane						
25	rac	7.59 ± 0.20	8.77 ± 0.60	13.03 ± 0.33	16.09 ± 0.79	17.87 ± 0.53
	exch	2.88 ± 0.06*	3.50 ± 0.13	5.05 ± 0.04	—	—
30	rac	9.76 ± 0.46	13.19 ± 0.34	16.09 ± 0.03	19.75 ± 1.30	27.75 ± 0.32
	exch	4.26 ± 0.41	5.68 ± 0.59	7.74 ± 0.06	—	10.55 ± 0.69
35	rac	15.73 ± 0.97	18.66 ± 0.88	24.19 ± 0.18	29.63 ± 0.31	34.25 ± 0.21
	exch	6.24 ± 0.69	7.82 ± 0.20	11.19 ± 0.40	—	15.32 ± 1.31
40	rac	23.00 ± 0.94	26.74 ± 0.25	34.39 ± 0.13	—	51.16 ± 0.01
	exch	8.60 ± 0.33*	—	16.42 ± 0.39*	—	26.54 ± 1.00*
45	rac	32.72 ± 0.43	40.29 ± 0.17	50.08 ± 0.05	58.83 ± 0.92	71.95 ± 1.57
1-Phenylbromoethane						
25	rac	2.67 ± 0.03	3.36 ± 0.01	4.70 ± 0.05	6.01 ± 0.06	7.42 ± 0.05
	exch	1.46 ± 0.15	—	2.33 ± 0.10	—	3.81 ± 0.09
30	rac	4.18 ± 0.02	5.26 ± 0.01	7.29 ± 0.02	9.20 ± 0.11	11.57 ± 0.11
	exch	2.09 ± 0.08	2.68 ± 0.12	3.66 ± 0.15	—	6.24 ± 0.25
35	rac	6.55 ± 0.02	8.18 ± 0.02	11.19 ± 0.04	14.23 ± 0.10	18.58 ± 0.17
	exch	3.24 ± 0.60	—	6.20 ± 0.07	—	9.49 ± 0.39
40	rac	9.86 ± 0.02	12.55 ± 0.08	16.90 ± 0.04	22.23 ± 0.19	28.66 ± 0.22
	exch	5.07 ± 0.03	—	8.74 ± 0.17*	—	14.68 ± 0.42*
45	rac	14.66 ± 0.11	18.79 ± 0.06	25.41 ± 0.07	32.72 ± 0.14	36.61 ± 0.17
1-(4-Bromophenyl)bromoethane						
25	rac	5.93 ± 0.30	7.98 ± 0.08*	11.88 ± 0.08*	—	—
	exch	2.09 ± 0.01	—	4.91 ± 0.06	—	8.07 ± 0.10*
30	rac	9.97 ± 0.50	12.45 ± 0.46	16.14 ± 0.66	—	—
	exch	4.52 ± 0.16	5.48 ± 0.38	8.44 ± 0.18	—	11.83 ± 1.60
35	rac	14.17 ± 0.04	18.07 ± 0.38	26.15 ± 0.98	—	—
	exch	6.89 ± 0.62	—	10.89 ± 1.08	—	20.43 ± 0.23
40	rac	21.49 ± 0.54	32.17 ± 2.14	43.25 ± 1.82	—	—
	exch	11.06 ± 0.14*	—	19.89 ± 0.17*	—	32.42 ± 0.24
1-(4-Nitrophenyl)bromoethane						
25	rac	11.59 ± 0.03*	—	20.57 ± 0.04*	25.61 ± 0.07*	32.62 ± 0.08*
	exch	—	—	8.73 ± 0.67	—	14.67 ± 0.16
30	rac	19.192 ± 0.004*	23.19 ± 0.06*	33.08 ± 0.07*	41.09 ± 0.27	52.53 ± 2.43
	exch	7.64 ± 1.55	10.43 ± 1.14	15.00 ± 0.72	—	21.16 ± 2.19
35	rac	29.46 ± 0.08	39.96 ± 0.16*	54.36 ± 0.15*	69.61 ± 1.98*	84.43 ± 1.02
	exch	13.32 ± 0.24	—	21.08 ± 1.96	—	—
40	rac	44.57 ± 0.14*	57.63 ± 0.20*	85.50 ± 0.13*	109.13 ± 0.77	—
	exch	20.82 ± 0.28*	—	38.26 ± 0.32*	—	63.15 ± 0.34
45	rac	69.21 ± 0.82*	90.87 ± 0.21	127.94 ± 0.35*	166.03 ± 0.53*	200.46 ± 1.50

* A single run was done.

hydration in gas phase substitutions by, for example, the hydroxide ion in methyl halides, found a marked rate retardation as the nucleophile is mono-, di-, or trihydrated. Similar rate retardations are observed for traces of water in aprotic, relatively nonpolar solvents. Holmgren and Beronius (12*b*), for example, report the rates of bromide exchanges in acetone as the water concentration is increased. The rate halves with the addition of about 0.4% water.

By contrast, for unimolecular processes in aprotic solvents, the addition of water commonly accelerates substitutions. Farinacci and Hammett (13*a*) reported nearly 50 years ago that addition of small amounts of water to the ethanol used in ethanolysis of diphenylmethyl chloride increased the solvolysis rate but left the product almost exclusively the ethyl ether.

TABLE 2. Typical alkyl bromide concentrations (all RBr concentrations have units × 10^{-2} *M*)

Compound used	Racemization studies	Exchanges at given [LiBr] 0.01 *M*	0.002 *M*	0.0005 *M*
4-Nitro	7.0	6.7	1.4	1.4
4-Bromo	9.0	6.5	1.4	1.4
Unsubstituted	7.5	7.4	1.6	1.6
4-Methyl	18.0	6.6	1.5	1.4
3,4-Dimethyl	23.0	6.0	1.4	1.4

Other workers (refs. 13*b*, *c*, and, for related discussion, ref. 13*d*) have reported similar accelerations and observed (13*a*) that, for S_N1 reactions in binary (aqueous) solvents, rate constants vary with the log of the water concentration for low water concentrations; the slope gives the number of water molecules involved.

This difference in behaviour for uni- and bimolecular processes presumedly arises principally because, in the former, the effective H-bonding solvation of the leaving group facilitates its departure as an anion whereas, in the latter, similar solvation of the nucleophile markedly reduces its nucleophilicity.

k_{rac}/k_{exch} *ratios*

In the introduction we indicated that the racemization rate could exceed twice the exchange rate if there was significant return with inversion. The average calculated ratio of k_{rac}/k_{exch} for unsubstituted 1-phenylbromoethane, for all LiBr concentrations at each temperature, ranges from 1.93 to 1.95 and averages 1.940 ± 0.069 overall. Clearly there is no evidence for ion-pair return with racemization here, nor is there for the compounds with bromo- or nitro-substituents, as perusal of the data reported in Table 1 will confirm.

As predicted, increasing the stability of the carbocation and hence of the ion pair by introducing a *para*-methyl substituent results in k_{rac}/k_{exch} ratios greater than 2. Averaged over the concentration range of LiBr, the ratio is 2.58 ± 0.07, 2.33 ± 0.23, 2.38 ± 0.14, and 2.23 ± 0.39 at 25, 30, 35, and 40°C respectively. The overall average for all values is 2.36 ± 0.24, a ratio that would be more convincing if the variation was less. However, that ratio means that racemization via an internal return pathway is over one-third as fast as substitution.

If one methyl is good, two should be better, so that (3,4-dimethylphenyl)bromoethane substrate was studied. With this compound great difficulty was experienced in, first, making half esters of the corresponding ethanol without dehydration and hence accomplishing the resolution of the alcohol until the current procedure (11) was developed, and, finally, in converting the alcohols to bromide without extensive racemization (11). In both the racemization and the exchange studies, reproducibility was a real problem. Elimination of HBr seems to be largely responsible for this lack of reproducibility. Even on storage in an evacuated sealed ampoule for a few days at −5 to −10°C, neat, optically active substrate begins to racemize at increasing rates. The liquid eventually becomes cloudy and, after months at room temperature, partially polymerized styrene separates out. The racemic material used for the exchange studies behaves similarly; it also had to be freshly made and (or) redistilled every few days.

In both sets of measurements, the concentration of the alkyl bromide was much higher than that of the lithium bromide. Exchange rates were determined by starting with ionic bromide containing ^{82}Br ions; the decreasing radioactivity of samples of

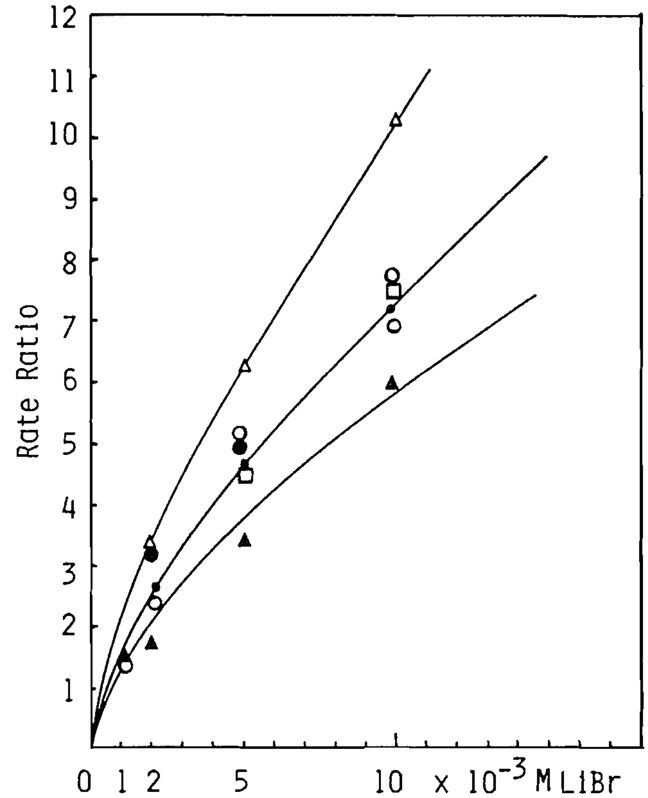

FIG. 1. Reaction rate ratios as a function of lithium bromide concentration. (Rate Ratio is the observed reaction rate divided by that for [LiBr] = 0.005 *M*, all at 30°C.) Racemizations: unsubstituted, ●; 4-methyl, ○; 4-nitro, □; and 3,4-dimethyl, △; and exchanges: 4-bromo, ⬤; and 3,4-dimethyl, ▲.

TABLE 3. Dissociation of LiBr in acetone*

T (°C)	K_{assoc}	Activity coeff. of Br^- at given [LiBr] 0.01	0.005	0.002	0.001	0.0005
25	4292	0.1957	0.2498	0.3438	0.4328	0.5346
30	4274	0.1971	0.2512	0.3453	0.4342	0.5360
35	4258	0.1985	0.2526	0.3467	0.4356	0.5373
40	4241	0.1999	0.2541	0.3482	0.4371	0.5387
45	4226	0.2014	0.2556	0.3497	0.4386	0.5401

*Calculated from data given by Beronius *et al.* in ref. 14.

the ionic bromide electrodeposited on silver discs at appropriate times was then used to follow ionic–covalent bromide exchange. In effect, isotopic dilution of ^{82}Br was occurring; the infinity value V_∞ corresponds to statistical distribution of ^{82}Br between RBr and ionic material, that is, $V_\infty = V_0$ ([LiBr]/[RBr] + [LiBr]). To get a reasonable variation in values through the reaction and minimize the effect of random errors, the concentration of the alkyl bromide had to be much larger than that of the lithium bromide. Concentration ratios of about 8:1 at the highest and 25:1 at the lowest LiBr concentration were used. For the racemizations, it was the measured initial rotation that dictated concentrations. For minimally acceptable signal-to-noise ratio, the initial rotation had to be 0.25° or more. Typical concentrations are given in Table 2. Because of the relatively low optical activities of the 3,4-dimethyl substrate, the concentrations had to be especially high in the racemization studies; here, the molar ratio of RBr to LiBr ranged from 23 to 460.

TABLE 4. Racemization results corrected for association of lithium bromide

T (°C)	Reaction order in Br^-	Corr. k_{rac} 10^{-3} L mol^{-1} s^{-1}	$\Delta H^{\ddagger}$ (kJ M^{-1})	$\Delta S^{\ddagger}$ J M^{-1} deg^{-1}
1-(3,4-Dimethylphenyl)bromoethane				
25	1.14 ± 0.04	21.57 ± 1.51		
30	1.18 ± 0.04	29.96 ± 0.65	44.6 ± 0.8	−127.3 ± 5.0
40	1.31 ± 0.02	53.75*		
1-(4-Methylphenyl)bromoethane				
25	1.08 ± 0.05	30.09 ± 1.56		
30	1.09 ± 0.04	43.11 ± 2.16		
35	1.08 ± 0.02	64.02 ± 1.06	55.0 ± 0.7	−95.5 ± 2.3
40	1.08 ± 0.02	91.99 ± 0.70		
45	1.11 ± 0.02	127.58 ± 2.32		
1-Phenylbromoethane				
25	0.986 ± 0.006	13.88 ± 0.13		
30	0.991 ± 0.006	21.35 ± 0.19†		
35	0.983 ± 0.015	33.31 ± 0.73	63.0 ± 1.7	−75.0 ± 5.5
40	0.965 ± 0.017	51.73 ± 1.36		
45	1.025 ± 0.022	71.02 ± 2.26		
1-(4-Bromophenyl)bromoethane‡				
25	1.00 ± 0.05	32.33 ± 2.38		
30	1.14 ± 0.03	39.50 ± 3.20		
35	0.96 ± 0.01	77.85 ± 1.32	72.2 ± 10.9	−73.9 ± 35.7
40	0.96 ± 0.05	128.85 ± 7.12		
1-(4-Nitrophenyl)bromoethane				
25	0.99 ± 0.01	60.33 ± 0.70		
30	0.98 ± 0.01	96.51 ± 1.65		
35	0.96 ± 0.03	162.75 ± 3.72	71.0 ± 1.44	−36.0 ± 4.7
40	0.92 ± 0.01	256.28 ± 5.46		
45	0.96 ± 0.01	360.26 ± 3.60		

*Only two data points, hence no error limits can be calculated.
†Rate constant becomes 21.340 ± 0.089 × 10^{-3} L mol^{-1} s^{-1} if the two data points (at 0.102 and 0.200 M LiBr) of Hughes *et al.* (25) are included in the calculations.
‡Relatively few concentrations of LiBr were used so that error limits are usually large.

Since elimination would liberate HBr, the bromide ion so produced would increase the bromide concentration and activity in the reaction mixture. At 0.002 M LiBr, 0.1% elimination could increase the bromide ion concentration by over 10% for the racemizations versus 0.7% for the exchanges. This additional bromide ion would accelerate the racemization and exchanges. The errors introduced from this source would be greatest at the lower concentrations of lithium bromide, so those rates and hence rate ratios are least secure.

For the 3,4-dimethyl compound, all values of the k_{rac}/k_{exch} ratios are less than the theoretical value of 2.00 for the S_N2 mechanism; at 30°C, they are 1.84, 1.98, 1.72, and 1.10 at 0.01, 0.005, 0.002, and 0.0005 M lithium bromide respectively and, for all the data points available, average 1.52 ± 0.39. Yet, because of the concentrations employed, any HBr in the added RBr should increase, not decrease that ratio. Consequently there has been a significant mechanistic change in going from the 4-methyl- to the 3,4-dimethyl compounds.

Effect of LiBr concentration

In Fig. 1, rate ratios, the reaction rate at the appropriate concentration, that is $k \times$ [LiBr], divided by the rate at [LiBr] = 0.0005 M, are plotted as a function of LiBr concentration at 30°C. All the compounds but (1-(3,4-dimethylphenyl)bromoethane fall on, or very near, the curve for the unsubstituted compound. For the 3,4-dimethyl compound, the racemization rate increases much more rapidly, the exchange less rapidly than for the other substrates, as the concentration of LiBr is increased.

In our discussion above, we indicated that any elimination of HBr and the concomitant increase in rate should have been most significant for the lowest lithium bromide concentrations. For the racemization studies with the 3,4-dimethyl compound, however, the deviations are just the opposite—either the rates for high LiBr concentrations are "excessive" or that at the lowest is far too low. Exchanges deviate in the opposite sense. For both reactions, like the reactions of the other compounds, the rates are clearly dependent upon the concentration of the inorganic bromide. They are not unimolecular processes.

Beronius *et al.* have determined the dissociation constants for lithium bromide in acetone (14). Using their equilibrium data and applying similar data analysis, our observed racemization rates can be corrected for the activity of the bromide ion. The results obtained are summarized in Tables 3 and 4. Several features stand out. Firstly, the reaction order in nucleophile reported in Table 4, i.e. the slope of a plot of the log of the observed rate $k_{rac} \times$ [LiBr] vs. the log of the calculated bromide ion activity from Table 3, should be unity. It is per-

TABLE 5. Eliminations in acetone with added lutidine

Compound	T (°C)	[LiBr] (M)	[Lutidine] (M)	k_{elim}* 10^{-6} s^{-1}	k_{rac}† 10^{-6} s^{-1}
3,4-DiMe	30	0.002	0.0343	0.673 ± 0.008	15.92
4-Me	30	0.002	0.0343	0.266 ± 0.003	27.4
3,4-DiMe	45	0.002	0.0343	4.46 ± 0.14	84.2‡
4-Me	45	0.002	0.0343	1.41 ± 0.011	100.2
Unsubst.	45	0.002	0.0343	0.0645 ± 0.0001§	50.82
3,4-DiMe	45	0.01	0.0686	4.38 ± 0.49	293.7‡
4-Me	45	0.01	0.0686	1.64 ± 0.08	372.2

* *Pseudo*-first-order elimination rate constant with added lutidine.
† Corresponding *pseudo*-first-order racemization rate constant in the absence of lutidine.
‡ Calculated.
§ Reaction was followed for only 190 h or to 5% completion.

haps significantly above one for the *p*-methyl substrate and averages 1.2 for the 3,4-dimethyl substrate. Thus, as we noted earlier, for the latter compound, the rate of racemization increases more rapidly with lithium bromide concentration than it should for a S_N2 process.

Another feature of the results in Table 4 is worth comment. Despite the fact that reaction rates for the 3,4-dimethyl compound are somewhat unexpectedly lower than the 4-methyl rates, the progressive decrease in $\Delta H^{\ddagger}$ continues as the carbocation stability increases. The markedly more negative $\Delta S^{\ddagger}$ accounts for the rate falloff. This variation in the activation parameters, using values not corrected for association of LiBr and preliminary results for the 3,4-dimethyl substrate, has already been discussed (15).

Elimination rates

We have already considered the effect of elimination of HBr from a small portion of the substrate prior to its addition to the acetone – lithium bromide mixture. The possibility of elimination being a competing reaction has not yet been considered. What would be the expected effect of a parallel elimination process?

For a bimolecular nucleophilic substitution process, the racemization rate should be twice that of exchange. Elimination of HBr would, of course, give achiral alkene with loss of one, not two, units of optical activity. The liberated bromide ion would result in isotopic dilution of the *radio*-labelled lithium bromide solution and, hence, be indistinguishable from an exchange. For elimination, apparent "racemization" and "exchange" rates would be equal.

A reaction mixture in which both substitution and elimination were occurring would, at first glace, seem to explain a lot of our observations for the 3,4-dimethyl compound. The k_{rac}/k_{exch} ratio would be expected to fall between the value of 2 for the S_N2 and 1 for the elimination pathway. Solvation effects, principally about the proton and bromide eliminated, could account for the large negative entropy of activation. Explaining the higher than unity reaction order in bromide is a problem unless the elimination process is very sensitive to ionic strength.

There are other problems, however, with this facile explanation. We have not considered the effect of the liberated halide ion on the rates of racemization and exchange—it should increase the rates of both. There should be an autocatalytic effect as the reaction proceeds and the halide ion concentration increases. None was observed. Nonetheless, the rate of elimination was examined.

Over three or four half-lives for the racemization reactions, it was not possible to detect any consistent decrease in the area of the alkyl bromide peak by glc for the unsubstituted, or for the methyl-, bromo-, or nitro-substituted species (10). When lutidine was added to the acetone solutions, determination of elimination rates became possible. Some are presented in Table 5. The rate of elimination is apparently independent of bromide ion concentration and, at 0.002 M LiBr for the 3,4-dimethyl compound, corresponds to about 5% of the racemization rate. It must be kept in mind that this is in the presence of added base. In butyl tosylate solvolysis, Dannenberg *et al.* (16), found that the amount of 2-butene increased with the concentration of trifluoroacetate ion in the CF_3CO_2Na/CF_3CO_2H buffer. Similarly, in the solvolysis of 1-(4-methylphenyl)-1-chloroethane in 50:50 TFE/H_2O, Richard and Jencks (17) report that the fraction of the product represented by 4-methylstyrene increases linearly with added sodium acetate, even for such weakly basic acetates as chloro- and trifluoroacetates. Thus even extremely weak base is enough to divert the reactions towards elimination. With lutidine added in excess, as it was for the results reported in Table 5, elimination could also have been accelerated. Consequently the elimination rates reported should be considered upper limits. Without lutidine, the eliminations were much slower and the bromide ion concentration tended to reach a plateau value a bit above the initial concentration, a value which varied considerably even in duplicate runs. Thus under the racemization and exchange conditions, elimination is apparently considerably slower and is apparently a reversible process. Addition of a large excess of an alkene, cyclohexene, had only a small retarding effect, so HBr was not intercepted to any extent under racemization conditions.

These results do not rule out the possibility of racemization via elimination followed by re-addition, all within a solvent cage or solvation sheath. Here though, unlike, say, the racemization of norbornyl brosylate (2) where only a small translation, the oxygen equilibration of esters (18) where only a small rotation, or the *cis–trans* isomerism through linear vinylic carbocations (19) where a facile rotation or migration is required, the HBr must migrate to the other side of the planar styrene. Here, unlike the situation for ion pairs, there would be no electrostatic attraction between the species involved and, especially in the presence of the added lutidine, it is unlikely the solvent cage lifetime would be sufficiently long for such a migration to occur to a significant extent. Consequently it can

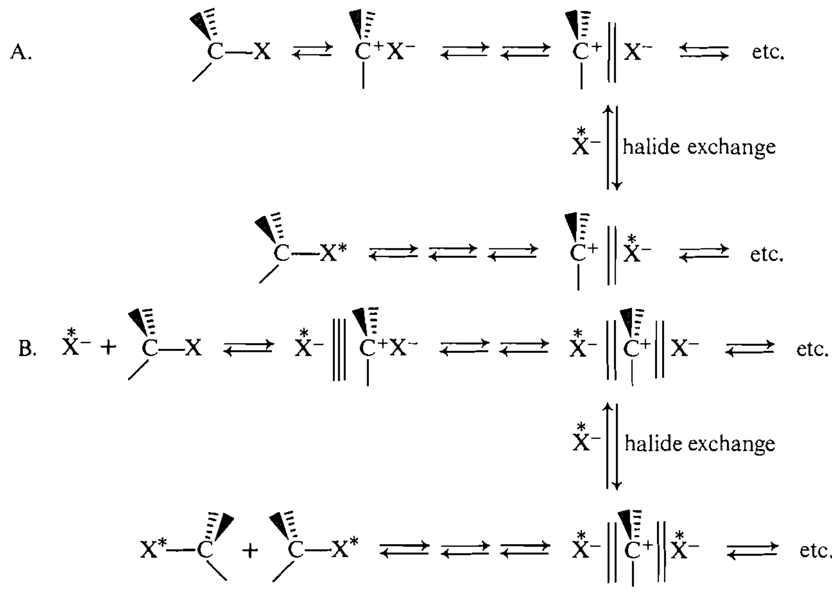

SCHEME 3

be concluded that elimination is a competing but much slower process that can not explain the observed racemization and exchange rate behavior.

A mechanistic explanation

As substituents on 1-phenylbromoethane are changed through the series p-NO_2, p-Br, none, p-CH_3 and 3,4-$(CH_3)_2$, the average value of the k_{rac}/k_{exch} ratio changes from essentially 2.00 for the first three to 2.36 and 1.52 for the last two compounds, respectively. The p-CH_3 rate ratio of greater than 2.00, the value predicted for the classical S_N2 mechanism, is easily accommodated by, and in fact is confirmatory of, the simple ion-pair mechanism depicted in Scheme 1. The ion-pair lifetime has become sufficient for carbocation inversion to occur before collapse, that is, for internal return with racemization to occur. Interestingly, Richard and Jencks, in their extensive study of the solvolyses of various 1-phenylethyl substrates, found that it was also the p-CH_3 substituted one which clearly showed internal return from an ion pair (17).

When the carbocation and hence the ion pair is further stabilized as with the 3,4-$(CH_3)_2$ substrate, the simple ion-pair scheme is not adequate in explaining the observations. The progressive change in activation parameters does not suggest a major mechanistic discontinuity (15); the enthalpy and entropy of activation decrease progressively, with the latter becoming markedly more negative, through the series of substrates as the expected carbocation/ion pair becomes more stable. Yet for the dimethyl compound, the k_{rac}/k_{exch} ratio is appropriate for a reaction of mixed mechanism, one about 50:50 classical S_N1/S_N2. The racemization, however, does not shift from first towards zeroth order in bromide ion; rather, the order increases to slightly over one. Clearly the S_N1-S_N2 mechanistic pair also are inadequate in explaining the results.

A logical modification to the ion-pair mechanism readily accommodates the observations. In a simplistic form, it is shown in Scheme 3A. Including exchange of leaving group with the anion pool allows for some retention of configuration with bromide exchange. Perhaps a more realistic version, with leaving group – anion pool exchange occurring through a solvated triple ion, is shown as Scheme 3B. Without getting involved in any controversy about the timing of nucleophilic involvement, that is, does it commence prior to (17, 20), concurrent with (21), or subsequent to (1*b*, 7, 8*a*) breaking of the substrate – leaving group bond to form the ion pair, the triple ion is quite analogous to the proposals of Jencks (17, 20) and of Bentley and Schleyer (21) and their respective co-workers. The nucleophilic involvement of solvent in the latter and of a good nucleophile in the former is replaced by that of a nucleophile identical to the leaving group to give a symmetrical species.

As pointed out by Bentley *et al.* (21), there is a marked tendency to treat the extended ion-pair scheme of Winstein (2), or as applied by Sneen (1), literally, that is, to ignore the fact that the reaction is occurring in a solvent, often with other added species present. Thus there are substrate–solvent (dipole–dipole) and ion pair – solvent (ion–dipole) interactions as well as substrate and ion-pair interactions with other species in solution, all of which are rarely shown or explicitly considered in mechanistic presentations. The "special salt effects" first noted by Winstein (2) confirm direct ion (or salt) involvement in ion-pair mechanisms. Added "inert" electrolyte at low concentration in relatively non-ionizing media can greatly promote dissociation of ion pairs. That this is through some sort of one-on-one interaction between the electrolyte and substrate is confirmed by the fact that, at higher salt concentrations where there is a generous supply of added ions, the rate acceleration becomes simply that of a normal salt effect. In more polar solvents, solvent dipole orientation can swamp the ion electric field in promoting dissociation. In our case, backside "nucleophilic assistance" (21) in ionization and (or) dissociation of the substrate would be by the $\delta(-)$ carbonyl oxygen of acetone and by Br^-. Li^+ might also play a role, for example, in facilitating the front-side leaving group – anion pool bromide exchange.

In any event, incorporation a leaving group exchange branch in the ion-pair mechanism allows for substitution—bromide exchange—with retention of configuration or, perhaps more accurately, collapse from triple ion to racemic substrate. Either would result in the k_{rac}/k_{exch} ratio falling below the S_N2 value of 2.00. The contribution to the racemization rate made by leaving group exchange at the triple ion—it should be second order in bromide ion—would also account for the changes in reaction order.

Conclusions

The results reported here strongly support the ion-pair mechanistic scheme for bimolecular displacement at saturated carbon. The effect of increasing the stability of the carbocation and hence the ease of ionization/separation is best explained through the ion-pair mechanism of Scheme 1, modified to include the ionization/separation assistance of other ions in solution as in Scheme 3B.

For the substrates lacking electron donating substituents, the ion pairs are not sufficiently stable and long lived to undergo the significant solvent separation required for inversion without exchange before collapse to starting material or rear-side attack by nucleophile. With moderate stabilization, as by the p-CH_3 group, the average point of nucleophilic attack is shifted sufficiently to the right, towards ion-pair separation, to permit internal return with racemization, and k_{rac}/k_{exch} becomes greater than the theoretical S_N2 value of 2.00. As the stability is further increased, as with our 3,4-dimethyl substrate, ion-pair lifetimes become still greater and exchange of anion involved in the ion pair with the anion pool can occur; exchange becomes more rapid. Relative exchange and racemization rates are intermediate between those predicted for the classical S_N2 and S_N1 mechanisms. This logical progression thus explains the observations reported in this paper.

The effects of solvent and isotopic substitution are currently under investigation.

Experimental

All solvents were reagent or Analar grade; the acetone was freshly distilled from Type 4A molecular sieves under dry tank nitrogen that was further dried by bubbling it through concentrated-H_2SO_4 followed by a column of Type 3A molecular sieves. The analytical grade (Merck or BDH) lithium bromide was oven dried at 225–250°C, the reagent grade (BDH) 2,6-dimethylpyridine (lutidine) was doubly vacuum distilled through a short column, and the silver nitrate was reagent grade.

Chiral substrates were prepared by the procedures described in the following paper (11), racemic ones by treating the corresponding racemic 1-phenylethanol instead of the resolved one with HBr in benzene or toluene. The racemic 1-phenylethanols, except the commercially available unsubstituted compound (Eastman), were made from the corresponding commercially available acetophenone by reduction with $NaBH_4$ in ice/aqueous methanol by procedures analogous to that reported for 1-(4-nitrophenyl)ethanol (11). The 1-phenylethanols were free of carbonyl absorptions in the ir, the bromides free of OH absorptions, and all gave clean nmr spectra in $DCCl_3$. Physical properties of the chiral materials have been reported (11); those of the racemic materials were almost identical.

For the kinetics reported in this paper, temperature control was better than 0.02°C for the longest runs, ±0.01°C in general. Standard linear regression analysis was done on the data; for the eliminations, the infinity value was determined iteratively. When a single run was done, the error range reported in Tables 1 and 5 is the standard deviation or σ of the linear regression. When duplicate or multi-runs were done, the standard deviation on the average value is reported. Generally the regression correlation coefficient was 0.99–0.99999, with polarimetry being near the upper end and exchanges and eliminations, which were aliquot methods with relatively few points, being nearer the lower end of the range. For all but the slowest reactions, two to three or more half-lives were used.

Kinetics of racemization were followed using a Perkin–Elmer model 141MC polarimeter as previously described (10). All solutions were prepared, stored, and transferred in a dry nitrogen-filled glove bag or box. the solution was prepared, and the jacketted cell was filled and quickly removed from the bag, connected to the constant temperature bath, and placed in the polarimeter. Rotations and times were measured from the graph of the potentiometric recorder with the first value taken some 5–8 min after the solution was initially prepared. Results are reported in Tables 1, 4, and 5.

Kinetics of exchange were followed as previously outlined (10). For 1-(3,4-dimethylphenyl)bromoethane the $Li^{82}Br$ was prepared by neutron bombardment of inactive salt in the reactors of Atomic Energy of Canada, Chalk River, Ontario; for the rest, the source was Aktiebolaget Atomenergi, Isotopservice, Nykoping, Sweden.

Kinetics of elimination were followed in anhydrous acetone with added lutidine as follows. Stock solutions of acetone 0.02000 ± 0.0005 M in LiBr were prepared and sealed in hypo-vials in a dry nitrogen-filled glove bag. This solution was diluted with freshly distilled acetone as required; 25 mL with 1 mL lutidine diluted to 250 mL gave a solution 2.00×10^{-3} M in LiBr and 34.3×10^{-3} M in lutidine. After 50 mL of this solution in a glass-stoppered volumetric flask had equilibrated to the desired temperature in the thermostatted bath, a weighed amount of the alkyl bromide, e.g. 0.1284 g of the p-methyl substrate, to give a 12.90×10^{-3} M solution, was added with a syringe, the reaction timer started, and the flask quickly removed, shaken, and returned to the bath. An aliquot, usually 3 mL, was removed with a pipet, the elapsed time noted, and the solution run into the upper of two chilled 50-mL separatory funnels which contained 15 mL of ice-cold, distilled water and 10 mL of cold ether. The funnel was immediately shaken for 10 s, allowed to settle for 30 s, and the aqueous layer drained into the second funnel, which contained 10 mL of ether. Shaking and settling were repeated, the aqueous layer drained into a small flask and 5, 10, or 15 mL pipetted into the cell of a Radiometer TTTld/SBR2C automatic titrator. The potentiometric titration of aqueous bromide ion was done with 5.00×10^{-3} M $AgNO_3$ using silver and calomel electrodes. The first aliquot could be removed at 60-s, subsequent ones at as little as 5-min intervals but, as most reactions were very slow, the 10–15 points were normally taken at much longer intervals and 2–5 runs were done simultaneously. Blanks were run without added RBr and, for slower runs, the first kinetic point agreed to within a few percent of the blank value and the least-squares calculated $t = 0$ value. For example, with the unsubstituted compound in 2.00×10^{-3} M LiBr at 45°C, reaction was only approximately 5% complete with the tenth and last point at 687 600 s—8 days—but gave $k = 6.54 \pm 0.01 \times 10^{-8}$ s^{-1} with R = 0.9997, blank zero 5.35; least-squares calculated $t = 0$, 5.313; value at 900 s, 5.40. Faster runs tended to behave better as a much larger fraction of reaction was available. Results are reported in Table 5.

Acknowledgements

The authors wish to thank Memorial University of Newfoundland, the Natural Sciences and Engineering Research Council of Canada, and the Swedish Natural Sciences Research Council for financial assistance; Umeå Universitet, Umeå, Sweden and Atomic Energy of Canada Ltd., Chalk River, Ontario, Canada for use of their facilities and equipment for the exchange studies; and the University of Auckland, Auckland, New Zealand for use of their laboratories and equipment for the elimination rate measurements. Dr. P. Beronius of Umeå Universitet and Dr. J. M. W. Scott of Memorial University are especially thanked, for assistance with the exchange studies and for performing some of the calculations on the data reported in this paper, respectively.

1. (*a*) R. A. SNEEN and J. W. LARSEN. J. Am. Chem. Soc. **91**, 363 (1969); **91**, 6031 (1969); (*b*) R. A. SNEEN. Acc. Chem. Res. **6**, 46 (1973).

2. S. WINSTEIN, B. APPEL, R. BAKER, and S. DIAZ. *In* Organic reaction mechanisms. Chem. Soc. Spec. Publ. No. 19, 1965, pp. 109–130.
3. T. H. LOWRY and K. S. RICHARDSON. Mechanism and theory in organic chemistry. 2nd ed. Harper and Row, Publishers, New York. 1981. p. 302 ff.; F. A. CAREY and R. J. SUNDBERG. Advanced organic chemistry. Part A. Structure and mechanism. 2nd ed. Plenum Press, New York. 1984. Chapt. 5.
4. J. L. GLEAVE, E. D. HUGHES, and C. K. INGOLD. J. Chem. Soc. 236 (1935).
5. E. D. HUGHES and C. K. INGOLD. J. Chem. Soc. 244 (1935).
6. (*a*) H. L. GOERING and H. HUMSKI. J. Org. Chem. **40**, 920 (1975), and reference cited therein; (*b*) H. L. PEETEIS and M. ANTENUNIS. J. Org. Chem. **40**, 307 (1975); **40**, 312 (1975); (*c*) F. G. BORDWELL, P. F. WILEY, and T. G. MECCA. J. Am. Chem. Soc. **97**, 132 (1975), and references cited therein; (*d*) J. M. W. SCOTT and R. E. ROBERTSON. Can. J. Chem. **50**, 167 (1972).
7. V. J. SHINER, JR., D. A. NOLLEN, and K. HUMSKI. J. Org. Chem. **44**, 2108 (1979).
8. (*a*) M. J. BLANDAMER, R. E. ROBERTSON, J. M. W. SCOTT, and A. VRIELINK. J. Am. Chem. Soc. **102**, 2585 (1980); (*b*) R. E. ROBERTSON and B. ROSSAL. Can. J. Chem. **49**, 1441 (1971); (*c*) J. M. SCOTT. Can. J. Chem. **48**, 3807 (1970).
9. P. BERONIUS. Trans R. Inst. Technol. Stockholm, No. 213 (1963).
10. ALLAN R. STEIN. J. Org. Chem. **41**, 519 (1976).
11. ALLAN R. STEIN, ROBERT D. DAWE, and JAMES R. SWEET. Can. J. Chem. **63**, 3442 (1985).
12. (*a*) D. K. BOHME and A. B. RAKSIT. J. Am. Chem. Soc. **106**, 3447 (1984); (*b*) A. HOLMGREN and P. BERONIUS. Acta. Chem. Scand. **26**, 3881 (1972).
13. (*a*) N. T. FARINACCI and L. P. HAMMETT. J. Am. Chem. Soc. **59**, 2542 (1937); (*b*) C. G. SWAIN. J. Am. Chem. Soc. **70**, 1119 (1948); (*c*) D. A. BROWN and R. F. HUDSON. J. Chem. Soc. 3352 (1953); (*d*) S. R. HARTSHORN. Aliphatic nucleophilic substitution. Cambridge University Press. 1973. pp. 20–25.
14. P. BERONIUS, U. ISACSSON, and A-M. NILSSON. Acta Chem. Scand. **24**, 189 (1970).
15. ALLAN R. STEIN, MICHAŁ TENCER, ELIZABETH A. MOFFATT, ROBERT DAWE, and JAMES SWEET. J. Org. Chem. **45**, 3539 (1980).
16. J. J. DANNENBERG, B. J. GOLDBERG, J. K. BARTON, K. DILL, D. H. WEINWURZEL, and M. O. LONGAS. J. Am. Chem. Soc. **103**, 7764 (1981).
17. J. P. RICHARD and W. P. JENCKS. J. Am. Chem. Soc. **106**, 1373 (1984); **106**, 1383 (1984).
18. H. L. GOERING, R. G. BRIODY, and G. SANDROCK. J. Am. Chem. Soc. **92**, 7401 (1970).
19. Z. RAPPOPORT and Y. APELOIG. J. Am. Chem. Soc. **96**, 6428 (1974).
20. W. P. JENCKS. Acc. Chem. Res. **13**, 161 (1980), and references therein.
21. T. W. BENTLEY, C. T. BOWEN, D. H. MORTEN, and P. v. R. SCHLEYER. J. Am. Chem. Soc. **103**, 5466 (1981), and references therein.
22. ALLAN R. STEIN. J. Org. Chem. **38**, 4022 (1973).
23. ALLAN R. STEIN. Tetrahedron Lett. 4145 (1974).
24. ALLAN R. STEIN. J. Org. Chem. **41**, 519 (1976).
25. E. D. HUGHES, F. JULIUSBURGER, A. D. SCOTT, B. TOPLEY, and J. WEISS. J. Chem. Soc. 1173 (1936).

Preparation of chiral 1-phenylethanols and bromides

ALLAN R. STEIN,[1] ROBERT D. DAWE, AND JAMES R. SWEET

Department of Chemistry, Memorial University of Newfoundland, St. John's Nfld., Canada A1B 3X7

Received March 29, 1985

ALLAN R. STEIN, ROBERT D. DAWE, and JAMES R. SWEET. Can. J. Chem. **63**, 3442 (1985).

A fast, convenient procedure for preparing and resolving moderate to large quantities of chiral secondary alcohols is described. The general procedure involves a one-pot conversion of the ketone (various acetophenones) to the half-ester of a diacid (succinic, phthalic...) and resolution with (+)- and (−)-1-phenylethylamines. Overall yields of the enantiomeric alcohols, the variously substituted 1-phenylethanols, are generally 65–85% with optical purities of approximately 90%. Properties and optical rotations of a number of chiral 1-phenylethanols and of the bromides made from them are tabulated. A discussion of optical purity determinations using nmr methods is included and absolute configurations are reported.

ALLAN R. STEIN, ROBERT D. DAWE et JAMES R. SWEET. Can. J. Chem. **63**, 3442 (1985).

On décrit une méthode simple et rapide de préparer et de résoudre en antipodes optiques des quantités importantes d'alcools secondaires chiraux. La méthode générale implique une conversion, dans un seul récipient, de la cétone (diverses acétophénones) en esters acides de diacides (acides succinique, phtalique...) puis une résolution par les phényl-1 éthylamines (+) et (−). Les rendements globaux en alcools énantiomériques, divers phényl-1 éthanols substitués, sont de l'ordre de 65 à 85% et les puretés optiques sont d'environ 90%. On rapporte les propriétés et les rotations optiques d'un certain nombre de phényl-1 éthanols chiraux ainsi que celles des bromures qui en résultent. On rapporte aussi une discussion relative à l'utilisation de la rmn pour la détermination des puretés optiques ainsi que les configurations absolues.

[Traduit par le journal]

For a continuing study of the ion-pair mechanism for nucleophilic displacement at saturated carbon (1), relatively large quantities of variously phenyl-substituted chiral 1-phenylbromoethanes were required. These were best made from the corresponding chiral 1-phenylethanols with hydrogen bromide in toluene or benzene. Since the optical resolutions evolved in this study are quite convenient and efficient, give a high optical purity, and can be extended to other substituents, halides, and carbon skeletons, they are reported in some detail.

Several of the chiral phenyl-substituted 1-phenylethanols have previously been resolved; the resolution of the parent compound, 1-phenylethanol itself, is a well-established process which nonetheless presents some difficulties. The classical Downer and Kenyon procedure (2) calls for the resolution of the mono- or half-ester of phthalic acid, i.e. (±)-1-phenylethyl hydrogen phthalate, in acetone with brucine, not the safest or most pleasant material to use in large quantities. Unless there are seed crystals available, obtaining the (−)-enantiomer of the half-ester instead of the racemic hydrogen phthalate salt of brucine can be quite a challenge! Even then, obtaining high optical purity requires removal of the racemic half-ester from the recovered chirally enriched hydrogen phthalate obtained by removal of the brucine from the precipitated salt through repeated large-volume acid extractions. This removal of the less soluble racemic half-ester is best accomplished by careful and repeated fractional crystallizations from carbon disulfide. The other enantiomer must be recovered from the somewhat enriched original mother liquor, again after removal of the unprecipitated brucine and by repeated crystallization and removal of the racemic ester from carbon disulfide. Obtaining moderate yields of resolved material requires repeated recycling of the recovered racemate.

At least the 1-(4′-nitrophenyl)ethanol analog has been made by electrophilic substitution on chiral unsubstituted 1-phenylethanol but yields of the 4-isomer were less than 25% (3). In addition, the optical purity was low and the desired product was accompanied by a higher yield of the 2-isomer. Selected chiral phenylethanols, generally the unsubstituted and occasionally the 4′-methyl analogue, have been made by asymmetric reduction of the corresponding acetophenones (4, 5) using metal hydrides complexed with naturally occurring chiral alcohols, for example, $LiAlH_3(OR^*)$, $LiAlH_2(OR^*)_2$, or $LiAlH(OR^*)_3$ where HOR* is *N*-methylephedrine, $C_6H_5CHOHCH(N(CH_3)_2)$-CH_3, or other chiral alcohol (4*b*). Needless to say, the required reagents are expensive to use for a large-scale preparation and usually only one of the enantiomeric alcohols is obtainable. Optical purities were generally 35–85%.

An enzymatic method that allows isolation of both enantiomeric alcohols in good yields and high activity has recently been published (5). It involves use of a carbonyl esterase as a stereoselective transesterification catalyst on the racemic alcohol and an excess of an ester. One enantiomer of the alcohol is recovered unreacted, the other after hydrolysis of the newly formed chiral ester. Should the method prove general, it alone may prove competitive with that published below for making relatively large quantities of both enantiomers of chiral alcohols with high optical purities.

Classically, optical purities were relative, that is, the optical rotation of a newly prepared sample was compared to the literature value, supposedly the highest optical activity yet achieved for the compound. More recently, the different chemical shifts exhibited by "diastereomeric species" in nuclear magnetic resonance spectroscopy have been utilized (6, 7). Most commonly the chiral substrate is an alcohol or an amine and the "diastereomeric species" is generated by use of a chiral H-bonding solvent (6*a*) or a chiral lanthanide paramagnetic nmr shift reagent, usually a europium(II) or phaseodymium(III) complex (6*b*), or by derivatizing with a chiral acid (6*c*).

Results and discussion

Since (+)- and (−)-phenylethylamines are commercially available, it seemed worthwhile to evolve procedures using these amines and the appropriate half-esters of the corresponding alcohols. The procedures finally arrived at for the various species are summarized below. Selected ones are presented in more detail in the experimental section.

[1] Author to whom correspondence may be addressed.

TABLE 1. Preparation and resolution of half-esters and 1-phenylethanols[a]

Substrate[b]	Recryst. solvent	Yield[c] (%)	Melting point (°C)	Diastereomeric salt[c,d] %(+)-Amine	Diastereomeric salt[c,d] %(−)-Amine	Chiral alcohol from salt[c] (+)-Amine[e]	Chiral alcohol from salt[c] (−)-Amine[e]
Unsubst.[f]	Benzene	96[f]	108.5–109.5	45.5[f]	47.0[f]	99/15 (+) 42.5%[f]	107/22 (−) 43.0%[f]
1-D-unsub.[f]	Benzene	74[f]	105–107	33.5[f]	33.5[f]	95/10 (+) 30.5[f]	106/20 (−) 29.0%[f]
4′-Methyl	pe[g]	88	118.5–120.5	44.0	40.5	76/2.2 (+) 42.0%	102/10 (−) 38.5%
1-D-4′-methyl	pe[g]	66[h]	—	—	—	—	95.5/7 (−) 38.0%[h]
3′,4′-Dimethyl	pe[g]	98	117.5–118.5	42.6	43.3	99/3.8 (+) 41.1%	103/4.4 (−) 39.5%
3′-Methyl	[i]	97	79–81.5	33.0	41.0	—	—
4′-Bromo[j]	Toluene	85	123.5–124.5	41.5	42.2	110/3.0 (+) 41.0%	116/5.2 (−) 42.0%
1-D-4′-bromo[k]	Toluene	60[h]	123.5–125.5	24.5[h]	23.4[h]	146/17 (+) 21.0%	—
4′-Nitro[f,l]	Toluene	90[f]	51–53	41.1[f]	39.3[f]	124/0.60 (+) 31.5%[f]	124/0.58 (−) 35%[f]

[a] Unless otherwise noted, phthalic acid half-esters were resolved in ether and base catalysis was used for their hydrolyses.
[b] 1-Phenylethanol prepared and resolved.
[c] Yields are based upon starting acetophenone except where otherwise noted. The total yield is the sum of the yields for the two diastereomeric salts.
[d] Salt of half-ester and (+)- or (−)-1-phenylethylamine.
[e] Boiling point in °C(uncorrected)/pressure in Torr, sign of rotation and yield respectively of the alcohol obtained from the diastereomeric salt of the indicated 1-phenylethylamine.
[f] The corresponding racemic 1-phenylethanol was used to make the half-ester. Yields are based upon this alcohol.
[g] 80–100°C petroleum ether.
[h] Yields based upon $LiAlD_4$.
[i] The viscous biphthalate half-ester crystallized after prolonged pumping and chilling. These crystals were repeatedly washed with pe[g].
[j] The resolving solvent was acetone.
[k] The resolving solvent was ethyl acetate.
[l] Succinic half-ester was used and the hydrolysis was acid catalyzed.

In general, the commercially available substituted acetophenones were reduced in anhydrous tetrahydrofuran (THF) with $LiAlH_4$ and $LiAlD_4$. A slight excess of purified anhydride, usually phthalic or succinic anhydride, was then added to the solution. (Commerical anhydrides contain small to moderate amounts of the diacids, which destroy the desired alcohol salt and markedly reduce yields of the half-ester.) Standard work-up and one or two recrystallizations generally gave yields of 85–98% (based upon starting acetophenone) in this one-pot reduction–esterification to half-ester.

Since the nitro group is also reduced by $LiAlH_4$, 4-nitroacetophenone was reduced to the corresponding ethanol with $NaBH_4$ in ice – aqueous methanol solution. The 4-nitrophenylethanol and phenylethanol itself, which is commercially available, were then converted to the half-ester by treating them with the appropriate acid anhydride and an excess of pyridine.

In the procedure for resolving the half-esters, a near-saturated solution of the half-ester in the solvent indicated in Table 1 was treated with about one-third of a molar equivalent of, for example, *d*-(+)-1-phenylethylamine. A precipitate formed, sometimes immediately, sometimes after some hours in a refrigerator—stubborn cases responded well to seed crystals once these were available. Filtering and washing gave varying amounts of diastereomeric salt. The mother liquor was extracted with acid to recover unprecipitated amine. Addition of slightly more than one-half of a molar-equivalent of the (−)-amine precipitated the other diastereomeric salt. Recycling gives near quantitative yields of the two salts.

Partition of the diastereomeric salt between ether and aqueous hydrochloric acid allowed isolation of the chiral half-ester from the ether layer. Subsequent hydrolysis, with acid or base catalysis, gave the chiral 1-phenylethanols. The combined yields of the enantiomeric phenylethanols were 60–85% based upon starting ketone. Well over 70% of the phenylethylamines could be recovered from the combined acidic aqueous solutions by basification with sodium hydroxide or carbonate followed by extractive work-up and distillation. If the intermediate acid extractions of unprecipitated amines were thoroughly done, the recovered 1-phenylethylamines had rotations unchanged from those of the original materials.

Conversion of the alcohols to the bromides was accomplished by bubbling hydrogen bromide into a benzene or toluene solution—the latter solvent tended to give severe foaming problems in the subsequent vacuum distillations—of the resolved alcohol, generally at −10 to 0°C. The 4-nitro alcohol reacted very slowly and required warming and prolonged contact. For the others, especially the 4-methyl- and the 3,4-dimethyl-substituted alcohols, contact times and temperatures had to be minimized and the vacuum distillation performed quickly and smoothly to prevent excessive racemization of the bromides. Hydrogen bromide in benzene or toluene proved more satisfactory than other recipes tried; both yields and optical activities were higher than for other procedures, including PBr_3 or PBr_5 in ether, triphenylphosphine and bromine, or *N*-bromosuccinimide in pyridine. Also the aromatic hydrocarbon solvents were much more satisfactory than solvents like hexane, chloroform, or carbon tetrachloride, presumedly because the solubility of the hydrogen bromide is higher in the aromatic hydrocarbon solvents.

Details of the synthesis and resolution of several of the alcohols are given in the experimental section. The acid anhydride, the solvents, and the hydrolysis procedures used for the specific alcohols are given in Table 1. The optical rotations of samples of the various 1-phenylethanols and of the bromides derived from them are reported in Table 2, the optical or enantiomeric purities of the alcohols in Table 3.

In all cases, the half-esters had rotations opposite to those of the 1-phenylethylamine used in their resolution; the resultant phenylethanols had the same sign of rotation as the amine used. Only for the 1-(4′-methyl- and 3′,4′-dimethylphenyl)ethanols are the signs of rotation of the ethanols and bromides made from them the same.

TABLE 2. Properties of the substituted 1-phenylethanols and bromides

Substituents present	Configuration	1-Phenylethanol: Optical rotation[a] 589	579	546	436	365 nm	1-Phenylbromoethane: Yield[b] (%)	Boiling point[c]	Optical rotation[a] 589	579	546	436	365 nm
None	(*S*)	−4.27	−4.47	−5.10	−8.84	−14.23	91	85/8.7	+1.93	+2.06	+2.38	+3.57	+8.36
4′-Methyl	(*R*)	+4.24	+4.43	+5.10	+8.93	+14.60	94	60/0.7	+0.47	+0.49	+0.69	+1.14	+2.27
1-D-4′-methyl		—	−4.26	−4.98	−8.63	−14.11	88	83/4.2	—	−0.17	−0.14	−0.50	−0.76
3-Methyl	(*S*)	−2.27	−2.38	−2.73	−4.66	−7.32	—	—	—	—	—	—	—
3′,4′-Dimethyl	(*R*)	+3.89	+3.91	+4.48	+7.38	+12.76	96	90/2.2	+0.36	+0.45	+0.66	+1.10	+2.30
4′-Bromo	(*S*)	−7.09	−7.31	−8.44	−15.09	−25.70	94	90/1.45	—	+1.62	+1.89	+3.64	+6.92
4′-Nitro	(*R*)	+4.89	+5.09	+5.87	+10.29	abs[d]	98.5	125/1.8	—	−2.05	−2.37	−4.70	abs[d]

[a]Optical rotation in degrees in a 1-cm cell of the neat liquid at 25°C and the wavelength indicated.
[b]Yields are based upon starting chiral 1-phenylethanol.
[c]Boiling point in °C, uncorrected/pressure in Torr.
[d]Absorption prevents measurement at this wavelength.

Optical purities

The results of determinations of optical purities of the resolved alcohols with the chiral shift reagent Eu-Opt[2] are summarized in Table 3. Cervinka *et al.* (8) and Okamoto *et al.* (9) previously used chiral nmr shift reagents to determine the optical purities of several of the same 1-phenylethanols. Based upon their measurements, the optical purity of our 1-phenylethanol was 93.6 or 92.5% respectively vs. our 99.7%. According to the former authors (8), our 4′-methyl derivative had an optical purity of 88.6%, almost identical to our determination. While the latter authors (9) also reported optical purities for 1-(4′-nitrophenyl)ethanol, it is not clear how they measured their optical activity so that we were unable to relate our activity to theirs.

With Eu-Opt[2] large shifts occurred; for example, with a molar ratio of 4:3 of 1-(3,4-dimethylphenyl)ethanol to shift reagent in $DCCl_3$ at 0°C on the 360-MHz machine, the aromatic proton multiplet was shifted from δ 7.16–7.08 to 7.65–7.27, the methine proton quartet from δ 4.82 to a pair of quartets centred at 5.965 and 5.935, the hydroxylic proton from δ 1.96 to 6.42, the aromatic methyl protons from δ 2.29 and 2.25 to 2.37 and 2.34, and the other methyl proton doublet at δ 1.48 to an ill-resolved "doublet" at 2.10. All signals are extensively broadened, the signal-to-noise ratio is degraded, and new signals due to the camphato residues of the shift reagent interfere with the region upfield of about δ 3. With decoupling from the α-methyl protons, the methine pair of quartets became two singlets at δ 5.965 for the (+)- and at δ 5.935 for the (−)-enantiomer. The overlap of the broadened peaks was such that, for the racemic mixture, the valley height was more than half the peak height, and for the (−)-alcohol, the (+)-enantiomer showed up as a very small blip on the upfield shoulder of the signal due to the major enantiomer. "Deconvolution" techniques had to be resorted to. Areas and hence enantiomeric purities have considerable uncertainty associated with them. Thus the determined ratio of (+)- to (−)-enantiomer for racemic mixtures ranged from as good as 48.4:51.6 to as bad as 43.1:56.7. Such uncertainties, with a standard deviation of 5.1 parts in 50 for the five racemic mixtures, reduce one's confidence in all of the results.

Despite a report in the literature that the purity of partially resolved 1-(4-nitrophenyl)ethanol was determinable (9), we were unable to separate any of the proton signals into contributions for the enantiomers even with substrate to shift reagent ratios as high as 1:2 at temperatures as low as −50°C on the high-field machine. The oxygens of the nitro group apparently compete very successfully with that of the hydroxyl for the Lewis acid shift reagent.

Commercial availability of resolved 2-methoxy-2-trifluoromethyl-2-phenylacetic acid, MTPA, facilitates determination of optical purities through use of the diastereomeric esters, the method of Dale and Mosher (6*c*). Their derivatization method has the advantage that several nuclei can be used; there are internal checks. Thus, with the 1-(4-methylphenyl)ethyl esters of (+)-MTPA, the methine proton (with decoupling from the methyl protons), the methoxy proton, the *para*-methyl and the aliphatic methyl protons (with decoupling from the methine proton), all could be used in proton, and the trifluoromethyl fluorines in fluorine, nmr.

[2]Eu-Opt is $Eu(C_{12}H_{14}F_3O_2)_3$, tris-[3-trifluoroacetyl-(+)-camphato]europium(III) available from the Alfa Division of Ventron Corporation.

TABLE 3. Optical purities of samples of 1-phenylethanols of Table 2

Substituent present	Optical purity or enantiomeric excess (as %) found based upon: Literature value[a]	Shift reagent[b]	Diastereomers ester[c] based upon: Methine	Methoxy	$ArCH_3$	RCH_3	Fluoro[d]	Average value
None	93.6 (8), 92.5 (9)	99.7	99.2	93.0	—	88.9	97.4	94.9 ± 4.0
4-Methyl	88.6 (9)	86.8	89.6	97.0	95.5	—	94.2	92.0 ± 4.2
3-Methyl	—	49.0	63.2	52.4	55.9	64.1	49.0	55.6 ± 6.7
3,4-Dimethyl	—	88.8	83.3	76.2[d]	—	—	85.6	83.5 ± 5.3
4-Bromo	—	88.6	92.8	93.0	—	86.4	93.0	90.8 ± 3.1
4-Nitro	—	—	74.8	67.4	—	67.4	79.4	72.3 ± 5.9

[a] Calculated purity based upon observed rotation and enantiomeric purity data given in the reference indicated.
[b] Chiral nmr shift reagent Eu-Opt in $DCCl_3$.
[c] Ester of (+)-2-methoxy-2-trifluoromethyl-2-phenylacetic acid in $DCCl_3$.
[d] Measured on the 80-MHz machine; the rest were done at 360 MHz.

TABLE 4. Nuclear magnetic resonance data for (4-nitrophenyl)ethyl esters of (+)-MTPA

Atoms(s)	Ar*H*	—C—*H*		—OCH_3		—C—CH_3		—CF_3	
Enantiomer	—	(+)	(−)	(+)	(−)	(+)	(−)	(+)	(−)
δ (ppm)	8.12, 7.34	6.05	6.02	3.401	3.502	1.516	1.568	—	—
Δδ (ppm)[a]	—	0.025		−0.079		−0.041		−0.118	
Character	Twin multiplets	Overlapping quartets[b]		Twin quartets[c]		Overlapping doublets[d]		Twin quartets[e]	
Area ratios									
(±)-Alcohol	—	47.2	52.8	54.4	45.5	55.1	44.8	49.7	50.3
(+)-Alcohol	—	87.4	12.6	83.7	16.3	83.7	16.3	89.7	10.3
1/3(±)- 2/3(+)- [f]	—	77.8	22.2	69.5	30.5	65.5	34.5	78.0	22.0

[a] Determined from an expanded spectrum as Δδ = (δ(+) − δ(−)) in ppm.
[b] Coupled to methyl protons, J = 6.6 Hz.
[c] Coupled weakly, J = 1.3 Hz, to fluorines.
[d] Coupled to methine proton, J = 6.6 Hz.
[e] Coupled to methoxy protons, J = 1.3 Hz.
[f] Calculated ratio from average of (+)-enantiomeric analysis values, 74.1% (+) and 25.9% (−).

The derivatization method with MTPA does have its disadvantages. It requires considerably more laboratory time but generally less effort on the spectrometer than the chiral shift reagent method. It depends upon quantitative conversion of, in our case, the alcohol to the ester. To minimize enantiomeric discrimination, minimal work-up and no separation of the diastereomeric esters is possible. Thus any impurities (grease, solvent and reagent residues, and the like) remain in the sample after preparation and extractive work-up. The aliphatic methyl proton signals, typically at δ 1.54–1.56 and 1.58–160, were especially prone to interference from trace impurities. Additionally, the MTPA used must be optically pure. It is prepared by resolving the acid with α-phenylethylamine (10) so that 100% optical purity is highly unlikely. Since enantiomers would have coincidental signals, the optical purities determined using MPTA are minimum values.

Since the chiral shift reagent method was found unsuitable for 4-nitrophenylethanol, the results using the diastereomeric esters prepared by derivatizing with (+)-MTPA are presented in Table 4. Overall, the results with MPTA show somewhat better internal agreement than do those with the shift reagent.

In Table 3, the determined optical purities or enantiomeric excesses of the particular samples of the alcohols of Table 2 are presented. Also included in Table 2 are the configurations of the alcohols. The configuration of (−)-phenylethanol has been related to (−)-lactic acid and consequently was assigned the (*S*) configuration (11). Dale and Mosher (6*c*) have established that MPTA esters can be used to assign configurations to alcohols. Using esters of (*R*)-(+)-MPTA, for (*S*)-phenylethanol the methyl group, as the medium sized group, is shielded by the phenyl of the acid residue. Thus these CH_3 protons appear at higher fields than those of the (*R*) configuration. Since substituents on the phenyl of the alcohol should enhance, not invert, the relative bulk of the aromatic vs. the methyl group, the same relative shifts would be predicted for our substituted phenylethanols. In all cases examined, the CH_3 protons for the ester of the (−)-alcohol wih *R*-(+)-MPTA were at higher fields and hence all are (*S*)-(−)-phenylethanols.

For the studies contemplated (1), the actual optical purity of the required bromides did not matter. Consequently no attempt was made to maximize the activities of the intermediate alcohols. Nor were the particular samples of the alcohols and their corresponding half-esters and bromides, for which physical properties, optical rotations, and optical purities are recorded, necessarily the ones with the highest purities; they simply reflect the particular samples of the alcohols used in the optical purity determinations. The use of more dilute solutions, a smaller mole fraction of chiral amine, and additional slurrying of the salt in the appropriate solvent increases the laboratory time but gives higher activities.

Finally, conversion of the alcohols to the bromides, especially for the methyl-substituted ones, leads to completely or nearly completely racemic products if care is not exercised. Consequently, considerable racemization almost certainly occurs in all cases. The optical purity of the bromide must not be equated to that of the alcohol used to prepare it; the alcohol purity merely establishes the maximum limit for bromide purity.

Experimental

Solvents

All solvents used were ACS or Reagent Grade. The THF was dried and purified by standing, with periodic shaking, over KOH pellets for several days before being refluxed for several hours over, and then distilled from $LiAlH_4$ under nitrogen, which itself had been further dried by bubbling through concentrated sulfuric acid followed by a column of Type 4A molecular sieves. The THF was distilled as required using oven-dried glassware.

Acetophenones

Commercial products were freshly vacuum distilled.

Acid anhydrides

Commercially available phthalic and succinic anhydrides from a variety of suppliers were found to contain 8–20% of the corresponding diacid. Purification is possible by repeated sublimations, but was more easily accomplished by recrystallization from chloroform. The diacid is almost totally insoluble whereas the anhydride is quite soluble. After drying briefly in a hood, the recrystallized anhydride was pumped for some hours at room temperature or with gentle heating. The anhydride was stored in an evacuated flask until required.

Melting and boiling points are uncorrected. Optical rotations were measured on a Perkin Elmer Model 141MC recording polarimeter using sodium (489 nm) and mercury vapour lamps as light sources.

Preparation of the half-esters

To illustrate the generalized procedures, the preparation of two particular half-esters, one from the acetophenone in one pot, the other via the phenylethanol, are presented here.

1-(4'-Methylphenyl)ethyl hydrogen phthalate

Under dried N_2, THF (approximately 250 mL) was distilled into an oven-dried flask containing a magnetic stirrer bar and 6.3 g (0.166 mol) of $LiAlH_4$. With stirring, chilling in ice, and still under N_2, 80.2 g (0.598 mol) of 4-methylacetophenone was added over a 40-min period. The mixture was then refluxed gently for 4 h. After cooling to ice temperature, 89.2 g (0.602 mol) of phthalic anhydride was added in four batches over 20–30 min with stirring, which was continued as the reaction was slowly heated and refluxed overnight.

Work-up consisted of removing the bulk of the THF on a rotatory evaporator (rot. evap.) and taking up the residue in about 400 mL of diethyl ether and 250 mL of 3.5 *M* HCl. The ethereal layer was washed several times with more dilute acid, water, and then saturated aqueous NaCl before being dried briefly over Na_2SO_4. The aqueous fractions were reextracted with ether, which was similarly treated and added to the first ethereal layer. The ether was removed, leaving a viscous cloudy oil, which was transferred to a 2-L Erlenmeyer flask. About 750 mL of 80–100°C petroleum ether was added and heated to boiling. The solution was decanted carefully from the undissolved half-ester into a 1-L Erlenmeyer flask. After cooling and chilling, the solvent was decanted from the crystalline product back into the first flask and the procedure repeated until only white crystals of phthalic acid (5.5 g, corresponding to 5.5% of the starting anhydride) remained in the original flask. The yield of half-ester was 149.2 g, 88%, mp 118.5–120.5°C. The deuterium-labelled analog was made on a 0.1-molar scale using $LiAlD_4$ as the limiting reagent.

1-(4'-Nitrophenyl)ethyl hydrogen succinate

To 130.0 g (0.788 mol) of 4-nitroacetophenone in a 1-L flask, about 250 g of ice and 400 mL of methanol were added. With magnetic stirring, 9.25 g (0.244 mol) of $NaBH_4$ was added in four batches over a half-hour period. After another half hour, the mixture, with continued stirring, was slowly heated to reflux and refluxed overnight. Once the bulk of the methanol had been removed on the rot. evap., ether and about a 50% excess of hydrochloric acid were added to the two-phase mixture. After washing with several portions of each of 1 *M* HCl, water, and saturated aqueous NaCl and drying over Na_2SO_4, the ethereal layer, combined with the ethereal layers from reextracting the aqueous fractions, was concentrated. Two vacuum distillations at 127.5°C and 0.65 Torr (1 Torr = 133.3 Pa) gave (4'-nitrophenyl)ethanol (113.3 g, 86%). It was not, however, necessary to isolate the alcohol; addition of benzene to the concentrate from the ethereal layers and azeotroping the water from the mixture allowed the crude product to be used directly, as was done in the following steps.

To the benzene–alcohol solution (or to the isolated alcohol) were added 100 mL of pyridine and 85.7 g (0.855 mol) of recrystallized succinic anhydride. The mixture was heated to 75–80°C with magnetic stirring overnight, the bulk of the excess pyridine removed on the rot. evap., 250 mL of ether added, and the mixture repeatedly extracted with ice-cold 2–3 *M* HCl to remove the remaining pyridine. The ethereal layer was combined with that from reextracting the various aqueous fractions, washed with water and saturated aqueous NaCl several times, dried, and concentrated on the rot. evap. The residue was taken up in 600 mL of hot toluene, decolorized with a generous amount of charcoal, and allowed to cool with periodic scratching to induce crystallization. A second and third crop of half-ester was obtained by concentrating the toluene phase. Based upon *p*-nitroacetophenone, the total yield of half-ester was 183 g (87%) without, 160 g (76%) with isolation of the alcohol.

Preparation of diastereomeric salts of half-esters and (+)- and (−)-1-Phenylethylamine

To illustrate the procedures employed, resolutions in a water insoluble solvent (ether) and in a water soluble one (acetone) are outlined.

Resolution of the 4'-methyl half-ester

In a 1-L Erlenmeyer flask, 147.5 g (0.519 mol) of the phthalate half-ester was dissolved in 400 mL of the ether by stirring and gentle warming. After chilling to ice temperatures, with sitrring, 27.0 g (0.223 mol) of (+)-phenylethylamine was added in 1- to 2-mL portions to minimize overheating and boiling. After several minutes, snow-like crystals formed ever faster until the solution gelled, and, despite continued cooling, considerable ether boiled off due to the heat of crystallization. The flask was placed in a freezer for 5 h, the solid was broken up with a stirring rod, and the thick slurry suction filtered. The solid was twice returned to the flask and slurried with fresh ether, chilled, and refiltered to give 82.1 g or 78% of the theoretical amount of salt based upon the chiral amine.

The combined filtrates were extracted with several 250-mL portions and several smaller portions of ice-cold 1.5 *M* HCl, water, and saturated NaCl. The volume of the ethereal layer, combined with that from reextracting the various aqueous phases, was reduced to about 600 mL and 28.4 g (0.234 mol) of (−)-amine added as before. Similar boiling occurred. Filtering and washing as before gave 86.9 g or 82.5% of the ammonium salt based on the starting chiral amine.

The combined ethereal washes and filtrates were treated as before except that they were reduced to approximately 300 mL before 10.5 g (0.086 mol) of the (+)-amine was added. The usual work-up gave 23.1 g for a total of 105.2 g or 100% of the (+)-amine diastereomeric salt based upon the starting racemic half-ester. (An estimated 5–6 g of the product was amine salt of phthalic acid from impurities in, and from hydrolysis of, the half-ester.) A second crop of the (−)-amine salt was obtained by adding 7.0 g of the amine to a concentrated ethereal phase after the usual work-up. The yield of the salt was 10.0 g, giving a total yield of the other diastereomeric salt of 96.9 g or 92.1%.

The combined yield of the diastereomeric salts was 84.5% based upon starting 4-methylacetophenone. (Approximately 80% of the unprecipitated chiral amines was recovered by neutralizing the first acid wash fractions with NaOH pellets, ether extraction, washing, drying, and vacuum distillation.) The salts were stored until required.

Resolution of the 4'-bromo half-ester

With cooling and stirring, 27.8 g (0.229 mol) of (−)-1-phenylethylamine was added to the solution of 175 g (0.501 mol) of 1-(4'-bromophenyl)ethyl hydrogen phthalate in 400 mL of acetone. After a half hour the solution was seeded with a crystal of the salt (or scratched repeatedly the first time) and placed in a freezer. The next morning, the slurry was filtered and the salt, returned to the flask, slurried with, then refiltered from, fresh fractions of chilled acetone three times. After drying, 53.0 g of the (−)-amine salt was obtained.

The combined acetone fractions were stripped of acetone on the rot. evap. and the residue taken up in ether, which was in turn extracted with aqueous acid etc. as in the previous example. After drying, the ether was removed on the rot. evap., the residue taken up in about 400 mL of acetone, and 30.0 g (0.248 mol) of (+)-amine added. After standing in a freezer overnight, work-up as before gave 90.5 g of the (+)-amine salt. The filtrate was treated as before except that the residue from the ether was taken up in only 250 mL of acetone and 15.2 g (0.125 mol) of the (−)-amine was added to give 49.9 g of the salt. Recycling with 8.9 g (0.073 mol) of the (+)-amine gave 24.5 g of salt. Finally 6.25 g (0.052 mol) of the (−)-amine was used to obtain 14.1 g of salt.

The combined yields of the two diastereomeric ammonium biphthalate salts were 117.0 g or 99.4% and 115.0 g or 97.6% of the (−)- and (+)-amine salts, respectively, or a total of 98.5% based upon the half-ester. Based upon 4-bromoacetophenone the combined yield of the resolved ammonium salts was 83.0%.

Isolation of the chiral alcohols

Only a generalized procedure is outlined since, with the exception of the nitro substrates, all were treated similarly.

The diastereomeric amine salt was partitioned between ether and ice-cold 2 *M* HCl by stirring magnetically for 15–60 min. The ethereal layer was reextracted with several more portions of chilled acid, washed several times with water, and concentrated on the rot. evap. About two molar equivalents of 3 *M* NaOH were added and the solution heated at gentle reflux with stirring for several hours, usually overnight. After chilling, the organic layer was extracted with several fractions of ether, which in turn was washed several times with 1 *M* base, water, and saturated aqueous NaCl before being dried over K_2CO_3. Concentration, followed by vacuum distillation, gave the chiral 1-phenylethanol, typically in 95–98.5% yield based upon the salt. Boiling points and yields are given in Table 1. The chiral amine was recovered from the original aqueous acid phases by basification, extraction with ether, and vacuum distillation, with about 75% recovery of material with an optical activity the same as, and on occasion even slightly higher than, the starting amine.

NOTE: The base-catalyzed hydrolysis of the nitro substrate gave intractable tars. Acid-catalyzed hydrolysis with the obvious modifications in procedure was done for this case. Acid catalysis is, of course, possible for the other compounds but the fact that the diacid produced is soluble in the aqueous phase in the case of base hydrolysis simplified the work-up and makes that the preferred method.

Optical purities of the ethanols

Chiral shift reagent, Eu-Opt

Analogous procedures were used for all of the cases examined so that only the 1-(3',4'-dimethylphenyl)ethanol compound is discussed.

To a nmr tube containing 20 μL (approx. 1.3×10^{-4} mol) of 1-(3',4'-dimethylphenyl)ethanol in 400 μL of $DCCl_3$, the amount of a solution of Eu-Opt (0.1797 g, 0.201 mmol/mL in $DCCl_3$) added was incrementally increased. A multi-scan nmr spectrum was obtained after each Eu-Opt addition. The α-H quartet centred at 4.81 δ in the absence of shift reagent was progressively shifted and separated into overlapping quartets. With 50 μL of added shift solution the separation was moderately good and the temperature was lowered to 0°C—the pair of quartets was then centred at δ 5.965 and 5.935. Decoupling from the methyl protons resolved that signal into an incompletely resolved pair of singlets with an area ratio of 47.8:52.2. Running the spectrum of the (−)-alcohol at the same shift reagent concentration and temperature gave a "clean" quartet at δ 5.93, which, on decoupling from the methyl protons, gave a broad singlet (δ 5.925) with a small up-field shoulder (δ 5.96) due to traces of the other enantiomer. Deconvolution gave the area ratio 5.6:94.4 for the (+)- and (−)-enantiomers respectively. The optical purity of the (−)-3,4-dimethylphenylethanol is thus approximately 89%. Mixed samples of the racemic and (−)-alcohols were also run to check the consistency of the determinations. For example, a mixture of 10 μL of each of (±)- and (−)-alcohols gave the area ratio 25.4:74.6 versus the calculated ratio 27.8:72.2 based upon the just determined purity of the (−)-alcohol.

Diastereomeric esters of (+)-MTPA (6*c*, 10)

(+)-MTPA (Sigma Chemical Company) was converted to the acid chloride with freshly distilled thionyl chloride (10). In oven-dried vials equipped with a screw cap and a Teflon-lined septum, about 0.10 mmol of the alcohol (12–15 μL depending upon its molar mass and density), 300 μL of each of molecular sieve dried pyridine and carbon tetrachloride, and 25 μL (34 mg, 0.14 mmol) of the (+)-MTPA-Cl were injected, shaken, and allowed to stand overnight (12–14 h). An excess, 25 μL (21 mg, 0.20 mmol) of 3-dimethylaminopropylamine was added to convert any excess (+)-MTPA-Cl into the aqueous acid soluble aminoamide. After shaking and standing for 30–90 min, the contents of the vial were quantitatively transferred to a 25-mL separatory funnel, taken up in 10 mL of ether, and the ethereal layer extracted successively with two chilled 10- to 15-mL portions of each of 3 *M* HCl, concentrated K_2CO_3, and saturated salt solution. The ethereal layer was poured onto a layer of molecular sieves in a small flask, stoppered, and allowed to stand with occasional swirling for several hours.

The solution was pipetted into a pear-shaped flask and the ether removed on a rot. evap. Three small portions of $DCCl_3$ were added and stripped off to ensure that the last traces of ether were removed and the residue was taken up in 400 μL of $DCCl_3$ for nmr analysis.

In the proton spectrum, the aliphatic methyl (δ ~1.6), the aromatic methyl if present (δ ~2.3), the methoxy (δ ~3.5), and the methine (δ ~6.1) protons were expanded, decoupled if necessary, and, if separation was adequate, the relative areas for the signals of the two diastereomeric components determined. Fluorine nmr was also used. Results for 4-nitrophenylethanol are reported in Table 4 and selected results are summarized in Table 3.

Preparation of chiral substituted 1-phenylbromoethanes

The chiral 1-phenylethanol was added to about eight volumes of benzene or toluene and chilled in an ice–acetone bath to well below 0°C for all except the 4'-bromo and 4'-nitro compounds, which were run near 0 and 40°C respectively. Hydrogen bromide gas was bubbled in at a relatively slow rate to reduce heating effects; the rate was such that the solution was saturated in HBr in about 5 min. With continuous slow bubbling or periodic resaturation with HBr, the methyl-substituted materials were allowed to stand less than 5, the unsubstituted, about 10, the bromo-substituted, about 20 min, and the nitro-substituted, several hours, before the lower aqueous layer was removed with a dropping pipet and the excess HBr removed at aspirator pressures and the same temperature as that at which the reaction was run. A nitrogen bleed was used to prevent bumping. After a few minutes, the solution was decanted from the remaining water into a clean pear-shaped flask and the remaining HBr and aromatic solvent removed on a vacuum pump. The product was then vacuum distilled as quickly and smoothly as possible to minimize racemization. Heating was best done with a micro-burner for speed. The boiling points and pressures are tabulated in Table 2. Using 5–8 g of the alcohols, yields of 85–95% of the corresponding bromide, which showed no OH-absorption in the infrared, were obtained. The nmr spectra were clean. The optical activities of the alcohol and of the bromide made from that particular batch of the alcohol are presented in Table 2.

Acknowledgements

The authors wish to thank Memorial University of Newfoundland and the Natural Sciences and Engineering Research

Council of Canada for financial support, and the Atlantic Provinces Interprovincial Committee for the Sciences for a summer studentship for J.R.S. We also thank Mr. Avery Earle of Memorial (Bruker 80-MHz spectrometer) and Mr. Bruce MacDonald of the Atlantic Region Magnetic Resonance Centre, Halifax, N.S. (Nicolet 360 NB 360-MHz spectrometer) for obtaining the nmr data used in calculating enantiomeric purities.

1. (*a*) ALLAN R. STEIN, MICHAL TENCER, ELIZABETH A. MOFFATT, ROBERT D. DAWE, and JAMES SWEET. J. Org. Chem. **45**, 3539 (1980); (*b*) ALLAN R. STEIN. Tetrahedron Lett. 4145 (1974); (*c*) ALAN R. STEIN and ELIZABETH A. MOFFATT. Can. J. Chem. **63**, 3433 (1985).
2. (*a*) E. DOWNER and J. KENYON. J. Chem. Soc. (London), 1156 (1939); (*b*) R. MCLEOD, F. J. WELCH, and H. S. MOSHER. J. Am. Chem. Soc. **82**, 876 (1960).
3. A. H. FORD-MOORE and H. N. RYDON. J. Chem. Soc. (London), 679 (1946).
4. (*a*) J. P. VIGNERON and I. JACQUET. Tetrahedron, **32**, 939 (1976); I. JACQUET and J. P. VIGNERON. Tetrahedron Lett. 2065 (1974); (*b*) S. R. LANDOV, B. J. MILLER, and A. R. TATCHELL. J. Chem. Soc. Chem. Commun. 197 (1967); 2280 (1966); S. TERASHIMA, N. TANORO, and K. KOGA. Chem. Lett. 981 (1980); N. COHEN, R. J. LOPVESTI, C. NEUKON, and G. SAVEY. J. Org. Chem. **45**, 582 (1980); A. I. MEYERS and A. M. KENDALL. Tetrahedron Lett. 1337 (1974); R. NOYORI, I. TOMINO, and Y. TAMIMOTO. J. Am. Chem. Soc. **101**, 1691 (1979); G. GIACOMELLI, L. LARDICCI, F. PALLA, and A. M. CAPORUSSO. J. Org. Chem. **49**, 1725 (1984).
5. B. CAMBOU and A. M. KLIBANOV. J. Am. Chem. Soc. **106**, 2687 (1984).
6. (*a*) W. H. PIRKLE and D. J. HOOVER. *In* Topics in Stereochemistry. Vol. 13. *Edited by* N. L. Allinger and E. I. Eliel. 267, Wiley Interscience, New York. 1982. p. 267; (*b*) G. R. SULLIVAN. *In* Topics in stereochemistry. Vol. 10. *Edited by* N. L. Allinger and E. I. Eliel. Wiley Interscience, New York. 1978. p. 287; (*c*) J. A. DALE and H. S. MOSHER. J. Am. Chem. Soc. **95**, 512 (1973).
7. P. L. RINALDI. *In* Progress in NMR spectroscopy. Vol. 15. Pergamon Press, London. 1982. p. 291.
8. (*a*) O. CERVINKA and O. BELOVSKI. Collect. Czech. Chem. Commun. **32**, 3897 (1967); (*b*) O. CERVINKA, P. MALON, and P. TRSKA. Collect. Czech. Chem. Commun. **38**, 1358 (1973); **38**, 3299 (1973); (*c*) O. CERVINKA and J. FUSEK. Collect. Czech. Chem. Commun. **38**, 441 (1973).
9. K. OKAMOTO, T. KINOSHITA, Y. TAKEMURA, and H. YONEDA. J. Chem. Soc. Perkin trans. 2, 1426 (1975).
10. J. A. DALE, D. L. DULL, and H. S. MOSHER. J. Org. Chem. **34**, 2543 (1969).
11. W. KLYNE and J. BUCKINGHAM. Atlas of stereochemistry. Chapman and Hall, London. 1974. p. 26.

The use of homogeneous and heterogeneous Lewis acids to catalyse the photoisomerizations of phenols

SATISH K. CHADDA AND RONALD F. CHILDS[1]
Department of Chemistry, McMaster University, Hamilton, Ont., Canada L8S 4M1

Received April 22, 1985

SATISH K. CHADDA and RONALD F. CHILDS. Can. J. Chem. **63**, 3449 (1985).

The reaction of methyl substituted phenols with CH_2Cl_2 solutions of Al_2Br_6 leads to the formation of two types of complexes. In both of these the aluminum is bound to the oxygen atom of the phenol but they differ in that the OH proton can either remain on oxygen, oxonium complex, or migrate to one, usually the *para*, ring carbon, keto complex. The equilibrium position between the two types of complex depends on the position of the methyl groups. Irradiation of a complex of the keto type leads initially to the formation of a complexed bicyclo[3.1.0]hexenone and subsequently to the formation of an isomeric complexed phenol. Only in the case of the tetramethylphenols is the yield of the bicyclic ketone high enough to warrant the use of this photoisomerization as a preparative procedure, although the technique can be used to isomerize a range of phenols to their 4-substituted isomers. The photoisomerizations are not restricted to the use of a homogeneous Lewis acid such as Al_2Br_6 but heterogeneous aluminosilicates can also be used. The adsorption of 2,3,5,6-tetramethylphenol, **1***h*, on an aluminosilicate was monitored quantitatively and it was shown that a monolayer was formed in which the phenol was at least partially present in the keto form. Irradiation of **1***h* in the presence of stirred slurries of the aluminosilicate led to the formation of 2,3,4,6-tetramethylphenol. No bicyclic ketones were present in the contacting solution but traces were detected on the catalyst when the irradiations were carried out on adsorbed material in the absence of a solvent. In the case of heterogeneous acids, the selectivity in the adsorption of the starting phenol and the photoproducts is important in determining the composition of the final mixture.

SATISH K. CHADDA et RONALD F. CHILDS. Can. J. Chem. **63**, 3449 (1985).

La réaction de phénols substitués par des groupements méthyles avec des solutions de Al_2Br_6 du CH_2Cl_2 conduit à la formation de deux types de complexes. Dans chacun de ces complexes, l'aluminium est lié à l'atome d'oxygène du phénol; toutefois, ils diffèrent par le fait que le proton du OH peut soit demeurer sur l'oxygène, complexe onium, soit migrer sur l'un, généralement celui en *para*, des carbones du cycle, complexe céto. La position de l'équilibre entre ces deux types de complexes dépend de la position des groupements méthyles. L'irradiation d'un complexe de type céto conduit initialement à la formation d'une bicyclo[3.1.0]hexènone complexée et subséquement en un phénol complexé isomère. Il n'y a que dans les cas des tétraméthylphénols que les rendements en cétones bicycliques sont suffisamment élevés pour justifier l'utilisation de cette photoisomérisation comme méthode préparative, même si cette technique peut être utilisée pour transformer un grand nombre de phénols en leurs isomères substitués en position 4. Les photoisomérisations ne sont pas restreintes à l'usage d'un acide de Lewis homogène, comme le Al_2Br_6; on peut aussi utiliser des aluminosilicates hétérogènes. On a déterminé les taux d'adsorption du tétraméthyl-2,3,5,6 phénol, **1***h*, sur un aluminosilicate et on a montré qu'il se forme une monocouche dans laquelle le phénol est présent, au moins en partie, sous la forme céto. L'irradiation de **1***h* en présence de suspensions agitées d'aluminosilicates conduit à la formation de tétraméthyl-2,3,4,6 phénol. On n'a pas trouvé de cétones bicycliques dans la solution en contact; toutefois, on en a détectée sur le catalyseur lorsqu'on a effectué des irradiations sur des matériaux adsorbés, en l'absence de solvant. Dans les cas des acides hétérogènes, la sélectivité dans l'adsorption du phénol de départ et des photoproduits est importante dans la détermination de la composition du mélange final.

[Traduit par le journal]

Phenols are relatively basic molecules that can be protonated readily in a variety of strong and super-acid media (1). Two types of cations can be formed, with protonation occurring either on oxygen to form an oxonium ion or on one of the ring carbons to give a protonated ketone structure. The preferred site of protonation depends both on the nature of the acid medium used and on the substituents on the phenol.

Ring protonated phenols have been shown to isomerize on irradiation to yield protonated bicyclo[3.1.0]hex-3-en-2-ones (2). This facile photoisomerization of the C-protonated phenols stands in marked contrast to the general lack of photochemical reactivity of the parent phenols or their oxygen protonated counterparts. Protonated bicyclo[3.1.0]hexenones are photochemically labile and undergo further reaction on irradiation, Scheme 1. With appropriate wavelength control of the illumination system it is possible to stop these reactions at either the bicyclic ketone or isomeric phenol stage.

This photochemical isomerization of *para*-protonated phenols is analogous to the photoisomerizations of 2,5-cyclohexadienones (3) and as such it is potentially a very useful method of preparing a wide variety of bicyclo[3.1.0]hexenones with one or two hydrogens at C6 (4). In addition to their potential synthetic utility, these photoreactions of protonated phenols hold promise as candidates for a photochemical latent heat storage system (5).

The principal disadvantage of these photoisomerization reactions, which prevents their widespread use for either synthetic purposes or solar energy storage, lies in the need to use strong acids as solvents. These acids must be neutralized to recover the products, and the scale-up of these vigorously exothermic reactions is always difficult.

We have sought ways around this problem of the use of strong protic acids and report here the results of a study of two related approaches. These involve the use of a Lewis acid to catalyse the photoisomerizations and, secondly, the use of heterogeneous acids as photocatalysts. The latter possibility would be particularly attractive in terms of energy storage.

Results and discussion

Homogeneous Lewis acids

Koptyug *et al.* have investigated the reactions of aluminum trichloride and tribromide with various methyl substituted phe-

[1] Author to whom correspondence should be addressed.

TABLE 1. ¹H nuclear magnetic resonance and ultraviolet spectra of Al_2Br_6 complexes of phenols[a]

Phenol or ketone	Predominant complex formed	Chemical shift (ppm)							Ultraviolet	
		H1	H2	H3	H4	H5	H6	OH	λ_{max} (nm)	log ε
1*a*	2*a*		(2.40)	—	6.95	—	(2.40)	7.8	300	2.41
									271	3.23
									278	3.21
1*b*	3*b*		(2.10)	7.85	3.74	(2.41)	7.17	—	298	3.04
1*c*	3*c*		6.95	(2.50)	3.85	(2.50)	6.95	—	303	2.37
1*d*	2*d*		(2.39)[b]	7.06	(2.27)[b]	7.0d	7.30d	8.0	298	2.27
1*e*	2*e*		7.13	(2.20)	(2.20)	7.13d	7.13d	nd	262	2.87
1*f*	2*f*		(2.40)	6.95	(2.28)	6.95	(2.40)	7.8	283	3.23
1*g*	3*g*		(2.25)	2.35	3.80	6.90	(2.25)	—	314	2.76
1*h*	3*h*		(2.25)	(2.45)	3.85	(2.45)	(2.35)	—	322	3.16
1*i*	2*i*		(2.26)[b]	(2.32)[b]	(2.10)[b]	6.95	(2.18)[b]	7.8	324	2.91
4	5	(1.55)	—	(1.51)	(1.70)	(2.26)	1.62d, 2.38d		324	3.78
									250	4.21

[a] Solvent CH_2Cl_2 or CD_2Cl_2; nd, not detected; d = doublet, m = multiplet.
[b] Assignment may be reversed.

[1] 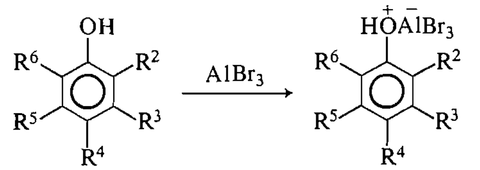

1 2

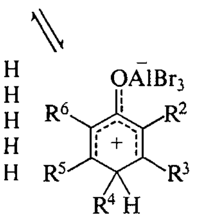

3

a $R^2 = R^6 = CH_3$; $R^3 = R^4 = R^5 = H$
b $R^2 = R^5 = CH_3$; $R^3 = R^4 = R^6 = H$
c $R^3 = R^5 = CH_3$; $R^2 = R^4 = R^6 = H$
d $R^2 = R^4 = CH_3$; $R^3 = R^5 = R^6 = H$
e $R^3 = R^4 = CH_3$; $R^2 = R^5 = R^6 = H$
f $R^2 = R^4 = R^6 = CH_3$; $R^3 = R^5 = H$
g $R^2 = R^3 = R^6 = CH_3$; $R^4 = R^5 = H$
h $R^2 = R^3 = R^5 = R^6 = CH_3$; $R^4 = H$
i $R^2 = R^3 = R^4 = R^6 = CH_3$; $R^5 = H$

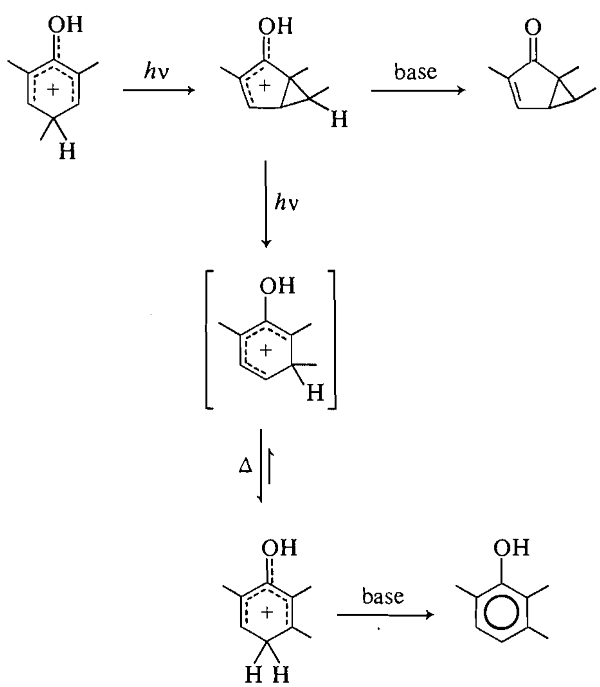

SCHEME 1

nols and found that two types of complexes can be formed, eq. [1] (6). In each of these complexes the Lewis acid is bound to the oxygen of the phenol but the OH proton can either remain on oxygen, **2**, or migrate to the *para* ring carbon, **3**. The position of the equilibrium established between **2** and **3** was shown to depend both on the substituents on the phenol and also on the ratio of Lewis acid to phenol used. It was found necessary to have at least one methyl group in a *meta* position in order for the keto type complex **3** to be the major species present.

We have reexamined the reactions of phenols **1***a*–*c* with Al_2Br_6 and have confirmed the results of Koptyug *et al.* (6). In each case the phenol was reacted with a slight molar excess of the Lewis acid in CH_2Cl_2 (or CD_2Cl_2) solution and the ¹H nmr (nuclear magnetic resonance) and uv (ultraviolet) spectra obtained (Table 1). Complexes of the hydroxy form, **2**, were the major species present in phenols **1***a*, *d*, *e*, *f*, and *i*, while the keto complexes, **3**, predominated with **1***b*, *e*, *g*, and *h*. In general, under the conditions used here, it was found that not only was it important to have a methyl group in the *meta* position for the formation of the keto form **3** of these complexes but also that the *para* position should be unsubstituted. This pattern of substituent effects is understandable in terms of the stabilizing effect of a methyl group on benzenium cations (7). In the case of **1***i* it would seem that the effect of two methyl

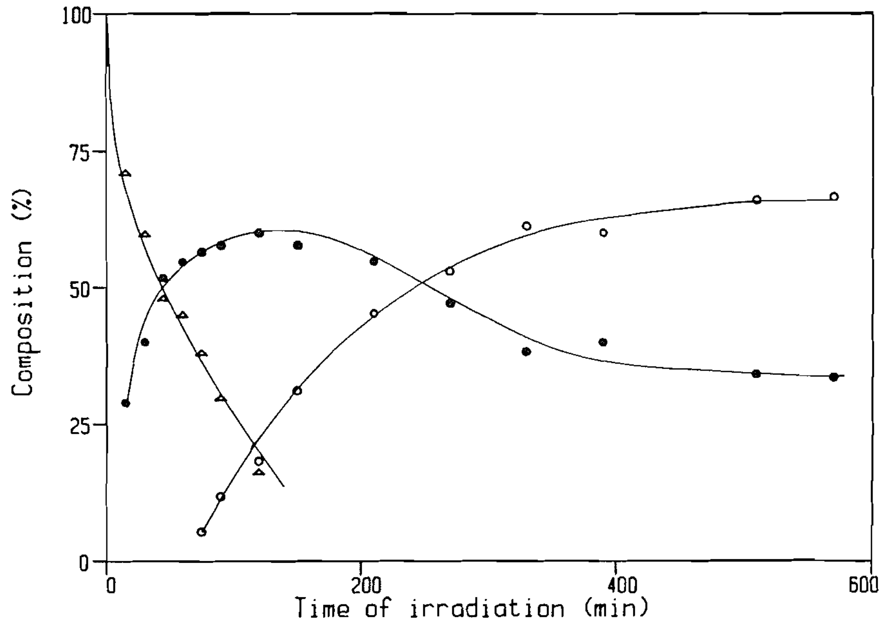

FIG. 1. Change in composition on irradiation of **1***h*; △, **1***h*; ●, **1***i*; ○, **4**.

groups in the *meta* positions outweighs the expected destabilizing effect that the *para* methyl group exerts on the keto complexes. The uv spectra of the various complexes are given in Table 1. It can be seen from these data that the keto complexes exhibit quite different uv spectra from those of the hydroxy complexes. Typically the keto complexes have strong adsorption maxima at wavelengths above 300 nm. Similar uv spectra have been reported for protonated 2,5-cyclohexadienones (8) and *para* protonated phenols (2).

Photoisomerizations

Unless otherwise specified, all irradiations were carried out using a Rayonet photoreactor and 300-nm lamps, conditions which have been shown to generally maximize the formation of bicyclic products. The reactions were followed by obtaining ^{1}H nmr spectra of the irradiated solutions and subsequently more detailed product analyses were carried out by gc (gas chromatography) after neutralization of the Lewis acids. Control reactions were carried out in each case to ensure that the observed reactions were photochemical rather than thermally induced.

The simplest cases present are the result of the irradiation of solutions of **1***f*, **1***a*, **1***d*, and **1***c*, as no photoisomerizations were observed. The $AlBr_3$ complexes of each of these phenols are primarily in the oxonium form (**2***f*, **2***a*, **2***d*, and **2***e*, respectively) and the failure to undergo photoisomerization is entirely consistent with the corresponding lack of reactivity of these oxonium ions in strong acid solutions (2, 4).

Irradiation of a solution of **1***h* in the presence of an equivalent amount of $AlBr_3$ led to the formation of **4** and subsequently **1***i*, eq. [2]. The identity of **4** was established by

[2] 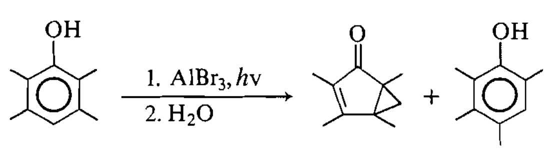

1*h* **4** **1***i*

comparison with authentic material using ^{1}H nmr and gc (4). The maximum conversion of **1***h* to **4** was ca. 60% and this was reached relatively early in the reaction, Fig. 1. Eventually a photostationary state appeared to be set up between **4** and **1***i*. To confirm this, a solution of **1***i* in the presence of $AlBr_3$ was irradiated. A mixture of **4** and **1***i* was obtained with a similar ratio to that reached starting with **1***h*. During the early stages of this reaction small amounts of **1***h* were detected in the reaction mixture. The $AlBr_3$ complex of the bicyclic ketone **4** was shown to be thermally stable under the reaction conditions. Irradiation of a CH_2Cl_2 solution of this complex led to the formation of the $AlBr_3$ complex of **1***i*. The effect of the variation in the molar ratio of Lewis acid to phenol **1***h* used in these reactions was examined. No difference in the composition of the resulting products was observed as the ratio was changed from 1 : 1 to 1 : 2 to 1 : 4 (phenol/$AlBr_3$). No photoisomerization of **1***h* or **1***i* could be detected in the absence of $AlBr_3$.

These results clearly indicate that it is possible to catalyze the photoreactions of these tetramethylphenols using a strong Lewis acid. The reactions observed are directly comparable to the reactions observed in FSO_3H or CF_3SO_3H solutions and can be understood in terms of the interrelationships shown in Scheme 2. The distribution of products observed in these reactions of the $AlBr_3$ complexes of **1***h* is different from that obtained in protic acid solution in that a much higher limiting concentration of **1***i* is obtained. This can be readily understood in terms of the thermodynamic preference for the complex of **1***i* to be in the photochemically inert oxonium form, with only small amounts being in the photochemically active dienone form. The importance of this equilibrium is more pronounced in the photoreactions of some of the other phenols described below.

Irradiation of **1***g* in the presence of $AlBr_3$ led to the formation of **1***f* and only traces (<4% maximum concentration) of materials which were possibly isomeric bicyclo[3.1.0]hexenones, although these materials were not isolated and characterized in view of the small amounts present. As has already been shown, **1***f* is inert when irradiated in the presence of $AlBr_3$ because it preferentially exists as the oxonium complex. The photoisomerization of **1***g* can be understood in terms of the sequence of reactions shown in the top part of Scheme 2. The difference

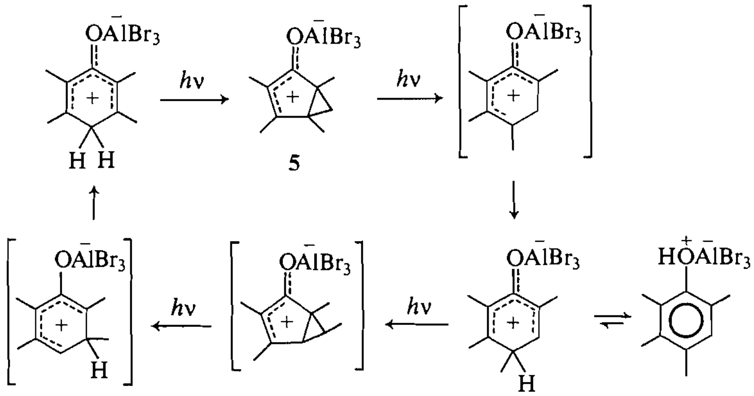

SCHEME 2

in this case is that the Lewis acid complex of 1*f* is in the photochemically inert oxonium form and this serves as the sink for the reaction.

The photochemical behaviour of 1*b* in the presence of $AlBr_3$ was similar to that of 1*g* described above in that the major products were again isomeric phenols, eq. [3]. In this case these photoproducts were identified as 1*a* and 1*e*. Traces of other unidentified products were present.

[3] 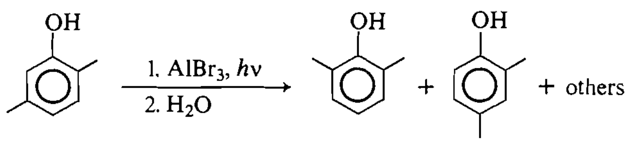

1*b* 1*a* 21% 1*d* 76% 3%

In the case of 1*c*, irradiation in the presence of $AlBr_3$ led to the formation of two major products, which were identified as 1*e* and 1*b*. Traces of materials (<2.5%) that could be bicyclic ketones were detected by gc, and also small amounts of 1*a*, eq. [4]. As 1*b* is photochemically active when complexed, the amount of 1*b* present decreased with longer irradiation times.

The $AlBr_3$ catalysed photoisomerizations of 1*b* and 1*c* differ from the reactions described above in that a net migration of a methyl group from the *meta* to the *ortho* position has occurred. These reactions were shown to be photochemically rather than thermally initiated. One possible route whereby this could occur would be if, in addition to the C4 protonated complexes present as the predominant species in solution of 1*b* and 1*c* and $AlBr_3$, smaller amounts of the two *ortho* C-protonated forms were present. These species, by analogy with the protonated 2,4-cyclohexadienones, photoisomerize as shown in Scheme 3 (3, 9).

[4] 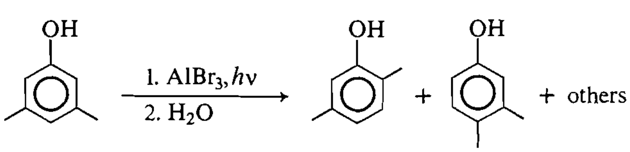

1*c* 1*b* 14% 1*e* 82% 4%

Careful examination of the ^1H nmr spectra of solutions of 1*b* and 1*c* in the presence of $AlBr_3$ did not show any evidence for the presence of *ortho* protonated complexes. If these species were present they were either in rapid exchange with the major *para* protonated complexes, 3*b* and 3*c* respectively, or in such small amounts that they were below nmr detection limits.

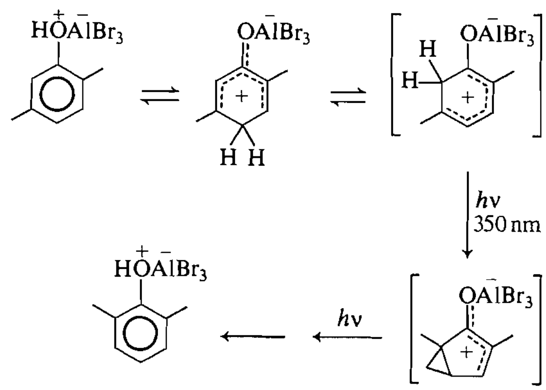

SCHEME 3

The uv spectra of protonated 2,4-cyclohexadienones exhibit bands at substantially longer wavelengths than protonated 2,5-cyclohexadienones (8, 9) and, if comparable *ortho* protonated complexes were present, it should be possible to detect them in the uv spectra of 1*b* and 1*c*/$AlBr_3$ solutions. No distinct band could be observed in their spectra that could be attributed to the *ortho* protonated complexes but it should be noted that there is a very large band associated with the *para* protonated complexes, which trails into the region expected for the *ortho* protonated complexes, and small amounts of these materials would not be detected. However, if these *ortho* complexes were involved, then the yields of the products from any *ortho* protonated species should be increased as longer wavelength light is used. This is indeed the case, as is evident from the data in Table 2. For example, irradiation of 1*b* in the presence of $AlBr_3$ using 350-nm lamps led to the exclusive formation of 1*a*. These results give strong support to the sequence of events depicted in Scheme 3.

Solid Acid Catalysts

Aluminosilicates contain both Bronsted and Lewis acid sites. These materials can be very acidic when dry and they should be capable of either protonating or complexing with a phenol (9).

The adsorption of 1*h* on an aluminosilicate containing 12% Al_2O_3 was followed quantitatively by gc and the results shown in Fig. 2. It would seem that a monolayer coverage of the catalyst occurs with about 0.4 mmol of 1*h*/g of catalyst being adsorbed. As the concentration of 1*h* in the contacting cyclohexane solution was increased beyond 2×10^{-2} *M*, a gradual increase in amount absorbed was noted. The phenol 1*h* was recovered unchanged on treatment of the catalyst or reaction mixture with water.

TABLE 2. Photoisomerization of phenols in presence of $AlBr_3$[a]

Starting phenol	Wavelength (nm)	Total isomerization (%)	Products[b]	
			Phenols (%)	Other[c] (%)
1*a*	300	0	—	—
1*d*	300	0	—	—
1*e*	300	0	—	—
1*b*	300	62	**1***a* (21) **1***d* (76)	(3)
1*b*	350	26	**1***a* (100)	—
1*c*	300	68	**1***e* (82), **1***b* (14), **1***a* (1)	(3)
1*c*	350	21	**1***b* (100)	—
1*f*	300	0	—	—
1*g*	300	37	**1***f* (89)	(11)
1*h*	300	52	**1***i* (65)	**4** (35)
1*i*	300	36	**1***g* (50)	**4 (50)**
4	300	81	**1***i* (77)	(5)

[a] Samples irradiated for 24 h.
[b] Expressed as a percentage of total products.
[c] Unidentified unless otherwise specified.

TABLE 3. Irradiation of **1***h* in the presence of Al_2O_3/SiO_2[a]

Starting concentration of **1***h* (M) ($\times 10^3$)	**1***h* (g/g catalyst)[c] ($\times 10^3$)	Length of irradiation (h)	Total recovery (% **1***h* + **1***i*)	Composition (% **1***i*)	
				Solution	Catalyst
10.14	35.45	10	71	15	20
10.52	34.67	15	71	25	30
10.78	35.11	20	75	34	32

[a] Irradiations carried out at 300 nm in glass apparatus with ca. 1 g of catalyst and 25 mL of cyclohexane as solvent.

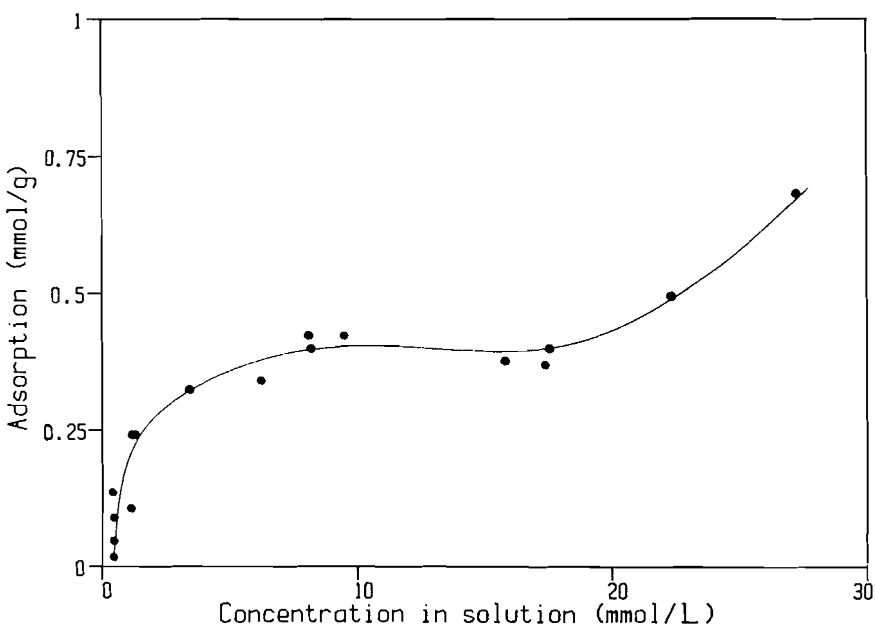

FIG. 2. Adsorption of **1***h* on aluminosilicate.

In order to characterize the nature of the adsorbed species, the uv spectra of slurries of the catalyst were examined in the presence of CH_2Cl_2 solutions of the phenol **1***h*. A new strong absorption band was found at 322 nm, which was absent in either the spectrum of the phenol itself in CH_2Cl_2 or the catalyst slurry in CH_2Cl_2 in the absence of the phenol. It was not possible to make reliable quantitative measurements of the new band but clearly the position of its absorption maximum is entirely consistent with the formation of ring protonated (keto type) complexes of **1***h*.

Irradiation of **1***h* in the presence of the aluminosilicate was carried out at 300 nm while stirring the cyclohexane/catalyst mixtures. The composition of the solution in contact with the catalyst and the composition of the materials adsorbed on the catalyst were determined by gc. The only photoproduct detected, in both the solution in contact with the catalyst and also

TABLE 4. Effect of catalyst loading on the photoisomerization of **1***h*

1*h* (g/g catalyst) ($\times 10^3$)	Initial concentration of **1***h* (*M*) ($\times 10^3$)	Total yield of **1***i*[b] (%)	**1***i* (g/g catalyst) ($\times 10^3$)
6.9	1.46	93	6.4
9.4	1.33	97	9.2
25.6	7.27	38	9.7
35.3	5.30	39	13.8
45.5	5.66	23	10.5
51.7	7.48	15	7.6
69.0	9.35	10	6.9
99.4	9.15	7	7.4
146.4	13.69	5	6.6
197.2	20.49	4	7.5

[a] All irradiations carried out in cyclohexane (50 mL) using 300-nm lamps for 24 h and Pyrex apparatus.
[b] Total yield of **1***i* in the resulting solution and adsorbed on the catalyst.

adsorbed on the catalyst, was **1***i*. As can be seen from Table 3, the proportion of **1***i* in solution and adsorbed on the catalyst was approximately the same throughout the course of the irradiation, suggesting that the two phenols are adsorbed to about the same extent on the aluminosilicate.

The effect of concentration of the phenol **1***h* on the photoreaction was examined (Table 4). It is clear from these data that quite high substrate/catalyst loadings can be used and the photoreaction still proceeds to give **1***i*. There appears to be an optimum loading in terms of efficiency of the photoreaction in the region of 0.035 g of **1***h*/g of catalyst; however, it should be noted that the conversions to **1***i* in the cases with low catalyst loadings are very high and the recorded conversions are limited by the amount of **1***h* present.

It should be stressed that no photoreactions of **1***h* were observed in the absence of the aluminosilicate and no isomerization of **1***h* to **1***i* could be detected in the presence of the catalyst but the absence of light. The isomerizations observed are clearly photochemical reactions that are occurring on the catalyst surface. The photoreaction is not limited to **1***h*. The conversion of **1***g* to **1***f* was also observed on irradiation of a cyclohexane solution in the presence of the aluminosilicate.

While it would seem most likely that the aluminosilicate functions in a comparable manner to the homogeneous Lewis or Bronsted acid catalyst with photoisomerizations of phenols, the question arises as to why, in the case of this heterogeneous acid, no bicyclic ketone, **4**, is produced in these reactions. One possibility is that the ketone is more strongly adsorbed to the catalyst surface than either of the phenols and that it undergoes further photoisomerization to give **1***i*. In order to check for this, competitive adsorptions of **1***h* and **4** were carried out (Table 5). From the data given in this table it can be seen that **4** is indeed much more strongly adsorbed than **1** on aluminosilicate. In view of the facility with which protonated or complexed **4** can undergo photoisomerization to **1***i*, it is likely that the adsorbed ketone undergoes a comparable photoreaction.

It is interesting to note that when **1***h* is vacuum deposited in low surface concentration on aluminosilicate and then irradiated, low concentrations (6%) of **4** can be detected in the presence of **1***i* (94%) at relatively low total conversions of **1***h*. It would seem clear that the overall chemistry occurring on the catalyst surface is very similar to that occurring in solutions of these phenols containing strong Bronsted or Lewis acids.

Conclusion

The results presented here confirm our original suggestion that Lewis acids and heterogeneous acid surfaces could function as catalysts for the photoiosmerization of phenols. However, apart from one case (**1***h* with $AlBr_3$), these reactions do not provide a convenient synthetic route to bicyclo[3.1.0]-hexenones. The major cause of this failure would seem to lie in the relative basicities of the bicyclic ketones as compared to the phenols, coupled with the photochemical inertness of the secondary photoproducts of these bicyclic materials. The exception to this generalization is the case of **4**, where **1***i*, its photoproduct, is still photochemically active and converted back to **4**. The importance of the relative basicities of starting material and product in Lewis acid catalysed photoreactions has been previously noted (10).

Experimental

Materials

All solvents were dried and distilled in oven-dried glassware under nitrogen immediately before use. The phenols were obtained commercially and purified by distillation. Aluminum bromide was sublimed before use. Aluminosilicate pellets (Stern chemicals) containing 12% Al_2O_3 were powdered and dried under vacuum at 350°C for 24 h before use.

General

The ^{1}H nmr spectra were obtained on a Varian EM390 instrument. The uv spectra were recorded on a Pye Unicam SP8-100 spectrometer. Gas chromatography was carried out using a Varian 3700 or a Hewlett Packard 5790A instrument, coupled with Varion CDS111 and HP3390A integrators, respectively. Columns used were 8 ft × 1/8 in. copper column packed with 10% PEGA on Chromosorb W and 10 ft × 1/8 in. stainless steel column packed with 10% Fluorad FC431 on Chromosorb W.

Photochemical procedures

Irradiations were carried out using a Rayonet photoreactor (Southern New England Ultraviolet Company) with ten lamps.The lamps used were RPR 3000 Å or RPR 3500 Å, depending on the wavelength desired.

For nmr work, the samples were prepared in 5-mm nmr tubes sealed with plastic caps and Teflon tape. Pyrex tubes of 1.5-cm diameter were used for preparative work. The reaction mixtures were stirred with magnetic stirrer during irradiation.

Preparation of solutions of complexes

All the manipulations were carried out in a nitrogen-filled glove bag. Solutions of the complexes were prepared by adding the purified phenols to a suspension of $AlBr_3$ in methylene chloride at −78°C. The reaction mixture was slowly brought to room temperature. The ratio of phenol to $AlBr_3$ was controlled by weighing both components. Unless otherwise stated, a 1.1 to 1.2 molar excess of the Lewis acid was used.

Adsorption studies were carried out using weighed samples of dried Al_2O_3/SiO_2 catalyst and varying amounts of **1***h* in dry cyclohexane. The uptake of **1***h* was followed by analyzing the solution by gc, using naphthalene as an internal standard. The adsorption was followed until no further change in concentration was observed. Competitive adsorption of **1***h* and its photoisomers was carried out by adding a known amount of phenol and its photoisomer to dried Al_2O_3/SiO_2 catalyst in 25 mL of cyclohexane. After 24 h stirring, the composition of isomers in the solution and on the catalyst was determined by analytical gc.

Desorption

The composition of products on Al_2O_3/SiO_2 after irradiation was determined by stirring the catalyst for 2 h in the presence of water and extracting the organic materials with CH_2Cl_2.

TABLE 5. Competitive adsorption of **1**h and its photoisomers on Al_2O_3/SiO_2[a]

Starting composition ($g \times 10^3$)			Final composition ($g \times 10^3$)						
			Solution			Catalyst			
1h	**4**	**1**i	**1**h	**4**	**1**i	**1**h	**4**	**1**i	K_1/K_2[b]
11.1	8.0	—	10.7	4.7	—	0.4	3.3	—	19
10.3	15.3	—	9.5	5.4	—	0.8	9.9	—	22
34.9		5.9	17.4		2.8	17.5		3.1	1.1
30.6		6.0	16.9		2.8	13.7		3.2	1.4

[a]Volume of cyclohexane used, 25 mL.

[b]$K_1/K_2 = \dfrac{\text{adsorbed } \mathbf{4} \text{ or } \mathbf{1}i \text{ (g)}}{\text{solution } \mathbf{4} \text{ or } \mathbf{1}i \text{ (g)}} \times \dfrac{\text{solution } \mathbf{1}h \text{ (g)}}{\text{adsorbed } \mathbf{1}h \text{ (g)}}$

Analysis of products

Phenols **1**a–e were converted to their benzoates using benzoyl chloride while phenols **1**h and **1**i were converted to trimethylsilylaryl ethers using bis(trimethylsilyl)trifluoroacetamide, BSTFA. Products were identified by comparison with derivatives of authentic samples, and quantitively determined by gc using naphthalene as an internal standard.

The products were recovered from the $AlBr_3$ reaction mixtures by adding the mixtures slowly to water – methylene chloride mixture at 0°C. The methylene chloride layer was separated and washed well with water. The dried solutions (Na_2SO_4) were filtered and the CH_2Cl_2 was removed by evaporation through a Vigreux column.

Benzoates were prepared by adding 0.1 g of product to 5 mL of 5% NaOH solution. To this 0.5 mL benzoyl chloride was slowly added and the mixture stirred for 1 h. After leaving the reaction mixture for 12 h at room temperature, it was extracted with ether. The ether extract, after washing with water, gave the appropriate benzoates.

Trimethylsilyl aryl ethers were prepared by adding 100 μL BSTFA to a solution of 100 μL reaction mixture in dry cyclohexane and 10 μL pyridine in a screw cap septum reacti-vial. The reaction mixture was allowed to stand at room temperature for 1 h to obtain the silyl ethers.

Control experiments were run with both procedures using mixtures of phenols with known compositions in order to ensure that the assay methods were reliable.

Acknowledgement

This work was supported by the Natural Sciences and Engineering Research Council of Canada.

1. R. F. CHILDS and B. D. PARRINGTON. Can. J. Chem. **52**, 3303 (1974); A. J. KRESGE, G. W. BARRY, K. R. CHARLES, and Y. CHIENG. J. Am. Chem. Soc. **84**, 4343 (1962); T. BIRCHALL, A. N. BOURNS, R. J. GILLESPIE, and P. J. SMITH. Can. J. Chem. **42**, 1433 (1964); R. W. ALDER and F. J. TAYLOR. J. Chem. Soc. B, 845 (1970); M. P. HARTSHORN, K. E. RICHARDS, J. VAUGHAN, and G. J. WRIGHT. J. Chem. Soc. B, 1624 (1971); S. M. BLACKSTOCK, K. E. RICHARDS, and G. J. WRIGHT. Can. J. Chem. **52**, 3313 (1974); K. E. HINE and R. F. CHILDS. J. Am. Chem. Soc. **93**, 2323 (1971); G. A. OLAH and Y. K. MO. J. Org. Chem. **38**, 353 (1973).
2. R. F. CHILDS, B. D. PARRINGTON, and M. ZEYA. J. Org. Chem. **44**, 4912 (1979); B. D. PARRINGTON and R. F. CHILDS. J. Chem. Soc. Chem. Commun. 1581 (1970).
3. R. F. CHILDS. J. Chem. Soc. Chem. Commun. 946 (1969); D. I. SCHUSTER. Acc. Chem. Res. **11**, 65 (1978); P. J. KROPP. Org. Photochem. **1**, 1 (1967); K. SCHAFTNER. Adv. Photochem. **4**, 81 (1966); H. ZIMMERMAN. Adv. Photochem. **1**, 183 (1963).
4. R. F. CHILDS, G. S. SHAW, and A. VARADARAJAN. Synthesis, 198 (1982); R. F. CHILDS, B. D. PARRINGTON, and M. ZEYA. J. Org. Chem. **44**, 4912 (1979).
5. R. F. CHILDS, D. L. MULHOLLAND, M. ZEYA, and A. K. GOYAL. solar Energy **30**, 155 (1983); R. F. CHILDS and D. L. MULHOLLAND. J. Am. Chem. Soc. **105**, 96 (1983).
6. V. A. KOPTYUG and A. V. GOLOUMIN. Zh. Org. Khim. **8**, 607 (1972); V. A. KOPTYUG, T. P. ANDREEVA, and V. I. MAMATYUK. Zh. Org. Khim. **6**, 1848 (1970).
7. H. H. PERKAMPUS. Adv. Phys. Org. Chem. **4**, 195 (1966); D. M. BROUWER, E. L. MACKOR, and C. MACLEAN. *In* Carbonium ions. Vol. 2. *Edited by* G. A. Olah and P. von R. Schleyer. Wiley Interscience, New York, NY. 1970. p. 837.
8. E. C. FRIEDRICH. J. Org. Chem. **33**, 413 (1968); V. P. VITULLO. J. Org. Chem. **34**, 224 (1969); A. J. WARING. J. Chem. Soc. Perkin. Trans. 2, 84 (1973); B. D. PARRINGTON and R. F. CHILDS. J. Chem. Soc. Chem. Commun. 1581 (1970).
9. E. C. FRIEDRICH. J. Org. Chem. **33**, 413 (1968); B. D. PARRINGTON and R. F. CHILDS. J. Chem. Soc. Commun. 1581 (1970); N. FILIPESCU and J. W. PAVLIK. J. Am. Chem. Soc. **92**, 6062 (1970); J. W. PAVLIK and R. J. PASTERIS. J. Am. Chem. Soc. **96**, 6107 (1970).
10. R. F. CHILDS, B. DUFFEY, and A. MIKA-GIBALA. J. Org. Chem. **49**, 4352 (1984).

Preparation, infrared spectra, and crystal structure of two modifications of the (thymidinato-N^3)methylmercury(II) complex

FRANCE GUAY AND ANDRÉ L. BEAUCHAMP[1]

Département de Chimie, Université de Montréal, C.P. 6210, Succ. A, Montréal (P.Q.), Canada H3C 3V1

Received June 20, 1984[2]

FRANCE GUAY and ANDRÉ L. BEAUCHAMP. Can. J. Chem. **63**, 3456 (1985).

Reaction of CH_3HgOH with thymidine (HT) yielded the neutral CH_3HgT complex crystallizing as a hydrated or an anhydrous material, depending on preparation conditions. Both forms were examined by X-ray diffraction. The anhydrous variety is monoclinic, space group $P2_1$, a = 4.798(6), b = 14.270(8), c = 10.390(4) Å, β = 102.74(9)°, and Z = 2 molecules per cell. The structure was refined on 1552 nonzero MoKα reflections to a conventional R factor of 0.034. The hydrated form belongs to the orthorhombic space group $P2_12_12_1$, a = 10.484(3), b = 14.633(3), c = 18.538(5), Z = 8. The structure was refined on 1816 nonzero MoKα reflections to R = 0.036. In both forms, the CH_3Hg^+ ion is linearly bonded to the deprotonated N(3) site of thymidine. The water molecules and hydroxyl groups in the ribose unit participate in a hydrogen bonding network, in which the carbonyl groups are involved as acceptors. The infrared spectra of the two forms differ significantly only by the absorptions due to the water molecules. By comparing with the spectrum of thymidine, diagnostic regions for complexation with deprotonated thymidine have been proposed.

FRANCE GUAY et ANDRÉ L. BEAUCHAMP. Can. J. Chem. **63**, 3456 (1985).

La réaction de CH_3HgOH avec la thymidine (HT) conduit au complexe neutre CH_3HgT, qui cristallise sous forme hydratée ou anhydre, selon les conditions de préparation. Les deux formes ont été étudiées par diffraction des rayons X. La forme anhydre est monoclinique, groupe spatial $P2_1$, a = 4,798(6), b = 14,270(8), c = 10,390(4) Å, β = 102,74(9)°, Z = 2 molécules par maille. La structure a été affinée au moyen de 1552 réflexions MoKα significativement observées jusqu'à un facteur R conventionnel de 0,034. La forme hydratée appartient au groupe orthorhombique $P2_12_12_1$, a = 10,484(3), b = 14,633(3), c = 18,538(5) Å, Z = 8. La structure a été affinée au moyen de 1816 réflexions MoKα significativement observées jusqu'à R = 0,036. Dans les deux sortes de cristaux, l'ion CH_3Hg^+ est linéairement lié au site N(3) déprotoné de la thymidine. Les molécules d'eau et les groupes hydroxyles du ribose participent à des liaisons hydrogène, pour lesquelles les groupes carbonyles jouent le rôle d'accepteurs. Les spectres infrarouges des deux formes ne diffèrent appréciablement que dans les régions associées à la molécule d'eau. Par comparaison avec le spectre de la thymidine, on identifie des régions diagnostiques pour la complexation avec la thymidine déprotonée.

Introduction

It has been shown by various methods that mercury reacts with N(1)-blocked uracil and thymine ligands by displacing the acidic N(3)-H proton (1–7). Substitution by the less electron-attracting metal atom is expected to increase the basic character of the nearby carbonyl groups. In agreement with this assumption, when CH_3HgMT (where MT^- = deprotonated 1-methylthymine) is allowed to precipitate in the presence of simple salts, mixed compounds such as $CH_3HgMT\cdot NaClO_4$ (8) and $CH_3HgMT\cdot \frac{1}{2}NaNO_3$ (7) are obtained. The carbonyl groups of the thymine unit have been shown to interact with the Na^+ ions in these mixed compounds. In order to determine whether such Na^+–carbonyl interaction are retained when good hydrogen-bond donors are simultaneously present, attempts were made to obtain mixed compounds containing the similar CH_3HgT complex, in which the ligand would be the deoxynucleoside thymidine HT. No mixed complexes could be prepared, but two forms of the neutral CH_3HgT complex have been isolated. They are discussed in the present paper.

Experimental section

Preparation

CH_3HgT

Thymidine (Het-Chem, 0.243 g, 1 mmol) was mixed with 1.0 mL of 1 *M* aqueous CH_3HgOH (Alfa) in 30 mL of hot 95% ethanol. After evaporation at room temperature to dryness, the solid was washed with absolute ethanol and dried *in vacuo*. Yield: 0.34 g. *Anal.* calcd. for $C_{11}H_{16}N_2O_5Hg$: C 28.92, H 3.53, N 6.13, Hg 43.91; found: C 29.37, H 3.67, N 6.08, Hg 43.68.

$CH_3HgT\cdot 0.69H_2O$[3]

Thymidine and CH_3HgOH were mixed (same proportions as above) in 30 mL of hot water. The mixture was allowed to evaporate at room temperature to a volume of 10 mL. The solid was filtered and dried *in vacuo*. Yield: 0.33 g, 70%. *Anal.* calcd. for $C_{11}H_{16}N_2O_5Hg$, $0.69H_2O$: C 28.15, H 3.73, N 5.97, Hg 42.74; found: C 28.41, H 3.90, N 5.95, Hg 42.37.

Infrared spectroscopy

The spectra were recorded on KBr pellets with a Digilab FTS-15 C/D Fourier-transform infrared spectrometer equipped with a Globar source and a wide-band mercury cadmium telluride detector (Infrared Associates, New Brunswick, NJ). Typically, 100 interferograms of 4096 points recorded with an optical velocity of 1.2 cm s^{-1} and maximum optical retardation of 0.5 cm were co-added, apodized with a boxcar function, and Fourier transformed with 4 levels of zero filling resulting in a spectral resolution of 2 cm^{-1}. The apparatus was purged with nitrogen during the experiment.

Crystallographic measurements and structure resolution

CH_3HgT

$C_{11}H_{16}HgN_2O_5$ fw = 456.8

Monoclinic, $P2_1$, a = 4.798(6) Å, b = 14.270(8) Å, c = 10.390(4) Å, β = 102.74(9)°, V = 693.9 Å^3, D_o = 2.16(2) g cm^{-3}, Z = 2, D_c = 2.186 g cm^{-3}, λ(MoK$\bar{\alpha}$) = 0.71069 (graphite monochromator), t = 20°C, μ(MoKα) = 110.9 cm^{-1}, crystal thickness (mm) between pairs of faces: 0.64 ($0\bar{1}0$–010) × 0.06 ($00\bar{1}$–001) × 0.06 ($01\bar{1}$–$0\bar{1}1$) × 0.10 ($0\bar{1}\bar{1}$–011), transmission range: 0.33–0.60, average fluctuation of standard reflections: ±1.6%.

Space group was determined from precession and cone axis photographs. The systematic absences ($0k0$, $k \neq 2n$) were consistent with space groups $P2_1$ and $P2_1/m$, but the latter was rejected as inconsis-

[1] To whom all correspondence should be addressed.
[2] Revision received June 3, 1985.

[3] Formula based on an occupancy factor of 0.38 for water molecule W(2).

tent with the presence of asymmetric centers in the D-deoxyribose unit. The intensity data were collected with an Enraf-Nonius CAD4 diffractometer, following a procedure described elsewhere (9). A set of 2099 *hkl* and $hk\bar{l}$ reflections in a reflection sphere limited by 2θ = 60° was collected. The 1552 reflections significantly above backgrounds ($I > 3\sigma(I)$) were retained for structure resolution.

The structure was solved by the heavy-atom method and refined on $|F_o|$ by full-matrix least-squares in the early stages. The *x* and *z* coordinates of Hg were determined from a Patterson synthesis, whereas the *y* coordinated was arbitrarily set to 0.25 to fix the origin along *b*. The difference Fourier map (ΔF) phased on Hg showed $P2/m$ symmetry as expected, but the pyrimidine ring and both carbonyl oxygens from one of the two overlapping images could be unambiguously assembled. A subsequent ΔF map phased on the known portion of the structure revealed the positions of all the remaining non-hydrogen atoms. Isotropic refinement converged to $R = \Sigma||F_o| - |F_c||/\Sigma|F_o| = 0.120$ and $R_w = [\Sigma w(|F_o| - |F_c|)^2/\Sigma w|F_o|^2]^{1/2} = 0.143$. At this stage, it was checked that the D-deoxyribose unit had the correct absolute configuration. Refinement was continued by block-diagonal least squares. The hydrogen atoms (except that of O(5′A)) were located from the ΔF map. They were introduced into the structure at idealized positions (B = 6.0 Å^2, C—H = 0.95 Å). The hydrogen parameters were not refined, but the coordinates were recalculated after each least-squares cycle. Anisotropic refinement of all non-hydrogen atoms reached convergence for R = 0.034 and R_w = 0.038. The goodness-of-fit ratio was 1.27. The final ΔF map showed a general background below ±0.7 e/Å^3, with a few extra peaks in the range 0.9–2.6 e/Å^3 near mercury.

CH_3HgT hydrate

$C_{11}H_{16}HgN_2O_5$, 0.69 H_2O fw = 469.28

Orthorhombic, $P2_12_12_1$, a = 10.484(3) Å, b = 14.633(3) Å, c = 18.538(5) Å, V = 2844.0 Å^3, D_o = 2.18(2) g cm^{-3}, Z = 8, D_c = 2.193 g cm^{-3}. λ(MoK$\bar{\alpha}$) = 0.71069 Å, t = 20°C, μ(MoKα) = 108.1 cm^{-1}, thickness (mm) between pairs of faces: 0.30 ($001-00\bar{1}$) × 0.24 ($20\bar{1}-\bar{2}01$) × 0.20 ($010-0\bar{1}0$), transmission range: 0.06–0.23; average fluctuation of standards: ±1.4%.

Space group was unambiguously defined from the systematic absences ($h00$, $h \neq 2n$; $0k0$, $k \neq 2n$; $00l$, $l \neq 2n$) noted on precession films. A set of 2684 independent *hkl* reflections in a sphere limited 2θ = 49° was collected, of which 1816 were retained as significantly above background ($I > 3\sigma(I)$).

The structure was solved by the heavy-atom method and refined on $|F_o|$ by full-matrix least-squares in the early stages. Both non-equivalent Hg atoms were located from a Patterson map, and the non-hydrogen atoms were progressively identified from structure factor calculations and ΔF maps. Electron density was found at suitable positions for all non-hydrogen atoms of both independent CH_3HgT units and two water molecules. Isotropic refinement converged to R = 0.064 and R_w = 0.069. Absolute configuration was checked at this point. Mercury was then refined anisotropically. It was then noticed that O(5′B) and water molecule W(2) had very high thermal motion. In addition, the ΔF map showed a residual peak properly located to correspond to an alternate position for O(5′B). Thus, two positions O(5′B) and O(5″B) were assigned to this terminal hydroxyl group with half occupancies.

Refinement was continued by full-matrix least-squares as above, except that besides the coordinates and isotropic temperature factors, occupancy factors were also refined for O(5′B), O(5″B), and W(2). For these atoms, only 20% of the calculated shifts were applied at each cycle to stabilize the convergence process. The occupancy factors converged to 0.40(5), 0.61(4), and 0.33(5) for W(2), O(5′B), and O(5″B), respectively. As total occupancy for O(5′B) and O(5″B) must be unity, the corresponding factors were normalized to 0.65 and 0.35, respectively, and kept constant in the subsequent steps of the refinement, whereas the occupancy factor of W(2) remained an adjustable parameter. The last steps were carried out by block-diagonal least squares. The hydrogens attached to C(8) and the ribose carbons were visible in the ΔF map and they were fixed at idealized positions (B = 6.0 Å^2, C—H = 0.95 Å). Their parameters were not refined, but their

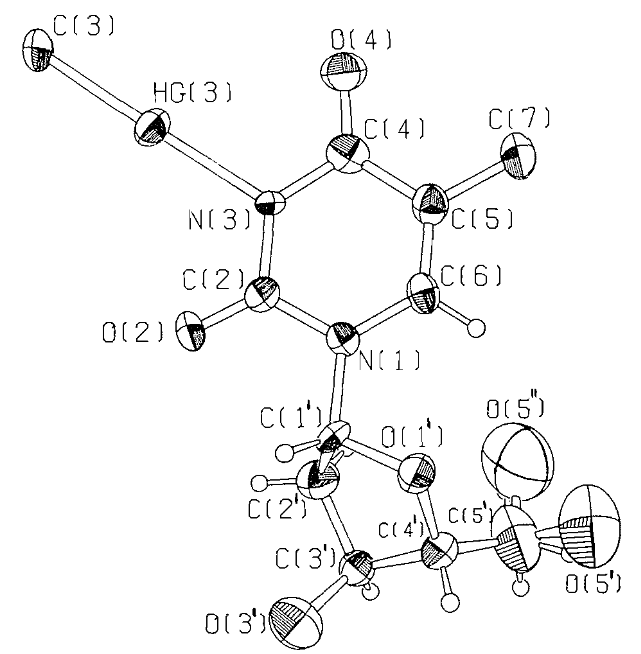

FIG. 1. ORTEP drawing of the CH_3HgT molecule B in the hydrated ($P2_12_12_1$) compound. Ellipsoids correspond to 50% probability. The two disordered positions for the terminal 5′ hydroxyl of molecule B are shown, O(5″) corresponding to the minor component (occupancy factor = 0.33(5)). No disorder is found for molecule A (anhydrous compound) and molecule C (hydrated compound).

coordinates were recalculated after each least-squares cycle. The methyl and hydroxyl hydrogens were not detected in the ΔF map. All non-hydrogen atoms were anisotropically refined and convergence was reached for R = 0.036, R_w = 0.038 and a goodness-of-fit ratio of 1.21. As a check on the validity of the occupancy factors for O(5′B) and O(5″B), extra cycle were calculated including the occupancy factors of these atoms in the refinement. The parameters of the remaining non-hydrogen atoms shifted by <0.05σ. The occupancy factor of O(5′B) and O(5″B) returned to the values found earlier (σ = 0.04), while their temperature factors changed slightly as expected. Therefore, the parameters obtained with the normalized values for these occupancy factors were retained. The general background in the final ΔF map was below ±0.9 e/Å^3. Some peaks near Hg were in the range ±0.9–1.2 e/Å^3.

The refined coordinates for both structures are listed in Table 1. Tables of temperature factors and structure factor amplitudes are provided in the supplementary material.[4] The form factors used were those of Cromer and Waber (10), except for hydrogen (11). The anomalous dispersion terms of Hg (12) were included in structure factor calculations. The programs used are listed elsewhere (13).

Results and discussion

Description of the structures

These two structures contain three non-equivalent CH_3HgT units: the hydrated compound consists of two independent molecules (B and C), whereas the molecules in the anhydrous form are all equivalent (type A). In all cases, the CH_3Hg^+ ion is

[4] Distances and angles in the thymidine ligands, tables of structure factor amplitudes, temperature factors, calculated hydrogen coordinates, least-squares plane calculations, distances and angles around oxygen atoms, as well as copies of the infrared spectra for both compounds may be purchased from the Depository of Unpublished data, CISTI, National Research Council of Canada, Ottawa, Ont., Canada K1A 0S2.

TABLE 1. Refined coordinates and equivalent temperature factors

(*a*) anhydrous CH_3HgT ($P2_1$) ($x, y, z \times 10^4$, Hg $\times 10^5$; $U_{eq} \times 10^3$)

Atom	*x*	*y*	*z*	U_{eq}[c]
Hg(3A)	9974(8)	25000	23115(4)	39
N(1A)	55(19)	−453(6)	2797(8)	29
C(2A)	1066(21)	455(7)	2986(12)	32
O(2A)	3284(18)	648(6)	3818(9)	46
N(3A)	−454(22)	1133(7)	2219(9)	36
C(3A)	2357(46)	3837(11)	2345(16)	73
C(4A)	−3039(24)	967(8)	1316(11)	34
O(4A)	−4344(19)	1644(6)	755(9)	46
C(5A)	−3912(21)	2(7)	1112(10)	30
C(6A)	−2373(22)	−651(7)	1853(11)	30
C(7A)	−6548(24)	−220(9)	89(12)	42
C(1′A)	1611(20)	−1213(7)	3592(11)	29
O(1′A)	2570(16)	−1835(5)	2734(8)	34
C(2′A)	−303(23)	−1801(8)	4301(11)	33
C(3′A)	1162(25)	−2762(7)	4384(11)	35
O(3′A)	3379(19)	−2756(5)	5542(8)	47
C(4′A)	2295(21)	−2795(6)	3116(12)	29
C(5′A)	491(25)	−3320(10)	1977(12)	42
O(5′A)	−2404(18)	−3020(7)	1742(9)	50

(*b*) Hydrated CH_3HgT ($P2_12_12_1$) ($x, y, z \times 10^4$, Hg $\times 10^5$; $U_{eq} \times 10^3$)

Atom	*x*	*y*	*z*	U_{eq}[c]
Hg(3B)	8929(7)	7486(5)	7548(4)	35
Hg(3C)	26474(7)	−10282(5)	15559(4)	40
N(1B)	−1565(12)	1304(9)	2546(7)	25
C(2B)	−1153(16)	1145(13)	1845(9)	35
O(2B)	−1845(11)	1139(9)	1326(6)	38
N(3B)	141(11)	987(10)	1788(7)	26
C(3B)	1667(18)	488(16)	−251(10)	49
C(4B)	1019(16)	970(12)	2343(10)	36
O(4B)	2146(11)	807(9)	2205(7)	46
C(5B)	526(17)	1154(13)	3059(9)	35
C(6B)	−731(17)	1310(12)	3118(9)	31
C(7B)	1439(18)	1168(15)	3688(10)	50
C(1′B)	−2919(16)	1572(12)	2587(9)	30
O(1′B)	−3111(11)	2040(9)	3242(6)	37
C(2′B)	−3841(17)	741(15)	2614(11)	48
C(3′B)	−4966(16)	1137(13)	3039(10)	36
O(3′B)	−5651(14)	1722(10)	2554(8)	61
C(4′B)	−4274(18)	1761(13)	3596(9)	38
C(5′B)	−4112(25)	1261(19)	4300(14)	92
O(5′B)[b]	−3572(30)	1810(22)	4775(15)	122
O(5″B)[b]	−3066(69)	780(50)	4264(36)	145
N(1C)	−260(13)	−1530(10)	3168(7)	29
C(2C)	947(18)	−1453(12)	2863(9)	33
O(2C)	1932(13)	−1488(11)	3204(7)	58
N(3C)	961(13)	−1336(9)	2113(7)	29
C(3C)	4228(20)	−677(15)	984(11)	58
C(4C)	−111(18)	−1292(12)	1685(10)	40
O(4C)	30(12)	−1170(9)	1025(6)	43
C(5C)	−1351(17)	−1381(13)	2036(10)	37
C(6C)	−1345(16)	−1496(12)	2753(9)	27
C(7C)	−2552(18)	−1348(14)	1586(11)	53
C(1′C)	−340(20)	−1658(14)	3957(11)	50
O(1′C)	−1295(11)	−2300(9)	4109(7)	45
C(2′C)	−708(16)	−775(12)	4336(9)	37
C(3′C)	−1596(16)	−1060(13)	4931(10)	37
O(3′C)	−808(14)	−1260(11)	5557(7)	71
C(4′C)	−2128(19)	−1996(14)	4692(10)	46
C(5′C)	−3468(20)	−1904(16)	4394(12)	60

TABLE 1. (*Continued*)

Atom	*x*	*y*	*z*	U_{eq}[c]
O(5′C)	−3624(12)	−1146(10)	3942(8)	60
W(1)	4567(15)	−1518(11)	2942(8)	69
W(2)[a]	3835(42)	2661(41)	5054(25)	116

[a] Occupancy factor, 0.40(5).
[b] Occupancy factors for O(5′B) and O(5″B) refined to 0.61(4) and 0.33(5), normalized to 0.65 and 0.35, respectively.
[c] $U_{eq} = (\Sigma_i \Sigma_j U_{ij} a_i^* a_j^* a_i a_j)/3$.

TABLE 2. Selected interatomic distances and bond angles[a]

Bond	Distance (Å) A	B	C
Hg(3)—N(3)	2.07(1)	2.10(1)	2.10(1)
Hg(3)—C(3)	2.01(2)	2.07(2)	2.03(2)
Bonds	**Angle (deg) A**	**B**	**C**
C(3)—Hg(3)—N(3)	178.3(6)	178.5(7)	176.8(7)
Hg(3)—N(3)—C(2)	121.2(8)	118(1)	122(1)
Hg(3)—N(3)—C(4)	115.5(8)	115(1)	113(2)
C(2)—N(3)—C(4)	123(1)	127(1)	125(2)

[a] Molecule A in the anhydrous compound ($P2_1$), B and C in the hydrated compound ($P2_12_12_1$).

bonded to the deprotonated N(3) site of the pyrimidine ring (Fig. 1), in the same manner as in the corresponding 1-methylthymine complex (7). The usual linear coordination of mercury is observed (Table 2). The departure from linearity in molecule C is significant (C(3C)—Hg(3C)—N(3C) = 176.8(7)°), although relatively small and not unprecedented. The Hg—N and Hg—C bond lengths (averaging 2.09(1) and 2.04(2) Å, respectively) correspond within experimental errors with those found in similar compounds (6, 7).

Linearly coordinated mercury usually forms a variable number of weaker bonds or contacts with donor atoms in the region of the equatorial plane (assuming the H_3C—Hg—N direction to be axial). In the present case, the carbonyl groups O(2) and O(4) fill some of the space in the equatorial region, and it is not clear whether these intramolecular Hg…O contacts (Table 3) have significant bonding character, even if some of them are below the 3.0 Å limit corresponding to the sum of the van der Waals radii (14). Indeed, the C=O…Hg angles are ~70°, and electron density along this direction is not expected to be high (15). The intramolecular Hg—O distances are shorter with O(4) than with O(2), and this would be consistent with the greater basicity of the former. However, these differences may simply reflect distortions imposed by packing on the tube-like CH_3Hg^+ group extending far into the structure. The best Hg…O contacts are intermolecular and they involve the O(1′) atom of the ribose rings: Hg(3B)—O(1′C) = 2.90(1) Å and Hg(3C)—O(1′B) = 2.89(1) Å. They play an important part in packing for the hydrated complex (*vide infra*).

The distances and angles in the pyrimidine rings are provided in the supplementary material. Within the experimental errors (σ ~ 0.02 Å on distances and ~1° on angles), they compare well with those of free thymidine (16). The six-membered ring is planar within 0.04 Å (4σ) for molecule A and within 0.01 Å

TABLE 3. Selected hydrogen-bonding distances and Hg...O contacts

(*a*) Hg...O contacts

Atoms	Distance (Å)	Atoms	Distance (Å)
Hg(3A)—O(4A)	2.96(1)	Hg(3B)—O(4C)	2.99(1)
Hg(3A)—O(3′A)[a]	3.09(1)	Hg(3B)—O(1′C)[f]	2.90(1)
Hg(3A)—O(2A)	3.14(1)	Hg(3C)—O(4B)	2.99(1)
Hg(3B)—O(2B)	3.11(1)	Hg(3C)—O(4C)	2.92(1)
Hg(3B)—O(4B)	2.99(1)	Hg(3C)—O(1′B)[e]	2.89(1)

(*b*) Hydrogen bonds

Bond	Distance (Å)	Bond	Distance (Å)
O(2A)—O(3′A)[a]	2.77(1)	O(5′C)—W(1)[g]	2.71(2)
O(4A)—O(5′A)[b]	2.74(1)	O(2B)—O(3′C)[j]	2.85(2)
O(3′A)—O(2A)[c]	2.77(1)	O(2C)—W(1)	2.81(2)
O(5′A)—O(4A)[d]	2.74(1)	O(4B)—O(3′B)[k]	2.75(2)
O(3′B)—O(4B)[g]	2.75(2)	O(4C)—W(2)[l]	3.06(5)
O(3′B)—W(1)[f]	2.96(2)	W(1)—O(5′C)[k]	2.71(2)
O(3′C)—O(2B)[h]	2.85(2)	W(1)—O(2C)	2.81(2)
O(5′B)—O(4C)[h]	2.93(3)	W(1)—O(3′B)[e]	2.96(2)
O(5′B)—W(2)[i]	2.66(6)	W(2)—O(4C)[m]	3.03(6)
O(5′B)—W(2)[g]	3.03(6)	W(2)—O(5′B)[k]	2.66(6)
O(5″B)—O(5′C)	2.94(7)	W(2)—O(5′B)[n]	3.03(6)
O(5′C)—O(5″B)	2.94(7)		

[a] $1 - x, 1/2 + y, 1 - z$.
[b] $-1 - x, 1/2 + y, - z$.
[c] $1 - x, -1/2 + y, 1 - z$.
[d] $-1 - x, -1/2 + y, - z$.
[e] $-x, -1/2 + y, 1/2 - z$.
[f] $-x, 1/2 + y, 1/2 - z$.
[g] $-1 + x, y, z$.
[h] $-1/2 - x, -y, 1/2 + z$.
[i] $-1/2 + x, 1/2 - y, 1 - z$.
[j] $-1/2 - x, -y, -1/2 + z$.
[k] $1 + x, y, z$.
[l] $1/2 - x, -y, -1/2 + z$.
[m] $1/2 - x, -y, 1/2 + z$.
[n] $1/2 + x, 1/2 - y, 1 - z$.

TABLE 4. Selected torsion angles (deg)

Bonds	Angle A	Angle B	Angle C	Thymidine (16)
O(1′)—C(1′)—N(1)—C(6)	62(1)	15(2)	40(2)	39(2)
C(2′)—C(1′)—O(1′)—C(4′)	−19(1)	−16(2)	−13(2)	−7(1)
C(3′)—C(2′)—C(1′)—O(1′)	33(1)	33(2)	23(3)	28(1)
C(4′)—C(3′)—C(2′)—C(1′)	−33(1)	−37(2)	−22(2)	−37(1)
O(1′)—C(4′)—C(3′)—C(2′)	23(1)	29(2)	15(2)	33(1)
C(1′)—O(1′)—C(4′)—C(3′)	−3(1)	−8(2)	−1(2)	−17(1)
O(1′)—C(4′)—C(5′)—O(5′)	−70(1)	66(3)	−73(2)	56(1)
C(3′)—C(4′)—C(5′)—O(5′)	50(1)	−177(3)	42(3)	172(1)
O(1′)—C(4′)—C(5′)—O(5″)		−33(4)		
C(3′)—C(4′)—C(5′)—O(5″)		86(4)		

(1σ) for molecules B and C. In molecules A and C, the CH_3Hg^+ group significantly deviates from the plane. The atom-to-plane distances are Hg(3A), 0.1915(4); C(3A), 0.38(2); Hg(3C), 0.255(1); C(3C), 0.58(2) Å. This supports the existence of packing effects on this linear group, which would normally lie in the plane and form equal Hg—N—C angles. Other exocyclic atoms also depart from the plane of the ring, namely O(4A) (0.12(1) Å), C(1′B) (0.15(2) Å), and O(4C) (0.03(1) Å).

The conformation of the ribose portion in nucleosides has been discussed by Sundaralingam (17). The rings for the three complexes have a C(3′)-*exo* conformation, the C(3′) atom being 0.46(1), 0.53(2), and 0.30(2) Å above the C(1′)—O(1′)—C(2′)—C(4′) plane for molecules A, B, and C, respectively. The torsion angles given in Table 4 show that the conformation of thymidine is not drastically changed in the complexes. The relative orientation of the pyrimidine moiety with respect to the deoxyribose ring corresponds to the *anti*

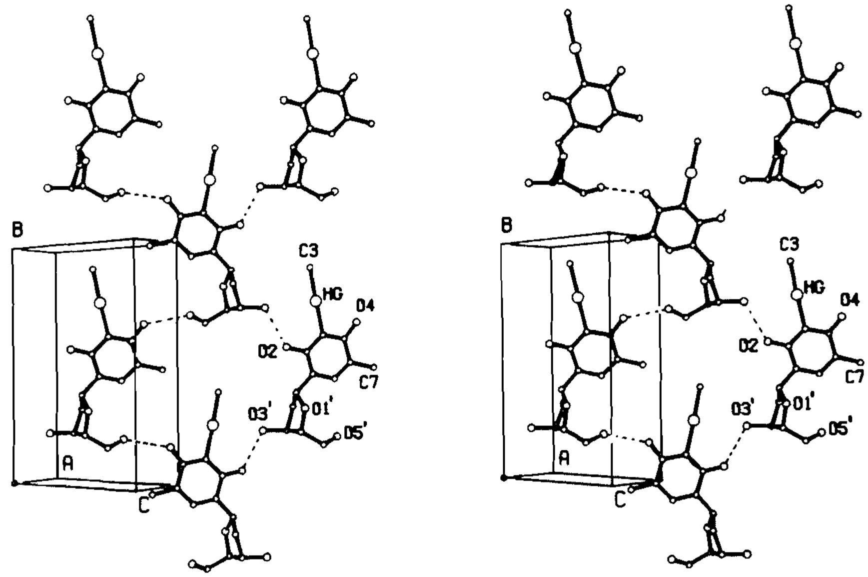

FIG. 2. Stereo view of the unit cell of the anhydrous compound ($P2_1$). The cell origin is shown as a black dot. Some atoms are labelled in one of the molecules. The others can be identified by comparison with Fig. 1. Dashed lines correspond to hydrogen bonds.

configuration as in thymidine, but the C(6)—N(1)—C(1′)—O(1′) angle spans a range of ±23° about the value of 39° found in thymidine. This angle is very sensitive to ring stacking and H-bonding. The orientation of the terminal O(5′) hydroxyl group is not a highly restricted variable in this structure, and the torsion angle about C(4′)—C(5′) seems to adjust to H-bonding opportunities.

A packing pattern for the anhydrous compound is shown in Fig. 2. The structure consists of layers in which each CH_3HgT molecule is anchored to four neighbors by strong hydrogen bonds (O...O = 2.74–2.77 Å) (Table 3). Each molecule provides two H-bond donors (O(3′A) and O(5′A) hydroxyl groups) and two acceptor sites (O(2A) and O(4A) carbonyl groups). These superimposed layers interact mainly by normal van der Waals contacts. The only particular contact involving Hg(3A) is established with an adjacent O(3′A) group at 3.09(1) Å, which is already strongly hydrogen-bonded with the O(2A) carbonyl oxygen.

In the anhydrous form, the O(1′) atom plays no particular role in hydrogen bonds or contacts with mercury. Its role is more important in the hydrated form. The structure can be described as irregular columns of molecules stacked along the *b* direction (Fig. 3). Molecules of type B alternate with molecules of type C along the column. They are grouped in pairs by means of two complementary Hg...O(1′) contacts of 2.89 Å. In both cases, the geometry is favorable: O(1′) lies near the equatorial plane of mercury, whereas the Hg—O(1′) direction defines roughly equal Hg—O(1′)—C(1′) and Hg—O(1′)—C(4′) angles. Between these pairs is found another pair of complementary Hg...O contacts, this time with O(4). They are longer (2.99 Å) than those with O(1′) and they compare well with those found for the columns of CH_3HgMT molecules in the crystal of the hemihydrate (7). B...C pairs belonging to adjacent columns are joined in the *a* direction (Fig. 3) by a pattern of four hydrogen bonds centered on the non-disordered water molecule W(1), acting as a donor to O(2C) and O(3′B), and as an acceptor from O(5′C). The pattern is completed with an extra O(3′B)—H...O(4B) interaction. Therefore, in the *ab* plane, cohesion is achieved through Hg...O contacts along *b*

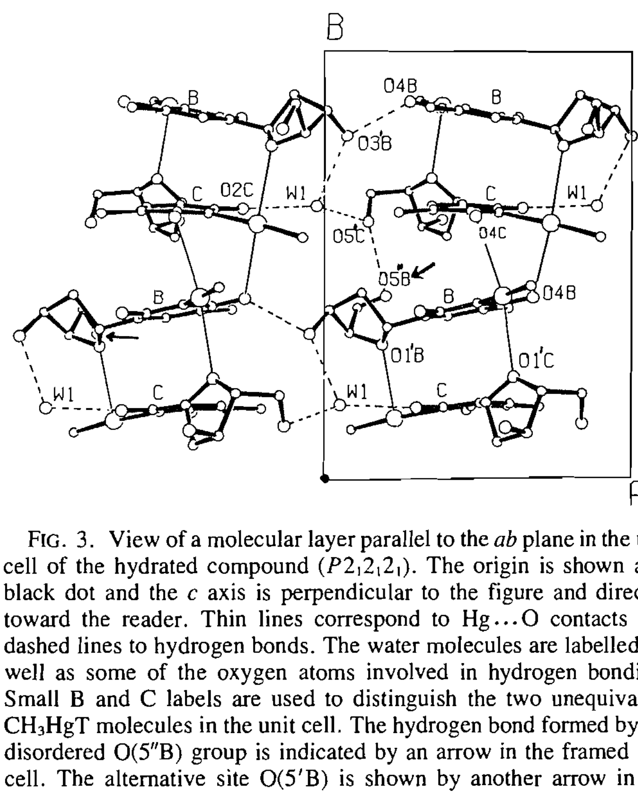

FIG. 3. View of a molecular layer parallel to the *ab* plane in the unit cell of the hydrated compound ($P2_12_12_1$). The origin is shown as a black dot and the *c* axis is perpendicular to the figure and directed toward the reader. Thin lines correspond to Hg...O contacts and dashed lines to hydrogen bonds. The water molecules are labelled, as well as some of the oxygen atoms involved in hydrogen bonding. Small B and C labels are used to distinguish the two unequivalent CH_3HgT molecules in the unit cell. The hydrogen bond formed by the disordered O(5″B) group is indicated by an arrow in the framed unit cell. The alternative site O(5′B) is shown by another arrow in the unframed unit cell.

and by hydrogen bonding along *a*. Part of the time, the O(5′) group of molecule B in its minor orientation O(5″B) contributes to cohesion within the columns by forming an O(5″B)—H...O(5′C) bond of 2.94(7) Å (indicated by an arrow in the framed unit cell, Fig. 3, right). It should be noted that in its major orientation O(5′B), this group assumes no particular role in the *ab* plane (see unframed cell, left of Fig. 3).

The columns along *b* and the intervening hydrogen-bond network define layers parallel to the *ab* plane, which are viewed down the *b* axis in Fig. 4. These layers are centered at

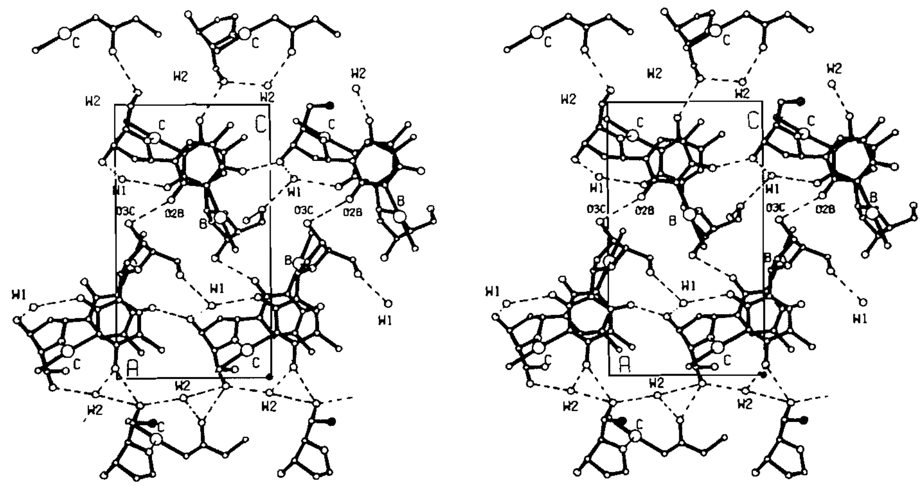

FIG. 4. Stereo view of the unit cell of the hydrated ($P2_12_12_1$) CH_3HgT compound down the b axis. The origin is indicated by a black dot. The b axis in perpendicular to the drawing and directed toward the reader. Hg...O contacts are shown as thin lines and hydrogen bonds as dashed lines. No disorder is present in the inter-layer region at $z \sim 1/2$. In the $z \sim 0$ (or ~ 1) region, occupancy for W(2) is only 0.37 and the O(5′) group of molecule B is disordered over the sites O(5′B) (occupancy 0.63, white spheres) and O(5″B) (occupancy 0.37, black spheres). All O...O contacts shorter than 3.1 Å are shown in the $z \sim 0$ region. The local hydrogen-bonding patterns proposed to explain the disorder are shown in the $z \sim 1$ region. An enlarged view of this region with atoms labelled is given in Fig. 5.

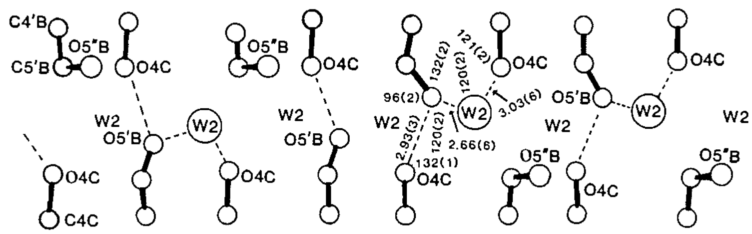

FIG. 5. Model proposed for the hydrogen-bonding pattern in the $z \sim 0$ (or ~ 1) inter-layer region of the unit cell of the hydrated compound. The circled W2 sites are those actually occupied.

$z \sim \frac{1}{4}$ and $\sim \frac{3}{4}$. They are symmetry equivalent, but the two inter-layer regions, at $z \sim 0$ (or ~ 1) and $\sim \frac{1}{2}$, respectively, are not. In the $z \sim \frac{1}{2}$ region, there is no disorder and besides normal van der Waals contacts, an O(3′C)—H...O(2B) hydrogen bond of 2.85(2) Å provides packing interactions.

The other inter-layer region is more complex. All the atomic positions for W(2), O(5′B), and O(5″B) are shown in the $z \sim 0$ layer in Fig. 4, together with the O...O contacts shorter than 3.1 Å. The occupancy values are 0.40, 0.65, and 0.35 (σ = 0.05), respectively, for these three atom types. Interpretation in terms of local hydrogen-bonding patterns is not unambiguous. We are retaining the following model, which is based on the fact that the occupancy factors for W(2) and O(5″B) are not significantly different. The average value (0.37) will be used for both in the following discussion. We are also assuming that the occupancy of these two sites is correlated, that is, the occupancy of a W(2) site (37% of the time) forces the O(5″B) orientation for an equal number of terminal O(5′) groups in B molecules. The assumed pattern is shown in the right portion of the $z \sim 1$ layer (Fig. 4), which is schematically represented in Fig. 5, with atom labels, distances and angles. A link in created between two O(4C) carbonyl groups by means of a W(2) water molecule and an O(5′B) hydroxyl group. The angles are all favorable and the W(2)—H...O(5′B) interaction of 2.66(6) Å is particularly strong. Another nearby O(5′B) position at 3.03(6) Å from the same W(2) molecule is not in a favorable orientation to hydrogen bond. This hydroxyl group is assumed to possess the O(5″B) orientation, thus forming a hydrogen bond with O(5′C) in the b direction as discussed earlier (Fig. 3), with an O...O separation of 2.94(7) Å and more favorable angles. When the O(5″B) site is occupied, the next W(2) molecule is deprived from its best hydrogen-bonding partner and, for this reason, this W(2) site would be vacant. This is the basic unit of the hydrogen-bond pattern.

In this unit, half of the W(2) sites are occupied. As the occupancy factor of W(2) is less than 0.50, there must be gaps between the units as they are repeated along c. If every fifth W(2) site is also vacant, as shown in Fig. 5, the vacant (V) and occupied (O) W(2) sites would be distributed along c as follows:

—(O—V—O—V)—V—(O—V—O—V)—V—

This would correspond to 0.40 occupancy for W(2), and also for O(5″B) since the presence of a W(2) molecule is assumed to force the O(5″B) orientation for the adjacent hydroxyl group. In fact, these occupancies are slightly lower (0.37), indicating that the gaps occur, on the average, slightly more often than 20% of the time. It should be noted that the present model does not imply a periodic pattern: strings of successive units without gaps may be longer than 2, and the gaps may consist of more than one missing W(2) molecule.

The above discussion takes care of only some of the O(5′B) sites, those which are part of the basic unit defined above (i.e. 0.37). The remaining O(5′B) sites are those facing the gaps, where consecutive W(2) sites are vacant. this is represented in Fig. 4 (layer $z \sim 1$, left) and in Fig. 5 (middle). In this case,

TABLE 5. Wavenumbers (cm^{-1}) of the infrared spectra

HT	CH_3HgT	HT	CH_3HgT	HT	CH_3HgT
1515 vw	1505 vw, sh	1172 w	1146 w	853 m	—
1477 s	1464 s	1121 s	1136 w	804 vw	—
1454 w	1451 s	1099 s	1097 s	—	799 w
1435 s	—	1067 vs	1061 w	794 vw	790 w
1401 m	1396 m	—	1053 w, sh	767 w	775 w
1391 m	1386 m	1025 m	1022 w	758 w	764 w
1363 w	1374 m	1010 m	990 m	734 w	712 vw
1352 w	1345 vw	1001 s	981 m	674 w	672 vw
1318 m	1305 s	971 m	947 w	627 m	628 w
1287 s, sh	1296 s, sh	959 m	934 w	578 vw	577 vw
1274 s	1288 s	905 m	—	562 vw, sh	563 vw
1254 m	—	897 m	896 vw	550 w	544 vw
1224 m	1238 m, br	883 w	885 w	—	505 w
—	1202 m	871 m	872 vw		
1197 w	1194 m				

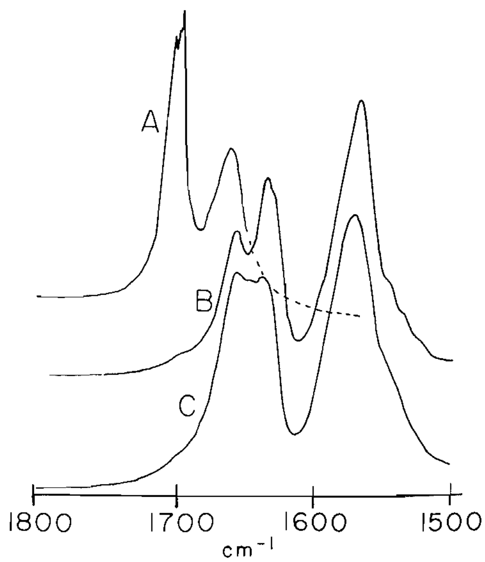

FIG. 6. Infrared spectra (1800–1500 cm^{-1}) of thymidine (A) and the methylmercury complexes (B = anhydrous $P2_1$ form; C = hydrated $P2_12_12_1$ form).

the hydroxyl group occupying an O(5′B) site is hydrogen-bonded to O(4C) as it is within the basic unit, but does not participate in other H-bonding interactions.

Infrared spectroscopy

The infrared spectra of thymidine and its CH_3Hg^+ complex are compared in Fig. 6 and Table 5. Copies of the spectra are provided in the supplementary material.[4]

The vibrations of the pyrimidine and sugar units have been discussed by several authors (18–21). However, owing to the absence of a detailed analysis for thymidine itself, the present discussion will be restricted to a few spectral features found to be useful as diagnostic for N(3) complexation in the methyl–thymine system (22).

The presence of the CH_3Hg^+ group is evident from the characteristic methyl C—H stretching band at 2925 cm^{-1}, which has become the dominant feature in the ν(C—H) region for the complexes. The medium band at 1202 cm^{-1} probably originates from the $\delta(CH_3)$ mode of the same group. The $\rho(CH_3)$ (~800 cm^{-1}) and Hg—C modes (~560 cm^{-1}) usually observed in infrared (22) are masked here by ligand bands.

The spectra show that the N(3)—H proton has been substituted. The broad absorption underlying the ν(C—H) region for thymidine (2600–3400 cm^{-1}) and containing a contribution (~3100 cm^{-1}) (22) from ν(N—H) motion, is removed from the spectra of the complexes. The remaining strong band in this region arises from the deoxyribose OH groups (and water molecules). The disappearanc of the γ(N—H) mode simplifies the spectrum at ~900 cm^{-1}, but the presence of deoxyribose bands in this region complicates the analysis. As to the δ(N—H) mode, it has been calculated to occur ca. 1453 cm^{-1} and thymidine indeed contains a band at this position, which disappears in the complexes. Another nearby band is shifted from 1477 to 1464 cm^{-1} by complexation. Similar displacements have been noted in Raman upon CH_3Hg^+ complexation of uridine (4) and TMP (2), and in infrared and Raman, for 1-methylthymine (22). This shift could be due to loss of coupling with N—H motion for a ring mode.

The 1500–1800 cm^{-1} spectral region (Fig. 6) is devoid of strong absorptions from the sugar moiety. Free thymidine shows a triplet at 1704 cm^{-1} mainly due to C(2)=O(2) stretching (18, 23). A broad band at 1650, together with a weak component at ~1630 cm^{-1} (masked here, but observed in D_2O solutions of TMP (2)) originate mainly from coupled motion of the C(5)=C(6) and C(4)=O(4) bonds. The changes introduced by complexation have been discussed in the case of 1-methylthymine (22). Three well-separated bands are observed at 1639, 1618, and 1579 cm^{-1}. The latter band is believed to arise mainly from the C(4)=O(4) bond, having lost some double bond character. A similar effect on C(2)=O(2) produces a negative shift of the absorption originally found at 1704 cm^{-1} in thymidine, so that the pair of bands at 1639/1618 cm^{-1} results from coupled C(5)=C(6) and C(2)=O(2) motions.

A few spectral changes are in good agreement with those observed in the Raman spectra of similar systems. For instance, a weak, but clearly observed, band of thymidine at 1254 cm^{-1} seems to shift to higher wavenumber and coalesce with the strong 1288 cm^{-1} band for the complexes. Similar shifts were observed in Raman for TMP (1239 to 1247 cm^{-1}) (2) and 1-methylthymine (1241 to 1262 cm^{-1}) (22). Another example is the disappearance of the band at 1172 cm^{-1}, possibly centered in the N(1)—C(1′) glycosidic bond (21), which is apparently displaced to 1145 cm^{-1}. Similarly, a band at 1172 cm^{-1} disappears from the Raman spectrum of TMP after complex formation, whereas significant intensity increase is noted at 1140 cm^{-1} (2).

The presence of water in the hydrated compound produces a $\delta(H_2O)$ peak at 1649 cm^{-1} (spectrum C, Fig. 6), superimposed on the double bond stretching bands. Besides, a doublet at 947/934 cm^{-1} for the anhydrous compound occurs as 933/928 cm^{-1} in the hydrated complex. This spectral region contains several bands originating from the deoxyribose unit (20, 21) and the observed shift reflects the difference in hydrogen bonding in the two compounds.

Conclusion

Both forms of the present CH_3Hg—thymidine compound show the characteristics already noted for the analogous 1-methylthymine compound (7), namely, binding to the deprotonated N(3) site and minimal interactions with the adjacent carbonyl groups. The oxygen donors in the deoxyribose moiety do not affect this general behavior, thus confirming the low affinity of CH_3Hg^+ for this component of DNA. The same solid phases were obtained in all our attempts to prepare "adducts" with $NaNO_3$, $NaClO_4$ and other salts, which had been found to form such "adducts" with the CH_3Hg–methylthymine complex (7, 8). This suggests that carbonyl groups forming H-bonds with deoxyribose hydroxyl groups provide good stabilization to the crystal and that their affinity for hard cations like Na^+ is not very strong.

Acknowledgments

We wish to thank M. J. Olivier who collected the X-ray data and J. C. Bolduc who recorded the infrared spectra. Financial support from the Natural Sciences and Engineering Research Council of Canada and the Ministère de l'Education du Québec is gratefully acknowledged.

1. A. J. CANTY and R. S. TOBIAS. Inorg. Chem. **18**, 413 (1979).
2. R. W. CHRISMAN, S. MANSY, H. J. PERESIE, A. RANADE, T. A. BERG, and R. S. TOBIAS. Bioinorg. Chem. **7**, 245 (1977).
3. S. MANSY and R. S. TOBIAS. Inorg. Chem. **14**, 287 (1975).
4. S. MANSY, T. E. WOOD, J. C. SPROWLES, and R. S. TOBIAS. J. Am. Chem. Soc. **96**, 1762 (1974).
5. R. B. SIMPSON. J. Am. Chem. Soc. **86**, 2059 (1964).
6. L. D. KOSTURKO, C. FOLZER, and R. F. STEWART. Biochemistry, **13**, 3949 (1974).
7. F. GUAY and A. L. BEAUCHAMP. Inorg. Chim. Acta, **66**, 57 (1982) and references therein.
8. F. GUAY and A. L. BEAUCHAMP. To be published.
9. F. BÉLANGER-GARIÉPY and A. L. BEAUCHAMP. J. Am. Chem. Soc. **102**, 3461 (1980).
10. D. T. CROMER and J. T. WABER. Acta Crystallogr. **18**, 104 (1965).
11. R. F. STEWART, E. R. DAVIDSON, and W. T. SIMPSON. J. Chem. Phys. **42**, 3175 (1965).
12. D. T. Cromer. Acta Crystallogr. **18**, 17 (1965).
13. M. AUTHIER-MARTIN and A. L. BEAUCHAMP. Can. J. Chem. **55**, 1213 (1977).
14. J. E. HUHEEY. Inorganic chemistry. Harper and Row, New York. 1975. pp. 184, 185.
15. R. BONACCORSI, A. PULLMAN, E. SCROCCO, and J. TOMASI. Theor. Chem. Acta, **24**, 51 (1972).
16. D. W. YOUNG, P. TOLLIN, and H. R. WILSON. Acta Crystallogr. B**25**, 1423 (1969).
17. M. SUNDARALINGAM. Biopolymers, **7**, 821 (1969).
18. H. SUSI and J. S. ARD. Spectrochim. Acta, **30**A, 1843 (1974).
19. M. TSUBOI, S. TAKAHASHI, and I. HARADA. Physico-chemical properties of nucleic acids. Vol. 2. *Edited by* J. Duchesne. Academic Press, London. 1973. pp. 91–145.
20. M. TSUBOI and Y. KYOGOKU. Synthetic procedures in nucleic acid chemistry. Vol. 2. *Edited by* W. W. Zorbach and R. S. Tipson. Wiley, New York. 1973. pp. 213–265.
21. E. W. SMALL and W. L. PETICOLAS. Biopolymers, **10**, 1377 (1971).
22. F. GUAY, A. L. BEAUCHAMP, C. GILBERT, and R. SAVOIE. Can. J. Spectrosc. **28**, 13 (1983).
23. R. C. LORD and G. J. THOMAS, JR. Spectrochim. Acta, **23**A, 2551 (1967).

Composite ZSM-5 zeolite/asbestos catalysts

RAYMOND LE VAN MAO,[1] PIERRE LÉVESQUE, BERNARD SJIARIEL, AND PETER HANS BIRD
Concordia University, Department of Chemistry, 1455 de Maisonneuve Blvd. West, Montreal, P.Q., Canada H3G 1M8

Received April 30, 1985

RAYMOND LE VAN MAO, PIERRE LÉVESQUE, BERNARD SJIARIEL, and PETER HANS BIRD. Can. J. Chem. **63**, 3464 (1985).

A procedure has been developed which allows growth of the zeolite ZSM-5 in chrysotile (asbestos) fibers which have previously had magnesium partially leached out. The resulting materials, when used as catalysts in the conversion of methanol into hydrocarbons showed very interesting product selectivities: i.e., (*a*) at high magnesium leaching degree (MLD), relatively larger amounts of aromatics and isoparaffins were produced; and (*b*) at low MLD, light olefins were the main products in the gaseous phase.

From NH_3 absorption/temperature programmed desorption studies, it was suggested that at lower MLD (higher magnesium content) the dual acidic and basic adsorption sites were responsible for the enhanced production of light olefins from methanol conversion.

RAYMOND LE VAN MAO, PIERRE LÉVESQUE, BERNARD SJIARIEL et PETER HANS BIRD. Can. J. Chem. **63**, 3464 (1985).

On a développé un procédé de cristallisation de la zéolite ZSM-5 dans les fibres d'amiante chrysotile dont une partie du magnésium a été lixiviée. Le matériel résultant, utilisé comme catalyseurs de conversion du méthanol en hydrocarbures, présente d'intéressantes sélectivités en produits; c'est-à-dire: (*a*) à un haut degré de lixiviation (MLD), les aromatiques et les isoparaffines se forment en quantités relativement larges; et (*b*) à un MLD inférieur, les oléfines légères sont les produits principaux dans la phase gazeuse.

Des études d'adsorption et de désorption à température programmée de l'ammoniac, il a été suggéré qu'à un MLD inférieur (ou à un contenu supérieur en magnésium), les sites acides et basiques en "duo" étaient responsables de cette augmentation de production des oléfines légères à partir du méthanol.

Introduction

The zeolite ZSM-5 has received great attention in recent years because of its high shape selectivity in many industrially important reactions. These include xylene isomerization, toluene disproportionation, aromatic alkylation, and methanol conversion to gasoline (1). The shape selectivity is attributed to its tridimensional channel network, and a pore size intermediate between the small pore (A type) and large pore (X and Y type) zeolites.

Doping or coating the pure ZSM-5 zeolite with inorganic materials can lead to an enhanced product selectivity (2, 3). The same phenomenon was observed by aggregation of the ZSM-5 microcrystals (4). Effects at the pore openings were suggested (4).

In the present paper, the preparation of a composite ZSM-5 zeolite/asbestos catalyst is described. It consists of partially leaching the magnesium out of the chyrsotile asbestos fibers and then growing the ZSM-5 zeolite into the leach asbestos macrostructure (5).

The composite catalysts were characterized by usual physico-chemical techniques and were tested in the catalytic conversion of methanol. The data for some "ZSM-5/asbestos" catalysts were compared to data obtained by using pure ZSM-5 catalysts with similar characteristics.

Experimental

Preparation of the catalysts (5)

Chrysotile fibers were first subjected to the Mg leaching operation. Mineral and organic acids were used as leaching agents. In general, the asbestos fibers (7 TF-12 short fiber grade[2]) were digested with a mineral acid solution (usually HCl) at 80°C for several hours. After dilution with cool water, the suspension was allowed to settle for a while, then filtered, washed with water and finally dried at 120°C. The experimental parameters for the preparation of the leached asbestos (Alix) are reported in Table 1.

The resulting solid materials (Alix) were mixed with aqueous solutions containing tetrapropylammonium bromide (TPA, Br), NaOH, and sodium aluminate in proportions shown in Table 2. The suspensions were loaded in an autoclave and heated at 170°C (±5°C) for 10 days. After unloading, the suspensions were filtered and the solids were washed thoroughly with distilled water, dried, and finally calcined at 550°C for 10 h. Thereafter, the solids were submitted to NH_4^+ ion-exchange using NH_4Cl aqueous solution (1 *M*). The NH_4^+ forms when activated at 550°C for at least 10 h, yielded the acid forms (or H-forms) of the catalysts.

The acid forms of the catalysts were intimately mixed with bentonite (20% by weight) and made into pastes with water. The pastes were pressed into 1 mm od extrudates.

Physico-chemical characterization

Elemental analysis, X-ray diffraction powder pattern determination, scanning electron microscopy (SEM), the adsorption of water and *n*-hexane, and the adsorption/temperature programmed desorption of ammonia, were techniques used to characterize our samples.

(a) Elemental analysis

Common techniques via atomic absorption were used for Si, Al, Na, Mg, and Fe concentration measurements.

Two derived quantities were particularly significant.

The first, the magnesium leaching degree (MLD), is defined as:

$$(\mathrm{MLD}) = \frac{(\mathrm{MgO})_i - (\mathrm{MgO})_f}{(\mathrm{MgO})_i} \times 100\ (\%)$$

where $(MgO)_i$ and $(MgO)_f$ are, respectively, the initial and final magnesium contents (on the dried oxide basis).

The second is the (Mat/Al) atom ratio:

$$(\mathrm{Mat/Al}) = \frac{(\mathrm{Si}) + (\mathrm{Al}) + (\mathrm{Na}) + (\mathrm{Mg}) + (\mathrm{Fe})}{(\mathrm{Al})}$$

where (Si), (Al), (Na), (Mg), (Fe) are the numbers of atoms of each element in a dehydrated sample.

In the case of our composite catalysts, this ratio can be seen as proportional to the reciprocal of the aluminum atom concentration, and thus acid site concentration.

[1]To whom all correspondence should be addressed.

[2]Chemical composition (dried oxide basis): SiO_2 = 42.8% wt/wt, MgO = 50.2%, Fe_2O_3 = 6.6% (as FeO and Fe_3O_4 forms); Al_2O_3 = 0.1% and Na_2O = 0.1%.

TABLE 1. Preparation of leached asbestos (Alix)

Alix	Amount of 7TF-12 asbestos (g)	HCl solution N	HCl solution mL	Heating time (80°C)	Product (Dehyd) (g)	SiO_2 (%)	Al_2O_3 (%)	Na_2O (%)	MgO (%)	Fe_2O_3 (%)	MLD (%)
001/2	100	3.0	1000	7.0 h	40	98.2	0.36	0.14	1.06	0.28	98
013	100	2.4	1000	4.5 h	44	89.0	0.51	0.14	4.14	6.22	92
025	200	3.0	2000	5.0 h	87	90.6	0.32	0.14	2.95	2.57	94
020/2	100	2.4	1000	4.0 h	42	91.8	0.38	0.14	3.38	4.35	93
024	120	2.4	1200	3.5 h	53	88.0	0.35	0.13	5.88	5.65	88
018/1	100	2.4	1000	3.5 h	45	85.2	0.36	0.16	6.60	7.65	87
018/2	100	2.4	1000	3.5 h	43	86.1	0.32	0.14	6.23	7.15	88
027	150	2.4	1500	2.5 h	71	82.6	0.43	0.19	9.39	7.68	81
030	150	2.4	1500	2.5 h	69	83.7	0.22	0.16	8.99	6.98	82
017	100	2.4	1000	2.5 h	41	81.8	0.45	0.12	10.10	7.59	80
016	100	2.4	1000	1.25 h	47	82.0	0.18	0.13	10.53	7.20	80

TABLE 2. Synthesis of ZSM-zeolite from silica gel and Alix*

Catalyst precursor	Alix	W (g)	Silica gel (g)	Na aluminate (g)	TPA bromide (g)	NaOH (g)	Added water (mL)	Synthesis T (°C)	Synthesis Time (days)	Product(3) (g)
P-38	(ZSM5)	—	44(1)	1.5	40	2.5	160	170	10	22.4
P-68	(ZSM5)	—	25(2)	1.8	40	2.5	160	170	10	24.4
A-39	001/2	24.0	—	1.5	40	2.5	180	170	10	20.0
A-45	013	24.1	—	1.5	40	2.5	180	170	10	19.4
A-62	025	35.0	—	2.0	40	2.5	180	170	10	30.3
A-56	020/2	25.0	—	1.5	40	2.5	180	170	10	21.3
A-58	024	45.0	—	2.7	40	2.5	180	170	10	46.5
A-49	018/1	25.0	—	1.5	40	2.5	180	170	10	21.1
A-54	018/2	30.0	—	1.8	40	2.5	180	170	10	25.3
A-64	027	35.0	—	2.0	40	2.5	180	170	10	30.7
A-69	030	66.0	—	4.2	80	5.0	360	170	10	56.7
A-48	017	25.0	—	1.5	40	2.5	180	170	10	20.4
A-60	016	35.0	—	2.0	40	2.5	180	170	10	31.8

*Silica gel Baker: (1) = 60% in SiO_2; (2) = 90% in SiO_2; (3) the product was dried 12 h at 120°C and then further 12 h at 550°C.

TABLE 3. *n*-Hexane and water adsorption = operating conditions

Adsorbate	Critical diameter (Å)	Vaporization temperature (°C)	Vapor pressure (Torr)	Adsorption temperature (°C)	Time required
n-Hexane	4.9	0	45	25	3 h
Water	2.8	22	22	25	Overnight

$$(\mathrm{Mat/Al}) = \frac{\text{constant}}{(\mathrm{Al})} \simeq \frac{\text{constant}}{(\mathrm{H^+})}$$

The (Mat/Al) atom ratio is equivalent to the (Si/Al) ratio commonly used for pure zeolites.

(b) X-ray powder diffraction

The ZSM-5 zeolite was identified by means of its characteristic of diffraction pattern (6). The degree of crystallinity (DC) in ZSM-5 zeolite structure of the samples was determined by a procedure similar to that of Kulkarni *et al.* (7). However, to ensure that the measurement did not depend on sample preparation, we used $BaCl_2$ as internal standard: this compound exhibits a strong diffraction peak at 2θ = 31.0–32.5°. The pure ZSM-5 zeolite sample (HP-38) was assigned a 100% value of crystallinity.

(c) Scanning Electron Microscopy (SEM)

Using the Hitachi Model S-20 SEM, it was possible to follow the morphological change of our samples: original asbestos fibers → leached fibers (Alix) → ZSM-5/asbestos catalyst. The SEM observations were necessary for ascertaining that our samples were not simply mechanical mixtures of "ZSM-5" and "unconverted asbestos".

(d) Adsorption of water and n*-hexane*

The adsorbates used were water and *n*-hexane. The technique adopted has been described elsewhere (8, 9). The operating conditions are reported in Table 3. Adsorption measurements were done on both the catalyst H-forms, and the magnesium leached asbestos (Alix) which had been used for the catalyst preparation. The relative adsorption affinity index (RAI) was defined as the volume ratio of adsorbed *n*-hexane to adsorbed water in zeolites. This index was used to evaluate the hydrophobic character of the ZSM-5 based materials (8–10).

(e) Adsorption/temperature programmed desorption of ammonia (A/TPD)

In order to study the acid strength and density of our samples, ammonia was adsorbed on the catalyst (final form) at 373 K and at room temperature, and then desorbed in a temperature programmed way (up to 723 K, heating rate = 5 K/min). The procedure used was similar to that described in reference (11). To minimize the phenomenon of physi-sorption, most likely with the adsorption performed at room temperature, vigorous flushing with nitrogen was carried out prior to the desorption phase. During the NH_3 desorption operation, the nitrogen stream which carried the desorbed ammonia was bubbled into a solution of diluted HCl. After the desorption step, this HCl solution was titrated with NaOH and the amount of NH_3 desorbed was calculated knowing the NaOH titer, and original HCl concentration. The amount of ammonia adsorbed at 100°C and then desorbed was believed to be related to acid sites of medium and strong character (11), while that adsorbed at room temperature should be related to the overall acidity which should include indeed weak sites.

Catalytic experiments

Catalytic tests were performed by injecting methanol using an injection syringe on an infusion pump into a methanol vaporizer gas mixer. Nitrogen gas was supplied to the methanol vaporizer and gas mixer from a cylinder connected in-line with a flowmeter. The vaporized methanol was then carried by the nitrogen gas through a catalyst bed set in a catalytic reactor contained inside an oven which was thermoregulated. A chromel–alumel thermocouple was placed in the catalyst bed and was used, in conjunction with a digital thermometer unit, to monitor the temperature of the catalyst bed. The gaseous mixture flowing out of the catalytic reactor was run through a series of condensors maintained at 5–10°C, to a liquid collector immersed in an ice bath followed by a cylinder from which gas sampling was carried out.

Following a pre-run of 10 min, the liquid products were collected and the gaseous ones were analyzed periodically by gas chromatography using a 3.5 m long column packed with Chromosorb P coated with 20% by weight of Squalane. The GC used was a dual FID Hewlett-Packard Model 5790. It was equipped also with a capillary column (length: 50 m; PONA type fused silica coated with a cross-linked polymer) which was used for accurate analyses of the liquid fractions after a run was completed. The composition of the aqueous layer was also determined by gc using a methanol in water calibration standard.

Table 4 reports the reaction conditions used in the experiments.

TABLE 4. Reaction conditions

Parameter	Value
Catalyst weight (dehydrated)	4 g
Temperature (°C)	350–500
Total pressure	1 atm
Methanol pressure	0.9 atm
Inert gas (stripping gas)	Nitrogen
W.H.S.V.*	2.4 h
Reaction duration	4 h

* Weight hourly space velocity.

$$\text{W.H.S.V.} = \frac{\text{g of injected methanol per hour}}{\text{g of catalyst}}\ (h^{-1})$$

Results and discussion

Table 5 reports the main physico-chemical characteristics of the sample studied. In this table, the label HA represents catalysts prepared from the 7T12 asbestos fibers and HP stands for catalysts made from pure ZSM-5 zeolite. The characteristics shown are: the magnesium leaching degree (MLD) in % wt/wt, the (Mat/Al) atom ratio, the iron content FC (% by weight), the degree of crystallinity, DC, in %. Table 6 reports the sorptive capacities, in % wt/wt, and in particular the RAI values, of our samples and of their Alix precursors. Table 7 reports the acidity measurements (as obtained through ammonia adsorption and desorption) of our samples and their alix precursors. Figures 1, 2, and 3 are the electron micrographs of samples (acid form) HA-39, HA-49, and HA-48, respectively (with magnifications as indicated).

Tables 8 and 9 report the catalytic conversion and product selectivities of all our catalysts at 400°C, and of the HP-38 and HA-60 samples at various temperatures, respectively. The methanol conversion is the C atom based yield in hydrocarbons. The balance (in C atoms) includes volatile gases (CO_2, H_2, etc.), dimethyl ether and methanol found in the liquid phase and C deposited onto the catalyst.

It can be expressed as follows:

$$\text{Conversion} = \frac{(NC)_{Prod}}{(NC)_{feed}} \times 100$$

where $(NC)_{feed}$ is the number of C atoms in the (methanol) feed and $(NC)_{Prod}$ is the number of C atoms in the (hydrocarbon) products.

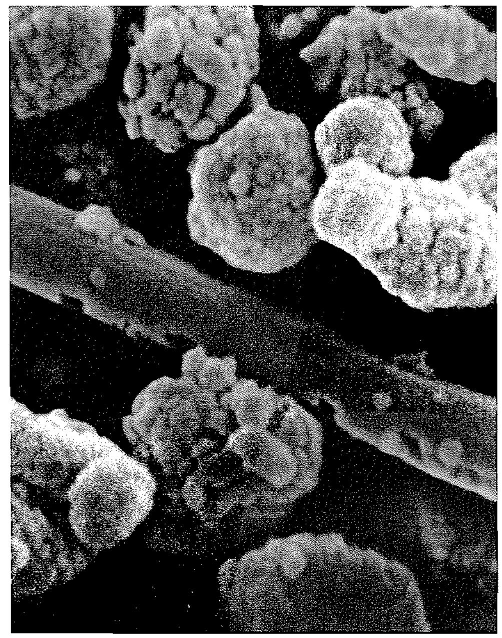

FIG. 1. SEM of the HA-39 sample (MLD = 97%). Magnification ×20 000.

The product selectivity is expressed as follows:

$$\text{PS (\%)} = \frac{\Sigma_i C_i}{\Sigma C} \times 100$$

where ΣC and $\Sigma_i C_i$ are the sums of all hydrocarbons produced and of the selected products, respectively.

If we compare the degree of crystallinity in the ZSM-5 zeolite structure, and the (Mat/Al) ratio of our samples, they are very close to each other. Scanning electron microscopy studies showed that while the leached asbestos (Alix) kept the fibrous form of the original chrysotile asbestos even at a high magnesium leaching degree (Alix 001/2, MLD = 98%), the composite ZSM-5/asbestos samples had a clearly degraded structure. Submicron ZSM-5 zeolite particles were embedded in the asbestos remnants, which resembled blocks, a few microns in size (see Figs. 1, 2, and 3). Moreover, these submicron zeolite particles decreased in size as the magnesium leaching degree decreased (approximate size of ZSM-5 particles in the HA-60 sample (80% MLD) = 0.02 micron). The RAI values decreased at lower MLD (see Table 6). This suggested that the

TABLE 5. Physical and chemical properties of ZSM-5 and composite catalysts

Catalyst*	SiO_2 (%)	Al_2O_3 (%)	Na_2O (%)	MgO (%)	Fe_2O_3 (%)	MLD (%)	Mat/Al	DC† (%)
HP-38 } pure	98.14	3.03	0.09	—	—	—	28.1	100
HP-68 } ZSM5	97.17	2.57	0.17	—	—	—	32.7	100
HA-39	95.11	2.94	0.08	1.33	0.54	97.4	28.7	86
HA-45	90.92	2.40	0.12	3.12	3.44	93.8	34.9	91
HA-62	91.26	3.23	0.27	3.10	2.13	93.8	26.0	100
HA-56	90.06	3.82	0.12	3.65	2.33	92.7	22.0	86
HA-58	86.03	2.91	0.17	5.99	4.90	88.1	28.8	88
HA-49	84.32	3.49	0.14	6.29	5.80	87.5	23.9	90
HA-54	83.53	3.02	0.17	6.85	6.43	86.4	27.6	86
HA-64	85.66	2.28	0.16	7.50	4.43	85.1	36.8	96
HA-69	81.70	3.41	0.15	7.90	6.84	84.2	24.5	99
HA-48	82.98	3.55	0.14	7.95	5.38	84.2	23.8	84
HA-60	81.15	2.23	0.35	9.87	6.20	80.4	38.1	83

* Acid form, dried oxide basis.
† Crystallinity.

TABLE 6. Water and *n*-hexane sorptive capacities of the HP and HA samples

Catalyst	MLD (%)	*n*-Hexane (% wt/wt)	H_2O (% wt/wt)	RAI*
HP-68	—	5.35	8.04	1.01
HA-39	97	8.86	7.03	1.91
HA-45	94	9.24	7.34	1.91
HA-56	93	7.88	7.91	1.51
HA-58	88	8.30	9.24	1.36
HA-54	86	7.78	10.37	1.14
HA-60	80	5.95	6.10	1.47
Alix 001/2	98	7.20	6.58	1.66
Alix 020/2	93	10.28	9.78	1.59
Alix 013	92	5.88	5.48	1.63
Alix 024	88	7.51	7.47	1.52
Alix 018/2	88	7.63	8.26	1.40
Alix 016	80	7.63	8.12	1.42

*RAI = *n*-hexane/H_2O (vol/vol) of relative adsorption affinity index.

TABLE 7. NH_3 adsorption/temperature programmed desorption studies

		Z_a = amount of NH_3 adsorbed*			
Catalyst	MLD (%)	Room $t°$ ($\times 10^4$)	Z_a/Z_{Al}†	At 100°C ($\times 10^4$)‡ (3)	Z_a/Z_{Al}†
HP-68	—	1.36	0.27	1.51	0.30
HA-39	97	0.99	0.17	1.05	0.18
HA-45	94	2.57	0.55	1.27	0.27
HA-56	93	2.79	0.37	1.55	0.21
HA-58	88	3.14	0.55	1.79	0.31
HA-54	86	4.06	0.69	1.82	0.31
HA-48	84	5.61	0.81	2.07	0.30
HA-60	80	5.76	1.32	2.30	0.53
Alix 001/2	98	2.22		0.34	
Alix 020/2	93	1.40		1.17	
Alix 013	92	1.36		0.00	
Alix 024	88	1.02		0.51	
Alix 018/2	88	3.20		0.00	
Alix 017	80	0.79		0.60	
Alix 016	80	1.03		0.50	

* Expressed in 10^{-4} mol of NH_3/g of catalyst.
† Z_a/Z_{Al} is the ratio of the molar amount of NH_3 adsorbed to the molar amount of Al present in 1 g of catalyst.
‡ With HP and HA samples = circa 95% NH_3 desorbed at 423–473 K and circa 5%, at 673–723 K.

hydrophobicity of the composite catalyst was closely dependent upon the magnesium content, e.g. a higher magnesium content, a lower hydrophobicity. A similar behavior observed with the Alix samples strongly supports this statement (Table 6). With the composite samples, the NH_3 adsorption was higher at lower magnesium leaching degree both for room temperature and 100°C operations while the Alix samples exhibited low adsorption of NH_3 (see Table 7). This behavior of the composite catalysts could not be accounted for on the basis of an enhanced acidity due to the formation of a larger amount of mixed oxides (SiO_2–MgO) at low MLD, although acidity was said to exist in mixed oxides (e.g. SiO_2–MgO) (12). Increased NH_3 adsorption at low MLD was better related to the presence of basic sites (from MgO) along with the acid sites. (The Bronsted sites were probably located on the external surface of the zeolite particles. The amount of such acid sites increased with the external surface area and corresponding particle size decrease, e.g. at low MLD as observed through the SEM.) In fact, NH_3 was expected to be dissociated into $\bar{N}H_2$ and H^+ when adsorbed onto both basic and acidic sites (12) (see also Fig. 4). Upon heating, these species would recombine and be desorbed as gaseous NH_3. Such an increased NH_3 adsorption was not observed with the Alix samples because they had only basic sites. No acid sites existed which could adsorb the $\bar{N}H_2$ species from the dissociated ammonia.

Table 8 shows that when the MLD was higher than 90%, the composite catalysts exhibited catalytic properties quite similar to those of a pure ZSM-5 based catalyst. However, when the MLD was less than 90%, more light olefins were produced at the expense of the paraffins (primarily) and the aromatics. A possible explanation could be the effect of the smaller zeolite particles at higher MLD, in provoking the lack of selectivity (to hydrocarbons higher than light olefins) in the reaction. However, it seems unlikely that a small change in crystallite size could

TABLE 8. Catalytic data of the HP and HA catalysis at 400°C

Catalyst	MLD (%)	Methanol conversion into hydrocarbons (%)	Product selectivities (%) C_1–C_4 paraffins	C_2–C_4 olefins (OLE)	Aromatics (AR)	Nonaromatic (C_5^+)	AR + OLE (%)	OLE + liquids (%)	OLE/ (Liq + Par)
HP-38	H-ZSM5	99	35	15	26	24	41	65	0.18
HP-68	H-ZSM5	99	31	22	26	21	48	69	0.28
HA-39	97	99	37	13	29	21	42	63	0.15
HA-45	94	99	37	15	27	21	42	63	0.18
HA-62	94	99	28	24	25	23	49	72	0.32
HA-56	93	99	34	17	28	21	45	66	0.21
HA-58	88	99	26	26	24	24	50	74	0.35
HA-49	87	99	20	33	20	27	53	80	0.49
HA-54	86	99	17	37	19	27	56	83	0.59
HA-64	85	99	16	39	18	27	57	84	0.64
HA-69	84	99	17	38	18	27	56	83	0.61
HA-48	84	98	16	39	16	29	55	84	0.64
HA-60	80	98	12	44	15	29	59	88	0.79

TABLE 9. Catalytic data of the HP-38 and HA-60 (MLD = 80%) at various reaction temperatures

Catalyst	T (°C)	CH_3OH conversion into hydrocarbon (%)	Product selectivity (%) C_1–C_4 paraffins (Par)	C_2–C_4 olefins (Ole)	Aromatics (AR)	Nonaromatics (C_5^+)	Ole + Liq (Liq = Ar + C_5^+)	Ole + Ar	Ole/ (Liq + Par)
HP-38 (H-ZSM5)	375	98	31	17	26	26	69	43	0.21
HA-60 (80% MLD)	375	80	9	41	14	36	91	55	0.70
HP-38	400	99	35	15	26	24	65	41	0.18
HA-60	400	98	12	44	15	29	88	59	0.79
HP-38	450	96	24	38	19	19	76	57	0.61
HA-60	450	98	5	63	13	19	95	76	1.70
HA-60	500	99	4	73	11	12	96	84	2.70

FIG. 2. SEM of the HA-49 sample (MLD = 90%). Magnification ×20 000.

FIG. 3. SEM of the HA-48 (MLD = 84%). Magnification ×10 000.

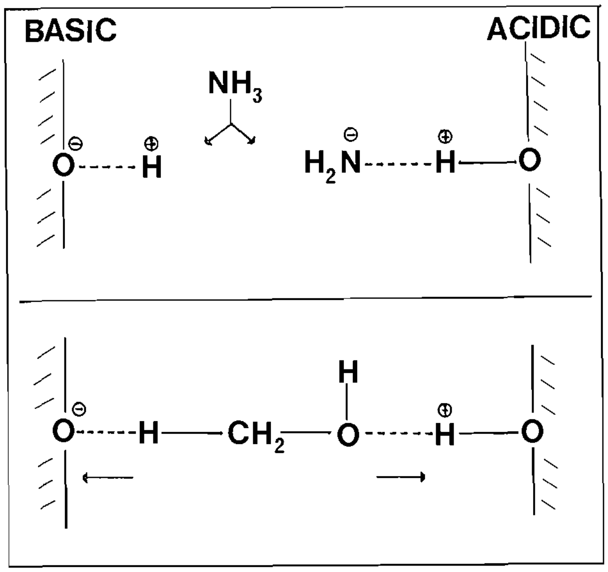

FIG. 4. Effects of simultaneous presence of acidic (zeolite) and basic sites (MgO) on NH_3 adsorption and on methanol conversion into olefins.

bring about such a large variation in the product spectrum (see Table 8).

Thus a possible explanation should be found in the two most probable effects of MgO on the Bronsted acid sites which were mainly located on the external surface of the tiny zeolite particles embedded in the asbestos remnants.

The first effect of the MgO could be a "partial neutralization" of the acid sites with a subsequent decrease in the medium and strong acidity (see Table 7, column "temperature 100°C", cases of samples HA-39 and HA-45 with 97% and 94% as MLD, respectively; e.g. low Mg contents). Such a MgO effect was fairly well supported by the fact that, though the acid sites were located at the external surface of the zeolite particles (e.g. there was no beneficial effect in terms of coking prevention, from the shape-selective framework of the ZSM-5 zeolite), the carbon deposit onto the composite catalysts was very low (less than 1% wt/wt for 4-hour runs at 400°C) while the pure ZSM-5 based catalyst like the HP-68 received about 2% wt/wt of coking under the same reaction conditions. This seemed to be in fair agreement with the work of Chang *et al.* (13) which showed an increased production of light olefins with a decreasing Bronsted acidity (high SiO_2/Al_2O_3).

However, according to our ammonia adsorption data (Table 7), composite catalysts which were very selective in olefin formation (MLD lower than 90%) exhibited also a high NH_3 adsorption both at room temperature and at 100°C. Such a phenomenon could be explained by a dissociative adsorption of NH_3 on dual acid-basic sites (see Fig. 4). The regular distribution of the MgO sites facing the SiO_2 sites in the original asbestos fibers could be assumed to remain non significantly changed when Bronsted acid sites (H^+--^-Al) were introduced into the zeolite particles following the crystallization of the SiO_2 component of the asbestos. Therefore, a plausible explanation, different from the "acid–base neutralization" and which could be applied to our data has been given by Swabb and Gates (14) who studied the dehydration of methanol over H-mordenite at 155–240°C, and detected traces of olefin at 240°C. Olefin formation was explained by an α-elimination mechanism (see also the mechanistic review by Chang (15)) and the methanol bond scission was said to be facilitated by cooperative action of acidic and basic sites in the zeolite lattice (14) (see Fig. 4). This mechanistic view could bring our catalytic data over methanol, very close to ammonia sorption results: basically, methanol does not greatly differ in terms of adsorption from ammonia.

Conclusion

With pure ZSM-5 based catalysts, for the conversion of methanol, olefins were regarded as the initial products followed by their conversion into paraffins and aromatics (16) and their production was mainly related to the existence of acid sites having a certain acid strength (17). However, the high olefins yield observed with our composite ZSM-5 (asbestos catalysts having a magnesium leaching degree less than 90% (see Tables 8 and 9)) could be better explained by the simultaneous presence (in addition to the acid sites inside the zeolite pores) of acid sites on the external surface of the small zeolite particles and of basic sites due to the MgO of the asbestos remnants. This interaction led to the formation in larger yields of olefins which did not undergo further transformation. This hypothesis of the dual presence of acidic and basic sites was strongly supported by greater adsorption of ammonia on these composite catalysts which had higher MgO contents. Such an enhanced NH_3 sorptive behavior was not observed either on leached asbestos precursors (Alix) (only basic sites due to the MgO) nor on pure ZSM-5 (large sized crystals with no basic sites). The regular increase in olefins formation and in ammonia adsorption which was parallel to the regular decrease in zeolite particle size (i.e., a parallel increase in zeolite external surface in contact with the asbestos remnants) suggested a strong interaction of the "microstructural" support (asbestos remnants) and the sub-micron size zeolite particles. Therefore, these phenomena were quite different from the effects observed with the ZSM-5 zeolites on which Mg (18) or P (18, 19) was deposited. These Mg or P bearing zeolites were very selective to the *para*-isomer in the alkylation reaction of alkylaromatics probably due to a change in diffusion resistance (18, 19).

Moreover, the microstructural support (asbestos remnants) could "bear" transition metal ions leading to a composite catalyst which was found to be very selective to the simultaneous production of olefins and aromatics (20).

Acknowledgements

Financial supports from l'Institut de l'Amiante, NSERC of Canada, and FCAC are gratefully acknowledged.

We thank Dr. N. N. Kapoor for preparing the scanning electron micrographs, Dr. R. H. Zienius for helpful discussion, and Ms. Nguyen Dothi for technical assistance.

1. P. B. WEISZ. Pure Appl. Chem. **52**, 2091 (1980).
2. N. Y. CHEN, W. W. KEADING, and F. G. DWYER. J. Am. Chem. Soc. **101**, 6783 (1979).
3. J. C. VEDRINE, A. AUROUX, P. DEJAIFVE, V. DUCARME, H. HOSER, and S. ZHOU. J. Catal. **73**, 147 (1982).
4. R. L. V. MAO, V. RAGAINI, G. LEOFANTI, and R. FOIS. J. Catal. **81**, 418 (1983).
5. R. L. V. MAO and P. H. BIRD. US Patent 4, 511,667. April 16, 1985.
6. R. J. ARGAUER and G. R. LANDOLT. U.S. Pat. 3702886. 1972.
7. S. B. KULKARNI, V. P. SHIRALKAR, A. N. KOTASTHANE, R. B. BORADE, and P. RATNASAMY. Zeolites. Vol. 2. 1982. p. 313.
8. R. L. V. MAO. React. Kinet, Catal. Lett. **12**, 69 (1979).
9. R. L. V. MAO, O. PILATI, A. MARZI, G. LEOFANTI, A. VILLA,

and V. RAGAINI. React. Kinet. Catal. Lett. **15**, 293 (1980).
10. E. C. DEROUANE. Catalysis on the energy scene. *Edited by* S. Kaliaguine and A. Mahay. Elsevier Publisher. 1984. p. 1.
11. C. V. HIDALGO, H. ITOH, T. HATTORI, M. NIWA, and Y. MURAKAMI. J. Catal. **85**, 362 (1984).
12. K. TANABE. Catalysis science and technology. Vol. 2. *Edited by* J. R. Anderson, and J. Boudart. Springer-Verlag. 1981. p. 231 and references therein.
13. C. D. CHANG, C. W. CHU, and R. F. SOCHA. J. Catal. **86**, 289 (1984).
14. F. A. SWABB and B. C. GATES. Ind. Eng. Chem. Fundam. **11**, 540 (1972).
15. C. D. CHANG. Hydrocarbons from methanol. Marcel Dekker Inc. 1983. p. 50 and references therein.
16. P. DEJAIFVE, J. C. VEDRINE, V. BOLIS, and E. G. DEROUANE. J. Catal. **63**, 331 (1980).
17. T. INUI, H. MATSUDA, and Y. TAKEGAMI. Proceedings of the VI International Conference. *Edited by* D. Olson and A. Bisio. Reno, U.S.A. p. 316.
18. N. Y. CHEN, W. W. KAEDING, and F. G. DWYER. J. Am. Chem. Soc. **101**, 6783 (1979).
19. W. W. KAEDING, C. CHU, L. B. YOUNG, and S. A. BUTTER. J. Catal. **69**, 392 (1981).
20. R. L. V. MAO. Can. and U.S. Pat. Appl. Jan. 3, 1985.

Pd/SiO_2–$AlPO_4$ systems. Influence of the preparation variables on their catalytic activity[1]

A. ALBA, M. A. ARAMENDIA, V. BORAU, C. JIMENEZ, AND J. M. MARINAS
Department of Organic Chemistry, Faculty of Sciences, Córdoba University, 14005-Córdoba, Spain

Received June 25, 1984[2]

A. ALBA, M. A. ARAMENDIA, V. BORAU, C. JIMENEZ, and J. M. MARINAS. Can. J. Chem. **63**, 3471 (1985).

A study on the liquid phase hydrogenation of cyclohexene over a series of Pd catalysts supported on various SiO_2–$AlPO_4$ systems (using a concentration of 2.47 *M*, with methanol as solvent, the initial hydrogen pressure is 5 bar and reaction temperature 300 K) is reported in this paper. The reaction has been studied as a standard in order to determine the most suitable preparation conditions for these catalysts.

We have also studied the influence of other factors such as the kind of support, the nature of the metal precursor, the previous calcination of the precursor, the addition of alkaline hydroxides, and the catalyst reduction with various agents, on the catalytic activity of different Pd-supported systems.

A. ALBA, M. A. ARAMENDIA, V. BORAU, C. JIMENEZ et J. M. MARINAS. Can. J. Chem. **63**, 3471 (1985).

On a étudié l'hydrogénation en phase liquide du cyclohexène sur un série de catalyseurs de Pd supportés par divers systèmes de SiO_2–$AlPO_4$ (utilisant une concentration de 2,47 *M*, le méthanol comme solvant, une pression initiale d'hydrogène de 5 bar et une température de réaction de 300 K). Cette étude a été réalisée comme modèle pour déterminer les conditions les plus appropriées pour la préparation de ces catalyseurs.

Nous avons aussi étudié l'influence de faceurs tels que la nature du support, la nature du précurseur du métal, les calcinations antérieures du précurseur, l'addition d'hydroxydes alcalins et la nature des agents de réduction du catalyseur sur l'activité catalytique de divers systèmes catalytiques portant du Pd.

[Traduit par le journal]

Introduction

The catalytic activity of a supported metal depends on a series of variables such as the texture, acid–base and redox properties of the supports used, as well as on the metal dispersion, metal–support interaction, etc. On the other hand, most of these characteristics depend, in turn, on the conditions used in the preparation of the metal-supported catalyst.

In this context, several authors have studied the effect of the preparation procedure on the surface properties of various metal-supported catalysts. Thus, Hyde and Rudhan (1) have recently reported on rhodium supported on γ-alumina, and Hanika *et al.* (2) have studied the relationship between the preparation conditions and the activity of supported platinum catalysts.

In earlier papers we have shown the usefulness of aluminium orthophosphate ($AlPO_4$), $AlPO_4$–Al_2O_3, and SiO_2–$AlPO_4$ systems as supports for dispersed metals such as Ni (3, 4), Pd (5, 6), Pt (7, 8), and Rh (9, 10). Since these supports have acidic and basic sites likely to take part in the catalytic process, the metal systems are bifunctional catalysts which can act simultaneously as acid–base or metal catalysts able to catalyze both C—C bond cleavage (11) and hydrogenation (or dehydrogenation) of hydrocarbons.

On the other hand, it has been pointed out that the catalyst activity might be determined by the interaction between metal particle and support, which is known as the "support effect" (12).

As for nickel supported on phosphate-containing materials such as aluminium phosphate (13), mixed alumina–aluminium phosphate (14), and mixed magnesia – alumina – aluminium phosphate (15), it has been proved that these systems suppress the hydrogen chemisorption characteristic of a strong metal–support interaction (SMSI) state.

We have shown (4, 16) that for nickel, the metal–support interaction follows the trend

$$Ni/SiO_2 < Ni/SiO_2\text{–}AlPO_4 < Ni/AlPO_4$$

We have recently studied in our laboratory (17) the hydrogenation of 1-hexene following several procedures for preparing the Ni/$AlPO_4$ supported catalysts and comparing the tendency of various precursors to yield different crystallite diameters for the catalyst. On the other hand, the prior impregnation of the support with alkali cations greatly influences the catalyst activity, with no change in the real rate of the catalyzed reaction.

This paper deals with the liquid-phase catalytic hydrogenation of cyclohexene as a standard reaction which Boudart and co-workers (18) have convincingly shown to be structure-insensitive, and which we have studied by hydrogenation over new Pd catalysts supported on SiO_2–$AlPO_4$.

The purpose of the present study is to systematically investigate the effect of various pretreatment steps and controllable preparation variables on the catalytic activity of the resulting systems. Among these variables, we have taken into account the kind of support, the nature of the metal precursor (either inorganic salts or organometals), the addition of alkaline hydroxides, the calcination or the lack thereof prior to the metal reduction and its nature (either with hydrogen or by various chemicals).

Experimental

Supports

Supports denominated APS_1, APS_2. APS_3, and APS_4 have been synthesized by procedures reported elsewhere (19, 20). They consist of SiO_2–$AlPO_4$, 80:20 in weight, and their texture properties, summarized in Table 1, have been described previously.

[1] All correspondence concerning this paper should be adressed to: Prof. J. M. Marinas Rubio, Dpto. Química Orgánica, Facultad de Ciencias, Universidad de Córdoba, Avda. Medina Azahara, s/n 14005-Cordoba (España).

[2] Revision received May 1, 1985.

TABLE 1. Texture properties of the supports

Supports	Chemical composition	Gelling medium	$S_{esp} \pm 15$ ($m^2\ g^{-1}$)	$V_p \pm 0.05$ ($mL\ g^{-1}$)	$\bar{r}_p$ (Å)	I.P.
APS_1	SiO_2–$AlPO_4$ (80:20)	Propylene oxide	465	0.56	35	4.3
APS_2	SiO_2–$AlPO_4$ (80:20)	Ammoniacal	310	0.52	35	3.2
APS_3[b]	SiO_2–$AlPO_4$ (80:20)	Propylene oxide	410	0.56	35	4.0
APS_4[b]	SiO_2–$AlPO_4$ (80:20)	Ethylene oxide	420	0.58	32	3.8
AP	$AlPO_4$	Ammoniacal	156	0.49	40	3.2
S	SiO_2	Commercial	395	0.55	28	1.0

[a] S_{esp}, specific surface; V_p, total pore volume; I.P., isoelectric point or zero point of charge; $\bar{r}_p$, average pore radius.
[b] After obtaining the supports they are soaked in isopropyl alcohol.

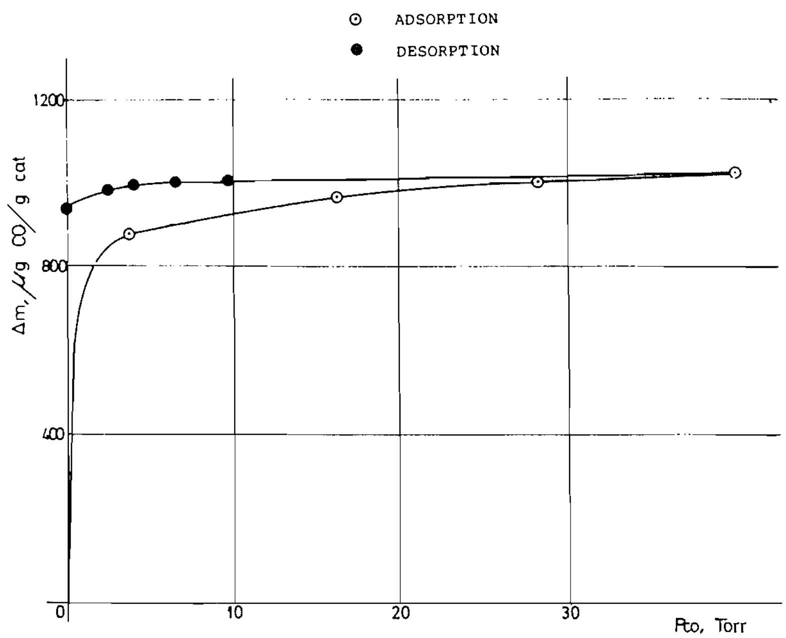

FIG. 1. CO adsorption–desorption isotherm for catalyst $Pd_{0.68}S^+$ C.

Support AP is made of pure aluminium phosphate synthesized as reported in ref. 21. A summary of its texture properties has been included in Table 1.

The silica used was supplied by Merck, ref. 7734. All supports were sieved through 70-230 mesh.

Metal systems

Catalysts have been obtained either by impregnation or by ion exchange.

Catalysts $Pd_{0.68}S^+$, Pd_xAPS^+, and $Pd_{0.97}AP^+$ have been synthesized by cation exchange between $Pd(NH_3)_4^{2+}$ and the corresponding support: S, APS_x, AP (see above); catalysts Pd_3 support K, N, M, O, P, and Q have been obtained by impregnation of the corresponding support with a solution of $PdCl_2$, $Pd(NH_3)_4^{2+}$, Na_2PdCl_4, $Pd(NO_3)_2$, palladium(II) acetylacetonate and palladium(II) acetate, respectively, with H_2O as solvent for the first three reagents and *N*,*N*-dimethylformamide for the rest. In all cases, the subscripts in the labels of the catalysts stand for the metal loading (% weight).

The precursor systems were dried at 393 K for 24 h, then heated from 293 K in air at a constant heating rate of 1 deg min^{-1}, the final temperature being kept constant for 15 min. A similar treatment up to and at 573 K in a hydrogen stream (60 mL min^{-1}) was then given. When naming the catalysts, C and NC stand for samples calcined or uncalcined before reduction, respectively. The type and amount of alkaline hydroxide added (NaOH, KOH, etc.) is also indicated.

When the metal precursor has been chemically reduced, the reducing agent used in each case is indicated.

Chemicals

All chemicals were either Fluka or Merck puris.

Procedure

Specific area and pore volume

The specific surface area (S_{BETN_2}, A_{N_2} = 16.2 Å^2) of the supports was determined on a volumetric adsorption apparatus. The pore volume was obtained from the desorption branch of the nitrogen adsorption–desorption isotherm, following the Innes method as modified by Lippens *et al.* (22). An average pore radius ($\bar{r}_p$, Table 1) was obtained directly from the experimental plots.

Metal loading

The chemical analysis of the metal loading was performed by atomic absorption spectrometry at λ = 247.8 nm, using a Perkin–Elmer 370 instrument with a hollow cathode lamp. An aqueous solution (5%) of lanthanum oxide was added in order to eliminate the interference from aluminium.

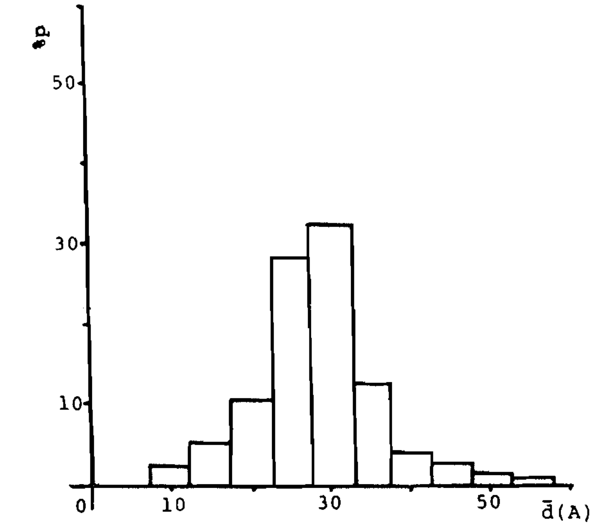

FIG. 2. Metal particle size distribution for catalyst $Pd_{0.68}S^+$ C.

Metal surface area

The metal surface area has been determined by CO chemisorption, transmission electron microscopy (TEM), and X-ray diffraction for catalysts with a metal loading equal to or less than 1%. Prior to carrying out X-ray measurements, these catalysts were subject to a procedure for enriching the sample with metal loading, involving the dissolution of the support into hydrofluoric acid in much the same way as in the extractive replica method used to prepare the samples for TEM measurements. In an earlier work it was shown that this treatment does not modify the results obtained by the X-ray technique (9). The remainder of metal catalysts were assayed by X-ray diffraction.

Carbon monoxide chemisorption

CO chemisorption measurements have been carried out by means of a thermogravimetric procedure, using a Cahn RG thermobalance. Prior to starting the measurements, the systems was subject to an operation involving the cleaning of the metal surface by applying a high vacuum (10^{-4}–10^{-5} Torr) at 448 K for 10 h.

The adsorption isotherm was run with high-purity (over 99.97%) CO supplied by the "Societé de l'Air Liquide". Before being introduced into the storage flask of the gravimetric system, the gas was passed through a purifying train and condensed at the temperature of liquid nitrogen. An adsorption temperature of 301 K and pressures ranging from 10^{-4}–40 Torr were used. The isotherm was recorded under these conditions by plotting Δm (μg adsorbed CO/g catalyst) vs. CO pressure. Figure 1 shows the shape of the isotherm obtained for catalyst $Pd_{0.68}S^+$ C.

The amount of chemisorbed gas was assessed by extrapolating the desorption branch of the isotherm to zero.

Blank isotherms were recorded for all the supports in order to make the corrections corresponding to the adsorption of CO on the support. In our case, the extent of adsorption was nil, and therefore, weighing fluctuations fell in the experimental error range. A value of 1.15 was chosen for the stoichiometric coefficient of CO following recommendations from other authors (23–25). A spherical particle model was assumed to calculate the average metal particle size ($\bar{d}_{CO}$).

TEM measurements

Transmission electron microscopy measurements were carried out on a Philips AM-300 instrument working at 100 kV. Samples were prepared by an extractive replica method, and metallic size distribution was determined by counting 1400–3000 particles. Figure 2 shows the distribution particle as a function of their size for catalyst $Pd_{0.68}S^+$ C. The average diameter ($\bar{d}_{TEM}$) was obtained from the volume/surface ratio.

X-ray diffraction measurements

X-ray diffractograms were recorded on a Philips 1130/00/60 apparatus by using the CuKα radiation, with λ = 1.5418 Å. The half-peak width was graphically measured, at an angle 2θ = 40.10° corresponding to plane (111) of Pd, and a value of 0.89 was taken for constant C of the Debye–Scherrer equation (26).

TABLE 2. Influence of the support on the catalyst activity[a]

Catalysts	$\bar{d}_{CO}$ (Å)	$\bar{d}_{TEM}$ (Å)	$\bar{d}_{X-R}$ (Å)	$10^5\ r'_0$(mol s^{-1} m_{Pd}^{-2})
$Pd_{0.74}APS_1^+$ C	31	33	34	1.46
$Pd_{0.77}APS_2^+$ C	32	32	39	1.90
$Pd_{0.74}APS_3^+$ C	44	43	46	0.93
$Pd_{0.75}APS_4^+$ C	38	34	44	2.37
$Pd_{0.97}AP^+$ C	31	33	36	0.12
$Pd_{0.68}S^+$ C	18	18	27	3.07

[a] T = 300 K; V_T = 20 mL; C = 2.47 M; 5 × 10^{-4} g Pd. r'_0, initial reduction rate as calculated by using the surface data obtained by CO chemisorption; $\bar{d}_{CO}$, average metallic particles diameter (Å) as measured by CO chemisorption; $\bar{d}_{TEM}$, average metallic particles diameter (Å) as measured by TEM; $\bar{d}_{X-R}$, average metallic particles diameter (Å) as measured by X-ray diffraction.

Catalytic activity

Hydrogenation runs were carried out in a conventional low-pressure Gerhardt hydrogenator equipped with a manometer which showed hydrogen pressure in the reaction vessel. Reactions were accomplished in a 2.47 M solution (20 mL) at 300 K, under an initial hydrogen pressure of 5 bar. A fresh 5 × 10^{-4} g Pd sample of catalyst was used for each experiment. The reaction temperature was controlled by pumping water from a thermostatic bath through the vessel jacket.

The reaction rate was calculated by taking the initial slope of the plot of the decrease in the hydrogen pressure at the manometer versus time. Blank tests were performed prior to obtaining kinetic data in order to check the absence of phenomena other than those inherent in the catalytic process. Neither the support nor any other parts of the reactor used proved to be active in the reduction of cyclohexene. No diffusion phenomena, which might distort the results obtained, were observed under the present reaction conditions.

The rate of the hydrogen transfer from the gas-phase to the reaction medium was shown not to be the rate-determining step of the process. Under our working conditions we have shown that the initial rate of reaction increases linearly with the amount of catalyst used.

Product analysis

The reaction products were analyzed by using a Hewlett-Packard 5830 A gas chromatograph fitted with a H-P18850 GC terminal; the column was packed with 5% Carbowax 20 M on 80/100 chromosorb G-AWDMCS. Under our experimental conditions the only product detected in the hydrogenation of cyclohexene was cyclohexane. The nature of the products was confirmed by coupling the gc apparatus to a Hewlett-Packard 5992B mass spectrometer.

Results and discussion

Table 1 lists the texture properties and the isoelectric points of the different supports used. All these supports have a high specific surface (as determined by the BET method) and an average pore radius to allow the occurrence of ion exchange inside the pores.

From the study of the Z potential curves (6, 27) it can be concluded that at pH's above the isoelectric point all the supports can act as cation exchangers. The complex $Pd(NH_3)_4Cl_2$, in which the metal nucleus is in a cation form, was used with this purpose.

Table 2 gathers the average metal particle diameters found by CO chemisorption, transmission electron microscopy, and X-ray diffraction. The particle size values obtained by the three procedures are very much alike. In fact, only catalyst $Pd_{0.68}S^+$

TABLE 3. Influence of the nature of the metal precursor and calcination on the catalytic activity of the system[a]

Catalyst	Solvent[b]	$\bar{d}_{X-R}$ (Å)	$10^3\ r_0$ (mol s^{-1} g_{Pd}^{-1})	$10^5\ r_0'$ (mol s^{-1} m_{Pd}^{-2})
Pd_3APS_2K NC	H_2O	84	2.06	3.43
Pd_3APS_2K C	H_2O	89	2.37	4.23
Pd_3APS_2N NC	H_2O	57	1.72	1.96
Pd_3APS_2N C	H_2O	79	1.88	2.98
Pd_3APS_2M NC	H_2O	111	1.38	3.07
Pd_3APS_2M C	H_2O	44	8.60	7.53
Pd_3APS_2M NC	DMF	57	7.00	7.95
Pd_3APS_2M C	DMF	43	10.00	8.62
Pd_3APS_2O NC	DMF	51	15.67	15.99
Pd_3APS_2O C	DMF	53	13.00	13.83
Pd_3APS_2P NC	DMF	20	15.83	6.33
Pd_3APS_2P C	DMF	23	13.83	6.37
Pd_3APS_2Q NC	DMF	68	7.83	10.58
Pd_3APS_2Q C	DMF	68	8.67	11.71

[a] T = 300 K; V_T = 20 mL; C = 2.47 M; 5 × 10^{-4} g Pd; r_0, initial reduction rate; r_0', initial reduction rate as calculated by using the surface data obtained by X-ray diffraction; $\bar{d}$, average metallic particles diameter as determined by X-ray diffraction.

[b] As used for the impregnation of the support.

C, which has a very small particle size (as determined by CO chemisorption), represents a higher extent of dispersion from the results obtained. As a rule, particle sizes obtained by CO chemisorption and TEM are practically the same, whereas those found by X-ray diffraction are slightly larger as compared to catalysts with a small particle size. This is a not surprising finding, considering the fact that no small crystallites can be observed by the X-ray diffraction technique.

The specific activity of the catalysts obtained by ion exchange was determined in the hydrogenation reaction of cyclohexene (Table 2), using the values of metal surface found by CO chemisorption. As can be seen, it is the silica support which yields the most disperse and active systems. Those supported on SiO_2-AlPO_4 show medium activities. The system obtained over $AlPO_4$, although with a similar particle size to that of SiO_2-AlPO_4 supports, show a low specific activity. This fact can be attributed to a strong metal–support interaction (16).

Table 3 shows the results of average metal particle diameter and catalytic activity found for the catalysts synthesized from various precursor salts over support APS_2, using either water or dimethylformamide (DMF) as impregnating solvent, depending on the solubility of the different salts employed.

The best dispersed system is obtained from Pd(II) acetylacetonate, which is logical in view of the type of interaction between this precursor and the OH groups of the supports, yielding a great extent of dispersion according to several authors (28).

$$—OH + Pd(AcAc)_2 \rightleftharpoons —O—Pd(AcAc) + AcAcH\ (ads)$$

The influence of the metal precursor is drastic. Thus, whilst Na_2PdCl_4 (which yields PdO after calcination) can be reduced at room temperature, resulting in good dispersion, it sinters easily above 573 K. Conversely, $Pd(NH_3)_4Cl_2$ cannot be reduced below 373 K, but yields good dispersion even at high temperatures. This type of precursor may be interesting if the catalyst should remain at high temperatures for a long time, as in our hydrogen-transfer reduction reactions. The high stability of the $Pd—NH_3$ bond makes it obviously difficult to reduce this precursor. Analogous results have been found by Gubitosa *et al.* (29).

TABLE 4. Promoting effect of NaOH and comparison between various alkaline hydroxides[a]

10^4 additive (mol g_{Cat}^{-1})	$\bar{d}_{X-R}$ (Å)	$10^3\ r_0$ (mol s^{-1} g_{Pd}^{-1})
—	89	2.37
5.56 NaOH	88	2.58
8.34 NaOH	26	16.83
11.12 NaOH	35	14.97
13.90 NaOH	38	14.38
16.68 NaOH	42	10.92
22.24 NaOH	47	6.45
11.12 LiOH	88	7.38
11.12 KOH	57	8.47

[a] Catalyst: Pd_3APS_2K C; T = 300 K; V_T = 20 mL; C = 2.47 M; 5 × 10^{-4} g Pd; $\bar{d}$, average particles diameter as determined by X-ray diffraction; r_0, initial reduction rate.

On the other hand, we have found that the reduction with Na_2PdCl_4 (PdO) at 373 K is not complete, but takes place in two steps: a first one at room temperature and a subsequent one around 503 K for all supports except AP, for which it occurs at approximately 593 K. Vasudevan *et al.* (30) have found similar results on the study of $Pd/\gamma-Al_2O_3$ catalysts, the two reduction steps occurring at room temperature and at 513 K, respectively. This fact may be due to the formation of various types of oxides with different ease of reduction.

As to the use of organometals (palladium acetate and acetylacetonate) as metal precursors, literature (30) indicates they do not yield bulky oxides when the systems are calcined at temperatures below 573 K, giving rise to high mononodal dispersion. In our case, the palladium acetate and acetylacetonate employed can be partially reduced with H_2 at room temperature, finding optimum reaction conditions similar to those of Na_2PdCl_4, as long as a temperature of 573 K is not exceeded.

The higher metal dispersion provided by the acetylacetonate as opposed to that of the acetate, may be due to the larger volume of the ligand of the former. As can be observed, the calcination prior to the reduction has a varying influence on the metal particle size according to the precursor salt.

TABLE 5. Influence of the reducer on the catalyst activity[a]

Reducer		$10^3\ r_0$ (mol s^{-1} g_{Pd}^{-1})	X (% 2h)
H_2		0.78	5.1
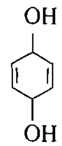 Hydroquinone	→ 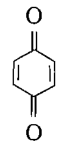 + H_2	0.03	0.3
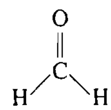 Formaldehyde	→ $CO + H_2$	0.28	2.1
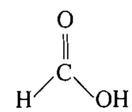 Formic acid	→ $CO_2 + H_2$	0.13	1.1
$NH_2-NH_2\cdot H_2O$ Hydrazine hydrate	→ $N_2 + H_2O + 2H_2$	0.50	2.9
$2NH_2OH\cdot HCl$ Hydroxylamine	→ $N_2 + 2HCl + 2H_2O + H_2$	1.37	7.8
$NaBH_4$	→ $BNa + 2H_2$	1.40	10.2
$(N_2H_5)_2SO_4$ Hydrazine sulphate	→ $H_2SO_4 + 2N_2 + 4H_2$	0.10	0.8
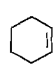 Cyclohexene	→ 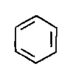 + $2H_2$	13.83	82.2

[a]Catalyst: Pd_1APS_3N C; T = 300 K; V_T = 20 mL; C = 2.47 M; 5 × 10^{-4} g Pd; r_0, initial reduction rate; X (% 2h), conversion of cyclohexene to cyclohexane, in wt.%, after 2 h reaction.

On comparing the catalytic activity values found, the results are different if expressed by square meter or by gram of Pd. Although no generalization can be made, calcination usually results in more active catalysts, even though the best specific activity results are obtained using Pd(II) nitrate reduced uncalcined.

A more marked influence of the particle size and catalytic activity is observed when adding alkaline hydroxides in the preparation of the catalyst. This is of special interest since their effect has been described to show in: (a) increasing the selectivity or specificity of a reaction; (b) increasing the catalyst activity; and (c) lengthening the catalyst lifetime.

The order in which the metal precursor and the alkaline metal are added onto the support has been shown to be important on the final activity of the systems; thus, with Co/γ-Al_2O_3 systems, Lycourghiotis *et al.* (31) have observed that the worst results are obtained if cobalt is first added and the alkaline metal is added in a second step, after calcination. We have used three different methods: Method 1, the support is first impregnated with an aqueous solution of $PdCl_2$, then filtered, dried, and calcined, and a second impregnation with aqueous NaOH is then performed. Method 2, the support is first impregnated with aqueous NaOH, and then with $PdCl_2$. Method 3, only one

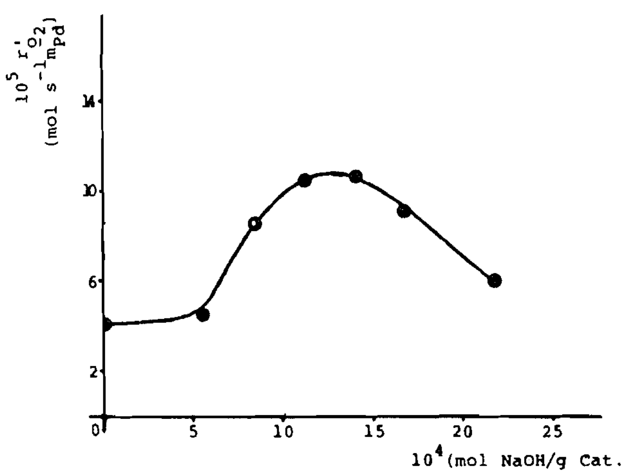

FIG. 3. Specific activity of catalyst Pd_3APS_2K C as a function of the amount of NaOH added.

impregnation with an aqueous solution containing NaOH and $PdCl_2$ is carried out.

Similar to the results reported by Lycourghiotis *et al.* (31), method 1 yields very low metal dispersion. As methods 2 and

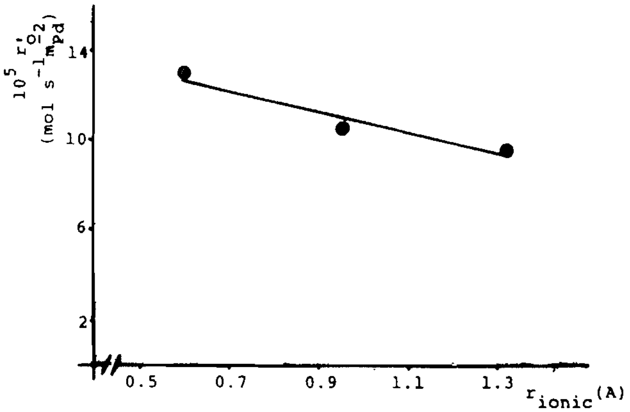

FIG. 4. Specific activity of catalyst Pd_3APS_2K C as a function of the radius of the alkaline cation added.

3 lead to similar results, method 3 is chosen.

Table 4 gathers the values of particle size and catalytic activity per g of metal found for catalysts to which various amounts of alkaline hydroxides are added. As can be seen, the catalyst with the greatest activity and most suitable particle size is that containing 8.34×10^{-4} mol of NaOH per g of catalyst.

Figure 3 reflects a similar behaviour in the plot of the specific catalytic activity as a function of the amount of sodium hydroxide added. For a given amount of alkali added, the specific catalytic activity decreases with increasing ionic radius of the alkaline metal (Fig. 4). Insofar as the specific catalytic activity is not directly related to the particle size, it must be a function of parameters involved in (1) change in the number of active centres of the catalyst or in the surface morphology; and (2) modification of the metal–support interactions.

Mross (32), in a comprehensive review on the effect of the addition of alkaline hydroxides to heterogeneous catalysts in different reactions, suggests several reasons to account for such an effect: (*a*) the alkali may act as an active component; (*b*) acid centres may be neutralized; (*c*) the population of basic centres may increase; (*d*) an electronic interaction between the metal and the alkali may occur; (*e*) the active component of its precursors may be rendered less volatile. In this context, we have shown (33) the gradual addition of alkaline hydroxides up to a given ratio result both in a significant increase in the population of basic centres and in a decrease in the number of oxidizing centres, whereas acidic and reducing centres remain practically unaltered.

The reducing agent used is another variable affecting the synthesis of Pd catalysts. In every case, the reductant was used dissolved in methanol (V_t = 20 mL), employing 20 mol of the agent per mol of $Pd(NH_3)_4Cl_2$ and reducing in reflux (358 K) for 8 h. The results thus obtained are listed in Table 5 and compared with those found for the catalyst reduced in a hydrogen stream under conditions identical with those in Table 3. The best results are obtained for the catalyst reduced with cyclohexene. Hydroxylamine and $NaBH_4$ also yield acceptable results from a catalytic point of view, better than those obtained by reducing the precursor with gaseous hydrogen. The remaining reductants used yield poor results, especially for hydrazine sulphate. We cannot rule out an inhibitory effect exerted by some of the chemical agents used to reduce the catalyst. On the other hand, this potential effect cannot be eliminated by successive washing of the catalysts. Therefore, we have opted for providing the activity per g of Pd and conversion after 2 h for such catalysts instead of their specific activity.

In summary, we can state that the nature of the support, the type of metal precursor used, the addition of alkaline hydroxides, and the reductant of the precursor are potential factors exerting a significant influence on the activity of the resulting catalyst. Therefore, no accurate prediction of a catalyst activity can be made unless every synthetic variable is individually optimized.

Acknowledgement

This study has been carried out with a grant from the "Comisión Asesora de Investigación Científica y Técnica", Project number: 0249/81.

1. E. A. HYDE and R. RUDHAM. J. Chem. Soc. Faraday Trans. I, **79**, 2105 (1983).
2. J. HANIKA, L-H. HAO, and V. RUCICKA. Collect. Czech. Chem. Commun. **48**, 3079 (1983).
3. J. M. CAMPELO, D. LUNA, and J. M. MARINAS. Rev. Roum. Chim. **26**, 867 (1981).
4. J. M. CAMPELO, A. GARCIA, D. LUNA, and J. M. MARINAS. Appl. Catal. **3**, 315 (1982).
5. M. A. ARAMENDIA, M. S. CLIMENT, C. JIMENEZ, and J. M. MARINAS. React. Kinet. Catal. Lett. **14**, 489 (1980).
6. M. A. ARAMENDIA, V. BORAU, C. JIMENEZ, J. M. MARINAS, and J. A. PAJARES. J. Catal. **78**, 188 (1982).
7. M. A. ARAMENDIA, V. BORAU, C. JIMENEZ, and J. M. MARINAS. Acta Chim. Acad. Sci. Hung. **110**, 97 (1982).
8. M. A. ARAMENDIA, V. BORAU, C. JIMENEZ, and J. M. MARINAS. Bull. Soc. Chim. Belg. **91**, 743 (1982).
9. J. M. CAMPELO, A. GARCIA, D. LUNA, and J. M. MARINAS. Colloids Surf. **5**, 227 (1982).
10. J. M. CAMPELO, A. GARCIA, D. LUNA, and J. M. MARINAS. React. Kinet. Catal. Lett. **21**, 209 (1982).
11. M. A. ARAMENDIA, V. BORAU, C. JIMENEZ, and J. M. MARINAS. React. Kinet. Catal. Lett. **19**, 233 (1982).
12. M. A. VANNICE and R. L. GARTEN. J. Catal. **63**, 255 (1980).
13. G. MARCELIN and R. F. VOGEL. J. Catal. **82**, 482 (1983).
14. G. MARCELIN, R. F. VOGEL, and H. E. SWIFT. J. Catal. **83**, 42 (1983).
15. G. MARCELIN, R. F. VOGEL, and H. E. SWIFT. Ind. Eng. Chem. Prod. Res. Dir. **23**, 41 (1984).
16. J. M. CAMPELO, A. GARCIA, D. LUNA, and J. M. MARINAS. Bull. Soc. Chim. Belg. **91**, 131 (1982).
17. J. M. CAMPELO, A. GARCIA, J. M. GUTIERREZ, D. LUNA, and J. M. MARINAS. Appl. Catal. **7**, 307 (1983).
18. E. SEGAL, R. J. MADON, and M. BOUDART. J. Catal. **52**, 45 (1978).
19. C. JIMENEZ, J. M. MARINAS, R. PEREZ-OSSORIO, and J. V. SINISTERRA. An. Quím. **73**, 1164 (1977).
20. J. V. SINISTERRA, C. JIMENEZ, V. BORAU, and J. M. MARINAS. Proc. Vth Iberoamerican Symposium on Catal. 1976. p. 259.
21. A. ALBEROLA and J. M. MARINAS. An. Quím. **65**, 1001 (1969).
22. B. C. LIPPENS, B. G. LINSEN, and J. H. DE BOER. J. Catal. **3**, 32 (1967).
23. R. FARRAUTO. AIChe Symp. Ser. 70 (N. 143) 9 (1974).
24. T. MALLAT and J. PETRO. React. Kinet. Catal. Lett. **11**, 307 (1979).
25. T. A. DORLING and R. L. MOSS. J. Catal. **7**, 378 (1967).
26. R. L. MOSS. Experimental methods in catalytic research. Vol. 2. *Edited by* R. B. Anderson and P. T. Dawson. Academic Press, New York. 1976. p. 43.
27. J. R. BRUNELLE. Pure Appl. Chem. **50**, 1211 (1978).
28. J. P. BOITIAUX, J. COSYNS, and S. VASUDEVAN. *In* Preparation of catalysts. III. Elsevier, Amsterdam. 1983. p. 123.
29. G. GUBITOSA, A. BERTON, M. CAMIA, and N. PERNICONE. *In* Preparation of catalysts. III. Elsevier, Amsterdam. 1983. p. 431.

30. S. VASUDEVAN, J. COSYNS, E. LESAGE, E. FREUND, and H. DEXPERT. *In* Preparation of catalysts. III. Elsevier, Amsterdam. 1983. p. 463.
31. A. LYCOURGHIOTIS, C. DEFOSSE, F. DELANNAY, J. LEMAITRE, and B. DELMON. J. Chem. Soc. Faraday Trans. I, **76**, 1677 (1980).
32. W. D. MROSS. Catal. Rev. Sci. Eng. **25** (4), 591 (1983).
33. J. M. CAMPELO, A. GARCIA, J. M. GUTIERREZ, D. LUNA, and J. M. MARINAS. J. Colloid. Interf. Sci. **95**, 544 (1983).

Sélectivité du transport de Ca^{2+}/Mg^{2+} à travers une membrane liquide par A.23187 (calcimycine) et son dérivé N-méthyle

JEAN BOLTE, COLETTE DEMUYNCK ET GEORGES JEMINET
Laboratoire de Chimie Organique Biologique, ERA 392 du CNRS, Université de Clermont II, B.P. 45, 63170 Aubière, France

Reçu le 14 janvier 1985

JEAN BOLTE, COLETTE DEMUYNCK et GEORGES JEMINET. Can. J. Chem. **63**, 3478 (1985).

Le transport préférentiel de Ca^{2+}/Mg^{2+} par A.23187 est mis en évidence dans une cellule eau/$CHCl_3$/eau. Par des mesures de flux d'extraction et de flux de libération dans une demi-cellule eau/$CHCl_3$, on montre que la sélectivité du transport est liée à une cinétique de libération nettement différente pour les deux ions, qui pourrait s'expliquer par la structure des complexes dimériques formés, si on se réfère aux études cristallographiques correspondantes. La méthylation du groupement —$NHCH_3$ entraîne une inversion de la sélectivité de transport.

JEAN BOLTE, COLETTE DEMUYNCK, and GEORGES JEMINET. Can. J. Chem. **63**, 3478 (1985).

Operating in a cell of water/$CHCl_3$/water, it is shown that there is a preferential transport of Ca^{2+}/Mg^{2+} by A.23187. On the basis of measurements of flux of extraction and of flux of liberation in a half-cell of water/$CHCl_3$, it is shown that the selectivity of the transport is related to the kinetics of liberation, which is markedly different for the two ions and which could be explained by the structure of the complex dimers that are formed, according to the corresponding crystallographic studies. The methylation of the —$NHCH_3$ entails an inversion of the selectivity in the transport.

[Traduit par le journal]

Introduction

L'étude du transport cationique induit par les antibiotiques polyéthers carboxyliques, à travers une membrane liquide épaisse, a été abordée au laboratoire dans le cadre plus général d'une recherche menée sur le mode d'action de ces composés.

Un premier travail consacré aux ionophores X.537A, A.23187 et X.14547A (1), classés comme des transporteurs des ions divalents (2), avait permis de mettre en évidence dans le système triphasique eau/$CHCl_3$/eau: (*i*) l'existence d'une courbe sigmoïdale de transport reliant le flux ionique $J_{Ca^{2+}}$ au pH du compartiment d'extraction, et (*ii*) le décalage des courbes d'un ionophore à l'autre, attribué aux différences de stabilité des associations formées aux interfaces avec H^+ et Ca^{2+}.

Récemment, une étude semblable a été abordée d'une manière approfondie pour des polyéthers couronnes de synthèse portant une ou deux fonctions —COOH (3).

Des trois ionophores cités, A.23187 (composé **1**, fig. 1) est le seul qui transporte préférentiellement les cations divalents et particulièrement Ca^{2+} et Mg^{2+} présents "in vivo" dans les compartiments cellulaires (4). Il paraissait donc intéressant d'étudier dans le système modèle évoqué la sélectivité de transport de ces deux ions et d'en préciser l'origine. Dans les conditions expérimentales utilisées mettant ou non en compétition les deux ions, on observe que $J_{Ca^{2+}} > J_{Mg^{2+}}$ quel que soit le pH. J représente le nombre de moles transportées par s et par cm^2. Le même transport préférentiel a été mentionné dans des vésicules de D.M.P.C. (5), des B.L.M. (6), ou dans la membrane mitochondriale (7). Une étude récente fait apparaître une augmentation de cette sélectivité pour un analogue bromé sur le cycle benzénique de A.23187 (8). Par opposition, le présent travail montre qu'une méthylation du groupement —$NHCH_3$ (composé **2**, fig. 1) entraîne une inversion de cette sélectivité.

Les valeurs des constantes thermodynamiques de complexation mesurées dans le méthanol ne permettent pas de prévoir les sélectivités observées; la détermination des cinétiques d'échange dans une demi-cellule eau/chloroforme autorise une interprétation des résultats en relation avec la structure des complexes dimériques connus à l'état cristallin.

A. *Étude de la sélectivité Ca^{2+}/Mg^{2+} pour A.23187* **1**. *Transport dans une cellule eau/$CHCl_3$/eau*

Les variations du flux ionique J en fonction du pH du compartiment d'extraction sont représentées sur la fig. 1.

Pour Ca^{2+}, J est inférieur à 10^{-12} mol s^{-1} cm^{-2} (limite de sensibilité de la méthode) lorsque pH < 6,6, puis il augmente jusqu'à pH 9 sans atteindre un palier distinct. Pour Mg^{2+}, on ne décèle aucun transport à pH < 7,4, au-delà duquel le flux reste faible. Il existe donc un transport préférentiel en faveur de Ca^{2+} qui se trouve confirmé si les deux cations sont présents en compétition dans la phase aqueuse d'extraction, la mesure du flux à pH 8,5 montre alors un transport exclusif de Ca^{2+} avec une valeur $J = 1 \times 10^{-11}$ mol s^{-1} cm^{-2}.

Une telle sélectivité n'est pas apparente pour les constantes de formation des complexes 1:1 et 2:1 mesurées dans le méthanol (1) exprimées sous la forme:

$$[1]\quad A^- + M^{2+} \overset{\beta_{AM^+}}{\rightleftharpoons} AM^+$$

$$\log \beta_{ACa^+} = 8{,}2 \qquad \log \beta_{AMg^+} = 7{,}6$$

$$[2]\quad 2A^- + M^{2+} \overset{\beta_{A_2M}}{\rightleftharpoons} A_2M$$

$$\log \beta_{A_2Ca} = 16{,}2 \qquad \log \beta_{A_2Mg} = 15{,}9$$

ou pour l'équation globale de l'échange:

$$[3]\quad 2AH + M^{2+} \overset{\beta'_{A_2M}}{\rightleftharpoons} A_2M + 2H^+$$

$$\beta'_{A_2Ca} = 2{,}09 \times 10^{-6} \qquad \beta'_{A_2Mg} = 1{,}04 \times 10^{-6}$$

La différence de flux ionique doit donc se créer au cours des échanges aux interfaces dans le processus global représenté sur la fig. 2 pour un transport par l'intermédiaire d'un complexe 2:1.

Pour préciser ce point nous avons utilisé une approche expérimentale en étudiant les cinétiques d'échange dans une demi-cellule eau/$CHCl_3$, à partir de l'acide libre, pour obtenir une information sur l'entrée de M^{2+} dans la phase organique ou, à partir du complexe 2:1, pour la libération du cation dans la phase aqueuse. Ces conditions expérimentales diffèrent donc

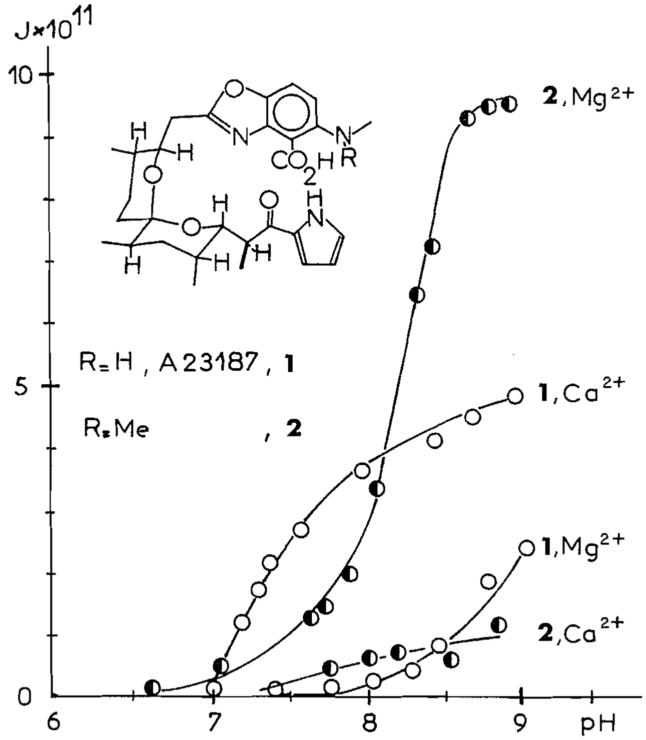

FIG. 1. Transport non compétitif de Ca^{2+} et Mg^{2+} par **1** (○) et **2** (◐), dans une cellule eau/$CHCl_3$/eau. Variations du flux J en mol s^{-1} cm^{-2} en fonction du pH de la phase aqueuse d'extraction. Conditions initiales: [ionophore]$_{org.}$ = 4×10^{-4} M, $[M^{2+}]_{aq.}$ = 10^{-2} M.

nécessairement du processus dynamique qui s'établit au cours du transfert triphasique. L'information recueillie sous cette forme permet cependant de proposer une explication à la discrimination Ca^{2+}/Mg^{2+} qui s'opère.

Cinétique d'extraction dans une demi-cellule eau/$CHCl_3$

On mesure la cinétique d'entrée de Ca^{2+} ou Mg^{2+} dans la phase organique contenant l'antibiotique (4×10^{-4} M) à partir d'une solution aqueuse 10^{-2} M de ces cations tamponnée à pH 8,5 qui correspond à un maximum d'extraction. La pente des droites représentant la quantité de cation extrait en fonction du temps permet d'accéder aux flux initiaux d'entrée qui sont respectivement:

$$J_{Ca^{2+}} = 1,1 \times 10^{-10} \text{ mol s}^{-1} \text{ cm}^{-2}$$

$$J_{Mg^{2+}} = 1,2 \times 10^{-10} \text{ mol s}^{-1} \text{ cm}^{-2}$$

Ces valeurs ne reflètent aucune différence notable entre les deux cations.

Cinétique de libération dans une demi-cellule eau/$CHCl_3$

La cinétique d'apparition de Ca^{2+} ou Mg^{2+} dans la phase aqueuse tamponnée à pH 7,0 est mesurée à partir des sels cristallisés de A.23187 dissous dans la phase organique à la concentration 2×10^{-4} M. Les courbes ainsi obtenues sont représentées sur la fig. 3. La différence entre les vitesses de libération des deux ions est apparente, les flux initiaux sont respectivement:

$$J_{Ca^{2+}} = 4,5 \times 10^{-10} \text{ mol s}^{-1} \text{ cm}^{-2}$$

$$J_{Mg^{2+}} = 3,5 \times 10^{-11} \text{ mol s}^{-1} \text{ cm}^{-2}$$

soit un rapport $J_{Ca^{2+}}/J_{Mg^{2+}} \sim 13$. Le même type de courbe est obtenu dans l'intervalle de pH 7,0–1,0. Les flux initiaux mesu-

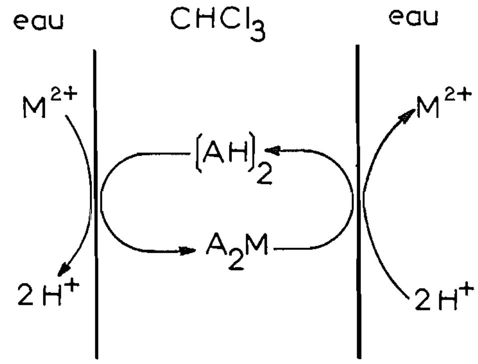

FIG. 2. Représentation du mécanisme d'échange $M^{2+} \leftrightarrow 2H^+$ aux interfaces, dans le transport à travers une membrane liquide épaisse.

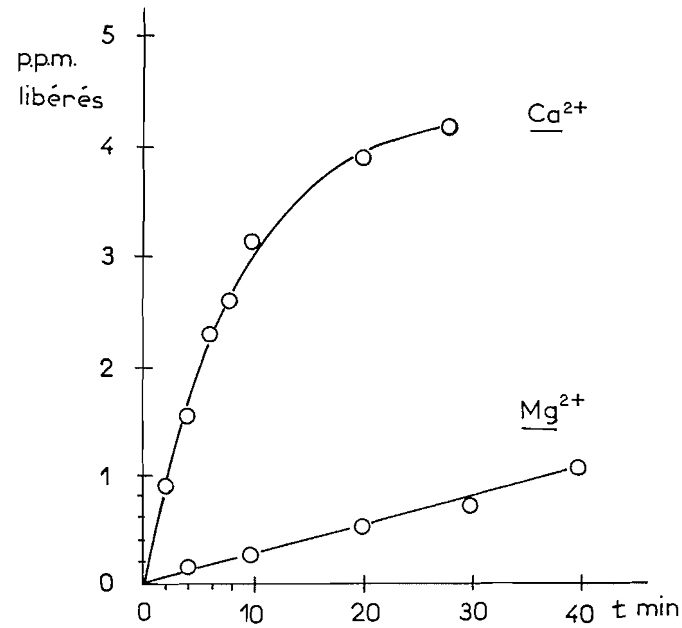

FIG. 3. Libération non compétitive de Ca^{2+} et Mg^{2+} dans la phase aqueuse, à partir des complexes cationiques dimères de la Calcimycine dissous dans la phase chloroformique, pour un système eau/$CHCl_3$. Conditions initiales: [complexe] = 2×10^{-4} M, pH de la phase aqueuse = 7,0.

rés sont indépendants de $[H^+]$ dans la phase aqueuse.

Les premières études cinétiques entreprises en phase homogène dans le méthanol ou le mélange méthanol 70/eau 30 (w/w) par des techniques de flux stoppé ou saut de température (9) donnent pour la constante cinétique globale de dissociation du complexe 1:1 qui constitue l'étape limitante (en s^{-1}):

Ca^{2+}	MeOH	2,2 ± 1,4	Mg^{2+}	MeOH	0,3 ± 0,2
MeOH 70/eau 30		>600		MeOH 70/eau 30	89 ± 20

Ceci conduit les auteurs à admettre que si l'étape limitante dans le transport est la libération du cation, on doit attendre une sélectivité de l'ordre de 8 en faveur de Ca^{2+}. Les résultats mentionnés dans ce travail qui décrivent une cinétique globale de libération à l'interface eau/$CHCl_3$ sont en accord avec cette proposition.

Les différences de propriétés des ions Ca^{2+} et Mg^{2+} en biologie ont été fréquemment discutées notamment par Williams (10). Il note que Ca^{2+} (1,06 Å) s'associe aux ligandes avec un indice de coordination minimum de 6 mais plus fréquemment 7 ou 8 dans une géométrie irrégulière (angles et longueurs de liaison), alors que Mg^{2+} (0,78 Å) est généralement hexacoordiné dans une géométrie proche de l'octaèdre. Pour l'assemblage moléculaire très particulier que représente le dimère de A.23187 la proposition de Williams est respectée si l'on compare l'heptacoordination irrègulière de Ca^{2+} (11) et l'hexacoordination octaédrique de Mg^{2+} (12). Cet aspect a été examiné récemment par Gresh et Pullman (13) au moyen de simulations théoriques à partir des données cristallographiques. Ils montrent que la présence d'une molécule d'eau observée dans le cristal du complexe avec Ca^{2+} comme 7ème site coordinant (11) est nécessaire pour assurer au complexe une stabilité comparable à celle du complexe avec Mg^{2+}; la possibilité d'un co-transport de molécules d'eau dans la migration intramembranaire est envisagée par les auteurs.

Ces différences structurales observées à l'état cristallin constituent un argument en faveur d'une différenciation entre les vitesses de libération des ions Ca^{2+} et Mg^{2+} à partir de leurs complexes, si l'on admet des structures comparables en solution. Il serait intéressant de préciser le mécanisme de cette discrimination cinétique. Dans un premier temps nous nous proposons d'étudier la présence éventuelle de molécules d'eau dans l'espèce qui assure le transport; cela nécessite la mise au point d'un processus expérimental approprié.

B. *Sélectivité Ca^{2+}/Mg^{2+} pour N-Me A.23187* **2**

Les deux substituants —$NHCH_3$ et —COOH (ou —COO^-) dans A.23187 (fig. 1, R = H) présentent une chélation intramoléculaire —NH (CH_3)···O=C(···) qui les maintient dans le plan du benzoxazole, si l'on se rapporte aux résultats radiocristallographiques donnés sur l'acide libre (14) et les sels complexes (11, 12). L'introduction d'un deuxième groupement méthyle sur —$NHCH_3$ (15) (fig. 1, R = CH_3) supprime cette possibilité de chélation et entraîne une modification des propriétés d'association avec les cations qui apparaît à l'examen des constantes de formation des complexes 1:1 et 2:1 dans le méthanol (16) (équilibres [1]–[3]).

$$\log \beta_{A'Ca^+} = 4{,}7 \qquad \log \beta_{A'_2Ca} = 8{,}5$$
$$\log \beta_{A'Mg^+} = 5{,}2 \qquad \log \beta_{A'_2Mg} = 9{,}5$$
$$\beta'_{A'_2Ca} = 1{,}26 \times 10^{-13}$$
$$\beta'_{A'_2Mg} = 1{,}25 \times 10^{-12}$$

où l'on observe une nette déstabilisation des associations formées.

Les résultats du transport cationique dans un système eau/$CHCl_3$/eau par cet ionophore modifié sont représentés sur la fig. 1. L'ion Mg^{2+} est transporté préférentiellement à Ca^{2+}, le flux maximun atteint étant supérieur à celui de Ca^{2+} pour A.23187 bien que la stabilité des complexes soit très inférieure. On avait déjà observé un phénomène semblable pour X.537A (1).

Lorsque les deux cations sont présents en compétition dans la phase d'extraction, les flux initiaux mesurés à pH 8,5 sont respectivement

$$J_{Ca^{2+}} = 0{,}2 \times 10^{-11} \text{ mol s}^{-1} \text{ cm}^{-2}$$
$$J_{Mg^{2+}} = 2{,}3 \times 10^{-11} \text{ mol s}^{-1} \text{ cm}^{-2}$$

La faible modification introduite sur la structure naturelle a donc pour effet d'inverser la sélectivité du transport Ca^{2+}/Mg^{2+} dans ce système membranaire.

Comme précédemment, les flux initiaux correspondant aux phénomènes d'extraction et de libération des cations dans une demi-cellule eau/$CHCl_3$ ont été mesurés; on obtient les valeurs suivantes:

Flux d'extraction	Flux de libération
$J_{Ca^{2+}} = 1{,}7 \times 10^{-11}$	$J_{Ca^{2+}} = 8 \times 10^{-11}$
$J_{Mg^{2+}} = 5{,}3 \times 10^{-11}$	$J_{Mg^{2+}} = 15 \times 10^{-11}$

Les flux d'entrée sont plus faibles si l'on se réfère à A.23187. Par ailleurs, tant à l'entrée qu'à la sortie de la phase organique les valeurs des flux sont en faveur de Mg^{2+} ce qui peut entraîner un transport global préférentiel de ce cation. Ainsi la transformation de —$NHCH_3$ en —$N(CH_3)_2$ suffit pour créer des effets stériques et électroniques autour du —CO_2H qui modifient la structure des complexes dimériques formés et par voie de conséquence les cinétiques d'échange aux interfaces, confirmant ainsi les observations faites pour A.23187.

En conclusion, il est nécessaire d'insister sur le fait que ces résultats ne sont pas nécessairement transposables systématiquement à d'autres phases membranaires, en particulier à la membrane mitochondriale (4) où un bon ionophore des cations divalents doit posséder des constantes d'associations élevées avec ces cations, compte tenu de la compétition avec les sites propres de la mitochondrie; c'est le cas de A.23187, mais c'est un transporteur lent (9).

Les premiers résultats obtenus avec N-Me A.23187 qui forme des complexes moins stables montrent effectivement que c'est un ionophore peu efficace dans cet organite.[1]

Le transport préférentiel de Ca^{2+}/Mg^{2+} mis en évidence pour A.23187 dans différentes conditions expérimentales (5–7) est très vraisemblablement attribuable à une cinétique de libération différente pour ces deux ions comme dans la membrane liquide chloroformique qui constitue sur ce point un modèle intéressant.

Partie expérimentale

Produits

L'antibiotique A.23187 **1** est isolé à partir d'une culture en fermenteur de 20 L de la souche NRRL 3882 (*Streptomyces chartreusis*) (1). La préparation du dérivé **2** est décrite dans la réf. 15.

Les sels de Ca^{2+} et Mg^{2+} sont préparés et isolés selon la technique de Deber et Pfeiffer (17). Le complexe cristallisé obtenu avec Mg^{2+} a servi conjointement pour les déterminations radiocristallographiques (12). Pour la N-méthylcalcimycine **2**, les sels de Ca^{2+} et Mg^{2+} sont préparés *in situ* en agitant au vortex une solution chloroformique 2×10^{-4} *M* du dérivé et une solution aqueuse tamponnée à pH 10,3 des sels $Mg(ClO_4)_2$ ou $Ca(ClO_4)_2$ Merck, 10^{-2} *M*. La formation du complexe 2:1 dans la phase chloroformique est totale, elle est vérifiée sur une quantité aliquote par libération des cations à l'aide d'HCl 0,1 *N* et mesure de leur concentration par absorption atomique (appareil Perkin–Elmer 420).

Les solutions aqueuses sont tamponnées par un mélange tricine–triéthanolamine Merck 10^{-2} *M*, le pH est ajusté avec une précision de 0,02 unités.

Transport triphasique eau/$CHCl_3$/eau (fig. 1)

La cellule utilisée et les conditions du transport ont été décrites précédemment (1). La phase chloroformique est préalablement saturée d'eau, elle contient l'ionophore **1** ou **2** à la concentration 4×10^{-4} *M*. La phase aqueuse d'extraction ou d'entrée est une solution 10^{-2} *M* de $Ca(ClO_4)_2$ ou $Mg(ClO_4)_2$ Merck.

On mesure les flux ioniques exprimés en mol s^{-1} cm^{-2} à l'établissement du régime quasi-stationnaire dans la phase aqueuse de libération ou de sortie, maintenue à pH 7,0, pour chaque valeur du pH

[1] J. Guyot, travaux non publiés.

de la phase d'entrée. Pour cela, un échantillon de 1 mL est prélevé dans la phase de sortie à intervalles de temps réguliers et dosé par absorption atomique, la même quantité de phase aqueuse tamponnée est introduite dans la cellule en compensation.

Le pH de la phase d'entrée est contrôlée en permanence.

Cinétiques de libération eau/$CHCl_3$ (fig. 3)

Une solution chloroformique (6 mL) préalablement saturée d'eau contenant le complexe de Ca^{2+} ou Mg^{2+} des composés **1** ou **2** à la concentration 2×10^{-4} *M* et 6 mL d'une solution aqueuse à pH 7,0 (tampon tricine 10^{-2} *M*) sont mis en contact dans une cellule cyclindrique thermorégulée à 25°C (diamètre intérieur 2 cm, hauteur 6 cm).

La phase organique est agitée par un agitateur magnétique tournant à 600 tours/min et la phase aqueuse par une baguette de verre (diamètre 3 mm) terminée par une pale rectangulaire de 6 × 3 mm mue par un moteur électrique synchrone tournant à 600 tours/min. La concentration des cations dans la phase aqueuse est mesurée par absorption atomique.

Cinétiques d'extraction eau/$CHCl_3$

La même cellule que précédemment est utilisée. Une solution chloroformique (6 mL) de **1** ou **2** à la concentration 2×10^{-4} *M* et 6 mL d'une solution tamponnée à pH 8,5 (triéthanolamine–tricine) de $Ca(ClO_4)_2$ ou $Mg(ClO_4)_2$ 10^{-2} *M* sont mis en contact et agitées comme ci-dessus.

La vitesse d'apparition du cation dans la phase organique est mesurée en prélevant 1 mL de celle-ci que l'on traite par 1 mL de HCl 0,1 *N* pour libérer le cation et le doser. Pour faire des mesures en fonction du temps on opère avec une série de cellules synchronisées. Les valeurs de flux initiaux mentionnés portent sur trois mesures.

Remerciements

Ce travail a été effectué dans le cadre de la R.C.P. 80/605 du C.N.R.S.

1. J. BOLTE, C. DEMUYNCK, G. JEMINET, J. JUILLARD et C. TISSIER. Can. J. Chem. **60**, 981 (1982).
2. J. W. WESTLEY (*Editor*). Polyether antibiotics. Vol. 1. Biology. M. Dekker, New York. 1982.
3. L. M. DULYEA, T. M. FYLES et D. M. WHITFIELD. Can. J. Chem. **62**, 498 (1984).
4. J. GUYOT, G. JEMINET et R. DEBISE. Experientia, **40**, 551 (1984).
5. M. A. KOLBER et D. H. HAYNES. Biophys. J. **36**, 369 (1981).
6. Y. N. ANTONEUKO et L. S. YAGUZHINSKY. FEBS Lett. **163**, 42 (1983).
7. D. R. PFEIFFER and H. A. LARDY. Biochemistry, **15**, 937 (1976).
8. M. DEBONO, R. M. MOLLOY, D. E. DORMAN, J. W. PASCHAL, D. F. BABCOCK, C. M. DEBER et D. R. PFEIFFER. Biochemistry, **20**, 6865 (1981).
9. G. KRAUSE, E. GRELL, A. M. ALBRECHT-GARY, D. W. BOYD et J. P. SCHWING. Stud. Phys. Theor. Chem. **24**, 255 (1983).
10. R. J. P. WILLIAMS. *In* Calcium in biological systems. Cambridge Univ. Press. 1976. pp. 1–17.
11. G. D. SMITH et W. L. DUAX. J. Am. Chem. Soc. **98**, 1578 (1976).
12. M. ALLÉAUME et Y. BARRANS. Can. J. Chem. **63**, 3482 (1985).
13. N. GRESH et A. PULLMAN. Int. J. Quantum Chem. **10**, 215 (1983).
14. M. O. CHANEY, P. V. DEMARCO, N. D. JONES et J. L. OCCOLOWITZ. J. Am. Chem. Soc. **96**, 1932 (1974).
15. M. PRUDHOMME et G. JEMINET. Experientia, **39**, 256 (1983).
16. J. BOLTE, S. CAFFAREL-MENDES, C. DEMUYNCK et G. JEMINET. Stud. Phys. Theor. Chem. **24**, 247 (1983).
17. C. M. DEBER et D. R. PFEIFFER. Biochemistry, **15**, 132 (1976).

Structure cristalline du complexe de magnésium de la calcimycine (A. 23187)

MARC ALLÉAUME[1] ET YVETTE BARRANS

Laboratoire de cristallographie, U.A. 144, C.N.R.S., Université de Bordeaux I, 33405 Talence Cédex, France

Reçu le 14 janvier 1985

MARC ALLÉAUME et YVETTE BARRANS. Can. J. Chem. **63**, 3482 (1985).

Le complexe de magnésium 1:2 de l'antibiotique calcimycine (A. 23187) cristallise dans le groupe spatial $P2_1$, avec des paramètres de maille a = 11,152(2), b = 27,684(2), c = 10,168(2) Å, β = 107,02(2)° et Z = 2. La structure a été affinée jusqu'à un facteur de reliabilité R = 0,063 pour 3473 réflexions observées. La coordination octaédrique de l'ion Mg^{2+} est hautement symétrique. Chaque ion calcimycine est lié à Mg^{2+} par un oxygène carbonyle, un oxygène carboxyle et l'azote du cycle benzoxazole. Les distances Mg—O sont respectivement de 2,00 Å et 2,06 Å, les distances Mg—N sont de 2,23 Å ($\sigma \simeq$ 0.01 Å).

MARC ALLÉAUME and YVETTE BARRANS. Can. J. Chem. **63**, 3482 (1985).

The 1:2 magnesium ion complex of the antibiotic calcimycine (A. 23187) crystallizes in the space group $P2_1$ with cell dimensions a = 11.152(2), b = 27.684(2), c = 10.168(2) Å, β = 107.02(2)°, and Z = 2. The structure was refined to an R = 0.063 based on 3473 observed reflections. The octahedral coordination of the Mg^{2+} ion is highly symmetrical. Each calcimycine ion is bound to Mg^{2+} through a carboxyl oxygen, a carbonyl oxygen, and the nitrogen of the benzoxazole ring system. The Mg—O distances are respectively 2.00 Å and 2.06 Å, the Mg—N distances 2.23 Å ($\sigma \simeq$ 0.01 Å).

La calcimycine ou A. 23187 est un polyéther monocarboxylique doué de propriétés ionophores: il complexe et transporte essentiellement les cations divalents Ca^{2+}, Mg^{2+}.

Plusieurs structures cristallines de la calcimycine[2] ont été déterminées: calcimycine, acide libre (1); 2[calci]$^-$ Ca^{2+}, 2 éthanol (2); 2[calci]$^-$ Ca^{2+}, H_2O (3); et, plus récemment, 2[calci]$^-$ Fe^{2+}, 2 éthanol (4). Nous publierons prochainement la structure du complexe 2[calci]$^-$ Mn^{2+}.

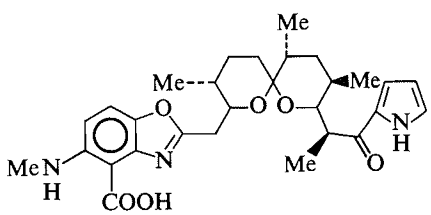

Calcimycine = A.23187

Les conditions d'extraction et de purification de la calcimycine à partir de la souche de *Streptomyces chartreusensis* sont précisées dans l'article suivant (5).

Partie expérimentale

Les cristaux du complexe 2[calci]$^-$ Mg^{2+} ont été obtenus par cristallisation d'une solution dans un mélange méthanol + acétone. Le cristal utilisé pour la collection des données était une aiguille prismatique de dimensions 0,20 × 0,30 × 0,25 mm³. Toutes les données cristallographiques—paramètres cristallins et intensités diffractées—ont été mesurées sur un diffractomètre Enraf–Nonius CAD-4 équipé d'un monochromateur au graphite ($\lambda K_{\alpha 1}$ = 1,5405 Å). Le tableau 1 résume les données cristallographiques et les conditions de mesure.

Affinement de la structure

Sur les 5207 réflexions indépendantes mesurées, 3473 réflexions "observées" ($I > 3\sigma(I)$) ont été utilisées dans la suite des calculs, après correction de Lorentz et de polarisation. Aucune correction d'absorption n'a été appliquée ($\mu R < 0{,}002$). La structure a été déterminée par méthodes directes en utilisant le programme MULTAN. Les 2/3 des atomes "lourds" sont apparus sur la première carte de densité électronique. Après 7 cycles d'affinement isotrope portant sur les 77 atomes "lourds", 3 cycles d'affinement anisotrope furent conduits avant l'introduction des atomes d'hydrogène. Tous les atomes d'hydrogène ont été affectés d'un coefficient d'agitation thermique isotrope. Les hydrogènes portés par les groupements méthyle n'ont pas été introduits dans l'affinement. Trois nouveaux cycles d'affinement sur ces 119 atomes ont conduit à un facteur de reliabilité R = 0,063 pour les 3473 réflexions observées ($R = \Sigma\|F_o| - |F_c\|/\Sigma|F_o|$), et un paramètre d'accord $s = \left(\frac{\Sigma w\Delta^2}{m-n}\right)^{1/2} = 1{,}52$. La densité électronique résiduelle sur la carte de Fourier-différence finale est inférieure à 0,30 e Å^{-3}. Les coordonnées atomiques (tableau 2), les paramètres d'agitation thermique anisotrope[3] ou isotrope (atomes d'hydrogène) ont été affinés par moindres carrés, en bloc diagonal; valeur minimisée $\Sigma\, w(|F_o| - |F_c|)^2$; schéma de pondération: $\sqrt{w} = 1$ si $|F_o| < p$ et $\sqrt{w} = p/F_o$ si $|F_o| > p$ avec $p = [F^2_{o(max)}/10]^{1/2}$; facteurs de diffusion de International Tables for X-Ray Crystallography (1974) pour les atomes lourds et de Stewart *et al.* (6) pour les atomes d'hydrogène.

Discussion

Comme dans le complexe de Ca^{2+}, 2 ions [calci]$^-$ s'associent tête-bêche pour créer une cavité complexante fermée. Chaque ion [calci]$^-$ forme une demi-coquille (fig. 1). Les 2 demi-coquilles identiques qui encagent le cation Mg^{2+} se déduisent l'une de l'autre par un pseudo-axe binaire $\psi(A_2)$ passant par le cation (fig. 1). Deux liaisons hydrogène identiques N(32)—H(321)... O(73) et N(72)—H(721)... O(33), avec N—O quasi identiques (2,84 Å et 2,85 Å), complètent la stabilisation de ce système complexant. Il faut cependant remarquer que les angles OH... N sont voisins de 150° ($\sigma \simeq$ 10°), ce qui implique une liaison hydrogène moins forte que ne l'indiquent les seules distances N... O.

1. *Ions calcimycine*

À l'exception des distances autour des carbones homologues

[1]À qui doit être adressé toute correspondance sur ce travail.

[2]Dans la suite de cet article, nous désignerons sous l'abréviation [calci]$^-$ l'ion résultant de la déprotonation de la molécule de calcimycine.

[3]Les coefficients d'agitation thermique et les facteurs de structures observés et calculés ont été déposés; on peut les acheter en s'adressant au Dépôt des données non publiées, ICIST, Conseil national de recherches du Canada, Ottawa (Ont.), Canada K1A 0S2.

TABLEAU 1. Données cristallographiques et conditions de mesure

Formule chimique: $(C_{29}H_{36}N_3O_6)_2Mg$
M: 1069,5

(a) Groupe spatial $P2_1$

$Z = 2$	$a = 11{,}152\ (2)$ Å
	$b = 27{,}684\ (2)$ Å
$F_{000} = 1136$	$c = 10{,}168\ (2)$ Å
$D_x = 1{,}18$ mg × m^{-3}	$\beta = 107{,}02°\ (2)$
$\mu = 0{,}66$ cm^{-1}	$V = 3001{,}7$ Å^3

(b) Balayage $\theta - \omega$; rapport de vitesse $\theta/\omega = 1/2$
$\theta_{min} = 1°$; $\theta_{max} = 65°$
Réflexions de contrôle: 240; $\bar{2}12$; périodicité 5400 s

TABLEAU 2. Coordonnées atomiques (× 10^4), et B équivalents des atomes lourds*

Atome	x	y	z	B_{eq}
Mg(80)	0,7431(3)	−0,3798	0,4024(3)	4,7
C(1)	0,9157(10)	−0,4530(4)	0,6067(10)	5,1
C(2)	0,8126(9)	−0,4837(3)	0,6241(9)	3,9
C(3)	0,8375(11)	−0,5254(4)	0,7130(10)	5,6
C(4)	0,7375(11)	−0,5535(4)	0,7289(11)	5,3
C(5)	0,6158(12)	−0,5446(4)	0,6621(12)	6,7
C(6)	0,5943(10)	−0,5040(4)	0,5712(11)	5,3
C(7)	0,6864(10)	−0,4752(3)	0,5539(9)	5,1
C(8)	0,5107(10)	−0,4494(4)	0,4198(10)	5,4
C(9)	0,4063(10)	−0,4297(4)	0,3048(11)	6,7
C(10)	0,4123(9)	−0,4517(4)	0,1699(10)	5,0
C(11)	0,3044(10)	−0,4391(4)	0,0429(11)	7,6
C(12)	0,3248(10)	−0,4650(5)	−0,0795(11)	7,0
C(13)	0,3435(10)	−0,5186(4)	−0,0520(11)	5,8
C(14)	0,4451(10)	−0,5297(4)	0,0821(11)	5,2
C(15)	0,4492(11)	−0,5842(4)	0,1221(12)	6,6
C(16)	0,5711(11)	−0,5964(4)	0,2334(12)	10,3
C(17)	0,6873(11)	−0,5790(4)	0,1978(12)	7,9
C(18)	0,6718(10)	−0,5245(4)	0,1707(10)	5,9
C(19)	0,7779(9)	−0,4982(4)	0,1325(11)	7,8
C(20)	0,7433(9)	−0,4444(4)	0,1354(10)	6,1
C(21)	0,6798(10)	−0,4198(4)	0,0078(10)	6,0
C(22)	0,6596(10)	−0,4333(4)	−0,1287(10)	6,5
C(23)	0,5862(12)	−0,3983(4)	−0,2071(11)	6,9
C(24)	0,5625(11)	−0,3633(4)	−0,1183(11)	8,4
C(25)	0,9886(13)	−0,5755(5)	0,8848(14)	14,3
C(26)	0,1737(10)	−0,4512(5)	0,0681(13)	8,6
C(27)	0,3328(13)	−0,5980(5)	0,1748(17)	15,2
C(28)	0,7070(13)	−0,6062(4)	0,0704(13)	10,3
C(29)	0,9074(10)	−0,5078(5)	0,2364(12)	6,6
N(30)	0,9583(9)	−0,5376(4)	0,7833(10)	5,3
N(31)	0,6300(7)	−0,4392(3)	0,4561(8)	4,3
N(32)	0,6202(8)	−0,3771(3)	0,0085(8)	6,9
O(33)	0,8839(6)	−0,4133(2)	0,5392(6)	4,5
O(34)	1,0262(7)	−0,4639(3)	0,6558(9)	10,7
O(35)	0,4809(7)	−0,4880(3)	0,4868(8)	6,4
O(36)	0,4227(6)	−0,5031(2)	0,1907(7)	5,6
O(37)	0,5594(6)	−0,5163(2)	0,0599(6)	5,2
O(38)	0,7628(6)	−0,4242(2)	0,2470(6)	4,4
C(41)	0,5335(9)	−0,3086(4)	0,2495(10)	5,4
C(42)	0,5273(9)	−0,2809(3)	0,3710(10)	4,6
C(43)	0,4435(10)	−0,2416(4)	0,3653(11)	5,5
C(44)	0,4376(11)	−0,2167(4)	0,4815(13)	6,0
C(45)	0,5190(12)	−0,2291(5)	0,6142(13)	7,0
C(46)	0,6009(10)	−0,2663(4)	0,6184(11)	6,3
C(47)	0,6056(9)	−0,2921(3)	0,5030(10)	4,8
C(48)	0,7518(9)	−0,3192(4)	0,6805(11)	4,8
C(49)	0,8654(10)	−0,3387(4)	0,7800(10)	5,2

TABLEAU 2. (*Suite*)

Atome	x	y	z	B_{eq}
C(50)	0,9784(10)	−0,3153(4)	0,7553(11)	4,8
C(51)	1,1035(11)	−0,3276(4)	0,8634(12)	5,9
C(52)	1,2062(12)	−0,2989(5)	0,8259(13)	7,8
C(53)	1,1766(11)	−0,2436(5)	0,8140(14)	5,5
C(54)	1,0474(11)	−0,2333(4)	0,7239(12)	5,1
C(55)	1,0042(11)	−0,1813(4)	0,7379(15)	6,9
C(56)	0,8954(14)	−0,1671(5)	0,6113(16)	10,6
C(57)	0,9103(13)	−0,1791(4)	0,4679(15)	9,7
C(58)	0,9400(11)	−0,2335(4)	0,4761(13)	7,6
C(59)	0,9603(11)	−0,2560(4)	0,3475(13)	8,2
C(60)	0,9708(10)	−0,3106(4)	0,3774(10)	5,3
C(61)	1,0924(11)	−0,3330(4)	0,4255(12)	7,1
C(62)	1,2088(11)	−0,3165(5)	0,4335(14)	8,8
C(63)	1,2929(11)	−0,3524(5)	0,5012(14)	8,9
C(64)	1,2258(11)	−0,3893(4)	0,5334(12)	8,9
C(65)	0,2809(14)	−0,1866(5)	0,2192(16)	11,9
C(66)	1,1017(13)	−0,3187(5)	1,0124(13)	8,2
C(67)	0,9712(13)	−0,1721(5)	0,8741(16)	8,7
C(68)	1,0173(18)	−0,1497(5)	0,4371(20)	16,8
C(69)	0,8515(13)	−0,2463(5)	0,2119(13)	11,0
N(70)	0,3627(9)	−0,2279(4)	0,2424(10)	7,8
N(71)	0,7041(8)	−0,3262(3)	0,5480(8)	4,7
N(72)	1,1036(8)	−0,3780(3)	0,4849(9)	7,4
O(73)	0,6008(6)	−0,3463(3)	0,2690(7)	5,4
O(74)	0,4767(8)	−0,2945(3)	0,1320(8)	10,1
O(75)	0,6919(7)	−0,2832(3)	0,7295(7)	7,2
O(76)	0,9547(6)	−0,2634(3)	0,7554(7)	5,4
O(77)	1,0507(7)	−0,2438(3)	0,5872(8)	6,1
O(78)	0,8725(7)	−0,3322(2)	0,3675(7)	7,0

*$B_{eq} = \frac{4}{3}(a^2\beta_{11} + b^2\beta_{22} + c^2\beta_{33} + bc\beta_{23} + ca\beta_{31} + ab\beta_{12})$. Les coordonnées atomiques et les B isotropes des atomes d'hydrogène ont été déposés (Tableau 2′).

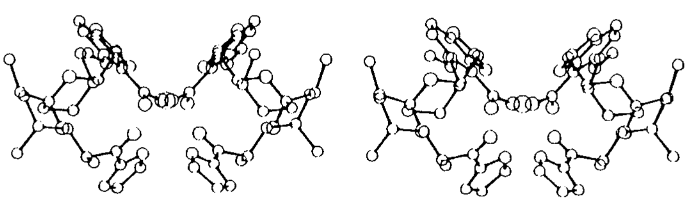

FIG. 1. Projection stéréographique du complexe sur un plan passant par $\psi(A_2)$.

C(5) et C(45), aucune variation significative n'apparaît entre les ions $[\text{calci}]_I^-$ et $[\text{calci}]_{II}^-$. La figure 2 donne les valeurs moyennes des distances et des angles.[4]

Cette identité conformationnelle des ions I et II est confirmée par l'accord entre les deux séries d'angles de torsion χ (tableau 3) ($(\delta\chi)_{max} = 4°$, $(\delta\chi)_{moy} = 2{,}3°$, $\sigma(\delta_{moy}) = 1{,}5°$)). Il faut noter que dans le complexe de Ca^{2+} (3) les variations d'angles de torsion entre les ions I et II sont beaucoup plus importantes ($(\delta\chi)_{max} = 20°$; $(\delta\chi)_{moy} = 6{,}4°$; $\sigma(\delta_{moy}) = 4{,}2°$).

Le tableau 4 donne les écarts significatifs aux groupements plans benzoxazole et cétopyrrole. L'écart de l'atome C(9) est dû aux contraintes stériques imposées par le spiroacétal. La variation de position des méthyles C(25)I et C(65)II pourrait

[4]Les figures 2′ et 2″ donnant respectivement les longueurs de liaisons et les angles de valence de chacun des 2 ions $[\text{calci}]^-$ ont été déposées; on peut les acheter en s'adressant au Dépôt des données non publiées, ICIST, Conseil national de recherches du Canada, Ottawa (Ont.), Canada K1A 0S2.

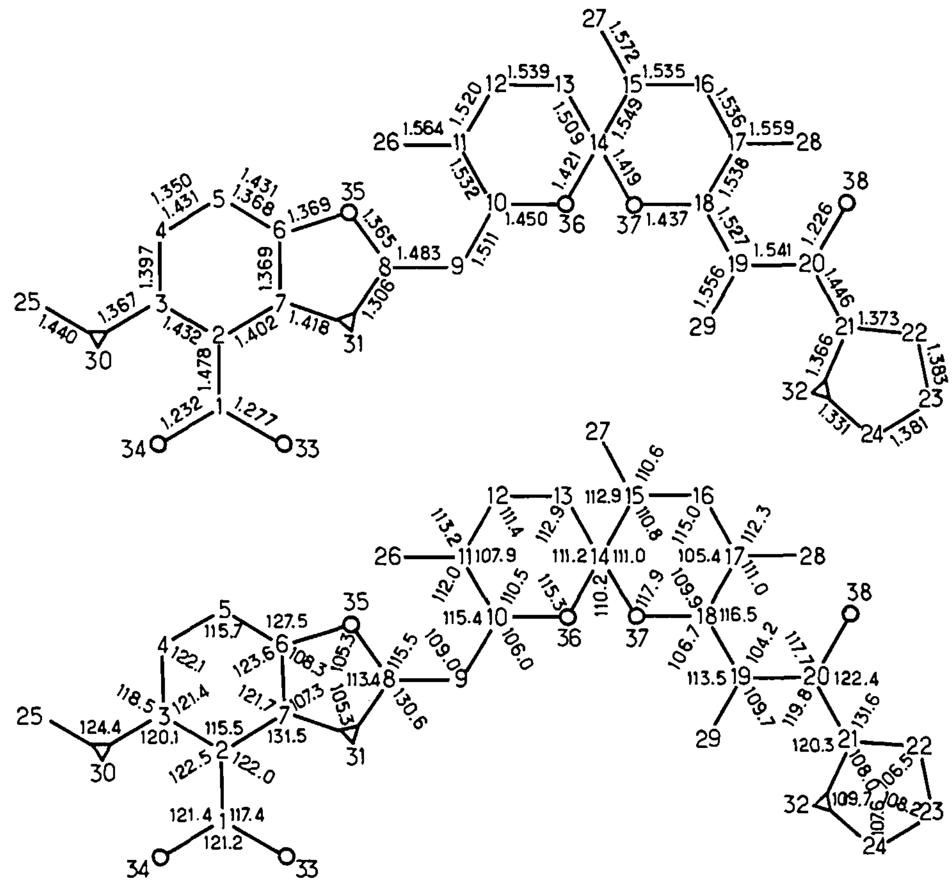

FIG. 2. Valeurs moyennes des distances et des angles. σ_{C-C} = 0,007–0,015 Å; $\sigma_{C-O} \simeq$ 0,07 Å; $\sigma_{C-N} \simeq$ 0,07 Å; $\sigma_{C-C-C} \simeq$ 0,7°; σ_{C-O-C}, $\sigma_{C-N-C} \simeq$ 0,5°.

TABLEAU 3. Angles de torsion (°) des ions $[calci]_I^-$ et $[calci]_{II}^-$; $\sigma \simeq$ 1°

χ	$[calci]_I^-$	$[calci]_{II}^-$
O(35) C(8) C(9) C(10)	−95	−99
N(31) C(8) C(9) C(10)	76	73
C(8) C(9) C(10) O(36)	50	52
C(8) C(9) C(10) C(11)	174	173
O(37) C(18) C(19) C(20)	67	63
C(17) C(18) C(19) C(20)	−171	−173
C(18) C(19) C(20) C(21)	−98	−98

être liée aux variations de distances autour du carbone C(5) signalées plus haut.

Il faut noter que l'ion Mg^{2+} est toujours voisin du plan du cycle, ce qui correspond à la géométrie la plus favorable de l'interaction ion–ligande pour les 3 ligandes O(carboxyle), O(carbonyle), N(pyrrole).

2. *Environnement du cation*

La complexation hexacoordonnée de l'ion Mg^{2+} est assurée par 4 atomes d'oxygène et 2 atomes d'azote, chacun des 2 ions $[calci]^-$ apportant la même contribution à cette complexation (tableau 5). Ces 6 ligandes forment un octaèdre quasi parfait autour de Mg^{2+}. La figure 3 donne une représentation schématique de cet octaèdre, le pseudo-axe binaire $\psi(A_2)$ étant dans le plan de la figure.

Si l'on admet que les distances cation–ligande sont pratiquement égales à la somme (rayon ionique + rayon de van der Waals), et que pour les atomes impliqués dans ces coordinations octaédriques, les contacts $[calci]_I^-$ – $[calci]_{II}^-$ (comme N(31) .... N(71) ou O(38) ... O(73)) sont de type contacts de van der Waals, on est conduit à prendre les valeurs suivantes: $R_{Mg^{2+}}$ = 0,60 Å; $R_{O\ carboxyle}$ = 1,40 Å; $R_{O\ carbonyle}$ = 1,46 Å; R_N = 1,65 Å.

Les valeurs que nous proposons sont légèrement différentes de celles habituellement admises (7, 8). Le tableau 5, colonnes (a) et (b), montre qu'elles donnent, pour le complexe étudié, un excellent accord entre les distances "observées" et les distances calculées à partir de nos propres valeurs. Il en est de même pour d'autres complexes hexacoordonnés de Mg^{2+}. La structure de Mg-malate pentahydrate (9) donne des résultats comparables: Mg^{2+} ... O de 2,02 à 2,11 Å. Ces valeurs sont aussi en accord avec les distances cation–ligande observées dans le complexe de Ca^{2+} monohydraté (3), à condition de prendre un rayon ionique $R_{Ca^{2+}} \simeq$ 0,90 Å. Les distances cation–ligande calculées vont de 2,30 Å à 2,55 Å, les distances moyennes observées étant de 2,27 Å à 2,63 Å.

De plus, ces deux séries de valeurs calculées pour les complexes de Mg^{2+} et de Ca^{2+} sont identiques aux valeurs obtenues par minimisation d'énergie (10). La comparaison des distances cation–ligande dans ces deux structures permet d'affirmer que la première structure de complexe publiée (2) a été interprétée incorrectement: il ne s'agit pas d'un complexe de Ca^{2+}, mais bien d'un complexe de Mg^{2+}. Les distances cation–ligande vont de 1,92 Å à 2,22 Å. Ces valeurs, voisines de celles produites par le présent travail, ne peuvent être attribuées à des distances Ca^{2+}–ligande, qui sont de 0,30 Å plus grandes.

Conclusions

Les deux traits majeurs du complexe $2[calci]^- Mg^{2+}$ à l'état cristallin sont (*i*) l'identité conformationnelle des 2 ions

TABLEAU 4. Écarts aux plans moyens des groupements benzoxazole et cétopyrrole

Atomes définissant le plan	Atome						
	Écart au plan (Å) ($\sigma \leq 0{,}01$ Å)						
Plan 1, I							
C(2), C(3), C(4), C(5), C(6)	C(1)	(C9)	C(25)	N(30)	O(33)	O(34)	Mg(80)
C(7), C(8), N(31), O(35)	0,00	0,28	−0,02	0,09	−0,21	0,17	−0,14
Plan 1, II							
C(42), C(43), C(44), C(45), C(46)	C(41)	C(49)	C(65)	N(70)	O(73)	O(74)	Mg(80)
C(47), C(48), N(71), O(75)	0,01	−0,26	−0,22	−0,06	0,21	−0,20	0,12
Plan 2, I							
C(20), C(21), C(22), C(23)	C(19)	O(38)	Mg(80)				
C(24), N(32)	−0,41	0,13	0,12				
Plan 2, II							
C(60), C(61), C(62), C(63)	C(59)	C(78)	Mg(80)				
C(64), N(72)	−0,41	0,10	0,05				

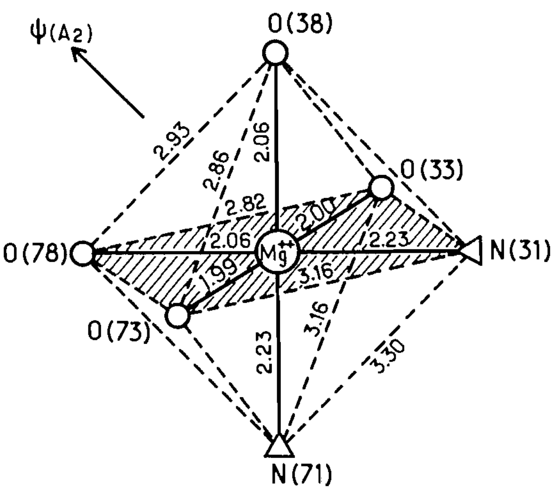

FIG. 3. Environnement octaèdrique de l'ion Mg^{2+}.

TABLEAU 5. Distances observées (a) et calculées (b) pour l'octaèdre de coordination

Atomes	(a) Distance (Å)	(b) Distance (Å)
Mg—N(3)	2,235(9)	2,20
Mg—N(71)	2,228(9)	
Mg—O(33)	1,996(7)	2,00
Mg—O(73)	1,990(8)	
Mg—O(38)	2,064(7)	2,06
Mg—O(78)	2,060(8)	
N(31)—N(71)	3,30(1)	3,30
N(31)—O(73)	3,16(1)	3,16
N(71)—O(33)	3,16(1)	
O(33)—O(78)	2,82(1)	2,86
O(73)—O(38)	2,86(1)	
O(38)—O(78)	2,93(1)	2,92

TABLEAU 6. Angles autour du cation Mg^{2+}

Atomes	Angles (°)
N(31)—Mg—O(33)	82,7(3)
N(31)—Mg—O(38)	86,7(3)
N(31)—Mg—N(71)	95,4(3)
N(31)—Mg—O(73)	96,6(3)
N(31)—Mg—O(78)	170,5(3)
O(33)—Mg—O(38)	91,0(3)
O(33)—Mg—N(71)	96,5(3)
O(33)—Mg—O(73)	178,8(3)
O(33)—Mg—O(78)	88,2(3)
O(38)—Mg—N(71)	172,4(3)
O(38)—Mg—O(73)	89,9(3)
O(38)—Mg—O(78)	90,7(3)
N(71)—Mg—O(73)	82,6(3)
N(71)—Mg—O(78)	88,3(3)
O(73)—Mg—O(78)	92,5(3)

[calci]$^-$; et (*ii*) la symétrie octaèdrique quasi parfaite des 6 ligandes qui assurent la complexation de l'ion Mg^{2+}.

La grande symétrie du complexe de Mg^{2+} ne se retrouve pas dans le complexe de Ca^{2+}; nous pensons que ces caractéristiques structurales, si elles se conservent en solution, pourraient être liées au transport préférentiel du Ca^{2+} par rapport au Mg^{2+} (5). La décomplexation du cation est, avec ce type de complexe, une opération de "rupture de symétrie", que favoriserait une dissymétrie préexistante, comme celle que présente le complexe de Ca^{2+}.

Remerciement

Ce travail a été mené dans le cadre de la Recherche Coopérative sur Programme 80/605 du C.N.R.S.

1. M. O. CHANEY, P. V. DEMARCO, N. D. JONES, et J. L. OCCOLOWITZ. J. Am. Chem. Soc. **96**, 1932 (1974).
2. M. O. CHANEY, N. D. JONES, et M. J. DEBONO. J. Antibiot. **29**, 424 (1976).
3. G. D. SMITH et W. L. DUAX. J. Am. Chem. Soc. **98**, 1578 (1976).
4. E. BAKER, E. N. MASLEN, K. J. WATSON et A. H. WHITE. J. Am. Chem. Soc. **106**, 2860 (1984).
5. J. BOLTE, C. DEMUINCK, et G. JEMINET. Can. J. Chem. **63**, 3478 (1985).
6. R. F. STEWART, E. R. DAVIDSON, et W. T. SIMPSON. J. Chem. Phys. **42**, 3175 (1965).
7. L. H. AHRENS. Geochim. Cosmochim. Acta, **2**, 155 (1952).
8. L. PAULING. The nature of the chemical bond. 3è ed. Cornell University Press, Ithaca, NY. 1960. p. 538.
9. W. VAN HAVERE et T. H. LENSTRA. Acta Crystallogr. Sect. B, **36**, 2424 (1980).
10. N. GRESH et A. PULLMAN. Int. J. Quantum Chem. Quantum Biol. Symp. **10**, 215 (1983).

An evaluation of the kinetic data for the hydrogen transfer reactions: $CH_3 + CH_3COCH_3$, $CD_3 + CD_3COCD_3$ and $CH_3 + CH_3NNCH_3$

NEVILLE L. ARTHUR AND PAULA J. NEWITT
Department of Physical Chemistry, La Trobe University, Melbourne, Victoria, Australia, 3083

Received June 20, 1985

NEVILLE L. ARTHUR and PAULA J. NEWITT. Can. J. Chem. **63**, 3486 (1985).

An evaluation of the kinetic data for the reactions

[2] $CH_3 + CH_3COCH_3 \rightarrow CH_4 + CH_3COCH_2$

[7] $CD_3 + CD_3COCD_3 \rightarrow CD_4 + CD_3COCD_2$

[11] $CH_3 + CH_3NNCH_3 \rightarrow CH_4 + CH_3NNCH_2$

has been undertaken, and the following rate constants, based on the value $10^{13.34}$ cm^3 mol^{-1} s^{-1} for the recombination of CH_3 and CD_3 radicals, are recommended:

$$\log k_2 = (11.54 \pm 0.03) - (40490 \pm 280)/19.145T$$

$$\log k_7 = (11.78 \pm 0.08) - (48500 \pm 690)/19.145T$$

$$\log k_{11} = (11.05 \pm 0.07) - (33390 \pm 560)/19.145T$$

$$\log k_{11}(\text{corr}) = (11.21 \pm 0.08) - (34570 \pm 590)/19.145T$$

where k is in cm^3 mol^{-1} s^{-1}, E is in J mol^{-1}, the error limits are standard deviations, and k_{11}(corr) refers to the rate constant corrected for the intramolecular elimination of C_2H_6 in the photolysis of CH_3NNCH_3.

NEVILLE L. ARTHUR et PAULA J. NEWITT. Can. J. Chem. **63**, 3486 (1985).

On a procédé à une évaluation des données cinétiques relatives aux réactions

[2] $CH_3 + CH_3COCH_3 \rightarrow CH_4 + CH_3COCH_2$

[7] $CD_3 + CD_3COCD_3 \rightarrow CD_4 + CD_3COCD_2$

[11] $CH_3 + CH_3NNCH_3 \rightarrow CH_4 + CH_3NNCH_2$

et, en se basant sur la valeur de $10^{13.34}$ cm^3 mol^{-1} s^{-1} pour la recombination des radicaux CH_3 et CD_3, on recommande les constantes de vitesses suivantes:

$$\log k_2 = (11{,}54 \pm 0{,}03) - (40490 \pm 280)/19{,}145T$$

$$\log k_7 = (11{,}78 \pm 0{,}08) - (48500 \pm 690)/19{,}145T$$

$$\log k_{11} = (11{,}05 \pm 0{,}07) - (33390 \pm 560)/19{,}145T$$

$$\log k_{11}(\text{corr}) = (11{,}21 \pm 0{,}08) - (34570 \pm 590)/19{,}145T$$

dans lesquelles k est en cm^3 mol^{-1} s^{-1}, E est en J mol^{-1}, les limites d'erreur sont les déviations standards et k_{11}(corr) se réfère à la constante de vitesse corrigée pour l'élimination intramoléculaire de C_2H_6 lors de la photolyse du CH_3NNCH_3.

[Traduit par le journal]

Introduction

A vast quantity of kinetic data on the hydrogen transfer reactions of CH_3 and CD_3 radicals has been gathered over the past thirty years (1, 2). This has been made possible by the availability of convenient, clean, sources of radicals: the photolyses of acetone, acetone-d_6, and azomethane.

For kinetic studies of this kind, the key reactions in the photolysis of acetone (3) are:

[1] $CH_3COCH_3 + h\nu \rightarrow 2CH_3 + CO$

[2] $CH_3 + CH_3COCH_3 \rightarrow CH_4 + CH_3COCH_2$

[3] $2CH_3 \rightarrow C_2H_6$

and the rate constant for reaction [2] is evaluated relative to that for [3] from the expression

[4] $k_2/k_3^{\frac{1}{2}} = R_{CH_4}[2]/(R_{C_2H_6}^{\frac{1}{2}}[CH_3COCH_3])$

where R represents the rate of formation. When acetone is photolyzed in the presence of a substrate, CH_4 is also formed:

[5] $CH_3 + RH \rightarrow CH_4 + R$

Provided that k_2 is known, that part of the total CH_4 resulting from reaction [2] can be calculated from $R_{C_2H_6}$, and subtraction gives $R_{CH_4}[5]$. $k_5/k_3^{\frac{1}{2}}$ is then obtained from

[6] $k_5/k_3^{\frac{1}{2}} = R_{CH_4}[5]/(R_{C_2H_6}^{\frac{1}{2}}[RH])$

k_2 and k_5 can be evaluated by inserting a value of k_3 from the literature.

In the case of acetone-d_6, two isotopically distinguishable methanes are formed:

[7] $CD_3 + CD_3COCD_3 \rightarrow CD_4 + CD_3COCD_3$

[8] $CD_3 + RH \rightarrow CD_3H + R$

k_8 can be evaluated by means of an expression analogous to eq. [6], or the ratio k_8/k_7 can be obtained from

$$[9] \quad k_8/k_7 = R_{CD_3H}[CD_3COCD_3]/(R_{CD_4}[RH])$$

and substitution for k_7 gives a value for k_8.

The relevant reactions in the photolysis of azomethane are

$$[10] \quad CH_3NNCH_3 + h\nu \rightarrow 2CH_3 + N_2$$

$$[11] \quad CH_3 + CH_3NNCH_3 \rightarrow CH_4 + CH_3NNCH_2$$

$$[3] \quad 2CH_3 \rightarrow C_2H_6$$

and a relation similar to eq. [4] allows k_{11} to be evaluated from R_{CH_4} and $R_{C_2H_6}$. However, there is a considerable amount of evidence (5, 6) that suggests that about 0.9% of the N_2 formed in the photolysis is produced by the intramolecular elimination reaction

$$[12] \quad CH_3NNCH_3 + h\nu \rightarrow C_2H_6 + N_2$$

and the expression for k_{11}, corrected for the occurrence of reaction [12], therefore becomes

$$[13] \quad k_{11}(\text{corr})/k_3^{\frac{1}{2}} = R_{CH_4}[11]/\{(R_{C_2H_6} - 0.009R_{N_2})^{\frac{1}{2}} \times [CH_3NNCH_3]\}$$

When azomethane-substrate mixtures are photolyzed, reaction [5] must be added to those above. k_5 may be evaluated, either by the analogue of eq. [6], ignoring the small correction for reaction [12], or, taking it into account, by means of the relation

$$[14] \quad k_5/k_3^{\frac{1}{2}} = R_{CH_4}[5]/\{(R_{C_2H_6} - 0.009R_{N_2})^{\frac{1}{2}}[RH]\}$$

where $R_{CH_4}[5]$ is calculated from $k_{11}(\text{corr})$ via eq. [13].

It can be seen from the above that rate constants for a particular hydrogen transfer reaction can only be evaluated if rate constants for attack on the radical source have previously been measured. In order to determine whether a particular set of data for abstraction from the radical source falls within acceptable limits, and therefore whether subsequent data collected in the same system can be regarded as reliable, best values for the Arrhenius parameters for attack on the radical source must be established.

Because of the limited amount of published rate constant data available for attack on CH_3COCH_3, CD_3COCD_3, and CH_3NNCH_3, previous evaluations (1, 4) have been confined to the averaging of Arrhenius parameters. We have obtained a large quantity of additional data by communicating with the authors, or by reference to theses, and the evaluation presented here is therefore based on a sounder statistical approach than has previously been used.

Evaluation procedure

The handling of the large amount of data involved in this work was greatly facilitated by the availability of an interactive computer-based storage, retrieval, and analysis system developed in this laboratory (7). For each investigation of a particular reaction, an input file in a standard format is created, containing the following information: authors, bibliographical reference, radical source, reference reaction, temperature and pressure ranges, comments, the rate constant versus temperature data, and the Arrhenius parameters resulting from a least-squares treatment of the data.[1]

The information contained in the files can be retrieved according to reaction type (attacking radical), reaction, author or reference, and the data from selected files can be combined into a single large set. A least-squares analysis of the data is then carried out to yield the Arrhenius parameters and their standard deviations; the output includes a value for the deviation of each data point from the line of best fit, and the data point furthest from the line is identified. This, or any other, point can be temporarily deleted and the remainder of the set reanalysed, a process which can be repeated at the discretion of the evaluator. To assist in the visual interpretation of the data analysis, the option of a hard copy Arrhenius plot is available at any stage of the analysis procedure.

Results and discussion

CH_3 attack on acetone

Of the 40 studies of abstraction from acetone by CH_3 radicals in the open literature, only 21 contain rate constant data. We obtained a further 12 sets of data from the authors or from theses, leaving only 7 studies for which data are not now available. All of the results are summarized in Table 1, together with the corresponding temperature ranges, and also rate constants evaluated at 400 K. The Arrhenius parameters quoted have been recalculated by us from the original data by the method described in the previous section, but without eliminating any of the data points. A number of discrepancies between these values and those originally reported were noticed, especially in the work done before electronic calculators and computers came into common use.

Most of the data fall within the temperature range 393–523 K (120–250°C), and data outside of this range were excluded. Three reasons contributed to this decision: the Arrhenius plot is known to be nonlinear at temperatures below about 393 K (3); product analyses outside these limits are less reliable than within (at high temperatures much more CH_4 is formed than C_2H_6, whereas at low temperatures C_2H_6 predominates); and, because the points are at the ends of the line, inclusion of the small number of rate constants involved would have had a disproportionate effect on the calculated Arrhenius parameters. In addition to these data, those contained in ref. 14 were also omitted because in that case CH_3 radicals were generated by means of the thermal decomposition of di-*tert*-butyl peroxide, rather than by the photolysis of acetone.

The combined data set edited in this way consisted of 395 points in 31 individual sets. Analysis by the method described in the previous section showed that 4 points were greater than 4 standard deviations from the line of best fit. After these points had been deleted, and taking the value of k_3 to be $10^{13.34}$ cm^3 mol^{-1} s^{-1} (48, 49), analysis of the remaining 391 points (in 31 sets) gave

$$[15] \quad \log k_2 = (11.54 \pm 0.03) - (40490 \pm 280)/19.145T$$

where k_2 and A_2 are in cm^3 mol^{-1} s^{-1} and E is in J mol^{-1}. The data points and the line represented by eq. [15] are shown in Fig. 1.

The averages of the Arrhenius parameters listed in Table 1 (omitting the very low results of ref. 9 and those from experiments in which di-*tert*-butyl peroxide was the radical source (14, 18)) are: $\log A = (11.48 \pm 0.23)$ and $E = (39.84 \pm 1.57)$ kJ mol^{-1}, where the error limits are standard deviations from the mean. These values are slightly lower than those suggested by Kerr and Parsonage (1), $\log A = (11.54 \pm 0.2)$, $E = (40.6 \pm 2.1)$ kJ mol^{-1} and Arthur *et al.* (4), $\log A = 11.54$, $E = 40.29$ kJ mol^{-1}. In view of the much larger quan-

[1]A complete set of these data files is available and may be purchased from the Depository of Unpublished Data, CISTI, National Research Council of Canada, Ottawa, Ont., Canada K1A 0R6.

TABLE 1. Hydrogen abstraction from CH_3COCH_3 by CH_3 radicals

Temp. (K)	log A (A/cm^3 mol^{-1} s^{-1})	E (kJ mol^{-1})	log k (400 K)	Ref.	Temp. (K)	log A (A/cm^3 mol^{-1} s^{-1})	E (kJ mol^{-1})	log k (400 K)	Ref.
394–573	11.53±0.05	40.76±0.45	6.21	8[a]	405–565	11.43	40.0	6.21	28[c]
299–395	9.41	25.28	6.11	9[a]	406–408	—	—	6.27[d]	29
397–523	11.37±0.04	38.59±0.35	6.33	10[a]	415–499	11.36±0.05	38.81±0.46	6.29	30[a]
298–395	—	40.2	—	11	386–573	11.55±0.04	41.27±0.32	6.16	31[a]
398–448	10.88±0.38	35.00±3.08	6.31	12[a]	413–493	11.47±0.16	41.06±1.39	6.11	32[a]
400–565	11.46±0.10	39.29±0.83	6.33	13[a]	403–503	11.42±0.04	39.51±0.34	6.26	33[a]
400–448	11.09±0.12	38.36±0.96	6.08	14[a,b]	403–521	11.37±0.10	39.61±0.90	6.20	34[a]
405–565	11.43±0.06	39.74±0.55	6.24	15[a]	394–571	11.34±1.67	39.50±1.46	6.18	35
558–688	—	40.6	—	16	399–524	11.53±0.03	40.30±0.25	6.27	36[a]
403–563	11.42	39.71	6.23	17[a]	389–478	11.66±0.03	41.41±0.24	6.25	[a,e]
403–427	11.8	39.7±1.3	6.62	18[b]	395–525	11.62±0.03	41.11±0.29	6.25	38[a]
544–712	11.39±0.12	38.62±1.41	6.35	19[a]	423–498	12.37±0.90	38.49±2.09	7.34	39
378–557	11.44±0.07	40.06±0.63	6.21	20[a]	343–534	11.49±0.14	40.29±1.12	6.23	40[a]
399–511	11.24±0.05	38.45±0.41	6.22	21[a]	381–543	11.51±0.28	40.17±2.74	6.26	41[a]
428–642	11.57±0.08	41.26±0.82	6.18	22[a]	400–513	11.65±0.17	41.60±1.42	6.22	42[a]
300–685	11.32±0.16	38.05±1.27	6.35	23[a]	398–521	11.61±0.05	40.49±0.45	6.32	43[a]
473–623	11.79±0.04	42.77±0.43	6.20	24[a]	383–598	11.57±0.06	40.09±0.48	6.33	44[a]
473–748	11.09±0.31	35.00±3.90	6.52	25[a]	395–517	11.52±0.02	40.59±0.17	6.22	45[a]
395–526	11.33±0.08	39.87±0.67	6.12	26	373–465	11.50±0.03	40.31±0.26	6.24	46[a]
396–574	11.69±0.08	41.56±0.68	6.26	27[a]	398–522	11.54±0.02	40.00±0.22	6.32	47[a]

[a]Reevaluated.
[b]Di-*tert*-butyl peroxide was employed as the radical source.
[c]The authors reworked the data of ref. 15, allowing for three different light intensities.
[d]Average value at 406–408 K.
[e]N. L. Arthur and J. C. Biordi. Unpublished data, 1969.

tity of data involved in the present evaluation, the more rigorous approach employed, and the errors found in some of the reported Arrhenius parameters, the agreement between the Arrhenius parameters proposed in the earlier evaluations and those recommended here must be regarded as fortunate.

It is our opinion that the performance of a particular experimental system can be considered satisfactory only if the data obtained with it for CH_3 attack on acetone yield Arrhenius parameters that lie within four standard deviations of the values given in eq. [15]. Our recommended values for the Arrhenius parameters for this reaction are therefore log A = (11.54 ± 0.12) and E = (40.49 ± 1.12) kJ mol^{-1}. On this basis the error limits suggested by Kerr and Parsonage are rather too generous.

CD_3 attack on acetone-d$_6$

Of the 19 studies of deuterium abstraction from CD_3COCD_3 by CD_3 radicals in the literature, only 9 include rate constant – temperature data. We have secured a further 6 sets of data through correspondence with the authors.

A summary of the Arrhenius parameters is presented in Table 2. Before the combined data were analysed, rate constants outside the range 393–523 K were excluded, leaving 183 of the original 242 points in 14 individual sets. Least-squares analysis of these data, together with the same value for k_3 as for CH_3 recombination (49), yielded

$$[16] \quad \log k_7 = (11.78 \pm 0.08) - (48500 \pm 690)/19.145T$$

where the units are the same as before. An Arrhenius plot of the data is shown in Fig. 2. All of the data points were found to be within four standard deviations of the line of best fit. It is interesting to note that with one exception, the only values of the Arrhenius parameters for the individual studies more than four standard deviations from the values in eq. [16] come from

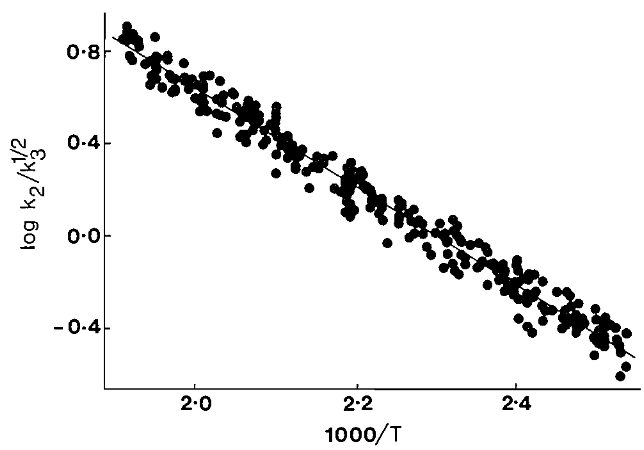

FIG. 1. Hydrogen abstraction from acetone by CH_3 radicals.

work undertaken prior to 1955, before samples of acetone-d_6 of high isotopic purity became available commercially.

The arithmetic means of the Arrhenius parameters from Table 2 are log A = (11.61 ± 0.22) and E = (46.71 ± 2.20) kJ mol^{-1}. These values are somewhat lower than those in eq. [16] as a result of the influence on them of several low values derived from a small number of points. The values recommended by Kerr and Parsonage, log A = (11.68 ± 0.2) and E = (47.7 ± 2.1) kJ mol^{-1}, and by Arthur *et al.*, log A = 11.69 and E = 47.99 kJ mol^{-1}, would also have been similarly affected.

We consider that Arrhenius parameters which fall more than four standard deviations outside the values given in eq. [16] are almost certainly unreliable, and therefore our recommended values are log A = (11.78 ± 0.32) and E = (48.50 ± 2.76) kJ mol^{-1}.

TABLE 2. Deuterium abstraction from CD_3COCD_3 by CD_3 radicals

Temp. (K)	log A (A/cm^3 mol^{-1} s^{-1})	E (kJ mol^{-1})	log k (400 K)	Ref.
411−565	11.29±0.06	43.21±0.56	5.65	8[a]
416−558	11.41±0.16	43.77±1.48	5.69	10[a]
407−569	11.41±0.12	44.60±1.11	5.59	15[a]
407−569	11.76	48.44	5.43	16
403−563	11.37	44.25	5.59	17[a]
373−563	11.76±0.10	46.26±0.80	5.72	50[a]
739−798	—	—	—	51[c]
398−475	11.48±0.24	45.77±1.99	5.50	21[a]
471−472	—	—	6.39[b]	52
473−623	12.09±0.17	50.37±1.71	5.51	53[a]
353−523	11.66±0.03	47.86±0.21	5.41	54
371−571	11.63±0.06	48.02±0.48	5.36	[a,d]
404−470	11.53±0.07	49.94±0.56	5.40	32[a]
410−520	11.62±0.08	48.49±0.66	5.29	34[a]
395−532	11.79±0.03	48.51±0.28	5.46	38[a]
396−496	11.63±0.02	46.48±0.21	5.56	56
472−582	11.84±0.07	48.90±0.65	5.45	57[a]
298−573	11.27±0.13	43.51±1.11	5.59	58[a]
385−499	11.80±0.08	48.69±0.67	5.44	42[a]

[a]Reevaluated.
[b]Average rate constant value at 471 K.
[c]Pyrolysis of acetone/acetone-d_6 mixture.
[d]G. Grieg. Private communication.

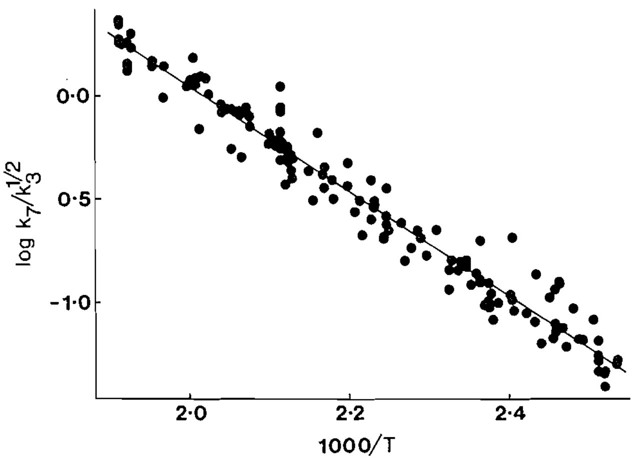

FIG. 2. Deuterium abstraction from acetone-d_6 by CD_3 radicals.

Kinetic isotope effect for CH_3 attack on CH_3COCH_3/CD_3COCH_3

If it is assumed that the reactivities of CH_3 and CD_3 radicals are equal (47, 51), the kinetic isotope effect for attack on CH_3COCH_3 and CD_3COCD_3 can be evaluated from

$$[17] \quad \log(k_H/k_D) = (\log A_H - \log A_D) + (E_D - E_H)/19.145T$$

Substituting our recommended values into this equation leads to $A_H/A_D = 0.58$, $E_D - E_H = 8.01$ kJ mol^{-1}, and $k_H/k_D = 6.4$ at 400 K.

Experimental kinetic isotope effects are usually compared with those predicted by the simple model that assumes the bond being attacked is broken in forming the transition state (4). According to this model, the ratio of A factors, A_H/A_D, is 1, and the difference in activation energies, $E_D - E_H$, is identified with the difference in zero-point energies of the C—H and C—D bonds, Δzpe. k_H/k_D is therefore given by

$$[18] \quad \log(k_H/k_D) = \Delta\text{zpe}/19.145T$$

The vibrational frequencies of these bonds in CH_3COCH_3 and CD_3COCD_3 are 2937 cm^{-1} and 2123 cm^{-1}, respectively (59), from which Δzpe = 4.87 kJ mol^{-1}, and hence $k_H/k_D = 4.3$ at 400 K. Comparison of the predicted and experimental values shows that $E_D - E_H > \Delta$zpe, $A_H/A_D < 1$, and $k_H/k_D > 4.3$ at 400 K. This may be due to the occurrence of quantum mechanical tunnelling (60), or to the loss of bending vibrations in the transition state (61).

CH_3 attack on azomethane

We have traced 31 studies of the reaction of CH_3 radicals with azomethane, but in only 10 of these were rate constant – temperature data reported. Although we have obtained a further 8 sets of data from the authors, the proportion of the total for which data are now available is still more than 20% less than for CH_3 attack on acetone and acetone-d_6.

The Arrhenius parameters for each study, together with the corresponding temperature ranges, are summarized in Table 3. As before, the Arrhenius parameters have been recalculated from the orginal data wherever possible.

We conducted two evaluations of the combined data: one of rate constants uncorrected for the intramolecular elimination of C_2H_6, reaction [12]; and the other of corrected data. In each case only rate constants within the temperature range 333–463 K (60–190°C) were considered, and the data of ref. 62 and 69 were omitted because of their unusually high degree of scatter.

After pruning the data in this way, 12 sets of rate constants uncorrected for reaction [12] remained, containing 166 points. Least-squares analysis of these data, with the same value of k_3 as before, gave

$$[19] \quad \log k_{11} = (11.05 \pm 0.07) - (33390 \pm 560)/19.145T$$

An Arrhenius plot of the data is shown in Fig. 3. The simple averages of the Arrhenius parameters for these 12 sets of data, taken from Table 3, are log A = (10.89 ± 0.30) and E = (32.56 ± 1.96) kJ mol^{-1}. These values are somewhat lower than those obtained in a similar way by Kerr and Parsonage: log A = (11.05 ± 0.03) and E = (33.1 ± 2.1) kJ mol^{-1}. Again, the agreement between these values and those given in eq. [19] is rather fortuitous, especially since Kerr and Parsonage did not distinguish between Arrhenius parameters corresponding to corrected and uncorrected rate constants. On the basis that Arrhenius parameters that fall outside four standard deviations from the values given in eq. [19] are suspect, we recommend the values log A = (11.05 ± 0.28) and E = (33.39 ± 2.24) kJ mol^{-1}.

Fifteen studies have reported Arrhenius parameters derived from rate constants corrected for the intramolecular elimination of C_2H_6. Of these only 8 contained tables showing the rate of

TABLE 3. Hydrogen abstraction from CH_3NNCH_3 by CH_3 radicals

Temp. (K)	log A (A/cm^3 mol^{-1} s^{-1})	E (kJ mol^{-1})	log k (400 K)	Ref.	Temp. (K)	log A (A/cm^3 mol^{-1} s^{-1})	E (kJ mol^{-1})	log k (400 K)	Ref.
297–464	10.12±0.11	27.32±0.81	6.55	62[a]	337–431	10.84±0.17	32.68±1.24	6.57	79[a]
	10.45±0.13	29.34±0.91	6.62	62[a,b1]	298–437	11.55±0.10	36.40±0.84	6.80	80[b2]
300–400	10.49	30.50	6.51	63	369–457	11.26±0.17	34.72±1.34	6.73	81[a]
301–406	10.54±0.07	30.71±0.47	6.53	64[a]		11.25±0.18	34.55±1.36	6.74	81[a,b1]
	10.55±0.09	30.76±0.57	6.53	64[a,b1]	298–453	11.6±0.3	36.0±2.1	6.90	82[b3]
296	—	—	5.40[c1]	65	344–526	11.1	31.8	6.95	83[b2]
360–452	—	35.1±1.3	—	66	323–470	11.13±0.07	32.87±0.55	6.84	56[a]
226–323	8.85±0.22	20.41±1.03	6.18	67[a]	366–447	11.01±0.05	32.18±0.35	6.81	84[a]
363–448	10.93±0.11	32.80±0.80	6.65	68		11.03±0.05	32.26±0.35	6.82	84[a,b1]
423	—	—	6.95[c2]	69	372–441	10.67±0.09	30.39±0.67	6.70	[a,e]
380–450	10.94±0.26	32.64±1.67	6.68	70		10.70±0.09	30.57±0.68	6.71	[a,b1,e]
287–468	10.97±0.04	32.76±0.33	6.69	71	352–450	11.48±0.13	36.44±1.01	6.72	86[a]
333	—	—	6.00[c3]	72	301	—	—	5.29[c4]	87[b4]
298–453	10.70±0.05	31.10±0.36	6.64	73[a]	298–491	11.16±0.25	33.68±1.84	6.76	37[b2]
393–448	11.03±0.06	34.31±0.42	6.55	74	323–453	12.00±0.18	40.78±1.32	6.67	55[a,b5]
391–453	10.84±0.08	32.75±0.64	6.56	75[a]	320–450	11.08±0.03	33.75±0.24	6.67	85
	10.84±0.09	32.73±0.72	6.57	75[a,b1]		11.10±0.04	33.89±0.25	6.67	85[b1]
393–448	10.9	32.6	6.64	76	334–463	10.98±0.02	32.55±0.16	6.73	47[a]
373–473	10.97±0.04	32.97±0.33	6.66	77		11.04±0.02	32.97±0.18	6.73	47[a,b1]
323–453	11.5	36.4	6.75	78[b2]					

[a]Reevaluated.
[b]Corrected for the intramolecular elimination of ethane: 1(0.009), 2(0.007), 3(0.012), 4(0.013), 5(0.0092).
[c]Average rate constant value at: 1(296 K), 2(423 K), 3(333 K), 4(301 K).
[d]Approximate temperature range.
[e]P. Gray and L. J. Leyshon. Private communication.

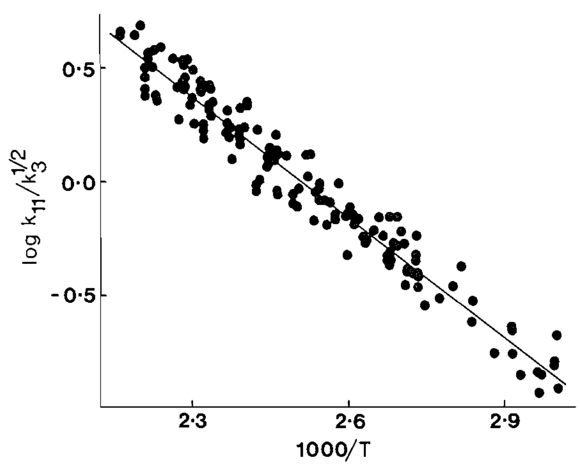

FIG. 3. Hydrogen abstraction from azomethane by CH_3 radicals.

nitrogen formation, R_{N_2}, and hence only for these could rate constants and Arrhenius parameters be recalculated. Analysis of the 128 points involved gave

$$[20] \quad \log k_{11}(\text{corr}) = (11.21 \pm 0.08) - (34570 \pm 590)/19.145T$$

These values are slightly higher than those corresponding to the uncorrected data. The simple averages of the 8 pairs of Arrhenius parameters are log A = (11.00 ± 0.46) and E = (33.09 ± 3.33) kJ mol^{-1}. We recommend that only Arrhenius parameters which fall within the range log A = (11.21 ± 0.32) and E = (34.57 ± 2.36) kJ mol^{-1} should be considered satisfactory.

1. J. A. KERR and M. J. PARSONAGE. Evaluated kinetic data on gas phase hydrogen transfer reactions of methyl radicals. Butterworths, London. 1976.
2. J. A. KERR and S. J. MOSS. Handbook of bimolecular and termolecular gas reactions. Vol. I. CRC Press, Boca Raton. 1981.
3. S. W. BENSON. The foundations of chemical kinetics. McGraw-Hill, New York. 1960.
4. N. L. ARTHUR, K. F. DONCHI, and J. A. MCDONNELL. J. Chem. Soc. Faraday Trans. 1, **71**, 2431 (1975).
5. S.-L. CHENG, J. NIMOY, and S. TOBY. J. Phys. Chem. **71**, 3075 (1967).
6. P. C. DURBAN and R. M. MARSHALL. Int. J. Chem. Kinet. **12**, 1031 (1980).
7. G. S. PAXINOS. B.Sc. (Hons) Thesis, La Trobe University, Australia, 1975.
8. A. F. TROTMAN-DICKENSON and E. W. R. STEACIE. J. Chem. Phys. **18**, 1097 (1950).
9. L. M. DORFMAN and R. GOMER. Chem. Rev. **46**, 499 (1950).
10. A. F. TROTMAN-DICKENSON, J. R. BIRCHARD, and E. W. R. STEACIE. J. Chem. Phys. **19**, 163 (1951).
11. A. J. C. NICHOLSON. J. Am. Chem. Soc. **73**, 3981 (1951).
12. R. GOMER and G. B. KISTIAKOWSKY. J. Chem. Phys. **19**, 85 (1951).
13. F. A. RAAL and E. W. R. STEACIE. J. Chem. Phys. **20**, 578 (1952).
14. M. T. JACQUISS, J. S. ROBERTS, and M. SZWARC. J. Am. Chem. Soc. **74**, 6005 (1952).
15. T. G. MAJURY and E. W. R. STEACIE. Can. J. Chem. **30**, 800 (1952).
16. E. WHITTLE and E. W. R. STEACIE. J. Chem. Phys. **21**, 993 (1953).
17. T. G. MAJURY and E. W. R. STEACIE. Disc. Faraday Soc. **14**, 45 (1953).
18. G. O. PRITCHARD, H. O. PRITCHARD, and A. F. TROTMAN-DICKENSON. J. Chem. Soc. 1425 (1954).
19. L. MANDELCORN and E. W. R. STEACIE. Can. J. Chem. **32**, 331 (1954).
20. L. MANDELCORN and E. W. R. STEACIE. Can. J. Chem. **32**, 79 (1954).

21. H. G. OSWIN, R. REBBERT, and E. W. R. STEACIE. Can. J. Chem. **33**, 472 (1955).
22. F. S. DAINTON and D. E. MCELCHERAN. Trans. Faraday Soc. **51**, 657 (1955).
23. J. CHANMUGAN and M. BURTON. J. Am. Chem. Soc. **78**, 509 (1956).
24. F. S. DAINTON, K. J. IVIN, and F. WILKINSON. Trans. Faraday Soc. **55**, 929 (1959).
25. R. K. BRINTON. J. Am. Chem. Soc. **83**, 1541 (1961).
26. J. C. T. THYNNE and P. GRAY. Trans. Faraday Soc. **58**, 2403 (1962).
27. I. B. BURKLEY and R. E. REBBERT. J. Phys. Chem. **67**, 168 (1963).
28. H. O. PRITCHARD and G. O. PRITCHARD. Can. J. Chem. **41**, 3042 (1963).
29. R. E. MARCH and J. C. POLANYI. Proc. R. Soc. Ser. A, **273**, 360 (1963).
30. T. W. SHANNON and A. G. HARRISON. Can. J. Chem. **41**, 2455 (1963).
31. M. CHER and C. S. HOLLINGSWORTH. Anal. Chem. **38**, 353 (1966).
32. G. GRIEG and J. C. J. THYNNE. Trans. Faraday Soc. **62**, 379 (1966).
33. L. ENDRENYI and D. L. LEROY. J. Phys. Chem. **71**, 1334 (1967).
34. P. GRAY and A. A. HEROD. Trans. Faraday Soc. **64**, 1568 (1968).
35. H. SHAW and S. TOBY. J. Phys. Chem. **72**, 2337 (1968).
36. N. L. ARTHUR and P. GRAY. Trans. Faraday Soc. **65**, 424 (1969).
37. R. E. BERKLEY, I. SAFARIK, H. E. GUNNING, and O. P. STRAUSZ. J. Phys. Chem. **77**, 1734 (1973).
38. P. GRAY and L. J. LEYSHON. Trans. Faraday Soc. **65**, 780 (1969).
39. R. SRINIVASAN and F. I. SONNTAG. Can. J. Chem. **47**, 1627 (1969).
40. K. C. FERGUSON and J. T. PEARSON. Trans. Faraday Soc. **66**, 910 (1970).
41. S. SATO, C. TAKAHASHI, and S. TSUNASHIMA. Bull. Chem. Soc. Jpn. **43**, 1319 (1970).
42. T. R. DONOVAN, W. DORKO, and A. G. HARRISON. Can. J. Chem. **49**, 828 (1971).
43. N. L. ARTHUR and M. S. LEE. Aust. J. Chem. **29**, 1483 (1976).
44. L. F. DAVID. M.Sc. Thesis, La Trobe University, Australia, 1976.
45. N. L. ARTHUR and P. J. NEWITT. Aust. J. Chem. **32**, 1025 (1979).
46. M. G. DUKE and K. A. HOLBROOK. J. Chem. Soc. Faraday Trans. 1, **76**, 1232 (1980).
47. H. ARICAN and N. L. ARTHUR. Aust. J. Chem. **36**, 2185 (1984).
48. A. SHEPP. J. Chem. Phys. **24**, 939 (1956).
49. D. A. PARKES, D. M. PAUL, and C. P. QUINN. J. Chem. Soc. Faraday Trans. 1, **72**, 1935 (1976).
50. M. H. J. WIJNEN. J. Chem. Phys. **22**, 1074 (1954).
51. J. R. MCNESBY, T. W. DAVIS, and A. S. GORDON. J. Am. Chem. Soc. **76**, 823 (1954).
52. J. F. HENDERSON and E. W. R. STEACIE. Can. J. Chem. **38**, 2161 (1960).
53. G. A. CREAK, F. S. DAINTON, and K. J. IVIN. Trans. Faraday Soc. **58**, 326 (1962).
54. R. SHAW and J. C. J. THYNNE. Trans. Faraday Soc. **62**, 104 (1966).
55. P. C. DURBAN and R. M. MARSHALL. Int. J. Chem. Kinet. **12**, 1031 (1980).
56. J. A. KERR, A. STEPHENS, and J. C. YOUNG. Int. J. Chem. Kinet. **1**, 339 (1969).
57. J. A. KERR and D. TIMLIN. J. Chem. Soc. A, 1241 (1969).
58. T. N. BELL and A. E. PLATT. Int. J. Chem. Kinet. **3**, 307 (1971).
59. T. SHIMANOUCHI. Tables of molecular vibrational frequencies. Vol. I. NSRDS-NBS 39 (1972).
60. I. W. M. SMITH. Kinetics and dynamics of elementary gas reactions. Butterworths, London, Boston. 1980.
61. M. SALOMON. Can. J. Chem. **42**, 610 (1964).
62. M. H. JONES and E. W. R. STEACIE. J. Chem. Phys. **21**, 1018 (1953).
63. P. AUSLOOS and E. W. R. STEACIE. Can. J. Chem. **32**, 593 (1954).
64. P. AUSLOOS and E. W. R. STEACIE. Can. J. Chem. **33**, 47 (1955).
65. J. G. CALVERT and J. T. GRUVER. J. Am. Chem. Soc. **80**, 1313 (1958).
66. S. TOBY and K. O. KUTSCHKE. Can. J. Chem. **37**, 672 (1959).
67. S. TOBY. J. Am. Chem. Soc. **82**, 3822 (1960).
68. P. GRAY and J. C. J. THYNNE. Trans. Faraday Soc. **59**, 2275 (1963).
69. R. E. REBBERT and P. J. AUSLOOS. J. Phys. Chem. **67**, 1925 (1963).
70. P. GRAY and J. C. J. THYNNE. Trans. Faraday Soc. **60**, 1047 (1964).
71. J. C. J. THYNNE. Trans. Faraday Soc. **60**, 2207 (1964).
72. M. CHER. J. Phys. Chem. **68**, 1316 (1964).
73. S. TOBY and B. H. WEISS. J. Phys. Chem. **68**, 2492 (1964).
74. P. GRAY, A. JONES, and J. C. J. THYNNE. Trans. Faraday Soc. **61**, 474 (1965).
75. P. GRAY and A. JONES. Trans. Faraday Soc. **61**, 2161 (1965).
76. P. GRAY and A. JONES. Trans. Faraday Soc. **62**, 112 (1966).
77. G. GRIEG and J. C. J. THYNNE. Trans. Faraday Soc. **62**, 3388 (1966).
78. S. TOBY and J. NIMOY. J. Phys. Chem. **70**, 867 (1966).
79. J. A. KERR, D. H. SLATER, and J. C. YOUNG. J. Chem. Soc. A, 104 (1966).
80. A. GOOD and J. C. J. THYNNE. Trans. Faraday Soc. **63**, 2708 (1967).
81. P. GRAY and A. A. HEROD. Trans. Faraday Soc. **63**, 2489 (1967).
82. D. G. L. JAMES and R. D. SUART. Trans. Faraday Soc. **65**, 175 (1969).
83. E. R. MORRIS and J. C. J. THYNNE. J. Phys. Chem. **73**, 3294 (1969).
84. P. GRAY, A. A. HEROD, and L. J. LEYSHON. Can. J. Chem. **47**, 689 (1969).
85. P. NEWITT. Ph.D. Thesis, La Trobe University, Australia, 1982.
86. A. L. BULLEN. B.Sc. (Hons) Thesis, La Trobe University, Australia, 1970.
87. R. S. KONAR and B. DEB. DARWENT. Can. J. Chem. **48**, 2280 (1970).

Étude statistique des effets de solvant. III.[1] Calcul et interprétation de paramètres empiriques de polarité à partir de propriétés physicochimiques des solvants purs

M. CHASTRETTE
Laboratoire de chimie organique physique, UA 463, Université Lyon 1, 43 Boulevard du 11 Novembre 1918, 69622 Villeurbanne Cédex, France

ET

J. CARRETTO
Ecole Normale Supérieure, 92260 Fontenay aux Roses, France

Reçu le 14 juin 1985

M. CHASTRETTE et J. CARRETTO. Can. J. Chem. **63**, 3492 (1985).

Le calcul et l'interprétation des paramètres empiriques de polarité des solvants sont abordés dans cet article à l'aide de méthodes statistiques multivariées. L'importance de l'échantillon traité (57 solvants aprotiques et 24 solvants protiques) garantit une bonne représentativité de l'ensemble des solvants. Les données recueillies sur les solvants sont des constantes physiques (constante diélectrique, moment dipolaire, indice de réfraction, réfraction molaire, température d'ébullition, paramètre δ de Hildebrand) ou des grandeurs théoriques (niveaux d'énergie des orbitales frontières). Les méthodes utilisées sont l'analyse factorielle et la régression multiple. Les résultats obtenus montrent que le paramètre E_T mesure la polarité, la polarisabilité et la cohésion du solvant dans les proportions respectives de 43, 39 et 18% pour les solvants aprotiques. Pour π^* ces proportions sont de 53, 18 et 29%. Dans le cas des solvants protiques E_T est expliqué par les mêmes variables, sauf pour 5 solvants plus acides que l'eau, par suite de la basicité de l'oxygène de la bétaïne qui sert à définir E_T.

M. CHASTRETTE and J. CARRETTO. Can. J. Chem. **63**, 3492 (1985).

Using multivariational statistical methods, the calculation and interpretation of empirical parameters of the polarity of solvents has been reexamined. The size of the sample used (57 aprotic solvents and 24 protic solvents) assures that it is representative. For each solvent, the data tabulated include some physical constants (dielectric constants, dipole moments, refractive indices, molar refractions, boiling points, Hildebrand's δ parameters) or theoretical values (energy levels of frontier orbitals). The methods used are factorial analysis and multiple regression. The results obtained show that, for the aprotic solvents, the parameter E_T is a measure of the polarity, of the polarizability, and of the cohesion of the solvent to the extent of 43, 39, and 18% respectively. For the parameter π^*, these proportions are respectively 53, 18, and 29%. For the protic solvents, the parameter E_T is explained by the same variables except for 5 solvents more acidic than water; this anomaly is explained by the basicity of the oxygen of the betaine used to define E_T.

[Journal translation]

Introduction

Dans les approches quantitatives de l'effet des solvants sur les processus chimiques, une propriété mesurant cet effet est considérée comme une fonction linéaire, soit d'un ou plusieurs paramètres empiriques, soit d'une ou plusieurs grandeurs physicochimiques du solvant, soit de combinaisons des deux types de variable.

De nombreuses échelles empiriques ont été proposées pour rendre compte: (*i*) de la polarisabilité et de la polarité des solvants, comme E_T (1) et E_T^N (2), Z (3) et π^* (4); (*ii*) de leur acidité et de leur basicité de Lewis, comme par exemple AN et DN (5) ou ΔH BF_3 (6); (*iii*) de leur basicité (en tant qu'accepteurs de liaisons H), comme B (7) ou β (8*a*). Taft et coll. (8*b*) ont aussi défini une échelle d'acidité des solvants en tant que donneurs de liaisons H avec α.

Ces échelles ont en commun d'être définies par la variation de propriétés spectroscopiques d'une ou plusieurs molécules-sondes (ou de propriétés thermodynamiques de réactions modèles) quand on passe d'un solvant à un autre. C'est d'ailleurs ce qui limite leur efficacité quand on veut les utiliser seules dans des conditions trop différentes de celles dans lesquelles elles ont été définies (9, 10*a*).

Pour améliorer les résultats en essayant de prendre en compte toutes les interactions soluté–solvant, plusieurs auteurs ont préconisé une approche multiparamétrique (4, 5, 13, 14). Certains autres (9, 11, 15) ont fait intervenir dans leurs relations à la fois des paramètres empiriques et des grandeurs physiques caractéristiques des solvants.

Les difficultés rencontrées pour attribuer un sens physique précis aux paramètres empiriques et pour les utiliser valablement dans des conditions variées ont conduit à n'utiliser (16) que des grandeurs physicochimiques. De même le paramètre π^* de Taft et Kamlet a été calculé (17, 18) à partir de fonctions de la constante diélectrique et de l'indice de réfraction des solvants.

À partir de nombreuses données cinétiques, thermodynamiques et spectroscopiques, C. G. Swain *et al.* (19*a*) ont calculé les deux paramètres A et B nommés "acité" et "basité". D'après ces auteurs, A mesure la capacité d'un solvant à solvater les anions et B sa capacité à solvater les cations, ce que contestent Taft *et al.* (19*b*).

La notion de polarité d'un solvant étant la plus largement utilisée dans la pratique quotidienne des chimistes, il est important de savoir ce que mesurent les paramètres empiriques de polarité. Or (20, 21), il y a encore un grand fossé à combler pour établir les fondements théoriques de l'interprétation des interactions entre molécules-sondes et solvants. Dans un précédent article (12) nous avons montré que les paramètres E_T, Z et AN peuvent être calculés correctement à partir de quatre propriétés physicochimiques des solvants purs (moment dipolaire μ, constante diélectrique ϵ, réfraction molaire RM et paramètre δ de Hildebrand). Dans le présent article nous étendons cette étude à un nombre beaucoup plus élevé de solvants (81 au total)

[1] Articles précédents; voir références 11 et 12.

TABLEAU 1. Solvants SLH: variables physicochimiques et paramètres empiriques

Solvants SLH		KIR	RM	μ	δ	n_D	T_c	E_T	π*	Z
Hexane	+×	0,185	29,9	0	7,27	1,375	69	33,1	−0,081	
Cyclohexane	+×	0,202	27,7	0	8,19	1,426	81	33,2	0	60,1
Triéthylamine	+×	0,243	33,1	2,9	7,42	1,401	90	33,7	0,14	
Sulfure de carbone		0,261	21,3	0	10	1,626	46	33,9	0,514	
Sulfolane	+×	0,483	27,2	16,05	12,5	1,482	287	44	0,98	77,5
Diméthylsulfoxyde	+×	0,484	20,1	13	13	1,478	189	45	1	71,1
Diméthylformamide	+×	0,48	19,9	12,88	11,79	1,431	152	43,8	0,88	68,4
Diméthylacétamide	+×	0,48	24,2	12,41	10,8	1,438	166	43,7	0,88	66,9
HMPT	×	0,475	47,7	18,48	8,9	1,458	235	40,9	0,87	62,8
N-Méthylpyrrolidone	+×	0,478	27	13,64	11,3	1,47	204	42,2	0,92	
Tétraméthylurée		0,469	32,2	11,58	9,5	1,449	175	41	0,83	
Nitrométhane	×	0,479	12,5	11,88	12,9	1,381	101	46,3	0,85	71,2
Acétonitrile	×	0,48	11,1	11,48	12,11	1,344	82	46	0,75	71,3
Butyronitrile	×	0,464	21,2	13,58	10,17	1,384	118	43,1	0,71	67,8
Propionitrile		0,473	15,8	11,91	10,73	1,366	97	43,7	0,71	
Acétone	+×	0,465	16,2	9,54	9,62	1,359	56	42,2	0,71	65,7
Méthyléthylcétone	+×	0,461	20,7	9,21	9,45	1,379	80	41,3	0,67	64
Diéthylcétone		0,457	25,2	9,41	9,06	1,392	102	39,3		
Cyclohexanone	+×	0,46	27,9	10,04	10,42	1,451	156	39,8	0,76	
Cyclopentanone	+×	0,446	23,2	9,44	10,4	1,437	131	39,4	0,76	
Oxyde de diéthyle	+×	0,345	22,1	4,34	7,53	1,352	35	34,6	0,27	
Oxyde de dibutyle	+×	0,291	40,8	3,94	7,76	1,399	142	34	0,24	60,1
Oxyde de diisopropyle	+×	0,329	31,7	4,2	7,06	1,368	68	34,4	0,27	
THF	+×	0,407	19,9	5,84	9,32	1,407	66	37,4	0,58	58,8
Dioxanne	×	0,223	21,6	1,5	10,13	1,422	101	36	0,55	64,6
1,2-Diméthoxyéthane	×	0,403	24,1	5,7	8,3	1,38	85	38,2	0,53	62,1
Anhydride acétique	+	0,465	22,4	9,41	10,65	1,39	140	43,9	0,76	
Acétate de méthyle	+×	0,396	17,6	5,37	9,46	1,361	56	40	0,6	
Acétate d'éthyle	+×	0,385	22,3	6,27	8,91	1,372	77	38,1	0,55	59,4
Carbonate de diéthyle		0,274	28,4	3,63	8,8	1,385	127	38,4		
Carbonate de propanediol	×	0,489	21,6	16,7	13,5	1,421	242	46,6	0,81	72,4
Benzène		0,23	26,2	0	9,16	1,501	80	34,8	0,59	54
Toluène		0,24	31,1	1,43	8,93	1,497	111	33,8	0,54	
o-Xylène		0,258	35,8	2,07	9,06	1,505	144	34,3		
m-Xylène		0,241	36	1,22	8,9	1,497	139	34,6	0,47	
p-Xylène		0,232	36	0	8,83	1,496	138	33,5	0,43	
Mésitylène		0,23	40,8	0	8,88	1,499	165	33,7	0,41	
Fluorobenzène		0,373	26,1	4,9	9,11	1,468	85	38,1	0,62	60,2
Chlorobenzène		0,377	31,2	5,14	9,67	1,525	132	37,5	0,71	58
Bromobenzène		0,373	33,7	5,17	9,87	1,56	156	37,5	0,79	59,2
Iodobenzène		0,354	39,2	4,64	10,13	1,62	188	37,9	0,81	
o-Dichlorobenzène		0,428	35,9	7,57	10,04	1,552	181	38,1	0,8	60
m-Dichlorobenzène		0,364	36	5,74	9,8	1,546	172	36,4	0,67	
Pyridine		0,442	24,1	7,91	10,62	1,51	115	40,2	0,87	64
Nitrobenzène		0,479	32,7	13,44	10,4	1,553	211	42	1,01	
Benzonitrile		0,471	31,6	13,51	10,7	1,528	191	42	0,9	65
Acétophénone		0,458	36,3	9,87	10,58	1,534	202	41,3	0,9	
Oxyde de diphényle		0,321	52,8	3,87	10,1	1,589	258	35,3	0,66	
Anisole		0,345	33	4,17	9	1,52	154	37,2	0,73	
Phénétole		0,341	37,6	4,54	9,2	1,507	170	36,4		58,9
Benzoate d'éthyle		0,385	42,5	6,67	9,75	1,501	213	38,1	0,74	
Tétrachlorométhane		0,226	25,8	0	8,55	1,46	77	33,6	0,28	
Dichlorométhane		0,42	16	5,17	9,88	1,424	40	41,1	0,82	64,2
1,2-Dichloroéthane		0,431	21	6,2	9,86	1,445	84	41,9	0,81	63,4
Trichloroéthylène		0,309	25,5	2,7	9,16	1,478	87	35,9	0,53	
1,1-Dichloroéthane		0,429	21,2	6,87	8,92	1,417	57	39,4		62,1
Chloroforme		0,359	21	3,84	9,16	1,445	61	39,1	0,58	63,2

Note: Les valeurs des grandeurs physicochimiques sont tirées des références 4, 10*e*, 26, 45–48.

et de propriétés (6 au lieu de 4). Nous cherchons à déterminer non seulement la nature mais aussi l'importance relative des variables physicochimiques dont dépendent les paramètres de polarité E_T, Z et π*.

I. Choix des variables et méthodes

Choix des solvants

Nous avons choisi le nombre maximum de solvants de fonctions chimiques variées, capables ou non de donner des

TABLEAU 2. Variables physicochimiques et paramètres de Reichardt pour 24 solvants ALH

Solvants ALH	KIR	RM	μ	δ	n_D	T_e	E_T
Formamide	0,493	10,6	11,24	19,2	1,448	211	56,6
N-Méthylformamide	0,496	15,3	12,88	16,1	1,432	180	54,1
N-Méthylacétamide	0,496	19,8	14,65	13,6	1,425	206	52
Eau	0,49	3,7	6,07	23,53	1,333	100	63,1
Méthanol	0,477	8,2	5,67	14,5	1,328	65	55,5
Ethanol	0,47	12,8	5,77	12,78	1,361	78	51,9
Butanol-1	0,458	22,1	5,84	11,6	1,399	118	50,2
Ethylèneglycol (*)	0,481	14,4	7,61	17,05	1,432	198	56,3
Isopropanol	0,463	17,5	5,54	11,44	1,377	82	48,6
Butanol-2	0,456	22,1	5,54	11,08	1,397	100	47,1
Diéthylèneglycol	0,477	28,4	7,71	14,24	1,448	245	53,8
Propanol-1	0,464	17,4	5,54	12,18	1,386	97	50,7
Isobutanol	0,459	22,2	5,97	11,24	1,396	108	49
Isopentanol	0,451	26,7	6,07	11,09	1,407	131	49
Pentanol-2	0,448	26,8	5,54	10,77	1,406	119	46,5
Pentanol-3	0,445	26,8	5,47	10,16	1,41	115	45,7
Pentanol-1	0,448	26,8	5,94	10,9	1,41	138	49,1
Hexanol-1	0,446	31,4	5,12	10,7	1,418	158	48,8
Octanol-1	0,431	40,7	5,81	10,3	1,429	195	48,3
Cyclohexanol	0,452	28,7	6,2	11,4	1,464	161	46,9
Trifluoroéthanol (*)	0,472	12,4	8,41	12,4	1,291	77	59,5
Méthoxy-2 éthanol (*)	0,457	19,2	6,81	11,4	1,402	125	52,3
Acide acétique (*)	0,387	12,9	5,6	13,01	1,372	118	51,7
Acide formique (*)	0,487	8,6	4,62	14,7	1,371	101	54,3

Note: Les valeurs des grandeurs physicochimiques sont tirées des références 4, 10*e*, 26, 45–48.

liaisons hydrogène, pour lesquels nous avons pu rassembler à la fois les valeurs des propriétés physiques retenues et celles des paramètres E_T, Z et π^*. Pour E_T l'échantillon comporte 81 solvants, répartis en 57 solvants ne pouvant donner de liaison hydrogène (appelés ici SLH) et 24 solvants donneurs de liaisons hydrogène (appelés ici ALH). Les 57 solvants SLH comportent 20 aromatiques et 6 aliphatiques chlorés (tableau 1). Les solvants ALH comportent l'eau, 18 alcools, 2 acides carboxyliques et 3 amides (tableau 2).

Choix des variables physicochimiques et de la forme des fonctions utilisées

En plus de ϵ et de n_D, liés respectivement à la polarité et à la polarisabilité, nous avons retenu le moment dipolaire μ, la réfraction molaire RM (produit du volume moléculaire par la fonction $(n^2 - 1)/(n^2 + 2)$), la température d'ébullition T_e, et le paramètre de solubilité δ de Hildebrand (22). Il serait sans doute préférable d'utiliser la pression interne P_i plutot que δ. En effet δ est définit à partir de la densité d'énergie de cohésion et donc à partir de l'énergie mise en jeu pour vaporiser le solvant en supprimant toutes les interactions. Au contraire P_i est définie comme la variation d'énergie interne lors d'un expansion élémentaire du liquide, au cours de laquelle toutes les interactions entre molécules (et en particulier les liaisons hydrogène) ne sont pas rompues (23). P_i traduit donc mieux la situation créée par l'introduction d'une molécule de soluté, mais comme on n'en connaît la valeur que pour un nombre insuffisant des solvants que nous étudions ici, nous avons utilisé δ.

Le moment dipolaire μ, le paramètre de solubilité δ et la température d'ébullition T_e ont été utilisés directement. La constante diélectrique ϵ peut intervenir sous forme de différentes fonctions analysées par Taft et coll. (réf. 24, pp. 488–500). L'un de nous (25) a étudié le degré de similitude de ces fonctions pour des valeurs de ϵ comprises entre 2 et 80. Pour $\epsilon > 6$ toutes les fonctions sont proportionnelles, sauf celle de Block–Walker, $\theta(\epsilon)$, qui surestime sans doute l'importance de l'effet de saturation. Une variable tenant compte de la séparation des effets d'orientation et de polarisation électronique a été utilisée dans des corrélations (18, 26) sans avantage très déterminant sur les expressions classiques. Nous avons donc retenu la fonction de Kirkwood–Onsager, $(\epsilon - 1)/(2\epsilon + 1)$, que nous appelons KIR dans la suite.

En ce qui concerne l'indice de réfraction n_D, nous avons vérifié que les différentes fonctions dans lesquelles il intervient généralement sont très bien corrélées avec lui: ainsi $r = 0,998$ pour $(n^2_D - 1)/(n^2_D + 1)$ et $(n^2_D - 1)/(2n^2_D + 1)$; $r = 0,999$ pour $(n^2_D - 1)/(n^2_D + 2)$. Nous avons donc utilisé simplement n_D.

Les deux échantillons SLH et ALH ont été traités séparément. Les six variables physicochimiques appelées X_i dans la suite sont présentées dans les tableaux 1 et 2.

Méthodes statistiques

Aucune hypothèse n'est faite a priori sur la dépendance entre un paramètre particulier et les variables que sont les propriétés des solvants purs. Dans un premier temps on tente, par une analyse en composantes principales (12, 35), de définir les relations entre les variables, puis de les remplacer par des facteurs qui en sont des combinaisons linéaires. Ensuite, on cherche si l'information associée aux facteurs permet de rendre compte de la variation des paramètres empiriques, en effectuant une régression de ces derniers sur les facteurs. Enfin, une régression multiple d'un paramètre empirique sur les propriétés du solvant pur permet de préciser la signification de ce paramètre.

2. Résultats

2.1. *Solvants SLH*

Cas de E_T

Le paramètre E_T a été utilisé dans de très nombreuses corrélations avec des vitesses de réaction (10). Il est curieux de

TABLEAU 3. Coefficients de corrélation entre facteurs et variables pour 57 solvants SLH

Variable	F_1	F_2	F_3	F_4	F_5	F_6
KIR	0,920	0,162	0,139	0,304	0,120	0,027
RM	0,286	0,882	0,358	0,014	0,067	0,085
μ	0,950	0,026	0,262	0,057	0,152	0,045
δ	0,862	0,052	0,440	0,229	0,059	0,063
n_D	0,053	0,841	0,457	0,279	0,055	0,008
T_e	0,520	0,803	0,156	0,227	0,001	0,094

constater la variété des interprétations qui en sont données. E_T a été considéré uniquement comme une mesure des propriétés électrophiles du solvant par plusieurs auteurs parmi lesquels Krygowski (15, 27–29), Mayer (30) et Koppel et Pal'm (7, 13); ces derniers ont en effet défini leur échelle d'acidité de Lewis à partir de E_T en lui enlevant la contribution de la polarité et de la polarisabilité. Ce point de vue a été contesté (31, 12). Taft et coll. (32) considèrent E_T comme un paramètre de polarité/polarisabilité contenant une contribution importante des propriétés électrophiles des solvants. D'autres ont noté de fortes corrélations de E_T avec le paramètre de solubilité de Hildebrand, δ (12), ou avec δ^2 ou avec ln δ (33). Enfin, récemment, le role des forces de dispersion déjà signalé (9) a été mis en évidence par Haak et Engberts (34). Il nous a semblé intéressant de comparer les importances relatives de ces différentes variables dans le calcul et l'interprétation de E_T.

Il est possible, en utilisant les six variables physicochimiques X_i précisées plus haut, d'étudier 57 solvants SLH (tableau 1). Dans un premier temps il fallait vérifier que les variables X_i retenues fournissaient bien une information suffisante pour déterminer E_T. Pour ce faire, tenant compte de ce que ces variables X_i ne sont pas indépendantes les unes des autres, nous avons effectué une analyse en composantes principales normée (11, 35*a*) permettant de définir à partir des variables X_i six facteurs F_i totalement indépendants. Le tableau 3 présente les valeurs des coefficients de corrélation entre les facteurs F_i et les grandeurs physiques X_i. Cette analyse permet de sélectionner les facteurs qui portent le plus d'information. Dans le cas des 57 solvants SLH, les trois premiers facteurs contiennent 94,2% de l'information totale.

E_T peut être calculé par une regression orthogonalisée (35*b*) sur ces trois facteurs. Le coefficient de F_3 n'est pas significatif;[2] on obtient l'équation [1]:

$$[1] \quad E_T = 38,79\ (\pm 0,12) + 2,11\ (\pm 0,07)\ F_1 - 0,658\ (\pm 0,08)\ F_2$$

$n = 57$; $r = 0,971$; $s = 0,87$; $F = 297$. Cette équation rend compte de 94,3% de la variance de E_T[3] (87,8% pour F_1 seul). D'après le tableau 3 on constate qu'il est difficile d'attribuer une signification physique aux différents facteurs retenus. F_1 est très lié aux variables de polarité (KIR, μ et δ) alors que F_2 est lié aux variables de polarisabilité (RM et n_D). La signification de F_3 reste obscure mais il n'intervient pas dans E_T. L'équation [1] montre que l'analyse de E_T en termes de variables physicochimiques du solvant pur est possible (l'information totale est suffisante).

Il nous paraît préférable d'utiliser directement les variables physicochimiques, pour obtenir une interprétation claire.

Pour les 57 solvants SLH considérés, la régression entre E_T et les valeurs de X_i est la suivante:[4]

$$[2] \quad E_T = 35,58\ (\pm 2,75) + 22,11\ (\pm 1,86)\ \text{KIR} + 1,358\ (\pm 0,127)\ \delta - 12,63\ (\pm 1,91)\ n_D$$

$n = 57$; $r = 0,971$; $s = 0,86$; $F = 301$. Les coefficients de RM, μ et T_e ne sont pas significatifs. L'équation [2] rend compte de 94,4% de la variance de E_T (89,8% à partir de KIR et δ; et 81,5% à partir de KIR seul).[3]

Pour préciser l'importance relative des trois variables physicochimiques dans la détermination de E_T on dispose d'une méthode employée par Gore (36), Krygowski (27) et plus récemment par Maccarone et Perrini (37) qui consiste à pondérer les coefficients de la régression par les écarts-types des variables. On trouve ainsi que KIR est le plus important (43,2%), suivi de δ (38,5%) et de n_D (18,3%). L'équation [2] montre que E_T est lié (*i*) à la polarité du solvant par l'intermédiaire de KIR. KIR et μ étant bien corrélés ($r = 0,913$), il est normal qu'une seule des variables apparaisse dans [2]; (*ii*) à la polarisabilité, à travers l'indice de réfraction n_D avec un coefficient de régression négatif indiquant que E_T croit lorsque la polarisabilité du solvant diminue; (*iii*) à la cohésion, par l'intermédiaire du paramètre δ de Hildebrand. On ne doit pas s'étonner que E_T, qui apparaît comme un bon paramètre de polarité/polarisabilité, dépende aussi nettement de δ car les échelles empiriques de polarité peuvent toutes faire intervenir plus ou moins l'énergie de cohésion du solvant. Cette dépendance multiple explique que l'échelle de Dimroth et Reichardt soit employée avec succès pour rendre compte des effets de la polarité des solvants (10*b*).

Pour déterminer l'influence du choix des solvants sur les résultats obtenus, nous avons traité séparément une sous-population de 19 solvants aliphatiques non halogénés (que Taft *et al.* nomment "select solvents"). Ces solvants ont été choisis parce que communs à notre échantillon et à la liste de "select solvents" donnée par Taft et coll. dans une publication récente (38) (ils sont marqués d'un signe + dans le tableau 1). La régression de E_T sur les variables physicochimiques conduit à retenir l'équation:

$$[3] \quad E_T = 60,68\ (\pm 11,7) + 11,53\ (\pm 4,77)\ \text{KIR} + 2,22\ (\pm 0,36)\ \delta - 33,86\ (\pm 9,5)\ n_D$$

$r = 0,980$; $n = 19$; $s = 0,835$; $F = 124$.

On constate que les variables significatives restent les mêmes que pour l'échantillon entier mais surtout qu'il est nécessaire de faire intervenir la cohésion du solvant pour obtenir une corrélation acceptable (avec seulement KIR, $r = 0,922$; avec δ seul, $r = 0,922$; avec KIR et δ, $r = 0,963$). L'introduction du paramètre δ rend inutile l'emploi dans la corrélation de termes croisés (comme par exemple le produit KIR $\times$ n_D).

Par ailleurs, il est connu que E_T est bien corrélé avec AN (2) mais nous avons montré que AN était non seulement une mesure de l'acidité mais aussi une bonne mesure de la polarité des solvants (12). Ceci est confirmé par la bonne corrélation observée entre AN et π^* (38, 39). Pour vérifier si E_T dépend réellement de l'acidité de Lewis des solvants, nous avons étudié la

[2] Les coefficients de régression sont considérés comme significatif quand leur probabilité critique est inférieure à 5%. Le plus souvent elle est inférieure à 0,1%.

[3] Les valeurs de E_T ne sont pas normalisées.

[4] Dans le cas des solvants SLH, pour le calcul de E_T, le résultat obtenu en remplaçant δ par δ^2 dans le groupe de variables δ, KIR et n_D est pratiquement le même qu'avec δ.

corrélation entre E_T et l'énergie de la plus basse orbitale non occupée, LUMO. En effet, Sabatino *et al.* (40) ont montré que l'énergie de l'orbitale LUMO et AN se comportaient de manière tout à fait semblable dans des corrélations avec des vitesses de réaction et des énergies de solvatation. Pour 53 solvants SLH de notre échantillon dont les valeurs de LUMO sont connues (25), le coefficient de corrélation entre E_T et LUMO est $r = 0,423$. E_T n'est donc pratiquement pas lié à l'acidité de Lewis des solvants SLH.

Cas de Z

L'étude de Z a été menée pour 29 solvants SLH (ceux de l'échantillon de 57 solvants pour lesquels Z est connu). Le calcul de Z n'a été effectué qu'à partir des variables physicochimiques (tableau 1). Les corrélations entre ces différentes variables sont du même ordre que pour l'ensemble des 57 solvants SLH. L'équation [4] permet de rendre compte de 87% de la variance de Z:

$$[4] \quad Z = 104,1\ (\pm 10,70) - 0,499\ (\pm 0,059)\ \mathrm{RM} - 26,30\ (\pm 7,97)\ n_D + 0,082\ (\pm 0,007)\ T_e$$

$n = 29$; $r = 0,933$; $s = 3,925$; $F = 56$.

Il faut noter que δ, dont le coefficient dans la régression multiple n'est pas significatif, est le paramètre qui, considéré seul, présente la plus forte corrélation avec Z ($r = 0,828$). Parmi les trois variables dont dépend Z, l'importance de l'indice de réfraction est nettement la plus grande: 62,7%, contre 20,7% pour la température d'ébullition et 16,6% pour la réfraction molaire. Z semble donc dépendre principalement de la polarisabilité du solvant: quand celle-ci augmente, Z diminue. Comme pour E_T, aucune corrélation significative n'existe entre Z et LUMO.

Cas de π^*

Les valeurs de π^* sont connues pour 52 des 57 solvants de notre échantillon de solvants SLH (tableau 1). Les trois premiers facteurs obtenus par analyse en composantes principales normée à partir des X_i portent 94,5% de l'information totale. Mais l'équation obtenue par régression de π^* sur ces trois facteurs ne rend compte que de 81,3% de la variance de π^*. En considérant les quatre premiers facteurs on obtient l'équation [5] qui ne permet d'expliquer que 88,6% de la variance de π^*:

$$[5] \quad \pi^* = 0,647\ (\pm 0,011) + 0,889\ (\pm 0,05)\ F_1 + 0,212\ (\pm 0,059)\ F_2 + 0,477\ (\pm 0,107)\ F_3 + 0,936\ (\pm 0,17)\ F_4$$

$n = 52$; $r = 0,941$; $s = 0,007$; $F = 92$.

La prise en compte du cinquième facteur n'apporte pas d'amélioration sensible ($r = 0,947$; $s = 0,006$; $F = 80$). Attribuer une signification physique aux facteurs F_i est tout aussi complexe que dans le cas de E_T et nous avons préféré établir la régression multiple qui permet de calculer π^* en fonction des propriétés physiques elles-mêmes:

$$[6] \quad \pi^* = -2,419\ (\pm 0,249) + 1,85\ (\pm 0,173)\ \mathrm{KIR} + 0,043\ (\pm 0,011)\ \delta + 1,33\ (\pm 0,249)\ n_D$$

$n = 52$; $r = 0,946$; $s = 0,006$; $F = 138$.

L'équation [6] rend compte de 89,6% de la variance de π^* (64,8% avec KIR seul; 61% avec δ seul). D'après [6], π^* est lié, comme E_T, à la polarité, à la polarisabilité et à la cohésion du solvant. C'est le paramètre de Kirkwood qui est ici le plus important dans la détermination de π^* (53,2%), suivi de n_D (28,5%) et de δ (18,3%). À partir des variables physicochimiques choisies, même en gardant près de 99% de l'information, on ne peut pas calculer π^* de façon satisfaisante. Pour 48 des 52 solvants pour lesquels on connaît les valeurs de LUMO, le coefficient de corrélation simple entre π^* et LUMO est $r = 0,715$. π^* apparaît donc très faiblement lié à l'acidité de Lewis du solvant. En faisant intervenir ce paramètre dans l'équation de régression on obtient:

$$[7] \quad \pi^* = -1,929\ (\pm 0,291) + 1,697\ (\pm 0,182)\ \mathrm{KIR} + 0,035\ (\pm 0,011)\ \delta + 1,006\ (\pm 0,197)\ n_D - 0,015\ (\pm 0,005)\ \mathrm{LUMO}$$

$n = 48$; $r = 0,955$; $s = 0,006$; $F = 113$.

Cette équation rend compte de 91,2% de la variance de π^*. En effectuant le même calcul pour E_T, on constate que le coefficient de LUMO dans l'équation de régression n'est pas significatif.

Suivant Bekarek (17) nous avons repris le calcul de π^* en fonction des variables physicochimiques pour, respectivement, 25 solvants aliphatiques non-halogénés et 18 solvants aromatiques, appartenant tous à notre échantillon de 52 solvants SLH. Dans les deux cas, le calcul de π^* se trouve nettement amélioré. Pour les 18 solvants aromatiques, la régression fait intervenir KIR, RM et n_D ($r = 0,964$, $s = 0,002$). Dans le cas des 25 solvants aliphatiques non halogénés (repérés par le signe × dans le tableau 1), π^* peut être calculé à partir de KIR, δ et n_D:

$$[8] \quad \pi^* = -2,616\ (\pm 0,649) + 2,082\ (\pm 0,258)\ \mathrm{KIR} + 0,040\ (\pm 0,014)\ \delta + 1,409\ (\pm 0,488)\ n_D$$

$n = 25$; $r = 0,963$; $s = 0,007$; $F = 90$.

Pour 36 solvants "select", dont 23 figurent aussi dans notre échantillon, Abboud *et al.* (26) ont obtenu l'équation:

$$[9] \quad \pi^* = -0,95\ (\pm 0,28) + 1,19\ (\pm 0,09)\ A_1 + 5,05\ (\pm 1,43)\ A_2$$

$n = 36$; $r = 0,983$; $s = 0,05$; $F = 472$, avec

$$A_1 = (\epsilon - 1)/(\epsilon + 2) - (n^2_D - 1)/(n^2_D + 2)$$
$$\text{et } A_2 = (n^2_D - 1)/(2n^2_D + 1)$$

Les fonctions A_1 et A_2 (de ε et de n_D) conviennent donc mieux au calcul de π^* que KIR et n_D lui-même.

2.2. *Solvants ALH*

En raison de la faible taille des échantillons de solvants ALH pour lesquels on connaît π^* ou Z, nous avons mené cette étude uniquement pour E_T. L'échantillon de 24 solvants considéré comprend l'eau, 18 alcools primaires ou secondaires, 3 amides non tertiaires et 2 acides carboxyliques (tableau 2). Une étude similaire à celle qui a été effectuée pour les solvants SLH a été réalisée pour ces solvants qui peuvent participer à des liaisons hydrogène. Une analyse factorielle normée effectuée sur les six variables physicochimiques X_i fournit six facteurs F_i indépendants. Il faut considérer les 4 premiers facteurs pour rendre compte de 96,2% de l'information totale. La régression orthogonalisée sur ces quatre facteurs conduit à:

$$[10] \quad E_T = 51,708\ (\pm 0,474) + 2,27\ (\pm 0,299)\ F_1$$

$n = 24$; $r = 0,85$; $s = 5,40$; $F = 57,5$, les coefficients des autres facteurs n'étant pas significatifs. Cette relation n'explique que 72% de la variance de E_T. De plus, les tests de qualité de la régression [10] (41) (variance des écarts (42*a*); test

TABLEAU 4. Coefficients de corrélation entre facteurs et variables pour 19 solvants ALH

Variable	F_1	F_2	F_3	F_4	F_5	F_6
KIR	0,820	0,218	0,266	0,456	0,029	0,022
RM	0,817	0,483	0,099	0,145	0,234	0,114
μ	0,574	0,624	0,399	0,343	0,013	0,065
δ	0,874	0,050	0,460	0,021	0,102	0,111
n_D	0,272	0,891	0,170	0,133	0,288	0,051
T_e	0,059	0,955	0,189	0,076	0,147	0,149

ψ d'Exner (42*b*)) ne sont pas satisfaisants. Reichardt (10*c*) reconnaît que la principale limite de l'échelle de polarité définie par E_T réside dans le fait que les valeurs de E_T ne sont pas mesurables dans les solvants acides. En effet, toute addition d'acide à une solution contenant la bétaïne de Dimroth provoque la protonation de l'oxygène phénolique. Nous avons donc repris ce calcul après avoir éliminé de notre échantillon les solvants plus acides que l'eau, c'est-à-dire les acides formique et acétique (pK_a = 3,75 et 4,75), le trifluoroéthanol (pK_a = 12,4 (43), l'éthylèneglycol (pK_a = 14,2) et le méthoxy-2 éthanol (pK_a = 14,8 (44)). L'étude effectuée sur les 19 solvants ALH restant (tableau 2, solvants sans*) à partir des trois premiers facteurs qui portent 96,6% de l'information totale, conduit à:

$$[11] \quad E_T = 50{,}89\ (\pm 0{,}27) + 2{,}117\ (\pm 0{,}157)\ F_1 + 2{,}672\ (\pm 0{,}436)\ F_3$$

r = 19; n = 0,967; s = 1,40; F = 73.

La qualité de la régression se trouve sensiblement améliorée puisque l'équation [11] explique 93% de la variance de E_T (F_1 seul en explique 77%). Dans ce cas, comme dans celui des solvants SLH, il n'est pas possible de faire le lien de façon univoque entre un facteur F_i et une propriété caractéristique des solvants (tableau 4). Le calcul à partir des propriétés des solvants purs limité aux 19 solvants finalement retenus conduit à l'équation:

$$[12] \quad E_T = 126{,}60\ (\pm 18{,}15) + 0{,}93\ (\pm 0{,}079)\ \delta - 66{,}28\ (\pm 13{,}24)\ n_D + 0{,}038\ (\pm 0{,}009)\ T_e$$

n = 19; r = 0,982; s = 0,765; F = 138.

La relation [12] rend compte de 96,4% de la variance de E_T (δ seul en explique 90,5%). C'est δ qui a l'importance relative la plus grande (41,9%), suivi par l'indice de réfraction n_D (31,5%) puis par la température d'ébullition T_e (26,6%). Ceci montre que, pour les 19 solvants ALH pas trop acides, E_T est lié à la cohésion et à la polarisabilité du solvant. L'existence d'une faible corrélation (r = 0,791) entre δ et KIR suggère un lien plus faible avec la polarité. Il n'existe pas de corrélation significative entre E_T et LUMO pour les 17 solvants ALH de notre échantillon pour lesquels les valeurs de LUMO sont connues. Par contre, nous avons constaté que l'introduction du paramètre α de Taft dans l'équation de régression de E_T améliore nettement le résultat obtenu pour des solvants d'acidité variée (acide acétique, formamide, alcools, eau) (pour $E_T = f(\text{KIR}, \delta, \alpha)$, n = 10, r = 0,989, s = 0,64). Mais, α étant connu (32) pour 10 seulement des 24 solvants ALH, ce résultat n'a pas une grande portée.

3. Discussion

Pour les solvants SLH, ce sont les mêmes variables physicochimiques KIR, δ et n_D qui interviennent dans les équations de régression de E_T et π^*. Les deux paramètres empiriques apparaissent donc liés à la polarité et à la polarisabilité comme l'ont déjà observé de nombreux chercheurs. Nous montrons de plus que E_T et π^* contiennent une contribution importante de la cohésion de solvant, par l'intermédiaire du paramètre δ de Hildebrand. Ce paramètre permet de tenir compte de l'énergie nécessaire pour former dans le solvant une cavité où loger le soluté. Il convient donc de comparer les différents paramètres de polarité en tenant compte de ces trois aspects et non plus seulement des deux premiers. L'importance relative des trois variables n'est pas la même pour E_T et pour π^* (tableau 5) et, de plus, le signe du coefficient de n_D dans la régression est différent.

TABLEAU 5. Importances relatives de KIR, δ et n_D dans le calcul de E_T et π^* (solvants SLH)

	Nb. solv.	KIR	δ	n_D
E_T	57	43,2%	38,5%	18,3%
E_T	52	44,7%	38,3%	17,0%
π^*	52	53,2%	18,3%	28,5%

Il est possible d'intepréter la contribution plus élevée de δ pour E_T que pour π^* en considérant que la bétaïne utilisée pour définir E_T est bien plus volumineuse que les composés utilisés dans la définition de π^*.

Si l'on admet (18 et références citées) que l'énergie de solvatation due à la polarisation électronique est donnée par l'équation:

$$\Delta E = \frac{\mu^2_E - \mu^2_G}{r^3} \times \frac{n^2_D - 1}{2n^2_D + 1}$$

(où μ_E et μ_G sont respectivement les moments dipolaires des états excité et fondamental) on peut rendre compte du signe du coefficient de régression de n_D qui est celui de la différence $\mu^2_E - \mu^2_G$. En effet, d'après Reichardt (10*d*) les moments dipolaires à l'état excité et à l'état fondamental de la *p*-nitro-*N*,*N*-diéthyl aniline, qui a servi parmi d'autres composés semblables à la définition de π^*, sont respectivement de 12,9 et 5,1 D, ce qui correspond à $\mu^2_E - \mu^2_G = 140{,}4$. Pour le bétaïne de Dimroth, les moments dipolaires à l'état excité et fondamental sont respectivement de 6 et 14,7 D, ce qui correspond à $\mu^2_E - \mu^2_G = -180{,}1$. Il est donc normal de trouver que le coefficient de régression pour la variable n_D est positif pour π^* et négatif pour E_T.

Pour les 52 solvants SLH communs aux deux études, E_T et π^* ne présentent qu'une corrélation très moyenne (r = 0,788). Kamlet, Abboud et Taft (réf. 24, p. 573) ont aussi constaté ce fait et l'attribuent à un dosage de polarisabilité et de polarité différent pour les deux paramètres empiriques, ce qui est vérifié si l'on considère le tableau 5. D'ailleurs, nous constatons que la corrélation entre E_T et π^* est nettement meilleure quand l'équation de régression fait intervenir n_D (r = 0,933, s = 0,008, n = 50), lié à la polarisabilité. Taft et coll. (4) obtiennent aussi une nette amélioration de la corrélation entre E_T et π^* en étudiant séparément des familles de solvants de même type (aliphatiques non chlorés, aliphatiques polychlorés, aromatiques) ayant des caractéristiques de polarisabilité communes.

Pour les solvants ALH, E_T peut être calculé à partir des grandeurs physicochimiques, à condition de ne pas prendre en considération les solvants les plus acides (pK_a < 15). Ceci correspond au caractère basique de la bétaïne de Dimroth dont

TABLEAU 6. Importances relatives de quatre variables physicochimiques dans le calcul de E_T

	δ	n_D	KIR	T_c
57 solvants SLH	38,5%	18,3%	43,2%	—
19 solvants ALH	41,9%	31,5%	—	26,6%

les solvants les plus acides provoquent la protonation de l'oxygène phénolique (10*c*). Pour les deux types de solvants, E_T dépend significativement de la polarisabilité, à travers l'indice de réfraction, et de la cohésion, par l'intermédiaire de δ. KIR, bien corrélé avec le moment dipolaire, intervient dans l'expression de E_T pour les solvants SLH. Par contre, ni KIR ni μ ne figurent dans l'expression de E_T pour les solvants ALH. Il faut toutefois noter que, dans ce dernier cas, il existe une corrélation faible ($r = 0,791$) entre δ et KIR. Pour E_T, δ a une importance relative notable et remarquablement proche pour les deux types de solvants (cf. tableau 6). Ceci montre l'influence très importante du processus de création d'une cavité dans le solvant et donc la nécessité de prendre en compte une grandeur liée à la cohésion du solvant dans tout traitement des effets de solvant.

Conclusion

Dans cette étude qui généralise la précédente (12) nous avons calculé E_T uniquement à partir de variables physicochimiques caractéristiques des solvants purs. Cette démarche nous a permis, pour un nombre raisonnable de solvants (57 SLH et 19 ALH), de rendre compte de plus de 94% de la variance de E_T et de conclure que l'échelle empirique de Dimroth et Reichardt est bien une échelle de polarité–polarisabilité avec une forte influence de la cohésion et une très faible influence de l'acidité du solvant.

En ce qui concerne π^* et Z, et pour les échantillons de solvants SLH correspondants (52 pour π^*, 29 pour Z), une conclusion plus nuancée s'impose bien que les mêmes effets soient mis en évidence.

1. K. DIMROTH, C. REICHARDT, T. SIEPMANN et F. BOHLMANN. Justus Liebigs Ann. Chem. **661**, 1 (1963).
2. C. REICHARDT et E. HARBUSCH. Justus Liebigs Ann. Chem. **5**, 721 (1983).
3. E. M. KOSOWER. J. Am. Chem. Soc. **80**, 3253 (1958).
4. M. J. KAMLET, J. L. M. ABBOUD et R. W. TAFT. J. Am. Chem. Soc. **99**, 6027 (1977).
5. U. MAYER, Y. GUTMANN et W. GERGER. Monatsh. Chem. **106**, 1235 (1975).
6. P. C. MARIA et J. F. GAL. J. Phys. chem. À paraitre.
7. I. A. KOPPEL et Y. A. PAL'M. *Dans* Advances in linear free energy relationship. *Édité par* N. B. Chapman et J. Shorter. Plenum Press, London. 1972. Chap. V.
8. (*a*) M. J. KAMLET et R. W. TAFT. J. Am. Chem. Soc. **98**, 377 (1976); **98**, 2886 (1976); (*b*) T. YOKOHAMA, R. W. TAFT et M. J. KAMLET. J. Am. Chem. Soc. **98**, 3233 (1976).
9. F. W. FOWLER, A. R. KATRITZKY et J. D. RUTHERFORD. J. Chem. Soc. B, 460 (1971).
10. C. REICHARDT. Solvent effects in organic chemistry. Verlag Chemie, Weinheim, New York. 1979. (*a*) p. 257; (*b*) p. 253; (*c*) p. 244; (*d*) pp. 193–194; (*e*) pp. 270–272.
11. M. CHASTRETTE. Tetrahedron, **35**, 1441 (1979).
12. M. CHASTRETTE et J. CARRETTO. Tetrahedron, **38**, 1615 (1982).
13. I. A. KOPPEL et Y. A. PAL'M. Org. React. (NY, Engl. Transl.) **8**, 296 (1971).
14. P. SVOBODA, O. PYTELA et M. VEČEŘA. Collect. Czech. Chem. Commun. **48**, 3287 (1983).
15. W. R. FAWCETT et T. M. KRYGOWSKI. Can. J. Chem. **54**, 3283 (1976).
16. R. C. DOUGHERTY. Tetrahedron Lett. 385 (1975).
17. V. BEKAREK. J. Phys. Chem. **85**, 722 (1981).
18. J. E. BRADY et P. W. CARR. J. Phys. Chem. **86**, 3053 (1982).
19. (*a*) C. G. SWAIN, M. S. SWAIN, A. L. POWELL et S. ALUNNI. J. Am. Chem. Soc. **105**, 502 (1983); (*b*) R. W. TAFT, J. L. M. ABBOUD et M. J. KAMLET. J. Org. Chem. **49**, 2001 (1984).
20. DAO CONG DONG et M. A. WINNIK. Photochem. Photobiol. **35**, 17 (1982).
21. C. REICHARDT. Angew. Chem. Int. Ed. Engl. **18**, 98 (1979).
22. J. HILDEBRAND et R. SCOTT. The solubility of non-electrolytes. 3e éd. Reinhold Publishing Corp., New York. 1949.
23. M. R. J. DACK. Aust. J. Chem. **28**, 1643 (1975).
24. M. J. KAMLET, J. L. M. ABBOUD et R. W. TAFT. Prog. Phys. Org. Chem. **13**, 485 (1981).
25. M. CHASTRETTE, M. RAJZMANN, M. CHANON et K. F. PURCELL. J. Am. Chem. Soc. **107**, 1 (1985).
26. J.-L. M. ABBOUD, G. GUIHENEUF, M. ESSTAR, R. W. TAFT et M. J. KAMLET. J. Phys. Chem. **88**, 4414 (1984).
27. T. M. KRYGOWSKI et W. R. FAWCETT. J. Am. Chem. Soc. **97**, 2143 (1975).
28. T. M. KRYGOWSKI, J. P. RADOMSKI, A. RZESZOWIAK, P. K. WRONA et C. REICHARDT. Tetrahedron, **37**, 119 (1981).
29. T. M. KRYGOWSKI, E. MILCZAREK et P. K. WRONA. J. Chem. Soc. Perkin Trans. 2, 1563 (1980).
30. U. MAYER. Monatsh. Chem. **109**, 421 (1975); **109**, 775 (1975).
31. S. GLIKBERG et Y. MARCUS. J. Solution Chem. **12**, 255 (1983).
32. M. J. KAMLET, J.-L. M. ABBOUD, M. H. ABRAHAM et R. W. TAFT. J. Org. Chem. **48**, 2877 (1983).
33. C. G. GEBELIN. Org. Coat. Plastics Chem. **39**, S.524 (1978).
34. J. R. HAAK and J. B. F. N. ENGBERTS. J. Org. Chem. **49**, 2387 (1984).
35. P. DAGNELIE. Analyse statistique à plusieurs variables. Presses agronomiques de Gembloux. 1977. (*a*) pp. 191–244; (*b*) pp. 185–190.
36. W. L. GORE. Statistical methods for chemical experimentation. Interscience, New York. 1952. p. 141.
37. E. MACCARONE and G. PERRINI. J. Chem. Soc. Perkin Trans. 2, 1605 (1983).
38. J. L. M. ABBOUD, R. W. TAFT et M. J. KAMLET. J. Chem. Research (S), 98 (1984).
39. R. W. TAFT, N. J. PIENTA, M. J. KAMLET et E. M. ARNETT. J. Org. Chem. **46**, 661 (1981).
40. A. SABATINO, G. LA MANNA et L. PAOLONI. J. Phys. Chem. **84**, 2641 (1980).
41. J. SHORTER. Correlation analysis of organic reactivity. Research Study Press, John Wiley, Chichester. 1982.
42. (*a*) N. DRAPER et H. SMITH. Applied regression analysis. 2e *Éd.* John Wiley, New York. 1981. p. 299; (*b*) O. EXNER. Collect. Czech. Chem. Commun. **31**, 3222 (1966).
43. R. W. TAFT, D. GURKA, L. JORIS, P. v. R. SCHLEYER et J. W. RAKSHYS. J. Am. Chem. Soc. **91**, 4801 (1969).
44. E. J. KING. Equilibrium properties of electrolyte solutions. Vol. 4. Acid–base equilibria. Pergamon Press, Oxford. 1965.
45. B. J. BARKER. Angew. Chem. Int. Ed. Engl. **18**, 503 (1979).
46. A. F. M. BARTON. Chem. Rev. **75**, 731 (1975).
47. H. BURELL. Polymer handbook. 2e éd. Vol. IV. Interscience, New York. 1975. p. 337.
48. R. C. WEAST (*Éditeur*). Handbook of chemistry and physics. 48e éd. The Chemical Rubber Publishing Co., Cleveland. 1967–1968.

Synthèses et analyses structurales de perchlorates anhydres d'In(III) et de Tl(III) $M(ClO_4)_3$ et $ClO_2M(ClO_4)_4$; (M = In, Tl)

MOHIEDDINE FOURATI, MONCEF CHAABOUNI ET HASSINE FERID AYEDI
École Nationale d'Ingénieurs de Sfax, Laboratoire de Chimie Physique et Inorganique, B.P.W. 3038 Sfax, Tunisie

ET

JEAN-LOUIS PASCAL ET JACQUELINE POTIER[1]
Laboratoire des Acides Minéraux, U. A. 79 C.N.R.S., Université des Sciences et Techniques du Languedoc, Place Eugène Bataillon, 34060 Montpellier Cédex, France

Reçu le 20 mars 1985

MOHIEDDINE FOURATI, MONCEF CHAABOUNI, HASSINE FERID AYEDI, JEAN-LOUIS PASCAL et JACQUELINE POTIER. Can. J. Chem. **63**, 3499 (1985).

Les réactions du trioxyde de chlore (Cl_2O_6) sur les $InCl_3$ et $TlCl_3$ anhydres ou $InCl_3,4H_2O$ ont conduit à deux nouveaux perchlorato métallates de chloryle $ClO_2In(ClO_4)_4$ et $ClO_2Tl(ClO_4)_4$. Par dégradation thermique sous vide dynamique, ces deux sels de chloryle donnent respectivement, vers 80°C, $In(ClO_4)_3$ et $Tl(ClO_4)_3$. $Tl(ClO_4)_3$ se transforme dès 95°C en $TlO_{0.5}(ClO_4)_2$ alors que $In(ClO_4)_3$ est stable jusqu'à 272°C. $In(ClO_4)_3$ et $Tl(ClO_4)_3$ cristallisent dans le même groupe d'espace $P\bar{3}$. La meilleure interprétation des spectres de vibration ir et Raman peut être effectuée en considérant une molécule polymère de type AsI_3. Les groupes (ClO_4) sont bidentés en pont et fortement liés au métal. Les composés $ClO_2M(ClO_4)_4$ (M = In, Tl) sont des complexes définis comportant le cation ClO_2^+ en interaction avec l'anion $M(ClO_4)_4^-$. Il existe dans cet anion des groupes (ClO_4) monodentés et bidentés.

MOHIEDDINE FOURATI, MONCEF CHAABOUNI, HASSINE FERID AYEDI, JEAN-LOUIS PASCAL, and JACQUELINE POTIER. Can. J. Chem. **63**, 3499 (1985).

Reactions of chlorine trioxide (Cl_2O_6) with anhydrous $InCl_3$, $TlCl_3$, and $InCl_3\cdot4H_2O$ have been investigated. They give two chloryl perchlorato metallates: $ClO_2In(ClO_4)_4$ and $ClO_2Tl(ClO_4)_4$, which can be decomposed on heating (80°C) under dynamic vacuum. They yield respectively $In(ClO_4)_3$ and $Tl(ClO_4)_3$. $Tl(ClO_4)_3$ appears to have weaker thermal stability than $In(ClO_4)_3$, which is stable up to 272°C; the former decomposes starting at 95°C to give $TlO_{0.5}(ClO_4)_2$. $In(ClO_4)_3$ and $Tl(ClO_4)_3$ have the same space group $P\bar{3}$. The best assignment of their ir and Raman vibrational spectra can be made on the basis of a polymeric structure (AsI_3 type) with bridging bidentate perchlorato groups strongly bonded to the metal. The $ClO_2M(ClO_4)_4$ (M = In, Tl) salts are well defined. The cation ClO_2^+ is unambiguously characterized; it interacts with the anion $M(ClO_4)_4^-$, which has monodentate and bidentate perchlorate groups.

Introduction

L'utilisation d'agents perchloratants efficaces tels que Cl_2O_6, $HClO_4$, $ClClO_4$,... a permis à Schmeisser et Brandle (1), Rosolovskii et coll. (2), Christe et coll. (3) et nous-mêmes (4) de préparer plusieurs complexes perchlorato anhydres des métaux de transition et d'éléments du bloc p.

Dans la colonne III, il a été mis en évidence des complexes de type $MCl(ClO_4)_2$ (M = B (5)); $MCl_2(ClO_4)$ (M = B (5) et Ga (6)); $M(ClO_4)_3$ (M = B (5), Al (2*a*) et Ga (6)); $A_nM(ClO_4)_{3+n}$ (M = B, n = 1, A = alcalin, NH_4^+, NO_2^+; M = Al, n = 1, A = ClO_2^+; $1 < n < 3$, A = alcalin, NH_4^+, NO_2^+; M = Ga, n = 1, A = ClO_2^+ (5–11). Aucun perchlorate anhydre d'In(III) ou de Tl(III) analogue aux précédents n'est connu. Seuls sont signalés dans la littérature des perchlorates In(I) et de Tl(I) (12*a*, 13) ainsi que des complexes de type $ML_x(ClO_4)_z$; M = In, Tl, L = base organique (12*b*, 13).

L'étude des structures de $Sn_3O_2Cl_4(ClO_4)_4$, $Sb_2Cl_6(O)(OH)(ClO_4)$ par RX (rayons X) (14, 15) et des complexes de type $M(ClO_4)_2$ (M = Cu (16*a*), Co, Ni (16*b*)) par EXAFS (Extended X-Ray Absorption Fine Structure) a permis d'affiner les données de la spectroscopie de vibration.

On a pu établir d'une façon rigoureuse les corrélations: fréquences des vibrations ↔ longueurs des liaisons et nombre de vibrations ↔ géométrie du ligand (*monodenté, bidenté en pont, tridenté en pont.*)

Nous présentons ici le mode de préparation des perchlorates anhydres d'indium(III) et de thallium(III) et proposons une analyse structurale des composés obtenus. Cette analyse repose sur les données de la spectroscopie de vibration ir et Raman, des diagrammes de poudre X et de récents résultats en EXAFS sur $Ga(ClO_4)_3$ (17).

Partie expérimentale

Attention: Le trioxyde de chlore et les perchlorates anhydres sont des composés très réactifs, particulièrement au contact des matières organiques ou sous les chocs. Les réactions doivent être surveillées attentivement. Les complexes sont extrêment hygroscopiques; ils sont manipulés sur une ligne de vide (18) ou dans une boîte à gant contenant de l'azote très sec.

Produits de base

La préparation et la purification du trioxyde de chlore ont déjà été décrites (19). $InCl_3$ (Alfa Ventron ou Merck pour analyse) et $TlCl_3$ (Cerac (99,9)) sont utilisés sans purification préalable.

$InCl_3,4H_2O$ est obtenu par recristallisation dans l'eau de $InCl_3$ anhydre et chauffage sous vide à 50–60°C jusqu'à poids constant.

Méthodes d'analyse

Les appareils d'analyse ir, Raman et RX sur poudre ainsi que les méthodes d'échantillonnage sont présentées par ailleurs (4, 5).

Pour l'analyse chimique, la mise en solution des perchlorates anhydres est effectuée avec beaucoup de précautions (4). Les dosages de In (20), Tl (20), de ClO_2^+ (4, 21) et de ClO_4^- (22) sont effectués généralement de façon classique comme indiqué dans la légende du tableau 1. Seule l'analyse de ClO_4^- dans les complexes du thallium fait l'objet d'une méthode originale mise au point au cours de ce travail.

Par suite d'une réaction de complexation secondaire (23), les complexes du thallium ne peuvent pas être titrés par potentiométrie grâce

[1] Auteur à qui adresser la correspondance.

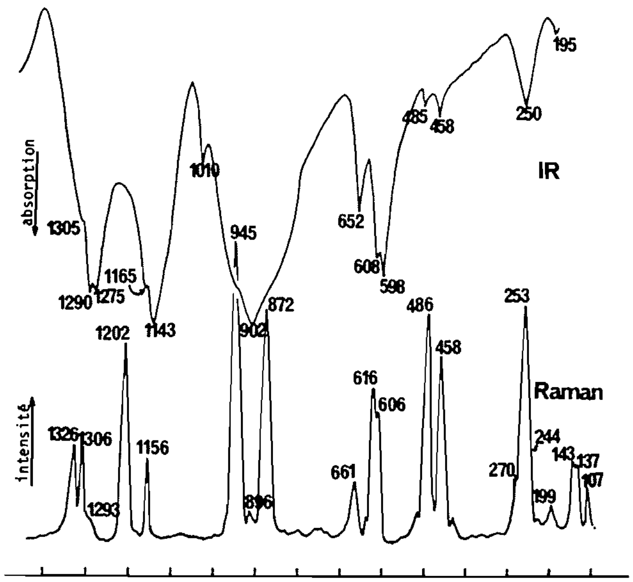

FIG. 1. Spectres ir et Raman de $In(ClO_4)_3$.

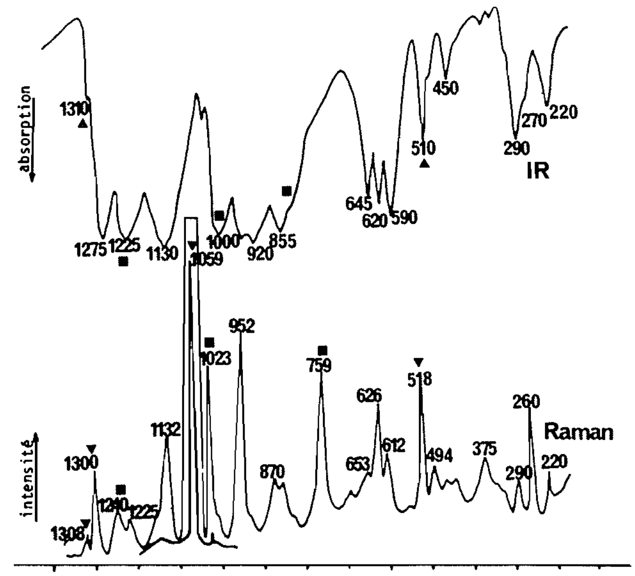

FIG. 3. Spectres ir et Raman de $ClO_2In(ClO_4)$. ▲ ClO_2^+; ■ groupe ClO_4 monodenté.

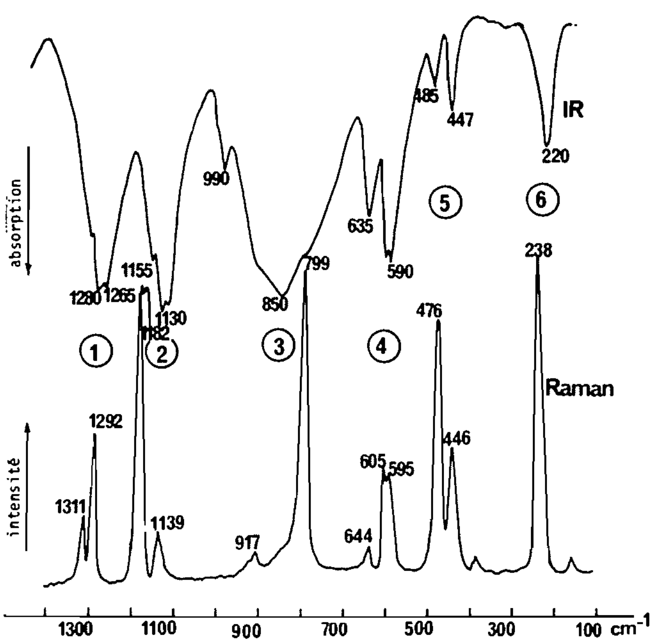

FIG. 2. Spectres ir et Raman de $Tl(ClO_4)_3$. (1) ν_{as} ClO_t; (2) ν_s ClO_t; (3) ν_s, ν_{as} ClO_p; (4) ρ_r, ρ_w et δ ClO_t; (5) ρ_t et δ ClO_p; (6) ν_s, ν_{as} $[TlO_6]$.

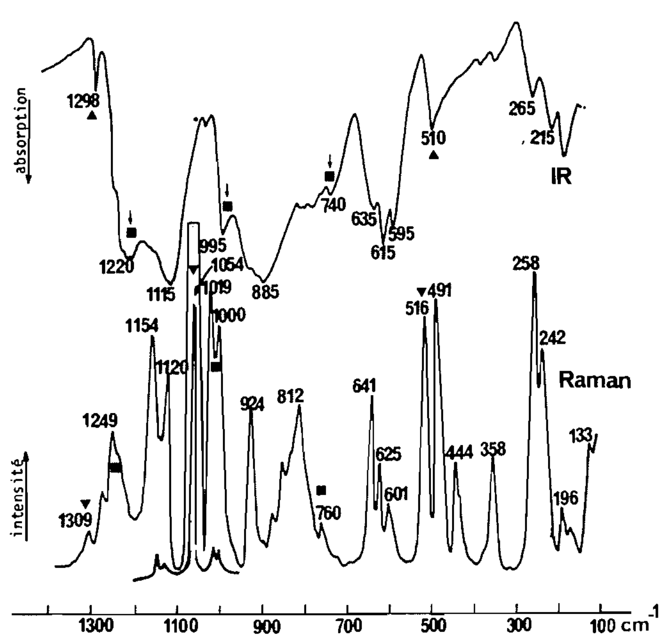

FIG. 4. Spectres ir et Raman de $ClO_2Tl(ClO_4)_4$. ▲ et ■, cf. figure 3. ↓ en ir indique les vibrations proches de celles de Cl_2O_6 liquide $(—ClO_2—ClO_4—)_n$, réf. 31.

au chlorure de tétraphényl-arsonium (22).

La concentration en ClO_4^- est déterminée en utilisant une courbe d'étalonnage préalablement établie à partir des potentiels d'électrode de plusieurs solutions étalons de perchlorates de potassium ($5 \times 10^{-4} < M < 5 \times 10^{-2}$). Pour tous les échantillons la force ionique est maintenue constante par addition de $(NH_4)_2SO_4$.

Synthèse des complexes perchlorato d'indium et de thallium

Les mécanismes de synthèses et de décomposition obeissent à des règles déjà rencontrées (4):

(*i*) À partir d'un chlorure anhydre:

[1] $MCl_3 + 4Cl_2O_6 \rightarrow ClO_2M(ClO_4)_4 + 3ClO_2 + 3/2Cl_2$

[2] $ClO_2M(ClO_4)_4 \rightarrow M(ClO_4)_3 + Cl_2O_6$

(*ii*) À partir d'un chlorure hydraté:

[3] $MCl_3 \cdot nH_2O + 3Cl_2O_6 \rightarrow M(ClO_4)_3\, nH_2O + 3ClO_2 + 3/2Cl_2$

[4] $M(ClO_4)_3 \cdot nH_2O + (n + 1)Cl_2O_6 \rightarrow ClO_2M(ClO_4)_n + nHClO_3 + nHClO_4$

Contrairement au bore (5) et au gallium (6), on n'obtient jamais avec l'indium et le thallium, dans un premier stade, des complexes de type $MCl_{n-1}(ClO_4)_n$.

Dans une expérience classique on distille à −180°C sur 0,5 à 6 × 10^{-3} mole de chlorure, un excès de Cl_2O_6 (2 à 5 fois plus). On laisse ensuite rechauffer doucement ce mélange jusquà 10°C, puis on agite plusieurs heures (de 3 à 8 h) jusqu'à ce que le maximum de trioxyde de chlore soit consommé. Durant l'agitation on note un fort dégagement de ClO_2, O_2, Cl_2. Ces gaz doivent être éliminés périodiquement sous vide dynamique du milieu réactionnel. Après avoir enlevé par pompage l'excès de Cl_2O_6, on aboutit un composé orange qui enrobe souvent des particules de chlorure qui n'ont pas réagi. On broit ce mélange en boîte à gant puis on le retraite par Cl_2O_6. Le

TABLEAU 1. Synthèse des complexes perchlorato d'indium et de thallium

Produit de base[a]		Cl_2O_6[a]	T[b]	Produit obtenu	Couleur	Analyse (%)[c] M	ClO$_4$	ClO$_2$	G[a,c,d]
$InCl_3$ $InCl_3,4H_2O$	(0,615) (1,672)	16 12	10	$ClO_2In(ClO_4)_4$	s. orangé	20,9 (19,79)	68,20 (68,57)	10,64 (10,60)	
$TlCl_3$	(0,165)	5	10	$ClO_2Tl(ClO_4)_4$	s. orangé	30,41 (30,52)	59,20 (59,40)	10,44 (10,07)	
$TlO_{0,5}(ClO_4)_2$	(0,6558)	1,5	15	$ClO_2Tl(ClO_4)_4$	s. orangé	—	—	—	1,0654 (1,0669)
$ClO_2In(ClO_4)_4$	(0,4614)	—	85	$In(ClO_4)_3$	s. blanc	27,00 (27,78)	71,81 (72,21)	— —	0,3389 (0,3286)
$ClO_2Tl(ClO_4)_4$	(1,2363)	—	80	$Tl(ClO_4)_3$[e]	s. blanc ivoire ou s. jaune orangé	38,89 (40,65)	59,85 (59,35)	— —	0,9281 (0,9273)
$ClO_2Tl(ClO_4)_4$	(2,8164)	—	95	$TlO_{0,5}(ClO_4)_2$[f]	s. jaune clair	—	—	—	1,7298 (1,7243)
$In(ClO_4)_3$	(0,1056)	—	272	$In(ClO_4)_3$	s. blanc	—	—	—	0,0964 (0,1056)

[a] Quantité en g (expérience type).
[b] Température de la réaction ou de la décomposition (°C).
[c] Les valeurs attendues sont données entre parenthèses. Analyse: In par complexométrie (20); Tl(III) sous forme de Tl(I) par iodométrie (20); ClO_4^- dans les complexes d'In par potentiométrie (22); pour ceux de Tl, cf. texte; ClO_2^+ sous forme de ClO_3^- par réduction au sel ferreux (21).
[d] G: thermogravimétrie.
[e] Quelque soit sa couleur, $Tl(ClO_4)_3$ a les mêmes propriétés (ir, Raman, RX).
[f] Le diagramme de poudre X et le spectre Raman indiquent qu'il s'agit d'un mélange. On relève l'existence de $Tl(ClO_4)_3$, Tl_2O_3 et d'un oxoperchlorato non identifié comportant des groupes ClO_4 monodentés fortement liés et des groupes ClO_4 bidentés faiblement liés.

TABLEAU 2. Diagramme de poudre

$In(ClO_4)_3$ I	d obs	d calc.	$Tl(ClO_4)_3$ I	d obs	d calc.	Indexation	$ClO_2In(ClO_4)_4$ I	d obs	$ClO_2Tl(ClO_4)_4$[a] I	d obs
15	7,69	7,67	30	7,74	7,74	003	20	7,39	m	7,25
15	7,23	7,18	20	7,26	7,23	100	5	7,10		
10	5,22	5,24	30	5,28	5,28	103	20	5,98	m	5,79
2	4,17	4,14	10	4,18	4,17	110	10	5,57	m	5,50
100	3,65	3,65	100	3,67	3,67	113	20	4,72	m	4,92
(sh)	3,60	3,59	10	3,61	3,62	200	25	4,64	sh	4,87
15	3,36	3,36	30	3,39	3,39	114	10	4,05	m	4,72
15	3,25	3,25	25	3,27	3,28	203	5	3,86	w	3,78
30	2,82	2,81	60	2,83	2,84	116	30	3,80	m	3,74
10	2,71	2,71	10	2,73	2,73	210	20	3,78	s	3,48
5	2,61	2,62	15	2,63	2,64	206	100	3,52	m	3,44
5	2,55	2,57	15	2,57	2,58	009	15	3,45	m	3,09
20	2,39	2,39	25	2,41	2,41	300	10	3,33	m	2,99
15	2,28	2,29	25	2,30	2,30	303	20	3,14	m	2,91
							15	3,09	w	2,83
							5	3,04	w	2,77
a = 8,296,		c = 23,013	a = 8,352,		c = 23,232		15	2,98	m	2,73
							10	2,92	m	2,56
							40	2,78	w	2,51
							15	2,63	w	2,38
							35	2,56	w	2,34
							10	2,50	w	2,33
							10	2,40	w	2,27
							5	2,32		
							10	2,28		

[a] Les échantillons de $ClO_2Tl(ClO_4)_4$ sont protégés par une feuille en Kapton; elle ne permet pas de faire de bonnes mesures d'intensités relatives. La signification de s, m, w est donnée dans le tableau 3.

produit final est un sel de chloryle pur, $ClO_2M(ClO_4)_4$. Par chauffage sous vide dynamique du sel de chloryle on obtient $M(ClO_4)_3$. Cette dernière opération doit être menée **avec précaution**, avec le sel de thallium pour éviter la formation d'un oxo perchlorato complexe.

Les caractéristiques des réactions, l'analyse des composés isolés sont reportées dans le tableau 1. On doit remarquer que $In(ClO_4)_3$ est stable jusqu'à 272°C.

Résultats

Analyse structurale

Les composés synthétisés sont anhydres car les spectres ir et Raman (figures 1–4) ne présentent aucune bande ou raie dans les domaines de vibrations du vibrateur O—H (3600–3000 cm^{-1} et 1800–1500 cm^{-1}).

In(ClO₄)₃

La similitude des spectres ir et Raman de $In(ClO_4)_3$ et $Ga(ClO_4)_3$ (fig. 1 et réf. 6) indique que l'environnement du métal et la symétrie locale sont identiques dans les deux complexes.

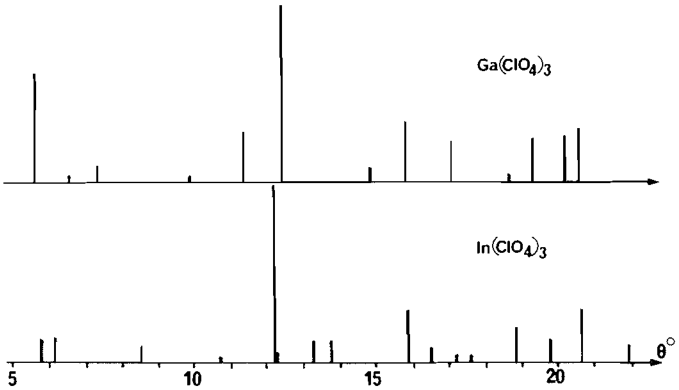

Leurs diagrammes de poudre sont cependant différents. Il est possible d'indexer les raies de celui de $Ga(ClO_4)_3$ à partir du groupe $R\bar{3}$ (17). Pour $In(ClO_4)_3$ on est conduit à adopter le groupe $P\bar{3}$ pour lequel les arrangements dans la maille sont voisins (tableau 2). On reste ainsi cohérent avec les données de la spectroscopie de vibration.

Une étude structurale par EXAFS de $Ga(ClO_4)_3$ (17) a montré que sa structure dérive de celle de AsI_3 (24). C'est un polymère à structure lamellaire, la distance Ga—Ga est de 4,71 Å. Les groupes ClO_4 sont bidentés en pont (fig. 5 et réf. 17).

Autour de chaque atome de métal la symétrie locale est D_3. Dans le cristal le groupe facteur est S_6. Ceci conduit au tableau de corrélation 3*a* pour le squelette MO_6.

TABLEAU 3*a*

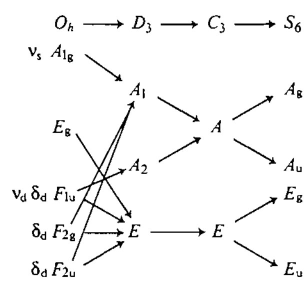

Pour les groupes ClO_4 on peut dresser le tableau de corrélation 3*b*.

TABLEAU 3*b*

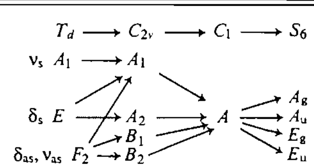

Il est bien évident que l'on ne pourra observer, pour les 6 molécules contenues dans la maille, les $((3 \times 16 \times 6) - 3 = 285)$ vibrations attendues. Par contre, on peut rendre compte des perturbations et effets de multiplicité pour les groupes ClO_4 et des vibrations du squelette métal–oxygène.

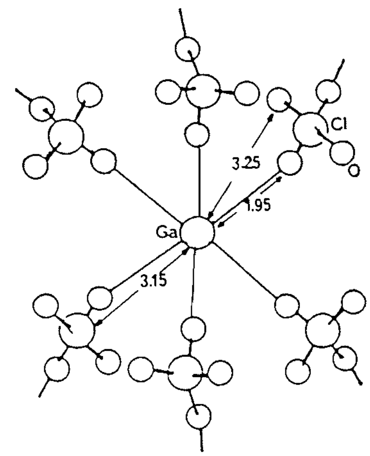

FIG. 5. Environnement de Ga dans $Ga(ClO_4)_3$ d'après réf. 17.

On note, pour les 18 modes de vibration attendus du groupe ClO_4 entre 1400 et 400 cm^{-1}, 14 composantes principales en Raman et 12 en ir. L'activité sélective ir–Raman prévue est vérifiée en particulier dans le domaine des vibrations de valence ClO_t (O_t = oxygène terminal) (fig. 1).

La présence de ligands ClO_4 bidentés est confirmée par 4 groupes de bandes ou raies dans le domaine des vibrations de valence (18, 25) (cf. tableau 4). Sous l'effet du groupe facteur (tableau 3*b*) chacun de ces modes de vibrations se dédouble en deux composantes A_g et E_g en Raman et A_u et E_u en ir (tableau 4). Par exemple ν_{as} ClO_t est observé à 1326 et 1306 cm^{-1} en Raman et 1290 et 1275 cm^{-1} en ir et ν_s ClO_t apparait à 1202 et 1156 cm^{-1} en Raman et 1165 et 1143 cm^{-1} en ir. L'effet de multiplicité dû à la présence de 6 motifs dans la maille permet d'expliquer, notamment les composantes à 1305 cm^{-1} en ir et à 1293 cm^{-1} en Raman. La plus faible résolution dans le domaine des modes de déformation de ClO_4 (700–400 cm^{-1}) ne permet pas de voir l'ensemble des composantes attendues (fig. 1). Les attributions les plus logiques sont données dans le tableau 4.

Quatre raies en Raman (autour de 241 cm^{-1}) et deux bandes en ir (vers 222 cm^{-1}) caractérisent les vibrations de valence du squelette.

Bien que le groupe ClO_4 soit fortement lié au métal, d(In—O) = 2,19 Å (17), les fréquences moyennes ν In—O ($\simeq$230 cm^{-1}) sont inférieures à celles notées pour l'acétylacétonate, ν_s: 444 cm^{-1} (27), les acétates, ν_s: 300 cm^{-1} (28) ou d'autres complexes organo métalliques signalés dans la littérature (29). Ceci est bien sur lié à la faible basicité du groupe ClO_4.

En dessous de 150 cm^{-1} on attend les vibrations de déformation de l'octaèdre et les modes de réseau. Une attribution spécifique semble délicate, cependant, sans ambiguïté, les raies à 143, 137 et 107 cm^{-1} doivent plutôt décrire des modes de déformation de symétrie A_g et E_g.

Tl(ClO₄)₃

La comparaison des diagrammes de poudre de $In(ClO_4)_3$ et $Tl(ClO_4)_3$ (tableau 2) montre que ces deux complexes cristallisent dans le même groupe d'espace. Leurs spectres ir sont identiques, ainsi qu'une grande partie de leurs spectres Raman. Par contre, le domaine des vibrations de valence ClO_p présente en Raman une grande différence. Pour l'indium on relève trois raies à 872, 945 et 896 cm^{-1} et deux pour le thallium à 799 et 917 cm^{-1}. Les vibrations du pont étant les plus affectées par le mode de coordination, on pourrait expliquer ces différences par

TABLEAU 4. Attributions des bandes ir et des raies Raman de $In(ClO_4)_3$ (s: fort, m: moyen, w: faible, sh: épaulement)

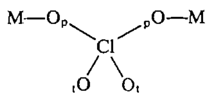

Raman	Infrarouge	Attributions
1326 (15) (A_g)		
1306 (15) (E_g)	1305 (sh)	
1293 (sh)		ν_{as} ClO_t
	1290 (s) (A_u)	
	1275 (s) (E_u)	
1202 (45) (A_g)		
	1165 (sh) (A_u)	ν_s ClO_t
1156 (15) (E_g)		
	1143 (s) (E_u)	
	1010 (m) ($E_u + A_u$)	
945 (100) ($A_g + E_g$)		ν_s ClO_p
	902 (s, br) ($E_u + A_u$)	
896 (10) (E_g)		ν_{as} ClO_p
872 (70) (A_g)		
661 (15) ($A_g + E_g$)		ρ_r
	652 (m) ($A_u + E_u$)	
616 (35) ($A_g + E_g$)		ρ_w
	608 (s) ($A_u + E_u$)	
606 (30) ($A_g + E_g$)		δ ClO_t
	598 (s) ($A_u + E_u$)	
514 (5)		
486 (65) ($A_g + E_g$)		ρ_t
	485 (w) ($A_u + E_u$)	
458 (40) ($A_g + E_g$)		δ ClO_p
	455 (w) ($A_u + E_u$)	
430 (3)		
270 (10) (E_g)		
253 (80) (A_g)		
	250 (m, br) ($A_u + E_u$)	ν GaO_6
244 (sh) (A_g)		
199 (3) (E_g)		
	195 (w) (E_u)	
143 (20)		
137 (20)		δ GaO_6
107 (10)		
89 (sh)		
80 (sh)		Réseau
52 (sh)		

l'existence de groupements $Tl(ClO_4)_3$ discrets comportant des groupes ClO_4 bidentés chelatants. Cependant, ce type d'engagement est rare (26). En l'absence de toute autre information, on conservera pour $Tl(ClO_4)_3$ le même type d'analyse que précédemment. On admet que l'évolution des vibrations ν ClO_p est liée aux différences de masse et de rayon ionique de l'élément central. La moyenne des fréquences ν ClO_p (889 cm^{-1}) dans $Tl(ClO_4)_3$ subit un déplacement normal par rapport aux complexes de la même série $Al(ClO_4)_3$: 935 cm^{-1}, $Ga(ClO_4)_3$: 901 cm^{-1}, $In(ClO_4)_3$: 906 cm^{-1}.

Comme attendu, les vibrations de valence ν MO du squelette TlO_6 apparaissent à des fréquences plus basses que celui de InO_6: $\Delta\nu_s = -18$ cm^{-1}. Les principales attributions sont notées sur le spectre (fig. 2).

$ClO_2M(ClO_4)_4$ (M = In, Tl)

Les diagrammes de poudre (tableau 2) montrent que ces sels sont des complexes définis puisque on n'y retrouve pas les raies de $M(ClO_4)_3$. Les spectres ir et Raman sont donnés sur les figures 3 et 4. On note une certaine similitude.

Le cation ClO_2^+ est défini par les bandes ou raies caractéristiques vers 1300 (ν_{as}), 1055 (ν_s) et 515 (δ) cm^{-1}.

Sur les spectres on relève des composantes à des fréquences voisines de celle observées pour le perchlorato métal correspondant. Elles sont attribuées à des groupes ClO_4 bidentés en pont. Il apparaît en outre des bandes et raies supplémentaires, par exemple pour l'indium, dans le domaine des vibrations de valence à 1225 (ir), 1240 (R), 1000 (ir), 1023 (R), 855 (ir) et 759 (R). Elles sont caractéristiques de groupes ClO_4 monodentés, ainsi que la raie à 375 cm^{-1} (balancement de ClO_3) (18).

L'existence des deux types de ligand est confirmé par la présence de trois bandes dans le domaine des vibrations ν MO alors qu'on en observe au plus deux pour le perchlorato métal (par exemple, pour les complexes d'indium, on a respectivement en ir: 290, 270, 220 et 250, 195 cm^{-1}).

On doit noter que à la différence du ligand NO_3 (30) le ligand ClO_4 ne parait pas apte à donner une environnement 8 pour Tl.

La raie Raman vers 760 cm^{-1} attribuée à ν_s Cl—O_p du groupe ClO_4 monodenté est caractéristique d'une coordination forte entre le métal et le ligand. Ceci devrait se traduire par l'apparition, vers 1300 cm^{-1}, de bandes correspondant à ν_{as} Cl—O_t (5). Ici cette vibration est relevée autour de 1220 (ir), 1240 cm^{-1} (R), alors que pour $ClO_2Ga(ClO_4)_4$ elle est observée vers 1235 cm^{-1}. Pour le complexe du gallium, ce déplacement vers les basse fréquences a été expliqué par une interaction métal–perchlorate supplémentaire conduisant à une semi-coordination (18). Il semblerait plus logique d'admettre une interaction entre ClO_2^+ et les groupes ClO_4 monodentés dans $M(ClO_4)_4^-$. Ceci tendrait à recréer des enchaînements comparables à ceux rencontrés dans Cl_2O_6 liquide (31). Cette hypothèse n'est pas aberrante puisque des interactions ClO_2^+–anion ont été observées lors de l'étude structurale de $ClO_2Sb_2F_{11}$, ClO_2GeF_5 et ClO_2BF_4 (32). Elle permet de plus, de rendre compte du mécanisme réactionnel de la transformation relativement facile de $ClO_2M(ClO_4)_4$ en $M(ClO_4)_3$ avec élimination de ClO_2ClO_4.

Conclusion

Grâce à ce travail, on a pu compléter l'étude des complexes perchlorato des éléments du groupe IIIB. L'action de Cl_2O_6 sur $InCl_3$ (ou $InCl_3,4H_2O$) et $TlCl_3$ conduit à la formation de quatre nouveaux perchlorates anhydres, deux perchlorato-métal $M(ClO_4)_3$ et deux sels de chloryle $ClO_2M(ClO_4)_4$ (M = In, Tl).

L'analyse structurale par spectroscopie de vibration infrarouge et Raman et diagrammes de poudre RX a permis de montrer que les perchlorato métal, $M(ClO_4)_3$ (M = In, Tl) ont des structures proches de celle de $Ga(ClO_4)_3$. Ce sont des polymères avec des groupes ClO_4 bidentés en pont où tous les groupes ClO_4 sont en interactions forte avec le métal, alors que dans $ClO_2In(ClO_4)_4$ et $ClO_2Tl(ClO_4)_4$ il faut distinguer des groupes ClO_4 de même nature que les précédents et des groupes ClO_4 monodentés présentant une interaction importante avec l'ion chloryle. Par ailleurs, on a pu mettre en évidence les évolutions des fréquences de vibration ν ClO_p et ν MO dans la colonne IIIB pour la série $M(ClO_4)_3$ (M = Al, Ga, In et Tl). Elles sont directement liées aux rayons ioniques et à la masse de l'élément central.

Remerciements

Ce travail a été réalisé dans le cadre d'accords de coopération CNRS (France) – DRST (Tunisie). Les auteurs du mémoire remercient ces organismes pour les liens qu'ils ont su renforcer entre les deux laboratoires et l'aide financière qu'ils leur ont apporté.

1. M. SCHMEISSER et K. BRANDLE. Adv. Inorg. Chem. Radiochem. **5**, 41 (1963).
2. (*a*) Z. K. NIKITINA, A. I. KARELIN et V. YA. ROSOLOVSKII. Russ. J. Inorg. Chem. (Trad. Anglaise), **25**, 71 (1980); et références citées; (*b*) V. P. BABAEVA et V. YA. ROSOLOVSKII. Zh. Neorg. Khim. **29**, 2731 (1984).
3. C. J. SHACK, D. PILIPOVICH et K. O. CHRISTE. J. Inorg. Nucl. Chem. Supp. **76**, 207 (1976).
4. J. L. PASCAL, J. POTIER et C. S. ZHANG. J. Chem. Soc. Dalton Trans. 297 (1985), et références citées.
5. T. CHAUSSE, J. L. PASCAL, A. POTIER et J. POTIER. Nouv. J. Chim. **5**, 261 (1981), et références citées.
6. M. CHAABOUNI, J. L. PASCAL et J. POTIER. J. Chem. Res. (S), 80 (1977).
7. Z. K. NIKITINA, A. I. KARELIN et V. Y. ROSOLOVSKII. Bull. Acad. Sci. USSR (Trad. Anglaise), **22**, 705 (1973).
8. T. CHAUSSE. Thèse Docteur Ingénieur Université des Sciences et Techniques du Languedoc, Montpellier. 1980.
9. T. CHAUSSE, A. POTIER et J. POTIER. J. Chem. Res. (S), 316 (1980).
10. Z. K. NIKITINA et V. YA. ROSOLOVSKII. Russ. J. Inorg. Chem. (Trad. Anglaise), **23**, 1293 (1979), et références citées.
11. Z. K. NIKITINA et V. YA. ROSOLOVSKII. Bull. Acad. Sci. USSR (Trad. Anglaise), **27**, 449 (1978).
12. (*a*) M. ASHRAF, A. MAZBZ et J. B. HEDDRIDGE. J. Chem. Soc. Dalton Trans. 170 (1977); (*b*) A. J. CARTY et D. G. TUCK. Prog. Inorg. Chem. **19**, 243 (1975), et références citées.
13. P. PASCAL. Compléments du Nouveau Traité de Chimie Minérale 11, 64 (1978). Masson, Paris.
14. C. BELIN, M. CHAABOUNI, J. L. PASCAL, J. POTIER et J. ROZIERE. J. Chem. Soc. Chem. Commun. 105 (1980).
15. C. BELIN, M. CHAABOUNI, J. L. PASCAL et J. POTIER. Inorg. Chem. **21**, 3557 (1982).
16. (*a*) J. L. PASCAL, J. POTIER, D. J. JONES, J. ROZIERE et A. MICHALOWICZ. Inorg. Chem. **23**, 2068 (1984); (*b*) **24**, 238 (1985).
17. (*a*) J. L. PASCAL, J. POTIER, A. SEIGNEURIN, D. J. JONES, J. ROZIERE, J. POTIER et A. MICHALOWICZ. Communication aux Journées EXAFS Lure–Orsay, 6–7 Décembre 1984; (*b*) Progress in X-ray studies by synchroton radiation. Strasbourg. avril 1985.
18. M. CHAABOUNI. Thèse, Montpellier, 1979.
19. A. C. PAVIA, J. L. PASCAL et A. POTIER. C.R. Acad. Sci. Paris Ser. C, **272**, 1495 (1971).
20. G. CHARLOT. Chimie analytique quantitative. Masson, Paris. 1974.
21. H. MATHIEU. Analyse quantitative. Masson, Paris. 1946.
22. (*a*) R. J. BACZUCK et W. G. BOTTELER. Anal. Chem. **40**, 687 (1968); (*b*) Guide des méthodes analytiques. 9e éd. Orion Research. 1979.
23. W. T. SMITH, JR. Anal. Chem. **20**, 937 (1948).
24. J. TROTTER. Z. Kristallogr. **121**, 81 (1965).
25. B. J. HATHAWAY et A. E. UNDERHILL. J. Chem. Soc. 3091 (1961).
26. E. A. GENKINA, V. P. BABAEVA et V. YA. ROSOLOVSKII. Koord. Khim. **10**, 1415 (1984).
27. R. E. ESTER et R. A. PLANE. Inorg. Chem. **3**, 513 (1964).
28. J. J. HABEEB et D. G. TUCK. J. Chem. Soc. Dalton Trans. 243 (1973).
29. E. MASLOWSKY. Vibrational spectra of organo-metallic compounds. John Wiley and Son, New York. 1977.
30. D. W. AMOS. J. Chem. Soc. Chem. Commun. 19 (1970).
31. (*a*) J. L. PASCAL. Thèse Université des Sciences et Techniques du Languedoc, Montpellier. 1978; (*b*) J. L. PASCAL, A. C. PAVIA, J. POTIER, J. M. BENY et B. SOMBRET. VIth International Conference on Raman Spectroscopy, Bangalore, Inde. Septembre, 1978.
32. A. J. EDWARDS et R. J. C. SILLS. J. Chem. Soc. Dalton Trans. 1776 (1974); T. E. MALLOUK, B. DESBAT et N. BARTLETT. Inorg. Chem. **23**, 3160 (1984); T. E. MALLOUK, G. L. ROSENTHAL, G. MULLER, R. BRUSASCO et N. BARLETT. Inorg. Chem. **23**, 3167 (1984).

Acidity measurements in THF. V.[1] Heteroaromatic compounds containing 5-membered rings

ROBERT R. FRASER, TAREK S. MANSOUR, AND SYLVAIN SAVARD
Ottawa–Carleton Institute for Graduate Studies and Research in Chemistry, University of Ottawa, Ottawa, Ont., Canada K1N 9B4

Received March 18, 1985

ROBERT R. FRASER, TAREK S. MANSOUR, and SYLVAIN SAVARD. Can. J. Chem. **63**, 3505 (1985).

The pK_a's of 13 heterocyclic aromatic compounds have been measured in tetrahydrofuran (THF) using ^{13}C nmr spectroscopy. The acidifying effect of a nitrogen heteroatom is seen to be quite large (4–6 pK units versus C—H) on an adjacent C—H bond but small on a more remote hydrogen. Most of these aromatic heterocycles are sufficiently acidic, pK_a < 34, to be completely deprotonated by lithium tetramethylpiperidide in THF. Benzoxazole appears to be an extremely strong carbon acid, its ring-opened isomer having a pK_a of less than 15.7.

ROBERT R. FRASER, TAREK S. MANSOUR et SYLVAIN SAVARD. Can. J. Chem. **63**, 3505 (1985).

Faisant appel à la rmn du ^{13}C et opérant dans le tétrahydrofuranne (THF), on a mesuré les pK_a de 13 composés hétérocycliques aromatiques. L'effet produit par l'acidification d'un azote hétéroatomique est assez important (4–6 unités de pK par rapport à un C—H) pour une liaison C—H adjacente; toutefois, cet effet n'est pas important pour les hydrogènes plus éloignés. La plupart de ces hétérocycles aromatiques sont suffisamment acides, pK_a < 34, pour être déprontonés par le tétraméthylpipéridure dans le THF. Le benzoxazole semble être une acide carboné extrèmement fort; le pK_a de son isomère à cycle ouvert est plus bas que 15,7.

[Traduit par le journal]

In recent times, the metalation of organic compounds has become an exceedingly useful component of synthetic methodology, the current reagent of choice being lithium diisopropylamide, (LDA) (1), or lithium tetramethylpiperidide, (LTMP) (2). Use of these and other lithiated dialkylamines (3) is preferable to direct treatment of a weak organic acid with butyl or methyllithium, as their selectivity in deprotonation avoids harmful side reactions. Nevertheless, alkyllithiums are still often employed in instances in which LDA or its counterparts might be more effective. To determine how strong a base is required for a given deprotonation, one simply requires knowledge of the pK_a of the proton to be removed. Then, lithiation of an amine less acidic by at least 4 pK units will provide the requisite base. For this reason, the measurement of acidities of weak carbon acids in THF is of considerable practical importance to organic chemists. Until recently, most of the accumulated data on weak carbon acid acidities have been obtained in DMSO (4) or cyclohexylamine (5) as solvent. However, it has been established that there are often significant solvent effects on acidity that are not completely predictable (5, 6). We have therefore recently undertaken a series of determinations of pK values in THF. Those compounds studied included arylmethanes (7), benzene derivatives (8), hindered amines (9), and alkylpyridines (10). In this paper we wish to describe pK measurements on a series of 5-membered aromatic heterocycles and some of their benz-fused derivatives.

Method of pK_a *measurement*

As in previous studies, we have used ^{13}C nmr to measure the relative concentrations of all four species in equilibrium, eq. [1],

$$[1] \quad HA_1 + A_2^- \rightleftharpoons A_1^- + HA_2$$

from which $K = K_1/K_2$ and thus yields a $\Delta pK = -\log K = pK_1 - pK_2$ (5). In most cases the measurements were done on a mixture of the heterocyclic compound and an equivalent of lithiated amine after equilibration at room temperature. In addition to LTMP and LDA we have used five other lithiated amines whose acidities vary from 25.8 to 39.5 (9) and thereby provide a wide accessibility of measurable pK. Certain of the lithiated heterocycles proved to be unstable at room temperature, in which cases we have carried out the pK_a determination at −60°C.[2] When decomposition persisted at the lower temperature, we carried out the measurement of the heterocycle in equilibrium with a second carbon acid of appropriate acid strenth.[3] For comparison, both types of equilibrium measurements were done with benzothiophene. There was a 1-unit difference in pK between the two methods. For two other compounds, *N*-methylpyrrole and dimethylaminopyrrole, the difference was negligible. As a verification of the nmr method, we routinely examined a sample of each heterocyclic compound after quenching the equilibrium mixture with methanol-*O-d*. The % deuterium content, as measured by mass spectrometry, was slightly lower (5–10%) than the % metalation measured by nmr. Such differences were not enough to alter the value for the pK_a beyond the experimental error of 0.2 pK units, and the lower ms value probably reflects traces of proton impurity in the medium, i.e. slight excess of amine or uptake of moisture in methanol-*O-d*. The results appear in Table 1.[4]

[1] This is the fifth in a series of papers describing acidity measurements in tetrahydrofuran (THF). Parts III and IV are assigned to refs. 11 and 9 respectively.

[2] In all cases that we have examined, there has been no observable change in ΔpK over this 90° temperature range (11). We earlier observed no pK change for a 5-fold change in concentration (7).

[3] Decomposition prevented us from studying benzothiazole in equilibrium with its lithio derivative. Nevertheless, we were able to assess its pK from low temperature experiments in which it was either completely deprotonated or untouched in the presence of lithiated amines (see Table 1). Extensive use of 2-lithiobenzothiazole in synthesis has been reported by Corey and Boger (12). Unfortunately, lack of solubility prevented us from obtaining any acidity data for n-propylbenzimidazole.

[4] As mentioned in our first paper (7), these pK values likely represent ion-pair or ion-aggregate acidities. The extent of aggregation has recently been found to vary considerably with structure (33). Since it can also vary with solvent and thereby influence pK, we feel the data in THF, though representing uncertain species, are the most useful to organic chemists.

TABLE 1. Heteroaromatic proton acidities (pK_1)

Acid$_1$		Reference acid (pK_2)	K_{eq}	$-\log K$	pK_1
1	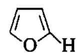	DIPA (35.7)	1.3	−0.1	35.6
2	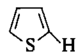	$(CH_3)_3C—N(H)—Si(CH_3)_3$ (33.6)	4	−0.6	33.0
3	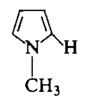	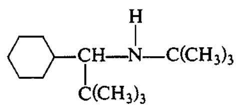 (39.5)	1.0	0	39.5[a]
		$C_6H_5SCH_3$ (38.1)	.027	+1.6	39.7
4	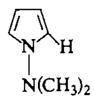	$C_6H_5SCH_3$ (38.1)	14.4	−1.2	36.9
		TMP (37.3)	1.7	−0.2	37.1
5	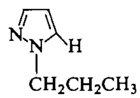	Furan (35.6)	0.45	+0.3	35.9
6	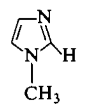	$(CH_3)_3C—N(H)—Si(CH_3)_3$ (33.6)	0.84	+0.1	33.7
7	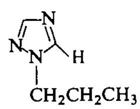	$(CH_3)_3Si—N(H)—Si(CH_3)_3$ (25.8)	0.4	+0.4	26.2[b]
8	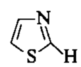	$(CH_3)_3Si—N(H)—Si(CH_3)_3$ (25.8)	<0.003	+2.5	>28.3[c]
9	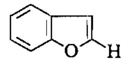	Thiophene (33.0)	0.6	+0.2	33.2
10	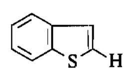	Thiophene (33.0)	4.6	−0.6	32.4
		$(CH_3)_3CCH_2N(H)—Si(CH_3)_3$ (33.2)	0.5	+0.3	33.5
11	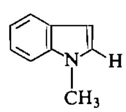	$C_6H_5—SCH_3$ (38.1)	0.95	0	38.1
12	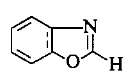	$C_6H_5—CH_2CN$ (18.7)	>10^3	<−3	<15.7[d]
13	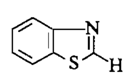	$(CH_3)_3Si—N(H)—Si(CH_3)_3$ (25.8)	<0.01	>+2	>27.8[c]
		$CH_3CH_2CH_2—N(H)—Si(CH_3)_3$ (30.9)	>100	<−2	<28.9[c]

[a]Due to slow equilibration K_{eq} was estimated by extrapolation, and verified by the second determination below.
[b]The value for K measuring the deuterium content of a sample quenched with CH_3OD at 5°C.
[c]Determined at −60°C. All other metalated amines caused decomposition at this temperature.
[d]As explained in the text, the pK being measured is that of *o*-isocyanophenol.

Discussion of results

The data in Table 1 reveal several qualitative correlations between structure and acidity. For the monocyclic 5-membered heterocycles, there is a significant acid strengthening effect of the heteroatom on the adjacent C—H bond (α) with S > O > N in acidifying influence (i.e. **2** > **1** > **3** in acidity). The effect of a second nitrogen heteroatom is appreciable (**6** vs. **3**) when α, causing a 4–6 pK unit decrease, but becomes smaller (**5** vs. **3**) when β. An attached benzene ring has a small, somewhat variable, acidifying effect of up to 3 pK units, and tends to decrease the effect of the heteroatom, for example in benzothiophene, **10**, vs. benzofuran, **9**. Table 3 summarizes all the pK data.

TABLE 2. ^{13}C chemical shifts (ppm from THF = 69.00)

Compound	X	C2	C3	C4	C5	*N*-alkyl
1	H	144.1	110.8	110.8	144.1	
	Li	165.0	123.1	108.6	145.1	
2	H	128.3	126.5	126.5	128.3	
	Li	174.0	137.4	130.8	127.7	
3	H	122.7	109.5	109.5	122.7	36.6
	Li	173.7	121.8	109.0	123.1	41.1
4	H	117.3	107.1	107.1	117.3	49.3
	Li	157.6	112.3	109.2	117.1	49.9
5	H	—	139.9	106.0	130.1	54.9, 25.4, 12.2
	Li	—	137.9	116.0	186.4	57.8, 26.4, 12.6
6	H	139.6	—	130.5	121.7	
	Li	171.5	—	129.1	118.9	

Compound	X	C2	C3	C4	C5	C6	C7	C8	C9
9	H	146.8	108.8	122.6	124.2	125.7	112.7	n.o.	n.o.
	Li[a]	n.o.	119.3	119.8	120.1	121.1	110.5	n.o.	n.o.
10	H	127.9	125.4	125.2	125.7	125.6	124.0	144.5	141.5
	Li	175.7	132.2	122.5	122.2	121.3	119.9	146.1	150.0
11	H	130.2	102.2	122.6	120.5	122.0	110.6	138.6	130.5
	Li	175.9	113.4	118.1	117.2	117.7	108.3	134.3	142.3
	H	154.8		122.0	126.9	125.9	112.3	151.9	142.2
12	Li	167.0		131.2	128.7	122.8	113.9	165.8	119.0
	R[b]	164.8		131.4	128.2	121.2	115.8	165.4	118.5
	H	155.7		125.1	127.5	126.9	123.5	135.7	155.4
13	Li	n.o.		122.3	124.0	122.3	120.5	139.6	159.0
	R[b]	164.8		126.1	134.7	129.3	122.5	132.0	146.5

[a] Signals for the lithio derivative were slightly broadened, so that quaternary carbons were not observed (n.o.) in some cases.
[b] R represents the shifts calculated for the ring-opened isomer. In these two cases the numbering system does not apply.

From the data in Tables 1 and 3 it can be seen that benzothiazole (pK_a = 28–29)[3] is about 4 pK units more acidic than benzothiophene. For comparison, the pK values for the same two compounds in cyclohexylamine were 28.1 and 37.0, the latter being clearly sensitive to the change in solvent, as are the acidities of thiophene and benzofuran (38.2 and 36.8 respectively, in cyclohexylamine (13)). These are the only examples for which data on another solvent are available. However, there are some data on the kinetic acidities of several of the heterocycles and related derivatives. Wherever comparisons can be made, our acidity data are in agreement with the data on rates of isotopic exchange. Grieco and co-workers recently reported that the presence of an *N*-dimethylamino group in pyrrole improved the ease of ring lithiation and subsequent substitution reactions (14). Though the exchange rates of imidazole and pyrazole are not known, their azolium salts differed by a factor of 3×10^4, the imidazolium salt reacting faster (15). Olofson *et al.* (16) showed that the replacement of a carbon in thiazole by one or more nitrogen atoms increased the exchange rate by a factor of 10^4. And while the order of exchange rates was thiazole > oxazole > imidazole in the base-catalyzed process (17), the condensed ring derivatives showed a reversal, benzoxazole being deuterated 30 times faster than benzothiazole (18).

In view of the exchange data we would expect benzoxazole to be more acidic than benzthiazole. Nevertheless, it was surprising to find that benzoxazole was completely deprotonated even by lithiated phenylacetonitrile, whose pK we have determined to be 18.7.[5] Benzoxazole then appears to have a pK_a of less than 16! That this value is not a true pK was indicated by the ^{13}C nmr shifts for its lithio derivative. These values appear in Table 2 along with the chemical shifts calculated for 2-isocyanophenoxide ion on the basis of the reported shifts for isocyanobenzene (19) and phenoxide ion (20). The excellent agreement shows that deprotonation of benzoxazole leads to formation of the ring-opened phenoxide ion. Several examples of similar equilibria for oxazoles (21, 22) and oxazolines (23) have been reported. We have further corroborated this point by isolating, after addition of trimethylsilyl chloride, the silyl ether of 2-isocyanophenol. Interestingly, the addition of dimethyl sulfate produces not only 2-isocyanoanisole (86%) but also 14% of 2-methylbenzoxazole, presumably by competitive C-alkylation of trace amounts of the ring-closed tautomer. Protonation also reforms benzoxazole. We have a clear indication that lithiated benzothiazole does not ring open in the same way. First of all, the ^{13}C shifts for the lithiated compound do not correspond closely to those calculated for 2-isocyanobenzenethiolate ion (see Experimental for thiophenoxide shifts). Secondly, reaction of the anion with trimethylsilyl

[5] By stepwise comparisons beginning with bistrimethylsilylamine and 3-methylpentyne, the following pK's were determined: 3-methylpentyne, 23.6; phenylacetylene, 21.6; indene, 20.9; and phenylacetonitrile, 18.7.

TABLE 3. Summary of pK data

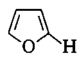	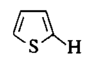	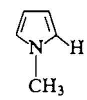	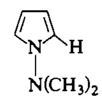
35.6	33.0	39.5	37.1
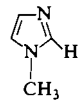	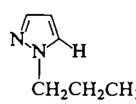	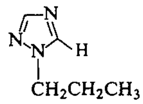	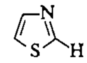
33.7	35.9	26.2	>28.3
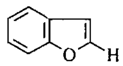	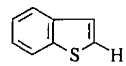	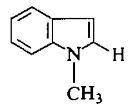	
33.2	32.4(33.5)	38.1	
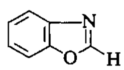	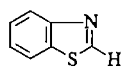		
<15.7[a]	~28		

[a] Actually represents o-isocyanophenol.

chloride gave only 2-trimethylsilylbenzothiazole.

From the synthetic point of view, the data in Table 1 allow the following conclusions to be drawn. Thiophene, N-methylimidazole, and 1-propyl-1,2,4-triazole will give >97% lithiation on treatment with LDA in THF, as will all benz derivatives except N-methylindole. Furan can be completely metalated by the strong base utilized in evaluating the acidity of N-methylpyrrole. N-methylpyrrole and its dimethylamino derivative are insufficiently acidic for complete metalation by any lithiated amine.

In every example studied, the sole site of lithiation has been at the carbon adjacent to the heteroatom or in between two heteroatoms, whenever such a position is present. It is clear that the metalation of heterocycles under our conditions (of equilibration) gives different results from metalation using an alkyllithium (24). There are several examples in which more than one site is attacked under the latter condition, e.g. thiazole, methylimidazole. In those cases, as in the ortholithiation of monosubstituted benzenes (8), there is a directing effect of the basic substituent that enhances the rate of metalation of the secondary less acidic site.

Experimental

The preparation of samples for nmr was the same as given below except those few cases in which a second carbon acid was used instead of an amine as the reference acid.

Each sample was prepared in a 10-mm septum-capped nmr tube (Wilmad Glass, Buena, NJ) fitted with an argon inlet and outlet. To a solution of 1.5 mequiv. of amine in 2 mL of freshly distilled THF at 0°C was added 1.5 mequiv. of methyllithium in ether. After 15 min a solution of 1.5 mequiv. of hydrocarbon in 1 mL of THF was added at 0°C. The cap was wrapped in Parafilm and the tube then warmed and transferred to the probe of a Varian FT-80 nmr spectrometer operating at 27°C. In a few instances metalation and spectral acquisition were done at low temperature to avoid decomposition. Spectra were accumulated using a small pulse angle (30°) and a 2-s repetition rate. That differential relaxation times were unimportant was shown by extending repetition rate to 3 s without affecting integral ratios. Other factors of quantitative influence, such as differential nOe's (nuclear Overhauser enhancements), were eliminated by using an empirically derived correction factor. For example, this factor applied to the methylene signals of TMP and LTMP was arrived at by measuring the integral for TMP prior to, then after, the addition of 0.5 equiv. of methyllithium as well as that of the LTMP produced, both relative to naphthalene present as an internal standard. We estimate the accuracy of K to be ±30%, leading to an uncertainty in ΔpK of ±0.2 pK units or less. Mass spectral measurements were carried out using a VG 707-E mass spectrometer.

Most of the heterocyclic compounds used herein were purchased from Aldrich Chemical Company and were purified and dried prior to use when necessary. N-propyl pyrazole and n-propyl-1,2,4-triazole, however, were made by alkylation of the parent heterocycle.

The site of metalation, as indicated in Table 1, was in each instance determined by comparison of the ^{13}C spectrum of a sample quenched with methanol-O-d with that of the starting material. The assignments to individual signals in the ^{13}C spectra were available from previous literature, except for the triazole **1**. In the fully coupled spectrum of this compound, C5 was clearly differentiated from C2 by its long range coupling to a CH_2 group. The ^{13}C shifts for all compounds and their lithio derivatives are summarized in Table 2. The shifts in tetrahydrofuran did not differ greatly from those reported in $CDCl_3$ for furan (25), thiophene (25), N-methylpyrrole, (26) N-methylimidazole (26), N-propylpyrazole (26, 27), indoles (28), benzofuran (29), benzothiophene (29, 30), benzoxazole (31), and benzothiazole (32). The ^{13}C shifts for lithium thiophenoxide, as determined in THF (0.5 M), were 148.9(C1), 134.0(C2), 128.5(C3), and 121.8(C4).

Reactions of lithiated benzoxazole

Metalation of 2 mequiv. benzoxazole was carried out using 2 mequiv. of lithiated bis-trimethylsilylamine in 2 mL of THF at 0°C. Addition of 2 mequiv. of trimethylsilyl chloride gave, after 15 min at room temperature, the trimethylsilyl ether of O-isocyanophenol as the only detectable product (by ^1H and ^{13}C nmr). The crude product showed a strong bond in the ir at 2130 cm^{-1}; ms, P^+ 191; ^{13}C nmr ($CDCl_3$): 153.0 (q), 131.7, 129.2, 123.4, 122.4. The products of the reaction carried out similarly with dimethylsulfate (2 days at room temperature) were identified as 2-isocyanoanisole, ir, 2130 cm^{-1} (strong); ms, P^+ 133; ^{13}C nmr ($CDCl_3$): 156.7 q, 132.0, 129.1, 122.0, 113.7, 57.1; ^1H nmr ($CDCl_3$): CH_3 singlet at 3.95; and 2-methylbenzthiazole, ms, P^+ 133; ^1H nmr ($CDCl_3$): CH_3 singlet at 2.62. The ratio of low field to high field methyl singlets was 86.14.

Reaction of lithiated benzothiazole

Treatment of 1 mequiv. of benzothiazole with 1 mequiv. of LDA in 5 mL of THF at −74°C and subsequent addition of 1.1 mequiv. of trimethylsilyl chloride yielded a crude liquid product (>90% pure by ^1H nmr) whose mass spectrum showed a parent peak at 207, in accord with a silyl derivative. The ^{13}C spectrum (THF): 158.2(C2), 125.0(C4), 127.2(C5), 126.7(C6), 123.2(C7), 155.6(C8), 137.9(C9) −0.3(Si-CH_3) is consistent with the ring-closed derivative (see Table 2, benzthiazole, for comparison).

Acknowledgments

The authors thank the Natural Sciences and Engineering Research Council of Canada (NSERC) for financial support. S. Savard thanks NSERC for a post-doctoral fellowship.

1. I. SASSON and J. LABOVITZ. J. Org. Chem. **40**, 3670 (1975).
2. R. A. OLOFSON and C. M. DOUGHERTY. J. Am. Chem. Soc. **95**, 582 (1973).
3. J. C. STOWELL. Carbanions in organic synthesis. John Wiley and Sons Inc., New York. 1975. p. 13.
4. W. N. OLMSTEAD, Z. MARGOLIN, and F. G. BORDWELL. J. Org. Chem. **45**, 3295 (1980), and references therein.
5. A. STREITWIESER, JR., E. JUARISTI, AND L. L. NEBENZAHL. Equilibrium carbon acidities in solution. *In* Comprehensive carbanion chemistry, Part A. *Edited by* E. Buncel and T. Durst. Elsevier – North Holland, Amsterdam. 1980. p. 323.
6. W. S. MATTHEWS, J. E. BARES, J. E. BARTMESS, F. G. BORDWELL, F. J. CORNFORTH, G. E. DRUCKER, Z. MARGOLIN, R. J. MCCALLUM, G. J. MCCOLLUM, and N. R. VANIER. J. Am.

Chem. Soc. **97**, 7006 (1975).
7. R. R. FRASER, M. BRESSE, and T. S. MANSOUR. J. Chem. Soc. Chem. Commun. 620 (1983).
8. R. R. FRASER, M. BRESSE, and T. S. MANSOUR. J. Am. Chem. Soc. **105**, 7790 (1983).
9. R. R. FRASER and T. S. MANSOUR. J. Org. Chem. **49**, 3442, 1984; **49**, 5284 (1984).
10. R. R. FRASER, T. S. MANSOUR, and S. SAVARD. J. Org. Chem. **50**, 3232 (1985).
11. R. R. FRASER, M. BRESSE, N. CHUAQUI-OFFERMANNS, K. N. HOUK, and N. G. RONDAN. Can. J. Chem. **61**, 2729 (1983).
12. E. J. COREY and D. L. BOGER. Tetrahedron Lett. 5 (1978).
13. A. STREITWIESER, JR. and J. L. SCANNON. J. Am. Chem. Soc. **95**, 6273 (1973).
14. G. R. MARTINEZ, P. A. GRIECO, and C. V. SRINIVASAN. J. Org. Chem. **46**, 3760 (1981).
15. P. HAAKE, L. P. BAUSHER, and W. B. MILLER. J. Am. Chem. Soc. **91**, 1113 (1969).
16. R. A. OLOFSON, J. M. LANDESBURG, K. N. HOUK, and J. S. MICHELMAN. J. Am. Chem. Soc. **88**, 4265 (1966).
17. J. A. ELVIDGE, J. R. JONES, C. O. O'BRIEN, E. A. EVANS, and H. C. SHEPPARD. Adv. Heterocycl. Chem. **16**, 1 (1974).
18. O. ATTANASI, P. BATTISTONI, and G. FAVA. Phosphorus Sulfur, **5**, 305 (1979).
19. D. KNOL, N. J. KOOLE, and M. J. A. DE BIE. Org. Magn. Reson. **8**, 213 (1976).
20. J. B. STOTHERS. C-13 NMR spectroscopy. Academic Press, New York, NY. 1972. p. 197.
21. R. SCHRÖDER, U. SCHÖLLKOPF, E. BLUME, and J. HOPPE. Ann. Chem. 183 (1975).
22. P. A. JACOBI, S. UENG, and D. CARR. J. Org. Chem. **44**, 2042 (1979).
23. A. I. MEYERS and E. W. COLLINGTON. J. Am. Chem. Soc. **92**, 6676 (1970).
24. H. W. GSCHWEND and H. R. RODRIGUEZ. Org. React. **26**, 1 (1979).
25. T. F. PAGE, JR., T. ALDER, and D. M. GRANT. J. Am. Chem. Soc. **87**, 5333 (1965).
26. J. ELGUERO, C. MARZIN, and J. D. ROBERTS. J. Org. Chem. **39**, 357 (1974).
27. W. ADAM, A. GRIMISON, and G. RODRIGUEZ. Tetrahedron, **23**, 2513 (1967).
28. R. R. FRASER, S. PASSANNANTI, and F. PIOZZI. Can. J. Chem. **54**, 2915 (1976).
29. N. PLATZER, J. J. BASSELIER, and P. DEMERSMAN. Bull. Soc. Chim. Fr. 905 (1974).
30. P. GENESTE, J. L. OLIVÉ, S. N. UNG, M. E. A. EL-FAGHI, J. W. EASTON, H. BEIERBECK, and J. K. SAUNDERS. J. Org. Chem. **44**, 2887 (1979).
31. L. F. JOHNSON and W. C. JANKOWSKI. ^{13}C NMR spectra. John Wiley and Sons, Inc., New York, NY. 1972.
32. S. N. SAWHNEY and D. W. BOYKIN. J. Org. Chem. **44**, 1136 (1979).
33. W. BAUER and D. SEEBACH. Helv. Chim. Acta, **67**, 1972 (1984).

The mechanism of an intramolecular Michael addition: a MNDO study

GRAHAM W. L. ELLIS, DONALD F. TAVARES, AND ARVI RAUK[1]
Department of Chemistry, University of Calgary, Calgary, Alta., Canada T2N 1N4

Received July 2, 1985

GRAHAM W. L. ELLIS, DONALD F. TAVARES, and ARVI RAUK. Can. J. Chem. **63**, 3510 (1985).

The 5-*endo-trig* cyclization reactions of α'-hydroxy α,β-unsaturated carbonyl compounds to form the 3-furanone ring system has been investigated by means of MNDO calculations. In acid medium, the activation energy for ring formation is reduced by protonation of the carbonyl oxygen and by electron-releasing β-substituents, both of which facilitate torsion about the α,β-CC bond. Rotation about the α,β-CC bond is essentially complete when the transition structure is achieved. In reverse ring opening, heterolytic rupture of the C—O bond is aided by prior enolization since induced polarization of the enol π system acts to stabilize the developing cationic centre at the β-carbon. In basic medium, ring closure is hindered by the combined effects of the intrinsic barrier to cyclization and solvation of the intermediate alkoxide. Ring opening in basic medium is prevented by prohibitively high intrinsic barriers except when a strongly electron-releasing group such as *p*-O(−)-phenyl is at the β-carbon.

GRAHAM W. L. ELLIS, DONALD F. TAVARES et ARVI RAUK. Can. J. Chem. **63**, 3510 (1985).

Faisant appel à des calculs MNDO, on a étudié les réactions de cyclisation du type *endo*-5 *trig* des composés carboxylés α,β-insaturés, portant un groupement d'hydroxy en position α', qui conduisent au système cyclique de la furanone-3. En milieu acide, la protonation de l'oxygène du carboxyle ainsi que la présence de substituants électrodonneurs en position β, qui toutes deux facilitent la rotation autour de la liaison carbone–carbone, réduisent l'énergie d'activation de la réaction. La rotation autour de la liaison carbone–carbone en α,β est totale au moment de la transition de structure. Contrairement à l'ouverture de cycle, l'énolisation préalable facilite la scission hétérolytique de la liaison C—O puisque la polarisation induite des systèmes énoliques π agit de façon à stabiliser le centre cationique en voie de formation au niveau du carbone en position β. En milieu basique, les effets combinés de la barrière intrinsèque à la cyclisation et la solvatation de l'alcoolate intermédiaire empêchent la cyclisation. La haute barrière intrinsèque inhibe l'ouverture de cycle en milieu basique mais la présence de groupements fortement électrodonneurs tels le *p*-O(−)-phényl au niveau du carbone en position β annule cet effet.

[Traduit par le journal]

Introduction

The role of stereoelectronic factors in controlling organic ring-forming and ring-breaking reaction pathways is a subject of current experimental (1–8) and theoretical (9–11) interest. In the case of smaller rings (less than eight atoms) where entropy considerations are not dominant, the formation of rings is governed largely by two interrelated factors. First, the atoms to be bonded must be able to approach each other sufficiently closely to initiate bond formation. Secondly, the approach path must be more or less compatible with the electronic requirements of the nucleophilic and electrophilic functionalities. The first factor includes angular and torsional strain that must be overcome. For 3- and 4-membered rings, even in the absence of substituents, strain energy may add substantially to the activation energy of the ring-forming step and correspondingly facilitate the reverse process. That the electronic (orientational) factor is important in chemical reactions has been demonstrated in the classic studies of Hughes, Ingold, and Rose (12), who established the antiperiplanar requirement in E2 eliminations. The collinear backside approach, which results in Walden inversion in the S_N2 reaction, is similarly well established. The latter reaction is a ready route to cyclic systems. Baldwin has introduced a general set of rules governing ring-closure reactions (1, 2). Of particular interest in the present context are those pertaining to the formation of 5-membered rings by nucleophilic addition to trigonal carbon, namely, the processes 5-*exo-trig* and 5-*endo-trig*, in Baldwin's terminology (1, 2).

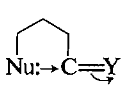

5-*exo-trig*

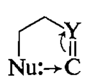

5-*endo-trig*

The former is a "favoured" process whereas the latter is "disfavoured", ostensibly because the trajectory (or approach vector) required by electronic factors can be achieved for the former but is sterically inaccessible for the latter (10). The approach vector (10) required for addition to a double bond has been deduced from crystallographic data (13) and from experimental (4, 8, 14, 15) and theoretical (9, 14, 16–18) studies of nucleophilic additions to the carbonyl group.

Cyclizations of the type **1** to **2** are of special interest. The ring closure of **1** to **2** is nominally a "disfavoured" 5-*endo-trig* cyclization, but has characteristics of the "favoured" 5-*exo-trig* process to the extent that the structure **3** is important for the

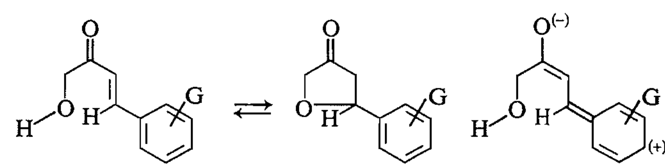

1 **2** **3**

description of **1**. Under conditions of basic catalysis for intermolecular Michael additions, neither the forward nor reverse transformation, **4** ⇌ **5**, is observed (3).

However, in acidic medium, the reaction proceeds quite readily. Presumably, under acid catalysis, the barrier to rotation of the α,β-CC bond may be reduced due to protonation of the carbonyl oxygen and by involving canonical structures **6** and **7** (5, 7). That this is the case is supported by the fact that electron-donating groups on the phenyl ring accelerate the reaction, giving a negative ρ value for the cyclization (5, 7). However, contributions of structures **6** and **7** restrict the approach of the nucleophilic hydroxy group by imposing double bond character internal to the incipient ring. Evidently, it is the rotation about the α,β-CC bond that is important. This question was

[1] Author to whom correspondence may be addressed.

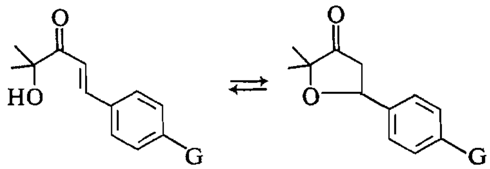

4 5

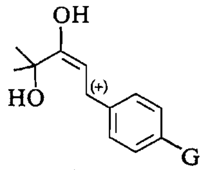

6

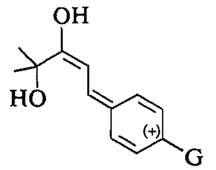

7

addressed in an earlier MNDO study by Perkins *et al.* on the model systems, **8** and **9**. Protonation of the carbonyl oxygen was calculated to lower the barrier to rotation about the α,β-CC bond by 100 kJ/mol (11).

In order to examine more closely the cyclization process, we report here the results of a MNDO investigation of the mechanism of interconversion of **10** and **11**, where R may be hydrogen atom or phenyl group.

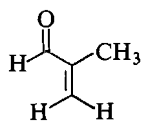

8

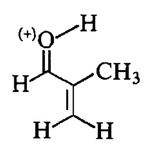

9

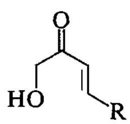

10

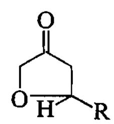

11

Method

Calculations were carried out using the MNDO program (19). The reaction coordinate was taken to be R_{CO}, the distance between the oxygen nucleophile and the β carbon atom. At selected fixed values of R_{CO} all remaining geometric parameters were optimized. The calculated heat of formation (ΔH_f) at each value of R_{CO} serves to define the potential energy profile of the reaction. For most species, two minima were located in the potential energy profile, corresponding to equilibrium structures of the cyclized species and a conformation of the acyclic species that is closest to the cyclic species. The transition structures were determined reasonably closely. While absolute energy changes cannot be compared directly with free energy changes since solvation effects are not included in the calculation, it will be seen that examination of structural changes that take place along the reaction coordinate lends important insight into the extent and timing of bond making and breaking during the cyclization process.

Results and discussion

*Acid catalyzed cyclization **10** ⇌ **11***

In acid medium, two alternate or competing pathways may be envisioned for the 5-*endo-trig* process for molecules such as **1**, **4**, or **10**. These are shown in Scheme 1.

We consider the reaction first in the forward direction, **10** (R = H) → **11** (R = H), via **12**, **13**, and **14**. The potential energy profile and selected structures for the rate-determining step, **12** (R = H) → **13** (R = H), are shown in Fig. 1. Numerical data are presented in Table 1. In the acyclic structure, **12** (R = H), the protonated enone portion of the molecule is planar and the hydroxyl group is rotated out of the plane by about 60°. The oxygen to β-carbon distance, R_{CO}, shown by a dashed line, is 3.25 Å. Rotation about the α,β-CC bond is pronounced at R_{CO} 2.5 Å (**12***a*), ΔH_f = 35 kJ/mol, and becomes rapid as the transition structure is approached (**12***b* → **T.S.**). The transition structure is 117 kJ/mol higher in energy and has R_{CO} = 1.95 Å. While the β-methylene group is still almost planar, rotation is essentially complete. Descent from the transition structure to the equilibrium cyclic protonated enol (**T.S.** → **13***a* → **13** (R = H) is accompanied by rapid rehybridization of the β carbon. The ring is almost planar in the transition structure and becomes planar by the time the R_{CO} value reaches 1.85 Å (**13***a*). The calculated equilibrium value of R_{CO} for **13** (R = H) is 1.49 Å. The transformation **11** (R = H) is completed by deprotonation of the ether oxygen, **13** (R = H) → **14** (R = H), followed by ketonization, **14** (R = H) → **11** (R = H), which may involve several protonation and deprotonation steps.

Ring opening must follow the same sequence of events in reverse by the principle of microscopic reversibility. It is noteworthy that ring opening of **13** (R = H) proceeds by in-plane stretching of the C—O bond. No resonance stabilization of the developing cationic centre by the adjacent enol π orbitals is possible until the transition structure is achieved. Instead, the developing cationic centre is stabilized by induced polarization of the enol π system. Mulliken population analysis reveals that this is the case. As one proceeds from **13** (R = H) to the point, **13***a*, where rotation about the α,β-CC bond begins, the buildup

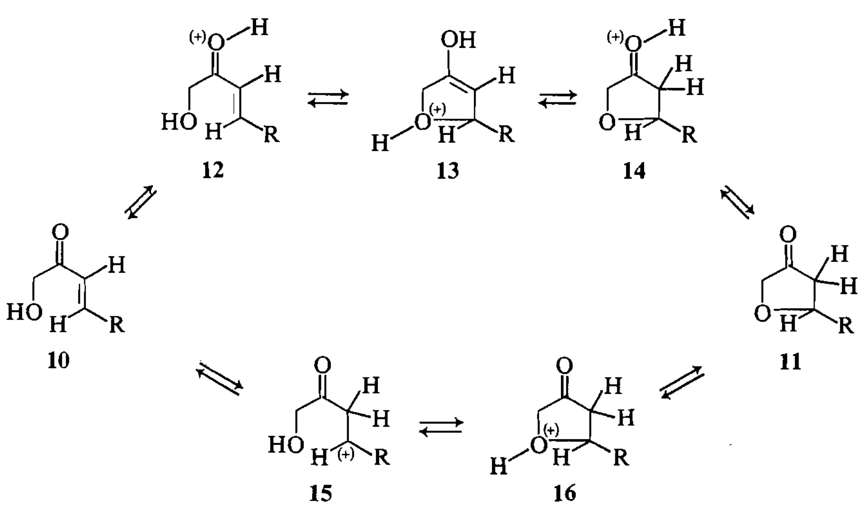

SCHEME 1

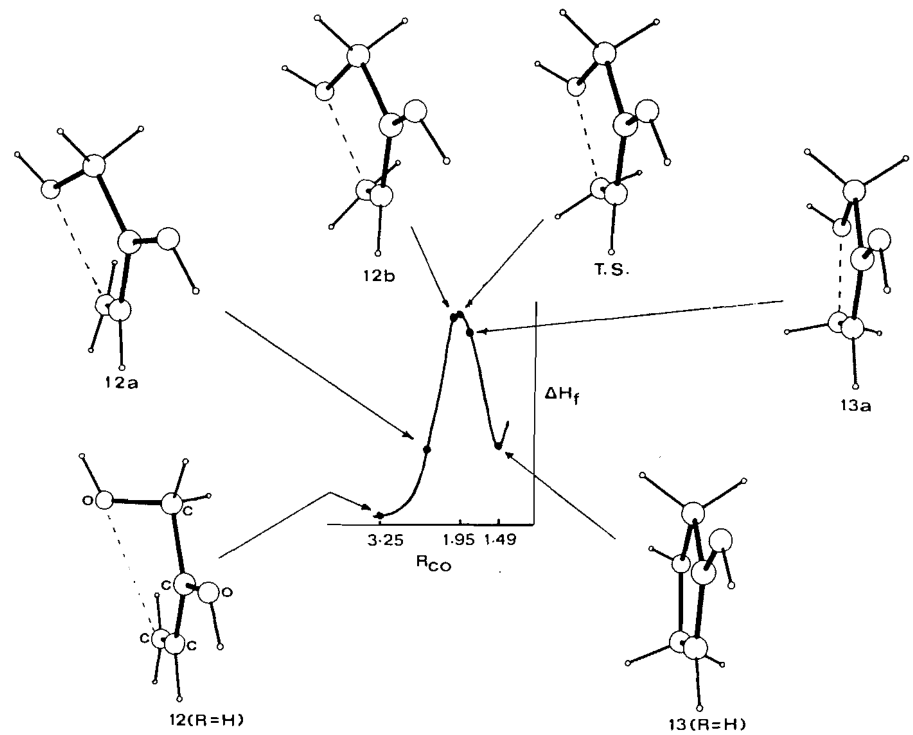

FIG. 1. The reaction coordinate and selected structures for **12** (R = H) $\rightleftharpoons$ **13** (R = H). The dashed line is the reaction coordinate R_{CO}.

TABLE 1. Calculated results for equilibrium and transition structures[a]

			Transition structures			
Compound	ΔH_f	R_{CO}	$A \rightleftharpoons B$	R_{CO}	$E_a(A \rightarrow TS)$	$E_a(TS \leftarrow B)$
10 (R = H)	−275	3.14				
11 (R = H)	−353	1.41				
12 (R = H)	422	3.25				
13 (R = H)	460	1.49	**12** $\rightleftharpoons$ **13**	1.95	118	79
15 (R = H)	588	2.73				
16 (R = H)	459	1.48	**15** $\rightleftharpoons$ **16**	2.73	129	~0
17 (R = H)	−258	3.40				
18 (R = H)	−359	1.42	**17** $\rightleftharpoons$ **18**	2.05	89	227
20 (R = H)	−48	1.65	**10** $\rightleftharpoons$ **20**	1.65	227	~0
10 (R = Ph)	174	3.42				
11 (R = Ph)	−218	1.42				
12 (R = Ph)	476	3.40				
13 (R = Ph)	557	1.52	**12** $\rightleftharpoons$ **13**	1.90	109	28
15 (R = Ph)	555	2.89				
16 (R = Ph)	561	1.51	**15** $\rightleftharpoons$ **16**	—	—	—
17 (R = Ph)	−160	3.44				
18 (R = Ph)	−275	1.43	**17** $\rightleftharpoons$ **18**	2.05	87	202
20 (R = Ph)	79	1.52	**10** $\rightleftharpoons$ **20**	1.52	253	~0

[a] Distances in angstroms, energies in kilojoules per mole.

of charge on the cationic centre, by +0.236 to +0.474, is partially compensated by an increase in charge at the α-carbon, by −0.106 to −0.355. Thus prior enolization of the ketone would seem to be necessary for facile rupture of the C—O bond even though the π orbitals cannot participate in resonance delocalization of the developing charge at the cationic centre.

The alternative mechanism, **10** → **15** → **16** → **11**, avoids the enolization step but requires prior protonation of the α-carbon atom of the enone system whose basicity is expected to be very low compared to that of the carbonyl oxygen. Structure **15** (R = H), shown in Fig. 2, is on the edge of the flat portion of the potential curve and has distance R_{CO} = 2.735 Å. The cationic centre is rotated to position the OH group over it in such a way as to maximize the attractive interaction between the empty $2p$ orbital of the cationic site with a nonbonded orbital of the oxygen atom. While **15** (R = H) has a twisted structure, the skeleton can become essentially planar and the —OH can approach the cationic centre at the β-carbon to within 2.0 Å with little gain in energy, arriving at structure **15***a*. Subsequently, shortening of R_{CO} from 2.0 Å to the equi-

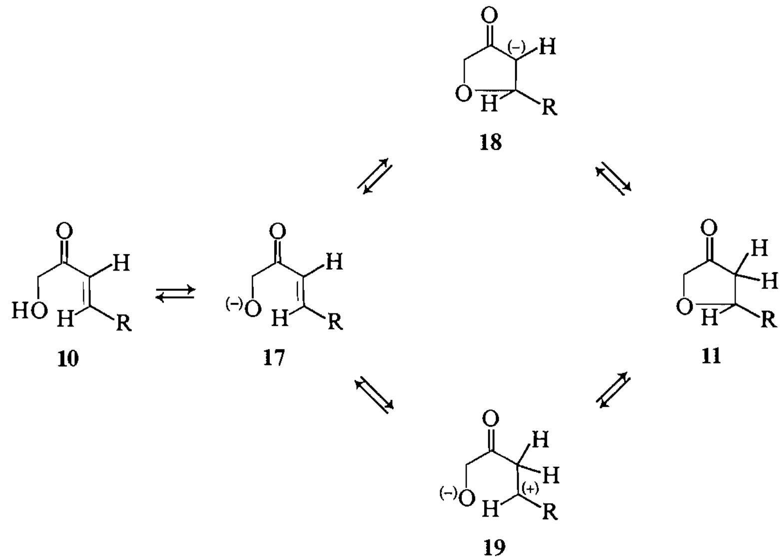

SCHEME 2

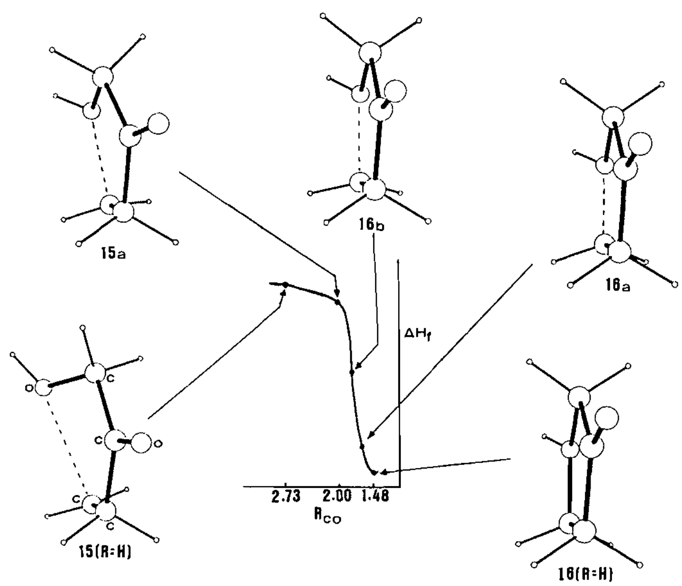

FIG. 2. The reaction coordinate and selected structures for **15** (R = H) $\rightleftharpoons$ **16** (R = H). The dashed line is the reaction coordinate R_{CO}.

librium distance, 1.48 Å, **16** (R = H), is accompanied by rapid rehybridization of the β-carbon (see **16***b* and **16***a*). Most of the increase in internal stability occurs at this stage. The heavy atom skeleton of the protonated furanone, **16** (R = H), is planar.

The rate-limiting factor for the forward reaction, **10** → **15** → **16** → **11**, may very well be the production of **15**. It is expected that, in solution, **15** will transfer a proton or will cyclize essentially without activation to **16**. Selected points along the reaction profile, **15** (R = H), shown in Fig. 2, confirm this view. The heat of formation of the protonated furanone, **16** (R = H), 460 kJ/mol, is calculated to be the same as the enolic form, **13** (R = H). By contrast, the α-C protonated form, **15** (R = H), is higher in energy than the O protonated form, **12** (R = H), by 166 kJ/mol. Indeed, **15** (R = H) is higher in energy than **T.S.** (Fig. 1) for the process **12** (R = H) → **13** (R = H) by 49 kJ/mol.

*Acid catalyzed cyclization **12** (R = Ph) $\rightleftharpoons$ **13** (R = Ph)*

The geometrical details for the acid catalyzed cyclization, **12** (R = Ph) $\rightleftharpoons$ **13** (R = Ph), are given in Table 1. The presence of the phenyl group has a negligible effect on the barrier to ring closure, 109 kJ/mol, but greatly facilities the reverse, 28 kJ/mol. The difference is due to preferential stabilization of the dienol form, **12** (R = Ph). In **12** (R = Ph), all of the atoms of the protonated enone moiety and the phenyl group are coplanar. The hydroxy group is almost perpendicular to the plane at R_{CO} = 3.40 Å. Rotation about the α,β-CC bond as R_{CO} decreases is significantly more advanced in the early stages of the cyclization than at a comparable point along the reaction coordinate for **10** (R = H) → **11** (R = H). As in that case, the geometry at the β-carbon atom remains planar and the phenyl group also lies in the plane. The transition structure has nearly a planar ring with R_{CO} = 1.9 Å. The cyclic structure, **13** (R = Ph), has a planar ring with R_{CO} = 1.52 Å. The equilibrium orientation of the phenyl group is perpendicular to the C—O bond. In this orientation, interaction between the phenyl π system and the low-lying σ^* orbital of the C—O bond is maximized. Electron release from the phenyl results in partial occupancy of the σ^*_{CO} and accounts for the slightly longer C—O bond length and the greater ease of bond dissociation.

The alternate route via **15** (R = Ph) and **16** (R = Ph) is calculated to be energetically more favourable than in the case where R = H. The presence of the electron-releasing phenyl group reduces the requirement of enol π polarization for the stabilization of the developing cationic β centre (by rotation about the α,β-CC bond in **12**, or by heterolytic dissociation of the labile bond in **13** → **12**). We have not explored the reaction profile for **15** (R = Ph) → **16** (R = Ph) but have determined the equilibrium geometries and energies of these species. The calculated heat of formation of **16** (R = Ph) is only 6 kJ/mol higher than that of **15** (R = Ph).

As in the case of the R = H species, the energies of the ether-oxygen protonated keto (**16** (R = Ph)) and enol (**13** (R = Ph)) forms are very similar, the latter being calculated to be 4 kJ/mol more stable. The acyclic α-C protonated structure, **12** (R = Ph), is computed to be 80 kJ/mol less stable than the O protonated species, **15** (R = Ph).

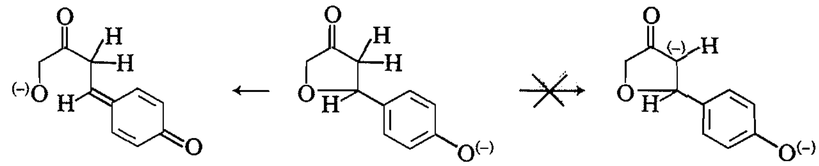

19 (R = p-O$^{(-)}$-Ph) **11** (R = p-O$^{(-)}$-Ph) **18** (R = p-O$^{(-)}$-Ph)

*The reaction in basic medium: **10** ⇌ **11***

In basic medium, the cyclization reaction may proceed by the two pathways shown in Scheme 2. The route **10** → **17** → **18** → **11** is analogous to the path **10** → **12** → **13** → **11** in acidic medium (Scheme 1). Similarly, the route **10** → **17** → **19** → **11** corresponds to the path **10** → **15** → **16** → **11** of Scheme 1.

As stated in the Introduction, neither the forward nor the reverse transformation takes place in basic medium in the case of **4** (G = H) or **4** (G = OCH_3) or similar compounds (3). The failure to react has been shown to be due to a high barrier to interconversion rather than to an unfavourable equilibrium (3). The large barrier to ring opening was attributed to the orthogonality of the C—O bond and the enolate π system. Ring closure was said to be prevented by the inability of the O(−) nucleophile to achieve the required approach vector. The calculated results for **17** (R = H) ⇌ **18** (R = H) and **17** (R = Ph) ⇌ **18** (R = Ph) are given in Table 1 and do not entirely support this view. The ring opening of both **18** (R = H) and **18** (R = Ph) is hindered by very large barriers, 227 kJ/mol and 202 kJ/mol, respectively, in agreement with experiment. However, the reverse cyclization, **17** → **18**, in each case, is hindered by barriers of the same magnitude as found for the acid catalyzed cyclization, namely 89 kJ/mol (R = H) and 87 kJ/mol (R = Ph). The reason for the large difference in the barriers to the forward and reverse reactions is the greater stability of the enolate anion over the alkoxide anion. Bearing in mind that the calculation is performed for an isolated anion in vacuum, the calculated differences, 138 kJ/mol (R = H) and 115 kJ/mol (R = Ph), between alkoxide and enolate forms, are probably not unreasonable. Preferential solvation of the alkoxide in protic solvents would reduce the free energy difference between the two anions and simultaneously increase the barrier hindering cyclization.

The alternative route, via **19**, is unlikely unless the formal cationic β-C centre of **19** can be stabilized by R. Since **4** (G = OCH_3) and **5** (G = OCH_3) do not interconvert in basic medium, a p-methoxyphenyl group is not sufficiently electron releasing to allow the reaction to proceed by either mechanism. However, with G = OH, **5** is smoothly converted to **4** in NaOMe/MeOH. In this medium, the prevalent form is not **5** (G = OH) but **5** (G = O(−)). In the present context, prior ionization of **11** (R = p-OH—Ph) to **11** (R = p-O(−)—Ph) increases the ease of transformation to **19** (R = p-O(−)—Ph) and decreases the probability of a second proton abstraction to form **18** (R = p-O(−)—Ph), which is a dianion.

*The reaction in neutral medium: **10** → **20***

The forward transformation is not observed under neutral conditions. The calculations indicate that the zwitterionic forms, **20** (R = H) and **20** (R = Ph), lie 227 kJ/mol and 253 kJ/mol, respectively, above the starting materials, **10** (R = H) and **10** (R = Ph). While the energy differences will be decreased in polar medium, it would remain highly unlikely that a structure such as **20** could be achieved in the absence of acids or bases. The calculations suggest little or no activation energy for the ring opening of **20**.

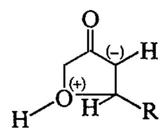

20

Conclusions

The 5-*endo-trig* cyclization of structures such as **1**, **4**, or **10** proceeds readily in acid medium via structures, e.g., **12**, in which the carbonyl oxygen is protonated. The reaction is facilitated by the lowered barrier to rotation about the α,β-CC bond that ensues from protonation of the carbonyl oxygen and by participation of electron-releasing substituents at the β position. Rotation about the bond is essentially complete in the transition structure. In the reverse step, **13** → **12**, the barrier to heterolytic bond rupture is lowered as a result of stabilization of the developing carbocation by polarization of the π system of the enol. The results of the calculations do not rule out the possibility that cyclization may proceed via the alternate pathway (i.e., via **15** and **16**) if sufficiently electron-releasing substituents are present at the β carbon.

In basic medium, the reaction does not proceed in either direction except when R = p-O(−)—Ph. The calculations indicate that an intrinsically high barrier is the operative factor preventing ring opening from the enolate (**18** → **17**). The reverse cyclization is not hindered by a prohibitively high barrier in the absence of selective stabilization of the alkoxide, **17**, in polar solvents. It is likely that the ring opening observed (3) when R = p-O(−)—Ph takes place via the alternate route involving **19** (R = p-O(−)—Ph).

Acknowledgements

This work was supported by the Natural Sciences and Engineering Research Council of Canada. Receipt of generous amounts of computing time from The University of Calgary at modest cost is gratefully acknowledged.

1. J. E. Baldwin, R. C. Thomas, L. I. Kruse, and L. Silberman. J. Org. Chem. **42**, 3846 (1977).
2. J. E. Baldwin. J. Chem. Soc. Chem. Commun. 734 (1976).
3. J. E. Baldwin, J. Cutting, W. Dupont, L. Silberman, and R. C. Thomas. J. Chem. Soc. Chem. Commun. 736 (1976).
4. C. L. Perrin and G. M. L. Arrhenius. J. Am. Chem. Soc. **104**, 2839 (1982).
5. G. W. L. Ellis, C. D. Johnson, and D. N. Rogers. J. Chem. Soc. Chem. Commun. 36 (1982).
6. J. P. Bradley, T. C. Jarvis, C. D. Johnson, P. D. McDonnell, and T. A. P. Weatherstone. Tetrahedron Lett. **24**, 2851 (1983).
7. G. W. L. Ellis, C. D. Johnson, and D. N. Rogers. J. Am. Chem. Soc. **105**, 5090 (1983).

8. F. M. MENGER and D. Y. WILLIAMS. Tetrahedron Lett. 3879 (1982).
9. P. DESLONGCHAMPS. Tetrahedron, **31**, 2463 (1975).
10. J. E. BALDWIN. J. Chem. Soc. Chem. Commun. 738 (1976).
11. M. J. PERKINS, P. C. WONG, J. BARRETT, and G. DHALIWAL. J. Org. Chem. **46**, 2196 (1981).
12. E. D. HUGHES, C. K. INGOLD, and J. B. ROSE. J. Chem. Soc. 3839 (1953).
13. J. D. DUNITZ. X-ray analysis and the structure of organic molecules. Cornell University Press, Ithaca, NY. 1979. Chapt. 7.
14. H. B. BURGI, J. D. DUNITZ, J. M. LEHN, and G. WIPFF. Tetrahedron, **30**, 1563 (1974).
15. H. B. BURGI. Angew. Chem. Int. Ed. Engl. **14**, 460 (1974).
16. H. B. BURGI, J. M. LEHN, and G. WIPFF. J. Am. Chem. Soc. **96**, 1956 (1974).
17. J. M. LEHN and G. WIPFF. J. Am. Chem. Soc. **102**, 1347 (1980).
18. S. J. WEINER, U. C. SINGH, and P. A. KOLLMAN. J. Am. Chem. Soc. **107**, 2219 (1985).
19. W. THIEL. QCPE, **11**, 353 (1978).

Structural studies of organoboron compounds. XXII.[1] Preparation and crystal and molecular structure of tetramethylammonium-2,4,6,6-tetraphenyl-1,3,5-trioxa-2,4-dibora-6-boratacyclohexane

W. KLIEGEL AND H.-W. MOTZKUS

Institut für Pharmazeutische Chemie, der Technischen Universität Braunschweig, 3300 Braunschweig, Beethovenstraße 55, Bundesrepublik Deutschland

AND

STEVEN J. RETTIG AND JAMES TROTTER

Department of Chemistry, University of British Columbia, 2036 Main Mall, Vancouver, B.C., Canada V6T 1Y6

Received April 12, 1985

W. KLIEGEL, H.-W. MOTZKUS, STEVEN J. RETTIG, and JAMES TROTTER. Can. J. Chem. **63**, 3516 (1985).

Details of the preparation and physical properties of $(Me_4N)^+ (Ph_4B_3O_3)^-$ are given. Crystals of tetramethylammonium 2,4,6,6-tetraphenyl-1,3,5-trioxa-2,4-dibora-6-boratacyclohexane are orthorhombic, a = 18.130(2), b = 11.9745(7), c = 12.5187(5) Å, Z = 4, space group $Pna2_1$. The structure was solved by direct methods and was refined by full-matrix least-squares procedures to R = 0.056 and R_w = 0.064 for 1460 reflections with $I \geq 2\sigma(I)$. The crystal structure consists of discrete tetramethylammonium cations and tetraphenylboroxinate anions, the first such anion to be structurally characterized. The six-membered B_3O_3 ring is significantly non-planar, having a flattened O(1)-envelope conformation (maximum deviation from the mean plane = 0.074(4) Å for O(1)). The boroxine ring in the anion shows significant deviations from the D_{3h} symmetry observed for neutral boroxines. Important mean structural parameters: $B(sp^3)$—O = 1.494(2), $B(sp^2)$—O[$B(sp^3)$] = 1.320(9), $B(sp^2)$—O[$B(sp^2)$] = 1.389(3) Å, O—$B(sp^3)$—O = 110.5(5), O—$B(sp^2)$—O = 121.7(6), $B(sp^2)$—O—$B(sp^2)$ = 118.9(5), and $B(sp^3)$—O—$B(sp^2)$ = 122.9(1)°.

W. KLIEGEL, H.-W. MOTZKUS, STEVEN J. RETTIG et JAMES TROTTER. Can. J. Chem. **63**, 3516 (1985).

On rapporte les détails relatifs à la préparation et aux propriétés physiques du composé $(Me_4N)^+ (Ph_4B_3O_3)^-$. Les cristaux du tétraphényl-2,4,6,6 trioxa-1,3,5 dibora-2,4 borata-6 cyclohexane de tétraméthylammonium sont orthorhombiques, avec a = 18,130(2), b = 11,9745(7), c = 12,5187(5) Å, Z = 4 et groupe d'espace $Pna2_1$. On a résolu la structure par des méthodes directes et on l'a affinée par la méthode des moindres carrés (matrice entière) jusqu'à des valeurs de R = 0,056 et R_w = 0,064 pour 1460 réflexions indépendantes avec $I \geq 2\sigma(I)$. La structure comporte des cations tétraméthylammonium et des anions tétraphenylboroxinates individuels; dans ce dernier cas, il s'agit du premier tel anion à être caractérisé. Le cycle B_3O_3 à six chaînons dévie considérablement de la planéité; il existe sous une conformation O(1)-enveloppe aplatie (la déviation maximale du plan moyen = 0,074(4) Å pour le O(1)). Le cycle boroxine de l'anion dévie considérablement de la symétrie D_{3h} qui a été observée dans le cas des boroxines neutres. Les paramètres structuraux moyens importants sont: $B(sp^3)$—O = 1,494(2), $B(sp^2)$—O[$B(sp^3)$] = 1,320(9), $B(sp^2)$—O[$B(sp^2)$] = 1,389(3) Å, O—$B(sp^3)$—O = 110,5(5), O—$B(sp^2)$—O = 121,7(6), $B(sp^2)$—O— $B(sp^2)$ = 118,9(5) et $B(sp^3)$—O—$B(sp^2)$ = 122,9(1)°.

Introduction

X-ray crystallographic analyses of heterocyclic boron compounds containing BOBON ring systems such as **1** (1) and **2** (2) or of polycyclic compounds such as **3**, which contain the same BOBON ring system (3–5), reveal a remarkably short B—O distance between the tricoordinated boron atom and the oxygen atom within the $B(sp^2)$—O—$B(sp^3)$ moiety in each case. This indicates a strong $pp(\pi)$-interaction between the tricoordinate boron atom and the oxygen atom (6, 7) at this site of the BOBON ring which represents an anhydridic bond between a boronic acid and a tetracoordinated borinic (**1** and **2**) or boronic acid (**3**). Replacement of the N—O unit (hydroxylamine component) in **1** or **2** by an O—B—O unit (a second boronic acid component) should lead to a boroxine ring system with one negatively charged tetrahedral boron atom and two very short B—O bonds of the type described above (cf. formula **4**).

It was thus of special interest to determine whether it would be possible to prepare and isolate a mixed anhydride of phenylboronic and diphenylborinic acids having an anionic boroxine structure. For "external" compensation of the negative charge, a tetraalkylammonium cation was chosen in order to produce a salt soluble in organic solvents. To the best of our knowledge, no tetraaryl- or tetraalkylboroxine salts have been reported in the literature to date. If donor–acceptor complexes of boroxines and Lewis bases (O, N, or P donors "D") of the general formula **5** are excluded, compound **4** would be the first example of a tetrakis(organyl)boroxine salt. Structure analyses of compounds of the type **5** have recently been reported by Yalpani and Boese (8). In solutions of **5** an equal participation of the three boron atoms in the donor–acceptor bond suggests intramolecular fluctuation (8, 9).

For the synthesis of **4**, two equivalents of phenylboronic acid were reacted with one equivalent of diphenylborinic acid in the presence of tetramethylammonium hydroxide. A high-melting crystalline product was obtained, the elemental composition and spectral data being consistent with the proposed structure **4**. An X-ray crystallographic analysis was undertaken to provide unambiguous proof.

Experimental

Tetramethylammonium 2,4,6,6-tetraphenyl-1,3,5-trioxa-2,4-dibora-6-boratacyclohexane, 4

Oxybis(diphenylborane) (0.87 g, 2.5 mmol) and phenylboronic acid (1.22 g, 10 mmol) were dissolved in 5 mL ethanol. After the addition of tetramethylammonium hydroxide (5 mmol, 20% solution in methanol), the mixture was evaporated *in vacuo*. The remaining oil was crystallized by cooling and the addition of ether. Yield: 2.33 g (100%). After recrystallization from acetone at −10°C there remained

[1]Previous paper in this series: Can. J. Chem. **63**, 509 (1985).

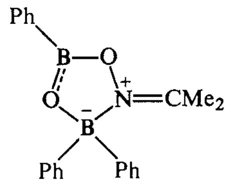

1

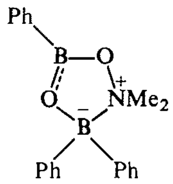

2

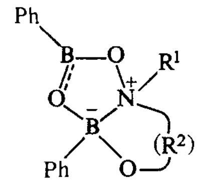

3

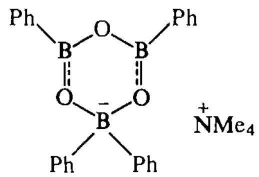

4

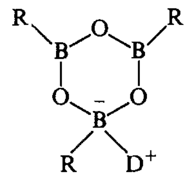

5

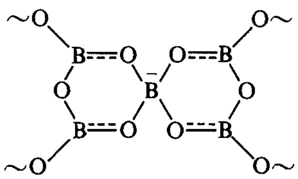

6

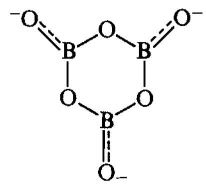

7

1.0 g (43%) of colorless crystals. Mp. 290–296°C (decomp.). *Anal.* calcd. for $C_{28}H_{32}B_3NO_3$: C 72.63, H 6.97, N 3.03; found: C 72.61, H 6.92, N 3.04. ^{1}H nmr (90 MHz, DMSO-d_6): δ(ppm) = 2.97 (s, NMe_4), 7.10 (m, 6 H, *m*- and *p*-H of Ph_2B), 7.47 (m, 6 H, *m*- and *p*-H of 2 PhB), 7.70 (m, 4 H, *o*-H of Ph_2B), 8.17 (m, 4 H, *o*-H of 2 PhB).

The substance gives a blue-colored solution upon reaction (10) with diphenylcarbazone in methanolic solution, indicating the presence of a Ph_2B grouping. Crystals suitable for X-ray analysis were obtained by recrystallization from acetone at low temperature.

X-ray crystallographic analysis

A crystal bounded by the 12 faces (followed by the distances in mm between parallel faces): ±(−1 0 2), 0.30, ±(1 0 2), 0.32, ±(−1 0 1), 0.36, ±(1 0 1), 0.30, ±(0 1 −1), 0.51, ±(0 1 1), 0.52 was mounted in a general orientation. Unit-cell parameters were refined by least-squares on 2 sin θ/λ values for 25 reflections (2θ = 40–50°) measured on a diffractometer with Cu-*K*α radiation ($\lambda(K\alpha_1)$ = 1.540562, $\lambda(K\alpha_2)$ = 1.544390 Å). Crystal data at 22°C are:

$C_{28}H_{32}B_3NO_3$ f.w. = 463.0
Orthorhombic, a = 18.130(2), b = 11.9745(7), c = 12.5187(5) Å, V = 2717.7(4) Å^3, Z = 4, ρc = 1.132 Mg m^{-3}, $F(000)$ = 984, μ(Cu-*K*α) = 5.21 cm^{-1}. Absent reflections: $0kl$, $k + l$ odd, and $h0l$, h odd, space group $Pna2_1$ (C^9_{2v}, No. 33) from structure analysis.

Intensities were measured with graphite-monochromated Cu-*K*α radiation on an Enraf-Nonius CAD4-F diffractometer. An ω−2θ scan at 0.72–10.06° min^{-1} over a range of (0.80 + 0.15 tan θ) degrees in ω (extended by 25% on both sides for background measurement) was employed. Data were measured to 2θ = 150°. The intensities of 3 check reflections, measured every 3600 s throughout the data collection, showed only small random fluctuations. Of the 2925 independent reflections measured and processed,[2] 1460 (49.9%) had intensities greater than or equal to $2\sigma(I)$ above background where $\sigma^2(I) = S + 2B + (0.03(S - B))^2$ with S = scan count and B = normalized background count. The paucity of data, partially a result of the washout of high-angle reflections, seems to be characteristic of light-atom structures consisting primarily of planar rings.

The noncentrosymmetric space group $Pna2_1$ was indicated by the *E*-statistics and by the number of molecules in the unit-cell. The structure was solved by direct methods, the coordinates of all non-hydrogen atoms being determined from an *E*-map. Refinement of the non-hydrogen atoms with anisotropic thermal parameters gave R = 0.083. The hydrogen atoms were introduced as fixed contributors in idealized positions (staggered methyl groups, C(sp^2)—H = 0.97, C(sp^3)—H = 0.98 Å), recalculated after each cycle of refinement. The large thermal parameters obtained for the carbon atoms of the tetramethylammonium cation [C(1)—C(4)] may actually represent thermal motion or may result from minor disordering, such being often noted for structurally isolated tetrahedral moieties. The scattering factors of ref. 11 were used for non-hydrogen atoms and those of ref. 12 for hydrogen atoms. The weighting scheme $w = 1/\sigma^2(F)$, where $\sigma^2(F)$ is derived from the previously defined $\sigma^2(I)$, gave uniform average values of $w(|F_o| - |F_c|)^2$ over ranges of both $|F_o|$ and sin θ/λ and was employed in the final stages of full-matrix refinement of variables. Reflections with $I < 2\sigma(I)$ were not included in the refinement. Convergence was reached at R = 0.056 and R_w = 0.064 for 1460 reflections with $I \geq 2\sigma(I)$. For all 2925 reflec-

TABLE 1. Final positional (fractional × 10^4) and isotropic thermal parameters ($U \times 10^3$ Å^2) with estimated standard deviations in parentheses

Atom	x	y	z	U_{eq}
O(1)	3393(2)	3781(3)	7582	97
O(2)	3810(2)	2127(3)	6744(5)	80
O(3)	4179(2)	2441(3)	8532(5)	98
N	1532(3)	786(4)	7441(6)	93
B(1)	3729(4)	3482(5)	8632(8)	83
B(2)	3379(4)	3083(6)	6757(7)	79
B(3)	4209(4)	1847(5)	7654(8)	75
C(1)	1104(6)	−253(8)	7501(10)	166
C(2)	1067(12)	1708(10)	7213(18)	325
C(3)	2024(11)	606(12)	6584(16)	316
C(4)	1911(10)	994(10)	8413(15)	252
C(5)	3065(4)	3252(5)	9479(7)	82
C(6)	3107(4)	2458(6)	10273(8)	99
C(7)	2500(6)	2254(6)	10967(8)	118
C(8)	1890(6)	2851(9)	10918(9)	126
C(9)	1837(5)	3647(8)	10148(10)	129
C(10)	2414(5)	3848(6)	9444(8)	108
C(11)	4249(3)	4498(5)	9043(7)	89
C(12)	4175(4)	5580(6)	8664(8)	109
C(13)	4611(5)	6452(6)	9041(11)	133
C(14)	5124(5)	6239(9)	9813(10)	134
C(15)	5223(4)	5187(9)	10209(8)	119
C(16)	4787(5)	4335(6)	9821(7)	113
C(17)	2860(3)	3307(5)	5780(7)	76
C(18)	2297(4)	4110(5)	5803(8)	105
C(19)	1804(4)	4239(6)	5012(11)	121
C(20)	1843(5)	3589(8)	4115(10)	121
C(21)	2364(4)	2795(7)	4045(7)	105
C(22)	2892(4)	2649(6)	4871(7)	96
C(23)	4698(3)	770(4)	7582(7)	70
C(24)	4751(4)	118(6)	6690(7)	113
C(25)	5159(6)	−837(7)	6644(9)	143
C(26)	5558(4)	−1137(5)	7489(10)	105
C(27)	5548(5)	−539(6)	8387(8)	129
C(28)	5114(4)	395(6)	8428(8)	110

U_{eq} = (1/3) trace(diagonalized U).

[2]The computer programs used include locally written programs for data processing and locally modified versions of the following: MULTAN 80, multisolution program by P. Main, S. J. Fiske, S. E. Hull, L. Lessinger, G. Germain, J. P. Declercq, and M. M. Woolfson; ORFLS, full-matrix least-squares, and ORFFE, function and errors, by W. R. Busing, K. O. Martin and H. A. Levy; FORDAP, Patterson and Fourier syntheses, by A. Zalkin; ORTEP II, illustrations, by C. K. Johnson.

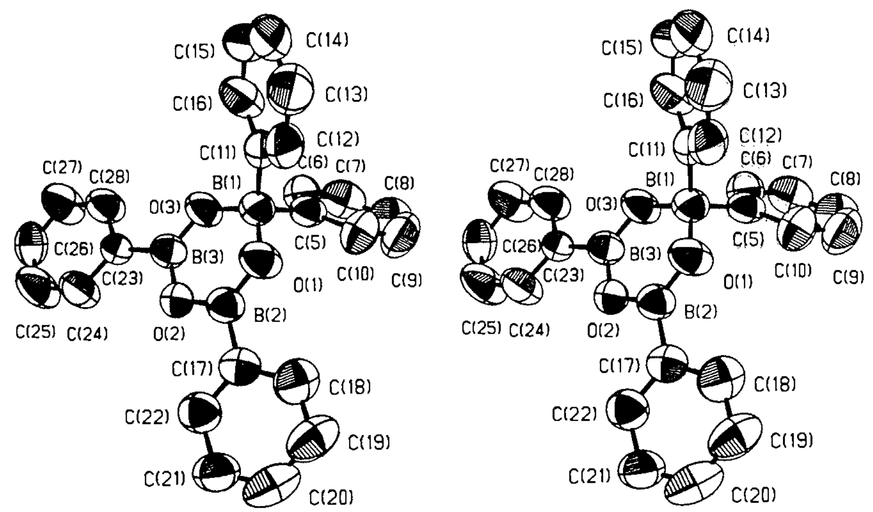

FIG. 1. Stereoscopic view of the $[(C_6H_5)_4B_3O_3]^-$ anion; 50% probability thermal ellipsoids are shown.

tions $R = 0.145$. The function minimized was $\Sigma w(|F_o| - |F_c|)^2$, $R = \Sigma||F_o| - |F_c||/\Sigma|F_o|$ and $R_w = (\Sigma w(|F_o| - |F_c|)^2/\Sigma w|F_o|^2)^{1/2}$.

On the final cycle of refinement the mean and maximum parameter shifts corresponded to 0.01 and 0.14σ, respectively. The mean error in an observation of unit weight was 2.977. A final difference map showed maximum fluctuations of ± 0.18 e $Å^{-3}$. The final positional and thermal parameters appear in Tables 1 and 6[3], respectively. Measured and calculated structure factors have been placed in the Depository of Unpublished Data.[3] Bond distances, bond angles, and intraannular torsion angles appear in Table 2–4, respectively. Calculated hydrogen parameters (Table 5) and a complete listing of torsion angles (Table 7) are included as deposited material.

Results and discussion

The structure consists of discrete Me_4N^+ cations and $[(C_6H_5)_4B_3O_3]^-$ anions, separated by normal van der Waals distances. There are no interionic H···H contacts less than 2.4 Å and the minimum cation–cation, cation–anion, and anion–anion contacts are >4.0, 3.56(2) [C(3)···C(10) $(1/2 - x, y - 1/2, z - 1/2)$], and 3.61(2) Å [O(2)···C(14) $(1 - x, 1 - y, z - 1/2)$], respectively. The isolated tetraphenylboroxinate anion reported here is the first such to be structurally characterized. The only related structures in the literature to date are a pair of triphenylboroxine–amine adducts (8) and a N→B coordinated polycyclic ring system ("tribenzotaralene") containing a nearly planar boroxine ring (13). In the latter case, only the N—B distance was reported in a brief communication.

Electron diffraction studies indicate that trimethylboroxine, $(MeB{=}O)_3$ (14), and boroxine, $(HB{=}O)_3$ (15), both contain planar ring systems with equal B—O distances of 1.39(2) and 1.376(2) Å, respectively. Among the borates and boric acid derivatives which have been studied by X-ray diffraction methods, several contain partial boroxine structures or have the boroxine skeleton. In general the boroxine ring is found to be planar, or nearly so, and to possess approximate D_{3h} symmetry.

The presence of the tetracoordinated boron atom induces a marked geometrical distortion of the boroxine ring, similar to,

TABLE 2. Bond lengths (Å) with estimated standard deviations in parentheses

Bond	Length (Å)	Bond	Length (Å)
O(1)—B(1)	1.492(9)	C(9)—C(10)	1.389(12)
O(1)—B(2)	1.329(8)	C(11)—C(12)	1.386(9)
O(2)—B(2)	1.386(7)	C(11)—C(16)	1.392(10)
O(2)—B(3)	1.392(8)	C(12)—C(13)	1.391(11)
O(3)—B(1)	1.495(7)	C(13)—C(14)	1.366(12)
O(3)—B(3)	1.311(8)	C(14)—C(15)	1.366(11)
N —C(1)	1.468(9)	C(15)—C(16)	1.378(10)
N —C(2)	1.417(14)	C(17)—C(18)	1.402(9)
N —C(3)	1.413(14)	C(17)—C(22)	1.386(9)
N —C(4)	1.419(14)	C(18)—C(19)	1.343(11)
B(1)—C(5)	1.627(11)	C(19)—C(20)	1.368(13)
B(1)—C(11)	1.624(9)	C(20)—C(21)	1.344(10)
B(2)—C(17)	1.565(10)	C(21)—C(22)	1.420(10)
B(3)—C(23)	1.566(8)	C(23)—C(24)	1.366(9)
C(5)—C(6)	1.378(9)	C(23)—C(28)	1.375(9)
C(5)—C(10)	1.380(9)	C(24)—C(25)	1.364(10)
C(6)—C(7)	1.422(11)	C(25)—C(26)	1.330(11)
C(7)—C(8)	1.319(11)	C(26)—C(27)	1.332(11)
C(8)—C(9)	1.359(12)	C(27)—C(28)	1.369(9)

but of greater magnitude than those noted for the triphenyl boroxine – amine adducts (8). These distortions involve distances and angles in the B_3O_3 ring as well as the planarity of the boroxine ring, reducing the symmetry of the anion to approximately C_{2v}.

The mean[4] $B(sp^3)$—O, $B(sp^2)$—O[$B(sp^3)$], and $B(sp^2)$—O[$B(sp^2)$] distances in **4** of 1.494(2), 1.320(9), and 1.389(3) Å may be compared to the corresponding values of 1.458(14) and 1.457(8), 1.353(3) and 1.357(2), 1.389(1) and 1.392(7) Å for the two triphenylboroxine–amine adducts (8). The differences result from the relatively greater strength of the B—C bond in **4** relative to the N→B interactions in the adducts (B—N = 1.663(8) and 1.714(10) Å). The very short B(2)—O(1) and B(3)—O(3) bonds in **4** are not unexpected and are comparable to bonds in analogous $B(sp^2)$—O—$B(sp^3)$ systems: **1** (1); 1.333(4); **2** (2); 1.340(3); **3** (3–5); 1.337(2), 1.341(3), 1.334(2) Å. Similar B—O bonding

[3]The structure factor table, Table 6 (anisotropic thermal parameters), and other material mentioned in the text are available, at a nominal charge, from the Depository of Unpublished Data, CISTI, National Research Council of Canada, Ottawa, Ont., Canada K1A 0S2.

[4]Here and elsewhere in this report mean values refer to weighted means with rms deviations from the mean in parentheses.

TABLE 3. Bond angles (deg) with estimated standard deviations in parentheses

Bonds	Angle (deg)	Bonds	Angle (deg)
B(1)—O(1)—B(2)	122.8(4)	C(8)—C(9)—C(10)	121.2(8)
B(2)—O(2)—B(3)	118.9(5)	C(5)—C(10)—C(9)	122.3(7)
B(1)—O(3)—B(3)	123.0(6)	B(1)—C(11)—C(12)	122.4(7)
C(1)—N —C(2)	110.9(9)	B(1)—C(11)—C(16)	121.6(6)
C(1)—N —C(3)	104.1(8)	C(12)—C(11)—C(16)	116.0(6)
C(1)—N —C(4)	111.1(10)	C(11)—C(12)—C(13)	122.0(8)
C(2)—N —C(3)	109.9(15)	C(12)—C(13)—C(14)	119.1(8)
C(2)—N —C(4)	108.9(9)	C(13)—C(14)—C(15)	121.2(8)
C(3)—N —C(4)	111.8(13)	C(14)—C(15)—C(16)	118.7(8)
O(1)—B(1)—O(3)	110.5(5)	C(11)—C(16)—C(15)	122.9(7)
O(1)—B(1)—C(5)	108.3(5)	B(2)—C(17)—C(18)	122.6(6)
O(1)—B(1)—C(11)	109.6(5)	B(2)—C(17)—C(22)	121.3(6)
O(3)—B(1)—C(5)	108.5(5)	C(18)—C(17)—C(22)	115.9(6)
O(3)—B(1)—C(11)	109.5(5)	C(17)—C(18)—C(19)	123.2(8)
C(5)—B(1)—C(11)	110.5(5)	C(18)—C(19)—C(20)	120.4(7)
O(1)—B(2)—O(2)	121.1(6)	C(19)—C(20)—C(21)	119.5(7)
O(1)—B(2)—C(17)	120.8(5)	C(20)—C(21)—C(22)	120.9(7)
O(2)—B(2)—C(17)	118.1(6)	C(17)—C(22)—C(21)	120.1(6)
O(2)—B(3)—O(3)	122.3(5)	B(3)—C(23)—C(24)	123.9(6)
O(2)—B(3)—C(23)	116.5(6)	B(3)—C(23)—C(28)	122.3(6)
O(3)—B(3)—C(23)	121.2(6)	C(24)—C(23)—C(28)	113.8(5)
B(1)—C(5)—C(6)	123.1(6)	C(23)—C(24)—C(25)	123.5(7)
B(1)—C(5)—C(10)	121.6(6)	C(24)—C(25)—C(26)	119.2(7)
C(6)—C(5)—C(10)	115.3(7)	C(25)—C(26)—C(27)	121.2(6)
C(5)—C(6)—C(7)	121.1(7)	C(26)—C(27)—C(28)	118.6(7)
C(6)—C(7)—C(8)	121.8(8)	C(23)—C(28)—C(27)	123.6(6)
C(7)—C(8)—C(9)	118.2(9)		

TABLE 4. Intra-annular torsion angles (deg) standard deviations in parentheses

Atoms	Value (deg)
B(2)—O(1)—B(1)—O(3)	13.0(8)
B(1)—O(1)—B(2)—O(2)	−13.9(10)
B(3)—O(2)—B(2)—O(1)	6.0(9)
B(2)—O(2)—B(3)—O(3)	1.6(8)
B(1)—O(3)—B(3)—O(2)	−1.3(9)
B(3)—O(3)—B(1)—O(1)	−5.4(8)

arrangements are found in the roughly comparable cyclic structures of pentaborates having spiro-fused boroxine rings as a basic structural unit as in **6**. This basic framework, built up from a BO_4 tetrahedron and four BO_3 triangles, has been established by structure determinations of various monoanionic pentaborates and combined polyborates (16). In these compounds the B(sp^2)—O bonds of B(sp^2)—O—B(sp^3) moieties are generally slightly shorter than the other B(sp^2)—O bonds. Thus in ammonium pentaborate (lardellite) the mean endocyclic B—O distance is 1.34 Å for B(sp^2)—O[B(sp^3)] bonds while the remaining B(sp^2)—O bonds average 1.39 Å and the B(sp^3)—O bonds 1.47 Å (17). Comparable short B(sp^2)—O distances also occur for exocyclic B—O bonds of anionic nature such as those in potassium metaborate (18), which has the boroxine structure **7**. The $B_3O_6^-$ anion shows exocyclic B—O distances of 1.331(10) Å and endocyclic distances of 1.398(5) Å (18). The calculated π-bond order for a B—O bond of 1.33 Å is about 0.6 (6), the bond energy being 130 kcal/mol (19).

The considerable π-bond character of the B(2)—O(1) and B(3)—O(3) bonds in **4** suggests a more important contribution of resonance form **4**d to the resonance hybrid **4**$a \leftrightarrow$ **4**$b \leftrightarrow$ **4**$c \leftrightarrow$ **4**d than that of **4**b or **4**c. This is supported by the length of the B(sp^3)—O bonds which are comparable in length to those in **1** (1.495(4) Å), **2** (1.487(3) Å), and those in other diphenylboron chelates with one or two oxygen ligands (1.476(2) − 1.580(3) Å) (20−27). In further support of the π-bonding argument, the longer of the two bonds (B(2)—O(1)) is observed where there is a larger local deviation from planarity (see Table 4). The B—O distances in the tetrahedral BO_4 groupings of various borates have been compiled (28, 29) and range from 1.470 to 1.510 Å. The B(sp^3)—O distances in the triphenylboroxine−amine adducts are in the range 1.444(6) to 1.472(8) Å (8).

The O—B—O and B—O—B angles in the unsubstituted boroxine molecule (15) are all 120.0(6)°. The presence of the tetrahedral B atom in **4** induces changes in all intracyclic bond angles. The O—B(1)—O angle is reduced to 110.5(5)° and

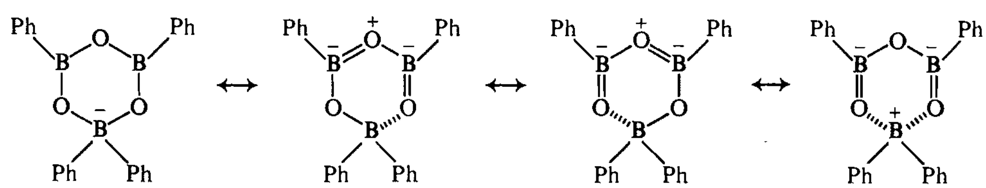

4a **4**b **4**c **4**d

the opposite angle at O(2) to 118.9(5)°, the remaining four angles increase to mean values of 122.9(1)° at O and 121.7(6)° at B. Angular distortions in the triphenylboroxine–amine adducts are similar but of lesser magnitude (e.g. 113.0(5) and 113.5(5)° at the tetrahedral B atom). Even smaller angles at B (106.9–107.5°) have been observed in other six-membered diphenylboron O—B—O chelate rings (23, 24).

The boroxine ring in **4** is significantly non-planar ($\chi^2 = 497$, maximum deviation from the mean plane = 0.074(4) Å for O(1)), having a flattened O(1)-envelope conformation. The two amine adducts (8) once again show intermediate parameters, the boroxine rings being planar to within 0.034 Å. All four phenyl rings are planar to within experimental error. The phenyl rings bonded to the two trigonal planar boron atoms are rotated out of the B(2) and B(3) coordination planes by 0.7(4) and 11.2(4)°, these values being normal for trigonal planar $PhBO_2$ moieties.

As noted for **1** (1), **2** (2), **3** (3–5), and the triphenylboroxine–amine adducts (8), the B(sp^3)—C bonds are significantly longer than the B(sp^2)—C bonds. This once again demonstrates the delocalization of aromatic π-electron density into the trigonal planar boron system and the impediment of such an interaction with tetrahedral boron. The mean B(sp^3)—C(Ph) distance of 1.626(2) Å is near the high end of the range of 1.598 to 1.639 Å observed for diphenylboron chelates.

The bond lengths and angles in the phenyl rings show the patterns characteristically induced by B-substitution (ref. 30 and references therein) although some of the distances are shortened as a result of thermal motion. The inequality of the N—C distances of the Me_4N^+ cation (Table 2) is also an artifact of thermal motion, the longer bond being associated with the one carbon atom (C(1)) which has relatively low thermal motion.

Acknowledgments

We thank the Natural Sciences and Engineering Research Council of Canada and the Fonds der Chemischen Industrie, Frankfurt am Main, for financial support and the University of British Columbia Computing Centre for assistance.

1. W. KLIEGEL, D. NANNINGA, S. J. RETTIG, and J. TROTTER. Can. J. Chem. **61**, 2329 (1983).
2. W. KLIEGEL, H.-W. MOTZKUS, S. J. RETTIG, and J. TROTTER. Can. J. Chem. **62**, 838 (1984).
3. S. J. RETTIG, J. TROTTER, W. KLIEGEL, and H. BECKER. Can. J. Chem. **54**, 3142 (1976).
4. W. KLIEGEL, S. J. RETTIG, and J. TROTTER. Can. J. Chem. **62**, 515 (1984).
5. W. KLIEGEL, D. NANNINGA, S. J. RETTIG, and J. TROTTER. Can. J. Chem. **62**, 845 (1984).
6. C. A. COULSON and T. W. DINGLE. Acta Crystallogr. Sect. B, **24**, 153 (1968).
7. W. BIFFAR, H. NÖTH, H. POMMERING, and B. WRACKMEYER. Chem. Ber. **113**, 333 (1980); B. WRACKMEYER and R. KÖSTER. Chem. Ber. **115**, 2022 (1982).
8. M. YALPANI and R. BOESE. Chem. Ber. **116**, 3347 (1983).
9. A. MELLER. Gmelin Handbuch der Anorganischen Chemie, Ergänzungswerk zur 8. Aufl., Bd. 44, Springer-Verlag. Berlin-Heidelberg-New York. 1977. pp. 119–239.
10. R. NEU. Z. Anal. Chem. **176**, 334 (1960); B. FRIESE and F. UMLAND. Anal. Chim. Acta, **96**, 303 (1978).
11. D. T. CROMER and J. B. MANN. Acta Crystallogr. Sect. A, **24**, 321 (1968).
12. R. F. STEWART, E. R. DAVIDSON, and W. T. SIMPSON. J. Chem. Phys. **42**, 3175 (1965).
13. E. B. FLEISCHER and R. DEWAR. Tetrahedron lett. 363 (1970).
14. S. H. BAUER and J. Y. BEACH. J. Am. Chem. Soc. **63**, 1394 (1941).
15. C. H. CHANG, R. F. PORTER, and S. H. BAUER. Inorg. Chem. **8**, 1689 (1969).
16. G. HELLER. Gmelin Handbuch der Anorganischen Chemie, Ergänzungswerk zur 8. Aufl., Bd. 28, Springer-Verlag. Berlin-Heidelberg-New York. 1975. pp. 1–220.
17. S. MERLINO and F. SARTORI. Acta Crystallogr. Sect. B, **25**, 2264 (1969).
18. W. SCHNEIDER and G. B. CARPENTER. Acta Crystallogr. Sect. B, **26**, 1189 (1970).
19. J. KROGH-MOE. Acta Chem. Scand. **17**, 843 (1963).
20. S. J. RETTIG, J. TROTTER, and W. KLIEGEL. Can. J. Chem. **52**, 2531 (1974).
21. S. J. RETTIG, J. TROTTER, W. KLIEGEL, and D. NANNINGA. Can. J. Chem. **56**, 1676 (1978).
22. W. KLIEGEL, D. NANNINGA, S. J. RETTIG, and J. TROTTER. Can. J. Chem. **61**, 2493 (1983).
23. S. J. RETTIG and J. TROTTER. Can. J. Chem. **60**, 2957 (1982).
24. S. J. RETTIG and J. TROTTER. Can. J. Chem. **54**, 1168 (1976).
25. S. J. RETTIG and J. TROTTER. Can. J. Chem. **51**, 1288 (1973).
26. S. J. RETTIG and J. TROTTER. Can. J. Chem. **54**, 3130 (1976).
27. S. J. RETTIG and J. TROTTER. Can. J. Chem. **61**, 2334 (1983).
28. W. H. ZACHARIASEN. Acta Crystallogr. **16**, 385 (1963).
29. C. T. GRAINGER. Acta Crystallogr. Sec. B, **37**, 563 (1981).
30. A. DOMENICANO, P. MURRAY-RUST, and A. VACIAGO. Acta Crystallogr. Sect. B, **39**, 457 (1983).

Vibrational spectral studies of solutions at elevated temperatures and pressures. VII. Raman spectra and dissociation of nitric acid

C. I. RATCLIFFE AND D. E. IRISH

Guelph-Waterloo Centre for Graduate Work in Chemistry, Waterloo Campus, Department of Chemistry, University of Waterloo, Waterloo, Ont., Canada N2L 3G1

Received March 19, 1985

C. I. RATCLIFFE and D. E. IRISH. Can. J. Chem. **63**, 3521 (1985).

An exploratory study of the Raman spectra of nitric acid solutions up to 250°C has been undertaken. The decrease in the frequencies of the νN—(OH) and δNO_2 bands of HNO_3 as temperature and concentration increase have been interpreted in terms of the reduced strength of hydrogen bonding. Approximate values of the degree of dissociation α have been determined and show that nitric acid is a very much weaker acid at high temperatures.

C. I. RATCLIFFE et D. E. IRISH. Can. J. Chem. **63**, 3521 (1985).

On a entrepris une étude préliminaire des spectres Raman de solutions d'acide nitrique, à des températures allant jusqu'à 250°C. On a observé une diminution dans les fréquences des bandes νN—(OH) et δNO_2 du HNO_3; on interprète ces résultats en fonction d'une diminution dans la force de la liaison hydrogène. On a déterminé les valeurs approximatives du degré de dissociation α et elles démontrent que l'acide nitrique est un acide beaucoup plus faible à des températures plus élevées.

[Traduit par le journal]

Introduction

The study of processes in aqueous solutions at temperatures well above 100°C and at elevated pressures is currently of great interest because of its considerable importance in such areas as corrosion in power plants, aqueous subsurface extraction of oil and minerals, geothermal energy sources, and geological mineral formation (1). The dielectric constant of water decreases substantially as temperature increases and this property, in the absence of other factors, increasingly promotes ion association. As part of a larger program of research in this area we have studied the effects of increasing temperature on the Raman spectra of several acids in water, at pressures sufficient to maintain the liquid state. Perchloric acid remains a "strong" acid at high temperatures (2). However, for solutions of nitric and sulphuric acid, large increases occur in the populations of the ionogens (i.e.; the molecular forms (3)) as the temperature rises (this work and other works to be published). The following account presents some preliminary results concerning nitric acid to illustrate this effect and to further demonstrate the potential usefulness of the technique.

Experimental

Raman spectra between 3 and 250°C were obtained using the same furnace and spectrometer described in earlier papers in this series (2, 4, 5). Since the pressures used in this apparatus to maintain the liquid state at high temperatures are insufficient to keep the density constant it is most convenient to describe the solutions in terms of molality m (mol kg^{-1} H_2O) or stoichiometric mole ratio N ($=H_2O:HNO_3$) which are density independent. The two solutions studied were $N = 1.493$ (37.21 m) and $N = 5.063$ (10.97 m) which, at 25°C, are roughly 15.6 and 8.1 molar. We will refer to the two as $N = 1.5$ and 5. When attempts were made to go much above 100°C for $N = 1.5$ and 250°C for $N = 5$, the additional heat absorbed from the laser beam caused local instabilities in the liquid (presumably due to formation and collapse of small bubbles) which made it impossible to obtain reliable spectra.

Results and discussion

It is well known that at room temperature aqueous solutions of nitric acid contain a significant population of undissociated HNO_3 molecules especially for $N < 12$ (6–9); therefore bands of both NO_3^- and molecular HNO_3 appear in the spectra of the two concentrated solutions studied here, even at 3°C. Although the HNO_3 molecule strictly has C_s symmetry the bands of the O′—NO_2 unit in solution behave as though the molecule were a C_{2v} species, i.e., (HO)—NO_2 where (HO) is treated as a single unit. This is reflected in the polarisation behaviour of the modes, exemplified for the $N = 1.5$ solution in Fig. 1. Only those modes which would be polarised under C_{2v} symmetry show any appreciable polarisation. The bands have all been assigned previously (though not without debate (10–16)) and mode descriptions and frequencies at the extremes of temperature studied here are given in Table 1. The modes of NO_3^- are assigned according to D_{3h} symmetry; in aqueous nitrate solutions the degeneracy of the $\nu_3(E')$ mode is lifted because of distortions caused by aquation (17, 18), but the weakness of the two component bands and the overlap with the intense 1302 cm^{-1} band of HNO_3 prevents the detection of the ca. 1340 cm^{-1} component.

The effects of increasing temperature are shown in Figs. 2 and 3. In Fig. 3 the same series of spectra have been normalised in two ways to emphasize those bands which (a) increase in intensity with increasing temperature (i.e. HNO_3) and (b) those which decrease in intensity with increasing temperature (i.e. NO_3^-). The changes are very prominent; nitric acid is seen to be a very much weaker acid at high temperature.

The overtone of the out-of-plane bending mode of NO_3^- and the NO_2 antisymmetric stretch of HNO_3 overlap considerably in the 1600–1700 cm^{-1} region, but it is quite clear from the effects of temperature (Fig. 3) and the polarisation behaviour that both are present. It may also be inferred, at least from the spectra at $N = 1.5$ or at high temperature, that the NO_3^- mode has the lower frequency. Although the bending mode of H_2O should also occur in this region it is expected to be much weaker.

A striking feature of the effect of increasing temperature (Fig. 3) is the large decrease in frequency of the N—O′ stretching mode (from 966 cm^{-1} to 940 cm^{-1} for $N = 5$) and the NO_2 scissors bending mode (from 697 cm^{-1} to 679 cm^{-1} for $N = 5$) of HNO_3. Similar behaviour has been observed for the S—O′

[1]Present address: Chemistry Division, National Research Council of Canada, Ottawa, Ont., Canada K1A 0R6.

TABLE 1. Mode descriptions and frequencies (cm^{-1}) at low and high temperatures for nitric acid solutions

HNO_3	C_s	C_{2v}	$N = 5$ 3°C	$N = 5$ 250°C	$N = 1.5$ 3°C	$N = 1.5$ 100°C
νO—H	A'	—	← Not investigated here →			
$\nu_{asym.}$—NO_2	A'	B_1		1662	1673	1670
2 × δ out-of-plane	A'	A_1	~1570sh	1553	1558	1553
δN—O—H or 2 × δNO_2	A'	—	← Not detected →			
ν_{sym}—NO_2	A'	A_1	1302	1304	1304	1302
νN—O′	A'	A_1	966	940	955	948
δ out-of-plane	A''	B_2	← Not detected →			
δ O—N—O (scissors)	A'	A_1	~697	679	688	683
δ O—N—O′ (rock)	A'	B_1	641	640sh	640	640
τ OH (torsion)	A''	—	← Not detected →			

NO_3^-	D_{3h}	$N = 5$ 3°C	$N = 5$ 250°C	$N = 1.5$ 3°C	$N = 1.5$ 100°C
2 × δ_2 out-of-plane	A'	~1648sh	*	~1648sh	*
$\nu_{3\ asym}$ NO_3	E'	1428	~1425w sh	~1430	1425
$\nu_{1\ sym}$ NO_3	A'	1047	1042	1046	1044
δ_2 out-of-plane	A_2''	← Not observed (ir-active) →			
δ_4 O—N—O	E'	719	v.w.sh	~720w.sh	~720w.sh

*Masked by 1662 or 1670 cm^{-1} bands.

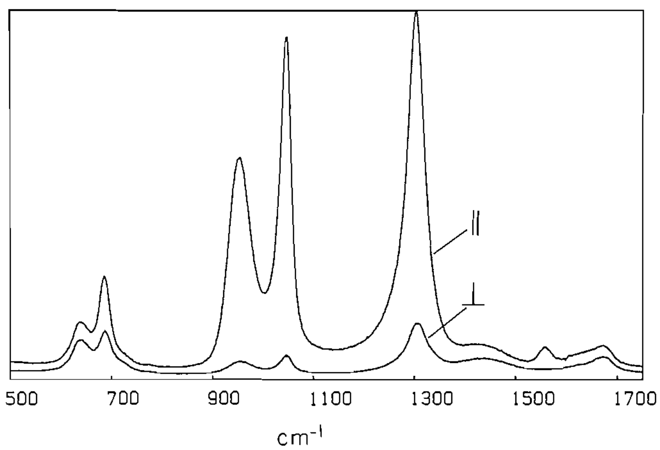

FIG. 1. Polarised spectra of N = 1.5 nitric acid solution at 25°C.

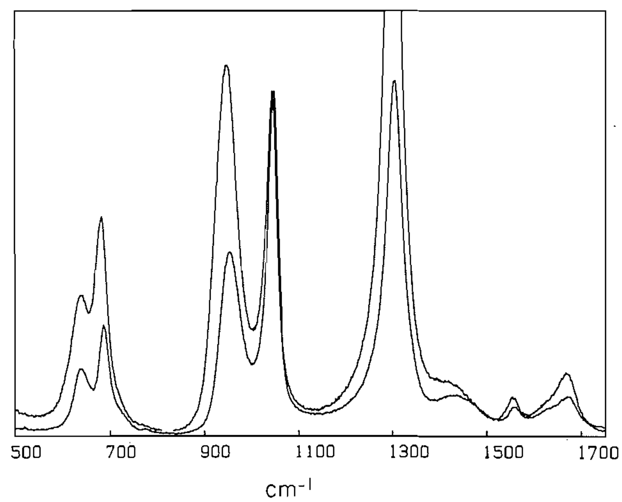

FIG. 2. Superimposed spectra of N = 1.5 nitric acid solution at 3°C (lower) and 100°C (upper), normalised on the symmetric stretching band of NO_3^- to show the increase in intensity of the HNO_3 bands.

stretching mode of HSO_4^- (19). Appreciable reductions in frequency also occur for the same two modes as N decreases. This shift is attributed to changing hydrogen bond strengths between the N—O—H bond and the surrounding medium. From a comparison of the structures of HNO_3 and NO_3^- (20), it is clear that the N—O′ bond is longer and hence should be weaker than the bonds of NO_3^-; thus the N—O′ bond is expected to have a lower stretching frequency. If the proton of HNO_3 is pulled further away from the oxygen as in a hydrogen bonding interaction the —O′—NO_2 grouping should tend towards becoming more like an NO_3^- ion. This would lead to a strengthening of the N—O′ bond and a reduction in the NO_2 angle, and thus to higher frequencies for the N—O′ stretching mode and the —NO_2 scissors bending mode. Evidence in favour of this may be found in the frequencies reported for HNO_3 in the vapour (13) and in matrix isolation studies (16, 21), Table 2. In the non-hydrogen bonded states, i.e. vapour or isolated monomer, the frequencies have their lowest values; they increase as soon as hydrogen bonding occurs either as HNO_3---HNO_3 or H_2O---HNO_3. Comparison of the frequencies of the nitric acid dimer versus the monohydrate complex, and for the liquid (10, 11, 13) versus solutions also indicates that the hydrogen bonding between HNO_3 and H_2O and/or $(H_{aq})^+$ is stronger than to other HNO_3 molecules; see Table 2. We can thus account for the behaviour as N increases; i.e., as $[HNO_3]$ decreases and $[H_2O]$ increases, the medium becomes more strongly hydrogen bonding. Increasing the temperature promotes ion association and thus $[HNO_3]$ increases and the medium becomes less strongly hydrogen bonding. In addition, increased temperature is expected to cause a general reduction in the strength of hydrogen bonding, an effect which is well

TABLE 2. Frequencies (cm^{-1}) of ν N—O' and δ NO_2 modes of HNO_3 in different environments

State of molecular HNO_3		ν N—O'	δ NO_2	Ref.
Vapour	(ir)	879	647	13*
Matrix Isolated Monomer in N_2	(ir)	902	660	16
Matrix Isolated Monomer in Ar	(ir)	893	—	21
Matrix Isolated Dimer in N_2	(ir)	939	666	16
Matrix Isolated Dimer in Ar	(ir)	927	—	21
Matrix isolated $H_2O \cdot HNO_3$ in Ar	(ir)	947	—	21
Liquid	(Raman)	926	677	10, 13*
			680	11
Solutions at 3°C $N=5$	(Raman)	966	697	This work
Solutions at 3°C $N=1.5$	(Raman)	955	688	This work

*Note that the authors (13) originally interchanged the labelling of the two modes, but the current labelling was later shown to be correct (16).

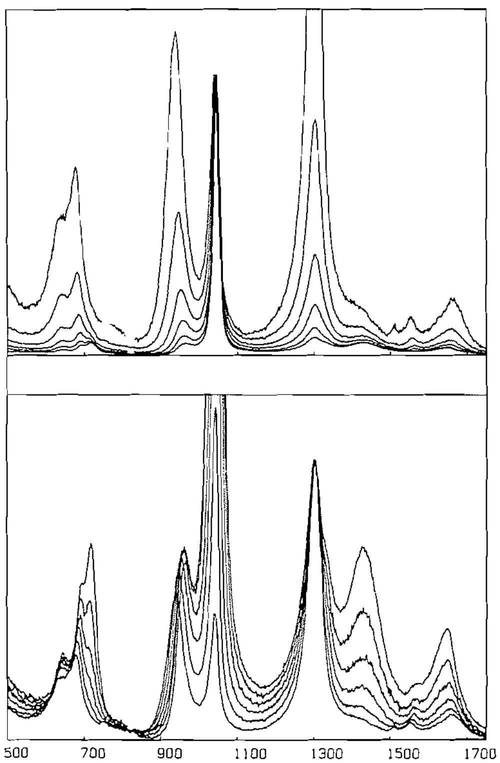

FIG. 3. Superimposed spectra of $N = 5$ nitric acid solution at 3, 50, 100, 150, 200, and 250°C. Top frame: spectra normalised on the symmetric stretching band of NO_3^-, temperature increases from bottom to top. Lower frame: spectra normalised on the —NO_2 symmetric stretching band of HNO_3, temperature increases from top to bottom.

known for water (5). On average the increased thermal motion causes fewer intermolecular configurations to be optimum for hydrogen bonding.

Dissociation of HNO_3 in solution

The dissociation of nitric acid has been the subject of a number of earlier studies, including one from this laboratory (7), using spectroscopic and other techniques (8, 9, 22–29). Of these only the salt solubilities measured by Marshall and Slusher (28, 29) have been studied at temperatures above 90°C,

TABLE 3. Estimated values of α

N	Temperature °C	Referenced to Raman (8, 9) NO_3^-†	Referenced to Raman (8, 9) HNO_3‡	Referenced to ir (6) NO_3^-†	Referenced to ir (6) HNO_3‡	Calculated from M−S equation
5	3	0.69	0.64	0.83	0.75	0.93
5	25	0.63*	0.63*	0.75*	0.75*	0.89
5	50	0.59	0.55	0.71	0.68	0.86
5	100	0.48	0.43	0.57	0.56	0.67
5	150	0.34	0.33	0.40	0.43	0.46
5	200	0.21	0.21	0.25	0.26	0.35
5	250	0.10	0.12	0.12	0.12	0.23
1.5	3	0.19	0.17	0.23	0.20	
1.5	25	0.17*	0.17*	0.20*	0.20*	
1.5	100	0.11	0.12	0.13	0.11	

*These values obtained from previous studies are used to reference the new results.
†Results based on the integrations normalised on the peak of ν_{sym} NO_3^-;
‡Results based on the integrations normalised on the peak of ν_{sym} (NO_2) of HNO_3, as described in the text.

and we shall compare their results with those of the present study. We shall consider the overall dissociation

$$\underset{(1-\alpha)m}{HNO_3} + nH_2O \rightleftharpoons (H_{aq})^+ + \underset{\alpha m}{NO_3^-}$$

though an intermediate step involving ion-pair formation and dissociation is thought to occur (7); evidence of bands due to the associated species H_2O---HNO_3 and H_3O^+---NO_3^- have been reported in a Raman study of the $N = 1$ liquid and glass (30), and at very high concentrations, ($4HNO_3 \cdot H_2O$), evidence for $[NO_3 \cdot 3HNO_3]^-$ has been presented (31).

These preliminary studies allow us to obtain reasonable estimates of α, the degree of dissociation, at different temperatures, but only by relating parameters derived from the spectra to α values determined in other studies for one or two specific concentrations and temperatures. Values of α at room temperature and the two concentrations studied here can be obtained from the tables or plots given in previous ir (6) and Raman (8, 9) work. We will use both sets independently since they are not completely in agreement (the ir results give slightly larger α values than the Raman results); specifically for $N = 5$, $\alpha = 0.75$ and for $N = 1.5$, $\alpha = 0.2$ from ir (6) and $\alpha = 0.63$ and 0.17, respectively, from Raman (8, 9) both at room temperature. (Accuracy is limited by ability to read the published graphs.) We initially attempted to use the *ratio* of the peak heights of $\nu_{sym}(NO_3^-)$ and ν_{sym}(—NO_2 of HNO_3) since this should have the simple dependence on α:

$$R = C\alpha/(1-\alpha)$$

where C is a constant, assuming the two peak heights are proportional to the amounts of the two species they represent. However, the value of C obtained by substituting previously known α's was substantially different for the two concentrations. We finally chose the following method of obtaining approximate α values. After subtracting an appropriate linear baseline over the 200–1400 cm^{-1} range, we obtained the total integral for each spectrum. These integrals were then scaled so as to effect a normalisation on the peak of the $\nu_{sym}(NO_3^-)$ band. We then made a number of assumptions: that there are only two species present in significant amounts which contribute to the spectra (NO_3^-/HNO_3), that the two species contribute intensity proportional to the amount present, and that the *peak* intensity of the NO_3^- band is proportional to the quantity of NO_3^- present. The normalised integrals (I) will then be the sum of a constant contribution (X) from NO_3^- and a variable contribution from HNO_3 (dependent on α):

$$I = X + \frac{Y(1-\alpha)}{\alpha}$$

X and Y can be determined by substituting the previously known values of α at room temperature for the two concentrations, and then α at other temperatures can be obtained. Alternatively we can normalise on the $\nu_{sym}NO_2$ (HNO_3) peak (instead of NO_3^-) and with appropriate changes to the equation again arrive at α values. The results are given in Table 3, from which it may be seen that the values of α based on integrations normalised in either way are in quite reasonable agreement, but as expected the two sets of values referenced to the previous ir or Raman results retain a significant difference.

Marshall and Slusher (28) express their results concerning the ionisation of nitric acid in the range up to 350°C in terms of the extended Debye–Hückel equation

$$\log Q_n = \log K_n + 2S\sqrt{I}/(1 + 1.6\sqrt{I}) \qquad \text{(their equation [25])}$$

where $2S$ is the Debye–Hückel limiting slope for a particular temperature (given in ref. 32), and I is the ionic strength given by

$$I = 0.5 \sum_i m_i z_i^2$$

where m_i = molality of ion, z_i = charge of ion. They found that the temperature variation of the ionisation constant can be fitted to the equation (in molal terms):

$$\log K_n = 5.424 - 134.37/T - 0.01199T \qquad \text{(their equation [32])}$$

The equations apply for the reaction $HNO_3 \rightleftharpoons H^+ + NO_3^-$ for which

$$Q_n = \frac{m\alpha \cdot m\alpha}{m(1-\alpha)} \text{ and } I = m\alpha$$

Hence

$$\log (m\alpha^2/(1-\alpha)) = \log K_n + 2s\sqrt{m\alpha}/(1 + 1.6\sqrt{m\alpha})$$

from which α can be calculated for various molalities and temperatures. The results for the $N = 5$ sample are included in Table 3; they are significantly different from the spectroscopic values. A lack of agreement is not unexpected. Marshall and Slusher's (28) values of K_n were determined from measurement of the solubility of $CaSO_4$ in HNO_3/H_2O mixtures with concentrations of acid less than 3.4 m, with the exception of two samples. Their extended Debye–Hückel formulations cannot be expected to apply to the two high concentrations studied spectroscopically, and thus only the estimates for the $N = 5$ sample are given in Table 3 to show the trend. Their analysis also neglects contributions from the ion pairs $CaNO_3^+$ and $CaSO_4$ which must form in their solutions; the inclusion of these equilibria in the data refinement will alter the values of K_n somewhat.

A careful study of the molal intensities of NO_3^- and HNO_3 at different temperatures is required to better quantify the Raman data. It is well known that proton exchange affects the bandwidths (33, 34), and that there is a finite concentration of the intermediate ion pair $H_3O^+ \cdot NO_3^-$ (7). All of these factors must be taken into account to obtain more reliable values of α.

We conclude with a few remarks about the "weakness" of nitric acid. Leuchs and Zundel (6) visualise the ionisation process in terms of a double well hydrogen bonding potential between the H_2O and HNO_3 molecules. For $N < 1$ solutions the well at the HNO_3 end is deeper (Zundel's proton boundary structure **I**) but as N increases the deeper well moves to the H_2O side, thus stabilising H_3O^+ (proton boundary structure **II**). In isolation the molecular complex $H_2O \cdot HNO_3$ is observed to be the stable form (21), rather than $H_3O^+NO_3^-$, since more water molecules are necessary to hydrogen bond and thus to stabilise H_3O^+. Recent *ab initio* calculations (35) substantiate this but furthermore indicate that in the isolated complex there is only one well in the H_2O---HNO_3 hydrogen bond potential, situated at the HNO_3 end. This implies that the double minimum potential forms only for the condensed medium, where even for $N < 1$ there are always other HNO_3 or H_2O molecules to accept hydrogen bonds. We might visualise the effect of increasing temperature as a shift from proton boundary structure **II** back to **I**, caused by a destabilisation of H_3O^+ as the general hydrogen bonding to other molecules decreases.

Acknowledgement

This research was supported by grants from the Natural Sciences and Engineering Research Council of Canada.

1. T. W. SWADDLE. Chem. Can. **32**, 21 (1980).
2. C. I. RATCLIFFE and D. E. IRISH. Can. J. Chem. **62**, 1134 (1984).
3. R. M. FUOSS. J. Chem. Educ. **32**, 527 (1955).
4. D. E. IRISH, T. JARV, and C. I. RATCLIFFE. Appl. Spectrosc. **36**, 137 (1982).
5. C. I. RATCLIFFE and D. E. IRISH. J. Phys. Chem. **86**, 4897 (1982).
6. M. LEUCHS and G. ZUNDEL. J. Phys. Chem. **82**, 1632 (1978).
7. D. E. IRISH and O. PUZIC. J. Solution Chem. **10**, 377 (1981).
8. A. A. KRAWETZ. Ph.D. Thesis. University of Chicago, Chicago, IL. 1955.
9. T. F. YOUNG, L. F. MARANVILLE, and H. M. SMITH. *In* The structure of electrolytic solutions. *Edited by* W. J. Hamer. Wiley and Sons, New York. 1959. Chapt. 4.
10. O. REDLICH and L. E. NIELSON. J. Am. Chem. Soc. **65**, 654 (1943).
11. C. K. INGOLD and D. J. MILLEN. J. Chem. Soc. 2612 (1950).
12. R. A. MARCUS and J. M. FRESCO. J. Chem. Phys. **27**, 564 (1957).
13. G. E. MCGRAW, D. L. BERNITT, and I. C. HISATSUNE. J. Chem. Phys. **42**, 237 (1965).
14. A. PALM and A. CASTELLI. Spectrochim. Acta, **24A**, 1658 (1968).
15. E. KOZLOWSKA. C.R. Acad. Sci. Paris, **267B**, 696 (1968).
16. W. A. GUILLORY and M. L. BERNSTEIN. J. Chem. Phys. **62**, 1058 (1975).
17. D. E. IRISH and A. R. DAVIS. Can. J. Chem. **46**, 943 (1968).
18. T. J. V. FINDLAY and M. C. R. SYMONS. J. Chem. Soc. Faraday 2, **72**, 820 (1976).
19. B. S. W. DAWSON, D. E. IRISH, and G. E. TOOGOOD. J. Phys. Chem. In press.
20. F. A. COTTON and G. WILKINSON. *In* Advanced inorganic chemistry. 2nd ed. Interscience, New York. 1966. p. 351.
21. G. RITZHAUPT and J. P. DEVLIN. J. Phys. Chem. **81**, 521 (1977).
22. O. REDLICH and J. BIGELEISEN. J. Am. Chem. Soc. **65**, 1883 (1943).
23. O. REDLICH. Chem. Rev. **39**, 333 (1946).
24. G. C. HOOD, O. REDLICH, and C. A. REILLY. J. Chem. Phys. **22**, 2067 (1954).

25. G. C. HOOD and C. A. REILLY. J. Chem. Phys. **32**, 127 (1960).
26. V. N. EGOROV and I. E. KUZINETS. Russ. J. Inorg. Chem. **20**, 1762 (1975).
27. V. N. EGOROV and I. E. KUZINETS. Russ. J. Phys. Chem. **49**, 1688 (1975).
28. W. L. MARSHALL and R. SLUSHER. J. Inorg. Nucl. Chem. **37**, 1191 (1975).
29. W. L. MARSHALL and R. SLUSHER. J. Inorg. Nucl. Chem. **37**, 2165 (1975).
30. M. H. HERZOG-CANCE, J. POTIER, A. POTIER, P. DHAMELINCOURT, B. SOMBRET, and F. WALLART. J. Raman Spectrosc. **7**, 303 (1978).
31. M. PHAM-THI, M. H. HERZOG-CANCE, A. POTIER, and J. POTIER. J. Raman Spectrosc. **11**, 96 (1981).
32. W. L. MARSHALL and E. V. JONES. J. Phys. Chem. **70**, 4028 (1966).
33. H. STREHLOW, I. WAGNER, and P. HILDEBRANDT. Ber. Bunsenges. Phys. Chem. **87**, 516 (1983).
34. D. E. IRISH. *In* Proceedings of the Sixth International Conference on Raman Spectroscopy, Bangalore, India, 4–9 Sept., 1978. *Edited by* E. D. Schmid, R. S. Krishnan, W. Kiefer, and H. W. Schrötter. Heyden, London. 1978. p. 245.
35. J. S. TSE. To be published.

Trapping of *o*-quinodimethane with *p*-quinones: synthesis of tetrahydro-1,4-anthracenediones

SYED ASKARI, SUSAN LEE, ROBERT R. PERKINS, AND JOHN R. SCHEFFER[1]
Department of Chemistry, University of British Columbia, Vancouver, B.C., Canada V6T 1T6

Received January 7, 1985[2]

SYED ASKARI, SUSAN LEE, ROBERT R. PERKINS, and JOHN R. SCHEFFER. Can. J. Chem. **63**, 3526 (1985).

Previous work from our laboratory has been concerned with investigating the photochemical reactivity of the tetrahydro-1,4-napthalenedione system, both in solution and the solid state. The results obtained prompted us to extend our studies to the analogous tetrahydro-1,4-anthracenedione system. The most direct method of synthesis of the desired compounds is through Diels–Alder addition of *o*-quinodimethane to *p*-quinones. Because of the ease with which the adducts would be expected to undergo bis-enolization to the corresponding hydroquinones, their preparation requires mild, neutral conditions. After much experimentation, success was achieved using the Durst–Charlton sulfur dioxide extrusion method for generating *o*-quinodimethane from 3,6-dihydro-1,2-oxathiin-2-oxide. *In situ* trapping using *p*-benzoquinone and other substituted *p*-quinones afforded the desired adducts in reasonable yields. In the case of duroquinone and 2,3-dimethyl-1,4-naphthalenedione, fluoride ion-catalyzed generation of *o*-quinodimethane from [*o*-[α-(trimethylsilyl)methyl]benzyl]trimethylammonium bromide by the method of Ito also gave acceptable results; however, the bis-enolizable adducts were not stable under these eaction conditions.

SYED ASKARI, SUSAN LEE, ROBERT R. PERKINS et JOHN R. SCHEFFER. Can. J. Chem. **63**, 3526 (1985).

Dans un travail antérieur réalisé dans notre laboratoire, on a examiné la réactivité photochimique du système tétrahydronaphtalènedione-1,4 tant en solution qu'à l'état solide. Les résultats obtenus nous ont incité à étendre nos études au système analogue de la tétrahydroanthracènedione-1,4. La méthode la plus directe de synthèse des composés désirés implique une addition de Diels–Alder du *o*-quinodiméthane sur des *p*-quinones. Compte tenu du fait qu'il est à prévoir que les adduits subiront facilement une bis-énolisation conduisant aux hydroquinones correspondantes, il est important d'utiliser des conditions neutres et douces pour leur préparation. Après beaucoup d'expérimentation, on a fait appel à la méthode de Durst–Charlton d'extrusion du bioxyde de soufre pour générer avec succès le *o*-quinodiméthane à partir de l'oxyde-2 de la dihydro-3,6 oxathiine-1,2. La réaction *in situ* de ce dérivé avec de la *p*-benzoquinone et d'autres *p*-benzoquinones substituées a permis d'obtenir les produits désirés, avec des rendements raisonnables. Dans les cas de la duroquinone et de diméthyl-2,3 naphtalènedione-1,4, il a aussi été possible d'obtenir des résultats acceptables en utilisant la méthode de I to qui implique une génération, catalysée par les ions fluorures, du *o*-quinodiméthane à partir du bromure de [*o*-[α-(triméthylsilyl)méthyl] benzyl]triméthylammonium; toutefois, dans ces conditions, les produits bis-énolisables n'étaient pas stables.

[Traduit par le journal]

Introduction

The Diels–Alder adducts formed between *p*-quinones and cyclic as well as acyclic 1,3-dienes have served, as a result of their photochemical rearrangements, as a rich source of novel polycyclic ring systems (1–13). Three representative examples are shown in Scheme 1. Because, among other things, the presence of an aromatic double bond at the 6,7–position would be expected to affect the formation of photoproducts analogous to **3**, **6**, and **8**, we decided to prepare and photolyze the 6,7-benzo analogue of ene-dione **1**, namely *cis*-4a,9a,9,10-tetrahydro-1,4-anthracenedione, **12** (Table 1). This paper reports the synthesis of compound **12** and five of its methylated and benzannelated derivatives; the photochemistry of these systems will be reported in a separate publication.

The most direct synthesis of the desired tetrahydro-1,4-anthracenediones is through Diels–Alder addition of *p*-quinones to the diene *o*-quinodimethane. Despite the enormous body of literature dealing with the generation and both the intermolecular (14–19) and intramolecular (20–22) Diels–Alder reactions of *o*-quinodimethane and its derivatives, there are very few reports which use simple *p*-benzoquinones as the trapping agents (23). This is largely due to the fact that, until recently, the reaction conditions required to generate *o*-quinodimethanes were such that the initial adducts (e.g., **12**) were not stable. Ene-diones analogous to **12** enolize readily at elevated temperatures or in the presence of acid or base to afford the corresponding hydroquinones. These hydroquinones, in turn, are oxidized readily to the fully aromatic 1,4-anthracenediols.

Results and discussion

We have investigated three methods for the synthesis of *cis*-4a,9a,9,10-tetrahydro-1,4-anthracenedione (**12**) and its derivatives. All three involve relatively mild and, at least in the initial stages of reaction, neutral conditions. Each is discussed separately below.

The first procedure was based on the work of Han and Boudjouk (24*a*; see also ref. 24*b*). These authors showed that *o*-quinodimethane can be generated by treatment of α,α-dibromo-*o*-xylene (**9**) with powdered zinc under conditions of ultrasound sonication at room temperature; trapping with maleic anhydride, dimethyl maleate, methyl acrylate, and methyl vinyl ketone provided the corresponding adducts in good yield. We found, however, that when mixtures of α,α-dibromo-*o*-xylene, zinc powder, and either *p*-benzoquinone or duroquinone were subjected to ultrasound treatment, no adducts were formed, and the dibromoxylene could be recovered unchanged. This difference in reactivity can be attributed to involvement of the zinc in reducing the quinones rather than participating in *o*-quinodimethane formation.

The second procedure that we tested for its suitability in preparing *o*-quinodimethane under sufficiently mild conditions was the fluoride ion-catalyzed decomposition of [*o*[α-(trimethylsilyl)methyl]benzyl]trimethylammonium bromide (**10***a*) reported by Ito, Nakatsuka, and Saegusa (16, 17). These workers showed that treatment of ammonium salt **10***a* with tetrabutyl-

[1]Author to whom correspondence may be addressed.
[2]Revision received July 26, 1985.

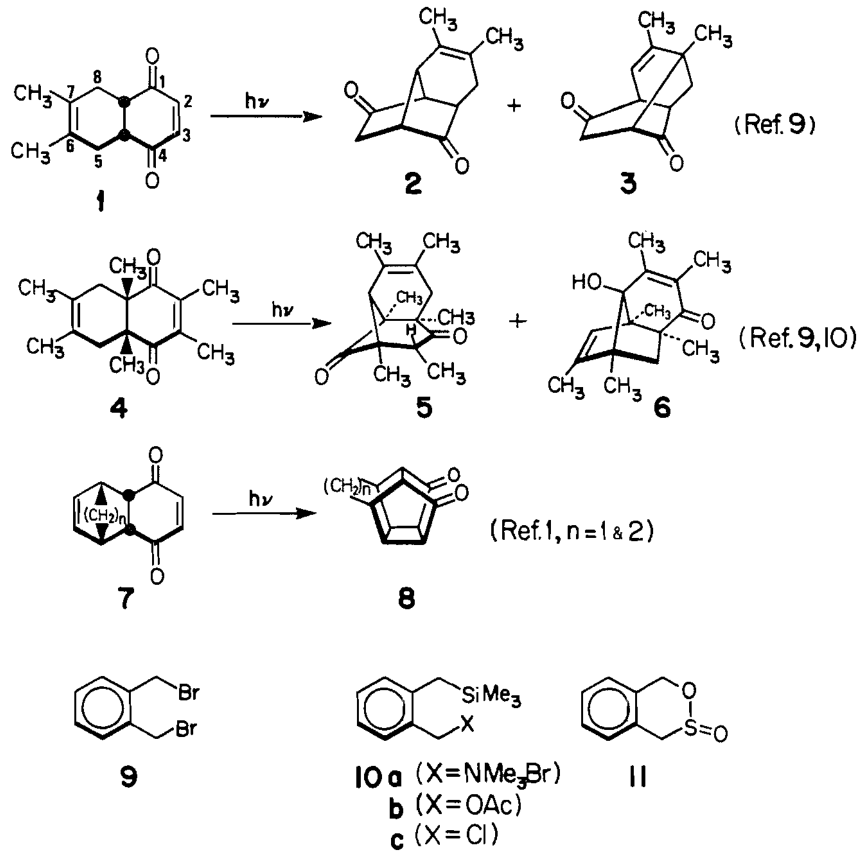

SCHEME 1

ammonium fluoride (TBAF) at room temperature is an efficient source of *o*-quinodimethane. Indeed, when an acetonitrile solution containing the ammonium salt **10***a*, TBAF, and either duroquinone or 2,3-dimethyl-1,4-naphthalenedione was allowed to react, the Diels–Alder adducts **16** and **17** were formed in modest yields (Table 1). Our initial apprehension, subsequently justified, was that the trimethylamine generated in this procedure would be capable of catalyzing the bis-enolization of the adducts bearing only hydrogen atoms at positions 4a and 9a (e.g., **12**). Thus, when *p*-benzoquinone or 2-methyl-*p*-benzoquinone were used as the dienophiles, no ene-dione-containing products could be isolated. A control experiment using 6,7-dimethyl-1,4-naphthalenedione (**1**) verified that small amounts of tertiary amines are, in fact, capable of inducing aromatization to the corresponding 5,8-dihydro-1,4-naphthalenediols. We next reasoned that this problem could be overcome by changing the nature of the leaving group in the *o*-quinodimethane precursor from trimethylamine to the less basic acetate ion. The required precursor **10***b* was readily available by conventional procedures, but despite the fact that **10***b* gave an even better yield of adduct **16** than **10***a* (61% vs. 44%), when treated with TBAF in the presence of duroquinone, it nevertheless proved totally ineffective in the preparation of the desired adduct **12**. Similar negative results were obtained with *p*-benzoquinone when the leaving group was chloride ion (precursor **10***c*). With these results, we finally decided to check the stability of similar 4a,9a hydrogen-containing adducts such as **1** to TBAF in acetonitrile. To our surprise, this caused adduct **1** to undergo rapid bis-enolization, even under the most anhydrous conditions we were able to achieve. Furthermore, the use of the Ito method with 2,5-dimethyl-*p*-benzoquinone as the dienophile afforded a 20% yield of the *trans*-adduct **14***t* rather than the *cis* isomer **14***c* (Table 1). With the successful preparation of the *cis*-adduct **14***c* (*vide infra*), we were able to verify that *cis* to *trans* isomerization of **14***c* does take place under the Ito reaction conditions.

We were finally successful in preparing the bis-enolizable adducts **12**, **13**, and **15** (Table 1) using 3,6-dihydro-1,2-oxathiin-2-oxide (**11**) as the *o*-quinodimethane precursor. Jung, Molin, Van den Elzen and Durst (25) were the first to synthesize sultine **11**. They showed, using maleic anhydride as the trapping agent, that **11** decomposes smoothly in refluxing benzene to *o*-quinodimethane and sulfur dioxide. An improved procedure for the synthesis of sultine **11** has been developed recently by Charlton and Durst (26). This sequence, involving as the key step the trapping of the photoenol of *o*-tolualdehyde by sulfur dioxide (27), provided us with gram quantities of sultine **11** on a routine basis. In addition to ene-diones **12**, **13**, and **15**, sultine **11** could be used to prepare adducts **14***c* and **16** (and presumably adduct **17**, although this was not tried). In general, the sultine method afforded higher yields (50–60%) than the trimethylsilyl ammonium salt method (20%). The one exception to this rule was duroquinone, which showed greater reactivity under the latter conditions (44% vs. 26%). That duroquinone reacts at all under these mild conditions is remarkable in view of the high temperature, sealed tube conditions required to bring about the Diels–Alder reaction between duroquinone and 2,3-dimethylbutadiene (28); this is presumably a testimony to the high reactivity of *o*-quinodimethane. Interestingly, tetraethyl-*p*-benzoquinone failed to react with *o*-quinodimethane generated by the trimethylsilyl ammonium salt procedure.

The solution phase and solid state photochemistry of adducts **12**–**17** is under active investigation.

TABLE 1. Structures, yields, and melting points of adducts synthesized

Adduct structure	Adduct mp	Quinone	*o*-Quinodimethane precursor	Yield
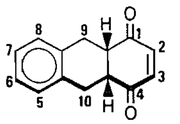 **12**	122–123°C	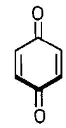	**11**	48%
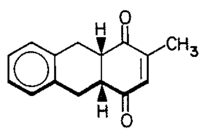 **13**	110–111°C	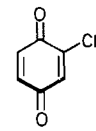	**11**	60%
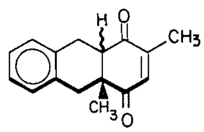 **14c**[a]	80–81°C	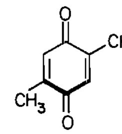	**11**	62%
14t[b]	119–120°C		**10a**	19%
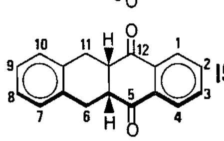 **15**	156–157°C	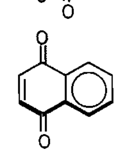	**11**	52%
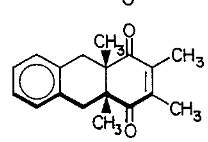 **16**	84–85°C	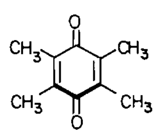	**11**	26%
			10a	44%
			10b	61%
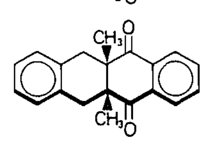 **17**	101–102°C	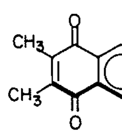	**10a**	20%

[a] *Cis*-4a,9a configuration.
[b] *Trans*-4a,9a configuration.

Experimental

General

Melting points were determined on a Fisher–Johns hot stage apparatus and are uncorrected. Infrared (ir) spectra were obtained on a Perkin–Elmer 710B instrument using KBr discs and are reported as ν_{max} in cm^{-1}. ^{1}H nuclear magnetic resonance (nmr) spectra were recorded at 400 MHz on a Bruker WH-400 instrument using $CDCl_3$ as the solvent and TMS as the internal standard; signal positions are given in δ, and their multiplicities, integrated areas, coupling constants, and assignments are indicated in parenthesis. Mass spectra (ms) were obtained with a Kratos MS-50 instrument operating at 70 eV; the relative intensity of each ion is given in parentheses. The elemental analyses were carried out in the departmental microanalytical laboratory by Mr. P. Borda. Flash chromatography was done using Merck 9385 silica gel with the columns being slurry-packed in the eluting solvent.

Acetonitrile was distilled from calcium hydride and stored over 4 Å molecular sieve. Tetrabutylammonium fluoride was prepared by the method of Kuwajima, Murofushi, and Nakamura (29), freeze dried, and stored in vacuum-sealed tubes under argon over P_2O_5 in a vacuum desiccator. Quinones were purified by sublimation, recrystallization, or both. [*o*-[α-(Trimethylsilyl)methyl]benzyl]trimethylammonium bromide (**10***a*) was prepared by the method of Ito, Nakatsuka, and Saegusa (16), and sultine **11** was prepared according to the procedure of Charlton and Durst (26).

cis-4a,9a,9,10-Tetrahydro-1,4-anthracenedione (12)

A solution of 1.00 g (5.95 mmol) of sultine **11** (26, 27) and 0.96 g (8.92 mmol) of freshly sublimed *p*-benzoquinone in 10 mL of anhydrous benzene was refluxed for 1.75 h. Benzene was removed *in vacuo* to give an orange solid which, after two recrystallizations from methanol, afforded 0.60 g (48%) of adduct **12** as off-white needles, mp 122–123°C; ν_{max} (KBr): 1680 cm^{-1} (C=O); δ ($CDCl_3$, 400 MHz): 7.18–7.06 (m, 4H, aromatics), 6.72 (s, 2H, vinyls), 3.40 (m, 2H, 4a,9a methines), 3.22 (dd, J = 18 and 6 Hz, 2H, benzylic hydrogens), 2.92 (dd, J = 18 and 4 Hz, 2H, benzylic hydrogens); m/e (relative intensity): 212 (M^+, 100), 195 (69), 184 (32), 165 (75), 152 (65), 141 (30), 128 (75), 115 (45). *Anal.* calcd. for $C_{14}H_{12}O_2$: C 79.23; H 5.70; found: C 79.00, H 5.50.

2-Methyl-cis-4a,9a,9,10-tetrahydro-1,4-anthracenedione (13)

The reaction between 1.00 g (5.95 mmol) of sultine **11** and 1.02 g (8.37 mmol) of toluquinone was carried out as described above to afford, after recrystallization from methanol, 0.80 g (60%) of adduct **13** as light yellow needles, mp 110–111°C; ν_{max} (KBr): 1690, 1675 cm^{-1} (C=O); δ($CDCl_3$, 400 MHz): 7.15–7.06 (m, 4H, aromatics), 6.58 (br s, 1H, vinyl), 3.42–3.30) (m, 2H, 4a,9a methines), 3.45–3.26 (m, 2H, benzylic hydrogens), 2.97–2.86 (m, 2H, benzylic hydrogens), 2.02 (d, J = 2 Hz, 3H, methyl); m/e (relative intensity): 226 (M^+, 44), 211 (33), 198 (100), 183 (46), 165 (72), 152 (33), 141 (30), 128 (90), 115 (55). *Anal.* calcd. for $C_{15}H_{14}O_2$: C 79.62, H 6.24; found: C 79.83, H 6.29.

2,4a-Dimethyl-cis-4a,9a,9,10-tetrahydro-1,4-anthracenedione (14c)

Reaction, as before, between 1.00 g (5.95 mmol) of sultine **11** and 1.21 g (8.92 mmol) of 2,5-dimethyl-*p*-benzoquinone gave, after recrystallization of the crude reaction mixture from methanol, 0.88 g (62%) of adduct **14***c*, mp 80–81°C; ν_{max} (KBr): 1680 cm^{-1} (C=O); δ($CDCl_3$, 400 MHz): 7.17–7.00 (m, 4H, aromatics), 6.52 (q, J = 1.5 Hz, 1H, vinyl), 3.38 (dd, J = 17 and 5 Hz, 1H, benzylic hydrogen at 9), 3.17 (d, J = 16 Hz, 1H, benzylic hydrogen at 10), 3.06 (m, 1H, 9a methine), 2.93 (dd, J = 17 and 6 Hz, 1H, benzylic hydrogen at 9), 2.53 (d, J = 16 Hz, 1H, benzylic hydrogen at 10), 2.00 (d, J = 1.5 Hz, 3H, vinyl methyl), 1.35 (s, 3H, 4a methyl); m/e (relative intensity): 240 (M^+, 18), 225 (16), 212 (85), 197 (100), 179 (28), 128 (47). *Anal.* calcd. for $C_{16}H_{16}O_2$: C 79.97; H 6.71; found: C 80.01, H 6.60.

cis-5a,11a,6,11-Tetrahydro-5,12-naphthacenedione (15)

Reaction, as before, using 1.00 g (5.95 mmol) of sultine **11** and 1.30 g (8.22 mmol) of 1,4-naphthalenedione afforded, after recrystallization from methanol, 0.80 g (52%) of adduct **15**, mp 156–157°C; ν_{max} (KBr): 1680 cm^{-1} (C=O); δ($CDCl_3$, 400 MHz): 8.08 (dd, J = 6 and 3 Hz, 2H, aromatics 1 and 4), 7.75 (dd, J = 6 and 3 Hz, 2H, aromatics 2 and 3), 7.17–7.07 (m, 4H, aromatics 7–10), 3.62–3.54 (m, 2H, 5a,11a, methines), 3.35–3.25 (m, 2H, benzylic hydrogens), 3.04–2.94 (m, 2H, benzylic hydrogens); m/e (relative intensity): 262 (M^+, 100), 245 (59), 244 (89), 215 (46), 202 (13), 128 (15). *Anal.* calcd. for $C_{18}H_{14}O_2$: C 82.42, H 5.38; found: C 82.15, H 5.29.

2,3,4a,9a-Tetramethyl-cis-4a,9a,9,10-tetrahydro-1,4-anthracenedione (16)

To a stirred solution of 2.44 g (7.72 mmol) of [*o*-[α-(trimethylsilyl)methyl]benzyl]trimethylammonium bromide (**10***a*) (16) and 3.80 g (23.2 mmol) of duroquinone in 50 mL of anhydrous acetonitrile was added, over a period of 30 min, 4.04 g (15.4 mmol) of tetrabutylammonium fluoride (29) in 15 mL of anhydrous tetrahydrofuran. After stirring under nitrogen overnight at room temperature, 10 mL of water was added, and the organic layer was extracted with ether, dried over sodium sulfate, and concentrated in *vacuo* to afford 3.68 g of dark oil. Purification by flash chromatography using 1:4 ethyl acetate – petroleum ether (30–60°C) gave 1.16 g of light yellow solid. Recrystallization from 1:1 ethyl acetate – hexane afforded adduct **16** (0.94 g, 44%) as nearly colorless crystals, mp 84-85°C; ν_{max} (KBr): 1664 cm^{-1} (C=O); δ ($CDCl_3$, 400 MHz): 7.12–7.02 (m, 4H, aromatics), 3.35 (d, J = 17 Hz, 2H, benzylic hydrogens), 2.55 (d, J = 17 Hz, 2H, benzylic hydrogens), 1.98 (s, 6H, vinyl methyls), 1.22 (s, 6H, 4a,9a methyls); m/e (relative intensity): 268 (M^+, 34), 253 (14), 240 (68), 225 (100), 210 (20), 207 (30). *Anal.* calcd. for $C_{18}H_{20}O_2$: C 80.56, H 7.51; found: C 80.45, H 7.51.

5a,11a-Dimethyl-cis-*5a,11a,6,11-tetrahydro-5,12-naphthacenedione (17)*

Reaction, as above, between 4.00 g (21.5 mmol) of 2,3-dimethyl-1,4-naphthalenedione, 6.80 g (21.5 mmol) of ammonium salt **10***a*, and 8.41 g (32.2 mmol) of TBAF in 60 mL of anhydrous acetonitrile afforded, after chromatography and recrystallization from 30–60°C petroleum ether, 1.20 g (20%) of crystalline adduct **17**, mp 101–102°C; ν_{max} (KBr): 1680 cm^{-1} (C═O); δ ($CDCl_3$, 400 MHz): 8.05 (dd, J = 6 and 3 Hz, 2H, aromatics 1 and 4), 7.73 (dd, J = 6 and 3 Hz, 2H, aromatics 2 and 3), 7.17–7.04 (m, 4H, aromatics 7–10), 3.42 (d, J = 16 Hz, 2H, benzylic hydrogens), 2.65 (d, J = 16 Hz, 2H, benzylic hydrogens), 1.33 (s, 6H, methyls); m/e (relative intensity): 290 (M^+, 16), 275 (9), 262 (100), 247 (44), 229 (11). *Anal.* calcd. for $C_{20}H_{18}O_2$: C 82.73, H 6.25; found: C 82.47, H 6.31.

2,4a-Dimethyl-trans-*4a,9a,9,10-tetrahydro-1,4-anthracenedione (14*t*)*

Reaction, as above, between 0.86 g (6.32 mmol) of 2,5-dimethyl-*p*-benzoquinone, 1.00 g (3.82 mmol) of rigorously dried ammonium salt **10***a*, and 1.65 g (6.32 mmol) of anhydrous TBAF in 50 mL of anhydrous acetonitrile afforded, after flash chromatography and recrystallization of the crude product from 30–60°C petroleum ether, 0.15 g (19%) of adduct **14***t*, mp 119–120°C; ν_{max} (KBr): 1680 and 1660 cm^{-1} (C═O); δ ($CDCl_3$, 400 MHz): 7.20–7.13 (m, 4H, aromatics), 6.57 (br d, J = 2Hz, 1H, vinyl), 3.21–2.95 (m, 5H, benzylic hydrogens and methine at 9a), 2.06 (d, J = 2 Hz, 3H, vinyl methyl), 1.15 (s, 3H, 4a methyl); m/e (relative intensity): 240 (M^+, 100), 225 (99), 212 (25), 197 (44), 179 (19), 141 (17), 128 (43), 115 (23), 96 (11), 69 (31). *Anal.* calcd. for $C_{16}H_{16}O_2$: C 79.97, H 6.71; found: C 80.00, H 6.62.

*[*o*-[α-(Trimethylsilyl)methyl]benzyl]acetate (10*b*)*

To a stirred solution of sodium acetate (0.2 g, 2.4 mmol) in 50 mL of freshly distilled acetic anhydride was added 5.00 g (22.5 mmol) of [*o*-[α-(trimethylsilyl)methyl]benzyl]dimethylamine (16). After refluxing for 24 h, acetic anhydride was removed *in vacuo* and the resulting crude product dissolved in ether. The ether solution was washed with 10% aqueous sodium bicarbonate solution dried over sodium sulfate, and concentrated in *vacuo* to give a brown oil which was distilled at 55°C and 0.3 Torr (1 Torr = 133.3 Pa) to afford 3.99 g (77%) of acetate **10***b* as a colorless liquid: ν_{max} ($CHCl_3$): 1720 cm^{-1} (C═O); δ ($CDCl_3$, 400 MHz): 7.34–7.02 (m, 4H, aromatics, 5.08 (s, 2H, —OCH_2), 2.18 (s, 2H, —$SiCH_2$), 2.10 (s, 3H, methyl), 0.03 (s, 9H, —$SiMe_3$); m/e (relative intensity): 236 (M^+, 58), 221 (44), 117 (22), 104 (100), 73 (55). *Anal.* calcd. for $C_{13}H_{20}O_2Si$: C 66.05, H 8.52; found: C 66.30, H 8.60. The reaction between compound **10***b* (100 mg, 0.43 mmol), duroquinone (208 mg, 1.26 mmol), and TBAF (0.22 g, 0.84 mmol) followed by the usual work-up afforded 69 mg (61%) of adduct **16** whose properties were identical to those reported above. Neither **10***b* nor **10***c* (compound **10***c* is reported by Ito *et al.* (16) without experimental detail) gave any trace of adduct **12** when decomposed by anhydrous TBAF in the presence of *p*-benzoquinone.

Acknowledgments

Financial support by the Natural Sciences and Engineering Research Council of Canada is gratefully acknowledged. Special thanks are due Professor James L. Charlton, University of Manitoba, for experimental details on the improved synthesis of sultine **11** prior to publication.

1. R. C. COOKSON, E. CRUNDWELL, R. R. HILL, and J. HUDEC. J. Chem. Soc. 3062 (1964).
2. R. C. COOKSON, R. R. HILL, and J. HUDEC. J. Chem. Soc. 3043 (1964).
3. J. C. BARBORAK, L. WATTS, and R. PETTIT. J. Am. Chem. Soc. **88**, 1328 (1966).
4. N. FILIPESCU and J. M. MENTER. J. Chem. Soc. B, 616 (1969).
5. P. E. EATON and S. A. CEREFICE. J. Chem. Soc. Chem. Commun. 1494 (1970).
6. A. S. KUSHNER. Tetrahedron Lett. 3275 (1971).
7. J. S. MCKENNIS, L. BRENER, J. S. WARD, and R. PETTIT. J. Am. Chem. Soc. **93**, 4957 (1971).
8. A. P. MARCHAND and T-C. CHOU. J. Chem. Soc. Perkin Trans. 1, 1948 (1973).
9. J. R. SCHEFFER, K. S. BHANDARI, R. E. GAYLER, and R. A. WOSTRADOWSKI. J. Am. Chem. Soc. **97**, 2178 (1975).
10. J. R. SCHEFFER, B. M. JENNINGS, and J. P. LOUWERENS. J. Am. Chem. Soc. **98**, 7040 (1976).
11. R. N. WARRENER, I. W. MCCAY, and M. N. PADDON-ROW. Aust. J. Chem. **30**, 2189 (1977).
12. G. MEHTA, A. SRIKRISHNA, A. VEERA REDDY, and M. S. NAIR. Tetrahedron, **37**, 4543 (1981).
13. A. WEISZ, M. KAFTORY, I. VIDAVSKY, and A. MANDELBAUM. J. Chem. Soc. Chem. Commun. 18 (1984).
14. I. L. KLUNDT. Chem. Rev. **70**, 471 (1970).
15. P. G. SAMMES. Tetrahedron, **32**, 405 (1976).
16. Y. ITO, M. NAKATSUKA, and T. SAEGUSA. J. Am. Chem. Soc. **104**, 7609 (1982).
17. Y. ITO, Y. AMINO, M. NAKATSUKA, and T. SAEGUSA. J. Am. Chem. Soc. **105**, 1586 (1983).
18. M. PFAU, S. COMBRISSON, J. E. ROWE, JR., and N. D. HEINDEL. Tetrahedron, **34**, 3459 (1978).
19. M. PFAU, J. E. ROWE, and N. D. HEINDEL. Tetrahedron, **34**, 3469 (1978).
20. R. L. FUNK and K. P. C. VOLLHARDT. Chem. Soc. Rev. 41 (1980).
21. W. OPPOLZER. Synthesis, 793 (1978).
22. G. QUINKERT and H. STARK. Angew. Chem. Int. Ed. Engl. **22**, 637 (1983).
23. T. KAMETANI and F. FUKOMOTO. Med. Res. Rev. **1**, 23 (1981).
24. (*a*) B. H. HAN and P. BOUDJOUK. J. Org. Chem. **47**, 751 (1982); (*b*) G. M. RUBOTTOM and J. E. WAY. Synth. Commun. **14**, 507 (1984).
25. F. JUNG, M. MOLIN, R. VAN DEN ELZEN, and T. DURST. J. Am. Chem. Soc. **96**, 935 (1974).
26. J. L. CHARLTON and T. DURST. Tetrahedron Lett. **25**, 5287 (1984).
27. J. L. CHARLTON and T. DURST. Tetrahedron Lett. **25**, 2663 (1984).
28. M. F. ANSELL, B. W. NASH, and D. A. WILSON. J. Chem. Soc. 3012 (1963).
29. I. KUWAJIMA, T. MUROFUSHI, and E. NAKAMURA. Synthesis, 602 (1976).

Complexes of hybrid ligands. Pd^{2+} and Pt^{2+} complexes of new fluoro-alcohol thioether ligands; the use of thioether inversions to make structural assignments[1]

RENÉ T. BOERÉ AND CHRISTOPHER J. WILLIS

Department of Chemistry, The University of Western Ontario, London, Ont., Canada N6A 5B7

Received April 17, 1985

RENÉ T. BOERÉ and CHRISTOPHER J. WILLIS. Can. J. Chem. **63**, 3530 (1985).

The fluorinated alcohol–thioethers $RSCH_2C(CF_3)_2OH$ (R = Me, Ph) have been synthesized by the reaction of $RSCH_2Li$ with $(CF_3)_2CO$. By ionization of the fluoroalcohol group, these may act as bidentate, uninegative, ligands L^-. The presence of the soft thioether function in the hybrid ligand stabilizes the bond to the harder fluoro-alkoxy group, and complexes with soft transition metals are formed. Neutral complexes PdL_2 and PtL_2 have been synthesized, and, by the use of nmr, the geometry of the complexes is assigned as *cis* for Pt complexes, while both *cis* and *trans* are observed for Pd.

The barrier to inversion at coordinated thioether is studied by dynamic nmr, and observation of coalescence temperatures leads to values of $\Delta G‡$ of 73–74 kJ/mol for *cis*-PdL_2, 67–69 kJ/mol for *trans*-PdL_2, and 89 ± 1 kJ/mol for *cis*-PtL_2.

RENÉ T. BOERÉ et CHRISTOPHER J. WILLIS. Can. J. Chem. **63**, 3530 (1985).

On a synthétisé des thioéthers alcools fluorés, $RSCH_2C(CF_3)_2OH$ (R=Me, Ph), en faisant réagir du $RSCH_2Li$ sur la $(CF_3)_2CO$. Par ionisation du groupement fluoroalcool, ces composés peuvent agir comme des ligands, L^-, bidentates et mononégatifs. La présence, dans le ligand hybride, de la fonction thioéther molle permet de stabiliser la liaison avec le groupement fluoroalkoxy qui est plus dur et il y a formation de complexes avec les métaux de transition mous. On a synthétisé les complexes neutres PdL_3 et PtL_2 et, faisant appel à la rmn, on a établi que la géométrie des complexes du Pt est *cis* alors que, dans le cas des complexes du Pd, on retrouve des complexes *cis* ainsi que des complexes *trans*.

Faisant appel à la rmn dynamique, on a étudié la barrière à l'inversion au niveau des thioéthers coordonnées; l'observation des températures de coalescences permet d'établir les valeurs des $\Delta G‡$, qui sont 73–74 kJ/mol pour le PdL_2-*cis*, 67–69kJ/mole pour le PdL_2-*trans* et 89±1 kJ/mol pour le PtL_2-*cis*.

[Traduit par le journal]

Introduction

In previous studies on highly fluorinated alkoxides of transition elements, we have concentrated on bidentate or multidentate ligands in which the potential donor sites comprise one or more fluorinated alkoxy groups, $C(CF_3)_2O^-$, in conjunction with other hard donors coordinating through oxygen or nitrogen (2). Such ligands preferentially form stable complexes with the first-row transition metal ions of hard or intermediate character, but we have recently extended their range of application by the synthesis of a number of Pt^{2+} complexes in which the chelating perfluoropinacolato dianion, $^-OC(CF_3)_2C(CF_3)_2O^-$ (PFP^{2-}), is present in conjunction with soft coligands containing phosphine or thioether donors (3). Thus, alkoxides of metal ions which are soft acids in the Pearson HSAB classification (4) may be prepared, with the PFP^{2-} ligand imposing *cis*-geometry on $L_2M—O—C(CF_3)_2C(CF_3)_2—O$ (**1**, L = SR_2 or PR_3; M = Pd or Pt).

In this paper, we describe the synthesis and application of new "hybrid" ligands $RS—CH_2—C(CF_3)_2—OH$, (**2**, R = Me; **3**, R = Ph), in which the thioether function is combined with a highly fluorinated tertiary alkoxide in a molecule suitable for chelation to metals in a five-membered ring. Neutral bis-complexes of the deprotonated ligands may then be prepared:

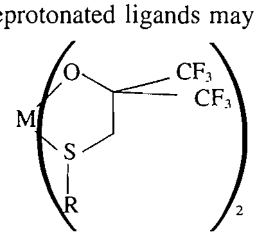

R = Me, M = Pd (**4**) or Pt (**5**); R = Ph, M = Pd (**6**) or Pt (**7**)

These complexes are capable of existing in either *cis* or *trans* geometrical isomers (using the terms with reference to the orientation of two soft donor sites). However, the presence of two pyramidal coordinated thioethers means that these geometric forms may each exist as diasteroeomeric pairs, the substituents on sulfur being either on the same side of the coordination plane ("*syn*") or on opposite sides ("*anti*"). From nmr studied reported here, we demonstrate that all four of these isomers coexist in the palladium complexes **4** and **6**, but that the platinum complexes **5** and **7** are found in the *cis*-form only under the conditions of the experiment. We have furthermore used dynamic nuclear magnetic resonance (DNMR) measurements to establish the relative barriers to inversion at coordinated sulfur in assigning the isomers. Although such inversion is a well-established phenomenon in thioether coordination chemistry (5 – 7), there has only been one previous example of its use as the primary means of assigning geometrical structures (8).

Experimental section

General information

Microanalysis was performed by Guelph Analytical Laboratories, Guelph, Ontario; all analytical data are in Table 1.[2] Solution molecular weights were determined by Malissa-Reuter Laboratories, West Germany. Infrared spectra were recorded on a Beckmann 4250 spectrometer, mass spectra on a Varian MAT 311A instrument, and nmr spectra on a Varian XL-100 spectrometer at 100.1 MHz for ^1H and 94.1 MHz for ^{19}F. Chemical shifts are reported from TMS or $CFCl_3$; positive shifts are downfield. Variable-temperature nmr spectra were recorded over the range −20 to +160°C; temperature settings of the spectrometer were checked with a Doric Trendicator 400 type T digital thermometer calibrated to ±0.5°C at the ice-point.

[1]Taken in part from ref 1(*a*). A preliminary account was presented in ref. 1(*b*).

[2]Table 1 may be purchased from the Depository of Unpublished Data, CISTI, National Research Council of Canada, Ottawa, Ont., Canada K1A 0S2.

Volatile compounds were manipulated on a conventional vacuum line. Glass apparatus and solvents were rigorously dried before use for ligand preparation. Air-sensitive materials were transferred using serum caps and syringes. *n*-Butyl lithium, thioethers, *N,N,N',N'*-tetramethylethylenediamine (TMED), and 1,4-diazabicyclo[2.2.2]-octane (DABCO) were commercial samples (Aldrich).

Ligand synthesis

(*i*) 2-Methylthio-1,1-bis(trifluoromethyl)ethanol, **2**. The procedure was based on that of Petersen (9), modified for handling the gaseous ketone. A 100 mL two-necked flask was attached to a stopcock arranged to permit alternate evacuation and pressurization (~10 cm Hg above atmospheric) with argon. It was equipped with a magnetic stirrer and serum cap, evacuated, and filled with dry argon. *n*-Butyl lithium (50 mL) in hexane solution (1.55 *M*, 78 mmol) was added by syringe, followed by 11.8 mL (78 mmol) of TMED. With stirring, dimethyl thioether (6.0 mL, 82 mmol) was added and the resulting white suspension stirred at 25°C for 4 h. Meanwhile anhydrous ether (75 mL) was introduced into a 250 mL two-necked RB flask equipped with magnetic stirrer and serum cap, the solvent outgassed and cooled to −196°C, then hexafluoroacetone (13.0 g, 78 mmol; Matheson) condensed in. The flask was warmed to −78°C in a CO_2/acetone cooling bath with stirring to dissolve hexafluoroacetone, then brought to atmospheric pressure with argon.

Using a 36" 16 gauge stainless-steel double-ended argon-filled needle extending through the serum caps, the lithium methyl − thioether suspension was transferred into the hexafluoroacetone solution at −78°C with continuous stirring. Reaction was vigorous at this temperature and a deep orange color appeared. Stirring was continued during 30 min at −78°C, then the suspension allowed to warm slowly to about 0°C, then poured into a mixture of concentrated HCl (100 mL) and ice (100 g). The product was extracted with ether, dried ($MgSO_4$) and distilled to give ligand **2**, bp 113°C/760 mm, 11.0 g (62% yield), characterized by analysis, mass spectrum (parent ion m/e = 228), and nmr ($CDCl_3$ solution; ^1H, s, δ = 4.46 (1 H); s, δ = 3.14 (2 H); s, δ = 2.20 (3 H) ppm; ^{19}F, s, δ = −78.14 ppm).

(*ii*) 2-Phenylthio-1,1-bis(trifluoromethyl)ethanol, **3**. The lithiation of thioanisole was carried out, using DABCO instead of TMED, according to the procedure of Corey and Seebach (10). THF was used as solvent throughout; other conditions, and workup, were the same as used in the preparation of **2**. The product **3** was distilled under vacuum (bp 60°C/1−2 Torr,); repeated distillation was necessary to remove traces of unreacted thioanisole, reducing the yield of pure product to 33%. Characterized by analysis, mass spectrum (parent ion m/e = 290), and nmr ($CDCl_3$ solution, ^1H m, δ = 7.24 − 7.46 (5 H); s, δ = 4.29 (1 H); s, δ = 3.54 (2 H) ppm; ^{19}F, s, δ = −77.5 ppm).

For convenient reference, the anionic forms of the ligands will be abbreviated in this paper to Me—S—O^- and Ph—S—O^-.

Preparation of complexes. (*i*) Reactions using 2-thiomethyl-2,2-bis(trifluoromethyl)ethanol, **2**.

The palladium complex was prepared by dissolving $PdCl_2$ (0.200 g, 1.13 mmol) in dimethylformamide (DMF, 40 mL) and adding ligand **2** (0.52 g, 2.26 mmol) followed by the stoichiometric amount of KOH (2.26 mmol) in ethanol. (In this and the following reactions, it was found convenient to measure out KOH volumetrically using a standardized solution, about 0.09 *M*, in ethanol.) Precipitated KCl was removed by centrifugation and the orange-red solution stirred 15 h, then solvents removed by vacuum evaporation at 25°C, and the residue extracted with acetone. Crystallization from ether gave the palladium bis-complex, Pd(Me—S—O)$_2$, **4**, as orange platelets, mp 199−201°C.

The platinum analogue was prepared by dissolving K_2PtCl_4 (1.01 g, 2.43 mmol) in DMF (50 mL) and adding ligand **2** (1.11 g, 4.90 mmol) followed by KOH (4.90 mmol) in ethanol, After stirring 6 days/25°C, precipitated KCl was removed, then solvents removed by vacuum evaporation at 25°C. The residue was extracted with warm acetone, the solution reduced in volume and chloroform added to precipitate the platinum bis-complex, Pt(Me—S—O)$_2$, **5**. Recrystallization from acetone/chloroform gave a pale yellow solid whose infrared spectrum showed the presence of water. An anhydrous analytical sample was obtained by vacuum sublimation at ~200°C.

(*ii*) Reactions using 2-phenylthio-2,2-bis(trifluoromethyl)ethanol, **3**. The palladium bis-complex, Pd(Ph—S—O)$_2$, **6**, was prepared by the same route as its methylthio analogue; pale orange platelets from ether, mp 198−199°C.

The platinum bis-complex, Pt(Ph—S—O)$_2$, **7**, was prepared by the same route as its methythio analogue, except that CH_2Cl_2 was used for the extraction of the solid residue and the product recrystallized from chloroform/acetone to give the complex as yellow needles, mp 190−191°C.

Characterization

Analytical data are given in Table 1.[2] All of the new complexes had infrared spectra consistent with their proposed structures. Mass spectra showed a parent ion for each neutral complex and similar fragmentation patterns. In order to eliminate the possibility of spurious nmr data resulting from association of the complexes ML_2, molecular weights for **4** and **5** were determined osmometrically in acetone. Three different concentrations in the range 0.006 to 0.03 *M* were used in each case, and results showed no significant association or concentration dependence of mw. (Found for **4**: 547 ± 8, calcd. 528. Found for **5**: 653 ± 7, calcd. 617.) Nuclear magnetic resonance spectra, which formed the principal means of characterization and structure determination, are discussed in detail below.

Results and discussion

Ligand synthesis

The lithium derivatives of thioethers have been extensively studied by Petersen and co-workers (9). We have restricted our study to derivatives of methyl-thioethers R—S—CH_3, where the CH_3 group is lithiated, but the reaction is capable of wide variation both in the nature of the R group and through the lithiation of alkyl groups other than methyl. However, little use has been made of these reagents for introducing a thioether function into a potential ligand system. In view of the highly electrophilic nature of hexafluoroacetone, we had little doubt that it would react with the intensely nucleophilic lithium derivatives of the thioethers. These are prepared by the deprotonation of methyl thioethers using *n*-butyl lithium in the presence of multidentate nitrogen bases:

$$\mathrm{CH_3\text{-}S\text{-}R} + {}^{n}\mathrm{Bu\text{-}Li} \xrightarrow[\text{hexane, 25°C}]{\text{(B)}} \mathrm{LiCH_2\text{-}S\text{-}R(B)} + \mathrm{C_4H_{10}}$$

$$\Big\downarrow \;\; (1)\ \mathrm{(CF_3)_2CO} \quad (2)\ \mathrm{H^+/H_2O}$$

$$\mathrm{HO\text{-}C(CF_3)_2\text{-}CH_2\text{-}S\text{-}R}$$

[(B) = TMED or DABCO]

We find that reaction of these lithium reagents with hexafluoroacetone is extremely vigorous, and cooling to dry-ice temperature is essential to obtain good yields of the fluorinated alcohol−thioethers. Choice of solvent is important in these syntheses because of the tendency of fluorinated alcohols to form stable complexes with some ethers. Ligand **2** was prepared in diethyl ether; ligand **3** in THF.

Our principal aim in the study reported in this paper was to prepare neutral complexes in which two molecules of the bifunctional ligand (in the ionized form) are coordinated to a dipositive metal atom. The divalent ions of the nickel triad were used in an attempt to make square-planar complexes. The synthetic approach initially used was that which had been successful in previous preparations of fluorinated alkoxides of transition metals; the addition of base to a 2:1 mixture of ligand and metal chloride in ethanol solution. With Ni^{2+}, an inter-

TABLE 2. Nuclear magnetic resonance data on complexes[a]

			CF₃ groups			CH₂ group			R—S	
t Compound	Solvent[b]	T (°C)	δ (ppm)	Δ_{AB} (Hz)	J_{AB} (Hz)	δ (ppm)	Δ_{AB} (Hz)	J_{AB} (Hz)	δ (ppm)	^3J(Pt,H) (Hz)
$Pt(Me—S—O)_2$, **5**										
cis–syn (48%)	A	32	−76.0	126	9.8	3.49	29.6	14.5	2.89	52.9
cis–anti (52%)	A	32	−75.9	58	9.3	3.51	23.2	14.0	2.93	54.7
cis–syn	D	32	[c]	121	9.75				2.72	53.5
cis–anti	D	32		62	9.75				2.80	56.0
cis	D	146		~100 (broad d)					2.76	53.0
$Pt(Ph—S—O)_2$, **7**										
cis–syn (54%)	A	32	−75.8	145	9.5	3.68	55	14	7.1–8.2	
cis–anti (46%)	A	32	−75.5	~35	~9	3.74	47	13		
cis–syn	D	32		157	9.5	3.69	74	14	7.1–8.1	
cis–anti	D	32		60	~9	3.76	70	13.5		
$Pd(Me—S—O)_2$, **4**										
cis–syn (24%)	A	0	−75.2	74	10				2.78	
cis–anti (34%)	A	0	−75.0	~4	—				2.82	
trans–syn (23%)	A	0	−75.8	81	9.7				2.69	
trans–anti (19%)	A	0	−75.4	0	—				2.75	
cis–syn (~21%)	A	32	−76.07	71.5	9.75	3.54	32.4	13	2.77	
cis–anti (~29%)	A	32	−76.04	~5	—	3.60	19.3	13	2.81	
trans (~50%)	A	32	(obscured)			(obscured)			2.71	
cis (38%)	A	65	(broad singlet)			(broad d of d)			2.78	
trans (62%)	A	65				3.42 (coalesced)			2.71	
cis–syn	D	30		61	9.5					
cis–anti[d]	D	30		7	—					
cis–syn	D	50				3.53	28	13	2.60[e]	
cis–anti	D	50				3.59	13.3	13	2.66	
trans	D	50				3.45 (broad s)			2.60[e]	
cis	D	110				3.53 (broad s)			2.64	
trans	D	110				3.42 (broad s)				
$Pd(Ph—S—O)_2$, **6**										
cis–syn	A	32	−75.7	133	9.5	3.75	50	13.0	7.3–8.2	
cis–anti	A	32	~−75.7	~5	—	3.87	35.7	14.0		
trans	A	32	−75.7	s (W^f = 7.5 Hz)			(broad s[g])			
cis–syn	D	32		143	~9	3.77	69.4	15		
cis–anti	D	32		~7	—	3.86	49.8	13		
trans	D	32		s (W^f = 3 Hz)			(broad s[h])			

[a]Chemical shifts from TMS (¹H) or $CHCl_3$ (¹⁹F). See text for assignment of isomers. Most CH_2 spectra have been assigned *only* on the basis of integrations relative to the identified CH_3 or CF_3 signals.
[b]A = d_6–acetone, D = d_6-dimethyl sulfoxide.
[c]No $CFCl_3$ standard was added to DMSO solutions intended for high-temperature studies.
[d]No *trans*-isomer observed.
[e]Overlapping peaks.
[f]W is the width at half-height in Hz.
[g]Singlet at 3.69 ppm at 60°C.
[h]Singlet at 3.76 ppm at 80°C.

action appeared to be occurring, but well-defined products could not be isolated. By employing dimethylformamide as solvent for the metal halides, stable, well-characterized, Pd^{2+} and Pt^{2+} complexes were obtained. The preferential formation of stable complexes with the heavier metals of the triad indicates the dominant effect of the soft thioether function in the O_2S_2 donor set.

Nuclear magnetic resonance studies and the identification of isomers

The nmr spectra of all four complexes have been obtained in d_6-acetone and d_6-DMSO (the latter for high-temperature work); sufficient concentrations could not be obtained with less polar solvents. The data are summarized in Table 2; the spectra are strongly temperature-dependent, and data are generally given for the limits of slow and fast exchange, unless further detail is warranted (as with compound **4**).

For the complex $Pt(Me—S—O)_2$, **5**, it is immediately apparent from both ¹H and ¹⁹F spectra at ambient temperature that two isomers are present. The $CH_3—S$ signals are at 2.93 and 2.89 ppm, with ^3J(Pt,H) values of 54.7 and 52.9 Hz, respectively. The similarity in the values of the coupling constants shows that these species are not due to *cis–trans* isomerism of the O_2S_2 donor set, which should give a large difference in ^3J. For example, in the complex $PtCl_2(SMe_2)_2$ the values of ^3J(Pt,H) are 49.0 and 40.0 Hz for the *cis* and *trans* isomers respectively (11). The two isomers of **5** therefore differ only in the orientation of the Me—S groups.

The ^{19}F spectrum consists of two sets of doublets of quartets, indicating non-equivalent CF_3 groups in each isomer; this would be expected from the presence of the pyramidal coordinated thioether in the chelate ring. Coupling constants between fluorine atoms in each set are in the range 9–10 Hz, typical for geminal CF_3 groups.

The suggestion that these two forms of the complex are diastereomers related by inversion at the thioether ligand is supported by variable-temperature nmr studies. When a solution in d_6-DMSO is heated, the separate CH_3—S signals collapse and coalesce together around 128°C, and further heating to 146°C produces a sharp singlet. The ^{195}Pt satellites remain throughout, showing that the thioether remains coordinated to the metal. Behaviour of this type is typical of a complex in which inversion at the thioether ligands is becoming rapid on the nmr time-scale, leading to effective equivalence of the CH_3—S groups. The same trend is apparent in the ^{19}F spectra, but the coalescence temperature is higher (because of the greater value of the chemical shift difference for the CF_3 groups) and cannot be reached before significant sample decomposition has occurred.

In the phenyl-containing complex, $Pt(Ph—S—O)_2$, **7**, the nmr data are less informative because of the absence of the CH_3 probe with its associated coupling to ^{195}Pt. However, the ^{19}F signals for **7** are entirely analogous to those of **5**, consisting of one well-separated doublet of quartets, and another which has strong second-order character. We interpret this to mean that **7** also exists as two diasteromers of a single geometric isomer. Because of the greater solubility of this complex, well-resolved ligand resonances were observed in both d_6-acetone and d_6-DMSO solutions, and these are clearly attributable to two overlapping AB type resonances. On heating the solutions, decomposition occurred before coalescence had been reached in either the fluorine or proton (CH_2 region) spectra. At no point in the variable-temperature nmr studies, below or above ambient temperature, was any evidence seen for a third species.

The situation for the palladium complex **4** is quite different. Variable-temperature ^1H spectra at equilibrium are presented in Fig. 1.

Both ^1H and ^{19}F spectra are strongly temperature-dependent, but is is clear that there are four separate $—SCH_3$ resonances at 0°C, labelled 1–4; on warming to ambient temperature, the signals labelled 3 and 4 collapse to a broad singlet. Our interpretation of this spectrum has been assisted by its time-dependence at 32°C. In a freshly-prepared solution in d_6-acetone, the peaks labelled 1 and 2 are present in a 60:40 ratio, and the CH_2 region can be clearly identified as two overlapping AB signals (Table 2), giving a situation parallel to that of the platinum complex **5**. The peak labelled 3,4 is extremely small if the spectrum is recorded immediately after sample dissolution. After about 1 h, the equilibrium spectrum of Fig. 1 is attained, and the CH_2 region becomes obscured by the presence of a broad resonance associated with 3,4. Cooling produces the lower trace in the figure, while warming to 65°C causes 1 and 2 to coalesce, and alters the proportions of the isomers. The ^{19}F spectra show similar behaviour, with freshly-prepared samples showing two sets of doublets of quartets, one with a large value of Δ_{AB} and the other a very small value. On equilibrating and cooling to 0°C, signals corresponding to four species are observed.

These observations may be rationalized on the assumption

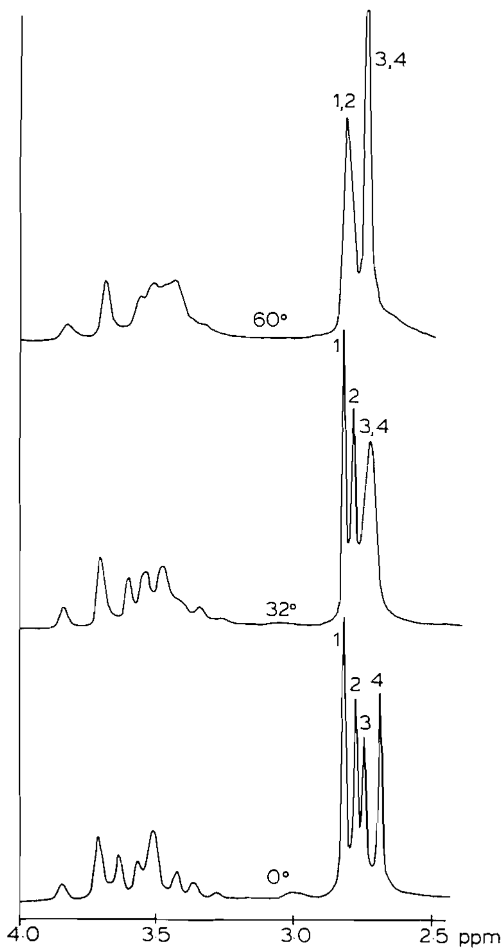

FIG. 1. Variable-temperature ^1H spectra of $Pd(Me—S—O)_2$, **4**.

that $Pd(Me—S—O)_2$ exists in solution as an equilibrium mixture of the four possible isomers: *cis–syn*, *cis–anti*, *trans–syn*, and *trans–anti*. We have previously demonstrated, in PFP^{2-} complexes of type **1**, that the *trans* effect of the $—C(CF_3)_2O^-$ group on the barrier to thioether inversion is considerably less than that of chloride (3). For example, in the SEt_2 complex $Pt(PFP)(SEt)_2$, $\Delta G‡$ is 75.5 kJ mol^{-1}, whereas in *cis*- and *trans*-$PtCl_2(SEt_2)_2$ $\Delta G‡$ values of 70.3 and 58.2 kJ mol^{-1}, respectively, have been reported (12). Assuming the validity of this *trans*-effect series for palladium, we would expect the *trans*-form of **4** to have the lower coalescence temperature for thioether inversion. This conclusion also depends on the relative separation of the signals in the two isomers, and we have calculated the actual values of $\Delta G‡$ (see below), which are in the expected order. We therefore assign peaks 1 and 2 in the figure to the *cis*-geometrical isomer, while 3 and 4 are diastereomers of the *trans*-isomer.

Complex **4** is thus probably *cis* in the solid state, undergoing rapid equilibration on dissolution in acetone to give the equilibrium *cis–trans* mixture. The proportion of *trans* increases from 40% at 0°C to 62% at 65°C, giving a ΔH value of 10.6 kJ mol^{-1} for the *cis*→*trans* interconversion.

Because of the greater chemical shift of the CH_2 and CF_3 spectra, their signals broadened but did not coalesce at 65°C, the highest temperature obtainable in acetone solution. When spectra were run in DMSO in order to reach higher temperatures, an immediate difference was observed in the behaviour of the complex: no signal for the *trans*-isomer appeared at ambient temperature. However, additional signals assignable to the *trans*-isomer (undergoing rapid *syn*−*anti* isomerization) began to appear at 50°C in the CH_3—S, CH_2, and CF_3 regions of the spectra. At 90°C, the ^{19}F spectrum consisted of a very broad coalesced peak for the *cis*-isomer and a sharp singlet for *trans*. By 110°C, the CH_2 region still showed separate peaks for *cis* and *trans*, but the CH_3—S signal had collapsed to a singlet, indicating rapid interconversion of all four isomers. The CH_2 signal also coalesced at higher temperature, but sample decomposition interfered with further measurements.

In view of the small differences in energy between the various isomers of complex **4**, it is not surprising that their proportions in the mixture are solvent-dependent. The preferential formation of the *cis*-isomer in going from acetone to DMSO would be expected from the greater polarity of the latter (13).

Assignment of the diastereomers

We have demonstrated that Pd(Me—O—S)$_2$, **4**, exists as a mixture of *cis*- and *trans*-isomers, and that the *cis*-isomer is thermodynamically the more stable form. On the basis of the barrier heights to inversion, $\Delta G\ddagger$, and the magnitude of the coupling ^3J(Pt,H) for **5**, in conjunction with our previous studies of PFP^{2-} complexes of Pt^{2+} with thioethers (3), we suggest that the sole isomeric species for **5** and **7** is in each case the *cis*-isomer. Complex **5** therefore consists of *cis*−*syn* and *cis*−*anti* isomers, and their approximately equal populations at ambient temperature show that there is little difference in energy between them. Assignment of the *syn* and *anti* forms cannot be made with certainty, but the spectra provide some evidence.

Consideration of molecular models shows a significant degree of steric interaction between the CH_3—S groups in the *syn*-isomer, which is minimized by the adoption of an "overall-envelope" configuration; that is, both of the chelate rings are in an envelope configuration on the same side of the coordination plane of the metal and opposed to the two R—S substituents. This locks the rings into a specific orientation which increases the difference in the environment of the pseudo-axial and -equatorial CF_3 groups, resulting in a larger difference in chemical shift, Δ_{AB}, between them. No such restraint applies in the *anti*-isomer, and the difference in environment between the CF_3 groups is therefore smaller. Since one species shows a value of 126 Hz for Δ_{AB} and the other of only 58 Hz, we assign the former as *cis-syn* and the latter as *cis*−*anti*. Similar steric arguments have been used by Abel to assign isomers of chelating dithioether complexes (14).

We have assigned the *syn*- and *anti*-forms of Pt(Ph—S—O)$_2$ on the same basis. The species with the larger value of Δ_{AB} for the CF_3 groups is assigned as the *cis-syn* form, the other as the *cis*−*anti*. For both **5** and **7**, the ^1H spectra have been tentatively assigned *from* the ^{19}F spectra using relative integration.

For the palladium complexes **4** and **6**, we have used the same configurational reasoning to assign the *syn* and *anti* forms of the *cis*-isomer as shown in Table 2. Such an assignment suggests a slight preference for the anti configuration in the temperature range studied, consistent with our postulate of greater steric repulsion for the *syn* form. However, the differences are not large, and no great weight can be attached to these results.

For the *trans*-isomer of **4** at 0°C, the ^{19}F spectrum indicates one species with equivalent CF_3 groups ($\Delta_{AB} = 0$), while the other is separated into quartets ($\Delta_{AB} = 81$ Hz). In this geometric form, the *anti*-isomer has the higher symmetry, and is more likely to correspond to the singlet CF_3 resonance. The ^1H spectra are tentatively assigned by integration, and in each case the *anti* configuration has CH_3—S resonances slightly to low field of the *syn*.

For the complex Pd(Ph—S—O)$_2$, **6**, the nmr spectra give less information because of the absence of the CH_3—S probe. At ambient temperature, the ^{19}F spectra in both acetone and DMSO shows three sets of signals, which may be analyzed in a similar manner to those of previous complexes studied. A doublet of quartets with a large value of Δ_{AB} (133 Hz) may be assigned to the *cis*−*syn* isomer, while a second-order multiplet with Δ_{AB}(effective) = ~5−7 Hz is assigned to the *cis*−*anti* isomer. The *trans*-isomer consists of a rapidly-inverting *syn*−*anti* mixture giving a sharp singlet; the proportion of the *trans*-isomer is ~30% in acetone and ~15% in DMSO.

The CH_2 region of the spectrum of **6** may be analyzed in terms of AB doublets as before. At ambient temperature in acetone, the signal for the *trans*-isomer is not observed because of exchange broadening, but it appears as a singlet at 3.69 ppm at 60°C. In DMSO, the spectra in this region are similar. The signals from the *cis*-isomers coalesce on heating, and an average singlet due to *syn*−*anti* interconversion is seen at 80°C; the *cis*/*trans* ratio is approximately 70/30.

Thioether inversion studies

Inversion at a single sulfur atom in complexes **4** and **5** will result in the interconversion of the diastereomeric isomers. Since these are species with different energies and populations, the process is classified as *non-mutual inversion*, and it may be followed by dynamic nmr. We have discussed the treatment of data previously in connection with perfluoropinacol−thioether complexes (3), and a comprehensive account is given by Sandström (15).

The rate constants for the major—minor (k_A) and minor—major (k_B) interconversion reactions may be estimated from the half-height linewidths at coalescence, w^*, using the equations:

$$k_A = P_A \frac{2\pi w^*}{X} \qquad k_B = P_B \frac{2\pi w^*}{X}$$

where the factor X depends on the ratio of the populations of the two forms, P_A and P_B. From the rate constants, the free energy of activation, $\Delta G\ddagger$, may then be found using the Eyring equation. Since $\Delta S\ddagger$ has consistently been found to be equal to zero or near zero for thioether inversion (16), little error is incurred by comparing $\Delta G\ddagger$ at different temperatures for different molecules. The calculations and results are summarized in Table 3.

The populations P_A and P_B are, as much as possible, extrapolations from the observable low-temperature region to the coalescence point. In the Pt complex **5**, the populations at T_c become fortuitously equal, so the classical equation of Gutowsky and Holm (17) has been used to obtain k ($=k_A = k_B$).

We are now able to justify the assignment of the stereochemistry of the complexes. Considering first the thioether inversion energies in Table 3, it is clear that, for the *cis*-isomer of the Pd complex **4**, the barrier to inversion is lower than in the *cis* Pt complex **5**. This is a general effect; for example, differences of 9 kJ mol^{-1} have been observed between Pd and Pt for the complexes MX_2L_2, where L is a monodentate cyclic thioether (18), 10−15 kJ mol^{-1} for various chelating dithioether complexes of PdX_2 and PtX_2 (14), and 5 kJ mol^{-1} for *trans*-$MX_2[S(CH_2SiMe_3)_2]_2$ (19). In each case, the barrier is lower for Pd than for Pt. In the following discussion, we adopt the classical mechanism of pyramidal inversion, with a planar

TABLE 3. Thioether inversion in $M(Me—S—O)_2$ complexes

Complex	*cis*-Pd(Me—S—O)$_2$, **4**	*trans*-Pd(Me—S—O)$_2$, **4**	*cis*-Pt(Me—S—O)$_2$, **5**
P_A	0.58[a]	0.54[b]	0.50
P_B	0.42[b]	0.46[a]	0.50
Δ_P	0.16	0.08	0
x	1.822	1.668	—
w^*, Hz	4.0	~5	9.0
k_A,[c] s^{-1}	5.8	8.7	20
k_B[d] s^{-1}	8.0	10	—
T_C, K	322±5	305±5	401±5
$\Delta G‡_A$, kJ mol^{-1}	74±1	69±1	89±1
$\Delta G‡_B$, kJ mol^{-1}	73±1	67±1	—

[a]*syn*-isomer.
[b]*anti*-isomer.
[c]Rate constant for conversion from major to minor.
[d]Rate constant for conversion from minor to major.

transition state, which has long been proposed for the inversion of tri-coordinate compounds of nitrogen, sulfur, and other main-group elements (20, 21). This model has recently come to be adopted for compounds of transition elements (5, 6). Two factors may be invoked to explain the lower barriers to inversion in Pd^{2+}. The first is the difference in electronegativity between the two metals: values are 1.44 for Pt and 1.35 for Pd (22). An increase in the electronegativity of the atom bonded to sulfur in a thioether complex increases the *s*-character of the remaining lone pair on the sulfur atom in the ground state, thus raising the barrier to inversion (20). A second factor, operating in the same direction, is that the stability of the intermediate with planar sulfur is increased by the more efficient π-overlap between S and Pd ($3p-4d$) than between S and Pt ($3d-5d$). A much smaller difference has been reported between isostructural chromium(0) and tungsten(0) complexes, for which these two factors work in opposite directions (6).

When a thioether function is incorporated into a chelate ring, there is generally an increase in the barrier to inversion. This probably occurs because there is a greater departure from the ideal 120° angle in the transition state when the sulfur atom is in a ring. A comparison of data on the Pt complex **5** with other complexes containing similar donor sets supports this trend. Our results on perfluoropinacolato (PFP^{2-}) complexes of Pt give $\Delta G‡$ values of 75.5 ± 1 kJ mol^{-1} for $Pt(PFP)(SEt_2)_2$, where the thioether is not chelated, and 86.5 ± 1 kJ mol^{-1} for Pt(PFP)(DTH) (3). Precise structural data are not available for the latter, but a reasonable estimate for the bond angle at sulfur in chelated dithiahexane, based on known values for chelated thioethers (7), would be 104°. In related Pt complexes of $Me—S—O^-$, we have found bond angles at sulfur averaging 97° (23). The value of $\Delta G‡$ is thus found to increase as the size of the chelate ring is reduced, due to an angle-strain effect on the transition state. Thus $\Delta G‡$ is about 13 kJ higher for the Me—S—O ring than for the unstrained SEt_2 complex of PFP^{2-}. From the series quoted earlier, a difference of 18 kJ is found between similar complexes where R_fO^- and R_2S are *trans* to a thioether. The hypothetical $\Delta G‡$ for *trans*-Me—S—O would thus be about 70 kJ. Thus predicted thioether inversion barriers allow us to assign the *cis* geometry to these complexes.

Precedent would suggest that *cis* geometry is more likely for an O_2S_2 donor set on platinum. The bis(monothio-β-diketonates) of both Pd^{2+} and Pt^{2+} are known to be *cis* (24), as is $(CH_3COO)_2Pt(SEt_2)_2$ (8). Values of ^3J(Pt,H) for the CH_3—S groups in **5** are fully consistent with *cis* geometry, which would of course place them *trans* to the fluorinated alkoxy groups. In the perfluoropinacol complex $Pt(PFP)(SMe_2)_2$, which has the same donor set on the metal in unambiguously *cis* geometry, ^3J is 44.0 Hz (3). However, other results show that the coupling to ^{195}Pt is often increased when the thioether is incorporated into a chelate ring. For example, in the 2,5-dithiahexane complex Pt(PFP)(DTH), ^3J is increased to 47–48 Hz (3). In related studies on other chelated Pt(Me—S—O) complexes (25), ^3J is 60.5 Hz for CH_3—S *trans* to Cl^-, 50.0 Hz *trans* to SEt_2, and ~41 Hz *trans* to phosphines. We have demonstrated that the $—C(CF_3)_2O^-$ group has a *trans* influence intermediate between Cl^- and R_2S (3), so the ^3J values of 53–55 Hz observed in $Pt(Me—S—O)_2$ are in the expected region for *cis* geometry. The value of ^3J has been shown to vary in a Karplus-type manner in $PtCl_2\{S(CH_2Ph)_2\}_2$, with $J(trans) \approx 55.7$ Hz and $J(gauche) \approx 29.3$ Hz (12). In complexes of S-methyl-cysteine, containing an S,N-coordinated five-membered ring, ^3J was found to be ~55 Hz with Cl^- *trans* to the S—CH_3 function and 44–51 Hz with NH_3 or en *trans* (26).

In the palladium complexes, the differences between the activation energies for thioether inversion of the *cis*- and *trans*-forms are only 5 to 6 kJ mol^{-1}. This is much less than for the platinum complexes discussed above, implying that ring effects may make a larger contribution to the size of $\Delta G‡$ than *trans*-effects. However, the absolute range of $\Delta G‡$ values for Pd are found to be much smaller, and these smaller differences are fully consistent with those of other palladium complexes which we have studied (25).

Conclusions

The use of the new hybrid ligands has enabled us to prepare some interesting analogues to the earlier type **1** complexes. We have demonstrated that the Pt^{2+} complexes **5** and **7** exist as syn and anti forms of the *cis*-isomer on the basis of the calculated ΔG values and the size of the coupling constants in **5**. Similarities in the ^{19}F spectra then allow us to transfer to the latter conclusions reached for the former. The observation of *cis*–*trans* isomerism for the Pd^{2+} complexes, with the *cis*-isomer being more stable, supports our contention that the platinum complexes must be *cis*, in agreement with the greater influence of antisymbiosis in the softer metal ion (4).

The presence of two independent nmr probes, ^1H and ^{19}F, has also enabled us to attempt assignments of the diastereomers in solution; although not definitive in every case, this has shown the potential of using multinuclear nmr in making structural assignments of coordination compounds.

Acknowledgement

We are grateful for financial support of this work provided by the Natural Sciences and Engineering Research Council of Canada through an operating grant to C.J.W. and a post-graduate scholarship to R.T.B.

1. R. T. BOERÉ, Ph.D. thesis, University of Western Ontario. 1984; (*b*) 10th International Symposium on Fluorine Chemistry, Vancouver, B.C. 1982. J. Fluorine Chem. **21**, 18 (1982).
2. E. KONEFAL, S. J. LOEB, D. W. STEPHAN, and C. J. WILLIS. Inorg. Chem. **23**, 538 (1984), and references therein.
3. R. T. BOERÉ and C. J. WILLIS. Inorg. Chem. **24**, 1059 (1985).
4. R. G. PEARSON. Inorg. Chem. **12**, 712 (1973).
5. E. W. ABEL, G. W. FARROW, K. G. ORRELL, and V. SIK. J. Chem. Soc. Dalton Trans. 42 (1977).
6. E. W. ABEL, G. D. KING, K. G. ORELL, and V. SIK. Polyhedron, **2**, 1363 (1983).
7. S. G. MURRAY and F. R. HARTLEY. Chem. Rev. **81**, 365 (1981).
8. J. KUYPER. Inorg. Chem. **18**, 1484 (1979).
9. (*a*) D. J. PETERSON. J. Org. Chem. **32**, 1717 (1967); (*b*) D. J. PETERSON. Organomet. Rev. A, **7**, 295 (1972).
10. E. J. COREY and D. SEEBACH. J. Org. Chem. **31**, 4097 (1966).
11. R. ROULET and C. BARBEY. Helv. Chim. Acta, **56**, 2179 (1973).
12. P. HAAKE and P. C. TURLEY. J. Am. Chem. Soc. **89**, 4611 (1967); **89**, 4617 (1967).
13. J. A. DEAN (*Editor*). Lange's Handbook of Chemistry. 12 ed. McGraw-Hill, New York. 1972. pp 5–45.
14. E. W. ABEL, S. K. BHARGAVA, K. KITE, K. C. ORRELL, V. SIK, and B. C. WILLIAMS. Polyhedron, **1**, 289 (1982).
15. J. SANDSTRÖM, Dynamic NMR spectroscopy. Academic Press, New York. 1982. p 77.
16. (*a*) R. L. BATSONE-CUNNINGHAM, H. W. DODGEN, J. P. HUNT, and D. M. ROUNDHILL. J. Chem. Soc. Dalton Trans. 1473 (1983); (*b*) E. W. ABEL, G. D. KING, K. G. ORRELL, and V. SIK. Polyhedron, **2**, 1363 (1983).
17. H. S. GUTOWSKY and C. H. HOLM. J. Chem. Phys. **25**, 1228 (1956).
18. E. W. ABEL, M. BOOTH, and K. G. ORRELL. J. Chem. Soc. Dalton Trans. 1994 (1979).
19. E. W. ABEL, G. W. FARROW, K. G. ORRELL, and V. SIK. J. Chem. Soc. Dalton Trans. 47 (1977).
20. J. M. LAMBERT. Top. Stereochem. **6**, 19 (1971).
21. A. RAUK, L. C. ALLEN, and K. MISLOW. Angew. Chem. Int. Edn. **12**, 712 (1970).
22. E. J. LITTLE and M. M. JONES. J. Chem. Educ. **37**, 231 (1960).
23. R. T. BOERÉ, N. C. PAYNE, and C. J. WILLIS. Unpublished results.
24. (*a*) S. E. LIVINGSTONE. Coord. Chem. Rev. **7**, 59 (1971); (*b*) E. A. SHUGAN *et al.* J. Struct. Chem. **8**, 490 (1967); (*c*) M. DAS. Inorg. Chim. Acta, **36**, 79 (1979).
25. R. T. BOERÉ and C. J. WILLIS. To be published.
26. L. E. ERICKSON, J. W. MCDONALD, J. K. HOWIE, and R. P. CLOW. J. Am. Chem. Soc. **90**, 6371 (1968).

Comment: Discussion on ^{13}C nuclear magnetic resonance spectra of nucleoside derivatives. Reflection of structural alterations on ^{13}C chemical shifts

JUN UZAWA AND KENTARO ANZAI[1]

The Institute of Physical and Chemical Research, Wako-shi, Saitama 351, Japan

Received April 30, 1985

(Ref.: Can. J. Chem. **62**, 1555 (1984))

Ambiguity in assigning C2′ and C3′ of the ribose residue of nucleic acid compounds in ^{13}C nmr spectra was pointed out in 1972 by Stothers (1), and the early assignments of C2′ and C3′ by Jones *et al.* (2) were revised by Mantsch and Smith (3) based on $^{31}POC^{13}C$ coupling in nucleotides. The usefulness of selective ^{1}H-decoupling was shown by Kainosho (4) using 2′,3′- or

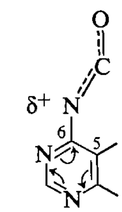

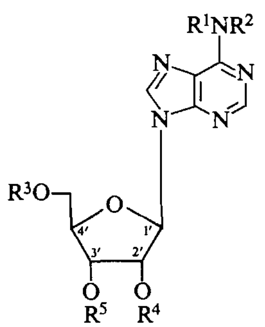

1 R¹, R², R³, R⁴, R⁵ = H
2 R¹, R² = H, R³ = *p*-$CH_3C_6H_4CO$
R⁴, R⁵ = $(CH_3)_2C<$
3 R¹ = H, R², R³ = *p*-$CH_3C_6H_4CO$
R⁴, R⁵ = $(CH_3)_2C<$
4 R¹, R², R³ = *p*-$CH_3C_6H_4CO$
R⁴, R⁵ = $(CH_3)_2C<$

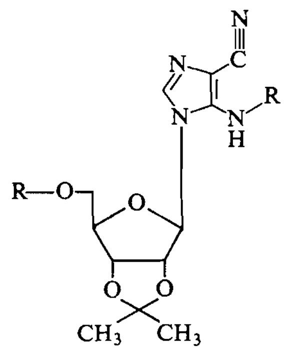

5 R = *p*-$CH_3C_6H_4CO$

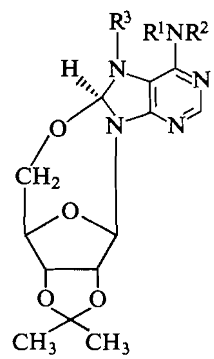

6 R¹ = H
R², R³ = C_6H_5OCO
7 R¹, R², R³ = C_6H_5OCO

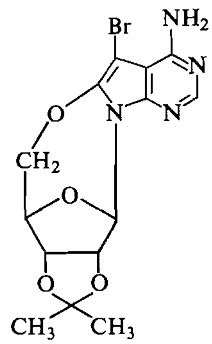

8

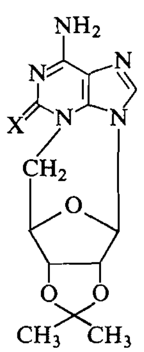

9 X = O
10 X = NH

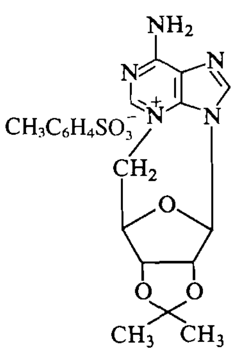

11

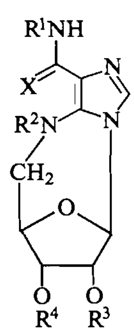

12 R¹, R², R³, R⁴ = H
X = NH
13 R¹ = C_6H_5CO, R² = H
R³, R⁴ = $(CH_3)_2C<$
X = NH
14 R¹, R², R³, R⁴ = H
X = O
15 R¹ = C_6H_5CO, R² = CHO
R³, R⁴ = $(CH_3)_2C<$
X = O

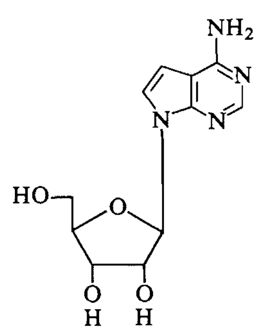

16

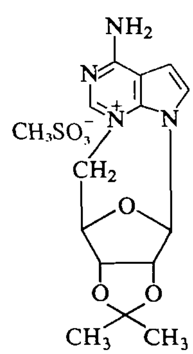

17

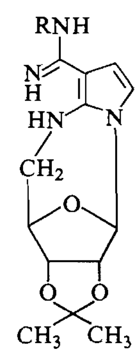

18 R = C_6H_5CO

[1]Author to whom correspondence may be addressed.

TABLE 1. ^{13}C chemical shifts of nucleosides and cyclonucleosides related to adenosine ($^{1}J_{C,H}$)

Carbon	Compound 1	2	3	4	5	6	7	8	9	10	11	12	13	14	15	16	17	18
2	152.6	152.8	151.5	152.0	—	154.6	153.8	151.7	155.5	116.9	149.1	—	—	—	—	151.7	149.2	—
	(197.8)	(200.0)	(206.3)	(208.7)		(205.1)	(206.3)	(200.2)			(215.8)					(197.7)	(213.8)	
4	149.2	148.8	150.7	152.0	133.4	156.6	156.0	144.0	141.9	145.5	140.4	144.1	135.7	143.9	131.7	150.0	138.9	147.4
5	119.5	119.3	125.7	126.4	109.5	111.0	117.2	98.8	113.3	113.3	119.5	112.0	115.4	115.8	127.3	103.3	104.7	100.0
6	156.3	156.2	150.7	152.0	113.7	142.1	138.3	156.1	158.4	163.8	156.5	158.6	163.1	166.5	159.1	157.7	158.3	165.0
7	—	—	—	—	—	—	—	70.2	—	—	—	—	—	—	—	99.7	103.1	103.0
																(177.0)	(181.6)	(170.9)
8	140.2	139.8	142.6	143.9	133.7	99.1	98.0	144.3	133.3	131.0	139.1	133.9	131.0	129.1	133.5	122.6	124.0	115.3
	(213.6)	(213.6)	(214.8)	(216.1)	(216.1)	(186.1)	(188.0)		(216.1)	(214.8)	(220.7)	(216.1)	(214.8)	(213.6)	(214.8)	(189.2)	(195.3)	(190.4)
1′	88.1	89.4	89.6	89.5	92.5	91.9	91.4	86.2	90.1	89.8	90.7	93.5	89.6	92.5	91.5	87.8	92.2	93.4
	(164.8)	(167.2)	(166.0)	(168.4)	(171.4)	(172.9)	(173.3)	(168.5)	(172.1)	(169.9)	(175.8)	(167.2)	(167.2)	(167.2)	(169.7)	(162.4)	(172.9)	(166.0)
2′	73.7	83.3	83.3	83.0	85.1	84.6	85.2	84.9	85.3	85.1	85.2	77.4	85.1	77.1	85.1	73.9	85.0	85.2
	(146.5)	(163.6)	(161.1)	(163.6)	(159.7)	(161.2)	(161.1)	(161.1)	(162.1)	(161.1)	(164.1)	(152.4)	(161.1)	(151.4)	(159.9)	(146.5)	(163.1)	(162.4)
3′	70.8	81.0	81.0	80.6	81.1	82.0	82.2	81.3	80.6	81.6	79.3	72.4	81.6	71.6	81.7	70.9	79.9	82.5
	(150.1)	(158.7)	(159.9)	(161.1)	(158.3)	(158.3)	(158.7)	(159.9)	(159.2)	(160.2)	(160.2)	(151.4)	(161.1)	(151.4)	(158.7)	(150.1)	(160.2)	(158.7)
4′	86.1	83.7	83.9	83.7	84.0	88.2	89.2	85.2	84.5	84.9	84.1	88.4	85.0	87.7	85.4	85.3	83.2	85.7
	(148.9)	(151.4)	(153.8)	(152.6)	(153.9)	(152.4)	(152.6)	(153.8)	(154.3)	(155.3)	(156.3)	(153.8)	(152.6)	(151.4)	(148.9)	(147.7)	(155.3)	(146.5)
5′	61.9	64.2	64.0	63.7	63.7	69.1	69.5	76.0	50.9	49.3	57.3	49.6	49.0	49.4	45.0	62.1	58.0	49.6
	(141.0)	(150.1)	(150.1)	(147.7)	(150.0)	(146.5)	(146.5)	(151.4)	(146.5)	(140.4)	(146.5)	(140.4)	(137.9)	(137.9)	(140.4)	(140.4)	(145.3)	(138.0)
															(146.5)			
>C<	—	113.6	113.7	113.7	114.7	112.7	113.0	111.3	112.0	116.6	112.4	—	111.4	—	113.2	—	112.2	112.3
CH_3	—	25.3	25.2	25.2	25.0	24.3	24.7	24.3	24.2	24.1	24.3	—	24.1	—	24.3	—	24.1	24.4
CH_3	—	27.0	27.0	27.0	26.8	25.9	26.3	26.0	25.8	25.9	25.7	—	25.8	—	25.9	—	25.6	26.1

3′,5′-cyclic nucleotides and by one of the present authors (5) using naturally occurring nucleosides.

Accumulation of ^{13}C nmr data has shown that C2′ of a nucleoside always exhibits a lower chemical shift than C3′, contrary to the recent announcement by Chang *et al.* (6) who assigned ^{13}C chemical shifts of methylated nucleosides based on wrong assignments of C2′ and C3′ of adenosine.

We encountered difficulty in assigning C2′ and C3′ of cyclonucleoside derivatives (7), whose H-2′ and H-3′ signals in ^{1}H nmr spectra were found to be a pair of doublets, exhibiting no coupling with H-1′ and H-4′. Thus, our early assignments of C2′ and C3′ of 8,5′-*O*-cycloadenosine derivatives by selective ^{1}H-decoupling were based on the fact that, in many nucleoside derivatives, H-2′ exhibited a lower chemical shift than H-3′.

Now unambigous assignments of H-2′ have been achieved using nOe (nuclear Overhauser enhancement) difference spectra irradiating H-1′, giving 4−8% nOe to H-2′. Subsequent selective ^{1}H-decoupling led to identification of C2′ and C3′ peaks, and our earlier assignments thus required revision.

In the case of isopropylidene derivatives of nucleosides, the signal of C2′ given as a doublet was always found to have a narrower line width than those of C3′ and C4′, reflecting the number of hydrogens which caused the long-range (two and three bond) C—H couplings.

The ^{13}C chemical shifts of several adenosine derivatives, including 8,5′-*O*- and 3,5′-*N*-cycloadenosine derivatives, are listed in Table 1. Throughout these compounds the C2′ signals were always located at lower magnetic fields than the C3′ signals, showing that ^{13}C chemical shifts of C2′ and C3′ were insensitive to the structural alterations of the base moiety.

However, chemical shifts of C5′ were found to reflect the nucleoside and cyclonucleoside structures: ^{13}C—O—H δ 62; ^{13}C—O—R (R = acyl) δ 64; ^{13}C—O—R (R = alkyl) δ 69; ^{13}C—O—N δ 49−51; ^{13}C—O—N^+ δ 57−58.

When the ^{13}C chemical shifts of C5 and C6 of compounds **2** and **3** were compared, it was evident that introduction of an acyl group at N6 of the adenine ring caused considerable increase in the C5−C6 bond polarity, i.e., shielding at C6 accompanied by deshielding at C5. However, in the case of the ring-cleaved compounds **12** and **13**, this trend was no longer observed, suggesting a contribution of the 6π-electrons of the pyrimidine ring to increase the C5—C6 bond polarity.

Similarly, affording positive charge at N3 of adenosine derivatives resulted in shielding at C4, to a considerable extent, as was shown by comparison of **1** with **11** as well as **16** with **17**.

Numbering of the compounds

The original numbering of adenosine is maintained in all the compounds listed here for the reader's convenience.

Experimental

Preparation of the compounds

Consult the following papers (reference numbers in parentheses): **2−4** (9), **5** (8), **6** (8 and 15), **7** (8 and 15), **8** (10), **9** and **10** (11), **11** (13), **12** and **13** (11 and 12), **14** and **15** (12), **17** (14), **18** (12).

Method

The nmr spectra were recorded by JEOL GX-400 and FX-100 spectrometers. ^{13}C chemical shift assignments were made based upon homo-spin decoupling on ^{1}H nmr, followed by selective decoupling and long-range selective decoupling (LSPD) on ^{13}C nmr in the case of **1**, **12**, **14**, and **16**. Assignments of H-2′, in the case of isopropylidene derivatives of nucleosides, were made based on nOe difference spectra, 4−8% nOe being observed for H-2′ {H-1′}.

Solvent

$CDCl_3$ for **5**, **6**, **7**, **15**, and **18**; DMSO-d_6 for other compounds. Difference of ^{13}C chemical shifts in these two solvents is less than 1 ppm in most cases.

1. J. B. STOTHERS. Carbon-13 NMR spectroscopy. Academic Press, New York. 1972. p. 468.
2. A. J. JONES, D. M. GRANT, M. W. WINKLEY, and R. K. ROBINS. J. Am. Chem. Soc. **92**, 4079 (1970).
3. H. H. MANTSCH and I. C. P. SMITH. Biochem. Biophys. Res. Commun. **46**, 808 (1972).
4. M. KAINOSHO. Org. Magn. Reson. **12**, 548 (1979).
5. J. UZAWA and M. URAMOTO. Org. Magn. Reson. **12**, 612 (1979).
6. C. CHANG, D. J. ASHWORTH, L. CHERN, J. D. GOMES, C. LEE, P. W. MOU, and R. NARAYAN. Org. Magn. Reson. **22**, 671 (1984).
7. J. UZAWA and K. ANZAI. Can. J. Chem. **62**, 1555 (1984).
8. K. ANZAI and J. UZAWA. J. Org. Chem. **47**, 5076 (1984).
9. K. ANZAI and M. MATSUI. Bull. Chem. Soc. Jpn. **46**, 3228 (1973).
10. K. ANZAI and M. MATSUI. Bull. Chem. Soc. Jpn. **47**, 417 (1974).
11. K. ANZAI. Agric. Biol. Chem. Jpn. **40**, 373 (1976).
12. K. ANZAI and M. MATSUI. Agric. Biol. Chem. Jpn. **37**, 301 (1973).
13. R. KUHN and W. JAHN. Ber. **98**, 1699 (1965).
14. K. ANZAI and K. MATSUI. Bull. Chem. Soc. Jpn. **46**, 618 (1973).
15. K. ANZAI, J. B. HUNT, G. ZON, and W. EGAN. J. Org. Chem. **47**, 4281 (1982).

The cleavage of aspirin by α- and β-cyclodextrins in basic aqueous solution

OSWALD S. TEE[1] AND BRYAN K. TAKASAKI[2]

Department of Chemistry, Sir George Williams Campus, Concordia University, Montreal, P.Q., Canada H3G 1M8

Received May 1, 1985

OSWALD S. TEE and BRYAN K. TAKASAKI. Can. J. Chem. **63**, 3540 (1985).

The deacetylation of aspirin is promoted by α- and β-cyclodextrins (αCD and βCD) in basic aqueous solution. From saturation kinetics the dissociation constants (K_d) for the aspirin anion − CD complexes are 12 m*M* (αCD) and 20 m*M* (βCD). At pH 12.25 the limiting rate constant for ester cleavage is 14 times (αCD) and 7 times (βCD) that in the medium alone. For the 4-chloroaspirin anion (K_d = 3.8 m*M*) the cleavage induced by αCD is 240 times that in the medium, but 5-chloroaspirin shows a very small effect. The results are discussed in terms of a model derived from that of Bender and co-workers (1967) and are compared to earlier work. For the αCD anion, the 4-chloroaspirin anion is almost as good as "substrate" as *m*-chloro- and *m*-*tert*-butylphenyl acetates. Compared to hydroxide ion, the αCD anion is better at cleaving 4-chloroaspirin (2000×) and aspirin (36×).

OSWALD S. TEE et BRYAN K. TAKASAKI. Can. J. Chem. **63**, 3540 (1985).

Dans des solutions aqueuses de base, la déacétylation de l'aspirine est facilitée par les cyclodextrines α et β. En se basant sur des cinétiques à saturation, on a pu établir que les constantes de dissociation (K_d) des complexes anion de l'aspirine/CD sont 12 m*M* (αCD) et 20 m*M* (βCD). À un pH de 12,25, les constantes limites de vitesse pour la coupure de l'ester sont respectivement 14 fois (αCD) et 7 fois (βCD) celle observé dans le milieu réactionnel seul. Dans le cas de l'anion chloro-4 aspirine (K_d = 3,8 m*M*), la coupure induit par la αCD est 240 fois plus rapide que celui observé dans le milieu réactionnel seul; toutefois, avec la chloro-5 aspirine, l'effet observé est petit. On discute des résultats en fonction d'un modèle dérivé de celui proposé par Bender et coll. (1967) et on les compare à ceux obtenus dans un travail antérieur. Pour l'anion de la αCD, l'anion de la chloro-4 aspirine est un substrat qui est pratiquement aussi bon que les acétates des *m*-chloro et *m*-*tert*-butylphényles. Par comparaison avec l'ion hydroxyle, l'anion de la αCD provoque des coupures beaucoup plus rapides de la chloro-4 aspirine (2000×) et de l'aspirine (36×).

[Traduit par le journal]

The solubility of aspirin (*O*-acetylsalicylic acid, ASA) in water is quite low (1 g/300 mL) (1). However, it can be increased substantially by the addition of the complexing agents α- and β-cyclodextrin, the effect of the latter being greater (2). β-Cyclodextrin also stabilizes solid aspirin (3). Any attempts to use these effects for pharmaceutical purposes (2, 3) should take into account the ability of cyclodextrins to promote the deacylation of phenyl acetates in aqueous solution (4). In the strictest sense of the word, cyclodextrins do not *catalyze* the hydrolysis of these esters since their deacylation results in the formation of an acetylcyclodextrin, which undergoes hydrolysis relatively slowly (4).

The seminal studies carried out by Bender and co-workers (4, 5) included *m*- and *p*-carboxyphenyl acetates (**2**, **3**) but not,

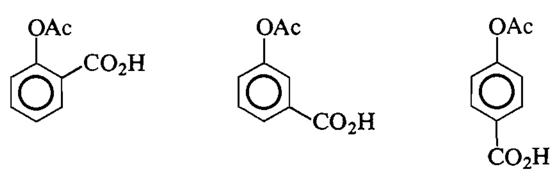

1   **2**   **3**

1^- = anion 2^- = anion 3^- = anion

surprisingly, ASA (**1**) (4). In view of the lack of a prior study and the potential interest of its results, it seemed worthwhile to examine the behavior of ASA under hydrolytic conditions in the presence of cyclodextrins. For comparative purposes, 4-chloro- and 5-chloroaspirin were also studied briefly.

TABLE 1. Rate constants for the cleavage of aspirin in presence and absence of α- and β-cyclodextrin at various pHs[a]

	k_{obs} (s^{-1})		
pH	No CD	αCD	βCD
13.55	0.116	0.137	0.123
13.25		0.0981	0.0580
12.85	0.0242	0.0747	0.0351
12.55		0.0652	0.0261
12.25	0.00570	0.0401	0.0165
11.85	0.00188	0.0198	0.00990
11.51		0.0102	

[a]At 25°C, *I* = 1.0 *M* (NaCl), $[ASA]_o$ = 0.5 m*M*, [CD] = 10 m*M*.

Results and discussion

The rate of hydrolysis of aspirin is very slow at intermediate pHs but it rises monotonically with hydroxide ion in aqueous base (6). For the sake of convenience we chose the pH range 11−14 which is close to that used by Bender and co-workers (4, 5). Moreover, within this range lie the apparent pK_as of the secondary hydroxyls of cyclodextrins that are involved in ester cleavage (4, 5, 7).

Table 1 and Fig. 1 show pH−rate data for the deacylation of ASA in the absence of and in the presence of α- and β-cyclodextrin (αCD and βCD). As expected from earlier work (6), the rate constant for hydrolysis in the absence of cyclodextrin simply increases linearly with [OH^-]. However, with αCD or βCD present the cleavage is faster at lower pH, the effect levelling off above pH 12 until by pH 13.5 normal

[1]Author to whom correspondence should be addressed.
[2]N.S.E.R.C. summer student, 1984.

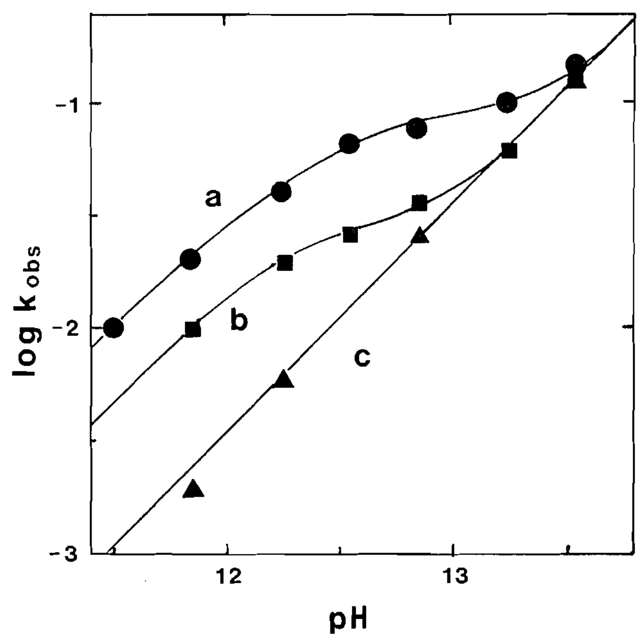

FIG. 1. pH–rate profiles for the cleavage of aspirin anion: (a) with 10 mM αCD; (b) with 10 mM βCD; (c) with no CD.

TABLE 2. Rate constants for the cleavage of aspirin as a function of cyclodextrin concentration[a]

[CD] (mM)	$10^3\ k_{obs}$ (s^{-1}) αCD	$10^3\ k_{obs}$ (s^{-1}) βCD
0	5.70	5.70
1.0	11.8	7.23
2.0	16.9	8.67
4.0	25.8	11.2
6.0	31.9	13.1
8.0	37.7	15.2
10.0	40.1	16.5

[a]At 25°C, I = 1.0 M (NaCl), pH = 12.25, $[ASA]_o$ = 0.25 mM.

hydrolysis by OH^- is dominant. This behaviour parallels that seen earlier for other phenyl esters (4, 5), the levelling-off being due to the cyclodextrin pK_as around 12.1 (4, 5, 7).

At fixed pH and varying CD concentration the observed first-order rate constants (k_{obs}) (Table 2) vary in a curvilinear manner (Fig. 2) appropriate to Michaelis–Menten type kinetics (8*a*). The simplest model that fits this behaviour involves reaction via a substrate–CD complex (7), as depicted below in eq. [1].

$$[1] \quad \mathrm{S} + \mathrm{CD} \underset{K_d}{\rightleftharpoons} \mathrm{S\cdot CD} \xrightarrow{k_c}$$
$$\downarrow k_u$$

For this reaction scheme the expected form of k_{obs} is:

$$[2] \quad k_{obs} = \frac{k_u K_d + k_c[\mathrm{CD}]}{(K_d + [\mathrm{CD}])}$$

where k_u is the "uncatalyzed" rate constant (in the absence of CD), k_c is that for the ASA–CD complex, and K_d is the dissociation constant of the complex. Analysis of the data in terms of eq. [2] was carried out in four ways: (a) linear regression $1/(k_{obs} - k_u)$ vs. $1/[\mathrm{CD}]$, a Lineweaver–Burk approach (7);

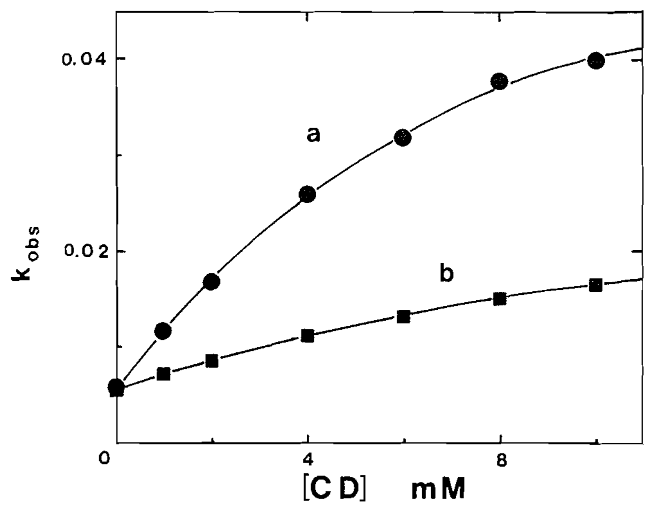

FIG. 2. Rate of cleavage of aspirin anion as a function of cyclodextrin concentration: (a) αCD; (b) βCD.

TABLE 3. Constants for the cleavage of phenyl acetates by cyclodextrins in aqueous solution

Substrate	CD	K_d (M)	$10^3 \cdot k_u$ (s^{-1})	$10^3 \cdot k_c$ (s^{-1})	k_c/k_u	Note
$\mathbf{1}^-$(ASA anion)	α	0.012	5.70	82.3	14	a
	β	0.020	5.70	38.0	6.7	a
$\mathbf{2}^-$	α	0.11	0.815	55.5	68	b
$\mathbf{3}^-$	α	0.15	1.25	6.7	5.3	b
PhOAc	α	0.022	0.804	21.9	27	b
$\mathbf{4}^-$	α	0.0038	14.0	3510	240	a
m-ClPhOAc	α	0.0056	0.505	78.9	160	c

[a]This work. At 25°C, I = 1.0 M (NaCl), pH 12.25.
[b]Bender and co-workers (4). At 25°C, I = 0.2 M, pH 10.60, 0.5% acetonitrile.
[c]As previous, but pH 10.01.

(b) linear regression of $(k_{obs} - k_u)$ vs. $(k_{obs} - k_u)/[\mathrm{CD}]$, an Eadie–Hofstee approach (7); (c) non-linear fitting of eq. [2] keeping k_u fixed at the experimental value; and (d) likewise, but treating k_u as a fitting parameter. All four approaches gave excellent fits and very similar values for k_c and K_d. In the following we simply present the values obtained by (b) since the Eadie–Hofstee type of analysis is statistically superior to (a), even though the latter usually gives better looking linear plots (9).

Table 3 contains values of k_u, k_c, and K_d obtained at pH 12.25 in this study, together with some relevant values from Bender and co-workers (4), obtained at slightly lower pHs. Note that in these basic media the carboxyl-bearing substrates **1**, **2**, **3**, and **4** (see below) will be present as their respective anions $\mathbf{1}^-$, $\mathbf{2}^-$, etc.

The anion of aspirin ($\mathbf{1}^-$) binds fairly well to αCD and βCD (K_d = 12 and 20 mM), about 10 times more strongly than its *m*- and *p*-isomers. Presumably this is because the four unsubstituted positions of $\mathbf{1}^-$, which should be relatively hydrophobic, can reside in the cavities of the cyclodextrins, while the polar carboxylate and ester groups are in a largely aqueous environment (see Scheme 1). In contrast, both of the anions $\mathbf{2}^-$ and $\mathbf{3}^-$ must have one or other of their polar groups in the hydrophobic cavity. With phenyl acetate, where this problem does not arise, the binding is stronger and comparable to that of the ASA anion (Table 3).

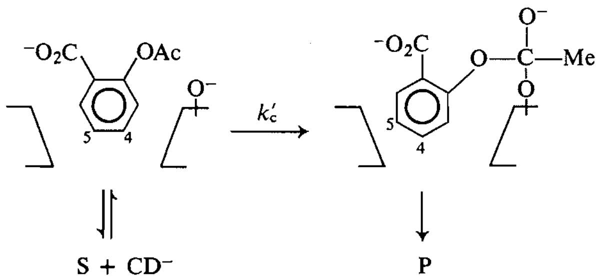

SCHEME 1

The rate enhancements (see k_c/k_u, Table 3) for the cleavage of aspirin by αCD and βCD are modest[3] and they parallel the binding of the substrate: for αCD the value of k_c/k_u and the binding are twice as large as for βCD. These differences are small but they may reflect the larger cavity size of βCD (7) in which **1**⁻ may sit deeper, but less snugly, so that the acetoxyl group is less accessible to the secondary hydroxyls that induce cleavage (4, 5, 7).

Despite showing much weaker binding to αCD, both **2**⁻ and **3**⁻ show comparable k_c/k_u values to the ASA anion. Thus, as is now generally recognized, good substrate binding is not of overriding importance in facilitating catalysis. Of more importance is the binding of transient intermediates and the transition states that flank them (10). The "catalytic" effect for the *meta*-substituted substrate **2**⁻ is about 5 times that for **1**⁻, which in turn is twice as large as that for the *p*-isomer **3**⁻. It was found by Bender and co-workers (4, 5, 7) that in general *m*-isomers show larger effects than *p*-isomers, a point which will arise again later. Phenyl acetate, which binds about as strongly as the ASA anion to αCD, shows a similar rate enhancement (Table 3).

Scheme 1 shows a depiction of the principal steps envisaged for the cleavage of the aspirin anion **1**⁻ by a cyclodextrin. In a guest–host complex (3, 7) formed from **1**⁻ and CD, the aspirin anion sits with its carboxylate and acetoxyl groups outside the cavity. The rate-limiting step is nucleophilic attack by an ionized secondary hydroxyl to give a tetrahedral intermediate, which undergoes fast phenolate loss to give acetylated cyclodextrin (4).

To provide support from Scheme 1 we have studied the behaviour of 4-chloro- and 5-chloroaspirin (**4** and **5**) with αCD.

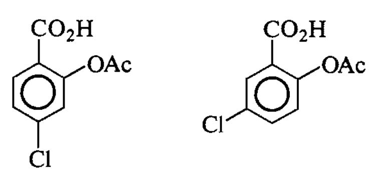

4 **5**

With the 4-chloro derivative one expects better substrate binding *and* better "catalysis," as the acetoxyl group should be held close to the secondary hydroxyl groups. On the other hand, with the 5-chloroaspirin the acetoxyl group should be held further from these OHs and so weaker "catalysis" is expected. These expectations, which are based on the earlier findings for *m*- and *p*-substituted phenyl acetates (4), were fully realized.

[3]The values for ASA given in Table 3 are for pH 12.25, close to the apparent pK_as of the CDs. At lower pHs the rate enhancements should be about twice as large.

TABLE 4. Rate constants for the cleavage of 4-chloroaspirin in the presence and absence of α-cyclodextrin[a]

pH	k_{obs} (s^{-1}) No CD	k_{obs} (s^{-1}) 10 m*M* CD
13.55	0.302	5.41
13.25		6.26
12.85	0.0542	6.17
12.55		4.70
12.25	0.0140	2.97
11.85	0.00526	1.27

[a]At 25°C, I = 1.0 *M* (NaCl), [4Cl-ASA]$_0$ = 0.5 m*M*.

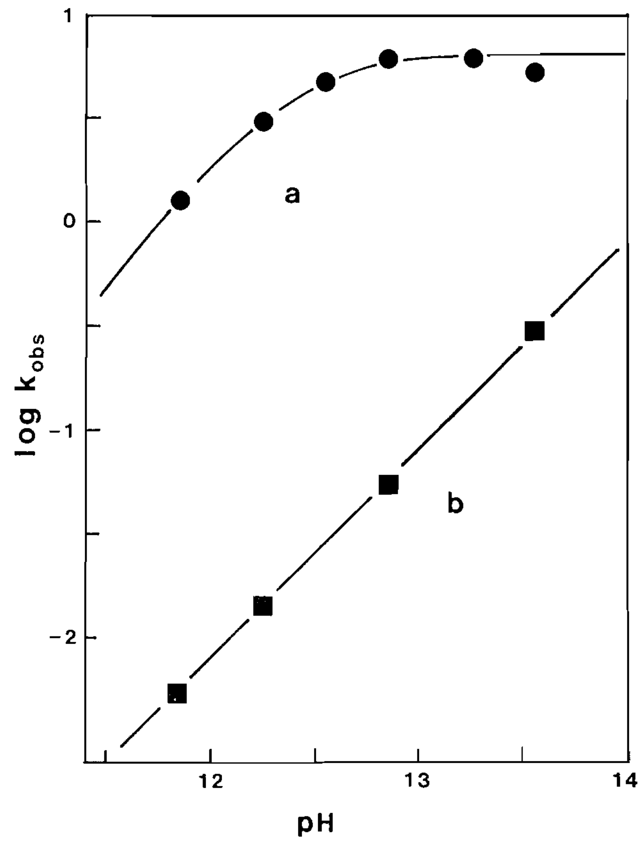

FIG. 3. pH–rate profiles for the cleavage of 4-chloroaspirin anion: (a) with 10 m*M* αCD; (b) with none.

TABLE 5. Rate constants for the cleavage of 4-chloroaspirin as a function of α-cyclodextrin concentration[a]

[αCD] (m*M*)	k_{obs} (s^{-1})
0	0.0147
1.0	0.739
2.0	1.21
4.0	1.88
6.0	2.22
8.0	2.41
10.0	2.45

[a]At 25°C, I = 1.0 *M* (NaCl), pH = 12.25, [4Cl-ASA]$_0$ = 0.5 m*M*.

TABLE 6. Constants for the attack of hydroxide ion and cyclodextrin anions on aspirin and other phenyl acetates[a]

Substrate	CD	k_{OH} (M^{-1} s^{-1})	k_c' (s^{-1})	k_c'/k_{OH} (M)	k_2' (M^{-1} s^{-1})	k_2'/k_{OH}
1^-(ASA anion)	α	0.326	0.141	0.433	12	36
	β	0.326	0.0649	0.199	3.3	10
4^-	α	0.787	6.00	7.62	1600	2000
PhOAc	α	2.02	0.714	0.354	32	16
m-ClPhOAc	α	4.94	9.78	1.98	1750	350

[a]Rate constants are: k_{OH}, attack of OH^-; k_c' reaction within ester·CD anion complex; k_2', apparent value for attack of CD anion on ester (= k_c'/K_d).

Table 4 and Fig. 3 show pH−rate data for 4-chloroaspirin with and without added αCD. Clearly, there is substantially faster cleavage in the presence of αCD (~200×) at the lower pHs. In contrast, for 5-chloroaspirin a very small effect was observed: at pH 12.25, k_{obs} = 0.0134 s^{-1} with no CD added and 0.0174 s^{-1} with 10 mM αCD. In view of this small rate increase (30%), we did not attempt to measure saturation kinetics for **5**. However, for **4** we obtained the rate data given in Table 5, from which were obtained the values of k_c and K_d given in Table 3.

Just as a *m*-chloro substitutent increases the binding of phenyl acetate (3.9×), the 4-chloro substituent increases the binding of the ASA anion (3.2×). The effect on the rate of cleavage is, however, larger. For *m*-ClPhOAc the ratio k_c/k_u is 5.9 times that for PhOAc whereas for 4^- the ratio is 17 times that for the unsubstituted aspirin anion. Moreover, the k_c/k_u ratio for 4^- is larger (240×) than found for *m*-ClPhOAc (160×). At lower pH, away from the pK_a of the CD hydroxyls, the effect for 4^- would be larger still.[3]

To take explicit account of pH and the ionization of the CD hydroxyls (4, 5) a more complete rate equation is required. The reaction outlined in Scheme 1 may be represented by eq. [3],

$$[3] \quad S + CD \underset{K_d}{\rightleftharpoons} S.CD \overset{K_a}{\rightleftharpoons} S.CD^- \overset{k_c'}{\rightarrow}$$

which also suffices to define appropriate constants. For this pathway the expected form of k_{obs} as a function of acidity and CD concentration is:[4]

$$[4] \quad k_{obs} = \frac{k_c'K_a[CD]}{(K_d[H^+] + [CD](K_a + [H^+]))}$$

If we impose limiting (saturation) conditions, $[CD] \gg K_d$, so that k_{obs} becomes equal to k_c (see eq. [2]), then eq. [4] simplies to eq. [5]. This equation, through appropriate rearrangement,

$$[5] \quad k_c = k_c'K_a/(K_a + [H^+])$$

allows us to correct results obtained at different pHs to a common basis, namely, the rate constant (k_c') for reaction within the substrate·CD anion complex (see eq. [3] and Scheme 1). Values of k_c', thus obtained, are presented in Table 6.

For the aspirin anion 1^- reacting with αCD (or βCD) the value of k_c' is appreciably lower than that for phenyl acetate with αCD. Also for the 4-chloro anion 4^- k_c' is slightly lower than that for *m*-ClPhOAc. However, these comparisons ignore the intrinsic reactivities of the different substrates for which k_{OH}, the rate constant for attack of hydroxide ion, provides a measure. If we "normalize" k_c' by division by k_{OH} (Table 6), a different picture emerges: cleavage of 4^- by αCD anion is clearly superior to that of *m*-ClPhOAc and cleavage of 1^- is comparable to that of PhOAc.

The data in Table 6 also provide for one further comparison, which emphasizes the effect of complexation on the rate of ester cleavage. We define $k_2' = k_c'/K_d$, which is the apparent second-order rate constant for the attack of the CD anion on the ester substrate[5] (see eq. [6]). The values of k_2' in

$$[6] \quad S + CD^- \overset{k_2'}{\rightarrow}$$

Table 6 provide a measure of the reactivity of the cyclodextrin anion towards the various substrates, i.e. its "substrate specificity".[6] From this viewpoint, the 4-chloroaspirin anion and *m*-ClPhOAc are very similar and are 50−100 times better substrates for αCD than PhOAc and the ASA anion. The values of k_2' (3.3−1750 M^{-1} s^{-1}) fall within the range of k_{cat}/K_m values (0.13−3 × 10^5 M^{-1} s^{-1}) found for chymotrypsin with various amide and ester substrates (8*d*). The "best" substrate found by Bender's group (4, 5) was *m-tert*-butylphenyl acetate, for which k_2' = 2100 (αCD) and 3.1 × 10^4 M^{-1} s^{-1} (βCD). Much larger specificities have been found subsequently by Breslow's group, using carefully designed substrates (11).

Table 6 also lists values of k_2'/k_{OH}, which account for the different substrate reactivities and measure the superiority of the CD anion over hydroxide ion in promoting ester cleavage. This ratio is largest for the 4-chloroaspirin anion (2000), similar to that found for *m-t*-BuPhOAc (1700) with αCD (5). Again, larger ratios can be found in Breslow's work (11).[7]

Experimental

Commercial aspirin was recrystallized from water before use. 4-Chloro and 5-chloroaspirins (12) were made by acetylation (13) of the corresponding chlorosalicylic acids obtained from Aldrich. Cyclodextrins (Aldrich) were used as received.

[4]The derivation of eq. [4] assumes $[CD] \gg [S]$, which is true for most of the experiments and certainly for the limiting condition $[CD] \gg K_d$. It is also implicit that ionization of one of the secondary hydroxyls of the CD does not significantly alter K_d. For convenience also, we ignore the contribution from normal hydrolysis since it is negligible when the limiting conditions are imposed.

[5]For reaction of the ester·CD anion complex: rate = $k_c'[S.CD^-]$, whereas for reaction of the ester with the CD anion: rate = $k_2'[S][CD^-]$ (see eq. [6]). Equating these two expressions leads to $k_2' = k_c'/K_d$. This approach was used earlier by Bender and coworkers (5) and is equivalent to the use of k_{cat}/K_m for enzymes (8*b*,*c*).

[6]One frequent use of k_{cat}/K_m is as a measure of substrate specificity (8*c*).

[7]After acceptance of this paper we became aware of previous work on the cleavage of ASA by CDs: see ref. 16. This paper, which is mainly concerned with aryl phosphate cleavage, contains results which are compatible with the present study.

Substrate solutions were prepared by dilution of an aliquot of a stock 0.01 *M* aspirin solution into a cyclodextrin solution, all in 1.0 *M* aqueous NaCl solution. For kinetic experiments these were mixed (1:1) in a stopped-flow apparatus (14) with aqueous NaOH + NaCl solutions (total $I = 1.0$ *M*). Initial concentrations (after mixing) of substrate were 0.25 or 0.50 m*M*, of CD were 0–10 m*M*, and final pHs were calculated from the final $[OH^-]$ and an activity correction for $I = 1.0$ *M*.

Kinetics were measured at 25.0 ± 0.1°C using an Aminco DW-2 spectrophotometer + stopped flow accessory (14) by monitoring salicylate ion appearance at 310 nm. Fast runs used the data acquisition described previously (15). For slower runs the output voltage (2 V/abs. unit) of the DW-2 was captured by a Cyborg Isaac 91a interfaced to an Apple II microcomputer.

Rate constants were calculated from least-squares analysis of ln $(A_\infty - A)$ vs. time for data covering >90% reaction, A_∞ being obtained after 10 half-lives. Excellent straight lines ($r > 0.9995$) were obtained and the quoted rate constants are the average of 4–5 determinations.

Acknowledgement

The authors thank the Natural Sciences and Engineering Research Council of Canada for an operating grant to O.S.T. and a Summer Studentship to B.K.T. Preliminary experiments were kindly carried out by Miss J. M. Bennett.

1. M. WINDHOLZ (*Editor*). The Merck index. 9th ed. Merck and Co., Rahway, NJ. 1976. p. 114.
2. J. L. LACH and J. COHEN. J. Pharm. Sci. **52**, 137 (1963).
3. W. SAENGER. Angew. Chem. Int. Ed. Engl. **19**, 344 (1980).
4. R. L. VAN ETTEN, J. F. SEBASTIAN, G. A. CLOWES, and M. L. BENDER. J. Am. Chem. Soc. **89**, 3242 (1967).
5. R. L. VAN ETTEN, G. A. CLOWES, J. F. SEBASTIAN, and M. L. BENDER. J. Am. Chem. Soc. **89**, 3253 (1967).
6. T. ST. PIERRE and W. P. JENCKS. J. Am. Chem. Soc. **90**, 3817 (1968).
7. M. L. BENDER and M. KOMIYAMA. Cyclodextrin chemistry. Springer Verlag, New York. 1978.
8. A. FEHRST. Enzyme structure and mechanism. W. H. Freeman, Reading, U.K. 1977; (*a*) Chapt. 3; (*b*) Chapt. 10; (*c*) Chapt. 11, (*d*) pp. 248, 249.
9. J. E. DOWD and D. S. RIGGS. J. Biol. Chem. **249**, 863 (1965).
10. R. L. SCHOWEN. *In* Transition states of biochemical processes. *Edited by* R. D. Gandour and R. L. Schowen. Plenum Press, New York, 1978. Chapt. 2; J. R. KNOWLES and W. J. ALBERY. Acc. Chem. Res. **10**, 105 (1977).
11. R. BRESLOW. Acc. Chem. Res. **13**, 170 (1980); Science, **218**, 532 (1982); R. BRESLOW, G. TRAINOR, and A. UENO. J. Am. Chem. Soc. **105**, 2739 (1983), and references therein.
12. A. R. FEHRST and A. J. KIRBY. J. Am. Chem. Soc. **89**, 4853 (1967).
13. A. I. VOGEL. A textbook of practical organic chemistry. 3rd ed. Longmans, London, U.K. 1961. p. 996.
14. O. S. TEE, D. C. THACKRAY, and C. G. BERKS. Can. J. Chem. **56**, 2970 (1978).
15. O. S. TEE, M. TRANI, R. A. MCCLELLAND, and N. E. SEAMAN. J. Am. Chem. Soc. **104**, 7219 (1982).
16. K. MOCHIDA, Y. MATSUI, Y. OTA, K. ARAKAWA, and Y. DATE. Bull. Chem. Soc. Jpn. **49**, 3119 (1976).

Oxidation of hydrocarbons. 15. A study of the oxidation of alkenes by methyltributylammonium permanganate

JOAQUIN F. PEREZ-BENITO AND DONALD G. LEE[1]
Department of Chemistry, University of Regina, Regina, Sask., Canada S4S 0A2

Received February 27, 1985

JOAQUIN F. PEREZ-BENITO and DONALD G. LEE. Can. J. Chem. **63**, 3545 (1985).

A study of the reduction of methyltributylammonium permanganate by a large number of alkenes in methylene chloride has dispelled a current uncertainty concerning the nature of the inorganic product obtained. It is colloidal manganese dioxide and not a manganate(V) cyclic diester as previously supposed. This product is stabilized in methylene chloride solutions by adsorption of the alkene, which decreases its polarity at the solvent interphase. The solubility of the colloid is therefore a function of both the concentration and the identity of the alkene. In certain (atypical) cases, where acidic compounds are present, the product is further reduced to manganese(III).

JOAQUIN F. PEREZ-BENITO et DONALD G. LEE. Can. J. Chem. **63**, 3545 (1985).

En se basant sur une étude de la réduction du permanganate de méthyltributylammonium par un grand nombre d'alcènes dans le chlorure de méthylène, on a pu éliminé un doute concernant la nature de produit inorganique obtenu. Il s'agit du dioxyde de manganèse à l'état colloïdal et non pas un diester cyclique du manganèse(V) tel qu'il avait été suggéré antérieurement. Dans des solutions de chlorure de méthylène, ce produit est stabilisé par une adsorbtion de l'alcène qui en diminue la polarité à l'interface du solvant. La solubilité du colloïde est donc fonction à la fois de la concentration et de la nature de l'alcène. Dans certains cas qui ne sont pas typiques et dans lesquels il existe des composés acides, le produit est alors réduit en manganèse(III).

[Traduit par le journal]

Introduction

When alkenes are oxidized by permanganate ion, an intermediate can be detected under certain conditions. For example, Wiberg, Deutsch, and Roček (1) observed that a reactive species could be detected spectrophotometrically when crotonic acid and permanganate were allowed to react in a neutral aqueous medium. Lee and Brownridge (2) also detected an intermediate during the oxidation of cinnamic acid in acidic aqueous solutions and it was assumed that this species was likely a cyclic manganese(V) diester, **1**, that had been previously proposed as an intermediate for this reaction (3).

[1] 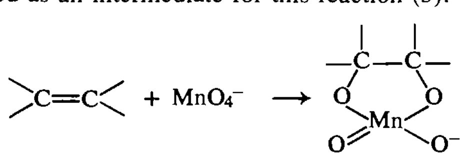

1

However, attempts by Simándi and Jáky (4) to determine the oxidation state of the intermediate led them to conclude that the detected species was a soluble manganese(IV) compound, H_2MnO_3. Unfortunately these results were not unequivocal and it was later pointed out (5) that they were also consistent with the intermediate being a manganese(V) species such as **1**.

Under certain conditions, a semi-stable product having approximately the same spectral properties as the intermediate is formed. For example, Freeman and his co-workers (6) found that the oxidation of uracils at pH 6.7 gave a long-lived intermediate, which was determined to have an oxidation state between +3.3 and +3.8. More recently, it has been observed that the product produced when alkenes are oxidized by quaternary ammonium permanganates in nonaqueous solvents is remarkably similar to the intermediate detected by Freeman (5, 7). Because of the stability of this product, we have made an attempt to characterize it and thus dispel the uncertainty regarding its nature that now exists.

[1] Author to whom correspondence may be addressed.

As described in the following paper, our results provide compelling evidence that the product obtained from the oxidation of most alkenes is a colloid of manganese(IV) oxide.

Experimental

Absorbances were measured and the spectra recorded by use of a Hewlett–Packard 8450A uv–vis spectrophotometer.

Anhydrous methylene chloride, purified by double distillation over 4A molecular sieves, was used in all experiments except those in which the effect of water on the reaction was studied.

The oxidant, methyltributylammonium permanganate, was obtained by reaction of an aqueous solution of methyltributylammonium bromide with potassium permanganate (8). All of the reducing agents are commercially available compounds.

The concentration of permanganate was approximately 3×10^{-4} *M* in all experiments. The ratio [reductant]/[oxidant] was about 5 in the experiments in which the final oxidation state of manganese was determined, and about 25 for experiments in which the isosbestic points and final spectra were recorded. The oxidation state of manganese in the brown-yellow species formed from the reduction of methyltributylammonium permanganate by the different reducing agents was determined iodometrically. In a typical experiment a 50-mL flask containing 1-decene (1.5×10^{-3} *M*) in dry methylene chloride was placed in a water bath at 25.0 ± 0.1°C until thermal equilibrium had been attained. Solid methyltributylammonium permanganate (5×10^{-3} g) was then added and the solution stirred until homogeneous. An approximately 2-mL aliquot was immediately transferred to a cuvette in the thermostated cell compartment of the spectrophotometer, and the progress of the reaction was followed by sequentially scanning the solution at constant intervals. When the spectrum showed that all of the permanganate had been reduced, 2 mL of a freshly prepared solution of tetrabutylammonium iodide in methylene chloride (3×10^{-2} *M*) and 5 mL of glacial acetic acid were added to 2.0 mL of the reaction product. An immediate reaction (producing a dark yellow solution) occurred. The color was so intense that dilution (to 50 mL) was required before the concentration of the iodine liberated could be assayed spectrophotometrically.

The spectrum of the quaternary ammonium triiodide (QI_3) exhibited maxima at 365 and 294 nm in methylene chloride solutions. The absorbance at 365 nm, the peak used for these analyses, obeyed Beer's Law and exhibited a molar absorptivity of 2.62×10^4.

TABLE 1. Data for the reduction of methyltributylammonium permanganate by several olefinic compounds in methylene chloride

Compound	Oxidation state[a]	Isosbestic point (nm)	Slope[b]
Butyl vinyl ether	3.97	488	[c]
Cyclododecene	4.05	483	[c]
Cyclooctene	3.93	482	4.70
1-Decene	4.05	485	5.04
cis-2-Decene	3.95	483	5.04
2,3-Dihydrofuran	4.02	481	4.11
2,3-Dimethyl-2-butene	3.94	482	4.70
1-Eicosene	3.98	485	4.93
trans-2-Heptene	4.02	486	[c]
1,5-Hexadiene	3.99	484	5.06
Isoprene	3.90	483	5.21
β-Methoxystyrene	4.05	488	[c]
2-Methyl-1-butene	4.05	485	[c]
2-Methyl-2-butene	3.99	483	4.55
Methyl cinnamate	4.01	483	4.09
cis-4-Methyl-2-pentene	4.03	488	[c]
α-Methylstyrene	4.00	484	5.11
β-Methylstyrene	3.95	484	4.72
1-Octene	4.02	485	4.82
trans-2-Octene	3.99	484	5.00
2,2,4,6,6-Pentamethyl-3-heptene	4.02	485	[c]
trans-4-Phenyl-3-buten-2-one	3.90	484	4.42
trans-1-Phenyl-1-pentene	3.95	484	[c]
cis-Stilbene	4.03	485	[c]
Styrene	4.03	484	4.49
1-Tetradecene	4.03	484	3.85

[a] Oxidation state of the product.
[b] Slope for plots of −log (absorbance) vs. log λ.
[c] Precipitation occurred.

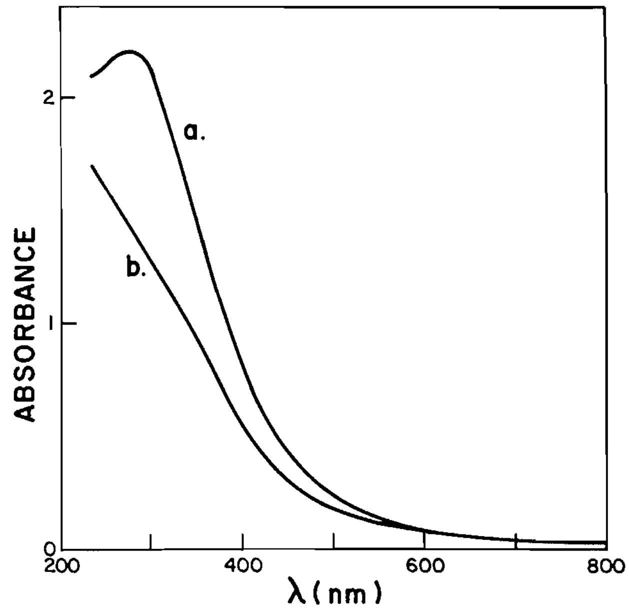

FIG. 1. Absorption spectrum of the product obtained from the reduction of methyltributylammonium permanganate (3.00×10^{-4} *M*) by 2,3-dihydrofuran (7.94×10^{-3} *M*). Spectrum "a" was obtained immediately after all of the permanganate had been reduced. Spectrum "b" was obtained after aging the product solution for 2 days.

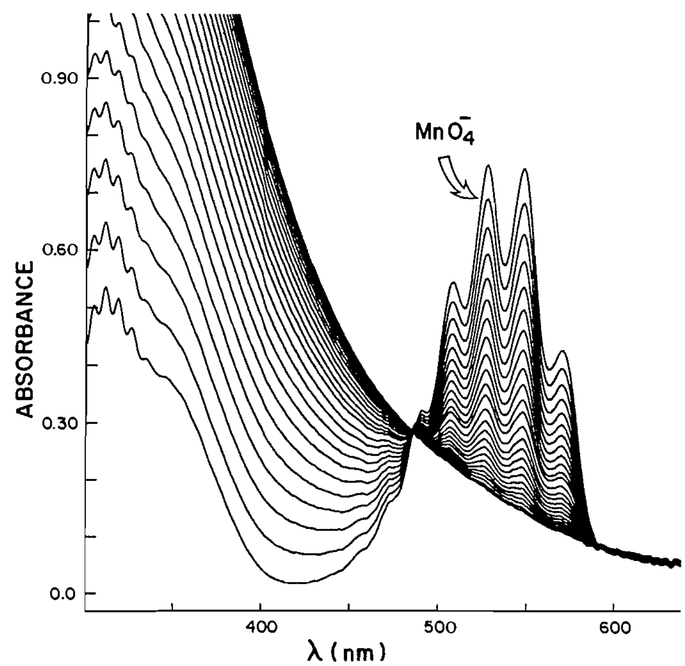

FIG. 2. Successive scans at 5-min intervals for the reduction of methyltributylammonium permanganate (2.84×10^{-4} *M*) by 2-methyl-1-butene (7.41×10^{-3} *M*) in methylene chloride at 25°C.

Application of this iodometric method to the titration of methyltributylammonium permanganate solutions of various concentrations indicated its reliability. The results from 19 different experiments confirmed that manganese is reduced by iodide ion to the +2 oxidation state under these conditions, and the results presented in Tables 1–3 are all based on this conclusion.

Results

The oxidation states of the products obtained from the reduction of methyltributylammonium permanganate by 26 different alkenes are summarized in Table 1. Also included in Table 1 is a list of the isosbestic points observed when the solutions were scanned sequentially as the reactions progressed.

The spectrum of the product obtained immediately following the completion of the reaction exhibited an absorption band with a maximum at about 280 nm (Fig. 1a). However, on standing, this band slowly disappeared and the final spectrum resembled that of a colloid, where energy loss from the incident uv–vis radiation is due to scattering rather than absorption (9) (Fig. 1b).

Sharp isosbestic points were observed when the rate of permanganate reduction was fast relative to the rate of flocculation of the colloidal product (Fig. 2). However, when the rate of flocculation was comparable to the rate of reduction, the isosbestic point was less sharply defined (Fig. 3). In any event, the occurrence of isosbestic points indicates that no long-lived intermediates are formed as the reaction proceeds.

The oxidation states of the products obtained from the reduction of methyltributylammonium permanganate by a representative alkyne, amine, and alcohol (given in Table 2) confirm that a similar product is formed regardless of the nature of the reductant.

Discussion

The results presented in Table 1 clearly indicate that the oxidation state of the initial product obtained from the reduction of permanganate by alkenes is +4. This product exhibits an absorption maximum (at about 280 nm) superimposed on

TABLE 2. Data for the reduction of methyltributylammonium permanganate by non-olefinic compounds in methylene chloride

Compound	Oxidation state[a]	Isosbestic point (nm)	Slope[b]
1-Decyne	3.97	486	5.18
Tributylamine	4.04	484	[c]
1-Tridecanol	3.97	488	4.97

[a] Oxidation state of the product.
[b] Slope for plots of −log (absorbance) vs. log λ.
[c] Precipitation occurred.

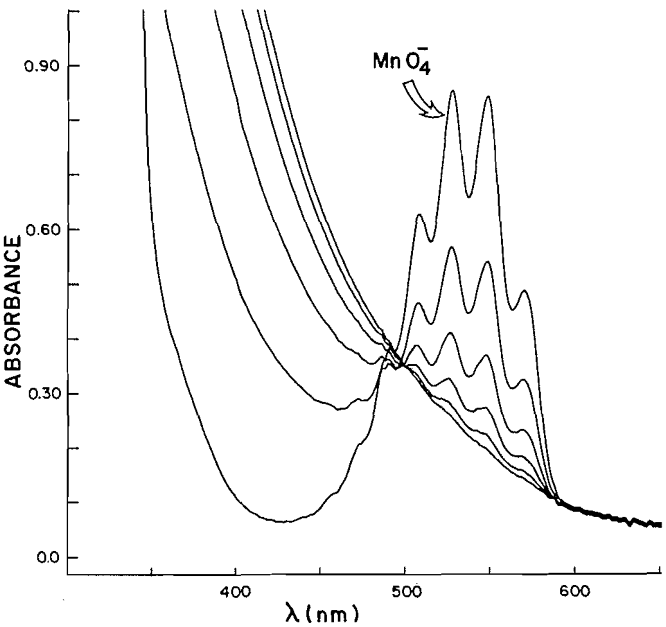

FIG. 3. Successive scans at 10-min intervals for the reduction of methyltributylammonium permanganate (3.24×10^{-4} *M*) by *cis*-stilbene (7.54×10^{-3} *M*) in methylene chloride at 25°C.

what appears to be a spectrum resulting from the scattering of light by a colloid. On standing, this absorption band slowly disappears and, for several alkenes, the spectrum of the resulting solution conforms quite closely to Rayleigh's Law for light scattering (9) (Fig. 1). This change in the spectrum is accompanied by a reduction in the measured oxidation state of the product from +4 to about +3.6.

An attractive explanation for these observations is that the absorption band at 280 nm is due to a π-bond between the alkene and MnO_2, the capacity of manganese dioxide to strongly adsorb organic molecules being well known (10). Such complexation would help to solubilize a colloid of MnO_2 in methylene chloride by providing an external lipophilic surface to the solvent. With time, however, oxidation of the alkene would lower the average oxidation state of the manganese.

The latter was demonstrated by adding an excess of 1-tetradecene to the colloidal product obtained from the reduction of methyltributylammonium permanganate. Iodometric titrations showed that this otherwise stable product was gradually reduced from an oxidation state of +3.96 to +3.60 (Fig. 4). The failure to obtain complete reduction (to +3.0) is probably a consequence of the inaccessibility of much of the MnO_2 to complexation with the alkenes.

A linear relationship between log (absorbance) and log λ

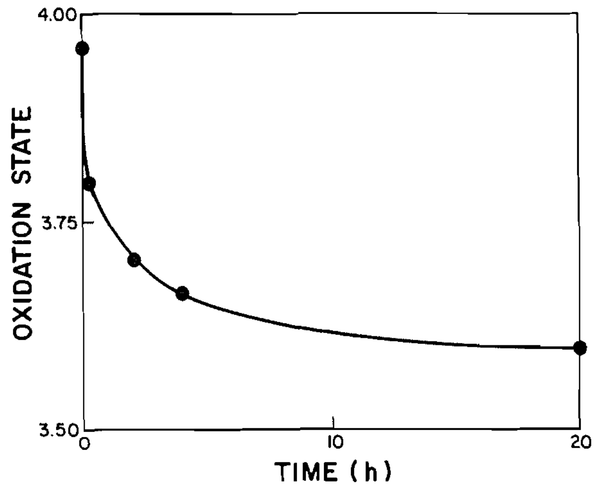

FIG. 4. Oxidation state vs. time when an excess of 1-tetradecene was added to the product freshly obtained from the reduction of methyltributylammonium permanganate (3.09×10^{-4} *M*) by 1-tetradecene (1.58×10^{-3} *M*).

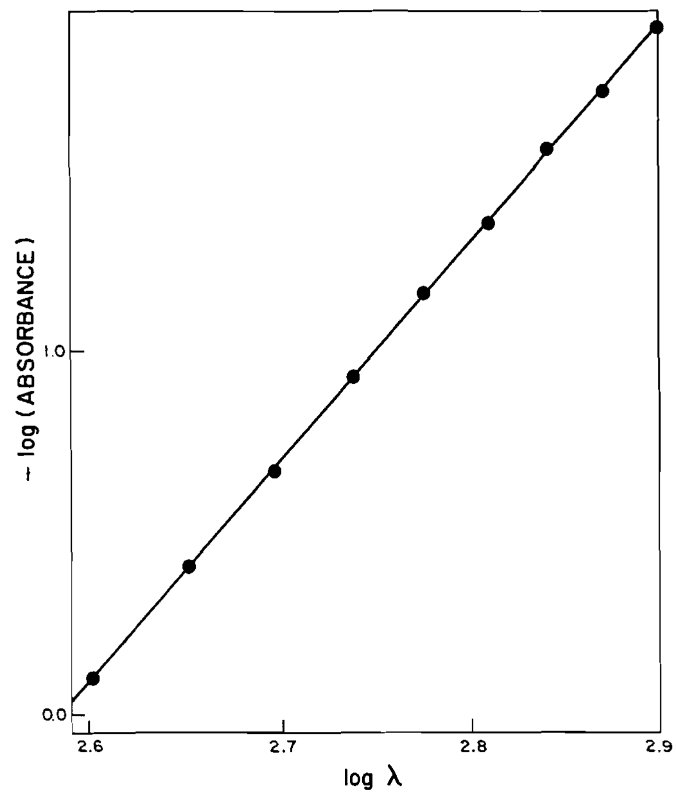

FIG. 5. Log *A* vs. log λ for the product obtained from the reduction of methyltributylammonium permanganate (2.74×10^{-4} *M*) by α-methylstyrene (7.69×10^{-3} *M*) in methylene chloride at 25°C.

would be expected if the product is present in the form of colloidal particles, i.e., if all of the energy lost is due to light scattering. This is a consequence of Rayleigh's Law, which can be written as in eq. [2],

$$[2] \quad A = C/\lambda^4$$

where *A* is the absorbance, λ the wavelength, and *C* a constant depending on the polarizability, mass, and concentration of the colloidal particles.

A typical plot of $-\log A$ vs. $\log \lambda$ has been reproduced in Fig. 5. Although these plots were all linear, with correlation coefficients of 0.99 or better, the slopes in every case were somewhat greater than the theoretical value of 4. Table 1 contains a summary of the slopes observed in those cases where precipitation did not occur. Consequently, it can be seen that all of the evidence available is in reasonably good agreement with the suggestion that the product is actually colloidal.

Although precipitation of manganese dioxide eventually occurs with some reducing agents, no turbidity could be detected at the end of the reactions. It seems likely that the solubility of the colloid is increased by adsorption of alkenes on its surface (thus decreasing the polarity of the colloid/solvent interphase). This suggestion is supported by the observation that the stability of the colloid in solution depends on the nature and the concentration of the alkene used in its preparation. For example, when 1-tetradecene is used as the reducing agent a 3-fold excess of alkene is sufficient to keep the colloid in solution; only when the ratio [alkene]/[$QMnO_4$] is less than 3 can precipitation be observed. However, in the case of 1-octene a 7-fold excess of alkene is necessary to keep the colloid in solution, and in the case of *cis*-stilbene even a 250-fold excess cannot prevent manganese dioxide from precipitating shortly after the end of the reaction.

The dependence of the solubility of the colloid on the nature of the reducing agent used in its preparation can be most easily explained by adsorption, which is well known to be a very specific process (11). Its dependence on the concentration of alkene must be a consequence of the adsorption isotherm, which determines the amount of adsorbate present on the colloid surface as a function of its concentration in solution.

Since there is an overwhelming abundance of evidence (3) that these reactions are initiated by the formation of a cyclic manganese(V) diester, **1**, it has previously been suggested that the detected product of the reaction could actually be a dimer or a polymer of **1** (5). This possibility appears, however, to be inconsistent with an oxidation state of +4, and with the observation that products of similar properties are also obtained from the reduction of permanganate by alkynes, alcohols, and amines under these conditions (Table 2).

No spectral evidence for the existence of an intermediate such as **1** can be found in the scans reproduced in Figs. 2 and 3. This means that the intermediate, assuming it exists, must either be present in very low concentration or else transparent in the spectral region scanned. In order to investigate the latter possibility an attempt was made to detect it iodometrically as the reaction progressed. Since the concentration of permanganate can be determined spectrophotometrically, the total concentration of product plus any intermediate can be obtained from the difference between the initial amount of permanganate and the amount present at any given time. The average oxidation state of the product plus any intermediate can then be determined from the magnitude of the iodine titer. As the results summarized in Table 3 indicate, the residual oxidation state remains close to 4 throughout the reaction. Consequently, it must be assumed that **1** is rapidly reduced to the observed product, colloidal manganese dioxide, most likely by abstraction of a hydrogen atom from the solvent.

Additional evidence for the colloidal nature of the product can be demonstrated by monitoring the absorbances of the solution at 418 and 526 nm simultaneously. Given that both reactant and product absorb light at 526 nm, the absorbance at this wavelength will be:

TABLE 3. Oxidation state of the product obtained from the reduction of methyltributylammonium permanganate (3.39×10^{-4} *M*) by cyclododecene (1.56×10^{-3} *M*) in methylene chloride at 25.0°C

% Reaction[a]	Oxidation state
16	3.73
29	3.91
41	4.07
53	4.03
64	4.14
75	4.12
85	4.09
98	3.97

[a] Defined as: $100[QMnO_4]_{consumed}/[QMnO_4]_{initial}$.

$$[3] \quad A(526) = \epsilon_R^{526}\, c + \epsilon_P^{526}\, (c_0 - c)$$

where ϵ_R^{526} and ϵ_P^{526} are, respectively, the extinction coefficients at 526 nm for the reactant, $QMnO_4$, and the product, and c and c_0 are permanganate concentrations at a particular time and initially. Since it has been demonstrated that no intermediates are present in the system in any appreciable amount, the concentration of the product can be assumed to be $c_0 - c$.

Due to the transparency of permanganate at 418 nm, the absorbance at this wavelength will be:

$$[4] \quad A(418) = \epsilon_P^{418}\, (c_0 - c)$$

where ϵ_P^{418} is the extinction coefficient of the product at 418 nm.

From eqs. [3] and [4] it is easy to derive eq. [5].

$$[5] \quad A(526) = \epsilon_R^{526}\, c_0 - [(\epsilon_R^{526} - \epsilon_P^{526})/\epsilon_P^{418}]\, A(418)$$

Equation [5] implies that a linear relationship should exist between $A(526)$ and $A(418)$. However, Fig. 6a shows that a slightly concave curve is actually obtained for the oxidation of *cis*-stilbene by permanganate in anhydrous methylene chloride solutions. A linear relationship was found only when the same reaction was followed in the presence of excess methyltributylammonium chloride (Fig. 6b). On the other hand, addition of a small amount of water to the solution caused the concavity of the curve to increase dramatically (Fig. 6c). This was accompanied by turbidity due to precipitation of manganese dioxide.

The three different situations reflected in Fig. 6 are a consequence of the colloidal nature of the product. Flocculation of the colloidal particles explains the slight concavity of the curve when the reaction was followed in the absence of both water and methyltributylammonium chloride (Fig. 6a). Flocculation would provoke an increase in the size of the colloidal particles and, consequently, an increase in the radiation scattered. According to eq. [5], if the extinction coefficients of the product, ϵ_P^{526} and ϵ_P^{418}, increase as the reaction is progressing, the absolute value of the slope of the $A(526)$ vs. $A(418)$ plot will decrease, and a concave curve will be obtained.

If this interpretation is correct, the effect of an addition of methyltributylammonium chloride or water is simply to decrease or increase the rate of flocculation. When the reaction is followed in the presence of water, the rapidity of the flocculation process can explain not only the concave curve shown in Fig. 6c, but also the precipitation of manganese dioxide that is observed experimentally.

The organic products produced under these conditions may be isolated by treatment of the brown-yellow methylene chlo-

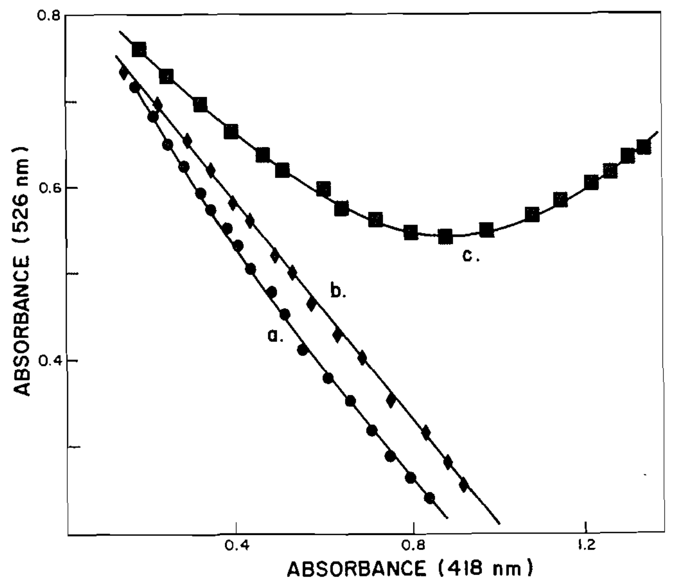

FIG. 6. Absorbance at 526 nm vs. absorbance at 418 nm for the reduction of methyltributylammonium permanganate (3.06×10^{-4} *M*) by *cis*-stilbene (1.50×10^{-3} *M*). "a", no additives; "b", methyltributylammonium chloride (2.53×10^{-2} *M*) added; "c", water (2.56×10^{-2} *M*) added.

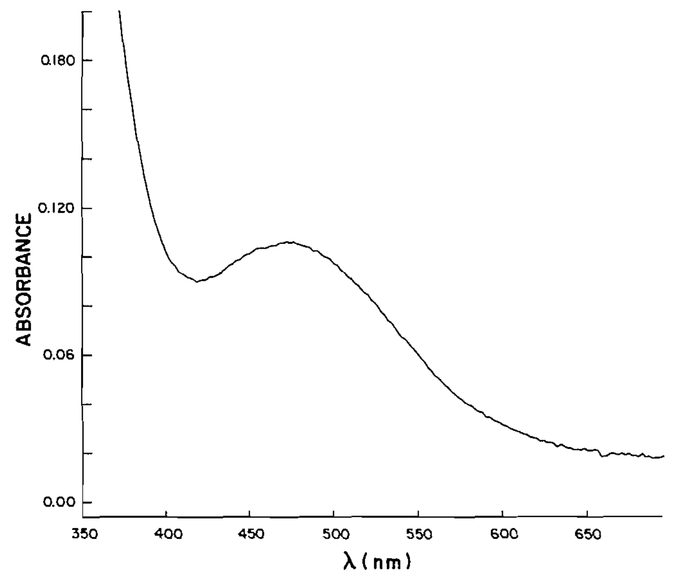

FIG. 7. Spectrum of the product obtained from the reduction of methyltributylammonium permanganate (2.70×10^{-4} *M*) by oleic acid (7.59×10^{-3} *M*) in methylene chloride at 25°C.

ride solutions with either dilute aqueous base or acid. If this aqueous solution is basic, diols are obtained; if it is acidic, cleavage products (aldehydes or ketones) are produced (7). Thus, it appears as if manganese dioxide cleaves diols under acidic conditions, a conclusion that is entirely consistent with the fact that MnO_2 is known to have a much higher reduction potential under acidic conditions than it has under basic conditions (12).

During the course of this study it was observed that the reduction of methyltributylammonium permanganate by two unsaturated compounds produced unusual products. When oleic acid was used as the reductant, the product had an apparent oxidation state of +3.25 and exhibited a spectrum quite differ-

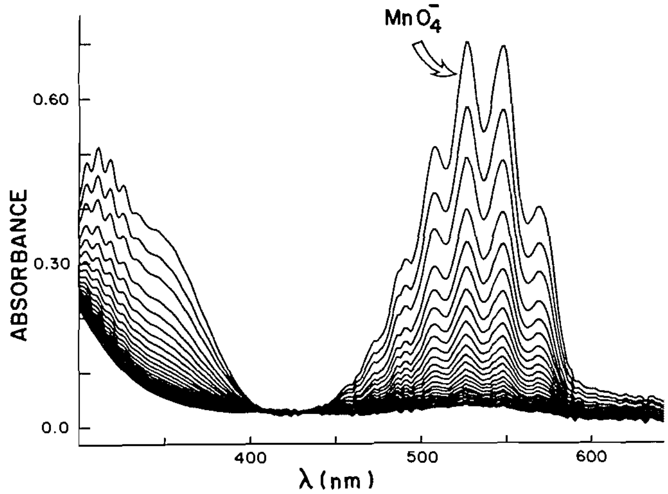

FIG. 8. Successive scans at 2-min intervals for the reduction of methyltributylammonium permanganate (2.67×10^{-4} *M*) by perfluorocyclohexene (1.65×10^{-3} *M*) in methylene chloride at 25°C.

ent from those previously described (Fig. 7). Since manganese(III) is known to have an absorption maximum at 470 nm (coincident with that in Fig. 7), it appears as if the product is a mixture of Mn^{3+} and MnO_2 with the former predominating. The more complete reduction observed in this case could be related to the presence of acidic compounds in the solution.

The other reductant that produced an atypical product was perfluorocyclohexene (Fig. 8). The lower oxidation state of the product of this reaction (+3.25), which is similar to that previously reported for the oxidation of 5-fluorouracil (6), may also have been caused by the presence of acidic molecules in the solution. The initially formed product, **2**, would readily release HF to the solution as in eq. [6].

[6]
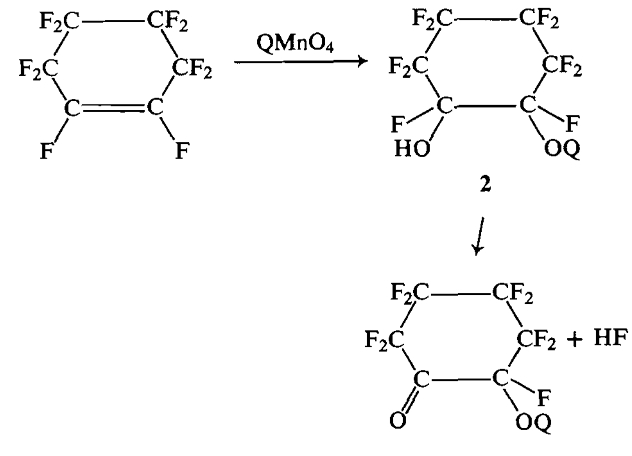

Summary

In conclusion, the results described herein establish that the brown-yellow product of these reactions is actually a soluble form of manganese dioxide. It is not a manganese(V) compound, as has been presumed in previous publications (5). The properties of this product indicate that it is a colloid, and flocculation appears to be responsible for the lack of good isosbestic points under certain conditions. For example, it can be seen from Fig. 3 that the crossover points near 490 nm move progressively to higher wavelengths—exactly the effect expected if flocculation of the MnO_2 particles was occurring as the redox reaction progressed. When a large excess of alkene

is present flocculation is suppressed, presumably because the colloidal manganese dioxide particles are stabilized by complexation with unsaturated compounds.

The presence of small amounts of water dramatically increases the rate of flocculation, whereas an excess of quaternary ammonium ion has the converse effect (Fig. 6).

Finally, when acidic compounds are present, manganese is reduced to a lower oxidation state and the spectral changes observed as the reaction progresses are greatly changed (Fig. 8).

Acknowledgments

J. F. Perez-Benito wishes to thank the Spanish Ministry of Education and Science for a grant to study in Canada, thus making possible his participation in this project. Financial assistance from the Natural Sciences and Engineering Research Council of Canada is gratefully acknowledged.

1. K. B. WIBERG, C. J. DEUTSCH, and J. ROČEK. J. Am. Chem. Soc. **95**, 3034 (1973).
2. D. G. LEE and J. R. BROWNRIDGE. J. Am. Chem. Soc. **95**, 3033 (1973); **96**, 5517 (1974).
3. G. WAGNER. J. Russ. Phys. Chem. Soc. **27**, 219 (1895); K. B. WIBERG and K. A. SAEGEBARTH. J. Am. Chem. Soc. **79**, 2822 (1957); R. STEWART. *In* Oxidation in organic chemistry. Part A. Academic Press, New York. 1965. p. 42; D. G. LEE. *In* Oxidation in organic chemistry. Part D. Academic Press, New York. 1982. p. 175.
4. L. I. SIMÁNDI and M. JÁKY. J. Am. Chem. Soc. **98**, 1995 (1976).
5. D. G. LEE and K. C. BROWN. J. Am. Chem. Soc. **104**, 5076 (1982).
6. F. FREEMAN, C. O. FUSELIER, and E. M. KARCHEFSKI. Tetrahedron Lett. 2133 (1975); L. I. SIMÁNDI, M. JÁKY, F. FREEMAN, C. O. FUSELIER, and E. M. KARCHEFSKI. Inorg. Chim. Acta, **31**, L457 (1978); F. FREEMAN, C. O. FUSELIER, C. R. ARMSTEAD, C. E. DALTON, P. A. DAVIDSON, E. M. KARCHEFSKI, D. E. KROCHMAN, M. N. JOHNSON, and N. K. JONES. J. Am. Chem. Soc. **103**, 1154 (1981).
7. T. OGINO and K. MOCHIZUKI. Chem. Lett. 443 (1979); T. OGINO. Tetrahedron Lett. **21**, 177 (1980).
8. H. KARAMAN, R. J. BARTON, B. E. ROBERTSON, and D. G. LEE. J. Org. Chem. **49**, 4509 (1984).
9. G. M. BARROW. Physical chemistry. 2nd ed. McGraw–Hill, New York. 1966. p. 803.
10. M. FIESER and L. F. FIESER. Reagents for organic synthesis. Vol. 1. Wiley, New York. 1967. p. 943.
11. W. S. BREY. Principles of physical chemistry. Appleton, New York. 1958. p. 251.
12. D. ARNDT. Manganese compounds as oxidizing agents in organic chemistry. Open Court, La Salle, Illinois. 1981. p. 27.

Charge distributions and chemical effects. XXXIX. Atomization energies and *in situ* atomic orbitals in ethylenic hydrocarbons

SÁNDOR FLISZÁR, GIUSEPPE DEL RE,[1] AND MICHEL COMEAU
Département de Chimie, Université de Montréal, C.P. 6210, Succ. A, Montréal, (P.Q.), Canada H3C 3V1

Received May 9, 1985

SÁNDOR FLISZÁR, GIUSEPPE DEL RE, and MICHEL COMEAU. Can. J. Chem. **63**, 3551 (1985).

A simple expression already used with success for computing atomization energies of alkanes and other molecules has been applied to alkenes. This has required evaluation of a term F which had been taken equal to zero in previous applications of the same equation. In order to explain the physical meaning of this novelty, we have been led to introduce a "principle" stating that the electrostatic potential created by σ electrons associated to any given atom of a molecule is well reproduced by a single charge centered at the nucleus and that the special behavior of alkenes is associated with residual π AO-centroid displacements with respect to the carbon nuclei. Direct computation of *in situ* valence AO's from optimized 4-31G* molecular orbitals yields a *pd* hybridization of the π AO's of the carbon atoms which does account for most of the expected F value. This indicated that use of simple equations derived from general theory and the application of simple principles or rules to the analysis of sophisticated molecular computations can yield a simple and quantitatively satisfactory picture of molecular reality.

SÁNDOR FLISZÁR, GIUSEPPE DEL RE et MICHEL COMEAU. Can. J. Chem. **63**, 3551 (1985).

On applique aux alcènes l'expression simple qui a permis de calculer les énergies d'atomisation des alcanes et d'autres molécules. Cette nouvelle utilisation implique l'évaluation d'un terme F qui avait été considéré nul dans les applications antérieures de cette équation. Dans le but d'expliquer la signification physique de cette nouvelle approche, nous sommes conduits à introduire un "principe" qui veut que le potentiel électrostatique créé par les électrons σ associés à n'importe quel atome d'une molécule est bien reproduit par une charge unique centrée sur le noyau. De plus, le comportement particulier des alcènes est associé à des déplacements par rapport aux noyaux des carbones, de centroides d'OA π. Les calculs des OA de valence in situ à partir des orbitales moléculaires optimisées 4-31G* conduisent à une hybridation *pd* des OA π des atomes de carbone qui rend compte des valeurs de F attendues. Ceci indique que l'utilisation d'équations simples dérivées de la théorie générale et l'application de principes ou de règles simples à l'analyse des calculs moléculaires compliqués peuvent conduire de façon satisfaisante à une image simple et quantitative de la réalité moléculaire.

[Traduit par le journal]

Introduction

Chemical bonds play an important role in the description of molecular systems. They are best investigated at 0 K, with reference to equilibrium molecules in their hypothetical vibrationless state (1). The corresponding atomization energy

$$[1] \quad \Delta E_a^* = \Sigma\epsilon_{ij} + \Delta E_{nb}$$

is conveniently partitioned into a non-bonded part, ΔE_{nb}, and a sum in which each ϵ_{ij} describes the energy contribution of an individual bonded atom pair ij. Estimates of ΔE_{nb} in σ systems (1–4) indicate that ΔE_{nb} is ~0.02–0.05% of ΔE_a^*. Hence, the theory of ΔE_a^* is essentially a theory of bond energies, at least in most organic molecules. Typical ethylenic carbon–carbon double bonds and related topics of fundamental importance in the theory of chemical bonding are the subject of the work reported here.

The scope of this study is best outlined by briefly reviewing relevant earlier results. Reference bond energies, ϵ_{ij}^0, can be deduced (2, 5) from appropriately selected reference molecules, e.g. $\epsilon_{C=C}^0 = 139.27$ kcal mol^{-1} for ethylene (6) and $\epsilon_{C-C}^0 = 69.633$, $\epsilon_{CH}^0 = 106.806$ kcal mol^{-1} for ethane (2). Straightforward addition of reference bond energies does not provide correct descriptions of alkanes or alkylsubstituted ethylenes, since molecular electroneutrality is not automatically ensured in this manner (1, 2). Charge normalization adds a term to $\Sigma\epsilon_{ij}^0$, thus leading to correct values of ΔE_a^*, the correction being of great numerical as well as theoretical importance. The present investigation is devoted to the approach that has permitted to bridge the gap between $\Sigma\epsilon_{ij}^0$ and ΔE_a^* in terms of changes in nuclear–electronic interactions accompanying charge normalization.

The key to the charge renormalization effects is provided by the quantity ΔV_{nc}, viz. the total change in the nuclear–electronic potential energy occurring when the valence-electron population of each atom i changes from N_i^0 (the value in the reference molecule) to $N_i = N_i^0 + \Delta N_i$, with the constraint that $\Sigma_i N_i$ should satisfy molecular electroneutrality. In the spirit of the Politzer–Parr core-valence separation (7), we write (1, 2)

$$[2] \quad \Delta V_{nc} = -\sum_i Z_i^{eff}\Big[N_i\langle r_i^{-1}\rangle - N_i^0\langle r_i^{-1}\rangle^0 + \sum_{j\neq i}(N_j\langle r_{ij}^{-1}\rangle - N_j^0\langle r_{ij}^{-1}\rangle^0)\Big]$$

where the Z_i^{eff}'s are "effective" nuclear charges (e.g., 4 for carbon). The quantities appearing in the square brackets are defined in terms of a suitable partitioning of the molecular electron density into atomic contributions ρ_i and of the equilibrium coordinates, $\boldsymbol{r}_i$, of the nuclei, i.e.,

$$[2a] \quad \begin{aligned} &\int \frac{\rho_i(\boldsymbol{r})}{|\boldsymbol{r}-\boldsymbol{r}_i|}\,d\boldsymbol{r} = N_i\langle r_i^{-1}\rangle \text{ with } \int\rho_i(\boldsymbol{r})\,d\boldsymbol{r} = N_i \\ &\int \frac{\rho_j(\boldsymbol{r})}{|\boldsymbol{r}-\boldsymbol{r}_i|}\,d\boldsymbol{r} = N_j\langle r_{ij}^{-1}\rangle \text{ with } \int\rho_j(\boldsymbol{r})\,d\boldsymbol{r} = N_j \end{aligned}$$

Thus, $\langle r_i^{-1}\rangle$ and $\langle r_{ij}^{-1}\rangle$ can be interpreted as the average inverse distances from Z_i^{eff} to the centers of the electron populations N_i and N_j, respectively; the superscript zero indicates the corresponding expressions for the reference molecule. Considering, where appropriate, also modifications in bond lengths, the ac-

[1] Visiting scientist. Permanent address: Cattedra di Chimica Teorica della Facoltà di Scienze, Via Mezzocannone 4, I-80134, Napoli, Italia.

companying change in nuclear repulsion can be added to the above expression in the form

$$[3] \quad 2(V_{nn} - V_{nn}^0) = \sum_i \sum_j Z_i^{eff} Z_j^{eff} [\langle R_{ij}^{-1}\rangle - \langle R_{ij}^{-1}\rangle^0]$$

where the summation extends over all bonded atom pairs. Combining eqs. [2] and [3], we obtain $\Delta(V_{nc} + 2V_{nn})$, i.e., the change in $(V_{nc} + 2V_{nn})$ resulting from changes in electron populations and bond lengths. Following Politzer's well documented approximation, $E \simeq (3/7)(V_{nc} + 2V_{nn})$, for the total molecular energy (5, 8), we can thus easily deduce energy changes resulting from modifications in orbital shapes and equilibrium distances. The general expression obtained from eqs. [1]–[3] is

$$[4] \quad \Delta E_a^* = \Sigma\epsilon_{ij}^0 + F + \sum_{i \neq j} \sum_j a_{ij}\Delta q_i + \Delta E_{nb}$$

where $\Sigma_i\Sigma_j a_{ij}\Delta q_i$ is the energy associated with the changes, Δq_i, of the net atomic charges with respect to the reference molecule. The calculation of all the terms of eq. [4] but F has been described elsewhere (1, 2, 6) and will not be discussed here. Attention is focussed on

$$[5] \quad F = -\frac{3}{7}\sum_i \sum_j Z_i^{eff} q_j(\langle r_{ij}^{-1}\rangle - \langle r_{ij}^{-1}\rangle^0) - \frac{3}{7}\sum_i \sum_j Z_i^{eff} Z_j^{eff}[\langle R_{ij}^{-1}\rangle - \langle R_{ij}^{-1}\rangle^0 - (\langle r_{ij}^{-1}\rangle - \langle r_{ij}^{-1}\rangle^0)]$$

which contains information regarding orbital shapes and internuclear distances. In [5], $q_j = Z_j^{eff} - N_j$ is the net atomic charge of atom j bonded to i.

Physical interpretation of F

First of all, let us point out that calculations of ΔE_a^* assuming F to be negligible have given agreement with experiment to within ~0.2 kcal mol^{-1} (average deviation) for over 70 saturated hydrocarbons with energies ranging between 400 and 4000 kcal mol^{-1} (1, 2). This is a strong indication that F is in fact negligibly small in saturated hydrocarbons. With this point in mind, let us define the external electrostatic potential at atom i as

$$[6a] \quad V_i = -\sum_j (N_j\langle r_{ij}^{-1}\rangle - Z_j^{eff}R_{ij}^{-1})$$

Let us also introduce the corresponding expression obtained when the electron populations are kept at their proper values in the molecule under study, but the inverse-distance terms referring to the bonded partners j are replaced by their values in the reference molecule, i.e.,

$$[6b] \quad V_i^{nr} = -\sum_j [N_j\langle r_{ij}^{-1}\rangle^0 - Z_j^{eff}(R_{ij}^{-1})^0]$$

Then, clearly,

$$[7] \quad F = -\frac{3}{7}\sum_i Z_i^{eff}(V_i - V_i^{nr})$$

The condition that F should vanish can be satisfied either because the various atomic contributions to F cancel, or because the individual terms in the summation over i vanish. Since it seems unlikely that cancellation of terms associated to different atoms would take place systematically in a large number of molecules, we shall assume that the results obtained for alkanes mean that, to a good approximation,

$$[8] \quad V_i \simeq V_i^{nr}$$

for any atom of any saturated hydrocarbon.

The most direct interpretation of eq. [8] follows from the observation, suggested by eqs. [6a], [b], that F is essentially a "relaxation" term. In fact, $V_i - V_i^{nr}$ represents the difference between the electrostatic potential at the ith nucleus in the given molecule and the potential which the same nucleus would feel if the atomic orbitals and the equilibrium distances remained the same as in the reference molecule in spite of the change in electron populations. With this picture in mind, eq. [8] reads: "Whenever the atoms under consideration in a given molecule are in the same valence states as in the reference molecule, the relaxation process is such that the potential created by the other atoms at the ith nucleus is the same as would be predicted by leaving the pertinent internuclear distances and the shapes of atomic electron densities as they are in the reference molecule, the electron populations being changed as required by the new situation". This may mean that changes in the nuclear positions and in the centroids of the atomic orbitals always take place so as to leave the ratio between the expectation value $\langle r_{ij}^{-1}\rangle$ and R_{ij}^{-1} the same as in the reference molecule or, at least, that changes are insignificant. It is impossible to decide which alternative applies from a study of the paraffins, since their bond distances and atomic orbitals are expected to be practically constant.

In contrast, consideration of ethylene could provide an instructive test. Computation of its atomization energy with $F = 0$ yields a result larger than the experimental one by ~9.6 kcal mol^{-1}. Similarly, an error of ~19.2 kcal mol^{-1} would be made in the computation of tetramethylethylene. Although estimates of this type are not free from difficulties, which are discussed in detail further below, the uncertainty they carry does not exceed a few tenths of a kcal mol^{-1} for one CH or CC bond, meaning that the discrepancies between theory and experiment are certainly real. Therefore, we have investigated the possibility that they may be associated with changes in valence states resulting in $F \neq 0$.

The ethylenic C=C bond

A simple way of satisfying eq. [8] consists in assuming that

$$[9] \quad \langle r_{ij}^{-1}\rangle \simeq R_{ij}^{-1}$$

when all bonds are σ bonds at their equilibrium geometries,[2] as in our calculations on the alkanes. Defining a density $\rho_{\mu j}$ and an electron population $N_{\mu j}$ associated with each valence atomic orbital μ of atom j, such that[3]

$$[10] \quad \int \frac{\rho_{\mu j}(\boldsymbol{r})}{|\boldsymbol{r} - \boldsymbol{r}_i|} d\boldsymbol{r} = N_{\mu j}\langle r_{\mu ij}^{-1}\rangle$$

we can write

[2] This simplifying hypothesis is supported by examination of SCF potentials at the nuclei, showing that eq. [9] holds at least to within ~5%, both for CH and CC bonds (to be published). It is especially useful here because it permits one to isolate the relevant conceptual points in a straightforward manner within the simple framework of the point-charge approximation.

[3] Definition [10] implies that orbital products can be well approximated in the average by some Mulliken-type expansion (9, 10). This does not imply that the populations introduced are gross Mulliken populations (11).

$$[11]\quad \sum_{\mu} \frac{N_{\mu j}}{N_j} \langle r_{\mu ij}^{-1} \rangle = 1/R_{ij}$$

Equation [11] reads: the average of the expectation values of $|r - r_i|^{-1}$ for the various valence AO's of atom j, weighted by the ratios of the orbital populations to the total atomic population of atom j equals the inverse of the i–j distance. For all their simplicity, eqs. [10] and [11] cannot be tested numerically by direct calculation. The reason is that the partitioning of the total electron density into atomic contributions is still an open question, in spite of an important conceptual step forward due to Parr (12). A practical step in the same direction is the construction of suitable *in situ* valence atomic orbitals (VAO) from accurate *ab initio* computations (13), as advocated a long time ago by Mulliken (14) and discussed by one of us (15). As will be seen, such *in situ* VAO's do provide useful information, but they are of no help in solving the additional problem of assigning suitable populations to the orbitals and of dividing overlap populations into atomic contributions. In view of this situation, we take eq. [8] and the sufficient (not necessary) condition [11] as statements whose validity rests on empirical evidence, at least for saturated hydrocarbons. Their extension to unsaturated hydrocarbons remains a problem, even though the success of approximations of molecular properties in terms of point charges located at the nuclei could be traced back to a general principle of that kind, as suggested long ago (16). A solution can be found by the following argument.

In paraffins, the bonds formed by carbon are either CH or CC single bonds; of course, the electron density around C is not exactly spherical, but special multipole contributions appear to vanish to the extent that one can regard that the CH electron density adjusts to that of CC, and conversely, so that electrostatic effects are adequately described by a point charge located at C. Now suppose that one bond to hydrogen is removed and replaced by a π bond of the same atom to another carbon atom. Changes in geometry and hybridization will, of course, occur but, at least to first order, the resulting π atomic orbital will not be able to participate in a possible mutual readjustment of the AO centroids, due to its different symmetry. Thus, we have to expect that condition [11] also applies to the simple mono-olefins considered here, with the restriction that it only concerns σ orbitals. In other words, ethylenic carbon atoms will obey a "principle" of σ-bond electrostatic balancing, i.e.,

$$[12]\quad N_j\langle r_{ij}^{-1}\rangle = \int \frac{\rho_j(\boldsymbol{r})}{|\boldsymbol{r}-\boldsymbol{r}_i|}\,\mathrm{d}\boldsymbol{r} = \sum_{\mu}\int \frac{\rho_{\mu j}(\boldsymbol{r})}{|\boldsymbol{r}-\boldsymbol{r}_i|}\,\mathrm{d}\boldsymbol{r}$$
$$= \frac{N_j - N_{j\pi}}{R_{ij}} + N_{j\pi}\langle r_{\pi ij}^{-1}\rangle$$

Let us now consider $\langle r_{\pi ij}^{-1}\rangle$. A π atomic orbital is essentially a pure p orbital; if there is any polarization (as will be discussed below), this will involve a very small displacement, $\Delta \boldsymbol{r}_{\pi j}$, of the centroid of the orbital. Then a monopole approximation of the π term of eq. [12] suffices, giving

$$[13]\quad \langle r_{ij}^{-1}\rangle = \frac{1 - N_{j\pi}/N_j}{R_{ij}} + \frac{N_{j\pi}/N_j}{|\boldsymbol{r}_j + \Delta\boldsymbol{r}_{\pi j} - \boldsymbol{r}_i|}$$

If this simple expression is sufficient to account for the discrepancies observed in calculations of olefins based on alkane reference bonds, we can claim that the "principle" [11] is, indeed, satisfied by ethylenic hydrocarbons.

Turning now to direct theoretical evaluations, we consider $|\Delta \boldsymbol{r}_{\pi j}|$ as the displacement (on the C═C axis) of the centroid of the π orbital with respect to the center j. Of course, such a displacement can differ from zero only if some hybridization is allowed which, in the case of a π orbital, must consist in admixture of the suitable $d\pi$ orbital. We have determined the hybrid in question from 4-31G calculations with d polarization functions for carbon and optimization of all scale factors, followed by a calculation of *in situ* valence orbitals, and of their characteristics, according to refs. 13, 17[4] (Appendix I).

TABLE 1. A calculation of atomization energies, eq. [4], using ethane C—H and C—C reference bonds with and without SCF π-AO centroids

	ΔE_a^*, kcal mol^{-1}		
Molecule	$F = 0$	Eqs. [4], [5], [13]	Exptl.[a]
Ethylene	571.80	564.12	562.10
Propene	870.62	861.02	858.56
Tetramethylethylene	1765.94	1749.58	1746.64

[a] Extracted from ref. 6.

In ethylene, the centroid of the π orbital is found to lie 0.0292 Å from the carbon atom, on the C═C axis. In propene, the centroid inward shifts, $\Delta r_{\pi j}$, are 0.0281 Å from C-1 and 0.0299 Å from C-2. The shift is 0.0280 Å in tetramethylethylene. Using the ethylene reference populations $N_{j\pi} = 1$ and $N_j = 3.9923$ e (6), we calculate the appropriate $\langle r_{ij}^{-1}\rangle$'s from eq. [13] and the experimental geometries indicated in ref. 18, as explained in Appendix II. Finally, F is deduced from eq. [5] and used in the calculation of ΔE_a^* by means of eq. [4]. The results are given in Table 1.

The following should be considered in an assessment of the approach having led to these results. In the first place, π orbital centroids deduced from SCF calculations clearly support the validity of the first-order approximation, eq. [13]: $\langle r_{ij}^{-1}\rangle$ values estimated in this manner lead to acceptable energies. In the present approach, improvements in the SCF wave functions consistently improve the agreement with experimental energies,[5] thus suggesting that, in fact, the quality of eq. [13] may even be better than what could be inferred at first sight from Table 1. It is also important to point out that the approximation involved in the definition [5] of F itself is excellent.[6] Therefore, the quality of the energies calculated from eq. [4] rests now primarily with the proper evaluation of $\langle r_{ij}^{-1}\rangle$. Tentatively, assuming that $\langle r_{ij}^{-1}\rangle$ is, indeed, adequately described by eq. [13], a 0.036 Å inward shift of the π orbital centroid can be shown to yield energies which are at the level of experimental accuracy. The true merits of this fine-tuning, which appears to be a realistic one when compared to its SCF counterpart, ~0.03

[4] An analysis of the σ orbitals will be presented separately. Here, we only point out that the σ hybrid AO's of carbon in ethylene, as obtained with the input data of Table 2 and Boys' localization criterion, appear to satisfy eq. [11] with entirely reasonable populations: the position vectors of their centroids give a zero population-weighted average if the CH hybrids are assigned ~0.96 e, and the CC hybrid 1.07 e.

[5] The use of standard exponents in the calculation of ethylene, for example, leads to $\Delta r_{\pi j} = 0.026$ Å, $\langle r_{ij}^{-1}\rangle = 0.49007$ au, $F = -6.82$, and $\Delta E_a^* = 564.98$ kcal mol^{-1}, which represents a worsening of the final result by 0.86 kcal mol^{-1} with respect to a fully optimized calculation.

[6] This approximation rests with the factor (3/7) which is used instead of its exact counterpart (5, 8). The latter, deduced from Hartree–Fock calculations, differs from 3/7 by no more than 0.5% for the molecules under scrutiny (1).

Å, are best illustrated by the following numerical examples, both as regards its practical aspects in applications of this theory to actual chemical problems and its conceptual simplicity disclosing a new insight into the nature of the chemical bond.

Energy calculations at the level of experimental accuracy

No test of a theory could be more severe than a direct comparison with experimental results. All the parameters required in energy calculations of saturated hydrocarbons were deduced from theory (1, 2). The only minor adjustment has concerned the ethane carbon net charge, selected as reference, in that the value 35.1 me was preferred over that derived from optimized 4-31G calculations with configuration interaction, 37.8 me — an adjustment which is easily justifiable on theoretical grounds (19). In view of the quality of the results thus obtained, we have no hesitation in treating the alkyl parts of ethylenic hydrocarbons in precisely the same manner, using the parameters and the charges described earlier (1, 2, 6). Namely, we use

$$[14] \qquad \epsilon_{ij} = \epsilon_{ij}^{0} + a_{ij}\Delta q_i + a_{ji}\Delta q_j$$

with ϵ_{CH}^{0} = 106.806 kcal mol^{-1}, $a_{HC} = -1.007$, and $a_{CH} = -0.394$ au for ethane-like CH bonds, and ϵ_{CC}^{0} = 69.633 kcal mol^{-1}, $a_{CC} = -0.777$ au for sp^3–sp^3 CC bonds.

The problem encountered here lies in the evaluation of CH and CC bonds formed by an ethylenic sp^2 carbon, because the corresponding a_{ij} values, $a_{CH} = -0.335$ and $a_{CC} = -0.718$ au, respectively, differ from those involving a sp^3 carbon atom. Tentatively taking the averages of the appropriate a_{ij}'s, we obtain for the CH and C(sp^2)—C(sp^3) bonds formed by an ethylenic carbon with net charge 7.7 me (1 au = 627.51 kcal mol^{-1}),

$$[15a] \qquad \epsilon_{CH} = 106.806 + \frac{1}{2}(-0.394 - 0.335) \times (-27.4 \times 10^{-3}) \times 627.51 = 113.07 \text{ kcal mol}^{-1}$$

$$[15b] \qquad \epsilon_{CC} = 69.633 + \frac{1}{2}(-0.777 - 0.718) \times (-27.4 \times 10^{-3}) \times 627.51 = 82.49 \text{ kcal mol}^{-1}$$

The increase in electron population, 27.4 me, accompanying the replacement of the ethane carbon by that of ethylene has thus been taken care of. In spite of minor uncertainties, eqs. [15*a*], [*b*] appear to be reasonably accurate. (Indeed, their use yields excellent results in the calculation of benzenoid CH bonds and of CC single bonds like that found in toluene, for a collection of 36 benzenoid hydrocarbons (20).) While the energy change associated with π-bond formation is included in $\epsilon_{C=C}^{0}$ = 139.27 kcal mol^{-1}, the effects related to the centroid shift of the atomic π orbitals still need to be evaluated.

In principle, one can resort to calculations of F — a task which is not free from difficulties, particularly at a level approaching that of experimental accuracy. It is simpler to proceed as follows, by taking advantage of the results indicated in Table 1. The theoretical contributions to F (Appendix II) are −1.92 for each ethylene CH and −4.09 kcal mol^{-1} for each tetramethylethylene CC single bond; the corresponding contributions of the bonds formed by the propene C-2 atom are −1.76 and −4.31 kcal mol^{-1}. The combined contributions are virtually the same in both cases. Similarly, three ethylene CH plus one tetramethylethylene CC single bond total −9.85 kcal mol^{-1} — an approximation which is reasonably close to the theoretical value, F = −9.60 kcal mol^{-1}, deduced for propene. The regularities are striking, despite the marked differences both in geometrical parameters and in the SCF Δr values between the molecules involved in this comparison. Capitalizing now on these regularities, we propose the following simple approximation which is consistent with the essential theoretical features disclosed in this study. Assuming an inward shift of 0.036 Å for a π orbital and R_{ij}'s of 1.08 and 1.53 Å for the CH and CC single bonds, respectively, at an angle of ~123° with the double bond, eq. [13] yields $\langle r_{HC}^{-1}\rangle = 0.48758$ and $\langle r_{CC}^{-1}\rangle = 0.34463$ au. The F values deduced from eq. [5] are thus −2.39 for *one* CH bond and −4.80 kcal mol^{-1} for *one* C(sp^2)—C(sp^3) bond. Finally, including these results into the ϵ_{ij}'s calculated above, eqs. [15*a*], [*b*], one obtains

$$[16a] \qquad \epsilon_{CH}^{0} = 110.68 \text{ kcal mol}^{-1}$$

$$[16b] \qquad \epsilon_{CC}^{0} = 77.69 \text{ kcal mol}^{-1}$$

for the new reference bonds involving an ethylenic C(sp^2) atom, with net charge 7.7 me. The hydrogen and C(sp^3) net charges are still those of ethane, −11.7 and 35.1 me, respectively. As regards the values (16*a*], [*b*], it is clear that their derivation is well within the limits of uncertainty set by our SCF analysis of charge centroids and by eq. [13].

The new ϵ_{ij}^{0}'s described in eqs. [16*a*], [*b*] were tailored to include the characteristic features of the sp^2 carbon of ethylene, as regards both the magnitude and the location of its charge. The use of these reference bond energies in the construction of the $\Sigma\epsilon_{ij}^{0}$ part of eq. [4] considerably simplifies the calculation of atomization energies because, under these circumstances, F should again be expected to vanish.[7] Indeed, for a collection of ~50 olefins calculated in this approach (6, 21), the average deviation between theoretical and experimental atomization energies is ~0.25 kcal mol^{-1}. Briefly, we are back at the point which has initiated our argument, eq. [8]: the use of the appropriate set of reference bond energies, incorporating the particular characteristics regarding charge centroids, suffices in the calculation of ΔE_a^* energies, at least within the present limits of experimental accuracy. This holds true also for benzenoid hydrocarbons (20), ethers, aldehydes, and ketones (3). The validity of eq. [8] is gratifying because it measures, in a way, the degree of transferability of basic bond properties — a transferability which appears to be pronounced, indeed.

Conclusion

The discussion and results reported above are to some extent a further step toward solving a persistent problem of theoretical chemistry: bridging the gap between the apparent simplicity of observed molecular behavior and the intricacies and ambiguities which plague the translation of accurate quantum mechanical results into simple chemical concepts and rules. The extraordinary accuracy with which eq. [4] allows prediction of atomization energies is a strong indication that hidden regularities can be discovered as a result of patient processing of general theory, but the price to be paid is that the use of final equations such as [4] often rests on simplifying assumptions

[7] The following may serve as an example. Using the ethylene-H net charge, −3.85 me (corresponding to its C charge of 7.7 me), i.e., Δq_H = 7.85 me, it results that $a_{HC}\Delta q_H = -4.96$ and, from [16*a*], ϵ_{CH} = 105.72 kcal mol^{-1}. Four of these CH bonds, plus the theoretical $\epsilon_{C=C}^{0}$ = 139.27 double bond contribution, lead to $\Delta E_a^*(C_2H_4)$ = 562.15 kcal mol^{-1}, in good agreement with its experimental counterpart, 562.22 kcal mol^{-1}.

which cannot be proven *a priori* to be of minor import. In the case at hand, those approximations are (*i*) the proportionality between the nuclear–electronic potential energy and the total (BO) energy and (*ii*) the point-charge model of a saturated hydrocarbon molecule. The agreement within experimental accuracy of over 170 predicted and experimental atomization energy values provides an *a posteriori* argument for claiming that those approximations are in fact very good ones. But then, as has been shown above, they must be interpreted as general rules which the partitionings of electron densities obtained from accurate electronic wavefunctions must obey. This is especially important in problems like the extension of eq. [4] to cover olefins as well as paraffins; for that extension, as has been seen, requires explicit introduction of the $\sigma-\pi$ separation. As a consequence, the point-charge approximation must be reformulated as a "principle" valid for the averages of electrostatic potentials of the σ orbitals of any given atom in a hydrocarbon molecule. This has two distinct practical advantages: it suggests a very simple numerical correction which allows application to ethylenic hydrocarbons of the same scheme as used for paraffins and assigns that correction an extremely simple physical interpretation (that of π centroid displacement) susceptible of numerical evaluation from accurate *ab initio* computations. On the other hand, it involves three important conceptual features: (*i*) the notion of *in situ* atomic orbitals, which must now be introduced explicitly, (*ii*) the postulate that there is a Mulliken-type partitioning of the molecular electron density into atomic orbital contributions which obeys the "principle of orbital balancing", and (*iii*) the implication that a CH bond or a CC bond in an olefin have the same basic properties as in a paraffin, except for the effective net charges of the atoms involved.

The internally coherent picture thus obtained, together with the excellent agreement with experiment also holding for olefins, provide a strong indication that the analysis of accurate *ab initio* computations into models, rules, and properties meaningful to chemists should be carried out precisely along the lines emerging from the above remarks. This conclusion, in addition to the concrete formulation of a principle valid within an atomic orbital picture, and to the explanation of the apparent deviation of the atomization energies of ethylenic hydrocarbons from the scheme valid for paraffins, seems to us a very important outcome of the application of eq. [4]: it points the way to a revised version of the elementary LCAO picture (whose merits are undeniable) where highly sophisticated computations provide the numerical support of an otherwise simple interpretational scheme.

Acknowledgements

The financial assistance given by the National Research Council of Canada is gratefully acknowledged. G.D.R. also thanks the CNR (Rome) and MPI (Rome) for support of the research projects within which this work has been carried out.

1. S. FLISZÁR. Charge distributions and chemical effects. Springer–Verlag, New York, NY. 1983.
2. S. FLISZÁR. J. Am. Chem. Soc. **102**, 6946 (1980).
3. S. FLISZÁR and M.-T. BÉRALDIN. Can. J. Chem. **60**, 792 (1982).
4. G. DEL RE. Gazz. Chim. Ital. **102**, 929 (1972).
5. S. FLISZÁR. Int. J. Quantum Chem. **26**, 743 (1984).
6. M.-T. BÉRALDIN and S. FLISZÁR. Can. J. Chem. **61**, 197 (1983).
7. P. POLITZER and R. G. PARR. J. Chem. Phys. **61**, 4258 (1974); P. POLITZER and R. G. PARR. J. Chem. Phys. **64**, 4634 (1976); S. FLISZÁR and H. HENRY. J. Chem. Phys. **67**, 2345 (1977); S. FLISZÁR. J. Chem. Phys. **79**, 3874 (1983).
8. P. POLITZER. J. Chem. Phys. **64**, 4239 (1976); R. G. PARR and S. R. GADRE. J. Chem. Phys. **72**, 3639 (1980); S. FLISZÁR, M. FOUCRAULT, M.-T. BÉRALDIN, and J. BRIDET. Can. J. Chem. **59**, 1074 (1981).
9. G. DEL RE, P. OTTO, and J. LADIK. Isr. J. Chem. **19**, 265 (1980).
10. Z. B. MAKSIĆ and K. RUPNIK. Croat. Chem. Acta, **56**, 461 (1983).
11. K. JUG. Theoret. Chim. Acta, **31**, 63 (1973).
12. R. G. PARR. Int. J. Quant. Chem. **26**, 687 (1984).
13. G. DEL RE and C. BARBIER. Croat. Chem. Acta, **57**, 787 (1984).
14. R. S. MULLIKEN. J. Am. Chem. Soc. **88**, 1849 (1966).
15. G. DEL RE. Adv. Quant. Chem. **8**, 95 (1974), and Sections IV and VII therein.
16. G. DEL RE. J. Chem. Soc. London, 4031 (1958).
17. C. BARBIER and G. DEL RE. Folia Chim. Theor. Lat. Madrid, **12**, 27 (1984).
18. (*a*) K. KUCHITSU. J. Chem. Phys. **44**, 906 (1966); (*b*) D. R. LIDE and D. CHRISTENSEN. J. Chem. Phys. **35**, 1374 (1961); (*c*) S. W. EISMA, C. ALTONA, H. J. GEISE, F. C. MIJLHOFF, and G. H. RENES. J. Mol. Struct. **20**, 251 (1974); (*d*) L. S. BARTELL, K. KUSHITSU, and R. J. DENUI. J. Chem. Phys. **35**, 1211 (1961); D. E. SHAW, D. W. LEPARD, and H. L. WELSH. J. Chem. Phys. **42**, 3736 (1965).
19. C. MIJOULE, J.-M. LECLERCQ, S. ODIOT, and S. FLISZÁR. Can. J. Chem. **63**, 1741 (1985).
20. S. FLISZÁR, G. CARDINAL, and N. A. BAYKARA. Can. J. Chem. In press.
21. S. FLISZÁR and G. CARDINAL. Can. J. Chem. **62**, 2748 (1984).
22. H. HENRY and S. FLISZÁR. J. Am. Chem. Soc. **100**, 3312 (1978).

Appendix I

Table 2 indicates relevant details concerning the basis and SCF results.

As concerns the calculation of *in situ* VAO's, we illustrate the procedure for the π bond, the one we are mainly interested here, and which is especially simple. Using the standard GO-SCF notation (cf. Table 2), the contribution of one carbon atom to the occupied π MO of ethylene has the form

$$[\mathrm{A1}] \quad c_\pi|\overline{p\pi}\rangle = 0.35975\,|2p_y\rangle + 0.32403\,|3p_y\rangle - 0.02715\,|4d_{yz}\rangle$$

where $|\overline{p\pi}\rangle$ and c_π denote that single normalized π atomic orbital and that coefficient which satisfy the equality [A1]. As is well kown, the p components of the right-hand term of eq. [A1] are not mutually orthogonal: their overlap is $S_{pp'}$ = 0.54632. Using this value, it is easy to see that

$$c_\pi = (0.35972^2 + 0.32403^2 + 0.02715^2 + 2 \times 0.35972 \times 0.32403 \times 0.54632)^{1/2} = 0.60209$$

and, consequently, that

$$[\mathrm{A2}] \quad |\overline{p\pi}\rangle = 0.59750\,|2p_y\rangle + 0.53817\,|3p_y\rangle - 0.04510\,|4d_{yz}\rangle$$

is the π hybrid orbital whose centroid we want to find. For the position vector of the centroid with respect to the center of the Gaussian functions entering [A2] we have

$$[\mathrm{A3}] \quad \Delta\boldsymbol{r} = \langle\overline{p\pi}|x|\overline{p\pi}\rangle\,\boldsymbol{i} + \langle\overline{p\pi}|y|\overline{p\pi}\rangle\,\boldsymbol{j} + \langle\overline{p\pi}|z|\overline{p\pi}\rangle\,\boldsymbol{k}$$

with $\boldsymbol{i}, \boldsymbol{j}, \boldsymbol{k}$ the standard unit vectors of the coordinate system. By symmetry, only the last term of the right-hand side of eq. [A3] is nonzero, and straightforward calculation of the appropriate linear combination of integrals over the gaussian functions entering [A2] gives the required result.

TABLE 2. Optimized results for ethylene, propene, and tetramethylethylene, from a 4-31G basis with d polarization functions on the olefinic carbon atoms

Molecule	E (au)[a]	Parameter	Scale factor Standard	Scale factor Optimized[b]	$C^{d}_{p\pi}$ [c]
C_2H_4	−77.957137	C s_K	1.00	1.00700	0.04510
		C $s_{L'}$ p'	1.00	0.99727	
		C $s_{L''}$ p''	1.04	1.00895	
		C d	1.00	0.95007	
		H s'	1.20	1.20650	
		H s''	1.15	1.14864	
C_3H_6	−116.938151	C_1 s_K	1.00	1.00699	0.04330
		C_1 $s_{L'}$ p'	1.00	0.99835	
		C_1 $s_{L''}$ p''	1.04	1.00680	
		C_1 d	1.00	0.94816	
		C_2 s_K	1.00	1.00703	0.04619
		C_2 $s_{L'}$ p'	1.00	0.99339	
		C_2 $s_{L''}$ p''	1.04	1.00812	
		C_2 d	1.00	0.95089	
		C_3 s_K	1.00	0.99939	
		C_3 $s_{L'}$ p'	1.00	0.99730	
		C_3 $s_{L''}$ p''	1.04	1.06972	
		H_c—(C_1) s	1.20	1.20339	
		H_c—(C_1) s''	1.15	1.14144	
		H_t—(C_1) s'	1.20	1.20408	
		H_t—(C_1) s''	1.15	1.14432	
		H—(C_2) s'	1.20	1.20567	
		H—(C_2) s''	1.15	1.13608	
		H_s—(C_3) s'	1.20	1.18868	
		H_s—(C_3) s''	1.15	1.11353	
		H_a—(C_3) s'	1.20	1.19029	
		H_a—(C_3) s''	1.15	1.11545	
C_6H_{12}	−233.868609	C_1 s_K	1.00	0.999	
		C_1 $s_{L'}$ p'	1.00	0.997	
		C_1 $s_{L''}$ p''	1.04	1.070	
		C_1 s_L	1.00	1.007	0.04322
		C_2 $s_{L'}$ p'	1.00	0.993	
		C_2 $s_{L''}$ p''	1.04	1.008	
		C_2 d	1.00	0.951	
		H_2 s'	1.20	1.190	
		H_2 s''	1.15	1.114	

[a] The energies obtained from the standard 4-31G basis are −77.921985, −116.901343, and −233.827831 au for C_2H_4, C_3H_6, and C_6H_{12}, respectively; with added standard d polarization functions, they are −77.953501, −116.934217, and −233.864190 au.

[b] The scale factors of tetramethylethylene were estimated from the optimized results obtained for propene.

[c] $C^{d}_{p\pi}$ is the d coefficient in the expansion of the normalized π hybrid of the olefinic carbon atom. Input geometries are from ref. 22. The use of experimental geometries leads to slightly higher SCF energies, with virtually no change in the centroids.

TABLE 3. The calculation of $\langle r_{ij}^{-1} \rangle$ from eq. [13] and of F from eq. [5][a]

Molecule	Bond $i-j$	R_{ij} (Å)	α (deg)	(R_{ij}^{-1}) (au)	Δr (Å)	$\langle r_{ij}^{-1}\rangle$ (au)	F^{bond} (kcal mol^{-1})
Ethylene	HC	1.076	121.7	0.49164	0.0292	0.48987	−1.92
Propene	H_t—C_1	1.081	121.5	0.48936	0.0281	0.48769	−1.81
	H_c—C_1	1.091	120.5	0.48488	0.0281	0.48328	−1.72
	H—C_2	1.090	119.0	0.48532	0.0299	0.48369	−1.76
	C(sp^3)—C_2	1.501	124.3	0.35250	0.0299	0.35151	−4.31
Tetramethylethylene	C(sp^3)—C	1.505	125	0.35150	0.0280	0.35056	−4.09

[a] The conversion factors 1 bohr = 0.529 Å and 1 hartree = 627.51 kcal mol^{-1} were used.

Appendix II

The calculation of F is presented here in a bond-by-bond approach, giving the individual contributions, F^{bond}; F is simply their sum over the 4 bonds formed by the two ethylenic carbons. Equation [5] is used with $(R_{ij}^{-1})^0 = \langle r_{ij}^{-1} \rangle^0$, taking ethane as reference, i.e., $(R_{\mathrm{CH}}^{-1})^0 = 0.48266$ au (corresponding to $R_{\mathrm{CH}} = 1.096$ Å) and $(R_{\mathrm{CC}}^{-1})^0 = 0.34553$ au (corresponding to $R_{\mathrm{CC}} = 1.531$ Å). The quantity $|\boldsymbol{r}_j + \Delta \boldsymbol{r}_{\pi j} - \boldsymbol{r}_i|$ of eq. [13] is

$$|\boldsymbol{r}_j + \Delta \boldsymbol{r}_{\pi j} - \boldsymbol{r}_i| = [R^2 + (\Delta r)^2 - 2R\,\Delta r \cos \alpha])^{1/2}$$

where R is the length of the C(sp^2)—i bond and α the angle it forms with C=C. The theoretical shift of the π-AO centroid (lying on C=C) is $\Delta \boldsymbol{r}$. Experimental geometries are from ref. 18, including that of ethane. The input parameters for use in, and the results deduced from, eq. [13] are indicated in Table 3, as well as the F^{bond} results derived from eq. [5].

The crystal field strength of the nitro ligand and the chemistry of the hexanitrocobaltate(III) anion

RICHARD J. BUIST, STEVE C. F. AU-YEUNG, AND DONALD R. EATON[1]
Department of Chemistry, McMaster University, Hamilton, Ont., Canada L8S 4M1

Received April 29, 1985

RICHARD J. BUIST, STEVE C. F. AU-YEUNG, and DONALD R. EATON. Can. J. Chem. **63**, 3558 (1985).

The chemical and spectroscopic properties of the hexanitrocobaltate(III) anion are not in accord with the classification of the N-bonded nitrite ion as a strong field ligand. The nitro groups are rapidly displaced by other ligands, including water, and in dilute aqueous solution spontaneous reduction to Co(II) occurs. Comparison of solid state and solution vibrational and ^{59}Co nmr spectra demonstrates that the principal species in solution is the same as in the solid. All ligands are N-bonded. However, within 2 or 3 min of dissolution new species appear. An electron transfer mechanism for ligand exchange is suggested. It is shown that the band at 480 nm arises from the first $d-d$ transition of the pentanitroaquacobaltate(III) ion and not from a hexanitrocobaltate(III) transition. The composition of the aged solutions has been studied by ^{59}Co, ^{14}N, and ^{17}O nmr. At least 10 different species are apparent in the ^{59}Co spectra. They have been assigned to mixed nitro/nitrito/aqua ions. Electron transfer can also lead to the formation of Co^{2+} and NO_3^- ions, both ions being detected by ^{14}N and ^{17}O nmr spectroscopy. The Co complexed nitro ligand has been detected for the first time in the ^{14}N nmr spectrum. Analysis of ^{59}Co chemical shifts shows that the crystal field strength of the nitro ligand falls steadily with the number of nitro groups in the molecule. The *cis* groups are four times more effective than the *trans* groups in causing this change. The cyano ligand shows the opposite behaviour — the crystal field strength increases with substitution and *trans* groups have a larger effect than *cis* groups. The reactions of the hexanitrocobaltate(III) ion with ethylenediamine and with cyanide ions have been studied by ^{59}Co nmr. Mixed nitro complexes are formed with ethylenediamine but mixed nitrito complexes predominate with cyanide.

RICHARD J. BUIST, STEVE C. F. AU-YEUNG et DONALD R. EATON. Can. J. Chem. **63**, 3558 (1985).

Les propriétés chimiques et spectroscopiques de l'anion hexanitrocobaltate(III) ne correspondent pas à la classification de l'ion nitrite lié par l'azote comme une ligand de champ fort. Les groupements nitro sont rapidement remplacés par d'autres ligands, y compris l'eau, et, en solutions aqueuses diluées, il se produit une réduction spontanée en Co(II). Une comparaison des spectres vibrationnels ainsi que rnm du ^{59}Co, tant à l'état solide qu'en solution, démontre que les principales espèces en solution sont les mêmes qu'à l'état solide. Tous les ligands sont liés par l'azote. Toutefois, il apparaît de nouvelles espèces en moins de trois minutes après leur dissolution. On suggère que l'échange de ligand se produit par un mécanisme impliquant un transfert d'électron. On démontre que la bande à 480 nm provient de la première transition $d-d$ de l'ion pentanitroaquacobaltate(III) et non pas d'une transition de l'hexanitrocobaltate(III). Faisant appel à la rmn du ^{59}Co, du ^{14}N et du ^{17}O, on a étudié la composition de solutions qui avaient vieilli. On peut déceler la présence d'au moins dix espèces différentes à l'aide de la rmn du ^{59}Co. On les a attribuées à des ions mixtes nitro/nitrito/aqua. Les transferts d'électrons peuvent aussi conduire à la formation des ions Co^{2+} et NO_3^- et ces deux ions ont pu être détectés par rmn du ^{14}N et du ^{17}O. Grâce à la rmn du ^{14}N, on a pu détecter pour la première fois la présence d'un ligand nitro complexé à un Co. L'analyse des déplacements chimiques du ^{59}Co démontre que la force du champ cristallin du ligand nitro diminue régulièrement avec le nombre de groupements nitro dans la molécule. Les groupements *cis* sont quatre fois plus efficace que les groupements *trans* pour provoquer ce changement. Avec les groupements cyano, on observe un comportement inverse — la force du champ cristallin augmente avec la substitution et les groupements *trans* ont un effet qui est plus grand que les groupements *cis*. Faisant appel à la rmn du ^{59}Co, on a étudié les réactions de l'ion hexanitrocobaltate(III) avec l'éthylènediamine et les ions cyanures. Il se forme des complexes nitro avec l'éthylènediamine; toutefois, avec les ions cyanures, il se forme des complexes nitrito.

[Traduit par le journal]

Introduction

Ligand field theory provides a convenient framework for the discussion of the chemistry of most transition metal complexes in which the metal is in one of its "normal" oxidation states. The spectrochemical series serves to systematize much of this chemistry. In writing down such a series the underlying assumption is that the bonding characteristics, and hence the relative crystal field splitting ability, of a given ligand will remain constant with changes of the metal ion and of the other ligands. The present paper will discuss a series of complexes for which the crystal field splitting of one ligand depends on the other ligands present.

A large number of transition metal complexes containing the nitro group have been reported. The area has been reviewed recently by Hitchman and Rowbottom (1). There are several possible modes of coordination for this ligand of which the most common are unidentate bonding by an oxygen to give a nitrito complex and unidentate binding through the nitrogen to give a nitro complex. The N-bonded nitro group is usually described as a strong field ligand. Thus Lever (2) places it between ethylenediamine and cyanide in the spectrochemical series with a ligand field strength approximately equal to that of bipyridyl or *o*-phenanthroline. Basolo and Pearson (3) attribute the high ligand field strength of the N-bonded nitro group to π donation from the metal ion. Most of the data used to reach these conclusions have been obtained from spectroscopic studies of Co(III) complexes since the Cr(III) compounds, for example, are usually O-bonded. Thus Wentworth and Piper (4) obtained D_q values in the range 3100−3200 cm^{-1} from the spectra of mono- and di-nitroCo(III) amines. This value may be compared with those of 3600 cm^{-1} for cyanide and 2530 cm^{-1} for ethylenediamine in Co(III) complexes.

The spectroscopy of Co(III) complexes containing more than two nitro groups is less well understood and the cobaltinitrite

[1]Author to whom correspondence should be addressed.

ion, $Co(NO_2)_6^{3-}$, in particular has been the subject of some disagreement. Most early papers assign a weak band around 480 nm to the $^1A_{1g} \rightarrow {}^1T_{1g}$ ligand field transition and this value has been used in all the reported correlations with ^{59}Co chemical shifts. Caulton and Fenske (5) pointed out that this value is inconsistent with the high D_q values quoted above and suggested that the band was a spin-forbidden ligand-to-metal charge transfer transition. Garnier (6) disagreed with this assignment, was able to move the band maximum to higher energy by some 4500 cm^{-1} by Gaussian analysis of the overlapping bands, and concluded that the $d-d$ transitions of all Co(III) nitro/ammine complexes were consistent with the rule of average environment. Barnes, Duncan, and Peacock (7) in a solid state study do not specifically refer to this band and suggest a rather different energy level scheme to that of Caulton and Fenske.

There have been numerous reports of the ^{59}Co nmr spectrum of the $Co(NO_2)_6^{3-}$ ion (8−14). Proctor and Yu (8) reported two lines and suggested that the less intense line probably arose from an isomeric molecule. Interestingly this is the first literature report of two separate nmr resonances from a single sample. Gasser and Richards (9) studied the temperature and nitrite ion concentration dependence of the relative intensities of the two lines and concluded that the high frequency line represented a mixture of an aquated hydrolysis product and a nitrito isomer. Several of these papers correlated the chemical shift of the more intense line with the 480 nm absorption band and reported satisfactory agreement with theory. More recently Rose and Bryant (14) found only a single ^{59}Co line which decreased in intensity with time. They also examined the ^{14}N spectrum showing that nitrate ion was present and inferred the existence of Co^{2+} from line broadening. The ^{59}Co nmr spectra of the series of complexes $Co(NH_3)_n(NO_2)_{6-n}$ have been reported by Juranic *et al.* (15) and by Pujar (16, 17). There is reasonable agreement between the two sets of experimental data. On increasing NO_2^- substitution the chemical shifts move to higher field, reach a maximum and then return to lower field. Juranic points out that this behaviour indicates a deviation from the rule of "average environment" for transition metal complexes. These authors also showed that the first absorption bands for the nitro/ammine complexes showed a parallel trend. Ethylenediamine/nitro complexes show similar behaviour. An earlier paper from this laboratory (18) proposed a simple point charge model for estimating ^{59}Co chemical shifts which gave satisfactory results for some 70 complexes involving a wide variety of ligands. If the nitro parameter obtained from the penta-ammine nitro complex is used to calculate the shift of the hexanitro complex a value of 5139 ppm is obtained compared with the experimental value of 7470 ppm. Clearly this simple model is unsatisfactory.

There are also anomalies in the aqueous chemistry of the cobaltinitrite ion. Crystal field theory predicts that strong field ligand will stabilize the d^6 Co(III) configuration relative to d^7 Co(II). Thus cobaltocyanide is a strong reducing agent and cobalticyanide shows no oxidizing properties. Cobalt amine complexes show similar, though less pronounced, oxidation/reduction properties. The spontaneous decomposition of cobaltinitrite solution to give Co^{2+} observed by Rose and Bryant (14) and by other authors is therefore unexpected. Slow ligand exchange is also the rule for strong field octahedral Co(III) complexes. Thus $Co(NH_3)_6^{3+}$ shows no ligand exchange in aqueous ammonia in 162 days (19) and $Co(CN)_6^{3+}$ is similarly inert. In contrast Matsko *et al.* (20) found half-lives of less than 10 min for the isotopic exchange between nitrite ions and cobaltinitrite. The replacement of nitro groups by amino acids has a very similar half-life (21).

The present paper is concerned with the origin of these spectroscopic and chemical anomalies. We have considered two main possibilities: (*a*) The major species in aqueous solution may not be the octahedral nitro complex. Interaction with the solvent may have led to isomerization, aquation, or some other chemical reaction which results in a product having properties different from those expected for the hexanitrocobaltate(III) anion. (*b*) The bonding properties and crystal field splitting of the nitro group may differ significantly in the Co hexanitro complex from the corresponding properties in complexes with only one or two nitro groups.

Possibility (*a*) will be discussed first.

Solid and solution spectra

The structure of the cobaltinitrite ion in the solid has been determined by X-ray crystallography (22). It is a regular octahedron with T_h symmetry with all of the nitro groups N bonded. If the structure in solution was different, the difference should be made apparent by a comparison of solid and solution spectra. Vibrational and ^{59}Co nmr spectra have been used for this purpose.

The infrared and Raman spectra of solid sodium cobaltinitrite have been measured. Both agree well with the spectra reported in the literature (23, 24). The Raman spectrum of aqueous sodium cobaltinitrite has also been measured and is in agreement with literature reports (23, 25). All the major peaks are shifted by no more than a few wavenumbers from the solid state frequencies.

The ^{59}Co nmr has been measured in the solid state. A single resonance is observed which shows some field dependent structure due to second order quadrupolar effects. The chemical shift is 7601 ± 3 ppm compared with 7470 ppm for the most intense resonance in aqueous solution. An analysis of the field dependent structure, which will be reported elsewhere, gives only a small quadrupole coupling constant as anticipated for a basically octahedral species. It would be desirable to obtain the spectrum in non-aqueous solution but low solubility limits the choice of solvents. In a 2.5:1 (w/w) mixture of acetonitrile and water the observed chemical shift is 7589 ppm and in a 1:1.5 (w/w) mixture of DMSO and water the shift is 7584 ppm. In each case and in a 1:1 (w/w) mixture of methanol and water the shift is 7546 ppm. In each case the shift in the non-aqueous solvent mixture is closer to the solid state value. These differences are compatible with hydrogen bonding effects. Shifts of 100−300 ppm to high field have been reported in hydrogen bonding solvents for cobalticyanide anions (26). Interaction with the hydrogen removes negative charge, encourages π back bonding and leads to a "stronger" field ligand. Thus the chemical shifts indicate the most hydrogen bonding in aqueous solution and the least in the solid state. The chemical shift in the solid is even less consistent with a strong field ligand than that in solution.

Solutions of cobaltinitrite are unstable below pH 4 decomposing with the evolution of N_2O_4. They are also unstable in basic solutions since cobalt hydroxides are precipitated. There is no significant variation of the ^{59}Co chemical shift over the accessible pH range.

We conclude that the major species in aqueous solutions of sodium cobalticyanide is the $Co(NO_2)_6^{3-}$ ion, that the resonance at 7470 ppm is correctly assigned to this species and that the

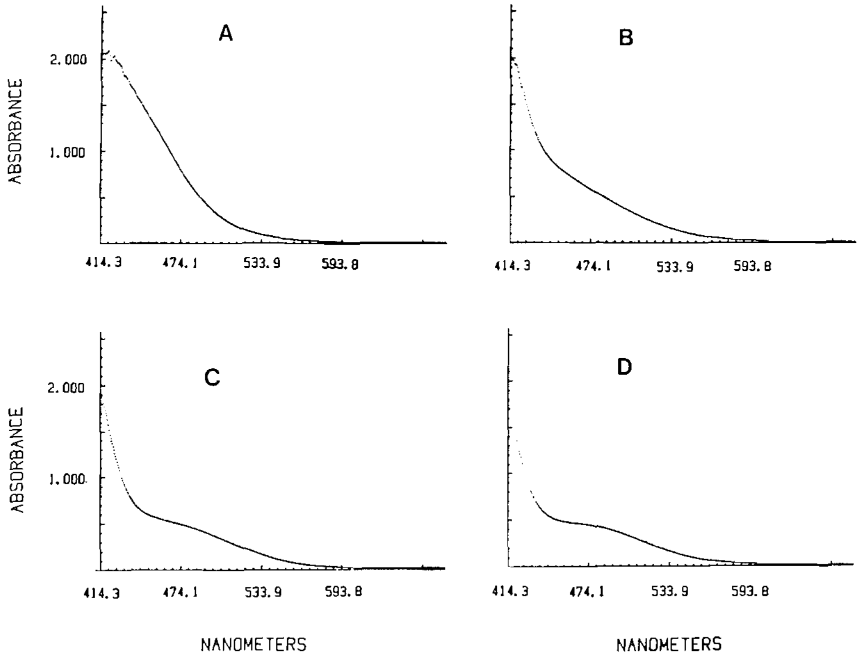

FIG. 1. Electronic spectra of 2.7 mM aqueous cobaltinitrite (l = 1 cm) for varying lengths of time after dissolution (A) t = 2 min, (B) t = 4 min, (C) t = 6 min, (D) t = 9 min.

perturbations due to hydrogen bonding or protonation produce only a modest high field shift.

The electronic spectrum of cobaltinitrite solutions

The above assignment of the ^{59}Co chemical shift raises the question of the correct assignment of the 480 nm band in the electronic spectrum. This band does not appear clearly in the solid state spectrum (7). The usual correlation between chemical shifts and the energy of the $d-d$ transition leads to a prediction of 460 nm for the $d-d$ transition which is slightly high but not decisively so. Figure 1 shows spectra of a 2.7 mM solution of sodium cobaltinitirite taken 2, 4, 6, and 9 min after dissolution. The intensity of the 480 nm band is clearly increasing with time and is zero at time zero. There is a parallel decrease in the intensity of the strong band at 355 nm. The half life for this process is of the order of 2 or 3 min. The 480 nm band does not therefore arise from $Co(NO_2)_6^{3-}$ but from a decomposition product. The nature of this decomposition product will be considered below.

$Co(NO_2)_6^{3-}$ has a centre of symmetry and the intensity of the $d-d$ transition would be expected to be about an order of magnitude less than that for a molecule without a centre of symmetry. Examination of Fig. 1A shows that the absorbance at 460 nm from the wing of the charge transfer band is greater than 1.0 for a 2.7 mM solution. The $d-d$ transition will therefore not be directly observable.

^{59}Co nmr spectra

In agreement with previous reports we find that the most intense line in the spectrum of a freshly prepared solution of sodium cobaltinitrite has a chemical shift of 7470 ppm. This line has a half width of 55 Hz, corresponding to a T_2 of 5.6 ms. The T_1, measured by inversion recovery, is 37.5 ms. The difference between T_1 and T_2 arises from scalar relaxation of the second kind as suggested by Rose and Bryant (14). If scalar coupling to six equivalent nitrogens contributes to the relaxation rate theory (27) predicts:

$$\frac{1}{T_2} - \frac{1}{T_1} = 16\pi^2 J^2 T_{1N}$$

The T_1 of the ^{14}N has been measured directly using a high power instrument. A value of 150 μs was obtained. The above formula gives a value of 80 Hz for the Co—N spin−spin coupling constant. This is compatible with literature values (28) for coupling between ^{15}N and ^{59}Co. The linewidth of the cobaltinitrite resonance therefore arises largely from scalar relaxation and can have only a small quadrupolar contribution. This provides further evidence for a symmetric N-bonded structure in solution.

On standing a variety of other lines appear in the ^{59}Co spectrum as illustrated in Fig. 2 and listed in Table 1. The most intense of thes new lines is at 8052 ppm. Figure 3 shows plots of the decrease in intensity of the 7470 line and the increase in the intensity of the 8052 line. Both curves are exponential in character with the half-life for the decay of the 7470 line measured as 150 s and that for the increase of the 8052 line as 180 s. These half-lives are very similar to the rate of appearance of the 480 nm band shown in Fig. 1. The relative intensity of the 8052 line compared to the 7470 line increases with dilution and decreases with the addition of sodium nitrite. Table 1 contains data illustrating these observations which are consistent with an equilibrium involving dissociation of the cobaltinitrite ion. These data indicate a dissociation constant of around 0.1 M. On further standing the intensity of the 8052 line decreases and the other lines in Fig. 2 gain intensity. A ^{59}Co chemical shift of 8052 ppm correlates very well with a $d-d$ transition at 480 nm. Thus, for example, $Co(NH_3)_6^{3+}$ has a chemical shift of 8175 ppm and a $d-d$ band at 476 nm. We assign the 8052 line to $Co(NO_2)_5H_2O^{2-}$ formed by dissociation of the cobaltinitrite ion. The assignment of the other lines in Table 1 will be discussed below.

^{14}N nmr of cobaltinitrite solutions

A set of ^{14}N spectra of cobaltinitrite solutions of various concentrations and after varying aging periods is shown in

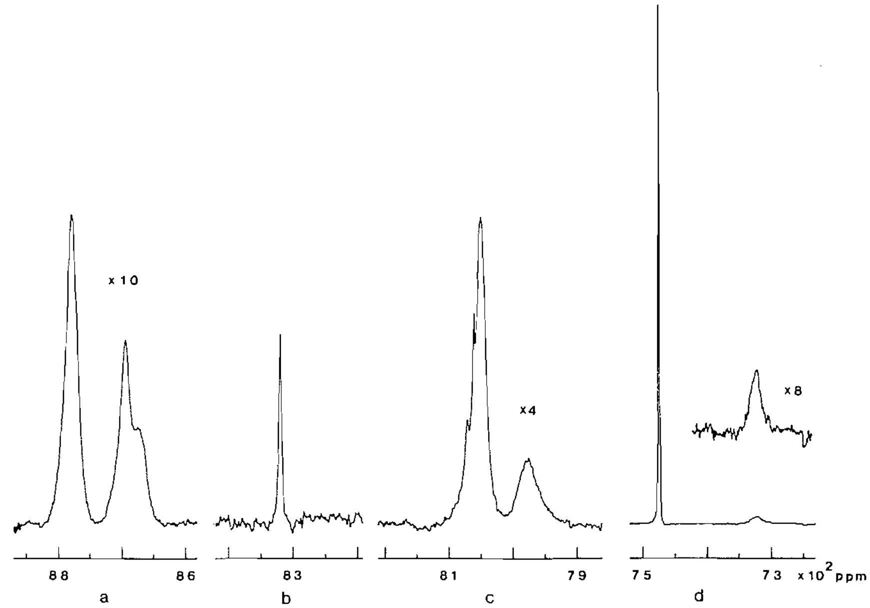

FIG. 2. ^{59}Co nmr spectra of $Na_3Co(NO_2)_6$ aqueous solutions. The assignments of the lines are given in Table 1. The initial spectrum shows the line at 7470 ppm. The other lines appear on aging. The line at 8815 ppm is only observed in concentrated solution (0.9 *M*).

TABLE 1.
(*a*) ^{59}Co spectrum of aqueous sodium cobaltinitrite

Observed chemical shift (ppm)	Linewidth (Hz)	Assignment	Calculated chemical shift (ppm)
7318	1650	$Co(NO_2)_5(ONO)^{3-}$	7573
7470	55	$Co(NO_2)_6^{3-}$	7511
7970	3300	*cis*-$Co(NO_2)_4(ONO)_2$	7816
		trans-$Co(NO_2)_4(ONO)_2$	7811
8052	1550	$Co(NO_2)_5(H_2O)^{2-}$	8108
8065	220	or $Co(NO_2)_5(OH)^{3-}$	8092
8074	300		
8315	175	*cis*-$Co(NO_2)_4(H_2O)(ONO)$	8331
8693	[a]		
8670	[a]	*cis*-$Co(NO_2)_4(H_2O)_2^{2-}$	8846
8790	2100		

[a]Overlapping lines.

(*b*) Relative intensities 8052 and 7470 lines at different $Co(NO_2)_6^{3-}$ concentrations

$[Co(NO_2)_6]$ (*M*)	Relative intensity
0.9	0.389
0.5	0.418
0.1	3.19
0.1 *M* + 1.0 *M* $NaNO_2$	0.329

Fig. 4. Three lines are apparent. The sharp line at zero ppm is the nitrate resonance. The line at 235 ppm, half-width 170 Hz, is assigned to free nitrite by comparison with the spectrum of sodium nitrite. The broad line, chemical shift 95 ppm line width 2200 Hz, is complexed nitrite. Rose and Bryant (14) in their report of the ^{14}N spectrum did not detect the very broad complexed resonance and assigned the complex to the free nitrite peak. Earlier authors (29) had assigned the sharp nitrate resonance to complexed nitrite. The chemical shift for complexed nitrite may be compared with the value of 44–46 ppm reported for a nitro rhodium complex (30) and with 4 ppm for nitromethane.

These spectra show several features of interest. The ratio of free nitrite to complexed nitrite increases with dilution as expected for a dissociative equilibrium. At high concentration this ratio does not change considerably with aging up to 28 days. The nitrate peak appears only with aging and most noticeably with dilute solutions. Its appearance is accompanied by a downfield shift and broadening of the free nitrite resonance. There is no similar shift or broadening of the complexed nitrite peak. Oxidation of nitrite to nitrate is plausibly accompanied by the reduction of Co(III) to Co(II) (14) and the inter-

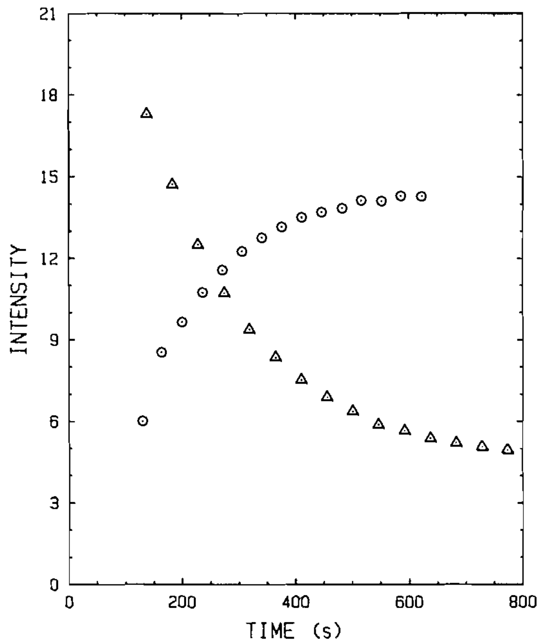

FIG. 3. ^{59}Co nmr spectra as a function of time after dissolution. $[Na_3Co(NO_2)_6]$ = 0.10 *M*. Circles represent intensity of δ 7470 peak (measured at 5.9 T); triangles that of δ 8052 peak (measured at 9.4 T).

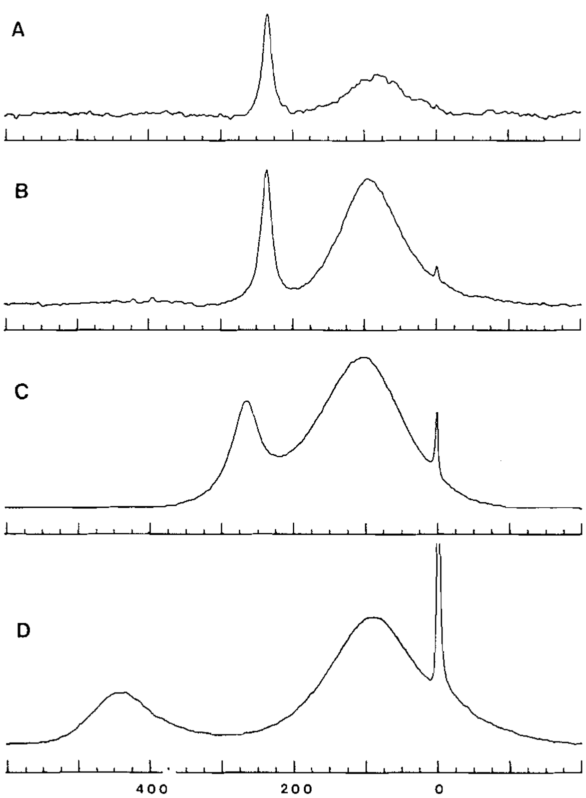

FIG. 4. ^{14}C nmr spectra obtained at 4.7 T (*A*) 0.1 *M* cobaltinitrite, aged 5 min, (*B*) 0.5 *M* cobaltinitrite, aged 5 min, (*C*) 1.1 *M* cobaltinitrite, aged 4 h, (*D*) same solution as (*C*), aged 28 days.

action of the nitrite ions with the paramagnetic Co ions causes the observed effect. This was confirmed by an experiment in which Co^{2+} ions were added to a solution of sodium nitrite. Addition of sodium nitrite to the cobaltinitrite solution enhances the intensity of the free nitrite peak as expected but also suppresses the formation of nitrate indicating that the aqua species is a necessary intermediate in the oxidation/reduction reaction.

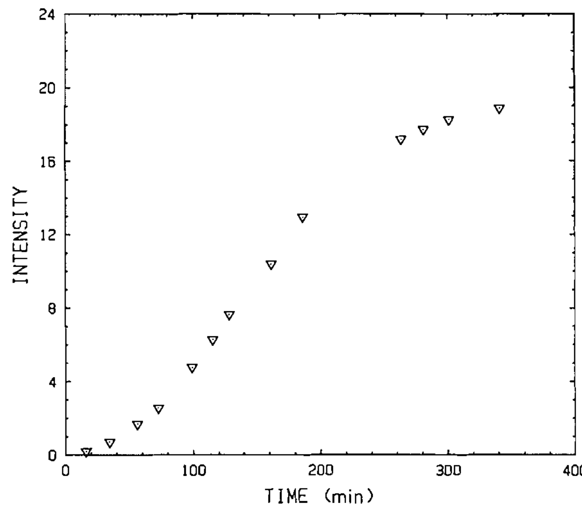

FIG. 5. ^{17}O nmr (9.7 T) intensity as a function of time after dissolution $[Na_3Co(NO_2)_6]$ = 0.9 *M*.

The ^{17}O spectrum of cobaltinitrite solutions

Spectra have been obtained from solutions containing ^{17}O in natural abundance and from solutions in water enriched to 18% in ^{17}O. In the natural abundance experiments the most intense line arises from water. This line shifts downfield and broadens with aging of the solution. The rate at which this occurs is comparable to the rate of the shift and broadening of the ^{14}N resonance of free nitrite and can be ascribed to a similar cause, complexing of the water to Co^{2+} from the reduction of the cobaltinitrite. In 0.9 *M* cobaltinitrite solutions additional lines, each with about 10% of the water line intensity, are observed at 168 ppm (linewidth 175 ± 10 Hz) and at 691 ppm (linewidth 1100 Hz). Sodium nitrite gives a line at 660 ppm (linewidth 135 ± 10 Hz). The 168 ppm signal shifts and broadens with time in a manner similar to the water signal and must therefore be a ligand capable of complexing to Co^{2+}. Its assignment is uncertain. The broad 691 ppm signal is reasonably assigned to complexed nitrite.

The sample dissolved in enriched ^{17}O water initially shows only the water resonance and a signal at −70 ppm which is assigned to complexed water in the pentanitroaqua compound. On standing a signal at 690 ppm (linewidth 1550 Hz) with a shoulder at 660 ppm increases in intensity with time. The time dependence is shown in Fig. 5. This result demonstrates a process by which ^{17}O from the water is incorporated in the nitrite ion. The shape of the curve of Fig. 5 shows that there is an induction period of approximately an hour before the rate of exchange reaches its highest value. The pH of the solution dropped from 5.2 to 4.3 on standing for 8 h due to the formation of nitrous and nitric acids. Isotopic oxygen exchange between nitrite ions and water has been studied by several groups (31, 32). The most recent study (32) indicates a half-life of approximately 24 h for the acid catalyzed exchange at pH 6.26. A rough calculation indicates that the data of Fig. 5 can be accomodated by ^{17}O exchange with free nitrite if allowance is made for the pH change but exchange with complexed nitrite cannot be completely ruled out.

TABLE 2. ^{59}Co chemical shifts of $Co(NH_3)_nX_{6-n}$ complexes[a]

	X = CN^-			X = NO_2^-		
	Observed	Calculated		Observed	Calculated	
n	(ref. 18)	*1*	*2*	(refs. 15, 37)	*1*	This work
0	0	4.545	−92	7470	2.711	7511
1	1168	4.469	1141			7182
cis 2	2457	4.330	2370	6880	2.893	7061
trans 2	2744	4.533	2726	6815	2.918	6935
mer 3	3991	4.364	3940	6981	2.969	7024
fac 3	3314	4.378	3596	7205	2.885	7122
cis 4	5132	4.236	5150	7277	3.001	7272
trans 4	5498	4.484	5481	7207	3.072	7204
5	6675	4.203	6675	7625	3.096	7625

[a] *1*, shift parameter in units of 10^5; *2*, using eq. [1].

The ^{59}Co nmr of complexes with ammonia, nitro, and cyano ligands

In an earlier publication (18) we suggested an empirical formula for calculating ^{59}Co chemical shifts in hexacoordinated Co(III) complexes, namely

$$\delta = \frac{1}{3}\left(\frac{1}{S_1 + S_2} + \frac{1}{S_3 + S_4} + \frac{1}{S_5 + S_6}\right) - 11000$$

In this formula S_1 and S_2 are parameters characteristic of the ligands on the x axis, S_3 and S_4 similar parameters for the ligands on the y axis, and S_5 and S_6 refer to the ligands on the z axis. The shifts are given in ppm and a single set of S parameters, one for each type of ligand, sufficed to calculate the chemical shifts of some 80 complexes with a standard deviation of less than 1% of the total shift range. The validity of the rule of average environment is implicit in the use of this formula. The chemical shifts of nitro complexes cannot be fitted to this formula if a constant shift parameter is assumed. The fit for cyano complexes is less satisfactory than for other ligands — three out of the four complexes for which the discrepancies between observed and calculated shifts were greater than 200 ppm involved this ligand.

These problems are illustrated by the data of Table 2 for mixed ammine complexes. For the nitro series increasing nitro substitution first results in a high field shift but with more than three nitro ligands the shifts return to low field. Juranic (15) pointed out that this behaviour is inconsistent with the rule of average environment. There are also other problems. For all other reported complexes the *trans* isomer has a larger shift than the *cis* isomer and the *mer* isomer a larger shift than the *fac* isomer. The converse is true in the nitro/ammine series. It is usually possible to distinguish the different isomers from the line width considerations (18) — *cis* complexes give narrower lines than *trans* and *fac* isomers narrower lines than *mer*. For this series the linewidths are very similar and do not provide a convenient criterion for assignments. It seems probable though that the literature assignments are correct since the method of preparation is specific for the *cis* compound (33) and crystal structures have been reported for both the *mer* and *fac* complexes (34, 35). The reversal of the chemical shifts must therefore be accepted. For the cyano compounds the discrepancies are less obvious but a good fit cannot be obtained with a single CN parameter. In Table 2 the results of calculating the values of S_{NO_2} and S_{CN} for each complex assuming the value of S_{NH_3} given previously are tabulated. With increasing nitro or cyano substitution a steady decrease in the nitro parameter and a steady increase in the cyano parameter is apparent. In both cases the effect of introducing a *cis* ligand is different from the effect of introducing a *trans* ligand. The parameters can be reasonably fitted by the equations:

$$[1] \quad \begin{aligned} S_{NO_2} &= (3.096 - 0.093n_{cis} - 0.023n_{trans}) \times 10^{-5} \\ S_{CN} &= (4.203 + 0.020n_{cis} + 0.301n_{trans}) \times 10^{-5} \end{aligned}$$

where n_{cis} is the number of NO_2 or CN ligands *cis* to the NO_2 or CN ligand for which the shift parameter is required and n_{trans} is the corresponding number of *trans* ligands. The shifts resulting from the use of these formulae are given as the calculated values in Table 2. We note that these calculations correctly predict the order of the *cis* and *trans* and *mer* and *fac* chemical shifts.

The implications of the above formulae are that increasing the number of nitro ligands makes each successive nitro group a weaker field ligand and that substituting a nitro ligand *cis* has a four times larger effect than substituting one *trans*. A recent paper (42) has considered the effect of nephelauxetism on ^{59}Co chemical shifts and has shown that in theory the energy of the first $d-d$ transition should be multiplied by the nephelauxetic ratio to obtain a correlation with ^{59}Co chemical shifts. Deviations in the chemical shift could therefore be ascribed either to a change in $10D_q$ or to a change in β or to changes in both. The linear correlation with the unweighted optical data reported by Juranic (15) argues that changes in $10D_q$ are most important. Since both $10D_q$ and β reflect the bonding properties of the ligand it is clear that these properties are changing with increasing substitution. We have also considered the possible contributions of charge transfer transitions to ^{59}Co chemical shifts but there does not seem to be any strong reason to invoke such an effect in the present case. Steric considerations provide a possible explanation of this observation. The negative charge on the nitro group has been shown (22) to be predominantly on the oxygen atoms and repulsive interactions between NO_2 ligands, particularly when they are *cis* to each other, must be anticipated. This will weaken the crystal field splitting of successive nitro substituents. For the cyano ligands increasing substitution results in larger crystal field splitting with *trans* ligands having a greater effect than *cis* ligands. It seems unlikely that this effect has a steric origin.

The assignment of the nmr spectra of cobaltinitrite solutions

The ^{59}Co chemical shift parameters for the nitro group obtained above can now be used to assign the lines in the cobaltinitrite spectrum of Fig. 2. The calculated chemical shifts of 8108 ppm for the pentanitroaqua complex or 8092 ppm for the pentanitrohydroxo complex are consistent with the assignment of the 8052 line already made. The neighboring lines at 8065 and 8074 ppm possibly arise from isomers of the monoaqua complex differing in the relative orientations of the nitro substituents. This suggestion is consistent with the observation that the chemical shifts are very similar, since the ligands are the same, but the line widths, depending on quadrupole relaxation and hence on the electric field gradients, are quite different. The possibility that hydrogen bonding could affect the orientation of the nitro groups is supported by the crystallographic structures of *mer* and *fac* $Co(NO_2)_3(NH_3)_3$ (34, 35) in which the NO_2 groups are twisted by 20−30° from their orientations in the hexanitro complex by interactions with the other ligands. The data of Table 1 were obtained on the WM400 instrument and it is notable that these lines are much less well resolved at lower fields, suggesting that chemical exchange due to rotation of the nitro groups may be occurring. From the frequency separation of the lines a lifetime of greater than 2×10^{-4} s would be required. There seems to be little precedent for estimating the barrier for rotation about a Co—N bond. We are unable to suggest alternative assignments for these lines. The line at 7970 probably does not belong to this group since its intensity varies with time in a manner different from its neighbours. It increases in intensity more slowly and remains longer suggesting that it is a later product in the reaction scheme. Assignment to *trans*-$[Co(NO_2)_4(ONO)_2]^{3-}$ is suggested on the basis of the calculated shift of 7811 ppm. The *cis*-tetranitrodiaqua complex has a calcualted shift of 8846 ppm and the lines at 8670, 8693, and 8790 can be plausibly assigned to isomers of this species differing in the nitro group orientations. It is notable that higher aquated species are all predicted to occur at shifts greater than 9000 ppm and are definitely not observed. Since the hexaqua Co(III) ion is reduced even by water it is reasonable that trisaqua and more highly aquated species would be reduced by the nitrite ion to give Co^{2+} and NO_3^- as indicated by the ^{14}N spectra. The remaining lines of Fig. 1 can best be ascribed to complexes containing the nitrito ligand. Thus the line at 8315 ppm can be assigned to the *cis*-tetranitroaquanitrito compound (calculated 8331 ppm) or less likely the *trans* isomer (calculated 8456 ppm). The only remaining line is at 7318 ppm. This is best assigned as the pentanitronitrito complex although the agreement with calculation (7573 ppm) is not particularly good. Thus all of the lines in this spectrum can be satisfactorily assigned to the combined effects of hydrolysis and isomerization involving nor more than two nitro ligands.

The mechanism of ligand exchange

The observed half lives for the aquation of the cobaltinitrite ion from the visible spectra (2.7 m*M* concentration) and the nmr (0.5 *M* concentration) correspond to a first order rate constant of approximately 4×10^{-3} s^{-1}. This anomalously high rate suggests that a mechanism other than simple dissociation may be involved. An attractive possibility is a rate determining step of electron transfer from NO_2^- to Co^{3+}, followed by rapid ligand exchange of the resulting labile Co^{2+} complex, with the reaction being completed by rapid reverse electron transfer from Co^{2+} to NO_2, i.e.

[1]	$LCo^{3+}NO_2^-$	$= LCo^{2+} + NO_2$	Slow
[2]	$LCo^{2+} + L'$	$= L'Co^{2+} + L$	Fast
[3]	$L'Co^{2+} + NO_2$	$= L'Co^{3+}NO_2^-$	Fast
[4]	$NO_2 + NO_2 + H_2O$	$= NO_3^- + NO_2^- + 2H^+$	Slow

An electron transfer mechanism for Co^{3+} ligand exchange was first suggested to account for rapid base catalysed hydrolyses (36) but did not achieve great popularity. More recently (37) a very similar mechanism has been convincingly demonstrated for the ligand substitution reactions of peroxo/ammine complexes of Co(III). Interestingly the rate reported in this latter paper (4.9×10^{-3} s^{-1}) is very similar to that given above. Since NO_2^- is an oxidizable ligand this mechanism provides a ready rationalization of the difference from ligand exchange mechanisms involving non-oxidizable ligands such as CN^- and NH_3. Reaction [4] is well established and competes with reaction [3] leading to irreversible oxidation/reduction. Thus all of the observed products can be accounted for by a single mechanism and the very similar rates reported for aquation, nitrite exchange (20), and substitution by other ligands (21) are explained as arising from a common rate determining step. Subsequent hydrolysis steps to give diaqua and more highly substituted species are slower as would be anticipated from the smaller number of nitro groups available to donate electrons.

Reactions with ethylenediamine and cyanide

The observation that nitro ligands are readily replaced by water in the hexanitro complex suggest that replacement by other ligands may be equally facile. The reactions with ethylenediamine and with cyanide ion have therefore been investigated by ^{59}Co nmr.

Figure 6 shows a spectrum obtained from a mixture of 0.1 *M* $Co(NO_2)_6^{3-}$ and 0.41 *M* ethylenediamine which has been allowed to equilibrate for 7 days. There is actually relatively little change in the spectrum after 30 min of reaction. The principal difference is that a line at 7530 ppm, which appears quite strongly in the initial spectrum, disappears on standing. It may be noted that even though the ethylenediamine is present in stoichiometric excess the very stable trisethylenediamine complex is not the major product. The observed chemical shifts and linewidths are given in Table 3 together with calculated and literature values. The five high field lines of Fig. 6 are assigned to the expected species $Co(NO_2)_6^{3-}$, $Co(en)_3^{3+}$, $Co(en)(NO_2)_4^-$, *cis*-$Co(en)_2(NO_2)_2^+$, and *trans*-$Co(en)_2(NO_2)_2^+$. It is notable that the lines of the nitro complexes are all found to rather higher field than expected from the calculations and the linewidths are considerably greater than would have been anticipated. It is suggested that the excess ethylenediamine is present as a second sphere ligand hydrogen bonded to the nitro ligands. High field shifts (26) and line broadening (38) are the expected results of such hydrogen bonding. The low intensity lines at 9356, 9342 ppm are assigned to conformational or to *cis−trans* isomers of $Co(en)_2(OH)_2^+$ (calculated 9309 ppm) or the corresponding aqua complex. Yajima *et al* (39) assigned the *cis* and *trans* isomers with only a very small chemical shift difference (9300 and 9280) but this is unexpected and we have some preference for assigning the two lines to conformational isomers of the *cis* compound. The line at 8510 ppm is best ascribed to $Co(en)_2(H_2O)(ONO)^{2+}$ (calculated 8787 but possibly H bonded) although it is perhaps a little surprising that this complex does not rapidly convert to the nitro isomer. These are presumably products of the reaction of en with the hydrolysis products of $Co(NO_2)_6^{3-}$ which accounts for their low intensity. The remaining features are the intense line at 7785 ppm and the weaker line at 7530 ppm. These are best assigned to the *mer* and *fac* isomers of $Co(NO_2)_3(en)(H_2O)$ or the hydroxy equivalents. The relative line widths suggest that the 7785 ppm

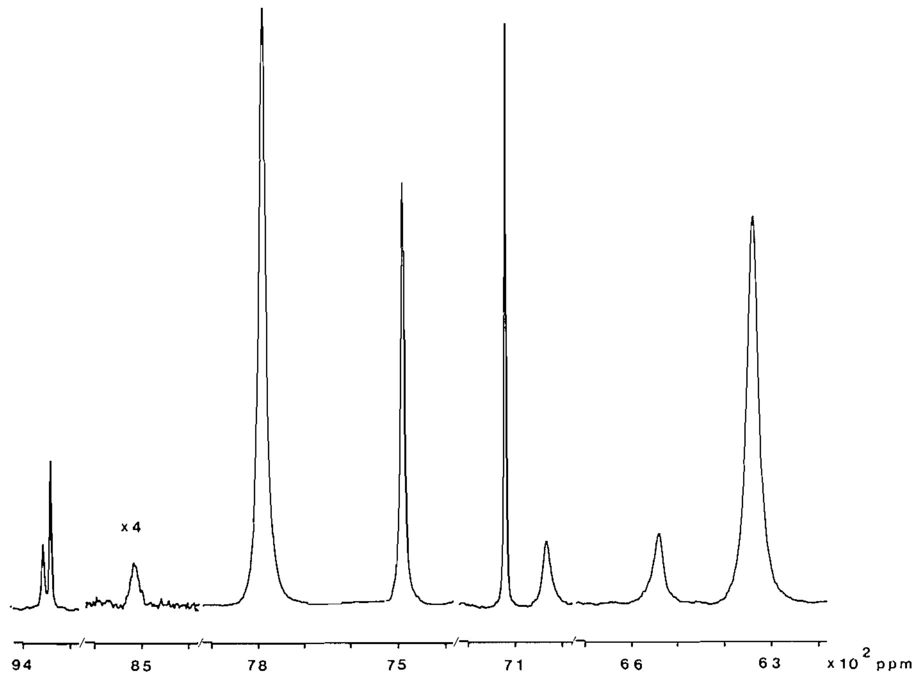

FIG. 6. ^{59}Co nmr (5.9 T) spectrum of reaction mixture of 0.1 *M* sodium cobaltinitrite and 0.41 *M* en in water aged 7 days.

TABLE 3. ^{59}Co nmr spectrum from the reaction of ethylenediamine and sodium cobaltinitrite

Observed chemical shift (ppm)	Linewidth (Hz)	Relative intensity	Assignment	Chemical shift: Refs. 15, 39, 40	Chemical shift: Calculated
9356	260	12	*cis*-$Co(en)_2(H_2O)_2$	9150	9310
			cis-$Co(en)_2(OH)_2$	9300	
9342	150		*trans*-$Co(en)_2(H_2O)_2$	9100	9780
			trans-$Co(en)_2(OH)_2$	9280	
8510	1350	2.3	$Co(en)_2(H_2O)(ONO)$		8781
7785	840	100	*mer*-$Co(NO_2)_3enH_2O$		7607
7530	150		*fac*-$Co(NO_2)enH_2O$		7669
7483	395	40	$Co(NO_2)_6$	7470	7510
7123	115	24	$Co(en)_3$	7146	7149
7035	1000	11	$Co(en)(NO_2)_4$	6795	6737
6539	1477	36	*cis*-$Co(en)_2(NO_2)_2$	6551	6627
6337	1453	103	*trans*-$Co(en)_2(NO_2)_2$	6323	6552

resonance is the *mer* isomer since it is much broader. The loss of the 7530 line on standing is presumably due to isomeric conversion to the more stable *mer* compound. The calculated shifts (*mer* 7603, *fac* 7669) are very similar but suggest the opposite assignment. Assignment of the more intense line to the *mer* isomer is consistent with the widely reported preferential formation of *mer*-$Co(NO_2)_3(NH_3)_3$.

The reaction of cobaltinitrite with cyanide produces the ^{59}Co spectra of Fig. 7*a* (0.2 *M* cobaltinitrite + 1.0 *M* cyanide) and 7*b* (0.05 *M* cobaltinitrite + 0.1 *M* cyanide). Data obtained from three different mixtures are presented in Table 4. Even with 5 mol of cyanide to 1 mol of cobaltinitrite, cobalticyanide is not the major product. The most intense line is at 1630 ppm and is best assigned as $Co(CN)_5(ONO)^{3-}$ (calculated 1372 ppm). The pentacyanonitro complex has been observed in other experiments at 609 ppm (40) but is definitely not seen in these mixtures. The other line at 2550 ppm can be assigned to the *cis*-tetracyanodinitrito complex (calculated 2835 ppm). A mixture of 1.0 *M* in cobaltinitrite and 1.0 *M* in cyanide ion also showed a line at 3621 ppm assigned to *trans*-$Co(CN)_4(ONO)_2^{3-}$ (calculated 3601 ppm). We find no evidence for mono or dinitro/cyano complexes. This observation is analogous to the report (41) that the pentacyano isothiocyanato Co(III) complex is formed in preference to the thiocyanato isomer in some reactions. In the solution most dilute in cyanide, lines at 6614 ppm and 6477 ppm can be assigned to *mer*-$Co(NO_2)_3(CN)(ONO)(H_2O)$ and *cis*-$Co(NO_2)_4(CN)(H_2O)$. The remaining lines in Table 4 are assigned to species not containing cyanide ligands. The multiplicity of lines with similar chemical shifts suggests conformational isomerism. The ^{14}N nmr spectra of these mixtures have also been examined. Separate resonances for free nitrite, coordinated nitrite, free cyanide, and complexed cyanide are observed but the different complexes are not distinguished.

Conclusion

The crystal field strength of the nitro ligand varies according to the number of nitro groups in the complex. If only one or two nitro ligands are present it is a strong field ligand. By the time the cobaltinitrite ion is reached it is a significantly weaker

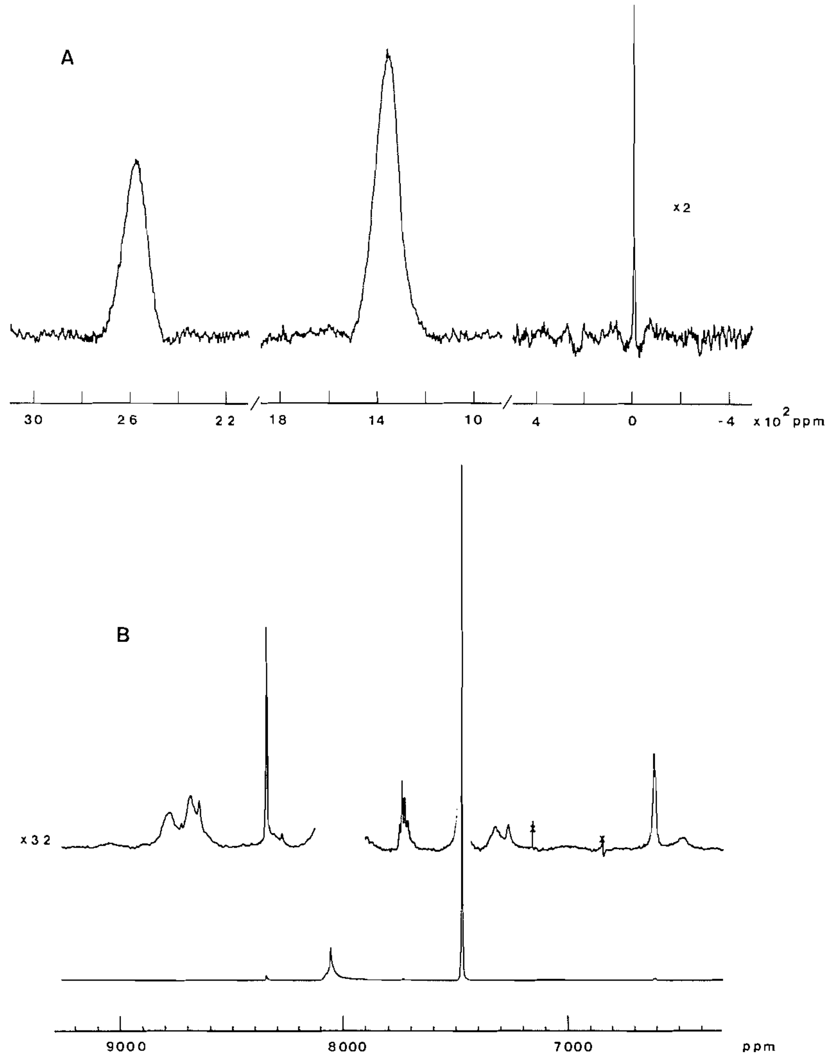

FIG. 7. ^{59}Co nmr spectra of fresh (aged 1 h) mixtures of sodium cobaltinitrite and sodium cyanide in water. (*A*) $[Na_3Co(NO_2)_6]$ = 0.2 *M*, [NaCN] = 1.0 *M*, B_0 = 5.9 T. (*B*) $[Na_3Co(NO_2)_6]$ = 0.5 *M*, [NaCN] = 0.1 *M*, B_0 = 4.7 T. Spikes are marked with crosses.

TABLE 4. ^{59}Co nmr spectrum from the reaction of sodium cyanide and sodium cobaltinitrite

A	*B*	*C*	Assignment	Calculated chemical shift
0			$Co(CN)_6^{3-}$	−92
1340			$Co(CN)_5(ONO)^{3-}$	1372
2550			*cis*-$Co(CN)_4(ONO)_2^{3-}$	2835
	3621		*trans*-$Co(CN)_4(ONO)_2^{3-}$	3601
		6477	*cis*-$Co(NO_2)_4(CN)(H_2O)^{2-}$	6558
		6614	*mer*-$Co(NO_2)_3(CN)(ONO)$	6625
		7266	$Co(NO_2)_5(ONO)^{3-}$	7573
	7470	7470	$Co(NO_2)_6^{3-}$	7511
		7689		
	7711	7709	*cis*-$Co(NO_2)_4(ONO)_2^{3-?}$	7811
		7715	*trans*-$Co(NO_2)_4(ONO)_2^{3-?}$	7816
	7725	7725		
	7733	7733		
	8052	8052	$Co(NO_2)_5(H_2O)^{2-}$	8108

[a]*A*, 0.2 *M* $Co(NO_2)_6^{3-}$ + 0.1 *M* CN^-; *B*, 1.0 *M* $Co(NO_2)_6^{3-}$ + 1.0 *M* CN^-; *C*, 0.5 *M* $Co(NO_2)_6^{3-}$ + 0.1 *M* CN^-.

ligand and the spectroscopic and chemical properties reflect this change. Ligand exchange is facile and irreversible reduction takes place slowly. ^{59}Co nmr can readily detect these changes in crystal field strength. In aqueous solutions of cobaltinitrite a variety of Co(III) species are present. All contain at least four nitro ligands with the remaining two positions being filled by aqua or nitrito groups. Electron transfer leads to the reduction of Co^{3+} to Co^{2+} and the oxidation of NO_2^- to NO_2 which is then hydrolysed to give NO_2^- and NO_3^-. These species have been detected by ^{14}N and ^{17}O nmr.

^{59}Co nmr is also a very convenient technique for following ligand exchange reactions. Such reactions may give surprisingly complex mixtures of products as is demonstrated by the reactions of cobaltinitrite with ethylenediamine and with cyanide ion. The products may not be those initially anticipated, e.g., nitrito rather than nitro isomers. With the added sensitivity and dispersion of high field FT NMR spectrometers, large numbers of resonances can be observed. Thus in the case of cobaltinitrite solutions we report 10 lines where only two had been seen previously. ^{59}Co nmr is therefore a powerful technique for investigating the solution chemistry of Co(III). The problem lies in assigning the multiplicity of lines. The point charge model developed previously is helpful in this respect but a fair amount of empirical data collecting will likely be required to establish the pattern of the chemical shifts.

Experimental

Sodium cobaltinitrite was purchased from Fisher (reagent grade liquid and solid) and was used without further purification. ^{59}Co nmr spectra were obtained at various fields — 2.14 T (Bruker WH90), 4.7 T (Bruker CXP 200), 5.9 T (Bruker WM 250), and 9.5 T (Bruker WM 400). The temperature is each case was 21 ± 1°C. Potassium cobalticyanide, saturated ammonium nitrate (NO_3^- resonance), and distilled water were used as external calibration standards for the ^{59}Co, ^{14}N, and ^{17}O spectra, respectively. A Tracor-Northern 6050 instrument, which is equipped with a diode detector array, was used to obtain the spectra of Fig. 1. Infrared spectra were run in KBr discs using a Perkin-Elmer 283 instrument and Raman spectra on a Spex model 14018 spectrometer equipped with a helium–neon laser. ^{17}O nmr spectra were obtained on the WM 400 instrument. The enriched sample gave a S/N ratio of 729 on the water peak with only eight scans. The best ^{14}N spectra were obtained on the CXP 200 instrument using a high power probe. On this probe, the 90° pulse width is 5–10 μs. These short pulse widths are necessary to obtain good spectra for resonances such as coordinated nitrite which have very short relaxation times.

Acknowledgements

We are indebted to the Natural Sciences and Engineering Research Council of Canada for financial support of this research and to the S.W. Ontario High Field NMR Centre for the use of the CXP 200 and WM 400 instruments.

1. M. A. HITCHMAN and G. L. ROWBOTTOM. Coord. Chem. Rev. **42**, 55 (1982).
2. A. B. P. LEVER. Inorganic electronic spectroscopy. Elsevier, New York. 1968.
3. F. BASOLO and R. G. PEARSON. Mechanisms of inorganic reactions. 2nd ed. John Wiley, New York. 1967.
4. R. A. D. WENTWORTH and T. S. PIPER. Inorg. Chem. **4**, 709 (1965).
5. K. G. CAULTON and R. G. FENSKE. Inorg. Chem. **6**, 562 (1967).
6. A. GARNIER. J. Chim. Phys. Physiochim. Biol. **67**, 1440 (1970).
7. J. C. BARNES, C. S. DUNCAN, and R. D. PEACOCK. J. Chem. Soc. Dalton, 1875 (1972).
8. W. G. PROCTOR and F. C. YU. Phys. Rev. **81**, 20 (1951).
9. R. P. H. GASSER and R. E. RICHARDS. Mol. Phys. **3**, 163 (1960).
10. R. FREEMAN, G. W. MURRAY, and R. E. RICHARDS. Proc. R. Soc. London, A**242**, 455 (1957).
11. S. S. DHARMATTI and C. R. KANEKAR. J. Chem. Phys. **31**, 1436 (1959).
12. A. YAMASAKI, F. YAJIMA, and S. FUJIWARA. Inorg. Chim. Acta, **2**, 39 (1968).
13. H. HARTMANN and H. SILLESCU. Theor. Chim. Acta, **2**, 371 (1964).
14. K. D. ROSE and R. G. BRYANT. Inorg. Chem. **18**, 2130 (1979).
15. N. JURANIC, M. B. CELAP, D. VUCELIC, M. J. MALINAR, and P. N. RADIVOJSA. Spectrochim. Acta, **35**A, 997 (1979).
16. M. A. PUJAR. J. Ind. Chem. Soc. **57**, 345 (1980).
17. M. A. PUJAR and N. S. BIRADAR. J. Ind. Chem. Soc. **57**, 783 (1980).
18. S. C. F. AU-YEUNG and D. R. EATON. Can. J. Chem. **61**, 2431 (1983).
19. D. R. LLEWELLYN, C. J. O'CONNOR, and A. L. ODELL. J. Chem. Soc. 196 (1964).
20. I. V. MATSKO, YU. E. SELYANINOV, and G. A. SHAGISULTANOVA. Russ. J. Inorg. Chem. **12**, 351 (1967).
21. M. B. CELAP, T. J. JANJIC, and P. N. RADIVOJSA. Rev. Chim. Min. **10**, 607 (1973).
22. S. OHBA, K. TORIUMI, S. SATO, and Y. SAITO. Acta Crystallogr. B**34**, 3535 (1978).
23. W. KRASSER. Z. Naturforsch. A**24**, 1667 (1969).
24. I. NAKAGAWA and T. SHIMANOUCHI. Spectrochim. Acta **23**A, 2099 (1967).
25. K. KANAMORI, T. MORIKAWA, and K. KAWAI. Bull. Chem. Soc. Jpn. **53**, 2787 (1980).
26. D. R. EATON, C. V. ROGERSON, and A. C. SANDERCOCK. J. Phys. Chem. **86**, 1365 (1982).
27. T. C. FARRAR and E. D. BECKER. Pulse and Fourier transform NMR. Academic Press, New York. 1971. p. 60.
28. A. YAMASAKI, Y. MIYAKOSHI, M. FUJITA, Y. YOSHIKAWA, and H. YAMATERA. J. Inorg. Nucl. Chem. **41**, 473 (1979).
29. R. BRAMLEY, B. N. FIGGIS, and R. S. NYHOLM. J. Chem. Soc. A, 861 (1967).
30. L. K. BELL, J. MASON, D. M. P. MINGOS, and D. G. TEW. Inorg. Chem. **22**, 3497 (1983).
31. C. A. BUNTON, D. R. LLEWELLYN, and G. STEDMAN. J. Chem. Soc. 568 (1959).
32. R. L. VAN ETTEN and J. M. RISLEY. J. Am. Chem. Soc. **103**, 5633 (1981).
33. H. SIEBERT. Z. Anorg. Allg. Chem. **441**, 47 (1978).
34. M. LAING, S. BAINES, and P. SOMMERVILLE. Inorg. Chem. **10**, 1057 (1971).
35. B. NUBER, H. SIEBERT, K. WEIDENHAMMER, J. WEISS, and M. L. ZIEGLER. Acta Crystallogr. B**35**, 1020 (1979).
36. R. D. GILLARD. J. Chem. Soc. A, 917 (1967).
37. T. SASAKI, K. Z. SUSUKI, A. MATSUMOTO, and K. SAITO. Inorg. Chem. **21**, 1825 (1982).
38. S. C. F. AU-YEUNG and D. R. EATON. J. Magn. Reson. **52**, 366 (1983).
39. F. YAJIMA, Y. KOIKE, A. YAMASAKI, and S. FUJIWARA. Bull. Chem. Soc. Jpn. **47**, 1442 (1974).
40. S. C. F. AU-YEUNG and D. R. EATON. J. Magn. Reson. **52**, 351 (1983).
41. D. F. GUTTERMAN and H. B. GRAY. J. Am. Chem. Soc. **91**, 3105 (1969).
42. R. BRAMLEY, M. BRORSON, A. M. SARGESON, and C. E. SCHAFFER. J. Am. Chem. Soc. **107**, 2780 (1985).

Infrared spectra of hydrogen bonded adducts of 2,6-dichlorophenols and oxygen bases

R. WOLNY, A. KOLL, AND L. SOBCZYK
Institute of Chemistry, University of Wroclaw, 50-383 Wroclaw, Poland

Received January 25, 1985

This paper is dedicated to Professor Camille Sandorfy on the occasion of his 65th birthday

R. WOLNY, A. KOLL, and L. SOBCZYK. Can. J. Chem. **63**, 3568 (1985).

Infrared spectra of hydrogen bonded complexes of 2,6-dichlorophenol derivatives and oxygen bases have been studied over a broad ΔpK_a range (from −10.55 to +1.69). For the complexes of 1:1 stoichiometry typical evolution of spectra, similar to those for other hydrogen bonded systems, have been found. With an increase of ΔpK_a, the hydroxyl group stretching vibration band shifts to lower frequencies until the inversion region is reached, where hydrogen bonded (HB) and proton transfer (PT) forms occur in equilibrium, then a broad background absorption is observed. The centre of gravity of the broad protonic bands, ν_{cg}, calculated from the integrated intensity over the whole infrared region have been correlated with ΔpK_a and the contribution of the PT form. It has been shown that the minimum on the plot ν_{cg} vs. ΔpK_a is reached close to the inversion point, where $K_{PT} = 1$. The observed correlations and the change in the shape of the broad protonic absorption are consistent with expectations of theories based on the concept of the double minimum potential function and the stochastic mechanisms of band broadening.

R. WOLNY, A. KOLL et L. SOBCZYK. Can. J. Chem. **63**, 3568 (1985).

Utilisant un large intervalle de ΔpK_a (allant de −10,55 à +1,69), on a étudié les spectres infrarouges des complexes des dérivés du dichloro-2,6 phénol et des bases oxygénées liés par des liaisons hydrogènes. Dans le cas des complexes du type 1:1, on a trouvé une évolution typique des spectres semblable à celle des autres systèmes liés par des liaisons hydrogènes. Lorsque le ΔpK_a augmente, la bande de vibration d'élongation du groupe hydroxyle glisse vers les basses fréquences jusqu'à atteindre la région d'inversion où les formes hydrogène lié (HL) et transfert de proton (TP) existent à l'équilibre; on observe alors une large absorption de fond. On a établi une corrélation entre le centre de gravité des bandes protoniques larges, ν_{cg}, calculé à partir de l'intensité intégrée sur toute la région infrarouge, avec le ΔpK_a et la contribution de la forme TP. On montre que l'on atteint le minimum de la courbe ν_{cg} en fonction du ΔpK_a près du point d'inversion où $K_{PT} = 1$. Les corrélations observées et le changement de forme de l'absorption protonique large sont en accord avec les attentes des théories fondées sur le concept de la fonction de potentiel du minimum double et sur le mécanisme stochastique de l'élargissement de la bande.

[Traduit par le journal]

Introduction

There is a number of papers dealing with infrared behaviour of hydrogen bonded adducts containing oxygen bases with various proton donors. Among them, are the results obtained by Hadži *et al.* (1−3), Szafran *et al.* (4−7), and Gramstad *et al.* (8−10). The complexes of oxygen bases appeared to be a convenient object for the studies of hydrogen bonding and its spectroscopic features due to a broad range of the proton acceptor properties and relatively high stability. However, the interpretation of the ir spectroscopic behaviour can be difficult because of the formation of adducts of varying composition, including ionic states with homoconjugated cations and anions. In some papers, the influence of the ΔpK_a of interacting components on the ir behaviour has been reported (7, 11, 12). However, the data available so far are not sufficient for formulating more general conclusions concerning the relationship between the donor−acceptor properties of interacting components and spectroscopic features of hydrogen bonded adducts. The aim of the present work was the study of ir spectra of hydrogen bonded adducts composed of oxygen bases and 2,6-dichlorophenol derivatives. For such systems there are informations available on the complexation equilibria (13) and the charge distribution within the hydrogen bridge expressed by the dipole moment increment (14). The magnitude of this increment correlates with the equilibrium constant of the intracomplex proton transfer and the ΔpK_a value of interacting components. In addition, the dipole moment increment describes semiquantitatively the potential for the proton motion and, in particular, informs about the so-called inversion point corresponding to the situation with either an equal population of two protonic states (pseudosymmetric hydrogen bond in the dynamical sense) or with one broad potential minimum for the proton motion. Such a situation, as can be suspected, should be reflected markedly in ir spectra.

Experimental

The ir spectra were recorded on a Perkin Elmer 180 spectrophotometer at room temperature in CCl_4 solutions contained in KBr cells of 2 mm thickness. To get the spectra of complexes of 1:1 compositon, equal concentrations of base and phenol 0.01 *M* were used. In such conditions, the contribution of complexes other than those of 1:1 composition can be neglected. The excess of oxygen bases shifts the equilibrium towards homoconjugated cations $[OHO]^+$, while an excess of phenol causes the formation of complexes of various composition $(AH)_nB$, the most stable being that with $n = 2$. The concentrations used in the ir studies were similar to those for the study of complexation equilibria (13) and dipole moments (14). The studies at relatively low concentrations allowed to avoid, to a large extent, the self-association of strongly polar complexes. The osmometric studies performed on most polar TBNO · DCNP adducts in CCl_4 showed that the association degree under experimental conditions used in this work reaches about 10%. For the complexes of lower polarity the association degree is much smaller.

The origin of the compounds investigated was the same as in previous studies. Their list, with the abbreviations used, is presented in Table 1. All operations connected with the preparation of the solutions and the cell filling were performed in a dry box.

Results and discussion

The informations about the systems investigated are collected in Table 1. They contain the ΔpK_a values, defined as $pK_a(BH^+) - pK_a(AH)$, the position of the high frequency protonic band ν_3OH (stretch) and the position of the centre of gravity, ν_{cg}, of the whole protonic broad bands (intergrated over the whole ir region). ν_{cg} defined as

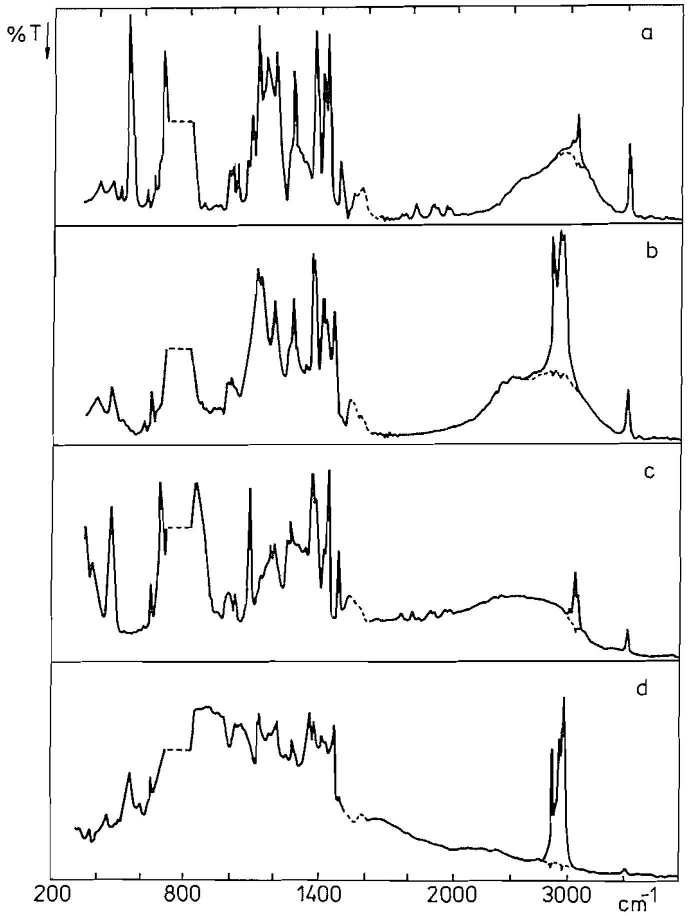

FIG. 1. Evolution of the ir spectra for the complexes of oxygen bases with PCP: (*a*) TPPO · PCP (ΔpK_a = −5.88), (*b*) TOPO · PCP (ΔpK_a = −4.22, (*c*) TPASP · PCP (ΔpK_a = −2.11), (*d*) TBNO · PCP (ΔpK_a = 0.49).

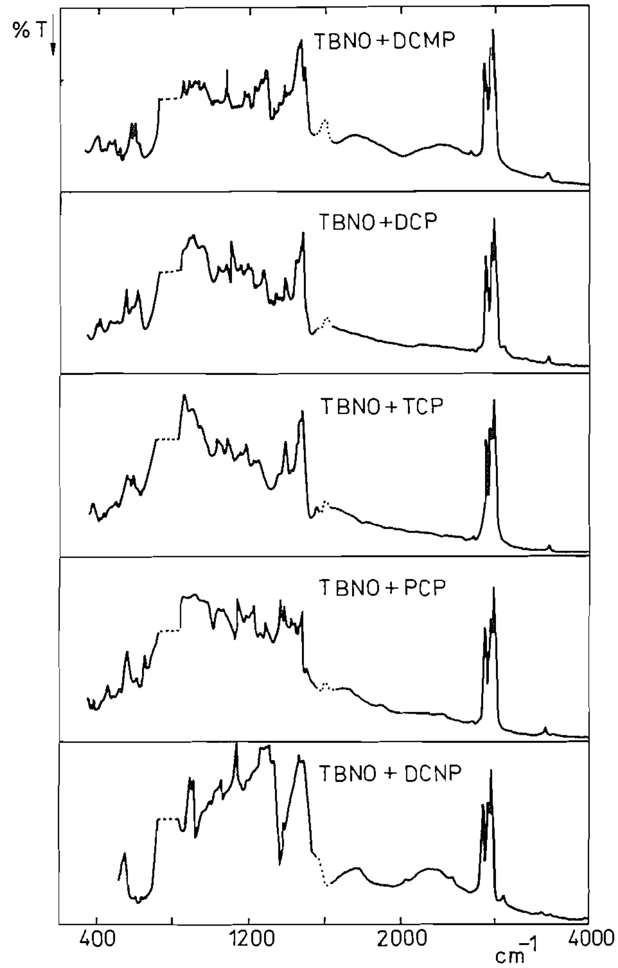

FIG. 2. Behaviour of the broad protonic absorption for TBNO complexes.

$$[1] \quad \nu_{cg} = \int \log\left(\frac{I_0}{I}\right) \nu d\nu \Big/ \int \log\left(\frac{I_0}{I}\right) d\nu$$

was calculated by using a computer.

The evolution of the absorption related to the protonic vibrations is illustrated taking selected PCP complexes as examples (Fig. 1). Most characteristic is the fact that close to the inversion point, which for the investigated systems corresponds to $\Delta pK_a \simeq -0.3$, the ν_s(OH) band becomes very broad and overlaps with a new low frequency broad absorption creating a "continuum". For the complexes directly in the inversion range, the band assignable to the OH stretching vibrations is shifted to lower frequencies, has a doublet character (the minimum is always located at about 2000 cm^{-1}) and a low intensity. The lowest intensity occurs at ΔpK_a = −1.15. The situation is illustrated by the behaviour of TBNO complexes, for which the proton transfer equilibrium was previously detected (Fig. 2) (13). The boundary systems, i.e., TBNO · DCMP and TBNO · DCNP, correspond to an almost complete shift of the proton transfer equilibrium to OH...O and O^-...HO^+ states, respectively. Their spectra are very similar in both the high frequency (the doublet) and the low frequency (background absorption) range. The high frequency doublet practically vanishes for complexes of TCP and DCP, while in the case of PCP complex, for which the PT state exceeds 60%, it appears clearly again. The proton transfer situation in the systems studied, derived from dipole moments and uv spectra, is illustrated in Fig. 3. There is only a little discrepancy for the two independent methods. The inversion point corresponding to 50% of PT state is located at $\Delta pK_a \simeq -0.3$.

Plotting the ν_{cg} value against ΔpK_a we obtain the curve with characteristic minimum close to the inversion point (Fig. 4). The anomaly on the $\nu_{cg} = f(\Delta pK_a)$ plot appears a little bit before reaching the inversion point, which seems to be understandable in the light of the following reason. The dipole moment increment of the contribution of the proton transfer state is related to the equilibrium process governed by the free energy change ΔF_{PT}. It means that the two minima for the proton motion in the free energy scale with a contribution of the entropy effect evoked by the reorganisation of the solvent molecules may be different to those in the potential energy scale for the adiabatic motion of protonic vibrations. The confirmation of such an argumentation is found in studies of the entropy effect based on the measurements of K_{PT} as a function of T. The ΔS_{PT} in all the cases investigated so far is characterised by negative values (15, 16).

In the interpretation of the results one should consider a possible contribution in the recorded spectra of homoconjugated $[OHO]^+$ and $[OHO]^-$ ions. The detailed analysis of equilibria based on uv and ir (in the overtone region) indicates that under experimental conditions the contribution of these ions can be neglected. This conclusion is supported by the results of dielectric (14), electric conductivity (17), and osmometric

TABLE 1. ΔpK_a,[a] position of the $\nu_s(OH)$ band maximum and ν_{cg} value (centre of gravity of protonic absorption) for investigated systems

	2,6-Dichloro-4-methylphenol (DCMP)			2,6-Dichlorophenol (DCP)			2,4,6-Trichlorophenol (TCP)			Pentachlorophenol (PCP)			2,6-Dichloro-4-nitrophenol (DCNP)		
Oxygen base	ΔpK_a	ν_{OH}[b]	ν_{cg}[b]	ΔpK_a	ν_{OH}	ν_{cg}	ΔpK_a	ν_{OH}	ν_{cg}	ΔpK_a	ν_{OH}	ν_{cg}	ΔpK_a	ν_{OH}	ν_{cg}
Diphenylsulphoxide (DPSO)	−10.55	—	—	−10.15	3210	3169	−9.82	3180	3129	−8.18	3140	3076	−6.98	3105	2988
Dibenzylsulphoxide (DBESO)	−9.63	—	—	−9.23	3160	3085	−8.90	3140	3072	−7.26	3095	3000	−6.06	3050	2910
Triphenylphosphine oxide (TPPO)	−8.25	3105	3024	−7.85	3085	3022	−7.52	3020	2961	−5.88	2948	2868	−4.68	2910	2802
Diphenylethylphosphine oxide (DPEPO)	−7.88	3080	3001	−7.48	3060	2995	−7.15	3000	2917	−5.51	2940	2832	−4.31	2885	2712
Diphenyloctylphosphine oxide (DPOPO)	−7.49	3070	2978	−7.09	3050	2967	−6.76	2995	2901	−5.12	2930	2815	−3.92	2880	2708
Diphenylselene oxide (DPSEO)	−7.26	3045	2947	−6.86	3020	2923	−6.53	2980	2825	−4.89	2920	2739	−3.69	2860	2553
Trioctylphosphine oxide (TOPO)	−6.59	3035	2909	−6.19	3000	2871	−5.86	2920	2777	−4.22	2820[d]	2682	−3.02	2670[d]	2464
Triphenylarsine oxide (TPASO)	−4.48	2920	2729	−4.08	2720[d]	2697	−3.75	2660[d]	2361	−2.11	2530	2151	−0.91	2520	1968
Tri-*n*-butylamine-N-oxide (TBNO)	−1.88	2400[c]	1493	−1.48	—	1270	−1.15	—	1178	+0.49	—	1109	+1.69	2350[c]	1536

[a] Defined in refs. 13 and 14.
[b] In cm^{-1}.
[c] Longwave length part of a doublet.
[d] Central position of two bands.

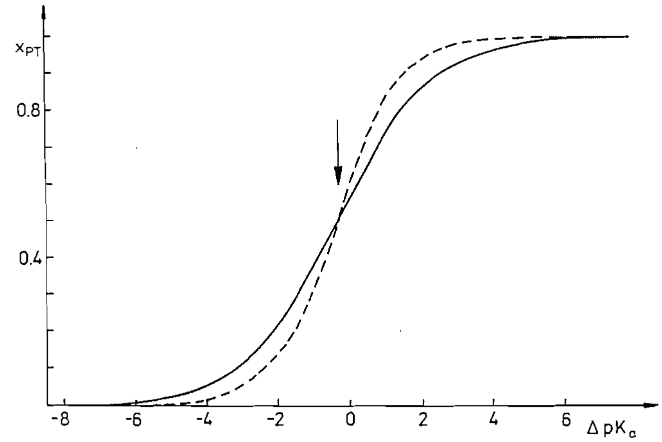

FIG. 3. Percentage of the PT state calculated from uv spectroscopic data (solid line) and dipole moment studies (dotted) with indicated inversion point ($\Delta pK_a = -0.3$).

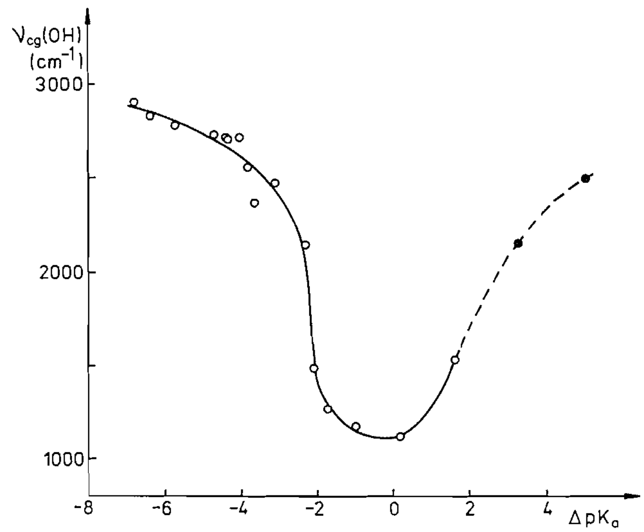

FIG. 4. ν_{cg} plotted against ΔpK_a values for the complexes over the inversion range. Full points refer to TBNO complexes with 2-Cl-4,6-NO_2-phenol and trinitrophenol.

studies. The last two methods, in particular, eliminate the involvement of 2:2 complexes which have been detected for some other systems with oxygen bases (18). This is most probably due to the essential steric hindrance in 2,6-dichlorophenols, which does not allow the formation of homoconjugated anions in this case. The formation of such anions is also excluded for $(AH)_2B$ complexes, even for the strongest proton donors and acceptors. The second phenol molecule is attached to 1:1 species via relatively weak hydrogen bond (13, 14). Based on the infrared spectra themselves it is very difficult to exclude the presence of $[OHO]^-$ homoconjugated anions because of the great similarity of background absorption for the 1:1 and 2:1 species.

In Fig. 5 ($a-d$) we compare the spectra of solid complexes (which can be easily isolated in crystalline state) $TBNO_1 \cdot DCNP_1$ and $(TBNO)_2 \cdot DCNP$, in CCl_4 solutions. For 2:1 adducts in the solid state the high frequency absorption above 1600 cm^{-1} almost completely disappears. In the solution there remains very weak high frequency doublet which could indicate that some of 1:1 complex is present in equilibrium. Some difference is visible in the backgorund absorption consisting in

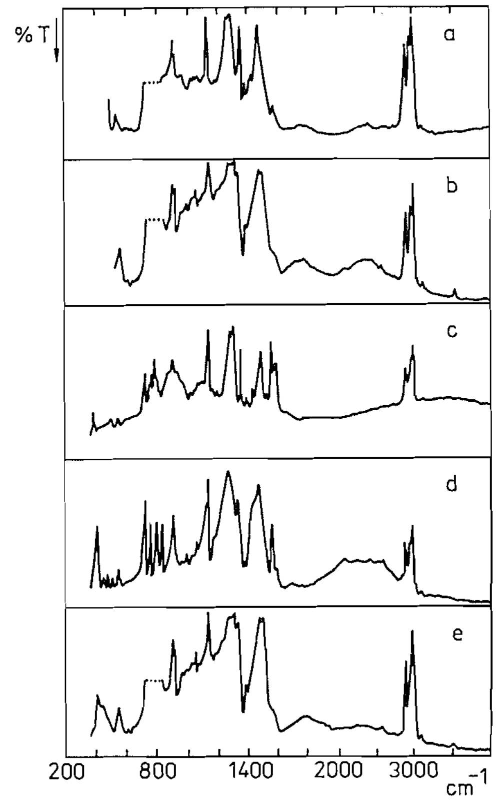

FIG. 5. Infrared spectra of TBNO · DCNP complexes: (a) 0.02 M TBNO and 0.01 M DCNP in CCl_4, d = 2 mm, (b) 0.01 M TBNO and 0.01 M DCNP in CCl_4, d = 2 mm, (c) solid $TBNO_2 \cdot DCNP_1$ in KBr, (d) solid $TBNO_1 \cdot DCNP_1$ in KBr, (e) 0.01 M TBNO and 0.01 M DCNP in CCl_4, d = 2 mm, deuterated at about 75%.

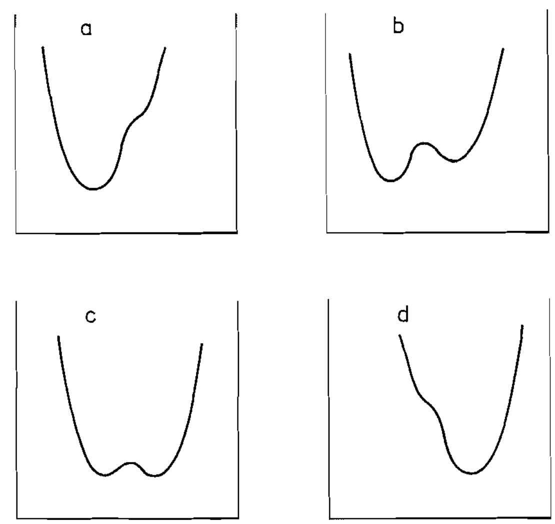

FIG. 6. Expected shapes of the potential for the proton motion in the investigated systems: (a) pK_a less than −4, (b) for intermediate range of ΔpK_a, (c) ΔpK_a equal to about −0.3, (d) ΔpK_a above 4.

larger extension of this absorption towards low frequency. On the other hand, we find a distinct difference in the spectra of the 1:1 complexes in the solid state and in solution. This difference arises from the fact that the crystalline state favours the proton transfer ionic state. Already in the solution the PT equilibrium is shifted towards the ion pairs, but in the solid state purely ionic form $O^- \ldots H—O^+$ is reached with the hydrogen bridge which is a mirror image of the usual non-proton-transfer hydrogen bond. They correspond to the boundary potential curves *a* and *d* shown in Fig. 6.

It seems that just using the anticipated evolution of the potential energy curves shown schematically in Fig. 6, one can also understand the evolution of ir spectra of the complexes under investigation. The particular spectroscopic properties of complexes belonging to the inversion range result most probably from the appearance of the second minimum for the proton motion a strong anharmonicity of the potential. The appearance of a second minimum on the level similar to the first one causes additional protonic transitions of similar intensities and widths. The analysis of the shape of the protonic bands, assuming a double minimum potential, performed in two somewhat different ways leads to quite similar results. In the semiempirical approach proposed by Romanowski and Sobczyk (19, 20), the evolution of ir spectra for OHO bridges of varying length has been calculated by assuming the coupling of protonic vibrations with low frequency, strongly damped, bridge vibrations. These authors showed that a flow frequency background absorption appears for sufficiently short bridges with double minimum for the proton motion. In the case of strong symmetrical bonds the high frequency absorption almost completely disappears. Similar results have been obtained by Zundel, Weidemann, and co-workers (21, 22). They calculated the shape of protonic bands by assuming the fluctuations of electric field and bridge length and showed that this shape can be substantially changed for various hydrogen bonds. In particular, the intensities of low and high frequency parts of the broad absorption are very sensitive to the hydrogen bond strength. The interpretation based on the assumption of a double minimum potential for the complexes of inversion range is supported by the isotopic effect. The calculations performed by Zundel *et al.* (23) showed, that in the case of broad "continuous" protonic absorption the total effect consists of the narrowing on both sides of the band and a drop of intensity. Such effect is observed in the case of complexes belonging to the inversion region. This is well demonstrated in Fig. 5 where the spectrum of the non-deuterated $TBNO_1 \cdot DCNP_1$ complex (*b*) is compared with that of the deuterated (75%) one (*e*). Quite similar features are reported for other complexes where nearly symmetrical double minimum potential for the proton motion is expected (11, 12, 24).

1. D. HADŽI. J. Chem. Soc. A, 5128 (1962).
2. D. HADŽI. J. Pure App. Chem. **11**, 435 (1965).
3. D. HADŽI and N. KOBILAROV. J. Chem. Soc. A, 439 (1966).
4. B. BRYCKI and M. SZAFRAN. Pol. J. Chem. **52**, 2247 (1978).
5. B. BRYCKI, Z. DEGA-SZAFRAN, and M. SZAFRAN. Adv. Mol. Relax. Inter. Proc. **15**, 71 (1979).
6. B. BRYCKI, Z. DEGA-SZAFRAN, and M. SZAFRAN. Pol. J. Chem. **54**, 221 (1980).
7. Z. DEGA-SZAFRAN and M. SZAFRAN. J. Chem. Soc. Perkin II, 195 (1982).
8. T. GRAMSTAD. Acta Chem. Scan. **15**, 1337 (1961).
9. T. GRAMSTAD. Spectrochim. Acta, **91**, 829 (1963).
10. T. GRAMSTAD and G. VANBINST. Spectrochim. Acta, **22**, 1681 (1966).
11. S. DETONI, D. HADŽI, R. SMERKOLJ, J. HAWRANEK, and L. SOBCZYK. J. Chem. Soc. A, 2852 (1970).
12. M. ROSPENK, A. KOLL, and L. SOBCZYK. Adv. Mol. Relax. Inter. Proc. **11**, 129 (1977).
13. R. WOLNY, A. KOLL, and L. SOBCZYK. J. Phys. Chem. **89**, 2053 (1985).
14. R. WOLNY, A. KOLL, and L. SOBCZYK. Bull. Soc. Chim. Belg. **93**, 99 (1984).
15. G. S. DENISOV and V. M. SCHREIBER. Vestnik LGU, **4**, 61 (1976).
16. A. KOLL. Bull. Soc. Chim. Belg. **92**, 313 (1983).
17. R. WOLNY and A. KOLL. Bull. Acad. Polon. Sci. Ser. Sci. Chim. **29**, 377 (1982).
18. Z. DEGA-SZAFRAN and M. SZAFRAN. J. Mol. Struct. **45**, 33 (1978).
19. H. ROMANOWSKI and L. SOBCZYK. Chem. Phys. **19**, 361 (1977).
20. H. ROMANOWSKI and L. SOBCZYK. Acta Phys. Polon. A**60**, 545 (1981).
21. R. JANOSCHEK, E. WEIDEMANN, and G. ZUNDEL. J. Chem. Soc. Faraday Trans. 2, **69**, 505 (1973).
22. A. HAYD, E. G. WEIDEMANN, and G. ZUNDEL. J. Phys. Chem. **70**(1), 86 (1979).
23. R. JANOSCHEK, A. HAYD, E. G. WEIDEMANN, M. LEUCHES, and G. ZUNDEL. J. Chem. Soc. Faraday Trans. II, **74**, 1238 (1978).
24. Z. MALARSKI, M. ROSPENK, L. SOBCZYK, and E. GRECH. J. Phys. Chem. **86**, 401 (1982).

Zn(II), Cd(II), and Hg(II) complexes of 6-amino-3-methyl-5-nitrosouracil

J. M. SALAS-PEREGRIN[1]
Department of Inorganic Chemistry, Faculty of Science, University of Granada, 18071 – Granada, Spain

M. N. MORENO-CARRETERO
Department of Inorganic Chemistry, University College, 23071 – Jaen, Spain

AND

E. COLACIO-RODRIGUEZ
Department of Inorganic Chemistry, Faculty of Science, University of Granada, 18071 – Granada, Spain

Received October 16, 1984[2]

J. M. SALAS-PEREGRIN, M. N. MORENO-CARRETERO, and E. COLACIO-RODRIGUEZ. Can. J. Chem. **63**, 3573 (1985).

The preparation and spectral properties of the complexes of 6-amino-3-methyl-5-nitroso-uracil (HAMNU) with Zn(II), Cd(II), and Hg(II) ions are reported. The results suggest that the exocyclic oxygen and nitrogen atoms have a much greater tendency to bind to these ions than the ring nitrogen atoms. In Zn(II) and Cd(II) complexes, the ligand is N,O-coordinated through the 5-nitroso and 6-oxide groups of (AMNU) in nitrosophenolic anionic form. In the Hg(II) complexes, the ligand seems to be bound in neutral form. Tetrahedral structures are proposed in all cases.

J. M. SALAS-PEREGRIN, M. N. MORENO-CARRETERO et E. COLACIO-RODRIGUEZ. Can. J. Chem. **63**, 3573 (1985).

On rapporte la préparation et les propriétés spectrales des complexes de l'amino-6 méthyl-3 nitroso-5 uracile (AMNU) avec les ions Zn(II), Cd(II) et Hg(II). Les résultats suggèrent que les atomes d'oxygène et d'azote exocycliques tendent à se lier plus facilement à ces ions que les atomes d'azote du cycle. Dans les complexes de Zn(II) et de Cd(II), la coordination-N,O du ligand est assumée par les groupements nitroso-5 et oxyde-6 du AMNU existant sous la forme anionique nitroso-phénolique. Dans les complexes du Hg(II), le ligand semble être lié à la forme neutre. Dans tous les cas, on suggère l'existence de structures tétraédriques.

[Traduit par le journal]

Introduction

The work of Rosenberg and the discovery of the antitumor action of some platinum(II) complexes (1, 2) have aroused extraordinary investigations into the interaction between metal ions and the nucleic acids, and their constituents, the nucleosides and nucleotides.

The pyrimidine bases that are found in living systems have a large number of positions to bind a metal ion, using, generally, their heterocyclic and amidic nitrogen atoms to make covalent bonds with several metal ions.

The exocyclic oxygen and nitrogen atoms of some pyrimidine derivatives share in selective reactions with metal ions as is shown in the "platinum pyrimidine blues" (3, 4). On the other hand, the exocyclic groups of pyrimidine bases, besides playing an important role in the formation of metal–pyrimidine bonds, can operate as acceptors or donors in hydrogen bonds, which help to stabilize the crystal structure of the complexes.

Investigations determing the binding sites of pyrimidine derivatives to metal ions are the first steps for the understanding of the biological role of some of these complexes (5–8) and have been the subject of several review articles (9, 10). As an extension of these studies, we report the preparation and spectral study of complexes of 6-amino-3-methyl-5-nitroso-uracil (HAMNU) with Zn(II), Cd(II), and Hg(II) ions.

Experimental

6-Amino-3-methyl-5-nitrosouracil was prepared by hydrolysis of 4-amino-1,6-dihydro-1-methyl-2-methoxy-5-nitroso-6-oxopyrimidine according to the method previously reported (11). All the chemicals used in this work were analytical reagent grade.

The complexes were prepared as follows: $Zn(AMNU)_2 \cdot 4H_2O$: a solution of zinc acetate (4 mmol) in water (10 mL) was added slowly and with stirring to a hot aqueous solution (100 ml) of the ligand (2 mmol). The resulting red solution was allowed to cool slowly to room temperature. Red crystals appeared after a few days.

$Cd(AMNU)_2 \cdot 2H_2O$ and $Cd(AMNU)_2$: These compounds were obtained by mixing hot solutions containing 2 mmol of HAMNU and 8 mmol of cadmium chloride, respectively. By evaporating at room temperature for 24 h, an orange powder was obtained. From the filtrate solution, red crystals can be isolated after a few days.

$HgCl_2(HAMNU)_2 \cdot 2H_2O$ and $HgCl_2(HAMNU)_2 \cdot H_2O$: An aqueous solution containing 8 mmol of $HgCl_2$ was added slowly and with stirring, to a hot concentrated aqueous solution of the ligand (2 mmol). After standing for about 2 days, red crystals were isolated. From the resulting filtrate solution, a pale rose powder was obtained after a few days.

All the compounds were filtered, washed with water and ethanol, and dried with diethyl ether.

Chemical analysis of C, H, and N was performed with a Carlo Erba 1106 Microanalyzer. Determination of Zn and Cd was carried out by atomic absorption spectrometry using a Perkin Elmer model 290 spectrophotometer and Hg analyzed using a Perkin Elmer 5000 apparatus. The percentage of water in the isolated complexes was determined by thermographic techniques, using a Mettler TG-50 thermobalance. The heating rate was 10°C min^{-1}. For zinc and cadmium complexes a static atmosphere of air was used. For mercury complexes, a dynamic atmosphere of nitrogen (100 ml min^{-1}) was utilized. The results obtained are listed in Table 1.

The absorption spectra in the uv–visible region (200–700 nm) were recorded on a Beckman Acta C-III spectrophotometer.

Infrared spectra were recorded in KBr pellets (4000–200 cm^{-1}) and polyethylene pellets (650–200 cm^{-1}) on a Beckman-4250 spectrophotometer.

^1H nmr spectra were recorded on a Hitachi Perkin Elmer model R-600 FT-NMR spectrometer, using dimethylsulfoxide-d_6 as solvent and TMS as internal reference.

Results and discussion

The 4-keto-5-nitroso portion of 6-amino-3-methyl-5-nitrosouracil (HAMNU) may exist in several tautomeric forms: dike-

[1] To whom all correspondence should be addressed.
[2] Revision received June 20, 1985.

TABLE 1. Analytical and thermogradimetric data*

Compound	Colour	C(%)	H(%)	N(%)	M(%)	H_2O(%)
$Zn(AMNU)_2 \cdot 4H_2O$	Red	25.8(25.3)	3.7(3.8)	23.3(23.6)	12.9(13.7)	15.1(15.1)
$Cd(AMNU)_2 \cdot 2H_2O$	Orange	25.1(24.7)	2.9(2.9)	22.6(23.0)	22.8(23.1)	7.5(7.4)
$Cd(AMNU)_2$	Red	26.6(26.6)	2.1(2.2)	25.2(24.8)	24.8(24.9)	—
$HgCl_2(HAMNU)_2 \cdot 2H_2O$	Red	18.9(18.5)	2.4(2.4)	17.9(17.3)	30.5(31.0)	5.6(5.6)
$HgCl_2(HAMNU)_2 \cdot H_2O$	Rose	19.4(19.1)	1.8(2.2)	16.9(17.7)	31.4(31.8)	3.0(2.9)

*Calculated values in parentheses.

TABLE 2. Electronic spectra of HAMNU and its isolated complexes*

	Maxima of absorption (nm)		
Compound	$\pi \rightarrow \pi^*$ ring	$\pi \rightarrow \pi^*$ R—NO	$n \rightarrow \pi^*$ R—NO
HAMNU	222 (1.50)	315 (1.75)	523
$Zn(AMNU)_2 \cdot 4H_2O$	221 (3.06)	315 (5.20)	485
$Cd(AMNU)_2 \cdot 2H_2O$	222 (2.70)	313 (4.94)	485
$Cd(AMNU)_2$	222 (1.62)	313 (3.32)	485
$HgCl_2(HAMNU)_2 \cdot 2H_2O$	223 (2.68)	316 (2.36)	518
$HgCl_2(HAMNU)_2 \cdot H_2O$	222 (2.06)	315 (1.80)	520

*Values in parentheses are $\epsilon \times 10^{-4}$.

TABLE 3. ^1H nmr chemical shifts (δ, ppm) for HAMNU and its complexes of Zn(II), Cd(II), and Hg(II)*

Compound	N_3—CH_3	H_2O	—NH_2	=N—H	N_1—H
HAMNU	3.2	—	7.8	—	11.4
$Zn(AMNU)_2 \cdot 4H_2O$	3.2	3.4	—	8.1	9.7
$Cd(AMNU)_2 \cdot 2H_2O$	3.2	3.3	—	7.8	10.5
$Cd(AMNU)_2$	3.3	—	—	7.8	10.5
$HgCl_2(HAMNU)_2 \cdot 2H_2O$	3.3	3.3	8.3	—	11.7
$HgCl_2(HAMNU)_2 \cdot H_2O$	3.2	3.2	8.3	—	11.7

*All signals are singlets.

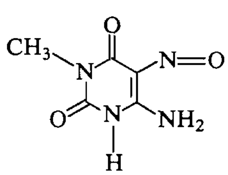

I

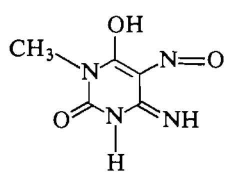

II

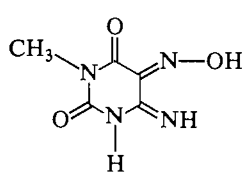

III

tonic (**I**), nitroso–phenolic (**II**), and keto–oximic (**III**) forms. Infrared data of HAMNU indicate that, in solid phase, the diketonic form is the most stable (11). Nevertheless, when this ligand is coordinated to metal ions in anionic form, nitroso–phenolic and keto–oximic forms are favoured because both have easily dissociable hydrogen atoms and the formation of a chelate can occur most readily.

The absorption maxima of these complexes in the ultraviolet–visible region are given in Table 2 and the assignment of the bands has been established according to bibliographic data (12–16).

A marked difference between the visible spectra of these complexes and the visible spectrum of free HAMNU is the hypsochromic shift (38 nm) of the band corresponding to the absorption of the chromophore group that takes place in the case of Zn(II) and Cd(II) complexes. It may indicate that the nitroso group is bound to the metal, whilst in the visible spectra of Hg(II) complexes, this displacement barely exists. These observations are in agreement with those found for some metal complexes with 6-amino-5-nitrosouracil (17, 18).

In Table 3 are given the ^1H nmr data of HAMNU and its isolated complexes. The signals between 9.7 and 11.7 ppm have been assigned to the resonance of N_1—H protons (17–19) and their presence indicates that the ligand is not bound to metal ions through the N_1 atom. On the other hand, this signal appears shifted with respect to its position in the ^1H nmr spectra of the free ligand, following two behavior types clearly defined. When the ligand is coordinated in anionic form (Zn(II) and Cd(II) complexes), this signal is shifted upfield, probably because of the increase of electronic density in the pyrimidine ring as a result of deprotonation (20). If HAMNU acts as a neutral ligand ((Hg(II) complexes), this signal appears shifted downfield, since coordination produces a decrease of negative charge density in the pyrimidine ring (21). Moreover, the ^1H nmr spectra show a signal at about 8 ppm, which has been assigned to the iminic proton, in the Zn(II) and Cd(II) complexes, and to the aminic hydrogens in the Hg(II) complexes (17).

The $Zn(AMNU)_2 \cdot 4H_2O$, $Cd(AMNU)_2 \cdot 2H_2O$, and $Cd(AMNU)_2$ complexes show practically the same infrared spectra. These show two bands in the 3400–3100 cm^{-1} range. The band at higher wavenumber corresponds to the ν(N—H) stretching vibration of the imino group and the other may be assigned to the $\nu(N_1$—H) stretching vibration. The position of these bands is similar to those found for other analogous complexes with 6-amino-5-nitrosouracil derivatives (17, 18, 22). The ν(C=O) band is shifted approximately 60 cm^{-1} to lower wavenumber from its position in the ir spectrum of free HAMNU (11), which can be a result of the change of the electronic density in the ring after coordination. This has also been observed in analogous pyrimidine derivative complexes (23). Likewise, we observe a band at about 1500 cm^{-1}, which corresponds to the ν(N=O) stretching vibration of the nitroso group. The presence of this band and the band corresponding to the ν(N—H) vibration of the imino group indicate that the coordination of HAMNU to Zn(II) and Cd(II) ions takes place through the tautomer anionic form **II**.

Two new bands in the 600–200 cm^{-1} region, corresponding to ν(ML) vibrations, are certainly assignable to ν(M—N) modes (18, 24–26). Likewise, there are no bands due to the existence of coordinated water molecules.

On the basis of the obtained data, we suggest that, in the Zn(II) and Cd(II) complexes, the ligand is bound to metal ion in iminic anionic form **II**, through the nitrogen and oxygen atoms of 5-nitroso and 6-oxide groups, respectively. This coordination mode coincides with the one found, from X-ray structural studies on analogous 5-nitrosopyrimidine derivative complexes (27–29).

This binding mode could be supported in the ir spectra by the appearance of the band corresponding to ν(C—O) stretching vibration. However, this band has not been observed since, due to the delocalization of negative charge by conjugation, this C—O bond may show an appreciable double bond contribution. Consequently, this band must appear at around 1300 cm^{-1} (30) and could be masked by the ν(C—N) bands of the ligand (18, 21). The lack of a shift of the ν(N=O) band to lower wavenumber in the ir spectra of $Zn(AMNU)_2 \cdot 4H_2O$ and $Cd(AMNU)_2$ can be also explained by the above-mentioned conjugation, since the loss of electronic density of the nitrogen atom as consequence of the coordination may be counteracted by the delocalization of free negative charge of the oxygen atom of 6-oxide group and thus loses the single character of the C—O whereas the electronic density of the N=O bond remains practically unaffected.

Finally, in view of the fact that the water molecules are out of the coordination sphere, it is reasonable to conclude that for these three complexes the most probably structure is a distorted tetrahedron.

The ir spectra of the Hg(II) complexes show that at about 3300 cm^{-1}, a broad band can be assigned to the ν(N—H) stretching vibration of an amino group. This band is confirmed by the band around 1660 cm^{-1} that corresponds to δ(N—H) in-plane deformation of this group. Bands at 3170 cm^{-1} ($HgCl_2(HAMNU)_2 \cdot 2H_2O$) and 3200 cm^{-1} ($HgCl_2(HAMNU)_2 \cdot H_2O$) can be assigned to $\nu(N_1$—H) vibration. The displacement to lower wavenumber of the bands corresponding to ν(C=O) and ν(N=O) stretching vibrations is smaller than that observed in the Zn(II) and Cd(II) complexes, which agrees with the interaction in the neutral form of HAMNU. This assumption is also corroborated by the ^1H nmr data of these complexes.

TABLE 4. Infrared data (cm^{-1}) of HAMNU and its isolated complexes

Compound	ν(O—H)	ν(N—H)	ν(C=O)	δ(N—H)	ν(C=N)	δ(O—H)	ν(C=C)	ν(N=O)	ν(M—N)*	ν(M—Cl)§
HAMNU	—	3200a	1740	1680	—	—	1640	1505	—	—
$Zn(AMNU)_2 \cdot 4H_2O$	3550	3260 3160	1675	—	†	1585a	†	1505	255 230	—
$Cd(AMNU)_2 \cdot 2H_2O$	3440	3310 3140	1685	—	†	1590a	†	1495	230 210	—
$Cd(AMNU)_2$	—	3400 3210	1675	—	1635	—	1605	1520	245 225	—
$HgCl_2(HAMNU)_2 \cdot 2H_2O$	3515	3300a 3170	1725	1660	—	1610a	†	1505	‡	225 210
$HgCl_2(HAMNU)_2 \cdot H_2O$	3510	3310a 3200	1735	1655	—	1610a	†	1480	‡	‡

* Broad band.
† Not observed due to overlapping with δ(O—H).
‡ Not observed.
§ In polyethylene pellets.

The far ir spectrum of $HgCl_2(HAMNU)_2 \cdot 2H_2O$ shows two bands at 225 and 210 cm^{-1}, which may be assigned to the ν(Hg—Cl) stretching vibrations (31). Moreover, there are no bands assignable to $\nu(Hg—OH_2)$ mode. The presence of two bands for ν(Hg—Cl) mode suggests three structural possibilities for this complex: *cis*-planar, octahedral polymeric with chlorine bridging and tetrahedral.

The first is improbable because of the electronic configuration of metal ion (d^{10}). The octahedral polymeric structure is not normal in Hg(II) complexes and is present only in some adducts of mercury chloride with solvents such as methanol (32, 33), pyridine (34), and 1,4-dioxane (35).

For these reasons, and taking into account the similarity of spectral data for both Hg(II) complexes, it seems logical to propose for them a distorted tetrahedral structure, in which the HAMNU acts as a monodentate ligand (tautomer form **I**). In view of the several occasions in which crystal structure determinations proved that binding site assignments made on the basis of spectral evidence for pyrimidine metal complexes were incorrect (29, 36–38), it would be rather naive to reach even a tentative conclusion favoring some atom of the exocyclic substituents over another one as the binding site of HAMNU in these Hg(II) complexes with this ligand.

Acknowledgments

We are indebted to Drs. A. Sánchez-Rodrigo and M. Nogueras-Montiel for their collaboration in the record of the ^{1}H nmr spectra.

1. B. ROSENBERG, L. VAN CAMP, J. E. TROSKO, and V. H. MANSOUR. Nature, **222**, 385 (1969).
2. B. ROSENBERG and L. VAN CAMP. Cancer Res. **30**, 1799 (1970).
3. B. ROSENBERG. Cancer Chemother. Rep. **59**, 589 (1975).
4. B. LIPPERT. J. Clin. Hematol. Oncol. **7**, 26 (1977).
5. J. A. CARBON, L. HUNG, and D. S. JONES. Proc. Natl. Acad. Sci. USA, **53**, 979 (1965).
6. J. A. CARBON, H. DAVID, and H. H. STUDIER. Science, **161**, 1146 (1968).
7. C. B. LOZZIO. Exp. Cell. Res. **69**, 377 (1971).
8. L. S. GOODMAN AND A. GILMAN. The pharmacological basis of therapeutics. 6th ed. *Edited by* Medica Suramericana. 1980.
9. L. G. MARZILLI. Prog. Inorg. Chem. **23**, 255 (1977).
10. D. J. HODGSON. Prog. Inorg. Chem. **23**, 211 (1977).
11. M. N. MORENO-CARRETERO, J. M. SALAS-PEREGRIN, A. SÁNCHEZ-RODRIGO, and M. NOGUERAS-MONTIEL. An. Quim. **79B**, 547 (1983).
12. S. F. MASON. J. Chem. Soc. 2071 (1954).
13. L. F. CAVALIERI and A. BENDICH. J. Am. Chem. Soc. **70**, 3875 (1948).
14. L. F. CAVALIERI and A. BENDICH. J. Am. Chem. Soc. **72**, 2587 (1950).
15. K. L. WIERZCHOWSKI, E. LITONSKA, and D. SHUGAR. J. Am. Chem. Soc. **87**, 4621 (1965).
16. P. LARDENOIS, M. SELIM, and M. SELIM. Bull. Soc. Chim. Fr. **5**, 1858 (1971).
17. J. M. SALAS-PEREGRIN, M. N. MORENO-CARRETERO, M. A. ROMERO-MOLINA, and E. COLACIO-RODRIGUEZ. Rev. Chim. Miner. **21**, 233 (1984).
18. J. M. SALAS-PEREGRIN, M. N. MORENO-CARRETERO, J. D. LÓPEZ-GONZÁLEZ, and A. GARCÍA-RODRÍGUEZ. An. Quim. **80B**, 437 (1984).
19. G. C. STOCCO, A. TAMBURELLO, and M. A. GIRASOLO. Inorg. Chim. Acta, **78**, 57 (1983).
20. P. CASTAN and J. P. LAURENT. Trans. Metal Chem. **5**, 154 (1980).
21. M. N. MORENO-CARRETERO, A. M. MARTÍNEZ-GARZÓN, R. LÓPEZ-GARZÓN, and J. M. SALAS-PEREGRIN. Rev. Chim. Miner. In press.
22. J. S. GARCÍA-MINO, J. D. LÓPEZ-GONZÁLEZ, M. N. MORENO-CARRETERO, and J. M. SALAS-PEREGRIN. An. Quim. **77B**, 335 (1981).
23. M. N. MORENO-CARRETERO. Ph.D. Thesis, University of Granada. 1983.
24. M. D. CHILD, G. A. FOULDS, G. D. PERCY, and D. A. THORNTON. J. Mol. Struct. **75**, 191 (1981).
25. D. M. L. GOODGAME and I. JEEVES. Inorg. Chim. Acta 32, 157 (1979).
26. J. ABBOT, D. M. L. GOODGAME, and I. JEEVES. J. Chem. Soc. Dalton, 880 (1978).
27. M. N. MORENO-CARRETERO and J. M. SALAS-PEREGRIN. Acta Crystallogr. To be published.
28. M. A. ROMERO-MOLINA, J. D. MARTÍN-RAMOS, J. D. LÓPEZ-GONZÁLEZ, and C. VALENZUELA-CALAHORRO. An. Quim. 79B, 200 (1983).
29. C. RUIZ-VALERO, A. MONGE, E. GUTIÉRREZ-PUEBLA, and E. GUTIÉRREZ-RIOS. Acta Crystallogr. C40, 811 (1984).
30. J. RUIZ-SÁNCHEZ. Thesis of Licenciate. University of Granada. 1984.
31. J. R. FERRARO. Low frequency vibrations of inorganic and coordination compounds. Plenum Press, New York. 1971.
32. H. BRUSET and F. MADAULE-AUBRY. Bull. Soc. Chim. Fr. 3121 (1965).
33. F. MADAULE-AUBRY and H. GILLIER-PANDRAUD. C.R. **260**, 6613 (1965).
34. D. GRDENIC and I. KRSTANOVIC. Archiv. Kemi. **27**, 143 (1955).
35. O. HASSEL and J. HVOSLEF. Acta Chem. Scand. **8**, 1653 (1954).
36. M. A. ROMERO-MOLINA, J. M. SALAS-PEREGRIN, J. D. LÓPEZ-GONZÁLEZ, and C. VALENZUELA-CALAHORRO. An. Quim. **79B**, 383 (1983).
37. C. RUIZ-VALERO, A. MONGE, E. GUTIÉRREZ-PUEBLA and E. GUTIÉRREZ-RIOS. Acta Crystallogr. C**39**, 1214 (1983).
38. J. D. LÓPEZ-GONZÁLEZ, M. A. ROMERO-MOLINA, J. M. SALAS-PEREGRIN, and C. VALENZUELA-CALAHORRO. An. Quim. **79B**, 477 (1983).

Simulation of edge effects in electroanalytical experiments by orthogonal collocation. Part V. Chronoamperometry at ultramicroelectrode ensembles

JOHN CASSIDY, JAMAL GHOROGHCHIAN, FERESHTEH SARFARAZI, AND STANLEY PONS[1]
Chemistry Department, University of Utah, Salt Lake City, UT 84112, U.S.A.

Received March 14, 1985

JOHN CASSIDY, JAMAL GHOROGHCHIAN, FERESHTEH SARFARAZI, and STANLEY PONS. Can. J. Chem. **63**, 3577 (1985).

The use of orthogonal collocation in the treatment of the problem of an array of ultramicroelectrodes is presented and compared to existing digital simulation techniques.

JOHN CASSIDY, JAMAL GHOROGHCHIAN, FERESHTEH SARFARAZI et STANLEY PONS. Can. J. Chem. **63**, 3577 (1985).

On rapporte les résultats obtenus lors de l'usage de collocations orthogonales dans l'examen du problème d'un arrangement d'ultramicroélectrodes et on les compare aux résultats obtenus par les techniques existantes de simulation digitale.

[Traduit par le journal]

Introduction

The geometries and methods of construction of ultramicroelectrodes have been approached in many ways since the pioneering work in the area by Bindra *et al.* (1) at Southampton in the early 1970's. The analytical theoretical characterizations of some of the geometries have been developed and are just now beginning to appear in the literature. Although several electrode geometries hold great promise in terms of ease of construction, performance and ease of mass transport description, the round disk electrode has maintained popularity in use, primarily because of the convenience in preparing them in the 10 to 50 μm diameter range (2, 3). These comparatively large microelectrodes have significant analytical applications and characterization of their behavior is important. We provide characterization of some arrays of this type of ultramicroelectrode in this report by orthogonal collocation simulation.

The effect of the magnitude of the circumference to surface area ratio of disk electrodes embedded in insulators on the response of conventional electrochemical techniques has been studied by a number of groups, including ourselves, in the earlier parts of the series (4–7). In the limit, when the surface area approaches atomic dimensions, the ratio becomes large and hemispherical diffusion becomes predominant. Under such conditions, the mass transport coefficient varies as $1/r$ where r is the radius of the ultramicroelectrode at small dimensions. Heterogeneous rate measurements and stochastic process studies may be greatly facilitated (1) under these conditions. Reaction mechanistic studies are also facilitated but without the benefit of spectroelectrochemistry and direct product analysis due to the extremely small amounts of electrogenerated species formed. This problem may be mitigated by the construction of clusters or arrays of ultramicroelectrodes arranged so that their individual diffusion fields are isolated on the timescale of the experiment. Thus processes which normally occur at individual electrodes at high mass transport rates are essentially amplified to a level where analyses by product isolation or conventional spectroelectrochemical techniques are easily implemented. The possibilities of using microelectrodes in the form of colloidal particles as heterogeneous catalysts and fluidized bed reactors have also been examined (8–10). Work has proceeded on a variety of ultramicroelectrode array geometries, including cross sections of epoxy embedded reticulated carbon arrays (11, 12) and arrays for liquid chromatography detectors (13). Geometries include those created by photoresist images (14, 15), carefully placed contiguous carbon fibers (13), sites of inactive oxides on metal substrates (16, 17), metal mesh (18), and platinum particles dispersed in polymer films (19, 20). A variety of new geometries which may be able to be prepared at the 100 Å level has been reported (21).

Disk electrodes, embedded in an insulator, exhibit uneven nonlinear diffusion unless the edge of the electrode is confined by the perpendicular walls of the cell. Since the flux at the edge is greater than that towards the center, the overpotential near the edge will be greater than at the center. There will also be a reduction in overpotential caused by the resistance to charge transfer across the face of the electrode (22). The resulting secondary or tertiary current distribution must be considered in any full analytical treatment of the disk electrode. Whereas the iR drop through the solution is small at a microelectrode due to the small current, the effect on potential distribution across the face of the electrode may still be considerable because of the very uneven current distribution. When this is taken into account along with the activation and transport overpotentials then the resulting "quaternary distribution" may be defined. These complications are currently under investigation using an iterative procedure.

Theory

The original analytical approach for the array, reviewed by Gueshi *et al.* (14), assumed that a steady state current was reached, and the resulting Laplace equation could be solved. For the rather large diameter electrodes used in most work today (>5 μm) this is not a valid assumption since the rate of reaction will vary across the surface of a disk. The electrode is non-uniformly accessible. Reller *et al.* (23) used a digital simulation approach similar to that of Feldberg (24) to examine chronoamperometry at an array of microelectrodes and showed that while the original analytical solutions were correct at long and short times, at intermediate times they were not because of the "steady state" assumption. More recently Shoup and Szabo used a hopscotch algorithm and presented an equation for a general solution (25). Comparison between the regular hexagon model (Fig. 1*a*) and various reticulated arrays has been made (26). Although the hexagonal model is most popular because of its symmetrical advantages (14, 25, 27), disks have also been positioned in square arrays (28) and strips (29). Numerous electrochemical techniques have been considered, including chronopotentiometry (30), cyclic voltammetry (23, 31), Faradaic impedance (32), and chronoamperometry (14, 27) which is considered here.

[1]To whom all correspondence should be addressed.

Orthogonal collocation techniques approximates the concentration profiles by utilization of orthogonal polynomials. The differential equation is accurately satisifed at certain points — the zeros or roots of the approximation polynomials. The problem is ultimately reduced to a system of coupled ordinary differential equations which are simultaneously solved by conventional means. In the case of cylindrical co-ordinates, the following trial function in two dimensions x and r is chosen:

$$[1]\quad C(x,r,t) = \sum_{l=1}^{N_r+2} \sum_{j=1}^{N_x+2} \lambda_{j,l} x^{j-1} r^{l-1}$$

where $C(x,r,t)$ is the concentration at a distance x above the electrode and radial distance r away from the center of the electrode as shown in Fig. 1*b*. N_r and N_x are the number of internal collocation points and $\lambda_{j,l}$ is determined by the number of points and the type of polynomial chosen (*vide infra*). After differentiation and substitution the following relations are found, where $A_{i,j}$, $B_{i,j}$, $C_{l,k}$, $D_{l,k}$ are constants, the values of which are detailed in earlier papers (4–7), and need only to be calculated once for a given geometry and polynomial.

$$[2]\quad \begin{aligned} \left(\frac{\partial C}{\partial x}\right)_{x_i,r_k} &= \sum_{j=1}^{N_x+2} A_{ij} C(x_j,r_k,t) \\ \left(\frac{\partial^2 C}{\partial x^2}\right)_{x_i,r_k} &= \sum_{j=1}^{N_x+2} B_{ij} C(x_j,r_k,t) \\ \left(\frac{\partial C}{\partial r}\right)_{x_j,r_k} &= \sum_{l=1}^{N_r+2} C_{l,k} C(x_j,r_l,t) \\ \left(\frac{\partial^2 C}{\partial r^2}\right)_{x_j,r_k} &= \sum_{l=1}^{N_r+2} D_{l,k} C(x_j,r_l,t) \end{aligned}$$

In this paper, the model due to Gueshi (14) is used (see Fig. 1*a*). The geometry is characterized by many contiguous unit cells, each an image of the other, so that there is perfect symmetry maintained in the macroscopic sense. The following simple electron transfer reaction is examined:

$$[3]\quad \mathrm{A} \underset{+ne^-}{\overset{-ne^-}{\rightleftarrows}} \mathrm{B} \qquad E^0$$

The diffusion equation in cylindrical coordinates is

$$[4]\quad \frac{\partial C_A}{\partial t} = D_A\left[\frac{\partial^2 C_A}{\partial x^2} + \frac{1}{r}\frac{\partial C_A}{\partial r} + \frac{\partial^2 C_A}{\partial r^2}\right]$$

Given that the diffusion coefficients of the two species are similar, and the fraction of the surface covered with electrodes is θ, the boundary conditions are the following:

$$[5]\quad t = 0,\ x \geq 0,\ r \geq 0 \qquad \begin{aligned} C_A(x,r,0) &= C_A{}^0 \\ C_B(x,r,0) &= 0 \end{aligned}$$

$$[6]\quad t > 0,\ x \to \infty,\ r \geq 0 \qquad \begin{aligned} C_A(\infty,r,t) &= C_A{}^0 \\ C_B(\infty,r,t) &= 0 \end{aligned}$$

$$[7]\quad t > 0,\ x = 0,\ 0 < r < r_0 \qquad \frac{C_B(0,r,t)}{C_A(0,r,t)} = \exp\left[\frac{nF}{RT}(E^0 - E)\right]$$

$$[8]\quad t > 0,\ x = 0,\ 0 < r < r_0 \qquad C_A(0,r,t) = 0$$

$$[9]\quad t > 0,\ x = 0,\ 0 < r < r_0 \qquad \left(\frac{\partial C_A}{\partial x}\right)_{x=0} = -\left(\frac{\partial C_B}{\partial x}\right)_{x=0}$$

$$[10]\quad t > 0,\ x = 0,\ r_0 < r < r_0' \qquad \left(\frac{\partial C_A}{\partial x}\right)_{x=0} = \left(\frac{\partial C_B}{\partial x}\right)_{x=0} = 0$$

$$[11]\quad t > 0,\ \text{at all } x,\ r = r_0' \qquad \left(\frac{\partial C_A}{\partial r}\right)_{r=r_0'} = \left(\frac{\partial C_B}{\partial r}\right)_{r=r_0'} = 0$$

$$[12]\quad t > 0,\ \text{at all } x,\ r = 0 \qquad \left(\frac{\partial C_A}{\partial r}\right)_{r=0} = \left(\frac{\partial C_B}{\partial r}\right)_{r=0} = 0$$

As before the cylindrical geometry is divided into the space above the electrode surface and above the insulator where the concentrations are C_1 and C_2, respectively. At the interface the following equations hold for all species

$$[13]\quad t > 0,\ x \geq 0,\ r = r_0 \qquad \begin{aligned} C_1(x,r_0,t) &= C_2(x,r_0,t) \\ \left(\frac{\partial C_1}{\partial r}\right)_{r=r_0} &= \left(\frac{\partial C_2}{\partial r}\right)_{r=r_0} \end{aligned}$$

r_0 is the radius of the active disk and the total area of a hexagon unit is approximated by a disk of area $\pi r_0'^2$. The radii are therefore related by

$$[14]\quad \theta = 1 - (r_0/r_0')^2$$

The transformations to converted the problem to dimensionless units and to a space between 0 and 1 are as follows:

$$[15]\quad \begin{aligned} X &= \frac{x}{L} \\ C_A^* &= \frac{C_A}{C_A{}^0} \\ R &= \frac{r}{r_0} \\ R' &= \frac{r' - r_0}{r_0' - r_0} \\ T &= \frac{Dt}{r_0^2} \end{aligned}$$

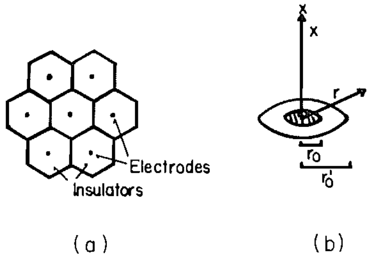

FIG. 1. (*a*) Hexagonal array model; the shaded area is active. (*b*) Cylindrical co-ordinates.

L is some distance into solution where no diffusion occurs during the time of the experiment. The dimensionless diffusion equations are:

(a) Above the active surface

$$[16] \quad \frac{\partial C^*_{A_1}}{\partial T} = \beta \frac{\partial^2 C^*_{A_1}}{\partial X^2} + \frac{1}{R}\frac{\partial C^*_{A_1}}{\partial R} + \frac{\partial^2 C^*_{A_1}}{\partial R^2}$$

where A_1 denotes the species A above the active area. An identical equation results for C_{B_1}.

(b) Above the insulator

$$[17] \quad \frac{\partial C^*_{A_2}}{\partial T} = \beta \frac{\partial^2 C^*_{A_2}}{\partial X^2} + \frac{1}{\gamma(R'\gamma + 1)}\left(\frac{\partial C^*_{A_2}}{\partial R'}\right) + \frac{1}{\gamma^2}\left(\frac{\partial^2 C^*_{A_2}}{\partial R'^2}\right)$$

and

$$\beta = (r_0/L)^2 \text{ and } \gamma = \left(\frac{1}{\sqrt{1-\theta}} - 1\right)$$

where A_2 denotes the species A above the insulator. An identical equation results for B_2. Legendre polynomials have been used for discretization in both the x and r directions. The summations [2] may be substituted into the original diffusion equations.

After substitution, expressions for the time derivative of the concentration of the species as a function of the concentration at the collocation points are obtained. For example, for species A above the active area,

$$[18] \quad \frac{dC^*_{A_1}}{dT} = \beta B_{i,N_X+2} + \sum_{j=2}^{N_X+1} B_{i,j} C^*_{A_1}(X_j,R_k,T) + \sum_{l=2}^{N_R+1} \frac{1}{C_{1,1}V} \times (-\gamma G_l I_{N_R+2,k} + V I_{l,k}) C^*_{A_1}(X_i,R_l,T) + \sum_{l=2}^{N_R+1} - \frac{H_l I_{N_R+2,k}}{VC_{1,1}} C^*_{A_2}(X_i,R_l,T)$$

where $I_{l,k} = E_{l,k}C_{1,1} - E_{1,k}C_{l,1}$

$$V = (H_1 + \gamma G_{N_R+2})$$

$$[19] \quad G_l = \frac{C_{1,N_R+2}C_{l,1}}{C_{1,1}} - C_{l,N_R+2}$$

$$H_l = C_{l,1} - \frac{C_{N_R+2,1}C_{l,N_R+2}}{C_{N_R+2,N_R+2}}$$

This system of ordinary differential equations is solved simultaneously, and the concentrations at the collocation points found. The current is evaluated as

$$[20] \quad i = nFD_0 \int_0^{r_0} \left(\frac{\partial C_A}{\partial x}\right)_{x=0} 2\pi r dr$$

and the dimensioned flux is

$$[21] \quad \frac{i}{\pi r_0'^2} = \frac{2nFC_A{}^0 D_0 \sqrt{\beta}(1-\theta)}{r_0} \int_0^{r_0} \left(\frac{\partial C_A}{\partial x}\right)_{x=0} r dr$$

where the integral is evaluated by a Gaussian quadrature technique in a manner similar to that described earlier in the series (4−7, 33).

Results and discussion

At short times, diffusion to the array will be controlled by the diffusion to the individual microelectrodes, i.e., the diffusion is highly nonlinear. At long times, the "near" hemispherical diffusion fields of adjacent microelectrodes will overlap and the mass transport resembles diffusion to a planar electrode. Practically at long times ($Dt/r_0^2 > 3 \times 10^{-2}$) convection occurs (6).

The value of β, which is a function of L, is given by

$$[22] \quad \beta = \left(\frac{r_0}{L}\right)^2$$

The simulated current is a function of β which is chosen from the following inequality

$$[23] \quad \beta \leq \frac{0.1}{T_{max}}$$

where T_{max} is the total dimensionless time of the experiment (Dt/r_0^2). This condition allows stable integration by the DHPCGL (SSP Library) subroutine, and an iterative change in β for each time step such as [24] was found to be no more effective.

$$[24] \quad \beta_{n+1} = \frac{T_n \beta_n}{T_{n+1}}$$

With the number of internal points equal to six, the C.P.U. time for a complete run from $1/t = 100$ s^{-1} to $1/t = 2$ s^{-1} is about 120 s.

A rule of thumb for natural convection to occur in this case is given by:

$$[25] \quad \begin{cases} \text{At short times:} \\ \quad R_a > 67.94 \text{ for convection to occur (34).} \\ \text{At long times:} \\ \quad R_a > 1100.65 \text{ for convection to occur (35).} \end{cases}$$

Where R_a is the Rayleigh number

$$[26] \quad R_a = \frac{l^4 g}{\mu D}\left(\frac{d\rho}{dx}\right)$$

where D is the diffusion coefficient, ρ the density, g, gravity, and μ is the viscosity. At short times l is the radius of the unit cell and at long times l represents a characteristic dimension of the macroscopic array such as the array radius, if the array takes the form of a disk. R_a is a function of the dimension to the fourth power and for a unit cell convection is very unlikely to occur. However, this is not the case when the macroscopic electrode is considered.

Depending on the value chosen for θ, and r_0 the microelectrodes may be far enough apart to be isolated from each other, or close enough that their diffusion layers overlap. In the former case convection is unlikely to occur and this property has been used in flow rate independent detectors. Results for both these situations are presented.

In Fig. 2 the results of the present technique are compared to those calculated by Lindemann and Landsberg and Reller *et al.*

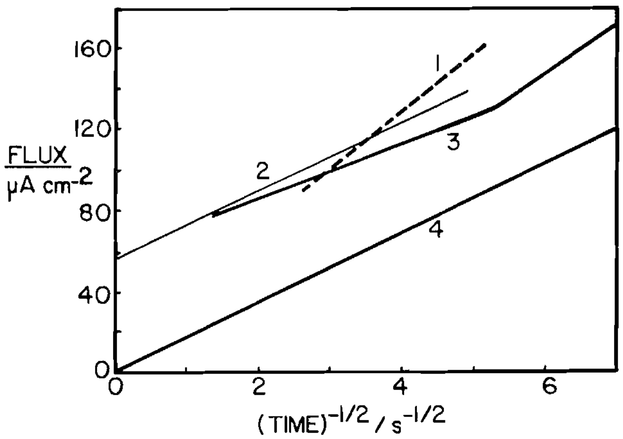

FIG. 2. Flux per total area vs. $t^{-1/2}$. Curve *1*: Lindemann and Landsberg result from ref. 27; curve *2*: result from Reller *et al.* from ref. 27; curve *3*: collocation result with $\theta = 0.99$, $r = 19.9$ μm, $C^0 = 0.01$ *M*, $D = 1 \times 10^{-5}$ cm²/s, $\beta = 1.9$; curve *4*: flux per total area by Cottrell equation.

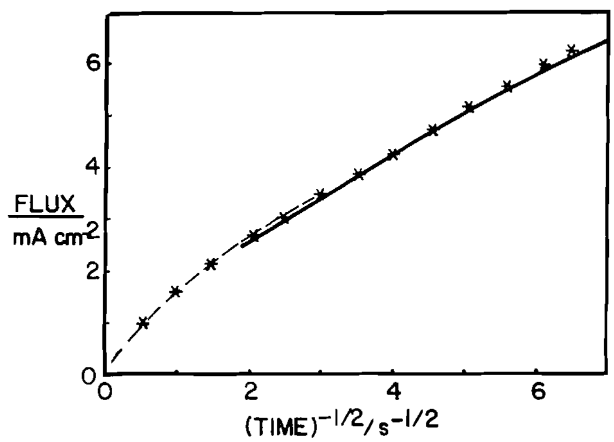

FIG. 3. Flux per total area vs. $t^{-1/2}$. *: estimated from Reller *et al.* in ref. 27; ---: calculated from equation from Shoup and Szabo, Table 2 in ref. 25 with $\theta = 0.528$, —— orthogonal collocation result with $C^0 = 0.01$ *M*, $D = 1 \times 10^{-5}$ cm²/s, $\theta = 0.53$, $\beta = 0.1$, $r = 43.9$ μm.

in ref. 27 for a highly blocked surface, i.e., 99% inactive, ($\theta = 0.99$, $r_0' = 199.9$ μm, $r_0 = 19.9$ μm). Our results agree with those of Reller *et al.* and extrapolation to infinite time, in the absence of convection, yields a finite current, characteristic of individual hemispherical diffusion at each microelectrode. The current per unit area is seen to be greater for active sites distributed in an insulator than for the pure semi-infinite linear diffusion. In Fig. 3 our results are compared with those of Reller *et al.* from Ref. 27 and Shoup and Szabo from ref. 25. In this case the blocked area is of the same order as the active area and at $1/\sqrt{t} = 2$ s$^{-1/2}$ the diffusion layers of the microelectrodes have overlapped forming a blanket diffusion layer. Thus convection is likely to be able to complicate the mass transport. As can be seen, however for intermediate times there is excellent agreement among the three simulations. In all the results presented, six internal collocation points were used and β was found using the inequality (23).

In Fig. 4 a comparison is made between the experimental results from curve 1 in ref. 36, the calculated results from ref. 25 with $\theta = 0.841$ and our calculations. Our results compare well with the experimental results and those of Reller *et al.* in ref. 27. However, at long time periods the outer boundary conditions are violated. This problem is alleviated using a greater number of collocation points which is only necessary for larger values of θ.

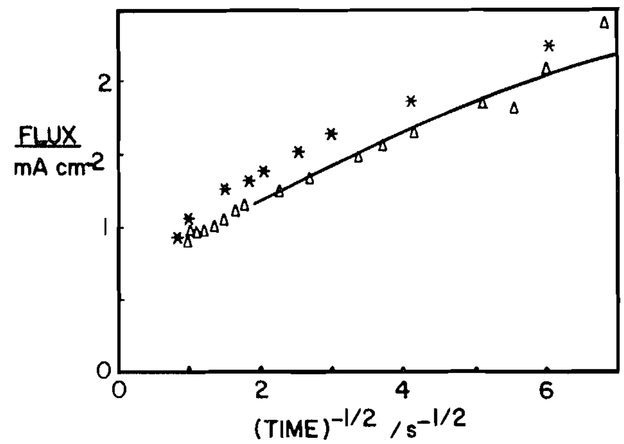

FIG. 4. Flux per total area vs. $t^{-1/2}$. *: calculated from Table 7 in ref. 25, with $\theta = 0.841$; △: experimental data estimated from curve *1* in ref. 36; ——: result from orthogonal collocation, $D = 6.8 \times 10^{-6}$ cm²/s, $C = 0.01$ *M*, $\theta = 0.84$, $r = 12.5$ μm, $\beta = 0.01$.

Since heterogeneous kinetics can be observed more readily at arrays of microelectrodes due to the accelerated rate of mass transport, other electrochemical experiments are useful in the kinetic analysis. Cyclic voltammetry is one useful technique for these studies, and is currently under investigation.

Comparison of calculation times between the orthogonal collocation technique and explicit or implicit fixed and variable grid finite difference methods still supports the conclusion reached in earlier reports; the calculation time required for the collocation method is still at least an order of magnitude faster than the finite difference schemes for the same local error. The initial mathematical rigor, however, is somewhat more demanding.

Conclusion

Orthogonal collocation was used to simulate the diffusion process at an array of ultramicroelectrodes. Despite the fact that no account was taken of the current and potential distributions across the face of each electrode, the simulated curves compare well with the experimental results. A more complete solution, taking into account current and potential distributions across the face of the electrode is necessary for cyclic voltammetry. As can be seen in Fig. 2, the enhancement of current compared to that of semiinfinite linear diffusion can be used for more efficient recovery of metals or catalysts. The next logical progression in the series is three dimensional arrays of ultramicroelectrodes in the form of bipolar fluidized bed reactors which are currently under consideration.

Acknowledgment

The authors thank the Office of Naval Research for support of this work.

1. R. BINDRA, A. P. BROWN, M. FLEISCHMANN, and D. PLETCHER. J. Electroanal. Chem. **58**, 31 (1975); **58**, 39 (1975).
2. A. M. BOND, M. FLEISCHMANN, and J. ROBINSON. J. Electroanal. Chem. **168**, 299 (1984).
3. J. PONCHON, R. CESPUGLIO, F. GONON, M. JOUVET, and J. PUJOL. Anal. Chem. **51**, 1483 (1979).

4. B. SPEISER and S. PONS. Can. J. Chem. **60**, 1352 (1982).
5. B. SPEISER and S. PONS. Can. J. Chem. **60**, 2463 (1982).
6. B. SPEISER and S. PONS. Can. J. Chem. **61**, 156 (1983).
7. J. CASSIDY, S. PONS, A. S. HINMAN, and B. SPEISER. Can. J. Chem. **62**, 716 (1984).
8. W. J. ALBERY and P. N. BARTLETT. J. Electroanal. Chem. **131**, 137 (1982).
9. W. J. ALBERY and P. N. BARTLETT. J. Electroanal. Chem. **131**, 145 (1982).
10. M. FLEISCHMANN, S. PONS, and J. GHOROGHCHIAN. To be published.
11. N. SLEASZYNSKI, J. OSTERYOUNG, and M. CARTER. Anal. Chem. **56**, 130 (1984).
12. D. J. CURREN and T. P. TOUGAS. Anal. Chem. **56**, 672 (1984).
13. W. LOWRY CAUDILL, J. O. HOWELL, and R. M. WIGHTMAN. Anal. Chem. **54**, 2532 (1982).
14. T. GUESHI, K. TOKUDA, and H. MATSUDA. J. Electroanal. Chem. **89**, 247 (1978).
15. K. AOKI and J. OSTERYOUNG. J. Electroanal. Chem. **125**, 315 (1981).
16. U. OESCH and J. JANATA. Electrochim. Acta, **28**, 1237 (1983).
17. U. OESCH and J. JANATA. Electrochim. Acta, **28**, 1247 (1983).
18. G. F. BLACKBURN, M. LEVY, and J. JANATA. Appl. Phys. Lett. **43**, 700 (1983).
19. W.-H. KAO and T. KUWANA. J. Am. Chem. Soc. **106**, 473 (1984).
20. K. DOBLEHOFER and W. DURR. J. Electrochem. Soc. **127**, 1041 (1980).
21. S. PONS and M. FLEISCHMANN. To be published.
22. N. IBL. *In* Comprehensive treatise of electrochemistry. *Edited by* E. Yeager, J. O'M. Bockris, B. E. Conway, and S. Sarangapani. Plenum Press, New York. 1983. p. 175.
23. H. RELLER, E. KIROWA-EISNER, and E. GILEADI. J. Electroanal. Chem. **161**, 247 (1984).
24. S. FELDBERG. *In* Electroanalytical chemistry, a series of advances. Vol. 3. *Edited by* A. J. Bard. Marcel Dekker, New York. 1969. p. 199.
25. D. SHOUP and A. SZABO. J. Electroanal. Chem. **160**, 19 (1984).
26. D. E. WEISSHAAR and D. E. TALLMAN. Anal. Chem. **55**, 1146 (1983).
27. H. RELLER, E. KIROWA-EISNER, and E. GILEADI. J. Electroanal. Chem. **138**, 65 (1982).
28. E. LEVANT, D. SCHUHMANN, and O. CONTAMIN. J. Electroanal. Chem. **70**, 117 (1976).
29. C. AMATORE, J. M. SAVEANT, and D. TESSIER. J. Electroanal. Chem. **147**, 39 (1983).
30. J. LINDEMANN and R. LANDSBERG. J. Electroanal. Chem. **29**, 261 (1971).
31. T. GUESHI, K. TOKUDA, and H. MATSUDA. J. Electroanal. Chem. **101**, 29 (1979).
32. K. TOKUDA, T. GUESHI, and H. MATSUDA. J. Electroanal. Chem. **102**, 41 (1979).
33. S. PONS. *In* Electroanalytical chemistry, a series of advances. Vol. 13. *Edited by* A. J. Bard. Marcel Dekker, New York. 1984.
34. E. L. CUSSLER. Diffusion, mass transfer in fluid systems. Cambridge University Press. 1984. p. 312.
35. S. CHANDRASEKHAR. Hydrodynamic and hydromagnetic stability. Oxford University Press, 1961. p. 43.
36. J. LINDEMANN and R. LANDSBERG. J. Electroanal. Chem. **30**, 79 (1971).

Substituent effects in carbocations CX^+, $CHX^{+\bullet}$, and CH_2X^+, and in singlet and triplet carbenes CHX. Proton affinities of singlet carbenes

A. C. HOPKINSON
Department of Chemistry, York University, Downsview, Ont., Canada M3J 1P3

AND

M. H. LIEN
Department of Chemistry, National Chung-Hsing University, Taichung, Taiwan 400

Received May 14, 1985

A. C. HOPKINSON and M. H. LIEN. Can. J. Chem. **63**, 3582 (1985).

Ab initio molecular orbital calculations with a 6-31G* basis set have been used to optimise structures for CX^+, $CHX^{+\bullet}$, CHX (both singlets and triplets), H_2CX^+ and H_3CX (X = H, CH_3, NH_2, OH, F, CN, and NC). Single point calculations were then performed on the 6-31G* optimised structures using a configuration interaction method involving all single and double excitations from the valence shell. Stabilisation energies for the carbocations are compared with those already reported for H_2CX^+. For the carbenes the single-triplet energy gap is examined as a function of substituent and the stabilisation energies of the singlet carbenes are compared with those of the isoelectronic carbocations H_2CX^+. Proton affinities are reported for the singlet carbenes and are compared with the proton affinities of similarly substituted ethylenes, $H_2C{=}CHX$.

A. C. HOPKINSON et M. H. LIEN. Can. J. Chem. **63**, 3582 (1985).

On a utilisé des calculs d'orbitales moléculaires *ab initio* avec une base 6-31G* pour optimiser des structures pour CX^+, $CHX^{+\bullet}$, CHX (tant sous forme de singulets que de triplets), H_2CX^+ et H_3CX (X = H, CH_3, NH_2, OH, F, CN et NC). Faisant appel à une méthode d'interaction de configuration impliquant toutes les excitations simples et doubles des couches de valence, on a alors effectué des calculs à point unique sur des structures optimisées en 6-31G*. On a comparé les énergies de stabilisation des carbocations avec celles rapportées antérieurement pour le H_2CX^+. Dans le cas des carbènes, on a examiné la différence d'énergie singulet/triplet en fonction du substituant; de plus, on compare les énergies de stabilisation des carbènes singulets avec celles des carbocations isoélectroniques H_2CX^+. On rapporte les affinités protoniques des carbènes triplets et on les compare avec les affinités protoniques des éthylènes $H_2C{=}CHX$ substitués d'une façon similaire.

[Traduit par le journal]

It has long been established that increasing the substitution at a carbocation centre increases the stability of the ion. Tertiary cations, RR′R″C$^+$, then, are the most stable and the primary carbenium ions, RCH_2^+, are the least stable. In tertiary cations all three groups are potential π-donors and the tertiary ions $(CH_3)_2CX^+$ show considerably less substituent dependence than the primary ions H_2CX^+ (1−6). Indeed, the highest substituent sensitivity ever observed is for the formation of H_2CX^+ from electron impact on H_3CX in the gas phase (7).

Substituents containing a heteroatom with a lone pair of electrons in the α-position (X = NH_2, OH, and F) function both as strong π-donors to the "vacant" p-orbital on C^+ and also as σ-acceptors. This class of substituents is the most effective at stabilising carbenium ions. Recently there has been considerable interest, both experimental (8−12) and theoretical (1,2,4−6) in carbenium ions containing an α-substituent which is usually both σ- and π-electron-withdrawing (X = NO_2, CHO, COOR, CN).[1] Here the substituents are destabilising, but in primary carbenium ions the destabilisation is less than expected on the basis of inductive electron-withdrawal. Calculations (5, 6) have shown that in these ions the substituents function as π-donors to the "vacant" *p*-orbital on the electron-deficient carbocation carbon.

All the theoretical studies to date have focussed on substituent effects in ions in which the cationic carbon has three σ bonds. Having observed that primary carbocations are more substituent dependent than tertiary carbocations it seemed possible that ions $CHX^{+\bullet}$ and CX^+ would have even greater substituent dependence. We now report our *ab initio* molecular orbital study of ions CX^+, $CHX^{+\bullet}$, and H_2CX^+ where X is H, CH_3, NH_2, OH, F, CN, and NC.

Carbenes, CHX, also contain an electron-deficient carbon atom and α-substituents having a lone pair of electrons are known to stabilise the singlet state (13−20). Here there is no positive charge to assist in attracting the lone pair to the carbene centre and substituent effects are therefore smaller than in the carbocations. Carbenes have previously been examined at various levels of theory (15−20) and we have included them here to permit comparison with the carbocations.

All molecules and ions were subjected to geometry optimisation at the 6-31G* level of theory (21) using the gradient techniques (22, 23) in the MONSTERGAUSS program (24). Single point calculations were then performed with a CI program using the direct CI method (25) and including all single and double excitations from the valence shell to all the virtual orbitals.

Results

(a) Carbocations

The effect of X in the carbocations relative to its effect in methane can be assessed from reactions [1], [2], and [3] using the total energies reported in Table 1. A positive energy for these reactions (i.e. an endothermic reaction) indicates that the substituent is more stabilising in the cation than in methane and we define the substituent stabilisation energy as ΔE for reactions [1]−[4]. With the exception of the cyano group, all the substituents are stabilising (Table 2), with the largest effect being in CX^+ and the smallest in H_2CX^+.

[1] $CX^+ + CH_4 \rightarrow H_3CX + CH^+$

[2] $HCX^{+\bullet} + CH_4 \rightarrow H_3CX + CH_2^{+\bullet}$

[1] Indirectively-destabilised carbocations have been reviewed in ref. 12.

TABLE 1. Total energies for CX^+, $CHX^{+\cdot}$, CH_2X^+, CH_3X, CHX (singlets), and CHX (triplets)

Molecular species	H	CH_3	NH_2	OH	F	CN	NC
(a) 6-31G//6-31G**							
CX^+	−37.89554	−77.02090	−93.09283	−112.91439	−136.84773	−129.61935	−129.69246
$HCX^{+\bullet}$	−38.56396	−77.65475	−93.72133	−113.50108	−137.43147	−130.27789	−130.29860
H_2CX^+	−39.23064	−78.31123	−94.38318	−114.15648	−138.09379	−130.94257	−130.95426
H_3CX	−40.19517	−79.22876	−95.20983	−115.03542	−139.03461	−131.92753	−131.89436
HCX (singlet)	−38.87237	−77.92189	−93.97435	−113.78351	−137.75453	−130.61785	−130.60529
HCX (triplet)	−38.91658	−77.95816	−93.94815	−113.76994	−137.76036	−130.65546	−130.62529
*(b) CI//6-31G**							
CX^+	−37.98847	−77.24932	−93.34746	−113.18016	−137.10454	—	—
$HCX^{+\bullet}$	−38.65214	−77.88014	−93.97874	−113.76645	−137.85748	—	—
H_2CX^+	−39.34271	−78.55733[a]	−94.66173	−114.44117	−138.36614	—	—
H_3CX	−40.34672	−79.50395	−95.50828	−115.34229	−139.33209	—	—
HCX (singlet)	−38.99094	−78.16765	−94.25069	−114.06810	−138.02880	—	—
HCX (triplet)	−39.01840	−78.18841	−94.20537	−114.03541	−138.01529	—	—

[a]At the 6-31G*//6-31G* level the open cation is the more stable while at the CI//6-31G* level the symmetrically bridged ion has the lower energy (29). At both levels of theory the two structures are very close in energy and we report energies for the open cation here.

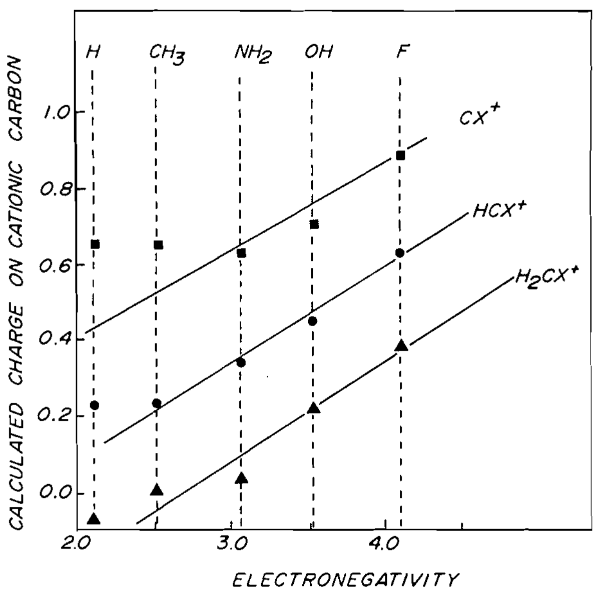

FIG. 1. Plot of calculated charge on the cationic carbon (6−31G*//6-31G*) against the electronegativity (Allred-Rochow electronegativities from ref. 27) of the heteroatom atom attached to the cationic carbon.

[3] $H_2CX^+ + CH_4 \rightarrow H_3CX + CH_3^+$

Inclusion of correlation energy increases all the stabilisation energies by 10−12 kcal/mol. As in other carbocations, π-donors produce the most dramatic stabilisation with the amino group being the most effective. The cyano group is destabilising in *all* the carbocations, with the destabilisation being smallest in CCN^+ and largest in H_2CCN^+. From these results then we find the increase in substituent stabilisation with the decrease in ion size, as first noted for ions $(CH_3)_2CX^+$, CH_3CHX^+, and CH_2X^+, is continued as the size of the ion is further decreased to $CHX^{+\bullet}$ and CX^+.

In all the cations hydrogen is the least electronegative element attached to the cationic carbon and most of the positive charge of the ion is carried by the hydrogens. Consequently for a given substituent X the positive charge on the cationic carbon is largest in CX^+ and smallest in CH_2X^+ (e.g. when X is NH_2 the charge on C^+ is +0.624 in CNH_2^+, +0.324 in $HCNH_2^{+\bullet}$, and +0.038 in $H_2CNH_2^+$). For each series of carbocations the total charge on C^+ increases roughly linearly with the electronegativity of the heteroatom (27) (Fig. 1). The amino group is the strongest π-donor (Table 2) but for *each* substituent the amount of π-donation increases slightly on going from CX^+ to $CHX^{+\bullet}$ to H_2CX^+, notwithstanding the increasing separation between C^+ and X along this series of ions. The total positive charge on X decreases from CX^+ to H_2CX^+, and since π-donation is smallest in CX^+, then in the three types of carbocations —C^+ must be the strongest σ-acceptor and —CH_2^+ the weakest.

(b) Carbenes

Methylene is a ground state triplet (**1***a*), lying ~10 kcal/mol below the singlet state (**1***b*) (28). If the substituent X is a

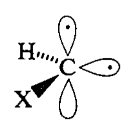

1*a*

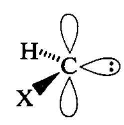

1*b*

π-donor then, as in carbocations, the singlet structure is stabilised by donation into the "vacant" *p*-orbital on the carbene carbon. This interaction has been studied previously at various levels of theory (17−20) and while our calculations used a larger basis set than in most studies, the overall trends and conclusions which we find are in agreement with the literature. At the 6-31G*//6-31G* level the singlet−triplet splitting (S−T gap) is negative for the two strongest π-donors, NH_2 and OH, indicating that the singlet states are lower in energy (Table 3). At the CI//6-31G* level, as expected due to the larger correlation energy of the singlets, all the singlets are lowered in energy relative to the triplets and at this level the singlet state is now lower than the triplet for CHF.

In the carbenes studied here π-donation, where possible, is the dominant interaction and clearly stabilises the singlet relative to the triplet. However, the cyano substituent, which usually functions as both a σ- and π-acceptor, is also weakly stabilising (by 4 kcal/mol at 6-31G*//6-31G*) and here again the stabilisation can be attributed to π-effects. In singlet cyanomethylene, as in carbocations, the cyano group functions as a π-donor, although the magnitude of the donation is smaller

TABLE 2. Bond lengths, charge distribution, and stabilisation energies in carbocations

Ion	C—X distance[a,b]	Total charge on cationic carbon[a,c]	π-density on cationic carbon[a,c]	Stabilisation energies from reactions [1], [2], and [3]	
				6-31G*	CI
HC^+	1.105	+0.650	0	0	0
$H_2C^{+\bullet}$	1.080	+0.234	0	0	0
H_3C^+	1.078	−0.072	0	0	0
H_3CC^+	1.378	+0.653	0.139[e]	57.6	65.0
$H_3CCH^{+\bullet}$	1.423	+0.233	0.147	35.9	42.3
$H_3CCH_2{}^+$	1.432	+0.013	0.161	29.5	36.0
H_2NC^+	1.234	+0.624	0.495	114.6	126.6
$H_2NCH^{+\bullet}$	1.248	+0.324	0.514	89.6	101.5
$H_2NCH_2{}^+$	1.263	+0.038	0.533	86.5	98.8
$HOCH^+$	1.141	+0.680	0.318	112.1	123.1
$HOCH^{+\bullet}$	1.210	+0.447	0.354	60.8	72.5
$HOCH_2{}^+$	1.232	+0.207	0.382	53.7	64.7
FC^+	1.144	+0.868	0.227[e]	70.8	82.0
$FCH^{+\bullet}$	1.195	+0.622	0.233	17.6	27.6
$FCH_2{}^+$	1.220	+0.382	0.241	14.9	23.9
NCC^+	1.383	+0.766	0.154[e]	−5.4	—
$NCCH^{+\bullet}$	1.350	+0.362	0.261	−11.5	—
$NCCH_2{}^+$	1.373	+0.009	0.264	−12.8	—
CNC^+	1.228	+0.707	0.265[e]	61.3	—
$CNCH^{+\bullet}$	1.247	+0.446	0.328	22.4	—
$CNCH_2{}^+$	1.278	+0.168	0.342	15.3	—

[a]From 6-31G*//6-31G* level.
[b]Distances are in Å.
[c]Charges are in electrons.
[d]Stabilisation energies are in kcal/mol.
[e]Molecule defined to be in xz plane and only π_y used.
[f]The gas phase reaction $H_3CX + e \rightarrow H_2CX^+ + H + 2e$ gives the following substituent stabilisation energies: CH_3, 35 kcal/mol; NH_2, 95 kcal/mol; OH, 60 kcal/mol; F, 26 kcal/mol; CN, −10 kcal/mol. (7)

TABLE 3. Carbene singlet−triplet energy gaps and stabilisation energies[a] from eq. [4]

X	E(S)−E(T)		Stabilisation energies: Singlet		Stabilisation energies: Triplet	
	6-31G*//6-31G*	CI//6-31G*	6-31G*//6-31G*	CI//6-31G*	6-31G*//6-31G*	CI//6-31G*
H	27.7	17.2	0.0	0.0	0.0	0.0
CH_3	22.8	13.0	10.0	12.2	5.0	8.0
NH_2	−16.4	−28.4	54.8	61.6	10.6	15.9
OH	−8.5	−20.5	44.5	51.2	8.2	13.5
F	3.7	−8.5	26.8	32.9	2.7	7.2
CN	23.6	—	8.3	—	4.2	—
NC	12.6	—	21.3	—	6.1	—

[a]All energies in kcal/mol.

than in carbocations (in HC(CN) the π-population of the carbene p-orbital is 0.109e, compared with the π-population of 0.261e on the cationic carbon of $HC(CN)^{+\bullet}$). In triplet cyanomethylene the cyano group reverts to its normal role as a π-acceptor, although the π-donation from the carbene carbon is very small (0.036e).

The S−T gap for a large number of carbenes has been found to correlate with Δq_π, the change in π-electron density of benzene on introducing the substituent X (20). We find that the S−T gap from our calculations correlates with Δq_π (correlation coefficient 0.965 at 6-31G*//6-31G*, 0.995 at CI//6-31G*), and also shows a similar linear correlation with the π-density of the "vacant" p-orbital on the carbene carbon of the singlet (correlation coefficients 0.954 at 6-31G*//6-31G* and 0.995 at CI//6-31G*). For both plots the cyano and isocyano substituents deviate the most and as these two substituents were not considered at the CI level, then the correlations with the CI data are better.

Reaction [4] has been used to estimate substituent stabilisation of carbenes over and above any stabilisation in methane (17). All substituents are stabilising in

[4] $HCX + CH_4 \rightarrow CH_2 + H_3CX$

both the singlets and the triplets, but the only large effects are for π-donors in the singlets (see Table 3). As with the carbocations inclusion of correlation energy increases the stabili-

TABLE 4. Proton affinities (kcal/mol) of singlet carbenes CHX and alkenes $H_2C{=}CHX$

X	Carbenes 6-31G*//6-31G*	Carbenes CI//6-31G*	Alkenes 6-31G*//3-21G
H	224.6	220.7	174.7
CH_3	244.3[a]	244.5[a]	194.1
NH_2	256.5	257.9	240.8
OH	234.0	234.1	211.3
F	212.7	211.7	182.8
CN	203.8	—	156.5
NC	219.0	—	179.9

[a]Using the bridged $C_2H_5^+$ ion, the proton affinities are 243.2 kcal/mol (6-31G*//6-31G*) and 247.9 kcal/mol (CI//6-31G*).

sation energies by between 2 and 10 kcal/mol. For singlet carbenes containing π-donors the stabilisation is smaller than in the cations H_2CX^+ when X is NH_2 (61.6 kcal/mol compared with 98.8 kcal/mol) and X is OH (51.2 kcal/mol compared with 64.7 kcal/mol), but the stabilisation of CHF is greater than that of H_2CF^+(32.9 kcal/mol compared with 23.9 kcal/mol). Also the cyano group which is destabilising in all carbocations is weakly stabilising in both singlet and triplet carbenes.

(c) Proton affinities of singlet carbenes

The proton affinity of a carbene is the negative of the enthalpy of the reaction described by reaction [5]. The parent carbene (X = H) has a proton affinity of 224.6 kcal/mol at the 6-31G*//6-31G* level and 220.7 kcal/mol at CI//6-31G*

[5] $CHX + H^+ \rightarrow H_2CX^+$

(Table 3). These are considerably higher than the proton affinity of ethylene (reaction [6], X = H) which is calculated to be 175 kcal/mol at the 6-31G*//6-31G* level (6).

[6] $H_2C{=}CHX + H^+ \rightarrow H_3C{-}CHX^+$

The product of protonation of ethylene, the ethyl cation $CH_3CH_2^+$, is stabilised by hyperconjugation between the methyl group and the cationic carbon (at the 6-31G*//3-21G level the stabilisation is 30 kcal/mol (6). This stabilisation is measured relative to that afforded by the hydrogen atom in CH_3^+, so the high proton affinity of singlet CH_2 relative to that of C_2H_4 results from the high energy of singlet CH_2.

The inclusion of correlation energy in the protonation reaction has little effect on the calculated proton affinities of any of the five carbenes examined. π-Donating substituents are weakly stabilising in ethylene (28) but are strongly stabilising in α-X-ethyl cations (6), with the result that the proton affinities of alkenes $H_2C{=}CHX$ are larger for π-donors and are very substituent dependent (Table 4). The cyano group is weakly stabilising in acrylonitrile, $H_2C{=}CH(CN)$ (28), and is destabilising in $CH_3CH(CN)^+$ (6) and consequently the proton affinity of acrylonitrile is 18.2 kcal/mol less than that of ethylene. By comparison, in the protonation of singlet carbenes, both CHX and CH_2X^+ are strongly stabilised by π-donors and the proton affinities of the carbenes are therefore less substituent dependent than those of the ethylenes. For example, the strongest π-donor, the NH_2 group, increases the proton affinity of methylene by 31.9 kcal/mol compared with an increase of 66.1 kcal/mol in ethylene.

Conclusions

The increase in dependence on substituents previously observed on going from a tertiary carbenium ion to a primary carbenium ion is continued when the coordination at the cationic carbon is reduced from three. The stabilisation energies of ions $CHX^{+\bullet}$ are all larger than those of CH_2X^+ but the differences are less than 7 kcal/mol, reflecting the fact that the electronic structures at the cationic carbons are similar in the two classes of ions ("sp^2 hybridised" with a vacant p-orbital which interacts with π-donors). In CX^+ the carbon atom is "sp hybridised" and there are two vacant p-orbitals available to interact with the substituent; the substituent effects in ions CX^+ are therefore much larger than in $CHX^{+\bullet}$ and CH_2X^+. Using the amino-substituted carbocations as an example then the stabilisation energies (kcal/mol) on going from the tertiary carbenium ion to CX^+ are 63.4 for $(CH_3)_2C^+NH_2$, 72.3 for $(CH_3)HC^+NH_2$, 86.5 for $H_2C^+NH_2$, 89.6 for $HCNH_2^{+\bullet}$, and 114.6 for CNH_2^+ (all calculations at 3-31G* level). In carbocations the α-cyano group is a weak π-donor but the overall effect is destabilising even in CCN^+. Nevertheless the destabilisation by cyano is smallest in CCN^+ (stabilisation energy is -5.4 kcal/mol) and becomes progressively larger up to $(CH_3)_2C^+CN$ (stabilisation energy -19.5 kcal/mol).

Substituents are only weakly stabilising in triplet carbenes, CHX, but in the corresponding singlets there is strong $\pi \rightarrow p$ stabilisation as in carbocations. For the strongest π-donors, NH_2 and OH, and also for CH_3 which interacts with adjacent vacant p-orbitals through hyperconjugation, the substituent stabilisation is larger in $CHX^{+\bullet}$ than in CHX. However, for the other substituents the stabilisation is larger in the singlet carbenes CHX and the cyano group, which destabilises all carbocations, is weakly stabilising.

Acknowledgements

We thank the Natural Sciences and Engineering Research Council of Canada for financial support and York University Computer Centre for generous allotments of computer time.

1. M. H. LIEN, A. C. HOPKINSON, and M. A. MCKINNEY. J. Mol. Struct. Theochem. **105**, 37 (1983).
2. M. N. PADDON-ROW, C. SANTIAGO, and K. N. HOUK. J. Am. Chem. Soc. **102**, 6561 (1980).
3. Y. APELOIG, P. V. R. SCHLEYER, and J. A. POPLE. J. Am. Chem. Soc. **99**, 1291 (1977).
4. J. B. MOFFAT. J. Am. Chem. Soc. **104**, 3949 (1982).
5. D. A. DIXON, R. A. EADES, R. FREY, P. G. GASSMAN, M. L. HENDEWERK, M. N. PADDON-ROW, and K. N. HOUK. J. Am. Chem. Soc. **106**, 7863 (1984).
6. M. H. LIEN and A. C. HOPKINSON. J. Mol. Struct. Theochem. In press.
7. R. W. TAFT, R. H. MARTIN, and F. W. LAMPE. J. Am. Chem. Soc. **87**, 2490 (1965).
8. P. G. GASSMAN and J. J. TALLEY. J. Am. Chem. Soc. **102**, 1214 (1980); **102**, 4138 (1980).
9. X. CREARY and C. C. GEIGER. J. Am. Chem. Soc. **104**, 4151 (1982).
10. A. C. HOPKINSON, L. H. DAO, P. DUPERROUZEL, M. MALEKI, and E. LEE-RUFF. J. Chem. Soc. Chem. Commun. 727 (1983).
11. G. A. OLAH, M. ARVANAGHI, and G. K. S. PRAKASH. J. Am. Chem. Soc. **104**, 1628 (1982).
12. P. G. GASSMAN and T. T. TIDWELL. Acc. Chem. Res. **16**, 279 (1983); J. P. BEGUE and M. CHARPENTIER-MORIZE. Acc. Chem. Res. **13**, 207 (1980).
13. A. J. MERER and D. N. TRAVIS. Can. J. Phys. **44**, 525 (1966); **44**, 1541 (1966).
14. C. W. MATHEWS. Can. J. Phys. **45**, 2355 (1967).
15. R. HOFFMANN, G. D. ZEISS, and G. W. VAN DINE. J. Am. Chem. Soc. **90**, 1485 (1968).

16. R. GLEITER and R. HOFFMANN. J. Am. Chem. Soc. **90**, 5457 (1968).
17. N. C. BAIRD and K. F. TAYLOR. J. Am. Chem. Soc. **100**, 1333 (1978).
18. D. FELLER, W. T. BORDEN, and E. R. DAVIDSON. Chem. Phys. Lett. **71**, 22 (1980).
19. C. W. BAUSCHLICHER, H. F. SCHAEFER III, and P. S. BAGUS. J. Am. Chem. Soc. **99**, 7106 (1976).
20. P. H. MUELLER, N. G. RONDAN, K. N. HOUK, J. F. HARRISON, D. HOOPER, B. H. WILLEN, and J. F. LIEBMAN. J. Am. Chem. Soc. **103**, 5049 (1981).
21. P. C. HARIHARAN and J. A. POPLE. Theor. Chim. Acta, **28**, 213 (1973).
22. H. B. SCHLEGEL. Ph.D. Thesis, Queen's University. 1975.
23. W. C. DAVIDON. Math Programming, **9**, 1 (1975).
24. M. R. PETERSON and R. A. POIRIER. MONSTERGAUSS. University of Toronto, Toronto, Ont. 1980.
25. N. C. HANDY, J. D. GODDARD, and H. F. SCHAEFER III. J. Chem. Phys. **71**, 426 (1979).
26. J. F. HARRISON, R. C. LIEDTKE, and J. F. LIEBMAN. J. Am. Chem. Soc. **101**, 7162 (1979).
27. F. A. COTTON and G. WILKINSON. Advanced inorganic chemistry. 3rd ed. Wiley Interscience, New York. 1972. p. 115.
28. J. D. DILL, A. GREENBERG, and J. F. LIEBMAN. J. Am. Chem. Soc. **101**, 6814 (1979).
29. K. RAGHAVACHARI, R. A. WHITESIDE, J. A. POPLE, and P. V. R. SCHLEYER. J. Am. Chem. Soc. **103**, 5649 (1981).

Pressions de vapeur des mélanges eau – nitrate d'éthylammonium à 298,15 K. Propriétés thermodynamiques des milieux eau – sel fondu

M. BIQUARD ET P. LETELLIER[1]
Laboratoire de physicochimie des solutions, E.N.S.C.P., 11 Rue Pierre et Marie Curie, 75231 Paris Cédex 05, France

ET

M. FROMON
Laboratoire d'électrochimie, Université Pierre et Marie Curie, 4, Place Jussieu, 75230 Paris Cédex 05, France

Reçu le 3 janvier 1985[2]

M. BIQUARD, P. LETELLIER et M. FROMON. Can. J. Chem. **63**, 3587 (1985).

L'activité et le coefficient d'activité de l'eau dans les mélanges eau – nitrate d'éthylammonium (NEA) entre l'eau pure et le sel pur fondu ont été déterminés par des mesures de pressions de vapeur à 298,15 K. Le comportement de l'eau dans la gamme de fraction molaire du sel, comprise entre 0,3 et 1 peut être décrit au moyen d'une relation linéaire entre le logarithme du coefficient d'activité de l'eau γ_E, la fraction molaire, X du sel et l'enthalpie libre de dilution de l'eau à dilution infinie dans le NEA pur, $\Delta G_E^{\ominus}$:

$$\ln \gamma_E = \frac{\Delta G_E^{\ominus}}{RT} X$$

L'interprétation des résultats expérimentaux a également été tentée à l'aide de l'équation B.E.T. Il apparaît que dans les mélanges eau–NEA, le terme énergétique relatif à l'adsorption de l'eau est voisin de zéro. On montre que dans ce cas précis, la relation empirique proposée et l'équation B.E.T. conduisent à une même description du comportement de l'eau et du sel, tant au plan de l'enthalpie libre qu'à celui des volumes.

M. BIQUARD, P. LETELLIER, and M. FROMON. Can. J. Chem. **63**, 3587 (1985).

The activity and activity coefficient of water in water and ethylammonium nitrate (EAN) mixtures were determined by vapor pressure measurements between pure water and pure fused salt at 298.15 K. For a wide range of mole fractions of salt, ($0.3 < X \leq 1$) the behaviour of water can be described very accurately by a "one parameter" empirical equation which involves activity coefficient, γ_E, mole fraction of EAN, and limiting Gibbs energy of the dilution of water in pure fused salt, $\Delta G_E^{\ominus}$:

$$\ln \gamma_E = \frac{\Delta G_E^{\ominus}}{RT} X$$

Interpretation of experimental results was also attempted by use of the B.E.T. equation. It appears that the energy, $\Delta E_d = E - E_L$, in those solutions is very low. Partial molar volumes of water and salt are also discussed in relation to empirical and B.E.T. equations. It can be shown that the two equations lead to similar results.

Introduction

L'utilisation d'un sel fondu à la température ambiante, le nitrate d'éthylammonium, NEA, (T_f = 14°C), miscible à l'eau en toute proportion, permet l'étude thermodynamique à 298,15 K des interactions qui s'établissent entre un électrolyte et l'eau, pour une gamme de composition étendue, comprise entre l'eau pure et le sel pur fondu.

Il a déjà été exposé, dans une publication antérieure (1), une étude volumétrique des mélanges eau–NEA au cours de laquelle il a été montré que le volume molaire partiel de l'eau varie linéairement avec sa fraction molaire dans le milieu.

Afin de juger de la généralité de cette dernière propriété et de ses implications sur les autres grandeurs thermodynamiques, la détermination des activités de l'eau et du sel a été entreprise dans ces mêmes milieux en utilisant une méthode précise de mesure de pressions de vapeur.

I. Technique expérimentale et résultats expérimentaux

Technique expérimentale

(a) Le nitrate d'éthylammonium (NEA) a été préparé par une technique proche de celle proposée par Evans *et al.* (2): Une solution d'éthylamine à 33% (Prolabo) est neutralisée par de l'acide nitrique de densité égale à 1,33 (Prolabo) dans un becher refroidi dans un bain de glace. La solution saline est concentrée à l'évaporateur rotatif à 60°C pendant 3 h et l'eau de la solution concentrée est éliminée par séchage sous vide pendant 3 jours en présence de P_2O_5. Le point de fusion du sel a été trouvé égal à 14°C.

(b) Les tensions de vapeur ont été mesurées à l'aide d'une jauge de précision Texas Instrument (3). Après dégazage par congélation et fusion successives, les solutions sont plongées dans un bain thermostaté à 298,15 K. La précision obtenue sur les tensions de vapeur est de $\pm 1 \times 10^{-2}$ Torr (1 Torr = 133.3 Pa).

(c) Les solutions ont été préparées par gravimétrie à partir d'eau bidistillée et de sel fondu pur.

Résultats expérimentaux

Les pressions de vapeur mesurées au-dessus des différentes solutions de fraction molaire X en NEA sont reportées dans le tableau 1.

La tension de vapeur de l'eau pure, P_E^0, a été déterminée à 298,15 K et trouvée égale à 23,75 Torr, ce qui correspond à la valeur généralement admise (4).

Les mesures réalisées avec le sel pur conduisent à une pression de vapeur inférieure à 4×10^{-2} Torr. Il est donc légitime de considérer que la pression de vapeur mesurée au-dessus des solutions correspond uniquement à celle de l'eau.

L'activité et le coefficient d'activité de l'eau, référés à l'eau pure, ont été calculés au moyen des relations:

$$a_E = \frac{P}{P_E^0} \quad \text{et} \quad \gamma_E = \frac{P}{P_E^0(1-X)}$$

où X est la fraction molaire du sel dans la solution. Il n'a été apporté aucune correction de fugacité des gaz dans le calcul des activités de

[1] Auteur à qui adresser la correspondance.
[2] La revision reçue le 20 juin 1985.

TABLEAU 1. Pressions de vapeur, activités et coefficients d'activité de l'eau dans les mélanges eau–NEA. Les deux valeurs entre parenthèses pour $X = 1$ correspondent à l'exploitation de la relation [9]

	X										
Paramètre	0	0,0247	0,111	0,147	0,220	0,330	0,500	0,648	0,801	0,942	1
P_E (Torr)	23,75	22,73	19,85	18,88	16,75	13,99	9,78	6,63	3,50	1,02	~0,04
a_E	1	0,957	0,836	0,795	0,705	0,589	0,412	0,279	0,147	0,043	0
ln a_E	0	−0,0439	−0,1794	−0,2295	−0,3492	−0,5292	−0,8872	−1,2760	−1,9148	−3,1478	—
γ_E	1	0,981	0,940	0,932	0,904	0,879	0,824	0,793	0,741	0,747	(+0,69)
ln γ_E	0	−0,0189	−0,0615	−0,0704	−0,1007	−0,1288	−0,1936	−0,2324	−0,3004	−0,2918	(−0,37)

l'eau, le coefficient de fugacité étant très proche de l'unité dans les conditions expérimentales.[3] Les valeurs de a_E et γ_E sont également regroupées dans le tableau 1.

II. Interprétation

L'analyse des résultats expérimentaux sera envisagée dans le cadre de différents modèles de solution exposés dans la littérature.

Toutefois ce travail faisant suite à une étude se rapportant aux volumes molaires partiels de l'eau et du NEA dans leurs différents mélanges, il est indispensable de prendre en compte les résultats obtenus à cette occasion. À ce titre, le paragraphe ci-dessous sera consacré aux conséquences, sur les potentiels chimiques, des principales relations expérimentales établies pour les volumes molaires partiels.

Comportement de l'eau dans les mélanges eau–NEA

Il a été montré (1) que les variations du volume molaire partiel de l'eau, dans les solutions salines de fraction molaire X supérieure à 5×10^{-2} pouvaient être décrites au moyen de la relation empirique:

$$[1] \quad \bar{V}_E = V_E^0 + (V_E^\ominus - V_E^0)\, X$$

dans laquelle V_E^0 et $V_E^\ominus$ sont respectivement les volume molaire et volume molaire partiel de l'eau infiniment diluée dans le NEA. L'expression du potentiel chimique, de l'eau, référé à

$$[2] \quad \mu_E = \mu_E^0 + RT \ln(1 - X) + RT \ln \gamma_E$$

l'eau pure permet d'établir, par dérivation par rapport à la pression, à *température et composition constantes*, une relation entre le coefficient d'activité γ_E et le volume molaire partiel de l'eau.

$$[3] \quad \bar{V}_E = V_E^0 + RT \left[\frac{\partial \ln \gamma_E}{\partial P}\right]_{T,X}$$

L'identification des relations [1] et [3] conduit à:

$$[4] \quad \left[\frac{\partial \ln \gamma_E}{\partial P}\right]_{T,X} = \left[\frac{V_E^\ominus - V_E^0}{RT}\right] X$$

Les potentiels chimiques normaux de l'eau pure, μ_E^0, et de l'eau infiniment diluée dans le NEA, $\mu_E^\ominus$, peuvent être introduits dans l'équation [4]

$$\left[\frac{\partial \ln \gamma_E}{\partial P}\right]_{T,X} = \frac{X}{RT}\left[\frac{\partial(\mu_E^\ominus - \mu_E^0)}{\partial P}\right]_{T,X}$$

soit encore si l'on convient de noter $\Delta G_E^\ominus$, l'enthalpie libre de dilution de l'eau à dilution infinie dans le sel pur:

$$\Delta G_E^\ominus = \mu_E^\ominus - \mu_E^0$$

$$[5] \quad \left[\frac{\partial \ln \gamma_E}{\partial P}\right]_{T,X} = \frac{X}{RT}\left[\frac{\partial \Delta G_E^\ominus}{\partial P}\right]_{T,X}$$

Si l'on suppose la validité de l'équation [5] vérifiée pour toute pression, son intégration en fonction de cette variable peut être envisagée à fraction molaire et température constantes, entre la pression atmosphérique et une pression non définie de référence:

$$[6] \quad \ln \gamma_E = \frac{\Delta G_E^\ominus}{RT} X + f(X)$$

$f(X)$ est une constante d'intégration, dont la valeur dépend de la pression choisie en référence; $f(X)$ est susceptible de varier avec la composition du mélange et la température. Sa valeur est fixée pour le sel pur ($X = 1$). Dans ce milieu, l'eau apparaît comme un soluté possédant les propriétés de l'état infiniment dilué. Par définition, son coefficient d'activité, par rapport à cette dernière référence est égal à l'unité, et son coefficient d'activité référé à l'eau pure tend vers une limite finie.

$$[7] \quad \lim_{X \to 1} (\ln \gamma_E) = \frac{\Delta G_E^\ominus}{RT}$$

La relation [6] permet de retrouver cette condition avec:

$$[8] \quad \lim_{X \to 1} f(X) = 0$$

La relation [6] montre qu'une variation linéaire, observée pour les volumes molaires partiels, n'implique pas nécessairement une propriété identique pour les potentiels chimiques. Afin de juger de l'importance relative des quantités intervenant dans l'équation [6], les valeurs de ln γ_E ont été reportées sur la figure 1 en fonction de la fraction molaire du NEA.

Compte tenu de l'incertitude inhérente aux valeurs des coefficients d'activité de l'eau, particulièrement pour les mélanges les plus riches en sel, il apparaît que les points expérimentaux pour $0,3 < X \leq 1$ se placent convenablement sur une droite de pente égale à $-0,370$ passant par l'origine.

Cette propriété permet d'être assuré que la constante d'in-

[3] La relation entre le coefficient de fugacité et le premier terme de l'équation du viriel B_{11} pour une phase vapeur pure est:

$$\Gamma_i = \frac{f_i}{p_i} = \exp\left(-\frac{B_{11} P_i}{RT}\right)$$

Dans le cas de l'eau:

$$B_{11} = -1056 \text{ mL mol}^{-1}$$

soit pour l'eau *pure* à 298,15 K:

$$\Gamma_i = 1,0013$$

Les pressions de vapeur d'eau des mélanges eau–sel étant inférieures à celle de l'eau pure, les coefficients de fugacité en seront d'autant plus proches de l'unité.

TABLEAU 2. Pressions de vapeur de l'eau: expérimentales et calculées au moyen des équations [11] et [23] en fonction de la fraction molaire du sel

	X										
Pression (Torr)	0	0,0247	0,111	0,147	0,220	0,330	0,500	0,648	0,801	0,942	1
P_E exp	23,75	22,73	19,85	18,88	16,75	13,99	9,78	6,63	3,50	1,02	~0,04
P_E calc. [11]	—	22,95	20,26	19,18	17,07	14,08	9,86	6,57	3,50	0,96	—
P_E calc. [23]	—	22,92	20,17	19,08	16,96	13,97	9,81	6,57	3,53	0,98	—

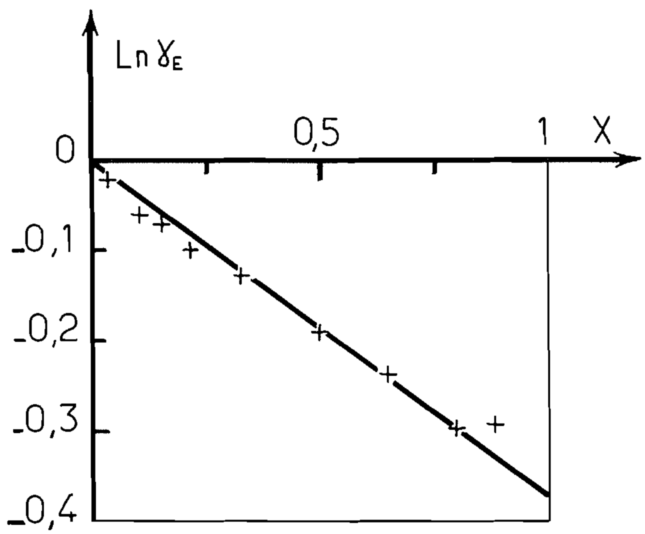

FIG. 1. Variation de ln γ_E avec la fraction molaire du sel dans le mélange eau–NEA.

tégration $f(X)$, nulle dans le sel pur, garde une valeur suffisamment faible pour être négligée dans la gamme $0{,}3 < X \leq 1$. Dans ce domaine de concentration les valeurs du coefficient d'activité de l'eau, référé à l'eau pure, sont décrites par:

$$[9] \quad \ln \gamma_E = \frac{\Delta G_E^\ominus}{RT} X$$

dans laquelle $\Delta G_E^\ominus = -919$ Joules. La relation [9] constitue un cas particulier de l'équation [6] pour une pression, une température et un domaine de composition donnés. L'activité de l'eau, a_E, peut ainsi être calculée à partir de la relation:

$$[10] \quad a_E = (1 - X)\, e^{\frac{\Delta G_E^\ominus}{RT} X}$$

et sa pression de vapeur par:

$$[11] \quad P_E = P_E^0 (1 - X)\, e^{\frac{\Delta G_E^\ominus}{RT} X}$$

Les valeurs de P_E calculées au moyen de l'équation [11] sont reportées dans le tableau 2 en regard de celles déterminées expérimentalement et l'on conviendra de leur excellent accord dans la gamme de composition considérée.

Les courbes de pression de vapeur de l'eau correspondantes à l'équation [11] (courbe a), aux lois des solutions idéales pour le sel non dissocié (courbe b) et totalement dissocié (courbe c) sont reportées sur la figure 2. Les points expérimentaux se placent sur la courbe a dans la gamme des fractions molaires $0{,}3 < X \leq 1$.

L'équation [11] permet de déterminer la valeur de la constante de Henry de l'eau dans le sel pur fondu. Elle correspond à la valeur de la tangente à la courbe $P_E = f(1 - X)$ pour $X = 1$:

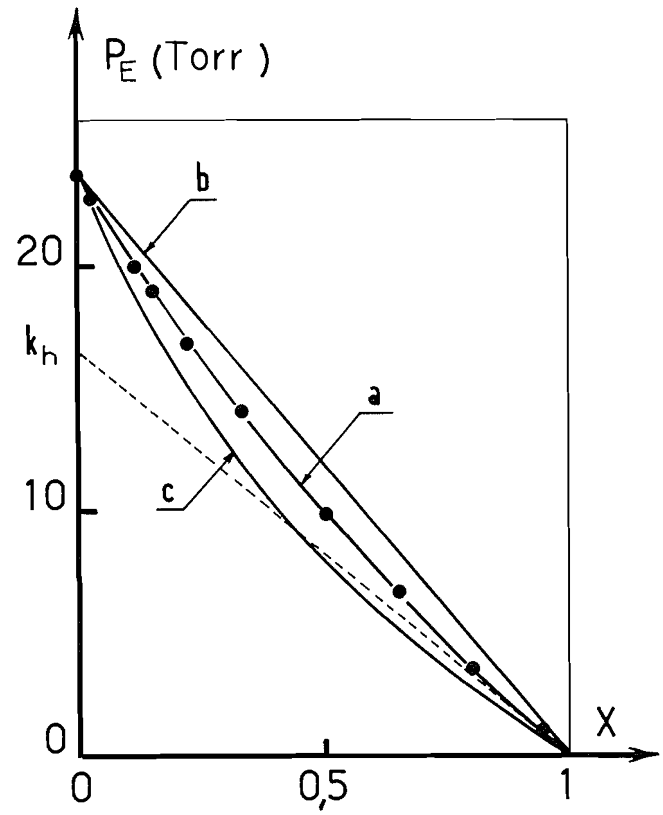

FIG. 2. Variation de la pression de vapeur de l'eau en fonction de X. Courbe a, calculée à partir de l'équation [11]. Courbe b, comportement idéal pour le sel non dissocié. Courbe c, comportement idéal pour le sel totalement dissocié. Les points expérimentaux sont figurés par des cercles.

$$[12] \quad k_h = \lim_{X \to 1} \left[\frac{\partial P_E}{\partial(1 - X)}\right] = P_E^0\, e^{\frac{\Delta G_E^\ominus}{RT}}$$

soit dans le cas présent k_h (Torr, X) = 16,4. La droite de Henry est tracée en pointillés sur la figure 2.

Comportement du sel dans les mélanges eau–NEA dans la gamme de composition $0{,}3 < X \leq 1$

Le potentiel chimique du sel μ_S peut être calculé en fonction de X, en utilisant la relation de Gibbs–Duhem.

Le potentiel chimique de l'eau s'écrit (relations [2] et [9]):

$$[13] \quad \mu_E = \mu_E^0 + RT \ln(1 - X) + \Delta G_E^\ominus X$$

La relation de Gibbs–Duhem implique que:

$$(1 - X)\, d\mu_E + X\, d\mu_S = 0$$

soit:

$$[14] \quad d\mu_S = (RT - \Delta G_E^\ominus) \frac{dX}{X} + \Delta G_E^\ominus\, dX$$

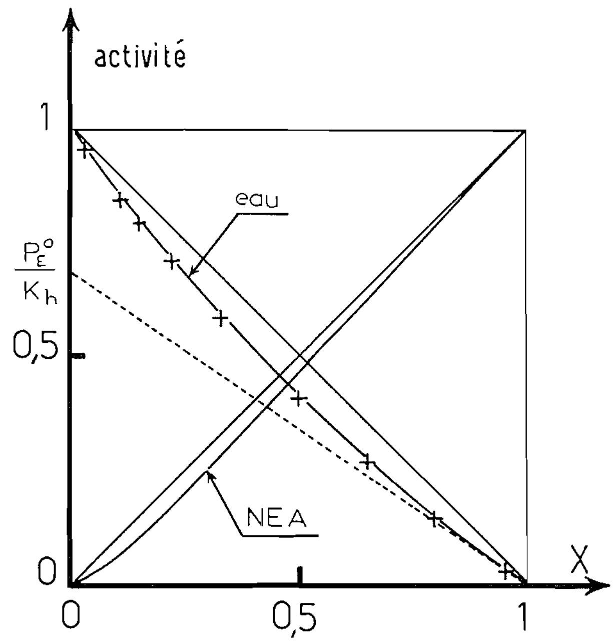

FIG. 3. Variation des activités de l'eau et du NEA avec X (calculées au moyen des équations [9] et [16]). Les points expérimentaux sont figurés par des croix.

L'intégration par rapport à X de l'équation [14], en se fixant comme borne l'état correspondant au sel lorsqu'il est pur ($X = 1$; $\mu_S = \mu_S^0$), conduit à:

$$[15] \quad \mu_S = \mu_S^0 + RT\left[1 - \frac{\Delta G_E^\ominus}{RT}\right]\ln X - \Delta G_E^\ominus (1 - X)$$

Le coefficient d'activité du sel référé au sel pur γ_S s'écrit alors:

$$[16] \quad \ln \gamma_S = -\frac{\Delta G_E^\ominus}{RT}(\ln X + (1 - X))$$

Les variations de l'activité de l'eau et du sel sont représentées sur la figure 3. Les points reportés correspondent aux résultats expérimentaux obtenus pour l'eau. On remarque que le sel présente un comportement quasi idéal pour X supérieur à 0,80.

Conclusion

Comme on a pu le constater, les propriétés de l'eau et du NEA dans leurs mélanges $0{,}3 < X \leq 1$ sont remarquablement décrites tant au plan de l'enthalpie libre qu'à celui des volumes molaires partiels, par *l'équation [9] et ses conséquences.* Toutefois l'examen de modèles de solution déjà établis montre que les résultats expérimentaux peuvent être décrits dans la même zone de composition avec une précision comparable par d'autres systèmes d'équations.

Comportements modèles

L'équation B.E.T.

D'une manière générale, l'interprétation du comportement de l'eau et du sel dans les solutions salines concentrées s'effectue au moyen de différents modèles dérivant de celui proposé initialement par Brunauer, Emmett et Teller (équation B.E.T.) (5). L'équation B.E.T. a été adaptée par Stokes et Robinson (6) pour décrire les propriétés de l'eau dans les solutions d'électrolyte concentré:

$$[17] \quad \frac{a_E \cdot X}{(1 - X)(1 - a_E)} = \frac{1}{Cr} + \frac{C - 1}{Cr} a_E = Y$$

On conviendra de noter Y cette fonction. Dans cette relation, C est donné approximativement par:

$$[18] \quad C = e^{-\frac{E - E_L}{RT}} = e^{-\frac{\Delta E_d}{RT}}$$

E est l'énergie molaire d'adsorption de l'eau sur un site disponible dans le sel fondu; E_L est l'énergie molaire de condensation de l'eau; r est le rapport du nombre de sites disponibles, au nombre de moles de sel dans le sel pur. La validité de cette relation a été discutée pour de très nombreux systèmes (à titre d'exemples 7–12).

Lorsqu'elle est vérifiée, l'équation B.E.T. fait intervenir des paramètres liés aux grandeurs thermodynamiques caractéristiques de la dilution de l'eau pure à dilution infinie dans le sel fondu. En effet, lorsque le sel devient pur ($X = 1$), le coefficient d'activité γ_E de l'eau tend vers une limite finie (éq. [7]).

$$[19] \quad \lim_{X \to 1} (\gamma_E) = \frac{1}{Cr} = e^{\frac{\Delta G_E^\ominus}{RT}}$$

soit encore en tenant compte de l'équation [18]:

$$[20] \quad \ln r = -\frac{1}{RT}(\Delta G_E^\ominus - \Delta E_d)$$

Si l'on considère de plus que l'énergie $\Delta E_d = E - E_L$ peut ne constituer dans le cas général qu'une partie de l'enthalpie de dilution de l'eau dans le sel fondu (on supposera que le terme relatif au travail est suffisamment faible pour être négligé), le bilan thermique relatif à cette opération prend la forme:

$$\Delta H_E^\ominus = H_E^\ominus - H^0 = \Delta E_d + \Delta H_E^i$$

ΔH_E^i représente l'éventuelle contribution thermique des interactions autres que celles impliquées par l'adsorption. L'équation [20] devient alors:

$$\ln r = -\frac{1}{RT}(\Delta G_E^\ominus - \Delta H_E^\ominus + \Delta H_E^i)$$

et si l'on convient de noter $\Delta S_E^\ominus$ l'entropie de l'eau à dilution infinie:

$$[21] \quad \ln r = +\frac{\Delta S_E^\ominus}{R} - \frac{\Delta H_E^i}{RT}$$

ou encore:

$$[22] \quad r = \frac{e^{\Delta S_E^\ominus / R}}{e^{\Delta H_E^i / RT}}$$

La vérification de la validité de l'équation B.E.T. a été tentée à partir des valeurs de l'activité de l'eau déterminées pour les mélanges eau–NEA.

La quantité Y est reportée sur la figure 4 en fonction de l'activité de l'eau. Le tracé obtenu correspond à une droite horizontale dans la gamme de composition $0{,}3 \leq X \leq 1$ dont l'ordonnée à l'origine est égale à:

$$Y_0 = 0{,}705$$

Si l'on s'en tient aux hypothèses à l'origine de l'équation B.E.T., cette propriété indique que le terme d'adsorption possède une valeur très faible ($C \approx 1$; $\Delta E_d \approx 0$).

L'équation B.E.T. se réduit alors à:

$$\gamma_E \times \frac{X}{1 - a_E} = \frac{1}{r}$$

Dans ce cas particulier les variations du coefficient d'activité de

TABLEAU 3. Volumes molaires partiels de l'eau ($\bar{V}_E$) et du sel ($\bar{V}_S$) expérimentaux, calculés au moyen des relations [1] puis [24] dans les mélanges eau–NEA

Volume molaire partiel (cm^3 mol^{-1})	X								
	0	4,22 × 10^{-2}	0,100	0,186	0,336	0,441	0,625	0,819	1
$\bar{V}_E$ exp	18,07	18,0	17,9	17,8	17,5$_5$	17,4	17,2	16,9	16,7
$\bar{V}_E$ calc. [1]	—	18,0	17,9	17,8	17,6	17,5	17,2	16,9	—
$\bar{V}_E$ calc. [24]	—	18,0	17,9	17,7	17,5	17,3	17,1	16,9	—
$\bar{V}_S$ exp	82,8	85,6	87,2	88,1	88,7	89,0	89,2	89,3	89,3

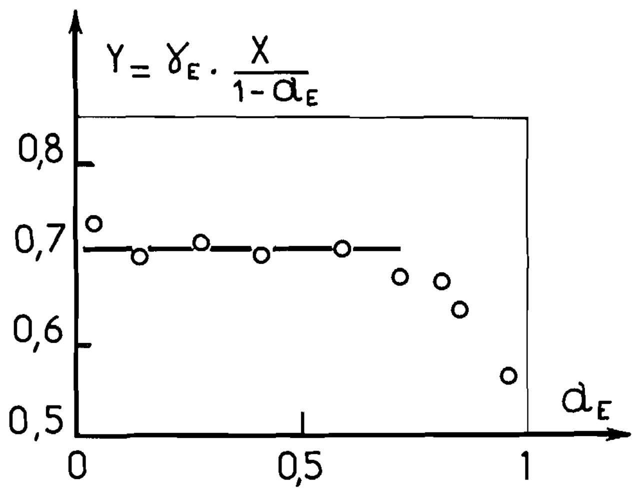

FIG. 4. Vérification de la validité de l'équation B.E.T. (éq. [17]).

l'eau sont décrites par:

$$[23] \quad \gamma_E = \frac{1}{1 + X(r-1)}$$

avec:

$$[23'] \quad r = e^{-\frac{\Delta G_E^{\ominus}}{RT}} = 1{,}42$$

soit $\Delta G_E^{\ominus}$: -865 J. La chaleur de dilution de l'eau à dilution infinie dans le sel pur a été mesurée par Mirejovsky et Arnett (13); elle s'identifie pour les mélanges eau–NEA à l'enthalpie d'interaction:

$$\Delta H_E^i = \Delta H_E^{\ominus} = 1339 \text{ J}$$

Le terme entropique est donc égal à $\Delta S_E^{\ominus} = 7{,}4$ J K^{-1}. Bien que d'origine totalement différente, on remarquera que la valeur $\Delta G_E^{\ominus}$ obtenue par l'équation B.E.T. est tout à fait comparable à celle déterminée dans le précédent paragraphe.

De la même manière que précédemment les valeurs de γ_E et des pressions de vapeur ont été recalculées à partir de la relation [23] (tableau 2). Malgré leurs formes très éloignées, les équations [11] et [23] conduisent à des valeurs comparables, si ce n'est le plus souvent identiques, et décrivent tout aussi bien l'une que l'autre la réalité expérimentale. Cette caractéristique se conserve lors de la dérivation avec la pression.

Le potentiel chimique de l'eau peut être écrit sous la forme:

$$\mu_E = \mu_E^0 + RT \ln(1 - X) - RT \ln(1 + X(r-1))$$

Si l'on suppose que r est un paramètre qui dépend de la pression,

$$\bar{V}_E = V_E^0 - RT \frac{X}{1 + X(r-1)} \left(\frac{\partial r}{\partial P}\right)_{T,X}$$

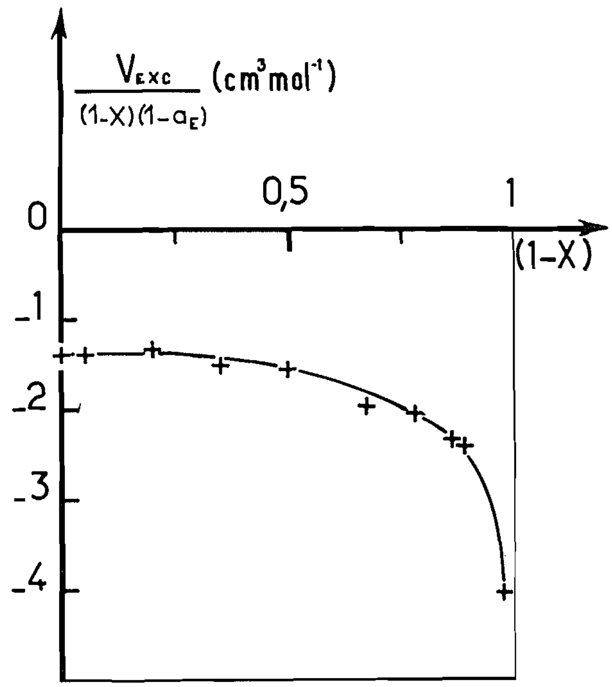

FIG. 5. Vérification de la relation proposée par Abraham (relation [25]).

Lorsque X tend vers l'unité, $\bar{V}_E$ s'identifie à $V_E^{\ominus}$

$$V_E^{\ominus} = V_E^0 - \frac{RT}{r}\left(\frac{\partial r}{\partial P}\right)_{T,X}$$

soit:

$$[24] \quad \bar{V}_E = V_E^0 + (V_E^{\ominus} - V_E^0)\frac{rX}{1 + (r-1)X}$$

Les valeurs expérimentales de $\bar{V}_E$ ainsi que celles calculées par les relations [1] et [24], avec la valeur de $r = 1{,}42$, sont reportées dans le tableau 3.

Comme pour l'enthalpie libre les deux systèmes d'équations décrivent avec une égale précision les propriétés de l'eau dans la solution. Il faut toutefois remarquer que l'on ne peut les identifier, et cela apparaît clairement dans l'expression [24] où le terme $r/[1 + (r-1)X]$ ne peut être constant et égal à l'unité lorsque la composition du milieu se modifie. Il s'en éloigne cependant suffisamment peu pour que l'on ne puisse pas mettre en évidence un écart significatif sur la valeur de $\bar{V}_E$ calculée.

Relation proposée par Abraham (14)

À partir d'un calcul impliquant l'équation B.E.T. et une hypothèse (différente de celle développée par Kodejš et Sacchetto (15)) concernant les contributions volumiques au volume total de la solution, de l'eau adsorbée et de l'eau libre, Abraham établit une relation entre le volume d'excès, V_{exc}, d'un mélange eau–sel et l'activité de l'eau dans ce même milieu.

$$[25] \quad V_{exc} = (1 - X)(1 - a_E)[V_E^{\ominus} - V_E^0 + A(1 - X)]$$

dont le domaine d'application a été fixé par l'auteur à $0 < (1 - X) < 0{,}5$. La vérification de la validité de cette relation pour les mélanges eau–NEA a pu être tentée à partir des valeurs de $\bar{V}_E$ précédemment déterminées (1) et la figure 5 représente les variations de la quantité $V_{exc}/(1 - X)(1 - a_E)$ en fonction de la fraction molaire de l'eau.

Comme on peut le constater, les valeurs reportées, relatives il est vrai à un domaine de composition plus étendu que celui proposé par l'auteur, ne conduisent pas au tracé d'une droite mais à celui d'une courbe qui s'identifie pour les fractions molaires de l'eau les plus faibles, à une horizontale ($A = 0$) d'ordonnée à l'origine ($V_E^{\ominus} - V_E^0$). On peut à ce titre remarquer que le terme $A(1 - X)$ n'a été introduit dans l'équation [25] par l'auteur que pour rendre compte des résultats expérimentaux analysés, mais que les démonstrations exposées ne l'impliquent nullement.

Il semble ainsi que les hypothèses à la base du modèle d'interaction développé par Abraham soient justifiées pour les solutions les plus concentrées en sel.

Nos résultats expérimentaux montrent également que la procédure de détermination de $V_E^{\ominus}$ au moyen de la méthode d'extrapolation linéaire proposée par l'auteur, peut entraîner une incertitude d'autant plus importante que le domaine d'étude concerne des solutions dont la composition s'éloigne de celle du sel pur.

1. M. HADDED, M. BIQUARD, P. LETELLIER et R. SCHAAL. Can. J. Chem. **63**, 575 (1985).
2. D. F. EVANS, A. YAMAUCHI, R. ROMAN et E. Z. CASASSA. J. Colloïd Interface Sci. **88**, 89 (1982).
3. C. TREINER. J. Chim. Phys. **70**, 1183 (1973).
4. Handbook of Chemistry. 61^e ed. D 196. 1980–1981.
5. S. BRUNAUER, P. H. EMMETT et E. TELLER. J. Am. Chem. Soc. **60**, 309 (1938).
6. R. H. STOKES et R. A. ROBINSON. J. Am. Chem. Soc. **70**, 1870 (1948).
7. A. N. CAMPBELL et B. G. OLIVER. Can. J. Chem. **47**, 2671 (1969).
8. M. C. TRUDELLE, M. ABRAHAM et J. SANGSTER. Can. J. Chem. **55**, 1713 (1977).
9. J. SANGSTER, M. C. ABRAHAM et M. ABRAHAM. Can. J. Chem. **56**, 348 (1978).
10. M. C. ABRAHAM, M. ABRAHAM et J. SANGSTER. Can. J. Chem. **56**, 635 (1978).
11. M. ABRAHAM. Electrochim. Acta, **26**, 1937 (1981).
12. H. BRAUNSTEIN et J. BRAUNSTEIN. J. Chem. Thermodyn. **3**, 419 (1971).
13. D. MIREJOVSKY et E. M. ARNETT. J. Am. Chem. Soc. **105**, 1112 (1983).
14. M. ABRAHAM. J. Chim. Phys. **81**, 207 (1984).
15. Z. KODEJŠ et G. A. SACCHETTO. J. Chem. Soc. Faraday Trans. 1, **78**, 3529 (1982).

Gas-phase photolysis of spiropentane at 147.0 nm

M. PALLER
Department of Chemistry, University of Miami, Coral Gable, FL 33124, U.S.A.

AND

R. D. DOEPKER
Department of Chemistry, Eastern Washington University, Cheney, WA 99004, U.S.A.

Received December 5, 1984[1]

M. PALLER and R. D. DOEPKER. Can. J. Chem. **63**, 3593 (1985).

The gas-phase photolysis of spiropentane has been investigated using xenon (147.0 nm) resonance radiation. Major products observed in order of decreasing importance are ethylene, allene, methylacetylene, 1,2-butadiene, acetylene, propylene, and vinylacetylene. Nitric oxide was used as a radical scavenger while hydrogen sulfide and hydrogen iodide were employed as radical interceptors in the determination of the relative importance of radical and molecular processes. CH_3/CH_2 and $CH_3C{\equiv}C\cdot$ radicals were identified and quantified. Seven primary reaction channels were postulated of which those involving the "elimination" of ethylene were the most predominant accounting for 71% of the photodecomposition.

M. PALLER et R. D. DOEPKER. Can. J. Chem. **63**, 3593 (1985).

Utilisant la résonance de radiation du Xénon (147,0 nm), on a examiné la photolyse en phase gazeuse du spiropentane. Les produits principaux observés, par ordre décroissant d'importance, sont: l'éthylène, l'allène, le méthylacétylène, le butadiène-1,2, l'acétylène, le propylène et le vinylacétylène. On a utilisé de l'oxyde nitrique comme piège de radicaux alors que l'on a utilisé du sulfure d'hydrogène et l'iodure d'hydrogène pour intercepter les radicaux dans la détermination des quantités relatives des processus radicalaires et moléculaires. On a identifié et mesuré les radicaux CH_3/CH_2 et $CH_3C{\equiv}C\cdot$. Le mécanisme réactionnel fait appel à sept voies primaires; celles impliquant l'"élimination" de l'éthylène prédominent puisqu'elles tiennent compte de 71% de la photodécomposition.

[Traduit par le journal]

Introduction

Throughout the years, a series of investigations have been carried out in order to identify the primary and secondary reaction channels for the neutral excited (8.4 eV and 10.0 eV) alkyl-substituted cyclopropane molecule. The most recent previous study in this series examined the photolysis of 1,1-dimethylcyclopropane (1) and disclosed that a methylene elimination process, reaction [1], was of major importance, with a quantum efficiency of 0.34 at 147.0 nm. Tang and Yeh (2) examined the 147.0 nm photolysis of spiropentane but

[1] 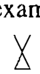 $+ h\nu \rightarrow CH_2 + \text{iso-}C_4H_8$

were unable to identify any C_4 products or the presence of methane and/or ethane in their photolysis mixture. These authors concluded that methylene elimination reaction channel was unfavorable and thereby negligable in the 147.0 nm photolysis of spiropentane.

From examination of the methylene elimination process for other alkyl-substituted cyclopropanes determined in the laboratories at the University of Miami (1, 3) and other laboratories (4, 5), it was learned that a quantum yield of around 0.30 might well be expected for the methylene elimination process from spiropentane. In order to evaluate better the role of the methylene elimination process in the alkyl-substituted cyclopropane systems, the 147.0 nm photolysis of spiropentane was reinvestigated.

Experimental

Materials

A commercial sample of spiropentane was purified by vapor chromatography using a 12 ft column of 30% squalane on Chromosorb P held at 50°C. A second purification was necessary due to an unidentified impurity near the retention time of the spiropentane. This purification (also by vapor chromatography) involved a 6 ft aluminum column at 95°C. The resulting spiropentane showed no impurities at levels greater than 0.005%. Low temperature trap-to-trap distillation techniques were employed to purify HI, NO, and H_2S while other additives obtained commercially were used without futher purification.

Irradiation and analysis

The vacuum–ultraviolet photolyses were carried out at 25°C (room temperature) in a static system using a 600 cm^3 reaction vessel and a titanium "gettered" Xenon (147.0 nm) resonance lamp equipped with a LiF window. Irradiation procedures have been reported previously (3). Analysis was performed by vapor chromatography (25 ft, 30% squalane at 60°C).

Actinometry

The chemical actiometers used at 147.0 nm were 1,1-dimethylcyclopropane $\Phi_{C_2H_4} = 0.26$) (1), and cyclopentene ($\Phi_{C_2H_4} = 0.24$) (6).

Results

The quantum yields of the observed major products of the photolyses of spiropentane at 147.0 nm are reported in Tables 1–3. This datum is representative of that collected under a variety of experimental conditions. In addition, the following observations and controls should be reported. (*1*) Irradiation times were selected in order to hold the total conversion of spiropentane below 0.05% for all experiments where quantum yields were obtained. (*2*) Small amounts of ethane ($\Phi_{C_2H_6} = 0.02$) were obtained when the photolyses were carried out without scavenger. (*3*) Extensive use of the radical interceptors H_2S (7) and HI (8) was employed in this investigation with those involving HI given in Table 3, and those involving H_2S summarized below: A maximum quantum yield for methane was obtained when the photolysis mixture contained from 10–15% H_2S. *No* increase in quantum yields was observed for any other products (including methyl acetylene and allene) for

[1] Revision received August 14, 1985.

TABLE 1. Photolysis of spiropentane at 147.0 nm

Product	Quantum yields with spiropentane in Torr and additive in Torr						
	0.3	0.5		1.0	3.0		5.0
	NO, 0.03	NO, 0.5	None	NO, 0.1	NO, 0.3	None	NO, 0.5
C_2H_2	0.10	0.10	0.09	0.10 ± 0.013[a]	0.09	0.09	0.10
C_2H_4	0.74	0.72	0.71	0.71 ± 0.046	0.74	0.78	0.71
C_3H_6	0.06	0.05	0.05	0.08 ± 0.013	0.08	0.08	0.08
C_3H_4[b]	0.15	0.11	0.11	0.14 ± 0.02	0.16	0.17	0.15
C_3H_4[c]	0.24	0.26	0.27	0.28 ± 0.026	0.29	0.31	0.28
C_4H_4[d]	0.05	0.03	0.05	0.05 ± 0.009	0.06	0.04	0.04
C_4H_6[e]	0.04	0.04	0.03	0.03 ± 0.009	0.05	0.06	0.04
C_4H_6[f]	0.11	0.09	0.13	0.14 ± 0.034	0.12	0.11	0.14

[a] Standard deviation, 12 photolyses.
[b] Methylacetylene.
[c] Allene.
[d] Vinylacetylene.
[e] Cyclobutene.
[f] 1,2-Butadiene.

TABLE 2. Photolysis of spiropentane at 147.0 nm

Product	Quantum yields, with spiropentane at 1 Torr, NO at 0.1 Torr, and moderator in Torr					
	N_2, 44	N_2, 53	Ar, 55	Ar, 105	Ar, 150	Ar, 200
C_2H_2	0.10	0.11	0.16	0.16	0.16	0.17
C_2H_4	0.69	0.70	0.71	0.71	0.69	0.68
C_3H_6	0.05	0.08	0.06	0.07	0.07	0.05
C_3H_4[a]	0.16	0.12	0.15	0.11	0.13	0.14
C_3H_4[b]	0.31	0.29	0.27	0.28	0.29	0.27
C_4H_4[c]	0.06	0.06	0.06	0.07	0.04	0.05
C_4H_6[d]	0.02	0.01	0.01	0.01	0.01	0.00
C_4H_6[e]	0.15	0.15	0.14	0.14	0.11	0.12

[a] Methylacetylene.
[b] Allene.
[c] Vinylacetylene.
[d] Cyclobutene.
[e] 1,2-Butadiene.

a 1 Torr spiropentane – 0.15 Torr H_2S photolysis mixture. The same results were observed for the above mixture even with the addition of 50 Torr of Ne. The maximum quantum yield of CH_4 observed was $\Phi_{CH_4} = 0.15$. (*4*) No products were found that could be identified as C_5. No real attempt was made to establish the presence or absence of C_6 hydrocarbons nor were hydrogen yields obtained.

Discussion

The most abundant stable product of the 147.0 nm photolysis of spiropentane is ethylene $\Phi_{C_2H_4} = 0.71$. Since ethylene quantum yields are independent of pressure and additive it can be assumed that it is produced through one or more primary reaction channels. The formation of ethylene along with allene (reaction [2])

[2]  $+ h\nu \rightarrow C_2H_4 + CH_2{=}C{=}CH_2$

has been observed in thermal (9), photochemical (10), and chemical excitation (11) studies. Tang and Yeh (2) also postulated that reaction [2] is of major importance in the 147.0 nm photolysis of spiropentane but did not attempt to quantify its quantum yield. These authors did report quantum yields of $\Phi_{C_2H_4} = 1.11 \pm 0.16$, $\Phi_{allene} = 0.525$, and $\Phi_{methylacetylene} = 0.152$.

In the studies of Flowers and Frey (9*a*) and Burkhardt (11*c*), methylenecyclobutane was reported as a competitive product at high pressure while methylenecyclobutane was not observed by Tang and Yeh (2) nor was it observed in the present study for the 147.0 nm photolysis. Since methylenecyclobutane was not observed with pressure up to 200 Torr (argon), coupled with the absence of a pressure effect observed on the quantum yields of ethylene, allene, and methylacetylene, it may be concluded that excited molecule(s) leading to the formation of C_2H_4 and C_3H_4 must have a life-time of but a few molecular vibrations, but also long enough to permit rearrangements to occur leading to the production of methylacetylene (reaction [3]).

[3]  $+ h\nu \rightarrow C_2H_4 + CH_3C{\equiv}CH$

If it can be assumed that all the allene and the methylacetylene formed in the absence of HI originates from reactions [2] and [3] respectively then $\phi_2 = \Phi_{C_3H_4}$ (allene) = 0.29 and $\phi_3 = \Phi_{C_3H_4}$ (methylacetylene) = 0.14. The total C_3H_4 production of 0.43 when compared to $\Phi_{C_2H_4} = 0.71$ indicates yet another primary reaction channel for the formation of C_2H_4. Table 3 reveals that the quantum yield of methylacetylene increased by approximately 0.21 when HI was present while allene was unaffected. An increase in the total yield of C_3H_4 products, with the addition of HI, points to the presence of C_3H_3 radicals. It is apparent though, that the C_3H_3 radical is not propargyl ($\cdot CH_2{-}C{\equiv}CH \rightleftarrows CH_2{=}C{=}CH\cdot$) since this species should lead to both allene and methylacetylene (12). As only methylacetylene is formed by the addition of HI, the methylethynyl ($CH_3{-}C{\equiv}C\cdot$) radical must be the precursor to the increased methylacetylene, reactions [4] and [5]).

[4]  $+ h\nu \rightarrow C_2H_4 + H + CH_3C{\equiv}C\cdot$

[5] $CH_3C{\equiv}C\cdot + HI \rightarrow CH_3C{\equiv}CH + I$

If it can be assumed that all C_3H_3 radicals are intercepted at 1 Torr pressure, the quantum yield of reaction [4] may be set equal to the increase in quantum yield for methylacetylene when HI is present. That is, $\phi_4 = \Phi_{C_3H_3} = \Phi(CH_3C{\equiv}CH)_{total} - \Phi(CH_3C{\equiv}CH)_{with\ NO} = 0.21$. Table 3 appears to show a decrease in C_3H_3 formation with an increase in total pressure.

TABLE 3. Photolysis of spiropentane at 147.0 nm

	Quantum yields with spiropentane at 1.0 Torr and additive(s) in Torr				
Product	HI, 0.05	HI, 0.1	HI, 0.15	HI, 0.1; Ar, 50	HI, 0.1; Ar, 100
CH_4	0.18	0.20	0.20	0.23	0.25
C_2H_2	0.10	0.10	0.10	0.12	0.13
C_2H_4	0.70	0.71	0.71	0.75	0.70
C_3H_6	0.08	0.08	0.08	0.08	0.08
C_3H_4[a]	0.30	0.32	0.36	0.25	0.19
C_3H_4[b]	0.29	0.30	0.31	0.32	0.29
C_4H_4[c]	0.06	0.07	0.06	0.08	0.07
C_4H_6[d]	0.02	0.01	0.00	0.00	0.00
C_4H_6[e]	0.13	0.13	0.13	0.15	0.15

[a] Methylacetylene.
[b] Allene.
[c] Vinylacetylene.
[d] Cyclobutene.
[e] 1,2-Butadiene.

This effect is not accompanied by an increase in allene nor a general pressure effect on methylacetylene in the presence of NO. It must be concluded, therefore, if this pressure effect is not an experimental artifact, that the intermediate responsible must not be simply a "hot" C_3H_4 species. Secondly since no C_5-products were observed, speculation of the nature of this intermediate is not warranted.

The total of the quantum yields of ethylene formation from reactions [2], [3], and [4] of 0.64 still points to an additional reaction channel leading to the formation of ethylene. The key to this reaction channel may well involve an expected methylene elimination process. It may be noted that the methylene elimination processes from methylcyclopropane (3*a*), 1,1-dimethylcyclopropane (1), ethylcyclopropane (3*c*), and vinylcyclopropane (3*d*) all indicate that nearly 30% of the primary processes involve the elimination of methylene.

It can be noted in Tables 1–3 that vinylacetylene is independent of pressure and unaffected by addition of additives. The formation of vinylacetylene may occur with the elimination of methylene, ring opening and $2H/H_2$ elimination (reaction [6]).

[6]  $+ h\nu \rightarrow CH_2 + 2H/H_2 + C_4H_4$

The quantum yield of reaction channel [6] can be assigned a value equal to the quantum yield of vinylacetylene $\phi_5 = \Phi_{C_4H_4} = 0.06$. A second process that certainly involves a CH_2 elimination is the formation of 1,2-butadiene. Reaction [7], may be postulated for this reaction channel. If it can be assumed that reaction [7]

[7]  $+ h\nu \rightarrow CH_2 + CH_3C{=}C{=}CH_2$

is the sole source of 1,2-butadiene, then the quantum yield of reaction [7] may be equated to the quantum yield of 1,2-butadiene, $\phi_6 = \Phi_{C_4H_6\text{-}1,2} = 0.14$. Cyclobutene formation shows a decided pressure sensitivity as well as a sensitivity to the presence of HI/H_2S. The formation of cyclobutene therefore must be associated with a secondary reaction channel which at present remains unknown.

On the other hand, propylene $\Phi_{C_3H_6} = 0.08$ is seen to be independent of pressure and unaffected by HI/H_2S additives. Two possible pathways may be postulated, both involving a rearrangement of the excited intermediate. The total quantum yield of propylene production may be distributed between

[8*a*]  $+ h\nu \rightarrow H + C_2H + C_3H_6$

TABLE 4. Quantum yields for the primary reaction channels of the 147.0 nm photolysis of spiropentane

Reaction	Quantum yield
 $+ h\nu \xrightarrow{[2]} C_2H_4 + H_2C{=}C{=}CH_2$	0.29
$\xrightarrow{[3]} C_2H_4 + H_3C{-}C{\equiv}CH$	0.14
$\xrightarrow{[4]} C_2H_4 + H_3C{-}C{\equiv}C\cdot + H$	0.21
$\xrightarrow{[6]} CH_2 + 2H/H_2 + H_2C{=}CH{-}C{\equiv}CH$	0.06
$\xrightarrow{[7]} CH_2 + CH_3CH{=}C{=}CH_2$	0.14
$\xrightarrow{[8]} \left\{\begin{matrix} H + C_2H + C_3H_6 \\ C_2H_2 + C_3H_6 \end{matrix}\right\}$	0.08
$\xrightarrow{[9]} \left\{\begin{matrix} CH_2 + C_2H_2 + C_2H_4 \\ CH_3 + C_2H + C_2H_4 \end{matrix}\right\}$	0.07
Total	0.99

[8*b*] $\rightarrow C_2H_2 + C_3H_6$

reactions [8*a*] and [8*b*] which are indistinguishable without hydrogen yields. The ethynyl radical is not expected to be scavenged by NO (13) but may abstract a hydrogen from a hydrocarbon (14) to produce acetylene. The total quantum yield of acetylene shows a constant low pressure value of 0.10 and a pressure dependent component increasing to a value of 0.17 at 200 Torr Ar. The yield of acetylene associated from reaction [8] is insufficient to account for the total acetylene found in the photolysis of spiropentane. Coupling this "excess" acetylene with the unaccounted ethylene, the following primary reaction channels may be postulated. Based on ethylene yields, the quantum yield for eaction [9]

[9*a*]  $+ h\nu \rightarrow C_2H_4 + C_2H_2 + CH_2$

[9*b*] $\rightarrow C_2H_4 + C_2H + CH_3$

should be $\phi_9 = \Phi_{C_2H_4} - \phi_2 - \phi_3 - \phi_4 = 0.71 - 0.29 - 0.14 - 0.21 = 0.07$.

An examination of all the above postulated mechanisms reveals a predicted CH_2/CH_3 quantum yield equal to $\phi_6 + \phi_7 + \phi_9 = 0.06 + 0.14 + 0.07 = 0.27$. This value of 0.27 is within reasonable agreement to the experimental value of $\Phi_{CH_2/CH} = 0.25$ obtained through the use of HI in the photolysis mixture. Since it is not possible to distinguish between methyl radicals formed through a rearrangement (reaction [9*b*]) and a triplet methylene abstraction process, with the data available, this yield can not be used to distinguish between the two pathways in reaction [9]. A total methylene elimination of approximately 0.27 ($\phi_6 + \phi_7 + \phi_9$) appears to be constant with these values obtained for the other substituted cyclopropanes (1, 3, 4 and 5).

Summary and conclusion

The vacuum–ultraviolet (147.0 nm) photolysis of spiropentane may be described by seven primary reaction channels. Quantum efficiencies of these pathways are summarized in Table 4. Although it is apparent that certain possibly informative data is missing from this study, the quantitative conclusions appear to be compatible with previous studies in the vacuum–ultraviolet photolysis of alkyl substituted cyclopropanes.

1. J. B. BINKEWICZ, M. KAPLAN, and R. D. DOEPKER. Can. J. Chem. **59**, 537 (1981).
2. Y-N. TANG and C-T. YEH. J. Chinese Chem. Soc. **25**, 21 (1978).
3. (*a*) R. D. DOEPKER. J. Phys. Chem. **73**, 8219 (1969); (*b*) K. L. HILL and R. D. DOEPKER. J. Phys. Chem. **76**, 3153 (1972); (*c*) E. LOPEZ and R. D. DOEPKER. J. Phys. Chem. **82**, 752 (1978); (*d*) E. LOPEZ and R. D. DOEPKER. J. Phys. Chem. **83**, 573 (1979); (*e*) T. S. PENDLETON, M. KAPLAN, and R. D. DOEPKER. J. Phys. Chem. **84**, 472 (1980).
4. (*a*) A. K. DHINGRA and R. D. KOOB. J. Phys. Chem. **74**, 4490 (1970); (*b*) K. DEES and R. D. KOOB. J. Phys. Chem. **77**, 759 (1973).
5. (*a*) G. J. COLLIN. J. Chim. Phys. **74**, 302 (1977); (*b*) G. J. COLLIN, H. GAGNAN-DESLAURIERS, M. SUGUET, K. BOKKA, and J. L. SIMARD. J. Photochem. **9**, 449 (1978).
6. C.-K. TU and R. D. DOEPKER. J. Photochem. **3**, 13 (1974).
7. (*a*) P. AUSLOOS and S. G. LIAS. J. Chem. Phys. **44**, 521 (1966); (*b*) G. J. COLLIN and P. M. PERRIN. Can. J. Chem. **50**, 2823 (1972).
8. P. AUSLOOS, R. E. REBBERT, and S. G. LIAS. J. Photochem. **2**, 267 (1973).
9. (*a*) M. C. FLOWERS and H. M. FREY. J. Chem. Sci. 5550 (1960); (*b*) M. C. FLOWERS and A. R. GI-BONS. J. Chem. Sci. 362 (1971); 612 (1971).
10. G. R. DEMARE. J. Photochem. **9**, 4 (1978).
11. (*a*) Y-N. TANG and Y. Y. SU. J. Chem. Phys. **57**, 4048 (1972); (*b*) Y. Y. SU and Y-N. TANG. J. Phys. Chem. **76**, 2187 (1972); (*c*) P. J. BURKHARDT. Ph.D. Dissertation, University of Oregon. 1962.
12. R. WALSH. Trans. Faraday Soc. **67**, 2085 (1971).
13. A. G. SHERWOOD and H. E. GUNNING. J. Phys. Chem. **69**, 1732 (1965).
14. A. M. TAN, O. P. STRAUSZ, and H. E. GUNNING. Trans. Faraday Soc. **62**, 1221 (1966).

Infrared and Raman polarized spectra of ammonium hydrogen bis(trichloroacetate) single crystal

VENETA VIDENOVA-ADRABINSKA
Institute of Inorganic Chemistry and Metallurgy of Rare Elements, Technical University of Wrocław, Smoluchowskiego 23, 50-372 Wrocław, Poland

JAN BARAN AND HENRYK RATAJCZAK
Laboratory of Theoretical Chemistry and Chemical Physics, Institute of Chemistry, Wrocław University, F. Joliot-Curie 14, 50-383 Wrocław, Poland

AND

WILLIAM J. ORVILLE-THOMAS
Department of Chemistry and Applied Chemistry, University of Salford, Salford M5 4WT, Great Britain

Received August 16, 1984[1]

This paper is dedicated to Professor Camille Sandorfy on the occasion of his 65th birthday

VENETA VIDENOVA-ADRABINSKA, JAN BARAN, HENRYK RATAJCZAK, and WILLIAM J. ORVILLE-THOMAS. Can. J. Chem. **63**, 3597 (1985).

The polarized infrared and Raman spectra of ammonium hydrogen bis(trichloroacctate) single crystal have been investigated in the 4000–350 cm^{-1} and 4000–10 cm^{-1} range, respectively. The infrared spectra have been measured at room and low temperatures. An assignment of the bands in terms of approximate type of motion is given. The asymmetric stretching vibration, ν_aOHO, of the strong hydrogen bond gives rise to a very broad infrared absorption, with a maximum around 800 ± 50 cm^{-1}, which is polarized strictly along a tetragonal $Z(c)$ direction of this crystal. For this vibration a correlation field (Davydov or factor group) splitting is not observed. The out-of-plane deformation vibration, γOHO, obeys selection rules for the C_2 site symmetry group. This result and also an interpretation of the νC=O vibration strongly suggest that a potential energy function of the strong hydrogen bond has a single symmetric minimum.

VENETA VIDENOVA-ADRABINSKA, JAN BARAN, HENRYK RATAJCZAK et WILLIAM J. ORVILLE-THOMAS. Can. J. Chem. **63**, 3597 (1985).

Opérant respectivement dans les intervalles de fréquence allant de 4000 à 350 cm^{-1} et de 4000 à 10 cm^{-1}, on a étudié les spectres infrarouges et Raman polarisés d'un monocristal de bis(trichloroacétate) acide d'ammonium. On a mesuré les spectres infrarouges à la température ambiante et à des températures plus basses. On propose une attribution des bandes en fonction du type approximatif de mouvement. La vibration d'élongation asymétrique ν_aOHO de la liaison hydrogène forte donne lieu à absorption infrarouge qui est très large, qui présente un maximum à environ 800 ± 50 cm^{-1} et qui est polarisée selon une direction tétragonale $Z(c)$ du cristal. Dans le cas de cette vibration, on n'a pas observé de dédoublement du champ de corrélation/facteur de Davidov ou de groupe. La vibration de déformation hors-plan, γOHO, suit les règles de sélection du groupe de symétrie C_2. Ce résultat ainsi qu'une interprétation de la vibration νC=O suggèrent fortement qu'une fonction d'énergie potentielle de la liaison hydrogène forte ne possède qu'un seul minimum symétrique.

[Traduit par le journal]

Introduction

The structural and dynamic aspects of hydrogen bonds have always attracted considerable attention. Most studies are on the solid state. Knowledge of the structure of hydrogen bonds and their environment obtained from diffraction methods are very useful not only for classification purposes but also for the interpretation of vibrational spectra, particularly when polarized light is used. In the case of very strong hydrogen bonds the main problem is the symmetry of the hydrogen bond potential. The diffraction methods give only the average position of atoms but the distinction between either dynamic or statistical disorder (double minima potential) and a true symmetry (centred single minimum) might possibly be obtained from infrared and Raman spectroscopy. Most spectroscopic work has been done on acid salts of carboxylic acids of the general formula Me^+[RCOOHOOCR]$^-$ by Hadži *et al.* (1–11, 16). The main results of the investigations may be summarized as follows (8): systems having an O—O distance of about 2.45 Å show a broad and strong infrared absorption between 500 and 1200 cm^{-1}. This was attributed to the asymmetric stretching ν_aOHO vibration. The number and symmetry character of the transitions connected with the OHO vibrations would be most relevant to the problem of the symmetry of the hydrogen bond potential function but much uncertainty is brought in by their bandwidth in infrared spectra and their weakness in Raman spectra even when transitions are allowed. Very large correlation splittings of the ν_aOHO vibration have been found only in the cases of KH–biphenylacetate and KH–dibenzoate (6) and KH–bis(dibromoacetate) (12). Information on the symmetry of the potential function may be obtained from an analysis of the νC=O modes. Although the selection rules appear to be operative in the cases where the centre of the hydrogen bond is on the C_i site, some extra bands in the νC=O region have also been detected in both polarized infrared and Raman spectra (5, 10). Therefore we decided to measure polarized infrared and Raman spectra of ammonium hydrogen bis(trichloroacetate) (AHTCA) and its potassium analogue (KHTCA). Both belong to the same space group ($I\bar{4}2d$, tetragonal system) and contain very strong crystallographically symmetric, C_2, hydrogen bonds with O—O distances of 2.46(2) Å and 2.456(4) Å in KHTCA and AHTCA (13, 14), respectively. The ^{35}Cl nqr studies (15) have shown that in these crystals the

[1]Revision received June 11, 1985.

TABLE 1. Vibrational analysis of the ammonium hydrogen bis(trichloroacetate) crystal ($I\bar{4}2d = D_{2d}^{12}$, $Z = 8$)[a]

D_{2d}	N_i	T_a	T	R	n_i	ν_aOHO	δOHO	γOHO	νC=O	Activity[b] Infrared	Raman
A_1	29	0	4	4	21	0	0	1	1	f	$xx + yy$, zz
A_2	30	0	4	4	22	1	1	0	1	f	f
B_1	29	0	4	4	21	0	0	1	1	f	$xx - yy$
B_2	30	1	3	4	22	1	1	0	1	Z	xy
E	61	1	9	10	41	1	1	1	2	X, Y	yz, zx

[a] N_i, number of degrees of freedom belonging to i species; T_a, number of overall translations; T, number of translational vibrations; R, number of rotational vibrations; n_i, number of intramolecular vibrations; ν_aOHO, δOHO, γOHO, asymmetric OHO stretching, in-plane, and out-of-plane bending vibrations; νC=O, C=O stretching vibrations.
[b] f, forbidden; x, y, z, principal axes of the polarizability derivative tensor; X, Y, Z, principal axes of optic indicatrix; Z is parallel to the tetragonal c direction; $X = Y$.

hydrogen bond potential might be either a single symmetrical or a double symmetrical with a dynamical disorder.

Experimental

The $NH_4H(Cl_3CCOO)_2$ was prepared by dissolving stoichiometric amounts of trichloroacetic acid and ammonium carbonate in water. The single crystals suitable for infrared and Raman spectra measurements were obtained by the slow evaporation method at a constant temperature of 20°C. The crystal was oriented with the aid of the X-Ray method and a polarizing microscope. A plate about 4 mm thick parallel to the optic axis Z was cut. The optic axis Z is parallel to the tetragonal c direction. The plate was stuck to the KBr window and polished until the measurement of polarized spectra was possible. The infrared spectra were measured with the electric vector of radiation parallel and perpendicular to the optic axis Z, respectively. The infrared spectra were measured with a Perkin-Elmer M180 spectrophotometer equipped with a wire grid polarizer. A CTI-Cryogenics low temperature cryostat was used to obtain infrared spectra at 20 K temperature. For the Raman spectra measurement a single crystal cubic sample was prepared. The edges of this cube were parallel to the $X(a)$, $Y(b)$, and $Z(c)$ directions. The spectra were measured with a Cary 82 Raman spectrometer using the 514 nm line of an argon-ion laser.

Discussion

Crystal structure and selection rules

The crystal of AHTCA belongs to the space group $I\bar{4}2d$ ($=D_{2d}^{12}$) of the tetragonal system (14). A primitive unit cell contains four molecular units. Two trichloroacetic acid groups are connected by a very strong crystallographically symmetric (twofold symmetry, with the C_2 axis perpendicular to the tetragonal $Z(c)$ axis) hydrogen bond with an O—O distance of 2.456(6) Å. Ammonium cations are situated on the C_2 symmetry axes which are parallel to the tetragonal $Z(c)$ axis. Other heavy atoms occupy the C_1 positions. The results of a factor group analysis are given in Table 1. The correlation diagram between a site symmetry group C_1 of trichloroacetic group and a C_2 ($\perp Z$) site symmetry group of the $H(Cl_3CCOO)_2$ anion and a factor group D_{2d} is given in Table 2. Every internal vibration of the trichloroacetic group should split into two components of A and B type symmetry as a result of an interaction inside the $H(Cl_3CCOO)_2$ anion. Interaction between the internal vibrations of the four $H(Cl_3CCOO)_2$ anions in the primitive unit cell leads to a correlation (Davydov or factor group) splitting.

Let us suppose that protons lie on the C_2 symmetry axes which are perpendicular to the tetragonal Z axis. In this case the asymmetric stretching ν_aOHO and the in-plane deformation

TABLE 2. Correlation chart for the internal vibrations of trichloroacetates[a] in the ammonium hydrogen bis(trichloroacetate) crystal[b]

Site symmetry group C_1	Site symmetry group of dimer $C_2(\perp Z)$	Unit cell group D_{2d}[c]	Activity Infrared	Raman
A	A	A_1	f	$xx + yy$, zz
		B_1	f	$xx - yy$
		E	X, Y	yz, zx
	B	A_2	f	f
		B_2	Z	xy
		E	X, Y	yz, zx

[a] Vibrations of hydrogen bonds: ν_aOHO and δOHO correlate as B representation of the C_2 site group; γOHO as A representation.
[b] Abbreviations similar as those in Table 1.
[c] Unit cell group is equivalent to the factor group.

δOHO vibrations transform according to the B type representation of the C_2 site symmetry group (see Table 2). Similarly, the out-of-plane γOHO vibration transforms according to the A type representation. The correlation coupling between the vibrations of the four protons in the primitive unit cell gives two infrared modes ($B_2(Z)$, $E(X,Y)$) for the ν_aOHO and two infrared modes ($B_2(Z)$, $E(X,Y)$) for the δOHO vibrations. Only one infrared mode of E type symmetry is expected for the γOHO vibrations. The B_2 type modes are supposed to interact with radiation polarized parallel to the tetragonal $Z(c)$ axis. The E type modes should interact with radiation polarized perpendicular to the tetragonal $Z(c)$ axis.

Band assignment

The polarized infrared spectra of the AHTCA single crystal are shown in Fig. 1. The polarized Raman spectra are presented in Fig. 2. The wavenumbers of the bands, their relative intensities, and a tentative assignment are listed in Table 3.

The bands observed in the interval 4000–300 cm^{-1} arise from: (*i*) the vibrations of the protons in the strong hydrogen bonds, (*ii*) the internal vibrations of the trichlororacetic acid residues, and (*iii*) the internal vibrations of the ammonium groups. In the assignment of the bands the characteristic group frequencies (17), the polarization properties of the bands (compared with those predicted on the base of the bond moment polar model (19)) and the correlation chart diagram (Table 2) were used. The infrared spectra of the AHTCA are very similar to the spectra of the potassium analogue (20). They are differ-

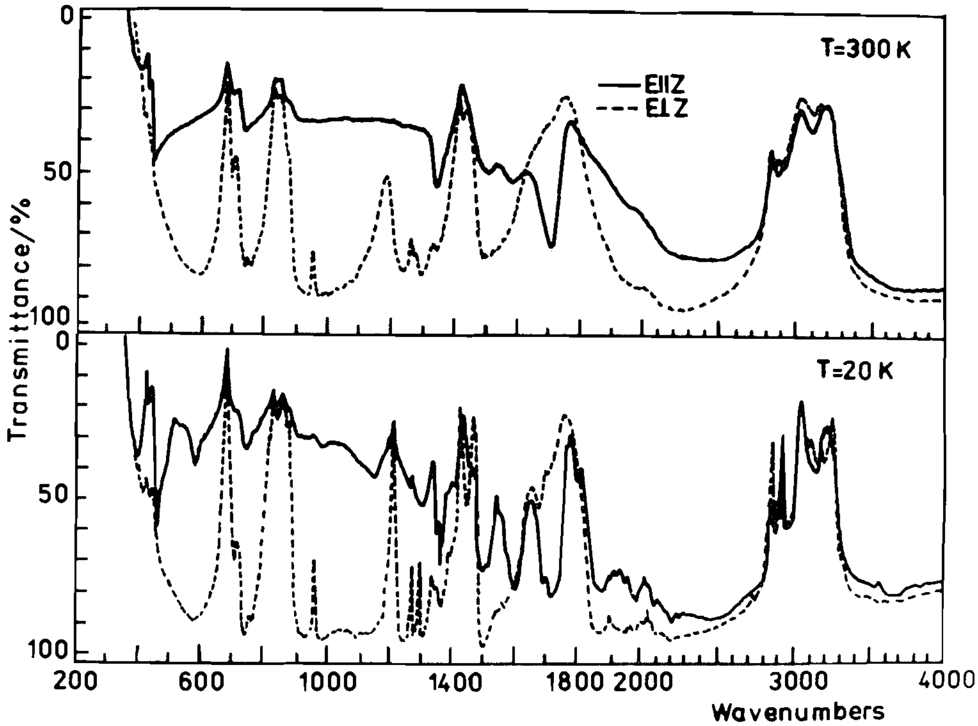

FIG. 1. The polarized infrared spectra of the ammonium hydrogen bis(trichloroacetate) single crystal at room temperature (upper) and low temperature (lower). Solid line, electric vector is parallel to the tetragonal $Z(c)$ axis; dashed line, electric vector is perpendicular to the tetragonal $Z(c)$ axis.

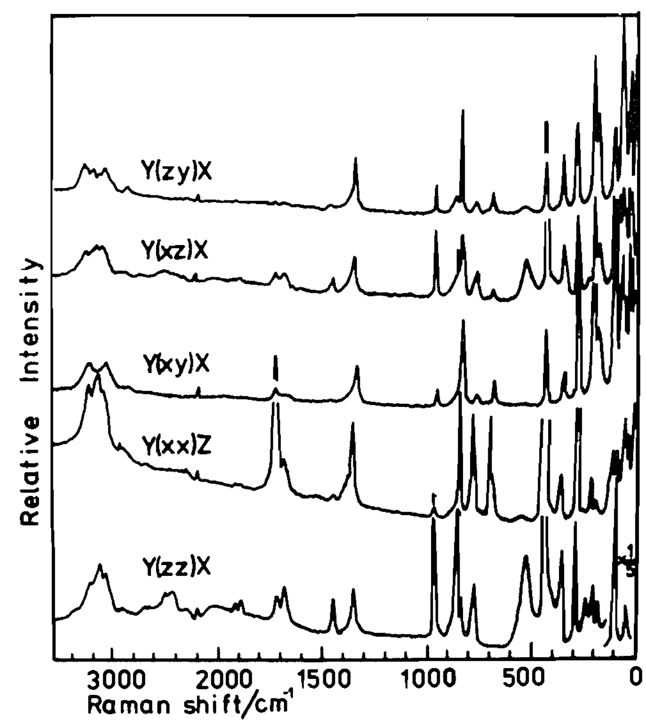

FIG. 2. The polarized Raman spectra of the ammonium hydrogen bis(trichloroacetate) single crystal at room temperature.

ent only in the region of the NH_4^+ group vibrations whose detailed interpretation will be given elsewhere.

Hydrogen bond vibrations

The asymmetric stretching vibration

The most characteristic feature of the powder infrared spectrum is a broad and strong absorption observed in the region between 1500−400 cm^{-1} with a maximum at 850 ± 30 cm^{-1}. This strong and broad absorption appears only in the spectrum polarized parallel to the tetragonal $Z(c)$ axis. Only four "transmission windows" at 1722, 1348, 728, and 445 cm^{-1} are observed in this absorption. The top of this absorption is very flat in the spectrum measured at room temperature. At low temperature (20 K) its maximum is at about 800 ± 50 cm^{-1}. This absorption would correspond to the B_2 type mode of the ν_aOHO. The E type mode is expected in the spectrum polarized perpendicular to the Z axis. In perpendicular spectrum a resonance transmission feature at 1500 cm^{-1} is observed at low temperature. This may indicate the presence of a broad absorption in this region. A careful investigation shows a slightly higher background in the region between ~1100−1900 cm^{-1} in the spectrum polarized perpendicular to the Z axis measured at room temperature. However, it is difficult to accept that this feature is arising from the E type mode of the ν_aOHO vibration. A background is not observed in the infrared spectrum of KHTCA crystal (20), polarized perpendicular to the Z axis (both crystals are isomorphous). We think that the background observed in the spectrum of ammonium salt arises from an overlapping of broad bands observed in the region between 1900−1100 cm^{-1}. Observed low-temperature decreasing of the background may be a result of a narrowing of the bands which appear in this region. Hence the resonance type transmission feature observed at 1500 cm^{-1} may be accidental. If this is true, then we may suggest that the correlation (Davydov) splitting of the ν_aOHO vibration is not observed in this crystal. From this experimental fact it follows that the ν_aOHO transition dipole moment is parallel to the tetragonal Z axis of the crystal. Now we may determine an orientation of this dipole transition moment with respect to the molecular structure of the dimer with hydrogen bond using Fig. 3. A line between carbon atoms of the two carboxylic groups bonded by the O···H···O hydro-

TABLE 3. Frequencies (cm^{-1}) of the bands observed in the infrared and Raman polarized spectra of ammonium hydrogen bis(trichloroacetate)

Infrared[a]				Raman[b]		Tentative assignment of the bands
$E \parallel Z(c)$		$E \perp Z(c)$		Room temperature		
$T = 300$ K	$T = 20$ K	$T = 300$ K	$T = 20$ K	$\Delta\bar{\nu}$	Relative intensity	
				3388	$zz(1)$	
				3272	$zy(2)$	
		3230vs	3243vs	3223	$xz(3)$, $zy(3)$	
3215vs	3208vs			3216	$xx(8)$, $xy(3)$	$\nu_3NH_4^+$
	3190s					
		3162vs	3162vs	3163	$zy(2)$, $xz(2)$	
			3139s			
			3110s	3115	$zz(6)$, $xx(8)$, $xz(3)$, $zy(2)$	Combinations
		3092ssh	3092s			
				3075	$zz(4)$	
				3063	$xz(3)$	
3050vs	3038vs	3050vs	3038vs	3055	$xx(6)$	$\nu_1NH_4^+$
				3052	$xy(2)$, $zy(3)$	
2915m	2915s	2920m	2920m	2917	$xx(2)$	$2\times\nu_4'(B)$ NH_4^+
				2910	$zz(1)$	
			2898m	2894	$xy(1)$	
			2885msh			
	2870m		2870wsh			
2850m	2850m					$2\times\nu_4(A)$ NH_4^+
		2838m	2840s	2838	$xy(1)$, $zy(1)$	$\nu_4(A)+\nu_4''(B)$
	2720vw	2720wsh	2720vwsh			
2690vw	2690vw		2690vw	2690	$zz(1)$	
				2680	$xz(1)$	
				2590	$xz(1)$	
				2488	$zz(2)$	
				2430	$zz(2)$, $xz(1)$	
	2365w					γOH overtone
	2340w					
				2290	$zz(1)$, $xx(1)$	
				2280	$xz(1)$	
	2118w					
			2075vw			
		2050vw	2050vw	2050	$zz(1)$, $xz(1)$	
	2038vw					
	2020vw		2020vw			
	2005vw		2005vw			
	1962w		1962vw			
	1935w		1940vw			
	1915w		1915wsh			
	1900w		1900w	1908	$zz(1)$, $xz(1)$	
1890msh		1892wsh		1886	$zz(1)$	
	1815s					
			1805wsh			
1780 vs	1775vs		1770ssh			
	1760ssh	1760vs				νC=O
1722[c]	1715[c]			1716	$zz(2)$, $xx(13)$, $xy(1)$, $xz(1)$	
		1695ssh	1695s			
				1676	$zz(4)$, $xx(3)$, $xy(1)$, $xz(1)$	
		1660ssh	1660msh			
	1655m		1653m			
1640s	1640msh		1645msh			$\nu_2NH_4^+$
	1628msh		1628msh	1625	$xy(1)$, $zy(1)$	
	1579wsh					
	1572wsh					
	1560msh		1560vw			
	1545msh					
1540s	1540m		1540vw			δOHO
	1533msh					

TABLE 3. (*Continued*)

Infrared[a]				Raman[b]		Tentative assignment of the bands
$E\parallel Z(c)$		$E\perp Z(c)$		Room temperature		
$T = 300$ K	$T = 20$ K	$T = 300$ K	$T = 20$ K	$\Delta\bar{\nu}$	Relative intensity	
1503ssh	1508w		1508vw			
	1495wsh					
	1485wsh					
	1472msh		1472ssh			
		1455s	1465s	1445	$zz(16)$, $xz(4)$	$\nu_4'(B)$ NH_4^+
			1459ssh			
			1440msh			
1425vs	1435s		1432msh			$\nu_4(A)NH_4^+$
	1425vssh					$\nu_4''(B)NH_4^+$
		1422vs	1424s			
1405ssh	1405m		1405wsh			
	1385m		1385w	1385	$xx(2)$	
1375msh			1375wsh	1373	$xx(2)$	
				1370	$xz(1)$	
	1365wsh					νC—O
1348[c]	1360[c]			1348	$xy(2)$	
	1352m		1352m			
	1335s	1335w	1338vw	1344	$zz(2)$, $xx(8)$, $xy(4)$, $xz(5)$, $zy(6)$	
1315ssh						
	1305msh					
	1294m		1294w			
		1280wsh				
1270ssh	1270m	1268w	1270w			
	1242msh					
	1212s		1212vs			γOHO
	1185ssh	1185s	1185wsh			
	1175ssh		1175wsh			
		1145wsh	1145w			
		1045vw	1045vw			
	1035s					
		952vw	959w	956	$zz(13)$, $xx(1)$, $xy(1)$,	
					$xz(5)$, $zy(7)$	νC—C
	879s	873msh	879s			
	860vs		860ssh	860	$xy(2)$, $zx(2)$	
850vs			855msh	850	$zz(11)$, $xz(4)$	ν_aCCl_3
	845vssh		843vs			
835vs	835vssh	835vssh	835vs	835	$xx(11)$, $xy(9)$, $zy(9)$	
	830vw		830vs	832	$zz(5)$, $xy(7)$	
815ssh	815vs		815s			
805ssh	805ssh					
770ssh	770s			770	$zz(6)$, $xx(9)$, $xy(1)$, $xz(2)$	
	748ssh					
	720ssh	720m	720wsh	725	$xy(1)$	δCOO
710s	710s		712w	713	$xy(1)$, $zy(1)$	
				687	$xx(10)$, $xy(3)$, $xz(2)$, $zy(2)$	
675vs	675vs	675vs	675vs			ν_sCCl_3
668vssh	665vs					
			635wsh			
			620wsh			
	600ssh					
	550s?					
				536	$zz(9)$, $xx(1)$, $xy(1)$	?ν_sO···O
				527	$xz(3)$, $zy(1)$	
435w	438s	438vw	440m	437	$zz(100)$, $xx(100)$, $xy(18)$	δ_sCCl_3
					$xx(28)$, $zy(4)$	
420s	425vs	420vw	425m	410	$zz(6)$, $xx(1)$	ρOCO
		395vw	395m			

TABLE 3. (*Concluded*)

Infrared[a]				Raman[b]		
$E\parallel Z(c)$		$E\perp Z(c)$		Room temperature		Tentative assignment of the bands
$T=300$ K	$T=20$ K	$T=300$ K	$T=20$ K	$\Delta\bar{\nu}$	Relative intensity	
				356	*zz*(10), *xz*(5)	Lattice modes
				353	*xx*(5)	
				350	*xy*(3)	
				330	*zz*(4)	
				291	*zz*(12)	
				285	*xx*(34), *xy*(20), *zy*(4)	
				250	*xx*(1), *xy*(1)	
				242	*zz*(5)	
				236	*xy*(3)	
				207	*zz*(16), *xx*(3), *xy*(21), *zy*(16)	
				189	*xy*(9), *xz*(5), *zy*(9)	
				183	*zz*(3), *xx*(2)	
				181	*xy*(7)	
				119	*zy*(7)	
				112	*xx*(5)	
				110	*xy*(24)	
				108	*xy*(26), *xx*(8)	
				103	*zz*(88), *xz*(26)	
				87	*xx*(6)	
				75	*xy*(15), *xz*(10), *zy*(20)	
				50	*zz*(24), *xx*(10)	
				47	*xz*(10)	
				34	*xz*(10), *zy*(10)	
				28	*xy*(26)	

[a]Abbreviations: v very, s strong, m medium, w weak, sh shoulder, t transmission window.
[b]The Damen–Porto–Tell notation is used in single crystal Raman work. Intensities relative to the band at 437 cm^{-1} (100) are given in parentheses.

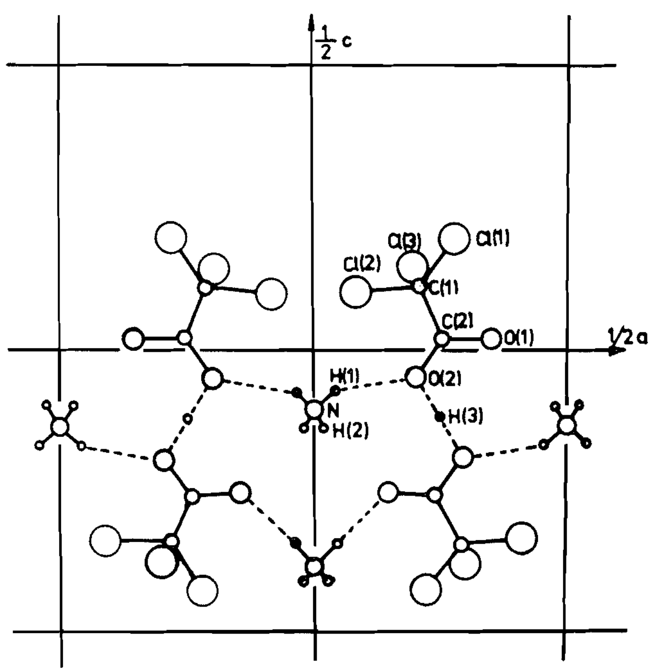

FIG. 3. Projection of the crystal structure of ammonium hydrogen bis(trichloroacetate) on the *ac* plane. The *c* tetragonal direction is parallel to the optic axis *Z*.

gen bond is parallel to the tetragonal $Z(c)$ direction. Hence the transition dipole moment of the ν_aOHO vibration is parallel to this line and makes an angle of about 30° with the O···O hydrogen bond direction. Similar behaviour of this broad absorption band has been observed in the other cases (10).

The out-of-plane deformation vibration

The well-shaped band at 1185 cm^{-1} in the spectrum polarized perpendicular to the *Z* axis has been assigned to the out-of-plane deformation vibration. Its polarization corresponds very well to that expected for the assumption that protons occupy the C_2 site symmetry. At low temperatures this band is very narrow and its maximum is at 1215 cm^{-1} with two shoulders at 1175 and 1185 cm^{-1}.

The in-plane deformation vibration

It is very difficult to assign a band to this vibration because of the presence of bending bands of the NH_4^+ group in the expected region. However, as with the potassium salt (20) a band at 1540 cm^{-1} polarized parallel to the *Z* axis has been assigned to this vibration. At low temperatures the shape of this band is highly varying.

The symmetric stretching ν_sO···O vibration

The selection rules allow this vibration in the infrared and Raman spectra. In the expected region, below 250 cm^{-1}, one observes many bands which are related to the lattice vibrations. Hadži *et al.* (16) have assigned, in the Raman spectra of RbHTCA, a band at 133 cm^{-1} to the symmetric stretching ν_sO···O vibration. However, there is no band at this frequency in our spectra. It is interesting to note that in Raman spectra of AHTCA there is a band at 536 cm^{-1} with the strongest *zz* component. The origin of this band is not clear. No band was found in this region in the infrared spectra at room temperatures. The bands at 550 and 512 cm^{-1} observed in the low temperature spectrum polarized parallel to the *Z* axis are uncertain since a change of gratings in this region takes place in the spectrophotometer. However, a Raman band of similar shape appears in the spectra of the other acid salts (20). It is worth noting that a "transmission window" at 573 cm^{-1} is observed at low temperatures in the infrared spectrum polarized parallel to the Z axis measured. It may be the result of an interaction of this vibration with the ν_aOHO vibration.

Internal vibrations of the trichloroacetic acid group

The νC=O stretching vibration

The bands associated with this vibration may give very useful information on the symmetry of the hydrogen bond potential function. A general discussion on the νC=O and νC—O stretching vibrations has been given by Svanfeldt *et al.* (21). Taking into account a correlation (Davydov) splitting, one can expect two infrared bands polarized perpendicular to the tetragonal Z axis and one band polarized parallel to the Z axis. Five bands are expected in the Raman spectra. Three Raman bands should have similar frequencies to the frequencies of the infrared bands (see Table 2). In the infrared spectrum polarized parallel to the Z axis a very strong band at 1780 cm^{-1}, asymmetric from the high frequency side and a deep transmission "hole" from its low frequency side (at 1722 cm^{-1}), is observed. In the spectrum polarized perpendicular a very strong band at 1760 cm^{-1} with shoulders at 1695 and 1660 cm^{-1} appears. In the Raman spectra there are two bands at 1716 cm^{-1} and at 1676 cm^{-1} in this region. They are observed in all Raman spectra but their intensity is strongest for the *xx* and *zz* components, respectively. The latter Raman band and infrared shoulder at 1660 cm^{-1} have been assigned to the ν_2 vibration of the ammonium ion. The former Raman band corresponds to the νC=O stretching vibration. Its frequency is close to that found for a band observed in the powder Raman spectra of potassium and rubidium analogues (16). Hence the correlation splitting expectation is not met by the experimental Raman data. The other possibility is to consider only coupling between the two C=O groups belonging to the acid groups bonded by the hydrogen bond. In this case the theory predicts two bands in the Raman and infrared spectra at similar frequencies. However, one may expect that the Raman band corresponding to the B type mode of the C_2 site group could be very weak. The infrared band corresponding to the A type component may have very weak intensity and should be polarized perpendicular to the tetragonal Z axis. The infrared polarization behaviour of the B component may depend on an orientation of the transition dipole moment of the νC=O vibration with respect to the C=O bond. In AHTCA crystal the C=O bonds are almost perpendicular to the tetragonal Z axis (Fig. 3). It is known that the transition dipole moment of the νC=O vibration may be as far as 40° out of the C=O bond direction (6). Hence the B type νC=O vibration may be observed in both polarized infrared spectra. We think that the shoulder at 1695 cm^{-1} in the infrared spectrum polarized perpendicular to the Z axis and the Raman band at 1716 cm^{-1} correspond to the A type component of the νC=O vibration. The infrared band at 1780 cm^{-1} polarized parallel and the band at 1760 cm^{-1} polarized perpendicular to the Z axis arise from the B type component of the νC=O vibration. One has to explain the different frequencies of these two bands. We suggest that this may be a result of an interaction of the B component of the νC=O vibration with the ν_aOHO broad absorption. Since the ν_aOHO transition dipole moment is polarized parallel to the Z direction but the B type transition moment of the νC=O is not perpendicular nor parallel to the Z direction, this interaction may have the character proposed by Marzocchi *et al.* (18). As a result of this interaction a dispersive type of "transmission window" with a minimum at 1722 cm^{-1} and a maximum at 1780 cm^{-1} appears. At low temperature the asymmetric band polarized parallel to the Z axis changes into an almost symmetric band with a maximum at 1775 cm^{-1}, a side band at 1810 cm^{-1}, and a shoulder at 1760 cm^{-1}. The band polarized in the perpendicular direction changes much less. The shoulder at 1695 cm^{-1} is better resolved and the shoulder at 1660 cm^{-1} is a well-resolved band.

The C—O stretching vibration

In the Raman spectra a depolarized band at 1344 cm^{-1} has been assigned to this vibration. It has the strongest intensity in the *xx* spectrum. In the infrared spectrum polarized parallel to the Z axis close to this frequency, a "transmission window" at 1348 cm^{-1} occurs. At low temperature a band at 1335 cm^{-1} is observed. A weak band at 1335 cm^{-1} is observed in the spectrum polarized perpendicular to the Z axis.

The other internal vibrations of the acid group

Bands at 835, 850, 675, and a shoulder at 875 cm^{-1} have been assigned to the $\nu_a CCl_3$ and $\nu_s CCl_3$ vibrations. These bands are very strong in the spectrum polarized perpendicular to the Z axis. In the Raman spectra there are bands at very similar frequencies. It is possible that the Raman band at 771 cm^{-1} and a shoulder in infrared spectrum polarized parallel to the Z axis at 770 cm^{-1} also arises from the stretching νCCl vibration (17). The bands observed at 710 and 720 cm^{-1} have been assigned to the deformation vibration of the COO groups. It is worth emphasizing that the Raman bands at 686 and 676 cm^{-1} are the strongest in the *xx* spectrum and are not observed in the *zz* Raman spectrum. The strongest depolarized Raman band at 437 cm^{-1} may be assigned to the $\nu_s CCl_3$ symmetric bending vibration (17). In the infrared spectra two bands at 438 and 420 cm^{-1}, polarized parallel to the Z axis, are observed. Following Hadži *et al.* (16), the former may be assigned to the ρOCO rocking vibration.

The νC—C stretching vibration gives rise to a very weak infrared band at 952 cm^{-1}, which is polarized perpendicular to the Z axis. There is no band nor "transmission window" in the absorption polarized parallel to the Z axis. Although the C—C bond is at an angle of 28° to the Z axis, one could expect the appearance of a band or "transmission window" in this spectrum. In the Raman spectra this vibration gives rise to the band at 956 cm^{-1}, which is the strongest in the *zz* spectrum.

Conclusion

It has been shown that the ν_aOHO vibration gives rise to a very broad absorption which is polarized parallel to the tetragonal $Z(c)$ axis. We do not observe any similar feature in the spectrum polarized perpendicular to the $Z(c)$ axis. Hence, we may suggest that for the ν_aOHO vibration a correlation field (Davydov or factor group) splitting is not observed.

For the out-of-plane deformation γOHO vibration, the correlation field coupling and the site group ($C_2 \perp Z$) symmetry predictions are similar for the infrared spectra. In either case only one band polarized perpendicular to the $Z(c)$ axis is expected. The appearance of only one infrared band polarized perpendicular to the $Z(c)$ axis allows us to confirm that protons occupy a site of C_2 symmetry, hence, the hydrogen bond potential is symmetrical with a single minimum.

This suggestion finds also confirmation in the analysis of the νC=O stretching vibration. If one takes into account only the infrared data, the agreement with a theoretical prediction on the basis of a correlation field coupling is surprisingly good. Two bands polarized perpendicular (E type) and one band polarized parallel (B_2 type) to the $Z(c)$ axis are observed in the polarized infrared spectra. The $\nu C{=}O$ band polarized parallel to the $Z(c)$ axis has a characteristic shape. A similar shape of the $\nu C{=}O$ band is observed in polarized infrared spectra of other acid salts (10, 22) in which a strong and broad absorption appears. This shape is characterized by a "transmission window" around 1700 cm^{-1} and an asymmetry observed on the high frequency side. We suggest that this feature may be connected with an interaction between the broad ν_aOHO absorption and the $\nu C{=}O$ mode of B_2 symmetry, when the correlation field coupling appears, or B symmetry, when only the coupling between the $\nu C{=}O$ vibrations inside the hydrogen-bonded dimer occurs. We suppose that the latter case is more reasonable because the correlation splitting of the $\nu C{=}O$ vibration is not observed in the polarized Raman spectra. Hence, the B type $\nu C{=}O$ mode, being a result of the out-of-phase coupling between the $\nu C{=}O$ vibrations inside the dimer (whose site group symmetry is C_2) interacts with the ν_aOHO vibrations. Since the transition dipole moment of this B type $\nu C{=}O$ mode is neither parallel nor perpendicular to the ν_aOHO transition dipole moment, a result of its interaction would be a "transmission window" at 1722 cm^{-1} and a dispersive shape of the $\nu C{=}O$ band observed in the infrared spectrum, in which a broad absorption occurs. This interaction may have a character similar to that proposed by Marzocchi *et al.* (18) and it may be responsible for the different frequencies of the $\nu C{=}O$ bands, arising from the B type mode, which are observed in the infrared spectra polarized parallel and perpendicular to the $Z(c)$ axis.

1. D. HADŽI and A. NOVAK. Nuovo Cim. Suppl. **2**, 715 (1955).
2. D. HADŽI, A. NOVAK, and B. OREL. Spectrochim. Acta, **29**A, 1745 (1973).
3. A. NOVAK. J. Chim. Phys. **69**, 1615 (1972).
4. D. HADŽI and B. OREL. J. Mol. Struct. **18**, 227 (1973).
5. L. ANGELONI, M. P. MARZOCCHI, D. HADŽI, B. OREL, and G. SBRANA. Spectrochim. Acta, **33**A, 735 (1977).
6. B. OREL and D. HADŽI. Chem. Scripta, **11**, 102 (1978).
7. B. OREL and D. HADŽI. Spectrochim. Acta, **31**A, 169 (1975).
8. D. HADŽI and B. OREL. Indian J. Pure Appl. Phys. **16**, 376 (1978).
9. L. ANGELONI, M. P. MARZOCCHI, D. HADŽI, B. OREL, and G. SBRANA. Chem. Phys. Lett. **28**, 201 (1974).
10. L. ANGELONI, M. P. MARZOCCHI, S. DETONI, D. HADŽI, B. OREL, and G. SBRANA. Spectrochim. Acta, **34**A, 253 (1978).
11. B. OREL and D. HADŽI. Spectrochim. Acta, **32**A, 1731 (1976).
12. V. VIDENOVA, J. BARAN, and H. RATAJCZAK. To be published.
13. L. GOLIC and F. LAZARINI. Cryst. Struct. Commun. **3**, 635 (1974).
14. L. GOLIC and F. LAZARINI. Cryst. Struct. Commun. **4**, 487 (1975).
15. H. RATAJCZAK, W. J. ORVILLE-THOMAS, and I. CHOŁONIEWSKA. Chem. Phys. Lett. **45**, 208 (1977).
16. D. HADŽI, M. OBRADOVIC, B. OREL, and T. SOLMAJER. J. Mol. Struct. **14**, 439 (1972).
17. E. SPINNER. J. Chem. Soc. 4217 (1964).
18. M. P. MARZOCCHI, L. ANGELONI, and G. SBRANA. Chem. Phys. **12**, 346 (1976).
19. J. OVEREND. *In* IR spectroscopy and molecular structure. *Edited by* M. Davies. Elsevier, London. 1963. p. 373.
20. V. VIDENOVA. Ph.D. Thesis, Wrocław University, Wrocław, Poland. 1979.
21. R. J. SVANFELDT, J. LINDGREN, and I. GRENTHE. Acta Chem. Scand. A**28**, 1129 (1975).
22. M. M. ILCZYSZYN. Ph.D. Thesis, Wrocław University, Wrocław, Poland. 1981.

Étude cinétique de l'ouverture thermique de la liaison C—C d'aziridines et d'époxydes dipôles-1,3 potentiels. II. Influence des substituants

AÏCHA DERDOUR ET FERNAND TEXIER

Laboratoire de synthèse organique, ONRS 75B/033, Institut de Chimie, Université d'Oran, Es-Sénia, Algérie

Reçu le 25 septembre 1984[1]

AÏCHA DERDOUR et FERNAND TEXIER. Can. J. Chem. **63**, 3605 (1985).

L'étude cinétique de l'ouverture thermique de la liaison C—C des cyano-2 aziridines **1**, des alcoxycarbonyl-2 aziridines **2**, des aroyl-2 aziridines **3** et des dicyano-2,2 époxydes **4** diversement substitués en 1 et 3 montre que (*i*) la stéréochimie des carbones cycliques a peu d'influence sur la vitesse d'ouverture électrocyclique; (*ii*) un substituant aryle en 1 favorise la réaction par rapport à un alkyle et d'une manière générale, la réaction est facilitée par des substituants qui rapprochent les niveaux d'énergie du doublet P de l'hétéroatome et l'OM $\sigma^*_{C\text{-}2-C\text{-}3}$. Elle est également favorisée par la dissymétrie de substitution des carbones 2 et 3. Les résultats sont discutés dans le cadre de la théorie des relaxations.

AÏCHA DERDOUR and FERNAND TEXIER. Can. J. Chem. **63**, 3605 (1985).

A kinetic study concerning the thermal opening of the C—C bond of 2-cyanoaziridines (**1**), 2-alkoxycarbonylaziridines (**2**), 2-aroylaziridines (**3**), and 1,3-substituted 2,2-dicyanoepoxides (**4**) has shown that (*i*) the stereochemistry of the cyclic carbon atoms has little influence on the rate of the electrocyclic opening; (*ii*) the presence of an aryl substituent in position 1, as opposed to an alkyl substituent, favors this reaction and, in general, the reaction is favored by the presence of substituents which produce energy levels closer to those of the P doublet of the heteroatom and of the $\sigma^*_{C\text{-}2-C\text{-}3}$ MO. This reaction is also favored by a dissymmetry of the substitution on the 2 and 3 carbons. The results are discussed in terms of the theory of relaxations.

[Journal translation]

Les facteurs qui favorisent l'ouverture thermique des hétérocycles isoélectroniques de l'anion cyclopropyle (aziridines, époxydes...) en dipôles-1,3 correspondants ne semblent pas être complètement dégagés, malgré quelques travaux expérimentaux (1–3) et les explications basées sur la méthode des relaxations (4).

Afin de préciser l'influence des substituants sur la réaction péricyclique, nous avons étudié, à l'aide des méthodes décrites dans l'article précédent (5), la cinétique d'ouverture de la liaison C—C des aziridines **1**, **2** et **3** et des époxydes **4**.

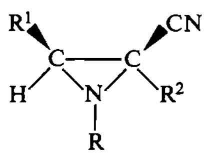

1

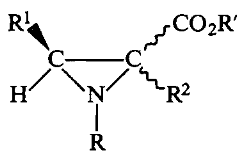

2

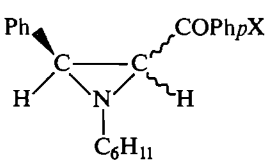

3

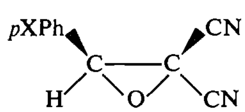

4

L'objet de ce mémoire est d'examiner l'influence de la configuration relative des carbones cycliques de l'aziridine et celle de divers substituants sur la réaction d'ouverture électrocyclique schématisée comme suit:

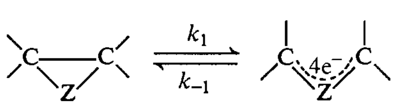

Aziridine ------ Ylure d'azométhine (Z = N—R)
Epoxyde ------ Ylure de carbonyle (Z = O)

[1] Revision reçue le 30 juillet 1985.

Résultats expérimentaux

1. *Influence de la configuration relative des carbones cycliques de l'aziridine*

Huisgen *et al.* ont montré que la stéréochimie *cis* ou *trans* des deux aziridines isomères **2***d* (*cis*) et **2***e* (*trans*) influe peu sur leur vitesse d'ouverture électrocyclique (3*a*):

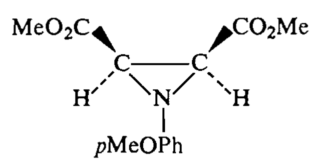

2*d* (*cis*)

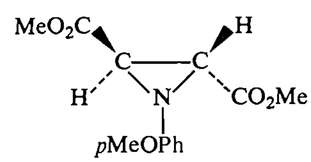

2*e* (*trans*)

Nous avons montré qu'il en était de même pour les deux aziridines isomères **3***a* (*cis*) et **3***b* (*trans*), quelle que soit la température de la réaction. Les résultats rassemblés dans le tableau 1 indiquent que la configuration relative des carbones cycliques ne joue qu'un rôle mineur sur la vitesse d'ouverture du cycle, contrairement à ce qui est observé lors de la transformation de dérivés cyclopropaniques en cations allyles, puisque dans ces cas, la stéréochimie joue un rôle prépondérant sur la vitesse de la réaction (6).

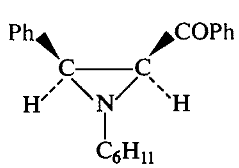

3*a cis*

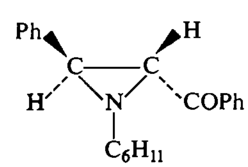

3*b trans*

2. *Influence du substituant de l'azote* (cas des aziridines)

Oehlschlager *et al.* ont montré que l'ouverture des *N*-arylaziridines **5** en ylures d'azométhine **6** à 110°C est favorisée par des substituants X et X′ électrodonneurs (2).

Pour notre part, nous avons montré que l'ouverture de l'aziridine est favorisée par substituant phényle comparé à un alkyle.

TABLEAU 1. Constantes cinétiques d'ordre 1 (k_1, 10^4 s^{-1}) et paramètres d'activation correspondant à l'ouverture thermique des aziridines **3** (solvant: toluène)

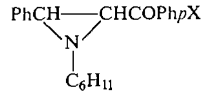

3

3: à l'exception de **3***a*, les substituants des carbones sont *trans*

		k_1 (10^4 s^{-1})							
N°	X	T:[b] 80,2	101,2	121,5	140	$\Delta H^{\ddagger a}$	log A_{ex}	$\Delta S^{\ddagger}$	$\Delta G^{\ddagger}$
3*a* (*cis*)	H	1,45	9,1	43,4	200	22	10,3	−14	28
3*b*	H	1,25	8,9	35,8	109,2	22,5	10,5	−13	27
3*c*	MeO	1,05	2,68	15,60	68,5	23,5	11	−11	27,5
3*d*	NO_2	3,16	15,7	57,2	156,1	19	8,6	−21	26,5

[a]Les $\Delta H^{\ddagger}$ sont exprimées en kcal mol^{-1} (précision ±1,5 kcal mol^{-1}) et les $\Delta S^{\ddagger}$ en unités d'entropie (précision ±5 ue).
[b]T, ±0,2°C.

TABLEAU 2. Constantes cinétiques d'ordre 1 (k_1, 10^4 s^{-1}) et paramètres d'activation correspondant à l'ouverture thermique des aziridines **2** (solvant: toluène)

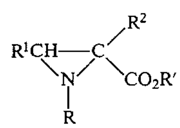

2

2 (R′ = Me sauf pour **2***b*, R′ = Et)

				k_1 (10^4 s^{-1})						
N°	R	R¹	R²	T:[a] 60	105	121,5	$\Delta H^{\ddagger b}$	log A_{ex}	$\Delta S^{\ddagger b}$	$\Delta G^{\ddagger}$
2*a*	C_6H_{11}	Ph	CO_2Me	—	—	6,35	[c]	[c]	[c]	[c]
2*b*	Ph	Ph	CO_2Et	2,9	34,0	100	17	7,5	−26	26,5
2*c*	Ph	CO_2Me	CO_2Me	0,25	4,3	10,3	17	7,00	−29	28
2*d*	*p*MeO Ph	H	CO_2Me				28,5[d]		−1,5	29
2*e*	*p*MeO Ph	H	CO_2Me	[d]	[d]	[d]	29,5[d]		+0,5	29

[a]T, ±0,2°C.
[b]Les $\Delta H^{\ddagger}$ sont mesurées à partir de constantes de vitesse déterminées en vitesse initiale (réf. 5); la précision est ±2 kcal mol^{-1}. Les $\Delta S^{\ddagger}$ sont obtenues avec précision de ±5 ue.
[c]Compte tenu de la difficulté à obtenir la constante de vitesse (réf. 5) nous avons renoncé à déterminer les paramètres d'activation.
[d]Ces aziridines ont été étudiées par Huisgen et Mader (3*a*), dans l'acétate d'éthyle. Les aziridines étudiées au cours de ce travail ont des $\Delta S^{\ddagger}$ largement négatives; ceci est dû en partie à une solvatation spécifique des aziridines dans les solvants aromatiques (1).

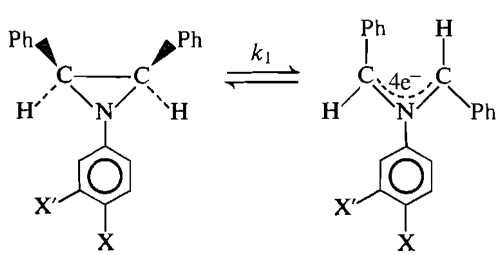

5 (*cis*) **6** (*trans*)

Ainsi à la température de 121,5°C, l'aziridine **2***b* dont l'azote est substitué par un phényle s'ouvre 16 fois plus vite (k_1 (**2***a*) = 6,35 × 10^{-4} s^{-1}; k_1 (**2***b*) = 100 × 10^{-4} s^{-1}) que l'aziridine **2***a* dont l'azote est substitué par un cyclohexyle.

Il en est de même pour l'ouverture des cyano-2 aziridines **1***i*, et **1***k*; la réaction électrocyclique est favorisée par un phényle

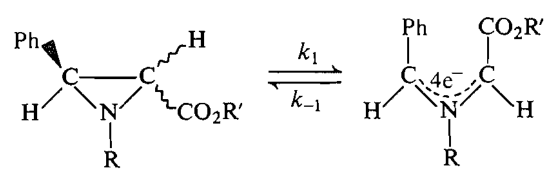

2*a*: R = C_6H_{11}; R′ = Me (*cis* par rapport au phényle)
2*b*: R = Ph; R′ = Et (*trans* par rapport au phényle)

comparé au cyclohexyle; ainsi à T = 121,5°C: k_1 (**1***i*) = 0,86 × 10^{-5} s^{-1} et k_1 (**1***k*) = 1,5 × 10^{-5} s^{-1}.

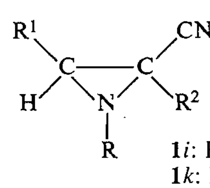

1*i*: R¹ = Me; R² = H; R = C_6H_{11}
1*k*: R¹ = H; R² = Me; R = Ph

TABLEAU 3. Constantes cinétiques d'ordre 1 (k_1, 10^4 s^{-1}) et paramètres d'activation correspondant à l'ouverture thermique des aziridines **1***a*, **1***i*, **1***j* et **1***h* (solvant: toluène)

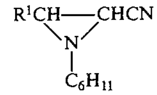

1

N°	R^1	k_1 (10^4 s^{-1}) T:[a] 120	130	140	160	$\Delta H^{\ddagger}$	$\log A_{ex}$	$\Delta S^{\ddagger}$	$\Delta G^{\ddagger}$
1*a*	Ph	2,92	7,3	12,5	44	27	11,6	−7	30
1*i*	Me	0,09	0,24	1,07	5,30	28	10,8	−11	33
1*j*	H	0,35	0,60	1,30	4,00	27,5	11,2	−10	32
1*h*	Me_2CH—	0,01	0,04	0,08	—	29	10,6	−12	34

[a] T, ±0,2°C.

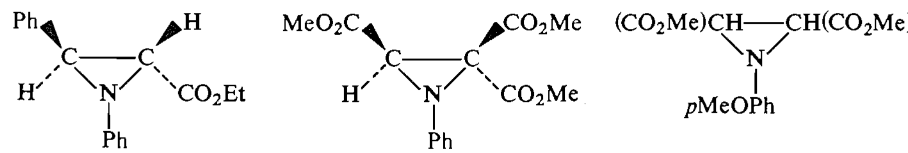

2*b* **2***c* **2***d cis* **2***e trans*

k_1 10^4 (s^{-1}), T = 120°C: 100,0 > 10,3 > 4,6 3,9

3. *Influence des substituants des carbones cycliques*

3.1. *Influence des groupements fonctionnels substituant le* C_2

Selon la littérature, la formation d'un ylure d'azométhine à partir d'une aziridine est favorisée par un groupement électro-attracteur activant, ester, cétone ou nitrile, substituant le(s) carbone(s) cyclique(s) (7). La comparaison de la vitesse d'ouverture des aziridines **1**, **2** et **3** substituées en 1 par un cyclohexyle et en 3 par un phényle montre que la constante k_1 suit l'aptitude du groupement fonctionnel à stabiliser une charge négative: À T = 121,5°C, dans le toluène, k_1 (**3***a*): $43{,}4 \times 10^{-4}$ s^{-1} > k_1 (**2***a*): $6{,}35 \times 10^{-4}$ s^{-1} > k_1 (**1***a*): $2{,}92 \times 10^4$ s^{-1}.

Si l'on considère les aziridines **3** dont le phényle lié au carbonyle est substitué en *para* par un groupement X, nous remarquons que l'effet du substituant X est modéré, mais lorsqu'il est électrodonneur, il ralentit l'ouverture, alors qu'il l'accélère quand il est électroattracteur, comme le montrent les résultats rassemblés dans le tableau 1.

Les paramètres d'activation correspondant à l'ouverture des aziridines **2** sont rassemblés dans le tableau 2. Ils montrent que le composé **2***c* s'ouvre plus facilement que les aziridines **2***d* et *e* étudiées par Huisgen *et al.* (3*c*), malgré la présence du méthoxy sur le phényle lié à l'azote. Il faut noter toutefois que l'aziridine **2***b* s'ouvre plus aisément que les composés **2***c* et **2***d*. À titre d'exemple, nous avons reporté ci-dessous les k_1 observées à T = 120°C.

3.2. *Substitution en position 3 par des groupements alkyles et aryles*

3.2.1. Dans une publication préliminaire, nous avons montré que l'ouverture thermique des cyano-2 aziridines en ylures d'azométhine est favorisée en remplaçant l'hydrogène en 3 par un phényle (1). Les résultats rassemblés dans le tableau 3 concernant les paramètres d'activation des aziridines **1***a*, *i*, *j* et *h*, montrent que la facilité de formation de l'ylure d'azométhine suit la séquence: R^1 = Ph > H > Me > Me_2CH. Ainsi, à la température de 120°C, la constante k_1 est divisée par environ un facteur 10 lorsque l'on remplace le phényle par un hydrogène et par un facteur 40 lorsque R^1 = Me. Toutefois, la variation de log k_1 en fonction des σ^* de Taft (8) n'est pas une relation linéaire.

3.2.2. *Cas des* N-*cyclohexyl-cyano-2* p*X phényl-3 aziridines*

Les résultats concernant l'ouverture d'une série de phényl-3 aziridines **1** dont le phényle est substitué en *para* par un groupement X (Me_2N—, MeO—, H, Cl, Br, CN, NO_2) sont rassemblés dans le tableau 4.

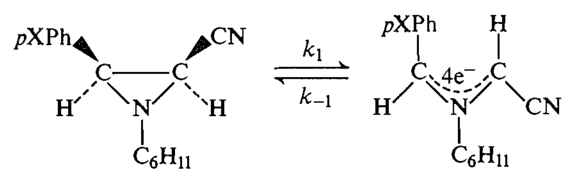

Contrairement à ce qui était attendu, la réaction électrocyclique est favorisée par un substituant X électrodonneur et défavorisée par un groupement X électroattracteur. Si l'on prend la constante de vitesse d'ouverture de l'aziridine **1***a* (X = H) égale à l'unité, nous obtenons les valeurs relatives suivantes (T = 121,5°C, solvant: toluène): k_1^{rel} (X = H) = 1,00; Me_2N— = 4,41; MeO— = 1,97; Cl = 0,95; Br = 0,94; C≡N = 0,89; NO_2 = 0,86.

L'influence du substituant X est donc modérée, mais elle est l'inverse de celle observée avec les aroyl aziridines dont le phényle lié au carbonyle est substitué en *para*. La figure 1 représentant log k_1 en fonction des σ de Hammett (8) montre que les substituants ayant un σ positif sont correctement alignés (ρ = −0,08); le diméthylamino et le méthoxy sont également alignés avec H, mais la droite n'a pas la même pente (ρ = −0,38).

3.2.3. *Cas des dicyano-2,2 phényl-3 époxydes* **4**

Les résultats relatifs à l'ouverture thermique des époxydes **4** en ylures de carbonyle correspondants sont rassemblés dans le tableau 5.

Ils sont analogues à ceux obtenus avec les aziridines **1**;

TABLEAU 4. Constantes cinétiques d'ordre 1 (k_1, 10^5 s^{-1}) et paramètres d'activation correspondant à l'ouverture des *N*-cyclohexy, cyano-2, *p*X phenyl-3, aziridines (solvant: toluène)

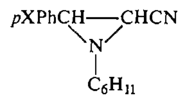

1

N°	X	k_1 (10^5 s^{-1}) T:[a] 81	121,5	130	140	$\Delta H^{\ddagger}$	log A_{ex}	$\Delta S^{\ddagger}$	$\Delta G^{\ddagger}$
1*a*	H	0,5	29,5	73	125	27	11,6	−7	30
1*b*	Cl	0,2	27,8	—	101	27	11,5	−8	30
1*c*	MeO[b]	1,0	57,5	—	165	24[b]	10,3[b]	−14[b]	29,0[b]
1*d*	NO_2	0,08	25,1	—	101	27	12	−7	30,5
1*e*	CN	0,5	26,2	—	—	27	12	−7	30,5
1*f*	Me_2N	9,3	129	210,7	—	16,5	6,7	−30	28

[a] T, ±0,2°C.

[b] Lorsque la réaction est effectuée dans le CCl_4, les paramètres d'activation deviennent: $\Delta H^{\ddagger} = 25$ kcal mol^{-1}; log $A_{ex} = 12$; $\Delta S^{\ddagger} = -7$ ue et $\Delta G^{\ddagger} = +27$ kcal mol^{-1}.

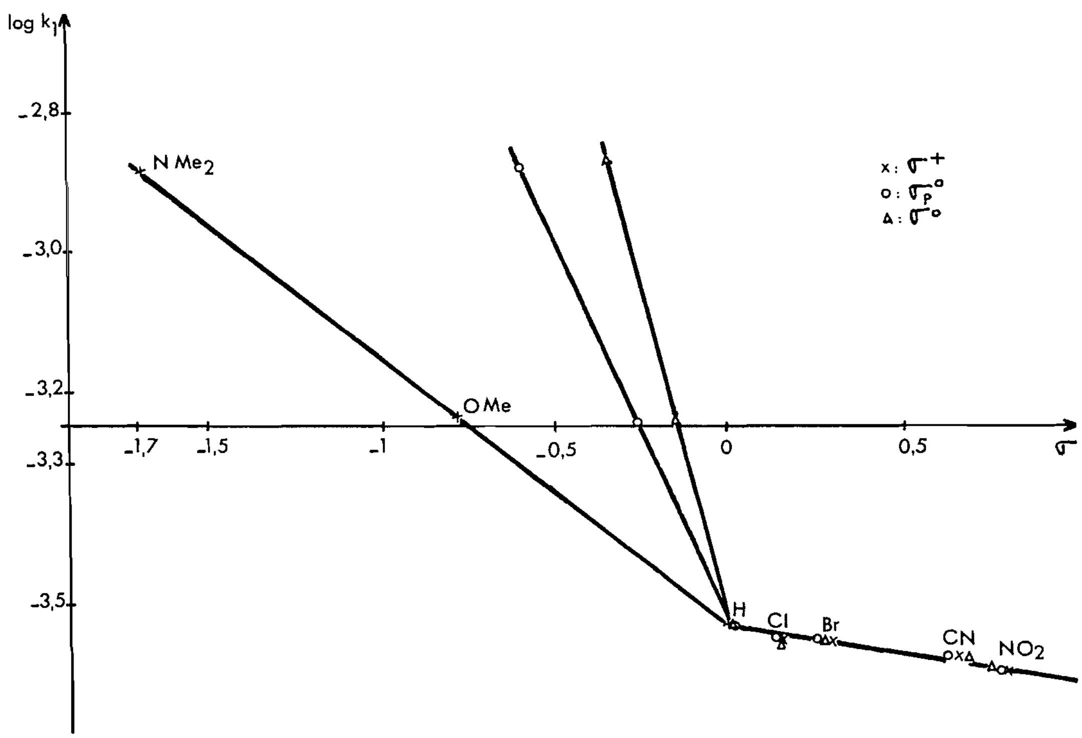

FIG. 1. Variations de log k_1 en fonction des σ de Hammett dans les cas des aziridines **1**; T = 121,5°C.

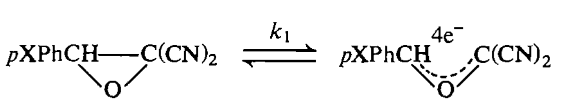

4

l'ouverture est favorisée par un substituant X électrodonneur tel que MeO et défavorisée par un substituant électroattracteur: k_1^{rel} (T = 121,5°C, solvant: CCl_4) H = 1,00; MeO = 4,00; Cl = 0,91; NO_2 = 0,70.

3.2.4. *Paramètres d'activation*

Si nous considérons l'ensemble des paramètres d'activation obtenus pour l'ouverture d'aziridines diversement substituées (tableaux 1−5), nous remarquons que l'enthalpie d'activation $\Delta H^{\ddagger}$ varie en sens inverse du facteur de fréquence log A_{ex} qui est relié simplement au $\Delta S^{\ddagger}$. Plus l'ouverture de l'aziridine est facile (cas de l'aziridine **2***b* par rapport à **1***a* ou **3***a*) et moins la constante de vitesse est dépendante de la température, ce qui se traduit par un facteur de fréquence log A_{ex} faible et par voie de conséquence un $\Delta S^{\ddagger}$ largement négatif.

Les valeurs largement négatives des $\Delta S^{\ddagger}$ peuvent paraître surprenantes. Toutefois, il faut remarquer que la faible évolution des constantes de vitesse (pour une série donnée, le $\Delta G^{\ddagger}$ varie peu) est dûe à la compensation de l'entropie d'activation.

Ce phénomène semble être une caractéristique des réactions unimoléculaires puisque une évolution analogue des $\Delta H^{\ddagger}$ et log A_{ex} a été observée lors d'isomérisations unimoléculaires effectuées en phase gazeuse (9).

De plus, il a été montré à l'aide de la rmn (résonance ma-

TABLEAU 5. Constantes cinétiques d'ordre 1 (k_1) d'ouverture des époxydes **4** dont le phényle est substitué en *para* par X; solvant: CCl_4; T = 121,5 ± 0,2°C

	X			
	MeO	H	Cl	NO_2
k_1	76,7	19,2	17,5	13,6
$\log k_1$	−3,12	−3,72	−3,76	−3,87

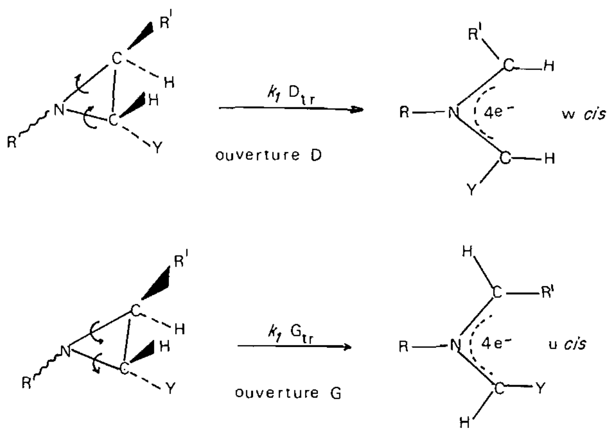

SCHÉMA 1. Ouverture conrotatoire d'une aziridine *trans*.

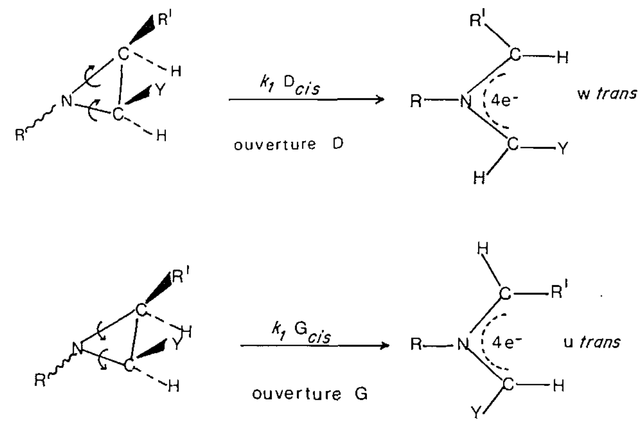

SCHÉMA 2. Ouverture conrotatoire d'une aziridine *cis*.

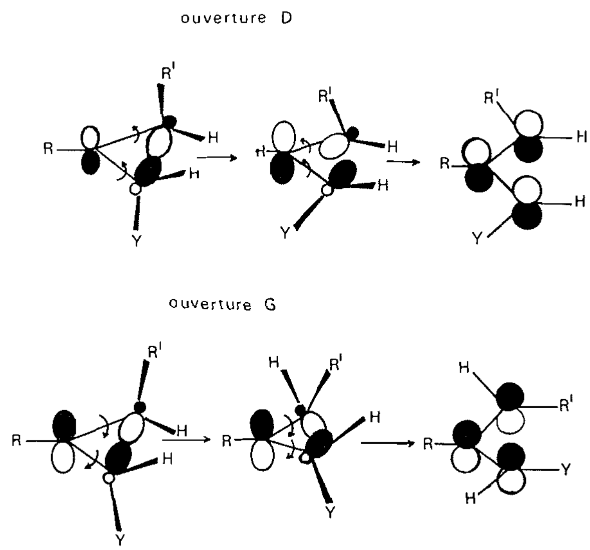

SCHÉMA 3. Interactions orbitalaires lors de l'ouverture conrotatoire d'une aziridine avec azote plan.

gnétique nucléaire) que si une aziridine est dissoute dans un solvant benzénique, le noyau aromatique a tendance à se placer le plus loin possible du doublet de l'azote (10). C'est pourquoi il a été envisagé une interaction spécifique entre les OF du solvant aromatique et l'OM σ^*_{C-C} destinée à se rompre (1). La solvatation spécifique des aziridines dans le toluène est donc en partie à l'origine des $\Delta S^{\ddagger}$ largement négatifs (11).[2] En effet, les paramètres d'activation de l'aziridine **1***c* mesurés dans le CCl_4 sont plus classiques (tableau 4, note de base de tableau), le $\Delta S^{\ddagger}$ est moins négatif; dans un tel solvant, il n'y a pas de solvatation spécifique.

Discussion

1. *Influence de la stéréochimie des aziridines*

L'ouverture conrotatoire d'une aziridine peut se faire, "a priori", de deux manières (droite ou gauche) conduisant ainsi à deux configurations *U* et *W* de l'ylure d'azométhine correspondant, selon les schémas 1 et 2.

La constante de vitesse d'ouverture d'une aziridine de stéréochimie donnée est la somme des constantes de vitesse de formation des deux configurations de l'ylure d'azométhine correspondant:

$$k_1\ (\text{Az. }trans) = k_1\ (\text{D }tr) + k_1\ (\text{G }tr)$$
$$k_1\ (\text{Az. }cis) = k_1\ (\text{D }cis) + k_1\ (\text{G }cis)$$

Ces différentes configurations *U* et *W* n'étant pas détectables par l'expérience, les mesures expérimentales ne peuvent distinguer k_1 (D) et k_1 (G).

D'après nos résultats et ceux de Huisgen *et al.* (3*c*), k_1 (Az. *trans*) ≃ k_1 (Az. *cis*). Un raisonnement basé sur la minimisation des contraintes stériques dans l'ylure formé (12) permet de montrer que le mode d'ouverture le plus facile est celui qui conduit à l'ylure *W cis*

$$k_1\ (\text{D }trans) > k_1\ (\text{D }cis) \text{ ou } k_1\ (\text{G }cis)$$

Cependant, la stéréochimie de l'ouverture des cations et anions cyclopropyles n'est pas gouvernée par des interactions stériques, mais par les propriétés des orbitales (13). Lors de la solvolyse des dérivés cyclopropaniques, des deux modes d'ouverture disrotatoires possibles "a priori", un seul a lieu effectivement: il correspond à celui pour lequel l'énergie de relaxation est la plus grande en valeur absolue (4).

L'explication de la formation préférentielle d'un ylure d'azométhine à l'aide des interactions stériques ne tient que dans la mesure où les interactions orbitalaires pour les deux modes d'ouvertures, D ou G, sont équivalentes. Ceci serait toujours vérifié quels que soient les substituants portés par les carbones de l'aziridine, si l'azote était plan dans l'état de transition. Quel que soit le mode d'ouverture conrotatoire D ou G, l'énergie de relaxation dûe au transfert de charge P→ σ^*_{C-C} serait la même (voir schéma 3). Si on se limite aux interactions entre les

[2] Le changement de solvant aromatique entraîne une modification des paramètres d'activation de l'aziridine **1***a*: ainsi, le remplacement du toluène par le nitrobenzène entraîne une diminution du $\Delta H^{\ddagger}$ (de 27 à 24,5 kcal mol^{-1}) et une diminution du $\Delta S^{\ddagger}$ (de −7 à −14 ue). Ces résultats sont en accord avec la règle générale; lorsque $\Delta H^{\ddagger}$ décroît, $\Delta S^{\ddagger}$ décroît algébriquement.

TABLEAU 6. Charges totales sur les atomes de l'ylure d'azométhine non substitué

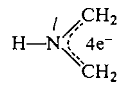

l (Å)	q_C	q_N
1,24	−0,246	+0,288
1,26	−0,243	+0,266
1,28	−0,239	+0,251
1,30	−0,236	+0,222
1,32	−0,231	+0,222

orbitales frontières, cette énergie est représentée par l'équation [1] (4):

$$[1] \quad \Delta E = \frac{H^2_{\mathrm{HO-BV}}}{E_{\mathrm{HO}} - E_{\mathrm{BV}}}$$

Elle serait la même pour les deux modes d'ouverture.

Toutefois, comme l'ont montré les calculs *ab initio* effectués sur l'ouverture de l'anion cyclopropyle (14) ainsi que les calculs MINDO effectués sur l'ouverture d'une aziridine (15), l'azote ne doit pas être plan dans l'état de transition et le doublet P n'est pas symétrique. Ceci entraîne que les interactions orbitalaires ne sont pas équivalentes des deux côtés du plan du cycle en train de s'ouvrir. Ce raisonnement implique que pour des aziridines dissymétriques, l'un des deux modes d'ouverture conrotatoire doit être privilégié (16).

2. *Influence des substituants*

Le concept de stablisation de charges partielles ne permet pas d'expliquer la stéréochimie de l'ouverture électrocyclique et nous ne pensons pas qu'il puisse expliquer les effets des substituants observés. En effet, il faudrait admettre que dans l'état de transition il se développe une charge partielle positive sur le carbone 3. Or les calculs CNDO/2 effectués sur les ylures d'azométhine montrent que lors de l'ouverture de l'aziridine, l'azote initialement négatif devient positif alors que les carbones initialement positifs deviennent négatifs (voir partie expérimentale et tableau 6).

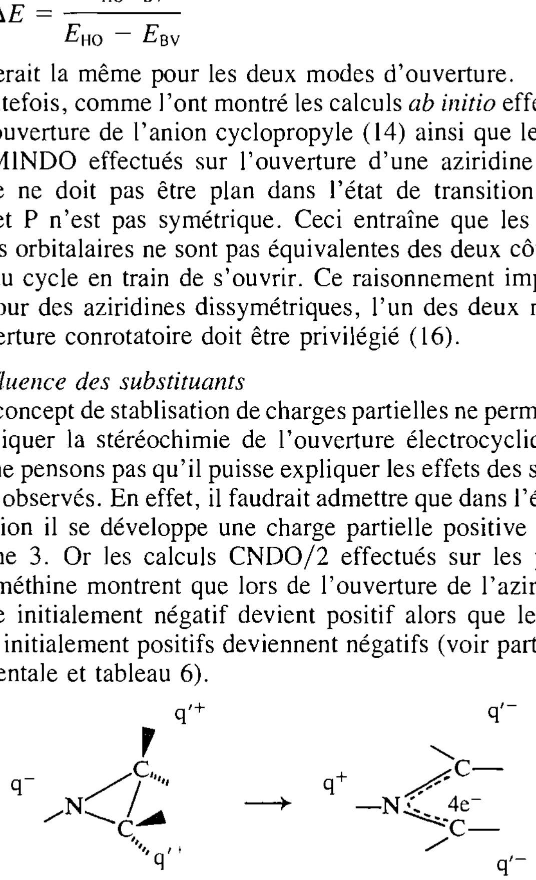

Compte tenu du fait que l'équilibre aziridine ⇌ ylure d'azométhine ou époxyde ⇌ ylure de carbonyle est considérablement déplacé vers l'hétérocycle fermé, selon le principe de Hammond, l'état de transition doit avoir une structure proche du dipôle-1,3 final. Des calculs *ab initio* effectués sur l'ouverture de l'anion cyclopropyle ont montré qu'il en devait être ainsi, tout au moins pour les longueurs de liaison (14).

Si l'on admet que la force motrice de la réaction est le transfert de charge du doublet de l'hétéroatome sur l'OM σ^*_{C-C} et que la réactivité est correctement interprétée par la théorie des relaxations, l'ouverture est d'autant plus aisée que l'énergie de relaxation (4) est grande en valeur absolue (éq. [1]).

2.1. *Substituants en position 1*

Dans des séries distinctes d'hétérocycles (aziridines et époxydes) ou dans des séries d'hétérocycles portant les mêmes

4*a*

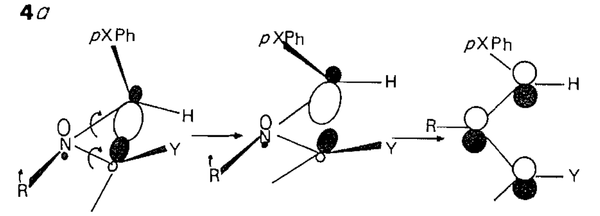

4*b*

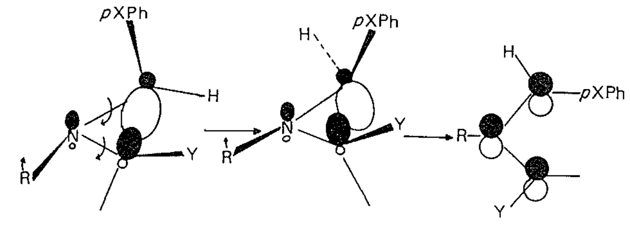

SCHÉMA 4. Interactions orbitalaires lors de l'ouverture conrotatoire d'une aziridine. État de transition.

substituants sur les carbones, la différence d'énergie entre le doublet de l'hétéroatome et l'OM σ^*_{C-C} destinée à se rompre, gouverne l'aptitude à l'ouverture.

La réactivité comparée des aziridines et époxydes a été discutée précédemment (1, 4) et nos résultats sont en accord avec le fait qu'à substituants identiques sur les carbones, les aziridines s'ouvrent plus aisément que les époxydes (17, 18). L'énergie du doublet de l'oxygène est plus basse que celle du doublet de l'azote (19), ce qui entraîne un transfert de charge du doublet P sur l'OM σ^*_{C-C} plus important dans le cas des aziridines.

L'influence des substituants donneurs sur le phényle lié à l'azote des aziridines **5** a été expliquée de la même manière (4).

La plus grande réactivité des aziridines *N*-phényles par rapport aux aziridines *N*-alkyles observée expérimentalement s'explique par la méthode des relaxations, puisque l'énergie d'interaction du doublet P avec l'OM σ^* est la plus grande lorsque le substituant de l'azote est un phényle.[3]

La facilité d'ouverture du cycle suit la facilité d'inversion de l'azote; en effet, la barrière d'inversion est plus faible dans le cas d'une aziridine *N*-phényle que dans le cas des aziridines *N*-alkyles; la différence est de l'ordre de 5 kcal mol^{-1} (20).

2.2. *Substituants en 2 et 3*

L'examen des tableaux montre que l'ouverture de la liaison C—C est facilitée par une substitution dissymétrique des carbones 2 et 3. Parmi les aziridines étudiées, **2***b* est la plus réactive. Puisque l'influence des substituants sur l'énergie des OM est additive en première approximation, ceci indique que dans une série d'hétérocycles de structures peu différentes, lorsque l'on passe d'un composé à l'autre, la variation du numérateur de l'équation [1] l'emporte sur celle du dénominateur. En effet, si la réactivité péricyclique était gouvernée uniquement par la différence d'énergie entre le doublet P et l'OM σ^*_{C-C}, la réactivité de **2***b* devrait se situer entre celle de **2***e* et **5**.

Cela n'a de sens que si l'on admet que l'azote qui passe de la forme pyramidale à la forme plane n'est pas encore plan dans l'état de transition (schéma 4).[4]

[3] O. Henri-Rousseau et N. Nafi. Communication personnelle.

[4] Dans le cas des époxydes, l'un des doublets joue le rôle du doublet de l'azote alors que l'autre joue le rôle de la liaison N—R.

Lorsque les substituants des carbones sont différents, l'OM σ^* est alors polarisée et les coefficients C_2 et C_3 sont d'autant plus différents que l'on a d'une part un substituant électro-attracteur et d'autre part un substituant électrodonneur (effet "push–pull"). Dans ces conditions, quel que soit le mode d'ouverture conrotatoire privilégié *a* ou *b*, plus l'OM est dissymétrique et plus H^2_{HO-BV} est important et plus l'ouverture est aisée.

La séquence de réactivité des aziridines **1***a*, **2***a* et **3***a* suit l'augmentation de la polarisation de l'OM σ^* due au substituant Y. L'influence des substituants X sur la polarisation de cette OM permet de comprendre la réactivité des aziridines et des époxydes dont le phényle en 3 est substitué: plus X est donneur et plus la dissymétrie de l'OM σ^* augmente entrainant un accroissement de l'hamiltonien d'interaction H^2_{HO-BV}. Dans les composés **1** et **4**, les substitants X ont deux effets antagonistes: (*i*) un substituant électrodonneur, en relevant l'énergie de l'OM σ^*, défavorise le transfert de charge $P_N \rightarrow \sigma^*_{C-C}$; (*ii*) ce même substituant en augmentant la dissymétrie de l'OM σ^* favorise la réaction. L'antagonisme des deux effets pourrait expliquer que l'influence des substituants X est globalement faible, mais nos résultats expérimentaux indiquent que l'influence d'un tel substituant sur la dissymétrie (numérateur de l'équation [1]) l'emporte sur la variation du niveau d'énergie (dénominateur de l'équation [1]).

Dans les composés **3**, X substitue le phényle lié au carbonyle et, dans ces conditions, les deux effets vont dans le même sens; ainsi, le groupement NO_2 abaisse l'énergie de l'OM σ^* et accroit la polarisation de cette OM, favorisant la réaction électrocyclique.

L'influence d'un méthyle en 3 comparé à un hydrogène (cas des aziridines **1***i*, R = Me, et **1***j*, R = H) s'explique de la même manière. Un carbone sp^3 étant plus électronégatif que l'hydrogène, le méthyle compense partiellement l'influence du nitrile sur la dissymétrie de l'OM σ^*_{C-C} et de ce fait diminue la vitesse d'ouverture, par rapport à l'hydrogène.

Nos résultats semblent en accord avec les prévisions d'Épiotis qui, dans une approche théorique différente, prévoyait une augmentation de la réactivité péricyclique avec l'augmentation de la polarité de l'état de transition (21).

Le raisonnement qui précède permet de comprendre l'ouverture aisée des hétérocycles **7**, **9** et **11**. L'effet $-I$ des substituants en 2 et 3, en abaissant l'énergie de l'OM σ^* et la forte dissymétrie de cette OM due à l'effet "push–pull" des substituants +M en 3 et −M en 2, favorise le transfert de charge $P_N \rightarrow \sigma^*_{C-C}$ et, partant, l'ouverture du cycle.

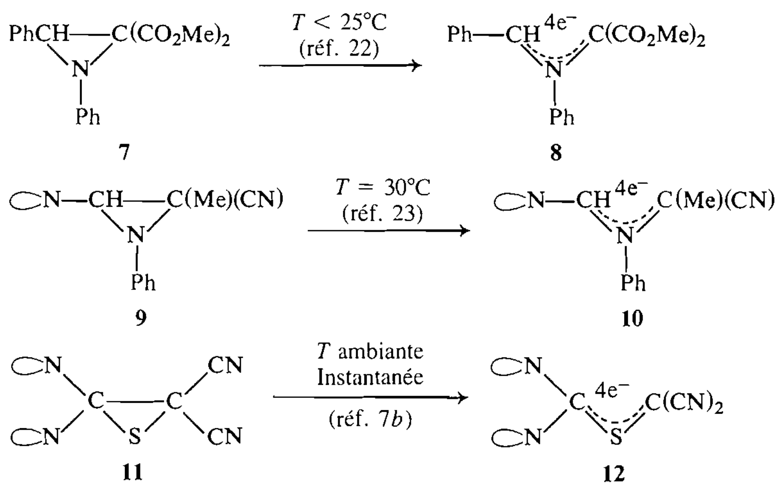

D'après ce travail, on peut prévoir que quand deux aziridines portent des substituants identiques, celle qui présente la plus grande dissymetrie doit donner plus aisément l'ylure d'azométhine correspondant.

En conclusion, cette étude permet de dégager les points essentiels suivants: (*i*) la configuration relative des carbones cycliques a peu d'influence sur la vitesse d'ouverture électrocyclique des aziridines; (*ii*) l'ouverture est globalement favorisée par des substituants qui rapprochent les niveaux d'énergie du doublet P d'une part et de l'OM σ^*_{C-C} d'autre part. Toutefois, la dissymétrie de substitution des carbones 2 et 3 joue un rôle important; au fur et à mesure qu'elle croit, la vitesse d'ouverture augmente.

Partie expérimentale

1. *Détermination des constantes de vitesse* k_i

Les constantes cinétiques concernant l'ouverture électrocyclique des composés **1**, **2**, **3** et **4** étudiées au cours de ce travail sont déterminées en suivant la disparition de l'hétérocycle au cours de la réaction d'addition à l'ACDM. Le dosage des cyano-2 aziridines **1** est effectué à l'aide de l'ir (disparition de la bande $\nu_{C\equiv N}$ vers 2240 cm^{-1}) et celui des autres composés, à l'aide de la chromatographie en phase liquide selon le mode opératoire décrit dans un mémoire précédent (5).

2. *Détermination des paramètres d'activation*

Les paramètres d'activation, $\Delta E^{\ddagger}$, $\Delta H^{\ddagger}$, $\Delta S^{\ddagger}$ et $\Delta G^{\ddagger}$ sont déterminés à l'aide de méthodes standard (9), après avoir mesuré la constante de vitesse d'ouverture k_1 à, *au moins*, 5 températures différentes.

La pente de la droite (coefficient de corrélation r = 0,996), représentant le log k_1 en fonction de $1/T$, permet de calculer l'énergie d'activation $\Delta E^{\ddagger}$. L'ordonnée à l'origine correspond à log A_{ex}.

Compte tenu des diverses gammes de température étudiées en fonction des substituants du cycle, le $\Delta H^{\ddagger}$ est calculé, dans chaque cas, à la température moyenne, alors que le $\Delta S^{\ddagger}$ est toujours calculé pour T = 100°C. Dans les tableaux, nous n'avons reporté que les constantes de vitesse obtenues aux mêmes températures, dans une série donnée. Les résultats rassemblés dans les tableaux sont donnés avec un pourcentage de confiance de 90%.

3. *Calculs CNDO/2*

Les calculs CNDO/2 ont été effectués sur les aziridines **7** et **8** en considérant les angles du cycle égaux à 60°, l'azote étant pyramidal et les longueurs de liaison C—N = 1,487 Å, C—C = 1,509 Å. Les valeurs des charges ainsi obtenues sont reportées ci-dessous.

La géométrie des ylures d'azométhine n'étant pas connue, les angles de liaison sont pris égaux à 120° pour les carbones terminaux du dipôle et de l'azote central.

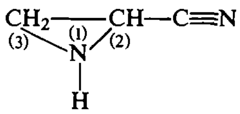

7

$q_1 = -0{,}157$
$q_2 = +0{,}04$
$q_3 = +0{,}016$

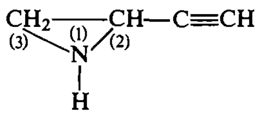

8

$q_1 = -0{,}163$
$q_2 = +0{,}065$
$q_3 = +0{,}007$

Les calculs rassemblés dans le tableau 6 ont été effectués sur l'ylure d'azométhine non substitué pour diverses longueurs de la liaison C—N; ils montrent que les charges évoluent peu.

Les calculs CNDO/2 concernant les ylures d'azométhine résultant de l'ouverture des aziridines **2*b*** nous ont été aimablement communiqués par Monsieur le Professeur R. Carrié (Université de Rennes) que nous remercions vivement.

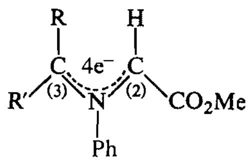

R = Ph R′ = H, $q_2 = -0{,}264$ $q_3 = -0{,}061$
R = H R′ = Ph, $q_2 = 0{,}245$ $q_3 = -0{,}073$

1. A. DERDOUR et F. TEXIER. C.R. Acad. Sci. Sér. C, **291**, 101 (1980).
2. A. C. OEHESCHLAGER, A. S. YIM et M. H. AKHTAR. Can. J. Chem. **56**, 273 (1978).
3. (*a*) R. HUISGEN et H. MADER. J. Am. Chem. Soc. **93**, 1777 (1971); (*b*) R. HUISGEN. Angew. Chem. Int. Ed. Engl. **16**, 572 (1977); (*c*) R. HUISGEN, W. SCHEER et H. MADER. Angew. Chem. Int. Ed. Engl. **8**, 602 (1969).
4. O. HENRI-ROUSSEAU, P. PUJOL et F. TEXIER. Bull. Soc. Chim. Fr. II, 496 (1980).
5. A. DERDOUR et F. TEXIER. Can. J. Chem. **63**, 2245 (1985).
6. T. S. SORENSEN et A. RAUK. Pericyclic reactions. Vol. 2. 1ère éd. *Édite par* A. P. Marchand et R. E. Lehr. Academic Press, New York. 1977. p. 1.
7. (*a*) J. W. LOWN. Rec. Chem. Prog. **32**, 51 (1971); (*b*) R. M. KELLOGG. Tetrahedron, **32**, 2165 (1976).
8. L. H. HAMMETT. Physical organic chemistry. *Dans* Series in advanced chemistry. McGraw–Hill, New York. 1970. p. 347.
9. S. N. BENSON. The foundations of chemical kinetics. *Dans* Series in advanced chemistry. McGraw–Hill, New York. 1960. p. 252.
10. T. YONEZAIRE, I. MORISHIMA et K. FUKUTA. Bull. Soc. Chim. Jpn. **41**, 2297 (1968).
11. A. DERDOUR. Thèse, Oran. 1982.
12. R. HUISGEN et H. MADER. Angew. Chem. Int. Ed. Engl. **8**, 604 (1969).
13. (*a*) R. B. WOODWARD et R. HOFFMANN. The conservation of orbital symmetry. Verlag Chemie, Berlin. 1970; (*b*) NGUYEN TRONG ANH. Les règles de Woodward et Hoffmann. Ediscience, Paris. 1970.
14. P. MERLET, S. PEYERIMHOFF, R. BUENKER et S. SHIH. J. Am. Chem. Soc. **96**, 959 (1974).
15. J. SAUER. Tetrahedron, **35**, 2109 (1979).
16. A. DERDOUR et F. TEXIER. C.R. Acad. Sci. Sér. C, **296**, 553 (1983).
17. R. HUISGEN, W. SCHEER, G. SZEIMIES et H. HUBER. Tetrahedron Lett. 397 (1966).
18. V. MARKOWSKI et R. HUISGEN. Chem. Commun. 439 (1977).
19. W. JORGENSEN et L. SALEM. The organic chemist's book of orbitals. Academic Press, New York. 1973. pp. 156 et 159.
20. J. L. PIERRE, P. BARET et P. ARNAUD. Bull. Soc. Chim. Fr. 3619 (1971).
21. N. D. EPIOTIS. Angew. Chem. Int. Ed. Engl. **13**, 751 (1974).
22. F. TEXIER et R. CARRIÉ. Bull. Soc. Chim. Fr. 310 (1974).
23. F. TEXIER et J. BOURGOIS. J. Heterocycl. Chem. **12**, 505 (1975).

Design and reactivity of organic functional groups—utility of imidazolylsulfonates in the synthesis of monobactams and 3-amino nocardicinic acid[1]

STEPHEN HANESSIAN,[2] CLAUDE COUTURE, AND HEINZ WYSS
Department of Chemistry, Université de Montréal, Montréal (Qué.), Canada H3C 3V1

Received May 30, 1985

STEPHEN HANESSIAN, CLAUDE COUTURE, and HEINZ WYSS. Can. J. Chem. **63**, 3613 (1985).

The imidazolylsulfonate group has been found to be a versatile leaving group in the intramolecular cyclization of *p*-methoxyphenyl amides and related derivatives of *N*-substituted L-serine to give the corresponding β-lactams.

STEPHEN HANESSIAN, CLAUDE COUTURE et HEINZ WYSS. Can. J. Chem. **63**, 3613 (1985).

Le groupement imidazolylsulfonate est un excellent groupe partant dans des réactions de cyclisation intramoléculaire des *p*-méthoxyphényle amides et d'autres dérivés de la L-sérine. Les produits de cyclisation sont les β-lactames correspondants.

Since the emergence of the monobactam family of monocyclic β-lactam antibiotics (1, 2) much effort has been devoted to their total synthesis (3–5), particularly since they have demonstrated potent antibacterial activity and high stability toward β-lactamases (6). Several reports have also been concerned with the synthesis of 2-oxo-azetidines (7), 4-substituted-2-azetidinones (8), 2-amino-4-substituted-2-azetidinones (9), and related compounds (10). The same monocyclic β-lactam system occurs also in the structure of the nocardicin group of antibiotics (11). Several elegant syntheses of this class of natural products and their components in optically active (12, 13) and racemic forms (14) have been reported. Some relevant structures are shown in Scheme 1. New types of 3-amino-2-azetidinones are continually being discovered from fermentation sources (15). We recently reported the total and stereocontrolled synthesis of 4-substituted 3-amino-2-azetidinones (16), which are known to be immediate precursors to potent antibotics in this series (9).

As already discussed (1, 2), a practical access to the monobactams in general could take advantage of the chiron approach (17) utilizing *N*-substituted L-serine or related amino acid derivatives as templates. A high degree of convergence in functionality and sense of chirality can thus be achieved with the intended target while utilizing the same number of required carbon atoms (Scheme 2). Ring closure by intramolecular attack of the amine nitrogen with a suitable leaving group on the hydroxyl terminus, as previously demonstrated for β-halopropionamides (7) or related derivatives (3–5), would complete the task of assembling the diminutive yet important synthetic intermediate. In spite of the seemingly trivial nature of this exercise, it should be noted that racemization, elimination, and intramolecular reactions could effectively compete with ring closure (5) and loom as major threats to such a strategy.

Most of the current syntheses of monobactams rely on using an *N*-alkoxy hydroxamate or *N*-sulfonic acid derivative, in which the NH is significantly acidic, hence more reactive in the internal displacement reaction (4).

We wish to report an exceptionally mild and efficient ring closure reaction of *N*-substituted serine amides, based on a novel activation of the hydroxyl group as the imidazolylsulfonate (imidazylate) (18; for a preliminary announcement of a portion of this work, see also ref. 19). This method leads to the efficient syntheses of (*S*)-3-amino-2-azetidinone and 3-amino nocardicinic acid. Thus, treatment of *N*-[(benzyloxy)-carbonyl]-L-serine *p*-(methoxyphenyl) amide **2***a* or the corresponding N-Boc derivative **2***b* with *N*,*N*-sulfuryl diimidazole (20) in DMF, and adding sodium hydride at −40°C, resulted in sequential *O*-imidazolysulfonylation and ring closure to give the crystalline azetidinones **3***a* and **3***b* in 70 and 85% yields, respectively, isolated by direct crystallization (Scheme 3). Bose and co-workers (5) have reported the successful application of the Mitsunobu reaction (21) to the toluidide derived from *N*-benzyloxycarbonyl L-serine, and the isolation of a β-lactam in 53% yield. Cleavage of the *p*-anisyl group with ceric ammonium nitrate (22) led to the known crystalline azetidinone derivatives **4***a* and **4***b*, respectively, in 70% yield. The isolation of these compounds in good yields indicates that the internal cyclization via the imidazolylsulfonates (Scheme 3) proceeded without racemization, elimination, or aziridine formation (5). The transformation of **4***a* and **4***b* into biologically active monobactams has been described elsewhere (3). Application of the same reaction conditions to the L-threonine series (Scheme 4) gave a poor yield of the expected cyclization product, with aziridine formation being prevalent. Since the imidazolylsulfonate is known to be an excellent leaving group in displacement reactions of secondary alcohols (18), it is likely that aziridine formation in the L-threonine derivatives is the result of the prevalence of a particular conformation in solution that favors attack by the carbamate nitrogen. Related examples can also be encountered in other work (5).

We then turned our attention to the prospects of utilizing the *O*-imidazolylsulfonyl group in the intramolecular cyclization of a precursor to 3-amino nocardicinic acid (Scheme 5). Thus, *N*-phthalimido L-serine **5** (23) was converted into the corresponding dipeptide derivative **6** (24) and the latter was subjected to ring closure via the imidazylate procedure. Under conditions that led to smooth cyclization, in the case of **2***a* or **2***b*, little if any reaction took place. However, gradual warming of the reaction mixture to 0°C led to the expected cyclization to give the diastereomeric β-lactams **8** and **9** (1 : 1) in 46% yield. It was found that simple treatment of **6** with fluoride ion in the presence of *N*,*N*-sulfuryl diimidazole resulted in the desired ring closure to give **8** and **9** in 63% yield as a 1 : 1 mixture of diastereomers. Thus, even though the conditions for cyclization were extremely mild and essentially neutral, considerable epimerization had occurred at the highly susceptible benzylic carbon, which is not unexpected in this series (13*b*). Again, little if any β-elimination was observed, in contrast to the results of the Mitsunobu reaction under some conditions

[1] Presented in part at the Xth European Symposium on Heterocyclic Chemistry, Kaiserslautern, Germany, Oct. 2–4, 1984. See also ref. 19.

[2] Author to whom correspondence may be addressed.

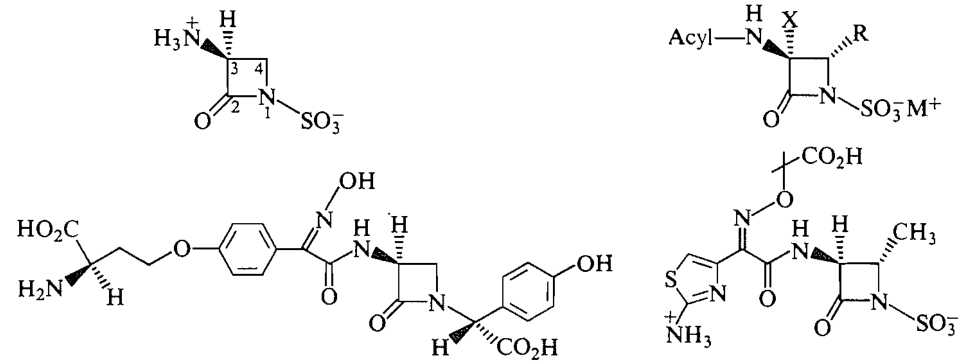

Nocardicin A

Azthreonam
(SQ 26,776)

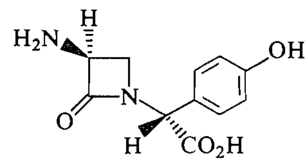

Amino nocardicinic acid

SCHEME 1

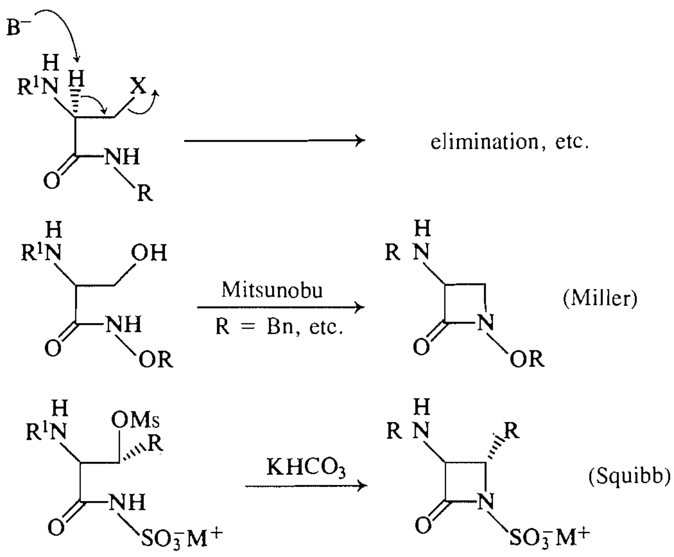

SCHEME 2

(13*b*). It should be noted, however, that Townsend and Nguyen had succeeded in considerably improving the ratio of **8** and **9** by utilizing tri-n-butylphosphine in the Mitsunobu reaction (13*b*). Catalytic debenzylation of the mixture of **8** and **9** led to **10** and **11**, from which the desired natural isomer **10** could be separated by direct fractional crystallization. The mother liquors were subjected to repeated equilibration in the presence of triethylamine to give **10** in 67% yield. The final mother liquors consisted of a 1:2 mixture of **10** and **11**, respectively. The overall yield of **10** from *N*-phthalimido L-serine **5** was ~33%. The conversion of **10** into (−)-3-amino nocardicinic acid by sequential deprotection has been previously described (13*a*).

Experimental

Melting points are uncorrected. Optical rotations were measured on a Perkin–Elmer automatic spectropolarimeter model 141. The ^{1}H nmr spectra were recorded on Bruker WH 900 and 400 MHz instruments with tetramethylsilane as internal standard in deuteriochloroform as solvent. Mass spectra were recorded on a VG 1212 low resolution mass spectrometer by the direct chemical ionization technique (DCI). Column chromatography was done by the flash technique. EDAC.HCl is the abbreviation for 1-ethyl-3-(3-dimethylaminopropyl) carbodiimide hydrochloride.

N-*Benzyloxycarbonyl* L-*serine* (N-p-*methoxyphenyl)amide* (**2**a)

To a solution of **1***a* (1.5 g, 6.28 mmol) in 8 mL of THF were added, in succession, 960 mg (1.1 equiv.) of 1-ethyl-3-(3-dimethylaminopropyl) carbodiimide hydrochloride (EDAC.HCl) (25) in 8 mL of dichloromethane. The solution was stirred for 1 h, the solvents were evaporated, and the residue was suspended in ethyl acetate. Washing with dilute aqueous hydrochloric acid, aqueous sodium bicarbonate, then water, and processing the organic phase in the usual manner gave a colorless solid. Trituration with a mixture of ethyl acetate and hexanes (1:1) gave 1.79 g (83%) of the title compound, which was used as such in the next step. Recrystallization of a portion from ethyl acetate gave an analytical sample, mp 146–147°C; $[\alpha]_D$ −16° (*c* 1, THF); λ_{max}: 1660 (amide) cm^{-1}; ms: 345 (M + 1), etc. *Anal.* calcd. for $C_{18}H_{19}N_2O_5$: C 62.79, H 5.81, N 8.14; found: C 62.86, H 5.79, N 8.17.

N-tert-*Butoxycarbonyl* L-*serine* (N-p-*methoxyphenyl)amide* (**2**b)

A solution containing **1***b* (8.85 g, 43 mmol), 5.83 g (1.1 equiv.) of *p*-anisidine, and 9.07 g (1.1 equiv.) of EDAC.HCl in a total of 75 mL of THF and 25 mL of dichloromethane was stirred and processed as described for **2***a*. The title compound was obtained as a colorless solid in 68.6% yield (9.18 g). Recrystallization from ethyl acetate gave pure product, mp 105–106°C; $[\alpha]_D$ −76° (*c* 1, $CHCl_3$); λ_{max}: 1660 (amide) cm^{-1}; ms: 311 (M + 1), etc. *Anal.* calcd. for $C_{15}H_{21}N_2O_5$: C 58.06, H 7.10, N 9.03; found: C 58.14, H 7.12, N 8.92.

(S)-3-N-[(*Benzyloxycarbonyl)amino]-1*-p-*methoxyphenyl-2-azetidinone* (**3**a)

A solution containing **2***a* (2 g, 5.81 mmol) in 30 mL of DMF was added dropwise at 0°C to 5 mL of DMF containing 348 mg (1.5 equiv.) of sodium hydride (60% suspension in mineral oil) that was previously washed with hexanes. The mixture was cooled to −40°C and 1.72 g (1.5 equiv.) of *N*,*N*-sulfuryl diimidazole in 7 mL

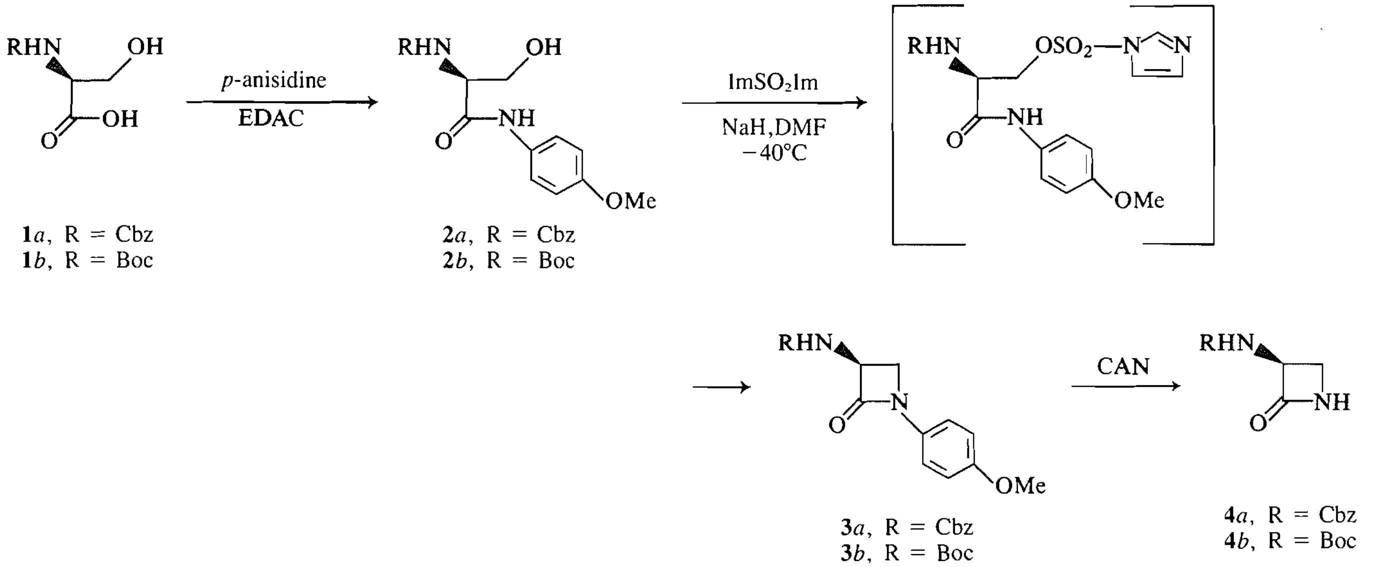

SCHEME 3

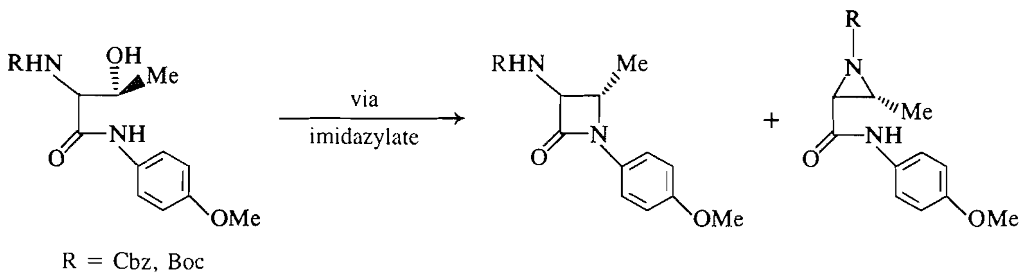

SCHEME 4

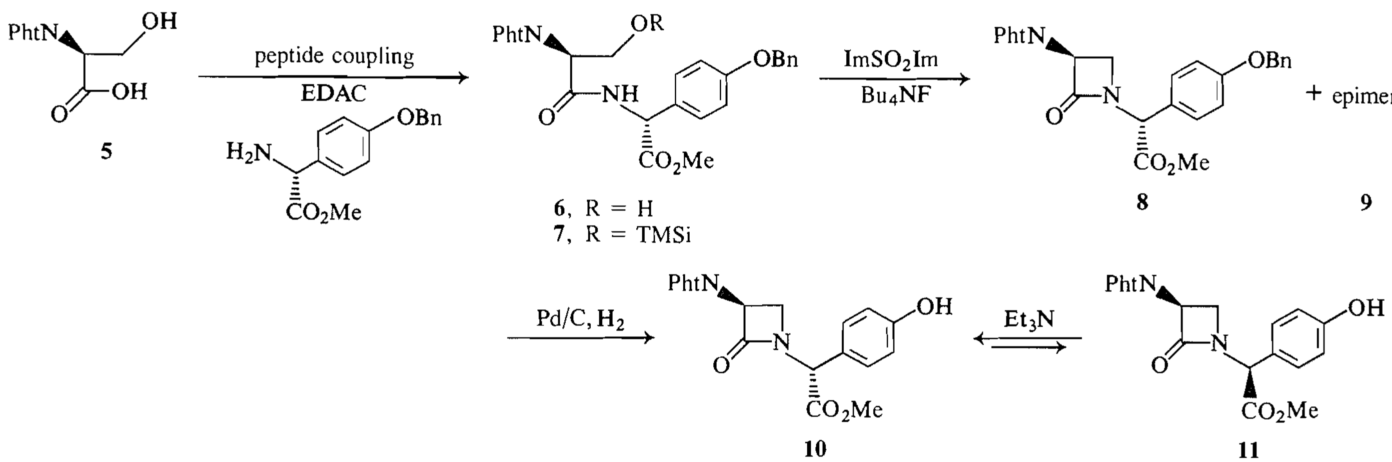

SCHEME 5

of DMF was added with efficient stirring under argon over a period of 25 min. After stirring for a further 30 min, the solution was allowed to warm up to room temperature, methanol (0.5 mL) and chloroform (100 mL) were added, and the solution was washed with saturated brine, then with water. Processing the organic phase gave a colorless solid, which when triturated with ethyl acetate gave 1.42 g (75%) of the desired product **3*a***. Recrystallization from a mixture of ethyl acetate and dichloromethane gave an analytical sample, mp 178°C; $[\alpha]_D$ +35.8° (*c* 1, $CHCl_3$); λ_{max}: 1740 (β-lactam C═O), 1700 (urethane C═O) cm^{-1}; ^1H nmr (90 MHz) ppm: 3.50 (dd, H4β, J = 2.3, 5.3 Hz), 3.73 (s, 3H, OCH_3), 3.88 (t, H4α, J = 5.3 Hz), 4.90 (dd, H3), 5.09 (s, 2H, OCH_2Ph), 5.8 (bd, N*H*, J ~ 8 Hz), 7, 7.3 (arom); ms: 327 (M + 1), etc. *Anal.* calcd. for $C_{18}H_{17}N_2O_4$: C 66.26, H 5.52, N 8.59; found: C 66.16, H 5.53, N 8.42.

*(S)-3-[(*tert*-Butoxycarbonyl)amino]-1-*p*-methoxyphenyl-2-azetidinone (3b)*

A solution containing 0.5 g (1.61 mmol) of **2*b***, 96.8 mg (1.5 equiv.) of sodium hydride, and 480 mg (1.5 equiv.) of *N*,*N*-sulfuryl diimidazole in a total of 13 mL of DMF was stirred at −20°C (addition done at −20°C) under argon for 1 h. Work-up as described above gave a solid, which was recrystallized from ethyl acetate to give 406 mg (85%) of the title compound, mp 180–180.5°C; $[\alpha]_D$ +48.5° (*c* 1.30, $CHCl_3$); λ_{max}: 1750 (β-lactam C═O), 1680 (urethane C═O) cm^{-1}; ^1H nmr (90 MHz) ppm: 1.46 (s, 9H, *tert*-butyoxycarbonyl), 3.51 (dd, H4β, J = 2.3, 5.3 Hz), 3.79 (s, 3H, OCH_3), 3.86 (t, H4α, J = 5.3 Hz), 4.90 (m, H3), 5.54 (dd, NH, J ~ 7 Hz), 7.6 (arom); ms: 293 (M + 1), etc. *Anal.* calcd. for $C_{15}H_{19}N_2O_4$: C 61.64, H 6.85, N 9.59; found: C 61.72, H 6.81, N 9.60.

(S)-3-[Benzyloxycarbonyl)amino]-2-azetidinone (4a)

To a cooled solution of **3***a* (760 mg, 2.33 mmol) in 60 mL of acetonitrile was added a solution of ceric ammonium nitrate (3.8 g, 3 equiv.) in 15 mL of water, dropwise and with stirring. After 30 min at 0°C, the solution was allowed to warm up to room temperature, diluted with water, and extracted with ethyl acetate (100 mL × 3). Processing the organic phase in the usual manner and decolorization with 10% aqueous sodium sulfite gave the title compound as a colorless solid. Trituration with ethyl acetate and hexanes (1:1) gave 360 mg (70%) of **4***a*, mp 164–165°C; $[\alpha]_D$ −17.6° (*c* 1.4, MeOH) (lit. (3) mp 163–164°C; $[\alpha]_D$ −17.8°). The overall yield from L-serine was ~40%; ^{1}H nmr (90 MHz) ppm: 3.33 (dd, H4β, *J* = 2.3, 5.3 Hz), 3.60 (t, H4α, *J* = 5.3 Hz), 4.83 (m, H3), 5.1 (s, 3H, OCH_3), 5.43 (m, NH β-lactam C=O); ms: 221 (M + 1), etc. *Anal.* calcd. for $C_{11}H_{11}N_2O_3$: C 60.00, H 5.45, N 12.73; found: C 59.95, H 5.39, N 12.52.

(S)-3-[(tert-Butoxycarbonyl)amino]-2-azetidinone, (4b)

A solution of **3***b* (800 mg, 2.74 mmol) in 70 mL of acetonitrile was treated with ceric ammonium nitrate (1.65 g, 3 equiv.) in 5 mL of water as described for **4***a*. Processing of the reaction mixture gave the title compound **4***b* (350 mg) in 70% yield after recrystallization from ethyl acetate and hexanes (5:1), mp 172–173°C; $[\alpha]_D$ −18.9° (*c* 1, MeOH) (lit. (3) mp 173–175°C; $[\alpha]_D$ −23.5°; lit. (13*c*) mp 171.5–172.5°C; $[\alpha]_D$ −19.8°); λ_{max}: 1760 (β-lactam C=O) cm^{-1}; ^{1}H nmr (90 MHz) ppm: 1.43 (s, 9H, *tert*-butoxycarbonyl), 3.26 (dd, H4β, *J* = 2.3, 5.3 Hz), 3.54 (t, H4α, *J* = 5.3 Hz), 4.76 (m, H3), 5.43 (dd, *J* ~ 8 Hz, NH β-lactam), 6.9 (m, urethane NH); ms: 189 (M+), etc.

Preparation of dipeptide 6

To a solution of *N*-phthalimido L-serine (86 mg, 0.37 mmol) in 0.5 mL of THF were added successively 109 mg (1.1 equiv.) of 4-*O*-benzyl-*p*-hydroxyphenyl L-glycine methyl ester (13*d*) in 0.5 mL of THF and 77 mg (1.1 equiv.) of EDAC.HCl suspended in 5 mL of dichloromethane. After stirring for 2.5 h at room temperature the solution was evaporated to dryness, the residue was dissolved in dichloromethane, and the solution was washed with aqueous acid, then aqueous bicarbonate, and finally with water. Processing of the organic phase gave 140 mg (78.5%) of the desired dipeptide **6** as a colorless solid. Recrystallization from a mixture of ethyl acetate and hexanes gave pure material (103 mg, 58%); compare 48% with a DCC coupling (24); mp 185–186°C; $[\alpha]_D$ −115.5° (*c* 1, $CHCl_3$) (lit. (24) mp 189–191°C; $[\alpha]_D$ −188°); ^{1}H nmr (90 MHz) ppm: 3.39 (bs, OH), 3.65 (s, 3H, CO_2CH_3), 3.7–4.9 (m, 3H, H3, H 4.4′), 5.00 (s, 2H, OCH_2Ph), 5.47 (d, 1H, *J* = 6 Hz, *CH*—CO_2CH_3), 7.34 (NH), 7.38–7.78 (arom). A single isomer was detected when the spectrum was recorded in the presence of a shift reagent [Eu(hfc)$_3$]; ms: 489 (M + 1).

Intramolecular cyclization of 6 to a mixture of 8 and 9

A solution of **6** (370 mg, 0.76 mmol) in 15 mL of THF was treated with 1.14 mL (1.5 equiv.) of a 1 *M* solution of tetra-n-butylammonium fluoride in THF, then with 225 mg (1.5 equiv.) of *N,N*-sulfuryl diimidazole. After stirring overnight, a few drops of aqueous acetic acid were added, the solvent was evaporated, and the residue was dissolved in dichloromethane. Washing with aqueous hydrochloric acid, then water, and usual processing gave a syrup that was chromatographed (ethyl acetate – hexanes 1:1) to give a mixture of **8** and **9** (224 mg, 63%) as a colorless solid, mp 55–65°C; $[\alpha]_D$ −110.5° (*c* 1, $CHCl_3$); λ_{max}: 1745 (β-lactam C=O), 1760 (phthalimido), 1720 (CO_2CH_3) cm^{-1}; ^{1}H nmr (90 MHz) ppm: 2.10–3.60 (dd, H4β), 3.8, 3.82 (s, H, CO_2CH_3), 3.70–4.08 (t, H4α), 5.07 (s, 2H, OCH_2Ph), 5.32–5.55 (dd, H3), 5.69, 5.76 (s, *C*HCO_2CH_3), etc; ms: 471 (M + 1), etc.

(S)-3-(Phthalimido)-1-(p-hydroxyphenyl-L-glycinyl methyl ester)-2-azetidinone 10 and its epimer 11

A solution containing 231 mg (0.6 mmol) of a mixture of **8** and **9** in a mixture of methanol and acetic acid (1:1, 15 mL) was hydrogenated in the presence of 150 mg of 10% palladium-on-charcoal. After an overnight treatment, the catalyst was filtered, washed with methanol, and the filtrate was coevaporated with benzene several times to remove all the residual acetic acid. The residue thus obtained (quant.) showed a 2:1 mixture (nmr) of **10** and **11**, respectively. Fractional recrystallization from ethyl acetate – hexanes (4:1) gave 68 mg of **10** as colorless crystals, mp 169–171°C; $[\alpha]_D$ −238.5° (*c* 0.58, MeOH) (lit. (24) mp 169–170°C; $[\alpha]_D$ −239°; lit. (13*d*) mp 203–204°C; $[\alpha]_D$ −236°; λ_{max}: 1770 (β-lactam C=O), 1750 (phthalimido), 1730 (CO_2CH_3) cm^{-1}; ^{1}H nmr (90 MHz), ppm: 3.46 (dd, H4β, *J* = 2.9, 5.5 Hz), 3.79 (s, 3H, CO_2CH_3), 3.95 (t, H4α, *J* = 5.5 Hz), 5.51 (dd, *J* = 2.9, 5.5 Hz), 7.1–7.76 (arom.); ms: 381 (M + 1), etc.

Treatment of the mother liquors of recrystallization overnight with dichloromethane containing ~10% triethylamine, evaporation to dryness, and chromatography (ethyl acetate – hexanes 2:1) gave a mixture of **10** and **11** in a ratio of 2:1. After recrystallization, a further 75 mg of **10** was obtained, for a total of 142 mg (67%). The final mother liquors gave 28 mg of a 1:2 mixture of **10** and **11**, respectively.

Acknowledgements

We wish to acknowledge the generous financial assistance of the Natural Sciences and Engineering Research Council of Canada, Sandoz (Vienna), and Le Ministère de l'éducation du Québec. We thank Mr. M. Evans for recording the mass spectra.

1. C. M. Cimarusti and R. B. Sykes. Med. Res. Rev. **4**, 1 (1984); Chem. Br. 302 (1983).
2. R. B. Sykes, C. M. Cimarusti, D. P. Bonner, K. Bush, D. M. Floyd, N. H. Georogopapadakou, W. Koster, W. C. Liu, W. L. Parker, P. A. Principe, M. L. Rathum, W. A. Slusarchyk, W. H. Trejo, and J. S. Well. Nature, **291**, 489 (1981); A. Imada, K. Kitano, K. Kintaka, M. Muroi, and M. Asai. Nature, **289**, 590 (1981); C. M. Cimarusti and R. B. Sykes. Chem. Br. 302 (1983).
3. W. L. Parker, W. H. Koster, C. M. Cimarusti, D. M. Floyd, W. Liu, and L. Rathum. J. Antibiot. **35**, 189 (1982); W. L. Parker and M. L. Rathum. J. Antibiot. **35**, 300 (1982); C. M. Cimarusti, H. E. Applegate, H. W. Chang, D. M. Floyd, W. H. Koster, W. A. Slusarchyk, and M. G. Young. J. Org. Chem. **47**, 179 (1982); D. M. Floyd, A. W. Fritz, and C. M. Cimarusti. J. Org. Chem. **47**, 176 (1982); E. M. Gordon, M. A. Ondetti, J. Pluscec, C. M. Cimarusti, D. P. Bonner, and R. B. Sykes. J. Am. Chem. Soc. **104**, 6053 (1982); D. M. Floyd, A. W. Fritz, J. Pluscec, E. R. Weaver, and C. M. Cimarusti. J. Org. Chem. **47**, 5160 (1982).
4. M. J. Miller, P. G. Mattingly, M. A. Morrison, and J. F. Kerwin, Jr. J. Am. Chem. Soc. **102**, 7026 (1980).
5. (*a*) A. K. Bose, M. S. Manhas, D. P. Sahu, and V. R. Hegde. Can. J. Chem. **62**, 2498 (1984); (*b*) D. P. Sahu, P. Mashava, M. S. Manhas, and A. K. Bose. J. Org. Chem. **48**, 1142 (1983); (*c*) A. K. Bose, D. O. Sahu, and M. S. Manhas. J. Org. Chem. **46**, 1229 (1981).
6. C. M. Cimarusti. J. Med. Chem. **27**, 247 (1984).
7. H. H. Wasserman, D. J. Hlasta, A.-W. Tremper, and J. S. Wu. Tetrahedron Lett. 549 (1979).
8. G. Georg and T. Durst. J. Org. Chem. **48**, 2092 (1983); H. Matsunaga, T. Sakamaki, H. Naguaka, and Y. Yamada. Tetrahedron Lett. **24**, 3009 (1983); M. J. Miller, J. S. Bajna, P. G. Mattingly, and K. Peterson. J. Org. Chem. **47**, 4928 (1982); M. A. Morrison and M. J. Miller. J. Org. Chem. **48**, 4421 (1983).
9. A. Mishida, M. Shibasaki, and S. Ikegami. Tetrahedron Lett. **25**, 765 (1984); S. R. Woulfe and M. J. Miller. Tetrahedron Lett. **25**, 3293 (1984).
10. H. P. Isenring and W. Hofheinz. Synthesis, 385 (1981).
11. H. Aoki, H. Sakai, M. Kohsaka, T. Konomi, J. Hosada, J. Kubochi, and E. Igushi. J. Antibiot. **29**, 492 (1976); M. Hashimoto, T. Komori, and T. Kamiya. J. Antibiot. **29**, 890 (1976).

12. T. KAMIYA. *In* Recent advances in the chemistry of β-lactam antibiotics. *Edited by* J. Elks. Spec. Publ. No. 28, Chem. Soc. London. 1977. pp. 281–294. T. KAMIYA, H. AOKI, and Y. MINE. *In* Chemistry and biology of β-lactam antibiotics. Vol. 2. *Edited by* R. B. Morin and M. Gorman. Academic Press, New York. 1982. pp. 165–226.
13. (*a*) H. P. ISENRING and W. HOFHEINZ. Tetrahedron, **39**, 2591 (1983); (*b*) C. A. TOWNSEND and L. T. NGUYEN. Tetrahedron Lett. **23**, 4859 (1982); (*c*) P. G. MATTINGLY and M. J. MILLER. J. Org. Chem. **46**, 1557 (1981); **45**, 410 (1979); (*d*) T. KAMIYA, M. HASHIMOTO, O. NAKAGUCHI, and T. OKU. Tetrahedron, **35**, 323 (1979); (*e*) T. KAMIYA, T. OKU, O. NAKAGUCHI, H. TAKENO, and M. HASHIMOTO. Tetrahedron Lett. 5119 (1978); (*f*) G. A. KOPPEL, L. MCSHANE, F. JOSE, and R. D. G. COOPER. J. Am. Chem. Soc. **100**, 3933 (1978).
14. H. H. WASSERMAN, D. J. HLASTA, A. W. TREMPER, and J. S. WU. J. Org. Chem. **46**, 2999 (1981); K. CHIBA, M. MORI, and Y. BAN. J. Chem. Soc. Chem. Commun. 770 (1980).
15. W. L. PARKER, W. H. KOSTER, C. M. CIMARUSTI, D. M. FLOYD, W. C. LIU, and M. L. RATHNUM. J. Antibiot. **35**, 189 (1982).
16. S. HANESSIAN and S. P. SAHOO. Can. J. Chem. **62**, 1400 (1984).
17. S. HANESSIAN. Total synthesis of natural products: the 'chiron' approach. *Edited by* J. E. Baldwin. Pergamon Press, Oxford, England. 1983.
18. S. HANESSIAN and J.-M. VATELE. Tetrahedron Lett. **22**, 3579 (1981).
19. S. HANESSIAN, S. SAHOO, C. COUTURE, and H. WYSS. Bull. Soc. Chim. Belg. **7**, 571 (1984).
20. H. STAAB. Angew. Chem. Int. Ed. Engl. **1**, 351 (1962).
21. O. MITSUNOBU. Synthesis, 1 (1981).
22. D. R. KRONENTHAL, C. T. HAN, and M. F. TAYLOR. J. Org. Chem. **47**, 2765 (1982).
23. G. H. L. NEFKENS, G. I. TESSER, and R. I. F. NIVARD. Recl. Trav. Chim. Pays-Bas, **79**, 688 (1960); R. S. HODGES and R. B. MERRIFIELD. J. Org. Chem. **39**, 1870 (1974).
24. C. A. TOWNSEND, A. M. BROWN, and L. T. NGUYEN. J. Am. Chem. Soc. **105**, 919 (1983).
25. J. C. SHEEHAN, J. PRESTON, and P. A. CRUICKSHANK. J. Am. Chem. Soc. **87**, 2491 (1965).

The geometry of 4-(1-ethoxyethylidene)-5-oxazolones and thiazolones: ^{1}H and ^{13}C studies and the crystal structure of 4-[(Z)-1-ethoxyethylidene]-2-phenyl-5-oxazolone

R. A. BELL,[1] R. FAGGIANI, C. J. L. LOCK, AND R. A. MCLEOD

Department of Chemistry and the Institute for Materials Research, McMaster University, Hamilton, Ont., Canada L8S 4M1

Received June 12, 1984[2]

R. A. BELL, R. FAGGIANI, C. J. L. LOCK, and R. A. MCLEOD. Can. J. Chem. **63**, 3618 (1985).

A series of *E* and *Z* isomers of substituted 4-(1-ethoxyethylidene)-5-oxazolones and thiazolones have been prepared and their ^{1}H and ^{13}C spectra recorded. The vinylic methyl ^{1}H chemical shifts showed minimal differences between *E* and *Z* isomers whereas the vinylic OCH_2 ^{1}H signals differed by 0.15−0.43 ppm, with the *Z* isomer being consistently the more deshielded. Both vinylic methyl and OCH_2 groups showed different ^{13}C resonances for each isomer, with the *Z* isomers being the more deshielded. The *Z* geometry was conclusively defined for one isomer of 4-(1-ethoxyethylidene)-2-phenyl-5-oxazolone, **5**, by X-ray crystallography and this was sufficient to assign the geometry of the remaining pairs of *E* and *Z* isomers. Oxazolone **5** has the space group $P2_1/n$ and cell dimensions a = 9.219(3), b = 19.899(5), c = 7.459(1) Å, β = 118.01(2)°, and has four formula units in the unit cell. Intensities were measured with use of MoKα radiation and a Nicolet P3 diffractometer. The crystal structure was determined by standard methods and refined to R_1 = 0.0709, R_2 = 0.0696 based on 1419 independent reflections. The molecule is essentially planar and most bond lengths and angles are normal. Exceptions are the very short C(olefin)—O(ether) bond (1.339(4) Å) and the large ether C—O—C angle (122.1(3)°) caused by extreme delocalization in the O(ether)CCCO(carbonyl) system. The planarity causes a number of strong intramolecular repulsive interactions, causing an exceptionally small external olefin angle, O(ether)CC(methyl), of 108.1(4)°. The ethoxyl side chain of **5** adopts a conformation in the solid state which places the methylene of the OCH_2 group adjacent to the oxazole ring nitrogen. This conformation is proposed to persist in solution phases and is consistent with the observed ^{13}C chemical shifts and known γ and δ substituent effects.

R. A. BELL, R. FAGGIANI, C. J. L. LOCK et R. A. MCLEOD. Can. J. Chem. **63**, 3618 (1985).

On a préparé une série d'isomères *E* et *Z* des (éthoxy-1 éthylidène)-4 oxazolones-5 et thiazolones-5 et on a enregistré leurs spectres rmn du ^{1}H et du ^{13}C. En rmn du ^{1}H, les déplacements chimiques des méthyles vinyliques ne présentent que des différences minimales entres les isomères *E* et *Z* alors que les déplacements chimiques des OCH_2 vinyliques diffèrent par 0,15−0,43 ppm; dans tous les cas, l'isomère *Z* est le plus déblindé. En rmn du ^{13}C, les groupements méthyles ainsi que les OCH_2 vinyliques de chacun des isomères présentent tous des résonances différentes; les isomères *Z* sont toujours les plus déblindés. Utilisant la diffraction des rayons-X, on a défini d'une façon non ambigue la géometrie *Z* de l'isomère **5** de la (éthoxy-1 éthylidène)-4 phényl-2 oxazolone-5 et cette démonstration est suffisante pour attribuer la géométrie des autres paires d'isomères *E* et *Z*. L'oxazolone **5** cristallise dans le group d'espace $P2_1/n$ avec a = 9,219(3), b = 19,899(5), c = 7,459(1) Å, β = 118,01(2)° et quatre molécules par maille. On a mesuré les intensités à l'aide de la radiation MoKα et un diffractomètre Nicolet P3. On a déterminé la structure cristalline par les méthodes usuelles et on l'a affinée jusqu'à des valeurs de R_1 = 0,0709 et R_2 = 0,0696 pour 1419 réflexions indépendantes. La molécule est essentiellement planaire et la plupart des longueurs et des angles sont normaux. La liaison C(oléfine)—O(éther) qui est très courte (1,339(4) Å) et l'angle de l'éther C—O—C qui est très grand (122,1(3)°) sont des exceptions qui sont causées par une délocalisation extrême dans le système O(éther)-CCCO(carbonyle). La planéité provoque un grand nombre d'interactions répulsives intramoléculaires qui font que l'angle oléfinique externe, O(éther)CC(méthyle), est extrèmement petit (108,1(4)°). À l'état solide, la chaîne latérale éthoxyle du composé **5** adopte une conformation telle que le groupement OCH_2 se trouve dans une position adjacente de l'azote du cycle oxazole. On croit que cette conformation persiste en solution et qu'elle est en accord avec les déplacements chimiques ainsi que les effets γ et δ de substituants observés en rmn du ^{13}C.

[Traduit par le journal]

Introduction

4-(1-Alkoxyethylidene)-5-oxalozones and the corresponding 5-thiazolones can exist as geometric isomers. Potentially one should be able to differentiate between *E* and *Z* isomers by examining the ^{1}H nmr chemical shifts of protons at positions a, a′, b, b′, c, c′, d, and d′ (see Fig. 1). In practice, however, positions b, b′, c, and c′ are the more important. This arises because in many compounds of interest the protons at both the a and a′ positions are substituted by other atoms and the difference in shifts of protons at d and d′ is too small to be of practical use.

Nevertheless, examination of shifts of protons at a and a′ is of interest since they can be correlated with the shifts of protons at b, b′, c, and c′, and much work has been done on the ^{1}H nmr of the isomers of compounds of type **1** (Fig. 2) where at least one H substituent is present and the other substituent is alkyl or aryl. The majority of the assignments have been made by correlation of the spectra of the oxazolones **1** (R^1 or R^2 = H) with the spectra of the base catalysed hydrolysis products of **2** (1−5). The problem of the unambiguous assignment of the *E* and *Z* geometry to a particular series of compounds has been solved by combined ^{1}H nmr and crystallographic studies. The structures of the oxazolone **3** and the ring opened product **4** have been determined by X-ray diffraction (6,7). It has been established (8) that the thermodynamic product, obtained by the Plochl−Erlenmeyer synthetic route (9,10) is of *Z* geometry, whereas the *E* geometry is obtained by photo-irradiation, or acid promoted isomerization of the *Z* isomer (8,11). From this, ^{1}H nmr assignments have been made for the olefinic protons in the *E* and *Z* isomers of the oxazolones **1** and their hydrolysis products **2**. These resonances of the olefinic protons in **1** and **2** (R^1 or R^2 = H) are at higher field for the *Z* isomer (8). This assignment has, in turn, allowed the assignment of

[1]Author to whom correspondence may be addressed.
[2]Revision received July 30, 1985.

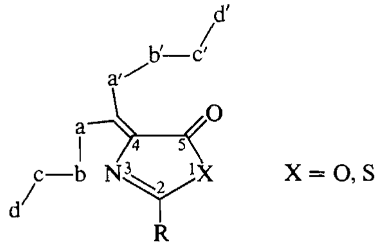

FIG. 1. General structure of 4-alkylidene-5-oxazolones and 4-alkylidene-5-thiazolones. Symbols a–d and a'–d' represent potential atom positions.

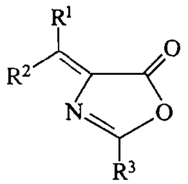

1

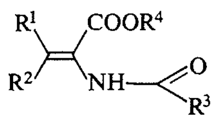

2

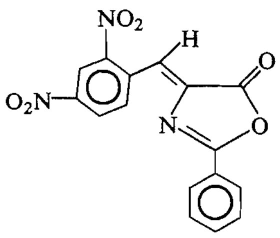

3

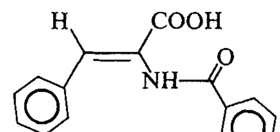

4

FIG. 2. Structures of 4-alkylidene-5-oxazolones and their derived α-amino-acrylamide derivatives. R^1 or R^2 = H, alkyl, or aryl; R^3 = alkyl or aryl; R^4 = H or alkyl.

the resonances of the allylic protons in **1** and **2** (b and b' in Fig. 1) (4).

Attempts to extrapolate the data to systems where neither R^1 nor R^2 = H have met difficulties. Recently two different research groups have assigned *E* and *Z* geometries to isomers of compounds of type **1** and **2** that are contrary to extrapolation from the work described above. The first group (12) (for **1** and **2**, $R^1 = CH_3$, $R^2 = CH_2CH_3$ and $R^1 = CH_2CH_3$, $R^2 = C_6H_5$ or CH_3) based their assignments on ^{1}H nmr solvent shifts, and the second group (13, 14) (for **1** and **2**, $R^1 = CH_3$, $R^2 = C_6H_5$ and $R^1 = C_6H_5$, $R^2 = CH_3$) based their assignments on the relative chemical shift positions, assuming that the methyl group closest to the carbonyl group was the more deshielded. Our own interest is in isomerism in 4-(1-alkoxyethylene)-5-oxazolones and the corresponding 5-thiazolones. Two isomers have been reported previously for 2-benzyl-4-methoxymethylene-5-oxazolone; the first was prepared by the penaldate method and the second by the addition of diazomethane to the hydroxymethylene derivate (15). Two isomers have also been reported for 4-(1-ethoxyethylidene)-2-phenyl-5-oxazolone, **5** (16, 17). No attempts were made to assign a particular structure to any of the above isomers.

In the work described here, two series of isomers of a number of 4-(1-alkoxyethylidene)-5-oxazolone and thiazolone compounds have been prepared (see Fig. 3), and it has proved possible to differentiate between the two series of isomers by ^{1}H and ^{13}C nmr spectroscopies. Nevertheless, in light of the

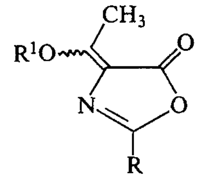

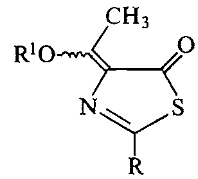

Compound	R	R'	Compound	R	R'
5	C_6H_5	Et	**13**	SBz	Et
6	Bz	Et	**14**	SCH_3	Et
7	*t*-Bu	Et	**15**	OEt	Et
8	*p*-Br-C_6H_5	Et	**16**	SBz	H
9	*p*-Cl-C_6H_5	Et	**17**	SBz	CH_3
10	Ph	CH_3	**18**	SCH_3	CH_3
11	*p*-Cl-C_6H_5	H			
12	Ph	H			

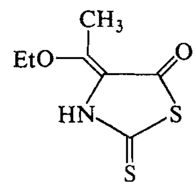

19

FIG. 3. 5-Oxazolone and 5-thiazolone derivatives prepared.

ambiguity caused by the extrapolation mentioned above, it seemed unwise to assign the structures on the basis of the work on compounds **1** (R^1 or R^2 = H), particularly because of the greater electronegativity of the oxygen atom. Thus we have examined the structure of one of our compounds by X-ray diffraction, and this has allowed the assignment of specific structures to each series.

Results

Syntheses

The 4-(1-alkoxyethylidene)-5-oxazolones and 5-thiazolones used in this work are listed in Fig. 3. The majority were prepared by the reaction of triethyl orthoacetate and acetic anhydride with the appropriate *N*-acyl or *N*-aroyl glycinate, for the oxazolones, or *N*-dithiocarbalkyl or *N*-thiocarbalkoxy glycinate, for the corresponding thiazolones. The synthetic processes are summarized in Schemes 1–3. In general, the orthoacetate – acetic anhydride procedure gave an equilibrium mixture of the *E* and *Z* isomers in a ratio which varied from 1:5 to 1:3 (*E*/*Z*). The only exceptions to this were the 2-alkyl-4-(1-ethoxyethylidene)-5-oxazolones **6** and **7**, which gave only the *Z* isomer from this reaction. The *E* isomers of **6** and **7**, as for other compounds with the exception of 4-(1-ethoxyethylidene)-2-thioxo-5-thiazolidinone, **19**, and the hydroxyethylidene compounds **11**, **12**, and **16**, were available either by photo-irradiation of the *Z* isomers, or by acid catalysed exchange. The *E* and *Z* isomers were separable, and able to be purified, by flash column chromatography on silica gel supports.

The 1-hydroxyethylidene oxazolone, **11**, was prepared by the action of acetic anhydride and 3-methylpyridine on sodium *N*-benzoylglycinate, and the 1-hydroxyethylidene oxazolone, **12**, by hydrolysis of the corresponding 1-ethoxyethylidene derivative, **5**, with concentrated hydrobromic acid (see Scheme 1). The 1-hydroxyethylidene thiazolone, **16**, was prepared by the hydroxide ion hydrolysis of the 1-ethoxyethylidene compound, **14** (see Scheme 2). The 1-methoxyethylidene oxazo-

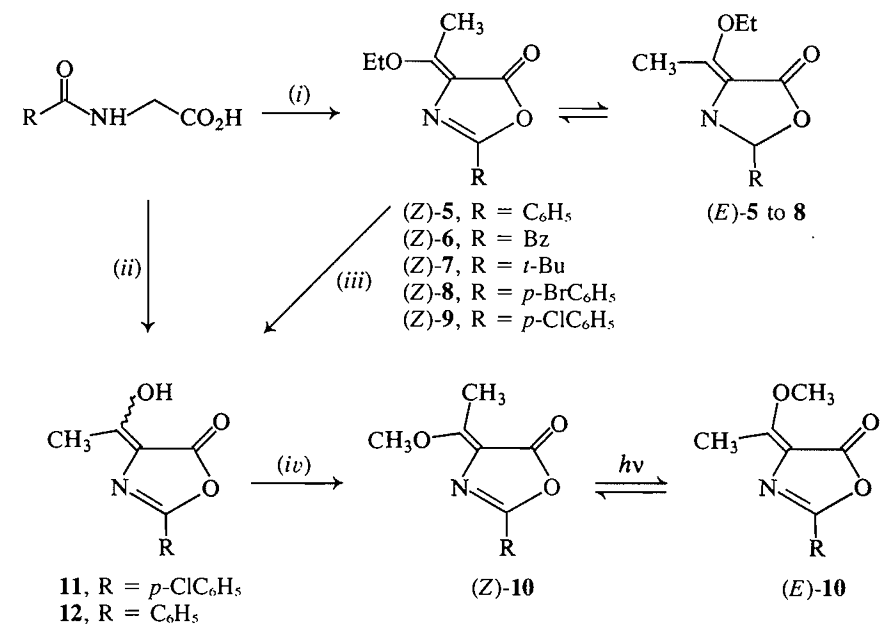

Reagents: (*i*) $CH_3C(OEt)_3$, Ac_2O, Δ; (*ii*) β-picoline, Ac_2O, Δ; (*iii*) $HBr_{(aq)}$; (*iv*) CH_2N_2, ether

SCHEME 1

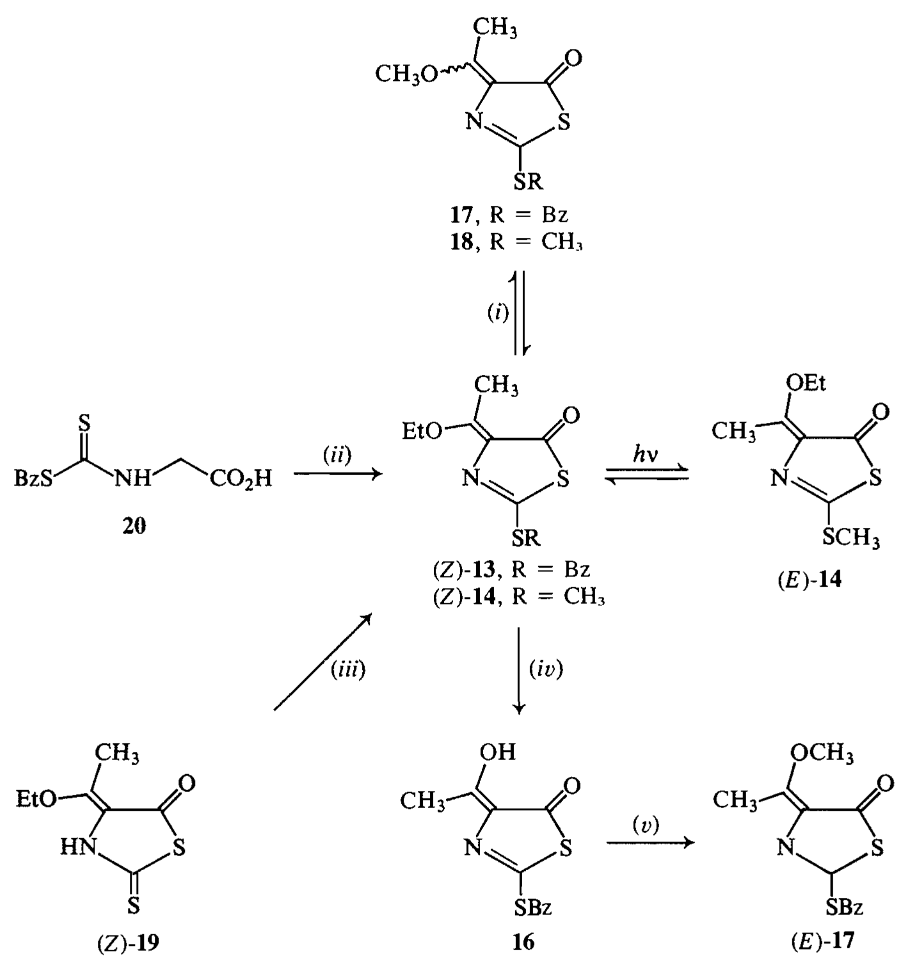

Reagents: (*i*) HCl, MeOH, 25°C; (*ii*) $CH_3C(OEt)_3$, Ac_2O, *p*-TsOH, Δ; (*iii*) K_2CO_3, acetone, BzBr or CH_3I, 25°C; (*iv*) KOH, EtOH, Δ; (*v*) CH_2N_2, ether

SCHEME 2

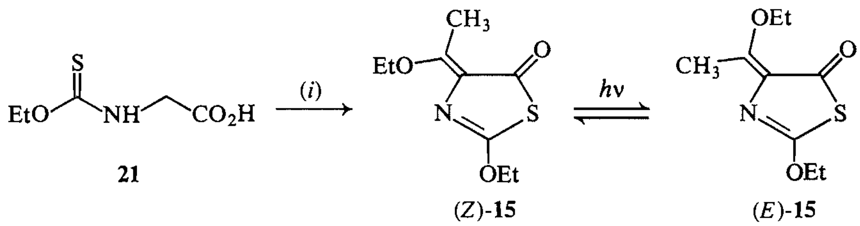

Reagents: (*i*) $CH_3C(OEt)_3$, Ac_2O, *p*-TsOH, Δ

SCHEME 3

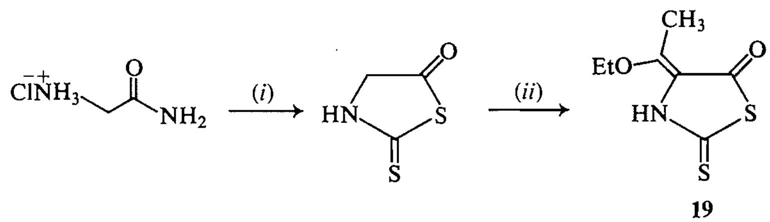

Reagents: (*i*) OH^- (1 equiv.), K_2CO_3, CS_2; then 50% H_2SO_4; (*ii*) $CH_3C(OEt)_3$, Ac_2O, Δ

SCHEME 4

lone, **10**, and the corresponding thiazolone, **17**, were both obtained by the reaction of diazomethane on the hydroxy compounds **12** and **16**, respectively. These reactions led to the formation of only one isomer in each case: **10** being assigned the *Z* geometry and **17** the *E* (see Discussion).

The 2-thioxo-thiazolidinone derivative **19** was synthesized from glycinamide hydrochloride and carbon disulphide as outlined in Scheme 4. The orthoacetate – acetic anhydride procedure gave only one isomer, (*Z*)-**19**.

Spectroscopic data

Selected ^1H and ^{13}C nmr data are summarized in Table 1. The remaining chemical shift data are given in the experimental section under each compound. The protons of an OCH_2 group (C(8)) (hydrogens on a carbon atom at sites b or b′ in Fig. 1) showed the greatest differences in chemical shift between the *E* and *Z* geometric isomers, the trend being consistent for all compounds examined. The vinylic CH_3 protons (hydrogens on a carbon atom at sites a or a′, C(7)) showed very small chemical shift changes and are included in Table 1 for comparison. The vinylic CH_3 carbon, on the other hand, showed a consistent trend in the ^{13}C chemical shift differences between the two isomers, as did the carbon of the OCH_2 group. These consistent trends, together with the absolute geometry of the 4,6-double bond in 4-[(Z)-1-ethoxyethylidene]-2-phenyl-5-oxazolone, **5**, as determined by X-ray crystallography, were used to assign the geometric isomers in both the oxazolone and the thiazolone series. The assignments are included in Table 1.

X-ray structural data

The crystal data for 4-[(Z)-1-ethoxyethylidene]-2-phenyl-5-oxazolone, (Z)-**5**, are given in Table 2. The atomic positional parameters and temperature factors for non-hydrogen atoms are given in Table 3 and selected interatomic distances and angles are given in Table 4. Tables of hydrogen atom positional and thermal parameters, bond lengths and angles involving hydrogen atoms, best planes and dihedral angles have been deposited.[3]

Discussion

E *and* Z *geometry assignment*

The geometry assignments of the 4-(1-alkoxyethylidene)-5-oxazolones and the 4-(1-alkoxyethylidene)-5-thiazolones prepared in this work were made on the basis of the consistent ^1H and ^{13}C chemical shift differences observed for the protons and carbon atom of the vinylic OCH_2 group (C(8)), and the carbon atom of the vinylic CH_3 group (C(7)), together with the structure of one compound, 4-[(Z)-1-ethoxyethylidene]-2-phenyl-5-oxazolone, (Z)-**5**, as determined by X-ray diffraction. For all compounds studied, one isomer, the thermodynamically more stable isomer, was always less polar in its chromatographic behaviour than the other isomer. The less polar isomers consistently showed the C(8) protons to be deshielded by 0.2–0.4 ppm relative to the more polar isomers (see Table 1). There was further consistency in the ^{13}C nmr spectra, where the less polar isomers showed C(8) to be deshielded by 0.6–1.8 ppm relative to the more polar isomer. The only exception to the trend in the C(8) ^{13}C chemical shifts was noted for compound **13** where the spectrum, recorded in acetone-d_6, showed both isomers with identical chemical shifts. Since both oxazolones and thiazolones exhibited the same trends, defining the geometry of one isomer was sufficient to assign the geometry of both series or compounds. The less polar isomer of compound **5** was subjected to X-ray diffraction analysis and this was found to be the *Z*-geometric isomer.

[3]Tables of hydrogen atom positional and thermal parameters, bond lengths and angles involving hydrogen atoms, best planes, dihedral and torsion angles, and the moduli of F_o and F_c have been deposited and may be purchased from the Depository of Unpublished Data, CISTI, National Research Council of Canada, Ottawa, Ont., Canada K1A 0S2.

TABLE 1. Selected ^{1}H and ^{13}C nmr chemical shifts*,†

	Vinyl CH_3 (C(7))				Vinyl OCH_2 (C(8))			
	δ, ^{1}H		δ, ^{13}C		δ, ^{1}H		δ, ^{13}C	
Compound	*E*	*Z*	*E*	*Z*	*E*	*Z*	*E*	*Z*
5	2.51	2.49	15.8	17.6	4.30	4.73	66.4	69.0
8	2.53	2.51	15.9	17.6	4.35	4.72	66.5	69.1
9	2.55	2.52	15.9	17.5	4.37	4.74	66.5	69.1
6	2.41	2.44	15.9	16.5	4.29	4.57	66.3	68.1
7	2.43	2.42	—	(16.8)‡	4.30	4.64	—	(68.8)‡
13	2.54	2.44	(16.5)‡	17.4 (16.5)‡	4.27	4.55	65.8 (65.9)	68.3 (68.2)‡
14	2.56	2.45	16.8	17.7	4.26	4.53	65.9	68.5
15	2.40	2.40	16.0	17.5	4.20	4.50	65.0	67.9
10	2.53	2.53	—	16.3	4.04	4.29	—	59.6
17	2.58	2.48	(15.4)‡	(16.1)‡	4.00	4.15	(56.9)‡	(59.0)‡

*Relative to tetramethylsilane as internal standard.
†Data were obtained from $CDCl_3$ solutions.
‡Data from acetone-d_6 solutions.

TABLE 2. Crystal data for 4-[(*Z*)-1-ethoxyethylidene]-2-phenyl-5-oxazolone

$C_{13}H_{13}NO_3$	fw = 231.3

Crystal size (mm), rough tetragonal prisms, 0.16 × 0.20 × 0.60, monoclinic $P2_1/n$,* a = 9.219(3), b = 19.899(5), c = 7.459(1) Å, β = 118.01(2)°, V = 1208.1(6) Å^3, Z = 4, ρ_{calc} = 1.272, ρ_{obs} = 1.26(2) (22°C, MoK_α, λ = 0.71069); linear abs. coeff. 0.983 cm^{-1}, reflections collect. h, k, $+l$, max 2θ = 45°, standard reflections, e.s.d.,† 2 3 $\bar{4}$ (0.0137), 2 4 $\bar{4}$ (0.0163), independent reflections 1584, no. with $I > 0$, used in refinement, 1419; final R_1‡ = 0.0709, R_2 = 0.0696, final shift/error, max. 0.141, ave. 0.012; secondary extinction, x = 0.00685, final diff. map, peak, 0.21 e Å^{-3}, valley −0.18 e Å^{-3}, wtg., $w = (\sigma_F^2 + 0.000519\ F_0^2)^{-1}$, error in obs. of unit wt. 0.85, no. of variables, 207, F(000) = 488.

*This cell can be transformed to the standard $P2_1/c$ cell, a = 9.219(3), b = 19.899(5), c = 8.720(2) Å, β = 130.96(2) by the matrix (100/0−10/−10−1).
†Measured after every 48 reflections.
‡$R_1 = \Sigma \| F_o| - |F_c\| / \Sigma |F_o|$; $R_2 = \{\Sigma w(|F_o| - |F_c|)^2 / \Sigma w F_o^2\}^{1/2}$

The ^{1}H chemical shift of the C(7) methyl group (positions a or a′ in Fig. 1) showed very small differences between the *E* and *Z* isomers. In general, the *E* isomer was the more deshielded, by 0.01−0.11 ppm, than the *Z* isomer, but compound **15** showed equality of the two methyl shifts and compound **6** (Table 1) showed the methyl of the *Z* isomer to be the more deshielded by 0.03 ppm. The vinylic methyl ^{1}H nmr shifts in the 4-alkoxyethylidene series cannot therefore be used to define unambiguously the stereochemistry of the geometric isomers. In view of this, and of the very small shifts observed for the corresponding 4-alkylidene-5-oxazolones, it is not surprising that previous authors have arrived at divergent isomer assignments when basing their arguments on the relative shifts of vinylic methyl or alkyl groups (4, 8, 12−14). The shielding/deshielding regions about the 5-carbonyl group and the ring N atom are fortuitously similar for the vinylic alkyl site and must not be used for isomer assignment. However, for protons on atoms one further out from the double bond, at the b or b′ site in Fig. 1, the spatial anisotropies about the 4,6-double bond are different for compounds of the 1-alkoxyethylidene type and distinct chemical shift changes are observed. This should be contrasted with the 1-methylpropylidene structures where atom a (or a′) is a carbon atom and where protons on b (or b′) atoms show small chemical shift differences (ca. 0.02 ppm) (12). We attribute this alteration in spectroscopic behaviour to the preferred conformations adopted by the 1-alkoxyethylidene compounds (see X-ray section below).

The two hydroxy compounds **12** and **16** were interesting in that they were obtained as single isomers, but the oxazolone **12** existed as the *Z* isomer whereas the thiazolone **16** existed as the *E* isomer. These geometries were demonstrated by trapping the isomers with diazomethane, when **12** gave (*Z*)-**10** and **16** gave (*E*)-**17**, as determined by a comparison of the ^{1}H and ^{13}C nmr chemical shifts of these methyl ethers with other compounds listed in Table 1. Evidently the presence of an O atom or an S atom in the ring causes subtle changes in the relative basicities of the ring N atom and the carbonyl O, with an oxygen causing the N atom to be more basic and hydrogen bond to the hydroxyl group of **12** more effectively than the carbonyl O. The reverse was true in the thiazolone **16**.

Compound **19** was assigned the thioamide structure and not the thiazolone tautomer on the basis of its ^{1}H nmr spectrum, which showed a hydrogen bonded N-H proton at 9.31 ppm, its ^{13}C spectrum, which gave a C(1) signal at 184 ppm (or 186 ppm), and its infrared spectrum, which showed a characteristic N—H stretch at 3110 cm^{-1}.

Synthesis

The general synthetic approaches and interrelationship of the 4-(1-ethoxyethylidene)-5-oxazolones and the 5-thiazolones are shown in Schemes 1−3. The orthoester − acetic anhydride procedure led to mixtures of *E* and *Z* isomers with the *Z* isomer predominating. These pairs of isomers were separable by flash column chromatography on silica gel. The acetic anhydride − 3-methylpyridine reagent used for the preparation of the 1-hydroxyethylidene compound, **11**, gave a single isomer.

Two methods have been used to isomerize (*Z*)-4-phenylmethylene-5-oxazolones to the less stable *E* geometry (8, 11). Strong acids, such as polyphosphoric acid or concentrated aqueous hydrobromic acid, can be used, or photo-irradiation employed. In our hands the acid procedures were found to be unsuccessful in carrying out the isomerization of the oxazolones (*Z*)-**5** and (*Z*)-**9**. When a mixture of (*E* and *Z*)-**9** was treated with hydrobromic acid, dissolution occurred and the *E*

TABLE 3. Atomic positional parameters and temperature factors (Å^2)

Atom	x	y ($\times 10^4$)	z	U_{11}	U_{22}	U_{33} ($\times 10^3$)	U_{12}	U_{13}	U_{23}
O(1)	2328(3)	5410(1)	4000(4)	51(2)	70(2)	93(2)	9(1)	25(1)	−4(1)
C(2)	942(4)	5007(2)	2987(5)	54(2)	64(2)	60(2)	8(1)	23(2)	−1(2)
N(3)	−413(3)	5290(1)	2588(4)	51(2)	56(2)	68(2)	5(1)	26(1)	2(1)
C(4)	−16(4)	5948(2)	3344(5)	52(2)	53(2)	66(2)	4(2)	29(2)	−1(2)
C(5)	1745(5)	6029(2)	4277(6)	67(3)	64(3)	85(3)	10(2)	27(2)	2(2)
O(2)	2708(3)	6475(1)	5138(5)	73(2)	75(2)	141(3)	−9(2)	22(2)	−19(2)
C(6)	−1058(5)	6450(2)	3215(5)	66(3)	65(2)	64(2)	7(2)	33)2)	−6(2)
C(7)	−534(7)	7159(2)	3972(9)	102(4)	56(2)	96(4)	−3(2)	46(3)	−7(2)
O(3)	−2698(3)	6419(1)	2388(4)	65(2)	65(2)	99(2)	−2(1)	38(2)	−2(1)
C(8)	−3580(5)	5809(2)	1590(8)	66(3)	62(3)	88(3)	6(3)	32(2)	4(2)
C(9)	−5374(6)	5964(3)	926(14)	61(3)	90(4)	155(6)	−3(4)	36(4)	7(3)
C(10)	1222(4)	4325(2)	2505(5)	60(2)	63(2)	55(2)	7(2)	24(2)	7(2)
C(11)	−116(5)	3902(2)	1503(6)	61(3)	75(3)	78(3)	−0(2)	31(2)	12(2)
C(12)	89(6)	3252(2)	1042(7)	81(3)	79(3)	88(3)	−11(2)	36(3)	2(3)
C(13)	1669(6)	3017(2)	1583(7)	100(4)	76(3)	82(3)	1(3)	47(3)	23(3)
C(14)	2994(6)	3425(2)	2608(7)	76(3)	91(3)	92(3)	4(3)	5(3)	23(3)
C(15)	2774(5)	4078(2)	3040(6)	60(3)	79(3)	77(3)	4(2)	33(2)	13(2)

TABLE 4. Selected interatomic distances (Å) and angles (deg)

Bond	Distance	Bond	Distance	Bond	Distance
O(1)—C(2)	1.393(4)	C(2)—N(3)	1.272(4)	N(3)—C(4)	1.405(4)
C(4)—C(5)	1.444(5)	C(5)—O(1)	1.397(4)	C(5)—O(2)	1.206(4)
C(4)—C(6)	1.358(4)	C(6)—C(7)	1.511(5)	C(6)—O(3)	1.339(4)
O(3)—C(8)	1.427(4)	C(8)—C(9)	1.519(6)	C(2)—C(10)	1.457(5)
C(10)—C(11)	1.387(5)	C(11)—C(12)	1.374(5)	C(12)—C(13)	1.396(6)
C(13)—C(14)	1.364(6)	C(14)—C(15)	1.377(6)	C(15)—C(10)	1.383(5)

Bond	Angle	Bond	Angle	Bond	Angle
C(5)—O(1)—C(2)	105.6(3)	O(1)—C(2)—N(3)	114.9(3)	C(2)—N(3)—C(4)	106.1(3)
N(3)—C(4)—C(5)	108.6(3)	C(4)—C(5)—O(1)	104.8(3)	O(1)—C(5)—O(2)	119.3(4)
C(4)—C(5)—O(2)	135.9(4)	N(3)—C(4)—C(6)	127.9(3)	C(5)—C(4)—C(6)	123.4(3)
C(4)—C(6)—C(7)	124.6(4)	C(4)—C(6)—O(3)	127.3(3)	C(7)—C(6)—O(3)	108.1(4)
C(6)—O(3)—C(8)	122.1(3)	O(3)—C(8)—C(9)	106.4(4)	O(1)—C(2)—C(10)	116.5(3)
N(3)—C(2)—C(10)	128.5(3)	C(2)—C(10)—C(11)	118.9(3)	C(2)—C(10)—C(15)	122.6(3)
C(15)—C(10)—C(11)	118.5(4)	C(10)—C(11)—C(12)	121.0(4)	C(11)—C(12)—C(13)	119.3(5)
C(12)—C(13)—C(14)	120.1(4)	C(13)—C(14)—C(15)	120.1(4)	C(14)—C(15)—C(10)	120.9(4)

isomer was converted to the Z material for short reaction periods. Longer reaction times resulted in hydrolysis to compound **11**. Since **9** had very poor water solubility, its solution in concentrated HBr suggested that it became highly protonated and that this state further increased the thermodynamic stability of the Z isomer. The experiment unfortunately does not define the site of protonation.

Photo-irradiation proved to be generally applicable in isomerizing both the oxazolone and thiazolone series of compounds. Photostationary states were formed from which both E and Z isomers could be isolated. The only alkoxyethylidene compound which did not undergo isomerization to an isolable E isomer in chloroform solution with 300-nm wavelength radiation was 4-(1-ethoxyethylidene)-2-thioxo-5-thiazolidinone, **19**. The only isolated, or detected, isomer of **19** was assigned the Z geometry because short term, base catalysed methylation with methyl iodide led to the kinetic formation of (Z)-**14** (see Table 1), while longer reaction times in the presence of base gave a mixture of (E and Z)-**14**.

X-ray and conformational analysis

The molecule, (Z)-**5**, is shown in Fig. 4 and selected interatomic distances given in Table 4. The molecule (except for hydrogen atoms) is essentially planar, although there are minor deviations, the largest distances out of the oxazolone ring plane being C(6) 0.055(4), C(7) 0.136(6), O(3) 0.065(3), and C(9) −0.087(9) Å. The geometry is Z and there is evidence of some very strong repulsive interactions. One can compare bond distances and angles observed here with those observed in the structure of the related 4-(2,4-dinitro)benzylidene-2-phenyloxazolin-5-one, **3** (7). Bond angles within the oxazolone and phenyl rings of both compounds are not significantly different, nor are the bond lengths within the phenyl ring. There are significant differences in the two compounds for bond lengths within the oxazolone rings and in the olefinic bonds that are consistent with less delocalization in the C(4)—N(3)—C(2)—O(1) system of **5** and more delocalization in the C(6)—C(4)—C(5)—O(2) system of **5** than in the corresponding systems of **3**. This is caused by the interaction of the C(6)—C(4)—C(5)—O(2) system of **5** with O(3). The multiple bond character in the C(6)—O(3) bond is considerable. This bond is short (1.339(4) Å) and at the low end of the range of values of 1.35−1.73 Å observed in CH_3—O—aryl (ref. 18, and references therein) or aryl—O—aryl ethers (ref. 19, and

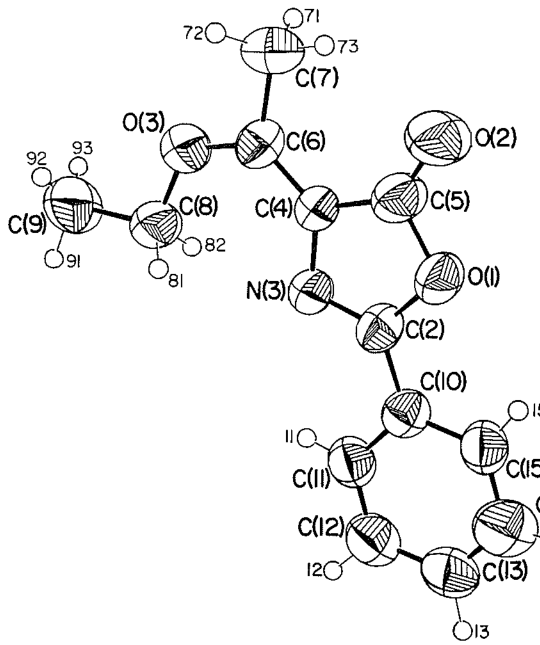

FIG. 4. The molecule 4-[(2)-1-ethoxyethylidene]-2-phenyl-5-oxazolone showing the atom numbering. Hydrogen atoms are indicated by affixes only and smaller numbers.

references therein). Further, the C(6)—O(3)—C(8) angle (122.1(3)°) is much larger than the angles usually found in CH_3—O—aryl ethers (range 116−119°) and is comparable to the value found in the ditropylium ether cation (123.6(5)°) and diaryl ethers (20). That the angle is so large must be caused by very extreme delocalization and strong π bonding to O(3), since there is obvious crowding at C(6). The crowding can be seen best by comparison with **3** and is caused by the repulsive interaction between the C(8) methylene group and N(3) together with the repulsive interaction between the C(7) methyl group and O(2). These effects cause the angles C(5)—C(4)—C(6) and C(4)—C(6)—C(7) to be larger than corresponding angles in **3** (123.4(3)°, 124.6(4)° versus 120.8°, 119°). N(3)— C(4)—C(6) and C(4)—C(6)—O(3) (127.9(3)°, 127.3(3)°) are much larger than the expected olefinic angle of 120°, because of the repulsive interaction of C(8) and the oxazolone ring. Nevertheless, they are significantly less than those observed in **3** (131.2°, 128.9°) because the two hydrogen atoms H(8, 1), H(8, 2) fit around the N(3) atom rather than pointing straight at it as does the phenyl hydrogen in **3**, and this allows a closer approach of C(8). Further evidence of crowding is shown by the very small C(7)—C(6)—O(3) angle of 108.1(4)°. While such angles at the ends of olefins have been observed when the attached atoms are part of a ring, such as N(3)—C(4)—C(5) (108.6°) and the corresponding angle in **3** (108.0°), to our knowledge angles this small have not been observed in normal olefins.

Once these restraints are put in place, the complete arrangement of the molecule is determined. The methyl group at C(7) is oriented such that H(7,1) and H(7,2) fit on either side of O(3) giving a short H(7,3)—O(2) distance (2.26 Å). Nevertheless, this is comparable to the O(1)—H(15) distance of 2.39 Å; apparently the greater electronegativity of oxygen allows much shorter C—H . . . O distances than in C—H . . . N, possibly because of weak hydrogen bonding. Similarly the CH_2 group at C(8) is oriented to put H(8, 1) and H(8, 2) on either side of N(3), giving H . . . N distances (H(8, 1) 2.45 Å; H(8, 2), 2.63 Å) comparable to N(3)—H(11) 2.60 Å and those in **3**, and ensuring C(9) is essentially coplanar with the remainder of the molecule.

Because a molecule is planar in the solid state does not mean it remains so in solution. Nevertheless, physical and spectroscopic data (see below) suggest that (*Z*)-**5** and related oxazolone isomers do indeed retain a preferred planar conformation in solution. We assume that this is caused by the very strong delocalization on to O(3). In addition there would be a substantial barrier to the C(8) methylene group moving past the C(7) methyl group, largely because of the extraordinarily small C(7)—C(6)—O(3) angle. In the most favourable orientation, and using the parameters herein, the C(7) . . . C(8) distance would be 2.58 Å, much less than the sum of the van der Waals radii. Similarly, the calculated H . . . H distance of 1.68 Å is much less than the van der Waals distance of 2.58 Å. Similar calculations show why this *Z* isomer is more stable than the *E* isomer. The calculated O(3) . . . O(2) distance of 3.17 Å in the *E* isomer is acceptable, but the C(7)—H . . . N(3) distances, ranging from 1.77 to 1.79 Å depending on the orientation, are very much shorter than typical values of 2.45−2.6 Å. Even a change in the angles at the olefin to shorten the O(2) . . . O(3) distance and increase the N . . . H distances does not give as favourable an arrangement as that observed for the *Z* isomer.

The packing of the molecules in the unit cell is shown in Fig. 5. Molecules are arranged in stacks along the **c** direction at $x = 1/2$, $y = 1/4, 3/4$. Adjacent molecules in a particular stack are related by the **c** glide plane so they are arranged head-to-tail and are roughly parallel, which maximizes the $\pi-\pi$ interactions. The molecules in a particular stack are tilted with respect to the stack direction, the tilt being in opposite directions in the stacks at $z = 1/4$ and $z = 3/4$. There is some overlap between these stacks in the **b** direction. In the **a** direction contact between stacks occurs near the **bc** plane and is between pairs of ethoxy groups and also between the phenyl ring on one molecule and the oxazolone ring on the adjacent molecule. All interactions are of the van de Waals type.

That the conformation adopted by the ethoxy side chain in (*Z*)-**5** (Fig. 3) in the solid state and, by analogy, the other (*Z*) isomers, is most likely preserved in solution phases was suggested by two pieces of experimental evidence: firstly, (*Z*)-**5** showed low polarity on chromatographic supports in contrast to the *E* isomer, and secondly, the relatively large deshielding (0.2−0.4 ppm) of the OCH_2 protons in the ^{1}H nmr spectrum of (*Z*)-**5** in comparison (*E*)-**5**, together with the downfield shift of the OCH_2 carbon (C(8)) in the ^{13}C nmr spectrum of (Z)-**5**. The low polarity of (*Z*)-**5** is consistent with the N(3) eclipsed conformation being the preferred conformation in solution, since this conformation has the N(3) atom effectively buried by the two hydrogen atoms attached to C(8) and therefore no longer a polar site in the molecule. Adsorption on a silica gel surface is thus restricted to the carbonyl and lactone oxygens, O(1) and O(2). The *E* isomer, on the other hand, has N(3) buttressed by a methyl group but with the lone pair still available for interaction with a silica surface and this, together with O(1) and O(2), gives the *E* isomer three polar interacting sites and thus higher chromatographic polarity. If the *Z* isomer were to possess significant conformer populations, with the ethyl fragment of the ethoxy group either out of the oxazolone ring plane or with C(8) adjacent to the C(7) methyl (see Fig. 6(a)), N(3) would lose its steric shielding and be free to interact with a silica surface. The chromatographic polarity of both *E* and *Z* isomers would then be expected to be similar.

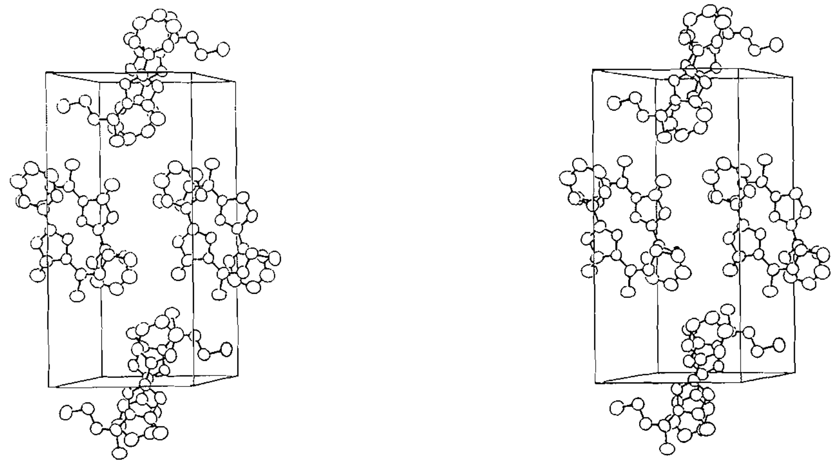

FIG. 5. The packing of the molecule within the unit cell. **a** and **b*** are parallel to the bottom and side of the page respectively and the view is down **c***. Hydrogen atoms have been omitted for clarity.

The [1]H nmr spectrum of (Z)-**5** showed the OCH_2 protons to be deshielded by 0.43 ppm relative to those in (*E*)-**5**. This large deshielding is again consistent with (Z)-**5** retaining the solid state, N(3) eclipsed, conformation in solution. Significant population of conformations either with C(8) out of the oxazolone plane or with C(8) close to the C(7) methyl would reduce the intense deshielding effects arising from the C(2)−N(3) double bond and the N(3)... CH_2 hydrogen steric compressions. Comparison with the *E* isomer shows that the OCH_2 group can take up conformations where C(8) is either adjacent to O(2) or to C(7) or slightly out of the oxazolone ring plane (see Fig. 6(b) and (C)). The first two conformations show strong steric compressions and the C(8)... O(2) arrangement expected to show intense deshielding arising from the carbonyl group anisotropy. The C(8) protons in the *E* isomer, occurring at 4.30 ppm, are thus anticipated to be deshielded relative to an unhindered ethoxy − vinyl ether system (for example, in (Z)-4-ethoxypent-3-en-2-one the ethoxy CH_2 signal occurs at 4.11 ppm (21)). The greater deshielding experienced by the *Z* isomer CH_2 (ca. 4.5 ppm) is therefore strong evidence for the N(3) eclipsed conformation being preferred in solution.

The [13]C nmr spectra of (Z)-**5** and (*E*)-**5** provide further compelling evidence for the conformational preference of the ethoxy group in solution. Comparison of the chemical shift of C(8) in both isomers shows the *Z* isomer C(8) resonance to be 2.6 ppm downfield from that of the *E* isomer. This is consistent with (Z)-**5** retaining the N(3) eclipsed conformation since N(3) is an atom which is in a δ-position with respect to C(8) and such arrangements are known to produce deshielding effects (22). If the conformation with the C(8) CH_2 group adjacent to the C(7) methyl (see Fig. 6(a)) were significantly populated, then an upfield shift would be anticipated because these two carbons are in a γ-relationship to each other (22). Any other conformation with C(8) out of the oxazolone ring plane would likewise reduce the deshielding effect of N(3). The chemical shift of C(8) in the *E* isomer is probably dominated by the shielding γ-effect arising from the conformation with C(8) and the C(7) methyl juxtaposed (Fig. 6(c)). The conformation with C(7) adjacent to O(2) is equivalent to a δ-interaction and little is known of such interactions. They are most likely deshielding in nature by analogy with O and N atom δ-effects (23).

It is interesting to note that the chemical shift of the C(7) methyl group in the series of *E* and *Z* isomers is consistent with the expected γ and δ effects of N and O atoms (see Table 1). Thus the *Z* isomers, with O(2) in a δ-position with respect to C(7), show the C(7) signals to be deshielded, while the *E* isomers, with N(3) in a γ-position with respect to C(7), show the C(7) signals to be shielded.

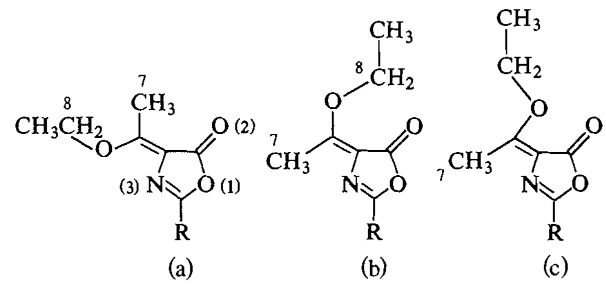

FIG. 6. Possible conformations of the ethoxy side chain in (a), (*Z*)-4-(1-ethoxyethylidene)-5-oxazolones, and (b), (c), (*E*)-4-(1-ethoxyethylidene)-5-oxazolones.

Experimental

Melting points were recorded on a Kofler micro hot stage apparatus and are uncorrected. Proton magnetic resonance ([1]Hmr) spectra were recorded on a Varian EM-390 spectrometer in deuteriochloroform using tetramethylsilane (TMS) as internal standard except where noted otherwise. The abbreviations s = singlet, d = double, t = triplet, q = quartet, and m = multiplet are used in the description of the spin−spin splitting patterns present in the spectra. The natural abundance carbon-13 magnetic resonances ([13]Cmr) were recorded on a Bruker WP80 instrument (at 20.115 MHz) in deuteriochloroform with TMS as the internal standard except where noted. Low resolution mass spectra (ms) and high resolution mass spectra (hrms) were recorded at 70 eV on a Micromass 7070F double focusing mass spectrometer, the samples being introduced through a direct inlet system. Infrared spectra (ir) were recorded on a Perkin Elmer 283 spectrometer. Liquid ir samples were run neat, while solids were prepared in potassium bromide discs (unless indicated otherwise). The symbols (s) = strong, (m) = medium, and (w) = weak are used in recording of ir data to indicate the intensity of the recorded bands.

Diazomethane was prepared by the method of de Boer and Backer (24) using ethereal *N*-methyl-*N*-nitroso-*p*-toluenesulfonamide (Diazald) in alcoholic sodium hydroxide.

Column chromatography was carried out using silica gel 60 (E. Merck Co. suppliers) of 0.063−0.200 mm particle size (70−230 mesh ASTM). Samples of low solubility were introduced onto the chromatographic column in a minimum volume of chloroform.

Silica gel 60 F_{254} (F. Merck Co.) plates of 0.2-mm thickness were used for analytical thin layer chromatography (tlc).

Collection of diffraction data

A homogeneous prismatic crystal was used for the X-ray studies and precession photographs showed the crystal was monoclinic. The cell parameters were obtained by least-squares refinement from the setting angles of 15 automatically centred reflections ($17° < 2\theta < 27°$) on a Nicolet P3 diffractometer with use of graphite monochromatized MoKα radiation (λ 0.71069 Å). Crystal data and other numbers related to the data collection are given in Table 2. The density was measured by flotation in aqueous zinc bromide solution. Intensity data were measured with used of the P3 diffractometer and a coupled θ(crystal) − 2θ(counter) scan. The methods of selection of scan rates and initial data treatment have been described (25, 26) (limits, from 4.88 to 29.3 deg min^{-1}). Corrections were made for Lorentz polarization effects, but not for absorption. This will introduce a maximum error in F_o of <0.1%.

Solution of the structure

The phases were determined by direct methods with use of 50 reflections with $|E| > 1.5$ and 12 sets of starting phases. A series of full-matrix least-squares refinements followed by electron density difference syntheses revealed all the atoms. In all further refinements the positional parameters of all atoms, isotropic temperature factors of hydrogen atoms, and anisotropic temperature factors of all other atoms were varied. Full-matrix least-squares refinement, which minimized the function $\Sigma w(|F_o| - |F_c|)^2$, was terminated when the maximum shift/error was <0.2. Corrections were made for secondary extinction by the method used in SHELX.[4] Scattering curves were taken from Cromer and Waber (27) and did not include corrections for anomalous dispersion effects.

2-Benzylthio-4-[E and Z-1-ethoxyethylidene]-5-thiazolone, ***13***

The method of Knott (28) for the preparation of **13** was used with some modifications.

To 0.75 mL of acetic anhydride were added 50.5 mg (0.27 mmol) of *N*-dithiocarbobenzyloxyglycine, **20** (29). This mixture was swirled and warmed on a steam bath until dissolution of the solid. The mixture was removed from the heat source and one crystal of toluenesulfonic acid (approximately 1 mg) was added. Immediately following this, 42 μL (37 mg. 0.27 mmol) triethyl orthoacetate was added, the mixture swirled to ensure homogeneity and replaced on the steam bath for 10 min. Upon removal from the heat, the mixture was diluted with 1 mL saturated sodium bicarbonate solution and 5 mL water and extracted twice with chloroform. The chloroform layer was dried with anhydrous sodium sulfate, filtered, and the volatiles removed, initially by rotoevaporator distillation and, finally, by evacuation at 0.5 Torr (1 Torr = 133.3 Pa) overnight. This left 61 mg of **13** as a yellow oil (quantitative yield) with a 5:1 ratio of *Z*/*E* isomers as indicated by ^{1}Hmr spectroscopy. This mixture was sufficiently pure for further experiments. Small quantities of **13** were purified by Kugelrohr distillation at 190−200°C and 0.3 Torr (lit. (28) bp 208°C at 1 Torr) without substantial losses because of polymerization. Otherwise, purification and isomer separation were effected by flash column chromatography on silica gel (7% ethyl acetate in 30−60 petroleum ether). An experiment using 233 mg of **20**, after chromatography through a 2 mm × 0.15 m column of silica gel, gave 192 mg of pure *Z* isomer (67% yield). Compound **13** showed: tlc (25% ethyl acetate in petroleum ether): R_f 0.65 (*Z*) 0.33 (*E*); ir, ν_{max}: 2986 (m), 1694 (s) (C=O), 1640 (m) (C=N), 1602 (m, shoulder), and 1574 (s) (exocyclic C=C) cm^{-1}; ^{1}Hmr, Z, δ: 1.39 (t, *J* = 7 Hz, 3H, ether CH_3), 2.44 (s, 3H, vinyl CH_3), 4.40 (s, 2H, benzyl CH_2), 4.55 (q, *J* = 7 Hz, 2H, ester CH_2), 7.22−7.44 (m, 5H, aromatic); *E*, δ: 1.43 (t, *J* = 7 Hz, 3H, ether CH_3), 2.54 (s, 3H, vinyl CH_3), 4.27 (q, *J* = 7 Hz, 2H, ether CH_2), and 7.22−7.44 (m, 5H, aromatic); ^{13}Cmr, (*Z*), δ: 154.0(152.6) (C-2), 129(128.2) (C-4), 193.3(192.3) (C-5), 165.2(165.9) (C-6), 17.4(16.5) (C-7), 68.3(68.2) C-8), 15.4(14.9) (C-9), 35.2(34.8) (benzyl CH_2), 136.5(137.0) (*ortho* C), 129.0(129.1) (*meta* C), 128.7(128.5) (*para* C), 127.6(127.4) (subst. C) (shifts in parentheses were recorded in acetone-d_6 solvent); (*E*), δ: 169.7 (C-6), 16.5 (C-7), 65.8 (C-8), 14.9 (C-9), 34.8 (benzyl CH_2), 137.0 (*ortho* C), 129.1 (*meta* C), 128.5 (*para* C), 127.4 (subst. C) (signals for C-2, 4, and 5 were too weak to be observed above noise); hrms calcd. for $C_{14}H_{15}NO_2S_2$: 293.0477; found: 293.0521; ms, *m*/*z* (RI%): 293 (25) and 91 (100).

*2-Ethoxy-4-[(Z)-1-ethoxyethylidene]-5-thiazolone, (Z)-**15***

The method of Knott (28) for the preparation of **13** was used with some modification.

To 14 mL of acetic anhydride was added 0.870 g (5.34 mmol) of *N*-thiocarbethoxyglycine (30). This mixture was swirled and warmed on a steam bath until dissolution of the solid. The mixture was removed from the heat source, after which 8 mg (0.05 mmol) of toluenesulfonic acid and 1.5 mL (1.3 g, 8.0 mmol) of triethyl orthoacetate were added in rapid succession. The solution was swirled to ensure homogeneity and replaced on a steam bath for 5 min. After removal from the steam bath, the volatiles were removed by rotoevaporator distillation with strong heating (forced air heater) and then by evacuation for 30 min. Flash column chromatography of the residue on silica gel (7.5% ethyl acetate in petroleum ether) gave 0.288 g (25%) of pure (*Z*)-**15** as a pale yellow oil. Some *E* isomer was also present in the crude reaction mixture, as evidenced by tlc. Separation of this isomer was not possible from other side-products by the chromatography method employed. The *E*/*Z* ratio in the crude mixture was not determined. Compound (*Z*)-**15** showed: ir, ν_{max}: 1699 (s) (CO), 1606 (s) (C=N), and 1570 (s) (C=C) cm^{-1}, ^{1}Hmr, δ: 1.38 (t, *J* = 7 Hz, 6H, both ethyl CH_3's), 2.40 (5, 3H, vinyl CH_3), 4.43 (q, *J* = 7 Hz, 2H, 2-ethoxy CH_2), and 4.50 (q, *J* = 7 Hz, 2H, vinyl ethoxy CH_2); ^{13}Cmr (acetone-d_6), (*Z*), δ: 157.7 (C-2), 126.7 (C-4), 191.4 (C-5), 162.7 (C-5), 162.7 (C-6), 17.5 (C-7), 67.9 (C-8), 15.2 (C-9), 65.5 (ethoxy CH_2), 14.0 (ethoxy CH_3); (*E*), δ: 158.0 (C-2), 129.1 (C-4), 194.2 (C-5), 164.5 (C-6), 16.0 (C-7), 65.0[a] (C-8), 14.8 (C-9), 65.4[a] (ethoxy CH_2), 14.0 (ethoxy CH_3); ((a), assignments may be reversed); hrms calcd. for $C_9H_{13}NO_3S$: 215.0616; found: 215.0613; ms, *m*/*z* (RI%): 215 (95) [M^+]. 187(40), 172(15), 159(100) [$M^+ - C_3H_4O$], 141(60), 71(75), 70(35), and 56(30).

4-[(Z)-1-Ethoxyethylidene]-2-thiono-5-thiazolinone, ***19***

The method of Cook *et al.* (31), with modification, was used for the preparation of the 4-ethoxymethylene analogue.

After dissolution of 92.2 mg (0.69 mmol) of 2-mercapto-4*H*-5-thiazolone (see the following preparation) in 2 mL warm acetic anhydride, 79 μL (83 mg, 1.38 mmol) were added in rapid succession. Immediately, the reaction flask was swirled to ensure homogeneity and placed on a steam bath for 10 min. On removal from the steam bath, the volatiles were removed by rotoevaporator distillation (25 Torr) with strong heating (forced-air heater). The solid residue was recrystallized from absolute ethanol (decolourizing charcoal) to give 80.2 mg (57%) of **19**, the pure *Z* isomer, as tan crystals, mp 185−186°C. Compound **19** showed: ir, ν_{max}: 1703 (s) (C=O), 1682 (m) (C=N), and 1607 (s) (C=C) cm^{-1}; ^{1}Hmr ($CDCl_3$, δ: 1.42 (t, *J* = 7 Hz, 3H, ester CH_3), 2.46 (s, 3H, vinyl CH_3), 4.24 (q, *J* = 7 Hz, 2H, ester CH_2); (acetone-d_6), δ: 1.38 (t, *J* = 7 Hz, 3H, ester CH_3), 2.20 (s, 1H, SH), 2.51 (s, 3H, vinyl CH_3), and 4.36 (q, *J* = 7 Hz, 2H, ether CH_2); ^{13}Cmr (acetone-d_6), (*Z*), δ: 184.1 (C-2),[a] 120.7 (C-4), 186.1 (C-5),[a] 155.2 (C-6), 12.2 (C-7), 65.5 (C-8), 14.4 (C-9); ((a), assignments may be reversed). Observation of long-range coupling between the 15.0 and 66.1 ppm resonances during a gated decoupling experiment definitively assigned the two methyl signals. hrms calcd. for $C_7H_9NO_2S_2$: 203.0075; found: 203.0082; ms, *m*/*z* (RI%): 203(100), 175(45), 141(50), 113(20), and 71(35).

2-Mercapto-4H-5-thiazolone

2-Mercapto-4*H*-5-thiazolone was prepared by the method of Cook *et al.* (31) from glycinamide and also directly from the commercially

---

[4]All calculations were carried out on CYBER 170/730 and 815 computers. Initial data treatment used the XRAY 76 package (39). Structure solution and refinement was done by use of the SHELX package (40), and diagrams were prepared with use of ORTEP II (41).

available glycinamide hydrochloride as described below.

Glycinamide hydrochloride (1.00 g, 9.05 mmol), potassium carbonate (1.25 g, 9.06 mmol), and potassium hydroxide (0.51 g, 9.1 mmol) were dissolved in 5 mL water. Into this solution was added 0.60 mL (0.76 g, 10 mmol) carbon disulfide. The mixture was stirred vigorously for 5.5 h at room temperature after which 2.0 mL 50% sulfuric acid was added rapidly (**caution: effervescence!**) with continued stirring. After about 30 s, as a yellow precipitate was formed, the solution was diluted with 5 mL water. Stirring continued a further 30 min after which the precipitate was filtered, washed with water, and dried *in vacuo*, giving 0.509 g of product (42%). This sample was sufficiently pure for subsequent preparations; mp (dec.) >300°C (lit. (31) mp (dec.) >300°C); ^{1}Hmr (acetone-d_6), δ: 2.75 (br s, 1H, —SH) and 4.70 (s, 2H, methylene).

2-Benzyl-4-[(Z)-1-ethoxyethylidene]-5-oxazolone, (Z)-6

The preparation of 4-(1-ethoxyethylidene)-5-oxazolones (or, in general, 4-(1-akloxyalkylidene)-5-oxazolones) by the action of triethyl orthoacetate (or other orthoesters) and acetic anhydride on *N*-acylglycines is well documented in the literature (15, 16, 32).

To a hot solution of *N*-(phenylacetyl)glycine (33) (1.04 g, 5.39 mmol) in 12 mL acetic anhydride was added 3.0 mL triethyl orthoacetate (2.6 g, 16 mmol) and the solution heated on a steam bath for 20 min. After this, the solvent was removed with strong heating (forced-air heater) at reduced pressure (25 Torr). The crude product, after eluting through a 20 mm × 0.18 m silica gel column with 10% ethyl acetate in petroleum ether, provided 0.580 g of pure **6** (44%) as a pale yellow oil that solidified on standing overnight (mp 37–41°C).

Compound (Z)-**6** showed: ir, ν_{max}: 2990 (m), 2932 (m), 1795 (m), 1762 (s) (C=O), 1693 (s) (C=N), 1604 (s), and 1595 (s) (exocyclic C=C) cm^{-1}; ^{1}Hmr, δ: 1.39 (t, J = Hz, 3H, ether CH_3), 2.44 (s, 3H, vinyl CH_3), 3.83 (s, 2H, benzyl CH_2), 4.57 (q, J = 7 Hz, 2H, ether CH_2), and 7.33 (br s, 5H, aromatic); ^{13}Cmr, δ: 158.2 (C-2), 114.3 (C-4), 168.7 (C-5), 166.5 (C-6), 16.5 (C-7), 68.1 (C-8), 15.2 (C-9), 35.6 (C-10), 134.2 (C-11), 128.8 (C-12), 129.1 (C-13), 127.3 (C-14); hrms calcd. for $C_{14}H_{15}NO_3$: 245.1052; found: 245.1023; ms, m/z (RI%): 245 (10), 118 (35), 91 (100), and 65 (25).

2-(1,1-Dimethylethyl)-4-[(Z)-1-ethoxyethylidene]-5-oxazolone, (Z)-7, 4-[(Z)-1-ethoxyethylidene]-2-phenyl-5-oxazolone, (Z)-5, 2-(4-bromophenyl)-4-[(E and Z)-1-ethoxyethylidene]-5-oxazolone, 8, and 2-(4-chlorophenyl)-4-[(E and Z)-1-ethoxyethylidene]-5-oxazolone, 9

The products (Z)-**7**, (Z)-**5**, **8**, and **9** were obtained from *N*-pivaloylglycine, (prepared as in ref. 34; recrystallized from acetone – petroleum ether), *N*-benzoyglycine (Eastman suppliers), *N*-(4-bromobenzoyl)glycine (35, 36), and *N*-(4-chlorobenzoyl)glycine (35, 36), respectively, using the procedure described above (for the *Z*-benzyl analogue) with the following changes:

In the preparation of (Z)-**7**, the *N*-pivaloylglycine in acetic anhydride was heated on a steam bath for 5 min before triethyl orthoacetate addition. Column chromatographic purification utilized 5% ethyl acetate in petroleum ether. Yield of (Z)-**7** from 222 mg of pivaloylglycine was 188 mg (64%) of a light yellow oil, which solidified in the refrigerator on storage (mp 35–38°C).

In the preparation of **5** both *E* and *Z* isomers were present in the crude mixture in a ratio of 1:5 (*E*/*Z* as indicated by ^{1}Hmr spectroscopy). The pure *Z* isomer was obtained by recrystallization from absolute ethanol or ethanol–water (mp 111–112°C; lit. (16, 17) mp 112–113°C, (32) mp 113°C). A yield of 1.34 g (52%) was obtained from 2.0 g (11 mmol) *N*-benzoylglycine.

In the preparation of **8**, both *E* and *Z* isomeric products cocrystallized on recrystallization of the crude mixture from absolute ethanol, giving a 1:4 ratio of *E* to *Z* (as determined by ^{1}Hmr spectroscopy; yellow-orange plates, mp 116–124°C). A yield of 0.341 g (65%) was obtained from 0.441 g (1.7 mmol) of *N*-(4-bromobenzoyl)-glycine. Flash chromatography of 0.278 g of this mixture of isomers (10% ethyl acetate in petroleum ether as the eluant) gave 0.215 g (45%) of pure *Z* isomer (yellow-orange plates from absolute ethanol, mp 128.5–129.5°C) and 55 mg (12%) of the pure *E* isomer (cream-coloured needles from absolute ethanol, mp 142.0–143.0°C); tlc of (*E* and *Z*)-**8** (developed with 10% ethyl acetate in petroleum ether) gave R_f 0.08 (*E*) and 0.36 (*Z*).

Similarly, 1.39 g (6.53 mmol) of *N*-(4-chlorobenzoyl)glycine gave 1.32 g (76%) of a co-crystalline mixture of *E* and *Z* isomers of **9** (1:4 ratio as determined by ^{1}Hmr spectroscopy). Flash chromatography of 0.503 g of this mixture (20% ethyl acetate in petroleum ether as eluant) gave 0.398 g *Z* isomer (orange plates from absolute ethanol, mp 122.5–123.0°C, 60% yield) and 90.8 mg *E* isomer (colourless needles from absolute ethanol, mp 130–132°C, 14%); tlc of (*E* and *Z*)-**9** (developed with 30% ethyl acetate in petroleum ether) gave R_f 0.18 (*E*) and 0.52 (*Z*).

Compound (Z)-**7** showed: ir, ν_{max}: 1788 (s) (C=O), 1764 (s) (C=O), 1643 (s) (C=N), and 1598 (s) cm^{-1}; ^{1}Hmr, δ: 1.28 (s, 9H, *tert*-butyl), 1.38 (t, J = 7 Hz, 3H, ether CH_3), 2.42 (s, 3H, vinyl CH_3), and 4.64 (g, J = 7 Hz, 2H, ether CH_2); ^{13}Cmr (acetone-d_6), δ: 165.2 (C-2),[a] 113.8 (C-4), 168.6 (C-5), 165.5 (C-6),[a] 16.8 (C-7), 68.8 (C-8), 14.9 (C-9), 33.6 (C-9), 33.6 (C-10), 26.9 (C-11); ((a), assignments may be reversed); hrms calcd. for $C_{11}H_{17}NO_3$: 211.1208; found: 211.1217; ms, m/z (RI%): 211 (15), 183 (10), 168 (15), 167 (15), and 57 (100).

Compound (Z)-**5** showed: ir, ν_{max}: 1786 (m), 1758 (s) (C=O), 1640 (s) (C=N), 1602 (m), and 1587 (s) (exocyclic C=C) cm^{-1}; ^{1}Hmr δ: 1.43 (t, J = 7 Hz, 3H, ether CH_3), 2.49 (s, 3H, vinyl CH_3), 4.73 (q, J = 7 Hz, 2H, ether CH_2), 7.36–7.53 (m, 3H, aromatic), and 7.92–8.07 (m, 2H, aromatic); ^{13}Cmr, δ: 155.4 (C-2), 116.4 (C-4), 168.6 (C-5), 166.9 (C-6), 17.6 (C-7), 69.0 (C-8), 15.3 (C-9), 127.0 (C-10), 127.0 (C-11), 128.7 (C-12), 131.3 (C-13).

Compound (*E*)-**8** showed: ir, ν_{max}: 1793 (s), 1770 (m), 1645 (s), 1597 (s), and 1584 (s) cm^{-1}; ^{1}Hmr δ: 1.45 (t, J = 7 Hz, 3H, ether CH_3), 2.53 (s, 3H, vinyl CH_3), 4.35 (q, J = 7 Hz, 2H, ether CH_2), 7.58 and 7.84 (AA′ BB′, J_{ortho} = 9 Hz, 2H and 2H, aromatic); ^{13}Cmr, δ: 154.9 (C-2), 118.4 (C-4), 169.4 (C-5), 163.5 (C-6), 15.9 (C-7), 66.5 (C-8), 15.2 (C-9), 125.9 (C-10),[a] 128.4 (C-11), 132.0 (C-12), 126.1 (C-13);[a] ((a) assignments may be reversed); hrms calcd. for $C_{13}H_{12}NO_3Br$: 309.0000; found: 309.0046; ms, m/z (RI%): 283 (20), 281 (20), 265 (20), 263 (20), 185 (100), 183 (100), 157 (30), 155 (30), 104 (10), 76 (30), and 75 (20).

Compound (Z)-**8** showed: ir, ν_{max}: 1792 (s), 1762 (m), 1637 (s), 1592 (s), and 1581 (s) cm^{-1}; ^{1}Hmr, δ: 1.45 (t, J = 7 Hz, 3H, ether CH_3), 2.51 (s, 3H, vinyl CH_3), 4.72 (q, J = 7 Hz, 2H, ether CH_2), 7.58 and 7.85 (AA′ BB′, J_{ortho} = 9 Hz, 2H and 2H, aromatic); ^{13}Cmr, δ: 154.5 (C-2), 114.9 (C-4), 168.2 (C-5), 167.4 (C-6), 17.6 (C-7), 69.1 (C-8), 15.2 (C-9), 125.5 (C-10), 128.5 (C-11), 132.0 (C-12), 126.3 (C-13); hrms calcd. for $C_{13}H_{15}NO_3Br$: 309.0000; found: 309.0059; ms: indistinguishable from the *E* isomer.

Compound (*E*)-**9** showed: ir, ν_{max}: 1792 (s) (C=O), 1769 (m) (C=O), 1644 (s) (C=N), 1599 (m), and 1583 (s) cm^{-1}; ^{1}Hmr, δ: 1.47 (t, J = 7 Hz, 3H, ether CH_3), 2.55 (s, 3H, vinyl CH_3), 4.37 (q, J = 7 Hz, 2H, ethyl CH_2), 7.43 and 8.94 (AA′ BB′, J_{ortho} = 9 Hz, 2H and 2H, aromatic); ^{13}Cmr, δ: 154.9 (C-2), 118.4 (C-4), 169.2 (C-5), 163.6 (C-6), 15.9 (C-7), 66.5 (C-8), 15.2 (C-9), 125.5 (C-10), 128.2 (C-11), 129.1 (C-12), 137.6 (C-13); hrms calcd. for $C_{13}H_{12}NO_3Cl$: 265.0506; found: 265.0502; ms, m/z (RI%): 267 (5) and 265 (15) [M^+], 239 (3), 237 (10), 221 (3), 219 (10), 141 (30), 139 (100), 113 (10), 111 (30), and 75 (15).

Compound (Z)-**9** showed: ir, ν_{max}: 1791 (s) (C=O), 1762 (m) (C=O), 1637 (s) (C=N), 1596 (m), 1580 (s) cm^{-1}; ^{1}Hmr, δ: 1.44 (t, J = 7 Hz, 3H, ether CH_3), 2.52 (s, 3H, vinyl CH_3), 4.74 (q, J = 7 Hz, 2H, ether CH_2), 7.43 and 8.95 (AA′ BB′, J_{ortho} = 9 Hz, 2H and 2H, aromatic); ^{13}Cmr, δ: 154.5 (C-2), 115.0 (C-4), 168.3 (C-5), 167.4 (C-6), 17.5 (C-7), 69.1 (C-8), 15.3 (C-9), 125.2 (C-10), 128.4 (C-11), 129.1 (C-12), 137.8 (C-13); hrms calcd. for $C_{13}H_{12}NO_3Cl$: 265.0506; found: 265.0554; ms: indistinguishable from the *E* isomer.

4-[(Z)-1-Methoxyethylidene]-2-phenyl-5-oxazolone, (Z)-10

The oxazolone (Z)-**10** (mp 101–102°C from 95% ethanol, lit. (ref. 15, p. 830) 101–102°C from petroleum ether) was prepared by the action of diazomethane on the hydroxymethylene analogue (ref. 15, p. 830), which, in turn, was prepared by the method of

Attenburrow *et al.* (37) from acetic anhydride and sodium hippurate. Compound (Z)-**10** showed: ^{1}Hmr, δ: 2.55 (s, 3H, vinyl CH_3), 4.30 (s, 3H, OCH_3) 7.45–7.55 (m, 3H, aromatic), and 7.98–8.15 (m, 3H, aromatic); ^{13}Cmr, δ: 167.2 (C-2), 115.8 (C-4), 168.4 (C-5), 155.4 (C-6), 16.3 (C-7), 59.6 (C-8), 126.6 (C-10), 127.3 (C-11), 128.8 (C-12), 131.8 (C-13).

*2-Benzylthio-4-[(E)-1-hydroxyethylidene]-5-thiazolone, **16***

Hydrolysis of the 4-(1-alkoxyalkylidene) side chain of 5-thiazolones is analogous to those in the literature for the oxazolone series (15, 38). To thiazolone, (Z)-**13** (35 mg, 0.12 mmol), was added, with stirring, 2 mL of 2 *M* potassium hydroxide in 95% ethanol. The mixture was heated on a hot plate until most of the solid dissolved. The solution was cooled and decanted from the remaining residue and acidified (to litmus) with 1 *M* hydrochloric acid. The solution was diluted with 5 mL of water, extracted twice with chloroform, and the chloroform layer dried over anhydrous sodium sulfate. After removal of solvent (rotoevaporator and then vacuum; 0.5 Torr, 30 min), a light pinkish solid of the hydroxymethylene oxazolone **16** remained. After recrystallization from acetone–water a yield of **19** mg (60%) was obtained (mp 102–104°C). Compound **16** showed: ir, ν_{max}: 1680 (s) (C=O), 1655 (m) (C=N), 1578 (s), and 1570 (s) cm^{-1}; ^{1}Hmr, δ: 2.44 (s, 3H, CH_3), 4.35 (s, 2H, benzyl CH_2), 7.27–7.41 (m, 5H, aromatic), and 9.85 (br s, 1H, OH); hrms calcd. for $C_{12}H_{11}NO_2S_2$: 265.0231; found: 265.0217; ms, *m/z* (RI%): 265 (25) and 91 (100).

*2-Benzylthio-4-[(E)-1-methoxyethylidene]-5-thiazolone, (E)-**17***

Thiazolone **16** (10.2 mg, 38.5 mol) was dissolved in excess diazomethane in ether. After 10 min, the excess diazomethane was removed by passing a stream of nitrogen through the solution. Removal of solvent (by rotoevaporator) and purification by silica gel column chromatography (10% ethyl acetate in petroleum ether eluant) gave 4.4 mg (41%) of (*E*)-**17** as an oil. This was assigned the *E* stereochemistry from its ^{1}Hmr spectrum. Compound (*E*)-**17** showed: ^{1}Hmr, δ: 2.54 (s, 3H, vinyl CH_3), 4.01 (s, 3H, OCH_3), 4.36 (s, H, benzyl CH_2), and 7.26–7.40 (m, 5H, aromatic); ms, *m/z* (RI%): 279 (25) and 91 (100).

*4-[(E and Z)-1-ethoxyethylidene]-2-methylthio-5-thiazolone, **14***

Potassium carbonate (304 mg, 2.2 mmol), **19** (149 mg, 0.734 mmol), and methyl iodide (0.14 mL, 312 mg, 2.2 mmol) were stirred in 2 mL of acetone for 30 min. Following this, the mixture was diluted with 10 mL of water, extracted twice with chloroform, the chloroform layer dried over anhydrous sodium sulfate, and the solvent removed by rotoevaporator and then vacuum (0.5 Torr, 60 min) to give 145 mg (91%) of (Z)-**14** as an oil that solidified to tan coloured needles (mp 35.0–37.5°C) on standing. This product was one isomer only and was assigned the *Z* geometry from its ^{1}Hmr spectrum. When the reaction time was longer (approximately 14 h), an equilibrium mixture of the *E* and *Z* isomers was obtained (7:2 = *Z*/*E* as determined by ^{1}Hmr spectroscopy) as an oil. Compound **14** showed: ir, *Z*, ν_{max}: 3024 (s), 3000 (m), 2936 (m), 1695 (s) (C=O), 1672 (s) (C=N), and 1570 (exocyclic C=C) cm^{-1}; ^{1}Hmr, *Z*, δ: 1.40 (t, *J* = 7 Hz, 3H, ether CH_3), 2.45 (s, 3H, vinyl CH_3), 2.59 (s, 3H, SCH_3), and 4.53 (q, *J* = 7 Hz, 2H, ethyl CH_2); *E*, δ: 1.40 (t, *J* = 7 Hz, 3H, ethyl CH_3), 2.56 (s, 3H, vinyl CH_3), 2.59 (s, 3H, SCH_3), and 4.26 (q, *J* = 7 Hz, 2H, ether CH_2); ^{13}Cmr, (Z)-**14**, δ: 165.0 (C-2), 128.9 (C-4), 193.6 (C-5), 155.2 (C-6), 17.6 (C-7), 68.5 (C-8), 15.5 (C-9), 13.7 (C-10); (*E*)-**14** (acetone-d_6), δ: 165.9 (C-2), 128.5 (C-4), 153.9 (C-6), 17.1 (C-7), 68.8 (C-8), 15.1 (C-9), 13.0 (C-10); C-5 signal too weak to assign; hrms calcd. for $C_8H_{11}NO_2S_2$: 217.0231; found: 217.0251; ms, *m/z* (RI%): 217 (50), 189 (45), 142 (35), and 91 (100).

The three methyl resonances were definitively assigned by observation of long-range coupling between the 15.5 and 68.5-ppm resonances during a gated coupling experiment.

*2-Benzylthio-4-[(Z)]-1-ethoxyethylidene)-5-thiazolone, (Z)-**13** from **19***

With the same procedure as that given above, (Z)-**13** was prepared from potassium carbonate (44 mg, 0.37 mmol), **19** (25 mg, 0.123 mmol), and benzyl bromide (37 μL, 55 mg, 0.32 mmol) in 92% yield (23 mg). The product so prepared was identical by tlc and ^{1}Hmr spectroscopy to the Z isomer obtained by the action of triethyl orthoacetate on **20**.

*2-Benzylthio-4-[(EandZ)-(1-methoxyethylidene]-5-thiazolone, **17** and 4-[(E and Z)-1-methoxyethylidene]-2-methylthio-5-thiazolone, **18**, by alcoholic exchange*

Precedence for acidic exchange reactions of the alkoxy substituent of 4-(1-alkoxyethylidene)-5-thiazolones is given in the work of Knott (28).

The oxazolone (Z)-**14** (11.2 mg, 52 mmol) was dissolved in 1 mL of methanol and a stream of hydrogen chloride gas was passed through the solution for approximately 30 s (the resulting acid concentration was not determined). After 1 h at room temperature, the reaction was quenched with 5 mL saturated sodium bicarbonate and the resulting mixture extracted twice with chloroform, the chloroform layer dried over anhydrous sodium sulfate, and the solvent removed by rotoevaporation and evacuation at 0.5 Torr. The residue (10.1 mg, 96%) was a 1:3 ratio (as determined by ^{1}Hmr spectroscopy) of *E* to *Z* isomers of **18** (mp 83–90°C). These were the only products observed by tlc and ^{1}Hmr spectroscopy. Compound **18** showed: tlc (20% ethyl acetate in pet. ether): R_f 0.15 (*E*), 0.34 (Z); ir, ν_{max}; 1678 (s) (CO), 1655 (m) (CN), 1595 (s), 1572 (s) cm^{-1}); ^{1}Hmr (DMSO-d_6), *E*, δ: 2.58 (s, 3H, vinyl CH_3), 2.58 (s, 3H, SCH_3), and 3.98 (s, 3H, OCH_3); *Z*, δ: 2.50 (s, 3H, vinyl CH_3), 2.58 (s, 3H, SCH_3), and 4.09 (s, 3H, OCH_3); ms, *m/z* (RI%): 203 (50) [M^+], 174 (10), 156 (15) [$M^+ - SCH_3$], 91 (100) [CH_3SCS^+].

Similarly, a 1:3 ratio f *E* to *Z* isomers of **17** were prepared using the procedure above. Compound **17** showed: tlc (25% ethyl acetate – pet. ether): R_f 0.16 (*E*), 0.49 (*Z*); ir, ν_{max}: 1682 (s) (C=O), 1678 (s) (C=N), 1600 (m, shoulder), 1582 (s) cm^{-1}; ^{1}Hmr, δ: 2.54 (s, 3H, vinyl CH_3), 4.01 (s, 3H, OCH_3), 4.36 (s, H, benzyl CH_2), and 7.26–7.40 (m, 5H, aromatic); *Z*, δ: 2.48 (s, 3H, vinyl CH_3), 4.15 (s, 3H, OCH_3), 4.42 (s, 2H, benzyl CH_2), and 7.26–7.40 (m, 5H, aromatic); ^{13}Cmr, (Z)-**17**, δ: 16.1 (C-7), 59.0 (C-8), 34.8 (C-10), 129.3 (C-12), 128.8 (C-13), 127.7 (C-14); signals for C-2, C-4, C-5, C-6, and C-11 too weak for definitive assignment; (*E*)-17, δ: 15.4 (C-7), 56.9 (C-8), 34.8 (C-10), 129.3 (C-12), 128.8 (C-13), 127.7 (C-14); signals for C-2, C-4, C-5, C-6, and C-11 too weak for definitive assignment; hrms calcd. for $C_{13}H_{13}NS_2O_2$: 279.0342; found: 279.0341; ms, *m/z* (RI%): 279 (25) [M^+] and 91 (100).

*Photoisomerization of **5**, **6**, **7**, **10**, **14**, and **15** and isolation of (E)-**6**, (E)-**5**, and (E)-**15***

Photoisomerization of phenylmethylene oxazolones have been reported (11).

Irradiations were carried out in a Rayonet Photochemical reactor with 300-nm lighting.

On approximately 30-μmol scale, compounds **5**, **6**, **7**, **10**, **14**, and **15** were irradiated in 5-mm nmr tubes (4-mm id) in 0.5 mL $CDCl_3$. The isomerizations were monitored by ^{1}Hmr. Photostationary states were obtained after 2 days of irradiation, giving a 2:3 ratio of *E* to *Z* isomers for **5**, **6**, and **10** and a 1:2 ratio for **7** and **15**. Compound **14** required the presence of solid potassium carbonate for a photostationary state (with an *E* to *Z* ratio of 1:3). The same photostationary ratio of **14** was obtained on irradiation in petroleum ether. In all the irradiations, the two isomeric products were the only products observed as indicated by tlc and ^{1}Hmr spectroscopy.

On a preparative scale, pure (Z)-**6** (0.220 g, 0.898 mmol) was dissolved in 8 mL of chloroform and place din a 10-mm od tube (9-mm id) and irradiated for 26 h. Solvent was removed and flash chromatography (initially with 20% ethyl acetate in petroleum ether until elution of the *Z* isomer, then 30% ethyl acetate to elute the *E* isomer) gave 142 mg of recovered (Z)-**6** (65%) and 68 mg (*E*)-**6** (31%), both as pale yellow oils.

Similarly, when (Z)-**5** (0.148 g, 0.642 mmol) was irradiated for 18 h, 58.0 mg (39%) of pure (*E*)-**5** was obtained (mp 132.0–134.5°C from absolute ethanol, lit. (16) mp 136–138°C) with 84.8 mg (57%) (Z)-**5** recovered after flash chromatography (elution with 15% ethyl acetate – petroleum ether).

Similarly when (Z)-**15** (150.1 mg, 0.698 mmol) was irradiated for

6 h, 44.9 mg (30%) of pure (*E*)-**15** was obtained (as a pale yellow oil) with 98.0 mg (65%) (*Z*)-**15** recovered after flash chromatography (elution with 7.5% ethyl acetate − petroleum ether).

For these compounds, the following tlc data were obtained with ethyl acetate (shown as per cent) in petroleum ether: **6** (30%): R_f 0.15 (*E*), 0.47 (Z); **10** (30%): R_f 0.15 (*E*), 0.35 (Z); **14** (15%): R_f 0.19 (*E*), 0.53 (Z); **7** (20%): R_f 0.26 (*E*), 0.62 (Z); **15** (15%): R_f 0.28 (*E*), 0.51 (Z).

Compound (*E*)-**5** showed: ^{1}Hmr, δ: 1.43 (t, J = 7 Hz, 3H, ether CH_3), 2.51 (s, 3H, vinyl CH_3), 4.30 (q, J = 7 Hz, 2H, ethyl, CH_2), 7.36−7.53 (m, 3H, aromatic), and 7.92−8.07 (m, 2H, aromatic); ^{13}Cmr, δ: 155.8 (C-2), 118.5 (C-4), 168.7 (C-5), 163.9 (C-6), 15.8 (C-7), 66.4 (C-8), 15.2 (C-9), 126.7 (C-10), 127.2 (C-11), 128.7 (C-12), 131.6 (C-13).

Compound (*E*)-**6** showed: ir, ν_{max}: 1805 (s) (C=O), 1770 (s) (C=O), 1665 (s) (C=N), 1606 (m), 1588 (m) cm^{-1}; ^{1}Hmr, δ: 1.37 (t, J = 7 Hz, 3H, ethyl CH_3), 2.41 (s, 3H, vinyl CH_3), 3.80 (s, 2H, benzyl CH_2), 4.29 (q, J = 7 Hz, 2H, ethyl CH_2), 7.33 (br s, 5H, aromatic); ^{13}Cmr, δ: 158.4 (C-2), 117.4 (C-4), 168.2 (C-5), 164.1 (C-6), 15.9 (C-7), 66.3 (C-8), 15.2 (C-9), 35.8 (C-10), 134.2 (C-11), 128.8 (C-12), 129.1 (C-13), 127.3 (C-14); hrms calcd. for $C_{14}H_{15}NO_3$: 245.1052; found: 245.1057; ms: indistinguishable from that of (Z)-**6**.

Compound (*E*)-**7** showed: ^{1}Hmr, δ: 1.27 (s, 9H, *tert*-butyl), 1.40 (t, J = 7 Hz, 3H, ethyl CH_3), 2.43 (s, 3H, vinyl CH_3), 4.30 (q, J = 7 Hz, 2H, ethyl CH_2).

Compound (*E*)-**10** showed: ^{1}Hmr, δ: 2.53 (s, 3H, vinyl CH_3), 4.04 (s, 3H, OCH_3), 7.45−7.55 (m, 3H, aromatic), and7.98−8.15 (m, 3H, aromatic); ^{13}Cmr (acetone-d_6), δ: 165.2 (C-2),[a] 113.8 (C-4), 168.6 (C-5), 165.5 (C-6),[a] 16.8 (C-7), 68.8 (C-8), 14.9 (C-9), 33.6 (C-10), 26.9 (C-11); ((a), assignments may be reversed).

Compound (*E*)-**15** showed: ir, ν_{max}: 1704 (s) (C=O), 1608 (s) (C=N), and 1573 (s) (C=C) cm^{-1}; ^{1}Hmr, δ: 1.38 (t, J = 7 Hz, 6H, both ethyl CH_3's), 2.40 (s, 3H, vinyl CH_3), 4.20 (q, J = 7 Hz, 2H, vinyl CH_2); ^{13}Cmr (acetone-d_6), δ: 158.0 (C-2), 129.1 (C-4), 194.2 (C-5), 164.5 (C-6), 16.0 (C-7), 65.0 (C-8),[a] 14.8 (C-9), 65.4 (C-10),[a] 14.0 (C-11); ((a), assignments may be reversed); ms: indistinguishable from that of (Z)-**15**.

Attempted oxazolone isomerization with concentrated HBr; preparation of 2-(4-chlorophenyl)-4-(1-hydroxyethylidene)-5-oxazolone, 11

4-Phenylmethylene-5-oxazolone isomerization of Z to E geometry has been accomplished by the action of concentrated aqueous hydrobromic acid solution (8).

A mixture of the two isomers of **9** (33 mg, 0.12 mmol) as prepared directly from *N*-(4-chlorobenzoyl)glycine was suspended in 48% hydrobromic acid solution at 0°C. Anhydrous hydrogen bromide was bubbled into the solution. After 10 min, the compound completely dissolved and after hydrogen bromide saturation (another 10 min), the flask was stoppered and left in the refrigerator (−2°C) for 7 h. The resulting precipitate was filtered and washed with water and dried *in vacuo*, yielding 16.2 mg (55%) of a light yellow powdery solid (mp 204−205°C, melts and immediately evaporates) assigned structure **11**.

In a similar experiment, 5 min following dissolution of the azalactone, the solution was quenched by the addition of ice-water and 10% aqueous potassium carbonate. A precipitate was formed, which was extracted with dichloromethane, the dichloromethane layer dried over anhydrous sodium sulfate and then removed by rotoevaporation. The product on analysis by both tlc and ^{1}Hmr spectroscopy showed no (*E*)-**9**; ^{1}Hmr showed (Z)-**9** (approximately 90%) and **11** (approximately 10%).

Compound **11** showed: ir, ν_{max}: 1784 (s), 1607 (m), and 1560 (s) cm^{-1}; ^{1}Hmr (DMSO-d_6), δ: 2.39 (s, 3H, CH_3), 7.58 and 7.93 (AA′BB′, J_{ortho} = 9 Hz, 2H and 2H, aromatic); hrms calcd. for $C_{11}H_8NO_3Cl$: 237.0192; found: 237.0161; ms, m/z (RI%): 239 (10) and 237 (30) (M^+), 221 (2) and 219 (5) [$M^+ - H_2O$], 141 (30), 139 (100), 113 (10), 111 (30), and 75 (15).

Acknowledgements

We acknowledge, with thanks, financial support from the Natural Sciences and Engineering Research Council of Canada and the McMaster University Science and Engineering Research Board.

1. K. Brocklehurst, H. S. Price, and K. Williamson. Chem. Commun. 884 (1968).
2. A. P. Morgenstern, C. Schnitij, and W. T. Nauta. J. Chem. Soc. D, Chem. Commun. 321 (1969).
3. A. Maquestiau, Y. Van Haverbeke, and R. N. Muller. Bull. Soc. Chim. Belg. **83**, 259 (1974).
4. J. M. Riordan and C. H. Stammer. J. Org. Chem. **39**, 654 (1974).
5. A. G. Brown and T. C. Smale. J. Chem. Soc. D, Chem. Commun. 1489 (1969).
6. K. Brocklehurst, R. P. Bywater, R. A. Palmer, and R. Patrick. Chem. Commun. 632 (1971).
7. A. W. Hanson. Acta Crystallogr. Sect. B, **33**, 594 (1977).
8. Y. S. Rao and R. Filler. Synthesis, 749 (1975).
9. J. Plöchl. Chem. Ber. **16**, 2815 (1883).
10. E. Erlenmeyer. Ann. Chem. **275**, 1 (1893).
11. R. Filler and Y. S. Rao. Adv. Heterocycl. Chem. **21**, 175 (1977).
12. J. Sekacis, I. E. Khatskevich, J. Kalnina, and J. Pumpure. Latv. PSR Zinat. Akad. Vestis, Kim. Ser. 368 (1978); Chem. Abstr. **89** 162925v (1979).
13. C. Cativiela and E. Meléndez. Synthesis, 832 (1978).
14. P. Kumar, H. D. Mishra, and A. K. Mukerjee. Synthesis, 836 (1980).
15. J. W. Cornforth. *In* The chemistry of Penicillin. *Edited by* H. T. Clarke, J. R. Johnson, and R. Robinson. Princeton University Press, Princeton, NJ. 1949. pp. 688−848.
16. S. I. Lur'e and G. A. Ravdel. Dokl. Akad. Nauk SSSR, **83**, 97 (1952); Chem. Abstr. **47**, 2167f (1953).
17. S. I. Lur'e and G. A. Ravdel. Sb. Statei Obshch. Khim. Akad. Nauk SSSR, **1**, 498 (1953); Chem. Abstr. **49**, 1009e (1955).
18. (*a*) A. Buroway, M. Cais, J. T. Chamberlain, F. Liversedge, and A. R. Thompson. J. Chem. Soc. 3727 (1955); (*b*) H. G. Norment and I. L. Karle. Acta Crystallogr. **15**, 873 (1962); (*c*) C. Romers. Acta Crystallogr. **17**, 1287 (1964); (*d*) R. F. Childs, B. D. Dickie, R. Faggiani, C. A. Fyfe, C. J. L. Lock, and R. E. Wasylishen. J. Crystallogr. Spectrosc. Res. **15**, 73 (1985).
19. R. Gopal, W. D. Chandler, and B. E. Robertson. Can. J. Chem. **58**, 658 (1980).
20. R. F. Childs, R. Faggiani, C. J. L. Lock, and C. V. Rogerson. J. Org. Chem. **48**, 3043 (1983).
21. J. Dabrowski and M. Tencer. Bull. Chem. Soc. Jpn. **49**, 981 (1976).
22. F. W. Wehrli and T. Wirthlin. Interpretation of carbon-13 NMR spectra. Heyden and Son Ltd., London. 1976. pp. 39−40.
23. J. G. Batchelor. J. Magn. Reson. **18**, 212 (1975).
24. Th. J. de Boer and H. J. Backer. Recl. Trav. Chim. Pays-Bas, **73**, 229 (1954).
25. R. P. Hughes, N. Krishnamachari, C. J. L. Lock, J. Powell, and G. Turner. Inorg. Chem. **16**, 314 (1977).
26. B. Lippert, C. J. L. Lock, B. Rosenberg, and M. Zvagulis. Inorg. Chem. **16**, 1525 (1977).
27. D. T. Cromer and J. T. Waber. International tables for X-ray crystallography. Vol. IV. *Edited by* J. A. Ibers and W. C. Hamilton. Kynoch Press, Birmingham, England. 1974. Table 2.2B. pp. 99−101.
28. E. B. Knott. J. Chem. Soc. 1482 (1954).
29. A. H. Cook, G. Harris, I. Heilbron, and G. Shaw. J. Chem. Soc. 1056 (1948).
30. L. P. Kulev and G. M. Stepnova. Izvt. Sib. Otd. Akad. Nauk SSSR, 73 (1960); Chem. Abstr. **55**, 516f (1961).

31. A. H. COOK, I. HEILBRON, and A. L. LEVY. J. Chem. Soc. 201 (1948).
32. J. D. KENDALL, G. F. DUFFIN, and ILFORD LTD. Brit. Patent 633736 (1949); Chem. Abstr. **44**, 7175d (1950).
33. J. H. FORD. J. Am. Chem. Soc. **71**, 3842 (1949).
34. G. PROTA, F. CHIOCCARA, and A. PREVIERO. Biochimie, **53**, 51 (1971).
35. N. J. NOVELLO, S. R. MIRIAM, and C. P. SHERWIN. J. Biol. Chem. **67**, 555 (1926).
36. A. W. INGERSOLL and S. H. BABCOCK. Org. Synth. Coll. Vol. II. p. 328. 1943.
37. J. ATTENBURROW, D. F. ELIOTT, and G. F. PENNY. J. Chem. Soc. 310 (1948).
38. J. W. CORNFORTH. *In* Heterocyclic compounds. Vol. 5. *Edited by* R. C. Elderfield. John Wiley and Sons, New York. 1957. pp. 298–417.
39. J. M. STEWART. Tech. Rept. TR-446. Computer Science Centre, University of Maryland, College Park, Maryland. 1976.
40. G. M. SHELDRICK. SHELX. Program for crystal structure determination. Cambridge University, U.K. 1976.
41. C. K. JOHNSON. Report ORNL-5138. Oak Ridge National Laboratory, Oak Ridge, Tennessee. 1976.

COMMUNICATION

An analysis of bond length information for oxygen atoms adsorbed on well-defined metal surfaces

K. A. R. MITCHELL AND SUSAN A. SCHLATTER
Department of Chemistry, University of British Columbia, 2036 Main Mall, Vancouver, B.C., Canada V6T 1Y6

Received August 15, 1985

K. A. R. MITCHELL and SUSAN A. SCHLATTER. Can. J. Chem. **63**, 3631 (1985).

New bond valence – bond length relations deduced by Brown and Altermatt for solid state structures have been used for rationalizing O—M interatomic distances, measured by various surface crystallographic techniques, for O atoms chemisorbed on well-defined metal (M) surfaces. The advantages of this approach, over the Pauling–Schomaker–Stevenson approach used previously, are especially apparent for initial rationalizations of new information on the nearest-neighbor and next-nearest-neighbor bond lengths for O adsorbed on long-bridge sites of (110) surfaces of face-centered cubic metals.

K. A. R. MITCHELL et SUSAN A. SCHLATTER. Can. J. Chem. **63**, 3631 (1985).

On a utilisé les nouvelles relations entre les valences de liaison et les longueurs des liaisons qui ont été déduites par Brown et Atermatt pour des structures à l'état solide pour rationaliser les distances interatomiques O—M, mesurées par diverses techniques cristallographiques de surface, pour des atomes de O liés par chemisorption sur des surfaces métalliques (M) bien définies. Les avantages de cette approche, par rapport à celle de Pauling–Schomaker–Stevenson qui a été utilisée antérieurement, sont spécialement apparents lors des rationalisations initiales de nouvelles informations relatives à des longueurs de liaison avec le plus proche voisin ainsi que le suivant pour des O adsorbés sur des sites de surfaces (110) impliquant de longs ponts sur des métaux cubiques à face centrée.

[Traduit par le journal]

Introduction

An understanding of bond lengths in chemisorption is required as one step in the development of atomistic models of chemical processes at surfaces. A recent review of bond length data available from the methods of surface crystallography (e.g., LEED, SEXAFS, photoelectron diffraction and ion scattering) suggested that good levels of correspondence can now be reached when different techniques are applied to surfaces involving the chemisorption of atoms (X) on well-defined surfaces of metals (M) (1). Hitherto most discussions in the literature have related measured surface X—M interatomic distances to values obtained either by packing "hard spheres" of listed radii (2), or to values measured from other areas of structural chemistry (3), but without regard in either case to the actual structural arrangements or chemical bonding involved. Nevertheless the recent survey (1) by one of the present authors showed that many measured X—M interatomic distances can apparently be interpreted to a fair degree with bond order – bond length relations of the type used by Pauling in combination with the Schomaker–Stevenson approach for determining single bond lengths (4). The latter provides empirical evidence that the chemisorption bonding can, at least to a first approximation, be treated analogously to the chemical bonding schemes which are well-established in the other main categories of structural chemistry, namely discrete molecules and the triperiodic solid state. Even so, the match up between measured and predicted X—M surface bond lengths is not always satisfactory (1); in some instances this may be because of errors in the earlier experimental analyses, but in other cases (e.g., for O on the (111) surface of aluminum) the Pauling–Schomaker–Stevenson (PSS approach appears deficient.

This present paper explores a refinement to the earlier interpretation of surface bond lengths (1). The approach initiated here uses the bond length correlations proposed very recently by Brown and Altermatt (5) for particular combinations of oxygen and M atoms. Such systems were chosen for this exploratory purpose because some new surface structural data, which have just become available for oxygen chemisorption on (110) surfaces of face-centered cubic (fcc) metals, suggest that the PSS approach may be less reliable for discussing bond distances between O atoms and second-layer metal atoms (insufficient information was available previously for discussing this topic in ref. 1). Also the bond length relations just produced by Brown and Altermatt (5) cover most O—M combinations for which surface structural data are currently available.

Calculations

Brown and Altermatt (5) proposed the use of expressions with the form

$$[1] \quad r = r_0 - 0.85 \log s$$

for a particular interatomic distance of bond valence s, where r_0 is the corresponding distance for a bond of unit valence (6). These authors listed values of r_0 for various combinations of atoms as deduced from analyses of large amounts of structural information, especially from X-ray crystallography. When values of r_0 are given for more than one oxidation state of M that for the lowest state is taken for estimating surface bond distances. The specific values used are detailed in Table 1, where O—M interatomic distances measured by surface crystallographic techniques are compared with those predicted both with the PSS approach used in ref. 1 and with the approach of Brown and Altermatt. For the latter, in situations where inequivalent O—M bonds can occur, a range of O—M interlayer spacings is considered, and the favoured interlayer spacing is fixed (and correspondingly the predicted bond lengths) by the condition that the sum of bond valences at each O atom is two according to eq. [1]. The calculations reported in Table 1 assume the same adsorption site as reported in the structural determination; they also assume that the structure of the metal

TABLE 1. O—M interatomic distances predicted by both the PSS approach used in ref. 1 and by eq. [1], and compared with values measured by surface crystallography

			O—M distance (Å)		
Surface	n	r_0 (Å)[p]	PSS	Eq. [1]	Surface crystallography
Ag(110)	2	1.842	2.07	2.05	2.06[a]
	2		2.27	2.15	2.17[a]
Al(111)	3	1.651	1.97	1.80	1.79,[b] 1.81,[c] 1.76[d]
Co(100)	4	1.692	2.00	1.95	1.94[e]
Cu(100)	4	1.679	2.01	1.94	1.92,[f] 1.94[g]
Cu(110)	2	1.679	1.88	1.84	1.84[h]
	2		2.21	2.06	2.00[h]
Fe(100)	4	1.734	2.10	2.10	2.08[i]
	1		1.98	1.98	2.02[i]
Ni(100)	4	1.654	1.99	1.91	1.98,[j] 1.96[k]
Ni(110)	2	1.654	1.86	1.80	1.78[l]
	2		2.22	2.06	1.95[l]
Ni(111)	3	1.654	1.89	1.80	1.88[m]
W(110)	3	1.917	2.02	2.07	2.08[n]
Zr(0001)	6	1.928	2.39	2.33	2.31[o]

[a]Reference 7.
[b]Reference 8.
[c]Reference 9.
[d]Reference 10.
[e]Reference 11.
[f]Reference 12.
[g]Reference 13.
[h]Reference 14.
[i]Reference 15.
[j]Reference 16.
[k]Reference 17.
[l]Reference 18.
[m]Reference 19.
[n]Reference 20.
[o]Reference 21.
[p]Values from ref. 5 for use in eq. [1].

is neither reconstructed nor relaxed (except a relaxation is included for Zr(0001) where O is indicated (21) to incorporate into the metal structure, at least to the depth probed by LEED).

In Table 1, n indicates the number of O—M bonds of each type; for example, for adsorption on a hollow site of three-fold coordination on a fcc(111) surface there are three equal bond lengths, whereas for adsorption on the long-bridge sites of a fcc(110) surface two pairs of O—M bond lengths occur, corresponding to bonds from O to M atoms in the top metal layer and to those in the second metal layer. Various important adsorption geometries are illustrated in ref. 22.

Discussion

In most cases the use of eq. [1] with the tabulated values (5) for r_0 gives an encouraging correspondence to the O—M bond lengths measured by surface crystallography, although the predicted O—Ni values appear slightly short for both (100) and (111) surfaces. The advantages of the new relations over the PSS approach (1) are particularly noticeable for O adsorbed on the long-bridge sites of fcc(110) surfaces. The recent analyses with SEXAFS for O chemisorbed on Ag(110) (7) and Cu(110) (14) indicate that the surfaces remain unreconstructed on adsorption, however the structure with Ni(110) has been controversial (18). Initially O was believed to adsorb on the short-bridge site of the unreconstructed metal surface (19), but the then reported O—Ni distance of 1.91 Å is clearly inconsistent with the value (1.65 Å) from eq. [1] as well as that (1.75 Å) from the PSS approach. The recent experimental information for Ni(110) suggests that O adsorbs on the long-bridge sites, but with missing nickel atoms in alternate [001] rows of the top metal layer (18). The bond lengths reported for this surface in Table 1 are from a low-energy ion scattering experiment which indicates the O atoms are held 0.25 Å above the Ni surface. The driving force for the missing-row model presumably depends on strong O—Ni bonds being formed at the expense of neighboring Ni—Ni bonding in the topmost metal layer.

TABLE 2. O—M bond valences for O adsorbed on long-bridge sites and center sites of some fcc(110) surfaces[a]

M	Long-bridge		Center	
Ag	0.57(2)	0.43(2)	0.16(4)	1.37(1)
Cu	0.65(2)	0.35(2)	0.22(4)	1.12(1)
Ni	0.67(2)	0.34(2)	0.23(4)	1.08(1)

[a]The number of bonds of each type are given in parentheses. In each case the height of the adsorbed atom above the surface is chosen so that the sum of bond valences to O is 2 according to eq. [1].

For many examples in Table 1, the O atoms adsorb on those sites which provide maximum coordination and equal bond valences in the various bonds. However, a compromise appears necessary at the fcc(110) surfaces. At these surfaces, adsorption on a center site would enable bonding to four atoms in the topmost metal layer and to one in the second layer (total five), whereas on a long-bridge site, which is the favored site for the examples in Table 1, each O atom bonds to a total of just four M atoms. The data in Table 2 for O—M bond valences predicted with eq. [1] for these sites therefore suggest that more-balanced O—M bond valences in combination with a less-than-maximum coordination number for O (as for long-bridge site) is favored over the situation which combines less-balanced bond valences with the maximum coordination number (as for center site). As more structural data become available, such analyses should aid the development of insight into why particular adsorption sites are favored in individual cases (incidentally, in examples available so far, both S and Se appear to adsorb on the center sites of fcc(110) surfaces (1)).

In summary, this work indicates that the bond length – bond valence relations given by Brown and Altermatt have helpful applications to interpreting structural information for the chemisorption of oxygen on well-defined metal surfaces. Extensions to wider-ranging combinations of X and M, as suitable data become available for systematic study, may be useful for two purposes: (*i*) to discuss aspects of chemisorption bonding, especially in relation to the bonding occurring in similar bonds in the other more-established branches of structural chemistry; and (*ii*) to provide a framework for assessing the general reasonableness, or otherwise, of structural information as produced by the methods of surface crystallography.

Acknowledgements

We thank Dr. I. D. Brown for supplying information in ref. 5 prior to publication. We also gratefully acknowledge the support of this research provided by the Natural Sciences and Engineering Research Council of Canada.

1. K. A. R. MITCHELL. Surface Sci. **149**, 93 (1985).
2. P. M. MARCUS. *In* Characterization of metal and polymer surfaces. Vol. 1. Metal surfaces. *Edited by* L. H. Lee. Academic Press, New York. 1977.

3. M. A. VAN HOVE. *In* The nature of the surface chemical bond. *Edited by* T. N. Rhodin and G. Ertl. North-Holland, Amsterdam. 1978.
4. L. PAULING. The nature of the chemical bond. Cornell University Press, Ithaca, NY. 1960.
5. I. D. BROWN and D. ALTERMATT. Acta Crystallogr. B, **41**, 244 (1985).
6. I. D. BROWN. *In* Structure and bonding in crystals. Vol. 2. *Edited by* M. O'Keefe and A. Navrotsky. Academic Press, New York. 1981. p. 1.
7. A. PUSCHMANN and J. HAASE. Surface Sci. **144**, 559 (1984).
8. J. STÖHR, L. I. JOHANSSON, S. BRENNAN, M. HECHT, and J. N. MILLER. Phys. Rev. B, **22**, 4052 (1980).
9. F. SORIA, V. MARTÍNEZ, M. C. MUÑOS, and J. L. SACEDÓN. Phys. Rev. B, **24**, 6926 (1981).
10. D. NORMAN, S. BRENNAN, R. JAEGER, and J. STÖHR. Surface Sci. **105**, L297 (1981).
11. M. MAGLIETTA, E. ZANAZZI, U. BARDI, F. JONA, D. W. JEPSEN, and P. M. MARCUS. Surface Sci. **77**, 101 (1978).
12. J. G. TOBIN, L. E. KLEBANOFF, D. H. ROSENBLATT, R. F. DAVIS, E. UMBACH, A. G. BACA, D. A. SHIRLEY, Y. HUANG, W. M. KANG, and S. Y. TONG. Phys. Rev. B, **26**, 7076 (1982).
13. U. DÖBLER, K. BABERSCHKE, J. STÖHR, and D. A. OUTKA. Phys. Rev. B, **31**, 2532 (1985).
14. U. DÖBLER, K. BABERSCHKE, J. HAASE, and A. PUSCHMANN. Phys. Rev. Lett. **52**, 1437 (1984).
15. K. O. LEGG, F. JONA, D. W. JEPSEN, and P. M. MARCUS. Phys. Rev. B, **16**, 5271 (1977).
16. J. E. DEMUTH, D. W. JEPSEN, and P. M. MARCUS. Phys. Rev. Lett. **31**, 540 (1973); M. VAN HOVE and S. Y. TONG. J. Vacuum Sci. Technol. **12**, 230 (1975); G. HANKE, E. LANG, K. HEINZ, and K. MÜLLER. Surface Sci. **91**, 551 (1980).
17. J. STÖHR, R. JAEGER, and T. KENDELEWICZ. Phys. Rev. Lett. **49**, 142 (1982); S. Y. TONG, W. M. KANG, D. H. ROSENBLATT, J. G. TOBIN, and D. A. SHIRLEY. Phys. Rev. B, **27**, 4632 (1983).
18. H. NIEHUS and G. COMSA. Surface Sci. **151**, L171 (1985) and references therein.
19. P. M. MARCUS, J. E. DEMUTH, and D. W. JEPSEN. Surface Sci. **53**, 501 (1975).
20. M. A. VAN HOVE and S. Y. TONG. Phys. Rev. Lett. **35**, 1092 (1975).
21. K. C. HUI, R. H. MILNE, K. A. R. MITCHELL, W. T. MOORE, and M. Y. ZHOU. Solid State Commun. **86**, 83 (1985).
22. G. A. SOMORJAI. Chemistry in two dimensions: Surfaces. Cornell University Press, Ithaca, NY. 1981.